PERGAMON

Polyhedron 21 (2002) 1–6

POLYHEDRON

www.elsevier.com/locate/poly

Synthesis and spectroscopic characterisation of cobalt(III) complexes with *S*-benzyl-β-*N*-(5-methylpyrazole-3-yl)methylenedithiocarbazate (H_2L): X-ray structures of $[Co(HL)_2]NO_3 \cdot EtOH$ (**1**) and $[Co(HL)(L)] \cdot H_2O$ (**2**)

Pulakesh Bera [a], Ray J. Butcher [b], Siddhartha Chaudhuri [c], Nityananda Saha [a,*]

[a] *Department of Chemistry, University of Calcutta, 92 Acharya Prafulla Chandra Road, Kolkata 700009, India*
[b] *Department of Chemistry, Howard University, 2400 Sixth Street, N.W., Washington, DC 20059, USA*
[c] *RSIC, Bose Institute, Kolkata 700009, India*

Received 16 May 2001; accepted 6 September 2001

Abstract

Two new cobalt(III) complexes with *S*-benzyl-β-*N*-(5-methylpyrazole-3-yl)methylenedithiocarbazate (H_2L), $[Co(HL)_2]NO_3 \cdot EtOH$ (**1**) and $[Co(HL)(L)] \cdot H_2O$ (**2**), have been synthesised and characterised using single-crystal X-ray diffraction and spectroscopic (electronic, IR and NMR) techniques. The structure of **1** consists of $[Co(HL)_2]^+$ cation and NO_3^- anion linked by an ethanol solvent molecule, that of **2** consists of neutral monomeric species [Co(HL)(L)] with one mole water of crystallisation where the two ligand molecules are uniquely non-equivalent. In both the complexes the coordination geometry about cobalt is distorted octahedral and the two ligands are in the *mer* configuration (S and tertiary N atom *cis* to each other and the iminic N atoms *trans*). © 2002 Elsevier Science Ltd. All rights reserved.

Keywords: Co(III) complexes; Pyrazole; Dithiocarbazate; Synthesis; Spectroscopy; X-ray crystal structures

1. Introduction

Recent studies [1–4] have attempted a correlation between the structural nature of transition metal ion complexes of heterocyclic thiosemicarbazones and *S*-alkyl/aryl dithiocarbazates and their wide spectrum therapeutic uses. This has prompted further research in this specific area with the great expectation that structural variation of the ^{4}N substituent on the thiosemicarbazone moiety as well as modification of the heterocyclic ring might prove beneficial and will lead to dramatic enhancement of the biological activity of such new metal ion complexes which might also provide unique structural information. As a part of our comprehensive efforts [5–10] towards synthesis and structural characterisation of the new materials containing *N*-heterocycles with proven bioactivity, we report, herein, the synthesis, spectroscopy and crystallographic characterisation of two new cobalt(III) complexes with the title ligand (H_2L), viz. $[Co(HL)_2]NO_3 \cdot EtOH$ (**1**) and $[Co(HL)(L)] \cdot H_2O$ (**2**).

2. Experimental

All the materials used at different stages for the preparation of the cobalt(III) complexes reported were of GR/AR quality and were used without further purification. Spectrograde solvents were used for spectral and conductance measurements. Solvent DMSO-d_6 (Sigma) was used for recording NMR data.

* Corresponding author. Present address: University of Kalyani, 741235, India. Fax: +91-33-582-8282.
E-mail address: nsaha@cucc.ernet.in (N. Saha).

0277-5387/02/$ - see front matter © 2002 Elsevier Science Ltd. All rights reserved.
PII: S0277-5387(01)00933-0

2.1. Synthesis of ligand S-benzyl-β-N-(5-methylpyrazole-3-yl)methylenedithiocarbazate (H_2L)

The title ligand, H_2L (Fig. 1), has been synthesised and thoroughly characterised for the first time as reported earlier [7].

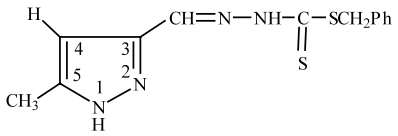


Fig. 1. *S*-Benzyl-β-*N*-(5-methylpyrazole-3-yl)methylenedithiocarbazate (H_2L).

Table 1
Crystal data and structural refinement parameters for **1** and **2**

	$[Co(HL)_2NO_3]\cdot$ EtOH (**1**)	$[Co(HL)(L)]\cdot H_2O$ (**2**)
Empirical formula	$C_{26}H_{26}CoN_8S_4\cdot NO_3\cdot C_2H_5OH$	$C_{26}H_{25}CoN_8S_4\cdot H_2O$
Formula weight	745.80	654.73
Temperature (K)	293(2)	293(2)
Wavelength (Å)	0.71073	0.71073
Crystal system	triclinic	monoclinic
Space group	$P\bar{1}$	$P2_1/c$
Unit cell dimensions		
a (Å)	8.484(10)	12.6215(10)
b (Å)	14.381(2)	15.1030(10)
c (Å)	14.522(2)	16.0430(10)
α (°)	89.940(10)	
β (°)	76.940(10)	103.690(10)
γ (°)	77.340(10)	
V (Å^3)	1681.8(4)	2971.2(4)
Z	2	4
D_{calc} (Mg m^{-3})	1.473	1.464
Absorption coefficient (mm^{-1})	0.807	0.894
$F(000)$	772	1352
Crystal size (mm)	$0.46\times0.10\times0.06$	$0.53\times0.41\times0.11$
θ Range for data collection (°)	1.43–22.38	2.14–27.50
Index ranges	$0\le h\le9$, $-15\le k\le15$, $-15\le l\le15$	$0\le h\le14$, $0\le k\le19$, $-20\le l\le20$
Reflections collected	4905	7080
Independent reflections	4394 $[R_{int}=0.0160]$	6549 $[R_{int}=0.0067]$
Absorption correction	empirical	empirical
Max. and min. transmission	0.9413 and 0.9202	0.8470 and 0.2683
Observed reflections	2660	6549
Number of parameters	488	469
Number of restraints	4	0
Goodness-of-fit on F^2	0.889	0.867
Final R indices $[I>2\sigma(I)]$	$R_1=0.0473$, $wR_2=0.0956$	$R_1=0.0464$, $wR_2=0.0842$
Largest difference peak and hole (e Å^{-3})	0.589 and −0.553	0.381 and −0.288

2.2. Synthesis of $[Co(HL)_2]NO_3\cdot EtOH$ (**1**)

To a boiling ethanolic solution (40 cm^3) of the ligand (0.29 g, 1 mmol) was added a solution (10 cm^3) of $Co(NO_3)_2\cdot6H_2O$ (0.14 g, 0.5 mmol) in the same solvent, followed by the addition of 0.5 cm^3 HNO_3 (1:1) to make the solution acidic (pH ~ 3); the mixture was stirred for 30 min in water-bath temperature. Upon slow evaporation, microcrystalline complex was obtained (ca. 80%). A recrystallisation from water–ethanol (1:14 v/v) afforded needle shaped reddish brown crystals.

2.3. Preparation of $[Co(HL)(L)]\cdot H_2O$ (**2**)

A hot ethanolic solution (30 cm^3) of the ligand (0.29 g, 1 mmol) was mixed with a solution of $CoBr_2\cdot6H_2O$ (0.16 g, 0.5 mmol) in the same solvent and the resulting clear reddish brown solution was stirred for 30 min around 90 °C. Upon slow evaporation, well-shaped crystals were obtained (yield: ca. 75%). The composition of the complex, as evidenced from elemental analyses, did not contain the expected bromide ion, and was established by X-ray analysis.

2.4. Physical measurements

Elemental analyses (C, H and N) were carried out at IACS, Kolkata with a Perkin–Elmer CHNS/O analyser 2400. The cobalt content of the complexes was determined gravimetrically as anhydrous $CoSO_4$. The molar conductance values of the complexes were measured in methanolic solution with a Systronics model 304 digital conductivity meter. The electronic spectra of the complexes in DMF solution (ca. 30 °C) were recorded in a Hitachi model UV 2000 spectrophotometer (250–1100 nm). IR spectra (4000–200 cm^{-1}) were recorded in a Perkin–Elmer model 833 infrared spectrophotometer with KBr pellets and magnetic measurements were made in the polycrystalline state in a PAR 155 sample vibrating magnetometer at IACS, Kolkata. NMR spectra were recorded in DMSO-d_6 with a Bruker AM300L(300 MHz) super conducting FTNMR.

2.5. Structure determination

Suitable crystals of **1** and **2** were used for X-ray diffraction data collection on a Siemens P4S diffractometer using Mo–Kα radiation. The relevant crystal data are summarised in Table 1. The data were corrected for Lorentz and polarisation effects and empirical absorption corrections were carried out using ψ-scan data of some selected reflections. The structures were solved by direct methods and refined by full-matrix least-squares based on $|F_{obs}|^2$ using the program SHELXL-97 [11]. The non-hydrogen atoms were refined

anisotropically while the hydrogen atoms, except those of a water molecule in structure **2**, were included in their idealised positions. The water hydrogen atoms in **2** were located from a difference electron density map and were restrained to maintain a fixed distance from the oxygen atom. Neutral atom scattering factors were taken from Cromer and Weber [12] and anomalous dispersion effects were included in F_{calc} [13].

3. Results and discussion

Satisfactory C, H and N analyses were obtained (Table 2) for both **1** and **2** for the empirical composition $C_{28}H_{32}CoN_9O_4S_4$ and $C_{26}H_{27}CoN_8OS_4$, respectively. Both the cobalt(III) complexes reported are diamagnetic at room temperature, while $[Co(HL)_2]NO_3{\cdot}EtOH$ (**1**) is an 1:1 electrolyte ($\Lambda_m = 78.2$ $\Omega^{-1}\,cm^2\,mol^{-1}$), the $[Co(HL)(L)]{\cdot}H_2O$ (**2**) is a non-electrolyte ($\Lambda_m = 17.0$ $\Omega^{-1}\,cm^2\,mol^{-1}$).

3.1. Vibrational, electronic and NMR spectra

Assignments of the selected characteristic IR bands of H_2L and its cobalt(III) complexes are given in Table 3. The characteristic IR bands (4000–200 cm^{-1}) for the free ligand (H_2L) when compared with those of its complexes provide significant indications regarding the bonding sites of the primary ligand molecule and the information are in conformity with our earlier results [7]. A negative shift in ν(C=N) (1580 cm^{-1}) in the spectrum of the free ligand to approximately 1560 cm^{-1} in its complexes is consistent with coordination of the azomethine nitrogen to the central cobalt(III) ion; the IR band at approximately 470 cm^{-1} is then assignable to ν(Co–N) [14]. A second band around 1600 cm^{-1}, assignable to ν(C=N) is expected in the spectra of the complexes, since the anionic ligand while coordinated to Co(III) generates a double bond between ^{2}N and ^{3}C (i.e. $-^1N-^2NH-^3C(S)-SCH_2Ph$) as the proton attached to ^{2}N atom of dithiocarbazate moiety is lost during complexation. An intensive strong band at 845 cm^{-1} in the free ligand spectrum is due to ν(C=S) which has been found to shift to lower frequency by ~ 50 cm^{-1} in the complexes, pointing to the coordination of the thiol sulfur to cobalt(III) atom; moreover, a new band at 375 and 390 cm^{-1} in complexes **1** and **2**, respectively, is assignable to ν(Co–S). The free ligand band at 1535 and 650 cm^{-1} assignable to the ν(C=N) (ring) and the inplane deformation of the pyrazole ring, respectively, are shifted to higher wave number ($\delta\nu = 25$ cm^{-1} in **1**, 40 cm^{-1} in **2** and $\delta\nu = 15$ cm^{-1} in **1**, 20 cm^{-1} in **2**, respectively); these data suggest that the tertiary ring nitrogen atom (^{2}N) as a possible bonding site in terms of earlier findings on crystallographic studies [7,15–18].

The electronic spectra (in DMF) of complexes **1** and **2** show bands (Table 3) in the regions 32 365–37 245 and 22 730–23 530 cm^{-1} and are attributed to intraligand charge transfer ($n \rightarrow \pi^*$) and d–d transition ($^1A_{1g} \rightarrow {}^1T_{2g}$) of a d^6 system, respectively [18]. However, diffuse reflectance spectra exhibit four bands in the region 8860–8895, 9650, 11 725 and 23 255–23 475 cm^{-1} which may be assigned as $^1A_{1g} \rightarrow {}^3T_{1g}$, $^1A_{1g} \rightarrow {}^3T_{2g}$, $^1A_{1g} \rightarrow {}^1T_{1g}$ and $^1A_{1g} \rightarrow {}^1T_{2g}$ transitions, respectively, in an octahedral symmetry.

Table 4 gives selected ^{1}H and ^{13}C NMR assignments for the ligand and the cobalt(III) complexes in order to compare the coordinated, anionic ligand species in the complex with the free ligand molecule (H_2L). The ^{1}H

Table 2
Colours, conductivity, magnetic moments and analytical data

Compound	Colour	Λ [a]	μ	%C found (calc)	%H found (calc)	%N found (calc)	%M found (calc)
$[Co(HL)_2]NO_3{\cdot}EtOH$	reddish brown	78.2	diamagnetic	45.0 (45.1)	4.3 (4.2)	17.0 (15.0)	7.8 (7.8)
$[Co(HL)(L)]{\cdot}H_2O$	reddish brown	17.0	diamagnetic	46.9 (47.7)	3.9 (4.1)	16.2 (17.1)	9.0 (9.1)

[a] Molar conductance ($\Omega^{-1}\,cm^2\,mol^{-1}$) of 10^{-3} M solution in DMF.

Table 3
Selected IR bands (cm^{-1}) and electronic spectral data for the cobalt(III) complexes

Compound	IR/far IR data (cm^{-1})						State	Electronic spectra ν (cm^{-1})
	ν_{NH}	$\nu_{C=N(azom)}$	$\nu_{N-N(pz)}$	$\nu_{Co-N(pz)}$	$\nu_{Co-N(azom)}$	ν_{Co-S}		
$[Co(HL)_2]NO_3{\cdot}EtOH$	3300–3200	1560	1030	270	470	370	Nujol	23 255; 11 725; 9650; 8860
							DMF	32 360; 23 530; 22 730
$[Co(HL)(L)]{\cdot}H_2O$	3300–3150	1560	1030	280	478	370	Nujol	23 475; 11 725; 9650; 8900
							DMF	37 240; 32 260; 23 530

Table 4
NMR data of ligand and its cobalt(III) complexes; values given (in δ ppm) relative to TMS

Compound	Imino proton	Pyrazole ring protons			Methine proton	Benzyl proton	^{13}C assignments		
		1	**4**	**5**(CH_3)			Thioamide carbon	Azomethine carbon	^{3}C (pyrazole)
H_2L	12.93, 8.81	13.20	6.31	2.21	7.41	4.45	202.0	136.6	142.5
$[Co(HL)_2]NO_3{\cdot}EtOH$	–	14.28	6.77	2.25	8.93	4.53	209.6	146.7	153.1
$[Co(HL)(L)]{\cdot}H_2O$	–	14.27	6.77	2.24	8.94	4.49	209.7	146.6	153.2

NMR spectra of the complexes (Table 4) when compared with those of the free ligand point out: (i) $-SCH_2-$ peak showing slightly downfield shift ($\delta =$ 4.45–4.53) is ascribed to coordination of the thiol sulfur to Co(III) resulting in reduced electron density at $-SCH_2-$; (ii) maximum downfield shift occurs with the methine proton appearing at approximately $\delta = 8.93$ in the complex molecule(s) corresponding to $\delta = 7.41$ ppm in the free ligand as expected due to coordination of the azomethine nitrogen to the central Co(III); and (iii) the shifting of ^{4}CH (the pyrazole ring) from $\delta = 6.77$ in the complexes is reasonable with the proposition that ^{2}N (pyrazole) coordinates with Co(III) ion. Comparison of the ^{13}C NMR spectra of the uncomplexed ligand with its cobalt complexes shows that the thioamide carbon shifts slightly downfield by $\delta = 7.6$ (e.g. $\delta = 202.0$ in free ligand to ca. $\delta = 209.6$ in complexes) showing a coordination through thioamide sulfur. The significant downfield shift occurs with azomethine carbon appearing at approximately $\delta = 146.7$ in the complex molecules corresponding to approximately $\delta = 136.6$ in the free ligand as expected due to coordination of the azomethine nitrogen to the central cobalt atom and the maximum downfield shifting of ^{3}C ring (pyrazole) carbon from $\delta = 142.5$ (free ligand) to approximately $\delta =$ 153.3 in complexes is quite reasonable with the proposition that neighbouring ^{2}N (pyrazole) coordinates strongly with the central atom.

3.2. Crystal structures of $[Co(HL)_2]NO_3{\cdot}EtOH$ (1) and $[Co(HL)(L)]{\cdot}H_2O$ (2)

ORTEP [19] diagrams of $[Co(HL)_2]NO_3{\cdot}EtOH$ (**1**) and $[Co(HL)(L)].H_2O$ (**2**) together with the atom numbering schemes are shown in Fig. 2 (a) and (b). In both the complexes the Co(III) atom is coordinated, as slightly distorted octahedron, to two deprotonated ligands through the thiol sulfur atoms [S(1A), S(1B)], the tertiary pyrazolyl nitrogen atoms [N(1A), N(1B)], and the hydrazinic nitrogen atoms [N(3A), N(3B)]. The crystallographic asymmetric unit in complex **1** consists of a $[Co(HL)_2]^+$ cation, a NO_3^- anion and a molecule of ethanol of crystallisation. The corresponding unit in complex **2** consists of a neutral [Co(HL)L] moiety and a molecule of water of crystallisation. During complexation in **2**, the secondary pyrazolyl nitrogen, N(2A), of one of the ligands has been deprotonated resulting in an extra negative charge which renders it unnecessary to have a counter anion like NO_3^- as in complex **1**, or as the Cl^- ion in another complex with the same ligand reported earlier [7]. The nitrate ion and the ethanol of crystallisation in complex **1** show some degree of disorder; two of the oxygen atoms of the nitrate group [O(1) and O(2)] and the carbon atoms [C(1S) and C(2S)] of the ethanol molecule vibrate between two alternate sets of positions, identified by the suffices A and B.

The bond distances and angles around the Co(III) atoms for both the complexes are shown in Table 5. In both complexes, two molecules (designated as A and B) of the tridentate *S*-benzyl-β-*N*-(5-methylpyrazole-3-yl)methylenedithiocarbazate ligand (H_2L) coordinate to the Co(III) atom to form four five-membered chelate rings [Co–S(1A)–C(5A)–N(4A)–N(3A), Co–S(1B)–C(5B)–N(4B)–N(3B), Co–N(1A)–C(3A)–C(4A)–N(3A) and Co–N(1B)–C(3B)–C(4B)–N(3B)].

The bond distances and angles involving the Co(III) atoms in both the complexes compare well with those observed in other similar structures [20–22]. The endocyclic angle N(1)–N(2)–C(1) in ligand A of complex **2** is 106.7(3)°; the corresponding angle in ligand B is 112.0(3)° while those in complex **1** are 111.2(4)° and 111.0(4)°, respectively. This clearly indicates the deprotonation of the secondary pyrazolyl ring nitrogen of ligand A in complex **2**. It is interesting to note that in complex **2**, the Co–N(1A) bond is approximately 0.02 Å shorter than the Co–N(1B) bond, this can be reasonably attributed to the stronger coordination of the harder base N(1A), owing to deprotonation of the adjacent N(2A), with the hard acid Co(III). As a corollary to this, the Co–S(1A) bond in complex **2**, which is *trans* to the Co–N(1A) bond [N(1A)–Co–S(1A) angle is 166.5(1)°], is observed to be shorter by approximately 0.03 Å than the Co–S(1B) bond.

In both the complexes, the two almost planar ligand molecules approach the central Co(III) atom in orthogonal orientation; the interligand diheral angle is

88.87(4)° in complex **1** and 87.70(4)° in complex **2**. The two azomethine nitrogen atoms [N(3A) and N(3B)] are *trans* to each other while the sulfur atoms [S(1A) and S(1B)] are in the *cis* position. The pyrazole rings, C(1)–C(2)–C(3)–N(1)–N(2), and the two five-membered chelate rings, Co–N(1)–C(3)–C(4)–N(3) and Co–S(1)–C(5)–N(4)–N(3), are individually planar with very small dihedral angles between the two planes. In complex **1**, the maximum dihedral angle of 7.5(1)° is between the pyrazole ring and its second neighbouring chelate ring, Co–S(1A)–C(5A)–N(4A)–N(3A); in complex **2**, the same pair of rings have the maximum dihedral angle of 6.0(1)°.

Table 6 gives the details of the hydrogen bonding patterns in the two structures. In complex **1**, the pyra-

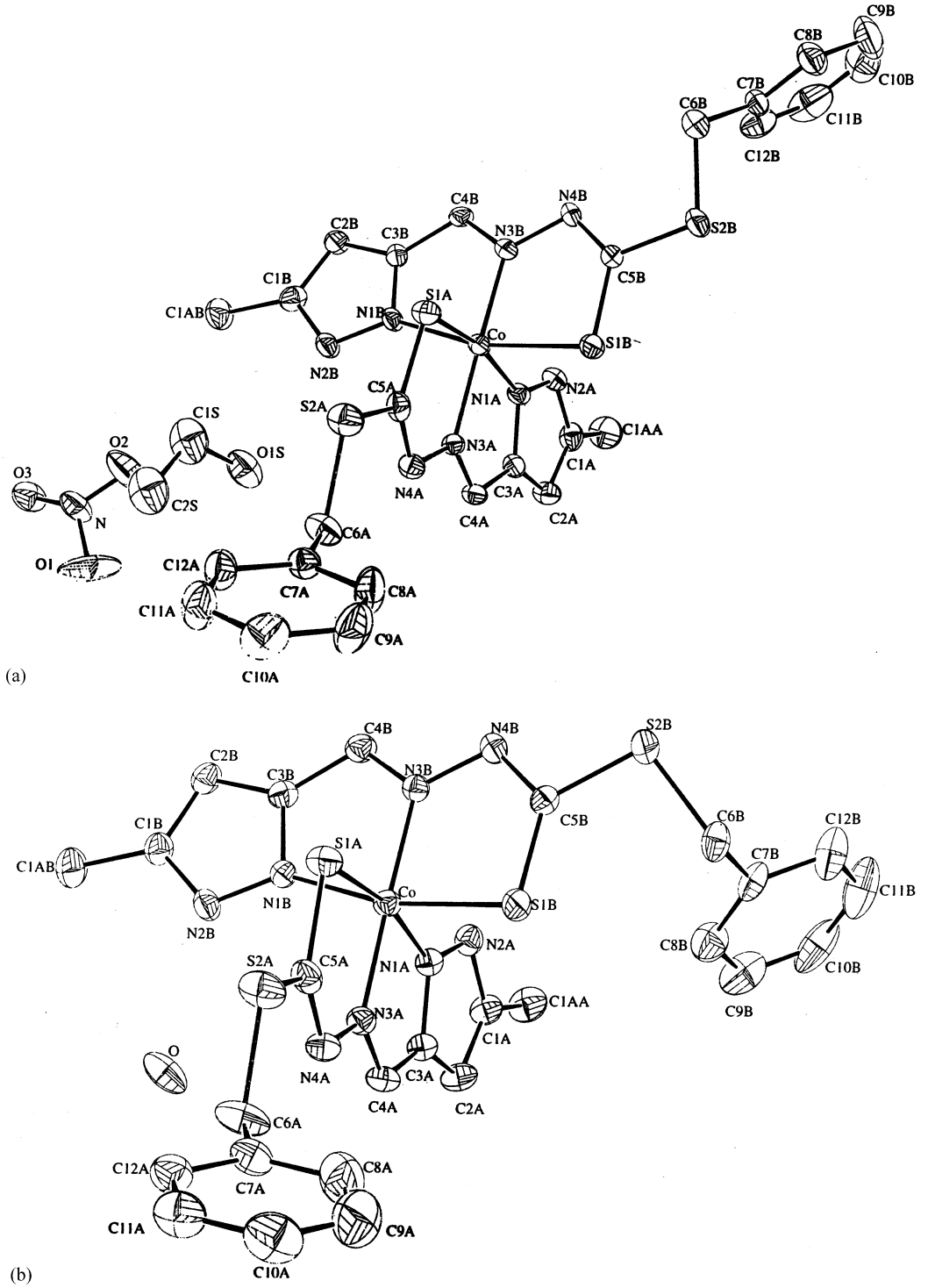


Fig. 2. (a) ORTEP diagram of $[Co(HL)_2]NO_3 \cdot EtOH$ (**1**) showing the atom labelling scheme. (b) ORTEP diagram of $[Co(HL)(L)] \cdot H_2O$ (**2**) showing the atom labelling scheme.

Table 5
Bond distances (Å) and bond angles (°) involving the Co(III) ions

	$[Co(HL)_2NO_3]\cdot EtOH$ (**1**)	$[Co(HL)(L)]\cdot H_2O$ (**2**)
Bond distances		
Co–N(1A)	1.964(4)	1.927(3)
Co–N(1B)	1.963(4)	1.945(3)
Co–N(3A)	1.901(4)	1.901(3)
Co–N(3B)	1.894(4)	1.901(3)
Co–S(1A)	2.234(2)	2.257(1)
Co–S(1B)	2.233(2)	2.220(1)
Bond angles		
N(3B)–Co–N(3A)	178.4(2)	177.2(1)
N(3A)–Co–N(1A)	80.8(2)	82.0(1)
N(3B)–Co–N(1A)	97.6(2)	95.2(1)
N(3B)–Co–N(1B)	81.1(2)	81.2(1)
N(3A)–Co–N(1B)	98.7(2)	99.0(1)
N(1A)–Co–N(1B)	92.0(2)	91.8(1)
N(3A)–Co–S(1B)	94.9(1)	94.3(1)
N(3B)–Co–S(1B)	85.3(1)	85.5(1)
N(1A)–Co–S(1B)	90.4(1)	90.1(1)
N(3B)–Co–S(1A)	96.0(1)	98.3(1)
N(1A)–Co–S(1A)	166.3(1)	166.5(1)
S(1B)–Co–S(1A)	89.7(6)	90.7(4)
N(1B)–Co–S(1B)	166.4(1)	166.7(1)
N(3A)–Co–S(1A)	85.6(1)	84.5(1)
N(1B)–Co–S(1A)	91.1(1)	90.5(1)

Table 6
Details of hydrogen bonding distances (Å) and angles (°)

D–H···A	D–H	D···A	H···A	∠D–H···A
Complex ***1***				
N(2B)–H(2B)···O(1S)	0.860(5)	2.777(9)	1.938(7)	164.7(4)
N(2A)–H(2A)···O(3) [a]	0.860(5)	2.844(6)	1.990(3)	171.6(3)
Complex ***2***				
N(2B)–H(2B)···O	0.860(3)	2.792(4)	1.936(3)	173.2(2)

[a] Symmetry equivalent: $-x, -y+1, -z+1$.

zolyl nitrogen atom N(2) of ligand A is the donor in a N–H···O hydrogen bond with the oxygen atom O(3) of the nitrate group, while the same atom of ligand B is the donor in a N–H···O hydrogen bond with the oxygen atom O(1S) of the solvent ethanol molecule. In complex **2**, the oxygen atom O of the water of crystallisation accepts a proton from the nitrogen atom, N(2), of the pyrazole ring of ligand B to form a N–H···O hydrogen bond.

4. Supplementary material

Crystallographic data for the structural analysis have been deposited with the Cambridge Crystallographic Data Centre, CCDC Nos. 153634 and 153635 for compounds **1** and **2**, respectively. Copies of this information may be obtained free of charge from The Director, CCDC, 12 Union Road, Cambridge, CB2 1EZ, UK (fax: +44-1223-336033; e-mail: deposit@ccdc.cam.ac.uk or www: http://www.ccdc.cam.ac.uk).

Acknowledgements

One of us (P.B.) is grateful to the Council of Scientific and Industrial Research (CSIR), New Delhi for the financial support (project 9/28(358)92/EMR-1) during the tenure of the work. The authors are also thankful to Professor (Mrs.) A. Chatterjee, Programme Coordinator, CAS on natural products, Calcutta University for providing NMR spectra and to Professor A. Patra of the Department of Chemistry, Calcutta University for useful discussion on NMR.

References

[1] M.A. Ali, S.E. Livingstone, Coord. Chem. Rev. 13 (1974) 101.
[2] W.K. Subsezynski, J.S. Hyde, D.H. Petering, J. Am. Chem. Soc. 109 (1987) 46.
[3] I. Haidu, G. Silvestru, Coord. Chem. Rev. 99 (1990) 253.
[4] D.X. West, S.B. Padhye, P.B. Sonawane, Struct. Bonding 76 (1991) 1.
[5] N. Saha, N. Mukherjee, Polyhedron 3 (1984) 1135.
[6] N. Saha, N. Mukherjee, Synth. React. Inorg. Met.-Org. Chem. 14 (1984) 1151.
[7] A. Mitra, T. Banerjee, P. Roychowdhury, S. Chaudhuri, P. Bera, N. Saha, Polyhedron 16 (1997) 3735.
[8] P. Bera, R.J. Butcher, N. Saha, Chem. Lett. (1998) 559.
[9] P. Bera, N. Saha, S. Kumar, D. Banerjee, R. Bhattacharya, Transition Met. Chem. 24 (1999) 425.
[10] N. Adhiikari, S. Chaudhuri, R.J. Butcher, N. Saha, Polyhedron 18 (1999) 1323.
[11] G.M. Sheldrick, SHELXL-97, Program for the Refinement of Crystal Structure, University of Göttingen, Göttingen, Germany, 1997.
[12] D.T. Cromer, J.T. Weber, International Tables for X-ray Crystallography, vol. IV, The Kynoch Press, Birmingham, England, 1994 (Table 2.2A).
[13] J.A. Ibers, W.C. Hamilton, Acta Crystallogr. 17 (1964) 781.
[14] D.X. West, C.S. Carlson, A.E. Liberta, J.P. Scovill, Transition Met. Chem. 15 (1990) 383.
[15] R.C. Agarwal, T.R. Rao, J. Inorg. Nucl. Chem. 40 (1978) 1177.
[16] J.R. Ferraro, Appl. Spectrosc. 23 (1969) 160.
[17] C.W. Reimann, A. Santoro, A.D. Mighell, Acta Crystallogr., Sect. B 26 (1970) 521.
[18] N. Saha, A. Saha, S. Chaudhuri, T.C.W. Mak, T. Banerjee, P. Roychowdhury, Polyhedron 11 (1992) 2341.
[19] L.J. Farrugia, J. Appl. Crystallgr. 30 (1997) 565 (ORTEP-3).
[20] M.B. Ferrari, G.G. Fava, M. Lanfranchi, C. Pelizzi, P.J. Tarasconi, J. Chem. Soc., Dalton Trans. (1991) 1951.
[21] A. Castineiras, D.X. West, H. Gebremedhin, T.J. Romack, Inorg. Chim. Acta 216 (1994) 229.
[22] M.B. Ferrari, G.G. Fava, G. Pelosi, M.C. Rodriguez-Arguelles, P. Tarasconi, J. Chem. Soc., Dalton Trans. (1995) 3035.

PERGAMON

Polyhedron 21 (2002) 7–17

POLYHEDRON

www.elsevier.com/locate/poly

Synthesis, reactivity, crystal and molecular structure of [5,14-dihydro-7,16-bis(2-oxo-3*H*-furan-5-yl)-6,8,15,17-tetramethyldibenzo[b,i][1,4,8,11]tetraazacyclotetradecinato(2-)-κ^4N]nickel(II)

Julita Eilmes [a,*], Marcin Ptaszek [a], Krzysztof Wozniak [b]

[a] *Department of Chemistry, Jagiellonian University, Ingardena 3, 30-060 Krakow, Poland*
[b] *Department of Chemistry, University of Warsaw, Pasteura 1, 02-093 Warsaw, Poland*

Received 4 June 2001; accepted 24 September 2001

Abstract

The reaction of the Ni(II) complex of 5,14-dihydro-6,8,15,17-tetramethyldibenzo[b,i][1,4,8,11]tetraazacyclotetradecine with succinyl dichloride leads to di- and monosubstituted derivatives bearing β,γ-unsaturated-γ-lactonic rings at the *meso* positions of the macrocycle. An aminolytic cleavage of these lactonic substituents gives rise to open-chain pendant groups containing the corresponding amide functions. A range of new complexes have been synthesized in this way with use of primary and secondary aliphatic and heterocyclic amines. The new products have been characterized by elemental analyses, ^{1}H, ^{13}C NMR, IR and ESI-MS spectral data. Single crystal X-ray studies revealed that the saddle-shaped molecules of [5,14-dihydro-7,16-bis(2-oxo-3*H*-furan-5-yl)-6,8,15,17-tetramethyldibenzo[b,i][1,4,8,11]tetraazacyclotetradecinato(2-)-κ^4N]nickel(II) act as receptors with molecules of toluene forming 1:1 supramolecular complexes. © 2002 Elsevier Science Ltd. All rights reserved.

Keywords: Dibenzotetraaza[14]annulenes; Macrocyclic Ni(II) complexes; Succinyl dichloride; Crystal structures; Solid state supramolecular complexes

1. Introduction

Recent studies on the chemistry of Ni(II) complexes of dibenzotetraaza[14]annulenes have revealed their diverse reactivity involving *meso* positions of the ring [1]. Some of these transformations were found to differ remarkably from that typical for the corresponding non-coordinated organic molecules [2–6]. These observations well support common opinion suggesting influence of the metal center on the coordinated ligand reactivity [7,8]

Herein we report on the metal center mediated reactivity of the dibenzotetraaza[14]annulene Ni(II) complex **1** towards succinyl dichloride, leading to *meso* di- and monosubstituted products, equipped with 2-oxo-3*H*-furan-5-yl substituents (**2a** and **2b**, Scheme 1). It has further been found that these β,γ-unsaturated-γ-lactonic groups easily undergo an aminolytic cleavage giving the open-chain amide-type pendant substituents. The procedure proved to be applicable to a wide variety of primary and secondary amines, thus showing its practical significance in the preparation of purpose-designed ligand superstructures. Schemes 1 and 2 outline the reactions performed.

Apart from being studied as fairly reactive coordinated ligands, dibenzotetraaza[14]annulene complexes have been recently appreciated as versatile supramolecular receptors. Thus, the host–guest inclusion complexes with toluene [9], benzene [10] as well as with molecules of C_{60} and C_{70} [11,12] have been described. In this paper we report crystallographic results showing

* Corresponding author. Tel.: +48-12-6336-377x2994; fax: +48-12-6340-515.
E-mail address: jeilmes@chemia.uj.edu.pl (J. Eilmes).

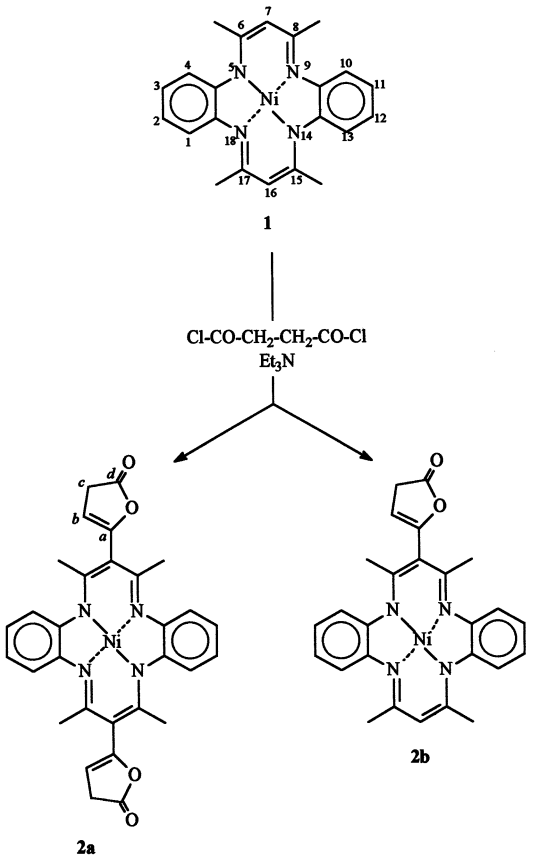
0277-5387/02/$ - see front matter © 2002 Elsevier Science Ltd. All rights reserved.
PII: S0277-5387(01)00962-7

that molecules of [5,14-dihydro-7,16-bis(2-oxo-3*H*-furan - 5 - yl) - 6,8,15,17 - tetramethyldibenzo[b,i][1,4,8,11]-tetraazacyclotetradecinato(2-)-κ^4N]Ni(II) (**2a**) forms the 1:1 solid state inclusion complex with molecules of toluene.

2. Experimental

2.1. Materials and equipment

Elemental analyses were performed with the use of an Euro-EA (EuroVector) microanalyser. The IR spectra were recorded in KBr and hexachlorobutadiene with a BRUKER IFS 48 spectrometer. ^{1}H and ^{13}C NMR spectra were run on a BRUKER AMX. instrument operating at 500 MHz, with TMS as internal standard. ESI-MS and MALDI-TOF spectra were taken on Finnigan MAT 95 and Voyager-Elite (PerSeptive Biosystems Inc.) mass spectrometers, respectively. The parent complex **1** was prepared by a procedure described in the literature [13]. All solvents were dried using standard methods and freshly distilled before use. Amines were purchased from commercial sources (Fluka, Aldrich) and used as received. 1-Ethoxycarbonylpiperazine was prepared according to Ref. [14]. Succinyl dichloride (Fluka) was distilled before use. Silica gel 60 (Fluka) (0.063–0.2 mm) and aluminum oxide 507 C (Fluka) were used for the column chromatography.



Scheme 1.

2.2. Synthesis of the complexes *2a* and *2b*

Succinyl dichloride (1 ml, 2.5 mmol) was added to a solution of the complex **1** (1 g, 2.5 mmol) and triethylamine (3 ml) in dry toluene (80 ml). The deep green reaction mixture was refluxed for 2 h with stirring and was protected from moisture. The reaction mixture was left aside to cool, triethylamine hydrochloride was filtered off and the filtrate was evaporated to dryness under reduced pressure. The green residue dissolved in a small quantity of methylene dichloride was chromatographed on a column of silica gel. Two fractions—the monosubstituted complex **2b** and the disubstituted **2a** were eluted successively using toluene–methylene chloride (1:1) and methylene dichloride–acetone (20:1) as eluents. The deep-violet crystals suitable for X-ray measurements were obtained by recrystallization of the complex **2a** from toluene.

2.3. Synthesis of the complexes *3–12* (general procedure)

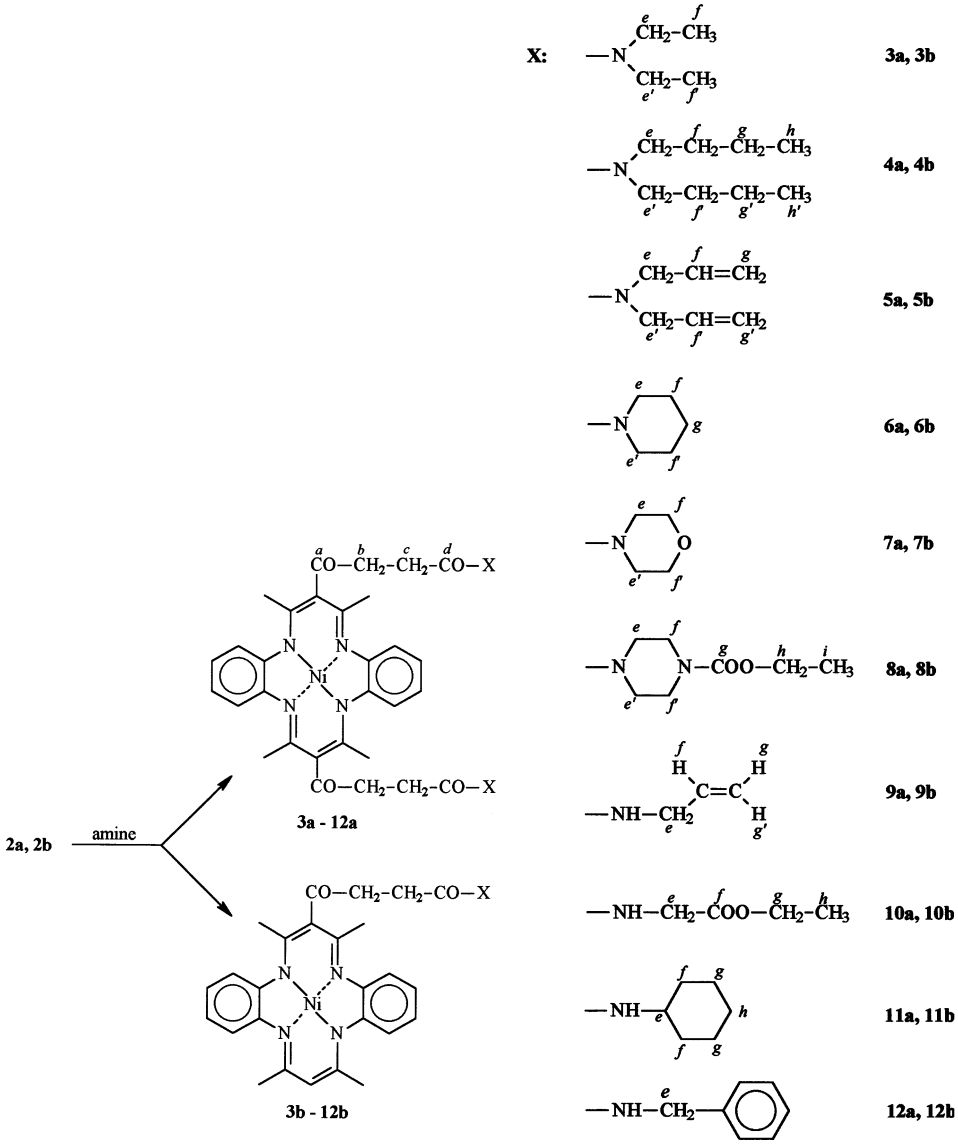
A deep green slurry consisting of the complex **2a** or **2b** (1 mmol), appropriate amine (10 mmol) and toluene (50 ml) was heated under gentle reflux for 1 h. Further procedures had to be adapted to the solubilities of the products, therefore two different methods have been employed.

Method A (for separation of the products **3**–**8** and **9b**–**12b**): the reaction mixture was evaporated to dryness under reduced pressure and the green residue was chromatographed on a column of Al_2O_3 using toluene–acetone (10:1) as eluent. The main fraction was separated to afford the corresponding amide-type product.

Method B (for separation of the products **9a**–**12a**): unlike the products described above, the disubstituted complexes **9a**–**12a** appeared in the reaction mixture as abundant, sparingly soluble, green precipitates. They were filtered off, washed thoroughly with toluene, acetone, water and acetone again. The green products thus obtained gave satisfactory results for elemental analyses.

2.4. Crystallography

Single crystal X-ray diffraction data were collected on a KUMA4CCD κ-axis diffractometer with the use of graphite monochromated Mo Kα radiation applying ω–2θ and ω scan techniques. The crystal was positioned at 65 mm from the KM4CCD camera. 576



Scheme 2.

frames were measured at 0.8° intervals with a counting time of 25 s. The data were corrected for Lorentz, polarization effects and variation of the reference frame. No absorption correction was applied. Data reduction and analysis were carried out with the Kuma diffraction (Wroclaw, Poland) programs. The structure was solved by direct methods [15] and refined using SHELXTL [16]. The refinement was based on F^2 for all reflections except those with very negative F^2. Weighted R factors wR and all goodness-of-fit S values are based on F^2. Conventional R factors are based on F with F set to zero for negative F^2. The $F_o^2 > 2s(F_o^2)$ criterion was used only for calculating R factors and is not relevant to the choice of reflections for the refinement. The R factors based on F^2 are about twice as large as those based on F. Anisotropic temperature factors were used to describe the thermal motions of non-hydrogen atoms (with the exception of toluene atoms). Most of the hydrogen atoms were located in idealized averaged geometrical positions, allowed to ride on the heavy atoms and rotate around C–C bonds. The toluene molecule is difficult to refine. Although its shape is clearly seen from differential maps we were unable to refine the carbon atoms using anisotropic ADPs. Additionally, we had to reduce atomic site occupation factors and constrain the ring. All this is due to really weak interactions of toluene with the host molecule. It tends to escape from crystals although the crystals seem to keep the structure and this is why some larger variation of reference frames (ca. 6% in total) had to be corrected for. Atomic scattering factors for C, H and O were derived from wave functions tabulated in Tables 6.1.1.4 and 4.2.4.2 from Ref. [17]. The average standard deviation for bonds is ca. 0.015 Å which means that

Table 1

Complex	Yield (%)	M.p. (°C)	Molecular formula	Molecular weight	Mass spectra (m/z)	IR ν (cm^{-1})	Elemental analysis (%)					
							Found			Calculated		
							C	H	N	C	H	N
2a	56	>330	$C_{30}H_{26}N_4O_4Ni$	564.19	565.5	1785 (C=O)	64.38	4.55	9.69	63.75	4.68	9.92
2b	30	>330	$C_{26}H_{24}N_4O_2Ni$	482.19	483.2	1798 (C=O)	64.36	5.23	11.38	64.63	5.00	11.59
3a	76	135	$C_{38}H_{48}N_6O_4Ni$	710.37	711.4	1693 (C^a=O), 1636 (C^d=O)	63.90	6.80	11.50	64.16	6.75	11.82
3b	75	132	$C_{30}H_{35}N_5O_2Ni$	555.28	556.0	1687 (C^a=O), 1630 (C^d=O)	64.41	6.36	12.35	64.78	6.30	12.60
4a	76	87	$C_{46}H_{64}N_6O_4Ni$	822.50	823.4	1692 (C^a=O), 1646 (C^d=O)	66.89	7.85	9.80	67.10	7.78	10.21
4b	72	130	$C_{34}H_{43}N_5O_2Ni$	611.34	612.3	1689 (C^a=O), 1637 (C^d=O)	66.50	7.17	11.10	66.73	7.03	11.44
5a	82	98	$C_{42}H_{48}N_6O_4Ni$	758.37	759.5	1692 (C^a=O), 1651 (C^d=O)	66.19	6.40	10.80	66.43	6.32	11.07
5b	83	102	$C_{32}H_{35}N_5O_2Ni$	579.28	580.2	1687 (C^a=O), 1643 (C^d=O)	66.03	5.90	11.77	66.24	6.08	12.08
6a	75	155–157	$C_{40}H_{48}N_6O_4Ni$	734.37	735.2	1687 (C^a=O), 1636 (C^d=O)	65.02	6.78	11.78	65.36	6.54	11.44
6b	73	178	$C_{31}H_{35}N_5O_2Ni$	567.28	568.1	1687 (C^a=O), 1630 (C^d=O)	65.27	6.23	12.13	65.53	6.16	12.33
7a	92	125–130	$C_{38}H_{44}N_6O_6Ni$	738.33	739.3	1692 (C^a=O), 1641 (C^d=O)	61.85	6.36	11.17	61.73	5.96	11.37
7b	88	174	$C_{30}H_{33}N_5O_3Ni$	569.26	570	1693 (C^a=O), 1630 (C^d=O)	63.00	5.80	12..01	63.24	5.80	12.30
8a	85	138	$C_{44}H_{54}N_8O_8Ni$	880.40	881.7 [a]	1693 (C^a=O), 1651 (C^d=O)	59.95	6.46	12.44	59.95	6.13	12.72
8b	82	200 (dec.)	$C_{33}H_{38}N_6O_4Ni$	640.29	641.4 [a]	1697 (C^a=O), 1651 (C^d=O)	61.62	6.00	12.90	61.81	5.93	13.11
9a	65	235	$C_{36}H_{40}N_6O_4Ni$	578.25	579.5 [a]	3264 (N–H), 1676 (C^a=O), 1636 (C^d=O)	63.82	6.12	12.41	63.64	5.93	12.37
9b	88	131	$C_{29}H_{31}N_5O_2Ni$	639.18	540.4 [a]	3340 (N–H), 1697 (C^a=O), 1646 (C^d=O)	64.17	5.90	12.78	64.47	5.78	12.96
10a	72	163	$C_{38}H_{44}N_6O_8Ni$	770.26	771.2	3264 (N–H), 1732 (C^f=O), 1671 (C^a=O), 1636 (C^d=O)	59.16	5.91	10.62	59.16	5.75	10.89
10b	81	116–118	$C_{30}H_{33}N_5O_4Ni$	585.19	586.3	3324 (N–H), 1747 (C^f=O), 1676 (C^a=O)	61.23	5.50	11.72	61.46	5.67	11.94
11a	70	242–244	$C_{42}H_{52}N_6O_4Ni$	762.34	763.2 [a]	3259 (N–H), 1681 (C^a=O), 1631 (C^d=O)	65.82	6.95	10.88	66.06	6.86	11.01
11b	79	187	$C_{32}H_{37}N_5O_2Ni$	581.23	581.3	3304 (N–H), 1697 (C^a=O), 1641 (C^d=O)	65.58	6.33	11.88	66.00	6.40	12.03
12a	71	229–231	$C_{44}H_{44}N_6O_4Ni$	778.28	780.1	3237 (N–H), 1687 (C^a=O), 1636 (C^d=O)	67.46	5.77	10.62	67.79	5.69	10.78
12b	83	215	$C_{33}H_{33}N_5O_2Ni$	590.3	590.3	3314 (N–H), 1692 (C^a=O), 1651 (C^d=O)	67.35	5.26	11.59	67.14	5.63	11.86

[a] MALDI-TOF.

Table 2

^{1}H NMR, δ (ppm), $CDCl_3$

Complex	Macrocycle	Succinedioyl	Amine
2a	2.14 (s, 12H, CH_3), 6.68 (m, AA′BB′, 8H, *o*-C_6H_4)	3.36 (d, $J = 2.3$ Hz, 4H, H^c), 5.44 (b.s., 2H, H^b)	
2b	2.08 (s, 6H, CH_3), 2.13 (s, 6H, CH_3), 4.83 (s, 1H, C^{16}-H), 6.58–6.67 (m, 6H, *o*-C_6H_4), 6.72 (m, 2H, *o*-C_6H_4)	3.35 (d, $J = 2.3$ Hz, 2H, H^c), 5.40 (t, $J = 2.2$ Hz, 1H, H^b)	
3a	2.04 (s, 12H, CH_3), 6.64 (m, AA′BB′ 8H, *o*-C_6H_4)	2.67 (t, $J = 6.3$ Hz, 4H, H^c), 3.17 (t, $J = 6.3$ Hz, 4H, H^b)	1.13 (t, $J = 7.1$ Hz, 6H, H^f), 1.24 (t, $J = 7.1$ Hz, 6H, $H^{f'}$), [3.39 (q, $J = 7.1$ Hz), 3.42 (q, $J = 7.1$ Hz), 8H, $H^{e,\ e'}$]
3b	2.03 (s, 6H, CH_3), 2.06 (s, 6H, CH_3), 4.82 (s, 1H, C^{16}–H), 6.54–6.61 (m, 4H, *o*-C_6H_4), 6.64 (d, $J = 7.8$ Hz, 2H, *o*-C_6H_4), 6.68 (d, $J = 7.8$ Hz, 2H, *o*-C_6H_4)	2.64 (t, $J = 6.3$ Hz, 2H, H^c), 3.14 (t, $J = 6.3$ Hz, 2H, H^b)	1.12 (t, $J = 7.1$ Hz, 3H, H^f), 1.25 (t, $J = 7.1$ Hz, 3H, $H^{f'}$), [3.40 (q, $J = 7.1$ Hz), 3.44 (q, $J = 7.1$ Hz) 4H, $H^{e,\ e'}$]
4a	2.02 (s, 12H, CH_3), 6.67 (m, AA′BB′, 8H, *o*-C_6H_4)	2.64 (t, $J = 6.3$ Hz, 4H, H^c), 3.14 (t, $J = 6.3$ Hz, 4H H^b)	0.91 (t, $J = 7.3$ Hz, 6H, H^h), 0.97 (t, $J = 7.3$ Hz, 6H, $H^{h'}$), 1.29 (m, 4H, H^g), 1.36 (m, 4H, $H^{g'}$), 1.50 (m, 4H, H^f), 1.62 (m, 4H, $H^{f'}$), 3.33 (m, 8H, $H^{e,\ e''}$)
4b	2.03 (s, 6H, CH_3), 2.07 (s, 6H, CH_3), 4.82 (s, 1H, C^{16}–H), 6.53–6.61 (m, 4H, *o*-C_6H_4), 6.64 (dd, $J_1 = 7.8$ Hz, $J_2 = 1.4$ Hz, 2H, *o*-C_6H_4), 6.69 (dd, $J_1 = 7.9$ Hz, $J_2 = 1.3$ Hz, 2H, *o*-C_6H_4)	2.64 (t, $J = 6.2$ Hz, 2H, H^c), 3.13 (t, $J = 6.1$ Hz, 2H, H^b)	0.91 (t, $J = 7.3$ Hz, 3H, H^h), 0.97 (t, $J = 7.3$ Hz, 3H, $H^{h''}$), 1.30 (m, 2H, H^g), 1.36 (m, 2H, $H^{g'}$), 1.50 (m, 2H, H^f), 1.62 (m, 2H, $H^{f'}$), [3.32 (t, $J = 6.8$ Hz), 3.34 (t, $J = 6.9$ Hz), 4H, $H^{e,\ e'}$]
5a	2.02 (s, 12H, CH_3), 6.62(m, AA′BB′, 8H, *o*-C_6H_4)	2.66 (t, $J = 6.2$ Hz, 4H, H^c), 3.15 (t, $J = 6.2$ Hz, 4H, H^b)	4.01 (dd, $J_1 = 4.1$ Hz, $J_2 = 1.5$ Hz, 8H, $H^{e,\ e'}$), 5.11–5.19 (m, 4H, H^g), 5.24 (m, 4H, $H^{g'}$), 5.77 (m, 2H, H^f), 5.85 (m, 2H, $H^{f'}$)
5b	2.03 (6H, s, CH_3), 2.07 (6H, CH_3), 4.83 (s, 1H, C^{16}–H), 6.56–6.60 (m, 4H, *o*-C_6H_4), 6.65 (dd, $J_1 = 7.80$ Hz, $J_2 = 1.2$ Hz, 2H, *o*-C_6H_4), 6.70 (dd, $J_1 = 7.9$ Hz, $J_2 = 1.1$ Hz, 2H, *o*-C_6H_4)	2.68 (3H, t, $J = 6.2$ Hz, H^c), 3.14 (3H, t, $J = 6.3$ Hz, H^b)	4.02 (4H, d, $J = 4.1$ Hz, H^e), 5.13–5.16 (m, 2H, H^g), 5.23–5.25 (m, 2H, $H^{g'}$), 5.76 (m, 1H, H^f), 5.84 (m, 1H, $H^{f'}$)
6a	2.03 (s, 12H, CH_3), 6.64 (m, AA′BB′, 8H, *o*-C_6H_4)	2.67 (t, $J = 6.4$ Hz, 4H, H^c), 3.14 (t, $J = 6.4$ Hz, 4H, H^b)	1.55 (m, 4H, H^g), 1.65 (m., 8H, $H^{f,\ f'}$), 3.50 (t, $J = 5.2$ Hz, 4H, H^e), 3.56 (t, $J = 5.5$ Hz, 4H, $H^{e'}$)
6b	2.04 (s, 6H, CH_3), 2.06 (s, 6H, CH_3), 4.81 (s, 1H, C^{16}–H), 6.54–6.61 (m, 4H, *o*-C_6H_4), 6.64 (d, $J = 7.8$ Hz, 2H, *o*-C_6H_4), 6.68 (d, $J = 7.7$ Hz, 2H, *o*-C_6H_4)	2.66 (t, $J = 6.4$, 2H, H^c), 3.13 (t, $J = 6.4$, 2H, H^b)	1.55 (m, 2H, H^g), 1.64 (m, 4H, $H^{f,\ f'}$), 3.50 (t, $J = 5.2$, 2H, H^e), 3.56 (t, $J = 5.5$, 2H, $H^{e'}$)
7a	2.04 (s, 12H, CH_3), 6.62 (m, AA′BB′, 8H, *o*-C_6H_4)	2.66 (t, $J = 6.2$ Hz, 2H, H^c), 3.16 (t, $J = 6.2$ Hz, H^b)	3.54 (m, 4H, H^e), 3.59 (m, 4H, $H^{e'}$), 3.68 (m, 4H, H^f), 3.74 (m, 4H, $H^{f'}$)
7b	2.04 (s, 6H, CH_3), 2.08 (s, 6H, CH_3), 4.84 (s, 1H, C^{16}–H), 6.54–6.60 (m., 4H, *o*-C_6H_4), 6.63 (d, $J = 7.8$ Hz, 2H, *o*-C_6H_4), 6.67 (d, $J = 7.4$ Hz, 2H, *o*-C_6H_4)	2.66 (t, $J = 6.2$, 2H, H^c), 3.15 (t, $J = 6.2$ Hz, 2H, H^b)	3.59 (m, 2H, H^e), 3.64 (m, 2H, $H^{e'}$), 3.68 (m, 2H, H^f), 3.72 (m, 2H, $H^{f'}$)
8a	2.02 (s, 12H, CH_3), 6.62 (m, AA′BB′, 8H, *o*-C_6H_4)	2.67 (t, $J = 6.1$ Hz, 4H, H^c), 3.18 (t, $J = 6.1$ Hz, 4H, H^b)	1.27 (t, $J = 7.1$ Hz, 6H, H^i), 3.47–3.62 (m, 16H, $H^{e–f}$), 4.18 (q, $J = 7.1$ Hz, 4H, H^h)
8b	2.03 (s, 6H, CH_3), 2.07 (s, 6H, CH_3), 4.82 (s, 1H, C^{16}–H), 6.55–6.62 (m, 4H, *o*-C_6H_4), 6.65 (dd, $J_1 = 7.8$ Hz, $J_2 = 1.3$ Hz, 2H, *o*-C_6H_4), 6.69 (dd, $J_1 = 7.9$ Hz, $J_2 = 1.2$ Hz, 2H, *o*-C_6H_4)	2.67 (t, $J = 6.1$ Hz, 2H, H^c), 3.14 (t, $J = 6.2$ Hz, 2H, H^b)	1.28 (t, $J = 7.1$ Hz, 3H, H^i), 3.45–6.63 (m, 8H, $H^{e–f}$), 4.16 (q, $J = 7.1$ Hz, 2H, H^h)
9a	1.98 (s, 12H, CH_3), 6.64 (m, AA′BB′, 8H, *o*-C_6H_4)	2.54 (t, $J = 6.0$ Hz, 6H, H^c), 3.13 (t, $J = 6.0$ Hz, 6H, H^b)	3.91 (m, 4H, H^e), 5.15 (d, $J = 10.0$ Hz, 2H, H^g), 5.27 (d, $J = 17.8$ Hz, 2H, $H^{g'}$), 5.82 (b.s. 2H, N–H), 5.85 (m, 2H, H^f)
9b	1.99 (s, 6H, CH_3), 2.07 (s, 6H, CH_3), 4.82 (s, 1H, C^{16}H), 6.57 (m, 4H, *o*-C_6H_4), 6.64 (d, $J = 7.8$ Hz, 2H, *o*-C_6H_4), 6.69 (d, $J = 7.8$ Hz, 2H, *o*-C_6H_4)	2.53 (t, $J = 6.1$ Hz, 2H, H^c), 3.10 (t, $J = 6.2$ Hz, 2H, H^b)	3.89 (dd, $J_{He–NH} = 5.6$ Hz, $J_{He–Hf} = 5.6$ Hz, 2H, H^e), 5.13 (dd, $J(H^g–H^f) = 10.3$ Hz, $J(H^g–H^{g'}) = 1.2$ Hz, 1H, H^g), 5.22 (dd, $J(H^{g'}–H^f) = 17.2$ Hz, $J(H^{g'}–H^g) = 1.3$ Hz, 1H, $H^{g'}$), 5.82 (b.s, 1H, N–H), 5.65 (m, 1H, H^f)

Table 2 (*Continued*)

Complex	Macrocycle	Succinedioyl	Amine
10a	1.99 (s, 12H, CH_3), 6.63 (m, AA′BB′, 8H, *o*-C_6H_4)	2.60 (t, $J = 6.3$ Hz, 4H, H^e), 3.11 (t, $J = 6.3$ Hz, 4H, H^b)	1.29 (t, $J = 7.2$ Hz, 6H, H^h), 4.04 (d, $J = 5.2$ Hz, 4H, H^e), 4.22 (q, $J = 7.1$ Hz, 4H, H^g), 6.24 (b.s, 2H, N–H)
10b	2.00 (s, 6H, CH_3), 2.07 (s, 6H, CH_3), 4.82 (s, 1H, C16–H), 6.62 (m, 4H, *o*-C_6H_4), 6.64 (dd, $J_1 = 7.8$ Hz, $J_2 = 1.1$ Hz, 2H, *o*-C_6H_4), 6.72 (dd, $J_1 = 7.4$ Hz, $J_2 = 1.0$ Hz, 2H, *o*-C_6H_4)	2.59 (t, $J = 6.2$ Hz, 2H, H^e), 3.11 (t, $J = 6.3$ Hz, 2H, H^b)	1.29 (t, $J = 7.1$ Hz, 3H, H^h), 4.05 (d, $J = 5.1$ Hz, 2H, H^e), 6.28 (b.s., 1H, N–H)
11a	1.98 (s, 12H, CH_3), 6.62 (m, AA′BB′, 8H, *o*-C_6H_4)	2.48 (t, $J = 6.0$ Hz, 4H, H^e), 3.10 (t, $J = 6.0$ Hz, 4H, H^b)	1.16 (m, 8H, CH_2), 1.35 (m, 4H, CH_2), 1.71 (m, 4H, CH_2), 1.90 (m, 4H, CH_2), 3.75 (m, 2H, H^e), 5.64 (d, $J = 7.1$ Hz, 2H, N–H)
11b	2.02 (s, 6H, CH_3), 2.08 (s, 6H, CH_3), 4.82 (s, 1H, $C^{16}H$), 6.55 (m, 4H, *o*-C_6H_5), 6.63 (dd, $J_1 = 7.8$ Hz, $J_2 = 1.3$ Hz, 2H, *o*-C_5H_4), 6.68 (dd, $J_1 = 7.9$ Hz, $J_2 = 1.1$ Hz, 2H, *o*-C_6H_4)	2.47 (t, $J = 6.1$ Hz, 2H, CH_2), 3.08 (t, $J = 6.2$ Hz, 2H, H^b),	1.15 (m, 2H, CH_2), 1.34 (m, 2H, CH_2), 1.60 (m, 4H, CH_2), 1.88 (m 2H, CH_2), 3.74 (m, 1H, H^e), 5.68 (d, $J = 8.1$ Hz, 1H, N–H)
12a	1.96 (s, 12H, CH_3), 6.63 (m, AA′BB′, 8H, *o*-C_6H_4)	2.56 (t, $J = 6.1$ Hz, 4H, H^e), 3.15 (t, $J = 6.1$ Hz, 4H, H^b)	4.46 (d, $J = 5.7$ Hz, 4H, H^e), 6.05 (b.s, 2H, N–H) 7.31 (m, 10H, C_6H_5)

most of the differences between bonds is within the level of errors.

$C_{30}H_{26}N_4O_4Ni{\cdot}C_7H_8$ (**2a**), formula weight = 657.39; temperature = 293 K; wavelength = 0.71073 Å; monoclinic; space group *Cc*; unit cell dimensions: $a = 25.252(5)$ Å, $b = 9.394(2)$ Å, $c = 15.356(3)$ Å, $\beta = 120.21(3)°$, $V = 3148(1)$ Å^3; $Z = 4$; $D_{calc} = 1.387$ Mg m^{-3}; absorption coefficient = 0.664 mm^{-1}; $F(000) = 1376$; crystal size = 0.20 × 0.25 × 0.30 mm; theta range for data collection = 3.65–21°; index ranges: $-25 \leq h \leq 25$, $-9 \leq k \leq 9$, $-15 \leq l \leq 15$; reflections collected = 15695; independent reflections = 3349 [$R_{int} = 0.0418$]; refinement method: full-matrix least-squares on F^2; data/restraints/parameters = 3349/3/368; goodness-of-fit on $F^2 = 1.100$; final R indices [$I > 2\sigma(I)$]: $R_1 = 0.0728$, $wR_2 = 0.1583$; R indices (all data): $R_1 = 0.2106$, $wR_2 = 0.0794$, largest difference peak and hole = 0.41 and −0.55 e A^{-3}.

3. Results and discussion

3.1. Syntheses

The reaction of the complex **1** and succinyl dichloride in a 1:3 molar ratio was performed in boiling toluene in the presence of triethylamine. In this way the di- and monosubstituted products **2a** and **2b** were obtained in 56 and 15% yields, respectively (Scheme 1). A 1:1 molar ratio of the reagents gave rise to the mixture of approximately equal amounts of the parent complex **1**, di- and monosubstituted products **2a** and **2b**. Aminolysis was accomplished by refluxing of the complexes **2a** and **2b** in toluene with an excess of the appropriate amines for 1 h to afford amide products in yields ranging from 65 to 92%. Analytical data and physical properties of the new complexes **2**–**12** are collected in Table 1.

Succinyl dichloride, similarly to other dicarboxylic acid dichlorides, is commonly considered to be a typical difunctional electrophilic reagent, often used in organic synthesis as a powerful linker in the preparation of dimers and polymeric products [18,19]. However, we have recently observed anomalous behavior of oxalyl dichloride in the reaction with dibenzotetraaza[14]annulene Ni(II) complexes [5]. The key step of the mechanism was postulated to involve a chloro-α-dioxo intermediate, formed as a result of electrophilic attack of oxalyl dichloride at the methine position of the macrocycle. Reactivity of this intermediate was found to be crucial for the final product formation.

Our experiments with succinyl dichloride showed that reaction with the complex **1** led to monomeric products **2a** and **2b**, equipped with β,γ-unsaturated-γ-lactonic rings at the *meso* positions. The reaction seems to proceed via a two-step mechanism involving acylation of the *meso* methine carbon by one of two electrophilic centers of succinyl dichloride, followed by intramolecular *O*-acylation within chlorosuccinoyl groups. Enolization of the ketomethylene part of the chlorosuccinoyl group presumably takes place prior to the lactonic ring closure. The procedure used was found to give a reasonable yield without recourse to the high dilution technique. Moreover, the reaction failed when applied to the corresponding dibenzotetraza[14]annulene ligand, allowing the starting material only to be recovered from the reaction mixture. In view of the above, we suppose that the metal center promotion takes place in the course of the reaction. It seems reasonable to believe in this case again, that reactivity of the open-chain monoacylated intermediate is essential for the

Table 3

^{13}C NMR, δ (ppm), $CDCl_3$

Complex	Macrocycle	Succinedioyl	Amine
2a	20.22 (CH_3), 109.43 (C^7, C^{16}), 121.87, 122.86, 147.29 (o-C_6H_4), 156.53 (C=N)	34.95 (C^c), 106.46 (C^b), 156.90 (C^a), 176.95 (C=O)	
2b	20.47 (CH_3), 21.79 (CH_3), 109.31 (C^7), 111.20 (C^{16}), 120.82, 121.71, 122.00, 123.04, 147.20, 147.46 (o-C_6H_4), 155.36, 155.42 (C=N)	34.99 (C^c), 106.26 (C^b), 157.02 (C^a), 177.06 (C=O)	
3a	19.75 (CH_3), 121.65, 122.59 (o-C_6H_4), 124.39 (C^7, C^{16}), 147.31 (o-C_6H_4), 152.46 (C=N)	26.73 (C^c), 40.36 (C^b), 170.48 (C^d=O), 208.8 (C^a=O)	13.05 (C^f), 14.22 ($C^{f'}$), 41.97 (C^e), 42.03 ($C^{e'}$)
3b	19.91 (CH_3), 21.77 (CH_3), 111.20 (C^{16}), 120.79, 121.67, 121.72 (o-C_6H_4), 124.11 (C^7), 147.21, 147.30 (o-C_6H_4), 152.49, 155.30 (C=N)	26.71 (C^c), 40.33 (C^b), 170.50 (C^d=O), 209.0 (C^a=O)	13.05 (C^f), 14.21 ($C^{f'}$), 41.95 (C^e), 42.02 ($C^{e'}$)
4a	19.79 (CH_3), 121.69, 122.62 (o-C_6H_4), 124.44 (C^7, C^{16}), 147.35 (o-C_6H_4), 152.49 (C=N)	26.84 (C^c), 42.16 (C^b), 170.89 (C^d=O), 208.86 (C^a=O)	13.82 (C^h), 13.85 ($C^{h'}$), 20.14 (C^g), 20.25 ($C^{g'}$), 29.90 (C^f), 31.05 ($C^{f'}$), 45.94 (C^e), 47.70 ($C^{e'}$)
4b	19.92 (CH_3), 21.77 (CH_3), 111.20 (C^{16}) 120.80, 121.69, 121.74, 122.73 (o-C_6H_4), 124.13 (C^7) 147.22, 147.34 (o-C_6H_4), 152.52, 155.30 (C=N)	26.82 (C^c), 42.12 (C^b), 170.90 (C^d=O), 209.05 (C^a=O)	13.82 (C^h), 13.88 ($C^{h'}$), 20.14 (C^g), 20.17 ($C^{g'}$), 30.88 (C^f), 31.08 ($C^{f'}$), 45.92 (C^e), 47.76 ($C^{e'}$)
5a	19.65 (CH_3), 121.55, 122.54 (o-C_6H_4), 124.20 (C^7, C^{16}), 147.18 (o-C_6H_4), 152.34 (C=N)	26.62 (C^b), 41.88 (C^c), 171.64 (C^d=O), 208.53 (C^a=O)	48.01 (C^e), 49.20 ($C^{e'}$), 116.58 (C^g), 116.87 ($C^{g'}$), 132.71 (C^f), 133.02 ($C^{f'}$)
5b	19.93 (CH_3), 21.76 (CH_3), 111.25 (C^{16}), 120.83, 121.73, 121.78, 122.79 (o-C_6H_4), 124.14 (C^7) 147.29, 147.41 (o-C_6H_4), 152.60, 155.31 (C=N)	26.83 (C^b), 42.05 (C^c), 171.62 (C^d=O), 208.80 (C^a=O)	48.19 (C^e), 49.37 ($C^{e'}$), 116.72 (C^g), 117.00 ($C^{g'}$), 132.95 (C^f), 133.24 ($C^{f'}$)
6a	19.94 (CH_3), 121.66, 122.63 (o-C_6H_4), 124.45 (C^7, C^{16}), 147.32 (o-C_6H_4), 152.45 (C=N)	26.80 (C^c), 41.97 (C^b), 169.58 (C^d=O), 208.81 (C^a=O)	24.55 (C^g), 25.52 (C^f), 26.37 ($C^{f'}$), 42.92 (C^e), 46.49 ($C^{e'}$)
6b	19.95 (CH_3), 21.90 (CH_3), 111.25 (C^{16}), 120.83, 121.70, 121.75, 122.77 (o-C_6H_4), 124.17 (C^7), 147.24, 147.36 (o-C_6H_4), 152.51, 155.33 (C=N)	26.81 (C^c), 41.96 (C^b), 169.64 (C^d=O), 209.02 (C^a=O)	24.56 (C^g), 25.53 (C^f), 26.38 ($C^{f'}$), 42.92 (C^e), 46.50 ($C^{e'}$)
7a	19.75 (CH_3), 121.69, 122.72 (o-C_6H_4), 124.30 (C^7, C^{16}), 147.29 (o-C_6H_4), 152.49 (C=N)	26.57 (C^c), 41.73 (C^b), 170.2 (C^d=O), 208.44 (C^a=O)	42.17 (C^e), 45.90 ($C^{e'}$), 66.56 (C^f), 66.83 ($C^{f'}$)
7b	19.53 (CH_3), 21.50 (CH_3), 111.21 (C^{16}), 120.73, 121.38, 122.45(o-C_6H_4), 123.88 (C^7), 147.13, 147.28 (o-C_6H_4), 152.40, 155.27 (C=N)	26.46 (C^c), 41.64 (C^b), 170.16 (C^d=O), 208.53 (C^a=O)	42.05 (C^e), 45.80 ($C^{e'}$), 66.45 (C^f), 66.70 ($C^{f'}$)
8a	19.76 (CH_3), 121.69, 122.73 (o-C_6H_4), 124.27 (C^7, C^{16}), 147.30 (o-C_6H_4), 152.46 (C=N)	26.77 (C^c), 41.58 (C^b), 170.20 (C^d=O), 208.45 (C^a=O)	14.62 (C^i), 41.78 (C^e), 43.52 (C^f, $C^{f'}$), 45.24 ($C^{e'}$), 61.68 (C^h), 155.38 (C^g=O)
8b	19.76 (CH_3), 21.73 (CH_3), 111.25 (C^{16}), 120.82, 121.04, 121.71, 122.83 (o-C_6H_4), 123.90 (C^7), 147.21, 147.36 (o-C_6H_4), 152.49, 155.34 (C=N)	26.79 (C^c), 41.56 (C^b), 170.21 (C^d=O), 208.64 (C^a=O)	14.58 (C^i), 41.71 (C^e), 43.48 (C^f, $C^{f'}$), 45.24 ($C^{e'}$), 61.54 (C^h), 155.34 (C^g=O)
9a	19.75 (CH_3), 121.75, 122.83 (o-C_6H_4), 123.80 (C^7, C^{16}), 147.31 (o-C_6H_4), 152.82 (C=N)	30.46 (C^c), 42.04 (C^b), 171.51 (C^d=O), 209.20 (C^a=O)	42.16 (C^e), 116.40 (C^g), 134.15 (C^f)
9b	19.91 (CH_3), 20.61 (CH_3), 111.30 (C^{16}), 120.89, 121.78, 122.93 (o-C_6H_4), 123.84 (C^7), 147.20, 147.40 (o-C_6H_4), 152.47, 155.42 (C=N)	30.48 (C^c), 40.02 (C^b), 171.58 (C^d=O), 209.17 (C^a=O)	42.18 (C^e), 116.35 (C^g), 134.14 (C^f)
10a	19.77 (CH_3), 124.10 (C^7, C^{16}), 121.71, 122.79, 147.24 (o-C_6H_4), 152.46 (C=N)	30.00 (C^c), 41.51(C^b), 171.81 (C^d=O) 208.58 (C^a=O)	14.14 (C^h), 41.85 (C^e), 61.54 (C^g), 169.89 (C^f=O)
10b	19.91 (CH_3), 21.77 (CH_3), 111.29 (C^{16}), 120.86, 121.77, 122.90, 147.21, 147.40 (o-C_6H_4), 152.53, 155.40 (C=N)	30.11 (C^c), 41.52 (C^b), 171.87 (C^d=O), 208.88 (C^a=O)	14.13 (C^h), 41.89 (C^e), 61.46 (C^g), 169.87 (C^f=O)
11a	19.76 (CH_3), 121.72, 122.80 (o-C_6H_4), 124.17 (C^7, C^{16}), 147.27 (o-C_6H_4), 152.43 (C=N)	30.72 (C^c), 42.34 (C^b), 170.70 (C^d=O), 209.05 (C^a=O)	24.81 (C^h), 25.54 (C^g), 33.10 (C^f), 48.26 (C^e)
11b	19.90 (CH_3), 21.80 (CH_3), 111.26 (C^{16}), 120.86, 121.74, 122.89 (o-C_6H_4), 123.81 (C^7), 147.15, 147.34 (o-C_6H_4), 152.39, 155.38 (C=N)	30.71 (C^c), 42.34 (C^b), 170.76 (C^d=O), 209.3 (C^a=O)	24.79 (C^h), 25.51 (C^g), 33.06 (C^f), 48.20 (C^e)
12a [a]			
12b	19.86 (CH_3), 21.80 (CH_3), 111.27 (C^{16}), 120.86, 121.74, 122.89 (o-C_6H_4), 123.71 (C^7), 147.13, 147.34 (o-C_6H_4), 152.39, 155.38 (C=N)	29.65 (C^c), 42.15 (C^b), 171.64 (C^d=O), 209.2 (C^a=O)	43.65 (C^e), 127.42, 127.72, 128.67, 138.24 (C_6H_5)

[a] Compound sparingly soluble in organic solvents.

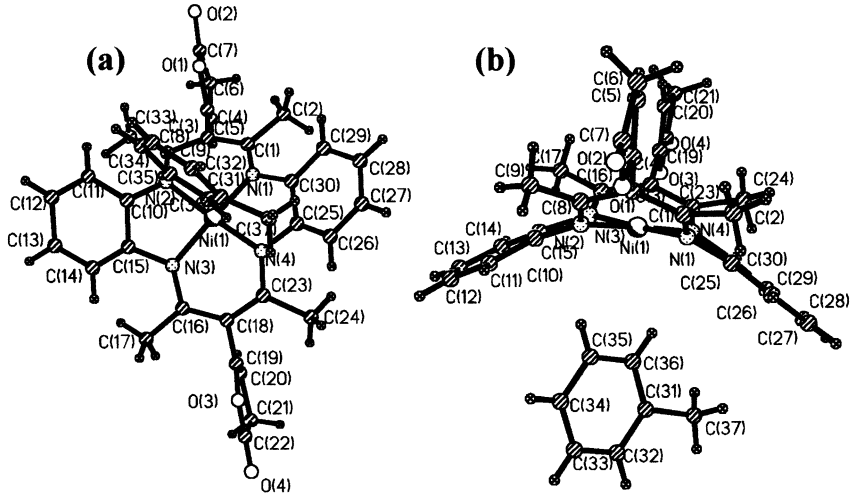


Fig. 1. Two projections of the complex **2a**—labelling of non-hydrogen atoms. Hydrogen atom label numbers are the same as the ones carried by their parental carbons.

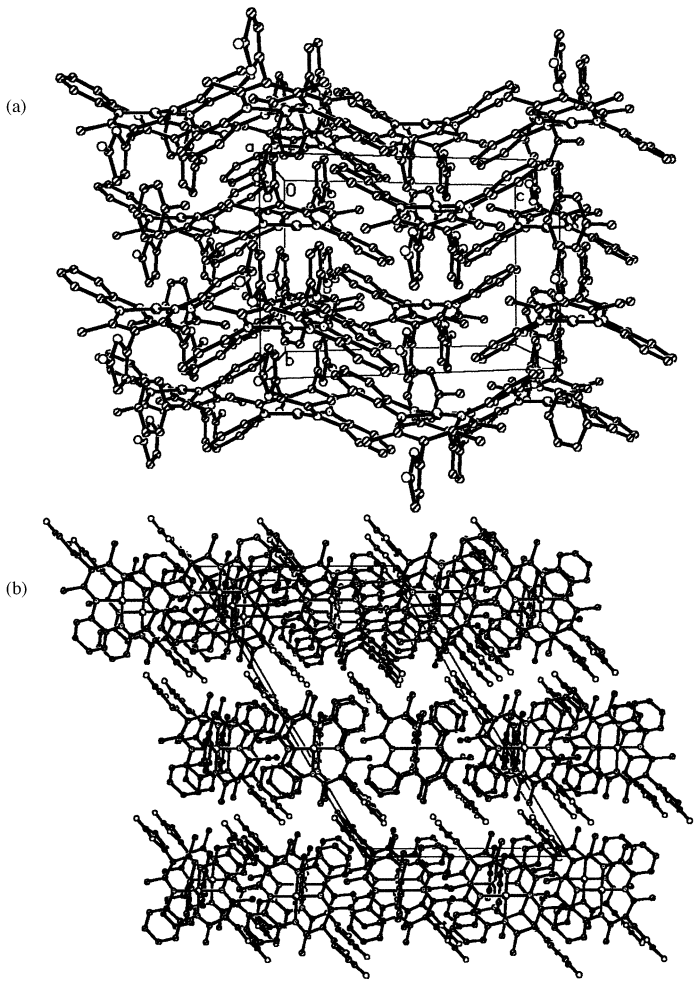


Fig. 2. 3D packing of molecules in the crystal lattice of **2a**: (a) view along the *X*-axis, (b) view along the *Y*-axis. Hydrogen atoms omitted for clarity.

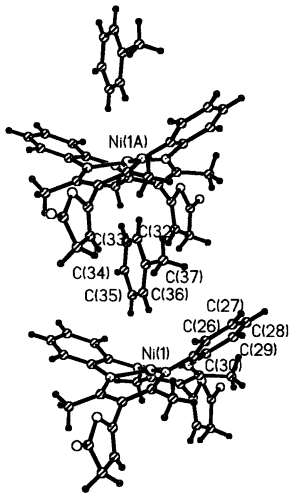


Fig. 3. Columns formed by **2a** and toluene molecules. Hydrogen atoms omitted for clarity.

formation of the final product. One could assume further that intramolecular interactions of pendant chlorosuccinoyl groups with the metal center prevents the intermolecular acylation that could result in a polymer formation. The saddle-like structure of the macrocyclic ring seems to additionally enhance this tendency. Such reasoning, taking into account the metal center role, is in fact not very far from that presented by Collman [20] and Nonhebel and Smith [21] in their first papers on the acylation of transition metal β-diketonates. It should be mentioned here that we have already reported similar reactivity involving glutaryl dichloride [6] and that analogous intramolecular lactonization was also observed in the metal centered reaction of both succinyl and glutaryl dichlorides with molybdenum and tungsten organometallic complexes [22].

The new complexes **3**–**12** have been synthesized in the course of the reactions of the products **2a** and **2b** with primary and secondary amines. The reaction can be explained in terms of nucleophilic attack of the base on the carbonyl carbon within the *meso* substituents of the macrocycle. The β,γ-unsaturated-γ-lactones are known to be susceptible to aminolytic cleavage usually leading to the open-chain amides [23,24], although pyrrolidine derivatives have also been isolated in some cases in the reactions with primary amines [25,26]. Our experiments showed the first type of the reactivity to be unique for the lactonic substituents of the complexes **2a** and **2b**. The open-chain amide-type derivatives **3**–**12** have been achieved in fair yields ranging from 65 to 92%. The structure assignment of the new complexes is based on elemental analyses, ^{1}H and ^{13}C NMR, IR and MS data. The ^{1}H and ^{13}C NMR signals and their detailed assignments as well as analytical, MS and IR data of the products **2**–**12** are summarized in Tables 1–3.

Table 5
Selected bond lengths (Å) and valence angles (°)

Bond lengths			
Ni(1)–N(1)	1.79(1)	Ni(1)–N(4)	1.81(1)
Ni(1)–N(2)	1.87(1)	Ni(1)–N(3)	1.89(1)
N(1)–C(1)	1.34(2)	N(1)–C(30)	1.41(2)
N(2)–C(8)	1.29(2)	N(2)–C(10)	1.41(2)
N(3)–C(16)	1.36(2)	N(3)–C(15)	1.46(2)
N(4)–C(23)	1.37(2)	N(4)–C(25)	1.43(2)
O(1)–C(7)	1.41(2)	O(1)–C(4)	1.43(2)
O(2)–C(7)	1.27(2)	O(3)–C(22)	1.38(2)
O(3)–C(19)	1.39(2)	O(4)–C(22)	1.12(2)
C(1)–C(3)	1.44(2)	C(3)–C(8)	1.41(2)
C(3)–C(4)	1.47(2)	C(4)–C(5)	1.34(2)
C(5)–C(6)	1.41(2)	C(6)–C(7)	1.48(3)
C(16)–C(18)	1.39(2)	C(18)–C(23)	1.38(2)
C(18)–C(19)	1.51(2)	C(19)–C(20)	1.25(2)
C(20)–C(21)	1.52(2)	C(25)–C(30)	1.33(2)
Valence angles			
N(1)–Ni(1)–N(4)	83.7(6)	N(1)–Ni(1)–N(2)	93.4(6)
N(4)–Ni(1)–N(3)	94.8(5)	N(2)–Ni(1)–N(3)	88.1(6)
C(7)–O(1)–C(4)	106(1)	C(22)–O(3)–C(19)	107(2)
N(1)–C(1)–C(3)	122(1)	C(8)–C(3)–C(1)	124(1)
C(5)–C(4)–O(1)	108(1)	C(4)–C(5)–C(6)	114(2)
C(5)–C(6)–C(7)	101(1)	O(1)–C(7)–C(6)	110(1)
N(2)–C(8)–C(3)	118(1)	N(2)–C(10)–C(15)	117(1)
C(10)–C(15)–N(3)	111(1)	N(3)–C(16)–C(18)	118(1)
C(23)–C(18)–C(16)	127(1)	C(20)–C(19)–O(3)	115(1)
C(19)–C(20)–C(21)	107(1)	C(22)–C(21)–C(20)	103(1)
O(3)–C(22)–C(21)	108(1)	N(4)–C(23)–C(18)	124(1)
C(30)–C(25)–N(4)	111(1)		

3.2. Crystallography

The crystal structure of [5,14-dihydro-7,16-bis(2-oxo-3*H* - furan - 5 - yl) - 6,8,15,17 - tetramethyldibenzo[b,i]-

Table 4
The least-square planes and angles between them

Nu	Atoms defining the best plane	Angle between planes	Angle (°)
1	C1, C3, C8	1 and 2, 1 and 3	92.5, 76.5
2	O1, C4, C5, C6, C7	2 and 4	2.0
3	C16, C18, C23	3 and 4	90.2
4	C19, C20, C21, C22		
5	C10, C11, C12, C13, C14, C15	5 and 6	64.5
6	C25, C26, C27, C28, C29, C30		
7	N1, N2, N3, N4, Ni1	7 and 1, 7 and 2, 7 and 3, 7 and 4, 7 and 5, 7 and 6	41.5, 90.0, 35.0, 91.9, 33.3, 31.2

[1,4,8,11]tetraazacyclotetradecinato(2-)-κ^{4}N]Ni(II) toluene solvate (**2a**·toluene) crystallizes in the monoclinic *Cc* space group with one molecule in the independent part of the unit cell. The molecule adopts a saddle-shaped conformation in which phenylene rings and pentanediiminato fragments are tilted in opposite directions to relieve steric constrain (Fig. 1). The distortion from planarity is typical of 6,8,15,17-substituted dibenzotetraaza[14]annulenes and their metal complexes [27–29]. The structure consists of columns of stacked molecules **2a**, mixed with the molecules of toluene locked in cavities formed by the host moieties (Figs. 2 and 3). The molecules of toluene are well fitted sitting at the top of one saddle host molecule along N2–Ni1–N4 bonds and being topped by the other one—the closest in the stack. The nearest C(toluene)···Ni contacts are close to 3.5 Å. All Ni–N bond lengths are quite typical ranging from 1.79 to 1.89 Å. Also the values of the valence angles around the central Ni ion are close to 90° (from 84 up to 95°). The geometry of the saddle is defined by a number of angles between the best planes calculated for particular molecular fragments. It appears that the angle between the aromatic rings and the central planar N1N2N3N4Ni1 fragment is equal approximately 32°, whereas the C1C3C11 and C18C25C26—the other walls of cavities—have angles equal to 41.5 and 35° with the central NNNNNi plane. The best planes of the lactonic rings are almost perpendicular to the delocalized fragments of the macrocyclic ring and the central NNNNNi fragment. The atoms defining the best least-squares planes as well as the angles between them are defined in Table 4. Numerical values of the most important structural parameters are given in Table 5.

The 'upper' and 'lower' halves of the molecule **2a** (as seen in the Fig. 1) appeared to differ slightly. This seems likely to be due to asymmetric intermolecular interactions involving the guest molecule (toluene) (in particular weak CH···N and CH···π bonds). The most striking differences in the bond lengths are those for C1C3, C3C8 and C16C18, C18C23. The first pair of bonds being approximatley 1.41 and 1.44 Å whereas the other pair are equal to 1.39 and 1.39 Å. Also the possibly symmetric bonds to the nitrogens are different (C1N1 = 1.34 and N2C8 = 1.29 Å whereas the topologically equivalent bonds to N3 and N4 are equal to 1.36 and 1.37 Å, respectively. Furthermore, the β,γ-unsaturated-γ-lactonic *meso* substituents have different C=O (1.27 and 1.12 Å) and double C=C bonds (1.34 and 1.25 Å).

4. Conclusions

The reaction of the Ni(II) complex of dibenzotetraaza[14]annulene **1** with succinyl dichloride afforded new derivatives equipped with β,γ-unsaturated-γ-lactonic groups at the *meso* positions. The intramolecular cyclization of the succinoyl groups seems to involve a metal-center mediated mechanism, supported additionally by the non-planar conformation of the macrocyclic framework. The lactonic substituents of **2a** and **2b** proved to be useful synthons of amide-type ligand superstructure. The X-ray crystallography showed that the saddle-shaped molecules of **2a** form solid state 1:1 supramolecular complexes with toluene.

5. Supplementary material

Crystallographic data (excluding structural factors) for the structure reported in this paper have been deposited with the Cambridge Crystallographic Data Centre, CCDC No. 157217. Copies of this information may be obtained free of charge from The Director, CCDC, 12 Union Road, Cambridge, CB2 1EW, UK (fax: +44-1233-336-033; e-mail: deposit@ccdc.cam.ac.uk or www: http://www.ccdc.cam.ac.uk).

Acknowledgements

This work was supported by the grant BW/44/2001 from the Jagiellonian University. The X-ray measurements were performed at the Crystallographic Unit of the Physical Chemistry Laboratory at the Chemistry Department of the University of Warsaw.

References

[1] P. Mountford, Chem. Soc. Rev. 27 (1998) 105 and references therein.
[2] M.C. Weiss, G.C. Gordon, V.L. Goedken, J. Am. Chem. Soc. 101 (1979) 857.
[3] P. Kofod, P. Moore, N.W. Alcock, H.J. Clase, J. Chem. Soc., Chem. Commun. (1992) 1261.
[4] L. Giannini, E. Solari, S. De Angelis, T.R. Ward, C. Floriani, A. Chiesi-Villa, C. Rizzoli, J. Am. Chem. Soc. 117 (1995) 5801.
[5] J. Eilmes, M. Ptaszek, K. Zielinska, Polyhedron 20 (2001) 143.
[6] J. Eilmes, Polyhedron 6 (1987) 423.
[7] C.J. Hipp, D.H. Busch, in: A.E. Martell (Ed.), Coordination Chemistry, Ch. 2–3, vol. 2, ACS Monographs 174, Washington, DC, 1978.
[8] E.C. Constable, Metals and Ligand Reactivity, Ch. 4–5, VCH, Weinheim, 1996.
[9] P.C. Andrews, J.L. Atwood, L.J. Barbour, P.D. Croucher, P.J. Nichols, N.O. Smith, B.W. Skelton, A.H. White, C.L. Raston, J. Chem. Soc., Dalton Trans. (1999) 2927.
[10] J. Eilmes, O. Michalski, K. Wozniak, Inorg. Chim. Acta 317 (2001) 103.
[11] P.C. Andrews, J.L. Atwood, L.J. Barbour, P.J. Nichols, C.L. Raston, Chem. Eur. J. 4 (1998) 1384.
[12] P.D. Croucher, J.M.E. Marshall, P.J. Nichols, C.L. Raston, Chem. Commun. (1999) 193.
[13] F.A. L'Eplattenier, A. Pugin, Helv. Chim. Acta 58 (1975) 917.

[14] T.S. Moore, M. Boyle, V.M. Thorn, J. Chem. Soc. (1929) 39.
[15] G.M. Sheldrick, Acta Crystallogr., Sect. A 46 (1990) 467–473.
[16] G.M. Sheldrick, SHELXL-93. Program for the Refinement of Crystal Structures, University of Göttingen, Germany.
[17] A.J.C. Wilson (Ed.), International Tables for Crystallography, vol. C, Kluwer, Dordrecht, 1992.
[18] H.A. Staab, Chem. Ber. 90 (1957) 1326.
[19] J. Baker, W. Hodges, J.W. Timberlake, J. Heterocycl. Chem. 20 (1983) 855.
[20] J.P. Collman, Angew. Chem., Int. Ed. Eng. 4 (1965) 132.
[21] D.C. Nonhebel, J. Smith, J. Chem. Soc. (C) (1967) 1919.
[22] A. Wong, R.L. Morgan, J.M. Golder, G.E. Quimbita, R.V. Pawlick, Organometallics 8 (1989) 844.
[23] N.H. Cromwell, P.L. Creger, K.E. Cook, J. Am. Chem. Soc. 78 (1956) 4412.
[24] N.H. Cromwell, K.E. Cook, J. Am. Chem. Soc. 80 (1966) 1059.
[25] J.B. Jones, J.H. Young, Can. J. Chem. 44 (1966) 1059.
[26] Y.S. Rao, Chem. Rev. 76 (1976) 625 and references therein.
[27] V.L. Goedken, J.J. Pluth, S.M. Peng, B. Bursten, J. Am. Chem. Soc. 98 (1976) 8014.
[28] F.A. Cotton, J. Czuchajowska, Polyhedron 9 (1990) 2553.
[29] J. Eilmes, M. Basato, G. Valle, Inorg. Chim. Acta 290 (1999) 14.

PERGAMON

Polyhedron 21 (2002) 19–26

POLYHEDRON

www.elsevier.com/locate/poly

Magneto-structural studies and thermal analysis of *n*-ethylpyridinium ($n = 2$, 3, 4) tetrabromocuprate(II) complexes

Antonio Luque *, Jon Sertucha, Oscar Castillo, Pascual Román

Departamento de Química Inorgánica, Universidad del País Vasco, Apartado 644, E-48080 Bilbao, Spain

Received 18 June 2001; accepted 24 September 2001

Abstract

Three *n*-ethylpyridinium salts of the tetrabromocuprate(II) anion [$n = 2$ (**1**), 3 (**2**) and 4 (**3**)] were prepared by air evaporation of an ethanolic solution of the aromatic amine base, HBr and $CuBr_2$ in a molar ratio 2:2:1. The compounds were characterized by elemental analysis, IR, UV–Vis and ESR spectroscopies, thermal analysis and variable-temperature magnetic susceptibility measurements. The crystal structures of **2** and **3** were determined by means of single-crystal X-ray diffraction methods. The $[CuBr_4]^{2-}$ anion (with C_2 symmetry for **2**) is connected to two organic cations through N–H···Br hydrogen bonds to form cation–anion–cation motifs which are held together by means of offset face-to-face interactions between the aromatic rings to give zig–zag one-dimensional chains in **2** and a dimeric entity in **3**. The dimeric units of **3** are joined by means of weak Br···Br contacts to give one-dimensional chains as well. The X-band ESR spectra show quasi-axial signals which are clearly resolved operating at Q-band, with $g_{\parallel} \gg g_{\perp} > 2.0$, characteristic of a flattened $[CuBr_4]^{2-}$ tetrahedral complex. The magnetic susceptibility measurements of powdered samples show that compounds behave as low-dimensional magnetic systems with weak antiferromagnetic exchange interactions. Thermal decomposition of the compounds yield copper(II) oxide and metallic Cu as stable final residues in synthetic air and dinitrogen atmospheres, respectively. © 2002 Elsevier Science Ltd. All rights reserved.

Keywords: Crystal structures; Magnetic properties; Thermal properties; Tetrabromocuprate(II); *n*-Ethylpyridinium

1. Introduction

We report herein on the preparation and solid-state properties of the compounds (2-ethylpyridinium)$_2$[$CuBr_4$] (**1**), (3-ethylpyridinium)$_2$[$CuBr_4$] (**2**) and (4-ethylpyridinium)$_2$[$CuBr_4$] (**3**). This work is a part of our studies of hybrid organic/inorganic materials based on organoammonium salts of copper(II) halides, in which we are attempting to analyse the influence of the organic cation features (size, shape and nature and position of the substituent) on the packing interactions that govern the crystal organisation and, as a consequence, the properties of this kind of complex [1–3]. In these compounds, structural units are held together by means of hydrogen-bonds and aromatic–aromatic interactions. These non-covalent interactions control many molecular recognition and self-assembly processes in both solution and solid-state, exercise important effects on the organization and properties of natural and artificial systems [4], and play an important role on the properties of many materials in areas such as biology [5], crystal engineering [6] and material science [7].

2. Experimental

2.1. Reagents and physical measurements

All chemicals were procured commercially and used without subsequent purification. Microanalyses of carbon, nitrogen and hydrogen were performed on a Perkin–Elmer 2400 C-, H-, N-analyser. Copper analysis was made on a Perkin–Elmer 360 atomic absorption/flame emission spectrometer. The densities were measured by flotation in $CHBr_3$–CCl_4 mixtures [8]. IR spectra were recorded in the 4000–200 cm^{-1} range on

* Corresponding author. Tel.: +34-94-6012-701; fax: +34-94-4648-500.

E-mail address: qipluara@lg.ehu.es (A. Luque).

0277-5387/02/$ - see front matter © 2002 Elsevier Science Ltd. All rights reserved.
PII: S0277-5387(01)00961-5

a IR Perkin–Elmer 283 spectrometer as Nujol suspensions. UV–Vis spectra were recorded on a Shimazu 260 spectrometer. Thermoanalytical measurements were made on a Setaram Tag 24 S16 thermobalance (TG/DTA) using dynamic synthetic air and dry dinitrogen atmospheres (flow rate of 50 $cm^3\ min^{-1}$) and a heating rate of 5 °C min^{-1}. ESR polycrystalline spectra were measured on a Bruker ESP300 spectrometer, operating at X- (ca. 9.5 GHz) and Q-band (ca. 34 GHz). Magnetic susceptibility measurements were performed on polycrystalline samples of the compounds with a Quantum Design SQUID susceptometer covering the temperature range 2–300 K and using an applied magnetic field $H = 0.1$ T. Diamagnetic corrections terms were estimated from Pascal's constants [9] and experimental magnetic susceptibility data were also corrected for temperature-independent paramagnetism (60×10^{-6} $cm^3\ mol^{-1}$ per Cu^{II}) and magnetisation of the sample holder.

2.2. Syntheses

All manipulations were carried out in an open atmosphere; exposure to air (O_2) is necessary for the synthesis of bromocuprate(II) complexes in HBr media, since preparation under anaerobic conditions led to the formation of mixed-valence Cu(II)/Cu(I) compounds [10]. Copper(II) bromide (1.00 g, 4.4 mmol) dissolved previously in ethanol, was added dropwise to a stirred ethanolic solution containing equimolecular amounts of concentrated HBr (1 ml, 8.8 mmol) and the corresponding aromatic amine. After heating for approximately 4 h at 60 °C, the resulting black solutions were filtered off and then allowed to stand at room temperature. Overnight, the complexes were obtained as black polycrystalline powders which were filtered off, washed with diethylether and dried in a dinitrogen stream. For compounds **2** and **3** polyhedral dark-violet crystals suitable for single-crystal X-ray crystallographic studies were grown by slow diffusion of *n*-hexane (20 ml) into a ethanol solution (5 ml) of the complexes (0.2 mmol) transferred previously to a 15-mm diameter glass tube. Crystals were filtered off, washed with diethylether and dried in a stream of dry dinitrogen. Crystals were essentially opaque due to the absorption of light in the visible region (ca. 560 nm) and showed metallic lustre. They were found to be quite stable to light and X-ray exposure, but after 3 weeks they lost crystallinity and gradually showed green powder on their surfaces. All our attempts to obtain single-crystals of the compound **1** were unsuccessful and led to the crystallization of twinned specimens with a density value of 2.06(1) g cm^{-3}.

2.2.1. (2-Ethylpyridinium)$_2$[CuBr$_4$] (**1**)

Yield 1.93 g, 75% based on copper. *Anal.* Found: C, 28.1; H, 3.3; N, 4.7; Cu, 10.6. Calc. for $C_{14}H_{20}Br_4CuN_2$: C, 28.1; H, 3.4; N, 4.7; Cu, 10.6%. Main IR data (cm^{-1}): 3200w, 3060m, 3050w, 2970m, 1635s, 1615vs, 1600s, 1505vs, 1445m, 1390w, 1215m, 1185m, 1035s, 795s, 760s, 650m, 230w, 220w and 210w. UV–Vis [EtOH/HBr, λ_{max} nm (ε, $M^{-1}\ cm^{-1}$)]: 560 (500), 335 (2800), 250 (10500), 215 (9000).

2.2.2. (3-Ethylpyridinium)$_2$[CuBr$_4$] (**2**)

Yield 1.93 g, 75% based on copper. *Anal.* Found: C, 28.1; H, 3.3; N, 4.6; Cu, 10.6. Calc. for $C_{14}H_{20}Br_4CuN_2$: C, 28.1; H, 3.4; N, 4.7; Cu, 10.6%. Main IR data (cm^{-1}): 3215w, 3170w, 3120w, 3050m, 2980w, 1625m, 1605s, 1545s, 1430m, 1385m, 1225m, 1195m, 1120s, 800s, 740s, 675f, 230w, 220w and 210w. UV–Vis [EtOH/HBr, λ_{max} nm (ε, $M^{-1}\ cm^{-1}$)]: 565 (500), 340 (2550), 275 (7950), 215 (2150).

2.2.3. (4-Ethylpyridinium)$_2$[CuBr$_4$] (**3**)

Yield 1.85 g, 70% based on copper. *Anal.* Found: C, 28.2; H, 3.3; N, 4.7; Cu, 10.5. Calc. for $C_{14}H_{20}Br_4CuN_2$: C, 28.1; H, 3.4; N, 4.7; Cu, 10.6%. Main IR data (cm^{-1}): 3205w, 3065m, 3045m, 2970m, 1635vs, 1620s, 1595s, 1500vs, 1435m, 1380w, 1225m, 1195s, 1030s, 815vs, 770s, 655m, 490m, 230w, 220w and 210w. UV–Vis [EtOH/HBr, λ_{max} nm (ε, $M^{-1}\ cm^{-1}$)]: 570 (450), 340 (2900), 255 (12500), 220 (9500).

The purity and homogenity of the samples of **1**–**3** used for physical measurements were checked by IR spectroscopy, elemental analysis and by the comparison between the observed X-ray powder diffraction patterns and those generated from the single crystal X-ray data (for compounds **2** and **3**). The magnetic and thermal data were reproducible between different preparations.

2.3. X-ray single-crystal analysis

Diffraction data were performed with an Enraf–Nonius CAD4 automatic four-circle diffractometer using graphite-monochromated Mo Kα radiation ($\lambda = 0.71069$ Å) (**2**) and Cu Kα radiation ($\lambda = 1.54180$ Å) (**3**) and operating in the ω–2θ scan mode. Crystal parameters and refinement results for both compounds are summarised in Table 1. The data were processed and corrected for Lorentz-polarization and absorption effects [11]. Crystal structures were solved by the SIR-92 program [12] and refined by full-matrix least-squares on F^2 including all reflections (SHELXL-93) [13]. Scattering factors for neutral atoms and anomalous dispersion were taken from the literature [14]. All calculations were performed using the WINGX crystallographic software package [15]. Anisotropic thermal parameters were given to all the non-hydrogen atoms. All hydrogen atoms were located on a Fourier difference map but

Table 1
Crystallographic data for compounds **2** and **3**

	2	**3**
Empirical formula	$C_{14}H_{20}Br_4CuN_2$	$C_{14}H_{20}Br_4CuN_2$
M_r	599.47	599.47
Crystal system	monoclinic	triclinic
Space group	$C2/c$	$P\bar{1}$
Crystal colour, habit	dark violet, prism	dark violet, prism
Crystal dimensions (mm^3)	$0.20\times0.20\times0.15$	$0.10\times0.08\times0.07$
Unit cell dimensions		
a (Å)	15.626(1)	8.320(1)
b (Å)	9.010(1)	8.994(1)
c (Å)	14.053(2)	15.721(2)
α (°)	90.0	93.42(2)
β (°)	91.33(1)	103.49(2)
γ (°)	90.0	115.41(3)
U ($Å^3$)	1978.0(4)	1016.0(2)
Z	4	2
D_{calc} (g cm^{-3})	2.013	1.959
D_m (g cm^{-3})	2.00(1)	1.97(1)
$F(000)$	1148	574
Radiation	Mo Kα	Cu Kα
λ (Å)	0.71069	1.54180
μ (mm^{-1})	9.180	10.687
θ_{max}	30	60
No. of data collected	3002	3168
No. of unique data	2878	3032
R_{int}	0.0490	0.0656
No. observed data ($I\geq2\sigma(I)$)	1712	1474
No. of variables	116	197
S (all data) [a]	1.013	1.024
R ($I\geq2\sigma(I)$) [b]	0.0482	0.0466
R_w (all data) [c]	0.1163	0.1014

[a] $S=[\Sigma\, w(|F_o|-|F_c|)^2/(N_{obs}-N_{var})]^{1/2}$.
[b] $R=\Sigma||F_o|-|F_c||/\Sigma|F_o|$.
[c] $R_w=[\Sigma\, w(|F_o|^2-|F_c|^2)^2/\Sigma\, w(|F_o|^2)^2]^{1/2}$.

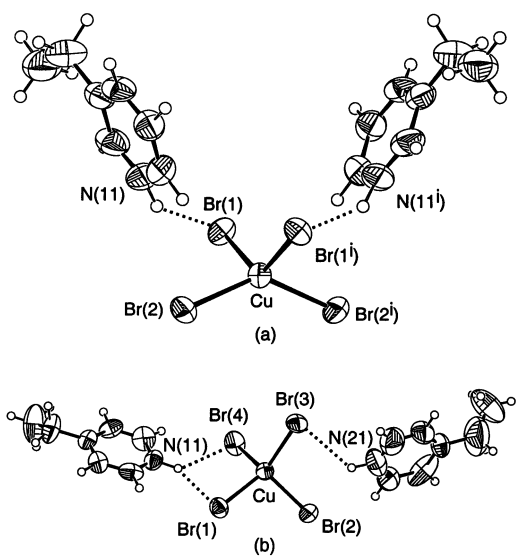


Fig. 1. Thermal ellipsoid plots (50% probability level) showing the N–H···Br hydrogen bonds (dotted lines) among the cations and the $[CuBr_4]^{2-}$ anion in **2** (a) and **3** (b).

only the pyridinic hydrogen atoms in **2** and those attached to the nitrogen atoms of **3** were refined isotropically.

3. Results and discussion

3.1. Crystal structures of *2* and *3*

The crystal structures of compounds **2** and **3** contain the same basic structural unit that consists of a discrete $[CuBr_4]^{2-}$ anion (a) bonded by two organic cations (c), as seen in Fig. 1. The c–a–c molecular units are built through the formation of N–H···Br hydrogen bonds from the pyridinium nitrogen atoms to the bromine atoms on the anions. The molecular unit of compound **2** has a C_2 symmetry and the copper atom sits on a crystallographic twofold axis. Selected bond lengths and angles, and hydrogen contacts are listed in Table 2.

As far as the geometry of the $[CuBr_4]^{2-}$ anions is concerned, the Cu–Br bond lengths are in the range 2.36–2.40 Å, being similar to those usually found for analogous compounds [1–3,16,17]. The tetrabromocuprate(II) anions present a compressed tetrahedral geometry with two bond angles distinguishing their high values (124°–140°) from the rest (96°–101°). These values show that the geometry is intermediate between square-planar (D_{4h}) and regular tetrahedral (T_d). A quantitative description of the distortion from the tetrahedral geometry has been evaluated by the Muetterties and Guggenberger [18] method [$\Delta D=0$ for regular tetrahedron and $\Delta D=100$ for a D_{4h} geometry] and the obtained values are listed in the Table 2. It has been pointed out that hydrogen bonding interactions are among the factors which determine a deviation from T_d symmetry in the tetrahalocuprate(II) anions to a near D_{2d} symmetry [1,17]. Presumably, this is due to a reduction of the effective charge on the halide ions, thus reducing the electrostatic repulsion between the bromide ions within the $[CuBr_4]^{2-}$ species. Two different types of hydrogen bonds are found (see end of the Table 2). The first cation [N(11)–C(18)] in **3** shares its N–H proton between two Br acceptors. The N···Br distances are approximately equal suggesting that the cation has established two nearly symmetric bifurcated hydrogen bonds. The two aromatic cations of **2** and the second pyridinic cation [N(21)–C(28)] in **3** only form a monofurcated hydrogen-bond with one bromine atom. The two aromatic cations around the tetrabromocuprate(II) anion are not coplanar and make dihedral angles of 52° and 81° for **2** and **3**, respectively.

In both cases the c–a–c molecular entities are held together by means of offset face-to-face aromatic stacking interactions between the rings of adjacent units. The most significant parameters of these interactions are listed in Table 3. The packing patterns of the com-

Table 2
Selected bond lengths (Å), bond angles (°) and hydrogen bonds (Å, °) for **2** and **3**

Compound ***2***			
Cu–Br(1)	2.3885(7)	Br(1)–Cu–Br(1^{i})	124.51(5)
Cu–Br(2)	2.3726(7)	Br(1)–Cu–Br(2)	99.47(2)
ΔD (%)	19.3	Br(1)–Cu–Br(2^{i})	100.73(2)
		Br(2)–Cu–Br(1^{i})	100.73(2)
		Br(2)–Cu–Br(2^{i})	135.75(5)
		Br(1^{i})–Cu–Br(2^{i})	99.47(2)
Hydrogen bonds	N···Br	H···Br	∠N–H···Br
N(11)–H(11)···Br(1)	3.382(6)	2.73(11)	134(7)
Compound ***3***			
Cu–Br(1)	2.396(2)	Br(1)–Cu–Br(2)	139.23(8)
Cu–Br(2)	2.369(2)	Br(1)–Cu–Br(3)	96.94(6)
Cu–Br(3)	2.368(2)	Br(1)–Cu–Br(4)	96.75(6)
Cu–Br(4)	2.377(2)	Br(2)–Cu–Br(3)	98.14(7)
ΔD (%)	28.1	Br(2)–Cu–Br(4)	98.37(7)
		Br(3)–Cu–Br(4)	135.67(8)
Hydrogen bonds	N···Br	H···Br	∠N–H···Br
N(11)–H(11)···Br(1)	3.426(9)	2.69(11)	144(6)
N(11)–H(11)···Br(4)	3.458(12)	2.80(6)	134(8)
N(21)–H(21)···Br(3^{ii})	3.341(16)	2.56(7)	147(7)

Symmetry transformations used to generate equivalent atoms: (i) $-x$, y, $-z+1/2$; (ii) $x+1$, y, z.

pounds are quite different. In the crystal structure of **2**, anions and cations are packed forming infinite zig–zag one-dimensional chains (Fig. 2a) with a…cac… sequence and an M···M···M angle of 120.5° between three successive copper atoms along the chain. The intrachain Cu···Cu distances is 11.96 Å. There are no other important interactions in the crystal structure, the centroid–centroid distance between parallel aromatic cations from two neighbouring is longer than 5 Å and the shortest interchain Br···Br contact is 4.31 Å. In **3**, the c–a–c molecular entity is connected to an inversion-related counterpart through face-to-face interactions involving the first aromatic ring [N(11)–C(16)] and forming a dimeric group with a Cu···Cu distance of 11.53 Å (Fig. 2b). The separation between the planes of the second aromatic cations [N(21)–C(26)] from adjacent dimeric units is longer than 3.8 Å and no graphite-like interactions may be considered. However, a Br(3)···Br(3) contact of 4.06 Å links the dimers together into chains along the [$\bar{1}$01] direction. The Cu–Br···Br angle is 141.9°. These chains are essentially isolated in

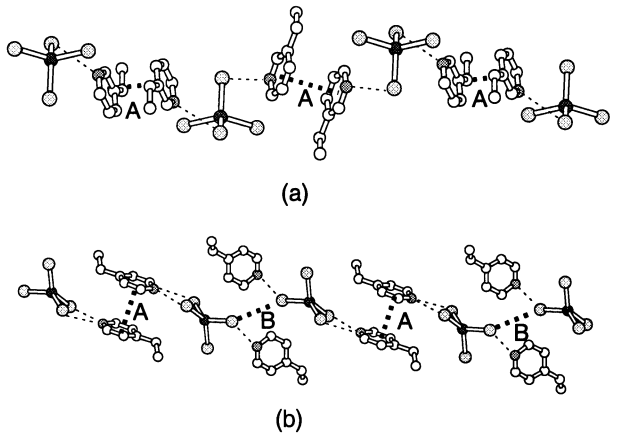


Fig. 2. (a) Fragment of the one-dimensional chain formed by the anions and cations in **2**. A denotes π-stacking interaction (see Table 3). Hydrogen bonds (dotted lines). (b) Alternated one-dimensional chain in **3**. A and B denote π-stacking interaction and Br···Br contact, respectively.

the crystal structure and the shortest interchain Br···Br and Cu···Br distances are 4.46 and 6.06 Å, respectively. So it is quite likely that the interchain interactions are only due to electrostatic effects.

3.2. Infrared and UV–Vis spectroscopies

The infrared spectra of the complexes are consistent with the structural data presented above. The IR spectra of the salts in the range 3300–600 cm^{-1} are dominated by the internal vibrations of the pyridinic ring and the aromatic and alkyl C–H bend peaks [19]. The far-IR region shows three weak bands at 230, 220 and 210 cm^{-1} due to the Cu–Br stretching vibrations, which are similar to those observed for other tetrabromocuprate(II) salts [20]. The UV–Vis spectra show strong bands below 280 nm, assigned to the $\pi \rightarrow \pi^*$ and $n \rightarrow \pi^*$ transitions of the *n*-ethylpyridinium cations which are not affected by the complex anion [21]. Two weak bands appear around 340 and 565 nm which, according to the literature, are associated with ligand-to-metal charge-transfer transitions [22], since the d–d transitions are expected in the near-IR region in the case of the $[CuBr_4]^{2-}$ chromophore [23]. The broad band at 565 nm is responsible for the compounds' dark-violet colour.

Table 3
Structural parameters of the π-stacking interactions for compounds **2** and **3**

Compound	Interaction	Ring	DC	ANG	DZ	DXY	θ
2	A	1–1^{i}	3.66	0.0	3.64	0.52	8.2
3	A	1–1^{ii}	3.65	0.0	3.51	1.01	16.1

Symmetry transformations used to generate equivalent atoms: (i) $-x+1/2$, $-y+1/2$, $-z+1$; (ii) $-x+1$, $-y+1$, $-z$. Interaction: see Fig. 2. Ring: 1 contains the N(11) atom. DC: centroid–centroid distance (Å). ANG: interplanar angle (°) between the rings. DZ: interplanar distance (Å). DXY: lateral offset of the rings (Å). θ: angle between the DC vector and the normal of the first ring plane.

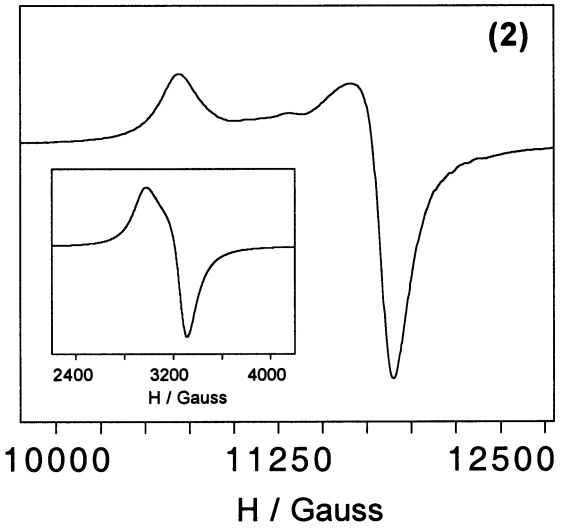


Fig. 3. Q- and X-band (inset) powder ESR spectra at room temperature for compound **2**.

Table 4
ESR and magnetic data for **1**–**3**

	1	2	3
Q-band ESR data			
$g_{\parallel}$	2.281	2.280	2.242
$g_{\perp}$	2.057	2.060	2.057
$\langle g \rangle$	2.13	2.14	2.12
Curie–Weiss fit			
C	0.44	0.42	0.43
Θ (K)	−2.10	−1.10	−4.60
Magnetic model fit			
J (cm^{-1})		−0.85	−1.50
J/k (K)		−1.22	−2.16
α			0.8
g		2.13	2.13
$R \times 10^5$		2.0	3.1

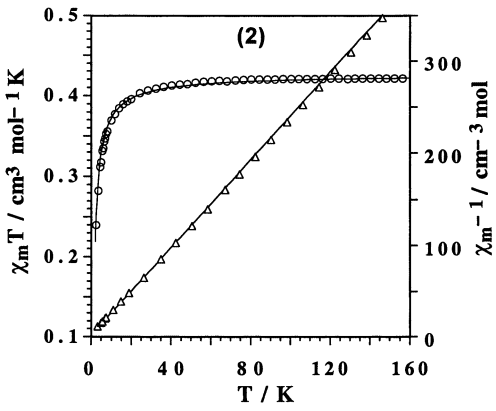


Fig. 4. Thermal variation of the reciprocal magnetic susceptibility (△) and $\chi_m T$ (○) for compound **2**. Solid lines correspond to the best theoretical fits.

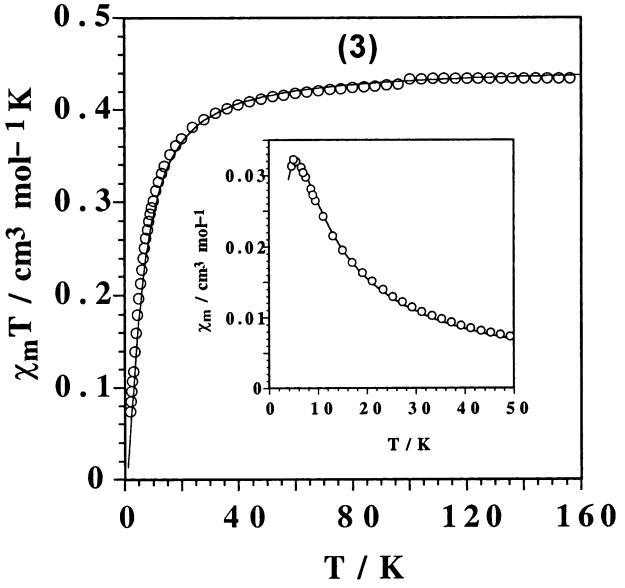


Fig. 5. Thermal dependence of $\chi_m T$ for compound **3**: (○) experimental data; (—) best theoretical fit (see text). The inset shows the region of the susceptibility maximum in the χ_m vs. T plot.

3.3. ESR spectroscopy and magnetic susceptibility

ESR spectra of the compounds were recorded at room temperature on powdered samples at both X- and Q-bands. The X-band spectra show a quasi-axial signal which is clearly resolved operating at Q-band (Fig. 3). The axial spectra are consistent with the compressed tetrahedral stereochemistry of the $[CuBr_4]^{2-}$ chromophore and the relation $g_{\parallel} \gg g_{\perp} > 2.0$ indicates a $b_1(d_{x^2-y^2})$ ground state [17].

Variable temperature magnetic susceptibility measurements (2.0–300 K) were carried out on powdered samples of the complexes taken from the same uniform batches used for the chemical and structural characterizations. The room temperature magnetic moments range from 1.83 to 1.85μ_B and are typical for one non-interacting d^9 copper(II) ion. The magnetic susceptibility data for all compounds follow a Curie–Weiss law at $T > 40$ K (Table 4). Thermal variations of reciprocal susceptibility and the $\chi_m T$ product of **2** are shown in Fig. 4. The overall appearance of the $\chi_m T$ versus T curves are indicative of weak antiferromagnetic interactions between the Cu(II) centres. The χ_m versus T curve of compound **3** exhibits a maximum at 5 K (Fig. 5).

Considering the structural features of compound **2**, the experimental data were analysed using the Heisenberg model with exchange interaction between pairs of Cu(II) ions with spins S_i and S_j of the form:

$$H = -2\sum_{i>j} J_{ij} S_i S_j \quad (1)$$

where we assumed interactions between nearest neighbour copper ions on a chain (i.e. $J_{ij} = J$ for $j = i \pm 1$ and $J_{ij} = 0$ otherwise). In order to evaluate the magnitude of the exchange coupling constant we have used the polynomial expression developed by Hall to describe the results graphically presented by Bonner and Fisher [24] for a uniformly spaced chain of spins with $S = 1/2$:

$$\chi_m = \frac{Ng^2b^2}{kT}\left[\frac{A + Bx + Cx^2}{1 + Dx + Ex^2 + Fx^3}\right] \quad (2)$$

where $x = |J|/kT$, N and k are the Avogadro and Boltzmann constants, β is the Bohr magneton, $A = 0.250$, $B = 0.150$, $C = 0.3009$, $D = 1.9862$, $E = 0.6885$ and $F = 6.0626$. The least-squares best-fit results are listed in Table 4. R is the agreement factor defined as $R = \Sigma_i[(\chi_m)_{obs}(i) - (\chi_m)_{calc}(i)]^2/\Sigma_i[(\chi_m)_{obs}(i)]^2$. The calculated g and J values are in good agreement with those deduced from the ESR spectra and Curie–Weiss fit, respectively. At high temperatures ($|J|/kT \ll 1$) Eq. (2) becomes a Curie–Weiss law with $\Theta = 1.38 \times J/k$, and from the observed Θ value a J/k exchange parameter of -0.80 K should be expected, practically the calculated one. Therefore, as expected, the 1D Heisenberg model gives a good representation for the magnetic behaviour of this compound. The overlap between adjacent aromatic rings and the hydrogen bond interactions most likely provides the exchange pathways for the small antiferromagnetic coupling observed. In this respect, weak magnetic couplings across aromatic (pyrazolyl and 2,2′-bipyridine rings) π-stacking interactions have been reported [25] and hydrogen bonding has been demonstrated extensively to be a powerful tool for generating magnetic interactions and for propagating them in both inorganic [26] and organic solids [27].

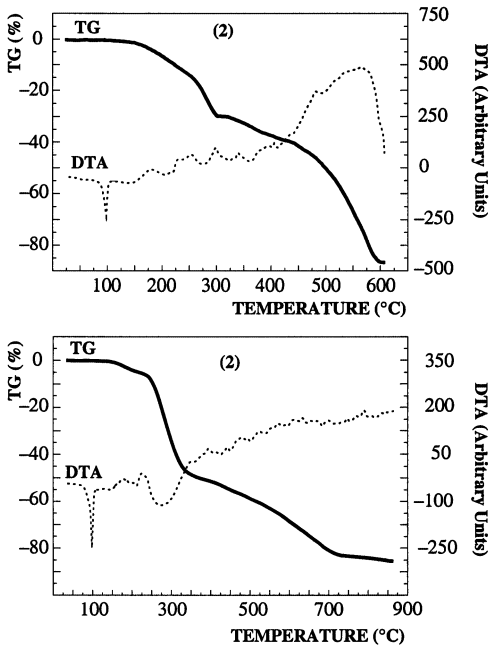


Fig. 6. Thermoanalytical curves (TG and DTA) for compound **2** in air (top) and dinitrogen (bottom) atmospheres.

In the case of **3**, the dimeric units are held together in a one-dimensional chain by means of Br···Br contacts and consequently we have analysed its magnetic data through an antiferromagnetic Heisenberg alternating chain model [28] which was derived through the Hamiltonian of Eq. (3)

$$H = -2J\Sigma[S_{2i}S_{2i-1} + \alpha S_{2i}S_{2i+1}] \quad (3)$$

where α is the alternating parameter and $S_{2i-1} = S_{2i} = S_{2i+1} = 1/2$. The expression derived for the susceptibility is

$$\chi_m = \frac{Ng^2b^2}{kT}\left[\frac{A + Bx + Cx^2}{1 + Dx + Ex^2 + Fx^3}\right] \quad (4)$$

where $x = |J|/kT$ and the coefficients A–F, all functions of α, are found in the above-referenced paper by Hatfield and co-workers [28]. The best-fit parameters are given in the Table 4.

From the point of view of the magnetic properties of copper(II)–bromide compounds, the examination of the Br···Br contacts is important [29]. The unpaired electron density in Cu(II) halide complexes is substantially delocalized out onto the orbitals of the halide ions. This is particularly true for bromide complexes, since the smaller difference in the energy between the copper d and Br p orbitals (as compared to the chloride complexes) enhances the delocalization. Hence, substantial overlap of the magnetic orbitals can occur and lead to the establishment of unusual and, on the surface, unexpected magnetic exchange pathways [30]. Although it has been observed experimentally [31,32] and confirmed theoretically [33] that the strength of these interactions, which are invariable antiferromagnetic, decrease rapidly with the Br···Br distance d, typically as d^{-10}, exchange couplings in excess of $|J/K| = 50$ K have been observed [31]. The magnitude of the interaction depends also on the geometry of the superexchange pathway through such parameters as the mean *trans* angle of the distorted $CuBr_4$ tetrahedra and the dihedral angle between the two Cu–Br···Br planes [34,35].

3.4. Thermal analysis

The thermal behaviour of the compounds have been deduced from its TG/DTA curves in both synthetic air and dinitrogen atmospheres. The data show the occurrence of three consecutive steps: melting point, organic cation pyrolysis and inorganic residue evolution (Fig. 6). No phase transitions were observed in the thermal evolution of the compounds **1**–**3** from room temperature to their melting points at 110 (**1**), 100 (**2**) and 85 °C (**3**). The melting enthalpies are 35 (**1**), 30 (**2**) and 25 kJ mol^{-1} (**3**). The melting points, the enthalpies and the density values are in the order **1** > **2** > **3**. The melt-

ing processes do not show significant dependence on the nature of the environmental gas, but the decomposition pathway of the liquid and the final residues are affected by the surrounding atmosphere. Under air atmosphere, the compounds decompose endothermically at 140 (**1**), 120 (**2**) and 155 °C (**3**) with the oxidation of the organic units to give copper(II) bromide followed by a strong exothermic loss of bromine to yield copper(II) oxide as final product above 610 °C. No other peak belonging to Cu or another copper oxide were found in the X-ray powder patterns of the final stable residues. In dinitrogen atmosphere, all degradation processes are endothermic and they lead, without stable intermediate species, to powdered metallic copper as the final product above 700 °C. No peaks corresponding to $CuBr_2$ or CuBr could be identified. These results suggest that organic cation pyrolysis under inert atmosphere can produce, direct or indirectly, the reduction of Cu(II) to Cu(0). It has been suggested that the thermal degradation of organoammonium halometalate complexes in inert atmospheres is an excellent method of obtaining powdered metals of great reactivity [36].

4. Supplementary material

Crystallographic data for the structural analysis have been deposited with the Cambridge Crystallographic Centre, CCDC Nos. 164530 for compound **2** and 164531 for compound **3**. Copies of this information may be obtained free of charge from The Director, CCDC, 12 Union Road, Cambridge, CB2 1EZ, UK (fax: +44-1233-336-033; e-mail: deposit@ccdc.cam.ac.uk or www: http://www.ccdc.cam.ac.uk).

Acknowledgements

We gratefully acknowledge financial support from the Universidad del País Vasco/Euskal Herriko Unibertsitatea (UPV/EHU) (project 169.310-EA857/2000). JS thanks the Spanish Government for a doctoral fellowship (grant no. AP94.42172547).

References

[1] J. Sertucha, A. Luque, F. Lloret, P. Román, Polyhedron 17 (1998) 3875.
[2] A. Luque, J. Sertucha, L. Lezama, T. Rojo, P. Román, J. Chem. Soc., Dalton Trans. (1997) 847.
[3] P. Román, J. Sertucha, A. Luque, L. Lezama, T. Rojo, Polyhedron 15 (1996) 1253.
[4] (a) A. Angeloni, A.G. Orpen, Chem. Commun. (2001) 343;
(b) K.M. Guckian, B.A. Schweitzer, R.X.F. Ren, C.J. Sheils, D.C. Tahmassebi, E.T. Kool, J. Am. Chem. Soc. 122 (2000) 2213;
(c) C. Janiak, J. Chem. Soc., Dalton Trans. (2000) 3885;
(d) K. Müller-Dethlefs, P. Hobza, Chem. Rev. 100 (2000) 143.
[5] G.R. Desiraju, T. Steiner, The Weak Hydrogen Bond in Structural Chemistry and Biology, Oxford University Press, Oxford, 1999.
[6] (a) L. Brammer, J.C. Mareque Rivas, R. Atencio, S. Fang, F.C. Pigge, J. Chem. Soc., Dalton Trans. (2000) 3855;
(b) F.H. Allen, V.J. Hoy, J.A.K. Howard, V.R. Thalladi, G.R. Desiraju, C.C. Wilson, G.J. McIntyre, J. Am. Chem. Soc. 119 (1997) 3477.
[7] J.M.A. Robinson, D. Philp, K.D.M. Harris, B.M. Kariuki, New J. Chem. 24 (2000) 799.
[8] P. Román, J.M. Gutiérrez–Zorrilla, J. Chem. Educ. 62 (1985) 167.
[9] A. Earnshaw, Introduction to Magnetochemistry, Academic Press, London, 1968.
[10] (a) R.D. Willett, K. Halvorson, Acta Crystallogr., Sect. A 44 (1988) 2068;
(b) A. Bencini, F. Mani, Inorg. Chim. Acta 87 (1984) L9.
[11] N. Walker, D. Stuart, Acta Crystallogr., Sect. A 39 (1983) 158.
[12] A. Altomare, M. Cascarano, C. Giacovazzo, A. Guagliardi, J. Appl. Crystallogr. 26 (1993) 343.
[13] G.M. Sheldrick, SHELXL-93, Program for the Refinement of Crystal Structures, Universitat of Göttingen, Germany, 1993.
[14] International Tables for X-ray Crystallography, vol. 4, Kynoch Press (present distributor: D. Reidel, Dordrecht), Birmingham, UK, 1974.
[15] L.J. Farrugia, WINGX, A Windows Program for Crystal Structure Analysis, University of Glasgow, Glasgow, 1998.
[16] (a) S. Haddad, R.D. Willett, Inorg. Chem. 40 (2001) 2457;
(b) T.J. Coffey, C.P. Landee, W.T. Robinson, M.M. Turnbull, M. Winn, F.M. Woodward, Inorg. Chim. Acta 303 (2000) 54;
(c) G. Pon, R.D. Willett, B.A. Prince, W.T. Robinson, M.N. Turnbull, Inorg. Chim. Acta 255 (1997) 325.
[17] M.R. Sunberg, R. Kikeväs, J. Ruiz, J.M. Moreno, E. Colacio, Inorg. Chem. 31 (1992) 1062.
[18] E.L. Muetterties, L.J. Guggenberger, J. Am. Chem. Soc. 96 (1974) 1748.
[19] C.J. Pouchert, The Aldrich Library of FT-IR Spectra, Aldrich Chemical, Milwaukee, 1985.
[20] (a) K. Nakamoto, Infrared and Raman Spectra of Inorganic and Coordination Compounds, Wiley, New York, 1997;
(b) G. Marcotrigiano, L. Menabue, G.C. Pellacani, Inorg. Chem. 5 (1970) 2333.
[21] R.C. Weast, M.J. Astle (Eds.), CRC Handbook of Chemistry and Physics, 59th ed., CRC Press, Boca Raton, FL, 1978.
[22] (a) R. Valiente, F. Rodriguez, J. Phys.: Condens. Matter 10 (1998) 9525;
(b) R. Valiente, M.C. Marco de Lucas, F. Rodriguez, J. Phys.: Condens. Matter. 7 (1995) 3881.
[23] M.J. Llopis, G. Alzuet, A. Martin, J. Borrás, S. García-Granda, R. Díaz, Polyhedron 12 (1993) 2499.
[24] (a) J.W. Hall, PhD thesis, University of North Carolina, USA, 1977;
(b) J.C. Bonner, M.E. Fisher, Phys. Rev. A 135 (1964) 640.
[25] (a) M.C. Muñoz, M. Julve, F. Lloret, J. Faus, M. Andruh, J. Chem. Soc., Dalton Trans. (1998) 3125;
(b) A.J. Amoroso, J.C. Jeffery, P.L. Jones, J.A. McCleverty, P. Thornton, M.D. Ward, Angew. Chem., Int. Ed. Engl. 34 (1995) 1443.
[26] (a) E. Escrivá, J. Server-Carrió, J. García-Lozano, F.V. Folgado, F. Sapina, L. Lezama, Inorg. Chim. Acta 279 (1998) 58;
(b) Y. Yamada, N. Ueyama, T. Okamura, W. Mori, A. Nakamura, Inorg. Chim. Acta 276 (1998) 43.
[27] N. Daro, J.P. Sutter, M. Pink, O. Khan, J. Chem. Soc., Perkin Trans. 2 (2000) 1087.

[28] J.W. Hall, W.E. Marsh, R.R. Weller, W.E. Hatfield, Inorg. Chem. 20 (1981) 1033.
[29] (a) C.P. Landee, M.M. Turnbull, C. Galeriu, J. Giantsidis, F.M. Woodward, Phys. Rev. B 63 (2001) 100402;
(b) T. Matsumoto, Y. Miyazaki, S.A. Albrecht, C.P. Landee, M.M. Turnbull, M. Sorai, J. Phys. Chem. B 104 (2000) 9993.
[30] G.S. Long, M. Wei, R.D. Willett, Inorg. Chem. 36 (1997) 3102.
[31] G.V. Rubenacker, S. Waplak, S.L. Hutton, D.N. Haines, J.E. Drumheller, J. Appl. Phys. 57 (1985) 3341.
[32] L.O. Snively, D.N. Haines, K. Emerson, J.E. Drumheller, Phys. Rev. B 26 (1982) 5245.
[33] P. Straatman, R. Bloch, L. Jensen, Phys. Rev. B 29 (1984) 1414.
[34] B.R. Patyal, B.L. Scott, R.D. Willett, Phys. Rev. B 41 (1990) 1657.
[35] P. Zhou, J.E. Drumheller, G.V. Rubenacker, K. Halvorson, R.D. Willett, J. Appl. Phys. 69 (1991) 5804.
[36] J.R. Allan, Thermochim. Acta 200 (1992) 355.

PERGAMON

Polyhedron 21 (2002) 27–31

POLYHEDRON

www.elsevier.com/locate/poly

Synthesis of new chiral diimine palladium(II) and nickel(II) complexes bearing oxazoline- and myrtanyl-based nitrogen ligands. Crystal structure of the C_2-symmetric complex [{(1*R*,2*S*)-*inda*-*box*}$PdCl_2$]

Adnan S. Abu-Surrah [a,*], Mika Kettunen [b], Kristian Lappalainen [b], Ulla Piironen [b], Martti Klinga [b], Markku Leskelä [b]

[a] *Department of Chemistry, Hashemite University, P.O. Box 150459, Zarqa-13115, Jordan*
[b] *Laboratory of Inorganic Chemistry, Department of Chemistry, University of Helsinki, P.O. Box 55, FIN-00014, Helsinki, Finland*

Received 3 July 2001; accepted 25 September 2001

Abstract

A synthesis of new chiral dihalo palladium(II)-(**5**, **7**) and nickel(II) (**6**, **8**) complexes bearing the ligands *N*,*N*′-bis{(−)-(*cis*)-myrtanyl}butylene-2,3-diimine (BMDI, **3**) and the conformationally constrained bisoxazoline ligand ((1*R*,2*S*)-*inda*-*box*, **4**) is described. Reaction of [(TMEDA)Pd(CH_3)Cl] (TMEDA: *N*,*N*,*N*′,*N*′-tetramethylethylenediamine) with **4** followed by chloride abstraction with $NaB(Ar_f)_4$ in the presence of CH_3CN afforded the solvent stabilized, monoalkyl complex [(**4**)Pd($NCCH_3$)(CH_3)]$B(Ar_f)_4$ (**9**) (Ar_f: 3,5-bis(trifluoromethyl)benzene). The solid state structure of the dichloro palladium(II) complex [{(1*R*,2*S*)-*inda*-*box*}$PdCl_2$] (**7**) was determined by X-ray structure analysis. © 2002 Elsevier Science Ltd. All rights reserved.

Keywords: Palladium; Nickel; Chirality; Bidentate nitrogen ligands; Crystal structures

1. Introduction

Numerous publications describing the coordination chemistry of phosphorous donor ligands and the application of their complexes in homogeneous catalysis have been disclosed [1]. In contrast, less has occurred for the organic nitrogen ligands, maybe because their complexes have not been used extensively for synthetic organic applications.

Recently, some research groups have highlighted the use and application of nitrogen donors, particularly because they are more easily obtained from the 'chiral pool' [2]. These reports included the application of different transition metal coordinating catalysts, which are based on the chiral and C_2-symmetric bisoxazoline ligands, in the field of catalytic asymmetric organic synthesis such as enantioselective C–C bond forming reactions [3], oxidation [4], reduction [5], and carbonylation of alkenes [6]. Furthermore, chiral and achiral Pd(II) and Ni(II) complexes bearing bidentate nitrogen donors have attracted interest due to their application as catalysts for homo- and copolymerization of linear and cyclic olefins with carbon monoxide [7,8] and for polymerization of functionalized olefins [9].

As an extension to our studies on both the coordination chemistry of chiral and C_2-symmetric heteroatom-containing ligands and the catalytic application of their metal complexes [10,11], we report here on the synthesis of new chiral diimine-palladium(II) and nickel(II) complexes containing the nitrogen ligands bis(myrtanyl)diimine (BMDI) and the C_2-symmetric bisoxazoline ligand (1*R*,2*S*)-*inda*-*box* [12]. The solid state structure of the chiral and C_2-symmetric palladium(II) complex [{(1*R*,2*S*)-*inda*-*box*}$PdCl_2$] (**7**) was determined by X-ray structure analysis.

* Corresponding author. Tel.: +962-5382-6600x4315; fax: +962-5382-6613.
E-mail address: asurrah@hu.edu.jo (A.S. Abu-Surrah).

0277-5387/02/$ - see front matter © 2002 Elsevier Science Ltd. All rights reserved.
PII: S0277-5387(01)00952-4

2. Experimental

2.1. Materials

All reactions were carried out under argon by using standard Schlenk techniques. [$(PhCN)_2PdCl_2$] [13], [(DME)$NiBr_2$] (DME: 1,2-dimethoxyethane) [14], and [(TMEDA)$Pd(CH_3)Cl$] (TMEDA: *N*,*N*,*N*′,*N*′-tetra methylethylenediamine) [15] were prepared according to literature procedures. (−)-(*cis*)-Myrtanylamine and bisoxazoline ([3*aR*-[2(3′*aR**, 8′*aS**),3′*a*β, 8′*a*β]]-(+)-2,2′-methylenebis [3*a*, 8*a*-dihydro-8H-indeno[1,2-*d*]oxazole]) were purchased from Aldrich. The hydrocarbon and ether solvents were purified by distillation over $LiAlH_4$. CH_2Cl_2 was distilled from CaH_2. MeCN and Me_2CO were dried over K_2CO_3 and $CaSO_4$, respectively. Reagent grade chemicals were used as received unless otherwise stated.

2.2. Physical measurements

Elemental analyses were performed at the Pharmacology Department, University of Helsinki (EA 1110 CHNS-O CE instrument). ^1H and ^{13}C NMR spectra were recorded on a Varian Gemini 200 spectrometer operating at 200 MHz and at 50.286 MHz, respectively. Infrared spectra were measured on BIO-RAD FTS-7 FT-IR spectrometer using KBr pellet. Mass spectra (EI) were acquired with a JEOL JMS-SX102 mass spectrometer.

2.3. Synthesis of compounds

2.3.1. (BMDI) (**3**)

To a solution of 2,3-butandione (1.0 g, 11.6 mmol) was added with continuous stirring a solution of (−)-(*cis*)-myrtanylamine (3.56 g, 23.2 mmol) in MeOH (50 ml) at room temperature. A white precipitate started to form after 15 min. After stirring for 3 h the product was filtered, washed with methanol (2 × 3 ml) and dried under vacuum.

Yield: 2.1 g (51%), m.p.: 73 °C. Found: C, 80.95; H, 11.67; N, 7.77. *Anal*. Calc. for $C_{24}H_{40}N_2$: C, 80.83; H, 11.30; N, 7.85%. ^1H NMR (200 MHz, $CDCl_3$): δ 3.46–3.37 (m, 2 H, N–CH_2), 2.58–2.31 (m, 2H, N–CH_2), 2.05 (s, 6H,), 1.98–1.86 (m, 14H), 1.65–1.50 (m, 2H, ring), 1.20 (2, 6H, $H_{Me-myrt.}$), 1.06 (s, 6H, $H_{Me-myrt.}$), 0.98 (m, 2H). ^{13}C NMR (200 MHz, $CDCl_3$): δ 168 (C=N), 59.1 (C–N), 13.2 (Me-bridge). IR (KBr, cm^{-1}): 1639 (m) (C=N).

2.3.2. [(BMDI)$PdCl_2$] (**5**)

A filtered solution of the ligand (**3**) (1.02 g, 2.87 mmol) in acetone (50 ml) was added to a filtered solution of $(PhCN)_2PdCl_2$ (1.0 g, 2.61 mmol) in acetone (50 ml) with continuous stirring. Upon addition, an orange–yellow solid was formed. After 5 h stirring, the precipitate was filtered, washed with acetone (2 × 5 ml), Et_2O (2 × 10 ml) and dried in vacuum.

Yield: 0.87 g (63%), m.p. (dec.): 230 °C. Found: C, 53.75; H, 8.01; N, 5.28. *Anal*. Calc. for $C_{24}H_{40}N_2PdCl_2$: C, 53.99; H, 7.55; N, 5.24%. EI MS; *m*/*e* (rel. int.): 467 (10.0%, $M^+ - 2Cl$), 356 (30%, $M^+ - Pd2Cl$). ^1H NMR (200 MHz, $CDCl_3$): δ 3.87 (m, 2H, N–CH_2), 2.80 (m, 2H, N–CH_2), 2.34 (8H,), 2.05–1.85 (m, 12H) 1.44 (m, 2H, ring), 1.19 (s, 6H, $H_{Me-myrt.}$), 1.07 (s, 6H, $H_{Me-myrt.}$), 0.98 (m, 2H). ^{13}C NMR (200 MHz, $CDCl_3$): δ 179 (C=N), 60.1 (C–N), 15.3 (Me-bridge). IR (KBr, cm^{-1}): 1635 (m) (C=N).

2.3.3. [(BMDI)$NiBr_2$] (**6**)

A filtered solution of the ligand BMDI (**3**) (1.27 g, 3.56 mmol) in CH_2Cl_2 (50 ml) was added to a suspension of (DME)$NiBr_2$ (1.0 g, 3.23 mmol) in the same solvent (50 ml) with continuous stirring. Upon addition, a red–orange solid was formed. Stirring was continued for 5 h, and the precipitate was filtered, washed with acetone (2 × 5 ml), Et_2O (2 × 10 ml) and dried in vacuum.

Yield: 1.43 g (77%), m.p.(dec.): 110 °C. Found: C, 49.81; H, 7.42; N, 4.93. *Anal*. Calc. for $C_{24}H_{40}N_2NiBr_2$: C, 50.12; H, 7.01; N, 4.87%. EI MS; *m*/*e* (rel. int.): 495 (30.0%, $M^+ - Br$), 412 (100.0%, $M^+ - 2Br$), 354 (30%, $M^+ - Ni2Br$). IR (KBr, cm^{-1}): 1636 (m) (C=N).

2.3.4. [{(1*R*,2*S*)-inda-box}$PdCl_2$] (**7**)

A filtered solution of the bisoxazoline ligand (**4**) (0.95 g, 2.87 mmol) in CH_2Cl_2 (50 ml) was added to a filtered solution of $(PhCN)_2PdCl_2$ (1.0 g, 2.61 mmol) in acetone (50 ml) with continuous stirring. Upon addition, a white solid was formed. After stirring for 18 h the precipitate was filtered, washed with acetone (2 × 5 ml), Et_2O (2 × 10 ml) and dried under vacuum. Orange crystals suitable for X-ray analysis were formed by crystallization from acetone.

Yield: 0.60 g (45%), m.p. (dec.): 183 °C. Found: C, 49.37; H, 3.85; N, 5.57. Anal. Calc. for $C_{21}H_{18}N_2O_2PdCl_2$: C, 49.68; H, 3.57; N, 5.52%. ^1H NMR (200 MHz, $CDCl_3$): δ 8.60 (m, 2H, $CH_{2\text{-bridge}}$), 7.39–7.26 (m, 8H, $H_{arom.}$), 5.38 (dt, 2H, 13 Hz), 6.27 (d, 2H, 6Hz) 3.38 (d, 4H). IR (KBr, cm^{-1}): 1652 (m) (C=N).

2.3.5. [{(1*R*,2*S*)-inda-box}$NiBr_2$] (**8**)

To a suspension of (DME)$NiBr_2$ (0.60 g, 1.94 mmol) in CH_2Cl_2 (50 ml) was added a filtered solution of the ligand (**4**) (0.77 g, 2.33 mmol) in the same solvent (50 ml) with continuous stirring. Upon addition, the colour changed from orange to red. Stirring was continued for 12 h at room temperature. After which, the precipitate was filtered, washed with acetone (2 × 5 ml), Et_2O (2 × 10 ml) and dried in vacuum.

Yield: 0.62 g (58%), m.p. (dec.): 200 °C. Found: C, 44.24; H, 3.63; N, 4.58. Anal. Calc. for $C_{21}H_{18}N_2O_2NiBr_2 \cdot H_2O$: C, 44.49; H, 3.56; N, 4.94%. EI MS; *m/e* (rel. int.): 468 (25.0%, $M^+ - Br$), 388 (50.0%, $M^+ - 2Br$), 330 (20%, $M^+ - Ni2Br$). IR (KBr, cm^{-1}): 1670 (m) (C=N).

Table 1
Crystallographic data and parameters for data collection and refinement of **7**

Formula	$C_{21}H_{18}Cl_2N_2O_2Pd$
Formula weight	507.67
Temperature (K)	193(2)
Crystal system	monoclinic
Space group	$P2_1$
Unit cell dimensions	
a (Å)	7.633(2)
b (Å)	8.807(2)
c (Å)	14.664(3)
α (°)	90
β (°)	97.22(3)
γ (°)	90
V (A^3)	978.0(4)
Z	2
D_{calc} ($Mg\,m^{-3}$)	1.724
Absorption coefficient (mm^{-1})	1.242
Crystal size (mm)	$0.30 \times 0.20 \times 0.10$
θ range (°)	2.69–25.00
Scan mode	$\omega/2\theta$
Scan range (°)	$1.40 + 0.40 \tan\theta$
Number of data collected	1986
Number of unique data	1841 [$R_{int} = 0.0238$]
Number of data refined	1841
Observed criterion	$F > 4\sigma(F)$
Number of parameters	253
R [a]	0.0269
wR_2 [b]	0.0650

[a] $R = \Sigma\|F_o| - |F_c\|/\Sigma|F_o|$.
[b] $wR_2 = [\Sigma[w(F_o^2 - F_c^2)^2]/\Sigma[w(F_o^2)^2]^{1/2}$.

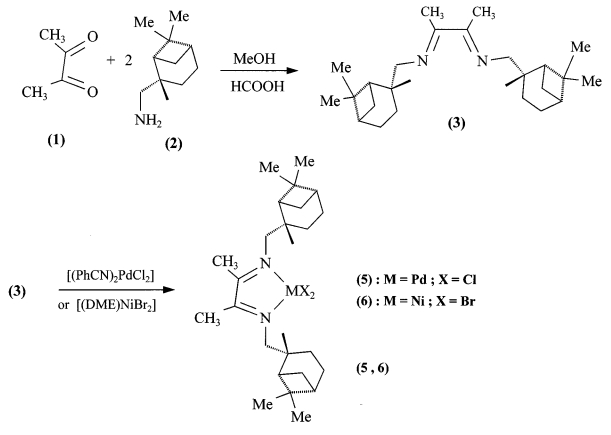


Fig. 1. Synthesis of the ligand BMDI (**3**) and its palladium(II)- and nickel(II) dihalide complexes (**5** and **6**).

*2.3.6. [{(1R,2S)-inda-box}Pd(NCCH$_3$)(CH$_3$)]·B(Ar$_f$)$_4$ (**9**)*

To a solution of [(TMEDA)Pd(CH_3)Cl] (0.17 g, 0.61 mmol) in toluene (20 ml) and CH_2Cl_2 (15 ml) was added with continuous stirring a solution of the ligand (**4**) (0.20 g, 0.61 mmol) in CH_2Cl_2 (30 ml). After 28 h stirring, the product was precipitated with diethylether and filtered. The residue was dissolved in CH_2Cl_2 (35 ml) and CH_3CN (15 ml) and $NaB(Ar_f)_4$ (0.44 g, 0.49 mmol) was added. After stirring for 24 h, the mixture was filtered and the solvent was evaporated to dryness. The isolated yellow product was extracted with CH_2Cl_2 (10 ml), filtered and dried in vacuum.

Yield: 0.41g (62%), m.p. (dec.): 83 °C. Found: C, 47.27; H, 2.92; N, 3.25. *Anal.* Calc. for $C_{56}H_{36}N_3O_2BF_{24}Pd \cdot 3H_2O$: C, 47.69; H, 3.00; N, 2.98%. EI MS; *m/e* (rel. int.): 437 (85.0%, $M^+ - C_{35}H_{18}NBF_{24}$). IR (KBr, cm^{-1}): 2362 (m) ν(C≡N), 1659 (m) (C=N), 1125 (s) ($B(Ar_f)$).

*2.4. X-ray structure determinations for **7***

Crystal data of compound (**7**) were collected on a Rigaku AFC7S single-crystal diffractometer at 193(2) K using graphite monochromatized Mo Kα radiation (0.71073 Å). The intensities were corrected for Lorentz and polarization effects [16]. An experimental absorption correction (psi-scan) was performed [17]. The structure was solved by direct methods (SHELX-97) [18]. All non-hydrogen atoms were refined anisotropically and hydrogen atoms isotropically on calculated positions. Final calculations were performed with SHELX-97 and SHELXTL/PC [19] program systems. The cell parameters and specific data collection parameters are summarized in Table 1.

3. Results and discussion

3.1. Ligand and complexes synthesis

The condensation reaction of the commercially available 2,3-butandione (**1**) with 2 equiv. of the enantiomerically pure amine (−)-*cis*-myrtanylamine (**2**) in MeOH at 25 °C afforded the bidentate diimine ligand, *N*,*N*′-bis((−)-*cis*-myrtanyl)butylene-2,3-diimine (BMDI, **3**) in a moderate yield (Fig. 1). The presence of a medium to strong band at around 1639 cm^{-1} in the IR-spectra of the Schiff base ligand and the disappearance of the peak due to the carbonyl group of the starting material indicate the formation of the desired diimine. The ^{13}C NMR spectrum of the diimine **3**, exhibits a resonance at 168 ppm which can be ascribed to the imine group (C=N). A singlet at 13.2 ppm has also been observed which can be attributed to the methyl groups in the backbone of the ligand.

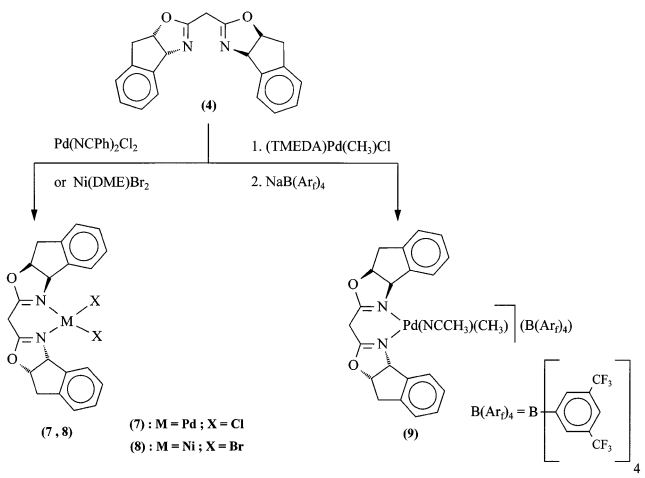


Fig. 2. Synthesis of the dihalide and the monocationic, monoalkyl complexes (**7**, **8**, **9**) of the bisoxazoline ligand (**4**).

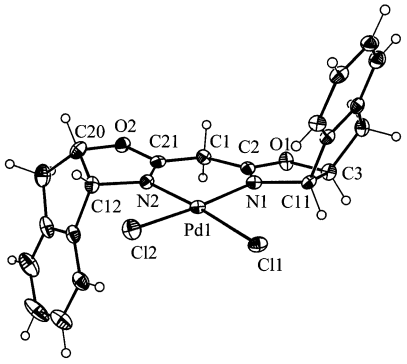


Fig. 3. Molecular structure of complex **7** with 30% probability thermal ellipsoids depicted.

Table 2
Selected bond lengths (Å) and bond angles (°) for complex **7**

Bond lengths			
Pd1–N1	2.046(4)	Cl2–Pd1–Cl1	87.47(6)
Pd1–N2	2.055(5)	C2–N1–Pd1	126.1(4)
Pd1–Cl2	2.2905(17)	C21–N2–Pd1	125.8(4)
Pd1–Cl1	2.2945(16)	C12–N2–Pd1	127.4(4)
		C11–N1–Pd1	126.9(3)
Bond angles			
N1–Pd1–N2	89.97(18)	C21–C1–C2	116.9(5)
N1–Pd1–Cl2	174.21(14)	O1–C2–C1	112.2(5)
N2–Pd1–Cl2	91.69(14)	O2–C21–C1	112.7(5)
N1–Pd1–Cl1	91.32(14)	N1–C2–C1	129.5(5)
N2–Pd1–Cl1	175.20(15)	N2–C21–C1	130.0(6)

The square-planar palladium(II) dihalide complexes [(BMDI)$PdCl_2$] (**5**) and {(1*R*,2*S*)-*inda-box*}$PdCl_2$ (**7**) as well as the nickel(II) complexes (BMDI)$NiBr_2$ (**6**) and {(1*R*,2*S*)-*inda-box*}$NiBr_2$ (**8**) were prepared in moderate yields by treating the complexes [$(NCPh)_2PdCl_2$] or [(DME)$NiBr_2$] with the corresponding ligands in acetone or CH_2Cl_2 at room temperature (Figs. 1 and 2).

Pd(II) complexes, like **5** and **7**, can be used as catalysts for CO/alkene copolymerization after conversion of the dichlorides to the solvent stabilized cationic species (Fig. 2) [20]. The monoalkyl complex [{(1*S*,2*R*)-*inda-box*}$Pd(NCCH_3)(CH_3)]\cdot B(Ar_f)_4$ (**9**) was prepared by the reaction of [(TMEDA)$Pd(CH_3)Cl$] with **4** in CH_2Cl_2 followed by chloride abstraction with $NaB(Ar_f)_4$ in the presence of CH_3CN.

To confirm the identity of the complexes prepared in the present study, a variety of techniques including elemental analysis, mass spectroscopy (EI), infrared spectroscopy, ^1H and ^{13}C NMR have been used. In addition, complex **7** was a subject to single-crystal X-ray diffraction study. The isolated complexes are microcrystalline and stable at atmospheric conditions, except compound **9** which is moisture sensitive. Compared to the palladium(II) complexes, the corresponding dibromo nickel(II) complexes (**6** and **8**) showed lower solubility in deuterated organic solvents such as $CDCl_3$, CD_3CN, and CD_3COCD_3.

3.2. Crystal structure of complex (7)

Suitable crystals of the chiral and C_2-symmetric palladium(II) complex [Pd(*inda-box*)Cl_2] (**7**) (Fig. 3) were obtained by crystallization from acetone. Selected bond lengths and angles are given in Table 2. The palladium atom is at the center of approximately square-planar arrangement with two chlorine atoms (Cl1 and Cl2) and two nitrogen atoms (N1 and N2) of the bidentate ligand. The compound crystallizes in the monoclinic space groups $P2_1$ (No. 4) with $a = 7.633(2)$ Å, $b = 8.807(2)$ Å, $c = 14.664(3)$ Å, $\beta = 97.22(3)°$, $V = 978.0(4)$ Å^3 and $Z = 2$.

The results of X-ray analysis indicate the desired C_2-symmetric form for complex **7** in the solid state. This is also the case in solution, since only one set of resonances for protons related by a C_2-symmetric axis can be detected. The significant bond lengths and angles in **7** are similar for the ones reported for the structures of the C_2-symmetric [(1,2-bis(*N*-indolinyl)ethane)$PdCl_2$] [21] and [(2,2′-bipyridine)$PdCl_2$] [22] which indicates electronic similarity of the nitrogen sites in both complexes.

4. Supplementary material

Crystallographic data for the structural analysis have been deposited with the Cambridge Crystallographic Data Centre, CCDC No. 166715. Copies of this information may be obtained free of charge from The Director, CCDC, 12 Union Road, Cambridge, CB2 1EZ, UK (fax: +44-1223-336033; e-mail: deposit@ccdc.cam.ac.uk or www: http://www.ccdc.cam.ac.uk).

Acknowledgements

Financial support from Fortum Oy and Magnus Ehrnrooth foundation are gratefully acknowledged.

References

[1] (a) E.C. Alyea, Catalytic aspects of metal phosphine complexes, Adv. Chem. Ser. (1982) 196;
(b) in: L.H. Pignolet (Ed.), Homogeneous Catalysis With Metal Phosphine Complexes, Plenum, New York, 1983.
[2] I. Ojima (Ed.), Catalytic Asymmetric Synthesis, Wiley–VCH, New York, 1993.
[3] E.J. Corey, N. Imai, H. Zhang, J. Am. Chem. Soc. 113 (1991) 728.
[4] Y. Uozumi, K. Kato, T. Hayashi, J. Am. Chem. Soc. 119 (1997) 5063.
[5] H. Nishiyama, S.-B. Park, K. Itoh, Tetrahedron: Asymmetry 3 (1992) 1029.
[6] M. Brookhart, M.I. Wagner, J. Am. Chem. Soc. 116 (1994) 3641.
[7] (a) N. Seehof, C. Mehler, S. Breunig, W. Risse, J. Mol. Catal. 76 (1992) 219;
(b) C.M Killian, D.J. Tempel, L.K. Johnson, M. Brookhart, J. Am. Chem. Soc. 118 (1996) 11664.
[8] (a) A.S. Abu-Surrah, B. Rieger, Top. Catal. 7 (1999) 165;
(b) A.S. Abu-Surrah, B. Rieger, Angew. Chem., Int. Ed. Engl. 35 (1996) 2475.
[9] L.K. Johnson, S. Mecking, M. Brookhart, J. Am. Chem. Soc. 118 (1996) 267.
[10] A.S. Abu-Surrah, K. Lappalainen, T. Repo, M. Klinga, M. Leskelä, H.A. Hodali, Polyhedron 19 (2000) 1601.
[11] (a) A.S. Abu-Surrah, B. Rieger, J. Mol. Catal. A 128 (1998) 239;
(b) A.S. Abu-Surrah, U. Thewalt, B. Rieger, J. Organomet. Chem. 587 (1999) 58.
[12] (a) J. Hall, J-M. Lehn, A. De Cian, J. Fischer, Helv. Chim. Acta 74 (1991) 1;
(b) A.K. Ghosh, P. Mathivanan, J. Cappiello, Tetrahedron Lett. 37 (1996) 3815.
[13] J.R. Doyle, P.E. Slade, H.B. Jonassen, Inorg. Synth. 6 (1960) 216.
[14] L.G.L. Ward, Inorg. Synth. 12 (1972) 154.
[15] W. De Graf, J. Boersma, W.J.J. Smeets, A. Spek, G. Van Koten, Organometallics 8 (1989) 2907.
[16] Molecular Structure Corporation, TEXSAN, Single Crystal Structure Analysis Software, Version 1.6. MSC, 3200 Research Forest Drive, The Woodlands, TX 77381, USA, 1993.
[17] A.C.T. North, D.C. Phillips, F.S. Mathews, Acta Crystallogr., Sect. A A24 (1968) 351.
[18] G.M. Sheldrick, SHELX-97, Program for the solution and refinement of crystal structures, University of Göttingen, Göttingen, Germany, 1997.
[19] G.M. Sheldrick, SHELXTL/PC, Siemens Analytical X-ray Instruments Inc., Madison, Wisconsin, USA, 1990.
[20] (a) A. Sen, T.W. Lai, J. Am. Chem. Soc. 104 (1982) 3520;
(b) A. Sen, Z. Jiang, Macromolecules 26 (1993) 911.
[21] A.S. Abu-Surrah, R. Fawzi, M. Steimann, B. Rieger, J. Organomet. Chem. 512 (1996) 243.
[22] A.J. Canty, B.W. Skelton, P.R. Traill, A.H. White, Aust. J. Chem. 45 (1992) 417.

PERGAMON

Polyhedron 21 (2002) 33–37

POLYHEDRON

www.elsevier.com/locate/poly

Design and properties of mixed-metal multinuclear molecules. Part II. Novel heterotrinuclear complexes of $[Ag(PPh_3)_2]_2[Cu(mtm)_2]$ and $[Ag_2(dppm)_2][Cu(mtm)_2]$ (mtm = [bis(methylthio)methylene]malonate and dppm = bis(diphenylphosphino)methane)

Young Jun Park [a], Youngkyu Do [b,*], Kwan Mook Kim [c], Moon-Gun Choi [a], Moo-Jin Jun [a,*], Cheal Kim [d]

[a] *Department of Chemistry, Yonsei University, Seoul 120-749, South Korea*
[b] *Department of Chemistry and Center for Molecular Science, Korea Advanced Institute of Science and Technology, Taejon 305-701, South Korea*
[c] *Inorganic Chemistry Laboratory, Korea Institute of Science and Technology, Seoul 136-791, South Korea*
[d] *Department of Chemistry, Seoul National University of Technology, Seoul 139-743, South Korea*

Received 22 May 2001; accepted 26 September 2001

Abstract

Novel trinuclear disilver(I)–copper(II) complexes, $[Ag(PPh_3)_2]_2[Cu(mtm)_2]$ (**1**) and $[Ag_2(dppm)_2][Cu(mtm)_2]$ (**2**) (mtm = [bis(methylthio)methylene]malonate, dppm = bis(diphenylphosphino)methane) have been prepared and characterized by a single-crystal X-ray structure analysis. In the complex **1**, a silver atom is coordinated to each of the two carboxylate oxygens with different bond distances of 2.325(5) Å (Ag–O(1)) and 2.653(6) Å (Ag–O(2)). In the case of the complex **2**, two silver atoms are bridged by two dppm ligands separated by 3.0130(9) Å and Ag(1) has bonded to O(5) (2.442(5) Å). Interestingly, Ag(2) has bonded to O(4) (2.325(5) Å) which is not a coordinated carboxylate oxygen bonded to copper(II) atom. Interaction between silver(I)–thioether group was not observed in **1** and **2**. © 2002 Published by Elsevier Science Ltd.

Keywords: Trinuclear complexes; Single crystal structures; Copper(II); Silver(I); Carboxylate; Thioether

1. Introduction

Since Coucouvanis and coworkers synthesized an interesting class of polynuclear adducts between $M(PPh_3)_2$ (M = Ni, Cu) and anionic metal complexes in 1974 [1], some derivatives have been reported. For example, Kawamura and coworkers have reported the structures of Pt and Pd derivatives containing tri(*n*-butyl)phosphine silver complexes [2]. Very recently, our group has reported the structure of $[Ag(PR_3)_2]_2[Ni(mnt)_2]$ (R = Me, Et, Cy and mnt = maleonitriledithiolate) and $[Ag_2L_2][Ni(mnt)]_2$ (L = dppf and dppm) [3]. The structures reported so far having $[M(PR_3)_2[M'(L)_2]$ type formulae contain only mnt as a ligand except one example. In 1998, Healy and coworkers have reported the structure using thiosalicylate having O and S donor set during their electrochemical reactions [4].

The study on the bonding modes of the potentially multidentate ligands provide various synthetic routes for synthesizing magnetic materials, catalysts and biological model compounds. Ylidenemalonate ligands containing both sulfur and oxygen exhibit versatile coordination chemistry and are capable of forming polymeric and molecular metal complexes having interesting structural and magnetic properties [5,6]. In particular, the ligand mtm (mtm = [bis(methylthio)methyl-

* Corresponding authors. Tel.: +82-2-2123-2639; fax: +82-2-364-7050 (M.-J.J.).
E-mail address: mjjun@yonsei.ac.kr (M.-J. Jun).

0277-5387/02/$ - see front matter © 2002 Published by Elsevier Science Ltd.
PII: S0277-5387(01)00951-2

ene]malonate) has been shown to be useful in linking two different metal ions to afford a ferrimagnetic compound. The heterobimetallic layered compounds of manganese(II) and copper(II) metal ions [5], and the polymeric (μ-oxo)diferric chain complex, all of which include the ligand mtm, have shown unique magnetism [6]. Such sulfur-containing ligands with diverse potentials have prompted our interest in synthesizing new multinuclear metal complexes, not only to search out the novel strategy to design multinuclear magnetic materials, but also to investigate their coordination modes and structural properties. Here, we report the synthesis of novel heterotrinuclear complexes of $[Ag(PPh_3)_2]_2$-$[Cu(mtm)_2]$ and $[Ag_2(dppm)_2][Cu(mtm)_2]$ and their unique structural properties.

2. Experimental

2.1. Materials and instrumentation

Triphenylphosphine (Aldrich) and dppm (bis(-diphenylphosphino)methane) (Aldirch) were used as received without further purification. The mtm ligand was synthesized by slight modification of literature methods [7a]. Infrared spectra were recorded in a Nicolet Avatar 360 FT-IR spectrometer. Elemental analyses were performed at the Korea Basic Science Institute Seoul Branch Lab.

2.1.1. $[Ag(PPh_3)_2]_2[Cu(mtm)_2]$ (1)

$CuSO_4$ (0.08 g, 0.5 mmol) and $(NH_4)_2SO_4$ (0.07 g, 0.5 mmol) were added to a solution of $Ba(mtm)\cdot 2H_2O$ (0.34 g, 1 mmol) in water (200 ml). The mixture was stirred for 2 h. The precipitate $BaSO_4$ was removed by filtration, the filtrate was treated with Ag_2SO_4 (0.16 g, 0.5 mmol), and the mixture was stirred for 24 h in the dark. The resulting pale green precipitate was collected on a sintered glass filter and washed successively with water (100 ml), ethanol (20 ml) and ether (20 ml) and dried in vacuo. To this pale green solid suspended in $CHCl_3$ (50 ml) was added PPh_3 (0.52 g, 2 mmol). The mixture was stirred for 24 h. Unreacted solid was removed by filtration, and the resulting blue solution was concentrated to approximately 10 ml under reduced pressure and layered with ether. Blue crystals formed after 24 h were collected on a sintered glass filter. They lost their crystallinity when removed from the mother liquor. Washing with ether and hexane produced blue solids. Yield is 69% based on PPh_3. Elemental analysis was performed after vacuum drying at room temperature (r.t.). *Anal.* Calc. for $[Ag(PPh_3)_2]_2[Cu(mtm)_2]$: C, 57.95; H, 4.16; S, 7.36. Found: C, 57.65; H, 4.25; S, 7.32%. IR (cm^{-1}, KBr disc) 3051(s), 2918(m), 1629(vs), 1586(sh), 1480(s), 1433(s), 1303(vs), 1096(s), 748(s), 592(s), 506(s).

2.1.2. $[Ag_2(dppm)_2][Cu(mtm)_2]$ (2)

The procedure was similar to that used to prepare compound **1**, except that 2 equiv. of dppm were used in place of PPh_3. Recrystallization with CH_2Cl_2/acetone/ether solvent system yielded blue needle crystals (yield 65%). They lost their crystallinity when removed from the mother liquor. Elemental analysis was performed after vacuum drying at r.t. *Anal.* Calc. for $[Ag_2(dppm)_2][Cu(mtm)_2]$: C, 50.99; H, 3.86; S, 8.78. Found: C, 51.02; H, 3.92; S, 8.57%. IR (cm^{-1}, KBr disc) 3050(m), 2918(m), 1612(vs, sh), 1483(m), 1434(s), 1098(s), 778(s), 740(s), 693(s) 586(m), 511(m), 474(m).

2.1.3. X-ray analysis of $[Ag(PPh_3)_2]_2[Cu(mtm)_2]\cdot 2CHCl_3$ (1) and $[Ag_2(dppm)_2][Cu(mtm)_2]\cdot 2CH_2Cl_2\cdot$acetone (2)

X-ray crystallographic data were collected in an Enarf–Nonius CAD 4 automatic diffractometer with graphite-monochromated Mo Kα ($\lambda = 0.71073$ Å) at ambient temperature for compound **1**, $[Ag(PPh_3)_2]_2$-$[Cu(mtm)_2]\cdot 2CHCl_3$, and a Siemens three-circle diffractometer with a CCD area detector (SMART system) [8] under nitrogen flow using a LT-2 low-temperature system at 233 K for compound **2**, $[Ag_2(dppm)_2]$-$[Cu(mtm)_2]\cdot 2CH_2Cl_2\cdot$acetone. The structures were solved by the direct methods (SHELXS-97) and were refined by full-matrix least-squares techniques (SHELXL-97) [9]. Crystal parameters and procedural information corresponding to data collection and structure solution are given in Table 1.

3. Results and discussion

The reaction of $CuSO_4$ along with $(NH_4)_2SO_4$ and barium salts of [bis(methylthio)methylene]malonate (mtm) in distilled water gives a deep green solution at room temperature. The addition of silver sulfate to this deep green solution affords a pale green precipitate. Treatment of this compound with PPh_3 in chloroform results in the formation of a blue solution from which $[Ag(PPh_3)_2]_2[Cu(mtm)_2]\cdot 2CHCl_3$ (**1**) has been crystallized. The molecular structure of **1** as determined by single-crystal X-ray structure analysis is shown in Fig. 1. Relevant bond distances and angles are listed in Table 2. The copper(II) ion is coordinated in a square-planar geometry by four carboxylate oxygens from two mtm ligands (see Scheme 1). Each of the two Ag (I) cations is coordinated in a distorted tetrahedral arrangement by two PPh_3 ligands and two carboxylate oxygens (Ag–O(1) = 2.325(5) Å) and (Ag–O(2) = 2.653(6) Å) that form a bridging to the Cu(II) center. As a result, the interaction of the $Ag(PPh_3)_2^+$ cations with the $Cu(mtm)_2^-$ complex anions occurs at the CuO_4 moiety. The plane which is made up of C(2), C(2_1), C(3), C(4), S(1), S(2) of mtm ligand is bent by 65° from

the mean square-plane calculated by copper and four carboxylate oxygen atoms resulting in an overall chair-like conformation.

The reaction of the pale green precipitate with 2 equiv. of bis(diphenylphosphino)methane (dppm) led to the formation of trinuclear complex $[Ag_2(dppm)_2]$-$[Cu(mtm)_2]$ (**2**). The crystal structure of complex **2** is shown in Fig. 2. Selected bond distances and angles are listed in Table 3. In striking contrast to the complex **1** described above, this complex has an unsymmetric structure. The two silver atoms, bridged by two dppm ligands and separated by 3.0130(9) Å, show some weak Ag–Ag bonding character [10]. One silver (Ag(1)–O(5) = 2.442(5) Å) is coordinated to a carboxylate oxygen that bridges to the Cu(II) center, while the other silver (Ag(2)–O(4) = 2.325(5) Å) is coordinated by the carbonyl oxygen that is not coordinated to the copper(II) atom. The coordination geometry

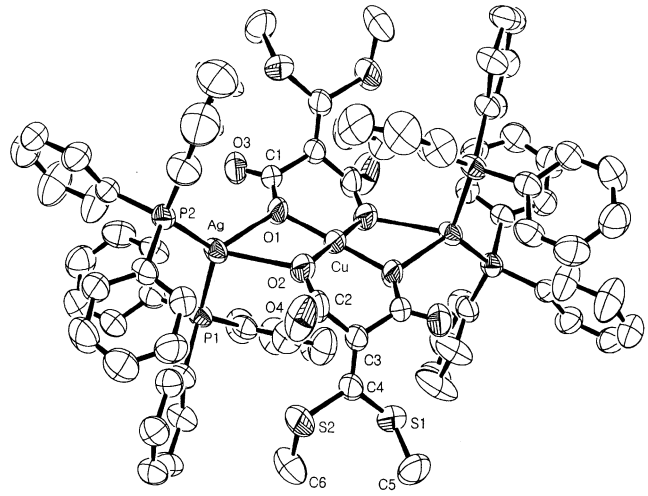


Fig. 1. ORTEP drawing of $[Ag(PPh_3)_2]_2[Cu(mtm)_2]\cdot 2CHCl_3$ (**1**) showing the atomic labeling scheme and thermal ellipsoids at the 50% level. The hydrogen atoms and solvent molecules are omitted for clarity.

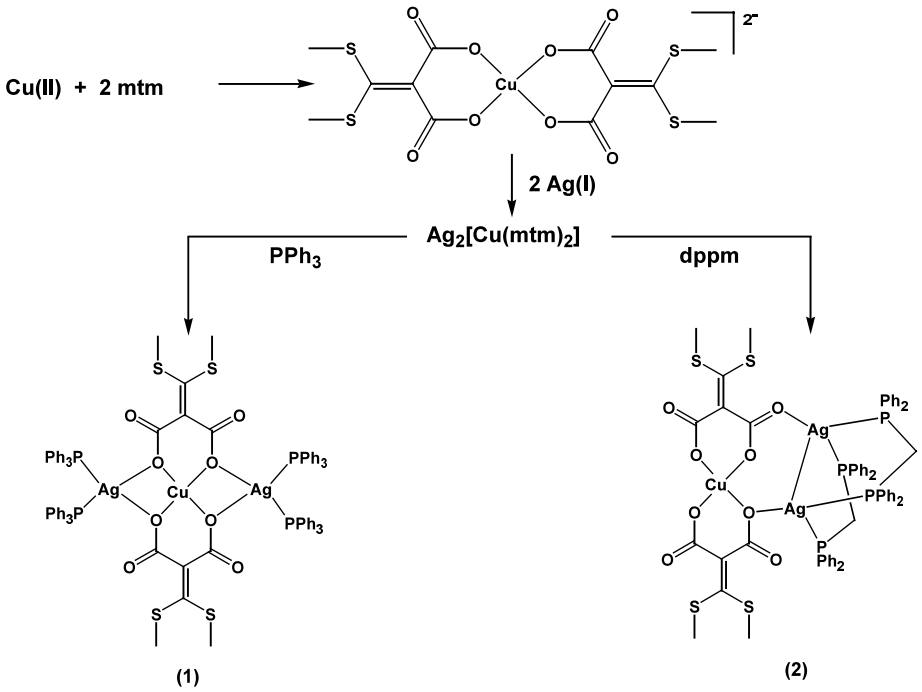
Table 1
Crystal data and structure refinement parameters for $[Ag(PPh_3)_2]_2$-$[Cu(mtm)_2]\cdot 2CHCl_3$ (**1**) and $[Ag_2(dppm)_2][Cu(mtm)_2]\cdot 2CH_2Cl_2\cdot$acetone (**2**)

	$[Ag(PPh_3)_2]_2$-$[Cu(mtm)_2]\cdot 2CHCl_3$	$[Ag_2(dppm)_2]$-$[Cu(mtm)_2]\cdot 2CH_2Cl_2\cdot$acetone
Empirical formula	$C_{86}H_{74}Ag_2Cl_6CuO_8P_4S_4$	$C_{67}H_{66}Ag_2Cl_4CuO_9P_4S_4$
Formula weight	1979.66	1688.49
Temperature (K)	293(2)	233(2)
Crystal system	triclinic	monoclinic
Space group	$P\bar{1}$	$P2_1/n$
Unit cell dimensions		
a (Å)	13.128(2)	12.67180(10)
b (Å)	13.849(7)	18.6778(3)
c (Å)	14.951(4)	31.2740(5)
α (°)	111.65(3)	
β (°)	104.942(19)	101.0080(10)
γ (°)	104.52(3)	
V (Å^3)	2252.9(13)	7265.78(17)
Z	1	4
D_{calc} (g cm^{-3})	1.475	1.535
Absorption coefficient (mm^{-1})	1.058	1.226
$F(000)$	1013	3384
Crystal size (mm)	$0.4\times0.35\times0.2$	$0.4\times0.2\times0.2$
Theta range for data collection (°)	1.59–24.98	1.28–26.42
Reflections collected/unique	5732	42 002
Unique reflections	5473 [$R_{int}=0.0255$]	14 863 [$R_{int}=0.1024$]
Completeness to $2\theta=24.98$ (%)	68.8	96.5
Data/restraints/parameters	5473/0/520	14 863/0/855
Final R indices [$I>2\sigma(I)$]	$R_1=0.0636$, $wR_2=0.1607$	$R_1=0.0797$, $wR_2=0.1500$
R indices (all data)	$R_1=0.0662$, $wR_2=0.1629$	$R_1=0.1566$, $wR_2=0.1749$
Goodness-of-fit on F^2	1.141	1.086

Table 2
Selected bond lengths (Å) and bond angles (°) for $[Ag(PPh_3)_2]_2$-$[Cu(mtm)_2]\cdot 2CHCl_3$ (**1**)

Bond lengths	
Ag–O(1)	2.324(5)
Ag–P(2)	2.3957(19)
Ag–P(1)	2.4426(19)
Ag–O(2)	2.653(6)
Ag–Cu	3.4844(15)
Cu–O(1)$^{\#1}$	1.898(5)
Cu–O(1)	1.898(5)
Cu–O(2)	1.901(6)
Cu–O(2)$^{\#1}$	1.901(6)
Bond angles	
O(1)–Ag–P(2)	126.46(16)
O(1)–Ag–P(1)	101.67(17)
P(2)–Ag–P(1)	128.67(6)
O(1)–Ag–O(2)	61.19(18)
P(2)–Ag–O(2)	111.15(14)
P(1)–Ag–O(2)	106.78(14)
O(1)–Ag–Cu	30.59(12)
P(2)–Ag–Cu	132.08(5)
P(1)–Ag–Cu	98.08(5)
O(2)–Ag–Cu	32.66(13)
O(1)$^{\#1}$–Cu–O(1)	180.0
O(1)$^{\#1}$–Cu–O(2)	95.7(2)
O(1)–Cu–O(2)	84.3(2)
O(1)$^{\#1}$–Cu–O(2)$^{\#1}$	84.3(2)
O(1)–Cu–O(2)$^{\#1}$	95.7(2)
O(2)–Cu–O(2)$^{\#1}$	180.0
O(1)$^{\#1}$–Cu–Ag	141.45(15)
O(1)–Cu–Ag	38.55(15)
O(2)–Cu–Ag	48.85(17)
O(2)$^{\#1}$–Cu–Ag	131.15(17)

$\#1$: $-x$, $-y$, $-z$



Scheme 1.

around the copper(II) atom is distorted square planar. The resulting chelation mode forms a seven-membered ring made up of two Ag(I), three oxygens, one carbon and one Cu(II). It is remarkable that the addition of PPh_3 into the $[Cu(mtm)_2]^{2-}$ moiety produced the symmetric complex **1**, while the addition of dppm to the same moiety resulted in the formation of the unusual unsymmetric complex **2**. Such tactic could be employed for synthesizing symmetric and unsymmetric complexes by switching the phosphine ligands. Two dppm molecules should react with two Ag(I) to produce an $Ag_2(dppm)_2^{2+}$ adduct [11], which is then, unlike the case of complex **1**, unsymmetrically coordinated to two oxygens (O(4) and O(5)) of the carboxylates of $[Cu(mtm)_2]^{2-}$. For complex **1**, each silver(I) is coordinated by two PPh_3 ligands to afford two $Ag(PPh_3)_2^+$ units and these $Ag(PPh_3)_2^+$ units are then coordinated symmetrically to two oxygens of CuO_4 moiety.

Another important feature in the molecular structures is the binding modes in complexes **1** and **2**. It has been well documented that the silver(I) ion is able to form coordination complexes with a variety of donor atoms (e.g. S, P, N and O) [12], and the complexes of silver(I) with carboxylic acid can adopt various bonding modes which may be monomeric or extended to dimeric, olygomeric or polymeric one through a carboxylate bridging [13]. Moreover, the thioether function of the mtm ligands is a non-innocent donor set to the coordination process [7b]. For example, the mtm ligand and its derivatives containing both two sulfur and two oxygen donors may coordinate to Pt(II) ion via one of the three distinct modes of O,O′-, O,S′-, and S,S′-chelation [7]. For both complexes **1** and **2** only O,O′-chelation to Cu(II) has been observed. The Cu(II) ion is regarded on the borderline in the hard–soft acid–base concept [14] and can interact with both oxygen and sulfur of the mtm ligand during the reaction. It is noted that in our work only oxygen donor atoms coordinated to Cu(II) ion. It is very interesting

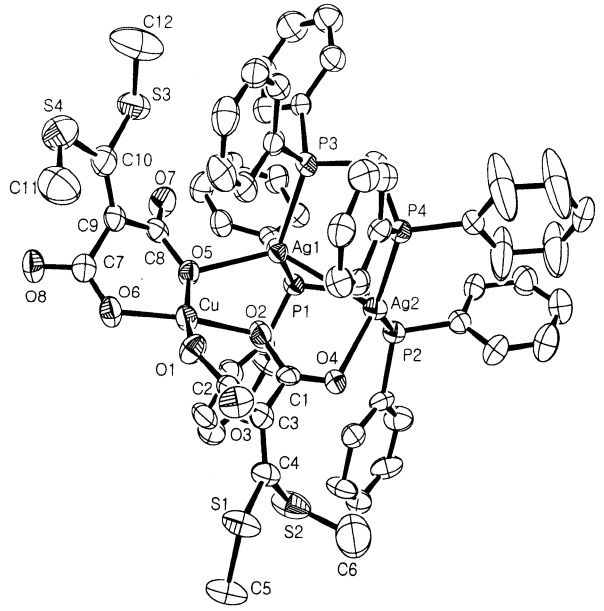


Fig. 2. ORTEP drawing of $[Ag_2(dppm)_2][Cu(mtm)_2]\cdot 2CH_2Cl_2\cdot$acetone (**2**) showing the atomic labeling scheme and thermal ellipsoids at the 50% level. The hydrogen atoms and solvent molecules are omitted for clarity.

Table 3
Selected bond lengths (Å) and bond angles (°) for $[Ag_2(dppm)_2][Cu(mtm)_2]\cdot 2CH_2Cl_2\cdot$acetone (**2**)

Bond lengths			
Ag(1)–P(1)	2.439(2)	Ag(2)–P(4)	2.435(2)
Ag(1)–O(5)	2.442(5)	Ag(2)–Cu	5.0060(11)
Ag(1)–P(3)	2.451(2)	Cu–O(6)	1.898(5)
Ag(1)–Ag(2)	3.0131(9)	Cu–O(5)	1.904(5)
Ag(1)–Cu	3.5864(11)	Cu–O(1)	1.918(5)
Ag(2)–O(4)	2.325(5)	Cu–O(2)	1.945(5)
Ag(2)–P(2)	2.431(2)		
Bond angles			
P(1)–Ag(1)–O(5)	110.86(13)	P(4)–Ag(2)–Cu	95.14(6)
P(1)–Ag(1)–P(3)	131.90(7)	Ag(1)–Ag(2)–Cu	45.147(18)
O(5)–Ag(1)–P(3)	109.11(13)	O(6)–Cu–O(5)	91.9(2)
P(1)–Ag(1)–Ag(2)	86.95(5)	O(6)–Cu–O(1)	92.6(2)
O(5)–Ag(1)–Ag(2)	126.98(12)	O(5)–Cu–O(1)	164.7(2)
P(3)–Ag(1)–Ag(2)	89.82(5)	O(6)–Cu–O(2)	169.1(2)
P(1)–Ag(1)–Cu	122.89(5)	O(5)–Cu–O(2)	85.2(2)
O(5)–Ag(1)–Cu	29.78(12)	O(1)–Cu–O(2)	92.9(2)
P(3)–Ag(1)–Cu	105.07(5)	O(6)–Cu–Ag(1)	130.92(16)
Ag(2)–Ag(1)–Cu	98.30(2)	O(5)–Cu–Ag(1)	39.58(15)
O(4)–Ag(2)–P(2)	114.11(14)	O(1)–Cu–Ag(1)	132.13(17)
O(4)–Ag(2)–P(4)	110.34(14)	O(2)–Cu–Ag(1)	48.28(15)
P(2)–Ag(2)–P(4)	134.60(7)	O(6)–Cu–Ag(2)	167.31(16)
O(4)–Ag(2)–Ag(1)	95.92(13)	O(5)–Cu–Ag(2)	75.44(15)
P(2)–Ag(2)–Ag(1)	93.33(5)	O(1)–Cu–Ag(2)	99.69(17)
P(4)–Ag(2)–Ag(1)	90.89(5)	O(2)–Cu–Ag(2)	13.98(15)
O(4)–Ag(2)–Cu	52.34(13)	Ag(1)–Cu–Ag(2)	36.555(15)
P(2)–Ag(2)–Cu	119.01(5)		

to observe that, in complexes **1** and **2**, the silver(I) cation coordinated to two oxygens instead of two sulfurs, even though the high preference of Ag(I) for sulfur has been reported with the mixed cyclic ether 1,4-thioxane [12]. Complexes **1** and **2** also possess unusual coordination modes between Ag^+ cations and $[Cu(mtm)_2]^{2-}$. The complex **1** involves silver(I) cations bound to two oxygens coordinated to Cu(II) cation, whereas the complex **2** has bridging through both the oxygen of carbonyl moiety and the oxygen coordinated to Cu(II) center. The bidentate dithiolene ligand containing sulfur donor atom is often used to produce polynuclear complexes. For example, the dithiolene complexes of Group 10 metals react with Ag(I) to form mixed-metal complexes of the type $[M(mnt)_2\{Ag(PR_3)_2\}_2]$ (M = Ni, Pd, Pt; mnt = maleonitriledithiolate) [1–3]. These structures show slightly longer Ag–S distances than the normal and shorter M–Ag distances than van der Waals contact. These results imply bonding interaction between M and Ag atoms. In the structures of these mixed-metal complexes the silver atoms are located above and below the MS_4 planes. Entirely different from the complexes of the $[M(mnt)_2\{Ag(PR_3)_2\}_2]$ described above, our trinuclear adducts of $[Cu(mtm)_2][Ag(PPh_3)_2]_2$ (**1**) and $[Cu(mtm)_2][Ag_2(dppm)_2]$ (**2**) do not exhibit bonding interaction between Cu(II) centers and Ag(I) (Ag–Cu = 3.4845(15) in **1** and Ag(1)–Cu = 5.0060(11) in **2**).

4. Supplementary material

Crystallographic data for the structural analysis have been deposited with the Cambridge Crystallographic Data Centre, CCDC Nos. 157084 and 157085 for compounds **1** and **2**, respectively. Copies of this information may be obtained free of charge from The Director, CCDC, 12 Union Road, Cambridge, CB2 1EZ, UK (fax: +44-1223-336033; e-mail: deposit@ccdc.cam.ac.uk or www: http://www.ccdc.cam.ac.uk).

Acknowledgements

The authors wish to acknowledge the financial support of the Korea Research Foundation made in the program year of 1997 (Grant No. 1997-011-D00018).

References

[1] (a) D. Coucouvanis, N.C. Baenziger, S.M. Johnson, Inorg. Chem. 13 (1974) 1191;
(b) M.L. Caffery, D. Coucouvanis, J. Inorg. Nucl. Chem. 37 (1975) 2081;
(c) F.J. Hollander, Y.L. Ip, D. Coucouvanis, Inorg. Chem. 15 (1976) 2230.
[2] M. Ebihara, M. Tsuchiya, M. Yamada, K. Tokoro, T. Kawamura, Inorg. Chim. Acta 231 (1995) 35.
[3] K.-T. Youm, Y. Kim, Y. Do, M.-J. Jun, Inorg. Chim. Acta 310 (2000) 203.
[4] R.C. Bott, P.C. Healy, D.S. Sagatys, Chem. Commun. (1998) 2403.
[5] J. Kim, J.M. Lim, Y.-K. Choi, Y. Do, Angew. Chem., Int. Ed. Engl. 35 (1996) 998.
[6] C.S. Hong, J. Kim, N.H. Hur, Y. Do, Inorg. Chem. 35 (1996) 5110.
[7] (a) Y.S. Sohn, K.M. Kim, S.-J. Kang, O.-S. Jung, Inorg. Chem. 35 (1996) 4274;
(b) K.M. Kim, S.S. Lee, O.-S. Jung, M.-J. Jun, Y.S. Sohn, Inorg. Chim. Acta 256 (1997) 217;
(c) S.S. Lee, M.J. Jun, K.M. Kim, O.-S. Jung, Y.S. Sohn, Polyhedron (1994) 1397.
[8] SMART Area-Detector Software Package, Siemens Analytical Instrumentation Inc., Madison, WI, 1995.
[9] (a) G.M. Shedrick, SHELXS-97: A Program for Structure Determination, University of Göttingen, Göttingen, Germany, 1997;
(b) G.M. Shedrick, SHELXL-97: A Program for Structure Refinement, University of Göttingen, Göttingen, Germany, 1997.
[10] V.W.-W. Yam, W.K.-M. Fung, K.-K. Cheung, Organometallics 16 (1997) 2032.
[11] D.M. Ho, R. Bau, Inorg. Chem. 22 (1983) 4073.
[12] H.A. Buchholz, G.K.S. Prakash, J.F.S. Vaughan, R. Bau, G.A. Olah, Inorg. Chem. 35 (1996) 4076 (and references therein).
[13] (a) G. Smith, D.E. Lynch, C.H.L. Kennard, Inorg. Chem. 35 (1996) 2711;
(b) P. Wei, T.C.W. Mak, D.A. Atwood, Inorg. Chem. 37 (1998) 2605.
[14] J.E. Huheey, E.A. Keiter, R.L. Keiter, Inorganic Chemistry: Principles of Structure and Reactivity, 4th ed., Harper-Collins, New York, 1993, p. 347.

PERGAMON

Polyhedron 21 (2002) 39–48

POLYHEDRON

www.elsevier.com/locate/poly

Cyclopalladated compounds derived from [C,N,O] terdentate ligands: synthesis, characterization and reactivity

Alberto Fernández [a,*], Esther Pereira [a], Jesús J. Fernández [a], Margarita López-Torres [a], Antonio Suárez [a], Roberto Mosteiro [a], José M. Vila [b,*]

[a] *Departamento de Química Fundamental, Universidad de La Coruña, E-15071 La Coruña, Spain*

[b] *Departamento de Química Inorgánica, Universidad de Santiago de Compostela, E-15782 Santiago de Compostela, Spain*

Received 1 June 2001; accepted 1 October 2001

Abstract

Treatment of the Schiff base ligands 2-$ClC_6H_4C(H)=NCH_2(C_4H_7O)$ (**a**) and 3,4-$(MeO)_2C_6H_3C(H)=NCH_2(C_4H_7O)$ (**b**) with palladium(II) acetate in toluene or glacial acetic acid gave the dinuclear cyclometallated complexes $[Pd\{2\text{-}ClC_6H_3C(H)=NCH_2(C_4H_7O)\}(\mu\text{-}OAc)]_2$ (**1a**) and $[Pd\{3,4\text{-}(MeO)_2C_6H_2C(H)=NCH_2(C_4H_7O)\}(\mu\text{-}OAc)]_2$ (**1b**) with the ligand bonded to the palladium atom through the imine nitrogen and the C6 carbon atom. The ^1H and $^{13}C-\{^1H\}$ NMR spectra of the complexes show the occurrence in solution of three pairs of enantiomers. The acetato-bridged cyclometallated complex $[Pd\{3,4\text{-}(MeO)_2C_6H_2C(H)=NCH_2(C_4H_7O)\}(\mu\text{-}OAc)]_2$ (**1c**) was prepared from the enantiopure ligand (*R*)-3,4-$(MeO)_2C_6H_3(H)=NCH_2(C_4H_7O)$ (**c**). The NMR spectra of **1c** showed the existence of only two diastereomers in the solution. The reaction of **1a** and **1b** with aqueous sodium chloride gave the chloro-bridged complexes $[Pd\{2\text{-}ClC_6H_3C(H)=NCH_2(C_4H_7O)\}(\mu\text{-}Cl)]_2$ (**2a**) and $[Pd\{3,4\text{-}(MeO)_2C_6H_2C(H)=NCH_2(C_4H_7O)\}(\mu\text{-}Cl)]_2$ (**2b**) after a metathesis reaction. The reaction of **2a** with PPh_3 in acetone gave the mononuclear cyclometallated complex $[Pd\{2\text{-}ClC_6H_3C(H)=NCH_2(C_4H_7O)\}(Cl)(PPh_3)]$ (**3a**) in a bridge-splitting reaction. Treatment of **3a** with silver triflate gave the cyclometallated complex $[Pd\{2\text{-}ClC_6H_3C(H)=NCH_2(C_4H_7O)\}(PPh_3)][CF_3SO_3]$ (**4a**) in which the palladium atom is bonded to four different atoms C, N, O and P. When complex **2a** was reacted with silver triflate in acetone complex $[Pd\{2\text{-}ClC_6H_3C(H)=NCH_2(C_4H_7O)\}((CH_3)_2CO)][CF_3SO_3]$ (**5a**) was obtained with the ligand as [C,N,O] coordinated. The reaction of complexes **2a** and **2b** with the diphosphine dppp in a complex–phosphine 1:1 molar ratio gave the dinuclear cyclometallated complexes $[\{Pd[2\text{-}ClC_6H_3C(H)=NCH_2(C_4H_7O)](Cl)\}_2(\mu\text{-}Ph_2P(CH_2)_3PPh_2)]$ (**8a**) and $[\{Pd[3,4\text{-}(MeO)_2C_6H_2C(H)=NCH_2(C_4H_7O)](Cl)\}_2(\mu\text{-}Ph_2P(CH_2)_3PPh_2)]$ (**5b**) with the diphosphine bridging the two palladium atoms. Reaction of complexes **2a** and **2b** with the phosphines dppp and *cis*-dppe in a 1:2 molar ratio gave the mononuclear complexes $[Pd\{2\text{-}ClC_6H_3C(H)=NCH_2(C_4H_7O)\}\{Ph_2P(CH_2)_3Ph_2\text{-}P,P\}][ClO_4]$ (**6a**), $[Pd\{3,4\text{-}(MeO)_2C_6H_2C(H)=NCH_2(C_4H_7O)\}\{Ph_2P(CH_2)_3Ph_2\text{-}P,P\}][ClO_4]$ (**3b**) and $[Pd\{2\text{-}ClC_6H_2C(H)=NCH_2(C_4H_7O)\}(cis\text{-}Ph_2PCH=CHPh_2\text{-}P,P)][Cl]$ (**4b**). The treatment of **2a** with the triphosphine bis(2-diphenylphosphinoethyl)phenylphosphine in 1:2 molar ratio, followed by treatment with sodium perchlorate gave $[Pd\{3,4\text{-}(MeO)_2ClC_6H_3C(H)=NCH_2(C_4H_7O)\}\{(PPh_2CH_2CH_2)_2PPh\text{-}P,P,P\}][ClO_4]$ (**7a**) in which the palladium atom is bonded to the triphosphine through the three phosphorus atoms and to the Schiff base ligand through one carbon atom and the imine nitrogen. © 2002 Elsevier Science Ltd. All rights reserved.

Keywords: C–H activation; Cyclometallation; Phosphorus ligands; Schiff bases; Palladium

1. Introduction

The study of cyclometallated compounds has attracted much attention over the last three decades [1–5]. They present numerous applications in organic and organometallic synthesis [6], in insertion reactions [7], in optical resolution [8], in the determination of the enantiomeric excess [9], in the synthesis of new metal mesogenic compounds [10], biologically active compounds [11,12], in catalytic materials [13], in the building of new self assembly supramolecular species [14], and to promote unusual coordination environments [15].

* Corresponding authors. Fax: +34-981-595-012 (J.M.V.); 34-981-167-065 (A.F.).

E-mail addresses: qiluaafl@udc.es (J.M. Vila), qideport@usc.es (A. Fernández).

0277-5387/02/$ - see front matter © 2002 Elsevier Science Ltd. All rights reserved.
PII: S0277-5387(01)00970-6

Our interest in cyclometallated complexes has been, in part, focused on the study of compounds derived from potentially [C,N,X] (X = O, S, N) terdentate ligands, such as semicarbazones [16,17], thiosemicarbazones [18,19] or Schiff bases [20–23] which react with palladium(II) and platinum(II) or palladium(0) to give cyclometallated complexes with two fused rings at the metal. In spite of the large number of [C,N,N] derivatives reported [24], relatively few [C,N,O] derivatives are known [25].

Semicarbazones are known to react readily with $M_2[PdCl_4]$ (M = Li, K) to give mononuclear cyclometallated complexes; however, complexes derived from thiosemicarbazones show tetranuclear structures.

In the present paper we report the synthesis of new cyclometallated compounds derived from the potentially terdentate Schiff bases 2-$ClC_6H_4C(H)$=NCH_2-(C_4H_7O) (**a**) and 3,4-$(MeO)_2C_6H_3C(H)$=$NCH_2(C_4H_7O)$ (**b**). We have found that direct reaction with Pd(II) or Pd(0) salts did not yield the expected complex with the ligand in a [C,N,O] terdentate fashion. Thus, in an oxidative addition reaction, treatment of **a** with $[Pd_2(dba)_3]$, in benzene under reflux, gave an untreatable mixture which was not further investigated, and reaction of **a** or **b** with palladium(II) acetate, in glacial acetic acid, only yielded the dimeric acetato-bridged complexes **1a** and **1b** with the corresponding ligand as [C,N] bidentate. However, the vacant site produced in the coordination sphere of the palladium atom, upon reaction of the cyclometallated halogen-bridged dimer complexes with a Ag(I) salt, promotes formation of the Pd–O bond. The reactivity of the cyclometallated complexes with mono-, di- and triphosphines is reported, and we also describe a new type of stereoisomerism arising from the folded open-book disposition of the cyclometallated ligands in the acetato-bridged dimers **1a** and **1b**.

2. Experimental

Safety note: Caution: perchlorate salts of metal complexes with organic ligands are potentially explosive. Only small amounts of these materials should be prepared and handled with great caution.

2.1. General procedures

Solvents were purified by standard methods [26]. Chemicals were reagent grade. The phosphines PPh_3, *cis*-Ph_2PCH=$CHPPh_2$ (*cis*-dppe), $Ph_2P(CH_2)_3PPh_2$ (dppp) and $(Ph_2PCH_2CH_2)_2PPh$ (triphos) were purchased from Aldrich-Chemie. Microanalyses were carried out using a Carlo–Erba elemental analyzer, model 1108. IR spectra were recorded as Nujol mulls or KBr discs on a Perkin–Elmer 1330 and on a Mattson spectrophotometers. NMR spectra were obtained as $CDCl_3$ solutions and referenced to $SiMe_4$ (^1H, $^{13}C-\{^1H\}$) or 85% H_3PO_4 ($^{31}P-\{^1H\}$) and were recorded on a Bruker AC-2005 spectrometer. All chemical shifts were reported downfield from standards. The FAB mass spectra were recorded using a Quatro mass spectrometer with a Cs ion gun; 3-nitrobenzyl alcohol was used as the matrix. Conductivity measurements were made on a CRISON GLP 32 conductivimeter using 10^{-3} mol dm^{-3} solutions in dry acetonitrile.

The syntheses of 2-$ClC_6H_4C(H)$=$NCH_2(C_4H_7O)$ (**a**) and 3,4-$(MeO)_2C_6H_3C(H)$=$NCH_2(C_4H_7O)$ (**b**) were performed by heating chloroform solutions of the appropriate quantities of tetrahydrofurfurylamine and 2-chlorobenzaldehyde or 3,4-dimethoxybenzaldehyde, respectively, in a Dean–Stark apparatus under reflux. Schiff base ligand (*R*)-3,4-$(MeO)_2C_6H_3C(H)$=NCH_2-(C_4H_7O) (**c**) was prepared similarly using enantiopure (*R*)-tetrahydrofufurylamine. IR (ν_{max}/cm^{-1}) (C=N) 1640s (**a**), 1645s (**b**, **c**). $^{13}C-\{^1H\}$ NMR for ligand **a**: (50.28 MHz, $CDCl_3$): δ 158.9 (C=N); δ 135.0 (C1); δ 129.6 (C6); δ 131.1 (C2); δ 126.8 (C5); δ 128.3, 131.4 (C3, C4); δ 78.3 (C8); δ 68.1 (C11); δ 65.8 (C7); δ 29.2, 25.7 (C9, C10). $^{13}C-\{^1H\}$ NMR for ligand **b, c**: δ 161.9 (C=N); δ 151.3, 149.2 (C3, C4); δ 129.4 (C1); δ 123.1 (C6); δ 110.3, 108.8 (C2, C5); δ 78.5 (C8); δ 68.1 (C11); δ 65.7 (C7); δ 29.3, 25.6 (C9, C10); δ 55.8 (OCH_3).

2.2. Syntheses

2.2.1. *[Pd{2-$ClC_6H_3C(H)$=$NCH_2(C_4H_7O)$}(μ-OAc)]$_2$ (1a)*

A pressure tube containing 2-$ClC_6H_4C(H)$=NCH_2-(C_4H_7O) (**a**) (150 mg, 0.67 mmol), palladium(II) acetate (150 mg, 0.67 mmol) and 25 cm^3 of dry toluene was sealed under argon. The resulting mixture was heated at 60 °C for 3 h. After cooling to room temperature (r.t.) the orange precipitate formed was filtered off and dissolved in chloroform. The red solution obtained was filtered through Celite to remove the black palladium formed. The solvent was removed under vacuum to give an orange solid which was chromatographed on a column packed with silica gel. Elution with dichloromethane–methanol (1%) afforded the final product after concentration. Yield 44%. *Anal.* Found: C, 43.2; H, 4.2; N, 3.6. Calc. for $C_{28}H_{32}N_2O_6Cl_2Pd_2$: C, 43.3; H, 4.1; N, 3.6%. IR: ν(C=N), 1610s cm^{-1}; ν_{as}(COO), 1560s cm^{-1}; ν_s(COO), 1410s cm^{-1}. $^{13}C-\{^1H\}$ NMR: (50.28 MHz, $CDCl_3$): δ 171.6, 171.7 (C=N); δ 156.9, 156.7 (C6); δ 143.2, 143.0 (C1); δ 131.0 (C2); δ 124.6, 124.7 (C5); δ 130.1, 130.2, 130.3, 130.4 (C3, C4); δ 76.6 (C8); δ 68.5 (C11); δ 63.6, 61.6 (C7); δ 29.1, 28.4, 25.9, 25.5 (C9, C10); δ 173.0 (CH_3COO); δ 24.4 (CH_3COO). FAB MS: m/z = 776 $[M]^+$; 717 $[M-AcO]^+$.

Complexes **1b** and **1c** were prepared similarly.

*2.2.2. [Pd{3,4-(MeO)$_2$C$_6$H$_2$C(H)=NCH$_2$-(C$_4$H$_7$O)}(μ-OAc)]$_2$ (**1b**)*

Yield 56%. *Anal*. Found: C, 46.2; H, 5.2; N, 3.3. Calc. for $C_{32}H_{42}N_2O_{10}Pd_2$: C, 46.4; H, 5.1; N, 3.4%. IR: ν(C=N), 1608m cm^{-1}; ν_{as}(COO), 1570s cm^{-1}; ν_s(COO), 1415s cm^{-1}. ^{13}C–{^{1}H} NMR: (50.28 MHz, $CDCl_3$): δ 173.8, 173.7, 172.5, 172.4 (C=N); δ 149.3, 149.0 (C6); δ 149.4, 146.0 (C3, C4); δ 137.8, 137.4 (C1); δ 114.1, 109.9 (C2, C5); δ 76.9 (C8); δ 68.3, 67.8 (C11); δ 62.7, 60.1 (C7); δ 29.1, 28.6, 25.8, 25.4 (C9, C10); δ 181.1, 180.0 (CH_3COO); δ 24.4, 24.3 (CH_3COO); δ 56.2, 55.7 (OCH_3).

*2.2.3. (R)-[Pd{3,4-(MeO)$_2$C$_6$H$_2$C(H)=NCH$_2$-(C$_4$H$_7$O)}(μ-OAc)]$_2$ (**1c**)*

Yield 65%. *Anal*. Found: C, 45.7; H, 5.4; N, 3.2. Calc. for $C_{32}H_{42}N_2O_{10}Pd_2$: C, 46.4; H, 5.1; N, 3.4%. IR: ν(C=N), 1608m cm^{-1}; ν_{as}(COO), 1570s cm^{-1}; ν_s(COO), 1415s cm^{-1}. ^{13}C–{^{1}H} NMR: (50.28 MHz, $CDCl_3$): δ 173.8, 172.4 (C=N); δ 149.3 (C6); δ 149.4, 146.0 (C3, C4); δ 137.8, 137.4 (C1); δ 114.1, 109.9 (C2, C5); δ 76.9 (C8); δ 68.3, 67.8 (C11); δ 62.7, 60.1 (C7); δ 29.1, 28.6, 25.8, 25.4 (C9, C10); δ 181.1, 180.0 (CH_3COO); δ 24.4, 24.3 (CH_3COO); δ 56.2, 55.7 (OCH_3).

*2.2.4. [Pd{2-ClC$_6$H$_3$C(H)=NCH$_2$(C$_4$H$_7$O)}(μ-Cl)]$_2$ (**2a**)*

An aqueous solution of NaCl (ca. 10^{-2} M) was added dropwise to a solution of **1a** (200.0 mg, 0.257 mmol) in 10 cm^3 of acetone. The resulting mixture was stirred for 6 h. The yellow precipitate formed was filtered off, washed with water and dried under vacuum. Yield 86%. *Anal*. Found: C, 39.9; H, 3.3; N, 3.7. Calc. for $C_{24}H_{26}N_2O_2Cl_4Pd_2$: C, 39.5; H, 3.6, N, 3.8%. IR: ν(C=N), 1615s cm^{-1}. ^{13}C–{^{1}H} NMR: (50.28 MHz, $CDCl_3$): δ 174.4 (C=N); δ 155.2 (C6); δ 143.3 (C1); δ 131.1 (C2); δ 125.4 (C5); δ 131.3, 131.7 (C3, C4); δ 76.7 (C8); δ 68.2 (C11); δ 63.7 (C7); δ 28.9, 25.8 (C9, C10). FAB MS: $m/z = 765$ $[M + Cl]^+$; 693 $[M - Cl]^+$.

Complex **2b** was prepared similarly as a yellow solid.

*2.2.5. [Pd{3,4-(MeO)$_2$C$_6$H$_2$C(H)=NCH$_2$-(C$_4$H$_7$O)}(μ-Cl)]$_2$ (**2b**)*

Yield 91%. *Anal*. Found: C, 43.4; H, 4.3; N, 3.7. Calc. for $C_{28}H_{36}N_2O_6Cl_2Pd_2$: C, 43.1; H, 4.6, N, 3.6%. IR: ν(C=N), 1610m cm^{-1}. FAB MS: $m/z = 780$ $[M]^+$; 745 $[M - Cl]^+$.

*2.2.6. [Pd{2-ClC$_6$H$_3$C(H)=NCH$_2$(C$_4$H$_7$O)}(Cl)(PPh$_3$)] (**3a**)*

PPh_3 (22.0 mg, 0.082 mmol) was added to a suspension of **2a** (30.0 mg, 0.041 mmol) in acetone (15 cm^3). The mixture was stirred for 12 h and the white precipitate formed filtered off, dried under vacuum and recrystallized from chloroform–hexane. Yield 74%. *Anal*. Found: C, 57.1; H, 4.9; N, 2.3. Calc. for $C_{30}H_{28}NOCl_2PdP$: C, 57.5; H, 4.5; N, 2.2%. IR: ν(C=N), 1620m cm^{-1}. ^{13}C–{^{1}H} NMR: (50.28 MHz, $CDCl_3$): δ 175.0 (d, C=N, $JPC = 4.2$ Hz); δ 160.0 (C6); δ 145.0 (C1); δ 131.3 (C2); δ 124.8 (C5); δ 131.0, 131.9 (C3, C4); δ 77.5 (C8); δ 67.9 (C11); δ 65.6 (C7); δ 28.8, 25.8 (C9, C10). P-phenyl: δ 135.4 (d, C_o, $JPC = 12.1$ Hz); δ 128.0 (d, C_m, $JPC = 11.3$ Hz); δ 130.8 (d, C_p, $JPC = 2.8$ Hz); δ 130.7 (d, C_i, $JPC = 42.5$ Hz). FAB MS: $m/z = 627$ $[M]^+$; 590 $[M - Cl]^+$.

*2.2.7. [Pd{2-ClC$_6$H$_3$C(H)=NCH$_2$(C$_4$H$_7$O)}-(PPh$_3$)][CF$_3$SO$_3$] (**4a**)*

A suspension of **3a** (24.0 mg, 0.020 mmol) in acetone (15 cm^3) was treated with silver trifluoromethanesulfonate (5.2 mg, 0.020 mmol) and stirred for 24 h. The resulting solution was filtered through Celite to eliminate the AgCl precipitate and the solvent removed to give a yellow solid, which was recrystallized from chloroform–hexane. Yield 60%. *Anal*. Found: C, 50.1; H, 3.7; N, 2.1. Calc. for $C_{31}H_{28}NO_4F_3ClSPdP$: C, 50.3; H, 3.8; N, 1.9%. IR: ν(C=N), 1620m cm^{-1}. ^{13}C–{^{1}H} NMR: (50.28 MHz, $CDCl_3$): δ 173.6 (d, C=N, $JPC = 3.5$ Hz); δ 151.3 (C6); δ 145.5 (C1); δ 127.7 (C2); δ 126.3 (C5); δ 128.7 (C3, C4); δ 81.9 (C8); δ 69.7 (C11); δ 61.7 (C7); δ 28.4 (C9, C10). P-phenyl: δ 134.9 (d, C_o, $JPC = 12.1$ Hz); δ 129.0 (d, C_m, $JPC = 10.6$ Hz); δ 131.8 (d, C_p, $JPC = 2.8$ Hz); δ 132.4 (d, C_i, $JPC = 48.2$ Hz). FAB MS: $m/z = 592$ $[M - CF_3SO_3]^+$. Specific molar conductivity, $\Lambda_m = 156.4$ ohm^{-1} cm^2 mol^{-1} (in acetonitrile).

*2.2.8. [{Pd[2-ClC$_6$H$_3$C(H)=NCH$_2$(C$_4$H$_7$O)](Cl)}$_2$-(μ-Ph$_2$P(CH$_2$)$_3$PPh$_2$)] (**8a**)*

$Ph_2P(CH_2)_3PPh_2$ (dppp) (17.0 mg, 0.041 mmol) was added to a suspension of **2a** (30.0 mg, 0.041 mmol) in acetone (15 cm^3). The mixture was stirred for 12 h and the precipitate formed filtered off and dried under vacuum to give a white solid which was recrystallized from chloroform–hexane. Yield 51%. *Anal*. Found: C, 49.1; H, 4.3; N, 2.3. Calc. for $C_{51}H_{52}N_2O_2Cl_4Pd_2P_2.CHCl_3$: C, 49.5; H, 4.2; N, 2.2%. IR: ν(C=N), 1623m cm^{-1}.

Compound **5b** was prepared similarly as a white solid.

*2.2.9. [{Pd[3,4-(MeO)$_2$C$_6$H$_2$C(H)=NCH$_2$-(C$_4$H$_7$O)](Cl)}$_2$(μ-Ph$_2$P(CH$_2$)$_3$PPh$_2$)] (**5b**)*

Yield 55%. *Anal*. Found: C, 55.1; H, 5.0; N, 2.3. Calc. for $C_{55}H_{62}N_2O_6Cl_2Pd_2P_2$: C, 55.4; H, 5.2; N, 2.3%. IR: ν(C=N), 1615m cm^{-1}.

*2.2.10. [Pd{2-ClC$_6$H$_3$C(H)=NCH$_2$(C$_4$H$_7$O)}-(Ph$_2$P(CH$_2$)$_3$Ph$_2$–P,P)][ClO$_4$] (**6a**)*

$Ph_2P(CH_2)_3Ph_2$ (dppp) (34.0 mg, 0.082 mmol) was added to a suspension of **2a** (30.0 mg, 0.041 mmol) in

acetone (20 cm^3). The mixture was stirred for 1 h, after which an excess of sodium perchlorate was added. The complex was then precipitated out by addition of water, filtered off and dried in vacuo. Recrystallization from chloroform–hexane gave the final compound as a white solid. Yield 85%. *Anal*. Found: C, 55.1; H, 4.2; N, 3.0. Calc. for $C_{39}H_{39}N_2O_5Cl_2P_2Pd$: C, 54.8; H, 4.6; N, 3.3%. IR: ν(C=N), 1617m cm^{-1}. Specific molar conductivity, $\Lambda_m = 113.5$ ohm^{-1} cm^2 mol^{-1} (in acetonitrile).

Complex **3b** was synthesized similarly as a yellow solid.

2.2.11. [Pd{3,4-(MeO)$_2$C$_6$H$_3$C(H)=NCH$_2$(C$_4$H$_7$O)}-(Ph$_2$P(CH$_2$)$_3$Ph$_2$–P,P)][ClO$_4$] (3b)

Yield 85%. *Anal*. Found: C, 56.1; H, 5.0; N, 1.9. Calc. for $C_{41}H_{44}NO_7ClPdP_2$: C, 56.8; H, 5.1; N, 1.6%. IR: ν(C=N), 1615m cm^{-1}. Specific molar conductivity, $\Lambda_m = 140.3$ ohm^{-1} cm^2 mol^{-1} (in acetonitrile).

2.2.12. [Pd{3,4-(MeO)$_2$C$_6$H$_2$C(H)=NCH$_2$(C$_4$H$_7$O)}-(cis-Ph$_2$PCH=CHPh$_2$–P,P)][Cl] (4b)

cis-$Ph_2PCH{=}CHPh_2$ (*cis*-dppe) (30.0 mg, 0.074 mmol) was added to a suspension of **2b** (29.0 mg, 0.037 mmol) in acetone (20 cm^3). The mixture was stirred for 1 h. The complex was then precipitated out by addition of water, filtered off and dried in vacuo. Recrystallization from chloroform–hexane gave the final compound as a white solid. Yield 62%. *Anal*. Found: C, 48.8; H, 4.5; N, 2.0. Calc. for $C_{40}H_{40}NO_3ClP_2Pd{\cdot}2CHCl_3$: C, 49.2; H, 4.1; N, 1.4%. IR: ν(C=N), 1606m cm^{-1}. Specific molar conductivity, $\Lambda_m = 90.3$ ohm^{-1} cm^2 mol^{-1} (in acetonitrile).

Complex **7a** was synthesized as a yellow solid using a similar procedure to the one described for complex **6a**.

2.2.13. [Pd{2-ClC$_6$H$_3$C(H)=NCH$_2$(C$_4$H$_7$O)}-{(PPh$_2$CH$_2$CH$_2$)$_2$PPh–P,P,P}][ClO$_4$] (7a)

Yield 95%. *Anal*. Found: C, 52.0; H, 4.5; N, 1.5. Calc. for $C_{46}H_{46}NO_5Cl_2P_3Pd{\cdot}CHCl_3$: C, 52.1; H, 4.4; N, 1.3%. IR: ν(C=N), 1615m cm^{-1}. $^{13}C-\{^1H\}$ NMR: (50.28 MHz, $CDCl_3$): δ 168.8 (d, C=N, $JPC = 5.0$); δ 139.6 (C1); δ 135.4 (C2); δ 124.5 (C5); δ 77.7 (C8); δ 67.9 (C11); δ 63.1 (C7); δ 28.8, 25.8 (C9, C10). FAB MS: $m/z = 862.2$ $[M - ClO_4]^+$. Specific molar conductivity, $\Lambda_m = 146.3$ ohm^{-1} cm^2 mol^{-1} (in acetonitrile).

2.2.14. [Pd{2-ClC$_6$H$_3$C(H)=NCH$_2$(C$_4$H$_7$O)}-((CH$_3$)$_2$CO)][CF$_3$SO$_3$] (5a)

A suspension of **2a** (30.0 mg, 0.041 mmol) in acetone (8 cm^3) was treated with silver trifluoromethanesulfonate (22.0 mg, 0.082 mmol) and stirred for 24 h. The resulting solution was filtered through Celite to eliminate the AgCl precipitate and the solvent removed to give a hygroscopic yellow solid which was recrystallized from dichloromethane–hexane and stored under nitrogen. Yield 65%. *Anal*. Found: C, 36.1; H, 3.3; N, 2.1. Calc. for $C_{16}H_{19}NO_5F_3ClSPd$: C, 35.8; H, 3.6; N, 2.6%. IR: ν(C=N), 1608m cm^{-1}. $^{13}C-\{^1H\}$ NMR: (50.28 MHz, $CDCl_3$): δ 174.1 (C=N); δ 151.3 (C6); δ 143.3 (C1); δ 131.4 (C2); δ 126.1 (C5); δ 132.0, 129.8 (C3, C4); δ 79.6 (C8); δ 70.1 (C11); δ 62.4 (C7); δ 28.5, 25.6 (C9, C10); δ 31.2, 29.7 ($CH_3C{=}O$). Specific molar conductivity, $\Lambda_m = 240.2$ ohm^{-1} cm^2 mol^{-1} (in acetonitrile).

3. Results and discussion

For the convenience of the reader the compounds and reactions are shown in Scheme 1. The compounds described in this paper were characterized by elemental analysis (C, H, N) and by IR spectroscopy (data in Section 2) and by ^1H, $^{31}P-\{^1H\}$ (see Table 1) and, in part, $^{13}C-\{^1H\}$ NMR spectroscopy and FAB mass spectrometry (Section 2).

Reaction of the Schiff base ligands 2-$ClC_6H_4C(H){=}NCH_2(C_4H_7O)$ (**a**) and 3,4-$(MeO)_2C_6H_3C(H){=}NCH_2(C_4H_7O)$ (**b**) with palladium(II) acetate in toluene gave the dinuclear cyclometallated complexes [Pd{2-$ClC_6H_3C(H){=}NCH_2(C_4H_7O)$}(μ-OAc)]$_2$ (**1a**) and [Pd{3,4 - $(MeO)_2C_6H_2C(H){=}NCH_2(C_4H_7O)$}(μ - OAc)]$_2$ (**1b**), respectively, which were fully characterized. The IR spectra of **1a** and **1b** showed the ν(C=N) stretch at 1610 and 1608 cm^{-1}, respectively, shifted to lower wavenumbers (as compared to the free ligand) due to N-coordination of the imine [27,28]. The IR spectra also showed strong bands assigned to the symmetric and asymmetric ν(COO) vibrations, in agreement with those expected for bridging acetate ligands [29] (see Section 2). The resonance corresponding to the HC=N proton in the ^1H NMR spectra was shifted to lower frequency consequent upon coordination of the imine group to the palladium atom *via* the lone pair of the nitrogen atom [30]. The assignment of the aromatic proton resonances unequivocally showed that metallation had taken place at the C6 carbon atom for both compounds (see Table 1).

A noticeable feature of the ^1H NMR spectra of **1a** and **1b** is the number of signals for the HC=N and aromatic protons. Four singlets for the HC=N protons were assigned in each case. For complex **1a** a multiplet was assigned to the H^3, H^4 and H^5 resonances, whereas for complex **1b** two singlets were assigned to each one of the H^2 and H^5 protons. We reasoned that the splitting could be caused by the presence of the *syn* and *anti* conformations, as acetato-bridged dimers exist in a folded arrangement which gives rise to two isomers: the *anti* isomer with C_2 symmetry and the *syn* isomer with C_s symmetry (see Fig. 1). By far, the *anti* disposition is the most frequent [31].

If both isomers were present two resonances would be expected for the HC=N protons and three for the

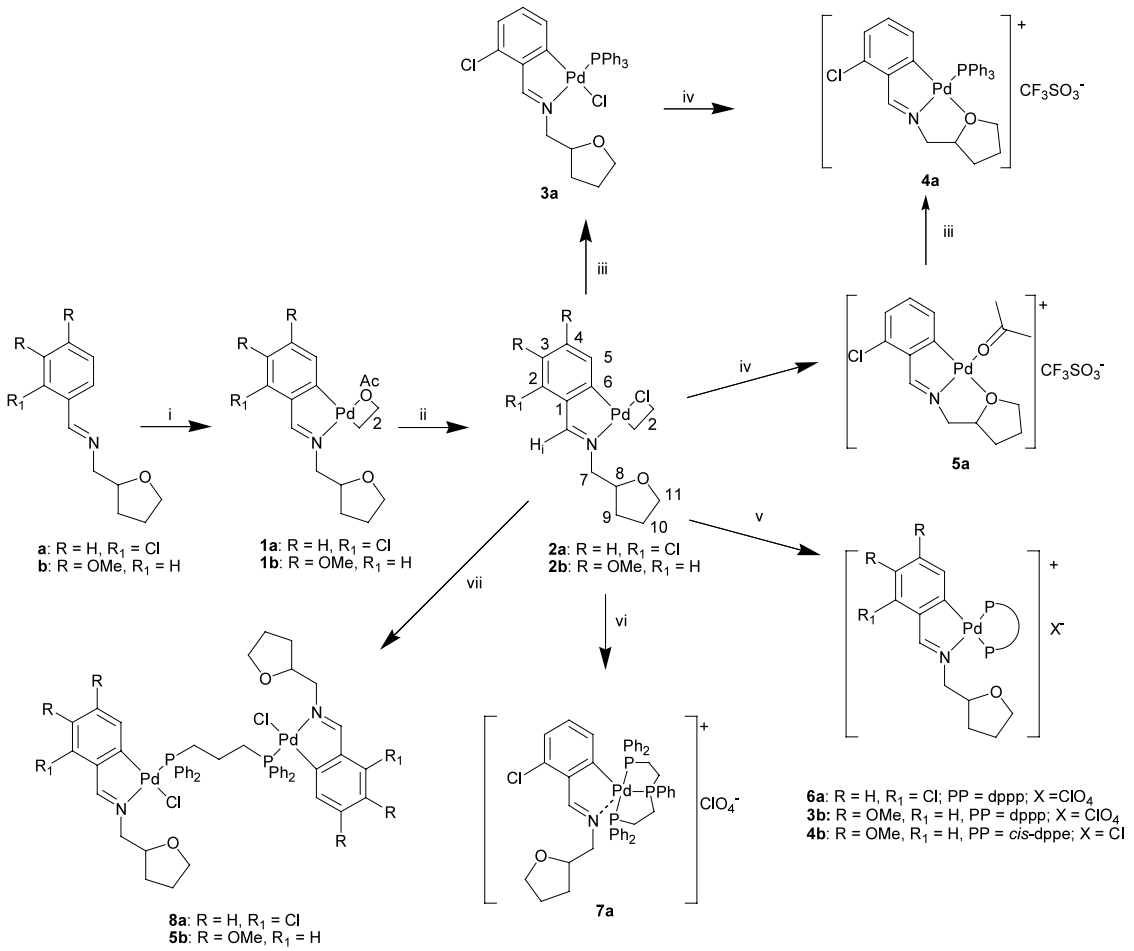
acetate MeCOO protons (one for the *anti* isomer and two for the *syn* separated by approximately 0.2 ppm [32]). However in the ^{1}H NMR spectra of **1a** and **1b** only two resonances, separated by approximately 0.02 ppm, were assignable to the acetate methyl groups.

Therefore, we believe that the number of signals found may be due to the presence of several diastereoisomers in solution.

Because the syntheses of ligands **a** and **b** were performed by heating a chloroform solution of (*R*,*S*)-tetrahydrofurfurylamine with 2-chlorobenzaldehyde or 3,4-dimethoxybenzaldehyde, as appropriate, the ligands would in fact be equimolar mixtures of both enantiomers and the cyclopalladated compounds **1a** and **1b** would yield a mixture of three pairs of enantiomers (see Fig. 2).

The NMR spectra of each pair of enantiomers are identical, but obviously different from those of their correspondent diastereoisomers. One set of signals is expected for enantiomers **I** and **II**, and another set for enantiomers **III** and **IV**; however, **V** and **VI** should give two groups of resonances for the protons of each cyclometallated unit of the acetate dimer. Thus, four signals could be assigned to the HC=N protons in the ^{1}H NMR spectra of the complexes, two resonances for the aromatic protons and two for the acetate methyl protons. The intensities of the signals for **V** and **VI** are the same as those for the **I**–**IV** enantiomers. Due to their similar solubility we were not able to separate the three pairs of enantiomers. Surprisingly, none of the other derivatives of ligands **a** and **b** showed splitting of the NMR signals. We attribute these findings to the folded structure of the acetato-bridged complex which brings close together the cyclometallated units. The asymmetric C8 carbon atom of one unit is situated close to the neighboring cyclometallated ligand, thus experiencing a different chemical environment in each diastereomer. Since the folded structure brings the HC=N proton close to the C8 carbon, the chemical differences between the diastereoisomers are most evident in the HC=N resonances.

In order to confirm this we synthesized the enantiopure ligand **c** by reaction of (*R*)-tetrahydrofufurylamine with 3,4-dimethoxybenzaldehyde. The ^{1}H NMR spectra



Scheme 1. (i) $Pd(AcO)_2$ (toluene or acetic acid); (ii) NaCl (acetone/water); (iii) PPh_3 (acetone); (iv) $AgCF_3SO_3$ (acetone); (v) dppp, $NaClO_4$ or *cis*-dppe (acetone, 1:2 molar ratio); (vi) triphos (acetone 1:2 molar ratio); (vii) dppp (acetone, 1:1 molar ratio).

Table 1
^{31}P and ^{1}H NMR

Compound	^{31}P	Aromatic	Others
a		8.03[d, 1H, H^6, 5.86 [a]] 7.3[m, 3H, H^3, H^4, H^5]	8.71[s, 1H, H_i] 4.21[m, 1H, H^8] 3.65[m, 4H, H^7, H^{11}] 1.8[m, 4H, H^9, H^{10}]
1a [b]		6.9[m, 6H, H^3, H^4, H^5]	7.76, 7.73, 7.69, 7.64 [s, 2H, H_i] 4.30[m, 2H, H^8] 3.75[m, 4H, H^{11}] 4.04[m, 2H, H^7] 3.30[m, 2H, H^7] 1.9[m, 8H, H^9, H^{10}]
2a		7.23[m, 2H, H^3] 6.97[m, 4H, H^4, H^5]	8.21[s, 2H, H_i] 4.41[m, 2H, H^8] 3.46[m, 2H, H^7] 3.85[m, 6H, H^7, H^{11}] 1.93[m, 8H, H^9, H^{10}]
3a	43.0s	6.82[d, 1H, H^3, 7.3 [a]] 6.43[t, 1H, H^4, 7.3 [a]] 6.25[dd, 1H, H^5, 6.4 [d]]	8.62[d, 1H, H_i, 8.3 [d]] 4.60[m, 2H, H^7, H^8] 3.40[m, 1H, H^7] 3.87[m, 2H, H^{11}] 1.90[m, 4H, H^9, H^{10}]
4a	39.60s	6.93[dd, 1H, H^3, 7.8 [a], 0.98 [c]] 6.51[t, 1H, H^4, 7.8 [a]] 6.23[m, 1H, H^5, 5.9 [d]]	8.62[d, 2H, H_i, 7.8 [d]] 4.40[m, 1H, H^8] 4.05, 3.90, 3.72 [m, 3H, H^7, H^{11}] 3.36[m, 1H, H^7] 2.3–1.7 [m, 4H, H^9, H^{10}]
5a [e]		6.98, 6.92 [m, 3H, H^3, H^4, H^5]	8.07[s, 1H, H_i] 4.40[m, 1H, H^8] 4.05, 3.90, 3.80 [m, 3H, H^7, H^{11}] 3.49[m, 1H, H^7] 2.0 [m, 4H, H^9, H^{10}]
6a	25.2d, −2.9d, 58.2 [f]	6.86[d, 1H, H^3, 7.4 [a]] 6.40m[s, 1H, H^4, H^5]	8.74[d, 1H, H_i, 7.0 [d]] 4.50[m, 1H, H^8] 3.7[m, 4H, H^7, H^{11}] 1.90[m, 4H, H^9, H^{10}]
7a	89.3t, 45.4d, 27.1 [f]	6.91[d, 1H, H^3, 7.8 [a]] 6.36[dd, 1H, H^4, 7.8 [a], 0.98 [c]] 5.76[t, 1H, H^5, 7.8 [d]]	8.37[s, 1H, H_i] 3.48, 3.24 [m, 5H, H^8, H^7, H^{11}]
8a	33.3s	6.80[d, 1H, H^3, 7.8 [a]] 6.46[t, 1H, H^4, 7.8 [a]] 6.22[dd, 1H, H^5, 5.9 [d]]	8.52[d, 1H, H_i, 7.8 [d]] 4.47[m, 2H, H^7, H^8] 3.52[m, 1H, H^7] 3.87[m, 2H, H^{11}] 2.10–1.70[m, 4H, H^9, H^{10}]
b, **c**		7.34[d, 1H, H^2, 1.9 [c]] 7.06[dd, 1H, H^5, 8.3 [a]] 7.76[d, 1H, H^6]	8.10[s, 1H, H_i] 4.20[m, 1H, H^8] 3.65, 3.55 [m, 4H, H^7, H^{11}] 1.9[m, 8H, H^9, H^{10}] 3.83, 3.79[s, 6H, OMe]
1b[b]		6.71, 6.69, 6.55, 6.53[s, 4H, H^2, H^5]	7.43, 7.42, 7.33, 7.29[s, 2H, H_i] 4.29[m, 2H, H^8] 1.9[m, 8H, H^9, H^{10}] 3.86, 3.79[s, 12H, OMe]
2b		6.80, 6.89[2, 4H, H^2, H^5]	7.75[s, 2H, H_i] 4.38[m, 2H, H^8] 3.46[m, 2H, H^7] 3.80[m, 6H, H^7, H^{11}] 1.92[m, 8H, H^9, H^{10}] 3.92, 3.81[s, 12H, OMe]
3b	27.0d, −2.0d, 56.0 [f]	7.0[s, 1H, H^2] 6.08[dd, 1H, H^5, 6.3, 8.8 [d]]	8.24[d, 1H, H_i, 7.3[d]] 1.9[m, 8H, H^9, H^{10}] 3.81, 2.91 [g] [s, 6H, OMe]
4b	63.5d, 51.0d, 10.2 [f]	7.13[s, 1H, H^2] 6.36[dd, 1H, H^5, 6.3, 8.7 [d]]	8.32[d, 1H, H_i, 6.8 [d]] 4.30[m, 1H, H^8] 3.77, 2.12 [g] [s, 6H, OMe] 1.9[m, 8H, H^9, H^{10}]

Table 1 (*Continued*)

Compound	^{31}P	Aromatic	Others
5b	33.2s	6.90[s, 1H, H^2] 5.86[d, 1H, H^5, 6.3 [d]]	8.03[d, 1H, H_i, 7.8 [d]] 4.2[br, 1H, H^8] 1.9[m, 8H, H^9, H^{10}] 3.78, 2.87 [g] [s, 6H, OMe]
1c		6.71, 6.69, 6.55, 6.53[s, 4H, H^2, H^5]	7.44 7.30[s, 2H, H_i] 4.29[m, 2H, H^8] 1.9[m, 8H, H^9, H^{10}] 3.87, 3.80[s, 12H, OMe]

^{31}P NMR: in $CDCl_3$ unless otherwise stated. Measured at 80.9 MHz (ca. ± 20 °C); chemical shifts (δ) in ppm (± 0.1) to high frequency of 85% H_3PO_4. ^1H NMR: in $CDCl_3$. Measured at 200 MHz (ca. ± 20 °C); chemical shifts (δ) in ppm (± 0.01) to high frequency of $SiMe_4$. Coupling constants in Hz. s, singlet; d, doublet; dd, doublet of doublets; t, triplet; m, multiplet; br, broad.

[a] ^3JHH.

[b] $\delta(CH^{acetate}) = 2.14$, 2.11[s, 6H] (compound **1a**); 2.14, 2.13[s, 6H] (compound **1b**).

[c] ^4JHH.

[d] JPH.

[e] δ [$(CH_2)_2CO$] = 2.5 br, ppm.

[f] JPP.

[g] C4–(OMe).

of **c** was identical to the one recorded for **b**. The cyclometallated acetato-bridged complex **1c** was prepared following an analogous procedure to that used for **1b**. The ^1H NMR spectrum of **1c** showed only two resonances for the HC=N proton at δ 7.44 and 7.30, indicating the presence of only two distinct diastereoisomers in solution (**I** and **III**).

The $^{13}C-\{^1H\}$ spectra of the complexes showed the signals assigned to the C6, C=N, and C1 resonances shifted to higher frequency confirming that metallation had occurred [20]. The signals exhibited the splitting due to the mixture of diastereoisomers (see Section 2). Four signals were observed for the C=N carbon atom due to the three pairs of enantiomers present in solution, as opposed to only two signals for the C=N carbon in the spectrum of complex **1c**.

The mass FAB spectrum of **1a** showed a cluster of peaks, centered at 776 and 717 amu which correspond to $[M]^+$ and $[M-AcO]^+$, respectively. The isotopic pattern is in good agreement with the expected dinuclear structure.

The reaction of **1a** and **1b** with aqueous sodium chloride gave the chloro-bridged complexes [Pd{2-$ClC_6H_3C(H)=NCH_2(C_4H_7O)$}(μ-Cl)]$_2$ (**2a**) and [Pd{3,4-$(MeO)_2C_6H_2C(H)=NCH_2(C_4H_7O)$}(μ-Cl)]$_2$ (**2b**), respectively, which were fully characterized (see Table 1 and Section 2). The IR spectra showed the absence of the ν(COO) bands. The ^1H NMR spectra of **2a** and **2b** showed the HC=N resonance at δ 8.21 and δ 7.75, respectively. The aromatic proton resonances of **2a** were at δ 7.23 (H^3) and δ 6.97 (H^4, H^5), as multiplets, whereas two singlets were observed for the H^2, H^5 resonances at δ 6.80 and 6.89, respectively, for compound **2b**. In the $^{13}C-\{^1H\}$ spectra the C=N, C1 and C6 carbon resonances were shifted to higher frequency as compared to the free ligands. The FAB mass spectra showed the peaks which were assigned to the $[M]^+$ and $[M-Cl]^+$ fragments; a similar fragmentation of cyclometallated chloro-bridged complexes has been reported [33].

Reaction of **2a** with PPh_3 in acetone gave the mononuclear cyclometallated complex [Pd{2-$ClC_6H_3C(H)=NCH_2(C_4H_7O)$}(Cl)($PPh_3$)], **3a**, in a typical bridge-splitting reaction. In the ^1H NMR spectra the HC=N and H^5 resonances showed coupling to the phosphorus nucleus [δ 8.62 ($JPH = 8.3$ Hz) and δ 6.25 ($JPH = 6.4$ Hz), respectively]; in the $^{31}P-\{^1H\}$ spectrum the resonance of the coordinated phosphine was a singlet at δ 43.0; these findings are in agreement with a phosphorus *trans* to nitrogen arrangement [34–37]. The FAB mass spectrum showed peaks centered at 627 and 590 amu for the $[M]^+$ and $[M-Cl]^+$ fragments, respectively.

Treatment of **3a** with silver triflate gave the complex [Pd{2-$ClC_6H_3C(H)=NCH_2(C_4H_7O)$}($PPh_3$)][$CF_3SO_3$] (**4a**) after the removal of the AgCl precipitate formed. The most noteworthy differences in the ^1H NMR spectrum of **4a** as compared to **3a**, were in the THF proton resonances, although overlapping of these resonances made an exact assignment difficult, especially in the

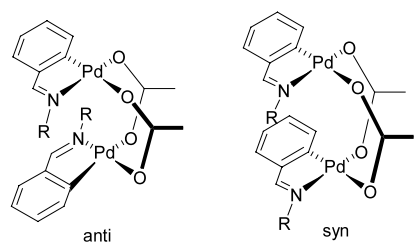


Fig. 1.

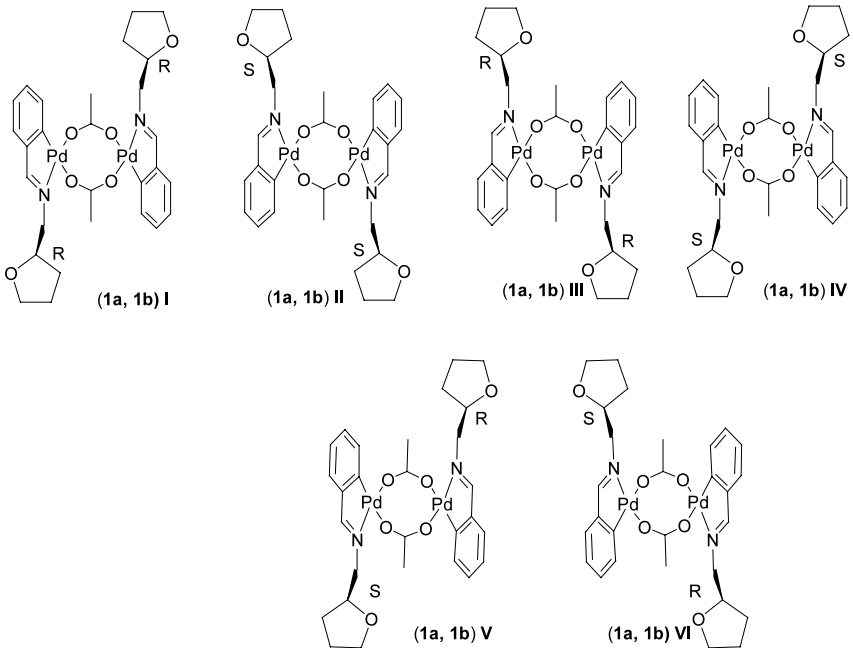


Fig. 2.

splitting pattern shown by the H^7, H^8, and H^{11} protons. Furthermore, the $^{13}C-\{^1H\}$ spectrum of **4a** showed the signal assigned to C8 at δ 81.9, downfield shifted consequent upon Pd–O bond formation (cf. δ 78.6, **a**, and δ 77.5, **3a**). Compound **4a** is a 1:1 electrolyte, as shown by molar conductivity measurements. The FAB-mass spectrum showed a set of peaks centered at 592 amu for the $[M-CF_3SO_3]^+$ fragment.

Pd–O bond formation could also be achieved by reacting **2a** with silver triflate in acetone which gave the complex $[Pd\{2\text{-}ClC_6H_3C(H)=NCH_2(C_4H_7O)\}((CH_3)_2CO)][CF_3SO_3]$ (**5a**) after AgCl removal. The IR spectra supports the presence of the $[CF_3SO_3]^-$ anion, which contains the characteristic stretching bands of the free anion [38], approximately 1274, 1251, 1170 and 1031 cm^{-1}. The ^1H NMR spectrum showed the HC=N resonance at δ 8.07 and the signals corresponding to the H^2, H^3 protons and H^4 as multiplets at δ 6.98 and 6.92, respectively. The splitting pattern and chemical shift resonances for the THF ring are clearly different from those observed in the spectrum of **2a**. In the $^{13}C-\{^1H\}$ spectrum of **4a** the C8 resonance appeared at δ 79.6, downfield shifted upon Pd–O bond formation. Molar conductivity measurements were in agreement with the ionic nature of the complex.

Treatment of complexes **2a** and **2b** with $Ph_2P(CH_2)_3PPh_2$, dppp, in a complex/phosphine 1:1 molar ratio gave the dinuclear cyclometallated complexes $[\{Pd[2\text{-}ClC_6H_3C(H)=NCH_2(C_4H_7O)](Cl)\}_2(\mu\text{-}Ph_2P(CH_2)_3PPh_2)]$ (**8a**) and $[\{Pd[3,4\text{-}(MeO)_2C_6H_2C(H)=NCH_2(C_4H_7O)](Cl)\}_2(\mu\text{-}Ph_2P(CH_2)_3PPh_2)]$ (**5b**) which were fully characterized (see Section 2 and Table 1). The $^{31}P-\{^1H\}$ NMR spectra only showed a singlet resonance in accordance with the centrosymmetric nature of this dinuclear complexes.

In the ^1H NMR spectra of complex **5b**, the C(4)–OCH_3 resonance was shifted towards lower frequency by approximately 0.8 ppm, as compared complex **2b**, due to the shielding effects of the phosphine phenyl ring, in agreement with a N–Pd–P *trans* geometry [16,21,39]. This arrangement was confirmed by the coupling of the HC=N and H^5 proton resonances to the phosphorus nucleus.

Reaction of complexes **2a** and **2b** with the diphosphines $Ph_2P(CH_2)_3Ph_2$, dppp, and $Ph_2PCH=CHPh_2$, *cis*-dppe, in a 1:2 molar ratio gave the mononuclear complexes $[Pd\{2\text{-}ClC_6H_3C(H)=NCH_2(C_4H_7O)\}\{Ph_2P(CH_2)_3Ph_2\text{-}P,P\}][ClO_4]$ (**6a**), $[Pd\{2\text{-}(MeO)_2C_6H_3C(H)=NCH_2(C_4H_7O)\}\{Ph_2P(CH_2)_3Ph_2\text{-}P,P\}][ClO_4]$ (**3b**) and $[Pd\{2\text{-}ClC_6H_3C(H)=NCH_2(C_4H_7O)\}(cis\text{-}Ph_2PCH=CHPh_2\text{-}P,P)][Cl]$ (**4b**) as air-stable solids which were fully characterized (see Table 1 and Section 2).

The $^{31}P-\{^1H\}$ NMR spectra showed two doublets for the two unequivalent phosphorus nuclei. The resonance at lower frequency was assigned to the phosphorus nucleus *trans* to the phenyl carbon atom in accordance with the higher *trans* influence of the latter with respect to the C=N nitrogen atom [40]. The *H*C=N resonance was only coupled to the ^{31}P nucleus *trans* to nitrogen. This was confirmed by selective decoupling experiments on the ^{31}P atoms. The H^5 resonance showed coupling to both phosphorus atoms. Measurements of the specific molar conductivity have shown the complexes to be 1:1 electrolytes.

Reaction of **2a** with the triphosphine bis(2-diphenylphosphinoethyl)phenylphosphine in 1:2 molar ratio, followed by treatment with sodium perchlorate gave [Pd{2-$ClC_6H_3C(H)$=$NCH_2(C_4H_7O)$}{$(PPh_2CH_2CH_2)_2PPh$-*P*,*P*,*P*}][ClO_4] (**7a**). The phosphorus resonances in the $^{31}P-\{^1H\}$ NMR spectrum were downfield shifted from their values in the free phosphine suggesting coordination of the three phosphorus atoms to the metal centre. A triplet resonance at δ 89.3 was assigned to the central ^{31}P nucleus, *trans* to the phenyl carbon atom, and a doublet at δ 45.4 was assigned to the two equivalent mutually *trans* phosphorus nuclei. The latter signal appeared at lower frequency in accordance with the high *trans* influence of the phosphine ligand [11]. The resonance of the proton in the *ortho* position to the metallated carbon appeared as a triplet showing coupling to the central ^{31}P atom [J(PH) 7.8 Hz]; no coupling was observed to the terminal phosphorus nuclei. These data are in accordance with a disposition in which the metallated ring is nearly perpendicular to the plane defined by the three phosphorus atoms; these observations were confirmed by selective decoupling experiments. The shift of the ν(C=N) stretching vibration to lower wavenumbers [27,28] as well as the upfield shift of the HC=N proton resonance in the ^1H NMR spectra [30] indicates the existence of palladium–nitrogen interaction in solution. These results strongly agree with those previously obtained by us in related pentacoordinated palladium(II) species, and hence we propose a similar disposition of the triphos ligand in this case [15]. The C=N signal in the $^{13}C-\{^1H\}$ spectrum at δ 168.8 coupled to the central phosphorus ($JPC = 5.0$ Hz) was also indicative of Pd–N interaction.

Molar conductivity measurements have shown that complex **7a** is a 1:1 electrolyte. The FAB mass spectrum showed a set of peaks centered at 862 amu assigned to the $[M - ClO_4]^+$ fragment.

Acknowledgements

We thank the Ministerio de Educación y Cultura (Proyecto PB98-0638-C02-01/02), the Xunta de Galicia (Proyecto PGIDT99PXI20907B) and the Universidad de la Coruña for financial support.

References

[1] I. Omae, Organometallic Intramolecular-Coordination Compounds, Elsevier Science, Amsterdam, 1986.
[2] V.V. Dunina, O.A. Zalevskaya, V.M. Potapov, Russ. Chem. Rev. 571 (1984) 250.
[3] G.R. Newkome, W.E. Puckett, W.K. Gupta, G.E. Kiefer, Chem. Rev. 86 (1986) 451.
[4] A.D. Ryabov, Chem. Rev. 90 (1990) 403.
[5] M. Pfeffer, Recl. Trav. Chim. Pays-Bas 109 (1990) 567.
[6] M. Pfeffer, J.P. Sutter, M.A. Rottevel, A. de Cian, J. Fischer, Tetrahedron 48 (1992) 2427.
[7] A.D. Ryabov, R. van Eldik, G. Le Borgne, M. Pfeffer, Organometallics 12 (1993) 1386.
[8] S.B. Wild, Coord. Chem. Rev 166 (1997) 291.
[9] S.Y.M. Chooi, P.H. Leung, C.C. Lim, K.F. Mok, G.H. Quek, K.Y. Sim, M.K. Tan, Tetrahedron Asymmetry 3 (1992) 529.
[10] P. Espinet, M.A. Esteruelas, L.A. Oro, J.L. Serrano, E. Sola, Coord. Chem. Rev. 17 (1992) 215.
[11] C. Navarro-Ranninger, I. López Solera, J. Rodríguez, J.L. García-Ruano, P.R. Raithby, J.R. Masaguer, C. Alonso, J. Med. Chem. 36 (1993) 3795.
[12] C. Navarro-Ranninger, I. López-Solera, V.M. Gonzalez, J.M. Pérez, A. Alvarez-Valdes, A. Martin, P.R. Raithby, J.R. Masaguer, C. Alonso, Inorg. Chem. 35 (1996) 5181.
[13] A. Bose, C.H. Saha, J. Mol. Catal. 49 (1989) 271.
[14] M. López-Torres, A. Fernández, J.J. Fernández, S. Castro-Juiz, A. Suárez, J.M. Vila y, M.T. Pereira, Organometallics 20 (2001) 1350.
[15] J.M. Vila, M.T. Pereira, J.M. Ortigueira, J.J. Fernández, A. Fernández, M. López-Torres, H. Adams, Organometallics 18 (1999) 5484.
[16] J.M. Vila, T. Pereira, J.M. Ortigueira, M. López-Torres, A. Castiñeiras, D. Lata, J.J. Fernández, A. Fernández, J. Organomet. Chem. 556 (1998) 21.
[17] A. Fernández, M. López-Torres, A. Suárez, J.M. Ortigueira, T. Pereira, J.J. Fernández, J.M. Vila, H. Adams, J. Organomet. Chem. 598 (2000) 1.
[18] J.M. Vila, M.T. Pereira, J.M. Ortigueira, M. López-Torres, D. Lata, M. Graña, A. Suárez, J.J. Fernández, A. Fernández, J. Chem. Soc., Dalton Trans. (1999) 4193.
[19] D. Vázquez-García, A. Fernández, J.J. Fernández, M. López-Torres, A. Suárez, J.M. Ortigueira, J.M. Vila, H. Adams, J. Organomet. Chem. 595 (2000) 199.
[20] J.M. Vila, M. Gayoso, M.T. Pereira, M. López-Torres, J.J. Fernández, A. Fernández, J.M. Ortigueira, J. Organomet. Chem. 532 (1997) 171.
[21] J.M. Vila, M.T. Pereira, J.M. Ortigueira, D. Lata, M. López-Torres, J.J. Fernández, A. Fernández, H. Adams, J. Organomet. Chem. 566 (1998) 93.
[22] A. Fernández, J.J. Fernández, M. López-Torres, A. Suárez, J.M. Ortigueira, J.M. Vila, H. Adams, J. Organomet. Chem. 612 (2000) 85.
[23] A. Fernández, P. Uría, J.J. Fernández, M. López-Torres, A. Suárez, D. Vázquez-García, M.T. Pereira, J.M. Vila, J. Organomet. Chem. 620 (2001) 8.
[24] J.M. Vila, M.T. Pereira, A. Suárez, J.J. Fernández, J.M. Ortigueira, A. Fernández, M. López-Torres, C. Rodríguez, Trends Organomet. Chem. 3 (1999) 71 and references therein.
[25] (a) M. Nonoyama, J. Inorg. Nucl. Chem. 42 (1980) 297;
(b) M. Nonoyama, Inorg. Chim. Acta 145 (1988) 53;
(c) S. Tollari, G. Palmisano, F. Demartin, M. Grassi, S. Magnaghi, S. Cenini, J. Organomet. Chem. 488 (1995) 79;
(d) M. Nonoyama, Inorg. Nucl. Chem. Lett. 14 (1978) 337;
(e) M. Nonoyama, M. Sugimoto, Inorg. Chim. Acta 35 (1979) 131;
(f) J. Albert, A. González, J. Granell, R. Moragas, C. Puerta, P. Valerga, Organometallics 16 (1997) 3775;
(g) M. Sugimoto, M. Nonoyama, Inorg. Nucl. Chem. Lett. 15 (1979) 405;
(h) G. Zhao, Q. Wang, C.W. Mak, Organometallics 17 (1998) 3437;
(i) G. Zhao, Q. Wang, C.W. Mak, J. Chem. Soc., Dalton Trans. (1998) 3785;
(j) G. Zhao, Q. Wang, C.W. Mak, J. Organomet. Chem. 574 (1999) 311;

(k) H. Yang, A. Masood, M.N. Kenneth, J. Chem. Soc., Chem. Commun. (1992) 210;
(l) P. Ghosh, A. Pramanik, N. Bag, K. Lahiri, A. Chakravorty, J. Organomet. Chem. 454 (1993) 237;
(m) A. Yoneda, M. Ouchi, T. Hakushi, G.R. Newkome, F.R. Fronczek, Chem. Lett. (1993) 709;
(n) A. Yoneda, G.R. Newkome, Y. Morimoto, Y. Higuchi, N. Yasuoka, Acta Crystallogr., Sect. C 49 (1993) 476;
(o) A. Yoneda, T. Hakushi, G.R. Newkome, Y. Morimoto, N. Yasuoka, Chem. Lett. (1994) 175;
(p) A. Yoneda, T. Hakushi, G.R. Newkome, F.R. Fronczek, Organometallics 13 (1994) 4912;
(q) D.R. Billodeaux, F.R. Fronczek, A. Yoneda, G.R. Newkome, Acta Crystallogr., Sect. C 54 (1998) 1439;
(r) C. Cativiela, L.R. Falvello, J.C. Ginés, R. Navarro, E.P. Urriolabeitia, New J. Chem. 25 (2001) 344.

[26] D.D. Perrin, W.L.F. Armarego, Purification of Laboratory Chemicals, 4th ed., Butterworth–Heinemann, London, 1996.

[27] H. Onoue, I. Moritani, J. Organomet. Chem. 43 (1972) 431.

[28] H. Onoue, K. Minami, K. Nakagawa, Bull. Chem. Soc. Jpn. 43 (1970) 3480.

[29] K. Nakamoto, IR and Raman Spectra of Inorganic and Coordination Compounds, 5th ed., Wiley, New York, 1997.

[30] Y. Ustynyuk, V.A. Chertov, J.V. Barinov, J. Organomet. Chem. 29 (1971) C53.

[31] B. Teijido, A. Fernández, M. López-Torres, S. Castro-Juiz, A. Suárez, J.M. Ortigueira, J.M. Vila, J.J. Fernández, J. Organomet. Chem. 598 (2000) 71.

[32] B.J. O'Keefe, P.J. Steel, Organometallics 17 (1998) 3621.

[33] M. Lousame, A. Fernández, M. López-Torres, D. Vázquez-García, J.M. Vila, A. Suárez, J.M. Ortigueira, J.J. Fernández, Eur. J. Inorg. Chem. (2000) 2055.

[34] R. Bosque, J. Granell, J. Sales, M. Fon-Bardiá, X. Solans, J. Organomet. Chem. 453 (1994) 147.

[35] J.M. Vila, M. Gayoso, M.T. Pereira, M. López-Torres, G. Alonso, J.J. Fernández, J. Organomet. Chem. 445 (1993) 287.

[36] J.M. Vila, M. Gayoso, M.T. Pereira, A. Romar, J.J. Fernández, M. Thornton-Pett, J. Organomet. Chem. 401 (1991) 385.

[37] R. Bosque, J. Granell, J. Sales, M. Fon-Bardiá, X. Solans, Organometallics 14 (1995) 1393.

[38] G.A. Lawrance, Chem. Rev. 86 (1986) 17.

[39] M. Vila, M. Gayoso, A. Fernández, N.A. Bailey, H. Adams, J. Organomet. Chem. 448 (1993) 233.

[40] P.S. Pregosin, R.W. Kuntz, ^{31}P and ^{13}C NMR of transition metal phosphine complexes, in: P. Diehl, E. Fluck, R. Kosfeld (Eds.), NMR, vol. 16, Springer, Berlin, 1979.

PERGAMON

Polyhedron 21 (2002) 49–54

POLYHEDRON

www.elsevier.com/locate/poly

Synthesis and enhanced photosensitization ability of a 4-carboxy-2,2′:6′,2″-terpyridine complex of ruthenium(II)

Charles Mikel [1], Pierre G. Potvin *

Department of Chemistry, York University, 4700 Keele Street, North York, Ont., Canada M3J 1P3

Received 20 April 2001; accepted 2 October 2001

Abstract

The new ligand 4-carboxy-4′-*p*-tolyl-2,2′:6′,2″-terpyridine (HttpyA) was prepared in complexed form via the methyl ester (ttpyE), which was elaborated from methyl isonicotinate in two-steps and in good yields. The homoleptic complex $[Ru(ttpyE)_2](PF_6)_2$ was prepared, characterized, and hydrolyzed to produce the diacid complex, $H_2[Ru(ttpyA)_2]^{2+}$. Once ionized to the neutral $[Ru(ttpyA)_2]^0$, there are no long-range electrostatic repulsions with the electron acceptor methyl viologen (MV^{2+}), and the surface COO^- groups are suitably disposed for a close-range, 1:1 supramolecular pre-association with MV^{2+}. $H_2[Ru(ttpyA)_2]^{2+}$ was indeed a significantly better photosensitizer in effecting electron transfer to MV^{2+} in CH_3CN than was the non-carboxylated dicationic analogue, $Ru(ttpy)_2^{2+}$ (ttpy is 4′-*p*-tolyl-2,2′:6′,2″-terpyridine). © 2002 Elsevier Science Ltd. All rights reserved.

Keywords: Photoinduced electron transfer; Cyclic voltammetry; Supramolecular pre-association; Ruthenium(II) complexes; 2,2′:6′,2″-Terpyridine; 4′-*p*-Tolyl-2,2′:6′,2″-terpyridine-4-carboxylic acid

1. Introduction

The photophysical and photochemical properties of the 2,2′-bipyridine-4,4′-dicarboxylate complexes of Ru(II) have been studied in some detail [1], in part because of the Coulombic advantages available to ionizable complexes in photo-induced electron transfers to cationic electron acceptors such as methyl viologen (MV^{2+}). Another manifestation of this advantage is the photo-induced injection of electrons into semiconductors even if the sensitizer excited states are extremely short-lived [2], and this has been attributed to attractive surface interactions involving COO^- groups on the sensitizer surface.

Terpyridines are superior to bipyridines in terms of symmetry and synthetic simplicity, but ionizable terpyridine complexes are relatively unknown. We are particularly interested in complexes able to enter into supramolecular associations with MV^{2+} through negatively charged groups on the ligand periphery. If it occurs prior to photoexcitation, this affords an additional, entropic advantage over dicationic sensitizers. Molecular models suggested that placing a COO^- group at the 4-position of each ligand in a bis(terpyridine) Ru(II) complex would afford a geometry and an inter-carboxylate distance conducive to a 1:1 association with MV^{2+} (Fig. 1).

The previously reported preparations of carboxyterpyridine ligands are either arduous or ill-suited for our objective [3]. We wish to report the facile Kröhnke synthesis [4] of a novel methyl terpyridine-4-carboxylate ligand (ttpyE), preparation of its Ru(II) complex $[Ru(ttpyE)_2]^{2+}$ and its hydrolyzed form $H_2[Ru(ttpyA)_2]^{2+}$, and the testing of the latter in photo-induced electron transfer to MV^{2+}.

2. Experimental

2.1. Preparation of methyl 2-acetylisonicotinate (*1*)

Methyl isonicotinate (8.2 g, 60.0 mmol) was added to a solution of excess paraldehyde (40 g) in CH_3CN (140

* Corresponding author. Tel.: +1-416-736 2100x66140; fax: +1-416-736 5936.

E-mail address: pgpotvin@yorku.ca (P.G. Potvin).

[1] Formerly Charles M. Chamchoumis.

0277-5387/02/$ - see front matter © 2002 Elsevier Science Ltd. All rights reserved.
PII: S0277-5387(01)00959-7

ml) at room temperature (r.t.). To this solution was added $FeSO_4 \cdot 7H_2O$ (0.28 g, 1.00 mmol), TFA (7 g) and 70% ^{t}BuOOH (15 g), and the mixture was heated to reflux for 4 h. This was freed of solvent under reduced pressure, and the residue was taken up in saturated aqueous Na_2CO_3 (100 ml), then extracted with $PhCH_3$ (3×75 ml). The combined organic fractions were dried ($MgSO_4$) and freed of solvent under reduced pressure. The dark brown residue was purified on a short column (silica, 30:70 P.E.–EtOAc). The main fraction was freed of solvent under reduced pressure, and the yellow residue was recrystallized from pentane to give white needles (9.8 g, 91%). The ^{1}H NMR spectrum agreed with that in the literature [5].

2.2. Preparation of N-[2-oxo-2-(2-(4-methoxycarbonylpyridyl))ethyl]pyridinium iodide (2a)

Methyl 2-acetylisonicotinate (**1**, 0.24 g, 1.34 mmol) was added to a warmed solution of I_2 (0.35 g, 1.38 mmol) in anhydrous pyridine (10 ml) and the resulting solution was heated to reflux under argon for 3 h. The precipitate which formed upon cooling was collected by vacuum filtration and washed with $CHCl_3$ (25 ml) and Et_2O (25 ml), and then dried, yielding a tan powder (0.300 g, 58% as **2a**). ^{1}H NMR (DMSO-d_6): δ 9.08 (d, 1H, H-6), 8.95 (d, 2H, H-2′), 8.72 (t, 1H, H-4′), 8.34 (s, 1H, H-3), 8.28 (t, 2H, H-3′), 8.21 (d, 1H, H-5), 6.51 (s, 2H, CH_2), 3.94 (s, 3H, OCH_3) ppm. FAB MS m/z (%): 257 (70) [M − I]. The product was contaminated with a small quantity ($< 6\%$) of the free acid analogue **2b** identified by additional ^{1}H NMR signals at 12–13 (bs), 9.10 (d) and 8.25 (d) ppm, as well as a FAB MS peak at m/z (%) 243 (30) [M − I].

2.3. Preparation of 4-methoxycarbonyl-4′-p-tolyl-2,2′:6′,2″-terpyridine (ttpyE)

3-*p*-Tolyl-1-(2-pyridyl)-2-propenone (**3**) [6] (0.18 g, 0.81 mmol) and **2a** (0.40 g, nominally 1.0 mmol as pure **2a**) were added to a solution of excess NH_4OAc (2.0 g) in CH_3OH (2 ml) and the resulting solution was heated to reflux for 4 h. The precipitate which formed upon cooling was collected by filtration, and triturated successively with CH_3OH (2×5 ml), $CHCl_3$ (2×5 ml) and Et_2O (2×5 ml). The $CHCl_3$ extract was set aside while the remaining solid was dried, then taken up in $SOCl_2$ (10 ml) and heated to reflux under argon for 1 h. The reaction mixture was freed of excess $SOCl_2$ in vacuo and the residue was taken up in dry CH_3OH and heated to reflux under argon for 1 h. Once the excess CH_3OH was removed under reduced pressure, the residue was taken up in 1:1 Et_3N–$CHCl_3$ (25 ml) and combined with the $CHCl_3$ extract from the original filtration. This was filtered on a short column (alumina–*N*-$CHCl_3$). The collected fraction was freed of solvent and recrystallized ($CHCl_3$–CH_3OH) to give tan flakes (0.226 g, 73%). Melting point (m.p.): 181–2 °C. ^{1}H NMR ($CDCl_3$): δ 9.17 (1H, s, H-3′/5′), 8.87 (1H, d, $J = 4.9$, H-6), 8.77 (1H, s, H-5′/3′), 8.75 (1H, d, $J = 1.4$, H-3), 8.74 (1H, d, $J = 4.5$, H6″), 8.70 (1H, d, $J = 7.9$, H3″), 7.91 (1H, dt, $J = 1.6$, 7.9, H4″), 7.89 (1H, d, $J = 4.9$, H-5), 7.82 (2H, d, Ar-H-2(6)), 7.37 (1H, dd, $J = 4.9$, 7.7, H-5″), 7.33 (2H, d, Ar-H-3(5)), 4.05 (3H, s, OCH_3), 2.45 (3H, s, Ar-CH_3) ppm. ^{13}C NMR ($CDCl_3$): δ 166.0, 157.6, 156.2, 155.2, 155.1, 150.3, 149.9, 149.1, 139.2, 138.4, 136.9, 135.4, 129.7, 127.2, 123.9, 122.7, 121.5, 120.7, 119.1, 118.9, 52.8, 21.3 ppm. FAB MS m/z (%): 382 (100) [M + H], 364 (10) [M − CH_3]. Elemental analysis: *Anal.* Calc. for $C_{24}H_{19}N_3O_2$ (M_W 381.42) (%): C, 75.57; H, 5.03; N, 11.02. Found: C, 75.45; H, 5.03; N, 10.94%.

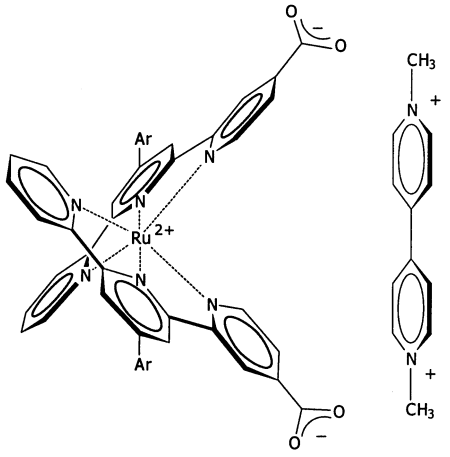
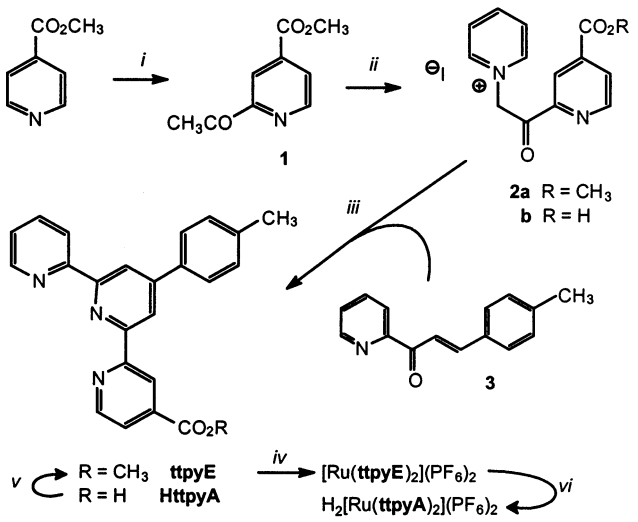


Fig. 1. Two-point supramolecular association of a 4-carboxylated terpyridine complex with MV^{2+} (Ar is *p*-tolyl).

2.4. Preparation of [Ru(ttpyE)$_2$](PF$_6$)$_2$

The ligand (ttpyE) (32.5 mg, 0.085 mmol) was added to a solution of $RuCl_3$ (8.8 mg, 0.034 mmol as the trihydrate) in CH_3OH and the resulting solution was heated to reflux for 16 h. The reaction mixture was rid of solvent in vacuo. The resulting residue was re-dissolved in a minimal quantity of CH_3CN, filtered to remove unreacted starting materials, and treated with an excess of a saturated aqueous solution of NH_4PF_6. The collected precipitate was purified by column chromatography (silica, 14:1:0.5 CH_3CN–satd. aq. KNO_3–H_2O). The minor, purple-colored, fore-fraction was discarded. The major, red-colored, fraction was collected and freed of solvent under reduced pressure, redissolved in a minimal quantity of CH_3CN, and again precipitated with NH_4PF_6, as above. The collected red powder (33 mg, 85% based on $RuCl_3 \cdot 3H_2O$) crystallized as red plates using vapor diffusion methods (CH_3CN–acetone). ^{1}H NMR (CD_3CN): δ 9.16 (1H, s, H-3′/5′), 9.10 (1H, s, H-3), 9.03 (1H, s, H-5′/3′), 8.60 (1H, d, H-3″/6″), 8.15 (2H, d, Ar-H-2(6)), 7.96 (1H, dd, H-4″/



Scheme 1. Reagents and conditions: (i) 70% aq. ^{t}BuOOH (2 equiv.), TFA (1 equiv.), $FeSO_4$ (1/60 equiv.), paraldehyde (22 equiv. of CH_2O), r.t. in CH_3CN, 4 h; (ii) I_2 (1 equiv.), reflux in pyridine, 3 h; (iii) NH_4OAc (24 equiv.), reflux in MeOH, 1 h; (iv) reflux in $SOCl_2$, 1 h, then reflux in MeOH, 1 h; (v) 0.4 equiv. $RuCl_3$, reflux in MeOH, 16 h; (vi) 2:5 0.78 N aq. NaOH–DMF, reflux, 8 h; excess 60% HPF_6.

5″), 7.59 (4H, m, Ar-H-3(5), H-5, H-6), 7.42 (1H, d, H-6″/3″), 7.18 (1H, dd, H-5″/4″), 3.98 (3H, s, OCH_3), 2.55 (3H, s, Ar-CH_3) ppm. ^{13}C NMR (CD_3CN): δ 164.5, 160.3, 158.9, 156.3, 155.9, 154.4, 153.4, 149.8, 142.1, 139.6, 139.3, 134.6, 131.2, 128.7, 128.5, 127.0, 125.5, 124.2, 122.9, 122.6, 53.8, 21.3 ppm. FAB MS m/z (%): 1008 (100) [$M-PF_6$], 863 (90) [$M-2PF_6$]. Elemental analysis: *Anal.* Calc. for $C_{48}H_{38}F_{12}N_6O_4P_2Ru$ (M_W 1153.87): C, 49.96; H, 3.32; N, 7.28. Found: C, 49.57; H, 3.37; N, 7.17%.

2.5. Preparation of $H_2[Ru(ttpyA)_2](PF_6)_2$

$[Ru(ttpyE)_2](PF_6)_2$ (11.0 mg, 9.5 μmol) was dissolved in DMF (5 ml) to which was added 2 ml of 0.775 N NaOH. This was heated at reflux overnight, cooled, then neutralized with excess 60% aq. HPF_6. The collected precipitate was washed with H_2O and dried under vacuum to give a red powder (10.1 mg, 94%). ^{1}H NMR (CD_3CN + TFA-*d*): δ 9.14 (1H, s, H-3′/5′), 9.08 (1H, s, H-3), 9.01 (1H, s, H-5′/3′), 8.64 (1H, d, H-3″/6″), 8.13 (2H, d, Ar-H-2(6)), 7.94 (1H, t, H-4″/5″), 7.56 (4H, m, H-5, H-6, Ar-H-3(5)), 7.41 (1H, d, H-6″/3″), 7.17 (1H, t, H-5″/4″), 2.52 (3H, s, CH_3) ppm. MALDI-MS m/z (%): 790.2 (11) [$M-2PF_6-CO_2-2H$], 747.1 (100) [$M-2PF_6-2CO_2-2H$].

2.6. Electrochemistry

Cyclic voltammetry was run at 298 K in CH_3CN containing 0.1 M $^{n}Bu_4NPF_6$, with a Pine Instruments RDE-3 potentiostat and Houston Instruments model 100 X-Y recorder, and used a three-electrode system, consisting of a quasi-reference Ag/AgCl wire electrode and working and auxiliary electrodes of Pt wire. The CH_3CN was dried via distillation over P_2O_5. Ferrocene served as a reference (Fc/Fc^+ +0.45 V vs. SSCE in CH_3CN) [7].

2.7. Electron transfer measurements

Sample solutions (2.5 ml) containing $H_2[Ru(ttpyA)_2](PF_6)_2$ (3.77×10^{-5} M) or $[Ru(ttpy)_2](PF_6)_2$ (3.99×10^{-5} M), $MV(PF_6)_2$ (MV, 9.45×10^{-3} M) and triethanolamine (5×10^{-2} M) in CH_3CN were prepared in 3 ml cuvettes for measurements and data treatment as detailed elsewhere [8]. The absorbance due to $MV^{\bullet+}$ (λ_{max} 600 nm, ϵ_{max} 10 060 M^{-1} cm^{-1} [9]) was monitored over time first under irradiation, then in the dark, and this cycle was repeated twice more with each sample. After converting the absorbance data to $MV^{\bullet+}$ concentrations, the average maximum $MV^{\bullet+}$ yields were measured, and the average initial growth rates were converted to first-order constants (k_{init} = rate/$[MV^{2+}]_0$). The pseudo-first-order rate constants for the formation (k_f) and quenching (k_q) of $MV^{\bullet+}$ were obtained from application of the kinetic model [8]:

$$d[MV^{\bullet+}]_t/dt = k_f[MV^{2+}]_0 - (k_f + k_q + k_{d1})[MV^{\bullet+}]_t - k_{d2}[MV^{\bullet+}]_t^2 \quad (1)$$

using k_d parameter values measured from a prior analysis of the subsequent aerobic decays in the dark (where $k_f = k_q = 0$).

3. Results and discussion

The Kröhnke synthesis [4] of ttpyE (Scheme 1) necessitated the preparation of ketone ester **1** as a means of introducing the desired functionality. The acetylation of methyl isonicotinate provided **1** in near quantitative yield through a modification of a recently reported procedure [5].

In the Kröhnke method, the desymmetrizing functionality on unsymmetrical terpyridines is normally introduced as part of a propenone synthon, but this approach failed in the present case. Indeed, attempted formation of the requisite propenone by Claisen condensation of **1** with *p*-tolualdehyde under basic conditions resulted in hydrolysis of the ester group. The alternate approach, via pyridinium salt **2a**, was, therefore, adopted and this represents one of the few examples of a Kröhnke synthesis employing a functionalized pyridinium salt [10]. Ester **1** was converted in 58% yield to salt **2a** which, without purification, was condensed with the known propenone **3** [6] in the presence of excess NH_4OAc to afford ttpyE. Despite rigorous con-

trol of all reaction conditions, the crude product contained variable but small quantities ($<6\%$) of a polar material that we suppose was the product of hydrolysis, the acid HttpyA, but this was easily separated by trituration with $CHCl_3$. The presence of residual hydrolyzed material was traced back to a contamination of **2a** by a variable but small quantity ($<6\%$) of acid salt **2b** (detected by ^1H NMR and FAB MS). This proved to be inseparable from the ester salt **2a**, but the presence of **2b** was inconsequential, as we were able to convert the putative HttpyA to ttpyE to improve the overall yield of pure ttpyE to 73%.

The putative HttpyA was too insoluble to undergo complexation under standard conditions. The insolubility is likely because it adopts a zwitterionic form, a problem encountered with other carboxyl-bearing tridentates [11]. Instead, the diester form $[Ru(ttpyE)_2](PF_6)_2$ was prepared in 85% isolated yield from ttpyE and $RuCl_3$, followed by anion exchange and column chromatography. The use of $Ru(DMSO)_4Cl_2$ [12] resulted in a lower yield (63%) [13]. Although the NMR spectra of both ttpyE and $[Ru(ttpyE)_2](PF_6)_2$ were complicated by low symmetry, COSY spectra allowed for the assignment of all H resonances. The most notable effect of complexation was the 1.3 ppm upfield migrations of H-6 and H-6″ (and smaller migrations for H-5 and H-5″) amidst generally downfield shifts, due to the ring current of the perpendicular ligand.

The room temperature electronic spectra and cyclic voltammogram of $Ru(ttpyE)_2^{2+}$ were obtained and compared to those of the parent complex $Ru(ttpy)_2^{2+}$ (Table 1). Two quasi-reversible reduction waves were found. When compared to $Ru(ttpy)_2^{2+}$, $Ru(ttpyE)_2^{2+}$ shows more positive potentials for all waves, more so for the first reduction wave ($\Delta E_{1/2}^{2+/+}$ 210 mV) than for the oxidation wave ($\Delta E_{1/2}^{3+/2+}$ 140 mV), and this is consistent with the electron-withdrawing ester groups stabilizing the ligand-centred π* (LUMO) level to a larger extent than the metal-centred d (HOMO) orbital. There is a rough correlation among Ru(II) terpyridine complexes between MLCT energies and $E_{1/2}^{3+/2+} - E_{1/2}^{2+/+}$, [14] which $Ru(ttpyE)_2^{2+}$ also obeys. The smaller $E_{1/2}^{3+/2+} - E_{1/2}^{2+/+}$ gap with $Ru(ttpyE)_2^{2+}$ is reflected in the red shift of the MLCT absorbance to one of the longest wavelengths measured in such complexes, accompanied by a broadening of the MLCT envelope due to the lower symmetry here than in $Ru(ttpy)_2^{2+}$, and the consequent loss of orbital degeneracy. The effects of ester groups were therefore very similar here as in a 4,4′-disubstituted 2,2′-bipyridine complex, [15] and are analogous to the effects of other electron-withdrawing substituents in tpy complexes [16].

The hydrolysis of $[Ru(ttpyE)_2](PF_6)_2$ by NaOH, followed by acidification with HPF_6, afforded the diacid complex $H_2[Ru(ttpyA)_2](PF_6)_2$ as a red powder in 94% yield. Except for the absence of an ester OCH_3 signal, its ^1H NMR spectrum was very similar to that of $[Ru(ttpyE)_2](PF_6)_2$.

The dilute CH_3CN solutions of this complex used in UV–Vis spectroscopy and in the photochemical experiments (vide infra) were homogeneous but, in concentrated solutions appropriate for crystallization and NMR, this acidic complex developed a precipitate that was subsequently insoluble in the usual solvents for Ru(II) complexes (CH_3CN, DMF) and only sparingly soluble in MeOH or H_2O. Similarly, the evaporation of solutions of $H_2[Ru(ttpyA)_2](PF_6)_2$ and redissolution left an insoluble residue. The residue could be solubilized in methanolic HCl or with TFA, and a drop of TFA-*d* in the CD_3CN sample for NMR prevented that precipitation. We believe that this insoluble material resulted from the loss of the elements of HPF_6, as had occurred with the PF_6^- salts of previous carboxyl-bearing Ru(II) complexes [17]. Since the pK_a values governing the deprotonations of each COOH group are likely very similar, this would probably generate the neutral $[Ru(ttpyA)_2]^0$. We cannot exclude the formation of a singly deprotonated $H[Ru(ttpyA)_2]PF_6$ but we note that COO^- groups are unable to hydrogen-bond with the solvent whereas COOH groups can. When, during synthesis, the acidification step following the NaOH digestion was omitted, the product was similarly insoluble and could only be analyzed in TFA solutions, i.e. in a protonated and charged state. Since the COO^- groups lie on the outer surface of the complex, they remain accessible for close-range electrostatic interactions with external cations, even if the complex is electrostatically indifferent at long range (or, in the case of $H[Ru(ttpyA)_2]PF_6$, repulsive). As they are disposed on one side of the complex, the COO^- groups on one molecule can interact with the opposite, positively

Table 1
Ground-state MLCT absorption maxima [a], electrochemical potentials [b], yields of photogenerated $MV^{\bullet+}$ and associated kinetic parameters

	$Ru(ttpy)_2^{2+}$	$Ru(ttpyE)_2^{2+}$	$H_2Ru(ttpyA)_2^{2+}$
λ_{max} (nm)	490	498	492
ϵ ($\times 10^{-4}$ M^{-1} cm^{-1})	1.55	1.35	1.30
$E_{1/2}^{3+/2+}$	1.25 [c]	1.39	
$E_{1/2}^{2+/+}$	−1.24 [c]	−1.03	
$E_{1/2}^{+/0}$	−1.42 [d]	−1.26	
$[MV^{\bullet+}]_\infty$ ($M\times 10^5$)	0.55(5)		1.3(2)
k_{init} ($s^{-1}\times 10^5$)	0.84(1)		1.72(4)
k_f ($s^{-1}\times 10^5$)	1.12(1)		1.86(3)
k_q ($s^{-1}\times 10^3$)	8.8(6)		5.9(18)

e.s.d. values in brackets.
[a] 5×10^{-5} M in MeOH at 298 K.
[b] CH_3CN, 0.1 M $^nBu_4NPF_6$, 298 K, in V vs. SSCE.
[c] Ref. [18].
[d] In DMSO (Ref. [19]).

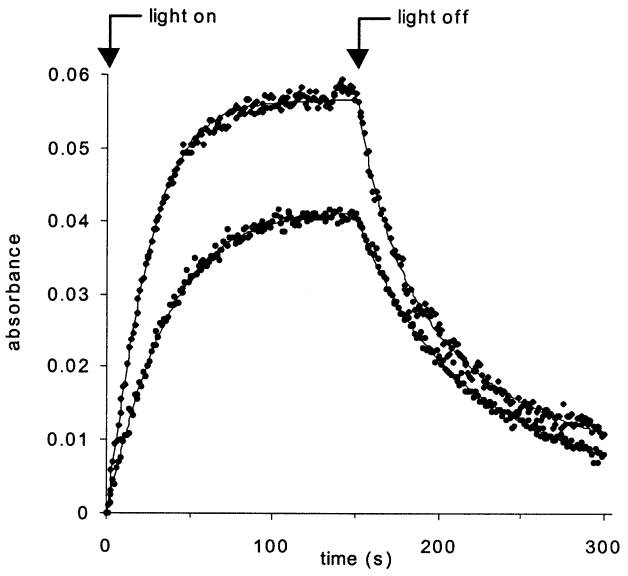


Fig. 2. Typical time courses of the absorbance at 600 nm with $H_2[Ru(ttpyA)_2](PF_6)_2$ (upper trace) and $[Ru(ttpy)_2](PF_6)_2$ (lower trace). Samples were in CH_3CN at 4×10^{-5} M and contained 9.45×10^{-3} M $MV(PF_6)_2$ and 0.05 M TEOA. The solid lines are the least-squares fits according to Eq. (1).

charged hemisphere of another, and the insolubility may therefore reflect the formation of an infinite chain of electrostatically ordered molecules, e.g. $\{[Ru(ttpyA)_2]\}_n$.

Although no satisfactory analytical sample of $H_2[Ru(ttpyA)_2](PF_6)_2$ could thus be prepared, its purity (as shown by its ^1H NMR spectrum) and its stability in dilute solutions were more than adequate for the photochemical experiments (vide infra).

The electronic spectrum of $H_2[Ru(ttpyA)_2](PF_6)_2$ was very similar to that of the diester, but with a blue shift of the MLCT λ_{max}. A similar shift had been recorded for a 2,2′-bipyridine-4,4′-dicarboxylic acid complex [1]. This attests to the weaker electron-withdrawing effect of COOH groups.

Methodology developed earlier [8] was used to comparatively assess the abilities of $H_2[Ru(ttpyA)_2](PF_6)_2$ and $[Ru(ttpy)_2](PF_6)_2$ to sensitize the production of cation radical ($MV^{\bullet+}$) from the electron acceptor (MV^{2+}) by oxidative quenching, under continuous irradiation in CH_3CN and with triethanolamine (TEOA) as sacrificial reductant. Fig. 2 presents typical results and Table 1 reports the pertinent findings: under continuous irradiation, there is an initial rapid rise of $[MV^{\bullet+}]$ (monitored at 600 nm), followed by a steady-state plateau. The rate of rise (rate constant k_{init}) and the steady-state yield of $MV^{\bullet+}$ were significantly higher than with $[Ru(ttpy)_2](PF_6)_2$. Kinetic analysis according to Eq. (1) suggested that this improvement arose from a 66% increase in the rate of $MV^{\bullet+}$ formation (larger k_f) while the $MV^{\bullet+}$ quenching rate constant (k_q) was, within experimental error, similar.

In the presence of TEOA, $H_2[Ru(ttpyA)_2](PF_6)_2$ should be in a deprotonated form. While the effects of $COOH/COO^-$ groups on the excited-state lifetimes (τ) of bpy complexes is ambiguous, [1,20] it is generally agreed that electron-withdrawing groups lengthen τ [1,15,16,20,21]. COO^- groups are weakly electron-withdrawing and therefore not expected to significantly increase τ beyond that previously measured for $[Ru(ttpy)_2]^{2+}$ (τ 0.95 ns in nitrile solvent [22]). Instead, the COO^- groups must play another role.

It may be that the TEOA-deprotonated complex is the neutral $[Ru(ttpyA)_2]^0$ (or $H[Ru(ttpyA)_2]PF_6$) and that this remains soluble at the low concentration employed in the photochemical experiments. If so, the improvement in photosensitization ability can be attributed to a simple electrostatic advantage over $[Ru(ttpy)_2]^{2+}$ of the kind invoked with other carboxylated complexes, [1] wherein the electrostatic repulsions experienced by photoexcited $[Ru(ttpy)_2]^{2+}$ in its encounters with MV^{2+}, repulsions that the solvent can poorly abate, are absent (or reduced) with TEOA-deprotonated $H_2[Ru(ttpyA)_2](PF_6)_2$. But, just as the insolubility of the material that $H_2[Ru(ttpyA)_2](PF_6)_2$ spontaneously deposits at higher concentrations is believed to result from intermolecular electrostatic interactions involving the surface COO^- groups, it is likely that the TEOA-generated COO^- groups here remain intimately associated with the co-generated $HTEOA^+$ ions through electrostatic and hydrogen bonding, both attractive interactions that can occur at close enough range to overcome the repulsions with the more distant metal centre. In this case, the TEOA-deprotonated complex is better described as a $(HTEOA)PF_6$ adduct, $(HTEOA)_2[Ru(ttpyA)_2](PF_6)_2$ or $H(HTEOA)[Ru(ttpyA)_2](PF_6)_2$. We had earlier obtained an analogous bis-$NaPF_6$ adduct with a diacidic complex [23]. There is no electrostatic advantage over $[Ru(ttpy)_2]^{2+}$ with such adducts, but they can undergo cation exchange with MV^{2+}. At the very least, such cation exchange provides encounters between the excited state and MV^{2+}. At best, the two COO^- moieties constitute a two-point binding site for MV^{2+} in 1:1 supramolecular interaction, as illustrated in Fig. 1. We have earlier described an analogous supramolecular association between MV^{2+} and a deprotonated tetra-acidic complex [17]. More importantly, such cation exchange or supramolecular association can occur prior to the photoevent and, once photoexcitation has taken place, would render the electron transfer a unimolecular process, thereby entropically enhancing the rate of transfer and reducing the dependence on τ. After the electron transfer has taken place, the electrostatic attractions with the photoproduct $MV^{\bullet+}$ are weaker and further weakened by enhanced repulsions from the Ru(III) centre. This promotes a dissociation that allows $MV^{\bullet+}$ to avoid the reverse electron transfer and accumulate. This notion of

electrostatic or supramolecular assistance of photosensitization is under further investigation in this and other systems.

Acknowledgements

The authors thank Phuong Uyen Luyen for conducting the photogeneration experiments and the Natural Sciences and Engineering Research Council (Canada) for funding.

References

[1] (a) G.L. Gaines, J. Phys. Chem. 83 (1979) 3088;
(b) S. Anderson, E.C. Constable, K.R. Seddon, J.E. Turp, J.E. Baggott, M.J. Pilling, J. Chem. Soc., Dalton Trans. (1985) 2247.
[2] (a) N. Vlachopoulos, P. Liska, J. Augustynski, M. Grätzel, J. Am. Chem. Soc. 110 (1988) 1216;
(b) O. Kohle, S. Ruile, M. Grätzel, Inorg. Chem. 35 (1996) 4779;
(c) R. Argazzi, C.A. Bignozzi, G.M. Hasselmann, G.J. Meyer, Inorg. Chem. 37 (1998) 4533.
[3] (a) V.-M. Mukkala, M. Helenius, I. Hemmilä, J. Kanare, H. Takalo, Helv. Chim. Acta 76 (1993) 1361;
(b) K.T. Potts, K.A. Gheysen Raiford, M. Keshavarz-K, J. Am. Chem. Soc. 115 (1993) 2793;
(c) A.P. deSilva, H.Q.N. Gunaratne, T.E. Rice, Angew. Chem., Int. Ed. Engl. 35 (1996) 2116.
[4] F. Kröhnke, Synthesis (1976) 1.
[5] M. Ishihara, T. Tsuneya, M. Shiga, S. Kawashima, K. Yamagishi, F. Yoshida, H. Sato, K. Uneyama, J. Agric. Food Chem. 40 (1992) 1647.
[6] C.M. Chamchoumis, P.G. Potvin, J. Chem. Res. (M) (1998) 0870; J. Chem. Res. (S) (1998) 180.
[7] A.J. Bard, L.R. Faulkner, Electrochemical Methods, Wiley, New York, 1980, p. 227.
[8] P.G. Potvin, P.U. Luyen, F. Al-Mutlaq, New J. Chem. 25 (2001) 839.
[9] E.M. Kosower, J.L. Cotter, J. Am. Chem. Soc. 86 (1964) 5524.
[10] (a) For other examples see: E.C. Constable, J. Lewis, Polyhedron 1 (1982) 303;;
(b) G.R. Newkome, D.C. Hager, G.E. Kiefer, J. Org. Chem. 51 (1986) 850;;
(c) R.-A. Fallahpour, E.C. Constable, J. Chem. Soc., Perkin Trans. 1, 16 (1997) 2263.
[11] J. Zadykowicz, P.G. Potvin, J. Org. Chem. 63 (1998) 235.
[12] B.R. James, R.S. McMillan, Inorg. Nucl. Chem. Lett. 11 (1975) 837.
[13] C.M. Chamchoumis, Ph.D. Thesis, York University, 1999.
[14] A.B.P. Lever, Inorg. Chem. 29 (1990) 1271.
[15] W.F. Wacholz, R.A. Auerbach, R.H. Schmehl, Inorg. Chem. 25 (1986) 227.
[16] M. Maestri, N. Amaroli, V. Balzani, E.C. Constable, A.M.W. Cargill Thompson, Inorg. Chem. 34 (1995) 2759.
[17] J. Zadykowicz, P.G. Potvin, Inorg. Chem. 38 (1999) 2434.
[18] K. Kalyanasundaram, M.K. Nazeeruddin, M. Grätzel, G. Viscardi, P. Savarino, E. Barni, Inorg. Chim. Acta 198 (1992) 831.
[19] (a) E.C. Constable, A.M.W. Cargill Thompson, D.A. Tocher, M.A.M. Daniels, New J. Chem. 16 (1992) 855;
(b) E.C. Constable, A.M.W. Cargill Thompson, N. Amaroli, V. Balzani, M. Maestri, Polyhedron 20 (1992) 2707;
(c) E. Amouyal, M. Mouallem-Bahout, G. Calzaferri, J. Phys. Chem. 95 (1991) 7641.
[20] J.-P. Sauvage, J.-P. Collin, J.-C. Chambon, S. Guillerez, C. Coudret, V. Balzani, F. Barigelletti, L. De Cola, L. Flamigni, Chem. Rev. 94 (1994) 993.
[21] Y. Luo, Ph.D. Thesis, York University, 1993.
[22] J.-P. Collin, S. Guillerez, J.-P. Sauvage, F. Barigelletti, L. De Cola, L. Flamigni, V. Balzani, Inorg. Chem. 30 (1991) 4230.
[23] R.P. Thummel, V. Hedge, Y. Jahng, Inorg. Chem. 28 (1989) 3264.

PERGAMON

Polyhedron 21 (2002) 55–59

POLYHEDRON

www.elsevier.com/locate/poly

Electrochemical studies of copper(II) complexes with Schiff-base ligands

Santiago Zolezzi [a], Evgenia Spodine [a,b], Antonio Decinti [a,*]

[a] *Departamento de Química Inorgánica y Analítica, Facultad de Ciencias Químicas y Farmacéuticas, Universidad de Chile, Casilla 233 Santiago, Chile*

[b] *Facultad de Ciencias Químicas y Farmacéuticas, Centro de Investigación Interdisciplinaria Avanzada en Ciencias de los Materiales, Universidad de Chile, Casilla 233 Santiago, Chile*

Received 9 May 2001; accepted 2 October 2001

Abstract

The electrochemical reduction of copper(II) complexes with salen Schiff-base ligands derived from ethylenediamine or (*R*,*R*) or (*S*,*S*)-1,2-diphenylethylenediamine and 5-methoxy, 5-bromo and 5-nitrosalicylaldehyde have been studied by cyclic voltammetry in the potential range +1 to −2.3 V in dimethyl sulfoxide (DMSO) as a solvent. The resulting voltammograms consist of a single quasi-reversible one-electron transfer attributable to the couple [Cu(II)L]/[Cu(I)L]$^-$. Trends in cathodic peak potential (E_{pc}) values are observed which can be correlated with the electronic effects of the 5-substituents of the Schiff-base ligands. Changes in the basicity of the ligand groups are determinant for such electrochemical trends. © 2002 Elsevier Science Ltd. All rights reserved.

Keywords: Salen Cu(II) complexes; Schiff-base ligands; Cyclic voltammetry; Hammett substituent constants

1. Introduction

Transition metal complexes with tetradentate Schiff-base ligands have been extensively investigated as catalysts for a number of organic redox reactions and electrochemical reduction processes [1–5]. Salen complexes have also been recently used as catalytically active materials to develop surface-modified electrodes for sensoring applications [6,7]. Cyclic voltammetry has been a useful tool to investigate the mechanisms of catalysis by Schiff-base metal complexes as well as to study the structure–reactivity relationships in these compounds [3,5,8]. We have previously studied the syntheses and spectroscopic characterisation of copper(II) complexes of salen Schiff bases derived from ethylenediamine, (1*R*,2*R*)- and (1*S*,2*S*)-1,2-diphenylethylenediamine, and 5-nitro, 5-bromo and 5-methoxysalicylaldehyde [9]. Electronic spectra of these complexes in the d–d region suggest that the ligand field strength varies as a function of the 5,5′-substituents according to the sequence $NO_2 < Br < H < OCH_3$. Hence, it should be expected that the thermodynamic stabilities of such complexes follow a similar order which, in turn, should influence both their electrochemical properties and potential catalytic behaviour. Properties of these complexes, as potential catalysts for epoxidation of olefins are being tested at present in our laboratory. In connection with such studies, herein, we report an electrochemical study of the above mentioned Schiff-base ligands and their respective copper(II) complexes in dimethyl sulfoxide (DMSO) as a solvent. Copper(II) complexes whose electrochemical characterisation has been reported previously [10,11] have been included in this report in order to parallel both Schiff-base ligand series, the ethylenediamine and the 1,2-diphenylethylenediamine derivatives.

2. Experimental

Reagent grade chemicals were obtained from Aldrich and were used as provided. HPLC grade DMSO was

* Corresponding author. Tel.: +56-2-6782851; fax: +56-2-7370567.

E-mail address: mroa@ciq.uchile.cl (A. Decinti).

0277-5387/02/$ - see front matter © 2002 Elsevier Science Ltd. All rights reserved.
PII: S0277-5387(01)00960-3

dried over molecular sieve previously dried at 105 °C under vacuum, redistilled and stored under N_2 over molecular sieve before use. The Schiff bases and copper(II) complexes under study have been prepared previously [9]. For comparative purposes, the redox couple Cu(II)/Cu(I) of $Cu(ClO_4)_2$ in DMSO was also considered. Moreover, in the cases of sparing solubility in DMSO, dimethylformamide (DMF) was used. Cyclic voltammetry was carried out under pure dry nitrogen in a three-electrode cell with a vitreous carbon working electrode, a platinum counter electrode and an aq. saturated AgCl/Ag reference electrode ($E = -0.0474$ V vs. the saturated calomel electrode). Supporting electrolyte was 0.05 M n-Bu_4NClO_4 (TBAP). Cyclic voltammograms were scanned at room temperature (r.t.) in the potential range of $+1$ to -2.3 V, at sweep rates (v) between 25 and 1000 mV s^{-1}, and were recorded with a Metrohm VA-693 potentiostat equipped with a VA-694 stand and connected to a personal computer. Oxidative CV measurements were not performed because, according to literature data on copper(II) complexes with similar coordination spheres [8], the CV wave for the process Cu(II)/Cu(III) falls at potentials near $+1.48$ V, i.e. outside the potential range allowed by the electrode–solvent system here used. Coulometric measurements were carried out at r.t., under pure dry nitrogen, with a Princeton Applied Research (PARC) model 173 potentiostat coupled to a PARC model 179 digital coulometer, with a platinum mesh working electrode, a platinum coil counter electrode and an aq. saturated AgCl/Ag reference electrode. Controlled-potential electrolysis measurements were performed at r.t., under pure dry nitrogen, with a Wenking POS 88 potentioscan, using an electrochemical cell modified for spectrophotometric measurements (optical path length, 1 cm). Here a platinum coil working electrode, a platinum coil counter electrode and an aq. saturated AgCl/Ag reference electrode were used. Absorption spectra were recorded in the visible region on a UV3 Unicam spectrometer.

Table 1
Labelling for the Schiff-base ligands and their copper(II) complexes

Ligand	Complex	Substituents	
		5,5′	8,8′
Ethylenediamine derivatives			
1	Cu1	OCH_3	H
2	Cu2	H	H
3	Cu3	Br	H
4	Cu4	NO_2	H
1,2-Diphenylethylenediamine derivatives			
1R	Cu1R	OCH_3	$(R,R)C_6H_5$
1S	Cu1S	OCH_3	$(S,S)C_6H_5$
2R		H	$(R,R)C_6H_5$
2S	Cu2S	H	$(S,S)C_6H_5$
3R	Cu3R	Br	$(R,R)C_6H_5$
4R	Cu4R	NO_2	$(R,R)C_6H_5$

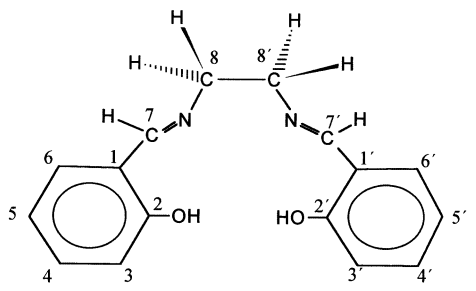


Fig. 1. Atom labelling scheme for salen copper(II) complexes.

3. Results and discussion

The ligands and metal complexes under study were labelled as shown in Table 1 by use of the atom-labelling scheme given in Fig. 1. The voltammetric parameters obtained for the ligands and their respective copper(II) complexes are listed in Table 2. Moreover, typical voltammograms of a given ligand and its respective copper(II) complex are shown in Fig. 2.

3.1. Schiff-base ligands

For all Schiff-base ligands studied, except compounds **4** and **4R** (nitro derivatives), cyclic voltammograms at 100 mV s^{-1} consist of a single cathodic peak at potentials ranging from -1.6 to -2.0 V; no anodic wave occurs in the reverse scan. This behaviour was observed for a wide range of scan rates from 25 to 1000 mV s^{-1}. Hence, such a reduction process should correspond to a totally irreversible electron transfer. Voltammograms of compounds **4** and **4R** show the above-mentioned cathodic peak at -1.13 V (Table 2). Additionally, they exhibit CV waves in the range -1.4 to -1.8 V, which may be ascribed to the reduction of the nitro groups [15]. Coulometric measurements of compound **2** in DMSO indicate that the cathodic wave observed corresponds to a two-electron transfer. In fact, the shapes of the cathodic waves suggest that they would consist of two overlapped one-electron processes. A similar result has previously been reported for this compound in DMF, but in the presence of 2 equiv. of acetic acid [12]. Such a requirement would arise from the fact that both the dielectric constant and the dipole moment of DMF are smaller than those of DMSO. For all Schiff bases under study, this irreversible reduction peak would be ascribed to an intramolecular reductive coupling of the two imine groups to yield a piperazine [12–14]. Such a process would involve self-protonation reactions where the phenolic hydroxyl groups act as proton donors.

Table 2
Cyclic voltammetric parameters for the Schiff-base ligands and their copper(II) complexes, and calculated values for $\Delta \log \beta = \log \beta(\mathrm{Cu(II)L}) - \log \beta(\mathrm{Cu(I)L^-})$

Ligand		*Complex*					
	E_{pc} (V)		E_{pc} (V)	$E_{1/2}$ (V)	ΔE_p (mV)	i_{pa}/i_{pc}	$\Delta \log \beta$
Ethylenediamine derivatives							
1	−1.97	Cu1	−1.26	−1.19	130	0.50	21.4
2	−1.79	Cu2	−1.23	−1.17	115	0.73	20.9
3	−1.62	Cu3 [a]	−1.14	−1.07	140	0.46	19.4
4	−1.13	Cu4	−0.91	−0.86	111	0.27	15.6
1,2-diphenylethylenediamine derivatives							
1R	−1.87	Cu1R	−1.28	−1.21	113	0.96	21.8
		Cu1S	−1.28	−1.23	100	1.01	21.8
2R	−1.85	Cu2S	−1.22	−1.17	101	0.97	20.9
3R	−1.69	Cu3R	−1.08	−1.05	91	0.80	18.5
4R	−1.13	Cu4R	−0.95	−0.91	94	0.88	16.3
$Cu(ClO_4)_2$ [b]			0.01	0.05	91	0.97	

[a] For Cu**3**, the solvent was DMF.
[b] CV parameters of $Cu(ClO_4)_2$ correspond to the couple Cu(II)/Cu(I). For the couple Cu(I)/Cu^0 $E_{pc} = -0.57$ V and $E_{1/2} = -0.26$ V.

On the other hand, in each series of ligands, the cathodic peak potential (E_{pc}) corresponding to the intramolecular reductive coupling of the imine groups varies as can be expected from the electronic effects of the substituents at positions 5,5′. Thus, E_{pc} becomes less negative according to the sequence $OCH_3 < H < Br < NO_2$, i.e. in order of an increase in both electron-withdrawing and π-acceptor qualities of the substituents. In fact, for both ethylenediamine and 1,2-diphenylethylenediamine derivatives, Hammett type relationships were found between the E_{pc} values and the appropriate *para*-substituent parameters [16]. Such correlations are shown in Fig. 3. However, since the substituents at positions 5,5′ are indeed *para*- to the respective phenolic hydroxyl groups, the occurrence of these Hammett type correlations would indicate that the E_{pc} for the reductive coupling of the imine groups actually varies as a function of the acidity of the hydroxyl group through the ligand series. This fact agrees with a mechanism involving self-protonation reactions for the electrochemical reduction of the imine groups in the Schiff bases under study.

3.2. Copper(II) complexes

The cyclic voltammetric curves for the electrochemical reduction of the studied copper(II) complexes (Table 2) exhibit a redox couple at potentials in the range of −0.91 to −1.28 V, which can be attributed to the reduction of the metal centre [10,11]. Voltammograms of complexes Cu4 and Cu4R show additional CV waves in the range of −1.5 to −1.8 V, which correspond to the reduction of the nitro groups. Moreover, for all complexes studied, the cathodic wave corresponding to the irreversible two-electron reduction of the imino groups is no longer observed. This fact indicates that, owing to the lack of transferable hydroxylic protons, the reduction potentials of the dianionic ligands have been shifted beyond the lower limit of the potential interval considered in the experimental measurements [12].

On the other hand, the ΔE_p data listed in Table 2, though being much larger than the theoretical value for an electrochemically reversible one-electron process, at least suggest that the reduction of copper(II) in the complexes under study should correspond to a one-electron charge transfer. Actually, this possibility has been corroborated through coulometric measurements on the system Cu2 in DMSO. The exceedingly large ΔE_p val-

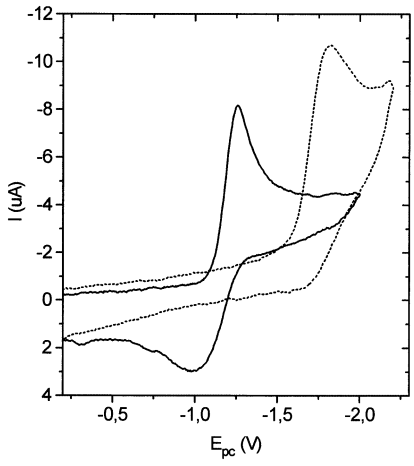


Fig. 2. Cyclic voltammograms recorded for the reduction of 1.0 mM ligand **2** (----) and 1.0 mM complex Cu2 (—) at a vitreous carbon electrode in DMSO containing 0.05 M TBAP. Scan rate, 0.1 V s^{-1}.

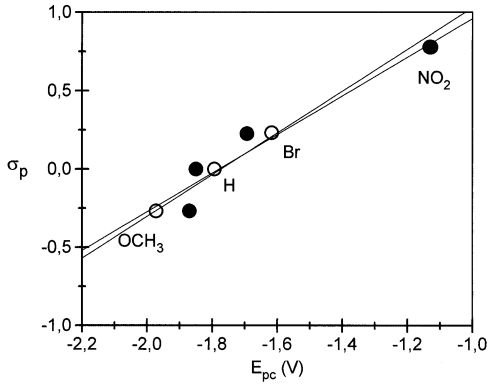


Fig. 3. Correlation between the E_{pc} values for Schiff-bases and the respective σ substituent constants (for *p*-substitution). Ethylenediamine derivatives (○) $r = 0.998$; 1,2-diphenylethylenediamine derivatives (●) $r = 0.960$.

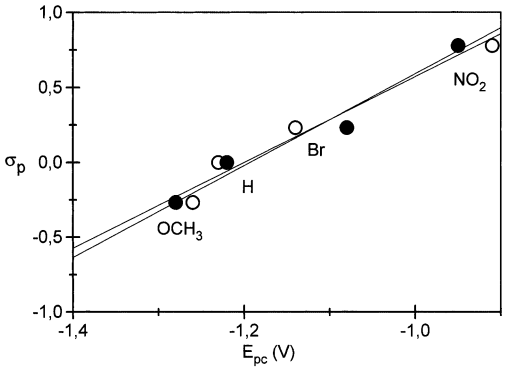


Fig. 4. Correlation between the E_{pc} values for copper(II) complexes with Schiff-base ligands and the respective σ substituent constants (for *p*-substitution). Ethylenediamine derivatives (○) $r = 0.982$; 1,2-diphenylethylenediamine derivatives (●) $r = 0.983$.

ues for the electrochemical reduction of copper(II) in these complexes would be due to both a quasi-reversible behaviour of the couple $[Cu(II)L] + e^- = [Cu(I)L]^-$ under the v conditions here adopted and the non-aq. nature of the systems [8,17]. For all complexes, CV measurements at different v, in the range 25–1000 mV s^{-1}, indicate that the E_{pc} values are only slightly dependent upon the v. Furthermore, in all cases a linear relationship between the cathodic peak current (i_{pc}) and the square root of the v ($v^{1/2}$) was observed. This fact implies that these electrochemical processes are mainly diffusion-controlled.

As can be noticed in Table 2, the E_{pc} and $E_{1/2}$ values for the copper complexes are more negative by 1.1–1.7 V compared with the respective values for the $Cu(ClO_4)_2$ couple in DMSO. This indicates that, for the Schiff-base ligands herein studied, the chelates of copper(II) are considerably more stable than the respective chelates of copper(I). Accordingly, the differences between the logarithms of the formation constants (β) of these complexes were estimated through the expression:

$$\Delta\log\beta = \log\beta(Cu(II)L) - \log\beta(Cu(I)L^-) = (E^{\circ\prime} - E)/0.059$$

where $E^{\circ\prime}$ stands for the reduction potential of the reference Cu(II)/Cu(I) redox couple and E for the reduction potential of the couple $[Cu(II)L]/[Cu(I)L]^-$. In such calculations, the approximation $E^{\circ\prime} - E = E_{pc}[Cu(ClO_4)_2] - E_{pc}[Cu(II)L]$ was taken. The parameters $\Delta\log\beta$ thus calculated are included in Table 2. As can be seen in this table, E_{pc} becomes less negative in the sequence $OCH_3 < H < Br < NO_2$ and, hence, $\Delta\log\beta$ decreases according to $OCH_3 > H > Br > NO_2$, i.e. in a sequence of increasing electron-withdrawing effects of the substituents at positions 5,5′. Similar results have been reported previously for analogous copper(II) and nickel(II) systems, and have been interpreted by assuming that the strong electron-withdrawing effects stabilise the lower oxidation state [8]. However, another possibility would be that, owing to the decrease in donor ability of the ligand groups (mainly the phenoxy groups) the stabilities of both [Cu(II)L] and $[Cu(I)L]^-$ decrease through the above mentioned sequence, but for the latter to a lesser extent. This would be a consequence of an increase in the flexibility of the coordination sphere over such a series, which should favour the stability of the copper(I) complex. Moreover, for both metal complex series, Hammett type relationships were found between E_{pc} and the appropriate *para*-substituent parameters [16] which reflect the variation of the electrode potential as a function of the electron-withdrawing ability of the substituents at positions 5,5′. Such correlations are shown in Fig. 4. These results indicate that the decrease in basicity of the phenoxy group through the sequence $OCH_3 > H > Br > NO_2$ would be determinant for the electrochemical trends observed.

On the other hand, since the $\Delta\log\beta$ data indicate that, for each system the Cu(II) complex should be considerably more stable than the Cu(I) one, a less negative electrode potential for the couple $[Cu(I)L]^-/Cu^0$ than for the couple $[Cu(II)L]/[Cu(I)L]^-$ should be expected. Hence, it should also be expected that the electrochemical reduction of the copper(II) complexes occurs through a two-electron charge transfer, i.e. by an EE or EC mechanism. Reduction of [Cu(II)L] to Cu^0 has not been observed, not even in the coulometric experiments. Thus, the copper(I) complexes would behave as kinetically inert to both cathodic heterogeneous charge transfer and disproportionation. Nevertheless, if the solution resulting from the coulometric experiment on the complex Cu2 is allowed to stand overnight under pure dry nitrogen, a partial recovery of its original colour is observed. This suggests that, at least for the mentioned complex, disproportionation of $[Cu(I)L]^-$ occurs to a some extent. This fact has been confirmed by means of spectroelectrochemical measure-

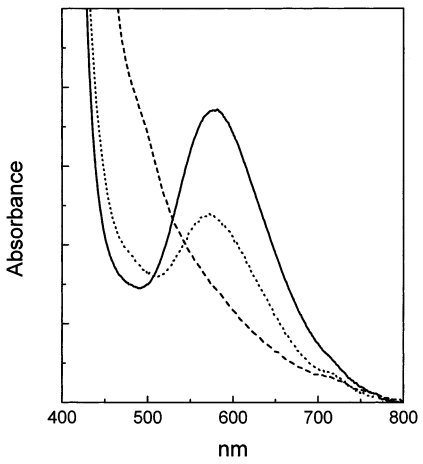


Fig. 5. Absorption spectrum in the d–d band region of 1 mM Cu2 in DMSO containing 0.05 M TBAP, (—) before electrochemical reduction; (----) after reduction; and (···) allowed to stand for 15 h after reduction, under pure dry nitrogen, at r.t.

ments on the complexes Cu2 and Cu4. Results obtained for Cu2 are shown in Fig. 5. Such results can be related with the i_{pa}/i_{pc} data listed in Table 2. Accordingly, for complexes with 8,8′-diphenyl substituted Schiff-base ligands the ratio of i_{pa}/i_{pc} takes values close to one, as required for a reversible or quasi-reversible charge transfer without coupled chemical reactions. Instead, for complexes with Schiff-base ligands derived from ethylenediamine $i_{pa}/i_{pc} < 1$ is always observed. This fact suggests that the electrochemical reduction of these complexes involves an EC mechanism consisting of a reversible or quasi-reversible one-electron heterogeneous charge transfer followed by an irreversible chemical reaction, i.e. the disproportionation of $[Cu(I)L]^-$. It has previously been suggested that the ratio i_{pa}/i_{pc} smaller than unity observed for complex Cu2 in DMF can be attributed to the presence of traces of water in the solvent-supporting electrolyte [10]. Accordingly, additional experiments performed in our laboratory have shown that, on increasing the water concentration of the Cu1S system from traces to 5 M, the peak-current ratio decreases from 1.01 to 0.87. However, as can be seen in Table 2, peak-current ratios for complexes with Schiff-base ligands derived from ethylenediamine are smaller than 0.87. Thus, the somewhat different behaviour of copper(II) complexes with 8,8′-diphenyl substituted Schiff-base ligands can be ascribed to a greater kinetic inertness to disproportionation of the respective copper(I) complexes. Since the disproportionation reaction of Cu(I) complexes should involve a bimolecular process, it could be assumed that such a greater kinetic inertness arises from the occurrence of steric hindrance effects involving the phenyl substituents in the transition state.

Acknowledgements

Financial support from FONDAP, project 11980002, is gratefully acknowledged.

References

[1] L. Canali, D.C. Sherrington, Chem. Soc. Rev. 28 (1998) 85.
[2] A.A. Isse, A. Gennaro, E. Vianello, J. Electroanal. Chem. 444 (1998) 241.
[3] D. Pletcher, H. Thompson, J. Electroanal. Chem. 464 (1999) 168.
[4] T. Okada, K. Katou, T. Hirose, M. Yuasa, I. Sekine, J. Electrochem. Soc. 146 (1999) 2562.
[5] L.J. Klein, K.S. Alleman, D.G. Peters, J.A. Karty, J.P. Reilly, J. Electroanal. Chem. 481 (2000) 24.
[6] P.H. Aubert, A. Neudeck, L. Dunsch, P. Audebert, P. Capdevielle, M. Maumy, J. Electroanal. Chem. 470 (1999) 77.
[7] L. Mao, K. Yamamoto, W. Zhou, L. Jin, Electroanalysis 12 (2000) 72.
[8] E.G. Jäger, K. Schuhmann, H. Görls, Inorg. Chim. Acta 255 (1997) 295.
[9] S. Zolezzi, A. Decinti, E. Spodine, Polyhedron 18 (1999) 897. (Owing to typing errors in the original manuscript, in this reference, page 900, right-hand column, line 18, it says: "… $NO_2 > Br > H > OCH_3$. Hence, the π-donor character...". It should say: "… $NO_2 < Br < H < OCH_3$. Hence, the σ-donor character...". Moreover, in page 903, figure 5, in the wave number-axis it says: '17000' and '18000'; it should say: "17" and "18").
[10] M.J. Samide, D.G. Peters, J. Electroanal. Chem. 443 (1998) 95.
[11] M.M. Bhadbhade, D. Srinivas, Inorg. Chem. 32 (1993) 6122.
[12] A.A. Isse, A. Gennaro, E. Vianello, Electrochim. Acta 42 (1997) 2065.
[13] T. Shono, N. Kise, E. Shirakawa, H. Matsumoto, E. Okazaki, J. Org. Chem. 56 (1991) 3063.
[14] N. Kise, H. Oike, E. Okazaki, M. Yoshimoto, T. Shono, J. Org. Chem. 60 (1995) 3980.
[15] J.A. Squella, G. Jimenez, S. Bollo, L.J. Núñez-Vergara, Electrochim. Acta 42 (1997) 2305.
[16] H.H. Jaffé, Chem. Rev. 53 (1953) 191.
[17] C.L. Bailey, R.D. Bereman, D.P. Rillema, R. Nowak, Inorg. Chem. 23 (1984) 3958.

PERGAMON

Polyhedron 21 (2002) 61–68

POLYHEDRON

www.elsevier.com/locate/poly

Synthesis, spectroscopic characterization, electrochemical and photochemical properties of ruthenium(II) polypyridyl complexes with a tertiary amine ligand

Hideo Konno [1], Yuji Ishii, Kazuhiko Sakamoto, Osamu Ishitani *

Graduate School of Science and Engineering, Saitama University, 255 Shimo-Okubo, Saitama 338-8570, Japan

Received 18 June 2001; accepted 2 October 2001

Abstract

A series of ruthenium(II) polypyridine complexes were synthesized with a tertiary aliphatic amine ligand, $[Ru(4,4'\text{-}X_2bpy)_2(DMAEPy)]^{2+}$ (**1a**; X = H, **2**; X = CF_3), $[Ru(tpy)(N\text{–}N)Cl]^{+}$ (**3a**; N–N = DMAEPy, **3c**; N–N = DEAEPy) and $[Ru(tpy)(DMAEPy)(MeCN)]^{2+}$ (**4**) where DMAEPy = 2-(2′-dimethylaminoethyl)-pyridine, DEAEPy = 2-(2′-diethylaminoethyl)-pyridine, tpy = 2,2′:6′,2″-terpyridine and bpy = 2,2′-bipyridine. The spectroscopic, electrochemical and photochemical properties of these complexes are studied and compared to those of the corresponding primary-amine complexes $[Ru(bpy)_2(AEPy)]^{2+}$ (**1b**) and $[Ru(tpy)(AEPy)Cl]^{+}$ (**3b**) where AEPy = 2-(2′-aminoethyl)-pyridine. The MLCT bands in the UV–Vis absorption spectra of the tertiary-amine complexes were blue-shifted (8–9 nm), and their redox potentials for the $Ru^{II/III}$ couples were more positive than expected (90–100 meV) compared to the corresponding primary-amine complexes. Irradiation of an acetonitrile solution of the complexes causes selective photochemical ligand substitution of the tertiary-amine ligand even under aerated conditions, giving the corresponding solvento complex $[Ru(4,4'\text{-}X_2bpy)_2(MeCN)_2]^{2+}$ or $[Ru(tpy)(MeCN)_2Cl]^{+}$. © 2002 Elsevier Science Ltd. All rights reserved.

Keywords: Tertiary amines; Ruthenium complexes; Photochemistry; Electrochemistry

1. Introduction

Oxidative dehydrogenation of amines is an important metabolic process in vivo. In the case of amine oxidase (EC 1.4.3.6) it is known that Cu^{II} is present at the active site and plays an important role in amine dehydrogenation [1]. The inorganic chemistry of the oxidative dehydrogenation of primary and secondary aliphatic amines coordinated to ruthenium(II) has been also investigated by many researchers [2]. Meyer and co-workers reported that primary-amine complexes such as $[Ru(bpy)_2(en)]^{2+}$ (en = ethylenediamine), underwent four-electron oxidation either electrochemically or chemically, giving the corresponding diimine complexes $[Ru(bpy)_2(dim)]^{2+}$ (dim = 1,2-diiminoethane) [3]. Formation of these diimine complexes is initiated by the oxidation of the central Ru^{II} to Ru^{III}, and oxidation of the amine ligand couples to the deprotonation process from the amine. Ford and co-workers reported that the oxidation of $[(NH_3)_4Ru(AMPy)]^{2+}$ (AMPy = 2-(2′-aminomethyl)-pyridine) gives the stable Ru^{III} complex at low pH, while on increasing the pH oxidation of the AMPy ligand takes place, and the imine complex $[(NH_3)_4Ru(IMPy)]^{2+}$ (IMPy = 2-(2′-iminomethyl)-pyridine) is produced [4]. Photochemical oxidation of the primary-amine complexes has also been reported: irradiation of an aerated water or acetonitrile solution of $[Ru(bpy)_2(en)]^{2+}$ or $[Ru(bpy)_2(tn)]^{2+}$ (tn = 1,3-propylenediamine) gives the corresponding α,α′-diimine complexes [5].

Although metal complexes that are coordinated by a tertiary amine, such as triethylamine or triethanolamine, are important intermediates in photocat-

* Corresponding author. Tel.: +81-488-583-733; fax: +81-488-583-818.

E-mail address: ishitani@apc.saitama-u.ac.jp (O. Ishitani).

[1] Present address: National Institute of Advanced Industrial Science and Technology (AIST), 16-1 Onogawa, Tsukuba 305-8569, Japan.

0277-5387/02/$ - see front matter © 2002 Elsevier Science Ltd. All rights reserved.
PII: S0277-5387(01)00969-X

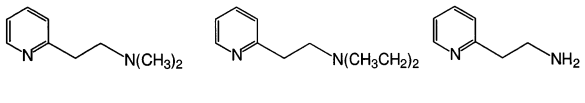
Table 1
Analytical data for the ruthenium complexes

Complex	Elemental analysis (%) [a]			ESI-MS (m/z)
	C	H	N	
1a $[Ru(bpy)_2(DMAEPy)](PF_6)_2$	41.03 (40.81)	3.49 (3.54)	9.68 (9.85)	709 [**1a**–PF_6^-]$^+$, 282 [**1a**–$(PF_6^-)_2$]$^{2+}$
2 $[Ru(4,4'\text{-}CF_3bpy)_2(DMAEPy)](PF_6)_2$	35.45 (35.21)	2.41 (2.33)	7.58 (7.47)	982 [**2**–PF_6^-]$^+$, 418 [**2**–$(PF_6^-)_2$]$^{2+}$
3a $[Ru(tpy)(DMAEPy)Cl](PF_6)$	43.47 (43.35)	3.74 (3.79)	10.28 (10.53)	520 [**3a**–PF_6^-]$^+$
3b $[Ru(tpy)(AEPy)Cl](PF_6)$	41.79 (41.49)	3.53 (3.32)	11.35 (11.00)	492 [**3b**–PF_6^-]$^+$
3c $[Ru(tpy)(DEAEPy)Cl](PF_6)\cdot Me_2CO$	46.28 (46.37)	4.52 (4.70)	9.19 (9.32)	548 [**3c**–Me_2CO–PF_6^-]$^+$
4 $[Ru(tpy)(DMAEPy)(MeCN)](PF_6)_2\cdot 1/2H_2O$	37.86 (37.87)	3.39 (3.43)	10.05 (10.19)	671 [**4**–$1/2H_2O$–(PF_6^-)]$^+$ 263 [**4**–$1/2H_2O$–$(PF_6^-)_2$]$^{2+}$

[a] Calculated values are in parentheses.

alytic reactions [6–8], only a few ruthenium polypyridine complexes with a tertiary-amine ligand have been isolated [9,10]. Information on the photochemical and electrochemical properties of the tertiary amine complexes is therefore very limited [10]. For example, we reported that $[Ru(tpy)(bpy)(py)]^{2+}$ (tpy = 2,2′:6′,2″-terpyridine, bpy = 2,2′-bipyridine, py = pyridine) photocatalyzes selective hydride reduction of an $NAD(P)^+$ model compound, and the tertiary-amine complex $[Ru(tpy)(bpy)(NEt_3)]^{2+}$ is presumed to be an important intermediate [6]. However, little information is available on the properties of the amine complex because it is not stable enough to be isolated.

We report here that five new tertiary-amine complexes were synthesized successfully using bidentate tertiary-amine ligands such as 2-(2′-dimethylaminoethyl)-pyridine (DMAEPy) and 2-(2′-diethylaminoethyl)-pyridine (DEAEPy), i.e. $[Ru(4,4'\text{-}X_2bpy)_2(DMAEPy)]^{2+}$ (**1a**; X = H, **2**; X = CF_3), $[Ru(tpy)(N–N)Cl]^+$ (**3a**; N–N = DMAEPy, **3c**; N–N = DEAEPy) and $[Ru(tpy)(DMAEPy)(MeCN)]^{2+}$ (**4**). Electrochemical and photochemical properties of the complexes are also reported.



DMAEPy DEAEPy AEPy

2. Experimental

2.1. Physical measurements and instrumentation

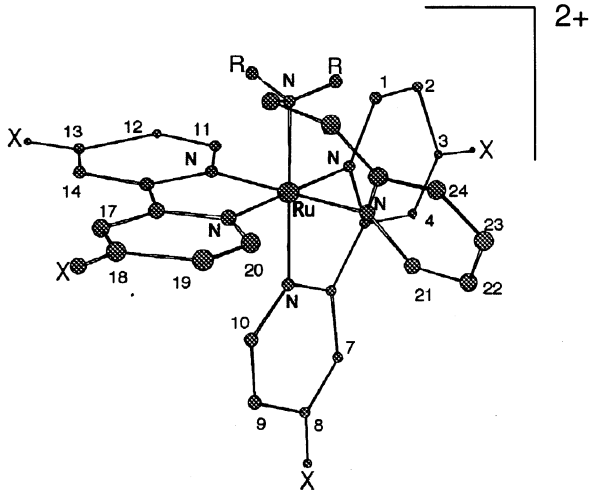
Proton NMR spectra were recorded on JEOL 500 NMR (500 MHz) and Bruker ARX-400 NMR (400 MHz) spectrometers at 25 °C. Both COSY and NOESY NMR techniques were used for unambiguous assignment of the resonances of the complexes. Electrospray ionization mass spectra (ESI-MS) were measured using a Hitachi M-1200 mass spectrometer with an M-1206 ES probe. The positive ion ESI-MS spectra were measured with 10–30 V drift voltages by a procedure reported elsewhere [11]. Electronic absorption spectra were recorded using an Otsuka–Denshi Photal MCPD-2000 multi channel spectrometer with a D_2/I_2 mixed lamp (± 1 nm resolution). The cyclic voltammograms of the complexes were measured in an acetonitrile solution containing tetra-*n*-buthylammonium tetrafluoroborate (0.1 M) as a supporting electrolyte using an ALS/CHI CHI-620 electrochemical analyzer with a Pt disk working electrode, a $Ag/AgNO_3$ (0.01 M) reference electrode and a Pt counter electrode.

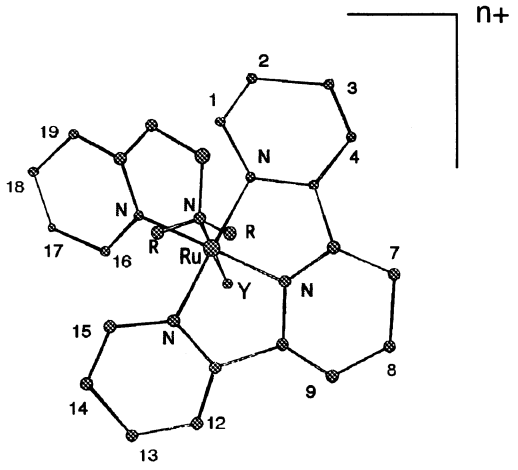
2.2. Materials

Acetonitrile was distilled over P_2O_5 three times, and then once over CaH_2 just before use. Tetra-*n*-buthylammonium tetrafluoroborate was recrystallized from ethyl acetate-benzene, and then dried in vacuo at 120 °C over night prior to use. The ligands: 2-(2′-dimethylaminoethyl)-pyridine (DMAEPy); 2-(2′-diethylaminoethyl)-pyridine (DEAEPy) [12] and the complexes: *cis*-$Ru(bpy)_2Cl_2\cdot 2H_2O$ [13]; $Ru(tpy)Cl_3$ [14]; *cis*-$Ru(4,4'\text{-}CF_3bpy)_2Cl_2$ [15]; $[Ru(bpy)_2(AEPy)](PF_6)_2$ (**1b**) [3] were prepared according to literature methods. The purities of the synthesized complexes were confirmed by ^1H NMR and ESI-MS and elementary analysis (Table 1). The structures of the complexes are illustrated in Scheme 1.

2.2.1. *[Ru(bpy)$_2$(DMAEPy)](PF$_6$)$_2$ (1a)*

An $EtOH/H_2O$ (1/1:v/v, 28 ml) solution containing *cis*-$Ru(bpy)_2Cl_2\cdot 2H_2O$ (0.505 g, 0.971 mmol) and DMAEPy (0.279 g, 1.86 mmol) was refluxed under an Ar atmosphere for 2 h. The color of the solution changed from purple to reddish orange. After the reaction mixture was cooled to room temperature (r.t.), the solution was concentrated to ~ 5 ml under reduced pressure and then a saturated NH_4PF_6 aqueous solution was added to it. The precipitated orange solid of **1a** was collected by filtration, recrystallized from





1a ; X = H, R = CH_3

1b; X = H, R = H

2; X = CF_3, R = CH_3

3a ; Y = Cl, R = CH_3, n = 1

3b ; Y = Cl, R = H, n = 1

3c ; Y = Cl, R = CH_2CH_3, n = 1

4 ; Y = MeCN, R = CH_3, n = 2

Scheme 1.

CH_3CN–diethyl ether, and then dried in vacuo. Yield: 74%. ^{1}H NMR (acetone-d_6): δ 9.32 (d, $J = 5.8$ Hz, H-1); 8.83 (d, $J = 7.9$ Hz, H-4, 17); 8.81 (d, $J = 5.6$ Hz, H-20); 8.65 (d, $J = 8.2$ Hz, H-7, 14); 8.37 (dd, $J = 7.9$, 7.6 Hz, H-3); 8.35 (dd, $J = 7.9$, 7.6 Hz, H-18); 8.13 (d, $J = 5.7$ Hz, H-10); 8.09 (dd, $J = 8.2$, 7.6 Hz, H-8); 7.96 (dd, $J = 8.2$, 7.6 Hz, H-13); 7.91 (dd, $J = 7.9$, 7.6 Hz, H-23); 7.88 (dd, $J = 7.6$, 5.6 Hz, H-19); 7.83 (dd, $J = 7.6$, 5.8 Hz, H-2); 7.75 (d, $J = 7.9$ Hz, H-24); 7.50 (dd, $J = 7.6$, 5.7 Hz, H-9); 7.39 (d, $J = 5.8$ Hz, H-11); 7.35 (d, $J = 6.0$ Hz, H-21); 7.29 (dd, $J = 7.6$, 5.8 Hz, H-12); 7.00 (dd, $J = 7.6$, 6.0 Hz, H-22); 3.57–3.66 (m, CH_2CH_2, 4H); 2.73 (s, CH_3, 3H); 1.83 (s, CH_3, 3H).

2.2.2. *[Ru(4,4′-CF_3bpy)$_2$(DMAEPy)](PF$_6$)$_2$ (**2**)*

An acetonitrile solution (30 ml) containing *cis*-Ru(4,4′-CF_3bpy)$_2Cl_2$ (0.197 g) and $AgPF_6$ (0.137 g, 0.54 mmol) was refluxed under Ar in the dark for 4 h. After the reaction mixture was cooled to r.t., precipitated AgCl was filtered out using celite layer. The solvent was evaporated under vacuum. One ml of saturated NH_4PF_6 solution was added to the solution and cooled at a refrigerator over night. Precipitated brown solid of [Ru(4,4′-CF_3bpy)$_2$(MeCN)$_2$](PF$_6$)$_2$ was collected by filtration and then washed with cold methanol. An EtOH/H_2O (1/1:v/v, 4 ml) solution containing the brown solid (0.0548 g) and DMAEPy (0.0293 g) was refluxed under an Ar atmosphere for 55 h. After the reaction mixture was cooled to r.t., a saturated NH_4PF_6 aqueous solution was added to it. The complex **2** was collected as brown solid by filtration. It was recrystallized from MeCN–diethyl ether. Yield: 40%. ^{1}H NMR (acetone-d_6): δ 9.69 (d, $J = 6.2$ Hz, H-1); 9.47 (s, H(4, 17)); 9.28 (s, H(7, 14); 9.15 (d, $J = 5.9$ Hz, H-20); 8.66 (d, $J = 5.9$ Hz, H-10); 8.23 (d, $J = 5.9$ Hz, H-19); 8.17 (d, $J = 6.2$ Hz, H-2); 7.96 (dd, $J = 7.7$, 7.0 Hz, H-23); 7.93 (d, $J = 6.6$ Hz, H-11); 7.81 (d, $J = 7.7$ Hz, H-24); 7.78 (d, $J = 5.9$ Hz, H-9); 7.57 (d, $J = 6.6$ Hz, H-21); 7.38 (d, $J = 6.6$ Hz, H-12); 6.97 (dd, $J = 7.0$, 6.6 Hz, H-22); 3.67-3.76 (m, CH_2CH_2, 4H); 2.80 (s, CH_3, 3H); 1.92 (s, CH_3, 3H).

2.2.3. *[Ru(tpy)(DMAEPy)Cl](PF$_6$) (**3a**)*

An EtOH/H_2O (2/1:v/v, 36 ml) solution containing Ru(tpy)Cl_3 (0.207 g, 0.47 mmol), DMAEPy (0.147 g, 0.98 mmol) and LiCl (0.200 g, 4.7 mmol) was refluxed under an Ar atmosphere for 8 h. After the reaction mixture was cooled to r.t., the solution was slowly concentrated to half volume under reduced pressure at r.t. A saturated NH_4PF_6 aqueous solution was added to it, and then the precipitated black solid was collected by filtration. The complex **3a** was isolated by column chromatography with basic alumina and 2:1 toluene/CH_3CN eluent to remove a by-product $[Ru(tpy)_2]^{2+}$. It was recrystallized from acetone–diethyl ether. Yield: 30%. ^{1}H NMR (acetone-d_6): δ 9.94 (d, $J = 5.9$ Hz,

H-16); 8.62 (d, $J = 8.1$ Hz, H-7, 9); 8.61 (d, $J = 8.1$ Hz, H-4, 12); 8.52 (d, $J = 5.5$ Hz, H-1, 15); 8.10 (dd, $J = 7.6$, 7.7 Hz, H-18); 8.08 (dd, $J = 7.6$, 8.1 Hz, H-3, 13); 8.02 (t, $J = 8.1$ Hz, H-8); 7.79 (d, $J = 7.7$ Hz, H-19); 7.64 (dd, $J = 5.5$, 7.6 Hz, H-2, 14); 7.56 (dd, $J = 5.9$, 7.6 Hz, H-17); 3.35–3.38 (m, CH_2CH_2, 2H); 2.50–2.53 (m, CH_2CH_2, 2H); 1.54 (s, $N(CH_3)_2$, 6H).

2.2.4. [Ru(tpy)(AEPy)Cl](PF$_6$) (**3b**) and [Ru(tpy)(DEAEPy)Cl](PF$_6$)·CH$_3$COCH$_3$ (**3c**)

These complexes were synthesized using procedures analogous to the method for **3a**, except for use of AEPy or DEAEPy instead of DMAEPy. **3b**: Yield: 14%. ^{1}H NMR (acetone-d_6): δ 10.25 (d, $J = 5.9$ Hz, H-16); 8.53 (d, $J = 8.1$ Hz, H-4, 12); 8.50 (d, $J = 8.1$ Hz, H-7, 9); 8.42 (d, $J = 5.5$ Hz, H-1, 15); 8.08 (dd, $J = 7.5$, 7.7 Hz, H-18); 8.00 (d, $J = 7.9$, 8.1 Hz, H-3, 13); 7.91 (t, $J = 8.1$ Hz, H-8); 7.71 (d, $J = 7.7$ Hz, H-19); 7.59 (dd, $J = 5.9$, 7.5 Hz, H-17); 7.56 (dd, $J = 5.5$, 7.9 Hz, H-2, 14); 3.14–3.19 (m, CH_2CH_2, 2H); 2.98 (brs, NH_2, 2H); 2.46–2.54 (m, CH_2CH_2, 2H). **3c**: Yield: 13%. ^{1}H NMR (acetone-d_6): δ 9.84 (d, $J = 5.9$ Hz, H-16); 8.62 (d, $J = 8.1$ Hz, H-4, 12); 8.61 (d, $J = 8.1$ Hz, H-7, 9); 8.56 (d, $J = 5.5$ Hz, H-1, 15); 8.06 ~ 8.12 (m, H-3, 13, 18, 3H); 7.99 (t, $J = 8.1$ Hz, H-8); 7.79 (d, $J = 7.7$ Hz, H-19); 7.67 (dd, $J = 5.5$, 7.7 Hz, H-2, 14); 7.50 (dd, $J = 5.9$, 7.5 Hz, H-17); 3.53–3.57 (m, CH_2CH_2, 2H); 2.72–2.76 (m, CH_2CH_2, 2H); 2.10 (q, $J = 7.0$ Hz, $N(CH_2CH_3)_2$, 4H); 2.08 (s, CH_3COCH_3, 6H); 0.43 (t, $J = 7.0$ Hz, $N(CH_2CH_3)_2$, 6H).

2.2.5. [Ru(tpy)(DMAEPy)(MeCN)](PF$_6$)$_2$·1/2H$_2$O (**4**)

This complex was synthesized in a manner similar to the reported method for [Ru(tpy)(bpy)(MeCN)](PF$_6$)$_2$ except for use of DMAEPy instead of bpy [16] Yield: 40%. ^{1}H NMR (acetone-d_6): δ 9.36 (d, $J = 5.9$ Hz, H-16); 8.79 (d, $J = 8.1$ Hz, H-7, 9); 8.75 (d, $J = 8.1$ Hz, H-4, 12); 8.58 (d, $J = 5.5$ Hz, H-1, 15); 8.35 (t, $J = 8.1$ Hz, H-8); 8.29 (dd, $J = 7.7$, 8.1 Hz, H-3, 13); 8.19 (dd, $J = 7.5$, 7.7 Hz, H-18); 7.87 (d, $J = 7.7$ Hz, H-19); 7.79 (dd, $J = 5.5$, 7.7 Hz, H-2, 14); 7.68 (dd, $J = 5.9$, 7.5 Hz, H-17); 3.41–3.46 (m, CH_2CH_2, 2H); 2.86 (brs, 1/2H$_2$O); 2.69–2.74 (m, CH_2CH_2, 2H); 2.10 (s, CH_3CN, 3H); 1.68 (s, $N(CH_3)_2$, 6H).

3. Results and discussion

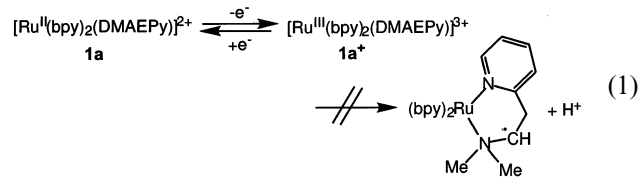
3.1. Synthesis and characterization

We successfully synthesized and purified tertiary-amine complexes **1a**, **2**, **3a**, **3c** and **4** using the bidentate tertiary-amine ligands DMAEPy and DEAEPy (Scheme 1). Complexes with the corresponding monodentate tertiary amine, such as triethylamine, are not stable enough to be isolated. This result clearly shows that use of bidentate tertiary-amine ligands is a good method for synthesis of metal complexes with a relatively bulky tertiary amine. Another tertiary amine complex, $[Ru(bpy)_2(DEAEPy)]^{2+}$ was also synthesized, although it could not be isolated using the same procedure as for **1a** because it decomposed very fast, even at room temperature. Similarly, $[Ru(bpy)_2(N,N,N',N'$-tetraethylethylenediamine$)]^{2+}$ was not stable, but $[Ru(bpy)_2(tmen)]^{2+}$ (tmen = N,N,N',N'-tetramethylethylenediamine) with the methyl group of the tertiary-amine ligand was isolated easily [10]. Steric repulsion between the hydrogen at position 1 on the bpy ligand (see the structures of **1** and **2** illustrated in Scheme 1) and the ethyl group of the amine ligand could cause these complexes to be unstable.

There are two possible structural isomers for each of **3a**, **3c** and **4**, in which the tertiary amine part of the bidentate ligand is in the *cis* or *trans* position relative to the monodentate ligand. As an example, the aromatic region of the ^{1}H NMR spectrum of **3c** is illustrated in Fig. 1. The resonance at 9.84 ppm, which is attributable to the proton at the position 16, is shifted down significantly by 1.38 ppm in magnetic field compared to the corresponding proton on 'free' DEAEPy, while the other aromatic protons on the DEAEPy ligand are only shifted slightly from the values for 'free' DEAEPy. If **3c** were the *cis* isomer, the chemical shift of the proton at position 16 should be observed at higher fields because of the shielding effect of the tpy ligand [17]. On the other hand, the chemical shift of the ethyl protons of the DEAEPy ligand was observed at ~0.5 ppm higher field than that of 'free' DEAEPy. It is plausible that the pyridine rings of the tpy ligand of the *trans* isomer shield the ethyl group magnetically. It follows that **3c** must be the *trans* isomer. The other complexes **3a**, **3b** and **4** had similar ^{1}H NMR characteristics. The structure of $[Ru(tpy)(DMAMPy)Cl]^+$ (DMAMPy = 2-(2′-dimethylaminomethyl)-pyridine) was recently determined by X-ray crystallographic analysis [18], showing that the dimethylamino group and the Cl ligand are in *trans* positions relative to each other. This complex has similar ^{1}H NMR characteristics to those of **3** and **4** described here.

3.2. Electrochemistry and UV–Vis absorption spectra

Fig. 2(A) illustrates the cyclic voltammogram (CV) of **1a** measured for an acetonitrile solution. A reversible redox wave attributable to a $Ru^{II/III}$ couple was observed at $E_{1/2} = 0.88$ V (Eq. (1)).



(1)

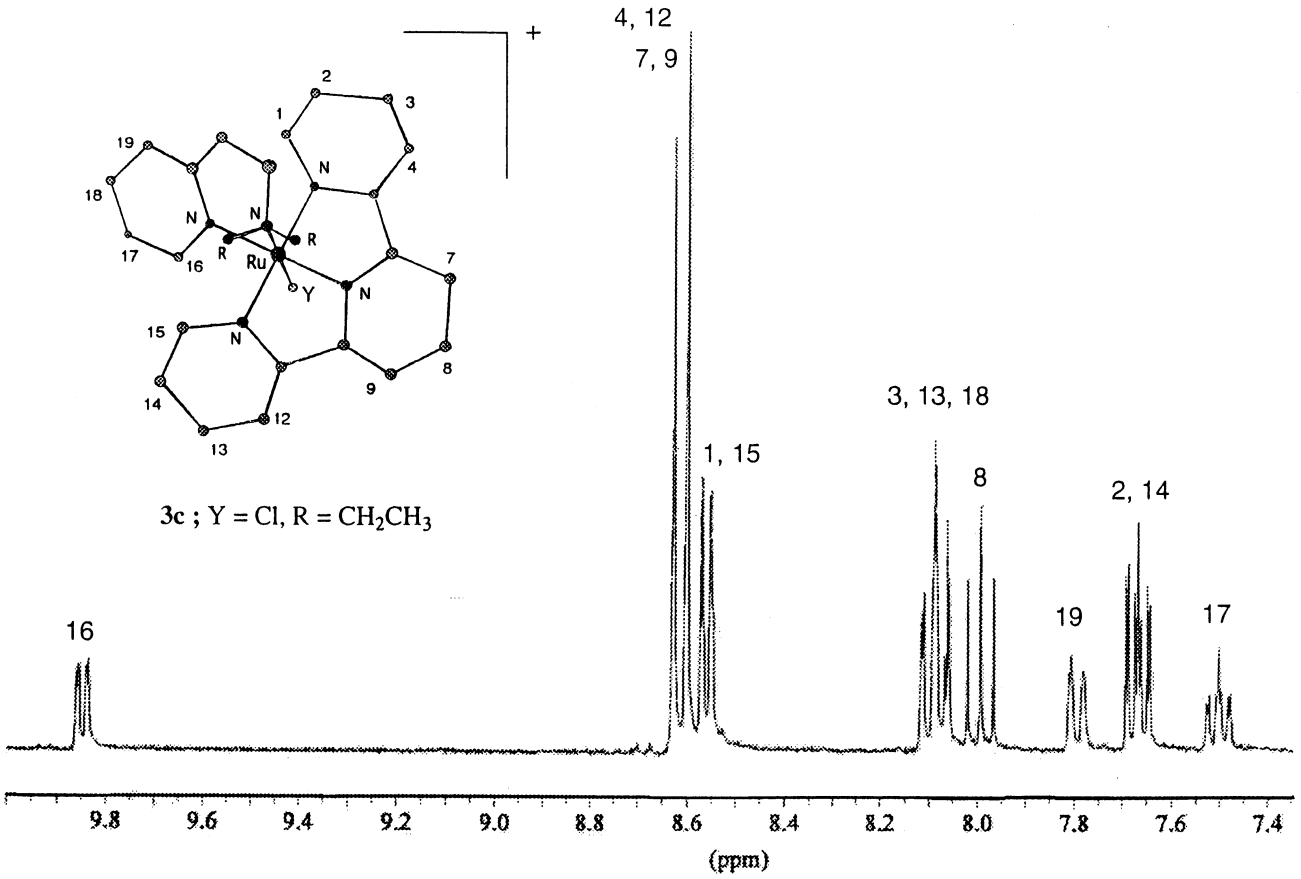
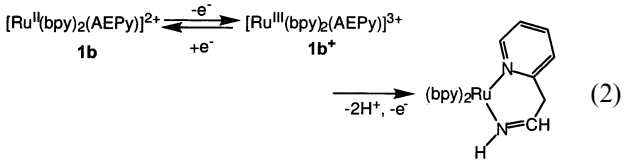


Fig. 1. Aromatic region of the ^{1}H NMR spectrum of **3c** measured in acetone-d_6 at 25 °C.

Addition of a base such as pyridine did not affect the reversibility. This finding is in sharp contrast to the corresponding primary-amine complex **1b**, for which oxidation is irreversible as shown in Fig. 2(B). Meyer and co-workers have reported that oxidation of primary-amine complexes occurs on the central Ru^{II} to give Ru^{III}, and is followed by rapid deprotonation from the primary amine ligand and additional one-electron oxidation to give the corresponding imine complex (Eq. (2)) [3].



(2)

It is well known that oxidation of 'free' tertiary amines such as NEt_3 and $N(CH_2CH_2OH)_3$ causes the loss of two electrons and also one proton from the α-carbon of the amine, to give the iminium cation (Eq. (3))[19,20].[2] The stability of the oxidized complex $\mathbf{1a}^+$ implies that deprotonation from the DMAEPy ligand on Ru^{III} is too slow, even in the presence of the base, to be converted to the corresponding iminium cation, at least during the CV measurement.

$$NEt_3 \xrightarrow{e^-} (NEt_3)^{+\bullet} \xrightarrow{-H^+} Et_2N\dot{C}HCH_3 \xrightarrow{e^-} Et_2N^+{=}CHCH_3 \quad (3)$$

In contrast to the oxidation, the one-electron reduction wave of **3a** was irreversible (this is the solid line in Fig. 2(C)). The chloride ligand of $\mathbf{3a}^-$ is substituted with the solvent molecule to give the acetonitrile complex **4**, for which the CV is shown as the dotted line in Fig. 2(C) (Eq. (4)).

$$[\underset{\mathbf{3a}}{Ru(tpy)(DMAEPy)Cl}]^+ \xrightarrow{e^-} [\underset{\mathbf{3a}^-}{Ru(tpy^{-\bullet})(DMAEPy)Cl}]^+$$
$$\xrightarrow{MeCN} [\underset{\mathbf{4}^-}{Ru(tpy^{-\bullet})(DMAEPy)(MeCN)}]^+ + Cl^- \quad (4)$$

Similar ligand substitution reactions occurred for the other chlorido complexes **3b** and **3c**. On the other hand, reversible waves attributable to (bpy/bpy$^{-\bullet}$) were observed for **1a** and **2**.

The redox potentials of the $Ru^{II/III}$ couples of **3a** and **3c** are more positive than that of **3b**, and reduction of **1a** also occurred at a more positive potential than for **1b** even though DMAEPy and DEAEPy have stronger electron donating abilities than AEPy, as shown in Table 2.

[2] The $Ru^{II/III}$ couple of **3b** is also reversible even though the primary amine AEPy coordinates to the Ru center. The central Ru^{III} of $\mathbf{3b}^+$ is probably unable to oxidize the AEPy ligand because the redox potential for $Ru^{II/III}$ in **3b** is much more negative than that in **1b** (Table 2).

For all complexes the lowest energy absorption band is attributable to the metal-to-X_2bpy ligand charge transfer (MLCT) transition, as summarized in Table 2. The UV–vis absorption spectra of the DMAEPy and DEAEPy reveal some unexpected features in comparison to the AEPy complexes. The tertiary-amine complexes have higher energy MLCT bands than those of the primary amine complexes, i.e. E_{MLCT}(**1a**) > E_{MLCT}(**1b**), E_{MLCT}(**3a**) and E_{MLCT}(**3c**) > E_{MLCT}(**3b**). These observations might be caused by distortion of the

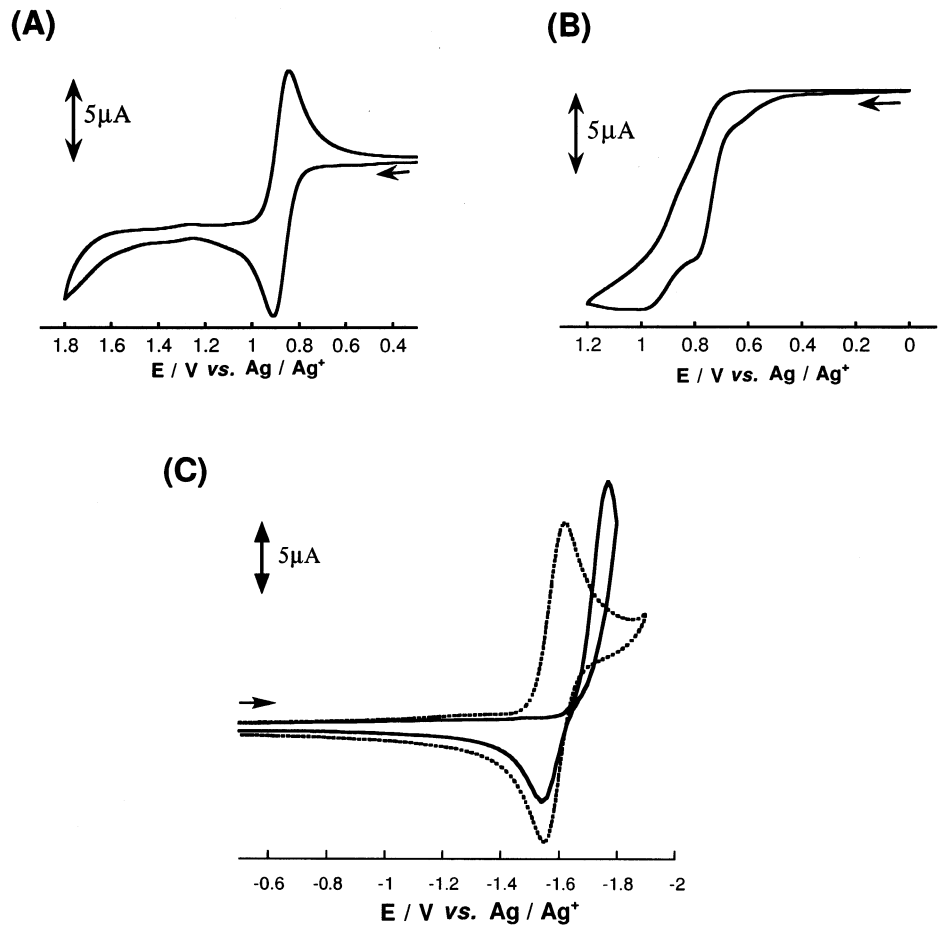


Fig. 2. Cyclic voltammograms for (A) **1a**, (B) **1b**, and (C) **3a** (the solid line) and **4** (the dotted line) in acetonitrile solutions containing $Bu^n_4NBF_4$ (0.1 M) under an Ar atmosphere at scan rates of (A, B) 0.05 V s^{-1} and (C) 0.2 V s^{-1}.

Table 2
Electrochemical and UV–Vis absorption data for the complexes and some amine ligands measured in an acetonitrile solution

Complex or ligand	$E_{1/2}$ (V vs. $Ag/AgNO_3$) [a]		λ_{MLCT} (nm)
	Oxidation	Reduction	(ε, M^{-1} cm^{-1})
1a $[Ru(bpy)_2(DMAEPy)](PF_6)_2$	0.88 (60)	−1.65 (60), −1.89 (70)	472 (10 000)
1b $[Ru(bpy)_2(AEPy)](PF_6)_2$	0.80 [b]	−1.73 (60), −1.95 (60)	476 (9400)
2 $[Ru(4,4'\text{-}CF_3bpy)_2(DMAEPy)](PF_6)_2$	1.21 (70)	−1.15 (70), −1.38 (60)	493 (9900)
3a $[Ru(tpy)(DMAEPy)Cl](PF_6)$	0.47 (70)	−1.79 [b]	509 (4900)
3b $[Ru(tpy)(AEPy)Cl](PF_6)$	0.38 (70)	−1.88 [b]	518 (4600)
3c $[Ru(tpy)(DEAEPy)Cl](PF_6)\cdot Me_2CO$	0.48 (70)	−1.75 [b]	510 (4400)
4 $[Ru(tpy)(DMAEPy)(MeCN)](PF_6)_2\cdot 1/2H_2O$	0.96 (70)	−1.58 (70), −2.00 [b]	479 (4800)
DMAEPy	0.76 [b]	< −2.1	
DEAEPy	0.85 [b]	< −2.1	
AEPy	>1.5	< −2.1	

[a] Pt-disk working (1.6 mm i.d.) and Pt-wire counter electrodes were used. Values in parentheses are peak-to-peak separations in mV.
[b] Peak potentials of irreversible waves.

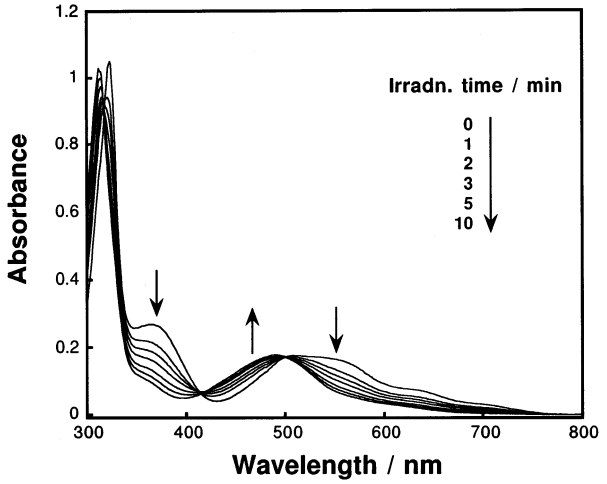


Fig. 3. UV–Vis absorption spectral change in an acetonitrile solution containing **3a** (0.039 mM) during irradiation.

complexes due to the steric bulkiness of the alkyl amine parts components of DMAEPy and DEAEPy [10].

3.3. Photochemistry

Irradiation of acetonitrile solutions containing **1a**, **2**, **3a** and **3c** caused quantitative substitution of the tertiary amine ligands with the solvent molecules. As an example, Fig. 3 shows the UV–vis absorption spectral change in an acetonitrile solution containing **3a** (0.039 mM) during irradiation with a high pressure Hg lamp through a $CuSO_4$ aqueous solution filter. Irradiation caused a rapid hypsochromic shift of the MLCT absorption maximum from 509 to 490 nm, accompanied by a set of isosbestic points. Immediately after irradiation the solution underwent ESI-MS analysis: the peak corresponding to the $[Ru(tpy)(MeCN)_2Cl]^+$ ($m/z =$ 452) was observed, but another possible product, $[Ru(tpy)(^1\eta\text{-DMAEPy})(MeCN)Cl]^+$, was not detected at all. Similar experimental results were obtained for other tertiary-amine complexes. The photochemical ligand substitution reaction also occurred even in the presence of a base or under aerated conditions. These observations clearly demonstrate that irradiation of the tertiary-amine complexes causes quantitative photochemical ligand substitution (Eq. (5)), but that oxidation of the tertiary-amine ligands does not proceed.

$$[Ru(tpy)(\underset{\mathbf{3a}}{DMAEPy})Cl]^+ \xrightarrow[MeCN]{h\nu} [Ru(tpy)(MeCN)_2Cl]^+ + DMAEPy \quad (5)$$

This results is in sharp contrast to the case of the primary-amine complexes $[Ru(bpy)_2(AMPy)]^{2+}$ and $[Ru(bpy)_2(en)]^{2+}$ (AMPy = 2-(2′-aminomethyl)-pyridine), for which irradiation under aerated conditions causes oxidation of the primary-amine ligand to give the corresponding imine complex [5,21,22]. Deprotonation from the α-carbons of the DMAEPy ligand on the central Ru^{III} of the MLCT excited states should be too slow, even in the presence of the base, for conversion to the corresponding iminium cation.

Acknowledgements

We acknowledge Drs Kazuhide Koike and Koji Takeuchi (AIST) for support of the ESI-MS analyses. We thank the Kojima Chemical Co. for the gift of $RuCl_3 \cdot 3H_2O$. This work was partially supported by the Asahi Glass Foundation and Kawamura Institute of Chemical Research.

References

[1] (a) A.J. Barrett, C.R. Cantor, C. Liébecq, G.P. Moss, W. Saenger, N. Sharon, K.F. Tipton, P. Venetianer, J.F.G. Vliegenthart, Enzyme Nomenclature, Academic Press, New York, 1992; (b) P.D. Boyer, H. Lardy, K. Myrbäck (Eds.), The Enzymes, vol. 8, Academic Press, New York, 1963.
[2] F.R. Keene, Coord. Chem. Rev. 187 (1999) 121.
[3] G.M. Brown, T.R. Weaver, F.R. Keene, T.J. Meyer, Inorg. Chem. 15 (1976) 190.
[4] V.E. Alvarez, R.J. Allen, T. Matsubara, P.C. Ford, J. Am. Chem. Soc. 96 (1974) 7686.
[5] M.A. Ollino, A.J. Rest, J. Photochem. Photobiol. A: Chem. 69 (1992) 73.
[6] O. Ishitani, N. Inoue, K. Koike, T. Ibusuki, J. Chem. Soc., Chem. Commun. (1994) 367.
[7] H. Hori, F.P.A. Johnson, K. Koike, K. Takeuchi, T. Ibusuki, O. Ishitani, J. Chem. Soc., Dalton. Trans. (1997) 1019.
[8] H. Hori, J. Ishihara, K. Koike, K. Takeuchi, T. Ibusuki, O. Ishitani, J. Photochem. Photobiol. A: Chem. 120 (1999) 119.
[9] D.A. Bardwell, J.C. Jeffery, E. Schatz, E.E.M. Tilley, M.D. Ward, J. Chem. Soc., Dalton Trans. (1995) 825.
[10] N. Aydin, C.W. Schlaepfer, Polyhedron 20 (2001) 37.
[11] H. Hori, J. Ishihara, K. Koike, K. Takeuchi, T. Ibusuki, O. Ishitani, Chem. Lett. (1997) 273.
[12] H.E. Reich, R. Levine, J. Am. Chem. Soc. 20 (1955) 4913.
[13] B.P. Sullivan, D.J. Salmon, T.J. Meyer, Inorg. Chem. 17 (1978) 3334.
[14] B.P. Sullivan, J.M. Calvart, T.J. Meyer, Inorg. Chem. 19 (1980) 1404.
[15] P.A. Anderson, R.F. Anderson, M. Furue, P.C. Junk, F.R. Keene, B.T. Patterson, B.D. Yeomans, Inorg. Chem. 39 (2000) 2721.
[16] S.C. Rasmussen, S.E. Ronco, D.A. Mlsna, M.A. Billadeau, W.T. Pennington, J.W. Koils, J.D. Petersen, Inorg. Chem. 34 (1995) 821.
[17] N.C. Fletcher, F.R. Keene, J. Chem. Soc., Dalton. Trans. (1998) 2293.
[18] M. Yamaguchi, T. Iida, T. Yamagishi, Inorg. Chem. Commun. 1 (1998) 299.

[19] P.J. DeLaive, B.P. Sullivan, T.J. Meyer, D.G. Whitten, J. Am. Chem. Soc. 101 (1979) 4007.
[20] P.J. DeLaive, T.K. Foreman, C. Giannotti, D.G. Whitten, J. Am. Chem. Soc. 102 (1980) 5627.
[21] R. Arakawa, S. Tachiyashiki, T. Matsuo, Anal. Chem. 67 (1995) 4133.
[22] R. Arakawa, S. Mimura, G. Matsubayashi, T. Matsuo, Inorg. Chem. 35 (1996) 5725.

PERGAMON

Polyhedron 21 (2002) 69–79

POLYHEDRON

www.elsevier.com/locate/poly

Synthesis and characterisation of uranyl substituted malonato complexes
Part I. Structural diversity with dimethylmalonate and different counter-cations

Yingjie Zhang [a,*], Francis R. Livens [b], David Collison [b], Madeleine Helliwell [b], Frank Heatley [b], Annie K. Powell [c], Sigrid Wocadlo [c], Harry Eccles [d]

[a] *Australian Nuclear Science and Technology Organization, PMB 1, Menai 2232, NSW, Australia*
[b] *Department of Chemistry, The University of Manchester, Oxford Road, Manchester M13 9PL, UK*
[c] *Institut für Anorganische Chemie, Universität Karlsruhe, Engesserstrasse Gelo 30.45, 76128 Karlsruhe, Germany*
[d] *Research and Technology, BNFL, Springfields, Salwick, Preston PR4 0XJ, UK*

Received 16 July 2001; accepted 3 October 2001

Abstract

Uranyl dimethylmalonato complexes with different metal to ligand ratios and connectivity, 1:2 monomeric, dimeric and 2:3, 3:4 infinite chain structures have been prepared and characterised by elemental analysis, thermal analysis, IR and ^{13}C CPMAS NMR spectroscopy, and X-ray crystallography. The different structural types are isolated by the use of different counter-cations. Two new kinds of binding mode of malonate with uranyl have been identified, tridentate (μ_2 1,3-bidentate and 1,5-bidentate) and tetradentate (1,3-bidentate with both carboxylate groups). A basis for the prediction of structural type from the results of ^{13}C CPMAS NMR spectroscopy is proposed. The structures of the crystallographically characterised products can be rationalised in terms of templating by the counter-cations, which appears to be influenced by the size of the counter-cations and the tendency to maximise hydrogen bonding in the lattice. © 2002 Elsevier Science Ltd. All rights reserved.

Keywords: Uranyl; Dimethylmelonate; Counter-cation; CPMAS ^{13}C NMR; X-ray crystallography

1. Introduction

In the solid state, pentagonal bipyramidal geometry appears to be favoured in malonato complexes of uranyl crystallised with NH_4^+, Sr^{2+} or Ba^{2+} [1–3]. In each case, one malonate is terminally 1,5-bidentate to a uranium atom, giving rise to a six-membered ring. The second malonate is also 1,5-bidentate through both carboxylate groups to the same uranium atom, but the other oxygen atom from one carboxylate group μ_1 bridges to the neighbouring uranium atom, producing an infinite chain of $[UO_2(C_3H_2O_4)_2]_n^{2n-}$. In the equatorial plane the U–O bonds are similar, with U–O distances between 2.31(1) and 2.41(1) Å and O–U–O angles ranging from 68.2(4) to 75.3(3)°. The conformations of the six-membered rings are different with different cations, and this is attributed to the size of the cations and the incorporation of non-bonded carboxylate oxygen atoms into the coordination spheres of Sr^{2+} or Ba^{2+}. For the ammonium derivative, the nitrogen atoms, carboxylate oxygen atoms and H_2O molecules are involved in numerous short contacts between 2.74 and 3.08 Å. Most of these contacts are probably involved in hydrogen bonding, which link the uranyl malonate chains into a three-dimensional network.

Although numerous investigations involving crystal structures of actinide complexes have provided data on coordination geometry and spatial arrangements, there is no coherent data set allowing identification of the

* Corresponding author. Tel.: +61-2-9717-9156; fax: +61-2-9543-7179.
E-mail address: yingjie.zhang@ansto.gov.au (Y. Zhang).

0277-5387/02/$ - see front matter © 2002 Elsevier Science Ltd. All rights reserved.
PII: S0277-5387(01)00964-0

effects of counter-cations and of systematic subtle change of the proligand. Therefore, we have initiated a study of the interactions between uranyl and malonates to delineate structural types and to assess spectroscopic methods for their characterisation. By varying appropriate substituent groups of the selected proligand, malonic acid, we might produce predictable trends in the properties of the resulting malonate complexes. Ultimately, it should be possible to predict the properties of similar homologous series. Malonates were selected as the ligand series because some crystallographic information was already available. Previously we have reported the synthesis and structural characterisation of monomeric and dimeric uranyl dimethyl malonato compounds [4]. In the present studies, dimethylmalonic acid was used as proligand and the counter-cations varied to explore further possible effects on structural diversity and bonding modes.

2. Experimental

2.1. Materials

All chemicals were reagent grade, purchased from Strem Chemicals, Aldrich or Lancaster and used without further purification.

2.2. Physical methods

Elemental analyses were performed by the Microanalysis Lab, Department of Chemistry, The University of Manchester. IR spectra were recorded on an ATI Mattson Genesis Series FTIR Spectrometer. TG/DT analyses were made on a Seiko (TG/DTA 220) thermal analyser at a heating rate of 10 °C min^{-1} and an air flow rate of 100 cm^3 min^{-1}. High resolution solid state ^{13}C NMR spectra were recorded using a Varian Associates Unity 300 spectrometer operating at 75.4 MHz using the cross polarisation-magic angle spinning (CP-MAS) technique. The acquisition time was 0.05 s, the spectral width was 30007.5 Hz, the contact time was 1.5 ms, the recycle time was 5 s and the spinning speed was approximately 4 kHz. The chemical shift scale was referenced by setting the CH_3 peak in a sample of solid hexamethylbenzene, run using the same conditions, to 16.5 ppm.

2.3. Syntheses

2.3.1. Preparation of tetramethylethylenediammonium tris(dimethylmalonato) bis[dioxouranate(VI)]

$(C_6H_{18}N_2)[(UO_2)_2(C_5H_6O_4)_3]$ (**1**): a solution of uranyl nitrate hexahydrate (1.00 g, 2 mmol in 10 cm^3 H_2O) was added to a solution of dimethylmalonic acid and tetramethylethylenediamine (0.52 g, 4 mmol and 0.60 cm^3, 4 mmol in 30 cm^3 H_2O). A yellow crystalline product formed after a week, and was collected by filtration and dried in air, yield 70%. *Anal.* Found: C, 23.90; H, 3.55; N, 2.65; U, 45.22. Calc. for $C_{21}H_{36}N_2O_{16}U_2$: C, 24.05; H, 3.46; N, 2.67; U, 45.40%. TG/DTA (°C): 231(−22.4%, *endo*, cation + ligand = 22.9%), 410 (53.2%, *exo*, UO_3 = 52.7%). IR (KBr disk), ν (cm^{-1}): 3458 vs (br), 1601 vs, 1571 w, 1520 m, 1478 m, 1416 m, 1384 m, 1200 s, 930 vs, 721 s, 602 m.

2.3.2. Preparation of dimethylpiperazinium di-aqua tetrakis(dimethylmalonato) tris[dioxouranate(VI)] trihydrate

$(C_6H_{16}N_2)[(UO_2)_3(C_5H_6O_4)_4(H_2O)_2]\cdot 3H_2O$ (**2**): a solution of uranyl nitrate hexahydrate (1.00 g, 2 mmol in 10 cm^3 H_2O) was added to a solution of dimethylmalonic acid and dimethylpiperazine (0.52 g, 4 mmol and 0.56 cm^3, 4 mmol in 30 cm^3 H_2O). EtOH (5 cm^3) was added. A yellow crystalline product, formed after a week, was collected by filtration and dried in air, yield 85%. *Anal.* Found: C, 21.00; H, 3.40; N, 1.76; U, 46.95. Calc. for $C_{26}H_{50}N_2O_{27}U_3$: C, 20.3; H, 3.3; N, 1.8; U, 46.5%. TG/DTA (°C): 96 (−6.0%, *endo*, $-5H_2O$ = 5.8%), 233 (−21.5%, *endo*, cation + ligand = 21.9%), 384 (55.2%, *exo*, UO_3 = 54.8%). IR (KBr disk), ν (cm^{-1}): 1637 m, 1617 s, 1584 w, 1542 w, 1517 m; 1467 m, 1440 w, 1406 m, 1365 w, 1321 w; 1193 s; 932 vs; 718 m; 609 m.

2.3.3. Preparation of ethylenediammonium aqua bis(dimethylmalonato) dioxouranate(VI) monohydrate

$(C_2H_{10}N_2)[UO_2(C_5H_6O_4)_2\ (H_2O)]\cdot H_2O$ (**3**): a solution of uranyl nitrate hexahydrate (1.00 g, 2 mmol in 15 cm^3 H_2O) was added to a solution of dimethylmalonic acid and ethylenediamine (0.51 g, 4 mmol and 0.28 cm^3, 4 mmol in 35 cm^3 H_2O). A yellow crystalline product formed after few days and was collected by filtration and dried in air, yield 85%. *Anal.* Found: C, 23.03; H, 4.16; N, 4.38; U, 37.65. Calc. for $C_{12}H_{26}N_2O_{12}U$: C, 22.94; H, 4.17; N, 4.46; U, 37.88%. TG/DTA (°C): 140 (−2.8%, *endo*, $-H_2O$ = 2.9%), 187 (*endo*), 330 (46.0%, UO_3 = 45.5%). IR (KBr disk) ν (cm^{-1}): 3476 s (br), 1615 s (br), 1586 w, 1549 w, 1468 m, 1414 s, 1357 m, 1204 m, 910 vs, 695 m, 593 m.

2.3.4. Preparation of bis[hexaaminecobalt(III) bis(dimethylmalonato) dioxouranate(VI)] di-chloride heptahydrate

$\{[Co(NH_3)_6][UO_2(C_5H_6O_4)_2]\}_2Cl_2\cdot 7H_2O$ (**4**): the preparation has been reported previously [4].

2.3.5. Preparation of piperazinium bis(dimethylmalonato) dioxouranate(VI) pentahydrate

$(C_4H_{12}N_2)[UO_2(C_5H_6O_4)_2]\cdot 5H_2O$ (**5**): a solution of uranyl nitrate hexahydrate (1.00 g, 2 mmol in 15 cm^3 H_2O) was added to a solution of dimethylmalonic acid and piperazine (0.51 g, 4 mmol and 0.76 g, 4 mmol in

35 cm^3 H_2O). A yellow crystalline product formed after few days and was collected by filtration and dried in air, yield 75%. *Anal.* Found: C, 23.94; H, 4.95; N, 3.91; U, 33.58%. Calc. for $C_{14}H_{34}N_2O_{15}U$: C, 23.73; H, 4.84; N, 3.95; U, 33.60%. TG/DTA (°C): 24 (-2.2%, *endo*, $-H_2O = 2.5\%$), 119 (-12.3%, *endo*, $-4H_2O = 12.7\%$), 194 (*exo*), 257 (*exo*), 317 (*exo*), 452 (41.2%, *exo*, $UO_3 = 40.4\%$). IR (KBr disk) ν (cm^{-1}): 3478 vs (br), 1608 vs, 1585 w, 1539 m, 1466 w, 1414 m, 1386 m, 1327 m, 1201 m, 1089 w, 905 vs, 710 s, 594 s.

2.3.6. Preparation of triethylenediammonium bis(dimethylmalonato) dioxouranate(VI)

$(C_6H_{14}N_2)[UO_2(C_5H_6O_4)_2]$ (**6**): a solution of uranyl nitrate hexahydrate (1.00 g, 2 mmol in 15 cm^3 H_2O) was added to a solution of dimethylmalonic acid and 1,4-diazabicyclo[2.2.2] octane (triethylenediammonium) (0.51 g, 4 mmol and 0.44 cm^3, 4 mmol in 35 cm^3 H_2O). A yellow crystalline product formed after few days and was collected by filtration and dried in air, yield 70%. *Anal.* Found: C, 29.08; H, 4.00; N, 4.20; U, 37.02. Calc. for $C_{16}H_{26}N_2O_{10}U$: C, 29.23; H, 4.07; N, 4.35; U, 36.94. TG/DTA (°C): 255 (-37.7%, *exo*, cation + ligand = 37.9%), 404 (45.0%, *exo*, $UO_3 = 44.4\%$). IR (KBr disk) ν (cm^{-1}): 3471 m (br), 1591 vs, 1530 m, 1413 m, 1359 mw, 1192 m, 912 s, 714 m, 593 m.

2.3.7. Preparation of tetraethylethylenediammonium tris(dimethylmalonato) bis[dioxouranate(VI)]

$(C_{10}H_{26}N_2)[(UO_2)_2(C_5H_6O_4)_3]$ (**7**): a solution of uranyl nitrate hexahydrate (1.00 g, 2 mmol in 10 cm^3 H_2O) was added to a solution of dimethylmalonic acid and tetraethylethylenediammonium (0.52 g, 4 mmol and 0.88 cm^3, 4 mmol in 30 cm^3 H_2O). A yellow crystalline product formed after a week and was collected by filtration and dried in air, yield 75%. *Anal.* Found: C, 27.45; H, 4.10; N, 2.69; U, 43.50. Calc. for $C_{25}H_{46}N_2O_{17}U_2$: C, 27.18; H, 4.01; N, 2.54; U, 43.10%. IR (KBr disk), ν (cm^{-1}): 3419 br, w, 1606 s, 1571 w, 1550 w, 1520 s, 1471 m, 1430 w, 1409 w, 1360 w, 1334 w, 1197 m, 930 vs, 716 m, 602 w, 574 w.

2.3.8. Preparation of propanediammonium aqua bis(dimethylmalonato) dioxouranate(VI) monohydrate

$(C_7H_{20}N_2)[UO_2(C_5H_6O_4)_2(H_2O)]\cdot 2H_2O$ (**8**): the preparation has been reported previously [4].

2.4. Crystallography

The crystallographic data for compounds **2**, **3** and **7** are listed in Table 1. The intensities for **2** were measured on a Rigaku AFC5R diffractometer with graphite monochromated Mo Kα radiation ($\lambda = 0.71073$ Å) in ω–2θ mode at 17 °C. The cell parameters were refined by least squares from the angular positions of 25 for carefully centred reflections. An empirical absorption correction was applied, based on azimuthal scans of three reflections. The data were corrected for Lorentz and polarization effects. The structure was solved by direct methods with SIR-92 [5], and expanded using Fourier techniques with DIRDIF-94 [6]. Disordered solvent molecules were refined isotropically, whilst all other, non-hydrogen atoms were refined anisotropically. Hydrogen atoms were added in calculated positions. All calculations were performed using the TEXSAN [7] crystallographic software package (Molecular Structure Corporation).

The diffraction data for **3** and **7** were measured on a Rigaku Raxis II diffractometer with graphite monochromated Mo Kα radiation ($\lambda = 0.71073$ Å) at 20 °C. The structures were solved by conventional direct methods for **3** and Patterson methods for **7** and were refined by the full-matrix least-squares method on all F^2 data with SHELXTL 5.03 package [8]. Non-hydrogen atoms were refined anisotropically. Hydrogen atoms were fixed in calculated positions.

3. Results and discussion

3.1. Crystal structures

Selected bond lengths and angles for **3**, **7** and **2** are given in Tables 2–4, respectively. The anionic structure of **3** is shown in Fig. 1. The uranium atom has pentagonal bipyramidal geometry. The two-malonate groups are both terminal 1,5-bidentate on the same uranyl ion with the fifth equatorial position of the uranium atom occupied by a H_2O molecule, forming a monomeric anion structure. The uranyl group is nearly linear with an O(1)–U–O(2) angle of 177.57(12)° and normal U–O distance [1.770(3) Å]. The U–O distances in the equatorial plane are separated into three groups, 2.311(2) Å for O(5), average 2.363(3) Å for O(3) and O(7), and average 2.430(3) Å for O(9) and O(11). The adjacent equatorial O–U–O angles range from 69.75(8) to 75.15(9)°. The deviations of the donor atoms from the mean equatorial plane are from -0.079 Å for O(5) to 0.117 Å for O(9). The packing diagram along crystallographic *b* axis is shown in Fig. 2. Several short contacts between a N atom and carboxylic oxygen atoms [2.725(4)–2.921(4) Å] suggest that cation–anion interactions are via H-bonding, which links the monomeric structures into a three-dimensional framework.

The anionic structure of the asymmetric unit for **7** is shown in Fig. 3. It has two crystallographically distinct uranyl groups and three ligands. Both U atoms have a hexagonal bipyramidal environment. The two ligands which form the central $(UO_2)_2(DMMA)_2$ unit are both 1,3-bidentate through one carboxylate group to one U atom and one of the oxygen atoms bridges μ_2 to the

Table 1
Crystallographic data for compounds **3**, **7** and **2**

	3	**7**		**2**
Formula	$C_{12}H_{26}N_2O_{12}U$	$C_{25}H_{44}N_2O_{16}U_2$		$C_{26}H_{44}N_2O_{28}U_3$
M_r	628.38	1104.68		1546.72
Crystal system	monoclinic	monoclinic		triclinic
Space group	$P2_1/n$	$P2_1/c$		$P\bar{1}$ (no. 2)
Unit cell dimension				
a (Å)	10.469(2)	8.590(2)		11.393(1)
b (Å)	13.910 (3)	18.090(4)		11.466(2)
c (Å)	13.754(3)	22.701(5)		8.7819(9)
α (°)	90	90		97.64(1)
β (°)	94.85(3)	90.57(3)		94.081(9)
γ (°)	90	90		79.79(1)
U (Å^3)	1995.7(7)	3527.5(12)		1117.6(2)
Z	4	4		1
D_{calc} (g cm^{-3})	2.078	2.080		2.298
$F(000)$	1184	2080		714
Crystal size (mm)	$0.19\times0.13\times0.06$	$0.15\times0.10\times0.06$		$0.15\times0.30\times0.38$
θ Range for data collection (°)	2.09–24.71	2.42–24.90	Cell determination (2θ range)	25 (35.3–40.9)
Limiting indices	$0\le h\le12$, $-16\le k\le16$, $-16\le l\le16$	$0\le h\le10$, $-21\le k\le21$, $-25\le l\le25$	Scan rate (° min^{-1})	32.0
μ (cm^{-1})	81.94	92.39		109.3
No. reflections collected	6185	11293		4172
Unique reflections	3375 ($R_{int}=0.022$)	5897 ($R_{int}=0.026$)		3953 ($R_{int}=0.020$)
Reflection/restraints/parameters	3375/0/245	5897/0/407	Observations/variables [$I>3\sigma(I)$]	3241/280
Final R_1, wR_2 [$I>2\sigma(I)$] [a]	0.018, 0.050	0.028, 0.068	R, R_w [b]	0.026; 0.026
R_1, $wR2$ (all data)	0.025, 0.052	0.035, 0.071		
Extinction coefficient	0.0037(2)	0.00126(10)	Transmission factors	0.69–1.00
Largest difference peak and hole (e Å^{-3})	0.931; −0.829	1.040; −1.694		1.04; −1.47
Goodness-of-fit on F^2	1.06	1.00	Goodness-of-fit on F	1.67

[a] $R_1=\Sigma\big||F_o|-|F_c|\big|\Sigma|F_o|$; $wR_2=[\Sigma\, w(F_o^2-F_c^2)^2|\Sigma\, w(F_o^2)^2]^{1/2}$.
[b] $R=\Sigma\big||F_o|-|F_c|\big|/\Sigma|F_o|$; $R_w=(\Sigma\, w(|F_o|-|F_c|)^2/\Sigma\, wF_o^2)^{1/2}$.

other U atom, and another carboxylate group is monodentate to the other U atom as well, forming a bridging structural unit with two uranyl groups and two ligands. These structural units are linked together by the third ligand through bis(1,3-bidentate) bonding of two carboxylate groups, forming infinite chains. The two uranyl groups are quite normal with O–U–O angle 178.1(2)° and U–O distance averaging 1.751(4) Å for U(1), 178.6(2)° and 1.752(4) Å for U(2). The equatorial U–O distances for U(1) are quite different, with 2.380(3) Å for O(11), 2.431(3) Å for O(3), 2.471(3) Å for O(7), average 2.503(3) Å for O(4) and O(9) and 2.544(4) Å for O(10), and the adjacent equatorial O–U–O angles range from 50.18(11)° (1,3-bidentate) to 68.13(12)°. The deviations of donor atoms from the mean equatorial plane for U(1) are significant, from −1.270 Å for O(3) to 0.602 Å for O(4), which accounts for the first experimental observation of donor atoms well outside the equatorial plan for uranyl. Similarly the equatorial U–O distances for U(2) are also quite different, 2.311(4) Å for O(13), average 2.453(3) Å for O(5), O(6) and O(9), 2.505(3) Å for O(7) and 2.559(4) Å for O(8), and the adjacent equatorial O–U–O angles range from 50.23(11)° (1,3-bidentate) to 69.03(12)°. Compared with U(1), U(2) has a more planar environment. The deviations of donor atoms from the equatorial plane are within ±0.08 Å. The packing diagram along crystallographic a axis is shown in Fig. 4. The short contacts [2.738(7)–2.764(7) Å] between N and carboxylate O atoms suggest cation–anion interactions via H-bonding, linking the infinite chains into a two-dimensional network.

Table 2
Selected bond lengths (Å) and bond angles (°) for **3**

Bond lengths			
U1–O1	1.771(3)	U1–O7	2.364(2)
U1–O3	2.362(3)	U1–O5	2.311(2)
U1–O11	2.438(3)	U1–O9	2.422(2)
U1–O2	1.768(3)		
Bond angles			
O1–U1–O2	177.57(12)	O3–U1–O11	75.15(9)
O7–U1–O9	69.75(8)	O5–U1–O9	72.27(8)
O5–U1–O3	70.44(9)	O7–U1–O11	72.59(8)

Table 3
Selected bond lengths (Å) and bond angles (°) for **7**

Bond lengths			
U1–O1	1.751(4)	U1–O10	2.544(4)
U1–O3	2.431(3)	U2–O9	2.444(3)
U1–O9	2.505(3)	U2–O7	2.505(3)
U2–O15	1.758(4)	U1–O11	2.380(3)
U2–O5	2.458(3)	U1–O4	2.501(3)
U2–O13	2.311(4)	U2–O16	1.747(4)
U1–O2	1.751(4)	U2–O6	2.456(3)
U1–O7	2.471(3)	U2–O8	2.559(4)
Bond angles			
O1–U1–O2	178.1(2)	O15–U2–O16	178.6(2)
O3–U1–O4	52.40(11)	O6–U2–O5	52.28(11)
O9–U1–O10	50.18(11)	O7–U2–O8	50.23(11)
O13–U2–O5	69.03(12)	O11–U1–O4	68.13(12)
O6–U2–O8	63.88(11)	O3–U1–O10	65.34(11)
O11–U1–O7	66.20(12)	O13–U2–O9	66.26(12)
O7–U1–O9	58.20(11)	O9–U2–O7	58.54(11)

Table 4
Selected bond lengths (Å) and bond angles (°) for **2**

Bond lengths			
U(1)–O(3)	2.471(5)	U(2)–O(6)	2.415(5)
U(1)–O(12)	2.474(5)	U(2)–O(10)	1.745(6)
U(2)–O(5)	2.528(5)	U(1)–O(11)	1.751(5)
U(2)–O(9)	1.744(6)	U(2)–O(2)	2.445(5)
U(1)–O(4)	2.493(5)	U(2)–O(7)	2.327(5)
U(2)–O(1)	2.492(5)		
Bond angles			
O(3)–U(1)–O(4)	51.9(2)	O(1)–U(2)–O(5)	63.2(2)
O(1)–U(2)–O(2)	51.9(2)	O(6)–U(2)–O(6)	59.1(2)
O(5)–U(2)–O(6)	50.1(2)	O(4)–U(1)–O(12)	64.1(2)
O(9)–U(2)–O(10)	178.8(3)	O(2)–U(2)–O(7)	70.6(2)
O(3)–U(1)–O(12)	64.0(2)	O(6)–U(2)–O(7)	66.5(2)

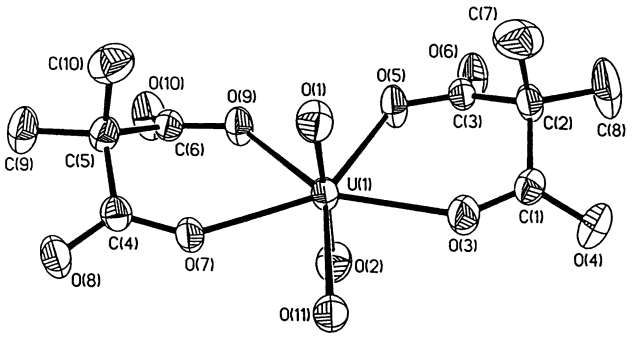


Fig. 1. An ORTEP drawing of the anionic structure for **3**, ellipsoids are drawn at the 50% probability level.

In the case of **2**, the uranium containing fragment in the asymmetric unit bonds together to form an infinite chain. U(1) lies on a centre of symmetry. The anionic structure in the asymmetric unit is shown in Fig. 5. The compound has two crystallographically unique uranyl groups. U(1) has hexagonal bipyramidal geometry, with two *trans* equivalent H_2O ligands and two dimethyl-

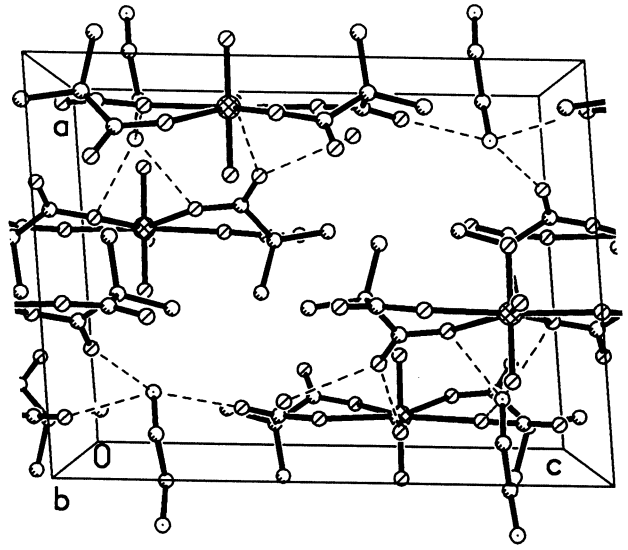


Fig. 2. Packing diagram along crystallographic *b* axis for **3**.

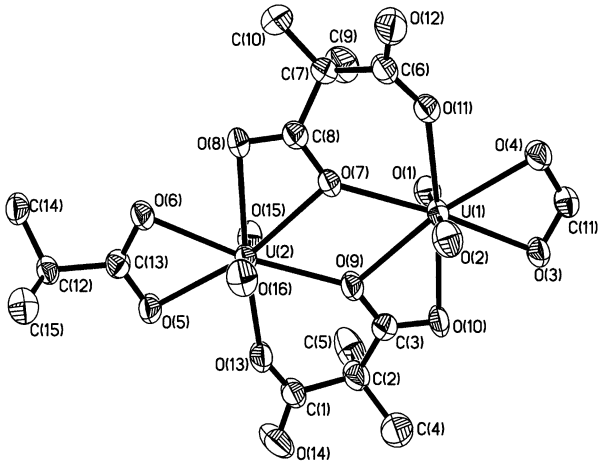


Fig. 3. An ORTEP drawing of the anion part of the asymmetric unit for **7**, ellipsoids are drawn at the 50% probability level.

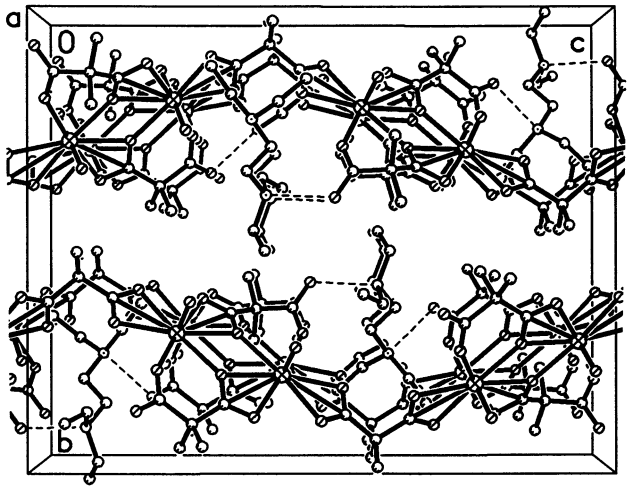


Fig. 4. Packing diagram along crystallographic *a* axis for **7**.

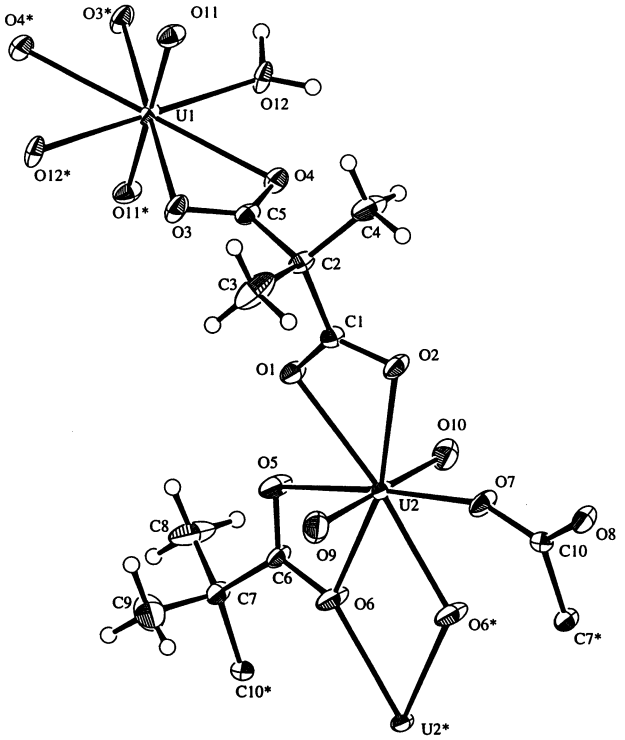


Fig. 5. An ORTEP drawing of the anion part of the asymmetric unit for **2**, ellipsoids are drawn at the 50% probability level.

malonate ligands that are each 1,3-bidentate. U(2) also has hexagonal bipyramidal geometry. Two symmetric crystallographically equivalent U(2) atoms are bridged together by two μ_2 carboxylate oxygen atoms from two crystallographically equivalent ligands (μ_2 1,3- and 1,5-bidentate arrangement). The infinite structure in the lattice is formed by bis(1,3-bidentate) dimethylmalonate ligands linking U(1) and U(2). The uranyl groups are nearly linear with normal U–O distance [average 1.751(5) Å for U(1) and 1.744(6) Å for U(2)]. The equatorial U–O distances for U(1) range from 2.471(5) to 2.493(5) Å with average 2.479(5) Å and the adjacent equatorial O–U–O angles range from 51.9(2)° (1,3-bidentate) to 64.1(2)°. The deviations from the mean equatorial plane for U(1) are within ± 0.025 Å. The equatorial U–O distances for U(2) are quite different, ranging from 2.327(5) Å for O(7) to 2.528(5) Å for O(5) with 2.415(5) Å for O(6), 2.492(5) Å for O(1) and 2.445(5) Å for O(2), average 2.456(5) Å and the adjacent equatorial O–U–O angles range from 50.1(2)° (1,3-bidentate) to 70.6(2)°. The deviations from the mean equatorial plane for U(2) are significant with -0.31 Å for O(1) and 0.13 Å for O(2). The packing diagram along crystallographic *c* axis is shown in Fig. 6. The short non-bonded contacts indicate that the oxygen atoms from non-bonded carboxylate groups, H_2O and EtOH molecules may be involved in H-bonding linking the chains in three dimensions. The distance of 2.732(9) Å between a non-bonded carboxylate O atom and a N atom implies that the cation–anion interactions are via H-bonding.

3.2. Infrared spectra

Compounds **3**–**6** and **8** [4] have very similar IR spectra, ν(OH) and ν(NH) between 3418 and 3478; ν_{as}(COO) between 1520 and 1654; ν_s(COO) between 1313 and 1478; ν_{as}(OUO) between 903 and 912; δ(C=O) between 695 and 721 and π(C=O) between 574 and 609 cm^{-1}. The IR spectra of compounds **1**, **2** and **7** differ mainly in the presence of a shifted ν_{as}(OUO) at 930, 932 and 930 cm^{-1}, respectively. Crystallographic studies confirmed that compounds **3**, **4** [4] and **8** [4] have pentagonal bipyramidal uranium centres and compounds **2** and **7** have hexagonal bipyramidal uranium centres. This seems to suggest that for the group of compounds studied, ν_{as}(OUO) at around 930 indicates the presence of a hexagonal bipyramidal uranium centre and ν_{as}(OUO) at around 900 indicates the presence of a pentagonal bipyramidal uranium centre. Thus compounds **5** and **6**, with ν_{as}(OUO) values at 905 and 912 cm^{-1}, respectively, are most likely to have pentagonal bipyramidal uranium centres and by contrast, compound 1 probably has a hexagonal bipyramidal uranium centre.

3.3. Thermal analysis

Compounds **1**, **6** and **7** first lost their counter-cations and one ligand, then the remaining ligands to give the final product, UO_3, at about 450 °C.

Compound **2** first lost its solvent molecules, then counter-cations and one ligand, finally the remaining ligands to give the final product, UO_3, at about 400 °C.

Compounds **3**, **5** and **8** [4] lost their final H_2O molecules at 106–140 °C. Since **3** and **8** [4] have a monomeric anion structure with one coordinated H_2O molecule, it is likely that **5** has a similar monomeric anion structure with a coordinated H_2O molecule.

3.4. ^{13}C CPMAS NMR spectroscopy

3.4.1. Compounds of known structure

^{13}C CPMAS NMR spectroscopy has been widely used to study the interactions of metals with ligands [9,10]. Unfortunately very little work has been done for uranium complexes [11,12]. Based on the specific patterns of carbonyl chemical shifts, compounds with known crystal structures can be used as model compounds to study the relationship between structural types and ^{13}C CPMAS NMR spectroscopic data. The ^{13}C CPMAS NMR spectra of **3**, **7** and **2**, together with the expanded carbonyl regions, are shown in Figs. 7–9.

3.4.1.1. Structure type 1: monomeric anion structure with no symmetry (see Fig. 1). Compound **3** has a monomeric anion structure with no crystallographically imposed symmetry, and in principle should give four carbonyl peaks. Experimentally only two peaks were observed at 183.3 and 180.9 ppm with approximately equal intensities (see Fig. 7), suggesting that the four carbonyls fall into two groups of two closely similar environments. Evidently the deviation from C_2 rotational symmetry is small. The peak at 48.4 ppm is assigned to the quaternary carbons (C_q) in the ligand and the broad peak at 34 ppm is assigned to the CH_2 carbons in the counter-cation. The CH_3 carbons in the ligand are assigned to the group of four closely spaced peaks at 24.0, 22.7, 21.0 and 18.7 ppm, indicating that all four CH_3 carbons are different.

3.4.1.2. Structure type 2: monomeric anion structure with C_2 rotational symmetry. Compound **8** [4] also has a monomeric anion structure but with a C_2 axis along the U(1)–O(6) direction. It is required to have two non-equivalent carboxylate groups, in agreement with the ^{13}C CPMAS NMR spectrum which shows two carbonyl peaks at 189.0 and 184.4 ppm, and two CH_3 peaks at 24.1 and 20.6 ppm. The peak at 48.7 ppm is assigned to C_q in the ligand, the broad peak at 52.5 ppm is assigned to the CH_2N cation carbons, the peaks at 42.6 and 39.8 ppm are assigned to the NCH_3 cation carbons, and the shoulder at ca. 19 ppm to the CCH_2C cation carbon.

3.4.1.3. Structure type 3: dimeric anion structure. Compound **4** [4] has a dimeric anion structure and shows three carbonyl peaks at 188.0, 184.2 and 182.5 ppm with an approximate intensity ratio of 1:1:2. It is likely that this pattern arises from non-equivalent carbonyl carbons in the bridging ligand (188.0 and 184.2 ppm) and equivalent carbonyls in the terminal 1,5-bidentate ligand (182.5 ppm). The peak at 51.5 is assigned to C_q and the peaks at 25.6 and 23.3 ppm to CH_3 carbons in the ligand, the CH_3 peak showing a barely resolved splitting indicating different CH_3 environments.

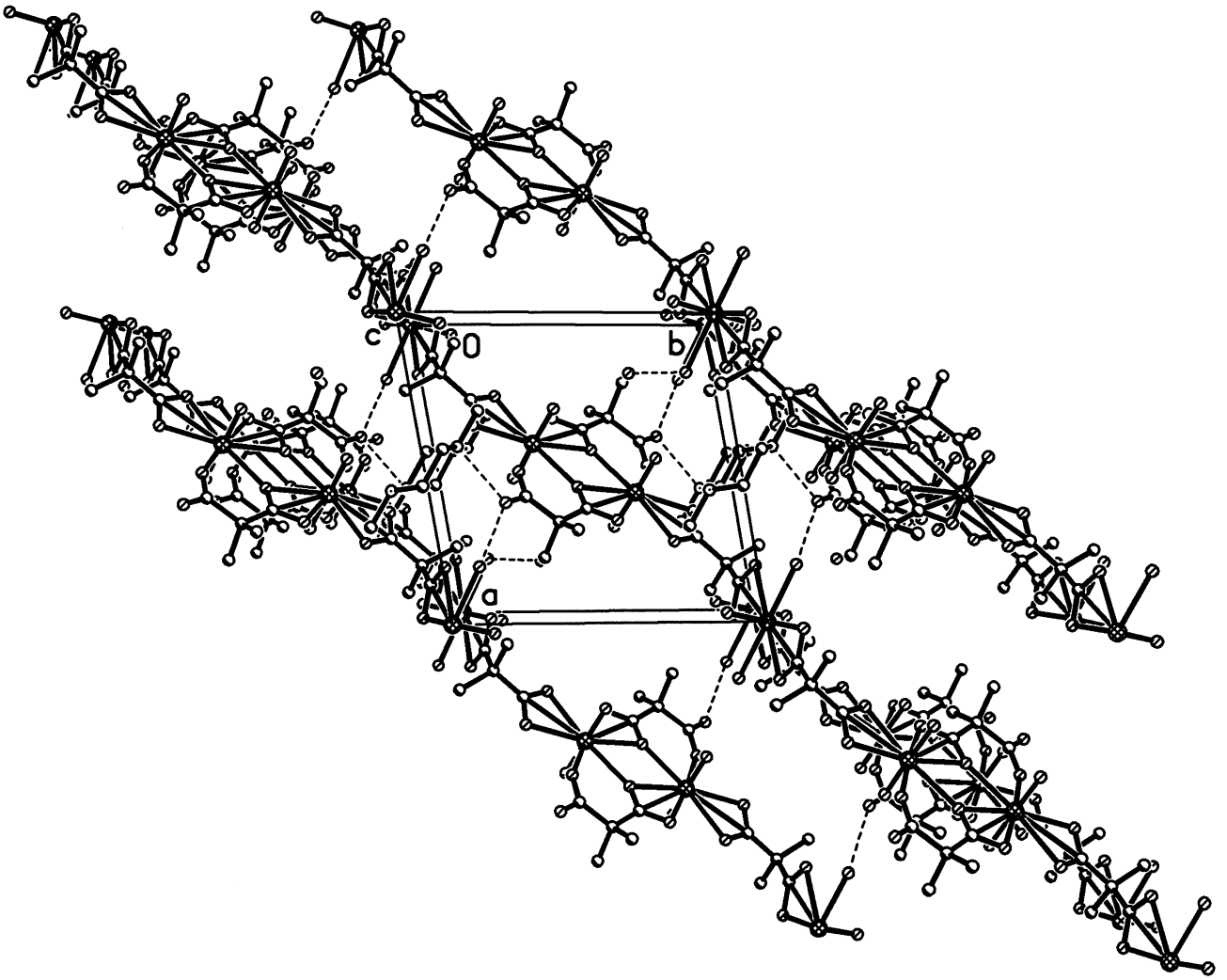


Fig. 6. Packing diagram along crystallographic *c* axis for **2**.

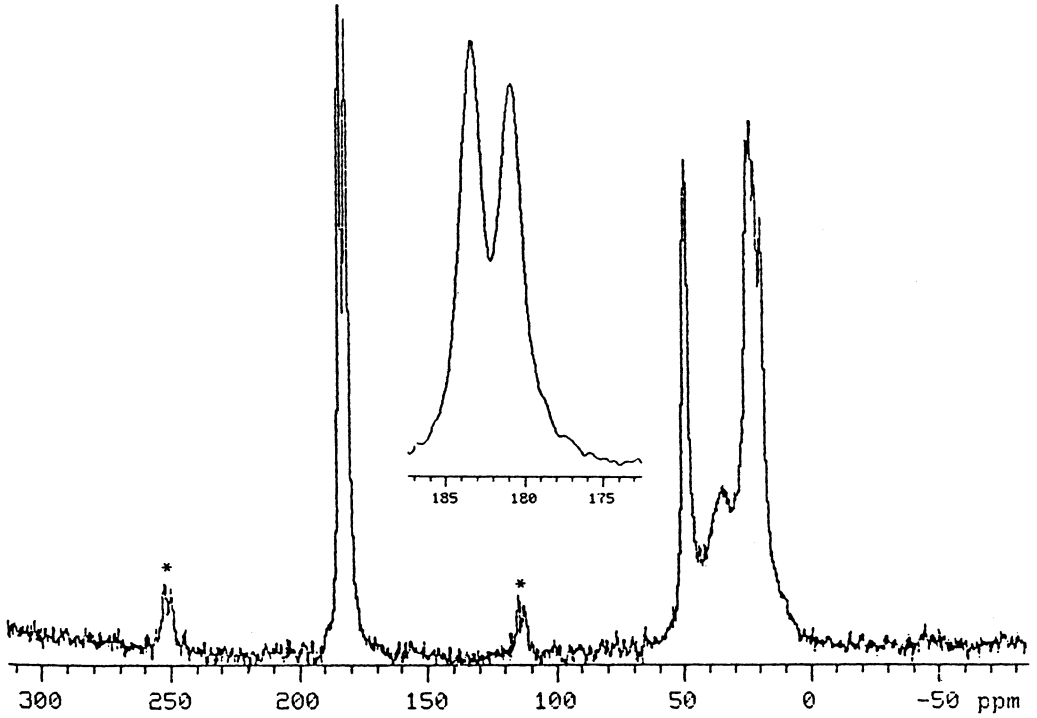


Fig. 7. ^{13}C NMR CPMAS spectrum with carbonyl expansion for **3** (* spinning sidebands).

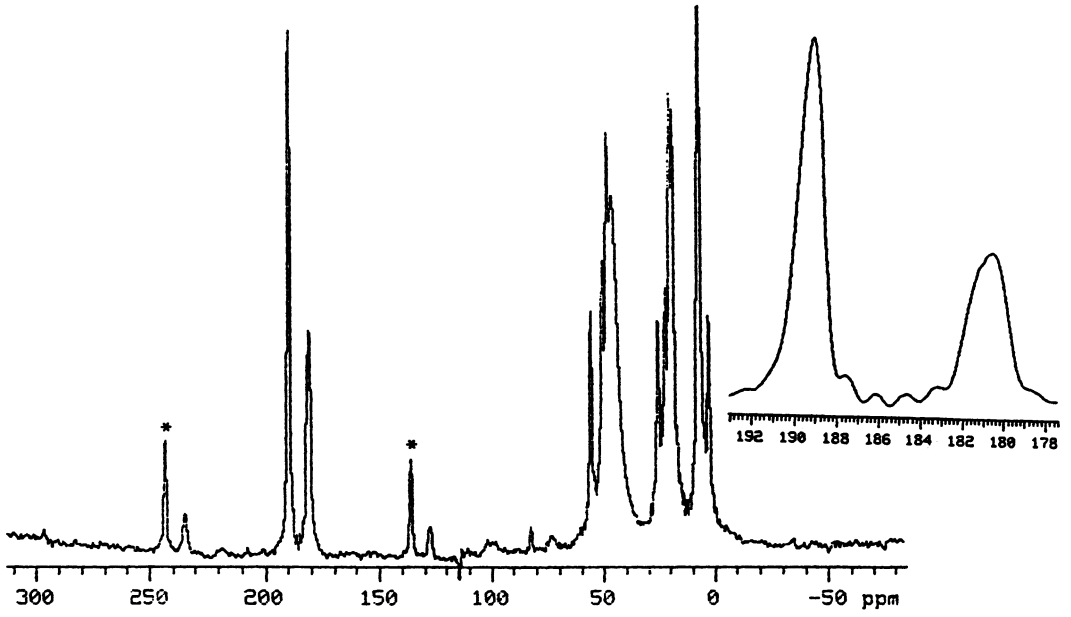


Fig. 8. ^{13}C NMR CPMAS spectrum with carbonyl expansion for **7** (* spinning sidebands).

3.4.1.4. Structure type 4: novel infinite chain (2:3) structure (see Fig. 3). Compound **7** has a novel 2:3 ratio infinite chain anion structure. It shows two well separated carbonyl peaks at 189.4 and 180.7 ppm with approximately 2:1 intensity ratio (see Fig. 8). These are tentatively assigned to 1,3-bidentate carboxylate groups (C(3), C(8), C(11) and C(13) in Fig. 2) and to monodentate carboxlate groups (C(1) and C(6) in Fig. 3), respectively. The peaks at 25.3, 21.9, 19.9 and 18.5 ppm with relative intensities approximately 1:1:2:2 arise from CH_3 carbons in the ligand, the first two being assigned to the [C(14), C(15)) pair and the last two to the (C(4), C(5)) and (C(9), C(10)] pairs. The sharp peaks at 55.7, 50.3 and 48.3 ppm are assigned to C_q in the ligands; evidently all three C_q in the repeat unit are non-equivalent. The broad peak at 46.4 ppm is assigned

to the CH_2 carbons in the counter-cation and then peaks at 6.7 and 2.4 ppm are assigned to CH_3 carbons in the counter-cation.

3.4.1.5. Structure type 5: novel infinite chain (3:4) structure (see Fig. 5). Compound **2** possesses a novel 3:4 ratio infinite chain anion structure. Four carbonyl peaks of equal intensity are observed at 191.6, 190.1, 187.7 and 184.6 ppm (see Fig. 9) as expected from the stoichiometry and symmetry of the asymmetric unit (Fig. 5). The peak at 56.2 ppm is assigned to C_q in the ligands, the peaks at 48.9 and 40.1 to CH_2 and CH_3 carbons, respectively, in the counter-cation, and the peaks at 25.5 and 20.9 ppm to CH_3 carbons in the ligands.

3.4.2. Structural predictions

There are three major factors which influence the carbonyl chemical shifts in the solid state: (i) the chemical structure of the anion, including factors such as $U-O_{eq}$ distances, conformations of chelate rings and H-bonding involving carboxylate oxygen atoms; (ii) the chemical structure of the cation; (iii) crystallographic symmetry and solid-state packing. Unfortunately, there are at present insufficient data to separate the contributions of all these factors. For the five compounds of known crystal structure, the ^{13}C carbonyl peaks span some 10 ppm and the number of peaks observed is consistent with the number of structurally distinct carbonyl groups. However the chemical shifts do not seem to show a regular relationship with the type of bonding. For example, compounds **3** (Fig. 7) and **8** [4] both have anions of similar structure with 1,5-bidentate ligands, but the carbonyl shifts of **3** are 180.8 and 183.3 ppm and those of **8** [4] are 184.4 and 189.0 ppm. Evidently subtle differences in anion, cation or crystal structure may have a significant effect on the chemical shifts. Nevertheless, tentative predictions of the structure of those compounds not characterised by X-ray diffraction have been made on the basis of comparisons of their carbonyl CPMAS NMR spectra (not shown) with those of the compounds of known structure:

1. The spectrum of compound **1** is similar to that of **7**, having two well-separated carbonyl peaks at 190.1 and 181.8 ppm of relative intensity 2:1. Its structure is predicted to be type 4 (2:3 novel infinite chain), see Scheme 1.
2. The spectrum of compound 5 has three carbonyl peaks at 185.6, 183.9 and 182.2 ppm with intensity ratio approximately 1:2:1. The form of this spectrum resembles that of **4** [4], though the peaks are more closely spaced and the order of intensities is different. The structure of **5** is tentatively identified as a dimer.
3. The spectrum of compound **6** is similar to that of **4** [4], having three carbonyl peaks at 186.7, 184.3 and 179.1 ppm with relative intensity 1:1:2. Its structure is predicted to be type 3 (dimer), see Scheme 1.

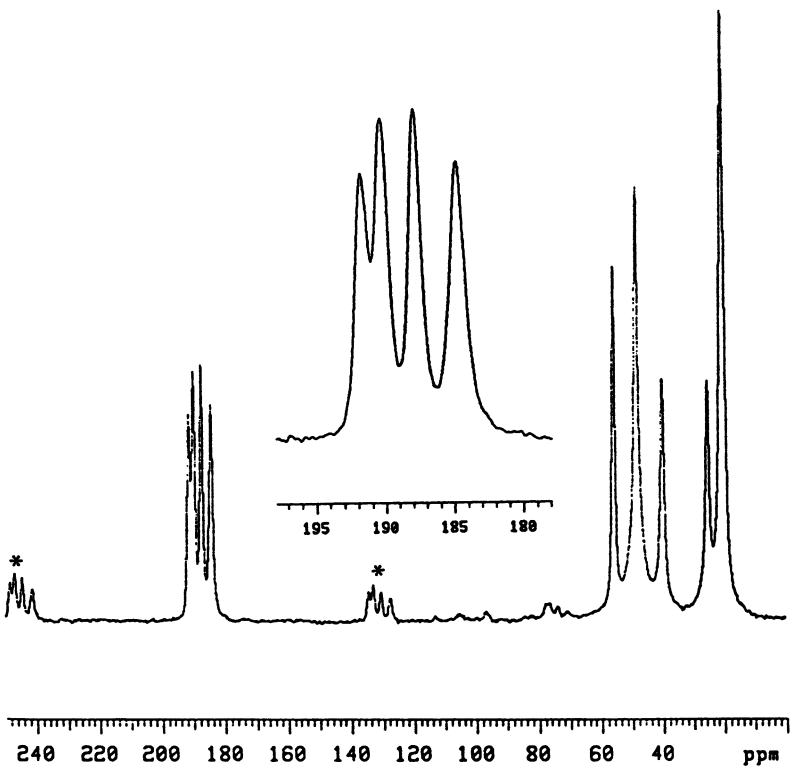
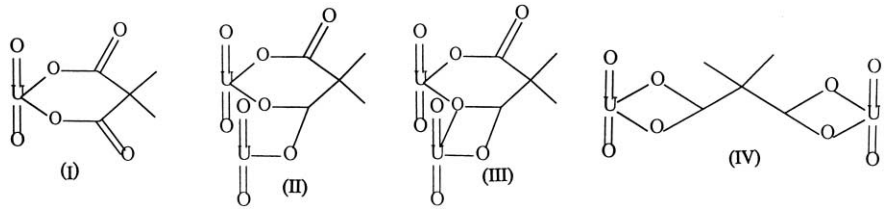


Fig. 9. ^{13}C NMR CPMAS spectrum with carbonyl expansion for **2** (* spinning sidebands).



Scheme 1. Bonding modes of malonate with uranyl.

These predictions are consistent with the elemental analysis and IR spectroscopic results.

3.5. Bonding modes of malonate with uranyl

Two bonding modes for malonate with the uranyl ion have been previously published [2]. These are bidentate (terminal 1,5-bidentate) (I), and tridentate (1,5-bidentate and μ_1 3-monodentate) (II), see Scheme 1. Two new type of bonding modes have been identified in this study, shown in Scheme 1, tridentate (μ_2 1,3-bidentate and 1,5-bidentate) (III) and tetradentate (1,3-bidentate through both carboxylate groups) (IV).

3.6. Effects of counter-cations and H-bonding

Infinite chain structures have previously been found for uranyl bis(malonato) complexes with different cations (Sr^{2+}, Ba^{2+} and NH_4^+) [2–4]. However, in the present studies, it appears that the steric bulk of the organic cations (ionic radii: Sr^{2+} 1.12 Å, Ba^{2+} 1.34 Å; N–N distances about 2.88 Å for piperazinium and about 3.76 Å for ethylenediammonium calculated from CSD relevant structures) prevents uranyl bis(malonate) units from bridging to form infinite chains, instead forming monomeric or dimeric structures with ethylenediammonium, piperazinium, triethylenediammonium and propanediammonium (**3**, **5**, **6** and **8** [4]). In addition the use of protonated amines as counter-cations encourages extensive H-bonding between counter-cations and the anions (ligating H_2O molecules and non-ligating O atoms of carboxylate groups). The hydrophobic effect of counter-cations probably is another factor, which may influence the equilibria in solutions and the resultant products in solid state.

When changing piperazine to dimethylpiperazine, ethylenediamine to tetramethylethylenediamine or tetraethylethylenediamine, 2:3 or 3:4 oligomeric compounds with infinite chain structures are formed. It is obvious that oligomeric compounds are favoured by methylation of the cations because that restricts the possibilities for H-bonding between cations and anions (complexes) and thereby encourages bridging between the anion and the ligand.

On the basis of these results, it appears that: (i) monomer formation is favoured by use of protonated, primary acyclic amines as counter-cations; (ii) dimer formation is directed by protonated alicyclic or secondary diamines; and (iii) protonated tertiary cyclic or alicyclic amines give rise to polymeric chains.

4. Conclusions

Eight uranyl dimethylmalonato compounds have been synthesised and characterised by elemental analysis, thermal analysis, IR and CP/MAS ^{13}C NMR spectroscopy and five of them by X-ray crystallography. Monomeric, dimeric and infinite chain motifs have been identified. ^{13}C CPMAS NMR has been shown to be a useful method to distinguish structural types and predict structures for related non-crystalline compounds.

So far unrecognised structural diversity for uranyl dicarboxylate complexes can be achieved by varying counter-cations and slightly modification of the substituent groups on the proligand. Two new kinds of bonding mode of malonate for uranyl have been identified in this study, tridentate (μ_2 1,3- and 1,5-bidentate) and tetradentate (1,3-bidentate through both carboxylate groups).

5. Supplementary material

Crystallographic data for the structural analysis have been deposited with the Cambridge Crystallographic Centre, CCDC Nos. 166052–166054. Copies of this information may be obtained free of charge from The Director, CCDC, 12 Union Road, Cambridge, CB2 1EZ, UK (fax: +44-1233-336-033; e-mail: deposit@ccdc.cam.ac.uk or www: http://www.ccdc.cam.ac.uk).

Acknowledgements

We are grateful to M. Hart (Manchester University) for microanalyses; J. Friend (Manchester University) for ^{13}C CPMAS NMR; to BNFL (Y.J.Z. and F.R.L.) and CVCP (Y.J.Z.) for their financial support.

References

[1] K.S. Rajan, A.E. Martell, J. Inorg. Nucl. Chem. 29 (1967) 523.
[2] R.M. Rojas, A. Del Pra, G. Bombieri, F. Benetollo, J. Inorg. Nucl. Chem. 41 (1979) 541.
[3] G. Bombieri, F. Benetollo, E. Forsellini, A. Del Pra, J. Inorg. Nucl. Chem. 42 (1980) 1423.
[4] Y.-J. Zhang, D. Collison, F.R. Livens, M. Helliwell, H. Eccles, N. Tinker, J. Alloys Compounds 271 (1998) 139.
[5] S.I.R.92: A. Altomare, M. Cascarano, C. Giacovazzo, A. Guagliardi, J. Appl. Crystallogr. 26 (1993) 343.
[6] P.T. Beurskens, G. Admiraal, G. Beurkens, W.P. Bosman, R. de Gelder, R. Israel, J.M.M. Smits, DIRDIF-94: the DIRDIF-94 program system. Technical Report of the Crystallography Laboratory, University of Nijmegen, The Netherlands, 1994.
[7] TEXSAN: Crystal Structure Analysis Package, Molecular Structure Corporation, The Woodlands, TX, 1985 and 1992.
[8] SHELXTL 5.03 program system; Siemens Analytical X-ray Instruments, Madison, WI, 1995.
[9] F.J. Martinez-Martinez, A. Ariza-Castolo, V. Ramos-Nava, N. Barba-Behrens, R. Contreras, Mag. Res. Chem. 31 (1993) 832.
[10] S. Aime, G. Digilio, R. Gobetto, P. Cecchi, G. Lobbia, M. Camalli, Polyhedron 13 (1994) 2695.
[11] G.C. Campbell, F.A. Cotton, J.F. Haw, W. Schwotzer, Organometallics 5 (1986) 274.
[12] N.A. Chumaevskii, G.A. Razgonyaeva, V.I. Privalov, Zh. Neorg. Khim. 40 (1995) 2009.

PERGAMON

Polyhedron 21 (2002) 81–96

POLYHEDRON

www.elsevier.com/locate/poly

Synthesis and characterisation of uranyl substituted malonato complexes
Part II: ^{13}C CPMAS NMR spectroscopy related to structural diversity

Yingjie Zhang [a,*], David Collison [b], Francis R. Livens [b], Madeleine Helliwell [b], Frank Heatley [b], Annie K. Powell [c], Sigrid Wocadlo [c], Harry Eccles [d]

[a] *Australian Nuclear Science and Technology Organisation, PMB 1, Menai 2234, NSW, Australia*
[b] *Department of Chemistry, The University of Manchester, Oxford Road, Manchester M13 9PL, UK*
[c] *Institut für Anorganische Chemie, Universität Karlsruhe, Engesserstrasse Gelo 30.45, 76128 Karlsruhe, Germany*
[d] *Research and Technology, BNFL, Springfields, Salwick, Preston PR4 0XJ, UK*

Received 16 July 2001; accepted 3 October 2001

Abstract

The reaction of aliphatic diamine with malonic or substituted malonic acid and uranyl nitrate in the ratio 2:2:1 in aqueous media leads in most cases to one predominant product, usually with a metal–ligand ratio of 1:2, but in a few cases it leads to oligomers with metal–ligand ratios of 2:3, 3:4 and 3:5. The crystalline products are salts with diprotonated diamines as cations, but crystals can also be formed with salts of hexaaminecobalt(III). Representative structures have been determined by single crystal X-ray diffraction for: $(C_4H_{12}N_2)[UO_2(C_4H_4O_4)_2(H_2O)]\cdot 1.5H_2O$ (**5**); $(C_4H_{14}N_2)[UO_2(C_4H_4O_4)_2(H_2O)]\cdot 2H_2O$ (**7**); $(C_4H_{12}N_2)[UO_2(C_7H_{10}O_4)_2(H_2O)]\cdot H_2O$ (**9**); $(C_{10}H_{26}N_2)[UO_2(C_7H_{10}O_4)_2(H_2O)]\cdot 2H_2O$ (**10**); $(C_{10}H_{26}N_2)[(UO_2)_3(C_7H_{10}O_4)_5]\cdot 2H_2O$ (**11**) and $\{[Co(NH_3)_6][UO_2(C_4H_4O_4)(C_5H_6O_4)]\}_2Cl_2\cdot 6H_2O$ (**20**). Compounds **5**, **7**, **9** and **10** possess similar, monomeric anion structures. The anion in **11** has an infinite zigzag chain structure containing three distinct types of U centres, linked by three kinds of bridging ligands. Compound **20** has a dimeric anion structure. Three new types of bonding mode have been identified in this study, tridentate (μ_2-1,3-bidentate and 1,5-bidentate), tetradentate (1,3-bidentate through both carboxylate groups) and tridentate (1,3-bidentate through one carboxylate group and 1-monodentate through the other). Several types of carbonyl environments have been identified by X-ray crystallography in the present and recent previous work [Zhang et al., Polyhedron 21 (2002) 69; Zhang et al., J. Alloys Compounds 271 (1998) 139; Tilley et al., unpublished data] and a general correlation between isotropic chemical shift values in the ^{13}C CPMAS NMR spectra and the carbonyl type has been identified. © 2002 Elsevier Science Ltd. All rights reserved.

Keywords: Uranyl; Malonato complexes; CPMAS ^{13}C NMR; X-ray crystallography

1. Introduction

Our earlier work on malonato and substituted malonato complexes of uranyl has indicated that considerable structural diversity is present in solids which have been isolated from the ternary system uranyl/proligand/diamine in aqueous solution [1–3]. Thus, when using malonic acid (H_2MA), although a pentagonal bipyramidal geometry is produced based upon 1,5-bidentate ligation by the dianion, monomeric or dimeric complexes may be formed in addition to the well known chain polymeric anions found when $[NH_4]^+$ or Group II cations are employed [4–6]. In contrast, with dimethylmalonic acid (H_2DMMA) as proligand, as well as similar monomeric and dimeric complexes, the equatorial coordination number can increase to six with the concomitant formation of polymeric anions even using diprotonated diamines as counter-cations. The purposes

* Corresponding author. Tel.: +61-2-9717-9156; fax: +61-2-9543-7179.
E-mail address: yingjie.zhang@ansto.gov.au (Y. Zhang).

0277-5387/02/$ - see front matter © 2002 Elsevier Science Ltd. All rights reserved.
PII: S0277-5387(01)00965-2

of this further study are to investigate the effects of both intermediate and greater bulk within the malonic acids by using methylmalonic (H_2MMA), diethylmalonic (H_2DEMA) and phenylmalonic (H_2PMA) acids, to extend the range of diamine pro-cations and hence to search for other new structural types. The effect of unsymmetrical substitution within the malonate ligand will also be investigated. There have been indications in our previous work that ^{13}C CPMAS NMR spectroscopy might be able to identify bonding modes in uranyl-malonato complexes from the number and nature of the carboxylate carbon resonances and the present study will add further to this database of spectroscopic information.

2. Experimental

2.1. Materials

All chemicals were reagent grade, purchased from Strem Chemicals, Aldrich or Lancaster and used without further purification.

2.2. Physical methods

Elemental analyses were performed by the Microanalysis Lab, Department of Chemistry, The University of Manchester. IR spectra were recorded on an ATI Mattson Genesis Series FTIR Spectrometer. TG/DT analyses were made on a Seiko (TG/DTA 220) thermal analyser at a heating rate of 10 °C min^{-1} and an air flow rate of 100 cm^3 min^{-1}. High resolution solid state ^{13}C NMR spectra were recorded using a Varian Associates Unity 300 spectrometer operating at 75.4 MHz using the cross polarisation-magic angle spinning (CP-MAS) technique. The acquisition time was 0.05 s, the spectral width was 30007.5 Hz, the contact time was 1.5 ms, the recycle time was 5 s and the spinning speed was approximately 4 kHz. The chemical shift scale was referenced by setting the CH_3 peak in a sample of solid hexamethylbenzene, run using the same conditions, to 16.5 ppm.

2.3. Syntheses

In general, a solution of uranyl nitrate hexahydrate was added to a solution of a ligand and a diamine in the molar ratio of 1:2:2. The yellow crystalline product formed after a week, and was collected by filtration and dried in air.

2.3.1. Synthesis of hexaaminecobalt(III) tris(malonato)hydromalonato bis[dioxouranate(VI)] dihydrate

$[Co(NH_3)_6][(UO_2)_2(C_3H_2O_4)_3(C_3H_3O_4)]\cdot 2H_2O$ (**1**): a solution of uranyl nitrate hexahydrate (0.50 g, 1 mmol in 5 cm^3 H_2O) was added to an aqueous solution of malonic acid (0.21 g, 2 mmol in 25 cm^3 H_2O), fresh sodium hydroxide solution (0.32 g, 8 mmol) and hexaaminecobalt(III) chloride (0.27 g, 1 mmol) in the ratio of 1:4:1. An orange, solid product formed after 1 h and was collected by filtration and dried in air, yield 85%. *Anal.* Found: C, 12.27; H, 3.00; N, 7.32; Co, 4.99; U, 41.85. Calc. for $C_{12}H_{31}N_6O_{22}CoU$: C. 12.57; H, 2.72; N, 7.33; Co, 5.14; U, 41.53%. TG/DTA (°C) 129 (-3.2% *endo*, $-2H_2O = 3.1\%$), 248 (*endo*), 296 (*exo*), 322 (58.0%, *exo*, $Co_2O_3 + UO_3 = 57.1\%$). IR (KBr disk) ν (cm^{-1}): 3430 vs (br), 1604 vs (br), 1561 s, 1440 w, 1406 w, 1385 m, 1357 w, 1272 m, 907 s, 705 s, 534 w.

2.3.2. Synthesis of *N*,*N*,*N*′,*N*′-tetramethylbutanediammonium bis(malonato) dioxouranate(VI) dihydrate

$(C_8H_{22}N_2)[UO_2(C_3H_2O_4)_2]\cdot 2H_2O$ (**2**), yield 80%. *Anal.* Found: C, 26.00; H, 4.74; N, 4.51; U, 36.19. Calc. for $C_{14}H_{30}N_2O_{12}U$: C, 25.62; H, 4.57; N, 4.27; U, 36.26%. TG/DTA (°C) 78 (-5.4% *endo*, $-2H_2O = 5.5\%$), 200 (*endo*), 282 (*exo*), 329 (44.0% *exo*, $UO_3 = 43.6\%$). IR (KBr disk) ν (cm^{-1}): 3444 vs (br), 1637 s, 1615 m, 1561 w, 1416 w, 1384 s, 913 s, 704 w.

2.3.3. Synthesis of *N*,*N*′-dimethylpiperazinium bis(methylmalonato) dioxouranate(VI)

$(C_6H_{16}N_2)[UO_2(C_4H_4O_4)_2]$ (**3**), yield 80%. *Anal.* Found: C, 27.14; H, 3.97; N, 4.63; U, 38.40. Calc. for $C_{14}H_{24}N_2O_{10}U$: C, 27.19; H, 3.91; N, 4.53; U, 38.49%. TG/DTA (°C) 299 (44.6% *exo* $UO_3 = 44.0\%$). IR (KBr disk) ν (cm^{-1}): 3420 m (br), 1649 s, 1563 vs (br), 1453 m, 1417 s, 1277 s, 1151 w, 1083 w, 1019 w, 906 vs, 710 s, 649 w, 533 w.

2.3.4. Synthesis of ethylenediammonium bis(methylmalonato)aqua dioxouranate(VI)

$(C_2H_{10}N_2)[UO_2(C_4H_4O_4)_2(H_2O)]$ (**4**), yield 80%. *Anal.* Found: C, 20.38; H, 3.45; N, 4.72; U, 40.69. Calc. for $C_{10}H_{20}N_2O_{11}U$: C, 20.06; H, 3.46; N, 4.81; U, 40.88%. TG/DTA (°C) 160 (-3.2% *endo*, $-1H_2O = 3.1\%$), 214 (*endo*), 228 (-23.1% *exo* ligand = 23.0%), 308 (*exo*), 451 (*exo*), 505 (49.4% *exo*, $UO_3 = 50.8\%$). IR (KBr disk) ν (cm^{-1}): 3415 m, 3145 s (br), 1616 vs, 1571 s, 1467 w, 1416 s, 1289 m, 1221 w, 912 vs, 714 m.

2.3.5. Synthesis of piperazinium bis(methylmalonato)aqua dioxouranate(VI) 1.5 hydrate

$(C_4H_{12}N_2)[UO_2(C_4H_4O_4)_2(H_2O)]\cdot 1.5H_2O$ (**5**), yield 55%. *Anal.* Found: C, 22.38; H, 4.12; N, 4.47; U, 37.07. Calc. for $C_{12}H_{25}N_2O_{12.5}U$: C, 22.37; H, 4.07; N, 4.35; U, 36.94%. TG/DTA (°C) 122 (-7.3% *endo*, $-2.5H_2O = 7.1\%$), 230 (*exo*), 253 (-39.4% *exo*, $-$ cation-ligand = 39.2%), 316 (*exo*), 500 (45.6% *exo*, $UO_3 = 45.0\%$). IR (KBr disk) ν (cm^{-1}): 3460 s (br),

1587 vs (br), 1436 w, 1408 m, 1336 w, 1275 m, 1119 w, 1089 w, 1011 w, 912 vs, 714 s, 598 w, 571 w.

2.3.6. Synthesis of piperazinium bis(methylmalonato)aqua dioxouranate(VI) tetrahydrate

$(C_4H_{12}N_2)[UO_2(C_4H_4O_4)_2(H_2O)]\cdot 4H_2O$ (**5a**): the yellow crystalline product formed as described above (**5**) coexists with a light yellow cubic crystalline product after standing for 2 weeks. The mixture was collected by filtration and dried in air. The compound **5a** was separated manually, yield 40%. *Anal*. Found: C, 21.49; H, 4.25; N, 4.22; U, 34.74. Calc. for $C_{12}H_{30}N_2O_{15}U$: C, 21.18; H, 4.44; N, 4.12; U, 34.98%. TG/DTA (°C) 93 (-11.0% *endo*, $-4H_2O = 10.9\%$), 236 (*endo*), 433 (43.3% *exo*, $UO_3 = 43.2\%$). IR (KBr disk) ν (cm^{-1}): 3468 vs (br), 1638 s, 1581 vs (br), 1460 m, 1432 w, 1410 w, 1384 m, 1318 w, 1291 m, 1086 w, 915 vs, 712 m, 580 w, 539 w.

2.3.7. Synthesis of triethylenediammonium bis(methylmalonato)aqua dioxouranate(VI)

$(C_6H_{14}N_2)[UO_2(C_4H_4O_4)_2(H_2O)]$ (**6**), yield 75%. *Anal*. Found: C, 26.40; H, 4.02; N, 4.39; U, 37.17. Calc. for $C_{14}H_{24}N_2O_{11}U$: C, 26.51; H, 4.13; N, 4.42; U, 37.52%. TG/DTA (°C) 128 (-3.0% *endo*, $-1H_2O = 2.8\%$), 207 (-21.3% *endo*, $-$cation $= 20.8\%$), 330 (45.6% *exo*, $UO_3 = 45.1\%$). IR (KBr disk) ν (cm^{-1}): 3442 s (br); 1609 vs, 1547 m, 1462 w, 1409 m, 1283 m, 910 vs, 710 m, 571 m.

2.3.8. Synthesis of N,N′-dimethylethylenediammonium bis(methylmalonato)aqua dioxouranate(VI) dihydrate

$(C_4H_{14}N_2)[UO_2(C_4H_4O_4)_2(H_2O)]\cdot 2H_2O$ (**7**), yield 50%. *Anal*. Found: C, 21.94; H, 4.31; N, 4.19; U, 36.82. Calc. for $C_{12}H_{28}N_2O_{13}U$: C, 22.30; H, 4.36; N, 4.33; U, 36.82%. TG/DTA (°C) 125, 150 (-7.3% *endo*, $-2.5H_2O = 7.1\%$), 194 (-40.8% *endo*, $-$cation-ligand $= 40.2\%$), 293 (*exo*), 437 (45.0% *exo*, $UO_3 = 44.2\%$). IR (KBr disk) ν (cm^{-1}): 3456 s (br); 3069 w, 2723 w, 1586 vs (br), 1463 w, 1431 m, 1384 w, 1320 m, 1291 m, 1126 w, 911 vs, 715 m, 546 m.

2.3.9. Synthesis of N,N,N′,N′-tetramethylethylenediammonium bis(diethylmalonato) dioxouranate(VI)

$(C_6H_{18}N_2)[UO_2(C_7H_{10}O_4)_2]$ (**8**), yield 65%. *Anal*. Found: C, 34.76; H, 5.33; N, 3.91; U, 34.28. Calc. for $C_{20}H_{38}N_2O_{10}U$: C, 34.98; H, 5.58; N, 4.08; U, 34.66%. TG/DTA (°C) 386 (40.5% *exo*, $UO_3 = 40.6\%$). IR (KBr disk) ν (cm^{-1}): 3449 s (br), 1626 s, 1602 w, 1544 ms, 1464 w, 1409 s, 1280 s, 1200 w, 908 vs, 808 s, 698 s, 576 m.

2.3.10. Synthesis of piperazinium bis(diethylmalonato) aqua dioxouranate(VI) monohydrate

$(C_4H_{12}N_2)[UO_2(C_7H_{10}O_4)_2(H_2O)]\cdot H_2O$ (**9**), yield 85%. *Anal*. Found: C, 30.75; H, 5.21; N, 3.96; U, 33.39. Calc. for $C_{18}H_{36}N_2O_{12}U$: C, 30.43; H, 5.11; N, 3.94; U, 33.50%. TG/DTA (°C) 129 (-2.4% *endo*, $-2H_2O = 2.5\%$), 183 (*endo*), 227 (*exo*), 414 (40.46% *exo*, $UO_3 = 40.3\%$). IR (KBr disk) ν (cm^{-1}): 3413 s (br), 1543 vs (br), 1460 m, 1422 w, 1380 m, 1322 w, 1289 m, 1178 w, 1094 w, 906 vs, 817 s, 707 m, 604 m, 583 w.

2.3.11. Synthesis of N,N,N′,N′-tetraethylethylenediammonium bis(diethylmalonato) dioxouranate(VI) dihydrate

$(C_{10}H_{26}N_2)[UO_2(C_7H_{10}O_4)_2(H_2O)]\cdot 2H_2O$ (**10**), yield 85%. *Anal*. Found: C, 35.59; H, 6.10; N, 3.35; U, 28.95. Calc. for $C_{24}H_{52}N_2O_{13}U$: C, 35.38; H, 6.43; N, 3.44; U, 29.22%. TG/DTA (°C) 106 (-6.5% *endo*, $-3H_2O = 6.6\%$), 209 (-47.2% *exo*, $-$cation-ligand $= 47.4\%$), 402 (35.8% *exo*, $UO_3 = 35.4\%$). IR (KBr disk) ν (cm^{-1}): 3461 s (br), 1619 s, 1585 w, 1543 m, 1456 m, 1411 m, 1289 w, 1230 w, 906 vs, 818 s, 703 m, 582 m.

2.3.12. Synthesis of N,N,N′,N′-tetraethylethylenediammonium pentakis(diethylmalonato) tris[dioxouranate(VI)] dihydrate

$(C_{10}H_{26}N_2)_2[(UO_2)_3(C_7H_{10}O_4)_5]\cdot 2H_2O$ (**11**), yield 75% at 30 °C. *Anal*. Found: C, 33.55; H, 5.47; N, 2.51; U, 35.76. Calc. for $C_{55}H_{106}N_4O_{28}U_3$: C, 33.27; H, 5.34; N, 2.82; U, 35.99%. TG/DTA (°C) 106 (-1.6% *endo*, $-2H_2O = 1.8\%$), 197 (-28.0% *exo*, -2 cations-ligand $= 27.3\%$), 402 (43.8% *exo*, $UO_3 = 43.2\%$). IR (KBr disk) ν (cm^{-1}): 3457 vs (br), 2972 m, 2363 w, 1626 s, 1598 w, 1548 m, 1507 w, 1463 m, 1383 s, 1319 m, 1296 m, 1180 w, 931 s, 919 m, 819 m, 710 m, 593 w.

2.3.13. Synthesis of N,N,N′,N′-tetramethylethylenediammonium bis(phenylmalonato) dioxouranate(VI)

$(C_6H_{18}N_2)[UO_2(C_9H_6O_4)_2]$ (**12**), yield 90%. *Anal*. Found: C, 38.60; H, 4.02; N, 3.57; U, 32.17. Calc. for $C_{24}H_{30}N_2O_{10}U$: C, 38.70; H, 4.06; N, 3.75; U, 31.97%. TG/DTA (°C) 134 (-21.2% *endo*, -2 phenyl $= 21.0\%$), 251 (-50.2% *exo*, $-$cation-ligand $= 50.0\%$), 487 (38.3% exo, $UO_3 = 38.4\%$). IR (KBr disk) ν (cm^{-1}): 3466 s (br), 1598 s, 1569 w, 1550 s, 1406 s, 1381 m, 1333 w, 1264 m, 909 vs, 794 m, 735 s, 697 m.

2.3.14. Synthesis of N,N′-dimethylpiperazinium bis(phenylmalonato) dioxouranate(VI) monohydrate

$(C_6H_{16}N_2)[UO_2(C_9H_6O_4)_2]\cdot H_2O$ (**13**), yield 85%. *Anal*. Found: C, 37.94; H, 3.69; N, 3.46; U, 31.44. Calc. for $C_{24}H_{30}N_2O_{11}U$: C, 37.90; H, 3.98; N, 3.68; U, 31.30%. TG/DTA (°C) 142 (-22.7% *endo*, $-H_2O$, -2 phenyl $= 22.6\%$), 270 (-51.4% *exo*, $-$cation-ligand $= 51.3\%$), 457 (37.0% *exo*, $UO_3 = 37.6\%$). IR (KBr disk) ν (cm^{-1}): 3455 vs (br), 1657 s, 1567 vs (br), 1455 w, 1382 s, 1323 w, 1286 w, 1133 w, 1072 w, 1006 w, 907 vs, 730 vs, 548 w.

2.3.15. Synthesis of ethylenediammonium bis(phenylmalonato) aqua dioxouranate(VI) dihydrate

$(C_2H_{10}N_2)[UO_2(C_9H_6O_4)_2(H_2O)]\cdot 2H_2O$ (**14**), yield 84%. *Anal*. Found: C, 33.83; H, 3.69; N, 3.66; U, 33.56. Calc. for $C_{20}H_{28}N_2O_{13}U$: C, 34.01; H, 3.96; N, 3.96; U, 33.69%. TG/DTA (°C) 70 (-5.0% *endo*, $-3H_2O = -5.0\%$), 156 (-15.3% *endo*, -2 phenyl = 15.6%), 258 (-35.1% *exo*, $-$cation-ligand = 34.8%), 484 (40.0% *exo*, $UO_3 = 39.5\%$). IR (KBr disk) ν (cm^{-1}): 3414 s (br), 1613 s (br), 1562 s (br), 1377 m, 1268 m, 922 vs, 801 m, 730 s, 693 m.

2.3.16. Synthesis of bis[hexaaminecobalt(III)] pentakis(phenylmalonato) bis[dioxouranate(VI)] decahydrate

$[Co(NH_3)_6]_2[(UO_2)_2(C_9H_6O_4)_5(H_2O)]\cdot 10H_2O$ (**15**): a solution of uranyl nitrate hexahydrate (1.00 g, 2 mmol in 15 cm^3 H_2O) was added to a solution of phenylmalonic acid and fresh NaOH solution (0.72 g, 4 mmol and 0.32 g, 8 mmol in 40 cm^3 H_2O). A solution of hexaaminecobalt(III) chloride (0.54 g, 2 mmol) in 5 cm^3 H_2O was added to the above solution. An orange precipitate formed immediately and an orange crystalline product formed under the precipitate after a few days. The crystalline product was collected manually and dried in air, yield 25%. *Anal*. Found: C, 27.79; H, 4.28; N, 8.40; Co, 5.97; U, 24.42. Calc. for $C_{45}H_{86}N_{12}O_{34}Co_2U_2$: C, 27.96; H, 4.48; N, 8.69; Co, 6.10; U, 24.63%. TG/DTA (°C) 101 (-10.0% *endo*, $-10H_2O = 9.3\%$), 170 (-30.0% *exo*, -5 phenyl = 29.2%), 260 (*exo*), 371 (*exo*), 500 (38.5% *exo*, $Co_2O_3 + UO_3 = 39.2\%$). IR (KBr disk) ν (cm^{-1}: 3434 s (br), 3260 s (br), 1610 vs, 1597 vs, 1385 s, 1327 m, 1265 w, 907 m, 730 m, 696 w.

2.3.17. Synthesis of hexaaminecobalt(III) tris(phenylmalonato) bis[dioxouranate(VI)] phenylmalonic acid undecahydrate

$[Co(NH_3)_6][(UO_2)_2(C_9H_6O_4)_3](C_9H_7O_4)\cdot 11H_2O$ (**15a**): a solution of uranyl nitrate hexahydrate (0.50 g, 1 mmol in 10 cm^3 H_2O) was added to a solution of phenylmalonic acid and hexaaminecobalt(III) chloride (0.54 g, 3 mmol and 0.28 g, 1 mmol in 40 cm^3 H_2O). The solution was then neutralised by the addition of fresh NaOH solution (0.20 g, 5 mmol in 5 cm^3 H_2O). An orange cubic crystalline product formed after 2 weeks and was collected by filtration and dried in air, yield 40%. *Anal*. Found: C, 27.10; H, 3.92; N, 4.99; Co, 3.80; U, 29.71. Calc. for $C_{36}H_{65}N_6O_{31}CoU_2$: C, 26.81; H, 4.06; N, 5.21; Co, 3.65; U, 29.52%. TG/DTA (°C) 105 (-12.2% *endo*, $-11H_2O = 12.3\%$), 179 (-31.0% *exo*, -4 phenyl = 31.4%), 272 (*exo*), 390 (*exo*), 451 (41.8% *exo*, $Co_2O_3 + UO_3 = 40.6\%$). IR (KBr disk) ν (cm^{-1}): 3444 vs (br), 1590 vs (br), 1401 vs, 1347 m, 1268 w, 922 vs, 733 s, 691 m.

2.3.18. Synthesis of tetrakis[hexaaminecobalt(III)] decakis(phenylmalonato) bis(hydroxy) pentakis[dioxouranate(VI)] octatriacontahydrate

$[Co(NH_3)_6]_4[(UO_2)_5(C_9H_6O_4)_{10}(OH)_2]\cdot 38H_2O$ (**15b**): a solution of uranyl nitrate hexahydrate (1.00 g, 2 mmol in 15 cm^3 H_2O) was added to a solution of phenylmalonic acid and hexaaminecobalt(III) chloride (0.72 g, 4 mmol and 0.54 g, 2 mmol in 50 cm^3 H_2O). The above solution was then neutralised by the addition of fresh NaOH solution (0.32 g, 8 mmol in 5 cm^3 H_2O). An orange crystalline product formed after an hour and was collected by filtration and dried in air, yield 75%. *Anal*. Found: C, 24.10; H, 4.56; N, 7.25; Co, 5.29; U, 26.28. Calc. for $C_{90}H_{212}N_{24}O_{90}Co_4U_5$: C, 24.04; H, 4.75; N, 7.47; Co, 5.24; U, 26.47%. TG/DTA (°C) 78 (-15.8% *endo*, $-38H_2O$, $-2OH = 16.0\%$), 173 (*endo*), 266 (*exo*), 361 (*exo*), 504 (39.4% *exo*, $Co_2O_3 + UO_3 = 39.2\%$). IR (KBr disk) ν (cm^{-1}): 3443 s (br), 1594 s (br), 1384 s, 1330 w, 1266 w, 913 s, 732 m, 693 w.

2.3.19. Synthesis of piperazinium bis(phenylmalonato) dioxouranate(VI) monohydrate

$(C_4H_{12}N_2)[UO_2(C_9H_6O_4)_2]\cdot H_2O$ (**16**), yield 90%. *Anal*. Found: C, 36.29; H, 3.55; N, 3.85; U, 32.25. Calc. for $C_{22}H_{26}N_2O_{11}U$: C, 36.07; H, 3.58; N, 3.82; U, 32.50%. TG/DTA (°C) 52 (-2.7% *endo*, $-1H_2O = 2.5\%$), 158 (-23.5% *endo*, -2 phenyl = 23.5%), 263 (-48.5% *exo*, $-$cation-ligand = 61.1%), 455 (40.4% *exo*, $UO_3 = 39.0\%$). IR (KBr disk) ν (cm^{-1}): 3445 s (br), 1621 vs, 1566 vs, 1452 w, 1402 m, 1385 s, 1250 w, 1085 w, 914 vs, 734 w, 707 m, 587 w.

2.3.20. Synthesis of triethylenediammonium bis(phenylmalonato) uranyl monohydrate

$(C_6H_{14}N_2)[UO_2(C_9H_6O_4)_2]\cdot H_2O$ (**17**), yield 90%. *Anal*. Found: C, 38.10; H, 3.79; N, 3.79; U, 31.29. Calc. for $C_{24}H_{28}N_2O_{11}U$: C, 38.00; H, 3.72; N, 3.69; U, 31.38%. TG/DTA (°C) 100 (-2.5% *endo*, $-1H_2O = 2.4\%$), 142 (-13.0% *endo*, $-$phenyl = 12.6%), 298 (-50.8% *exo*, $-$cation-ligand = 51.0%), 451 (38.0% *exo*, $UO_3 = 37.7\%$). IR (KBr disk) ν (cm^{-1}): 3476 m, 3414 s, 1637 s, 1617 s, 1557 m, 1418 w, 1386 w, 1320 w, 911 s, 731 m, 705 w, 618 m.

2.3.21. Synthesis of N,N,N′,N′-tetramethylbutane-diammonium bis(phenylmalonato) dioxouranate(VI)

$(C_8H_{26}N_2)[UO_2(C_9H_6O_4)_2]$ (**18**), yield 75%. *Anal*. Found: C, 39.80; H, 5.03; N, 3.83; U, 30.37. Calc. for $C_{26}H_{38}N_2O_{10}U$: C, 40.22; H, 4.89; N, 3.60; U, 30.65%. TG/DTA (°C) 119 (-19.6% *endo*, -2 phenyl = 19.4%), 282 (-51.2% *exo*, $-$cation-ligand = 51.0%), 458 (36.3% *exo*, $UO_3 = 36.0\%$). IR (KBr disk) ν (cm^{-1}): 3435 s (br), 1619 s, 1595 m, 1470 w, 1386 s, 1324 w, 1238 w, 903 vs, 743 m, 686 w.

2.3.22. Synthesis of bis[N,N′-dimethylethylenediammonium] tetrakis(phenylmalonato) bis[dioxouranate(VI)] trihydrate

$(C_4H_{14}N_2)_2[(UO_2)_2(C_9H_6O_4)_4]\cdot 3H_2O$ (**19**), yield 85%. *Anal.* Found: C, 35.66; H, 3.76; N, 3.75; U, 32.24. Calc. for $C_{44}H_{58}N_4O_{23}U_2$: C, 35.98; H, 3.98; N, 3.81; U, 32.41%. TG/DTA (°C) 71 (-3.6% *endo*, $-1.5H_2O = 3.7\%$), 169 (-24.2% *endo*, -2 phenyl $= 24.0\%$), 280 (*exo*), 522 (39.0% *exo*, $UO_3 = 38.0\%$). IR (KBr disk) ν (cm^{-1}): 3424 m (br), 1579 s (br), 1534 m, 1396 m, 1335 w, 1270 w, 913 vs, 736 m, 696 w, 625 w.

2.3.23. Synthesis of bis[hexaaminecobalt(III) methylmalonato dimethylmalonato dioxouranate(VI)] di-chloride hexahydrate

$\{[Co(NH_3)_6][UO_2(C_4H_4O_4)(C_5H_6O_4)]\}_2Cl_2\cdot 6H_2O$ (**20**): a solution of uranyl nitrate hexahydrate (0.50 g, 1 mmol in 5 cm^3 H_2O) was added to an aqueous solution of methylmalonic acid and dimethylmalonic acid (0.12 g, 1 mmol; 0.13 g, 1 mmol, respectively, in 25 cm^3 H_2O), fresh NaOH solution (0.16 g, 4 mmol in 10 cm^3 H_2O) and hexaaminecobalt(III) chloride (0.13 g, 0.5 mmol in 5 cm^3 H_2O) in the molar ratio of 4:8:1. An orange, crystalline product formed after a few days and was collected by filtration and dried in air, yield 60%. *Anal.* Found: C, 15.07; H, 4.42; N, 11.58; Co, 7.86; U, 32.02. Calc. for $C_{18}H_{74}N_{12}O_{26}Co_2Cl_2U_2$: C, 14.78; H, 4.68; N, 11.49; Co, 8.06; U, 32.25%. TG/DTA (°C) 93 (-7.1% *endo*, $-6H_2O = 7.0\%$), 221 (*endo*), 304 (*exo*), 320 (*exo*), 425 (*exo*) 500 (52.6% *exo*, $Co_2O_3 + U_3O_8 = 53.0\%$). IR (KBr disk) ν (cm^{-1}): 3438 vs (br), 3265 s (br), 1620 vs (br), 1561 m, 1473 w, 1409 m, 1384 s, 1354 w, 1326 m, 1196 m, 903 s, 817 w, 707 w.

2.4. Crystallography

The crystallographic data for compounds **5**, **7**, **9**, **10**, **11** and **20** are summarised in Table 1. The intensities were measured on a Rigaku AFC5R diffractometer with graphite monochromated Mo Kα radiation ($\lambda = 0.71073$ Å) in ω–2θ mode at 23 °C for **5** and **9**, Cu Kα radiation ($\lambda = 1.54178$ Å) in ω–2θ mode at 23 °C for

Table 1
Crystallographic data for **5**, **7**, **9**, **10**, **11** and **20**

	5	**7**	**9**	**10**	**11**	**20**
Formula	$C_{12}H_{23}N_2O_{12.5}U$	$C_{12}H_{28}N_2O_{13}U$	$C_{18}H_{36}N_2O_{12}U$	$C_{24}H_{46}N_2O_{12}U$	$C_{55}H_{106}N_4O_{28}U_3$	$C_9H_{28}N_6O_{13}ClCoU$
M_r	633.35	646.39	710.52	792.66	1985.53	760.78
Colour, habit	yellow needle	yellow needle	yellow needle	yellow plate	yellow needle	orange plate
Crystal system	triclinic	orthorhombic	monoclinic	monoclinic	monoclinic	triclinic
Space group	$P\bar{1}$ (no. 2)	*Pbcn* (no. 60)	$C2/c$ (no. 15)	$P2_1/n$ (no. 14)	$P2_1/c$ (no. 14)	$P\bar{1}$ (no. 2)
Unit cell dimensions						
a (Å)	12.761(3)	11.625(2)	27.180(7)	9.966(2)	22.325(5)	9.310(2)
b (Å)	17.000(4)	16.723(2)	13.512(8)	15.873(3)	12.309(3)	10.294(2)
c (Å)	9.285(3)	10.660(2)	16.631(4)	19.955(4)	27.316(6)	15.279(3)
α (°)	94.03(2)	90	90	90	90	107.95(3)
β (°)	100.98(2)	90	123.95(2)	92.76(3)	99.21(3)	92.70(3)
γ (°)	84.32(2)	90	90	90	90	110.84(3)
U (Å^3)	1964.9(9)	2072.1(5)	5066(3)	3153.0(11)	7410(3)	1281.5(5)
Z	4	4	8	4	4	2
D_{calc} (g cm^{-3})	2.141	2.072	1.863	1.670	1.780	1.972
F(000)	1204.00	1240.00	2768.00	1568.00	3856.00	728.00
Crystal size (mm)	$0.20\times0.15\times0.30$	$0.10\times0.1\times0.10$	$0.1\times0.1\times0.28$	$0.2\times0.1\times0.08$	$0.1\times0.0\times0.06$	$0.2\times0.1\times0.08$
Transmission factors	0.49–1.00	0.83–1.00	0.79–1.00	0.67–1.00	0.84–1.00	0.68–1.00
Cell determination (2θ range) (°)	15 (15.5–17.1)	25 (41.5–58.9)	22 (15.0–20.6)	18 (14.7–21.4)	17 (16.3–18.9)	23 (15.1–17.6)
μ (cm^{-1})	83.3	226.6	64.7	52.1	66.2	71.2
No. reflections collected	7282	2167	4778	16474	23350	6286
Unique reflections	6940 ($R_{int} = 0.037$)	2167	4671 ($R_{int} = 0.093$)	5058 ($R_{int} = 0.040$)	12029 ($R_{int} = 0.021$)	3958 ($R_{int} = 0.054$)
No. variables	496	129	298	353	811	284
No. observations	4600 [$I>3\sigma(I)$]	1209 [$I>3\sigma(I)$]	3074 [$I>3\sigma(I)$]	4226 [$I>2\sigma(I)$]	9885 [$I>2\sigma(I)$]	3652 [$I>2\sigma(I)$]
R [a]	0.036	0.041	0.041	0.022 (R_1)	0.030 (R_1)	0.041 (R_1)
R_w	0.028	0.041	0.028	0.057 (wR_2)	0.081 (wR_2)	0.116 (wR_2)
Goodness-of-fit	1.63	2.54	1.41	1.04	1.26	1.08
Largest difference peak and hole (e A^{-3})	0.99 and -1.29	1.67 and -3.16	1.24 and -0.96	0.68 and -0.78	1.00 and -1.16	4.13 and -1.34

[a] $R = \Sigma||F_o|-|F_c||/\Sigma|F_o|$; $R_w = (\Sigma\, w(|F_o|-|F_c|)^2/\Sigma\, wF_o^2)$; $R_1 = \Sigma||F_o|-|F_c||/\Sigma|F_o|$; $wR_2 = [\Sigma\, w(F_o^2-F_c^2)|^2/\Sigma\, w(F_o^2)^2]$.

Table 2
Selected bond lengths (Å) and bond angles (°) for **5**

Bond lengths			
U(1)–O(1)	2.338(6)	U(2)–O(12)	2.323(7)
U(1)–O(8)	2.346(7)	U(2)–O(19)	2.338(7)
U(1)–O(11)	2.430(7)	U(2)–O(22)	2.440(7)
U(2)–O(16)	2.313(8)	U(1)–O(5)	2.329(7)
U(2)–O(21)	1.739(7)	U(1)–O(10)	1.760(6)
U(1)–O(4)	2.314(7)	U(2)–O(15)	2.349(7)
U(1)–O(9)	1.758(6)	U(2)–O(20)	1.731(7)
Bond angles			
O(1)–U(1)–O(4)	70.3(2)	O(15)–U(2)–O(16)	72.7(2)
O(5)–U(1)–O(8)	70.0(2)	O(12)–U(2)–O(15)	71.2(2)
O(12)–U(2)–O(22)	72.7(2)	O(4)–U(1)–O(5)	75.9(2)
O(19)–U(2)–O(22)	72.6(2)	O(9)–U(1)–O(10)	176.9(3)
O(1)–U(1)–O(11)	73.2(2)	O(16)–U(2)–O(19)	70.7(2)
O(8)–U(1)–O(11)	71.5(2)	O(20)–U(2)–O(21)	177.5(4)

Table 3
Selected bond lengths (Å) and bond angles (°) for **7**

Bond lengths			
U(1)–O(1)	2.386(10)	U(1)–O(5)	1.778(8)
U(1)–O(6)	2.39(1)	U(1)–O(4)	2.381(8)
Bond angles			
O(1)–U(1)–O(4)	70.7(3)	O(1)–U(1)–O(6)	72.4(2)
O(5)–U(1)–O(5)	177.2(6)	O(4)–U(1)–O(4)	73.8(4)

Table 4
Selected bond lengths (Å) and bond angles (°) for **9**

Bond lengths			
U(1)–O(1)	2.311(7)	U(1)–O(9)	1.760(6)
U(1)–O(8)	2.315(6)	U(1)–O(5)	2.346(6)
U(1)–O(11)	2.507(5)	U(1)–O(10)	1.743(7)
U(1)–O(4)	2.365(6)		
Bond angles			
O(1)–U(1)–O(4)	69.2(2)	O(8)–U(1)–O(11)	74.4(2)
O(5)–U(1)–O(8)	69.7(2)	O(4)–U(1)–O(5)	79.1(2)
O(1)–U(1)–O(11)	67.7(2)	O(9)–U(1)–O(10)	179.1(3)

Table 5
Selected bond lengths (Å) and bond angles (°) for **10**

Bond lengths			
U(1)–O(11)	1.777(3)	U(1)–O(2)	2.353(3)
U(1)–O(1)	2.350(3)	U(1)–O(5)	2.275(3)
U(1)–O(9)	2.485(3)	U(1)–O(6)	2.396(3)
U(1)–O(10)	1.793(3)		
Bond angles			
O(11)–U(1)–O(10)	176.90(14)	O(5)–U(1)–O(1)	76.54(10)
O(1)–U(1)–O(2)	69.00(9)	O(5)–U(1)–O(6)	68.91(10)
O(2)–U(1)–O(9)	74.44(10)	O(6)–U(1)–O(9)	71.19(10)

7. The cell parameters were refined by least-squares from the angular positions of 15 (for **5**), 22 (for **9**) and 25 (for **7**) carefully centred reflections, respectively. An empirical absorption correction was applied, based on azimuthal scans of three reflections. The data were corrected for Lorentz and polarisation effects. Linear decay correction factors were applied for **5**. The structure for **7** was solved with SIR-92 [7], **9** with ORIENT [8] by direct methods and **5** with PATTY [9]. Non-hydrogen atoms were refined anisotropically. Hydrogen atoms were added in calculated or difference map positions. Neutral atom scattering factors were taken from Cromer and Waber [10]. Anomalous dispersion effects were included in F_{calc} [11]; the values for $\Delta f'$ and $\Delta f''$ were those of Creagh and McAuley [12]. The values for the mass attenuation coefficients were those of Creagh and Hubbell [13]. All calculations were performed using the TEXSAN [14] crystallographic software package (Molecular Structure Corporation). The diffraction data for **10**, **11** and **20** were measured on a Rigaku Raxis IIc diffractometer with graphite monochromated Mo Kα radiation ($\lambda = 0.71073$ Å) at 20 °C. The structures were solved by conventional direct methods for **10** and **20**, and Patterson methods for **11** and were refined by the full-matrix least-squares method on all F^2 data with the SHELXTL 5.03 package [15]. Non-hydrogen atoms were refined anisotropically. Hydrogen atoms were fixed in calculated positions.

3. Results and discussion

3.1. Crystal structures

3.1.1. Crystal structures for compounds *5*, *7*, *9* and *10*

Compounds **5**, **7**, **9** and **10** have similar monomeric structures. Their selected bond lengths and angles are listed in Tables 2–5. The asymmetric unit of **5** contains two pairs of ions and three H_2O molecules. Both anions are monomeric structures with two terminal 1,5-bidentate methylmalonates and the seventh coordination positions of U atoms being occupied by H_2O molecules. The anion structures for **5** are shown in Fig. 1. Both uranyl groups are nearly linear with ordinary U–O distances. The U–O distances in the equatorial plane for U(1) are separated into two groups with average 2.331(7) Å for O(1), O(4), O(5) and O(8), and 2.430(7) Å for the water molecule O(11); similarly for U(2) with average 2.331(8) Å for O(12), O(15), O(16) and O(19), and 2.440(7) Å for the water molecule O(22). The presence of short O–O [2.667(10) Å] and O–N [2.659(12)–3.121(12) Å] contacts suggests that H_2O molecules, carboxylate oxygen atoms and cations are involved in extensive H-bonding and that cation–anion interactions are via H-bonding.

The anion structure for **7** is shown in Fig. 2. The asymmetric unit consists of half the molecule, related to the other half by twofold symmetry. The uranyl group is quite normal with O–U–O angle 177.2(6)° and U–O distance 1.778(8) Å. The U–O distances in the equato-

rial plane are 2.381(8) Å for O(4), 2.386(10) Å for O(1) and 2.39(1) Å for O(6). The water molecules and carboxylate oxygen atoms, O(1), O(2) and O(3) are involved in extensive H-bonding and lead the monomeric structures into a three-dimensional framework. The short contacts, 2.942 Å for a N atom to O(2) and 2.745 Å for it to O(3) indicate that the cation–anion interactions are via H-bonding.

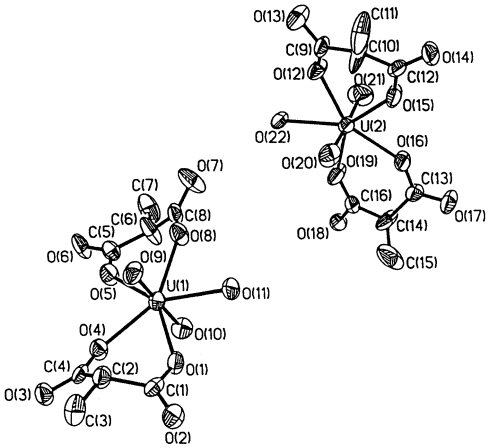


Fig. 1. An ORTEP drawing of the anionic structures for $(C_4H_{12}N_2)$-$[UO_2(C_4H_4O_4)_2(H_2O)]\cdot 1.5H_2O$ (**5**) (50% probability ellipsoids).

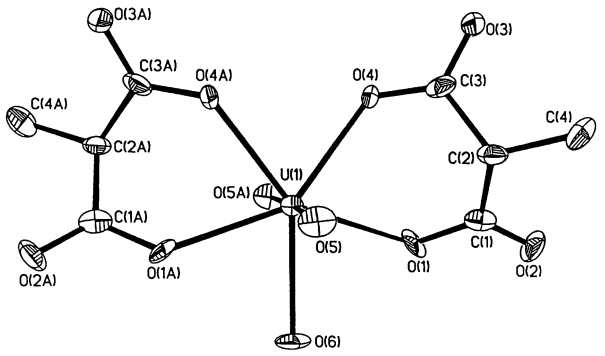


Fig. 2. An ORTEP drawing of the anionic structure for $(C_4H_{14}N_2)$-$[UO_2(C_4H_4O_4)_2(H_2O)]\cdot 2H_2O$ (**7**) (50% probability ellipsoids).

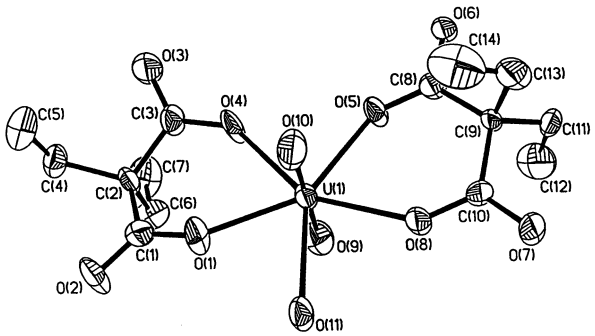


Fig. 3. An ORTEP drawing of the anionic structure for $(C_4H_{12}N_2)$-$[UO_2(C_7H_{10}O_4)_2(H_2O)]\cdot H_2O$ (**9**) (50% probability ellipsoids).

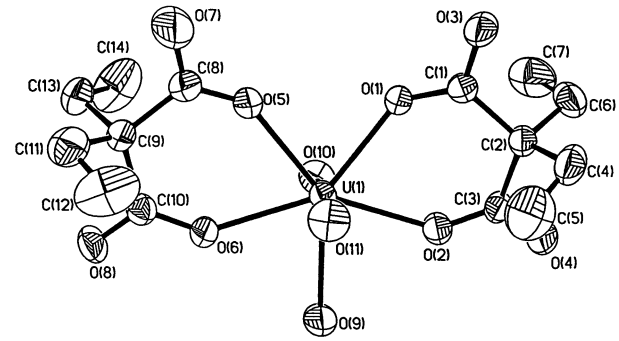


Fig. 4. An ORTEP drawing of the anionic structure for $(C_{10}H_{26}N_2)[UO_2(C_7H_{10}O_4)_2(H_2O)]\cdot 2H_2O$ (**10**) (50% probability ellipsoids).

The monomeric anion structure for **9** is shown in Fig. 3. The uranyl ion is almost linear with an average U–O distance of 1.752(7) Å. The equatorial U–O distances are separated into two groups with average 2.334(7) Å for O(1), O(4), O(5) and O(8), and 2.507(5) Å for the coordinated water molecule O(11). Several short contacts between O and O atoms [from 2.881(11)–2.895(10) Å] suggest that the carboxylate O atoms, lattice and coordinated H_2O molecules are involved in H-bonding.

The asymmetric unit for **10** contains a whole molecule. The monomeric anion structure for **10** is shown in Fig. 4. The uranyl ion is unusual, with two different U–O distances [1.776(3) and 1.792(3) Å]. The equatorial U–O distances range from 2.273(3) Å for O(5), average 2.350(3) Å for O(1) and O(2), 2.394(3) Å for O(6) and 2.485(3) Å for the coordinated H_2O molecule O(9). H-bonding between a N atom and O(3), a N atom and O(4), O(4) and O(9) links the monomeric structures into a one-dimensional chain along the crystallographic *b* axis.

*3.1.2. Crystal structure for compound **11***

Selected bond lengths and angles for **11** are listed in Table 6. The anionic structure for **11** is shown in Fig. 5. The anion part of the asymmetric unit has five ligands and three uranyl groups. U(2) and U(3) are linked together by two bridging ligands which are both 1,3-bidentate through one carboxylate group to one U atom and one of the oxygen atoms bridges μ_2 to the other U atom. Another carboxylate group is monodentate to the other U atom as well, forming a structural unit with two uranyl groups and two ligands. Both U atoms have a hexagonal bipyramidal environment. U(1) has a pentagonal bipyramidal environment with a terminal 1,5-bidentate ligand. U(1) and the structural unit containing U(2) and U(3) are linked together by two kinds of linear ligands, tetradentate (1,3-bidentate through both carboxylate groups) and tridentate {1,3-bidentate to the structural unit [U(2), U(3)] and 1-monodentate through the other carboxylate group to

U(1)}, forming an infinite zigzag chain. The three uranyl groups are quite normal with average U–O distances 1.756(6) Å for U(1), 1.751(6) Å for U(2), 1.746(5) Å for U(3) and O–U–O angles 178.2(2)° for U(1), 177.9(3)° for U(2) and 178.5(2)° for U(3). The equatorial U–O distances range from 2.308(5) Å to 2.447(5) Å for U(1), 2.284(5) Å to 2.590(4) Å for U(2) and 2.338(5) Å to 2.510(5) Å for U(3) and the O–U–O angles in the equatorial planes range from 52.3(2)° (1,3-bidentate) to 82.3(2)° for U(1), 49.70(14)° (1,3-bidentate) to 71.3(2)° for U(2) and 49.7(2)° (1,3-bidentate) to 70.8(2)° for U(3). The deviations of donor atoms from the equatorial planes are quite different, between −0.30 Å [O(7)] and 0.33 Å [O(4)] for U(1), and from −0.10 Å [O(14)] to 0.08 Å [O(13)] for U(2) and within ±0.08 Å for U(3). The terminal 1,5-bidentate ligand on U(1) is so puckered that no typical conformation can be assigned to it and the two tridentate bridging ligands are fairly planar. There are extensive H-bonding interactions between N atoms and non-bonded carboxylate oxygen atoms [2.654(8)–2.723(8) Å] within the infinite one-dimensional chains.

Table 6
Selected bond lengths (Å) and bond angles (°) for **11**

Bond lengths			
U(1)–O(1)	1.748(5)	U(1)–O(11)	2.308(5)
U(1)–O(3)	2.325(4)	U(1)–O(7)	2.473(4)
U(2)–O(15)	1.767(6)	U(2)–O(13)	2.466(5)
U(2)–O(14)	2.473(4)	U(2)–O(21)	2.590(4)
U(3)–O(26)	1.763(5)	U(3)–O(21)	2.440(4)
U(3)–O(10)	2.498(4)	U(3)–O(18)	2.505(4)
U(1)–O(2)	1.763(6)	U(1)–O(4)	2.334(4)
U(1)–O(8)	2.447(5)	U(2)–O(16)	1.735(6)
U(2)–O(17)	2.284(5)	U(2)–O(18)	2.481(4)
U(2)–O(23)	2.537(5)	U(3)–O(25)	1.729(5)
U(3)–O(22)	2.338(5)	U(3)–O(9)	2.469(4)
U(3)–O(20)	2.510(5)		
Bond angles			
O(1)–U(1)–O(2)	178.2(2)	O(13)–U(2)–O(23)	63.6(2)
O(11)–U(1)–O(8)	79.7(2)	O(25)–U(3)–O(26)	178.5(2)
O(16)–U(2)–O(15)	177.9(3)	O(9)–U(3)–O(10)	51.6(2)
O(13)–U(2)–O(14)	52.1(2)	O(20)–U(3)–O(18)	49.7(2)
O(23)–U(2)–O(21)	49.7(2)	O(4)–U(1)–O(3)	71.4(2)
O(22)–U(3)–O(10)	70.8(2)	O(8)–U(1)–O(7)	52.3(2)
O(21)–U(3)–O(18)	58.5(2)	O(17)–U(2)–O(14)	71.3(2)
O(11)–U(1)–O(4)	82.3(2)	O(18)–U(2)–O(21)	56.87(14)
O(3)–U(1)–O(7)	74.3(2)	O(22)–U(3)–O(21)	66.7(2)
O(17)–U(2)–O(18)	66.7(2)	O(9)–U(3)–O(20)	63.0(2)

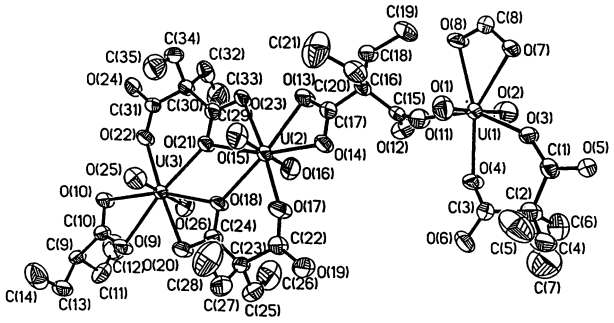


Fig. 5. The anionic part of the asymmetric unit for $(C_{10}H_{26}N_2)[(UO_2)_3(C_7H_{10}O_4)_5]\cdot 2H_2O$ (**11**) (50% probability ellipsoids).

Table 7
Selected bond lengths (Å) and bond angles (°) for **20**

Bond lengths			
U(1)–O(2)	1.778(6)	U(1)–O(7)	2.371(6)
U(1)–O(3)	2.343(6)	U(1)–O(4)	2.312(6)
U(1)–O(8)	2.431(6)	U(1)–O(10)	2.412(6)
U(1)–O(1)	1.786(6)		
Bond angles			
O(2)–U(1)–O(1)	176.5(3)	O(7)–U(1)–O(8)	68.1(2)
O(4)–U(1)–O(10)	74.5(2)	O(3)–U(1)–O(7)	73.3(2)
O(4)–U(1)–O(3)	70.5(2)	O(10)–U(1)–O(8)	73.7(2)

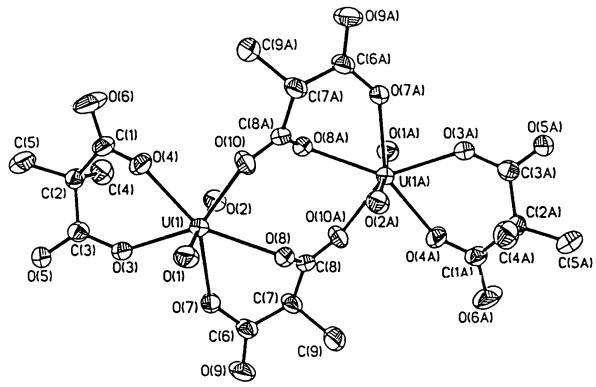


Fig. 6. An ORTEP drawing of the anionic structure for $\{[Co(NH_3)_6][UO_2(C_4H_4O_4)(C_5H_6O_4)]\}_2Cl_2\cdot 6H_2O$ (**20**) (50% probability ellipsoids).

3.1.3. Crystal structure for compound *20*

Selected bond lengths and angles for **20** are listed in Table 7. The asymmetric unit for **20** consists of half of the U complex anion, together with two half $[Co(NH_3)_6]^{3+}$ ions, with each of the Co atoms on a centre of symmetry. In each case, the other halves are generated by inversion. In addition, the asymmetric unit contains a Cl^- ion and three water molecules. The anionic structure is shown in Fig. 6. The dimethylmalonate ligand is terminal whilst the methylmalonate ligand links to the adjacent uranium atom through a third oxygen atom of one carboxylate group to give a dimeric, centrosymmetric structure for the anion. The uranyl unit is quite normal with U–O distances averaging 1.782(6) Å and an axial O–U–O angle 176.5(3)°. The equatorial U–O distances range from 2.312(6) Å for O(4) to 2.431(6) Å for O(8). Short intermolecular contacts indicate H-bonding interactions among the water molecules, the carboxylate oxygen atoms, chlorine atoms and the ammonia ligands in the countercation which links the dimeric structures into a

three-dimensional framework. Each hexaaminecobalt(III) ion has two symmetry-related Cl^- ions on each side. The Cl^- ions are involved in H-bonding and also play a charge balancing role. The extensive short O–N contacts [2.872(12)–3.232(10) Å] suggest that the cation–anion interactions are via H-bonding.

Crystals were obtained for **15** and were shown to be monoclinic, $C2/c$, $a = 36.608(7)$, $b = 13.602(3)$, $c = 30.649(6)$ Å, $\alpha = 105.51(3)°$, $Z = 8$, $V = 14706(6)$ A^3, $F(000) = 7536$, but only a low resolution refinement ($R_1 = 0.060$, $wR_2 = 0.186$) could be obtained. However, a monomeric structure containing two adjacent $\{UO_2\}$ centres was apparent. Both centres had pentagonal bipyramidal geometry with two chelating 1,5-bidentate malonate ligands. The coordination of one U was completed with a H_2O molecule and the second U by a single oxygen atom of a phenyl malonate, the other carboxylic group taking part in H-bonding interactions with other complexes in the lattice. This is consistent with the structure proposed below on the basis of spectroscopic and analytical data.

3.1.4. U–O bond lengths

The average U–O_{ax} and U–O_{eq} distances of pentagonal (P) and hexagonal (H) bipyramidal uranium centres for the uranyl compounds which have been crystallographically characterised in the present work and others in this series[1–6] are shown in Fig. 7. This scatter diagram gives two well defined and well separated footprints with U–O_{eq} distances ranging from 2.34 to 2.38 Å for P and 2.45 to 2.49 Å for H. For C.N. 8 (H), U–O_{ax} remains fairly constant as U–O_{eq} varies, in contrast to C·N. 7 (P) where the correlation of the equatorial and axial U–O distances is not obvious. The two 'bottom left hand' points which separate from the rest of the C·N. 7 data correspond to the unusually short U–O_{ax} distances in **5** and $Ba[UO_2(C_3H_2O_4)_2]\cdot 3H_2O$. Compared to the average U–O distances for the uranyl malonato compounds discussed here, the average U–O distances for uranyl carboxylato compounds [16], especially those for uranyl dicarboxylato compounds [17] are less well correlated. This would be expected since these data are from a variety of sources (different ligands and different types of complexes) and of variable quality.

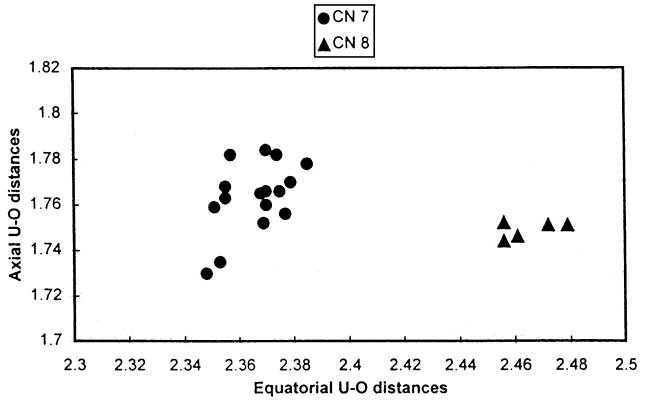


Fig. 7. Average U–O distances for uranyl malonato and substituted malonato compounds.

3.2. Structural comparisons

A variety of structural types [monomeric, dimeric for 1:2 (M:L) ratio compounds; infinite chains for 2:3, 3:4 and 3:5 (M:L) ratio compounds] for uranyl malonato and substituted malonato compounds has been identified by X-ray crystallography and these will be discussed by structural types.

3.2.1. Dimeric structure

The dimeric compounds $\{(C_6H_{18}N_2)[UO_2(C_3H_2O_4)_2]\}_2\cdot(CH_3OH)_2$, $\{(C_4H_{12}N_2)[UO_2(C_3H_2O_4)_2]\}_2\cdot 6H_2O$ and $\{[Co(NH_3)_6][UO_2(C_5H_6O_4)_2]\}_2Cl_2\cdot 7H_2O$ have centrosymmetric dimeric anion structures and have been described previously [2,3]. Compound **20** is very similar to $\{[Co(NH_3)_6][UO_2(C_5H_6O_4)_2]\}_2Cl_2\cdot 7H_2O$ [2] except one of the dimethylmalonate ligands is replaced by a methylmalonate ligand. They have very similar IR and TG/DTA results. The similarities and differences between these two compounds are summarised in Table 8. From a structural point of view, these two dimeric complexes are very similar. The only obvious differences are that **20** has axial and equatorial U–O distances about 0.02 Å longer and an O(10)–U(1)–O(8)–C(8) torsion angle about 2° wider.

3.2.2. Monomeric structures

Compounds **5**, **7**, **9**, **10** and $(C_6H_{16}N_2)[UO_2(C_3H_2O_4)_2(H_2O)]\cdot 2H_2O$ [3], $(C_2H_{10}N_2)[UO_2(C_5H_6O_4)_2(H_2O)]\cdot 2H_2O$ [1] and $(C_7H_{20}N_2)[UO_2(C_5H_6O_4)_2\cdot(H_2O)]\cdot 2H_2O$ [1] have monomeric anion structures and their similarities and differences are summarised in Table 9. The monomeric compounds have U–O_{ax} distances between 1.747(7) and 1.782(6) Å and except for **7**, U–O(malonate) distances between 2.320(6) and 2.365(3) Å, U–O(H_2O) distances between 2.435(7) and 2.507(7) Å and O–U–O angles from 110° to 118°. Compound **7** has a relatively shorter U–O(H_2O) distance [2.39(1) A], longer U–O(malonate) distances [2.384(10) Å] and narrower C–C–C angle (108°). All the malonate ligands have boat or skew boat conformations. Compound **7** and $(C_7H_{20}N_2)[UO_2(C_5H_6O_4)_2\cdot(H_2O)]\cdot 2H_2O$ both have a C_2 axis along the U–O(H_2O) direction and a more planar equatorial coordination environment than the others.

3.2.3. Infinite chain structures

Compounds $(C_{10}H_{26}N_2)[(UO_2)_2(C_5H_6O_4)_3]$ [1], $(C_6H_{16}N_2)[(UO_2)_3(C_5H_6O_4)_4(H_2O)_2]\cdot 2(C_2H_5OH)$ [1] and

Table 8
Comparison of compound **20** with $\{[Co(NH_3)_6][UO_2(C_5H_6O_4)_2]\}_2Cl_2\cdot 7H_2O$ [2]

	20	$\{[Co(NH_3)_6][UO_2(C_5H_6O_4)_2]\}_2Cl_2\cdot 7H_2O$
Mean U–O_{ax} distances (Å)	1.782(6)	1.763(6)
Mean U–O_{eq} distances (Å)	2.374(6)	2.355(6)
O_{eq}–U–O_{eq} angles (°)	68.1–74.5(2)	67.9–74.6(2)
Mean C–O distances (Å)	1.256(11)	1.254(10)
C–C–C angles (°)	110.4(7) (T), 111.1(7) (B)	111.0(7) (T), 114.6(7) (B)
Conformations of the six-rings	boat (T), puckered (B)	Boat (T), puckered (B)
Deviations of donor atoms from the equatorial planes (Å)	$-0.662 \rightarrow 0.789$	$-0.648 \rightarrow 0.782$
O–U–O–C torsion angles (°)	−118.2	−116.0
Space group	$P\bar{1}$ (no. 2)	$P\bar{1}$ (no. 2)
Unit cell parameters [a, b, c (Å); α, β, γ (°)]	9.310(2), 10.294(2), 15.279(3); 107.95(3), 92.70(3), 110.84(3)	10.362(4), 15.207(3), 9.274(2); 92.42(2), 110.95(2), 108.16(2)
Peaks in ^{13}C CPMAS NMR carbonyl region	190.0, 184.9	188.9, 185.1, 183.4

T, terminal ligand; B, bridging ligand.

11 are sub-stoichiometric products (metal–ligand = 2:3, 3:4 and 3:5) and they all possess infinite chain structures containing a similar 2:2 structural unit (two uranyl groups linked together by two μ_2 bridging ligands, 1,3-bidentate to one uranyl group and 1,5-bidentate to the other). In the case of $(C_{10}H_{26}N_2)[(UO_2)_2(C_5H_6O_4)_3]$, the structural units are linked together by linear tetradentate ligands (1,3-bidentate through both carboxylate groups) forming the infinite chain structure. For $(C_6H_{16}N_2)[(UO_2)_3(C_5H_6O_4)_4(H_2O)_2]\cdot 2(C_2H_5OH)$, the structural unit is centrosymmetric and the two uranyl groups and the two bridging ligands are equivalent. There is a second type of uranyl group *trans*-coordinated by two H_2O molecules. The two kinds of uranyl groups are linked together by linear tetradentate ligands (1,3-bidentate through both carboxylate groups) forming the infinite chain structure. For **11**, there is a third uranyl group with 1,5-bidentate coordination by a ligand. The structural units and the third uranyl groups are linked by two kinds of linear bridging ligands, a tetradentate (1,3-bidentate through both carboxylate groups) and a tridentate (1,3-bidentate through one carboxylate group and 1-monodentate through the other) forming the zigzag infinite chain structure.

3.3. Effects of substituent groups, size of counter-cations and H-bonding

With malonic acid and mono-substituted malonic acids (methylmalonic acid and phenyl malonic acid) as ligands, only compounds with a ratio of metal–ligand of 1:2 have been isolated and monomeric and dimeric structures dominate the products. This seems to suggest that mono-substitution of the ligands has little effect on the coordination of uranyl by malonate. In those cases the structural types are mainly controlled by the size of counter-cations. With ethylenediammonium, piperazinium and triethylenediammonium as counter-cations, di-substituted malonates all give products with metal–ligand ratio of 1:2. On increasing the size of the counter-cations, for example tetramethyl- or tetraethyl-ethylenediammonium and dimethyl-piperazinium, a variety of 2:3, 3:4 and 3:5 sub-stoichiometric compounds with polymeric structures are formed. These could be solely effects of counter-cations or combined effects of counter-cations and di-substituted groups of malonate.

Many short O–N contacts clearly indicate the strong H-bonding that would be expected from protonated amines. The tendency to maximise the H-bonding between ligands and protonated amines undoubtedly have a bearing on the solid state structure, including the role of the ligands, since carboxylate oxygen atoms have been involved in the H-bonding. Thus, the size of the protonated amines may not necessarily be as significant as the H-bonding networks they can accommodate.

3.4. Bonding modes of malonate with uranyl

Two bonding modes for malonate with the uranyl ion have been previously published [5,6]. These are bidentate (terminal 1,5-bidentate) (I), and tridentate (bridging 1,5-bidentate and μ_1 3-monodentate) (II). Three new types of bonding mode have been identified in this study, tridentate (μ_2 1,3-bidentate and 1,5-bidentate) (III), tetradentate (1,3-bidentate through both carboxylate groups) (IV) and tridentate (1,3-bidentate through one carboxylate group and 1-monodentate through the other) (V). These bonding modes are summarised in Scheme 1.

3.5. Infrared spectra

IR spectroscopy has been of limited value in indicating metal–ligand bonding for this group of uranyl compounds because the ligands coordinated to uranyl have low symmetry and the multiple features of anti-

Table 9
Structural comparisons of monomeric compounds

	$(C_6H_{16}N_2)[UO_2(C_3H_2O_4)_2(H_2O)]\cdot 2H_2O$ [3]	**5**	**7**	$(C_2H_{10}N_2)[UO_2(C_5H_6O_4)_2(H_2O)]\cdot 2H_2O$ [1]	$(C_7H_{20}N_2)[UO_2(C_5H_6O_4)_2(H_2O)]\cdot 2H_2O$ [1]	**9**	**10**
U–O_{ax} (Å)	1.768(3)	1.747(7)	1.778(8)	1.770(3)	1.782(6)	1.752(7)	1.752(3)
U–O (malonate) (Å)	2.334(3)	2.332(7)	2.384(10)	2.365(3)	2.320(6)	2.334(7)	2.344(3)
U–O (H_2O) (Å)	2.438(3)	2.435(7)	2.39(1)	2.438(3)	2.503(7)	2.507(5)	2.485(3)
C–O distances(Å)	1.249(6)	1.25(1)	1.25(2)	1.253(4)	1.238(9)	1.25(1)	1.254(6)
C–C–C angles (°)	116.4, 117.2	U1: 113.4, 115.2; U2: 118, 117	108	109.9, 110.6	113.7	113.9, 116.9	115.2, 116.8
O_{eq}–U–O_{eq} angles (°)	70.5–74.9	70.0–75.9	70.7–73.8	69.75–75.15	70.0–76.4	67.7–79.1	68.91–76.54
Conformations of chelate rings and C–C torsion angles (°)	1-skew boat [55.1, −30.2; −16.7, 46.4]	boat [45, −49; −40, 41; −29, 38; −36, 36]	boat [59.1, 59.7]	boat [45.9, −55.8; −43.0, 58.1]	skew boat [31.7, −46.7]	skew boat [−24, 43; 2, −8]	1-boat [14.4, 9.7; −5.0, −20.3]
Deviations of donor atoms (Å)	−0.108 → 0.111	U1: −0.159 → 0.174; U2: ±0.02	±0.018	−0.079 → 0.117	±0.006	±0.09	±0.06

symmetric and symmetric carboxylate stretching frequencies makes it almost impossible to identify the nature of the carboxylate groups with confidence. However, the coordination number of $\{UO_2\}^{2+}$ may be determined from the value of ν_{as}(OUO).

All of the compounds in this and previous work[1–3] except $(C_6H_{18}N_2)[(UO_2)_2(C_5H_6O_4)_3]$, $(C_6H_{16}N_2)[(UO_2)_3(C_5H_6O_4)_4(H_2O)_2]\cdot 2(C_2H_5OH)$, $(C_{10}H_{26}N_2)[(UO_2)_2(C_5H_6O_4)_3]$ and **11** have very similar IR spectra, ν(OH) and/or ν(NH) at 3418–3478; ν_{as}(COO) at 1520–1654; ν_s(COO) at 1313–1478; ν_{as}(OUO) at 900–922, δ(C=O) at 695–721 and p(C=O) at 574–609 cm^{-1}. The IR spectra of those four compounds differ mainly in the presence of a shifted ν_{as}(OUO) at 930, 932, 930, 931 and 919 cm^{-1}, respectively. Crystallographic studies [1–3] confirmed that uranyl malonato compounds with pentagonal bipyramidal uranium centres $(\{(C_6H_{18}N_2)[UO_2(C_3H_2O_4)_2]\}_2\cdot(CH_3OH)_2$, $(C_6H_{16}N_2)[UO_2(C_3H_2O_4)_2(H_2O)]\cdot 2H_2O$, $\{(C_4H_{12}N_2)[UO_2(C_3H_2O_4)_2]\}_2\cdot 6H_2O$, **5**, **7**, $(C_2H_{10}N_2)[UO_2(C_5H_6O_4)_2(H_2O)]\cdot 2H_2O$, $(C_7H_{20}N_2)[UO_2(C_5H_6O_4)_2\cdot(H_2O)]\cdot 2H_2O$, **9** and **10**) have ν_{as}(OUO) at 900–920 cm^{-1} and compounds with hexagonal bipyramidal uranium centres $(C_6H_{16}N_2)[(UO_2)_3(C_5H_6O_4)_4(H_2O)_2]\cdot 2(C_2H_5OH)$ and $(C_{10}H_{26}N_2)[(UO_2)_2(C_5H_6O_4)_3]$ have ν_{as}(OUO) both at 932 and 930 cm^{-1}. This seems to suggest that for the group of compounds studied, ν_{as}(OUO) at around 930 cm^{-1} may indicate the presence of a hexagonal bipyramidal uranium centre and ν_{as}(OUO) at 900–920 cm^{-1} may indicate the presence of a pentagonal bipyramidal uranium centre. Evidently **11** has both pentagonal and hexagonal bipyramidal uranium centres and it has ν_{as}(OUO) at 931 and 919 cm^{-1}. Thus, $(C_6H_{18}N_2)[(UO_2)_2(C_5H_6O_4)_3]$ most likely has hexagonal bipyramidal uranium centres, together with 2:3 (M:L) stoichiometry suggesting an infinite chain anionic structure as has $(C_{10}H_{26}N_2)[(UO_2)_2(C_5H_6O_4)_3]$. By contrast, the

Scheme 1. Bonding modes for malonate with the uranyl ion (I–V) and associated carbonyl environments (a, a′, a″, b, c, d, e). Type I, terminal 1,5-bidentate; type II, tridentate (bridging 1,5-bidentate and μ_1 3-monodentate); type III, tridentate (μ_2-1,3-bidentate and 1,5-bidentate); type IV, tetradentate (1,3-bidentate through both carboxylate groups); and type V, tridentate (1,3-bidentate through one carboxylate group and 1-monodentate through the other).

rest of the 1:2 (M:L) non-X-ray characterised compounds probably have pentagonal bipyramidal uranium centres, suggesting monomeric or dimeric structures.

3.6. Thermal analysis

The main use of TG/DTA in this work has been to identify the nature of H_2O molecules in those compounds isolated from aqueous solution. Three main types of H_2O are present in the structurally characterised compounds in this series, viz. ligand, weakly bound in the lattice, strongly bound in the lattice. For monomeric bis(malonato) complexes, where the fifth equatorial coordination position comprises a H_2O ligand and there is a characteristic endothermic process at >100 °C. Weakly bound lattice H_2O is generally lost in an endothermic process at <90 °C. However, there is some overlap between the temperature ranges over which ligand and strongly bound H_2O is removed. Compounds $\{(C_4H_{12}N_2)[UO_2(C_3H_2O_4)_2]\}_2\cdot 6H_2O$, **5**, **5a**, $(C_4H_{12}N_2)[UO_2(C_5H_6O_4)_2]\cdot 5H_2O$, **9** and **16** all have a metal–ligand ratio of 1:2 with the same counter-cation, piperazinium. The decomposition temperatures decrease with larger substituent groups on the malonate, about 205 °C for malonate and methylmalonate, 190 °C for dimethylmalonate, 180 °C for diethylmalonate and 150 °C for phenylmalonate as ligands. Thus, there are several general features of the thermal analysis for this group of compounds: (i) the final residue for the compounds with organic counter-cations is UO_3 at about 480 °C and U_3O_8 at over 570 °C. (ii) The final residue for the compounds with hexaaminecobalt(III) as counter-cation at over 570 °C is Co_2O_3 and U_3O_8. (iii) Hydrated compounds (except with phenylmalonate as ligand) lose their solvent molecules first, then counter-cations or one ligand or cation plus one ligand and finally the remaining ligands. (iv) Hydrated compounds with phenylmalonate as ligand lose their solvent molecules first, then phenyl groups, cations plus ligands, finally the remaining ligands. (v) The temperature, above or below 100 °C, at which compounds lose their final water molecules may be used to identify the presence of coordinated water molecules.

3.7. ^{13}C CPMAS NMR spectroscopy

As indicated in the preceding paper, based on the specific patterns of carbonyl chemical shifts, compounds with known crystal structures can be used as model compounds to study the relationship between structural types and ^{13}C CPMAS NMR spectroscopic data.

3.7.1. Compounds of known structure

$(C_6H_{16}N_2)[UO_2(C_3H_2O_4)_2(H_2O)]\cdot 2H_2O$ has a monomeric structure [3] and the ^{13}C NMR spectrum contains two carbonyl peaks (at 179.2 and 176.1 ppm) with a 1:3 intensity ratio, which suggests that the chemical environment of one carbonyl atom is different from the other three. That is consistent with the unusually short U–O distance, U(1)–O(7). The broad peak at 47.1 ppm is assigned to the CH_2 carbons in the counter-cation and the broad peak at 40.2 ppm to the CH_2 carbons in the ligands. $(C_4H_{12}N_2)[UO_2(C_4H_4O_4)_2(H_2O)]\cdot 1.5H_2O$ (**5**) has a pair of monomeric anion structures in the asymmetric unit (see Fig. 1) and the ^{13}C NMR spectrum contains two carbonyl peaks (at 179.9 and 177.8 ppm) of approximately equal intensity. The peaks at 45.9 and 43.8 ppm are assigned to CH_2 carbons in the counter-cation, those at 41.5 and 37.9 ppm to the CH carbons in the ligands and those at 17.3, 14.2, 9.8 and 8.5 ppm to the CH_3 carbons. $(C_4H_{14}N_2)[UO_2(C_4H_4O_4)_2(H_2O)]\cdot 2H_2O$ (**7**) has a monomeric anion structure with a C_2 axis along the U–O(H_2O) direction (see Fig. 2). The two U–O(malonate) distances are not significantly different. The ^{13}C CPMAS NMR spectrum has one carbonyl peak at 178.1 ppm, demonstrating the near equivalence of the carbonyl carbons. The peak at 46.7 ppm is assigned to the CH_2 carbons in the counter-cation, those at 40.0 and 30.0 ppm to the CH carbons and those at 8.7 and 4.1 ppm to the CH_3 carbons. $(C_4H_{12}N_2)[UO_2(C_7H_{10}O_4)_2(H_2O)]\cdot H_2O$ (**9**) has a monomeric anion structure with no crystallographically imposed symmetry (see Fig. 3). Experimentally only two carbonyl peaks are observed in the ^{13}C NMR spectrum (184.8 and 182.4 ppm), with an intensity ratio of approximately 1:3. The peak at 58.4 ppm is assigned to the C_q carbons in the ligands, those at 34.7 and 33.1 ppm to the CH_2 carbons and the peak at 8.3 ppm to the CH_3 carbons. $(C_{10}H_{26}N_2)[UO_2(C_7H_{10}O_4)_2(H_2O)]\cdot 2H_2O$ (**10**) has a monomeric anion structure with no crystallographically imposed symmetry (see Fig. 4). As in the cases of **2**, **13** and **21**, two carbonyl peaks were expected on the basis of X-ray crystallography. Experimentally, four carbonyl peaks at 185.0, 182.1, 179.8 and 177.6 ppm of approximately equal intensities were observed in the ^{13}C NMR spectrum. The peak at 58.2 is assigned to CH_2N carbons in the counter-cations, that at 43.6 ppm to the C_q carbons in the ligands, that at 30.5 ppm to the CH_2CH_3 carbons in the counter-cations, and those at 9.2, 7.3, 5.0 and 2.8 ppm to the CH_3 carbons.

$(C_{10}H_{26}N_2)[(UO_2)_3(C_7H_{10}O_4)_5]\cdot 2H_2O$ (**11**) possesses a rather complicated 3:5 ratio infinite chain anion structure. A single uranium atom, with one 1,5-bidentate ligand, and the dimeric structural unit encountered in compounds $(C_{10}H_{26}N_2)[(UO_2)_2(C_5H_6O_4)_3]$ [1] and $(C_6H_{16}N_2)[(UO_2)_3(C_5H_6O_4)_4(H_2O)_2]\cdot 2(C_2H_5OH)$ [1] are linked together by two distinct types of ligands, one tetradentate (1,3-bidentate through both carboxylate groups) and the other tridentate (1,3-bidentate to the dimeric unit and 1-monodentate to the single uranium atom to form a zigzag, 3:5 infinite chain. This com-

Table 10
Isotropic chemical shifts for different carbonyl environments

Compound	$\delta_{C=O}$ (ppm) and intensity ratios	Structural type	Carbonyl type [b]
H_2MA–	171.5 (169.2) [a]		
H_2MMA–	175.1(171.8) [a]		
H_2DMMA–	176.7(174.0) [a]		
H_2DEMA–	175.8		
H_2PMA–	174.9, 170.2(169.8) [a]		
7	178.1	monomeric	a
$(C_7H_{20}N_2)[UO_2(C_5H_6O_4)_2.(H_2O)]\cdot 2H_2O$	186.2, 181.6 (1:1)	monomeric [1]	a
$(C_2H_{10}N_2)[UO_2(C_5H_6O_4)_2(H_2O)]\cdot 2H_2O$	183.3, 180.9	monomeric [1]	a
$(C_6H_{16}N_2)[UO_2(C_3H_2O_4)_2(H_2O)]\cdot 2H_2O$	179.2, 176.1 (1:3)	monomeric [3]	a
5	179.9, 177.8	monomeric	a
9	184.8, 182.4 (1:3)	monomeric	a
$\{(C_6H_{18}N_2)[UO_2(C_3H_2O_4)_2]\}_2\cdot(CH_3OH)_2$	181.6, 179.0, 176.0, 173.8 (1:1:1:1)	dimeric [1]	a, a′, b
$\{(C_4H_{12}N_2)[UO_2(C_3H_2O_4)_2]\}_2\cdot 6H_2O$	181.5, 177.8, 175.4 (1:1:2)	dimeric [1]	a, a′
$Ba[UO_2(C_3H_2O_4)_2]\cdot 3H_2O$	181.4, 177.4, 176.2 (2:1:1)	infinite chain [4]	a, a′, b
$(C_{10}H_{26}N_2)[(UO_2)_2(C_5H_6O_4)_3]$	189.4, 180.7 (2:1)	infinite chain	a″, c, d
$(C_6H_{16}N_2)[(UO_2)_3(C_5H_6O_4)_4(H_2O)_2]\cdot 2(C_2H_5OH)$	191.6, 190.1, 187.7, 184.6	infinite chain	a″, c, d
11	190.5, 187.3, 184.5, 183.0, 180.2, 175.3	infinite chain [1]	a, a″, c, d, e

–H_2MA = malonic acid, H_2MMA = methylmalonic acid, H_2DMMA = dimethylmalonic acid, H_2DEMA = diethylmalonic acid, H_2PMA = phenylmalonic acid.

[a] The values in brackets are solution ^{13}C NMR data from Aldrich [18].

[b] Carbonyl type is in Scheme 1.

pound has six carbonyl peaks in the ^{13}C CPMAS NMR spectrum at 190.5, 187.3, 184.5, 183.0, 180.2 and 175.3 ppm, indicating that the six kinds of carbonyl groups in the asymmetric unit can be distinguished by ^{13}C CP-MAS NMR. The peaks at 61.1, 59.6, 58.2 and 57.5 ppm are assigned to the four non-equivalent C_q carbons in the ligands, those two broad peaks at 43.8 and 30.6 ppm to the CH_2 carbons and those at 9.3, 7.4, 4.9 and 2.7 ppm to the CH_3 carbons.

Several types of carbonyl environments identified by X-ray crystallography are shown in Scheme 1(I–V). The isotropic chemical shifts (ICS) of carbonyl carbons for the ligands and some structurally characterised compounds are summarised in Table 10. For the ligands generally, there are differences of 2–4 ppm between solid and solution NMR but overall the trend in values is reasonably consistent (see Table 10). In the solid state, $\delta_{C=O}$ moves to higher values with an increase in the number of substituent alkyl groups (electron withdrawal leads to the carbonyl carbon being more deshielded) on the malonate. The occurrence of two values of $\delta_{C=O}$ for H_2PMA could be the effect of solid state packing.

Because monomeric structures only have 1,5-bidentate ligands, carbonyl type a (see Scheme 1) should have ICS values of 176–186 ppm. The ICS for dimeric and 1:2 (M:L) infinite chain structures suggests that a, a′ should be at 176–182 ppm which is within the range defined from monomeric structures and the bridging carbonyl type b should be at 173–176 ppm. The ^{13}C CPMAS NMR spectrum of $(C_{10}H_{26}N_2)[(UO_2)_2(C_5H_6O_4)_3]$ indicates that carbonyl types c and d have ICS values over 189 ppm and type a″ at 181 ppm. The data from $(C_6H_{16}N_2)[(UO_2)_3(C_5H_6O_4)_4(H_2O)_2]\cdot 2(C_2H_5OH)$ and **11** confirm that carbonyl types c and d have ICS values over 189 ppm. The ICS at 175.3 ppm for **11** could be the characteristic ICS for carbonyl type e. Thus, there is a rough correlation between ICS value and the carbonyl type: a, a′, a″ 176–186 ppm; b, e 173–176 ppm; c, d >189 ppm.

3.7.2. Structural predictions

The structural characterisation of the compounds in this series which have not been determined by single crystal X-ray diffraction can be attempted using a combination of ^{13}C MAS NMR and IR spectroscopy, together with the thermal and microanalytical data. Inspection of Tables 11 and 12 indicates that these spectroscopic and physical properties lead to a consistent interpretation of monomeric or dimeric structures based on a pentagonal bipyramidal coordination geometry at U for most of these compounds. The exceptions are **11** and **14**, which may have polymeric structures with a mixture of hexagonal and pentagonal equatorial geometry.

These data provide an opportunity to test the principles suggested in Part I of this paper. Table 14 summarises the known or spectroscopically inferred structures and provides a comparison with predicted ones based purely on counter-cations. In 11 out of 21 cases, the predicted and actual or inferred structural types are the same and, of the ten examples where there is disagreement, the predicted connectivity is more complex than actually observed in all cases. Since the

Table 11
^{13}C CPMAS NMR data for the compounds of unknown structure

Compound	$\delta_{C=O}$	δ_{arom}	Chemical shifts (ppm), δ_{Cq} or δ_{CH} or δ_{CH_2N}	δ_{CH_2}	δ_{CH_3}
1	183.1, 178.8, 177.3 (1:1:2)		43.5, 39.7		
2	181.1, 177.8, 176.2, 172.9 (1:1:1:1)		53.6, 53.1, 49.3 (CH_2N)	41.9, 40.3, 37.6	18.8
3	182.0, 177.9, 175.6 (2:1:1)		47.7 (CH_2N), 41.4 (CH)		15.4, 12.6
4	179.0, 178.2 (1:1)		46.6 (CH_2N), 34.3 (CH)		10.3
5a	183.1, 180.1, 178.8 (overlapped)		47.7 (CH_2N), 38.5 (CH)		14.3, 10.4
6	182.7, 177.2 (1:1)		47.5 (CH_2N)	60.7, 59.2, 52.6, 49.6 (C_q)	12.5
8	186.4, 182.6, 181.6, 179.3 (1:1:1:1)		42.0, 39.1, 32.3, 29.7		8.2, 6.5
12	183.8, 182.2, 180.6, 174.5	135.1, 127.8	84.1, 76.8	59.8, 58.2, 49.7, 41.4, 39.7	25.8
13	185.2, 179.0, 177.6, 172.9 (1:1:1:1)	135.5, 129.3	83.4, 77.0	61.1, 59.5, 48.4, 42.0	24.0
14	184.3, 178.1 (1:1)	132.2, 125.5	57.7	34.8	
15	181.2, 179.4, 178.4, 177.1				
16	183.3, 180.6, 177.1 (1:1:2)	134.6, 132.4, 126.1	75.0, 58.0	38.9	24.3
17	182.7, 181.7, 178.2, 175.2	135.0, 132.4, 127.0	87.0, 84.2, 78.8, 61.4, 59.2	40.1	
18	180.8, 177.4, 176.1	135.9, 134.8, 128.6, 125.8	60.3, 57.9, 53.0	45.0, 41.6, 39.9, 36.7	24.5, 21.7, 17.8
19	multi-feature (174.7–183.4)	133.6, 126.2	74.5, 67.2, 59.6	42.5, 30.0	8.1

$[Co(NH_3)_6][(UO_2)_2(C_3H_2O_4)_3].(C_3H_3O_4)\cdot 2H_2O$ (**1**); $(C_8H_{22}N_2)[UO_2(C_3H_2O_4)_2]\cdot 2H_2O$ (**2**); $(C_6H_{16}N_2)[UO_2(C_4H_4O_4)_2]$ (**3**); $(C_2H_{10}N_2)[UO_2(C_4H_4O_4)_2]\cdot H_2O$ (**4**) $(C_4H_{12}N_2)[UO_2(C_4H_4O_4)_2]\cdot 5H_2O$ (**5a**); $(C_6H_{14}N_2)[UO_2(C_4H_4O_4)_2]\cdot H_2O$ (**6**); $(C_6H_{18}N_2)[UO_2(C_7H_{10}O_4)_2]$ (**8**); $(C_6H_{18}N_2)[UO_2(C_9H_6O_4)_2]$ (**12**); $(C_6H_{16}N_2)[UO_2(C_9H_6O_4)_2]\cdot H_2O$ (**13**); $(C_2H_{10}N_2)[UO_2(C_9H_6O_4)_2]\cdot 3H_2O$ (**14**); $[Co(NH_3)_6]_2[(UO_2)_2(C_9H_6O_4)_5]\cdot 10H_2O$ (**15**); $(C_4H_{12}N_2)[UO_2(C_9H_6O_4)_2]\cdot H_2O$ (**16**); $(C_6H_{14}N_2)[UO_2(C_9H_6O_4)_2]\cdot H_2O$ (**17**); $(C_8H_{26}N_2)[UO_2(C_9H_6O_4)_2]$ (**18**); $(C_4H_{14}N_2)[UO_2(C_9H_6O_4)_2]\cdot 1.5H_2O$ (**19**).

Table 12
Structural prediction for uranyl malonato and substituted malonato compounds

Compound	Carbonyl chemical shift (ppm)	Nature of H_2O from TG/DTA	Equatorial coordination from IR	Predicted structural type by ^{13}C CPMAS NMR
1	183.1, 178.8, 177.3 (1:1:2)	ligand	pentagonal	dimeric type 2
2	181.1, 177.8, 176.2, 172.9 (1:1:1:1)	lattice	pentagonal	dimeric type 1
3	182.0, 177.9, 175.6 (2:1:1)	anhydrous	pentagonal	dimeric type 2
4	179.0, 178.2 (1:1)	ligand	pentagonal	monomeric type 2 or 3
5a	183.1, 180.1, 178.8 (shoulder)	ligand + lattice	pentagonal	dimeric type 2
6	182.7, 177.2 (1:1)	ligand	pentagonal	monomeric type 2 or 3
A [a]	190.1, 181.8 (2:1)	anhydrous	pentagonal + hexagonal	2:3 infinite chain
B [a]	183.9, 182.2 (3:1)	ligand + lattice	pentagonal	monomeric type 4
C [a]	186.7, 184.3, 179.0 (2:1:1)	anhydrous	pentagonal	dimeric type 2
D [a]	185.3, 180.5 (1:1)	ligand + lattice	pentagonal	monomeric type 2 or 3
8	186.4, 182.6, 181.6, 179.3 (1:1:1:1)	anhydrous	pentagonal	dimeric type 1
12	183.8, 182.2, 180.6, 174.5	anhydrous	pentagonal	dimeric type 1
13	185.2, 179.0, 177.6, 172.9	ligand + lattice	pentagonal	dimeric type 1
14	184.3, 178.1 (1:1)	ligand + lattice	pentagonal + hexagonal	monomeric type 2 or 3
15	181.2, 179.4, 178.4, 177.1	lattice	pentagonal	dimeric type 2
16	183.3, 180.6, 177.1	lattice	pentagonal	dimeric type 2
17	182.7, 181.7, 178.2, 175.2	lattice	pentagonal	dimeric type 1
18	180.8, 177.4, 176.1	anhydrous	pentagonal	dimeric type 1
19	multi-feature (174.7-183.4)	lattice	pentagonal	dimeric type 1

[a] $(C_6H_{18}N_2)[(UO_2)_2(C_5H_6O_4)_3]$ (**A**); $(C_4H_{12}N_2)[UO_2(C_5H_6O_4)_2]\cdot 5H_2O$ (**B**); $(C_6H_{14}N_2)[UO_2(C_5H_6O_4)_2]$(**C**); $(C_8H_{22}N_2)[UO_2(C_5H_6O_4)_2]\cdot 4H_2O$ (**D**).

Table 13
Summary of chemical and structural information for the compounds

Cations	Proligands				
	H_2MA	H_2MMA	H_2DMMA	H_2DEMA	H_2PMA
H_2TMED	(1:2) X-D	no	(2:3) P-IC #	**8** (1:2) P-D #	**12** (1:2) P-D #
H_2DMP	(1:2) X-M	**3** (1:2) P-D #	(3:4) X-IC	no	**13** (1:2) P-D #
H_2ED	no	**4** (1:2) P-M #	(1:2) X-M	no	**14** (1:2) P-M #
HAC	**1** (2:4) P-D #	no	(1:2) X-D	no	**15** (2:5) P-D #, **15a** (2:4) X, **5b** (5:10) X
H_2PIP	(1:2) X-D	**5** (1:2) X-M, **5a** (1:2) X-D #	(1:2) X-M #	**9** (1:2) X-M	**16** (1:2) P-D #
H_2DABCO	no	**6** (1:2) X-M #	(1:2) P-D #	no	**17** (1:2) P-D #
H_2TEED	no	no	(2:3) X-IC	**10** (1:2) X-M, **11** (3:5) X-IC	no
H_2TMPD	no	no	(1:2) X-M	no	no
H_2TMBD	**2** (1:2) P-D #	no	(1:2) X-M #	no	**18** (1:2) P-D #
H_2DMED	no	**7** (1:2) X-M	no	no	**19** (1:2) P-D #

The ratio of metal-to-ligand in the product is given in parentheses. Data from this work identify each compound by a number and other data come from Refs. [1–3]. H_2MA, malonic acid; H_2MMA, methylmalonic acid; H_2DMMA, dimethylmalonic acid; H_2DEMA, diethylmalonic acid; H_2PMA, phenyl malonic acid; H_2TMED, *N*,*N*,*N*′,*N*′-tetramethylethylenediammonium; H_2DMP, *N*,*N*′-dimethylpiperazinium; H_2ED, ethylene-diammonium; HAC, hexaaminecobalt(III); H_2PIP, piperazinium; H_2DABCO, 1,4-diazabicyclo[2.2.2]octane (triethylene-diammonium); H_2TEED, *N*,*N*,*N*′,*N*′-tetraethylethylenediammonium; H_2TMPD, *N*,*N*,*N*′,*N*′-tetramethyl-1,3-propanediammonium; H_2TMBD, *N*,*N*,*N*′,*N*′-tetramethyl-1,4-butanediammonium; H_2DMED, *N*,*N*′-dimethylethylenediammonium; X, crystalline; P, powder; no, no solid product obtained; D, dimer; M, monomer; IC, infinite chains; #, predicted by ^{13}C CPMAS NMR, IR, thermal and elemental analyses.

Table 14
Comparison of structural types determined by XRD or inferred from spectroscopic and thermoanalytical data (the latter in parentheses) with predictions based on principles proposed in part I of this paper

Compound	Structural type	Prediction type	Compound	Structural type	Prediction type
1	(D)	D	**11**	IC	IC
2	(D)	D	**12**	(D)	IC
3	(D)	IC	**13**	(D)	IC
4	(M)	M	**14**	(M)	M
5	M	D	**15**	(D)	D
5a	(D)	D	**16**	(D)	D
6	(M)	D	**17**	(D)	D
7	M	D	**18**	(D)	IC
8	(D)	IC	**19**	(D)	D
9	M	D	**20**	D	D
10	M	IC			

principles defined in Part I of this paper exclude any effects of ligand chemistry, this level of disagreement is not surprising. In spite of the large size and aromaticity of the phenyl-substituted ligand, the structures of the phenylmalonato complexes (**12**–**19**) are predicted even better than those of complexes with other ligands. The tendency to overpredict structural complexity perhaps reflects a preference for simpler structural types with large cations and bulky ligands, and suggests that structures with high connectivity may be the exception rather than the rule.

4. Conclusions

The reaction of aliphatic diamine with malonic or substituted malonic acid and uranyl nitrate in the ratio 2:2:1 and in aqueous media leads in most cases to one predominant product, often crystalline, and with a range of stoichiometries and structures throughout the series (see Table 13). ^{13}C MAS NMR spectroscopy gives resonances for the carboxylate carbon ligands in the range 172–192 ppm which appear to be characteristic of structural type. Metal–ligand ratios are 1:2 for malonate and methylmalonate ligands and only differ from this in a few cases when larger substituent groups are present (i.e. dimethylmalonate, diethylmalonate, phenylmalonate). Thus, the stoichiometry of products is affected primarily by the bulk of the ligand and not by the bulk of the dipositive counter-cation, but the latter's bulk and ability to form hydrogen bonds affects the nuclearity of the anionic product. In the case of

phenylmalonate, although the compounds form slowly from solution, we have been unable to obtain diffraction quality crystals of sufficient quality to complete a structural refinement, but the spectroscopic and analytical data are indicative of simple monomeric or dimeric species based on pentagonal bipyramidal geometry. Direct evidence for the influence of the bulk of the substituents on the ligand comes from the mixed ligand complex with methyl- and dimethyl-malonates, which is dimeric and the bulkier ligand is terminal whilst the mono-substituted ligand is bridging. However, the choice of counter-cation does not appear to dictate the production of a given structural type, viz. monomer, dimer, polymeric chain. The tendency to maximise H-bonding in the lattice undoubtedly has a significant effect on the structure in the solid state. Although more than thirty uranyl malonato compounds have been studied (see Table 13) there remains no evidence for the isolation of oligomeric anions, $\{UO_2(\text{ligands})\}_n^{x-}$, of intermediate nuclearity, i.e. where $2 < n < \infty$, despite the identification of several new types of bonding mode for malonate with uranyl.

5. Supplementary material

Crystallographic data for the structural analysis have been deposited with the Cambridge Crystallographic Centre, CCDC Nos. 166055–166060. Copies of this information may be obtained free of charge from The Director, CCDC, 12 Union Road, Cambridge, CB2 1EZ, UK (fax: +44-1233-336-033; e-mail: deposit@ccdc.cam.ac.uk or www: http://www.ccdc.cam.ac.uk).

Acknowledgements

We are grateful to M Hart (Manchester University) for microanalyses; J Friend (Manchester University) for ^{13}C CPMAS NMR; to BNFL (Y.J.Z. and F.R.L.) and CVCP (Y.J.Z.) for their financial support.

References

[1] Y.-J. Zhang, D. Collison, F.R. Livens, M. Helliwell, F. Heatley, A.K. Powell, S. Wocadlo, H. Eccles, Polyhedron 21 (2002) 69.
[2] Y.-J. Zhang, D. Collison, F.R. Livens, M. Helliwell, H. Eccles, N. Tinker, J. Alloys Compounds 271 (1998) 139.
[3] G. Tilley, Y.-J. Zhang, D. Collison, F.R. Livens, M. Helliwell, K.M.A. Malik, M.B. Hursthouse, unpublished data.
[4] K.S. Rajan, A.E. Martell, J. Inorg. Nucl. Chem. 29 (1967) 523.
[5] R.M. Rojas, A. Del Pra, G. Bombieri, F. Benetollo, J. Inorg. Nucl. Chem. 41 (1979) 541.
[6] G. Bombieri, F. Benetollo, E. Forsellini, A. Del Pra, J. Inorg. Nucl. Chem. 42 (1980) 1423.
[7] S.I.R.92: A. Altomare, M. Cascarano, C. Giacovazzo, A. Guagliardi, J. Appl. Crystallogr. 26 (1993) 343.
[8] P.T. Beurskens, G. Admiraal, G. Beurskens, W.P. Bosman, S. Garcia-Granda, R.O. Gould, J.M.M. Smits, C. Smykalla, ORIENT: the DIRDIF-94 program system, Technical Report of the Crystallography Laboratory, University of Nijmegen, The Netherlands, 1992.
[9] P.T. Beurskens, G. Admiraal, G. Beurskens, W.P. Bosman, S. Garcia-Granda, R.O. Gould, J.M.M. Smits, C. Smykalla, PATTY: the DIRDIF-94 program system, Technical Report of the Crystallography Laboratory, University of Nijmegen, The Netherlands, 1992.
[10] D.T. Cromer, J.T. Waber, International Tables for X-ray Crystallography, Table 2.2 A, vol. IV, The Kynoch Press, Birmingham, UK, 1974.
[11] J.A. Ibers, W.C. Hamilton, Acta Crystallogr. 17 (1964) 781.
[12] D.C. Creagh, W.J. McAuley, in: A.J.C. Wilson (Ed.), International Tables for Crystallography, Table 4.2.6.8, vol. C, Kluwer Academic Publishers, Boston, MA, 1992, pp. 219–222.
[13] D.C. Creagh, J.H. Hubbell, in: A.J.C. Wilson (Ed.), International Tables for Crystallography, Table 4.2.4.3, vol. C, Kluwer Academic Publishers, Boston, MA, 1992, pp. 200–206.
[14] TEXSAN: Crystal structure analysis package, Molecular Structure Corporation, The Woodlands, TX, 1985 and 1992.
[15] SHELXTL 5.03 program system, Siemens Analytical X-ray Instruments, Madison, WI, 1995.
[16] J. Leciejewicz, N.W. Alcock, T.J. Kemp, Struct. Bond. 82 (1995) 43.
[17] Y.-J. Zhang, PhD thesis, University of Manchester 1998, and references therein.
[18] G.C. Pouchert, J. Behnke, The Aldrich Library of ^{13}C and ^{1}H FT NMR Spectra, 1st ed., Aldrich, St. Louis, MO, 1993, p. 1.

PERGAMON

Polyhedron 21 (2002) 97–104

POLYHEDRON

www.elsevier.com/locate/poly

Synthesis, structure and redox properties of isomeric $[RuCl_2(L)_2]$ (L = *N*-aryl-1,2-arylenediimine) complexes formed by the oxidative dimerization of coordinated aromatic amines

Amrita Saha [a], Chayan Das [a], Kedar N. Mitra [a], Shie-Ming Peng [b], G.H. Lee [b], Sreebrata Goswami [a,*]

[a] *Department of Inorganic Chemistry, Indian Association for the Cultivation of Science, Calcutta 700 032, India*
[b] *Department of Chemistry, National Taiwan University, Taipei, Taiwan, ROC*

Received 11 July 2001; accepted 4 October 2001

Abstract

The di-arylamino complex $[RuCl_2(ArNH_2)_2L]$ ($ArNH_2$ = aromatic monoamine and L = *N*-aryl-1,2-diimino arene) reacts spontaneously with aqueous H_2O_2 to produce two isomers of $[RuCl_2(L)_2]$ via oxidative dimerization of the two coordinated aromatic amines. The geometries of two isomers are *cis* with respect to two chlorides and are *trans*, *cis*(tc) and *cis*, *cis*(cc) in the following sequence: NH(imine), HN(imine) and ArN(imine), ArN(imine). Of the above two, the tc-$[RuCl_2(L)_2]$ forms good X-ray quality crystals. The structure of a representative has been solved by X-ray diffraction. The geometry of the cc-$[RuCl_2(L)_2]$ is, however, revealed by the spectral data. The tc-isomer possesses a C_2-symmetry axis and the two-coordinated diimine ligands are magnetically equivalent. As a result, a single NH resonance in tc-$[RuCl_2(L)_2]$ appeared at approximately δ 12.40. By contrast, the cc-isomer is unsymmetrical and a complex pattern of ^1H NMR was observed in this case. Thus, there were two NH resonances observed in the range approximately δ 14.11–11.88. A semi-empirical extended Hückel MO calculations on a representative example showed strong metal–ligand overlap. A highly intense electronic transition that appeared in the visible range spectra of the complexes was assigned to a transition involving two molecular orbitals with considerable metal and ligand contributions. Both the isomers of the complex showed a high potential anodic response (0.8 V) due to the Ru^{III}/Ru^{II} couple. The trivalent congeners $[RuCl_2(L)_2]^+$ were generated in solution which showed characteristic rhombic EPR for the low spin d^5 ions. The distortion parameters have been computed using the observed *g* values. The axial distortion (Δ) in each case is found to be stronger than the rhombic (V) distortion. © 2002 Elsevier Science Ltd. All rights reserved.

Keywords: Ruthenium promoted reactions; Dimerization of aromatic amines; 1,2-Diimine; Structures; Redox

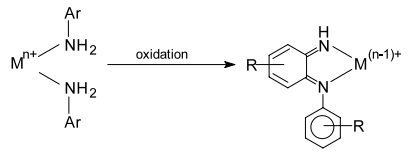
1. Introduction

Metal complexes of redox non-innocent dioxolene ligand series together with their nitrogen analogues are of considerable interest [1–3] because of their exceptionally rich redox and spectroscopic behavior, which originate from a strong degree of orbital mixing between metal ($d\pi$) and ligand ($p\pi$) frontier orbitals. Since the first report [4] of the ruthenium complex of bqdi, $[Ru(bqdi)_3](PF_6)$ (benzoquinonediimine) by Warren, the ruthenium complexes of bqdi and its redox partners have been the focus of many recent studies [5,6].

As a part of our ongoing work [7,8] in the area of metal promoted assembly of diimine complexes based on oxidation of aromatic amines we report herein the synthesis [7c], characterization, crystal structure and redox properties of isomeric $RuCl_2(L)_2$ (L = *N*-aryl-1,2-arylenediimine). The diimine ligand L is generated in situ by the oxidative dimerization of two coordinated aromatic amines (Scheme 1). It is proposed that the metal ion mediates these transformations by holding the amine residues in close proximity and also by taking part in the redox processes. In the present study two di-arylamino complexes [7b] of ruthenium of gen-

* Corresponding author. Tel.: +91-33-473-4971; fax: +91-33-473-2805.
E-mail address: icsg@mahendra.iacs.res.in (S. Goswami).

0277-5387/02/$ - see front matter © 2002 Elsevier Science Ltd. All rights reserved.
PII: S0277-5387(01)00963-9



Scheme 1.

eral formula $[RuCl_2(ArNH_2)_2(L)]$ were chosen for the study of oxidation reaction. Oxidative deprotonation [9] of coordinated aromatic amines leading to the formation of metal–imido complexes was known in the literature. However, oxidative dimerization of coordinated amines of above type has been noted by us only in the recent past [7]. Furthermore, the transformation described in this work represents an example of an oxidation reaction, which led to the oxidation of internal substrate. Such reactions are important but are scanty [10].

2. Experimental

The solvents and chemicals used for synthesis were of analytical grade. The supporting electrolyte tetraethylammonium perchlorate (TEAP) and solvents for electrochemical work were obtained as before [11].

2.1. Physical measurements

A Shimadzu UV 2100 UV–Vis spectrophotometer was used to record electronic spectra. The IR spectra recorded with a Perkin–Elmer 783 spectrophotometer. ^1H NMR spectra in $CDCl_3$ were recorded with a Bruker Advance DPX300 spectrophotometer. $SiMe_4$ was used as internal standard. A Perkin–Elmer 240C elemental analyzer was used to collect microanalytical data (C,H,N). Electrochemical measurements were performed under dry nitrogen with an EG&G PARC model 273A potentiostat/galvanostat based electrochemistry system. All potentials, reported in this work, are referenced to the saturated calomel electrode (SCE) and are uncorrected for junction contributions. EPR measurements were made with a Varian 109C E-line X-band spectrometer fitted with a flat cell. Spectra were calibrated with the help of DPPH ($g = 2.0037$). Electronic spectra were recorded on a JASCO V-570 spectrophotometer.

2.1.1. Synthesis of dianiline dichloro N-phenyl-1,2-benzoquinone diimine ruthenium(II) $[RuCl_2(L^a)(PhNH_2)_2]$ (**1a**)

A sample of $RuCl_3 \cdot 3H_2O$ (0.25 g, 0.95 mmol) was added to 0.5 ml of aniline, and the mixture was heated on an oil bath at 140 °C for 30 min. The brown color changed gradually to violet and then an intense red solution resulted. The crude mass was extracted with dichloromethane and was washed thoroughly with 1 M hydrochloric acid and finally washed with water. The acid free solution was dried over anhydrous sodium sulfate. Hexane was then layered over the red solution and after 2 days shiny brown crystals were obtained. Yield 60%. Calc. for $C_{24}H_{24}Cl_2N_4Ru$ (540): C, 53.33; H, 4.44; N, 10.37. *Anal.* Found: C, 53.46; H, 4.50; N, 10.52%.

A similar reaction using *p*-toluidine instead of aniline afforded (**1b**) in 65% yield. Calc. for $C_{28}H_{32}Cl_2N_4Ru$ (596): C, 56.37; H, 5.37; N, 9.39. *Anal.* Found: C, 56.48; H, 5.27; N, 9.50%.

2.1.2. Synthesis of dichloro bis(N-phenyl-1,2-benzoquinone diimine)ruthenium(II), tc-$[RuCl_2(L^a)_2]$ and cc-$[RuCl_2(L^a)_2]$ (**2a**)

To a dichloromethane solution of $[RuCl_2(PhNH_2)_2(L^a)] \cdot CH_2Cl_2$ (0.108 g, 0.2 mmol), 0.5 ml 30% weight/volume hydrogen peroxide solution was added and the mixture was stirred at room temperature for 30 min. An intense blue color resulted, which was evaporated at room temperature. The crude product, thus obtained, was purified on a TLC plate. Two intense blue bands moved with a 25% chloroform–acetonitrile mixture. The two geometrical isomers were collected by evaporation of the solvent at room temperature. The first blue isomer (tc-) was crystallized by slow diffusion of dichloromethane tetrahydrofuran solution of the complex into hexane. Analysis and yields of the two isomers are given below:

tc-$[RuCl_2(L^a)_2]$ (first blue), yield (35%). Calc. for $C_{24}H_{20}N_4Cl_2Ru$ (537): C, 53.63; H, 3.72; N, 10.43. *Anal.* Found: C, 53.65; H, 3.43; N, 10.52%.

cc-$[RuCl_2(L^a)_2]$ (second blue), yield (35%). Calc. for $C_{24}H_{20}N_4Cl_2Ru$ (537): C, 53.63; H, 3.72; N, 10.43. *Anal.* Found: C, 54.02; H, 3.33; N, 10.62%.

The tc and cc isomers of $[RuCl_2(L^b)_2]$ (**2b**) were similarly prepared following the above procedure.

tc-$[RuCl_2(L^b)_2]$, yield 32%. Calc. for $C_{28}H_{28}N_4Cl_2Ru$ (592): C, 56.76; H, 4.73; N, 9.46. *Anal.* Found: C, 56.85; H, 4.32; N, 9.45%.

cc-$[RuCl_2(L^b)_2]$, yield 32%. Calc. for $C_{28}H_{28}N_4Cl_2Ru$ (592): C, 56.76; H, 4.73; N, 9.46. *Anal.* Found: C, 56.76; H, 4.35; N, 9.36%.

2.2. Crystal structure determination

The crystallographic data for the compound tc-$[RuCl_2(L^a)_2]$ (**2a**) are collected in Table 1. Slow diffusion of a dichloromethane–THF solution of tc-$[RuCl_2(L^a)_2]$ in hexane yielded thin needle like crystals ($0.50 \times 0.05 \times 0.04$ mm^3). Intensity data were collected on a SMART CCD diffractometer with graphite-monochromated Mo Kα radiation ($\lambda = 0.7107$

Table 1
Crystallographic data for $[RuCl_2(L^a)_2]\cdot THF$

Empirical formula	$C_{28}H_{28}Cl_2N_4ORu$
M_r	608.51
Crystal system	monoclinic
Space group	$P2_1/c$
Unit cell dimensions	
a (Å)	11.5638(7)
b (Å)	20.5507(11)
c (Å)	11.8331(7)
β (°)	96.062(2)
U (Å^3)	2796.3(3)
Z	4
D_{calc} (Mg m^{-3})	1.445
R_1 $[I>2\sigma(I)]$	0.0698
wR_2 $[I>2\sigma(I)]$	0.1520
Goodness-of-fit	1.033

Å). A total of 13 424 unique reflections were collected and 5719 with $I \geq 2\sigma(I)$ were used in the refinement [12]. Refinement of positional and anisotropic thermal parameters for all non-hydrogen atoms converged to $R = 0.0698$. The final Fourier difference maps showed residual extrema at 0.591, -0.570 e Å^{-3}.

3. Results and discussion

3.1. The starting compounds and synthesis

Hydrated ruthenium(III) chloride reacts [7b] with neat $ArNH_2$ at 130 °C to yield the brown complex, $[RuCl_2(ArNH_2)_2L]$ [$ArNH_2$ = aniline, L = L^a and $ArNH_2$ = *p*-toluidine, L = L^b, Eq. (1)], which was used as the starting complex for carrying out the synthesis.

$$RuCl_3\cdot nH_2O \xrightarrow[130-135\ ^\circ C]{ArNH_2} \underset{\mathbf{1}}{[RuCl_2(ArNH_2)_2L]} \quad (1)$$

$ArNH_2$	**L**	**1**
aniline	L^a	1a
p-toluidine	L^b	1b

The complex **1** is poorly soluble in common organic solvents. A suspension of **1** in CH_2Cl_2, however, reacts instantaneously [7c] with 5% aqueous H_2O_2 at room temperature (300 K) to afford $[RuCl_2L_2]$ (**2**) (Eq. (2)):

$$[RuCl_2(ArNH_2)_2L] \xrightarrow{H_2O_2} [RuCl_2L_2] \quad (2)$$

Preliminary work up followed by chromatographic purification yielded the two geometrical isomers of $[RuCl_2L_2]$ (vide infra). In this reaction, the two coordinated amine residues have undergone oxidative coupling to give a 1,2-diamino ligand. This transformation, **1** → **2** is a combination of many operations: (i) isomerization of the starting complex **1** in order to bring two $ArNH_2$ in close proximity (*trans* → *cis*); (ii) oxidative coupling of two $ArNH_2$ residues to *ortho*-semidine (C–N bond making); and (iii) further oxidative dehydrogenation, *ortho*-semidine → 1,2-diimine (diamine → diimine).

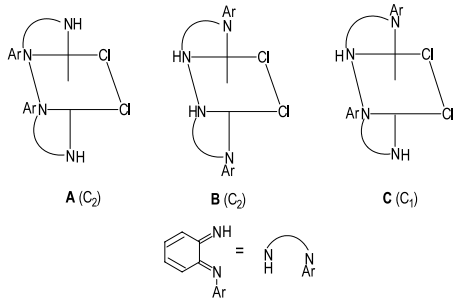
3.2. Formulation and spectral characterization of isomeric $[RuCl_2(L)_2]$

The crude product, obtained from the reaction (1), contained two major blue fractions, which were separated on a preparative TLC plate. These were obtained in almost identical yields (ca. 35% each). FAB mass spectra of these two compounds are nearly identical which indeed confirm that these two are isomers. Due to the unsymmetric nature of L, there exist [13] five geometrical possibilities for $[RuCl_2L_2]$. The present complexes are characterized by two sharp and medium Ru–Cl stretches in the region 310–350 cm^{-1} (Table 2). Thus, the $RuCl_2$ fragments in these complexes are *cis* and three geometries A–C are possible (Scheme 2). The relative orientations (*trans*/*cis*) of the coordinated imine nitrogen atoms [N(H), N(H)] and aryl substituted imine nitrogen atoms [N(Ar), N(Ar)] in the isomeric $[RuCl_2(L)_2]$ are *trans*, *cis* and *cis*, *cis* respectively (vide infra). We shall refer these two isomers as tc- (first blue) and cc- (second blue) isomers. Of the above two com-

Table 2
IR and NMR data

Compound	IR [a] (cm^{-1})			^{1}H NMR [b] (ppm)	
	ν(N–H)	ν(C=N)	ν(Ru–Cl)	δMe	δN–H(imine)
tc-$[RuCl_2(L^a)_2]$	3160	1540	360, 350		12.47
cc-$[RuCl_2(L^a)_2]$	3150	1545	360, 355		12.46, 12.00
tc-$[RuCl_2(L^b)_2]$	3160	1550	360, 345	2.33, 2.023	12.33
cc-$[RuCl_2(L^b)_2]$	3165	1560	360, 340	2.38, 2.32, 2.03, 1.94	14.11, 11.88
$[RuCl_2(ArNH_2)_2(L^a)]$ [c]	3300, 3100	1580	360, 340		14.66
$[RuCl_2(ArNH_2)_2(L^b)]$ [c]	3310, 3140	1580	350, 340	2.17, 2.08, 1.97, 1.96	14.51

[a] In KBr.
[b] In $CDCl_3$.
[c] δN–H(–NH_2) appeared at 5.09, 4.84; 5.07, 4.80 ppm.



Scheme 2.

pounds, the tc-$[RuCl_2(L^a)_2]$ formed suitable crystals for X-ray structure determination. The geometry of the cc-isomer was however, revealed by the spectral data.

The complexes showed well resolved ^1H NMR spectra in $CDCl_3$ at 300 MHz, chemical shift data are listed in (Table 2) and the spectra of two representatives are shown in Fig. 1. The spectrum of the tc-isomer is simpler than that of the cc-isomer. Each kind of proton in the tc-isomer gave rise to only one signal (singlet or multiplet), which indicates that the two L ligands in this isomer are magnetically equivalent. By contrast, the corresponding cc-isomer showed two signals for each kind of protons. In this geometry the two ligands are magnetically inequivalent and their spectral pattern is as expected. For comparison, while the tc-$[RuCl_2L_2]$ showed only one NH resonance [7d] at δ 12.40, the

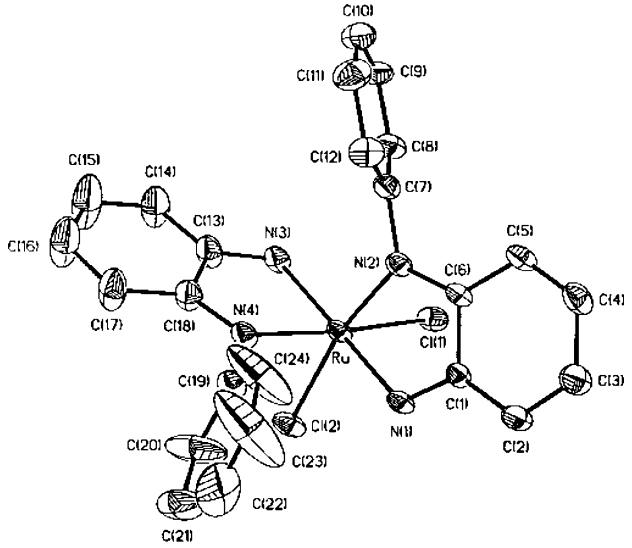


Fig. 2. Molecular structure and atom numbering scheme for tc-$[RuCl_2(L^a)_2]$.

corresponding cc-$[RuCl_2L_2]$ displayed two such resonances at approximately δ 14.11 and 11.88. The two isomers of the complex with methyl substituted ligand, $[RuCl_2(L^b)_2]$ showed two (tc-) and four (cc-) methyl resonances, respectively, in the range δ 2.38–1.94. The ^1H NMR together with the IR spectral data, thus confirms the geometries of the two isomers of $[RuCl_2L_2]$.

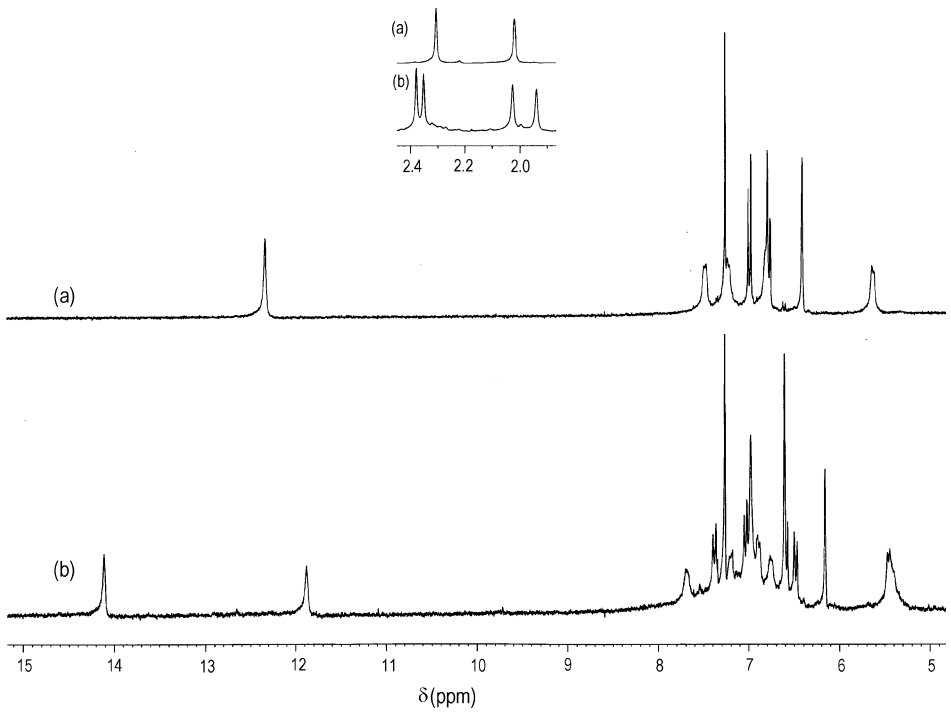


Fig. 1. NMR spectra of (a) tc-$[RuCl_2(L^b)_2]$ and (b) cc-$[RuCl_2(L^b)_2]$ in $CDCl_3$. Inset: resonances due to methyl protons.

3.3. Crystal structure, tc-[$RuCl_2(L^a)_2$]

The first blue fraction of $RuCl_2(L^a)_2$ formed suitable X-ray quality crystals for structure determination. A view of the molecule is shown in Fig. 2, which shows that one of the *N*-phenyl rings is disorder. Selected bond parameters are collected in (Table 3). The coordination sphere involves $RuCl_2N_4$. Two chlorides are *cis* to each other and the aryl substituted imine nitrogens are also in relative *cis* positions. The imine C–N bond lengths, average 1.316 Å are within the range of values expected for the diimine oxidation state of L [5e,7]. These bonds are much shorter than the two C–N single bonds, viz. C(7)–N(2) and C(19)–N(4), average 1.434 Å. Moreover, the C–C lengths (average 1.348 Å) at positions that would have localized double bond for the diimine form of the ligands are significantly shorter than the other C–C lengths (average 1.432 Å) in the same ring. The Ru–Cl lengths in this complex compare well with the corresponding lengths in the related complexes. The overall gross structural features of this conforms well with those of a related osmium(II) complex [7a], tc-[$OsBr_2(L^a)_2$]. Moreover, the average of Ru–N lengths in the present complex (average 1.995 Å) significantly smaller than Ru^{II}–N single bonds. For comparison, the Ru–N bond distances [10,11] in Ru^{II}–NH_3 and Ru^{II}–bpy (bpy = 2,2′-bipyridine) lie in the range 2.14–2.06 Å; which are appreciably longer than [9,12] Ru(II)–N(azo) lengths (ca. 1.98 Å) in [$RuCl_2(pap)_2$] complex where very strong metal (dπ) and ligand (pπ) interactions were noted. Thus the short Ru–N distances in the tc-[$RuCl_2(L^a)_2$] complex confirms strong dπ–pπ interactions. This effect has also been reflected in the high metal based anodic potentials (vide infra).

3.4. Electronic spectra and redox properties

From the crystallographic data it is obvious that in the ruthenium complexes, under consideration, there exist strong metal–ligand dπ–pπ interactions. In order to have some insight into the nature of redox and spectroscopically relevant orbitals, a standard extended Hückel MO calculation using the crystallographic parameters was performed on tc-[$RuCl_2(L^a)_2$] using the CACAO programme [14] by Mealli and Proserpio. A partial energy level scheme is shown in Fig. 3. In this complex, the molecular orbitals, LUMO and HOMO-1 are heavily mixed orbitals where as HOMO is almost a pure ruthenium orbital. Pictorial representations of these three molecular orbitals are deposited as supplementary information.

The electronic spectral data are collected in (Table 4). Two representative spectra of isomeric (tc- and cc-) [$RuCl_2(L^a)_2$] are shown in Fig. 4. There are two major transitions in the range 1600–250 nm. The lowest energy transitions, occurring in the near IR region, is weak (λ, ca. 950 nm; ε, ca. 950 M^{-1} cm^{-1}) and broad compared to the next highly intense transition (λ, ca. 600 nm; ε, ca. 23 100 M^{-1} cm^{-1}) in the visible region. However, the intensity of NIR transition for the present complex is too intense for a d–d transition. This transition may be ascribed to HOMO Ru(dπ) → LUMO transition. The next highly intense transition at approximately 590 nm is due to a transition between two heavily mixed metal–ligand orbitals, LUMO and HOMO-1. This type of transitions are known to exist in other related complexes [7d,15] and their intensities are

Table 3
Selected bond lengths (Å) for tc-[$RuCl_2(L^a)_2$]

Ru–Cl(1)	2.402(2)	C(1)–C(2)	1.429(9)
Ru–Cl(2)	2.388(2)	C(2)–C(3)	1.360(10)
Ru–N(1)	1.996(5)	C(3)–C(4)	1.422(11)
Ru–N(2)	2.005(5)	C(4)–C(5)	1.337(11)
Ru–N(3)	1.982(6)	C(5)–C(6)	1.413(9)
Ru–N(4)	1.999(6)	C(6)–C(1)	1.453(9)
C(1)–N(1)	1.314(8)	C(13)–C(14)	1.429(12)
C(6)–N(2)	1.333(8)	C(14)–C(15)	1.332(14)
C(13)–N(3)	1.302(10)	C(15)–C(16)	1.420(2)
C(18)–N(4)	1.314(9)	C(16)–C(17)	1.362(14)
C(7)–N(2)	1.436(9)	C(17)–C(18)	1.445(11)
C(19)–N(4)	1.432(8)	C(18)–C(13)	1.447(10)

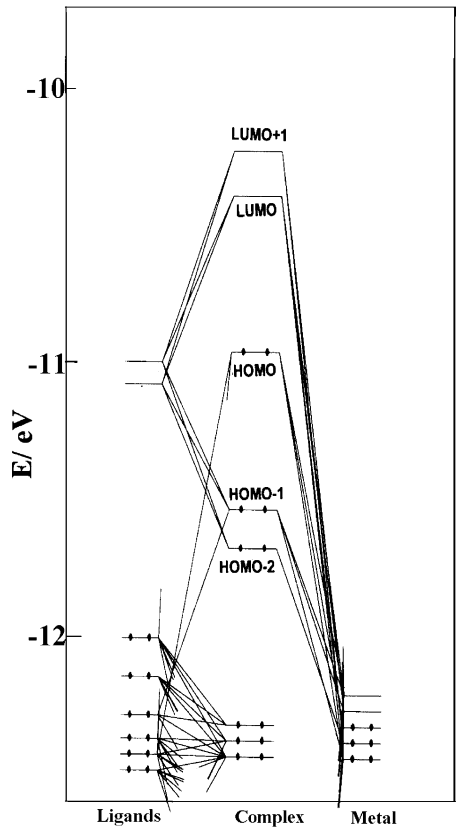


Fig. 3. Partial energy level diagram of tc-[$RuCl_2(L^a)_2$].

Table 4
Electronic spectral data

Compound	Absorption [a] λ_{max} [nm (ε ($M^{-1}cm^{-1}$))]
tc-$[RuCl_2(L^a)_2]$	948 [b] (950), 590 (22682), 486 [b] (6993), 432 [b] (5748)
cc-$[RuCl_2(L^a)_2]$	970 [b] (942), 598 (23124), 482 [b] (6350), 432 [b] (5642)
tc-$[RuCl_2(L^b)_2]$	930 [b] (850), 592 (19500), 475 [b] (9580), 406 [b] (9933)
cc-$[RuCl_2(L^b)_2]$	930 [b] (840), 598 (20100), 476 [b] (9240), 419 [b] (9870)
$[RuCl_2(ArNH_2)_2(L^a)]$	585 [b] (2070), 492 (6840), 365 (2650)
$[RuCl_2(ArNH_2)_2(L^b)]$	590 [b] (6750), 495 (15350), 380 (5390)

[a] Data obtained from absorption spectra.
[b] Shoulder.

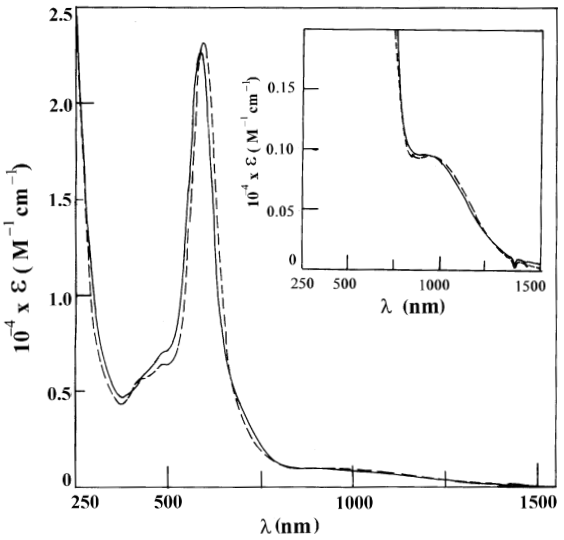


Fig. 4. Solution spectra of tc-$[RuCl_2(L^a)_2]$ (—) and cc-$[RuCl_2(L^a)_2]$ (---) in dichloromethane.

Table 5
Cyclic voltammetric data

Compound	Oxidation $E_{1/2}$ (V) [a]	Reduction $E_{1/2}$ (V) [a]
tc-$[RuCl_2(L^a)_2]$	0.81	−0.66 [b], −1.41 [b]
cc–$[RuCl_2(L^a)_2]$	0.80	−0.65 [b], −1.41 [b]
tc-$[RuCl_2(L^b)_2]$	0.70	−0.75 [b], −1.48 [b]
cc-$[RuCl_2(L^b)_2]$	0.70	−0.78 [b], −1.55 [b]
$[RuCl_2(ArNH_2)_2(L^a)]$	0.60	−0.73 [b]
$[RuCl_2(ArNH_2)_2(L^b)]$	0.52	−0.82 [b]

[a] Experiments were carried out in CH_3CN at 298 K using TEAP as supporting electrolyte. The reported data correspond to a scan rate of 50 mV s^{-1}.
[b] Irreversible cathodic response, the potential corresponds to E_{pc}.

generally very high. For example, a similar transition at approximately 620 nm was noted [7a] for a related osmium complex, $[OsBr_2(L^a)_2]$. The spectral patterns of the two isomers of $[RuCl_2(L)_2]$ are nearly identical except the minor differences in band positions and intensities.

The redox properties of the ruthenium complexes have been studied by cyclic voltammetry with a platinum-working electrode in the range 1.8 to −1.5 V. Voltammetric data are collected in (Table 5) and representative voltammograms are displayed in Fig. 5. All the potentials are referenced to the saturated calomel electrode (SCE). Both the isomers of $[RuCl_2(L)_2]$ show almost identical voltammograms. The difference in geometry seems to have negligible effects on the redox potentials. The complexes exhibited a reversible anodic response near 0.80 V and two irreversible cathodic responses in the potential range −0.60 to −1.60 V. The oxidation process in these complexes occurs at HOMO, which is primarily a metal orbital. One-electron coulometric oxidation of both the isomers of $[RuCl_2(L^a)_2]$ afforded reddish–brown solutions. The voltamograms of the electrogenerated trivalent complexes are superposable (initial scan cathodic) on those of the corresponding isomers of $[RuCl_2(L^a)_2]$ (initial scan anodic) showing that the metal redox processes are reversible. The EPR of the Ru(III) complexes were studied in acetonitrile–toluene glass at 77 K, which display rhombic EPR spectra with three distinct resonances (Table 6). The spectrum of a representative example cc-$[RuCl_2(L^a)_2]^+$ is shown in Fig. 6. The trivalent ruthenium complexes may also be generated by the chemical oxidation of the bivalent complexes by Br_2. Unfortunately, the oxidized complexes are not stable

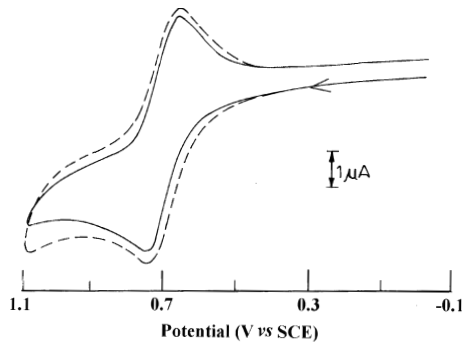


Fig. 5. Cyclic voltammograms (scan rate 50 mV s^{-1}, solvent CH_3CN, 0.1 M TEAP) of tc-$[RuCl_2(L^a)_2]$ (—) and cc-$[RuCl_2(L^a)_2]$ (---).

Table 6
EPR g-values [a] and derived parameters of the complex $[RuCl_2(L^a)_2]^+$

Compound	Derived energy parameters [b] (cm^{-1})				
	g_1	g_2	g_3	Δ	V
tc-$[RuCl_2(L^a)_2]^+$	2.404	2.256	1.882	5529	2014
cc-$[RuCl_2(L^a)_2]^+$	2.469	2.272	1.909	6676	3136

[a] In 1:1 dichloromethane–toluene solution at 77 K.
[b] Taking the value of the spin–orbit coupling constant (λ) for Ru(III) as equal to 1000 cm^{-1}.

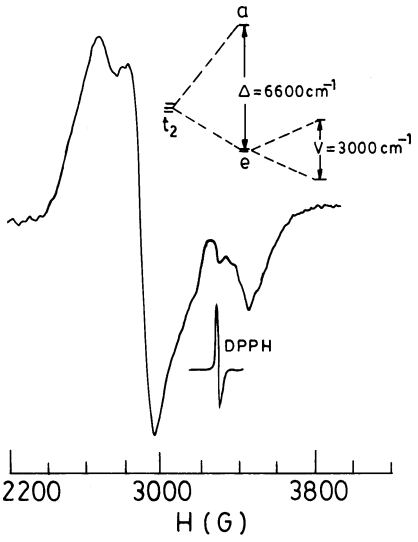


Fig. 6. EPR spectrum of cc-$[RuCl_2(L^a)_2]^+$ in frozen 1:1 dichloromethane–toluene solution at 77 K, showing computed splittings of t_2 orbitals. DPPH = diphenylpicrylhydrazyl.

enough for their isolation. They revert to the parent divalent complexes rapidly. The observed rhombicity of the EPR spectra in the present cases is understandable in terms of the gross molecular symmetry of these complexes, containing three non-equivalent axes. The distortion parameters have been computed [16] using the observed g values. The axial distortion (Δ, which split t_2 into a and e) is indeed much stronger than the rhombic distortion (V, which splits e). Thus the EPR spectral data of the complexes indicate significant distortion from ideal octahedral arrangements which indeed in line with the observed structure of the parent bivalent complexes.

In conclusion it may be stated that the present work further demonstrates that aromatic primary amines are susceptible to metal mediated oxidative dimerization processes via the formation of a C–N bond. The isomeric complexes, $RuCl_2L_2$, thus formed, represent an interesting family of ruthenium–diimines that show strong metal d(π)–ligand p(π) interactions. Chemical reactions including the chloride substitution at $[RuCl_2(L)_2]$ are now under scrutiny.

4. Supplementary material

Crystallographic data for the structural analysis have been deposited with the Cambridge Crystallographic Data Centre, CCDC No. 160040. Copies of this information may be obtained free of charge from The Director, CCDC, 12 Union Road, Cambridge, CB2 1EZ, UK (fax: +44-1233-336-033; e-mail: deposit@ccdc.cam.ac.uk or www: http://www.ccdc.cam.ac.uk).

Acknowledgements

Financial support received from the Council of Scientific and Industrial Research, New Delhi is gratefully acknowledged.

References

[1] C.G. Pierpont, C.W. Lange, Prog. Inorg. Chem. 41 (1994) 331.
[2] A.B.P. Lever, H. Masui, R.A. Metcalfe, D.J. Stufkens, E.S. Dodsworth, P.R. Auburn, Coord. Chem. Rev. 125 (1993) 317.
[3] S.I. Gorelsky, E.S. Dodsworth, A.B.P. Lever, A.A. Vlcek, Coord. Chem. Rev. 174 (1998) 469.
[4] L.F. Warren, Inorg. Chem. 16 (1977) 2814.
[5] (a) S.-M. Peng, C. Chen, D.-S. Liaw, C.-I. Chen, Y. Wang, Inorg. Chim. Acta 101 (1985) L31;
(b) S.-M. Peng, K. Peters, E. Peters, A. Simon, Inorg. Chim. Acta 101 (1985) L35;
(c) D. Liaw, S.-M. Peng, Inorg. Chim. Acta 101 (1986) L11;
(d) M. Hsieh, M. Cheng, S.-M. Peng, Inorg. Chim. Acta 145 (1988) 1;
(e) P.-H. Cheng, H.-Y. Cheng, C.-C. Lin, S.-M. Peng, Inorg. Chim. Acta 169 (1990) 90;
(f) H.-Y. Cheng, S.-M. Peng, Inorg. Chim. Acta 169 (1990) 23.
[6] (a) R.A. Metcalfe, A.B.P. Lever, Inorg. Chem. 36 (1997) 4762 and references therein;
(b) C.J. Cunha, S.S. Fielder, D.V. Stynes, M. Masui, P.R. Auburn, A.B.P. Lever, Inorg. Chim. Acta 242 (1996) 293;
(c) R.A. Metcalfe, L.C.G. Vasconcellos, H. Mirza, D.W. Franco, A.B.P. Lever, J. Chem. Soc., Dalton Trans. (1999) 2653;
(d) H. Masui, A.L. Freda, M.C. Zerner, A.B.P. Lever, Inorg. Chem. 39 (2000) 141.
[7] (a) K.N. Mitra, S. Goswami, Inorg. Chem. 36 (1997) 1322;
(b) K.N. Mitra, P. Majumdar, S.-M. Peng, A. Castiñeiras, S. Goswami, Chem. Commun. (1997) 1267;
(c) K.N. Mitra, S.-M. Peng, S. Goswami, Chem. Commun. (1998) 1685;
(d) K.N. Mitra, S. Choudhury, A. Castiñeiras, S. Goswami, J. Chem. Soc., Dalton Trans. (1998) 2901;
(e) K.N. Mitra, S. Goswami, Proc. Indian Acad. Sci. (Chem. Sci.) 111 (1999) 461;
(f) A.K. Ghosh, K.N. Mitra, G. Mostafa, S. Goswami, Eur. J. Inorg. Chem. (2000) 1961.
[8] A.K. Ghosh, S.-M. Peng, R.L. Paul, M.D. Ward, S. Goswami, J. Chem. Soc., Dalton Trans. (2001) 336.
[9] S.-M. Au, W.-H. Fung, J.-S. Huang, K.-K. Cheung, C.-M. Che, Inorg. Chem. 37 (1998) 6564.
[10] C.X. Zhang, H.-C. Liang, E.-I. Kim, Q.-F. Gan, Z. Tyekla'r, K.-C. Lam, A.L. Rheingold, S. Kaderli, A.D. Zuberbuhler, K.D. Karlin, Chem. Commun. (2001) 631 and references therein.
[11] (a) S. Goswami, R. Mukherjee, A. Chakravorty, Inorg. Chem. 22 (1983) 2825;
(b) S. Goswami, A.R. Chakravarty, A. Chakravorty, Inorg. Chem. 22 (1983) 602.
[12] G.M. Sheldrick, SHELXS-86, Program for the solution of crystal structures, University of Göttingen, 1986.
[13] S. Choudhury, M. Kakoti, S. Goswami, Polyhedron 11 (1992) 3183.

[14] C. Mealli, D.M. Proserpio, J. Chem. Educ. 67 (1990) 399.

[15] (a) A.B.P. Lever, H. Masui, R.A. Metcalfe, D.J. Stufkens, E.S. Dodsworth, P.R. Auburn, Coord. Chem. Rev. 125 (1993) 317;
(b) G.A. Mines, J.A. Roberts, J.T. Hoop, Inorg. Chem. 31 (1992) 125.

[16] (a) B. Bleany, M.C.M. O'Brien, Proc. Phys. Soc. Lond., Sect. B 69 (1956) 1216;
(b) J.S. Griffith, The Theory of Transition Metal Ions, Cambridge University Press, London, 1961, p. 364;
(c) S. Bhattacharyya, A. Chakravorty, Proc. Indian Acad. Sci. 95 (1985) 159;
(d) P.H. Rieger, Coord. Chem. Rev. 135/136 (1994) 203.

PERGAMON

Polyhedron 21 (2002) 105–113

POLYHEDRON

www.elsevier.com/locate/poly

Formation and cleavage of platinacycles containing a fluorinated imine. Crystal structure of [PtMe(3,4,5-$C_6HF_3CH{=}NCH_2C_6H_5$)PPh_3]

Margarita Crespo [a,*], Mercè Font-Bardía [b], Xavier Solans [b]

[a] *Departament de Química Inorgànica, Facultat de Química, Universitat de Barcelona, Diagonal 647, E-08028 Barcelona, Spain*
[b] *Departament de Cristal.lografia, Mineralogia i Dipòsits Minerals, Universitat de Barcelona, Martí i Franquès s/n, E-08028 Barcelona, Spain*

Received 3 August 2001; accepted 5 October 2001

Abstract

The reaction of [$Pt_2Me_4(\mu\text{-}SMe_2)_2$] with the ligand 3,4,5-$C_6H_2F_3CH{=}NCH_2C_6H_5$ (**L**) yielded the cyclometallated platinum(II) compound [PtMe(3,4,5-$C_6HF_3CH{=}NCH_2C_6H_5$)SMe_2] (**1**), in which the imine acts as a [C,N]-bidentate ligand. Compounds [PtMe(3,4,5-$C_6HF_3CH{=}NCH_2C_6H_5$)DMSO] (**2**) (DMSO = dimethyl sulfoxide) and [PtMe(3,4,5-$C_6HF_3CH{=}NCH_2C_6H_5$)PPh_3] (**3**) were obtained from a displacement reaction of SMe_2 for DMSO or PPh_3, respectively. Oxidative addition of methyl iodide to compounds **1**–**3** produced, respectively, [$PtMe_2I$(3,4,5-$C_6HF_3CH{=}NCH_2C_6H_5$)SMe_2] (**4a**/**4b**) as two isomers, [{$PtMe_2I$(3,4,5-$C_6HF_3CH{=}NCH_2C_6H_5$)}$_2$] (**5**) and [$PtMe_2I$(3,4,5-$C_6HF_3CH{=}NCH_2C_6H_5$)PPh_3] (**6**). Platinum(II) metallacycles can be cleaved upon reaction with an excess of PPh_3 or with the diphosphine dppe to yield, respectively, compounds [PtMe(3,4,5-$C_6HF_3CH{=}NCH_2C_6H_5$)$(PPh_3)_2$] (**7**) and [PtMe(3,4,5-$C_6HF_3CH{=}NCH_2C_6H_5$)dppe] (**8**) in which the imine acts as a monodentate [C] ligand. Analogous compounds could not be obtained for platinum(IV) since in this case neither PPh_3 nor dppe can cleave the metallacycle. The reaction of **4a**/**4b** with dppe produced [{$PtMe_2I$(3,4,5-$C_6HF_3CH{=}NCH_2C_6H_5$)}$_2$dppe] (**11**), a binuclear compound in which the diphosphine bridges two platinum(IV) moieties with the imine acting as a [C,N]-bidentate ligand. All compounds were characterised by analytical and spectroscopic techniques and compound **3** was also characterised crystallographically. © 2002 Elsevier Science Ltd. All rights reserved.

Keywords: Platinum; Cyclometallation; Imine; Fluorine; Phosphine; Crystal structures

1. Introduction

Cyclometallated complexes of the Group 10 elements have generated considerable interest due to their numerous applications and interesting properties. Previous results showed that the reactions with phosphines could be taken as a criterion for the stability of metallacycles [1]. Moreover, it has been shown that steric crowding in the co-ordination sphere of the metal favoured the cleavage of metallacycles upon reaction with triphenylphosphine. In particular, the presence of a fluorine [2–4] or a chlorine [5,6] atom in the position adjacent to the M–C(aryl) bond seems to be decisive. On the other hand, both palladium(II) [7] and platinum(II) [6,8,9] metallacycles are cleaved easily with diphosphines such as 1,2-bis(diphenylphosphino)-ethane, which can be explained by the chelating nature of this ligand. Nevertheless, examples in which the formation of either compounds containing a bridging diphosphine [10] or ionic compounds with a chelate diphosphine [11] is favoured over cleavage of the metallacycles have also been reported.

In this paper we report new cyclometallated platinum compounds containing the imine 3,4,5-$C_6H_2F_3CH{=}NCH_2C_6H_5$ and their reactions with phosphines in order to analyse the factors governing the cleavage of the formed metallacycles.

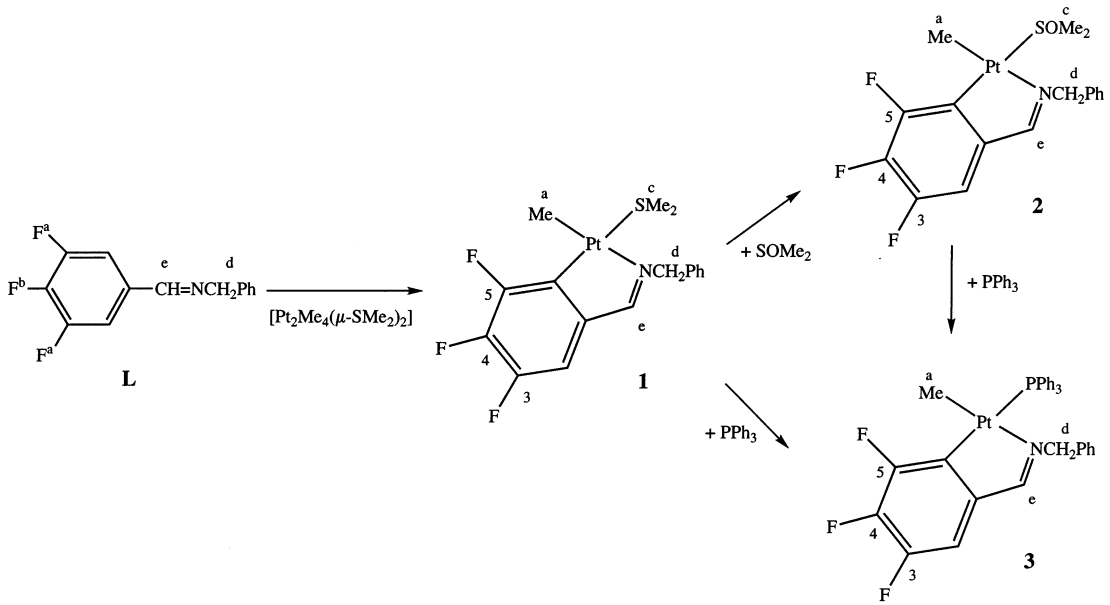
* Corresponding author. Fax: +34-93-4907-725.
E-mail address: margarita.crespo@qi.ub.es (M. Crespo).

0277-5387/02/$ - see front matter © 2002 Elsevier Science Ltd. All rights reserved.
PII: S0277-5387(01)00971-8

2. Results and discussion

The reaction of $[Pt_2Me_4(\mu\text{-}SMe_2)_2]$ with ligand 3,4,5-$C_6H_2F_3CH{=}NCH_2C_6H_5$ (**L**) yielded the cyclometallated platinum(II) compound [PtMe(3,4,5-$C_6HF_3CH{=}NCH_2$-C_6H_5) SMe_2] (**1**) by *ortho* metallation with loss of methane, as reported for analogous systems [3,4]. Compound **1** reacted with an excess of dimethylsulfoxide (DMSO) or with PPh_3 in a 1:1 molar ratio to yield respectively compounds [PtMe(3,4,5-$C_6HF_3CH{=}NCH_2$-C_6H_5)DMSO] (**2**) and [PtMe(3,4,5-$C_6HF_3CH{=}NCH_2$-C_6H_5)PPh_3] (**3**) which result from a displacement reaction of SMe_2 for DMSO or PPh_3. The reaction of compound **2** with PPh_3 gave compound **3** which indicates the lability order $SMe_2 > DMSO > PPh_3$ for these platinum(II) compounds. Compounds **1**–**3**, shown in Scheme 1, were characterised by elemental analysis and NMR spectroscopies. In the ^1H NMR spectra, the methyl group bound to platinum is coupled to the fluorine atom in position five of the aryl ring, thus revealing a through-space interaction; additional coupling to the phosphorous atom is observed for compound **3**. The methyl, the imine and the methylene hydrogens are coupled to ^{195}Pt and the values of the coupling constants are characteristic of this kind of cyclometallated platinum(II) compounds. For compound **2**, the $J(H{-}Pt)$ value of the protons of DMSO [12] and the $\delta(^{195}Pt)$ value [13] indicate that DMSO is S-bonded to platinum; this is further confirmed by a strong band at 1110 cm^{-1} in the IR spectrum. A process involving oxidative cycloplatination and sulfur deoxygenation has been reported in the reaction between (*E*)-2-methyl-1-phenylbutan-1-one oxime and *cis*-$[PtCl_2(DMSO)_2]$ in refluxing methanol [14]; however, compound **2** was recovered unchanged when treated under such conditions. The presence of the PPh_3 ligand in **3** is confirmed by ^{31}P NMR spectroscopy and the value of the coupling constant to platinum ($J(P{-}Pt) = 2631$ Hz) is in the expected range for a phosphine with a fluorinated aryl group in *trans*. In the ^{19}F NMR spectra, three distinct resonances appear in the aromatic region and the values of the coupling constants are in the range expected for analogous compounds [15].

Compound **3** was also characterised crystallographically. Suitable crystals were grown from acetone solution. The crystal structure is composed of discrete molecules separated by van der Waals interactions. A view of the molecule is shown in Fig. 1. Selected bond lengths and angles are given in Table 1. As expected from spectroscopic characterisation, the methyl group is *trans* to the nitrogen atom, the C=N group is *endo* to the cycle and the imine adopts an (*E*)-configuration, the torsion angle C(6)–C(7)–N–C(8) being $-173.99(4)°$. The platinum atom displays a tetrahedral distorted planar co-ordination and the following displacements (Å) are observed from the least-squares plane of the co-ordination sphere: Pt, -0.0264; P, 0.1658; N, -0.1785; C(1), 0.2074; C(15), -0.1683. The metallacycle is approximately planar; the largest deviation from the mean plane determined by the five atoms is -0.0628 Å for C(1). The dihedral angle between the metallacycle and the co-ordination plane is larger (10.24°) than those reported for [PtMe(2,3,4-$C_6HF_3CH{=}NCH_2C_6H_5$)PPh_3] (4.6°) [3] and [PtMe-(2,3,4-$C_6HF_3CH{=}NCH_2CH_2NMe_2$)] (0.28°) [4]. A larger deviation from coplanarity reduces the steric interaction between the methyl group and the fluorine substituent



Scheme 1.

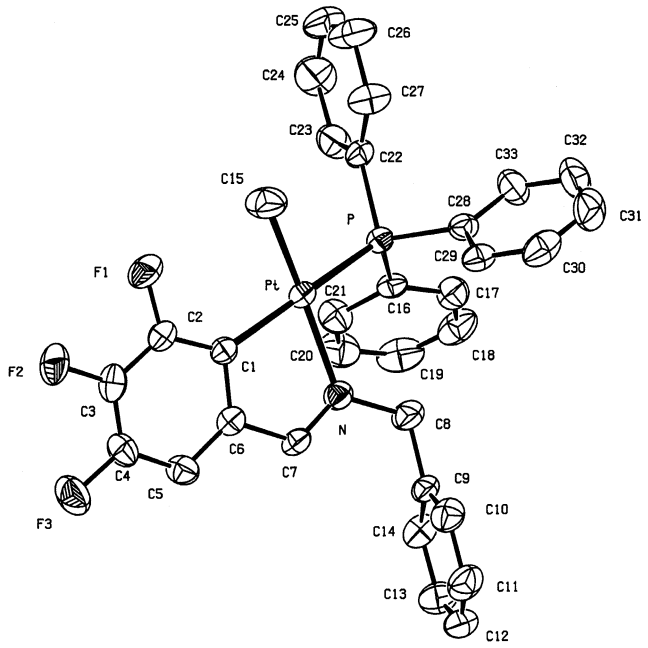


Fig. 1. Molecular structure of compound **3**.

Table 1
Selected bond lengths (Å) and bond angles (°)

Bond lengths			
Pt–C(15)	2.053(6)	Pt–C(1)	2.064(5)
Pt–N	2.144(4)	Pt–P	2.2815(12)
P–C(28)	1.816(5)	Pt–C(16)	1.824(5)
P–C(22)	1.833(5)	F(1)–C(2)	1.360(6)
F(2)–C(3)	1.344(6)	F(3)–C(4)	1.354(6)
N–C(7)	1.279(6)	N–C(8)	1.489(7)
C(1)–C(2)	1.384(7)	C(1)–C(6)	1.409(7)
C(2)–C(3)	1.379(7)	C(3)–C(4)	1.360(8)
C(4)–C(5)	1.366(8)	C(5)–C(6)	1.388(7)
C(6)–C(7)	1.451(7)	C(8)–C(9)	1.498(7)
C(13)–C(12)	1.349(9)	C(13)–C(14)	1.373(8)
C(12)–C(11)	1.359(9)	C(11)–C(10)	1.387(8)
C(10)–C(9)	1.368(8)	C(9)–C(14)	1.366(8)
Bond angles			
C(15)–Pt–C(1)	94.8(2)	C(15)–Pt–N	169.3(2)
C(1)–Pt–N	79.08(17)	C(15)–Pt–P	90.58(18)
C(1)–Pt–P	167.76(13)	N–Pt–P	97.17(11)
C(28)–P–C(16)	106.5(2)	C(28)–P–C(22)	101.6(2)
C(16)–P–C(22)	101.7(2)	C(28)–P–Pt	117.48(16)
C(16)–P–Pt	110.25(15)	C(22)–P–Pt	117.67(17)
C(7)–N–C(8)	119.3(4)	C(7)–N–Pt	113.6(3)
C(8)–N–Pt	126.6(3)	C(2)–C(1)–C(6)	112.3(4)
C(2)–C(1)–Pt	135.0(4)	C(6)–C(1)–Pt	112.3(3)
C(3)–C(2)–C(1)	124.3(5)	C(4)–C(3)–C(2)	120.2(5)
C(3)–C(4)–C(5)	119.9(5)	C(4)–C(5)–C(6)	118.2(5)
C(5)–C(6)–C(1)	125.0(5)	C(5)–C(6)–C(7)	119.1(4)
C(1)–C(6)–C(7)	115.8(4)	N–C(7)–C(6)	118.3(4)
N–C(8)–C(9)	116.4(4)		

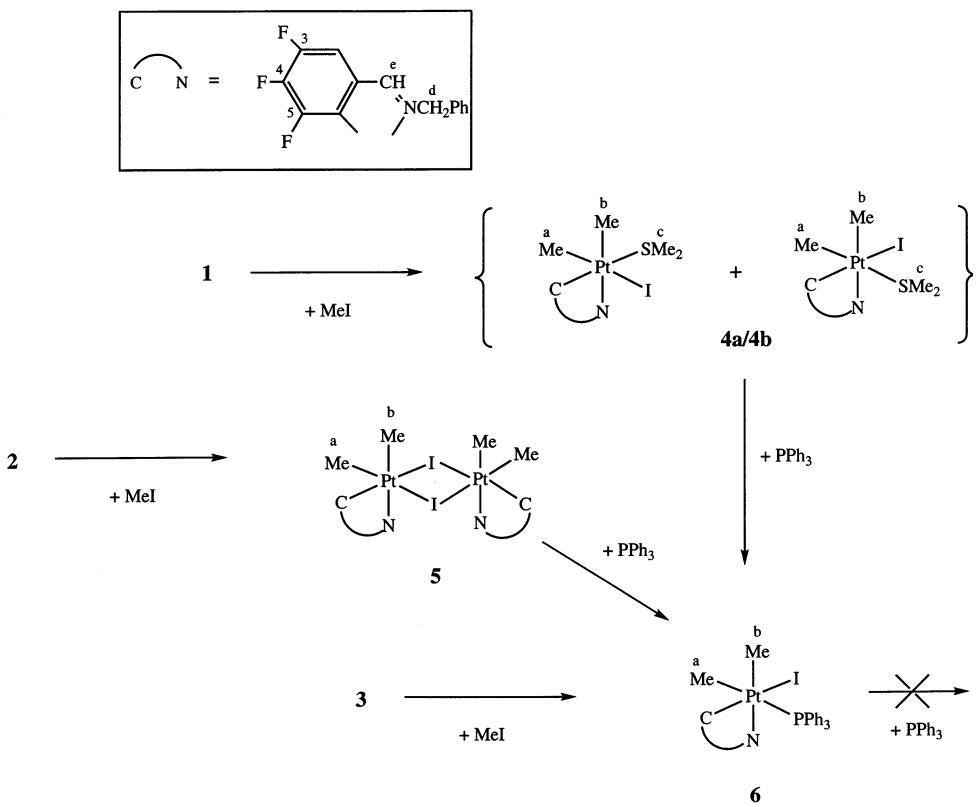
in a position adjacent to the Pt–C(aryl) bond. Nevertheless, the distance C(15)···F(1) of 2.929 Å can be taken as an indication of a short contact between the methyl group and the fluorine, which are close enough for the van der Waals radii to overlap. The coupling between the methyl protons and ^{19}F in the NMR spectrum implies that this interaction persists in solution. Bond lengths and angles are well within the range of values obtained for analogous compounds [3,4,16]. The 'bite' angle C(1)–Pt–N of 79.08(17) is characteristic of cyclometallated platinum(II) complexes [17].

Oxidative addition of methyl iodide to compound **1** carried out in $CDCl_3$ at NMR scale produced a mixture of two isomers of platinum(IV) compound $[PtMe_2I(3,4,5\text{-}C_6HF_3CH{=}NCH_2C_6H_5)SMe_2]$ (**4a**/**4b**) in nearly equal amounts together with a very small amount (less than 5% of the reaction mixture) of compound **5** (see below). The spectral parameters for compounds **4** are in good agreement with those reported in the literature for analogous compounds [18] and are assigned to the isomers depicted in Scheme 2, which differ only in having a SMe_2 or an I *trans* to the axial methyl. For both isomers only the equatorial methyl is coupled to the fluorine at position five of the aryl ring. Oxidative addition of methyl iodide to compound **2** gave compound **5** as a pale yellow solid which was characterised by NMR and FAB spectroscopies. Of the two methyl resonances—both coupled to platinum—the one at lower field is assigned to the equatorial methyl which is also coupled to the fluorine atom F^5. The absence of coordinated S– or O–DMSO in the ^1H and IR spectra points to an iodide bridged platinum(IV) dimer, a structure that is confirmed by FAB mass spectrometry. Moreover, since resonances due to SMe_2 are not observed, the formation of dimethylsulfide from DMSO within the co-ordination sphere of platinum as described in the literature for analogous systems[14] can be ruled out. The low affinity of the DMSO ligand for platinum(IV) has already been shown in the reaction of *cis*-$[PtMe_2(DMSO)_2]$ with methyl iodide which yields the platinum(IV) tetramer $[\{PtMe_3(\mu_3\text{-}I)\}_4]$ [19]. The $\delta(^{195}Pt)$ value obtained for **5** (-2700 ppm) is similar to that reported in the literature for the tetramer (-2769 ppm) [20]. Oxidative addition of methyl iodide to compound **3** produced cyclometallated platinum(IV) compound $[PtMe_2I(3,4,5\text{-}C_6HF_3CH{=}NCH_2C_6H_5)(PPh_3)]$ (**6**) which was characterised by elemental analyses and NMR spectra. Two methyl resonances appear at $\delta = 1.38$ ($^2J(Pt–H) = 60$ Hz) and $\delta = 2.20$ ($^2J(Pt–H) = 69$ Hz) both coupled to ^{195}Pt and ^{31}P ($^3J(P–H) = 8$ Hz). The small value of the coupling constant of the axial methyl with platinum suggest a *trans* arrangement of this group and the PPh_3 ligand, as reported previously for analogous compounds [8]. The equatorial methyl is also coupled to the fluorine atom at position five of the aryl ring. The $J(P–Pt)$ value is in the range expected for platinum(IV) compounds, which is considerably reduced compared to that of the platinum(II) compound. Alternatively, compound **6** could be prepared upon reaction of com-

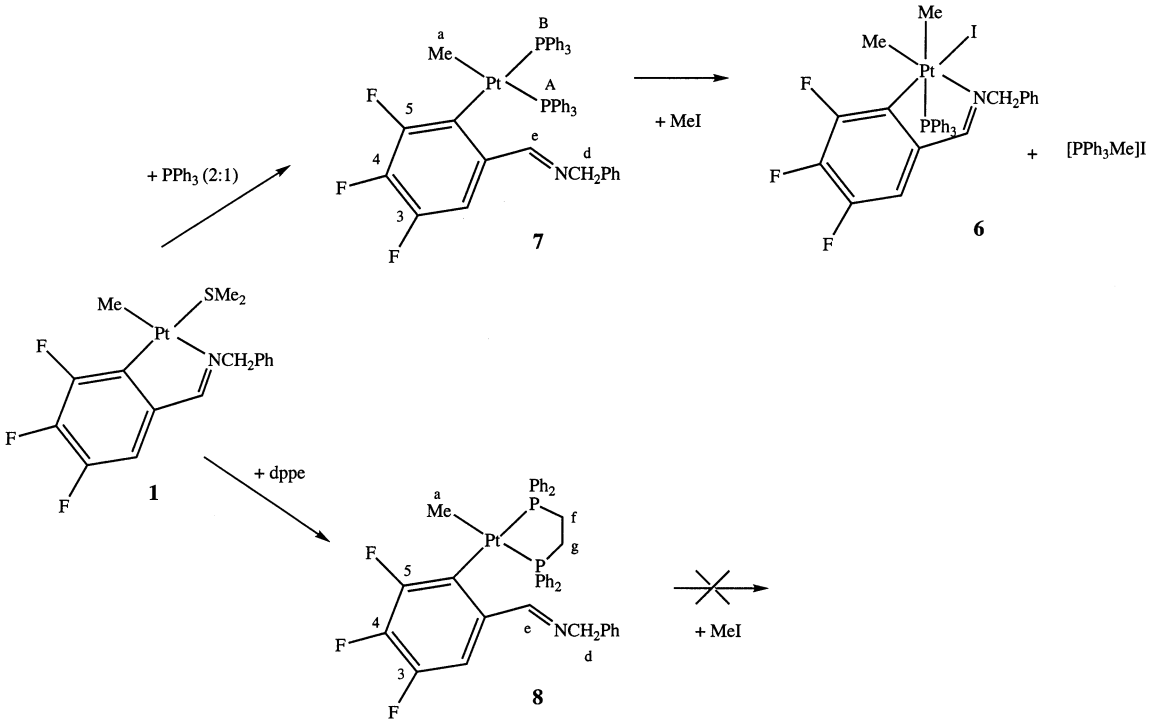
pounds **4a**/**4b** or **5** obtained in situ in acetone with the equivalent amount of triphenylphosphine and all preparative methods lead to the same stereoisomer in which the bulky triphenylphosphine is in an axial position. The lability order $DMSO > SMe_2 > PPh_3$ is deduced for platinum(IV) compounds.

Cleavage of the metallacycle in platinum(II) compounds was achieved upon reaction of compound **1** with two equivalents of PPh_3 or with one equivalent of the bidentate phosphine 1,2-bis(diphenylphosphino)ethane (dppe) to yield, respectively, compounds [PtMe(3,4,5-$C_6HF_3CH{=}NCH_2C_6H_5$)(PPh_3)$_2$] (**7**) and [PtMe(3,4,5-$C_6HF_3CH{=}NCH_2C_6H_5$)dppe] (**8**) (see Scheme 3) which were obtained as white solids and characterised by elemental analyses and NMR spectroscopies. In both cases, the methyl resonance is coupled to two non-equivalent phosphorus atoms and the value of the coupling constants with ^{195}Pt are reduced (^2J(Pt–H) = 65 Hz (**7**) or 67 Hz (**8**)) when compared to that of cyclometallated compound **3** (83 Hz). Moreover, the imine proton is not coupled to ^{195}Pt and the ^{31}P NMR spectra show two sets of resonances due to two non-equivalent phosphorus atoms, both coupled to platinum. These results indicate that two phosphorus atoms are present in the co-ordination sphere of platinum(II) and therefore the imine is acting as a monodentate ligand through the aryl carbon. As observed previously for analogous compounds [3,4], the ^3J(Pt–F^5) values are much larger (412 Hz (**7**) and 385 Hz (**8**)) than those obtained for cyclometallated compounds **1** (140 Hz), **2** (98 Hz) and **3** (87 Hz). The large value of the coupling constant may arise from a perpendicular orientation of the aryl group to the co-ordination plane [21]. The methyl group consistently does not couple with the fluorine in position five of the aryl ring.

In spite of the easy cleavage of the metallacycle reported above for platinum(II) compounds, cyclometallated platinum(IV) compound **6** did not react further with triphenylphosphine even when large excesses were used. Other attempts to obtain triphenylphosphine platinum(IV) derivatives in which the imine acts as a monodentate [C] ligand were also unsuccessful. For instance, the reaction of platinum(II) compound [PtMe(3,4,5-$C_6HF_3CH{=}NCH_2C_6H_5$)(PPh_3)$_2$] (**7**) with methyl iodide gave a mixture of cyclometallated platinum(IV) compound **6**, characterised as above, and the phosphonium salt [PPh_3Me]I, for which ^{1}H and ^{31}P NMR data are consistent with the values given in the literature [22]. In this process, oxidative addition of methyl iodide took place along with co-ordination of the dangling imine nitrogen to platinum and dissociation of the phosphine, which gave the phosphonium salt. This result can be related to the higher affinity of platinum(IV) for nitrogen than for phosphorus donor ligands due to its harder nature.



Scheme 2.



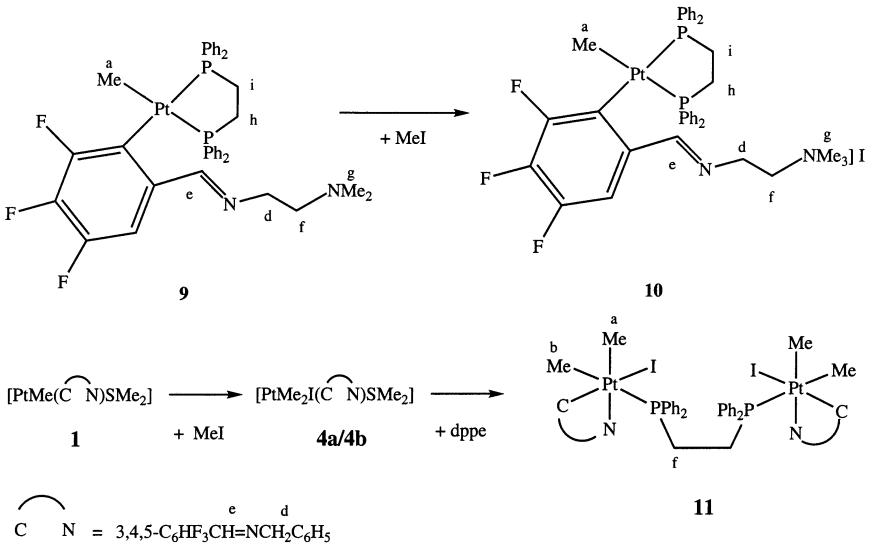
Scheme 3.

On the other hand, compound [PtMe(3,4,5-$C_6HF_3CH{=}NCH_2C_6H_5$)dppe] (**8**) did not react with methyl iodide even after 48 h when evidence of decomposition was observed. For the purpose of comparison, the reaction with methyl iodide was also tested for compound [PtMe(3,4,5-$C_6HF_3CH{=}NCH_2CH_2NMe_2$)(dppe)] (**9**) obtained from [PtMe(3,4,5-$C_6HF_3CH{=}NCH_2CH_2NMe_2$)] [4] in which the terdentate imine 3,4,5-$C_6HF_3CH{=}NCH_2CH_2NMe_2$ acts as a monodentate [C] ligand. The reaction of compound **9** with methyl iodide is shown in reaction 1 and produced the ionic compound [PtMe(3,4,5-$C_6HF_3CH{=}NCH_2CH_2NMe_3$)(dppe)]I (**10**) resulting from methylation of the amine group. NMR data are similar to those obtained for **9** except for the fact that the amine protons are shifted towards higher fields ($\delta = 3.43$ ppm) and integrate nine hydrogen atoms. An analogous process in which methyl iodide is added to the dangling NMe_2 moiety but not to the platinum centre has been described for compound [PtMe(3-$C_6H_3ClCH{=}NCH_2CH_2NMe_2$)(dppe)] [6].

In view of these results, the reaction of compounds **4a**/**4b**—obtained in situ from **1**—with dppe in the ratio 2:1 was also tested. A yellow non-electrolyte solid was obtained and was characterised as binuclear platinum(IV) compound [{$PtMe_2I$(3,4,5-$C_6HF_3CH{=}NCH_2C_6H_5$)}$_2$(dppe)] (**11**) by NMR and FAB Mass spectra. Compound **11** could not be isolated in a pure form due to decomposition processes during attempted crystallisation in several solvents. In the ^{1}H NMR spectrum two methyl resonances appear at $\delta = 1.05$ (^2J(Pt–H) = 59 Hz) and $\delta = 1.83$ (^2J(Pt–H) = 69 Hz) both coupled to ^{195}Pt and to one phosphorus atom (J(Pt–P) ca. 7–8 Hz), and the equatorial methyl also coupled to the fluorine atom at position five of the aryl ring. As in compound **6**, these values suggest a *trans* arrangement of the axial methyl and the phosphorus atom and a *fac*-PtC_3 stereochemistry. The imine proton is also coupled to ^{195}Pt (^{3}J(Pt–H) = 47 Hz) indicating that the metallacycle has not been cleaved. Two resonances appear in the ^{31}P NMR spectrum at $\delta = -10.4$ (J(Pt–P) = 1049 Hz) and $\delta = -10.9$ (J(Pt–P) = 1048 Hz); these values are characteristic of phosphines bound to platinum(IV) and *trans* to a methyl group [9], and can only be assigned to two different conformations of compound **11**. When larger amounts of diphosphine were used the main products are compound **11** and free diphosphine or its oxide. No evidence of formation of compounds containing chelate diphosphine was observed in the ^{1}H or in the ^{31}P NMR; the formation of such compounds requires dissociation of either nitrogen or iodide, and it is likely that such processes are not favoured for platinum(IV) compounds.

In conclusion, while platinum(II) metallacycles derived from imine 3,4,5-$C_6H_2F_3CH{=}NCH_2C_6H_5$ can be opened up using a diphosphine or an excess of a monodentate phosphine, platinum(IV) metallacycles are much more resistant to cleavage. Moreover, oxidative addition to platinum(II) compound [PtMe(3,4,5-$C_6HF_3CH{=}NCH_2C_6H_5$)(PPh_3)$_2$] (**7**) in which the imine acts as a [C] ligand favours the co-ordination of the

imine nitrogen to yield a [C,N] platinum(IV) cyclometallated compound. These results could be explained by the higher affinity of platinum(IV) for nitrogen donor ligands when compared to the softer platinum(II).



3. Experimental

^{1}H, ^{19}F, $^{31}P-\{^{1}H\}$ and ^{195}Pt NMR spectra were recorded by using Varian Gemini 200 (^{1}H, 200MHz), Varian 300 (^{19}F, 282.2 MHz; ^{195}Pt, 64.2 MHz) and Bruker 250 (^{31}P, 101.25 MHz) spectrometers, and referenced to $SiMe_4$ (^{1}H), CCl_3F (^{19}F), H_3PO_4 (^{31}P) and H_2PtCl_6 (^{195}Pt). δ values are given in ppm and J values in Hz. IR spectra were recorded as KBr disks on a Nicolet 520 FT-IR spectrometer. Conductivity measurements were carried out to a Crison 2000 equipment. Microanalyses and FAB mass spectra were performed by the Serveis Científico-Tècnics de la Universitat de Barcelona.

3.1. Preparation of the compounds

Compounds $[Pt_2Me_4(\mu\text{-}SMe_2)_2]$ [23] and [PtMe(3,4,5-$C_6HF_3CH{=}NCH_2CH_2NMe_2$)] [4] were prepared as reported.

The ligand 3,4,5-$C_6H_2F_3CH{=}NCH_2C_6H_5$ (**L**) was prepared by the reaction of 0.5 g (3.1×10^{-3} mol) of the corresponding aldehyde with an equimolecular amount (0.33 g) of benzylamine in refluxing ethanol. The mixture was refluxed for 2 h, and the solvent was removed in a rotary evaporator to yield a yellow oil. Yield 0.65 g (83%). ^{1}H NMR ($CDCl_3$): $\delta = 4.82$ [s, H^d]; 7.42 [m, aromatics]; 8.24 [s, H^e]. ^{19}F NMR ($CDCl_3$): $\delta = -140.09$ [dd, $J(F^a-F^b) = 20$, $J(F^a-H) = 8$, F^a]; -163.14 [tt, $J(F^a-F^b) = 20$, $J(F^b-H) = 6$, F^b].

Compound [PtMe(3,4,5-$C_6HF_3CH{=}NCH_2C_6H_5$)SMe_2] (**1**) was obtained by the reaction of 100 mg (1.74×10^{-4} mol) of compound $[Pt_2Me_4(\mu\text{-}SMe_2)_2]$ with 87.6 mg (3.52×10^{-4} mol) of the ligand 3,4,5-$C_6H_2F_3CH{=}NCH_2C_6H_5$ in acetone (20 ml). After continuous stirring during 16 h, the solvent was removed in a rotary evaporator and the resulting orange solid was washed with hexane (2×10 mL) and dried under vacuum. Yield 140 mg (77%). ^{1}H NMR (acetone-d^6): $\delta = 1.13$ [d, $^{2}J(Pt-H) = 80$, $J(F-H) = 6$, Me^a]; 1.90 [s, $^{3}J(Pt-H) = 36$, Me^c]; 5.19 [s, $^{3}J(Pt-H) = 13$, H^d]; {7.28–7.38 [m], aromatics}; 8.96 [s, $^{3}J(Pt-H) = 56$, H^e]. ^{19}F NMR (acetone-d^6): $\delta = -122.61$ [dt, $J(Pt-F^5) = 140$, $J(F^5-F^4) = 23$, $J(F^5-F^3) = J(F^5-H) = 5$, F^5]; -146.95 [m, F^3]; -159.89 [ddd, $J(Pt-F^4) = 100$, $J(F^4-F^5) = 24$, $J(F^4-F^3) = 20$, $J(F^4-H) = 7$, F^4]. *Anal.* Found: C, 39.4; H, 3.6; N, 2.9. Calc. for $C_{17}H_{18}F_3NSPt$: C, 39.23; H, 3.49; N, 2.69%.

Compound [PtMe(3,4,5-$C_6HF_3CH{=}NCH_2C_6H_5$)-DMSO] (**2**) was obtained by adding two drops of DMSO to 50 mg (9.6×10^{-5} mol) of compound **1** in dichloromethane (20 ml). After continuous stirring during 1 h, the solvent was removed in a rotary evaporator and the oily residue was washed with diethylether (3×5 ml). The obtained yellow solid was dried in vacuum. Yield 35 mg (68%). ^{1}H NMR ($CDCl_3$): $\delta = 0.95$ [d, $^{2}J(Pt-H) = 80$, $J(F-H) = 6$, Me^a]; 2.78 [s, $^{3}J(Pt-H) = 20$, Me^c], 5.28 [s, $^{3}J(Pt-H) = 5$, H^d]; {7.14 [m, 1H]; 7.30–7.41 [m, 5H], aromatics}; 8.62 [s, $^{3}J(Pt-H^e) = 62$, H^e]. ^{19}F NMR ($CDCl_3$): $\delta = -120.91$ [dt, $J(Pt-F^5) = 98$, $J(F^5-F^4) = 22$, $J(F^5-F^3) = J(F^5-H) = 7$, F^5]; -142.97 [dt, $J(F^3-F^4) = 18$, $J(F^3-F^5) = J(F^3-H) = 7$, F^3]; -156.46 [m, $J(Pt-F^4) = 43$, $J(F^4-F^5) = 22$, $J(F^4-F^3) = 18$, $J(F^4-H) = 6$, F^4]. ^{195}Pt NMR ($CDCl_3$): $\delta = -3982$ [s]. IR (KBr): 1110 cm^{-1} (ν(SO)). FAB(+) MS (NBA, m/z): 521 ($[M-Me]^+$); 443 ($[M-Me-SOMe_2]^+$). *Anal.* Found: C, 37.6; H, 3.4; N, 2.6. Calc. for $C_{17}H_{18}F_3NOPtS$: C, 38.06; H, 3.38; N, 2.61%.

Compound [PtMe(3,4,5-$C_6HF_3CH{=}NCH_2C_6H_5$)-PPh_3] (**3**) was obtained from the reaction of 50 mg (9.6×10^{-5} mol) of compound **1** with the equimolecular amount (25 mg) of PPh_3 in acetone (20 ml). After continuous stirring during 2 h, the solvent was removed in a rotary evaporator and the resulting yellow solid was washed with hexane (2×5 ml), and diethylether (2×5 ml) and dried under vacuum. Yield 55 mg (80%). ^{1}H NMR (acetone-d^6): $\delta=0.97$ [dd, ^2J(Pt–H) = 83, ^3J(P–H) = 9, J(F–H) = 6, Me^a]; 4.22 [s, ^3J(Pt–H) = 8, H^d]; {6.79 [m, 1H]; 7.40 [m], 7.64 [m], aromatics}; 8.63 [s, ^3J(Pt–H^e) = 55, H^e]. ^{19}F NMR (acetone-d^6): $\delta=-122.62$ [m, J(Pt–F^5) = 87, J(F^5–F^4) = 24, J(P–F^5) = J(F^5–F^3) = J(F^5–H) = 7, F^5]; -146.01 [m, F^3]; -159.80 [m, F^4]. ^{31}P NMR (acetone-d^6): $\delta=29.79$ [dd, J(Pt–P) = 2631, J(P–F^5) = 10, J(P–F^4) = 7]. *Anal.* Found: C, 54.7; H, 3.8; N, 2.0. Calc. for $C_{33}H_{27}F_3NPPt$: C, 55.00; H, 3.78; N, 1.94%.

Compound [PtMe(3,4,5-$C_6HF_3CH{=}NCH_2C_6H_5$)-$(PPh_3)_2$] (**7**) was obtained as a white solid by an analogous procedure using 100 mg (1.9×10^{-4} mol) of PPh_3. Yield 80 mg (85%). ^{1}H NMR (acetone-d^6): $\delta=$ 0.27 [dd, ^2J(Pt–H) = 65, ^3J(P^A–H) = 8, ^3J(P^B–H) = 7, Me^a]; {4.74 [d], 4.87 [d], J(H–H) = 13, AB pattern, H^d}; 7.13–7.24 [m, aromatics]; 9.40 [s, H^e]. ^{19}F NMR (acetone-d^6): $\delta=-113.96$ [ddd, J(Pt–F^5) = 412, J(F^5–F^4) = 30, J(P–F^5) = 15, J(F^5–F^3) = 3, F^5]; -148.54 [m, F^3]; -164.33 [ddt, J(F^5–F^4) = 30, J(F^4–F^3) = 19, J(P–F^4) = J(F^4–H) = 7, F^4]. ^{31}P NMR (acetone-d^6): $\delta=25.38$ [d, J(Pt–P^A) = 1908, J(P^A–P^B) = 15, P^A]; 26.01 [td, J(Pt–P^A) = 2311, J(P^B–P^A) = J(P^B–F^5) = 15, J(P^B–F^4) = 8, P^B]. *Anal.* Found: C, 61.9; H, 4.3; N, 1.4. Calc. for $C_{51}H_{42}F_3NP_2Pt$: C, 62.32; H, 4.31; N, 1.44%.

Compound [PtMe(3,4,5-$C_6HF_3CH{=}NCH_2C_6H_5$)-(dppe)] (**8**) was obtained as a white solid by an analogous procedure using 38 mg (9.5×10^{-5} mol) of dppe. Yield 70 mg (85%). ^{1}H NMR (acetone-d^6): $\delta=$ 0.48 [t, ^2J(Pt–H) = 67, ^3J(P^A–H) = ^3J(P^B–H) = 6, Me^a]; 2.44 [m, H^{f,g}]; 4.36 [s, H^d]; {7.12–7.32 [m], 7.45–7.55 [m], 7.70–7.79 [m], 7.89–7.98 [m], aromatics}; 8.65 [s, H^e]. ^{19}F NMR ($CDCl_3$): $\delta=-114.20$ [dd, J(Pt–F^5) = 385, J(F^5–F^4) = 27, J(P–F^5) = 11, F^5]; -147.38 [m, F^3]; -163.92 [ddt, J(F^5–F^4) = 29, J(F^4–F^3) = 20, J(P–F^4) = J(F^4–H) = 8, F^4]. ^{31}P NMR (acetone-d^6): $\delta=46.58$ [s, J(Pt–P^A) = 1718, P^A]; 47.36 [m, J(Pt–P^B) = 2287, P^B]. *Anal.* Found: C, 57.4; H, 4.4; N, 1.6. Calc. for $C_{41}H_{36}F_3NP_2Pt$: C, 57.48; H, 4.24; N, 1.63%.

Compound [PtMe(3,4,5-$C_6HF_3CH{=}NCH_2CH_2$-NMe_2)(dppe)] (**9**) was obtained as a white solid by an analogous procedure from 50 mg (1.14×10^{-4} mol) of the compound [PtMe(3,4,5-$C_6HF_3CH{=}NCH_2CH_2$-NMe_2)] and 45 mg of dppe. Yield 80 mg (84%). ^{1}H NMR (acetone-d^6): $\delta=0.46$ [t, ^2J(Pt–H) = 68, ^3J(P^A–H) = ^3J(P^B–H) = 7, Me^a]; 2.15 [s, Me^g]; {2.20–2.45 [m], 3.26 [t, J(H–H) = 7, H^{d,f,h,i}} 7.14–7.76 [m, aromatics]; 8.52 [s, H^e]. ^{19}F NMR ($CDCl_3$): $\delta=-109.17$ [dd, J(Pt–F^5) = 390, J(F^5–F^4) = 30, J(P–F^5) = 16, F^5]; -144.31 [m, F^3]; -161.64 [m, F^4]. ^{31}P NMR (acetone-d^6): $\delta=46.37$ [s, J(Pt–P^A) = 1718, P^A]; 47.27 [dd, J(Pt–P^B) = 2274, J(P^B–F^5) = 16, J(P^B–F^4) = 8, P^B]. $\Lambda_M=2.3\ \Omega^{-1}\ cm^2\ mol^{-1}$ (10^{-3} M in acetone). *Anal.* Found: C, 53.9; H, 4.7; N, 3.2. Calc. for $C_{38}H_{39}F_3N_2P_2Pt$: C, 54.48; H, 4.69; N, 3.34%.

Compound [PtMe$_2$I(3,4,5-$C_6HF_3CH{=}NCH_2C_6H_5$)-(SMe_2)] (**4a**/**4b**) was obtained from 20 mg of compound **1** (3.84×10^{-5} mol) and 10 μL of methyl iodide in 0.7 ml of $CDCl_3$ in a 5 mm NMR tube and was characterised by NMR spectra. ^{1}H NMR ($CDCl_3$): $\delta=$ {0.81 [s, ^2J(Pt–H) = 68], 1.46 [s, ^2J(Pt–H) = 70], Me^a}; {1.72 [d, ^2J(Pt–H) = 68, J(F–H) = 6], 2.10 [d, ^2J(Pt–H) = 68, J(F–H) = 7], Me^b}; 2.21 [s, ^3J(Pt–H) = 15, Me^c]; 5.25–5-50 [m, H^d]; {8.12 [s, ^3J(Pt–H) = 47], 8.30 [s, ^3J(Pt–H) = 42], H^e}.

Compound [{PtMe$_2$I(3,4,5-$C_6HF_3CH{=}NCH_2C_6H_5$)}$_2$] (**5**) was obtained as a pale yellow solid from the reaction of an excess of methyl iodide (0.1 ml) with 50 mg (9.3×10^{-5} mol) of compound **2** carried out in acetone (20 ml). The mixture was stirred for 3 h, and the solvent was removed under vacuum. The residue was washed with diethylether (3×5 ml) and dried under vacuum. Yield 35 mg (63%). ^{1}H NMR ($CDCl_3$): $\delta=1.27$ [s, ^2J(Pt–H) = 75, Me^a]; 2.94 [d, ^2J(Pt–H) = 69, J(F–H) = 8, Me^b]; {5.63 [d], 5.92 [d], J(H–H) = 16, AB pattern, H^d}; {7.01 [m, 1H]; 7.37–7.57 [m, 5H], aromatics}; 8.05 [s, ^3J(Pt–H^d) = 45, H^e]. ^{19}F NMR ($CDCl_3$): $\delta=-127.90$ [dt, J(F^5–F^4) = 21, J(F^5–F^3) = J(F^5–H) = 8, F^5]; -142.59 [m, F^3]; -153.64 [td, J(F^4–F^3) = J(F^4–F^5) = 20, J(F^4–H) = 7, F^4]. ^{195}Pt NMR ($CDCl_3$): -2700 [s]. FAB(+) MS (NBA, m/z): 1200 ($[M]^+$); 1073 ($[M-I]^+$); 1043 ($[M-I-2Me]^+$); 1028 ($[M-I-3Me]^+$); 779 ($[M-I-3Me-L]^+$). *Anal.* Found: C, 31.8; H, 2.5; N, 2.3. Calc. for $C_{32}H_{30}F_6I_2N_2Pt_2$: C, 32.01; H, 2.52; N, 2.33%.

Compound [PtMe$_2$I(3,4,5-$C_6HF_3CH{=}NCH_2C_6H_5$)-(PPh_3)] (**6**) was obtained as a white solid by an analogous procedure from 50 mg (6.9×10^{-5} mol) of compound **3**. Yield 50 mg (83%). ^{1}H NMR ($CDCl_3$): $\delta=1.38$ [d, ^2J(Pt–H) = 60, ^3J(P–H) = 8, Me^a]; 2.20 [t, ^2J(Pt–H) = 69, ^3J(P–H) = J(F–H) = 8, Me^b]; {4.58 [d], 5.52 [d], J(H–H) = 17, *AB* pattern, H^d}; {6.86 [m, 4H]; 7.31–7.58 [m], 7.64 [m], aromatics}; 7.69 [s, ^3J(Pt–H^d) = 44, H^e]. ^{19}F NMR ($CDCl_3$): $\delta=-127.35$ [dt, J(F^5–F^4) = 21, J(F^5–F^3) = J(F^5–H) = 7, F^5]; -144.57 [m, F^3]; -153.62 [td, J(F^4–F^3) = J(F^4–F^5) = 21, J(F^4–H) = 6, F^4]. ^{31}P NMR ($CDCl_3$): $\delta=-11.32$ [s, J(Pt–P) = 1001]. *Anal.* Found: C, 47.2; H, 3.5; N, 1.6. Calc. for $C_{34}H_{30}F_3INPPt$: C, 47.34; H, 3.51; N, 1.62%.

Compound [PtMe(3,4,5-$C_6HF_3CH{=}NCH_2CH_2$-NMe_3)(dppe)]I (**10**) was obtained as a yellow solid from the reaction of an excess of methyl iodide (0.1 ml) with 35 mg (4.18×10^{-5} mol) of compound **9** carried out in acetone. The mixture was stirred for 3 h, and the

solvent was removed under vacuum. Yield 35 mg (85%). ^{1}H NMR (acetone-d^6): $\delta = 0.43$ [t, ^2J(Pt–H) = 69, $^3J(P^A–H) = {}^3J(P^B–H) = 7$, Me[a]; 3.43 [s, Me[g]; {3.60–3.90 [m], H [d,f,h,i]}; 7.13–7.84 [m, aromatics]; 8.53 [s, H[e]. ^{19}F NMR ($CDCl_3$): $\delta = -108.75$ [ddd, J(Pt–F[5]) = 390, $J(F^5–F^4) = 30$, $J(P–F^5) = 15$, $J(F^5–F^3) = 4$, F[5]; –143.75 [m, F[3]; –160.30 [m, F[4]. ^{31}P NMR (acetone-d^6): $\delta = 47.28$ [s, $J(Pt–P^A) = 1711$, P[A]; 47.39 [dd, $J(Pt–P^B) = 2293$, $J(P^B–F^5) = 15$, $J(P^B–F^4) = 8$, P[B]. $\Lambda_M = 103\ \Omega^{-1}\ cm^2\ mol^{-1}$ (10^{-3} M in acetone). *Anal.* Found: C, 46.0; H, 4.5; N, 2.7. Calc. for $C_{39}H_{42}F_3IN_2P_2Pt{\cdot}2H_2O$: C, 46.12; H, 4.56; N, 2.76%.

[{$PtMe_2I(3,4,5\text{-}C_6HF_3CH{=}NCH_2C_6H_5)$}$_2$dppe] (**11**) was obtained using the following procedure: 50 mg (9.6×10^{-5} mol) of compound **1** was treated with an excess of methyl iodide (0.1 ml) in acetone (20 ml) with continuous stirring for 30 min. The solvent was removed in a rotary evaporator and the residue was treated with 19 mg (4.7×10^{-5} mol) of dppe in acetone (20 ml). The mixture was stirred for 1 h and the solvent was removed under vacuum. The residue was washed with hexane (3×5 ml) and the resulting white solid was dried under vacuum. Yield 63 mg (82%). ^{1}H NMR (acetone-d^6): $\delta = 1.05$ [d, ^2J(Pt–H) = 59, ^3J(P–H) = 8, Me[a]; 1.83 [t, ^2J(Pt–H) = 69, J(P–H) = J(F–H) = 7, Me[b]; 2.43 [m, H[f]; {4.27 [d], 5.47 [d], J(H–H) = 15, AB pattern, H[d]}; 7.18–7.35 [m, aromatics]; 8.04 [s, ^3J(Pt–H[e]) = 47, H[e]. ^{19}F NMR (acetone-d^6): $\delta = -128.07$ [m, F[5]; –144.03 [m, F[3]; –153.92 [m, F[4]. ^{31}P NMR (acetone-d^6): $\delta = -10.4$ [s, J(Pt–P) = 1049]; –10.9 [s, J(Pt–P) = 1048]. $\Lambda_M = 3\ \Omega^{-1}\ cm^2\ mol^{-1}$ (10^{-3} M in acetone). FAB(+) MS (NBA, m/z): 1471 ($[M-I]^+$); 1456 ($[M-I-Me]^+$); 1441 ($[M-I-2Me]^+$); 1344 ($[M-2I]^+$); 1299 ($[M-2I-3Me]^+$); 1192 ($[M-I-2Me-L]^+$); 1179 ($[M-I-3Me-L]^+$).

Table 2
Crystallographic details

Formula	$C_{33}H_{27}F_3NPPt$
F_w	720.62
Temperature (K)	293(2)
Wavelength, Å	0.71069
Crystal system	triclinic
Space group	$P\bar{1}$
Unit cell dimensions	
a (Å)	9.0350(10)
b (Å)	11.2170(10)
c (Å)	14.2390(10)
α (°)	90.63
β (°)	105.299(10)
γ (°)	92.62
V (Å^3)	1390.1(2)
Z	2
D_{calc} (Mg m^{-3})	1.722
Absorption coefficient (mm^{-1})	5.148
F(000)	704
θ Range for data collection (°)	2.37–24.95
No. of reflections collected/unique	7346/4108 [$R_{int} = 0.0219$]
No. of data/restraints/parameters	4108/0/432
Goodness-of-fit on F^2	1.076
$R_1(I>2\sigma(I))$	0.0259
wR_2 (all data)	0.0668
Largest difference peak and hole (e Å^{-3})	0.710, –0.642

3.2. X-ray structure analysis: data collection

A prismatic crystal ($0.1 \times 0.1 \times 0.2$ mm) was selected and mounted on a MAR345 diffractometer with an image plate detector. Unit cell parameters were determined from automatic centring of 6890 reflections ($3 < \theta < 31°$) and refined by least-squares method. Intensities were collected with graphite monochromatized Mo Kα radiation. 7346 reflections were measured in the range $2.37 < \theta < 24.95°$, 4108 of which were non-equivalent by symmetry (R_{int} (on I) = 0.021). A total of 3820 reflections were assumed as observed applying the condition $I > 2\sigma(I)$. Lorentz polarisation and absorption corrections were made.

3.3. Structure solution and refinement

The structure was solved by direct methods, using SHELXS computer program [24], and refined by the full-matrix least-squares method, with the SHELXL-97 computer program [25] using 4108 reflections (very negative intensities were not assumed). The function minimised was $\Sigma\, w||F_o|^2 - |F_c|^2|^2$, where $w = [\sigma^2(I) + (0.0374P)^2 + 3.1998P]^{-1}$ and $P = (|F_o|^2 + 2|F_c|^2)/3$. f, f' and f'' were taken from the International Tables of X-ray Crystallography [24]. 20 H were located from a difference synthesis and refined with an overall isotropic temperature factor and 7 H atoms were computed and refined, using a riding model, with an isotropic temperature factor equal to 1.2 times the equivalent temperature factor of the atom to which they are linked. Further details are given in Table 2.

4. Supplementary material

Crystallographic data for the structural analysis have been deposited with the Cambridge Crystallographic Centre, CCDC No. 167426. Copies of this information may be obtained free of charge from The Director, CCDC, 12 Union Road, Cambridge, CB2 1EZ, UK (fax: +44-1233-336-033; e-mail: deposit@ccdc.cam.ac.uk or www: http://www.ccdc.cam.ac.uk).

Acknowledgements

This work was supported by the DGICYT (Ministerio de Educación y Cultura, Spain, BQU2000-0652) and from the Generalitat de Catalunya (project 1997-SGR-00174).

References

[1] J. Albert, M. Gómez, J. Granell, J. Sales, Organometallics 9 (1990) 1405.
[2] J. Albert, J. Granell, R. Moragas, J. Sales, M. Font-Bardía, X. Solans, J. Organomet. Chem. 494 (1995) 95.
[3] M. Crespo, X. Solans, M. Font-Bardía, Organometallics 14 (1995) 355.
[4] O. López, M. Crespo, M. Font-Bardía, X. Solans, Organometallics 16 (1997) 1233.
[5] M. Crespo, X. Solans, M. Font-Bardía, J. Organomet. Chem. 518 (1996) 105.
[6] M. Crespo, C. Grande, A. Klein, M. Font-Bardía, X. Solans, J. Organomet. Chem. 563 (1998) 179.
[7] R. Bosque, J. Granell, J. Sales, M. Font-Bardía, X. Solans, J. Organomet. Chem. 453 (1993) 147.
[8] M. Crespo, X. Solans, M. Font-Bardía, J. Organomet. Chem. 483 (1994) 187.
[9] C. Anderson, M. Crespo, M. Font-Bardía, X. Solans, J. Organomet. Chem. 604 (2000) 178.
[10] (a) A. Bayler, A.J. Canty, P.G. Edwards, B.W. Skelton, A.H. White, J. Chem. Soc., Dalton Trans. (2000) 3325;
(b) J.M. Vila, M. Gayoso, T. Pereira, C. Rodríguez, J.M. Ortigueira, J.F. Fernández, M. López Torres, J. Organomet. Chem. 479 (1994) 37.
[11] J.M. Vila, M. Gayoso, A. Fernández, N.A. Bailey, H. Adams, J. Organomet. Chem. 448 (1993) 233.
[12] (a) A. Doppiu, G. Minghetti, M.A. Cinellu, S. Stoccoro, A. Zucca, Organometallics 20 (2001) 1148;
(b) R. Romeo, L. Monsù-Scolaro, N. Nastasi, B.E. Mann, G. Bruno, F. Nicolò, Inorg. Chem. 35 (1996) 7691;
(c) G.W.V. Cave, F.P. Fanizzi, R.J. Deeth, W. Errington, J.P. Rourke, Organometallics 19 (2000) 1355.
[13] (a) P.S. Pregosin, Coord. Chem. Rev. 44 (1982) 247;
(b) A.P.S. Fontes, A. Oskarson, K. Lövqvist, N. Farrell, Inorg. Chem. 40 (2001) 1745.
[14] A.D. Ryabov, G.M. Kazankov, I.M. Panyashkina, O.V. Grozovsky, O.G. Dyachenko, V.A. Polyakov, L.G. Kuz'mina, J. Chem. Soc., Dalton Trans. (1997) 4385.
[15] (a) W.W. Paudler, Nuclear Magnetic Resonance: General Concepts and Applications, Wiley, New York, 1987;
(b) C. Crocker, R.J. Goodfellow, J. Gimeno, R.J. Usón, J. Chem. Soc., Dalton Trans. (1977) 1448.
[16] (a) S. Stoccoro, M.A. Cinellu, A. Zucca, G. Minghetti, F. Demartin, Inorg. Chim. Acta 215 (1994) 17;
(b) C. Navarro-Ranninger, I. López-Solera, A. Alvarez-Valdés, J.M. Rodríguez-Ramos, J.R. Massaguer, J.L. García Ruano, X. Solans, Organometallics 12 (1993) 4104;
(c) M. Crespo, X. Solans, M. Font-Bardía, J. Organomet. Chem. 509 (1996) 29;
(d) M. Crespo, X. Solans, M. Font-Bardía, Polyhedron 17 (1998) 1651.
[17] M. Ghedini, D. Pucci, A. Crispini, G. Barberio, Organometallics 18 (1999) 2116.
[18] C. Anderson, M. Crespo, M. Font-Bardía, A. Klein, X. Solans, J. Organomet. Chem. 601 (2000) 22.
[19] E. Rotondo, A. Giannetto, S. Lanza, J. Organomet. Chem. 396 (1990) 115.
[20] J.D. Kennedy, W. McFarlane, R.J. Puddephatt, P.M. Thompson, J. Chem. Soc., Dalton Trans. (1976) 874.
[21] (a) J. Forniés, J.C. Fortuño, M.A. Gómez, B. Menjón, E. Merdtweck, Organometallics 12 (1993) 4368;
(b) J.M. Casas, J. Forniés, A. Martín, B. Menjón, Organometallics 12 (1993) 4376.
[22] (a) J. Hendrickson, Tetrahedron 20 (1964) 449;
(b) T.A. Albright, J. Am. Chem. Soc. 97 (1975) 940.
[23] G.S. Hill, M.J. Irwin, L.M. Rendina, R.J. Puddephatt, Inorg. Synth. 32 (1998) 149.
[24] G.M. Sheldrick, SHELXS-97: A Computer Program for Crystal Structure Determination, University of Göttingen, Germany, 1997.
[25] J.A. Ibers, W.C. Hamilton, Eds., International Union of Crystallography, International Tables of X-ray Crystallography, vol. IV, Kynoch Press, Birmingham, UK, 149, 1974, pp. 89–100.

PERGAMON

Polyhedron 21 (2002) 115–118

POLYHEDRON

www.elsevier.com/locate/poly

Backscatter Fe-57 Mössbauer studies of iron(II) phthalocyanine

Norman A. Bell [a,*], John S. Brooks [a], Susan D. Forder [a], Jacqueline K. Robinson [a], Stephen C. Thorpe [b]

[a] *Materials Research Institute, Sheffield Hallam University, Howard Street, Sheffield S1 1WB, UK*
[b] *Health and Safety Laboratory, Broad Lane, Sheffield S3 7HQ, UK*

Received 3 August 2001; accepted 5 October 2001

Abstract

Phthalocyanines are established gas sensitive materials. We have successfully recorded backscatter conversion electron Mössbauer spectra (CEMS) of iron(II) phthalocyanine. Further, we have shown that the introduction of nitrogen dioxide, a typical analyte for these materials, into the detector system can be achieved without deleterious effects. The method allows surface sensitive spectra of these materials to be recorded under normal sensor operating conditions of temperature and pressure. The high vacuum conditions of other surface sensitive techniques used to study materials of this type are not required by this method.
© 2002 Elsevier Science Ltd. All rights reserved.

Keywords: Iron(II) phthalocyanine; Backscatter Mössbauer spectroscopy; Gas sensing

1. Introduction

Phthalocyanines are well-known for their gas sensing properties [1–5]. When electron acceptor gases such as NO_2 interact with solid organic or organometallic compounds with delocalised π-electron systems, charge transfer between the solid and the absorbed gas is believed to lead to charge-carrier generation and large increases in electrical conductivity. Metal phthalocyanines have a high chemical and physical stability and show large conductivity increases which allow electrophilic gases such as NO_2 to be detected in the parts per million (ppm) range. However, the exact mechanisms for the gas sensing actions are not well understood [6] and hence our interest in iron(II) phthalocyanine (FePc) as a model system which can be studied by Fe-57 Mössbauer spectroscopy. Although iron phthalocyanine is not an optimised gas sensor it nevertheless has gas sensing properties which are typical of metal phthalocyanines. It exhibits polymorphism due to relatively weak intermolecular forces allowing a variety of stacking arrangements. In the α-form iron lies at the centre of a square of four nitrogen atoms coordinated to the metal whereas in the β-polymorph there are additionally two other longer nitrogen bonds in the octahedral positions from neighbouring molecules [7,8]. Transmission Mössbauer and variable temperature studies of the α- and β-phases of FePc have been reported elsewhere [9]. This paper presents the results from a series of backscatter conversion electron Mössbauer spectroscopy (CEMS) experiments, designed to observe in-vitro behaviour of the surface of a sample of iron(II) phthalocyanine when exposed to reactive gases.

2. Experimental

Crude FePc has been prepared in the laboratory based on the method of Tomoda et al. [10] by the

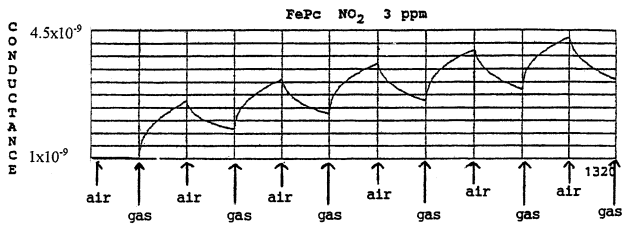


Fig. 1. Conductance response of FePc to 3 ppm NO_2.

* Corresponding author. Tel.: +44-114-225-3002; fax: +44-114-225-3066.
E-mail address: n.a.bell@shu.ac.uk (N.A. Bell).

0277-5387/02/$ - see front matter © 2002 Elsevier Science Ltd. All rights reserved.
PII: S0277-5387(01)00972-X

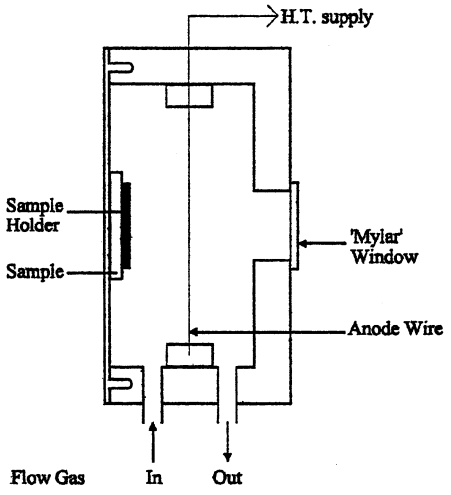


Fig. 2. Schematic diagram of a backscatter detector.

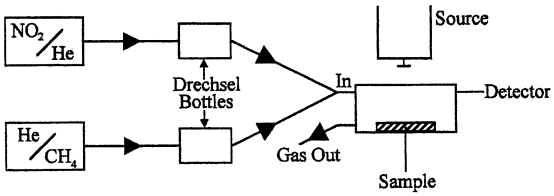


Fig. 3. Schematic diagram of dilution and delivery of NO_2/He to the CEMS detector.

reaction of iodine and iron powder in ethanol, followed by the addition of a mixture of phthalonitrile and 1,5-diazabicyclo[4,3,0]non-5-ene. The α-FePc phase was prepared by vacuum sublimation onto a water-cooled finger[8]. The β-FePc phase was isolated as purple needle-like crystals from crude FePc by entrainer sublimation [11]. The response of FePc to NO_2 was verified using a conventional interdigitated electrode. The sensor consisted of a 3 mm × 3 mm × 0.5 mm alumina substrate with an electrode pattern on one side and a platinum heater on the other. Approximately 500 nm films of FePc were vacuum sublimed onto the interdigitated electrode pattern. The sensor was exposed to two minutes of air, followed by two minutes of gas and this sequence repeated. The results of gas exposure were plotted as conductance against time during cyclic exposure to air and gas with typical results shown in Fig. 1.

3. Mössbauer spectroscopy

Conventional transmission Mössbauer spectra have been recorded for both phases and the experimental arrangement, computer fitting strategies and results have been previously reported [9]. Backscatter Mössbauer spectroscopy can be performed following the resonant absorption of the 14.4 keV γ-ray by an Fe-57 nucleus by either detecting the re-emitted 14.4 keV γ-ray photon, or the 6.3 keV X-ray photon (conversion X-ray Mössbauer spectroscopy (CXMS)), or from the internal conversion at 7.3 keV or by detecting the associated KLL Auger electrons at 5.3 keV (CEMS), all of which result from the decay of the $I = \pm 3/2$ excited iron nucleus. The backscatter radiations are detected as a function of the conventional Doppler velocity to enable hyperfine interactions to be studied. Of particular interest in this work is the relative surface sensitivities of CXMS and CEMS and the detector design which enables in-vitro gas sensing experiments to be designed. Krakowski and Miller [12] have estimated theoretically that 65% of the 7.3 keV conversion electrons detected (from iron) would have arisen from within 45 nm of the surface. However, Swanson and Spijkerman have shown experimentally that 65% originate within 60 nm and 95% within 300 nm of the surface [13]. Detection of the conversion electrons therefore yields chemical information which is extremely surface sensitive (≤ 0.3 μm). Conversion X-rays have a much greater penetration depth ($\sim$ 10 μm) and yield chemical information which is characteristic of the near surface region.

The detector used for the backscatter experiments was a gas flow proportional counter where the sample material (fluorescor) was mounted inside the chamber behind the HT wire of the counter (Fig. 2). An informed choice of gas mixture in the detector allows the preferential detection of either the conversion electron or X-ray. Thus, a gas mixture of helium 95% and methane 5% was used for CEMS and argon 95%/methane 5% for CXMS. The gas flow detector was chosen in preference to the channeltron, which has a superior signal to noise performance but which operates under high vacuum, because it offered the potential for introducing reactive gas into the detector while recording a Mössbauer spectrum and thus mimicked sensor operating conditions. The aim of the experiment was to place an FePc sample in the backscatter detector and to allow NO_2 to flow through the detector so that in-vitro spectra could be accumulated before, during and after exposure to NO_2. The experiments were carried out at ambient temperature and pressure, normal gas sensor operating conditions. Cylinders containing 90 ppm NO_2 normally contain oxygen to prevent dissociation. However, the presence of oxygen would oxidize the anode wire in the CEMS detector and so was removed and replaced with helium which is the normal ionizing gas in the chamber. To ensure that dissociation had not occurred, tests using Drager tubes confirmed NO_2 in the range 80–90 ppm. A simple gas flow arrangement as shown in Fig. 3 combined the diluted reactive gas with the conventional ionization sensing gas to create within the detector 15-20 ppm of NO_2. Once conditions had stabilised, a backscatter Mössbauer spectrum was accumulated in the conventional way.

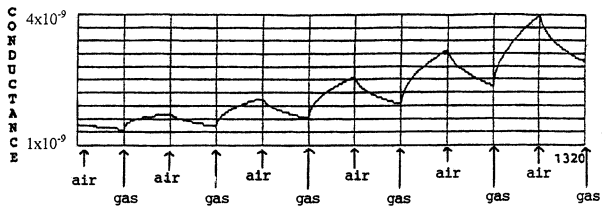


Fig. 4. Change in conductivity of FePc during exposure in 2 min intervals to 1–5 ppm NO_2.

4. Results and discussions

4.1. Gas sensing

The α-FePc film was exposed to 1–5 ppm NO_2, 3 ppm NO_2 and 5 ppm NO_2, diluted down from 90 ppm by mass flow controllers to show that the film would act as a sensor and to determine appropriate gas concentration levels. Fig. 4 shows the exposure to 1–5 ppm NO_2. The observed response is fast and approximately exponential and conductivity increases with increasing concentration of NO_2. The recovery is also fast but not to the original starting point with a gradual increase in the baseline with continued cyclic exposure. This response is characteristic of all metal phthalocyanines which behave as p-type semiconductors when exposed to electron acceptor gases [14].

4.2. Mössbauer spectroscopy

Previously published variable temperature studies ([9] and references therein) have shown that the α-FePc has a Debye temperature, θ_D of 143 K and a recoil free fraction at room temperature f_{300} of 0.14. The corresponding results for β-FePc are $\theta_D = 199$ K and $f_{300} = 0.36$. The starting point for a series of backscatter experiments was to record the spectra from the mixed phase FePc powder which was pressed onto double-sided sellotape to form a sample within the detector.

A similar CEMS backscatter spectrum was obtained for the purified β-phase as shown in Fig. 5. An attempt was made to obtain a backscatter spectrum from the α-phase but no emission could be detected after 6 days of accumulation. This in part can be explained by the low recoil free fraction of the α-phase. The fitting parameters for the backscatter spectra are compared to transmission parameters in Table 1.

To investigate the effect on the anode wire, the NO_2 flow experiment was repeated with a stainless steel sample. Identical spectra were recorded with and without NO_2 confirming that the operation of the detector is not affected by the NO_2. Transmission spectra were recorded of β-FePc and powder which had been exposed to 90 ppm NO_2 for 48 h. Identical spectra were recorded indicating that NO_2 had not chemically reacted with the bulk β-FePc.

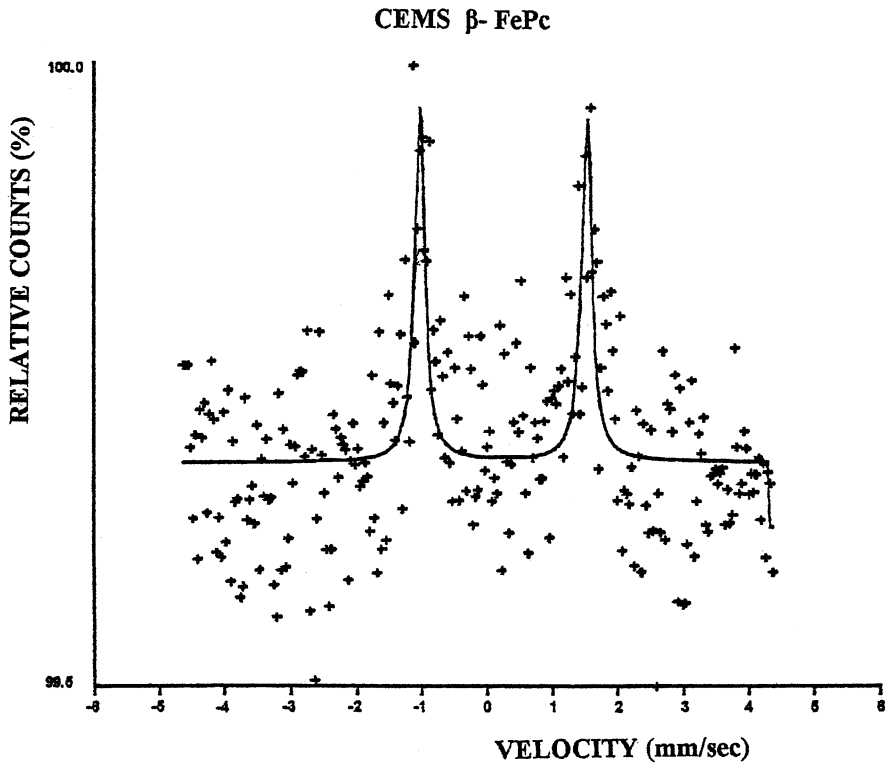


Fig. 5. CEMS Mössbauer spectrum of β-FePc.

Table 1
CEMS and transmission Mössbauer parameters of FePc

Sample	Isomer shift ± 0.02 mm s^{-1} (αFe)	Quadrupole split ± 0.02 mm s^{-1}
CEMS Crude FePc RT	0.39	2.61
Transmission-α RT	0.35	2.39
Transmission-β RT	0.37	2.53
CEMS β-FePc	0.37	2.56

Thus, we have demonstrated the ability to record backscatter spectra at ambient temperatures and pressure. We have also confirmed that the sample gas, NO_2 can be introduced to the backscatter detector with no deleterious effect on its operation. We now propose to collect backscatter spectra, CEMS and CXMS, in an attempt to elucidate the interaction between the sample gas and the phthalocyanine. Initial experiments suggest that long collection times are required and this may in part be due to adsorption of NO_2 on the FePc surface, and other surface characterisation techniques will be used to explore this possibility. ^{57}Fe enriched FePc might also be used and this might also allow spectra from β-FePc to be collected.

References

[1] B. Bott, T.A. Jones, Sensors and Actuators 5 (1984) 43.
[2] H. Laurs, G. Heiland, Thin Solid Films 149 (1987) 129.
[3] T.A. Jones, B. Bott, S.C. Thorpe, Sensors and Actuators 17 (1989) 467.
[4] S. Pizzini, G. Timo, M. Beghi, N. Butta, C. Mari, J. Faltenmaier, Sensors and Actuators 17 (1989) 481.
[5] S. Dogo, J. Germain, C. Maleysson, A. Nakajima, W. Nevin, Appl. Phys. Lett. 61 (1992) 2184.
[6] A. Wilson, G. Rigby, J. Wright, S.C. Thorpe, T. Terui, Y. Maruyama, J. Mater. Chem. 2 (1992) 303.
[7] S.E. Harrison, J.M. Assour, J. Chem. Phys. 40 (1964) 365.
[8] T.S. Srivastava, J.L. Przybylinski, A. Nath, Inorg. Chem. 13 (1974) 1562.
[9] N.A. Bell, J.S. Brooks, J.K. Robinson, S.C. Thorpe, J. Chem. Soc., Faraday Trans. 94 (1998) 3155.
[10] H. Tomoda, H. Saito, S. Ogawa, S. Shiraishi, Chem. Lett. (1980) 1277.
[11] J. Sharp, M. Larder, J. Phys. Chem. 72 (1968) 3230.
[12] R.A. Krakowski, R.B. Miller, Nucl. Inst. Methods 70 (1969) 36.
[13] K.R. Swanson, J.J. Spijkermann, J. Appl. Phys. Lett. 13 (1968) 11.
[14] T.A. Jones, B. Bott, Sensors and Actuators 9 (1986) 27.

PERGAMON

Polyhedron 21 (2002) 119–124

POLYHEDRON

www.elsevier.com/locate/poly

Determining substrate selectivity and regiochemistry of nitrilium phosphanylid tungsten complexes in cycloaddition reactions with terminal alkynes

Rainer Streubel *, Nils Hoffmann, Frank Ruthe, Peter G. Jones

Institut für Anorganische und Analytische Chemie der Technischen Universität Braunschweig, PO Box 3329, D-38023 Braunschweig, Germany

Received 3 August 2001; accepted 5 October 2001

Dedicated to Professor Kurt Dehnicke on the occasion of his 70th birthday

Abstract

Here we report reactions of intermediate nitrilium phosphanylid complexes, formed via reactions of a 2*H*-azaphosphirene complex, and 2-furanocarbonitrile, 2-thiopheno-carbonitrile or 2-cyano-1,5-dimethyl-pyrrole, and different alkynes. These examples show the dependencies of substrate selectivity and regiochemistry of this new reactive intermediate. Furthermore, we report on an unusual ^{13}C NMR coupling phenomena within the 2*H*-1,2-azaphosphole ring. © 2002 Elsevier Science Ltd. All rights reserved.

Keywords: P-Ligands; 2*H*-Azaphosphirene complexes; 2*H*-1,2-Azaphosphole complexes; Cyclisation; 1,3-Dipoles

1. Introduction

Recently, we developed the generation and trapping of the transient nitrilium phosphanylid complexes **II** as a novel and highly efficient synthesis of five-membered P-heterocycle complexes. Such intermediates are usually generated via thermal ring opening of 2*H*-azaphosphirene complexes **I** [1] or, more recently, via decomposition of 7-phosphanorbornadiene complexes **III** [2] in the presence of nitriles. Intermediates **II** can be trapped with a wide variety of different π-systems such as alkynes, [3] nitriles [4] and phosphaalkynes [5] to give complexes **IV** (Scheme 1). Furthermore, we showed that, in the case of complexes **I**, formal nitrile–nitrile exchange reactions of **II** occurred intermediately via [1 + 1]-addition of transiently formed terminal phosphanediyl complexes with a nitrile (*transylidation reactions*), thus offering novel applications of this method in heterocyclic synthesis [6].

Although we recently reported on trapping reactions of derivatives of **II** with various alkynes in some detail, the regiochemistry of **II** in [3 + 2]-cycloaddition reactions with acetylene ethylcarboxylate was only deduced from ^{13}C NMR spectroscopic data of the 2*H*-1,2-azaphosphole complexes thus obtained [6]. It is noteworthy that the metal complex fragment of the 2*H*-azaphosphirene complexes played an important role in such three-component reactions [6]. Whereas reactions of 2*H*-azaphosphirene chromium and tungsten complexes are in general selective, the analogous reactions of molybdenum are not and, furthermore, the products displayed lower stabilities towards chromatographic work-up procedures. We also showed that the reaction courses significantly depended on the alkyne substituents, thus leading to 2*H*-1,2-azaphosphole complexes if the employed alkyne has electron-withdrawing groups as substituents, as in dimethyl acetylenedicarboxylate or ethyl acetylenecarboxylate [6].

Since our interest in exploiting this three-component reaction methodology, we have started a new series of reactions using hetarene-substituted nitriles. Here we report first reactions using the 2*H*-azaphosphirene tungsten complex **1**, 2-furanonitrile (**2a**), 2-thiophenonitrile (**2b**) and 2-cyano-1,5-dimethyl-pyrrole (**2c**) as nitrile components and phenylacetylene (**3a**),

* Corresponding author. Tel.: +49-531-3917350; fax: +49-531-3915387.

E-mail address: r.streubel@tu-bs.de (R. Streubel).

0277-5387/02/$ - see front matter © 2002 Elsevier Science Ltd. All rights reserved.
PII: S0277-5387(01)00976-7

ethoxyacetylene (**3b**), acetylene ethylcarboxylate (**3c**) as trapping reagents.

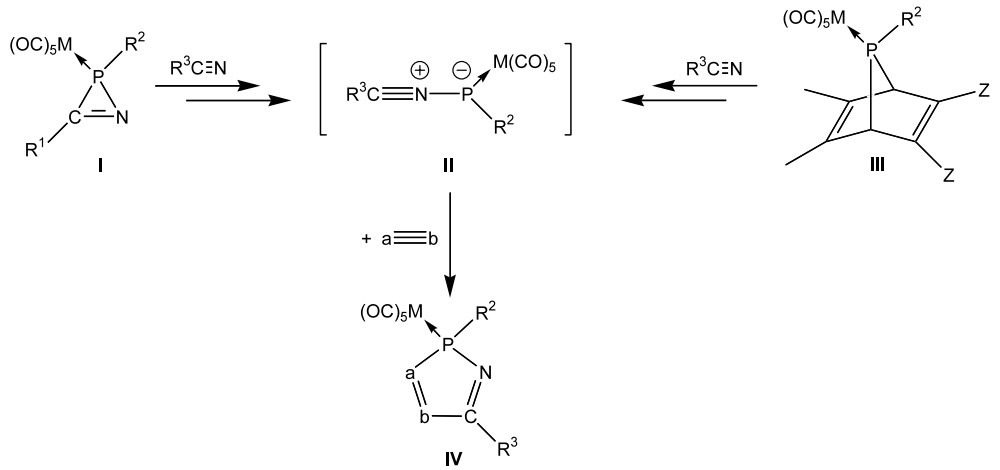
2. Results

Reactions of the 2*H*-azaphosphirene tungsten complex **1** [7] with the nitriles **2a**–**c** and phenylacetylene (**3a**) furnished exclusively the 1*H*-phosphirene complex **4a** [8] as the only phosphorus-containing product, which was readily identified by ^{31}P NMR spectroscopy (Scheme 2).

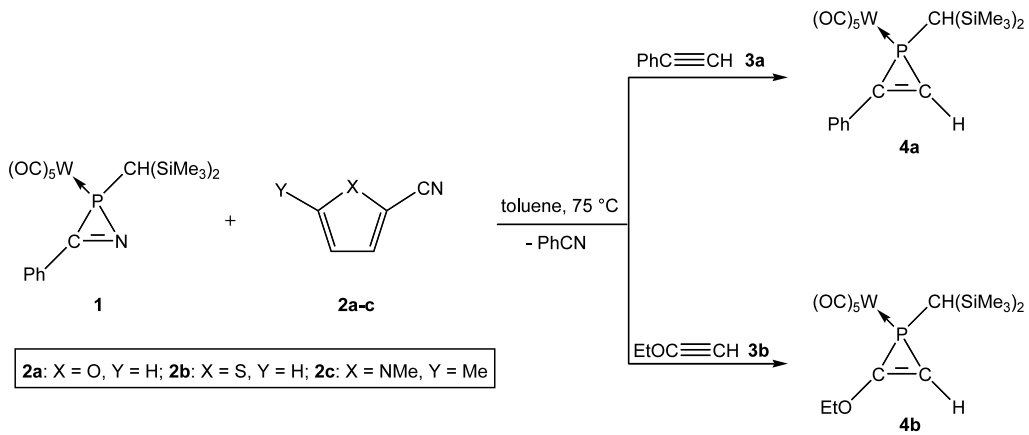
Using complex **1**, nitriles **2a**–**c** and ethoxyacetylene (**3b**), having an electron-donating group, the reactions afforded selectively the 1*H*-phosphirene complex **4b**; [9] neither was evidence for 2*H*-1,2-azaphosphole complex formation obtained in this case (Scheme 2).

The three-component reactions of complex **1**, nitriles **2a**–**c** and ethyl acetylenecarboxylate (**3c**) led to the formation of the regioisomeric 2*H*-1,2-azaphosphole complexes **5a**,**b** (ratio 3:1), **6a**,**b** (ratio 5:1) and **7a**,**b** (ratio 8:1) (Scheme 3); formation of a 1*H*-phosphirene complex was not observed in these reactions. Selected NMR data are given in Table 1. Whereas the 2*H*-1,2-azaphosphole complexes **5a**,**b** and **7a** were obtained in pure form, the derivatives **6a**,**b** were characterized as mixtures. Complex **7b** could not be characterized, because of the very low amounts formed; nevertheless, its identity can be deduced from its ^{31}P NMR spectrum.

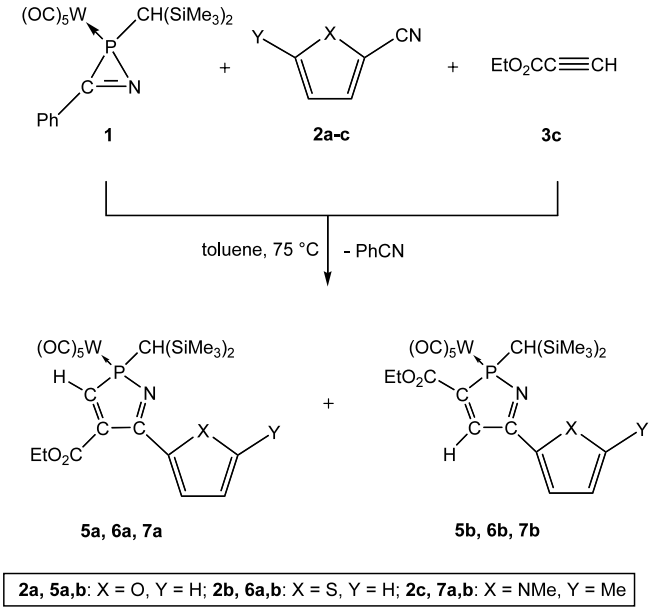
In all cases, the 4-ethoxycarbonyl-substituted 2*H*-1,2-azaphosphole complexes **5a**, **6a** and **7a** were formed predominantly, as established unambiguously by the X-ray structure analysis of the 2*H*-1,2-azaphosphole complex **7a**. The outcome of these reactions was completely unexpected, especially with regard to the ^{13}C NMR data of the regioisomeric 2*H*-1,2-azaphosphole complexes. The 4-ethoxy-carbonyl-substituted 2*H*-1,2-azaphosphole complex **7a** showed a greater phosphorus-coupling constant magnitude for the C^4-atom than for the C^3-atom of the 2*H*-1,2-azaphosphole ring, which was unambiguously shown through DEPT-NMR experiments. Assuming that there are no other contributions than through-bond couplings in this ring system, this would mean that the $|^{(1+4)}J(P,C^3)|$-value is



Scheme 1. 2*H*-azaphosphirene complexes **I**, 7-phosphanorbornadiene complexes **II**, nitrilium phosphanylid complexes **III** and phosphorus heterocycles **IV** (**I**–**IV**, R^1–R^3 = organic substituents).



Scheme 2. Attempted three-component reactions of 2*H*-azaphosphirene complex **1** with nitriles **2a**–**c** and alkynes **3a**,**b**.



Scheme 3. Synthesis of 2*H*-1,2-azaphosphole complexes **5**–**7**.

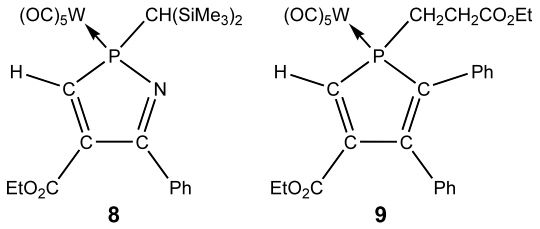


Fig. 1. Comparison of related 2*H*-1,2-azaphosphole and phosphole complexes.

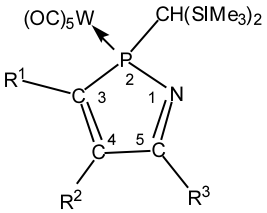
Table 2
Selected bond lengths in Å for compound **7a**

Bond	Compound **7a**
W–C1	2.009 (3)
W–P	2.5098(6)
P–C13	1.807(2)
P–N1	1.7042(19)
C13–C14	1.337(3)
N1–C15	1.312(3)
C14–C15	1.503(3)
C15–C20	1.439(3)

smaller than the $|^{(2+3)}J(P,C^4)|$-value, which is completely counterintuitive! Remarkable are also the significantly different $|^2J(P,H)|$- and $|^3J(P,H)|$-values determined by ^{1}H NMR spectroscopy, which therefore also provide structural information concerning the regioisomerism of complexes **5**–**7**. A comparison of the ^{1}H NMR data of complexes **6a**, **8** [10] and **9** [11] shows $|^2J(P,H)|$-values of 31.8 Hz (**6a**), 32.7 Hz [10] (**8**) and 33.3 Hz [11] (**9**) as the most valuable information; this is especially the case if the derivatives are closely related with respect to the nature of the substituents at C^4 and C^5 (Fig. 1). All other NMR and analytical data of the complexes **5a**,**b**, **6a**,**b** and **7a** are in agreement with the proposed structures.

The molecular structure of the diethyl ether solvate of complex **7a** (Fig. 2) shows bond lengths in the 2*H*-1,2-azaphosphole ring, which are typical for localized C_{sp^2}=C_{sp^2} (1.337(3) Å) [12] and N_{sp^2}=C_{sp^2} (1.312(3) Å) [12] double-bonds and are close to the values observed for {pentacarbonyl[2-bis(trimethylsilyl)methyl-4-ethoxycarbonyl-5-phenyl-2*H*-1,2-azaphosphol-κ*P*]-tungsten(0)} [6] (Table 2). The interplanar angle in **7a** of 14.8° should enable only weak, if any, electronic interactions between the two ring systems.

Table 1
Selected NMR spectroscopic data [a] of the 2*H*-1,2-azaphosphole complexes **5**–**7**



Compound	δ^{31}P	^1J(W,P)	$\delta^{13}C^3$	$^{(1+4)}J(P,C^3)$	$\delta^{13}C^4$	$^{(2+3)}J(P,C^4)$	$\delta^{13}C^5$	$^{(2+3)}J(P,C^5)$	$\delta^1H^{C3/4}$	$^{(2/3)}J(P,H^{C3/4})$
5a	97.8	229.4	160.1	8.2	149.7	23.8	157.8	7.5	8.23	32.6
5b	104.0	237.4	164.2	[b]	137.1	24.2	159.4	7.7	7.94	26.5
6a	92.3	229.0	162.2	8.1	139.5	21.9	163.2	5.3	8.23	31.8
6b	101.7	238.1	162.4	8.0	140.0	20.4	162.2	8.0	7.79	26.3
7a	94.8	232.4	156.8	8.8	140.2	23.6	159.8	[b]	7.84	32.9
7b	102.2	231.7	[c]	[c]	[c]	[c]	[c]	[c]	[c]	[c]

[a] In $CDCl_3$. δ values are given in ppm and J values in Hz.
[b] Not resolved.
[c] Not isolated.

3. Conclusions

These results provide new insights into substrate selectivity and the regiochemistry of nitrilium phosphanylid complexes **II** in [3 + 2]-cycloaddition reactions. Concerning the substrate selectivity this can understood in terms of favored reactions of intermediately formed terminal phosphanediyl complexes **I**, which are in some kind of equilibrium with nitrilium phosphanylid complexes **II**, with electron-rich alkynes and disfavored reactions of **I** with electron-poor alkynes. Regarding our earlier assignments cf. [6,10] of the ^{13}C NMR data of ethoxycarbonyl-substituted 2*H*-1,2-azaphosphole complexes and the associated regio-chemistry of **II** this means that they were most probably erroneous.

As we already pointed out for HOMO-dipole LUMO-dipolarophile-directed reactions of derivatives of **II** with nitriles [4], the reactions are regioselective, but in contrast to our former conclusions, the selectivity seems to be mainly determined by steric rather than electronic factors. This would also explain the formerly observed lower regioselectivity of C-phenyl-substituted nitrilium phosphanylid complexes, cf. [4]. New findings obtained very recently from reactions of derivatives of **II** with a *P*-chloro phosphaalkene [13] also substantiate this new conclusion.

The concertedness of [3 + 2]-cycloaddition reactions of nitrilium phosphanylid complexes will be subject of further investigations.

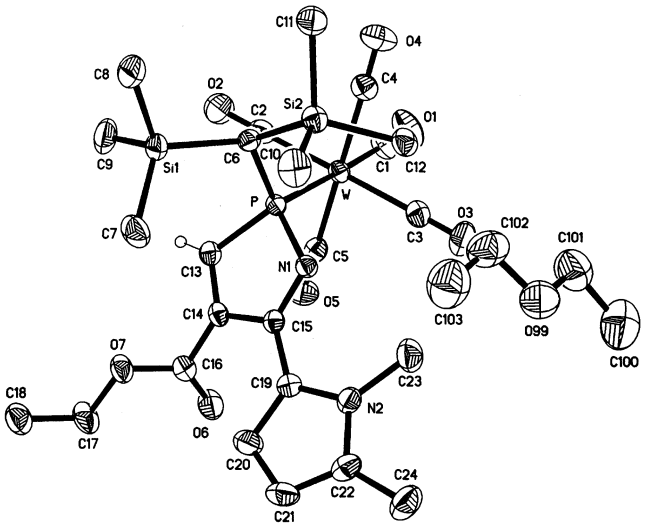


Fig. 2. Molecular structure of **7a** in the crystal. Ellipsoids represent 50% probability levels; hydrogen atoms, except for C(13)–H are omitted for clarity. Selected bond lengths (Å) and angles (°): W–C(1) 2.009(3), W–P 2.5098(6), P–N(1) 1.7042(19), P–C(13) 1.807(2), N(1)–C(15) 1.312(3), C(13)–C(14) 1.337(3), N(2)–C(19) 1.393(3); C(1)–W–P 178.19(9), W–P–C(13) 108.19(8), P–N(1)–C(6) 104.58(10), N(1)–P–C(13) 93.36(10), C(6)–P–W 117.4(8).

4. Experimental

4.1. General procedures

All reactions and manipulations were carried out under an atmosphere of deoxygenated dry nitrogen, using standard Schlenk techniques with conventional glassware, and solvents were dried according to standard procedures. NMR spectra were recorded on a Bruker AC-200 spectrometer (200 MHz for ^{1}H; 50.3 MHz for ^{13}C; 81.0 MHz for ^{31}P) using [D]chloroform and [D_6]benzene as solvent and internal standard; shifts are given relative to ext. tetra-methylsilane (^{1}H, ^{13}C) and 85% H_3PO_4 (^{31}P). Mass spectra were recorded on a Finigan Mat 8430 (70 eV); apart from *m*/*z*-values of the molecule ions, only *m*/*z*-values having intensities of more than 20% are given. Infrared spectra were recorded on a Biorad FT-IR 165 (selected data given). UV–Vis spectra were recorded on a Hewlett–Packard HP 8452. Melting points were obtained on a Büchi 535 capillary apparatus. Elemental analyses were performed using a Carlo Erba analytical gas chromatograph. The κP-notation in the nomenclature is intended to differentiate between P- and N-coordination of the appropriate heterocycle to the metal.

4.2. General procedure for the preparation of complexes 5–7

To the 2*H*-azaphosphirene complex **1** (0.62 g, 1 mmol), dissolved in 10 ml of toluene, 5 mmol of the nitriles **2a**–**c** and 2 mmol of the alkynes **3a**–**c** were added and, in each case, the solutions were heated at 75 °C for 5 h with slow stirring. Afterwards, all volatile components were removed in vacuo and the products separated by low-temperature column chromatography (SiO_2, −15 °C, 10 × 2 cm, *n*-pentane–diethyl ether 70/30).

4.3. {Pentacarbonyl[2-bis(trimethylsilyl)methyl-4-ethoxycarbonyl-5-(2-furanyl)-2H-1,2-azaphosphole-κP]tungsten(0)} (5a)

Evaporation of the second fraction yielded **5a:** orange crystals (200 mg, 30%); 83 °C (decomp.); ^{1}H NMR ($CDCl_3$) δ 0.26 (s, 9H, $SiMe_3$), 0.31 (s, 9H, $SiMe_3$), 1.41 (t, $^{3}J(H,H) = 7.2$ Hz, 3H, CH_2CH_3), 1.43 (d, $^{2}J(P,H) = 8.4$ Hz, 1H, $CH(SiMe_3)_2$), 4.45 (q, $^{3}J(H,H) = 7.1$ Hz, 2H, CH_2CH_3), 6.61 (m_c, 1H; CH_{aryl}), 7.35 (m_c, 1H, CH_{aryl}), 7.62 (m_c, 1H; CH_{aryl}), 8.23 (d, $^{2}J(P,H) = 32.6$ Hz, 1H, PC^3H); $^{13}C\{^{1}H\}$ NMR ($CDCl_3$) δ 2.2 (d, $^{3}J(P,C) = 2.9$ Hz, $SiMe_3$), 2.5 (d, $^{3}J(P,C) = 2.3$ Hz, $SiMe_3$), 14.0 (s, CH_2CH_3), 20.0 (d, $^{1}J(P,C) = 4.2$ Hz, $CH(SiMe_3)_2$), 62.1 (s, CH_2CH_3), 112.5 (s, C^3_{aryl}), 116.8 (s, C^4_{aryl}), 137.4 (d, $^{3}J(P,C) = 21.9$ Hz, C^2_{aryl}), 146.1 (s, C^5_{aryl}), 149.7 (d, $^{(2+3)}J(P,C) = 23.8$ Hz, PCC^4), 157.8

(d, ^2J(P,C) = 7.5 Hz, PN*C*^{5}), 160.1 (d, $^{(1+4)}J$(P,C) = 8.2 Hz, P*C*^{3}C), 164.3 (d, ^3J(P,C) = 17.5 Hz, *C*O$_2$Et), 196.3 (d, ^2J(P,C) = 6.5 Hz, *cis*-*C*O), 198.7 (d, ^2J(P,C) = 20.9 Hz, *trans*-*C*O); ^{31}P{^{1}H} NMR (CDCl$_3$) δ 97.8 (s, ^1J(P,W) = 229.4 Hz); UV–Vis (CH$_3$CN) λ (ln ε) 194 (4.46), 234 (4.83), 330 (4.19), 370 (4.68), 376 (3.61); IR (KBr) 2052 (s), 1977 (s), 1913 (s) cm^{-1} (CO); 1750 (s) cm^{-1} (CO$_2$); MS (70 eV, EI, ^{184}W); *m*/*z* 705 (12) [M$^+$], 677 (8) [(M–CO)$^+$], 649 (100) [(M–2CO)$^+$], 621 (4) [(M–3CO)$^+$], 593 (20) [(M–4CO)$^+$], 565 (50) [(M–5CO)$^+$·], 73 (74) [(SiMe$_3$)$^+$].

4.4. {Pentacarbonyl[2-bis(trimethylsilyl)methyl-3-ethoxycarbonyl-5-(2-furanyl)-2H-1,2-azaphosphole-κP]tungsten(0)} (**5b**)

Evaporation of the third fraction yielded **5b**: orange powder (60 mg, 3%); 93 °C (dec.); ^{1}H NMR (CDCl$_3$) δ 0.13 (s, 9H, SiMe$_3$), 0.41 (s, 9H, SiMe$_3$), 1.37 (d, ^2J(P,H) = 6.7 Hz, 1H, C*H*(SiMe$_3$)$_2$), 1.45 (t, ^3J(H,H) = 7.1 Hz, 3H, CH$_2$C*H*$_3$), 4.43 (m, 2H, C*H*$_2$CH$_3$), 6.67 (m$_c$, 1H; C*H*$_{aryl}$), 7.31 (m$_c$, 1H, C*H*$_{aryl}$), 7.70 (m$_c$, 1H; C*H*$_{aryl}$), 7.94 (d, ^3J(P,H) = 26.5 Hz, 1H, PCC^4*H*); ^{13}C{^{1}H} NMR (CDCl$_3$) δ 2.7 (d, ^3J(P,C) = 2.3 Hz, SiMe$_3$), 3.2 (d, ^3J(P,C) = 2.4 Hz, SiMe$_3$), 14.3 (s, CH$_2$*C*H$_3$), 20.6 (s, *C*H(SiMe$_3$)$_2$), 62.1 (s, *C*H$_2$CH$_3$), 113.0 (s, C3$_{aryl}$), 116.0 (s, C4$_{aryl}$), 137.1 (d, $^{(2+3)}J$(P,C) = 24.2 Hz, PC*C*^{4}), 146.6 (s, *C*$^5_{aryl}$), 150.2 (d, ^3J(P,C) = 22.6 Hz, *C*$^2_{aryl}$), 159.4 (d, $^{(2+3)}J$(P,C) = 7.7 Hz, PN*C*^{5}), 163.2 (d, ^2J(P,C) = 14.4 Hz, *C*O$_2$Et), 164.2 (s, P*C*^{3}C), 197.1 (d, ^2J(P,C) = 6.7 Hz, *cis*-*C*O), 198.9 (d, ^2J(P,C) = 22.7 Hz, *trans*-*C*O); ^{31}P{^{1}H} NMR (CDCl$_3$) δ 104.0 (s, ^1J(P,W) = 237.4 Hz); UV–Vis (CH$_3$CN) λ (ln ε) 234 (4.84), 246 (4.67), 270 (4.15), 274 (4.07), 284 (3.96), 340 (4.14), 386 (3.53), 392 (3.45); IR (KBr) 2047 (s), 1985 (s) cm^{-1} (CO); 1732 (s) cm^{-1} (CO$_2$); MS (70 eV, EI, ^{184}W); *m*/*z* 705 (7) [M$^+$], 677 (16) [(M–CO)$^+$], 649 (43) [(M–2CO)$^+$], 621 (7) [(M–3CO)$^+$], 593 (2) [(M–4CO)$^+$], 565 (74) [(M–5CO)$^+$], 73 (56) [(SiMe$_3$)$^+$].

Complexes **6a**,**b** were characterized as mixtures and, therefore, the assignment was made tentatively; UV–Vis-, IR- and MS-data are given for the 5:1 mixture.

Evaporation of the second fraction yielded **6a**,**b**: orange powder (220 mg, 32%).

4.5. {Pentacarbonyl[2-bis(trimethylsilyl)methyl-4-ethoxycarbonyl-5-(2-thienyl)-2H-1,2-azaphosphole-κP]tungsten(0)} (**6a**)

^{1}H NMR (CDCl$_3$) δ 0.13 (s, 9H, SiMe$_3$), 0.19 (s, 9H, SiMe$_3$), 1.28 (s, 1H, C*H*(SiMe$_3$)$_2$), 1.30 (t, ^3J(H,H) = 7.1 Hz, 3H, CH$_2$C*H*$_3$), 4.33 (q, ^3J(H,H) = 7.1 Hz, 2H, C*H*$_2$CH$_3$), 7.03 (m$_c$, 1H; C*H*$_{aryl}$), 7.45 (m$_c$, 1H, C*H*$_{aryl}$), 7.68 (m$_c$, 1H; C*H*$_{aryl}$), 8.23 (d, ^3J(P,H) = 31.8 Hz, 1H, PC^3*H*); ^{13}C{^{1}H} NMR (CDCl$_3$) δ 2.2 (d, ^3J(P,C) = 2.9 Hz, SiMe$_3$), 2.4 (d, ^3J(P,C) = 2.3 Hz, SiMe$_3$), 14.0 (s, CH$_2$*C*H$_3$), 19.9 (d, ^1J(P,C) = 4.5 Hz, *C*H(SiMe$_3$)$_2$), 62.2 (s, *C*H$_2$CH$_3$), 128.0 (s, *C*$^3_{aryl}$), 131.8 (s, *C*$^4_{aryl}$), 132.6 (s, *C*$^5_{aryl}$), 137.0 (d, ^3J(P,C) = 21.5 Hz, *C*$^2_{aryl}$), 140.0 (d, $^{(2+3)}J$(P,C) = 20.4 Hz, PC*C*^{4}), 162.2 (d, $^{(1+4)}J$(P,C) = 8.1 Hz, P*C*^{3}C), 163.2 (d, $^{(2+3)}J$(P,C) = 5.3 Hz, PN*C*^{5}), 164.2 (d, ^3J(P,C) = 17.3 Hz, *C*O$_2$Et), 196.2 (d, ^2J(P,C) = 6.5 Hz, *cis*-*C*O), 198.7 (d, ^2J(P,C) = 20.8 Hz, *trans*-*C*O); ^{31}P{^{1}H} NMR (CDCl$_3$) δ 92.3 (s, ^1J(P,W) = 229.0 Hz).

4.6. {Pentacarbonyl[2-bis(trimethylsilyl)methyl-3-ethoxycarbonyl-5-(2-thienyl)-2H-1,2-azaphosphole-κP]tungsten(0)} (**6b**)

^{1}H NMR (CDCl$_3$) δ 0.02 (s, 9H, SiMe$_3$), 0.30 (s, 9H, SiMe$_3$), 1.24 (d, ^2J(P,H) = 6.4 Hz, 1H, C*H*(SiMe$_3$)$_2$), 1.33 (t, ^{3}J(H,H) = 7.1 Hz, 3H, CH$_2$C*H*$_3$), 4.33 (m, 2H, C*H*$_2$CH$_3$), 7.11 (m$_c$, 1H; C*H*$_{aryl}$), 7.52 (m$_c$, 1H, C*H*$_{aryl}$), 7.59 (m$_c$, 1H; C*H*$_{aryl}$), 7.79 (d, ^2J(P,H) = 26.3 Hz, 1H, PCC^4*H*); ^{13}C{^{1}H} NMR (CDCl$_3$) δ 2.6 (d, ^3J(P,C) = 2.2 Hz, SiMe$_3$), 3.2 (d, ^3J(P,C) = 2.6 Hz, SiMe$_3$), 14.2 (s, CH$_2$*C*H$_3$), 20.7 (s, *C*H(SiMe$_3$)$_2$), 62.1 (s, *C*H$_2$CH$_3$), 127.6 (s, *C*$^3_{aryl}$), 128.5 (s, *C*$^4_{aryl}$), 131.4 (s, *C*$^5_{aryl}$), 132.5 (s, *C*$^2_{aryl}$), 133.0 (s, PC*C*^{4}), 140.0 (d, ^3J(P,C) = 20.4 Hz, P*C*C), 162.2 (d, ^2J(P,C) = 8.0 Hz, PN*C*), 163.2 (d, ^2J(P,C) = 5.3 Hz, *C*O$_2$Et), 195.6 (d, ^2J(P,C) = 6.4 Hz, *cis*-*C*O), 197.0 (d, ^2J(P,C) = 20.4 Hz, *trans*-*C*O); ^{31}P{^{1}H} NMR (CDCl$_3$) δ 101.7 (s, ^1J(P,W) = 238.1 Hz). 5:1-Mixture of **6a**,**b**: UV–Vis (CH$_3$CN) λ (ln ε) 232 (4.83), 282 (4.05), 336 (4.13), 368 (3.77), 384 (3.56); IR (KBr) 2073 (s), 1997 (s), 1952 (s), 1924 (s), 1903 (s) cm^{-1} (CO); 1730 (s) cm^{-1} (CO$_2$); MS (70 eV, EI, ^{184}W); *m*/*z* 721 (12) [M$^+$], 693 (10) [(M–CO)$^+$], 665 (26) [(M–2CO)$^+$], 637 (89) [(M–3CO)$^+$], 581 (100) [(M–5CO)$^+$], 73 (45) [(SiMe$_3$)$^+$].

4.7. {Pentacarbonyl[2-bis(trimethylsilyl)methyl-4-ethoxycarbonyl-5-(2-1,5-dimethylpyrryl)-2H-1,2-azaphosphole-κP]tungsten(0)} (**7a**)

Evaporation of the second fraction yielded **7a** as yellow crystals (160 mg, 23%); 115 °C (dec.); ^{1}H NMR (CDCl$_3$) δ 0.01 (s, 9H, SiMe$_3$), 0.06 (s, 9 H, SiMe$_3$), 1.14 (d, ^2J(P,H) = 8.2 Hz, 1H, C*H*(SiMe$_3$)$_2$), 1.15 (t, ^3J(H,H) = 7.1 Hz, 3H, CH$_2$C*H*$_3$), 2.13 (s, C$_{aryl}$–C*H*$_3$), 3.77 (s, N–C*H*$_3$), 4.18 (q, ^3J(H,H) = 7.1 Hz, 2H, C*H*$_2$CH$_3$), 5.79 (d, ^3J(H,H) = 4.0 Hz, 1H; C*H*$_{aryl}$), 6.40 (d, ^3J(H,H) = 4.1 Hz, 1H, C*H*$_{aryl}$), 7.84 (d, ^2J(P,H) = 32.9 Hz, 1H, PC^3*H*); ^{13}C{^{1}H} NMR (CDCl$_3$) δ 2.2 (d, ^3J(P,C) = 2.7 Hz, SiMe$_3$), 2.4 (d, ^3J(P,C) = 2.2 Hz, SiMe$_3$), 12.9 (s, C–*C*H$_3$), 14.0 (s, CH$_2$*C*H$_3$), 20.9 (d, ^1J(P,C) = 4.3 Hz, *C*H(SiMe$_3$)$_2$), 33.6 (s, N–*C*H$_3$), 62.0 (s, *C*H$_2$CH$_3$), 108.6 (s, *C*$^3_{aryl}$), 118.0 (s, *C*$^4_{aryl}$), 126.9 (d, ^3J(P,C) = 19.2 Hz, *C*$^2_{aryl}$), 139.0 (s, *C*$^5_{aryl}$), 140.2 (d, $^{(3+2)}J$(P,C) = 23.6 Hz, PC*C*^{4}), 156.8 (d, $^{(1+4)}J$(P,C) =

8.8 Hz, PC^{3}C), 159.8 (s, PNC^5), 165.8 (d, ^2J(P,C) = 17.5 Hz, CO_2Et), 196.8 (d, ^2J(P,C) = 6.7 Hz, *cis*-CO), 199.3 (d, ^2J(P,C) = 20.8 Hz, *trans*-CO); ^{31}P{^{1}H} NMR ($CDCl_3$) δ 94.8 (s, ^1J(P,W) = 232.4 Hz); UV–Vis (CH_3CN) λ (ln ε) 232 (4.78), 248 (4.58), 270 (4.20), 282 (4.00), 290 (3.91), 374 (4.15); IR (KBr) 2069 (s), 1986 (s), 1976 (s), 1934 (s), 1919 (s) cm^{-1} (CO); 1726 (s) cm^{-1} (CO_2); MS (70 eV, EI, ^{184}W); *m*/*z* 732 (16) [M$^+$], 704 (22) [(M–CO)$^+$], 676 (100) [(M–2CO)$^+$], 648 (48) [(M–3CO)$^+$], 620 (4) [(M–4CO)$^+$], 592 (70) [(M–5CO)$^+$], 517 (12) [(M–5CO–$SiMe_3$)$^+$], 408 (11) [(M–W(CO)$_5$)$^+$], 73 (40) [($SiMe_3$)$^+$]; *Anal.* Calc. for $C_{24}H_{33}N_2O_7PSi_2W$: C, 39.35; H, 4.54; N, 3.82. Found: C, 38.95; H, 4.43; N, 3.67%.

4.8. Crystal structure determination of **7a**·Et_2O, $C_{28}H_{43}N_2O_8PSi_2W$

Crystal data: triclinic, space group $P\bar{1}$, a = 1103.18(12), b = 1125.48(12), c = 1649.94(16) pm, α = 82.051(2), β = 71.975(2), γ = 65.999(2)°, U = 1.7794(3) nm^3, Z = 2, μ = 3.403 mm^{-1}, T = −130 °C. Data collection: a yellow crystal (ca. 0.35 × 0.13 × 0.11 mm) was used to record 29 869 intensities on a Bruker SMART 1000 CCD diffractometer (Mo Kα radiation, $2\theta_{max}$ 60°); 10 717 reflections were independent (R_{int} 0.0566). An absorption correction based on multiple scans was applied, with transmissions 0.72–1.00. Structure refinement: the structure was solved by the heavy-atom method and refined anisotropically on F^2 (program SHELXL-97, G.M. Sheldrick, University of Göttingen) to wR_2 0.0549, R_1 0.0307 for 392 parameters and 200 restraints; S = 0.953, max $\Delta\rho$ 1.178 e Å^{-3}. The hydrogen atoms were included using a riding model or rigid methyl groups, except for H13, which was freely refined.

5. Supplementary material

Atomic coordinates, bond lengths and angles, and thermal parameters have been deposited at the Cambridge Crystallographic Data Centre (CCDC). Any request to the CCDC for this data should quote the full literature citation and the reference number 163567. Copies of the data can be obtained free of charge on application to The Director, CCDC, 12 Union Road, Cambridge CB2 1EZ, UK (fax: +44-1223-336033; e-mail: deposit@chemcrys.cam.ac.uk or www: http://www.ccdc.cam.ac.uk).

Acknowledgements

We are grateful to the Fonds der Chemischen Industrie and the Deutsche Forschungsgemeinschaft for financial support.

References

[1] (a) R. Streubel, H. Wilkens, A. Ostrowski, C. Neumann, F. Ruthe, P.G. Jones, Angew. Chem., Int. Ed. Engl. 109 (1997) 1549;
(b) R. Streubel, H. Wilkens, A. Ostrowski, C. Neumann, F. Ruthe, P.G. Jones, Angew. Chem., Int. Ed. Engl. 36 (1997) 1492.
[2] R. Streubel, U. Schiemann, P.G. Jones, N.H. Tran Huy, F. Mathey, Angew. Chem., Int. Ed. Engl. 39 (2000) 3686.
[3] (a) U. Rohde, J. Jeske, F. Ruthe, P.G. Jones, R. Streubel, Angew. Chem. 111 (1999) 158;
(b) U. Rohde, J. Jeske, F. Ruthe, P.G. Jones, R. Streubel, Angew. Chem., Int. Ed. Engl. 37 (1999) 215.
[4] (a) H. Wilkens, J. Jeske, P.G. Jones, R. Streubel, Chem. Commun. (1997) 2317;
(b) H. Wilkens, F. Ruthe, P.G. Jones, R. Streubel, Chem. Eur. J. 4 (1998) 1542.
[5] H. Wilkens, F. Ruthe, P.G. Jones, R. Streubel, Chem. Commun. (1998) 1529.
[6] H. Wilkens, A. Ostrowski, J. Jeske, F. Ruthe, P.G. Jones, R. Streubel, Organometallics 18 (1999) 5627.
[7] (a) R. Streubel, A. Kusenberg, J. Jeske, P.G. Jones, Angew. Chem. 106 (1994) 2565;
(b) R. Streubel, A. Kusenberg, J. Jeske, P.G. Jones, Angew. Chem., Int. Ed. Engl. 36 (1997) 378.
[8] A. Ostrowski, J. Jeske, F. Ruthe, P.G. Jones, R. Streubel, Z. Anorg. Allg. Chem. 623 (1997) 1897.
[9] R. Streubel, H. Wilkens, F. Ruthe, P.G. Jones, Z. Anorg. Allg. Chem. 625 (1999) 102.
[10] R. Streubel, H. Wilkens, F. Ruthe, P.G. Jones, Chem. Commun. (1999) 2127.
[11] A. Espinosa Ferao, B. Deschamps, F. Mathey, Bull. Soc. Chim. Fr. 130 (1973) 695.
[12] F.H. Allen, O. Kennard, D.G. Watson, L. Brammer, A.G. Orpen, R. Taylor, J. Chem. Soc., Perkin Trans. II (1987) S1.
[13] R. Streubel, U. Schiemann, N. Hoffmann, P.G. Jones, Chem. Commun. (2001) 1334.

PERGAMON

Polyhedron 21 (2002) 125–131

POLYHEDRON

www.elsevier.com/locate/poly

Homopiperazine platinum(II) complexes containing substituted disulfide groups: crystal structure of $[Pt^{II}(homopiperazine)(diphenylsulfide)Cl]NO_3$

Mohammad S. Ali [a], Uday Mukhopadhyay [a], Shervin M. Shirvani [a], John Thurston [b], Kenton H. Whitmire [b], Abdul R. Khokhar [a,*]

[a] *Department of Experimental Therapeutics, Box 353, The University of Texas, M.D. Anderson Cancer Center, 1515 Holcombe Boulevard, Houston, TX 77030, USA*

[b] *Department of Chemistry, MS 60, Rice University, 6100 Main Street, Houston, TX 77005, USA*

Received 9 April 2001; accepted 9 October 2001

Abstract

A series of new cationic platinum(II) complexes of the type $[Pt(L)(R'R''S)Cl]NO_3$ (where L = homopiperazine or 1-methylhomopiperazine and R′R″S = dimethylsulfide, diethylsulfide, dipropylsulfide, diisopropylsulfide, dibutylsulfide, diphenylsulfide, dibenzylsulfide, methylphenylsulfide, or methyl *p*-tolylsulfide) were synthesized and characterized by elemental analysis and infrared, ^1H and ^{195}Pt nuclear magnetic resonance spectroscopy. Among the complexes synthesized, $[Pt^{II}(homopiperazine)(diphenylsulfide)Cl]NO_3$ was examined by single-crystal X-ray diffraction. The slightly distorted square plane of the platinum complex included the amino groups of the homopiperazine molecule in a *cis* orientation, the sulfur atom of diphenyl sulfide, and a chloride ion. The homopiperazine molecule adopts a boat conformation and forms five- and six-membered chelating rings with platinum. Hydrogen bonding plays an important part in holding the crystal together. © 2002 Elsevier Science Ltd. All rights reserved.

Keywords: Platinum(II); Homopiperazines; Disubstituted sulfides; Synthesis; Crystal structure

1. Introduction

The wide success of cisplatin in the treatment of a variety of human cancers [1], especially those of the testes, ovaries, head, and neck [2–5], has encouraged the search for new cisplatin derivatives in an effort to improve the therapeutic index of its compounds, which is reduced by dose-limiting toxic effects, namely, nephrotoxicity, myelotoxicity, neurotoxicity, nausea, and vomiting [6,7]. The clinical effectiveness of cisplatin has been improved by replacing the labile chloro ligands with other leaving groups of intermediate lability so as to alter the pharmacokinetics as well as by substituting stable amine ligands with cyclic or acyclic alkylamines [8]. Carboplatin (diammine-1,1-cyclobutanedicarboxylatoplatinum(II) [9,10], one of a number of cisplatin analogs developed in this way, is now used clinically. Many other compounds that have 1,2-diaminocyclohexane as a carrier ligand and chloride or carboxylate ion as a leaving group, such as oxaliplatin (*trans* - l - 1,2 - diaminocyclohexaneoxalatoplatinum(II) and L-NDDP [liposome-entrapped bis(neodecanoato)-(*trans*-1R,2R-diaminocyclohexane)platinum(II)] are now in clinical trials [10–12].

Platinum antitumor complexes like cisplatin and its analogs are neutral complexes that obey the general formula $[cis\text{-}Pt(Am)_2(X)_2]$ in which Am is an amine ligand having at least one NH group and X is a moderately strongly bound anionic leaving group, such as chloride [13,14]. These complexes are bifunctional in nature, which is probably necessary to form an intrastrand cross-link between two adjacent guanine bases in DNA [15,16]. However, two cationic classes of

* Corresponding author. Tel.: +1-713-792-2387; fax: +1-713-745-1176.

E-mail address: akhokhar@mdanderson.org (A.R. Khokhar).

0277-5387/02/$ - see front matter © 2002 Elsevier Science Ltd. All rights reserved.
PII: S0277-5387(01)00967-6

platinum complexes having antitumor properties have been described, both of which are much more soluble in water than the neutral complexes are. Such complexes have the general formula [*cis*-$Pt(NH_3)_2$(N-het)Cl]Cl (N-het = heterocyclic amine) or [Pt(diam)(R′R″SO)Cl]NO_3 (diam = bidentate diamine, R′R″SO = substituted sulfoxide) [17,18]. On the other hand, related monofunctional cationic complexes like [Pt(dien)Cl]Cl and $[Pt(NH_3)_3Cl]Cl$ are antitumor inactive [19,20]. Eventually, compounds having the formula [Pt(diam)-(R′R″SO)Cl]NO_3 or [Pt(diam)Cl_2] will form the same adduct with 5′GMP and d(GpG) [21]. In principle, the same adducts can be expected with DNA, therefore, the mechanisms of action of both types of compounds might well be related to each other but are unlikely to be the same as that of cisplatin [21].

Hollis et al. [17] reported on a series of cationic platinum(II) complexes whose antitumor activity violates some of the rules of classical structure-activity relationships. However researchers have known of cationic diammineplatinum(II) complexes with substituted sulfoxide for the past 2 decades [22,23]. It has been reported that these complexes have antitumor activity in certain tumor models [24,25]. We have been developing platinum complexes with diamines such as diaminocyclohexane as a carrier ligand and disulfides as leaving groups [26]. Complexes containing thioether groups can reduce cisplatin-induced nephrotoxicity when administered simultaneously with cisplatin [27]. Hence we report here the synthesis and characterization of cationic platinum(II) complexes of the type [PtL(R′R″S)Cl]NO_3 along with the crystal structure of [Pt^{II}(homopiperazine)(diphenylsulfide)Cl]NO_3.

2. Experimental

2.1. Chemicals

K_2PtCl_4 was purchased from Johnson Matthey, Seabrook, MA. Homopiperazine, 1-methylhomopiperazine, dimethylsulfide, diethylsulfide, dipropylsulfide, diisopropylsulfide, dibutylsulfide, diphenylsulfide, dibenzylsulfide, methylphenylsulfide, and methyl *p*-tolylsulfide were purchased from Aldrich Chemical Co., Milwaukee, WI. Silver nitrate was obtained from Fisher Scientific Co., Houston, TX. All chemicals obtained from commercial sources were used as supplied.

2.2. Physical measurements

Elemental analyses of the complexes were performed by Robertson Laboratory Inc., Madison, NJ. Infrared (IR) spectra in the range of 600–4000 cm^{-1} and far-IR spectra in the range of 150–600 cm^{-1} were recorded in KBr and polyethylene pellets, respectively, on a Perkin–Elmer 2000 spectrophotometer. ^1H nuclear magnetic resonance (NMR) spectra in MeOH-d_4 and ^{195}Pt NMR spectra in methanol were recorded using a Bruker Advance 300 spectrometer. ^1H spectra were recorded with a 5-mm tunable probe at 300.13 MHz, ^{195}Pt spectra were recorded at 43.055 MHz, and the shifts were measured relative to an external standard of 2.2 M Na_2PtCl_6 in D_2O at 0.00 ppm.

2.3. Preparation of {Pt(hpip)[$(CH_3)_2S$]Cl}NO_3 (hpip = homopiperazine) (complex **1**)

K_2PtCl_4 (20.76 g, 50 mmol) was dissolved in 250 ml of deionized water and filtered. KI (83.0 g, 0.5 mol) in 100 ml of water was added to it, and the reaction mixture was stirred for 10 min. Next, homopiperazine (8.5 g, 100 mmol) was added dropwise to the mixture while stirring to obtain a yellow precipitate of [Pt(hpip)I_2]. The stirring was continued for a further 30 min, and the precipitate was then collected by filtration. This compound was stirred in 100 ml of dimethylformamide, filtered, washed with water, ethanol, and acetone, and dried under vacuum (yield, 95%). [Pt(hpip)I_2] (12.38 g, 20 mmol) was suspended in an aqueous solution of silver nitrate (6.72 g, 39.8 mmol) in 250 mL of water. The reaction mixture was stirred for 24 h at room temperature (r.t.) in the dark. The AgI precipitate was filtered off, and a solution of NaCl was added dropwise to the filtrate with constant stirring until a yellow precipitate of [Pt(hpip)Cl_2] formed. The precipitate was filtered and recrystallized from dimethylformamide. The yellow crystals obtained were washed with water and acetone and dried under vacuum (yield, 75%). An equivalent amount of $AgNO_3$ (0.338 g, 2 mmol) dissolved in 100 ml of hot methanol was added to a slurry of [Pt(hpip)Cl_2] (0.872 g, 2 mmol) in 100 ml of methanol. An equivalent amount of dimethylsulfide (0.15 mg, 2 mmol) in 20 ml of methanol was added to this mixture. The reaction mixture was then stirred overnight in the dark. The AgCl precipitate was filtered off and the filtrate was evaporated to dryness under reduced pressure. A yellow solid was obtained, which was recrystallized from methanol and ether. Finally, the light yellow compound, [Pt(hpip)$(CH_3)_2S$)Cl]NO_3, was obtained, which was then dried under vacuum (yield, 70%).

Complexes **2**–**18** (Table 2) were prepared in a similar manner.

Complex **11** [Pt^{II}(hpip)(diphenylsulfide)Cl]NO_3 (100 mg) was dissolved in 100 ml of methanol, after which the volume of the solution was reduced to 50 ml and filtered. The filtrate was allowed to evaporate slowly at r.t. Within 2 weeks, colorless needle-shaped crystals were separated from the solution, which were used for X-ray crystallography.

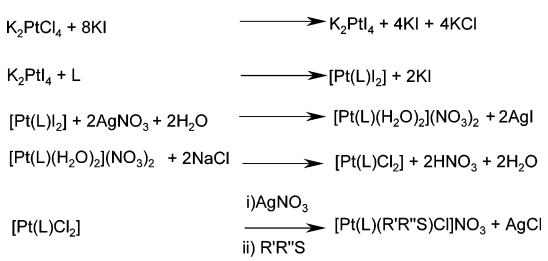
2.4. Single crystal X-ray crystallographic study

The experimental details of the X-ray data collection, the structure solution and refinement of the title compound are compiled in Table 1. A single crystal of [Pt^{II}(homopiperazine)(diphenylsulfide)Cl]NO_3 was coated with a thin layer of epoxy cement and glued to the end of a glass fiber. The fiber was mounted on the goniometer of a Bruker SMART 1K diffractometer equipped with a CCD area detector at 298 K. The orientation matrix and all data were collected at this temperature. The diffractometer is equipped with graphite monochromated Mo Kα radiation ($\lambda =$ 0.71073 Å) and the data was corrected for Lorentz and polarization effects. Absorption correction was applied using the program SADABS [28]. No appreciable decay of the crystal was detected during data collection.

Table 1
Crystal data and structure refinement for [Pt^{II}(homopiperazine)-(diphenylsulfide)Cl]NO_3

Empirical formula	$C_{17}H_{20}ClN_3O_3PtS$
Formula weight	576.96
Temperature (K)	293(2)
Wavelength (Å)	0.71073
Crystal system	monoclinic
Space group	$P2_1/c$
Unit cell dimensions	
a (Å)	17.666(4)
b (Å)	8.8116(18)
c (Å)	12.619(3)
β (°)	101.02(3)
V (Å^3)	1928.1(7)
Z	4
D_{calc} (Mg m^{-3})	1.988
Absorption coefficient (mm^{-1})	7.546
$F(000)$	1112
Crystal size (mm)	$0.318 \times 0.242 \times 0.163$
θ Range for data collection (°)	1.17–23.33
Limiting indices	$-19 \le h \le 17$, $-9 \le k \le 9$, $-12 \le l \le 13$
Reflections collected	8122
Independent reflections	2740 ($R_{int} = 0.0785$)
Refinement method	Full-matrix least-squares on F^2
Data/restraints/parameters	2740/0/235
Goodness-of-fit on F^2	1.057
Final R indices [$I > 2\sigma(I)$] [a]	$R_1 = 0.0400$, $wR_2 = 0.1035$
R indices (all data)	$R_1 = 0.0416$, $wR_2 = 0.1110$
Largest difference peak and hole (e Å^{-3})	1.865 and −1.319

[a] $R_1 = \Sigma||F_o|-|F_c||/\Sigma|F_o|$. $R_w = [\Sigma\, w(F_o^2-F_c^2)^2]/\Sigma[w(F_o^2)^2]^{1/2}$. $w = [\sigma^2(F_o^2)+(0.0833P)^2]^{-1}$. $P = (F_o^2+2F_c^2)/3$. $a = 0.0833$, $b = 0$.



Scheme 1.

The structure was solved using direct methods with the SHELXTL software package [28]. Scattering factors were taken from the literature [29]. Heavy atoms were located initially to set the correct phases for the model. All other atoms were located by successive Fourier maps and were refined using the full-matrix least-squares method on F^2. All non-hydrogen atoms were refined anisotropically. Hydrogen atoms were placed in calculated positions ($d_{C-H} = 0.96$ Å) and allowed to ride on the adjacent carbon atom. Refinement of positional and anisotropic parameters led to convergence.

3. Results and discussion

3.1. Synthesis of platinum complexes

The procedure used in the synthesis of complexes is shown in Scheme 1. [$PtLCl_2$] was prepared according to the method described by Dhara [30], which was adopted because it is rapid and easy and provides a much higher yield than when K_2PtCl_4 is treated directly with homopiperazines. K_2PtCl_4 mixed with an excess of KI produced K_2PtI_4 in solution. K_2PtI_4 was then reacted with one equivalent of hpip or mhpip (1-methylhomopiperazine) to precipitate [$PtLI_2$]. The reaction of [$PtLI_2$] with $AgNO_3$ led to the formation of [$PtL(H_2O)_2$]$(NO_3)_2$ in solution, which was further converted to [$Pt^{II}LCl_2$] by treating it with a NaCl solution. Finally [$Pt^{II}(L)Cl_2$] was reacted with one equivalent of $AgNO_3$ and subsequently with thioethers to form the required compounds of the type [Pt(L)(R′R″S)Cl]NO_3 in solution, while the insoluble AgCl was separated by filtration. The yellow solid [Pt(L)(R′R″S)Cl]NO_3 was obtained [26] upon removal of the solvent.

3.2. Characterization of platinum complexes

The complexes were characterized by elemental analysis and IR, ^{1}H NMR, and ^{195}Pt NMR spectroscopy. The composition of each complex as determined by elemental analysis showed good agreement between the theoretical and actual values. The analytical results are summarized in Table 2. The results of characterization by IR and ^{195}Pt NMR are shown in Table 3.

The IR spectra of the complexes in general showed a broad absorption between 3204 and 3009 cm^{-1}, which was due to the ν_{N-H} stretching vibrations of coordinated homopiperazine and 1-methylhomopiperazine. The intense band observed in the region 1331–1385 cm^{-1} was due to the ν_{S-C} stretching vibrations in all the complexes [31–33]. The ν_{Pt-S} stretching vibrations

Table 2
Elemental analysis of $[Pt^{II}(L)(R'R''S)Cl]NO_3$

Complex	Complex name	Observed (calculated)		
		C (%)	H (%)	N (%)
1	$[Pt^{II}$(hpip)(dimethylsulfide)Cl$]NO_3$	18.50 (18.72)	3.94 (4.01)	9.20 (9.36)
2	$[Pt^{II}$(1-mhpip)(dimethylsulfide)Cl$]NO_3$	20.33 (20.50)	4.20 (4.30)	8.80 (8.97)
3	$[Pt^{II}$(hpip)(diethylsulfide)Cl$]NO_3$	22.35 (22.37)	4.51 (4.56)	8.69 (8.70)
4	[Pt(1-mhpip)(diethylsulfide)Cl$]NO_3$	24.29 (24.17)	4.78 (4.87)	8.36 (8.34)
5	$[Pt^{II}$(hpip)(dipropylsulfide)Cl$]NO_3$	25.91 (25.85)	5.02 (5.09)	8.21 (8.22)
6	$[Pt^{II}$(1-mhpip)(dipropylsulfide)Cl$]NO_3$	27.38 (27.47)	5.23 (5.38)	7.91 (8.01)
7	$[Pt^{II}$(hpip)(diisopropylsulfide)Cl$]NO_3$	25.56 (25.85)	5.05 (5.09)	8.29 (8.22)
8	$[Pt^{II}$(1-mhpip)(diisopropylsulfide)Cl$]NO_3$	27.31 (27.47)	5.03 (5.38)	8.20 (8.01)
9	$[Pt^{II}$(hpip)(dibutylsulfide)Cl$]NO_3$	29.01 (31.41)	5.55 (6.04)	7.77 (6.04)
10	$[Pt^{II}$(hpip)(dibutylsulfide)Cl$]NO_3$	30.09 (30.41)	5.84 (5.83)	7.55 (7.60)
11	$[Pt^{II}$(hpip)(diphenylsulfide)Cl$]NO_3$	35.02 (35.26)	3.92 (3.80)	7.37 (7.26)
12	$[Pt^{II}$(1-mhpip)(diphenylsulfide)Cl$]NO_3$	36.76 (36.46)	4.14 (4.08)	7.08 (7.09)
13	$[Pt^{II}$(hpip)(dibenzylsulfide)Cl$]NO_3$	37.74 (37.59)	4.28 (4.14)	6.92 (6.80)
14	$[Pt^{II}$(1-mhpip)(dibenzylsulfide)Cl$]NO_3$	38.58 (38.68)	4.57 (4.54)	6.68 (6.77)
15	$[Pt^{II}$(hpip)(methylphenylsulfide)Cl$]NO_3$	27.86 (27.87)	3.87 (3.87)	8.13 (8.06)
16	$[Pt^{II}$(1-mhpip)(methylphenylsulfide)Cl$]NO_3$	29.69 (29.41)	4.20 (4.18)	7.77 (7.92)
17	$[Pt^{II}$(hpip)(methyl *p*-tolylsulfide)Cl$]NO_3$	30.02 (29.40)	4.24 (4.14)	7.82 (7.91)
18	$[Pt^{II}$(1-mhpip)(methyl *p*-tolylsulfide)Cl$]NO_3$	30.69 (30.87)	4.41 (4.44)	7.62 (7.72)

L = homopiperazine (hpip) or 1-methylhomopiperazine (1-mhpip).

were observed around 350–400 cm^{-1}, which were close to the values reported for such compounds [26,27,34,35]. The absorption for ν_{Pt-Cl} stretching vibrations were seen around 300 cm^{-1} [26,27,36].

The ^1H NMR spectra, which are shown in Table 4, were most informative with respect to the structures of the complexes. Platinum coordination at S atom of substituted disulfides in all complexes leads a downfield shift of S–CH protons relative to the free ligands. Hence, evidence of ^1H NMR spectra suggests the coordination of platinum(II) with sulfur atom.

The ^{195}Pt NMR data shown in Table 3 further confirmed the structures of these platinum complexes. The singlet observed in the range of -3178 to -3415 ppm indicated the coordination of amino nitrogens of homopiperazine, and 1-methylhomopiperazine to the two adjacent corners of square planar platinum(II), while the other two positions were bound to the chloride and sulfur atoms of the thioether group. Such chemical shifts are characteristic for the square planar platinum(II) complexes in which platinum(II) is bound by two nitrogen atoms, one sulfur atom, and one chlorine atom [26,27,37]. Fig. 1 shows the general structure of the complexes.

3.3. Crystal structure

Fig. 2 shows a view of the crystal structure of $[Pt^{II}$(hpip)(diphenylsulfide)Cl$]NO_3$. Selected bond lengths and bond angles are given in Table 5. In this molecule, the coordination environment around the platinum atom is a slightly distorted square planar one, with the angles ranging from 77.1(2) to 96.69(6)°. The distortion is caused by limitation in the bite distances of the chelating ligand.

In the platinum square plane, two adjacent corners are occupied by the two nitrogen atoms of the homopiperazine ligand, whereas the remaining two *cis* positions are coordinated with one chloride ion and one sulfur atom of the diphenylsulfide. All Pt–N, Pt–Cl, and Pt–S bond lengths are in the range normally

Table 3
IR and ^{195}Pt NMR data for $[Pt^{II}(L)(R'R''S)Cl]NO_3$

Complex	IR (cm^{-1})		^{195}Pt NMR (ppm)
	νN–H	νS–C	
1	3139	1384	−3415
2	3115	1331	−3192
3	3049	1383	−3215
4	3130	1337	−3210
5	3009	1384	−3144
6	3102	1331	−3208
7	3039	1384	−3144
8	3104	1338	−3208
9	3058	1384	−3173
10	3140	1338	−3178
11	3204	1384	−3138
12	3127	1340	−3151
13	3124	1385	−3165
14	3107	1338	−3098
15	3091	1384	−3153
16	3152	1337	−3105
17	3151	1384	−3160
18	3113	1335	−3145

Table 4
^{1}H NMR data for [Pt^{II}(L)(R′R″S)Cl]NO_3

Ligand/complex no.	S–CH_3	S–CH_2–	–CH_2–	–CH_2–	–CH_3	S–C–H	C_6H_5
Dimethylsulfide	2.07 s						
	2.50 s						
	2.45 s						
Diethylsulfide		2.52 q			1.22 t		
3		2.99 m			1.45 t		
4		2.98 m			1.43 t		
Dipropylsulfide		2.46 t	1.58 m		0.97 t		
5		3.00 m	1.92 m		1.11 t		
6		2.95 m	1.90 m		1.09 t		
Diisopropylsulfide					1.21 d	2.95 m	
7					1.52 d	3.35 m	
8					1.52 d	3.36 m	
Dibutylsulfide		2.49 t	1.54 m	1.42 m	0.91 t		
9		2.77 t	1.86 m	1.61 m	1.24 t		
10		3.04 m	1.80 m	1.54 m	0.99 t		
Diphenylsulfide							7.17 m
							7.25 m
11							7.53 m
							7.78 m
12							7.51 m
							7.76 m
Dibenzylsulfide		3.59 s					7.26 m
13		4.11 d					7.28 m
							8.35 m
14		4.11 d					7.45 m
		4.39 d					7.66 m
Methylphenylsulfide	2.42 s						7.08 m
							7.20 m
15	2.88 s						7.53 m
							7.93 m
16	2.86 s						7.53 m
							7.97 m
							C_6H_4
Methyl-*p*-tolylsulfide	2.25 s				2.38 s		7.02 d
							7.14 d
17	2.72 s				2.37 s		7.23 d
							7.72 d
18	2.83 s				2.38 s		7.33 d
							7.86 d

Chemical shift in ppm; ^{1}H NMR spectra were recorded in deuterated methanol. s = singlet, d = doublet, t = triplet, q = quartet, m = multiplet.

observed for platinum(II) complexes. The average Pt–N bond length of 2.041(5) Å is consistent with those found in homopiperazine containing complexes. For instance, this length is 2.02(10) Å in [Pt^{II}(hpip)-(pentadecanoate)$_2$] [38], 1.99(2) Å in Pt^{II}(1-methylhomopiperazine)(methylmalonato)]·$2H_2O$ [34], and 2.027(6) Å in [Pt^{II}(hpip)Cl_2] [39]. The Pt(1)–Cl(1) bond length of 2.3021(17) Å is normal as compared with the values observed in other Pt(II) dichloride complexes, e.g. 2.309 (2) Å in [Pt^{II}(hpip)Cl_2] [39] and 2.315(2) Å in [Pt(piperidine)Cl_2]·H_2O [40]. The Pt–S bond distance of 2.284(15) Å is not significantly different from the 2.279(7) Å observed in the sulfide complex [Pt(μ-SC_5H_9NM)Br [41].

Homopiperazine is in boat conformation and forms five- and six-membered chelating rings with platinum. The coordination structure of platinum with two ring nitrogens of homopiperazine is considerably strained, and the N(1)–Pt(1)–N(2) bond angle is contracted to 77.1(2)° due to geometric constraints imposed by the ligand. This angle is close to that reported for [Pt^{II}(hpip)Cl_2] (76.9 (3)°) [39], Pt^{II}(1-methylhomopiperazine)(methylmalonato)]·$2H_2O$ (77.8(8)° [36], and

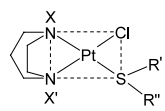


Fig. 1. Structure of [Pt(L)(R′R″S)Cl]. X = X′ = H = Homopiperazine (L). X = H, X′ = CH_3 = 1-methyl homopiperazine (L). R′, R″ = methyl, ethyl, propyl, isopropyl, butyl, phenyl or benzyl, in complexes **1**–**14**, R′ = methyl, R″ = phenyl in complexes **15** and **16**, R′ = methyl, R″ = *p*-tolyl in complexes **17** and **18**.

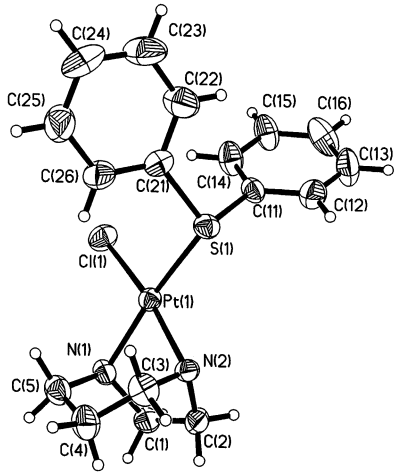


Fig. 2. ORTEP representation of [Pt^{II}(homopiperazine)(diphenylsulfide)Cl]NO_3. Counter ion omitted for clarity. Thermal ellipsoids drawn at 50% probability.

Table 5
Selected bond lengths (Å) and bond angles (°) for [Pt^{II}(homopiperazine)(diphenylsulphide)Cl]NO_3

Bond lengths			
Pt(1)–N(1)	2.042(5)	Pt(1)–S(1)	2.2846(15)
Pt(1)–N(2)	2.050(5)	Pt(1)–Cl(1)	2.3021(17)
Bond angles			
N(1)–Pt(1)–N(2)	77.1(2)	C(11)–S(1)–Pt(1)	114.6(2)
N(1)–Pt(1)–S(1)	168.82(16)	C(21)–S(1)–Pt(1)	110.1(2)
N(2)–Pt(1)–S(1)	92.53(15)	C(1)–N(1)–Pt(1)	107.3(4)
N(1)–Pt(1)–Cl(1)	93.67(16)	C(5)–N(1)–Pt(1)	107.9(4)
N(2)–Pt(1)–Cl(1)	170.77(15)	C(2)–N(2)–Pt(1)	106.7(4)
S(1)–Pt(1)–Cl(1)	96.69(6)	C(3)–N(2)–Pt(1)	109.2(4)

[Pt^{II}(hpip)(pentadecanoate)$_2$] (76.3(4)°) [38]. In addition, the contraction of the N1–Pt–N2 bond angle is compensated for with expansion of the N(2)–Pt(1)–S(1), N(1)–Pt(1)–Cl(1) and S(1)–Pt(1)–Cl(1) bond angles to 92.53(15)°, 93.67(16)° and 96.69(6)°, respectively. The Pt(1)–N(1)–C(1) and Pt(1)–N(1)–C(5) bond angles in the present study are 107.3(4)° and 107.9(4)°, respectively, these angles are 107.7(4)° and 109.0(4)°, respectively, in [Pt^{II}(hpip)Cl_2] [39], 105.9(8)° and 112.1(7)°, respectively, in [Pt^{II}(hpip)(pentadecanoate)$_2$] [38], and 104.3(14)° and 109.5(14)°, respectively, in Pt^{II}(1-methylhomopiperazine)(methylmalonato)]·$2H_2O$ [36]. The molecules in the crystal show a system of N–H···O hydrogen bonds (Fig. 3).

In summary, we have synthesized and characterized a series of new platinum(II) complexes containing homopiperazine or 1-methylhomopiperazine as nonleaving amine ligands and different sulfide groups as leaving ligands. The crystal structure of [Pt^{II}(hpip)(diphenylsulfide)Cl]NO_3 was determined by X-ray crystallography.

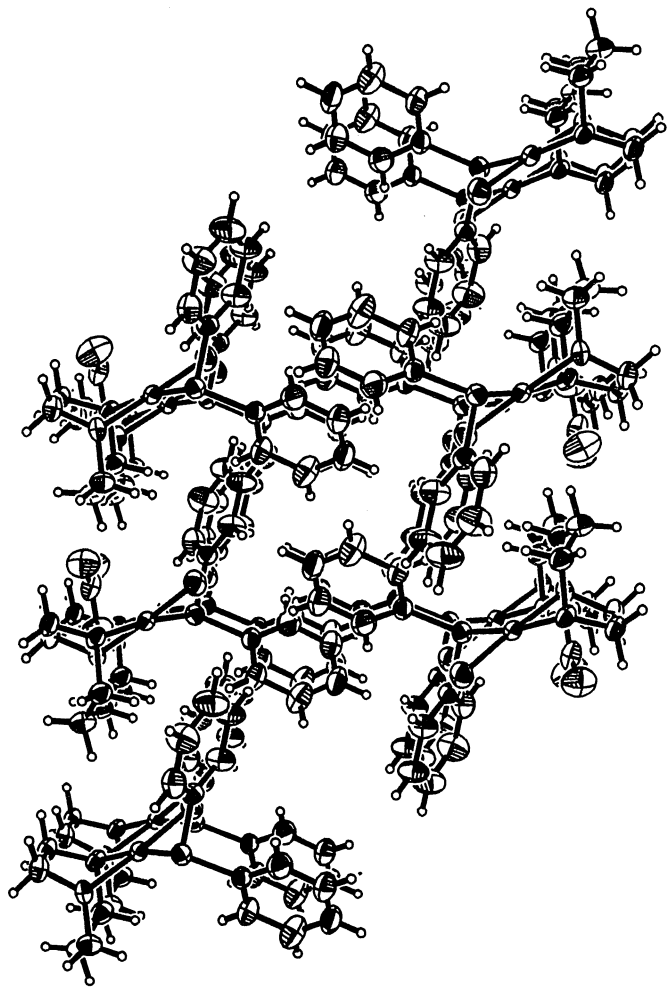


Fig. 3. Packing diagram of [Pt^{II}(homopiperazine)(diphenylsulfide)-Cl]NO_3. Orientation is along the 0 1 0 axis. Thermal ellipsoids drawn at 50% probability.

4. Supplementary material

Crystallographic data for the structural analysis have been deposited with the Cambridge Crystallographic Centre, CCDC No. 160939. Copies of this information may be obtained free of charge from The Director, CCDC, 12 Union Road, Cambridge, CB2 1EZ, UK (fax: +44-1233-336-033; e-mail: deposit@ccdc.cam.ac.uk or www: http://www.ccdc.cam.ac.uk).

Acknowledgements

This work was supported by grants CA-77332 and CA-82361 from the National Cancer Institute and by grant C0976 from the Robert A. Welch Foundation.

References

[1] P.J. Loehrer, L.H. Einhorn, Ann. Intern. Med. 100 (1984) 704.

[2] W.B. Pratt, R.W. Rudden, W.D. Ensminger, J. Maybaum, The Anticancer Drugs, Oxford University Press, New York, 1994, p. 133.
[3] I.H. Krakoff, Cancer Treat. Rep. 63 (1979) 1523.
[4] J.B. Vermorken, H.M. Pinedo, Neth. J. Med. 25 (1982) 270.
[5] D.D. Vonhoff, R. Schilsky, C.M. Reichart, Cancer Treat. Rep. 63 (1979) 1527.
[6] I.H. Krakoff, in: M. Nicolini (Ed.), Platinum and Other Metal Coordination Compounds in Cancer Chemotherapy: Clinical Application of Platinum Complexes, Martinus Nijhoff, Boston, MA, 1988, p. 351.
[7] P.J. Loehrer, S.D. Williams Sr, L.H. Einhorn, J. Natl. Cancer Inst. 80 (1988) 1373.
[8] M.J. Cleare, Coord. Chem. Rev. 12 (1974) 349.
[9] A.H. Calvert, S.J. Harland, D.R. Newell, Z.H. Siddik, K.R. Harrap, Cancer Treat. Rev. 12 (1985) 51.
[10] B.W. Booth, R.B. Weiss, A.H. Korzun, W.C. Wood, R.W. Carey, L.P. Panasci, Cancer Treat. Rep. 69 (1985) 919.
[11] R. Perez-Soler, G. Lopez-Berestein, J. Luthersztain, S. Al-Baker, K. Francis, D. Macias-Kiger, M.N. Raber, A.R. Khokhar, Cancer Res. 50 (1990) 4254.
[12] J.M. Extra, M. Espie, F. Calvo, C. Ferme, L. Mignot, M. Marty, Cancer Chemother. Phermacol. 25 (1990) 299.
[13] M.J. Cleare, P.C. Hydes, D.R. Hepburn, B.W. Malerbi, in: A.W. Prestayko, S.T. Crooke, S.K. Carter (Eds.), Cisplatin, Current Status and New Developments, Academic Press, New York, 1980, p. 149.
[14] A.H. Calvert, in: D.C.H. McBrien, T.F. Slater (Eds.), Biochemical Mechanisms of Platinum Antitumor Drugs, IRL Press, Washington, DC, 1986, p. 307.
[15] J. Reedijk, A.M.J. Fichtinger-Schepman, A.T. van Oosterom, P. van de Putte, Struct. Bond. (Berlin) 67 (1987) 53.
[16] A.L. Pinto, S.J. Lippard, Biochim. Biophys. Acta 780 (1985) 167.
[17] L.S. Holis, A.R. Amundsen, E.W. Stern, J. Med. Chem. 32 (1989) 128.
[18] N. Farrell, D.M. Kaley, W. Schmidt, M.P. Hacker, Inorg. Chem. 29 (1990) 397.
[19] (a) M.J. Cleare, J.D. Hoeschele, Bioinorg. Chem. 2 (1973) 187; (b) J.P. Macquet, J.-L. Butour, J. Natl. Cancer Inst. 70 (1983) 899.
[20] E.L.M. Lempers, M.J. Bloemink, J. Brouwer, Y. Kidani, J. Reedijk, J. Inorg. Biochem. 40 (1990) 23.
[21] E.L.M. Lempers, M.J. Bloemink, J. Reedijk, Inorg. Chem. 30 (1991) 201.
[22] (a) M.L. Tobe, A.R. Khokhar, J. Clin. Hemat. Oncol. 7 (1973) 114;
(b) P.D. Braddock, T.A. Connors, M. Jones, A.R. Khokhar, D.H. Melzack, M.L. Tobe, Chem. Biol. Interact. 11 (1975) 145.
[23] P.D. Braddock, A.R. Khokhar, R. Romeo, M.L. Tobe, in: T.A. Connors, J.J. Roberts (Eds.), Recent Results in Cancer Research: Platinum Coordination Complexes in Cancer Chemotherapy, vol. 48, Springer, Berlin, 1974, p. 14.
[24] (a) V. Fimiani, D. Minniti, Anticancer Drugs 3 (1992) 9;
(b) J. Landi, M.P. Hacker, N. Farrell, Inorg. Chim. Acta 202 (1992) 79.
[25] N. Farrell, D.M. Kiley, W. Schimdt, M.P. Hacker, Inorg. Chem. 29 (1990) 379.
[26] (a) A.R. Khokhar, S. Shamsuddin, S. Al-Baker, C. Shah, J. Coord. Chem. 36 (1995) 7;
(b) S.R. Ali Khan, A.R. Khokhar, J. Coord. Chem. 51 (2000) 323.
[27] M.M. Jones, M.A. Basinger, M.A. Holsher, Anticancer Res. 11 (1991) 449.
[28] SHELXTL 5.10, Bruker AXS, Madison, WI, 1997.
[29] The scattering factors are part of the SHELXTL package and can be found in the International Tables for X-ray Crystallography, vol. C, Kluwer, Dordrecht, The Netherlands, 1992.
[30] S.C. Dhara, Indian J. Chem. 8 (1970) 193.
[31] S. Shamsuddin, S. Al-baker, Z.H. Siddik, A.R. Khokhar, Inorg. Chim. Acta 241 (1996) 101.
[32] D. Gibson, G.M. Arvantis, H.M. Berman, Inorg. Chim. Acta 218 (1994) 11.
[33] A.R. Khokhar, S. Shamsuddin, S. Al-Baker, C. Shah, J. Coord. Chem. 36 (1995) 7.
[34] D.M. Adams, P.J. Chandler, J. Chem. Soc. A (1969) 588.
[35] F.A. Cotton, R. Francis, W.D. Horrocks, J. Phys. Chem. 64 (1960) 1534.
[36] M.S. Ali, K.H. Whitmire, T. Toyomasu, Z.H. Siddik, A.R. Khokhar, J. Inorg. Biochem. 77 (1999) 231.
[37] P.S. Pregsin, Coord. Chem. Rev. 44 (1982) 247.
[38] M.S. Ali, C.A. Powers, K.H. Whitmire, I. Guzman-Jimenez, A.R. Khokhar, J. Coord. Chem. 52 (2001) 273.
[39] E.C.H. Ling, G.W. Allen, T.W. Hambley, J. Am. Chem. Soc. 16 (1994) 2673.
[40] S.R. Ali Khan, I. Guzman-Jimenez, K.H. Whitmire, A.R. Khokhar, Polyhedron 19 (2000) 975.
[41] A. Jose-Antonio, P. Gonzalez-Duarte. J. Chem. Soc., Dalton Trans. (1990) 1793.

PERGAMON

Polyhedron 21 (2002) 133–140

POLYHEDRON

www.elsevier.com/locate/poly

Interaction of sulfur dioxide and cyanide with cobalt(II) tetrasulfophthalocyanine in aqueous media

Mamothibe Thamae, Tebello Nyokong *

Department of Chemistry, Rhodes University, Grahamstown 6140, South Africa

Received 13 August 2001; accepted 9 October 2001

Abstract

Kinetic and equilibrium studies for the coordination of cyanide or sulfur dioxide to the cobalt(II) tetrasulfophthalocyanine ($[CoTSPc]^{4-}$) complex are reported. The equilibrium constant for the coordination of the cyanide under pH 11 conditions and an oxygen atmosphere, and the formation of $[(CN^-)_2Co(III)TSPc]^{5-}$ species, was found to be 2.1×10^1 dm^3 mol^{-1} and the rate constant, k_f was found to be 7.4 dm^3 mol^{-1} s^{-1}. Similarly, the coordination of SO_2 to $[CoTSPc]^{4-}$ occurred with an equilibrium constant of 8.7×10^1 dm^3 mol^{-1} and a rate constant of 2.1×10^2 dm^3 mol^{-1} s^{-1}, at pH 11. These rate and equilibrium constants represent the coordination of the second cyanide or sulfur dioxide ligands to the $[CoTSPc]^{4-}$ species. Coordination of the first ligand occurred faster than that of the second ligand in both cases. The coordination is accompanied by the oxidation of the central Co(II) metal with the formation of a Co(III) tetrasulfophthalocyanine species. © 2002 Elsevier Science Ltd. All rights reserved.

Keywords: Cobalt; Phthalocyanine; Cyanide; Sulfur dioxide; Kinetics; Equilibria

1. Introduction

Analysis of cyanide and sulfur dioxide is of environmental importance. The oxidation of sulfur dioxide to higher oxidation states of sulfur is also of industrial importance. Metalloporphyrin (MP) complexes are known to react with SO_2 to give sulfonato metalloporphyrin complexes [1–3]. Coordination of SO_2 to metallophthalocyanine (MPc) complexes, FePc and CoPc, has been implicated during electrocatalytic oxidation of sulfur dioxide by these complexes [4]. Our reports on the photolysis of tin(IV) mono- and di-phthalocyanine ($(L)_2Sn(IV)Pc(-2)$ and $Pc(-2)Sn(IV)Pc(-2)$, respectively, where Pc(-2) is the phthalocyaninato dianion) complexes in the presence of SO_2 showed the reduction of the $(L)_2Sn(IV)Pc(-2)$ species to $[(L)_2Sn(IV)Pc(-3)]^-$, and the oxidation of the diphthalocyanine to $[Pc(-1)Sn(IV)Pc(-2)]^+$ [5,6]. Electron transfer reactions between SO_2 and MPc complexes could be useful in converting harmful sulfur complexes to their less harmful analogues.

There is a need to develop complexes that may act as antidotes for cyanide intoxication. Metalloporphrins and metallophthalocyanine complexes have sharp spectral features such as strong Q bands in the visible region for the MPc complexes and strong Soret or B bands for the MP complexes. The MPc and MP com-

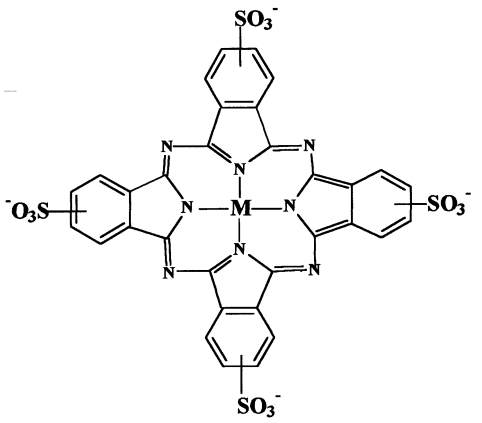


Fig. 1. Molecular structure of cobalt(II) tetrasulfophthalocyanine, ($[CoTSPc]^{4-}$).

* Corresponding author. Tel.: +27-46-603-8260; fax +27-46-622-5109.

E-mail address: t.nyokong@ru.ac.za (T. Nyokong).

0277-5387/02/$ - see front matter © 2002 Elsevier Science Ltd. All rights reserved.
PII: S0277-5387(01)00968-8

plexes may thus be used as sensitive spectrophotometric reagents for the detection of analytes. Interactions between cyanide and porphyrin complexes have been reported [7,8]. Reactions catalysed by MPc complexes are often mediated by axial ligation of the species to be catalysed. Kinetic and equilibrium studies for the coordination of cyanide to FePc [9,10], $FePc(Cl)_{16}$ [11] and RuPc [12] in non-aqueous media have been reported. Coordination of cyanide under these conditions occurred in a step-wise manner, with coordination of the first cyanide occurring much faster than that of the second one. The coordination of each cyanide ligand gave distinct spectroscopic changes [9]. Axial ligand substitution reactions in metallophthalocyanine and metalloporphrin complexes are dissociative with the formation of a highly reactive five-coordinate intermediate [9,13,14], prior to coordination of the ligands.

In this work, we investigate the interaction of cobalt(II) tetrasulfophthalocyanine ($[CoTSPc]^{4-}$), (Fig. 1) with cyanide and sulfur dioxide in aqueous basic media. We report on the kinetics and equilibria of this interaction. Studies on the coordination of cyanide or sulfur dioxide to MPc complexes have been mainly undertaken in non-aqueous media. The possibility of electron transfer from the $[CoTSPc]^{4-}$ species following the coordination of sulfur dioxide or cyanide is explored.

2. Experimental

2.1. Materials

Cobalt(II) tetrasulfophthalocyanine ($[CoTSPc]^{4-}$) was prepared and purified according to reported procedures [15]. The complex gave satisfactory spectroscopic and elemental analysis. $[CoTSPc]^{4-}$ complexes containing axially ligated cyanide or SO_2 were prepared by adding cyanide or SO_2 to aqueous solutions of $[CoTSPc]^{4-}$, allowing the reaction to proceed until there was a definite change in spectra, then evaporating off the solvent. Potassium cyanide (Merck) and SO_2 (Messer Grieshem) were used as received. Dimethyl sulfoxide (DMSO) was dried on alumina and 0.01 or 0.1 mol dm^{-3} (ionic strength, $\mu = 0.5$ mol dm^{-3} $NaClO_4$) tris(hydroxymethyl)aminomethane (Tris) buffer was employed for buffered solutions, pH 7.4 and 11. SO_2 stock solutions were prepared by bubbling SO_2 gas into aqueous solutions, the flasks containing SO_2 were closed with a tight fitting stopper. SO_2 concentrations were determined by treatment with standard iodine, followed by titration with standard aqueous sodium thiosulfite [16]. Potassium hexacyanoferrate, $K_3[Fe(CN)_6]$ was purchased from Merck and used as received. Distilled deionised Millipore water was employed for all studies in aqueous media, and dimethyl sulfoxide, DMSO in non-aqueous media. Cyanide determinations in non-aqueous media were done using silver nitrate [16].

UV–Vis spectra were recorded with the Cary 500 UV–Vis/NIR spectrophotometer. Infrared spectra (KBr discs) were recorded with the Perkin Elmer Spectrum 2000 FTIR spectrophotometer.

2.2. Kinetics and equilibria

Kinetic and equilibrium studies were run at 20 ± 0.5 °C and monitored with the spectrophotometer. We monitored the appearance of the spectra due to the products formed following the addition of cyanide or SO_2 solutions to $[CoTSPc]^{4-}$ dissolved in an appropriate buffer. Typically, a known volume of the solution of $[CoTSPc]^{4-}$ was added to a 1-cm path length spectrophotometric cell. Then a known volume of the aqueous solution of either cyanide or SO_2 in an appropriate buffer was added to the cell and changes in absorbance monitored with time. A comparison was made between the experiments performed in the presence of residual oxygen or when nitrogen or oxygen were bubbled through the solutions prior to kinetic studies. Spectroscopic changes were also recorded in DMSO. The concentration of the $[CoTSPc]^{4-}$ complex in water was estimated from the published molar extinction coefficient of 5.8×10^4 dm^3 mol^{-1} cm^{-1} [17]. The concentration of $[CoTSPc]^{4-}$ was kept constant at 1.0×10^{-5} mol dm^{-3}, while cyanide concentrations were varied from 2.5×10^{-3} to 8.7×10^{-2} mol dm^{-3}, and SO_2 concentrations from 2.0×10^{-3} to 1.6×10^{-2} mol dm^{-3}. Since the concentrations of cyanide and SO_2 were much larger than that of $[CoTSPc]^{4-}$, pseudo first-order conditions were assumed for kinetic studies.

3. Results and discussion

3.1. Interaction of cyanide with $[CoTSPc]^{4-}$

Electronic absorption spectra of $[CoTSPc]^{4-}$ complexes have been described in terms of the monomer dimer equilibrium [17,18]. This equilibrium is affected by conditions such as ionic strength, pH and temperature. The monomer peak for the $[CoTSPc]^{4-}$ species under pH 11 buffer conditions is observed as a broad shoulder near 666 nm, while the dimer peak is observed at 627 nm. On addition of cyanide to solutions of $[CoTSPc]^{4-}$ in pH 11 buffer, spectral changes shown in Fig. 2(a) were observed. pH 11 was chosen deliberately since at this pH it is expected that the CN^- species exist mainly in solution, hence avoiding complicating effects of HCN species. pK_a for $[HCN]/([CN^-][H^+]$ is 9.14 [8]. Spectral changes shown in Fig. 2(a) consisted of a decrease in the dimer peak at 627 nm, and an increase

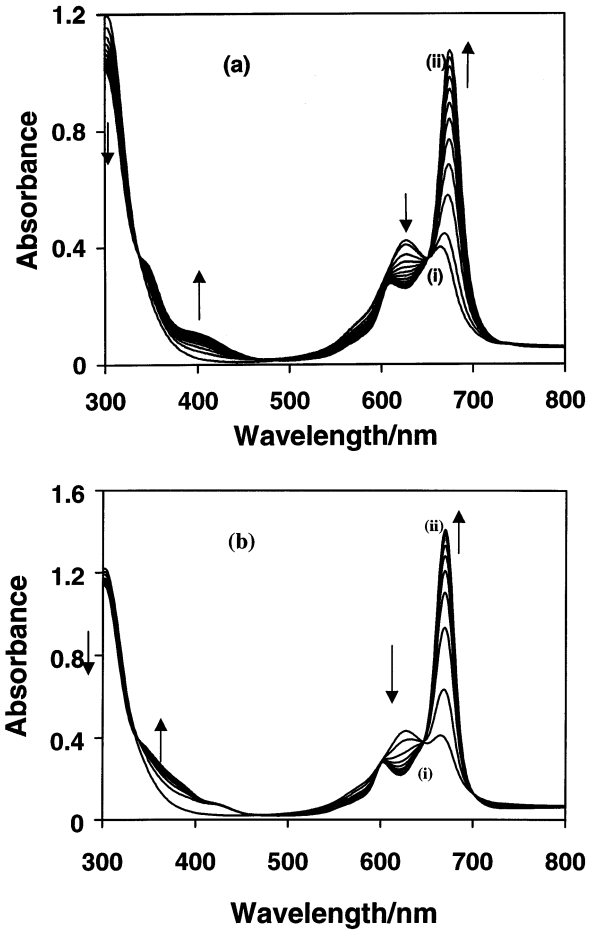


Fig. 2. Electronic absorption spectral changes observed on addition of (a) cyanide (1.8×10^{-4} mol dm^{-3}); (b) ferrocyanide (3.3×10^{-2} mol dm^{-3}) to solutions of $[CoTSPc]^{4-}$) in a pH 11 buffer. (i) Spectrum before addition of cyanide and (ii) final spectrum 2.5 min following the addition of cyanide.

accompanied by a shift in the monomer peak from 666 to 670 nm and finally to 676 nm. There were also new peaks at 610, 404 and 348 nm. The split in the Soret band with the shifting of one of the split peaks to wavelengths near 400 nm, is characteristic of cyanide coordination in MPc complexes [19,20]. Isosbestic points were observed at 652, 458 and 337 nm. The original spectrum before addition of cyanide did not go precisely through the isosbestic point at 458 nm, suggesting that there are more than two species in solution. The shifting of the monomer peak from 666 to 670 nm and finally to 676 nm also shows that there are more than two species in solution. The solution changed from blue to green as the spectral changes shown in Fig. 2(a) progressed. No further spectral changes were observed following the formation of the species with a Q band at 676 nm.

Weber and Busch [21] reported on the interaction of cyanide with $[Co(II)TSPc]^{4-}$ and concluded that a cyanocobalt phthalocyanine did not form when solutions of cyanide were added to $[Co(II)TSPc]^{4-}$, but that cyanocobalt(III) phthalocyanine complex was formed when ferricyanide was employed as a source of cyanide. Fig. 2(b) shows spectral changes obtained on addition of ferricyanide to solutions of $[Co(II)TSPc]^{4-}$ under pH 11 buffer conditions. Spectral changes similar to those shown in Fig. 2(a) were obtained, except that the monomer peak shifted only from 666 to 670 nm, with no further shift to 676 nm, which was observed in Fig. 2(a). There was evidence of coordination of cyanide by the split in the Soret band with a formation of a broad band near 400 nm as was observed in Fig. 2(a). Thus, these results show that cyanide coordination is observed when either cyanide or ferricyanide are added to the solutions of $[CoTSPc]^{4-}$ in basic media. Stable cyanocobalt(III) phthalocyanine complexes have been reported from addition of cyanide to other CoPc complexes [19,20] in non-aqueous media. Literature reports have thus shown that coordination of cyanide to Co(II)Pc complexes result in the oxidation of the central metal with the formation of Co(III)Pc complexes [19,20]. Autooxidation of $[CoTSPc]^{4-}$ is known to depend on the nature of the axial ligands [21,22].

The fact that the final Q band maxima in Fig. 2(a,b) are different yet in both cases coordination of cyanide occurs, as evidenced by split in the Soret band, suggests that different levels of axial ligand coordination occurs in the two situations. Since the final Q band maxima on addition of ferricyanide to $[CoTSPc]^{4-}$ is at the same wavelength as the Q band observed when cyanide is first added to the $[CoTSPc]^{4-}$ species, we propose that on addition of ferricyanide, only one cyanide ligand is coordinated, since further spectral changes to 676 nm were not observed. While in the case where cyanide (instead of ferricyanide) was added to the $[Co(II)TSPc]^{4-}$ solutions, Fig. 2(a), the first spectral changes with a Q band located at 670 nm are due to the coordination of the first cyanide in a similar manner (and with a similar Q band maxima) to when ferricyanide is added. The further shifting of the spectra to 676 nm in the case of addition of cyanide is due to the coordination of the second cyanide and the formation of the $[(CN^-)_2Co(III)TSPc]^{5-}$ species. The coordination of cyanide to CoPc complexes is known to result in dicyano complexes [19,20]. The coordination of the first cyanide to other MPc complexes (e.g. $(L)_2FePc$) is known to occur much faster than the coordination of the second cyanide [11]. In general coordination of the first axial ligands in MPc complexes occurs much faster than the coordination of the second ligands [9–12]. The fact that gradual spectral changes were not observed for the formation of the monocyano species with a Q band maxima at 670 nm on addition of cyanide, under aqueous conditions, even though gradual changes were observed when ferricyanide was employed as a source of cyanide, may be a result of the extent of cyanide availability in the latter. Gradual evolution of the 670

nm band was not observed even on addition of very small amounts of cyanide. Instantaneous formation of the species with a Q band centered at 670 nm was observed under all circumstances.

In order to confirm the step-wise coordination of cyanide to the $[CoTSPc]^{4-}$ species, we monitored spectral changes of this complex in the presence of cyanide using DMSO as a solvent. Spectral changes observed, Fig. 3, clearly showed the stepwise coordination of cyanide to the $[CoTSPc]^{4-}$ species. In DMSO the $[CoTSPc]^{4-}$ is in the monomeric form only. The spectral changes shown in Fig. 3(a) consisted of a decrease in the Q-band (located at 663 nm) accompanied by an isosbestic shift to 670 nm. When the solution that resulted in spectral changes of Fig. 3(a) is left for longer periods, or when larger cyanide concentrations, (0.03 mol dm^{-3}) were added to $[CoTSPc]^{4-}$ solutions, spectral changes of Fig. 3(b) were observed, which consisted of a shift of the Q band from 670 to 680 nm. Thus, in organic media, stepwise spectral changes were observed corresponding to the stepwise coordination of cyanide.

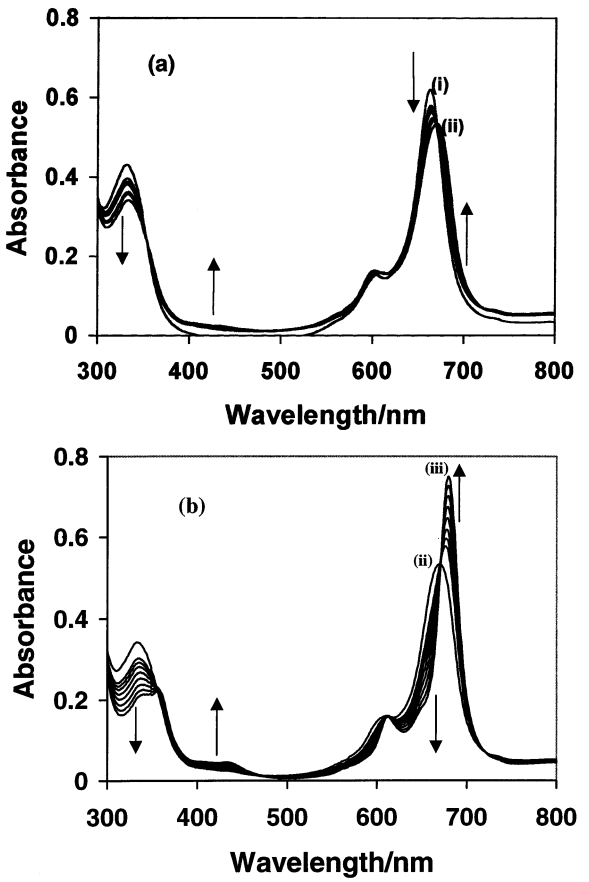


Fig. 3. Electronic absorption spectral changes observed on addition of cyanide (6.7×10^{-3} mol dm^{-3}) to solutions of $[CoTSPc]^{4-}$) in DMSO. (i) Spectrum before addition of cyanide, (ii) final spectrum 2.5 min following the addition of cyanide and (iii) spectra 6 h after the addition of cyanide. (a) and (b) represent the spectral changes for the coordination of the first and second cyanides, respectively.

Fig. 3(a) corresponds to the coordination of the first cyanide and Fig. 3(b) to the coordination of the second cyanide. The fact that these stepwise coordinations are observed in organic media and not in aqueous solutions is a result of the slower kinetics in the former.

It is suggested that coordination of cyanide to the $[Co(II)TSPc]^{4-}$ species occurs simultaneously with the oxidation of Co(II) to Co(III) and hence the formation of the $[(CN^-)_2Co(III)TSPc]^{5-}$ species in aqueous solutions. As mentioned above, oxidation of Co(II) to Co(III) occurs on addition of cyanide to CoPc complexes [19,20]. Addition of bromine to aqueous solutions of $[Co(II)TSPc]^{4-}$ resulted in the formation of the Q band at 670 nm (due to the formation of the $[Co(III)TSPc]^{3-}$ species) and the disappearance of the dimer band. Central metal oxidation in the $[Co(II)TSPc]^{4-}$ complex results in the disappearance of the dimer peak and the shifting of the Q band to longer wavelengths [13,23,24]. Addition of a reducing agents (e.g. sodium borohydride) at the end of the reaction between cyanide and $[CoTSPc]^{4-}$ and the formation of a species with a Q band located at 676 nm, resulted in regeneration of the original spectrum in Fig. 2(a), confirming that oxidation accompanies the coordination of cyanide to the $[Co(II)TSPc]^{4-}$ species and that cyanide binds reversibly to $[CoTSPc]^{4-}$.

The slight deviation from the isosbestic point at 458 nm of the spectra before addition of cyanide in Fig. 2(a) may be attributed to the presence of more than two species in solution, these being the dimer, monomer, monocyano and dicyano species.

The ligation of cyanide to $[CoTSPc]^{4-}$ was evidenced by IR spectra of the solid complex produced when cyanide was added to solutions of $[CoTSPc]^{4-}$ and then evaporating off the solvent. ν_{CN^-} was observed at 2130 cm^{-1}. This value is larger than that reported by Weber and Busch for the formation of cyanocobalt(III) phthalocyanine complex using ferricyanide as a source of cyanide [21], but is in the range reported for ν_{CN^-} (2120 cm^{-1}) in dicyanoiron phthalocyanine [11].

Earlier studies [13] have shown that bubbling oxygen through a solution of $[CoTSPc]^{4-}$ resulted in an increase in the monomer peak of the spectra of this complex, followed by a further shift to longer wavelengths. These spectral changes were attributed to formation of an adduct between oxygen and $[CoTSPc]^{4-}$. We did not observe any spectral changes for $[CoTSPc]^{4-}$ in the absence of cyanide, showing that residual oxygen present in water is not enough to oxidize $[CoTSPc]^{4-}$ in the absence of cyanide.

The relatively strong ligands, cyanide [21] and imidazoles [21,23] are known to facilitate central metal oxidation in $[CoTSPc]^{4-}$ by atmospheric oxygen. The spectral changes observed when oxygen was deliberately bubbled into the solution containing $[CoTSPc]^{4-}$ and cyanide are similar to those observed in the pres-

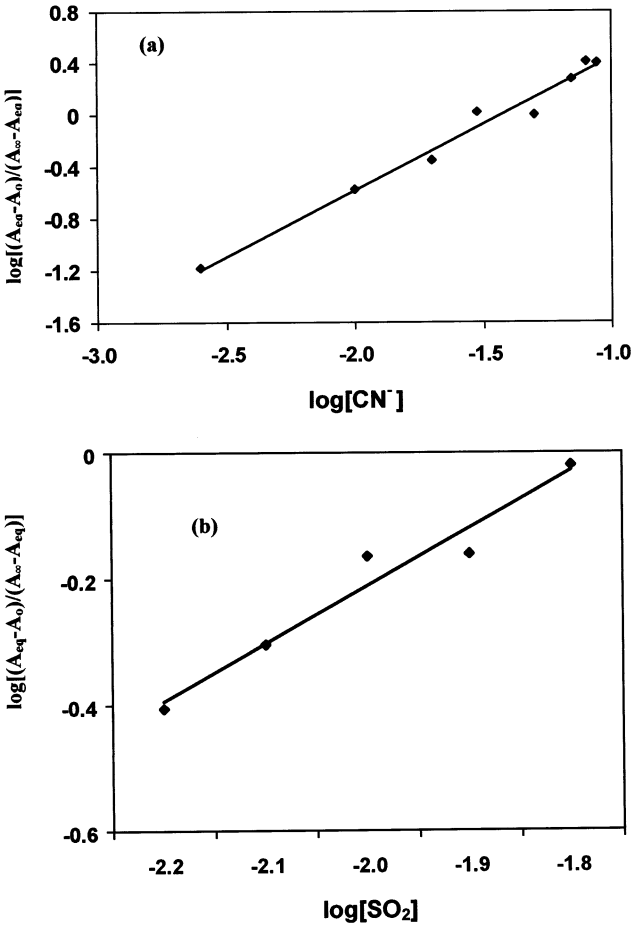


Fig. 4. Plots of $\log[(A_{eq}-A_0)/(A_\infty-A_{eq})]$ vs. (a) $\log[CN^-]$ and (b) $\log[SO_2]$. pH 11 buffer.

ence of residual oxygen, and as will be shown below, the rate of formation of products is much faster when oxygen is bubbled, clearly showing that oxygen is involved in the oxidation of $[CoTSPc]^{4-}$ on coordination of cyanide.

Assuming that two molecules of water are initially ligated to the $[CoTSPc]^{4-}$ forming $[(H_2O)_2CoTSPc]^{4-}$ as has been suggested before [18], the following mechanism for the coordination of cyanide to $[CoTSPc]^{4-}$ is suggested, Eqs. (1) and (2):

$$[(H_2O)_2Co(II)TSPc]^{4-} + CN^- \xrightarrow{O_2} [(H_2O)(CN^-)Co(III)TSPc]^{4-} + H_2O + O_2^- \quad (1)$$

$$[(H_2O)(CN^-)Co(III)TSPc]^{4-} + CN^- \rightarrow [(CN^-)_2Co(III)TSPc]^{5-} + H_2O \quad (2)$$

Eq. (1) is a result of the fast coordination of the first cyanide ligand with a Q band maxima cented at 670 nm in Fig. 2. Eq. (2) is proposed for the coordination of the second cyanide with gradual spectral changes in Fig. 2(a) and the final formation of a Q band at 676 nm.

We followed the kinetics and equilibria for the formation of the new species following addition of cyanide to $[CoTSPc]^{4-}$, by monitoring the spectra due to the product, $[(CN^-)_2Co(III)TSPc]^{5-}$, with a Q band at 676 nm, Fig. 2(a). The equilibrium data were analysed by standard spectrophotomeric method using Eq. (3):

$$\log[(A_{eq}-A_0)/(A_\infty-A_{eq})] = \log K + n\log[CN^-] \quad (3)$$

where A_{eq} is the equilibrium absorbance at 676 nm, A_0 is the absorbance at 676 nm before addition of cyanide. A_∞ was determined from the final absorbance at 676 nm in Fig. 2(a), following complete formation of the $[(CN^-)_2Co(III)TSPc]^{5-}$ complex. From the plot of $\log[(A_{eq}-A_0)/(A_\infty-A_{eq})]$ versus $\log[CN^-]$, Fig. 4(a), an equilibrium constant of $K = 2.1 \pm 0.1 \times 10^1$ dm^3 mol^{-1} was determined for the formation of $[(CN^-)_2Co(III)TSPc]^{5-}$ when oxygen was deliberately bubbled through the solution. A lower value of the equilibrium constant of $K = 6.0 \pm 0.1$ dm^3 mol^{-1} (Table 1) was observed when no oxygen was bubbled into solution (i.e. in the presence of residual oxygen in water). The number of moles of electrons transferred of near unity ($n = 0.9 \pm 0.1$) was obtained from the slope of the plot shown in Fig. 4(a) showing the coordination of one molecule of cyanide at this stage. As has been discussed above, the coordination of the second cyanide is responsible for the formation of a species with a Q

Table 1
Equilibrium and rate constants for the coordination of cyanide and SO_2 to MPc complexes

Complex	Ligand	Conditions [a]	K (dm^3 mol^{-1})	k_f (dm^3 mol^{-1} s^{-1})	k_r (s^{-1})	Ref. [b]
$[CoTSPc]^{4-}$ [c]	CN^-	pH 11	$2.1 \pm 0.1 \times 10^1$	7.4 ± 0.2	0.34 ± 0.01	tw
$[CoTSPc]^{4-}$ [d]	CN^-	pH 11	6.0 ± 0.1	5.9 ± 0.1	0.96 ± 0.01	tw
FePc	CN^-	DMSO	5.7×10^2	0.2	3.5×10^{-4}	[9]
$FePc(Cl)_{16}$	CN^-	DMSO	1.6×10^3	4.2×10^{-3}	2.3×10^{-6}	[11]
$[CoTSPc]^{4-}$	SO_2	pH 11	$8.7 \pm 0.2 \times 10^1$	$2.1 \pm 0.2 \times 10^2$	2.3 ± 0.1	tw
$[CoTSPc]^{4-}$	SO_2	pH 7.4	$1.3 \pm 0.2 \times 10^2$	$2.4 \pm 0.1 \times 10^2$	1.9 ± 0.02	tw

The data are for the coordination of second cyanide or sulfur dioxide ligands.
[a] Ionic strength = 0.5 M $NaClO_4$ for aqueous solutions. 0.01 mol dm^{-3} Tris buffer employed.
[b] tw = this work.
[c] Oxygen bubbled.
[d] Residual oxygen (no oxygen bubbled).

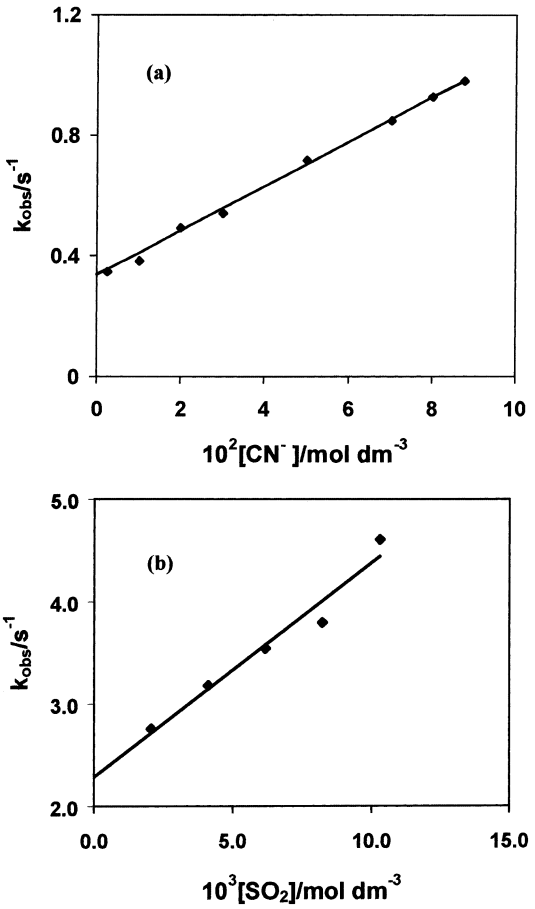


Fig. 5. Plots of k_{obs} (s^{-1}) vs. concentration for the coordination of (a) cyanide, (b) sulfur dioxide to $[CoTSPc]^{4-}$ species. pH 11 buffer.

band at 676 nm, hence the determined equilibrium constant is for the formation of $[(CN^-)_2Co(III)TSPc]^{5-}$ species by Eq. (2). The value of the equilibrium contant could be slightly affected by the initial formation of the monocyano species.

The plot of the observed rate constant (k_{obs}) versus cyanide concentration was linear, Fig. 5(a)) for the data shown in Fig. 2(a), showing that the coordination is first order in cyanide and obeys the following rate law, which is typical of coordination of axial ligands to MPc complexes:

$$k_{obs} = k_f[CN^-] + k_r \quad (4)$$

where k_f is the rate constant for the formation of $[(CN^-)_2Co(III)TSPc]^{5-}$ and is given by $k_1k_2/k_{-1}[CN^-]$. k_r is the rate constant for the dissociation of the complex. Least-square analysis of the data gave $k_f = 7.4 \pm 0.2$ dm^3 mol^{-1} s^{-1} from the slope and $k_r = 0.34 \pm 0.01$ s^{-1} from the intercept for the case when oxygen was bubbled through the solution, and $k_f = 5.9 \pm 0.2$ dm^3 mol^{-1} s^{-1} and $k_r = 0.96 \pm 0.01$ s^{-1}, in the presence of residual oxygen (i.e. no oxygen bubbled through the solution). Using the k_f and k_r values, the equilibrium constants were estimated to be $K \sim 2.2 \times 10^1$ and 6.0 dm^3 mol^{-1}, respectively, for situations when oxygen was bubbled or in the presence of residual oxygen. These values are in good agreement with the values determined from equilibrium data.

Rates and equilibrium constants are higher when oxygen was bubbled through the solution, hence showing that the formation of the oxidized $[(CN^-)_2Co(III)TSPc]^{5-}$ species is depended on oxygen. As has been mentioned above, it has been reported in the literature that cyanide facilitates central metal oxidation in $[CoTSPc]^{4-}$ by atmospheric oxygen [21]. The kinetics were not affected by varying the concentration of Tris buffer employed.

Table 1 compares the equilibrium and rate constants for the coordination of cyanide to $[CoTSPc]^{4-}$ complex, to the constants reported for the coordination of cyanide to FePc complexes. Table 1 shows that the rate constants for the coordination of cyanide to the $[CoTSPc]^{4-}$ complex in aqueous solutions is larger than those reported for the coordination of cyanide to FePc complexes in DMSO. The differences in the rate and equilibrium constants may be caused by the presence of different ring substituents, the nature of the central metal and also by differences in the solvents employed. Coordination of axial ligands (e.g. pyridine) to FePc was found [25] to occur faster than its coordination to CoPc complexes in DMSO solutions, suggesting faster axial ligand exchange reactions in FePc complexes compared to CoPc complexes. As has been mentioned above, in the presence of DMSO coordination of cyanide to $[CoTSPc]^{4-}$ occurred slower in DMSO (hence the observation of a stepwise cyanide coordination) than in water, thus the nature of the solvent plays an important role. The rate constants for the coordination of axial ligands to MPc complexes are a measure of the ease of dissociation of the bond between the central metal and the leaving ligand. As mentioned above, in aqueous solutions $[CoTSPc]^{4-}$ contains water molecules in axial positions (forming $[(H_2O)_2CoTSPc]^{4-}$), whereas the reported data for coordination of cyanide to FePc, DMSO was employed as a solvent, giving the $(DMSO)_2FePc$ species. The observation of higher rate constants for coordination of cyanide to $[CoTSPc]^{4-}$ in water when compared to its coordination to FePc in DMSO may reflect the ease of dissociation of the Co-water bond in the former complex, compared to the dissociation of the Fe–DMSO bond in the later. When DMSO is in the axial position, the metal–DMSO bond gets extra stability from π back-bonding due to the DMSO ligand, making it difficult to replace the DMSO compared to the replacement of water. The relative strength of the Fe–DMSO bond compared to the Co–water bond may be one of the reasons for a larger rate constants for the coordination of cyanide to the $[CoTSPc]^{4-}$ complex when compared to its coordination to FePc complexes. The rate

constants for the coordination of cyanide to CoPc in non-aqueous solutions have not been reported. The rate constant reported for the coordination of cyanide to the $[CoTSPc]^{4-}$ species is much lower than the rate constant of 3×10^4 dm^3 mol^{-1} s^{-1} reported for the coordination of cyanide to cobalt tetraphenyl porphyrin [26].

3.2. Interaction of sulfur dioxide with $[CoTSPc]^{4-}$

Fig. 6 shows spectral changes observed when sulfur dioxide solutions were added to solutions of $[CoTSPc]^{4-}$ under pH 11 buffer conditions in presence of residual oxygen (no oxygen bubbled). We chose basic solutions for this study in order to allow for comparison with the studies for cyanide coordination discussed above. The spectral changes shown in Fig. 6 are similar to those observed in Fig. 2(a) for the addition of cyanide to $[CoTSPc]^{4-}$ species, except that the final spectra showed a Q band at 673 nm, and not 676 nm, observed for cyanide coordination. The monomer peak shifted from 666 to 670 nm and finally to 673 nm, with clear isosbestic points at 710, 649, 502 and 341 nm. Similar spectral changes were observed in pH 7.4 buffer. The similarities between spectral changes on addition of SO_2 to $[CoTSPc]^{4-}$ to the changes observed on coordination of cyanide above, suggests that similar processes are taking place in both cases. Thus, coordination of SO_2 to $[CoTSPc]^{4-}$ is proposed for changes observed in Fig. 6, in a similar manner to coordination of cyanide, with coordination of the first SO_2 occurring fast, resulting in the Q band shift to 670 nm, and then the final spectral changes leading to the observation of the Q band at 673 nm, being due to the coordination of the second SO_2 molecule resulting in the formation of a disulfite complex, since SO_3^- is the prominent form of SO_2 in basic media. The exact nature of the complex formed is under investigation. However, the step-wise coordination of SO_2 to the $[CoTSPc]^{4-}$ species was confirmed by the observation of spectral changes (in DMSO) similar to those shown in Fig. 3 for the coordination of cyanide.

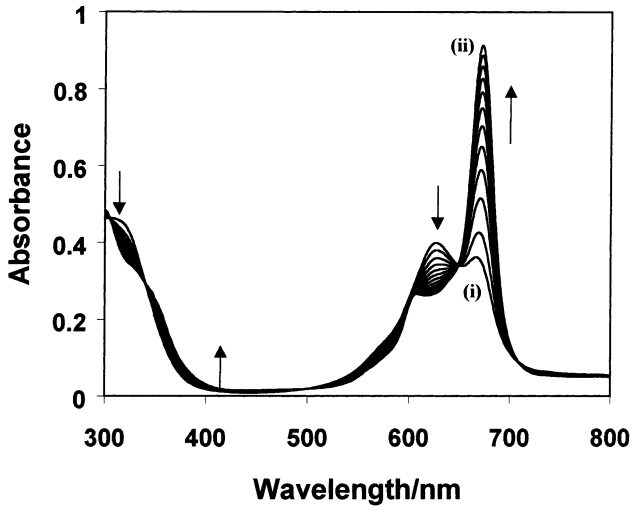


Fig. 6. Electronic absorption changes observed on addition of SO_2 (2.1×10^{-3} mol dm^{-3}) to solutions of $[CoTSPc]^{4-}$ in pH 11 buffer (i) spectrum before addition of sulfur dioxide and (ii) final spectrum, 2.5 min following the addition of SO_2.

In comparison with cyanide, it is likely that the coordination of SO_2 is also accompanied by electron transfer and oxidation of $[Co(II)TSPc]^{4-}$ to the $[Co(III)TSPc]^{3-}$ species. Earlier studies [27] showed that photochemical reduction of tin(IV) phthalocyanine complexes, $(OH)_2SnPc$ or $(Cl)_2SnPc$ in the presence of SO_2 resulted in the ring reduction of these SnPc complexes, whereas oxidation of Pc(-2)Sn(IV)Pc(-2) to the Pc(-1)Sn(IV)Pc(-2) species was observed on addition of sulfur dioxide [5].

The fact that the final spectra peak is observed at different wavelengths for cyanide ($\lambda_{Q\,band} = 676$ nm) and SO_2 ($\lambda_{Q\,band} = 673$ nm) coordination to $[CoTSPc]^{4-}$ confirms that different complexes are formed due to axial ligation.

Metalloporphyrin complexes are known to react with SO_2 to form porphyrin sulfate complexes [28,29], with the IR spectra of monocoordinated sulfate groups being observed at 1147, 1098 and 464 cm^{-1} [30]. IR spectra of the solid product formed following evaporation of the solvent from a solution containing SO_2 and $[CoTSPc]^{4-}$ showed an IR band at 1104 cm^{-1}. However, the IR spectra were complicated by the presence of vibrations from the SO_3^- groups attached to the phthalocyanine ring in the $[CoTSPc]^{4-}$ complex.

Equilibrium data for the formation of the SO_2 complex were determined as explained above using Eq. (3), with CN^- replaced by SO_2. We monitored the increase in the monomer peak in Fig. 6. In Eq. (3), A_{eq} is the equilibrium absorbance at 673 nm; A_0 is the absorbance at 673 nm before addition of SO_2. A_{∞}, the absorbance after complete formation of the complex, was determined from the final absorbance at 673 nm. From the plot of $\log[(A_{eq} - A_0)/(A_{\infty} - A_{eq})]$ versus $\log[SO_2]$, Fig. 4(b), an equilibrium constant of $K = 8.7 \pm 0.3 \times 10^1$ dm^3 mol^{-1} was determined for the formation of the proposed $[(SO_3^-)_2CoTSPc]^{5-}$ complex. The value of n was found to be near unity ($n = 1.1 \pm 0.1$) showing that the coordination of one molecule of SO_2, results in the observed spectral evolution with a Q band centred at 673 nm in Fig. 6. The plot of k_{obs} versus $[SO_2]$ for the data shown in Fig. 6 was linear, Fig. 5(b) with $k_f = 2.1 \pm 0.2 \times 10^2$ dm^3 mol^{-1} s^{-1} and $k_r = 2.3 \pm 0.2$ s^{-1}, under pH 11 conditions. Again using these values equilibrium constant was estimated to be $K \sim 9.0 \times 10^1$ dm^3 mol^{-1} in agreement with the value determined from equilibrium data. The plot in Fig. 5(b) confirms that a rate law similar to that shown by Eq. (4) is obeyed for

the coordination of SO_2 to the $[CoTSPc]^{4-}$ species and that the coordination is first-order in SO_2. Equilibrium and rate constants for the reaction between SO_2 and $[CoTSPc]^{4-}$ at pH 11 are shown in Table 1, and are compared with those obtained at pH 7.4. Similar rate constants are obtained at these two pH values. The equilibrium constant at pH 7.4 was slightly higher than that obtained at pH 11, but the difference was not significant. As discussed above, in basic media, it is expected that the predominant species for SO_2 is the SO_3^- species. Thus, at both pH 7.4 and 11, the same species (SO_3^-) is expected to coordinate to the $[CoTSPc]^{4-}$ complex, $pK_a = 1.81$ and 6.9 for H_2SO_3.

The rate and equilibrium constants for the coordination of cyanide to the $[CoTSPc]^{4-}$ complex are much lower than those obtained for the coordination of SO_2 (as SO_3^-). Due to the strong π acceptor abilities of cyanide which makes it easier to coordinate to the $[CoTSPc]^{4-}$ species by stabilization of the resulting complex through π back-bonding, one would have expected cyanide to exhibit larger rate and equilibrium constants compared to SO_2.

In conclusion we have shown in this work that cyanide and SO_2 coordinate to the $[CoTSPc]^{4-}$ species. The coordination is accompanied by oxidation of the central Co(II) metal forming a Co(III) species. The rate constants reported here for cyanide coordination to the $[CoTSPc]^{4-}$ complex are larger than those reported for the coordination of cyanide to FePc and RuPc complexes in non-aqueous media. The values of the forward rate constants are larger than the values for the reverse reactions for the coordination of both cyanide and SO_2, showing that the interaction between $[CoTSPc]^{4-}$ and these pollutants is highly favoured. This is an important observation since complexes which can react with these harmful molecules and hopefully counteract their toxic effects, are needed.

Acknowledgements

The National Research Foundation of South Africa supported this work. M.T. thanks the Mellon Foundation for a graduate bursary.

References

[1] A.R. Miksztal, J.S. Valentine, Inorg. Chem. 23 (1984) 3548.
[2] K. Shin, H.M. Goff, J. Chem. Soc., Chem. Commun. (1990) 461.
[3] N.R. Scheidt, Y.J. Lee, M.G. Finnegan, Inorg. Chem. 27 (1988) 4725.
[4] J.H. Zagal, Coord. Chem. Rev. 119 (1992) 89.
[5] N. Nensala, A. Nzimande, T. Nyokong, J. Photochem. Photobiol. A: Chem. 98 (1996) 129.
[6] T. Nyokong, J. Chem. Soc., Chem. Commun. (1994) 1983.
[7] S. Modi, V.P. Shedbalkar, D.V. Behere, Inorg. Chim. Acta 173 (1990) 9.
[8] P. Hampbright, Inorg. Chim. Acta 157 (1989) 95.
[9] T. Nyokong, J. Chem. Soc., Dalton Trans. (1993) 3601.
[10] A. Boffi, E. Ercolani, F. Monacelli, P. Ascenzi, Inorg. Chim. Acta 267 (1998) 109.
[11] T. Nyokong, Polyhedron 14 (1995) 643.
[12] T. Nyokong, J. Guthrie-Stracham, Inorg. Chim. Acta 208 (1993) 239.
[13] E. Pennesi, P. Ercolani, M. Ascenzi, F. Brunori, J. Monacelli, J. Chem. Soc., Dalton Trans. (1985) 1107.
[14] D.A. Sweigart, J. Chem. Soc., Dalton Trans. (1976) 1476.
[15] J.H. Weber, D.H. Busch, Inorg. Chem. 4 (1965) 469.
[16] A.I. Vogel, A Textbook of Quantitative Inorganic Analysis Including Elementary Instrumental Analysis, 3rd ed., Longman, London, 1968.
[17] L.C. Gruen, R.J. Blagrove, Aust. J. Chem. 26 (1973) 319.
[18] A.B.P. Lever, M.R. Hempstead, C.C. Leznoff, W. Liu, M. Melnik, N.A. Nevin, P. Seymour, Pure Appl. Chem. 58 (1986) 1467.
[19] M.J. Stillman, A.J. Thomson, J. Chem. Soc., Faraday Trans. II 70 (1974) 790.
[20] M.J. Stillman, T. Nyokong, in: C.C. Leznoff, A.B.P. Lever (Eds.), Phthalocyanines: Properties and Applications, vol. 1, VCH, New York, 1989.
[21] J.H. Weber, D.H. Busch, Inorg. Chem. 4 (1965) 472.
[22] R.J. Sundberg, R.B. Martin, Chem. Rev. 74 (1974) 496.
[23] S. Sekota, T. Nyokong, Polyhedron 16 (1997) 3279.
[24] N. Chebotareva, T. Nyokong, J. Coord. Chem. 46 (1999) 433.
[25] T. Nyokong, Polyhedron 14 (1995) 2325.
[26] P. Hambright, R. Langley, J. Inorg. Biochem. 32 (1988) 197.
[27] T. Nyokong, J. Chem. Soc., Chem. Commun. (1994) 983.
[28] W.R. Scheidt, Y.J. Lee, M.G. Finngan, Inorg. Chem. 27 (1988) 4725.
[29] K. Shin, H.M. Goff, J. Chem. Soc., Chem Commun. (1990) 461.
[30] A.R. Miksztal, J.S. Valentine, Inorg. Chem. 23 (1984) 3548.

PERGAMON

Polyhedron 21 (2002) 141–146

POLYHEDRON

www.elsevier.com/locate/poly

X-ray crystal structures, spectroscopic and magnetic measurements of dinuclear alkoxo-bridged copper(II) compounds with substituted bis(2-benzimidazolyl)alkane ligands. First X-ray structure of a copper(II) dinuclear propoxo-bridged compound

Gerard A. van Albada [a], Ilpo Mutikainen [b], Ivonne Riggio [a,1], Urho Turpeinen [b], Jan Reedijk [a,*]

[a] *Gorlaeus Laboratories, Leiden Institute of Chemistry, Leiden University, PO Box 9502, 2300 RA Leiden, The Netherlands*
[b] *Laboratory of Inorganic Chemistry, Department of Chemistry, PO Box 55 (A.I. Virtasen aukio 1), 00014 University of Helsinki, Helsinki, Finland*

Received 23 April 2001; accepted 2 August 2001

Abstract

The synthesis and characterization of three new alkoxo-bridged dinuclear copper(II) compounds are described, all having the general formula $[Cu_2(L)_2(RO^-)_2](ClO_4)_2(ROH)_y(H_2O)_z$, in which L = b2b (bis(2-benzimidazolyl)-2-butane) and b3b (bis(2-benzimidazolyl)-3-butane), ROH = MeOH, EtOH, 1-PrOH, $y = 1$ or 2, $z = 0$ or 3. The X-ray structure has been solved from two compounds; $[Cu_2(b2b)_2(OCH_3)_2](ClO_4)_2(CH_3OH)_2(H_2O)_3$ (**1**) and from compound $[Cu_2(b3b)_2(C_3H_7O)_2](ClO_4)_2(C_3H_7OH)_2$ (**3**). These two compounds consist of dinuclear Cu(II) units with bridging methoxo group for **1** and an unique bridging propoxo group for **3** with two ligands linked to each copper via N, providing square–planar CuN_2O_2 chromophores. The latter one is the first dinuclear Cu(II) X-ray structure with bridging propoxo groups. Both dinuclear compounds are diamagnetic. © 2002 Elsevier Science Ltd. All rights reserved.

Keywords: Copper(II); Alkoxo-bridged; Magnetism; Benzimidazoles; Crystal structures

1. Introduction

The co-ordination chemistry of azoles acting as ligands in copper(II) compounds in the context of modeling biological systems has gained much interest in the past decades [1–4]. In this respect bis(2-benzimidazoles) have received much attention for their wide-ranging antivirus activity [5,6] their importance in selective ion exchange resins [7,8] and the possibility to form supramolecular aggregates with d^{10} metal ions [9].

Previously, spectroscopic and magnetic properties, as well as some structures of copper(II) co-ordination compounds with bis(2-benzimidazolyl)alkanes and some substituted bis(2-benzimidazolyl)alkanes have been reported [10–18] by others and by us. In an earlier study, we synthesized and characterized copper(II) dinuclear alkoxo-bridged compounds with these bis(2-benzimidazolyl)alkanes [12,13]. So far only methoxo- and ethoxo-bridged Cu(II) dinuclear compounds were obtained. When using higher alcohols, like 1-propanol, only mononuclear species were obtained [15]. To the best of our knowledge so far no X-ray structures of Cu(II) propoxo-bridged compounds are reported; in fact with transition metals only one Fe(III) dinuclear propoxo-bridged X-ray structure has been solved [19]. To investigate whether there is an influence in varying the steric properties, a methyl group was introduced on two different positions in the alkyl chain, obtaining the ligands bis(2-benzimidazolyl)-2-butane (abbreviated as b2b), where a chiral C atom is present and bis(2-benz-

* Corresponding author. Tel.: +31-71-527-4459; fax: +31-71-527-4671.
E-mail address: reedijk@chem.leidenuniv.nl (J. Reedijk).
[1] Socrates exchange student from Department of Inorganic Chemistry, University of Palermo, Palermo, Italy.

0277-5387/02/$ - see front matter © 2002 Elsevier Science Ltd. All rights reserved.
PII: S0277-5387(01)00903-2

imidazolyl)-3-butane (abbreviated as b3b), which has a twofold symmetry axis. With Cu(II) and Co(II) halides, monomeric compounds with a tetrahedral geometry were obtained [20]. However, with other anions dinuclear species were formed. In this paper, we describe the synthesis and characterization of three new copper(II) alkoxo-bridged compounds with the general formula $[Cu_2(L)_2(RO^-)_2](ClO_4)_2(ROH)_y(H_2O)_z$, in which L = b2b and b3b, ROH = MeOH, EtOH, 1-PrOH, $y = 1$ or 2, $z = 0$ or 3. The X-ray structure has been solved from two compounds, i.e. $[Cu_2(b2b)_2(OCH_3)_2](ClO_4)_2(CH_3OH)_2(H_2O)_3$, a methoxo bridged Cu(II) dinuclear compound and $[Cu_2(b3b)_2(C_3H_7O)_2](ClO_4)_2(C_3H_7OH)_2$, which appears to be the first reported X-ray structure with a Cu-bridging propoxo group.

Table 1
Crystal data and details of the structure determination

	Structure (**1**)	Structure (**3**)
Crystal data		
Compound	$C_{40}H_{48}Cl_2Cu_2N_8O_{15}$	$C_{48}H_{64}Cl_2Cu_2N_8O_{12}$
Molecular weight	1078.8	1143.1
Crystal system	triclinic	monoclinic
Space group	$P\bar{1}$	$P2(1)/n$
a (Å)	11.893(2)	10.396(7)
b (Å)	12.363(3)	12.875(10)
c (Å)	9.718(3)	20.249(14)
α (°)	96.83(3)	90
β (°)	107.11(3)	101.26(5)
γ (°)	73.52(3)	90
V (Å^3)	1308.5(5)	2658(3)
Z	1	2
D_{calc} (g cm^{-3})	1.369	1.428
$F(000)$	556	1192
μ (cm^{-1})	9.82	9.67
Crystal size (mm)	$0.40 \times 0.30 \times 0.25$	$0.30 \times 0.20 \times 0.10$
Data collection and refinement		
Temperature (K)	193	193
θ min, θ max	2.65, 25.25	2.55, 23.25
Total data collected	4971	4038
Independent reflections (R_{int})	4728 (0.0331)	3797 (0.0875)
Observed reflections [$I > 2\sigma(I)$]	3497	1767
Number of refined reflections and parameters	4728, 337	3797, 334
Final $R1$, $wR2$ [$I > 2\sigma(I)$]	0.077, 0.210	0.099, 0.182
Goodness-of-fit on F^2	1.048	0.955
Min and max resd.dens. (e Å^{-3})	−0.604, 0.865	−0.377, 0.446

Weighting schemes: (**1**) $w = 1.0/[\sigma^2(F_o^2) + (0.0.1503P)^2 + 0.4290P]$, (**3**) $w = 1.0/[\sigma^2(F_o^2) + (0.0.0751P)^2$.

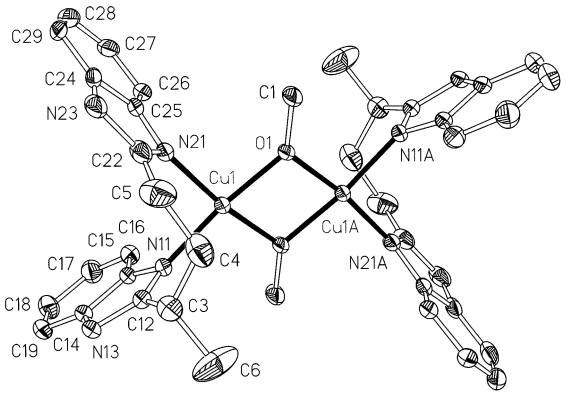


Fig. 1. ORTEP at 50% probability plot of the centrosymmetric cation of $[Cu_2(b2b)_2(CH_3O)_2](ClO_4)_2(CH_3OH)_2(H_2O)_3$ (**1**) with atom labeling scheme. H-atoms and non-coordinating methanol, water and perchlorate molecules are omitted for clarity. Atoms marked with an 'A' are generated by an inversion center.

Table 2
Selected bond distances (Å) and angles (°) for structure $[Cu_2(b2b)_2(CH_3O)_2](ClO_4)_2(CH_3OH)_2(H_2O)_3$ (**1**)

Bond distances	
Cu(1)–O(1)a	1.900(3)
Cu(1)–O(1)	1.910(3)
Cu(1)–N(21)	1.953(4)
Cu(1)–N(11)	1.958(4)
Cu(1)–Cu(1)a	2.9854(13)
Bond angles	
Cu(1)–O(1)–Cu(1)a	103.21(14)
O(1)a–Cu(1)–O(1)	76.79(14)
O(1)a–Cu(1)–N(21)	172.20(15)
O(1)–Cu(1)–N(21)	95.86(16)
O(1)a–Cu(1)–N(11)	97.24(16)
O(1)–Cu(1)–N(11)	173.26(15)
N(21)–Cu(1)–N(11)	90.23(17)
O(1)a–Cu(1)–Cu(1)a	38.51(9)
O(1)–Cu(1)–Cu(1)a	38.28(10)
N(21)–Cu(1)–Cu(1)a	134.08(12)
N(11)–Cu(1)–Cu(1)a	135.68(13)

$a = -x, -y, -z$; H-bond information is given in the text.

2. Experimental

2.1. Syntheses

All chemicals were used as received without further purification. The ligands b2b and b3b were synthesized as described before [20].

The coordination compounds were prepared according to the following general procedure: 1.2 mmol of the $Cu(ClO_4)_2$ and 1.2 mmol of the ligand were each dissolved in 10 ml of alcohol. The ligand solution was then added slowly to the Cu(II)-salt solution and filtered to remove any undissolved material. Usually, after a few days to at most 2 weeks, the product separates as crystals. These were isolated by filtration and dried in air, and characterized by elemental analysis and spectroscopic methods. Yield for both compounds was approximately 40%.

Table 3
Structural parameters for Cu(II) dinuclear bis(benzimidazole)alkane compounds

Compound [a]	Cu–Cu distance (Å)	Cu–O–Cu angle (°)	References
$[Cu_2(tbz)_2(CH_3O)_2](ClO_4)_2(CH_3OH)_2$	2.9827(6)	102.89(14)	[12]
$[Cu_2(tbz)_2(NO_3)(CH_3O)_2](NO_3)(CH_3OH)_2$	3.0072(4)	103.97(9)	[12]
$[Cu_2(tbz)_2(C_2H_5O)_2](ClO_4)_2(CH_3OH)_2$	3.0129	102.4(10)	[10,11]
$[Cu_2(mtbz)_2(CH_3O)_2](ClO_4)_2$	2.9872(16)	103.2(2)	[13]
$[Cu_2(mtbz)_2(CH_3O)_2(CF_3SO_3)](CF_3SO_3)$	2.9775(13) 2.9751(13)	101.7(3) 101.7(3)	[13]
$[Cu_2(b2b)_2(OCH_3)_2](ClO_4)_2(CH_3OH)_2(H_2O)_3$	2.9854(13)	103.21(14)	this work
$[Cu_2(b3b)_2(C_3H_7O)_2](ClO_4)_2(C_3H_7OH)_2$	3.003(3)	102.9(3)	this work

[a] tbz, bis(2-benzimidazolyl)propane); mtbz, bis(1-methyl-2-benzimidazolyl)propane; b2b, bis(2-benzimidazolyl)-2-butane; b3b, bis(2-benzimidazolyl)-3-butane.

2.2. Physical measurements

C, H, N determinations were performed on a Perkin–Elmer 2400 Series II analyzer. Metal analysis was performed by complexometric titration technique.

Ligand-field spectra were obtained on a Perkin–Elmer Lambda900 spectrophotometer using the diffuse-reflectance technique, with MgO as a reference.

X-band powder EPR spectra were obtained on a JEOL RE2× electron spin resonance spectrometer, using DPPH ($g = 2.0036$) as a standard.

FTIR spectra were obtained on a Perkin–Elmer Paragon 1000 FTIR spectrophotometer equipped with a Golden Gate ATR device, using the reflectance technique (4000–300 cm^{-1}, res. 4 cm^{-1})

Magnetic susceptibility measurements (5–250 K) were carried out using a Quantum Design MPMS-5 5T SQUID magnetometer (measurements carried out at 1000 G). Data were corrected for magnetization of the sample holder and for diamagnetic contributions, which were estimated from the Pascal constants.

2.3. Crystal structure determination and refinement of the structures

2.3.1. General

A crystal was selected for and mounted to the glass fiber using the oil-drop method, data were collected on a Rigaku AFC-7S diffractometer (graphite-monochromated Mo Kα radiation, ω–2θ scans). The intensity data were corrected for Lorentz and polarization effects, for absorption (psi-scan absorption correction) and extinction. The structures were solved by direct methods. The programs TEXSAN [21], SHELXS-97 [22], SHELXL-97 [23] were used for data reduction, structure solution and structure refinement, respectively. Refinement of F^2 was done against all reflections. The weighted R factor, wR, and goodness-of-fit S are based on F^2, the conventional R factor is based on F, with F set to zero for negative F^2. All non-H atoms were refined anisotropically.

2.3.2. Specific details for structure **1**

The H atoms of the disordered water molecule and the H atom of the lattice methanol O_2 atom were not located. The other H atoms were introduced in calculated positions and refined with fixed geometry with respect to their carrier atoms. The disordered perchlorate anion was refined on two positions as a rigid group.

2.3.3. Specific details for structure **3**

The H atoms were introduced in calculated positions and refined with fixed geometry with respect to their carrier atoms. The disordered methyl group on the propyl chain was refined in two positions (50/50).

Crystal data and numerical details of the structure determination of compounds **1** and **3** are given in Table 1.

3. Results and discussion

3.1. Description of the crystal structures $[Cu_2(b2b)_2(CH_3O)_2](ClO_4)_2(CH_3OH)_2(H_2O)_3$ (1)

The structure of the dinuclear cationic unit is depicted in Fig. 1, with relevant bond length and bond

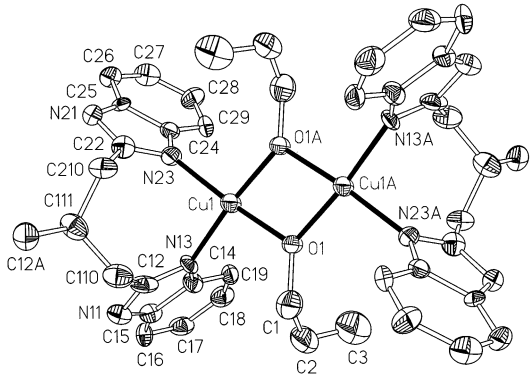


Fig. 2. ORTEP at 50% probability plot of $[Cu_2(b3b)_2(C_3H_7O)_2(ClO_4)_2]$-$(C_3H_7OH)_2$ (**3**) with atom-labeling scheme. H-atoms, the non-coordinating propanol and perchlorate molecules are omitted for clarity. Atoms marked with an 'A' are generated by an inversion center.

Table 4
Selected bond distances (Å), angles (°) and H-bond information for structure $[Cu_2(b3b)_2(C_3H_7O)_2(ClO_4)_2](C_3H_7OH)_2$ (**3**)

Bond distances				
Cu1–O1a	1.918(6)			
Cu1–O1	1.922(7)			
Cu1–N13	1.981(8)			
Cu1–N23	1.980(9)			
Cu1–Cu1a	3.003(3)			
Bond angles				
Cu1a–O1–Cu1	102.9(3)			
O1a–Cu1–O177	77.1(3)			
O1a–Cu1–N13173	173.6(3)			
O1–Cu1–N13	98.3(3)			
O1a–Cu1–N23	97.4(3			
O1–Cu1–N23	173.3(3)			
N13–Cu1–N23	87.5(3)			
O1a–Cu1–Cu1a	38.58(19)			
O1–Cu1–Cu1a	38.49(19)			
N13–Cu1–Cu1a	136.7(2)			
N23–Cu1–Cu1a	135.9(2)			
Hydrogen bonds				
	D–H	H···A	D···A	D–H···A
O_w2–H2B···O13 [3/2−x, 1/2+y, 1/2−z]	0.84	2.536	3.078	123 [a]
O_w2–H2B···O14 [3/2−x, 1/2+y, 1/2−z]	0.84	2.230	3.070	177 [a]
N11–H11A···O11	0.88	2.087	2.923	158 [a]
N21–H21A···O2 [1/2−x, −1/2+y, 1/2−z]	0.88	1.852	2.729	174

Symmetry transformations used to generate equivalent atoms: $a = -x, -y+1, -z$.
[a] Bifurcated H-bond system. O_w lattice water atom.

angle information given in Table 2. The unit cell contains one dinuclear methoxo-bridged copper(II) unit, two perchlorate molecules, two methanol molecules and three water molecules. The perchlorate anions and the water molecules are disordered.

The dinuclear unit has a center of symmetry located between two copper ions. Due to the chiral center in the ligand at C3, each molecule has two enantiomers of the ligand. The Cu–Cu distance within the dinuclear unit is 2.9854(13) Å; the ligand b2b acts as a didentate ligand with N(11) and N(21) as coordinating atoms.

The Cu atoms are square–planar coordinated with the basal plane formed by the two nitrogens of the ligand and two oxygens of two methoxo ligands. The angles (O(1)–Cu(1)–N(11) 173.26(15)°, O(1)a–Cu(1)–N(21) 172.20(15)°) deviate nearly 8° from linearity; the angle of the Cu–O–Cu bridge is 103.21(14)°. Axial ligands are not present at semi-coordinating distance (Cu–O distances are > 5 Å).

The Cu–Cu distance and the Cu–O–Cu angle can be well compared with other compounds with bis(benzimidazole)alkanes for which the X-ray structure is known (see Table 3).

The lattice structure is stabilized by stacking between the benzimidazole groups of different units (shortest ring–ring distances of 3.861 Å) and by a hydrogen-bonding network primarily consisting of the methanol oxygen atom to a water molecule (O2···O4 2.695 Å), and to an imidazole nitrogen atom (O2···N13 2.749 Å). Additional weaker H-bonds involve an oxygen atom of the perchlorate molecule (O2···O22 3.219 Å) and oxygen atoms of water molecules to oxygen of perchlorate molecules (O4···O22 2.975 Å, O4···O21 3.156 Å), and to imidazole nitrogen atom (O3···N23 2.654 Å, O31···N23 3.149 Å). Due to the disorder of the perchlorate and water molecule and as not all H-atoms could be located, no specific details of these hydrogen bondings have been obtained.

3.2. Description of crystal structure of $[Cu_2(b3b)_2(C_3H_7O)_2(ClO_4)_2](C_3H_7OH)_2$ (3)

The structure of the dinuclear cationic unit is depicted in Fig. 2, with relevant bond length and bond angle information given in Table 4. The unit cell con-

Table 5
Copper(II) dinuclear alkoxo-bridged compound with ligands b2b and b3b

Compound [a]	Color	LF maxima (diffuse reflectance) (10^3 cm^{-1})		Elemental analysis, Found (Calc.) (%)			
				C	H	N	Cu
$[Cu_2(b2b)_2(OCH_3)_2](ClO_4)_2(CH_3OH)_2$-$(H_2O)_3$ (**1**) [b]	brown–violet	28.5	19.0	44.9 (44.2)	4.9 (5.2)	11.8 (10.3)	11.2 (11.7)
$[Cu_2(b2b)_2(C_2H_5O)_2](ClO_4)_2(C_2H_5OH)$ (**2**)	dark brown–violet	27.0	18.0	45.9 (46.5)	5.3 (4.9)	10.7 (10.9)	12.1 (12.3)
$[Cu_2(b3b)_2(C_3H_7O)_2](ClO_4)_2(C_3H_7OH)_2$ (**3**) [b]	brown–violet	26.5	17.8	48.6	5.5	10.2	10.7

[a] b2b, bis(2-benzimidazolyl)-2-butane; b3b, bis(2-benzimidazolyl)-3-butane.
[b] X-ray crystal structure solved.

tains two-dinuclear methoxo-bridged copper(II) unit, two perchlorate molecules and two propanol molecules. The methyl group of the bis-benzimidazole was found to be disordered and has been refined in two positions (ratio 1:1). No axial coordination or semi-coordination is observed (Cu···O > 3.5 Å).

The dinuclear unit has a center of symmetry located between two copper ions. The Cu–Cu distance within the dinuclear unit is 3.003(3) Å; the ligand b3b acts as a didentate ligand with N(13) and N(23) as coordinating atoms.

The Cu atoms are square–planar coordinated with the basal plane formed by the two nitrogens of the ligand and two oxygens of two propoxo ligands. The angles (O1a–Cu1–N13 173.6(3)°, O1–Cu1–N23 173.3(3)°) deviate nearly 8° from linearity; the angle of the Cu–O–Cu bridge is 102.9(3)°. The Cu–Cu distance and the Cu–O–Cu angle can be well compared with other compounds with bis(benzimidazole)alkanes for which the X-ray structure is known (see Table 3).

The lattice structure is stabilized by stacking between the benzimidazole groups of different units (shortest ring–ring distances of 3.750 Å) and by a hydrogen-bonding system between the oxygen of the uncoordinating propanol molecule and the perchlorate anion and between the nitrogens of the benzimidazole ligand and the oxygens of the propanol molecule and the oxygens of the perchlorate molecules. The shortest contact being N···O 2.729 Å. Relevant details of this hydrogen bonding system are included in Table 4.

3.3. Electronic spectra

The diffuse-reflectance spectra of the powdered solids are given in Table 5.

From this table it is observed that the ligand field bands for compounds **1**, **2** and **3** are at $17.8–19.0 \times 10^3$ cm^{-1}, which are normal ligand field transitions for a CuN_2O_2 or a $CuN_2O_2(O)_x$ chromophore [24,25]. These bands are also comparable with the transitions found earlier for compounds with the chromophore $N_2Cu(OR)CuN_2$ [12,13]. In addition, a second very strong and sharp band is found for all these compounds at $28.4–26.6 \times 10^3$ cm^{-1}, which is characteristic for dinuclear copper(II) compounds, with a square–planar $Cu_2O_2N_4$ chromophore and has been assigned to an (O) → (Cu) charge-transfer band [12,13,26,27].

3.4. Magnetic properties

X-band EPR spectra of polycrystalline powders were taken at room temperature. All the alkoxo-bridged compounds are EPR silent and show even no traces of signals of monomeric impurities, a phenomenon often seen in other bis(benzimidazole)alkane compounds [12,13].

The magnetic susceptibility was measured as powders between 5 and 300 K and these measurements show a diamagnetic behavior below room temperature (above approximately 360 K, the compounds decompose). This diamagnetism results from strong antiferromagnetism and is in accordance with earlier magnetic investigations of alkoxo-bridged bis(benzimidazole)alkane compounds [12,13,28].

4. Concluding remarks

The results discussed above have shown that with the two new bis(benzimidazole) ligand b2b and b3b in the presence of weakly coordinating anions in alcoholic solution dinuclear copper(II) alkoxo-bridged compounds are formed. It appears that these ligands are basic enough to dehydronate the alcohol. The Cu–Cu distances and the Cu–O–Cu angles of the compounds, as determined by single-crystal X-ray analysis, are in the range known for other alkoxo-bridged compounds with bis(benzimidazolyl)alkane ligands. The spectroscopic and magnetic properties of our compounds also agree with theoretical expectations. Finally, the first X-ray structure of a Cu(II) dipropoxo-bridged dinuclear compound is reported.

5. Supplementary material

Crystallographic data (excluding structure factors) for the structures in this paper have been deposited with the Cambridge Crystallographic Data Centre as supplementary publication no. CCDC-159159 and no. CCDC-159160 for structures **1** and **3**, respectively. Copies of the data can be obtained free of charge on application to CCDC, 12 Union Road, Cambridge CB2 1EZ, UK (fax: +44-1223-336033, e-mail: deposit@ccdc.cam.ac.uk or www: http://www.ccdc.cam.ac.uk).

Acknowledgements

The work described in the present paper has been supported by the Leiden University Study group WFMO (Werkgroep Fundamenteel Materialen Onderzoek). Ivonne Riggio wishes to thank the Socrates student exchange program.

References

[1] J. Reedijk, in: G. Wilkinson, R.D. Gillard, J.A. McCleverty (Eds.), Comprehensive Coordination Chemistry, vol. 2, Pergamon Press, Oxford, 1987, p. 73.
[2] E. Bouwman, W.L. Driessen, J. Reedijk, Coord. Chem. Rev. 104 (1990) 143.

[3] T.N. Sorrell, Tetrahedron 45 (1989) 3.
[4] P. Zanello, S. Tamburini, P.A. Vigato, G.A. Mazzocchin, Coord. Chem. Rev. 77 (1987) 165.
[5] B. Çakir, E. Büyükbingöl, Ü. Uçucu, U. Abbasoğlu, N. Noyanalpan, J. Fac. Pharm. Gazi 5 (1988) 71.
[6] W.R. Roderick, C.W. Nordeen Jr., A.M. von Esch, R.N. Appell, J. Med. Chem. 15 (1972) 655.
[7] H.J. Hoorn, P. de Joode, W.L. Driessen, J. Reedijk, React. Funct. Polym. 27 (1995) 223.
[8] P.M. van Berkel, D.J. Dijkstra, W.L. Driessen, J. Reedijk, D.C. Sherrington, React. Funct. Polym. 28 (1995) 39.
[9] C. Piquet, J.-C.G. Bünzli, G. Bernardinelli, G. Hopfgartner, A.F. Williams, J. Alloys Comp. 225 (1995) 324.
[10] G. Bernardinelli, A. Kübel-Pollak, S. Rüttimann, A.F. Williams, Chimia 46 (1992) 155.
[11] G. Bernardinelli, A. Kübel-Pollak, S. Rüttimann, A.F. Williams, Z. Kristallogr. 203 (1993) 132.
[12] G.A. van Albada, M.T. Lakin, N. Veldman, A.L. Spek, J. Reedijk, Inorg. Chem. 34 (1995) 4910.
[13] G.A. van Albada, W.J.J. Smeets, A.L. Spek, J. Reedijk, Inorg. Chim. Acta 260 (1997) 151.
[14] G.A. van Albada, W.J.J. Smeets, A.L. Spek, J. Reedijk, Inorg. Chim. Acta 288 (1999) 220.
[15] G.A. van Albada, W.J.J. Smeets, N. Veldman, A.L. Spek, J. Reedijk, Inorg. Chim. Acta 290 (1999) 105.
[16] G.A. van Albada, W.J.J. Smeets, A.L. Spek, J. Reedijk, Inorg. Chim. Acta 299 (2000) 35.
[17] G.A. van Albada, N. Veldman, A.L. Spek, J. Reedijk, J. Chem. Crystallogr. 30 (2000) 69.
[18] G.A. van Albada, I. Riggio, I. Mutikainen, U. Turpeinen, J. Reedijk, J. Chem. Cryst. 30 (2000) 1.
[19] F. Le Gall, F. Fabrizia de Biani, A. Caneschi, P. Cinelli, A. Cornia, A.C. Fabretti, D. Gatteschi, Inorg. Chim. Acta 262 (1997) 123.
[20] I. Riggio, G.A. van Albada, D.D. Ellis, I. Mutikainen, A.L. Spek, U. Turpeinen, J. Reedijk, Polyhedron 20 (2001) 2659.
[21] TEXSAN. Single Crystal Structure Analysis Software, Version 1.6, Molecular Structure Corporation, The Woodlands, TX 77381, USA, 1993.
[22] G.M. Sheldrick, SHELXS-97, Program for Crystal Structure Determination, University of Göttingen, Germany, 1997.
[23] G.M. Sheldrick, SHELXL-97. Program for the Refinement of Crystal Structures, University of Göttingen, Germany, 1997.
[24] B.J. Hathaway, in: G. Wilkinson, R.D. Gillard, J.A. McCleverty (Eds.), Comprehensive Coordination Chemistry, vol. 5, Pergamon Press, Oxford, 1987.
[25] A.B.P. Lever, Inorganic Electronic Spectroscopy, 2nd ed., Elsevier, Amsterdam, 1984.
[26] M. Yamashita, H. Ito, T. Ito, Inorg. Chem. 22 (1983) 2102.
[27] S. Kida, Y. Nishida, M. Sakamoto, Bull. Chem. Soc. Jpn. 46 (1973) 2428.
[28] S. Amani Komaei, G.A. van Albada, I. Mutikainen, U. Turpeinen, J. Reedijk, Polyhedron 18 (1999) 1991.

PERGAMON

Polyhedron 21 (2002) 147–153

POLYHEDRON

www.elsevier.com/locate/poly

Synthesis and characterization of some new acetato complexes of molybdenum(IV), (V) and (VI). Crystal structures of $Na_2[Mo_2O_4(OCOCH_3)_6]\cdot NaOCOCH_3\cdot CH_3COOH$ and $K[MoO_2(OCOCH_3)_3]\cdot CH_3COOH$

Branka Korpar-Čolig, Marina Cindrić *, Dubravka Matković-Čalogović, Višnja Vrdoljak, Boris Kamenar

Chemistry Department, Laboratory of General and Inorganic Chemistry, Faculty of Science, University of Zagreb, Ulica Kralja Zvonimira 8, POB 153, 10001 Zagreb, Croatia

Received 20 July 2001; accepted 11 September 2001

Abstract

The acetato complexes of molybdenum(VI), (V) and (IV): $[MoO_2(OCOCH_3)_2]$ (**1**), $Na_2[Mo_2O_4(OCOCH_3)_6]\cdot NaOCOCH_3\cdot CH_3COOH$ (**2**), $K[MoO_2(OCOCH_3)_3]\cdot CH_3COOH$ (**3**), $[Mo_2O_3(OCOCH_3)_4]$ (**4**), $[Mo_3O_2(OCOCH_3)_6(H_2O)(OH)_2]\cdot 16H_2O$ (**5**) and $[Mo_3O_2(OCOCH_3)_6(H_2O)_3]Cl_2\cdot 14H_2O$ (**6**) have been prepared and characterized by chemical analyses, ESR and IR spectroscopy. The crystal structures of **2** and **3** have been determined by single-crystal X-ray crystallography. Both complexes contain octahedrally coordinated molybdenum atoms with bonds formed to two terminal oxo-oxygen atoms and four oxygen atoms from the acetate ligands. In **2** two acetate ligands are monodentately bonded to each molybdenum atom while the third one together with its centrosymmetrical pair acts as a bridging ligand between two molybdenum atoms. In **3** two acetate ligands are monodentately and one bidentately bonded to molybdenum. In both structures the acetic acid molecules are not involved in bonding to molybdenum but act as bridges over both (in **2**) or only one oxygen atom (in **3**) connecting centrosymmetrically related sodium and potassium ions, respectively. © 2002 Elsevier Science Ltd. All rights reserved.

Keywords: Molybdenum; Crystal structures; Cluster complexes; Acetates; Reduction

1. Introduction

The dimeric molybdenum(II) acetate, $[Mo_2(OCOCH_3)_4]$, prepared by the method described by E. Bannister and G. Wilkinson in 1960, was the first isolated acetato complex of molybdenum. However, the reaction yield was poor, amounting to 20% [1,2]. In 1978 A. Bino et al. showed that as well as $[Mo_2(OCOCH_3)_4]$, different trinuclear molybdenum(IV) compounds could be separated from the same solution by ion exchange chromatography [3]. A few years later, the same authors reported the isolation of six new complexes of the general formula $[Mo_3O_x(CCH_3)_{2-x}(OCOCH_3)_6(H_2O)_3]^{2+}$ containing a trinuclear cation capped either by oxygen atoms or alkylidyne ligands [4]. These findings opened a new area in the chemistry of molybdenum and so far a number of acetato complexes containing the trinuclear molybdenum(IV) core with different bridging units have been described [5].

The structural type of triangular metal–metal bonded cluster compounds basically depends upon the applied preparative procedure [6,7]. For instance, the reaction of MoO_4^{2-} with $Mo(CO)_6$ (or $Cr(CO)_6$) results in the formation of the most commonly found cluster of an

* Corresponding author. Tel.: +385-1-460-6653; fax: +385-1-461-1191.

E-mail address: marina@chem.pmf.hr (M. Cindrić).

0277-5387/02/$ - see front matter © 2002 Elsevier Science Ltd. All rights reserved.
PII: S0277-5387(01)00973-1

incomplete cubane type such as in $[Mo_3O_4(OCOCH_3)_8]^{4-}$ [8–11] or the monooxo-capped cluster as in the $[Mo_3O(OCOCH_3)_8]^{2-}$ anion [12]. In addition, the trimolybdenum clusters with two capping oxygen atoms (μ_3-O) of the general formula $[Mo_3O_2(OCOCH_3)_6X_3]^{2+}$ were prepared in the reaction of $Mo(CO)_6$ with acetic acid and acetic anhydride [3,4], or by reducing sodium molybdate in acetic anhydride with the use of $W(CO)_6$ [13], $[Mo_2(OCOCH_3)_4]$ [6] or zinc [7] as reducing agents. Until now, the molecular structures of some of these clusters such as $[Mo_3O_2(OCOCH_3)_6(H_2O)(OH)_2]\cdot 16H_2O$ [13], $[Mo_3O_2(OCOCH_3)_6(H_2O)_3]Br_2\cdot H_2O$ [4,14], $[Mo_3O_2(OCOCH_3)_6(H_2O)_3](CF_3SO_3)_2\cdot CF_3SO_3H\cdot H_2O$ [4,6,14] and $[Zn_2(OCOCH_3)_3][Mo_3O_2(OCOCH_3)_6(OCH_3)_3]\cdot 2H_2O$ [7] have been determined by single-crystal diffraction method.

However, in spite of many examples of such acetato complexes of molybdenum(IV) very little is known about such complexes with molybdenum in its higher oxidation states $+5$ and $+6$. Rare examples are dimeric complexes in which two molybdenum atoms are bridged either by one, $[Mo_2O_3(OCOR)_4]$ [15], or by two oxygen atoms $(NH_4)_2[Mo_2O_4(OCOCH_3)_4(H_2O)_2]$ [16]. Their structures, however, have been postulated only on the basis of chemical analyses and spectroscopic data. As far as we are aware of, the crystal structures of $[\{Mo_2ClO_3(OCOCH_3)_3\}_2]\cdot(CH_3CO)_2O$ [17] and of those of the general formula $[Mo_2(NTo)_2\{S_2P(OEt)_2\}_2(OCOCH_3)S(SR)]$ (To = *p*-tolyl) [18–20] are the only known examples of molybdenum acetates with molybdenum in its higher oxidation states.

In this paper we describe the preparation and characterization of the following acetato complexes of molybdenum(VI), (V) and (IV): $[MoO_2(OCOCH_3)_2]$ (**1**), $Na_2[Mo_2O_4(OCOCH_3)_6]\cdot NaOCOCH_3\cdot CH_3COOH$ (**2**), $K[MoO_2(OCOCH_3)_3]\cdot CH_3COOH$ (**3**), $[Mo_2O_3(OCOCH_3)_4]$ (**4**), $[Mo_3O_2(OCOCH_3)_6(H_2O)(OH)_2]\cdot 16H_2O$ (**5**) and $[Mo_3O_2(OCOCH_3)_6(H_2O)_3]Cl_2\cdot 14H_2O$ (**6**). Whereas, the complexes **1**–**4** and **6** are described here for the first time, for the known complex **5** we suggest a different procedure for its preparation. However, while all syntheses are of interest to understand more fully the reaction of MoO_4^{2-} with an excess of acetic anhydride, the identification of the reaction products helps to explain how the reduction of molybdenum depends upon the reaction conditions, starting materials and the type of reducing agents.

All prepared complexes were characterized by chemical analyses, ESR and IR spectroscopy, **2** and **3** additionally by single-crystal X-ray crystallography. Our X-ray determination of the structures **5** and **6** confirmed that they belong to the structural type already known from the literature [13,14].

2. Experimental

All reagents were of reagent grade and used as purchased. The starting compound $(NH_4)_2[Mo_2O_4(OH)_4(H_2O)_2]$ was prepared as described in the literature [21]. The Analytical Services Laboratory of Rudjer Bošković Institute, Zagreb, provided C and H analyses. Molybdenum [22], Na [23], K [24] and chlorine [23] were determined according to the methods described in literature. Infrared spectra were recorded with an FTIR 1600 Fourier transform spectrophotometer in the 4500–450 cm^{-1} region. The KBr discs of **2** and **3** were prepared in the dry box. Magnetic measurements were made by the standard Gouy method. pH measurements were done using a Mettler MP220 pH meter. The ESR spectra were recorded on a polycrystalline sample on a Varian E-109 spectrometer operating at 100 kHz modulation. DPPH (α,α′-diphenil-β-picrylhydrazyl) was used as an internal reference. All measurements were made at room temperature (r.t.). Paramagnetic (Mo^{5+}) concentration was determined by double integration of the spectrum and compared with the standard Varian strong pinch [25].

2.1. Synthesis and characterization of complexes

2.1.1. Dioxobis(acetato(O,O′))molybdenum(VI), $[MoO_2(OCOCH_3)_2]$ (1)

$MoO_3\cdot 2H_2O$ (2 g, 11.1 mmol) was added in several portions to the mixture of AcOH (10 ml) and Ac_2O (10 ml) and the suspension was heated for 2 h at 80 °C. The unreacted MoO_3 was filtered off and the obtained filtrate evaporated to the third of its volume. The resulting precipitate obtained upon standing of the solution at r.t. for 1 week was filtered off in dry atmosphere, rinsed with CCl_4 and stored in a dessicator.

Yield: 2.1 g, 78%. *Anal.* Calc. for $C_4H_6MoO_6$ (M_r = 246.026): C, 19.53; H, 2.46; Mo, 39.00. Found: C, 19.41; H, 2.61; Mo, 38.93%. IR data (KBr, cm^{-1}): 1575 (s), 1441 (s), 1431 (s), 1349 (m), 992 (m), 950 (s), 669 (m), 656 (m).

2.1.2. Sodium di-μ-oxo-bis(μ-acetato(O,O′))tetrakis-(acetato(O))-dioxodimolybdate(VI) sodium acetate acetic acid solvate (1/1/1), $Na_2[Mo_2O_4(OCOCH_3)_6]\cdot NaOCOCH_3\cdot CH_3COOH$ (2)

$Na_2MoO_4\cdot 2H_2O$ (3 g, 12.4 mmol) was dissolved in Ac_2O (15 ml) and the solution warmed up just below the boiling temperature until all the sodium molybdate was dissolved. The solution was cooled to r.t., the mixture allowed to settle overnight and the resulting precipitate filtered off. The resulting filtrate was left at r.t. and after a few days the obtained crystalline product was filtered off in dry atmosphere, rinsed with CCl_4 and dried in a dessicator.

Yield: 2.1 g, 42.3%. *Anal.* Calc. for $C_{14}H_{21}Mo_2Na_3O_{18}$ ($M_r = 738.16$): C, 22.78; H, 2.87; Mo, 25.99; Na, 9.34. Found (since the crystals rapidly lost AcOH they were left in a dessicator until they were a constant weight and the analysis was then performed using the unsolvated sample): C, 23.75; H, 2.98; Mo, 25.73; Na, 8.65%. IR data (KBr, cm^{-1}): 1557 (s, br), 1452 (s, br), 1272 (s), 1059 (m), 988 (m), 948 (s), 732 (s, br), 639 (m).

*2.1.3. Potassium bis(acetato(O))(acetato(O,O'))-dioxomolybdate(VI) acetic acid solvate (1/1), $K[MoO_2(OCOCH_3)_3]\cdot CH_3CO_2H$ (**3**)*

The preparation was performed as described above by dissolving K_2MoO_4 (3 g, 15.1 mmol) in Ac_2O (15 ml).

Yield: 2.3 g, 46.3%. *Anal.* Calc. for $C_6H_9KMoO_8$ ($M_r = 344.172$): C, 20.94; H, 2.64; K, 11.36; Mo, 27.88. Found (since these crystals were also rapidly losing AcOH the same analytical procedure was used as in **2**): C, 20.45; H, 2.34; K, 11.21; Mo, 27.39%. IR data (KBr, cm^{-1}): 1560 (s, br), 1444 (s, br), 1349 (s), 1049 (m), 990 (s), 949 (m), 885 (m, br), 638 (m).

*2.1.4. μ-Oxo-tetrakis(acetato(O,O'))-tetraoxodimolybdenum(V) $[Mo_2O_3(OCOCH_3)_4]$ (**4**)*

$(NH_4)_2[Mo_2O_4(OH)_4(H_2O)_2]$ (2 g, 5.1 mmol) was dissolved in Ac_2O (30 ml) and the solution warmed up for 3 h at 90 °C. The obtained olive brown product was filtered off, rinsed with CCl_4 and dried in a dessicator.

Yield: 1.8 g, 75%. *Anal.* Calc. for $C_8H_{12}Mo_2O_{11}$ ($M_r = 476.054$): C, 20.18; H, 2.54; Mo, 40.31. Found: C, 19.57; H, 2.52; Mo, 39.95%. IR data (KBr, cm^{-1}): 1538 (s, br), 1446 (s, br), 981 (s), 739 (s, br), 655 (m).

*2.1.5. Hexakis(μ-acetato(O,O'))di-μ_3-oxo-aquadihydroxytrimolybdenum(IV) hexadecahydrate (**3** Mo–Mo) $[Mo_3O_2(OCOCH_3)_6(H_2O)(OH)_2]\cdot 16H_2O$ (**5**) and hexakis(μ-acetato(O,O'))di-μ_3-oxo-triaqua-trimolybdenum(IV) chloride tetradecahydrate (**3** Mo–Mo) $[Mo_3O_2(OCOCH_3)_6(H_2O)_3]Cl_2\cdot 14H_2O$ (**6**)*

2.1.5.1. Procedure A. A mixture of $Na_2MoO_4\cdot 2H_2O$ (or K_2MoO_4) (0.5 g, 2 mmol), $SnCl_2\cdot 2H_2O$ (0.46 g, 2 mmol) and Ac_2O (20 ml) was warmed at 125 °C under Ar atmosphere for 15 h during which time a dark brown supernatant liquid and red precipitate were formed. The precipitate was isolated by filtration, rinsed with dry CCl_4 and dried in dessicator. It was hydrolysed in water (5 ml) and the obtained solution (pH approximately 5) left to evaporate slowly in an open vessel at r.t. After 2 days red crystals of **5** were filtered off and dried.

2.1.5.2. Procedure B. A mixture of M_2CO_3, where M = Na, K, Rb, Cs (2 mmol), $MoO_3\cdot 2H_2O$ (0.36 g, 2 mmol), $SnCl_2\cdot 2H_2O$ (0.46 g, 2 mmol) and Ac_2O (20 ml) was warmed at 125 °C under Ar atmosphere for 3 days until a dark brown solution was obtained. The solution was evaporated by vacuum distillation to one-third of its volume and cooled to r.t. Acetone (30 ml) was added and the obtained red powdered mixture was isolated by filtration, rinsed with CCl_4 and dried in a dessicator. It was hydrolysed in water (5 ml) and the resulting solution was left to evaporate slowly in air. After about 3 days crystals of **6** came out from the solution if the pH of the solution was maintained at about 3. However, if the pH was about five crystals of **5** instead of **6** were obtained. IR and elemental analyses proved that compound **5** prepared by procedure B was identical to that prepared by procedure A.

Compound **5**: Yield: 0.23 g, 45.6% (prepared by procedure A). Yield: 25–30% (prepared by procedure B). *Anal.* Calc. for $C_{12}H_{22}Mo_3O_{17}$ ($M_r = 726.112$): C, 19.85; H, 3.05; Mo, 39.64. Found (since the crystals were losing water of crystallization they were left in a dessicator until they were a constant weight so that the analysis was performed using an unsolvated sample): C, 19.4; H, 3.55; Mo, 39.10%. IR data (KBr, cm^{-1}): 3616 (m), 3475 (s, br), 1636 (m, br), 1556 (s), 1454 (s), 1354 (m), 1051 (w), 689 (s), 644 (m), 588 (m).

Compound **6**: Yield: 30–35%. *Anal.* Calc. for $C_{12}H_{24}Cl_2Mo_3O_{17}$ ($M_r = 799.034$): C, 18.04; H, 3.03; Cl, 8.87; Mo, 36.02. Found (since the crystals were losing water of crystallization the same procedure was used as in the case of **5**): C, 18.41; H, 3.25; Cl, 8.18; Mo, 36.66%. IR data (KBr, cm^{-1}): 3616 (m), 3447 (s, br), 2936 (w), 1636 (m, br), 1560 (s), 1454 (s), 1354 (m), 1052 (w), 893 (w), 691 (s), 644 (s), 591 (m).

2.2. X-ray crystallography

The well-developed, colourless single crystals of **2** and **3** were very difficult to handle due to rapid decomposition when exposed to air. They were stable if kept in a closed flask in mother liquor. They had to be transferred directly from the flask into a capillary and sealed. Data were collected at r.t. on a four-circle PW 1100 diffractometer (Stoe upgraded) with graphite-monochromated Mo Kα radiation ($\lambda = 0.71073$ Å) [26]. Lattice constants were obtained by least-squares refinement from the settings of 42 reflections ($10.3 \leq \theta \leq 18.8°$) for **2** and 38 reflections ($10.9 \leq \theta \leq 18.5°$) for **3**. Three reference reflections were monitored every 90 min. Both crystals were stable at the beginning of the data collection but the final decay amounted to 9 and 8% for **2** and **3**, respectively. The data were corrected for decay, Lorentz and polarization effects using the X-RED [27] program. Crystal data, experimental conditions, details of structure determination and final refinement parameters are given in Table 1.

In both structures the molybdenum atoms were located by the Patterson method and all non-hydrogen atoms in the subsequent difference Fourier maps. Refinement, in which non-hydrogen atoms were treated anisotropically, was performed by the full-matrix least-squares method based on the F^2 values against all reflections. The last Fourier maps revealed positions of all H atoms but some of them with poor geometry. Methyl-H was therefore calculated at positions that maximized the sum of their electron density, i.e. the torsion angles were refined while keeping the angles and distances fixed (C–H 0.96 Å and $U_{iso} = 1.5\ U_{eq}$). In both **2** and **3** the hydrogen atom bonded to the AcOH oxygen atom was found in the Fourier maps. In **2** it was kept fixed during the refinement with an occupancy of 0.5 since it belongs with 50% probability to either one of the centrosymmetrically related acetate ions thus forming AcOH–acetate pairs, while in **3** it was refined (Tables 2 and 3).

All calculations were done by SHELXS [28] and SHELXL [29], and the molecular graphics with PLATON [30].

Table 1
Crystallographic data for compounds **2** and **3**

Compound	**2**	**3**
Empirical formula	$C_{16}H_{25}Mo_2Na_3O_{20}$	$C_8H_{13}KMoO_{10}$
M_r	798.22	404.22
Crystal system and habit	triclinic, prism	monoclinic, prism
Space group	$P\bar{1}$	$P2_1/n$
a (Å)	8.997(3)	7.494(1)
b (Å)	9.183(3)	14.287(4)
c (Å)	10.031(4)	14.098(2)
α (°)	101.04(2)	
β (°)	98.51(2)	99.88(1)
γ (°)	114.32(2)	
V (Å^3)	717.0(4)	1487.0(5)
Z	1	4
D_{calc} (g cm^{-3})	1.849	1.806
μ (mm^{-1})	1.004	1.204
$F(000)$	398	808
Crystal dimensions (mm)	$0.20 \times 0.26 \times 0.42$	$0.33 \times 0.28 \times 0.43$
2θ Range for data collection (°)	4–60	4–60
h, k, l range	−12–12, −12–12, 0–11	−10–10, 0–20, 0–19
Scan type	θ–2θ	θ–2θ
Measured reflections	4073	4369
Observed reflections [$I \geq 2\sigma(I)$]	3374	2929
Independent reflections (R_{int})	3852 (0.025)	4282 (0.031)
Refined parameters	187	189
g_1, g_2 in w [a]	0.0353, 0.1397	0.0693, 0
R [b], wR [c] [$I \geq 2\sigma(I)$]	0.0256, 0.0661	0.0394, 0.0939
R, wR (all data)	0.0339, 0.0684	0.0699, 0.1052
Goodness-of-fit on F^2, S [d]	1.190	0.982
Max., min. electron density (e Å^{-3}) [e]	1.059, −0.963	1.137, −0.858
Extinction coefficients	0.008(1)	
Maximum Δ/σ	<0.001	0.001

[a] $w = 1/[\sigma^2(F_o^2) + g_1P + g_2P]$ where $P = (F_o^2 + 2F_c^2)/3$.
[b] $R = \Sigma\ ||F_o| - |F_c|| / \Sigma\ |F_o|$.
[c] $wR = [\Sigma\ (F_o^2 - F_c^2)^2 / \Sigma\ w(F_o^2)^2]^{1/2}$.
[d] $S = \Sigma\ [w(F_o^2 - F_c^2)^2 / (N_{obs} - N_{param})]^{1/2}$.
[e] In both structures the maximum electron density in the last difference Fourier map is near Mo.

Table 2
Selected bond lengths (Å) and angles (°) for **2**

Bond lengths	
Mo–O1	1.6798(17)
Mo–O2	1.6986(17)
Mo–O3	2.1685(17)
Mo–O4^i	2.2220(15)
Mo–O5	2.0233(17)
Mo–O7	2.0279(16)
Bond angles	
O1–Mo–O2	102.41(9)
O5–Mo–O3	81.30(7)
O7–Mo–O3	80.69(6)
O1–Mo–O4^i	172.16(7)
O2–Mo–O4^i	85.38(7)
O5–Mo–O4^i	82.00(7)
O7–Mo–O4^i	84.29(6)
O3–Mo–O4^i	79.32(6)
O1–Mo–O5	97.56(9)
O2–Mo–O5	98.14(8)
O1–Mo–O7	93.88(9)
O2–Mo–O7	96.41(8)
O5–Mo–O7	159.08(7)
O1–Mo–O3	92.87(8)
O2–Mo–O3	164.63(6)

Symmetry transformations used to generate equivalent atoms: i: $-x, -y, -z+1$.

3. Results and discussion

3.1. Synthesis and characterization of complexes

3.1.1. Synthesis of molybdenum(VI) complexes

$[MoO_2(OCOCH_3)_2]$ (**1**) was obtained by refluxing molybdenum(VI) oxide with the 1:1 mixture of acetic acid and acetic anhydride, $Na_2[Mo_2O_4(OCOCH_3)_6]\cdot NaOCOCH_3\cdot CH_3COOH$ (**2**) and $K[MoO_2(OCOCH_3)_3]\cdot CH_3CO_2H$ (**3**) were prepared by dissolving sodium and potassium molybdate, respectively, in acetic anhydride. As far as we know complexes **2** and **3** are the first structurally characterized examples of molybdenum acetato complexes with molybdenum in its +6 oxidation state. All complexes were extremely sensitive to moisture not only in the solid state but also in solution. The crystals of **1** exposed to light and moisture also showed photochromic behaviour changing colour from pale yellow to blue. Its ESR spectrum (Fig. 1) clearly

showed partial change of the Mo oxidation number from +6 to +5 [31].

3.1.2. Synthesis of molybdenum(V) complex

An olive green molybdenum(V) complex $[Mo_2O_3(OCOCH_3)_4]$ (**4**) was prepared by the reaction of $(NH_4)_2[Mo_2O_4(OH)_4(H_2O)_2]$ [21] with acetic anhydride. The diamagnetism of the complex is characteristic of an oxo bridged molybdenum(V) dimer, but due to its insolubility in all common solvents we were not able to prepare crystals suitable for X-ray analyses.

3.1.3. Synthesis of molybdenum(IV) complexes

The reduction of sodium or potassium molybdate with $SnCl_2{\cdot}2H_2O$ in hot acetic anhydride gave a mixture of a red powder and a colourless substance. Red crystals of $[Mo_3O_2(OCOCH_3)_6(H_2O)(OH)_2]{\cdot}16H_2O$ (**5**) were obtained if the precipitate was dissolved in water and the solution left to evaporate slowly. The same complex could be obtained by heating the mixture of MoO_3 and corresponding carbonate M_2CO_3 (M = Na, K, Rb, Cs) in acetic anhydride with $SnCl_2{\cdot}2H_2O$. However, the structural type of the obtained cluster depends upon the pH of the solution i.e. upon the amount of carbonate left over in the reaction solution. The crystals of $[Mo_3O_2(OCOCH_3)_6(H_2O)(OH)_2]{\cdot}16H_2O$ (**5**) and $[Mo_3O_2(OCOCH_3)_6(H_2O)_3]Cl_2{\cdot}14H_2O$ (**6**) were obtained from aqueous solution at pH 5 and 3, respectively. For both complexes the oxidation number +4 of molybdenum (actually +3.93 and +3.95 for **5** and **6**, respectively) was determined by titration with standard Ce(IV) solution [32]. The trimeric nature of **5** and **6** was also confirmed by X-ray diffraction [13,14].

Table 3
Selected bond lengths (Å) and angles (°) for **3**

Bond lengths	
Mo–O1	1.692(2)
Mo–O2	1.696(2)
Mo–O3	1.989(2)
Mo–O5	2.021(2)
Mo–O7	2.270(2)
Mo–O8	2.233(2)
Bond angles	
O1–Mo–O2	107.99(13)
O1–Mo–O3	96.81(9)
O2–Mo–O3	96.06(9)
O1–Mo–O5	95.72(9)
O2–Mo–O5	94.01(9)
O3–Mo–O5	160.66(9)
O1–Mo–O7	152.57(11)
O2–Mo–O7	99.39(11)
O3–Mo–O7	81.71(8)
O5–Mo–O7	80.38(8)
O8–Mo–O7	57.18(8)
O1–Mo–O8	95.40(11)
O2–Mo–O8	156.51(11)
O3–Mo–O8	82.88(8)
O5–Mo–O8	81.32(8)

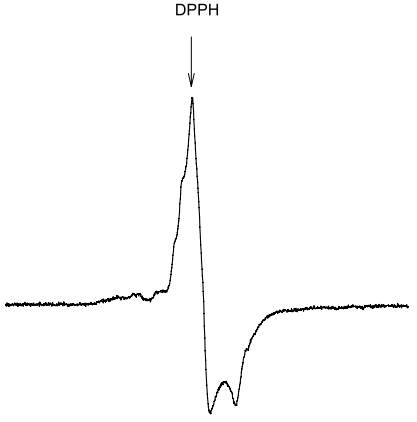


Fig. 1. EPR spectrum of $[MoO_2(OCOCH_3)_2]$.

The complexes were also characterized by IR spectroscopy. The strong bands characteristic of $\nu(Mo–O_t)$ were found at 995–950 cm^{-1} for the *cis*-dioxomolybdate(VI) unit and 938 cm^{-1} for μ-oxomolybdenum(V). Other characteristic strong bands appearing around 1575–1540 and 1455–1440 cm^{-1} (broad) were attributed to $\nu_{asym}(OCO)$ and $\nu_{sym}(OCO)$, respectively. The strong absorption found at 739 cm^{-1} is characteristic of $\nu(Mo–O_b)$, while those at 690 and 644 cm^{-1} were attributed to $\nu(Mo–O_3)$.

3.2. Structural studies

Structures of both $Na_2[Mo_2O_4(OCOCH_3)_6]{\cdot}NaOCOCH_3{\cdot}CH_3COOH$ (**2**) and $K[MoO_2(OCOCH_3)_3]{\cdot}CH_3COOH$ (**3**) contain octahedrally coordinated molybdenum atoms bonded to two terminal oxo-oxygen atoms and four oxygen atoms from the acetate ligands.

The crystal structure of **2** is built up of centrosymmetrical dinuclear complex $[Mo_2O_4(OCOCH_3)_6]^{2-}$ anions (Fig. 2) interconnected by sodium cations and centrosymmetrical pairs of acetate–acetic acid (Fig. 3). The terminal Mo=O bond lengths amount to 1.680(2) and 1.699(2) Å. Two acetate ligands are monodentately bonded to each molybdenum atom at 2.023(2) and 2.028(2) Å, while the third one together with its centrosymmetrical pair acts as a bridge with Mo–O distances of 2.169(2) and 2.222(2) Å. They are the longest Mo–O bonds due to the *trans* influence of the terminal oxo-oxygen atoms. The octahedron is distorted with angles at Mo atom ranging from 79.32(6) (involving two oxygens from the bridging acetate) to 102.41(9)° (formed by two oxo-oxygen atoms).

The crystal structure of **3** is built up of mononuclear complex $[MoO_2(OCOCH_3)_3]^-$ anions (Fig. 4) interconnected by potassium cations and acetic acid molecules. The Mo=O bonds are similar as in **2** (1.692(2) and 1.696(2) Å). The Mo–O bonds from the bidentately bonded acetate ligand are *trans* to the oxo-oxygen

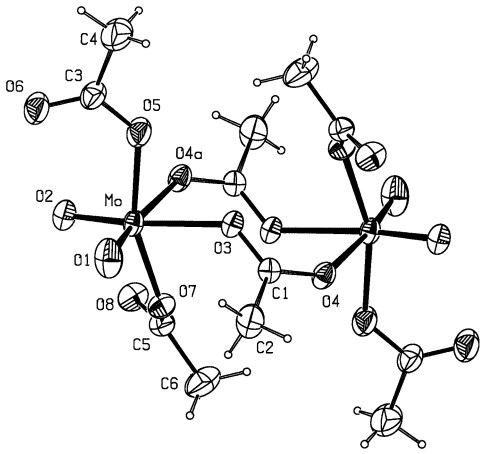


Fig. 2. Drawing of the $[Mo_2O_4(OCOCH_3)_6]^{2-}$ anion in **2** with the atom labelling scheme. The thermal ellipsoids are at the 50% probability level. Symmetry operations: $a = -x, -y, -z+1$.

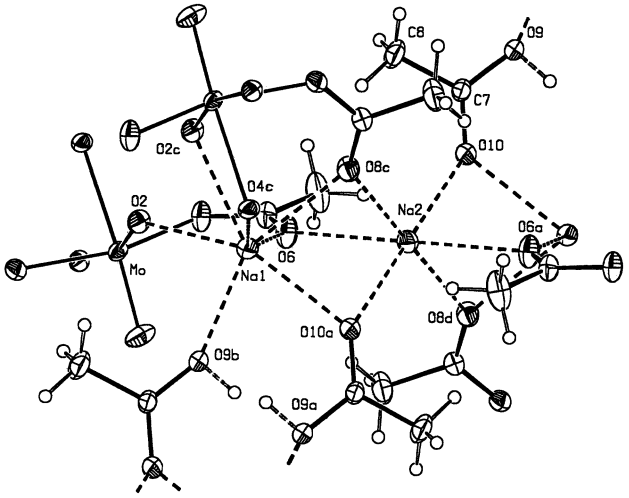


Fig. 3. The coordination polyhedron around the two sodium atoms is shown by dashed lines. Only the oxygen atoms within the sodium coordination sphere and the acetic acid–acetate ion atoms are labelled. The H atom on O9 is of 50% probability and the bond is shown by double broken lines. Symmetry operations: $a = 1-x, 1-y, -z$; $b = -1+x, y, z$; $c = -x, -y, -z$; $d = 1+x, 1+y, z$.

atoms and are again the longest ones (2.233(2) and 2.270(2) Å), even longer than in **2**. The two monodentately bonded acetates form Mo–O bonds of 1.989(2) and 2.021(2) Å, respectively. The coordination octahedron is even more distorted than in **2** with O–Mo–O angles ranging from 57.18(8) to 108.0(1)°, the largest angle is again that one involving the oxo-oxygen atoms and the smallest one involving oxygens from the bidentately bonded acetate ligand. In the chemistry of molybdenum there are not many examples of such structures with an acetato ligand bidentately bonded to one molybdenum atom. Actually molybdenum(IV) complexes $[Mo\{C_7H_2(CCH_3)_4\}(OCOCH_3)_2]$ [33] and $[Mo(OCOCH_3)(\eta^3\text{-}C_3H_5)_3]$ [34] are the only such examples with the Mo-to-acetate–oxygen bond lengths ranging from 2.144(2) to 2.264(2) Å. They are longer comparing to those in **2** and **3**.

By searching the Cambridge Structural Database for all Mo–O(acetate) bonds, 69 structures with 215 Mo–O bonds were found ranging from 2.057 to 2.264 Å. Only two molybdenum complexes with mondentately bonded acetate ligands were found: in one of them, $(Bu_4N)_2[Mo_6(\mu_3\text{-}Cl)_8(OCOCH_3)_6]$ [35], six acetate ligands are bound to a hexanuclear cluster with Mo–O distances ranging from 2.085 to 2.093 Å, while in the other one, $[Mo(H_2CPz)(CO)_2(NO)(OCOCH_3)]$, CPz = 3,5-dimethylpyrazol-1-yl [36], the acetate ions in two independent molecules are bonded with Mo–O distances of 2.095 and 2.152 Å. Therefore, the Mo–O bonds involving the monodentate acetate ligands in **2** and **3** are the shortest Mo–O(acetate) bonds found so far.

In both structures the acetic acid molecules are not involved in bonding to molybdenum but act as bridges either over both (as in **2**, Fig. 3) or over only one oxygen atom (as in **3**, Fig. 5) connecting centrosymmetrically related sodium and potassium ions, respectively. In **2** the acetic acid molecule and the acetate ion are centrosymmetrically related and connected by a hydrogen bond O9–H···O9($-x, 1-y, -z$) of 2.422(3) Å (O9–H 0.92, H···O9 1.51 Å, O9–H···O9 170.2°) with a positionally disordered hydrogen atom. The acetic acid molecule in **3** is linked to a neighbouring acetate ion by a hydrogen bond O10–H···O6 ($2-x, 1-y, -z$) of 2.638(4) Å (O10–H 0.71(4), H···O6 2.01(4) Å, O10–H···O6 148(1)°).

In **2** the two crystallographically independent sodium ions Na1 and Na2 are surrounded by seven and six oxygen atoms, respectively, with distances Na···O ranging from 2.316 (2) to 2.604 (2) Å, while the larger

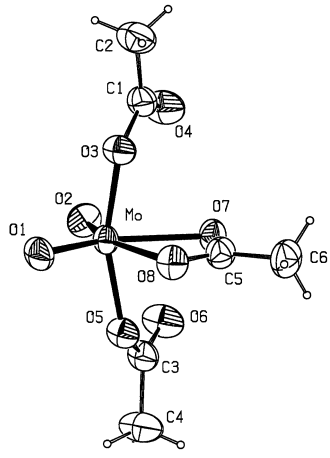


Fig. 4. Drawing of the $[MoO_2(OCOCH_3)_3]^-$ anion in **3** with the atom labelling scheme. The thermal ellipsoids are at the 50% probability level.

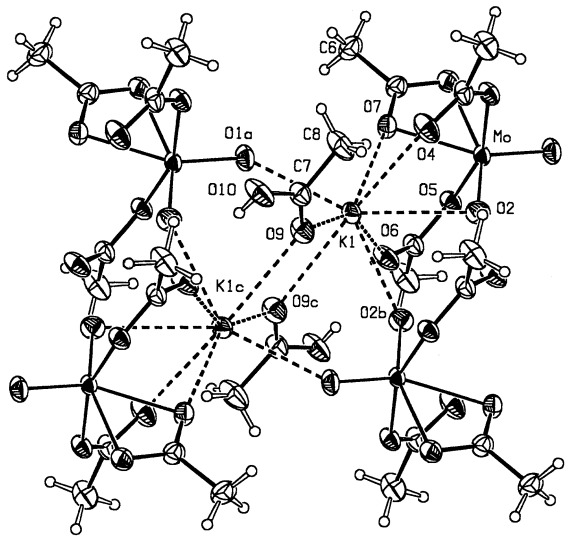


Fig. 5. The coordination polyhedron around the potassium atom is shown by dashed lines. Only the oxygen atoms within the potassium coordination sphere and the acetic acid atoms are labelled. Symmetry operations: $a = 1 + x, y, z$; $b = 1 - x, 1 - y, -z$; $c = 2 - x, 1 - y, -z$.

potassium ion in **3** is eight-coordinated with K···O distances from 2.778(2) to 3.047(3) Å.

4. Supplementary material

Crystallographic data for the structural analysis have been deposited with the Cambridge Crystallographic Data Centre, CCDC Nos. 166269 and 166270 for compounds **2** and **3**, respectively. Copies of this information may be obtained free of charge from The Director, CCDC, 12 Union Road, Cambridge, CB2 1EZ, UK (fax: +44-1223-336033; e-mail: deposit@ccdc.cam.ac.uk or www: http://www.ccdc.cam.ac.uk).

Acknowledgements

Financial support for this research was provided by the Ministry of Science and Technology of the Republic of Croatia (Grant No. 119407). We thank Dr Z. Veksli, Ruder Bošković Institute, Zagreb, for recording the ESR spectra.

References

[1] E. Bannister, G. Wilkinson, Chem. Ind. (London) (1960) 319.
[2] T.A. Stephenson, E. Bannister, G. Wilkinson, J. Chem. Soc. (1964) 2538.
[3] A. Bino, F.A. Cotton, Z. Dori, J. Am. Chem. Soc. 100 (1978) 5252.
[4] A. Bino, F.A. Cotton, Z. Dori, J. Am. Chem. Soc. 103 (1981) 243.
[5] F.A. Cotton, Polyhedron 5 (1986) 3.
[6] F.A. Cotton, Z. Dori, D.O. Marler, W. Schwotzer, Inorg. Chem. 22 (1983) 3104.
[7] A. Birnbaum, F.A. Cotton, Z. Dori, M. Kapon, Inorg. Chem. 23 (1984) 1617.
[8] L. Huang, X. Li, H. Jinshun, C. Wendan, H. Xiagoyin, H. Xin, Polyhedron 15 (1996) 2003.
[9] X. Li, L. Huang, Y. Duangcao, H. Jinshun, Z. Qianer, J. Am. Chem. Soc., Chem. Commun. (1993) 1507.
[10] L. Xu, Z. Li, J. Huang, Polyhedron 16 (1997) 1365.
[11] L. Xu, Z. Li, J. Huang, Inorg. Chem. 35 (1996) 5097.
[12] L. Xu, J. Huang, Q. Zhang, Polyhedron 16 (1997) 1407.
[13] A. Birnbaum, F.A. Cotton, Z. Dori, D.O. Marler, G.M. Reisner, W. Schwotzer, M. Shaia, Inorg. Chem. 22 (1983) 2723.
[14] M. Ardon, A. Bino, F.A. Cotton, Z. Dori, M. Kaftory, G. Reisner, Inorg. Chem. 21 (1982) 1912.
[15] A.L. Doadrio, M.T. Calabuig, A. Doadrio Lopez, An. Real. Acad. Farm. 52 (1986) 575.
[16] O.V. Klimov, M.A. Fedotov, D.I. Kuchubei, S.P. Degtyarev, A.N. Strasev, Russ. J. Coord. Chem. 21 (1995) 678.
[17] B. Kamenar, B. Korpar-Čolig, M. Penavić, J. Chem. Soc., Dalton Trans. (1981) 311.
[18] M.E. Noble, D.E. Williams, Inorg. Chem. 27 (1988) 749.
[19] R. Wang, M.S. Mashuta, J.F. Richardson, M.E. Noble, D.E. Williams, Inorg. Chem. 35 (1996) 3022.
[20] E.I. Koffi-Sokpa, D.T. Calfee, B.R.T. Allred, J.L. Davis, E.K. Haub, A.K. Rich, R.A. Porter, M.S. Mashuta, J.F. Richardson, M.E. Noble, Inorg. Chem. 38 (1999) 802.
[21] A.N. Strasev, O.V. Klimov, S.A. Shkuropat, M.A. Fedotov, S.P. Degtyarev, D.I. Kochubey, Polyhedron 13 (1994) 505.
[22] G.A. Parker, Analytical Chemistry of Molybdenum, Springer-Verlag, New York, 1983.
[23] W.W. Scott, Standard Methods of Chemical Analysis, D. Van Nostarand Company, Princeton, 1961.
[24] F.J. Welcher, Standard Methods of Chemical Analysis, D. Van Nostarand Company, Princeton, 1963.
[25] D. Čukman, J. Jadnačak-Bišćan, Z. Veksli, W. Haller, J. Colloid Interface Sci. 111 (1987) 357.
[26] Stoe and Cie, STADI4, Diffractometer Control Program for Windows, Darmstadt, Germany, 1995.
[27] Stoe and Cie, X-RED, Data Reduction Program for Windows, Darmstadt, Germany, 1995.
[28] G.M. Sheldrick, Acta Crystallogr., Sect. A 46 (1990) 467.
[29] G.M. Sheldrick, SHELXL-97, Program for the Refinement of Crystal Structures, University of Göttingen, Germany, 1997.
[30] A.L. Spek, Acta Crystallogr., Sect. A 46 (1990) C34.
[31] M. Cindrić, N. Strukan, V. Vrdoljak, M. Devčić, Z. Veksli, B. Kamenar, Inorg. Chim. Acta 304 (2000) 260.
[32] J.J. Stark, J. Chem. Educ. 64 (1969) 505.
[33] H. Strutz, J.C. Dewan, R.R. Schrock, J. Am. Chem. Soc. 107 (1985) 5999.
[34] R. Benn, S. Holle, P.W. Jolly, C. Kruger, C.C. Romao, M.J. Romao, A. Rufinska, G. Schroth, Polyhedron 5 (1986) 461.
[35] R.D. Adams, Gong Chen, Jianquan Huang, J. Cluster Sci. 4 (1993) 151.
[36] K.-B. Shiu, S.-T. Lin, D.-W. Fung, T.-J. Chan, S.-M. Peng, M.-C. Cheng, J.L. Chou, Inorg. Chem. 34 (1995) 854.

PERGAMON

Polyhedron 21 (2002) 155–165

POLYHEDRON

www.elsevier.com/locate/poly

Spectroscopic studies of the dodecanuclear chromium complex $Cr_{12}O_9(OH)_3(pivalate)_{15}$: confirmation of the presence of twelve Cr(III) centers and the crystal structure of $Cr_{12}O_9(OH)_3(pivalate)_{15}\cdot 2PrOH\cdot 9H_2O$

April C. Royer, Robin D. Rogers, David L. Arrington, Shane C. Street, John B. Vincent *

Department of Chemistry, The University of Alabama, Tuscaloosa, AL 35487-0336, USA

Received 11 June 2001; accepted 14 September 2001

Abstract

The complex originally reported to be '$Cr_{12}O_{12}(pivalate)_{15}$' has been examined by a number of spectroscopic techniques in order to elucidate the chromium valence states. By charge balance arguments, the complex could, for example, contain nine Cr(III) and three Cr(IV) centers, contain 11 Cr(III) and one Cr(VI) center or could possess three protons, not detected by X-ray crystallography, and 12 Cr(III) centers. While a recent neutron diffraction study has suggested the existence of three additional and disordered deuterons (and thus 12 Cr(III) centers), the complex has been studied by several complementary spectroscopic techniques which confirm the formula to be $Cr_{12}O_9(OH)_3(pivalate)_{15}$. © 2002 Elsevier Science Ltd. All rights reserved.

Keywords: Chromium; Pivalate; Mass spectrometry; Paramagnetic; NMR; X-ray photoelectron spectroscopy

1. Introduction

In 1991, Batsanov et al. reported the synthesis and X-ray diffraction (XRD) structure of a complex they tentatively assigned the formula '$Cr_{12}O_{12}(pivalate)_{15}$' [1]. Charge balance requirements necessitate that the complex be mixed valent containing Cr(III) and higher oxidation state chromium centers or that all the chromium centers be trivalent and three additional protons be present that could not be located by X-ray crystallography. To establish the chromium oxidations states, we set out to obtain a higher resolution X-ray structure and to characterize the complex by a series of spectroscopic techniques. While this work was in progress, Winpenny and co-workers [2] reported that the complex's formula should be $Cr_{12}O_9(OH)_3(pivalate)_{15}$ based on variable temperature magnetic susceptibility studies, high-field EPR studies, and most importantly neutron diffraction studies. The last technique disclosed the presence of three disordered half-weight deuterons bound to six of the μ_3-oxo ligands. Herein are reported our complementary spectroscopic studies, which confirm the formula as $Cr_{12}O_9(OH)_3(pivalate)_{15}$.

2. Experimental

2.1. Materials and physical measurements

The starting polymer $[Cr(OH)(O_2CC(CH_3)_3)_2]_n$ was prepared as described previously [1]. All chemicals were used as received; all operations were performed in air unless otherwise noted. Infrared spectra (mineral oil mulls) were recorded on a Perkin–Elmer 283B spectrophotometer, and ^1H NMR spectra were obtained using a Bruker AM-360 or a Bruker AM-500 spectrometer at 23 °C. Chemical shifts are reported on the δ scale (shifts downfield are positive) using the solvent

* Corresponding author. Tel.: +1-205-348-9203; fax: +1-205-348-9104.

E-mail address: jvincent@bama.ua.edu (J.B. Vincent).

0277-5387/02/$ - see front matter © 2002 Elsevier Science Ltd. All rights reserved.
PII: S0277-5387(01)00955-X

deuterio-component signal(s) as reference. Evans method solution susceptibility measurements [3] were performed using hexamethyldisiloxane as a chemical shift reference; diamagnetic contributions were corrected using Pascal's constants. A Hewlett–Packard 8451A spectrophotometer was used to record UV–Vis spectra. FAB and EI mass spectra were obtained using a VG Autospec high-resolution mass spectrometer. FAB mass spectra of the dodecanuclear complexes (**1** and **3**) were collected on mixtures made from 1.5 μl of the complex in *n*-propanol (10 μg ml^{-1}) and 1.5 μl of thioglycerol containing 1% trifluoroacetic acid. The FAB mass spectrum of **2** was collected on a 10 μg ml^{-1} solution of the complex in 3-nitrobenzyl alcohol. EPR spectra were collected on a Varian E-12 spectrophotometer equipped with an Oxford ESR 900 cryostat. X-ray photoelectron spectroscopy (XPS) measurements were performed using a Kratos Analytical Axis 165 XPS with monochromatic Al Kα radiation (1486.6 eV). The analyzer pass energy employed for high resolution spectra was 40 eV with 0.1 eV per step. The Cr-containing powder sample was placed onto carbon tape mounted on an analysis stub. The stub was then inserted into the chamber. The base pressure during XPS analysis remained below 10^{-9} Torr. A charge neutralizer was employed to supply electrons for charge compensation. The XPS spectra were referenced to aliphatic carbon in the C 1s region as 285.0 eV and carboxylate carbon to 289.3 eV. Data analysis and fitting using standard Shirley background correction was performed using Spectral Data Processor software (XPS International). Elemental analyses were performed by Galbraith Laboratories (Knoxville, TN).

2.2. $Cr_{12}O_9(OH)_3(O_2CC(CH_3)_3)_{15}\cdot 3\ 1/6\ HOPr\cdot 4H_2O$ (1)

$[Cr(OH)(O_2CC(CH_3)_3)_2]_n$ (2.0 g) was placed in a quartz boat within a reaction tube and heated under a slow purge of Ar in a 400 °C tube furnace for 1 h. The green sublimate, which was deposited in the end of the reaction tube, was taken up in a minimum amount of Et_2O, and an equal volume of MeCN was added. The solution was allowed to concentrate slowly, yielding dark green crystals. The crystals were collected by filtration and recrystallized from *n*-propanol producing dark green crystals of **1** in an average yield of 0.35 g (23% yield based on Cr). *Anal.* Calc. (Found) for $C_{84.50}H_{171.33}O_{49.17}Cr_{12}$: C, 39.06 (39.14); H, 6.65 (7.14); Cr, 24.01 (24.06%). Selected IR data (cm^{-1}): 1584 (s), 1564 (s), 1548 (s), 1233 (s), 690 (s), 624 (s), 467 (s). Visible spectrum (*n*-propanol): $\lambda_{max} = 444$ nm (ε/Cr = 69), $\lambda_{max} = 616$ nm (ε/Cr = 89).

2.3. $[Cr_3O(O_2CC(CH_3)_3)_6(H_2O)_3]^+$ (2)

Pivalic acid (1.02 g, 9.98 mmol) and 0.560 g (9.98 mmol) of potassium hydroxide were combined in 35 ml of stirred and gently warmed tetramethylene sulfone; stirring with low heat was continued until all the solid dissolved. To this solution, a solution of 2.00 g (7.51 mmol) chromium(III) chloride hexahydrate in 25 ml of warm tetramethylene sulfone was added. The reaction mixture was heated at reflux for 4.5 h and then allowed to cool to r.t. The resulting green solid was dissolved in acetone, filtered, and allowed to concentrate slowly to produce dark green crystals of the chloride salt of **2** in 22% yield (based on Cr). *Anal.* Calc. (Found) for $C_{30}H_{60}O_{16}Cr_3Cl$: C, 39.08 (38.59); H, 7.38 (7.24); Cl, 3.66 (4.03), Cr, 16.09 (15.75). Selected IR data (cm^{-1}): 1594 (s), 1487 (m), 1460 (s), 1432 (s), 1379 (s), 1297 (w), 1231 (s), 1148 (w), 1110 (w), 1035 (w), 942 (w), 906 (w), 789 (w), 724 (w), 670 (w), 623 (m), 490 (w), 469 (m). Visible spectrum (acetone): $\lambda_{max} = 441$ and 590 nm.

2.4. $Cr_{12}O_{12}(O_2CC(CH_3)_3)_{12.46}(O_2CCCl_3)_{2.54}\cdot HOPr\cdot 4H_2O$ (3)

$Cr_{12}O_9(OH)_3(O_2CC(CH_3)_3)_{15}\cdot 3\ 1/6\ HOPr\cdot 4H_2O$ (**1**) (0.25 g, 0.096 mmol) was dissolved in 35 ml of *n*-propanol. To this stirred solution was added 0.35 g, 2.2 mmol of Cl_3CCO_2H. The reaction mixture was heated at reflux for 9.5 h. The resulting solution was cooled, and slow concentration of the solution produced dark green crystals in 83% yield (0.20 g, 0.079 mmol). *Anal.* Calc. (Found) for $C_{79.38}H_{152.14}O_{50}Cr_{12}Cl_{7.62}$: C, 34.00 (34.04); H, 5.58 (5.57); Cl, 9.64 (9.63); Cr, 22.25 (22.25). Selected IR data: 1700 (m), 1650 (m), 1578 (s), 1234 (s), 1772 (w), 853 (m), 836 (m), 783 (w), 758 (w), 720 (m), 689 (s), 624 (s), 585 (m). Visible spectra (*n*-propanol): $\lambda_{max} = 446$ (ε/Cr = 42) and 611 nm (ε/Cr = 55).

2.5. X-ray crystallography and structure solution

X-ray crystallographic intensity data for complex **1** were collected on a green, hexagonal-shaped crystal, $0.1 \times 0.20 \times 0.20$ mm (Table 1). The crystal was mounted in a glass capillary, and intensity data were collected at −100 °C on a Siemens SMART diffractometer with a CCD area detector and with graphite-monochromated Mo Kα radiation in the range $\theta = 1.39°$–$27.87°$. The space group *R*32 was assigned on the basis of extinctions. A total of 22 694 reflections were collected of which 5575 were unique and 3520 were considered observed [$I > 1\sigma(I)$]. The structure was solved by direct methods using the computing package SHELXTL, Version 5 [4], and refined by full-matrix least-squares minimization of $w(F_o^2 - F_c^2)^2$ with anisotropic thermal parameters for all non-hydrogen

atoms. Final R factors were 0.0896 and 0.2233 for R_1 and wR_2, respectively.

In the refinement of **1**, solvent and ligand disorder was noted. The ligand t-butyl groups, in general, exhibited high thermal motion and were refined isotropically. Rotational disorder was resolved for one unique ligand and atoms C(8)–C(10) were refined in two alternate orientations with 50% occupancy each.

The solvent and water molecules exhibited very diffuse peaks making it difficult to refine effectively these atoms. The final refinement was nest modeled on two disordered n-PrOH molecules and nine disordered water molecules per formula unit. The high thermal motion and disorder of the solvent and ligand molecules on the periphery of the cluster resulted in high R values for the overall refinement. Nonetheless, the Cr and O atoms of the cluster were well behaved in the refinement, and the geometrical parameters of the core of the cluster gave reasonable e.s.d. Only this portion of the structure will be discussed.

Table 1
Crystal data and structure refinement

Color/shape	green/hexagonal
Empirical formula	$C_{81}H_{169}Cr_{12}O_{53}$
Formula weight	2615.16
Temperature (K)	173(2)
Crystal system	rhombohedral
Space group	$R32$
Unit cell dimensions (5774 reflections in full θ range)	
a (Å)	18.4460(3)
b (Å)	18.4460(3)
c (Å)	36.1138(5)
α (°)	90
β (°)	90
γ (°)	120
V (Å^3)	10641.6(3)
Z	3
D_{calc} (g cm^{-3})	1.224
Absorption coefficient (mm^{-1})	0.951
Reflections collected	22 694
Reflections observed ($I>2\sigma(I)$)	3520
Independent reflections	5575 [$R_{int}=0.0987$]
Data/restraints/parameters	5060/0/186
Final R indices [$I>2\sigma(I)$]	$R_1=0.0896$, $wR_2=0.2233$
R indices (all data)	$R_1=0.1503$, $wR_2=0.2875$
Goodness-of-fit on F^2	1.052
Largest difference peak and hole (e Å^{-3})	0.834 and −0.661

3. Results and discussion

3.1. Synthesis

The original synthesis of **1** by Bastanov et al. involved heating the starting polymer $[Cr(OH)(O_2CC(CH_3)_3)_2]_n$ in a 400 °C bath under a flow of argon; the resulting sublimate underwent extensive purification via a series of extractions and crystallizations. The yield after recrystallization from n-propanol, but before suitable crystals for X-ray crystallography were obtained from α-methylnapthalene, was approximately 37% [1]. A synthesis and purification involving fewer steps was desirable. In initial attempts to develop an alternate synthesis of **1**, the starting polymer was refluxed in a high-boiling-point solvent, tetramethylene sulfone (b.p. 285 °C). However, the subsequent reaction gave rise to the basic carboxylate trimer $[Cr_3O(O_2CC(CH_3)_3)_6(H_2O)_3]^+$ (**2**).

As an alternative, the starting polymer was heated to 400 °C in a reaction tube in a tube furnace under a flow of argon. Under these conditions, released pivalic acid was flushed from the reaction tube, and **1** deposited at the end of the tube, readily separating from the chromic oxide byproduct left in the quartz boat. Now the sublimate only had to be recovered by rinsing the reaction tube with an appropriate solvent; recrystallization from n-propanol gave crystals suitable for XRD studies. Winpenny and co-workers [2] have shown recently that a single recrystallization step (also using n-propanol) is all that is necessary after the first step of the original Bastanov procedure.

In order to test whether hydroxide bridges were present in **1**, an effort was made to substitute the pivalate ligands with another carboxylate with a very different electron donating ability. It was anticipated that substitution of the electron-donating t-butyl group of pivalate with the electron-withdrawing CCl_3 group of trichloroacetate might alter the acidity of any bridging hydroxide groups and give rise to a dodecamer bearing a negative charge. The addition of the more acidic acid, trichloroacetic acid, to a refluxing solution of **1** in n-propanol resulted in partial substitution of the pivalate ligands with trichloroacetate. The reaction presumably occurs in the same manner as for similar metal carboxylate assemblies [5] where the more acidic acid is believed to protonate the carboxylate ligand (from the weaker acid). The newly generated carboxylate replaces the newly formed acid. Why only partial substitution occurred is unclear as increasing the ratio of trichloroacetic acid to **1** and increasing the reaction time had little effect on the reaction.

3.2. Description of structure

In the structure of the Cr_{12} by Bastanov et al., the compound was found to crystallize in the space group $P2_1/c$ [1]. Partially because of the large number of atoms, the structure was refined to a precision of $R=$

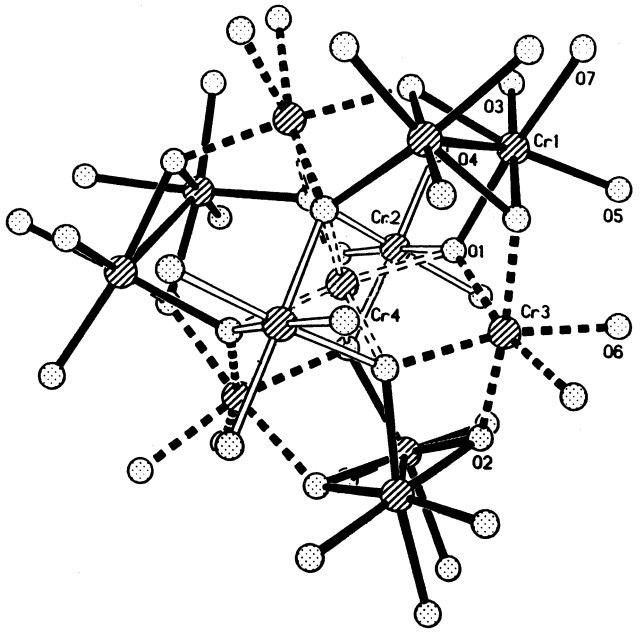


Fig. 1. Body-centered pentacapped trigonal antiprism core of $Cr_{12}O_9(OH)_3(pivalate)_{15}$ (**1**) with atom labels.

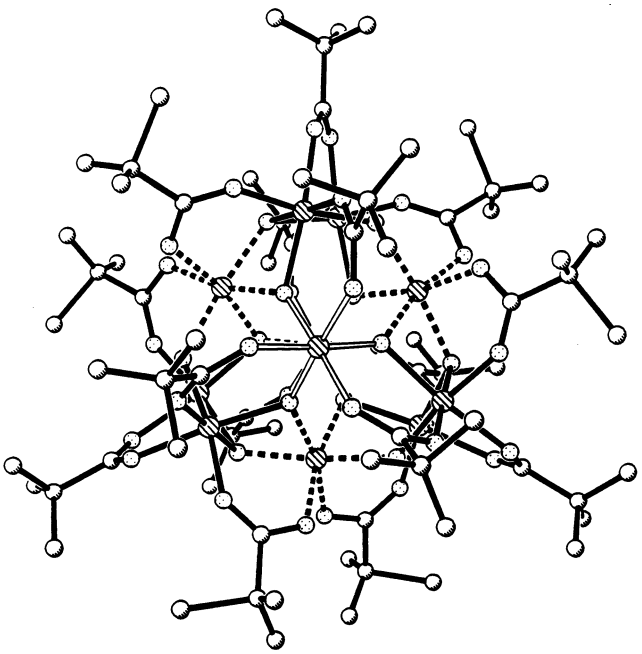


Fig. 2. Structure of $Cr_{12}O_9(OH)_3(pivalate)_{15}$ (**1**) viewed approximately along the C_3 axis.

0.059 ($R_w = 0.067$). It was hoped that obtaining crystals of the complex from another solvent could give rise to crystals with a different space group and whose molecular structure could be refined to a greater degree of precision. Greater precision might allow for the average Cr–O bond distances for the various chromium centers to be distinguished as would be expected if chromium existed in multiple oxidation states in the complex. The space group of **1** recrystallized from *n*-propanol was *R*32 with the molecule lying on a 32 site, imposing D_3 symmetry on the molecule. Consequently, the molecule possessed only four unique chromium sites with the others being generated by the symmetry elements. The molecule is nearly identical in terms of its metric parameters to the α-methylnaphthalene solvate. The formula found for the molecule from X-ray crystallography is the same as reported by Bastanov et al. [1]; three additional, disordered protons corresponding to the three additional deuterons found in the neutron diffraction study [2] could not be located. The 12 chromium centers are arranged in a body-centered pentacapped trigonal antiprism with a twist angle of 16.8° (Fig. 1), compared with 15.3° in the α-methylnaphthalene solvate [1]. The six chromium centers of type Cr1 form the trigonal antiprism. Two chromium centers (type Cr2) form caps 1.284 Å above the triangular bases, while three chromium centers, type Cr3, form caps 1.147 Å above the lateral faces. A unique center, Cr4, lies at the center of the trigonal antiprism. All 15 pivalate ligands are bidentate, bridging between two chromium atoms (Fig. 2).

The octahedron for each of the six Cr1 type chromium centers is completed by one pivalate bridge to a second Cr1 center, spanning the lateral edge of the prism, two μ_3-oxide bridges, which also coordinate to the Cr3 type centers on the adjacent lateral faces, one pivalate bridging to a type Cr2 center, one pivalate bridging to a Cr3 center, and one μ_4-oxide, which is also coordinated to a Cr2, a Cr3, and the Cr4 type center. The octahedron of each of the Cr2 type centers is completed by the pivalate bridging to each of the three type Cr1 centers forming a trigonal face and three μ_4-oxide ligands which bridge between a Cr1, Cr3, and Cr4 center. Octahedral coordination about the Cr3 centers is composed of two pivalate bridges, one each to opposing Cr1 centers such that they span the diagonal of a lateral face, two μ_3-oxide bridges which also coordinate Cr1 centers of the lateral face, and two μ_4-oxide bridges. The Cr4 center lying at the center of the prism is in an extremely novel environment, being surrounded by six μ_4-oxide bridges and capable of supporting a high valent chromium center theoretically.

Tables 2 and 3 list the important bond angles and bond distances for **1**. Examination of the bond lengths reveals all Cr–(μ_n-O) bond lengths to be virtually identical (1.982–2.027 Å). For example, the Cr–(μ_4-O(1)) bond lengths are 1.986(5) Å for the Cr1 type chromiums (corners of the antiprism), 1.994(5) Å for the Cr2 type chromiums (trigonal caps), 2.027(5) Å for the Cr3 type chromiums (lateral face caps), and 1.985(4) Å for the Cr4 type chromium lying at the center of the prism. The values for Cr1, Cr2, and Cr4 are all equivalent within the 3σ criterion. The value for the Cr3 type chromiums (lateral face caps) is considerably larger,

lying outside the 3σ difference. This difference is not, however, suggestive of Cr(IV) or Cr(VI) as bond lengths for Cr(IV)–O or Cr(VI)–O bonds would be shorter than the comparable Cr(III)–O bond length. The origin of the long Cr3–(μ_4-O) bond length is probably steric; the Cr3 centers have two μ_4-O interactions and two μ_3-O interactions, which prevent the center from fitting more closely into the $Cr_{12}O_9(OH)_3$ core. The Cr–(μ_4-O) bond lengths observed are consistent with reported Cr(III) to μ_4-oxide bond lengths in the range of 1.97–2.04 Å [6,7].

The observed Cr–(μ_3-O) bond lengths are 1.974(7) and 1.985(5) Å for the Cr1 type chromium centers and 1.982(6) Å for the Cr3 type chromium centers. These Cr–(μ_3-O) bond distances are slightly elongated relative to those cited for Cr(III)–(μ_3-O) bonds; Cr(III) to μ_3-oxide bond lengths are known to be in the range of 1.85–1.95 Å, although nearly all examples contain planar Cr_3O units rather than pyramidal [8–12]. Though elongated relative to Cr(III)–(μ_3-O) bonds, the observed bond lengths are not suggestive of Cr(IV)–(μ_3-O) or Cr(VI)–(μ_3-O) as these would be shorter than comparable Cr(III) bonds. These μ_3-'oxo' groups are the ones bound to the half-occupancy deuterons in the neutron diffraction study [2]. Thus, the long bond distances and pyramidal geometry are consistent with these sites being on average a mixture of μ_3-oxo and μ_3-hydroxo.

Evaluation of the Cr–(μ-$O_2CC(CH_3)_3$) bond lengths reveals these to be also virtually identical. The Cr–(μ-$O_2CC(CH_3)_3$) bond lengths are 1.940(8), 1.961(5), and 2.017(7) Å, for an average of 1.97(3) Å for the Cr1 type chromiums (corners of the antiprism), 1.985(6) Å for the Cr2 type chromiums (trigonal caps), and 1.989(6) Å for the Cr3 type chromiums (lateral face caps). Using the average value for the Cr1 type chromium atoms, all values are equivalent within the 3σ criterion. This value is consistent with the range of 1.97–2.01 Å reported for μ-carboxylates bound to chromium(III) [8,9,13]. Therefore, the crystallographic data is consistent with all chromium atoms being trivalent. It should be noted that examination of the Bastanov structure also reveals all Cr–O bond lengths to be virtually identical, in the range of 1.95–2.02 Å [1].

X-ray crystallographic data were collected on the trichloroacetic acid derivative $[Cr_{12}O_{12}(O_2CC(CH_3)_3)_{12.46}(O_2CCCl_3)_{2.54}]\cdot 4HOPr\cdot 4H_2O$ (**3**). Unfortunately, the partially substituted complex possessed extensive disorder making refinement very difficult; a

Table 2
Important bond lengths (Å) for compound **1**

Cr(1)–O(5)	1.940(8)
Cr(1)–O(2) # 1	1.974(7)
Cr(1)–O(1)	1.986(5)
Cr(1)–Cr(1) # 3	2.817(3)
Cr(1)–O(3)	1.961(5)
Cr(1)–O(2) # 2	1.985(5)
Cr(1)–O(7)	2.017(7)
Cr(2)–O(1)	1.994(5)
Cr(2)–O(4)	1.985(6)
Cr(2)–Cr(4)	2.632(2)
Cr(3)–O(2)	1.982(6)
Cr(3)–O(1)	2.027(5)
Cr(3)–O(6)	1.989(6)
Cr(3)–Cr(4)	2.738(2)
Cr(4)–O(1)	1.985(4)

Symmetry transformations used to generate equivalent atoms: # 1, $-y+1, x-y+1, z$; # 2, $x-y+2/3, -y+4/3, -z+1/3$; # 3, $y-1/3, x+1/3, -z+1/3$.

Table 3
Important bond angles (°) for compound **1**

O(5)–Cr(1)–O(3)	85.7(3)
O(3)–Cr(1)–O(2) # 1	91.8(3)
O(3)–Cr(1)–O(2) # 2	179.1(2)
O(5)–Cr(1)–O(1)	93.6(3)
O(2) # 1–Cr(1)–O(1)	94.8(2)
O(5)–Cr(1)–O(7)	85.6(4)
O(2) # 1–Cr(1)–O(7)	86.2(3)
O(1)–Cr(1)–O(7)	86.2(3)
O(5)–Cr(1)–O(2) # 1	171.5(3)
O(5)–Cr(1)–O(2) # 2	94.1(3)
O(2) # 1–Cr(1)–O(2) # 2	88.3(2)
O(3)–Cr(1)–O(1)	102.7(2)
O(2) # 2–Cr(1)–O(1)	78.2(2)
O(3)–Cr(1)–O(7)	87.4(3)
O(2) # 2–Cr(1)–O(7)	91.7(3)
O(4) # 4–Cr(2)–O(1)	95.5(2)
O(4) # 1–Cr(2)–O(1)	176.2(2)
O(1)–Cr(2)–O(1) # 1	80.8(2)
O(4)–Cr(2)–O(4) # 1	84.8(2)
O(4)–Cr(2)–O(1)	99.0(2)
O(1)–Cr(2)–O(1) # 4	80.8(2)
O(2)–Cr(3)–O(6) # 2	93.4(3)
O(6) # 2–Cr(3)–O(6)	81.2(3)
O(2) # 2–Cr(3)–O(1)	77.3(2)
O(6)–Cr(3)–O(1)	94.2(2)
O(2)–Cr(3)–O(2) # 2	174.3(3)
O(2)–Cr(3)–O(6)	90.9(3)
O(2)–Cr(3)–O(1)	98.7(2)
O(6) # 2–Cr(3)–O(1)	167.1(3)
O(1) # 2–Cr(3)–O(1)	92.7(3)
O(1) # 5–Cr(4)–O(1)	174.3(3)
O(1)–Cr(4)–O(1) # 1	81.2(2)
O(1) # 2–Cr(4)–O(1)	95.2(3)
O(1) # 3–Cr(4)–O(1)	102.7(3)
Cr(4)–O(1)–Cr(1)	122.4(2)
Cr(1)–O(1)–Cr(2)	120.5(2)
Cr(1)–O(1)–Cr(3)	96.4(2)
Cr(4)–O(1)–Cr(2)	82.8(2)
Cr(4)–O(1)–Cr(3)	86.1(2)
Cr(2)–O(1)–Cr(3)	141.7(3)
Cr(1) # 4–O(2)–Cr(3)	129.8(3)
Cr(3)–O(2)–Cr(1) # 2	97.9(2)
Cr(1) # 4–O(2)–Cr(1) # 2	90.7(2)

Symmetry transformations used to generate equivalent atoms: # 1, $-y+1, x-y+1, z$; # 2, $x-y+2/3, -y+4/3, -z+1/3$; # 3, $y-1/3, x+1/3, -z+1/3$; # 4, $-x+y, -x+1, z$; # 5, $-x+2/3, -x+y+1/3, -z+1/3$.

satisfactory structure solution for publication has not been obtained. The best refinement to date reveals the body-centered pentacapped trigonal antiprism core of $Cr_{12}O_{12}$ is maintained (Royer et al., unpublished results).

3.3. NMR spectroscopy

Paramagnetic ^{1}H NMR spectroscopy has been demonstrated to be of utility in the characterization of chromium(III) assemblies [9,13–17] For the d^3 chromic ion in an octahedral crystal field, one unpaired electron lies in each of the t_{2g} orbitals, which are directed between the chromium–ligand bonds. Hence, a π-delocalization mechanism is responsible for the paramagnetic shift in these chromium complexes [18]. The ^{1}H NMR spectrum of **1** contains one large, broad resonance centered at approximately 0.5 ppm (Fig. 3), readily assigned to the pivalate methyl hydrogens, the only hydrogen atoms in the complex. Although examination of the crystal structure reveals three distinct pivalate ligands, the ligands all bridge between two chromium centers and, therefore, have would be expected to have virtually identical chemical shifts if all the chromium centers involved are trivalent. The very small paramagnetic shift is not surprising considering that no good mechanism is available for unpaired electron density to be delocalized onto the ligand; the possibility of a π-delocalization mechanism playing a significant role in electron delocalization from the metal orbitals to the methyl groups of the ligand is negated by the quaternary carbon separating the carboxylate π-system from the methyl protons. Evans method solution susceptibility measurements revealed a magnetic moment per chromium of 3.20 B.M. This is significantly less than the expected spin-only value of 3.87 B.M. if all the centers are Cr(III), suggesting the Cr(III) centers within **1** are antiferromagnetically coupled. This is consistent with the results of variable temperature magnetic susceptibility studies that indicate the complex possesses antiferromagnetically coupled centers and an $S = 6$ ground state [2]. The ^{1}H NMR spectrum for **3** contained one paramagnetically broadened signal centered at 0.8 ppm, again assigned to the methyl protons of the pivalate ligands.

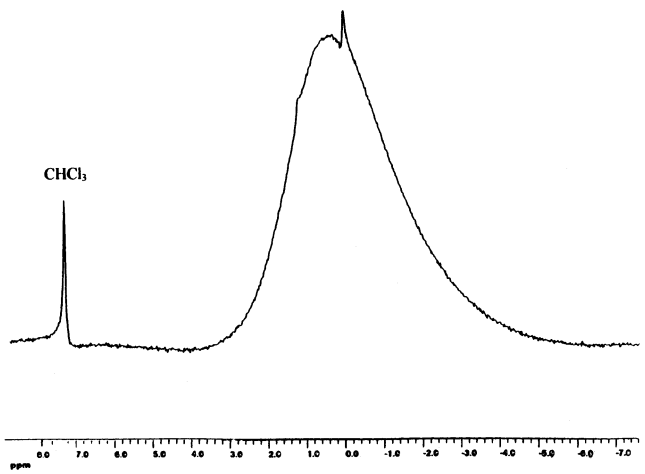


Fig. 3. ^{1}H NMR spectrum of **1** in *n*-propanol.

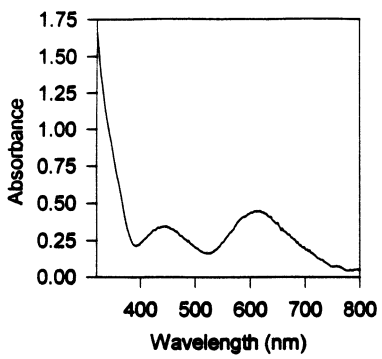


Fig. 4. Electronic spectrum of **1** in *n*-propanol.

The ^{1}H NMR spectrum of **2** contained one paramagneticaly broadened signal centered at 1.2 ppm assigned to the methyl protons of the pivalate ligands; again the lack of an appreciable paramagnetic shift is attributed to a lack of significant π-delocalization of the electron density. Evans method solution susceptibility measurements revealed a magnetic moment per chromium of 3.37 B.M. indicating the chromium atoms within **2** are antiferromagnetically coupled. This value is typical for Cr_3O complexes [8].

3.4. UV–vis spectroscopy

The electronic spectrum of complex **1** in *n*-propanol is shown in Fig. 4. The spectrum contains two major features, with maxima at 444 (ε/Cr = 69) and 616 nm (ε/Cr = 89), and two small shoulders between approximately 750–800 nm. The two strong, broad features at 444 and 616 nm are consistent with spin-allowed d–d transitions for chromic ions in a pseudo-octahedral environment. The two small shoulders between 750 and 800 nm are assigned tentatively to spin-forbidden (spin-flip) transitions that gain intensity from exchange coupling. Notably, there are no features assignable to chromium(IV) [19]. In terms of chromium(VI), oxo to chromium charge transfer bands would be expected, but no such features are observed. Therefore, the electronic spectrum is consistent with **1** possessing 12 chromic ions. The electronic spectrum of complex **3** in *n*-propanol is nearly identical to that of **1**, containing two major features with maxima at 446 and 611 nm.

The electronic spectrum of a saturated solution of complex **2** in acetone contains two major features with maxima at 441 and 590 nm, consistent with spin-allowed d–d transitions for chromic ions in a pseudo-oc-

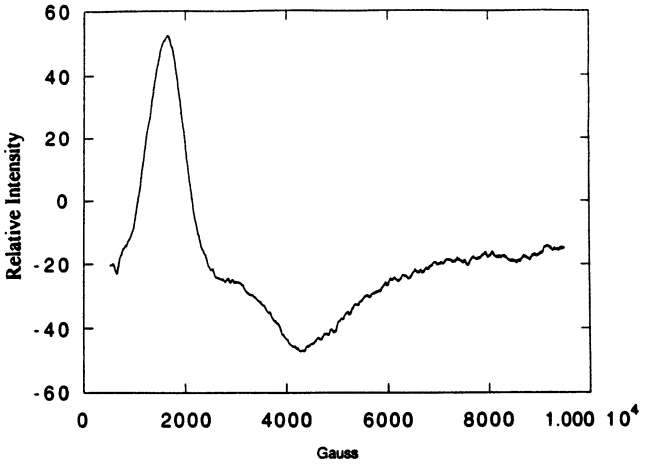


Fig. 5. X-band EPR spectrum of *n*-propanol glass of **1** at 100 K.

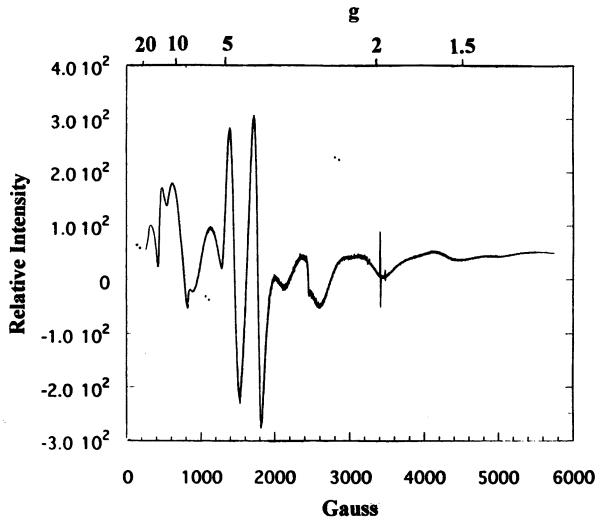


Fig. 6. X-band EPR spectrum of *n*-propanol glass of **1** at ~4 K.

tahedral environment, and three small shoulders at 358, 667, and 715 nm, assigned tentatively to spin-forbidden (spin-flip) transitions which gain intensity from exchange coupling. Because of the poor solubility of the trimer in common solvents, spectra were obtained on saturated solutions, preventing the calculation of extinction coefficients. The spectrum is nearly identical to that of other basic carboxylate type chromic assemblies with terminal oxygen ligands [8].

3.5. EPR spectroscopy

X-band EPR data were collected for complex **1** at 100 K (Fig. 5) and at approximately 4 K (Fig. 6). Twelve Cr(III) centers would give rise to an integer spin system, while the presence of three Cr(IV) or one Cr(VI) in the complex would give rise to half-integer spin systems. The 100 K spectrum, obtained as a saturated *n*-propanol glass, contained one major feature at $g = 3.78$. The 4 K spectrum, also obtained as a saturated *n*-propanol glass, was considerably more complex. Winpenny and co-workers have reported previously the EPR spectrum of the complex at 10 K at 34.11 and 89.21 GHz [2]. The higher field spectrum was simulated successfully assuming an $S = 6$ state. The X-band spectrum at 4 K is consistent with the higher field spectra and the existence of an integer spin-system and, thus, all 12 Cr centers being Cr(III).

3.6. Mass spectrometry

The EI mass spectrum of complex **1** (Fig. 7) contains the molecular ion (2336 mass to charge ratio) with m-(pivalic acid)$_n$ fragmentation signals, where $n = 1$–4, at mass values 2234 (54% intensity relative to the parent ion), 2132 (17%), 2029 (13%), 1928 (36%), respectively. The FAB mass spectrum of **1** confirmed the molecular ion at 2336 mass. This mass is consistent with the exact mass calculated for the complex formula $[Cr_{12}(OH)_3O_9(O_2CC(CH_3)_3)_{15}]$ having three additional protons relative to the originally proposed formula. Although the protonation of species to give positive ions in FAB MS is commonly observed, the mass to charge ratio of 2336 representative of $[Cr_{12}(OH)_3O_9(O_2CC(CH_3)_3)_{15}]$ is reproducible in both the EI and FAB spectra, and signals at 2331, representative of the originally proposed $[Cr_{12}O_{12}(O_2CC(CH_3)_3)_{15}]$, are not observed. The isotopic distribution for the mass ion at 2336 in the FAB spectrum agrees well with values calculated for the formula of the triprotonated complex, $[Cr_{12}(OH)_3O_9(O_2CC(CH_3)_3)_{15}]$, as shown in Fig. 8. Bastanov et al. reported that the mass spectrum of the complex contained the molecular ion and fragments from loss of one to five pivalate ligands. However, the technique used and the mass-to-charge ratios were not reported [1]. Given that the use of two standard techniques gives rise to the molecular ion corresponding to the hydroxide-containing formulation, interpretation of the report of Bastanov et al. (as Bastanov et al. use the formula based on 12 oxide ligands rather than nine oxide ligands and three hydroxo ligands, presumably the molecular ion mass they expect should be three units smaller) is difficult. Winpenny and co-workers have reported electrospray mass spectrometric studies on CH_2Cl_2–methanol solutions of the complex indicate that species of the form $Cr_{12}O_{12-x}(OH)_x(pivalate)_{15}$ were the only significant species present [2]; unfortunately, no other details were presented.

The EI mass spectrum of complex **3** (Fig. 9) reveals the nature of the disorder problem observed in the X-ray studies. While a feature consistent with the triprotonated formula, $[Cr_{12}(OH)_3O_9(O_2CC(CH_3)_3)_{12}(O_2CCCl_3)_3]$ (2519 m/z, 63% intensity relative to the most intense feature) was observed, higher mass ions corresponding to carboxylate ratios ($O_2CC(CH_3)_3$:

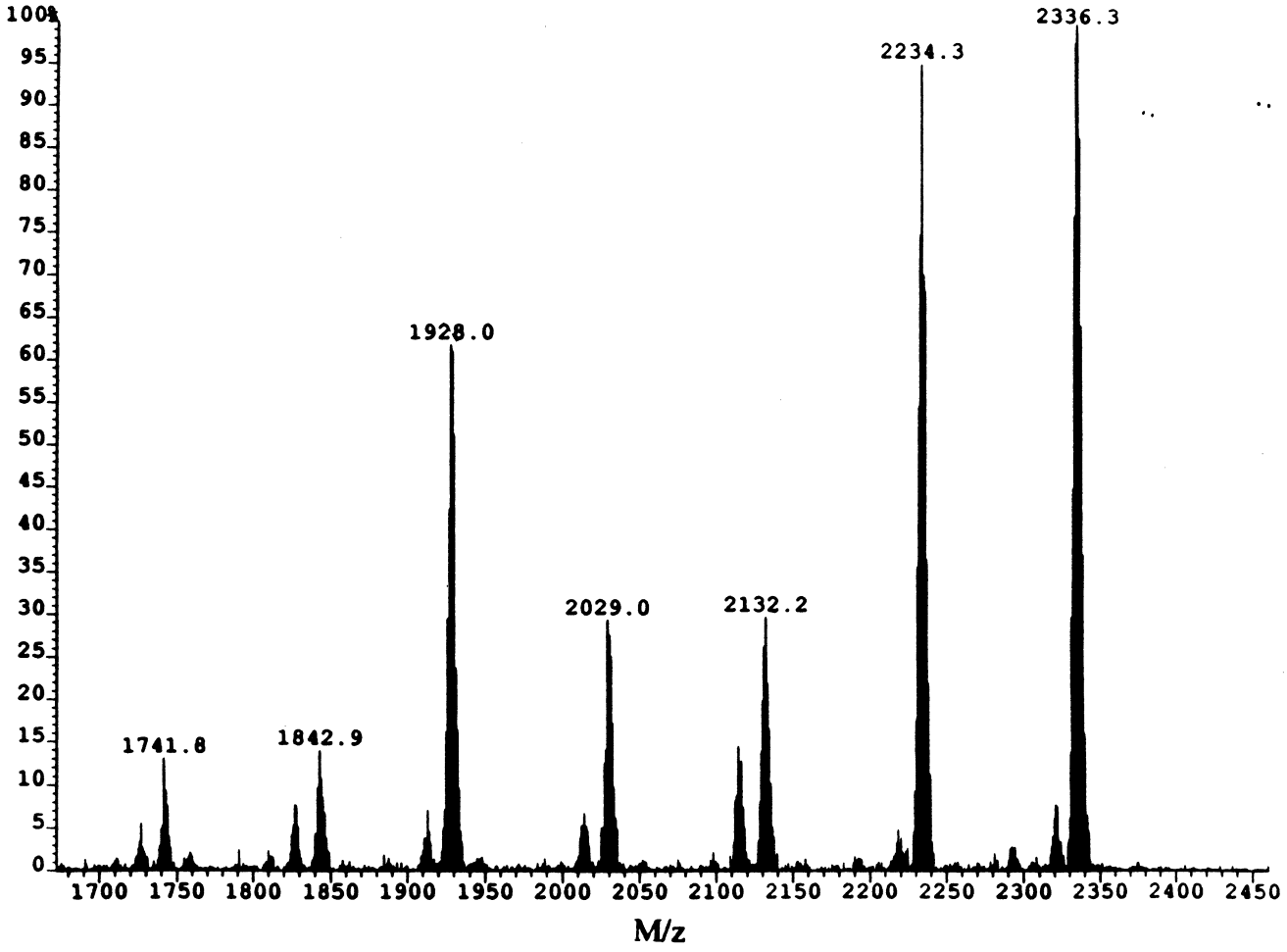


Fig. 7. EI mass spectrum of **1**.

O_2CCCl_3) of 11:4 (2581 m/z, 25%), and 10:5 (2641 m/z, 5%), as well as lower mass ions for ratios of 15:0 (2336 m/z, 31%), 14:1 (2397 m/z, 70%), and 13:2 (2458 m/z, 100%) were also observed. Each of these species produced additional signals resulting from both loss of one pivalate ligand loss or one trichloroacetate ligand. Evaluation of the relative abundance for each of these features revealed an average of 2.08 O_2CCCl_3 ligands in the complex. This difference, from the average number of 2.54 O_2CCCl_3 ligands in the complex from elemental analysis, could be the result of differing gas-phase stability of the various species and/or preferential loss of O_2CCCl_3 or $O_2CC(CH_3)_3$. The isotopic distribution for the mass ion at 2519 also agrees well with that calculated for the formula of the triprotonated complex, $Cr_{12}(OH)_3O_9(O_2CC(CH_3)_3)_{12}(O_2CCCl_3)_3$ (not shown).

The FAB mass spectrum for complex **2** contains the molecular ion, $[Cr_3O(O_2CC(CH_3)_3)_6]^+$ (778 mass), consistent with the proposed structure after loss of the three terminal water ligands. Loss of terminal water

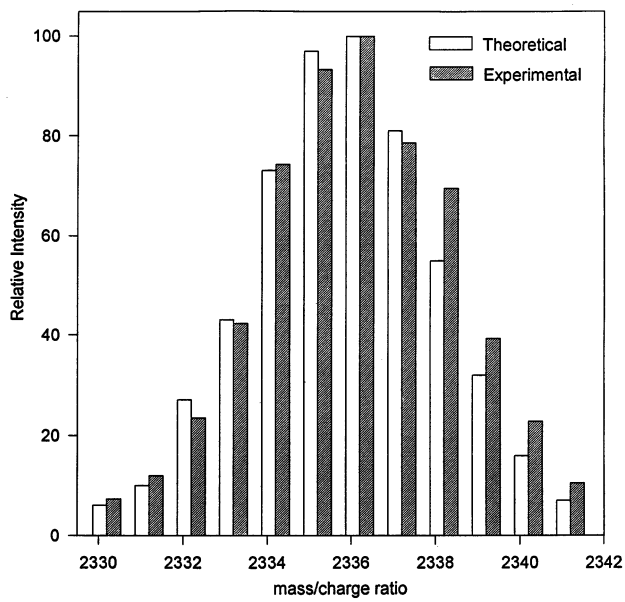


Fig. 8. Comparison of experimental and theoretical isotopic distribution pattern for molecular ion of **1**.

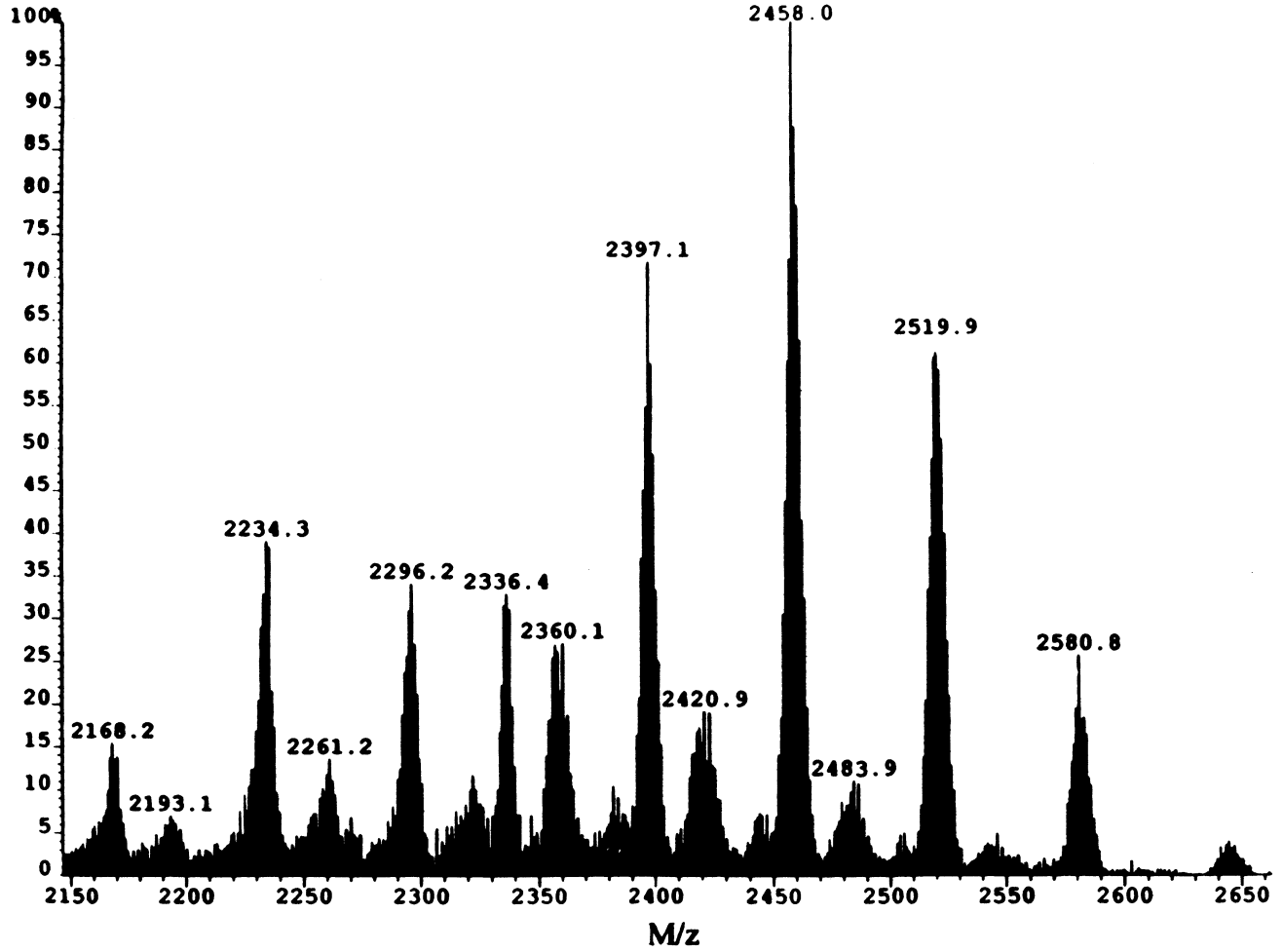


Fig. 9. EI mass spectrum of **3**.

molecules in FAB MS has been observed for other similar trinuclear complexes [20–22]. The spectrum also contains features from m-(pivalic acid)$_n$ fragmentation, where $n = 1–3$; this type of fragmentation has also been observed previously [20,21].

3.7. Photoelectron spectroscopy

The Cr 2p region was analyzed in the high-resolution mode, and the resulting spectrum is shown in Fig. 10. The binding energy value for the $2p_{3/2}$ feature is 576.2 eV (FWHM 3.8 eV). This value is indicative of a mid-range valence state of chromium (Cr^{+3} or Cr^{+4}) [23,24]. There appears to be some small ($< 10\%$) quantity of Cr metal present, probably the result of secondary electron reduction of the Cr under irradiation. This does not affect attribution of the oxidized Cr states. It can be concluded that there is no high valence chromium (Cr^{+6}) in the sample. Distinguishing between the Cr^{+3} and Cr^{+4} states is problematic. The separation between the two would be small (~ 0.5 eV). However, the peak analysis fits a single Gaussian–Lorentzian feature and is entirely consistent with all Cr^{+3} metal centers.

3.8. Infrared spectroscopy

As XPS demonstrated the presence of only chromic ions in **1**, three protons that cannot be observed by X-ray crystallography are necessary for charge balance. Either the triply bridging oxide ligands or bridging pivalate groups could be protonated. The IR spectrum of **1** contains stretches at 1584 (s), 1564 (s), and 1548 (s) cm^{-1} consistent with the symmetric and asymmetric C–O stretches of a bridging carboxylate. There is no evidence for the protonated form, pivalic acid. Thus, the spectrum is consistent with the neutron diffraction studies that indicated the partial protonation of the six symmetry-related triply-bridging oxide ligands. The possible presence of hydroxide ligands is masked by the presence of n-propanol and water solvate. The asymmetric Cr–O stretches expected at approximately 500–600 cm^{-1} are difficult to assign in these systems due to the presence in this region of modes from coordinated

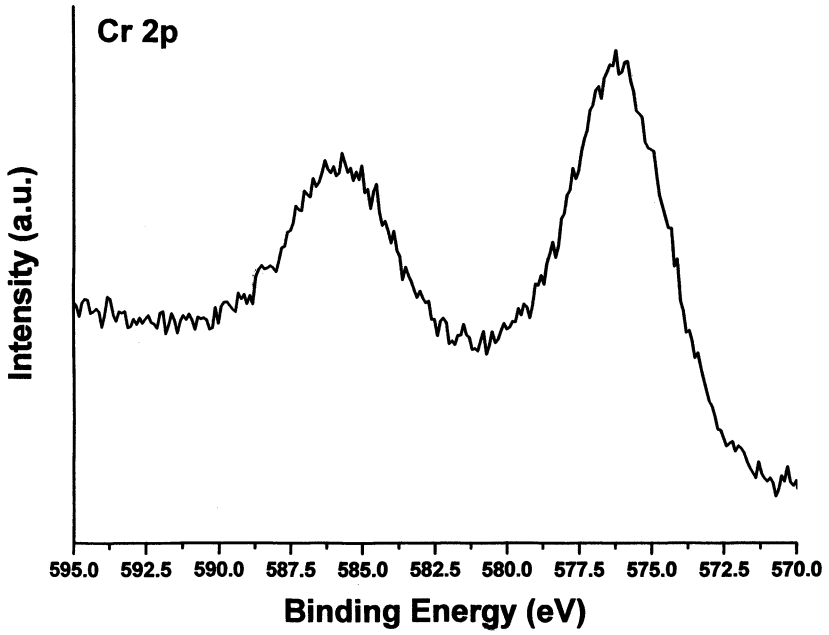


Fig. 10. X-ray photoelectron spectrum of **1**.

carboxylates [25]. The spectrum of the mixed-carboxylate complex (**3**) also displays no absorption in the region of the CO stretches of carboxylic acids.

3.9. Bond valence sum analysis

Finally the simple method of determining oxidation states of metal ions in a coordination complex termed bond valence sum (BVS) analysis was utilized [26]. The analysis in addition to bond lengths from the crystal structure only requires the value of a constant for each bond type (i.e. Cr(III)–O). For compound **1**, only Cr–O bonds are present, and fortunately the necessary constants, R_0, has previously been determined for Cr(II), Cr(III), and Cr(IV) [27]; an average value for approximation of the valence state when the Cr valence is unknown (1.724) has also been determined [27]. The range of calculated valances for the four unique chromium centers in complex **1** is from 2.85 to 3.03, strongly supporting the all Cr(III) oxidation state assignment.

4. Supplementary material

Crystallographic data for the structural analysis of **1** have been deposited with the Cambridge Crystallographic Data center, CCDC No. 164780. Copies of this material may be obtained free of charge from The Director, CCDC, 12 Union Road, Cambridge, CB2 1EZ, UK (fax: +44-1223-336033; e-mail: deposit@ccdc.cam.ac.uk or www: http://www.ccdc.cam.ac.uk).

Acknowledgements

The work was supported by NRICGP/USDA 97-35200-4259 (J.B.V.).

References

[1] A.S. Bastanov, G.A. Timko, Y.T. Struchkov, N.V. Gerbeleu, K.M. Indrichan, Koord. Khim. 17 (1991) 662.
[2] F.E. Mabbs, E.J.L. McInnes, M. Murrie, S. Parsons, G.M. Smith, C.C. Wilson, R.E.P. Winpenny, Chem. Commun. (1999) 643.
[3] D.F. Evans, J. Chem. Soc. (1959) 2003.
[4] SHELXTL, Version 5, Siemens Industrial Automation, Inc., Analytical Instrumentation Business Unit, Madison, WI, 1995.
[5] J.E. Sheats, R.S. Czernuszewicz, G.C. Dismukes, A.L. Rheingold, V. Petroleas, J. Stubbe, W.H. Armstrong, R.H. Beer, S.J. Lippard, J. Am. Chem. Soc. 109 (1987) 1435.
[6] I.M. Atkinson, C. Benelli, M. Murrie, S. Parsons, R.E.P. Winpenny, Chem. Commun. (1999) 285.
[7] W. Clegg, R.J. Errington, D.C.R. Hockless, A.D. Glen, D.G. Richards, J. Chem. Soc., Chem. Commun. (1990) 1565.
[8] R.D. Cannon, R.P. White, Prog. Inorg. Chem. 36 (1988) 195.
[9] M.K. Nagi, A. Harton, S. Donald, Y.-S. Lee, M. Sabat, C.J. O'Connor, J.B. Vincent, Inorg. Chem. 34 (1995) 3813.
[10] A. Bino, R. Chayat, E. Pederson, A. Schneider, Inorg. Chem. 30 (1991) 856.
[11] A.S. Batsanov, Y.T. Struchkov, N.V. Gerbeleu, G.A. Timko, O.S. Manole, Koord. Khim. 20 (1994) 833.
[12] C.E. Anson, N. Chai-Sa'ard, J.P. Bourke, R.D. Cannon, U.A. Jayasooriya, A.K. Powell, Inorg. Chem. 32 (1993) 1502.
[13] A. Harton, K. Terrell, J.C. Huffman, C. MacDonald, A. Beatty, S. Li, C.J. O'Connor, Inorg. Chem. 36 (1997) 4875.
[14] T. Ellis, M. Glass, A. Harton, J.C. Huffman, J.B. Vincent, Inorg. Chem. 33 (1994) 5522.
[15] S. Donald, K. Terrell, K. Robinson, J.B. Vincent, Polyhedron 14 (1995) 971.

[16] M.M. Glass, K. Belmore, J.B. Vincent, Polyhedron 12 (1993) 133.
[17] K. Belmore, X.J. Madison, A. Harton, J.B. Vincent, Spectrochim. Acta 50A (1994) 2365.
[18] K.F. Kingry, A.C. Royer, J.B. Vincent, J. Inorg. Biochem. 72 (1998) 79.
[19] A.B.P. Lever, Inorganic Electronic Spectroscopy, second ed., Elsevier, New York, 1984.
[20] A. Harton, M.C. Nagi, M.M. Glass, P.C. Junk, J.L. Atwood, J.B. Vincent, Inorg. Chim. Acta 217 (1994) 171.
[21] J.B. Vincent, Inorg. Chem. 33 (1994) 5604.
[22] A. van den Bergen, R. Colton, M. Percy, B.O. West, Inorg. Chem. 32 (1993) 3408.
[23] A.M. Salvi, J.E. Castle, J.F. Watts, E. Desimoni, Appl. Surf. Sci. 90 (1995) 333.
[24] J.F. Moulder, W.F. Stickle, P.E. Sobol, K.D. Bomben (Eds.), Handbook of X-ray Photoelectron Spectroscopy, Physical Electronics, Eden Prairie, MN, 1995.
[25] W.P. Griffith, J. Chem. Soc. (1969) 2270.
[26] M. O'Keefe, N.E. Brese, J. Am. Chem. Soc. 113 (1991) 3226 and references therein.
[27] R.M. Wood, K.A. Abboud, R.C. Palenik, G.J. Palenik, Inorg. Chem. 39 (2000) 2065.

PERGAMON

Polyhedron 21 (2002) 167–173

POLYHEDRON

www.elsevier.com/locate/poly

Complex formation equilibria of palladium(II) complexes involving *N*,*N*′-dimethylethylenediamine, DNA constituents and cyclobutane dicarboxylic acid. The catalysis of glycine methyl ester hydrolysis through complex formation

Mahmoud M.A. Mohamed [a], Mohamed M. Shoukry [b,*]

[a] *Department of Chemistry, Faculty of Education, Assuit University, New Valley, Egypt*
[b] *Department of Chemistry, Faculty of Science, Cairo University, Giza, Egypt*

Received 1 June 2001; accepted 24 September 2001

Abstract

Mixed-ligand complex formation equilibria of Pd(Me_2en)–CBDCA–DNA constituent have been investigated (Me_2en = *N*,*N*′-dimethylethylenediamine, CBDCA = cyclobutane dicarboxylic acid). The results show ring opening of CBDCA and monodentate complexation of the DNA constituent. Stoichiometries and stability constants of the complexes were determined at 25 °C and at constant 0.1 M ionic strength. The kinetics of base hydrolysis of glycine methyl ester in presence of $Pd(Me_2en)^{2+}$ complex was studied in aqueous solution at different temperatures, and in dioxane–water solutions of different compositions at 25 °C. © 2002 Elsevier Science Ltd. All rights reserved.

Keywords: Palladium(II) complexes; Bioligands; Glycine methyl ester hydrolysis

1. Introduction

cis-Platin, *cis*-diammine dichloroplatinum(II), is one of the most effective anticancer agents that are clinically active to solid tumors [1,2]. Cytotoxicity of this drug is regarded as the consequence of making a covalent 1,2-intrastrand adduct with N_7 of the guanine base of DNA.

Carboplatin, *cis*-diammine(1,1-cyclobutanedicarboxylate)platinum(II), is a widely used second-generation platinum anticancer drug [3]. It has less side effects than *cis*-platin [4]; for example, it does not cause the loss of high frequency hearing, or have significant renal or neural toxicity. This is attributed to lower reactivity of carboplatin due to the presence of the bidenate-chelated bis(carboxylato)ligand [5]. Some workers have suggested that carboplatin is merely a pro-drug for *cis*-platin [6], whereas others have postulated a ring-opening reactions [7] of carboplatin followed by reaction with guanosine 5′-monophosphate (5′-GMP) forming *cis*-[$Pt(NH_3)_2$(CBDCA-O)(5′-GMP)]. The ring opening reaction with DNA constituent was investigated from the kinetic point of view through studies of [Pd(amine)(CBDCA) with inosine 5′-monophosphate [8].

In order to save the inert kinetics of Pt(II) complexes and on the basis of the remarkable analogy of Pt(II) and Pd(II) coordination chemistry a variety of Pd(II) complexes have proved useful as models to obtain a reasonable view on the thermodynamic aspects of the reactions for closely related Pt(II) ones.

Work in our laboratory has focused on studies of complex formation of model (amine)palladium(II) complexes with bioligands [9–13]. We have recently studied the reaction of $[Pd(Me_2en)(H_2O)_2]^{2+}$ with amino acid, peptide and DNA constituent [14], and now we are concentrating our effort to study the ring opening of chelated CBDCA and monodentate chelation of DNA components in the Pd(Me_2en)–CBDCA–DNA system. Also, the hydrolysis of glycine methyl ester through

* Corresponding author. Tel.: +20-2-567-6562; fax: +20-2-572-7556.
E-mail address: shoukry@chem-sci-cairo.eun.eg (M.M. Shoukry).

0277-5387/02/$ - see front matter © 2002 Elsevier Science Ltd. All rights reserved.
PII: S0277-5387(01)00958-5

complex formation with $[Pd(Me_2en)(H_2O)_2]^{2+}$ was also investigated in dioxane–water solutions of different composition and at different temperatures.

2. Experimental

The complex $[Pd(Me_2en)Cl_2]$ was prepared as described [14]. The diaqua-complex $[Pd(Me_2en)(H_2O)_2](NO_3)_2$ was prepared in solution by stirring the chloro-complex with 2 equiv. of $AgNO_3$ overnight (with careful protection from light). The precipitated AgCl was removed by filtration and the filtrate was made up to the required volume in a standard flask. The glycine methyl ester hydrochloride was purchased from Fluka and converted to the corresponding hydronitrate by stirring with 1 equiv. of $AgNO_3$, filtering off the precipitated AgCl and making up to the desired volume in a standard flask. The ligands used were cyclobutane dicarboxylic acid, methylamine, imidazole, potassium dihydrogen phosphate (KH_2PO_4) and DNA constituents as inosine, uracil, uridine, thymine, thymidine. These materials were obtained from Sigma Chemicals Co.

Potentiometric measurements were made using a Metrohm 686 titroprocessor equipped with a 665 Dosimat. The electrode and titroprocessor were calibrated with standard buffer solutions prepared according to NBS specifications [15]. The pH meter readings were converted into hydrogen concentration by titrating a standard acid solution (0.01 M), the ionic strength of which was adjusted to 0.1 M with $NaNO_3$, with standard base (0.10 M) at 25 °C. The pH is plotted against p[H]. The relationship $pH - p[H] = 0.05$ was observed. The kinetics of hydrolysis was monitored using the titroprocessor operated with (SET) mode.

2.1. Kinetic measurements

Hydrolysis kinetics of glycine methyl ester (MeGly) in the presence and absence of $[Pd(Me_2en)(H_2O)_2]^{2+}$ was investigated by pH-stat techniques [16]. Hydrolysis of MeGly (1.25 mM) in the presence of the Pd(II) complex of equimolar molar concentration was studied at different temperatures (20–35 °C) and at 25 °C in dioxane–water solutions of different compositions. All solutions have a constant ionic strength 0.1 M $NaNO_3$.

After equilibrating $[Pd(Me_2en)(H_2O)_2]^{2+}$ solution at the required temperature under nitrogen flow, a solution of ester was added and the pH brought to the desired value by the addition of 0.05 M NaOH solution. The hydrolysis was then followed by the automatic addition of 0.05 M NaOH solution to maintain the given pH. The data fitting was performed with the OLIS KINFIT set of programs as described previously [17].

2.2. Equilibrium measurements

The acid dissociation constants of the ligands were determined by titrating 40 ml of ligand solution (1.25 mM). The formation constants of the complexes Pd(Me_2en)–(CBDCA)–(DNA) were determined by titrating solution mixtures of $[Pd(Me_2en)(H_2O)_2](NO_3)_2$ (1.25 mM), CBDCA and DNA constituents in concentration ratios of 1:1:1, 1:2:1 and 1:1:2. The titrating solution mixtures had a volume of 40 ml. The titrations were carried out at 25 °C by circulating thermostated water into the appropriate reaction cell and a slow and constant stream of N_2 passed over the test solution. The ionic strength was adjusted by $NaNO_3$ (0.1 M). A 0.05 M NaOH solution was used as titrant.

The equilibrium constants evaluated from the titration data (summarized in Table 1) are defined by Eqs. (1) and (2), where M, C, D and H stand for the $[Pd(Me_2en)(H_2O)_2]^{2+}$ ion, cyclobutane dicarboxylate, DNA constituent and proton, respectively.

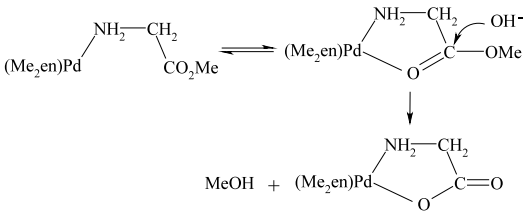
$$lM + pC + qD + rH \rightleftharpoons [M_lC_pD_qH_r] \quad (1)$$

$$\beta_{lpqr} = \frac{[M_lC_pD_qH_r]}{[M]^l[C]^p[D]^q[H]^r} \quad (2)$$

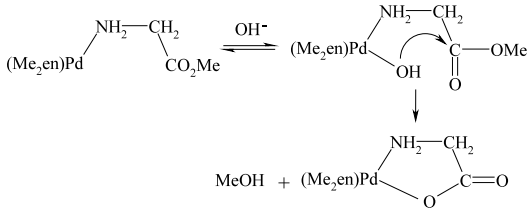
The calculations were obtained from ≈ 150 data points in each titration using the computer program [18] MINIQUAD-75. The stoichiometries and stability constants of the complexes formed were determined by trying various possible composition models. The model selected gave the best statistical fit and was chemically consistent with the titration data without giving any systematic drifts in the magnitudes of various residuals, as described elsewhere [18]. The accepted model was tested by comparing the experimental titration data with the theoretically simulated curve calculated from the acid dissociation constants of the ligand and formation constants of the complexes. The species distribution diagrams were obtained using the program SPECIES [19] under the experimental conditions used. The hydrolysis of the coordinated ester $[Pd(Me_2en)(ester)]^{2+}$ is monitored over the pH range 4.2–4.8. In this pH range the hydrolysis of free ester is negligible, as the free ester starts to hydrolyze above pH 10 [20]. The results are summarized in Tables 2–6.

3. Results and discussion

The hydrolysis of coordinated glycine methyl ester may proceed by mechanism (3) and/or mechanism (4). The first mechanism involves an initial rapidly established equilibrium in which the carbonyl oxygen of the ester group coordinates, followed by a rate-determining attack by OH^- (Eq. (3)).



(3)



(4)

The second mechanism involves rapid equilibrium formation of a Pd–OH complex, followed by intramolecular OH^- attack (Eq. (4)).

The kinetic data, the volume of base added to keep the pH constant versus time, could be fitted by one exponential as shown in Fig. 1. Various other kinetic

Table 1
Formation constants of $M_lC_pD_qH_r$ species [a]

System	l	p	q	r [b]	log β [c]
Pd(Me_2en)–OH	1	0	0	−1	−5.54(0.05)
	1	0	0	−2	−15.01(0.01)
	2	0	0	−2	−7.90(0.07)
1,1-Cyclobutane dicarboxylic acid	0	1	0	1	5.42(0.00)
	0	1	0	2	8.06(0.01)
	1	1	0	0	7.17(0.01)
	1	1	0	1	9.44(0.03)
Imidazole	0	0	1	1	7.04(0.01)
	1	0	1	0	7.92(0.06)
	1	0	2	0	14.64(0.04)
	1	1	1	0	14.20(0.10)
Methylamine	0	0	1	1	10.03(0.04)
	1	0	1	0	7.64(0.03)
	1	0	2	0	13.46(0.06)
	1	1	1	0	16.57(0.10)
KH_2PO_4	0	0	1	1	6.66(0.01)
	1	0	1	0	4.50(0.03)
	1	1	1	0	12.83(0.01)
Inosine	0	0	1	1	8.43(0.01)
	1	0	1	0	8.03(0.02)
	1	0	2	0	12.74(0.01)
	1	1	1	0	12.29(0.09)
	1	1	1	1	17.72(0.10)
Uridine	0	0	1	1	9.02(0.01)
	1	0	1	0	8.70(0.01)
	1	0	2	0	14.37(0.03)
	1	1	1	0	15.17(0.09)
Uracil	0	0	1	1	8.83(0.01)
	1	0	1	0	8.35(0.01)
	1	0	2	0	14.88(0.02)
	1	1	1	0	16.18(0.09)
Thymine	0	0	1	1	9.30(0.01)
	1	0	1	0	8.56(0.01)
	1	0	2	0	15.14(0.02)
	1	1	1	0	15.71(0.08)
Thymidine	0	0	1	1	9.28(0.01)
	1	0	1	0	8.75(0.01)
	1	0	2	0	14.53(0.02)
	1	1	1	0	16.26(0.10)

[a] Literature pk_a value [21] of KH_2PO_4 is 6.72. The pK_a of other ligands were taken from Ref. [14].
[b] The values l, p, q and r are the stoichiometric coefficients corresponding to Pd–Me_2en, cyclobutane 1,1′-dicarboxylate, DNA and H^+, respectively.
[c] Standard deviations are given in parentheses.

Table 2
Kinetics of hydrolysis of the coordinated glycine methyl ester at different temperatures in aqueous solution

Temperature	pH	10^{10} [OH] [a] (mol dm^{-3})	10^4 k_{obs} (s^{-1})
20	4.20	1.07	1.51
	4.40	1.70	1.90
	4.60	2.69	2.56
	4.80	4.27	3.48
25	4.20	1.58	2.39
	4.40	2.51	3.20
	4.60	3.98	4.25
	4.80	6.31	5.73
30	4.20	2.34	3.26
	4.40	3.72	4.30
	4.60	5.89	5.83
	4.80	9.33	8.70
35	4.20	3.31	4.10
	4.40	5.25	5.60
	4.60	8.32	7.80
	4.80	13.20	12.5

[a] pK_w 14.17 at 20 °C; 14.00 at 25 °C; 13.83 at 30 °C and 13.68 at 35 °C. These data were taken from Ref. [22].

Table 3
Kinetics of hydrolysis of the glycine methyl ester in different dioxane–water solutions of different compositions at 25 °C

Dioxane (%)	pH	10^5 [OH] [a] (mol dm^{-3})	$10^5 \times k_{obs}$ (s^{-1})
12.5	10.00	5.25	5.70
	10.25	9.33	6.24
	10.50	16.60	6.93
	10.75	29.50	7.99
25.0	10.00	1.90	4.79
	10.25	3.39	5.10
	10.50	6.03	5.90
	10.75	10.70	6.89
37.5	10.00	0.74	3.90
	10.25	1.32	4.20
	10.50	2.34	4.90
	10.75	4.17	5.80
50	10.00	0.35	3.50
	10.25	0.62	3.90
	10.50	1.10	4.40
	10.75	1.95	5.28
62.5	10.00	0.12	4.47
	10.25	0.36	4.90
	10.50	0.63	5.50
	10.75	1.22	6.50

[a] pK_w are 14.28, 14.72, 15.13, 15.46 and 15.70 for 12.5, 25.0, 37.5, 50.0 and 62.5% dioxane in water, respectively. These data were taken from Ref. [23].

models were tested without leading to satisfying fits of the data. Plots of k_{obs} versus the hydroxide ion concentration is linear, Fig. 2. The rate expression can therefore be given in the form, Fig. 5. The k_o term arises from the attack by water.

$$\text{Rate} = k_{obs}[\text{Pd(DME)(ester)}]$$

$$k_{obs} = k_o + k_{OH}[\text{OH}] \quad (5)$$

The linear dependence of rate on the OH^- concentration is consistent with the direct attack of OH^- ion on the coordinated ester carbonyl group as given in mechanism (3). On the other hand mechanism (4) requires that the plot of k_{obs} versus the hydroxide ion concentration is not linear. The catalysis ratio ($C = k_{OH}/k_{OH}^{ester}$) is calculated and found to be approximately

Table 4
Kinetics of hydrolysis of the coordinated glycine methyl ester in dioxane–water solutions at different compositions at 25 °C

Dioxane (%)	pH	10^{11} [OH] (mol dm^{-3})	$10^4 \times k_{obs}$ (s^{-1})
12.5	4.20	8.32	1.93
	4.40	13.20	2.62
	4.60	20.90	3.50
	4.80	33.10	4.69
25.0	4.20	3.02	1.47
	4.40	4.79	1.98
	4.60	7.59	2.75
	4.80	1.20	3.52
37.5	4.20	1.17	1.20
	4.40	1.86	1.46
	4.60	2.95	2.02
	4.80	4.68	2.65
50	4.20	0.55	0.98
	4.40	0.87	1.28
	4.60	1.38	1.70
	4.80	2.19	2.33
62.5	4.20	0.32	0.85
	4.40	0.50	1.04
	4.60	0.79	1.45
	4.80	1.26	2.01

Table 5
Rate constants (k/dm^3 mol^{-1} s^{-1}) for base hydrolysis of free and coordinated glycine methyl ester in dioxane–water solutions of different compositions at 25 °C

Dioxane (% V/V)	$10^{-5} \times k_{OH}$ (coord. ester)	$10^5 \times k_o$	$10^2 \times k_{OH}$ (free ester)	$10^6 \times C$
12.5	11.00	11.00	9.24	11.9
25.0	22.70	8.70	24.24	9.8
37.5	41.90	7.10	55.99	7.5
50.0	81.70	5.50	108.85	7.5
62.5	124.00	4.50	185.31	6.7

Table 6
Rate constants (k/dm^3 mol^{-1} s^{-1}) for base hydrolysis of coordinated glycine methyl ester at different temperatures

Temperature	$10^4 \times k_o$	$10^{-5} \times k_{OH}$
20	0.86	5.60
25	1.49	6.98
30	1.30	7.76
35	1.10	8.47

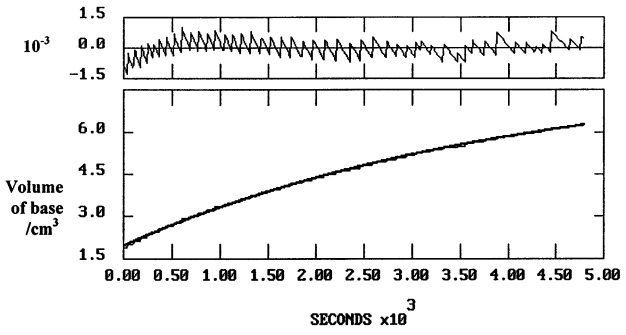


Fig. 1. Typical value of the base–time trace for the hydrolysis of coordinated glycine methyl ester fitted with one exponential function. The top of the figure shows the value of base difference between measured and calculated kinetics trace.

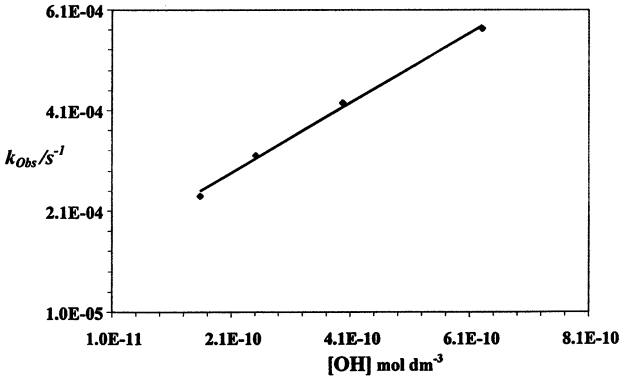


Fig. 2. Plots of k_{obs} vs. [OH^-] for the hydrolysis of coordinated glycine methyl ester in water solution at 25 °C.

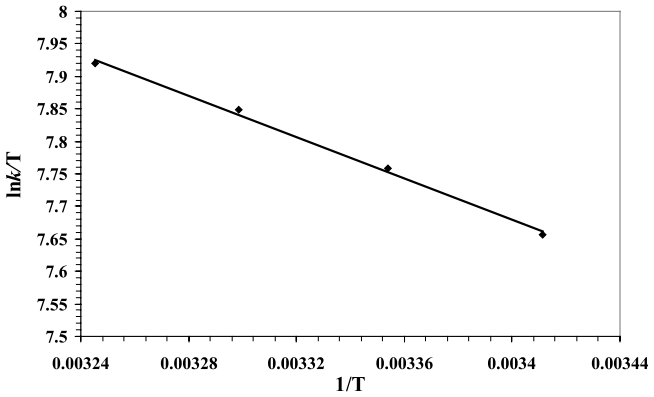


Fig. 3. Plots of $\ln k_{OH}$ vs. $1/T$ for the hydrolysis of coordinated of glycine methyl ester.

10^7, Table 5. The relatively high catalysis ratio is also consistent with the proposed mechanism.

The activation parameters for the hydrolysis of coordinated ester were determined using the Eyring plot of ($\ln k_{OH}/T$) versus $1/T$, Fig. 3, from which the values of $\Delta H^{\pm} = 13.2 \pm 0.4$ kJ mol^{-1}, $\Delta S^{\pm} = -88.7 \pm 0.5$ J K^{-1} mol^{-1} were calculated. For base hydrolysis of free glycine methyl ester the activation parameters were found [23] to be $\Delta H^{\pm} = 39.7$ kJ mol^{-1} and $\Delta S^{\pm} = -117$ J K^{-1} mol^{-1}. The enhanced rate for base hydrolysis of the ester incorporated in the complex is therefore due to contributions from a decreased $\Delta H^{\pm}$ and an increased $\Delta S^{\pm}$. The large increase in $\Delta S^{\pm}$ implies desolvation between the ground and transition states and is indicative of a mechanism involving nucleophilic attack by external OH^- on the complexed ester group as shown in mechanism (3).

Comparative values of k_{OH} [24] at 25 °C for the glycine methyl ester incorporated in $[Pd(en)L]^{2+}$ and $[Pd(Bpy)L]^{2+}$ are 6.3×10^4 and 2.0×10^5 dm^3 mol^{-1} s^{-1}, respectively. The k_{OH} value for $[Pd(Me_2en)L]^{2+}$ is lower than those of other Pd(II) complexes. This may be due to the steric interaction between the ester and the methyl substituent group of the amine. The high reactivity of $[Pd(Bpy)L]^{2+}$ complex is due to π-acceptor property of the pyridine ring, leading to an increase of electrophilicity of the metal center.

It is known that solutions in biochemical micro-environments such as active sites of enzymes and side chain in proteins have dielectric constant values of 30–50 [25–27]. It was suggested that these properties approximately correspond to those (or can be simulated by those) existing in the water–dioxane mixtures. Consequently, investigation of amino acid ester hydrolysis in water–dioxane mixture is of biological significance.

In order to examine the effect of organic solvent on the hydrolysis of the ester, the rate constants for the hydrolysis of free and coordinated ester were determined in various dioxane–water solutions of different compositions. The rate constant values are given in Table 5. The rate constant k_{OH} increases with increasing amount of dioxane. This may be explained on the premise that as the dioxane content increases the dielectric constant of the solution medium decreases. This will favor the interaction of negatively charged OH^- ion with the electropositive carbonyl carbon atom of

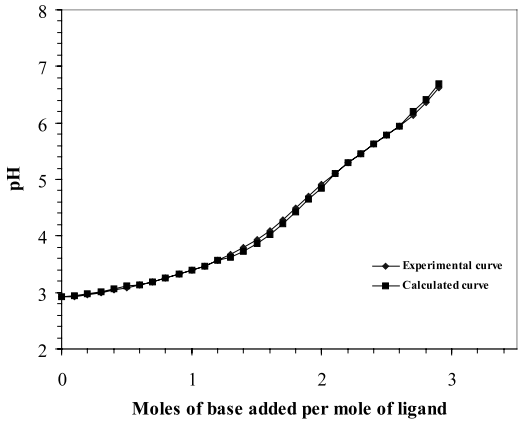


Fig. 4. Potentiometric titration curve of the Pd(DME)–CBDCA–inosine system.

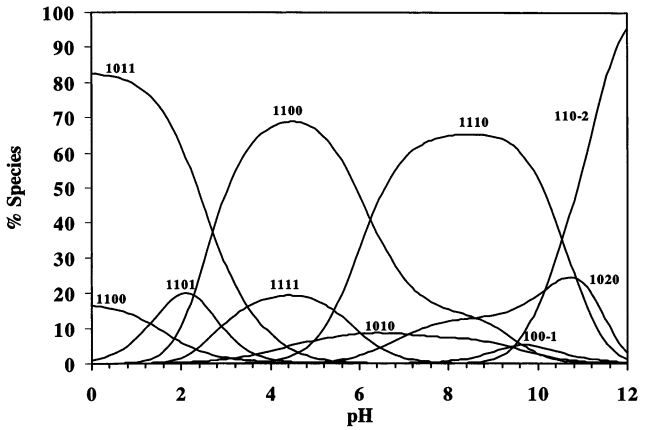


Fig. 5. Species distribution of various species as a function of pH in the Pd(DME)–CBDCA–inosine system (at concentration of 1.25 mM of each).

the ester. Consequently the hydrolysis will proceed faster.

3.1. Equilibrium studies

The potentiometric data of the system consisting of $[Pd(Me_2en)(H_2O)_2]^{2+}$, CBDCA and DNA constituent were fitted assuming the formation of the complexes of 1110 with uracil, uridine, thymine and thymidine. In addition to 1110 species inosine forms the species 1111. This result was verified by comparing the experimental potentiometric data with the theoretically calculated curve. Fig. 4 represents such a comparison for the inosine system. The experimental data coincide with the theoretical curve. This supports the formation of the quaternary complex.

The pyrimidines uracil, uridine, thymine and thymidine have only basic nitrogen (N_3). Consequently the pyrimidines ligate in the deprotonated form through this site and they do not form protonated complexes. Inosine has two binding centers N_1 and N_7 nitrogens. The pH-dependent binding of these *N*-donors has already been reported. The results showed that inosine forms the complexes 1110 and 1111. The species 1111 is formed in the acidic pH region and it corresponds to a N_7 coordinated complex, while the N_1 nitrogen is in a protonated form. The pK_a of the protonated form ($\log \beta_{1111} - \log \beta_{1110}$) amounts to 5.43. The lowering of pK_a of N_1H upon coordination was reported previously [28].

The ring opening reaction of carboplatin with 5′-GMP was characterized by NMR [29]. These studies conclude that CBDCA is attached through one carboxylate oxygen and 5′-GMP through N_7 of the purine base. Also such a reaction for [Pd(en)(CBDCA)] with thiourea, inosine 5′-monophosphate or iodide was mechanistically investigated [8].

It should be recognized that further studies are necessary to elucidate the ring opening of chelated CBDCA by DNA constituents, especially multinuclear NMR measurements. These aspects will be considered in future investigations.

Estimation of the concentration distribution of the various species in solution provides a useful picture of metal ion binding. To illustrate the main features observed in the species distribution plots in these systems the speciation diagram obtained for the $Pd(Me_2en)$–CBDCA–inosine system is shown in Fig. 5. The $Pd(Me_2en)$–CBDCA species (1100) predominates with a formation degree of 68% at pH 4.4. The $Pd(Me_2en)$–inosine species (1010) reaches the maximum concentration of 8% at pH 6.4. The quaternary species $Pd(Me_2en)$–CBDCA–inosine species (1110) attains a maximum of 60% in the pH range 7.6–8.8. This reveals that in the physiological pH range the ring opening of chelated CBDCA by DNA is quite feasible.

References

[1] B. Rosenberg, Cancer Chemother., Part 1 54 (1977) 739.
[2] J.P. Davidson, P.J. Faber, R.G. Fischer IV, S. Mansy, H.J. Peresie, B. Rosenberg, A.L. van Camp, Cancer Chemother., Part 1 59 (1975) 287.
[3] M. Nicolini (Ed.), Platinum and Other Metal Complexes in Cancer Chemotherapy, M. Martinus, Boston, MA, 1988.
[4] A.J. Wagstaff, A. Ward, P. Benfield, R.C. Heel, Drugs 37 (1989) 162.
[5] S. Neidle, I.M. Ismail, P.J. Sadler, J. Inorg. Biochem. 13 (1980) 205.
[6] N.D. Tinker, H.L. Sharma, C.A. McAuliffe, in: M. Nicolini (Ed.), Platinum and Other Metal Coordination Compounds in Cancer Chemotherapy, N. Martinus, Boston, MA, 1988.
[7] L. Canovese, L. Cattalini, G. Chessa, M.L. Tobe, J. Chem. Soc., Dalton Trans. (1988) 2135.
[8] A. Shoukry, T. Rau, M. Shoukry, R. van Eldik, J. Chem. Soc., Dalton Trans. (1998) 3105.
[9] M.M. Shoukry, H. Hohmann, R. Van Eldik, Inorg. Chim. Acta 198 (1992) 187.
[10] M.M. Shoukry, R. van Eldik, J. Chem. Soc., Dalton Trans. (1998) 2673.
[11] M.M. Shoukry, I.M. Kenawy, I.H. El-Haj, Transition Met. Chem. 16 (1991) 637.
[12] M.M. Shoukry, E.M. Khairy, A. Saeed, J. Coord. Chem. 17 (1988) 305.
[13] S.M. El-Medani, S.M. Shohayeb, M.M. Shoukry, Transition Met. Chem. 23 (1998) 287.
[14] M.M.A. Mohamed, M.M. Shoukry, Polyhedron 20 (2001) 343.
[15] R.G. Bates, Determination of pH—Theory and Practice, 2nd ed., Wiley Interscience, New York, 1975.
[16] R.W. Hay, C. You-Quan, Polyhedron 14 (1995) 869.
[17] OLIS KINFIT, Olis Inc., Bogart, GA.
[18] P. Gans, A. Sabatini, A. Vacca, Inorg. Chim. Acta 18 (1976) 237.
[19] L. Pettit, Personal Communication, University of Leeds.
[20] R.W. Hay, L.J. Porter, J. Chem. Soc., B (1967) 1261.
[21] M.L. Escoda, F. de la Torre, V. Salvado, Polyhedron 18 (1999) 2369.

[22] O. Al-Flaijj, M.R. Shehata, M.M.A. Mohamed, M.M. Shoukry, Monatsh. Chem. 132 (2001) 349.
[23] R.W. Hay, P.J. Morris, in: H. Sigel (Ed.), Metal Ions in Biological Systems, vol. 5, Marcel Dekker, New York, 1976, p. 173.
[24] R.W. Hay, A.K. Basak, J. Chem. Soc., Dalton Trans. (1982) 1819.
[25] O.O. Rees, J. Mol. Biol. 141 (1980) 323.
[26] N.K. Rogers, G.R. Roore, M.J.E. Strenberg, J. Mol. Biol. 182 (1985) 613.
[27] H. Sigel, R.B. Martin, R. Tribolet, U.K. Haring, R. Molini-Balakrish, Eur. J. Biochem. 152 (1985) 187.
[28] H. Sigel, S.S. Massoud, N.A. Corfu, J. Am. Chem. Soc. 116 (1994) 2958.
[29] U. Frey, J.D. Ranford, P.J. Sadler, Inorg. Chem. 32 (1993) 1333.

PERGAMON

Polyhedron 21 (2002) 175–179

POLYHEDRON

www.elsevier.com/locate/poly

Synthesis, structure and fluorescence of a 3-D polymer $\{(Mo_4O_{12})(4,4'\text{-bipy})_2\}_n$

Chuan-Peng Cui, Jing-Cao Dai, Wen-Xin Du, Zhi-Yong Fu, Sheng-Min Hu, Li-Ming Wu, Xin-Tao Wu *

State Key Laboratory of Structural Chemistry, Fujian Institute of Research on the Structure of Matter, Chinese Academy of Sciences Fuzhou, Fujian 350002, China

Received 15 June 2001; accepted 5 October 2001

Abstract

We report the synthesis, single-crystal X-ray structure, IR, TGA–DTA and fluorescence of a black MOF crystal $\{(Mo_4O_{12})(4,4'\text{-bipy})_2\}_n$, which has two channels. One channel along the [001] direction was formed by a metal–oxygen octatomic ring and the another one along the [010] direction was shaped by 4′4-bipy. © 2002 Elsevier Science Ltd. All rights reserved.

Keywords: Metal-organic frameworks (MOF); Synthesis; Crystal structures; TGA–DTA

1. Introduction

Enormous efforts have recently been made in synthesizing new coordination polymers with 1-D, 2-D, 3-D structures [1]. Incorporation of both organic and inorganic components in these compounds has created a new dimension in the search for functional materials that have desired structure and properties [2]. The significance of composite metal-organic frameworks organic/inorganic micro/meso porous solid-state material engineering [3], is based on their potential applications in catalysis [4], magnetism [5], photochemistry [6] and ion-exchange [7]. Using the organic ligands and inorganic ions for design and research of novel structures with micro/meso pores is our interest. The poly-functional rod-like ligand 4,4-bipy is an effective tether for construction of extended solids with diverse topologies [8], such as linear chain $[Cu(4,4'\text{-bipy})]^{+1}$, zigzag chain $\{Zn(SPh)_2(\mu\text{-bipy})\}_n$ [9], square or rectangular grids [M(bipy)] ($M = Zn^{2+}$ or Fe^{2+}; bipy = 4,4′-bipyridyl) [10], ladder $[Zn(4,4'\text{-bipy})(H_2O)_3(ClO_4)]^{+1}$ [11], diamondoid [12], honeycomb [13], T-shaped [14], brick wall [15] and molecular bilayer [16], etc.

Zubieta and coworkers have synthesized a series of molybdenum oxide organo-diamine compounds, such as: (i) a simple counter-ion compound as in $[4,4'\text{-bipyH}_2][Mo_7O_{22}]$ [17]; (ii) ligands covalently bound to the molybdenum oxide skeleton, as in $[MoO_3(4,4'\text{-bipy})]$ or $[Mo_3O_9(2,2'\text{-bpy})_2]$ [18] and the cross-linking 1-D molybdenum oxide chains and through hydrogen bonding of the pendant and protonated arm of the ligands forming a 2-D sheet, as in $[Mo_4O_{13}(Hbpa)_2]$ [19]; (iii) $[Co(2,2'\text{-bpy})Mo_3O_{10}]$ [20], the ligand to heterometal forming part of a bimetallic molybdenum oxide backbone; (iv) the compound $[\{Cu(4,4'\text{-bipy})\}_4Mo_{15}O_{47}]$ [21], which contains spacer ligands in a polymeric coordination complex cation providing charge compensation for the negatively charged metal oxide.

In this work we used the hydrothermal technique to obtain the title polymer and characterized the structure and physical properties of the polymer, which has a 3-D molecular network formed by the 4,4′-bipy ligands covalently bound to the 2-D molybdenum oxide square grids in the diagonal positions.

* Corresponding author. Tel.: +86-591-371-9238; fax: +86-591-371-4946.

E-mail address: wxt@ms.fjirsm.ac.cn (X.-T. Wu).

0277-5387/02/$ - see front matter © 2002 Elsevier Science Ltd. All rights reserved.
PII: S0277-5387(01)00975-5

2. Experimental

Chemicals were used as purchased. The crystal was synthesized by the hydrothermal technique. Infrared spectra were recorded on a Nicolet Magna 750 FT–IR spectrophotometer using KBr pellets. Elemental analyses were performed by Elementar (Germany) Vario EL III. The differential thermal analysis was measured by the Universal V2.4F TA Instrument. Fluorescence was obtained by RF-540 fluorometry.

2.1. Preparation of the compound $\{(Mo_4O_{12})(4,4'\text{-bipy})_2\}_n$ (1) and $(NH_4)_4(Mo_8O_{26})(4,4'\text{-bipy})_6$ (2)

$(NH_4)_6Mo_7O_{24}\cdot 4H_2O$ (1.25 g, 1.01 mmol) and distilled water (6 ml) were added to a 25 ml Teflon Lined Parr Autoclave. The autoclave was sealed and heated under static condition for 96 h at 200°; the velocity of heat up was 1° per 3 min from room temperature (r.t.). To facilitate crystal growth, the reaction was cooled to r.t. over 50 h. Black cube crystal $\{(Mo_4O_{12})(4,4'\text{-bipy})_2\}_n$ (0.265 g, 28.8%) was obtained and thoroughly washed with H_2O and C_3H_6O; at same time, we also got 0.20 g (27.35%) of red crystal $(NH_4)_4(Mo_8O_{26})(4,4'\text{-bipy})_6$ in this reaction.

Table 1
Crystal data refinement details for the structures of **1** and **2**

Complex	**1**	**2**
Empirical formula	$Mo_2O_6C_{10}N_2H_8$	$Mo_8O_{26}C_{60}N_{16}H_{64}$
M_t	444	2912
T (K)	293	293
Space group	$C2$	$P2/c$
a (Å)	7.447(4)	10.2839(12)
b (Å)	7.460(5)	18.988(4)
c (Å)	11.945(6)	18.893(8)
β (°)	108.07(4)	104.92(3)
V (Å^3)	630.9(6)	3564.9(17)
Z	2	2
D_{calc} (g cm^{-3})	2.058	1.970
$F(000)$	428	2018
μ (mm^{-1})	3.827	1.449
Absorption correction	SADABS	SADABS
Crystal size (mm)	$0.43\times0.28\times0.23$	$0.58\times0.30\times0.28$
Crystal appearance	cube	rectangle
Radiation Mo Kα (Å)	0.71073	0.71073
Scan type	ω	ω
h, k, l range	−7–8, −8–8, −12–14	−12–12, −22–13, −22–12
R_{int}	0.0282	0.0384
Reflections measured	1636	14 126
Observed reflections	1045	3713
Independent reflections	1067	6316
Parameters refined	92	2018
R*	0.038	0.0688
wR**	0.1053	0.1636
Goodness-of-fit on F^2	1.192	1.058
Max./min. $\Delta\rho$ (e Å^{-3})	1.25, −0.68	1.66, −1.22
Max./means shift in final cycle	0.000	0.002

2.2. Elemental analysis and IR spectrum

The elemental analysis was obtained using the combustion method. *Anal*. Calc. for $Mo_4O_{12}C_{20}N_4H_{16}$: C, 27.03; H, 1.8; N, 6.31; O, 21.62. Found: C, 27.36; H, 1.9; N, 6.11; O, 21.45%. *Anal*. Calc. for $C_{60}H_{64}Mo_8N_{16}O_{26}$: C, 32.85; H, 2.92; N, 10.22; O, 18.98. Found: C, 32.73; H, 3.02; N, 10.15; O, 19.16%. IR (KBr pellet, cm^{-1}): $\{(Mo_4O_{12})(4,4'\text{-bipy})_2\}_n$. $\nu_{Mo=O}$ 806(s), $\nu_{\mu\text{-}Mo\text{–}O}$ 924(m), $\nu_{\mu\text{-}Mo\text{–}N}$ 955(s); $(NH_4)_4(Mo_8O_{26})(4,4'\text{-bipy})_6$ Mo–O stretching region, 939(s), 912(s), 903(s), 841(w), 806(m), 712(s).

2.3. The TG–DTA and fluorescence

The thermogravimetric (TG) and differential thermal analyses (DTA) were performed using an Universal V2.4F TA Instrument. TGA–DTA were run with a temperature ramp of 10.0 °C min^{-1} between 20 and 700 °C. For compound **1** there is an endothermal peak at 420° and an exothermal peak at 495°. For compound **2**, there are three endothermal peaks at 140, 250, 390° and an exothermal peak at 495°. Using the RF-540 fluorometry with 320 nm Xe light as a pumping beam, starting at 350 nm and stopping at 600 nm, with a step of 1.00 nm and a dwell of 0.20 ns, we got fluorescence at 450 nm for compound $\{(Mo_4O_{12})(4,4'\text{-bipy})_2\}_n$ (**1**) and the count of this compound was about 3.5×10^3.

2.4. Crystal structure determination

The crystal data for compounds **1** and **2** are summarized in Table 1, together with some experimental details. Intensity data for the two compounds were obtained on a Siemens Smart/CCD area-detector diffractometer with graphite-monochromated Mo Kα ($\lambda = 0.71073$ Å) radiation. Data reductions and cell refinements were performed with SMART CCD software [22]. The structures were solved by direct methods with the SHELXTL-97 program [23]. Absorption corrections were carried out using SADABS [24]. Selected bond distances and angles of the title compound are shown in Table 2.

3. Results and discussion

3.1. Crystal structure of $\{(Mo_4O_{12})(4,4'\text{-bipy})_2\}_n$ (1) and $(NH_4)_4(Mo_8O_{26})(4,4'\text{-bipy})_6$ (2)

Compound **1** is a 3-D polymer and an ORTEP drawing of a portion of the polymeric structure is shown in Fig. 1. The Mo atom is coordinated by five O atoms

Table 2
Selected bond distances (Å) and angles (°) of compound **1**

Bond distances	
Mo1–O1	1.700(5)
Mo1–O2	1.918(9)
Mo1–O4	1.9185(17)
Mo1–O3	1.9176(18)
Mo1–O2 [a]	1.926(9)
Mo1–N1	2.460(6)
O2–Mo1 [b]	1.926(9)
O3–Mo1 [c]	1.9176(18)
O4–Mo1 [d]	1.9185(17)
Bond angles	
O1–Mo1–O2	99.2(9)
O1–Mo1–O4	99.2(3)
O2–Mo1–O4	88.5(3)
O1–Mo1–O3	99.8(3)
O2–Mo1–O3	88.2(3)
O4–Mo1–O3	161.04(4)
O1–Mo1–O2 [a]	99.7(9)
O2–Mo1–O2 [a]	161.08(4)
O4–Mo1–O2 [a]	88.4(3)
O3–Mo1–O2 [a]	88.7(3)
O1–Mo1–N1	179.8(13)
O2–Mo1–N1	80.7(7)
O4–Mo1–N1	80.63(17)
O3–Mo1–N1	80.41(17)
O2–Mo1 [a]–N1	80.4(7)
Mo1–O2–Mo1 [b]	159.5(3)
Mo1–O3 [c]–Mo1	160.0(5)
Mo1–O4–Mo1 [d]	159.6(4)
C1–N1–C5	118.7(8)
C1–N1–Mo1	121.0(11)
C5–N1–Mo1	120.2(11)

[a] $-x+1/2, y-1/2, 1-z'$.
[b] $-x+1/2, y+1/2, 1-z$.
[c] $1-x, y, 1-z$.
[d] $-x, y, 1-z$.

and one N atom from the 4,4-bipy molecule in a distorted octahedral geometry [the angles of O1–Mo1 to other O atoms around Mo1 are 99.3(7)–99.7(3)°, and the angle of O1–Mo1–N1 is 179.6(9)°], O(1) is a terminal oxo-oxygen. At the same time, the structure of $\{(Mo_4O_{12})(4,4'\text{-bipy})_2\}_n$ has a number of unusual and interesting features. Firstly, it contains a 2-D square grid formed by fused metal–oxygen octatomic rings as shown in Fig. 2. As far as we know, the metal–oxygen octatomic ring that formed the square grid in the MOF has not been reported previously, the dimensions of the square grid are 3.7×3.7 Å^2 and the length from Mo1a to Mo1c is 5.27 Å. Secondly, there are two N atoms of 4,4′-bipy molecules and two oxygen atoms in the diagonal position of the square grid. Thus a 3-D metal-organic framework is formed by the 4,4′-bipy connecting the 2-D square grids, the distance between the square grids being 11.987 Å. A channel with the dimensions of 11.98×5.27 Å^2, ignoring the space occupied by O and 4,4′-bipy, is shown in Fig. 3.

The anion of structure **2** is the β-isomer of $(Mo_8O_{26})^{4-}$, which has approximately C_{2h} symmetry and has eight edge-sharing MoO_6 octahedra. From the packing drawing (Fig. 4), the 4,4′-bipy molecule and NH_4^+ cation are dissociated from the $(Mo_8O_{26})^{4-}$ anion.

3.2. Thermal stability

Compound **1** underwent a two-step weight loss process and is thermally stable up to 350 °C, The on-set temperature of the weight losses are approximately 350 °C, the decomposition process being complete at approximately 495 °C. The demonstrated thermal sta-

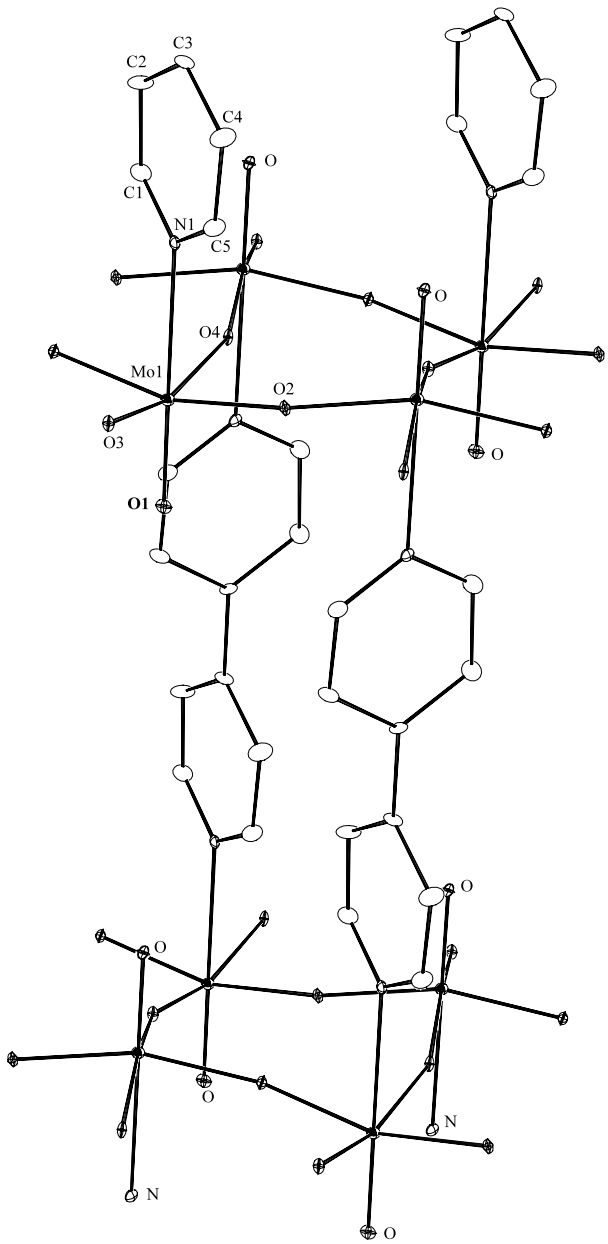


Fig. 1. The ORTEP drawing of a portion of $\{(Mo_4O_{12})(4,4'\text{-bipy})_2\}_n$.

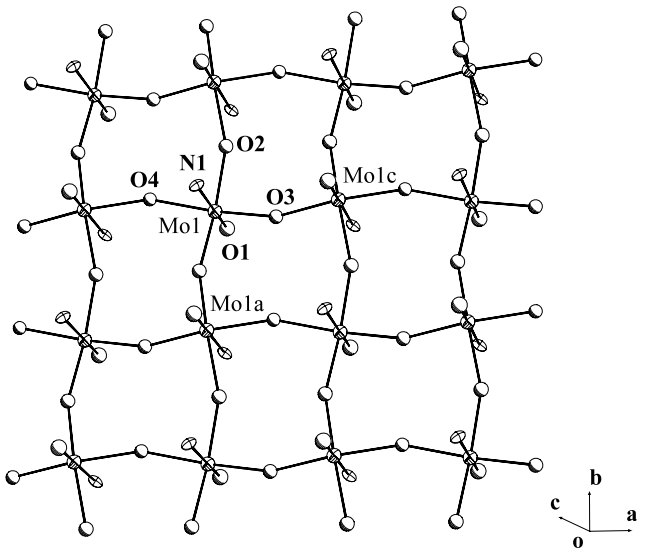


Fig. 2. 2-D square grids formed by the Mo–O octatomic ring.

bility of the polymer could be, at least partially, attributed to the weak π–π interactions between adjacent 4,4′-bipy molecules [25], which are parallel to each other. The distance between any two adjacent 4,4′-bipy is 5.270 Å which is subject to a weak π–π interaction that stabilizes the structure. The oxygen ligands may also enhance the stability of the structure. The weight loss curves clearly indicate that no water molecules are

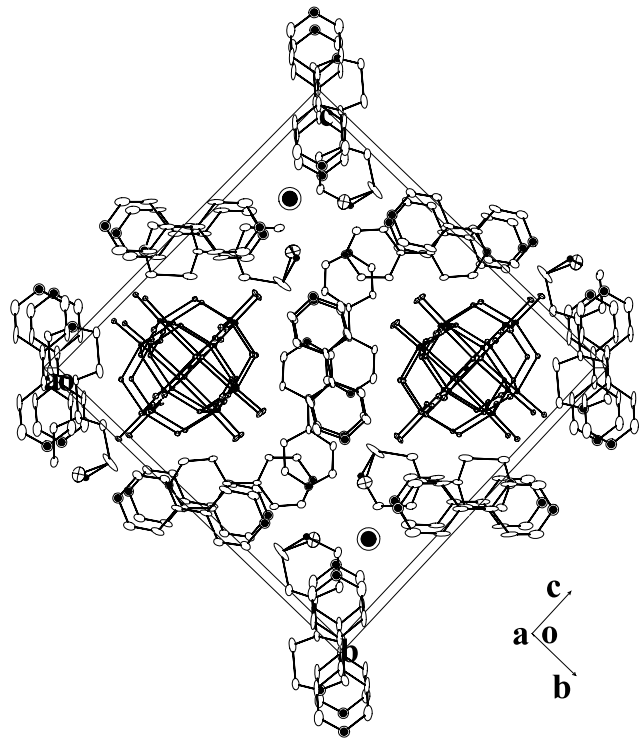


Fig. 4. The packing drawing of the compound $(NH_4)_4(Mo_8O_{26})(4,4'\text{-bipy})_6$.

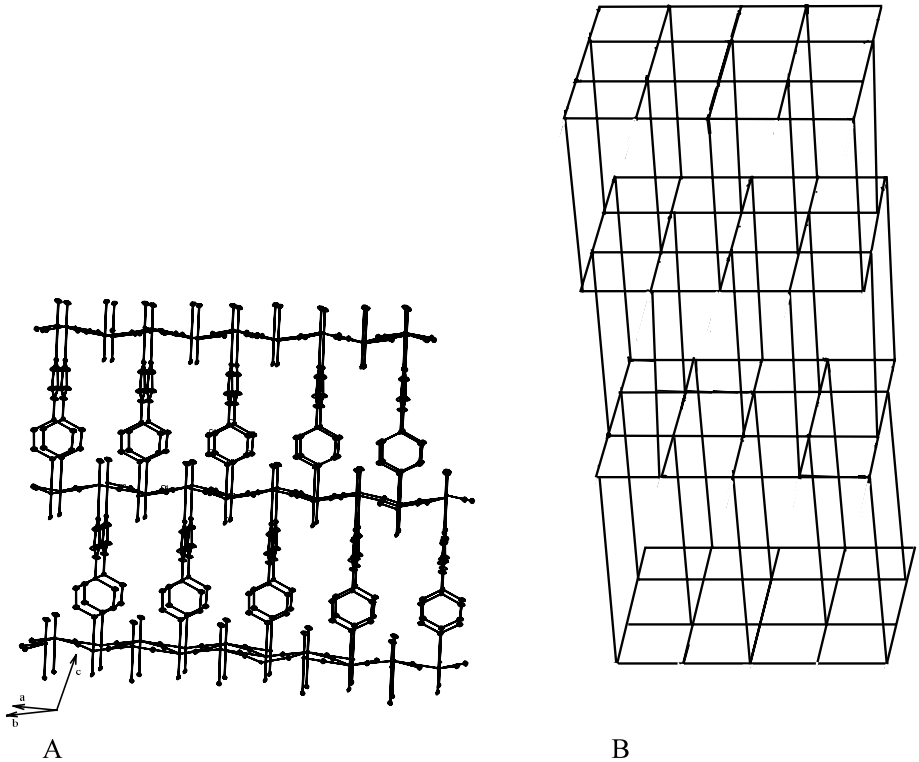


Fig. 3. (a) The points of intersection represent Mo; the long lines represent 4,4-bipy ligands and the short lines respresent O ligands; (b) the packing drawing of the compound $\{(Mo_4O_{12})(4,4'\text{-bipy})_2\}_n$ with a 3-D channel.

incorporated in the compounds through inclusion. The same situation has been noted in the hydrothermal synthesis of other compounds under similar experimental conditions [26]. Compound **2** has no weak π–π interactions between the 4,4′-bipy molecules; it underwent a four-step weight loss process and is thermally stable up to 100 °C, the on-set temperature of weight losses (actual weight loss 1.8%, Calculated for $4NH_4^+$ 1.1%). The decomposition process is completed at approximately 490 °C. The fluorescence in compound **1** may be caused by the π–π interaction of the 4,4′-bipy molecules.

4. Supplementary data

Crystallographic data for the structural analysis have been deposited with the Cambridge Crystallographic Data Centre, CCDC Nos. 162635 and 162634 for compounds **1** and **2**. Copies of this information may be obtained free of charge from The Director, CCDC, 12 Union Road, Cambridge, CB2 1EZ, UK (fax: +44-1223-336033; email: deposit@ccdc.cam.ac.uk or www: http://www.ccdc.cam.ac.uk).

Acknowledgements

This research was supported by grants from the State Key Laboratory of Structural Chemistry, Fujian Institute of Research on the Structure of Matter, CAS, the National Science Foundation of China (29333032, 29873053, 29571029) and the Science Foundation of the Chinese Academy of Sciences.

References

[1] (a) R. Robson, Comprehensive Supramolecular Chemistry, Pergamon, New York, 1996 Chapter 22;
(b) S.R. Batten, R. Robson, Angew. Chem., Int. Ed. Engl. 37 (1998) 1460;
(c) M. Zaworotko, R.D. Rogers, Synthesis of New Materials by Coordination Chemistry Self-Assembly and Template Formation, 217th National Meeting of the ACS, Anaheim, CA, 1999.
[2] J.Y. Lu, B.R. Cabrera, R.J. Wang, J. Li, Inorg. Chem. 38 (1999) 4608.
[3] (a) D. Hagrman, C. Zubieta, D.J. Rose, J. Zubieta, R.C. Huanshalter, Angew. Chem., Int. Ed. Engl. 36 (1997) 873;
(b) H. Li, M. Eddaoudi, M. O'Keeffe, O.M. Yaghi, Nature 402 (1999) 276.
[4] M. Fujita, Y.J. Kwon, S. Washizu, K. Ogura, J. Am. Chem. Soc. 116 (1994) 1151.
[5] M. Inoue, M. Kubo, Coord. Chem. Rev. 21 (1976) 1.
[6] N. Masciocchi, D. Cairati, L. Carlucci, G. Ciani, A. Sireni, J. Chem. Soc., Dalton Trans. (1996) 2793.
[7] J. Lu, Y. Lawandy, M.A.J. Li, T. Yuan, C.L. Lin, Inorg. Chem. 38 (1999) 2695.
[8] (a) F. Robinson, M.J. Zaworotko, J. Chem. Soc., Chem. Commun. (1995) 2143;
(b) G.M. Yaghi, H. Lie, J. Am. Chem. Soc. 118 (1996) 295;
(c) O.M. Yaghi, H. Li, J. Am. Chem. Soc. 117 (1995) 10401;
(d) O.M. Yaghi, G. Li, Angew. Chem., Int. Ed. Engl. 34 (1995) 207.
[9] J.T. Sampanthar, J.J. Vittal, J. Chem. Soc., Dalton Trans. (1999) 1993.
[10] (a) L. Carlucci, G. Ciani, D.M. Proserpio, A. Sironi, J. Chem. Soc., Dalton Trans. (1997) 1801;
(b) R.W. Sironi, B.F. Hosikin, R. Robson, J. Chem. Soc., Chem. Commun. (1990) 11677;
(c) D. Hagrman, C. Zubieta, D.J. Rose, J. Zubieta, R.C. Huashalter, Angew. Chem., Int. Ed. Engl. 36 (1997) 873;
(d) J. Li, H. Zeng, J. Chen, Q. Wang, X. Wu, J. Chem. Soc., Chem. Commun. (1997) 1213;
(e) L.R. MacGillivray, R.H. Groeneman, J.L. Atwood, J. Am. Chem. Soc. 120 (1998) 2676;
(f) L.-M. Zheng, K.-H. Li, H.-H. Song, X.-Q. Xin, H.-K. Fun, K. Chinnakali, I.A. Razak, J. Chem. Soc., Dalton Trans. (1999) 2311;
(g) Z. Wang, R.-G. Xiong, B.-M. Foxman, S.R. Wilson, W. Lin, Inorg. Chem. 38 (1999) 1523;
(h) C.V.K. Sharama, R.D. Rogers, Chem. Commun. (1999) 83.
[11] C.-M. Liu, X.-Z. You, W. Chen, J. Coord. Chem. 46 (1998) 183.
[12] (a) M. Hayashi, Y. Miyamoto, T. Inoue, N. Oguni, J. Chem. Soc., Chem. Commun. (1992) 1752;
(b) L.R. MacGillivray, S. Subramanian, M. Zaworotko, J. Chem. Soc., Chem. Commun. (1994) 1325;
(c) L. Carlucci, G.D.M. Proserpio, A. Sironi, J. Chem. Soc., Chem. Commun. (1994) 2755.
[13] G.B. Gardner, D. Venkataraman, J.S. Moore, Nature 374 (1995) 792.
[14] (a) O.M. Yaghi, H. Li, J. Am. Chem. Soc. 118 (1996) 295;
(b) F. Robinson, M.J. Zaworotko, J. Chem. Soc., Chem. Commun. (1995) 2413;
(c) H. Gudbjartson, K. Birasha, K.M. Poirier, M.J. Zaworotko, J. Am. Chem. Soc. 121 (1999) 2599.
[15] (a) R.W. Gable, B.F. Hoskins, R. Robson, J. Chem. Soc., Chem. Commun. (1990) 1677;
(b) M. Fujita, Y.J. Kwon, Y.O. Sasaki, K. Yamaguch, K. Ogura, J. Am. Chem. Soc. 117 (1995) 7287.
[16] K.N. Power, T.L. Hennigar, M.J. Zaworotko, New J. Chem. 22 (1998) 177.
[17] P.J. Zapf, R.C. Haushalter, J. Zubieta, Chem. Commun. (1997) 321.
[18] P.J. Zapf, R.C. Haushalter, J. Zubieta, Chem. Mater. 9 (1997) 2019.
[19] P.J. Zapf, R.L. LaDuca Jr., R.S. Rarig, K.M. Johnson III, J. Zubieta, Inorg. Chem. 37 (1998) 3411.
[20] P.J. Zapf, C.J. Warren, R.C. Haushalter, J. Zubieta, Chem. Commun. (1997) 1543.
[21] D. Hagram, C. Zubieta, D.J. Rose, J. Zubieta, R.C. Haushalter, Angew. Chem., Int. Ed. Engl. 36 (1997) 795.
[22] Siemens, Smart Version 4.0. User manual Siemens Analytical X-ray Instruments Inc., Madison, WI, 1994.
[23] G.M. Sheldrick, SHELX-97, Program for structure refinement, University of Göttingen, Germany, 1997.
[24] G.M. Sheldrick, SADABS, Program for Siemens area detector absorption correction, University of Göttingen, 1996.
[25] J.Y. Lu, M.A. Lawndy, J. Li, T. Yuen, C.L. Lin, Inorg. Chem. 38 (1999) 2695.
[26] (a) J.Y. Lu, B.R. Cabrera, R.-J. Wang, J. Li, Inorg. Chem. 37 (1998) 4480;
(b) J.Y. Lu, B.R. Cabrera, J. Li, Inorg. Chem. 38 (1999) 4068.

PERGAMON

Polyhedron 21 (2002) 181–185

POLYHEDRON

www.elsevier.com/locate/poly

Oxidation of 3,5-di-*tert*-butylcatechol by molecular oxygen catalysed by a copper(I) complex, $Cu_2(bdpdz)Cl_2$, bdpdz = 3,6-bis-(di-2-pyridilmethyl) pyridazine

Jorge Manzur [a,*], Ana M. García [a], Carolina Córdova [a], Olga Pizarro [a], Verónica Acuña [b], Evgenia Spodine [c]

[a] *Facultad de Ciencias Físicas y Matemáticas, Universidad de Chile, Casilla 2777, Santiago, Chile*

[b] *Facultad de Ciencias Naturales, Matemáticas y del Medio Ambiente, Universidad Tecnológica Metropolitana, Casilla 9845, Correo 21, Santiago, Chile*

[c] *Facultad de Ciencias Químicas y Farmacéuticas, Universidad de Chile, Casilla 233, Santiago, Chile*

Received 22 March 2001; accepted 9 October 2001

Abstract

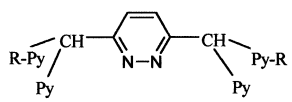
The syntheses, voltammetry and autoxidation of the binuclear copper(I) complex, $Cu_2(bdpdz)Cl_2$, (bdpdz = 3,6-bis-(di-2-pyridylmethyl)pyridazine) are reported. The complex catalyses the aerobic oxidation of 3,5-di-*tert*-butylcatechol, $DTBCH_2$, to 3,5-di-*tert*-butyl-*o*-benzoquinone. At constant catalyst concentration (5×10^{-5} M) the initial rate of oxygen uptake increases with increasing amounts of substrate reaching an asymptotic value. At constant $DTBCH_2$ (1×10^{-3} M) the reaction rate depends linearly on the concentration of catalyst with a rate constant k' equal to 8.8×10^{-3} s^{-1}. The relevance of the oxidation of $DTBCH_2$ by the copper(I)–dioxygen adduct becomes evident from the kinetic data reported in this work. © 2002 Elsevier Science Ltd. All rights reserved.

Keywords: Copper(I) complexes; Autoxidation; Kinetic data; Catalytic activity

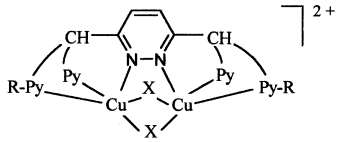
1. Introduction

The oxidation of catechol and in particular, 3,5-di-*tert*-butylcatechol ($DTBCH_2$), using copper(II) complexes as catalysts, has been studied widely as a model reaction for the catecholase activity of tyrosinase [1–10]. The reaction mechanism proposed by several authors includes an initial step leading to the formation of a reduced copper(I) complex as the active species towards molecular oxygen. The copper–oxygen adduct then would react with the catechol to give the quinone, or be oxidised to copper(II), which in turn reacts with the catechol in a ping–pong mechanism giving the corresponding quinone [11]. In this way the properties of the copper(I) complex should be as important as those of the copper(II) complex to determine the catalytic activity, depending on the rate-determining step.

We have reported the catalytic activity of copper(II) complexes with the ligand 3,6-bis-(di-2-pyridylmethyl) pyridazine, (bdpdz), and its methyl derivatives in the oxidation reaction of $DTBCH_2$ using methanol as a solvent [12]. Our results suggest an initial equilibrium between the copper(II) complex and the catechol instead of an irreversible reaction to give the reduced copper(I) species. This species is the active one towards molecular oxygen.



bdpdz ligands: R = H (bdpdz); 6-Me (mbdpdz)



Cu(II) bdpdz complexes: X = Cl; Br.

* Corresponding author. Fax: +56-2-699-4119.
E-mail address: jmanzur@dqb.uchile.cl (J. Manzur).

0277-5387/02/$ - see front matter © 2002 Elsevier Science Ltd. All rights reserved.
PII: S0277-5387(01)00966-4

In this work we report the syntheses, characterisation and autoxidation of the copper(I) complex, $Cu_2(bdpdz)Cl_2$, and its catalytic activity in the oxidation of $DTBCH_2$ by molecular oxygen. The electrochemical behaviour of solutions of CuCl with the ligand in methanol is also studied in order to gain information about the species present in solution, relevant to the reaction mechanism.

2. Experimental

2.1. Reagents

All reagents and solvents were of high purity grade and were purchased from commercial sources and used as received unless noted otherwise. 3,6-bis(di-2-pyridylmethyl) pyridazine, (bdpdz) was prepared as reported elsewhere [13].

The copper(I) complex, $Cu_2(bdpdz)Cl_2$, was prepared under anaerobic conditions by reaction of CuCl (2 mmol) dissolved in acetonitrile (4 ml) with the ligand (1mmol) dissolved in methanol (25 ml). The red–brown solid was filtered, washed with cold methanol and vacuum dried. Elemental analysis: Calc. for $Cu_2(bdpdz)Cl_2$: C, 50.81; H, 3.28; Cu, 20.68; N, 13.68. *Anal.* Found: C, 49.13; H, 3.15; Cu, 20.30; N, 12.3%.

2.2. Measurements

The C, H, N elemental analyses were performed at CEPEDEQ (University of Chile) on a Fison–Carlo Erba EA 1108 model analyser. Electronic spectra were recorded on a Perkin–Elmer Lambda 11 spectrophotometer using methanol (Chrom AR HPLC, Mallinckrodt) as solvent.

Electrochemistry was performed in methanol solution using 0.05 M $NaNO_3$ as electrolyte. The cyclic voltammograms were recorded at a glassy carbon electrode, with a saturated calomel reference electrode and a Pt wire as an auxiliary electrode, on a BAS CV 50W voltammetric analyzer. All potential values are reported versus SCE. The voltammograms were obtained for solutions of the prepared complex and also for mixtures of solutions of CuCl and the ligand in the appropriate ratio.

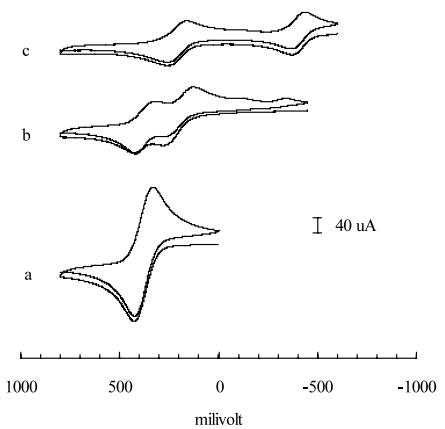


Fig. 1. Cyclic voltammogram of solutions of: (a) CuCl: 2×10^{-3} M. (b) CuCl: 2×10^{-3} M and L: 1×10^{-3} M. (c) CuCl: 2×10^{-3} M and L: 2×10^{-3} M.

Kinetic measurements were done following the oxygen uptake with a YSI (model 53) oxygen monitor, in a sealed thermostatted (28 °C) reaction cell. The oxygen concentration was adjusted to the desired value in the reaction cell. The copper(I) solution was injected by syringe into the stirred solution and the O_2 uptake was recorded. Kinetic data were obtained using a solution of the prepared complex as catalyst and also an in situ solution prepared by mixing solutions of CuCl and the ligand in the appropriate molar ratio. Both systems give the same results.

3. Results and discussion

Before studying the catalytic reaction of the complex, $Cu_2(bdpdz)Cl_2$, with $DTBCH_2$ it was of outmost importance to know the nature of the species in solution, because equilibrium of different species with varying stoichiometries is conceivable. In order to have an insight of the actual species present in solution we undertook a voltammetric study of solutions of CuCl and the ligand in methanol.

3.1. Electrochemistry

Fig. 1(a) shows the cyclic voltammogram of a solution of CuCl. It is compared with solutions of CuCl and the ligand in a 2:1, (Fig. 1(b)), and 1:1 ratios, (Fig. 1(c)). Fig. 1(a) shows the oxidation peak at 425 mV and the reduction peak at 330 mV for the Cu(I)/Cu(II) couple. Fig. 1(b) shows the first oxidation peak at 270 mV and a second one at 425 mV. The reverse scan shows a reduction peak at 330 mV, a second one at 130 mV and a third one at -345 mV. The quasi-reversible $E_{1/2} = 378$ mV couple (peak-to-peak separation equal to 95 mV) can be identified with the Cu(I)/Cu(II) redox pair. To understand the rest of the peaks, it is necessary to analyse Fig. 1(c). This voltammogram (1:1 ratio) can be explained by one-electron redox processes of the $L_2Cu(I)–Cu(I)$ species, formed by the reaction:

$$2Cu(I) + 2L \rightarrow L_2Cu(I)–Cu(I)$$

The oxidation peak at -375 mV corresponds to the formation of the mixed valence complex $L_2Cu(I)–Cu(II)$. The oxidation peak at 250 mV corresponds to the oxidation of the mixed valence complex to the dicupric species, $L_2Cu(II)–Cu(II)$. The corresponding

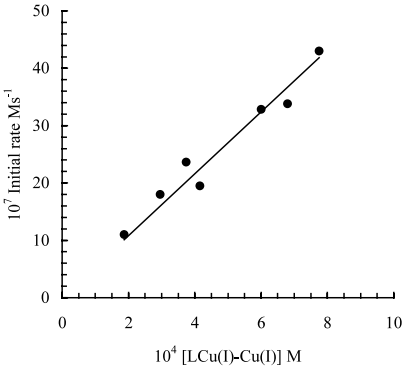


Fig. 2. Dependence of the initial rate of autoxidation of the copper(I) complex with its concentration.

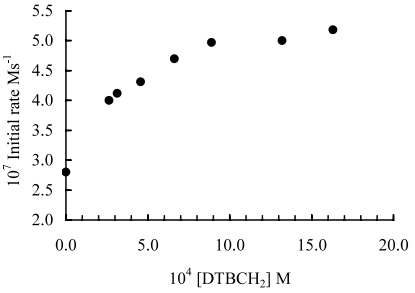


Fig. 3. Dependence of the initial rate of oxygen consumption on the concentration of $DTBCH_2$ at constant concentration of copper(I) complex equal to 5×10^{-5} M.

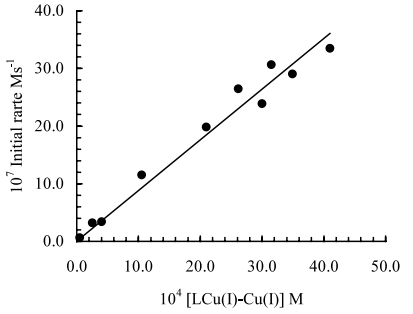


Fig. 4. Dependence of the initial rate of oxygen uptake with the concentration of copper(I) complex at constant concentration of $DTBCH_2$, 1×10^{-3} M.

reductions in the reverse scan appear at 150 and -445 mV.

The absence in the voltammogram of Fig. 1(b) of the oxidation peak at -375 mV is indicative of the non-existence of the $L_2Cu(I)–Cu(I)$ species when the ratio Cu(I)/L = 2:1. Then, the signal at 270 mV may be explained by the process:

$$LCu(I)–Cu(I) \rightarrow 1/2L_2Cu(II)–Cu(II) + Cu(I) + 1e$$

This species would generate the corresponding reduction at 130 mV.

$$L_2Cu(II)–Cu(II) + 1e \rightarrow L_2Cu(I)–Cu(II)$$

The fact that the signal corresponding to the reduction of the solvated cupric ion persists is indicative that the reaction:

$$1/2L_2Cu(II)–Cu(II) + Cu(II) \rightarrow LCu(II)–Cu(II)$$

is slow at the time scale of the voltammetric scan. The peak at -345 mV corresponds to the process:

$$1/2L_2Cu(II)–Cu(II) + Cu(I) + 1e \rightarrow LCu(I)–Cu(I)$$

A solution of the prepared cuprous complex gives a voltammogram identical to the one obtained for a mixture of solutions of CuCl and the ligand in a 2:1 ratio.

In conclusion it can be assessed that in the two to one copper to ligand ratio the species in solution is mainly LCu(I)–Cu(I) and not $L_2Cu(I)–Cu(I)$.

3.2. Kinetic studies

The kinetic data for the autoxidation of the cuprous complex were obtained following the initial oxygen uptake by the reaction mixture in methanol at 28 °C. The kinetic results were obtained using a solution of the in situ generated cuprous complex. Solutions of the solid prepared complex gave the same results.

The observed initial rate is linearly dependent on the copper(I) complex concentration with an experimental rate constant $k = 5.4 \pm 0.5 \times 10^{-3}$ s^{-1} (Fig. 2).

The addition of variable amounts of $DTBCH_2$ (0.2 to 4×10^{-3} M.) increases the rate of oxygen consumption (Fig. 3). When a 5×10^{-5} M solution of complex is used the rate tends to an asymptotic value of $5 \pm 0.2 \times 10^{-7}$ M s^{-1}, at concentration of $DTBCH_2$ above 8×10^{-4} M.

At a constant value of 1×10^{-3} M in $DTBCH_2$ the oxygen consumption has a linear dependence with the copper(I) complex (Fig. 4). A value of $k' = 8.8 \pm 1 \times 10^{-3}$ s^{-1} is obtained for this set of values.

In a previous paper we reported a kinetic study of this reaction, followed spectrophotometrically by the formation of the quinone [12]. The initial rate of quinone formation was found to be slower than the oxygen consumption observed in this work.

The following mechanism can account for the set of data given above:

$$Cu(I) - Cu(I) + O_2 \underset{k_{-1}}{\overset{k_1}{\rightleftarrows}} Cu(II) - O_2^{2-} - Cu(II) \quad (1)$$

$$Cu(II) - O_2^{2-} - Cu(II) \xrightarrow{k_2} Cu(II) - Cu(II) + O_2^{2-} \quad (2)$$

$$Cu(II) - O_2^{2-} - Cu(II) + DTBCH_2 \xrightarrow{k_2} DTB + Cu(I) - Cu(I) + H_2O_2 \quad (3)$$

Reaction (3) would account for the difference in reaction rates for the formation of the DTBQ and oxygen uptake. This reaction would also explain the observed dependence of the rate of oxygen consumption on the concentration of $DTBCH_2$.

Taking steps (2) and (3) as competitive reactions and applying the steady state to the oxygen adduct; the kinetic law for the initial oxygen consumption becomes:

$$V_{O_2} = \frac{k_1k_2[\text{Cu(I)}-\text{Cu(I)}][O_2] + k_1k_3[\text{Cu(I)}-\text{Cu(I)}][\text{DTBCH}_2][O_2]}{k_{-1}+k_2+k_3[\text{DTBCH}_2]} \quad (4)$$

At high $DTBCH_2$ concentration the rate of step (3) would be high enough to make reaction (1) to be rate-determining and the consumption becomes independent of $DTBCH_2$ concentration, as shown in Fig. 3.

At low $DTBCH_2$ concentration, it is possible to assume $k_3[\text{DTBCH}_2] \ll (k_{-1}+k_2)$. Therefore, at constant Cu(I)–Cu(I) concentration (5×10^{-5} M) a plot of V_{O_2} versus the concentration of $DTBCH_2$ should give a linear dependence, as was found. These data permit to estimate:

$$\frac{k_1k_2}{k_1+k_2} = 66\pm6 \text{ M s}^{-1}$$

$$\frac{k_1k_3}{k_{-1}+k_2} = 1.0\pm0.08\times10^5 \text{ s}^{-1}$$

In the absence of $DTBCH_2$, only steps (1) and (2) would be operative. In these conditions the kinetic law for the initial consumption of oxygen is:

$$V_{O_2} = \frac{k_1k_2[\text{Cu(I)}-\text{Cu(I)}][O_2]}{k_{-1}+k_2} \quad (5)$$

From the slope of Fig. 2 a value of 70 ± 7 M s^{-1} for the $k_1k_2/(k_{-1}+k_2)$ ratio was obtained. This value is the same as the one determined from the set of kinetic data with $DTBCH_2$.

The data presented above permit to estimate a value of k_3/k_2 close to 1.5×10^3. Then, for the experiments at constant concentration of $DTBCH_2$ equal to 1×10^{-3} M (Fig. 4) the $k_3[\text{DTBCH}_2]$ product is of the same order of magnitude as k_2. Under these conditions Eq. (4) applies for the rate of oxygen uptake. The plot of V_{O_2} versus the concentration of cuprous complex gives a linear dependence as expected.

The catalytic activity of the studied binuclear copper(I) complex can be compared with that of the binuclear copper(II) complexes informed by Chyn and Urbach [11], since these authors propose two alternative mechanism in which the cupric species are totally reduced by the catechol in an initial fast reaction, prior to the formation of the $Cu(II)–O_2^{2-}–Cu(II)$ adduct.

Mechanism I

$$\text{Cu(II)}-\text{Cu(II)} + \text{DTBCH}_2 \rightarrow \text{Cu(I)} - \text{Cu(I)} + \text{DTBQ} + 2\text{H}^+$$

$$\text{Cu(I)}-\text{Cu(I)} + O_2 \rightarrow \text{Cu(II)}-O_2^{2-}-\text{Cu(II)}$$

$$\text{Cu(II)}-O_2^{2-}-\text{Cu(II)} + 2\text{H}^+ \rightarrow \text{Cu(II)}-\text{Cu(II)} + H_2O_2$$

Mechanism II

$$\text{Cu(II)}-\text{Cu(II)} + \text{DTBCH}_2 \rightarrow \text{Cu(I)} - \text{Cu(I)} + \text{DTBQ} + 2\text{H}^+$$

$$\text{Cu(I)}-\text{Cu(I)} + O_2 \rightarrow \text{Cu(II)}-O_2^{2-}-\text{Cu(II)}$$

$$\text{Cu(II)}-O_2^{2-}-\text{Cu(II)} + \text{DTBCH}_2 \rightarrow \text{Cu(I)} - \text{Cu(I)} + \text{DTBQ} + H_2O_2$$

They assume that mechanism I is the correct one based on the fact that the μ-peroxo-dicopper(II) species would be rapidly protonated and would not exist long enough to oxidise $DTBCH_2$. Besides they find a zero-order dependence with respect to $DTBCH_2$ concentration. In our previous work we also informed a zero-order dependence with respect to $DTBCH_2$ [12]. However, when the concentration range is amplified, and lower concentration than 8×10^{-4} are used the consumption of oxygen begins to decrease. This fact together with the different rate in production of quinone (determined spectrophotometrically by following the absorption band at 400 nm) as stated above compared to the oxygen uptake (followed amperometrically with an oxygen sensor) permits to propose the mechanism based on steps (1) to (3).

Therefore, our results show that both mechanisms operate in parallel. This could be due to the fact that the catalytic activity was studied in methanol, while Chyn and Urbach used a solvent system of 1 to 1 methanol–water buffered at pH 6.4. In this mixed system the decomposition of the copper oxygen adduct would be faster than in pure methanol, thus promoting mechanism I.

Other authors have also shown the dependence of the catalytic activity on the substrate concentration, thus giving evidence of the existence of mechanism II [1,14]. Besides, Rockcliffe and Martell [15] have shown that a copper(I) dioxygen complex can act as an oxidising agent towards different substrates, including $DTBCH_2$. Our work together with the reported data in the literature, permits to conclude that both the solvent and the characteristics of the catalysts seem to be important in the existence of the reaction of the peroxo-dicopper(II) species with the catechol.

Acknowledgements

The financial support by the Consejo Nacional de Ciencia y Tecnología (project FONDECYT 1990185) is gratefully acknowledged.

References

[1] E. Monzani, L. Quinti, A. Perotti, L. Casellla, M. Gullotti, L. Randaccio, S. Geremia, G. Nardin, P. Faleschini, G. Tabbi, Inorg. Chem. 37 (1998) 553.

[2] N. Oishi, Y. Nishida, K. Ida, S. Kida, Bull. Chem. Soc. Jpn. 53 (1980) 2847.
[3] J.H. Satcher, M.W. Droege, T.J.R. Weakleay, R.T. Taylor, Inorg. Chem. 34 (1995) 3317.
[4] M.R. Malachowski, M.G. Davidson, Inorg. Chim. Acta 163 (1989) 199.
[5] U. Casellato, S. Tamburini, P.A. Vigato, A. De Stefani, M. Vidali, D.E. Fenton, Inorg. Chim. Acta 69 (1983) 45.
[6] M. Lubben, R. Hage, A. Meetsma, K. Byma, B.L. Feringa, Inorg. Chem. 34 (1995) 2217.
[7] F. Zippel, F. Ahlers, R. Werner, W. Haase, H.-F. Nolting, B. Krebs, Inorg. Chem. 35 (1996) 3409.
[8] L. Casella, M. Gullotti, C. Pessina, A. Pintar, Gazz. Chim. Ital. 116 (1986) 41.
[9] M.R. Malachowski, H.B. Huynh, L.J. Tomlinson, R.S. Kelly, J.W. Furbee Jun., J. Chem. Soc., Dalton Trans. (1995) 31.
[10] M.R. Malachowski, B. Dorsey, J.G. Sackett, R.S. Kelly, A.L. Ferk, R.N. Nardin, Inorg. Chim. Acta 249 (1996) 85.
[11] J.P. Chyn, F.L. Urbach, Inorg. Chim. Acta 189 (1991) 157.
[12] J. Manzur, A.M. García, B. Gómez, E. Spodine, Polyhedron 19 (2000) 2367.
[13] J. Manzur, A.M. García, R. Letelier, E. Spodine, O. Peña, D. Grandjean, M.M. Olmstead, B.C. Noll, J. Chem. Soc., Dalton Trans. (1993) 905.
[14] T.C. Woon, R. McDonald, S.K. Mandal, L.K. Thompson, S.P. Connors, A.W. Addison, J. Chem. Soc., Dalton Trans. (1986) 2381.
[15] D.A. Rockcliffe, A.E. Martell, Inorg. Chem. 32 (1993) 3143.

PERGAMON

Polyhedron 21 (2002) 187–191

POLYHEDRON

www.elsevier.com/locate/poly

Solid state metathesis synthesis of metal silicides; reactions of calcium and magnesium silicide with metal oxides

Artur M. Nartowski, Ivan P. Parkin *

Department of Chemistry, Christopher Ingold Laboratory, University College London, 20 Gordon Street, London WC1H OAJ, UK

Received 17 August 2001; accepted 10 October 2001

Abstract

Reactions of transition metal oxides (V_2O_3, V_2O_5, Nb_2O_5, $LiNbO_3$, Ta_2O_5, $LiTaO_3$, MoO_3 and Li_2MoO_4) with lithium silicide (Li_2Si) and calcium silicide–magnesium silicide mix ($CaSi_2$, Mg_2Si) could be initiated by grinding, flame, filament or bulk thermal methods to produce a range of single phase transition metal silicides (VSi_2, $NbSi_2$ and $TaSi_2$) in good yields (approximately 90%). The silicides were characterised by X-ray powder diffraction, scanning electron microscopy (SEM), energy dispersive analysis by X-rays (EDAX), electron probe, FTIR and microelemental analysis. © 2002 Elsevier Science Ltd. All rights reserved.

Keywords: Silicides; Solid state metathesis; Self-propagating

1. Introduction

Transition metal silicides are hard, inert and have high electrical and thermal stability [1]. Molybdenum disilicide is widely used as a high temperature heating element [2], whilst the other metal silicides show potential as interface diffusion barriers and in large scale integrated (VLSI) circuit technology [3]. Silicides are generally unaffected by strong acids including aqua-regia. Their resistance to oxidation, particularly at high temperatures is largely due to the formation of a tenacious oxide layer that passivates the surface to further attack [4].

Silicides are usually prepared by co-reduction of SiO_2 with aluminium or carbon or by direct elemental combination at elevated temperatures [4]. Russian researchers have shown that in certain reactions silicides can be made from elemental combination reactions that are self-propagating, a technique known as Self propagating High temperature Synthesis or SHS [5]. These reactions rely on the in-built exothermicity of the elemental combination, can often be initiated at a point source and proceed by passage of a synthesis wave, also known as a solid-flame. Such work has produced a range of metal silicides, including commercial production of $MoSi_2$ for use as furnace elements [5]. SHS has some associated problems with the speed of the reaction (over in approximately 2–20 s), exceptionally high temperatures generated (>2000 °C) and low density of the product. Control of product stoichiometry and purity can also be difficult [6]. Kaner [7] has shown that a variant of the SHS process can form a range of ceramic materials including metal silicides—solid state metathesis or SSM. In SSM the reaction involves the exchange of ions between reacting solids and is driven largely by the formation of a co-produced salt. To date all SSM reactions have involved the use of a metal halide (M) starting material and a main group metal—element (E) anion Eq. (1).

$$MCl_n + Na_nE \rightarrow ME + n\,NaCl \quad (1)$$

In the case of metal silicide formation Kaner [7] has shown that reaction of $MoCl_5$ with Mg_2Si leads to the formation of $MoSi_2$, Mo metal and $MgCl_2$. The magnesium halide is readily removed from the silicide product, simply by washing with water, however, the molybdenum metal was difficult to remove. We have extended the range of compounds that can be made in SSM reactions [8]. In silicide formation we have reported on a large survey of reactions involving lan-

* Corresponding author. Tel.: +44-207-679-4669; fax: +44-207-679-7463.

E-mail address: j.p.parkin@ucl.ac.uk (I.P. Parkin).

0277-5387/02/$ - see front matter © 2002 Elsevier Science Ltd. All rights reserved.
PII: S0277-5387(01)00974-3

thanide and transition metal halides with magnesium silicide [9]. All of these reactions were undertaken in sealed quartz ampoules under vacuum. In no instance was the reaction self-propagating and consequently no synthesis wave was observed. However, over 10 h at 850 °C a metathesis reaction occurred with formation of a range of products. Unfortunately single-phase metal silicide products were not formed in the reactions. Invariably mixed phase silicide products were formed such as $NbSi_2$ and Nb_5Si_3 and in some instances the products were also contaminated with elemental metal impurity [9].

Given the relative refractory nature of metal silicides and their resistance to oxidation we report here the metathesis formation of metal silicide utilising metal oxide starting materials. In particular, we show that by using a range of siliciding reagents, such as Li_2Si and $MgSi_2/CaSi_2$ the reactions can be made to proceed in the propagation mode by means of a solid-flame and that single-phase transition metal silicides can be synthesised.

2. Experimental

All chemicals were purchased from Aldrich Chemical Co and used as supplied. All powders were of 99.9% purity or better except calcium oxide which was 80%. No purity rating was available for the $CaSi_2$ used in the experiments (Aldrich), this was also used as provided. Manipulations and weighings were carried out in a Saffron Scientific nitrogen filled glove box. Ampoules were made from quartz (0.6 cm diameter, 15 cm long, 2–3 mm walls) and were annealed and flamed dried in vacuum prior to use. Dilute HCl (5%) was used for all triturations. After treatment with acid the remaining solids were always rinsed with distilled water and dried in vacuum. X-ray powder diffraction patterns were determined on a Siemens D5000 transmission powder diffractometer using germanium monochromated Cu Kα1 radiation ($\lambda = 1.5046$ Å). Patterns were indexed using TREOR or METRIC-LS programmes. SEM–EDAX was determined on a JEOL JSM820 microscope, equipped with a Kevex Quantum Detector Delta 4, and a Hitachi SEM S-570. Infra-red spectra were recorded on a Nicolet 205 spectrometer using KBr pressed discs. Electron probe measurements were made on a JEOL EMA. Reactions were initiated in one of four ways, flame, filament, grinding and bulk initiation. Flame initiation was carried out in air using a gas torch at 1000 °C, the pre-ground reaction mixture was placed in a line on a ceramic mat and initiated at one end. This encouraged a yellow propagation wave to move through the solid. Filament initiation was carried out analogously to flame initiation except that a hot nichrome filament (800 °C) was used. Initiation using grinding occurred simply by grinding the starting powders in a glove box. Bulk initiation was used in all reactions and was accomplished by adding the pre-ground powders to an ampoule. The ampoule was sealed in vacuo and heated in a Lenton Thermal designs programmable tube-furnace to 1000 °C at a ramp rate of 20 °C a minute.

2.1. Reactions of Li_2Si with V_2O_5, $NaVO_3$, Nb_2O_5, $LiNbO_3$, Ta_2O_5, $LiTaO_3$, MoO_3, Li_2MoO_4 and Li_2WO_4 inside ampoules

The same reaction scale and procedure were used for all reactions exemplified below for the reaction of Li_2Si and Nb_2O_5.

Niobium(V) oxide (0.200 g, 0.752 mmol) and lithium silicide (0.126 g, 3.00 mmol) were ground together and placed inside of an ampoule that was evacuated and sealed. The ampoule was placed in a tube furnace that was brought from room temperature (r.t.) to 1000 °C over 1 h. At 550 °C some white residue settled at the cooler part of the ampoule whilst the solid at the hottest part of the ampoule had turned black over a 20 s period. The ampoule was annealed at 1000 °C for 12 h. After annealing the ampoule was allowed to cool to room temperature, broken open and the contents triturated with dilute HCl (3×6 ml), rinsed with distilled water (3×10 ml) and then dried in vacuum. The resultant black solid was analysed using powder XRD, SEM–EDAX, FTIR and electron probe measurements, Table 1.

3. Results and discussion

3.1. Synthesis; reaction of metal oxides with magnesium–calcium silicides

Solid state metathesis reactions between transition metal oxides and a mixture of calcium silicide–magnesium silicide produced transition metal disilicides and calcium and magnesium oxide, Table 1, Eqs. (2) and (3). The reactions were promoted by three methods of initiation, bulk, flame and filament. Bulk initiation was studied in all systems. This involved heating pre-ground powders in a sealed ampoule. A thermal flash was noted in each system somewhere between 450 and 600 °C. This corresponded to the initiation of a reaction within the bulk powder. Flame initiation was accomplished in air using a gas flame. This induced an orange propagation wave that travelled through the solid at 5 mm s^{-1}. Filament initiation involved the use of a heated nichrome wire. It was only successful for the reaction of Ta_2O_5 with $Mg_2Si/CaSi_2$ mixture. In this case the reaction also proceeded with an orange synthesis wave of velocity 4 mm s^{-1}.

Neither filament nor flame initiations were annealed. The products from all three modes of initiation were analysed as made and after trituration with dilute hydrochloric acid and water. The as made products showed the presence of calcium and magnesium oxides. These were removed by the trituration treatment. Notably the method of initiation did have a bearing on the phase composition of the product.

The ratio of magnesium silicide to calcium silicide used in the initial starting mixture (normally 2:1 Mg_2Si–$CaSi_2$) was altered to make single-phase metal disilicide products Eqs. (2) and (3). This proved to be successful for bulk initiation. Flame initiation for M_2O_5 (M = Nb, Ta) also produced a small amount (approximately 10%) of a secondary phase M_5Si_3. This phase also correlated with some unreacted magnesium disilicide reagent in the as-formed product-mix. Trituration with acids removed this magnesium disilicide but could not remove the secondary M_5Si_3 phase.

$$M_2O_5 + 2Mg_2Si + CaSi_2 \rightarrow 2MSi_2 + 4MgO + CaO \quad (M = V,\ Nb,\ Ta) \tag{2}$$

$$2LiNbO_3 + 2Mg_2Si + CaSi_2 \rightarrow 2NbSi_2 + Li_2O + 4MgO + CaO \tag{3}$$

3.2. Synthesis; reaction of metal oxides and lithium silicide

Solid state metathesis reactions were also studied between metal oxides and lithium silicide, Table 1. The reactions of lithium silicide with $LiMO_3$ (M = Nb, Ta) and Li_2MoO_4 initiated more readily than the corresponding $CaSi_2$ and Mg_2Si reactions. In these two cases simply grinding the reagents together initiated the reaction. It was observed, conversely, that binary transition metal oxides such as M_2O_5 (M = V, Nb, Ta), V_2O_3 and MoO_3 could not be initiated on grinding with lithium silicide. All of the reactions of metal oxides with lithium silicide could be initiated in bulk by heating in an ampoule; a yellow thermal flash was noted at a point between 450 and 650 °C dependent on the specific reaction. In a number of cases initiation in the bulk produced single-phase metal silicides, Eqs. (4) and (5). The reactions that initiated on grinding produced a mixture of product phases.

$$Nb_2O_5 + 4Li_2Si \rightarrow 2NbSi_2 + 4Li_2O + 1/2O_2 \tag{4}$$

$$LiMO_3 + 2Li_2Si \rightarrow MSi_2 + 2.5Li_2O + 1/2O_2 \tag{5}$$

3.3. Characterisation

The samples produced after trituration in all reactions were black. The FT–IR spectra matched commercially available samples with a broad band at approximately 600 cm^{-1}. Elemental microanalysis of the silicides using powdered tin as a combustion aid showed negligible amounts of carbon, nitrogen and hydrogen.

X-ray powder diffraction showed that all modes of initiation; bulk heating, filament and grinding produced crystalline products without recourse to annealing (Fig. 1). The formed products were mixtures of co-formed salts (MgO, CaO and Li_2O) together with metal silicide. The washing procedure using dilute acid proved very effective in removing the co-formed oxide and in most cases left a single phase of metal silicide. Hence, from flame initiated reactions single phases of VSi_2 and $TaSi_2$ could be made in seconds from the reaction. Line broadening studies using the Scherrer equation indi-

Table 1
X-ray powder diffraction data of the products from the reactions of metal oxides and lithium silicide and calcium–magnesium silicide

Reaction	Initiation conditions	Products after trituration	a_{obs}, c_{obs} (Å) (± 0.004 Å) for principal phase
$V_2O_3 + Mg_2Si/CaSi_2$	bulk	VSi_2 [V_5Si_3]	$a = 4.565$, $c = 6.363$
$V_2O_5 + Mg_2Si/CaSi_2$	bulk	VSi_2	$a = 4.572$, $c = 6.373$
$V_2O_5 + Mg_2Si/CaSi_2$	flame	VSi_2	$a = 4.569$, $c = 6.369$
$Nb_2O_5 + Mg_2Si/CaSi_2$	bulk	$NbSi_2$	$a = 4.776$, $c = 6.555$
$Nb_2O_5 + Mg_2Si/CaSi_2$	flame	$NbSi_2$ [Nb_5Si_3]	$a = 4.801$, $c = 6.596$
$Nb_2O_5 + Li_2Si$	bulk	$NbSi_2$	$a = 4.787$, $c = 6.584$
$Nb_2O_5 + Li_2Si$	ground	Nb_5Si_3 [$NbSi_2$]	$a = 7.512$, $c = 5.247$
$LiNbO_3 + Li_2Si$	bulk	$NbSi_2$	$a = 4.792$, $c = 6.590$
$LiNbO_3 + Mg_2Si/CaSi_2$	flame	$NbSi_2$ [Nb_5Si_3]	$a = 4.796$, $c = 6.592$
$Ta_2O_5 + Mg_2Si/CaSi_2$	bulk	$TaSi_2$	$a = 4.778$, $c = 6.562$
$Ta_2O_5 + Mg_2Si/CaSi_2$	flame	$TaSi_2$	$a = 4.776$, $c = 6.560$
$Ta_2O_5 + Mg_2Si/CaSi_2$	filament	$TaSi_2$ [Si]	$a = 4.776$, $c = 6.561$
$LiTaO_3 + Li_2Si$	bulk	$TaSi_2$	$a = 4.777$, $c = 6.564$
$MoO_3 + Li_2Si$	ground	Mo, Mo_5Si_2, [$MoSi_2$]	
$Li_2MoO_4 + Mg_2Si/CaSi_2$	bulk	$MoSi_2$ [Mo_5Si_3, Mo]	$a = 3.199$, $c = 7.839$
$Li_2MoO_4 + Li_2Si$	flame	$MoSi_2$ [Mo_5Si_3]	$a = 3.198$, $c = 7.830$
$Li_2MoO_4 + Mg_2Si/CaSi_2$	flame	$MoSi_2$ [Mo]	$a = 3.203$, $c = 7.840$

[ ] Minor phases present.

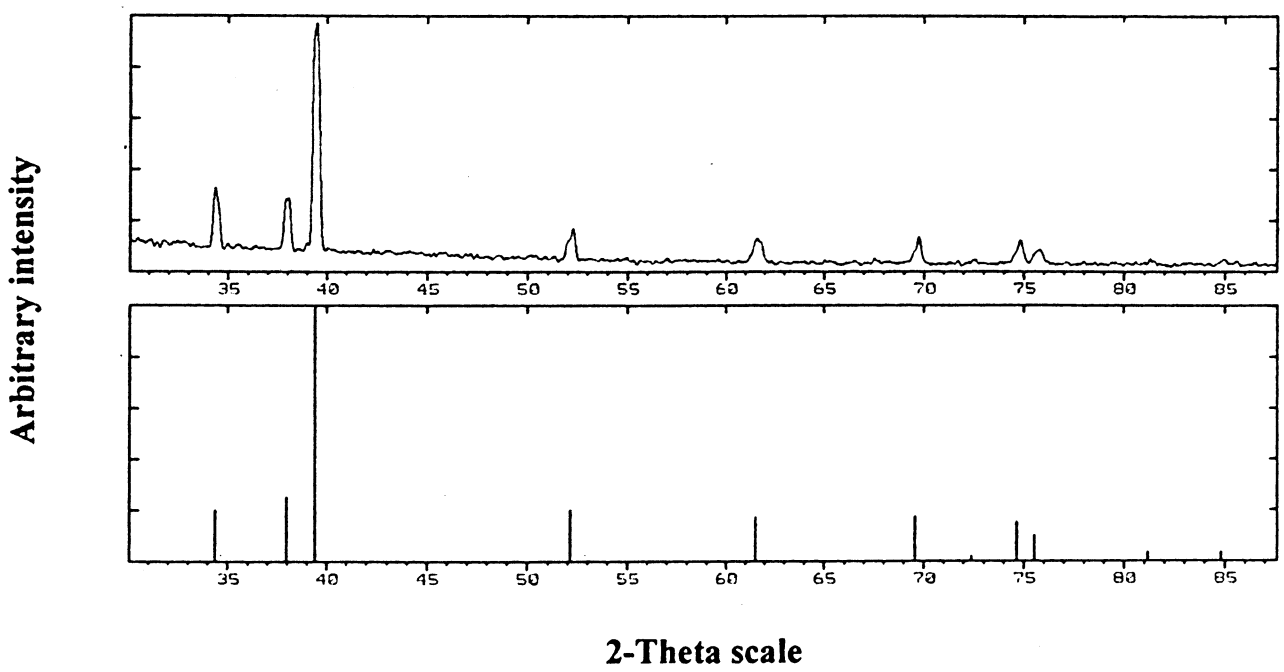


Fig. 1. Top trace; X-ray powder diffraction pattern of the product from reaction of Nb_2O_5 and calcium–magnesium silicide (bulk reaction, 1000 °C, 12 h), bottom trace XRD stick pattern for $NbSi_2$.

Table 2
ICCD [11] reference codes and unitcell data for comparison with Table 1

Compound	ICDD reference	*a* (Å)	*c* (Å)	Space group	Crystal system
VSi_2	38-1419	4.57230(16)	6.3730(4)	*P*6222	hexagonal
$NbSi_2$	8-450	4.7971	6.592	*P*6222	hexagonal
Nb_5Si_3	8-422	7.536	5.248	*P*63/*mcm*	hexagonal
$TaSi_2$	38-483	4.7851(7)	6.56980(16)	*P*6222	hexagonal
$MoSi_2$	41-612	3.2047(2)	7.8449(8)	*I*4/*mmm*	tetrahedral

Values in parentheses are e.s.d.'s, where these are available, corresponding to the least significant digits of entries. Note 8-422 vs 30-874 and 30-875 for Nb_5Si_3 and 41-612 vs 17-917 for $MoSi_2$.

cated that crystallite sizes were 500–600 Å irrespective of the mode of initiation [10]. The reactions involving molybdenum always produced mixed phase products irrespective of the starting silicide reagents. The reactions that initiated on grinding did not give single-phase silicide products. In this case it is probable that the reaction is too rapid for the formation of a single thermodynamic product. In all cases the X-ray powder patterns of the crystalline metal silicides indexed well with values within error limits of literature measurements (Table 2) [11].

EDAX analysis of the metal silicides, as formed from the SSM reactions showed that the pre-washed material contained calcium and magnesium oxide or lithium oxide in addition to metal and silicon. Trituration with dilute acid and water proved to be effective in removing the co-formed oxides. It was not effective in removing the free metal that was identified in some of the reactions. EDAX analysis of the triturated product correlated extremely well with the phases observed by XRD and gave the expected elemental ratios for silicon and transition metal over a number of surface spots. Electron-probe line-scan analyses were consistent with the EDAX results. Notably no calcium, magnesium or free silicon could be detected in the triturated products by either electron probe or EDAX. In the reactions involving molybdenum (Li_2MoO_4, MoO_3) some free metal was noted by both techniques, in agreement with the XRD results. SEM analysis revealed that the triturated products consisted of rough irregular particles with sharp surfaces. The products showed a narrow particle size distribution within the samples (Fig. 2(a and b)).

3.4. Thermodynamic considerations

Hesses law calculations indicate that the formation of transition metal silicide products from reaction of transition metal oxide and lithium silicide or calcium–mag-

nesium silicide is exothermic (typical exothermicities 300–500 kJ mol^{-1}) [12]. The driving force for the reaction is the formation of the co-formed oxides (MgO, CaO, Li_2O). This is analogous to traditional solid state metathesis reactions that are driven by the formation of co-formed salts (NaCl, LiCl, …). The reaction exothermicity is such that once the reaction is initiated it can be self-sustaining. In traditional SSM reactions an exothermicity of 300 kJ mol^{-1} is typically required for propagation [8,9], similar to that calculated for the oxide based metathesis reactions reported here. The temperature required to initiate a metathesis reactions often correlates with a phase change of one of the reagents. In the reactions studied here for silicides this does not seem readily applicable as the Li_2Si (760 °C), Mg_2Si (1085 °C) and $CaSi_2$ (980 °C) have melting points above the temperature at which the bulk reactions were noted to initiate (450–650 °C) [12]. It is possible that metal impurities, such as magnesium in the commercial Mg_2Si may initiate some of the reactions as magnesium melts at 645 °C. The maximum reaction temperature in the reactions is approximately 1000 °C as assessed by the colour of the synthesis flame. Full thermodynamic data on specific heat capacities could not be found for the silicide products, hence, a calculated maximum reaction temperature was not obtained [12].

4. Conclusions

A range of single-phase transition metal silicides can be made from solid state metathesis recations. This is the first report of the use of metal oxides as starting materials in SSM reactions. These have proven useful in silicide synthesis, in contrast attempts using metal halides formed mixed phase silicide products. In particular crystalline metal silicide powders can be made in seconds from solid state metathesis, in air, using a gas flame to initiate the process. Under all modes of reaction initiation crystalline products were produced without recourse to annealing.

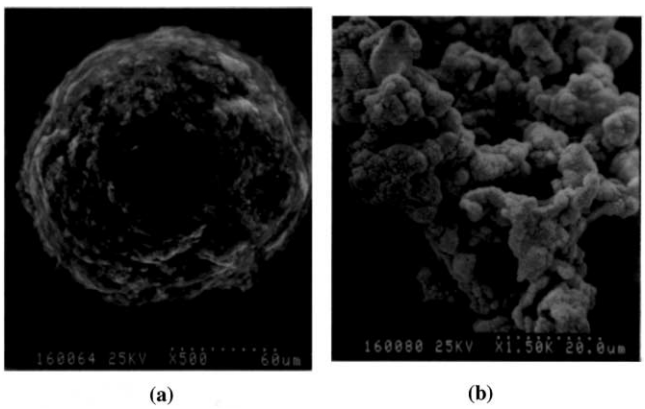


Fig. 2. SEM micrographs of $TaSi_2$ produced from SSM reaction of Ta_2O_3 and $CaSi_2/Mg_2Si$ at 1000 °C for 12 h. Reaction initiated at 500 °C.

Acknowledgements

I.P.P. and A.M.N. thank the EPSRC for a project studentship. Professor A.J. Craven and Dr M. McKenzie of Glasgow University are thanked for useful discussions.

References

[1] L. Topor, O.J. Kleppa, Met. Trans. A 17 (1986) 1217.
[2] N.N. Greenwood, A. Earnshaw, Chemistry of the Elements, Pergamon Press, Oxford, 1990.
[3] M.S. Chandrasekharaiah, J.L. Margrave, P.A.G. O'Hare, J. Phys. Chem. Ref. Data 22 (1993) 1459.
[4] (a) E.G. Rochow Jr., in: J.C. Bailar Jr., H.J. Emeléus, R. Nyholm, A.F. Trotman-Dickenson (Eds.), Comprehensive Inorganic Chemistry, vol. 1, Pergamon Press, Oxford, 1973;
(b) J.H. Weaver, A. Franciosi, V.L. Moruzzi, Phys. Rev. B 29 (1984) 3293.
[5] (a) H.C. Yi, J.J. Moore, J. Mater. Sci. 25 (1990) 1159;
(b) A.G. Merzhanov, Russ. Chem. Bull. 1 (1997) 8.
[6] (a) A.G. Merzhanov, in: Z.A. Munir, J.B. Holt (Eds.), Combustion and Plasma Synthesis of High Temperature Materials, VCH Publications, New York, 1990;
(b) A.G. Merzhanov, Int. J. SHS 4 (1993) 323.
[7] (a) J.B. Wiley, R.B. Kaner, Science 255 (1992) 1093;
(b) P.R. Bonneau, R.K. Shibao, R.B. Kaner, Inorg. Chem. 29 (1990) 2511;
(c) P.R. Bonneau, R.F. Jarvis, R.B. Kaner, Nature 349 (1991) 510;
(d) P.R. Bonneau, R.F. Jarvis, R.B. Kaner, Inorg. Chem. 31 (1992) 227;
(e) E.G. Gillan, R.B. Kaner, Chem. Mater. 8 (1996) 333;
(f) R.E. Treece, J.A. Conklin, R.B. Kaner, Inorg. Chem. 33 (1994) 5701;
(g) R.M. Jacubinas, R.B. Kaner, Mater. Res. Soc. Proc. 33 (1993) 133.
[8] (a) A.L. Hector, I.P. Parkin, Z. Naturforsch 49b (1994) 477;
(b) A.L. Hector, I.P. Parkin, J. Mater. Chem. 4 (1994) 279;
(c) J.C. Fitzmaurice, I.P. Parkin, A.T. Rowley, J. Mater. Chem. 4 (1994) 285;
(d) A.T. Rowley, I.P. Parkin, J. Mater. Chem. 3 (1993) 689;
(e) A.M. Nartowski, I.P. Parkin, M. MacKenzie, A.J. Craven, I. Macleod, J. Mater. Chem. 9 (1999) 1275;
(f) C.J. Carmalt, D.E. Morrison, I.P. Parkin, Main Group Metal Chem. 22 (1999) 263;
(g) C.J. Carmalt, D.E. Morrisen, I.P. Parkin, J. Mater. Chem. 8 (1998) 2209;
(h) A.M. Nartowski, I.P. Parkin, M. MacKenzie, A.J. Craven, Adv. Mater. 10 (1998) 805;
(i) M. Aguas, A.T. Nartowski, I.P. Parkin, A. Craven, M. Mckenzie, J. Mat. Chem. 8 (1998) 1875.
[9] J.C. Fitzmaurice, A.L. Hector, I.P. Parkin, A.T. Rowley, Phosphorus, Sulfur and Silicon 101 (1995) 47.
[10] H.P. Klug, L.E. Alexander, X-ray Diffraction Procedure for Polycrystalline and Amorphous Materials, 2nd ed., Wiley, New York, 1974.
[11] PDF-2 database on CD-ROM, International Centre for Diffraction Data, Swarthmore, PA 19081, USA, 1990.
[12] D.D. Wyman, W.H. Evans, V.B. Parker, R.H. Schumm, I. Harlow, S.M. Bailey, K.C. Chumey, R.L. Nuttal, The NBS Tables of Chemical Thermodynamics Properties, American Chemical Society, Washington DC, 1982.

PERGAMON

Polyhedron 21 (2002) 193–195

POLYHEDRON

www.elsevier.com/locate/poly

On the structure of heterometallic methoxide $Li_2(WO)_2(OMe)_{10}\cdot MeOH$

Zoya A. Starikova [a], Evgeniya P. Turevskaya [b,*], Nataliya Ya. Turova [b], Alexsandr I. Yanovsky [a]

[a] *A.N. Nesmeyanov Institute of Organoelement Compounds of Russian Academy of Sciences, 117813 Moscow, Russia*
[b] *Chemistry Department, M.V. Lomonosov Moscow State University, 119899 Moscow, Russia*

Received 3 August 2001; accepted 16 October 2001

Abstract

The crystalline $Li_2(WO)_2(OMe)_{10}\cdot MeOH$ (**I**) is formed as a side product in the process of anodic oxidation of tungsten in methanol in the presence of LiCl, which is used as a conductive additive. The structure of **I** as determined by the X-ray diffraction (XRD) method features infinite chains made up of two alternating tetranuclear species $[Li_2(WO)_2(OMe)_{10}]$ (**A**) and $[Li_2(WO)_2(OMe)_{10}(MeOH)_2]$ (**B**), linked via Li–O=W bridges involving the Li atom belonging to fragment **A** and tungstenyl group from fragment **B**. Each fragment occupies a special position in the crystallographic inversion center and has a metal–oxygen framework. All tungsten atoms have octahedral coordination, whereas all lithium vertices have five-coordinated trigonal bipyramidal environments. The H-bonds of the (A)W=O…HOMe(B) type in the crystal of **I** provide the links between the **A** and **B** fragments belonging to the different chains. © 2002 Published by Elsevier Science Ltd.

Keywords: Alkoxides; Crystal structures; Lithium; Tungsten; Methoxide

1. Introduction

Electrochemistry provides one of the most convenient synthetic routes to Mo and W alkoxides. The detailed studies of the processes of dissolution of Mo and W in alcohols in the presence of various conductive additives showed that along with the target products, i.e. the expected alkoxides, low yield side products may be often isolated from the electrolyte solutions. In most cases the latter represent heterometallic Li containing complexes. They are formed in the reactions between the Mo or W alkoxides and LiOR generated during the electrolysis of the electrolyte. The composition and structure of these complexes may vary depending on the particular metals and alcohols.

Thus, anodic dissolution of W in EtOH leads to crystallization of $WO(OEt)_4$ as the main product. However, after subsequent treatment of the mother electrolyte solution with $MeOC_2H_4OH$, the crystalline $[\{LiWO_2(OC_2H_4OMe)_3\}_2\cdot 2Li(HOC_2H_4OMe)_2]^{2+}[W_6O_{19}]^{2-}$ was isolated. Its structure comprises one neutral centrosymmetric molecule $\{Li_2W_2O_4(OR)_6\}$ and two cationic $\{Li(ROH)_2\}^+$ moieties linked into hexanuclear cationic aggregates $[\{Li_2W_2O_4(OR)_6\}\{Li(ROH)_2\}_2]^{2+}$ [1].

Electrochemical synthesis of Mo alkoxides in MeOH or EtOH yielded two side products, viz. $[LiMo_2^{V}O_2(OMe)_7\cdot MeOH]$ and $[LiMo_2^{VI}O_4(OPr^i)_4(OC_2H_4OMe)]_2$ (the latter precipitated upon the treatment of the mother liquor, from which $MoO(OEt)_4$ had been extracted, first with ^{i}PrOH, and then with methylcellosolve). In the crystals of the former, complex cationic and anionic residues, $[Li(MeOH)]^+$ and $[Mo_2O_2(OMe)_7]^-$, are linked into infinite chains via μ-OMe-groups. The anionic species represents a well-known motive in the alkoxide structural chemistry featuring M_2X_9 group, two octahedra sharing a common face. The dimeric molecule of the second side product is made up of two trinuclear $[LiMo_2O_2(OR)_5]$ fragments linked via two [Mo=O–Li] bridges [1].

The present paper reports the results of the structural study of complex $Li_2(WO)_2(OMe)_{10}\cdot MeOH$ (**I**) which was isolated in a small yield from the electrolyte, pre-

* Corresponding author.
E-mail address: turevsk@inorg.chem.msu.ru (E.P. Turevskaya).

0277-5387/02/$ - see front matter © 2002 Published by Elsevier Science Ltd.
PII: S0277-5387(01)00981-0

pared by the anodic oxidation of W in MeOH in the presence of LiCl [1,2]. No data on methoxotungstenates of lithium have ever been reported in literature (see discussions in [1,3]).

2. Experimental

The electrolysis was carried out for 9 h using direct current at 110 V and 0.1 A cm^{-2}, the concentration of the LiCl additive was 0.073 M, and the reaction mixture was kept at room temperature (r.t.). Upon completion of the process, the electrolyte turned dark-brown and then gradually changed to blue as the solution was left to stand for a week without atmospheric contact. After the solvent was removed in vacuo, the light-blue precipitate was treated with hexane. The most part of the precipitate was dissolved and a blue solution was formed. White non-transparent crystals of **I** were then slowly (in the course of approximately 1 week) reprecipitated on cooling to ~ 0 °C, the yield of the complex was 2–3%. The main products obtained by electrolysis—$W(OMe)_6$ and $WO(OMe)_4$ still remained in the solution.

3. Results and discussion

The structure of $Li_2(WO)_2(OMe)_{10}\cdot MeOH$ (**I**)[1] features zigzag-like infinite chains made up of two alternating fragments $[Li_2(WO)_2(\mu_3\text{-}OMe)_2(\mu\text{-}OMe)_4(OMe)_4]$ (**A**) and $[Li_2(WO)_2(\mu_3\text{-}OMe)_2(\mu\text{-}OMe)_4(OMe)_4(MeOH)_2]$ (**B**). Each of the fragments represents a tetranuclear centrosymmetric complex with coplanar metal atoms; this metal–oxygen framework is widely known in the alkoxide chemistry as the $Ti_4(OMe)_{16}$-type structure [4]. It is characterized by the presence of two distinct metal atom positions, which differ in the number of coordinated μ_3-O atoms. Indeed two of the four metal atoms are coordinated only by one μ_3-O whereas the other two are bonded to two μ_3-O atoms. In complex **I** the tungsten octahedra $[WO(\mu_3\text{-}OMe)(\mu\text{-}OMe)_2(OMe)_2]$ occupy the sites of the first kind in both fragments **A** and **B**; the lithium trigonal bipyramids $[LiO(\mu_3\text{-}OMe)_2(\mu\text{-}OMe)_2]$ and $[Li(\mu_3\text{-}OMe)_2(\mu\text{-}OMe)_2(MeOH)]$ occupy the sites of the second kind in the fragments of **A** and **B**, respectively. Table 1 lists selected bond lengths and angles within **I**. The fragments **A** and **B** are linked in the chains via Li–O=W bridges involving the Li atoms of the **A** fragments and the tungstenyl groups of the **B** fragments. The Li(1)–O(2)–W(2) angle is equal to 159.7(6)°.

Table 1
Selected bond lengths (Å) and angles (°) in the structure of **I**

Bond lengths			
W(1)–O(1)	1.734(7)	W(2)–O(12)	1.895(7)
W(1)–O(3)	1.946(6)	Li(1)–O(2)	2.023(15)
W(1)–O(4)	2.075(5)	Li(1)–O(3)	2.09(2)
W(1)–O(7)	1.899(7)	Li(1)–O(4)	1.99(2)
W(1)–O(8)	1.954(6)	Li(1)–O(4)$^{(i)}$	2.066(15)
W(1)–O(9)	1.891(7)	Li(1)–O(8)$^{(i)}$	2.06(2)
W(2)–O(2)	1.738(7)	Li(2)–O(5)	2.13(2)
W(2)–O(5)	2.078(6)	Li(2)–O(5)$^{(ii)}$	2.00(2)
W(2)–O(6)	1.938(6)	Li(2)–O(6)	2.090(15)
W(2)–O(10)	1.887(7)	Li(2)–O(11)$^{(ii)}$	2.07(2)
W(2)–O(11)	1.940(6)	Li(2)–O(13)	2.01(2)
Bond angles			
W(2)–O(2)–Li(1)	159.7(6)	W(2)–O(5)–Li(2)$^{(ii)}$	100.7(5)
W(1)–O(3)–Li(1)	101.5(5)	Li(2)–O(5)–Li(2)$^{(ii)}$	85.5(6)
W(1)–O(4)–Li(1)	100.5(5)	W(2)–O(6)–Li(2)	104.1(5)
W(1)–O(4)–Li(1)$^{(I)}$	100.4(5)	W(1)–O(8)–Li(1)$^{(i)}$	104.9(5)
Li(1)–O(4)–Li(1)$^{(i)}$	88.3(6)	W(2)–O(11)–Li(2)$^{(ii)}$	103.0(5)
W(2)–O(5)–Li(2)	97.9(5)		

Symmetry transformations: (i) $(-x, 2-y, 1-z)$; (ii) $(-x, 3-y, -z)$.

The existence of the W=O–Li bridges may be regarded as one of the most interesting features of the structure **I**. It is noteworthy that the W=O bond in the W=O–Li bridge in **I** (W(2)=O(2) 1.738(7) Å) is considerably longer than in $[WO(OMe)_4]_2$ (1.691 Å [5]), wherein the W=O bond is not involved in any additional interactions. The similar lengthening of the W=O bond is caused by its participation in the hydrogen bonding which is manifested in the long W(1)=O(1) bond in **I** (1.734(7) Å). At the same time the Li(1)–O(2) bond 2.023(15) Å does not show any lengthening as compared with other Li–O bonds in **I** (1.99–2.13 Å) or to the known Li–O distances, say, in LiOMe·2MeOH [6]. The Li–O bond lengths are in fact unaffected by the function of the O atom, which should be attributed to the predominantly ionic character of these bonds. On the other hand the lengths of the substantially covalent W–OR bonds show quite noticeable and regular increase with the increase of the number of oxygen atom neighbors (1.887–1.899 for the terminal OMe groups, 1.938–1.954 for μ_2-OMe and 2.075–2.078 Å for μ_3-OMe ligands).

The crystal structure of **I** supports the assumption that monomeric species $[LiWO(OMe)_5(MeOH)]_n$ and $[LiWO(OMe)_5(MeOH)_2]_2$ (the latter seems to be structurally analogous to the known sodium complex, $[NaWO(OEt)_5(EtOH)_2]_2$ [3]) indeed exist in the hydrocarbon solution. One may believe that elimination of one alcohol molecule and formation of the Li…O=W bridge occurs in the process of crystallization. (Fig. 1.)

[1] Crystal data for **I**: $C_{11}H_{34}Li_2O_{13}W_2$, $M = 755.96$, triclinic, space group $P\bar{1}$, $a = 8.664(5)$, $b = 10.974(8)$, $c = 13.416(11)$ Å, $\alpha = 77.88(6)$, $\beta = 72.18(5)$, $\gamma = 76.42(5)$°, $V = 1167.3(14)$ Å^3, $T = 213(2)$ K, $Z = 2$, λ(Mo Kα) = 0.71073 Å, 6165 reflections measured, 5735 unique ($R_{int} = 0.0786$) were used in all calculations. The final $wR(F^2)$ was 0.1514 for all data, $R(F)$ was 0.0550 for 4721 observed data with $I > 2\sigma(I)$.

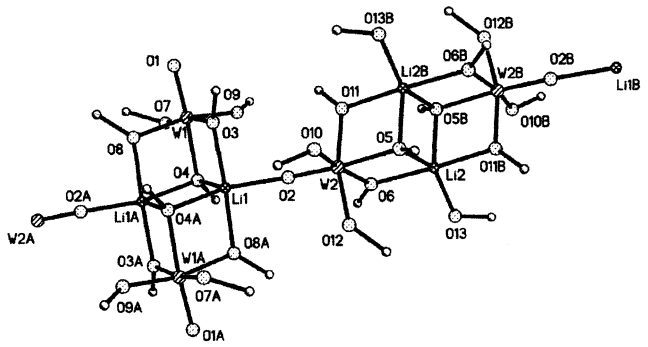


Fig. 1. The fragment of the infinite chain $[Li_2(WO)_2(OMe)_{10}\cdot MeOH]_n$ in the crystal of **I**.

The bridges of the M^{VI}=O–M^{I} type were observed previously in the structures of several Mo and W complexes. In particular such bridges were found in the above mentioned cation $\{[LiWO_2(OC_2H_4OMe)_3]_2\cdot 2Li(HOC_2H_4OMe)_2\}^{2+}$ (**2**), the neutral molecules $[LiMo_2^{VI}O_4(OPr^i)_4(OC_2H_4OMe)]_2$ (**3**) [1], and $[NaMo_2O_4(OPr^i)_5(^iPrOH)]_2$ (**4**) [3] as well as in the anionic species $[Mg_2Mo_8O_{22}(OMe)_6(MeOH)_4]^{2-}$ (**5**) [7]. It is noteworthy, however, that in all of the above mentioned literature results, in contrast to **I**, the M=O bond involved in the M=O–M bridge belongs to the MO_2 group. The lengthening of the M=O bond in all cases is similar to that observed in **I** [the M^{VI}=O(M^{I}) bond lengths are in the range of 1.72–1.76 Å]. At the same time the second M=O bond does not show any lengthening in **3** and **5**, (1.68–1.70 Å), whereas in **2** and **3** this bond is lengthened to the same extent as the one which takes part in the additional interaction. The bond angles M(VI)–O–M(I) in **1** and **3** (159.7(6) and 156.6°) are much wider than the corresponding angles in **2** and **4** (141.9 and 144.5°) which probably reflects the different degree of the sp^3–sp-rehybridization of the O atom.

It is worth mentioning, in conclusion, that the infinite chains built of the $[Ti_4(OMe)_{16}]$-type aggregates have been observed previously only in the structure of $[Na_2(MO_2)_2(OC_2H_4OMe)_6]_\infty$, M = Mo, W [3,8]. However, in these complexes the aggregates are linked via the bidentate ligand which coordinates the Na atoms of two neighboring tetranuclear fragments.

4. Supplementary material

Supplementary data for this compound are available on request from The Director, Cambridge Crystallographic Data Center, 12 Union Road, Cambridge CB2 1EZ, UK (fax: +44-1223-3360333; e-mail: deposit@ccdc.cam.ac.uk or www: http://www.ccdc.cam.ac.uk). CCDC deposition number, 167119.

References

[1] V.G. Kessler, A.N. Panov, N.Ya. Turova, et al., J. Chem. Soc., Dalton Trans. (1998) 21.
[2] S.I. Kucheiko, N.Y. Turova, V.A. Shreider, J. Gen. Chem. USSR 55 (1985) 2130.
[3] N.Y. Turova, V.G. Kessler, S.I. Kucheiko, Polyhedron 10 (1991) 2617.
[4] D.A. Wright, D.A. Williams, Acta Crystallogr., Sect. B 24 (1968) 1107.
[5] W. Clegg, R.J. Errington, P. Kraxner, C. Redshaw, J. Chem. Soc., Dalton Trans. (1992) 1431.
[6] Z.A. Starikova, E.P. Turevskaya, N.Ya. Turova, A.I. Yanovsky, J. Chem. Soc., Dalton Trans. (2000) 3237.
[7] M.Y. Antipin, Y.T. Struchkov, A.K. Shilova, L.M. Kachapina, L.P. Didenko, A.E. Shilov, Sov. J. Metalloorg. Chem. 2 (1989) 331.
[8] V.G. Kessler, D.E. Chebukov, N.Y. Turova, Russ. J. Inorg. Chem. 38 (1993) 23.

PERGAMON

Polyhedron 21 (2002) 197–203

POLYHEDRON

www.elsevier.com/locate/poly

Syntheses and characterization of lead(II) salts with 4,4′-bithiazole ligand: X-ray crystal structures of $[(BTZ)_2Pb(NO_3)_2]$ and $[(BTZ)Pb(SCN)_2]_n$ (a new polymeric compound)

Ali R. Mahjoub *, Ali Morsali

Department of Chemistry, School of Science, Tarbiat Modarres University, P.O. Box 14155-4838 Tehran, Iran

Received 3 August 2001; accepted 16 October 2001

Abstract

Complexes of lead(II) nitrate and lead(II) thiocyanate with 4,4′-bithiazole (BTZ) have been synthesized using a direct reaction of PbX_2 (X = nitrate and thiocyanate) and ligand. The complexes have been isolated and characterized by IR spectra and CHN elemental analysis. The structures of $[(BTZ)_2Pb(NO_3)_2]_2$ and $[(BTZ)Pb(SCN)_2]_n$ were confirmed by X-ray crystallography. The coordination polyhedron is different in the two complexes. The coordination number of Pb in $[(BTZ)_2Pb(NO_3)_2]$ is six (four by the chelating BTZ and two oxygen atoms of the two nitrate anions), whereas in $[(BTZ)Pb(NCS)_2]_n$ it is five with two different Pb environments, PbN_3S_2 (two by the chelating BTZ and three by SCN^- anions) and PbN_5 (two by BTZ and three by SCN^- anions). The coordination geometry of $[(BTZ)_2Pb(NO_3)_2]$ and $[(BTZ)Pb(NCS)_2]$ complexes show a gap around the Pb(II) ion, occupied possibly by a stereoactive lone pair of electrons on lead(II) and coordination around the lead atoms is hemidirected with a significant gap trans to chelating BTZ ligands, nitrate and thiocyanate anions. There is a π–π stacking interaction between the parallel aromatic rings belong to adjacent chains in $[(BTZ)Pb(NCS)_2]_n$ that may help to increase the 'gap' in the coordination geometry around the Pb(II) ion. © 2002 Elsevier Science Ltd. All rights reserved.

Keywords: BTZ ligands; X-ray crystallography; Pb(II) salts; π–π stacking interaction

1. Introduction

The most of the lead(II) issues are on macrocyclic ligands and recently a number of lead(II) complexes with different N-donor ligands have been synthesized and studied by X-ray crystallography [1–10]. These studies have provided a basis for a rather detailed analysis of the evidence for coordination sphere distortions, which may be a consequence of the presence of the lone pair on Pb^{2+}. It appears that in complexes of lead(II) [and probably in those of related species such as Tl(I) and Bi(III)], the nature and form of the coordination sphere is generally determined by a number of factors, possibly including lone pair–bond pair repulsions, of comparable influence, so that seemingly minor differences in ligands or in the crystal array can have quite marked effects upon the coordination stereochemistry. Since the presence of a lone pair is not directly detected but is inferred on the basis of the spatial distribution of atoms assumed to be donors to the central metal, the identification of these donor atoms is fundamental to the analysis of any particular system. In a recent report [2] on the crystal structure of $[Pb(phen)(O_2CCH_3)(O_2ClO_2)]$, the presence of a lone pair and its influence upon the coordination stereochemistry of the lead(II) ion and also π–π stacking interaction in polymeric structure was described.

In the present paper we want to show the nature of adducts formed between lead(II) salts (nitrate and thiocyanate anions) and the aromatic *N*,*N*′-bidentate ligand 4,4′-bithiazole (BTZ). This ligand is planar like 1,10-phenanthroline and 2,2′-bipyridyl, and can act as a bidentate ligand.

* Corresponding author. Tel.: +98-21-801-1001; fax: +98-21-800-6544.

E-mail address: mahjouba@net1cs.modares.ac.ir (A.R. Mahjoub).

0277-5387/02/$ - see front matter © 2002 Elsevier Science Ltd. All rights reserved.
PII: S0277-5387(01)00986-X

2. Experimental

2.1. Physical measurment

IR spectra were recorded as Nujol mulls using Perkin–Elmer 597 and Nicolet 510P spectrophotometers. Microanalyses were carried out using Carlo–Erba microanalyses.

2.2. Preparation of ligand

The BTZ ligand was prepared as described in the literature [11].

2.3. Preparation of $[(BTZ)_2Pb(NO_3)_2]$ (1)

(a) The complex $[(BTZ)_2Pb(NO_3)_2]$ was prepared by dissolving 0.331 g (1 mmol) lead(II) nitrate in distilled water and adding an alcoholic solution of BTZ (2 mmol). The resulting solution was stirred for 1 h at room temperature (r.t.); then it was allowed to stand for 2–3 days in a refrigerator. Colorless crystals of the desired product precipitated, which were filtered off, washed with C_3H_6O and ether, then air dried (yield 70%), m.p. 205 °C.

Anal. Found: C, 21.6; H, 1.2; N, 12.4. Calc. for $[(BTZ)_2Pb(NO_3)]_2$: C, 21.5; H, 1.19; N, 12.57%. The IR spectrum of the solid complex shows $\nu(NO_3)$ at 1378 cm^{-1} consistent with unidentate or unsymmetrical bidentate nitrate coordination.

(b) *Branched tube method:* 4,4′-Bithiazole (2 mmol) was placed in one arm of the branched tube and 0.331 g (1 mmol) lead(II) nitrate in the other. Methanol was carefully added to fill both arms, then the tube was sealed and the ligand-containing arm immersed in a bath at 60 °C while the other was at ambient temperature. After 15 days, white crystals, m.p. 205 °C had deposited in the cooler arm.

2.4. Preparation of $[(BTZ)Pb(NCS)_2]$ (2)

To a solution of BTZ (2 mmol) in hot MeOH was added a hot aq. solution of lead(II) nitrate (1 mmol) and excess of potassium thiocyanate. The final solution was allowed to cool slowly overnight, when crystals separated from the solution. The crystals were filtered,

Table 1
Crystal data and structure refinement for the two complexes

Compound	$[(BTZ)Pb(SCN)_2]$	$[(BTZ)_2Pb(NO_3)_2]$
Empirical formula	$C_{16}H_8N_8Pb_2S_8$	$C_{12}H_8N_6O_6PbS_4$
Formula weight	983.16	667.67
Temperature (K)	293(2)	153(2)
Wavelength (Å)	0.71073	0.71073
Crystal system	triclinic	monoclinic
Space group	$P\bar{1}$	$C2/c$
Unit cell dimensions		
a (Å)	9.672(4)	16.8571(19)
b (Å)	10.592(4)	13.3895(16)
c (Å)	13.386(5)	8.8706(11)
α (°)	103.77(3)	90
β (°)	101.78(3)	109.191(3)
γ (°)	92.65(3)	90
V (Å^3)	1297.4(8)	1890.9(4)
Z	2	4
D_{calc} (Mg m^{-3})	2.517	2.345
Absorption coefficient (mm^{-1})	13.627	9.410
$F(000)$	904	1264
Crystal size (mm)	$0.3 \times 0.2 \times 0.2$	$0.30 \times 0.15 \times 0.10$
θ range for data collection (°)	1.99–25.03	1.99–30.01
Index ranges	$0 \le h \le 11,\ -12 \le k \le 12,\ -15 \le l \le 15$	$-23 \le h \le 19,\ -18 \le k \le 18,\ -12 \le l \le 12$
Reflections collected	4678	10 968
Independent reflections	4381 [$R_{int} = 0.0485$]	2761 [$R_{int} = 0.0376$]
Completeness to theta (%)	95.5	99.9
Absorption correction	PSI-SCAN	SADABS
Max./min. transmission	0.856, 0.4856	1.00000, 0.54844
Refinement method	full-matrix least-squares on F^2	full-matrix least-squares on F^2
Data/restraints/parameters	4381/0/307	2761/0/148
Final R indices [$I > 2\sigma(I)$]	$R_1 = 0.0618,\ wR_2 = 0.1475$	$R_1 = 0.0199,\ wR_2 = 0.0499$
R indices (all data)	$R_1 = 0.0913,\ wR_2 = 0.1604$	$R_1 = 0.0210,\ wR_2 = 0.0504$
Goodness-of-fit on F^2	1.047	1.010
Largest difference peak and hole (e Å^{-3})	3.879 and −4.099	1.809 and −1.974

Table 2
Selected bond lengths (Å) and angles (°) for $[(BTZ)_2Pb(NO_3)_2]$

Bond lengths	
Pb(1)–N # 1	2.617(2)
Pb(1)–N(2)	2.617(2)
Pb(1)–N(3) # 1	2.636(2)
Pb(1)–N(3)	2.636(2)
Pb(1)–O(3) # 1	2.729(2)
Pb(1)–O(3)	2.729(2)
Pb(1)···O(1)	3.045
Pb(1)···O(1) # 2	3.110
Pb(1)···O(1) # 3	3.045
Pb(1)···O(1) # 4	3.110
Bond angles	
N(2) # 1–Pb(1)–N(2)	70.77(9)
N(2) # 1–Pb(1)–N(3) # 1	63.80(6)
N(2)1–Pb(1)–N(3) # 1	73.21(6)
N(2) # 1–Pb(1)–N(3)	73.21(6)
N(2)–Pb(1)–N(3)	63.80(6)
N(3) # 1–Pb(1)–N(3)	126.78(9)
N(2) # 1–Pb(1)–O(3) # 1	140.28(6)
N(2)–Pb(1)–O(3) # 1	70.54(6)
N(3) # 1–Pb(1)–O(3) # 1	112.23(6)
N(3)–Pb(1)–O(3) # 1	82.02(6)
N(2) # 1–Pb(1)–O(3)	70.54(6)
N(2)–Pb(1)–O(3)	140.28(6)
N(3) # 1–Pb(1)–O(3)	82.02(6)
N(3)–Pb(1)–O(3)	112.23(6)
O(3) # 1–Pb(1)–O(3)	148.98(6)

Symmetry transformations used to generate equivalent atoms: # 1 $-x, y+2, -z+1/2$; # 2 $-x, -y, -z$; # 3 $x, y, -z+1/2$; # 4 $-x, -y, z+1/2$.

washed with C_3H_6O and air dried (yield 80%), m.p. 250 °C. *Anal*. Found: C, 19.1; H, 1.2; N, 7.4. Calc. for $[(BTZ)Pb(SCN)_2]$: C, 19.3; H, 1.07; N, 7.53%. The IR spectrum of this complex shows ν(SCN) at 2040 cm^{-1}.

2.5. Crystallography

2.5.1. Crystal data and refinement details

*2.5.1.1. $[(BTZ)_2Pb(NO_3)_2]$ (**1**).* $C_{12}H_8N_6O_6PbS_4$, M 667.67, monoclinic, space group $C2/c$, a 16.8571(19), b 13.03895(16), c 8.8706(11) Å, β 109.191(3)°, V 1890.9(4) $Å^3$, D_{calc} ($Z = 4$ f.u.) 2.345 mg m^{-3}, F(000) 1264, specimen: $0.30 \times 0.15 \times 0.10$ mm, $T_{max,min}$ 1.00000, 0.54844, N 10 968, N_0 2761, R 0.0199, R_w 0.0499.

*2.5.1.2. $[(BTZ)Pb(SCN)_2]_2$ (**2**).* $C_{16}H_8N_8Pb_2S_8$, M 983.16, triclinic, space group $P\bar{1}$, a 9.672(4), b 10.592(4), c 13.386(5) Å, α 103.77(3), β 101.78(3), γ 92.65(3)°, V 1297.4(8) $Å^3$, D_{calc} ($Z = 2$ f.u.) 2.517 mg m^{-3}, F(000) 904, specimen: $0.3 \times 0.2 \times 0.2$ mm, $T_{max,min}$ 0.856, 0.4856, N 4678, N_0 4381, R 0.0618, R_w 0.1475.

2.5.2. Determination of the structures

Crystallographic measurements were made at 153(2) K using a Siemens R3m/V diffractometer. The intensity data were collected within the range $1.99° \leq \theta \leq 30.01°$ for compound **1** and $1.99° \leq \theta \leq 25.03°$ for compound **2** using graphite monochromated Mo Kα radiation ($\lambda = 0.71073$ Å). Accurate unit cell parameters and orientation matrix for data collection were obtained from least-squares refinements. Intensities of 10 968 for compound **1** and 4678 for compound **2** unique reflections were measured, from which 2649 for compound **1** and 4381 for compound **2** with $I > 2\sigma(I)$ were used in the refinement. The structures have been solved by direct methods and refined by full-matrix least-squares techniques on F^2.

The positions of hydrogen atoms were idealized and included in the calculations of the structure factors as fixed contributions. Each hydrogen atom was assigned an isotopic thermal parameter. R, R_w, with a goodness-of-fit on F^2 of 1.010, for compound **1** are 0.0199, 0.046 and for compound **2** are 0.0818, 0.1475. The final difference density map showed a maximum peak and hole of 1.809 and -1.947 e $Å^{-3}$ for compound **1**, 3.879 and -4.099 e $Å^{-3}$ for compound **2**. Corrections for the Lp as well as the empirical correction for absorption using the SADABS programs for compound **1**

Table 3
Selected bond lengths (Å) and angles (°) for the $[(BTZ)Pb(SCN)_2]_n$

Bond lengths	
Pb(1)–N(5)	2.441(13)
Pb(1)–N(1)	2.502(10)
Pb(1)–N(2)	2.549(11)
Pb(1)–N(6)	2.686(14)
Pb(2)–N(7) # 1	2.525(11)
Pb(2)–N(3)	2.531(11)
Pb(2)–N(4)	2.548(11)
Pb(2)–S(7)	3.021(4)
Pb(2)–S(6)	3.053(4)
S(1)–C(1)	1.676(15)
Bond angles	
N(5)–Pb(1)–N(1)	85.5(4)
N(5)–Pb(1)–N(2)	81.4(4)
N(1)–Pb(1)–N(2)	67.0(4)
N(5)–Pb(1)–N(6)	88.2(5)
N(1)–Pb(1)–N(6)	78.6(4)
N(2)–Pb(1)–N(6)	144.6(4)
N(7) # 1–Pb(2)–N(3)	77.5(4)
N(7) # 1–Pb(2)–N(4)	83.4(4)
N(3)–Pb(2)–N(4)	66.9(4)
N(7) # 1–Pb(2)–S(7)	90.0(3)
N(3)–Pb(2)–S(7)	82.7(3)
N(4)–Pb(2)–S(7)	149.63(3)
N(7) # 1–Pb(2)–S(6)	155.3(3)
N(3)–Pb(2)–S(6)	78.9(2)
N(4)–Pb(2)–S(6)	94.2(3)
S(7)–Pb(2)–S(6)	79.67(10)

Symmetry transformations used to generate equivalent atoms: # 1 $-x, -y+2, -z+1$.

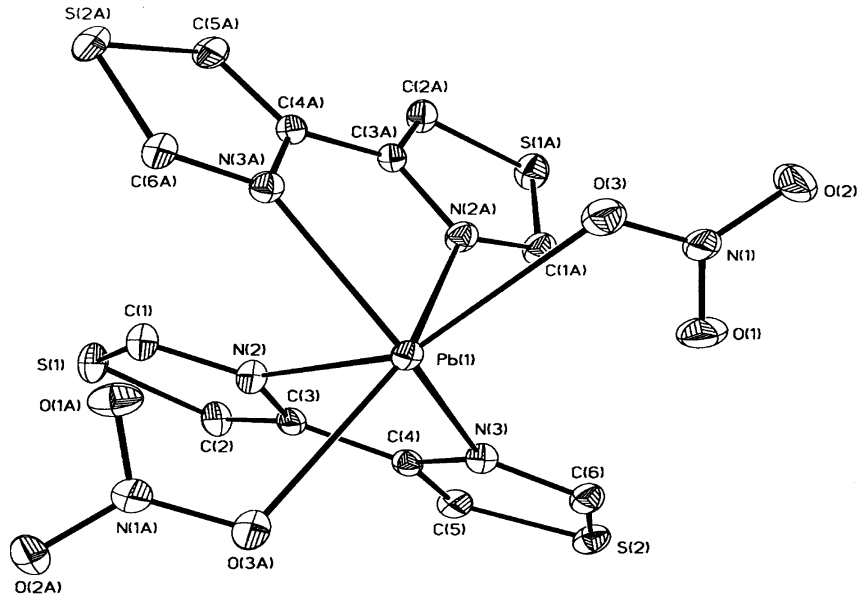


Fig. 1. ORTEP diagram of $[(BTZ)_2Pb(NO_3)_2]$. Hydrogen atoms are omitted for clarity.

and PSI-SCAN programs for compound **2** were applied. All structural calculations were carried out with a PDP—11/23+ computer using the SDP–PLUS program package [12,13].

Crystal data and structure refinement are given in Table 1. Selected bond lengths and angles are given in Tables 2 and 3. Anisotropy thermal parameters, observed and calculated structure factors, full lists of bond distances, bond angles and torsion angles are given in the Section 4. ORTEP diagrams and a perspective view of the packing in the unit cells are shown in Figs. 1–5.

3. Discussion

3.1. Synthesis

The method of synthesis of both complexes is the same and in preparing these two complexes, BTZ ligand and lead(II) nitrate have been reacted in a 2:1 ratio. In preparing $(BTZ)Pb(SCN)_2$, KSCN is used excess. The attempt to isolate $(BTZ)_2Pb(SCN)_2$ was not successful and each time the 1:1 adduct was isolated.

3.2. Crystal structure of $[(BTZ)_2Pb(NO_3)_2]$ (1)

The crystal structure of compound **1** consists of dimeric units of $[(BTZ)_2Pb(NO_3)_2]_2$. Each lead atom is chelated by the nitrogens of two BTZ ligands with a Pb–N distance of 2.617 and 2.636 Å, and the oxygen atoms of nitrate anions with a Pb–O distance of 2.729 Å. The coordination number in this complex is six (four from BTZ ligands and two from nitrate anions) and the weak interaction of lead(II) with oxygen atoms of an adjacent molecule produces dimer units in the solid state. In fact each Pb atom in this structure alone with six normal bonds forms four 'weak' Pb···O bonds. Only two of them are symmetry independent and the exact distances are Pb1···O1 = 3.045, Pb1···O1 $(-x, -y, -z) = 3.110$ Å, Pb1···O1 $(-x, y, 1/2-z) = 3.045$ and Pb1···O1 $(-x, -y, z+1/2) = 3.110$ Å (Table 2). The presence of a lone pair of electrons on the lead atom is apparently the reason why the bridging interactions cannot come closer together. If the stereochemically active lone pair was not present, it might create a

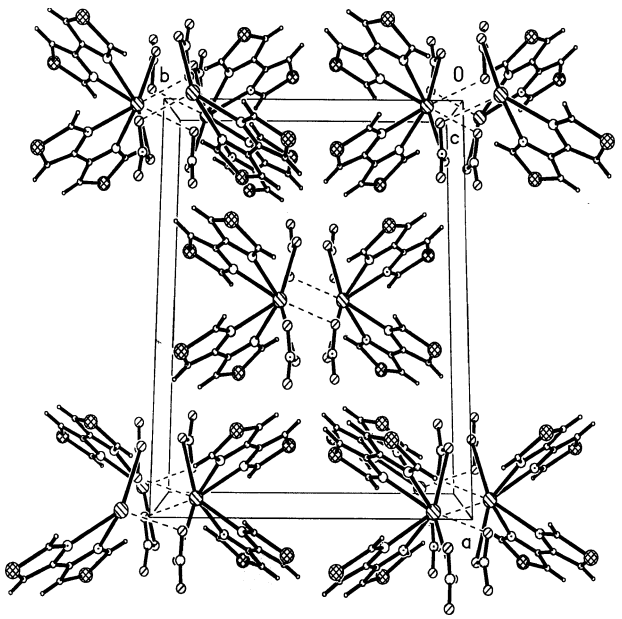


Fig. 2. The unit cell of $[(BTZ)_2Pb(NO_3)_2]_2$.

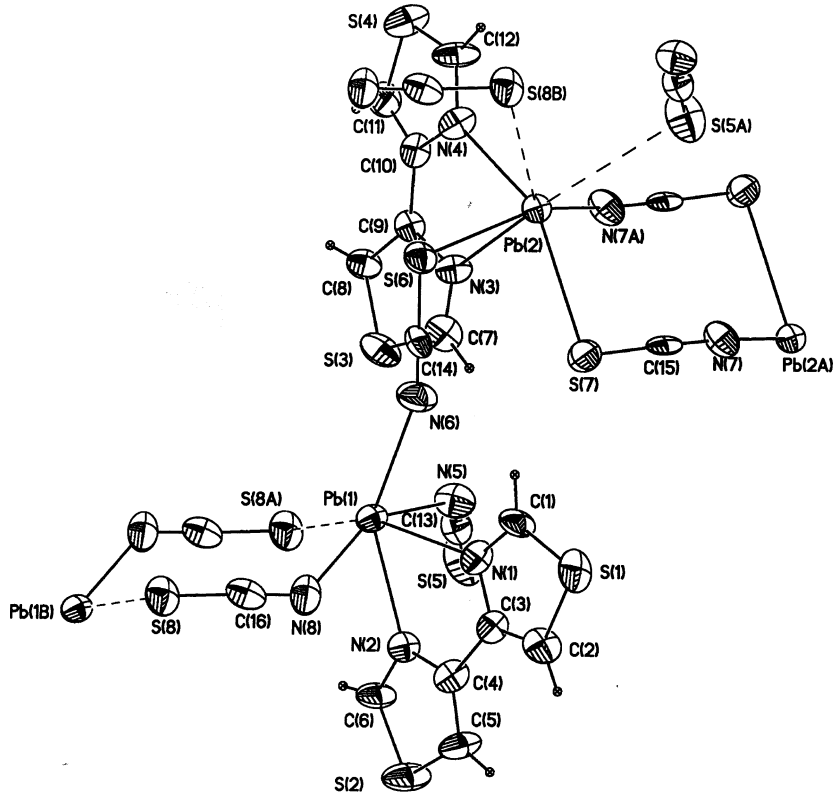


Fig. 3. ORTEP diagram of $[(BTZ)Pb(SCN)_2]_n$.

greater interaction between bridging atoms of lead(II) with the neighboring oxygens from nitrate anions. Consequently, this phenomenon could lead to more symmetry.

The arrangement of BTZ ligands and nitrate anions suggests a gap in the coordination geometry around the metal ion [O(3A)–Pb(1)–O(3) angle is 148.98°] (Table 2), occupied possibly by a stereoactive lone pair of electrons on lead(II). The observed shortening of the Pb–N bond on the side of Pb(II) ion opposite to the position of the putative lone pair (2.617 compared with 2.636 Å adjacent to the lone pair) supports the presence of this feature [4]. Hence, the geometry of the nearest

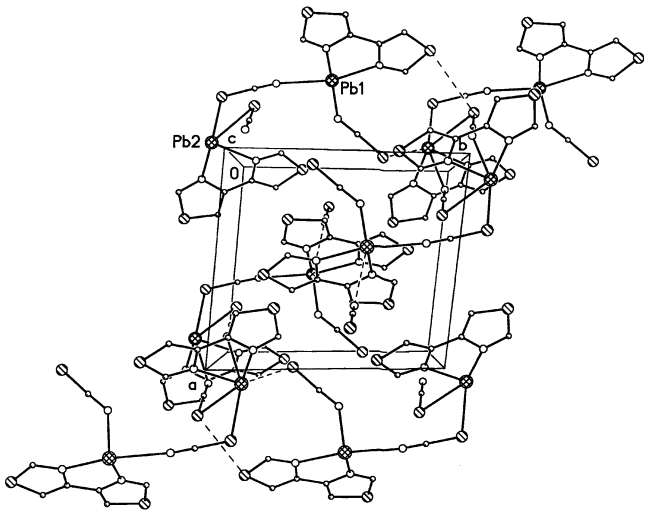


Fig. 4. The unit cell of $[(BTZ)Pb(SCN)_2]_n$.

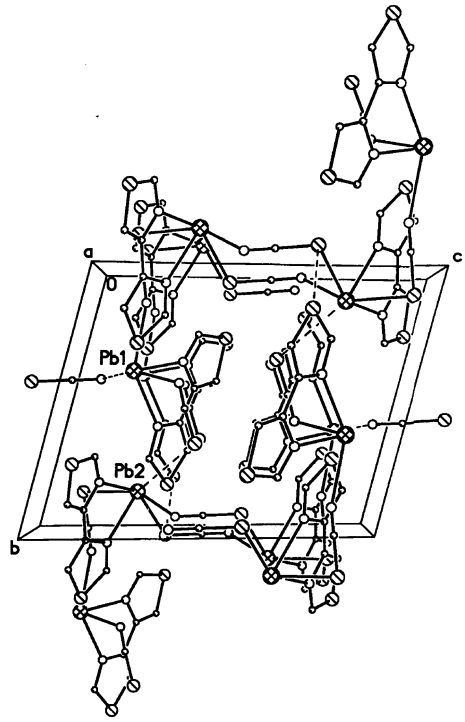


Fig. 5. Showing π–π stacking interaction in $[(BTZ)Pb(SCN)_2]_n$ with atom labelling.

coordination environment of every lead atom is likely caused by the geometrical constraints of coordinated BTZ ligands, nitrate anions and by the influence of a stereochemically active lone pair of electrons in a hybrid orbital on the metal atom. Such an environment leaves space for bonding of oxygen atoms of nitrate anions of an adjacent molecule (Fig. 2).

3.3. Crystal structure of [(BTZ)Pb(NCS)$_2$] (2)

The structure of compound **2** is polymeric as a result of thiocyanate ligand bridging (Fig. 3), with various similarities to polymeric (phen)Pb(SCN)$_2$ [10], in which the lead atoms are five coordinated with two different coordinate polyhedra, PbN_3S_2 (two by the chelating BTZ and three by SCN^- anions) and PbN_5 (two by BTZ and three by SCN^- anions).

The Pb(1) atoms are in a deformed pseudooctahedral arrangement with five nitrogen atoms, two from the bithiazole ligand and three from the thiocyanate anions (one lone pair of electrons occupying an equatorial site). The Pb(2) atoms are also in a deformed pseudooctahedral arrangement with two nitrogen atoms from the bithiazole ligand, two sulfur atoms and one nitrogen atom from the thiocyanate anions (one lone pair of electrons occupying an equatorial site).

The arrangement of the BTZ ligands and two SCN^- anions [N(2)–Pb(1)–N(6), N(7A)–Pb(2)–S(6) angles are 144.6° and 155.3°, respectively] (Table 3) suggests a gap in the coordinate geometry around the metal ions, occupied possibly by a stereoactive lone pair of electrons on the lead(II). The observed shortening of the Pb–N bond on side of the Pb(II) ion opposite to the position of the putative lone pair (2.441 compared with 2.686 Å adjacent to the lone pair) supports the presence of this feature [4]. Hence the geometry of the nearest coordination environment of every lead atom, the same as the compound **1**, is likely to be caused by the geometrical constraints of coordinated bithiazole ligands, thiocyanate anions and by the influence of a stereochemically active lone pair of electrons in an hybrid orbital on the metal atom, which occupies one equatorial coordination site of a pseudooctahedral. Such an environment leaves space for bonding of sulfur atoms (Fig. 3).

The possible stereochemically active lone pair of electrons in divalent lead compounds has recently been discussed by Shimoni-Livny et al., based on a thorough review of crystal data available in the Cambridge Structural Database (CSD) [14]. They classified lead complex coordination as holodirected or hemidirected. Holodirected refers to complexes in which the bonds to ligands are directed throughout the surface of an encompassing sphere, while hemidirected refers to those cases in which the bonds to ligands are directed throughout only part of the coordination sphere, leaving a gap in the distribution of bonds to the ligands. The latter is present in all Pb(II) compounds with coordination numbers 2–5, is quite common in Pb(II) complexes with coordination numbers 6, 7 and 8 and does not exist in lead complexes with higher coordination number, where holodirected geometry is the rule. For the structures described here, coordination around the lead atoms is hemidirected with a significant gap trans to the BTZ ligand, nitrate and thiocyanate anions. The strikingly different features of compound **2** compared to compound **1** is that there is a π–π stacking interaction (charge-transfer arrays) [15,16] between the parallel aromatic rings belong to adjacent chains, as shown in Fig. 5. It is a planar species in which the mean molecular planes are close to parallel and separated by a distance of ~3.5 Å, close to that of the planes in graphite. The 'gap' in $[(BTZ)Pb(NCS)_2]_n$ is more than that in $[(BTZ)_2Pb(NO_3)]_2$. In five reported compounds, $[Pb(phen)(CH_3COO)_2]_2$, $[Pb(phen)(NO_3)_2]_n$, $[Pb(bpy)(NO_3)_2]_n$ [10], $[Pb(phen)(CH_3COO)(ClO_4)]_n$ [2], $[Pb(phen)(CH_3COO)(NO3)]_n$ [17], and the reported compound here, $[(BTZ)Pb(SCN)_2]_n$, the ratio of ligand–metal is 1:1. There are π–π stacking interactions in all these compounds, but π–π stacking interactions are rarely observed in complexes with a ligand–metal ratio of 2:1 [10]. In both 1:1 and 2:1 complexes there is a gap but this gap is more for the 1:1 ratio. It may be that this increased gap is due to the influence of the π–π stacking of aromatic units upon Pb(II) coordination.

4. Supplementary material

Complete bond lengths and angles, co-ordinates and displacement parameters have been deposited with the Cambridge Crystallographic Data Centre, CCDC Nos. 162630 and 167891 for compounds **1** and **2**. Supplementary data are available on request from The Director, CCDC, 12 Union Road, Cambridge CB2 1EZ, UK (fax: +44-1223-336033; e-mail: deposit@ccdc.cam.ac.uk or www: http://www.ccdc.cam.ac.uk).

Acknowledgements

The Tarbiat Modarres University Research Council supported this work.

References

[1] L.M. Engelhard, D.L. Kepert, J.M. Patrick, A.H. White, Aust. J. Chem. 42 (1998) 329.
[2] A.K. Hall, J.M. Engelhard, A. Morsali, A.A. Soudi, A. Yanovsky, Crystallogr. Eng. Commun. (2000) 13.

[3] R.D. Hancock, in: A.F. Williams, C. Floriani, A.E. Merbach (Eds.), Perspectives in Coordination Chemistry, VCHA:VCH, Basel, 1992, p. 129.
[4] R.D. Hancock, M.S. Shaikjee, S.M. Dobson, J.C.A. Boeyens, Inorg. Chim. Acta 154 (1988) 229.
[5] P. Pyykkö, Chem. Rev. 88 (1988) 563.
[6] A. Bashall, M. Mcpartlin, B.P. Murphy, D.E. Fenton, S.J. Kitchen, P.A. Tasker, J. Chem. Soc., Dalton Trans. (1990) 505 and references therein.
[7] P. Schwerdtheger, G.A. Heath, M. Dolg, M.A. Bennett, J. Am. Chem. Soc. 114 (1992) 7518.
[8] K. Byriel, K.R. Dunster, L.R. Gahan, C.H.L. Kennard, J.L. Latten, I.L. Swann, P.A. Duckworth, Polyhedron 11 (1992) 1205.
[9] A. Andres, A. Bencini, A. Garachalios, A. Bianchi, P. Dapporto, E. Garcia-Espna, P. Paoletti, P. Paoli, J. Chem. Soc., Dalton Trans. (1993) 3507.
[10] (a) J.M. Harrowfield, H. Miyamae, B.W. Skelton, A.A. Soudi, A.H. White, Aust. J. Chem. 49 (1996) 1029;
(b) J.M. Harrowfield, H. Miyamae, T.M. Shand, B.W. Skelton, A.A. Soudi, A.H. White, Aust. J. Chem. 49 (1996) 1043;
(c) J.M. Harrowfield, H. Miyamae, T.M. Shand, B.W. Skelton, A.A. Soudi, A.H. White, Aust. J. Chem. 49 (1996) 1051;
(d) J.M. Harrowfield, H. Miyamae, B.W. Skelton, A.A. Soudi, A.H. White, Aust. J. Chem. 49 (1996) 1067;
(e) J.M. Harrowfield, H. Miyamae, B.W. Skelton, A.A. Soudi, A.H. White, Aust. J. Chem. 49 (1996) 1081;
(f) G.A. Bowmaker, J.M. Harrowfield, H. Miyamae, B.W. Skelton, A.A. Soudi, A.H. White, Aust. J. Chem. 49 (1996) 1089;
(g) I. Bytheway, L.M. Engelhardt, J.M. Harrowfield, D.L. Kepert, H. Miyamae, J.M. Patrick, B.W. Skelton, A.A. Soudi, A.H. White, Aust. J. Chem. 49 (1996) 1099;
(h) L.M. Engelhardt, J.M. Harrowfield, D.L. Kepert, H. Miyamae, J.M. Patrick, B.W. Skelton, A.A. Soudi, A.H. White, Aust. J. Chem. 49 (1996) 1111;
(i) J.M. Harrowfield, H. Miyamae, B.W. Skelton, A.A. Soudi, A.H. White, Aust. J. Chem. 49 (1996) 1121;
(j) J.M. Harrowfield, H. Miyamae, B.W. Skelton, A.A. Soudi, A.H. White, Aust. J. Chem. 49 (1996) 1127;
(k) L.M. Engelhardt, J.M. Harrowfield, D.L. Kepert, H. Miyamae, J.M. Patrick, B.W. Skelton, A.A. Soudi, A.H. White, Aust. J. Chem. 49 (1996) 1135;
(l) J.M. Harrowfield, D.L. Kepert, H. Miyamae, B.W. Skelton, A.A. Soudi, A.H. White, Aust. J. Chem. 49 (1996) 1147;
(m) J.M. Harrowfield, H. Miyamae, B.W. Skelton, A.A. Soudi, A.H. White, Aust. J. Chem. 49 (1996) 1157;
(n) J.M. Harrowfield, H. Miyamae, B.W. Skelton, A.A. Soudi, A.H. White, Aust. J. Chem. 49 (1996) 1165.
[11] H. Erlenmeyer, H. Ueberwasser, Helv. Chim. Acta 23 (1940) 1268.
[12] G. Ferguson, C. Glidewell, E.S. Lavender, Acta Crystallogr., Sect. B B55 (1999) 591.
[13] G.M. Sheldrick, SHLXTL-97 V5.10, Bruker AXS Inc., Madison, WI-53719, USA, 1997.
[14] L. Shimonni-Livny, J.P. Glusker, C.W. Bock, Inorg. Chem. 37 (1998) 1853.
[15] R. Foster (Ed.), Molecular Complexes, Paul Elek (Scientific Books), London, 1973.
[16] N.N. Greenwood, A. Earnshaw, Chemistry of the Elements, Pergamon Press, Oxford, 1984, pp. 235–236.
[17] A. Morsali, M. Payheghader, M.S. Salehi, submitted for publication in Zeitschrift fur anorganische und allgemeine Chemie.

PERGAMON

Polyhedron 21 (2002) 205–209

POLYHEDRON

www.elsevier.com/locate/poly

Metal-phosphine chalcogenide interactions. Crystal structures of palladium(II)/mercury(II) complexes with 1,2-bis(diphenylthiophosphinyl)ethane containing seven-membered metallacyclic rings

Tarlok S. Lobana [a,*], Renu Verma [a], Amarjeet Singh [a], Meenam Shikha [a], Alfonso Castineiras [b]

[a] *Department of Chemistry, Guru Nanak Dev University, Amritsar 143 005, India*
[b] *Departamento de Quimica Inorganica, Facultad de Farmacia, Universidad de Santiago, 15706 Santiago, Spain*

Received 24 April 2001; accepted 17 October 2001

Abstract

An organophosphorus ligand, namely, 1,2-bis(diphenylthiophosphinyl)ethane {$Ph_2P(S)–CH_2–CH_2–P(S)Ph_2$; $dppeS_2$} reacted with palladium(II) chloride in acetonitrile forming $[PdCl_2(dppeS_2)](CH_3CN)$ (**1**). Similarly, it reacted with mercury(II) bromide in acetone to yield $HgBr_2(dppeS_2)$ (**2**). In these compounds, Pd/Hg are bonded to two S atoms of chelating $dppeS_2$ ligand and to the respective halogen atoms. The geometry about Pd is distorted square planar with *trans*-bond angles S(1)–Pd–Cl(1) and S(2)–Pd–Cl(2) being 174.10(5)° and 172.85(5)°, respectively. The angles about Hg vary in the range 96.20(6)–124.56(4)°, suggesting highly distorted geometry about Hg. The bite angle S(1)–Hg–S(2) of the ligand is 118.85° in **2** versus 97.76° in **1**, and it demonstrates large flexibility of alkane moiety and stability of the seven-membered metallacyclic rings formed by $dppeS_2$.
© 2002 Elsevier Science Ltd. All rights reserved.

Keywords: Phosphine chalcogenide; Seven-membered; Palladium(II); Mercury(II); Metallacyclic rings; bis(diphenylthiophosphinyl)ethane

1. Introduction

Organophosphorus ligands such as tertiary phosphine oxides, sulphides, or selenides (I, II below) bearing O, S, or Se donor atoms have been the focus of several investigations related to their coordination chemistry, extractive metallurgy, catalytic properties, and structural chemistry [1,2].

$$\underset{\text{I}}{R_3P=E} \qquad \underset{\text{II}}{R_2P(E)–(CH_2)_m–P(E)R_2}$$

$\{E = O, S, Se;\ R = Ph, \text{etc.} \quad m = 1, 2, \text{etc.}\}$

In view of the importance of the study of metal–sulphur interactions, the structures and spectroscopic properties of a number of metal complexes of heterocyclic thiones, thiosemicarbazones, and tertiary phosphine chalcogenides have been reported in the literature [1–11]. As a part of our interest in investigating the structural chemistry of metal–phosphine chalcogenide interactions, particularly with bis(tertiary phosphine chalcogenides), we have reported the structures of the complexes, viz. $[HgCl_2\{Ph_2P(S)–CH_2–P(S)Ph_2\}]$ [11c] (compound **3**), $[HgI_2\{Ph_2P(S)–CH_2–PPh_2\}]$ [11b] (compound **4**), $[HgCl_2\{Ph_2P(S)–CH_2–CH_2–P(S)Ph_2\}]$ [11b] (compound **5**), $[HgPh_2\{Ph_2P(S)–CH_2–CH_2–P(S)Ph_2\}]$ [11a] (compound **6**), $[Cu_2(\mu\text{-}I)_2(Ph_3PSe)_2(MeCN)_2]$ [12](compound **7**), $[Cu_2(\mu\text{-}I)_2(Ph_3PS)_2{\cdot}(CH_3CN)_2]$ [13] (compound **8**), and $[Cu_2(\mu\text{-}Cl)_2(dppeSe_2)_2]$ [13] (compound **9**; $dppeSe_2$ is selenium analogue of $dppeS_2$), $[ZnI_2(dppmSe_2)]$ [14] (compound **10**, $dppmSe_2 = Ph_2P(Se)–CH_2–P(Se)Ph_2$). As regards palladium, there are only two complexes, $PdCl_2L_2$ {$L = PhEt_2PS$, *i*-Bu_3PS}, whose crystal structures are known and none

* Corresponding author. Tel.: +91-183-257604; fax: +91-183-258820.
E-mail address: tarlok@angelfire.com (T.S. Lobana).

0277-5387/02/$ - see front matter © 2002 Elsevier Science Ltd. All rights reserved.
PII: S0277-5387(01)00977-9

among bis(tertiary phsophine sulphides or selenides) [1,15,16].

In this paper, the structures of complexes of palladium(II)/mercury(II) with 1,2-bis(diphenylthiophosphinyl)-ethane are described which represent rare examples of seven-membered chelate ring formation among metal-phosphine sulphides or selenides [11b]. In a copper(I) complex, $[Cu_2Cl_2\{dppeS_2\}_2]$, $dppeS_2$ bridges two Cu atoms [13]. Furthermore, for palladium(II) it is the first structurally characterised complex with a bis(tertiary phosphine chalcogenide) [1,2,18].

2. Experimental

2.1. General materials

Palladium(II) chloride and mercury(II) bromide were of standard grade and used as such. The compound 1,2-bis(diphenylphosphino)ethane, $\{Ph_2P–CH_2–CH_2–PPh_2$, dppe$\}$, was prepared by lithiation of PPh_3 in dry tetrahydofuran followed by the reaction with dichloroethane [17]. Treatment of dppe with elemental sulphur (1:2 mole ratio) in benzene formed $Ph_2P(S)–CH_2–CH_2–P(S)Ph_2$ $\{dppeS_2\}$ [18].

2.2. Preparation of $[PdCl_2(dppeS_2)](CH_3CN)$ (1)

To a solution of palladium(II) chloride (0.100 g, 0.56 mmol) in hot acetonitrile (25 cm^3) was added to the solution of the ligand, $dppeS_2$ (0.260 g, 0.56 mmol), and the contents refluxed for 3 h. The solution was filtered and allowed to crystallise, whereupon light red-coloured crystals were formed. The crystals were separated and dried at room temperature (r.t.). Yield 70%; melting point (m.p.) 245–47 °C. *Anal.* Found: C, 49.4; H, 4.3; N, 1.97. Calc. for $C_{28}H_{27}Cl_2NPdS_2$: C, 49.4; H, 4.0; N, 2.05%. Main IR bands: 1098 cm^{-1} $\{\nu P–C\}$; 575 cm^{-1} $\{\nu P–S\}$; ligand band($dppeS_2$): 1097 cm^{-1} $\{\nu P–C\}$; 600 cm^{-1} $\{\nu P–S\}$.

2.3. Preparation of $[HgBr_2(dppeS_2)]$ (2)

To a solution of mercury(II) bromide (0.050 g, 0.14 mmol) in acetone (20 cm^3) was added the solution of the ligand, $dppeS_2$ (0.065 g, 0.14 mmol), in acetone (20 cm^3) and the contents were stirred for 1 h, followed by refluxing for half an hour. The solution was filtered and allowed to crystallise at r.t. whereupon colourless crystals were formed. The crystals were separated and dried at r.t. Yield 60%; m.p. 206–08 °C. *Anal.* Found: C, 39.2; H, 3.2. Calc., for $C_{26}H_{24}Br_2HgS_2$: C, 38.0; H, 2.9%. Main IR bands: 1110 cm^{-1} $\{\nu P–C\}$; 585 cm^{-1} $\{\nu P–S\}$; ligand band: 1097 cm^{-1} $\{\nu P–C\}$; 600 cm^{-1} $\{\nu P–S\}$.

2.4. Elemental analyses and spectroscopic techniques

The C, H, and N elemental analyses were obtained with a Carlo–Erba 1108 microanalyser. The melting points were determined with a Gallenkamp electrically heated apparatus. IR spectra were recorded using KBr pellets on a Pye-Unicam SP3-300 Infrared Spectrophotometer in the 4000–400 cm^{-1} range.

2.5. Crystal structure determinations

A red prismatic crystal of compound **1** (colourless for compound **2**) was mounted on a glass fibre and used for data collection. Cell constants and orientation matrices for data collection were obtained by least-squares refinement of the diffraction data from 25 reflections in the range of $21.513 < \theta < 45.145°$ for **1** and $4.682 < \theta < 20.743°$ for **2**, on an Enraf–Nonius CAD 4 automatic diffractometer [19]. Data were collected at 293 K using Cu Kα radiation ($\lambda = 1.54184$ Å) for **1** or Mo Kα radiation (0.71073 Å) for **2** and the ω scan technique and corrected for Lorentz and polarisation effects [20]. A semi-empirical absorption correction (ψ-scan) was made [21].

The structures were solved by direct methods [22] and subsequent difference Fourier maps and refined on F^2 by a full-matrix least squares procedure using anisotropic displacement parameters [23]. All hydrogen atoms were located from difference Fourier maps in their calculated positions (C–H, 0.93–0.97 Å) and were refined isotropically. Atomic scattering factors were used from International Tables for X-ray crystallography [24] and molecular graphics from PLATON 98 [25]. A summary of the crystal data, experimental details, and refinement results is given in Table 1.

3. Results and discussion

3.1. General comments

Reactions of $Ph_2P(S)–CH_2–CH_2–P(S)Ph_2\cdot\{dppeS_2\}$ with $PdCl_2(CH_3CN)_2$ in hot CH_3CN or with $HgBr_2$ in acetone (room temperature) formed 1:1 complexes, viz. $MX_2(dppeS_2)$, as revealed by the physical properties and analytical data. The IR spectra for the ligand and the complexes were different, and the diagnostic peak νP–S of free $dppeS_2$ at 600 cm^{-1} shifted to 575 cm^{-1} in compound **1** and to 585 cm^{-1} in compound **2**, and it clearly shows that $dppeS_2$ is coordinating to Pd(II)/Hg(II) metal centres via S donor atoms. The shift is more pronounced for Pd(II) vis-à-vis Hg(II) even though the latter is believed to be softer than the former in the terminology of the HSAB principle. The crystal structures of both the compounds are described below.

Table 1
Crystal data and structure refinement for compounds **1** and **2**

	1	**2**
Empirical formula	$C_{28}H_{27}Cl_2NP_2PdS_2$	$C_{26}H_{24}Br_2HgP_2S_2$
Formula weight (M)	680.87	822.92
Crystal system	monoclinic	monoclinic
Space group	$P2_1/n$ (no. 14)	$P2_1/c$ (no. 14)
Unit cell dimensions		
a (Å)	10.1009(3)	21.911(5)
b (Å)	20.905(2)	8.2046(7)
c (Å)	14.1048(6)	16.576(4)
β (°)	102.636(3)	107.066(17)
V (Å^3)	2906.2(4)	2848.6(10)
Z	4	4
D_{calc} (Mg m^{-3})	1.556	1.919
$F(000)$	1376	1568
Crystal size (mm)	$0.35\times0.15\times0.10$	$0.35\times0.25\times0.15$
θ Range for data collection (°)	3.85–75.95	2.47–27.97
Index ranges	$0\le h\le12$, $-26\le k\le0$, $-17\le l\le17$	$-28\le h\le27$, $0\le k\le10$, $0\le l\le21$
Reflections collected	6403	7097
Independent reflections	6057 [$R_{int}=0.0216$]	6856 [$R_{int}=0.0433$]
Max/min transmission	0.983 and 0.885	0.983 and 0.547
Data/restraints/parameters	6057/0/433	6856/0/298
Goodness-of-fit on F^2	1.033	0.924
Final R indices [$I>2\sigma(I)$]	$R_1=0.0474$, $wR_2=0.1209$	$R_1=0.0445$, $wR_2=0.0806$
R indices (all data)	$R_1=0.0833$, $wR_2=0.1370$	$R_1=0.2303$, $wR_2=0.1137$
Largest difference peak and hole (e Å^{-3})	1.951 and −1.247	0.746 and −2.217

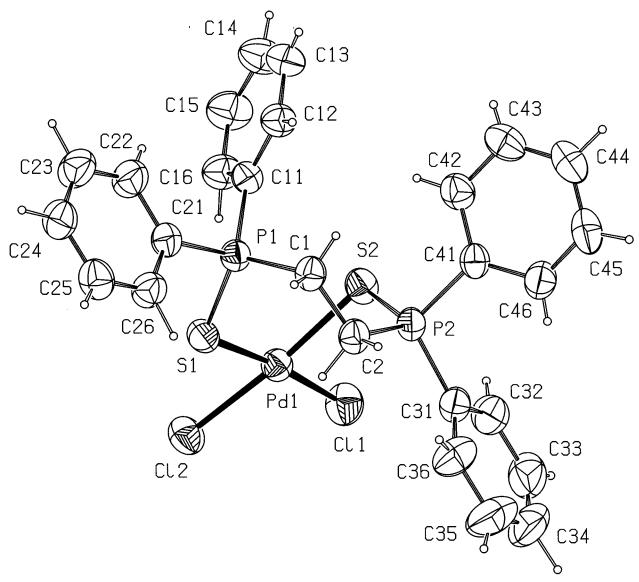


Fig. 1. Perspective view of the structure of compound [$PdCl_2$-($dppeS_2$)](CH_3CN) (**1**) with numbering scheme (CH_3CN lies in the lattice as a non-bonded molecule – not shown).

Table 2
Bond lengths (Å) and bond angles (°) for compounds **1** and **2**

Compound **1**		Compound **2**	
Bond distances			
Pd(1)–S(1)	2.3005(14)	Hg(1)–S(1)	2.678(2)
Pd(1)–S(2)	2.3018(13)	Hg(1)–S(2)	2.552(2)
Pd(1)–Cl(1)	2.3161(15)	Hg(1)–Br(1)	2.5592(11)
Pd(1)–Cl(2)	2.3347(14)	Hg(1)–Br(2)	2.5509(11)
P(1)–S(1)	2.0181(18)	P(1)–S(1)	1.990(3)
P(2)–S(2)	2.0089(18)	P(2)–S(2)	1.999(3)
P(1)–C(11)	1.803(5)	P(1)–C(11)	1.815(8)
P(1)–C(21)	1.804(5)	P(1)–C(21)	1.777(8)
P(1)–C(1)	1.832(5)	P(1)–C(1)	1.794(7)
P(2)–C(31)	1.799(6)	P(2)–C(31)	1.811(8)
P(2)–C(41)	1.802(5)	P(2)–C(41)	1.810(8)
P(2)–C(2)	1.808(5)	P(2)–C(2)	1.809(7)
C(1)–C(2)	1.531(7)	C(1)–C(2)	1.544(9)
Bond angles			
Pd(1)–S(1)–P(1)	113.54(7)	Hg(1)–S(1)–P(1)	108.96(11)
Pd(1)–S(2)–P(2)	105.11(7)	Hg(1)–S(2)–P(2)	104.79(11)
S(1)–Pd(1)–S(2)	97.76(5)	S(1)–Hg(1)–S(2)	118.85(8)
S(1)–Pd(1)–Cl(1)	174.10(5)	S(1)–Hg(1)–Br(1)	96.20(6)
S(2)–Pd(1)–Cl(1)	88.06(5)	S(2)–Hg(1)–Br(1)	110.40(6)
S(1)–Pd(1)–Cl(2)	83.19(5)	S(1)–Hg(1)–Br(2)	101.47(6)
S(2)–Pd(1)–Cl(2)	172.85(5)	S(2)–Hg(1)–Br(2)	105.81(6)
Cl(1)–Pd(1)–Cl(2)	91.17(5)	Br(1)–Hg(1)–Br(2)	124.56(4)
P(1)–C(1)–C(2)	117.2(4)	P(1)–C(1)–C(2)	112.8(5)
P(2)–C(2)–C(1)	115.0(4)	P(2)–C(2)–C(1)	112.9(5)
S(1)–P(1)–C(1)	114.35(19)	S(1)–P(1)–C(1)	111.5(3)
S(2)–P(2)–C(2)	112.00(19)	S(2)–P(2)–C(2)	111.7(3)

3.2. Description of crystal structures of compounds *1* and *2*

The atomic numbering schemes for [$PdCl_2$($dppeS_2$)]-(CH_3CN) (**1**) and $HgBr_2$($dppeS_2$) (**2**) are shown in Figs. 1 and 2, respectively. While Table 1 contains crystal data, experimental details, and refinement results, Table 2 contains important bond lengths and bond angles. Both compounds adopt a monoclinic crystal system similar to that of [$HgCl_2${$Ph_2P(S)–CH_2–CH_2–P(S)Ph_2$}] [11b]. The basic unit is [MX_2($dppeS_2$)] (X, M = Cl, Pd; Br, Hg) with no evidence for intermolecular interaction, and in compound **1**, CH_3CN lies in the lattice as a non-bonded molecule.

In compound **1**, palladium(II) is bonded to two S atoms of the chelating $dppeS_2$ ligand and two chlorine atoms. The *trans*-bond angles S(1)–Pd–Cl(1) and S(2)–Pd–Cl(2) are 174.10(5)° and 172.85(5)°, respectively, with the bite angle S(1)–Pd–S(2) of the ligand being 97.76°. Whereas Cl(1)–Pd–Cl(2) and S(2)–Pd–Cl(1) bond angles are close to 90°, the angle S(1)–Pd–Cl(2) of 83.19(5)° is unusually short. Thus the square planar geometry about Pd is severely distorted and is the consequence of the effect of the large bulk of the ligand and the tendency of the Pd metal to form square planar geometries. The angles at the S atom differ significantly [cf. Pd–S(1)–P(1), 113.54(7)°,

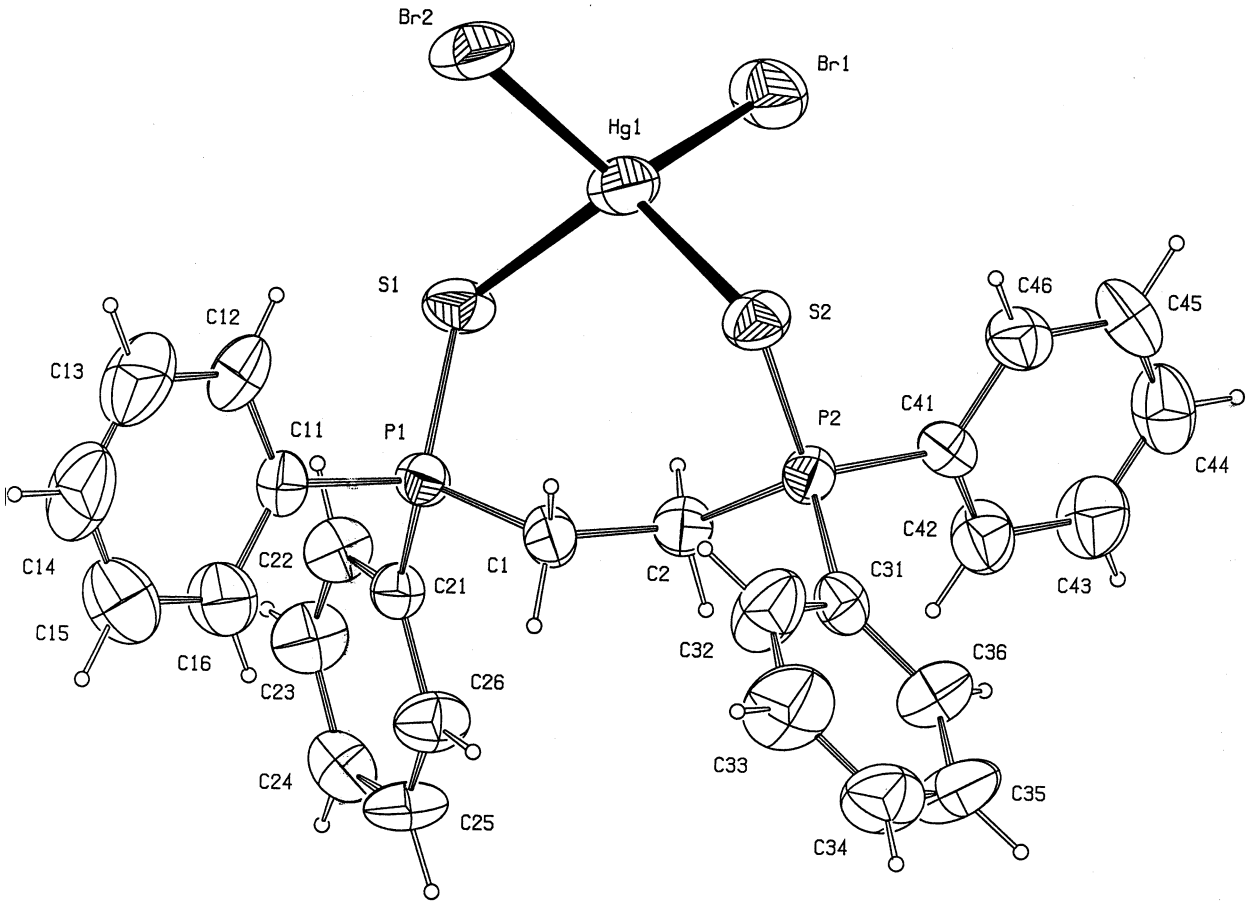
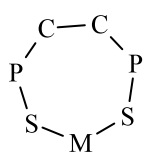


Fig. 2. Perspective view of the structure of compound $HgBr_2(dppeS_2)$ (**2**) with numbering scheme.

Pd–S(2)–P(2), 105.11(7)°]. Similarly, in compound **2** Hg is bonded to two S atoms of the chelating $dppeS_2$ ligand and two bromine atoms. The angles about Hg vary in the range 96.20(6)°–124.56(4)°, suggesting highly distorted geometry about Hg. The bite angle S(1)–Hg–S(2) of the ligand expands to 118.85(8)° in **2**, and interestingly this angle is still higher at 122.3(1)° in the analogous complex, $[HgCl_2(dppeS_2)]$ [11b] (compound **5**). This is clearly the effect of the bulky Br atoms, which has not only affected the bite angle S(1)–Hg–S(2) of the ligand, but also affected other bond angles. Note that the Br(1)–Hg–Br(2) bond angle of 124.56(4)° is much larger than the analogous Cl(1)–Hg–Cl(2) angle of 111.4(1)° in compound **5**. In the three examples of complexes of $dppeS_2$ discussed above {compounds **1**, **2**, **5**}, the flexibility of the alkane moiety is very apparent, which is tuning to the steric requirements of the metal or the anion. Thus the seven-membered metallacyclic rings (III) are interestingly stable and flexible.



III

The Pd–S bond distances, 2.3005(14) and 2.3018(13) Å, are shorter than those reported for $PdCl_2L_2$ {2.334, 2.350 Å for L = *i*-Bu_3PS, $PhEt_2PS$, respectively} [15,16]. The Pd–Cl bond distances are normal, though unequal. The P–S bond distances for **1** {2.0181(18), 2.0089(18) Å} are equal to those for the above Pd complexes [2.014, 2.013 Å, respectively [15,16]] and a bit longer than those found in **2**{1.990(3), 1.999(3) Å}. Other bond distances of the metallacyclic ring, namely P(1)–C(1) and P(2)–C(2), are also unequal, but similar for both the compounds (Table 2). In compound **2** Hg–S distances are unequal{2.678(2), 2.552(2) Å} and quite different from those for compound **5** {2.559(3), 2.546(3) Å} [11b]. The longer Hg–S distance in **2** is comparable to that observed in HgI_2L {Hg–S = 2.760 Å, L = Ph_2P–CH_2–P(S)Ph_2} [11b] for which a flattened tetrahedral structure was concluded. In **2** also, the sum of the bond angles of the trigonal plane formed by Hg, S(2), Br(1) and Br(2), is 340.77 Å [S(2)–Hg–Br(1), S(2)–Hg–Br(2), and Br(1)–Hg–Br(2)], similar to that in HgI_2L {353.7°} [11b]. The lengthening of the Hg–S(1) bond distance is reflected in the shorter P(1)–S(1) and P(1)–C(1) distances.

4. Supplementary material

Supplementary data are available from The Director, CCDC, 12 Union Road, Cambridge CB2 1EZ, UK (fax: +44-1223-336033; e-mail: deposit@ccdc.cam.ac.uk or www: http://www.ccdc.cam.ac.uk) on request, quoting the deposition numbers 166375 for compound **1**, 166374 for compound **2.**

Acknowledgements

Financial assistance from the CSIR [01(1444)/97/EMR-II] and laboratory facilities (to Renu Verma, Amarjeet Singh, Meenam Shikha) by the Guru Nanak Dev University, Amritsar 143 005 are gratefully acknowledged.

References

[1] T.S. Lobana, Prog. Inorg. Chem. 37 (1989) 495.
[2] T.S. Lobana, in: F.R. Hartley (Ed.), The Chemistry of Organophosphorus Compounds, vol. 2, Wiley, Chichetser, 1992, p. 409.
[3] E.S. Raper, Coord. Chem. Rev. 61 (1985) 115.
[4] E.S. Raper, Coord. Chem. Rev. 153 (1996) 199.
[5] E.S. Raper, Coord. Chem. Rev. 129 (1994) 91.
[6] E.S. Raper, Coord. Chem. Rev. 165 (1997) 475.
[7] M.J.M. Campbell, Coord. Chem. Rev. 15 (1975) 279.
[8] S.B. Padhye, G.B. Kauffman, Coord. Chem. Rev. 63 (1985) 127.
[9] D.X. West, S.B. Padhye, P.B. Sonawane, Struct. Bonding (Berlin) 76 (1991) 4.
[10] D.X. West, A.E. Liberta, S.B. Padhye, R.C. Chilate, P.B. Sonawane, A.S. Kumbhar, R.G. Yerande, Coord. Chem. Rev. 123 (1993) 49.
[11] (a) T.S. Lobana, M.K. Sandhu, E.R.T. Tiekink, J. Chem. Soc., Dalton Trans. (1988) 1401;
(b) T.S. Lobana, M.K. Sandhu, M.J. Liddell, E.R.T. Tiekink, J. Chem. Soc., Dalton Trans. (1990) 691;
(c) T.S. Lobana, R. Singh, M.K. Sandhu, E.R.T. Tiekink, J. Coord. Chem. 24 (1991) 29;
(d) T.S. Lobana, P.K. Bhatia, E.R.T. Tiekink, J. Chem. Soc., Dalton Trans. (1989) 749;
(e) T.S. Lobana, P.K. Bhatia, D.C. Povey, G.W. Smith, J. Cryst. Spect. Res. 21 (1991) 9;
(f) E.R.T. Tiekink, T.S. Lobana, R. Singh, J. Cryst. Spect. Res. 21 (1991) 205;
(g) T.S. Lobana, P.K. Bhatia, J. Chem. Soc., Dalton Trans. (1992) 1407;
(h) E. Horn, T.S. Lobana, R. Singh, E.R.T. Tiekink, Z. Kristallogr. 205 (1993) 291;
(i) T.S. Lobana, A. Sanchez, J.S. Casas, A. Castineiras, J. Sordo, M.S. Garica-Tasende, E.M. Vazquez-Lopez, J. Chem. Soc., Dalton Trans. (1997) 4289;
(j) T.S. Lobana, S. Paul, A. Castineiras, Polyhedron 16 (1997) 4023;
(k) T.S. Lobana, R. Verma, R. Singh, A. Castineiras, Transition Met. Chem. 23 (1998) 25;
(l) T.S. Lobana, R. Verma, A. Castineiras, Polyhedron 17 (1998) 3753;
(m) T.S. Lobana, S. Paul, G. Hundal, S. Obrai, Transition Met. Chem. 24 (1999) 202;
(n) T.S. Lobana, A. Sanchez, J.S. Casas, A. Castineiras, J. Sordo, M.S. Garica-Tasende, Polyhedron 17 (1998) 3701.
[12] T.S. Lobana, R. Verma, R. Mahajan, E.R.T. Tiekink, Z. Kristallogr. NCS 214 (1999) 513.
[13] T.S. Lobana, R. Mahajan, A. Castineiras, Transition Met. Chem. 26 (2001) 440.
[14] T.S. Lobana, R. Hundal, P. Turner, J. Coord. Chem. 53 (2001) 301.
[15] M.F. Richardson, Acta Crystallogr., Sect. C C41 (1985) 27.
[16] L.C. Satek, H.L. Ammon, J.M. Stewart, Acta Crystallogr., Sect. B 31 (1975) 2691.
[17] L. Maier, in: G.M. Kosolapoff, L. Maier (Eds.), Organic Phosphorus Compounds, vol. 4, Wiley-Interscience, New York, 1972 chapter 1.
[18] (a) S.S. Sandhu, T. Singh, Transition Met. Chem. (Weinheim, Germany) 1 (1976) 155;
(b) L. Maier, in: G.M. Kosolapoff, L. Maier (Eds.), Organic Phosphorus Compounds, vol. 4, Wiley-Interscience, New York, 1972 chapter 7.
[19] B.V. Nonius, CAD 4-EXPRESS Software, Ver. 5.1/1.2, Enraf–Nonius, Delft, The Netherlands, 1994.
[20] M. Kretschmar, GENHKL Program for the reduction of CAD4 Diffractometer data, University of Tübingen, Germany, 1997.
[21] A.C.T. North, D.C. Phillips, F.S. Mathews, Acta Crystallogr., Sect. A 24 (1968) 351.
[22] G.M. Sheldrick, Acta Crystallogr. A46 (1990) 467.
[23] G.M. Sheldrick, shelxl-97. Program for the Refinement of Crystal Structures, University of Goettingen, Germany, 1997.
[24] International Tables for X-ray Crystallography, vol. C, Kluwer Academic, Dordrecht, The Netherlands, 1995.
[25] A.L. Spek, PLATON. A Multipurpose Crystallographic Tool, Utrecht University, Utrecht, The Netherlands, 1999.

PERGAMON

Polyhedron 21 (2002) 211–218

POLYHEDRON

www.elsevier.com/locate/poly

Synthesis, structure, and reactivity of bis(*N*,*N*′-bis(2-hydroxybenzylidene)-2-hydroxyphenylmethanediaminato)zirconium(IV), a Schiff base complex with 6,4,6-membered chelate rings

Marvin L. Illingsworth [a,*], Leslie J. Schwartz [a,1], Andrew J. Jensen [a], Tong Zhu [a], Eric J. Knappenberger [a], Julie E. Sweet [a], Patricia S. Wilkinson [b], Beth E. Waltermire [c], Arnold L. Rheingold [c]

[a] *Department of Chemistry, Rochester Institute of Technology, Rochester, NY 14623, USA*
[b] *Bruker Instruments, Inc., 19 Fortune Drive, Manning Park, Billerica, MA 01821, USA*
[c] *Department of Chemistry and Biochemistry, University of Delaware, Newark, DE 19716, USA*

Received 6 April 2001; accepted 22 October 2001

Abstract

The title complex $Zr(dshpm)_2$ has been successfully prepared by heating a 1:2 mole ratio of $Zr(OBu^n)_4$ and the free ligand in absolute ethanol. It is mononuclear and eight-coordinate in the solid state with a dodecahedral coordination sphere. The two O,N,N,O donor atom quadridentate Schiff base ligands each form 6,4,6-membered chelate rings. As expected, the change in a chelate ring sizes from 6,5,6- to 6,4,6- resulted in significantly more labile complex, as indicated by TLC and NMR of heated solutions and its subsequent chemical reactions. The 0.010 Å shorter average Zr–N bond distance was not anticipated, and appears to result from the zirconium atom's preference that the oxygen atoms occupy certain locations. Preparations of two heteroleptic complexes from the title complex were undertaken to evaluate potential of the title compound as a synthon. A new fluorine-substituted homoleptic Schiff base Zr complex was also prepared, for comparison purposes. Despite the reasonable stability of $Zr(dshpm)_2$ in air, the decomposition of labilized Hdshpm(2-) ligand on silica gel and in heated solution interfered with the purifications of the desired heteroleptic products. © 2002 Published by Elsevier Science Ltd.

Keywords: Eight-coordinate; Schiff base; Zirconium complexes; X-ray crystal structure; Synthon; Heteroleptic

1. Introduction

The recent publication of articles dealing with early transition metal eight-coordinate complexes reflects a continuing interest in this subject, especially with regard to their structural aspects [1–6] intramolecular dynamics [7–10] and ligand exchange properties [11–14]. Our current interest is in the development of a more facile route to heteroleptic (mixed ligand) bis(quadridentate) complexes for use as polymer pendent groups [15]. Commercially available entry points for the preparation of zirconium(IV) complexes include zirconium tetraalkoxides and zirconium tetrachloride, which are polymeric to some degree and/or susceptible to atmospheric hydrolysis, and tetrakis(acetylacetonato)zirconium(IV), which can exhibit varying degrees of ligand substitution.

Bis(quadridentate) Schiff base complexes of zirconium(IV), which have fused 6,5,6-membered chelate rings and two O,N,N,O donor atom sets, are sufficiently inert that chromatographic separation on silica gel can be accomplished [15]. However, we have observed that the temperatures needed to overcome this inertness cause decomposition of the freed ligands in dimethyl sulfoxide. By choosing a quadridentate Schiff base ligand capable of forming fused 6,4,6-membered chelate rings

* Corresponding author. Tel.: +1-585-475-2497; fax: +1-585-475-7800.
E-mail address: mlish@rit.edu (M.L. Illingsworth).
[1] On leave from the Department of Chemistry, St. John Fisher College, Rochester, NY 14618, USA.

0277-5387/02/$ - see front matter © 2002 Published by Elsevier Science Ltd.
PII: S0277-5387(01)00979-2

upon coordination, we hoped to isolate a mononuclear complex with a convenient balance of ligand lability and air stability to serve as a new reaction intermediate (synthon). The increased lability would be a consequence of the greater ring strain, i.e. poorer overlaps, in the 4-membered chelate ring portion of the complex. The quadridentate Schiff base that we chose to use is *N*,*N*′ - bis(2 - hydroxybenzylidene) - 2 - hydroxyphenylmethanediamine, also called *N*,*N*′-bis(salicylidene)-2-hydroxy-α,α benzyldiamine, or more commonly *N*,*N*′-di(salicylidene) - 2 - hydroxyphenylmethanediamine, H_3dshpm. It can be made by mixing reagents found in most synthetic chemistry labs, ammonium hydroxide and salicylaldehyde, at room temperature [16,17]. This reaction is an example of one of the earliest known 'spontaneous assembly' reactions [18]. This compound allows facile modification of its structure [19–23] and is known to form complexes with other transition metals [24].

The synthesis, structural characterization and further reactions of the title complex, Zr(dshpm)$_2$, are reported here (Fig. 1).

2. Experimental

Zirconium *n*-butoxide (80% in *n*-butanol), salicylaldehyde, 3-fluorosalicylaldehyde, deuterated methylene chloride and deuterated dimethyl sulfoxide were obtained from Aldrich and used as received. The ammonium hydroxide and all solvents used were of reagent grade. Silica Gel (Merck), grade 60, 230–400 mesh, 60 Å pore size was obtained from Aldrich, and silica TLC plates were obtained from Kodak.

Prior to all TLC separations, silica plates were activated by heating at 110 °C for approximately 10 min, cooled in a desiccator for at least 5 min, and then stored for approximately 1 h or less in a glove bag filled with dry dinitrogen. Ligands and complexes were spotted while in the glove bag, and the plates returned to the oven for at least 2 min to drive away the spotting solvent.

Infrared spectra were obtained on a Perkin–Elmer FT-IR X spectrophotometer as KBr pellets using polystyrene for external calibration. ^{1}H NMR spectra for preliminary identification purposes were obtained on either a Nicolet NT-200 or a Bruker WP200 SY NMR instrument using tetramethylsilane as internal standard. ^{1}H, ^{19}F (using α,α,α-trifluorotoluene or internal referencing based on sample solvent), and all 2-D NMR spectra for detailed analyses were obtained on a Bruker Avance 400 NMR instrument.

X-ray crystallographic data for the title compound were obtained as follows: Large yellow block crystals were mounted on fine glass fibers and found to be monoclinic with systematic absences for *C* centering and a *c* glide along *b* indicating either *Cc* or *C*2/*c* as

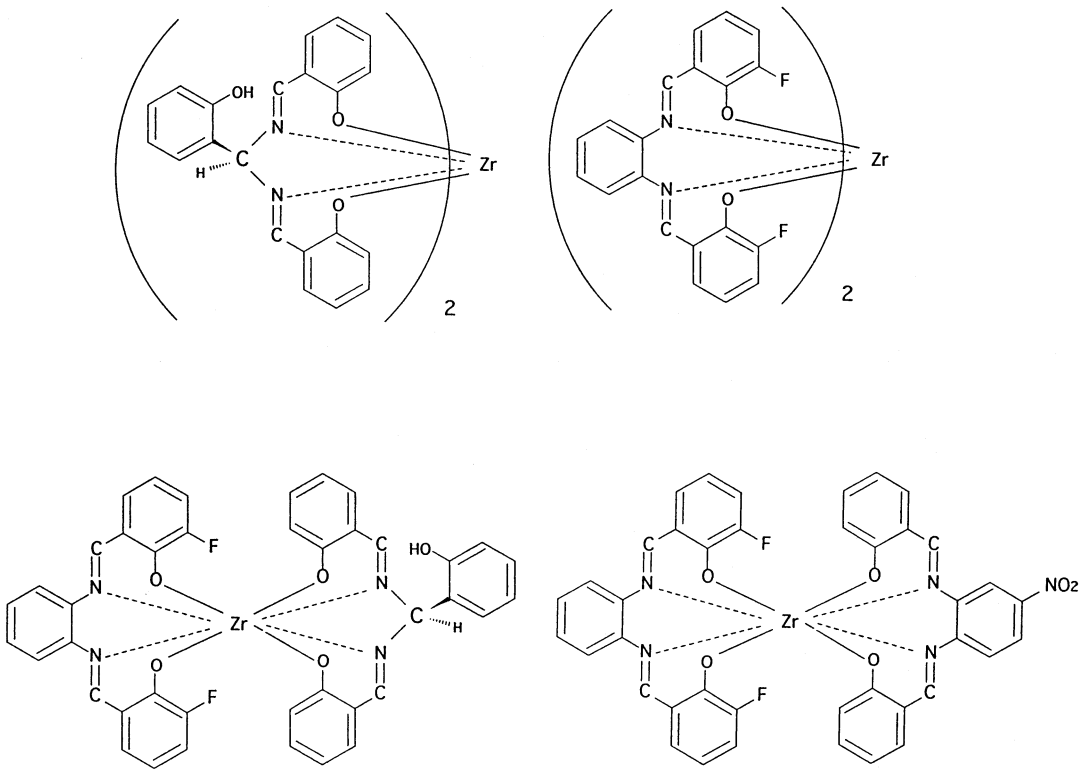


Fig. 1. Proposed structures for all new complexes in this report. Top left, Zr(dshpm)$_2$; top right, Zr(3-Fdsp)$_2$; bottom left, Zr(dshpm)(3-Fdsp); bottom right, Zr(ndsp)(3-Fdsp).

possible space groups. The latter was confirmed by the presence of a crystallographic twofold rotation axis in the Zr complex and the stability of the refinement in the centrosymmetric setting. The structure was solved by direct methods. All nonhydrogen atoms were refined anisotropically and hydrogen atoms were included as idealized isotropic contributions. All computations used the programs contained in the SHELXTL library (version 4, G. Sheldrick, Siemens XRD, Madison, WI).

2.1. *N,N′-di(salicylidene)-2-hydroxyphenylmethanediamine*, *H_3dshpm*

In a 125 ml Erlenmeyer flask was placed 20.5 g (0.168 mole) salicylaldehyde. Concentrated ammonium hydroxide was added almost to the top (ca. 115 ml), the flask stoppered and vigorously shaken. Bright yellow precipitate formed almost immediately. The flask was allowed to sit unopened for 3 days. At this point, the flask contained tamped-down, fused-looking yellow orange precipitate with a clear yellow supernate. The solution was gravity filtered, and the precipitate washed with ethyl ether. A powdery yellow solid containing some shiny orange spheres was obtained. Trituration of this product in 40 ml of absolute ethanol failed to completely remove the orange spheres. Yield, 13.0 g (66.9%).

A portion of this product was dissolved in acetone, petroleum ether added, and the volume of solvents reduced using rotary evaporation to induce recrystallization. After filtering, and washing with pertroleum ether, the fluffy yellow solid obtained lacked any visible orange component, and was only slightly soluble in methylene chloride; m.p. 159–160 °C. *Anal.* Calc. for $C_{21}H_{18}N_2O_3$: C, 72.8; H, 5.20; N, 8.09. Found: C, 72.58; H, 5.31; N, 8.09%. ^{1}H NMR (acetone-d_6): δ 13.1 (br) [1], 8.7 [2], 7.5–6.8 [12], 6.35 [1]. IR (cm^{-1}): 1628s, 1276m.

2.2. *Bis(N,N′-di(salicylidene)-2-hydroxyphenylmethanediaminato)zirconium(IV)*, *$Zr(dshpm)_2$*

A 1.69 g (4.86 mmol) portion of the yellow and orange H_3dshpm product was covered with 80 ml absolute ethanol in a 500 ml round bottom flask. Under a dinitrogen tmosphere, 0.50 ml (1.2 mmol) of $Zr(OBu^n)_4$ was then precipitated to the flask, causing the immediate formation of a cloudy, white precipitate. The flask was heated at reflux for 24 h, and filtered, to give a fine yellow powder; m.p. ca. 250 °C (slow dec.). Yield, 0.62 g (67%).

The sample submitted for elemental analysis was dried in vacuo at 100 °C for 3 days. *Anal.* Calc. for $C_{42}H_{32}N_4O_6Zr$: C, 64.7; H, 4.11; N, 7.19. Found: C, 64.56; H, 4.14; N, 6.97%. ^{1}H NMR (CD_2Cl_2): δ 9.5 (br) [2], 8.2 [2], 8.0 [2], 7.6–6.5 [28]. IR (cm^{-1}): 1638s, 1604s, 1310m, 1288m.

2.3. *N,N′-Di(3-fluorosalicylidene)-1,2-phenylenediamine*, *$H_2$3-Fdsp*

A 1:2 mole ratio of 1,2-phenylenediamine and 3-fluorosalicylaldehyde, respectively, were heated at reflux in absolute ethanol for 6 h, concentrated, and chilled to give an orange precipitate; m.p. 148–150 °C.

Anal. Calc. for $C_{20}H_{14}F_2N_2O_2$: C, 68.2; H, 3.98; N, 7.95. Found: C, 67.95; H, 3.86; N, 7.87%. ^{1}H NMR (CD_2Cl_2): δ 13.2 (br) [2], 8.9 [2], 7.5–6.9 [10]. ^{19}F NMR (CD_2Cl_2): -140.6. IR (cm^{-1}): 1620s, 1275m, 1250s, 1230s.

2.4. *Bis(N,N′-di(3-fluorosalicylidene)-1,2-phenylenediaminato)zirconium(IV)*, *$Zr(3\ Fdsp)_2$*

Under a dinitrogen atmosphere, 0.49 ml (0.52 g, 1.1 mmole) $Zr(OBu^n)_4$ were added to 0.80 g (2.3 mmole) $H_2$3-Fdsp in 50 ml absolute ethanol and heated at reflux for 1 h, suction filtered, washed with absolute ethanol, and allowed to dry to give a bright yellow powder; m.p. approximately 416 °C (422 °C dec.). Yield, 0.73 g (81%).

The sample submitted for elemental analysis was dried in vacuo at 100 °C for 3 days. *Anal.* Calc. for $C_{40}H_{24}F_4N_4O_4Zr$: C, 60.7; H, 3.06; N, 7.08. Found: C, 60.86; H, 3.03; N, 7.00%. ^{1}H NMR (CD_2Cl_2): δ 8.7 [4], 7.5–6.4 [20]. ^{19}F NMR (CD_2Cl_2): -137.4. IR (cm^{-1}): 1615s, 1320m, 1255m, 1240m.

2.5. *(N,N′-di(salicylidene)-2-hydroxyphenylmethanediaminato)(N,N′-di(3-fluorosalicylidene)-1,2-phenylenediaminato)zirconium(IV)*, *Zr(dshpm)(3-Fdsp)*

2.5.1. *Method 1*

In 200 and 100 ml portions of methylene chloride, 1.97 g (2.5 mmole) $Zr(dshpm)_2$ and 0.30 g (0.85 mmole) $H_2$3-Fdsp, respectively, were separately dissolved. The former solution was heated to reflux, and the latter added in five increments with 2 h intervals between additions, and reflux maintained overnight. TLC separation of the resulting solution (using methylene chloride eluent on silica) indicated that some unreacted Schiff base remained, whereupon 100 ml absolute ethanol was added. Reflux was maintained, periodically monitoring the reaction with TLC. A pale spot having a value of R_F clearly lower than those for the reactants or $Zr(3\text{-}Fdsp)_2$ or H_3dshpm appeared. After 22.5 h at reflux, TLC of the reaction solution revealed a spot due to $Zr(3\text{-}Fdsp)_2$, at which time the reaction was stopped. The volume was reduced by rotary evaporation to one half of its original volume, 80 ml absolute ethanol added, and concentrated again to induce precipitation. The impure product was redissolved in minimal methylene chloride and subjected to column chromatography

using methylene chloride eluent on silica gel. Fractions containing only the trailing spot (as shown by TLC) were combined, and the solvent evaporated to give a yellow product. Subsequent recrystallizations and column separations failed to produce a product having experimental elemental analyses within established limits from their theoretical values. ^{1}H NMR (CD_2Cl_2): δ 9.0 br [less than 1], 8.5 [1], 8.4 [1], 8.0 [2], 7.5–5.8 [ca. 29] ^{19}F NMR (CD_2Cl_2): -138.5, -133.5. IR (cm^{-1}): 1641s, 1616s, 1317m, 1300m, 1238m.

2.5.1.1. Derivative preparation. An impure sample of Zr(dshpm)(3-Fdsp) was mixed with *N*,*N*′-di(salicylidene)-4-nitro-1,2-phenylenediamine, H_2ndsp, in 30:70 methylene chloride and absolute ethanol, respectively, and heated at reflux. The reaction was monitored by TLC using the TLC system noted above. When the spots attributed to the starting materials were no longer apparent, the reaction solution was concentrated by rotary evaporation to give a red solid. A 0.1 g portion of this product was separated on a silica gel column using methylene chloride as eluent. Fractions having single spot TLCs which appeared to correspond with the desired product were consolidated and evaporated to give a red product. The sample submitted for elemental analysis was dried in vacuo at 100 °C for 3 days. *Anal.* Calc. for $C_{40}H_{25}F_2N_5O_6Zr$ [Zr(ndsp)(3-Fdsp)]: C, 60.0; H, 3.15; N, 8.74. Found: C, 61.24; H, 3.50; N, 8.60%. ^{1}H NMR (CD_2Cl_2): δ 8.6–8.2 [6], 7.5–5.9 [19]. These NMR signals matched those for a sample of Zr(ndsp)(3-Fdsp) prepared directly from $Zr(OBu^n)_4$ and the corresponding free Schiff base ligands, to be reported elsewhere (Found: C, 60.66; H, 3.44; N, 8.52%).

2.5.2. Attempted method 2

Under a dinitrogen atmosphere, 1:1:1 mole ratio amounts of H_3dshpm, $H_2$3-Fdsp, and $Zr(OBu^n)_4$ were heated at reflux in absolute ethanol for 7 h, until the TLC spot from H_3dshpm was no longer apparent (using a 16:1 petroleum ether to ethanol eluent). After being allowed to cool, the mixture was filtered to give a bright yellow powder.

2.5.3. Attempted method 3

Under a dinitrogen atmosphere, 1:1 mole ratio amounts of $Zr(dshpm)_2$ and $Zr(3\text{-}Fdsp)_2$ were separately dissolved in d^6-DMSO. The solutions were mixed, and heated for 20 h intervals at 40, 43, and 50 °C. Changes in the reaction solution were monitored by TLC (using a 16:1 petroleum ether–ethanol eluent), and compared with those for the separate complexes.

3. Results and discussion

The physical and spectroscopic data collected in this study are consistent with the following reaction schemes:

Reaction Scheme I.

$$3NH_3\ (aq) + 2\ \text{salicylaldehyde}\ (aq) \xrightarrow{(-3\ H_2O)} H_3\text{dshpm}\ (s)$$

$$2\ H_3\text{dshpm} + Zr(OBu^n)_4 \xrightarrow{(-4\ HOBu)} Zr(\text{dshpm})_2 \xrightarrow{(H_2\text{3-Fdsp})} Zr(\text{dshpm})(\text{3-Fdsp}) \xrightarrow{(H_2\ \text{ndsp})} Zr(\text{ndsp})(\text{3-Fdsp})$$

Reaction Scheme II.

$$\text{1,2-phenylenediamine} + 2\ \text{3-fluorosalicylaldehyde} \xrightarrow{(-2\ H_2O)} H_2\text{3-Fdsp}\ (s)$$

$$2\ H_2\text{3-Fdsp} + Zr(OBu^n)_4 \xrightarrow{(-4\ HOBu)} Zr(\text{3-Fdsp})_2$$

The 1628 and 1276 cm^{-1} infrared bands for H_3dshpm are comparable to those observed for the dsp-type ligands used in our previous studies [25,26] and are assigned to imine stretching and ring-to-oxygen stretching, respectively. The broad ^{1}H NMR signal at 13.1 ppm is assigned to exchangeable salicylidene O–H, the 8.7 ppm singlet to the two imine protons, 7.5–6.8 ppm multiplets to the 12 aromatic protons, and a singlet at 6.35 to a methine proton. The appearance of an orange component in the initial product, the variety of melting points reported [16,17,27] and the differences between the NMR spectra in deuterated acetone versus methylene chloride (of poor quality due to low solubility) indicate the presence of tautomeric forms of this material. Very similar observations were made for the ethyl ester substituted H_2dsp ligand, for which either tautomer gave the same product upon complexation [28].

3.1. Zr(dshpm)$_2$

The shift in salicylidene ring-to-oxygen vibration frequency from 1276 to 1310 cm^{-1} upon Zr complexation is analogous to those seen for all H_2dsp-type ligands studied previously by us [25,26]. The essentially non-shifted band at 1288 cm^{-1} is assigned to the phenyoxy ring-to-oxygen vibration since coordination does not take place at this site (vide infra). Either of the bands at 1638 or 1604 cm^{-1} could be assigned to an imine vibration. However, the former is more the likely, given the increase in frequency upon complexation noted above. The absence of a peak near 13.1 ppm in the ^{1}H NMR spectrum of $Zr(dshpm)_2$ is expected, as the Zr displaces the salicylidene O–H protons of each ligand.

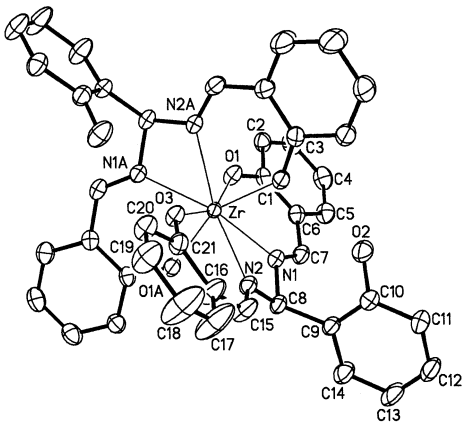


Fig. 2. Labeled thermal ellipsoid drawing for $Zr(dshpm)_2$.

The broad signal at 9.5 ppm, which integrates for a little less than two protons, is assigned to an exchangeable phenoxy proton on each ligand. The imine protons become nonequivalent upon complexation, giving singlets at 8.2 and 8.0 which each integrate for 2. The methine proton signal from each ligand occurs among the aromatic proton multiplets which extend from 7.6 to 6.5 ppm, the region integrating for 28 protons. The upfield shift upon Zr complexation, especially for the salicylidene protons *meta* to the oxygen, is comparable to those observed for all H_2dsp-type ligands studied by us [25,26]. The doublets at 7.0 and 6.8 ppm which have no apparent fine structure and integrate for one proton each, are most likely from the methine protons. If these assignments are accurate, as indicated by the 2-D COSY spectrum, then the salicylidene and/or phenyoxy rings must have different average positions in solution, e.g. an equilibrium could exist between coordinated phenoxy and salicylidene moieties, or, less likely, the short bite N–C–N moieties could span different edges in the coordination sphere in solution to create different methine proton environments.

Table 1
Selected bond lengths, bond angles, and coordination sphere parameters for $Zr(dshpm)_2$; see Fig. 2

Bond lengths (Å)					
Zr–O(1)	2.090(2)	O(1)–C(1)	1.323(5)	N(1)–C(7), imine	1.270(5)
Zr–O(3)	2.151(3)	O(3)–C(21)	1.324(4)	N(2)–C(15), imine	1.263(5)
Zr–N(1)	2.318(3)			N(1)–C(8), methine	1.468(4)
Zr–N(2)	2.334(3)	O(2)–C(10)	1.364(4)	N(2)–C(8), methine	1.476(5)
Bond angles (°)					
O(1)–Zr–O(3)	154.0(1)	Zr–O(1)–C(1)	142.1(2)	Zr–N(1)–C(7)	135.5(2)
O(1)–Zr–N(1)	74.2(1)	Zr–O(3)–C(21)	139.4(3)	Zr–N(1)–C(8)	102.0(2)
O(1)–Zr–N(2)	131.2(1)			Zr–N(2)–C(15)	135.6(3)
O(3)–Zr–N(2)	74.4(1)			Zr–N(2)–C(8)	101.0(2)
O(3)–Zr–N(1)	131.3(1)	C(7)–N(1)–C(8)	122.4(3)		
N(1)–Zr–N(2)	57.0(1)	C(15)–N(2)–C(8)	123.4(3)	N(1)–C(8)–N(2)	97.9(3)
Deviations from planarity (Å)					
O(1)–N(1)–N(2)–O(3)	0.0047(5)				
Zr–N(1)–N(2)–C(8)	0.2360(3) [a]	O(1)–N(1)–N(2)–O(3)–Zr	0.0211(3)		
'*a*' *Edges* [b] (Å)					
N(1)–N(2)	2.220(4)				
'*b*' *Edges* [b] (Å)					
O(1)–O(1a)	3.126(5)				
O(1)–O(3a)	3.096(5)				
'*m*' *Edges* [b] (Å)					
O(1)–N(1)	2.666(4)				
O(3)–N(2)	2.714(5)				
O(1a)–N(1a)	2.803(5)				
O(3a)–N(2a)	2.714(5)				
'*g*' *Edges* [b] (Å)					
O(1)–N(1a)	2.803(5)				
O(1)–N(2a)	2.757(5)				
O(3)–N(1a)	2.917(5)				
O(3)–N(2a)	2.835(5)				
Mean edge length ratios					
b/*a*	1.38				
b/*m*	1.14				
b/*g*	1.085				

[a] The deviation of C(8) from the N(1)–Zr–N(2) plane is away from the phenoxy group.
[b] Standard Hoard and Silverton symbolism [29]. The remaining dodecahedral edge lengths for $Zr(dshpm)_2$ are dictated by symmetry.

Results of X-ray crystallography on $Zr(dshpm)_2$ establish its solid state structure as eight-coordinate with a dodecahedral coordination sphere, point group $2/m$, and space group $C2/c$. A labeled thermal ellipsoid drawing is shown in Fig. 2. Important bond lengths, bond angles, and coordination sphere parameters are summarized in the Table 1. Comparisons with bis(*N*,*N*′-disalicylidene-1,2-phenylenediaminato)zirconium(IV), $Zr(dsp)_2$ [26] and bis(*N*,*N*′-disalicylidene-1,2-*trans*-diaminocyclohexanato)zirconium(IV), $Zr(trans\text{-}dsd)_2$ [25] which have fused 6,5,6-membered Schiff base ligands, reveal the following: While the mean Zr–O distances are approximately equal for each complex, the mean Zr–N distance for $Zr(dshpm)_2$ is approximately 0.010 Å shorter. Considering the ring strain normally associated with four-membered rings, poor bonding overlaps would justify longer bonds. In this case, the shorter bonds probably arise due to zirconium's preference for the oxygen atoms to be located in certain positions, the 'B' positions of a dodecahedron [29], which is consistent with theory for d^0 dodecahedral systems [30]. The imine bond is highly localized in $Zr(dshpm)_2$, as for the other complexes, and the methine-to-nitrogen bond lengths are ordinary. The O–Zr–O bond angles are larger for $Zr(dshpm)_2$ than for the other complexes, which indicates that the 6,4,6 ligands do not engulf the Zr as extensively. The N–Zr–N bond angle is the smallest for $Zr(dshpm)_2$, due to the limited reach of the methine diamine moiety versus those of the phenylenediamine and diaminocyclohexane moieties [25,26]. The above mentioned bond length and angle constraints produce a dodecahedron having the shortest N–N distance ('a edges'), and a Zr–N (ave.) to Zr–O (ave.) bond length ratio of 1.09. The latter is closer to the Hard Sphere Model (1.00) and Most Favorable Model (1.03) [29] than the other members of this series. The angle made between the trapezoidal O,N,N,O donor atom planes is 89.0° for $Zr(dshpm)_2$, which is comparable to those for $Zr(dsp)_2$ and $Zr(trans\text{-}dsd)_2$ [25,26]. The angle made between the phenoxy ring and the donor atom plane of the same ligand is 85.2°. The corresponding value for the other ligand is equivalent by symmetry.

In vitro tests conducted by the National Cancer Institute, Developmental Therapeutics Program (Sample and Test Identification NSC: 657558-U/0-1/38), indicated that this compound was inactive against nine cancers and HIV.

3.2. $Zr(3\text{-}Fdsp)_2$

The preparation of $Zr(3\text{-}Fdsp)_2$ was undertaken so that its spectral data could be compared with those of Zr(dshpm)(3-Fdsp) and Zr(ndsp)(3-Fdsp), see Reaction Scheme II and the final two legs of Reaction Scheme I (see Section 3). The method employed is well established [15,25,28]. The IR bands at 1615 and 1320 cm^{-1} are assigned to the imine and coordinated-oxygen-to-ring stretching vibrations, respectively [25,26], while the band at 1255 or 1240 cm^{-1} arises from a fluorine-to-ring stretching vibration. The absence of the proton NMR signal at 13.2 ppm, observed for the free ligand, is consistent with ligand coordination. The imine proton signals are virtually equivalent, and shifted upfield by approximately 0.15 ppm from that of the free ligand. Similar upfield shifts are observed in the $Zr(dsp)_2$ and $Zr(trans\text{-}dsd)_2$ systems [25,26]. Symmetrical multiplets at 7.5–7.4 ppm arise from the 1,2-phenylenediamine protons, as observed for $Zr(dsp)_2$ [26]. Nearly identical doublets at 7.1–7.0 arise from the salicylidene ring protons *para* to F and *meta* to O; less similar doublets at 6.9–6.7 arise from the salicylidene ring protons *ortho* to F and *meta* to O; and two distinct triplets at 6.5–6.4 arise from the salicylidene ring protons *meta* to F and *para* to O. Off diagonal features in the ROESY (with 400 ms mixing) and DQF COSY NMR experiments confirm these assignments and indicate interactions between the imine protons and aromatic protons of the phenylenediamine (α and β) and salicylidene (*para* to F) moieties.

3.3. Zr(dshpm)(3-Fdsp)

Method 2, the reaction of Zr butoxide and the free ligands in 1:1:1 mole ratio, has successfully been used to prepare heteroleptic complexes [15]. However, the yellow product obtained in this research was determined to be mostly $Zr(3\text{-}Fdsp)_2$, based on TLC and proton NMR analyses. Since the solubilities of $Zr(3\text{-}Fdsp)_2$ and the desired Zr(dshpm)(3-Fdsp) are very similar, recrystallization was precluded as an effective method of purification. Furthermore, since $Zr(dshpm)_2$ decomposes rapidly on a silica gel column (on the elution time scale) and is the fastest moving of the three Zr products, the Zr(dshpm)(3-Fdsp) band becomes contaminated. This precludes chromatography as a convenient method of purification. With purification proving to be difficult, Method 2 was deemed ineffective in this case.

While $Zr(3\text{-}Fdsp)_2$ withstood heating in d^6-DMSO up to 148 °C with no change in its TLC or proton NMR, $Zr(dshpm)_2$ was shown to undergo chemical change upon heating to only 40 °C. Heating a 1:1 mole ratio mixture of the two complexes, as per Method 3, resulted in labilization and decomposition of the H_3dshpm ligand at low temperature without any evidence of mixed ligand complex formation.

The relative success of Method 1 is, based upon stopping the addition of $H_2$3-Fdsp to $Zr(dshpm)_2$ as soon as $Zr(3\text{-}Fdsp)_2$ appears in the reaction solution's TLC. The approximately equal mixture of unreacted $Zr(dshpm)_2$ and Zr(dshpm)(3-Fdsp) which resulted

could be substantially purified due to the limited solubility of the former in absolute ethanol. However, despite repeated recrystallizations followed by a column separation, contamination of the desired product persisted, as reflected by the elemental analyses. The impurities, which are likely to arise from on-going labilization of Hdshpm(2-), probably contributed to our inability to grow a crystal suitable for X-ray crystallography. Fortunately, the composition of the new material could be established using IR and NMR spectroscopies, and by preparing chemical derivatives.

For the substantially purified product, infrared bands at 1641 and 1616 cm^{-1} are assigned as imine stretching vibrations arising from the Hdshpm(2-) and 3-Fdsp(2-) ligands, respectively, by analogy to the corresponding homoleptic complexes. The band at 1317 cm^{-1} and its shoulder are assigned as 'coordinated O-to-salicylidene ring' stretching vibrations for the two ligands. The band at 1238 cm^{-1} and/or its higher frequency shoulder are assigned as an aromatic ring-to-F vibration, analogous to that for $Zr(3\text{-}Fdsp)_2$. Thus, all IR assignments are consistent with the Zr(dshpm)(3-Fdsp) formulation.

While strong parallels between Zr(dshpm)(3-Fdsp) and the corresponding homoleptic complexes are readily apparent from the IR spectra of solid state samples, fewer parallels are evident from their solution ^1H NMR spectra. The absence of a signal around 13.2 ppm is consistent with the presence of coordinated ligands. Small singlets at 11.0 and 9.9 ppm match signals observed for salicylaldehyde, which is a likely decomposition by-product from the Hdshpm(2-) ligand. The broad signal at 9.0 ppm, which integrates for less than one proton, is assigned to an exchangeable phenoxy O–H and is consistent with the presence of one Hdshpm(2-) ligand. This chemical shift is 0.5 ppm upfield from the analogous signal for $Zr(dshpm)_2$, which, from examination of molecular models, could result from a nearby fluorine on the opposing 3-Fdsp(2-) ligand. The singlets at 8.5 and 8.4 ppm, which integrate for one proton each, are assigned to the imine protons of the 3-Fdsp(2-) ligand, protons which had been equivalent for $Zr(3\text{-}Fdsp)_2$ at 8.7 ppm. The singlet at 8.0 ppm, which integrates for two protons, is assigned to the imine protons of the Hdshpm(2-) ligand, protons which had been inequivalent for $Zr(dshpm)_2$ at 8.2 and 8.0 ppm. Signals in the 7.5–5.8 ppm range are assigned to the aromatic protons of the ligands. The upfield end of this range appears higher than observed for either of the homoleptic complexes, 6.4 ppm in both cases. The integration over this range, corresponding to approximately 29 protons, is higher than expected for 22 aromatic protons and one methine proton, and is consistent with the presence of some impurity, e.g. salicylaldehyde. We also note that the aromatic signals for Zr(dshpm)(3-Fdsp) appear poorly resolved in CD_2Cl_2, a poor H-bonding solvent, and appear strikingly different in d^6-DMSO, a good H-bonding solvent, while the imine proton signal at 8.0 ppm appears the same in each solvent. Furthermore, in the d^6-DMSO spectrum, the phenoxy O–H signal is a sharp singlet which integrates for one proton; the aromatic range extends down to 8.1 ppm; and, the integration of the aromatic region corresponds to 22.8 protons, which is much closer to the expected number of 23.

In addition to TLC evidence, rapid disproportionation of Zr(dshpm)(3-Fdsp) in solution to form a 1:1 mole ratio of homoleptic complexes was ruled out by observing the CD_2Cl_2 ^1H NMR spectrum of a mixture of separately prepared $Zr(3\text{-}Fdsp)_2$ and $Zr(dshpm)_2$. The spectrum showed all of the signals apparent in the spectra of the separate complexes with no perceptible shifts, i.e. with no sign of interaction.

The $^{19}F\{^1H\}$ NMR of the proposed Zr(dshpm)(3-Fdsp) product shows two proton decoupled signals, neither of which matches the ^{19}F signal from $Zr(3\text{-}Fdsp)_2$. The ^{19}F signal from a mixture of $Zr(3\text{-}Fdsp)_2$ and $Zr(dshpm)_2$ was identical with the latter. The coordinated Hdshpm(2-) ligand evidently imposes a different chemical environment on the two fluorines of the opposing 3-Fdsp(2-) ligand. $^1H\{^{19}F\}$ NMR (i.e. proton observe with decoupled ^{19}F using the above ^{19}F NMR frequencies) of the proposed Zr(dshpm)(3-Fdsp) product in CD_2Cl_2 solution indicates that each F atom couples with the nearest imine proton and nearest salicylidene protons (*ortho* and *meta*).

A plausible explanation for some of the observed NMR differences between Zr(dshpm)(3-Fdsp) and the corresponding homoleptic complexes is the presence of H bonding between the phenoxy O–H of Hdshpm(2-) and a fluorine atom on the opposing 3-Fdsp(2-). Such an interaction would render the ^{19}F NMR chemical shifts of the 3 Fdsp(2-) inequivalent. Since the above decoupling experiment established that each fluorine is coupled to the nearest imine proton, the different Zr(dshpm)(3-Fdsp) fluorine environments could explain the separate imine proton signals at 8.5 and 8.4 ppm. The imine protons for $Zr(3\text{-}Fdsp)_2$, where analogous H-bonding is not possible, gave a singlet at 8.5 ppm. However, alternate explanations for these observations, such as coordination sphere structure in solution and ligand puckering, cannot be ruled out.

3.4. Zr(ndsp)(3-Fdsp)

In light of the less-than-convincing elemental analysis for Zr(dshpm)(3-Fdsp), the inability to obtain a suitable single crystal, and the complexity of its NMR results, corroboration of its composition was sought using chemical means. In this case, the 6,4,6-chelating Hdshpm(2-) was replaced by the 6,5,6-chelating ndsp(2-). As expected, the proposed Zr(ndsp)(3-Fdsp) derivative

was demonstrated by NMR to be identical to the heteroleptic product from the 1:1:1 mole ratio reaction of H_2ndsp, $H_2$3-Fdsp, and $Zr(OBu^n)_4$. The latter had a satisfactory elemental analysis. Its NMR spectrum shows four proton signals in the imine proton region (8.6–8.3), attributed to the two imine protons and the two protons adjacent to the nitro group; the multiplet at 7.5–7.4 which integrates for five protons is attributed to the remaining phenylenediamine protons [four from 3-Fdsp(2-) and one from ndsp(2-), *meta* to the nitro group]; and the series of triplets and doublets over the 7.3–5.9 range, which each integrate for two protons each, are assigned to salicylidene ring protons, and correspond to the signals observed for the homoleptic complexes [31].

4. Conclusions

The title complex $Zr(dshpm)_2$ has been successfully prepared. Based on X-ray crystallographic results, it is mononuclear, and eight-coordinate in the solid state with a dodecahedral coordination sphere, as observed for other similar Schiff base Zr complexes [15,25,26]. The two quadridentate ligands employ O,N,N,O donor atoms to form 6,4,6-membered chelate rings, while the phenyoxy moieties are not coordinated. Although the coordination sphere dimensions of $Zr(dshpm)_2$ are closer to the Hard Sphere Model and the Most Favored Model [29] than previously studied 6,5,6- Schiff base Zr complexes [15,25,26], the change in chelate ring sizes resulted in a significantly more labile complex, as indicated by TLC, NMR of heated solutions, and chemical reactivity. The 0.010 Å shorter average Zr–N bond distance was not anticipated, and appears to result from the zirconium atom's preference that the oxygen atoms occupy certain locations.

Despite the respectable stability of the title complex in air, the decomposition of labilized ligands on silica gel and in heated solutions seriously detracts from its utility as a synthon. Complete purification of the two heteroleptic complexes prepared from it were not achieved. Zr complexes having more resilient 6,4,6-chelating ligands are expected to give more promising results.

5. Supplementary material

Crystallographic data for the structural analysis has been deposited with the Cambridge Crystallographic Data Center, reference number CCDC 150144. Copies of this information can be obtained free of charge from The Director, CCDC, 12 Union Road, Cambridge CB2 1EZ, UK (Fax: +44-1223-336-033; e-mail: deposit@ccdc.cam.ac.uk or www: http://www.ccdc.cam.ac.uk).

Acknowledgements

Acknowledgment is made to the Donors of the Petroleum Research Fund, administered by the American Chemical Society, for partial support of this research. Additional funding from the RIT College of Science and Department of Chemistry, and technical support from Astra Arcus USA, and Bruker are also gratefully acknowledged.

References

[1] M.Y. Reza, H. Matsushima, M. Koikawa, M. Nakashima, T. Tokii, Polyhedron 18 (1999) 787.
[2] F. Calderazzo, U. Englert, C. Maichle-Mossmer, F. Marchetti, G. Pampaloni, D. Petroni, C. Pinzino, J. Strahle, G. Tripepi, Inorg. Chim. Acta 270 (1998) 177.
[3] D.P. Steinhuebel, P. Fuhrmann, S.J. Lippard, Inorg. Chim. Acta 270 (1998) 527.
[4] E. Solari, C. Maltese, F. Franceschi, C. Floriani, A. Chiesi-Villa, C. Rizzoli, J. Chem. Soc., Dalton Trans. (1997) 2903.
[5] S. Ryu, D. Whang, H.-J. Kim, K. Kim, M. Yoshida, K. Hashimoto, K. Tatsumi, Inorg. Chem. 36 (1997) 4607.
[6] S.M. Harbert, P.D. Smith, R.L. Beddoes, D. Collison, C.D. Garner, Angew. Chem. Int. Ed. Engl. 36 (1997) 1897.
[7] R.C. Fay, Coord. Chem. Rev. 154 (1996) 99.
[8] R.C. Fay, J.K. Howie, J. Am. Chem. Soc. 101 (1979) 1115.
[9] R.A. Pribush, R.D. Archer, Inorg. Chem. 13 (1974) 2556.
[10] D.C. Bradley, C.E. Holloway, J. Chem. Soc. (A) (1968) 1316.
[11] R.C. Fay, R. Neil Lowry, Inorg. Chem. 13 (1974) 1309.
[12] T.J. Pinnavia, M.T. Mocella, B.A. Averill, J.T. Woodard, Inorg. Chem. 12 (1973) 763.
[13] T.J. Pinnavia, R.C. Fay, Inorg. Chem. 5 (1966) 233.
[14] A.C. Adams, E.M. Larsen, Inorg. Chem. 5 (1966) 228.
[15] L. He, S.R. Wagner, M.L. Illingsworth, A.J. Jensen, G.A. Yap, A.L. Rheingold, Chem. Mater. 9 (1997) 3005.
[16] E.W. Cottman, R.B. Moffett, S.M. Moffett, Proc. Indiana Acad. Sci. 47 (1938) 124 [Chemical Abstracts name: Phenol, 2,2′-[{(2-hydroxyphenyl)methylene}bis(nitrilomethylidyne)]bis-; RN: 99875-17-9 (for E,E) and 35832-40-7].
[17] M. Delepine, P. Rivals, Soc. Chimique 21 (1910) 939.
[18] M.A. Laurent Liebigs, Ann. Chem. 21 (1837) 130.
[19] T. Takajo, S. Kambe, W. Ando, Synthesis (1985) 344.
[20] T. Takajo, S. Kambe, Synthesis (1984) 256 and 259.
[21] T. Takajo, S. Kambe, Synthesis (1983) 564.
[22] T. Takajo, S. Kambe, Synthesis (1980) 833.
[23] T. Takajo, S. Kambe, K. Saito, T. Hayashi, A. Sakurai, H. Midorikawa, Synthesis (1975) 802.
[24] Y.-W. Wang, H.-L. Zhang, Gaodeng Xuexiao Huaxue Xuebao 15 (1994) 794.
[25] M.L. Illingsworth, B.P. Cleary, A.J. Jensen, L.S. Schwartz, A.L. Rheingold, Inorg. Chim. Acta 207 (1993) 147.
[26] R.D. Archer, R.O. Day, M.L. Illingsworth, Inorg. Chem. 18 (1979) 2908.
[27] N.A.R. Nabulsi, F.R. Fronczek, R.D. Gandour, Acta Crystallogr. Sect. C: Cryst. Struct. Commun. C44 (1988) 1086.
[28] M.L. Illingsworth, R.D. Archer, Polyhedron 1 (1982) 487.
[29] J.L. Hoard, J.V. Silverton, Inorg. Chem. 2 (1963) 235.
[30] R.J.H. Clark, J. Lewis, R.S. Nyholm, J. Chem. Soc. (1962) 2460.
[31] M.L. Illingsworth, A.L. Rheingold, Inorg. Chem. 26 (1987) 4312.

PERGAMON

Polyhedron 21 (2002) 219–223

POLYHEDRON

www.elsevier.com/locate/poly

Synthesis and spectral studies of binuclear ruthenium(II) carbonyl complexes containing bis(β-diketone) and their applications

R. Karvembu, K. Natarajan *

Department of Chemistry, Bharathiar University, Coimbatore 641-046, India

Received 5 February 2001; accepted 22 October 2001

Abstract

A series of new binuclear ruthenium(II) complexes of the type $\{[RuX(CO)(AsPh_3)_2]_2L\}$ (X = H or Cl; L = bis-β-diketone) have been synthesised by reacting $[RuHX(CO)(AsPh_3)_3]$ (X = H or Cl) with various bis(β-diketones) of the general formula [(RCO)(R′CO)CH–CH(R″)–CH(COR)(COR′)] (R = CH_3 or C_6H_5; R′ = CH_3 or C_6H_5; R″ = H, C_6H_5, 4-$(CH_3)C_6H_4$, 4-$(OCH_3)C_6H_4$ or 4-$N(CH_3)_2C_6H_4$) in 2:1 molar ratio in benzene. An octahedral structure has been tentatively proposed for all the new ligand bridged binuclear complexes. The new complexes have been subjected to the antibacterial and catalytic activity studies.
© 2002 Elsevier Science Ltd. All rights reserved.

Keywords: Ruthenium(II); Binuclear; Bis(β-diketone); Triphenylarsine; Syntheses; Antibacterial activity; Catalytic study

1. Introduction

Metal complexes of binucleating ligands are attractive as models for the coordination environments of metallobiomolecules. Binuclear complexes have also gained considerable interest in the recent past, because of their utility in promoting multi-electron redox reactions, in homogeneous catalysis as species capable of carrying out multi-step reactions, in photochemistry as sensitizers in energy transfer reactions and in magnetic exchange interactions.

Several bis(β-diketonato) bridged binuclear transition metal complexes are known [1–6] for its electrochemical and biological properties. Though many hydride, chloride and carbonyl complexes of ruthenium(II) containing bis(β-diketones) and tertiaryphosphine have been reported [7–11], analogues tertiaryarsine complexes are limited. In continuation of our systematic investigations on the ligand bridged binuclear ruthenium(II) and ruthenium(III) complexes [8–12], we report herein the synthesis, spectral, antibacterial and catalytic activity studies of bis(β-diketonato) bridged binuclear ruthenium(II) complexes containing triphenylarsine as one of the ligands. The general structure of the bis(β-diketone) ligands used in this study is shown in Fig. 1.

2. Experimental

2.1. Procedures and analyses

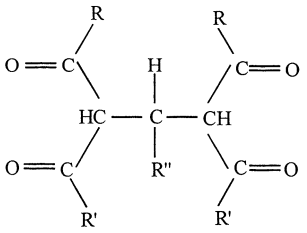
$RuCl_3 \cdot 3H_2O$ was purchased from Loba-Chemie and was used without further purification. Solvents were purified and dried according to standard procedure [13]. The starting compounds $[RuH_2(CO)(AsPh_3)_3]$ [14], $[RuHCl(CO)(AsPh_3)_3]$ [15] and bis(β-diketones) [16] were prepared by the literature methods.

C, H and N analysis were performed at the Central Salt and Marine Chemicals Research Institute, Bhavnagar. IR spectra of the complexes were recorded in KBr pellets with a Perkin–Elmer 597 infrared diffraction grating spectrophotometer in the range 4000–200 cm^{-1}. Electronic spectra were recorded in CH_2Cl_2 solution with a Systronics 119 spectrometer in the range of 800–200 nm. ^1H NMR spectra were recorded in Varian AMX 400 instrument using TMS as an internal standard. Melting points (m.p.) were recorded with a Boetius micro heating table and are uncorrected.

* Corresponding author. Tel.: +91-422-422-222; fax: +91-422-422-387.

E-mail address: karuppannannatarajan@yahoo.com (K. Natarajan).

0277-5387/02/$ - see front matter © 2002 Elsevier Science Ltd. All rights reserved.
PII: S0277-5387(01)00980-9



	R	R′	R″	Abbreviation
(i)	CH_3	CH_3	C_6H_5	H_2L1
(ii)	CH_3	CH_3	4-$N(CH_3)_2C_6H_4$	H_2L2
(iii)	C_6H_5	C_6H_5	H	H_2L3
(iv)	CH_3	CH_3	4-$(OCH_3)C_6H_4$	H_2L4
(v)	CH_3	CH_3	4-$(CH_3)C_6H_4$	H_2L5
(vi)	C_6H_5	C_6H_5	4-$N(CH_3)_2C_6H_4$	H_2L6
(vii)	C_6H_5	C_6H_5	C_6H_5	H_2L7

Fig. 1. Structure of the bis(β-diketones).

2.2. Synthesis of the complexes

To a solution of $[RuHX(CO)(AsPh_3)_3]$ (X = H or Cl) (0.1 g; 0.107–0.11 mmol) in benzene (25 cm^3), was added the appropriate bis(β-diketone) (0.015–0.032 g; 0.054–0.055 mmol) (molar ratio of ruthenium complex: bis(β-diketone) ligand was 2:1). The solution was heated under reflux for 6 h. Then, the solution was concentrated to a small volume (3 cm^3) and the new complex was separated from it by the addition of a small quantity (6 cm^3) of petroleum ether (60–80 °C). The product was filtered, washed with petroleum ether and recrystallized from CH_2Cl_2–petroleum ether (60–80 °C) mixture and dried in vacuo. Yield: 71–78%.

2.3. Antibacterial activity studies

Three pathogenic microbials were used to test the biological potential of the bis(β-diketones) and their ruthenium(II) complexes. They were (i) *Bacillus* sp. (ii) *Escherichia coli* and (iii) *Pseudomonas* sp.

The antibacterial activity of the compounds was determined by disc diffusion method [17]. The bacteria were cultured in nutrient agar medium and used as inoculam for the study. Bacterial cells were swabbed on to nutrient agar medium (prepared from NaCl 5.0 g, peptone 5.0 g, beef extract powder 3.0 g, yeast extract powder 3.0 g, agar 20.0 g in 100 cm^3 distilled H_2O; pH 7.5 ± 0.2) in Petri plates. The compounds to be tested were dissolved in DMF to a final concentration of 0.25 and 0.5% and soaked in filter paper discs (whatmann No. 4, 5 mm diameter). These discs were placed on the already seeded plates and incubated at 35 ± 2 °C for 24 h. The zones of inhibition around the discs were measured after 24 h. Streptomycin was used as a standard (Table 1).

2.4. Catalytic studies

The catalytic activity of ruthenium(II) complexes in aerial oxidation of benzaldehyde was followed spectrophotometrically by monitoring the increase in the benzoic acid absorbance as a function of time. A CH_2Cl_2 solution of the ruthenium(II) complex (2 cm^3, 1×10^{-4} M) and 2 cm^3 of 1×10^{-3} M freshly distilled benzaldehyde in CH_2Cl_2 were mixed in a 1 cm quartz cell at room temperature (r.t.; 26 °C) and the absorbance change at 279 nm was recorded.

3. Results and discussion

Bis(β-diketones) react with $[RuHX(CO)(AsPh_3)_3]$ (X = H or Cl) in 1:2 molar ratio in benzene to afford stable chelated diruthenium complexes as indicated below.

Table 1
Analytical data, melting points and electronic spectral data of the ruthenium(II) complexes

Complex	Melting points (°C)	Found (Calc.) (%)			λ_{max} (nm)
		C	H	N	
$\{[RuH(CO)(AsPh_3)_2]_2L1\}$	129	61.42 (61.70)	4.20 (4.55)		260, 234, 221
$\{[RuCl(CO)(AsPh_3)_2]_2L1\}$	155	59.02 (59.39)	3.89 (4.27)		262, 231, 221
$\{[RuH(CO)(AsPh_3)_2]_2L2\}$	142	61.69 (61.56)	4.49 (4.72)	0.69 (0.77)	260, 231, 222
$\{[RuCl(CO)(AsPh_3)_2]_2L2\}$	118	59.07 (59.31)	4.11 (4.44)	0.68 (0.74)	262, 231, 224
$\{[RuH(CO)(AsPh_3)_2]_2L3\}$	130	64.55 (64.89)	4.06 (4.36)		255, 231, 222
$\{[RuCl(CO)(AsPh_3)_2]_2L3\}$	150	62.31 (62.66)	3.87 (4.11)		267, 231, 222
$\{[RuH(CO)(AsPh_3)_2]_2L4\}$	117	61.07 (61.33)	4.17 (4.59)		265, 231, 217
$\{[RuCl(CO)(AsPh_3)_2]_2L4\}$	162	58.70 (59.08)	4.02 (4.31)		267, 231, 222
$\{[RuH(CO)(AsPh_3)_2]_2L5\}$	124	61.51 (61.89)	4.25 (4.63)		262, 231, 224
$\{[RuCl(CO)(AsPh_3)_2]_2L5\}$	139	59.10 (59.59)	4.12 (4.35)		265, 231, 222
$\{[RuH(CO)(AsPh_3)_2]_2L6\}$	145	65.45 (65.80)	4.21 (4.54)	0.60 (0.68)	258, 231, 224
$\{[RuCl(CO)(AsPh_3)_2]_2L6\}$	123	63.35 (63.67)	3.97 (4.30)	0.58 (0.66)	253, 231, 222
$\{[RuH(CO)(AsPh_3)_2]_2L7\}$	137	65.85 (66.01)	4.07 (4.39)		265, 231, 219
$\{[RuCl(CO)(AsPh_3)_2]_2L7\}$	144	63.49 (63.83)	3.87 (4.15)		267, 231, 222

Table 2
IR and ^{1}H NMR data for ruthenium(II) complexes (ν in cm^{-1} and δ in ppm)

Complex	ν(C≡O)	ν(C=O) and ν(C=C)	ν(Ru–H)	ν(Ru–Cl)	^{1}H NMR
{[RuH(CO)(AsPh$_3$)$_2$]$_2$L1}	1950	1590, 1550, 1490	2020		1.6–1.8 (bs, 4-CH$_3$), 3.5 (s, CH), 6.8–7.3 (m, aromatic), −12.0 (s, Ru–H)
{[RuCl(CO)(AsPh$_3$)$_2$]$_2$L1}	1940	1580, 1560, 1480		320	1.6–1.8 (bs, 4-CH$_3$), 3.04 (s, CH), 7.0–7.5 (m, aromatic)
{[RuH(CO)(AsPh$_3$)$_2$]$_2$L2}	1950	1600, 1550, 1490	2020		1.6–1.8 (bs, 4-CH$_3$), 2.6 (s, NMe$_2$), 3.1 (s, CH), 6.7–7.7 (m, aromatic), −20.14 (s, Ru–H)
{[RuCl(CO)(AsPh$_3$)$_2$]$_2$L2}	1960	1600, 1570, 1490		310	1.6–1.8 (bs, 4-CH$_3$), 2.7 (s, NMe$_2$), 3.1 (s, CH), 6.9–7.5 (m, aromatic)
{[RuH(CO)(AsPh$_3$)$_2$]$_2$L3}	1950	1600, 1560, 1480	2020		2.0 (s, CH$_2$), 6.7–7.8 (m, aromatic), −20.13 (s, Ru–H)
{[RuCl(CO)(AsPh$_3$)$_2$]$_2$L3}	1960	1570, 1480		310	2.04 (s, CH$_2$), 6.9–7.4 (m, aromatic)
{[RuH(CO)(AsPh$_3$)$_2$]$_2$L4}	1940	1560, 1500	2020		1.7–1.9 (bs, 4-CH$_3$), 3.5 (s, CH), 3.8 (s, OCH$_3$), 6.8–7.9 (m, aromatic), −14.9 (s, Ru–H)
{[RuCl(CO)(AsPh$_3$)$_2$]$_2$L4}	1960	1580, 1490		310	1.6–1.8 (bs, 4-CH$_3$), 3.2 (s, CH), 3.8 (s, OCH$_3$), 6.9–7.5 (m, aromatic)
{[RuH(CO)(AsPh$_3$)$_2$]$_2$L5}	1940	1560, 1545, 1508	2020		1.6–1.8 (bs, 4-CH$_3$), 1.3 (s, CH$_3$), 3.55 (s, CH), 7.3–7.9 (m, aromatic), −14.86 (s, Ru–H)
{[RuCl(CO)(AsPh$_3$)$_2$]$_2$L5}	1960	1580, 1490		320	1.6–1.8 (bs, 4-CH$_3$), 1.3 (s, CH$_3$), 3.56 (s, CH), 6.9–7.5 (m, aromatic)
{[RuH(CO)(AsPh$_3$)$_2$]$_2$L6}	1950	1590, 1550, 1490	2020		2.2 (s, NMe$_2$), 3.6 (s, CH), 6.7–7.7 (m, aromatic), −20.1 (s, Ru–H)
{[RuCl(CO)(AsPh$_3$)$_2$]$_2$L6}	1960	1580, 1480		310	2.7 (s, NMe$_2$), 3.5 (s, CH), 6.9–7.7 (m, aromatic)
{[RuH(CO)(AsPh$_3$)$_2$]$_2$L7}	1950	1590, 1520, 1480	2010		3.2 (s, CH), 6.9–7.8 (m, aromatic), −14.5 (s, Ru–H)
{[RuCl(CO)(AsPh$_3$)$_2$]$_2$L7}	1950	1580, 1480		310	3.2 (s, CH), 6.9–7.6 (m, aromatic)

$$2[RuHX(CO)(AsPh_3)_3] + [(RCO)(R'CO)CH{-}CH(R'')-CH(COR)(COR')](H_2L) \xrightarrow[\text{Reflux, 6 h}]{\text{Benzene}} \{[RuX(CO)(AsPh_3)_2]_2L\} + 2AsPh_3 + 2H_2 \quad (X = H \text{ or } Cl)$$

The new complexes are soluble in most of the common organic solvents. Molecular weight determination (Rast method) and elemental analysis data confirm the complexes to be binuclear.

3.1. ^{1}H NMR spectra

The NMR spectral data of the complexes are presented in Table 2. The presence of a sharp singlet at 3.04–3.6 ppm in the spectra of all the complexes is assigned as due to the methine proton. The multiplet observed in the region 6.1–7.9 ppm has assigned to the protons of the phenyl groups present in triphenylarsine and bis(β-diketone). In all the hydrido complexes, the metal hydride signal corresponding to two protons has been detected in the very high upfield region (-12.0 to -20.14 ppm), suggesting the identical environment around the hydride ligand in both the metal centers. In addition to the above signals, the resonances corresponding to CH_3, OCH_3, CH_2 and $N(CH_3)_2$ were also observed in the expected region (Table 2). The above spectral observations are in good agreement with the values reported for similar bis(β-diketonato) bridged binuclear ruthenium phosphine complexes [7,11].

3.2. IR spectra

The IR spectra of all the new complexes show two to three bands in the region 1480–1600 cm^{-1}, which are characteristic of the mixed modes of vibrations arising due to the normal coordinates having contribution from ν(C=O) and ν(C=C) of the coordinated β-diketone groups [18]. This coordination is further confirmed by the absence of a band at about 1700 cm^{-1} due to free carbonyl group of bis(β-diketone) ligand. The strong absorption around 1950 cm^{-1} has been assigned to the coordinated terminal carbonyl group [11]. In hydrido complexes, the ν(Ru–H) appeared in the region 2010/2020 cm^{-1} [11] and in chloride complexes ν(Ru–Cl) absorption has been found in the 310–320 cm^{-1} region [19]. Characteristic bands of $AsPh_3$ [20] are observed in the spectra of all the complexes at 1440, 1080, 740 and 680 cm^{-1}. Thus, the IR data reveal the dibasic tetradentate behavior of bis(β-diketone) moiety in all the new complexes.

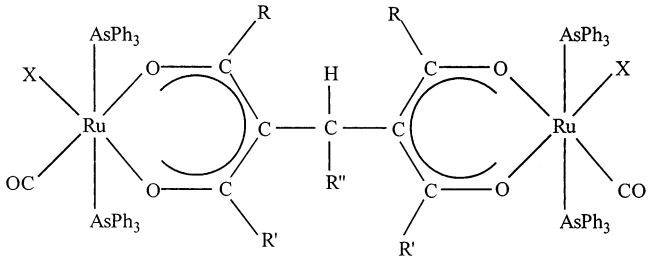


Fig. 2. Proposed structure of the Ru(II) complexes (where R, R′, R″ and X groups are as previously described).

3.3. Electronic spectra

All the new ruthenium complexes are diamagnetic, indicating the presence of ruthenium in the +2 oxidation state. The ground state of ruthenium(II) is $^1A_{1g}$ arising from the t_{2g}^6 configuration in an octahedral environment. The excited states corresponding to the $t_{2g}^5 e_g^1$ configuration are $^3T_{1g}$, $^3T_{2g,}$ $^1T_{1g}$ and $^1T_{2g}$. Hence, four bands corresponding to the transitions $^1A_{1g} \rightarrow {}^3T_{1g}$, $^1A_{1g} \rightarrow {}^3T_{2g}$, $^1A_{1g} \rightarrow {}^1T_{1g}$ and $^1A_{1g} \rightarrow {}^1T_{2g}$ are possible in the order of increasing energy.

The electronic spectra of all the complexes in CH_2Cl_2 displayed three bands in the region 220–270 nm. On the basis of high extinction coefficients ($\varepsilon = 15\,255$–$24\,360$ dm^3 mol^{-1} cm^{-1}), these bands have been assigned to charge transfer transitions arising from excitation of an electron from the metal t_{2g} level to an unfilled molecular orbital derived from the π* level of the ligands [21]. Similar assignments have been made for other octahedral ruthenium(II) complexes [22].

Thus, on the basis of elemental analysis, IR, electronic and ^{1}H NMR spectral data, the following octahedral structure has been tentatively proposed for the new binuclear ruthenium(II) complexes. The *trans* positions for the $AsPh_3$ groups have been assigned on the basis of the structures proposed for similar Ru(II) and Ru(III) phosphine complexes [7,27] (Fig. 2).

3.4. Antibacterial activity

Ligands H_2L1, H_2L2, H_2L4 and H_2L5 and their ruthenium(II) complexes yielded clear inhibition zones around the discs when treated against *Bacillus* sp. and *E. Coli* which clearly indicates the activity of the compounds. But all the compounds except {[RuCl(CO)-$(AsPh_3)_2]_2$L2} are inactive against *Pseudomonas* sp. From the results, it is concluded that the complexes possess more toxicity than their parent ligand and the toxicity increases with increase in concentration of the test solution containing new complexes. Though the complexes possess activity, it could not reach the effectiveness of the standard drug, Streptomycin. The variation in the effectiveness of different compounds against different organisms depends either on the impermeability of the cells of the microbes or differences in ribosomes of microbial cells [23] (Table 3).

3.5. Catalytic activity

The catalytic activities of {[RuH(CO)$(AsPh_3)_2]_2$L1}, {[RuCl(CO)$(AsPh_3)_2]_2$L1}, {[RuH(CO)$(AsPh_3)_2]_2$L2}, {[RuH(CO)$(AsPh_3)_2]_2$L6} and {[RuCl(CO)$(AsPh_3)_2]_2$-L6} were investigated for aerial oxidation of benzaldehyde to benzoic acid.

The course of the reaction was followed spectrophotometrically by monitoring the increase in benzoic acid absorbance at 279 nm as a function of time. Plots of the absorbance versus time are linear. The slope of the line is equal to the reaction rate constant [24], K, and the observed K values are given in Table 4. There is no

Table 3
Antibacterial activity data for selected complexes

Compound	Diameter of inhibition zone (mm)					
	Bacillus sp.		*E. coli*		*Pseudomonas* sp.	
	0.25%	0.5%	0.25%	0.5%	0.25%	0.5%
H_2L1	9	11	7	9		
{[RuH(CO)$(AsPh_3)_2]_2$L1}	12	15	10	12		
{[RuCl(CO)$(AsPh_3)_2]_2$L1}	11	15	10	13		
H_2L2	7	10	7	9		
{[RuH(CO)$(AsPh_3)_2]_2$L2}	10	14	9	12		
{[RuCl(CO)$(AsPh_3)_2]_2$L2}	10	13	10	12	6	8
H_2L4	8	10	8	11		
{[RuH(CO)$(AsPh_3)_2]_2$L4}	12	16	10	13		
{[RuCl(CO)$(AsPh_3)_2]_2$L4}	13	15	11	14		
H_2L5	8	11	7	10		
{[RuH(CO)$(AsPh_3)_2]_2$L5}	11	14	9	11		
{[RuCl(CO)$(AsPh_3)_2]_2$L5}	10	12	9	12		
Streptomycin	21	25	20	23	19	21

Table 4
Catalytic activity for selected complexes

Compound	K (M^{-1} s^{-1})
{[RuH(CO)($AsPh_3$)$_2$]$_2$L1}	2.103×10^{-3}
{[RuCl(CO)($AsPh_3$)$_2$]$_2$L1}	1.022×10^{-3}
{[RuH(CO)($AsPh_3$)$_2$]$_2$L2}	3.867×10^{-4}
{[RuH(CO)($AsPh_3$)$_2$]$_2$L6}	4.290×10^{-4}
{[RuCl(CO)($AsPh_3$)$_2$]$_2$L6}	5.210×10^{-5}

change in absorbance at 279 nm in the absence of complex, indicating the catalytic activity of the new complexes. The catalytic activity is found to decrease with an increase in size [25] of the X and R″ group. This may be due to the possibility of steric effect which hinders the formation of activated complex and thus reduces the rate of oxidation [26]. There is no appreciable change in rate constant with respect to R and R, moieties.

Acknowledgements

We thank the Council of Scientific and Industrial Research, New Delhi, India for financial assistance.

References

[1] A.W. Maverick, S.C. Buckingham, Q. Yao, J.R. Bradbury, G.G. Stanley, J. Am. Chem. Soc. 108 (1986) 7430.
[2] A.W. Maverick, F.E. Klavetter, Inorg. Chem. 23 (1984) 4129.
[3] A.W. Maverick, D.P. Martone, J.R. Bradbury, J.E. Nelson, Polyhedron 8 (1989) 1549.
[4] B.C. Whitmore, R. Eisenberg, Inorg. Chem. 23 (1984) 1697.
[5] P.J. Bonitatebus, Jr., S.K. Mandal, W.H. Armstrong, Chem. Commun. (1998) 939.
[6] R. Grybos, W. Paw, Polyhedron 9 (1990) 1397.
[7] S. Gopinathan, S.S. Deshpande, C. Gopinathan, Indian J. Chem. 27A (1988) 126.
[8] P. Viswanathamurthi, K. Natarajan, Transition Met. Chem. 25 (2000) 311.
[9] R. Ramesh, K. Natarajan, Indian J. Chem. 34A (1995) 535.
[10] V. Chinnusamy, K. Natarajan, Synth. React. Inorg. Met.-Org. Chem. 24 (1994) 553.
[11] G. Muthusamy, N. Jayakumar, B. Manonmani, R. Shantha, K. Natarajan, Synth. React. Inorg. Met. -Org. Chem. 22 (1992) 171.
[12] T. Hashimoto, A. Endo, N. Nagao, G.P. Sato, K. Natarajan, K. Shimizu, Inorg. Chem. 37 (1998) 5211.
[13] A.I. Vogel, Textbook of Practical Organic Chemistry, Longman, London, 1989.
[14] J.-Y. Kim, M.-J. Jun, W.-Y. Lee, Polyhedron 15 (1996) 3787.
[15] R.A. Sanchez-Delgado, W.-Y. Lee, S.R. Choi, Y. Cho, M.-J. Jun, Transition Met. Chem. 21 (1991) 241.
[16] D.F. Martin, M. Shamma, W.E. Ferrielius, J. Am. Chem. Soc. 80 (1958) 5851.
[17] C.H. Collins, P.M. Lyne, Microbial Methods, University Park Press, Baltimore, 1970.
[18] K. Nakamato, Infrared Spectra of Inorganic and Coordination Compounds, Wiley, New York, 1964.
[19] E. Alessio, G. Balducci, M. Calligaris, G. Costa, W.H. Attia, G. Mestoni, Inorg. Chem. 30 (1991) 609.
[20] D.S. Pandey, A.N. Sahey, O.S. Sisodiya, D.K. Gupta, U.C. Agarwala, Indian J. Chem. 37A (1998) 63.
[21] A.B.P. Lever, Inorganic Electronic Spectroscopy, Elsevier, New York, 1984.
[22] V. Chinnusamy, K. Natarajan, Synth. React. Inorg. Met. -Org. Chem. 23 (1993) 889.
[23] P.G. Lawrence, P.L. Harold, O.G. Francis, Antibiot. Chemother. (1980) 1597.
[24] A.S. Orabi, M.I. Ayad, A.E.M. Ramadan, Transition Met. Chem. 23 (1998) 391.
[25] R. Sreekala, K.K. Mohammed Yusuff, Indian J. Chem. 34A (1995) 994.
[26] N.K. Saran, M.N. Dash, R.C. Acharya, Indian J. Chem. 18A (1979) 994.
[27] O.K. Medhi, U. Agarwala, Inorg. Chem. 19 (1989) 1381.

PERGAMON

Polyhedron 21 (2002) 225–228

POLYHEDRON

www.elsevier.com/locate/poly

Linear coordination of Hg(II) by cysteamine

Chong-Hyeak Kim, Sean Parkin, Mohan Bharara, David Atwood *

Department of Chemistry, University of Kentucky, Lexington, KY 40506-0055, USA

Received 4 June 2001; accepted 22 October 2001

Abstract

Combination of the hydrochloride salt of cysteamine (**1**) with $HgCl_2$ in water affords the unique compound, $[Hg\{S(CH_2)_2NH_3\}_2](Cl)_2$ (**2**) in which the S–Hg–S angle is nearly linear. The ammonium portion of the molecule forms short hydrogen bonding contacts with the sulfur atoms. A related S···H bond is observed in the structure of the free ligand **1** indicating that such bonding does not require the presence of a metal. The compounds were characterized with spectroscopic (^1H NMR, IR) and physical techniques (Mp, CH-analysis) as well as X-ray diffractometry. © 2002 Elsevier Science Ltd. All rights reserved.

Keywords: Cysteamine; Cysteine; Sulfur; Hydrogen bonding

1. Introduction

The affinity of the amino acid cysteine for soft heavy metals is exploited in many metal binding proteins. For example, cysteine is found in the binding sites of the mercury metalloregulatory proteins, MerR [1] and MerP [2]. Due to the abundance and importance of cysteine in biological systems a great deal of research has been conducted to understand how the amino acid interacts with metals [3].

By comparison, the chemistry of cysteamine ($HS(CH_2)_2NH_2$), having the same sulfur-containing unit as cysteine, has not been examined in as much depth. This is despite the fact that cysteamine is a fairly common medicinal agent. It is approved by the US Food and Drug Administration for the treatment of the painful disease, cystinosis where its effect is to break up excess intracellular cysteine as a soluble cysteine–cysteamine complex that can be subsequently excreted [4]. It is also one of the best radioprotective agents [5].

Recently, a small-molecule model of the binding site for MerP has been prepared which incorporates two cysteamine units. The ligand, benzene (or pyridine) diaminoethanethiol (BDET) irreversibly binds mercury (and other metals) from aqueous sources, is totally insoluble, and does not release the bound metal under harsh conditions [6]. The nature of the interaction between free cysteamine and mercury has not yet been established and so little can be inferred about the remarkable stability of the BDET–Hg complex. The purpose of the work presented herein is to obtain some insight into the BDET–Hg interaction.

$[Hg\{S(CH_2)_2NH_3\}_2](Cl)_2$ (**2**), is prepared by combining cysteamine-hydrochloride (**1**) with $HgCl_2$ in

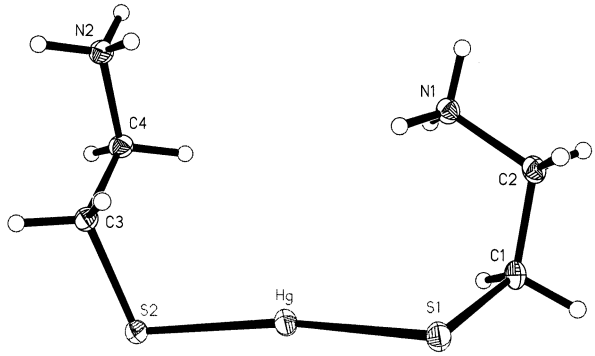


Fig. 1. ORTEP view of $[Hg(SCH_2CH_2NH_3)_2](Cl)_2$ (**2**). Selected bond distances (Å) and angles (°): Hg–S(1) 2.3330(9), Hg–S(2) 2.3380(9), S(1)–C(1) 1.832(3), C(1)–C(2) 1.512(4), C(2)–N(1) 1.489(4), S(2)–C(3) 1.830(3), C(3)–C(4) 1.518(4), C(4)–N(2) 1.499(4); S(1)–Hg–S(2) 168.53(3), Hg–S(l)–C(1) 105.5(1), S(1)–C(1)–C(2) 114.0(2), C(1)–C(2)–N(1) 113.0(3), Hg–S(2)–C(3) 100.6(l), S(2)–C(3)–C(4) 112.1(2), C(3)–C(4)–N(2) 108.8(2).

* Corresponding author. Tel.: +1-859-257-4741; fax: +1-859-323-1069.

E-mail address: datwood@pop.uky.edu (D. Atwood).

0277-5387/02/$ - see front matter © 2002 Elsevier Science Ltd. All rights reserved.
PII: S0277-5387(01)00978-0

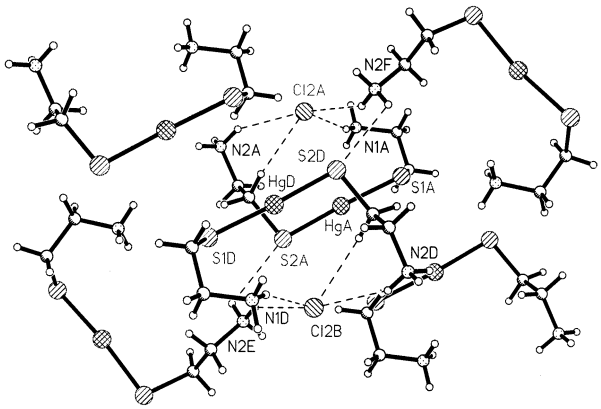


Fig. 2. Packing diagram of $[Hg(SCH_2CH_2NH_3)_2](Cl)_2$ (**2**) showing the hydrogen bond networks.

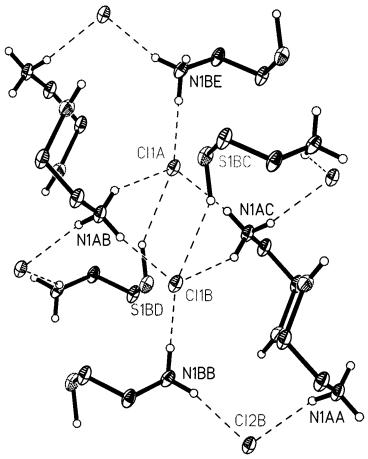


Fig. 3. ORTEP view of $[SHCH_2CH_2NH_3]Cl$ (**1**). Selected bond distances (Å) and angles (°): S(1)–H(1) 1.248, S(1)–C(1) 1.814(5), C(1)–C(2) 1.525(7), C(2)–N(1) 1.486(6); S(1)–C(1)–C(2) 114.4(4), C(1)–C(2)–N(1) 112.4(4).

water. After cooling for 2 weeks at 4 °C colorless X-ray quality crystals form in near quantitative yield. In the structure the Hg atom is coordinated to two sulfurs in a nearly linear fashion (168.53(3)°) and there are no secondary contacts to the mercury atom (Fig. 1). The structure is unique in that other related compounds feature either bridging and/or chelating cysteamine units [7]. For instance, the structures of soft metals bound by cysteamine and related molecules feature predominantly bidentate S-N coordination [8,9]. When employing cysteamine hydrochloride metals such as Cu [10] and Ag [11] form clusters with bridging (μ_2, μ_3 and μ_4) sulfur atoms. The only exception, and closest precedent to (**2**) is a rhenium-oxo compound which is coordinated by a single μ_1, cysteamine [12].

In general, structurally characterized molecules possessing a linear S–Hg–S geometry are rare [13]. This unit is observed in the cysteine compound, $Hg\{SCH_2CH(NH_3)COO\}$ $\{SCH_2CH(NH_3)COOH\}Cl{\cdot}0.5$ H_2O (**3**) (S–Hg–S = 170°) [14], and in $Hg\{SCN)_2$–Rb(SCN) (S–Hg–S = 154) [15]. The groups in $[MeHgSCMe_2CH(NH_3)](CO_2^-)$ (**4**) are also linear (C–Hg–S = 178°, Hg–S = 2.35 (**1**) Å) [16]. Most other Hg compounds that are linear have close secondary contacts [17,18]. This is true, for example, in $Hg\{SSi(O^tBu)_3\}_2$ (S–Hg–S = 180°, Hg–O ~ 2.8 Å) [19] and $Hg[(SPh)(OAc)]_2$ (S–Hg–S = 162°, Hg–O ~ 2.4–2.9 Å) [20]. Remarkably, the Hg–S distances in all of these compounds, including **2** are essentially the same at ~2.4 Å.

A unique feature that has been identified in **2**, in contrast to other synthetic mercury thiolates, is the presence of short S···H contacts (Fig. 2) [21]. The S···N distance is 3.26 Å (between S2A and N1D) implying a short hydrogen bond distance of ~2.2 Å (with the N–H fixed at 0.920 Å). This type of contact, although rare, has been found to be important in the structures of ferredoxins [22]. The common feature for **2** and the ferredoxins is the fact that the hydrogen bonding occurs in conjunction with the sulfur (either cysteamine for **2** or cysteine for the ferredoxin models) bound to the metal. It is possible that such a contact exists in MerP but the known structures are not of sufficient resolution to determine this.

In order to explore whether sulfur–hydrogen bond contacts are unique to the structure of **2** and possibly require a metal to be present, the structure of **1** was determined (Fig. 3). Hydrogen bonding is, indeed, observed for **1**, but between the S–H and a chloride. The S1BD···Cl1A distance is 3.78 Å implying a hydrogen bond contact of 2.75 Å (with an S–H distance of 1.25 Å (the hydrogens were found as peaks in the Fourier Difference map and then fixed in place)). The ammonium groups are hydrogen bonded to the chlorides (2.3–2.8 Å) but not to the sulfurs as in **2**. Clearly, chloride is the organizing force for the hydrogen bonding contacts in **1**.

2. Conclusion

With a linear S–Hg–S unit and S···H hydrogen bonding compound **2** may be viewed as a potential soluble model of the binding site of MerP in which two cysteine units coordinate a mercury atom in a linear manner [4]. It is possible that this is also occurring in the BDET–Hg complex [6]. Additionally, there is growing evidence that hydrogen bonding may be common in metal thiolate compounds. Compound **2** is the first mercury thiolate to demonstrate such bonding.

3. Experimental

3.1. General considerations

NMR data were obtained on JEOL-GSX-400 and -270 instruments operating at 270.17 and 399.78 MHz

and are reported relative to $SiMe_4$ and are in ppm. Elemental analyses were obtained on a Perkin–Elmer 2400 Analyzer. IR data were recorded as KBr pellets on a Matheson Instruments 2020 Galaxy Series spectrometer and are reported in cm^{-1}. X-ray data for **1** and **2** were collected on a Nonius Kappa-CCD unit using Mo Kα radiation. The structures were refined using the Siemens software package SHELXTL 4.0. All of the non-hydrogen atoms were refined anisotropically. The hydrogen atoms were put into calculated positions. Absorption corrections were not employed. Further details of the structure analyses are given in Table 1.

Isolation of $(SHCH_2CH_2NH_3)Cl$ (**1**): cysteamine hydrochloride (0.57 g, 5 mmol) was dissolved in hot 1-$C_4H_{10}O$ (15 ml) and filtered. The solution was allowed to stand for 2 weeks at 4 °C during which time colorless crystals formed in quantitative yield. Other alcohols, such as iso-C_3H_8O and *n*-C_3H_8O could be employed in a similar manner. Yield: 0.40 g (70%); m.p. 64–66 °C. ^1H NMR (D_2O, 200 MHz): δ 2.83 (t, 2H, CH_2N), 3.21 (t, 2H, CH_2S), 4.80 (s, residual water in the D_2O, HS, NH). IR (KBr; ν cm^{-1}): 3410w, 2955s, 2718w, 2660w, 2558w, 2504w, 1598s, 1499s, 1444m, 1423m, 1379s, 1321m, 1279m, 1244m, 1130s, 1079s, 1041s, 979m, 898s, 858s, 787w, 660w, 455m. *Anal.* Calc. for C_2H_8ClNS: C, 21.14; H, 7.10; N, 12.33; S, 28.22. Found: C, 21.33; H, 7.25; N, 12.19; S, 28.47%.

Preparation of $[Hg(SCH_2CH_2NH_3)_2](Cl)_2$ (**2**): to a stirring solution of cysteamine hydrochloride (1.14 g, 10 mmol) in deionized water (15 ml) was added mercury(II) chloride (1.36 g, 5 mmol). The resulting solution was allowed to stand for 2 weeks at 4 °C during which colorless crystals formed in near quantitative yield. Yield: 1.72 g (81%); m.p. 218–220 °C (dec.). ^1H NMR (D_2O, 400 MHz): δ 3.23 (m, 4H, CH_2N), 3.27 (m, 4H, CH_2S), 4.80 (br s, residual water in the D_2O and NH). ^{13}C NMR (D_2O, 100 MHz): δ 25.2 (CH_2S), 43.3 (CH_2N). IR (KBr; ν cm^{-1}): 3445w, 2991s, 2904s, 2720w, 2606w, 2532w, 2410w, 1604s, 1566s, 1491s, 1477s, 1420w, 1405m, 1366w, 1315m, 1264s, 1249m, 1134m, 1094m, 1077m, 1034m, 1015w, 933s, 882m, 802w, 787m, 724w, 653w, 453w. *Anal.* Calc. for $C_4H_{14}Cl_2HgN_2S_2$: C, 11.28; H, 3.32; N, 6.58; S, 15.06. Found: C, 11.39; H, 3.25; N, 6.70; S, 14.98%.

Table 1
Summary of X-ray data for compounds **1** and **2**

Chemical formula	C_2H_8ClNS	$C_4H_{14}Cl_2HgN_2S_2$
Formula weight	113.60	425.78
Temperature (K)	145(1)	145(1)
Crystal system	triclinic	monoclinic
Color/shape	colorless cube	colorless cube
Space group	$P\bar{1}$	$P2_1/c$
a (Å)	8.540(4)	7.746(1)
b (Å)	8.659(4)	12.138(1)
c (Å)	8.990(4)	12.023(1)
α (°)	107.12(3)	
β (°)	117.08(3)	103.61(1)
γ (°)	90.00(3)	
V (Å^3)	558.6(2)	1098.7(2)
Z	4	4
D_{calc} (g cm^{-3})	1.351	2.574
Absorption coefficient (mm^{-1})	0.900	14.823
Reflections	3277	4925
Independent	1912 unique ($R_{int} = 0.0417$)	2528 unique ($R_{int} = 0.0295$)
$R[F>4\sigma(F)]$	0.0634	0.0194
R(all data)	0.0634	0.0240

4. Conclusion

The presence of S···H contacts in **1** and **2** suggests that the thiol and sulfide form of the MerP protein are capable of hydrogen bonding. This hydrogen bonding is well-known in iron sulfide containing proteins but not established for either the MerP or MerR proteins. This may be due, in part, to the relative paucity of information on the later two proteins. Out of the synthetic mercury-sulfides known, including **3** and **4**, none are reported to have S···H contacts. Thus, compound **2** is unique in this regard.

5. Supplementary material

Crystallographic data for the structural analysis have been deposited with the Cambridge Crystallographic Data Centre, CCDC No. 15748 and 157479 for compounds **1** and **2** which includes full tables of bond lengths and angles, full atom-labeled ORTEP views, unit cell views and observed and calculated structure factor tables are available upon request. Copies of this information may be obtained free of charge from The Director, CCDC, 12 Union Road, Cambridge, CB2 1EZ, UK (fax: +44-1223-336033; e-mail: deposit@ccdc.cam.ac.uk or www: http://www.ccdc.cam.ac.uk).

Acknowledgements

NMR instruments used in this research were obtained with funds from the CRIF program of the National Science Foundation (CHE 997841) and from the Research Challenge Trust Fund of the University of Kentucky.

References

[1] (a) N.L. Brown, Trends Biol. Sci. (1985) 400;
(b) J.S. Wright, M.J. Natan, F.M. McDonnell, D.M. Ralston, T.V. O'Halloran, in: S.J. Lippard (Ed.), Prog. Inorg. Chem. Bioinorg. Chem, vol. 38, John Wiley and Sons, New York, 1990.

[2] (a) R.A. Steele, S.J. Opella, Biochemistry 36 (1997) 6885;
(b) H. Qian, L. Sahlman, P.-O. Eriksson, C. Hambraeus, U. Edlund, I. Sethson, Biochemistry 37 (1998) 9316;
(c) G. Veglia, F. Porcelli, T. Desilva, A. Prantner, S.J. Opella, J. Am. Chem. Soc. 122 (2000) 2389.
[3] M.J. Stillman, C.F. Shaw III, K.T. Suzuki (Eds.), Metallothioneins, VCH Publishers, New York, 1992.
[4] T.C. Markello, I.M. Bernardini, W.A. Gahl, New Eng. J. Med. 328 (1993) 1157.
[5] H.F. Mark, D.F. Othmer, C.G. Overberger, G.T. Seaborg (Eds.), Kirk-Othmer Encyclopedia of Chemical Technology, vol. 19, John Wiley & Sons, New York, 1982, p. 801.
[6] (a) M.M. Matlock, B.S. Howerton, K.R. Henke, D.A. Atwood, J. Haz. Mat. B82 (2001) 55;
(b) M.M. Matlock, B.S. Howerton, D.A. Atwood, J. Haz. Mat. 84B (2001) 73.
[7] For some recent examples as chelate: (a) G.G. Briand, N. Burford, T.S. Cameron, W. Kwiatkowski, J. Am. Chem. Soc. 120 (1998) 11374;
(b) J. Real, M. Pages, A. Polo, J.F. Piniella, A. Alvarez-Larena, Chem. Commun. (1999) 277;
For some recent examples as bridging ligand: (c) W. Su, R. Cao, M. Hong, J. Chen, J. Lu, Chem. Commun. (1998) 1389;
(d) R.G. Pritchard, R.V. Parish, Z. Salehi, J. Chem. Soc., Dalton Trans. (1999) 243.
[8] G. Fleissner, P.M. Kozlowski, M. Vargek, J.W. Bryson, T.V. O'Halloran, T.G. Spiro, Inorg. Chem. 38 (1999) 3523.
[9] G.G. Briand, N. Burford, T.S. Cameron, W. Kwiatkowski, J. Am. Chem. Soc. 120 (1998) 11374.
[10] Z. Salehi, R.V. Parish, R.G. Pritchard, J. Chem. Soc., Dalton Trans. (1997) 4241.
[11] W. Su, R. Cao, M. Hong, J. Chen, J. Lu, Chem. Commun. (1998) 1389.
[12] K.P. Maresca, F.J. Femia, G.H. Bonavia, J.W. Babich, J. Zubieta, Inorg. Chim. Acta 297 (2000) 98.
[13] I.G. Dance, Polyhedron 5 (1986) 1037.
[14] N.J. Taylor, A.J. Carty, J. Am. Chem. Soc. 99 (1977) 6143.
[15] G. Thiele, D. Messer, Z. Anorg. Allg. Chem. 421 (1976) 24.
[16] N.J. Taylor, Y.S. Wong, P.C. Chieh, A.J. Carty, J. Chem. Soc., Dalton Trans. (1975) 438.
[17] G. Krauter, B. Neumuller, V.L. Goedken, W.S. Rees Jr., Chem. Mater. 8 (1996) 360.
[18] X. Almagro, W. Clegg, L. Cucurull-Sanchez, P. Gonzalez-Duarte, M. Traveria, J. Organomet. Chem. 623 (2001) 137.
[19] W. Wojnowski, M. Wojnowski, H.G. von Schnering, Z. Anorg. Allg. Chem. 534 (1985) 153.
[20] C. Stalhandske, F. Zintl, Acta Cryst. C 42 (1986) 1731.
[21] G.R. Desiraju, T. Steiner, The Weak Hydrogen Bond, Oxford University Press, Oxford, 1999, p. 226.
[22] (a) E. Adman, K.D. Watenpaugh, L.H. Jensen, Proc. Natl. Acad. Sci. 72 (1975) 4854;
(b) N. Ueyama, Y. Yamada, T. Okamura, S. Kimura, A. Nakamura, Inorg. Chem. 35 (1996) 6473.

PERGAMON

Polyhedron 21 (2002) 229–238

POLYHEDRON

www.elsevier.com/locate/poly

Metal complexes of dipeptides containing the α-aminoisobutyric residue (Aib): preparation, characterization and crystal structures of copper(II) complexes with H–Aib–Aib–OH

Manolis Tiliakos [a,d], Dimitrios Raptis [b], Aris Terzis [c], Catherine P. Raptopoulou [c], Paul Cordopatis [a], Evy Manessi-Zoupa [d,*]

[a] *Department of Pharmacy, University of Patras, GR 265 04 Patras, Greece*
[b] *Technological Education Institute, GR 122 10 Egaleo Athens, Greece*
[c] *Institute of Materials Science, NCSR 'Demokritos', GR 153 10 Aghia Paraskevi Attikis, Greece*
[d] *Department of Chemistry, University of Patras, GR 265 04 Patras, Greece*

Received 8 August 2001; accepted 31 October 2001

Abstract

A systematic investigation of the reactions between metal ions and dipeptides containing the α-aminoisobutyric residue (Aib) was initiated. The solid complexes $[Cu(H_{-1}L)]_n$ (**1**, **2**) and $(LH_2)_n[CuCl_3]_n$ (**3**) were isolated and characterized by single-crystal X-ray crystallography, solid-state IR spectra and UV–Vis spectroscopy in solution ($H_{-1}L^{2-}$ is the dianionic form of H–Aib–Aib–OH). Of remarkable interest is the isolation of two complexes which have the same chemical formula, $[Cu(H_{-1}L)]_n$, but different structures. Complex **1** is a chain (1D) compound, while complex **2** is a 3D coordination polymer. The doubly deprotonated dipeptide behaves as a N(amino), N(peptide), O(carboxylate), O′(carboxylate) $\eta^1{:}\eta^1{:}\eta^1{:}\eta^1{:}\mu_2$ ligand in **1**. In **2** the $H_{-1}L^{2-}$ ligand binds to one Cu^{II} atom at its amino and peptide nitrogens and at one carboxylate oxygen, and to a second metal at the other carboxylate oxygen, while a third Cu^{II} atom is attached to the peptide oxygen. The structure of **3** consists of zigzag $(CuCl_3)_n^{n-}$ chains and protonated dipeptides (H_2L^+) which remain uncoordinated. Two neighbouring Cu^{II} atoms are bridged by two chloro ligands, while a terminal chloro ligand completes five coordination at each metal center. The IR data are discussed in terms of the nature of bonding and known structures. The UV–Vis spectra show that the solid-state structures of **1** and **2** do not persist in H_2O. © 2002 Elsevier Science Ltd. All rights reserved.

Keywords: α-Aminoisobutyryl-α-aminoisobutyric acid (H–Aib–Aib–OH); Copper(II) peptide complexes; Spectroscopic characterization; X-ray crystal structures

1. Introduction

The interaction of metal ions with small peptides has been a subject of increasing interest over the past three decades [1–3]. Among many reasons for the development of this area are: (a) many of these reactions provide simple models for much more complex biochemical reactions and processes of great importance, e.g. the investigation of the action of metalloenzymes or the storage and transport of trace metal ions through the human body [4,5]; (b) the mode of coordination has a major influence on the conformation of a peptide molecule, a fact that influences its reactivity and ability to interact with receptor sites. Hence, complex formation can have a significant influence on the biological activity of peptides and the metal ions can be regarded as catalysts for many reactions involving peptides [6,7]; and (c) the possibility that such metal complexes possess pharmacological activity [8].

We have recently initiated a systematic study of the coordination chemistry of dipeptides and tripeptides containing the α-aminoisobutyric residue [–HNC-$(CH_3)_2$CO–, Aib]. The occurrence of high proportions of Aib in microbial polypeptide antibiotics and the unusual ion conductance of membranes and artifi-

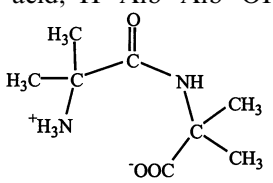
* Corresponding author. Tel./fax: +30-61-997-147.
E-mail address: emane@upatras.gr (E. Manessi-Zoupa).

0277-5387/02/$ - see front matter © 2002 Elsevier Science Ltd. All rights reserved.
PII: S0277-5387(01)00983-4

cial bilayers composed of these peptides [9,10] have stimulated studies concerning the effect of Aib unit on the conformations available to small peptides in solution and in the solid state. Theoretical and ^{1}H NMR investigations have shown that dimethyl alkylation of the α-carbon sterically restricts the conformational freedom of peptides containing the Aib unit [11–13]. The crystal structure of several peptides containing Aib residues show that a 3_{10}- or a-helical conformation is favoured [14–16]. Despite the special properties of Aib, there is a limited number of reports concerning the coordination chemistry of Aib-based small peptides [17–21].

Our interest in this chemistry is fourfold: (i) to redress the almost complete lack of structurally characterized metal complexes with Aib-containing peptides as ligands. To the best of our knowledge, only the X-ray crystal structure of the remarkable copper(III) complex $[Cu^{III}(H_{-2}Aib_3)]\cdot 2H_2O\cdot 1.5NaClO_4$, containing the trianion of tri-α-amino-isobutyric acid as ligand, has been determined [18]. We are particularly interested in investigating how the inductive and steric properties of α-carbon methyl groups affect the structures of the complexes in the solid state and their ability to bind metals of various sizes and oxidation states. We plan to use ligands which will introduce several coordination possibilities and a variety of steric and electronic effects. (ii) To compare the solid-state and solution structures of the peptide complexes using the appropriate physical and spectroscopic techniques. (iii) To investigate the possibility of creating helical complexes (helicates) and/or one-dimensional (1D), two-dimensional (2D) and three-dimensional (3D) coordination polymers. The unique steric properties of Aib and the variety of donor sites present in peptides containing Aib would favour the formation of such complexes. Syntheses of helicates containing two or more metal ions have attracted considerable attention in recent years as examples of self-assembly reactions [22]. Transition metals coordination polymers are of great interest as magnetic, electronic and photooptical materials [23]. (iv) To test the pharmacological activity, e.g. the antitumour activity of tin(IV) complexes [8], the antiinflammatory properties of copper(II) complexes [24,25], etc. of selective peptide complexes.

We wish to report here the initial results of our studies concerning the products from the reaction between copper(II) salts and the α-aminoisobutyryl-α-aminoisobutyric acid, H–Aib–Aib–OH (LH, **I**). Emphasis is given on the characterization of the products in the solid state.



LH, I

2. Experimental

2.1. General and physical measurements

All manipulations were performed under aerobic conditions using materials (reagent grade) and solvents as received.

Microanalyses (C, H, N) were performed by the University of Ioannina (Greece) Microanalytical Service using an EA 1108 Carlo Erba analyzer. Copper analysis was carried out by EDTA titration. M.p.s were taken on a Buchi SMP-20 capillary m.p. apparatus and are uncorrected. IR spectra (4000–500 cm^{-1}) were recorded on a Perkin–Elmer 16 PC FT spectrometer and a Jasco FT-IR 5300 spectrometer with samples prepared as KBr pellets. Solution electronic spectra (800–250 nm) were recorded on a Pharmacia-Biochrom 4060 instrument using H_2O as solvent.

2.2. Compound preparation

2.2.1. H–Aib–Aib–OH

The protected aminoacids Z–Aib–OH and *p*-TsA–Aib–OBzl were prepared according to the literature [26]. Coupling of Z–Aib–OH (0.71 g, 3 mmol) with 1.20 g (3.3. mmol) of *p*-TsA–Aib–Obzl via the PyBOP procedure [27], provided 1.05 g (85%) of Z–Aib–Aib–OBzl; m.p. 122–125 °C (recrystallized from EtOAc–petroleum ether); $R_f = 0.72$ in CH_2Cl_2–MeOH (9:1 v/v); $R_f = 0.68$ in EtOAc. The protecting groups were removed by catalytic hydrogenolysis (10% Pd on charcoal) in methanol. After 3 h the catalyst was filtered off and the solvent evaporated in vacuo. Complete removal was ensured by the addition of a few milliliters of methanol and repetition of the evaporation. The free dipeptide crystallized upon addition of AcOEt–petroleum ether. The product was further purified by column chromatography on Sephadex G-10 using AcOH (5%) as the eluant. Yield: 0.40 g (85%). $R_f = 0.53$ in *n*-BuOH:MeCOOH:Py:H_2O (4:1:1:2 v/v); m.p. 101–102 °C.

2.2.2. $[Cu(H_{-1}L)]_n$ (1)

A solution of LH (0.05 g, 0.26 mmol) in MeOH (3 ml) was added to a stirred green solution of $CuCl_2\cdot 2H_2O$ (0.02 g, 0.12 mmol) in the same solvent (8 ml). The color of the solution was immediately changed to pale blue. The pH of the solution was adjusted to ~6 with aqueous 0.1 N NaOH. The resultant dark blue solution was left for slow evaporation at room temperature. The blue residue obtained dissolved in 2 ml of a mixture

EtOH:Et_2O (50:50 v/v) and was left to a closed test tube. After 4 days, blue crystals suitable for X-ray crystallography formed; these were collected by filtration and dried in vacuo over P_4O_{10}. Yield: 34%. *Anal.* Found: C, 38.9; H, 5.6; Cu, 24.6; N, 11.0. Calc. for $C_8H_{14}O_3N_2Cu$: C, 38.5; H, 5.6; Cu, 25.4; N, 11.2%.

2.2.3. $[Cu(H_{-1}L)]_n$ (2)

LH (0.05 g, 0.26 mmol) was added to a blue solution of $[Cu_2(O_2CMe)_4(H_2O)_2]$ (0.06 g, 0.15 mmol) in H_2O (6 ml). The solid soon dissolved and EtOH (6 ml) was added to the solution. Upon slow evaporation at room temperature (r.t.), blue crystals of the product were precipitated, collected by filtration and dried in vacuo. Some of them were suitable for crystallographic studies. Yield: 37%. *Anal.* Found: C, 38.3; H, 5.5; Cu, 24.2; N, 11.0. Calc. for $C_8H_{14}O_3N_2Cu$: C, 38.5; H, 5.6; Cu, 25.4; N, 11.2%.

2.2.4. $(LH_2)_n)[CuCl_3]_n$ (3)

A solution of LH (0.02 g, 0.11 mmol) in MeOH (6 ml) was added to a stirred green solution of $CuCl_2{\cdot}2H_2O$ (0.02 g, 0.12 mmol) in the same solvent (2 ml). The pH of the resulting solution obtained was lowered to ~ 2 with aqueous 0.1 N HCl and this was left for slow evaporation at r.t. After complete evaporation, a yellow solid was obtained which was dissolved in EtOH (5 ml). Brown crystals suitable for crystallographic studies were obtained from the ethanolic solution by vapour diffusion with Et_2O. Yield: 46%. *Anal.* Found: C, 26.5; H, 4.7; Cu, 16.6; N, 7.5. Calc. for $C_8H_{17}O_3N_2Cl_3Cu$: C, 26.7; H, 4.8; Cu, 17.7; N, 7.8%.

2.3. X-ray crystallographic studies

Crystals of complexes **1**, **2** and **3** were mounted in air. Diffraction measurements were made on a Crystal Logic Dual goniometer diffractometer using graphite-monochromated Mo radiation. Complete crystal data and parameters for data collection and processing are reported in Table 1. Unit cell dimensions were determined and refined using the angular settings of 25 automatically centred reflections in the range $11 < 2\theta < 23°$. Three standard reflections, monitored every 97

Table 1
Crystallographic data for complexes **1**, **2**, and **3**

Parameter	1	2	3
Formula	$C_8H_{14}N_2O_3Cu$	$C_8H_{14}N_2O_3Cu$	$C_8H_{17}Cl_3N_2O_3Cu$
Formula weight	249.75	249.75	359.13
Crystal colour, habit	blue, prism	blue, prism	brown, prism
Crystal dimensions (mm)	$0.15\times0.30\times0.60$	$0.08\times0.15\times0.40$	$0.10\times0.50\times0.60$
Crystal system	hexagonal	orthorhombic	monoclinic
Space group	$P6_1$	$P2_12_12_1$	$P2_1/c$
Unit cell dimensions			
a (Å)	14.858(6)	10.101(10)	12.529(5)
b (Å)	14.858(6)	11.304(9)	6.084(2)
c (Å)	9.197(4)	8.690(8)	18.619(8)
α (°)	90	90	90
β (°)	90	90	91.09
γ (°)	120	90	90
V (Å^3)	1758.4(11)	992(2)	1419(1)
Z	6	4	4
D_{calc} (g cm^{-3})	1.415	1.672	1.681
Radiation, Mo Kα (λ, Å)	0.71073	0.71073	0.71073
Temperature (K)	298	298	298
Scan mode/speed (° min^{-1})	θ–2θ/2.2	θ–2θ/2.5	θ–2θ/2.5
$2\theta_{max}$ (°)	50.0	50.0	50.0
Reflections collected	2198	1946	2625
Unique reflections (R_{int})	1955 (0.0205)	1740 (0.0879)	2501 (0.0126)
Data with $I>2\sigma(I)$	1783	1700	2073
Parameters refined	144	183	222
$[\Delta/\sigma]_{max}$	0.080	0.001	0.001
$(\Delta\rho)_{max}$, $(\Delta\rho)_{min}$ (e Å^{-3})	0.786, −0.385	0.311, −0.376	0.628, −0.437
w [a]	$\alpha = 0.0568$, $b = 0.0000$	$\alpha = 0.0767$, $b = 0.6369$	$\alpha = 0.0389$, $b = 1.9613$
Goodness-of-fit (on F^2)	1.106	1.093	1.130
R_1 [b]	0.0351	0.0425	0.0370
wR_2 [c]	0.0909	0.1062	0.0956

[a] $w = 1/[\sigma^2(F_o^2)+(aP)^2+bP]$ and $P = (\max(F_o^2,0)+2F_c^2)/3$.
[b] $R_1 = \Sigma(||F_o|-|F_c||)/\Sigma(|F_o|)$.
[c] $wR_2 = \{\Sigma[w(F_o^2-F_c^2)^2]/\Sigma[w(F_o{}^2)^2]\}^{1/2}$.

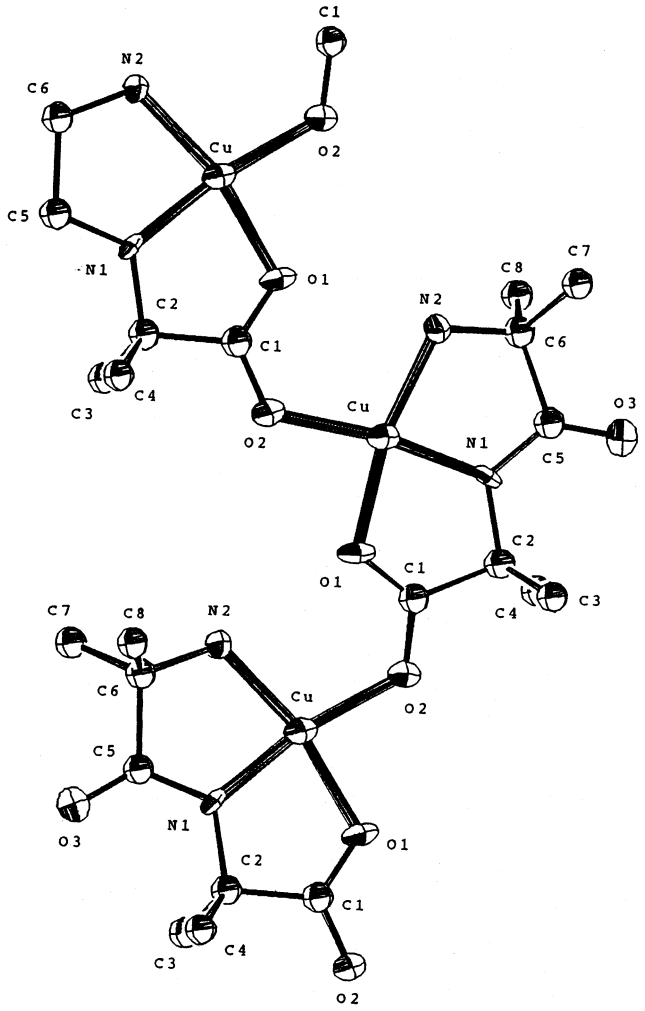


Fig. 1. A portion of one chain of complex **1** showing three metal centers.

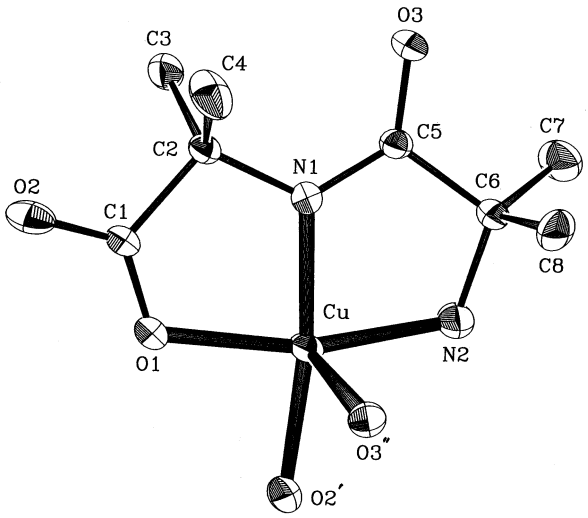


Fig. 2. Details of the structural unit in the 3D coordination polymer **2**. Atoms O(2′) and O(3″) are carboxylate and peptide oxygens, respectively, from two different neighbouring $H_{-1}L^{2-}$ ligands.

reflections, showed less than 3% intensity fluctuation and no decay. Lorenz polarization and Ψ-scan absorption corrections were applied using Crystal Logic software.

The structures were solved by direct methods using SHELXS-86 [28] and refined by full-matrix least-squares techniques on F^2 with SHELXL-93 [29]. For **2** and **3**, all hydrogen atoms were clearly visible in subsequent difference Fourier maps and refined with isotropic thermal parameters; in **1**, all hydrogen atoms were introduced at calculated positions as riding on bonded atoms. For all structures, all non-hydrogen atoms were refined using anisotropic thermal parameters.

3. Results and discussion

3.1. Syntheses

The case of blue complexes **1** and **2** is very interesting and as far as we are aware unique in metal–peptide chemistry. The two complexes have the same chemical formula, $[Cu(H_{-1}L)]_n$, but different structures. Complex **1** is a chain compound (1D) and complex **2** is a three-dimensional (3D) coordination polymer. Different inorganic starting materials were used for the preparation of the two complexes; $CuCl_2{\cdot}2H_2O$ for **1** and $[Cu_2(O_2CMe)_4(H_2O)_2]$ for **2**. Both reactions took place at pH ~ 6 in aqueous alcoholic media. The LH:Cu^{II} reaction ratio has no influence on the stoichiometry of the products. For example, complex **1** can be isolated using either a 2:1 or an 1:1 LH:$CuCl_2{\cdot}2H_2O$ ratio. The preparation of **1** and **2** is summarized in Eqs. (1) and (2), respectively.

$$n\,CuCl_2{\cdot}2H_2O + n\,LH + 2n\,NaOH \xrightarrow{MeOH/H_2O} \underset{\mathbf{1}}{[Cu(H_{-1}L)]_n} + 2n\,NaCl + 4n\,H_2O \quad (1)$$

$$[Cu_2(O_2CMe)_4(H_2O)_2] + 2n\,LH \xrightarrow{H_2O/EtOH} \underset{\mathbf{2}}{2[Cu(H_{-1}L)]_n} + 4n\,MeCO_2H + 2n\,H_2O \quad (2)$$

We believe that the solvent mixture used is the critical factor for the different structural identity of the two products.

The 1:1 reaction between $CuCl_2{\cdot}2H_2O$ and LH in $MeOH/H_2O$ under acidic conditions (pH ~ 2) yielded the ionic polymer **3**, in which the dipeptide is in its cationic form (LH_2^+) acting as a counter-ion (Eq. (3)).

$$n\,CuCl_2{\cdot}2H_2O + n\,LH + n\,HCl \xrightarrow{MeOH/H_2O} \underset{\mathbf{3}}{(LH_2)_n[CuCl_3]_n} + 2n\,H_2O \quad (3)$$

Despite our efforts, no copper(II) complexes containing the monoanionic (L^-) and neutral (LH) forms of the dipeptide could be obtained at intermediate acidity ($2 < pH < 6$) conditions.

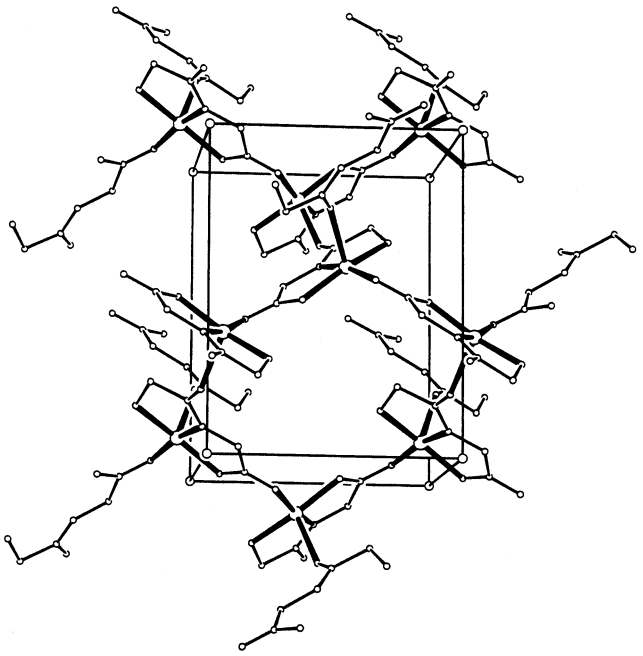


Fig. 3. A crystal packing diagram of complex **2**; the weak intermolecular hydrogen bond is not shown.

3.2. Description of structures

The structures of complexes **1**, **2** and **3** are shown in Figs. 1, 2 and 4, respectively. A crystal packing diagram of **2** is present in Fig. 3. The important metric parameters are listed in Tables 2–4.

The crystal structure of **1** consists of isolated 'flat' helical chains along the *c* axis. The helical chain develops along a twofold screw axis. The metal ion is chelated by the terminal amino [N(2)] nitrogen, the deprotonated peptide [N(1)] nitrogen and one of the carboxylate oxygens [O(1)] of the ligand. The fourth coordination site is occupied by a carboxylate oxygen [O(2)] of a neighbouring dipeptide dianion. The carboxylate bridging interaction with two neighbouring metal ions is of the *syn*, *anti* type. Thus, $H_{-1}L^{2-}$ behaves as $\eta^1{:}\eta^1{:}\eta^1{:}\eta^1{:}\mu_2$ ligand or in a $[2{\cdot}1_1 1_2 1_1 1_1]$ mode (as described using 'Harris' notation [30]). According to the latter, the binding mode of a ligand is referred to as $[X{\cdot}Y_1 Y_2 Y_3 \ldots Y_n]$, where X is the overall number of metals bound by the whole ligand and each value of Y refers to the number of metal atoms attached to the different donor atoms. The ordering of Y

Table 3
Selected bond lengths (Å) and bond angles (°) for complex **2** [a]

Bond lengths			
Cu–N(1)	1.911(4)	C(1)–O(1)	1.261(5)
Cu–N(2)	2.016(4)	C(1)–O(2)	1.259(5)
Cu–O(1)	1.988(3)	C(5)–O(3)	1.253(6)
Cu–O(2) # 1	1.959(3)	C(5)–N(1)	1.320(5)
Cu–O(3) # 2	2.362(3)		
Bond angles			
N(1)–Cu–O(1)	83.2(1)	O(3) # 2–Cu–N(2)	92.7(2)
N(1)–Cu–O(2) # 1	166.8(1)	C(1)–O(1)–Cu	114.3(3)
N(1)–Cu–N(2)	82.7(2)	C(1)–O(2)–Cu # 3	124.9(3)
N(1)–Cu–O(3) # 2	105.8(1)	C(5)–O(3)–Cu # 4	139.0(3)
O(1)–Cu–O(2) # 1	90.9(1)	C(2)–N(1)–Cu	117.1(3)
O(1)–Cu–N(2)	162.9(2)	C(5)–N(1)–Cu	120.2(3)
O(1)–Cu–O(3) # 2	100.5(1)	C(5)–N(1)–C(2)	122.7(4)
O(2) # 1–Cu–N(2)	100.7(2)	N(1)–C(2)–C(1)	105.4(3)
O(2) # 1–Cu–O(3) # 2	86.9(1)	C(6)–C(5)–N(1)	113.0(4)

[a] Symmetry transformations used to generate equivalent atoms: # 1 $-x+1/2, -y, z+1/2$; # 2 $x-1/2, -y+1/2, -z$; # 3 $-x+1/2, -y, z-1/2$; # 4 $x+1/2, -y+1/2, -z$.

Table 2
Selected bond lengths (Å), bond angles (°) and hydrogen bonding details for complex **1** [a]

Bond lengths				
Cu···Cu	5.045(1)	C(1)–O(1)	1.255(6)	
Cu–N(1)	1.888(4)	C(1)–O(2) # 1	1.250(6)	
Cu–N(2)	1.979(4)	C(5)–O(3)	1.247(6)	
Cu–O(1)	1.948(3)	C(5)–N(1)	1.324(6)	
Cu–O(2)	1.950(3)			
Bond angles				
N(1)–Cu–O(1)	83.1(1)	C(1) # 2–O(2)–Cu	125.0(3)	
N(1)–Cu–O(2)	168.2(2)	C(1)–O(1)–Cu	115.5(3)	
N(1)–Cu–N(2)	83.7(2)	C(2)–N(1)–Cu	117.4(3)	
O(1)–Cu–O(2)	88.6(1)	C(6)–N(2)–Cu	112.4(3)	
O(1)–Cu–N(2)	165.0(2)	C(5)–N(1)–C(2)	123.7(4)	
O(2)–Cu–N(2)	105.5(2)	N(1)–C(2)–C(1)	104.4(4)	
C(5)–N(1)–Cu	118.8(3)	C(6)–C(5)–N(1)	113.9(4)	
D–H···A	D–H	H···A	D–H···A	Symmetry equivalence of A
Hydrogen bonds				
N(2)–H(N2A)···O(3)	0.911	2.042	137.6	$x-y, x-1, -z$
N(2)–H(N2B)···O(1)	0.693	2.335	126.3	$-x+1, -y, z-1/2$

[a] Symmetry transformations used to generate equivalent atoms: # 1 $-x+1, -y, z-1/2$; # 2 $-x+1, -y, z+1/2$. A = acceptor; D = donor.

is listed by the Cahn–Ingold–Prelog priority rules, hence here O before N. In the case of chelating/bridging ligands, to distinguish between several alternatives, a subscript number is included to show to which metal ion the donor is attached.

A moderate distortion in the square planar environment of Cu^{II} is indicated by the observed *cis* bond angles which vary from 83.1(1) to 105.5(2)°. The deviation of the Cu^{II} atom from the best mean plane of the donor atoms N(1), N(2), O(1), O(2) is 0.10 Å. The $Cu^{II}–N_{peptide}$ bond [1.888(4) Å] is stronger than the $Cu^{II}–NH_2$ one [1.979(4) Å], as expected [1,2]. The two chelating rings are almost coplanar; the dihedral angle between the best mean planes CuN(1)C(2)C(1)O(1) and CuN(1)C(5)C(6)N(2) is 3.8°. Intermolecular hydrogen bonds involving the amino group and atoms O(1) and O(3) stabilize the crystal structure.

There is one very weak interaction between Cu and the peptide oxygen of a neighbouring chain, the dimension being Cu···O(3) $[x-y,\ y,\ z] = 2.959(1)$ Å.

Another 1D copper(II) dipeptide complex is structurally related to **1** in that it also exhibits a $\eta^1{:}\eta^1{:}\eta^1{:}\eta^1{:}\mu_2$ coordination mode of the ligand, namely $[Cu(H_{-1}L')]_n$ (L′H = L-trypthophyl-glycine) [31]. However, in the latter there are $Cu^{II}–\pi$ interactions that are provided by the 'sandwich' structure involving each Cu^{II} atom and two trypthophan residues from neighbouring molecules.

Although complexes **1** and **2** have the same chemical formula, their solid-state structures are quite different. Complex **2** is a 3D coordination polymer. The doubly deprotonated dipeptide binds copper(II) via the amino [N(2)] nitrogen atom, the deprotonated peptide [N(1)] nitrogen atom and a carboxylate oxygen atom [O(1)]. In addition there are two bonds from the peptide oxygen atom [O(3)] and the second carboxylate oxygen atom [O(2)] to two other Cu^{II} atoms. Thus, each peptide dianion participates in the coordination spheres of three Cu^{II} atoms and behaves as $\eta^1{:}\eta^1{:}\eta^1{:}\eta^1{:}\mu_3$ ligand or in a $[3{\cdot}1_1 1_2 1_3 1_1 1_1]$ mode [30]. Conversely, each copper is bonded to three different peptides; this is the view emphasized in Fig. 2. The Cu···Cu distances are 5.105(1) [through the carboxylate group] and 6.097(1) Å [through the deprotonated peptide bond].

The coordination number of Cu^{II} is five and its geometry is distorted square-pyramidal. Three of the basal coordination sites are occupied by the donor atoms of the same ligand O(1), N(1), N(2) and the fourth by the second carboxylate oxygen [O(2)] of an adjacent repeating unit. In the axial coordination position lies the peptide oxygen [O(3)] of a third unit. The metal lies 0.19 Å out of the least-squares basal plane, towards O(3). As expected the axial Cu–O(3) bond is approximately 0.4 Å longer than the Cu–O bond lengths in the basal plane. The $Cu–N_{amino}$, $Cu–N_{peptide}$ and $Cu–O_{carboxylate}$ bond lengths in **2** are distinctly longer than in **1**, as expected from the higher coordination number in the former. The two individually almost planar chelate rings CuN(1)C(2)C(1)O(1) and CuN(1)C(5)C(6)N(2) are slightly twisted out of coplanarity, the dihedral angle between their least-squares plane being 6.5°. The crystal structure is stabilized by a

Table 4
Selected bond lengths (Å), bond angles (°) and hydrogen bonding details for complex **3** [a]

Bond lengths				
Cu–Cl(1) # 1	2.268(1)	C(1)–O(1)	1.196(5)	
Cu–Cl(1)	2.529(1)	C(1)–O(2)	1.310(5)	
Cu–Cl(2) # 2	2.294(1)	C(3)–O(3)	1.221(4)	
Cu–Cl(2)	2.424(1)	C(3)–N(1)	1.327(5)	
Cu–Cl(3)	2.251(1)			
Bond angles				
Cl(1) # 1–Cu–Cl(1)	87.1(1)	Cl(2) # 2–Cu–Cl(3)	92.8(1)	
Cl(1) # 1–Cu–Cl(2)	90.6(1)	Cl(2)–Cu–Cl(3)	140.6(1)	
Cl(1) # 1–Cu–Cl(2) # 2	172.7(1)	Cu # 1–Cl(1)–Cu	93.0(1)	
Cl(1) # 1–Cu–Cl(3)	94.6(1)	Cu # 2–Cl(2)–Cu	96.5(1)	
Cl(1)–Cu–Cl(2)	99.9(1)	C(3)–N(1)–C(2)	123.2(3)	
Cl(1)–Cu–Cl(2) # 2	89.8(1)	N(1)–C(2)–C(1)	108.9(3)	
Cl(1)–Cu–Cl(3)	119.4(1)	C(4)–C(3)–N(1)	117.1(3)	
Cl(2) # 2–Cu–Cl(2)	83.5(1)			
D–H···A	D–H	H···A	D–H···A	Symmetry equivalence of A
Hydrogen bonds				
O(2)–H(O2)···O(3)	0.712	2.021	147.7	$-x+2,\ y+1/2,\ -z-1/2$
N(2)–H(N2A)···O(1)	0.890	2.028	167.9	$-x+2,\ y+1/2,\ -z-1/2$
N(1)–H(N1)Cl(1)	0.763	2.767	169.6	$x,\ -y+1/2,\ z-1/2$
N(2)–H(N2B)···Cl(3)	0.846	2.436	167.0	$-x+1,\ -y,\ -z$
N(2)–H(N2C)···Cl(2)	0.794	2.632	157.0	$x,\ y,\ z$

[a] Symmetry transformations used to generate equivalent atoms: # 1 $-x+1,\ -y,\ -z$; # 2 $-x+1,\ -y+1,\ -z$. A = acceptor; D = donor.

weak, intermolecular hydrogen bond involving the amino group and the carboxylate oxygen atom [O(1)], dimensions being: N(2)···O(1) [$-x+1/2$, $-y$, $z+1/2$] = 3.045 Å, H(N2B)···O(1) [$-x+1/2$, $-y$, $z+1/2$] = 2.510 Å and N(2)–H(N2B)···O(1) [$-x+1/2$, $-y$, $z+1/2$] = 118.4°.

The structure of **2**, as detailed in the above discussion and in Figs. 2 and 3, shows remarkable resemblance to those of $[Cu(H_{-1}L_A)]_n$, where L_AH = glycyl-L-methionine [32], glycyl-L-alanine [33], L-methionylglycine [34] and L-leucyl-L phenylalanine [35]. In all five complexes, the deprotonated peptide bond bridges two different Cu^{II} atoms through the oxygen and nitrogen atoms. This μ_2 coordination mode of the deprotonated peptide group is extremely rare in transition metal chemistry. It has also been observed in the dinuclear complex $[Pt_2(H_{-1}L_B)(NH_3)_4]\cdot(SO_4)$ [36], where L_BH = glycylglycine; however, one of the carboxylate oxygen atoms remains uncoordinated in the platinum(II) complex.

The crystal structure of **3** is composed of zigzag, polymeric chains of stoichiometry $(CuCl_3)_n^{n-}$ and protonated [at the amino nitrogen, N(2)] dipeptides which remain uncoordinated. There are two bridging chloro ligands between two neighbouring atoms, while a terminal chloro ligand [Cl(3)] completes five coordination at each metal centre. A regular alternation of two non-equivalent $Cu_2(\mu_2\text{-}Cl)_2$ units occurs in the chain. Both bridging Cu_2Cl_2 units are strictly planar with a crystallographic inversion centre in the middle of each Cu···Cu distance. The Cu···Cu separations are 3.483(1) Å through the Cl(1) bridges and 3.522(1) Å through the Cl(2) bridges. The bridging Cu–Cl bond distances range from 2.268(1) to 2.529(1) Å. As expected, the terminal Cu–Cl(3) bond distance [2.251(1) Å] is shorter than the bridging distances. These Cu–Cl distances are within the normal range observed [37] for other 1D polymeric complexes of the stoichiometry $ACuCl_3$ (A = cation).

Salts of stoichiometry $ACuCl_3$ often contain $[Cu_2Cl_6]^{2-}$ ions and large, e.g. Ph_4P^+, cations to keep the anions well separated; the $[Cu_2Cl_6]^{2-}$ ions are formed by two tetrahedra sharing an edge [38,39]. For smaller cations, the dimers become linked by long Cu–Cl bonds giving infinite chains with five- or six-coordinate Cu^{II} [38,39]. The chloro complex $CsCuCl_3$ is unique in forming infinite chains of distorted octahedra sharing opposite triangular faces [38].

The five donor atoms within bonding distances do not define a regular polyhedron around copper in **3**. Analysis of the shape-determining angles using the approach of Addison et al. [40] yields a value for trigonality index, τ, of 0.53 ($\tau = 0$ and 1 for perfect square pyramidal and trigonal bipyramidal geometries, respectively). Thus, the geometry about copper(II) is distorted significantly and can be described as either a distorted sp or a distorted tbp arrangement. With use of the tbp description, the apical sites are occupied by Cl(1) [$-x+1$, $-y$, $-z$] and Cl(2) [$-x+1$, $-y+1$, $-z$] with atoms Cl(1), Cl(2) and Cl(3) making up the equatorial plane; Cu lies 0.52 Å out of the equatorial plane. For the sp description the basal plane consists of atoms Cl(1) [$-x+1$, $-y$, $-z$], Cl(2), Cl(2) [$-x+1$, $-y+1$, $-z$] and Cl(3) with Cl(1) occupying the apical site. The four basal atoms are not coplanar; Cl(1) [$-x+1$, $-y$, $-z$] and Cl(2) [$-x+1$, $-y+1$, $-z$] lie 0.20 and 0.50 Å, respectively, above the best least-squares plane through the four atoms, while Cl(2) and Cl(3) lie 0.27 and 0.67 Å, respectively, below it. In the sp description, the bridging Cl(1) (or Cl(1) [$-x+1$, $-y$, $-z$]) atom simultaneously occupies a basal site at one Cu^{II} atom and the apical site of the neighbouring Cu^{II} atom. This is a common structural feature for dinuclear Cu^{II} units with two mono-atomic bridges. The copper(II) atom is 0.29 Å above the plane toward the apical donor atom. The distortions from the ideal tbp geometry appear greater than in the sp model; thus, the sp description is more preferred.

The presence of hydrogen bonds is a dominant feature in the crystal structure of **3** (see Fig. 4). The LH_2^+ peptide cations form dimers through the two hydrogen bonding interactions O(2)–H···O(3) [$-x+2$, $y+1/2$, $-z-1/2$] and N(2)–H(N2A)···O(1) [$-x+2$, $y+1/2$, $-z-1/2$]. Moreover, the chloro atoms of the $CuCl_3^-$ chains are hydrogen bonded to the dimeric LH_2^+ moieties through the N(1)–H···Cl(1)[(x, $-y+1/2$, $z-1/2$], N(2)–H(N2B)···Cl(3) [$-x+1$, $-y$, $-z$] and N(2)–H(N2C)···Cl(2) [x, y, z] interactions.

3.3. Spectroscopic studies

Table 5 gives diagnostic IR bands for the dipeptide LH and complexes **1**, **2** and **3**. Assignments have been made by studying extensive literature reports [34,41–48], noting spectral differences between the free, protonated and coordinated dipeptide and bearing in mind the known X-ray structures of the complexes.

The free dipeptide exists as zwitterion, as evidenced by the appearance of the typical $-NH_3^+$ and $-COO^-$ bands [34,42,45]. The simultaneous presence of the $-NH_3^+$ and characteristic –COOH bands [ν(C=O), ν(C–O), δ(OH)] in the spectrum of **3** confirms that the dipeptide is protonated, i.e. LH_2^+.

The extensive hydrogen bonding in LH and $H_{-1}L^{2-}$, and their difference in charge makes it difficult to rationalize frequency shifts upon copper(II) coordination. However, we observe the disappearance of the $\nu(NH_3^+)$, $\delta_d(NH_3^+)$ and $\delta_s(NH_3^+)$ bands associated with the zwitterionic structure in **1** and **2**, coupled with the appearance of two absorptions in the 3358–3150 cm^{-1} assigned to the antisymmetric and symmetric $-NH_2$ stretching modes. These changes and the relatively low frequency of the $\nu(NH_2)$ bands are in agree-

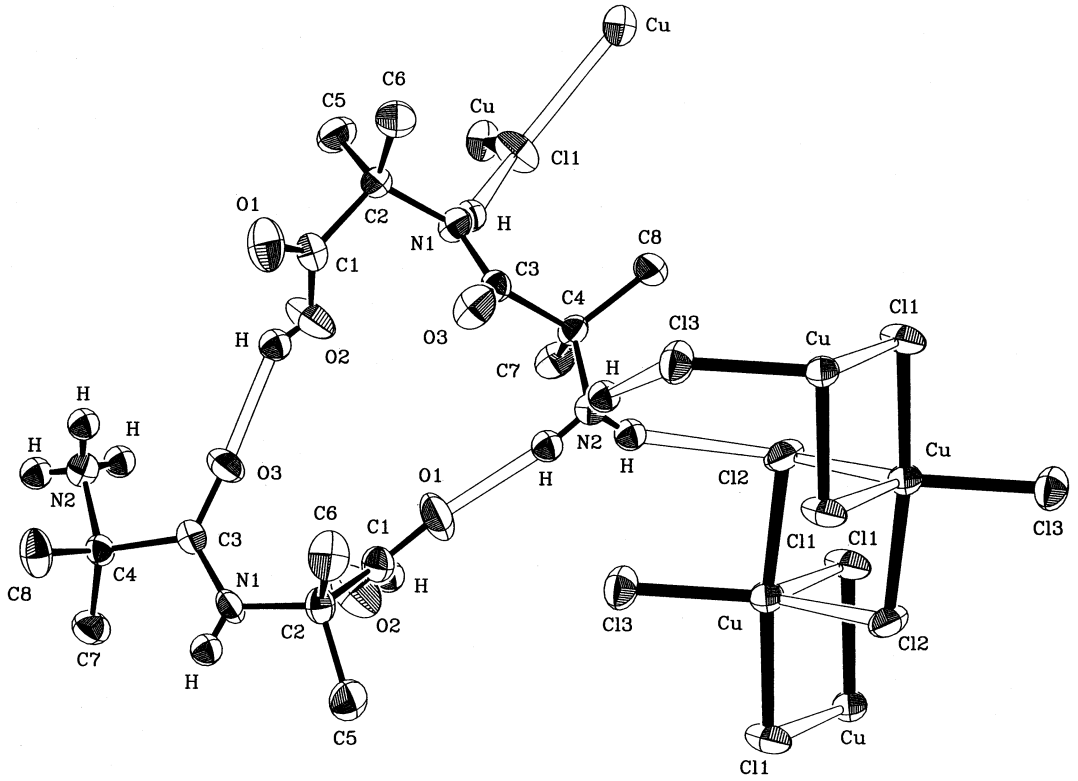


Fig. 4. A view of the structure of complex **3** showing a portion of the $(CuCl_3)_n^{n-}$ chain and two dipeptide counterions. Identical numbers are used for symmetry-generated atoms. Open bonds indicate weak coordination bonds or hydrogen bonds.

ment with the fact that the terminal amino group of $H_{-1}L^{2-}$ occupies one of the coordination sites of the metal ion [34]. The difference $\Delta[\Delta = \nu_{as}(CO_2) - \nu_s(CO_2)]$ for complexes **1** and **2** is less than that for the corresponding free zwitterionic dipeptide as expected for the bidentate bridging mode of carboxylate ligation [46].

The IR spectrum of the free dipeptide LH shows the characteristic bands of a hydrogen-bonded, trans secondary peptide group [41,48]. As would be expected from the stoichiometry, the $\nu(NH)_{peptide}$ band is absent in the spectra of **1** and **2**. Also the amide II and III bands are replaced by a new absorption at 1400 (**1**) and 1404 (**2**) cm^{-1}, which is characteristic for deprotonated secondary (in fact tertiary) peptide complexes [41]; this replacement might be expected, since on removal of the peptide proton the band becomes a pure C–N stretch. The $\nu(CO)_{peptide}$ [amide I] band appears at 1600 (**1**) and 1576 (**2**) cm^{-1}; this large low-frequency shift is typical of peptide N-bonding [34]. It is interesting to note, however, that this mode appears at lower frequencies in **2** (compared to **1**) which has been shown by X-ray crystallography to contain a μ_2 O,N-bound deprotonated peptide group. Thus, in the solid state, there is only indirect IR evidence that the peptide group in complex **2** is bound to the Cu^{II} atoms through both its deprotonated nitrogen and peptide oxygen.

Electronic spectra of aqueous solutions of **1** and **2** have been recorded. The longest wavelength absorption band of the peptide group itself occurs near 220 nm in the free dipeptides and this is due to an $n \rightarrow \pi^*$ transition [2]. Several transitions in the 210–280 nm region appear upon coordination of Cu^{II}; these intense absorption maxima are assigned [2,34] to $N \rightarrow Cu^{II}$ ligand-to-metal charge transfer (LMCT) transitions. Data in the 285–800 nm range are as follows: complex **1**, $\lambda_{max} =$ 292, 609 ($\varepsilon = 130$ l mol^{-1} cm^{-1}) nm; and complex **2**, $\lambda_{max} = 292$, 610 ($\varepsilon = 125$ l mol^{-1} cm^{-1}) nm. The d–d visible band is suggestive of approximately square pyramidal geometry with mixed O and N donors about the metal ion as observed in other copper(II) peptide complexes [49]. The approximately 290 nm band is tentatively assigned to a $COO^- \rightarrow Cu^{II}$ charge-transfer transition [34].

From our solution data it is evident that complexes **1** and **2**, which have a different solid-state geometry, have the same chromophore in water. We believe that the polymeric structures—observed for **1** and **2** in the solid state—do not persist in solution. Possibly, one of the carboxylate oxygens and the apical peptide oxygen (in **2**) are replaced by H_2O molecules when the crystals are dissolved in water [34]. Further evidence of the disruption of the solid-state structures upon dissolution is provided by the absence of a band in the 320–370 nm range in the solution spectra [34,50]; this LMCT band, which is observed when the COO^- group is bridging between two Cu^{II} ions and considered to be a diagnos-

Table 5
Most characteristic and diagnostic FT-IR data (cm^{-1}) of LH and complexes **1**, **2** and **3**

Assignment	LH	1	2	3
$\nu(NH)_{peptide}$	3384s			3360mb
$\nu_{as}(NH_2)$		3322m	3358m	
$\nu_s(NH_2)$		3150wb	3294w	
$\nu(NH_3^+)$	3096mb			3050mb
$\delta(NH_2)$		1620sh	1606w	
$\nu(C{=}O)_{-COOH}$				1719mb
$\nu(CO)_{peptide}$ [amide I]	1686s, 1667m	1600s	1576s	1668s
$\delta_d(NH_3^+)$	1648w, 1614m			1608sb
$\nu_{as}(CO_2)$ + amide II	1576sb			
$\nu_{as}(CO_2)$		1542s	1550s	
$\delta(NH)$ + $\nu(CN)_{peptide}$ [amide II]				1544m
$\delta_s(NH_3^+)$	1492s			1473m [a]
$\delta_d(CH_3)$	1454s	1454m	1462m	1473m [a]
$\nu_s(CO_2)$	1400s	1414s	1416m	
$\nu(CN)_{peptide}$		1400sh	1404m	
$\delta(OH)_{-COOH}$				1400m
$\delta_s(CH_3)$	1350s	1350w	1378w	1385sh
$\nu(C{-}O)_{-COOH}$				1280w
$\nu(CN)_{peptide}$ + $\delta(NH)$ [amide III]	1246s			1245s
$\rho_t(NH_2)$		1202sh	1194w	
$\rho_w(NH_2)$		1052w	1036m	
$\rho_r(NH_2)$		688w	686w	

Abbreviations: b, broad; m, medium; s, strong; sh, shoulder; w, weak.
[a] Overlapping bands.

tic property of the Cu^{II}–OCO–Cu^{II} linkage, has been attributed to the bridging π system that is delocalized over the carboxylate group and the Cu^{II} atoms.

4. Conclusions and perspectives

The Cu^{II}/LH reaction system fulfilled its promise as a source of new interesting copper(II) complexes. The most interesting point of this work is that complexes **1** and **2** have a completely similar chemical identity, i.e. $[Cu(H_{-1}L)]_n$, but a different structural identity; **1** is a chain (1D) polymer, whereas **2** is a 3D coordination polymer. This structural difference arises from the different ligation modes of the dianion $H_{-1}L^{2-}$ in the two complexes. Our results indicate that competition and cooperation between potential binding sites in the dipeptide used are rather complicated processes and support the view that 'fine-tuning' of the synthetic and crystallization conditions can bring remarkable changes in the structure of the copper(II)/Aib-based peptide complexes.

It is clear that a plethora of new experiments is required to fulfil the goals (i)–(iv) cited in the introduction. In addition to complexes **1**–**3** described above, a number of copper(II) and diorganotin(IV) complexes with other Aib–based peptides as ligands, i.e. Aib–Gly, Aib–Ala, Aib–Leu, Aib–Phe, etc. have been characterized or are under characterization at the time of writing. The products comprise a remarkably wide variety of structural types, emphasizing the capability of the dipeptides to adopt a number of ligation modes in their mono- or dianionic forms, both terminal and bridging, and both tridentate and polydentate. The complexes obtained to date, some of which have an impressive biological activity, will be reported in due course.

5. Supplementary material

Crystallographic data for the structural analysis have been deposited with the Cambridge Crystallographic Centre, CCDC Nos. 160947, 160948 and 160949 for complexes **1**, **2** and **3**, respectively. Copies of this information may be obtained free of charge from The Director, CCDC, 12 Union Road, Cambridge, CB2 1EZ, UK (fax: +44-1233-336-033; e-mail: deposit@ccdc.cam.ac.uk or www: http://www.ccdc.cam.ac.uk).

References

[1] H.C. Freeman, Adv. Protein Chem. 22 (1967) 257.
[2] H. Sigel, R.B. Martin, Chem. Rev. 82 (1982) 385.
[3] I. Sovago, in: K. Burger (Ed.), Biocoordination Chemistry, Ch. IV, Ellis Hoorwood, London, 1990.
[4] U. Herr, W. Spahl, G. Trojandt, W. Steglich, F. Thaler, R. van Eldik, Bioinorg. Med. Chem. 7 (1999) 699 and references therein.
[5] T. Gajda, B. Henry, A. Aubry, J.-J. Delpnech, Inorg. Chem. 35 (1996) 586 and references therein.
[6] L.D. Pettit, J.E. Gregor, H. Kozlowski, in: R.W. Hay, J.R. Dilworth, K.B. Nolan (Eds.), Perspectives on Bioinorganic Chemistry, vol. 1, Jai Press, London, 1991, pp. 1–41.
[7] L.D. Pettit, G. Formicka-Kozlowska, Neurosci. Lett. 50 (1982) 53.
[8] F. Huber, R. Barbieri, in: B.K. Keppler (Ed.), Metal Complexes in Cancer Chemotherapy, VCH, Weinheim, 1993, pp. 353–368.
[9] G. Jung, W.A. König, D. Leibfritz, T. Ooka, K. Janco, G. Boheim, Biochim. Biophys. Acta 433 (1976) 164.
[10] (a) R.C. Pandey, J. Carter Cook Jr, K.L. Rinehart Jr, J. Am. Chem. Soc. 99 (1977) 8469;
(b) R.C. Pandey, J. Carter Cook Jr, K.L. Rinehart Jr, J. Am. Chem. Soc. 99 (1977) 5203;
(c) R.C. Pandey, H. Meng, J. Carter Cook Jr, K.L. Rinehart Jr, J. Am. Chem. Soc. 99 (1977) 5205.
[11] R. Nagaraj, N. Shamala, P. Balaram, J. Am. Chem. Soc. 101 (1979) 16.
[12] Y. Paterson, S.M. Runsey, E. Benedetti, G. Nemethy, H.A. Scheraga, J. Am. Chem. Soc. 103 (1981) 2947.
[13] K. Ramnarayan, M.F. Chan, V.N. Balaji, S. Proffeta Jr, S.N. Rao, Int. J. Pept. Prot. Res. 45 (1995) 366.
[14] E. Benedetti, Biopolymers 40 (1996) 3 and references therein.
[15] I.L. Karle, R. Balaram, Biochemistry 29 (1996) 6747.
[16] I.L. Karle, Biopolymers 40 (1996) 157 and references therein.

[17] A.W. Hamburg, M.T. Nemeth, D.W. Margerum, Inorg. Chem. 22 (1983) 3535.
[18] L.L. Diaddario, W.R. Robinson, D.W. Margerum, Inorg. Chem. 22 (1983) 1021.
[19] S.T. Kirksey Jr, T.A. Neubecker, D.W. Margerum, J. Am. Chem. Soc. 101 (1979) 1631.
[20] J.P. Hinton, D.W. Margerum, Inorg. Chem. 25 (1986) 3248.
[21] B.E. Schwederski, D.W. Margerum, Inorg. Chem. 28 (1989) 3472.
[22] J.-M. Lehn, Supramolecular Chemistry, VCH, Weinheim, 1995, pp. 144–154.
[23] G. Denti, S. Serroni, S. Campagna, A. Juris, M. Ciano, Y. Balzani, in: A.F. Williams, C. Floriani, A.E. Merbach (Eds.), Perspectives in Coordination Chemistry, VCH, Weinheim, 1992, pp. 153–164.
[24] G.E. Jackson, P.W. Linder, A. Voye, J. Chem. Soc., Dalton Trans. (1996) 4605 and references therein.
[25] G.E. Jackson, L. Mkhonta-Gama, A. Vohe, M. Kelly, J. Inorg. Biochem. 79 (2000) 147.
[26] E. Schröder, K.L. Lübke, The Peptides, Academic Press, New York, 1965 (vol. 1), 1966 (vol. 2).
[27] J. Coste, D. Le Nguyen, B. Castro, Tetrahedron Lett. 31 (1990) 205.
[28] G.M. Sheldrick, SHELXS-86, Structure Solving Program, University of Göttingen, Germany, 1986.
[29] G.M. Sheldrick, SHELXL-93, Crystal Structure Refinement, University of Göttingen, Germany, 1993.
[30] R.A. Coxall, S.G. Harris, D.K. Henderson, S. Parsons, P.A. Tasker, R.E.P. Winpenny, J. Chem. Soc., Dalton Trans. (2000) 2349.
[31] O.R. Nascimento, A.J. Costa-Filho, D.I. De Morais, J. Ellena, L.F. Delboni, Inorg. Chim. Acta 312 (2001) 133.
[32] C.A. Bear, H.C. Freeman, Acta Crystallogr., Sect. B 32 (1976) 2534.
[33] H.C. Freeman, M.J. Healy, M.L. Scudder, J. Biol. Chem. 252 (1977) 8840.
[34] J. Dehand, J. Jordanov, F. Keck, A. Mosset, J.J. Bonnet, J. Galy, Inorg. Chem. 18 (1979) 1543.
[35] G. Maccarrone, G. Nardin, L. Randaccio, G. Tabbi, M. Rosi, A. Sgamellotti, E. Rizzarelli, E. Zangranto J. Chem. Soc., Dalton Trans. (1996) 3449.
[36] T.G. Appleton, J.R. Hall, T.W. Hambley, P.D. Prenzler, Inorg. Chem. 29 (1990) 3562.
[37] U. Geiser, R.M. Gaura, R.D. Willett, D.X. West, Inorg. Chem. 25 (1986) 4203.
[38] F.A. Cotton, G. Wilkinson, Advanced Inorganic Chemistry, 5th ed., Wiley, New York, 1988, pp. 766–767.
[39] S.R. Desjardins, D.E. Wilcox, R.L. Musselman, E.I. Solomon, Inorg. Chem. 26 (1987) 288.
[40] A.W. Addison, T.N. Rao, J. Reedijk, J. Rijn, G.C. Verschoor, J. Chem. Soc., Dalton Trans. (1984) 1349.
[41] S.P. Perlepes, T. Kabanos, V. Hondrellis, J.M. Tsangaris, Inorg. Chim. Acta 150 (1988) 13 and references therein.
[42] M.L. Bair, E.M. Larsen, J. Am. Chem. Soc. 93 (1971) 1140.
[43] A. Garoufis, M. Louloudi, S. Kasselouri, J. Hatiris, N. Hadjiliadis, Polyhedron 14 (1995) 1155.
[44] E. Manessi-Zoupa, S.P. Perlepes, V. Hondrellis, J.M. Tsangaris, J. Inorg. Biochem. 55 (1994) 217 and references therein.
[45] K. Nakamoto, Infrared and Raman Spectra of Inorganic and Coordination Compounds, 4th ed., Wiley, New York, 1986, pp. 233–244.
[46] G.B. Deacon, R.J. Phillips, Coord. Chem. Rev. 33 (1980) 227.
[47] S.P. Perlepes, E. Libby, W.E. Streib, K. Folting, G. Christou, Polyhedron 11 (1992) 923.
[48] H.O. Desseyn, in: S. Patai (Ed.), The Chemistry of Acid Derivatives, Ch. 7, vol. 2, Wiley, New York, 1992, pp. 291–294.
[49] A. Garcia-Raso, J.J. Fiol, B. Adrover, E. Molins, C. Miravitlles, Polyhedron 15 (1996) 1289.
[50] A.B.P. Lever, Inorganic Electronic Spectroscopy, 2nd ed., Elsevier, Amsterdam, 1984, pp. 627, 636–638.

PERGAMON

Polyhedron 21 (2002) 239–246

POLYHEDRON

www.elsevier.com/locate/poly

Dithiocarbamates of gallium(III) and indium(III): syntheses, spectroscopy, and structures

Dimple P. Dutta [a], Vimal K. Jain [a,*], Axel Knoedler [b], Wolfgang Kaim [b,*]

[a] *Novel Materials and Structural Chemistry Division, Bhabha Atomic Research Centre, Mumbai 400 085, India*
[b] *Institut für Anorganische Chemie, Universität Stuttgart, Pfaffenwaldring 55, D-70569 Stuttgart, Germany*

Received 9 August 2001; accepted 8 November 2001

Abstract

Several complexes of the type, $[M\{S_2CNR\}_3]$ (**1**) (M = Ga or In; R = $CH_2CH_2OCH_2CH_2$, $CH_2CH_2N(Me)CH_2CH_2$), $[MCl_2\{S_2CN(CH_2CH_2)_2O\}]$ (**2**) (M = Ga or In), $[MCl\{S_2CN(CH_2CH_2)_2O\}_2]$ (**3**) (M = Ga or In), $[Ga\{S_2CN(CH_2CH_2)_2O\}\{S_2P(OR)_2\}_2]$ (**4**) (R = Et, Pr^i) and $[M\{S_2CNR\}\{(SCH_2CH_2)_2O\}]$ (**5**) (M = Ga or In; R = $CH_2CH_2OCH_2CH_2$, $CH_2CH_2N(Me)CH_2CH_2$) have been prepared. All the complexes were characterized by elemental analysis, IR and NMR (^1H, $^{13}C\{^1H\}$) spectroscopy. ^{71}Ga NMR chemical shifts and half line widths are influenced by the coordination number of gallium and the substituents on the ligand moiety. Single crystal X-ray structures of two complexes $[M\{S_2CN(CH_2CH_2)_2O\}_3]$ (M = Ga, In) have been determined. © 2002 Published by Elsevier Science Ltd.

Keywords: Gallium; Indium; Dithiocarbamates; Dialkyldithiophosphates; ^{71}Ga NMR; Structures

1. Introduction

Compounds containing metal–sulfur bonds have attracted considerable attention during the last three decades due to their synthetic and structural aspects [1], spectroscopic and theoretical features [2] and their biochemistry [3]. More recently, their relevance in catalysis [4] and materials science [5] has been demonstrated. Among the sulfur ligands, the dithiocarbamate species ($RR'NCS_2^-$) form an important family of classical anionic ligands. These anions are 3-electron donors, capable of stabilising metal centres in a variety of oxidation states [6]. Besides their extensive technological applications [6], these ligands are still of topical interest as a potential source of novel structures.

The significance of III–VI materials (particularly those of Ga and In), formed in different stoichiometries [7,8], in various electronic applications has provided a stimulus for the current interest in the chemistry of Group 13 elements with chalcogen ligands. The ligands include thiolates [9], thiocarboxylates [10], xanthates [11], dithiophosphates [12,13], monothiocarbamates [14–16] and dithiocarbamates [17–20]. The gallium–indium complexes with the latter ligands have usually been isolated as tris-chelates. The ligands in general contain simple R groups on the nitrogen atom. The tris-chelates have been employed as molecular precursors for the preparation of M_2S_3 by us [20] and others [17–19]. These developments have motivated us to study the chemistry of gallium and indium complexes with internally functionalized ligands, viz. *N*-methylpiperazine and morpholine dithiocarbamates. The results of this work are reported herein.

2. Experimental

Except for the preparation of tris-complexes, all other reactions were carried out under anhydrous conditions using Schlenk techniques. High purity metal trichlorides (Trans Metal), 2-mercaptoethylether (Aldrich), morpholine, *N*-methylpiperazine, $Me_2NCS_2Na{\cdot}3H_2O$ and $Et_2NCS_2Na{\cdot}3H_2O$ were obtained from commercial sources. $[Ga(S_2CNR_2)_3]$ (R = Me, Et, Pr^i)

* Corresponding author. Tel.: +91-22-559-5095; fax: +91-22-550-5151.
E-mail address: jainvk@apsara.barc.ernet.in (V.K. Jain).

0277-5387/02/$ - see front matter © 2002 Published by Elsevier Science Ltd.
PII: S0277-5387(01)00990-1

[21] and morpholine and *N*-methylpiperazine dithiocarbamates [22,23] were prepared by literature methods. The infrared spectra were recorded as Nujol mulls between CsI plates on a Bomem MB-102 FT spectrometer. ^{1}H, $^{13}C\{^{1}H\}$, $^{31}P\{^{1}H\}$ and $^{71}Ga\{^{1}H\}$ NMR spectra were recorded in $CDCl_3$ solutions in 5 mm tubes on a Bruker DPX-300 NMR spectrometer operating at 300.13, 75.44, 121.44 and 91.53 MHz, respectively. Chemical shifts were referenced to the internal $CHCl_3$ peak (δ 7.26 and 77.0 ppm) for ^{1}H and ^{13}C, respectively, external 85% H_3PO_4 for ^{31}P and external $GaCl_3$ solution in D_2O (known to form $Ga(H_2O)_6^{3+}$ [24]) for ^{71}Ga.

2.1. Preparation of $[Ga\{S_2CN(CH_2)_4NMe\}_3]$ (**1a**)

To a methanolic solution (25 ml) of $GaCl_3$ (0.26 g, 1.47 mmol) (exothermic reaction), a solution of potassium salt of *N*-methylpiperazine dithiocarbamate (0.95 g, 4.43 mmol) in MeOH (25 ml) was added slowly and stirred for 3 h. The solvent was dried in vacuo and the residue was extracted with dry CH_2Cl_2 and filtered through a G-3 filtration unit using suction pump. The clear filtrate was evaporated in vacuo to give a white solid in 90% yield (0.79 g). Pertinent data are given in Table 1.

2.2. Preparation of $[Ga\{S_2CN(CH_2)_4O\}_3]$ (**1c**)

To a methanolic solution (20 ml) of $GaCl_3$ (0.37 g, 2.10 mmol), a solution of Na salt of morpholine dithiocarbamate (1.18 g, 6.37 mmol) in MeOH (25 ml) was added slowly and stirred for 3 h. The MeOH was evaporated in vacuo and the solid was extracted with dry $CHCl_3$. The solution was filtered and the clear filtrate was evaporated in vacuo to obtain a dirty white solid (1.09 g, 93%). The solid was recrystallized from dry CH_2Cl_2–C_6H_{14} in 81% yield.

In a similar manner, $[In\{S_2CN(CH_2)_4O\}_3]$ (**1d**) was prepared.

2.3. Preparation of $[GaCl_2\{S_2CN(CH_2)_4O\}]$ (**2a**)

A methanolic solution (25 ml) of Na salt of morpholine dithiocarbamate (0.60 g, 3.24 mmol) was added dropwise to a methanolic solution (20 ml) of $GaCl_3$ (0.57 g, 3.24 mmol) and the mixture was stirred for 3 h. The solution was evaporated in vacuo and the residual solid was extracted with dry $CHCl_3$. The solution was filtered and the clear filtrate evaporated to give a white solid (0.65 g, 66%).

$[InCl_2\{S_2CN(CH_2)_4O\}]$ (**2b**) was prepared using a similar method.

2.4. Preparation of $[GaCl\{S_2CN(CH_2)_4O\}_2]$ (**3a**)

To a solution (20 ml) of $GaCl_3$ (0.53 g, 3.0 mmol) in dry $CHCl_3$, a solution of $[Ga\{S_2CN(CH_2)_4O\}_3]$ (3.34 g, 6.0 mmol) in $CHCl_3$ was added and stirred for 3 h. The clear solution was evaporated in vacuo to obtain a white solid (3.80 g, 98% yield).

2.5. Preparation of $[InCl\{S_2CN(CH_2)_4O\}_2]$ (**3b**)

To a methanolic solution (20 ml) of $InCl_3$ (0.44 g, 1.99 mmol), a methanolic solution of Na salt of morpholine dithiocarbamate (0.73 g, 3.94 mmol) was added slowly and stirred for 3 h. The MeOH was evaporated in vacuo and the solid was extracted with dry $CHCl_3$. The solution was filtered and the clear filtrate was

Table 1
Yield and analytical data for morpholine and *N*-methylpiperazine dithiocarbamate complexes of Gallium(III) and Indium(III)

Compound	% Yield	M.p. (°C)	% Analysis found (Calc.)			
			C	H	N	Ga–In
$[Ga\{S_2CN(CH_2)_4NMe\}_3]$	91	262 [a]	36.1 (36.3)	5.4 (5.6)	14.1 (14.1)	11.6 (11.7)
$[In\{S_2CN(CH_2)_4NMe\}_3]$	99	226 [a]	33.5 (33.7)	5.1 (5.2)	12.9 (13.1)	17.9 (17.9)
$[Ga\{S_2CN(CH_2)_4O\}_3]$	92	212 [a]	32.3 (32.4)	4.3 (4.3)	7.4 (7.5)	12.4 (12.5)
$[GaCl\{S_2CN(CH_2)_4O\}_2]$	98	208	27.8 (27.9)	3.5 (3.7)	6.3 (6.5)	16.0 (16.2)
$[GaCl_2\{S_2CN(CH_2)_4O\}]$	66	220 [a]	19.6 (19.8)	2.6 (2.7)	4.6 (4.6)	22.9 (23.0)
$[In\{S_2CN(CH_2)_4O\}_3]$	86	>225	29.7 (29.9)	3.9 (4.0)	6.9 (7.0)	19.1 (19.1)
$[InCl\{S_2CN(CH_2)_4O\}_2]$	84	262 [a]	25.2 (25.3)	3.2 (3.4)	5.9 (5.9)	24.2 (24.2)
$[InCl_2\{S_2CN(CH_2)_4O\}]$	39	220 [a]	17.2 (17.3)	2.1 (2.3)	3.9 (4.0)	32.9 (33.0)
$[Ga\{S_2CN(CH_2)_4O\}\{S_2P(OEt)_2\}_2]$	95	Liquid				17.4 (17.6)
$[Ga\{S_2CN(CH_2)_4O\}\{S_2P(OPr^i)_2\}_2]$	88	Paste	31.1 (31.0)	5.3 (5.5)	2.1 (2.1)	10.6 (10.6)
$[Ga\{S_2CN(CH_2)_4NMe\}\{(SCH_2CH_2)_2O\}]$	95	170	31.2 (31.5)	5.1 (5.0)	7.0 (7.3)	18.2 (18.3)
$[In\{S_2CN(CH_2)_4NMe\}\{(SCH_2CH_2)_2O\}]$	95	167	28.1 (28.2)	4.3 (4.4)	6.5 (6.6)	26.9 (26.9)
$[Ga\{S_2CN(CH_2)_4O\}\{(SCH_2CH_2)_2O\}]$	96	198	29.1 (29.4)	4.3 (4.4)	4.2 (3.8)	18.8 (18.9)
$[In\{S_2CN(CH_2)_4O\}\{(SCH_2CH_2)_2O\}]$	97	80	26.2 (26.2)	3.9 (3.9)	3.5 (3.4)	27.5 (27.8)

[a] Decomposed.

Table 2
Crystal data and structural refinement for $[M\{S_2CN(CH_2CH_2)_2O\}_3]$

	M = Ga	M = In
Empirical formula	$C_{15}H_{24}GaN_3O_3S_6 \cdot CH_2Cl_2$	$C_{15}H_{24}InN_3O_3S_6 \cdot CH_2Cl_2$
Formula weight	641.38	686.48
Temperature (K)	173(2)	173(2)
Crystal size (mm)	$0.3 \times 0.2 \times 0.2$	$0.3 \times 0.3 \times 0.2$
Wavelength (Å)	0.71073	0.71073
Crystal system	triclinic	triclinic
Space group	$P\bar{1}$	$P\bar{1}$
Unit cell dimensions		
a (Å)	10.602(2)	10.710(2)
b (Å)	11.370(2)	11.460(2)
c (Å)	13.059(3)	13.065(3)
α (°)	104.49(3)	104.42(3)
β (°)	100.45(3)	99.96(3)
γ (°)	115.30(3)	115.53(3)
V (Å^3)	1301.1(5)	1327.3(5)
Z	2	2
D_{calc} (Mg m^{-3})	1.637	1.718
Absorption coefficient (mm^{-1})	1.768	1.587
$F(000)$	656	692
θ range of data collection (°)	1.71–30.00	6.81–21.97
Limiting indices	$0 \le h \le 14$, $-15 \le k \le 14$, $-18 \le l \le 18$	$-8 < h < 11$, $-12 < k < 10$, $-13 < l < 13$
Reflections collected	7967	2673
Independent reflections	7585 ($R_{int} = 0.0292$)	2509 ($R_{int} = 0.0535$)
Absorption correction	ψ scan	ψ scan
Refinement method	full-matrix least-squares on F^2	full-matrix least-squares on F^2
Data/restraints/parameters	7585/0/324	2509/0/307
Goodness-of-fit on F^2	1.470	1.083
Final R indices $[I > 2\sigma(I)]$	$R_1 = 0.0436$, $wR_2 = 0.1066$	$R_1 = 0.0642$, $wR_2 = 0.1552$
R indices (all data)	$R_1 = 0.0586$, $wR_2 = 0.1133$	$R_1 = 0.0912$; $wR_2 = 0.1758$
Largest difference peak and hole (e Å^{-3})	0.773 and −1.327	0.875 and −0.875

evaporated in vacuo to obtain a white solid (0.79 g, 84%).

2.6. Preparation of $[Ga\{S_2CN(CH_2)_4O\}\{S_2P(OEt)_2\}_2]$ (4a)

To a methanolic solution (20 ml) of $GaCl_3$ (1.17 g, 6.64 mmol), a solution of Na salt of morpholine dithiocarbamate (1.22 g, 6.59 mmol) in MeOH (25 ml) was added slowly and stirred for 3 h. The MeOH was evaporated in vacuo and the solid was suspended in dry $CHCl_3$. To it a $CHCl_3$ solution of ammonium diethyldithiophosphate (2.70 g, 13.30 mmol) was added and stirred which was continued for 4 h. The mixture was filtered and the clear filtrate evaporated in vacuo to yield an oily product (3.80 g, 95%).

$[Ga\{S_2CN(CH_2)_4O\}\{S_2P(OPr^i)_2\}_2]$ (**4b**) was prepared in a similar manner.

2.7. Preparation of $[Ga\{S_2CN(CH_2)_4NMe\}\{(SCH_2CH_2)_2O\}]$ (5a)

$[GaCl\{(SCH_2CH_2)_2O\}]$, prepared by stirring a C_6H_6 solution of $GaCl_3$ (1.89 g, 10.73 mmol) and $[(NaSCH_2CH_2)_2O\}]$ [obtained from $(HSCH_2CH_2)_2O$ (1.48 g, 10.72 mmol) and Na (0.49 g, 21.3 mmol) in MeOH and then dried in vacuo] for 3 h, was treated with potassium salt of *N*-methylpiperazine dithiocarbamate (2.30 g, 10.73 mmol). The whole was stirred at room temperature (r.t.) for 3 h. Precipitated salts were filtered off and the filtrate was evaporated in vacuo to give a dirty white solid (3.90 g, 95%).

$[In\{S_2CN(CH_2)_4NMe\}\{(SCH_2CH_2)_2O\}]$ (**5b**), $[Ga\{S_2CN(CH_2)_4O\}\{(SCH_2CH_2)_2O\}]$ (**5c**) and $[In\{S_2CN(CH_2)_4O\}\{(SCH_2CH_2)_2O\}]$ (**5d**) were prepared in an identical manner.

2.8. X-ray crystallography

X-ray data of the isostructural systems $[M\{S_2CN(CH_2CH_2)_2O\}_3]$ (M = Ga, In) which crystallize with a molecule of (disordered) dichloromethane (Table 2) were collected at 173(2) K on a Siemens P3 diffractometer using graphite monochromated Mo Kα radiation ($\lambda = 0.71073$ Å) employing the ω–2θ scan technique. The unit cell parameters were determined for 25 reflections measured by random search routine. The intensity data were corrected for Lp and absorption effects. The structures were solved using direct methods. The non-hydrogen atoms were refined anisotropically. A disorder model (ring inversion) was used for the N(3)–O(3) containing six-membered ring in the Ga compound (CCDC Nos. 167589 for Ga and 167588 for In).

3. Results and discussion

Several gallium(III) and indium(III) complexes with morpholine and *N*-methylpiperazine have been prepared. The reaction of MCl_3 with 3 equiv. of sodium–potassium salt of dithiocarbamate in methanol (for Ga) or water (for In) resulted in the formation of $[M(S_2CNR)_3]$ (**1**) (R = –$CH_2CH_2OCH_2CH_2$–, –$CH_2CH_2N(Me)CH_2CH_2$–) as colourless crystalline solids (Eq. (1)). Treatment of MCl_3 with sodium salt of morpholine dithiocarbamate in 1:1 and 1:2 molar ratio afforded chloro complexes $[MCl_2\{S_2CN(CH_2CH_2)_2O\}]$ (**2**) (M = Ga (**2a**), In (**2b**)) and $[MCl\{S_2CN(CH_2CH_2)_2O\}_2]$ (**3**) (M = Ga (**3a**), In (**3b**)), respectively

(Eq. (2)). However, similar reactions with $[KS_2CN(CH_2CH_2)_2NMe]$ yielded only **1**. Treatment of **2a** with ammonium dialkyldithiophosphate gave mixed ligand complexes, $[Ga\{S_2CN(CH_2)_4O\}\{S_2P(OR)_2\}_2]$ (**4**) (Eq. (3)). Yet another series of mixed ligand complexes $[M\{(SCH_2CH_2)_2O\}\{S_2CNR\}]$ (**5**) could be isolated by the reaction of MCl_3 with sodium salt of 2-mercaptoethylether followed by addition of dithiocarbamate in 1:1:1 stoichiometry (Eq. (4)). All the complexes **1**–**5** are colorless crystalline solids. They are soluble in common organic solvents, except **2** and **3**, which are sparingly soluble in chloroform and benzene.

$$MCl_3 + 3[KS_2CN(CH_2)_4NMe] \rightarrow [M\{S_2CN(CH_2)_4NMe\}_3] + 3KCl \quad (1)$$

$$MCl_3 + n[NaS_2CN(CH_2)_4O] \rightarrow [MCl_{3-n}\{S_2CN(CH_2)_4O\}_n] + n\,NaCl \quad (n = 1, 2, 3) \quad (2)$$

$$[GaCl_2\{S_2CN(CH_2CH_2)_2O\}] + 2[NH_4S_2P(OR)_2] \rightarrow [Ga\{S_2CN(CH_2)_4O\}\{S_2P(OR)_2\}_2] + 2NH_4Cl \quad (R = Et \text{ or } Pr^i) \quad (3)$$

$$MCl_3 + [NaSCH_2CH_2)_2O] + Na/KS_2CNR \rightarrow [M\{S_2CNR\}\{(SCH_2CH_2)_2O\}] + Na/KCl \quad (4)$$

The infrared spectra of these complexes exhibited strong bands in the regions 1155–1134 and 1009–980 cm^{-1} attributable to νCNC and ν C=S, respectively [25]. Interpretation of the ν M–Cl and ν M–S absorptions have been made by comparison of the infrared spectra of the free ligands, chloro complexes and the tris-derivatives. An absorption at 372 ± 2 (in $[GaCl_{3-n}L_n]$ ($n = 1$ or 2)) [12,21] and 327 cm^{-1} (in $[InCl_{3-n}L_n]$) [13,26], absent in the spectra of free ligands and in tris-complexes have been assigned to ν M–Cl stretchings. Similarly, absorptions in the region 316–370 (for gallium complexes) and 319–375 cm^{-1} (for indium complexes) absent in the spectra of free ligands may be assigned to ν M–S absorptions [26–29]. In the spectra of mixed thiolate complexes (**5**) two–three such absorptions appeared in these regions.

The ^1H and $^{13}C\{^1H\}$ NMR spectra of these complexes exhibited characteristic resonances due to the ligand protons–carbons at room temperature (Table 3). The dithiocarbamate ligand protons in the ^1H NMR spectra of 1–5 were little affected with other substituents (metal or chloride) as each set of resonances appeared in a narrow region. The methylene proton signals appeared as triplets. In the $^{13}C\{^1H\}$ NMR spectra the quarternary carbon resonance had low intensity as expected and in a few cases could not be resolved. This signal showed substituent dependance. It was deshielded on substituting chloride with dithiocarbamate ligands as in $[MCl_{3-n}\{S_2CN(CH_2)_4O\}_n]$ (M = Ga or In). However, other resonances were little affected either on changing the metal ion (e.g. Ga or In) or the chloride ligand with dithiocarbamate. The ^{31}P NMR spectra of $[Ga\{S_2CN(CH_2)_4O\}\{S_2P(OR)_2\}_2]$ displayed a single resonance. These values can be compared with the corresponding tris-dithiophosphates, $[Ga\{S_2P(OR)_2\}_3]$ [12]. The ^1H NMR spectra of $[M\{S_2CN(CH_2CH_2)_2O\}\{(SCH_2CH_2)_2O\}]$ exhibited four triplets due to methylene protons as expected. There is little change in the chemical shift on substituting gallium with indium. However, in the $^{13}C\{^1H\}$ NMR spectra, the CS_2 carbon resonance is deshielded on replacing gallium with indium.

Although there are only a few reports on ^{71}Ga ($I = 3/2$, natural abundance 39.6%) NMR spectroscopy [30], it would be an important probe to study the behaviour of gallium with simple and chelating ligands—a relatively underdeveloped area. The ^{71}Ga NMR chemical shifts cover rather a broad range (ca. 1500 ppm) with half line width at times as great as 37 kHz [31]. In order to throw some light on the solution behaviour of gallium dithiocarbamate complexes, $^{71}Ga\{^1H\}$ NMR spectra were recorded in $CDCl_3$ (Table 3). The ^{71}Ga NMR resonance for all the tris-complexes is considerably shielded relative to the six-coordinate hexa-aquo ion, $[Ga(H_2O)_6]^{3+}$. The effect of the organic groups of dithiocarbamate ligands are reflected on the ^{71}Ga NMR chemical shifts. The resonance is deshielded with increasing steric demand of the R group (i.e. Me < Et < Pr^i). The substituents effects are also seen on the half line width of the signal (Fig. 1). The $\Delta 1/2$ decreases with decreasing size of the R group (Me, Et, Pr^i). The ^{71}Ga signal for morpholine and *N*-methylpiperazine complexes appeared close to the signal for S_2CNEt_2 derivative, but with greater half line width. The X-ray structural analyses of $[Ga\{S_2CN(CH_2)_5\}_3]$ [21] and $[Ga\{S_2CN(CH_2CH_2)_2O\}_3]$ (see later) have revealed an octahedral geometry around gallium atom. The observed ^{71}Ga NMR shifts can be interpreted in terms of octahedral geometry around gallium atom.

The X-ray structure of $[GaCl\{S_2CNMe_2\}_2]$ [21] has shown a square pyramidal environment around gallium atom. It is likely that mono–chloro complexes with other dithiocarbamate ligands have a similar structure. The ^{71}Ga NMR spectrum of $[GaCl\{S_2CN(CH_2)_4O\}_2]$ displayed a broad resonance at δ 77.2 ppm. The signal is considerably downfield shifted ($\sim$150 ppm) from the hexa-coordinated complexes and is upfield ($\sim$150 ppm) from the four-coordinate regime (sodium gallate δ 223.3 ppm). This may be interpretated in terms of penta-coordinate structure for gallium in solution. The increased line width may be attributed to the asymmetry in the electric field gradient (efg) around the gallium nucleus due to the presence of different ligands. The ^{71}Ga measurements of $[GaCl_2\{S_2CN(CH_2)_4O\}]$ were

Table 3
^{1}H, $^{13}C\{^{1}H\}$ and $^{71}Ga\{^{1}H\}$ NMR data of dithiocarbamate complexes of gallium(III) and indium(III)

Complex [a]	^{71}Ga NMR data		$^{13}C\{^{1}H\}$ NMR data δ in ppm	^{1}H NMR data δ in ppm
	δ	$\Delta 1/2$ in Hz		
$[Ga(H_2O)_6]^{3+}$	0.0	28		
$Na[Ga(OH)_4]$	223.3	123		
$[Ga\{S_2CNMe_2\}_3]$	−94.6	1100	45.0 (s, N**Me**$_2$); 202.7 (s, S_2**C**–)	3.38 (s, N**Me**$_2$)
$[Ga\{S_2CNEt_2\}_3]$	−83.9	1730	12.0 (s, NCH$_2$**Me**); 49.4 (s, N**C**H$_2$–); 201.3 (s, S_2**C**–)	1.29 (t, 7.2 Hz, NCH$_2$**Me**); 3.77 (q, 7.2 Hz, NC**H**$_2$–)
$[Ga\{S_2CNPr^i_2\}_3]$	−64.5	2220	19.7 (s, NCH**Me**$_2$); 54.9 (br, N**C**H); 200.9 (s, S_2**C**–)	1.40 (br, NCH**Me**$_2$); 4.50 (br, NC**H**<)
$NaS_2CN(CH_2)_4O$ [b]			51.5 (s, –N**C**H$_2$–); 66.3 (s, –**C**H$_2$O); 209.4 (s, –S_2**C**N–)	3.71 (t, –NC**H**$_2$–); 4.31 (t, –C**H**$_2$O)
$[GaCl_2\{S_2CN(CH_2)_4O\}]$			51.8 (s, –N**C**H$_2$–); 65.9 (s, –**C**H$_2$O) [c]	3.79 (t, 4.9 Hz, –NC**H**$_2$–); 3.94 (t, 4.9 Hz, –C**H**$_2$O)
$[GaCl\{S_2CN(CH_2)_4O\}_2]$	77.2	3875	51.8 (s, –N**C**H$_2$–); 65.9 (s, –**C**H$_2$O); 198.7 (s, –S_2**C**N–)	3.79 (t, 4.8 Hz, –NC**H**$_2$–); 3.94 (t, 4.7 Hz, –C**H**$_2$O)
$[Ga\{S_2CN(CH_2)_4O\}_3]$	−76.2	2298	51.5 (s, –N**C**H$_2$–); 65.9 (s, –**C**H$_2$O); 203.0 (s, –S_2**C**N–)	3.74 (t, 4.8 Hz, –NC**H**$_2$–); 3.93 (t, 4.8 Hz, –C**H**$_2$O)
$[InCl_2\{S_2CN(CH_2)_4O\}]$			52.9 (s, –N**C**H$_2$–); 65.9 (s, –CH$_2$O); 200.1 (s, –S_2**C**N–)	3.79 (t, 4.9 Hz, –NC**H**$_2$–); 4.00 (t, 4.9 Hz, –C**H**$_2$O)
$[InCl\{S_2CN(CH_2)_4O\}_2]$			52.6 (s, –N**C**H$_2$–); 65.9 (s, –CH$_2$O); 202.4 (s, –S_2**C**N–)	3.76 (t, 4.9 Hz, –NC**H**$_2$–); 4.02 (t, 4.8 Hz, –C**H**$_2$O)
$[In\{S_2CN(CH_2)_4O\}_3]$			52.5 (s, –N**C**H$_2$–); 66.0 (s, –**C**H$_2$O); 203.3 (s, –S_2CN–)	3.76 (t, 4.8 Hz, –NC**H**$_2$–); 4.03 (t, 4.9 Hz, –C**H**$_2$O)
$KS_2CN(CH_2)_4NMe$			44.2 (s, –N**C**H$_3$); 50.5 (s, –S_2CN**C**H$_2$–); 53.6 (s, MeN**C**H$_2$–); 208.9 (s, –S_2**C**N–)	2.23 (s, –NC**H**$_3$); 2.47 (t, MeNC**H**$_2$–); peaks due to –S_2CNC**H**$_2$– merged with water resonance
$[Ga\{S_2CN(CH_2)_4NMe\}_3]$	−80.7	2822	45.5 (s, –N**C**H$_3$); 51.4 (s, –S_2CN**C**H$_2$–); 54.2 (s, MeN**C**H$_2$–); 202.4 (s, –S_2**C**N–)	2.33 (s, –NC**H**$_3$); 2.50 (t, 5.0 Hz, –C**H**$_2$NMe); 3.98 (t, 4.9 Hz, –S_2NC**H**$_2$–)
$[In\{S_2CN(CH_2)_4NMe\}_3]$			45.5 (s, –N**C**H$_3$); 52.4 (s, –S_2CN**C**H$_2$–); 54.3 (s, MeN**C**H$_2$–); 202.5 (s, –S_2**C**N–)	2.32 (s, –NC**H**$_3$); 2.51 (t, 5.0 Hz, –C**H**$_2$NMe); 4.06 (t, 4.9 Hz, –S_2NC**H**$_2$–)
$[Ga\{S_2CN(CH_2)_4O\}\{S_2P(OEt)_2\}_2]$ [d]			15.9 (d, 8 Hz, OCH$_2$**C**H$_3$); 51.6 (s, N**C**H$_2$); 64.3 (d, 5 Hz, O**C**H$_2$CH$_3$); 65.9 (s, –**C**H$_2$O)	1.37 (t, 7.0 Hz, OCH$_2$C**H**$_3$); 3.81 (t, 4.8 Hz, NC**H**$_2$); 3.92 (t, 4.3 Hz, OC**H**$_2$); 4.23 (q, 7.1 Hz, OC**H**$_2$CH$_3$)
$[Ga\{S_2CN(CH_2)_4O\}\{S_2P(OPr^i)_2\}_2]$ [e]			23.7 (d, 3.6 Hz, OCH**Me**$_2$); 51.5 (s, N**C**H$_2$); 66.0 (s, O**C**H$_2$); 73.1 (s, O**C**H<) [c]	1.38 (d, 6.1 Hz, OCH**Me**$_2$); 3.06 (t, 5 Hz, NC**H**$_2$); 3.21 (t, 5 Hz, OC**H**$_2$); 4.18 (m, OC**H**<)
$[Ga\{S_2CN(CH_2)_4O\}\{(SCH_2CH_2)_2O\}]$			26.3 (s, S**C**H$_2$CH$_2$O); 50.2 (s, –N**C**H$_2$–); 65.3 (s, –OCH$_2$–); 71.0 (s, SCH$_2$**C**H$_2$O); 199.3 (s, –S_2**C**N–)	2.90 (t, 5.2 Hz, SC**H**$_2$CH$_2$O) 3.73 (t, 3.1 Hz, SCH$_2$C**H**$_2$O) 3.77 (t, 5.5 Hz, –NC**H**$_2$–); 3.91 (t, 2.6 Hz, –OC**H**$_2$–)
$[In\{S_2CN(CH_2)_4O\}\{(SCH_2CH_2)_2O\}]$			27.2 (s, S**C**H$_2$CH$_2$O); 52.0 (s, –N**C**H$_2$–); 65.9 (s, –OCH$_2$–); 72.0 (s, SCH$_2$**C**H$_2$O); 201.9 (s, –S_2**C**N–)	2.98 (t, 5.0 Hz, SC**H**$_2$CH$_2$O) 3.75 (t, 4.8 Hz, SCH$_2$C**H**$_2$O) 3.78 (t, 5.3 Hz, –NC**H**$_2$–); 4.02 (t, 4.6 Hz, –OC**H**$_2$–)
$[Ga\{S_2CN(CH_2)_4NMe\}\{(SCH_2CH_2)_2O\}]$			26.9 (s, S**C**H$_2$CH$_2$O); 45.4 (s, –N**C**H$_3$); 50.8 (s, –S_2CN**C**H$_2$–); 53.7 (s, MeN**C**H$_2$–); 71.7 (s, SCH$_2$**C**H$_2$O); 199.3 (s, –S_2**C**N–)	2.32 (s, –NC**H**$_3$); 2.49 (t, 5.1 Hz, –C**H**$_2$NMe); 2.92 (t, 5.1 Hz, SC**H**$_2$CH$_2$O) 3.78 (t, 5.1 Hz, SCH$_2$C**H**$_2$O) 3.94 (t, 5.1 Hz, –S_2NC**H**$_2$–)
$[In\{S_2CN(CH_2)_4NMe\}\{(SCH_2CH_2)_2O\}]$			27.0 (s, S**C**H$_2$CH$_2$O); 45.5 (s, –N**C**H$_3$); 51.9 (s, –S_2CN**C**H$_2$–); 54.1 (s, MeN**C**H$_2$–); 72.2 (s, SCH$_2$**C**H$_2$O); 200.5 (s, –S_2**C**N–)	2.32 (s, –NC**H**$_3$); 2.50 (t, 5.1 Hz, –C**H**$_2$NMe) 2.97 (t, 5.0 Hz, SC**H**$_2$CH$_2$O) 3.77 (t, 5.0 Hz, SCH$_2$C**H**$_2$O) 4.03 (br, –S_2NC**H**$_2$–)

[a] Spectra were recorded in $CDCl_3$.
[b] In D_2O.
[c] CS_2 carbon resonance could not be resolved.
[d] δ $^{31}P\{^{1}H\}$ 93.9.
[e] δ $^{31}P\{^{1}H\}$ 89.7.

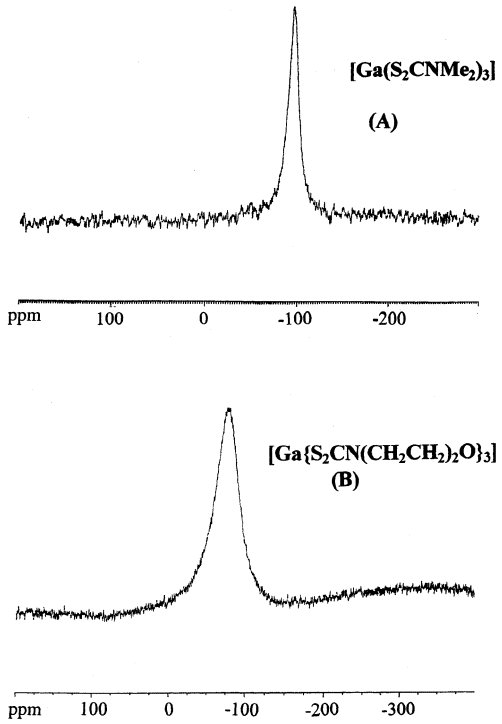


Fig. 1. $^{71}Ga\{^{1}H\}$ NMR spectra of: (A) $[Ga(S_2CNMe_2)_3]$; and (B) $[Ga\{S_2CN(CH_2CH_2)_2O\}_3]$.

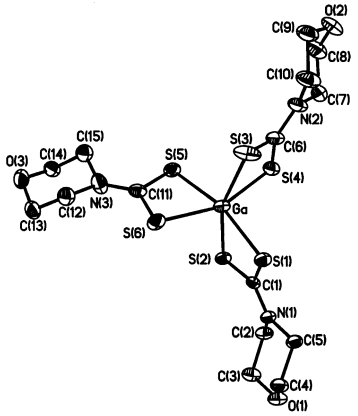


Fig. 2. Molecular structure of $[Ga\{S_2CN(CH_2CH_2)_2O\}_3]$ with atomic numbering scheme.

thwarted due to poor solubility of the complex coupled with extensive line broadening of the resonance. The ^{27}Al NMR chemical shifts have also been reported to depend on the coordination number of aluminium and deviation from spherical geometry around aluminium nucleus resulted in broadening of the resonances [32,33]. Unlike ^{27}Al NMR spectroscopy, deviation of chemical shifts with changes in coordination number and signal half line widths with ligand substituents are more pronounced in ^{71}Ga NMR spectroscopy.

The structures of $[In\{S_2P(OR)_2\}\{SCH_2CH_2)_2O\}]$ (R = Et or Pr^i) established by X-ray diffraction analyses showed a dimeric structure. The 2-mercaptoethylether dianion coordinates the indium atom using both sulfur atoms and the ether oxygen atom while at the same time one of the sulfur atoms bridges the second indium atom of the dinuclear species [29]. The dithiocarbamate complexes, $[M\{(SCH_2CH_2)_2O\}\{S_2CNR\}]$ (**5**), reported here are likely to have a similar structure since the R_2NCS_2 ligands are isoelectronic and isostructural to the dithiophosphates.

The molecular structures of $[M\{S_2CN(CH_2CH_2)_2O\}_3]$ (M = Ga, In) as shown in Figs. 2 and 3 (the CH_2Cl_2 solvate molecule is omitted) have been established unambiguously by single crystal X-ray diffraction analy-

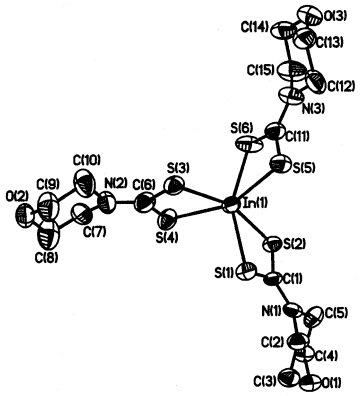


Fig. 3. Molecular structure of $[In\{S_2CN(CH_2CH_2)_2O\}_3]$ with atomic numbering scheme.

Table 4
Selected bond lengths (Å) and angles (°) for $[M\{S_2CN(CH_2CH_2)_2O\}_3]$

M = Ga		M = In	
Bond lengths			
Ga–S(1)	2.4256(15)	In–S(1)	2.586(2)
Ga–S(2)	2.4306(12)	In–S(2)	2.580(2)
Ga–S(3)	2.4496(10)	In–S(3)	2.585(2)
Ga–S(4)	2.4484(10)	In–S(4)	2.607(2)
Ga–S(5)	2.4223(13)	In–S(5)	2.615(2)
Ga–S(6)	2.4544(9)	In–S(6)	2.592(2)
S–C(av)	1.722	S–C(av)	1.727
N–C(av)	1.329	N–C(av)	1.330
Bond angles			
S(1)–Ga–S(2)	74.06(5)	S(1)–In–S(2)	69.91(7)
S(3)–Ga–S(4)	73.07(3)	S(3)–In–S(4)	69.47(6)
S(5)–Ga–S(6)	73.37(4)	S(5)–In–S(6)	69.47(7)
S(1)–Ga–S(4)	101.38(4)	S(1)–In–S(4)	100.78(7)
S(1)–Ga–S(5)	164.94(3)	S(1)–In–S(5)	95.07(7)
S(1)–Ga–S(3)	92.44(5)	S(1)–In–S(3)	96.04(7)
S(1)–Ga–S(6)	97.88(4)	S(1)–In–S(6)	154.10(7)
S(2)–Ga–S(3)	159.34(3)	S(2)–In–S(3)	160.28(7)
S(2)–Ga–S(4)	93.95(3)	S(2)–In–S(4)	98.85(7)
S(2)–Ga–S(5)	94.92(5)	S(2)–In–S(5)	105.27(6)
S(2)–Ga–S(6)	99.26(4)	S(2)–In–S(6)	93.57(7)
S(3)–Ga–S(5)	100.82(5)	S(3)–In–S(5)	89.29(6)
S(3)–Ga–S(6)	98.03(4)	S(3)–In–S(6)	104.13(7)
S(4)–Ga–S(5)	89.42(4)	S(4)–In–S(5)	154.56(5)
S(4)–Ga–S(6)	159.04(3)	S(4)–In–S(6)	101.42(8)

ses. Selected bond lengths and angles for the isostructural systems are given in Table 4. The six sulphur atoms from three chelating dithiocarbamate moeties in each molecule are arranged in a distorted octahedral environment around the central metal atom. The observed distortion from ideal geometry may be attributed to the small bite angle (< S–M–S being 73.5° for Ga and 69.6° for In) of the chelating dithio-ligand. Decreased ligand bite with increasing size of the metal atom results in opening of the S–C–S angle (115.9° in the Ga and 118.0° in the In derivative). The overall geometry of these complexes closely resembles those reported for related dithiocarbamates [20,34–36].

All six M–S distances are very similar and agree well with the reported values [13,34–39]. The C–S distances are also similar (close to 1.72 Å) within experimental error in the two molecules, indicating delocalization in the CS_2 skeleton. The C–N distances, which are close to 1.33 Å, are significantly shorter than the normal single bond, suggesting considerable double bond character, as expected for metal dithiocarbamates. The four-membered 'MS_2C' rings are planar while the six-membered heterocyclic rings adopt a puckered conformation; the angles between the SCS and CNC planes range from 4.6° to 9.4° for the non-disordered morpholine rings, confirming the efficient π electron conjugation.

4. Supplementary material

Crystallographic data for the structural analysis have been deposited with the Cambridge Crystallographic Data Centre, CCDC Nos. 167589 for Ga and 167588 for In. Copies of this information may be obtained free of charge from The Director, CCDC, 12 Union Road, Cambridge CB2 1EZ, UK (fax: +44-1223-336033; e-mail: deposit@ccdc.cam.ac.uk or www: http://www.ccdc.cam.ac.uk).

Acknowledgements

We thank Drs J.P. Mittal and P. Raj for encouragement of this work. We are grateful to the Head, Analytical Chemistry Division for providing microanalyses of the compounds. Support from the Indo-German exchange program WTZ 99/060 is gratefully acknowledged.

References

[1] (a) P.J. Blower, J.R. Dilworth, Coord. Chem. Rev. 76 (1987) 121;
(b) V.K. Jain, Coord. Chem. Rev. 135 (1994) 809;
(c) C. Silvestru, I. Haiduc, Coord. Chem. Rev. 147 (1996) 117;
(d) E.S. Raper, Coord. Chem. Rev. 153 (1996) 199.
[2] (a) P.J. Hauser, A.F. Schreiner, J.D. Gunter, W.J. Mitchell, M.K. DeArmond, Theor. Chim. Acta 24 (1972) 78;
(b) J.D. Lebedda, R.A. Palmer, Inorg. Chem. 10 (1971) 2704;
(c) J.D. Lebedda, R.A. Palmer, Inorg. Chem. 11 (1972) 484;
(d) A.F. Schreiner, P.J. Hauser, Inorg. Chem. 11 (1972) 2706.
[3] (a) L. Casella, M. Gullotti, R. Vigano, Inorg. Chim. Acta 121 (1988) 1124;
(b) M. Gullotti, P. Casello, A. Pinter, E. Suardi, P. Zanello, S. Mangani, J. Chem. Soc., Dalton Trans (1989) 1979;
(d) E. Block, H.Y. Kang, G. Ofori-Okai, J. Zubeita, Inorg. Chim. Acta 166 (1989) 155.
[4] J.C. Bayon, C. Claver, A.M. Masdeu-Bulto, Coord. Chem. Rev. 193–195 (1999) 73.
[5] M. Bochmann, Chem. Vap. Deposition 2 (1996) 85.
[6] D. Coucouvanis, Prog. Inorg. Chem. 26 (1979) 301.
[7] M. Lazell, P. O'Brien, D.J. Otway, J.-Ho. Park, J. Chem. Soc., Dalton Trans (2000) 4479.
[8] J.A. Hollingsworth, D.M. Poojary, A. Clearfield, W.E. Buhro, J. Am. Chem. Soc. 122 (2000) 3562.
[9] A.N. MacInnes, M.B. Power, A.F. Hepp, A.R. Barron, J. Organomet. Chem. 449 (1993) 95.
[10] G. Zhang, K. Kunze, M.J. Hampden-Smith, E.N. Duesler, Chem. Vap. Dep. 2 (1996) 242.
[11] V.G. Bessergenev, E.N. Ivanova, Y.A. Kovalevskaya, S.A. Gromilov, U.N. Kirichenko, S.V. Larionev, Inorg. Mater. 32 (1996) 592.
[12] D. Pahari, V.K. Jain, Main Group Metal Chem. 20 (1997) 691.
[13] D. Pahari, V.K. Jain, R.P. Patel, Main Group Metal Chem. 21 (1998) 261.
[14] W.M. Cleaver, M. Spath, D. Hynk, G. McMurdo, M.B. Power, M. Stuke, D.W.H. Rankin, A.R. Barron, Organometallics 14 (1995) 690.
[15] G.A. Horley, M. Chunggaze, P. O'Brien, A.J.P. White, D.J. Williams, J. Chem. Soc., Dalton Trans. (1998) 4205.
[16] G.A. Horley, M.R. Lazell, P. O'Brien, Chem. Vap. Dep. 5 (1999) 203.
[17] P. O'Brien, D.J. Otway, J.R. Walsh, Thin Solid Films 315 (1998) 57.
[18] S.W. Haggata, M.A. Malik, M. Motevalli, P. O'Brien, J.C. Knowles, Chem. Mater. 7 (1995) 716.
[19] M.R. Lazell, P. O'Brien, D.J. Otway, J.H. Park, Chem. Mater. 11 (1999) 3430.
[20] D.P. Dutta, V.K. Jain, S. Chauchury, E.R.T. Tiekink, Main Group Metal Chem. 24 (2001) 405.
[21] S. Bhattacharya, N. Seth, D. Srivastava, V.D. Gupta, H. Nöth, M.T. Albach, J. Chem. Soc., Dalton Trans. (1996) 2815.
[22] A. Zweirzak, M. Kluba, Tetrahedron 27 (1971) 3171.
[23] G. Marcotrigiano, G.C. Pellacini, C. Preti, J. Inorg. Nucl. Chem. 36 (1976) 3709.
[24] M.J. Taylor, Polyhedron 9 (1990) 207.
[25] M. Kilner, Spectroscopic Properties of Inorganic and Organometallic Compounds, in: N.N. Greenwood, J.R. Blackborow, J.H. Carpenter, K.D. Croskie, R. Greatrex, M. Kilner, B.E. Prater, B.P. Straughan, vol. 4, The Chemical Society, London, 1971, p. 430.
[26] N.N. Greenwood, J.W. Akitt, W. Errington, T.C. Gibb, B.P. Straughan, Spectroscopic Properties of Inorganic and Organometallic Compounds, vol. 1, 3, The Chemical Society, London, 1968.
[27] T. Maida, G. Yoshida, R. Okawara, J. Organomet. Chem. 44 (1972) 237.
[28] D.G. Tuck, M.K. Yang, J. Chem. Soc., Sect. A (1971) 214.
[29] D. Pahari, V.K. Jain, E.R.T. Tiekink, Main Group Metal Chem. 21 (1998) 293.
[30] J.W. Akitt, in: J. Mason (Ed.), Multinuclear NMR, Plenum Press, New York, 1987.

[31] Z. Cerny, J. Machacek, J. Fusek, B. Casensky, O. Kriz, T.G. Tuck, Inorg. Chim. Acta 247 (1996) 119.
[32] R.K. Iyer, S.B. Karveer, V.K. Jain, Mag. Reson. Chem. 27 (1989) 328.
[33] S.J.A. Faremi, Adv. Inorg. Chem. 36 (1991) 409.
[34] P.J. Hauser, J. Bordner, A.F. Schreiner, Inorg. Chem. 12 (1973) 1347.
[35] S. Bhattacharya, N. Seth, V.D. Gupta, H. Nöth, M. Thomann-Albach, Z. Naturforsch. Teil. B 49 (1994) 193.
[36] K. Dymock, G.J. Palenik, J. Slezak, C.L. Raston, A.H. White, J. Chem. Soc., Dalton Trans. (1976) 28.
[37] B.F. Hoskins, E.R.T. tiekink, R. Vecchiet, G. Winter, Inorg. Chim. Acta 90 (1984) 197.
[38] P. Coggon, J.D. Lebedda, A.T. McPhail, R.A. Palmer, Chem. Commun. (1970) 78.
[39] P.C. Andrews, S.M. Lawrence, C.L. Raston, B.W. Skelton, V. Tolhurst, A.H. White, Inorg. Chim. Acta 300–302 (2000) 56.

PERGAMON

Polyhedron 21 (2002) 247–253

POLYHEDRON

www.elsevier.com/locate/poly

Coordination geometries in bis(di-2-pyridylamine)copper(II) complexes. Crystal structures and spectroscopic properties of $[CuL_2(H_2O)_2](S_4O_6)$, $[CuL_2(CF_3SO_3)_2]$ and $[CuL_2(SO_4)]_2[CuL_2(H_2O)_2](PF_6)_2{\cdot}2H_2O$ (L = Di-2-pyridylamine)

Sujittra Youngme [a,*], Narongsak Chaichit [b]

[a] *Department of Chemistry, Faculty of Science, Khon Kaen University, Khon Kaen 40002, Thailand*
[b] *Department of Physics, Faculty of Science and Technology, Thammasart University Rangsit, Pathumthani 12121, Thailand*

Received 3 August 2001; accepted 13 November 2001

Abstract

The crystal structures of three compounds containing bis(di-2-pyridylamine)copper(II) complex units have been determined by X-ray crystallographic methods; $[Cu(dpyam)_2(OH_2)_2](S_4O_6)$ (**1**), $[Cu(dpyam)_2(CF_3SO_3)_2]$ (**2**) and $[Cu(dpyam)_2(SO_4)]_2[Cu(dpyam)_2(OH_2)_2](PF_6)_2{\cdot}2H_2O$ (**3**). In compound **1** the anions are uncoordinated, and each Cu(II) ion involves the elongated tetragonal octahedral geometry with two water molecules occupying the axial positions. Compound **2** consists of neutral mononuclear units, the Cu(II) environment being elongated tetragonal octahedral with two unidentate triflate anions coordinating in axial positions. Two crystallographically independent molecules are found in compound **3**, one complex unit being centrosymmetric and octahedrally elongated, with two water molecules coordinated in the axial positions, the other predominately close to the distorted square-based pyramidal (4 + 1) stereochemistry of the CuN_3ON' chromophore which is best described as square-pyramidal *cis*-distorted octahedral (4 + 1 + 1*). The latter complex unit of compound **3** is the first example containing a *cis*-distorted octahedral coordination among the copper(II) complexes with divalent oxyanions. © 2002 Elsevier Science Ltd. All rights reserved.

Keywords: Crystal structures; Copper complexes; Di-2-pyridylamine complexes; Tetrathionate complexes; Trifluoromethanesulfonate complexes; Sulfate complexes; Hexafluorophosphate complexes

1. Introduction

Copper(II) complexes are known to display a large variation of non-regular stereochemistries [1]. A large number of $[Cu(chelate)_2(OXO)]^+$ cations, where the chelate is di-2-pyridyl (bpy), 1,10-*o*-phenanthroline (phen) or di-2-pyridylamine (dpyam) and OXO is monovalent oxyanions: ONO^-, HCO_2^-, $CH_3CO_2^-$ or $CH_3CH_2CO_2^-$ have been well known and characterized as having *cis*-distorted octahedral stereochemistry [1,2]. There is no crystal structure of this geometry involving the divalent oxyanion has been found for the copper(II) complexes with chelating ligands.

The copper(II) complexes of $Cu(chelate)_2(OYO){\cdot}nH_2O$ and $Cu(chelate)_2X_2$, where OYO is divalent $S_4O_6^{2-}$, $S_3O_6^{2-}$, $S_2O_6^{2-}$ or SO_4^{2-} oxyanions and X is monovalent ClO_4^-, BF_4^-, PF_6^-, NO_3^- or Br^- anions, show different geometries with four-, five- and six-fold coordination. These complexes can be characterized as monomeric or polymeric chain structures. Previous work led to the characterization of a number of bpy, phen and dpyam ligands representing a sequence of increasingly flexible chelate nitrogen ligands. The four-coordinate $[Cu(chelate)_2](PF_6)_2$, where chelate = bpy [3], phen [4] and dpyam [5] and $[Cu(dpyam)_2]X_2$, where $X = ClO_4^-$ [6] and BF_4^- [7]; the five-coordinate $[Cu(bpy)_2(OH_2)](S_2O_6)$ [8] and six-coordinate $[Cu(dpyam)_2X_2]$, where $X = NO_3^-$ [5,9] and $Br^-{\cdot}2H_2O$ [10] and $[Cu(dpyam)_2(OH_2)_2](SO_4){\cdot}7H_2O$ [7] complexes,

* Corresponding author. Fax: +66-43-243-338.
E-mail address: sujittra@kku.ac.th (S. Youngme).

0277-5387/02/$ - see front matter © 2002 Elsevier Science Ltd. All rights reserved.
PII: S0277-5387(01)00993-7

belong to the mononuclear compounds, whereas the bridged $[Cu(bpy)_2(OYO)]$, where $OYO = S_4O_6^{2-}$ and $S_3O_6^{2-}$ [11], $[Cu(phen)_2(S_4O_6)]$ [12] and $[Cu(bpy)_2X]X$, where $X = ClO_4^-$ and BF_4^- [13] complexes correspond to the polymeric infinite chain structure.

Among this family of copper(II) complexes with dpyam ligand, six crystal structures of mononuclear compounds have been crystallographically characterized: $[Cu(dpyam)_2](ClO_4)_2$ [6], $[Cu(dpyam)_2](BF_4)_2$ [7], $[Cu(dpyam)_2](PF_6)_2$ [5], $[Cu(dpyam)_2(NO_3)_2]$ [5,9], $[Cu(dpyam)_2Br_2]\cdot 2H_2O$ [10] and $[Cu(dpyam)_2(OH_2)_2](SO_4)\cdot 7H_2O$ [7]. The continued interest in the more flexible dpyam ligand in this family of copper(II) complexes, has prompted us to examine more examples of three compounds containing bis(di-2-pyridylamine)-copper(II) complex units, namely diaqua-bis(di-2-pyridylamine)copper(II) tetrathionate (**1**), bis(di-2-pyridylamine)bis(trifluoromethanesulfonato-*o*)copper-(II) (**2**) and {bis[bis(di-2-pyridylamine)(sulfato-*o*,*o*′)-copper(II)][diaqua-bis(di-2-pyridylamine)copper(II) bis-(hexafluorophosphate)]}dihydrate (**3**).

These complexes were prepared and their structures determined crystallographically. Their IR, ESR and electronic spectra were investigated and discussed, along with the structural and spectral comparisons with those of the analogous complexes.

2. Experimental

All reagents were commercial grade materials and were used with out further purification. Elemental analysis (C, H, N) was performed by the Microanalytical Service of Science and Technological Research Equipment Centre, Chulalongkorn University on Perkin–Elmer PE2400 CHNS/O Analyzer. The Infrared spectra were recorded on a Biorad FTS-7/PC FTIR spectrophotometer as KBr pellets in the 4000–450 cm^{-1} region. Solid-state (diffuse reflectance) electronic spectra were recorded as polycrystalline samples on a Perkin–Elmer Lambda2S spectrophotometer over the range 8000–18 000 cm^{-1}. The X-band ESR spectra were recorded on polycrystalline samples at room temperature with a Jeol ESR JES-RE2X spectrometer.

2.1. Preparation

2.1.1. Preparation of $[Cu(dpyam)_2(H_2O)_2](S_4O_6)$ (1)

A warm solution of $Cu(BF_4)_2$ (237 mg, 1.0 mmol) in 10 ml water was added with stirring to a warm solution of dpyam (171 mg, 1.0 mmol) in 10 ml EtOH and $Na_2S_4O_6\cdot 2H_2O$ (306 mg, 1.0 mmol) in 20 ml DMSO yielding a light green solution with a small amount of the undissolved precipitates. Brownish-green crystals of **1** appeared upon slow evaporation of the filtrate at room temperature (r.t.). They were filtered off, washed with mother liquor and air-dried. Yield ca. 50%. *Anal.* Calc. for $C_{20}H_{22}CuN_6O_8S_4$: C, 36.06; H, 3.33; N, 12.62. Found: C, 36.11; H, 3.40; N, 12.58%.

2.1.2. Preparation of $[Cu(dpyam)_2(CF_3SO_3)_2]$ (2)

Compound **2** was obtained as a side product in the preparation of the dihydroxo-bridged complex $[Cu(dpyam)(OH)]_2(CF_3SO_3)_2]$ by adding a warm solution of dpyam (171 mg, 1.0 mmol) in 5 ml MeOH to a warm solution containing $Cu(CF_3SO_3)_2$ (362 mg, 1.0 mmol) in 20:10 ml of water–DMF mixed solvent and 1 ml of 1.0 N KOH solution. Greenish-brown needle-like crystals of **2** were deposited by slow evaporation at r.t. Yield ca. 85%. *Anal.* Calc. for $C_{22}H_{18}CuF_6N_6O_6S_2$: C, 37.53; H, 2.58; N, 11.94. Found: C, 37.44; H, 2.51; N, 12.01%.

2.1.3. Preparation of $[Cu(dpyam)_2(SO_4)]_2[Cu(dpyam)_2(H_2O)_2](PF_6)_2\cdot 2H_2O$ (3)

A warm solution of dpyam (342 mg, 2.0 mmol) and KPF_6 (92 mg, 0.5 mmol) in 40 ml EtOH was added with stirring to a warm solution of $CuSO_4\cdot 5H_2O$ (250 mg, 1.0 mmol) in 100 ml water. The rod-like green crystals were deposited from the solution after slow evaporation in air. Yield ca. 83%. *Anal.* Calc. for $C_{60}H_{58}Cu_3F_{12}N_{18}O_{12}P_2S_2$: C, 40.67; H, 3.53; N, 14.23. Found: C, 40.59; H, 3.58; N, 14.30%.

2.2. Crystallography

Reflection data for complexes **1**, **2** and **3** were collected at 293 K on a 1 K Bruker SMART CCD area-detector diffractometer using graphite monochromated Mo Kα radiation ($\lambda = 0.71073$ Å) at a detector distance of 4.5 cm and swing angle of $-35°$. A hemisphere of the reciprocal space was covered by combination of three sets of exposures; each set had a different ϕ angle (0, 88, 180°) and each exposure of 30, 15 and 35 s for **1**–**3**, respectively, covered 0.3° in ω. Data reduction and cell refinements were performed using the program SAINT [14]. An empirical absorption correction by using the SADABS [15] program was applied, which resulted in transmission coefficients ranging from 0.779 to 1.000 for **1**, 0.633 to 1.000 for **2** and 0.129 to 1.000 for **3**. The structures were solved by direct methods and refined by full-matrix least-squares method on F_{obs}^2 with anisotropic thermal parameters for all non-hydrogen atoms using the SHELXTL-PC V 5.03 [16] software package. All hydrogen atoms in **1** and **2** were located by difference synthesis and refined isotropically, except two hydrogens from different pyridyl ring in **2**. In **3**, all hydrogen atoms, except seven atoms from the pyridyl rings, were geometrically fixed and allowed to ride on the attached atoms. Atoms O(4), O(6) and O(7) of the tetrathionate group in **1** show disorder with occupancies of 0.55 and 0.45; 0.74 and 0.26; and 0.64

Table 1
Crystal and refinement data for complexes **1**, **2** and **3**

Complex	**1**	**2**	**3**
Molecular formula	$[Cu(dpyam)_2(H_2O)_2](S_4O_6)$	$[Cu(dpyam)_2(CF_3SO_3)_2]$	$[Cu(dpyam)_2(SO_4)]_2[Cu(dpyam)_2(H_2O)_2](PF_6)_2 \cdot 2H_2O$
Molecular weight	666.22	704.08	885.97
Temperature (K)	293(2)	293(2)	293(2)
Crystal system	monoclinic	triclinic	monoclinic
Space group	*Cc*	*P*1	$P2_1/c$
a (Å)	15.3413(3)	8.3428(2)	13.4941(2)
b (Å)	10.1378(2)	9.4958(2)	18.7462(3)
c (Å)	18.8657(4)	9.4977(2)	14.4010(10)
α (°)	90	88.48(2)	90
β (°)	113.11	76.69(2)	101.55(2)
γ (°)	90	65.89(2)	90
V (Å^3)	2698.59(9)	66.42(2)	3569.23(6)
Z	6	1	4
D_{calc} (g cm^{-3})	1.640	1.754	1.641
μ (mm^{-1})	1.175	1.070	1.093
F(000)	1364	355	1786
Crystal size (mm)	$0.28 \times 0.28 \times 0.10$	$0.15 \times 0.30 \times 0.15$	$0.18 \times 0.48 \times 0.15$
θ Range (°)	2.35–30.43	2.21–30.42	1.54–30.44
h/*k*/*l*	−11, 21/−14, 14/−26, 26	−11, 10/−13, 11/−13, 11	−8, 18/−26, 26/−19, 20
Reflection collected	9783	4983	25 737
No. of unique reflections	4933	4234	10 147
Reflection observed	3845	3482	1930
Absorption correction	Semi-empirical	Semi-empirical	Semi-empirical
Max/min transmission	1.000, 0.779	1.000, 0.633	1.000, 0.129
Data/restraints/parameters	4933/2/432	4234/3/460	10 147/0/522
Final *R* indices [$I>2\sigma(I)$]	$R_1 = 0.0322$, $wR_2 = 0.0806$	$R_1 = 0.0337$, $wR_2 = 0.0883$	$R_1 = 0.0879$, $wR_2 = 0.2126$
R indices (all data)	$R_1 = 0.0470$, $wR_2 = 0.0908$	$R_1 = 0.0435$, $wR_2 = 0.0940$	$R_1 = 0.2074$, $wR_2 = 0.2394$
Goodness-of-fit on F^2	1.017	1.032	0.490
Largest difference peak and hole (e Å^{-3})	0.409, −0.566	0.313, −0.512	1.212, −0.775

and 0.36, respectively. In **3**, the PF_6^- group (F(2) and F(6)) shows disorder with site occupancies of 0.47 and 0.53; and 0.45 and 0.55, respectively. The large molecule with disorder PF_6^- anion arise to the reasonably high *R* value in **3**. The molecular graphics were created by using SHELXTL-PC. The crystal and refinement details for complexes **1**–**3** are listed in Table 1. Selected bond lengths and angles are given in Tables 2–4. Figs. 1–3 illustrates the structures of **1**–**3**, respectively, and the atom numbering scheme used.

3. Results and discussion

3.1. Description of structure *1*

The crystal structure of **1** is composed of a $[Cu(dpyam)_2(H_2O)_2]^{2+}$ cation and a $S_4O_6^{2-}$ anion (Fig. 1). The six-coordinated copper ion is equatorially bonded to two bidentate dpyam ligands [Cu–N = 1.990(7), 1.992(7), 2.013(6) and 2.047(7) Å] and axially, weakly bonded to the water oxygens [2.460(6) and 2.437(6) Å]. The coordination geometry around each copper ion can be described as an elongated tetragonal octahedral of the CuN_4O_2 chromophore with the tetragonality of 0.82. The basal CuN_4 plane is planar with r.m.s.d. of 0.006 Å, resulted by the large dihedral angles, 40.1(3) and 41.8(3)° between the pyridine rings within one dpyam ligand. The N–Cu–N bite angles of the dpyam ligands are 86.4(3)° and 85.3(3)°, respectively.

Three oxygen atoms from two tetrathionate groups show disorder, resulting in a slight distortion from the

Table 2
Selected bond lengths (Å) and angles (°) with e.s.d.s. in parentheses of $[Cu(dpyam)_2(H_2O)_2](S_4O_6)$ (**1**)

Bond lengths			
Cu(1)–N(1)	1.990(7)	Cu(1)–N(2)	1.992(7)
Cu(1)–N(4)	2.013(6)	Cu(1)–N(5)	2.047(7)
Cu(1)–O(1)	2.460(6)	Cu(1)–O(2)	2.437(6)
Bond angles			
N(1)–Cu(1)–N(2)	86.4(3)	N(1)–Cu(1)–N(4)	179.0(3)
N(2)–Cu(1)–N(4)	93.8(3)	N(1)–Cu(1)–N(5)	94.6(3)
N(2)–Cu(1)–N(5)	178.9(4)	N(4)–Cu(1)–N(5)	85.3(3)
N(1)–Cu(1)–O(2)	88.7(3)	N(2)–Cu(1)–O(2)	88.5(3)
N(4)–Cu(1)–O(2)	90.4(3)	N(5)–Cu(1)–O(2)	90.9(3)
O(1)–Cu(1)–N(1)	92.1(3)	O(1)–Cu(1)–N(2)	92.3(3)
O(1)–Cu(1)–N(4)	88.4(3)	O(1)–Cu(1)–N(5)	88.5(3)
O(1)–Cu(1)–O(2)	178.5(4)		

Table 3
Selected bond lengths (Å) and angles (°) with e.s.d.s. in parentheses of $[Cu(dpyam)_2(CF_3SO_3)_2]$ **(2)**

Bond lengths			
Cu(1)–N(4)	1.983(7)	Cu(1)–N(2)	1.999(7)
Cu(1)–N(5)	2.022(7)	Cu(1)–N(1)	2.030(7)
Cu(1)–O(1)	2.498(7)	Cu(1)–O(4)	2.471(7)
Bond angles			
N(1)–Cu(1)–N(4)	178.9(4)	N(1)–Cu(1)–N(5)	93.0(3)
N(1)–Cu(1)–N(2)	85.8(3)	N(2)–Cu(1)–N(5)	95.2(3)
N(2)–Cu(1)–N(4)	95.2(3)	N(4)–Cu(1)–N(5)	85.9(3)
O(1)–Cu(1)–N(1)	94.1(3)	O(1)–Cu(1)–N(2)	91.7(3)
O(1)–Cu(1)–N(4)	86.3(3)	O(1)–Cu(1)–N(5)	87.8(3)
O(1)–Cu(1)–O(4)	178.7(4)	O(4)–Cu(1)–N(1)	86.7(3)
O(4)–Cu(1)–N(2)	87.2(3)	O(4)–Cu(1)–N(4)	93.1(3)
O(4)–Cu(1)–N(5)	93.3(3)		

Table 4
Selected bond lengths (Å) and angles (°) with e.s.d.s. in parentheses of $[Cu(dpyam)_2(SO_4)]_2[Cu(dpyam)_2(H_2O)_2](PF_6)_2{\cdot}2H_2O$ **(3)**

Molecule A			
Bond lengths			
Cu(1)–N(1)	2.014(6)	Cu(1)–N(4)	2.036(6)
Cu(2)–N(8)	1.999(6)	Cu(1)–N(5)	2.170(6)
Cu(1)–N(2)	2.041(6)	Cu(1)–O(1)	1.989(5)
Cu(1)–O(2)	2.981(6)		
Bond angles			
N(1)–Cu(1)–N(2)	89.4(3)	N(1)–Cu(1)–N(5)	98.7(3)
N(1)–Cu(1)–N(4)	171.4(2)	N(2)–Cu(1)–N(5)	101.7(2)
N(1)–Cu(1)–O(1)	89.2(2)	N(2)–Cu(1)–O(1)	163.0(2)
N(2)–Cu(1)–N(4)	93.5(2)	N(4)–Cu(1)–N(5)	88.6(2)
N(4)–Cu(1)–O(1)	85.7(2)	N(5)–Cu(1)–O(1)	89.2(2)
O(2)–Cu(1)–N(1)	83.6(2)	O(2)–Cu(1)–N(2)	109.9(2)
O(2)–Cu(1)–N(4)	87.8(2)	O(2)–Cu(1)–N(5)	148.4(2)
O(2)–Cu(1)–O(1)	53.1(3)		
Molecule B			
Bond lengths			
Cu(2)–N(7)	2.030(6)	Cu(2)–N(8)	1.999(6)
Cu(2)–O(5)	2.450(6)		
Bond angles			
N(7)–Cu(2)–N(8)	85.3(3)	N(7)–Cu(2)–N(8A)	94.7(3)
O(5)–Cu(2)–N(7)	93.6(3)	O(5)–Cu(2)–N(8)	93.5(2)
O(5)–Cu(2)–N(7A)	86.4(3)	O(5)–Cu(2)–N(8A)	86.5(3)

usual values [11,12,21] of some related bond lengths and angles [S–O, 1.364(8)–1.489(8) Å; S–S, 2.018(3)–2.130(3) Å]. The monomeric units are connected through the $(S_4O_6^{2-})O\cdots H–O(H_2O)$ and $N–H\cdots O$-$(S_4O_6^{2-})$ hydrogen bonds.

3.2. Description of structure *2*

The crystal structure of **2** is made up of discrete neutral $[Cu(dpyam)_2(CF_3SO_3)_2]$ units (Fig. 2). The copper ion exhibits an elongated tetragonal octahedral CuN_4O_2 chromophore with four pyridyl N atoms from the dpyam ligands occupying the equatorial plane and two axial oxygen atoms from each triflate group. The four equatorial Cu–N distances are not significantly different ranging from 1.983(7) to 2.030(7) Å. The two oxygen atoms from each triflate group weakly coordinated in the axial positions with the distances of 2.471(7) and 2.498(7) Å, giving the tetragonality of the CuN_4O_2 chromophore of 0.81. The basal CuN_4 plane is planar with r.m.s.d. of 0.002 Å, attributed to the large angles between the pyridine rings of 36.6(4)° and 38.2(5)°, respectively. The bite angles of the dpyam ligands are 85.8(3)° and 85.9(3)°.

The structure contains unidentate trifluoromethanesulfonate anions which are semi-coordinated to the copper ion. The bonding parameters for the CF_3SO_3 ligand are very close to those found for previously reported unidentate coordinated triflate groups [17–20]. In the present case these anions exhibit a staggered-ethane conformation about the S–C bond. The values of the O–S–O angles are greater than the C–S–O ones as predicted on the basis of bond-pair repulsion. The slight distortion in the S–O bond lengths from the expected values of the second triflate group may due to the involvement of the uncoordinated O atoms in strong N–H···O and C–H···O hydrogen bonds. However, the mean value of the S–O bond lengths involving the coordinated oxygen atoms (1.444 Å) is somewhat

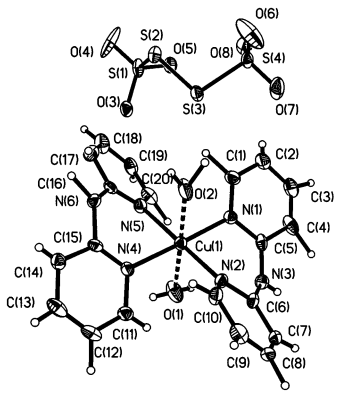


Fig. 1. The molecular structure of $[Cu(dpyam)_2(H_2O)_2](S_4O_6)$ (**1**).

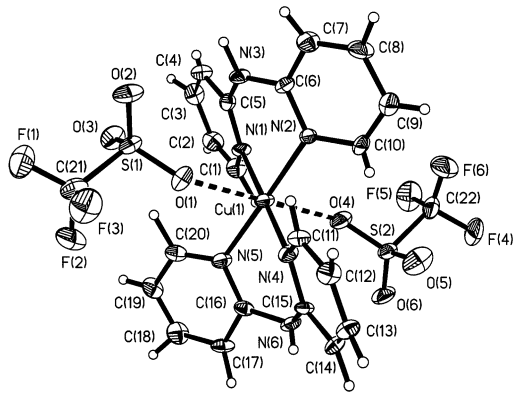


Fig. 2. The molecular structure of $[Cu(dpyam)_2(CF_3SO_3)_2]$ (**2**).

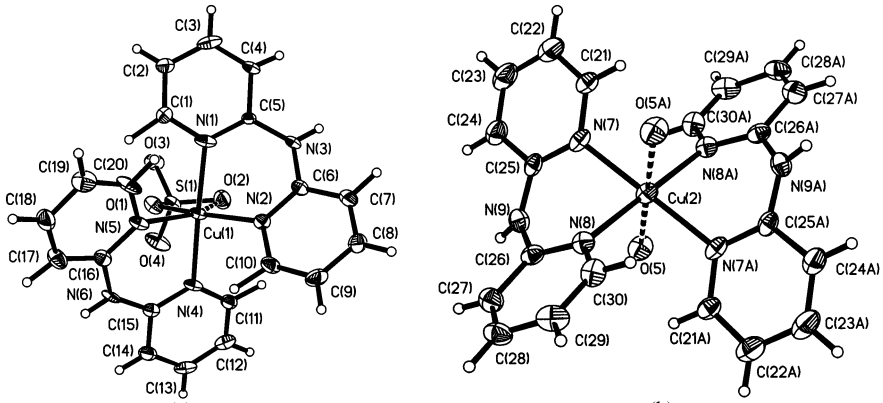


Fig. 3. The molecular structure of $[Cu(dpyam)_2(SO_4)]_2[Cu(dpyam)_2(H_2O)_2](PF_6)_2{\cdot}2H_2O$ (**3**).

longer than the average value of the uncoordinated ones (1.436 Å).

3.3. Description of structure *3*

The asymmetric unit of **3** contains two crystallographically independent units of $[Cu(dpyam)_2(SO_4)]$ and one-half $[Cu_{0.5}(dpyam)(H_2O)]$ moieties (the other half being inversion related), one hexafluorophosphate and one water molecule in the lattice. The two crystallographically independent Cu(II) ions are in totally different coordination geometries. The molecule A (Fig. 3(a)) of compound **3** involves a basic *cis*-distorted octahedral stereochemistry of the CuN_4O_2 chromophore with a marked asymmetric coordination of the sulfate anion. The Cu atom of the $[Cu(dpyam)_2(O_2SO_2)]$ unit is basically five-coordinate, but with the second O atom, O(2), of the sulfate group occupying a sixth-coordinate position at a distance greater than 2.6 Å, namely 2.981(6) Å, to give (4 + 1 + 1*)-type coordination [1,2]. The short Cu–O distance of 1.989(5) Å agrees well with the typical value of 2.00 Å [2]. However, the bidentate coordination of the sulfate group is highly asymmetric with a $\Delta O_{1,2}$ value of 0.99 Å, giving a square-pyramidal distorted octahedral stereochemistry of the six-coordinate CuN_4OO' chromophore [1,2]. The out-of-plane Cu–N(1) and Cu–N(4) distances [2.014(6) and 2.036(6) Å] are not significantly different. The in-plane Cu–N(2) and Cu–N(5) distances [2.041(6) and 2.170(6) Å] are significantly different with $\Delta N_{2,5} = 0.129$ Å and the out-of-plane N(1)–Cu–N(4) angle is 171.4(2)°. There is the in-plane angular distortion, the O(1)–Cu–N(2) and O(2)–Cu–N(5) angles are significantly $< 180°$ at 163.0(2) and 148.4(2)° and the O(1)–Cu–O(2) bite angle is significantly $< 90°$ at 53.1(2)°. However, the copper centre alternatively adopts distorted square-pyramidal stereochemistry if the weak interaction between Cu and O(2) is not considered, with atoms N(1), N(2), N(4) and O(1) forming the basal plane. The Cu atom is lifted out of the basal plane by 0.22 Å, in the direction of the N(5) atom. The basal plane has a slight tetrahedral distortion with a τ value of 0.14, which is relatively close to that of a square-pyrmidal CuN_3ON' chromophore ($\tau = 0$). However, O(2) is close enough to be involved in the off-axis weak semi-coordination to the Cu(II) ion [1,2], indicated by the geometry of the bidentate sulfate anion. The pyridine rings form dihedral angles of 25.2° and 10.6(4)° for the two dpyam ligands, respectively and the dpyam bite angles are 89.4(3)° and 88.6(2)°. The asymmetric bidentate chelating SO_4^{2-} anion shows a small deviation from tetrahedral symmetry, the S–O bonds involving coordinated and hydrogen bonded oxygen atoms, O(1) and O(3) being slightly longer (1.502(5) and 1.478(6) Å) compared to the other two bonds (1.468(5) and 1.457(6) Å), and the angle involving the coordinated oxygen atoms being slightly smaller (106.7(3)°) than the remaining angles (108.0(3)°–113.0(4)°). These correspond to the asymmetric bidentate coordination of the sulfate group [21].

In molecule B of compound **3** (Fig. 3(b)), the Cu(2) atom is in an octahedral environment with four nitrogen atoms from the two inversion related dpyam ligands occupying the basal plane (exactly planar). The axial positions in Cu(2) are occupied by the centrosymmetrically related water oxygens at 2.450(6) Å, giving the elongated tetragonal octahedral CuN_4O_2 chromophore with the tetragonality of 0.82. The Cu–N distances are not significantly different, 2.030(6) and 1.999(6) Å. As the basal plane is exactly planar, the dihedral angle between the pyridine rings is of high value, 40.9(2)° and the dpyam bite angle is 85.3(3)°. Two F atoms of the ionic PF_6^- group show disorder [F(2) and F(6)] so that the bond lengths and angles deriving from the disordered atoms are unusual [5]. The crystal structure of **3** is stabilized by a number of $(SO_4^{2-})O{\cdots}H{-}O(H_2O)$, $(SO_4^{2-})O{\cdots}H{-}N$, $N{\cdots}H{-}O(H_2O)$ and $N{-}H{\cdots}O(H_2O)$ hydrogen bonds involving both the coordinated and uncoordinated water molecules.

3.4. Structure comparison

The bis(dpyam) copper(II) complex with a divalent $S_4O_6^{2-}$ oxyanion of **1** differs from the monomeric five-coordinate $[Cu(bpy)_2(H_2O)](S_2O_6)$ [8] and the polymeric infinite chain structure of $[Cu(bpy)_2(S_4O_6)]$ [11], $[Cu(bpy)_2(S_3O_6)]$ [11] and $[Cu(phen)_2(S_4O_6)]$ [12]. The local geometry of the latter three complexes involves an elongated rhombic octahedron with a marked tetrahedral twist of the basal plane. The most relevant complexes to **1** are found in the elongated centrosymmetric octahedral geometry of $[Cu(dpyam)_2(H_2O)_2](SO_4)\cdot 7H_2O$ [7] and $[Cu(dpyam)_2(H_2O)_2](PF_6)_2$ complex unit of compound **3**, all of which display the planarity of the basal plane and the same tetragonality (0.81–0.82).

The ditriflate complex **2** is not centrosymmetric, but has a structure similar to the elongated centrosymmetric octahedral complexes $[Cu(dpyam)_2X_2]$ where $X = NO_3^-$ [5,9] and Br^- [10], the complex units $[Cu(dpyam)_2X_2]$, where $X = O$-tricyanoethyleneoate [22] and NCS^- [5] and also the related monomeric complexes $[Cu(dpyam)_2(H_2O)_2]X_2$, where $X = \frac{1}{2}(SO_4^{2-})$ [7], $\frac{1}{2}(S_4O_6^{2-})$ (**1**) and PF_6^- (**3**). The equatorial Cu–N distances in these eight complexes are not significantly different. The planarity of the basal CuN_4 plane is only possible because of the flexibility of the dpyam ligands which in these eight complexes are puckered such that the angles between the pyridine rings are quite large and comparable for all complexes [36.6° and 38.2° for **2**, 41.4° for the tricyanoethyleneoated unit, 40.0° for the thiocyanate unit, 37.4° for the nitrate complex, 39.4° for the bromide complex, 35.6° and 38.9° for the sulfate complex, 40.1° and 41.8° for **1** and 40.9° for the hexafluorophosphate complex unit of compound **3**]. The N–Cu–N bite angles within these complexes are also comparable [85.8° and 85.9°; 86.3°; 85.7°; 85.5°; 85.4°, 85.9° and 85.4°; 86.4° and 85.3°; and 85.3°, respectively]. The analogous coordination geometry has not been found in complexes with the less flexible bpy or phen ligand. These observations demonstrate a noticeable difference between the chelate functions of bpy or phen and the more flexible dpyam ligand.

However, these structures of compounds **1** and **2** and their analogous complexes above differ from those of the related complexes: (a) the compressed CuN_4 tetrahedron of $[Cu(chelate)_2](PF_6)_2$, where chelate = bpy [3] and phen [4], and $[Cu(dpyam)_2]X_2$, where $X = BF_4^-$ [7], ClO_4^- [6] and PF_6^- [5]; (b) the asymmetric *cis*-distorted CuN_4OO' octahedral complexes $[Cu(bpy)_2(NO_3)](NO_3)$ [23] and $[Cu(dpyam)_2(OXO)]Y$, where OXO = formate [24], acetate [5,24] and propionate [25–27].

The *cis*-distorted octahedral coordination in molecule A, $[Cu(dpyam)_2(SO_4)]$ of compound **3** is a rare example among copper(II) complexes with divalent oxyanions. However, the CuN_4OO' chromophore geometry is extremely asymmetric *cis*-distorted octahedral, comparable to those of the asymmetric *cis*-distorted octahedral complexes containing the dpyam ligand above. These complexes are slightly different from the less asymmetric *cis*-distorted octahedral complexes $[Cu(dpyam)_2(ONO)]X$ [28–30].

3.5. ESR, electronic and IR spectra

3.5.1. Complexes $[Cu(dpyam)_2(H_2O)_2](S_4O_6)$ (1) and $[Cu(dpyam)_2(CF_3SO_3)_2]$ (2)

The room temperature ESR spectra of **1** and **2** are of the axial type with $g_\parallel \gg g_\perp > 2.0 = 2.26 \gg 2.09 > 2.0$ for **1** and $2.18 \gg 2.06 > 2.0$ for **2**, corresponding to their elongated tetragonal octahedral CuN_4O_2 chromophores and the $d_{x^2-y^2}$ ground state [1,2].

The electronic reflectance spectra of **1** and **2** display a weak peak centred at 17 980 and 18 120 cm^{-1} and a poorly resolved shoulder at approximately 14 790 and 15 430 cm^{-1}, respectively, which correlate well with those of the most likely related complexes $[Cu(dpyam)_2(NO_3)_2]$ (17 870, 14 700(sh) cm^{-1}) [7,30], $[Cu(dpyam)_2(H_2O)_2](SO_4)\cdot 7H_2O$ (17 520, 14 500(sh) cm^{-1}) [7] and $[Cu(dpyam)_2Br_2]$ (17 200 cm^{-1}) [31].

The IR spectrum of **1** shows a strong band splitting into two peaks at 1235 and 1210 cm^{-1} and a medium band at 625 cm^{-1}, characteristic of the $S_4O_6^{2-}$ anion with a number of hydrogen bonds involved [11,12]. The IR spectrum of the triflate group in **2** indicates lowering of symmetry from C_{3v} to C_s as expected for unidentate sulfonate coordination. In C_s symmetry, the E modes are split and nine peaks would occur [17,18]. In fact, $\nu_4(E)$ is slightly split by 20 cm^{-1} (two SO_3 stretching modes at 1250 and 1230 cm^{-1} as strong absorptions) and $\nu_5(E)$ is not split (SO_3 deformation mode at 515 cm^{-1} as a strong peak), whereas no splitting is observed for $\nu_1(A_1)$ 1020, $\nu_2(A_1)$ 745 and $\nu_3(A_1)$ 625 cm^{-1}.

3.5.2. Complex $[Cu(dpyam)_2(SO_4)]_2[Cu(dpyam)_2(H_2O)](PF_6)_2\cdot 2H_2O$ (3)

The observed ESR spectrum of **3** is axial elongated with $g_\parallel \gg g_\perp > 2.0 = 2.47 \gg 2.08 > 2.0$, attributed to two different chromophore coordination. However, this feature is consistent with an elongated tetragonal octahedral CuN_4O_2 chromophore of the complex unit B and a square-pyramidal *cis*-distorted octahedral CuN_4OO' chromophore of the complex unit A in compound **3**, and a $d_{x^2-y^2}$ ground state ($g_\parallel \gg g_\perp > 2.0$) for both chromophores [1,2].

The diffuse reflectance spectra of **3** consists of two almost equally intense peaks at approximately 10 130 and 14 970 cm^{-1}, $\Delta E = 4840$ cm^{-1}, values that are typical and comparable to those reported for the *cis*-distorted octahedral stereochemistry [25–30]. This feature corresponds to the asymmetric *cis*-distorted octahedral unit A, $[Cu(dpyam)_2(O_2SO_2)]$ in compound

3. The observed electronic spectrum of **3** does not show the typical characteristic bands of the elongated tetragonal octahedral unit B, $[Cu(dpyam)_2(H_2O)_2](PF_6)_2$ in compound **3** as its weak band is superimposed under the higher intensity peaks developed from the unit A. This conclusion can be made reasonably by comparison to the weak bands found in the closely related complexes $[Cu(dpyam)_2(H_2O)_2](SO_4)\cdot 7H_2O$ [17 520(w) and 14 500(sh) cm^{-1}] and compound **1** [17 980(w) and 14 790(sh) cm^{-1}]. With a predominated $d_{x^2-y^2}$ ground state, these two observed d–d bands are consistent with the $d_{z^2} \rightarrow d_{x^2-y^2}$ and d_{xy}, d_{yz}, $d_{zx} \rightarrow d_{x^2-y^2}$ transitions for a low-energy shoulder and a higher-energy peak, respectively.

The hexafluorophosphate ion in **3** gives two IR-active bands at 845 cm^{-1} (ν_{PF},s) and 560 cm^{-1} (δ_{FPF}, s) which are in good agreement with those reported earlier for the ionic PF_6^- ion [31], while the coordinated SO_4^{2-} ion displays a strong band (ν_3) splitting into three peaks at 1165, 1150 and 1110 cm^{-1} and a medium band (ν_4) at 620 cm^{-1} attributed to the bidentately coordinated sulfate group [32–34].

4. Supplementary material

Crystallographic data for the structural analysis have been deposited with the Cambridge Crystallographic Data Centre, CCDC nos. 168976, 168977 and 168978 for compounds **1**, **2** and **3**. Copies of this information may be obtained free of charge from the CCDC, 12 Union Road, Cambridge, CB2 1EZ, UK (fax: +44-1223-336033; e-mail: deposit@ccdc.cam.ac.uk or www: http://www.ccdc.cam.ac.uk).

Acknowledgements

The authors would like to thank the National Research Council of Thailand and Khon Kaen University for research grant. Support of the Postgraduate Education and Research Program in Chemistry is also gratefully acknowledged.

References

[1] B.J. Hathaway, Comprehensive coordination chemistry, in: G. Wilkinson, R.D. Gillard, J.A. McCleverty (Eds.), The Synthesis, Reactions, Properties and Applications of Coordination Compounds, vol. 5, Pergamon Press, Oxford, 1987, pp. 533–774 Section 53.
[2] (a) B.J. Hathaway, Struct. Bonding 57 (1984) 55 and references; (b) B.J. Hathaway, D.E. Billing, Coord. Chem. Rev. 5 (1970) 143.
[3] J. Foley, S. Tyagi, B.J. Hathaway, J. Chem. Soc., Dalton Trans. (1984) 1.
[4] K. Amournjarusiri, B.J. Hathaway, Acta Crystallogr., Sect. C 47 (1991) 1383.
[5] J. Sletten, K. Svardal, A. SØrensen, Acta Chem. Scand. 47 (1993) 1091.
[6] J.E. Johnson, T.A. Beineke, R.A. Jacobson, J. Chem. Soc., Sect. A (1971) 1371.
[7] S. Youngme, K. Poopasit, K. Chinnakali, S. Chantrapromma, H.K. Fun, Inorg. Chim. Acta 292 (1999) 57.
[8] W.D. Harrison, B.J. Hathaway, Acta Crystallogr., Sect. B 36 (1980) 1069.
[9] M.C. Munoz, J.M. Lazaro, J. Faus, M. Julve, Acta Crystallogr., Sect. C 49 (1993) 1756.
[10] A. Camus, A. Facchinetti, N. Marsich, A.M.M. Lanfredi, F. Ugozzoli, Inorg. Chim. Acta 290 (1999) 180.
[11] W.D. Harrison, B.J. Hathaway, Acta Crystallogr., Sect. B 35 (1979) 2910.
[12] E. Freire, S. Baggio, R. Baggio, M.T. Garland, Acta Crystallogr., Sect. B 54 (1998) 464.
[13] J. Foley, D. Kennefick, D. Phelan, S. Tyagi, B. Hathaway, J. Chem. Soc., Dalton Trans. (1983) 2333.
[14] Siemens, SAINT, Version 4, Software Reference Manual, Siemens Analytical X-Ray Systems Inc., Madison, Wisconsin, USA, 1996.
[15] G.M. Sheldrick, SADABS, Program for Empirical Absorption correction of Area Detector Data, University of Göttingen, Germany, 1996.
[16] Siemens, SHELXTL, Version 5, Reference Manual, Siemens Analytical X-Ray Systems Inc., Madison, Wisconsin, USA, 1996.
[17] G.A. Lawrance, Chem. Rev. 86 (1986) 17.
[18] J.S. Haynes, S.J. Rettig, J.R. Sams, R.C. Thompson, J. Trotter, Can. J. Chem. 64 (1986) 429.
[19] J.S. Haynes, S.J. Rettig, J.R. Sams, J. Trotter, R.C. Thompson, Inorg. Chem. 27 (1988) 1237.
[20] J. Faus, M. Julve, J.M. Amigó, T. Debaerdemaeker, J. Chem. Soc., Dalton Trans. (1989) 1681.
[21] K. Nakamoto, Infrared, Raman Spectra of Inorganic, Coordination Compounds, Part B, 5th ed., Wiley, New York, 1997.
[22] C.C. Fuller, R.A. Jacobson, Inorg. Chim. Acta 48 (1981) 191.
[23] R.J. Fereday, P. Hodgson, S. Tyagi, B.J. Hathaway, J. Chem. Soc., Dalton Trans. (1981) 2070.
[24] S. Aduldecha, M.E. Keniry, P. Akhter, S. Tyagi, B.J. Hathaway, Acta Crystallogr., Sect. C 47 (1991) 1378.
[25] S. Youngme, K. Chandavong, C. Pakawatchai, Z.Y. Zhou, H.K. Fun, Acta Crystallogr., Sect. C 54 (1998) 199.
[26] S. Youngme, K. Poopasit, H.K. Fun, K. Chinnakali, I.A. Razak, S. Chantrapromma, Acta Crystallogr., Sect. C 54 (1998) 1221.
[27] (a) S. Youngme, C. Pakawatchai, K. Poopasit, K. Chandavong, A.H. White, unpublished work;
(b) K. Chandavong, M.Sc. Thesis, Khon Kaen University, Thailand, 1998.
[28] S. Youngme, N. Chaichit, N. Koonsaeng, submitted for publication.
[29] A. Walsh, B. Walsh, B. Murphy, B.J. Hathaway, Acta Crystallogr., Sect. B 37 (1981) 1512.
[30] (a) V. Koonsaeng, B.J. Hathaway, unpublished work;
(b) V. Koonsaeng, Ph.D. Thesis, University College Cork, Ireland, 1989.
[31] J.C. Lancaster, W.R. Mcwhinnie, P.L. Welham, J. Chem. Soc., Sect. A (1971) 1742.
[32] I.M. Procter, B.J. Hathaway, P.G. Hodgson, Inorg. Nucl. Chem. 34 (1972) 3698.
[33] J.C. Tedenac, N.D. Phung, C. Avinens, M. Maurin, Inorg. Nucl. Chem. 38 (1976) 85.
[34] S. Youngme, C. Pakawatchai, N. Chaichit, submitted for publication.

PERGAMON

Polyhedron 21 (2002) 255–263

POLYHEDRON

www.elsevier.com/locate/poly

Synthesis, characterization and electrochemistry of novel differently octasubstituted phthalocyanines

Mehmet Kandaz [a], Meryem N.U. Yaraşir [a], Atıf Koca [b], Özer Bekaroğlu [c,*]

[a] *Department of Chemistry, Sakarya University, 54100, Adapazarı, Sakarya, Turkey*
[b] *Chemical Engineering Department, Engineering Faculty, Marmara University, 81040, Kadıköy, Istanbul, Turkey*
[c] *Department of Chemistry, Istanbul technical University, Maslak, 80620 Istanbul, Turkey*

Received 3 July 2001; accepted 12 October 2001

Abstract

We describe the complete synthesis of differently substituted multifunctional metallo phthalocyanines (MPcs) (M = Ni, Zn, Co) bearing four 2′-aminophenylsulfanyl or 2-aminophenoxy moieties and four chloro atoms on peripheral positions. The synthesis started from the corresponding anhydrous metal salts and differently substituted [4-(2′-aminophenylsulfanyl)-5-chlorobenzene-1,2-dicarbonitrile] (**2a**) and [4-(2-aminophenoxy)-5-chlorobenzene-1,2-di-carbo nitrile] (**2b**), and the products were separated by HPLC. These multifunctional amino substituents serve as strong binding sites for further reactions after phthalocyanine formation, such as Schiff-bases, and provide solubility of the phthalocyanines in organic solvents (THF, $CHCl_3$ and CH_2Cl_2). The newly synthesized compounds have been characterized by elemental analysis, FTIR, ^{1}H NMR, MS (EI and FAB), UV–Vis and atomic absorption spectroscopy. Electrochemical studies reveal that CoPc (**6a**) has two metal and four ligand-based redox processes while NiPc (**4a**) and ZnPc (**5b**) show three ligand-based reduction processes. © 2002 Elsevier Science Ltd. All rights reserved.

Keywords: Phthalocyanines; Phthalonitrile derivatives; Electrochemistry; Nickel; Zinc; Cobalt

1. Introduction

Over the last few years, phthalocyanine's derivatives with purpose-designed functional substituents have been receiving more frequent attention due mainly to the utility of these species in a variety of new fields, such as molecular electronics [1,2], non-linear optics [3], liquid crystals [4,5], gas sensors [6], photosensitizers [7], catalysts and semiconductive materials [8,9], photovoltaic cells [10] and electrochromic displays [11,12].

The considerable interest in these macrocycles focuses our studies to this area. So we have been investigating peripherally reactive phthalocyanines having electron donating or electron withdrawing substituents on benzenoid rings of the phthalocyanines as precursors for the development of further applications [12–15]

Incorporation of functional moieties such as 2′-aminophenylsulfanyl, 2-aminophenoxy nitro and pyridyl groups to the peripheral position of the phthalocyanines can have stronger coupling ability to the macrocyclic core than do non-reactive moieties [13,16–19]. Using this strategy, it is possible to prepare reactive compounds in which the solubility, redox and electronic properties may be varied. This makes this family of the reactive phthalocyanine molecules an interesting target for the further development of new chemical reactions on phthalocyanine complexes.

In the present work, as a further part of our previous studies on phthalocyanines with octasubstituted multifunctional substituents [13], here it has been reported that, for the first time, a reproducible procedure on the preparation and characterization of novel 4,5-differently substituted functional phthalonitrile derivatives and their metallophthalocyanines carrying both 2′-aminophenylsulfanyl or 2-aminophenoxy and chloro substituents. In the substituent reactions, 4,5-bis (2′-aminosulfanylphenyl)-1,2-dicyanobenzene (**3a**) and 4,5-

* Corresponding author. Tel.: +90-212-285-3436; fax: +90-212-285-6386.
E-mail address: obek@itu.edu.tr (Ö. Bekaroğlu).

0277-5387/02/$ - see front matter © 2002 Elsevier Science Ltd. All rights reserved.
PII: S0277-5387(01)00982-2

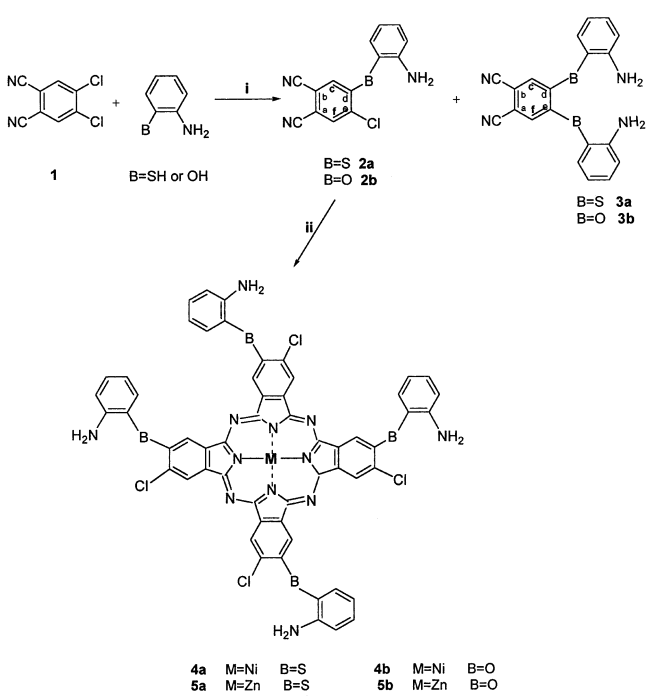
bis (2′-aminophenoxy)-1,2-dicyanobenzene (**3b**), as by-products formed during the course of the reaction, were separated from **2a** and **2b** by using HPLC preparative separation.

The functions of metallophthalocyanine derivatives are almost all based on their electron transfer properties. Thus, in this study, electrochemical analysis of **4a**, **5b** and **6a** were also carried out by cyclic voltammetric measurements.

2. Results and discussion

In the present study, nucleophilic aromatic displacement reactions have been used on either one or two chloro atoms of the 4,5-dichloro-1,2-dicyanobenzene (**1**) with the –SH or –OH function of the corresponding 2′-aminothiophenyl or 2-aminophenol nucleophiles at reflux temperature in tetrahydrofuran in the presence of Cs_2CO_3 (Scheme 1). Compounds **2a** and **2b** were separated from **3a** and **3b** by preparative HPLC. Because of the more acidic –SH groups, under similar conditions, the yields of **3a** and **2a** were found to be much greater than those of **2b** and **3b**.

In our group's previous studies when K_2CO_3 was used as a base, the chloro atoms were only partially substituted. However, in the case of Na_2CO_3 base, both chloro atoms were substituted in aliphatic structured starting materials [20,21]. Selective substitution of one of the two chloro atoms by 2-aminothiophenol or 2-aminophenol for the synthesis of **2a** and **2b** was not practical without forming **3a** and **3b** disubstituted side products in the case of the strong Cs_2CO_3 base-catalyzed reaction. According to these studies, displacement of one chloro atom might be a consequence of steric hindrance of the bulky groups, the acidic capacities of the displacement groups and the strength of the bases used in these reactions [20–22].



Scheme 1. Cs_2Co_3, thf **ii**, anhydrous quinoline or ethyleneglycol, anhydrous $NiCl_2$, $Zn(O_2CMe)_2$, $CoCl_2$.

Compounds **2a** and **2b** were converted into the desired phthalocyanines (**4a**–**6a** and **4b**, **5b**) by using anhydrous high-boiling solvents and metal salts ($NiCl_2$, $Zn(O_2CMe_2)_2$, $CoCl_2$). The blue–green cyclotetramerization products were purified by flash chromatography with sephadex in tetrahydrofuran [17,23].

In the case of **3a** and **3b**, the cyclotetramerization led to the octasubstituted phthalocyanines described in our previous studies, whereas the mixture of constitutional phthalocyanine isomers were obtained by the cyclization of **2a** or **2b** at approximately 195–200 °C in a sealed tube. Purification steps were tedious. All attempts to separate these isomers by column chromatography and also HPLC methods using different solvents were unsuccessful. Their presence were determined by a slight broadening both in ^{1}H NMR and UV–Vis spectra when compared with symmetrically octasubstituted phthalocyanines [13,20–22]. The solubilities of the zinc phthalocyanines are slightly higher than those of the others.

The structures of the phthalocyanine substances (**4a**–**6a** and **4b**, **5b**) were verified by elemental analysis, IR, ^{1}H NMR, UV–Vis and mass spectroscopy.

In the IR spectra of **2a** and **2b**, both the major strong –CN and $-NH_2$ peaks are at approximately 2220 and 3350–3450 cm^{-1} and the rest of the spectra are very similar. The most instinctive indicators of the presence of **2a** and **2b** are the signals belonging to the aromatic protons *ortho* to the cyano group in the lower field region of the ^{1}H NMR. In the phthalonitriles bearing two different substituents in 4,5-positions (**2a** and **2b**), the aromatic protons *ortho* to the –CN group appear at 7.64–7.34 and 7.78–7.47 ppm as two slightly broad singlets in the down field region of the ^{1}H NMR spectrum while broad deuterium exchangeable NH_2 protons appear at 5.33 and 5.55 ppm respectively. Also, the presence of **2a** and **2b** were confirmed by the mass spectra (EI) showing molecular ion peaks at m/z: 285.0 [M^+] and m/z: 269.0 [M^+], respectively, and the major fragment ions corresponding to the loss of Cl [$M-35]^+$, C_6H_5N [$M-93]^+$, C_6H_5NS [$M-124]^+$ and C_6H_5NO [$M-108]^+$ were identified easily.

The ^{1}H NMR spectra of the phthalocyanines bearing four 2′-aminophenylsulfanyl or 2-aminophenoxy moieties and four chloro atoms are almost identical, with small changes in shifts. The broad signals in the case of **4a**, **4b** (NiPc) rather than those in **5a**, **5b** (ZnPc) were probably due to the chemical exchange associated with

Table 1
Electronic spectral data for the phthalocyanine complexes in dimethylformamid

Compound	$\lambda_{max\ (nm)}$ (10^{-4} ε dm^3 mol^{-1} cm^{-1})			
	Q-band region		Soret region	
4a	708(11.20)	634(5.60)	440 [a](4.45)	330(14.04)
4b	670(6.85)	618(3.06)	445(3.04)	329(11.24)
5a	696(12.82)	642(4.3)		355(14.68)
5b	680(7.16)	638(3.58)		367(6.53)
6a	687(7.14)	628(3.20)		317(8.65)

[a] Shoulder.

aggregation–disaggregation equilibria which occurred at high concentrations used in the NMR measurements [13,22,24,25]. Differently substituted benzo units of the phthalocyanines result in the formation of positional isomers which in turn cause the splitting of the signals for the peripheral aromatic protons in the down field aromatic region. Slightly broad signals for Ar–NH_2 exchangeable protons of the phthalocyanines appear at 5.40 and 5.47 ppm, and disappear after addition of D_2O. ^{1}H NMR signals of the phthalocyanines (**4a**, **4b** and **5a**, **5b**) at 8.02, 7.78; 8.10, 7.85 and 8.07, 7.85; 8.17, 7.90 ppm, respectively, in the down field region of the spectrum are another indication of positional isomers.

The mass spectra by the FAB technique on the newly synthesized phthalocyanines (**5b**, **6a**) confirmed the proposed structures. Molecular ions in **5b** and **6a** were identified easily at m/z: 1143.1 $[M]^+$ and m/z: 1201 $[M+1]^+$ and as well as the fragment ions corresponding to loss of Cl $[M-35]$, C_6H_7NS $[M-124]^+$, C_6H_7NO $[M-93]^+$, $2\times C_6H_7NS$ $[M-249]^+$, $[M-Zn-1]^+$, $[M-Co\ -1]^+$.

The typical UV–Vis spectra of the phthalocyanine complexes **4**–**6** exhibited characteristic Q and B bands, one in the visible region at approximately 600–750 nm (Q-band) attributed to the π–π* transition from the highest occupied molecular orbital (HOMO) to the lowest unoccupied molecular orbital (LUMO) of the Pc^{2-} ring, and the other in the UV region at 300–400 nm (B-band) arising from the deeper π-levels → LUMO transition (Table 1). In the UV–Vis absorption spectra of all phthalocyanines (**4**–**6**) in dmf, the Q-band absorptions of the π–π* transition were observed as a single band of high intensity at 708, 670, 696, 680, 687 nm, respectively. There is also a shoulder at the slightly higher energy side for each phthalocyanine. In the phthalocyanines bearing 2′-aminophenylsulfanyl moieties (**4a**–**6a**) on the periphery, the wavelengths of the maximum of the Q-bands were shifted to a lower energy as a result of the electron-donating thioether substituents compared to those of phthalocyanines bearing 2′-aminophenoxy moieties (**4b** and **5b**). The position of the soret-like π–π* bands of all phthalocyanines were slightly shifted. Any increase in the concentration results in the aggregation of the phthalocyanine molecules, which are accompanied by a blue shift of the Q-band with a decrease in intensity. The extent of aggregation is slightly stronger for phthalocyanines bearing a low number of 2′-aminophenylsulfanyl or 2-aminophenoxy moieties on the periphery than those of octasubstituent ones [13].

3. Electrochemical measurements

The voltammograms of **4a**, **5b** and **6a** were recorded at different scan rates and are presented in Fig. 1. The reduction and oxidation potentials of these complexes are summarized in Table 2. The controlled potential coulometric (CPC) studies indicated that the number of electrons transferred for all electrochemical reactions of the complexes is one.

The cyclic voltammograms of complexes **6a**, **4a** and **5b** exhibited six, three and three redox processes in the $+1.10$ to -1.80 V range, respectively. Scanning the potential to the positive side, two irreversible oxidation processes of complex **6a** at 0.620 and 0.960 V are seen, and upon scanning cathodically, two reduction peaks with the corresponding anodic waves on the reverse step and two irreversible reduction waves were recorded at -0.610, -1.263, -1.037 and -1.618 V, respectively, at 0.05 V s^{-1} scan rate.

The reduction and oxidation behavior of metallophthalocyanine derivatives is due to the interaction between the phthalocyanine ring and the central metal. The redox properties of metallophthalocyanines have been studied by many authors [26–29]. First-row transition metal phthalocyanines differ from those of the main-group metal phthalocyanines due to the fact that metal 'd' orbitals may be positioned between the HOMO and LUMO of the phthalocyanine (Pc^{-2}) ligand. This has been well established by several papers published by Lever et al. [29–31]. According to these studies, the first oxidation and first reduction processes occur on the metal center in the metal phthalocyanines only for Mn, Fe and Co derivatives. According to Lever et al., for Ni, Cu and Zn phthalocyanines, redox processes take place on the phthalocyanine ring. As understood from these studies, in the case of **6a**, phthalocyanine ring oxidation occurs after the oxidation of the cobalt center, while the ring reductions follow the reduction of the central metal. So the first oxidation at 0.620 V and the first reduction at -0.610 V are attributed to the cobalt center while other redox processes are to the phthalocyanine ring system. All redox processes recorded for complexes **4a** and **5b** are also attributed to the phthalocyanine ring system. Peak potentials and differences between the first oxidation and reduction for the cobalt center and for the phthalocya-

nine rings are comparable to those given in the corresponding papers. In the case of **6a**, the phthalocyanine ring reduction recorded at a higher negative potential than the ring reduction of **4a** and **5b**. This difference may be due to the variation in the effect of the interaction between the central metal and phthalocyanine ring. Ring oxidations of **4a** and **5b** cannot be recorded with the available solvent/electrolyte range. It may be out of the solvent windows. The difference between the first reduction and oxidation of the phthalocyanine ring was given in the range 1.7–1.8 V in different studies. In the case of **4a** and **5b** first reductions were recorded at

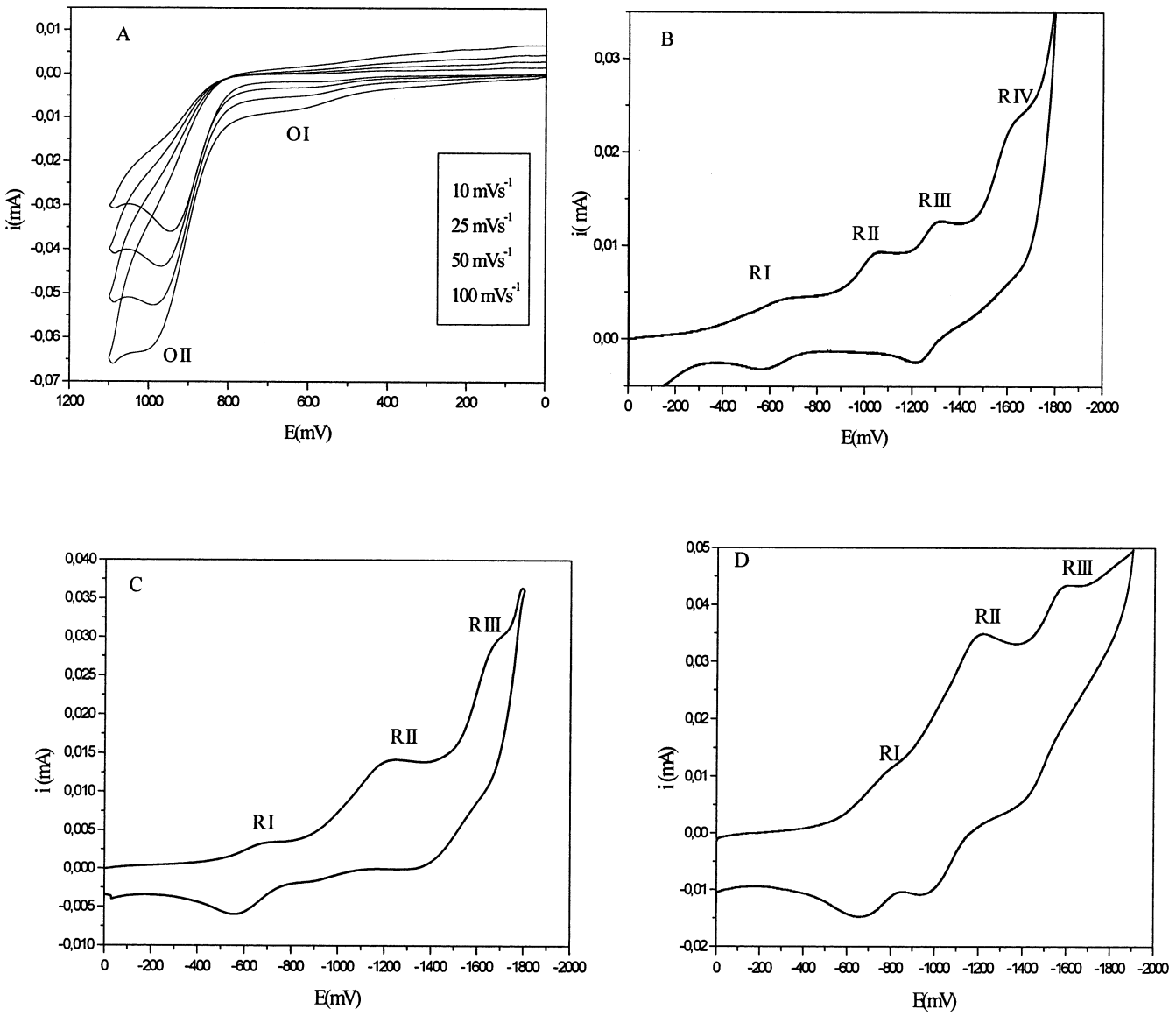


Fig. 1. Cyclic voltammograms of **4a**, **5b** and **6a** at 0.050 V s^{-1} scan rate (A and B: **6a**; C: **4a**; and D: **5b**).

Table 2
The reduction and oxidation potentials of **4a**, **5b** and **6a** at 0.05 V s^{-1} scan rate (5×10^{-4} mol dm^{-3} complex in 0.1 mol dm^{-3} TBAP/DMSO solution)

Pcs	Reduction, $E_{1/2}$ (ΔE) or E_{pc} (mV)				Oxidation, $E_{1/2}$ (ΔE) or E_{pa} (mV)	
	I. Red.	II. Red.	III. Red.	IV. Red.	I. Ox.	II. Ox.
4a	−615 (67)	−1210	−1668 (180)			
5b	−713 (63)	−1105 (112)	−1493 (73)			
6a	−609 (63)	−1037	−1263 (65)	−1618	605	950

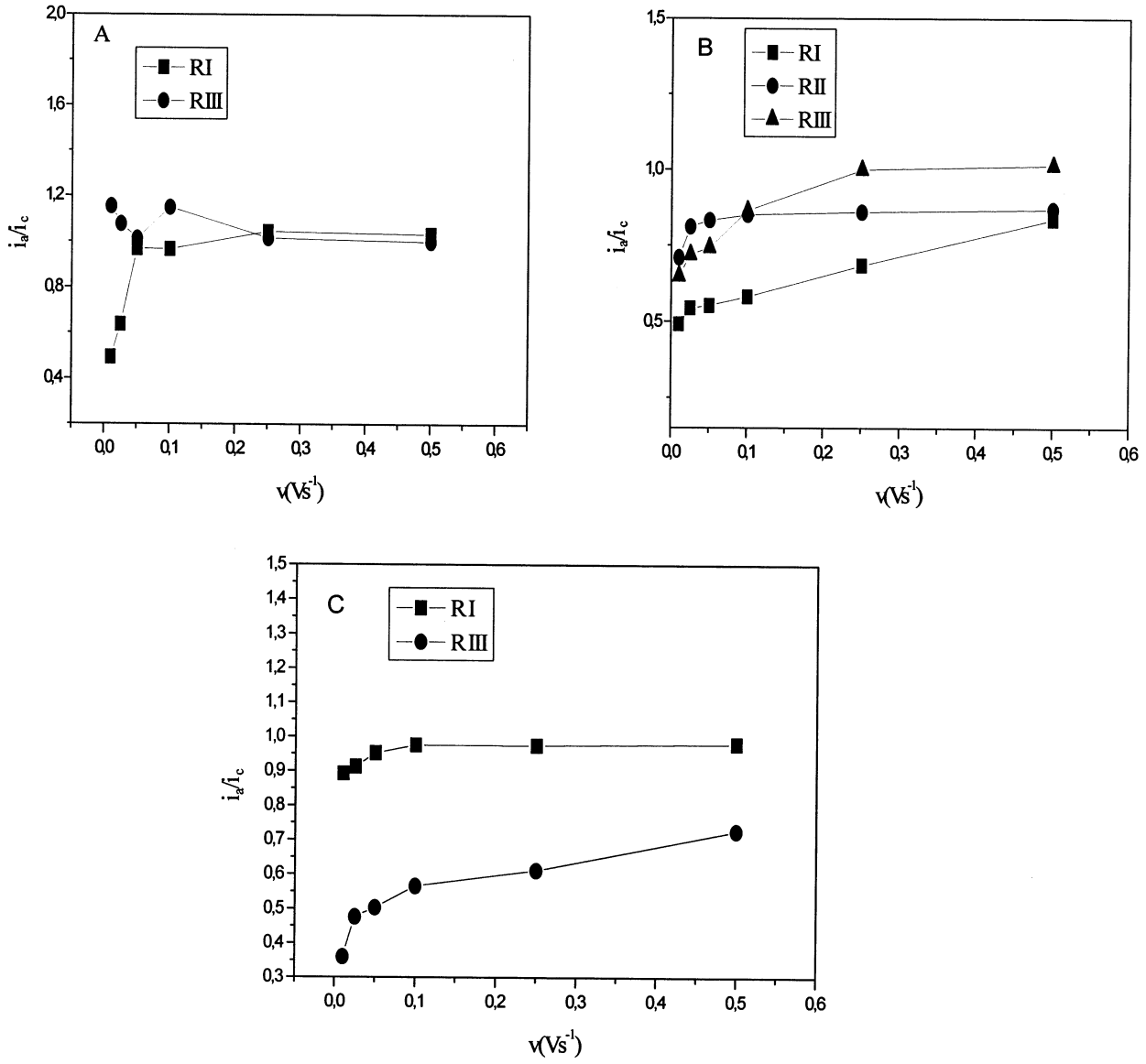


Fig. 2. The plot of $i_{pa}/i_{pc} - v$ for the reversible couple of the complexes (A: **6a**; B: **5b**; C: **4a**).

approximately -0.600 and -0.700 V, respectively. So oxidation should be observed at approximately 1.200–1.300 V which is out of our solvent/electrolyte range.

For the redox couples (peaks I and III) of **6a**, the peak separation ΔE_p, 63 and 65 mV, respectively, at 0.005 V s^{-1} scan rate, indicated that the first and third redox couples are reversible at this scan rate, but approach an irreversible case at higher scan rates (above 0.250 V s^{-1} scan rate). In the case of **5b**, at low scan rates all redox couples are reversible, but approach an irreversible case with higher scan rates. However, the third redox couple of **4b** shows quasi-reversible properties even at a very low scan rate and goes to an irreversible case at higher scan rates (Table 2). With the same approaches, the first one is also a reversible couple.

The linear dependence of the peak currents (i_{pc} (i_{pa} for oxidation)) of **6a** (except the ring oxidation process) to the scan rate is characteristic of a behavior that is associated with a diffusion process for solution species. The peak current of the ring oxidation is much bigger than the one of Co (II) oxidation and it is directly proportional to the scan rate (Fig. 1). This indicates the adsorption of the Co(II) oxidation's product on the electrode.

Fig. 2 shows the change in the ratio of the anodic to the cathodic peak current (i_{pa}/i_{pc}) of complexes **4a**, **5b** and **6a** with scan rate for the redox couples. The relationship between the i_{pa}/i_{pc} of a reversible couple with scan rate serves as a quick test for an electrochemical mechanism associated with a preceding or succeeding chemical reaction. In the case of the ratio of i_{pa}/i_{pc} at all scan rates being unity, it is a simple electron

transfer reaction. In the case of i_{pa}/i_{pc} decreasing with scan rate, it is assigned as a reversible electron transfer followed by a reversible chemical reaction. While for i_{pa}/i_{pc} increasing with scan rate, it is a chemical reaction preceding a reversible electron transfer reaction. It is shown that the i_{pa}/i_{pc} ratio is nearly unity at all scan rates for the first redox couple of **6a**. This is an indication of a simple electron transfer reaction. For redox process III, the i_{pa}/i_{pc} ratio increased with the scan rate. This indicates the existence of an irreversible chemical reaction succeeding the electron transfer reaction (Fig. 2A). The unit values of the i_{pa}/i_{pc} ratio indicated that the first couple of **4a** also shows a simple electron transfer reaction, while the third redox couple is an electron transfer reaction followed by an irreversible chemical reaction. For complex **5b**, the i_{pa}/i_{pc} ratio increased towards unity with scan rate for the first reversible couple. This indicates the existence of an irreversible chemical reaction followed by electron transfer reactions. For the other redox couples, the i_{pa}/i_{pc} ratios are near unity indicating simple electron transfer reactions.

4. Experimental

All organic solvents were dried and distilled before use. All reagents were freshly distilled or recrystallized and dried under reduced pressure before use. Melting points were determined using a Buchi melting apparatus. FTIR (KBr) were recorded on ATI a Unicom-Mattson 1000 spectrophotometer. Elemental analysis (C, H and N) was performed at the Instrumental Analysis Laboratory of TUBITAK Gebze Research Center. Electronic (UV–Vis) Absorption Spectra were recorded on a UnicamUV2 spectrophotometer. Nuclear Magnetic Resonance spectra were recorded on a Bruker (200 MHz) and Mass Spectra (IE and FAB) were recorded on a VG Zab-spectrometer. Chromatography was performed with silica gel (Merck grade 60 and sephadex) from Aldrich. The metal contents of the complexes were determined with a Hitachi 180-80 atomic absorption spectrophotometer in solution prepared by decomposition of the compounds in conc. HCI and conc. HNO_3 (3:1) solution followed by the dilution in water.

The homogeneity of the products was tested in each step by TLC (SiO_2, $CHCl_3$, DMF, methanol).

CV measurements were carried out with Princeton Applied Research Model 273 potentiostat controlled by an external PC, using the computer program HEADSTRT, utilizing a three-electrode configuration at 25 °C. ORIGIN.50 graph program was used to evaluate HEADSTRT data, to draw voltammograms and analyze them. A Pt wire served as the counter electrode. A saturated calomel electrode (SCE) was employed as the reference electrode and was separated from the bulk of the solution by a glass bridge. The working electrode was a Pt plate with an area of 1.0 cm^2. The surface of the working electrode was polished with a H_2O suspension of Al_2O_3 before each run. Electrochemical grade 0.1 mol dm^{-3} tetrabutylammoniumperchlorate (TBAP) in extra pure DMSO was employed as the supporting electrolyte. High purity nitrogen was used for deaeration and to maintain an N_2 blanket for at least 15 min prior to each run. For controlled potential coulometric (CPC) studies, a platinum gauze working electrode (10.5 cm^2 surface area), a Pt wire counter electrode separated by a glass bridge, a saturated calomel reference electrode, and a model 377/12 Synchronous stirrer were used.

5. Materials and synthesis

4,5-Dicholoro-1,2-benzenedicarboxylic acid was purchased from Aldrich Chemical Co. and used as received. 4,5-Dichloro-1,2-dicyanobenzene was synthesized according to the procedure in Ref. [6], by a multi-step reaction sequence; yield 75%, m.p. 182 °C. Owing to instability of the amines **2b** and **3b**, all the preparations described below require the use of freshly prepared and purified samples of these ligands.

*5.1. 4-(2′-Aminophenyl sulfanyl)-5-chloro-benzene-1,2-dicarbonitrile (**2a**)*

2-Aminothiphenol (0.64 g, 5.1 mmol) was dissolved in 50 cm^3 dry tetrahydrofuran under nitrogen. Finely ground anhydrous cesium carbonate ($\sim$2.0 g) was added to this solution. After stirring for 0.5 h efficiently, 0.5 g (2.53 mmol) 4,5-dichloro-1,2-dicyanobenzene was added dropwise over 1 h. After the reaction mixture was stirred under nitrogen at reflux temperature for 12 h, the solution was cooled to room temperature (r.t.). Having reduced the volume of the solvent to 20 cm^3 under reduced pressure, water was added to separate any inorganic residues and the aqueous phase was extracted with chloroform (3×25 cm^3). The combined extracts were first treated with sodium carbonate (5%), then with water (3×20 cm^3) and finally dried over anhydrous sodium sulfate. The solvent was distilled off and the resulting yellow–light-brown oily residue was crystallized from toluene. The light yellow powder mixture was dissolved in a minimum amount of tetrahydrofuran and purified by preparative HPLC (on Lichrospher reverse phase-18 (5 μm)) using acetonitrile as the mobile eluent. As the first fraction 0.28 g (39%) of **2a** and as the second fraction 0.16 g (16.45%) of **2b** was obtained.

2a: m.p: 190 °C *Anal.* Calc. for $C_{14}H_8ClN_3S$: C, 58.84; H, 2.80; N, 14.71. Found: C, 59.01; H, 2.76; N,

14.26%. IR (KBr disc) ν: 2230 (–CN), 3345–3450 (Ar–NH_2); ^{1}H NMR ([d_6]-DMSO) δ: 7.64 (s, 1H, *ortho* to Cl group), 7.34 (s, 1H, *meta* to Cl), 6.90–6.62 (m, superimposed 8H, Ar–H), 5.33 (s, br, 2H, Ar–NH_2). EI/MS: m/z (%): 285.0 (25) [M^+], 249.1, 234, 217.1, 204.1, 187.0, 125, 93.1.

5.2. 4-(2′-Aminophenoxy)-5-chloro-benzene-1,2-dicarbonitrile (**2b**)

The white compound was prepared by following the same procedure as described above, starting from 0.55 g, (5.1 mmol) 2-aminophenol and (0.5 g, 2.53 mmol) 4,5-dichloro-1,2-dicyanobenzene. Crude solid was collected by suction filtration and washed copiously with cold MeOH until the washings were clear. The white–yellow product was dissolved in a minimum of thf and purified by preparative HPLC (on LiChrosorp reverse phase-18 (5 μm)) 25 × 250 mm by using acetonitrile as eluent. The first fraction was determined to be **2b** (0.14 g, 20.57%). The second band was determined as **3b** (0.09 g, 10.40%).

2b: m.p.: 178 °C, *Anal*. Calc. for $C_{14}H_8ClN_3O$: C, 62.33; H, 2.97; N, 15.58. Found: C, 62.14; H, 3.18; N, 15.02%. IR (KBr disc) ν: 2230 cm^{-1} (–CN), 3350–3440 cm^{-1} (Ar–NH_2); ^{1}H NMR ([d_6]-DMSO) δ: 7.78 (s, 1H, *ortho* to Cl), 7.47 (s, 1H, *meta* to Cl), 6.98 (d, $^3J = 7.5$ Hz, 1H, phenyl H6), 6.83 (dd, $^3J = 7.4$ Hz, $^4J = 1.7$ Hz, 1H, phenyl H3), 6.78 (dd, $^3J = 7.5$, $^4J =$ 1.7 Hz, 1H, phenyl H4), 6.62 (d, $^3J = 7.0$ Hz, 1H, phenyl H5), 5.55 (s, br, 2H, Ar–NH_2); EI/MS: m/z (%): 269.0 (100) [M^+], 234.1, 206.1, 179.0, 161.0, 125.0, 108.0, 80.0.

5.3. 2,3,9,10,16,17,23,24-[Tetrakis (2′-aminophenyl-sulfanyl)]-tetrachloro-substituted-nickel(II) phthalocyanines (**4a**) or 2,3,9,10,16,17,23,24-[tetrakis-(2′-aminophenoxy)]-tetra-chloro-substituted-nickel(II) phthalocyanines (**4b**)

Compound **2a** (0.1 g, 0.35 mmol) or **2b** (0.07 g, 0.26 mmol) were dissolved in 0.2 cm^3 of dry quinoline in a sealed tube. Anhydrous $NiCl_2$ (0.012 g excess) was added to the reaction mixture under nitrogen atmosphere. The mixture was heated and stirred gently at 120 °C for approximately 1 h under nitrogen until the moisture was get rid of the sealed tube and then covered. After, stirring and heating for about another 3 h at 190–195 °C, the mixture was cooled to r.t. Ethanol was added to mixture in order to precipitate the crude product. The filtrated blue product was washed several times with ethanol, acetic acid and then ethanol again to remove unreacted inorganic and organic impurities (i.e. isoindoline derivative intermediates and unreacted metal salts). The crude product was further purified by acidification with HBr gas and then neutralization into the amino compound with aqueous KOH in ethanol medium. Precipitates were collected by suction of the filtrate, washed with methanol and dried in vacuo.

4a: yield 0.031g (30.72%), m.p. > 200 °C. *Anal*. Calc. for $C_{56}H_{32}Cl_4N_{12}S_4Ni$: C, 55.95; H, 2.66; N, 13.98. Found: C, 55.01; H, 2.68; N, 13.76%. IR (KBr disc) ν: 3350–3450 cm^{-1} (Ar–NH_2); ^{1}H NMR ([d_6]-DMSO) δ: 8.02 (s, 1H, *ortho* to Cl), 7.78 (s, 1H, *meta* to Cl), 7.25–6.86 (m, 16H, phenyl 4 × C_6H_4), 5.40 (s, br, 8H, Ar–NH_2).

4b: yield 0.015 g (% 20.1), m.p. > 200 °C. *Anal*. Calc. for $C_{56}H_{32}Cl_4N_{12}O_4Ni$: C, 59.10; H, 2.81; N, 14.76 Found: C, 58.84; H, 2.63; N, 14.30%. IR (KBr disc) ν: 3350–3450 cm^{-1}; ^{1}H NMR ([d_6]-DMSO) δ: 8.10 (s, 1H, C_6H_2, *ortho* to Cl), 7.85 (s, 1H, C_6H_2 *para* to Cl), 7.43–6.80 (m, 16 H, C_6H_4), 5.47 (s, Br, 8H, Ar–NH_2).

5.4. 2,3,9,10,16,17,23,24-[Tetrakis(2′-aminophenyl-sulfanyl)]-tetrachloro-substituted-zinc(II) phthalocyanines (**5a**) or 2,3,9,10,16,17,23,24-[tetrakis-(2′-aminophenoxy)]-tetrachloro-substituted-zinc(II) phthalocyanines (**5b**)

Compound **2a** (0.1 g, 0.35 mmol) or compound **2b** (0.7 g, 0.26 mmol) were dissolved in 0.2 cm^3 of anhydrous quinoline in a sealed tube under nitrogen atmosphere and ~0.017 g (0.18 5 mmol) of $Zn(OCMe)_2$ was added to the mixture. The colour of the mixture immediately turned into green–blue. The mixture was kept under nitrogen at 185–190 °C for 2 h, then the green–blue product was cooled to r.t. The subsequent procedure was carried out the same way as described in **4a** and **4b**.

5a: yield 0.025 g (24.65%), m.p. > 200 °C. *Anal*. Calc. for $C_{56}H_{32}Cl_4N_{12}S_4Zn$: C, 55.67; H, 2.65; N, 13.91. Found: C, 55.21; H, 2.58; N, 13.77%. IR (KBr disc) ν: 3350–3450 cm^{-1}; ^{1}H NMR ([d_6]-DMSO) δ: 8.07 (s, 4H, C_6H_2, *ortho* to Cl), 7.85 (s, 4H, C_6H_2 *meta* to Cl), 7.30–6.84 (m, 16 H, C_6H_4), 5.57 (s, Br, 8H, Ar–NH_2).

5b: yield 0.017 g (22.90%), m.p. > 200 °C. *Anal*. Calc. for $C_{56}H_{32}Cl_4N_{12}O_4Zn$: C, 58.79; H, 2.79; N, 14.69. Found: C, 58.77; H, 2.82; N, 14.28%. IR (KBr disc) ν: 3350–3450 cm^{-1}; ^{1}H NMR ([d_6]-DMSO) δ: 8.17 (s, 4H, C_6H_2, *ortho* to Cl), 7.90 (s, 4H, C_6H_2 *meta* to Cl), 7.45–6.99 (m, 16H, 4 × C_6H_4), 5.65 (s, Br, 8H, Ar–NH_2); MS (FAB): m/z (%): 1143.1 (5) [M]$^+$, 1106.3 (8) [M – Cl]$^+$, 1072 [$M - 2 \times$ Cl]$^+$, 1050 [$M - C_6H_6N$]$^+$, 1033 (2), [$M - C_6H_6NO$]$^+$, 998.1 (3) [$M - C_6H_6NO$ + Cl]$^+$, 958 (3) [$M - 2 \times C_6H_6N$]$^+$, 924 (2.5) [$M - 2 \times C_6H_6NO$]$^+$, 869 (5) [$M - 3 \times C_6H_6N$]$^+$, 777.1 (10) [$M - 4 \times C_6H_6N$]$^+$, 725 (5.5) [$M - 4 \times$ C_6H_6NO]$^+$.

5.5. 2,3,9,10,16,17,23,24-[Tetrakis-(2′-aminophenylsulfanyl)]-tetrachloro-substituted-cobalt(II) phthalocyanines (6a)

Compound **2a** (0.1 g, 0.35 mmol) and anhydrous $CoCl_2$ (0.012 g, 0.083 mmol) were dissolved in 20 cm^3 of anhydrous ethylene glycol in a two round-necked bottomed flask under nitrogen atmosphere. The reaction was continued at 180 °C for approximately 6h. The dark-green–blue product formed during the reaction was poured into ethanol (30 cm^3) after cooling to r.t. to precipitate the desired product. The green–blue product was filtered off and then washed successively with water, ethanol and several times with acetic acid and finally with again ethanol. Further purification was carried out by passing HBr gas through a tetrahydrofuran solution of the product and carefully neutralized with 1 M KOH. The precipitates formed after neutralization were centrifuged, washed with ethanol and dried in vacuo. The compound is soluble in dmf, dmso, quinoline and moderately in thf.

6a: yield 0.012 g (12.07%), m.p. > 200 °C. *Anal.* Calc. for $C_{56}H_{32}Cl_4N_{12}S_4Co$: C, 55.95; H, 2.66; N, 13.98. Found: C, 55.99; H, 2.70; N, 13.44%. IR (KBr disc) ν: 3350–3450 cm^{-1}; MS (FAB) m/z (%): 1202 (5) $[M+1]^+$, 1237.3 (10) $[M+Cl]^+$, 1166.3 (3) $[M-Cl]^+$ 1141.0 (2) $[M-Co-1]^+$, 1132.1 (6) $[M-2\times Cl]^+$, 1113 (7) $[M-C_6H_6N]^+$, 1076.2 (3) $[M-C_6H_6NS]^+$, 1016 (3) $[M-2\times C_6H_6N]^+$, 955 (7) $[M-2\times C_6H_6NS]^+$.

6. Conclusion

The present work introduces the preparation, characterization and electrochemical properties of novel phthalocyanines, which have been peripherally substituted with four 2-aminophenylsulfanyl or 2-aminophenoxy moieties through flexible S- or O-bridges. The design strategy for functional phthalonitriles substituted by the same or different substituents is based on mainly the size and the strength of the base, and the Lewis acidity of the aromatic thiols and phenols used during the reaction. The approach described here allows us to prepare a wide number of novel phthalonitriles and phthalocyanines having mixed substituents on the periphery.

Electrochemical studies indicated that the reduction and oxidation of compounds **4a**, **5b** and **6a** were due to the interaction between the phthalocyanine ring π electron system and the central metal atoms. The voltammograms of **6a** show considerably different and interesting voltammetric behaviors compared to **4a** and **5b**, probably owning to the interaction between the cobalt ions and the platinum electrode. The absorption process occurred for the first oxidation product of the **6a**. Electrode processes of all redox reactions were diffusion controlled (except the ring oxidation of **6a**) with one-electron transfers having succeeded chemical reactions.

Acknowledgements

ÖB is grateful to the Turkish Academy of Science (TUBA). MK thanks the Sakarya University for the Research Fund (SAÜ/2000-013) and Toprak Drug Company for HPLC measurements.

References

[1] J.J. Simon, H.J. Andre, Molecular Semiconductors, Springer, Berlin, 1985.
[2] M.J. Crossley, P.L. Burn, S.J. Langford, J.K. Prashar. J. Chem. Soc., Chem. Commun. (1995) 1991.
[3] M.A. Diaz Garcia, I. Ledoux, J.A. Duro, T. Tores, F. Agullo-Lopez, J. Zyss, J. Phys. Chem. 98 (1994) 8761.
[4] H. Eichhorn, D. Wöhrle, D. Presner, Liquid Cryst. 22 (1997) 643.
[5] D. Lelievre, M.A. Petit, J. Simon, Liquid Cryst. 4 (1989) 707.
[6] G.E. Collins, N.R. Amstrong, J.W. Pankow, C. Oden, R. Brina, C. Anbour, J.-P. Dodelet, J. Vac. Sci. Technol. A 11 (1993) 1383.
[7] I. Rosenthal, in: C.C. Leznoff, A.B.P. Lewer (Eds.), Phthalocyanines: Properties and Applications, vol. 4, VCH, New York, 1996, p. 485.
[8] K.K. Dailey, G.P.A. Yap, A.L. Rheingold, T.B. Rauchfuss, Angew. Chem., Int. Ed. Engl. 35 (1996) 1833.
[9] D. Wöhrle, J. Gitzel, G. Krawczyk, E. Tsuchida, H. Ohno, T. Nishisaka, J. Macromol. Sci. Chem. A 25 (1998) 1227.
[10] D. Wöhrle, D. Meissner, Adv. Mater. 3 (1991) 129.
[11] C.S. Frampton, J.M. O'Conner, J. Retevson, J. Silver, Display (1988) 174.
[12] A. Gürek, V. Ahsen, A. Gül, Ö. Bekaroğlu, J. Chem. Soc., Dalton Trans. (1991) 3367.
[13] M. Kandaz, Ö. Bekaroğlu, Chem. Ber. 135 (1997) 1833.
[14] D. Wöhrle, T. Buck, U. Hündorf, G. Schulz-Ekloff, A. Andreev, Macromol. Chem. 190 (1989) 961.
[15] C. Rager, G. Schmid, M. Hanack, Chem. Eur. J. 5 (1999) 280.
[16] M. Kandaz, Ö. Bekaroğlu, J. Porphyrin Phthalocyanines 3 (1999) 339.
[17] M. Kandaz A. Riza Ozkara, Ö. Bekaroğlu, Monatshefte Chem. 132 (2001) 1013.
[18] S. Dabak, Ö. Bekaroğlu, New J. Chem. 21 (1997) 271.
[19] M. Kimura, T. Hamakawa, K. Hanabusa, H. Shirai, N. Kobayashi, Inorg. Chem. 40 (2001) 4775.
[20] A. Gürek, Ö. Bekaroğlu, J. Porphyrins Phthalocyanines 1 (1997) 67.
[21] A. Gürek, Ö. Bekaroğlu, J. Porphyrins Phthalocyanines 1 (1997) 227.
[22] S. Merey, Ö. Bekaroğlu, J. Chem. Soc., Dalton Trans. (1999) 1.
[23] C.C. Leznoff, A.B.P. Lever, in: C.C. Leznoff, A.B:P. Lever (Eds.), Phthalocyanines: Properties and Applications, vols. 1–4, VCH, Weinheim, 1989–1996.
[24] M. Kandaz, İ. Yılmaz, Ö. Bekaroğlu, Polyhedron 19 (2000) 115.
[25] İ. Yılmaz, Ö. Bekaroğlu, Chem. Ber. 129 (1996) 967.
[26] A.R. Özkaya, A.I. Okur, A. Gül, Ö. Bekaroğlu, J. Coord. Chem. 33 (1994) 311.

[27] A.R. Özkaya, İ. Yılmaz, Ö. Bekaroğlu, J. Porphyrins Phthalocyanines 2 (1998) 483.
[28] A.B.P. Lever, S. Liccocia, P. Minor, B.S. Ramaswamy, S.R. Pickens, K. Magnell, J. Am. Chem. Soc. 103 (1981) 6800.
[29] A.B.P. Lever, P.C. Minor, Inorg. Chem. 20 (1980) 4015.
[30] A.B.P. Lever, Adv. Inorg. Chem. Radiochem. 7 (1965) 27.
[31] A.R. Özkaya, E. Musluoğlu, A. Gül, Ö. Bekaroğlu, J. Chem. Res. (S) (1995) 2721.

PERGAMON

Polyhedron 21 (2002) 265–274

POLYHEDRON

www.elsevier.com/locate/poly

Synthesis and characterisation of dipyridinated magnesium phthalocyaninato(2-) complex

Jan Janczak, Ryszard Kubiak *

W. Trzebiatowski Institute of Low Temperature and Structure Research, Polish Academy of Sciences, 2 Okólna Str., P.O. Box 1410, 50-950 Wroclaw, Okolna 2, Poland

Received 17 July 2001; accepted 19 October 2001

Abstract

A new complex of dipyridinated magnesium phthalocyanine has been synthesised in crystalline form by dissolving magnesium phthalocyanine in pyridine and heating at 160 °C. The crystals are formed during the slow cooling process. $MgPc(py)_2$ crystallises in the monoclinic system, space group $P2_1/c$ with two molecules in a unit cell. The structure was solved by direct and Fourier difference methods and refined by full-matrix least-squares techniques to $R = 0.0462$, $wR = 0.1210$ and $S = 1.012$ for 3856 independent reflections and 242 refined parameters. The magnesium cation coordinates four isoindole nitrogen atoms of the almost planar phthalocyaninato(2-) ligand and axially two nitrogen atoms of pyridine molecules. The coordination polyhedron around the magnesium atom approximates to a tetragonal bypyramid with relatively long bonds between the Mg atom and the axial base ligands. The thermal analysis shows that the crystals of $MgPc(py)_2$ are stable up to ~ 180 °C, at higher temperature the release of pyridine ligands is rapid. The UV–Vis and FT–IR and Raman spectra of $MgPc(py)_2$ are discussed in relation to its structure and compared with the spectral data of magnesium phthalocyanine. © 2002 Elsevier Science Ltd. All rights reserved.

Keywords: Magnesium phthalocyanines; Magnesium complexes; Crystal structures; IR spectroscopy; Raman spectroscopy; UV–Vis spectroscopy

1. Introduction

The chemistry of metallophthalocyaninato complexes (M(II)Pc) has been widely investigated [1]. Interest in these MPc complexes arise from their extensive electrochemical properties that make them useful in several fields where metalophthalocyanines find applications. Especially in the last 20 years, they have been used in industry as sensing elements, visual pigments in display devices, photochemical redox agents in solar conversion and photosensitisers for photodynamic cancer therapy [2–7]. Many of these applications depend on the nature of the metal ion incorporated at the centre of an 18π-electron phthalocyaninato(2-) macroring as well as on their solubility in a wide range solvents [8]. The studies of phthalocyanines in solutions have been hindered by their limited solubility in many solvents. Among of the four coordinate metal(II) phthalocyaninato complexes the magnesium phthalocyanine exhibits the highest solubility, especially in N- or O-donor solvents [9].

In the course of our studies of magnesium phthalocyanine we have stated, based on X-ray single crystal investigations, that in contrast to the metal(II) phthalocyaninato complexes of the metals of the d-block (Mn, Fe, Co, Ni, Cu and Zn) whose structures are stabilised by $4 + 2$ coordination of the central metal ion, MgPc in the crystal form dimerises $(MgPc)_2$ [10]. The dimers of magnesium phthalocyanine are stabilised by $4 + 1$ coordination of the magnesium ion, which is significantly deviated from the N_4-isoindole plane as a result of the intermolecular $Mg\cdots N_{azamethine}$ interaction. Additionally, we have stated that magnesium phthalocyanine in ambient atmosphere is unstable and interacting with the air molecules (O_2 as well as N_2) transforms into complexes with the composition of $(MgPc)_2O_2$ and $(MgPc)_2N_2$ [10,11]. The existence of the dimers in the crystal of magnesium phthalocyanine as subunits fully correlates with the composition of the complexes with

* Corresponding author. Tel.: +48-71-343-5021; fax: +48-71-441029.

E-mail address: kubiak@int.pan.wroc.pl (R. Kubiak).

0277-5387/02/$ - see front matter © 2002 Elsevier Science Ltd. All rights reserved.
PII: S0277-5387(01)00988-3

dioxygen or/and dinitrogen molecules. The formation process of $(MgPc)_2X_2$ (where X = O or N) is reversible and strongly depends on the temperature. This process take place by insertion of O_2 and/or N_2 between Pc planes of the $(MgPc)_2$ moiety, since the deviated magnesium ion from the N_4-isoindole plane with an effective ~ 0.5 positive charge interacts with more electronegative atoms of O_2 or N_2 molecules [12]. Continuing the studies on magnesium phthalocyanine we have obtained a new complex of magnesium phthalocyanine with two additional pyridine molecules, which are axially coordinated to the magnesium ion.

In the present paper, details concerning the synthesis and crystal structure of $MgPc(py)_2$ are described together with its stability, vibrational and electronic properties. Additionally, the relation between five- and six-coordinated magnesium phthalocyaninato(2-) complexes is discussed. Knowledge of the structures of magnesium containing phthalocyanine and its related complexes are of considerable interest because of their relationship to chlorophyll and can aid in the understanding of photosynthesis, spectroscopy and other properties. The complete structure may be useful as the first step for a theoretical study of the excited electronic states of $MgPc(py)_2$.

2. Experimental

2.1. Preparation

The MgPc used for the synthesis of $MgPc(py)_2$ was obtained by the procedure described elsewhere [10]. The single crystals of $MgPc(py)_2$ suitable for X-ray analysis were obtained by the following procedure. About 0.2 g of powder magnesium phthalocyanine was dissolved into 25 ml of twice distilled and dry pyridine. Next, the mixture of MgPc in pyridine was inserted into an evacuated glass ampoule and heated at 160 °C for 3 h. When the MgPc was fully dissolved, the ampoule was slowly cooled (2° h^{-1}) to room temperature (r.t.). During the cooling procedure the parallelepiped violet crystals of $MgPc(py)_2$ in various sizes (0.1–2 mm) were well formed. Elemental analysis was carried out on an energy dispersive spectrometer. *Anal.* Found: C, 72.67; Mg, 3.47; N, 20.08%. Calc. for $(C_{32}H_{16}N_8)$-$Mg(C_5H_5N)_2$: C, 72.58; H, 3.77; Mg, 3.51; N, 20.14%.

2.2. X-ray data collection

A violet single crystal of $MgPc(py)_2$ having dimensions $0.38 \times 0.16 \times 0.12$ mm^3 was used for data collection on a four-circle KUMA KM-4 diffractometer equipped with a two-dimensional area CCD detector. The graphite monochromatised Mo Kα radiation ($\lambda =$ 0.71073 Å) and the ω-scan technique with $\Delta\omega = 0.75°$ for one image were used for data collection. The 960 images for six different runs covering over 90% of the Ewald sphere were performed. Initially the lattice parameters were refined on 165 reflections obtained from 40 images for eight runs with different orientations in the reciprocal space. Finally, the lattice parameters were refined by least-squares methods based on 2250 reflections. One image was monitored as a standard after every 40 images. Integration of the intensities, correction for Lorenz and polarisation effects was performed using KUMA KM-4 CCD software [13]. The face-indexed analytical absorption was calculated using the SHELXTL program system [14], max. and min. transmission factors being 0.988 and 0.962. Three thousand eight hundred and fifty-six independent reflections (a total of 10 855 reflections were integrated, $R_{int} =$ 0.0407) were used for crystal structure solution and refinement.

2.3. Structure solution and refinement

The structure was solved by direct methods using SHELXS-97 program [15]. Fourier maps calculated from the $E \geq 1.8$ gave the positions of the magnesium and most of the nitrogen and carbon atoms of the phthalocyaninato(2-) ring. The remaining non-hydrogen atoms were located successfully by difference Fourier synthesis. Initially, the structure was refined with isotropic thermal displacement parameters. The hydrogen atoms were located from the $\Delta\rho$ maps, but in the final refinement their positions were constrained using HFIX 43 with the isotropic thermal parameters of $1.2U_{eq}$ of the carbon atoms linked directly to the H-atoms. In the final refinement all non-hydrogen atoms were refined anisotropically by full-matrix least-squares methods using the SHELXL-97 program [15]. The final unweighted and weighted agreement factors converged to $R[F^2 > 2\sigma(F^2)] = 0.0464$ and $wR(F^2) = 0.1210$, and the goodness-of-fit calculation resulted in a value of 1.012. The final difference map calculation showed no peaks of chemical significance; the largest were $+0.169$ and -0.191 e Å^{-3}. Scattering factors for neutral atoms and calculations for anomalous dispersion were as in SHELXL-97. Details of the data collection parameters, crystallographic data and final agreement factors are collected in Table 1. Selected bond lengths and angles are given in Table 2.

2.4. Spectroscopic measurements

IR spectra of the solid material (KBr pellets) were recorded at r.t. on a Bruker IFS 113 V FT–IR spectrometer (4000–400 cm^{-1}). The powder Fourier transform (FT) Raman spectrum was taken on a FRA-106 attachment to the Bruker ITS-88 spectrometer. Resolu-

tion was set to 2 cm^{-1}. A diode-pumped Nd^{3+}:YAG laser with a power of about 200 mW was used as the exciting source. Measurements of the electronic spectra were carried out at r.t. using a CARRY VARIAN/5E UV–Vis–NIR spectrometer. The UV–Vis spectra (200–1000 nm) were recorded from solution in pyridine and DMSO in 0.5 cm quartz cells.

2.5. Thermal measurements

Thermal analyses were carried out on a Lineis L81 thermobalance apparatus with Pt crucibles. Powdered Al_2O_3 has been used as a reference. The measurements on several samples have been performed under static air atmosphere on heating from r.t. to 300 °C at the heating rate of 2 °C min^{-1}.

3. Results and discussion

3.1. Synthesis and characterisation

Our preparation method of the single crystals of the dipyridinated magnesium phthalocyanine complex, $MgPc(py)_2$, presented here, is very fast and simple. A mixture of magnesium phthalocyanine with purificated pyridine was heated in an evacuated glass ampoule at 160 °C for 3 h. The molecular orbital calculations predict for the magnesium atom in magnesium porphyrin and related complexes about 0.5 positive charge [12]. This explains why during the heating process the molecule of MgPc interacts by its central magnesium atom with a lone electron pair of the nitrogen atom of the pyridine molecule. This interaction take place on both sides of the MgPc molecule and leads to the formation of the $MgPc(py)_2$ complex. During slow cooling (2° min^{-1}) violet crystals are formed. The first crystals of $MgPc(py)_2$ have been observed at about 140 °C; from this temperature point the cooling process was twice as slow (1° min^{-1}). The obtained crystals of $MgPc(py)_2$ are soluble in pyridine, DMF, DMSO an in other N- and O-donor solvents as well as in aromatic solvents like chloronaphthalene or quinoline. The complex of $MgPc(py)_2$ may also be obtained from a stirred suspension of pure MgPc in purified and dry pyridine at room temperature in approximately 2–3 days. However, at room temperature the complex of $MgPc(py)_2$ is formed only in powdered form. The elemental analysis of the powder product corresponds to the 1:2 adduct.

The crystals of $MgPc(py)_2$ are stable under dry atmosphere, but under conditions of moist atmosphere after several days they transform into a powder form. During this process, the complex of $MgPc(py)_2$ interacts

Table 1
Crystallographic data and final refinement parameters for $MgPc(py)_2$

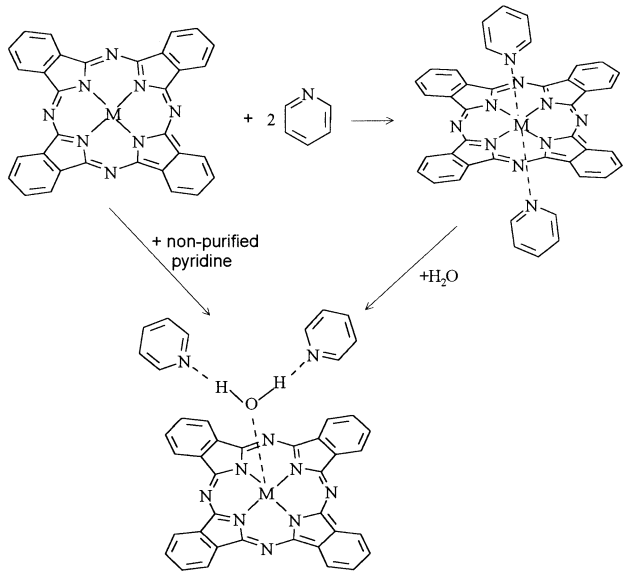
Chemical formula	$C_{42}H_{26}N_{10}Mg$
Molecular weight	695.04
Temperature (K)	298
Crystal system	monoclinic
Space group	$P2_1/c$
Unit cell dimensions	
a (Å)	9.918(2)
b (Å)	19.964(4)
c (Å)	9.141(2)
β (°)	111.89(3)
V (Å^3)	1679.4(6)
Z	2
D_{obs} (measured by flotation) (g cm^{-3})	1.37
D_{calc} (g cm^{-3})	1.374
Absorption coefficient, μ (mm^{-1})	0.102
Radiation, Mo Kα (Å)	0.71073
Reflections collected	10 855
Reflections observed	2274
Independent reflections	3856 ($R_{int} = 0.0407$)
Correction	Lorenz, polarisation, face-indexed analytical absorption, $T_{min} = 0.962$, $T_{max} = 0.988$
Refinement on F^2	
$R[F^2 > 2\sigma(F^2)]$ [a]	0.0462
$wR(F^2$ all reflections) [b]	0.1210
Goodness-of-fit, S	1.012
Residual electron density, $\Delta\rho_{max}$, $\Delta\rho_{min}$ (e Å^{-3})	+0.169, −0.191

[a] $R = \Sigma \||F_o| - |F_c|\| / \Sigma F_o$.
[b] $wR = \{\Sigma [w(F_o^2 - F_c^2)^2] / \Sigma wF_o^4\}^{1/2}$; $w^{-1} = \sigma^2(F_o^2) + (0.0589P)^2$ where $P = (F_o^2 + 2F_c^2)/3$.

Table 2
Selected bond lengths (Å) and angles (°) for $MgPc(py)_2$

Bond lengths			
Mg1–N1	2.006(2)	Mg1–N3	2.007(2)
Mg1–N5	2.376(2)	N1–C1	1.372(2)
N1–C8	1.365(2)	N2–C9	1.342(2)
N2–C8	1.349(2)	C1–C2	1.459(2)
C2–C3	1.378(2)	C2–C7	1.412(2)
C3–C4	1.386(3)	C4–C5	1.388(3)
C5–C6	1.381(3)	C6–C7	1.387(2)
C7–C8	1.455(2)	C9–C10	1.469(2)
C10–C11	1.386(2)	C10–C15	1.402(2)
C11–C12	1.379(3)	C12–C13	1.391(3)
C13–C14	1.383(3)	C14–C15	1.386(2)
C15–C16	1.459(2)	N3–C9	1.367(2)
N3–C16	1.365(2)	N4–C16	1.341(2)
N5–C17	1.336(2)	N5–C21	1.328(2)
C17–C18	1.369(3)	C18–C19	1.368(3)
C19–C20	1.367(3)	C20–C21	1.375(3)
Bond angles			
N1–Mg1–N3	89.37(6)		
N1–Mg1–N3^i	90.63(6)		
N1–Mg1–N5	91.01(5)		
N3–Mg1–N5	89.36(6)		
N1–Mg1–N5^i	88.99(5)		
N3–Mg1–N5^i	90.64(6)		

with water molecules and converts into an hydrated complex according to the equation (see Scheme 1) with the composition $MgPcH_2O{\cdot}2py$. This was proved by elemental analysis and by X-ray powder and single crystal diffraction methods. The speed of the conversion of $MgPc(py)_2 + H_2O \rightarrow MgPcH_2O{\cdot}2py$ takes place several times quicker in the solution of non-purified pyridine. It should be added that in a separate experiment part of the $MgPc(py)_2$ crystals obtained were dissolved in pyridine and then the solution was slowly evaporated to dryness in laboratory air. As a result the well described in the literature $MgPcH_2O{\cdot}2py$ crystals were obtained. Our observations are not only consistent with those observed by Fischer et al. [16] but also explain why they have obtained only the hydrated



Scheme 1.

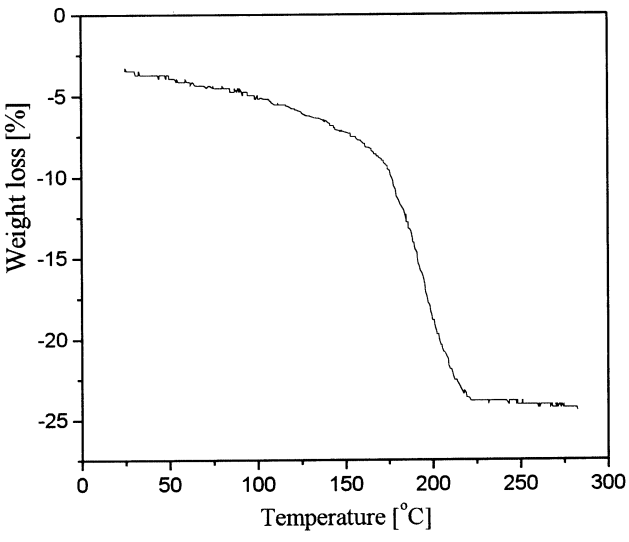


Fig. 1. Thermogram for the complex $MgPc(py)_2$. Speed rate 2 °C min^{-1}.

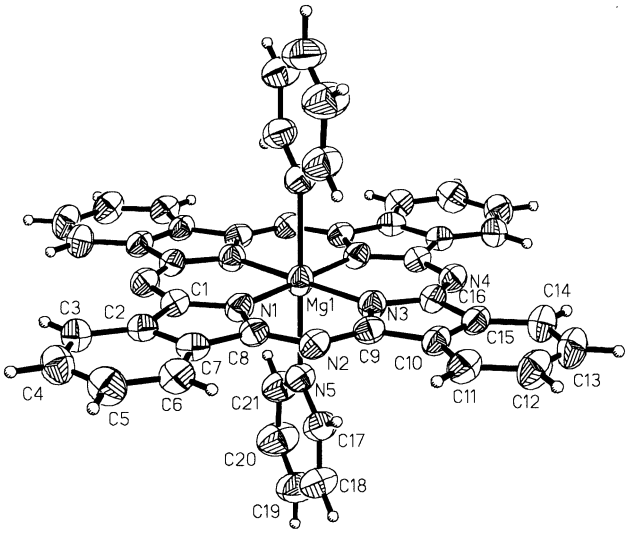


Fig. 2. Molecular structure of the $MgPc(py)_2$ molecule with labelling of the atoms. Displacement ellipsoids are drawn at the 50% probability level.

complex from the air-exposed solution of MgPc in pyridine. Contact of $MgPc(py)_2$ with dilute acids led to demetallation, yielding metal-free phthalocyanine (H_2Pc). As can be seen from the thermogram (Fig. 1) the complex of $MgPc(py)_2$ is relatively stable up to about 180 °C. Above this temperature point the 2 equiv. $Mg–N_{(py)}$ bonds in the complex of $MgPc(py)_2$ break, giving MgPc in crystalline form. Its powder diffraction pattern indicates the β-form. There was no evidence for the formation of the 1:1 adducts (MgPcPy) by thermal dissociation. Similar observations during thermal analysis have been noticed by Cariati et al. [17] for the equivalent cocomplex ($CoPc(py)_2$). However, the $MgPc(py)_2$ complex is much more stable, since the sharp thermal dissociation of both pyridine molecules take place at the temperature about 80 °C higher than in $CoPc(py)_2$.

3.2. Description of the structure

The molecular structure of the centrosymmetric dipyridinated magnesium phthalocyaninato complex is illustrated in Fig. 2. In contrast to the molecular structure of MgPc in which the magnesium cation is significantly displaced (~ 0.5 Å) from the plane defined by four *N*-isoindole atoms of the Pc(2-) ring [10], in this dipyridinated complex the magnesium cation lies closely on the N_4-isoindole plane. The phthalocyaninato(2-) macroring is almost planar. The greatest deviations from the N_4-isoindole plane are observed for the outermost carbon atoms of the phenyl rings; the displacement of C12 and C13 are equal to 0.12(1) and 0.11(1) Å, while C4 and C5 are displaced only by 0.02(1) and 0.03(1) Å, respectively. The two nitrogen atoms of the pyridine molecules are coordinated by

their lone electron pair to the magnesium atom with an effective ~ 0.5 positive charge forming a deformed octahedral complex. The sp^3d^2 hybridisation of the magnesium atom orbitals accommodates six donor nitrogen atoms, four of which are from the phthalocyaninato(2-) macroring and two of which belong to the pyridine molecules. The planes of the pyridine molecules are almost perpendicular to the phthalocyaninato(2-) ring and are positioned above and below this plane. Thus, the coordination polyhedron around the magnesium cation approximates to a tetragonal bipyramid with relatively long bonds between the magnesium atom and the axial base ligands. The four $Mg–N_{iso}$ bonds are shorter and almost equal, while the two axial $Mg–N_{py}$ bonds are longer by ~ 0.37 Å. Thus, the magnesium atom has $4+2$ coordination. A similar correlation between the short and long M–N bonds can be found in the cobalt phthalocyaninato(2-) complex with two axially coordinated molecules of 4-methylpyridine ($Co–N_{iso} \sim 1.94$ and $Co–N_{4Mepy} \sim 2.32$ Å) [18]. In the Co(II) complex with axially coordinated 4-methylpyridine molecules, the longer axial Co–N bond is likely to be due to an unpaired electron which is essentially localised on the d_z^2-orbital of the Co^{2+}. In the absence of this electron, as in an axially coordinated Co(III) porphyrin complex, both axial Co–N bond lengths decreases to ~ 1.94 Å [19]. The strength of the axial M–N bonds in Mg and Co complexes correlate with their stability as was mentioned above. A similar relation between the bonds of Mg–N in plane and perpendicular to the plane can be found in the crystal structures of $4+2$ coordinated porphyrinato(2-) complexes [20–22]. The difference in the Mg–L bond lengths in plane and perpendicular to the plane are significantly smaller in magnesium phthalocyaninato complexes in which the axial ligands are coordinated by oxygen atoms of methanol, water or 2-methoxyenthanol molecules [23–25]. This is likely due to the steric hindrance from the structural environment of the non-bonding contacts, which play an important role in the dipyridinated magnesium phthalocyaninato(2-) complex.

All C–C and C–N bond distances (Table 2) of the phthalocyaninato(2-) ring in $MgPc(py)_2$ are normal in the sense that their values are not very different from the corresponding values found in the various metallophthalocyaninato complexes [26,27]. However, it should be noted that the good accuracy of the present structure determinations and relatively small standard deviations indicate that differences between the average values of $C–N_{iso}$ (1.367(2) Å) and $C–N_{aza}$ (1.343(2) Å) are observable. These differences indicate an accumulation of charge density on the bridged aza-nitrogen atoms as well as on the outer carbon atoms of the pyrrole rings and therefore can be explained by an important electron donation from the free-electron pair of the pyridine nitrogen atom to the magnesium hybrid orbital. A similar correlation between the $C–N_{iso}$ and $C–N_{aza}$ bond lengths can be found in the crystals of other metallophthalocyaninato complexes [28], but no comment was made on this fact.

The orientation of the coordinated pyridine plane relative to the phthalocyaninato(2-) macroring is well described by the torsion angle of N1–Mg1–N5–C17. The rotation of the pyridine ligand around the Mg1–N5 axis would reduce the steric effect, i.e. the non-bonding distances between the carbon or hydrogen atoms of the axial pyridine ligand in *ortho* positions and the atoms of the phthalocyaninato(2-) macrocycle. In particular, if the rotation angle is equal to zero, the pyridine plane is parallel to the Mg1–N1 bond (or the equivalent position rotated by 90° where the pyridine plane is parallel to the Mg1–N3 bond) making the non-bonding C–C distances greater than 3 Å and the C–H distance greater than 2.5 Å. The second orientation (the rotation angle being 45°) makes the axial pyridine ligand plane parallel to the $Mg1–N_{aza}$ axis and reduces the non-bonding distance between the azamethine nitrogen atoms of the Pc(2-) ring and the hydrogen atoms of pyridine molecule in the *ortho* positions. This conformation of $MgPc(py)_2$ is the most stable conformation, since the greatest interactions between the *ortho* H-atoms of pyridine molecules and the N_{aza} atoms of Pc(2-) exist. The intermolecular interactions and crystal packing force present in the crystal makes the rotation angle of the axial pyridine plane have a value of 26.6(2)°. The architectural arrangement of the $MgPc(py)_2$ molecules in the unit cell is illustrated in Fig. 3. The structure is composed of isolated $MgPc(py)_2$ molecules, which form alternating sheets. In one sheet the planes of the Pc(2-) macrorings are parallel to each other while between the sheets the Pc(2-) planes are perpendicular. In one sheet the neighbouring molecules have two overlapping phenyl rings which are separated by about 3.38(2) Å. This value is comparable to the van der Waals distance (~ 3.4 Å) for aromatic carbon atoms and indicates weak interactions between the delocalised π-electron systems [29].

3.3. UV–Vis spectroscopy

Fig. 4 shows the UV–Vis spectra of the dipyridinated magnesium phthalocyaninato(2-) complex in solution in pyridine (a) and in DMSO (b). The experimentally observed electronic bands are collected in Table 3, which also comprises the electronic bands for the vapour-phase absorption spectrum for MgPc as well as those calculated for magnesium phthalocyanine. The UV–Vis spectra of solid and vapour-phase metal(II) phthalocyanines as well as for MgPc have been reported several times [30–34]. In the metal(II) phthalocyaninato(2-) complexes several theoretical calculations

predict five distinct electronic bands in the spectral region between 200 and 800 nm [35–37]. The description of the bands for porphyrin have been labelled as C, L, N, B and Q [32]. We adhere to this convention in explaining our results. The spectra of $MgPc(py)_2$ recorded in both solvents are very similar. However, the electronic bands recorded in DMSO are slightly hypsochromic shifted in relation to the spectrum recorded in pyridine. It is generally known that for a given phthalocyanine its Q-band appears at a shorter wavelength in non-aromatic solvents and at a longer wavelength in aromatic solvents [38]. The Q-band corresponds to the excitation between the HOMO—A_{1g} ground state ($(a_{1u}^2)(\pi)$) and the degenerate LUMO ($e_g(\pi^*)$)—the first excited singlet state which has E_u symmetry, from the ($a_{1u}^1 e_g^1$) configuration. As can be seen from Fig. 4 in both solvents the Q-band of the $MgPc(py)_2$ complex exhibits splitting, which has been mentioned in the literature and labelled as Q_1 and Q_2 [39,40]. The splitting value of the Q-band in $MgPc(py)_2$ is equal to about 65 nm and is likely due to the vibronic coupling in the excited state as suggested in the literature [41–43]. In the spectral region between 550 and 750 nm for the spectra of $MgPc(py)_2$ in both solvents, besides the two distinctly separated Q_1 and Q_2 bands, a shoulder is observed. This shoulder between the Q_1 and Q_2 bands is also observed in the vapour-phase spectrum of magnesium phthalocyanine [32]. The Q_1 and Q_2 bands observed on the $MgPc(py)_2$ spectra are slightly shifted in relation to the MgPc spectrum and can be attributed to the substitution effect of axially coordinated pyridine molecules. The B band region is more complicated. The B (or Soret) band is associated with the excitation between the $1a_{2u}(\pi)$ and the $1e_g(\pi^*)$ states. In addition to the B band, two other bands at lower wavelengths, have been observed. The N band results mainly from a transition $b_{2u}(\pi) \rightarrow e_g(\pi^*)$ while the L band results from a combination of $a_{2u}(\pi) \rightarrow e_g(\pi^*)$ and $b_{2u}(\pi) \rightarrow e_g(\pi^*)$ transitions.

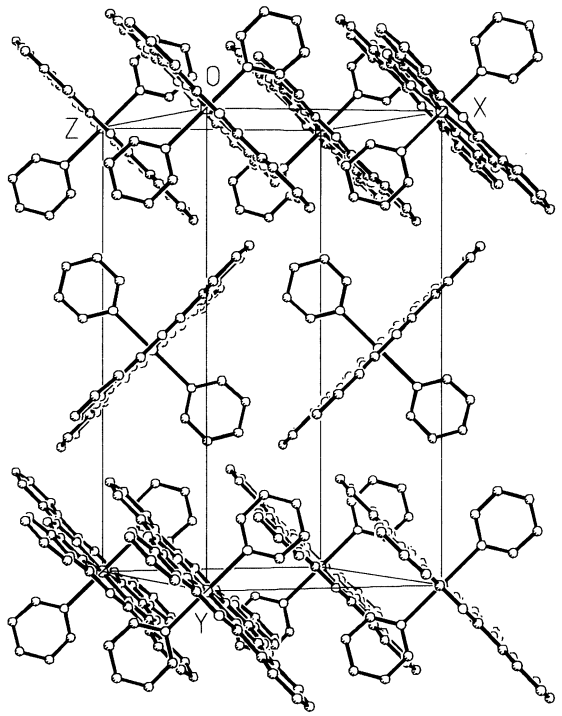


Fig. 3. Arrangement of the $MgPc(py)_2$ molecules in the unit cell.

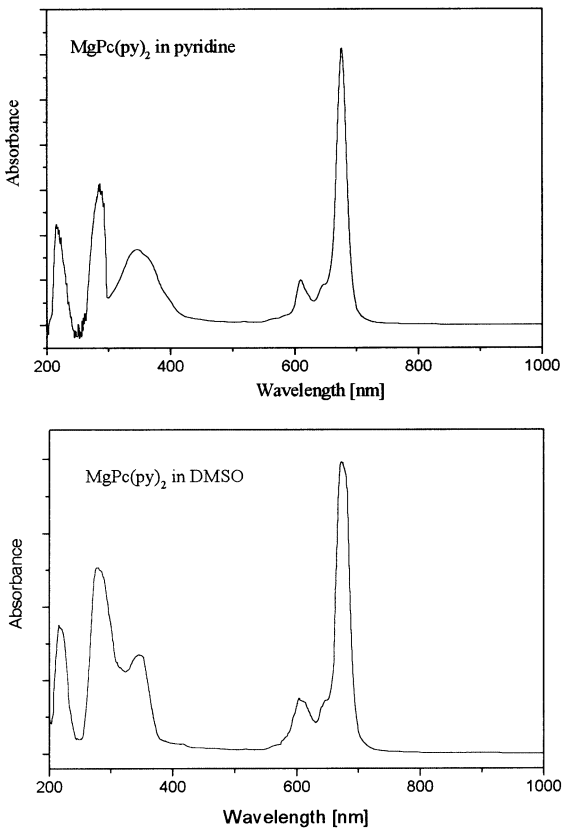


Fig. 4. UV–Vis spectrum of $MgPc(py)_2$ complex in pyridine (a) and in DMSO (b).

3.4. Vibrational spectroscopy

The equilibrium geometry of the $MgPc(py)_2$ molecule can be assumed to have a D_{2h} point group symmetry. Each $MgPc(py)_2$ molecule contains 79 atoms and 231 normal vibrational modes. The number of fundamentals of each irreducible representation are: $\Gamma = 39A_g + 31B_{1g} + 24B_{2g} + 20B_{3g} + 17A_u + 28B_{1u} + 35B_{2u} + 39B_{3u}$. IR active modes include $28B_u + 35B_{2u} + 39B_{3u}$ vibrational fundamentals, while Raman active modes include $39A_g + 31B_{1g} + 24B_{2g} + 20B_{3g}$. Seventeen modes with A_{1u} symmetry are inactive. Despite this large number of vibrational fundamentals the IR and Raman spectra of this dipyridinated magnesium phthalocyanine complex are composed of a small number of fundamentals as shown in Figs. 5 and 6. The positions of the most prominent IR and Raman bands are listed in Tables 4 and 5, respectively. The spectral data of MgPc are also

Table 3
Experimentally observed spectral data for $MgPc(py)_2$ as well as observed and calculated spectral data for MgPc, for a comparison

Compound	*Q*			*B*	*N*	*L*	*C*
$MgPc(py)_2$ in py	676	644	609	350	284		~220
$MgPc(py)_2$in DMSO	672	641	604	345	278		~220
MgPc-vapour phase [32]	666		610	332	280	242	219
MgPc/6-31G** [37]	725			305	257	236	221

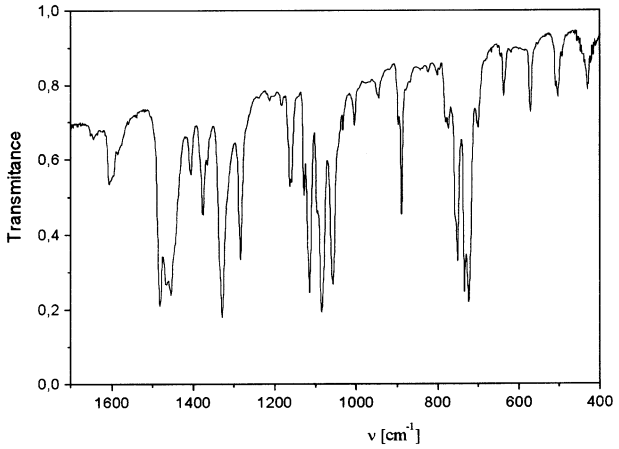


Fig. 5. Infrared spectrum of $MgPc(py)_2$ complex.

listed in the tables for comparison. The vibrational assignment of the observed IR and Raman bands can be discussed in terms of the following groups: vibrations of the macrocycle, isoindole moieties, axial pyridine ligands, C–H bending and magnesium–nitrogen vibrations.

The main IR bands correspond to the characteristic vibrations of the phthalocyanine molecule as well described in the literature for metal-free phthalocyanine and M(II)Pc complexes. In the spectral region 1500–1400 cm^{-1}, the spectrum of $MgPc(py)_2$ shows four slightly overlapped bands at frequencies of 1445, 1456, 1467 and 1482 cm^{-1}, while in the IR spectrum of MgPc in this spectral region only two bands at 1451 and 1479 cm^{-1} are observed [44,45], thus the bands at 1445 and 1467, as suggested Stymme et al. [46], could be attributed to the axially coordinated pyridine molecules. This assignment is also supported by the fact that relative strong intensity bands at about 1436 and 1478 cm^{-1} are observed in the IR spectrum of pyridine and several metallodipyridinated complexes [47]. The bands in the spectrum of $MgPc(py)_2$ at 1215, 1160, 1096 and 1033 cm^{-1} could be attributed to the axially coordinated pyridine molecules, since in this spectral region several other metallodipyridinated complexes have also displayed four bands at about 1215, 1160, 1070 and 1035 cm^{-1} [47]. The spectral region from 900 to 800 cm^{-1} shows two bands; one much more intense at 890 cm^{-1} attributed to a γ(C–H) vibration (also present in the IR spectrum of MgPc) and the second at

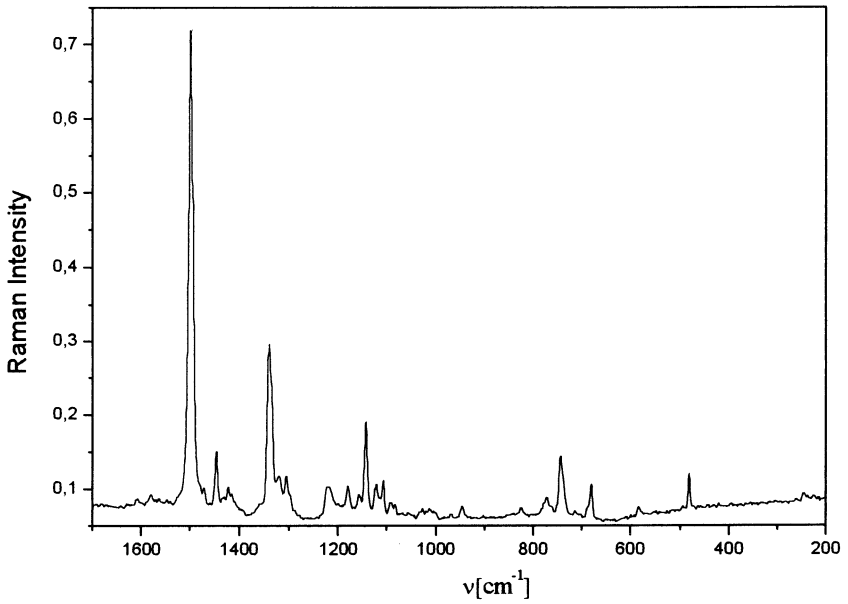


Fig. 6. Raman spectrum of $MgPc(py)_2$ complex.

Table 4
IR spectral data for $MgPc(py)_2$ (in cm^{-1})

$MgPc(py)_2$ [a]	MgPc [44,45]	Assignment
431 (m)	431	ϕ(C–C) macrocycle ring deformation
504 (m)	502	ϕ(C–C) macrocycle ring deformation
572 (m)	571	ϕ(C–C) macrocycle ring deformation
638 (m)	638	ϕ(C–C) macrocycle ring deformation
701 (m)		γ(C–H) in pyridine
724 (vs)	722	γ(C–H) out of plane deformation
734 (s)		γ(C–H) in pyridine
752 (s)		γ(C–H) in pyridine
775 (w)	771	ν(C–N) stretching
890 (m)	890	γ(C–H) out of plane deformation
898 (w)		γ(C–H) out of plane deformation
947 (w)		ν(C–N) in pyridine
1033 (w)	1027	β(C–H) bending in plane and in pyridine
1057 (s)	1058	β(C–H) in plane deformation
1086 (vs)	1082	ν(C–N) stretching in pyrrole
1096 (m)		ν(C–N) in pyridine
1116 (s)	1113	β(C–H) bending in plane
1160 (m)		β(C–H) bending in pyridine
1165 (m)	1163	ν(C–N) in plane
1215 (w)		ν(C–N) in pyridine
1286 (m)	1282	ν(C–N) in isoindole
1330 (s)	1327	ν(C–C) in isoindole
1366 (w)	1361	ν(C–C) in isoindole
1378 (m)		ν(C–C) in pyridine
1407 (m)		ν(C–C) in pyridine
1445 (m)		ν(C–C) in pyridine
1456 (s)	1451	ν(C–C) in isoindole
1467 (s)		ν(C–C) in pyridine
1482 (s)		ν(C–C) in pyridine
1585 (w)	1578	ν(C–C) in pyrrole
1606 (w)	1606	ν(C–C) in pyrrole and benzene

[a] v, very; s, strong; m, medium; w, weak.

898 cm^{-1} is attributed to the C–H out-of-plane vibration of axially coordinated pyridine molecules. In the last region, below 800 cm^{-1}, besides the bands also observed in the spectrum of MgPc ($\sim$775, 724, 638, 572, 504 and 431 cm^{-1}), two intense bands at $\sim$752 and 734 cm^{-1} and one weaker band at 701 cm^{-1} associated with the coordinated pyridine are observed. Comparing the IR spectrum of $MgPc(py)_2$ complex with the spectrum of MgPc we can see that they are very similar, excluding the bands attributed to the axially coordinated pyridine molecules as well as any reduction in vibrational degeneracy of the parent complex.

The most intense Raman band is observed at 1499 cm^{-1}. This band is assigned to the symmetric stretching vibration of the C_β–C_β bonds in the pyrrole groups.

Table 5
Raman vibrational frequencies for $MgPc(py)_2$ (in cm^{-1})

$MgPc(py)_2$ [a]	MgPc [48,49]	Assignment
1582 (w)	1595	(C–C) in benzene and (C–C) in pyrrole
1499 (vs)	1506	(C_β–C_β) pyrrole stretching
1448 (m)	1448	ν(C–N_{aza})
1424 (w)	1423	ν(C–$N_{pyrrole}$)
1341 (s)	1340	ν(C_α–C_β)
1320 (w)		(C–N) in pyridine
1308 (w)	1301	β(C–H) bending
1221 (w)	1216	β(C–H) bending
1181 (w)		β(C–H) bending in pyridine
1156 (w)		β(C–H) bending in pyridine
1143 (m)	1141	Pyrrole breathing
1112 (w)		β(C–H) bending in pyridine
1107 (w)	1106	β(C–H) in plane bending
1024 (w)	1030	β(C–H) in plane bending
947 (w)	945	(C–C) breathing of benzene
827 (w)	827	Macrocycle deformation, ν(C–N) stretching
775 (w)	775	Macrocycle deformation, ν(C–N)
746 (m)	744	Macrocycle deformation
682 (m)	682	Breathing vibration of macrocycle
585 (w)	588	Isoindole ring deformation
482 (m)	481	Isoindole ring deformation
247 (w)	221	Mg–$N_{isoindole}$

[a] v, very; s, strong; m, medium; w, weak.

The corresponding vibration in the Raman spectrum of MgPc complex is observed at 1506 cm^{-1} [48–50]. This assignment is supported by the fact that the corresponding vibration in the Raman spectrum of free indole is observed at 1509 cm^{-1} with a relative strong intensity [51]. In the Raman spectrum of metal-free phthalocyanine two bands are observed in this spectral region (1513 and 1534 cm^{-1}) [52]. The band at 1513 cm^{-1} assigned to the C–N stretching is not observed in the Raman spectrum of metallophthalocyanines [48–50]. Frequencies in the region $\sim$1400 cm^{-1} (1424 and 1448 cm^{-1}) could be attributed to the C–N stretching vibrations. The X-ray crystallographic studies showed that the aza C–N bonds with the average distance of 1.344(3) Å are shorter than the isoindole C–N bonds (average distance of 1.369(3) Å); thereby the stretching vibration of the aza group is expected at higher frequency than the C–N stretching vibration of the isoindole group. Thus, the band at 1448 cm^{-1} should be attributed to the C–N aza stretching vibration and the band at 1424 cm^{-1} to the C–N isoindole stretching vibration. The Raman band at 1341 cm^{-1} is a characteristic feature of the phthalocyaninato ring. It is assigned to the C_α–C_β stretching vibration of the pyrrole groups. This characteristic vibration is also present in the Raman spectrum of indole (at 1352 cm^{-1}) [51]. The breathing stretching vibration of pyrrole groups is ob-

served at 1143 cm^{-1}, while in MgPc it is at 1141 cm^{-1} and the corresponding breathing vibration of the benzene rings is observed at 947 cm^{-1} (for MgPc at 945 cm^{-1}). The Raman bands at 585 and 482 cm^{-1} in the spectrum of $MgPc(py)_2$ could be attributed to the deformation of the isoindole moieties. The equivalent Raman bands in the spectrum of MgPc are observed at 588 and 481 cm^{-1} [48,49]. The C–H in-plane bending vibrations of the isoindole groups are observed at 1024 and 1107 cm^{-1} and in the Raman spectrum of MgPc at 1030 and 1106 cm^{-1}. Similar frequencies are observed in the spectrum of metal-free phthalocyanine [52]. The $Mg–N_{isoindole}$ vibration in the Raman spectrum of $MgPc(py)_2$ is observed at 247 cm^{-1} while in the Raman spectrum of MgPc it is at 221 cm^{-1} [48,49]. A higher frequency value for the dipyridinated magnesium complex than that in MgPc is indicative of a stronger coordination, i.e. a larger force constant value. This relation is fully consistent with the X-ray single crystal structure analysis of $MgPc(py)_2$ described here and the structure of MgPc [10]. The $Mg–N_{isoindole}$ bond length in the $MgPc(py)_2$ complex is shorter (2.006(2)) Å, greater value of the force constant) than in the MgPc complex (2.026(2) Å). The Raman bands at 1320, 1181, 1156, 1112 and 947 cm^{-1} are associated with the vibrations of the axially coordinated pyridine molecules, since they are not observed in the Raman spectrum of MgPc [48,49].

4. Conclusion

Our investigations showed that the dipyridinated magnesium phthalocyanine complex could only be obtained by a solving MgPc in purified and dry pyridine. The crystals of $MgPc(py)_2$ (4 + 2 coordinated complex) are stable under dry atmosphere, while under moist conditions the $MgPc(py)_2$ complex interacts with water molecules and converts into 4 + 1 coordinated complex of $MgPcH_2O{\cdot}2py$, in which the water molecule is apically coordinated to the Mg atom and the pyridine molecules as solvated molecules are involved as acceptors in O–H···N hydrogen bonds. The $MgPc(py)_2$ complex is moderately stable up to about 180 °C. At higher temperatures $MgPc(py)_2$ loses both pyridine molecules and MgPc transforms into β-modification. This observation is in agreement with the vibrational spectroscopic data, which shows that most of the high intensity peaks of free pyridine are also seen with only minor shifts or splittings in the spectrum of $MgPc(py)_2$ complex. This fact indicates that the pyridine molecules are coordinated to the MgPc molecule without forming strong bonds. However, the Mg–N(pyridine) bonds in $MgPc(py)_2$ complex are much stronger than Co–N(pyridine) bonds in the equivalent dipyridinated cobalt phthalocyanine complex, which is stable only up to ~100 °C [17]. Additionally, we have not observed any evidence for the existence of the 1:1 complex (MgPcpy) as was suggested in the literature [45].

5. Supplementary material

Additional material comprising of atomic coordinates, anisotropic thermal parameters, a full list of bond lengths and angles for the $MgPc(py)_2$ complex have been deposited with the Cambridge Crystallographic Data Centre in CIF format as supplementary publications no. CCDC 166120. Copies of this information may be obtained free of charge from The Director, CCDC, 12 Union Road, Cambridge, CB2 1EZ, UK (fax: +44-1223-336033; e-mail: deposit@ccdc.cam.ac.uk or www: http://www.ccdc.cam.ac.uk).

Acknowledgements

This work was supported by a grant (No. 3 T09A 180 19) from the Polish State Committee for Scientific Research.

References

[1] C.C. Leznoff, A.B.P. Lever, Phthalocyanines: Properties and Applications, VCH Publishers, New York, vol. 1, 1989; vol. 2, 1993; vol. 3, 1993; vol. 4, 1996.
[2] (a) R.O. Loufty, A.M. Hor, G. DiPaola-Baranyi, C.K. Hasio, J. Imag. Sci. 29 (1985) 116;
(b) T. Saito, W. Sisk, T. Kobayshi, S. Suzuki, T. Ywayanagi, J. Chem. Soc. 97 (1993) 8026.
[3] J.L. Kahl, L.R. Faulkner, K. Dwarakanath, H. Tichikawa, J. Am. Chem. Soc. 108 (1986) 5434.
[4] (a) M. Hanack, M. Lang, Adv. Mater. 6 (1994) 819;
(b) M. Hanack, H. Heckmann, Eur. J. Inorg. Chem. (1998) 367.
[5] R. Bonnett, Chem. Soc. Rev. 24 (1995) 19.
[6] J. Mizuguchi, C. Rihs, H.R. Karfunkel, J. Phys. Chem. 99 (1995) 16217.
[7] (a) W.S. Chan, J.F. Marshall, G.Y.F. Lam, I.R. Hart, Cancer Res. 48 (1988) 3040;
(b) Q. Peng, J. Moan, J.M. Nesland, C. Remington, Int. J. Cancer 61 (1990) 719;
(c) R.W. Boyle, B. Paquette, J.S. van Lier, Br. J. Cancer 65 (1992) 813;
(d) C.S. Loh, J. Bedwell, A.J. MacRobert, H. Krasner, D. Phillips, S.G. Brown, Br. J. Cancer 66 (1993) 452.
[8] (a) F.H. Moser, A.L. Thomas, Phthalocyanine Compounds, Van Nostrand-Reinhold, Princeton, New York, 1963;
(b) L.J. Buchler, Coordination Chemistry of Macrocyclic Compounds, Plenum Press, New York, 1979.
[9] (a) A.B.P. Lever, Adv. Inorg. Chem. Radiochem. 7 (1965) 27;
(b) K. Kasuga, M. Tsutsui, Coord. Chem. Rev. 32 (1980) 67;
(c) K. Schweiger, M. Göldner, H. Hückstädt, H. Homborg, Z. Anorg. Allg. Chem. 625 (1999) 1693.
[10] J. Janczak, R. Kubiak, Polyhedron 20 (2001) 2901.
[11] R. Kubiak, J. Janczak, K. Ejsmont, Chem. Phys. Lett. 245 (1995) 249.

[12] M. Zerner, M. Gouterman, H. Kobayashi, Theor. Chim. Acta 6 (1966) 363.
[13] KUMA Diffraction, KM-4 CCD User Guide, Wroclaw, 1999.
[14] G.M. Sheldrick, SHELXTL-Program System, Siemens Analytical X-Ray Instruments Inc., Madison, WI, 1990.
[15] G.M.Sheldrick, SHELXTL-97, Program for the Solution and Refinement of Crystal Structures, University of Göttingen, Göttingen, 1997.
[16] M.S. Fischer, D.H. Templeton, A. Zalkin, M. Calvin, J. Am. Chem. Soc. 93 (1971) 2622.
[17] F. Cariati, D. Galizzoli, F. Morazzoni, C. Besetto, J. Chem. Soc., Dalton Trans. (1975) 556.
[18] F. Cariati, F. Morazzoni, M. Zocchi, J. Chem. Soc., Dalton Trans. (1978) 1018.
[19] J.W. Lauher, J.A. Ibers, J. Am. Chem. Soc. 96 (1974) 4452.
[20] R. Bonnett, M.B. Hursthouse, K.M.A. Malik, B. Marteen, J. Chem. Soc. Perkin Trans. 2 (1977) 2072.
[21] V. McKee, Ch.Ch. Ong, G.A. Roodley, Inorg. Chem. 23 (1984) 4242.
[22] M.P. Byrn, C.J. Curtis, Yu. Msiou, S.I. Kahn, P.A. Savin, S.K. Tendick, A. Terzis, C.J. Stouse, J. Am. Chem. Soc. 115 (1993) 9480.
[23] V. McKee, A.G. Roodley, Inorg. Chim. Acta 151 (1988) 233.
[24] A. Endo, S. Matsumoto, J. Mizuguchi, J. Phys. Chem., Sect. A 103 (1999) 8193.
[25] S. Matsumoto, A. Endo, J. Mizuguchi, Z. Kristallogr. 215 (2000) 182.
[26] B. Assmann, G. Ostendorp, G. Lehman, H. Homborg, Z. Anorg. Allg. Chem. 622 (1996) 1085.
[27] H. Hückstädt, Ch. Jaouen, M. Göldner, U. Cornelissen, A. Tutass, H. Homborg, Z. Anorg. Allg. Chem. 626 (2000) 671.
[28] (a) J. Janczak, R. Kubiak, J. Chem. Soc., Dalton Trans. (1993) 3809;
(b) J. Janczak, R. Kubiak, A. Jezierski, Inorg. Chem. 34 (1995) 3505;
(c) J. Janczak, R. Kubiak, F. Hahn, Inorg. Chim. Acta 281 (1998) 195;
(d) J. Janczak, R. Kubiak, Polyhedron 18 (1999) 1621;
(e) J. Janczak, R. Kubiak, J. Richter, H. Fuess, Polyhedron 18 (1999) 2775;
(f) J. Janczak, M. Razik, R. Kubiak, Acta Crystallogr., Sect. C 55 (1999) 359;
(g) J. Janczak, R. Kubiak, A. Jezierski, Inorg. Chem. 38 (1999) 2043;
(h) J. Janczak, R. Kubiak, Inorg. Chem. 38 (1999) 2429;
(i) J. Janczak, R. Kubiak, Polish J. Chem. 73 (1999) 1587;
(j) J. Janczak, R. Kubiak, F. Hahn, Inorg. Chim. Acta 287 (1999) 101;
(k) J. Janczak, R. Kubiak, Inorg. Chim. Acta 288 (1999) 174;
(l) R. Kubiak, J. Janczak, M. Razik, Inorg. Chim. Acta 293 (1999) 155;
(m) J. Janczak, Polish J. Chem. 74 (2000) 157;
(n) J. Janczak, R. Kubiak, I. Svoboda, A. Jezierski, H. Fuess, Inorg. Chim. Acta 304 (2000) 150.
[29] L. Pauling, The Nature of the Chemical Bonds, Cornell University Press, Ithaca, New York, 1960.
[30] D. Eastwood, L. Edwards, M. Gouterman, J. Steinfeld, J. Mol. Spectrosc. 20 (1966) 381.
[31] R.L. Ake, M. Gouterman, Theor. Chim. Acta 15 (1969) 20.
[32] L. Edwards, M. Gouterman, J. Mol. Spectrosc. 33 (1970) 292.
[33] A.M. Schaffer, M. Gouterman, R.E. Davidson, Theor. Chim. Acta 30 (1973) 9.
[34] J. Mack, S. Kirkby, E.A. Ough, M.J. Stillman, Inorg. Chem. 31 (1992) 1717.
[35] A. Henrikson, M. Soundbom, Theor. Chim. Acta 27 (1972) 213.
[36] A. Rosa, E.J. Baerends, Inorg. Chem. 33 (1994) 584.
[37] M.G. Cory, H. Hirose, M.C. Zerner, Inorg. Chem. 34 (1995) 2969.
[38] M.J. Stillman, T. Nykong, in: C.C. Leznoff, A.B.P. Lever (Eds.), Phthalocyanines: Properties and Applications, vol. 1, VCH Publishers, New York, 1989, pp. 133–289.
[39] A.J. McHugh, M. Gouterman, C. Weiss, Theor. Chim. Acta 24 (1972) 346.
[40] W.R. Browett, M.J. Stillman, Inorg. Chim. Acta 49 (1981) 69.
[41] T. Nozawa, N. Kobayshi, M. Hatamo, M. Ueda, M. Sogami, Biochim. Biophys. Acta 626 (1980) 282.
[42] T. Nykong, Z. Gasyna, M.J. Stillman, Inorg. Chem. 26 (1987) 1087.
[43] T.C. VanCott, J.L. Rose, G.M. Misener, B.E. Williamson, A.E. Schrimp, M.E. Boyle, P.N. Schatz, J. Phys. Chem. 93 (1989) 2999.
[44] H.F. Shurvell, L. Pinzuti, Can. J. Chem. 44 (1966) 125.
[45] F.X. Sauvage, M.G. DeBacker, B. Stymne, Spectrochim. Acta, Sect. A 38 (1982) 803.
[46] B. Stymme, F.X. Souvage, G. Wettermark, Spectrochim. Acta, Sect.A 36 (1980) 397.
[47] N.S. Gill, R.H. Nattall, D.E. Scaife, D.W.A. Sharp, J. Inorg. Nuclear Chem. 18 (1961) 79.
[48] C. Jennig, R. Aroca, A.M. Hor, R.O. Loutfy, J. Raman Spectrosc. 15 (1984) 34.
[49] R. Aroca, Z.Q. Zeng, J. Mink, J. Phys. Chem. Solids 51 (1990) 135.
[50] B.J. Palys, D.M.W. Ham, W. Brids, D. Feil, J. Raman Spectrosc. 26 (1995) 63.
[51] A. Lautie, M.F. Lautie, A. Gruger, S.A. Fakhri, Spectrochim. Acta, Sect. A 36 (1980) 85.
[52] R. Aroca, D.P. Dilleia, R.O. Loutfy, J. Phys. Chem. Solids 43 (1982) 707.

PERGAMON

Polyhedron 21 (2002) 275–280

POLYHEDRON

www.elsevier.com/locate/poly

Structural characterization of the 'lantern-shaped' platinum(III) complex $[Pt_2Cl_2\{N(H)C(Bu^t)O\}_4]$

Alessandro Dolmella [a], Francesco P. Intini [b], Concetta Pacifico [b], Giacomo Padovano [c], Giovanni Natile [b,*]

[a] *Dipartimento di Scienze Farmaceutiche, Università degli Studi di Padova, Via F. Marzolo 5, 35131 Padova, Italy*
[b] *Dipartimento Farmaco-Chimico, Università degli Studi di Bari, Via E. Orabona 4, 70125 Bari, Italy*
[c] *Dipartimento di Biologia e Chimica Agro-Forestale ed Ambientale, Università degli Studi di Bari, Via E. Orabona 4, 70125 Bari, Italy*

Received 18 July 2001; accepted 19 October 2001

Abstract

The synthesis of a new platinum(III) 'lantern-shaped' complex with amidate bridging ligands, $[Pt_2Cl_2\{N(H)C(Bu^t)O\}_4]$ (**1**), is described. Complex **1** has been structurally characterized by X-ray diffraction and compared with the related compound $[Pt_2I_2\{N(H)C(Me)O\}_4]$ (**2**). The two complexes exhibit very short N···O bite distances which are similar in the two cases but the Pt(III)–Pt(III) distance is significantly shorter in **1** than in **2**. © 2002 Elsevier Science Ltd. All rights reserved.

Keywords: Platinum(III) compounds; Lantern-type complexes; Amidate bridging ligands; X-ray structure

1. Introduction

Dinuclear platinum(III) complexes represent a topic of intense research not only from a theoretical point of view but also for their potential use in catalysis and biomedicine [1–4].

Starting from the early discovery of elusive platinum-blue materials [5], various types of amides and amidates have been used as terminal and bridging ligands, respectively [6]. In particular, the use of terminal amide ligands allowed the synthesis of the first Pt(III) dimer unsupported by covalent bridges [7,8]. A great number of platinum(III) dimers supported by two amidate bridges has been reported ([1,2] and references therein), in contrast the synthesis of platinum dimers with four bridging amidate ligands proved to be much more difficult and was accomplished only recently. The first fully characterized 'lantern-type' platinum(III) dimer with amidate bridging ligands was $[Pt_2I_2\{N(H)C(Me)O\}_4]$ (**2**) and it contains four acetamidate bridges and two axial iodo ligands [9]. In this paper, we report on the synthesis and X-ray structural characterization of a corresponding complex with chloro ligands in the axial positions, $[Pt_2Cl_2\{N(H)C(Bu^t)O\}_4]$ (**1**), for which the Pt–Pt distance has been found to be even shorter than in the previous case.

2. Experimental

2.1. Synthesis

2.1.1. Preparation of $[Pt_2Cl_2\{N(H)C(Bu^t)O\}_4]$ (1)

K_2PtCl_4 (445 mg) and K_2PtCl_6 (522 mg) were dissolved in water (40 ml) and treated with an excess of pivaloamide (6.30 g). The reaction mixture was kept under stirring for approximately 16 h at 90 °C. A sticky black precipitate separated from the solution. The solution was filtered off keeping the temperature high and the solid residue carefully washed with hot water to remove unreacted pivaloamide. The solid was then extracted with acetone and the solution evaporated to dryness in a rotary evaporator. The solid residue was transferred on a filter, washed twice with small quantities of ether (the washing ether became

* Corresponding author. Tel.: +39-080-544-2774; fax: +39-080-544-2230.
E-mail address: natile@farmchim.uniba.it (G. Natile).

0277-5387/02/$ - see front matter © 2002 Elsevier Science Ltd. All rights reserved.
PII: S0277-5387(01)00992-5

blue in color) and dried. The light-green solid can be crystallized from acetone–water to yield a mixture of yellow and green crystals. The two types of crystals differ for the solvent of crystallization they incorporate, which can be either acetone (one molecule of solvent per molecule of Pt dimer, light green crystals) or water (1.5 molecules of solvent per molecule of Pt complex, yellow crystals). *Anal.* Calc. for $[Pt_2Cl_2\{N(H)C(Bu^t)O\}_4]\cdot COMe_2$, $C_{23}H_{46}Cl_2N_4O_5Pt_2$: C, 30.0; H, 5.0; N, 6.1. Found: C, 30.4; H, 4.9; N, 5.9%.

2.1.2. Preparation of $[Pt_2Cl_2\{N(H)C(Me)O\}_4]$ (3)

K_2PtCl_4 (500 mg) and K_2PtCl_6 (590 mg) (molar ratio 1:1) were dissolved in water (25 ml) and treated with an excess of acetamide (3 g). The reaction mixture was kept under stirring for approximately 6 h at 90 °C. A yellow solid precipitated from the solution. The solution was filtered and the solid residue was carefully washed with water to remove unreacted acetamide, and dried. This product resulted to be insoluble in most solvents and was characterized only by IR and elemental analysis. *Anal.* Calc. for $[Pt_2Cl_2\{N(H)C(Me)O\}_4]\cdot 2H_2O$, $C_8H_{20}Cl_2N_4O_6Pt_2$: C, 13.2; H, 2.8; N, 7.7. Found: C, 12.5; H, 2.3; N, 7.7%. Fedova et al. [10] who first prepared this product by a similar procedure concluded that it had a lantern-shaped structure on the bases of XPS, IR and analytical data. No information about the isomer type was given.

2.1.3. Preparation of $[Pt_2I_2\{N(H)C(Me)O\}_4]$ (2)

This compound was obtained from the previously described chloro-complex by metathesis of the axial ligands. In a typical experiment 0.060 g of the chloro-complex, $[Pt_2Cl_2\{N(H)C(Me)O\}_4]\cdot 2H_2O$, were suspended in 5 ml of water, 0.500 g of KI were added and the reaction mixture heated at 90 °C for about 10 min, meanwhile the color turned red–brown. The filtered mother liquor, kept at 4 °C in a refrigerator, afforded red crystals of the desired compound. *Anal.* Calc. for $[Pt_2I_2\{N(H)C(Me)O\}_4]\cdot 8H_2O$, $C_8H_{32}I_2N_4O_{12}Pt_2$: C, 9.4; H, 3.2; N, 5.5. Found: C, 8.9; H, 2.9; N, 5.3%.

Table 1
Crystal data for $[Pt_2Cl_2\{N(H)C(Bu^t)O\}_4]\cdot 1.5H_2O$

Empirical formula	$C_{20}H_{40}Cl_2N_4O_4Pt_2\cdot 3/2H_2O$
Formula weight (g mol^{-1})	888.66
Wavelength (Å)	1.54178
Crystal system	monoclinic
Space group	$C2/c$
a (Å)	11.364(5)
b (Å)	15.767(7)
c (Å)	18.573(9)
β (°) [$\alpha = 90°$, $\gamma = 90°$]	98.45(7)
V (Å^3)	3292(3)
Z	4
D_{calc} (g cm^{-3})	1.793
Absorption coefficient (mm^{-1})	17.434
$F(000)$	1700
Crystal size (mm)	$0.12 \times 0.08 \times 0.06$
2θ max (°)	60.02
Reflections collected	2625
Independent reflections	1560 ($R_{int} = 0.0377$)
Data/restraints/parameters	1534/0/90
Final R indices [$I > 2\sigma(I)$]	$R_1 = 0.078$, $wR_2 = 0.20$
Goodness-of-fit on F^2	1.056
Largest difference peak and hole (e Å^{-3})	3.109 and −3.631

2.2. X-ray crystal structure determination

2.2.1. $[Pt_2Cl_2\{N(H)C(Bu^t)O\}_4]$

Yellow crystals of **1** were obtained by crystallization from acetone–water. The intensities were collected at 293(2) K on a Philips PW 1100 four-circle diffractometer operating in the θ–2θ scan mode, using Cu Kα monochromatized radiation ($\lambda = 1.54178$). Crystal data for compound **1** are reported in Table 1.

The structure was solved by direct methods, using the SHELXTL NT program [11], completed by subsequent difference Fourier syntheses, and refined by full-matrix least-square procedures on F^2 with the SHELXL-93 program [12]. The platinum, chlorine, O(1) and O(2) atoms were anisotropically refined, while the remaining atoms necessitated isotropic treatment in order to maintain satisfactory thermal displacement parameters. Refinement of the crystal structure was severely hampered by many factors. The crystal batch had inherent handling difficulties, but repeated attempts to obtain higher quality crystals were unsuccessful. The only remotely suitable sample, a very small gem-like block, for a single-crystal structure determination was substandard. The peaks were broad and the diffracting ability of the sample fell off rapidly with increasing Bragg angle and most of the higher angle data collected (up to $\theta = 60°$) were flagged as weak and bore negative intensities. As a consequence of the poor data set (2625 reflections), convergence was inhibited, but improved by omitting reflections with negative intensity from the final refinement cycles. In addition, the crystal was sensitive towards X-rays and decomposed after prolonged irradiation, as shown by the severe decay (up to 40%) in intensity of the three reference reflections throughout the data collection. Moreover, as there were no identifiable faces and no reflections of high intensity at χ approximately 90°, correction for absorption effects was not applied. The final R factor was 0.078, wR_2 was 0.200 and the goodness-of-fit was 1.056 for all 1534 observed ($I > 2\sigma(I)$) reflections, the number of parameters was 90. As expected, the final Fourier-difference map did show four major peaks (up to 3.1 e Å^{-3}), approximately 1.1 Å far from the Pt atom. Although bond distances and angles are affected by relatively high standard deviations, the structural analysis did attain the configuration of the organic ligands attached

Table 2
Selected bond lengths (Å) and angles (°) for $[Pt_2Cl_2\{N(H)C(Bu^t)O\}_4]$

Bond lengths			
Pt–PtA [a]	2.448(2)	Pt–O(2)	2.06(2)
Pt–Cl	2.427(5)	Pt–N(1)	1.97(2)
Pt–O(1)	2.03(1)	Pt–N(2)	2.05(2)
Bond angles			
Cl–Pt–PtA	178.8(1)	Cl–Pt–N(1)	92.2(5)
N(1)–Pt–N(2)	89.2(6)	Cl–Pt–N(2)	91.4(5)
N(1)–Pt–O(1A)	175.2(6)	Cl–Pt–O(1A)	92.6(4)
N(1)–Pt–O(2A)	91.6(6)	Cl–Pt–O(2A)	93.2(4)
N(2)–Pt–O(1A)	90.6(6)	PtA–Pt–N(1)	86.7(5)
N(2)–Pt–O(2A)	175.3(6)	PtA–Pt–N(2)	88.2(5)
O(1A)–Pt–O(2A)	88.2(6)	PtA–Pt–O(1A)	88.5(4)
O(1)–C(1)–N(1)	120(2)	PtA–Pt–O(2A)	87.2(4)
O(2)–C(6)–N(2)	126(2)		

[a] Symmetry operator A: $\frac{1}{2}-x, \frac{1}{2}-y, -z$.

to the platinum centers and selected bond lengths and angles are listed in Table 2.

2.3. Physical measurements

Elemental analyses were obtained by an Elementar Analyzer mod. 1106 Carlo Erba instrument. IR spectra were recorded on a spectrophotometer Perkin–Elmer Spectrum One using KBr pellets, ^1H and ^{195}Pt NMR spectra were recorded on a Bruker Avance DPX 300 WB spectrometer.

3. Results and discussion

3.1. $[Pt_2I_2\{N(H)C(Me)O\}_4]\cdot 8H_2O$

The X-ray crystal structure of **2** was solved by Fedotova et al. [9].

The asymmetric unit included a quarter of complex **2** and two independent water molecules. The two crystallographically independent water molecules were randomly disordered (with a refined occupancy factor of 0.50(5)), and gave rise to a complex network of hydrogen-bonds which serve to stabilize the crystal edifice.

The X-ray study showed one symmetrical isomer for complex **2** and, as a consequence, the ^1H NMR spectrum was expected to exhibit one signal for NH's and one signal for the methyl groups. In contrast, the ^1H NMR spectrum of a sample of **2** prepared by a similar procedure showed four NH's signals at 6.02, 5.62, 5.53 and 5.41 ppm. The intensity ratios between the signals at 6.02, 5.62 and 5.41 ppm were 2:1:1, respectively; moreover this intensity pattern remained constant in different samples in which, however, the intensity of the peak at 5.53 ppm, with respect to the previous set of three signals, had changed. Therefore, it is most likely that the set of three signals belongs to the same compound in which one Pt(III) atom has N_3O coordination of the four bridging amidates and the second Pt(III) atom has NO_3 coordination. For such an asymmetric isomer only two out of the four bridging amides are equivalent and therefore three signals of 2:1:1 intensity ratios, are expected. The fourth signal at 5.53 ppm must belong to a symmetrical isomer having N_2O_2 coordination of the amidates for both Pt(III) units. The presence of two isomers, one symmetrical and one non-symmetrical was confirmed by the ^1H resonances in the region for the methyl groups. Three methyl signals were observed at 2.19, 2.18, and 2.15 ppm. A NOESY spectrum proved that two NH's signals (at 5.62 and 5.53 ppm) couple with the signal at 2.18 ppm, which therefore must be the sum of two separate methyl signals. Therefore, it is possible to assign the signals at 2.19 and 2.15 ppm, and a portion of the signal at 2.18 ppm (intensity ratio between signals at 2.19 and 2.15 ppm of 1:2) to the asymmetric isomer and the remaining portion of the signal at 2.18 ppm to the symmetric isomer.

In principle two types of symmetrical isomers are possible, one with *cis* and one with *trans* geometry. There is no way for distinguishing between the two geometries on the basis of NMR data, but the X-ray structure has shown the geometry to be *cis*.

The ratio between the symmetrical and the non-symmetrical isomers was different for different samples while, for a given sample, the intensity ratios remain constant with time. Therefore, it is possible to conclude that there is no fast interconversion between the two isomers. It is rather surprising that the symmetrical isomer, which is the only one obtained in crystalline form, is generally the less abundant in solution.

The starting chloro-complex **3** from which **2** is obtained by substitution of iodide for chloride, is insoluble in most solvents. Therefore, it is not possible to decide if it is a mixture of different isomers, as shown for **2**, or, alternatively, it is a single isomer which

partially isomerizes during the halide ion metathesis and dissolution processes.

3.2. $[Pt_2Cl_2\{N(H)C(Bu^t)O\}_4]$

Complex **1** crystallizes incorporating molecules of solvent. This can be either acetone (light green crystals, IR absorption band at 1710 cm^{-1}) or water (yellow crystals). The X-ray analysis of the yellow crystals showed the presence of 1.5 molecules of water per molecule of complex.

The asymmetrical unit comprises half a molecule of the diplatinum complex and the structure is generated by the inversion center ($\frac{1}{4}$, $\frac{1}{4}$, 0) at the midpoint of the Pt–Pt bond (Fig. 1). Around the Pt_2Cl_2 stick are located four uninegative ligands, producing the 'lantern-shaped' structure. The Pt–Pt distance (2.448(2) Å) (Table 2) is very short and second only to the Pt(III)–Pt(III) distance observed in the quadruply bridged acetate complex $[Pt_2(H_2O)_2\{OC(Me)O\}_4]^{2+}$ for which the Pt(III)–Pt(III) distance is 2.390(1) Å [13].

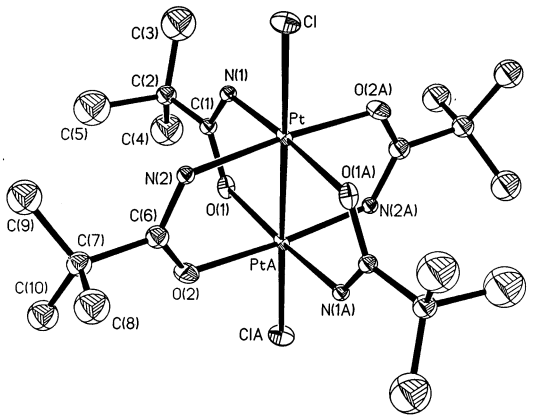


Fig. 1. View of the complex $[Pt_2Cl_2\{N(H)C(Bu^t)O\}_4]$ (**1**). The suffix **A** denotes atom at $\frac{1}{2}-x$, $\frac{1}{2}-y$, $-z$.

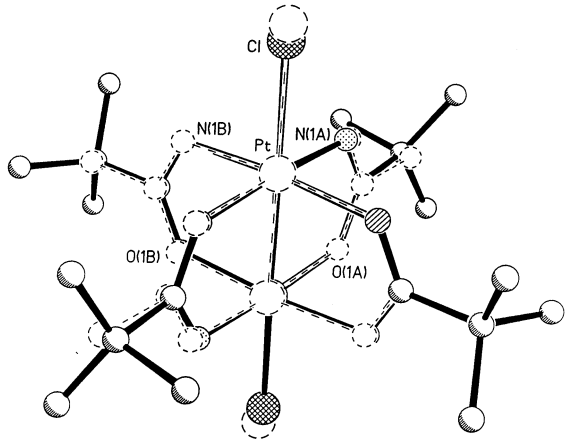


Fig. 2. Superimposition of $[Pt_2Cl_2\{N(H)C(Bu^t)O\}_4]$ and $[Pt_2I_2\{N(H)C(Me)O\}_4]$ complexes.

It is worth noting that the intermetallic distance in Pt(III) dimers is very sensitive to the bite of the covalently bridging ligands, this latter distance can range from 2.94 Å, as in the case of pyrophosphate bridging ligands, to 2.23 Å, as in the case of acetate bridges ([14] and references therein). The N···O bite distance for complexes **1** and **2** (average 2.28(2) Å) is also very short and comparable to that of the acetate ligand (2.26 Å) in $[Pt_2(H_2O)_2\{OC(Me)O\}_4]^{2+}$.

The platinum coordination squares are perfectly eclipsed (maximum twist angle 1.1°) and such a conformation allows the greatest separation between the platinum atoms. The platinum atoms are displaced from the equatorial coordination planes by 0.08 Å towards the axial chlorides, such a displacement being a measure of the strength with which the four bridging ligands pull together the two metal centers. The five-membered Pt–N–C–O–PtA rings (the suffix A denotes the symmetry-related atom at $\frac{1}{2}-x$, $\frac{1}{2}-y$, $-z$) are planar to within 0.01 Å and virtually orthogonal to each other (dihedral angle of 91.9(3)°).

The structures of **1** and **2** are superimposable (Fig. 2), the weighted root mean square deviation being only 0.04 Å when the fitting is performed upon the atoms common to the two structures. In the iodo complex **2** the Pt–Pt distance is slightly longer (2.473(2) Å) than in the chloro-complex **1** (2.448(2) Å), probably as a consequence of the greater *trans* influence of the iodo ligand with respect to the chloro ligand. The bond lengths between each platinum atom and the corresponding axial halogen ligand (2.427 and 2.73 Å for **1** and **2**, respectively) are much longer than analogous bond distances in 4-coordinate platinum(II) and 6-coordinate platinum(IV) complexes (2.32 and 2.61 Å for Cl and I, respectively [7,15]). This lengthening has been ascribed to a very strong *trans* influence exerted by the intermetallic bond on the *trans* halogen ligands.

The molecules of water (1.5 molecules per platinum dimer) fill the empty spaces of the crystal lattice (Fig. 3). Only the water molecule in a special position at $\frac{1}{2}$, y, $\frac{1}{4}$ is engaged in hydrogen bonds (Fig. 4) and its oxygen atom is equidistant (3.22 Å) from the Cl and N(1) atoms (probably a water hydrogen interacts with the axial chloride and the amide hydrogen interacts with the water oxygen).

Green crystals of **1**, containing one molecule of acetone per molecule of complex, can also be obtained. They are hexagonal in shape and the space group and cell parameters are $C2$, $a = 11.389(4)$, $b = 15.810(6)$, $c = 18.549(6)$ Å, $\beta = 98.52(3)°$.

Complex **1** was also investigated by ^1H and ^{195}Pt NMR spectroscopy in $CDCl_3$. Only one signal was observed for the *tert*-butyl groups of the amidate bridges (1.17 ppm), while four signals were observed in the region of NH protons (6.13, 5.81, 5.67 and 5.52 ppm). Intensity ratios of 2:1:1 were observed for three

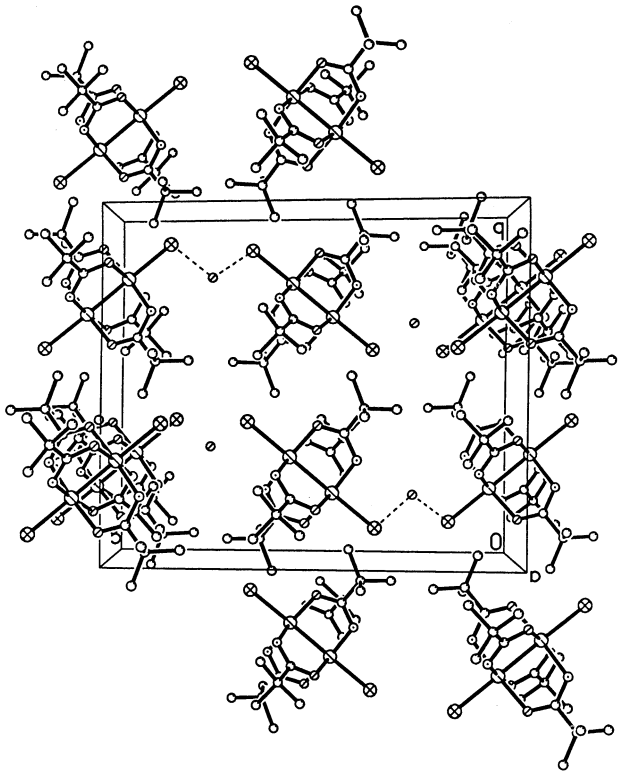


Fig. 3. Packing diagram of the unit cell for $[Pt_2Cl_2\{N(H)C(Bu^t)O\}_4]\cdot 3/2\ H_2O$.

NH's signals (6.13, 5.81 and 5.52 ppm, respectively) while the signal at 5.67 ppm had a much greater intensity. Therefore, also in the case of complex **1**, as already described for complex **2**, two isomers are present in solution: one symmetrical (NH signal at 5.67 ppm) and one non-symmetrical (NH signals at 6.13, 5.81 and 5.52 ppm). In the case of compound **1** the ratio between symmetrical and non-symmetrical isomers observed in various samples was of the order of 4:1, therefore much more in favor of the symmetrical isomer than in the case of compound **2**. The $\{^1H\}^{195}Pt$ spectrum showed a signal at $\delta = -82$ ppm (external reference H_2PtCl_6 in D_2O), the broad shape of this signal is probably due to the coordination to platinum of two N-donor ligands. The observation of only one ^{195}Pt resonance could either indicate a coincidence of chemical shift for the symmetrical and the non-symmetrical isomer, or, more probably, to a too small intensity for the signals of the non-symmetrical isomer which is present in small percentage and has unequivalent platinum atoms. This value of chemical shift falls in the range of those observed for platinum(III) dimers which, however, are spread over a wide range of values spanning from those of platinum(II) to those of platinum(IV) [2].

Also for compound **1**, as already described for **2**, the symmetrical isomer, having N_2O_2 coordination for both Pt(III) centers, has a *cis* configuration as proved by the X-ray analysis (Fig. 1).

4. Supplementary material

Crystallographic data for the structural analysis have been deposited with the Cambridge Crystallographic Data Centre, CCDC No. 149290 for compound **1**. Copies of this information may be obtained free of charge from The Director, CCDC, 12 Union Road, Cambridge, CB2 1EZ, UK (fax: +44-1223-336033; e-mail: deposit@ccdc.cam.ac.uk or www: http://www.ccdc.cam.ac.uk).

Acknowledgements

The authors acknowledge Dr A. Carrieri for X-ray data retrieval. This work was financially supported by the University of Bari, the Ministero della Università e della Ricerca Scientifica e Tecnologica (Cofin. 1998 no. 9803021072). Cooperation within COST chemistry

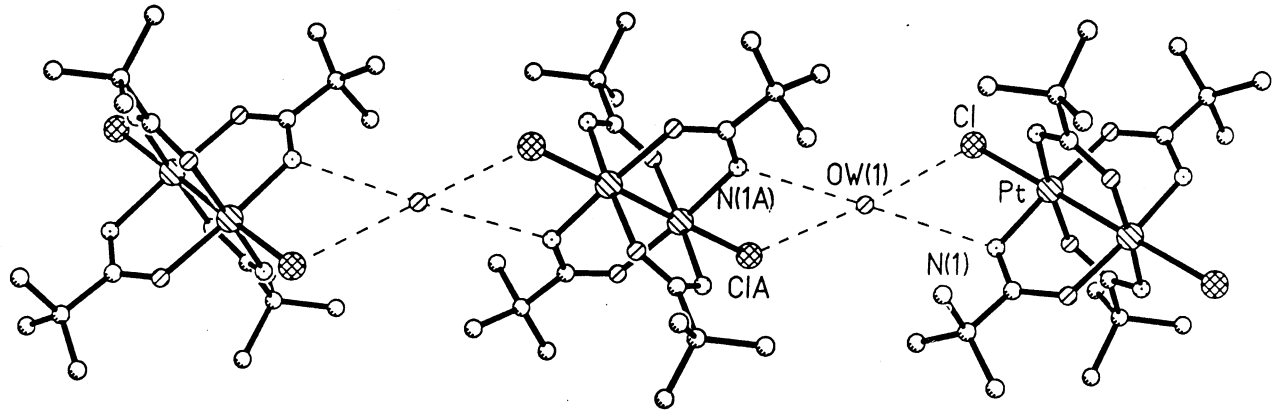


Fig. 4. Drawing of hydrogen bonds between the water molecule in a special position and the dinuclear complex in $[Pt_2Cl_2\{N(H)C(Bu^t)O\}_4]\cdot 3/2H_2O$.

projects D20/001/00 and D20/003/00 is gratefully acknowledged.

References

[1] G. Natile, F.P. Intini, C. Pacifico, in: B. Lippert (Ed.), Cisplatin: Chemistry and Biochemistry of a Leading Anticancer Drug, Verlag Helvetica Chimica Acta, Zurich, Switzerland, and WILEY-WCH, Weinheim, Germany, 1999, 429 pp.
[2] K. Matsumoto, K. Sakai, Adv. Inorg. Chem. 49 (2000) 375.
[3] (a) T.V. O'Halloran, P.K. Marascharak, I.D. Williams, M.M. Roberts, S.J. Lippard, Inorg. Chem. 26 (1987) 1261;
(b) R. Faggiani, C.J.L. Lock, R.J. Pollock, B. Rosemberg, G. Turner, Inorg. Chem. 20 (1981) 804;
(c) K. Matsumoto, H. Miyamae, H. Moriyama, Inorg. Chem. 28 (1989) 2959;
(d) K. Sakai, Y. Tanaka, Y. Tsuchiya, K. Hirata, T. Tsubomura, S. Iijima, A. Bhattacharjee, J. Am. Chem. Soc. 120 (1998) 8366.
[4] (a) G. Cervantes, M.J. Prieto, V. Moreno, Metal Based Drugs 4 (1997) 9;
(b) G.B. Onoa, G. Cervantes, V. Moreno, M.J. Prieto, Nucl. Acid Res. 26 (1998) 1473.
[5] K.A. Hofmann, G. Bugge, Berichte 41 (1908) 312.
[6] (a) L.S. Hollis, S.J. Lippard, J. Am. Chem. Soc. 103 (1981) 6761;
(b) L.S. Hollis, S.J. Lippard, Inorg. Chem. 22 (1983) 2605;
(c) T.V. O'Halloran, M.M. Roberts, S.J. Lippard, Inorg. Chem. 25 (1986) 957;
(d) D.P. Bancroft, F.A. Cotton, Inorg. Chem. 27 (1988) 4022;
(e) E.S. Peterson, D.P. Bancroft, D. Min, F.A. Cotton, E.H. Abbott, Inorg. Chem. 29 (1990) 229;
(f) K. Matsumoto, K. Harashima, Inorg. Chem. 30 (1991) 3032;
(g) T. Abe, H. Moriyama, K. Matsumoto, Inorg. Chem. 30 (1991) 4198;
(h) K. Matsumoto, J. Matsunami, K. Mizuno, H. Uemura, J. Am. Chem. Soc. 118 (1996) 8959.
[7] R. Cini, F.P. Fanizzi, F.P. Intini, G. Natile, J. Am. Chem. Soc. 113 (1991) 7805.
[8] G. Bandoli, P.A. Caputo, F.P. Intini, M.F. Sivo, G. Natile, J. Am. Chem. Soc. 119 (1997) 10370.
[9] T.N. Fedotova, Kh.L. Minacheva, G.N. Kuznetsova, V.G. Sakharova, M.I. Gel'fman, I.B. Baranovskii, Russ. J. Inorg. Chem. 42 (1997) 1838.
[10] T.N. Fedotova, G.N. Kuznetsova, Kh.L. Minacheva, I.B. Baranovskii, Russ. J. Inorg. Chem. 35 (1990) 840.
[11] G.M. Sheldrick, SHELXTL NT, Version 5.10. Bruker axs Inc., Madison, WI, USA, 1999.
[12] G.M. Sheldrick, SHELXL93, Program for the Refinement of Crystal Structures, University of Göttingen, Germany, 1993.
[13] T.G. Appleton, K.A. Byriel, J.R. Hall, C.H.L. Kennard, M.T. Mathieson, J. Am. Chem. Soc. 114 (1992) 7305.
[14] K. Umakoshi, Y. Sasaki, Adv. Inorg. Chem. 40 (1993) 187.
[15] F.P. Fanizzi, F.P. Intini, L. Maresca, G. Natile, C. Pacifico, Acta Crystallogr., Sect. C 55 (1999) 712.

PERGAMON

Polyhedron 21 (2002) 281–286

POLYHEDRON

www.elsevier.com/locate/poly

Alkylaluminium derivatives of 2,2′-di(hydroxymethyl)biphenyl: structural characterization of trinuclear complexes

Wanda Ziemkowska *

Faculty of Chemistry, Warsaw University of Technology, Koszykowa 75, 00-662 Warsaw, Poland

Received 9 August 2001; accepted 31 October 2001

Abstract

Reactions of 2,2′-di(hydroxymethyl)biphenyl with trimethyl-, triethyl- and tri-*iso*-butylaluminium yield tri-aluminium compounds $R_5Al_3(OCH_2C_{12}H_8CH_2O)_2$ [where R = Me (**1**), R = Et (**2**), R = *i*-Bu (**3**)]. Compounds **1**–**3** have been characterized by NMR spectroscopy, molecular weight measurements and elemental analysis. The crystal structures of the complexes **1** and **3** have been determined by X-ray crystallography. The geometry about the central aluminium atom in both compounds is a distorted trigonal-bipyramidal with two oxygen atoms occupying the axial positions. © 2002 Elsevier Science Ltd. All rights reserved.

Keywords: Aluminium; Diols; Trinuclear complexes; 2,2′-Di(hydroxymethyl)biphenyl; Crystal structures; Alkylaluminium diolates

1. Introduction

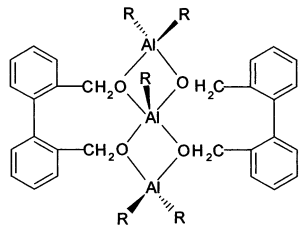
The reaction of alcohols with one equivalent of trialkylaluminium affords mainly dimeric complexes $[(R_2AlOR^1)_2]$ with four-coordinate aluminium atoms [1]. Dimethylaluminium- and diethylaluminium methoxide are trimeric due to the sterically undemanding alkoxide and alkyl ligands [2]. The interaction of carbonyl-, carboxyl-, alkoxyl- and hydroxyl-functionalized alcohols with aluminium trialkyls leads to the formation of a wide variety of organoaluminium O,O′-chelated complexes depending on the reactants molar ratio, the nature of the alkyl substituent R–Al and the nature of the O,O′-bifunctional ligands [3]. The structures of products obtained in the reactions of trialkylaluminium with diols mainly fall into two categories. The first may be characterized as a bimetallic alkylaluminium diolates of the formula $R_4Al_2[diol–(H)]_2$, in which the aluminium centres are four-coordinate and two O*H* protons form intra-molecular hydrogen bonding. Only one example of this group has been recently reported, a *tert*-butylaluminium complex with 2,2-dimethylpropane-1,3-diol [4]. The second category is trimetallic compounds $R_5Al_3[diol–(2H)]_2$ [where R = Me, Et, $CH(SiMe_3)_2$] with two four-coordinate aluminium atoms and one central five-coordinate aluminium atom [5–12]. Numerous examples of similar compounds have been obtained with the salen class of N_2O_2 tetradentate ligands [13]. Although an increasing number of the complexes $R_5Al_3[diol–(2H)]_2$ have been reported, only one example of the crystal structure of a methylaluminium diolate is known for 2,4-dimethylpentane-2,4-diol [10]. Barron et al. has recently reported the structure of *tert*-butylaluminium derivatives of 2,2-dimethylpropane-1,3-diol of the formula $[(t\text{-Bu})_4XAl_3(OCH_2C(CH_3)_2CH_2O)_2]$ [where X = H, Me, Cl] [4]. *iso*-Butylaluminium diolates are unknown. It is, therefore, the goal of this paper to present the crystal structure of methyl- and *iso*-butylaluminium complexes of 2,2′-di(hydroxymethyl)biphenyl. The ethylaluminium derivative has been also synthesised and characterized by spectroscopic methods.

2. Results and discussion

The reaction of three equivalents of R_3Al [where R = Me, Et, *i*-Bu] with two equivalents of 2,2′-di(hydroxymethyl)biphenyl yields trimetallic products [1–3]. The complex **1** is formed almost quantitatively. The complexes **2** and **3** were obtained with yields of about 70 and 50%, respectively.

* Tel.: +48-22-660-7316.
E-mail address: ziemkows@chemix.ch.pw.edu.pl (W. Ziemkowska).

0277-5387/02/$ - see front matter © 2002 Elsevier Science Ltd. All rights reserved.
PII: S0277-5387(01)01004-X



1 (R = Me), **2** (R = Et), **3** (R = *i*-Bu)

The complex **1** was isolated 10 days after the reaction as a colourless crystalline solid. The molecular structure of compound **1** has been determined by X-ray crystallography and is shown in Fig. 1(a). Data collection and structure analysis are presented in Table 1. Selected bond lengths and angles are given in Table 2. The molecule consists of a tetracyclic structure formed from two four-membered and two nine-membered rings. The geometry about the central aluminium atom is a distorted trigonal bipyramidal with O(2) and O(4) occupying the axial positions [O(2)–Al(1)–O(4) = 156.07°] and O(1), O(3) and C(29) defining the equatorial sites (Fig. 1(b)). The sum of the bond angles between the equatorial ligands is 359.98°. Compound **1** is the first alkylalu-

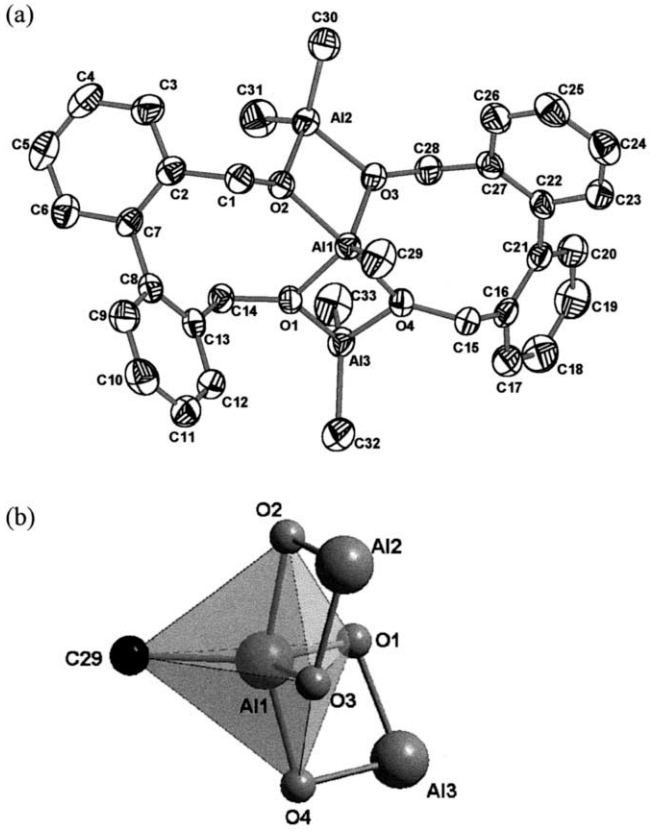


Fig. 1. $[Me_5Al_3(OCH_2C_{12}H_8CH_2O)_2]$ (**1**) (a) molecular structure. Thermal ellipsoids are given at the 50% level and hydrogen atoms are omitted for clarity. (b) View of the coordination sphere of the central aluminium atom showing distorted trigonal bipyramidal geometry with two oxygen atoms occupying the axial positions.

Table 1
Crystal data and data collection parameters for **1** and **3**

	1	**3**
Empirical formula	$C_{33}H_{39}Al_3O_4{\cdot}C_6H_5CH_3$	$C_{48}H_{69}Al_3O_4$
Formula weight	672.72	790.97
Temperature (K)	260(5)	293(2)
Wavelength (Å)	0.71073	0.71073
Crystal system	triclinic	orthorombic
Space group	$P\bar{1}$	*Pbca*
Unit cell dimensions		
a (Å)	12.374(3)	19.521(4)
b (Å)	13.439(3)	20.474(4)
c (Å)	14.647(3)	23.094(5)
α (°)	113.71(3)	90
β (°)	91.55(3)	90
γ (°)	116.68(3)	90
V (Å^3)	1927.5(7)	9230(3)
Z	2	8
D_{calc} (g cm^{-3})	1.159	1.138
Absorption coefficient (mm^{-1})	0.136	0.122
$F(000)$	716	3424
Crystal size (mm)	$0.25\times0.25\times0.30$	$0.30\times0.30\times0.25$
θ Range for data collection (°)	3.29 to 21.00	3.01 to 21.00
Index ranges	$-12\le h\le12$, $-13\le k\le13$, $-14\le l\le14$	$-12\le h\le19$, $-20\le k\le20$, $-23\le l\le23$
Reflections collected	20522	34626
Independent reflections	4123 [$R_{int}=0.0559$]	4942 [$R_{int}=0.1308$]
Refinement method	Full-matrix least-squares on F^2	Full-matrix least-squares on F^2
Data/restraints/parameters	4123/481/463	4942/0/527
Goodness-of-fit on F^2	1.067	1.062
Final R indices [$I>2\sigma(I)$]	$R_1=0.0464$, $wR_2=0.1186$	$R_1=0.0823$, $wR_2=0.1849$
R indices (all data)	$R_1=0.0646$, $wR_2=0.1310$	$R_1=0.1308$, $wR_2=0.2178$
Extinction coefficient	0.0000(17)	0.0000(3)
Largest difference peak and hole (e Å^{-3})	0.204 and −0.230	0.311 and −0.273

Table 2
Bond lengths (Å) and bond angles (°) for $Me_5Al_3(OCH_2C_{12}H_8CH_2O)_2$ (**1**)

Bond lengths			
Al(1)–O(1)	1.854(2)	Al(3)–O(4)	1.820(2)
Al(1)–O(3)	1.858(2)	Al(3)–O(1)	1.834(2)
Al(1)–O(2)	1.921(2)	Al(2)–O(2)	1.816(3)
Al(1)–O(4)	1.928(2)	Al(2)–O(3)	1.836(2)
Bond angles			
O(1)–Al(1)–O(3)	115.36(10)	O(1)–Al(1)–O(2)	90.34(10)
O(3)–Al(1)–O(2)	76.32(9)	O(1)–Al(1)–O(4)	76.33(9)
O(3)–Al(1)–O(4)	91.35(9)	O(2)–Al(1)–O(4)	156.07(10)
O(1)–Al(1)–C(29)	123.78(14)	O(3)–Al(1)–C(29)	120.84(14)
O(2)–Al(1)–C(29)	101.11(13)	O(4)–Al(1)–C(29)	102.82(13)
O(2)–Al(2)–O(3)	79.48(10)	O(4)–Al(3)–O(1)	79.54(9)

minium diolate with a trigonal-bipyramidal geometry at the central atom. The central metal atom of the trinuclear complexes noted in Section 1 adopts a square based pyramidal structure, in which four oxygen atoms occupy the basal sites. The sums of the angles about the O(1), O(2), O(3) and O(4) atoms are equal 358.21°, 356.05°, 359.42° and 358.25°, respectively, which indicates a lack of strain in the nine-membered cycles. The terminal aluminium centres in **1** are coordinated in a distorted tetrahedral fashion by two methyl groups and two oxygen atoms of the diol moiety.

The solvent plays an important role in the crystallisation of product **1**. From hexane and diethyl ether solutions the product precipitates as a powder. Single crystals suitable for X-ray structure analysis were obtained from a toluene solution and one molecule of solvent is present in the formula unit. The toluene molecules show complicated positional disorder. To avoid the loss of toluene from the lattice the X-ray measurement was performed at low temperature.

The CH_2 protons of ligands are inequivalent and appear as a pattern of four doublets in the ^1H NMR spectrum, in contrary to the earlier reported alkylaluminium diolates $Me_5Al_3(OCH_2C_6H_4CH_2O)_2$ [10], $Me_5Al_3[O(CH_2)_3O]_2$, $Me_5Al_3[O(CH_2)_4O]_2$ and Me_5Al_3-$[OCH_2C(CH_3)_2CH_2O]_2$ [9], which possess equivalent OCH_2 groups. The chemically different CH_2 groups of **1** are derived from the molecular structure with two groups below and two groups above the molecular plane.

The ethylaluminium derivative of 2,2′-di(hydroxymethyl)biphenyl **2** was separated by crystallisation from hexane, however, the crystals were unsuitable for X-ray diffraction studies. It was confirmed on the bases of NMR spectra that the structure of **2** is similar to that of complex **1**. The ^1H NMR spectrum reveals the signals of two C_2H_5Al groups *syn* and two C_2H_5Al groups *anti* (the triplets at 1.56 and 0.93, quartet at 0.60 and multiplet at -0.09 ppm) to the ethyl group bonded to the central aluminium atom.

The reaction of $(i\text{-Bu})_3Al$ with 2,2′-di(hydroxymethyl)biphenyl yields the product $[(i\text{-Bu})_5Al_3(OCH_2$-$C_{12}H_8CH_2O)_2]$ (**3**) and unidentified oligomeric products. Compound **3** was separated by crystallisation from hexane–dichloromethane. The molecular structure of **3** is shown in Fig. 2(a) and selected bond lengths and angles are given in Table 3. As with compound **1**, compound **3** consists of a tetracyclic structure with a central pentacoordinated aluminium atom. Also like compound **1**, the geometry at the central atom approximates trigonal bipyramidal with the oxygens O(1) and O(3) occupying the axial positions [O(1)–Al(1)–O(3) = 161.43°] (Fig. 2(b)). The sum of the bond angles between the equatorial ligands O(2), O(4) and C(29) is 360.0°. The oxygen atoms O(1) and O(3) are situated in the planes formed by Al(1), Al(3), C(1) and Al(1),

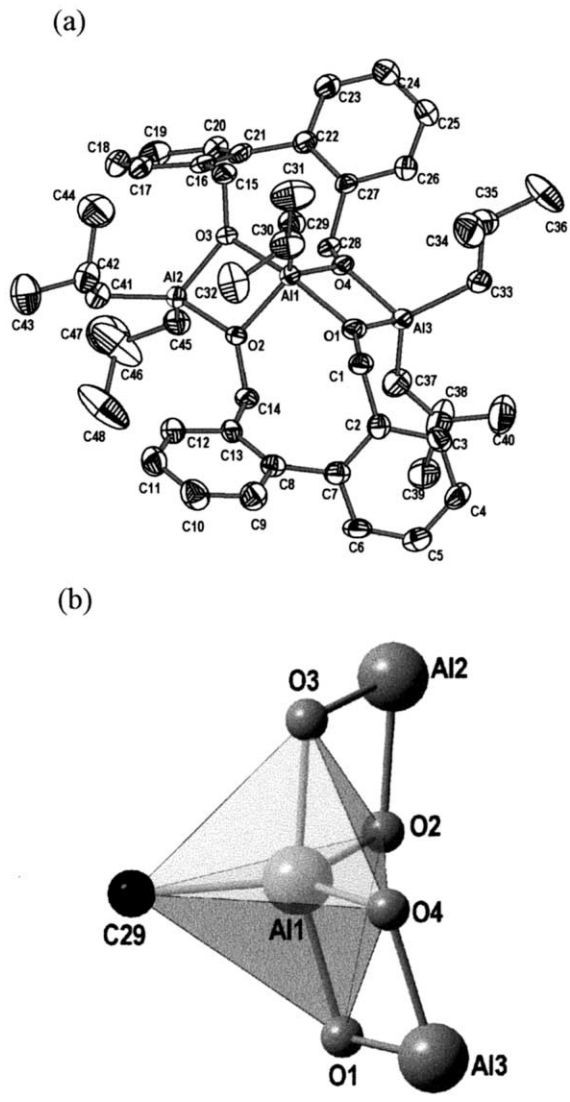


Fig. 2. $[i\text{-}Bu_5Al_3(OCH_2C_{12}H_8CH_2O)_2]$ (**3**) (a) molecular structure. Thermal ellipsoids are given at the 30% level and hydrogen atoms are omitted for clarity. (b) View of the coordination sphere of the central aluminium atom showing distorted trigonal bipyramidal geometry with two oxygen atoms occupying the axial positions.

Table 3
Bond lengths (Å) and bond angles (°) for $i\text{-}Bu_5Al_3$-$(OCH_2C_{12}H_8CH_2O)_2$ (**3**)

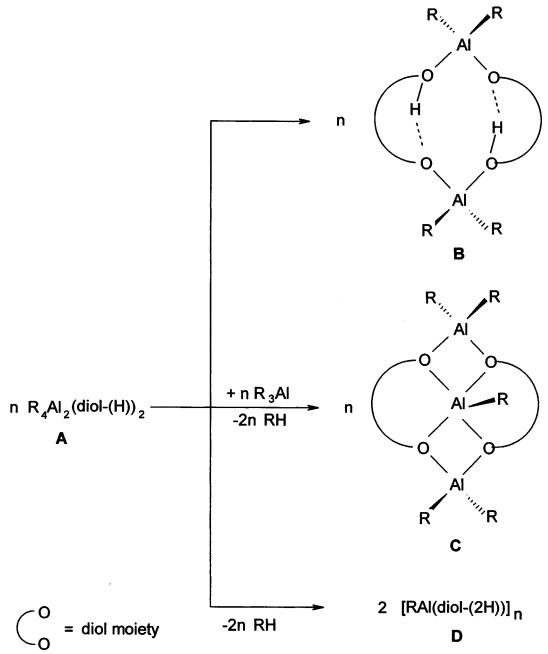
Bond lengths			
Al(1)–O(4)	1.860(4)	Al(1)–O(2)	1.861(4)
Al(1)–O(3)	1.920(4)	Al(1)–O(1)	1.936(4)
Al(1)–C(29)	1.966(7)	Al(2)–O(3)	1.824(4)
Al(2)–O(2)	1.860(4)	Al(3)–O(1)	1.816(4)
Al(3)–O(4)	1.853(4)		
Bond angles			
O(4)–Al(1)–O(2)	111.99(19)	O(4)–Al(1)–O(3)	92.36(17)
O(2)–Al(1)–O(3)	77.03(17)	O(4)–Al(1)–O(1)	76.56(18)
O(2)–Al(1)–O(1)	93.15(18)	O(3)–Al(1)–O(1)	161.43(19)
O(3)–Al(2)–O(2)	79.48(18)	O(1)–Al(3)–O(4)	79.74(19)

Al(2), C(15) atoms, respectively, because the three X–O(1)–Y angles and the three X–O(3)–Y angles sum about 360°. The sums of the angles about the O(2) and O(4) atoms are equal to 354.4° and 352.76°, respectively. It means that the O(2) and O(4) atoms deviate slightly from the C(14), Al(2), Al(1) and C(28), Al(3), Al(1) planes, contrary to the comparable oxygen atoms in compound **1**. The terminal aluminium atoms are coordinated in a highly distorted tetrahedral fashion by two carbons of *iso*-butyl groups and two oxygen atoms of the diol moiety.

Like compounds **1** and **2**, the ^{13}C NMR spectrum of **3** shows two kinds of inequivalent CH_2O groups (signals at 63.30 and 62.70 ppm). In the ^1H NMR spectrum the doublets of $(CH_3)_2CHCH_2$ and $(CH_3)_2CHCH_2$ protons are split, because the methyl groups of the *iso*-butyl substituents are diastereotopic.

Barron et al. have recently proposed the complex $R_4Al_2(diol–(H))_2$ with two intra-molecular hydrogen bonds as an intermediate product in the reactions of diols with trialkylaluminium compounds [4]. The complex might subsequently react with trialkylaluminium yielding the trimetallic product $R_5Al_3(diol–(2H))_2$. However, the bimetallic complex $[(t\text{-Bu})_4Al_2(OCH_2C(CH_3)_2CH_2OH)_2]$ showed low reactivity towards trialkylaluminiums and long heating in refluxing toluene was necessary for the inclusion of the third aluminium atom into the molecule. Alkylaluminium derivatives described above and other earlier reported trinuclear alkylaluminium diolates have been easy obtained in the temperature range from −78 to 20 °C [5–12]. Moreover, the compound $[(t\text{-Bu})_5Al_3(OCH_2C(CH_3)_2CH_2O)_2]$ could not be formed from the reaction of $[(t\text{-Bu})_4Al_2(OCH_2C(CH_3)_2CH_2OH)_2]$ with $(t\text{-Bu})_3Al$, although only little steric interaction was found between the bulky *tert*-butyl substituent on the central metal and diol moieties [4]. On the other hand the reaction of 1,2-catechol with $(t\text{-Bu})_3Al$ smoothly yields the tri-aluminium product $[(t\text{-Bu})_5Al_3(OC_6H_4O)_2]$ [14]. It seems that the first step of the reaction of R_3Al with diol is the formation of the dimeric intermediate product $R_4Al_2(diol–(H))_2$ (**A**) with two hydroxyl groups. Then the strong intra-molecular hydrogen bonding interaction competes with the reaction of OH groups with the excess of R_3Al and inclusion of the third metal atom to give the products **B** and **C**, respectively. Although examples were not found in the literature, the reaction of the hydroxyl groups with the next alkyl groups of the intermediate product and formation of $[RAl(diol–(2H))]_n$ type complexes (**D**) cannot be excluded (Scheme 1). Final products depend on many factors, steric bulk and the nature of R–Al substituents, acidity of O*H* groups, basicity of oxygen atoms from diol moieties and presumably on the substituents on the diol.

In conclusion, trimethyl-, triethyl- and tri-*iso*-butylaluminium react with 2,2′-di(hydroxymethyl)biphenyl to give trimetallic compounds $R_5Al_3(OCH_2C_{12}H_8CH_2O)_2$ [where R = Me (**1**), Et (**2**), *i*-Bu (**3**)]. The formation of the intermediate products with two OH groups and intra-molecular hydrogen bonding was not observed. Further studies on the effects of steric and electron changes in a subunit structure on the molecular and crystal structure of aluminium diolates are in progress.



Scheme 1. Possible reaction pathways and products in the reaction of trialkylaluminiums with diols.

3. Experimental

All manipulations were carried out using standard Schlenk techniques in anhydrous solvents under an inert gas atmosphere. Me_3Al, Et_3Al, $(i\text{-Bu})_3Al$ and 2,2′-di(hydroxymethyl)biphenyl were obtained from Aldrich. ^{27}Al NMR spectra were run on a Varian VXR 300 spectrometer, (standard $Al(acac)_3 = 0.0$ ppm). ^1H NMR spectra were recorded with a Mercury-400BB spectrometer, at 400.09 MHz. Chemical shifts were referenced to the residual proton signal of C_6D_6 (7.15 ppm). ^{13}C NMR spectra were run on the same instrument at 100.60 MHz (standard, benzene $^{13}CC_5D_6$, 128 ppm). The molecular weight of the compounds was determined by cryoscopy in benzene.

3.1. The synthesis of $[Me_5Al_3(OCH_2C_{12}H_8CH_2O)_2]$ (1)

A sample (0.446 g, 6.2 mmol) of Me_3Al in 10 cm^3 of diethyl ether was placed in a 250-cm^3 two-necked flask and cooled to −78 °C. A solution of 0.856 g (4.0 mmol) of 2,2′-di(hydroxymethyl)biphenyl in 100 cm^3 of

diethyl ether was then added drop by drop within 0.5 h. The reaction mixture was allowed to warm to room temperature (r.t.) within 2 h. Evolution of gases was observed during the course of the reaction. All volatiles were then removed from 10 cm^3 of the post-reaction mixture and the residue was characterized by NMR spectroscopy. After the reaction the ^1H and ^{13}C NMR spectra showed a mixture of two isomers **1a** [major product (65%, calculated on the basis of integration of Al–CH_3 signals)] and **1**.

The mixture of **1a** and **1**: ^1H NMR (C_6D_6): δ 6.8–7.8 (16H, H arom.), **1a**: {4.62 (d, ^2J(H–H) = 12.0 Hz), 4.37 (d, ^2J(H–H) = 12.0 Hz), 4.34 (d, ^2J(H–H) = 12.0 Hz), 4.27 (d, ^2J(H–H) = 12.0 Hz) [5.2H, CH_2]}, –0.30 (s, 1.95H, AlCH_3), –0.44 (s, 1.95H, AlCH_3), –0.69 (s, 1.95H, AlCH_3), –0.76 (s, 1.95H, AlCH_3), –1.11 (s, 1.95H, AlCH_3). **1**: {4.56 (d, ^2J(H–H) = 12.0 Hz), 4.43 (d, ^2J(H–H) = 12.0 Hz), 4.26 (d, ^2J(H–H) = 12.0 Hz), 4.22 (d, ^2J(H–H) = 12.0 Hz) [2.8H, CH_2]}, –0.07 (s, 2.1H, AlCH_3), –0.78 (s, 2.1H, AlCH_3), –0.99 (s, 1.05H, AlCH_3). ^{13}C NMR (C_6D_6): δ **1a**: 141.26, 140.44, 137.42, 136.65, 130.41, 130.24, 129.87, 129.02, 128.71, 128.69, 128.18 (*C* aromat.), 66.12, 64.01, (CH_2), –11.50, –11.85 (AlCH_3) ppm, **1**: the signals are the same as for the pure **1** (see below).

Over 10 days compound **1a** undergoes complete transformation to **1**. The solvent and the slight excess of Me_3Al were distilled off and the pure product **1** was obtained (yield 1.00g, 95%). X-ray quality, colourless crystals were crystallised from toluene.

1: ^1H NMR (C_6D_6): δ 6.8–7.8 (16H, H arom), 4.56 (d, ^2J(H–H) = 12.0 Hz), 4.43 (d, ^2J(H–H) = 12.0 Hz), 4.26 (d, ^2J(H–H) = 12.0 Hz), 4.22 (d, ^2J(H–H) = 12.0 Hz) [8H, CH_2], –0.07 (s, 6H, AlCH_3), –0.78 (s, 6H, AlCH_3), –0.99 (s, 3H, AlCH_3). ^{13}C NMR (C_6D_6): δ 141.20, 139.38, 138.03, 136.35 130.50, 130.07, 129.82, 128.96, 128.52, 128.49, 128.15 (*C* aromat.), 62.98, 61.84 (CH_2), –9.32, –10.30 (AlCH_3, broadened). ^{27}Al NMR (C_6D_6): δ 150 (Al four-coordinate), 57 Al five-coordinate) ppm. Molecular weight. *Anal.* Found: 600. Calc.: 580. Association degree: 1.03. Elemental *Anal.* Found: Al, 14.07; hydrolysable methyl groups, 12.52. Calc.: Al., 13.97; Me, 12.93 wt.%.

3.2. The synthesis of $[Et_5Al_3(OCH_2C_{12}H_8CH_2O)_2]$ (2)

Compound **2** was obtained as described in Section 3.1 using 0.856 g (4.0 mmol) of 2,2′-di(hydroxymethyl)biphenyl and 0.707 g (6.2 mmol) of Et_3Al. The solvent was removed under vacuum and the solid precipitated from hexane–methylene dichloride solution in the freezer (0.923 g, yield 71%). ^1H NMR (C_6D_6): δ 6.90–7.76 (16H, H arom.), 4.66 (2H, d, ^2J = 12.8 Hz, CH_2), 4.47 (2H, d, ^2J = 11.6 Hz, CH_2), 4.35 (2H, d, ^2J = 12.8 Hz, CH_2) 4.24 (2H, d, ^2J = 11.6 Hz, CH_2), 1.56 (6H, t, CH_3CH_2Al), 0.93 (6H, t, CH_3CH_2Al), 0.87 (3H, t, CH_3CH_2Al), 0.60 (4H, q, CH_3CH_2), –0.09 (4H, m, CH_3CH_2), –0.30 (2H, m, CH_3CH_2). ^{13}C NMR (C_6D_6): δ 141.08, 139.42, 137.83, 136.43, 130.51, 130.22, 130.09, 129.91, 129.06, 128.65, 128.46, 128.29 (*C* arom.), 63.16, 62.35 (CH_2), 9.59, 9.52, 9.05 (CH_3CH_2), 0.46, –0.14, –2.71 (CH_3CH_2). Molecular weight. *Anal.* Found: 655. Calc.: 650. Association degree: 1.00. Elemental *Anal.* Found: Al, 12.17; hydrolysable ethyl groups, 22.42. Calc.: Al., 12.46; Et, 22.31 wt.%.

3.3. The synthesis of $[(i\text{-}Bu)_5Al_3(OCH_2C_{12}H_8CH_2O)_2]$ (3)

Compound **3** was obtained as described in Section 3.1 using 1.070 g (5.0 mmol) of 2,2′-di(hydroxymethyl)biphenyl and 1.544 g (7.8 mmol) of $(i\text{-}Bu)_3Al$. The solvent was distilled off and a thick colourless liquid was obtained. The crude material was redissolved in hexane–methylene dichloride and placed in freezer. X-ray quality, colourless crystals were formed with the yield 0.948 g, 48%.

^1H NMR (C_6D_6): δ 7.91 (d, 2H ^3J(H–H) = 7.8 Hz, *H* aromat.), 7.61 (d, 2H ^3J(H–H) = 7.6 Hz, *H* aromat.), 7.30 6.90 (m, 12H, *H* aromat.) 4.79 (d, 2H, ^2J(H–H) = 12.8 Hz, CH_2O), 4.63 (d, 2H, ^2J(H–H) = 12.8 Hz, CH_2O), 4.62 (d, 2H, ^2J(H–H) = 11.7 Hz, CH_2O) 4.38 (d, 2H, ^2J(H–H) = 11.7 Hz, CH_2O), 2.38 (m, 2H, $(CH_3)_2CHCH_2$), 1.63 (m, 2H, $(CH_3)_2CHCH_2$), 1.55 (m, 1H, $(CH_3)_2CHCH_2$), 1.37 (d, 12H, ^3J(H–H) = 6.4 Hz, $(CH_3)_2CHCH_2$), 0.92, 0.90 [(d, ^3J(H–H) = 6.4 Hz), (d, ^3J(H–H) = 6.4 Hz), (12H, $(CH_3)_2CHCH_2$)], 0.72 (m, 6H, $(CH_3)_2CHCH_2$), 0.71 (d, 4H, ^3J = 6.6 Hz, $(CH_3)_2CHCH_2$)), –0.03 (m, 4H, $(CH_3)_2CHCH_2$), –0.20 (m, 2H, $(CH_3)_2CHCH_2$). ^{13}C NMR (C_6D_6): δ 141.23, 139.54, 137.43, 136.16, 130.92, 130.69, 130.58, 130.31, 129.18, 128.60, 128.44, 128.54 (*C* aromat.), 63.30, 62.70 (CH_2O), 29.03, 28.72, 25.65 (($CH_3)_2CHCH_2$), 27.94, 26.53, 22.94 (($CH_3)_2CHCH_2$), 20.07 (($CH_3)_2CHCH_2$, broad) ppm. Molecular weight. *Anal.* Found: 779. Calc.: 790. Association degree: 0.99. Elemental *Anal.* Found: Al, 10.02; hydrolysable *iso*-butyl groups, 36.24. Calc.: Al, 10.25; *i*-Bu, 36.08 wt.%.

3.4. X-ray crystal structure analysis

Crystal data regarding structures **1** and **3** are given in Table 1. All measurements of crystals were performed on a Kuma KM4CCD κ-axis diffractometer with graphite-monochromated Mo Kα radiation. The crystals were positioned at 65 mm from the KM4CCD camera. For compound **1** 748 frames were measured at 1.7° intervals with a counting time of 15 s. For compound **3** 288 frames were measured at 1.6° intervals with a counting time of 15 s. The data were corrected for Lorentz and polarization effects. No absorption correction was applied. Data reduction and analysis

were carried out with the Kuma Diffraction (Wroclaw) programs. The structure was solved by direct methods [15] and refined using SHELXL [16]. All hydrogen atoms were located from a differential map and refined isotropically. Scattering factors were taken from Tables 6.1.1.4 and 4.2.4.2 in Ref. [17].

4. Supplementary material

Crystallographic data for the structural analysis have been deposited with the Cambridge Crystallographic Centre, CCDC Nos. 161314 and 161315 for compounds **1** and **3**, respectively. Copies of this information may be obtained free of charge from The Director, CCDC, 12 Union Road, Cambridge, CB2 1EZ, UK (fax: +44-1233-336-033; e-mail: deposit@ccdc.cam.ac.uk or www: http://www.ccdc.cam.ac.uk).

References

[1] (a) E.G. Hoffmann, Trans. Faraday Soc. 58 (1962) 642;
(b) T. Mole, Aust. J. Chem. 19 (1966) 373;
(c) E.A. Jeffrey, T. Mole, J.K. Saunders, Aust. J. Chem. 21 (1968) 649;
(d) H. Schmidbaur, J. Organomet. Chem. 1 (1963) 28;
(e) H. Schmidbaur, F. Schindler, Chem. Ber. 99 (1966) 2178;
(f) P.J. Whetley, J. Chem. Soc. (1963) 2562;
(g) A.V. Grosse, J.M. Mavity, J. Org. Chem. 5 (1940) 106;
(h) K.B. Starowieyski, J. Organomet. Chem. 31 (1971) 149;
(i) H. Fujii, Macromol. Chem. 82 (1965) 32;
(j) H. Yasuda, J. Organometal. Chem. 49 (1973) 103;
(k) H. Yasuda, J. Polym. Sci., Polym. Ed. 11 (1973) 1421;
(l) S. Pasynkiewicz, K.B. Starowieyski, M. Skowrońska-Ptasińska, J. Organomet. Chem. 52 (1973) 269;
(m) R.M. Owens, J. Organomet. Chem. 55 (1973) 237;
(n) R. Benn, A. Rufińska, H. Lehmkuhl, E. Janssen, C. Krüger, Angew. Chem., Int. Ed. Engl. 22 (1983) 779;
(o) R. Benn, E. Janssen, H. Lehmkuhl, A. Rufińska, K. Angermund, P. Betz, R. Goddard, C. Krüger, J. Organomet. Chem. 411 (1991) 37;
(p) J.H. Rogers, A.W. Apblett, W.M. Cleaver, A.N. Tyler, A.R. Barron, J. Chem. Soc. Dalton Trans. (1992) 3179.

[2] (a) R. Tarao, Bull. Chem. Soc. Jpn. 39 (1966) 725;
(b) T. Hirabayashi, J. Organomet. Chem. 35 (1972) 19;
(c) C.A. Tolman, Chem. Rev. 77 (1977) 313;
(d) E.G. Hoffman, Liebigs Ann. Chem. 629 (1960) 104;
(e) N. Davidson, H.C. Brown, J. Am. Chem. Soc. 64 (1942) 316;
(f) D.A. Drew, A. Haaland, J. Weidlein, Z. Anorg. Allg. Chem. 398 (1973) 241.

[3] (a) J.A. Francis, C.N. McMahon, S.G. Bott, A.R. Barron, Organometallics 18 (1999) 4399;
(b) J.A. Francis, S.G. Bott, A.R. Barron, J. Organomet. Chem. 597 (2000) 29;
(c) U. Heinz, K. Hegetschweiler, P. Acklin, B. Faller, R. Lattmann, H.P. Schnebli, Angew. Chem, Int. Ed. 38 (1999) 2568;
(d) B.-T. Ko, F.-C. Wang, Y.-L. Sun, C.-H. Lin, C.-C. Lin, C.-Y. Kuo, Polyhedron 17 (1998) 4257;
(e) T.-L. Yu, C.-H. Huang, L.-F. Yang, B.-T. Ko, C.-C. Lin, J. Chin. Chem. Soc. 47 (2000) 1185;
(f) C.-H. Lin, B.-T. Ko, F.-C. Wang, C.-C. Lin, C.-Y. Kuo, J. Organomet. Chem. 575 (1999) 67;
(g) J. Lewiński, J. Zachara, B. Mańk, S. Pasynkiewicz, J. Organomet. Chem. 454 (1993) 5;
(h) J. Lewiński, J. Zachara, I. Justyniak, Organometallics 16 (1997) 3859;
(i) J. Lewinski, I. Justyniak, Z. Ochal, J. Zachara, J. Chem. Soc., Dalton Trans. (1999) 2909;
(j) J. Lewinski, J. Zachara, I. Justyniak, Chem. Commun. (1997) 1519;
(k) J. Lewiński, P. Goś, T. Kopeć, J. Lipkowski, R. Luboradzki, Inorg. Chem. Commun. 2 (1999) 374.

[4] C.N. McMahon, S.J. Obrey, A. Keys, S.G. Bott, A.R. Barron, J. Chem. Soc., Dalton Trans. (2000) 2151

[5] W. Ziemkowska, S. Pasynkiewicz, R. Anulewicz-Ostrowska, M. Fraczak, Main Group Metal Chem. 23 (2000) 169.

[6] S. Pasynkiewicz, W. Ziemkowska, J. Organomet. Chem. 423 (1992) 1.

[7] S. Pasynkiewicz, W. Ziemkowska, J. Organomet. Chem. 437 (1992) 99.

[8] W. Ziemkowska, S. Pasynkiewicz, E. Kalbarczyk, J. Organomet. Chem. 465 (1994) 93.

[9] W. Ziemkowska, S. Pasynkiewicz, J. Organomet. Chem. 508 (1996) 243.

[10] W. Ziemkowska, S. Pasynkiewicz, T. Głowiak, J. Organomet. Chem. 562 (1998) 3.

[11] W. Ziemkowska, S. Pasynkiewicz, T. Skrok, Main Group Metal Chem. 21 (1998) 105.

[12] W. Uhl, R. Gerding, A. Vester, J. Organomet. Chem. 513 (1996) 163.

[13] D.A. Atwood, M.J. Harvey, Chem. Rev. 101 (2001) 37.

[14] W. Ziemkowska, Main Group Metal Chem. 23 (2000) 389.

[15] G.M. Sheldrick, Acta Crystallogr., Sect. A 46 (1990) 467.

[16] G.M. Sheldrick, SHELXL-93. Program for the Refinement of Crystal Structures, University of Göttingen, Germany.

[17] A.J.C. Wilson (Ed.), International Tables for Crystallography, vol. C, Kluwer, Dordrecht, 1992.

PERGAMON

Polyhedron 21 (2002) 287–293

POLYHEDRON

www.elsevier.com/locate/poly

Structures and catalytic properties of triphenylphosphine oxide complexes of scandium and lanthanide triflates

John Fawcett [a], Andrew W.G. Platt [b,*], David R. Russell [a]

[a] *Department of Chemistry, University of Leicester, Leicester, LE1 7RH, UK*
[b] *School of Sciences, Staffordshire University, College Road, Stoke-on-Trent, ST4 2DE, UK*

Received 15 August 2001; accepted 6 November 2001

Abstract

The complexes $M(OTf)_3(Ph_3PO)_4$ where M = lanthanide metals and scandium have been prepared and characterised in the solid state by single crystal X-ray diffraction, infrared spectroscopy and elemental analysis. All the complexes have the ionic structure $[M(OTf)_2(Ph_3PO)_4]^+[OTf]^-$. Single crystal X-ray structures for M = Sc, Nd and Lu are reported. In the complexes of the early lanthanides (La–Nd) the metals are seven-coordinate with one monodentate, one bidentate triflate. The smaller lanthanide ions, and scandium, have six-coordinate structures with an approximate octahedral coordination about the metal where both triflates are bound as monodentate ligands. The solution structures have been analysed by electrospray mass spectrometry, which indicates that extensive ligand redistribution occurs. The complexes catalyse the Friedel Crafts acylation, alkenylation and alkylation of activated aromatics with modest increases in selectivity compared to the same reactions using scandium triflate. © 2002 Elsevier Science Ltd. All rights reserved.

Keywords: Triflates; Triphenylphosphine oxide complexes; Single crystal X-ray diffraction; Scandium and lanthanide; Catalysis

1. Introduction

Scandium and lanthanide triflates have been extensively studied as catalysts for a variety of organic reactions in protic [1,2] and aprotic [1,3] media, and the use of $Yb(OTf)_3$ and $Sc(OTf)_3$ in particular as water tolerant Lewis acid catalysts continues to attract considerable interest.

The coordination complexes of lanthanide triflates with Ph_3PO have previously been investigated in the solid state by infrared and electronic spectroscopy and elemental analysis, and in solution by conductivity [4]. No structural data for these compounds were reported.

Coordination complexes might be expected to display lower catalytic activity than the triflates themselves as the metal ion will be less available to the substrates in the reaction. This may be compensated to some extent if the resulting catalysts were more selective. Previous studies on the catalysis of Diels Alder reactions found that ytterbium triflate complexes with polyethers were more selective than those of polyethylene glycols and that the uncomplexed ytterbium triflate had intermediate selectivity [5a], and more recently chiral coordination complexes of scandium triflate have been shown to catalyse enantioselective Michael addition reactions [5b], and aldol reactions in aqueous media [5c]. We have thus examined the structures of the triphenylphosphine oxide complexes and the catalytic properties of the scandium complex in particular, and compared its activity and selectivity to that of uncomplexed scandium triflate.

2. Results and discussion

2.1. Solid state structures

Crystals suitable for single crystal X-ray diffraction study were obtained for the Sc, Nd and Lu complexes. Crystals of poorer quality for the La and Er complexes

* Corresponding author. Tel.: +44-1782-294-784; fax: +44-1782-294-000.
E-mail address: a.platt@staffs.ac.uk (A.W.G. Platt).

0277-5387/02/$ - see front matter © 2002 Elsevier Science Ltd. All rights reserved.
PII: S0277-5387(01)00987-1

have also allowed us to establish the atom connectivities in these compounds. The complexes are ionic containing $[M(OTf)_2(Ph_3PO)_4]^+$ and an uncoordinated triflate anion. The smaller lanthanide ions, Er and Lu and also Sc, are six-coordinate, whilst for the larger Nd and La, one of the triflates adopts a bidentate mode giving seven-coordinate geometries about the metal. The structures of the Nd and Sc complexes are shown in Fig. 1, selected interatomic distances and bond angles are given in Table 1 and details of the data collection and refinement in Table 2.

The structures are very similar to those of the complexes of lanthanide triflates with hexamethylphosphoramide, $[Ln(OTf)_2(HMPA)_4]^+[OTf]^-\cdot CHCl_3$ [6a], where a change from bidentate to monodentate triflate coordination is found, with the lanthanum complex containing one bidentate and one monodentate triflate whilst the cerium analogue has two monodentate triflates.

The scandium and lutetium complexes form slightly distorted octahedra, with bond angles at the metal $90 \pm 5°$. The increased steric effect of the bidentate triflate in the Nd complex forces the equatorial oxygen atoms of the phosphine oxides out of plane towards the mondentate triflate. The Ln–O(P) distances increase in line with the ionic radii of the metal ion, the 12% increase mirroring almost exactly the increased ionic size from Sc to Nd [7]. The Nd–O(triflate) distances are longer than expected, presumably as a result of the increased steric congestion caused by the bidentate ligand. The bidentate S–O(Nd) lengths are significantly longer than the S–O(Nd) monodentate. In general the S–O bond distances reflect the coordination state to the metal, with S–O(metal) distances being longer than S–O(terminal), an identical effect being observed in the HMPA complexes [6b].

The change from bidentate to monodentate triflate coordination presumably occurs later in our series of complexes as a result of lower steric strain from the less bulky triphenylphosphine oxide ligand.

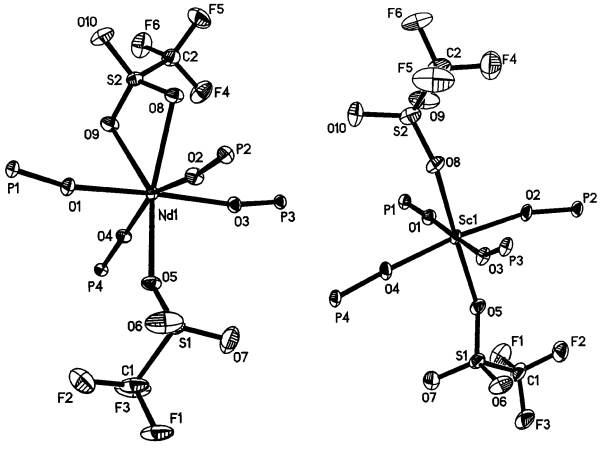


Fig. 1. The structures of the $[M(O_3SCF_3)_3(Ph_3PO)_4]^+$ cations M = Nd and Sc phenyl groups omitted for clarity.

Infrared spectroscopy in principle provides a means of identifying the coordination mode of the triflate ligand. The spectra were obtained as hexachlorobutadiene mulls and as KBr discs and showed no significant differences. This indicates that halide substitution, which is common for nitrate complexes, is not occurring here. The spectra themselves are complex with bands due to S–O and C–F not easily assigned. This is due to mixing of the vibrational modes [8], the presence of up to three different coordination modes in the same compound, and interference from phosphine oxide absorptions. It is, however, possible to deduce which complexes contain bidentate triflate by examination of their spectra. The spectra for the Nd and Sm complexes as KBr discs are shown in Fig. 2. Whilst only subtle differences are seen between the two spectra, the absorption at 1329 cm^{-1} in the Sm complex splits into two bands at 1342 and 1326 cm^{-1} in the Nd complex. Spectra for the complexes of the heavier lanthanides and scandium are essentially identical to that of the Sm complex. On this basis the transition from bidentate to monodentate coordination occurs at Nd with the complexes from Sm onwards being six-coordinate with two monodentate triflates.

2.2. Catalytic studies

Preliminary studies on the catalytic activity of several of the complexes have been carried out. Three of the phosphine oxide complexes were initially screened for activity in the acylation of anisole in nitromethane solution. The scandium complex was found to be most active, with erbium less so and the praseodymium complex showing no catalytic activity. $Sc(OTf)_3(Ph_3PO)_4$ was subsequently examined as a catalyst for the acylation, alkenylation [3a] and alkylation of activated aromatics. The reactions studied are shown in Scheme 1 and the results, together with some comparisons of the reactions using $Sc(OTf)_3\cdot 9H_2O$ as catalyst, in Table 3. The products were assigned using GC-mass spectrometry. The % conversions are based on GC measurements using benzophenone as an internal standard.

As expected, the activity of the triphenylphosphine oxide complex is considerably lower than that of the uncomplexed triflate salt. Some increase in selectivity is seen in reaction 1, whilst in reaction 3 the single substitution product is preferred when $Sc(OTf)_3(Ph_3PO)_4$ is used. These observations are presumably accounted for by the increased steric congestion around the metal centre, with extensive dissociation of the complexes accounting for the relatively modest increases in selectivity observed.

Table 1
Bond lengths (Å) and angles (°) for $M(O_3SCF_3)_3(Ph_3PO)_4$

Sc		Nd		Lu	
Bond lengths					
Sc(1)–O(1)	2.051(2)	Nd(1)–O(1)	2.304(2)	Lu(1)–O(1)	2.156(5)
Sc(1)–O(2)	2.0712(19)	Nd(1)–O(4)	2.317(2)	Lu(1)–O(4)	2.183(5)
Sc(1)–O(4)	2.079(2)	Nd(1)–O(3)	2.333(2)	Lu(1)–O(2)	2.192(5)
Sc(1)–O(3)	2.090(2)	Nd(1)–O(2)	2.339(2)	Lu(1)–O(3)	2.199(5)
Sc(1)–O(8)	2.111(2)	Nd(1)–O(5)	2.408(2)	Lu(1)–O(5)	2.202(6)
Sc(1)–O(5)	2.138(2)	Nd(1)–O(8)	2.553(2)	Lu(1)–O(8)	2.232(5)
		Nd(1)–O(9)	2.624(2)		
P(1)–O(1)	1.516(2)	P(1)–O(1)	1.513(2)	P(1)–O(1)	1.525(6)
P(2)–O(2)	1.514(2)	P(2)–O(2)	1.501(2)	P(2)–O(2)	1.508(5)
P(3)–O(3)	1.514(2)	P(3)–O(3)	1.517(2)	P(3)–O(3)	1.507(5)
P(4)–O(4)	1.511(2)	P(4)–O(4)	1.513(2)	P(4)–O(4)	1.511(5)
S(1)–O(5)	1.465(2)	S(1)–O(5)	1.458(2)	S(1)–O(5)	1.467(6)
S(1)–O(6)	1.419(2)	S(1)–O(6)	1.399(3)	S(1)–O(6)	1.403(8)
S(1)–O(7)	1.430(3)	S(1)–O(7)	1.420(3)	S(1)–O(7)	1.474(9)
S(1)–C(1)	1.828(3)	S(1)–C(1)	1.850(5)	S(1)–C(1)	1.773(13)
S(2)–O(8)	1.464(2)	S(2)–O(8)	1.461(3)	S(2)–O(8)	1.459(6)
S(2)–O(9)	1.408(3)	S(2)–O(9)	1.462(3)	S(2)–O(9)	1.417(7)
S(2)–O(10)	1.444(3)	S(2)–O(10)	1.415(3)	S(2)–O(10)	1.409(7)
S(2)–C(2)	1.795(4)	S(2)–C(2)	1.822(4)	S(2)–C(2)	1.825(12)
Bond angles					
O(1)–Sc(1)–O(2)	91.34(8)	O(1)–Nd(1)–O(2)	89.76(8)	O(1)–Lu(1)–O(2)	90.8(2)
O(1)–Sc(1)–O(4)	90.57(8)	O(1)–Nd(1)–O(4)	94.94(8)	O(1)–Lu(1)–O(4)	91.7(2)
O(1)–Sc(1)–O(3)	177.03(8)	O(1)–Nd(1)–O(3)	175.98(8)	O(1)–Lu(1)–O(3)	177.2(2)
O(1)–Sc(1)–O(5)	90.31(8)	O(1)–Nd(1)–O(5)	83.91(9)	O(1)–Lu(1)–O(5)	92.6(2)
O(1)–Sc(1)–O(8)	92.04(8)	O(1)–Nd(1)–O(8)	97.27(8)	O(1)–Lu(1)–O(8)	89.7(2)
O(2)–Sc(1)–O(3)	89.92(8)	O(2)–Nd(1)–O(3)	88.51(8)	O(2)–Lu(1)–O(3)	88.4(2)
O(2)–Sc(1)–O(8)	92.89(8)	O(2)–Nd(1)–O(8)	74.56(8)	O(2)–Lu(1)–O(8)	86.6(2)
O(2)–Sc(1)–O(5)	85.82(8)	O(2)–Nd(1)–O(5)	80.07(8)	O(2)–Lu(1)–O(5)	92.9(2)
O(3)–Sc(1)–O(8)	85.21(8)	O(3)–Nd(1)–O(8)	85.76(8)	O(3)–Lu(1)–O(8)	92.9(2)
O(3)–Sc(1)–O(5)	92.46(8)	O(3)–Nd(1)–O(5)	92.22(9)	O(3)–Lu(1)–O(5)	84.8(2)
O(4)–Sc(1)–O(2)	173.03(8)	O(4)–Nd(1)–O(2)	160.15(8)	O(4)–Lu(1)–O(2)	172.2(2)
O(4)–Sc(1)–O(3)	88.50(8)	O(4)–Nd(1)–O(3)	85.51(8)	O(4)–Lu(1)–O(3)	89.4(2)
O(4)–Sc(1)–O(8)	93.74(8)	O(4)–Nd(1)–O(8)	123.68(8)	O(4)–Lu(1)–O(8)	86.1(2)
O(4)–Sc(1)–O(5)	87.46(8)	O(4)–Nd(1)–O(5)	81.27(8)	O(4)–Lu(1)–O(5)	94.3(2)
O(5)–Sc(1)–O(8)	177.35(8)	O(5)–Nd(1)–O(8)	154.60(8)	O(5)–Lu(1)–O(8)	177.6(2)
P(1)–O(1)–Sc(1)	172.03(13)	O(1)–Nd(1)–O(5)	83.91(9)	P(1)–O(1)–Lu(1)	171.8(4)
P(2)–O(2)–Sc(1)	164.94(13)	O(1)–Nd(1)–O(9)	79.30(8)	P(2)–O(2)–Lu(1)	177.9(4)
P(3)–O(3)–Sc(1)	157.31(13)	O(4)–Nd(1)–O(9)	74.92(8)	P(3)–O(3)–Lu(1)	160.0(4)
P(4)–O(4)–Sc(1)	176.41(13)	O(3)–Nd(1)–O(9)	104.66(8)	P(4)–O(4)–Lu(1)	165.6(4)
S(1)–O(5)–Sc(1)	149.80(13)	O(2)–Nd(1)–O(9)	124.93(8)	S(1)–O(5)–Lu(1)	146.3(4)
S(2)–O(8)–Sc(1)	144.48(14)	O(5)–Nd(1)–O(9)	149.36(8)	S(2)–O(8)–Lu(1)	150.4(4)
		O(8)–Nd(1)–O(9)	54.13(7)		
		P(1)–O(1)–Nd(1)	167.71(15)		
		P(2)–O(2)–Nd(1)	171.16(15)		
		P(3)–O(3)–Nd(1)	165.93(15)		
		P(4)–O(4)–Nd(1)	166.99(14)		

2.3. Solution properties

The solution behaviour of the complexes has been examined by electrospray mass spectrometry (ES MS) [9]. ES MS has found increasing use as a means of examining solution speciation, where the relatively mild transfer of solvated ions in solution to the gas phase in many cases occurs with little fragmentation [10]. For lanthanide complexes it is a particularly powerful tool as other methods tend to give indirect information due to the lability and paramagnetism of many of the complexes. The ES MS were recorded on methanol solutions, the results are shown in Table 4.

The low cone voltage spectra in methanol clearly show that extensive ligand redistribution reactions involving both triflate and Ph_3PO occur on dissolution and that the solid state structure is not retained. Assignments are based on the calculated mass to charge ratio and comparison of the observed and calculated isotope distribution patterns. These are particularly in-

formative when assigning signals to multiply charged ions where a characteristic compression of the isotope profile is observed. Interestingly the pseudo-parent ion, $[Ln(OTf)_2(Ph_3PO)_4]^+$, observed in the solid state is only present in small concentration in solution. The spectra obtained from the scandium complex differ from those of the lanthanides in that at low cone voltage, no metal containing ions were observed with the spectrum dominated by ions derived from dissociated Ph_3PO and ions (H^+ and Na^+) present in the solvent. Thus peaks due to $[(Ph_3PO)_nH]^+$ and $[(Ph_3PO)_nNa]^+$ ($n = 1$–4) are the main features in the positive ion spectra. At higher cone voltages scandium containing ions such as $[Sc(OTf)(Ph_3PO)_3]^{2+}$ ($m/z = 514$), $[Sc(OTf)_2(Ph_3PO)_2]^+$ ($m/z = 899$) and $[Sc(OTf)_2(Ph_3PO)_3] + (m/z = 1177)$ are seen at low intensity.

On addition of excess triphenylphosphine oxide the relative abundances of the ions in solution as measured by ES MS changes. The formation of $[Ln(Ph_3PO)_6]^{3+}$ is favoured for the lighter lanthanides and forms the base peak for the La and Nd complexes. This is expected in view of the labile nature of lanthanide complexes with monodentate ligands.

ES MS has previously been used to identify intermediates in reactions of lanthanide ions in solution [11], thus direct observation of reactions 2 and 3 using about 10 mol% $Sc(OTf)_3(Ph_3PO)_4$ as catalyst was carried out in an attempt to directly observe any catalytic intermediates. It was anticipated that species such as $[Sc(OTf)_2(Ph_3PO)_4(PhCCH)]^+$ or $[Sc(OTf)_2(Ph_3PO)_4(Me_2C_6H_4)]^+$ might be present in sufficiently high concentration to be detectable. In both solutions the base peak was due to $[Ph_3POH]^+$ with $[(Ph_3PO)_2H]^+$ of similar intensity. The main scandium containing ions are $[Sc(OTf)(Ph_3PO)_4]^{2+}$ ($m/z = 653$) and $[Sc(OTf)(Ph_3PO)_3]^{2+}$ ($m/z = 514$) with $[Sc(OTf)(Ph_3PO)_2]^{2+}$ and $[Sc(OTf)_2(Ph_3PO)_n]^+$ ($n = 1$–3) being represented by much lower intensity signals. No peaks assigned to complexes of these ions with either phenylacetylene or aromatic were observed, and thus it is not possible to deduce which, if any, of the scandium containing ions observed, are the catalytically active species.

Table 2
Crystal data and structure refinement for $M(O_3SCF_3)_3(Ph_3PO)_4$

	Sc	Nd	Lu
Empirical formula	$C_{75}H_{60}F_9ScO_{13}P_4S_3$	$C_{75}H_{60}F_9NdO_{13}P_4S_3$	$C_{75}H_{60}F_9LuO_{13}P_4S_3$
Formula weight	1605.25	1704.53	1735.26
Temperature (K)	160(2)	160(2)	200(2)
Wavelength (Å)	0.71073	0.71073	0.71073
Crystal system	triclinic	triclinic	triclinic
Space group	$P\bar{1}$	$P\bar{1}$	$P\bar{1}$
Unit cell dimensions			
a (Å)	13.4303(15)	13.7208(15)	13.592(3)
b (Å)	14.5187(16)	14.9959(16)	14.738(3)
c (Å)	19.472(2)	19.362(2)	19.615(3)
α (°)	94.422(2)	94.123(2)	94.275(14)
β (°)	107.252(2)	109.101(2)	107.909(14)
γ (°)	91.545(2)	93.731(2)	91.877(19)
V (Å^3)	3610.4(7)	3738.1(7)	3722.3(12)
Z	2	2	2
D_{calc} (Mg m^{-3})	1.477	1.514	1.548
Absorption coefficient (mm^{-1})	0.365	0.948	1.581
$F(000)$	1648	1726	1748
Crystal size (mm)	$0.34 \times 0.31 \times 0.09$	$0.18 \times 0.14 \times 0.13$	$0.35 \times 0.20 \times 0.15$
Theta range for data collection (°)	1.10–27.00	1.12–27.00.	2.13–26.00
Index ranges	$-16 \le h \le 17$, $-18 \le k \le 19$, $-24 \le l \le 24$	$-17 \le h \le 17$, $-19 \le k \le 19$, $-24 \le l \le 24$	$-16 \le h \le 0$, $-18 \le k \le 18$, $-23 \le l \le 24$
Reflections collected	29 557	31 272	15 198
Independent reflections	15 346 [$R_{int} = 0.0365$]	15 961 [$R_{int} = 0.0258$]	14 557 [$R_{int} = 0.0658$]
Completeness to $\theta = 27.00°$	97.30%	97.80%	99.60%
Absorption correction	Empirical	Empirical	Psi-scan
Max./min. transmission	0.928, 0.514	0.862, 0.775	0.672, 0.571
Refinement method	Full-matrix least-squares on F^2	Full-matrix least-squares on F^2	Full-matrix least-squares on F^2
Data/restraints/parameters	15 346/0/1018	15 961/0/946	14 557/0/802
Goodness-of-fit on F^2	0.959	0.97	1.012
Final R indices [$I > 2\sigma(I)$]	$R_1 = 0.0596$, $wR_2 = 0.1569$	$R_1 = 0.0415$, $wR_2 = 0.1019$	$R_1 = 0.0662$, $wR_2 = 0.1410$
R indices (all data)	$R_1 = 0.0836$, $wR_2 = 0.1661$	$R_1 = 0.0527$, $wR_2 = 0.1044$	$R_1 = 0.1047$, $wR_2 = 0.1600$
Largest difference peak and hole (e Å^{-3})	2.318 and −1.142	1.830 and −1.873	2.853 and −1.574

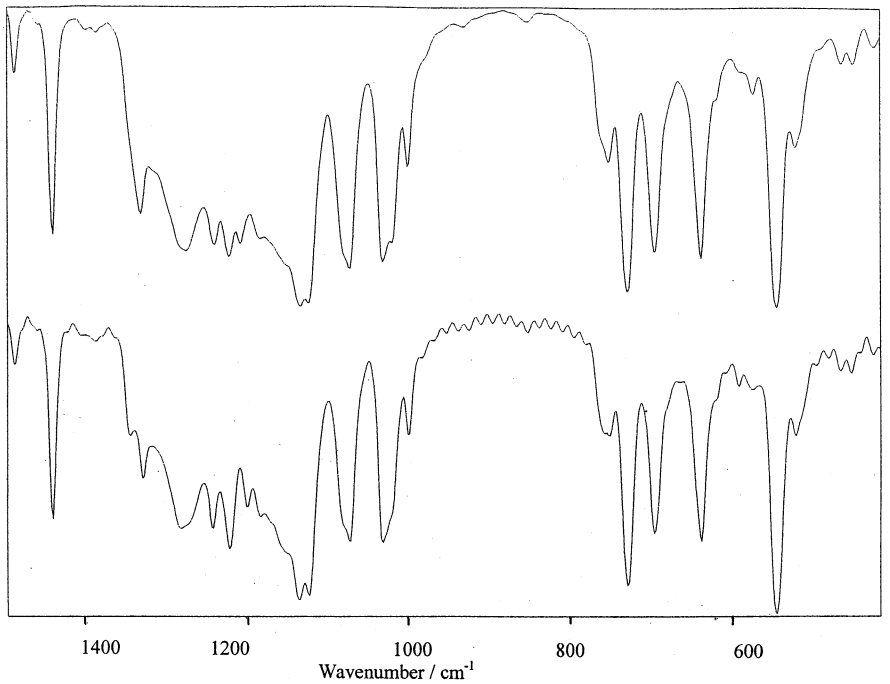


Fig. 2. Infrared spectra (KBr) of $Nd(OTf)_3(Ph_3PO)_4$ (lower) and $Sm(OTf)_3(Ph_3PO)_4$ (upper).

3. Experimental

The same general method of preparation was used with the exception of the La and Sc complexes, which are detailed separately below. The lanthanide triflate and slight excess of triphenylphosphine oxide were dissolved in EtOH and heated briefly to reflux. The solution was evaporated to dryness and the excess phosphine oxide removed by stirring with a little THF. The complexes generally show a marked decrease in solubility in THF with decreasing ionic radius, with the exception of the Sc complex, which has appreciable solubility. Thus the La complex is freely soluble in THF and could not be purified in this manner, and whilst the Nd complex is sufficiently soluble for the lilac colour of Nd^{3+} to be seen in solution it can be recovered in reasonable yield. Typical yields were in the region of 80% based on metal, all compounds analysed satisfactorily as $Ln(OTf)_3(Ph_3PO)_4$. The Sc and La complexes were crystallised from EtOH as described below.

3.1. $La(OTf)_3(Ph_3PO)_4H_2O$

Hydrated La triflate (1.48 g, 1.98 mmol) and triphenylphosphine oxide (2.38 g, 8.57 mmol) were suspended in 100 ml of EtOH heated to boiling until a clear solution was obtained. The resulting solution was reduced to about 20 ml and cooled to room temperature (r.t.) when crystallisation occurred. The crystals were filtered, washed with a little Et_2O and dried at the pump to give 2.95 g (87%) of the product as a white powder.

Anal. Calc. for $C_{75}H_{62}F_9LaO_{14}P_4S_3$: C, 52.47; H, 3.70. Found: C, 52.41; H, 3.64%.

3.2. $Sc(OTf)_3(Ph_3PO)_4$

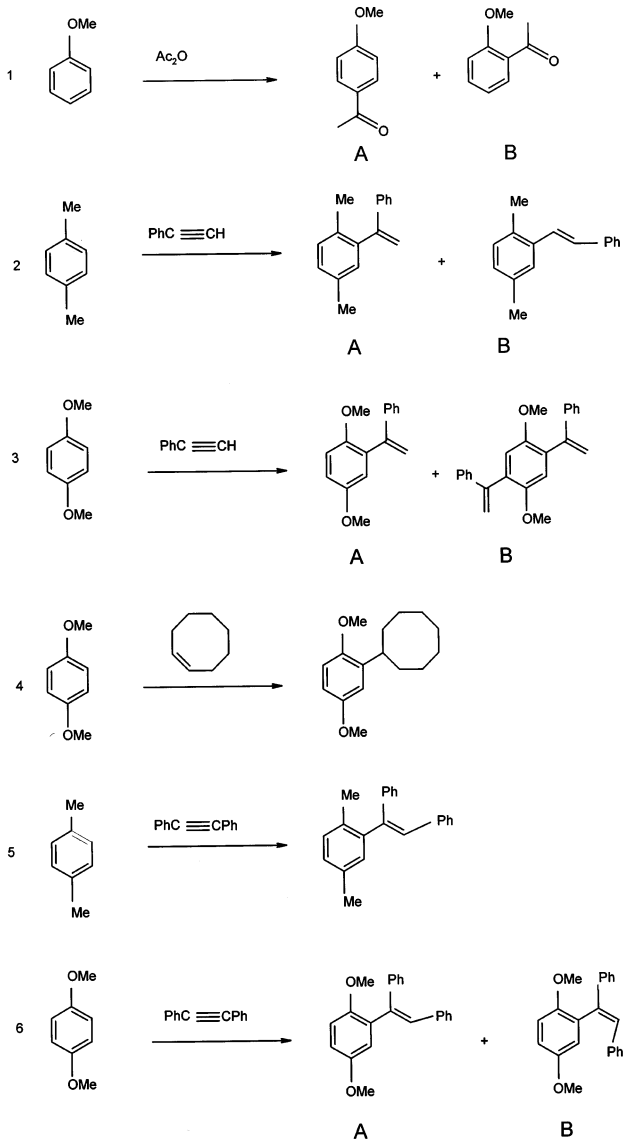
Hydrated scandium triflate (1.09 g, 1.66 mmol) in 40 ml EtOH was mixed with a solution of Ph_3PO (2.04 g, 7.35 mmol in 15 ml EtOH) The volume was reduced by boiling to 25 ml and the product crystallised on cooling to r.t. The solid was collected, washed with Et_2O and dried at the pump to give 1.61 g as a white powder. A second crop (0.29 g) was obtained on further concentration of the filtrate. Combined yield 72%.

Anal. Calc. for $C_{75}H_{60}F_9O_{13}P_4S_3Sc$: C, 56.12; H, 3.77. Found: C, 55.94; H, 3.79%.

Crystals for X-ray analysis formed spontaneously during the preparations for the Sc, La and Nd complexes. Crystals of the Er and Lu complexes were grown by slow evaporation of EtOH solutions. Whilst the bulk sample of the La complex analysed as the monohydrate the crystal chosen for X-ray analysis appears to have a higher hydration state and is probably not representative of the bulk sample.

4. Crystallography

Data for the Sc and Nd complexes were measured on a Bruker SMART diffractometer with a 2K CCD area



Scheme 1.

detector. Data for the Lu complex were measured on a Bruker P4 diffractometer. All data were collected using graphite monochromated Mo Kα radiation ($\lambda = 0.71073$ Å). Semi-empirical absorption corrections, based on comparison of Laue equivalents, were applied to the data sets. The structures were solved by direct methods and refined by full-matrix least-squares cycles on F^2 for all data, using SHELXTL [12]. All non hydrogen atoms were refined with anisotropic displacement parameters. All hydrogen atoms were included in refinement cycles riding on bonded atoms. For all structures the uncoordinated triflate ion exhibits high anisotropic displacement values and for the Sc complex this was resolved to disordered sites.

Catalytic reactions were carried out on 5 ml of approximately 2 M solutions of the reagents in nitromethane. The reactions were heated to reflux and monitored by GC-MS using a Carlo Erba MFC 500 gc linked to a Trio 1000 mass spectrometer.

Electrospray mass spectra were obtained by the EPSRC National Mass Spectrometry Service Centre at Swansea University. The spectra were recorded on a VG Quattro II triple quadrupole mass spectrometer. Samples were loop injected into a stream of MeOH passing through a steel capillary held at high voltage ($+3.5$ kV for positive mode and -3.0 kV for negative mode). Nebulisation of the resulting spray was pneumatically assisted by a flow of nitrogen bath gas and heated source (70 °C). Declustering and molecular fragmentation were promoted by increasing the cone voltage from 8 to 50 V.

5. Supplementary material

Crystallographic data for the structures reported in this paper have been deposited with the Cambridge Crystallographic Data Centre, CCDC nos. 168629, 168630, 168631, 168632 and 168633 for complexes Lu,

Table 3
$Sc(OTf)_3(Ph_3PO)_4$ catalysed Friedel Crafts reactions [a]

Reaction	Catalyst (mol%)	Reaction time (h)		% Conversion	Product ratio A:B
1	$Sc(OTf)_3(Ph_3PO)_4$	(0.6)	24	15	30:1
1	$Sc(OTf)_3{\cdot}9H_2O$	(0.6)	24	40	20:1
2	$Sc(OTf)_3(Ph_3PO)_4$	(0.6)	120	<5	9:1
2	$Sc(OTf)_3{\cdot}9H_2O$	(0.6)	16	<5	– [b]
3	$Sc(OTf)_3(Ph_3PO)_4$	(0.3)	168	30	60:1
3	$Sc(OTf)_3{\cdot}9H_2O$	(0.6)	16	75	20:1
4	$Sc(OTf)_3(Ph_3PO)_4$	(0.3)	330	40	– [b]
5	$Sc(OTf)_3(Ph_3PO)_4$	(0.3)	24	<5	– [b]
6	$Sc(OTf)_3(Ph_3PO)_4$	(0.3)	72	<5	8:1

[a] Under reflux in nitromethane.
[b] Only product A detected by GC-MS.

Table 4
Positive ion electrospray mass spectra [a] of $MTf_3(Ph_3PO)_4$

	ML_6^{3+}	ML_5^{3+}	$MTfL_5^{2+}$	$MTfL_4^{2+}$	$MTfL_3^{2+}$	$MTf_2L_4^{+}$	$MTf_2L_3^{+}$	$MTf_2L_2^{2+}$
Y	586.1(80)	493.4(100)	814.3(85)	700.3(40)		1499.0(10)	1271.1(5)	
La	602.8(75)	510.0(100)	839.3(80)	700.3(40)	561.0(20)	1549.2(10)	1271.1(5)	
Nd	604.8(60)	511.5(100)	841.8(50)	702.8(60)	563.6(80)	1554.2(5)	1276.3(<5)	
Nd [b]		511.5(60)	841.8(15)	702.5(90)	563.7(100)			
Sm	607.3(60)	514.6(100)	846.9(30)	704.9(65)	568.6(25)	1564.1(10)	1286.2(10)	1005.9(10)
Er	612.2(35)	519.4(100)	853.4(30)	714.3(60)	575.2(25)	1577.3(<5)	1301.1(10)	1023.2(5)
Lu		521.9(95)	Not observed [c]	718.2(75)	579.2(100)	1585.2(<5)	1307.2(5)	1029.2(10)

[a] In methanol at +20 V cone, m/z values quoted for highest intensity ion in the isotope profile. Relative intensity given in parenthesis.
[b] In nitromethane.
[c] Coincident with $[(Ph_3PO)_3Na]^+$.

Nd, Sc, La and Er, respectively. Copies of this information may be obtained free of charge from The Director, CCDC, 12 Union Road, Cambridge, CB2 1EZ, UK (fax: +44-1223-336033; e-mail: deposit@ccdc.cam.ac.uk or www: http://www.ccdc.cam.ac.uk).

Acknowledgements

Thanks are due to the EPSRC for the use of the Chemical data base service [13] at Daresbury and the National Mass Spectrometry Service at Swansea University.

References

[1] S. Kobayashi, Eur. J. Org. Chem. (1999) 15.
[2] (a) D. Liu, R.W. Giese, Tetrahedron Lett. 41 (2000) 2817;
(b) S. Kobayashi, T. Busujima, S. Nagayama, Chem. Commun. (1998) 19.
[3] (a) T. Tsuchimoto, T. Maeda, E. Shirakawa, Y. Kawakami, Chem. Commun. (2000) 1573;
(b) Y. Ma, C. Qian, Tetrahedron Lett. 41 (2000) 945;
(c) W.-C. Zhang, G.S. Viswanatha, C.-J. Li, Chem. Commun. (1999) 291;
(d) C.-J. Li, Chem. Commun. (1999) 291.
[4] F.L. Alencar, L.B. Zinner, K. Zinner, J.E.X. Matos, J. Coord. Chem. 46 (1999) 471.
[5] (a) H.C. Aspinall, J.L. Dwyer, N. Greeves, E.G. McIver, C.J. Woolley, Organometallics 17 (1998) 1884;
(b) M. Nakajima, Y. Yamaguchi, S. Hashimoto, Chem. Commun. (2001) 1596;
(c) S. Kobayashi, T. Hamada, S. Nagayama, K. Manabe, Org. Lett. 3 (2001) 165.
[6] (a) T. Imamoto, M. Nishiura, Y. Yamanoi, H. Tsuruta, K. Yamaguchi, Chem. Lett. 10 (1996) 875;
(b) K. Yamaguchi, Personal communication.
[7] M. Winter, WebElements, http://www.shef.ac.uk/chemistry/web-elements.
[8] G.A. Lawrance, Chem. Rev. 86 (1986) 17.
[9] P. Kebarle, T. Tang, Anal. Chem. 65 (1993) 972.
[10] R. Colton, A. D'Agostino, J.C. Traeger, Mass Spectrosc. Rev. 14 (1995) 79.
[11] K. Asakura, K. Yamaguchi, T. Imamoto, Chem. Lett. (2000) 424.
[12] SHELXTL, an integrated system for solving, refining and displaying crystal structures. Version 5.10, Bruker Analytical X-ray Systems, Madison, WI, USA, 1997.
[13] The United Kingdom Chemical Database Service: D.A. Fletcher, R.F. McMeeking, D. Parkin, J. Chem. Inf. Comput. Sci. 36 (1996) 746.

PERGAMON

Polyhedron 21 (2002) 295–303

POLYHEDRON

www.elsevier.com/locate/poly

Potentiometric and spectroscopic study of mixed-ligand copper(II) complexes with *N*,*N*,*N*′,*N*″,*N*″-pentamethyldiethylenetriamine and α- (or β-) alaninehydroxamic acids in water solution

Danuta Kroczewska [a], Katarzyna Bogusz [a], Barbara Kurzak [a,*], Julia Jezierska [b]

[a] *Institute of Chemistry, University of Podlasie, 3-Maja 54, 08-110 Siedlce, Poland*
[b] *Faculty of Chemistry, University of Wroclaw, 50-383 Wroclaw, Poland*

Received 11 July 2001; accepted 8 November 2001

Abstract

Stabilities of the mixed-ligand complexes of Cu^{2+} ion with *N*,*N*,*N*′,*N*″,*N*″-pentamethyldiethylenetriamine [*N*,*N*,*N*′,*N*″,*N*″-pentamethyl-{bis(2-aminoethyl)amine}, Me_5dien] as a primary ligand and α-alaninehydroxamic acid [2-amino-*N*-hydroxypropanamid, α-Alaha] or β-alaninehydroxamic acid [3-amino-*N*-hydroxypropanamid, β-Alaha] as a secondary ligand L and their absorption and EPR spectra at various pH values are reported. The visible spectra exhibit a characteristic red shift and a shoulder at lower energies indicating a five-coordinate structure of the formed complexes. The change of the EPR spectral parameters as a function of pH reflects two modes of an equatorial–axial chelation by the aminohydroxamic acid ligand L in the $[Cu(Me_5dien)(HL)]^{2+}$ and $[Cu(Me_5dien)(L)]^{+}$ species. © 2002 Elsevier Science Ltd. All rights reserved.

Keywords: Copper(II) complexes; Mixed-ligand complexes; Five-coordinate complexes; Aminohydroxamic acids; EPR spectra; Vis spectra

1. Introduction

The aim of this paper is to summarise our results on the mixed-ligand copper(II) complexes in which polyamines play a role as a primary ligand and aminohydroxamic acid as a secondary one [1–3]. However, we have extended this paper including *N*,*N*,*N*′,*N*″,*N*″-pentamethyldiethylenetriamine (Me_5dien) to investigate its complexing properties with copper(II) in binary and ternary systems. We were looking for an answer for the following question: is the geometry around copper(II) controlled first of all by polyamines? In order to find the answer we used different methods (pH-metric and spectroscopic: UV–Vis and EPR).

2. Experimental

2.1. Materials

α-Alaha and β-Alaha were prepared in our laboratory via the methyl ester of the respective amino acid as described in Ref. [4]. Me_5dien from Fluka was used without further purification and its purity was greater than 99%.

The exact concentrations of the stock solutions of the ligands used for potentiometric studies were determined by the Gran method [5]. The copper(II) chloride solution was purchased from Merck. Carbonate-free potassium hydroxide (the titrant) was prepared and standardized against a standard potassium hydrogenphtalate solution.

For clarity, the charges of the complexes are omitted in the tables. It has to be mentioned, however, that the fully deprotonated forms of aminohydroxamic acids are L^- while the *N*,*N*,*N*′,*N*″,*N*″,-pentamethyldiethylenetriamine is neutral.

* Corresponding author. Tel.: +48-25-643-1097; fax: +48-25-644-2045.
E-mail address: bkurzak@ap.siedlce.pl (B. Kurzak).

0277-5387/02/$ - see front matter © 2002 Elsevier Science Ltd. All rights reserved.
PII: S0277-5387(01)01001-4

2.2. Potentiometric measurements

A summary of the potentiometric experimental details is given in Table 1. The data for the Cu^{2+}–α-Alaha and Cu^{2+}–β-Alaha binary systems can be found in our early papers [4,6]. Data for the Cu^{2+}–Me_5dien binary system can be found in the literature [7], but for a comparison we had to determine stability constants under identical conditions to those of ternary systems, i.e. at 298 K and ionic strength of 0.2 M (KCl). For the binary system 1:1, 1:2 and 1:4 metal ion to ligand ratios were used. For the determination of the stability constants of the mixed-ligand complexes the concentration ratios of copper(II):Me_5dien: α-Alaha/β-Alaha were 1:1:1, 1:1:2, 1:2:1, 1:2:2, 2:1:1 and 2:2:1.

All the pH-metric titrations were carried out with carbonate-free KOH solution of known concentration (ca. 0.2 M). Titration emf data were used to calculate the hydrogen ion concentration, $[H^+]$. Stability constants $\beta_{pqrs} = [M_p(Me_5dien)_qL_rH_s]/[M]^p[Me_5dien]^q[L]^r[H]^s$ were calculated with the aid of the SUPERQUAD computer program [8]. The reported standard deviations were calculated by assuming random errors.

Table 1
Summary of experimental parameters for the potentiometric measurements

Systems	binary: Me_5dien with H^+ or Cu^{2+} in water solution ternary: Me_5dien and α-Alaha/β-Alaha with Cu^{2+} in water solution
Solution composition	[Me_5dien], [α-Alaha] and [β-Alaha] range—0.002–0.008 M, [Cu^{2+}] range—0.001–0.004 M; ionic strength—0.200 M; electrolyte KCl.
Experimental method	pH-metric titration of 2 or 5 cm^3 samples in the range of pH 2–11; $pK_w = 13.72$.
Instruments	MOLSPIN automatic titrator, micro combination pH electrode (Mettler–Toledo, type 2) or autoburette ABU 80, combination pH electrode (Russel).
Calibration	by periodic titrations of a HCl solution (1×10^{-2} M) against standard KOH solution; $I = 0.2$ M (KCl).
T (°C)	25.0 ± 0.1
n_{tot} [a]	100–150
n_{tit} [b]	6–8
Method of calculation	SUPERQUAD

[a] Number of titration points per titration.
[b] Number of titrations per metal-ligand (or metal–Me_5dien–α-Alaha/β-Alaha) systems.

Table 2
Overall protonation constants and dissociation constants of the ligands at 25 °C and $I = 0.2$ M (KCl) in water solutions

	Me_5dien	dien [b]	α-Alaha	β-Alaha
$\log \beta_1^H$	9.42(1)	9.97(1)	9.20(1)	9.74(1)
$\log \beta_2^H$	17.95(1)	19.05(1)	16.59(1)	18.21(1)
$\log \beta_3^H$	20.03(1)	23.40(1)		
pK_{H_3L}	2.08, 2.09 [a]	4.35		
pK_{H_2L}	8.53, 8.41 [a]	9.08	7.39	8.47
pK_{HL}	9.42, 9.22 [a]	9.97	9.20	9.77
$pK^{micro}_{NH_3^+}$			7.48 [c]	8.85 [c]
pK^{micro}_{NHOH}			7.90 [c]	8.47 [c]

[a] Ref. [18].
[b] Ref. [2].
[c] Ref. [9].

2.3. Spectroscopic measurements

The absorption spectra were recorded on a SPECORD M-40 spectrophotometer using 1-cm quartz cells at room temperature. The individual spectra of the copper(II) complexes were calculated. EPR measurements were performed on a Bruker 300E X-band spectrometer at 77 K in water/ethyleneglycol (4:1 v/v) solution. The metal ion concentrations for both spectroscopic measurements were 4×10^{-3} M and metal ion to ligands molar ratios were 1:1 and 1:2 for the binary systems and 1:2:1 for the Cu^{2+}–Me_5dien–α-Alaha/β-Alaha systems. pH-varied absorption spectra were obtained by the addition of 2 M KOH to the sample solutions so that the concentration (4×10^{-3} M) was not changed significantly. The pH of solutions was measured by employing an OP-208/1 Radelkis pH-meter with a Mettler–Toledo combined electrode.

3. Results and discussion

The acid dissociation constants of the ligands are given in Table 2, together with the macro- and microscopic dissociation constants of α- and β-alaninehydroxamic acids, which have been reported in our previous papers [9]. Me_5dien undergoes three acid dissociation processes during the potentiometric titration from pH 2 to 11. The pK values of these processes can be assigned to the three tertiary ammonium groups. Comparison of the pK values for Me_5dien with that of dien [2] (Table 2), shows that the substitution of hydrogen atoms of the $-NH_2$ group by $-CH_3$ groups decreases the pK values. The coordination tendencies of Me_5dien toward Cu^{2+} ions in aqueous solution were studied in the binary and ternary systems. In the course of the potentiometric titrations no precipitation at any metal ion to ligand ratios and concentrations applied in the studied pH range ($2 < pH < 11.5$). The best fits between the measured and calculated titrations curves were obtained by assuming the species given in Table 3 (for binary systems) and Table 4 (for ternary systems).

Table 3
Overall formation constants ($\log \beta$) for Cu^{2+} complexes formed with Me_5dien and dien (am) in binary systems at 25 °C and $I = 0.2$ M (KCl) in water solutions (the ion charges are omitted)

	Me_5dien	dien
$\log \beta$[Cu(am)]	12.47(1)	16.01(1)
$\log \beta$[Cu(am)H_{-1}]	3.49(1)	6.99(3)
$\log \beta$[Cu(am)$_2$]		20.94(1)
$\log \beta$[Cu(am)$_2$H]		29.36(3)
$\log \beta$[Cu(am)]$-\Sigma$ p$K_{(am)}$	−7.56	−7.39

Table 4
Overall stability constants ($\log \beta$) and deprotonation constants (pK) for Cu^{2+} complexes formed with triamine (Me_5dien) and α- (or β-) alaninehydroxamic acids (L) in ternary systems at 25 °C and $I = 0.2$ M (KCl) in water solutions (the ion charges are omitted)

Assignments	Cu–Me_5dien –α-Alaha	Cu–Me_5dien –β-Alaha
$\log \beta$[Cu(Me_5dien)]	12.47(1)	12.47(1)
$\log \beta$[Cu(Me_5dien)H_{-1}]	3.49(1)	3.49(1)
$\log \beta$[CuL]	10.32(2)	12.85(2)
$\log \beta$[$Cu_5L_4H_{-4}$]		46.66(6)
$\log \beta$[CuL_2]	19.65(1)	
$\log \beta$[$Cu_2L_2H_{-1}$]	20.88(3)	
$\log \beta$[CuL_2H_{-1}]	9.91(2)	
$\log \beta$[Cu(Me_5dien)LH_2]		34.01(2)
$\log \beta$[Cu(Me_5dien)LH]	27.09(9)	27.76(2)
$\log \beta$ [Cu(Me_5dien)L]	20.45(5)	18.91(2)
$\log \beta$[Cu(Me_5dien)LH] $-$ pK^{micro}_{NHOH}	19.07	19.29
pK[Cu(Me_5dien)LH_2]		6.25
pK[Cu(Me_5dien)LH]	6.64	8.85
σ [a]	1.98	1.83

[a] Ref. [8].

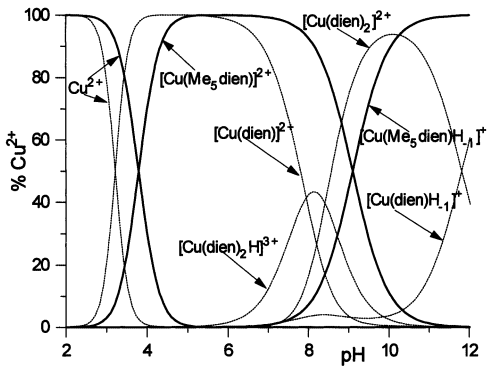


Fig. 1. Species distribution curves calculated for the Cu^{2+}–Me_5dien system (solid lines) and the Cu^{2+}–dien system (dashed lines), as a function of pH; $c_{Cu^{2+}} = 4 \times 10^{-3}$ M; Cu^{2+}:L = 1:2 molar ratio.

3.1. Cu^{2+}-complexation for binary systems

The values of the stability constants obtained for the complexes in the copper(II)–Me_5dien system are listed in Table 3 and the corresponding species distribution diagram is presented in Fig. 1. For comparison the data for the copper(II)–dien system [2] are included in the same table and figure. The studied system contains only equimolar complexes. The formation of bis complexes seems to be hindered because of a steric hindrance (as a result of the methylation of the $-NH_2$ groups in dien). In this system the concentration of the Cu^{2+} ions starts to drop at considerably higher pH values than in the case of dien. This indicates that dien is a noticeably stronger chelating agent than Me_5dien. The overall stability constants of the complexes are remarkably lower for Me_5dien species as compared to dien. However, the basicity-adjusted stability constants for 1:1 complexes, $\log K_{[Cu(am)]} - \Sigma$ pK_{am}, are −7.56 and −7.39, respectively. It means that the stabilities of these complexes are almost identical.

The Vis spectra at the maximum concentration distribution of $[Cu(Me_5dien)(H_2O)]^{2+}$ (pH 6.10) and $[Cu(dien)(H_2O)]^{2+}$ (pH 5.40) were obtained. The molar absorptivity (ε) for $[Cu(Me_5dien)(H_2O)]^{2+}$ ($\varepsilon = 225$ at $\lambda = 664$ nm) (Fig. 2) is much higher than that for $[Cu(dien)(H_2O)]^{2+}$ ($\varepsilon = 78$ at $\lambda = 614$ nm) [2]. It is difficult to correlate these results quantitatively with specific features, but they may indicate an increasing distortion of the complex geometry due to the bulkiness of the methyl groups. Similar results were obtained for Cu^{2+}–tren and Cu^{2+}–Me_6tren complexes [10].

3.2. Cu^{2+}-complexation for ternary systems

Analysis of the potentiometric titration data by the SUPERQUAD computer program allowed the determination of the main complex species in equilibrium. The overall formation constants are defined as: $\beta_{pqrs} = [M_p(Me_5dien)_qL_rH_s]/[M]^p[Me_5dien]^q[L]^r[H]^s$. The values of these constants are given in Table 4. The β_{pqrs} constant expresses the stability of the $[Cu(Me_5dien)L]^+$ species but does not represent directly the binding

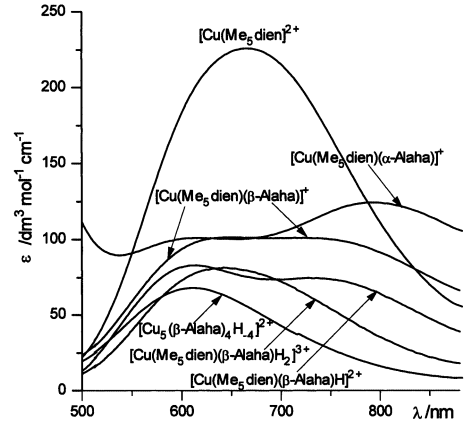


Fig. 2. Calculated electronic spectra of individual species.

Table 5
Derived equilibrium constants of Cu^{2+} mixed-ligand complexes of amino acids and their hydroxamic analogues at 25 °C and $I = 0.2$ M (KCl) in water solutions (the ion charges are omitted)

Assignments	L =			
	α-Ala	α-Alaha	β-Ala	β-Alaha
Reference	[18]	This work and [2]	[a]	This work and [2]
$[Cu(dien)]+L \rightleftharpoons [Cu(dien)L]$				
$\log K_{[Cu(dien)L]} = \log \beta^{Cu^{2+}}_{[Cu(dien)L]} - \log \beta^{Cu^{2+}}_{[Cu(dien)]}$	4.13	5.10	3.92	3.98
$[Cu(Me_5dien)]+L \rightleftharpoons [Cu(Me_5dien)L]$				
$\log K_{[Cu(Me_5dien)L]} = \log \beta^{Cu^{2+}}_{[Cu(Me_5dien)L]} - \log \beta^{Cu^{2+}}_{[Cu(Me_5dien)]}$	5.13	7.98	3.40	6.44
$\Delta\log K_{[Cu(dien)L]}$	−3.98	−5.75	−2.86	−8.91
$\Delta\log K_{[Cu(Me_5dien)L]}$	−2.98	−2.34	−3.38	−6.41
$\log K_{[Cu(dien)L]} - \Sigma\, pK_L$	−7.89	−11.44	−9.53	−14.40
$\log K_{[Cu(Me_5dien)L]} - \Sigma\, pK_L$	−6.89	−8.61	−10.05	−11.77

[a] B. Kurzak, D. Kroczewska, unpublished data.

strength between L and the Cu^{2+} ions. The equilibrium constant, $K_{[Cu(Me_5dien)L]}$, derived from the computed values of β_{pqrs} according to equation: $\log K_{[Cu(Me_5dien)L]} = \log \beta_{[Cu(Me_5)L]} - \log \beta_{[Cu(Me_5dien)]}$, shows how tightly L (aminohydroxamate) is bound to the simple $[Cu(Me_5dien)]^{2+}$ complex. Thus, the binding strength of α-Alaha or β-Alaha in the mixed-ligand complexes depends on the stability of the simple complex $[Cu(Me_5dien)]^{2+}$. Useful information can be obtained by considering equilibrium (1).

$$[Cu(Me_5dien)]^{2+} + [CuL]^{+} \rightleftharpoons [Cu(Me_5dien)L]^{+} + Cu^{2+} \quad (1)$$

$$\Delta\log K = \log \beta_{[Cu(Me_5dien)L]^{+}} - \log \beta_{[Cu(Me_5dien)]^{2+}} - \log \beta_{[CuL]^{+}} \quad (2)$$

Eq. (2) follows a criterion suggested by Sigel [11,12] to account for the stability of a mixed-ligand complex with respect to the corresponding simple ones. Since the aminohydroxamic acids coordinate more easily with the free Cu^{2+} ion than with the complexed metal ion, $[Cu(Me_5dien)]^{2+}$, $\Delta\log K$ should be negative. It can be seen, by viewing the $\Delta\log K$ values for different systems, that values of this factor for the Cu^{2+}–Me_5dien–α-Alaha and Cu^{2+}–Me_5dien–β-Alaha systems are low (−2.34 and −6.41, respectively). This effect of the mixed-ligand complex is due to a Cu^{2+} lower (than six) coordination number [13].

The Cu^{2+} mixed-ligand complexes of Me_5dien with α-Alaha or β-Alaha show larger $\log K_{[Cu(Me_5dien)L]}$ values, or less negative in $\Delta\log K$, compared with the corresponding dien systems (Table 5).

3.3. Cu^{2+}–Me_5dien–α-Alaha system

The stability constants obtained for the complexes formed in the Cu^{2+}–Me_5dien–α-Alaha system are given in Table 4. Concentration distribution curves for this system are presented in Fig. 3(a). From Table 4 it can be seen that the chemical model contains six simple species and two mixed-ligand ones: $[Cu(Me_5dien)(α\text{-Alaha})H]^{2+}$ and $[Cu(Me_5dien)(α\text{-Alaha})]^{+}$.

Absorption spectral data provide evidence for the presence of mixed-ligand complexes. These spectra exhibit an intense charge-transfer transition band in the near-UV region, which is not observed in the spectra of the $[Cu(Me_5dien)]^{2+}$ species (Fig. 2). In other words, the CT transition is observed when the hydroxamic ligand is coordinated. Additionally, a comparison between the species distribution curves (Fig. 3(a)) and the pH-dependent curves of the absorption (Fig. 4) clearly indicates that the spectral change shown in Fig. 3(a) is attributable to the formation and decay of the main mixed-ligand species.

The first mixed-ligand complex, $[Cu(Me_5dien)(α\text{-Alaha})H]^{2+}$, reaches a maximum concentration (ca. 70%) at pH 5.5 (Fig. 3(a)). The $pK_{[Cu(Me_5dien)(α\text{-Alaha})H]^{2+}}$ value characteristic of the deprotonation step for this complex is lower than the corresponding deprotonation constant and microscopic acid dissociation constant of the 'free' α-Alaha (Table 2) and it can be assigned to proton release from the amino group promoted by the copper(II) binding. Thus, the protonated H-α-Alaha coordinates to $[Cu(Me_5dien)]^{2+}$ by the hydroxamate group forming a five-membered chelate ring with {O, O} donor atoms and deprotonated α-Alaha gives a five-membered chelate ring but with $\{N_{amino}, N_{hydrox.}\}$ donor atoms. The proposed structures of the mentioned complexes are presented in Scheme 1(a).

In the visible region the Cu^{2+}–Me_5dien–α-Alaha system shows the existence a broad band which is assigned to the copper(II) d–d transitions. As the pH of the solution increases, the maximum in the longer wavelength region is greatly enhanced. The most evident changes are observed between pH 5.78 and 6.40 (5

and 6 spectra in Fig. 4(a)) which correspond to the formation of the $[Cu(Me_5dien)(\alpha\text{-Alaha})]^+$ species. From pH 8.50 to 9.50 absorption spectra are identical, what means that this complex is the predominant one in this pH range (see Fig. 3(a)). The studied spectra show well two noticeable maxima: at 609 nm (16 420 cm^{-1}) and at 790 nm (12 656 cm^{-1}). This absorption pattern, two peaks with one more intense being near the IR region, indicates a structural change around the Cu^{2+} ion towards five-coordinate copper(II) complexes [14–16]. Taking into account a bulky linear tridentate ligand with three tertiary amino groups (which have poor σ-donating properties [17], if compare with the amino groups of dien) we can see that such steric and electronic characters of the donors permit Me_5dien to easily form five-coordinate type copper(II) complexes with an intermediate geometry between square-pyramidal and trigonal-bipyramidal.

The analysis of the EPR spectra (Table 6) reveals a distinct difference between the spectral characteristic for the species formed between three partners: Cu^{2+}, aminohydroxamic acid and Me_5dien as compared to those for suitable simple complexes. For the ternary systems only a few spectra associated with the parallel

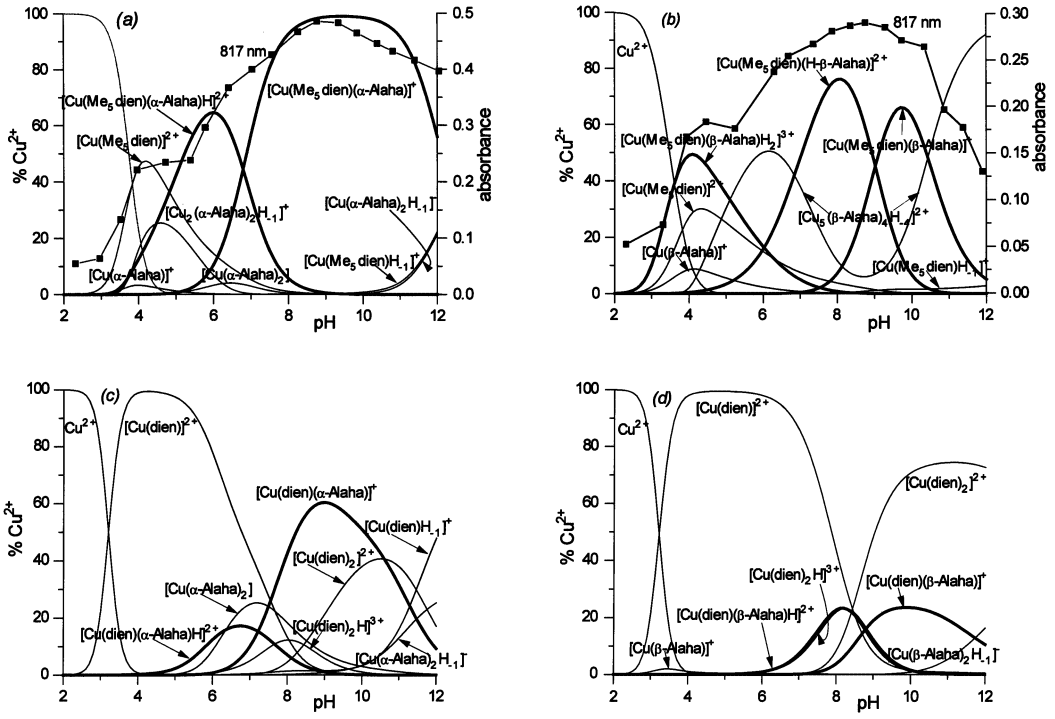


Fig. 3. Species distribution curves as a function of pH (—) and variations of visible absorption ($\lambda = 817$ nm) (···) for the Cu^{2+}–Me_5dien–α-Alaha (a) and Cu^{2+}–Me_5dien–β-Alaha (b) systems; species distribution curves as a function of pH for the Cu^{2+}–dien–α-Alaha (c) and Cu^{2+}–dien–β-Alaha (d) systems; $c_{Cu^{2+}} = 4 \times 10^{-3}$ M and Cu^{2+}:amine:L = 1:2:1 molar ratio (for all systems).

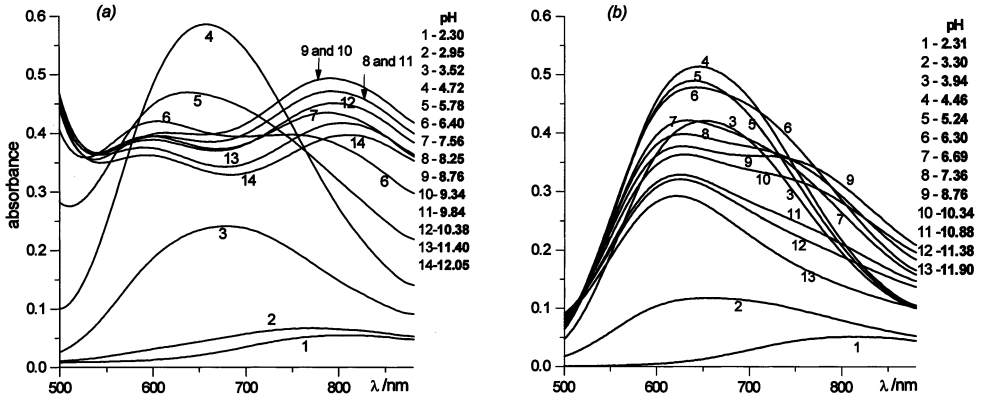
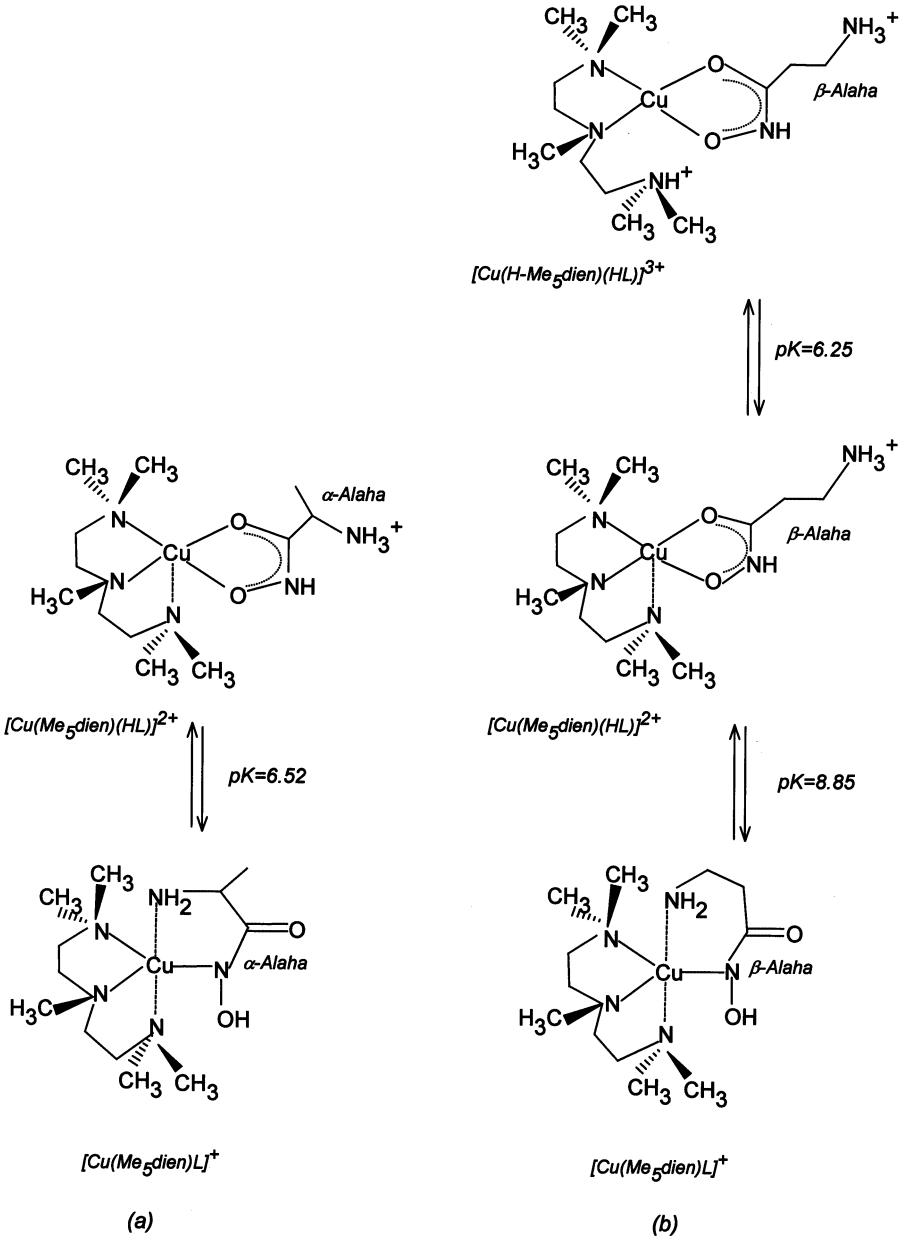


Fig. 4. pH-varied absorption spectra of the Cu^{2+}–Me_5dien–α-Alaha (a) and Cu^{2+}–Me_5dien–β-Alaha (b) systems; $c_{Cu^{2+}} = 4 \times 10^{-3}$ M and Cu^{2+}:amine:L = 1:2:1 molar ratio.



Scheme 1.

formation of the simple species are observed. At pH between 4 and 5, the spectrum has an orthorhombic character reflecting a distorted geometry of the $[Cu(Me_5dien)(H_2O)]^{2+}$ complex as a result of the effect of bulky *N*-methyl groups. This spectrum is observed for the mixed ligand system with α-Alaha alone and with β-Alaha in equilibrium with the spectrum assigned to the mixed-ligand species. The spectrum with strongly rhombically distorted parameters is typical for the complex geometry being intermediate between square-pyramidal and trigonal-bipyramidal [18,19]. The simple complexes with aminohydroxamic acids of tetragonal geometry, beside the species assigned to the first complex formed by α-Alaha and copper(II) [4] at pH 3.5, are not detected in the EPR spectra for the Cu^{2+}–Me_5dien–α-Alaha systems.

The comparison of the concentration distribution curves presented for the Cu^{2+}–Me_5dien–α-Alaha system in Fig. 3(a) together with those for the Cu^{2+}–dien–α-Alaha system (Fig. 3(c)) reveals that the coordination of α-Alaha towards $[Cu(Me_5dien)]^{2+}$ begins at a lower pH (pH ≈ 3) than towards $[Cu(dien)]^{2+}$ (pH ≈ 4.5). Additionally, Fig. 3(a) shows that the presence of Me_5dien does not suppress the formation of the dimeric $[Cu_2(\alpha\text{-Alaha})_2H_{-1}]^{+}$ species in the ternary system (in contrast to system with dien (Fig. 3(c) and [2]).

3.4. Cu^{2+}–Me_5dien–β-Alaha system

In the case of the Cu^{2+}–Me_5dien–β-Alaha system, the chemical model is different if compared to the system with α-Alaha (Table 4). Three mixed-ligand species (in addition to the simple ones) are observed in this case. Two of these are the same type, i.e. $[Cu(Me_5dien)LH]^{2+}$ and $[Cu(Me_5dien)L]^{+}$. However, in the system with β-Alaha $[Cu(Me_5dien)(\beta\text{-Alaha})H_2]^{3+}$ is formed additionally (Fig. 3(b)).

The effect of the formed mixed-ligand species is observed distinctly in the electronic spectral changes. A comparison between the species distribution curves (Fig. 3(b)) and the pH-dependent curves of the absorption (Fig. 4(b)) clearly indicates that the spectral change shown in Fig. 3(b) is attributable to the formation and decay of the mixed-ligand species. It is analogous as it was mentioned above in the system with α-Alaha.

The $[Cu(Me_5dien)(\beta\text{-Alaha})H_2]^{3+}$ species is observed in the pH range of 3–6 and is predominant at pH 4. Thus, all uncoordinated amino groups should be protonated. The deprotonation process of this species leads to the formation of $[Cu(Me_5dien)(\beta\text{-Alaha})H]^{2+}$ above pH 6. The deprotonation constant, $pK_{[Cu(Me_5dien)(\beta\text{-Alaha})H_2]^{3+}}$, is 6.25. This value is lower than the deprotonation constants of the 'free' ligands (Table 2). However, the second deprotonation step, having a $pK_{[Cu(Me_5dien)(\beta\text{-Alaha})H]^{2+}}$ value equal to 8.85 which is identical with the $pK^{micro}_{\beta\text{-Alaha}}(NH_3^+)$ microconstant value [9], supports that N_{amino} of β-Alaha is not involved in the coordination sphere probably because of steric reasons. So, the first deprotonation step can be assigned to the deprotonation of Me_5dien promoted by the copper(II) binding. Thus, the proposed binding mode for these mixed-ligand species is presented on Scheme 1(b).

Table 6
EPR parameters of the binary and ternary systems

	Cu–Me_5dien	Cu–Me_5dien –α-Alaha	Cu–Me_5dien –β-Alaha
pH	4.9	5.7–6.7	3.3–5.1
g_z	2.240	2.233	2.240
g_x	2.060	2.067	2.055
g_y	2.045	2.035	2.055
A_z	175	172	177
A_x	30	50	10
A_y	15	10	10
pH	9.2–11.8	8.1–11.1	6.1–8.9
g_z	2.250	2.230	2.233
g_x	2.195	2.165	2.060
g_y	2.054	2.040	2.030
A_z	150	172	173
A_x	72	86	40
A_y	20	20	15
pH			9.0–11
g_z			2.235
g_x			2.087
g_y			2.030
A_z			170
A_x			50
A_y			20

The anisotropic parameters are estimated on the basis of computer simulation of the experimental spectra measured at 77 K. Parameters A are given in 10^{-4} cm^{-1}.

This bonding mode may be supported by the d–d transition. The absorption curve for the $[Cu(Me_5dien)(\beta\text{-Alaha})H_2]^{3+}$ species (Fig. 2) exhibits a maximum at about 644 nm with a ε (molar absorptivity) value of ~ 78. A maximum or a shoulder in the region of 800 nm was not observed in the spectrum for this species. So, in the $[Cu(Me_5dien)(\beta\text{-Alaha})H_2]^{3+}$ species Me_5-dien occupies two equatorial positions only and the hydroxamic group, forming an{O, O} type chelate ring, occupies the two remaining equatorial positions. The values of its axial EPR parameters indicate involvement of two nitrogen donors and two oxygen donors in the Cu^{2+} coordination plane. Thus, two amino groups, one from Me_5dien and a second from β-Alaha, remain protonated (this type of species is not observed in the spectra recorded for the system with α-Alaha, which supports the species distribution model shown in Fig. 3).

The absorption curve for the next species, $[Cu(Me_5dien)(\beta\text{-Alaha})H]^{2+}$, which exhibits peaks at 610 nm (83) and 753 nm (75) is drastically different from that for $[Cu(Me_5dien)(\beta\text{-Alaha})H_2]^{3+}$ (Fig. 2). This spectral behaviour reveals a structural transformation around the copper(II) ion, strongly suggesting the formation of a five-coordinated mixed-ligand complex. The EPR spectra for $[Cu(Me_5dien)(\beta\text{-Alaha})H]^{2+}$ display parameters of slightly rhombic character and reveal the formation of a complex with a coordination mode of the ligands including two nitrogen and two oxygen donors in the Cu^{2+} plane (Table 6).

The values of $\log K_{[Cu(Me_5dien)LH]^{2+}} = \log \beta_{[Cu(Me_5dien)LH]^{2+}} - pK^{micro}_{NHOH}$ for $[Cu(Me_5dien)(\beta\text{-Alaha})H]^{2+}$ and $[Cu(Me_5dien)(\alpha\text{-Alaha})H]^{2+}$ are 19.29 and 19.07, respectively (Table 4). These values show that the complex formed with β-Alaha is slightly more stable than that formed with α-Alaha. The presence of the positive $-NH_3^+$ group in the side-chain (an electrostatic repulsion between the $-NH_3^+$ group and the coordinating Cu^{2+} ion) decreases the stability of these two complexes and the extent of the decrease depends on the distance between the $-NH_3^+$ group and the hydroxamate moiety [20].

Final liberation of the proton allows all the nitrogen donors to participate in the coordination sphere in the $[Cu(Me_5dien)(\beta\text{-Alaha})]^{+}$ species leading to the chelate rings twisting away followed by an apparent distortion of the geometry from square-pyramidal to trigonal-bipyramidal.

The EPR spectral characteristics for the $[Cu(Me_5dien)L]^+$ mixed-ligand complexes are observed between pH 8 and 11 for the species with α-Alaha, whereas for the complex with β-Alaha the final change of the spectrum is achieved at about pH 10.5 (Table 6). The spectra reveal an apparently stronger rhombic distortion in the case of mixed-ligand species with α-Alaha than that for the complex with β-Alaha and this effect appeared to be the highest for $[Cu(Me_5dien)H_{-1}]$ at pH 12. It is especially noteworthy that the spectrum of the ethanolic solution of the polycrystalline sample precipitated from the ethanol solution of the Cu–Me_5dien–α-Alaha system exhibits exactly the same parameters as that observed between pH 8.1 and 11 for this system in aqueous solution. This not accidental resemblance strongly supports the fact that the spectra are associated with the same thermodynamically $[Cu(Me_5dien)(α\text{-Alaha})]^+$ complex. The EPR spectral difference between both main mixed-ligand complexes may be only assigned to the dissimilar chelate rings formed by aminohydroxamic acid—a five-membered ring for the species with α-Alaha and a six-membered ring for the species with β-Alaha as is shown in the proposed structure (Scheme 1). It is remarkable that the spectral pattern consistent with a strictly trigonal-bipyramidal geometry of the complexes as observed for $[CuX(Me_6tren)^+]$, where Me_6tren is tris(2-dimethylaminoethyl)amine and X = Br, I) [21] is not reached and only an increasing distortion from square-pyramidal is observed in the following order: $[Cu(Me_5dien)(β\text{-Alaha})H]^{2+} < [Cu(Me_5dien)(α\text{-Alaha})H]^{2+}) < [Cu(Me_5dien)(β\text{-Alaha})]^+ < [Cu(Me_5dien)(α\text{-Alaha})]^+$

The basicity-adjusted stability constants, $\log K_{[Cu(Me_5dien)(α\text{-Alaha}/β\text{-Alaha})]} - \Sigma\, pK_L$, for $[Cu(Me_5dien)(α\text{-Alaha})]^+$ and $[Cu(Me_5dien)(β\text{-Alaha})]^+$ are −8.61 and −11.77, respectively (Table 5). These values show that the complex formed with α-Alaha is more stable than that formed with β-Alaha. It seems that the basicity of the coordinating donor groups is over-compensated by the chelating effect which is clearly seen in the case when the $\{N_{amino}, N_{hydrox.}\}$ donor set (provided by aminohydroxamate ligands) is involved in copper(II) chelation. Thus, due to the preference of Cu^{2+} for five- rather than six-membered chelation [22], the complex with α-Alaha is found to be more stable.

The comparison of the concentration distribution curves presented for the Cu^{2+}–Me_5dien–β-Alaha system in Fig. 3(b) together with those for Cu^{2+}–dien–β-Alaha (Fig. 3(d)) reveal that the coordination of β-Alaha towards $[Cu(Me_5dien)]^{2+}$ begins at a much lower pH (pH ≈ 2.50) than towards $[Cu(dien)]^{2+}$ (pH ≈ 6). In the latter system the presence of dien suppresses the formation of pentameric $[Cu_5(β\text{-Alaha})_4H_{-4}]^{2+}$ species whereas in the system with Me_5dien this species appears above pH 4 and reaches two maxima (ca. 50% at pH 6 and close to 100% above pH 12) and one minimum around pH 8.8 (Fig. 3(b)). In the binary system this complex is a main component in the whole pH range.

Very interesting information can be obtained from the comparison of the ternary systems with hydroxamic acids as against those with amino acids (Table 5). The relatively more favoured formation of the complexes involving the mixed bonding mode is showed by results obtained for the studied systems with dien. The order of decreasing stability ($\log K_{[Cu(dien)L]} - \Sigma\, pK_L$) is: $[Cu(dien)(α\text{ - Ala})]^+ > [Cu(dien)(β\text{ - Ala})]^+ > [Cu(dien)(α\text{-Alaha})]^+ > [Cu(dien)(β\text{-Alaha})]^+$ which corresponds to the existence of (N,O) > (N,O) > (N,N) > (N,N) chelate donors of the ligand L and (5) > (6) > (5) > (6) chelate rings of this ligand.

In the case of the systems with Me_5dien this fact is not confirmed. The order of decreasing stability ($\log K_{[Cu(Me_5dien)L]} - \Sigma\, pK_L$) is: $[Cu(Me_5dien)(α\text{-Ala})]^+ > [Cu(Me_5dien)(α\text{ - Alaha})]^+ > [Cu(Me_5dien)(β\text{ - Ala})]^+ > [Cu(Me_5dien)(β\text{-Alaha})]^+$ which corresponds to the existence of (N,O) > (N,N) > (N,O) > (N,N) chelate donors of the ligand L and (5) > (5) > (6) > (6) chelate rings of this ligand.

This order reflects that the chelate containing the pure five-membered rings are favoured over systems with the five- and six-membered rings in the mixed-ligand five coordination complexes with Me_5dien. It is well known that the formation of six-membered chelate rings generally results in a decrease of thermodynamic stability and distortion of coordination geometry of the complexes.

Our spectroscopic data show that the geometry of the mixed-ligand five-coordination complexes consisting of copper(II), Me_5dien and L is closer to trigonal-bipyramidal in the case when L = α-Alaha (see Fig. 2) and when L = β-Alaha the spectrum indicates that the geometry of this mixed-ligand complex is closer to square-pyramidal (see above).

In conclusion, both thermodynamic and structural parameters are rather sensitive functions of the sizes of linked chelate systems. On the other hand, it should be emphasised that there is not a strict relationship between the thermodynamic and structural parameters.

4. Conclusion

Studying the mixed-ligand complexes: $[Cu(en)(α\text{-Alaha})]^+$, $[Cu(dien)(α\text{-Alaha})]^+$, $[Cu(dien)(β\text{-Alaha})]^+$, $[Cu(dien)(Hisha)]^+$, $[Cu(dien)(Metha)]^+$, $[Cu(Me_5dien)(α\text{-Alaha})]^+$ and $[Cu(Me_5dien)(β\text{-Alaha})]^+$ we could see the phenomena of the plasticity of the coordination sphere of copper(II). In these complexes the geometry around the copper(II) atom is controlled first of all by the polyamine, i.e. by the number of nitrogen atoms

which may occupy coordination sites. In the case of $[Cu(en)(\alpha\text{-Alaha})]^+$ bidentate amine occupies two coordination sites and α-Alaha is coordinated in the same way as in the binary system; the mixed-ligand complex has a planar geometry and 4N coordination. The other above-mentioned complexes with tridentate amines are five-coordinate species but species with dien have a geometry slightly deviated from square-pyramidal whereas species with Me_5dien have a geometry closer to trigonal-bipyramidal probably because of steric reasons.

An increasing distortion of the $[Cu(Me_5dien)H_2O]^{2+}$ complex geometry in comparison with $[Cu(dien)H_2O)]^{2+}$ has no influence on their relative stability but results in higher stability of the mixed-ligand complexes with Me_5dien than those with dien ($\log K_{[Cu(Me_5dien)L]} > \log K_{[Cu(dien)L]}$). Murakami et al. [18] observed the same tendency for the ternary systems in which ligand L was replaced by an amino acid.

The present of additional groups in the side chain of the aminohydroxamic acids, i.e. a $CH_3–S–CH_2–$ group in methioninehydroxamic acid or an imidazole ring in histidinehydroxamic acid do not cause considerable deformations of the coordination geometry [3].

References

[1] B. Kurzak, D. Kroczewska, J. Coord. Chem. 34 (1995) 67.
[2] B. Kurzak, D. Kroczewska, J. Jezierska, Polyhedron 17 (1998) 1831.
[3] B. Kurzak, K. Bogusz, D. Kroczewska, J. Jezierska, Polyhedron 20 (2001) 2627.
[4] B. Kurzak, K. Kurzak, J. Jezierska, Inorg. Chim. Acta 125 (1986) 77.
[5] G. Gran, Acta Chem. Scand. 4 (1950) 599.
[6] B. Kurzak, E. Farkas, T. Glowiak, H. Kozlowski, J. Chem. Soc., Dalton Trans. (1991) 163.
[7] Stability Constants of Metal-Ion Complexes: Part B. Organic Ligands, IUPAC Chemical Data Series, No. 22, compiled by D.D. Perrin, Pergamon Press, UK, Wheaton & Co. Ltd., Exeter, 1983.
[8] P. Gans, A. Sabatini, A. Vacca, J .Chem. Soc., Dalton Trans. (1985) 1195.
[9] E. Farkas, T. Kiss, B. Kurzak, J. Chem. Soc., Perkin Trans. 2 (1990) 1255.
[10] F. Thaler, C.D. Hubbard, F.W. Heinemann, R. van Eldick, S. Schindler, I. Fabian, A.M. Dittler-Klingemann, F.E. Hahn, C. Orvig, Inorg. Chem. 37 (1998) 4022.
[11] H. Sigel, Angew. Chem., Int. Ed. Engl. 14 (1975) 394.
[12] H. Sigel, B.E. Fischer, B. Prijs, J. Am. Chem. Soc. 99 (1977) 4489.
[13] H. Sigel, Metal Ions in Biological Systems, vol. 2, Marcel Dekker, New York, 1973, pp. 105–107.
[14] S. Tyagi, B.J. Hathaway, J. Chem. Soc., Dalton Trans. (1981) 2029.
[15] S. Tyagi, B.J. Hathaway, S. Kremer, H. Stratemeier, D. Reinen, J. Chem. Soc., Dalton Trans. (1984) 2087.
[16] T. Murakami, T. Takei, Y. Ishikawa, Polyhedron 16 (1997) 89.
[17] D. Meyerstein, Coord. Chem. Rev. 185–186 (1999) 141.
[18] T. Murakami, K. Murata, Y. Ishikawa, Inorg. Chim. Acta 244 (1996) 51.
[19] N. Azuma, Y. Kohno, K. Izshizu, T. Takakuwa, S. Tsuboyama, K. Tsuboyama, K. Kobayashi, T. Sakurai, Inorg. Chim. Acta 215 (1994) 109.
[20] E. Farkas, E. Kozma, T. Kiss, I. Toth, B. Kurzak, J. Chem. Soc., Dalton Trans. (1995) 477.
[21] R. Barbucci, A. Bencini, D. Gatteschi, Inorg. Chem. 16 (1977) 2117.
[22] I. Sovago, D. Sanna, A. Dessi, K. Varnagy, G. Micera, J. Inorg. Biochem. 63 (1996) 99.

PERGAMON

Polyhedron 21 (2002) 305–312

POLYHEDRON

www.elsevier.com/locate/poly

1,4-Diaza-1,3-diene niobium chlorides: syntheses and X-ray crystal structures of (*t*-Bu-DAD)$NbCl_3$(THF), (*t*-Bu-DAD)$_2$NbCl, and [(*t*-Bu-DAD)$NbCl_4$](H_3N*t*-Bu)

Joachim Scholz [a,*], Helmar Görls [b]

[a] *Institut für Chemie, Universität Koblenz-Landau, Rheinau 1, D-56075 Koblenz, Germany*
[b] *Institut für Anorganische und Analytische Chemie der Friedrich-Schiller-Universität Jena, Lessingstraße 8, D-07743 Jena, Germany*

Received 18 July 2001; accepted 8 November 2001

Abstract

The new 1,4-diaza-1,3-diene niobium complexes (*t*-Bu-DAD)$NbCl_3$(THF) (**2**) and (*t*-Bu-DAD)$_2$NbCl (**3**) [*t*-Bu-DAD≡(*t*-Bu)N=CHCH=N(*t*-Bu)] have been prepared in 75–82% isolated yields by replacing of two or four chlorine atoms of $NbCl_5$ by the sterically demanding *t*-Bu-DAD ligand. In addition, we also describe the ionic Nb(V) complex [(*t*-Bu-DAD)$NbCl_4$](H_3N*t*-Bu) (**6**) which was formed as a byproduct during the preparation of **2**. The new compounds have been characterized in solution by NMR measurements as well as by X-ray analyses in solid state. The structural parameters within the *t*-Bu-DAD ligand of **6** are in agreement with a chelating enediamido dianion. On the other hand the N–C and C–C bond distances of the *t*-Bu-DAD ligand of **2** are rather comparable to those found in complexes having a radical–anionic *t*-Bu-DAD ligand. The higher steric crowding at the niobium center caused by two 1,4-diaza-1,3-diene ligands in **3** leads to a significant asymmetric distortion of the 1,3-diaza-2-niobacyclopent-4-ene rings. However, none of the 1,4-diaza-1,3-diene ligands of **2**, **3** or **6** is coordinated in the sterically less demanding η2-C,N bonding mode as found in the binuclear complex (*t*-Bu-DAD)$_5Nb_2$ (**4**). © 2002 Elsevier Science Ltd. All rights reserved.

Keywords: Niobium complexes; Heterodiene; 1,4-Diaza-1,3-diene; X-ray crystal structures

1. Introduction

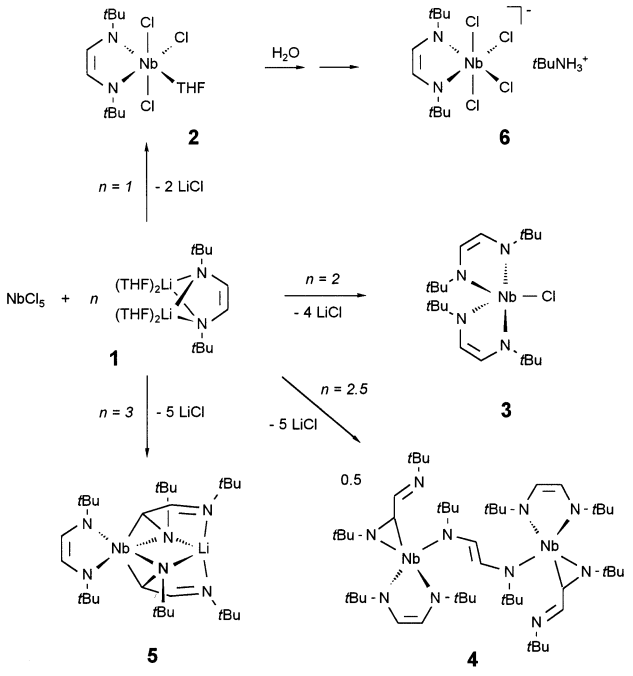
1,4-Diaza-1,3-diene (DAD) metal complexes have been shown to play an important role in homogeneous catalytic reactions. Ni(DAD) complexes, for instance, are very active catalysts for the homo and copolymerization of alkenes [1], Ru(DAD) complexes were used to catalyze the hydrogenation, the hydrosilylation and the isomerization of alkenes [2], whereas in other cases Fe(DAD) complexes are effective and selective catalysts for the cyclodimerization of 1,3-dienes [3]. The structural chemistry of 1,4-diaza-1,3-diene complexes of late transition metals is dominated by the versatile coordination behavior of this type of organic ligand [4]. This versatility arises from the ability of the 1,4-diaza-1,3-dienes to use both the lone pairs of the nitrogen atoms (σ-donor) and the π system of the two C=N bonds (π-acceptor) for coordination to a metal.

Recently, we reported about the novel niobium 1,4-diaza-1,3-diene complexes **4** and **5** (Scheme 1) [5]. With regard to the stability of the early transition metals in their highest oxidation state it is not surprising, that the 1,4-diaza-1,3-diene ligands in **4** and **5** as in other 1,4-diaza-1,3-diene complexes of Group 4 and 5 metals [6] formally have been double reduced to the dianion. Nevertheless, complexes **4** and **5** are the first examples which demonstrate that other coordination types than the ordinary chelate form are also possible for 1,4-diaza-1,3-diene ligands bound to early transition metals. Most spectacular is the molecular structure of the dinuclear niobium complex **4** which shows five 1,4-diaza-1,3-diene ligands in three different bonding situations.

In this paper, we complete the series of 1,4-diaza-1,3-diene niobium complexes by the chloride complexes

* Corresponding author. Tel.: +49-261-9119-328; fax: +49-261-9119-321.
E-mail address: scholz@uni-koblenz.de (J. Scholz).

0277-5387/02/$ - see front matter © 2002 Elsevier Science Ltd. All rights reserved.
PII: S0277-5387(01)00989-5



Scheme 1.

(*t*-Bu-DAD)$NbCl_3$(THF) (**2**) and (*t*-Bu-DAD)$_2$NbCl (**3**) [*t*-Bu-DAD=(*t*-Bu)N=CHCH=N(*t*-Bu)] which have been prepared by replacing of two or four halogen atoms of $NbCl_5$ by the sterically demanding *t*-Bu-DAD ligand. In addition, we also describe the ionic Nb(V) complex [(*t*-Bu-DAD)$NbCl_4$](H_3N*t*-Bu) (**6**) which was formed as a byproduct during the preparation of **2**.

2. Results and discussion

2.1. Syntheses of (t-Bu-DAD)$NbCl_3$(THF) (2), (t-Bu-DAD)$_2$NbCl (3) and [(t-Bu-DAD)$NbCl_4$][t-BuNH_3] (6)

The 1,4-diaza-1,3-diene niobium chloride complex (*t*-Bu-DAD)$NbCl_3$(THF) (**2**) was synthesized by reaction of the lithium 1,4-diaza-1,3-diene compound Li_2(*t*-Bu-DAD) (**1**) [7] with 1 equiv. of $NbCl_5$ in THF according to Scheme 1. Removal of the solvent after the reaction gave a dark red residue, from which **2** could be isolated by extracting with diethyl ether as purple crystals in good yield (75%). Complex **2** is thermally stable but very air-sensitive and only sparingly soluble in diethyl ether but moderately soluble in THF. Crystals suitable for an X-ray study were obtained by cooling a saturated THF solution of 2 to −20 °C for 1 week.

A minor byproduct (about 5%) formed during the synthesis of **2** was identified as [(*t*-Bu-DAD)$NbCl_4$][*t*-BuNH_3] (**6**). This complex probably arises from the reaction of **2** with traces of water which could have contaminated the ether solution during the purification of **2** but the details of the formation of **6** are not yet understood. Complex **6** is sparingly soluble in THF and crystals of **6** suitable for an X-ray diffraction study were found during an attempt to grow crystals of **2**.

A dark brown crystalline solid of (*t*-Bu-DAD)$_2$NbCl (**3**) (see Scheme 1) was isolated in high yield (82%) by reaction of $NbCl_5$ with 2 equiv. of **1** in THF, and crystallization from pentane and ether. In contrast to **2** complex **3** is highly soluble in aliphatic and aromatic solvents and is considerable volatile. The robustness of this complex is convincingly demonstrated by the fact that the molecular ion peak in the electron impact mass spectra appears as basis peak. Single crystals of **3** suitable for an X-ray diffraction study were grown from a saturated ether solution.

2.2. X-ray diffraction studies

Single-crystal X-ray studies on the compounds **2**, **3** and **6** were carried out in order to have a complete set of structural parameters for **1**–**6** and to determine to what extent the 1,4-diaza-1,3-diene bonding mode is influenced by changing the electronic and steric situation at the metal center. The molecular structures of **2**, **3**, and **6** with their atom labeling schemes are shown in Figs. 1–3. Selected intramolecular bond lengths and angles are listed in Tables 1–3. Table 4 contains the crystal data for these complexes.

Some general comments about these structures are warranted. The structural parameters and the NMR data we have obtained for the new complexes **2**, **3** and **6** are largely consistent with a bonding situation found in most other 1,4-diaza-1,3-diene complexes of early transition metals [6]. The heterodiene ligands are bonded as *N*,*N*-chelates forming five-membered rings which have a folded geometry with the niobium atom lying out of the plane of the NC=CN backbone. Usually the lack of planarity of the metallacyclic rings in

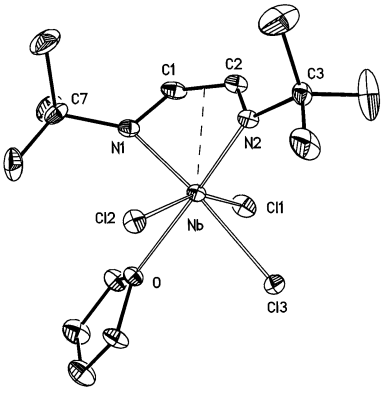


Fig. 1. Molecular structure of **2** (ORTEP drawing) with the atom numbering scheme. The thermal ellipsoides are scaled to enclose 50% probability.

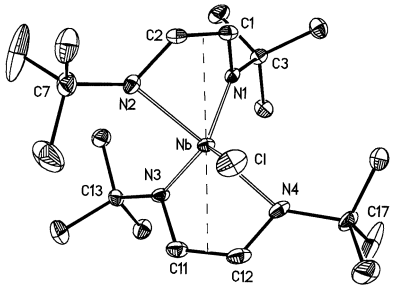


Fig. 2. Molecular structure of **3** (ORTEP drawing) with the atom numbering scheme. The thermal ellipsoides are scaled to enclose 50% probability.

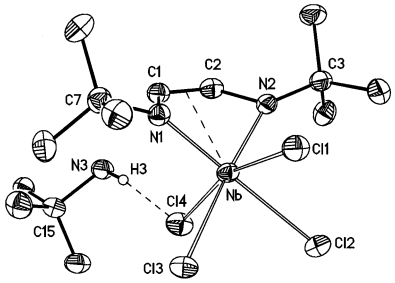


Fig. 3. Molecular structure of **6** (ORTEP drawing) with the atom numbering scheme. The thermal ellipsoides are scaled to enclose 50% probability.

Table 1
Selected bond lengths (Å) and angles (°) for (*t*-Bu-DAD)$NbCl_3$(THF) (**2**)

Bond lengths			
Nb–N1	1.973(3)	Nb–N2	1.961(3)
Nb–Cl1	2.397(1)	Nb–Cl2	2.408(1)
Nb–Cl3	2.465(1)	Nb–O	2.314(2)
Nb–C1	2.359(4)	Nb–C2	2.389(4)
N1–C1	1.298(5)	N2–C2	1.345(5)
C1–C2	1.414(5)		
Bond angles			
N1–Nb–N2	87.40(10)	Cl1–Nb–Cl2	160.17(4)
Cl1–Nb–Cl3	84.28(4)	Cl2–Nb–Cl3	83.94(5)
N1–Nb–Cl1	100.87(9)	N1–Nb–Cl2	89.93(9)
N1–Nb–Cl3	173.32(9)	N2–Nb–Cl1	82.67(10)
N2–Nb–Cl2	92.87(9)	N2–Nb–Cl3	95.52(8)
N1–Nb–O	91.94(10)	N2–Nb–O	174.23(9)
Cl1–Nb–O	81.66(7)	Cl2–Nb–O	81.39(7)
Cl3–Nb–O	84.56(6)		
(Nb, N1, N2)(N1, C1, C2, N2)	123.2(1)		
Sum of angles at N1	359.8(3)	N2	358.4(3)

these 1,4-diaza-1,3-diene complexes has been taken as proof of an enediamide ligand donating to a d^0 metal center and forming a metallacyclopentene ring and not a π-bonded 1,4-diaza-1,3-diene ligand. In both **2**, **3** and **6**, the ring folding moves the internal carbons, C1 and C2, of the 1,3-diaza-2-niobacyclopentene rings closer to the electrophilic niobium center. The corresponding Nb–C1 and Nb–C2 distances of 2.36–2.49 Å imply that these complexes could experience some stabilization from a weak attractive interaction between the filled π-orbital of the C1=C2 double bond and an empty metal orbital. However, the absence of any significant difference in the C1=C2 bond distances of the complexes **2** (1.414(5) Å) and **3** (1.386(6), 1.414(7) Å) and the fact that the folding angles are quite comparable (**2**: 123.2(1)°; **3**: 123.4(1)°, 122.4(2)°) and do not reflect the different coordination geometries of these two niobium complexes suggests that this type of π-interaction is probably not a major factor in determining the relative stability of the nonplanar structures.

*2.3. Solid state structures of (t-Bu-DAD)$NbCl_3$(THF) (**2**) and [(t-Bu-DAD)$NbCl_4$][H_3Nt-Bu] (**6**)*

The distorted octahedral coordination sphere about the niobium atom of complex **2** consists of the three chlorine atoms, the coordinated THF molecule, and the two nitrogen donors of a symmetrically-chelating *t*-Bu-DAD ligand. A small *trans* influence is observed when the niobium–chlorine distances are compared. The Nb–Cl1 (2.397(1) Å) and Nb–Cl2 (2.408(1) Å) bond lengths are typical and compare well to terminal Nb–Cl distances found in other Nb(V) complexes [8], while the Nb–Cl3 distance (*trans* to N1) is somewhat longer (2.465(1) Å). Surprisingly the C–N bond lengths within the *t*-Bu-DAD ligand of **2** (N1–C1 1.298(5), N2–C2 1.345(5) Å) do not fall within the range 1.38–1.42 Å, observed for related enediamide complexes that conform to the metallacyclopentene structure [6]. Accordingly the C1–C2 bond length (1.414(5) Å) is significantly longer than expected for a double bond and much closer to the C–C single bond of *t*-Bu-DAD [7b,9]. In contrast to the results of the NMR spectroscopic investigations (vide infra) which clearly demonstrate the presence of a diamagnetic d^0 enediamide niobium(V) complex these N–C and C–C bond distances are rather comparable to those found in complexes having a radical–anionic *t*-Bu-DAD ligand [10]. Furthermore it is remarkable, that the folding of the (N1, C1, C2, N2) plane relative to the (Nb, N1, N2) plane is not accompanied by a rehybridization of the nitrogen atoms to sp^3. The sum of angles at N1 (359.8(3)°) and N2 (358.4(3)°) demonstrates that the nitrogen atoms are arranged in the plane of the surrounding three atoms. This coordination geometry about the amido nitrogen atoms together with the relatively short Nb–N bond distances (Nb–N1 1.973(3), Nb–N2 1.961(3) Å) [11] suggests that these nitrogen atoms act as four-electron donors in this molecule.

On the other hand the homologous 1,4-diaza-1,3-diene niobium complex (*i*-Pr-DAD)$NbCl_3$(THF) (**7**), [*i*-Pr-DAD≡(*i*-Pr)N=CHCH=N(*i*-Pr)] (Scheme 2) [12],

Table 2
Selected bond lengths (Å) and angles (°) for (t-Bu-DAD)$_2$NbCl (**3**)

Bond lengths			
Nb–N1	1.962(4)	Nb–N2	2.110(3)
Nb–N3	1.978(4)	Nb–N4	2.111(4)
Nb–C1	2.432(4)	Nb–C2	2.492(4)
Nb–C11	2.429(4)	Nb–C12	2.471(5)
N1–C1	1.401(5)	N2–C2	1.365(5)
N3–C11	1.395(5)	N4–C12	1.325(7)
C1–C2	1.386(6)	C11–C12	1.414(7)
Nb–Cl	2.523(1)		
Bond angles			
N1–Nb–N2	86.3(1)	N3–Nb–N4	85.9(2)
(Nb, N1, N2)(N1, C1, C2, N2)	123.4(1)		
(Nb, N3, N4)(N3, C11, C12, N4)	122.4(2)		
(Nb, N1, N2)(Nb, N3, N4)	78.0(1)		
Sum of angles at			
N1	358.6(3)	N2	351.2(3)
N3	357.9(3)	N4	351.4(3)

Table 3
Selected bond lengths (Å) and angles (°) for [(t-Bu-DAD)NbCl$_4$][t-BuNH$_3$] (**6**)

Bond lengths			
Nb–N1	1.962(3)	Nb–N2	1.979(3)
Nb–Cl1	2.424(1)	Nb–Cl2	2.571(1)
Nb–Cl3	2.523(1)	Nb–Cl4	2.434(1)
Nb–C1	2.416(4)	Nb–C2	2.423(4)
N1–C1	1.373(5)	N2–C2	1.381(5)
C1–C2	1.395(6)	Cl4···H30	2.24(1)
Bond angles			
N1–Nb–N2	88.8(1)	Cl1–Nb–Cl2	84.02(4)
Cl1–Nb–Cl3	83.24(4)	Cl1–Nb–Cl4	162.54(4)
Cl2–Nb–Cl3	86.21(4)	Cl2–Nb–Cl4	82.77(4)
Cl3–Nb–Cl4	84.54(4)	N1–Nb–Cl1	92.2(1)
N3–H30–Cl4	163.6(10)		
(Nb, N1, N2)(N1, C1, C2, N2)	125.4(3)		
Sum of angles at			
N1	356.1(3)	N2	356.0(3)

exhibits ordinary Nb–N bond distances (2.048(2) and 2.057(2) Å) without any significant π-bonding contribution.

Moreover, in contrast to that of **2**, the five-membered ring (Nb–N–C=C–N) is hardly folded (6.3(2)°) and two chlorine atoms are found in the plane of the 1,4-diaza-1,3-diene. It is very surprising that an apparent unimportant change at the ligand periphery has such significant consequences for the structure of **7**. We found that these unusual structural parameters are caused by hydrogen bonds between the metal-bonded chlorine atoms and the methine hydrogen atoms of the isopropyl groups. To date there are hardly any compounds known in which chlorine atoms are covalently bound and nevertheless participate in C–H···Cl hydrogen bonds.

Complex **6** crystallizes as an ionic compound consisting of a niobate(V) anion and one *tert*-Butylammonium cation to balance the charge. The overall geometry of the [(t-Bu-DAD)NbCl$_4$]$^-$ anion and in particular the bonding parameters of the reduced heterodiene ligand are in close agreement with those of **2**. The environment about the niobium atom corresponds to a distorted octahedron with four chlorine ligands and the two N-donors of the t-Bu-DAD ligand. The *cis* chlorine–niobium–chlorine angles ranging from 82.77(4)° to 86.21(4)°, while the *trans* angle Cl1–Nb–Cl2 spans 162.54(4)°. Closer inspection of the crystal structure reveals that the *tert*-Butylammonium hydrogen atom H3 is hydrogen bonded to Cl4 (H3···Cl4 2.24(1) Å, N3–H3–Cl4 163.6(10)°). Nevertheless, the Nb–Cl4 distance (2.434(1) Å) which is not longer than those of Nb–Cl1 (2.424(1) Å), Nb–Cl2 (2.571(1) Å), and Nb–Cl3 (2.523(1) Å), implies that this interaction is rather weak. Moreover, the N–H3···Cl2 hydrogen bonding observed in **6** should not be viewed as unusual, since

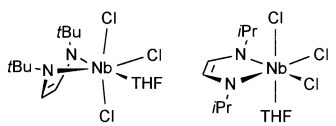
Table 4
Crystallographic data and details of data collection and refinement of **2**, **3** and **6**

Compound	**2**	**3**	**6**
Chemical formula	$C_{14}H_{28}Cl_3N_2NbO$	$C_{20}H_{40}ClN_4Nb$	$C_{18}H_{42}Cl_4N_3NbO$
Molecular weight (g mol^{-1})	439.64	464.92	551.26
Temperature (K)	293(2)	183(1)	183(1)
Crystal system	orthorhombic	monoclinic	monoclinic
Space group	*Pbca* (No. 61)	I_2/a (No. 15)	$P2_1/n$ (No. 14)
Cell parameter			
a (Å)	9.395(3)	19.360(4)	11.9195(8)
b (Å)	14.035(8)	12.748(6)	12.4925(5)
c (Å)	30.20(2)	19.734(2)	18.742(1)
β (°)		97.78(3)	105.557(2)
V (Å^3)	3982(4)	4825(2)	2688.5(3)
Number of formula units Z	8	8	4
D_{calc} (g cm^{-3})	1.466	1.280	1.362
Absorption coefficient μ (cm^{-1})	10.07	6.20	8.58
Crystal dimension (mm)	$0.40 \times 0.35 \times 0.34$	$0.40 \times 0.38 \times 0.36$	$0.35 \times 0.32 \times 0.28$
2θ Range (°)	2–55	2–55	2–55
Reflections collected	15398	5619	7049
Observed data [$I > 2\sigma(I)$]	1798	4635	2864
Number of variables	190	235	267
R_1	0.0703	0.069	0.0406
wR_2	0.1565	0.214	0.0942
Residual electron density (e Å^{-3})	1.574, −1.528	2.14, −3.24	0.422, −0.620

there are many other examples of related N–H···Cl–M complexes [8b,13].

2.4. Solid state structure of (t-Bu-DAD)$_2$NbCl (3)

Unlike the complexes **2** and **6** the Nb atom in **3** has the coordination number five if only the lone pair donor sites of the ligands are taken into account. Moreover, the binding of the *t*-Bu-DAD ligands is slightly asymmetric, as seen by different Nb–N bond distances (Nb–N1 1.962(4), Nb–N2 2.110(3), Nb–N3 1.978(4), Nb–N4 2.111(4) Å). According to this asymmetric bonding mode only the nitrogen atoms N1 and N3 which exhibit significantly shorter Nb–N bond distances maintain a planar sp^2 environment, as seen by the summation of angles about N1 and N3 (358.6(3)° and 357.9(3)°). The nitrogen atoms N2 and N4 tend appreciably more towards pyramidality, with angle sums of 351.2(3)° and 351.4(3)°. The dihedral angle between the planes containing the atoms Nb, N1, N2 and Nb, N3, N4 is 78.0(1)°. The slightly longer niobium–chlorine bond (2.523(1) Å) in **3** can be rationalized by the presence of the two heterodiene ligands and no other halogen atoms which make the central metal less electrophilic, relative to that in **2** or **6**. Consequently, a longer bond length of the chlorine atom to the niobium atom in **3** ensues.



2 **7**

Scheme 2.

2.5. Solution structures of 2 and 3

The ^{1}H NMR spectrum of **2** in THF-d_8 at room temperature (300 MHz) exhibits the HC=CH and the *t*-Bu signal as single peaks at δ 6.44 and δ 1.51, as well as a set of the THF proton signals. Their relative intensities indicate that **2** contains one coordinated THF molecule. Furthermore, the simplicity of the ^{1}H NMR spectrum at room temperature suggests that a dynamic process is occurring that in contrast to the solid state structure renders the two ends of the 1,4-diaza-1,3-diene ligand equivalent. On cooling the sample to −80 °C the low-temperature limiting spectrum is observed, with two separate resonances for the backbone protons at δ 6.69 and 6.64 as well as two signals for the *t*-Bu protons at δ 1.58 and 1.54. This observation is consistent with a rapid (NMR time scale) exchange process involving probably the inversion of the folded 1,3-diaza-2-niobacyclopentene ring and equilibrating the geminal protons of the ligand backbone and that of the *t*-Bu groups. The final limiting low-temperature spectra is totally consistent with the observed solid-state structure of **2**.

The ^{1}H NMR spectrum of complex **3** acquired at −80 °C contains four sharp signals for the *t*-Bu hydrogens (δ 1.38, 1.21, 1.15, and 0.98) and four doublets for the HC=CH groups which is in agreement with the lack of any symmetry of the solid structure of **3**. As the temperature is raised up to ambient temperature, both the *t*-Bu and the HC=CH resonances broaden and collapse into one signal, respectively (*t*-Bu δ 1.29, HC=CH δ 6.10). These NMR results of **3** coupled with the solid state geometry suggests that the enediamide units show a dynamic behavior passing through an apparent molecular plane of symmetry. In other words, we assume that the folded 1,3-diaza-2-niobacyclopentene rings undergo a ring inversion which is rapid on the NMR time scale at room temperature [6c,6e,6l].

3. Concluding remarks

Reaction of $NbCl_5$ with Li_2(*t*-Bu-DAD) offers a convenient synthetic route for the preparation of the 1,4-diaza-1,3-diene niobium halogenide complexes **2** and **3** in consistently good isolated yields and provide the opportunity to evaluate structural changes due to the stepwise replacement of chlorides by the heterodienes. X-ray studies completed by variable-temperature NMR measurements show that the 1,4-diaza-1,3-diene ligand in **2** is strongly bound as a *N*,*N*-chelate to the metal center with structural parameters consistent with a folded 1,3-diaza-2-niobacyclopentene ring bonding description. Furthermore, comparison of the structural data of **2** and **3** shows that the lower steric requirements of only one 1,4-diaza-1,3-diene ligand in **2** enhance the metals Lewis acidity and even permit the addition of one molecule THF. The higher steric crowding caused by two 1,4-diaza-1,3-diene ligands in **3** leads to a significant asymmetric distortion of the 1,3-diaza-2-niobacyclopentene rings. However, none of the 1,4-diaza-1,3-diene ligands is coordinated in the sterically less demanding η^2-C,N bonding mode as found in **4** [5] and in Cp*Ta(η^2-*t*-Bu-DAD)(S-*t*-Bu)2 [14]. Altogether, the complete series of niobium complexes **2**–**5** confirms that the 1,4-diaza-1,3-diene bonding mode in this type of compounds is mainly influenced by the sterical situation of the metal center.

4. Experimental

4.1. General procedures

All reactions were carried out under Ar with strict exclusion of moisture using standard Schlenk techniques [15]. Solvents were dried over and distilled from Na–benzophenone ketyl under Ar, except for CD_2Cl_2, which was distilled from activated molecular sieves (3 Å). $NbCl_5$ was purchased from Aldrich. *t*-Bu-DAD [16] and Li_2(*t*-Bu-DAD) [7] were prepared according to literature procedures.

NMR spectra were recorded on a Varian Gemini 300 BB spectrometer with deuterated solvents as an internal lock. ^{1}H (300 MHz) and ^{13}C NMR (75 MHz) shifts are referenced to internal solvent resonances and reported relative to TMS. MS studies were performed on a Intectra AMD 402 instrument with 70 eV electron impact ionization. Elemental analyses were carried out at the Mikroanalytisches Laboratorium of the Chemical Department at the Martin-Luther-Universität Halle-Wittenberg.

4.2. (*t*-Bu-DAD)$NbCl_3$(THF) (**2**)

To a solution of 6.42 g of $NbCl_5$ (23.8 mmol) in 100 ml THF cooled to −60 °C was added dropwise with stirring a solution of 23.8 mmol of Li_2(*t*-Bu-DAD) in 100 ml of THF prepared by addition of 0.33 g lithium (47.6 mmol) to a solution of 4.00 g *t*-Bu-DAD (23.8 mmol) in THF. The reaction mixture was allowed to warm to room temperature (r.t.) within 2 h whereupon a red brown color developed. After stirring for a further 12 h, the solvent was removed in vacuo and the residue was extracted several times with 100 ml of Et_2O. Cooling of the extract to −20 °C overnight afforded a purple crystalline material (7.87 g, 17.9 mmol, 75%). Single crystals suitable for X-ray crystallography were obtained by slow cooling of a solution of **2** in THF. ^{1}H NMR (d_8-THF) + 20 °C: δ 6.44 (s, 2H; *H*C=C*H*), 3.62 (m, 4H; OCH_2, THF), 1.77 (m, 4H; OCH$_2$CH_2, THF), 1.51 (s, 18H; CMe_3); −80 °C: δ 6.69 (d, ^3J(H,H) = 2.0 Hz, 1H; *H*C=C*H*), 6.64 (d, ^3J(H,H) = 2.0 Hz, 1H; *H*C=C*H*), 3.62 (m, 4H; OCH_2, THF), 1.80 (m, 4H; OCH$_2$CH_2, THF), 1.58 (s, 9H; CMe_3), 1.45 (s, 9H; CMe_3); (CD_2Cl_2) + 20 °C: δ 6.31 (s, 2H; *H*C=C*H*), 4.14 (m, 4H; OCH_2, THF), 1.95 (m, 4H; OCH$_2$CH_2, THF), 1.55 (s, 18H; CMe_3). ^{13}C NMR (d_8-THF) + 25 °C: δ 102.48 (d, ^1J(C,H) = 180.2 Hz, ^2J(C,H) = 10.4 Hz; H*C*=*C*H), 68.21 (t, OCH_2, THF), 64.85 (s; *C*Me$_3$), 29.69 (q, ^1J(C,H) = 127.2 Hz; CMe_3), 26.24 (t, ^1J(C,H) = 135.3 Hz; OCH$_2$*C*H$_2$, THF); (CD_2Cl_2) 25 °C: δ 101.01 (d, ^1J(C,H) = 178.5 Hz, ^2J(C,H) = 10.6 Hz; H*C*=*C*H), 71.07 (t, ^1J(C,H) = 146.7 Hz; OCH_2, THF), 65.26 (s; *C*Me$_3$), 29.70 (q, ^1J(C,H) = 128.8 Hz; CMe_3), 25.64 (t, ^1J(C,H) = 135.3 Hz; OCH$_2$*C*H$_2$, THF). EI MS (70 eV), *m*/*z* (%): 366 (5) [M^+ − THF], 331 (8) [M^+ − Cl − THF], 310 (8) [M^+ − THF − CMe_3], 254 (24) [$C_2H_2N_2Cl_2Nb^+$], 219 (12) [$C_2H_2N_2Cl_3^+$]. *Anal.* Calc. for $C_{14}H_{28}Cl_3N_2NbO$ (439.65 g mol^{-1}): C, 38.25; H, 6.42; N, 6.37. Found: C, 37.97; H, 6.40; N, 6.52%.

4.3. (t-Bu-DAD)$_2$NbCl (3)

To a solution of 4.11 g of $NbCl_5$ (15.2 mmol) in 100 ml THF cooled to −60 °C was added dropwise with stirring a solution of 30.4 mmol of Li_2(*t*-Bu-DAD) in 100 ml of THF prepared by addition of 0.42 g Li (60.8 mmol) to a solution of 5.12 g *t*-Bu-DAD (30.4 mmol) in THF. The reaction mixture was allowed to warm to r.t. and was stirred for 12 h. The solvent was removed by evaporation in vacuum, and the product was then extracted into C_5H_{12}. The extract was concentrated to 50 ml and cooled at −20 °C overnight to give a brown crystalline solid (5.72 g, 12.3 mmol, 81%). Suitable brown–red single crystals for X-ray studies were obtained from a saturated solution of **3** in C_5H_{12} at 0 °C. ^{1}H NMR (d_8-THF, 20 °C): $\delta = 6.10$ (br s, 4H; *H*C=C*H*), 1.29 (s, 36H; C*Me*$_3$); (CD_2Cl_2, −80 °C): $\delta = 6.60$ (d, ^3J(H,H)=2.3 Hz, 1H; =C*H*), 6.48 (d, ^3J(H,H) = 2.3 Hz, 1H; =C*H*), 5.84 (d, ^3J(H,H) = 2.5 Hz, 1H; =C*H*), 5.29 (d, ^3J(H,H) = 2.5 Hz, 1H; =C*H*), 1.38 (s, 9H; C*Me*$_3$), 1.21 (s, 9H; C*Me*$_3$), 1.15 (s, 9H; C*Me*$_3$), 0.98 (s, 9H; C*Me*$_3$). ^{13}C NMR (d_8-THF, 25 °C): $\delta = 107.50$ (br, H*C*=*C*H), 59.46 (*C*Me$_3$), 31.20 (br, C*Me*$_3$). EI MS (70 eV), *m*/*z* (%): 465 (100) [M^+], 450 (15) [$M^+ -$ Me], 407 (68) [$M^+ -$ CMe$_3$], 297 (30) [$C_{10}H_{20}N_2NbCl^+$], 185 (80) [$C_2H_4N_2NbCl^+$]. *Anal.* Calc. for $C_{20}H_{40}ClN_4Nb$ (464.92 g mol^{-1}): C, 51.67; H, 8.67; N, 12.05. Found: C, 50.88; H, 8.82; N, 12.30%.

4.4. [(t-Bu-DAD)NbCl$_4$][t-BuNH$_3$] (6)

^{1}H NMR (d_8-THF, 20 °C): $\delta = 7.77$ (br s, 3H, Me$_3$CN*H*$_3$), 6.34 (br s, 2H; H*C*=C*H*), 3.38 (q, 4H; OC*H*$_2$, Et$_2$O), 1.58 (s, 18H; C*Me*$_3$), 1.46 (s, 9H; *Me*$_3$CNH$_3$), 1.11 (t, 6H; OCH$_2$C*H*$_3$, Et$_2$O). ^{13}C NMR (d_8-THF, 25 °C): $\delta = 102.02$ (H*C*=*C*H), 66.26 (O*C*H$_2$, Et$_2$O), 64.64 (*C*Me$_3$), 53.37 (*C*Me$_3$), 30.02 (C*Me*$_3$), 28.04 (C*Me*$_3$), 15.60 (OCH$_2$*C*H$_3$, Et$_2$O). *Anal.* Calc. for $C_{18}H_{42}N_3OCl_4Nb$ (551.27 g mol^{-1}): C, 39.22; H, 7.68; N, 7.62. Found: C, 39.01; H, 7.66; N, 8.10%.

4.5. X-ray crystal structure determination of 2, 3 and 6

The intensity data for the compounds **2** and **3** were collected on a Nonius CAD4 diffractometer and for compound **6** on a Nonius Kappa CCD diffractometer using graphite-monochromated Mo Kα radiation (λ = 0.7107 Å). Data were corrected for Lorentz and polarization effects, but only for **2** and **3** for absorption [17,18]. The structures were solved by direct methods (SHELXS) [19] and refined by full-matrix least squares techniques against F_o^2 (SHELXL-97) [20]. For the compounds **3** and **6** the hydrogen atoms were located by difference Fourier synthesis and refined isotropically, the hydrogen atoms of the compound **2** were included at calculated positions with fixed thermal parameters. All nonhydrogen atoms were refined anisotropically [20]. XP (SIEMENS Analytical X-ray Instruments, Inc.) was used for structure representations. Cell constants and other pertinent data are collected and recorded in Table 4.

5. Supplementary material

Crystallographic data for the structural analysis have been deposited with the Cambridge Crystallographic Data Centre, CCDC Nos. 165574, 165575, and 165576 for compounds **2**, **3**, and **6**, respectively. Copies of this information may be obtained free of charge from The Director, CCDC 12 Union Road, Cambridge CB2 1EZ, UK (fax: +44-1223-336033; e-mail: deposit@ccdc.cam.ac.uk or www: http://www.ccdc.cam.ac.uk).

Acknowledgements

Professor D. Steinborn is kindly acknowledged for providing laboratory facilities. This work has been financially supported by the Deutsche Forschungsgemeinschaft and Bayer AG.

References

[1] (a) L.K. Johnson, C.M. Killian, M. Brookhart, J. Am. Chem. Soc. 117 (1995) 6414;
(b) C.M. Killian, L.K. Johnson, M. Brookhart, Organometallics 16 (1997) 2005;
(c) L.K. Johnson, S. Mecking, M. Brookhart, J. Am. Chem. Soc. 118 (1996) 267;
(d) A.S. Abu-Surrah, B. Rieger, Angew. Chem. 108 (1996) 2627; Angew. Chem., Int. Ed. Engl. 35 (1996) 2475;
(e) G.J.P. Britovsek, V.C. Gibson, D.F. Wass, Angew. Chem. 111 (1999) 448; Angew. Chem., Int. Ed. Engl. 38 (1999) 428.
[2] M. Brockmann, H. tom Dieck, J. Klaus, J. Organomet. Chem. 301 (1986) 209.
[3] (a) H. tom Dieck, I. Kleinwächter, E.T.K. Haupt, J. Organomet. Chem. 321 (1987) 237;
(b) H. tom Dieck, A.M. Lauer, L. Stamp, R. Diercks, J. Mol. Catal. 35 (1986) 317;
(c) H. tom Dieck, J. Dietrich, Angew. Chem. 97 (1985) 795; Angew. Chem., Int. Ed. Engl. 24 (1985) 781;
(d) H. tom Dieck, C. Munz, C. Müller, J. Organomet. Chem. 384 (1990) 243;
(e) R. van Asselt, C.J. Elsevier, J. Mol. Catal. 65 (1991) L13.
[4] (a) K. Vrieze, G. van Koten, Adv. Organomet. Chem. 21 (1982) 151;
(b) K. Vrieze, J. Organomet. Chem. 300 (1986) 307.
[5] B. Richter, J. Scholz, K.-H. Thiele, J. Sieler, Angew. Chem. 107 (1995) 2865; Angew. Chem., Int. Ed. Engl. 34 (1995) 2649.
[6] (a) St. L. Latesky, A.K. McMullen, G.P. Niccolai, I.P. Rothwell, Organometallics 4 (1985) 1896;
(b) F.G.N. Cloke, H.C. de Lemos, A.A. Sameh, J. Chem. Soc., Chem. Commun. (1986) 1344;

(c) L.R. Chamberlain, L.D. Durfee, Ph.E. Fanwick, L.M. Kobriger, St.L. Latesky, A.K. McMullen, B.D. Steffey, I.P. Rothwell, K. Folting, J.C. Huffman, J. Am. Chem. Soc. 109 (1987) 6068;
(d) B. Hessen, J.E. Bol, J.L. de Boer, A. Meetsma, J.H. Teuben, J. Chem. Soc., Chem. Commun. (1989) 1276;
(e) J. Scholz, M. Dlikan, D. Ströhl, A. Dietrich, H. Schumann, K.-H. Thiele, Chem. Ber. 123 (1990) 2279;
(f) C. Woitha, U. Behrens, V. Vergopoulos, D. Rehder, J. Organomet. Chem. 393 (1990) 97;
(g) H. tom Dieck, H.J. Rieger, G. Fendesak, Inorg. Chim. Acta 177 (1990) 191;
(h) J. Scholz, A. Dietrich, H. Schumann, K.-H. Thiele, Chem. Ber. 124 (1991) 1035;
(i) F.J. Berg, J.L. Petersen, Organometallics 10 (1991) 1599;
(j) F.J. Berg, J.L. Petersen, Organometallics 12 (1993) 3890;
(k) L.G. Hubert-Pfalzgraf, A. Zaki, L. Toupet, Acta Crystallogr., Sect. C 49 (1993) 1609;
(l) W.A. Herrmann, M. Denk, W. Scherer, F.-R. Klingan, J. Organomet. Chem. 444 (1993) C21;
(m) R. Goddard, C. Krüger, G.A. Hadi, K.-H. Thiele, J. Scholz, Z. Naturforsch. Teil. B 49 (1994) 519;
(n) J. Wunderle, J. Scholz, U. Baumeister, H. Hartung, Z. Kristallogr. 211 (1996) 423;
(o) L. Kloppenburg, J.L. Petersen, Organometallics 16 (1997) 3548;
(p) R. Leigh Huff, S.-Y.S. Wang, K.A. Abboud, J.M. Boncella, Organometallics 16 (1997) 1779;
(q) M.J. Scott, S.J. Lippard, Organometallics 16 (1997) 5857;
(r) K. Mashima, Y. Matsuo, K. Tani, Chem. Lett. (1997) 767;
(s) G.J. Pindado, M. Thornton-Pett, M. Bochmann, J. Chem. Soc., Dalton Trans. (1998) 393;
(t) T. Zippel, P. Arndt, A. Ohff, A. Spannenberg, R. Kempe, U. Rosenthal, Organometallics 17 (1998) 4429;
(u) K. Mashima, Y. Matsuo, K. Tani, Organometallics 18 (1999) 1471;
(v) H. Görls, J. Scholz, J. Organomet. Chem. 626 (2001) 168;
(w) J. Scholz, G.A. Hadi, K.-H. Thiele, H. Görls, R. Weimann, H. Schumann, J. Sieler, J. Organomet. Chem. 626 (2001) 243.

[7] (a) H. Görls, B. Neumüller, A. Scholz, J. Scholz, Angew. Chem. 107 (1995) 732; Angew. Chem., Int. Ed. Engl. 34 (1995) 673;
(b) M. Haaf, A. Schmiedl, T.A. Schmedake, D.R. Powell, A.J. Millevolte, M. Denk, R. West, J. Am. Chem. Soc. 120 (1998) 12714.

[8] Typical Nb–Cl bond distances in Nb(V) complexes: (a) $CpNbCl_4(PMePh_2)$: 2.4127(8), 2.4168(8), 2.4315(9), 2.3965(9) Å; J.C. Fettinger, D.W. Keogh, R. Poli, Inorg. Chem. 34 (1995) 2343;
(b) Nb(N*i*-Pr)$Cl_3(NH_2i$-Pr): 2.380(3), 2.369(3) Å; K.C. Jayaratne, G.P.A. Yap, B.S. Haggerty, A.L. Rheingold, C.H. Winter, Inorg. Chem. 35 (1996) 4910;
(c) $NbCl_3(OC_6H_3$-2,6-*i*-$Pr_2)_2$(py): 2.379(1), 2.373(1), 2.403(1) Å; J.R. Clark, A.L. Pulvirenti, Ph.E. Fanwick, M. Sigalas, O. Eisenstein, I.P. Rothwell, Inorg. Chem. 36 (1997) 3623;
(d) Nb(N*t*-Bu)Cl_3(dme): 2.400(3), 2.366(3), 2.424(3) Å; A.V. Korolev, A.L. Rheingold, D.S. Williams, Inorg. Chem. 36 (1997) 2647.

[9] Bond distances and bond angles of *t*-Bu-DAD: C=N 1.267(2) Å, C–C 1.467(2) Å. N–C–C 120.1(1)° C.J.M. Huige, A.L. Spek, J.L. de Boer, Acta Crystallogr., Sect. C 41 (1985) 113.

[10] N–C and C–C bond distances in complexes with singly reduced *t*-Bu-DAD ligands: (a) (*t*-Bu-DAD)$_2$Zn: N–C 1.321(6), 1.339(6) Å; C–C 1.400(8), 1.378(7) Å. (*t*-Bu-DAD)$_2$Li: N–C 1.317(6), 1.317(5) Å; C–C 1.399(7) Å; M.G. Gardiner, G.R. Hanson, M.J. Henderson, F.C. Lee, C.L. Raston, Inorg. Chem. 33 (1994) 2456;
(b) K[(*t*-Bu-DAD)$_2$Zn]: N–C 1.32(1), C–C 1.398(5) Å; E. Rijnberg, B. Richter, K.-H. Thiele, J. Boersma, N. Veldman, A.L. Spek, G. van Koten, Inorg. Chem. 37 (1998) 56;
(c) [(tren)Th(*t*-Bu-DAD)]: N–C 1.319(10), 1.317(10); C–C 1.408(12) Å; P. Scott, P.B. Hitchcock, J. Chem. Soc., Chem. Commun. (1995) 579.

[11] Sum of covalence radii of Nb (1.429 Å) and N (0.70 Å): 2.129 Å; L. Pauling, Die Natur der chemischen Bindung, 3. verb. Aufl., Verlag Chemie, Weinheim, 1976. Typical Nb–N bond distances in Nb(V) amide complexes: (a) [Nb(OC_6H_2-2,4-*t*-Bu_2-6-Ph)$_2$(NMe_2)$_3$]: 1.940(3)–2.036(3) Å; V.M. Vis-ciglio, Ph. E. Fanwick, I.P. Rothwell, Inorg. Chim. Acta 211 (1993) 203;
(b) [(*c*-Hex)$_2$N]$_2$Nb[η_2-C_6H_{10}N(*c*-Hex)]Cl: 1.977(5), 1.956(5), 1.984(5) Å; P. Berno, S. Gambarotta, Organometallics 14 (1995) 2159.

[12] T. Spaniel, H. Görls, J. Scholz, Angew. Chem. 110 (1998) 1962; Angew. Chem., Int. Ed. Engl. 37 (1998) 1862.

[13] (a) For representative examples, see C.H. Winter, C.H. Sheridan, P.H. Heeg, Inorg. Chem. 30 (1991) 1962;
(b) I.A. Guzei, C.H. Winter, Inorg. Chem. 36 (1997) 4415.

[14] H. Kawaguchi, Y. Yamamoto, K. Asaoka, K. Tatsumi, Organometallics 17 (1998) 4380.

[15] D.F. Shriver, M.A. Drezdon, The Manipulation of Air Sensitive Compounds, Wiley and Sons, New York, 1986.

[16] (a) J.M. Kliegmann, R.K. Barnes, Tetrahedron 26 (1970) 2555;
(b) J.M. Kliegmann, R.K. Barnes, J. Org. Chem. 35 (1970) 3140.

[17] MolEN, An Interactive Structure Solution Procedure, Enraf–Nonius, Delft, The Netherlands, 1990.

[18] Z. Otwinowski, W. Minor, Processing of X-ray diffraction data collected in oscillation mode, in methods in enzymology, in: C.W. Carter, R.M. Sweet (Eds.), Macromolecular Crystallography Part A, vol. 276, Academic Press, San Diego, CA, 1997, pp. 307–326.

[19] G.M. Sheldrick, Acta Crystallogr., Sect. A 46 (1990) 467.

[20] G.M. Sheldrick, SHELXL-97, University of Göttingen, Germany, 1993.

PERGAMON

Polyhedron 21 (2002) 313–319

POLYHEDRON

www.elsevier.com/locate/poly

Syntheses, spectroscopic and crystal structural studies of novel imidazo[4,5-f]1,10-phenanthroline derivatives and their Eu(III) ternary complexes with dibenzoylmethane

Zu-Qiang Bian, Ke-Zhi Wang *, Lin-Pei Jin

Department of Chemistry, Beijing Normal University, Beijing 100875, People's Republic of China

Received 6 August 2001; accepted 8 November 2001

Abstract

Two novel ligands, 2-(4′-dimethylaminophenyl)imidazo[4,5-f]1,10-phenanthroline (L1) and 3-ethyl-2-(4′-dimethylaminophenyl)imidazo[4,5-f]1,10-phenanthroline (L2), and their europium(III) complexes with dibenzoylmethanate (DBM), Eu(DBM)$_3$(L1) and Eu(DBM)$_3$(L2), were synthesized and characterized by IR, UV–Vis and fluorescence spectroscopy, and thermogravimetric and differential thermal analyses (TG–DTA). The fluorescent intensity of Eu(DBM)$_3$(L2) is 18 times that of Eu(DBM)$_3$(L1). The crystal structures of Eu(DBM)$_3$(L1) and L2 were determined by single crystal X-ray diffraction. Each europium atom is coordinated by six oxygen atoms of three bidentate DBM anions and two nitrogen atoms from one bidentate L1, forming a distorted square antiprism. Highly resolved fluorescence spectroscopy of Eu(DBM)$_3$(L1) at 77 K revealed one Eu(III) site. © 2002 Elsevier Science Ltd. All rights reserved.

Keywords: Europium complexes; X-ray crystallography; Luminescence property; Dibenzoylmethane; 2-(4′-Dimethylaminophenyl)imidazo[4,5-f]1,10-phenanthroline; 3-Ethyl-2-(4′-dimethylaminophenyl)imidazo[4,5-f]1,10-phenanthroline

1. Introduction

In the past three decades, Eu(III) β-diketonates have been intensively studied with respect to their applications for luminescence and laser materials since the first successful laser action in europium β-diketonate was reported by Lempicki and Samelson in 1963 [1]. Recently, Eu(III) complexes have attracted extensive interest in electroluminescent devices owing to their inherent extremely sharp emission bands and potentially high internal quantum efficiency [2–6]. These characteristics make Eu(III) complexes promising candidates for the next generation of flat-panel display with low-voltage drive. Among the Eu(III)-β-diketonate complexes studied as an emissive layer in EL devices, Eu(III) dibenzoylmethanate ternary complexes exhibited appealing and desirable EL properties. The formation of ternary complexes by the introduction of a second ligand into Eu dibenzoylmethanate complexes could improve the volatility, thermal stability and carrier-transport ability of the europium complexes, and thus greatly enhance the photoluminescent and electroluminescent properties [3,7,8]. In order to develop novel Eu(III) complex-based materials for EL devices with improved device performance, we synthesized two novel ligands, 2-(4′-dimethylaminophenyl)imidazo[4,5-f]1,10-phenanthroline and 3-ethyl-2-(4′-dimethylaminophenyl)imidazo[4,5-f]1,10-phenanthroline, and also their europium ternary complexes with dibenzoylmethanate. The synthetic details and spectroscopic and crystal structure results are reported in this paper.

2. Experimental

2.1. Materials and methods

Dimethylformamide (DMF) was purified by distillation over P_2O_5 and *n*-hexane over CaH_2. All other

* Corresponding author. Tel.: +86-10-6220-5522; fax: +86-10-6220-9940.

E-mail address: kzwang@bnu.edu.cn (K.-Z. Wang).

0277-5387/02/$ - see front matter © 2002 Elsevier Science Ltd. All rights reserved.
PII: S0277-5387(01)00995-0

reagents were commercially available and were used without further purification. Contents of carbon, hydrogen and nitrogen were determined using a Perkin–Elmer 240 elemental analyzer. Absorption spectra were recorded with a Shimadzu UV-3100 spectrophotometer. IR-spectra were recorded on a Perkin–Elmer 200-FTIR spectrophotometer in the range of 4000–400 cm^{-1} using KBr pellets. The ^1H NMR spectra were recorded on a Varian 500 MHz instrument using d_6-DMSO as solvent and Me_4Si as internal reference. Thermogravimetric and differential thermal analyses were carried out with a LCT-1 system, at an elevation temperature rate of 10° min^{-1} in an ambient atmosphere. Luminescence spectra were performed with a Hitachi F-4500 spectrophotometer. The highly resolved emission spectra and the time-resolved fluorescence measurements were performed at 77 K using a Nd–YAG pumped dye laser with RG 10 dye as the excitation source and a Spex 1403 double grating monochromator.

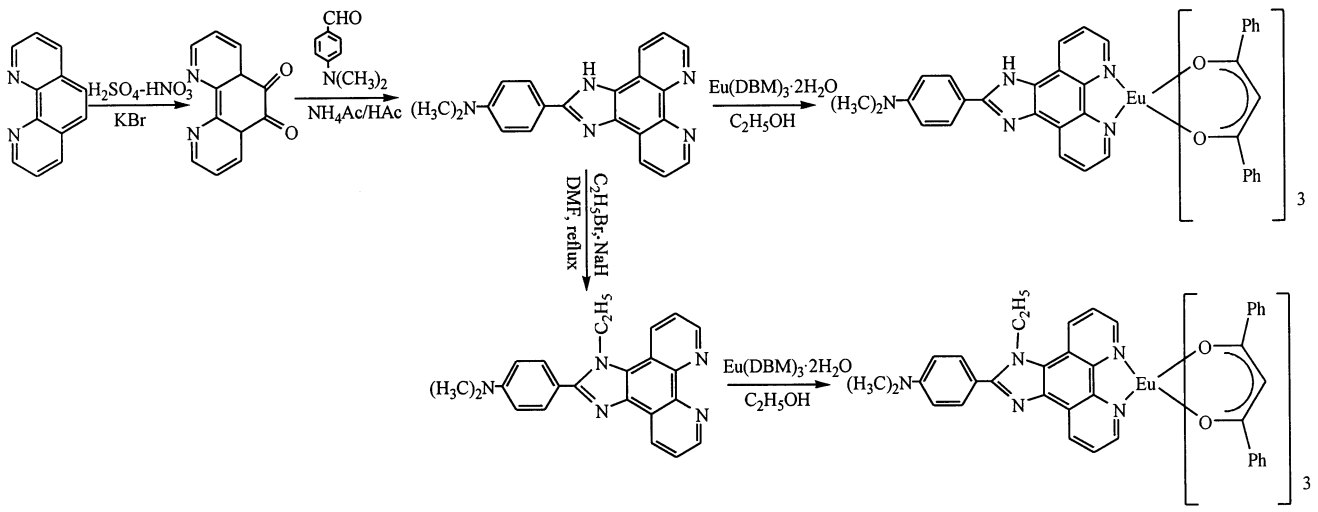
2.2. Syntheses

Synthetic routes of the ligands and their Eu(III) complexes are presented in Scheme 1.

2.2.1. Synthesis of ligands

2-(4′-Dimethylaminophenyl)imidazo[4,5-f]1,10-phenanthroline (**L1**) was synthesized by condensation of 1,10-phenanthroline-5,6-dione [9] and dimethylaminobenzaldehyde, according to a slightly modified imidazole ring preparation method [10,11]. The crude product was purified by recrystallization from a mixture of EtOH and water to get yellow crystals (yield 79%). *Anal.* Found: C, 66.17; H, 5.70; N, 17.05. Calc. for $C_{21}H_{17}N_5{\cdot}0.5C_2H_5OH{\cdot}2H_2O$: C, 66.17; H, 5.55; N, 16.78%. ^1H NMR, δ: 13.42 (s, 1H), 9.02 (d, 2H), 8.91 (q, 2H), 8.12 (d, 2H), 7.82 (d, 2H), 6.90 (d, 2H), 3.02 (s, 6H) ppm. UV–Vis in ethanol, λ_{max}/nm ($\varepsilon \times 10^{-4}$/$dm^3$ mol^{-1} cm^{-1}): 235 (2.34), 292 (2.33), 338 (2.60). IR in KBr pellet: 1718(vw), 1612(vs), 1560(w), 1527(m), 1489(s), 1440(s), 1396(w), 1370(m), 1352(m), 1202(m), 1070(w), 1030(w), 953(w), 812(w), 741(s) cm^{-1}. M.p. >300 °C.

3-Ethyl-2-(4′-dimethylaminophenyl)imidazo[4,5-f]1,10–phenanthroline (**L2**) was synthesized as follows: L1 (1.7 g, 5.0 mmol) in 20 ml of DMF was allowed to react with sodium hydride (0.288 g, 6.0 mmol, 50% dispersion in mineral oil), which was washed by *n*-hexane in order to remove the mineral oil, under a N_2 atmosphere. Upon heating to 100 °C, a vigorous reaction occurred with the evolution of H_2 gas and the color of the solution changed from pale yellow to brown. After the evolution of the gas has ceased, bromoethane (1.1 g, 10 mmol) was added dropwise and the resulting solution was further refluxed for 12 h. NaBr precipitated upon cooling was removed by filtration. An addition of a large amount of ether gave a yellow precipitate of the desired ligand, which was chromatographed on a silica gel column with CH_2Cl_2–MeOH (15:1, v/v) as an eluent and recrystallized from ethanol to get yellow crystals (58% yield). Crystals suitable for X-ray analysis were obtained from the mother liquor after 2 weeks at the room temperature (r.t.). *Anal.* Found: C, 75.19; H, 5.76; N, 19.06. Calc. for $C_{23}H_{21}N_5$: C, 74.83; H, 5.79; N, 18.53%. ^1H NMR, δ: 9.06 (d, 2H), 8.94 (q, 2H), 7.86 (d, 2H), 7.64 (d, 2H), 6.92 (d, 2H), 4.72 (m, 2H), 3.03 (s, 6H), 1.49 (m, 3H) ppm. UV–Vis in ethanol, λ_{max}/nm ($\varepsilon \times 10^{-4}$/$dm^3$ mol^{-1} cm^{-1}): 237 (2.38), 288 (2.65). IR in KBr pellet: 1612(vs), 1561(w), 1544(m), 1474(s), 1439(s), 1391(s), 1350(s), 1289(vw), 1227(vw), 1202(s), 1159(m), 1128(vw), 1097(vw), 1018(vw), 827(m), 748(m), 727(w) cm^{-1}. M.p. >250 °C.



Scheme 1. Synthetic routes of the ligands and their Eu(III) complexes.

Table 1
Experimental details and crystal data for $Eu(DBM)_3L1$ and L2

Chemical formula	$C_{66}H_{50}O_6N_5Eu$	$C_{23}H_{21}N_5$
Formula weight	1161.11	367.45
Temperature (K)	293	293
Radiation (Mo Kα) (Å)	0.71069	0.71073
Crystal system	orthorhombic	monoclinic
Space group	$P2_12_12_1$	$P2_1/c$
Unit cell dimensions		
a (nm)	1.8550(6)	0.96970(15)
b (nm)	2.2334(4)	0.97602(15)
c (nm)	1.3411(4)	1.9724(3)
β (°)		92.971(4)
V (nm^3)	5.556(2)	1.8642(5)
Z	4	4
D_{calc} (g cm^{-3})	1.388	1.309
Absorption coefficient (cm^{-1})	11.84	8.1
$F(000)$	2372.00	776
Crystal size (mm)	$0.20\times0.20\times0.30$	$0.20\times0.15\times0.10$
$2\theta_{max}$ (°)	50.0	50.0
Index ranges	$0\le h\le22$, $0\le k\le26$, $0\le l\le15$	$-11\le h\le6$, $-10\le k\le11$, $-23\le l\le23$
Reflections collected	5416	7557
Independent reflections	3254	3293
Data/restraints/parameters	3254/0/703	3293/0/254
Goodness-of-fit on F^2	1.29	1.033
Final R indices	$R=0.059$, $R_w=0.057$	$R=0.0629$, $R_w=0.1608$
Largest difference peak and hole (e Å^{-3})	1.16 and −1.07	0.577 and −0.225

2.2.2. Synthesis of complexes

Tris(dibenzoylmethanato){2-(4′-dimethylaminophenyl)imidazo[4,5 - f]1,10 - phe - nanthroline}europium(III) [$Eu(DBM)_3L1$] was synthesized as follows: $Eu(DBM)_3{\cdot}2H_2O$ [12] (0.170 g, 0.2 mmol) and L1 (0.080 g, 0.2 mmol) were refluxed in 20 ml of ethanol for 2 h. A yellow precipitate formed upon cooling was filtered and recrystallized from 30 ml of mixed solvents EtOH and THF (1:1, v/v). Crystals suitable for X-ray analysis were obtained from the mother liquor after 8 days at r.t. *Anal*. Found: C, 67.83; H, 4.14; N, 5.81. Calc. for $C_{66}H_{50}N_5O_6Eu$: C, 68.27; H, 4.34; N, 6.03%. UV–Vis in tetrahydrofuran, λ_{max}/nm ($\varepsilon\times10^{-4}$/dm^3 mol^{-1} cm^{-1}): 247 (6.08), 288 (3.51), 349 (8.02). IR in KBr pellet: 1610(s), 1594(s), 1547(vs), 1518(vs), 1479(vs), 1455(s), 1406(vs), 1359(m), 1312(m), 1284(m), 1222(w), 1199(w), 1073(m), 1024(w), 736(m), 687(m), 608(w) cm^{-1}.

Tris(dibenzoylmethanato){3 - ethyl - 2 - (4′ - dimethylaminophenyl)imidazo[4,5 - f]1,10 - phenanthroline}europium(III) [$Eu(DBM)_3$(L2)] was synthesized by following the procedure described above for $Eu(DBM)_3$(L1) except that L2 was used instead of L1. *Anal*. Found: C, 66.28; H, 4.74; N, 5.51. Calc. for $C_{68}H_{58}N_5O_8Eu$: C, 66.67; H, 4.77; N, 5.72%. UV–Vis in tetrahydrofuran, λ_{max}/nm ($\varepsilon\times10^{-4}$/dm^3 mol^{-1} cm^{-1}): 243 (4.77), 284 (3.69), 348 (4.32). IR in KBr pellet: 1595(vs); 1549(vs); 1518(vs); 1478(vs); 1457(s); 1410(vs); 1309(m); 1219(w); 1023(w); 722(m); 670(w) cm^{-1}.

2.3. X-ray crystallographic determination

X-ray data were collected in ω–2θ scan mode with a Rigaku AFC 7R diffractomer for $Eu(DBM)_3$(L1) and a CCD area detector Bruker SMART 2000 X-ray for L2 using Mo Kα radiation at 298 K. All calculations were performed using the TEXSAN [13] crystallographic software package. The intensity data were corrected for LP and empirical absorption corrections using the program DIFABS [14] were applied. Crystallographic data for the two compounds are listed in Table 1 and full details of the structure determination are given in the supporting information.

3. Results and discussion

3.1. The crystal structures of $Eu(DBM)_3$(L1) and L2

The perspective view of the molecular unit of $Eu(DBM)_3$(L1) is shown in Fig. 1. The selected bond lengths are tabulated in Table 2.

The central ion Eu(III) is eight-coordinated by six oxygen atoms of three bidentate DBM anions and two nitrogen atoms from one bidentate L1, forming a distorted square antiprism. Compared with the crystallographic data of $Eu(DBM)_3{\cdot}phen{\cdot}CH_3COCH_3$ [12] in which phen is 1,10-phenanthroline, the average Eu–O bond length of 2.35 Å for the former is equal to that for the latter and the mean Eu–N bond length of 2.60(2) Å for the former is slightly shorter than that [2.64(3) Å] for the latter although L1 is much more bulky than phen. The calculated results of the least square planes revealed that all of the atoms in the ligand L1 are almost coplanar and thus L1 is more conjugated than phen. The enhancement in coordinative ability of L1 compared to phen may be due to the presence of the electron donor dimethylamino group. In the β-diketone chelate rings, average distances for the carbon–carbon [C(28)–C(29), C(29)–C(30), C(43)–C(44), C(44)–C(45), C(58)–C(59), C(59)–C(60)] and carbon–oxygen [C(28)–O(1), C(30)–O(2), C(43)–O(3), C(45)–O(4), C(58)–O(5), C(60)–O(6)] bonds of 1.39 and 1.26 Å respectively, lie between the single- and double-bond distances, reflecting the delocalization of the π-electrons in the chelate ring system. The mean C–C–C angle is also compatible with the values reported for delocalized systems of β-diketonates [15].

The molecular structure of L2 is shown in Fig. 2. Similarly to the structure of L1, the molecular backbone of L2 mainly consists of an imidazo ring, a phenyl

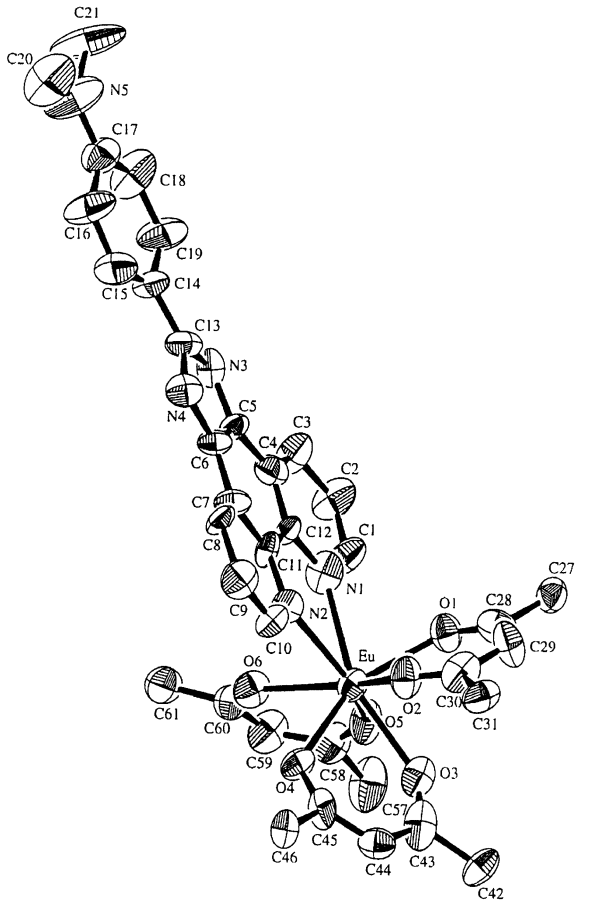


Fig. 1. Molecular structure of $Eu(DBM)_3L1$.

Table 2
Selected bond distances (Å) for $Eu(DBM)_3L1$

Eu–O(1)	2.32(1)	O(3)–C(43)	1.29(2)
Eu–O(2)	2.324(10)	O(4)–C(45)	1.30(2)
Eu–O(3)	2.34(1)	O(5)–C(58)	1.23(2)
Eu–O(4)	2.374(10)O(6)–	C(60)	1.30(2)
Eu–O(5)	2.34(1)	C(28)–C(29)	1.39(2)
Eu–O(6)	2.39(1)	C(29)–C(30)	1.46(3)
Eu–N(1)	2.59(2)	C(43)–C(44)	1.39(2)
Eu–N(2)	2.60(1)	C(44)–C(45)	1.36(2)
O(1)–C(28)	1.24(2)	C(58)–C(59)	1.38(2)
O(2)–C(30)	1.21(2)	C(59)–C(60)	1.38(2)

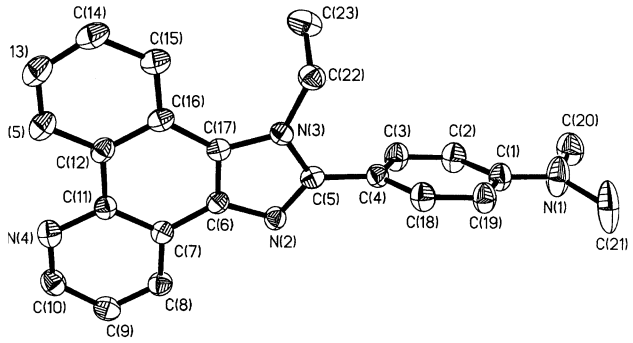


Fig. 2. Molecular structure of L2.

ring and a phenanthroline ring. The rings in the molecule do not show any unusual features and the bond lengths as well as bond angles are within the range of normal values. The only notable difference is that the moiety of imidazo[4,5-f]1,10-phenanthroline in L2 is not coplanar with the phenyl ring due to the grating of the ethyl group to the nitrogen atom on the imidazo ring in contrast to the structure of L1.

3.2. Absorption spectra

The UV spectrum of L1 showed three bands at 235, 292 and 338 nm attributed to $\pi-\pi^*$ transitions. While the former two bands were small red- or blue-shifted, the last one at the low-energy side was absent in the spectrum of L2. The difference obviously arose from the fact that L1 is more conjugated than L2, as revealed by X-ray crystal structural results. The UV spectrum of $Eu(DBM)_3{\cdot}2H_2O$ exhibited three ligand-centered $\pi-\pi^*$ transitions at 251, 280 and 355 nm which are dominant in the spectra of the two complexes [277, 288 and 349 nm for $Eu(DBM)_3(L1)$; 243, 284 and 348 nm for $Eu(DBM)_3(L2)$] so that the characteristic absorption of L1 and L2 were obscured. Interestingly, the molar extinction coefficient of the two complexes was larger than the sum of $Eu(DBM)_3{\cdot}2H_2O$ and L1 or L2, strongly supporting the occurrence of a coordination reaction between $Eu(DBM)_3{\cdot}2H_2O$ and L1 or L2.

3.3. IR spectra

The main IR data and their assignments are summarized in Table 3. The assignments are made by comparison with known related compounds and functional groups [16]. The C–H in-plane bending vibrations observed at 1396 cm^{-1} for L1, 1391 cm^{-1} for L2 and 1398 cm^{-1} for $Eu(DBM)_3{\cdot}2H_2O$ red shifted to 1406 cm^{-1} for $Eu(DBM)_3(L1)$ and 1410 cm^{-1} for $Eu(DBM)_3(L2)$, indicating that coordination of the ligands L1 and L2 to the europium ion has taken place. Two strong C–H out-of–plane bending vibrations appearing at 741 and 812 cm^{-1} for L1, and 748 and 827 cm^{-1} for L2 were obscured by following dominant absorption contributed by the $Eu(DBM)_3$ moiety: out-of-plane bending vibration π(C–H) at 784 cm^{-1}, phenyl ring out-of-plane bending C–H vibration $\phi\pi$(C–H) at 690 and 721 cm^{-1}. A ν(C=O) stretching vibration was observed at 1594 cm^{-1} for $Eu(DBM)_3(L1)$ and at 1595 cm^{-1} for $Eu(DBM)_3(L2)$, and a ν(C=N) stretching vibration was observed at 1610 cm^{-1} for $Eu(DBM)_3(L1)$ and at 1611 cm^{-1} for $Eu(DBM)_3(L2)$. However, the ν(C=O) and ν(C=N) stretching vibrations for the two complexes were merely subjected to minor red- or blue-shift compared to their counterparts, $Eu(DBM)_3{\cdot}2H_2O$, L1 and L2.

Table 3
IR data (cm^{-1}) of ligands and complexes and their assignments[a]

L1	L2	$Eu(DBM)_3 \cdot 2H_2O$	$Eu(DBM)_3L1$	$Eu(DBM)_3L2$	Assignments[b]
3443 (s)	3424 (m)	3434 (m)	3431 (m)	3440 (s)	ν(N–H) or ν(O–H)
3095 (w)	3040 (w)	3058 (w)	3053 (w)	3049 (w)	φν(C–H)
2910 (w)	2923 (w)		2911 (w)	2922 (w)	$\nu_{as}(CH_3)$
1612 (s)	1612 (s)		1611 (s)	1611 (s)	ν(C=N)
		1596 (s)	1595 (s)	1595 (s)	ν(C=O)
1527 (m)	1544 (m)	1520 (s)	1518 (s)	1518 (s)	ν_{as}(C=C)
1489 (s)	1474 (s)	1479 (s)	1479 (s)	1478 (s)	φν(C=C)
1440 (s)	1439 (s)	1454 (s)	1455 (s)	1457 (s)	ν_s(C=O) or δ(C–H)
1396 (m)	1391 (m)	1398 (s)	1406 (s)	1410 (s)	δ(C–H)
741 (s)	748 (m)	721 (s)	736 (m)	722 (m)	π(C–H)

[a] Relative intensity: s = strong, m = medium, w = weak.
[b] Assignment: ν = stretching, δ = in-plane bending, π = out-of-plane bending, s = symmetric, as = asymmetric, φ = phenyl vibrations.

3.4. Thermal analysis

Thermogravimetric and differential thermal analyses (TG–DTA) provide important information on vacuum-deposition behaviors of the materials. TG–DTA curves showed the complex $Eu(DBM)_3(L1)$ is chemically stable from the room temperature to 360 °C and no endothermic peak was observed on the corresponding differential thermal curve, indicating that there exist no melting point prior to decomposition. Over 360 °C the complex underwent a four-stage decomposition–oxidation process. Similarly, complex $Eu(DBM)_3(L2)$ also exhibited a four-stage decomposition–oxidation process without melting. However, $Eu(DBM)_3(L2)$ is thermodynamically less stable than $Eu(DBM)_3(L1)$ and has a lower decomposition temperature of 256 °C.

3.5. Luminescence spectra at room temperature

As shown in Fig. 3, powder of the free ligand L1 gave a broad band emission at $\lambda_{max} = 515$ nm with a shoulder at about 500 nm upon excitation at 370 nm, while that of L2 showed an emission band centered at about 432 nm upon excitation at 374 nm. It is noteworthy that the ligand emission characteristics totally vanished in the emission spectra of $Eu(DBM)_3(L1)$ and $Eu(DBM)_3(L2)$, showing that efficient energy transfer from the ligands L1 and L2 to Eu(III) has occurred. The emission spectra of the complexes, excited at 386 nm for $Eu(DBM)_3(L1)$ and 400 nm for $Eu(DBM)_3(L2)$, do not show any significant difference and both exhibit characteristic emissions of Eu(III) ions. As shown in Fig. 4, five narrow emission peaks centered at 580, 592, 612, 652 and 703 nm, assigned to $^5D_0 \rightarrow {}^7F_0$, $^5D_0 \rightarrow {}^7F_1$, $^5D_0 \rightarrow {}^7F_2$, $^5D_0 \rightarrow {}^7F_3$ and $^5D_0 \rightarrow {}^7F_4$ transitions, respectively, were obtained for the two complexes. Among the peaks, the emission at 612 nm from the $^5D_0 \rightarrow {}^7F_2$ electronic dipole transition is the strongest, suggesting low symmetry around the Eu(III) ion [17]. Because the forbidden $^5D_0 \rightarrow {}^7F_2$ electronic dipole transition is sensitive to the coordination environment of the Eu(III) ion, the asymmetric microenvironment causes the polarization of the Eu(III) ion under the influence of the electric field of the surrounding ligands and thus increases the probability for the electronic dipole transition. More interesting is that the luminescence intensity of Eu-

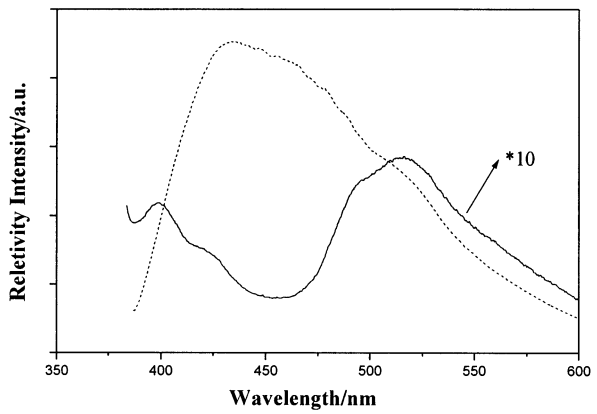


Fig. 3. The emission spectra of the ligands (solid line—L1, dashed line—L2).

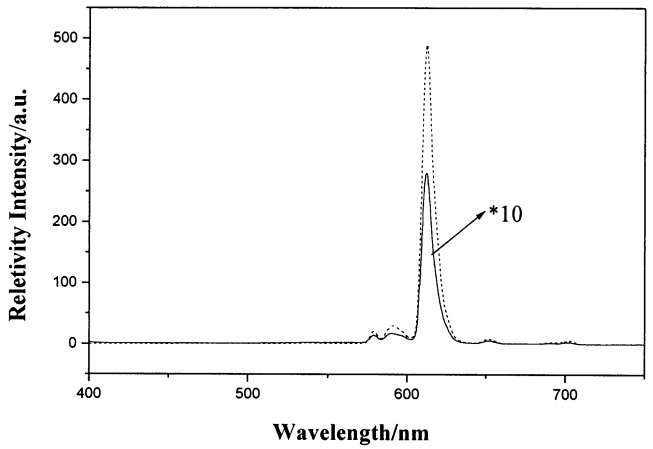


Fig. 4. The emission spectra of the complexes (solid line—Eu(-DBM)$_3$L1, dashed line—$Eu(DBM)_3L2$).

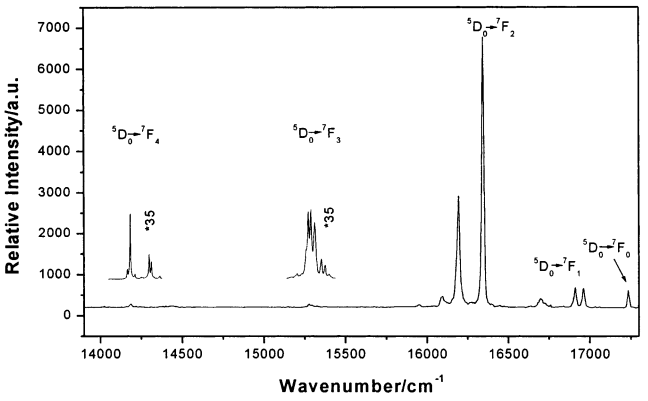


Fig. 5. The highly resolved emission spectrum of $Eu(DBM)_3L1$, $\lambda_{exc} = 335$ nm, 77 K.

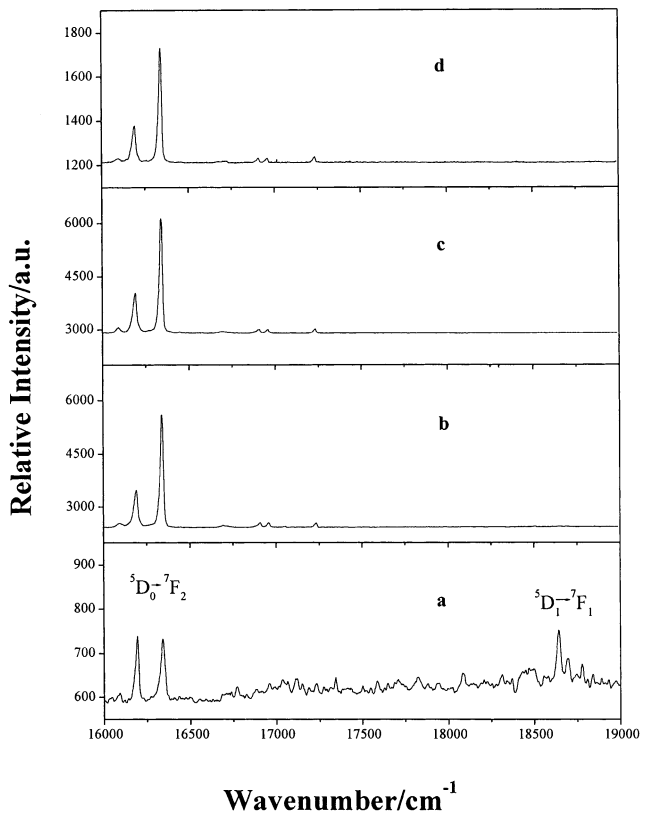


Fig. 6. The time resolved spectra of $Eu(DBM)_3L1$, $\lambda_{exc} = 335$ nm, 77 K. Delay time (a) 2 s; (b) 30 s; (c) 100 s; (d) 500 s.

$(DBM)_3(L2)$ is 18 times that of $Eu(DBM)_3(L1)$. Two reasons may account for the improved luminescence intensity observed. One is that the quenching effect of the luminescence by the non-radiative dissipation of energy on the high-energy N–H vibrations was removed after ethyl group substituted the hydrogen atom bonding with the nitrogen atom on the imidazole ring in $Eu(DBM)_3(L1)$. The other reason is that the energy transfer to Eu(III) from ligand L2 is more efficient than from ligand L1 on account of energy level and absorption factors.

3.6. Highly resolved luminescence spectra at 77 K and time-resolved luminescence spectra

In order to get information regarding the energy transfer mechanism and Eu(III) site symmetry in the crystal, time-resolved luminescence spectra and highly resolved luminescence spectra at 77 K were measured for $Eu(DBM)_3(L1)$ and $Eu(DBM)_3(L2)$. Unfortunately, irreproducible luminescence spectra were detected for $Eu(DBM)_3(L2)$ due to chemical unstability of $Eu(DBM)_3(L2)$ under the laser irradiation. Therefore, only highly resolved luminescence spectra (Fig. 5) and time–resolved luminescence spectra (Fig. 6) for $Eu(DBM)_3(L1)$ are reported here. The degeneracy of J manifolds of a Eu(III) ion can be split into the maximum $2J+1$ non-degenerate energy levels. One can determine through group theory whether a particular transition will be symmetry allowed or forbidden [18]. This has been well documented for Eu(III) compounds with different site symmetry [19]. It can be seen from Fig. 5 that no splitting of the singlet $^5D_0 \rightarrow {}^7F_0$ transition implies a single Eu^{3+} ion crystallographic site symmetry. Additionally, three peaks for the $^5D_0 \rightarrow {}^7F_1$ transition, four peaks for the $^5D_0 \rightarrow {}^7F_2$ transition, 5 peaks for the $^5D_0 \rightarrow {}^7F_3$ transition and seven peaks for the $^5D_0 \rightarrow {}^7F_4$ transitions with reasonable intensity were observed, corresponding to a C_{2v} site symmetry in a rhombic crystal system of eight-coordinated Eu(III) compounds. This is in agreement with the result of crystal structural determination.

The time-resolved photoluminescence spectra of $Eu(DBM)_3(L1)$ obtained using 355 nm excitation at 77 K are shown in Fig. 6. Emission lines of $^5D_1 \rightarrow {}^7F_1$ transition were observed when the delay time was 2 μs, but $^5D_1 \rightarrow {}^7F_1$ emission bands disappeared after 30 μs. However, the emission band intensity of $^5D_0 \rightarrow {}^7F_J$ transitions increases. This reveals that the lowest triplet state of the ligands is higher than the emission level $^5D_1$ of the Eu^{3+} ion and energy mostly transfers from the triplet state of the ligands DBM and L1 to the $^5D_1$ level of the Eu^{3+} ion followed by the $^5D_0$ emission level although it is not exclusive that energy directly transfers from the triplet state of the ligands to the lowest emission level $^5D_0$ of the Eu^{3+} ion, and then a $^5D_0 \rightarrow {}^7F_J$ transition occurs. This also indicates that the $^5D_1$ state of the Eu^{3+} ion is deactivated within 30 μs and the lifetime of the $^5D_1$ state is much shorter than that of the $^5D_0$ level of the Eu^{3+} ion in the complex. The lifetime of the $^5D_0$ level of the Eu^{3+} ion in the complex obtained from the delayed curve is 1.24 ms.

4. Conclusion

Two novel imidazo[4,5-f]1,10-phenanthroline-containing Eu(III)-dibenzoyl-methanate mixed ligand com-

plexes were designed and synthesized. Alkylation at the imidazo ring of the Eu(III) complex resulted in greatly enhanced emission. The work on electroluminescent devices based on vacuum deposited films of these two Eu(III) complexes is in progress.

5. Supplementary material

Crystallographic data for the structural analysis have been deposited with the Cambridge Crystallographic Centre, CCDC Nos. 153376 and 173284 for compounds $Eu(DBM)_3$(L1) and L2, respectively. Copies of this information may be obtained free of charge from The Director, CCDC, 12 Union Road, Cambridge, CB2 1EZ, UK (fax: +44-1233-336-033; e-mail: deposit@ccdc.cam.ac.uk or www: http://www.ccdc.cam.ac.uk).

Acknowledgements

This work is financed by the State Key Project of Fundamental Research (G1998061308), the National Natural Science Foundation of China (Z9971005 and 20071004) and the Scientific Research Foundation for Returned Overseas Chinese Scholars, State Education Ministry, to K.Z.W.

References

[1] A. Lempicki, H. Samelson, Phys. Lett. 4 (1963) 133.
[2] L.H. Wang, W. Wang, W.G. Zhang, E.T. Kang, W. Huang, Chem. Mater. 12 (2000) 2212.
[3] (a) L. Huang, K.Z. Wang, C.H. Huang, F.Y. Li, Y.Y. Huang, J. Mater. Chem. 11 (2001) 1790;
(b) X.C. Gao, H. Cao, C.H. Huang, S. Umitani, G.Q. Chen, P. Jiang, Synth. Met. 19 (1999) 127;
(c) G. Yu, Y.Q. Liu, X. Wu, D.B. Zhou, H.Y. Li, L.P. Jin, M.Z. Wang, Chem. Mater. 12 (2000) 2537;
(d) W.P. Hu, M. Matsumura, M.Z. Wang, L.P. Jin, Appl. Phys. Lett. 77 (2000) 4271.
[4] M.R. Robinson, M.B. O'Regan, G.C. Bazan, Chem. Commun. (2000) 1645.
[5] J. Kido, K. Nagai, Y. Okamoto, J. Alloys Compd. 30 (1993) 192.
[6] J. Kido, H, Hayase, K. Hongawa, K. Nagai, K. Okuyama, Appl. Phys. Lett. 65 (1994) 2124.
[7] T. Sano, M. Fujita, T. Fujii, Y. Hamada, K. Shibata, K. Kuroki, Jpn. J. Appl. Phys. 34 (4A) (1995) 1883.
[8] L. Liu, W.L. Li, Z.R. Hong, J.B. Peng, X.Y. Liu, C.J. Liang, Z.B. Liu, J.Q. Yu, D.X. Zhao, Synth. Met. 91 (1997) 267.
[9] C. Hiort, P. Lincoln, B. Norden, J. Am. Chem. Soc. 115 (1993) 3449.
[10] E.A. Steck, A.R. Day, J. Am. Chem. Soc. 65 (1943) 452.
[11] B. Jing, T. Wu, C. Tian, M. Zhang, T. Shen, Bull. Chem. Soc. Jpn. 73 (2000) 1749.
[12] J. Yu, X.Q. He, Z.Y. Zhou, L. Liu, Chin. J. Struct. Chem. 8 (1989) 187.
[13] Crystal Structure Analysis Package, Molecular Structure Corporation, USA, 1992.
[14] N. Walke, D. Stuart, Acta. Crystallogr., Sect. A 39 (1983) 158.
[15] (a) E.C. Lingafelter, R.L. Braun, J. Am. Chem. Soc. 88 (1966) 2951;
(b) D.J. Zhou, C.H. Huang, K.Z. Wang, G.X. Xu, Polyhedron 13 (1994) 987;
(c) K.Z. Wang, C.H. Huang, G.X. Xu, R.J. Wang, Polyhedron 14 (1995) 3669.
[16] (a) S. Misumi, N. Iwasaki, Bull. Chem. Soc. Jpn. 40 (1967) 550;
(b) C.Y. Liang, E.J. Schimischek, J.A. Trias, J. Inorg. Nucl. Chem. 32 (1970) 811;
(c) M.F. Richardson, W.F. Wagner, D.E. Sands, Inorg. Chem. 7 (1968) 2495;
(d) P.C. Mehta, S.S.L. Surana, S.P. Tandon, Can. J. Spectrosc. 18 (1973) 55.
[17] J.-C.G. Bünzli, G.R. Choppin, Lanthanide Probers in Life, Chemical and Earth Science, Elsevier, Amsterdam, 1989 Ch. 7.
[18] S. Hufner, Optical Spectra of the Transparent Rare Earth Compounds, Academic Press, New York, 1978.
[19] N.A. Stump, L.L. Pesterfield, G.K. Schweitzer, G.R. Pterson, J. Alloys Compd. 180 (1992) 141.

PERGAMON

Polyhedron 21 (2002) 321–332

POLYHEDRON

www.elsevier.com/locate/poly

Interactions of zinc(II), magnesium(II) and calcium(II) with aminomethane-1,1-diphosphonic acids in aqueous solutions

Ewa Matczak-Jon [a,*], Barbara Kurzak [b], Anna Kamecka [b], Paweł Kafarski [c]

[a] *Institute of Inorganic Chemistry, Wroclaw University of Technology, 50-370 Wroclaw, Poland*
[b] *Institute of Chemistry, University of Podlasie, 08-110 Siedlce, Poland*
[c] *Institute of Organic Chemistry, Biochemistry and Biotechnology, Wroclaw University of Technology, 50-370 Wroclaw, Poland*

Received 22 August 2001; accepted 8 November 2001

Abstract

Complex formation equilibria of the aminomethane-1,1-diphosphonic acids with Zn^{II}, Mg^{II} and Ca^{II} have been studied by potentiometric pH titrations and by means of NMR spectroscopy. The ligands exhibit a strong tendency to form protonated species over a wide range of pH. The most efficient binding mode in all the studied systems is the formation of the six-membered chelate ring involving oxygens of both phosphonate groups. An evident preference for the formation of multinuclear complexes is noted in the case of zinc(II). Magnesium demonstrates preference for mononuclear complexes, whereas calcium(II) tends to form insoluble species with most of the studied ligands. The structures of the main complex species are discussed with respect to the priorities in the hydrogen-bond network organization in solid state. © 2002 Elsevier Science Ltd. All rights reserved.

Keywords: Aminomethane-1,1-diphosphonic acids; Zinc(II) complexes; Magnesium(II) complexes; Calcium(II) complexes; Potentiometry; NMR

1. Introduction

Osteoporosis is the most common metabolic bone disease which affects 40–50% of the elderly female and 10–15% elderly male population. The disease involves the gradual loss of bone mass as a result of an imbalance between the bone resorption activity of osteoclasts and the bone formation activity of osteoblasts. Analogues of the inorganic pyrophosphate with non-hydrolysable P–C–P structure, commonly known as bisphosphonates, strongly inhibit bone resorption. For more than 20 years, they have been used successfully for the treatment of bone disorders such as Paget's disease, cancer-related hypercalcemia and post-menopausal osteoporosis, presently comprising nearly US$ 1 billion of the global pharmaceutical market [1–4]. Some of bisphosphonates have also been shown to act as inhibitors of matrix metalloproteases, thus additionally blocking the initiating step in the bone resorption process, i.e. degradation of connective tissues associated with peridontal diseases [5]. Surprisingly very little is known about the molecular mechanism of action of these compounds which are believed to act as complexing agents of bone calcium ions or affect enzyme essential metal ions. Quite unexpectedly the same bisphosphonates may form a basis for a new generation of anti-malarial compounds not only being active against *Plasmodium faciparum*, a causative agent for malaria, but also killing trypanosomes, *Leishmania* and *Toxoplasma gondii* [6]. Together these parasites infect over 500 million people annually worldwide, mostly in tropics.

The aminomethane-1,1-diphosphonic acids constitute an interesting class of bisphosphonates that exert herbicidal activity. However, similarly as in the case of bone disorder treatment, the molecular basis of their action still awaits elucidation. The available data suggest that they should be considered as an heterogenous group of compounds with various modes of action [7]. Their activity is most likely a result of their simultaneous action on several enzymes that are metal-dependent. The preliminary calculations of their interaction with

* Corresponding author. Tel.: +48-103371-320-2454; fax: +48-103371-328-4330.
E-mail address: jon@ichn.ch.pwr.wroc.pl (E. Matczak-Jon).

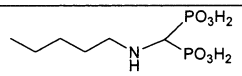
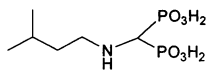
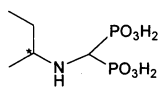
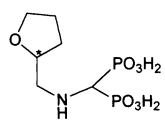
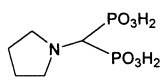
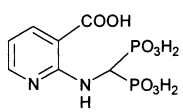
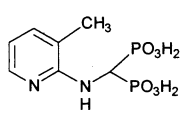
0277-5387/02/$ - see front matter © 2002 Elsevier Science Ltd. All rights reserved.
PII: S0277-5387(01)00996-2

farnesyl pyrophosphate synthase, glutamine synthetase and 3-deoxy-D-*arabino*-heptulosonate-7-phosphate synthase, suggested as molecular targets, have shown that their action most strongly depends on the complexation of the metal ion present in the active centre of the enzyme [8]. Thus, the understanding the complex-forming abilities of these compounds seems to be crucial for the proper interpretation of their physiological properties.

The most important structural feature that accounts for the complexation properties of the aminomethane-1,1-diphosphonic acids is an attachment of two phosphonate groups to the central $CH(P_2)$ carbon atom. It predisposes the ligands to exhibit greater diversity in coordination modes, when compared to the iminodimethylenediphosphonic acids [9]. X-ray data demonstrate that the *gem*-diphosphonate groups can either coordinate through as few as two oxygen donors to bidentately chelate metal ions [10–14] or can perform the multidentate bridging functions using a higher number (up to six) oxygen donors [15–25]. A peculiar coordination mode for this class of compounds is a 'doubly bidentate' chelation with one metal ion bound on the one side of the P–C–P plane and another on the opposite side of this plane [20–25].

This work is aimed at aqueous solution studies of the stability and coordination modes of the complexes of Zn^{II}, Mg^{II} and Ca^{II} with a series of aminomethane-1,1-

Table 1
Compounds used in this study

Compound	Structure	[M+ H^+]	Name
1		262.3 [Ref. 26]	N-*n*-pentylaminomethane-1,1-diphosphonic acid
2		262.3	N-*iso*-pentylaminomethane-1,1-diphosphonic acid
3		248.0	N-*sec*-butylaminomethane-1,1-diphosphonic acid
4		276.2	N-2-methylenetetrahydrofurylo aminomethane-1,1-diphosphonic acid
5		245.1 [Ref. 26]	N-pyrrolidinomethane-1,1-diphosphonic acid
6		312.2 [Ref. 26]	N-(3-carboxy-2-pyridyl)aminomethane-1,1-diphosphonic acid
7		283.2 [Ref. 26]	N-(3-methyl-2-pyridyl)aminomethane-1,1-diphosphonic acid

* chiral carbon centre.

diphosphonic acids having amino group substituted by various functional groups (Table 1). Our final goal is to shed some light on the general relations between the complexation mechanism in solution and the molecular organization in the solid state.

2. Experimental

2.1. Materials

The aminomethane-1,1-diphosphonic acids were obtained according to the previously described procedures [27–33]. Their identity and purity were confirmed with the use of ES-MS spectrometry (Table 1) and by the NMR method. The exact concentrations of the solutions of the ligands used for potentiometric studies were determined by the Gran method [34]. The concentrations of the zinc(II) and the alkaline-earth metal(II) chloride stock solutions were standardized by complexometric ethylenedinitrilotetraacetate (EDTA) titration. Carbonate-free potassium hydroxide (the titrant) was prepared and standardized against a standard potassium hydrogenphthalate solution.

2.2. Methods

2.2.1. Potentiometric measurements

The stability constants of the proton and metal(II) complexes were determined by pH-metric titration of 2 cm^3 samples except for the Zn^{II}–**2** and Zn^{II}–**4** systems for which the sample volumes were 5 and 3 cm^3, respectively. The ligand (L) concentration for the Zn^{II} systems was varied between 1×10^{-3} and 3×10^{-3} mol dm^{-3} and for Mg^{II} or Ca^{II} between 3.5×10^{-3} and 5×10^{-3} mol dm^{-3} (because of precipitation the ligand concentration for the zinc(II) system with **1** was 5×10^{-4} mol dm^{-3}). The metal-to-ligand molar ratios were 1: 1.5, 1: 2 and 1: 2.5 and the ionic strength was adjusted to 0.2 mol dm^{-3} with KCl in each case. The pH-metric titrations were performed with a carbonate-free KOH solution. For the Zn^{II} and Mg^{II} systems the measurements were made from pH 3 to $\sim$11. The exception were Zn^{II}–**7** and Mg^{II}–**7** measured from pH 4 to $\sim$11 due to a poor solubility of the ligand in acidic pH. For the majority of the Ca^{II} systems immediate precipitation of insoluble species, even in the case of the highest ligand excess, precluded the reliable titration curves at pH > 4.5 (ligands **1**–**3**) and pH > 6 (ligands **6**, **7**) being obtained. Only the Ca^{II}–**4** and Ca^{II}–**5** systems were titrated throughout the whole range pH 3–11. All titration solutions were thermostatted at 25 ± 0.1 °C using a constant-temperature water-bath.

The pH was measured with a MOLSPIN automatic titration system using a micro combination pH electrode (Mettler-Toledo, Type 2). Small amounts ($\Delta v =$ 0.001 cm^3) of titrant were added (total volume 0.1 or 0.2 cm^3). The electrode system was calibrated by periodic titrations of HCl solution (7.5×10^{-3} mol dm^{-3} in KCl) against standard KOH solution. The resulting titration data were used to calculate the standard electrode potentials, $E°$, and the dissociation constant for water ($pK_w = 13.74$). These values were then used to calculate the hydrogen ion concentration $[H^+]$ from emf readings [35]. The titrations were performed in triplicate and calculations were carried out using the SUPERQUAD computer program [36] with three titration curves for each system. The χ^2 values never exceeded the range 5–12. The standard deviations (σ values) quoted were computed by the program and refer to random errors only. They are, however, a good indication of the importance of the particular species in the equilibrium.

In the calculations of the equilibrium models hydrolysis was considered. The values of the hydrolysis constants for the most possible hydroxo complexes were taken from the literature [37].

The charges of the complexes have been omitted in the text and tables. However, for clarity, it should be mentioned that the fully deprotonated forms of **1**–**5** and **7** have negative charges L^{4-} and of **6** L^{5-}.

2.2.2. Mass spectrometry

Mass spectra were recorded in a positive-ion mode on a Finnigan Mat TSQ 700 triple quadrupole mass spectrometer operating with an ESI source. The spray voltage was 4.5 kV and the heated capillary temperature was maintained at 473 K.

2.2.3. NMR measurements

NMR spectra were recorded on a Bruker DRX spectrometer operating at 121.50 MHz for ^{31}P, 300.13 MHz for ^{1}H and 75.46 MHz for ^{13}C, at 300 K (unless otherwise noted), and are given in relation to 85% H_3PO_4 (^{31}P) and $SiMe_4$. The Bruker standard program was used to acquire [^{31}P–^{31}P] 2D spectra. All downfield shifts are denoted as positive.

Samples for NMR studies were prepared in deuteriated water with a metal(II) concentration of 1×10^{-2} mol dm^{-3} and M^{II} to ligand molar ratios of 1:1 and 1:2. Nitrate salts of Zn^{II}, Mg^{II} and Ca^{II} (Aldrich) were used as a source of the metal ions. The measurements were performed only for freshly prepared samples.

The pH of the samples was measured using a Radiometer pHM83 instrument equipped with a 2401 C combined electrode and given as meter readings without correction for p*D*.

Table 2
Protonation constants of aminomethane-1,1-diphosphonic acids ($\log \beta_n^H$) at 25 ± 0.1 °C and $I = 0.2$ mol dm^{-3} (KCl)

	1	2	3	4	5	6	7	
							Present work	Ref. [38]
$\log \beta_1^H$	12.3	12.4	12.4	11.92(2)	12.6	10.20(1)	10.49(1)	10.49
$\log \beta_2^H$	20.45(5)	20.57(3)	20.40(6)	19.91(2)	21.46(3)	17.95(1)	18.54(1)	18.54
$\log \beta_3^H$	25.44(5)	25.58(3)	25.19(6)	24.85(3)	25.15(3)	23.43(2)	23.85(1)	23.84
$\log \beta_4^H$						25.82(5)		
$pK_{(NH_2^+)}$	12.3	12.4	12.4	11.92	12.60			
$PK_{(PO_3H^-)}$	8.15	8.17	8.00	7.99	8.86	10.20	10.49	10.49
$pK_{(PO_3H^-)}$	4.99	5.01	4.79	4.94	3.69	7.75	8.05	8.05
$pK_{(NH_{pyr}^+)}$						5.48	5.31	5.30
$pK_{(COOH)}$						2.39		

3. Results and discussion

3.1. Solution properties of compounds 1–7

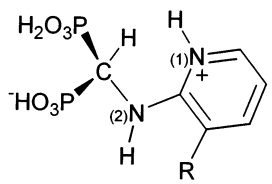
The fully protonated ligand forms contain five dissociable protons (H_5L^+) for **1**–**5** and **7** and six protons (H_6L^+) for **6** (because of the additional proton on the carboxylic group). The amino and imino nitrogen is protonated in compounds **1**–**4** and **5**, respectively. In compounds **6** and **7** the protonation of $N_{pyridine}$ instead of the amino group occurs [26]. On the other side, as shown in Table 2, the studied ligands in the measurable pH range release only three protons: two protons from the PO_3H^- groups and one proton from NRH_2^+ (**1**–**4**), $NH^+_{pyrrolidine}$ (**5**) or $NH^+_{pyridine}$ (**6**, **7**). An additional proton from COOH dissociates in **6**. This is due to the fact that the characteristic pK values for dissociation of one proton from each of the PO_3H_2 groups lie in the range 1.5–2.

The protonation constants for both phosphonic functions of **1**–**5** correspond well with those reported for the aminoethane-1,1-diphosphonic and *N*,*N*-dimethylaminomethane-1,1-diphosphonic acids [39–41]. Generally, the positively charged NH_2^+ (**1**–**4**) or NH^+ (**5**) nitrogen atom bound to the central $CH(P_2)$ carbon lowers the pK values of each PO_3H^- group by approximately 1–2 log units when compared to alkane-1,1-diphosphonic acids [42–44] and to compounds **6** and **7** (Table 2).

The ^{31}P NMR spectra of **1**–**7** exhibit the single resonance lines over the whole pH range studied except for compounds **3** and **4** that both represent chiral molecules used as racemate forms (Table 1). In these cases the spectra consist of two signals of close chemical shifts and 1:1 intensity ratio that are interpreted as belonging to the non-equivalent phosphonate groups. The two-bond coupling between the phosphorus nuclei confirmed by the ^{31}P–^{31}P correlation spectra is reflected as a slight broadening of the ^{31}P resonances of compound **3**. In the spectra of **4** the $^2J_{P-P}$ coupling constants of 1.2–2.1 Hz are detected in a narrow pH range 7–8.

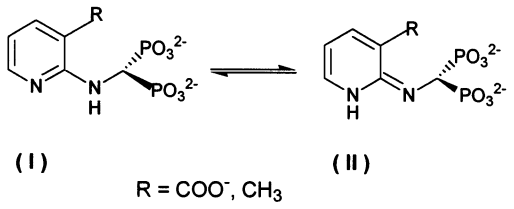
The solution behaviour of **1**–**5**, reflected in their ^{31}P NMR titration curves, does not depart significantly from that of the iminodimethylenediphosphonic acids [9]. The evident similarity, i.e. relatively small changes in the chemical shifts upon deprotonation of the PO_3H^- groups and a large ($\Delta\delta \sim 7$ ppm), commonly observed [9,45,46] downfield shifting upon deprotonation of NH_2^+, is detected for **4** bearing the most electronegative methylenetetrahydrofuryl moiety. Since as compared to **4**, the basicities of NH_2^+ in **1**–**3** and NH^+ in **5** are higher (Table 2) the appropriate ^{31}P NMR titration curves reflect the lower abundance of the completely deprotonated ligand form even under the pH titration limit (pH $\sim$13.5). Accordingly, in the ^{1}H NMR spectra of compounds **1**–**5** the methine proton resonance, appearing as a triplet, shifts gradually upfield upon increase of pH.

A number of distinct features is observed in the case of **6** and **7**. Both compounds crystallize in the solid state as *E* isomers (Fig. 1) and are also proved to preserve their configuration in solution [26]. In **6**, the internal molecular configuration is stabilised with the intramolecular hydrogen bonds involving amino N(2) hydrogen as a donor and two oxygens, one from the carboxylate and one from the phosphonate group, as the proton acceptors. In **7**, the same conformation of



6 R = COOH
7 R = CH_3

Fig. 1. Zwitterionic form of **6** and **7** with the amino proton in *trans* orientation with respect to the pyridine nitrogen (*E* isomer) [26,47].



Scheme 1.

the pyridyl moiety is constrained through a N(2)H···O(phosphonate) hydrogen bond and a N(2)H···CH_3 short contact.

The proton transfer toward the pyridine instead of to the amino nitrogen in the zwitterionic form (Fig. 1) is dictated by the tendency of these compounds to delocalise the lone pair on the amino nitrogen onto the electron deficient pyridyl ring π system. This is a general property of all 2-aminopyridine derivatives, conveniently described in terms of resonance between the mesomeric structures [48]. Due to the conjugation, the N(2)–C(2) bond bears partial double bond character. Consequently, the 2-aminopyridine portions of **6** and **7** are almost planar in any state of protonation.

In addition, in alkaline conditions at pH higher than 8–9 both **6** and **7**, contrary to the 5- or 6-pyridine substituted *N*-(2-pyridyl)aminomethane-1,1-diphosphonic acids, presumably exist as an equilibrium mixture of the amino (**I**) and imino (**II**) tautomers [26] (Scheme 1).

3.2. Complexation of zinc(II), magnesium(II) and calcium(II) with aminomethane-1,1-diphosphonic acids

The chemical models for the studied systems were considered taking into account on one side the potential ability of the ligands to form multinuclear complexes and on the other, revealed by the ^{31}P NMR titration curves, the strong preference to form exclusively protonated species over a wide range of pH. The best-fit models based on the potentiometric data calculations are given in Tables 3–5.

3.2.1. Zinc(II) complexes

The pH-metric titrations indicate that the extent of complex formation in the Zn^{II}–ligand systems is quite similar (Table 3). Each sample with a 1:2 metal to ligand molar ratio could be titrated without precipitation up to pH 11. However, functionalization of the ligands by structural modification of the amino moiety decides the peculiarity in their coordination capabilities.

The metal complex speciations derived from the potentiometric calculations carried out for compounds **1**–**5** do not differ considerably. Generally, the Zn^{II}–**1** system presented in Figs. 2 and 3 exhibits approximately the same distribution curves as those observed for **2**–**5**. Therefore, it can be considered as a representative for all the mentioned systems. The pH dependence of the ^{31}P chemical shifts (Fig. 3(b)) fits well the species distribution pattern, thus confirming a predominance of the protonated species up to pH of about

Table 3
Zinc(II) complex formation constants (log β) of aminomethane-1,1-diphosphonic acids at 25 ± 0.1 °C and $I = 0.2$ mol dm^{-3} (KCl)

	1	**2**	**3**	**4**	**5**	**6**	**7**
log β[Zn(H_2L)]	23.79(1)	23.75(3)	23.56(1)	22.71(8)	24.17(4)	21.71(5)	21.80(8)
log β[Zn(HL)]	19.13(1)	19.39(2)	19.40(1)	19.00(1)	19.89(2)	17.01(2)	17.35(2)
log β[ZnL]	10.55(4)	10.44(6)	10.16(9)	11.08(2)	10.74(5)	10.10(7)	10.32(4)
log β[ZnLH_{-1}]	0.64(4)	0.29(5)	−0.22(6)	0.60(4)	0.12(5)	1.04(6)	1.32(8)
log β[ZnLH_{-2}]	−9.85(10)	−11.55(14)	−11.54(4)	−10.95(4)			
log β[Zn(H_2L)$_2$]						43.20(6)	43.34(11)
log β[Zn(HL)$_2$]	36.53(3)	36.79(3)	36.53(1)	35.61(1)	37.55(3)	31.08(4)	32.31(3)
log β[Zn(HL)L]	26.31(15)	26.07(11)	26.00(6)				
log β[ZnL$_2$]				15.64(8)		14.50(4)	14.30(7)
log β[Zn$_4$L$_3$H$_3$]	69.23(4)	69.84(3)	68.59(2)				
log β[Zn$_3$L$_2$H$_2$]				45.03(2)	46.85(3)		
No. of points	334	197	332	280	159	196	190
p$K_{[Zn(H_2L)]}$	4.66	4.36	4.16	3.71	4.28	4.70	4.45
p$K_{[Zn(HL)]}$	8.58	8.95	9.24	7.92	9.15	6.91	7.03
p$K_{[ZnL]}$	9.91	10.15	10.38	10.48	10.62	9.06	9.00
p$K_{[ZnLH_{-1}]}$	10.49	11.84	11.32	11.55			
p$K_{[ZnLH_{-2}]}$	10.22	10.72	10.53				
log $K_{[ZnL]}$ − Σ pK	−14.89	−15.14	−15.03	−13.77	−14.41	−7.85 [a]	−8.22 [a]
log $\beta_{[Zn(HL)]}$ − p$K_{(NH_2^+)}$	6.83	6.99	7.00	7.08	7.29	6.81 [b]	6.86 [b]
log $K_{[ZnL]/[ZnL_2]}$				6.52		5.70	6.34

Charges are omitted for simplicity.

[a] log $K_{[ZnL]}$ − Σ p$K_{(PO_3H^-)}$ − p$K_{(PO_3H^-)}$.

[b] log $\beta_{[Zn(HL)]}$ − p$K_{(PO_3H^-)}$.

Table 4
Magnesium(II) complex formation constants ($\log \beta$) of aminomethane-1,1-diphosphonic acids at 25 ± 0.1 °C and $I = 0.2$ mol dm^{-3} (KCl)

	1	2	3	4	5	6	7
$\log \beta[Mg(H_2L)]$	22.98(1)	23.20(1)	22.61(2)	22.48(1)	23.20(5)	20.68(1)	21.34(1)
$\log \beta[Mg(HL)]$	17.41(1)	17.55(1)	17.23(1)	17.10(1)	17.60(2)	14.55(1)	15.33(2)
$\log \beta[MgL]$	6.43(2)	6.41(1)	6.12(3)	7.28(2)		5.88(2)	6.12(4)
$\log \beta[MgLH_{-1}]$				−4.79(8)		−4.88(6)	−5.89(12)
$\log \beta[Mg(HL)_2]$	32.23(4)	32.37(2)	32.22(4)	31.84(3)	32.73(6)	26.84(8)	27.83(11)
$\log \beta[Mg(HL)L]$				21.59(7)	21.18(10)	18.51(8)	
$\log \beta[MgL_2]$				10.46(6)		9.05(6)	8.65(8)
$\log \beta[Mg_3L_2H_2]$	39.67(10)	40.62(2)					
No. of points	238	316	220	345	113	133	273
$pK_{[Mg(H_2L)]}$	5.57	5.65	5.38	5.38	5.60	6.13	6.01
$pK_{[Mg(HL)]}$	10.98	11.14	11.11	9.82		8.67	9.21
$pK_{[MgL]}$				12.07		10.76	12.01
$PK_{[Mg(HL)_2]}$				10.25	11.55	8.33	
$pK_{[Mg(HL)L]}$				11.13		9.46	
$\log K_{[MgL]} - \Sigma pK$	−19.01	−19.17	−19.07	−17.57		−12.07 [a]	−12.42 [a]
$\log \beta_{[Mg(HL)]} - pK_{(NH_2^+)}$	5.11	5.15	4.83	5.18	5.00	4.35 [b]	4.84 [b]
$\log K_{[MgL]/[MgL_2]}$				4.10		2.71	3.59

Charges are omitted for simplicity.
[a] $\log K_{[MgL]} - \Sigma pK_{(PO_3H^-)} - pK_{(PO_3H^-)}$.
[b] $\log \beta_{[Mg(HL)]} - pK_{(PO_3H^-)}$.

Table 5
Calcium(II) complex formation constants ($\log \beta$) of aminomethane-1,1-diphosphonic acids at 25 ± 0.1 °C and $I = 0.2$ mol dm^{-3} (KCl)

	1	2	3	4	5	6	7
$\log \beta[Ca(H_2L)]$	22.70(3)	22.79(1)	22.30(2)	22.20(3)	23.40(4)	20.17(1)	20.87(1)
$\log \beta[Ca(HL)]$	17.06(2)		16.69(5)	16.76(2)	17.30(2)	13.97(2)	14.75(1)
$\log \beta[CaL]$				6.08(4)			
$\log \beta[Ca(HL)_2]$				30.92(6)			
$\log \beta[Ca(HL)L]$				21.55(4)	21.02(8)		
$\log \beta[CaL_2]$				9.28(15)			
No. of points	54	54	52	273	141	65	107
$pK_{[Ca(H_2L)]}$	5.64		5.61	5.44	6.10	6.20	6.12
$pK_{[Ca(HL)]}$				10.68			
$pK_{[Ca(HL_2)]}$				9.37			
$pK_{[Ca(HL)L]}$				12.27			
$\log K_{[CaL]} - \Sigma pK$				−18.77			
$\log \beta_{[Ca(HL)]} - pK_{(NH_2^+)}$	4.76		4.29	4.84	4.70		
$\log K_{[CaL]/[CaL_2]}$				2.88			

Charges are omitted for simplicity.

9–10. This is reflected in the relatively small chemical shift changes in the spectra of the ligand solutions upon addition of Zn^{II}, that indicate that formation of these complexes involves the ligand forms with the protonated nitrogen atom.

In the presented systems $[Zn(H_2L)]$ complexes are formed as the minor ones. The $pK_{[Zn(H_2L)]}$ values characteristic for the first deprotonation step for the $[Zn(H_2L)]$ complexes are of the same order of magnitude and are lower than the corresponding dissociation constants of the 'free' ligands (Table 2). Thus, they can be assigned to deprotonation of the phosphonic group promoted by the zinc(II) binding. In [Zn(HL)] the protonated ligand coordinates to zinc(II) in a bidentate

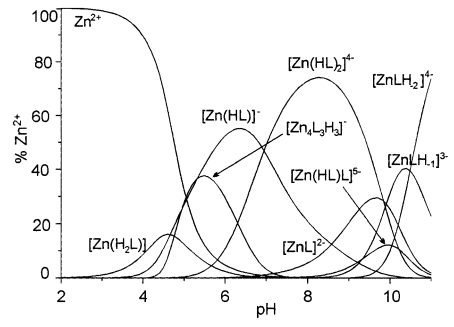


Fig. 2. Species distribution curves for the Zn^{II}–**1** system as a function of pH for the measurement conditions; $c_M = 2.5 \times 10^{-4}$, $c_L = 5 \times 10^{-4}$ mol dm^{-3}.

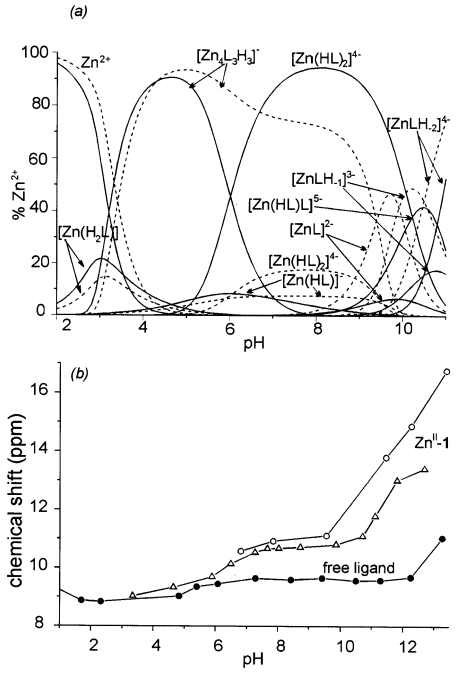
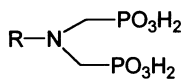


Fig. 3. (a) Species distribution curves for the Zn^{II}–**1** system as a function of pH simulated for conditions used in NMR studies; $c_M = 1 \times 10^{-2}$, $c_L = 2 \times 10^{-2}$ mol dm^{-3} (solid line); $c_M = c_L = 1 \times 10^{-2}$ (dashed line). (b) ^{31}P NMR chemical shifts as a function of pH for compound **1** (●) and for Zn^{II}–**1** 1:1 (○) and 1:2 (△) solutions.



8-a R = $(CH_3)_2CH(CH_2)_2$

8-b R = 

Scheme 2.

manner using one oxygen atom of each suitably positioned phosphonate group to form the six-membered chelate ring. The preference for such coordination is well documented in the literature [10–14]. The $\log K_{[Zn(HL)]} = \log \beta_{[Zn(HL)]} - pK_{(NH_2^+)}$ constants provide further evidence indicating increase in stability of the [Zn(HL)] complexes by about two to three orders of magnitude when compared to those formed by the iminodimethylenediphosphonic acids [9]. The latter compounds use phosphonate group(s) to bind zinc(II) monodentately or to form disadvantageous eight-membered chelate rings [49].

The striking feature of the Zn^{II} systems with ligands **1**–**5** is the formation of the protonated multinuclear species, which is strongly dependent upon the metal to ligand stoichiometry and the solution concentration (Figs. 2 and 3(a)). The ^{31}P NMR experiments clearly support this indication. A pronounced formation of the $[Zn_4L_3H_3]$ (or $[Zn_3L_2H_2]$) complexes demonstrated on the speciation diagrams (see Fig. 3(a) as example) is always accompanied with an exceptional broadening of the corresponding resonance line ($\nu_{1/2} \sim 200$–400 Hz). This feature is not observed when mononuclear protonated complexes predominate in solution ($\nu_{1/2} \sim 20$–25 Hz). A possible explanation can be the relatively slow, on the NMR time scale, exchange of the ligand between the multinuclear complex species. In the relevant ^{1}H NMR experiments the methine $CH(P_2)$ resonances are broad and shifted downfield with $\Delta\delta$ being about 0.1 ppm with respect to the HL species. According to our observations serious broadening of $CH(P_2)$ (one broad line with $\nu_{1/2} \sim 10$–40 Hz) appears to serve as a direct estimation of the incorporation of the *gem*-diphosphonate groups in the six-membered chelate ring.

The second deprotonation step, having $pK_{[Zn(HL)]}$ values much lower than $pK_{NH_2^+}$ (**1**–**4**) and pK_{NH^+} (**5**) of the 'free' ligands (Tables 2 and 3) may be attributed to Zn^{II}-promoted nitrogen deprotonation. This corresponds to our recent finding [9,45,46] that involvement of a nitrogen atom in zinc(II) chelation moves the pH region indicating a gradual downfield shifting of the ^{31}P resonances towards the acidic side by about 2–3 log units, when compared to 'free' ligand (Fig. 3(b)). Accordingly, the respective ^{1}H NMR spectra demonstrate an upfield shifting for the protons adjacent to the nitrogen donor. This allows anticipation that the [ZnL] complexes are very likely tridentate with both phosphonates and the nitrogen donor complexed to Zn^{II}. A tridentate binding mode is also reflected in the $\log K_{[ZnL]}$ values that are generally 3–4 log units higher than the $\log K_{[Zn(HL)]}$ values. In the particular case of **4** a tetrahydrofuryl moiety is also involved in coordination. This is seen from the comparison of the basicity-adjusted constant $\log K_{[ZnL]} - \Sigma pK$ for **4** (-13.77) with those for ligands **1**–**3** (-14.89, -15.14, -15.03, respectively). An increase in stability of about 1–1.4 log units can be explained by the presence of an additional chelate ring in the complex.

In addition, a comparison of the basicity-adjusted constants for **2** and **4** (see above) with the values found for their iminodimethylenediphosphonic acid counterparts which differ structurally but have the same functionalities, namely **8a** and **8b** (-14.01 and -11.53, respectively) [9] (Scheme 2), demonstrates that due to a higher rigidity imposed by the chelate rings the tridentate [ZnL] complexes formed by the aminomethane-1,1-diphosphonic acids are less stable than those formed by the iminodimethylenediphosphonic acids [9].

The two further deprotonation processes of [ZnL] can also be detected by potentiometry. At around pH 10–10.5 coordinated water molecules lose protons to yield $[ZnLH_{-1}]$ and $[ZnLH_{-2}]$. On the other side, at pH 9–13 the ^{1}H NMR spectra of the equimolar Zn^{II}–ligand solutions demonstrate different behaviour for

the protons placed on the opposite sides of the nitrogen donor. Specifically, the protons of the substituent which are placed in the neighbouring α position, namely CH_2 (**1**, **2**, **4**, **5**) or CH (**3**), appear as broad lines. Quite oppositely, $CH(P_2)$ of the methane-1,1-diphosphonate portion undergoes apparent narrowing upon increase of pH. Accordingly, the ^{31}P NMR spectra reveal the single, rather broad resonance lines except for the Zn^{II}–**3** system, which demonstrates two broad signals ($\delta_P =$ 20.28 ppm, $\delta_P = 11.77$ ppm, pH 12.48) coalescing at 320–330 K. These facts may indicate that one phosphonate group leaves the coordination sphere of the zinc(II) ion before a final release of the ligand, usually observed at pH ≥ 13.5.

The protonated bis complexes are also formed in the studied systems (Figs. 2 and 3(a)). Their formation does not lead to any distinct variation in the ^{31}P chemical shifts when compared to the equimolar solutions (Fig. 3(b)). Therefore, one can presume no variation in the coordination modes of ligand molecules in $[Zn(HL)_2]$ with respect to [Zn(HL)]. The deprotonation constants, $pK_{[Zn(HL)_2]}$, of the corresponding equilibrium: $[Zn(HL)_2] \rightleftharpoons [Zn(HL)L] + H^+$ for the systems with ligands **1**–**3** (10.22, 10.72 and 10.53, respectively) are considerably lower than are deprotonation constants of the amino nitrogen of the 'free' ligands. Thus, the most likely binding mode for [Zn(HL)L] is the mixed bidentate/tridenate chelation with the fully deprotonated ligand (L) providing both phosphonate oxygens and the nitrogen donor to coordinate zinc(II).

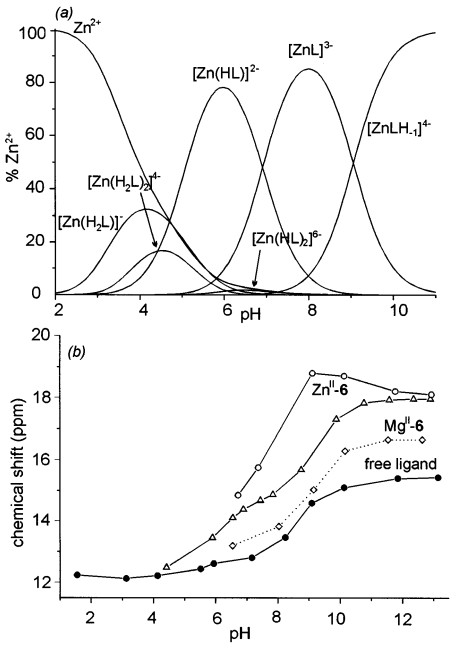


Fig. 4. (a) Species distribution curves for the Zn^{II}–**6** system as a function of pH simulated for conditions used in NMR studies; $c_M = c_L = 1 \times 10^{-2}$ mol dm^{-3}. (b) ^{31}P NMR chemical shifts as a function of pH for compound **6** (●) and for Zn^{II}–**6** 1:1 (○) and 1:2 (△) solutions; $c_M = 1 \times 10^{-2}$ mol dm^{-3}. For comparison, see the analogous NMR titration curve for the Mg^{II}–**6** 1:1 solution (dotted line).

Generally, the formation of the $[ZnL_2]$ complexes is disfavoured due to a strong inter-phosphonate electrostatic repulsion of highly charged phosphonate groups. In fact, the two fully deprotonated ligands would bring together a high negative charge density, 8-, around Zn^{II}. It is the reason why only **4** is capable of forming $[ZnL_2]$ (Table 3). In this case, an additional stabilisation induced by a coordination of the tetrahydrofuryl moiety may partly compensate the unfavourable effect of the electrostatic repulsion. The ratio of the stepwise stability constants $\log(K_{[ZnL]}/K_{[ZnL_2]})$ of 6.52 indicates, however, that the binding of the second ligand molecule is strongly hindered.

The most essential feature that preponderates the complex-forming properties of both **6** and **7** is a propensity of the amino nitrogen to delocalise the lone pair onto the pyridyl ring resulting in its sp^2-hybridization both in the solid [26,47] and in the solution state [26]. The consequent roughly planar 2-aminopyridine portion of the ligand as well as an inability of the amino nitrogen to coordinate metal ion are further substantiated in the chemical models for the Zn^{II}–**6** and Zn^{II}–**7** systems.

As shown on the species distribution diagram of the representative Zn^{II}–**6** system (Fig. 4(a)) the ligands form exclusively mononuclear complexes. The sets of complex species calculated from the potentiometric titrations are in both cases essentially identical (Table 3). Likewise, 1:1 and 1:2 molar ratio complexes are detected. The $[ZnL_2]$ species, as has been discussed above, are strongly disfavoured owing to the repulsion between the negatively charged phosphonate groups. The unfavourable conditions for their formation are expressed with high $\log(K_{[ZnL]}/K_{[ZnL_2]})$ values; 5.70 for Zn^{II}–**6** and 6.34 for Zn^{II}–**7**.

The stability constants of $[Zn(H_2L)]$ and [Zn(HL)] are lower than those of the analogous species formed by compounds **1**–**5** due to the lower $\log \beta_3^H$ values (Table 2). However, from the comparison of the values $\log K_{[Zn(HL)]} = \log \beta_{[Zn(HL)]} - pK_{(PO_2H^-)}$ for ligands **6** and **7** with the values $\log K_{[Zn(HL)]} = \log \beta_{[Zn(HL)]} - pK_{(NH_2^+)}$ for ligands **1**–**5**, which are of the same order of magnitude (Table 3), one can conclude that coordination in [Zn(HL)] is similar for all the studied ligands. Thus, in [Zn(HL)] the proton is most likely bound to the phosphonate group. Consequently, the deprotonation constant of [ZnL] can be assigned to the ionisation of a bound water molecule.

In contrast to the rest of the studied systems the ^{31}P spectra of either 1:1 or 1:2 Zn^{II}–ligand solutions exhibit relatively sharp resonance lines over the whole pH range. The chemical shift profiles for the representative Zn^{II}–**6** system are depicted alongside with the species

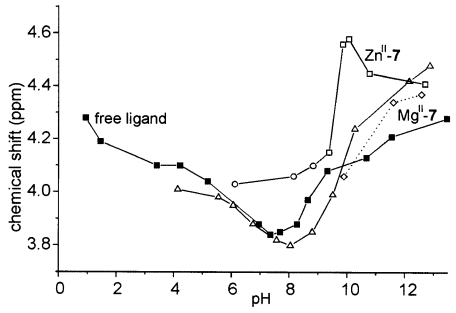


Fig. 5. ^{1}H NMR chemical shifts of $CH(P_2)$ as a function of pH for compound **7** (■) and for Zn^{II}–**7** 1:2 (△) and 1:1 (○, $T = 300$ K; □, $T = 330$ K, see text) solutions; $c_M = 1 \times 10^{-2}$ mol dm^{-3}. For comparison, see the analogous NMR titration curve for the Mg^{II}–**7** 1:1 solution (dotted line).

distribution diagram (Fig. 4(b)). The changes in δ_P observed for the 'free' ligand solutions reflect the deprotonation sequence determined by potentiometry (Table 2), indicating that the loss of the proton from the pyridyl nitrogen ($pK_{NH^+\,pyr} = 5.30$) has greater impact on the phosphorus chemical shift than the deprotonations of the PO_3H^- groups. Since the unfavourable position of pyridyl moiety (Fig. 1) precludes simultaneous coordination of both the pyridine nitrogen and the phosphonate groups the changes in chemical shifts upon complexation can be considered as resulting from the formation of only 'pure' phosphonate bonded complexes. Interestingly, this effect is larger from that produced upon formation of the phosphonate-bonded species by compounds **1**–**5** (Fig. 3(b)).

As we discussed already [26] the position of the methine $CH(P_2)$ resonance in the ^{1}H NMR spectrum can serve as a defining 'fingerprint' of the configurational preferences of *N*-(2-pyridyl)aminomethane-1,1-diphosphonic acids. The δ_P dependence on pH for **7** (*E* geometrical isomer) is depicted in Fig. 5. The extraordinary downfield shifts of the $CH(P_2)$ proton signal upon increase of pH to above 7 can be considered as resulting from a combination of two effects: the deshielding contributed by the electron lone pair of the deprotonated nitrogen in the proximate pyridine ring and the deshielding caused by the pyridine ring current (Fig. 1). The driving force that aligns the methine proton co-planar with respect to the pyridine ring is the enhancement of repulsion resulting from the additional negative charges on the deprotonated phosphonate groups. Quite oppositely, in the *Z* isomer of *N*-2-pyridylaminomethane-1,1-diphosphonic acid the $CH(P_2)$ proton is too distant to be affected by the pyridine nitrogen. Thus, under analogous conditions the proton will be affected exclusively by the deprotonation(s) of the functional group(s) and $CH(P_2)$ resonance will shift upfield, similarly as in the case of compounds **1**–**5**.

We studied carefully the behaviour of the $CH(P_2)$ resonance in the ^{1}H NMR spectra of the ligand solutions upon addition of zinc(II). Interestingly, at pH above 10 the line is too broad to be detected at 300 K. As shown for the Zn^{II}–**7** system (Fig. 5), the increase of the temperature to 320–340 K allows the separation of the signal located in close proximity to the position of the water resonance. This, in the context of the earlier discussion, demonstrates that the configuration of the ligand remains likely unchanged upon complexation of zinc(II). Analogous conclusions can also be drawn for the Zn^{II}–**6** system, which behaves similarly to Zn^{II}–**7**.

In addition, we presumed [26] that the splitting of the C-2 resonance in the ^{13}C NMR spectra ($\Delta\delta \sim 7$ ppm (**6**) and ~ 10 ppm (**7**)), observed when pH is higher than 8–9, might be an indication of the presence of both amino (upfield C-2 signal) and imino (downfield C-2 signal) tautomeric forms of the ligand (Scheme 1). An analogous pattern of the C-2 resonance signals is detected in the ^{13}C NMR spectra of either 1:1 or 1:2 Zn^{II}–ligand alkaline solutions with compounds **6** and **7** (see for example: Zn^{II}–**6**: 165.41 and 155.89 ppm, pH 10.72, 1:1 ratio; Zn^{II}–**7**: 166.70 and 157.69 ppm, pH 11.19, 1:1 ratio). This suggests that the tautomeric equilibrium is not induced by zinc(II) complexation and both amino and imino tautomeric forms (Scheme 1) may bind zinc(II) in a similar manner.

On the other hand, the positions of the carbon resonances do not differ markedly from those detected for the non-protonated 'free' ligand samples, confirming that only phosphonate oxygens participate in the complexation of zinc(II).

3.2.2. Magnesium(II) and calcium(II) complexes

The refined formation constants obtained from the best fit model data for the magnesium(II) systems with compounds **1**–**7** are presented in Table 4. The following species: $[Mg(H_2L)]$, $[Mg(HL)]$ and $[Mg(HL)_2]$ are found in all the systems studied. The formation of others species such as $[Mg_3L_2H_2]$, $[MgL]$, $[Mg(HL)L]$ and $[MgL_2]$ is dependent on the steric requirements and the coordination capabilities of each individual ligand. As an illustration the species distribution curves and the ^{31}P chemical shifts dependence on pH for the Mg^{II}–**4** system are presented in Fig. 6. Generally, a lesser tendency to form multinuclear complexes is noted as compared to zinc(II). $[Mg_3L_2H_2]$ is detected exclusively as the minor species throughout the pH range 4–7 in the solutions of Mg^{II}–**1** and Mg^{II}–**2**.

In the case of **1**–**5** the deprotonation of $[Mg(H_2L)]$ leading to $[Mg(HL)]$ can be assigned to the proton dissociation at the phosphonic group. A further deprotonation, giving $[MgL]$, corresponds to the proton dissociation at the amino group. The latter species is not formed in the Mg^{II}–**5** system at all. On the other hand, only **4** and **5** show a propensity to form $[Mg(HL)L]$, whereas $[MgL_2]$ is detected exclusively in the case of **4**. The increase in log $K_{[Mg(HL)]}$ values with respect to those

of the iminodimethylenediphosphonic acids [9] in the order of approximately 2.5 log units indicates that magnesium(II), similarly to zinc(II), prefers bidentate chelation. The relatively small changes in the ^{31}P NMR chemical shifts upon formation of the protonated species clearly confirm the binding mode(s) based on oxygen complexation. A comparison of the stability constants $\log K_{[MgL]}$ for **1**–**4** with equilibrium constants $\log \beta_{[Mg(HL)]} - pK_{(NH_2^+)}$ reveals increase in stability of approximately 1.3 log units in the case of **1**–**3** and 2.1 for **4**. This fact may indicate that in the [ML] complex the ligand coordinates by the phosphonate groups possibly involving also the amino nitrogen. The comparison of the basicity adjusted stability constants $\log K_{[MgL]} - \Sigma pK$ for **4** (-17.57) with those for **1**–**3** (-19.01, -19.17 and -19.07, respectively) reveals an increase in stability of about 1.5 log units which suggests some stabilising interaction between the magnesium(II) and the teterahydrofuryl oxygen. Accordingly, the metal ion promoted nitrogen deprotonation is accompanied by the downfield shifts of the ^{31}P NMR resonance lines in agreement with an increasing abundance of [ML], [ML(HL)] or [ML_2], in the species distribution diagrams. A slow chemical exchange similar to that of the Zn^{II}–**3** system is detected for the alkaline solutions of Mg^{II}–**3** and Mg^{II}–**4**.

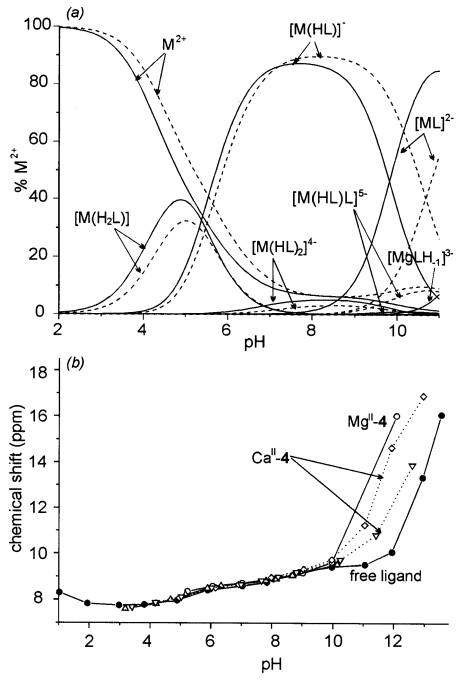


Fig. 6. (a) Species distribution curves for the M^{II}–**4** systems (Mg^{II}, solid line; Ca^{II}, dashed line) as a function of pH simulated for conditions used in NMR studies; $c_M = c_L = 1 \times 10^{-2}$ mol dm^{-3}. (b) Averaged ^{31}P NMR chemical shifts as a function of pH for compound **4** (●) and for Mg^{II}–**4** 1:1 (○) and 1:2 (△) solutions; $c_M = 1 \times 10^{-2}$ mol dm^{-3} (solid lines). For comparison, see the analogous NMR titration curves for the Ca^{II}–**4** 1:1 (◇) and 1:2 (▽) solutions (dotted lines).

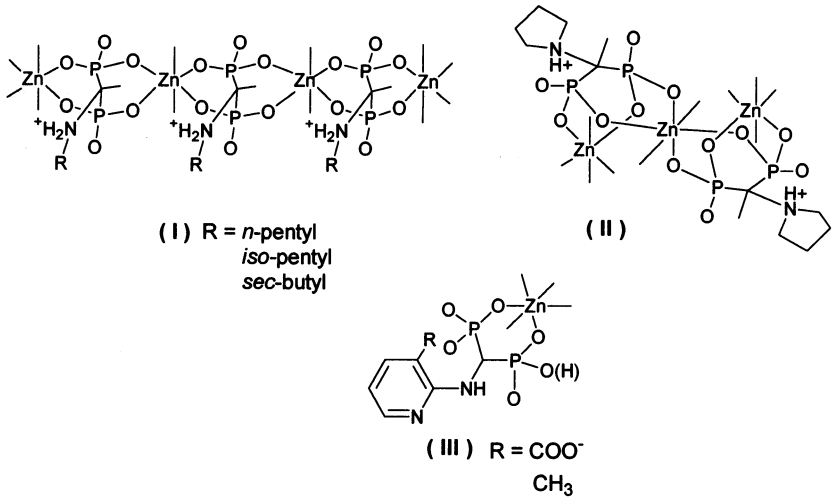
The coordination of Mg^{II} to **6** and **7** is similar to that discussed for the Zn^{II} systems (Tables 3 and 4). The changes in the ^{31}P chemical shifts upon complexation support no variation in the coordination modes for both protonated and non-protonated complexes with respect to those of zinc(II) (Fig. 4(b)). Similarly, magnesium(II) complexation does not tend to induce either a change in the configurational geometry of the ligand (Fig. 5) or the tautomeric equilibrium.

Calcium(II) behaves differently compared to magnesium(II). Among the studied ligands only Ca^{II}–**4** and Ca^{II}–**5** can be titrated over the whole pH range. Owing to the precipitation the pH-metric titrations of the rest of the Ca^{II} systems are confined to the acidic region of pH (see Section 2) that allows detecting only 1:1 protonated complexes (Table 5). No attempt was made to identify the precipitates. We can only speculate that several features that differentiate magnesium and calcium chemistry may have a critical impact on their formation. Calcium(II) is a bigger and a more flexible ion compared to magnesium(II) and prefers higher coordination numbers such as 7, 8. In addition, it forms more ionic, weaker M–L bonds [50,51]. These properties, combined with the peculiar steric requirements of the *gem*-diphosphonate groups allow the binding of several calcium ions to the same molecule [20,52] and enable formation of aggregate polynuclear complexes that deposit as solid materials under conditions when charge balance is achieved.

Functionalization of the aminomethane-1,1-diphosphonic core with either methylenetetrahydrofuryl (**4**) or pyrrolidine directly attached to the $CH(P_2)$ carbon (**5**) allows the formation of mononuclear complexes that are soluble. This can be primarily due to a dominance of steric factors imposed by the substituents. In addition, in **4,** a tetrahydrofuryl moiety decreases the basicity of the ligand and provides a potential coordination site for Ca^{II}. Both the potentiometric and NMR data indicate that coordination of Ca^{II} to **4** is very similar to that observed for the Mg^{II}–**4** system (Fig. 6). In the case of Ca^{II}–**5**, only the protonated, oxygen-bonded species are found from the calculations of the potentiometric titration data and based on NMR data. In general, Ca^{II} forms less stable complexes than Mg^{II} (Tables 4 and 5) even in the particular case of **4**. This is in contrast to the calcium(II) and magnesium(II) systems with compound **8b** where [CaL] has been demonstrated to be more stable than [MgL] [9].

4. Conclusion

There is a full consistency between the pH-metric and NMR spectroscopic studies indicating that the aminomethane-1,1-diphosphonic acids prefer formation of the protonated species over a wide range of pH. The



Scheme 3.

most efficient binding of Zn^{II}, Mg^{II} or Ca^{II} ions, dictated by the structural arrangement of the *gem*-diphosphonate groups, is the formation of the six-membered chelate ring involving oxygens of both phosphonate groups. Such a coordination is preferred in the protonated species of **1**–**5,** as well as in [M(HL)] and [ML] complexes of **6** and **7**. The role of the amino group in compounds **1**–**5** is to decrease the $pK_{PO_3H^-}$ of the phosphonate groups, thus enabling the formation of the [HL] ligand forms efficiently chelating metal ions.

The formation of the nitrogen bonded [ML] complexes by **1**–**5** is generally of lesser importance. They are detected at relatively high pH values and, contrary to the [M(HL)] species, are less stable than those formed by the iminodimethylenediphosphonic acids [9]. In the case of **4** the complexation of a sterically accessible tetrahydrofuryl oxygen promotes the nitrogen binding that results in a tetradentate coordination not only in [ZnL] and [MgL] but also in the [CaL] complex.

Some ligands demonstrate an evident preference for the formation of protonated, multinuclear complexes, that are soluble. This tendency is strongly dependent upon the metal to ligand stoichiometry and the concentration (Figs. 1 and 2) and is especially well expressed in the case of zinc(II). We already suggested [26] that it is also dependent upon the structural organization of the ligands and especially upon the strong capacity of the phosphonic (PO_3H_2) and/or phosphonate (PO_3H^-) groups to form intermolecular hydrogen bonds. On the other hand, the priorities in the hydrogen bond network organization are influenced by the structural peculiarities of each particular amino moiety.

Accordingly, the solid state ribbon aggregation via phosphonic–phosphonic and phosphonate–phosphonate interactions in compound **1** allows for the formation of multinuclear complexes of $[M_4L_3H_3]$ type in solution. The complex of $[M_3L_2H_2]$ type is detected for **5**, where due to phosphonic–phosphonate and phosphonate–phosphonate intermolecular interactions multimeric aggregates composed of two different dimeric units are formed. In the case of **7**, where only mixed phosphonic–phosphonate intermolecular hydrogen-bonding exist in the solid state, any metal ion coordination as well as deprotonation destroys the basic hydrogen-bonded network. Consequently, mononuclear complexes are explicitly formed which is proved by both potentiometry and NMR methods.

In the light of the above discussion it seems to be evident that prior crystal structural studies of the ligands themselves might be valuable in predicting the most likely binding modes. Three examples are presented in Scheme 3.

Structure **I** is presumed based on the molecular ribbon formed by **1**, provided that in all *N*-alkyl substituted aminomethane-1,1-diphosphonic acids the intermolecular hydrogen bond networks are similar. Structure **II** is based on the dimeric units that constitute the multimeric aggregates of ligand **5**. Structure **III** represents the mononuclear complex(es) formed preferentially with compounds **6** and **7**.

Magnesium(II) is worst as a template organizing the multinuclear complex forms. The $[M_3L_2H_2]$ species formed exclusively with **1** and **2** may be assumed, by analogy, as short forms of structure **I**.

Zinc(II), forming the strongest M–O bonds among all of the studied cations, prefers formation of multinuclear complexes, whilst Mg^{II} and Ca^{II} behave quite differently. Magnesium(II) demonstrates a preference for mononuclear species whereas calcium(II) tends to form insoluble complexes with most of the studied ligands.

References

[1] R. Rawls, Chem. Eng. News 94 (1998) 38.
[2] D.E. Hughes, M. Mian, D.F. Guilland-Cumming, R.G.G. Russell, Drugs Exp. Clin. Res. 17 (1991) 109.
[3] R.E. Coleman, Ann. Oncol. 11 (2000) 179.
[4] F.H. Ebetino, M.D. Francis, M.J. Rogers, R.G.G. Russell, Rev. Contemp. Pharmacother. 9 (1998) 233.
[5] H. Nakaya, G. Osawa, N. Iwasaki, G.L. Cochran, T.W. Oates, J. Peridontol. 71 (2000) 1158.
[6] M.B. Martin, J.S. Grimley, J.C. Lewis, H.T. Heath III, B.N. Bailey, H. Kendrick, V. Yardley, A. Caldera, R. Lira, J.A. Urbina, S.N.J. Moreno, R. Docampo, S.N. Crofs, E. Oldfield, J. Med. Chem. 44 (2001) 909.
[7] P. Kafarski, B. Lejczak, G. Forlani, Heteroatom Chem. 11 (2000) 449.
[8] L. Berlicki, P. Kafarski, Unpublished data.
[9] E. Matczak-Jon, B. Kurzak, A. Kamecka, W. Sawka-Dobrowolska, P. Kafarski, J. Chem. Soc., Dalton Trans. (1999) 3627.
[10] T.P. Haromy, W.B. Knight, D. Dunaway-Mariano, M. Sundaralingam, Inorg. Chem. 23 (1984) 2412.
[11] J.-P. Silvestre, N. El Messbahi, R. Rochdaoui, N.Q. Dao, M.-R. Lee, A. Neuman, Acta Crystallogr., Sect. C 46 (1990) 986.
[12] V.S. Sergienko, G.G. Aleksandrov, E.G. Afonin, Zh. Neorg. Khim. 42 (1997) 1291.
[13] E.G. Afonin, G.G. Aleksandrov, V.S. Sergienko, Koord. Khim. 23 (1997) 846.
[14] K.A. Lyssenko, V.M. Akimov, M.Yu. Antipin, P.N. Abakumov, Yu.T. Struchkov, V.G. Skvortsov, M.A. Ershov, Zh. Neorg. Khim. 42 (1997) 1283.
[15] C. Dufau, M. Benramdane, Y. Leroux, D. El Manouni, A. Neuman, T. Prangé, J.-P. Silvestre, H. Gillier, Phosphorus Sulfur Silicon Relat. Elem. 107 (1995) 145.
[16] R. Rochdaoui, J.-P. Silvestre, N.Q. Dao, M.-R. Lee, A. Neuman, Acta Crystallogr., Sect. C 48 (1992) 2132.
[17] V.S. Sergienko, G.G. Aleksandrov, E.G. Afonin, Zh. Coord. Khim. 25 (1999) 423.
[18] A. Neuman, A. Safsaf, H. Gillier, Y. Leroux, D. El Manouni, Phosphorus Sulfur Silicon Relat. Elem. 70 (1992) 273.
[19] L.M. Zheng, Ch. Y. Duan, X.R. Ye, L.Y. Zhang, Ch. Wang, X.Q. Xin, J. Chem. Soc., Dalton Trans. (1998) 905.
[20] V.A. Uchtman, J. Phys. Chem. 9 (1972) 1304 and references therein.
[21] Y. Leroux, A. Neuman, H. Gillier, D. El Manouni, Z. Abkhar, T. Prangé, Supramol. Chem. 5 (1995) 267.
[22] G.G. Aleksandrov, V.S. Sergienko, Crystallogr. Rep. 44 (1999) 991.
[23] G.G. Aleksandrov, E.G. Afonin, V.S. Sergienko, Zh. Coord. Khim. 26 (2000) 512.
[24] L.M. Zheng, H.H. Song, C.Y. Duan, X.Q. Xin, Inorg. Chem. 38 (1999) 5061.
[25] R. Bau, S.K.S. Huang, J.A. Feng, Ch.E. McKenna, J. Am. Chem. Soc. 110 (1998) 7546.
[26] E. Matczak-Jon, W. Sawka-Dobrowolska, P. Kafarski, V. Videnova-Adrabinska, New J. Chem. (2001) 1447.
[27] F. Suzuki, Y. Fujikawa, S. Yamamoto, H. Mizutani, T. Ohya, T. Ikai, T. Oguchi, Y. Ochiai, K Nakahara, Jpn. Kokai Tokkyo Koho (1979)79 37, 829; Chem. Abstr. 91 (1980) 103762h.
[28] F. Suzuki, Y. Fujikawa, S. Yamamoto, H. Mizutani, C. Funabashi, T. Ohya, T. Ikai, T. Oguchi, Ger. Offen. (1979) 28, 31, 578.
[29] B. Lejczak, B. Boduszek, P. Kafarski, G. Forlani, H. Wojtasek, P. Wieczorek, J. Plant Growth Regul. 15 (1996) 109.
[30] P. Kafarski, B. Lejczak, G. Forlani, R. Gancarz, C. Torreilles, J. Grembecka, A. Ryczek, P. Wieczorek, J. Plant Growth Regul. 16 (1997) 153.
[31] A.L. Chuiko, M.O. Lozinsky, I. Jasicka-Misiak, P. Kafarski, J. Plant Growth Regul. 18 (1999) 171.
[32] G. Forlani, B. Lejczak, P. Kafarski, P. Wieczorek, J. Plant Growth Regul. 16 (1997) 147.
[33] L. Maier, Phosphorus Sulfur Silicon Relat. Elem. 11 (1981) 311.
[34] G. Gran, Acta Chem. Scand. 4 (1950) 599.
[35] M. Molina, C. Melios, J.O. Tognalli, L.C. Luchiari, M. Jafelicci Jr, J. Electroanal. Chem. 105 (1979) 237.
[36] P. Gans, A. Sabatini, A. Vacca, J. Chem. Soc., Dalton Trans. (1985) 1195.
[37] Ch.F. Baes Jr, R.E. Mesmer, The Hydrolysis of Cations, Robert E. Krieger Publishing Company, Malabar, FL, 1986.
[38] B. Boduszek, M. Dyba, M. Jeżowska-Bojczuk, T. Kiss, H. Kozłowski, J. Chem. Soc., Dalton Trans. (1997) 973.
[39] M.N. Rusina, T.M. Balashova, B.V. Zhadanov, A. Yu. Tsitrina, I.A. Polyakova, Zh. Obsh. Khim. 47 (1977) 1721.
[40] (a) J.E. Bollinger, D.M. Roundhill, Inorg. Chem. 32 (1993) 2821; (b) J.E. Bollinger, D.M. Roundhill, Inorg. Chem. 33 (1994) 6421.
[41] L.H. Merwin, W.A. Dollase, G. Hägele, H. Blum, Phosphorus Sulfur Silicon Relat. Elem. 56 (1991) 117.
[42] M. Dyba, M. Jezowska-Bojczuk, E. Kiss, T. Kiss, H. Kozlowski, Y. Leroux, D. El Manouni, J. Chem. Soc., Dalton Trans. (1996) 1119.
[43] S. Lacour, V. Deluchat, J.-C. Bollinger, B. Serpaud, Environm. Technol. 20 (1999) 249.
[44] V. Deluchat, B. Serpaud, C. Caullet, J.-C. Bollinger, Phosphorus Sulfur Silicon Relat, Elem. 104 (1995) 81 and references therein.
[45] E. Matczak-Jon, B. Kurzak, W. Sawka-Dobrowolska, B. Lejczak, P. Kafarski, J. Chem. Soc., Dalton Trans. (1998) 161.
[46] E. Matczak-Jon, B. Kurzak, W. Sawka-Dobrowolska, P. Kafarski, B. Lejczak, J. Chem. Soc., Dalton Trans. (1996) 3455.
[47] W. Sawka-Dobrowolska, Private communication.
[48] A.R. Katritzky, Ch.W. Rees, Comprehensive Heterocyclic Chemistry, vol. 2 (Pt. 2A), Pergamon Press, Oxford, UK, 1984.
[49] (a) K. Sawada, T. Kanda, Y. Naganuma, T. Suzuki, J. Chem. Soc., Dalton Trans. (1993) 2557;
(b) K. Sawada, T. Miyagawa, T. Sakaguchi, K. Doi, J. Chem. Soc., Dalton Trans. (1993) 3777.
[50] O. Carugo, K. Djinović, M. Rizzi, J. Chem. Soc., Dalton Trans. (1993) 2127.
[51] A. Kaufman Katz, J.P. Glusker, S.A. Beebe, Ch.W. Bock, J. Am. Chem. Soc. 118 (1996) 5752.
[52] J.P. Räsänen, E. Pohjala, H. Nikander, T. Pakkanen, J. Phys. Chem. 100 (1996) 8230.

PERGAMON

Polyhedron 21 (2002) 333–342

POLYHEDRON

www.elsevier.com/locate/poly

The synthesis of small azamacrocycles bearing pendant aromatic functionalities. The crystal structures of $[Cu(\mathbf{L}_1)_2](PF_6)_2$, $[(\mathbf{L}_1)CuCl_2]$, $[Cu(\mathbf{L}_6)(NO_3)_2]$ and $[Cu_2(\mathbf{L}_7\text{–H})_2(OH_2)_2](PF_6)_2\cdot 3H_2O$ ($\mathbf{L}_1$ = *N*-(mesitylethyl)-1,4,7-triazacyclononane, $\mathbf{L}_6$ = *N*-(4-hydroxymethylbenzyl)-1,4,7-triazacylcononane, $\mathbf{L}_7$ = *N*-(4-benzylcarboxylic acid)-1,4,7-triazacylcononane)

Andrew C. Benniston [a,b,*], David Ellis [a], Louis J. Farrugia [a], Roselyn Kennedy [a], Robert D. Peacock [a,*], Sarah Walker [a]

[a] *Department of Chemistry, Joseph Black Building, The University of Glasgow, Glasgow G12 8QQ, UK*
[b] *Department of Chemistry, Bedson Building, University of Newcastle, Newcastle-upon-Tyne NE1 7RU, UK*

Received 24 September 2001; accepted 13 November 2001

Abstract

A simple synthetic procedure for the mono- or di-functionalization of tri- and tetra-azamacrocycles with electron rich arenes has been developed. Specifically, 1,4,7-triazacyclononane (tacn), 1,4,7,10-tetraazacyclododecane (cyclen) and 1,4,8,11-tetraazacyclotetradecane (cyclam) react with 2,4,6-trimethylstyrene in the presence of *n*-butyllithium to give, respectively *N*-(mesitylethyl)-1,4,7-triazacyclononane ($\mathbf{L}_1$), *N*-(mesitylethyl)-1,4,7,10-tetraazacyclododecane ($\mathbf{L}_4$), and *N*-(mesitylethyl)-1,4,8,11-tetraazacyclotetradecane ($\mathbf{L}_5$). In contrast, when styrene itself or *p*-vinylanisole are used as the Michael acceptor with 1,4,7-triazacyclononane, the *N′*,*N″* product is formed, respectively *N′*,*N″*-*bis*(phenylethyl)-1,4,7-triazacyclononane ($\mathbf{L}_2$) and *N′*,*N″*-*bis*(*p*-methoxyphenylethyl)-1,4,7-triazacyclononane ($\mathbf{L}_3$). Using conventional mono-functionalization techniques, the phenyl derivatives *N*-(4-hydroxymethylbenzyl)-1,4,7-triazacyclononane ($\mathbf{L}_6$) and *N*-(4-benzylcarboxylic acid)-1,4,7-triazacyclononane ($\mathbf{L}_7$) have also been synthesised. A series of transition metal complexes of $\mathbf{L}_1$ to $\mathbf{L}_7$ with Ni(II), Cu(II), Zn(II) and Co(II) have been prepared. The X-ray crystal structures of $[Cu(\mathbf{L}_1)_2](PF_6)_2$, $[(\mathbf{L}_1)CuCl_2]$, $[Cu(\mathbf{L}_6)(NO_3)_2]$ and $[Cu_2(\mathbf{L}_7\text{–H})_2(OH_2)_2](PF_6)_2\cdot 3H_2O$ are described. In all of these complexes, coordination to the metal takes place through the macrocycle nitrogens. The crystal structure of $[Cu_2(\mathbf{L}_7\text{–H})_2(OH_2)_2](PF_6)_2\cdot 3H_2O$ reveals that it is a coordinate-polymeric material. Attempts to coordinate the pendent arenes to Rh(I) are discussed. © 2002 Elsevier Science Ltd. All rights reserved.

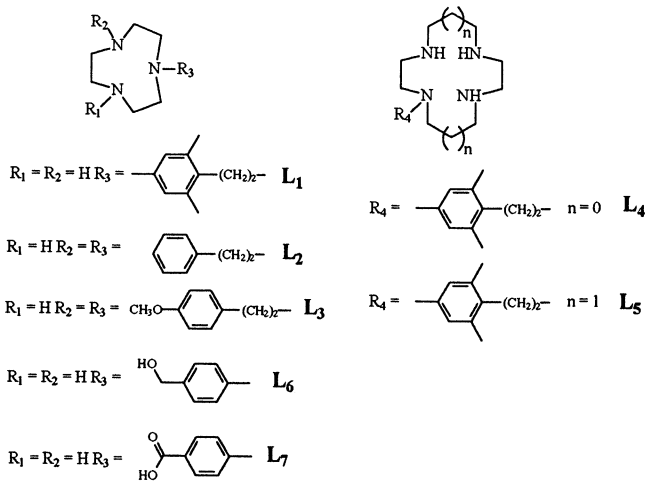
Keywords: Azamacrocycles; Aromatic pendant arms; Coordination compounds; Metallic polymer

1. Introduction

The chemistry of triazamacrocycles, *N*-functionalized with hard ligators, e.g. carboxylic acids [1], alcohols [2], amines [3], sulfates [4], phosphates [5], imidazoles [6] and pyridine [7] is now well established. More recently the chemistry has been extended to include more classic soft donors such as sulfides [8], alkenes [9], phosphines [10] and alkynes [11]. As part of our own research effort we have been exploring the possibility of introducing aromatic groups onto the macrocycle (Scheme 1), which are either electron rich so as to generate organometallic clusters, or have oxygen binding sites for further molecular recognition [12]. As a result we

* Corresponding authors. Tel.: +44-141-222-5706; fax: +44-141-222-6929.
E-mail address: a.c.benniston@ncl.ac.uk (A.C. Benniston).

0277-5387/02/$ - see front matter © 2002 Elsevier Science Ltd. All rights reserved.
PII: S0277-5387(01)00994-9

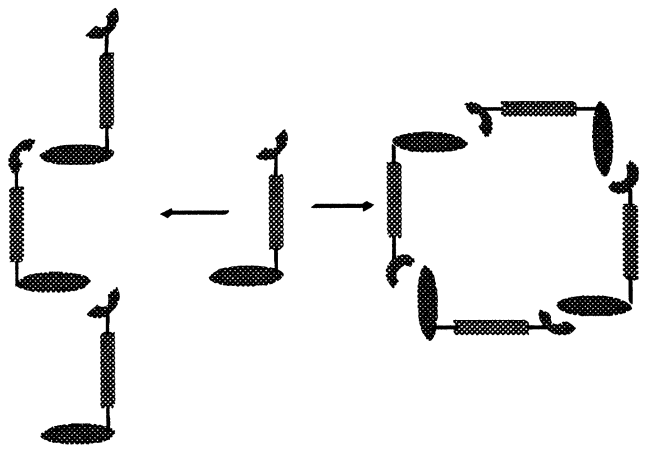


Scheme 1. List and numbering scheme of the macrocycles discussed in the text.

now present some of our work towards these goals. In particular, a high yielding procedure is reported for the monofunctionalization of tacn with the electron rich arene derived from 2,4,6-trimethylstyrene.

Syntheses of single pendent arm macrocycles are comparatively rare, and are often not straightforward, requiring chromatographic separation of the products. We have found that direct reaction of an excess of 2,4,6-trimethylstyrene with either of the macrocycles, tacn, cyclen or cyclam in the presence of *n*-butyllithium leads to good yields of the monosubstituted products without further separation. Under the same experimental conditions, the vinylaromatics styrene or *p*-vinylanisole give the *N′*,*N″* disubstituted products, in a similarly pure state.

Complexes of $\mathbf{L}_1$ with the metals, Cu(II), Ni(II), Co(II) and Zn(II) were synthesised and the X-ray crystal structures of $[Cu(\mathbf{L}_1)_2](PF_6)_2$ and $[(\mathbf{L}_1)CuCl_2]$ are described. It was anticipated that the pendent 'activated' arene of the coordinated ligand would react with soft metal centres, but no reaction was observed with Rh(I) [13] or Mo(0) [14] despite the use of forcing conditions. Complexes of $\mathbf{L}_6$ with the metals, Cu(II), Ni(II), Co(II) and $\mathbf{L}_7$ with Cu(II) were also prepared. In these two cases it was expected that the hydroxyl or carboxyl unit would play host to intermolecular bonding, and hence the construction of self-assembled molecular aggregates (e.g. polymers, boxes) as illustrated in Scheme 2.



Scheme 2. Pictorial representation of potential products from the self-assembly of an 'L' type motif.

2. Experimental

All chemicals unless otherwise stated were purchased from Aldrich and used as received. 1,4,7,10-Tetraazacyclododecane (cyclen) was purchased from Strem Chemicals. Solvents where necessary were dried by reported methods [15]. 1,4,7-Triazacyclononane (tacn) [16], 1,4,8,11-tetraazacyclotetradecane (cyclam) [17], 1,4,7-triazacyclo[5.2.1.^{04,10}]decane [18] and $[Rh(\mu\text{-}Cl)(COD)]_2$ [19] were synthesised according to literature procedures. ^{1}H and ^{13}C NMR spectra were recorded using a Bruker AM360 360 MHz spectrometer. UV–Vis spectra were recorded using a Shimadzu UV-3101 PC spectrophotometer. Mass spectra were obtained using a JEOL JMS 700 (The MStation) mass spectrometer. Combustion analysis was performed using in-house facilities.

2.1. Synthesis of *N*-(mesitylethyl)-1,4,7-triazacyclononane ($\mathbf{L}_1$)

^{n}BuLi (4 ml of a 2.5 M solution in hexanes, 10 mmol) was added dropwise to a solution of tacn (1.0 g, 7.8 mmol) dissolved in THF (20 ml). The reaction mix was stirred for 5 min, followed by the dropwise addition of 2,4,6-trimethylstyrene (3.4 g, 23.2 mmol) in THF (10 ml) and the solution stirred at 60 °C for 16 h. Water (1 ml) was added and the reaction mix stirred for 5 min. All volatiles were removed in vacuo. The residue was extracted into CH_2Cl_2 and the solution extracted with 2 M HCl (2 × 40 ml). The aq. phase was basified with NaOH (1 M) solution and the free ligand extracted into $CHCl_3$ (3 × 40 ml). The combined organic phases were dried over $MgSO_4$, filtered and the solvents removed in vacuo to leave a clear oil which slowly solidified. Yield: 1.1 g, 3.9 mmol, 50%. ^{1}H NMR ($CDCl_3$): $\delta = 6.80$ (s, 2H, $C_6H_2Me_3$), 2.98–2.60 (m, 18H, CH_2NH), 2.27 (s, 6H, *o*-$C_6H_2(CH_3)_2$), 2.21 (s, 3H, *p*-$C_6H_2CH_3$). ^{13}C NMR ($CDCl_3$): $\delta = 136.0$, 135.3, 133.3, 128.9 (phenyl–*C*), 55.6 (N–CH_2–CH_2–$C_6H_2Me_3$), 52.3, 46.7, 46.4 (N–CH_2–CH_2–N), 27.2 (N–CH_2–CH_2–$C_6H_2Me_3$), 20.8 (*p*-$C_6H_2CH_3$), 19.8 (*o*-$C_6H_2(CH_3)_2$). EI MS: $m/z = 273$ $[M-2H]^+$, 154 $[M-C_6H_2Me_3]^+$.

2.2. Synthesis of N-(mesitylethyl)-1,4,7,10-tetraazacyclododecane (L_4)

^{n}BuLi (1.6 ml of a 2.5 M solution in hexanes, 4.0 mmol) was added dropwise to a solution of cyclen (0.50 g, 3.0 mmol) in THF (20 ml). The reaction mixture was stirred for 5 min, followed by the addition of 2,4,6-trimethylstyrene (1.3 g, 9 mmol) in THF (10 ml) and the reaction mixture was stirred at 60 °C for 16 h. Water (5 ml) was added and the reaction mixture stirred for 5 min. All volatiles were removed in vacuo. The residue was dissolved in CH_2Cl_2 and the solution extracted into 2 M HCl (2×40 ml). The aq. phase was basified with NaOH (1 M) solution and the free ligand extracted into $CHCl_3$ (3×40 ml). The combined organic phases were dried over $MgSO_4$, filtered and the solvents removed in vacuo to leave a clear, yellow oil. Yield: 0.58 g, 1.8 mmol, 60%. ^{1}H NMR ($CDCl_3$): $\delta = 6.80$ (s, 2H, $C_6H_2Me_3$), 2.82–2.50 (m, 23H, CH_2,NH), 2.27 (s, 6H, o-$C_6H_2(CH_3)_2$), 2.21 (s, 3H, p-$C_6H_2CH_3$). ^{13}C NMR ($CDCl_3$): $\delta = 135.9$, 135.0, 133.2, 129.7 (phenyl–C), 53.0 (N–CH_2–CH_2–$C_6H_2Me_3$), 51.0, 46.9, 45.7, 45.3 (N–CH_2–CH_2–N), 26.8 (N–CH_2–CH_2–$C_6H_2Me_3$), 20.6 (p-$C_6H_2CH_3$), 19.5 (o-C_6H_2-$(CH_3)_2$). EI MS: $m/z = 185$ $[M - (CH_2)_2C_6$-$H_2Me_3]^+$, 147 $[(CH_2)_2C_6H_2Me_3]^+$, 133 $[CH_2C_6H_2Me_3]^+$.

2.3. Synthesis of N-(mesitylethyl)-1,4,8,11-tetraazacyclotetradecane (L_5)

Prepared similarly to $\mathbf{L}_1$ from cyclam (0.40 g, 2.0 mmol), ^{n}BuLi (1.1 ml of a 2.5 M solution in hexanes, 2.8 mmol) and 2,4,6-trimethylstyrene (1.2 g, 8.0 mmol). Yield: 0.30 g, 0.88 mmol, 44%. ^{1}H NMR ($CDCl_3$): $\delta = 6.73$ (s, 2H, $C_6H_2Me_3$), 2.72–2.51 (m, 23H, NH, N–CH_2–CH_2–N,N–CH_2–CH_2–CH_2–N), 2.23 (s, 6H, o-$C_6H_2(CH_3)_2$), 2.15 (s, 3H, p-$C_6H_2CH_3$), 1.67 (m, 4H, N–CH_2–CH_2–$C_6H_2Me_3$). ^{13}C NMR ($CDCl_3$): $\delta = 135.9$, 134.8, 133.4, 128.7 (phenyl–C), 54.0, 52.3, 50.9, 50.7, 50.5, 49.3, 49.1, 49.0, 48.9, 47.9, 28.9, 28.6, 26.3, 24.5 (CH_2), 20.7 (p-$C_6H_2CH_3$), 19.8 (o-$C_6H_2(CH_3)_2$). EI MS: $m/z = 213$ $[M - CH_2(C_6H_2Me_3]^+$, 147 $[(CH_2)_2C_6$-$H_2Me_3]^+$.

2.4. Synthesis of N′,N″-bis(phenylethyl)-1,4,7-triazacyclononane (L_2)

Prepared similarly to $\mathbf{L}_1$ from tacn (0.20 g, 1.58 mmol), ^{n}BuLi (1.0 ml of a 2.5 M solution in hexanes, 2.1 mmol) and styrene (0.50 g, 4.8 mmol). Yield: 0.24 g, 0.72 mmol, 45%. ^{1}H NMR ($CDCl_3$): $\delta = 7.29$–7.18 (m, 10H, C_6H_5), 2.79–2.62 (21H, CH_2 NH). ^{13}C NMR ($CDCl_3$): $\delta = 140.6$, 128.6, 128.3, 125.9 (phenyl–C), 59.1 (NH–CH_2–CH_2–C_6H_5), 53.0, 53.5, 46.7 (NH–CH_2–CH_2–NH), 34.1 (NH–CH_2–CH_2–C_6H_5). EI MS: $m/z = 335$ $[M]^+$, 246 $[M - CH_2C_6H_5]^+$, 105 $[C_6H_5(CH_2)_2]^+$.

2.5. Synthesis of N′,N″-bis(p-methoxyphenylethyl)-1,4,7-triazacyclononane (L_3)

Prepared similarly to $\mathbf{L}_1$ from tacn (0.21 g, 1.58 mmol), ^{n}BuLi (1.0 ml of a 2.5 M solution in hexanes, 2.1 mmol), and p-vinylanisole (0.64 g, 4.8 mmol). Yield: 0.28 g, 0.71 mmol, 45%. ^{1}H NMR ($CDCl_3$): $\delta = 7.09$ (d, 4H, C_6H_4, $J = 8.64$ Hz), 6.81 (d, 4H, C_6H_4, $J = 8.68$ Hz), 3.74 (s, 6H, CH_3), 2.71–2.58 (m, 21H, CH_2, NH). ^{13}C NMR ($CDCl_3$): 157.8, 132.2, 129.6, 113.7 (phenyl–C), 59.0 (N–CH_2–CH_2–C_6H_4OMe), 55.1 (CH_3), 52.3, 50.1, 45.8 (N–CH_2–CH_2–N), 33.0 (N–CH_2–CH_2–C_6H_4OMe). EI MS: $m/z = 396$ $[M]^+$, 276 $[M - CH_2C_6H_4OMe]^+$, 135 $[CH_2CH_2C_6H_4OMe]^+$.

2.5.1. Synthesis of A

To a one-necked flask flushed with dinitrogen and charged with 1,4,7-triazacyclo[5.2.1.^{04,10}]decane (0.69 g, 4.96 mmol) in dry THF (30 ml), was slowly added 4-bromomethylbenzyl alcohol (1 g, 4.98 mmol) in dry THF (20 ml). The reaction mixture was stirred overnight and the resultant white precipitate filtered washed with THF and dried. Yield: 1.03 g, 3.02 mmol, 61%. ^{1}H NMR (C_3H_6O-d_6): $\delta = 7.73$–7.72 (d, 2H, C_6H_4, $J = 7.9$ Hz), 7.54–7.52 (d, 2H, C6H_4, $J = 7.9$ Hz), 5.97 (s, 1H, N–CH), 4.75 (s, 2H, Ar–CH_2), 4.71 (s, 2H, ArCH_2), 4.04–3.98 (m, 2H, NCH_2), 3.81–3.70 (m, 4H, NCH_2), 3.50–3.42 (m, 2H, N–CH_2), 3.33–3.25 (m, 4H, N–CH_2).

2.6. Synthesis of N-(4-hydroxymethylbenzyl)-1,4,7-triazacyclononane (L_6)

Compound **A** (1.31 g, 3.85 mmol) was refluxed in water (40 ml) for 4 h followed by the addition of NaOH (0.54 g, 10 mmol). The resulting basic solution was refluxed for 24 h and the water removed with $C_6H_5CH_3$ using a Dean–Stark apparatus. Removal of the $C_6H_5CH_3$ afforded an oil which was sufficiently pure enough for metal ion complexation. Yield: 0.65 g, 2.6 mmol, 68%. ^{1}H NMR ($CDCl_3$): $\delta = 7.26$ (s, 4H, C_6H_4), 4.53 (s, 2H, N–CH_2–OH), 3.62 (s, 2H, CH_2–N), 2.65 (m, 4H, N–CH_2), 2.54 (m, 8H, N–CH_2). EI MS: $m/z =$ 250 $[M$H$]^+$.

2.6.1. Synthesis of B

This compound was prepared in a similar manner to that reported for compound **A**, using methyl-4-(bromomethyl)benzoate (1 g, 4.37 mmol) and 1,4,7-triazacyclo[5.2.1.^{04,10}]decane (0.69 g, 4.96 mmol). Yield: 1.1 g, 2.98 mmol, 68%. ^{1}H NMR (C_3H_6O-d_6): $\delta = 8.11$–8.09 (d, 2H, C_6H_4, $J = 8.1$ Hz), 7.91–7.88 (d, 2H, C_6H_4,

$J = 8.2$ Hz), 6.02 (s, 1H, NC*H*), 4.79 (s, 2H, Ar–CH_2), 3.98–3.93 (m, 2H, NCH_2), 3.90 (s, 3H, OCH_3), 3.82–3.75 (m, 4H, N–CH_2), 3.45–3.32 (m, 2H, NCH_2), 3.26–3.31 (q, 4H, NCH_2, $J = 6.7$ Hz).

2.7. Synthesis of N-(4-benzylcarboxylic acid)-1,4,7-triazacyclononane (L_7)

Compound **B** (1 g, 2.8 mmol) was dissolved in water (50 ml) and refluxed for 2 h followed by addition of NaOH (0.2 g, 5 mmol) and further refluxing for 4 h. The solution was cooled to room temperature and extracted with CH_2Cl_2 to remove organic impurities. The solution was made acidic with concd. HBr and the solvent removed on a rotary evaporator. The remaining solid was extracted with EtOH (3×50 cm^3) and the combined EtOH fractions removes on a rotary evaporator to afford a yellow solid, which was recrystallized from MeOH–Et_2O (1:5). Yield: 0.44 g, 1.7 mmol, 60%. ^{1}H NMR (DMSO-d_6): $\delta = 7.91$–7.88 (d, 2H, C_6H_4, $J = 8.0$ Hz), 7.57–7.54 (d, 2H, C_6H_4, $J = 8.1$ Hz), 4.42 (s, 2H, Ar–CH_2), 3.88 (m, 4H, N–CH_2), 3.13 (m, 4H, N–CH_2), 2.87 (m, 4H, N–CH_2). EI MS: $m/z = 264$ $[M\text{H}]^+$, 247 $[M - \text{OH}]^+$, 219 $[M - \text{CO}_2\text{H}]^+$.

2.8. Metal complexes

2.8.1. $[Cu(L_1)_2](PF_6)_2 \cdot 1/2CH_3CN$ (1)

The ligand $\mathbf{L}_1$ (150 mg, 0.55 mmol) in EtOH (2 ml) was added to $CuCl_2 \cdot 2H_2O$ (48 mg, 0.28 mmol) in EtOH (10 ml), containing NH_4PF_6 (230 mg). Stirring was continued for approximately 16 h. A blue precipitate was filtered off, washed with EtOH and ether, and air-dried. The compound was recrystallized from MeCN. Yield: 138 mg (50%). IR (cm^{-1}): 3142 $\nu_{(\text{N–H})}$, 843 $\nu_{(\text{P–F})}$. CHN Found (Calc.): C, 45.80 (45.45); H, 6.55 (6.48); N, 9.46 (9.84)%.

2.8.2. $[Co(L_1)_2](PF_6)_2$ (2)

The ligand $\mathbf{L}_1$ (256 mg, 0.93 mmol) in EtOH (5 ml) was added to $CoCl_2 \cdot 6H_2O$ (88 mg, 0.37 mmol) in degassed EtOH (20 ml), containing NH_4PF_6 (300 mg). The reaction mixture was stirred for approximately 16 h under nitrogen. A pink precipitate was filtered off, washed repeatedly with EtOH and dried in vacuo. Yield: 200 mg (60%). IR (cm^{-1}): 3200 $\nu_{(\text{N–H})}$, 845 $\nu_{(\text{P–F})}$. CHN Found (Calc.): C, 45.30 (45.39); H, 6.57 (6.50); N, 9.18 (9.34)%.

2.8.3. $[Zn(L_1)_2](PF_6)_2$ (3)

The ligand $\mathbf{L}_1$ (200 mg, 0.72 mmol) in EtOH (2 ml) was added to $ZnCl_2$ (48 mg, 0.36 mmol) in EtOH (20 ml) containing NH_4PF_6 (300 mg). The mixture was stirred for 2 h. A white precipitate was then filtered off, washed with EtOH and dried in vacuo. Yield: 183 mg (56%). IR (cm^{-1}): 3214 $\nu_{(\text{N–H})}$, 843 $\nu_{(\text{P–F})}$. CHN Found (Calc.): C, 44.9 (45.06); H, 6.52 (6.45); N, 9.23 (9.27)%. ^{1}H NMR (CD_3CN): $\delta = 6.87$ (s, 4H, phenyl–*H*), 3.31 (s, 4H, N*H*), 2.96–2.64 (m, 32H, CH_2), 2.25 (s, 12H, *o*-$C_6H_2(CH_3)_2$), 2.23 (s, 6H, *p*-$C_6H_2CH_3$). ^{13}C NMR (CD_3CN): 136.8, 131.6, 129.5, 117.8 (phenyl–*C*), 55.8, 49.1, 44.0, 43.2 (N–*C*H$_2$), 22.5 (*C*H$_2$-mesityl), 20.3 (*p*-$C_6H_2CH_3$), 19.5 (*o*-$C_6H_2(CH_3)_2$).

2.8.4. $[Ni(L_1)_2](PF_6)_2$ (4)

The ligand $\mathbf{L}_1$ (150 mg, 0.55 mmol) in EtOH (5 ml) was added to $NiCl_2 \cdot 6H_2O$ (60 mg, 0.25 mmol) in EtOH (20 ml), containing NH_4PF_6 (200 mg). The mixture was stirred for 4 h. A purple precipitate was filtered off and air-dried. Yield: 100 mg (44%). IR (cm^{-1}): 3270 $\nu_{(\text{N–H})}$, 841 $\nu_{(\text{P–F})}$. CHN Found (Calc.): C, 44.9 (45.4); H, 6.71 (6.50); N, 8.88 (9.34)%.

2.8.5. $[Cu(L_4)](ClO_4)_2 \cdot 1/2EtOH$ (5)

The ligand $\mathbf{L}_4$ (140 mg, 0.44 mmol) in EtOH (5 ml) was added to $Cu(ClO_4)_2 \cdot 6H_2O$ (130 mg, 0.35 mmol) in EtOH (20 ml). The solution was stirred for 24 h. A purple precipitate was filtered off, washed with EtOH and dried in vacuo. Yield: 114 mg (54%). IR (cm^{-1}): 3280 $\nu_{(\text{N–H})}$, 1100 $\nu_{(\text{Cl–O})}$. CHN Found (Calc.): C, 40.0 (39.77); H, 5.78 (6.17); N, 8.95 (9.28)%. UV–Vis (CH_3NO_2): λ_{max} (nm) (ε_{max}, mol^{-1} l cm^{-1}): 579 (334).

2.8.6. $[Zn(L_4)Cl](ClO_4)_2$ (6)

The ligand $\mathbf{L}_4$ (202 mg, 0.64 mmol) in EtOH (3 ml) was added to $ZnCl_2$ (69 mg, 0.51 mmol) in EtOH (20 ml) containing $LiClO_4$ (300 mg). Stirring was continued for approximately 24 h. The white precipitate was filtered off, washed with EtOH and ether and dried in vacuo. Yield: 120 mg (45%). ^{1}H NMR (CD_3CN): $\delta =$ 6.84 (s, 2H, phenyl–*H*), 3.11–2.69 (m, 23H, CH_2 N*H*), 2.27 (s, 6H, *o*-$C_6H_2(CH_3)_2$), 2.20 (s, 3H, *p*-$C_6H_2CH_3$). ^{13}C NMR (CD_3CN): 137.2, 132.8, 130.0, 118.3 (phenyl–*C*), 53.0 (N–*C*H$_2$–CH$_2$–mes), 50.2, 45.5, 44.6, 43.6 (N–*C*H$_2$–*C*H$_2$–N), 22.5 (*C*H$_2$–mes), 20.9 (*p*-$C_6H_2CH_3$), 19.9 (*o*-$C_6H_2(CH_3)_2$). IR (cm^{-1}): 3280 $\nu_{(\text{N–H})}$, 1090 $\nu_{(\text{Cl–O})}$. CHN Found (Calc.): C, 44.1 (44.6); H, 6.74 (6.71); N, 10.2 (10.9)%.

2.8.7. $[Ni(L_4)](ClO_4)_2 \cdot 1/2Et_2O$ (7)

The ligand $\mathbf{L}_4$ (301 mg, 0.94 mmol) in butan-1-ol (10 ml) was added to $Ni(ClO_4)_2 \cdot 6H_2O$ (278 mg, 0.76 mmol) in hot butan-1-ol (30 ml). The reaction mixture was stirred for 24 h. A green precipitate was filtered off, washed with butan-1-ol and dried in vacuo. Yield: 142 mg. The blue liquor was concentrated in vacuo to dryness to leave a yellow solid. This was washed repeatedly with ether and dried in vacuo. Yield: 280 mg (64%). IR (cm^{-1}): 3260 $\nu_{(\text{N–H})}$, 1100 $\nu_{(\text{Cl–O})}$. CHN Found (Calc.): C, 40.60 (41.14); H, 6.19 (6.41); N, 8.54 (9.14)%. UV–Vis (CH_3NO_2): λ_{max} (nm) (ε_{max}, mol^{-1} l cm^{-1}): 418 (40), 454 (26.1), 878 (27.9).

*2.8.8. [Cu(**L**$_5$)](ClO$_4$)$_2$·H$_2$O (**8**)*

The ligand **L**$_5$ (120 mg, 0.34 mmol) in EtOH (2 ml) was added to Cu(ClO$_4$)$_2$·6H$_2$O (100 mg, 0.27 mmol) in EtOH (10 ml). The reaction mixture was stirred for approximately 16 h. A purple precipitate was filtered off, washed with EtOH and ether, and dried in vacuo. Yield: 105 mg (63%). IR (cm^{-1}): 3230 $\nu_{(N-H)}$, 1100 $\nu_{(Cl-O)}$. CHN Found (Calc.): C, 40.7 (40.23); H, 6.38 (6.43); N, 9.33 (8.94)%. UV–Vis (MeOH): λ_{max} (nm) (ε_{max}, mol^{-1} l cm^{-1}): 516 (135).

*2.8.9. [Ni(**L**$_5$)](ClO$_4$)$_2$ (**9**)*

The ligand **L**$_5$ (150 mg, 0.43 mmol) in EtOH (5 ml) was added to Ni(ClO$_4$)$_2$·6H$_2$O (124 mg, 0.34 mmol) in EtOH (20 ml). The reaction mixture was stirred for approximately 16 h. A red precipitate was filtered off, washed with EtOH and ether, and dried in vacuo. Yield: 98 mg (50%). IR (cm^{-1}): 3210 $\nu_{(N-H)}$, 1100 $\nu_{(Cl-O)}$. CHN Found (Calc.): C, 41.3 (41.7); H, 6.24 (6.35); N, 9.28 (9.28)%. UV–Vis (MeOH): λ_{max} (nm) (ε_{max}, mol^{-1} l cm^{-1}): 463.5 (79).

*2.8.10. [Ni(**L**$_5$)Cl$_2$] (**10**)*

(a) The ligand **L**$_5$ (150 mg, 0.43 mmol) in EtOH (5 ml) was added to NiCl$_2$·6H$_2$O (93 mg, 0.39 mmol) in warm EtOH (20 ml). The reaction mixture was stirred for approximately 16 h. Diethyl ether was added and a mauve precipitate was filtered off, washed with ether and dried in vacuo. Yield: 23 mg (12%).

(b) LiCl (108 mg, 2.55 mmol) in C$_3$H$_6$O (10 ml) was added to **9** (150 mg, 0.207 mmol) in C$_3$H$_6$O (10 ml) with stirring. A mauve precipitate was filtered off, washed with C$_3$H$_6$O, and dried in vacuo. Yield: 23 mg (15%). IR (cm^{-1}): 3190 $\nu_{(N-H)}$. CHN Found (Calc.): C, 52.9 (53.0); H, 7.99 (8.06); N, 11.57 (11.77)%. UV–Vis (MeOH): λ_{max} (nm) (ε_{max}, mol^{-1} l cm^{-1}): 463 (90).

*2.8.11. Reaction of **L**$_1$ with [Rh(COD)]$^+$(PF$_6$)$^-$*

AgPF$_6$ (101 mg, 0.40 mmol) in MeCN (5 ml) was added under nitrogen to [Rh(μ-Cl)(COD)]$_2$ (100 mg, 0.20 mmol) in MeCN (10 ml). The yellow solution was separated from precipitated AgCl and added to **6** (362 mg, 0.40 mmol) in MeCN (10 ml). No reaction was observed by ^{1}H or ^{13}C NMR spectroscopy after prolonged heating and stirring. When **6** was substituted by free **L**$_1$, no reaction of the pendent arene group was observed.

*2.8.12. [Ni(**L**$_6$)$_2$](PF$_6$)$_2$ (**12**)*

The ligand **L**$_6$ (200 mg, 0.8 mmol) in EtOH (5 ml) was added to a solution of Ni(NO$_3$)$_2$·6H$_2$O (0.23 g, 0.79 mmol) in H$_2$O (5 ml) and stirred for 5 min. A saturated NH$_4$PF$_6$ solution was added and the product extracted with CH$_3$NO$_2$ (2 × 5 ml). The organic layer was separated and removed to give oil, which was recrystallized from CH$_3$CN–Et$_2$O (1:3). Yield: 100 mg (30%). IR (cm^{-1}): 3424 $\nu_{(N-H)}$, 2927 $\nu_{(C-H)}$, 843 $\nu_{(P-F)}$. FAB MS: $m/z = 701$ [Ni(**L**$_6$)$_2$](PF$_6$)$^+$, 555 [Ni(**L**$_6$)$_2$]$^+$. UV–Vis (CH$_3$CN): λ_{max} (nm) (ε_{max}, mol^{-1} l cm^{-1}): 885 (18), 533 (10), 316 (63).

*2.8.13. [Co(**L**$_6$)(NO$_3$)$_2$(OH$_2$)]·H$_2$O (**13**)*

The ligand **L**$_6$ (100 mg, 0.4 mmol) in EtOH (5 ml) was added to a solution of Co(NO$_3$)$_2$·6H$_2$O (116 mg, 0.4 mmol) in H$_2$O (5 ml) and stirred for 5 min. The solution was left to slowly evaporate until a precipitate formed, which was filtered off and purified by passing down a Sephadex column eluting with CH$_3$CN. Yield: 69 mg (40%). IR (cm^{-1}): 3527 ν_{OH}, 3272 ν_{NH}, 1480, 1318 ν_{NO_2}. FAB MS: $m/z = 370$ [Co(**L**$_6$)NO$_3$]$^+$. CHN Found (Calc.): C, 37.10 (37.34); H, 5.85 (5.60); N, 15.08 (15.55)%. UV–Vis (CH$_3$CN): λ_{max} (nm) (ε_{max}, mol^{-1} l cm^{-1}): 539 (119).

*2.8.14. [Cu(**L**$_6$)(NO$_3$)$_2$] (**14**)*

The ligand **L**$_6$ (97 mg, 0.39 mmol) in EtOH (5 ml) was added to a solution of Cu(NO$_3$)$_2$·3H$_2$O (94 mg, 0.39 mmol) in H$_2$O (5 ml) and stirred for 5 min. The solution was left to slowly evaporate until a precipitate was formed, which was filtered off and purified as described above. Yield: 85 mg (50%). IR (cm^{-1}): 3527 ν_{OH}, 3272 ν_{NH}, 1480, 1318 ν_{NO_2}. FAB MS: $m/z = 374$ [Cu(**L**$_6$)NO$_3$]$^+$. CHN Found (Calc.): C, 38.68 (38.48); H, 5.36 (5.31); N, 15.87 (16.03)%. UV–Vis (CH$_3$CN): λ_{max} (nm) (ε_{max}, mol^{-1} l cm^{-1}): 647 (59).

*2.8.15. [Cu(**L**$_7$)(Br$_2$)]·2H$_2$O (**15**)*

The ligand **L**$_7$·HBr (158 mg, 0.46 mmol) in H$_2$O (5 ml) was added to a solution of Cu(NO$_3$)$_2$·3H$_2$O (111 mg, 0.46 mmol) in H$_2$O (5 ml) and stirred for 5 min. The solution was left to slowly evaporate until a precipitate formed, which was filtered off and dried under vacuum. Yield: 89 mg (37%). IR (cm^{-1}): 3430 ν_{OH}, 3288 ν_{NH}, 2920 ν_{CH}, 1695 ν_{CO}. FAB MS: $m/z =$ 485 [Cu(**L**$_7$)Br$_2$]$^+$, 407 [Cu(**L**$_7$)Br]$^+$, 326 [Cu(**L**$_7$)]$^+$. CHN Found (Calc.): C, 31.79 (32.16); H, 4.12 (4.82); N, 8.55 (8.04)%. UV–Vis (H$_2$O): λ_{max} (nm) (ε_{max}, mol^{-1} l cm^{-1}): 650 (39).

*2.8.16. [Cu$_2$(**L**$_7$–H)$_2$(OH$_2$)$_2$](PF$_6$)$_2$·6H$_2$O (**16**)*

A saturated aq. solution of KPF$_6$ was added to a solution of [Cu(**L**$_7$)(Br$_2$)]·2H$_2$O (40 mg, 0.076 mmol) in H$_2$O (5 ml). The water was allowed to slowly evaporate until a blue crystalline solid precipitated, which was filtered off and dried under vacuum. Yield: 37 mg (95%). IR (cm^{-1}): 3430 ν_{OH}, 2925 ν_{CH}, 1609 ν_{CO}, 838 ν_{PF}. CHN Found (Calc.): C, 30.36 (30.96); H, 4.03 (4.79); N, 7.33 (7.74)%. FAB MS: $m/z = 326$ [Cu(**L**$_7$)]$^+$.

2.9. Crystallography

Details of the data collection and analysis of **1**, **14** and **16** are collected in Table 1. Single crystals were attached to a glass fibre using acrylic resin, and mounted on a goniometer head in a general position. Data were collected using an Enraf–Nonius CAD4 diffractometer (compound **1**) or a Bruker–Nonius Kappa CCD diffractometer (compounds **14** and **16**) using graphite-monochromated X-radiation ($\lambda =$ 0.71073 Å). The structures were solved by direct methods (SIR-92) [20]. All non-H atoms were allowed anisotropic thermal motion. Aliphatic CH hydrogen atoms were included at calculated positions with C–H = 0.96 Å. Refinement (SHELXL-97) [21] was by full-matrix least-squares on F^2. All crystals of **16**, which were examined proved to be twins. The crystal chosen was twinned according to a rotation of 180° about 010. Many reflections from both lattices are overlapped. Despite these problems, the overall identity of compound **16** was satisfactorily determined by the X-ray analysis. Neutral atom scattering factors, coefficients and anomalous dispersion and absorption coefficients were obtained from [22].

3. Results and discussion

3.1. Synthesis of the ligands

The ligands $\mathbf{L}_1$–$\mathbf{L}_5$ were synthesised according to a Michael type reaction [23]. An excess of the 'activated' vinylaromatic was added to a THF solution of the free macrocycle to which an excess of ^{n}BuLi had been added. After removal of solvents, the residue was converted to the hydrochloride salt, extracted into water then basified to liberate the free amine. In the case of those reactions involving 2,4,6-trimethylstyrene, the single pendent arm product was the only one isolated. When the Michael acceptor was styrene or *p*-vinylanisole, the *N*′,*N*″ disubstituted product was the only one isolated after work up. This variation is curious and no explanation is apparent. The ligands $\mathbf{L}_6$–$\mathbf{L}_7$ were prepared by the conventional mono-functionalization technique of reacting the appropriate arylalkyl halide with 1,4,7-triazacyclo[5.2.1.$^{04.10}$]decane followed by base hydrolysis (Scheme 3).

Table 1
Crystallographic data

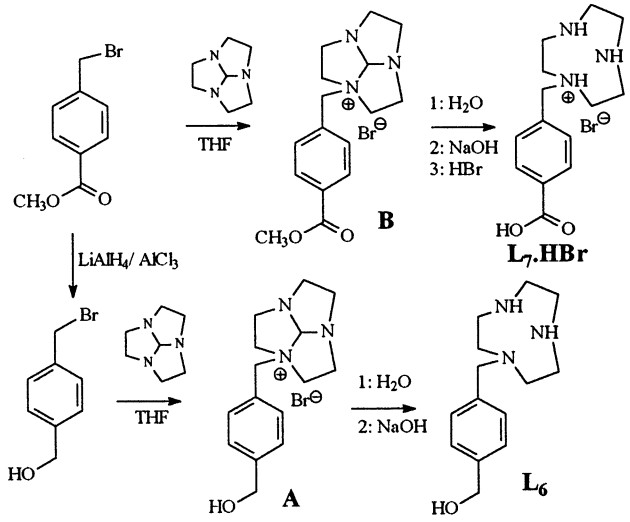
Compound	**1**	**14**	**16**
Chemical formula	$C_{68}H_{116}Cl_4Cu_3F_{12}N_{12}P_2$	$C_{14}H_{23}CuN_5O_7$	$C_{28}H_{50}N_6Cu_2O_9P_2F_{12}$
Formula weight	1724.09	436.91	1031.76
Temperature (°C)	291	−123	−173
Space group	$P\bar{1}$	$P\bar{1}$	$P\bar{1}$
Crystal system	triclinic	triclinic	triclinic
a (Å)	11.834(2)	7.3210(2)	10.2057(1)
b (Å)	13.114(3)	8.2780(2)	12.8715(2)
c (Å)	13.581(3)	16.3904(6)	16.6340(3)
α (°)	75.556(19)	80.800(1)	72.597(1)
β (°)	84.126(17)	89.262(1)	85.361(1)
γ (°)	75.980(17)	67.288(1)	81.907(1)
V (Å^3)	1978.3(7)	903.20(5)	2062.56(5)
Z	1	2	2
μ (mm^{-1})	1.05	1.258	1.218
Data collected	8050	12 462	18 679
Unique data	6951	4145	8927
R_{int}	0.0208	0.0356	0.0503
Final R_1	0.0545	0.0553	0.1207
Final R_w^2	0.161	0.142	0.3328

3.2. Synthesis of the complexes

The complexes were prepared by addition of the free ligand to ethanolic or water solutions of the appropriate metal salts. The solid complexes could be obtained as precipitates by addition of a suitable counter ion ($(PF_6)^-$ or $(ClO_4)^-$). In the case of the neutral complex **1**, the product was precipitated from ethanolic solution by the addition of diethyl ether. Crystals suitable for X-ray crystallography were obtained for complexes **1**, **14** and **16**.

3.3. Description of the crystal structures

The structure of the two different cations found in the unit cell of complex **1** are illustrated in Fig. 1. In the first case the Cu(II) metal ion is coordinated to the three nitrogens of the macrocycle with the two other sites occupied by chloride ions. The Cu–N bond lengths



Scheme 3. Reactions used in the preparation of *N*-funtionalized triazamacrocycles.

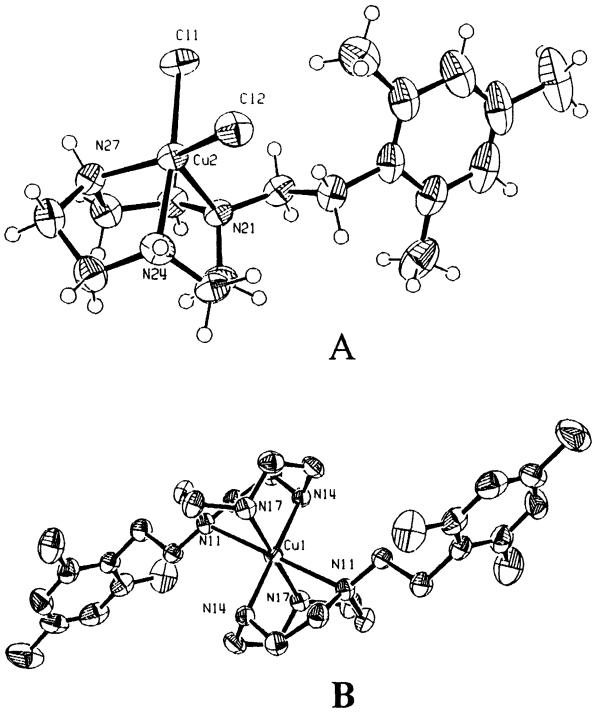


Fig. 1. ORTEP for Windows [30] plot of: (A) $[Cu(\mathbf{L}_1)Cl_2]$; and (B) $[Cu(\mathbf{L}_1)_2]^{2+}$ (thermal ellipsoids are shown at 50% probability and hexafluorophosphate anions are omitted or clarity); selected bond lengths (Å) and angles (°): Cu2–N21, 2.268(3); Cu2–N24, 2.045(4); Cu2–N27, 2.040(4); Cu2–Cl1, 2.295(1); Cu2–Cl2, 2.253(1); N27–Cu2–N24, 81.71(15); N27–Cu2–Cl2, 154.03(11); N24–Cu2–Cl2, 89.12(11); N27–Cu2–N21, 83.64(14); N24–Cu2–N21, 82.08(14); Cl2–Cu2–N21, 119.25(10); N27–Cu2–Cl1, 91.22(12); N24–Cu2–Cl1, 172.61(11); Cl2–Cu2–Cl1, 98.21(5); N21–Cu2–Cl1, 95.05(10); Cu1–N11, 2.571(4); Cu1–N14, 2.056(3); Cu1–N17, 2.023(4); N17–Cu1–N17, 180.00(18); N17–Cu1–N14, 82.54(15); N17–Cu1–N14, 97.46(15); N17–Cu1–N14, 97.46(15); N17–Cu1–N14, 82.54(15); N14–Cu1–N14, 180.0(2).

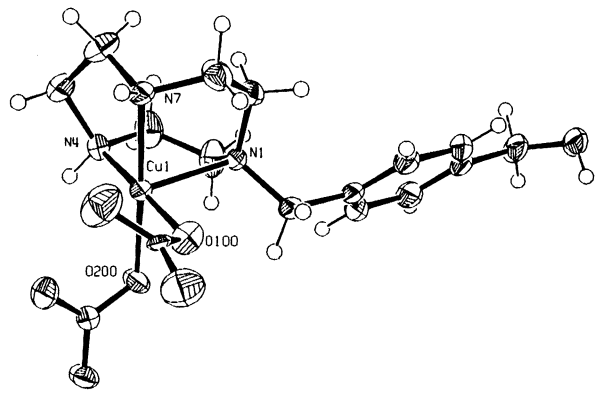


Fig. 2. ORTEP for Windows [30] plot of $[Cu(\mathbf{L}_6)(NO_3)_2]$ (thermal ellipsoids are shown at 50% probability); selected bond lengths (Å) and angles (°): Cu–N1, 2.243(3); Cu–N4, 2.005(3); Cu–N7, 2.016(3); Cu–O100, 1.952(3); Cu–O200, 2.018(3); O100–Cu1–N4, 177.77(13); O100–Cu1–N7, 97.27(13); N4–Cu1–N7, 84.65(13); O100–Cu1–O200, 85.63(13); N4–Cu1–O200, 92.47(13); N7–Cu1–O200, 176.90(12); O100–Cu1–N1, 94.16(12); N4–Cu1–N1, 84.88(12); N7–Cu1–N1, 84.46(11); O200–Cu1–N1, 96.47(10).

are consistent with a complex that is Jahn–Teller distorted, affording the cation a square-based pyramidal geometry. The pendant mesitylene is non-coordinated which is compatible with the 'soft' nature of the ligand. The second cation is a six coordinate centrosymmetric copper complex containing two macrocycles. Again the complex is Jahn–Teller distorted with two long bonds, the Cu–N (axial) bond length significantly greater than that found in the five coordinate complex. The pendant mesitylene group is well separated from the copper centre suggesting that steric hindrance is not a major factor in rationalising the lack of any reaction of the group with organometallic reagents (see later).

For complexes containing the ligands $\mathbf{L}_6$ and $\mathbf{L}_7$, the alcohol and carboxyl groups, respectively are, in contrast to most pendant arm macrocyclic ligands, not available for binding to the same metal ion centre. For complexes of the two ligands intermolecular bonding is however feasible, and hence affords a way to create well-defined supramolecular structures. Illustrated in Fig. 2 is the structure of the complex $[Cu(\mathbf{L}_6)(NO_3)_2]$, and collected is a list of selected bond lengths and angles. The complex is five-coordinate and, as observed for the previously discussed copper systems, has a Jahn–Teller distorted square-based pyramidal structure. The two nitrate ions act as monodentate ligands and the pendant aromatic group is well separated from the copper–tacn core. The oxygen of the benzylalcohol segment is disordered over two sites consistent with a lack of intermolecular bonding to an adjacent unit. Indeed, no weak forces such as H-bonding to the nitrate ions are evident in the crystal-packing diagram.

In contrast to the previous complex the structure of the Cu(II) system containing the ligand $\mathbf{L}_7$ displays a more interesting recognition phenomenon as depicted in Fig. 3. As before the three nitrogens of the macrocycle are all coordinated and the pendant aromatic is well separated from the Jahn–Teller distorted Cu(II) centre. Unlike the copper complex of $\mathbf{L}_6$ the carboxyl oxygen from a neighbouring unit coordinates to the copper so that the asymmetric unit contains a basic $[Cu_2(\mathbf{L}_7\text{–H})_2]^{2+}$ repeat unit. As a result, a one-dimensional coordination polymer is produced as illustrated in the packing diagram of Fig. 4. A water molecule completes the fifth coordination sphere of each copper and it is noted that these water molecules point in the same direction but do not hydrogen bond to the layer above. The 'L' motif of the complex has dimensions of approximately 9.5×11 Å^2, which leads to speculation that further self-assembly using an appropriate template could generate a tetracopper molecular box (Scheme 2). Such control of molecular self-assembly is currently of great interest but as of yet has not utilised triazamacrocycles containing pendant arms. Further coordination studies of ligands based on $\mathbf{L}_7$ are underway and will be reported at a later date.

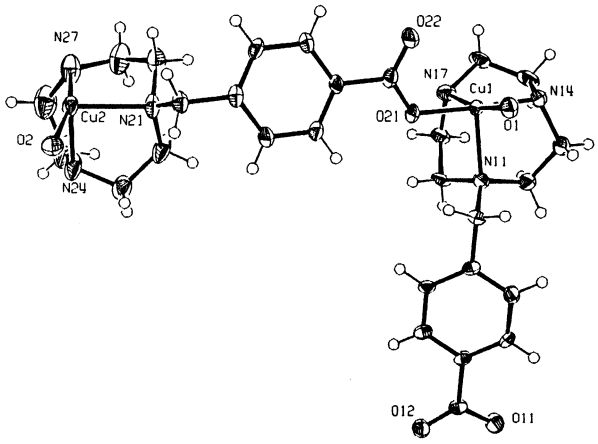


Fig. 3. ORTEP for Windows [30] plot of $[Cu_2(\mathbf{L}_7\text{–H})_2(H_2O)_2]^{2+}$ (thermal ellipsoids are shown at 50% probability and hexafluorophosphate anions and extraneous water molecules are omitted or clarity); selected bond lengths (Å) and angles (°): Cu1–N11, 2.235(6); Cu1–N14, 2.021(7); Cu1–N17, 2.035(7); Cu1–O1, 1.981(6); Cu1–O21, 1.946(6); Cu2–N21, 2.246(7); Cu2–N24, 2.024(8); Cu2–N27, 2.035(9); Cu2–O2, 1.978(7); Cu2–O11, 1.932(6); O21–Cu1–O1, 92.4(3); O21–Cu1–N14, 175.3(3); O1–Cu1–N14, 91.6(3); O21–Cu1–N17, 90.2(3); O1–Cu1–N17, 168.1(3); N14–Cu1–N17, 85.4(3); O21–Cu1–N11, 97.6(2); O1–Cu1–N11, 107.4(2); N14–Cu1–N11, 83.4(3); N17–Cu1–N11, 83.7(3); O11–Cu2–O2, 93.2(3); O11–Cu2–N24, 175.0(4); O2–Cu2–N24, 91.5(4); O11–Cu2–N27, 89.0(4); O2–Cu2–N27, 166.6(3); N24–Cu2–N27, 86.0(4); O11–Cu2–N21, 96.0(3); O2–Cu2–N21, 109.6(3); N24–Cu2–N21, 83.9(3); N27–Cu2–N21, 83.2(3).

3.4. Description of the metal complexes

3.4.1. L_1 complexes

The $\mathbf{L}_1$ complexes are all typical octahedral *bis* ligand species as expected for the metal ions concerned. As is described above, a second form of **1** is observed in the crystal, namely a neutral 1:1 dichloro-complex. This five coordinate species is analogous to the copper complex of *N*-(5-pent-2-yne)-1,4,7-triazacyclononane described elsewhere [11]. Solutions of the pale pink cobalt complex rapidly darken in air suggesting oxidation to Co(III), though no single species could be obtained from the dark solutions.

The 'hard' Lewis acidic metal centres in these complexes do not interact with the pendent arm arene groups, and coordination takes place exclusively through the ring nitrogens. For example, the ^{13}C NMR of the zinc complex **3** shows the signals due to the arene moiety to be essentially unshifted from those of the free ligand.

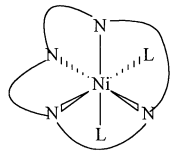


Fig. 5. Proposed folding of the cyclen macrocycle to generate a *cis*-complex.

3.4.2. L_4 complexes

The copper complex **5** is, as isolated in the solid state, a 1:1 species containing a four coordinate Cu(II) centre [24], though it may well become five coordinate in solution. When $\mathbf{L}_2$ in butan-1-ol is added to $Ni(ClO_4)_2{\cdot}6H_2O$ in hot butan-1-ol, a green solid precipitates from solution. This species shows three visible bands in nitromethane solution at 882, 586 and 443 nm, respectively. On this basis, we postulate a five- or six-coordinate nickel species. The size of the macrocyclic cavity in the 12 membered cyclen ring is such that square coplanar coordination of the metal is unlikely. The ligand rather is wrapped around the metal forming a *cis* complex [25], with the remaining coordination sites occupied by water (Fig. 5).

The blue liquor from the reaction yields, on removal of the solvent, a yellow solid. This dissolves in nitromethane or acetonitrile to give blue solutions. The yellow colour of the solid suggests a four-coordinate square coplanar environment for the nickel atom. This behaviour is well documented and Lincoln and coworkers [24] have described such a high spin-low spin equilibrium for the nickel complex of 1,4,7,10-tetramethyl-1,4,7,10-tetraazacyclododecane (tmc) (Eq. (1)).

1,4,7,10-tetraazacyclododecane (tmc) (equation 1).

$$[Ni(tmc)]^{2+} + H_2O \leftrightarrow [Ni(tmc)H_2O]^{2+} \quad (1)$$

low spin high spin

In addition, Fabbrizzi [26] has noted that in aqueous solutions of the nickel complex of cyclen, the normal blue colour of the octahedral high spin species becomes yellow on addition of 6 M $LiClO_4$ when heated, and the electronic spectrum, showing a new band at 23 000

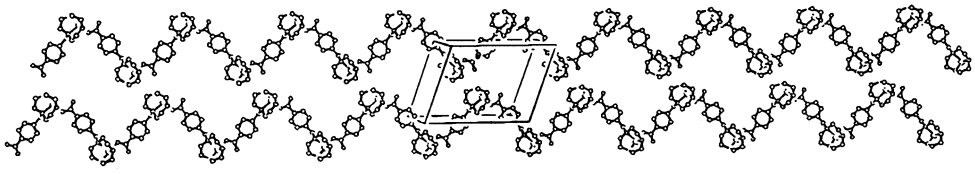


Fig. 4. ORTEP for Windows [30] view down the *a*-axis of the coordination polymer generated by the repeating $[Cu_2(\mathbf{L}_7\text{–H})_2(H_2O)_2]^{2+}$ moiety.

cm^{-1} becomes more typical of a low spin square planar species. Unfortunately, electronic spectra of the yellow form of **7** were not available in solution, as any solvent which led to dissolution, regenerated the octahedral form.

3.4.3. L_5 complexes

The macrocyclic cavity of the larger 14-membered ring is large enough to accommodate the metal ions Cu(II) and Ni(II) in square coplanar coordination. The UV–Vis spectrum of $[Ni(\mathbf{L}_5)](ClO_4)_2$ (**9**) in methanol ($\lambda = 463$ nm, $\varepsilon_{max} = 79\ mol^{-1}\ l\ cm^{-1}$) is consistent with a four coordinate complex. On addition of an excess of LiCl, a mauve solid separates from an acetone solution, which may be identified as $[Ni(\mathbf{L}_5)Cl_2]$ (**10**). This complex may also be prepared by addition of free ligand to $NiCl_2{\cdot}6H_2O$ in ethanol [27]. The UV–Vis spectrum of **10** in methanol is identical to that of **9** indicating the ionisation of the two chlorides in methanolic solution.

3.4.4. L_6 complexes

The complexation of $\mathbf{L}_6$ with Ni(II) produced a pale pink solid which exhibited three bands in the UV–Vis region at 885, 533 nm and a shoulder at 316 nm, respectively. The mass spectrum of the complex revealed a prominent ion at $m/z = 701$ which is assigned to the $[Ni(\mathbf{L}_6)_2](PF_6)^+$ ion. Interestingly a weaker peak as also observed in the mass spectrum at $m/z = 1547$ which can be attributed to a dimeric $[Ni(\mathbf{L}_6)_2]_2(PF_6)_3^+$ ion. It is possible that weak intermolecular H-bonds between the hydroxyl groups are responsible for the self-aggregation (Fig. 6).

The cobalt complex of $\mathbf{L}_6$ is dark claret in colour and displays one band at 539 nm in the UV–Vis region. The mass spectrum of the complex reveals a prominent ion at $m/z = 370$ which is compatible with the $[Co(\mathbf{L}_6)NO_3]^+$ ion. The IR and elemental analysis supports the existence of coordinated water so that as in the nickel case the complex is six-coordinate. Unlike the cobalt complex of $\mathbf{L}_1$ a solution of **13** exhibits no observable change in air suggesting that oxidation to Co(III) is slow.

3.5. Attempts to coordinate the pendent arene arm

Electron rich arenes such as mesitylene (1,3,5-trimethylbenzene) are excellent π acceptor ligands towards 'softer' transition metals. Such metal species as $[Rh(COD)]^+$, generated in situ from $[Rh(\mu\text{-}Cl)(COD)]_2$ (COD = 1,5-cyclooctadiene) and $AgPF_6$ react smoothly with arenes at room temperature to give η^6 arene complexes [28,29]. However, in our hands, reaction of either $\mathbf{L}_1$ or the zinc complex **3** with $[Rh(COD)](PF_6)$ in refluxing THF showed no reaction of the arene ring after 24 h. In the former case, ^1H NMR spectroscopy indicated reaction of the rhodium centre with the macrocycle ring nitrogens, but addition of further $[Rh(COD)](PF_6)$ did not lead to the formation of an η^6 complex. Clearly, the presence of the ring nitrogens must have a considerable deactivating effect on the arene moiety.

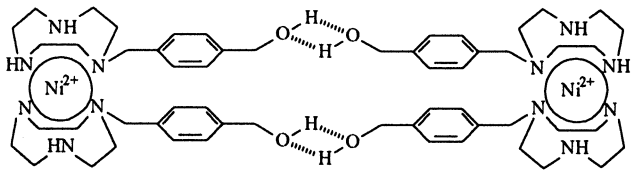


Fig. 6. Proposed dimerization of $[Ni(\mathbf{L}_6)_2]^{2+}$ by H-bonding of the alcohol groups.

4. Conclusions

A number of aromatic functionalized azamacrocycles have been prepared along with their metal complexes. Electron rich aromatics can be selectively incorporated into tri- and tetra-azamacrocycles in good yields using Michael-type chemistry. Complexation via the macrocycle nitrogens to hard metal ions is facile but unfortunately the π-rich aromatics do not react with soft metal ions to create mixed metal systems.

The Cu(II) complex of a single pendant arm benzylcarboxylic acid funtionalized 1,4,7-triazacyclononane macrocycle displays interesting self-assembly properties. This recognition phenomenon has the potential to be exploited in the creation of large superstructures with interesting magneto properties, and hence the generation of novel inorganic materials.

5. Supplementary data

Crystallographic data (excluding structure factors) for the structures in this paper have been deposited with the Cambridge Crystallographic Data Centre as supplementary publication nos. CCDC 166329 ,166330, 166331 for compounds **1**, **14** and **16**. Copies of the data may be obtained free of charge on application to The Director, CCDC, 12 Union Road, Cambridge, CB2 1EZ, UK (fax: +44-1223-336033; e-mail: deposit@ccdc.cam.ac.uk or www: http://www.ccdc.cam.ac.uk).

Acknowledgements

This work was supported by the University of Glasgow and the Engineering and Physical Sciences Research Council (EPSRC).

References

[1] (a) M. Takahashi, S. Takamoto, Bull. Chem. Soc. Jpn. 50 (1977) 3413;
(b) M.J. van der Merwe, J.C.A. Boeyens, R.D. Hancock, Inorg. Chem. 24 (1985) 1208.

[2] (a) B.A. Sayer, J.P. Michael, R.D. Hancock, Inorg. Chim. Acta 77 (1983) L63;
(b) R.D. Peacock, J. Robb, Inorg. Chim. Acta 121 (1986) L15;
(c) A.A. Belal, L.J. Farrugia, J. Robb, R.D. Peacock, J. Chem. Soc., Dalton Trans. (1989) 931;
(d) I.A. Fallis, L.J. Farrugia, N.M. Macdonald, R.D. Peacock, J. Chem. Soc., Dalton Trans. (1993) 2759.

[3] A. Hammershøi, A.M. Sargeson, Inorg. Chem. (1983) 3554.

[4] K. Weighardt, U. Bossek, M. Guttmann, J. Weiss, Z. Naturforsch., Teil. B 38 (1983) 81.

[5] M.I. Kabachnik, T.Ya. Medved, B.K. Shcherbakov, E.I. Sinyavskaya, Yu M. Polikarpov, K.B. Yatsimirskii, Russ. J. Inorg. Chem. 30 (1985) 1463.

[6] M. Di Vaira, F. Mani, P. Stoppioni, Inorg. Chim. Acta 303 (2000) 61.

[7] (a) G.A. McLachlan, G.D. Fallon, R.L. Martin, B. Moubaraki, K.S. Murray, L. Spiccia, Inorg. Chem. 33 (1994) 4663;
(b) G.A. McLachlan, G.D. Fallon, R.L. Martin, L. Spiccia, Inorg. Chem. 34 (1995) 254;
(c) G.A. McLachlan, S.J. Brudenell, G.D. Fallon, R.L. Martin, L. Spiccia, E.R.T. Tiekink, J. Chem. Soc., Dalton Trans. (1995) 439;
(d) G.D. Fallon, G.A. McLachlan, B. Moubaraki, K.S. Murray, L. O'Brien, L. Spiccia, J. Chem. Soc., Dalton Trans. (1997) 2765.

[8] (a) D.J. Evans, G. Garcia, G.J. Leigh, M.S. Newton, M.D. Sontana, J. Chem. Soc., Dalton Trans. (1992) 3229;
(b) D.J. Evans, G. Garcia, D.L. Hughes, G.J. Leigh, M.D. Santana, Acta Crystallogr., Sect. C C49 (1993) 905;
(c) K. Mockizyki, F. Kesting, T. Weyhermuller, K. Wieghardt, C. Butzlaff, A.X. Trautwein, J. Chem. Soc., Chem. Commun. (1994) 909;
(d) R.P. Houser, V.G. Young Jr., W.D. Tolman, J. Am. Chem. Soc. 118 (1996) 2101.

[9] L.J. Farrugia, P.A. Lovatt, R.D. Peacock, Inorg. Chim. Acta 246 (1996) 343.

[10] (a) D. Ellis, L.J. Farrugia, D.T. Hickman, P.A. Lovatt, R.D. Peacock, J. Chem. Soc., Chem. Commun. (1996) 1817;
(b) D. Ellis, L.J. Farrugia, P.A. Lovatt, R.D. Peacock, Eur. J. Chem. (2000) 1489.

[11] (a) D. Ellis, L.J. Farrugia, R.D. Peacock, Polyhedron 18 (1999) 1229;
(b) M.V. Baker, D.H. Brown, B.W. Skelton, A.H. White, J. Chem. Soc., Dalton Trans. (2000) 4607.

[12] S. Leininger, B. Olenyuk, P.J. Stang, Chem. Rev. 100 (2000) 853.

[13] G. Wilkinson, F.G.A. Stone, E.W. Abel (Eds.), Comprehensive Organometallic Chemistry, vol. 5, Pergamon, Oxford, Ch. 35 and references therein.

[14] G. Wilkinson, F.G.A. Stone, E.W. Abel (Eds.), Comprehensive Organometallic Chemistry, vol. 3, Pergamon, Oxford, Ch. 27.

[15] D.D. Perrin, W.L.F. Armarego, Purification of Laboratory Chemicals, 3 ed., Pergamon Press, England, 1988.

[16] T.J. Atkins, J.E. Richman, J. Am. Chem. Soc. 96 (1974) 2268.

[17] E.K. Barefiled, F. Wagner, A.W. Herlinger, A.R. Dahl, Inorg. Synth. 16 (1976) 220.

[18] T.J. Atkins, J. Am. Chem. Soc. 102 (1980) 6364.

[19] J. Chatt, L.M. Venanzi, J. Chem. Soc. (1957) 4735.

[20] SIR-92—a program for automatic solution of crystal structures by direct methods: A. Altomare, G. Cascarno, C. Giacovazzo, A. Gualiardi, J. Appl. Crystallogr. 27 (1994) 435.

[21] G.M. Sheldrick, SHELXL-97, a program for crystal structure refinement, University of Göttingen, Germany, 1997.

[22] Table 4.24.2, 4.2.6.8 and 6.1.1.4 from International Tables for Crystallography, Volume C Mathematical, Physical and Cemical Tables, Kluwer, Dordrecht, 1995.

[23] B.F. Ross, J.G. Grasselli, W.M. Ritchey, H.D. Kaesz, Inorg. Chem. 2 (1963) 1023.

[24] J.H. Coates, D.A. Hadi, S.F. Lincoln, Aust. J. Chem. 35 (1982) 903.

[25] Y. Iitaka, M. Shina, E. Kimura, Inorg. Chem. 13 (1974) 2886.

[26] L. Fabbrizzi, Inorg. Chem. 16 (1977) 2667.

[27] B. Bosnich, M.L. Tobe, G.A. Webb, Inorg. Chem. 4 (1965) 1109.

[28] M. Green, T.A. Kuc, J. Chem. Soc., Dalton Trans. (1972) 832.

[29] R.R. Schrock, J.A. Osborn, J. Am. Chem. Soc. 93 (1971) 3089.

[30] L.J. Farrugia, J. Appl. Crystallogr. 30 (1997) 565.

PERGAMON

Polyhedron 21 (2002) 343–348

POLYHEDRON

www.elsevier.com/locate/poly

The X-ray structure of bis(5,7-dimethyl-1,2,4-triazolo-[1,5α]-pyrimidinium) hexachloroplatinate(IV) and spectroscopic properties of Pt(II) and Pt(IV) chloride complexes with 1,2,4-triazolo-[1,5α]-pyrimidines

Edward Szlyk [a,*], Leszek Pazderski [a], Iwona Lakomska [a], Andrzej Surdykowski [a], Tadeusz Glowiak [b], Jerzy Sitkowski [c], Lech Kozerski [c]

[a] *Department of Chemistry, Nicholas Copernicus University, Gagarina 7, 87-100 Torun, Poland*
[b] *Institute of Chemistry, University of Wroclaw, F. Joliot-Curie 14, 50-383 Wroclaw, Poland*
[c] *Drug Institute, Chelmska 30/34, 00-725 Warsaw, Poland*

Received 18 July 2001; accepted 13 November 2001

Abstract

Pt(II) and Pt(IV) chloride complexes with 1,2,4-triazolo-[1,5α]-pyrimidines: *trans*-$[Pt(tp)_2Cl_2]$, *trans*-$[Pt(dmtp)_2Cl_2]$, *trans*-$[Pt(tp)_2Cl_4]$ and *trans*-$[Pt(dmtp)_2Cl_4]$ where tp = 1,2,4-triazolo-[1,5α]-pyrimidine and dmtp = 5,7-dimethyl-1,2,4-triazolo-[1,5α]-pyrimidine were synthesised and studied by ^1H, ^{13}C, ^{15}N, ^{195}Pt NMR and IR spectroscopies. Significant ^{15}N NMR upfield coordination shifts (92–96 ppm) were observed for the N(3) atom indicating that this nitrogen is the metallation site. The X-ray structure of an ionic pair $(dmtpH)_2[PtCl_6]$ {bis(5,7-dimethyl-1,2,4-triazolo-[1,5α]-pyrimidinium) hexachloroplatinate(IV)} was determined, exhibiting the presence of unique $(dmtpH)_2^{2+}$ dimeric cations, protonated at N(3), N(3′) atoms and linked by hydrogen bonding. © 2002 Elsevier Science Ltd. All rights reserved.

Keywords: Platinum chloride complexes; X-ray structures; N-donor ligands; ^{15}N NMR; 1,2,4-Triazolo-[1,5α]-pyrimidines

1. Introduction

1,2,4-triazolo-[1,5α]-pyrimidines are heterocycles isomeric to purines, their fused ring system differing in having the pyrimidine nitrogen atom in a bridge-head position (Fig. 1) [1,2]. The transition metal complexes with this class of N-donor ligands have been studied intensively, the researches concerned mainly with 1,2,4-triazolo-[1,5α]-pyrimidine (tp), 5,7-dimethyl-1,2,4-triazolo-[1,5α]-pyrimidine (dmtp) and 4,7-H-5-methyl-7-oxo-1,2,4-triazolo-[1,5α]-pyrimidine (HmtpO) [3]. Among them, a few coordination compounds with platinide metals have been also described: $[Pt^{II}(dmtp{-}N^3)_4][Pt^{IV}(SCN)_6]$, *trans*-$[Pd^{II}(dmtp{-}N^3)_2Br_2]\cdot CH_3OH$, *cis*-$[Pt^{II}(Hmtpo{-}N^3)_2Cl_2]\cdot 2H_2O$, *cis*-$[Pt^{II}(HmtpO{-}N^3)_2(NH_3)_2](NO_3)_2\cdot 2H_2O$, *mer*-$[Ru^{III}(dmtp{-}N^3)_2Cl_3(H_2O)]\cdot H_2O$ and *mer*-$[Ru^{III}(2\text{-amino-dmtp}{-}N^3)_2Cl_3(H_2O)]\cdot H_2O$ [4–9]. Recently we have characterised a series of *cis*-dichlorocomplexes of Pd(II) with tp, dmtp, 5,7-diphenyl-1,2,4-triazolo-[1,5α]-pyrimidine (dptp) and 5,7-di-*tert*-butyl-1,2,4-triazolo-[1,5α]-pyrimidine (dbtp), their general formula being *cis*-$[Pd^{II}L_2Cl_2]\cdot xH_2O$ where L = tp, dmtp, dptp, dbtp ($x = 0$, 1) [10]. The ^{15}N NMR measurements have shown that the coordination site in

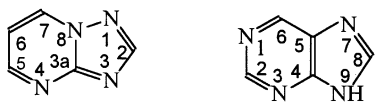


Fig. 1. 1,2,4-Triazolo-[1,5α]-pyrimidine (tp) and purine.

* Corresponding author. Tel.: +48-56-611-4304; fax: +48-56-654-2477.
E-mail address: eszlyk@dove.boa.uni.torun.pl (E. Szlyk).

0277-5387/02/$ - see front matter © 2002 Elsevier Science Ltd. All rights reserved.
PII: S0277-5387(01)01000-2

all triazolopyrimidine ligands has been N(3). We have reported also the X-ray structure of *cis*-[Pd^{II}(dbtp–N^3)$_2Cl_2$]·0.5C_2H_5OH that has been isostructural with the former compounds [10].

Strong N(3) coordination tendency of 1,2,4-triazolo-[1,5α]-pyrimidines, noted for the majority of their complexes with transition metals [3], is in favour of their usage as model ligands for metal–purine interactions. These heterocycles, however, differ in the strength of metal–nitrogen bonds, depending on the presence of substituents in the five and seven positions. In this paper we study four new Pt(II) and Pt(IV) coordination compounds with unsubstituted tp and its 5,7-dimethyl derivative dmtp: *trans*-[Pt^{II}(tp)$_2Cl_2$] (**1**), *trans*-[Pt^{II}(dmtp)$_2Cl_2$] (**2**), *trans*-[Pt^{IV}(tp)$_2Cl_4$] (**3**) and *trans*-[Pt^{IV}(dmtp)$_2Cl_4$] (**4**). It is the first report on Pt(IV) complexes with this class of heterocycles.

The present work is also a continuation of our ^{15}N NMR studies of the chloride complexes of diamagnetic transition metal ions with 1,2,4-triazolo-[1,5α]-pyrimidines. In our earlier reports we have described the correlation between the ^{15}N NMR coordination shifts and the type of a metal ion, the former researches concerning Zn(II) and Pd(II) compounds [10–12].

During the present studies we have solved the crystal and molecular structure of (dmtpH)$_2$[$PtCl_6$] (**5**). The molecule of this ionic pair seems to be interesting as there is a unique dimerization of the two N(3)-protonated dmtpH^+ cations resulting in the formation of a divalent $(dmtpH)_2^{2+}$ ion. Such a phenomenon has never been observed for 1,2,4-triazolo-[1,5α]-pyrimidines. In the only described X-ray structure with a protonated form of dmtp, (dmtpH)$_2$[$CdBr_4$]·2H_2O, the dmtpH^+ cations have not been dimerized [13].

2. Experimental

2.1. Materials

Pt of 99.9% purity was purchased from the Polish State Mint whereas tp and dmtp were from Aldrich. A water solution of H_2PtCl_6 was prepared using a standard procedure by the dissolution of Pt in aqua regia. K_2PtCl_4 was obtained by the reduction of H_2PtCl_6 with hydrazine to H_2PtCl_4 and neutralization by KOH.

2.2. Methods

The content of C, H, N in **1**–**4** was determined by elemental semi-microanalysis, whereas Pt was determined gravimetrically [14]. IR spectra were measured with a Perkin–Elmer spectrum 2000 FT IR spectrometer, using KBr (400–4000 cm^{-1}) and polyethylene discs (100–4000 cm^{-1}). ^1H, ^{13}C, ^{15}N, ^{195}Pt NMR spectra were performed on a Varian INOVA 500 spectrometer equipped with inverse Nalorac Z gradient shielded probe. ^{15}N NMR was detected by 2D ^1H–^{15}N gradient selected heteronuclear multiple quantum correlation (HMQC) in the absolute value mode. ^{195}Pt NMR of Pt(II) species was measured by a 1D technique optimised for fast relaxing nuclei (acquisition time 10 ms, relaxation delay 10 ms, flip angle 20°, spectral width 100 kHz) whereas that of Pt(IV) compounds was measured by phase-sensitive 2D ^1H–^{195}Pt HMQC. The solvent was dmf-d_7, the concentration of samples 0.05 M and the temperature 303 K. The reference standard was TMS for ^1H and ^{13}C; CH_3NO_2 for ^{15}N and K_2PtCl_6 for ^{195}Pt.

The X-ray data for **5** was collected for an $0.08 \times 0.10 \times 0.10$ mm orange crystal with a Kuma KM-4 diffractometer using Mo Kα radiation, $\lambda = 0.71069$ Å at 100(1) K, by 2θ method. The structure was solved with the Patterson method using SHELXS-86 [15] and refined with SHELXL-93 [16] giving $R = 0.038$, $wR_2 = 0.1009$ and goodness-of-fit on $F^2 = 1.046$ [$I > 2\sigma(I)$]. The atomic scattering factors were taken from the International Tables for Crystallography [17]. The geometry of **5** was compared to other compounds using the Cambridge Structural Database [18].

2.3. Synthesis

2.3.1. Complexes *1*–*4*

K_2PtCl_4 (1 mmol, for **1** and **2**) or H_2PtCl_6 (1 mmol, 30% water solution, for **3** and **4**) was dissolved in 10 ml of water and added to: (a) 2 mmol of tp in 20 ml of water (for **1** and **3**); (b) 2 mmol of dmtp in 20 ml of ethanol (for **2** and **4**). The mixture was stirred and left for 24 h at room temperature (r.t.). The obtained yellow precipitate was filtered, washed with ethanol and dried in air. The elemental analysis of **1** corresponded to Pt(tp)$_2Cl_2$ formula (%; calc. for $PtC_{10}H_8N_8Cl_2$/found): Pt (38.5/38.1), C (23.7/23.2), H (1.6/1.3), N (22.1/21.6); that of **2** to Pt(dmtp)$_2Cl_2$ (%; calc. for $PtC_{14}H_{16}N_8Cl_2$/found): Pt (34.7/34.4), C (29.9/29.8), H (2.9/3.1), N (19.9/19.8); that of **3** to Pt(tp)$_2Cl_4$ (%; calc. for $PtC_{10}H_8N_8Cl_4$/found): Pt (33.8/34.0), C (20.8/21.0), H (1.4/1.5), N (19.4/19.1); that of **4** to Pt(dmtp)$_2Cl_4$ (%; calc. for $PtC_{14}H_{16}N_8Cl_4$/found): Pt(30.8/31.0), C (26.6/27.0), H (2.5/2.7), N(17.7/17.3).

2.3.2. The ionic pair *5*

H_2PtCl_6 (1 mmol) and 2 mmol of dmtp were mixed in a strongly acidic (5 M HCl) water–ethanol (1:1) solution. The obtained (after 24 h) orange crystals were filtered, washed with 1 M HCl and ethanol, then dried over P_2O_5.

3. Results and discussion

3.1. The crystal structure of 5

The crystal structure data of **5** are listed in Table 1 and the selected bond lengths and angles are in Table 2. The perspective view of the molecule with its numbering scheme is shown in Fig. 2.

Complex **5** is an ionic pair consisting of two N(3)-monoprotonated dmtpH$^+$ cations and one $[PtCl_6]^{2-}$ anion. The unit cell, marked by eight Pt atoms, contains two triazolopyrimidinium ions related by the centre of symmetry $[-x, -y, -z]$. Each of those dmtpH$^+$ species is linked by hydrogen bonding {N(3)–H···N(4′) and N(4)···H–N(3′)} with an analogous ion, positioned in an adjacent unit cell and related by the centre of symmetry $[-x+1, -y+1, -z]$. Thus, in the crystal lattice there are unique dimeric and divalent $(dmtpH)_2^{2+}$ cations. It is interesting that the repulsion forces of the two positively charged triazolopyrimidinium ions are weaker than their attraction by hydrogen bonds.

Table 1
Crystal structure data for **5**

Compound	$(dmtpH)_2[PtCl_6]$
Empirical formula	$PtC_{14}H_{18}Cl_6N_8$
Molecular weight	706.15
Crystal system	triclinic
Space group	$P\bar{1}$
Unit cell dimensions	
a (Å)	7.884(2)
b (Å)	9.140(2)
c (Å)	9.427(2)
α (°)	63.38(3)
β (°)	66.55(3)
γ (°)	65.40(3)
V (Å^3)	533.2(2)
Z	1
D_{calc} (Mg m^{-3})	2.199
μ (mm^{-1})	7.352
Reflections collected/unique	3059/1822
Final R_1/wR_2 indices $[I>2\sigma(I)]$ (all data)	0.0380/0.1009

Table 2
Selected bond lengths (Å) and bond angles (°) for dmtpH$^+$ cation in **5**

Bond lengths			
N(8)–N(1)^{i}	1.393(9)	C(3a)–N(4)^{p}	1.335(9)
N(1)–C(2)^{i}	1.303(10)	N(4)–C(5)^{p}	1.343(10)
C(2)–N(3)^{i}	1.369(9)	C(5)–C(6)^{p}	1.410(10)
N(3)–C(3a)^{i}	1.340(9)	C(6)–C(7)^{p}	1.356(11)
N(8)–C(3a)^{i,p}	1.350(9)	C(7)–N(8)^{p}	1.364(10)
Bond angles			
C(3a)–N(8)–N(1)^{i}	110.9(6)	N(8)–C(3a)–N(4)^{p}	124.4(7)
N(8)–N(1)–C(2)^{i}	103.1(5)	C(3a)–N(4)–C(5)^{p}	115.4(6)
N(1)–C(2)–N(3)^{i}	113.0(6)	N(4)–C(5)–C(6)^{p}	121.0(7)
C(2)–N(3)–C(3a)^{i}	106.5(5)	C(5)–C(6)–C(7)^{p}	122.6(7)
N(3)–C(3a)–N(8)^{i}	106.5(6)	C(6)–C(7)–N(8)^{p}	114.1(6)
		C(7)–N(8)–C(3a)^{p}	122.3(6)

i, imidazole ring; p, pyrimidine ring.

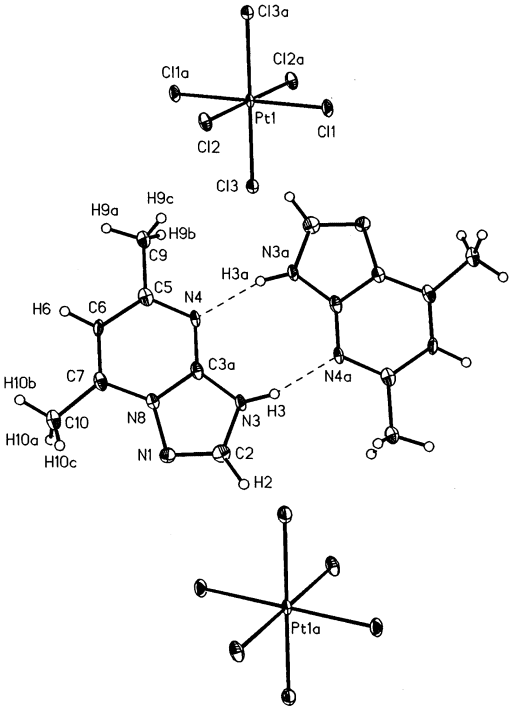


Fig. 2. ORTEP drawing of the $(dmtpH)_2[PtCl_6]$ (**5**) molecule.

In a single dmtpH$^+$ cation the triazolopyrimidine rings are planar, the rms. deviation from the best plane for the N(1)···N(8) moiety being 0.020 Å. The comparison of their geometry with that of solvated dmtp in the compound $[Pd(thiourea)_4]\cdot 2\ dmtp\cdot 2H_2O$ [19] shows that the protonation at N(3) results in an increase of the C(2)–N(3)–C(3a) angle {from 102.2(3)° to 106.5(5)°} and a decrease of adjacent angles N(1)–C(2)–N(3) {from 117.6(4)° to 113.0(6)°} and N(3)–C(3a)–N(8) {from 109.5(3)° to 106.5(6)°}. The N(3)–C(2) and N(3)–C(3a) bonds have been elongated upon protonation, from 1.333(5) to 1.369(9) Å and from 1.313(4) to 1.340(9) Å, respectively. Similar effects were described for another ionic pair, $(dmtpH)_2[CdBr_4]\cdot 2H_2O$ [13]. The formation of N(3)–H···N(4′) and N(4)···H–N(3′) hydrogen bonding has not affected the geometry of the pyrimidine ring, the C(3a)–N(4)–C(5) angle in **5** being the same as in solvated dmtp [19] (115.4(6)° compared to 115.6(3)°). The parameters of the H–bonds are as follows: N(3)–H(3) 0.86 Å, H(3)···N(4′) 1.98 Å, N(3)–H(3)···N(4′) 161.4°.

The $[PtCl_6]^{2-}$ anions are nearly octahedral, although some deviations from the ideal geometry occur. The lengths of Pt–Cl bonds vary from 2.317(2) to 2.324(2) Å and the Cl–Pt–Cl angles from 88.5(1)° to 91.5(1)°. Such a phenomenon is not unusual and has been described for $[N(CH_3)_4]_2[PtCl_6]$ [20], $[N(C_2H_5)_4]_2[PtCl_6]$ [21], $[NH_2(CH_3)_2]_2[PtCl_6]$ [22] and $(9\text{-MeGuH})_2[PtCl_6]$ [23] (9-MeGuH = 9-methylguaninium cation).

3.2. IR spectroscopy

For **1**–**4** the coordination of tp or dmtp molecules by Pt(II) or Pt(IV) ions results in very slight shifts of the absorption bands in the region 400–1700 cm^{-1}. The two most characteristic ones, assigned previously by us as the whole triazolopyrimidine ring skeletal vibration ($\nu_{tp} = 1621$ cm^{-1} for tp, 1637 cm^{-1} for dmtp) and the pyrimidine ring skeletal vibration ($\nu_{py} = 1525$ cm^{-1} for tp, 1550 cm^{-1} for dmtp) [12] are shifted by a maximum of 11 cm^{-1} (Table 3). There are no significant differences between the respective Pt(II) and Pt(IV) complexes.

In the case of **5** the observed shifts of those bands are much larger, approximately 10–20 cm^{-1} towards higher wave numbers. This phenomenon can be the result of both N(3) protonation and the formation of N(3)–H···N(4′) hydrogen bonding. In the IR spectrum of **5** there is also an intensive band of rich structure in the 2500–2700 cm^{-1} range, characteristic for the $(N–H)^+$ stretching vibration in the salts of tertiary ammines [24]. Its presence is in full agreement with the X-ray data revealing the protonated $dmtpH^+$ species in the solid phase of **5**.

Far-IR spectroscopy of **1**–**4** has exhibited one new absorption band of large intensity in a narrow range 338–347 cm^{-1} (Table 3). Its energy is similar to that found for some chloride complexes of Pt(II) and Pt(IV) with ammonia, pyridine (py) or imidazole (imH) {365 cm^{-1} for *trans*-$Pt(NH_3)_2Cl_2$, 345 and 331 cm^{-1} for *cis*-$Pt(NH_3)_2Cl_2$, 352 cm^{-1} for *trans*-$Pt(NH_3)_2Cl_4$, 353, 344 and 330 cm^{-1} for *cis*-$Pt(NH_3)_2Cl_4$ [25]; 342 cm^{-1} for *trans*-$Pt(py)_2Cl_2$, 343 and 329 cm^{-1} for *cis*-$Pt(py)_2Cl_2$ [26]; 350 cm^{-1} for *trans*-$Pt(imH)_2Cl_2$, 329 and 322 cm^{-1} for *cis*-$Pt(imH)_2Cl_2$ [27]}. Thus it derives, most likely, from a Pt–Cl stretching vibration. As only one band is active in the IR spectra, we can assume that **1**–**4** are *trans* isomers of symmetry C_{2h} (square-planar in **1** and **2**) or D_{4h} (pseudooctahedral in **3** and **4**) [28]. The Pt–N stretching vibrations, expected in the range 200–300 cm^{-1}, have not been detected, most probably due to overlapping with ligand internal modes, observed at 237 cm^{-1} (tp) or 286, 276, 236 cm^{-1} (dmtp).

In the far-IR spectrum of **5** one could expect two absorption bands analogous to those found at 342 and 183 cm^{-1} for K_2PtCl_6 [29]. In reality we have observed a group of heavily overlapped bands in the range 150–330 cm^{-1}.

Table 3
Selected IR bands (cm^{-1}) for **1**–**5** (coordination shifts, $\Delta\nu_{coord} = \nu_{compl} - \nu_{lig}$, in parentheses)

Compound	ν_{tp} (cm^{-1})	ν_{py} (cm^{-1})	ν(Pt–Cl) (cm^{-1})
1	1623 (+2)	1536 (+11)	338
2	1631 (−6)	1554 (+4)	343
3	1622 (+1)	1531(+6)	347
4	1630 (−7)	1554 (+4)	345
5	1649 (+12)	1571 (+21)	150–330

3.3. NMR spectroscopy

The ^1H and ^{13}C NMR spectra of tp and dmtp have been reported by many authors, however, the data concerned $CDCl_3$ or dmso-d_6 solutions [30–35]. Recently, we have completely assigned ^{15}N NMR signals of tp and dmtp in dmso-d_6 using heteronuclear correlation (HETCOR) methods [10–12]. During this work we had to perform all NMR measurements in dmf-d_7, due to insolubility or decomposition of the complexes in $CDCl_3$ and dmso-d_6. The assignment of the signals for tp, dmtp and **1**–**5** was based on analogous HETCOR techniques.

3.3.1. ^{15}N NMR

The ^{15}N NMR chemical shifts for tp, dmtp and **1**–**5** are listed in Table 4.

In the case of **1**–**4** the Pt(II) or Pt(IV) coordination most significantly affects the N(3) signal, shifting it upfield 92.6–92.9 or 94.7–95.4 ppm, respectively. Such a diamagnetic shift unambiguously indicates that the complexation occurs via N(3). The absolute values of the coordination shifts are larger than for analogous Pd(II) complexes (78–90 ppm) [10] which is consistent with the known fact that the shielding of nitrogen increases down a group of coordinating transition metals in the periodic table [36]. The increased shielding of the Pt(II)- or Pt(IV)-coordinated nitrogen nucleus is, most likely, the result of the decrease of the absolute value of the paramagnetic term in its ^{15}N NMR shielding constant. It is evident that this effect increases with the oxidation number of platinum.

For **5** the observed upfield shift of N(3) signal is only 10 ppm whereas the other resonances are nearly not

Table 4
^{15}N NMR chemical shifts for tp, dmtp and **1**–**5** in dmf-d_7 (coordination shifts, $\Delta\delta_{coord} = \delta_{compl} - \delta_{lig}$, in parentheses)

Compound	N(1)	N(3)	N(4)	N(8)
tp	−106.0	−151.3	−103.2	−154.3
dmtp	−111.9	−153.9	−115.8	−155.3
1	−106.9	−244.2	−108.7	−157.1
	(−0.9)	(−92.9)	(−5.5)	(−2.8)
2	−112.8	−246.5	−120.3	−158.4
	(−0.9)	(−92.6)	(−4.5)	(−3.1)
3	−106.3	−246.7	−109.1	−156.8
	(−0.3)	(−95.4)	(−5.9)	(−2.5)
4	−112.6	−248.6	−120.1	−158.6
	(−0.7)	(−94.7)	(−4.3)	(−3.3)
5	−111.9	−164.0	−116.4	−156.0
	(0.0)	(−10.1)	(−0.6)	(−0.7)

shifted. It is discussable if so moderated shielding can be regarded as a result of protonation as the common range for azoloazines is 80–150 ppm [37]. However, if to assume that the dmtpH$^+$ cations are dimerised also in dmf-d_7 solution, it is possible that the formation of N(3)–H···N(4′) hydrogen bonding results in an additional deshielding of N(3), this effect being opposite to that of protonation.

3.3.2. ^1H and ^{13}C NMR

The selected ^{1}H and ^{13}C NMR chemical shifts for tp, dmtp and **1**–**5** are listed in Table 5.

For **1**–**4** the chemical shifts changes pattern is very clear. The protons in heteroaromatic rings are generally deshielded, this effect being much more pronounced for H(2) (0.47–0.64 ppm) than for H(6) (0.06–0.19 ppm). The carbons adjacent to the N(3) metallation site, i.e. C(2) and C(3a), are shielded (0.7–4.6 ppm) whereas the others are deshielded (1.6–3.4 ppm). Those coordination shifts also increase with the oxidation number of platinum. Analogous results but of a smaller magnitude were described by us for Pd(II) complexes [10].

In the ^{1}H NMR spectrum of **5** an additional broad singlet occurs at 11 ppm. It disappears when D_2O is added which proves that it derives from the N(3)–H$^+$ protonated group. This observation reveals that in dmf-d_7 solution the dmtp molecules of **5** are also protonated (as it was in the solid state) although it is not clear if they appear as monomeric dmtpH$^+$ or in the dimerised $(dmtpH)_2^{2+}$ form.

3.3.3. ^{195}Pt NMR

The ^{195}Pt signals of **1** and **2** are observed at -2061 and -2058 ppm whereas those of **3** and **4** at -17 and -30 ppm. Such values of ^{195}Pt chemical shifts are typical for Pt(II) and Pt(IV) complexes in N-donor heteroaromatic compounds [38–42]. A characteristic 'oxidation shift' of approximately 2040 ppm (downfield, when comparing Pt(IV) with Pt(II) species) is very close to that described in literature (e.g. for Pt(bipy)Cl$_2$ and Pt(bipy)Cl$_4$ the $\delta(^{195}Pt)$ value increases from -2315 to -311 ppm) [43].

The ^{195}Pt signals of Pt(II) complexes (**1** and **2**) have been detected as broad singlets, their half-line widths being approximately 650–750 Hz. Such values are relatively high, comparing to those found for $[PtCl_4]^{2-}$ ions (ca. 110 Hz) [44], which can be explained, most likely, by the quadrupolar ^{195}Pt–^{14}N interactions between the Pt and N(3) nuclei.

In the case of Pt(IV) complexes (**3** and **4**) the ^{195}Pt–^{1}H spin–spin interactions have been observed in HMQC spectra between the Pt and H(2) nuclei. The measured values of $^3J_{Pt-H}$, approximately 11 Hz, are rather small comparing to those found for Pt(IV) complexes with ethylenediamine (26–28 Hz) [45].

The ^{195}Pt signal of **5**, observed at $+353.5$ ppm (half–line width 10–15 Hz) exhibits a characteristic shape with ^{35}Cl/^{37}Cl isotopic lines typical for the $[PtCl_6]^{2-}$ anion [46], which proves that this ion is present also in dmf-d_7 solution.

4. Conclusions

In the direct reactions of $[PtCl_4]^{2-}$ or $[PtCl_6]^{2-}$ with tp or dmtp the formation of *trans*-isomers is favoured in water–ethanol solutions, contrary to the case of $[PdCl_4]^{2-}$ where *cis*-forms have been obtained. ^{15}N NMR spectroscopy proves that the Pt(II) or Pt(IV) coordination by 1,2,4-triazolo-[1,5α]-pyrimidines occurs via N(3). Such a complexation mode can be regarded as representative for this class of heterocycles and analogous to the N(9) coordination of purines. The formation of Pt–N(3) bonding results in the increased shielding of this nitrogen nucleus as well as of the adjacent carbon atoms. The observed upfield shifts of N(3) signals are larger than for analogous Pd(II) complexes and increase with the oxidation number of platinum. The X-ray study of the ionic pair $(dmtpH)_2[PtCl_6]$ shows that in the solid state the dmtp molecules are protonated at N(3) and the formed dmtpH$^+$ cations are linked by N(3)–H···N(4′) hydrogen bonding into unique dimeric and divalent species $(dmtpH)_2^{2+}$. The ^{1}H and ^{195}Pt NMR measurements

Table 5
^{1}H and ^{13}C NMR chemical shifts for tp, dmtp and **1**–**5** in dmf-d_7 (coordination shifts, $\Delta\delta_{coord} = \delta_{compl} - \delta_{lig}$, in parentheses)

Compound	H(2)	H(6)	C(2)	C(3a)	C(5)	C(6)	C(7)
tp	8.72	7.47	156.7	156.0	156.1	111.6	138.0
dmtp	8.59	7.19	155.9	155.8	165.4	111.5	148.0
1	9.19 [a] (+0.47)	7.53 (+0.06)	156.0 (−0.7)	153.1 (−2.9)	158.7 (+2.6)	113.9 (+2.3)	139.6 (+1.6)
2	9.09 [a] (+0.50)	7.29 (+0.10)	155.1 (−0.8)	152.8 (−3.0)	168.4 (+3.0)	113.7 (+2.2)	149.7 (+1.7)
3	9.32 [b] (+0.60)	7.63 (+0.16)	153.7 (−3.0)	151.4 (−4.6)	159.3 (+3.2)	114.6 (+3.0)	140.7 (+2.7)
4	9.23 [b] (+0.64)	7.38 (+0.19)	152.9 (−3.0)	151.2 (−4.6)	168.8 (+3.4)	114.3 (+2.8)	150.7 (+2.7)
5	8.79 (+0.20)	7.33 (+0.14)	154.1 (−1.8)	154.4 (−1.4)	166.6 (+1.2)	112.3 (+0.8)	148.5 (+0.5)

[a] No ^{1}H–^{195}Pt couplings observed for the studied Pt(II) complexes.
[b] ^{1}H–^{195}Pt couplings observed for the studied Pt(IV) complexes, their $^3J_{HPt}$ being 11.4 Hz (**3**) or 11.0 Hz (**4**).

reveal that the $dmtpH^+$ and $[PtCl_6]^{2-}$ ions are present also in dmf-d_7, although it is not clear if the above described H-bonds also occur in the solution.

5. Supplementary material

Crystallographic data for the structural analysis have been deposited with the Cambridge Crystallographic Centre, CCDC No. 166796 for complex **5**. Copies of this information may be obtained free of charge from The Director, CCDC, 12 Union Road, Cambridge, CB2 1EZ, UK (fax: +44-1233-336-033; e-mail: deposit@ccdc.cam.ac.uk or www: http://www.ccdc.cam.ac.uk).

Acknowledgements

We thank the Polish Committee for Scientific Research for the grant 3T09A11616, supporting our studies.

References

[1] G. Fischer, Z. Chem. 30 (9) (1990) 305.
[2] G. Fischer, Adv. Het. Chem. 57 (1993) 81.
[3] J. Salas, M.A. Romero, M.P. Sanchez, M. Quiros, Coord. Chem. Rev 193–195 (1999) 1119.
[4] M. Biagini-Cingi, A.M. Manotti-Lanfredi, A. Tiripicchio, J.G. Haasnoot, J. Reedijk, Inorg. Chim. Acta 72 (1983) 81.
[5] R. Hage, R.A.G. de Graaff, J.G. Haasnoot, K. Kieler, J. Reedijk, Acta Crystallogr., Sect. C 46 (1990) 2349.
[6] J.A.R. Navarro, M.A. Romero, J.M. Salas, M. Quiros, Inorg. Chem. 36 (1997) 3277.
[7] J.A.R. Navarro, J.M. Salas, M.A. Romero, R. Vilaplana, F. Gonzalez-Vilchez, R. Faure, J. Med. Chem. 41 (1998) 332.
[8] A.H. Velders, L. Pazderski, F. Ugozzoli, M. Biagini-Cingi, A.M. Manotti-Lanfredi, J.G. Haasnoot, J. Reedijk, Inorg. Chim. Acta 273 (1998) 259.
[9] A.H. Velders, F. Ugozzoli, M. Biagini-Cingi, A.M. Manotti-Lanfredi, J.G. Haasnoot, J. Reedijk, Eur. J. Inorg. Chem. 2 (1999) 213.
[10] E. Szlyk, A. Grodzicki, L. Pazderski, A. Wojtczak, J. Chatlas, G. Wrzeszcz, J. Sitkowski, B. Kamieński, J. Chem. Soc., Dalton Trans. (2000), 867.
[11] A. Grodzicki, E. Szłyk, L. Pazderski, J. Sitkowski, Polish J. Chem. 72 (1998) 55.
[12] E. Szłyk, A. Grodzicki, L. Pazderski, E. Bednarek, B. Kamieński, Polyhedron 19 (2000) 965.
[13] J.M. Salas, M.A. Romero, A. Rahmani, R. Faure, G. Alvarez de Cienfuegos, E.R.T. Tiekink, J. Inorg. Biochem. 64 (1996) 259.
[14] A. Vogel, Textbook of Quantitative Inorganic Analysis Including Elementary Instrumental Analysis, Longman, London, 1978, pp. 474–475.
[15] G.M. Sheldrick, Acta Crystallogr., Sect. A 46 (1990) 467.
[16] G.M. Sheldrick, SHELXL-93, Program for Crystal Structure Refinement, University of Göttingen, Germany, 1993.
[17] International Tables for Crystallography, Kluwer Academic Publishers, Dordrecht, 1992.
[18] F.H. Allen, O. Kennard, Chem. Des. Automation News 8 (1993) 31.
[19] J.M. Salas, A. Rahmani, M.A. Romero, M. Quiros, E.R.T. Tiekink, J. Chem. Cryst. 24 (1994) 669.
[20] R.W. Berg, I. Sotofle, Acta Chim. Scand. A 32 (1978) 241.
[21] M.S.D. Elyouloi, M.H. Ben Ghozlen, Y. Milk, A. Daoud, Phys. Status Solidi A 98 (1986) 435.
[22] D.D. Makitova, O.N. Krasochka, L.V. Atormyan, I.P. Lavrentev, Yu.M. Shulga, L.V. Revenko, M.L. Khidekel, Koord. Khim. 13 (1987) 383.
[23] A. Terzis, D. Mentzafos, Inorg. Chem. 22 (1983) 1140.
[24] R.M. Silverstein, F.X. Webster, Spectrometric Identification of Organic Compounds, Wiley, New York, 1998, p. 103.
[25] K. Nakamoto, Infrared and Raman Spectra of Inorganic and Coordination Compounds, Wiley, New York, 1978, p. 204, 321.
[26] J.R. Durig, B.R. Mitchell, D.W. Sink, J.N. Willis, A.S. Wilson, Spectrochim. Acta 23A (1967) 1121.
[27] C.G. van Kralingen, J.K. de Ridder, J. Reedijk, Inorg. Chim. Acta 36 (1979) 69.
[28] K. Nakamoto, Infrared and Raman Spectra of Inorganic and Coordination Compounds, Wiley, New York, 1978, p. 319, 321.
[29] K. Nakamoto, Infrared and Raman Spectra of Inorganic and Coordination Compounds, Wiley, New York, 1978, p. 152, 156.
[30] E. Kleinpeter, R. Borsdorf, G. Fischer, H.-J. Hofmann, J. Prakt. Chem. 314 (1972) 515.
[31] T. La Noce, A.M. Giuliani, Tetrahedron 34 (1978) 2927.
[32] J.S. Bajwa, P.J. Sykes, J. Chem. Soc., Perkin Trans 1 (1979) 3085.
[33] M. Hori, K. Tanaka, T. Kataoka, H. Shimizu, E. Jimai, J. Chem. Soc., Perkin Trans. I (1985) 2333.
[34] R.J. Pugmire, J.C. Smith, D.M. Grant, B. Stanovnik, M. Tisler, B. Vercek, J. Het. Chem. 24 (1987) 805.
[35] J.W. Wiench, L. Stefaniak, G.A. Webb, Magn. Res. Chem. 32 (1994) 373.
[36] J. Mason, Chem. Rev. 81 (1981) 205.
[37] M. Witanowski, L. Stefaniak, G.A. Webb, Annual Reports on NMR Spectroscopy, vol. 25, Academic Press, London, 1993, p. 40.
[38] P.S. Pregosin, Transition Metal Nuclear Magnetic Resonance, Elsevier, Amsterdam, 1991, p. 250.
[39] P.S. Pregosin, Coord. Chem. Rev 44 (1982) 247.
[40] R.K. Harris, B.E. Mann, NMR and the Periodic Table, Academic Press, London, 1978, p. 249.
[41] P. Laszlo, NMR of Newly Accessible Nuclei, vol. 2, Academic Press, London, 1983, p. 404.
[42] G.A. Kirakosyan, Koord. Khim. (Russ.) 19 (1993) 507.
[43] E.G. Hope, W. Levason, N.A. Powell, Inorg. Chim. Acta 115 (1986) 187.
[44] J.J. Pesek, W.R. Mason, J. Magn. Res. 25 (1977) 519.
[45] T.G. Appleton, J.R. Hall, Inorg. Chem. 10 (1971) 1717.
[46] F.M. Ismail, S.J.S. Kerrison, P.J. Sadler, J. Chem. Soc., Chem. Commun. (1980) 1175.

PERGAMON

Polyhedron 21 (2002) 349–352

POLYHEDRON

www.elsevier.com/locate/poly

Preparation and crystal structures of new phenoxide derivatives of tungsten(VI) oxytetrachloride

Ari Lehtonen *, Reijo Sillanpää

Department of Chemistry, University of Turku, Fin-20014 Turku, Finland

Received 25 September 2001; accepted 22 November 2001

Abstract

Two oxotungsten(VI) complexes of the type $[WOCl_2(OAr)_2]$ (OAr = OC_6H_3–^{t}Bu-2-Me-6 or OC_6H_2–^{t}Bu-2-Br-4-Me-6) were prepared by the reaction of $WOCl_4$ with 2 equiv. of phenolic ligand precursors in a refluxing toluene solution. Both compounds form monomeric units, in which the tungsten ion has adopted a square pyramidal coordination geometry with the oxo ligand in the apical position and phenoxide groups bound in a *trans* orientation. © 2002 Elsevier Science Ltd. All rights reserved.

Keywords: Chloride ligands; Oxo ligands; Phenolates; Tungsten

1. Introduction

Aryloxide derivatives of oxotungsten(VI) are used commonly in production of unsaturated polymers using ROMP chemistry, as well as in the syntheses of cyclic compounds by the use of ring closing metathesis [1]. The general benefit of aryloxide ligands in these complexes is that altering the substituents on the aromatic ring can easily vary their electron-withdrawing properties and also modify steric effects in the close neighbourhood to the metal. The hard donor character of phenoxide ligand also stabilises the high oxidation state of tungsten ion. A standard procedure for the preparation of these complexes is the reaction of $WOCl_4$ (**1**) with a phenolic compound [2], which may also result in a mixture of species with varying numbers of aryloxide substituents [3,4]. Sometimes the use of lithium aryloxides is necessary to complete the reaction [5]. Although oxotungsten derivatives of type $[WOCl_2(OAr)_2]$ are frequently prepared and used as catalyst precursors, only few compounds have been structurally fully characterised [5–7]. In the context of a broader program aimed at developing transition metal catalysts for olefin metathesis, our laboratory has recently become interested in the chemical manipulation of tungsten aryloxide complexes [8]. To have more detailed knowledge about this chemistry, we are at present studying monomeric oxotungsten(VI) chloride phenoxides. In this paper, we report syntheses and X-ray crystal structures of two new potential catalyst precursors.

2. Experimental

$WOCl_4$ and 2-*tert*-butyl-4-bromo-6-methylphenol were prepared according to literature procedures [9,10]. 2-*tert*-Butyl-6-methylphenol was used as received from Aldrich. Solvents were distilled over sodium benzophenone ketyl prior to use. Syntheses and manipulations were performed using standard inert atmosphere techniques [11].

2.1. Syntheses

A suspension of **1** (340 mg, 1.0 mmol) in toluene (25 ml) was treated with 2 equiv. of phenol **2a** (330 mg) or **2b** (490 mg), respectively. These reaction mixtures were stirred at reflux temperature for 4 h to obtain intense red solutions. Evaporation of solvents afforded red microcrystalline solids, which were practically pure (according to ^{1}H NMR analyses) compounds **3a** and **3b**, respectively. These solids were extracted by C_6H_{14}, con-

* Corresponding author. Tel.: +358-2-333-6733; fax: +358-2-333-6700.

E-mail address: ari.lehtonen@utu.fi (A. Lehtonen).

0277-5387/02/$ - see front matter © 2002 Elsevier Science Ltd. All rights reserved.
PII: S0277-5387(01)00998-6

centrated and stored at −20 °C to obtain purple, moderate air-stable crystals. For **3a**: yield 370 mg (62%). NMR: δ_H ($CDCl_3$, standard $SiMe_4$): 7.35 (d, 2H, ArH), 7.20 (d, 2H, ArH), 6.97 (t, 2H, ArH), 2.55 (6H, ArCH_3), 1.58 (18H, C(CH_3)$_3$). IR: 1181 (vs, C–O), 997 (s, W=O) cm^{-1}. *Anal.* Found: C, 44.0; H, 5.0. $C_{22}H_{30}Cl_2O_3W$. Calc. for C, 44.2; H, 5.1%. For **3b**: yield 545 mg (72%). NMR: δ_H ($CDCl_3$, standard $SiMe_4$): 7.47 (2H, ArH), 7.34 (2H, ArH), 2.49 (6H, ArCH_3), 1.55 (18H, C(CH_3)$_3$). IR: 1196 (vs, C–O), 995 (s, W=O) cm^{-1}. *Anal.* Found: C, 35.2; H, 4.1. $C_{22}H_{28}Br_2Cl_2O_3W$. Calc. for C, 35.0; H, 3.7%.

2.2. Crystal structure determination

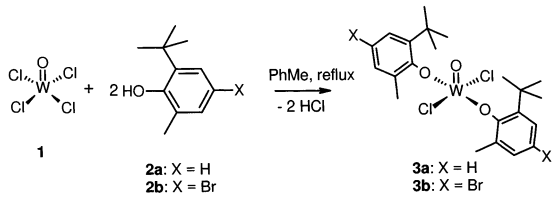
Single-crystal data collections were performed at ambient temperature on a Rigaku AFC5S diffractometer using graphite monochromatised Mo Kα radiation ($\lambda = 0.71069$ Å). The unit cell parameters were determined by least-squares refinement of 22 and 25 carefully centred reflections for **3a** and **3b**, respectively. Data reduction and subsequent calculations were performed with TEXSAN for Windows [12]. The data was corrected for Lorenz and polarisation effects, for absorption (PSI-scans [13]) and for decay. Crystal data for compounds **3a**–**3b** along with other experimental details, are summarised in Table 1.

Table 1
Crystal data and experimental details of the structure determination of **3a** and **3b**

	3a	**3b**
Empirical formula	$C_{22}H_{30}Cl_2O_3W$	$C_{22}H_{28}Br_2Cl_2O_3W$
M_r	597.21	755.01
Crystal system	monoclinic	monoclinic
Space group (no.)	$P2_1/n$ (14)	$P2_1/c$ (14)
a (Å)	10.986(2)	12.8565(17)
b (Å)	14.9008(13)	11.508(3)
c (Å)	14.8838(13)	18.287(3)
β (°)	90.990(11)	101.629(12)
U (Å^3)	2436.1(6)	2650.0(9)
Z	4	4
μ(Mo Kα) (cm^{-1})	49.79	75.96
Observed reflections	4272	4676
Parameters	253	271
R_1	0.109 (0.042) [a]	0.087 (0.042)
wR_2	0.095 (0.081)	0.104 (0.092)

$R_1 = \Sigma \, ||F_o| - |F_c|| / \Sigma \, |F_o|$; $wR_2 = \{\Sigma \, [w(F_o^2 - F_c^2)^2] / \Sigma \, [w(F_o^2)^2]\}^{1/2}$ and $w = 1/[\sigma^2(F_o^2) + (aP)^2 + bP)]$, where $P = (2F_c^2 + F_o^2)/3$.

[a] Values in parentheses for reflections with $[I > 2.0\sigma(I)]$.



Scheme 1.

The structures were solved by direct methods using the SIR-92 program [14] and full-matrix least-squares refinements on F^2 were performed using the SHELXL-97 program [15]. For both compounds all heavy atoms were refined anisotropically. The CH hydrogen atoms were included at the fixed distances with fixed displacement parameters from their host atoms. Figures were drawn with ORTEP-3 for Windows [16].

3. Results and discussion

3.1. Preparations and spectral characterisation

Studied compounds were prepared by known halide displacement reaction of $WOCl_4$ (**1**) [2]. A suspension of tungsten precursor **1** in toluene was reacted with 2 equiv. of 2-*tert*-butyl-6-methylphenol (**2a**) or 2-*tert*-butyl-6-4-bromo-methylphenol (**2b**) at reflux temperature for 4 h to obtain intense red solutions (Scheme 1). Evaporation of solvent and HCl coproduct afforded red solids, which were extracted by hexane, concentrated and stored at −20 °C to obtain purple, prismatic crystals. Complex **3b** crystallised nicely overnight, but the crystallisation of **3a** was unexpectedly slow, and about a week is needed to attain an acceptable recovery (> 50%) of compound. Both compounds **3** are very soluble in non-coordinating solvents, e.g. hexane, toluene and dichloromethane. They are soluble also in coordinating solvents, e.g. pyridine, acetone, thf and acetonitrile, but decompose quickly to form white deposit. Even small amounts of coordinating molecules in hexane solution can destroy these complexes, hence our attempts to prepare six-coordinated adducts $WOCl_2(OAr)_2L$ failed. Crystals of **3** are stable in air for a few hours, but can be stored for weeks under an inert atmosphere.

The ^{1}H NMR spectra of compounds showed typical resonances for aromatic and aliphatic protons. In principal, the unsymmetrical phenolato ligands could adopt different rotational isomers (two *syn*- and one *anti*-isomer). However, the ^{1}H NMR spectra of compounds **3** in $CDCl_3$ at room temperature contain only individual singlet resonances for the ^{t}Bu and Me substituents on the phenoxide group. Thus, on the NMR time-scale in solution at room temperature phenoxide groups are time-averaged and yield only one signal. X-ray structure determinations verified that these asymmetric phenolato ligands adopted a *syn* conformation in the solid state (see Section 3.2). The IR spectra of compounds **3a** and **3b** show strong absorption bands at 997 and 995, respectively, which were assigned as metal–oxygen stretching modes of terminal oxo ligands [17].

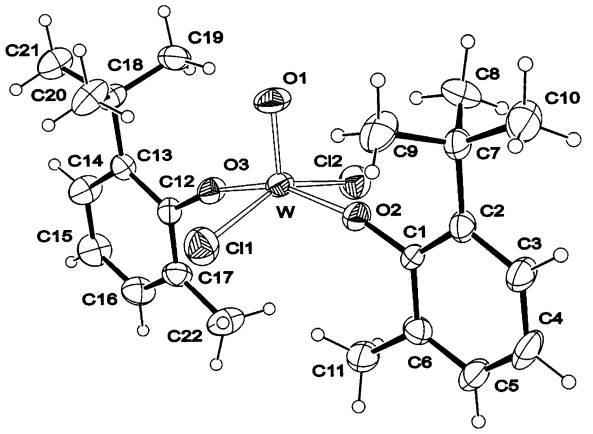


Fig. 1. Molecular structure of $[WOCl_2(OPh\text{-}2\text{-}^tBu\text{-}6\text{-}Me)_2]$ (**3a**). Thermal ellipsoids have been drawn by 30% probability.

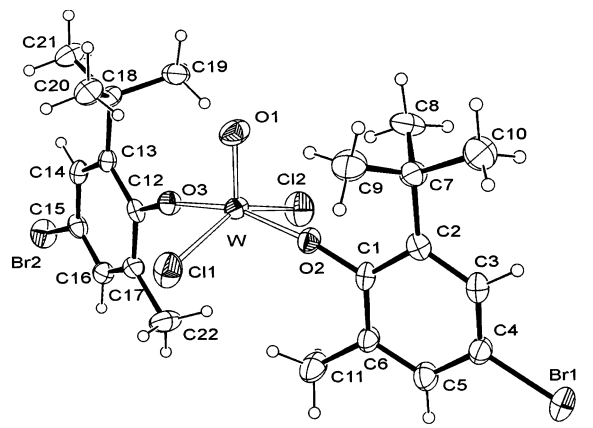


Fig. 2. Molecular structure of $[WOCl_2(OPh\text{-}2\text{-}^tBu\text{-}4\text{-}Br\text{-}6\text{-}Me)_2]$ (**3b**). Thermal ellipsoids have been drawn by 30% probability.

3.2. Structures

Nugent et al. [6] and Wagener and coworkers [7] have published some structures of oxotungsten derivatives of type $[WOCl_2(OAr)_2]$ bearing substituted 2,6-dibromophenoxide ligands. In these structures one bromine atom from phenoxide ligand has some interaction with the tungsten centre, which also makes these two phenoxide groups inequivalent. Thus the coordination sphere around W(VI) is virtually a distorted octahedron. X-ray crystallographic studies of **3** reveal that both compounds form monomeric units, in which the tungsten(VI) cation has adopted a square pyramidal coordination geometry with the oxo ligand in the apical position and phenoxide groups in a *trans* orientation, as shown in Figs. 1 and 2. In solid state, the both studied compounds have adopted similar conformation. The aryloxide ligands with *tert*-butyl and methyl groups are almost parallel in **3a** as the dihedral angle between the phenyl rings is 3.0(2)°, while in **3b** this dihedral angle is 27.4(4)°. This large difference can be related to the fact that in **3a** there is no π-stacking of the phenyl rings, but in **3b** one phenyl ring (C1, …, C6) is stacked with a phenyl ring ($C1^i$, …, $C6^i$) (symmetry code $i = 1-x, -y, 1-z$) at a distance of about 4.2 Å. Orientation of *tert*-butyl and methyl groups indicate the formation of only the *syn* isomer in both compounds. The possible reasons for the formation of this isomer are ($C^{t\text{-}}$Bu)H···O=W and (C^{Me})H···Cl hydrogen bonds, e.g. in **3a** the four shortest ($C^{t\text{-}Bu}$)H···O1 distances are from 2.760 to 2.894 Å and in **3b** from 2.592 to 2.959 Å (H atoms are in calculated positions). Relevant C···O distances vary from 3.669 to 3.778 Å in **3a** and in **3b** from 3.464 to 3.620 Å, respectively. For comparison, in organic molecules the weak C–H···O is observed if the appropriate C···O distances lie in the range of 3.00–4.00 Å [18]. The four shortest C–H···Cl distances are from 2.950 to 3.367 Å in **3a** (relevant C···Cl distances are from 3.844 to 3.952 Å) and from 2.965 to 3.286 Å in **3b** (C···Cl distances are 3.464–3.620 Å). Thus the intramolecular H-bonds seem to freeze molecules to the *syn* isomer. Consequently the structures above resemble the structure of the corresponding complex bearing two 2,6-diisopropylphenoxide ligands [5].

In the high-valent transition metal aryloxides the M–O distances are generally shorter than the values expected solely on the basis of σ-bonding. This indicates that π-bonding (electron donation from the p-orbital of oxygen to the d-orbitals of metal) is present. As a result, the relationship between the M–O bond distances and the degree of π-bonding for the terminal phenoxides has been widely discussed [19,20]. The value of the M–O–C angle can also, in theory, reflect the degree of π-donation to the metal, but it has been shown to be an extremely flexible parameter and primarily controlled by steric properties [20,21]. In the compounds studied now (see Table 2) the W–O–C angles vary from 161.6(5)° to 165.4(5)°. The relevant W–O bond lengths vary from 1.861(5) to 1.849(5) Å. However, no evident correlation between W–O distance and W–O–C angle can be seen, thus crystal-packing forces seem to have strong effects to the bending of these bonds.

4. Supplementary data

Crystallographic data (excluding structure factors) for the structures reported in this paper have been deposited with the Cambridge Crystallographic Data Centre CCDC No. 170998–170999 for compounds **3a** and **3b**, respectively. Copies of the data can be obtained free of charge on application to The Director, CCDC, 12 Union Road, Cambridge CB2 1EZ, UK (fax: +44-1223-336033; e-mail: deposit@ccdc.cam.ac.uk or www: http://www.ccdc.cam.ac.uk).

Table 2
Selected bond lengths (Å) and angles (°) for **3a** and **3b**

	3a	**3b**
Bond lengths		
W–O(1)	1.671(5)	1.661(6)
W–O(2)	1.849(5)	1.846(5)
W–O(3)	1.836(5)	1.861(5)
W–Cl(1)	2.325(3)	2.315(3)
W–Cl(2)	2.335(3)	2.321(3)
O(2)–C(1)	1.365(9)	1.364(9)
O(3)–C(12)	1.370(9)	1.366(8)
Bond angles		
O(1)–W–O(2)	101.8(3)	100.0(3)
O(1)–W–O(3)	101.3(3)	99.5(3)
O(1)–W–Cl(1)	104.1(3)	105.9(3)
O(1)–W–Cl(2)	104.2(2)	108.2(3)
O(2)–W–O(3)	156.9(2)	160.3(2)
O(2)–W–Cl(1)	87.77(19)	88.77(19)
O(2)–W–Cl(2)	87.20(19)	85.60(19)
O(3)–W–Cl(1)	87.0(2)	88.24(18)
O(3)–W–Cl(2)	86.8(2)	86.05(19)
Cl(1)–W–Cl(2)	151.70(11)	145.93(11)
C(1)–O(2)–W	165.4(5)	162.9(5)
C(12)–O(3)–W	165.1(5)	161.6(5)

References

[1] K.J. Ivin, J.C. Mol, Olefin Metathesis and Metathesis Polymerization, Academic Press, London, 1997.
[2] H. Funk, G. Mohaupt, Z. Anorg. Allg. Chem. 315 (1962) 204.
[3] D.R. Kelsey, D.L. Handlin, M. Narayna, B.M. Scardino, J. Polym. Sci. A: Polym. Chem. 35 (1997) 3027.
[4] M.W. Glenny, A.J. Nielson, C.E.F. Rickard, Polyhedron 17 (1998) 851.
[5] A. Bell, J. Mol. Catal. 76 (1992) 165.
[6] W. Nugent, J. Feldman, J.C. Calabrese, J. Am. Chem. Soc. 117 (1995) 8992.
[7] (a) F.J. Gómez, K.A. Abboud, K.B. Wagener, J. Mol. Catal. A: Chem. 133 (1998) 159;
(b) F.J. Gómez, M.S. Manak, K.A. Abboud, K.B. Wagener, J. Mol. Catal. A: Chem. 160 (2000) 145.
[8] (a) A. Lehtonen, R. Sillanpää, Inorg. Chem. Commun. 4 (2001) 108;
(b) A. Lehtonen, R. Sillanpää, Inorg. Chem. 40 (2001) 6047.
[9] R.H. Crabtree, G.G. Hlatky, Polyhedron 4 (1985) 521.
[10] G. Brunton, B.C. Gilbert, R.J. Mawby, J. Chem. Soc., Perkin Trans. 2 (1976) 1267.
[11] R.J. Errington, Advanced Practical Inorganic and Metalorganic Chemistry, Blackie Academic and Professional, London, 1997.
[12] TEXSAN for Windows, Structure Analysis Software, Molecular Structure Corporation, TX 77381, USA, 1997.
[13] A.C. North, D.C. Phillips, F.S. Mathews, Acta Crystallogr., Sect. A 24 (1968) 351.
[14] A. Altomare, G. Cascarano, C. Giacovazzo, A. Gualiardi, M.C. Burla, G. Polidori, M. Camalli, J. Appl. Crystallogr. 27 (1994) 435.
[15] G.M. Sheldrick, SHELXL-97, Program for Crystal Structure Refinement, University of Göttingen, Germany, 1997.
[16] L.J. Farrugia, J. Appl. Crystallogr. 30 (1997) 565.
[17] W.M. Nugent, J.M. Mayer, Metal–Ligand Multiple Bonds, Wiley-Interscience, New York, 1988.
[18] G.R. Desiraju, Acc. Chem. Res. 29 (1996) 441.
[19] M.H. Chisholm, I.P. Rothwell, in: G. Wilkinson, R.D. Gillard, J.A. McCleverty (Eds.), Comprehensive Coordination Chemistry, vol. 2, Pergamon, New York, 1987, pp. 335–364 Ch. 15.3.
[20] B.D. Steffey, P.E. Fanwick, I.P. Rothwell, Polyhedron 9 (1990) 963.
[21] N. Kanehisa, Y. Kai, Y. Kasai, H. Yasuda, Y. Nakayama, A. Nakamura, Bull. Chem. Soc. Jpn. 65 (1992) 1197.

PERGAMON

Polyhedron 21 (2002) 353–358

POLYHEDRON

www.elsevier.com/locate/poly

Synthesis and characterization of $K_6[Ti(H_2O)P_2MoW_{16}O_{61}]\cdot 17H_2O$, a Ti(IV) derivative of monolacunary Wells-Dawson 16-tungsto-molybdo-2-phosphate

Cristina Raţiu [a], Adrian-Raul Tomşa [a,b,*], Aglaia Koutsodimou [b], Polycarpos Falaras [b], Traian Budiu [a]

[a] *Institute of Chemistry 'Raluca Ripan', 30 Fântânele Street, RO-3400 Cluj-Napoca, Romania*
[b] *Institute of Physical Chemistry, NCSR 'Demokritos', 15310 Aghia Paraskevi Attikis, Greece*

Received 22 June 2001; accepted 31 October 2001

Abstract

Monolacunary Wells-Dawson 16-tungsto-molybdo-phosphate $[P_2MoW_{16}O_{61}]^{10-}$ reacts with $[Ti(H_2O)_6]^{4+}$ in aqueous solution to give the $[Ti(H_2O)P_2MoW_{16}O_{61}]^{6-}$ complex, isolated as the potassium salt. Optimal synthesis conditions were established by spectrophotometric and conductometric studies. The molecular formula of the complex was determined by elemental analysis, thermogravimetric analysis and basicity titration. The Ti(IV) complex was further characterized by UV, FTIR, Raman and ^{31}P NMR spectroscopies as well as cyclic voltammetry. Powder X-ray diffraction was used to obtain the lattice parameters for both ligand and complex. A modified Wells-Dawson structure for the new Ti(IV) polyoxometalate complex was inferred from the results. © 2002 Elsevier Science Ltd. All rights reserved.

Keywords: Polyoxometalates; Heteropolyanions; Ti(IV) complex; Wells-Dawson structure

1. Introduction

Polyoxometalates are a broad class of complexes of considerable interest from both theoretical and practical points of view [1]. Recently, the chemistry of Ti(IV) polyoxometalates became an attractive research field not only for fundamental reasons, due to the newly synthesized complexes [2–8], but also for the potential applications of these compounds as catalysts in oxidation reactions [9–13], or as antiviral agents [14–18].

According to the basic principles of polyoxometalate formation (ionic radius, ionic charge and availability of vacant 'd' orbitals to form π oxygen–metal bonds), Ti(IV) polyoxometalates can be classified as isopolytitanates or heteropolytitanates [19,20]. In isopolytitanates the structure consists only of TiO_6 octahedra, but in heteropolytitanates the Ti(IV) atom can act as the central heteroatom with tetrahedral geometry [21,22] or as an addendum with octahedral geometry [2,3]. In the last case, enhanced reactivity and very interesting properties are usually observed due to the presence of Ti(IV) as an addendum [11,17]. For that reason in the present study the synthesis and characterization of a new polyoxometalate complex formed by introducing one Ti(IV) atom into the monolacunary 16-tungsto-molybdo-2-phosphate polyoxoanion $[P_2MoW_{16}O_{61}]^{10-}$ is described.

2. Experimental

2.1. Physical measurements

Elemental analysis was performed upon decomposition of the complex in aq. alkaline solution at pH ~ 12. Ti(IV) was photocolorimetrically determined using H_2O_2 in the presence of H_2SO_4 [23]. A Baird I.C.P. 2070 optical emission spectrometer was used for phosphorus, tungsten and molybdenum determinations. Water content was determined thermogravimetrically

* Corresponding author. Fax: +40-64-420-441.
E-mail address: rtomsa@gmx.co.uk (A.-R. Tomşa).

0277-5387/02/$ - see front matter © 2002 Elsevier Science Ltd. All rights reserved.
PII: S0277-5387(01)00991-3

by means of a Paulik Erdely OD-102 type derivatograph, at a temperature range of 20–800 °C and a heating rate of 5 °C min^{-1}. Conductometric studies were performed with a Radelkis OK-102 type conductometer in an acetate buffer solution, pH 5.6, using Ti:P_2MoW_{16} molar ratios ranging from 0.2:1 up to 2.5:1. Conductometric titration of 10^{-3} M Ti(IV) derivative with 4.9×10^{-2} M thalium acetate established the basicity of the complex [24].

UV–Vis spectra were recorded on a Specord or a Unicam spectrophotometer. The absorbances of 1.2×10^{-5} M mixtures of Ti(IV) and $[P_2MoW_{16}O_{61}]^{10-}$ (in 1:1 molar ratio) at 33 800 and 40 800 cm^{-1} were measured in different reaction conditions. The pH of the solutions were adjusted between 4 and 7.5 using 5% KOH and 1 M HCl. IR spectra were recorded using KBr pellets on a FTIR–JASCO 610 spectrophotometer. Raman experiments were performed on solid powders at room temperature (r.t.), using a DILOR OMARS 89 Raman spectroscope equipped with a microscope, CCD detection and a 632.8 nm He–Ne laser (1–5 mW). ^{31}P (121.5 MHz) NMR spectra were recorded at r.t. on a Bruker AC-300 MHz spectrometer, using saturated solutions. Chemical shifts were referenced to 85% H_3PO_4. The main parameters used were: 32 K data domain size, 62 500 Hz spectral width, 2 s relaxation delay and 100 scans. X-ray diffraction (XRD) experiments were performed on a Philips Analytical X-ray PW 1050 Diffractometer using Cu Kα radiation.

Cyclic voltammetry measurements were made using a Vinci Technologies P/G STAT Z1 potentiostat, operating in conjunction with a 33120 A Hewlett Packard function/arbitrary waveform generator and with a Linseis LY 18100 X-Y recorder. A conventional (single-compartment) three electrode electrochemical cell was used, with a Metrohm planar platinum counter electrode and a Metrohm saturated calomel ($Hg–Hg_2Cl_2$) reference electrode (SCE). Pyrolytic graphite (Union Carbide, $\Phi \sim 3$ mm) was used as a working electrode (WE), which was polished with emery paper 4000 and cleaned in ultrasons prior to use. The WE was polarized in a 10^{-3} M solution of the complex in acetate buffer (pH 4.0–5.6) with a scan rate between 10 and 200 mV s^{-1}. The experiments were performed in deoxygenated solutions by passing purified Ar gas (99.9%) through the solutions. During the experiment the Ar was passed over the solution surface.

2.2. Materials

All chemicals were commercially available, of reagent grade quality and used as received. In all syntheses and studies distilled water was used. $K_{10}[P_2MoW_{16}O_{61}]\cdot 21H_2O$ was prepared according to the literature [25].

2.2.1. Preparation of $K_{10}[P_2MoW_{16}O_{61}]\cdot 21H_2O$

$K_6[P_2MoW_{17}O_{62}]\cdot 14H_2O$ (40 g, 8.4 mmol), prepared as described by Contant and Ciabrini [26], was dissolved in 142 ml of water and treated with 124 ml 1 M $KHCO_3$. When the solution became blue in color, the precipitate was filtered, washed with cold 1 M KCl, followed by MeOH and then air dried. The yield was 33 g (86%).

IR (cm^{-1}, KBr pellets, polyoxometalate region): 1083, 1049, 1018, 939, 916, 886, 805, 730, 600, 566, 525. Raman (cm^{-1}): 1016, 974, 964, 953, 939, 890, 586, 541, 520, 368, 332, 264, 229, 163, 126. ^{31}P NMR (D_2O) δ −6.12 (s), −13.28 (s).

2.2.2. Preparation of $K_6[Ti(H_2O)P_2MoW_{16}O_{61}]\cdot 17H_2O$

$TiCl_4$ (15.24 ml, 0.139 mol) was added dropwise to a solution of 0.1 M HCl (100 ml) under vigorous stirring while keeping cool at 5 °C (solution A). $K_{10}[P_2MoW_{16}O_{61}]\cdot 21H_2O$ (18 g, 3.71 mmol) was dissolved in 100 ml water and heated to 65–75 °C (solution B). Solution A (2.66 ml) was then added dropwise under vigorous stirring. A KOH solution (5%) was used to maintain the pH between 4 and 6. After addition of $[Ti(H_2O)_6]^{4+}$, the reaction mixture was kept at 65–75 °C for 20 min and then brought to boiling. The slight turbid solution was filtered while hot. After several days at r.t., white crystals were obtained from the filtrate which were further purified by recrystallization from distilled water. The yield was 3.48 g (20%).

Anal. Calc. for $K_6[Ti(H_2O)P_2MoW_{16}O_{61}]\cdot 17H_2O$: P, 1.32; Ti, 1.02; Mo, 2.04; W, 62.82; H_2O, 6.86. Found: P, 1.32; Ti, 1.05; Mo, 1.92; W, 62.45; H_2O, 6.99% (TGA). IR (cm^{-1}, KBr pellets, polyoxometalate region): 1086, 1015, 949, 917, 778, 598, 566, 527. Raman (cm^{-1}): 1021, 982, 967, 925, 901, 855, 784, 666, 539, 495, 463, 419, 378, 325, 305, 231, 205, 160, 121. ^{31}P NMR (D_2O) δ −9.26 (s), −12.87 (s).

3. Results and discussion

Conductometric titration of the ligand $[P_2MoW_{16}O_{61}]^{10-}$ with $[Ti(H_2O)_6]^{4+}$ was performed in order to establish the complex composition in solution. The titration curve presents a clear break point at 1 equiv. of Ti(IV) per equivalent of the ligand. Then the best synthesis conditions were spectrophotometrically determined by successively varying the reaction parameters (pH, temperature). The solution pH was adjusted between 4 and 7.5 and the absorbances of Ti(IV) and $[P_2MoW_{16}O_{61}]^{10-}$ mixtures (stoichiometric ratios of 1:1) at 33 800 and 40 800 cm^{-1} were measured under different reaction conditions. The optimum pH range for the complex formation was between 4 and 6 and the maximum absorption was observed for samples brought up to boiling.

The study of the polyoxometalate complex thermal behavior depicts four main processes, two endothermal and two exothermal, (see Supporting Information). In the DTA curve, the endothermal processes at 120 and 205 °C were assigned to water loss. The second process was faster than the first, as shown by the DTG curve. The first exothermal process, with a maximum at 590 °C on the DTA curve, was assigned to decomposition of the polyoxometalate while the second, with a maximum at 620 °C, may be assigned to the polymorph transformations of the oxides that resulted from the decomposition of polyoxometalate [27]. Based on the thermogravimetric study, it can be concluded that the polyoxometalate is thermally stable up to 500 °C and has a water content of 6.99%.

The elemental analysis found (P, 1.32; Ti, 1.05; Mo, 1.92; W, 62.45) is in excellent agreement with the calculated composition of the complex (P, 1.32; Ti, 1.02; Mo, 2.04; W, 62.82). Moreover, the basicity determination performed by thalium acetate titration, resulted in a 6^- charge for the polyoxometalate species in solution. Thus, taking into account the formation studies, elemental analyses, basicity determination and thermal behavior of the synthesized compound, the following reaction sequence is suggested:

$$[P_2MoW_{16}O_{61}]^{10-} + [Ti(H_2O)_6]^{4+} \rightarrow [Ti(H_2O)P_2MoW_{16}O_{61}]^{6-} + 5H_2O \quad (1)$$

The UV electronic spectra of the $K_6[Ti(H_2O)P_2MoW_{16}O_{61}]$ complex and the $K_{10}[P_2MoW_{16}O_{61}]$ ligand are similar in shape and number of bands (see Section 5: Supporting Information). The band at ~ 200 nm is assigned to $p_\pi - d_\pi$ transitions in $M-O_t$ bonds. The two shoulders at ~ 250 and ~ 290 nm are assigned to the electron transitions between the energy levels of $M-O_b-M$ (M = W, Mo) tricentric bonds [28]. In the spectrum of the complex, both bands are red shifted when compared to the corresponding bands of the monolacunary polyoxometalate, but the energy levels are higher than in the isocharge $K_6[P_2MoW_{17}O_{62}]$ polyoxometalate. This is due to distorsions introduced by the weaker Ti(IV) ion onto its neighbouring MO_6 octahedra (M = W, Mo).

It is important to notice that the IR spectrum of the $K_6[Ti(H_2O)P_2MoW_{16}O_{61}]$ polyoxometalate complex shows a frequency shift of the stretching vibrations towards higher wavelengths compared to that of the ligand. This is consistent with an increase of the anion cohesion by coordination of the Ti(IV) in the polyoxometalate framework [29]. Moreover, owing to the structural modifications, the band patterns of the bridge regions (950–700 cm^{-1}) are considerably changed. In the 1100–1000 cm^{-1} range, where the asymmetric stretch vibration of the P–O bond appears, a band splitting is seen, similar to the splitting normally observed in α-Dawson structures [30]. This is characteristic of lower symmetry for modified or lacunary polyoxometalate structures. The value of the band splitting can be considered as a measure of the deviation from the saturated structure symmetry [29]. The ν_{as}P–O (asymmetric stretching) band splitting of the ligand is diminished upon Ti(IV) coordination, implying an increase of the PO_4 tetrahedron symmetry as a result of vacancy completion. In the range 1000–700 cm^{-1} three other characteristic bands were observed and assigned to the asymmetric stretching vibrations of the bridges ($M-O_b-M$) and the terminal bonds ($M-O_t$) [29,30]. The bands appearing in the 600–500 cm^{-1} region assigned to the deformations δ P–O and stretching vibrations of the internal bonds ($M-O_i-M$) are not significantly influenced by the coordination of Ti(IV) (Figs. 1 and 2).

In a similar way, in the Raman investigation the main vibrations of the polyoxometalate complex are shifted towards higher energies suggesting an increase of the polyoxometalate stability [31]. The Raman spectrum of $K_6[Ti(H_2O)P_2MoW_{16}O_{61}]$ shows characteristic strong vibration bands at 982, 967 and 231 cm^{-1}, assigned to $\nu_s(M-O_t)$, $\nu_{as}(M-O_t)$ and $\nu_s(M-O_i)$, respectively. O_i represents the bridging oxygen between the

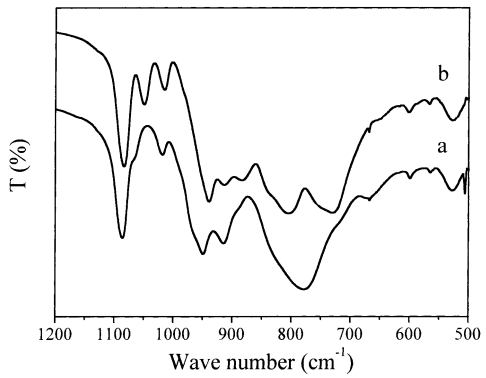


Fig. 1. FTIR spectra of $K_6[Ti(H_2O)P_2MoW_{16}O_{61}]$ complex (a) and $K_{10}[P_2MoW_{16}O_{61}]$ ligand (b).

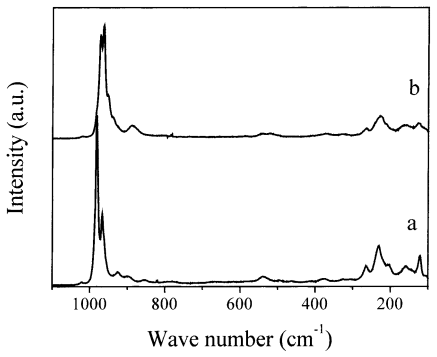


Fig. 2. Raman spectra of $K_6[Ti(H_2O)P_2MoW_{16}O_{61}]$ complex (a) and $K_{10}[P_2MoW_{16}O_{61}]$ ligand (b).

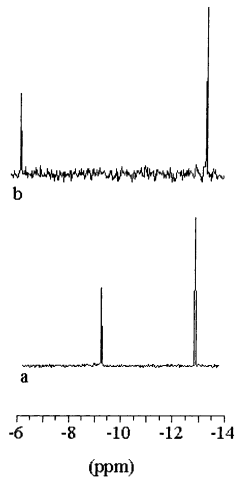


Fig. 3. ^{31}P NMR spectrum of $K_6[Ti(H_2O)P_2MoW_{16}O_{61}]$ complex (a) and $K_{10}[P_2MoW_{16}O_{61}]$ ligand (b) recorded in D_2O.

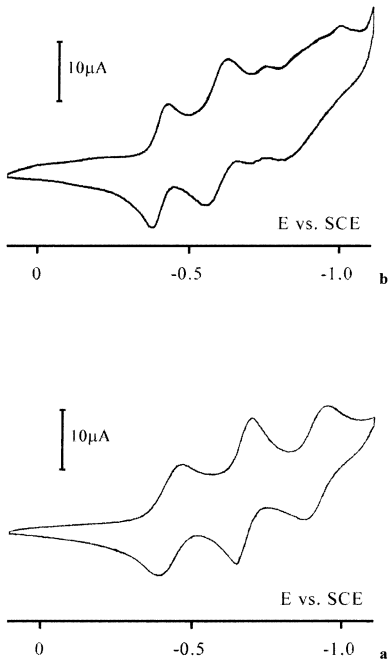


Fig. 4. Cyclic voltammograms of $K_6[Ti(H_2O)P_2MoW_{16}O_{61}]$ complex (a) and $K_{10}[P_2MoW_{16}O_{61}]$ ligand (b) recorded in acetate buffer solutions (pH 5.2), sweep rate 20 mV s^{-1}.

internal P heteroatom and external addenda (Mo, W or Ti). Other weak Raman lines appearing at 1021, 950, 924, 901 and 855 cm^{-1} can be assigned to $\nu_s(P–O_i)$, $\nu_{as}(P–O_i)$ and $\nu_{as}(M–O_b)$ [31].

The ^{31}P NMR spectrum in D_2O solution of $K_6[Ti(H_2O)P_2MoW_{16}O_{61}]$ consists of two sharp singlets at P(1) δ −9.26 and P(2) δ −12.87 indicative of two inequivalent phosphorus centers (Fig. 3). P(1) is the phosphorus atom closest to the substitution site while P(2) is further away. These resonances are different from the lacunary $K_{10}[P_2MoW_{16}O_{61}]$ (P(1) δ −6.12 and P(2) δ −13.28) and are close to $K_6[\alpha_2$-$P_2MoW_{17}O_{62}]$ species (P(1) δ −11.9 and P(2) δ −12.6) [32], suggesting the presence of Ti(IV) in a polar site.

To establish the electrochemical behavior of $K_{10}[P_2MoW_{16}O_{61}]$ and of the $K_6[Ti(H_2O)P_2MoW_{16}O_{61}]$ derivative, cyclic voltammogram experiments were performed in aqueous solutions and the results are reported on Fig. 4.

Three well defined oxidation–reduction pairs of waves were obtained for the Ti(IV) complex. A linear dependence between the peak current logarithm ($\log I_{pc}$) and the sweep rate logarithm ($\log v$) confirmed the reversibility of the three electron transfer processes (see Supporting Information). Such a behavior is not unusual. In fact, previous studies on a V(IV) complex with $K_{10}[P_2MoW_{16}O_{61}]$ [33], showed that the polyoxometalate anion in the negative potential range presented only three peaks instead of the four observed in the ligand. On the other hand, from literature data [34,35], the presence of both molybdenum and tungsten cations in the same polyoxometalate structure, first leads to electrochemical reduction of molybdenum (Mo^{VI}) and then to that of tungsten (W^{VI}). As a result, in the case of the $K_6[Ti(H_2O)P_2MoW_{16}O_{61}]$ complex, the first wave at $\sim$0.4 V was assigned to the Mo^{VI}–Mo^{V} redox reaction, while the other two waves were attributed to the W^{VI}–W^{V} redox processes. The formal potential $\varepsilon^{0\prime}$ (estimated as the average value of anodic and cathodic peak potentials) showed a negative shift with increasing values of pH (see Supporting Information). For all three peaks, the $\varepsilon^{0\prime}$ versus pH dependences are linear, with slopes of 38.70, 62.66 and 52.41 mV/ΔpH. The anodic to cathodic peak separation values (ΔE) and the described pH dependence are probably consistent with the fact that both a single electron and one proton are involved in parallel in each redox reaction [36].

Attempts to obtain single crystals of the complex were unsuccessful. However, powder XRD was used to obtain the lattice parameters for both the monolacunary $K_{10}[P_2MoW_{16}O_{61}]$ ligand and the Ti(IV) derivative (see Supporting Information). The lattice constants obtained ($K_{10}[P_2MoW_{16}O_{61}]$: $a = 14.25$, $b = 14.70$, $c = 18.76$ Å, $\alpha = \beta = 90$, $\gamma = 104°$, $Z = 2$; $K_6[Ti(H_2O)P_2MoW_{16}O_{61}]$: $a = 14.12$, $b = 14.744$, $c = 18.44$ Å, $\alpha = \beta = 90°$, $\gamma = 103.75°$, $Z = 2$), were characteristic of a monoclinic structural modification for both the ligand and the Ti(IV) complex.

4. Conclusion

A $K_6[Ti(H_2O)P_2MoW_{16}O_{61}]\cdot 17H_2O$ complex was prepared by reaction of $[Ti(H_2O)_6]^{4+}$ with $K_{10}[P_2MoW_{16}O_{61}]\cdot 21H_2O$ monolacunary polyoxometalate after establishing optimal synthesis conditions. Spectroscopic studies show that the structure of the

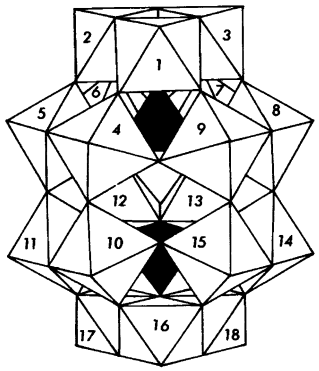


Fig. 5. The structure of the $K_6[Ti(H_2O)P_2MoW_{16}O_{61}]\cdot 17H_2O$ polyoxometalate (white octahedra represent MO_6 site. Black tetrahedra represent PO_4 sites).

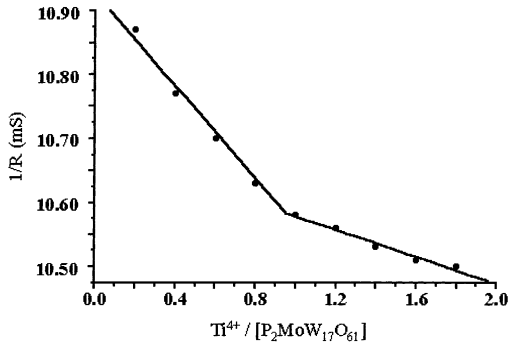
ligand is stabilized upon addition of the Ti(IV) atom. Cyclic voltammetry experiments clearly showed three single electron reversible reduction processes instead of four as obtained for the ligand. The complex belongs to the monoclinic system and adopts a modified Wells-Dawson structure as found by ^{31}P NMR and XRD data (Fig. 5), in which the Ti atom occupies a polar position (1, 2, 3, 16, 17 or 18) and the Mo atom is located on a belt site (4) [25].

5. Supporting information

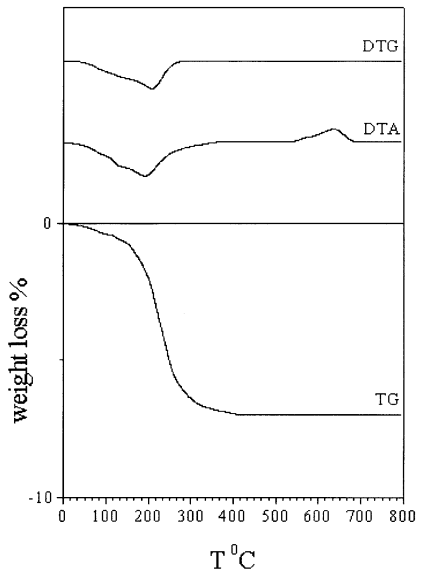
Schemes SI1–6.

Acknowledgements

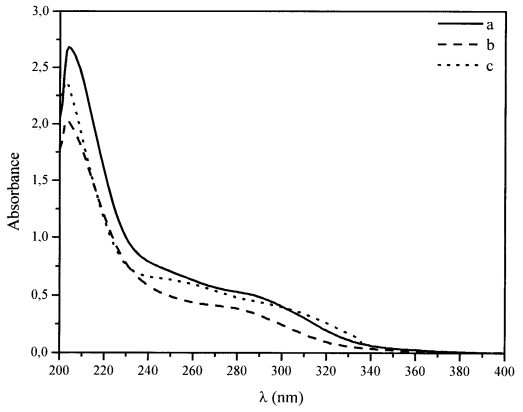
This work was partially founded by a Greek–Romanian bilateral cooperation project and A.R.T. is greatful to the GSRT (Greece) and NASTI (Romania) for financial support. The authors would like to thank Dr Marie-Claude Bernard (Université Pierre et Marie Curie, Paris) for recording the Raman spectra.



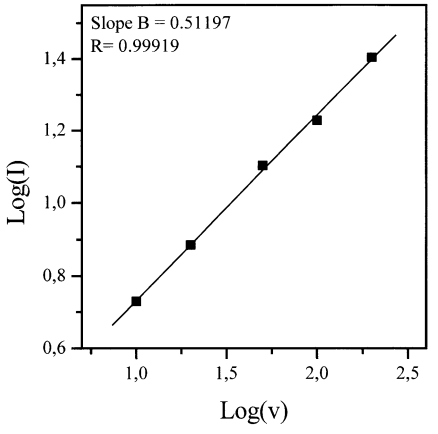
Scheme SI1. Plot of conductivity vs Tri:$K_{10}[P_2MoW_{16}O_{61}]$ molar ratio.



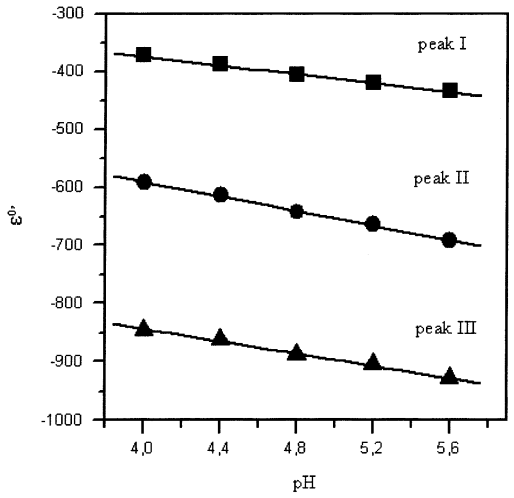
Scheme SI2. TG, DTA and DTG curves obtained for the $K_6[Ti(H_2O)P_2MoW_{16}O_{61}]$ complex.



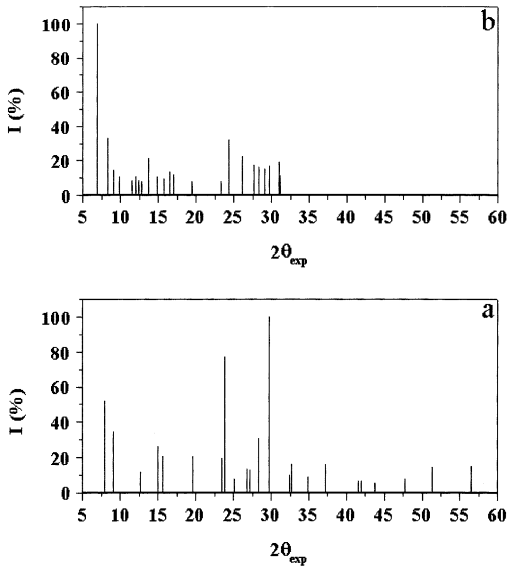
Scheme SI3. Electronic spectra of $K_6[Ti(H_2O)P_2MoW_{16}O_{61}]$ (a), $K_{10}[P_2MoW_{16}O_{61}]$ (b) and $K_6[P_2MoW_{17}O_{62}]$ (c) recorded in aqueous 10^{-5} M solutions.



Scheme SI4. Dependence of the peak current logarithm on the potential sweep rate logarithm for $K_6[Ti(H_2O)P_2MoW_{16}O_{61}]$ complex at pH = 4.0.



Scheme SI5. Dependence of the formal potential, $\varepsilon^{0\prime}$, on the pH (sweep rate 20 mV/s) for the $K_6[Ti(H_2O)P_2MoW_{16}O_{61}]$ complex.



Scheme SI6. Bare X-ray spectra of $K_6[Ti(H_2O)P_2MoW_{16}O_{61}]$ complex (a) and $K_{10}[P_2MoW_{16}O_{61}]$ ligand (b).

References

[1] C.L. Hill, Chem. Rev. 98 (1998) 1.
[2] W.H. Knoth, P.J. Domaille, D.C. Roe, Inorg. Chem. 22 (1983) 198.
[3] P.J. Domaille, W.H. Knoth, Inorg. Chem. 22 (1983) 818.
[4] M.T. Che, V.W. Day, L.C. Francesconi, M.F. Fredrich, W.G. Klemperer, W. Shum, Inorg. Chem. 24 (1985) 4055.
[5] W.H. Knoth, P.J. Domaille, R.D. Farlee, Organometallics 4 (1985) 62.
[6] M.T. Che, V.W. Day, L.C. Francesconi, W.G. Klemperer, D.J. Main, A. Yagasaki, O.M. Yaghi, Inorg. Chem. 31 (1992) 2920.
[7] Y. Lin, J.R. Weakley, B. Rapko, R.G. Finke, Inorg. Chem. 32 (1993) 5095.
[8] L.Y. Qu, Q.J. Shan, J. Gong, R.Q. Lu, D.R. Wang, J. Chem. Soc., Dalton Trans. (1997) 4525.
[9] T. Yamase, J. Chem. Soc., Dalton Trans. (1991) 3055.
[10] R.C. Chambers, C.L. Hill, Inorg. Chem. 30 (1991) 2776.
[11] O.A. Kholdeeva, G.M. Maksimov, R.I. Maksimovskaya, L.A. Kovaleva, M.A. Fedotov, V.A. Grigoriev, C.L. Hill, Inorg. Chem. 39 (2000) 3828.
[12] M.A. Chamblor, A. Corma, A. Martinez, J. Perez-Pariente, J. Chem. Soc., Chem. Commun. (1992) 589.
[13] J.S. Reddy, U.R. Khire, P. Ratnasamy, R.B. Mitra, J. Chem. Soc., Chem. Commun. (1992) 1234.
[14] N. Yamamoto, D. Schols, E. De Clercq, Z. Debyser, R. Pauwels, J. Balzarini, H. Nakashima, M. Baba, M. Hosoya, R. Snoeck, J. Neyts, G. Andrei, B.A. Murrer, B. Theobald, G. Bossard, G. Henson, M. Abrams, D. Picker, Mol. Pharmacol. 42 (1992) 1109.
[15] Y. Inouye, Y. Tokutake, J. Kunihara, T. Yoshida, T. Yamase, A. Nakata, S. Nakamura, Chem. Pharm. Bull. 40 (1992) 805.
[16] D.L. Barnard, C.L. Hill, T. Gage, J.E. Matheson, J.H. Huffman, R.W. Sidwell, M.I. Otto, R.F. Schinazi, Antiviral Res. 34 (1997) 27.
[17] J.W. Blasecki, Top. Mol. Org. Eng. 10 (1994) 373.
[18] S.X. Liu, B.T. Li, L. Wang, Y.Y. Liu, E.B. Wang, Chin. Chem. Lett. 7 (1996) 777.
[19] R. Schmid, A. Mosset, J. Galy, J. Chem. Soc., Dalton Trans. (1991) 1999.
[20] V.W. Day, T.A. Eberspacher, W.G. Klemperer, C.W. Park, F.S. Rosenberg, J. Am. Chem. Soc. 113 (1991) 8190.
[21] R. Văţulescu, T. Budiu, G. Marcu, Rev. Roum. Chim. 26 (1981) 851.
[22] R. Văţulescu, T. Budiu, G. Marcu, Rev. Roum. Chim. 26 (1981) 971.
[23] E.B. Sandell, Colorimetric Determination of Traces of Metals, third ed., Interscience Publ., Inc. New York, Interscience Publ., Ltd. London, 1959, pp. 870.
[24] G. Marcu, L. Ghizdavu, Rev. Roum. Chim. 21 (1976) 589.
[25] R. Contant, J.P. Ciabrini, J. Inorg. Nucl. Chem. 43 (1981) 1525.
[26] R. Contant, J.P. Ciabrini, J. Chem. Res. (M) (1977) 2601.
[27] E.A. Nikitina, N.A. Tsvetov, Zh. Neorgan. Khim. 7 (1962) 325.
[28] H. So, M.T. Pope, Inorg. Chem. 11 (1972) 1441.
[29] C. Rocchiccioli-Deltcheff, R. Thouvenot, Spectrochim. Acta 32A (1976) 587.
[30] C. Rocchiccioli-Deltcheff, R. Thouvenot, Spectrosc. Lett. 12 (1979) 127.
[31] C. Rocchiccioli-Deltcheff, R. Thouvenot, J. Chem. Res. Part S (Synop) (1977) 46.
[32] R. Massart, R. Contant, J.M. Fruchart, J.P. Ciabrini, Inorg. Chem. 16 (1977) 2916.
[33] L. David, C. Craciun, C.M. Rusu, O. Cozar, O.P. Ilea, D. Rusu, Polyhedron 19 (2000) 1917.
[34] M. Otake, Y. Komiyama, T. Otaki, J. Phys. Chem. 77 (1973) 2896.
[35] J.B. Tommasino, R. Contant, J.P. Michaut, J. Roncin, Polyhedron 17 (1998) 357.
[36] C. Rong, F.C. Anson, Inorg. Chem. 33 (1994) 1064.

PERGAMON

Polyhedron 21 (2002) 359–364

POLYHEDRON

www.elsevier.com/locate/poly

Synthesis of and magnetic interactions in binuclear Cu(II)–M(II) (M = Cu, Ni and Mn) complexes of macrocyclic oxamido ligands

En-Qing Gao [a,*], Hai-Ying Sun [a], Dai-Zheng Liao [b], Zong-Hui Jiang [b], Shi-Ping Yan [b]

[a] *Department of Chemistry, Qufu Normal University, Qufu, Shandong 273165, China*
[b] *Department of Chemistry, Nankai University, Tianjin 300071, China*

Received 16 July 2001; accepted 31 October 2001

Abstract

Six oxamido-bridged binuclear Cu(II)–M(II) (M = Cu, Ni and Mn) complexes containing macrocyclic oxamido ligands have been synthesized and characterized by IR, ESR and electronic spectra. They are of the formula $[Cu(L^2)M(L)_n](ClO_4)_2$, where H_2L^2 = 2,3-dioxo-5,6:13,14-dibenzo-7,12-bis(ethoxycarbonyl)-1,4,8,11-tetraazacyclotetradeca-7,11-diene, L = 2,2′-bipyridine and 1,10-phenanthroline (phen), $n = 1$ for M = Cu and $n = 2$ for M = Ni and Mn. The magnetic properties of the complexes with L = phen have been investigated and quantitatively interpreted using the Hamiltonian $\hat{H} = -2J\hat{S}_1 \cdot \hat{S}_2$, suggesting antiferromagnetic interactions through the oxamido bridge with $J = -210.2$, -53.9 and -14.1 cm^{-1} for the Cu_2, CuNi and CuMn complexes, respectively. Finally, the magnitudes of the Cu(II)–M(II) interactions with M = Cu, Ni and Mn have been compared and qualitatively justified. © 2002 Published by Elsevier Science Ltd.

Keywords: Macrocyclic compound; Binuclear complexes; Magnetic properties

1. Introduction

The design and magnetism of polynuclear complexes are of interest for designing new magnetic materials and for investigating the structure and the role of the polymetallic active sites in biological systems [1,2]. One of the best strategies to design polynuclear species is the 'complex as ligand' approach [3,4]. This approach has been widely employed to prepare oxamido-bridged bi- and polynuclear complexes, by using mononuclear *N*,*N*′-disubstituted oxamidocopper(II) complexes as ligands [5–13]. Recently, we have synthesized several copper(II) complexes of macrocyclic oxamides (Fig. 1, $[Cu(L^i)]$, $i = 1–4$) [14,15]. The mononuclear complexes contain unbridged oxamido groups so that they are potential bidentate chelating 'ligands'. Non-cyclic oxamides may adopt a *cis* or *trans* conformation on coordination, and this flexibility allows less control over the type of the complex formed [6–8], while the exclusive *cis* conformation of the macrocyclic oxamides allows us to synthesize polynuclear systems in a more controlled fashion. Along this line, we have reported some heterotetranuclear species of $[(CuL^i)_3M]$ type [M = Mn(II), Fe(III), Ni(II)] [15–17] and heterobinuclear species of $[(CuL^i)Ni(N_4)]$ type (N_4 = tetradentate terminal ligands [18] or a tridentate ligand plus NCS^- [19]). Robertson and co-workers have reported a trinuclear complex of $[(CuL^5)_2Cu]$ type (see also Fig. 1 for $[Cu(L^5)]$) [20].

As an extension of the investigation, here we report the synthesis, characterization and magnetism of new binuclear Cu(II)–M(II) (M = Cu, Ni and Mn) complexes derived from $[Cu(L^2)]$. They are of formulas $[Cu(L^2)Cu(L)](ClO_4)_2$ [L = 1,10-phenanthroline (phen)

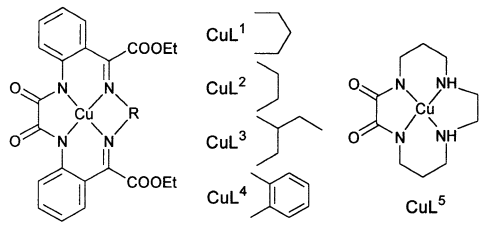


Fig. 1. Some mononuclear macrocyclic oxamido–copper(II) complexes.

* Corresponding author. Tel.: +86-537-445-5961.
E-mail address: eqgao@263.net (E.-Q. Gao).

0277-5387/02/$ - see front matter © 2002 Published by Elsevier Science Ltd.
PII: S0277-5387(01)01002-6

(**1**) and 2,2′-bipyridine (bpy) (**2**)] and $[Cu(L^2)M(L)_2](ClO_4)_2$ [M = Ni, L = phen (**3**) and bpy (**4**); M = Mn, L = phen (**5**) and bpy (**6**).

2. Experimental

2.1. Materials and syntheses

All chemicals were of A. R. grade and used as received. The mononuclear precursor, $[Cu(L^2)]$, was prepared as described elsewhere [15]. All attempts to grow single crystals of the binuclear complexes were unfortunately unsuccessful.

2.1.1. Caution

Although we have not encountered any problems, it should be kept in mind that perchlorate salts of metal complexes are potentially explosive and should be handled with care.

2.1.2. $[Cu(L^2)Cu(phen)](ClO_4)_2$ (*1*)

A solution of $Cu(ClO_4)_2 \cdot 6H_2O$ (0.3 mmol) in EtOH (6 ml) was added to a suspension of $[Cu(L^2)]$ (0.3 mmol) in EtOH (8 ml). The mixture was stirred for 10 min until it became a brownish red solution and then a solution of 1,10-phenanthroline (0.3 mmol) in the same solvent (6 ml) was added. The mixture was stirred at room temperature (r.t.) for 4 h and the resulting brownish yellow precipitate was filtered off, washed successively with EtOH and Et_2O, and then dried in vacuo over P_2O_5. Yield: 75%. *Anal.* Found: C, 44.4; H, 3.3; N, 8.5. Calc. for $C_{36}H_{30}Cl_2Cu_2N_6O_{14}$: C, 44.6; H, 3.1; N, 8.7%. IR (KBr, cm^{-1}): 1720s, 1620sh, 1593s, 1570s, 1550s, 1512w, 1478w, 1440sh, 1425m, 1345m, 1324m, 1270m, 1205s, 1172w, 1140sh, 1100s, 1075sh, 1035s, 1015sh, 915m, 848m, 770w, 750m, 720m. Molar conductance (MeCN, Ω^{-1} cm^2 mol^{-1}): 225.

2.1.3. $[Cu(L^2)Cu(bpy)](ClO_4)_2$ (*2*)

The complex was synthesized by a similar procedure, using 2,2′-bipyridine instead of 1,10-phenanthroline. Yellow powder. Yield: 83%. *Anal.* Found: C, 43.5; H, 3.0; N, 9.1. Calc. for $C_{34}H_{30}Cl_2Cu_2N_6O_{14}$: C, 43.2; H, 3.2; N, 8.9%. IR (KBr, cm^{-1}): 1735s, 1620sh, 1600s, 1570s, 1553s, 1475m, 1440s, 1350m, 1320m, 1270m, 1200s, 1170w, 1140sh, 1080s (br), 1035sh, 1010sh, 913w, 845w, 760m, 740sh, 725w. Molar conductance (MeCN, Ω^{-1} cm^2 mol^{-1}): 254.

2.1.4. $[Cu(L^2)Ni(phen)_2](ClO_4)_2$ (*3*)

This complex was synthesized by the following procedure: a solution of $Ni(ClO_4)_2 \cdot 6H_2O$ (0.2 mmol) in EtOH (5 ml) was added to a suspension of $[Cu(L^2)]$ (0.2 mmol) in EtOH (5 ml). The mixture was stirred for 10 min until it became a brownish red solution and then a solution of 1,10-phenanthroline (0.4 mmol) in the same solvent (5 ml) was added. The mixture was stirred at r.t. for 4 h and the resulting yellow brown precipitate was filtered off, washed successively with EtOH and Et_2O, and then dried in vacuo over P_2O_5. Yield: 81%. *Anal.* Found: C, 50.0; H, 3.4; Cu, 6.0; N, 10.0; Ni, 5.3. Calc. for $C_{48}H_{38}Cl_2CuN_8NiO_{14}$: C, 50.4; H, 3.4; Cu, 5.6; N, 9.8; Ni, 5.1%. IR (KBr, cm^{-1}): 1728s, 1625s, 1598s, 1575s, 1550s, 1515m, 1480m, 1440m, 1425s, 1345s, 1326m, 1272m, 1202s, 1170w, 1142m, 1080s (br), 1040sh, 1015w, 920w, 845m, 770w, 748m, 725s. Molar conductance (MeCN, Ω^{-1} cm^2 mol^{-1}): 228.

The other complexes were synthesized from $[Cu(L^2)]$, the appropriate hydrated metal perchlorate and terminal bidentate ligands by procedures similar to that for **3**.

2.1.5. $[Cu(L^2)Ni(bpy)_2](ClO_4)_2$ (*4*)

Brownish yellow powder. Yield: 78%. *Anal.* Found: C, 48.6; H, 3.5; Cu, 5.6; N, 10.3; Ni, 5.7. Calc. for $C_{44}H_{38}Cl_2CuN_8NiO_{14}$: C, 48.2; H, 3.5; Cu, 5.8; N, 10.2; Ni, 5.4%. IR (KBr, cm^{-1}): 1725s, 1625s, 1595s, 1572s, 1550s, 1478m, 1440s, 1345s, 1324m, 1270m, 1202s, 1170w, 1075s (br), 1040sh, 1005m, 920w, 863w, 808w, 760s, 745m, 730w. Molar conductance (MeCN, Ω^{-1} cm^2 mol^{-1}): 234.

2.1.6. $[Cu(L^2)Mn(phen)_2](ClO_4)_2$ (*5*)

Brownish yellow powder. Yield: 68%. *Anal.* Found: C, 50.2; H, 3.3; N, 10.1. Calc. for $C_{48}H_{38}Cl_2CuMnN_8O_{14}$: C, 50.6; H, 3.4; N, 9.8%. IR (KBr, cm^{-1}): 1735s, 1620sh, 1600s, 1575s, 1550m 1515m, 1475w, 1440m, 1425m, 1347m, 1326sh, 1265w, 1205s, 1170w, 1140w, 1080s (br), 1040sh, 1010w, 920w, 845m, 770w, 748m, 726m. Molar conductance (MeCN, Ω^{-1} cm^2 mol^{-1}): 249.

2.1.7. $[Cu(L^2)Mn(bpy)_2](ClO_4)_2$ (*6*)

Brownish orange powder. Yield: 74%. *Anal.* Found: C, 48.3; H, 3.4; N, 10.4. Calc. for $C_{44}H_{38}Cl_2CuMnN_8O_{14}$: C, 48.4; H, 3.5; N, 10.3%. IR (KBr, cm^{-1}): 1734s, 1624s, 1595s, 1570s, 1548s, 1474m, 1436s, 1340s, 1265m, 1200s, 1168m, 1135w, 1075s (br), 1040sh, 1010m, 920m, 855w, 810w, 765m, 745m, 730w. Molar conductance (MeCN, Ω^{-1} cm^2 mol^{-1}): 220.

2.1.8. Physical measurements

Elemental analysis (C, H, N) were performed on a Perkin–Elmer 240 analyzer. Conductivities of the complexes in MeCN were measured using a DDS-11A conductometer. IR spectra were recorded on a Shimadzu IR-408 spectrometer as KBr pellets, electronic spectra on Shimadzu UV-240 and Hitachi UV-330 recording spectrophotometers in MeCN, and solid-state X-band ESR spectra on a Bruker ER 200 D-SRC ESR spectrometer. Variable-temperature magnetic suscepti-

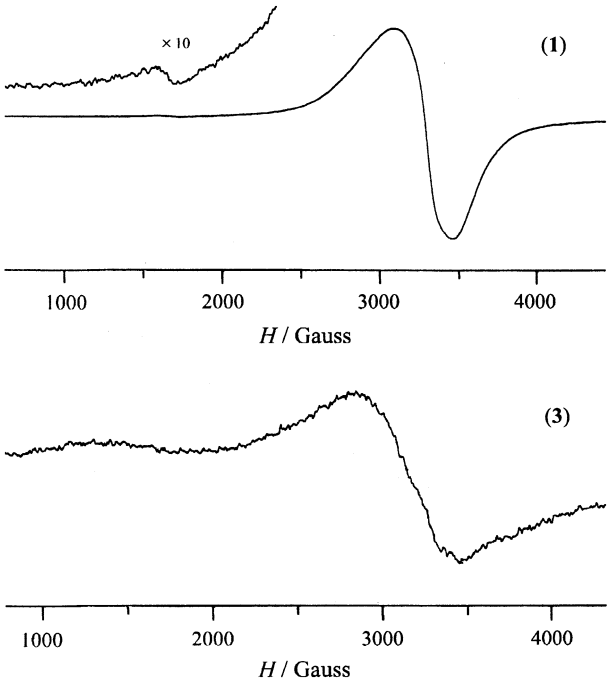


Fig. 2. Polycrystalline X-band ESR spectra of complexes **1** and **3** at room temperature.

bilities were measured on a Quantum Design MPMS-7 SQUID magnetometer. Diamagnetic corrections were made with Pascal's constants for all the constituent atoms [21].

3. Results and discussion

Elemental analysis confirmed that the complexes are of formula $[Cu(L^2)M(L)_n](ClO_4)_2$ ($n = 1$ for M = Cu; $n = 2$ for M = Ni and Mn). Their molar conductance values fall within the range expected for 1:2 electrolytes [22], indicating that the perchlorate ion is non-coordinated in acetonitrile solutions.

3.1. IR spectra

The IR spectra of the six complexes are quite similar. It would be informative to compare the spectra of the present binuclear complexes with those of the mononuclear $[Cu(L^2)]$ precursors [15] and the tetranuclear $[(CuL^2)_3M](ClO_4)_2$ (M = Ni, Mn) complexes [15,17]. The bands attributable to the ν(C=O) (ester carbonyl) and ν(C=N) vibrations appear at approximately 1730 and 1620 cm^{-1}, respectively, and show no significant shift in comparison with the mononuclear precursor. However, the ν(C=O) (oxamido carbonyl) band observed at 1650 cm^{-1} for the mononuclear precursor is significantly shifted to approximately 1575 cm^{-1}. The significant red shift suggests the coordination of the $[Cu(L^2)]$ precursor to M(II) through the oxamido carbonyl oxygen atoms and reflects the decrease in the C=O bond strength upon coordination. All binuclear complexes show a broad strong band at approximately 1080 cm^{-1}, indicating the presence of the perchlorate ion. Nearly all bands of the tetranuclear complexes can be found in the spectra of the binuclear complexes, with no significant shift. Complexes **1**, **3** and **5** exhibit several medium or strong bands at $\sim$1515, 1425, 845 and 725 cm^{-1}, which were not observed for the mono- and tetranuclear complexes. They are attributable to the phen ligand. Complexes **2**, **4** and **6** show two weak bands at $\sim$810 and 730 cm^{-1}, attributable to the bpy ligand. The other absorptions of bpy may be obscured by the bands of the $[Cu(L^2)]$ moiety and cannot be easily distinguished.

3.2. Electronic spectra

The electronic spectra of the binuclear complexes in acetonitrile exhibit an intense maximum absorption at approximately 355 ($\varepsilon > 10^4$ M^{-1} cm^{-1}) and two shoulders at approximately 410 nm ($\varepsilon \sim 5000$ M^{-1} cm^{-1}) and 530 nm ($\varepsilon = 200$–300 M^{-1} cm^{-1}). According to the intensities and positions, the first two bands should be due to intraligand or charge-transfer transitions, and the last band is attributable to the envelope of the d–d transitions of the Cu(II) ions. No other d–d transition absorptions were observed for the Cu(II)Mn(II) complexes, consistent with the spin-forbidden nature of the d–d transitions of the Mn(II) ion. The Cu(II)Ni(II) complexes **3** and **4** show a weak broad near-infrared absorption at 850–890 nm ($\varepsilon \sim 50$ M^{-1} cm^{-1}), assignable to the $^3A_{2g} \rightarrow {}^3T_{2g}$ transition of the Ni(II) ion in an octahedral environment. The other two spin-allowed transitions of the Ni(II) chromophore may be obscured by the d–d and charge-transfer bands of the Cu(II) ion.

3.3. ESR spectra

The X-band powder ESR spectra of complexes **1** and **3** at room temperature are shown in Fig. 2. Complex **1** presents an intense quasi-isotropic feature around 3280 G ($g = 2.06$) and a weak half-field signal at 1650 G ($g = 4.10$). These features are characteristic of magnetically coupled dicopper(II) pairs: the two signals arise from the $\Delta M_S = \pm 1(|0\rangle \leftrightarrow |\pm 1\rangle)$ and $\pm 2(|+1\rangle \leftrightarrow |-1\rangle)$ transitions, respectively, within the $S = 1$ excited state.

Complex **3** exhibits a broad intense band around $g = 2.14$ (3160 G) and a weak broad signal at $g = 4.98$ (1365 G), quite similar to the oxamido- and oxamato-bridged binuclear Cu(II)–Ni(II) complexes reported elsewhere [18,19], indicating the presence of magnetically coupled Cu(II)–Ni(II) pairs. The spectrum can be explained by the allowed $|S, +1/2\rangle \leftrightarrow |S, -1/2\rangle$ tran-

sitions within the doublet ground state ($S = 1/2$) and the quartet excited state ($S = 3/2$) [9,18].

The room temperature spectrum of **5** was also measured and was found to exhibit only a broad isotropic signal centered at $g = 2.01$, indicating the presence of magnetic exchange between Cu(II) and Mn(II).

According to the above discussion, together with magnetic studies (Section 3.4), the present complexes are proposed to have the molecular structure schematized in Fig. 3, in which Cu(II) and M(II) ions are bridged by an oxamido group.

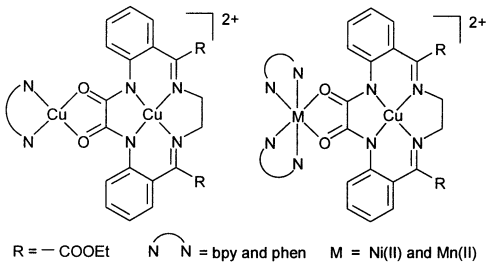


Fig. 3. The proposed molecular structure for the complexes.

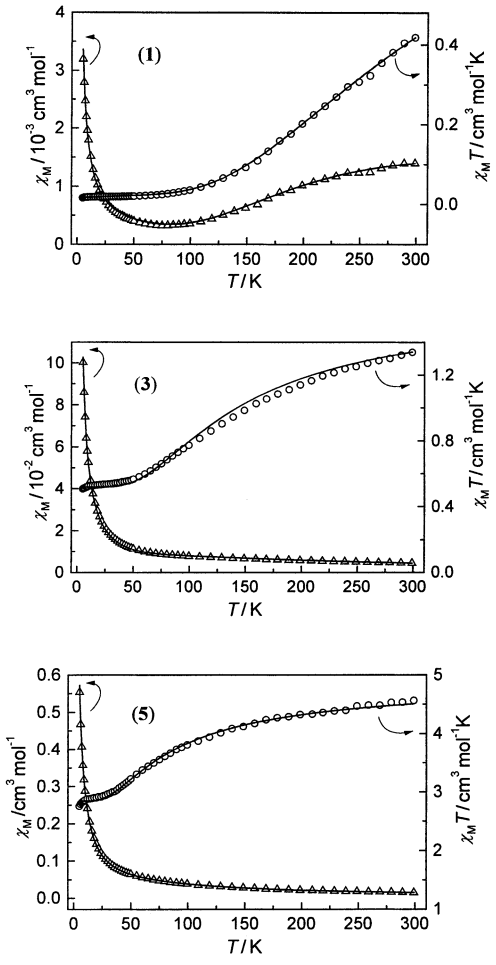


Fig. 4. χ_M versus T and $\chi_M T$ versus T plots for complexes **1**, **3** and **5**.

3.4. Magnetic properties

The temperature dependence of the molar magnetic susceptibility (χ_M) and its product with temperature ($\chi_M T$) for **1**, **3** and **5** are shown in Fig. 4.

The $\chi_M T$ product of **1** at room temperature is approximately 0.40 cm^3 mol^{-1} K, well below the spin-only value (0.75 cm^3 mol^{-1} K, assuming $g = 2.0$) expected for an uncoupled dicopper(II) system. Both χ_M and $\chi_M T$ decrease as the temperature is lowered from room temperature to approximately 75 K. This behavior is typical of discrete dicopper(II) pairs with a rather strong antiferromagnetic intramolecular interaction [23]. The increase of χ_M upon cooling further below 75 K indicates the presence of paramagnetic impurity. The impurity accounts for the plateau value of the $\chi_M T$ product in the low temperature region.

The $\chi_M T$ product of **3** at room temperature is approximately 1.33 cm^3 mol^{-1} K, less than the spin-only value (1.38 cm^3 mol^{-1} K) expected for an uncoupled Cu(II)–Ni(II) pair. The product decreases upon cooling and finally reaches a plateau below approximately 40 K with $\chi_M T = 0.52$ cm^3 mol^{-1} K. These features are quite typical of isolated Cu(II)–Ni(II) pairs with antiferromagnetic intramolecular interaction [9,18,19]. The plateaus below 30 K indicate that only the doublet ground state is thermally populated at low temperature.

The $\chi_M T$ product of **5** at room temperature is approximately 4.56 cm^3 mol^{-1} K, decreases as the temperature is lowered, reaches an approximate plateau between 25 and 10 K with $\chi_M T = 2.9$ cm^3 mol^{-1} K and finally decreases rapidly upon cooling further. This behavior indicates an antiferromagnetic interaction between the Cu(II) and Mn(II) ions. The plateaus indicate that only the quintet ground state is thermally populated below 25 K and the rapid decrease below 10 K may be due to secondary effects such as an antiferromagnetic intermolecular interaction and/or the zero-field splitting effect, which are operative only at very low temperature.

The magnetic data were fitted on the basis of the isotropic Heisenberg model $\hat{H} = -2J\hat{S}_1 \cdot \hat{S}_2$, where J is the interaction parameter between two spin carriers. The molar magnetic susceptibility for dicopper(II) complexes is expressed as

$$\chi_M = \frac{2N\beta^2 g^2}{kT}\left[\frac{1}{3+\exp(-2J/kT)}\right](1-\rho) + \frac{N\beta^2 g^2}{2kT}\rho + N\alpha$$

where ρ is the proportion of the paramagnetic impurity (presumably non-coupled monomeric copper(II) complex), $N\alpha$ is the temperature-independent paramagnetism (120×10^{-6} cm^3 mol^{-1}) and the other symbols

have their usual meaning. The simulation of the experimental data of **1** leads to $J = -210.2\ cm^{-1}$, $g = 2.29$ and $\rho = 0.016$. The agreement factor R defined as $R = \Sigma(\chi_{obsd} - \chi_{cacld})^2/\Sigma\chi^2_{obsd}$ is 1.1×10^{-3}. These large J values suggest that a very strong antiferromagnetic interaction between the two Cu(II) ions is mediated through the oxamido group.

For Cu(II)–Ni(II) complexes, the theoretical expression of the magnetic susceptibility is:

$$\chi_M = \frac{N\beta^2}{4kT}\left[\frac{g_{1/2}^2 + 10g_{3/2}^2\exp(3J/kT)}{1 + 2\exp(3J/kT)}\right]$$

where the g_S ($S = 1/2, 3/2$) factors are related to local g factors by $g_{1/2} = (4g_{Ni} - g_{Cu})/3$, and $g_{3/2} = (2g_{Ni} + g_{Cu})/3$. The simulations of the experimental data of **3** leads to $J = -53.9\ cm^{-1}$, $g_{Ni} = 2.27$, $g_{Cu} = 2.01$ with $R = 3.6 \times 10^{-4}$.

For Cu(II)–Mn(II) complexes,

$$\chi_M = \frac{2N\beta^2}{kT}\left[\frac{5g_2^2 + 14g_3^2\exp(6J/kT)}{5 + 7\exp(6J/kT)}\right]$$

where the g_S ($S = 2, 3$) factors are related to local g factors by $g_2 = (7g_{Mn} - g_{Cu})/6$, and $g_3 = (5g_{Mn} + g_{Cu})/6$. The simulations of the experimental data of **5** leads to $J = -14.1\ cm^{-1}$, $g_{Mn} = 1.99$, $g_{Cu} = 2.22$, with $R = 3.5 \times 10^{-4}$.

The antiferromagnetic interaction between Cu(II) and M(II) (M = Cu, Ni and Mn) can be easily understood in term of the non-zero overlap between the magnetic orbitals around Cu(II) and M(II) [24]. It has been demonstrated that, for oxalato-, oxamido- or oxamato-bridged copper(II) complexes, the magnitude of the magnetic interaction can be tuned by the coordination geometry around the metal ions [23,25–28]. Therefore, one can derive important structural information from the J parameter. The very strong antiferromagnetic interaction in the present dicopper complexes strongly suggest that the coordination planes of both Cu(II) ions are approximately coplanar with the oxamido bridge, as illustrated in Fig. 3. With such a geometry, the magnetic orbitals of both Cu(II) ions are favorably oriented and delocalized towards the bridging network to give a very large overlap, thus resulting in a very strong antiferromagnetic interaction. A similar structure has been determined for [Cu(oxpn)-Cu(bpy)]$(ClO_4)_2$ [oxpn = *N*,*N*′-bis(3-aminopropyl)-oxamido] [23], for which the J value ($-219.8\ cm^{-1}$) is comparable to the value reported here.

It should be worthwhile to compare the magnitude of the interaction in this series of binuclear Cu(II)–M(II) species containing the same bridging and terminal ligands but different M(II) ions. For the present series, we have $J_{CuCu} \approx 4J_{NiCu} \approx 15J_{MnCu}$. According to Kahn [24], the J_{CuM} parameter can be related to contributions from pairs of magnetic orbitals by $J_{CuM} = (\Sigma_\mu J_{\mu b_1})/n_M$, where n_M is the number of the magnetic orbitals (or unpaired electrons) around M, the index b_1 stands for the symmetry of the unique magnetic orbital ($d_{x^2-y^2}$) around Cu, and μ for the symmetry of the magnetic orbital around M, assuming a C_{2v} local symmetry for the Cu($C_2O_2N_2$)M bridging network. According to this relation, we have $J_{CuCu} = J_{b_1b_1}$, $J_{NiCu} = (J_{b_1b_1} + J_{a_1b_1})/2$ and $J_{MnCu} = (J_{b_1b_1} + J_{a_1b_1} + J_{a_1b_1} + J_{a_2b_1} + J_{b_2b_1})/5$. $J_{b_1b_1}$ involves the magnetic orbitals located in the plane of the bridging network and makes a predominant antiferromagnetic contribution. All other $J_{\mu b_1}$'s involve orthogonal magnetic orbitals and make small ferromagnetic contributions. Assuming that $J_{b_1b_1}$ is independent of M, it can be derived that $5|J_{MnCu}| < 2|J_{NiCu}| < |J_{CuCu}|$, where the $<$ signs are used to include the ferromagnetic contributions. This order is in agreement with the J_{MCu} values deduced from experimental magnetic data. Similar justification has been made for the MCu(obp)$(H_2O)_n$ [obp = oxamidobis(*N*,*N*′-propionato), M = Mn(II), Co(II) and Ni(II)] series [29]. However, the differences between the $n_M|J_{MCu}|$ values are so large that they cannot be only due to ferromagnetic contributions that are usually very small. It is difficult to estimate the ferromagnetic contributions in systems where the antiferromagnetic contribution predominates, but we can get some information from some similar Cu(II)Cr(III) systems where there are only ferromagnetic contributions [$J_{CrCu} = (J_{a_1b_1} + J_{a_2b_1} + J_{b_2b_1})/3 > 0$]. The J_{CrCu} values for several oxalato-bridged binuclear complexes and two oxamido-bridged Cu_3Cr species have been evaluated and are less than $7\ cm^{-1}$ [30–32]. The other origin of the differences between the $n_M|J_{MCu}|$ values lies in the antiferromagnetic contribution $J_{b_1b_1}$ itself, which is actually dependent on M. The dependence of $J_{b_1b_1}$ on M may be related to the following facts: (i) the 3d-orbital energy decreases in the order Mn > Ni > Cu due to the increased nuclear charge. A lower 3d energy means a smaller energy gap between the single-occupied 3d-orbital of M and the symmetry-adapted orbital of the bridging ligand; (ii) the M–O distance decreases in the same order. Both a smaller energy gap and a shorter M–O distance result in a stronger interaction between the metal and the ligand orbitals, and thus yield a magnetic orbital (the antibonding orbital) with enhanced ligand character, i.e. the delocalization of the magnetic orbital from M towards the bridge increases in the order Mn < Ni < Cu. It then follows that the overlap between the b_1-type magnetic orbitals of Cu and M and the resulting antiferromagnetic contribution $J_{b_1b_1}$ increase in the same order.

Acknowledgements

This work was supported by the Natural Science Foundation of China (No. 20071019).

References

[1] O. Kahn, Molecular Magnetism, VCH, New York, 1993.
[2] E.I. Solomon, T.C. Brunold, M.Z. Davis, J.N. Kemsley, S.-K. Lee, N. Lehnert, A.J. Skulan, Y.S. Yang, J. Zhou, Chem. Rev. 100 (2000) 235.
[3] S.J. Gruber, C.M. Harris, E. Sinn, J. Inorg. Nucl. Chem. 30 (1968) 1805.
[4] N.B. O'Brien, T.O. Maier, I.C. Paul, R.S. Drago, J. Am. Chem. Soc. 95 (1973) 6640.
[5] H. Ojima, K. Nonoyama, Coord. Chem. Rev. 92 (1988) 85.
[6] R. Ruiz, J. Faus, F. Lloret, M. Julve, Y. Journaux, Coord. Chem. Rev. 193–195 (1999) 1069.
[7] J.L. Sanz, R. Ruiz, A. Gleizes, F. Lloret, J. Faus, M. Julve, J.J. Borrás-Almenar, Y. Journaux, Inorg. Chem. 35 (1996) 7384.
[8] U. Casellato, P. Guerriero, S. Tamburini, P.A. Vigato, Inorg. Chim. Acta 260 (1997) 1.
[9] A. Escuer, R. Vicente, J. Ribas, R. Costa, X. Solans, Inorg. Chem. 31 (1992) 2627.
[10] Z.-Y. Zhang, D.-Z. Liao, Z.-H. Jiang, S.-Q. Hao, X.-K. Yao, H.-G. Wang, G.-L. Wang, Inorg. Chim. Acta 173 (1990) 201.
[11] J. Larionova, S.A. Chavan, J.V. Yakhmi, A.G. Frøystein, J. Sletten, C. Sourisseau, O. Kahn, Inorg. Chem. 36 (1997) 6374.
[12] F. Lloret, Y. Journaux, M. Julve, Inorg. Chem. 29 (1990) 3967.
[13] F. Lloret, M. Julve, R. Ruiz, Y. Journaux, K. Nakatani, O. Kahn, J. Sletten, Inorg. Chem. 32 (1993) 27.
[14] E.-Q. Gao, W.-M. Bu, G.-M. Yang, D.-Z. Liao, Z.-H. Jiang, S.-P. Yan, G.-L. Wang, J. Chem. Soc., Dalton Trans. (2000) 1431.
[15] E.-Q. Gao, G.-M. Yang, D.-Z. Liao, Z.-H. Jiang, S.-P. Yan, G.-L. Wang, H.-Z. Kou, Transition Met. Chem. 24 (1999) 244.
[16] E.-Q. Gao, G.-M. Yang, J.-K. Tang, D.-Z. Liao, Z.-H. Jiang, S.-P. Yan, Polyhedron 18 (1999) 3643.
[17] E.-Q. Gao, G.-M. Yang, D.-Z. Liao, Z.-H. Jiang, S.-P. Yan, G.-L. Wang, J. Chem. Res. (S) (1999) 278.
[18] E.-Q. Gao, J.-K. Tang, D.-Z. Liao, Z.-H. Jiang, S.-P. Yan, G.-L. Wang, Helv. Chim. Acta 84 (2001) 908.
[19] E.-Q. Gao, D.-Z. Liao, Z.-H. Jiang, S.-P. Yan, Polyhedron 20 (2001) 923.
[20] L. Cronin, A.R. Mount, S. Parsons, N. Robertson, J. Chem. Soc., Dalton Trans. (1999) 1925.
[21] C.J. O'Connor, Prog. Inorg. Chem. 29 (1982) 203.
[22] W.J. Geary, Coord. Chem. Rev. 7 (1971) 81.
[23] Y. Journaux, J. Sletten, O. Kahn, Inorg. Chem. 24 (1985) 4063.
[24] O. Kahn, Struct. Bonding (Berlin) 68 (1987) 89.
[25] O. Kahn, Angew. Chem., Int. Ed. Engl. 24 (1985) 834.
[26] A. Garcia, R. Costa, J. Ribas, T. Mallah, Y. Journaux, J. Sletten, X. Solans, V. Rodriguez, Inorg. Chem. 32 (1993) 3733.
[27] R. Costa, A. Garcia, R. Sanchez, J. Ribas, X. Solans, V. Rodriguez, Polyhedron 21 (1993) 2697.
[28] E.-Q. Gao, Q.-H. Zhao, J.-K. Tang, D.-Z. Liao, Z.-H. Jiang, S.-P. Yan, J. Chem. Soc., Dalton Trans. 9 (2001) 1537.
[29] A. Gulbrandsen, J. Sletten, K. Nakatani, Y. Pei, O. Kahn, Inorg. Chim. Acta 212 (1993) 71.
[30] M. Ohba, H. Tamaki, N. Matsumoto, H. Okawa, S. Kida, Chem. Lett. (1991) 87.
[31] M. Ohba, H. Tamaki, N. Matsumoto, H. Okawa, Inorg. Chem. 32 (1993) 5385.
[32] E.-Q. Gao, J.-K. Tang, D.-Z. Liao, Z.-H. Jiang, S.-P. Yan, Transition Met. Chem. 26 (2001) 473.

PERGAMON

Polyhedron 21 (2002) 365–370

POLYHEDRON

www.elsevier.com/locate/poly

Structure and spectral study of copper(II) pyridinecarboxylates: crystal and molecular structure of *trans*-diaqua-bis(*N*,*N*-diethylnicotinamide-*N*)bis(2-chloronicotinate-*O*)copper(II)

Ján Moncol' [a,*], Martina Palicová [a], Peter Segl'a [a], Marian Koman [a], Milan Melník [a], Marian Valko [b], Tadeusz Glowiak [c]

[a] *Department of Inorganic Chemistry, Slovak Technical University, Radlinského 9, SK-81237 Bratislava, Slovakia*
[b] *Department of Physical Chemistry, Slovak Technical University, Radlinského 9, SK-81237 Bratislava, Slovakia*
[c] *Institute of Chemistry, University of Wrocław, PL-50383 Wrocław, Poland*

Received 3 August 2001; accepted 2 November 2001

Abstract

New copper(II) pyridinecarboxylate compounds of the composition $[CuX_2(Et_2nia)_2(H_2O)_2]$ (where X = 2-methylthionicotinate (2-MeSnic), 2-chloronicotinate (2-Clnic), 2,6-dichloronicotinate (2,6-Cl_2nic), isonicotinate (isonic) and Et_2nia = *N*,*N*-diethylnicotinamide) have been prepared. All the $[CuX_2(Et_2nia)_2(H_2O)_2]$ compounds seem to possess octahedral copper(II) stereochemistry with differing tetragonal distortions. An X-ray analysis of $[Cu(2\text{-}Clnic)_2(Et_2nia)_2(H_2O)_2]$ was carried out and it featured a tetragonal-bipyramidal geometry around the copper(II) atom. The tetragonal plane is created by 2-chloronicotinate anions bonded to the copper(II) atom via the unidentate carboxylate oxygen atoms [Cu–O1 = 1.965(2) Å] and the pyridine ring nitrogen atoms of the neutral ligand *N*,*N*-diethylnicotinamide [Cu–N1 = 2.015(2) Å], whilst in axial positions are water molecules [Cu–O1w = 2.503(2) Å]. © 2002 Elsevier Science Ltd. All rights reserved.

Keywords: Copper(II) complexes; Spectral properties; Crystal structures; Pyridinecarboxylate complexes; Mononuclear complexes

1. Introduction

The interaction of the Cu(II) atom, which plays a vital role in a number of a quite different biological processes [1], with therapeutically administered drugs is a subject of considerable interest. Pyridinecarboxylic acid and its derivatives constitute an important group of antihelmintics and vitamins. It is known that the same drugs act via chelation [2] or via the inhibition of metalloenzymes [3], but little is known about modification of the activities of most drugs that are potential ligands.

Synthesis and spectral properties of various complexes $CuX_2{\cdot}nH_2O$ (where X = nicotinate (nic), isonicotinate (isonic), 2-methylthionicotinate (2-MeSnic), 2-chloronicotinate (2-Clnic) or 2,6-dichloronicotinate (2,6-Cl_2nic); $n = 0$–4) have been reported [4–9]. For complexes $Cu(nic)_2$ [8], $Cu(nic)_2{\cdot}4H_2O$ [9], $Cu(isonic)_2{\cdot}4H_2O$ [9] and $Cu(2\text{-}Clnic)_2{\cdot}H_2O$ [5] monomeric, dimeric and polymeric structures have been determined by X-ray analysis.

Some complexes of copper(II) carboxylates with *N*,*N*-diethylnicotinamide were also studied by X-ray. Structures of these complexes are dimeric [10] (similarly as for copper(II) acetate monohydrate [11]), polymeric [12] or monomeric [13–16], where carboxylate anions are bonded in an unidentate [13–15] or bidentate [16] manner, and *N*,*N*-diethylnicotinamide in all examples is a monodentate nitrogen donor ligand.

In order to better understand some aspects of copper(II) interactions with pyridine-carboxylates, we have studied the complexation of pyridine-4-carboxylate (isonicotinate) and 2-substituted derivatives of pyridine-3-carboxylate in the presence of *N*,*N*-diethylnicotinamide (Et_2nia). In the present paper, compounds of

* Corresponding author. Tel.: +421-2-593-25611; fax: +421-2-524-93198.
E-mail address: moncol@chtf.stuba.sk (J. Moncol').

0277-5387/02/$ - see front matter © 2002 Elsevier Science Ltd. All rights reserved.
PII: S0277-5387(01)01003-8

general composition, $[CuX_2(Et_2nia)_2(H_2O)_2]$ (where X = isonicotinate (isonic), 2-methylthionicotinate (2-MeSnic), 2-chloronicotinate (2-Clnic) or 2,6-dichloronicotinate (2,6-Cl_2nic)) are characterized by spectral methods. Moreover, the crystal structure of one of the complexes $[Cu(2\text{-Clnic})_2(Et_2nia)_2(H_2O)_2]$ has been studied by X-ray analysis. Based on the molecular structure the electronic, infrared and EPR spectra are discussed.

Table 1
Crystal data and structure refinement for $[Cu(2\text{-Clnic})_2(Et_2nia)_2(H_2O)_2]$ (**2**)

Empirical formula	$C_{32}H_{38}Cl_2CuN_6O_8$
Formula weight	769.12
Temperature (K)	293(2)
Wavelength (Å)	0.71073
Crystal system	triclinic
Space group	$P\bar{1}$ (no. 2)
Unit cell dimensions	
a (Å)	7.1740(10)
b (Å)	8.705(2)
c (Å)	14.329(3)
α (°)	97.02(3)
β (°)	97.47(3)
γ (°)	103.89(3)
V (Å^3)	850.3(3)
Z	1
D_{calc} (Mg m^{-3})	1.502
Absorption coefficient (mm^{-1})	0.859
$F(000)$	399
Crystal size (mm)	$0.23 \times 0.15 \times 0.4$
θ Range for data collection (°)	2.90–29.02
Index ranges	$-9 \le h \le 7$, $-11 \le k \le 11$, $-19 \le l \le 18$
Reflections collected	5949
Independent reflections	3841 [$R_{int} = 0.0283$]
Refinement method	Full-matrix least-squares on F^2
Data/restraints/parameters	3778/0/232
Goodness-of-fit on F^2	1.114
Final R indices [$I > 2\sigma(I)$]	$R_1 = 0.0616$, $wR_2 = 0.1540$
R indices (all data)	$R_1 = 0.0696$, $wR_2 = 0.1726$
Largest difference peak and hole (e Å^{-3})	0.439 and −0.587

Table 2
Selected bond lengths (Å) and bond angles (°) for $[Cu(2\text{-Clnic})_2(Et_2nia)_2(H_2O)_2]$ (**2**)

Bond lengths			
Cu–O1	1.965(2)	Cu–N1	2.015(2)
Cu–O1W	2.503(2)		
Bond angles			
O1–Cu–O1 #1	180.0	O1–Cu–N1	89.52(9)
N1–Cu–N1 #1	180.0	O1–Cu–O1W	91.1(1)
C7–N1–Cu	119.4(2)	N1–Cu–O1W	86.8(1)
C11–N1–Cu	122.1(2)	C1–O1–Cu	128.9(2)

Symmetry transformations used to generate equivalent atoms: #1 $-x$, $-y$, $-z$.

2. Experimental

2.1. Chemical reagents, analysis and spectral studies

All the chemicals used were of analytical grade (Aldrich or Sigma) and were used without further purification.

Copper was determined by electrolysis after mineralization of the complexes; carbon, hydrogen, nitrogen and sulfur were determined by microanalytical methods (Carlo Erba Instruments EA 1108). Besides the elemental analysis, the water content in hydrates was determined from thermogravimetrical curves.

Electronic spectra of the powdered samples in Nujol mulls were recorded at room temperature on a Specord M40 and Specord 200. IR spectra were recorded on a Magna 750 spectrophotometer at room temperature. Spectra of solid samples were obtained in nujol mulls, KBr and polyethylene pellets at a resolution of 1 cm^{-1}. EPR spectra of powdered samples were measured on a Bruker 200D SRC X-band (9.4 GHz) at room temperature.

2.2. X-ray crystallographic study

Data collection and cell refinement were carried out using Kuma CCD diffractometer and software [17]. Intensity data were corrected for Lorentz and polarization factors using KM4CCD software package [17]. The structure was solved by the heavy atom method with SHELXS-86 [18], and subsequent Fourier syntheses using SHELXL-93 [19], anisotropic thermal parameters were refined for all non-hydrogen atoms. Geometrical analysis was performed using SHELXL-93 [19]. The structure was drawn using ORTEP-3 [20]. The carbonyl oxygen atom of the carboxylic group is disordered occupying two statistical positions, represented by O2a and O2b with site occupancy factors of 0.44(7) and 0.56(7), respectively. The final parameters after refinement are summarized in Table 1. Selected interatomic distances and bond angles are given in Table 2.

2.3. Preparation of complexes $[Cu(2\text{-MeSnic})_2(Et_2nia)_2(H_2O)_2]$ (**1**), $[Cu(2\text{-Clnic})_2(Et_2nia)_2(H_2O)_2]$ (**2**), $[Cu(2,6\text{-}Cl_2nic)_2(Et_2nia)_2(H_2O)_2]$ (**3**) and $[Cu(isonic)_2(Et_2nia)_2(H_2O)_2]$ (**4**)

To the aqueous solutions (40 cm^3) of copper(II) sulfate (2 mmol), the aqueous solutions of the appropriate nicotinic acid (2-MeSnicH, 2-ClnicH or 2,6-Cl_2nicH) and equimolar quantities of sodium hydroxide (4 mmol) were slowly added and refluxed for 15 min. These reaction mixtures were left to stand at room temperature (r.t.) and the green $[CuX_2(H_2O)]_2$ (X = 2-MeSnic and 2-Clnic) or blue $[Cu(2,6\text{-}Cl_2nic)_2(H_2O)_2]$ products were isolated [4,5].

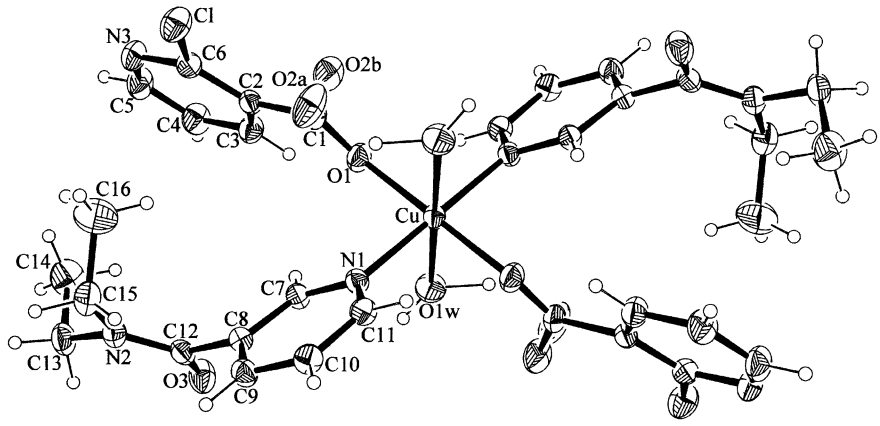


Fig. 1. Perspective view of the complex $[Cu(2\cdot Clnic)_2(Et_2nia)_2(H_2O)_2]$ (**2**), with atom numbering scheme. Thermal ellipsoids are drawn at the 30% probability level.

Compounds of the composition $[CuX_2(Et_2nia)_2(H_2O)_2]$ (**1**–**3**) were prepared by adding Et_2nia (5 cm^3) in excess to methanol solutions (20 cm^3) of appropriate $CuX_2\cdot nH_2O$ (1,25 mmol). The fine blue microcrystals produced on standing were separated, washed and dried in vacuo. Well-shaped single crystals of $[Cu(2\text{-}Clnic)_2(Et_2nia)_2(H_2O)_2]$ suitable for structure determination were obtained by recrystallizing in methanol. *Anal.* Calc. for $C_{34}H_{44}CuN_6O_8S_2$ (**1**): C, 51.5; H, 5.6; N, 10.6; S, 8.1; Cu, 8.0. Found: C, 51.9; H, 5.8; N, 10.9; S, 8.3; Cu, 8.2%. *Anal.* Calc. for $C_{32}H_{38}CuN_6O_8Cl_2$ (2): C, 50.0; H, 5.0; N, 10.9; Cu, 8.3. Found: C, 50.4; H, 5.0; N, 11.1; Cu, 8.0%. *Anal.* Calc. for $C_{32}H_{36}CuN_6O_8Cl_4$ (3): C, 45.9; H, 4.3; N, 10.0; Cu, 7.6. Found: C, 45.7; H, 4.4; N, 9.8; Cu, 7.4%.

Complex **4** was prepared only by adding Et_2nia (5 cm^3) in excess to the solid complex $[Cu(isonic)_2(H_2O)_4]$ (which was prepared as described earlier [7]). The resulting suspension was left to stand at r.t. After standing the suspension for 1 week, acetone (20 cm^3) was added to the resulting oil and blue crystals of complex **4** were collected by filtration, washed with ethanol and dried in vacuo. The analogous reaction of anhydrous $[Cu(nic)_2]$ [6] with Et_2nia under the same experimental conditions leads only to separation of unchanged starting complex. *Anal.* Calc. for $C_{32}H_{40}CuN_6O_8$ (4): C, 54.9; H, 5.8; N, 12.0; Cu, 9.1. Found: C, 55.3; H, 5.4; N, 12.2; Cu, 8.9%.

3. Results and discussion

3.1. Crystal structure description of complex (2)

The principal structural features of $[Cu(2\text{-}Clnic)_2(Et_2nia)_2(H_2O)_2]$ (**2**) are illustrated in Fig. 1. Selected bond lengths and angles of **2** are tabulated in Table 2. The coordination environment of the copper(II) atom is elongated tetragonal bipyramidal. The tetragonal plane is built up by a pair of unidentate 2-Clnic anions using carboxylate oxygen atoms (Cu–O1 = 1.965(2) Å) and by a pair of neutral *N*,*N*-diethylnicotinamide molecules using pyridine ring nitrogen atoms (Cu–N1 = 2.015(2) Å) in *trans* positions. The axial positions are occupied by water molecules (Cu–O1w = 2.503(2) Å). Intramolecular hydrogen bonding interactions involving an axial coordinated water molecule and disordered carboxylic oxygen atoms [O1w–H17···O2a, or O1w–H17···O2b, with O···O distances 2.652(10). and 2.736(8) Å, respectively] stabilize the molecular structure. The packing diagram of $[Cu(2\text{–}Clnic)_2(Et_2nia)_2(H_2O)_2]$ (**2**) perpendicular to the *bc* plane is shown in Fig. 2. All pyridine rings of *N*,*N*-diethylnicotinamide molecules coordinating to copper(II) ions are involved in offset face-to-face p–p stacking interactions by themselves (face-to-face distance 3.43 Å $[-x, -y+1, -z]$) [21], leading to supramolecular 1D chains propagating along the *b* axis. Supramolecular 1D chains are connected by intermolecular hydrogen bonds O1w–H18···O3 $[-x+1, -y+1, -z]$ with O···O distance 2.850(3) Å in the *ab* plane.

Table 3 shows selected bond distances of complex **2** and other complexes $[Cu(ArCO_2)_2L_2(H_2O)_2]$ (Ar = aryl; L = Et_2nia or nicotinamide (nia)), which have a similar centrosymetric molecular structure [13–16,22]. All five compounds have the same *trans*-$Cu^{II}O_2N_2\cdots O_2$ chromophore with a tetragonal bipyramidal geometry, axially elongated as predicted by the Jahn–Teller theorem. The values of the *T* parameter ($T = R_S/R_L$) [23], indicating the degree of tetragonal distortion about the copper(II) centers [23], decrease for the complexes in the sequence: 0.809 $[Cu(flu)_2(Et_2nia)_2(H_2O)_2] > 0.800$ $[Cu(4\text{-}O_2Nbz)_2(Et_2nia)_2(H_2O)_2] > 0.795$ $[Cu(2\text{-}Clnic)_2(Et_2nia)_2(H_2O)_2] > 0.775$ $[Cu(mef)_2(Et_2nia)_2(H_2O)_2] > 0.770$ $[Cu(4\text{-}HObz)_2(nia)_2(H_2O)_2]$, which follows the trend of the observed distortions. On the other hand, complex $[Cu(salicylate)_2(nia)_2(H_2O)_2]$ crystallizes in the non-centrosymmetric space group $P2_1$.

The geometrical environment around the copper(II) centre is asymmetric tetragonal bipyramidal, with significantly different axial bond distances Cu–Ow = 2.373(3) and 2.894(4) Å [24].

3.2. IR spectra

The IR spectra of all complexes under study show one or two strong absorption bands in the region from 3300 to 3500 cm^{-1}. These bands correspond to the antisymmetric and symmetric OH stretch and confirm the presence of water in the compounds. Moreover, the IR spectra exhibit characteristic bands at approximately 870 and 550 cm^{-1} assigned to rocking and wagging modes of the coordinate water molecule [25].

Extensive infrared studies have been made on metal complexes of carboxylic acids [25]. Each compound showed the carboxylate stretching frequencies

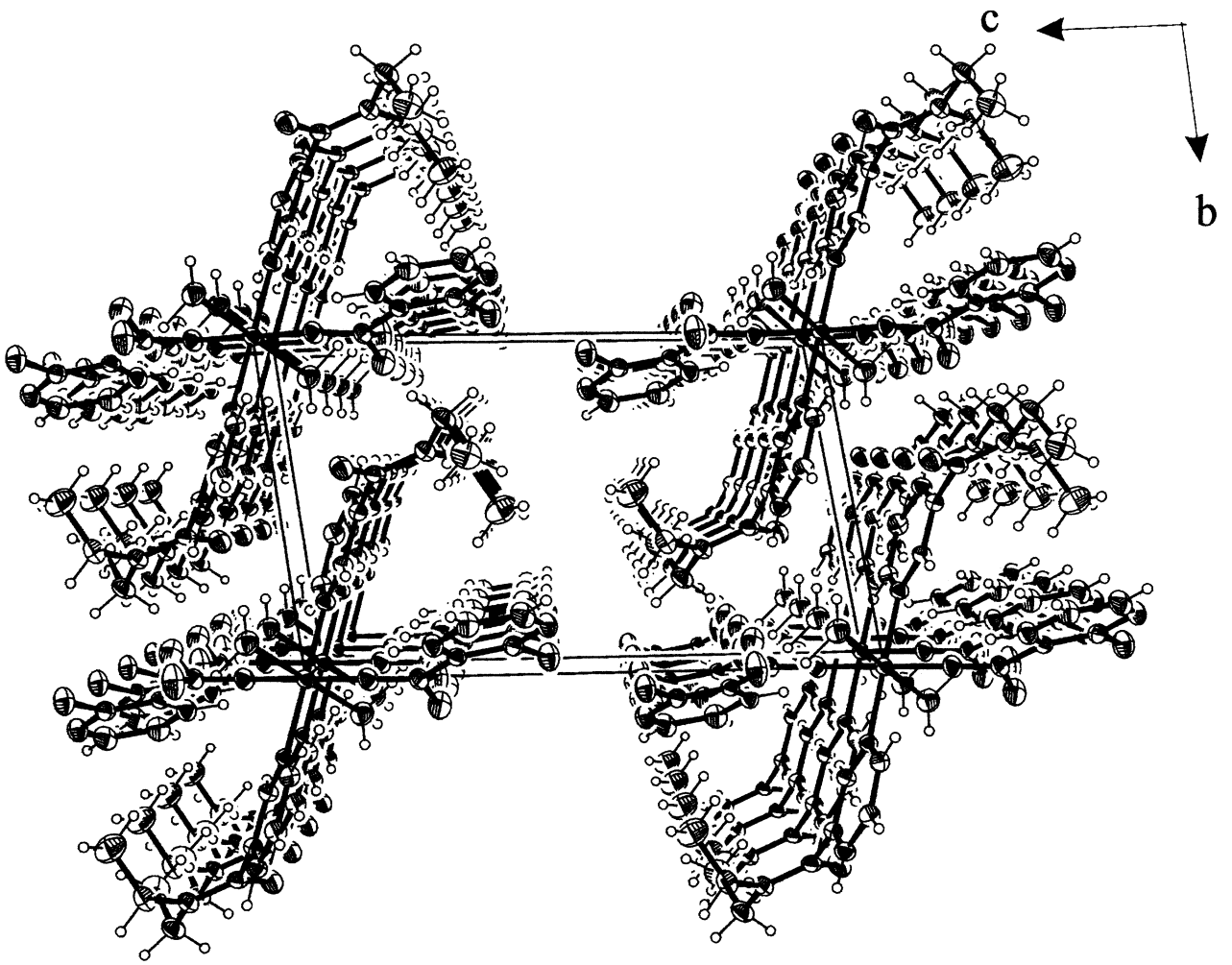


Fig. 2. The packing diagram of the complex $[Cu(2\cdot Clnic)_2(Et_2nia)_2(H_2O)_2]$ (**2**), viewed perpendicular to the *bc* plane.

Table 3
Selected bond lengths (Å) of similar complexes $[Cu(ArCO_2)_2L_2(H_2O)_2]$

Complex	$Cu–O_{eq}$	$Cu–N_{eq}$	$Cu–O_{ax}$	T [a]	Ref.
$[Cu(2\text{-}Clnic)_2(Et_2nia)_2(H_2O)_2]$	1.965(2)	2.015(2)	2.503(2)	0.795	this work
$[Cu(flu)_2(Et_2nia)_2(H_2O)_2]$	1.961(2)	2.001(2)	2.449(4)	0.809	[13]
$[Cu(4\text{-}O_2Nbz)_2(Et_2nia)_2(H_2O)_2]$	1.959(2)	2.019(2)	2.485(2)	0.800	[14]
$[Cu(mef)_2(Et_2nia)_2(H_2O)_2]$	1.936(3)	2.027(3)	2.557(3)	0.775	[15]
$[Cu(4\text{-}HObz)_2(nia)_2(H_2O)_2]$	1.956(2)	2.011(2)	2.575(2)	0.770	[22]

2-Clnic, 2-chloronicotinato; flu, flufenamato; 4-O_2Nbz, 4-nitrobenzoato; mef, mefanamato; 4-Hobz, 4-hydroxybenzoato; Et_2nia, *N*,*N*-diethylnicotinamide; nia, nicotinamide.

[a] $T = R_S/R_L$.

Table 4
Electronic spectra and EPR data for the complexes

No.	Complex	Electronic spectra (cm^{-1})	EPR			
			$g_\perp$	$g_\parallel$	g_{av}	G [b]
1	$[Cu(2\text{-}MeSnic)_2(Et_2nic)_2(H_2O)_2]$	15500br [a]	2.010	2.235	2.085	23.5
2	$[Cu(2\text{-}Clnic)_2(Et_2nic)_2(H_2O)_2]$	15300br	2.072	2.270	2.138	3.75
3	$[Cu(2,6\text{-}Cl_2nic)_2(Et_2nic)_2(H_2O)_2]$	15100br	2.019	2.240	2.093	12.63
4	$[Cu(isonic)_2(Et_2nic)_2(H_2O)_2]$	15700br	1.989	2.217	2.049	

[a] br, broad.
[b] $G = (g_\parallel - 2)/(g_\perp - 2)$.

$\nu_{as}(COO^-)$ and $\nu_s(COO^-)$. The broad bands at about 1620 cm^{-1} (assigned to the antisymmetric stretch $\nu_{as}(COO^-)$) are overlaped with the stretching vibrations of ν(C=O) (amide I) of *N*,*N*-diethylnicotinamide. The differences between the antisymmetric stretch $\nu_{as}(COO^-)$ and symmetric stretch $\nu_s(COO^-)$ (Δ) give information on the carboxylate bonding mode for the complexes after comparison with Δ values of complexes with ionic carboxylic groups. Paris et al. [26] have studied the IR spectra of pyridinecarboxylic acid and its sodium and potassium salts. For sodium nicotinate the Δ value is approximately 220 cm^{-1}. The greater Δ values for all complexes under study containing 2-substituted nicotinates or isonicotinate (from 253 to 275 cm^{-1}) are rather typical for unidentately bonded carboxylic groups.

The non-coordination of the pyridinecarboxylate ring of X^- in all $[CuX_2(Et_2nia)_2(H_2O)_2]$ complexes is in agreement with the positions of the absorption bands at about 400 cm^{-1}, which are due to out-of-plane deformation of the uncoordinated pyridine rings [25]. On the other hand, the positions of bands which correspond to pyridine ring deformation of *N*,*N*-diethylnicotinamide (the band due to out-of-plane pyridine ring deformation at 400 cm^{-1} for free Et_2nia are shifted to higher wavenumbers at about 430cm^{-1}) show that it is coordinated only through the nitrogen atom of the pyridine ring. The coordination of the pyridine ring is also indicated from the IR spectra by other typical shifts of bands of the pyridine ring which are characteristic for its coordination. Moreover, the absorption bands in the region of 270–283 cm^{-1} (assigned to ν(Cu–N)) confirm the coordination of the nitrogen atom of pyridine ring of *N*,*N*-diethylnicotinamide to the Cu(II) atom.

3.3. Electronic spectra

The solid state electronic spectra of all copper(II) complexes **1**–**4** exhibit a broad ligand field band with a maximum in the range of 15700–15100 cm^{-1} (Table 4). This type of spectrum is typical for tetragonal arrangement around copper(II) atoms corresponding to electron transfer from the one-electron orbital state $d_{x^2-y^2}$ [27]. Moreover, the suggested stereochemistry of the above complexes has also been confirmed by structure analysis in complex **2**. Maxima of the bands are consistent with the assignments for other copper(II) carboxylates with a *trans*-$Cu^{II}N_2O_2\cdots O_2$ chromophore [28].

3.4. EPR spectra

The EPR data for complexes **1**–**4** at ambient temperature are given in Table 4. The X-band spectra for complexes **1**–**4** are typical for axial type complexes. They exhibit two g values at room temperature with $g_\parallel > g_\perp$, suggesting a $d_{x^2-y^2}$ ground state which is consistent with the observed elongated octahedral stereochemistry [29]. The calculated G values [$G = (g_\parallel - 2)/(g_\perp - 2)$] show that the two g-value spectra with the lowest g-value (> 2.0) of complexes **1** and **3** are outside the range 3.5–5.0 and exchange coupling invalidates the observed g-values [30]. The spectral parameters are comparable to those of adducts of copper(II) carboxylates with *trans*-$Cu^{II}O_2N_2\cdots O_2$ chromophores [28]. The calculated G value of $[Cu(2\text{-}Clnic)_2(Et_2nia)_2(H_2O)_2]$ (**2**) indicates little resolution due to dipol–dipol interactions between copper atoms of neighboring molecules. It is in agreement with the X-ray results which reveal a mononuclear structure with a Cu···Cu distance of 7.174(4) Å, which is in the range, up to 11 Å [31], for which a magnetic exchange has been observed [32,33]. A similar magnetic exchange has been observed in the bis copper(II) carboxylate adducts with *trans*-$Cu^{II}O_2N_2\cdots O_2$ chromophores [Cu(acetylsalicylato-O,O′)$_2$(pyridine)$_2$] [34] with a Cu···Cu distance of 6.598(4) Å.

4. Supplementary material

Supplementary material including all atomic coordinates ($\times 10^4$), anisotropic displacement parameters for non-hydrogen atoms and all interatomic distances and bond angles have been deposited with the Cambridge Crystallographic Centre, CCDC No. 145984 for the

compound [Cu(2-Clnic)$_2$(Et$_2$nia)$_2$(H$_2$O)$_2$]. Copies of this information may be obtained free of charge from The Director, CCDC, 12 Union Road, Cambridge, CB2 1EZ, UK (fax: +44-1233-336-033; e-mail: deposit@ccdc.cam.ac.uk or www: http://www.ccdc.cam.ac.uk).

Acknowledgements

This work was financially supported by the grant 1/6106/99 of the Slovak Grant Agency for Science.

References

[1] D. Kovala-Demertzi, A. Theodorou, M.A. Demertzis, C.P. Raptoulou, A. Terzis, J. Inorg. Biochem. 65 (1997) 151.
[2] A. Albert, Selective Toxicity, The Physico-Chemical Basis of Therapy, 6th ed., Chapman and Hall, London, 1979.
[3] M.N. Hughes, The Inorganic Chemistry of Biological Processes, 2nd ed., Wiley, New York, 1981.
[4] D. Mikloš, P. Segla', M. Palicová, M. Kopcová, M. Melník, M. Valko, T. Glowiak, J. Mrozinski, M. Korabik, Polyhedron 20 (2001) 1867.
[5] J. Moncol', M. Korabik, P. Segla, M. Koman, M. Palicová, T. Glowiak, M. Melník, J. Mrozinski, Inorg. Chim. Acta, submitted for publication.
[6] M. Palicová, P. Segla', D. Mikloš, M. Kopcová, M. Melník, B. Dudová, D. Hudecová, T. Glowiak, Polyhedron 19 (2000) 2689.
[7] P. Segla', M. Palicová, M. Koman, D. Mikloš, M. Melník, Inorg. Chem. Commun. 3 (2000) 120.
[8] M.E. Chapman, P. Ayyappan, B.M. Foxman, G.T. Yee, W. Lin, Cryst. Growth Des. 1 (2001) 159.
[9] K. Waizumi, M. Takuno, N. Fukushima, H. Masuda, J. Coord. Chem. 44 (1998) 269.
[10] (a) Ch. Minacheva, T.S. Chodashova, M.A. Porai-Koshits, A.Yu. Tsivadze, Koord. Khim. 7 (1981) 455;
(b) T. Hökelek, H. Necefoglu, M. Balci, Acta Crystallogr., Sect. C 51 (1995) 2020;
(c) B. Kozlevcar, N. Lah, I. Leban, F. Pohleven, P. Šegedin, Croat. Chem. Acta 73 (2000) 733.
[11] P. de Meester, S.R. Fletcher, A.C. Skapsi, J. Chem. Soc., Dalton Trans. (1973) 2575.
[12] F. Valach, M. Dunaj-Jurco, M. Melník, M.M. Hoang, Z. Kristallogr. 209 (1994) 267.
[13] M. Melník, I. Potocnak, L. Macášková, D. Mikloš, C.E. Holloway, Polyhedron 15 (1996) 2159.
[14] T. Hökelek, K. Budak, H. Necefoglu, Acta Crystallogr., Sect. C 53 (1997) 1049.
[15] M. Melník, M. Koman, L'. Macášková, T. Glowiak, J. Coord. Chem. 44 (1998) 163.
[16] (a) T. Hökelek, H. Gunduz, H. Necefoglu, Acta Crystallogr., Sect. C 52 (1996) 2470;
(b) M. Koman, M. Melník, T. Glowiak, J. Coord. Chem. 44 (1998) 133.
[17] Kuma Diffraction, KM4CCD System Software, Version 1.149, Kuma Diffraction Instruments and Université de Lausanne, Switzerland, 1998.
[18] G.M. Sheldrick, SHELXS-86. (Crystallographic Computing 3, G.M. Sheldrick, C. Krueger and R. Goddard). Oxford University Press, Oxford, 1985, pp. 175–189.
[19] G.M. Sheldrick, SHELXL-93. Program for Refinement of Crystal Structure. University of Göttingen, Germany, 1994.
[20] L.J. Farrugia, J. Appl. Crystallogr. 30 (1997) 565.
[21] K.S. Min, M.P. Suh, Eur. J. Inorg. Chem. (2001) 449.
[22] T. Hökelek, T. Budak, K. Sendil, H. Necefoglu, Acta Crystallogr., Sect. C 54 (1998) 347.
[23] (a) M. Procter, B.J. Hathaway, P. Nicholls, J. Chem. Soc. A (1968) 1678;
(b) J. Gažo, I.B. Bersuker, J. Garaj, M. Kabešová, J. Kohout, H. Langfelderová, M. Melník, M. Serátor, F. Valach, Coord. Chem. Rev. 19 (1976) 253.
[24] N. Petrovčič, B. Kozlevčar, L. Golič, I. Leban, P. Šegedin, Acta Crystallogr., Sect. C 55 (1999) 176.
[25] K. Nakamoto, Infrared and Raman Spectra of Inorganic and Coordination Compounds, Part B, 5th ed., Willey, New York, 1997, p. 23, 53, 59.
[26] M. Paris, G. Thomas, J.C. Merlin, Bull. Soc. Chim. Fr. 28 (1961) 707.
[27] A.B.P. Lever, Inorganic Electronic Spectroscopy, Elevier, Amsterdam, 1984, pp. 308–313, 554–572.
[28] (a) L. Antolini, L.P. Battaglia, A. Bonamartini-Corradi, G. Marcotrigiano, L. Menabue, G.C. Pellacani, M. Saladini, Inorg. Chem. 21 (1982) 1391;
(b) A.L. Abuhijleh, C. Woods, J. Chem. Soc., Dalton Trans. (1992) 1249;
(c) C.P. Raptopoulou, S. Paschalidou, A.A. Pantazaki, A. Terzis, S.P. Perlepes, Th. Lialiaris, E.G. Bakalbassis, J. Mrozinski, D.A. Kyriakidis, J. Inorg. Biochem. 71 (1998) 15;
(d) A.L. Abuhijleh, C. Woods, E. Bogas, G. Le Guenniou, Inorg. Chim. Acta 195 (1992) 67.
[29] B.J. Hathaway, Coord. Chem. Rev. 35 (1981) 211.
[30] B.J. Hathaway, J. Chem. Soc., Dalton Trans. (1972) 1196.
[31] G. Psomas, C. Dendrinou-Samara, P. Philippakopoulos, V. Tangoulis, C.P. Raptopoulou, E. Samaras, D.P. Kessissoglou, Inorg. Chim. Acta 272 (1998) 24.
[32] T.D. Smith, J.R. Pilbrow, Coord. Chem. Rev. 13 (1974) 173.
[33] M. Melník, Coord. Chem. Rev. 42 (1982) 259.
[34] F.T. Greenaway, A. Pezeshk, A.W. Cordes, M.C. Noble, J.R.J. Sorenson, Inorg. Chim. Acta 93 (1984) 67.

PERGAMON

Polyhedron 21 (2002) 371–379

POLYHEDRON

www.elsevier.com/locate/poly

Tantalocene–hydride–phosphorus chemistry. Some new complexes and crystal structures of $[CpCp'TaH_2(PMe_2H)]PF_6$ ($Cp = C_5H_5$, $Cp' = C_5H_2^tBu(Me)_2$) and $Cp_2Ta(H)(\mu\text{-}PPh_2,H)Fe(CO)_3$

Gilles Boni, Olivier Blacque, Philippe Sauvageot, Nicolas Poujaud, Claude Moïse, Marek M. Kubicki *

Laboratoire de Synthèse et d'Electrosynthèse Organométalliques – UMR 5632, Faculté des Sciences, Université de Bourgogne, 9 Av. A. Savary, BP 47870, 21078 Dijon, France

Received 3 July 2001; accepted 14 November 2001

Abstract

The aim of this paper is to look for a better knowledge of the behaviour of bent tantalocenes that bear hydrides, phosphorus PR_2X (R = Me, Ph; X = H, lone pair) and cyclopentadienyl ($Cp = C_5H_5$, $Cp' = C_5H_2^tBu(Me)_2$, $Cp^* = C_5Me_5$) ligands. An orbital control of regioselectivity of insertion of the PR_2 phosphide fragment of chlorophosphines PR_2Cl into the central Ta–H bond of trihydrides Cp_2TaH_3 leading to the formation of metallophosphonium cations is discussed. Neutralisation of cationic complexes with strong bases leads either to the Ta(V)–phosphide or to the Ta(III)–phosphine species depending on the nature of the cyclopentadienyl ligand; good electron donor Cp′ and Cp* rings favour the formation of Ta(V)–phosphide species, while C_5H_5 orients neutralisation towards Ta(III)–phosphine ones. These trends are roughly confirmed by DFT calculations. The X-ray structure of the first tantalocene phosphonium ionic compound $[CpCp'TaH_2(PMe_2H)]PF_6$ ($Cp' = C_5H_2^tBu(Me)_2$) as well as that of the bimetallic complex $Cp_2Ta(H)(\mu\text{-}PPh_2,H)Fe(CO)_3$ are also reported. © 2002 Elsevier Science Ltd. All rights reserved.

Keywords: Tantalum; Metallocenes; Hydrides; Metallophosphines; Bimetallics; X-ray structures

1. Introduction

The search for binuclear complexes containing two different transition metals still attracts great interest [1]. In particular, the chemistry of heterobimetallic compounds stabilised by bridging phosphido groups has been widely studied [2]. Our group is involved in this field and we have developed synthetic strategies starting from metalloligands. These metallophosphines are obtained by reacting d^2 monohydrides $Cp_2M(L)H$ (M = Nb, Ta; L = two electron donor) [3] or d^0 dihydrides Cp_2MH_2 (M = Mo, W) [4] with chlorophosphines PR_2Cl. In keeping with our interest in phosphido derivatives, we turned our attention to the trihydrides Cp_2MH_3 (M = Nb, Ta; d^0) which are good precursors of highly reactive unsaturated intermediates $[Cp_2MH]$ and are therefore able to undergo coordination or insertion reactions with phosphines. Boni and coworkers [5] and Nikonov et al. [6] have shown that trihydrides Cp_2MH_3 give clean reactions with chlorophosphines PR_2Cl. In this paper we report on the syntheses and properties of some new mononuclear and dinuclear complexes with Ta–P bonds.

2. Results and discussion

2.1. Cationic complexes

It is experimentally established that chlorophosphines PR_2Cl react with tantalocene (and niobocene) trihydrides (**1**) leading to the formal insertion of the PR_2 unit into the central Ta–H bond with formation of

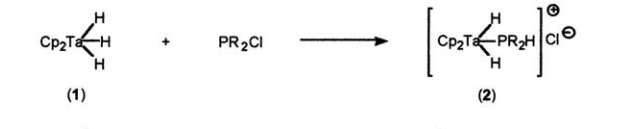
* Corresponding author.
E-mail address: marek.kubicki@u-bourgogne.fr (M.M. Kubicki).

0277-5387/02/$ - see front matter © 2002 Elsevier Science Ltd. All rights reserved.
PII: S0277-5387(01)01014-2

symmetrical metallophosphonium cations $[Cp_2TaH_2(PR_2H)]^+$ (**2**) ($Cp_2 = (C_5H_5)_2$ (**2**,**2**), $(C_5H_5)(C_5H_2'Bu(Me)_2)$ (**2**,**2′**), $(C_5H_5)(C_5Me_5)$ (**2**,**2***) and $(C_5Me_5)_2$ (**2***,**2***); R = Me, Ph) bearing both residual hydrides in lateral positions (Scheme 1).

Nikonov proposed recently a plausible general mechanism of an insertion process based on carbenoid behaviour of halophosphines [6c]. This model involves the HOMO and the LUMO of PR_2Cl molecules which represent, respectively, the canonical lone pair of phosphorus (LP), and the σ*(p) antibonding P–Cl molecular orbital. We calculated the shapes of these orbitals for PMe_2Cl with a semi-empirical PM3 method [7] and depicted them on Fig. 1. Their lobes of chemical interest have a high contribution of phosphorus and form an angle close to 60°.

The first step of this mechanism consists of an interaction between one of the three M–H bonds of the complex with the LUMO of the PR_2Cl reagent (hydride nucleophilic attack on the P atom of chlorophosphine). However, the regiochemistry of this interaction is not clear, because both the central and the lateral M–H bonds of Cp_2MH_3 may formally operate. Nikonov assumed that it is the central M–H_a bond that attacks the σ*(p)P–Cl orbital, because he knows the result of this action. The simplified energy diagrams of tantalocene trihydrides (Fig. 2), calculated at the DFT/



Cp_2TaH_3	Cp_2
(1,1)	$(C_5H_5)_2$
(1,1′)	$(C_5H_5)(C_5H_2{}^tBuMe_2)$
(1,1*)	$(C_5H_5)(C_5Me_5)$
(1*,1*)	$(C_5Me_5)_2$

$[Cp_2TaH_2PR_2H]Cl$	Cp_2	R
(2,2,Me) [5b]	$(C_5H_5)_2$	Me
(2,2,Ph) [5b]	$(C_5H_5)_2$	Ph
(2,2′,Me)	$(C_5H_5)(C_5H_2{}^tBuMe_2)$	Me
(2,2*,Me)	$(C_5H_5)(C_5Me_5)$	Me
(2*,2*,Me)	$(C_5Me_5)_2$	Me
(2*,2*,Ph)	$(C_5Me_5)_2$	Ph

Scheme 1.

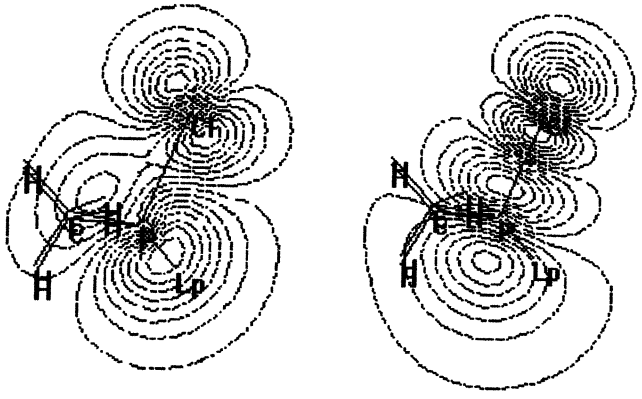


Fig. 1. Shapes of the HOMO (left) and the LUMO (right) for PMe_2Cl.

B3LYP level with Lanl2DZ basis[8], do not distinguish clearly which Ta–H bond ($2a_1$ or b_2) is preferentially responsible for the initial interaction with the σ*(p)P–Cl orbital. The $2a_1$ occupied molecular orbital of trihydride is mainly built of the Ta–H central bond, while the filled b_2 orbital contains contributions from the lateral ones. The HOMO for (**1**,**1**) is $2a_1$, thus indicating the reactivity of the central bond, but it lies only 0.25 eV over b_2. With a good electron donor permethylated ligands (**1***,**1***) the b_2 orbital builds the HOMO, thus suggesting a lateral interaction. However, the energy difference HOMO–HOMO-1 here is still smaller (0.15 eV) than for (**1**,**1**), and consequently, this electronic argument for lateral interaction may be contoured by steric hindrances in the transition state of insertion. If we consider the interaction of the $2a_1$ molecular orbital (central Ta–H bond of the trihydride) with the LUMO of PR_2Cl, we should assume that the HOMO of PR_2Cl (P lone pair) must be placed in the *xz* molecular plane defined by the Ta atom and the centres of the cyclopentadienyl rings (because of repulsions between the phosphorus lone pair and Ta–H bonds) and, consequently, should overlap with the b_1 empty metallic orbital (d_{xz}) located in this plane. On the other hand, if the lateral Ta–H bond (b_2) is implied in the interaction with the LUMO of PR_2Cl, the lone pair of this reagent should now interact with the metallic a_2 (d_{xy}) orbital. The d_{xz}–LP(P) ligand interaction consists of a direct metal–ligand overlap ('strong' interaction), whereas that involving d_{xy} is of lateral nature ('weak' interaction). Such an analysis of bonding favours a central coordination of the chlorophosphine. Moreover, the lateral interaction can lead to steric hindrances consisting of geometrical conflicts between R substituents of PR_2Cl and cyclopentadienyl rings. Thus, the participation of the b_1 metallic orbital (in the building of the transition state) may explain the observed regiochemistry of the insertion process.

It is worth noting that the tantalocene cationic species bearing the phosphine (PMe_2Ph) or the phosphite ($P(OMe)_3$) [9] in lateral sites, obtained by protonation of Ta(III) (d^2) $Cp_2Ta(L)H$ derivatives, are known and stable. However, the ligands in these last derivatives already occupy the lateral positions allowing the attack of the proton on the central lobe of the non-bonding HOMO in the d^2 system [10].

In order to confirm the stereochemistry of the insertion process we have carried out the experiments with a centrally deuteriated complex $(C_5H_5)(C_5H_2'Bu(Me)_2)TaH_2D$ [11]. Reaction of this freshly prepared complex in toluene with PMe_2Cl at low temperature (−78 °C) gives almost exclusively (90%) the phosphorus deuteriated salt $[(C_5H_5)(C_5H_2'Bu(Me)_2)TaH_2(PMe_2D)]Cl$ together with a small fraction of the metal deuteriated isotopomer $[(C_5H_5)(C_5H_2'Bu(Me)_2)TaHD(PMe_2H)]Cl$ (10%) (the ratios estimated from ^1H NMR data). The

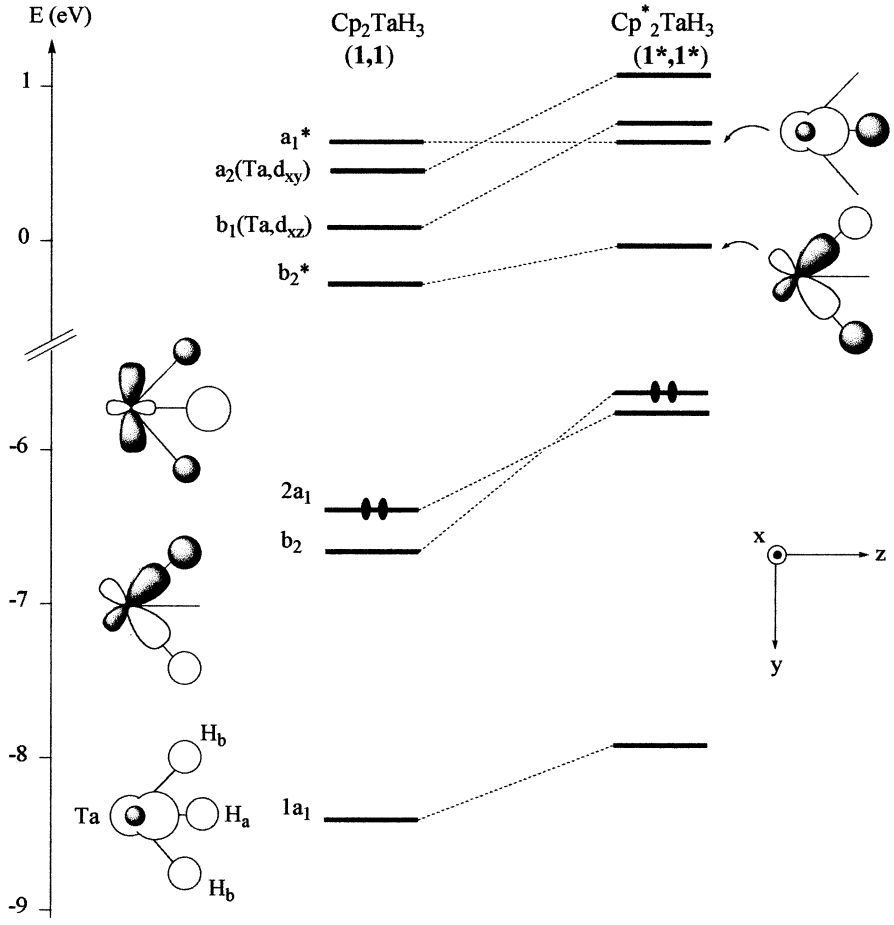


Fig. 2. Simplified energy diagram of the frontier molecular orbitals for C_5H_5 (**1**,**1**) and C_5Me_5 (**1***,**1***) trihydrides.

complex $[C_5H_5)(C_5H_2^tBu(Me)_2)TaH_2(PMe_2D)]Cl$ is stable in toluene solution under argon for several days with neither detectable H/D exchange nor the formation of isomers with the phosphine in the lateral position.

The use of the new ($C_5H_2^tBu(Me)_2$) ligand [12] allowed us to grow for the first time X-ray quality crystals of a Group 5 cationic metallocene bearing a secondary phosphine ligand (**2**,**2**′,**Me**). The crystal structure of (**2**,**2**′,**Me**) is built of organometallic cations and PF_6 anions. The cation has a structure similar to that reported for the neutral complex $Cp_2TaH_2PPh_2$ with a terminal phosphido ligand [6b]. The geometry of the cation may be regarded as a highly distorted trigonal bipyramid or as a tetrahedron one with one edge (H–H) capped with a phosphorus ligand (Fig. 3).

The Ta–P(PMe_2H) bond length of 2.533(1) Å in (**2**,**2**′,**Me**) is significantly shorter than that reported by Nikonov for the Ta(V) neutral complex with a terminal PPh_2 ligand $Cp_2Ta(H)_2PPh_2$ (2.595(3) Å) [6b]. Although, the substituents on the P atom (Me vs. Ph) are different it seems reasonable to assume that the presence of a diffused phosphorus lone electron pair in the neutral complex, instead of the hydrogen atom in

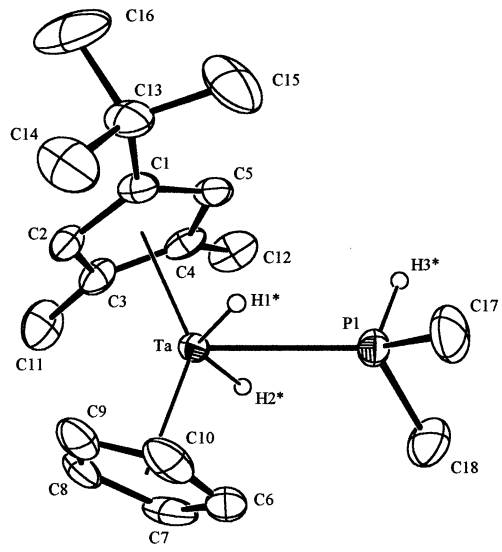


Fig. 3. ORTEP plotting (50% probability level) of the cation in (**2**,**2**′,**Me**). Selected bond lengths (Å) and angles (°): Ta–P1 2.533(1); Ta–H1 1.69(4); Ta–H2 1.73(6); Ta–CP′ 2.063; Ta–CP 2.059; H1–Ta–H2 135(2); H1–Ta–P1 70(1); H2–Ta–P1 66(2); CP′–Ta–CP 138.8.

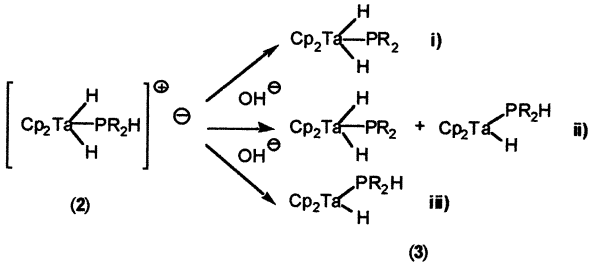
(**2**,**2′**,**Me**), is responsible for the long Ta–P bond observed in the neutral complex. The pure so called 'transition metal gauche effect' [3d,13] cannot be applied to the observed lengthening in the neutral complex because there is no non-bonding tantalum filled orbital in a formal (Ta(V), d^0) structure. However, the repulsions between the P lone pair and Ta–H bonds may easily operate therein.

2.2. Neutral complexes

It has been observed that the cationic metallophosphonium compounds of type **2** (Group 5 and 6 metallocenes) are easily deprotonated by strong bases [3–6,14,15]. In the case of Group 5 metals, like Ta(V) complexes, the neutralisation may lead either to the Ta(III)–phosphine or to the Ta(V)–phosphide species (complexes **3**, Scheme 2).

A similar phosphine (M–PPh_2H) versus phosphide (M–PPh_2) isomerism due to the nature of the second versus third row transition metal has been observed by Baker et al. [16] for Mo/W monocyclopentadienyl $Cp^*Mo(PMe_3)(PPh_2)(PPh_2H)$/$Cp^*W(PMe_3)(PPh_2)_2H$ and by Nikonov [6a,6b] for the Nb/Ta metallocene $Cp_2Nb(PPh_2H)(H)$/$Cp_2Ta(H)_2(PPh_2)$ series. This has been assigned to the stronger metal–hydrogen bonds for third row metals as compared to those from the second row [17]. We have also observed such an isomerism after deprotonation of molybdenocene phosphonium cations $[Cp_2Mo(H)(PR_2H)]^+$ (R = Me, Ph) which gives either the Mo^{II} $Cp_2Mo(PMe_2H)$ or the Mo^{IV} $Cp_2Mo(H)(PPh_2)$ neutral species; a process clearly depending on the nature of the coordinated secondary phosphine [15]. A similar behaviour is also observed for tantalocenes (**2**,**2**) (pathways (i) and (iii) in Scheme 2). Thus, the type of neutral complex (M, d^2-phosphine) or (M, d^0-phosphide) depends on the nature of M and on that of R.

The isomerism observed in the case of new neutralised 'tantalocene–PMe_2X (X = H or LP)' systems depends on a third factor: the nature of the substituted



i) $Cp_2 = (C_5H_5)_2$, R = Ph, (**3**,**3**,**Ph**) ; $Cp_2 = (C_5H_5)(C_5Me_5)$, R = Me, (**3**,**3***,**Me**)
ii) $Cp_2 = (C_5H_5)(C_5H_2Me_2{}^tBu)$, R = Me, (**3**,**3′**,**Me**)
iii) $Cp_2 = (C_5H_5)_2$, R = Me, (**3**,**3**,**Me**)

Scheme 2.

cyclopentadienyl ligands. Strong electron donor Cp ligands e.g. alkyl substituted cyclopentadienyl rings, ($C_5H_2'Bu(Me)_2$) and (C_5Me_5) versus non-substituted C_5H_5 favour the formation of Ta(V)–phosphide complexes when R = Me. Both isomers are formed with mixed Cp/Cp′ ligands (**3**,**3′Me**), but a sole Ta(V)–phosphide isomer is found for the mixed Cp/Cp* complex (**3**,**3***Me**). Note, however, that neutralisation of permethylated cations (**2***,**2***) (expected formation of Ta(V)–phosphide isomer) does not give the isolable defined product of the type (**3***,**3***Me**). This may be due to a very electron rich nature of the expected complex.

Because all neutral complexes (**3**), whatever their phosphine (Ta(III)) or phosphide (Ta(V)) nature, react with Group 6 and 8 metal carbonyls giving μ-phosphido bimetallics [14], we focussed our attention on the relative stabilities of different Ta(V) and Ta(III) neutral species ((**3**,**3**) and (**3**,**3***)). They have been estimated from total energies calculated for optimised geometries of extreme Ta(V) and Ta(III) cases with the DFT/B3LYP method with Lanl2DZ basis. The results are shown on Fig. 4.

The calculations indicate that for non-substituted (**3**,**3**) isomers (part *a*) on Fig. 4) the Ta(V)–phosphide structure should be more stable than that of Ta(III)–phosphine, but only by 0.35 eV (some 34 kJ mol^{-1}). Note, that the last one (Ta(III)–phosphine) is experimentally observed upon neutralisation of (**2**,**2**). In the (**3**,**3***) series (part *b*) on Fig. 4), the lowest energy Ta(V)–phosphide structure is more stable than that of Ta(III)–phosphine by 0.52 eV (50 kJ mol^{-1}). It agrees with experimental observation. Thus, one may conclude that the calculated trends roughly correspond to the experimental ones: the presence of a good electron donor Cp ligand stabilizes the Ta(V) isomer more than the Ta(III) isomer. The Me groups of the phosphide ligand in a stable geometry of the (**3**,**3***) system are found, with respect to the TaH_2P plane, on the side of the non-substituted Cp ligand (structure *x*). We also looked at what happens when the Me groups are placed on the other side of this plane (rotation by 180°), in the space of the Cp* ligand (structure *y*). A local minimum of energy has been effectively observed for this conformation (*y*), lying only 0.2 eV higher with respect to the structure (*x*). The Ta–P distances in optimised structures (**3**,**3**) and (**3**,**3***) remain roughly unchanged. However, one observes an increase of the Ta–P–Me angle in the (*y*) conformer (113.6°, Cp*–Me repulsions) with respect to the value (109.8°) calculated for (*x*). Thus, the P lone pair is pushed towards the unsubstituted Cp ring in (**3**,**3***). Such a tendency may lead to an energetically (and geometrically) unfavourable structure in the presence of two permethylated Cp* ligands and, consequently, may explain the experimental difficulties encountered upon neutralisation of (**2***,**2***) cations attempted for the isolation of (**3***,**3***) metallophos-

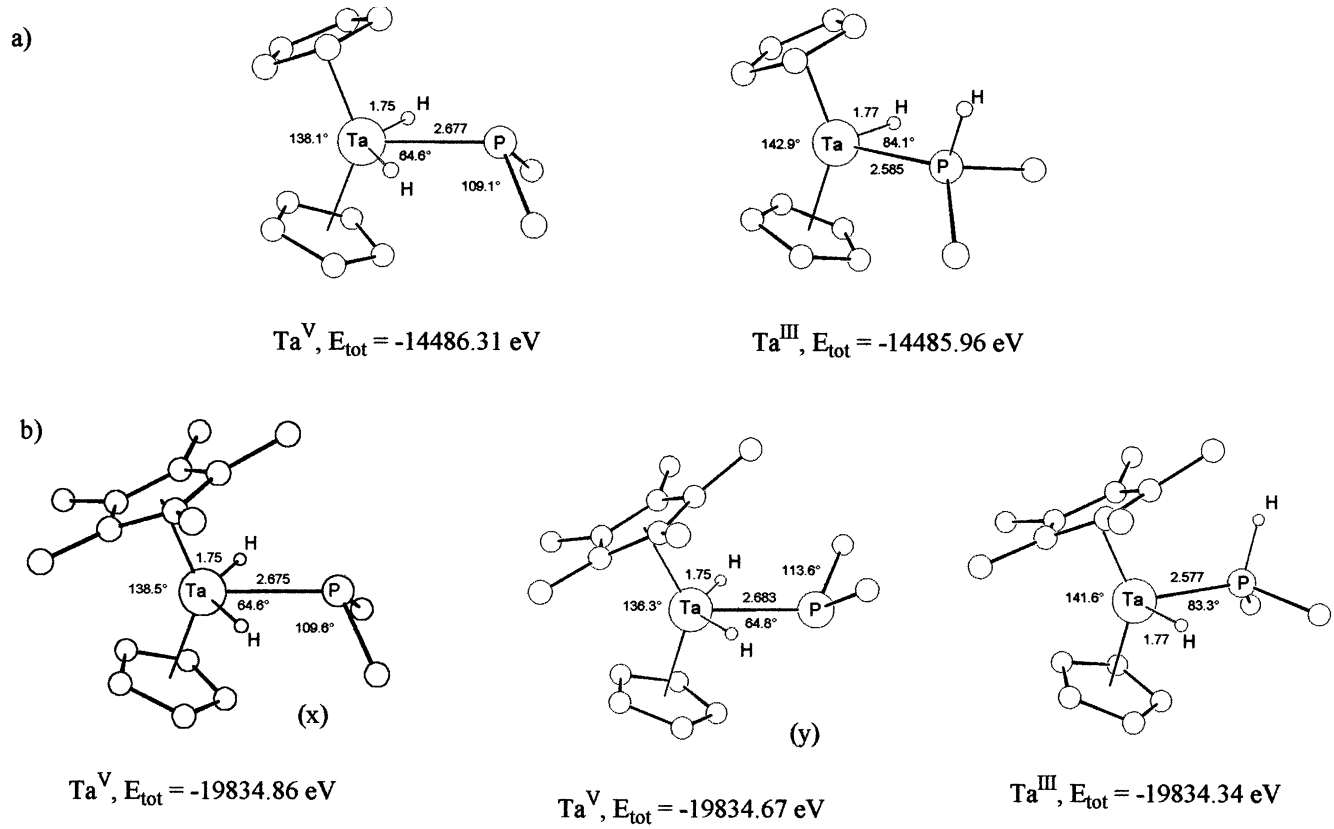


Fig. 4. Optimised geometries and total energies for Ta(V)–phosphide and Ta(III)–phosphine complexes. (a) $(C_5H_5)(C_5H_5)$, (b) $(C_5H_5)(C_5Me_5)$ series.

phides. For this last case, there are some indications on the ^{1}H NMR spectrum of the crude material that (**3***,**3***) is formed, but we were not able to isolate it. It is worth noting that the attempts of optimisation of permethylated metallocene Ta(V) or Ta(III) structures (**3***,**3***) failed with our standard computational DFT method. Another interesting observation arising from this study concerns the Ta–P bond lengths. The Ta–P optimised distances are shorter for Ta–PMe_2H bonds (2.58 Å) than for Ta–PMe_2 ones (2.68 Å), confirming the trends observed in crystal structures of (**2**,**2′**,**Me**) (phosphine, 2.53 Å) and of $Cp_2TaH_2PPh_2$ (phosphide, 2.59 Å) [6b].

2.3. Bimetallic phosphido bridged complexes

The neutral complexes (**3**) easily react with metal–carbonyls of Group 6 M′$(CO)_6$ (M′ = Cr, Mo, W) giving rise to the monobridged Ta(μ-PR_2)M′ (**4**) and the dibridged Ta (μ-PR_2, H) M′ (**5**) isolated species, while with $Fe(CO)_5$, $Fe_2(CO)_9$ or (BDA)$Fe(CO)_3$ the dibridged structures (**5**) are directly formed [14]. However, no crystal structure in the series of monobridged compounds $M^V(H)_2$(μ-PR_2)M′ has been reported to date, probably because they easily transform to the dibridged structures during crystallisation.

In the series of bimetallic dibridged complexes (μ-PR_2,H) we have already reported two crystal structures of Group 5 (d^0) metallocenes $Cp_2Ta(H)$(μ-PMe_2,H)Cr-$(CO)_4$ [5b] and $Cp_2Nb(H)$(μ-PPh_2,H)$W(CO)_4$ [18], and describe here the third member in this series, the Ta–Fe complex $Cp_2Ta(H)$(μ-PPh_2,H)$Fe(CO)_3$ (**5**,**5Fe**). There is one dinuclear organometallic and one solvent (acetone) molecule in the asymmetric unit of $P2_1/n$ space group. The metallic fragments have their usual pentacoordinated (Ta) and trigonal bipyramidal (Fe) geometries (Fig. 5). The Ta, H1, H2, P, Fe, C3 and O3 atoms roughly lie in the plane bisecting that of the Cp rings. The apical Fe–C3 (CO trans to H) distance of 1.71(2) Å in the iron polyhedron is apparently, but not significantly, shorter than the equatorial ones (1.75(2) Å). It may suggest, however, that a slight compression of iron bipyramide is due to the donor *trans* effect of the hydride [19]. These distances fall in a lower part of the range of Fe–CO bond lengths observed in $Fe(CO)_n$ units (1.73–1.81 Å; $n = 3$–5) [20] indicating a rather high electron density (due to the π-back bonding) retained on the $Fe(CO)_3$ fragment in (**5**,**5Fe**). Note, that the mean Fe–CO bond length reported for the structurally related electron rich discrete [*cis*-$HFe(CO)_3$-$P(OPh)_3]^-$ anion (1.73(1) Å) [20a] is essentially the same. The electron density on the $Fe(CO)_3$ fragment

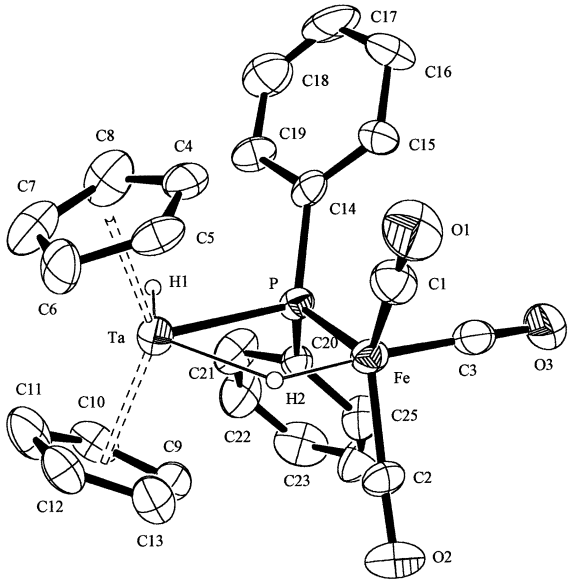


Fig. 5. ORTEP drawing of (**5**,**5Fe**) (30% probability level). Selected bond lengths (Å) and angles (°): Ta–Fe 3.111(2); Ta–P 2.548(3); Ta–H1 1.82(13); Ta–H2 2.01(12); Fe–P 2.168(4); Fe–H2 1.49(12); Fe–C1 1.740(17); Fe–C2 1.757(14); Fe–C3 1.708(16); Ta–CP1 2.059; Ta–CP2 2.068; H1–Ta–H2 124(5); H1–Ta–P 58(4); H2–Ta–P 67(3); Ta–P–Fe 82.1(1); Ta–H2–Fe 125(3); CP1–Ta–CP2 135.2.

is still higher in (**5**,**5*Fe**) as indicated by its ν(CO) IR data (see Section 4). All these observations argue for no (or little) direct electron density exchange between the metals. Effectively, the Ta–Fe separation in (**5**,**5Fe**) of 3.111(2) Å is longer than in $Cp_2Nb(\mu\text{-}PPh_2,CO)Fe(CO)_3$ for which a direct Nb–Fe bond (2.884(2) Å) has been postulated and confirmed by EHMO calculations [3c]. Thus, the electron density exchange (bonding) between the $Cp_2Ta(H)(\mu\text{-}PPh_2,H)$ and $Fe(CO)_3$ fragments in (**5**,**5Fe**) operates via the bridging atoms and not through a direct Ta–Fe bond. Such a difference may be rationalised in a frame of singular properties of 's' (bridging hydride) and 'p' (bridging carbon (CO)) atomic orbitals which are able to orient the phases (lobes) of metal atomic orbitals in these bimetallic systems either towards the 'in phase' (bonding M–M′) interaction (as in the case of $M(\mu\text{-}PR_2,CO)M'$) or towards the opposite phases (antibonding M–M′) as in the case of the hydride bridge in the $M(\mu\text{-}PR_2,H)M'$ system.

3. Conclusion

In this contribution we attempted to clarify the crucial points of tantalocene–hydride–phosphorus chemical systems: the regiochemistry of insertion of PR_2 (from PR_2Cl) into the central Ta–H bond of trihydrides Cp_2TaH_3 (formation of symmetrical metallophosphonium cations) and the influence of substitution on the cyclopentadienyl ring on the site (Ta–H or P–H) of neutralisation in these organometallic cations with strong bases. The proposed pathways for these reactions have been confirmed by DFT calculations. Good electron donor cyclopentadienyl ligands (Cp′ and Cp*) favour the formation of Ta(V)–phosphide structures when R is also a donor (Me). A supposition that the metal–phosphide (PR_2) bonds are longer than the metal–secondary phosphine (PR_2H) ones, because of a more diffuse nature of the phosphorus lone pair than that of the P–H bond, is also confirmed by DFT calculations.

4. Experimental

Nuclear magnetic resonance spectra were recorded on a Bruker AC 200 instrument at 200 MHz for ^1H and 81 MHz for ^{31}P. The chemical shifts are reported in ppm relative to $SiMe_4$ (^1H) and external H_3PO_4 (^{31}P–$\{^1H\}$). Infrared spectra were obtained with a Nicolet 250 spectrometer, with the sample in solution in thf. Elemental analyses were performed on a EA 1108 CHNS-O FISONS Instruments apparatus.

All manipulations were performed under a dry nitrogen atmosphere by standard techniques. Solvents were dried and deoxygenated by using conventional procedures. $Cp_2TaH_2(PPh_2)$ [5a,6b], $CpCp'TaH_3$ [12], $CpCp^*TaH_3$, $Cp^*_2TaH_3$ [21] and $Fe(CO)_3$(BDA) [22] were prepared according to literature methods.

4.1. Preparation of [CpCp*TaH$_2$(PMe$_2$H)]Cl (2,2*,Me)

To a $C_6H_5CH_3$ solution (30 ml) of Cp^*CpTaH_3 (0.19 g, 0.5 mmol) was added 1 equiv. of PMe_2Cl. After 15 min of stirring, a white precipitate was filtered, washed with $C_6H_5CH_3$ and C_5H_{12} and dried under vacuum (yield 0.22 g, 92%). ^1H NMR (200 MHz, CD_3COCD_3, 25 °C, TMS): $\delta = 5.69$ (s, Cp), 5.29 (dh, $^1J(H, P) = 348.4$ Hz, $^3J(H, H) = 6.5$ Hz, PH), 2.19 (s, Cp*), 1.76 (dd, $^2J(H, P) = 10.7$ Hz, $^3J(H, H) = 6.5$ Hz, Me), -0.58 (d, $^2J(H, P) = 75.1$ Hz, TaH). $^{31}P\{^1H\}$ NMR (81 MHz, CD_3COCD_3, 25 °C, TMS): $\delta = -43.1$ (s, PMe_2H).

4.2. Preparation of CpCp*TaH$_2$(PMe$_2$) (3,3*,Me)

A saturated aq. solution of KOH (10 ml) was added to the dried salt $[Cp^*CpTaH_2(PMe_2H)]Cl$ (0.24 g, 0.5 mmol). The mixture was stirred for 30 min. The product was extracted with $C_6H_5CH_3$ (2×15 ml) and the organic layer was evaporated under vacuum (yield 0.2 g, 90%). ^1H NMR (200 MHz, CD_3COCD_3, 25 °C, TMS): $\delta = 4.99$ (s, Cp), 2.02 (s, Cp*), 1.27 (d, $^2J(H, P) = 2.9$ Hz, Me), -0.67 (d, $^2J(H, P) = 56.1$ Hz, TaH). $^{31}P\{^1H\}$ NMR (81 MHz, CD_3COCD_3, 25 °C, TMS): $\delta = -81.3$ (s, PMe_2).

4.3. Preparation of $[Cp^*_2TaH_2(PMe_2H)]PF_6$ (**2***,**2***,**Me**)

To a $C_6H_5CH_3$ solution (30 ml) of $Cp^*_2TaH_3$ (0.23 g, 0.5 mmol) was added 1 equiv. of PMe_2Cl. After 15 min of stirring, a white precipitate was filtered, washed with $C_6H_5CH_3$ and C_5H_{12} and dried under vacuum. The resulting white powder was dissolved in water (10 ml). One equiv. of a water solution of NH_4PF_6 was added. A white precipitate was instantaneously formed which was filtered washed with water a dried under vacuum (yield 0.25 g 75%). ^{1}H NMR (200 MHz, CD_3COCD_3, 25 °C, TMS): $\delta = 5.15$ (dh, ^1J(H, P) = 344.0 Hz, ^3J(H, H) = 7.1 Hz, PH), 2.06 (s, Cp*), 1.67 (dd, ^2J(H, P) = 9.3 Hz, ^3J(H, H) = 7.3 Hz, Me), 0.00 (d, ^2J(H, P) = 77.1 Hz, TaH). ^{31}P{^{1}H} NMR (81MHz, CD_3COCD_3, 25 °C, TMS): $\delta = -50.2$ (s, PMe_2H), -146.3 (h, ^1J(P, F) = 703.2 Hz, PF_6).

4.4. Preparation of $[Cp^*_2TaH_2(PPh_2H)]PF_6$ (**2***,**2***,**Ph**)

The procedure was the same as above starting from $Cp^*_2TaH_3$ (0.23 g, 0.5 mmol) and 1 equiv. of PPh_2Cl (yield 0.27 g, 80%). ^{1}H NMR (200 MHz, $CDCl_3$, 25 °C, TMS): $\delta = 7.66$–7.30 (m, Ph), 6.86 (d, ^1J(H, P) = 356.2 Hz, PH), 1.97 (s, Cp*), 0.67 (d, ^2J(H, P) = 73.7 Hz, TaH). ^{31}P{^{1}H} NMR (200 MHz, $CDCl_3$, 25 °C, TMS): $\delta = 2.3$ (s, PPh_2H), -146.3 (h, ^1J(P, F) = 703.2 Hz, PF_6).

4.5. Preparation of $[CpCp'TaH_2(PMe_2H)]PF_6$ (**2**,**2′**,**Me**)

To a $C_6H_5CH_3$ solution (30 ml) of $Cp'CpTaH_3$ (0.2 g, 0.5 mmol) was added 1 equiv. of PMe_2Cl. After 15 min of stirring, a white precipitate was filtered, washed with $C_6H_5CH_3$ and C_5H_{12} and dried under vacuum. To a water solution (20 ml) of this salt was added 1 equiv. of NH_4PF_6. A white precipitate was instantaneously formed. After 10 min of stirring, it was filtered, washed with cold water and dried under vacuum (yield 0.22 g, 72%). Recrystallization from thf gave colourless crystals. *Anal.* Calc. for $C_{18}H_{31}F_6P_2Ta$: C, 35.81; H, 5.23. Found: C, 35.74; H, 5.16%. ^{1}H NMR (200 MHz, CD_3COCD_3, 25 °C, TMS): $\delta = 5.75$ (s, Cp), 5.21 (d, ^3J(H, P) = 3.5 Hz, CH), 5.54 (dh, ^1J(H, P) = 360 Hz, ^3J(H, H) = 6 Hz, PH), 2.33 (s, CH_3), 1.79 (dd, ^2J(H, P) = 9.7 Hz, ^3J(H, H) = 6 Hz, PMe), 1.27 (s, ^{t}Bu), -0.82 (d, ^2J(H, P) = 74 Hz, TaH). ^{31}P NMR (81 MHz, CD_3COCD_3, 25 °C, TMS): $\delta = -54.0$ (d, ^1J(H, P) = 360 Hz, PMe_2H), -141.0 (h, ^1J(P, F) = 708 Hz, PF_6).

4.6. Preparation of $CpCp'TaH(PMe_2H)$ and $CpCp'TaH_2(PMe_2)$ (**3**,**3′**,**Me**)

The procedure was the same as for (**3**,**3***,**Me**), starting from (**2**,**2′**,**Me**) (0.1 g, 0.2 mmol). The two complexes have not been separated from the mixture. The NMR data of each complex are given from the spectra of the mixture.

4.7. $Cp'CpTaH(PMe_2H)$ (60%)

^{1}H NMR (200 MHz, C_6D_6, 25 °C, TMS): $\delta = 5.10$ (dh, ^1J(P, H) = 309 Hz, ^3J(H, H) = 6 Hz, PH), 4.30 (d, J(P, H) = 2 Hz, Cp), 3.82 (dd, J(P,H) = 5Hz, J(H, H) = 3.3 Hz, CH) 3.41 (dd, J(P, H) = 3 Hz, J(H, H) = 3.3 Hz, CH), 1.96 (s, Me), 1.95 (s, Me), 1.28 (s, ^{t}Bu), 1.23 (dd, ^2J(P, H) = 7Hz, ^3J(H, H) = 6 Hz, PMe_2), 1.05 (dd, ^2J(P, H) = 6 Hz, ^3J(H, H) = 6Hz, PMe_2), -8.82 (d, ^2J(P, H) = 22 Hz, TaH). ^{31}P NMR (81 MHz, C_6D_6, 25 °C, TMS): $\delta = -46.8$ (d, ^1J(P, H) = 309 Hz, PMe_2H).

4.8. $Cp'CpTaH_2(PMe_2)$ (40%)

^{1}H NMR (200 MHz, C_6D_6, 25 °C, TMS): $\delta = 4.70$ (s, Cp), masked (CH), 2.08 (s, Me), 1.77 (d, ^2J(P, H) = 3.7 Hz, PMe_2), 1.27 (s, ^{t}Bu), -0.51 (d, ^2J(P, H) = 53 Hz, TaH). ^{31}P NMR (81 MHz, C_6D_6, 25 °C, TMS): $\delta = -113.7$ (d, ^2J(P, H) = 53 Hz, PMe_2).

4.9. Preparation of $Cp_2TaH(\mu\text{-}H)(\mu\text{-}PPh_2)Fe(CO)_3$ (**5**,**5**,**Fe**)

To a thf solution (30 ml) of $Cp_2TaH_2(PPh_2)$ (0.50 g, 1 mmol) was added 1 equiv. of $Fe(CO)_3$(BDA). The mixture was stirred for 2 h at room temperature (the reaction was monitored by IR spectroscopy). The solvent was removed under vacuum and the crude reaction product was chromatographed on silica gel with $C_6H_5CH_3$ as eluent affording a red bimetallic complex (72% yield). *Anal.* Calc. for $C_{25}H_{22}FeO_3PTa$: C, 47.05; H, 3.47. Found: C, 47.25; H, 3.32%. IR (thf): ν_{CO}, 1989, 1940, 1916 cm^{-1}. ^{1}H NMR (200 MHz, C_6D_6, 25 °C, TMS): $\delta = 8.16$–7.89 (m, Ph), 7.21–6.89 (m, Ph), 4.43 (s, Cp), -1.36 (dd, ^2J(H, H) = 8.9 Hz, ^2J(H, P) = 46.2 Hz, H), -10.11 (dd, ^2J(H, H) = 8.9 Hz, ^2J(H, P) = 43.3 Hz, H). ^{31}P{^{1}H} NMR (81MHz, C_6D_6, 25 °C, TMS): $\delta = 177.2$ (s, PPh_2). Crystals for X-ray analysis have been grown from acetone solution.

4.10. Preparation of $CpCp^*TaH(\mu\text{-}H)(\mu\text{-}PMe_2)Fe(CO)_3$ (**5**,**5***,**Fe**)

The procedure was the same as above starting from $Cp^*CpTaH_2(PMe_2)$. *Anal.* Calc. for $C_{20}H_{28}FeO_3PTa$: C, 41.12; H, 4.83. Found: C, 41.04; H, 4.81%. IR (thf): ν_{CO}, 1953, 1874, 1857 cm^{-1}. ^{1}H NMR (200 MHz, C_6D_6, 25 °C, TMS): $\delta = 4.46$ (s, Cp), 1.75 (d, ^3J(H, P) = 9.8 Hz, Me), 1.70 (d, ^3J(H, P) = 9.8 Hz, Me), 1.49

Table 1
Crystallographic data for $[CpCp'TaH_2(PMe_2H)]PF_6$ (**2**,**2′Me**) and $Cp_2Ta(H)(\mu\text{-}PPh_2,H)Fe(CO)_3,(CH_3)_2CO$ (**5**,**5Fe**) complexes

Complex	(**2**,**2′Me**)	(**5**,**5Fe**)
Empirical formula	$C_{18}H_{31}F_6P_2Ta$	$C_{28}H_{27}FeO_4PTa$
Formula weight	604.32	695.27
Colour, size (mm)	colourless, $0.25\times0.25\times0.20$	red, $0.4\times0.3\times0.15$
Crystal system	monoclinic	monoclinic
Space group	$P2_1/c$ (No. 14)	$P2_1/n$ (No. 14)
Unit cell dimensions		
a (Å)	8.878(1)	14.783(3)
b (Å)	13.303(2)	11.7922(17)
c (Å)	19.324(2)	17.198(4)
β (°)	97.877(8)	114.83(2)
V (Å^3)	2260.9(5)	2720.9(9)
Z, ρ_{calc}, Mg m^{-3}	4, 1.775	4, 1.697
$F(000)$	1184	1364
Radiation, λ(Mo Kα), Å	0.71073	0.71073
Linear absorption, μ (mm^{-1})	5.052	4.641
Scan	ω	ω–2θ
θ Range (°)	2.13–26.29	2.30–20.59
Index ranges	$0\le h\le11$, $-16\le k\le0$, $-24\le l\le-23$	$0\le h\le14$, $0\le k\le11$, $-16\le l\le14$
Reflections collected	4875	2311
Reflections unique [$I>2\sigma(I)$]	3697 [$R_{int}=0.019$]	1931 [$R_{int}=0.047$]
Linear decay (%)	−10, corrected	−28, corrected
Abs. corr., Ψ scan	69.48/99.77	64.5/99.78
Refinement method	Full-matrix least-squares on F^2	Full-matrix least-squares on F^2
Data/restraints/parameters	3697/0/263	1931/0/304
Final R indices [$I>2\sigma(I)$]	$R_1=0.026$, $wR_2=0.062$	$R_1=0.036$, $wR_2=0.086$
Goodness-of-fit F^2	1.025	1.052
ρ_{max}/ρ_{min} (e Å^{-3})	0.62/−0.84	0.63/−0.57

(s, Cp*), −1.36 (dd, ^2J(H, H) = 8.9 Hz, ^2J(H, P) = 46.2 Hz, H), −10.11 (dd, ^2J(H, H) = 8.9 Hz, ^2J(H, P) = 43.3 Hz, H). $^{31}P\{^1H\}$ NMR (81 MHz, C_6D_6, 25 °C, TMS): δ = 110.0 (s, PMe_2).

4.11. X-ray crystallography

All measurements have been carried out at 296 K on an Enraf–Nonius CAD4 diffractometer. The pertinent crystallographic data are given in Table 1. The unit cells have been determined from 25 randomly selected reflections (CAD4-Express) [23]. Intensity data have been reduced with PROCESS contained in MolEN package [24] with neutral–atom scattering factors. Both structures were solved by direct methods (SHELXS-97) [25] and refined by using the SHELXL-97 library [26]. All non-hydrogen atoms were refined with anisotropic thermal parameters. The hydrides in both structures and the hydrogen atom bound to phosphorus in (**2**,**2′**,**Me**) were found from difference Fourier synthesis and refined isotropically. All other hydrogen atoms were placed in calculated positions and included in refinements in a riding model with isotropic U(H) = 1.3 U_{eq}(C). The acetone molecule in (**5**,**5**,**Fe**) was refined isotropically.

5. Supplementary material

Crystallographic data for the structural analysis have been deposited with CCDC (12 Union Road, Cambridge CB2 1EZ, UK) and are available on request quoting the deposition numbers CCDC No. 147080 and 147081 for compounds **2**,**2′Me** and **5**,**5Fe**, respectively (fax: +44-1223-336033; e-mail: deposit@ccdc.cam.ac.uk or www: http://www.ccdc.cam.ac.uk).

References

[1] (a) L.H. Gade, H. Memmler, U. Kauper, A. Schneider, S. Fabre, I. Bezougli, M. Lutz, C. Galka, I.J. Scowen, M. McPartlin, Chem. Eur. J. 6 (2000) 692;
(b) M.A. Casado, J.J. Perez-Torrente, M.A. Ciriano, L.A. Oro, A. Orejon, C. Claver, Organometallics 18 (1999) 3035;
(c) T.W. Graham, A. Llamazares, R. McDonald, C. Martin, Organometallics 18 (1999) 3502.
[2] (a) V.G. Albano, L. Busetto, M. Monari, V. Zanotti, J. Organomet. Chem. 583 (1999) 28;
(b) D.G. Dick, D.W. Stephan, Organometallics 10 (1991) 2811;
(c) D.G. Dick, D.W. Stephan, Can. J. Chem. 69 (1991) 1146;
(d) E. Hey-Hawkins, M.F. Lappert, J.L. Atwood, S.G. Bott, J. Chem. Soc., Dalton Trans. (1991) 939;
(e) D.G. Dick, D.W. Stephan, Organometallics 9 (1990) 1910;
(f) R.T. Baker, T.H. Tulip, S.S. Wreford, Inorg. Chem. 24 (1985) 1379;

(g) R.T. Baker, J.F. Whitney, S.S. Wreford, Organometallics 2 (1983) 1049.
[3] (a) G. Boni, P. Sauvageot, E. Marpeaux, C. Moïse, Organometallics 14 (1995) 5652;
(b) G. Boni, P. Sauvageot, C. Moïse, J. Organomet. Chem. 489 (1995) C32;
(c) P. Oudet, M.M. Kubicki, C. Moïse, Organometallics 13 (1994) 4278;
(d) G. Bonnet, M.M. Kubicki, C. Moïse, R. Lazzaroni, P. Salvadori, G. Vitulli, Organometallics 11 (1992) 964;
(e) G. Bonnet, O. Lavastre, J.C. Leblanc, C. Moïse, New J. Chem. 12 (1988) 551–552.
[4] (a) C. Barré, P. Boudot, M.M. Kubicki, C. Moïse, Inorg. Chem. 34 (1995) 284;
(b) C. Barré, M.M. Kubicki, J.C. Leblanc, C. Moïse, Inorg. Chem. 29 (1990) 5244;
(c) M.M. Kubicki, R. Kergoat, M. Cariou, J.E. Guerchais, P. L'Haridon, J. Organomet. Chem. 322 (1987) 357.
[5] (a) G. Bonnet, O. Lavastre, G. Boni, J.C. Leblanc, C. Moïse, C.R. Acad. Sci. Paris (1994) t. 319, Série II, 1293;
(b) O. Lavastre, G. Bonnet, G. Boni, M.M. Kubicki, C. Moïse, J. Organomet. Chem. 547 (1997) 141.
[6] (a) G.I. Nikonov, D.A. Lemenovskii, J. Lorberth, Organometallics 13 (1994) 3127;
(b) G.I. Nikonov, L.G. Kuzmina, P. Mountford, D.A. Lemenovskii, Organometallics 14 (1995) 3588;
(c) G.I. Nikonov, Y.K. Grishin, D.A. Lemenovskii, N.B. Kazennova, L.G. Kuzmina, J.A.K. Howard, J. Organomet. Chem. 547 (1997) 183.
[7] HYPERCHEM, release 4, Hypercube Inc., 1994.
[8] (a) GAUSSIAN 94, Revision E.1, Gaussian Inc., Pittsburgh PA, 1995;
(b) R.G. Parr, W. Yang, Density Functional Theory of Atoms and Molecules, Oxford University Press, Oxford, UK, 1989;
(c) A.D. Becke, J. Chem. Phys. 98 (1993) 5648;
(d) T.H. Dunning Jr., P.J. Hay, in: H.F. Schaefer (Ed.), Modern Theoretical Chemistry, 3rd ed., Plenum Press, New York, 1976, p. 1.
[9] J.F. Leboeuf, O. Lavastre, J.C. Leblanc, C. Moïse, J. Organomet. Chem. 418 (1991) 359.
[10] J.W. Lauher, R. Hoffmann, J. Am. Chem. Soc. 98 (1976) 1729.
[11] P. Sauvageot, PhD thesis, Université de Bourgogne, Dijon, 1996.
[12] P. Sauvageot, C. Moïse, Bull. Soc. Chim. Fr. 133 (1996) 177.
[13] W.E. Buhro, B.D. Zwick, S. Georgiou, J.P. Hutchinson, J.A. Gladysz, J. Am. Chem. Soc. 110 (1988) 2427.
[14] G. Boni, M.M. Kubicki, C. Moïse, in: P. Braunstein, L.A. Oro, P.R. Raithby (Eds.), Metal Clusters in Chemistry, Wiley-VCH, 1999, 110 pp.
[15] C. Barré, M.M. Kubicki, C. Moïse, Phosphorus Sulfur Silicon 77 (1993) 49.
[16] R.T. Baker, J.C. Calabrese, R.L. Harlow, I.D. Williams, Organometallics 12 (1993) 830.
[17] D.S. Moore, S.D. Robinson, Chem. Soc. Rev. 12 (1983) 415.
[18] G. Bonnet, PhD thesis, University of Burgundy, Dijon, 1990.
[19] B. Jezowska-Trzebiatowska, B. Nissen-Sobocinska, L. Natkaniec, J. Organomet. Chem. 376 (1989) 67.
[20] (a) C.E. Ash, C.M. Kim, M.Y. Darensbourg, A.L. Rheingold, Inorg. Chem. 26 (1987) 1357;
(b) L.P. Battaglia, D. Delledonne, M. Nardelli, C. Pelizzi, G. Predieri, G.P. Chiusoli, J. Organomet. Chem. 330 (1987) 101;
(c) T.J. Kim, K.H. Kwon, S.C. Kwon, J.O. Baeg, S.C. Shim, D.H. Lee, J. Organomet. Chem. 389 (1990) 205;
(d) R. Glaser, Y.H. Yoo, G.S. Chen, C.L. Barnes, Organometallics 13 (1994) 2578;
(e) P.E. Riley, R.E. Davis, Inorg. Chem. 19 (1980) 159;
(f) T.J. Kim, S.C. Kwon, Y.H. Kim, N.H. Heo, M.M. Teeter, A. Yamano, J. Organomet. Chem. 426 (1991) 71;
(g) D. Braga, F. Grepioni, A.G. Orpen, Organometallics 12 (1993) 1481.
[21] V.C. Gibson, J.E. Bercaw, W.J. Bruton, R.D. Sanner, Organometallics 5 (1986) 976.
[22] J.A.S. Howell, B.F.G. Johnson, P.L. Josty, J. Lewis, J. Organomet. Chem. 39 (1972) 329.
[23] Enraf–Nonius, Delft, CAD4 EXPRESS, v. 5.1, The Netherlands, 1992.
[24] C.K. Fair, Enraf–Nonius, MolEN. An Interactive Intelligent System for Crystal Structure Analysis, Delft, The Netherlands, 1990.
[25] G.M. Sheldrick, SHELXS-97, Program for the Solution of Crystal Structures, University of Göttingen, Germany, 1997.
[26] G.M. Sheldrick, SHELXL-97, Program for the Refinement of Crystal Structures, University of Göttingen, Germany, 1997.

PERGAMON

Polyhedron 21 (2002) 381–387

POLYHEDRON

www.elsevier.com/locate/poly

Sulfido triosmium clusters containing bridging dppm ligand: crystal structures of $[Os_3(CO)_7(\mu_3\text{-}CO)(\mu_3\text{-}S)(\mu\text{-}dppm)]$ and the two isomers of $[Os_3(CO)_7(\mu_3\text{-}S)_2(\mu\text{-}dppm)]$

Kazi A. Azam [a,*], G.M. Golzar Hossain [b], Shariff E. Kabir [a], K.M. Abdul Malik [b,*], Md. Abdul Mottalib [a], Salina Perven [a], Nitai C. Sarker [a]

[a] *Department of Chemistry, Jahangirnagar University, Savar, Dhaka 1342, Bangladesh*
[b] *Department of Chemistry, Cardiff University, P.O. Box 912, Park Place, Cardiff, CF10 3TB, UK*

Received 5 September 2001; accepted 20 November 2001

Abstract

The reaction of $[Os_3(CO)_{10}(\mu\text{-}dppm)]$ (**1**) with H_2S at 110 °C leads to the known compound $[(\mu\text{-}H)_2Os_3(CO)_7(\mu_3\text{-}S)(\mu\text{-}dppm)]$ (**2**) (11%) and the new compound $[Os_3(CO)_7(\mu_3\text{-}CO)(\mu_3\text{-}S)(\mu\text{-}dppm)]$ (**3**) (65%). Treatment of **1** with thiourea at 110 °C gives **2** (70%). The analogous reaction of **1** with tetramethylthiourea at 110 °C yielded two 50 electron stereoisomeric compounds **4a** and **4b** with stoichiometry $[Os_3(CO)_7(\mu_3\text{-}S)_2(\mu\text{-}dppm)]$ in 16 and 64% yields, respectively. The new compounds **3**, **4a** and **4b** were characterized by spectroscopic data and X-ray diffraction studies. Compound **3** reacts with tetramethylthiourea at 110 °C to give **4a** and **4b**. Hydrogenation of **3** at 1 atmosphere pressure at 151 °C gives **2**. © 2002 Elsevier Science Ltd. All rights reserved.

Keywords: Triosmium cluster; Tetramethylthiourea; Desulfurization; Sulfido; X-ray structures

1. Introduction

There is considerable interest in the synthesis, structure and reactivity of sulfido triosmium carbonyl clusters. The most important simple sulfido triosmium clusters are $[Os_3(\mu_3\text{-}CO)(CO)_9(\mu_3\text{-}S)]$ (**5**) and $[Os_3(CO)_9(\mu_3\text{-}S)_2]$ (**6**) together with their corresponding dihydrides $[(\mu\text{-}H)_2Os_3(CO)_9(\mu_3\text{-}S)]$ (**7**) and $[(\mu\text{-}H)_2Os_3(CO)_8(\mu_3\text{-}S)_2]$ (**8**) [1,2]. The synthesis of sulfido triosmium clusters has been tackled from a number different routes including the cleavage of carbon–sulfur bond of the coordinated organosulfur ligands, direct reaction of $[Os_3(CO)_{12}]$ with elemental sulfur, with hydrogen sulfide or with carbon disulphide. For example, the cluster **5** along with **6** and various other Os_4 and Os_6 sulfido clusters have been synthesized by desulfurization of the coordinated thiolato ligand in $[(\mu\text{-}H)Os_3(CO)_{10}(\mu\text{-}SPh)]$ (**9**) [3]. The distribution of the products can be controlled by performing the reaction under a pressure of CO and at 120 atm it is possible to obtain just **6**, $[Os(CO)_5]$ and C_6H_6 [4]. However, the UV decomposition of **9** under CO is more useful and gives **5** in moderate yield [5]. The reaction mixture is purged with H_2 during photolysis to give **7** while treatment with COS gives **6** [5]. Another good route to the simple clusters is from *cyclo*-SCH_2CH_2, which reacts with $[Os_3(CO)_{12}]$ to give **5** and **6** [6]. Hydrogen sulfide (H_2S) reacts with $[Os_3(CO)_{12}]$ at 128 °C to give **7** in almost quantitative yields [7]. Elemental sulfur reacts with $[Os_3(CO)_{12}]$ at 128 °C to yield **6**, **8** and $[(\mu\text{-}H)_2Os_4(CO)_{12}(\mu_3\text{-}S)_2]$ [8]. Carbon disulfide (CS_2) reacts with $[Os_3(CO)_{12}]$ to form $[Os_3(CO)_8(\mu_3\text{-}S)_2(CS)]$ [9] and with the lightly-stabilized cluster $[(\mu\text{-}H)_2Os_3(CO)_8(\mu_3\text{-}S)(NCMe)]$ it yields $[(\mu\text{-}H)_2Os_3(CO)_8(\mu_3\text{-}S)_2(CS)]$ [10]. Sulfurdimide, $Me_3SiN{=}S{=}NSiMe_3$, reacts with $[Os_3(CO)_{12}]$ at 128 °C to give $[Os_3(CO)_9(\mu_3\text{-}S)(\mu_3\text{-}NSiMe_3)]$ [11]. Recently, it has been reported that *N*-(*p*-methoxybenzoyl)-*S*-benzoylsulphenamide reacts with $[Os_3(CO)_{10}(MeCN)_2]$ at room temperature to yield **5** and $[Os_6(CO)_{20}(\mu_4\text{-}S)(MeCN]$ [12] (Fig. 1).

* Corresponding authors. Tel.: +44-29-2087-4950; fax: +44-29-2087-4030.
E-mail address: malikka@cardiff.ac.uk (K.M. Abdul Malik).

0277-5387/02/$ - see front matter © 2002 Elsevier Science Ltd. All rights reserved.
PII: S0277-5387(01)00999-8

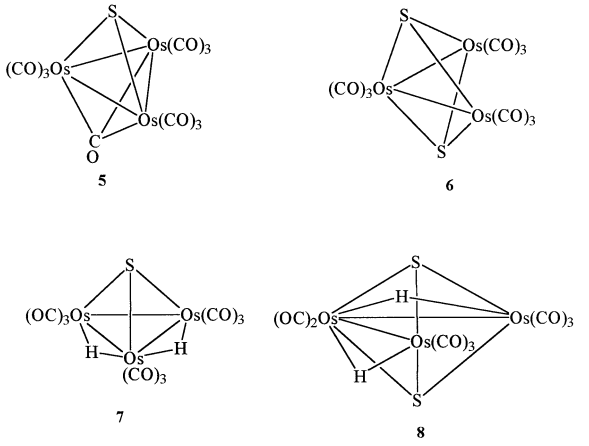
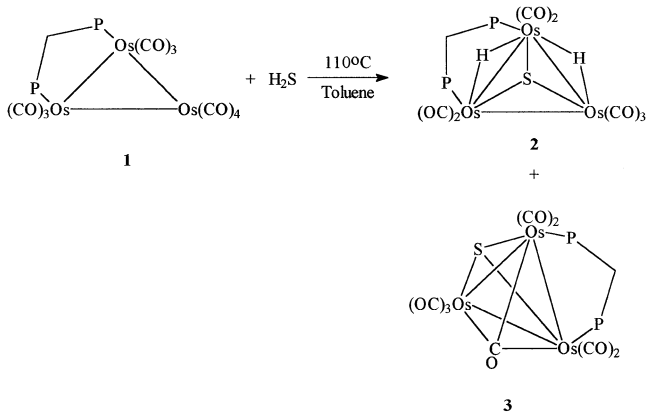


Fig. 1. Some simple sulfido triosmium clusters.



Scheme 1.

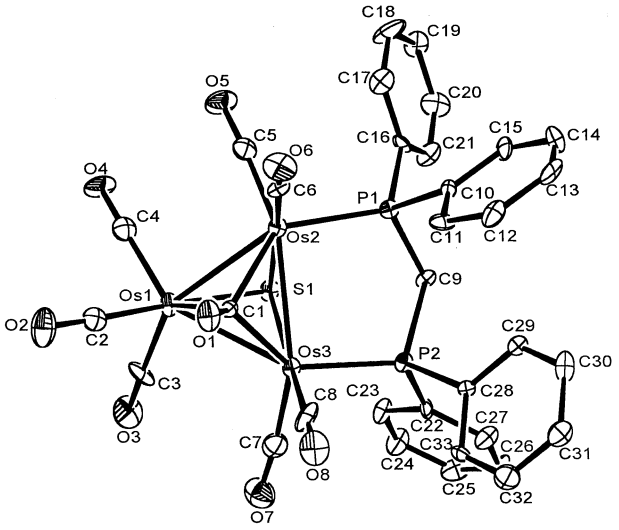


Fig. 2. The structure of one independent molecule of $[Os_3(CO)_7(\mu_3\text{-}CO)(\mu_3\text{-}S)(\mu\text{-}dppm)]$ **3** showing the atom labelling scheme. Thermal ellipsoids are drawn at 35% probability level. The hydrogen atoms are omitted for clarity.

The reactivity of thioureas with $Ru_3(CO)_{12}$ has extensively been studied by Süss-Fink and coworkers [13–20]. These reactions are associated with the cleavage of C–S, C–N, N–H and/or C–H bonds of the alkyl substituted derivatives, and they depend markedly on the substituent groups and also on the reaction conditions. For example, thiourea and its dimethyl derivative react with $[Ru_3(CO)_{12}]$ to give the N–H activated product $[(\mu\text{-}H)Ru_3(CO)_9(\mu_3\text{-}\eta^2\text{-}NRCSNHR)]$ (R = H or Me) [13] whereas the analogous reaction with di-*tert*-butylthiourea yields $[(\mu\text{-}H)Ru_3(CO)_8(\mu_3\text{-}S)(\eta^2\text{-}CH_2\text{-}CMe_2NHCNHBu^t)]$ and $[(\mu\text{-}H)Ru_3(CO)_9\{\mu_3\text{-}SRu(CO)_3\text{-}(\eta^2\text{-}CH_2CMe_2NHCNHBu^t)\}]$ in which both C=S and C–H bonds of the ligand have been cleaved [18]. In comparison to the extensive ruthenium carbonyl cluster chemistry of thiourea ligands, only a few examples concerning the reactivity of these ligands with triosmium carbonyl clusters are known [21–23]. For example, Azam et al. [22] and others [21] have reported that thiourea and its diphenyl analogue react with the lightly stabilized cluster $[Os_3(CO)_{10}(MeCN)_2]$ to give the edge and triply bridging clusters $[(\mu\text{-}H)Os_3(CO)_{10}(\mu\text{-}NRC\text{-}SNHR)]$ and $[(\mu\text{-}H)Os_3(CO)_9(\mu_3\text{-}\eta^2\text{-}NRCSNHR)]$ (R=H or Ph). We also reported that tetramethylthiourea reacts with $[Os_3(CO)_{12}]$ in presence of a methanolic solution of Me_3NO and H_2O at 80 °C to give $[Os_3(CO)_{11}\text{-}\{\eta^1\text{-}SC(NMe_2)_2\}]$, $[Os_3(CO)_9(\mu\text{-}OH)(\mu\text{-}OMeCO)\{\eta^1\text{-}SC(NMe_2)_2\}]$ and $[(\mu\text{-}H)Os_3(CO)_8(\mu_3\text{-}S)(\mu\text{-}OMeCO)\{\eta^1\text{-}SC(NMe_2)_2\}]$ [23]. As part of a study of the reactivity of thiourea ligands with trimetallic clusters, we have investigated the reactions of $[Os_3(CO)_{10}(\mu\text{-}dppm)]$ with thiourea, tetramethylthiourea and H_2S, and report here the synthesis, structures and reactivity of the sulphido triosmium clusters $[Os_3(CO)_7(\mu_3\text{-}CO)(\mu_3\text{-}S)(\mu\text{-}dppm)]$ and the two isomers of $[Os_3(CO)_7(\mu_3\text{-}S)_2(\mu\text{-}dppm)]$.

2. Results and discussion

The reaction of $[Os_3(CO)_{10}(\mu\text{-}dppm)]$ (**1**) with H_2S at 110 °C yielded $[(\mu\text{-}H)_2Os_3(\mu_3\text{-}S)(CO)_7(\mu\text{-}dppm)]$ (**2**) and $[Os_3(\mu_3\text{-}CO)(\mu_3\text{-}S)(CO)_7(\mu\text{-}dppm)]$ (**3**) (Scheme 1). Compound **2** was previously reported from the reaction of $[(\mu\text{-}H)_2Os_3(CO)_9(\mu_3\text{-}S)]$ with dppm and structurally characterized [24]. Compound **3** is now characterized by spectroscopic methods together with a crystal structure determination. In the crystals of **3**, there are two independent molecules in an asymmetric unit, one of which is shown in Fig. 2. Selected bond distances and angles in the two molecules are compared in Table 1. The structures of the two molecules are very similar with only minor differences in the orientations of the phenyl rings on the phosphorus atoms. For the sake of brevity, the bond lengths and angles in molecule 1 are quoted in the following discussion. The structure of **3**

Table 1
Selected bond lengths (Å) and angles (°) for **3**

	Molecule 1	Molecule 2
Bond lengths		
Os(1)–Os(2)	2.8245(10)	2.8259(11)
Os(1)–Os(3)	2.8378(11)	2.8370(10)
Os(2)–Os(3)	2.8323(11)	2.8383(11)
Os(1)–S(1)	2.385(4)	2.385(4)
Os(2)–S(1)	2.400(4)	2.395(4)
Os(3)–S(1)	2.393(4)	2.395(4)
Os(2)–P(1)	2.339(4)	2.340(4)
Os(3)–P(2)	2.345(4)	2.363(4)
Os(1)–C(1)	2.270(14)	2.248(15)
Os(2)–C(1)	2.16(2)	2.112(14)
Os(3)–C(1)	2.151(14)	2.15(2)
Os–C (terminal) [a]	1.91(2)	1.90(2)
C–O (average)	1.15(2)	1.14(2)
P–C (average)	1.84(1)	1.84(1)
Bond angles		
Os(1)–S(1)–Os(2)	72.37(10)	72.47(11)
Os(1)–S(1)–Os(3)	72.89(11)	72.80(10)
Os(3)–S(1)–Os(2)	72.46(10)	72.67(10)
O(1)–C(1)–Os(1)	127.2(10)	127.6(10)
O(1)–C(1)–Os(2)	133.0(11)	133.5(12)
O(1)–C(1)–Os(3)	134.7(11)	131.7(12)
Os(2)–C(1)–Os(1)	79.1(5)	80.7(5)
Os(3)–C(1)–Os(1)	79.8(5)	80.2(5)
Os(3)–C(1)–Os(2)	82.1(5)	83.4(5)
C(1)–Os(1)–S(1)	87.1(4)	86.3(4)
C(2)–Os(1)–S(1)	170.8(5)	170.8(4)
C(3)–Os(1)–S(1)	93.5(5)	96.2(4)
C(4)–Os(1)–S(1)	96.4(4)	95.5(5)
C(6)–Os(2)–S(1)	170.2(5)	172.5(5)
C(5)–Os(2)–S(1)	95.1(5)	95.3(5)
C(1)–Os(2)–S(1)	89.3(4)	89.2(4)
P(1)–Os(2)–S(1)	89.28(13)	90.85(13)
C(7)–Os(3)–S(1)	101.1(5)	96.0(5)
C(8)–Os(3)–S(1)	168.1(5)	169.0(5)
C(1)–Os(3)–S(1)	89.7(4)	88.2(4)
P(2)–Os(3)–S(1)	89.56(13)	88.89(12)

[a] Average value.

consists of an Os_3 triangle with three osmium–osmium bonds containing seven terminal and one triply bridging carbonyl ligands, a μ_3-sulphido ligand and a bridging dppm ligand. Two of the metal–metal bonds, Os(1)–Os(3) = 2.8378(11) Å and Os(2)–Os(3) = 2.8323(11) Å, are equal and only marginally longer than the third bond, Os(1)–Os(2) = 2.8245(10) Å. There are no significant differences between the bridged and unbridged edges. This is in contrast with the structure of **2**, where the unbridged Os–Os edge is significantly shorter than the two bridged Os–Os edges [2.7658(6) vs 2.8981(4) and 2.9212(6) Å] [24]. All three bonds in **3** are significantly shorter than those found in $[Os_3(CO)_{12}]$ {2.877(3) Å} [25]. The triply bridging carbonyl and the sulfido ligands lie on opposite sides of the Os_3 triangle resulting in a trigonal bipyramidal geometry for the $Os_3(S)(CO)$ core. The μ_3-S is bound to the Os_3 triangle in a symmetrically, with the Os–S distances lying in the narrow range, 2.385(4)–2.400(4) Å and the average value {2.393(4) Å} is comparable with those found for the triply bridging sulfido ligands in **5** {2.378(3) Å} [5], $[Os_4(CO)_{12}(\mu_3\text{-S})]$ {2.381(3) Å} [26] and $[(\mu\text{-H})_2Os_3(CO)_7(\mu_3\text{-S})(\mu\text{-dppm})]$ {2.389(2) Å} [24]. In contrast, the μ_3-CO group is bonded asymmetrically to the Os_3 triangle. Two of these distances Os(3)–C(1) = 2.151(14) Å and Os(2)–C(1) = 2.16(2) Å are equal, and the third Os(1)–C(1) = 2.270 (14) Å is significantly longer. These values are close to those involving the μ_3-CO ligand in **5**, which range from 2.157(12) to 2.188(12) Å [5]. As expected, the Os–C distances involving the terminal CO groups are considerably shorter {average value = 1.91(2) Å}. The Os–P bond distances in **3** {Os(2)–P(1) = 2.339 (4) and {Os(3)–P(2) = 2.345(4) Å} are comparable to those found in **1** {2.332(3) and 2.312(3) Å} [27]. Overall, the structure of **3** is similar to that of **5** [5] if one considers that an equatorial carbonyl group on each of the two osmium atoms is replaced by the Ph_2P groups of the dppm ligand. The complex contains 48 valence electrons and is electron precise with three metal–metal bonds.

The spectroscopic properties of **3** are consistent with the solid state structure being maintained in solution. The infrared spectrum shows, in addition to absorptions due to terminal carbonyls, a weak absorption at 1820 cm^{-1} indicating the presence of a triply bridging carbonyl ligand. In the ^1H NMR spectrum, the multiplets centered at δ 3.67 and 4.83 are assigned to the methylene protons while that at δ 7.31 is due to the phenyl protons of dppm ligand. The $^{31}P\text{-}\{^1H\}$ spectrum contains a singlet at δ 20.4 indicating equivalent ^{31}P nuclei. The mass spectrum displays the molecular ion peak at m/z 1210 and fragmentation peaks corresponding to the loss of up to eight carbonyl ligands. Compound **3** reacts with molecular hydrogen at 1 atmosphere pressure at 151 °C to give **2** in 50% yield. However, attempts to convert **2** into **3** by prolong thermolysis at 110 °C were not successful.

The reaction of **1** with thiourea at 110 °C gave **2** resulting from the oxidative cleavage of N–H and C=S bonds of thiourea. In order to explore the effect of alkyl substituent groups of thiourea ligands on their reactivity with **1**, we investigated the reaction of **1** with tetramethylthiourea. The reaction of **1** with tetramethylthiourea at 110 °C yielded two isomeric compounds **4a** and **4b** with stoichiometry $[Os_3(CO)_7(\mu_3\text{-S})_2(\mu\text{-dppm})]$, that were characterized by spectroscopic and crystallographic methods. The structure of **4a** (Fig. 3; Table 2) consists of an open cluster of three osmium atoms with two metal–metal bonds, Os(1)–Os(3) = 2.8620(2), Os(2)–Os(3) = 2.8251(8) Å, a bridging dppm ligand and two triply bridging sulfido ligands. The Os(1)···Os(2) distance at 3.6196(14) Å is clearly nonbonding and shorter than that observed in **6**

{3.662(1) Å} [28]. Two of the osmium atoms Os(1) and Os(2) are six-coordinate, whilst the third Os(3) is seven-coordinate. The Os–S distances to the seven-coordinated osmium atom in **4a** {Os(3)–S(1) = 2.430(3), Os(3)–S(2) = 2.432(3) Å} are slightly longer than those to the six-coordinate osmium atoms {2.392(3)–2.407(3) Å} and also than the corresponding values in **3**. The dppm ligand bridges the two basal osmium atoms in the axial positions and the Os–P bond distances {Os(1)–P(1) = 2.286(3) Å, Os(2)–P(2) = 2.302(3)} are slightly shorter than those found in **1** [27] and **3**. Overall, compound **4a** has a square pyramidal structure with the two bridged Os atoms and two sulfur atoms alternating in the basal plane and the third osmium atom at the apex of the pyramid.

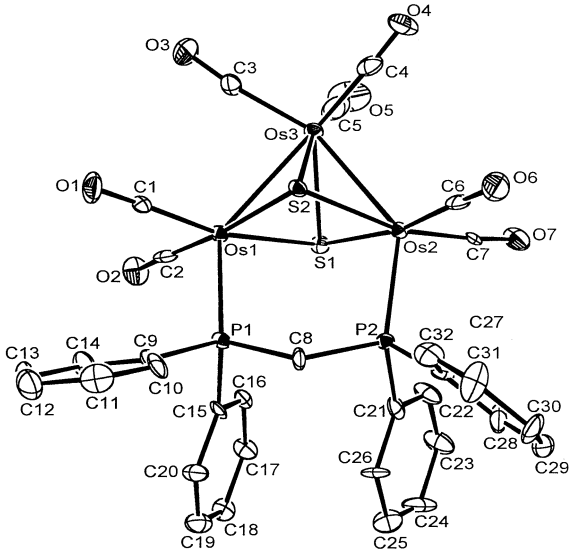


Fig. 3. Molecular structure of $[Os_3(CO)_7(\mu_3\text{-}S)_2(\mu\text{-dppm})]$ **4a** showing the atom labelling scheme. Thermal ellipsoids are drawn at 50% probability level. The hydrogen atoms are omitted for clarity.

Table 2
Selected bond lengths (Å) and angles (°) for **4a**

Bond lengths			
Os(1)–Os(3)	2.8620(12)	Os(2)–Os(3)	2.8251(8)
Os(1)···Os(2)	3.6196(14)	Os(1)–P(1)	2.286(3)
Os(1)–S(1)	2.392(3)	Os(1)–S(2)	2.400(3)
Os(2)–P(2)	2.302(3)	Os(2)–S(1)	2.392(3)
Os(2)–S(2)	2.407(3)	Os(3)–S(1)	2.430(3)
Os(3)–S(2)	2.432(3)	Os–C(CO) (average)	1.91(2)5
P–C (average)	1.84(2)	C–O (average)	1.14(2)
Bond angles			
Os(2)–S(1)–Os(1)	98.32(11)	Os(2)–S(1)–Os(3)	71.73(9)
Os(1)–S(1)–Os(3)	72.80(9)	Os(1)–S(2)–Os(2)	97.71(12)
Os(1)–S(2)–Os(3)	72.64(9)	Os(2)–S(2)–Os(3)	71.44(9)
S(1)–Os(1)–S(2)	80.07(11)	S(1)–Os(2)–S(2)	79.93(11)
S(1)–Os(3)–S(2)	78.69(11)	P(1)–Os(1)–S(1)	95.81(11)
P(1)–Os(1)–S(2)	93.68(11)	P(2)–Os(2)–S(1)	91.25(11)
P(2)–Os(2)–S(2)	94.60(11)		

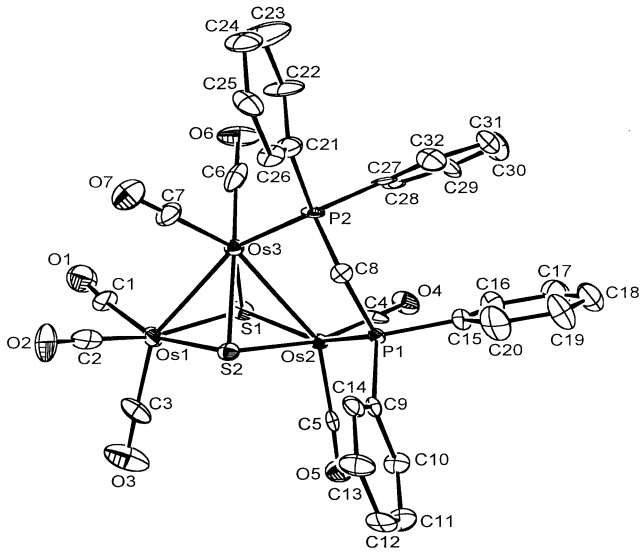


Fig. 4. Molecular structure of $[Os_3(CO)_7(\mu_3\text{-}S)_2(\mu\text{-dppm})]$ **4b** showing the atom labelling scheme. Thermal ellipsoids are drawn at 50% probability level. The hydrogen atoms are omitted for clarity.

Table 3
Selected bond lengths (Å) and angles (°) for **4b**

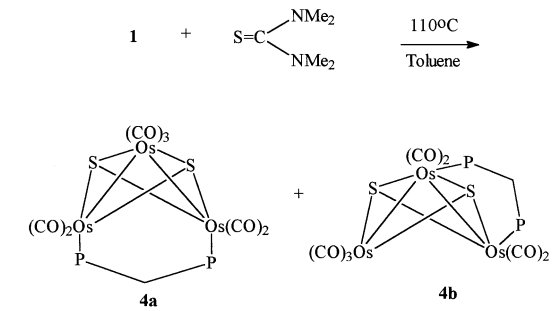
Bond lengths			
Os(1)–Os(3)	2.7910(11)	Os(2)–Os(3)	2.8412(12)
Os(1)···Os(2)	3.6760(14)	Os(1)–S(1)	2.386(4)
Os(1)–S(2)	2.411(4)	Os(2)–S(1)	2.363(4)
Os(2)–S(2)	2.428(4)	Os(3)–S(1)	2.432(4)
Os(3)–S(2)	2.466(4)	Os(2)–P(1)	2.362(4)
Os(3)–P(2)	2.316(4)	Os–C(CO) (average)	1.89(2)
P–C (average)	1.84(2)	C–O(average)	1.15(2)
Bond angles			
Os(2)–S(1)–Os(1)	101.5(2)	Os(2)–S(1)–Os(3)	72.66(11)
Os(1)–S(1)–Os(3)	70.80(11)	Os(1)–S(2)–Os(2)	98.86(14)
Os(1)–S(2)–Os(3)	69.80(11)	Os(2)–S(2)–Os(3)	70.97(12)
S(1)–Os(1)–S(2)	78.84(14)	S(1)–Os(2)–S(2)	78.95(14)
S(1)–Os(3)–S(2)	76.90(14)	P(1)–Os(2)–S(1)	152.66(14)
P(1)–Os(2)–S(2)	85.41(14)	P(2)–Os(3)–S(1)	128.64(14)
P(2)–Os(3)–S(2)	95.8(2)		

The structure of **4b** (Fig. 4; Table 3) consists of an Os_3 triangle involving two metal–metal bonds {Os(2)–Os(3) = 2.8412(12), Os(1)–Os(3) = 2.7910(11) Å} and a nonbonding osmium–osmium separation {Os(1)···Os(2) = 3.6760(14) Å}. In contrast to **4a**, the dppm ligand in **4b** bridges one of the bonded pair of osmium atoms Os(2) and Os(3) and the two Os–P distances are significantly different. The shorter Os(3)–P(2) distance {2.316(4) Å, axial position, *transoid* to Os} is comparable to those observed in **4a** where the dppm bridges the basal osmium atoms in the axial positions {Os–P = 2.286(3) and 2.302(3) Å}. In comparison, the Os(2)–P(1) distance {2.362(4) Å, equatorial, *transoid* to S} is significantly longer. This is consistent with the suggestion that the Os–P interaction in the Ru_3S_2 *indo* clusters suffers a short of *trans* effect [29]. The dppm substitution on Os(2)–Os(3) edge causes

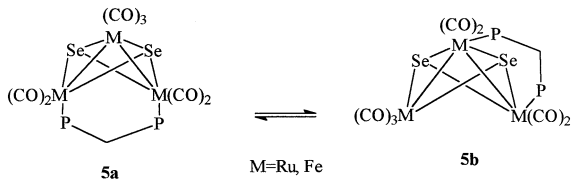
an important deformation in the cluster core, and the two Os–Os bond distances are significantly shorter than those in **4a**. The Os–S distances to the triply bridging sulfido ligands {Os(1)/Os(2)/Os(3)–S(1) = 2.386(4)/2.363(4)/2.432(4) and Os(1)/Os(2)/Os(3)–S(2) = 2.411(4)/2.428(4)/2.466(4) Å} are similar to those in **4a** and **6** [28], and as observed in **4a** the bonds with S(1) are slightly longer than those with the corresponding bonds to S(2).

The spectroscopic data of **4a** and **4b** are in accord with their solid state-structures. In the ^{31}P NMR spectra, as is expected, the minor isomer **4a** exhibits a singlet at δ 13.8 indicating equivalent ^{31}P nuclei while the major isomer **4b** shows two doublets at δ 9.5 and -20.3 indicating nonequivalence of the ^{31}P nuclei. In the ^{1}H NMR, in addition to the phenyl resonances, the isomer **4a** shows a triplet at δ 3.23 while the isomer **4b** shows two pseudo-quartets (dt, $J_{H-H} = 14.1$, $J_{H-P} = 10.5$ Hz) centered at δ 3.81 and 5.10. The pattern of ^{31}P NMR and ^{1}H NMR spectra of **4a** and **4b** is similar to that of $[Ru_3(CO)_7(\mu_3\text{-}Se)_2(\mu\text{-dppm})]$ which exists as an equilibrium mixture of two isomers in solution [30]. The mass spectrum of each isomer shows the molecular ion peak at m/z 1215 and fragment ions formed by the sequential loss of seven carbonyl groups. Compound **3** reacts with tetramethylthiourea at 110 °C affording **4a** and **4b**, which demonstrates that **3** is an earlier intermediate of **4a** and **4b** (Scheme 2).

In summary the reaction of the tetramethylthiourea with **1** provides a simple, one step route to the two isomers (**4a** and **4b**) of the open-triangular-nido cluster $[Os_3(CO)_7(\mu_3\text{-}S)_2(\mu\text{-dppm})]$ through oxidative transfer of the sulfur atoms to the low-valent osmium centres. The corresponding ruthenium and iron analogues $[M_3(CO)_7(\mu_3\text{-}Se)_2(\mu\text{-dppm})]$ have recently been reported



Scheme 2.



Scheme 3.

from the reaction of $[M_3(CO)_{12}]$ (M = Fe or Ru) with $dppmSe_2$ [31,32]. It was also suggested [29] that these compounds exist as a mixture of two isomers in solution because of the reversible migration of a metal–metal bond from one side of the open triangle to the basal plane resulting in the linking of the two metal atoms (Scheme 3). In the present work, we have successfully isolated the isomers **4a** and **4b** by careful chromatographic separation and characterized them structurally. It is also suggested that intramolecular fluxional processes are faster for ruthenium and iron compounds than for osmium. Another interesting aspect of the present study is the synthesis of **3** from the reaction of **1** with H_2S which reacts with tetramethylthiourea to give **4a** and **4b** and this shows that **3** is an earlier intermediate to **4a** and **4b**.

3. Experimental

All manipulations were carried out under N_2 atmosphere by employing standard Schlenk techniques. The solvents were of reagent grade and distilled from appropriate drying agents. The infrared spectra were recorded on a Shimadzu 8101 spectrophotometer. $^{31}P\{^{1}H\}$- and ^{1}H NMR spectra were obtained by use of a Bruker AC 200 spectrometer. Chemical shifts are referenced to internal TMS $\{^{1}H\}$ and to external 85% H_3PO_4 $\{^{31}P\}$. Mass spectra were recorded on a Varian Mat 312 mass spectrometer. Elemental analyses were carred out at the microanalytical Laboratory of the Institut für Anorganische and Analytical Chemie, Universität Freiburg, Germany. The cluster $[Os_3(CO)_{10}(\mu\text{-dppm})]$ was prepared according to the published procedure [33]. Tetramethylthiourea and thiourea were purchased from Aldrich and used as received.

3.1. Reaction of $[Os_3(CO)_{10}(dppm)]$ (1) with H_2S

Hydrogen sulphide gas was bubbled through a refluxing $C_6H_5CH_3$ solution (50 cm^3) of **1** (0.105 g, 0.085 mmol) for 2 h. The solvent was removed under vacuum and the residue chromatographed by TLC on silica gel. Elution with C_6H_{14}–CH_2Cl_2 (2:1, v/v) developed three bands. The first moving band gave unconsumed **1** (0.005 g), the second band gave $[(\mu\text{-}H)_2Os_7(CO)_7(\mu_3\text{-}S)(dppm)]$ (**2**) (0.011 g, 11%) and the third band yielded $[Os_3(\mu_3\text{-}CO)(CO)_7(\mu_3\text{-}S)(dppm)]$ (**3**) (0.067 g, 65%) as yellow crystals after recrystallization from C_6H_{14}–CH_2Cl_2 at room temperature (r.t.) by slow evaporation of the solvents. Spectroscopic and analytical data for **3**: (*Anal.* Calc. for $C_{33}H_{22}O_8Os_3P_2S$: C, 32.72; H, 1.83. Found: C, 32.81; H, 1.93%). IR (νCO, CH_2Cl_2): 2073s, 2017vs, 1995s, 1962m cm^{-1}; ^{1}H NMR ($CDCl_3$): δ 3.67 (m, 1H), 4.83 (m, 1H), 7.31 (m, 20H); $^{31}P\{^{1}H\}$ NMR: δ 20.4 (s); mass spectrum: m/z 1210.

Table 4
Crystal data and details of data collection and structure refinement for **3**, **4a** and **4b** [a]

	Compound **3**	Compound **4a**	Compound **4b**
Empirical formula	$C_{33}H_{22}O_8Os_3P_2S$	$C_{32}H_{22}O_7Os_3P_2S_2$	$C_{32}H_{22}O_7Os_3P_2S_2$
Formula weight	1211.11	1215.16	1215.16
a (Å)	8.943(3)	11.426(3)	10.041(3)
b (Å)	18.216(4)	11.665(2)	11.124(2)
c (Å)	22.122(4)	14.365(2)	17.723(4)
α (°)	107.972(13)	100.91(2)	73.800(14)
β (°)	98.02(2)	95.35(2)	84.47(2)
γ (°)	94.64(2)	114.90(2)	64.03(2)
V (Å^{-3})	3365(2)	1672.8(6)	1708.2(6)
Z	4	2	2
μ(Mo Kα) (mm^{-1})	11.51	11.63	11.39
Crystal size (mm)	$0.30\times0.10\times0.03$	$0.22\times0.12\times0.10$	$0.40\times0.25\times0.20$
Crystal color/shape	Yellow/plate-like	Yellow/prism	Yellow/prism
θ Range for data collection (°)	1.77–25.01	1.99–25.00	2.11–25.25
Reflections collected	14 174	6869	6914
Unique reflections (R_{int})	9296(0.0825)	4615(0.0805)	4693(0.1040)
Data/restraints/parameters	9296/126/751	4615/24/367	4693/24/367
Goodness-of-fit on F^2	0.937	1.095	0.963
Final R_1/wR_2 indices (all data)	0.0618/0.1078	0.0535/0.1263	0.0656/0.1373
R_1/wR_2 indices [$I>2\sigma(I)$] [b]	0.0454/0.1047	0.0493/0.1251	0.0529/0.1319

[a] Details in common: fast area detector, Mo Kα, $\lambda = 0.71069$ Å, 150 K, triclinic, space group $P\bar{1}$ full-matrix least-squares on F^2 (SHELXL-96).
[b] Number of data with [$I>2\sigma(I)$]:6881 (**3**), 4062 (**4a**), and 3652 (**4b**).

3.2. Reaction of **1** with thiourea

A $C_6H_5CH_3$ solution (25 cm^3) of **1** (0.110 g, 0.089 mmol) and thiourea (0.014 g, 0.184 mmol) was heated to reflux for 4 h. A similar chromatographic separation to that above afforded **2** (0.074 g, 70%).

3.3. Reaction of **1** with tetramethylthiourea

To a $C_6H_5CH_3$ solution (30 cm^3) of **1** (0.200 g, 0.162 mmol) was added tetramethylthiourea (0.107 g, 0.809 mmol) and the reaction mixture was heated to reflux for 6 h. Chromatographic separation as above gave two bands which afforded two isomeric compounds **4a** (0.031 g, 16%) and **4b** (0.126 g, 64%) as yellow crystals. Spectroscopic and analytical data for **4a**: *Anal*. Calc. for $C_{32}H_{22}O_7Os_3P_2S_2$: C, 31.63; H, 1.82. Found: C, 31.85; H, 1.93%. IR (νCO, CH_2Cl_2): 2072s, 2057m, 2002vs, 1985w, 1942m cm^{-1}; ^{1}H NMR ($CDCl_3$): δ 3.23 (t, 2H), 6.81–7.85 (m, 20H); ^{31}P{^{1}H}: δ 13.8 (s), mass spectrum: m/z 1215. Spectroscopic and analytical data for **4b**: *Anal*. Calc. for $C_{32}H_{22}O_7Os_3P_2S_2$: C, 31.63; H, 1.82. Found: C, 31.72; H, 1.90%. IR(νCO, CH_2Cl_2): 2071s, 2055m, 2002vs, 1987m, 1945m cm^{-1}; ^{1}H NMR ($CDCl_3$): δ 3.81 (dt, $J_{H-H} = 14.1$, $J_{H-P} = 10.5$ Hz, 1H), 5.10 (m, 1H), 6.81–7.85 (m, 20H); ^{31}P{^{1}H}: δ 9.5 (d, $J = 37.5$ Hz), -20.3 (d, $J = 37.5$ Hz); mass spectrum: m/z 1215.

3.4. Reaction of **3** with H_2

Hydrogen gas was bubbled through a refluxing $C_6H_5CH_3$ solution (20 cm^3) of **3** (0.025 g, 0.021 mmol) for 2 h. The solvent was removed under vacuum and the residue was chromatographed as above to give **2** (0.012 g, 50%).

3.5. Reaction of **3** with tetramethylthiourea

To a $C_6H_5CH_3$ solution (25 cm^3) of **3** (0.045 g, 0.037 mmol) was added tetramethylthiourea (0.024 g, 0.181 mmol) and the reaction mixture refluxed for 4 h. The solvent was removed under vacuum and the residue chromatographed to give **4a** (0.007 g, 19%) and **4b** (0.028 g, 76%).

3.6. X-ray crystallography

Crystallographic measurements for **3**, **4a** and **4b** were made at 150 K on a FAST TV area-detector diffractometer positioned at the window of a rotating anode generator, using Mo Kα radiation ($\lambda = 0.71069$ Å) in a manner described previously [34]. In all cases the unit-cell parameters were obtained by least-squares refinement of the diffractometer angles for 250 reflections. The crystallographic data and the data collection and refinement details are presented in Table 4. All data sets were corrected for absorption using DIFABS [35]. The structures were solved by direct methods (SHELXS-86)

[36], developed via difference syntheses, and refined on F^2 by full-matrix-least squares (SHELXL-96) [37] using all unique data with intensities greater than zero. In all cases, the phenyl rings were treated as idealized hexagon (C–C = 1.390 Å, C–C–C = 120.0°), the nonhydrogen atoms were anisotropic, and the hydrogen atoms included in calculated positions (Riding model).

4. Supplementary material

Crystallographic data for the compounds have been deposited with the Cambridge Crystallographic Data Centre, CCDC Nos. 169489 (**3**), 169490 (**4a**) and 169491 (**4b**). Copies of this information may be obtained free of charge from The Director, CCDC, 12 Union Road, Cambridge, CB2 1EZ, UK (fax: +44-1223-3360333 or e-mail: deposit@ccdc.cam.ac.uk or www: http://www.ccdc.cam.ac.uk).

Acknowledgements

The support of this research by the Ministry of Science and Technology, Government of the Peoples Republic of Bangladesh is gratefully acknowledged. K.M.A.M. is grateful to Professor M.B. Hursthouse for access to the EPSRC supported X-ray data collection Service.

References

[1] A.J. Deeming, in: E.W. Abel, F.G.A. Stone, G. Wilkinson (Eds.), Comprehensive Organometallic Chemistry II, vol. 7, Pergamon, Oxford, 1995, p. 648.
[2] R.D. Adams, Polyhedron 4 (1985) 2003.
[3] R.D. Adams, L.-W. Yang, J. Am. Chem. Soc. 104 (1982) 4115.
[4] R.D. Adams, I.T. Horvath, B.E. Segmüller, L.-W. Yang, Organometallics 2 (1983) 1301.
[5] R.D. Adams, I.T. Horvath, H.-S. Kim, Organometallics 3 (1984) 584.
[6] R.D. Adams, G. Chen, S. Sun, T.A. Wolfe, J. Am. Chem. Soc. 112 (1990) 868.
[7] A.J. Deeming, M. Underhill, J. Organomet. Chem. 42 (1972) C60.
[8] B.F.G. Johnson, J. Lewis, P.G. Lodge, P.R. Raithby, J. Chem. Soc., Chem. Commun. (1979) 719.
[9] P.V. Broadhurst, B.F.G. Johnson, J. Lewis, P.R. Raithby, J.R. Thornback, J. Organomet. Chem. 194 (1980) C35.
[10] P.V. Broadhurst, B.F.G. Johnson, J. Lewis, A.G. Orpen, P.R. Raithby, J.R. Thornback, J. Organomet. Chem. 187 (1980) 141.
[11] G. Süs-Fink, U. Thewalt, H.P. Klein, J. Organomet. Chem. 224 (1982) 59.
[12] S.M. Lee, K.K. Cheung, W.T. Wong, J. Organomet. Chem. 503 (1995) C19.
[13] U. Bodensieck, H. Stoeckli-Evans, G. Süss-Fink, Chem. Ber. 123 (1990) 1603.
[14] U. Bodensieck, H. Stoeckli-Evans, G. Rheinwald, G. Süss-Fink, J. Organomet. Chem. 433 (1992) 167.
[15] U. Bodensieck, H. Stoeckli-Evans, G. Süss-Fink, J. Organomet. Chem. 433 (1992) 149.
[16] U. Bodensieck, J. Santiago, H. Stoeckli-Evans, G. Süss-Fink, J. Chem. Soc., Dalton Trans. (1992) 255.
[17] U. Bodensieck, L. Hoferkamp, H. Stoeckli-Evans, G. Süss-Fink, J. Chem. Soc., Dalton Trans. (1993) 127.
[18] U. Bodensieck, H. Stoeckli-Evans, G. Süss-Fink, J. Chem. Soc., Chem. Commun. (1990) 267.
[19] U. Bodensieck, G. Miester, H. Stoeckli-Evans, G. Süss-Fink, J. Chem. Soc., Dalton Trans. (1992) 2131.
[20] G. Süss-Fink, U. Bodensieck, L. Hoferkamp, G. Rheinwald, H. Stoeckli-Evans, J. Cluster Sci. 3 (1992) 469.
[21] E.W. Ainscough, M.A. Brodie, S.L. Ingham, T.G. Kotch, A.J. Lees, J. Lewis, J.M. Waters, J. Chem. Soc., Dalton Trans. (1994) 1.
[22] K.A. Azam, R. Dilshad, S.E. Kabir, R. Miah, M. Shahiduzzaman, E. Rosenberg, K.I. Hardcastle, M.B. Hursthouse, K.M.A. Malik, J. Cluster Sci. 7 (1996) 49.
[23] S.M.T. Abedin, K.A. Azam, B.M. Hursthouse, S.E. Kabir, K.M.A. Malik, R. Mia, H. Vahrenkamp, J. Organomet.Chem. 564 (1998) 133.
[24] K.A. Azam, S.E. Kabir, A. Miah, M.W. Day, K.I. Hardcastle, E. Rosenberg, A.J. Deeming, J. Organomet. Chem. 435 (1992) 157.
[25] M.R. Churchill, B.G. DeBoer, Inorg. Chem. 16 (1977) 878.
[26] R.D. Adams, D.F. Foust, P. Foust, P. Mather, Organometallics 2 (1983) 990.
[27] K.A. Azam, M.B. Hursthouse, S.E. Kabir, K.M.A. Malik, M.A. Mottalib, J. Chem. Crystallogr. 29 (1999) 813.
[28] R.D. Adams, I.T. Horvath, B.E. Segmüller, Li-Wu. Young, Organometallics 2 (1983) 144.
[29] D. Cauzzi, C. Graiff, C. Massera, G. Predieri, A. Tiripicchio, D. Acquotti, J. Chem. Soc., Dalton Trans. (1999) 3515.
[30] D. Cauzzi, C. Graiff, G. Predieri, A. Tiripicchio, C. Vignali, J. Chem. Soc., Dalton Trans. (1999) 237.
[31] D. Cauzzi, C. Graiff, M. Lanfranchi, G. Predieri, A. Tiripicchio, J. Organomet. Chem. 536–537 (1997) 497.
[32] D. Cauzzi, C. Graiff, M. Lanfranchi, G. Predieri, A. Tiripicchio, J. Chem. Soc., Dalton Trans. (1995) 3221.
[33] A.J. Deeming, S.E. Kabir, J. Organomet. Chem. 340 (1988) 359.
[34] J.A. Darr, S.R. Drake, M.B. Hursthouse, K.M.A. Malik, Inorg. Chem. 32 (1993) 5704.
[35] N.P.C. Walker, D. Stuart, Acta Crystallogr. Sect. A 39 (1983) 158 adapted for FAST geometry by A.I. Karaulov, University of Wales 1991.
[36] G.M. Sheldrick, Acta Crystallogr. Sect. A 46 (1990) 467.
[37] G.M. Sheldrick, SHELXL-96, program for crystal structure refinement, University of Göttingen, Germany, 1996.

PERGAMON

Polyhedron 21 (2002) 389–394

POLYHEDRON

www.elsevier.com/locate/poly

Reaction of diperoxovanadate with vanadyl sulphate in presence of EDTA as an access to dinuclear peroxovanadates(V)

Swapnalee Sarmah, Pankaj Hazarika, Nashreen S. Islam *

Department of Chemical Sciences, Tezpur University, Tezpur 784 028, Assam, India

Received 18 July 2001; accepted 22 November 2001

Abstract

The reaction of alkali–metal diperoxovanadate with vanadyl sulphate in the presence of EDTA afforded the dinuclear heteroligand peroxovanadates(V), $A_4[V_2O_3(O_2)(EDTA)(SO_4)(H_2O)]\cdot 2H_2O$, A = Na (**1**) or K (**2**). The compounds were characterised by elemental analysis, magnetic susceptibility and spectral studies. The two vanadium(V) centres in the complex ion are bridged by an oxo group and a hexadentate EDTA ligand. One of the vanadium(V) centres of the dinuclear species contains a bidentate peroxide, whereas the other vanadium centre is bonded to a unidentate sulphate and water leading to hepta-co-ordination around each vanadium(V). Oxygen release reactions and molar conductance measurements revealed that the compounds were stable in solution. The compounds were resistant to catalase and were unable to oxidise NADH or bromide. It is proposed that this dinuclear complex species corresponds to the complex formed in solution responsible for EDTA induced inhibition of oxidation of NADH and bromide by a mixture of diperoxovanadate and vanadyl. © 2002 Published by Elsevier Science Ltd.

Keywords: Diperoxovanadate; Vanadyl; EDTA inhibition; EDTA bridged heteroligand peroxovanadates; Catalase resistance; Oxo-bridged peroxovanadates containing sulphate

1. Introduction

Diperoxovanadate is receiving importance as a biologically active vanadium compound. It mimicks insulin action [1] and was found to have antineoplastic activity [2,3]. An intermediate derived from diperoxovanadate was shown to stimulate oxidation of NADH [4]. It has been reported earlier by others [4–7] that diperoxovanadate (DPV) gains oxidant activity by complexing with vanadyl (V^{IV}) to form a highly reactive peroxo-bridged intermediate, $[OVOOVO(O_2)]^+$, which could act as oxidant species of NADH [4] and bromide [5], as well as inactivate glucose oxidase [6] or release oxygen as gas in the absence of any substrate [7]. Our studies on synthetic compounds with a 'VOOV' bridge of the type, $[V_2O_2(O_2)_3L_2]$ (L = amino acid or peptide) lent further support for such an intermediate as the powerful bromide oxidant at physiological pH [8,9].

One interesting finding of such studies was the inhibitory effect of certain organic ligating agents viz. EDTA, histidine, imidazole etc. on the above redox processes [4–9]. Such inhibition was found to be maximum in the presence of EDTA. EDTA induced inhibition was also reported to occur in the oxygen release reaction involving H_2O_2 and $VOSO_4$ [10]. The basis for such potent inhibition appeared to be the inactivation of the reactive peroxo intermediates by the ligands through complexation with V(V) and V(IV) centres. However, there has been a paucity of evidence on the exact identity of the actual species responsible for such an inhibitory effect [4–8].

We therefore, considered it worthwhile to investigate the reaction of DPV and VO^{2+} in presence of EDTA with an aim to ascertain the nature of the above inhibitory complex by attempting to isolate such species in the solid state. Moreover, it has been realised that any information related to the interaction of vanadate or vanadyl with ligands like EDTA may be relevant in addressing the role of vanadium in vanadate mediated inhibition or activation of enzymes [11,12]. In view of the continued search for stable peroxovanadate com-

* Corresponding author. Tel.: +91-3712-67173 (O)/24272 (R); fax: +91-3712-67006.

E-mail address: nsi@tezu.ernet.in (N.S. Islam).

0277-5387/02/$ - see front matter © 2002 Published by Elsevier Science Ltd.
PII: S0277-5387(01)01005-1

pounds suitable for therapeutic use [13–15], an additional goal of the present study was also to explore the possibility of gaining an access to newer heteroligand peroxovanadate compounds stable at physiological conditions.

We report here, an account of the reaction of alkali diperoxovanadate (ADPV) with $VOSO_4$ in presence of EDTA which led to the synthesis of novel dimeric peroxovanadates of the type $A_4[V_2O_3(O_2)(EDTA)(SO_4)(H_2O)]\cdot 2H_2O$ thought to correspond to the inhibitor complex in the above redox processes. The compounds have been subjected to dissolution and reactivity studies in order to determine their nature and stability in solution.

2. Experimental

The chemicals used were all reagent grade products. Catalase and NADH were obtained from Sigma–Aldrich Chemical Company. The water used for solution preparations was deionised and distilled.

2.1. Preparation of alkali metal diperoxovanadate, $A[VO(O_2)_2(H_2O)]$ (A = Na or K)

Alkali metal diperoxovanadate (ADPV) was prepared by adding an equal volume of H_2O_2 solution (40 mM) to a vanadate solution (20 mM) maintaining the pH at 7.0 by adding dilute alkali hydroxide solution. On addition of pre-cooled EtOH to this solution, a yellow microcrystalline product precipitated out which was separated by centrifugation, washed with EtOH and finally dried over conc. H_2SO_4. Analysis of the content of vanadium and peroxide agreed with the formula $A[VO(O_2)_2(H_2O)]$ (A = Na or K).

2.2. Reaction of $A[VO(O_2)_2(H_2O)]$ (A = Na or K) with $VOSO_4$ in presence of EDTA. Synthesis of $A_4[V_2O_3(O_2)\ (EDTA)\ (SO_4)\ (H_2O)]\cdot 2H_2O$

In a typical reaction the disodium or dipotassium salt of EDTA (2.5 mmol) was dissolved in approximately 5 ml of water by warming. To this $VOSO_4\cdot 5H_2O$ (0.42 g, 1.66 mmol) was added with constant stirring. The reaction mixture was stirred for approximately 5 min in an ice-bath. Alkali hydroxide pellets were added to this solution to raise the pH to 7. Solid $A[VO(O_2)_2(H_2O)]$ complex (2.5 mmol) was then added in one portion to the reaction mixture with constant stirring. The pH of the solution was ultimately raised to 8.5 by the further addition of AOH. The initial blue colour of the solution changed to green on addition of yellow ADPV and ultimately a deep red coloured clear solution was obtained within approximately 4 min. On addition of pre-cooled C_3H_6O in portions (approximately 5 ml) to the reaction solution under vigorous stirring, a red coloured pasty mass separated. The supernatant liquid was decanted off, and the oily residue was treated repeatedly with C_3H_6O under scratching until it became a microcrystalline solid. The product was separated by centrifugation, washed with EtOH and dried in vacuo over conc. H_2SO_4.

Anal. Calc. for $Na_4[V_2O_3(O_2)_3(EDTA)(SO_4)(H_2O)]\cdot 2H_2O$: C, 16.85; H, 2.52; N, 3.93; Na, 12.92; O_2^{2-}, 4.49; SO_4^{2-}, 13.48; V, 14.32. Found: C, 16.78; H, 2.58; N, 3.87; Na, 13.11; O_2^{2-}, 4.44; SO_4^{2-}, 13.41; V, 14.27%. Yield: approximately 55%.

Anal. Calc. for $K_4[V_2O_3\ (O_2)_3(EDTA)(SO_4)(H_2O)]\cdot 2H_2O$: C, 15.46; H, 2.31; K, 20.10; N, 3.60; O_2^{2-}, 4.12; SO_4^{2-}, 12.37; V, 13.14. Found: C, 15.41; H, 2.35; K, 20.13; N, 3.62; O_2^{2-}, 3.98; SO_4^{2-}, 12.30; V, 13.16%. Yield: approximately 30%.

The complexes in the solid state were found to be stable for several weeks stored dry at a temperature < 20 °C, but tended to be hygroscopic and decompose in a few days at a temperature ≥ 30 °C. The compounds were soluble in water.

2.3. Elemental analysis

The compounds were analysed for C, H, N, Na and K at the Regional Sophisticated Instruments Centre, North-Eastern Hill University, Shillong, India. Vanadium and peroxide were estimated by methods mentioned in earlier papers [16,17].

2.4. Physical and spectroscopic measurements

Spectra in the UV–Vis region were recorded on a Hitachi model 2001 recording spectrophotometer in 1 cm quartz cuvettes. The absorbance values are denoted as, e.g. A_{592}, A_{340}, at the wavelengths indicated. The infrared (IR) spectra were recorded with samples as KBr pellets in a Nicolet model 410 FTIR spectrophotometer and also in a Perkin–Elmer Model 983 spectrophotometer. The ^1H NMR spectra were recorded in deuterium oxide using a Varian EM-390 90 MHz spectrophotometer. Sodium salt of 3-(trimethylsilyl)-1-propane sulphonic acid was used as the internal standard. Magnetic susceptibilities were measured by the Gouy Method, using $Hg[Co(NCS)_4]$ as the calibrant.

2.5. Measurement of catalase-dependent oxygen release

A Gilson 5/6 H oxygraph fitted with a Clark oxygen electrode was used for measuring changes in dissolved oxygen (0.224 mM at 30 °C) in the medium and the changes were recorded in units of μM of dissolved oxygen. The rate and total amount of oxygen released from a 0.2 mM solution of the compound in phosphate

buffer (50 mM, pH 7.0) on adding catalase (0.08 mg protein ml^{-1}) were measured. The recorder pen was set in the middle of the chart paper for measuring the release of oxygen into the medium. The machine was standardised by the increases in dissolved oxygen obtained on adding catalase to buffered solutions containing known amounts of H_2O_2.

The effect of catalase on complexes was also studied by estimating the peroxide content of the compound **1** at different time intervals in a solution containing catalase. The reaction solution contained phosphate buffer (50 mM, pH 7.0), catalase (20 mg) and the compound **1** (50 mg). The volume of the reaction solution was kept at 25 ml. The solution was incubated at 30 °C. Aliquots of 5 ml were pipetted out and titrated for peroxide content at time 5, 10. 20, 30 and 40 min from starting the reaction.

2.6. Measurement of bromination activity

The method of de Boer et al. [18] of introducing four bromine atoms into the molecule of C_6H_5OH red ($\varepsilon^{433} = 19.7$ mm) to form the product, bromophenol blue ($\varepsilon^{592} = 67.4$ mm) was used to measure bromination activity. Phenol red acts as an efficient trap of active bromine species without influencing the rate of reaction until it is exhausted. The reaction mixture contained phosphate buffer (50 mM, pH 5.5), KBr (2 M) and C_6H_5OH red (20 μM). The redox activity was tested by adding the solid compounds and by monitoring the possible change in absorbance at 592 nm at 30 °C. The volume of the reaction mixture was kept at 25 ml in experiments where weighed amounts of solid peroxovanadate samples were added. Aliquots were transferred to the spectrophotometer immediately after mixing.

2.7. Measurement of oxidation of NADH

The absorbance at 340–380 nm by high concentrations of peroxovanadates had to be balanced by adding equivalent amounts in the blank and experimental cuvettes. Weighed samples of compound (20 mg/10 ml) were added to phosphate buffer (50 mM, pH 7.0). Only the experimental sample contained NADH (0.2 mM). Immediately after mixing, the sample was transferred to a cuvette and A_{340} was noted. No effect was observed on A_{340}.

3. Results and discussion

Based on their detailed investigations on V^{IV}–DPV reactions [4–8] and taking into account the redox chemistry of vanadyl, vanadate and peroxovanadates described earlier by Brooks and Sicilio [10] and Jaswal and Tracey [19], it was proposed by Ramasarma and co-workers that a short lived [$OVOOV(O_2)$] species is the intermediate shared by the processes: oxidation of NADH [4], formation of oxidised bromine species [5], inactivation of glucose oxidase [6] and release of oxygen [7]. Evidence was shown earlier for the participation of the peroxo-bridged divanadate compound in oxidising bromide ion at physiological pH [5,8,9]. Observing the inhibitory effect of EDTA and other organic ligands on each of the above-mentioned redox processes [4–7], we realised the distinct possibility of stabilising and isolating the proposed peroxo-bridged intermediate through complexation. Using this as a synthetic strategy, the reactions of alkali diperoxovanadate, EDTA and $VOSO_4$ were carried out at varying pH, ranging from 7 to 9. The success of obtaining the solid dinuclear heteroligand peroxovanadates containing SO_4^{2-} and EDTA as heteroligands, as sodium or potassium salts depended on the following essential components: maintenance of the molar ratio of DPV:VO^{2+}:EDTA at 1:0.75:1, order of addition of the reactants, pH of 8.5, maintenance of required reaction time as well as temperature at ≤ 4 °C. A solid product isolated at pH 7–8 was found to be EDTA peroxovanadate, which rendered inconsistent analysis.

The elemental analysis data provided crucial information regarding composition of the compounds. A ratio of 2:1 was ascertained for V:peroxide, V:EDTA, as well as for V:SO_4^{2-}. This suggested a dimeric nature of the complex species. The elemental analysis results and the molar conductance values obtained from measurement at ambient temperatures (510–522 Ω^{-1} cm^2 mol^{-1}) were in complete agreement with the formulation of the complexes as $A_4[V_2O_3(O_2)(EDTA)(SO_4)(H_2O)]\cdot 2H_2O$ (A = Na or K).

The electronic spectra of the complexes **1** and **2** displayed a broad band at 390–400 nm ($\varepsilon \approx 600$ mm) which has been assigned to the peroxo (LMCT) transition. According to previous studies [7], the absorbance at 780 nm of a blue coloured aqueous solution of $VOSO_4$ decreases progressively on adding batches of DPV to the solution. The complete absence of the 780 nm band in the spectra of the newly synthesised complexes indicated the oxidative loss of V^{IV} during complex formation. Occurrence of vanadium in the complexes **1** and **2** in its +5 oxidation state was further evident from their being diamagnetic at room temperature and ESR silent. The 8-band spectrum (hyperfine splitting **a** = 115 G) characteristic of V^{IV} of an aqueous solution of $VOSO_4$ was not observed in case of the complexes suggesting oxidation of V^{IV} to V^{V} during the course of the reaction.

The IR spectra of the complexes **1** and **2** displayed a rich but sufficiently well resolved spectral pattern significant features of which are summarised in Table 1. The bands observed for peroxo groups were in the

range characteristic of a triangularly bonded peroxide [15–17,20]. For the binuclear V–O–V unit the antisymmetric and symmetric stretchings were expected in the 700 and 500 cm^{-1} region [20]. Accordingly, a medium intensity band observed at approximately 712 cm^{-1} was assigned to a $\nu_{as}(V_2O)$ mode. The strong absorption at approximately 950 cm^{-1} was consistent with the presence of a terminally bonded V=O group in the complexes. This band was observed to be rather broad in the spectra probably owing to the presence of bridging oxo groups as well as co-ordinated sulphate in the complexes. The IR spectra of the complexes displayed a strong broad band with a maximum at approximately 1625 cm^{-1}, typical of co-ordinated carboxylato groups of EDTA [21a]. The broadening of the band was possibly caused by the additional OH deformation modes of the water molecules present in the complexes. No other band was observed in the vicinity of 1700 cm^{-1} which indicated the absence of free carboxylate groups, thereby suggesting the co-ordination of EDTA as a hexadentate ligand in the complexes. The corresponding $\nu_s(COO^-)$ band of EDTA was observed at approximately 1399 cm^{-1} which was shifted from the free ligand value (1412 cm^{-1}) as expected for unidentate carboxylate groups [21a]. The presence of water in the complexes was evident from the broad absorption at 3500–3400 cm^{-1}, due to ν(O–H). A band at approximately 755 cm^{-1}, assigned to the rocking mode of water, suggested the occurrence of co-ordinated water. The existence of co-ordinated sulphate in the complexes was evident from their IR spectra. The well-resolved splitting of the ν_3 and ν_4 modes of SO_4^{2-} into two bands each (Table 1) and appearance of a medium intensity ν_2 mode at approximately 465 cm^{-1} conclusively proved that the sulphate ligand binds the vanadium centre in an unidentate (C_{3v}) fashion [21b]. The ν_1 mode of an unidentately bonded SO_4^{2-} expected in the vicinity of 970 cm^{-1} could not be assigned decisively due to its possible mixing with the V=O stretching of terminal oxo groups. Significantly, the IR spectral pattern originating from co-ordinated sulphate in the complexes was observed to be very similar to that of vanadyl sulphate, $VO(SO_4)\cdot 5H_2O$. This observation led us to infer that the sulphate–vanadium co-ordination in $VOSO_4$ remained unaltered during its reaction with DPV in the presence of EDTA, being affected neither by the oxidation of V^{IV} to V^{V} nor by the complexation with EDTA leading to the formation of the newly synthesised complexes.

Table 1
Structurally significant IR bands of $A_4[V_2O_3(O_2)(EDTA)(SO_4)(H_2O)]\cdot 2H_2O$ (A = Na or K)

Compound	IR bands (cm^{-1})	Assignment
$Na_4[V_2O_3(O_2)(EDTA)(SO_4)(H_2O)]\cdot 2H_2O$	3434m	ν(O–H)
	1624s	ν_{as}(COO)
	1404s	ν_s(COO)
	1136s, 1103s	ν(S–O)(ν_3)
	641m, 614m, 464m	ν(S–O)(ν_4), ν(S–O)(ν_2)
	945s	ν(V=O)
	712m	$\nu_{as}(V_2O)$
	836m	ν(O–O)
	584s	$\nu_s(V–O_2)$
$K_4[V_2O_3(O_2)(EDTA)(SO_4)(H_2O)]\cdot 2H_2O$	3420m	ν(O–H)
	1631s	ν_{as}(COO)
	1399s	ν_s(COO)
	1138s, 1105s	ν(S–O)(ν_3)
	638, 612, 468	ν(S–O)(ν_4), ν(S–O)(ν_2)
	944	ν(V=O)
	712	$\nu_{as}(V_2O)$
	835	ν(O–O)
	578	$\nu_s(V–O_2)$

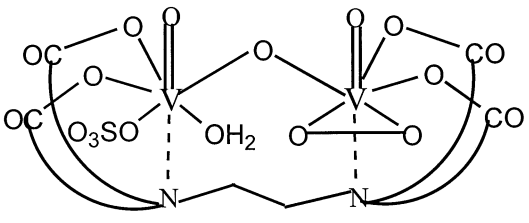


Fig. 1. Proposed structure of dinuclear heteroligand peroxovanadate(V) compounds, $A_4[V_2O_3(O_2)(EDTA)(SO_4)(H_2O)]\cdot 2H_2O$ (A = Na, K).

The ^{1}H NMR spectra of the complexes **1** and **2** exhibited a singlet at δ 2.71 and an AB quartet at δ 3.03 of intensity ratio 2:1. On the basis of previous studies on EDTA complexes, the AB quartet was assigned to the eight acetate protons and the singlet to the four ethylenic protons of the EDTA ligand [22]. The close analogy between the NMR spectra of the complexes **1** and **2** and that of a previously reported Mo–EDTA complex [22] containing bridging EDTA suggested the occurrence of the ligand in these complexes as a bridging one, as anticipated by us.

Based on the above observations a structure of the type shown in Fig. 1 has been envisaged for the complex species. An hexadentate EDTA ligand occupying three co-ordination positions around each of the oxo-bridged hepta co-ordinated vanadium(V) centres probably enhances the stability of the dinuclear complexes.

To us it appears that EDTA, which is known to undergo a facile condensation reaction with DPV [11,12] and also forms a stable complex with VO^{2+}, binds simultaneously to V^{V} and V^{IV} centres of the

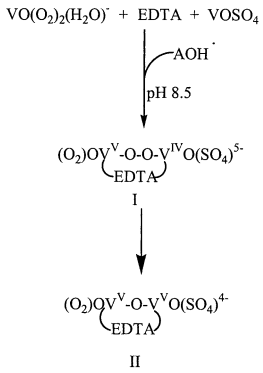


Fig. 2. Schematic representation of the formation of the dinuclear heteroligand peroxovanadate(V) complex, $[V_2O_3(O_2)(EDTA)(SO_4)(H_2O)]^{4-}$ from the reaction of diperoxovanadate with $VOSO_4$ in presence of EDTA. Hexa co-ordination of EDTA is not shown for simplicity. No attempt is made to show exact stoichiometry of reactions.

μ-peroxovanadate intermediate proposed to be formed in a solution of DPV and vanadyl (Fig. 2, complex I). This species then undergoes internal redox involving the reductive cleavage of the bridging peroxo group at the expense of oxidation of V^{IV} to V^{V} leading to formation of the stable dinuclear EDTA and oxo bridged complex (Fig. 2, complex II).

The stability of the complexes in solution has been studied by testing the possible oxygen release from a freshly prepared solution of the dinuclear peroxovandate **1** with the help of an oxygraph. However, no oxygen was found to be released on dissolution of the complex in water. Moreover, the single broad band observed in the 390–400 nm region in the electronic spectra of the complexes showed no change in its position or absorbance over a 2 h period. From these observations in combination with molar conductance values the stability of the complexes in water was implicit.

Having achieved the synthesis of these compounds we were interested in studying their activity in terms of their ability in bromide and NADH oxidation and action with the enzyme, catalase. On incubation with catalase DPV was found to be degraded releasing half the molecular equivalent of oxygen [23] at the rate of 36.0 μM min^{-1} from a solution of 0.2 mM. EDTA selectively inhibited this reaction of diperoxovandate with catalase [23]. For complexes **1** and **2**, a maximum of 0.5 O_2 per mole of the compound is expected to be released due to the presence of one peroxide group per molecule. However, no oxygen release took place from the solution of the complexes **1** and **2** in phosphate buffer (pH 7.0) on treatment with catalase and incubating at 30 °C for up to 30 min, confirming the resistance of the compounds to the enzyme. After 30 min, oxygen was found to be released from the solution at an extremely slow rate. The exceptional stability of the compounds to resist the catalase action is evidently owing to the extra stability imparted to the complex species by chelation, which probably interferes with the redox changes in the molecule necessary for catalase action.

The complexes were unable to bring about NADH oxidation as expected. Under the conditions given above, NADH was rapidly oxidised by a mixture of DPV and $VOSO_4$ [4]. We now find that addition of the solid compound **1** to solutions of NADH (0.2 mM) failed to oxidise it even at high concentration. There was no instant oxidation and A_{340} decreased at a negligible rate (results not shown).

Unlike our earlier experience with peroxo bridged dimeric compounds, $[V_2O_2(O_2)_3L_2]$ (L = amino acid or peptide) which led to the instant bromination of phenol red into its 592-absorbing brominated product, bromophenol blue, at physiological pH [8,9], with the complexes **1** and **2** no such activity was observed.

The above observations suggest that the factors such as absence of a μ-peroxo group in the complexes as well as their high stability due to chelation by EDTA are probably responsible for their lack of participation in the above redox processes thus resembling the inhibitor complex formed in solution.

In summary, with the examples of the newly synthesised compounds, the present investigation has established that it is possible to isolate the species formed in a solution of diperoxovanadate and VO^{2+} in presence of EDTA which is considered to be responsible for inhibiting the NADH and bromide oxidation and oxygen release reaction by a combination of DPV and VO^{2+}. Formation of the complex proceeds through steps where EDTA co-ordinates simultaneously to the V^{V} and V^{IV} centres of the proposed $[(O_2)OV^{V}OOV^{IV}O]^{+}$ intermediate. The peroxo bridged species then undergoes internal redox to produce the oxo and EDTA bridged dinuclear peroxovanadate(V) complex (Fig. 2, species II), which is resistant to further degradative loss of peroxide and can be isolated in the solid state as its Na^{+} or K^{+} salts. It is of interest to note that although SO_4^{2-} is not directly co-ordinated to the peroxovanadate centre, these complexes are probably the only known peroxovanadate compounds containing co-ordinated sulphate. The reaction may serve as a paradigm for the synthesis of stable dinuclear heteroligand peroxovanadates if carried out in the presence of suitable organic ligands in lieu of EDTA.

A significant finding in the present study is the high stability of the synthesised complexes at physiological pH and their resistance to catalase action. This may be relevant in the cellular milieu where H_2O_2 has little chance to survive abundant catalase and glutathione peroxidase. By forming peroxo complexes of the above type vanadate may provide a way of preserving cellular H_2O_2 in presence of abundant catalase and make it available for its functions.

Acknowledgements

Financial assistance from the Council of Scientific and Industrial Research, New Delhi, is gratefully acknowledged. We express our gratitude to Professor T. Ramasarma, Department of Biochemistry, Indian Institute of Science, Bangalore, for valuable discussion and for allowing us to use the Oxygraph.

References

[1] I.G. Fantus, S. Kodota, G. Deragon, B. Foster, B.I. Posner, Biochemistry 28 (1989) 8864.
[2] H.J. Thompson, N.D. Chasteen, L.D. Mecker, Carcinogenesis 5 (1984) 849.
[3] C. Djodjevic, G.L. Wampler, J. Inorg. Biochem. 251 (1985) 51.
[4] H.N. Ravishankar, T. Ramasarma, Arch. Biochem. Biophys. 316 (1995) 319.
[5] A.V.S. Rao, H.N. Ravishankar, T. Ramasarma, Arch. Biochem. Biophys. 334 (1996) 121.
[6] A.V.S. Rao, P.D. Sima, J.R. Kanofsky, T. Ramasarma, Arch. Biochem. Biophys. 369 (1999) 163.
[7] H.N. Ravishankar, M.K. Chaudhuri, T. Ramasarma, Inorg. Chem. 33 (1994) 3788.
[8] A.V.S. Rao, N.S. Islam, T. Ramasarma, Arch. Biochem. Biophys. 342 (1997) 289.
[9] S. Sarmah, N.S. Islam, J. Chem. Res. (M) (2001) 0536.
[10] H. Brooks, F. Sicilio, Inorg. Chem. 10 (1971) 2530.
[11] D.C. Crans, P.K. Shin, J. Am. Chem. Soc. 116 (1994) 1305.
[12] D.C. Crans, in: H. Sigel, A. Sigel (Eds.), Metal Ions in Biology, vol. 51, Wiley, New York, 1994, pp. 34–35.
[13] D. Rehder, Coord. Chem. Rev. 182 (1999) 297.
[14] A. Shaver, J.B. Ng, D.A. Hall, B.I. Posner, Mol. Cell. Biochem. 153 (1995) 5.
[15] C. Djordjevic, N. Vuletic, M.L. Renslo, B.C. Puryear, R. Alimard, Mol. Cell. Biochem. 153 (1995) 25.
[16] M.K. Chaudhuri, S.K. Ghosh, Inorg. Chem. 23 (1984) 534.
[17] M.K. Chaudhuri, N.S. Islam, Inorg. Chem. 24 (1985) 2706.
[18] E. de Boer, H. Plat, M.G.M. Tromp, R. Wever, M.C.R. Franssen, H.C. van der Plas, H.C. Meijer, H.E. Schoemaker, Biotech. Bioeng. 30 (1987) 607.
[19] J.S. Jaswal, A.S. Tracey, Inorg. Chem. 30 (1991) 3718.
[20] N.J. Campbell, A.C. Dengel, W.P. Griffith, Polyhedron 8 (1989) 1379.
[21] (a) K. Nakamoto, Infrared and Raman Spectra of Inorganic and Co-ordination Compounds, 5th ed., Wiley, New York, 1997, p. 68;
(b) K. Nakamoto, Infrared and Raman Spectra of Inorganic and Co-ordination Compounds, 5th ed., Wiley, New York, 1997, p. 81.
[22] L.V. Haynes, D.T. Sawyer, Inorg. Chem. 6 (1967) 2146.
[23] H.N. Ravishankar, A.V.S. Rao, T. Ramasarma, Arch. Biochem. Biophys. 321 (1995) 477.

PERGAMON

Polyhedron 21 (2002) 395–401

POLYHEDRON

www.elsevier.com/locate/poly

Synthesis and structural studies of the dien complexes of metal saccharinates, $[M(dien)_2]\cdot 2(sac)\cdot H_2O$ [M(II) = Ni(II), Cu(II) and Zn(II); dien = diethylenetriamine, $C_4H_{13}N_3$; sac = saccharinate, $C_7H_4NO_3S^-$], and $[Cd(dien)_2]\cdot 2(sac)$

Caroline A. Johns, K.M. Abdul Malik *

Department of Chemistry, Cardiff University, PO Box 912, Park Place, Cardiff CF10 3TB, Wales, UK

Received 24 September 2001; accepted 22 November 2001

Abstract

The synthesis and structural characterisation of a series of metal–saccrarinate complexes of formula $[M(dien)_2]\cdot 2(sac)\cdot H_2O$ [M(II) = Ni(II), Cu(II), Zn(II); dien = diethylenetriamine, $C_4H_{13}N_3$, sac = saccharinate, $C_7H_4NO_3S^-$] and $[Cd(dien)_2]\cdot 2(sac)$ are described. The Ni, Cu and Zn complexes are isostructural and belong to the monoclinic space group *Ia*, whilst the Cd complex crystallizes in the triclinic space group $P\bar{1}$. In each case, two tridentate dien ligands are bonded with the metal in a distorted octahedral arrangement, and the saccharinate anions remain outside the coordination sphere but participate in extensive hydrogen bonding network. The Ni, Cu and Zn complexes have a meridonal distribution of the dien ligands, whilst the Cd complex shows a facial configuration. © 2002 Elsevier Science Ltd. All rights reserved.

Keywords: Nickel; Copper; Zinc; Cadmium; Saccharinate; X-ray structures

1. Introduction

Chemistry of metal–saccharin complexes is an interesting area of research because of the potential biological significance of such compounds [1–3]. The saccharin molecule ($C_7H_5NO_3S$) contains an imino hydrogen which is acidic in nature and can easily be lost producing the anion $(C_7H_4NO_3S)^-$. This anion has several potential donor atoms, i.e. the imino nitrogen, one carbonyl and two sulphonyl oxygens, which can be utilised in forming coordination bonds with different metals ions. We and others have shown that all the divalent transition metal ions in the 1st transition series form an isostructural series of complexes with stoichiometry $[M(sac)_2(H_2O)_4]\cdot 2H_2O$ [sac = $(C_7H_5NO_3S)^-$] in which the sac anions are directly bonded to the metals through the nitrogen atom in a *trans* octahedral geometry [4–9]. There are also examples where one sac anion is bonded to the metal whereas the other anion remains outside the coordination sphere [10–12]. In a recent paper, we have shown that in some bipyridine derivatives belonging to this category, the whole complex can be taken as examples of the formation of 'cation–anion' pair [13]. Salt-like compounds where both the sac anions remain in the lattice are relatively few, but this type of situation appears to be preferred when the secondary ligand has got strong chelating properties [14]. In the present paper, we describe the synthesis, properties and structural characterisation of the Ni, Cu, Zn and Cd complexes of diethylenetriamine (dien) with saccharinate anions, and show that they form salt-like structures stabilised by extensive hydrogen bonded networks.

2. Experimental

2.1. General

Analar grade chemicals (BDH or E. Merck) were used as received. CHN analyses were done using an automatic microanalyser. The metal contents were de-

* Corresponding author: Tel: +44-29-2087-4950; fax: +44-29-2087-4030.

E-mail address: malikka@cardiff.ac.uk (K.M. Abdul Malik).

0277-5387/02/$ - see front matter © 2002 Elsevier Science Ltd. All rights reserved.
PII: S0277-5387(01)00997-4

termined by atomic absorption spectroscopy using a Shimadzu atomic absorption/flame emission spectrophotometer, model AA-680, and also by standard gravimetric (dimethylglyoximate) as well as complexometric (Na_2EDTA) methods. Melting point was measured on a heating device MEL-TEMP (II) with a FLUKE 51 thermometer. IR spectrum (KBr pillet) was recorded on a Shimadzu IR spectrophotometer, Model IR-470, range 4000–400 cm^{-1}.The UV–Vis spectrum was recorded on a Shimadzu UV–Vis spectrophotometer, range 200–100 nm. The magnetic susceptibility was measured at room temperature using a Curie–Chenevean magnetic balance.

2.2. Synthesis of the complexes

The complexes described in this work were all synthesised from the reactions of $[M(sac)_2(H_2O)_4]\cdot 2H_2O$ (M = Ni, Cu, Zn, Cd) with dien. The detailed procedure is described below for the nickel complex (**1**) and this was also adopted in other cases. The starting purely saccharinate complexes were prepared by following known methods [1,15].

$[Ni(sac)_2(H_2O)_4]\cdot 2H_2O$ (2.6558 g, 5 mmol) was dissolved in 150 ml of methanol and dien (1.08 ml, 10 mmol) was added. The color changed from light green to violet. The resulting solution was filtered, and the filtrate heated gently to about 50 °C on a water bath for 30 min and allowed to stand overnight at room temperature. Violet crystals of $[Ni(C_4H_{13}N_3)_2]\cdot 2(C_7N_4NO_3S)\cdot H_2O$ (**1**) were formed, which were collected by filtration, washed with methanol and dried over silica gel. Yield 84.3%, m.p. 236.8 °C. *Anal*. Calc. for $C_{22}H_{32}NiN_{16}O_7S_2\cdot H_2O$: C, 40.53, H, 5.55; N, 17.42; Ni, 8.99. Found. C, 40.82; H, 5.61; N, 17.31; Ni, 9.07%. I.R. (KBr disc), ν cm^{-1}, 3465 (s), 3440 (s), 3325(vs), 3264 (vs), 3200 (s), 2925 (s), 2872 (m), 1640 (vs), 1616 (vs), 1579 (vs), 1470 (vw), 1450 (m), 1330 (s), 1273 (sh), 1258 (vs), 1162 (sh), 1144 (vs) 1095 (m), 1062 (sh), 1051 (s), 1022 (vs), 996 (w), 981 (s), 950 (vs), 915 (w), 891 (s), 864 (w), 769 (m), 758 (s), 703 (m), 681 (s), 633 (s), 605 (vs), 579 (vw), 544 (s), 528 (s), 492 (vw), 455 (vw), 418 (vw). UV–Vis (λ_{max})/nm: 242 (π–π*), 356 (charge transfer), 532, 853 (d–d). $\mu_{eff} = 3.02$ BM.

The Cu complex $[Cu(C_4H_{13}N_3)_2]\cdot 2(C_7N_4NO_3S)\cdot H_2O$ (**2**) was obtained as navy blue crystals. Yield 92.6%, m.p. 134.7 °C. *Anal*. Calc. for $C_{22}H_{32}CuN_{16}O_7S_2.H_2O$: C, 40.45, H, 5.49; N, 17.25; Cu, 9.02. Found. C, 40.52; H, 5.56; N, 17.18; Cu, 9.74%. I.R. (KBr disc), ν cm^{-1}, 3454 (m), 3376 (m), 3316 (s), 3285 (vs), 3240 (vs), 3185 (s), 2915 (s), 2868 (s), 1644 (vs), 1615 (sh), 1578 (vvs), 1470 (sh), 1447 (m), 1328 (m), 1274 (sh), 1258 (vs), 1162 (sh), 1144 (vs), 1118 (m), 1083 (sh), 1050 (s), 1033 (s), 997 (sh), 972 (s), 949 (vs), 921 (w), 900 (m), 870 (vw), 858 (w), 827 (vw), 788 (m), 768 (sh), 758 (s), 703 (m), 681 (s), 633 (m), 604 (vs), 541 (sh), 529 (s), 467 (m), 456 (m), 422 (vw), 418 (vw). UV–Vis (λ_{max})/nm: 244 (π–π*), 352 (charge transfer), 646, (960) (d–d). $\mu_{eff} = 1.76$ BM.

The Zn complex $[Zn(C_4H_{13}N_3)_2]\cdot 2(C_7N_4NO_3S)\cdot H_2O$ (**3**) was obtained as colorless crystals. Yield 81.4%, m.p. 152.6 °C. *Anal*. Calc. for $C_{22}H_{32}ZnN_{16}O_7S_2\cdot H_2O$: C, 40.45, H, 5.50; N, 17.20; Zn, 9.42. Found. C, 40.40; H, 5.55; N, 17.13; Zn, 9.99%. I.R. (KBr disc), ν cm^{-1}, 3460 (s), 3408 (s), 3335 (vs), 3280 (vs), 3200 (sh), 2915 (s), 2880 (s), 1637 (vs), 1619 (sh), 1578 (vs), 1468 (sh), 1453 (m), 1380 (vw), 1331 (vs), 1263 (vs), 1144 (vs), 1120 (sh), 1050 (s), 1025 (s), 999 (s), 952 (vs), 904 (m), 883 (m), 824 (w), 789 (m), 768 (sh), 752 (vs), 702 (m), 678 (vs), 632 (m), 602 (vs), 569 (w), 541 (s), 528 (s), 506 (w), 498 (w), 453 (vw). UV–Vis (λ_{max})/nm: 243 (π–π*), 299 (n–π*).

The Cd complex $[Cd(C_4H_{13}N_3)_2]\cdot 2(C_7N_4NO_3S)$ (**4**) was also colorless crystals. Yield 78.5%, m.p. 123.2 °C. *Anal*. Calc. for $C_{22}H_{32}CdN_{16}O_7S_2$: C, 38.72, H, 4.95; N, 16.35; Cd, 15.76. Found. C, 38.68; H, 5.02; N, 16.40; Cd, 16.45. I.R. (KBr disc), ν cm^{-1}, 3455 (s), 3408 (s), 3360 (vs), 3330 (vs), 3280 (vs), 3185 (s), 2920 (s), 2880 (s), 1638 (vs), 1615 (vs), 1579 (vs), 1490 (sh), 1484 (sh), 1449 (m), 1333 (vs), 1272 (sh), 1252 (vvs), 1160 (sh), 1146 (vs), 1118 (sh), 1073 (m), 1062 (sh), 1040 (m), 1037 (m), 1013 (s), 972 (s), 958 (vs), 912 (vw), 891 (m), 864 (vw), 831 (vw), 798 (m), 788 (sh), 761 (vs), 703 (m), 680 (vs), 632 (s), 604 (vs), 540 (s), 531 (s), 505 (sh), 453 (w), 409 (vw). UV–Vis (λ_{max})/nm: 242 (π–π*), 295 (n–π*).

2.3. X-ray crystallography

Crystallographic measurements for the complexes **1**–**4** were made at 293 K on a CAD4 diffractometer using graphite monochromatised Mo Kα radiation, $\lambda =$ 0.71069 Å, and ω–2θ scan technique. The structures were solved by direct methods (SHELXS-86) [16] and refined by full-matrix least-squares on F (SHELX-80) [17] using the observed data [$F_o > 3\sigma(F_o)$]. The weighting scheme applied was of the form $w = 1/[\sigma^2(F_o) + g(F_o^2)]$ and the coefficients 'g' were chosen to five flat analyses of variance with $\sin\theta/\lambda$. For **1**–**3**, the hydrogen atoms belonging to the H_2O molecules were experimentally located but not refined; those on the saccharinate and dien ligands were included in calculated positions. For **4**, one of the carbon atoms [C(47)] in a CH_2CH_2 bridge was disordered between two positions, which were refined with partial occupancies of 0.70 and 0.30. In this structure, the hydrogen atoms on the disordered carbon were ignored, and others included in calculated positions. Anisotropic displacement coefficients were refined for all non-hydrogen atoms. Final difference maps did not show any residual electron density of stereochemical significance. The correct absolute structure for **1**–**3** was chosen on the basis of the fact that the this model gave slightly lower R/R_w values compared

with the corresponding inverted structure. The crystal data and refinement details are summarised in Table 1, and selected bond lengths and angles involving the metal atoms are collected together in Table 2. Dimensions of the hydrogen bonds and some significant short contacts are listed in Table 3. ORTEP drawings of the structures of **1** and **4** are shown in Figs. 1 and 2, respectively.

3. Results and discussion

The new complexes **1**–**4** were obtained as air-stable violet (Ni), blue (Cu) or colorless (Zn and Cd) crystals from the reaction of the respective metal saccharinates $[M(sac)_2(H_2O)_4]\cdot 2H_2O$ with diethylenetriamine (dien) in aqueous medium. All the complexes are soluble in water, alcohol, acetone and DMSO. The analytical and spectroscopic data are consistent with the proposed formulation of the complexes, and are confirmed by an X-ray study. The relatively low melting points of the complexes suggest that they are monomeric species. The magnetic data indicate the presence of two unpaired electrons on Ni(II) (high-spin, d^8 configuration) in **1** and one unpaired electron on Cu(II) (d^9 configuration) in **2**.

3.1. Spectral study of *1*–*4*

Some of the important peaks in the IR spectra of the complexes were assigned by comparing with related compounds [2]. There are several close peaks in the region 3465–3200 cm^{-1} which may be attributed to the ν(O–H) vibrations of the H_2O molecules and N–H vibrations of the dien NH_2 groups. Splitting and broadening of these peaks suggest that the H_2O molecules/NH_2 groups are coordinated and/or hydrogen bonded. Two close peaks at $\sim$2925–2880 cm^{-1} are due to the ring ν(C–H) vibrations. The ν(CO) peaks appears at 1640, 1644, 1637 and 1638 cm^{-1} with corresponding shoulders at 1616, 1615, 1619 and 1615 $cm^{-1}$for **1**–**4**, respectively. The peaks with medium intensity at 1579–1578 cm^{-1} may be attributed to the ring ν(CC) vibrations. The peaks at $\sim$1333–1328 cm^{-1} are due to the ν(CN) ring vibrations. The $\nu_{as}(SO_2)$ peaks appear as strong peaks at 1263–1252 cm^{-1} and also as shoulders at $\sim$1274–1272 cm^{-1} whilst the $\nu_{sy}(SO_2)$ bands appear as strong peaks at 1144–1146 cm^{-1}. The ring ν(CC) absorption band overlaps with the $\nu_{as}(SO_2)$ peak at 1267 cm^{-1}. The weak bands at 456–453 cm^{-1} may be assigned to the M–N (dien) vibrations. There are also other peaks in the spectra that are difficult to assign

Table 1
Crystal data and details of data collection and structure refinement for $[Ni(C_4H_{13}N_3)_2]\cdot 2(C_7N_4NO_3S)\cdot H_2O$ (**1**), $[Cu(C_4H_{13}N_3)_2]\cdot 2(C_7N_4NO_3S)\cdot H_2O$ (**2**), $[Zn(C_4H_{13}N_3)_2]\cdot 2(C_7N_4NO_3S)\cdot H_2O$ (**3**) and $[Cd(C_4H_{13}N_3)_2]\cdot 2(C_7N_4NO_3S)$ (**4**)

	1	**2**	**3**	**4**
Chemical formula	$C_{22}H_{36}N_8NiO_7S_2$	$C_{22}H_{36}N_8CuO_7S_2$	$C_{22}H_{36}N_8ZnO_7S_2$	$C_{22}H_{34}N_8CdO_6S_2$
Formula weight	647.41	652.25	654.09	683.10
Crystal system	monoclinic	monoclinic	monoclinic	triclinic
Unit cell dimensions				
a (Å)	8.232(3)	8.312(2)	8.261(2)	7.826(2)
b (Å)	40.000(9)	39.975(8)	40.203(8)	13.592(3)
c (Å)	8.720(4)	8.676(2)	8.721(3)	14.349(3)
α (°)	90	90	90	106.80(2)
β (°)	98.91(3)	98.63(2)	99.12(2)	77.73(2)
γ (°)	90	90	90	84.93(2)
V (Å^3)	2836.7	2850.2	2859.78	1409.37
Space group	*Ia* (no. 15)	*Ia* (no. 15)	*Ia* (no. 15)	$P\bar{1}$ (no. 2)
Z	4	4	4	2
Crystal size (mm)	$0.50\times0.30\times0.15$	$0.40\times0.30\times0.30$	$0.35\times0.30\times0.25$	$0.40\times0.40\times0.35$
Shape	parallelepiped	prism	Prism	prism
Colour	violet	blue	Colorless	colorless
θ Range for data collection (°)	1.5–24.0	1.5–24.0	1.5–23.0	1.5–25.0
Reflections collected	2477	2520	4392	5053
Unique reflections	2387	2392	2145	4953
Total observed	2245	2045	2077	4495
Significance test	$F_o>3\sigma(F_o)$	$F_o>3\sigma(F_o)$	$F_o>3\sigma(F_o)$	$F_o>3\sigma(F_o)$
R_{int}	0.0190	0.0090	0.0092	0.0094
Data/parameters in the refinement	2245/360	2045/3605	2077/360	4495/362
Weighting scheme coefficient 'g'	0.0018	0.0006	0.00015	0.0015
Final R/R_w [a] indices $[(F_o>3\sigma(F_o)]$	0.0244/0.0324	0.0643/0.0832	0.0245/0/0.0295	0.0291/0.0391
R/R_w indices for all data	0.0293/0.0327	0.0834/0.0839	0.0260/0.0296	0.0336/0.0394
$\rho_{min}-\rho_{max}$ (e Å$^3-$)	−0.22 to 0.27	−0.96 to 1.30	−0.37 to 0.51	−0.58 to 0.68

All measurements were done at 293(2) K.
[a] $w=1/[\sigma(F_o)+g(F_o^2)]$, $R=\Sigma(F_o-F_c)/\Sigma(F_o)$; $R_w=[\Sigma\, w(F_o-F_c)^2/\Sigma\, w(F_o)^2]^{1/2}$.

Table 2
Important bond lengths (Å) and bond angles (°) for **1**–**4**

	1	2	3	4
Bond lengths				
M–N(31)	2.150(6)	2.347(13)	2.244(5)	2.401(4)
M–N(32)	2.065(5)	2.021(12)	2.106(5)	2.431(4)
M–N(33)	2.192(6)	2.634(14)	2.286(6)	2.342(5)
M–N(41)	2.180(6)	2.107(12)	2.264(5)	2.357(4)
M–N(42)	2.079(6)	1.995(14)	2.136(5)	2.405(5)
M–N(43)	2.110(6)	2.042(14)	2.152(6)	2.327(5)
Bond angles				
N(31)–M–N(32)	81.9(2)	80.4(5)	80.0(2)	72.6(2)
N(31)–M–N(33)	162.5(2)	154.8(5)	158.6(1)	109.1(2)
N(32)–M–N(33)	80.8(3)	74.6(5)	79.1(2)	74.8(2)
N(31)–M–N(41)	92.8(1)	95.5(5)	93.0(2)	150.5(1)
N(32)–M–N(41)	98.9(2)	98.1(5)	99.2(2)	92.9(2)
N(33)–M–N(41)	87.2(3)	85.2(5)	86.1(2)	90.8(2)
N(31)–M–N(42)	93.4(2)	97.1(5)	93.7(2)	87.3(2)
N(32)–M–N(42)	175.3(2)	177.4(5)	173.2(1)	112.4(2)
N(33)–M–N(42)	103.9(3)	107.9(5)	107.0(2)	163.5(2)
N(41)–M–N(42)	80.6(2)	81.9(5)	78.4(2)	74.4(2)
N(31)–M–N(43)	94.5(3)	95.8(5)	96.4(2)	91.1(2)
N(32)–M–N(43)	98.5(2)	95.6(5)	102.1(2)	160.8(1)
N(33)–M–N(43)	90.7(3)	89.6(5)	92.1(3)	102.2(2)
N(41)–M–N(43)	161.9(2)	163.6(5)	157.9(1)	106.1(2)
N(42)–M–N(43)	82.5(2)	84.9(5)	81.1(2)	75.8(2)

unambiguously. It should be noted, however, that the IR spectra of the four complexes are strikingly similar in relative positions and intensities of the peaks, which suggests a close structural relationship among the compounds.

3.2. Crystal structural studies

X-ray crystal structural studies show that the Ni(II) (**1**), Cu(II) (**2**) and Zn(II) (**3**) complexes have the same stoichiometry $[M(dien)_2]\cdot 2(sac)\cdot H_2O$ and are isostructural (monoclinic, comparable cell dimensions, same space group, similar atom coordinates). The crystal structures consist of $[M(dien)_2]^+$ cations, $(sac)^-$ anions and H_2O molecules (1:2:1) held together by several hydrogen bonds and van der Waals' interactions. The coordination sphere around M(II) consists of two tridentate dien ligands with a meridonal configuration. The two sacchrinate anions and the H_2O molecule remain outside the coordination sphere, but these are linked with each other and also with the cation through several strong hydrogen bonds (Table 3). This is illustrated in Fig. 1, which shows the structure of the Ni complex **1** and represents the above isostructural series of three compounds. The H_2O molecule forms an acceptor hydrogen bond with the central amine group [N(32)–H(32)] of one of the dien ligands, and two donor bonds with the carbonyl oxygen atoms [O(11)] of two symmetry related saccharinate anions. Relatively short donor–acceptor distances (2.80–2.93 Å) and very favourable donor–hydrogen–acceptor angles (155–160°) indicate that these hydrogen bonds are quite strong and play crucial roles in the stabilisation of the crystal structural framework. Further stabilisation is achieved through additional hydrogen bonds involving the amine groups on the dien ligands and the nitrogen and sulfonyl oxygens of the saccharinate anions. In the Cd complex **4**, there is no water molecule to form any O–H···O hydrogen bond as observed in the other three complexes, but in this case there are several N–H···O hydrogn bonds involving the amine groups and the carbonyl/sulphonyl oxygen atoms of the saccharinate anions to hold the crystal structure together (Fig. 2 and Table 3). Further, the two tridentate dien ligands in this complex are arranged differently, i.e. in a facial mode, in contrast with the meridonal mode in the other complexes. The reasons for this different behaviour of the Cd complex are not clear, but a relatively larger size of Cd compared with Ni, Cu and Zn [18] could be a contributing factor.

The coordination polyhedron in each case shows large distortions from ideal octahedral geometry. The M–N (dien) bond distances vary from 2.065(5) to 2.192(6), 1.995(14) to 2.634(14), 2.106(5) to 2.286(6) and 2.327(5) to 2.431(4) Å in **1**–**4** respectively. Similar values and variations in the M–N(dien) distances have also been observed in other complexes, i.e. 2.083–2.166 in $[Ni(dien)_2]\cdot 2Cl\cdot H_2O$ [19], 2.096–2.133 in $[Ni(dien)_2]\cdot 2(CNS)$ [20], 2.027–2.459 in $[Cu(dien)_2]\cdot 2Br\cdot H_2O$ [21], 2.001–2.265 in $[Cu(dien)_2]\cdot 2(NO_3)$ [21], 2.126–2.283 in $[Zn(dien)_2]\cdot 2Br\cdot H_2O$ [22], 2.155–2.245 in $2[Zn(dien)_2]\cdot[Fe(CN)_6]\cdot 4H_2O$ [23], and 2.340–2.425 in the polymeric cluster $[Cd(dien)_2]\cdot[Cd(dien)_2]\cdot 3(CN)\cdot[Cd_8(CN)_{19}]\cdot 3H_2O$ [24]. In the present Ni, Zn and Cd complexes, one of the dien ligands has two short and one long, and the other one short and two long M–N bonds, but in the Cu complex there are four short Cu–N bonds in the coordination plane and two long bonds along the normal to the plane. The long bonds in this case are associated with the two terminal NH_2 groups of the same dien, but in other cases, each dien has both long and short M–N bonds. It is noticed that the shortest M–N bond involves the central –NH– group in each case.

The distortions in the coordination polyhdra are also evident from the N–M–N angles. Thus the mutually cis and mutually trans angles, respectively, range from 80.6(2)° to 103.9(3)° and 161.9(2)° to 175.3(2)° in **1**, 74.6(5)° to 107.9(5)° and 154.8(5)° to 177.4(5)° in **2**, 78.4(2)° to 107.0(2)° and 157.9(1)° to 173.2(1)° in **3**, and 72.6(2)° to 112.4(2)° and 150.5(1)° to 163.5(2)° in **4**. As expected the N–M–N bite angles in each complex are all acute due to the steric constraints imposed by the ethylene bridge, and those in the Cd complex are narrowest due to longer Cd–N bonds. Similarly, the narrowing down of the trans angles from ideal value of

Table 3
Dimensions of the hydrogen bonds in **1**–**4**

D–H···A	Compound	D–H	D···A	H···A	∠D–H···A
*Complexes **1**, **2** and **3*** [a]					
N(31)–H(31B)···O(13)	**1**	0.96	3.266	2.41	149
	2	0.96	3.171	2.34	145
	3	0.96	3.229	2.36	150
N(32)–H(32)···O(1)	**1**	0.96	2.934	2.02	159
	2	0.96	2.935	2.08	147
	3	0.96	2.935	2.03	156
N(33)–H(33B)···N(21)	**1**	0.96	3.250	2.30	169
	2	0.96	3.240	2.39	147
	3	0.96	3.261	2.31	172
N(41)–H(41B)···N(21)	**1**	0.96	3.273	2.44	146
	2	0.96	3.251	2.40	147
	3	0.96	3.243	2.39	148
N(43)–H(43B)···N(11)	**1**	0.96	3.081	2.14	165
	2	0.96	3.078	2.15	161
	3	0.96	3.099	2.15	171
C(45)–H(45B)···O(23)	**1**	0.96	3.376	2.52	149
	2	0.96	3.405	2.54	151
	3	0.96	3.368	2.52	148
O(1)–H(1A)···O(11)	**1**	0.90	2.808	1.95	161
	2	0.87	2.800	1.97	158
	3	0.96	2.810	1.89	161
C(16)–H(16)···O(21)^{i}	**1**	0.96	3.327	2.46	150
	2	0.96	3.274	2.39	152
	3	0.96	3.314	2.45	150
C(26)–H(26)···O(23)^{ii}	**1**	0.96	3.409	2.50	159
	2	0.96	3.372	2.44	163
	3	0.96	3.417	2.51	158
N(31)–H(31A)···O(12)^{iii}	**1**	0.96	3.176	2.32	149
	2	0.96	3.187	2.34	148
	3	0.96	3.201	2.34	149
N(41)–H(41A)···O(12)^{iii}	**1**	0.96	3.156	2.28	151
	2	0.96	3.138	2.28	149
	3	0.96	3.176	2.30	151
N(42)–H(42)···O(22)^{iv}	**1**	0.96	2.992	2.06	164
	2	0.96	2.995	2.05	168
	3	0.96	2.962	2.02	165
N(43)–H(43A)···O(21)^{v}	**1**	0.96	2.934	2.07	150
	2	0.96	2.980	2.13	147
	3	0.96	2.903	2.00	156
O(1)–H(1B···O(11)^{vi}	**1**	0.90	2.847	2.00	155
	2	1.04	2.862	1.90	153
	3	0.83	2.837	2.07	152
*Complex **4*** [b]					
N(31)–H(31A)···O(22)		0.96	3.305	2.41	155
N(31)–H(31B)···O(11)		0.96	2.994	2.07	162
N(33)–H(33B)···O(21)		0.96	3.080	2.18	155
N(42)–H(42)···O(11)		0.96	2.974	2.09	152
N(43)–H(33A)···O(22)		0.96	3.138	2.20	165
N(41)–H(41B)···N(11)^{I}		0.96	3.112	2.19	161
N(32)–H(32)···N(11)^{I}		0.96	3.130	2.22	157
N(43)–H(43B)···N(21)^{ii}		0.96	3.089	2.19	155
N(41)–H(41A)···O(23)^{ii}		0.96	2.999	2.14	148

Distances in (Å) and angles in (°). The e.s.d.s associated with the D–H, D···A, H···A distances and D–H···A angles are ~0.03, 0.04, 0.006 Å, and 2–3°, respectively.

[a] Symmetry code: (i) $-1+x, y, 1+z$; (ii) $x, -0.5-y, -0.5+z$; (iii) $1+x, y, z$; (iv) $x, y, 1+z$; (v) $-1+x, y, z$; (vi) $0.5+x, -y, z$.

[b] Symmetry code: (i) $1+x, y, z$; (ii) $1-x, 1-y, -z$.

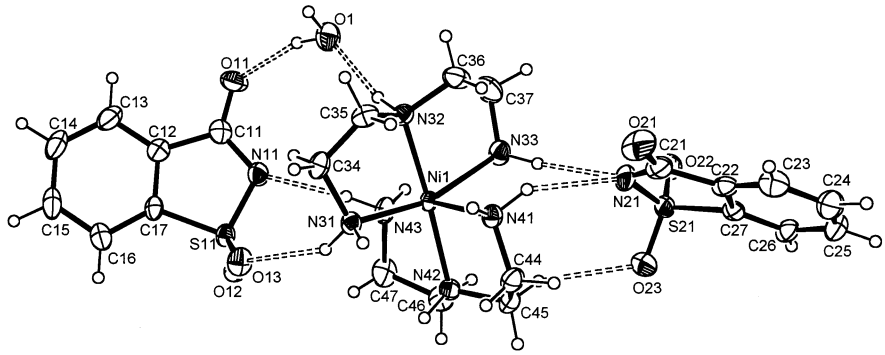


Fig. 1. X-ray structure of $[Ni(dien)_2]\cdot 2(sac)\cdot H_2O$ (**3**) showing the atom numbering scheme. The thermal ellipsoids are drawn at 35% probability level. The ring hydrogen atoms are omitted for clarity. The unique hydrogen bonds in the asymmetric unit are indicated by the dashed lines.

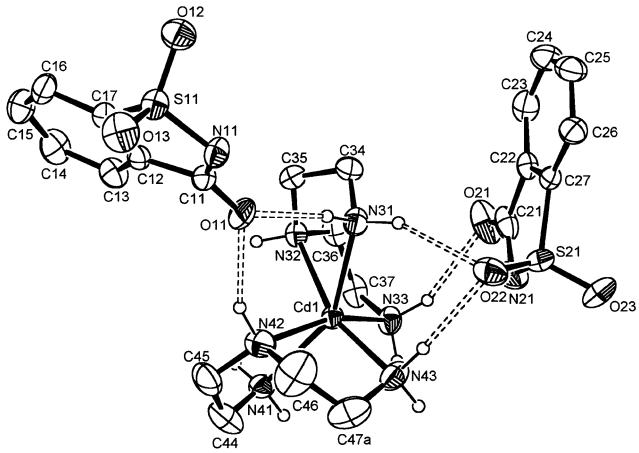


Fig. 2. X-ray structure of $[Cd(dien)_2]\cdot 2(sac)$ (**6**) showing the atom numbering scheme in the asymmetric unit. The thermal ellipsoids are drawn at 35% probability level. The ring hydrogen atoms are omitted for clarity. The unique hydrogen bonds in the asymmetric unit are indicated by the dashed lines.

180° may be explained by the steric restrictions of the tridentate ligands. In **1**–**3**, both the trien ligands adopt the same $\delta\lambda$ configuration. In **4**, however, one of them has only the $\lambda\lambda$ configuration whilst the other dien is disordered and adopt both the $\delta\lambda$ (70%) and $\lambda\lambda$ (30%) configurations. The N(31)–C(34)–C(35)–N(32), N(32)–C(36)–C(37)–N(33), N(41)–C(44)–C(45)–N(42) and N(42)–C(46)–C(47)–N(43) torsion angles (e.s.d.s 0.2–0.3°), respectively, are 56.8, −53.7, −52.8, 58.4 (**1**), 61.3, −57.4, −49.0, 52.0 (**2**), 58.0, −54.7, −54.5, 58.6 (**3**) and −57.7, −61.7, −51.3, 51.1 [C(47A)]/−35.0 [C47B)] (**4**).

The two saccharinate anions are both nearly planar with bond lengths and angles as expected. These dimensions are also comparable with the corresponding values in other metal–saccharin complexes [8,9].

4. Supplementary data

Crystallographic data for the structural analysis have been deposited with the Cambridge Crystallographic Centre, CCDC Nos. 155093 (**1**), 155094 (**2**), 155095 (**3**) and 155096 (**4**). Copies of this information may be obtained free of charge from The Director, CCDC, 12 Union Road, Cambridge, CB2 1EZ, UK (fax: +44-1233-336-033; e-mail: deposit@ccdc.cam.ac.uk or www: http://www.ccdc.cam.ac.uk).

Acknowledgements

C.A.J. is thankful to the EPSRC for a research studentship.

References

[1] S.Z. Haider, K.M.A. Malik, K.J. Ahmed, J. Bangladesh Acad. Sci. 5 (1981) 81.
[2] S.Z. Haider, K.M.A. Malik, J. Bangladesh Acad. Sci. 6 (1982) 119.
[3] S.Z. Haider, K.M.A. Malik, T. Wadsten, J. Bangladesh Acad. Sci. 7 (1983) 107.
[4] F.A. Cotton, L.R. Falvello, R. Llusar, E. Libby, C.A. Murillo, W. Schwotzer, Inorg. Chem. 25 (1986) 3423.
[5] F.A. Cotton, G.E. Lewis, C.A. Murillo, W. Schwotzer, G. Valle, Inorg. Chem. 23 (1984) 4038.
[6] B. Kamenar, G. Jovannovski, Cryst. Struct. Commun. 11 (1982) 257.
[7] K.J. Ahmed, A. Habib, S.Z. Haider, K.M.A. Malik, M.B. Hursthouse, Inorg. Chim. Acta 56 (1981) L37.
[8] S.Z. Haider, K.M.A. Malik, K.J. Ahmed, H. Hess, H. Riffel, M.B. Hursthouse, Inorg. Chim. Acta 72 (1983) 21.
[9] S.Z. Haider, K.M.A. Malik, S. Das, M.B. Hursthouse, Acta Crystallogr., Sect. C 40 (1984) 1147.
[10] K.B. Dillon, C. Bilton, J.A.K. Howard, V.J. Hoy, R.M.K. Deng, D.T. Sethatho, Acta Crystallogr., Sect. C 55 (1999) 330.
[11] A. Hergold-Brundic, O. Grupce, G. Jovanvski, Acta Crystallogr., Sect. C 47 (1991) 2659.
[12] R.M.K. Deng, C. Bilton, R.K. Dillon, J.A.K. Howard, Acta Crystallogr., Sect. C 56 (2000) 142.
[13] C.A. Johns, G.M.G. Hossain, K.M.A. Malik, S.Z. Haider, U.K.R. Romman, Polyhedron 20 (2001) 721.
[14] J.M. Li, J.Z. Sun, P.C. Chen, X.T. Wu, Cryst. Res. Technol. 30 (1995) 353.

[15] S.Z. Haider, K.M.A. Malik, K.J. Ahmed, Inorg. Synth. 23 (1985) 47.
[16] G.M. Sheldrick, Acta Crystallogr., Sect. A 46 (1990) 467.
[17] G.M. Sheldrick, SHELX-80, Program for Crystal Structure Refinement, University of Göttingen, Germany, 1980.
[18] J.E. Huheey, Inorganic Chemistry: Principles of Structure and Reactivity, 3rd ed., Harper & Row, New York, 1983, pp. 73–76.
[19] R.C. Hynes, C.J. Willis, J.J. Vittal, Acta Crystallogr., Sect. C 52 (1996) 1879.
[20] A.K. Mukherjee, S. Koner, A. Ghosh, N.R. Chaudhuri, M. Mukherjee, A.J. Welch, J. Chem. Soc., Dalton Trans. (1994) 2367.
[21] F.S. Stephens, J. Chem. Soc. A (1969) 2233.
[22] P.G. Hodgson, B.R. Penfold, J. Chem. Soc., Dalton Trans. (1974) 1870.
[23] I.A. Razak, S.S.S. Raj, H.-K. Fun, Y.-X. Tong, Z.-L. Lu, B.-S. Kang, Acta Crystallogr., Sect. C 56 (2000) 291.
[24] H. Kurihara, S. Nishikiori, T. Iwamoto, Chem. Lett. (1997) 61.

PERGAMON

Polyhedron 21 (2002) 403–408

POLYHEDRON

www.elsevier.com/locate/poly

Complexes of cobalt(II), nickel(II) and copper(II) with a thia ligand; 2,5-bis(2-pyridyl)-1,3,4-thiadiazole: structural identification

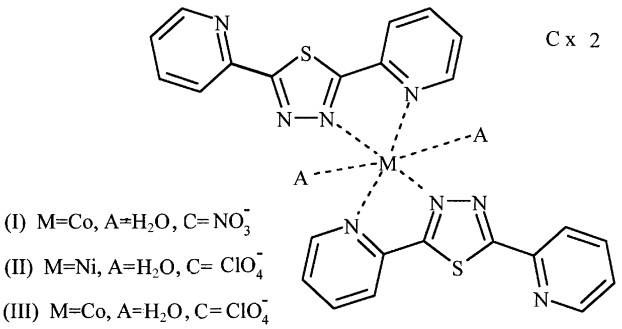
F. Bentiss [a], M. Lagrenée [a,*], J.P. Wignacourt [a], E.M. Holt [b]

[a] *Laboratoire de Cristallochimie et Physicochimie du Solide, CNRS UPRESA 8012, ENSCL, BP. 108, F-59652 Villeneuve d'Ascq Cedex, France*
[b] *Department of Chemistry, Oklahoma State University, Stillwater, OK 74078, USA*

Received 25 September 2001; accepted 22 November 2001

Abstract

A heterocycle, previously untested as a polydentate ligand, 2,5-bis(2-pyridyl)-1,3,4-thiadiazole, namely bptd, has been found to form the monomeric complexes, $Co(bptd)_2(H_2O)_2(NO_3)_2$ (**I**), $Ni(bptd)_2(H_2O)_2(ClO_4)_2$ (**II**), $Co(bptd)_2(H_2O)_2(ClO_4)_2$ (**III**), and $Cu(bptd)_2(NO_3)_2$ (**IV**) with Co(II), Ni(II) and Cu(II) in the presence of nitrate or perchlorate anions. Despite similar syntheses, nitrate serves as a ligand to Cu(II) in **IV** whereas, it is seen as a free ion in the cell of $Co(bptd)_2(H_2O)_2(NO_3)_2$ (**I**).

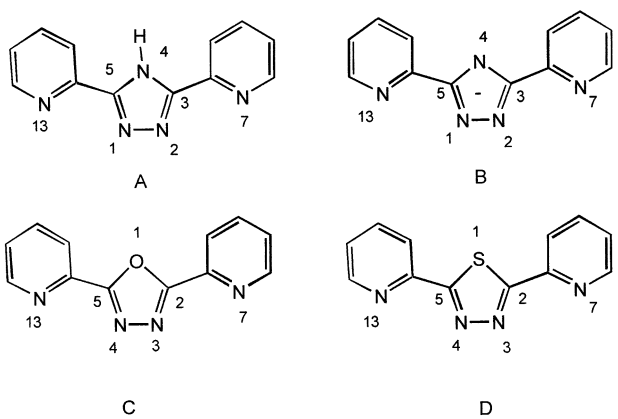


© 2002 Elsevier Science Ltd. All rights reserved.

Keywords: Thiadiazole; M = Co; M = Ni; M = Cu; Crystal structures; Monomeric complexes

1. Introduction

The associative magnetic properties of transition metal complexes in the solid state are influenced by the presence of close metal–metal distances, by the presence of bridging atoms or pathways and by the overall geometry of metals, bridging atoms and coordinated ligands. Thus there is interest in designing ligands capable of enforcing close metal contacts during the process of assembly or crystallization to form the solid state. Four heteroatom derivatives of 1,2-diazoles with *o*-pyridine substitution at the 3 and 5 positions have been of interest for such applications (Scheme 1A and B).



* Corresponding author. Tel.: +33-320-337-746; fax: +33-320-436-814.
E-mail address: michel.lagrenee@ensc-lille.fr (M. Lagrenée).

0277-5387/02/$ - see front matter © 2002 Elsevier Science Ltd. All rights reserved.
PII: S0277-5387(01)01012-9

The use of (1,3,4)-oxadiadiazoles with such substitution [2,5-bis(2-pyridyl)-1,3,4-oxadiazole] (1C) abbreviated as (bpo) however, has normally led to the crystallization of monomeric complexes without metal–metal interaction [1–3]. The only reported example of a multimetal complex with bpo is the polymeric species $[Cu(bpo)Cl_2]_\infty$ in which successive metal centers are indeed bridged by the tetradentate ligand. In this case the ligands show a large deviation from coplanarity, resulting in a large intermetal distance and EPR measurements show the copper atoms to have no interaction [3].

(1,2,4-Triazoles) with *o*-pyridine substitution at the 3 and 5 positions [3,5-bis(2-pyridyl)-4H-1,2,4-triazole] (bpt) may be used as ligands in neutral (1A) or anionic form (1B). When one of the three nitrogen atoms of the aromatic triazole ring bears a substituent, the ligand is neutral. When this substituent is absent, the ligand is in the anionic form. With one exception, the reported solid state complexes involving the neutral ligand and divalent transition metals are monomeric [4–8]. An exception to this generalization is the nickel dimer formed with 4-amino-1,2,4-triazole, water and chloride molecules. This neutral ligand forms a dimeric face to face complex with close Ni–Ni interactions [9].

Anionic forms of the ligand, on the other hand, are normally seen to bridge two metal atoms. When the pyridyl nitrogen atoms face in the same direction as the N1 and diazole rings, the four nitrogen atoms bond to two metal atoms and metal–metal distances of about 4 Å are seen [10]. However, one pyridine ring may rotate 180° to bond to a metal atom along with the nitrogen atom in the 4 position. A second metal is found on the opposite side of the ligand, bound to the nitrogen atom of the remaining pyridine ring and to the near nitrogen of the triazole ring [11].

There are no reports in the literature of the complexed form of the 2,5-bis(2-pyridyl)-thia derivative (**1D**). We begun exploration of the properties of the 1-thia-3,4-diazole species with ortho pyridine rings substituted at the 2 and 5 positions [2,5-bis(2-pyridyl)-1,3,4-thiadiazole (bptd)] as a molecular architect with transition metals. We report here the single crystal structures of several complexes formed by bptd with divalent Co (structures **I** and **III**), Ni (structure **II**) and Cu (structure **IV**).

Table 1
IR data (KBr, cm^{-1})

	Pyridine bands			Anion bands	
Ligand		1580	1560		
I	1650	1603	1560	1384	1315
II	1650	1603	1560	1090	
III	1634	1603	1560	1100	
IV	1649	1603	1560	1384	1323

2. Experimental

2,5-Bis(2-pyridyl)-1,3,4-thiadiazole was synthesized as described previously [12,13]. $Co(NO_3)\cdot 6H_2O$ (1.5 mmol, 0.44 g) in 8 ml of water was added to (0.42 mmol, 0.1 g) of ligand dissolved in 8 ml of EtOH. The solution was filtered and after 24 h the orange compound (**I**) crystallized at room temperature (r.t.). Crystals (**I**) were washed with water and dried under vacuum.

$Ni(ClO_4)\cdot 6H_2O$ (1.5 mmol, 0.55 g) in 8 ml of water was added to (0.42 mmol, 0.1 g) of ligand dissolved in 8 ml of EtOH. The solution was filtered and after 24 h the colorless compound (**II**) crystallized at r.t. Crystals were washed with water and dried under vacuum.

$Co(ClO_4)\cdot 6H_2O$ (1.5 mmol, 0.55 g) in 8 ml of water was added to (0.42 mmol, 0.1 g) of ligand dissolved in 8 ml of EtOH. The solution was filtered and after 24 h the colorless compound crystallized at r.t. Crystals of (**III**) were washed with water and dried under vacuum.

$Cu(NO_3)\cdot 2.5H_2O$ (1.5 mmol, 0.35 g) in 8 ml of water was added to (0.42 mmol, 0.1 g) of ligand dissolved in 8 ml of EtOH. The solution was filtered and after 24 h the blue compound (**IV**) crystallized at r.t. Crystals were washed with water and dried under vacuum.

Infrared spectra were recorded on a Nicolet FT Impact 400 D double-beam spectrometer. Solid samples were examined in the form of KBr pellets.

Intensity data were collected on a Bruker AXS SMART three-circle diffractometer using graphite monochromated Mo Kα radiation ($\lambda = 0.71073$ Å), equipped with a CCD two dimensional detector [14]. Crystal data are given in Table 2. All non-hydrogen atom positions were determined by direct methods [15]. Positional parameters and a scaling factor were refined to convergence [16] using first isotropic thermal parameters and then anisotropic displacement factors. Hydrogen atoms on the pyridyl rings were placed in idealized positions whereas those on the water molecules were identified from a difference Fourier synthesis. For (**II**) and (**III**), the perchlorate anion was found to be disordered over two principal orientations. Occupancy factors for these two positions were refined. Bond angles and distances are given in Table 3.

3. Discussion

The bonding mode of the ligands and anions can be deduced from the IR spectra of the complexes, see Table 1. The indicators for the ligand are the two intensive bands of the pyridine ring vibrations near

Table 2
Crystal data for compounds **I**, **II**, **III** and **IV**

Compound	**I**	**II**	**III**	**IV**
Empirical formula	$C_{12}Co_{0.5}H_{10}N_5O_4S$	$C_{12}Ni_{0.50}H_{10}ClN_4O_5S$	$C_{12}Co_{0.50}H_{10}ClN_4O_5S$	$C_{12}Cu_{0.50}H_8N_5O_3S$
Formula weight	349.77	387.11	387.21	334.06
Temperature (K)	293(2)	293(2)	293(2)	293(2)
Crystal system	triclinic	monoclinic	monoclinic	monoclinic
Space group	$P\bar{1}$	$P2_1/n$	$P2_1/n$	$P2_1/c$
a (Å)	7.749(3)	10.9085(15)	10.914(2)	7.7369(11)
b (Å)	7.896(3)	11.0524(15)	11.085(2)	8.9126(13)
c (Å)	11.995(4)	13.2823(19)	13.217(2)	19.191(3)
α (°)	88.166(6)	90	90	90
β (°)	79.723(5)	101.055(3)	100.608(4)	93.644(3)
γ (°)	83.329(6)	90	90	90
V (Å^3)	717.2(4)	1571.7(4)	1571.8(4)	1320.6(3)
Z	2	4	4	4
D_{calc} (Mg m^{-3})	1.620	1.636	1.636	1.680
μ (mm^{-1})	0.811	0.988	0.916	1.048
$F(000)$	357	788	786	678
Crystal size (mm)	$0.05\times0.1\times0.1$	$0.1\times0.1\times0.1$	$0.1\times0.1\times0.1$	$0.1\times0.1\times0.1$
Data collection range	$5.38<2\theta<46.68$	$4.44<2\theta<52.04$	$4.46<2\theta<60.04$	$5.04<2\theta<46.56$
Range of indices	$-8\le h\le8,\ -8\le k\le8,$ $-1\le l\le22$	$-13\le h\le13,$ $-13\le k\le13,\ -16\le l\le16$	$-15\le h\le15,$ $-15\le k\le15,\ -18\le l\le17$	$-8\le h\le8,\ -9\le k\le9,$ $-15\le l\le21$
Reflections measured	3075	9296	16953	4798
Unique reflections	1923	2687	4572	1639
Observed reflections $[I>2\sigma(I)]$	1743	1665	1385	1573
R_{int}	0.0289	0.0532	0.1185	0.0409
Weighting scheme	$1/[\sigma^2(F_o^2)+(0.1000P)^2$ $+0.0000P]$ where $P=(F_o^2+2F_c^2)/3$	$1/[\sigma^2(F_o^2)+(0.1000P)^2$ $+0.0000P]$ where $P=(F_o^2+2F_c^2)/3$	$1/[\sigma^2(F_o^2)+(0.1000P)^2$ $+0.0000P]$ where $P=(F_o^2+2F_c^2)/3$	$1/[\sigma^2(F_o^2)+(0.1000P)^2$ $+0.0000P]$ where $P=(F_o^2+2F_c^2)/3$
Number of parameters	214	257	260	197
Rgt	0.0565	0.0485	0.0478	0.0528
Rw/gt	0.1466	0.1235	0.1145	0.1435
Goodness-of-fit	1.22	0.836	0.670	1.137
Maximum peak in final ΔF map (e Å^{-3})	0.29	0.32	0.250	0.23
Minimum peak in final ΔF map (e Å^{-3})	−0.19	−0.28	−0.25	−0.20

1580 cm^{-1}. Upon pyridine coordination to a metal the higher one of these bands is shifted by about +20 cm^{-1} [17]. In all cases there are two IR bands in the 1600–1650 cm^{-1} range which can be assigned to one coordinated and one uncoordinated pyridine ring. This means that in these 2:1 complexes each thiadiazole ligand uses one pyridine nitrogen and probably one thiadiazole nitrogen for chelate binding, as was confirmed by the structure determination of complexes (see below). With respect to anion binding, the positions of the two nitrate stretching bands of (**IV**) point to unidentate nitrate coordination in this complex. The nitrate in (**I**) and perchlorate in (**II**) and (**III**) are free anions [18,19].

(**I**), (**II**), (**III**) and (**IV**) crystallize with the monomeric metal atom situated on a center of symmetry and with coordination to four nitrogen atoms plus the oxygen atoms of two water molecules [(**I**), (**II**) and (**III**)] or of two nitrate moieties (**IV**) (Figs. 1–4). In each structure, M [(**I**) and (**III**), M = Co, (**II**), M = Ni, (**IV**) M = Cu] is seen in a distorted octahedral geometry with the N3 and N7 atoms of each of two ligand molecules forming an equatorial plane on which the metal atom is found. The three rings forming the ligand are each individually planar within experimental limits. Ring, C6, N7, C8, C9, C10, C11, is close to coplanarity with ring S1, C2, N3, N4, C5; S.D. (**I**) 0.021, (**II**) 0.026, (**III**) 0.027, (**IV**) 0.022. In (**I**), ring C12, N13, C14, C15, C16, C17 subtends an angle of 2.0° with the plane of the other two rings. In (**II**), this angle is 18.0°, in (**III**), 19.0° and in (**IV**), 7.0°. This rotation may be attributed to packing influences, as there are no obvious hydrogen bonding or other influences seen.

Metal nitrogen distances average 2.125(3) Å (**I**), 2.076(4) Å (**II**), 2.107(3) Å (**III**), 2.035(4) Å (**IV**) and are normal for these metals.

Axial positions in (**I**), (**II**) and (**III**) are occupied by water molecules with M–O distances of 2.101(3) Å (**I**),

Table 3
Bond angles (°) and distances (Å) for $Co(bptd)_2(H_2O)_2(NO_3)_2$ (**I**), $Ni(bptd)_2(H_2O)_2(ClO_4)_2$ (**II**), $Co(bptd)_2(H_2O)_2(ClO_4)_2$ (**III**) and $Cu(bptd)_2(NO_3)_2$ (**IV**)

	I	II	III	IV
Bond lengths				
M–O11	2.101(3)	2.083(4)	2.087(4)	2.323(4)
M–N3	2.120(3)	2.049(3)	2.077(3)	2.026(4)
M–N7	2.130(3)	2.104(4)	2.137(3)	2.044(4)
N4–C5	1.297(5)	1.296(5)	1.289(5)	1.303(6)
N4–N3	1.376(4)	1.360(5)	1.367(5)	1.371(5)
N3–C2	1.301(5)	1.310(5)	1.315(5)	1.297(6)
C2–C6	1.465(5)	1.455(6)	1.463(6)	1.460(7)
C2–S1	1.715(4)	1.707(4)	1.700(4)	1.701(5)
S1–C5	1.728(4)	1.736(5)	1.725(4)	1.727(5)
C5–C12	1.464(5)	1.469(6)	1.471(6)	1.469(7)
C6–N7	1.338(5)	1.355(5)	1.345(5)	1.355(6)
C6–C11	1.374(5)	1.378(6)	1.375(6)	1.366(7)
N7–C8	1.333(5)	1.330(6)	1.335(5)	1.335(7)
C8–C9	1.378(6)	1.375(6)	1.371(6)	1.371(7)
C9–C10	1.357(7)	1.373(6)	1.372(6)	1.364(7)
C10–C11	1.379(6)	1.377(7)	1.367(6)	1.372(7)
C12–N13	1.334(5)	1.326(6)	1.334(6)	1.350(6)
C12–C17	1.387(5)	1.366(7)	1.360(6)	1.365(7)
N13–C14	1.335(5)	1.327(6)	1.343(6)	1.315(7)
C14–C15	1.366(6)	1.371(9)	1.359(8)	1.373(9)
C15–C16	1.368(6)	1.365(8)	1.362(7)	1.378(9)
C16–C17	1.382(6)	1.360(8)	1.370(7)	1.377(8)
N30–O21	1.209(6)			1.194(5)
N30–O22	1.217(5)			1.210(6)
N30–O23	1.227(5)			1.183(6)
Cl–O1		1.441(12)	1.420(6)	
Cl–O2		1.436(9)	1.396(6)	
Cl–O3		1.385(11)	1.347(8)	
Cl–O4		1.542(11)	1.434(5)	
Bond angles				
O11–M–N3^{i}	89.99(15)	89.17(15)	89.11(17)	87.04(18)
O11–M–N3	90.01(15)	90.83(15)	90.89(17)	92.96(18)
O11–M–N7^{i}	89.37(12)	88.84(16)	88.52(15)	88.64(16)
N3–M–N7^{i}	102.81(12)	100.79(14)	102.21(13)	99.40(15)
N3–M–N7	77.19(12)	79.21(14)	77.79(13)	80.60(15)
O11^{i}–M–N7^{i}	90.63(12)	91.16(16)	91.48(15)	91.36(16)
C5–N4–N3	111.2(3)	111.8(4)	111.7(4)	110.9(4)
C2–N3–N4	113.7(3)	113.7(4)	112.7(3)	113.8(4)
N3–C2–C6	119.9(3)	119.4(4)	119.0(4)	119.3(4)
N3–C2–S1	113.5(3)	113.4(3)	114.0(3)	113.9(4)
C6–C2–S1	126.6(3)	127.1(3)	127.0(3)	126.8(4)
C2–S1–C5	86.9(2)	86.9(2)	86.7(2)	87.0(2)
N4–C5–C12	125.5(3)	125.3(4)	124.2(4)	125.2(4)
N4–C5–S1	114.6(3)	114.1(3)	114.9(3)	114.4(4)
C12–C5–S1	119.9(3)	120.5(3)	120.9(3)	120.3(4)
N7–C6–C11	123.1(3)	122.2(4)	122.3(4)	122.8(4)
N7–C6–C2	113.6(3	113.8(4)	113.8(4)	113.2(4)
C11–C6–C2	123.4(3)		123.9(4)	123.9(4)
C8–N7–C6	117.1(3)	117.4(4)	118.2(4)	116.9(4)
N7–C8–C9	123.1(4)	123.3(4)	122.1(4)	123.1(5)
C10–C9–C8	119.2(4)	119.2(5)	119.4(4)	119.1(5)
C9–C10–C11	118.9(4)	118.5(5)	119.2(5)	119.2(5)
C6–C11–C10	118.7(4)	119.4(4)	118.8(4)	118.8(5)
N13–C12–C17	123.9(3)	123.4(5)	124.7(4)	124.2(5)
N13–C12–C5	115.1(3)	115.0(4)	113.7(4)	113.1(4)
C17–C12–C5	121.1(3)	121.5(4)	121.7(4)	122.7(5)
C12–N13–C14	117.0(3)	116.4(5)	116.0(5)	116.5(5)
N13–C14–C15	123.0(4)	124.3(6)	123.3(5)	123.8(6)
C14–C15–C16	119.6(4)	117.5(5)	118.7(5)	118.7(6)
C15–C16–C17	119.0(4)	119.5(6)	119.9(5)	119.0(6)
C16–C17–C12	117.5(4)	118.8(6)	117.4(5)	117.8(5)
O21–N30–O22	118.8(4)			123.9(5)
O21–N30–O23	119.2(5)			117.1(5)
O22–N30–O23	121.8(4)			118.8(5)
O1–Cl–O2			105.0(5)	
O1–Cl–O3			116.5(9)	
O1–Cl–O4			105.7(4)	
O2–Cl–O3			109.0(6)	
O2–Cl–O4			112.0(4)	
O3–Cl–O4			108.6(5)	

$i = -x, -y, -z$.

2.083(4) Å (**II**) and 2.087(4) Å (**III**). In (**IV**), the axial positions are occupied by monodentate nitrate oxygen atoms, Cu–O(nitrate) 2.323(4) Å. M bonds to the oxygen atoms are close to perpendicular as seen in the ranges of O–M–N angles which deviate only slightly from the theoretical value of 90°; (**I**) 89.37(12)–90.63(12), (**II**) 88.84(16)–91.16(16), (**III**) 88.52(15)–91.48(15), (**IV**) 87.0(2)–93.0(2)°.

Hydrogen bonding is seen between hydrogen atoms of the water molecule and in (**I**) H11b is 2.33 Å from O21 $(x, 1+y, -1+z)$ and 2.30 Å from O23 $(x, 1+y, -1+z)$ whereas H11c is 1.96 Å from O21 $(-1-x, -1-y, 1-z)$. In (**II**), bonding is seen to oxygen atoms of the perchlorate anion: H11b is 2.14 Å from O2$(0.5-x, -0.5+y, 0.5-z)$ and H11c is 1.92 Å from O3 $(x, -1+y, z)$. H11b of (**III**) is 2.114 Å from the perchlorate oxygen atom, O2 $(1/2-x, -1/2+y, 1/2-z)$ and H11c is 1.947 Å from O3 $(x, -1+y, z)$. Bonding details within nitrate and perchlorate ions are normal.

Both (**I**) and (**IV**) were prepared from the appropriate metal nitrate salts and ligand dissolved in water and ethanol, respectively and then mixed. Stoichiometry and crystallization conditions were equivalent, yet cobalt is seen with water molecules as axial ligands and two nitrate ions as a distant counter ions whereas copper has two nitrate ions as axial ligands and no solvent water molecules are found in the cell. This behavior is normal for Co(II). In 62 published structures in which Co(II), NO_3^- and H_2O are present in the cell, cobalt is ligated to neither Lewis base in 26 cases and only to water in 33 examples. A review of the 110 published Cu(II) crystal structures with both nitrate and water molecules present in the cell shows only the water molecule complexed in 56 structures and neither water nor nitrate complexed to Cu(II) in 21 other structures. There are 20 reported examples of Cu(II) coordination to both, but only seven in which copper is coordinated to two nitrate anions and not to water. Thus, structure (**III**), in which copper(II) is axially coordinated to two nitrate ions, is unusual. It remains

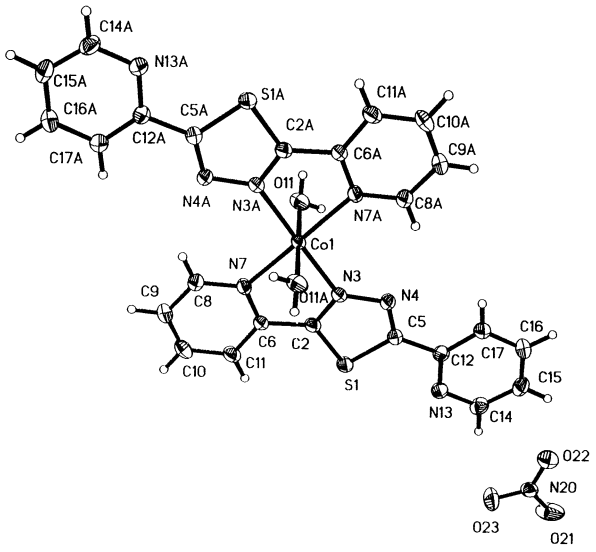


Fig. 1. Projection view of $Co(bptd)_2(H_2O)_2(NO_3)_2$ (**I**) (thermal ellipsoids are shown at the 50% probability level).

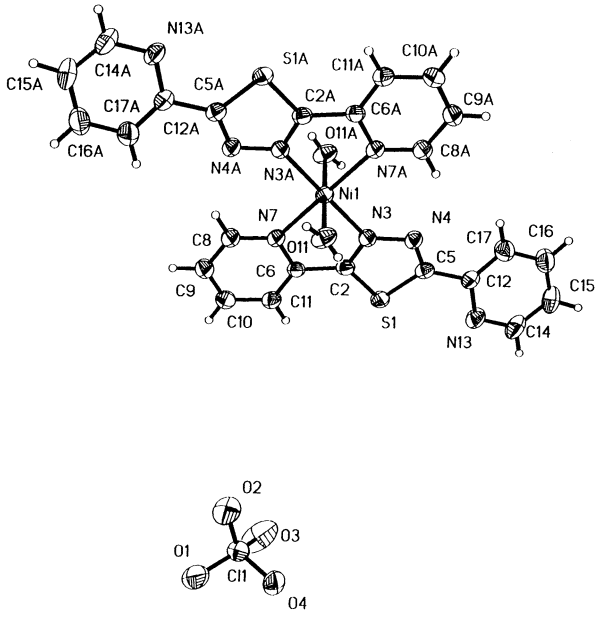


Fig. 2. Projection view of $Ni(bptd)_2(H_2O)_2(ClO_4)_2$ (**II**) showing one of two ClO_4^- molecules disordered about the Cl site (thermal ellipsoids are shown at the 50% probability level).

to be seen if copper complexation to nitrate has been influenced by some electronic or geometric influence of the bptd ligand.

In structures (**I**), (**II**), (**III**) and (**IV**), metal complexation under the synthetic conditions used and with the perchlorate and nitrate counter ions, follows the pattern of formation of monomeric complexes expected for neutral ligands of the bis(2-pyridyl) substituted oxadiazole and triazole family.

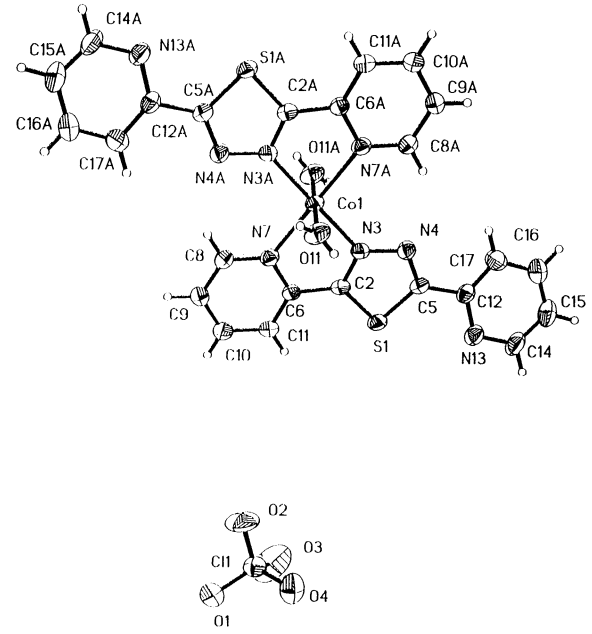


Fig. 3. Projection view of $Co(bptd)_2(H_2O)_2(ClO_4)_2$ (**III**) showing one of two ClO_4^- molecules disordered about the Cl site (thermal ellipsoids are shown at the 50% probability level).

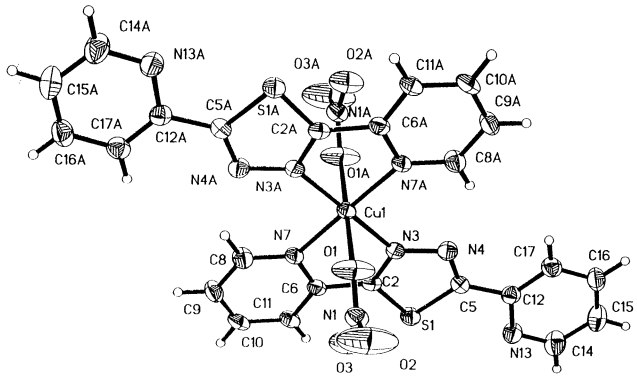


Fig. 4. Projection view of $Cu(bptd)_2(NO_3)_2$ (**IV**) (thermal ellipsoids are shown at the 50% probability level).

4. Supplementary material

The supplementary material is available from the Cambridge Crystallographic Data Center, 12 Union Road, Cambridge CB2 1EZ, UK on request quoting the deposition numbers 164806, 164807, 165314 and 164808 for compounds (**I**)–(**IV**), respectively and can be obtained by contacting the CCDC (quoting the article details and the corresponding SUP number) (fax: +44-1223-336033; e-mail: deposit@ccdc.cam.ac.uk or www:http://www.ccdc.cam.ac.uk).

References

[1] A. El Gueddi, B. Mernari, M. Giorgi, M. Pierrot, Acta Crystallogr. 56e (2000) 426.

[2] J.-P. Wignacourt, S. Sueur, M. Lagrenée, Acta Crystallogr., Sect. C 46 (1990) 394.
[3] M. Lagrenée, S. Sueur, J.-P. Wignacourt, B. Mernari, A. Boukhari, J. Chim. Phys. Phys. Chim. Biol. 88 (1991) 2075.
[4] P.J. van Koningsbruggen, K. Goubitz, J.G. Hassnoot, J. Reedijk, Inorg. Chim. Acta 268 (1998) 37.
[5] C. Faulman, P.J. van Koningsbruggen, R.A.G. de Graaf, J.G. Hassnoot, J. Reedijk, Acta Crystallogr., Sect. C 46 (1990) 2357.
[6] A.J. Jircitano, S.O. Sommerern, K.A. Abboud, Acta Crystallogr., Sect. C 53 (1997) 434.
[7] D. Zhu, Y. Song, Y. Liu, Y. Xu, Y. Zhang, X You, S.S.S. Raj, H.-K. Fun, Transition Met. Chem. 25 (2000) 589.
[8] P.J. Kunkeler, P.J. van Koningsbruggen, J.P. Cornelissen, A.N. van der Horst, A.M. van der Kraan, A.L. Spek, J.G. Haasnoot, J. Reedijk, J. Am. Chem. Soc. 118 (1996) 2190.
[9] F.S. Keijj, R.A.G. de Graaff, J.G. Haasnoot, J. Reedijk, J. Chem. Soc., Dalton Trans. (1984) 2093.
[10] R. Prins, P.J.M.W.L. Birker, J.G. Haasnoot, G.C. Verschoor, J. Reedijk, Inorg. Chem. 24 (1985) 4128.
[11] R. Hage, J.G. Haasnoot, H.A. Nieuwenhuis, J. Reedijk, D.J.A. DeRidder, J.G. Vos, J. Am. Chem. Soc. 112 (1990) 9245.
[12] A.R. Katritzky, A.J. Boulton, Advances in Heterocyclic Chemistry, vol. 9, Academic Press, New York and London, 1968, pp. 166–170.
[13] G. Mazzone, G. Puglisi, F. Bonina, A. Corsaro, J. Heterocyclic Chem. 20 (1983) 1399.
[14] Bruker AXS, SMART, Madison, Wisconsin, USA, 1998.
[15] G.M. Sheldrick, Acta Crystallogr., Sect. A 46 (1990) 467.
[16] G.M. Sheldrick, SHELXL-97. Program for the Refinement of Crystal Structures, University of Göttingen, Germany, 1997.
[17] M.M. da Mota, J. Rodgers, S.M. Nelson, J. Chem. Soc., Sect. A (1969) 2036.
[18] L.J. Bellamy, The Infrared Spectra of Complex Molecules, vol. I, Chapman and Hall, London, 1985.
[19] K. Nakamoto, Infrared and Raman Spectra of Inorganic and Coordination Compounds, 4th ed., Willey & Sons Interscience Publisher, New York, 1986.

PERGAMON

Polyhedron 21 (2002) 409–416

POLYHEDRON

www.elsevier.com/locate/poly

Tetrachlorocuprate(II) salts of heterocyclic aminoguanidonium (guanylhydrazonium) ions

Jesús Valdés-Martínez [a,*], James H. Alstrum-Acevedo [b], Rubén A. Toscano [a], Simón Hernández-Ortega [a], Georgina Espinosa-Pérez [a], Douglas X. West [c], Brian Helfrich [d]

[a] *Instituto de Química, Universidad Nacional Autónoma de México, Circuito Exterior, Ciudad Universitaria, Coyoacán 04510, Mexico*
[b] *Department of Chemistry, Illinois State University, Normal, IL 61790-4160, USA*
[c] *Department of Chemistry, 351700, University of Washington, Seattle, WA 98195-1700, USA*
[d] *Department of Chemistry, Kansas State University, Manhattan, KS 66506-3701, USA*

Received 12 February 2001; accepted 26 November 2001

Abstract

Condensation of aminoguanidine with 2-formylpyridine, 2-benzoylpyridine and 2,6-diacetylpyridine results in the aminoguanidones, HFogu, HBzgu and $H_2$2,6Acgu$_2$, respectively. Reaction of the heterocyclic aminoguanidone in a mixture of hydrochloric acid–ethanol with copper(II) chloride produces the following mixed salts: [H_3Fogu][$CuCl_4$], (**1**), [H_3Bzgu]$_2$[$CuCl_4$]Cl_2·H_2O, (**2**), and [$H_5$2,6Acgu$_2$][$CuCl_4$]Cl·H_2O, (**3**). Their crystal structures, as well as their ESR and UV spectra, have been obtained. The influence on the geometry of the $[CuCl_4]^{2-}$ of the N–H···Cl–Cu hydrogen bonds, in the context of charged compensation hypothesis, has been evaluated. © 2002 Elsevier Science Ltd. All rights reserved.

Keywords: Aminoguanidonium; Copper(II) halides; Crystal structures; Tetrachlorocuprate(II)

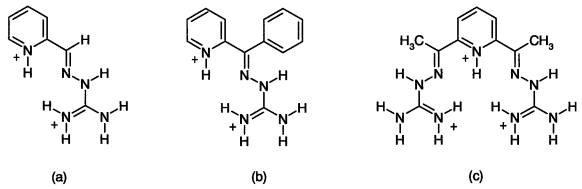
1. Introduction

There has been a continuous interest in the chemistry of copper(II) halides due to their stereochemical complexity and the magnetic and optical properties many of them display. The structural chemistry of more than 60 salts containing tetrachlorocuprate(II) ions were summarized a few years ago [1], and many others have been reported more recently [2]. The copper(II) halides reported show a wide variety of geometric complexity. Compounds with coordination numbers 4, 5 and 6 with several geometries for each coordination number have been reported. The bridging ability of the halides complicates even more the structural chemistry of these compounds. In addition to the simple mononuclear species, it is possible to obtain oligomeric units ranging from 2 to 14 Cu(II) ions, and infinite one- two- or three-dimensional polimeric species. Willett proposed that it is possible to have some reasonable rationalization for many of these structures through the application of some simple electrostatic arguments which he called 'charged compensation' [3]. According to this idea the observed structure of copper(II) halides salts can be visualized as a balance between crystal field stabilization effects and an electrostatic ligand–ligand repulsion effect. In four-coordinate compounds, the former favors a square-planar, and the latter a tetrahedral geometry. As long as hydrogen bonds tend to remove charge from the Cl atoms they will promote the $[CuCl_4]^{2-}$ ion to move toward a square-planar geometry.

In this paper we present the crystal and molecular structure as well as spectroscopic properties of chlorocuprate(II) salts with cations of heterocyclic derivatives of aminoguanidine with 2-formylpyridine, 2-benzoylpyridine and 2,6-diacetylpyridine, Scheme 1. The cations of these compounds have several N–H hydrogen bonding atoms, and therefore, we expect to have

* Corresponding author. Tel.: +52-55-5622-4514; fax: +52-55-5616-2217.
E-mail address: jvaldes@servidor.unam.mx (J. Valdés-Martínez).

0277-5387/02/$ - see front matter © 2002 Elsevier Science Ltd. All rights reserved.
PII: S0277-5387(01)01006-3



Scheme 1. (a) 2-formylpyridine aminoguanidone; (b) 2-benzoylpyridine aminoguanidone; (c) 2,6-diacetylpyridine aminoguanidone.

multiple N–H···Cl–Cu hydrogen bonds, which will allow us to evaluate the charged compensation hypothesis in systems with multiple hydrogen bonds.

2. Experimental

The aminoguanidones were prepared by reaction of a one molar equivalent of aminoguanidine bicarbonate per carbonyl functionality of the desired ketone or aldehyde. Prior to mixing with the aldehyde–ketone, an ethanolic solution of aminoguanidine bicarbonate was neutralized by the dropwise addition of concentrated H_2SO_4 until the evolution of CO_2 ceased. Representative of the preparations is the preparation of 2-benzoylpyridine aminoguanidone: 0.008 moles (1.46 g) of 2-benzoylpyridine was added to 30 ml of EtOH in a 100 ml round-bottom flask and stirred until dissolution occurred. To this solution, 0.008 mol (1.09 g) of neutralized aminoguanidine was added, followed by 2–3 drops of H_2SO_4 to catalyze the reaction. The mixture was refluxed for 5 h, slowly evaporated at approximately 35 °C and white HBzgu (m.p. = 206–208 °C) was isolated by suction filtration. HFogu (m.p. = 190–192 °C) is yellow and $H_2$2,6Acgu$_2$ (m.p. = 249–251 °C) is white. Their IR, ^{1}H and ^{13}C NMR, and mass spectra confirmed the identification of the aminoguanidones.

The chlorocuprate(II) salts were prepared by dissolving an aminoguanidone in approximately 50 ml of a 3:1 EtOH–HCl by volume, adding an equimolar amount of $CuCl_2$, and refluxing for 1 h. The resultant solution was decanted into a beaker, and left until crystals formed. The aldehyde–ketones and the aminoguanidine bicarbonate were purchased from Aldrich and used as received; other reagents were of the highest quality available.

IR spectra were recorded as nujol mulls between CsI plates using Nicolet 5SCX FT (4000–400 cm^{-1}) and Magna 850 (600–100 cm^{-1}) spectrometers. Solid state (i.e. nujol mulls on strips of filter paper) and solution (DMSO solutions in 1 cm cells) electronic spectra were recorded with a Cary 5E spectrometer. ESR spectra of the copper(II) complexes were recorded as solids at 298 and 3 mm Pyrex tubes on a Brucker EMX spectrometer.

2.1. X-ray data collection, structure solution and refinement

Crystals of the chlorocuprate(II) salts were mounted in a random orientation on glass fibers. Crystal data were collected at 293(2) K using a Siemens P4/PC four-circle diffractometer with graphite monochrometer Mo Kα ($\lambda = 0.71073$ Å) radiation. Crystal stability was monitored by measuring standard reflections every 97 reflections. Cell parameters were obtained from 35 accurately centered reflections. Data were collected using a ω–2θ scanning technique. Three reflections were chosen as intensity standards, being re-measured every 97 reflections, there were no significant variation in the intensity of these standards. Lorentz and polarization corrections were applied. The structures were solved by direct methods, and the non-hydrogen atoms were found by successive full-matrix least-squares refinement on F^2 and refined with anisotropic thermal parameters. Hydrogen atom positions were located from difference Fourier maps: and a riding model with fixed thermal parameters ($U_{iso} = 1.2\ U_{eq}$ for the atom to which they are bonded) was used for subsequent refinements. The weighting function applied was $w^{-1} = (\sigma^2(F_o^2) + (gP)^2)$ where $P = (F_o^2 + 2F_c^2)/3$. Scattering factors were taken from the International Tables for Crystallography (1974, vol. IV). The SHELXTL-97 package was used for data reduction and structure solution and refinement. Table 1 contains a summary of the crystallographic data for the three salts.

3. Results

Three aminoguanidones were synthesized from the condensation of aminoguanidine with 2-formylpyridine, HFogu; 2-benzoylpyridine, HBzgu; and 2,6-diacetylpyridine, $H_2$2,6Acgu$_2$, using one molar equivalent of aminoguanidine per carbonyl functionality. The compounds are stable to air and moisture, and melt without decomposition. Under acid conditions the first two compounds form dications and $H_2$2,6Acgu$_2$ a trication by protonation of the pyridyl and guanyl nitrogens, see Scheme 1. Their corresponding aminoguanidonium chlorocuprate(II) salts were prepared by the reaction of equimolar amounts of the aminoguanidone and $CuCl_2$ in EtOH–HCl: [H_3Fogu][$CuCl_4$] (**1**); [H_3Bzgu]$_2$[$CuCl_4$]$Cl_2\cdot H_2O$ (**2**), and [$H_5$2,6Acgu$_2$][$CuCl_4$]$Cl\cdot H_2O$ (**3**).

Details of data collections and structural refinements for **1**, **2** and **3** are given in Table 1. The molecular geometries, thermal ellipsoids (30%) and numbering schemes are shown in Figs. 1–3. Selected bond dis-

Table 1
Crystal data and structure refinement for **1**, **2** and **3**

Crystal data	**1**	**2**	**3**
Empirical formula	$C_7H_{11}Cl_{14}CuN_5$	$C_{26}H_{32}C_{16}CuN_{10}O$	$C_{11}H_{22}Cl_5CuN_9O$
Crystal size (mm)	$0.44\times0.20\times0.14$	$0.40\times0.36\times0.18$	$0.48\times0.42\times0.40$
Crystal system	monoclinic	monoclinic	orthorhombic
Space group	$P2_1/c$	$P2_1/n$	$Pna2_1$
a (Å)	8.101(1)	17.293(2)	13.790(1)
b (Å)	25.801(2)	8.521(1)	12.550(1)
c (Å)	7.210(1)	23.325(2)	12.488(1)
β (°)	108.18(1)	91.08(9)	
V (Å^3)	1431.8(3)	3436.4(6)	2161.2(3)
Z	4	4	4
D_{calc} (Mg m^{-3})	1.719	1.502	1.651
μ (Mo Kα), (mm^{-1})	2.257	1.140	1.651
2θ Range (°)	2.65–24.99	1.75–27.50	2.19–27.50
Index ranges	$-9\le h\le9,\ -30\le k\le1,$ $-1\le l\le8$	$0\le h\le22,\ 0\le k\le11,$ $-30\le l\le30$	$0\le h\le17,\ -16\le k\le0,$ $0\le l\le16$
Absorption coefficient (mm^{-1})	2.257	1.140	1.651
Reflections collected	3307	8134	2601
Independent reflections	2523, [$R_{int}=0.0254$]	7876, [$R_{int}=0.0300$]	2601, [$R_{int}=0.0000$]
Max/min transmission	0.7429, 0.4367	0.8211, 0.6584	0.5581, 0.5046
Absorption correction	Face indexed numerical		Semi-empirical
Data/restraints/parameters	2523/0/155	7876/0/398	2601/1/244
Goodness-of-Fit	0.801	0.985	1.028
Final R indices [$I>2\sigma(I)$]	$R_1=0.0333,\ wR_2=0.0794$	$R_1=0.0634,\ wR_2=0.1253$	$R_1=0.0399,\ wR_2=0.0842$
R indices (all data)	$R_1=0.0481,\ wR_2=0.0846$	$R_1=0.1513,\ wR_2=0.1610$	$R_1=0.0552,\ wR_2=0.0919$
Absolute structure parameter			$-0.01(2)$
Extinction coefficient		0.0034(3)	
Largest difference peak and hole (e Å^{-3})	0.435 and -0.437	0.404 and -0.682	0.392 and -0.320
Weighting function variables	0.0566	0.0581	0.0363
Completenes of data at maximum 2θ (%)	100	100	100

tances and angles are in Table 2 and intra- and intermolecular hydrogen bonds are in Table 3. The solid state electronic spectral bands and their assignments are shown in Table 4.

The asymmetric unit of **1** consist of a $[CuCl_4]^{2-}$ anion and a H_3Fogu^{2+} cation. The H_3Fogu^{2+} is protonated at the pyridyl nitrogen and the guanyl nitrogen (N3). Two intra-molecular H-bonds, N1–H···N2 and N5–H···N2, give planarity to the cation, the angle between the pyridine ring and the aminoguanidone moiety (N2–N3–C8–N4–N5) is 2.0(2). The copper(II) center has a coordination geometry intermediate between tetrahedral and square-planar with *trans* angles of 132.46(5)° and 124.94(4)° and the Cu–Cl bond distance ranges from 2.216(1) to 2.288(1) Å. Due to several N–H···Cl–Cu hydrogen bonds, pair wise ribbons are present in the crystal structure. The ESR spectra of **1** shows only a broad isotropic spectrum with $g_{iso}=2.205$ indicating considerable interaction between copper(II) centers.

The asymmetric unit of **2** contains two non-equivalent H_3Bzgu^{2+} ions, which are balanced by a $[CuCl_4]^{2-}$, two Cl^- ions and a hydrate water molecule. HBzgu is protonated in the pyridyl nitrogen and the guanyl nitrogen. The two H_3Bzgu^{2+} ions present in the asymmetric unit of **2** have significantly different distances in the 'equivalent' moieties. For example, the bond distances for N2–N3 and N22–N23 are 1.384(7) and 1.351(7) Å, and the related N2–C7–C2 and N22–C27–C22 bond angles, 112.6(5)° and 115.0(5)° respectively, Table 2. These differences likely result from the different hydrogen bonding interactions of the two ions; N5–H5B and N1–H1 hydrogen bond to O1W of the water molecule and O1W–H1W hydrogen bonds to N2, but the 'equivalent' N25–H25B and N21–H21

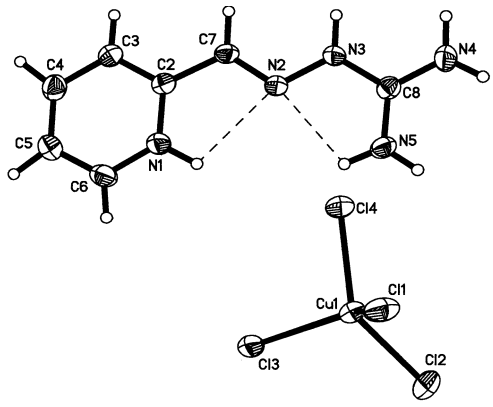


Fig. 1. Labeling scheme and thermal ellipsoid (30%) for **1**. Intramolecular hydrogen bonds are shown with dotted lines.

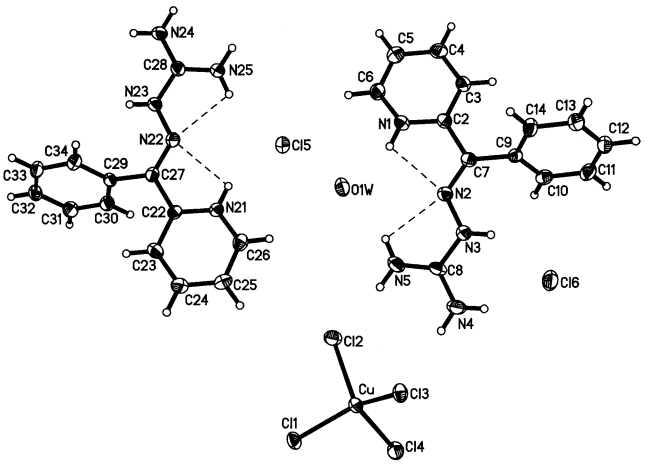


Fig. 2. Labeling scheme and thermal ellipsoid (30%) for **2**. Intramolecular hydrogen bonds are shown with dotted lines.

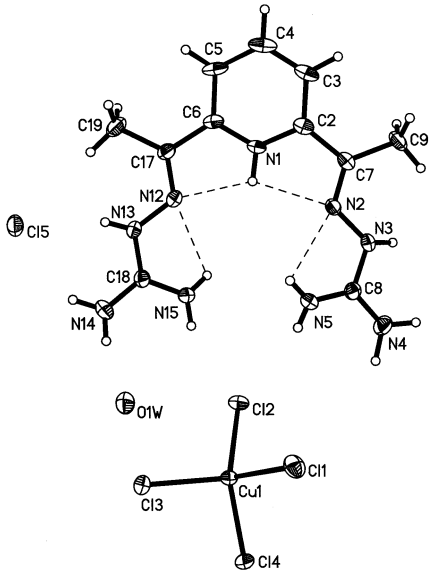


Fig. 3. Labeling scheme and thermal ellipsoid (30%) for **3**. Intramolecular hydrogen bonds are shown with dotted lines.

hydrogen bond to the chloride ion, Cl5. There are two intramolecular H-bond in each non-equivalent molecule, N1–H···N2, N5–H···N2 and N21–H···N22, N25–H···N22. The angle between the phenyl and pyridyl rings in the two forms, are 12.0(3)° and 8.9(3)° and may also be explained by the different modes of hydrogen bonding. The copper(II) center has a coordination geometry intermediate between tetrahedral and square-planar the *trans* angles are 135.44(7)° and 130.50(7)° and the Cu–Cl bond distances range from 2.232(2) to 2.269(2) Å. The ESR spectra of **2** has an axial signal having $g_{\|} = 2.336$, $g_{\perp} = 2.079$ and $g_{av} = 2.165$ indicating minimal distortion from a regular stereochemistry. Calculation of Racah covalency parameters for **2** gives $k_{\|} = k_{\perp} = 0.72$, which is significantly higher than found for aminopyridinium tetrachlorocuprate(II) salts [4] and indicates that there is minimal π-bonding in the anions.

The asymmetric unit of **3** contains one tetrachlorocuprate(II), a chloride ion, a hydrate water molecule and $H_5$2,6Acgu$_2^{3+}$, the latter resulting from protonation of the pyridyl nitrogen and the two guanyl nitrogens, Fig. 3. There are four intramolecular hydrogen bonds in the trication, N1–H···N2, N5–H···N2, N11–H···N12 and N15–H···N12. The angle between the pyridine ring and the aminoguanidone moieties, N2–N3–C8–N4–N5 and N12–N13–C18–N14–N15, are 23.6(2)° and 15.9(1)°, respectively. The copper(II) center has a coordination geometry intermediate between tetrahedral and square-planar, the *trans* angles are 138.86(8)° and 137.73(7)° and the Cu–Cl bond distance ranges from 2.211(1) to 2.265(2) Å.

The ESR spectra of **3** has a rhombic spectrum with $g_1 = 2.239$, $g_2 = 2.159$ and $g_3 = 2.092$ resulting in a $g_{av} = 2.163$, which is consistent with the two long and two short Cu–Cl bonds found by crystal structure determination.

4. Discussion

4.1. Structure of the aminoguanidonium cations

The heterocyclic aminoguanidonium ions have the same pattern of protonation in the three salts; the pyridyl nitrogen and guanyl nitrogen, N3 (or the equivalent N13 or N23). Protonation at the guanyl nitrogen results in two NH_2 groups being attached to the guanidine moiety's carbon atom, C8 (C18 or C28), and a formal double bond is present between this carbon atom and N3 (N13 or N23) resulting in a formal positive charge on N3 (N13 or N23), as found in previous studies [5,6]. However, the C–N bond distances to the two NH_2 groups, C8–N4 (C18–N14 or C28–N24) and C8–N5 (C18–N15 or C28–N25), are shorter than the C8–N3 'double' bond in the three salts indicating considerable π-character in the former bonds and suggesting that the formal bonding picture described above is very approximate.

The imine bond, C2–N7 (C12–N17 or C22–N27), in the three cations is the shortest carbon–nitrogen bond of these guanidonium moieties, and its distance is similar to the analogous bond of neutral thiosemicarbazones prepared from 2-formyl- [7], 2-benzoyl- [7] and 2,6-diacetylpyridine [8]. This suggests that protonation of both the pyridine ring and aminoguanidone moiety in these cations has little effect on the imine bond distance. This is consistent with the small distance changes of the imine bond on coordination except to the hardest metal ions [9].

Bond distances and angles within the guanidonium moieties are similar among the three salts, as well as the

two unique ions of H_3Bzgu^{2+} and the two moieties of $H_52,6Acgu_2^{3+}$. The N2–C7–C2 angle of H_3Fogu^{2+} is significantly larger than in the other cations, which was not observed for neutral heterocyclic thiosemicarbazones [7,8], but each of these angles is in the same range as found for the thiosemicarbazones. Also, the N2–N3 (N12–N13, N22–N23) bond distances are essentially the same in the present cations as they are in the neutral thiosemicarbazones [7,8].

4.2. Structure of the tetrachlorocuprate(II) ions

According to the charge compensation hypothesis, the hydrogen bonds tend to remove charge from the Cl atoms, and promote $[CuCl_4]^{2-}$ to have a more square-planar geometry [3]. In the present compounds the presence of multiple hydrogen bonds in the three structures, as well as chloride anions and hydrate water molecules in **2** and **3**, allow us to test this simple hypothesis in complex situations. Considering the short and intermediate intermolecular N–H···Cl–Cu contacts, Table 3, **1** has more contacts than **2** and **3** (**3** > **2**) and according to the above mentioned hypothesis a geometry more near to square-planar will be expected for **1**. Based on the *trans* angles the three compounds have distorted D_{2d} symmetry, but **1** is the nearest to tetrahedral symmetry, the opposite to the expected result. This indicate that other crystal forces, not considered in this simple model, have a substantial effect upon the geometries of the metal ions in this compounds [9].

4.3. Spectroscopic characterization

Bands above 40,000 cm^{-1} are assigned to $\pi \rightarrow \pi^*$ transitions of the pyridine ring and imine function. Since the pyridyl nitrogen is protonated in all three salts, the two bands in the 30,000 cm^{-1} region are assigned to the $n \rightarrow \pi^*$ transitions of the guanidonium moiety. 2-Acetylpyridine N(4)–dialkyl- or azacyclothiosemicarbazones exist in a bifurcated hydrogen bonding form, which results in conjugation in an analogous manner to the guanidonium moiety [10]. Conjugation of the thiosemicarbazone moiety results in strong bands in the 25,000 and 30,000 cm^{-1} range with the band at 25,000 cm^{-1} being assigned to the thioamide part of the thiosemicarbazone. Conjugation of the aminoquanidone moiety would be expected to produce a band at higher energy as assigned above. Although, there are five assignable Cl → Cu(II) charge transfer bands for tetrachlorocuprate(II) ions having D_{2d} sym-

Table 2
Selected bond lengths (Å) and angles (°) for **1**, **2** and **3**

	1	**2**	**3**
Bond lengths			
Cu1–Cl4	2.2287(9)	2.232(2)	2.211(1)
Cu1–Cl3	2.288(1)	2.269(2)	2.250(2)
Cu1–Cl2	2.216(1)	2.254(2)	2.264(2)
Cu1–Cl1	2.262(1)	2.252(2)	2.265(2)
Bond angles			
Cl1–Cu1–Cl3	124.93(4)	130.50(7)	138.86(8)
Cl2–Cu1–Cl4	132.46(5)	135.44(7)	137.73(7)
Cl2–Cu1–Cl1	101.25(5)	99.11(7)	98.64(7)
Cl4–Cu1–Cl1	99.72(4)	99.26(7)	96.38(7)
Cl3–Cu1–Cl2	103.19(4)	99.28(7)	98.74(7)
Cl4–Cu1–Cl3	98.72(4)	98.88(7)	95.28(7)

1		**2**				**3**			
Bond lengths									
N2–C7	1.280(4)	N2–C7	1.288(7)	N22–C27	1.291(7)	N2–C7	1.280(8)	N12–C17	1.281(8)
N2–N3	1.360(4)	N2–N3	1.384(7)	N22–N23	1.351(7)	N2–N3	1.356(7)	N12–N13	1.359(7)
N3–C8	1.352(4)	N3–C8	1.355(7)	N23–C28	1.365(7)	N3–C8	1.362(7)	N13–C18	1.341(8)
N4–C8	1.310(5)	N4–C8	1.307(8)	N24–C28	1.313(8)	N4–C8	1.327(8)	N14–C18	1.311(8)
N5–C8	1.318(4)	N5–C8	1.322(8)	N25–C28	1.305(7)	N5–C8	1.305(8)	N15–C18	1.316(9)
Bond angels									
N1–C2–C7	118.0(3)	N1–C2–C7	118.5(5)	N21–C22–C27	118.1(5)	N1–C2–C7	117.0(5)	N1–C6–C17	116.9(5)
N2–C7–C2	118.5(3)	N2–C7–C2	112.6(5)	N22–C27–C22	115.0(5)	N2–C7–C2	112.6(5)	N12–C1–C6	112.9(6)
C7–N2–N3	116.7(3)	C7–N2–N3	118.3(5)	C27–N22–N23	118.7(5)	C7–N2–N3	118.8(5)	C17–N12–N13	118.2(5)
C8–N3–N2	118.7(3)	C8–N3–N2	117.4(5)	N22–N23–C28	117.7(5)	N2–N3–C8	116.9(5)	C18–N13–N12	118.4(5)
N4–C8–N3	117.8(3)	N4–C8–N3	117.0(6)	N24–C28–N23	118.1(5)	N4–C8–N3	117.4(6)	N14–C18–N13	119.1(6)
N5–C8–N3	119.5(3)	N5–C8–N3	119.9(6)	N25–C28–N23	119.8(6)	N5–C8–N3	119.4(6)	N15–C18–N13	119.9(6)
N4–C8–N5	122.7(3)	N4–C8–N5	123.1(5)	N25–C28–N24	122.1(5)	N5–C8–N4	123.2(6)	N14–C18–N15	121.0(6)

Table 3
Intra- and inter-molecular hydrogen bonding interactions (Å) and (°) in **1**, **2** and **3**

	D–H	H···A	D···A	D–H···A	Symmetry
1					
N1–H1A···N2	0.86	2.37	2.706(4)	104	
N5–H5A···N2	0.86	2.32	2.653(4)	104	
N1–H1A···Cl1	0.86	2.35	3.151(3)	154	$-x, 1-y, -z$
N3–H3A···Cl3	0.86	2.45	3.258(3)	156	$1+x, y, z$
N4–H4A···Cl2	0.86	2.71	3.269(4)	124	$1+x, y, z$
N4–H4A···Cl3	0.86	2.62	3.394(4)	150	$1+x, y, z$
N4–H4B···Cl4	0.86	2.31	3.160(4)	169	
N5–H5A···Cl1	0.86	2.57	3.393(3)	161	$-x, 1-y, -z$
N5–H5B···Cl3	0.86	2.63	3.404(3)	150	
2					
N1–H1A···N2	0.86	2.30	2.645(7)	104	
N5–H5A···N2	0.86	2.32	2.656(7)	103	
N21–H21A···N22	0.86	2.34	2.680(7)	104	
N25–H25A···N22	0.86	2.33	2.653(7)	103	
N4–H4B···Cl3	0.86	2.35	3.167(6)	159	$1-x, 1-y, 1-z$
N5–H5B···Cl2	0.86	2.45	3.257(5)	156	$1-x, 1-y, 1-z$
N24–H24B···Cl1	0.86	2.44	3.239(5)	156	$3/2-x, 1/2+y, 1/2-z$
N25–H25B···Cl4	0.86	2.62	3.381(5)	148	$3/2-x, 1/2+y, 1/2-z$
N3–H3A···Cl6	0.86	2.44	3.192(5)	146	
N4–H4A···Cl6	0.86	2.33	3.104(5)	151	
N21–H21A···Cl5	0.86	2.27	3.067(5)	154	
N23–H23A···Cl6	0.86	2.69	3.401(5)	140	$1+x, y, z$
N24–H24A···Cl6	0.86	2.35	3.173(5)	159	$1+x, y, z$
N25–H25A···Cl5	0.86	2.39	3.192(5)	155	
N1–H1A···O1W	0.86	1.99	2.808(7)	158	
N5–H5A···O1W	0.86	2.12	2.930(7)	157	
3					
N1–H1A···N2	0.86	2.22	2.591(8)	106	
N1–H1A···N12	0.86	2.21	2.597(8)	107	
N5–H5A···N2	0.86	2.31	2.641(7)	103	
N15–H15A···N12	0.86	2.36	2.665(7)	101	
N5–H5B···Cl2	0.86	2.44	3.246(6)	155	
N15–H15A···Cl1	0.86	2.52	3.246(7)	142	$1/2+x, 1/2-y, z$
N15–H15B···Cl2	0.86	2.57	3.305(6)	144	
N14–H14A···Cl4	0.86	2.61	3.027(6)	111	$-x, -y, 1/2+z$
N4–H4A···Cl4	0.86	2.64	3.122(7)	117	$-x, -y, -1/2+z$
N4–H4B···Cl3	0.86	2.65	3.481(7)	163	$-x, -y, -1/2+z$
N3–H3A···Cl5[1]	0.86	2.37	3.175(5)	156	$x, y, -1+z$
N4–H4A···Cl5[1]	0.86	2.62	3.370(7)	147	$x, y, -1+z$
N5–H5A···Cl5	0.86	2.67	3.325(6)	134	$-x, 1-y, -1/2+z$
N13–H13A···Cl5	0.86	2.54	3.256(5)	141	
N14–H14A···Cl5	0.86	2.55	3.325(7)	151	
N14–H14B···O1W	0.86	2.06	2.854(9)	154	

metry [11], most are obscured by the higher energy bands of the cations in the salts of this study. These bands are very broad, but there are no resolvable shoulders present. However, the lowest energy Cl→Cu(II) bands in the 25,000 cm^{-1} range are present in the spectra of all three salts and, there is some resolution of this band for **3**.

While most studies of the various $[CuCl_4]^{2-}$ ions having D_{2d} symmetry have reported two bands for the d→d transitions in the spectral ranges 5800–6400 and 8900–9500 cm^{-1} ranges [4,12,13], D_{2d} symmetry allows for three or even four bands (i.e. when the excited ^2E level is split). We have been able to assign either three or four bands in the NIR region for these three salts although narrow bands due to various ν(NH) combination bands complicate the spectra. The assignments for the $^2B_2 \rightarrow {}^2A_1, \rightarrow {}^2B_1$ and $\rightarrow {}^2E$ transitions in D_{2d} symmetry are included in Table 4.

Table 4
UV–Vis-NIR (cm^{-1}) and ESR data for **1**, **2** and **3**

Mode	1	2	3
$\pi \rightarrow \pi^*$ (py)	40,500	41,590	41,280
$n \rightarrow \pi^*$ (gu)	31,600, 29,260	30,630, 28,130	34,300, 28,630
$Cl \rightarrow Cu(II)$	23,930	24,600	26,700, 25,530, 22,830
$^2B_2 \rightarrow {}^2A_1$	10,470	11,170	11,500
$^2B_2 \rightarrow {}^2B_1$	8670	10,170	10,300
$^2B_2 \rightarrow {}^2E$	5160	6100, 5680	7,600, 6,570
$g_{\|}$ or g_1		2.336	2.239
g_2			2.159
g_1 or g_3		2.079	2.092
g_{av} or g_{iso}	2.205	2.165	2.163

The nature of the powder ESR spectra of the three salts is different. These spectra correlate well with the ESR found for tetrachlorocuprate salts of 2-aminopyridinium ion, $g_{av} = 2.189$; 2-amino-5-picolinium ion, $g_{av} = 2.152$; and 2-amino-4,6-picolinium ion, $g_{av} = 2.164$ [13]. The higher energy $d \rightarrow d$ bands and g_{av} values at the lower end of the range found for related tetrachlorocuprate(II) salts [4] are in agreement that these salts having stronger hydrogen bonding interactions resulting in a greater $[CuCl_4]^{2-}$ planarity, particularly for **2** and **3**.

5. Conclusions

The C–N bond distances to the two NH_2 groups are shorter than the C8=N3 'double' bond in the three salts indicating considerable π-character in the former bonds. This indicates that the formal bonding picture, which considers a single bond between the C–NH_2 and a double bond between C8=N3, is very approximate.

As expected the crystal structure of the compounds present extended hydrogen bonding networks. Unfortunately, the presence of water molecules and Cl^- in two of these structures prevent an analysis of reproducible N–H···Cl–Cu hydrogen bonding patterns.

Due to the complicated hydrogen bond networks and crystal forces present in these compounds the charge compensation hypothesis fail to predict the geometry of the $[CuCl_4]^{2-}$ ions.

6. Supplementary material

Crystallographic data have been deposited with the Cambridge Crystallographic Data Centre, CCDC Nos. 157431 for **1**, 157432 for **2** and 157433 for **3**. Copies of the information may be obtained free of charge from the Director, CCDC, 12 Union Road, Cambridge CB2 1EZ, UK, (fax: +44-1223-336033 or e-mail: deposit@ccdc.cam.ac.uk or www: http://www.ccdc.cam.ac.uk).

Acknowledgements

Acknowledgement is made to the Universidad nacional Autónoma de México, the Donors of the Petroleum Research Fund, administered by the American Chemical Society and the National Science Foundation for the partial support of this research.

References

[1] K.E. Halvorson, C. Patterson, R.D. Willett, Acta Crystallogr., Sect. B 46 (1990) 508.
[2] (a) T.J. Coffey, C.P. Landee, W.T. Robinson, M.M. Turnbull, M. Winn, F.M. Woodward, Inorg. Chim. Acta 303 (2000) 54;
(b) I. Diaz, V. Fernandez, V.K. Belsky, J.L. Martinez, Z. Naturforsch. (B) 54 (1999) 718;
(c) A. Weselucha-Birczynska, B. Oleksyn, C. Paluszkiewicz, J. Sliwinski, J. Mol. Struct. 512 (1999) 301;
(d) M. Parvez, A.P. Sabir, Acta Crystallogr., Sect. C 53 (1997) 675;
(e) M. Parvez, A.P. Sabir, Acta Crystallogr., Sect. C 53 (1997) 678;
(f) M. Parvez, A.P. Sabir, Acta Crystallogr., Sect. C 53 (1997) 679;
(g) G.S. Long, M.Y. Wei, R.D. Willett, Inorg. Chem. 36 (1997) 3102;
(h) V. Fernandez, J.C. Doadrio, S. Garcia-Granda, P. Pertierra, Acta Crystallogr., Sect. C 52 (1996) 1412;
(i) Z.M. Wang, R.D. Willett, S. Molnar, K.J. Brewer, Acta Crystallogr., Sect. C 52 (1996) 581;
(j) G. Valle, Acta Crystallogr., Sect. C 51 (1995) 2273;
(k) R.D. Willett, Acta Crystallogr., Sect. C 51 (1995) 1517;
(l) B. Viossat, N.H. Dung, N. Rodier, Acta Crystallogr., Sect. C 51 (1995) 628;
(m) A. Mahoui, J. La Passet, J. More, T.P. Saint Gregoire, Z. Kristallogr. 210 (1995) 125;
(n) C.L. Bouchard, M.A. Hitchman, B.W. Skelton, A.H. White, Aust. J. Chem. 48 (1995) 771.
[3] R.D. Willett, Coord. Chem. Rev. 109 (1991) 181.
[4] (a) G. Marcotigiano, L. Menabue, G.C. Pellacani, Inorg. Chem. 15 (1976) 2333;
(b) G. Marcotigiano, L. Menabue, G.C. Pellacani, J. Coord. Chem. 5 (1976) 189;
(c) M. Hitchman, P.J. Cassidy, Inorg. Chem. 17 (1978) 1682;
(d) L.G. Battaglia, A. Bonamartini Corradi, G. Marcotigiano, L. Menabue, G.C. Pellacani, Inorg. Chem. 18 (1979) 148.
[5] A. Akella, D.A. Keszler, Acta Crystallogr., Sect. C 50 (1994) 1974.
[6] (a) J.M. Adams, Acta Crystallogr., Sect. B 33 (1977) 1513;
(b) D. Mullen, E. Hellner, Acta Crystallogr., Sect. B 34 (1978) 2789.
[7] D.X. West, G.A. Bain, R.J. Butcher, J.P. Jasinski, Y. Li, R.Y. Pozdniakiv, J. Valdés-Martínez, R.A. Toscano, S. Hernández-Ortega, Polyhedron 15 (1996) 665.
[8] G.F. de Sousa, D.X. West, C.A. Brown, J.K. Swearingen, J. Valdés-Martínez, R.A. Toscano, S. Hernández-Ortega, M. Hörner, A.J. Bortoluzzi, Polyhedron 19 (2000) 841.
[9] (a) D.X. West, J.K. Swearingen, J. Valdés-Martínez, S. Hernández-Ortega, A.K. El-Sawaf, F. van Meurs, A. Castiñeiras, I. Garcia, E. Bermejo, Polyhedron 18 (1999) 2919 and references therein;

(b) E. Bermejo, R. Carballo, A. Castiñeiras, R. Domininguez, C. Maichle-Mössmer, J. Strähle, D.X. West, Polyhedron 18 (1999) 3695 and references therein.
[10] D.W. Smith, Coord. Chem. Rev. 21 (1976) 93 and references therein.
[11] G. Marcotigiano, L. Menabue, G.C. Pellacani, M. Saladini, Inorg. Chim. Acta 34 (1979) 43.
[12] B.D. Bird, P. Day, J. Chem. Phys. 49 (1968) 392.
[13] R.M. Gaura, P. Stein, R.D. Willett, D.X. West, Inorg. Chim. Acta 60 (1982) 213.

PERGAMON

Polyhedron 21 (2002) 417–420

POLYHEDRON

www.elsevier.com/locate/poly

Synthesis and characterization of new di-*n*-butylhydroxytin(IV) derived compounds from 1,3-diketone malonates

David Aarón Nieto-Alvarez [a], Federico Jiménez-Cruz [b], Teresa Mancilla [a,*]

[a] *Departamento de Química, Centro de Investigación y de Estudios Avanzados del Instituto Politécnico Nacional, Apartado Postal 14-740, CP 07000 Mexico DF, Mexico*

[b] *Instituto de Química, Universidad Nacional Autónoma de México, Circuito Exterior, Ciudad Universitaria, CP 04500 Mexico DF, Mexico*

Received 8 March 2001; accepted 26 November 2001

Abstract

The synthesis of four new di-*n*-butylhydroxytin(IV) derivatives obtained from 1,3-diketone malonates **2a**–**2d** is reported. All compounds were characterized by ^{1}H, ^{13}C, ^{119}Sn NMR, infrared spectroscopy and mass spectrometry (FAB). The ^{119}Sn NMR spectra at room temperature showed that in $CDCl_3$ solution the tin atom is hexacoordinated. Moreover, the ^{119}Sn NMR spectra of compound **2a** at low temperature exhibits two signals in the range of hexacoordinated compounds, suggesting the existence of additional species in higher states of aggregation. © 2002 Elsevier Science Ltd. All rights reserved.

Keywords: Tin enolates; Diorganohydroxytin; Diorganotin; Sn(IV) complexes; Malonates; Di-*n*-butylhydroxytin(IV)

1. Introduction

Organotin reagents have been extensively studied in the context of carbon–carbon bond formation [1]. Organotin(IV)enolates in particular have been the subject of studies with electrophiles such as carbonyl compounds [2–4] and organic halides [5–9]. These reagents usually exist as mixture of *C*-stannyl ketone and *O*-stannylenolate, the ratio being dependent on structural factors [10–12]. NMR studies have indicated that tin(IV)enolates exhibit high-coordinated *O*-stannyl enolates in the presence of HMPA, which may be responsible for the selectivity observed in the reactions of α-haloketones [13]. Tin(IV)enolates have been prepared by transmetallation of lithium enolates, transesterification of enolates and hydrostannation of conjugate carbonyls [1]. In spite of the fact that tin(IV)enolates are relativity more stable than their lithium and silicium analogous there are few reports concerning their structures [14]. Our current interest in the synthesis of organotin(IV) compounds [15–17] prompted us to extend our investigations in the synthesis of new organotin(IV) enolates, which could have biological properties [18]. This paper describes the synthesis of new di-*n*-butylhydroxytin(IV) enolates **2a**–**2d** derived from 1,3-diketone malonates **1a**–**1d**, where the latter exist as enolates [19,20], (Fig. 1). All compounds were characterized by ^{1}H, ^{13}C, ^{119}Sn NMR, infrared spectroscopy and mass spectrometry (FAB).

2. Results and discussion

The reaction of 1,3-diketone malonates **1a**–**1d** with di-*n*-butyltin(IV) oxide led to di-*n*-butylhydroxytin(IV) enolates **2a**–**2d** (Fig. 1). The compounds were

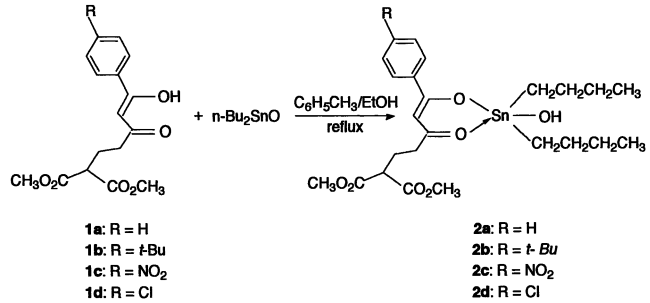


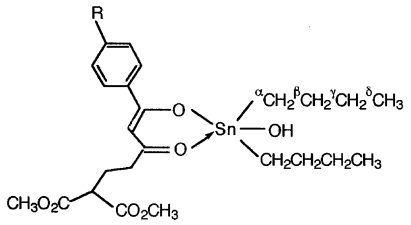
Fig. 1. Synthesis of di-*n*-butylhydroxytin(IV) enolates **2a**–**2d**.

* Corresponding author. Tel.: +(52-55)-57-47-37-23; fax: +(52-55)-57-47-71-13.

E-mail address: tmancill@mail.cinvestav.mx (T. Mancilla).

0277-5387/02/$ - see front matter © 2002 Elsevier Science Ltd. All rights reserved.
PII: S0277-5387(01)01010-5

Table 1
^{1}H and ^{119}Sn NMR data for compounds **2a**–**2d**



2a: R = H
2b: R = *t*-Bu
2c: R = NO_2
2d: R = Cl

Compound	*n*-BuSn	CH_2CO	CH_2CH	$CHCO_2$	CH_3CO	$CH_{vinylic}$	H_{arom}	δ^{119} Sn
2a	H_δ: 0.80 (t) $J = 7.3$ H_γ: 1.27 (m) H_β: 1:34 (m) H_α: 1.62 (b)	2.44 (b)	2.66 (q) $J = 7.2$	3.51 (t) $J = 7.4$	3.74 (s)	5.99 (br)	7.44 (m) 7.86 (d) $J = 7.2$	−383.82
2b [a]	H_δ: 0.81 (t) $J = 7.2$ $H_{\gamma,\beta}$: 1.27 (m) H_α: 1.63 (b)	2.45 (b)	2.33 (q) $J = 7.0$	3.55 (t) $J = 7.4$	3.76 (s)	5.99 (br)	7.47 (d) $J = 8.2$ 7.86 (d) $J = 8.2$	−386.82
2c	H_δ: 0.87 (m) H_γ: 1.25 (m) H_β: 1.36 (m) H_α: 1.64 (b)	2.53 (b)	2.30 (q) $J = 7.2$	3.52 (t) $J = 7.4$	3.77 (s)	6.09 (br)	8.05 (d) $J = 8.5$ 8.32 (d) $J = 8.5$	−378.53
2d	H_δ: 0.78 (t) $J = 7.1$ H_γ: 1.25 (m) H_β: 1.38 (m) H_α: 1.60 (b)	2.42 (b)	2.25 (m)	3.49 (m)	3.71 (s)	5.93 (br)	7.82 (d) $J = 8.4$ 7.35 (d) $J = 8.4$	−381.79

δ (^{1}H) relative to $Si(CH_3)_4$; δ(^{119}Sn) relative to $Sn(CH_3)_4$; in $CDCl_3$.
[a] The singlet at 1.36 ppm is assigned to the protons of the *t*-Bu group. b, broad; d, doublet; dd, doublet of doublets; m, unresolved pattern; q, quartet; s, singlet; t, triplet and IJI Hz.

obtained as yellow oils. The ^{1}H and ^{119}Sn NMR data of **2a**–**2d** are summarized in Table 1. An analysis of the ^{1}H NMR spectra showed that both the $(n\text{-Bu})_2Sn$ protons and those due to the ligands are in a 1:1 ratio. This requires that a OH group be bonded to the tin atom, although it is not observed, probably due to the formation of hydrogen bond or to the overlap with other signals. The CH_2CO and C=CH vinyl protons appear as broad signals (0.04 and 0.2 ppm) at higher field with respect to the free ligands, (**1a**–**1d**), which appear as triplet and singlet signals, respectively. This constitutes evidence for the formation of a Sn–O bond between the enolate moiety and C=O→Sn coordination bond, respectively. Their ^{119}Sn chemical shifts in chloroform are within the range of di-*n*-butyltin(IV) hexacoordinated compounds [21–25], suggesting the existance of additional aggregates in chloroformic solution (Fig. 2).

In order to obtain more information about the structure of these compounds, a variable-temperature NMR ^{119}Sn study of **2a** was undertaken. Thus the ^{119}Sn spectra in chloroform at 293 and 283 K showed only one peak at δ −383.75 and −383.97, respectively. However, upon lowering the temperature to 273 and 263 K the signal became broad at δ −384.67 and −384.06, respectively and the spectrum at 253 K exhibited two equally intense resonances at δ −383.94 and −385.16. The same result was observed at 240, 233 and 223 K. The temperature-dependent changes observed in the spectra are fully reversible, and the data could be indicative of a fast dynamic equilibrium, on the NMR time scale, between the aggregates shown in Fig. 2 and an additional species in a higher state of aggregation, where the tin atom is also hexacoordinated.

Table 2 shows the ^{13}C NMR data spectra for compounds **2a**–**2b**. The signals assigned to the C_5 (enolate)

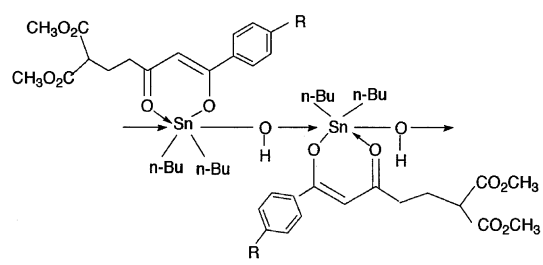
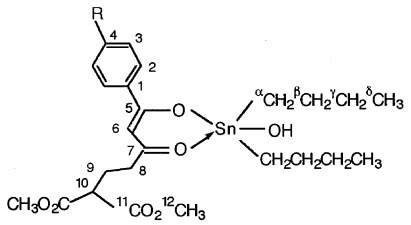


Fig. 2. State of aggregation of compound **2a** at low temperature.

Table 2
^{13}C NMR data for compounds **2a**–**2d**



Compound	2a	2b	2c [a]	2d
C_1	139.32	136.28	130.95	137.84
C_2	127.52	127.64	128.32	128.68
C_3	128.52	125.79	124.01	128.08
C_4	131.62	130.31	149.66	128.77
C_5	183.36	183.75	184.00	181.71
C_6	96.67	96.60	97.98	97.50
C_7	193.56	193.19	193.00	194.56
C_8	38.77	39.05	38.10	38.55
C_9	25.29	25.73	24.64	25.30
C_{10}	50.87	51.13	50.65	50.81
C_{11}	169.77	169.70	169.69	169.63
C_{12}	52.71	52.96	53.08	52.70
C_α	26.87	27.04	26.68	27.15
C_β	29.63	29.66	29.61	29.75
C_γ	26.25	26.28	26.19	27.12
C_δ	13.57	13.63	13.99	13.74

δ: (ppm); in $CDCl_3$.
[a] The quaternary carbons and methy I group of the *t*-Bu group appear at δ 35.38 and 31.56, respectively.

Table 3
IR data for compounds **2a**–**2d**

Compound	C–H_{arom}	C–H_{aliph}	C=O	C=C–C–O	Sn–O
2a	3100	2956 2866	1736	1542	432–318
2b	3110	2958 2866	1736	1551	444–314
2c	3089	2960 2928	1734	1558	438–302
2d	3107	2956 2928	1734	1558	442–316

v(cm^{-1}), $CHCl_3$.

and C_7 (carbonyl) appear broad and small, indicating again the formation of the Sn–OC bond of the enolate moiety and C=O→Sn coordination bond, respectively. While the C_{11} (carbonyl ester) exhibits a sharp signal, which indicates that this carbonyl group does not interact with tin atom. Characteristic IR bands of the investigated compounds are summarized in Table 3. Compounds **2a**–**2d** show the band due to the carbonyl function located between 1736 and 1734 cm^{-1}, a band due to the enolate group in the range of 1558–1541 cm^{-1} and broad bands due to the Sn–O group between 444–432 and 318–302 cm^{-1}.

The FAB mass spectra for **2a**, **2c** and **2d** exhibit a molecular ion corresponding to a dimeric structure and for all compounds other fragment ions are associated with an spiroostannolane ion, (Fig. 3). They also exhibit the fragment ion $[RC_6H_4CO]^+$ at $m/z = 105$ (13%), 161 (26%), 150 (7%) and 139 (15%), respectively.

3. Conclusions

The new diorganotin(IV) compounds **2a**–**2d** were obtained as enolate derivatives, according to their spectroscopic data they are aggregates in solution. The ^{119}Sn variable-temperature NMR study for compound **2a** indicated the existence of a dynamic equilibrium between aggregates, where the tin atoms are hexacoordinated. Their FAB mass spectra exhibit the molecular ion corresponding to a dimer structure, which supports the existence of a additional specie aggregated.

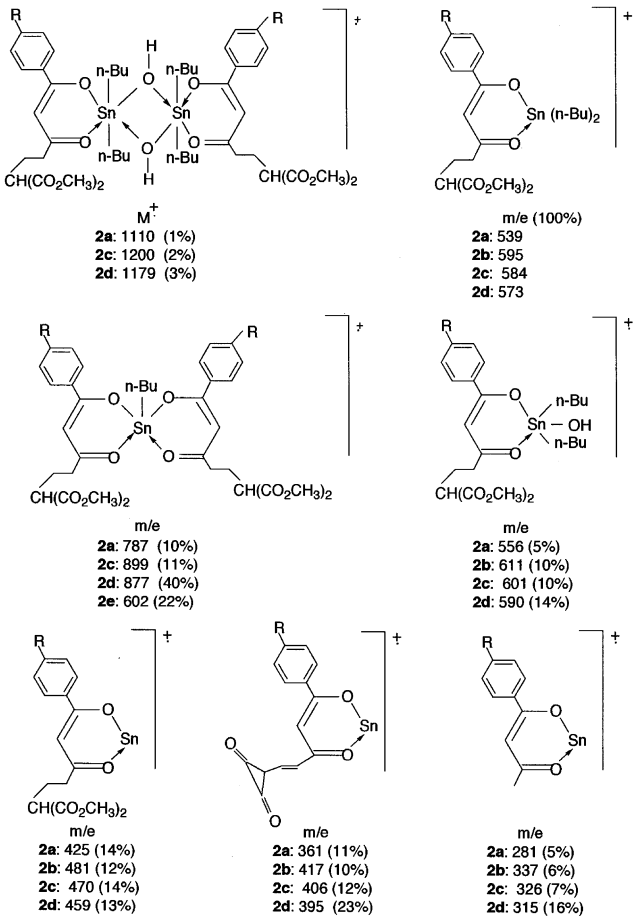


Fig. 3. Mass spectral data of compounds **2a**–**2d**.

4. Experimental

4.1. General procedure and measurements

Reagents were purchased from Aldrich Co. 1,3-Diketone malonates **1a**–**1d** were prepared according to the literature [18]. ^{1}H, ^{13}C and ^{119}Sn NMR spectra were recorded on Jeol GLX-270 JEOL Eclipse-400 and Bruker Avance 300-DPX spectrometers. All ^{1}H and ^{13}C resonances are reported relative to TMS in $CDCl_3$ being used as solvent. High resolution mass spectra (FAB) were obtained with a Jeol JMS-AX 505 mass spectrometer, and infrared spectra were recorded on a Perkin–Elmer 16F PC FT-IR spectrometer.

4.2. Preparation of compounds *2a*–*2d*

The procedure outlined in the following paragraph is general for the preparation of compounds **2a**–**2d**.

4.2.1. Synthesis of di-n-butylhydroxy[dimethyl 2-(3-oxo-5-phenylpenten-5-ato)malonate]tin(IV) (*2a*)

A solution of 0.10 g (0.33 mmol) of **1a**, in 100 ml of a 80/20 $C_6H_5CH_3$–EtOH mixture was placed in a flask equipped with a magnetic stirrer and a Dean-stark trap and 0.08 g (0.33 mmol) of di-*n*-butyltin(IV) oxide were added. The suspension was refluxed during 9 h and after cooling to room temperature (r.t.), the solvents were evaporated under vacuum and the residue was treated with $CHCl_3$. The solution was filtered and the solvent was evaporated under vacuum to yield 0.85 g (45%) of **2a** as a yellow oil.

4.2.2. Synthesis of di-n-butylhydroxy[dimethyl 2-{5-(4-tertbutylphenyl)-3-oxopenten-5-ato}malonate]-tin(IV) (*2b*)

A 0.07 g (0.28 mmol) amount of compound **1b** gave 0.70 g of compound **2b** (57%) as a yellow oil.

4.2.3. Synthesis of di-n-butylhydroxy[dimethyl 2-{5-(4-nitrophenyl)-3-oxopenten-5-ato}malonate]-tin(IV) (*2c*)

A 0.10 g (0.28 mmol) amount of compound **1c** gave 0.70 g of compound **2c** (54%) as a yellow sticky solid.

4.2.4. Synthesis of di-n-butylhydroxy[dimethyl 2-{5-(4-chlorophenyl)-3-oxopenten-5-ato}malonate]-tin(IV) (*2d*)

A 0.09 g (0.28 mmol) amount of compound **1d** gave 0.10 g of compound **2d** (59%) as a yellow oil.

Acknowledgements

The authors thank the 'Consejo Nacional de Ciencia y Tecnologia' (Conacyt-México) for financial support and for research scholarship to D.A.N.A. Thanks to Guillermo Uribe Rojas for recording the NMR spectra, Ing. Luis Velasco for recording the FAB-MS and to Dr Rosa Luisa Santillan B. for reading the manuscript and for her helpful comments.

References

[1] M. Pereyre, J.P. Quintard, A. Rahm, Tin in Organic Synthesis, Butterworth, London, 1987.
[2] J.G. Noltes, H.M.J.C. Creemers, G.J.M. Van der kerk, J. Organomet. Chem. 11 (1968) 21.
[3] S.S. Labadie, J.K. Stille, Tetrahedron 48 (1984) 2329.
[4] Y. Yamamoto, H. Yataggi, K. Maruyama, J. Chem. Soc., Chem. Commun. (1981) 162.
[5] Y. Odic, M. Pereyre, J. Organomet. Chem. 55 (1973) 273.
[6] M.E. Jung, R.B. Blum, Tetrahedron Lett. 43 (1977) 3791.
[7] M. Kosugi, I. Hagiwara, T. Sumiya, T. Migita, Bull. Chem. Soc. Jpn. 57 (1984) 242.
[8] M. Kosugi, I. Hagiwara, T. Migita, Chem. Lett. (1983) 839.
[9] M. Kosugi, M. Koshiba, A. Atoh, H. Sano, T. Migita, Bull. Chem. Soc. Jpn. 59 (1986) 677.
[10] M. Pereyre, B. Bellegarde, J. Mendelsohn, J. Valade, J. Organomet. Chem. 11 (1968) 97.
[11] I.F. Lutsenko, Y.I. Baukov, I.Y. Balavin, J. Organomet. Chem. 24 (1970) 359.
[12] K. Kobayashi, M. Kawanisi, I. Hitomi, S. Kozima, Chem. Lett. (1984) 497.
[13] M. Yasuda, Y. Katoh, I. Shibata, A. Baba, H. Matsuda, N. Sonada, J. Org. Chem. 59 (1994) 4386.
[14] I. Shibata, A. Baba, Org. Prep. Proc. Int. 26 (1994) 363.
[15] T. Mancilla, L. Carrillo, Main Group Met. Chem. 17 (1994) 363.
[16] T. Mancilla, D. Castillo, L. Carrillo, N. Farfán, Heteroatom Chem. 10 (1999) 133.
[17] T. Mancilla, L. Carrillo, L.S. Zamudio Rivera, C. Camacho Camacho, D. De Vos, R. Kiss, F. Darro, B. Mahieu, E.R.T. Tiekink, H. Rahier, M. Gielen, M. Kemmer, M. Biesemans, R. Willem, Appl. Organomet. Chem. 15 (2001) 593.
[18] A.J. Crowe, in: M. Gielen (Ed.), Metal-Based Antitumor Drugs, vol. 1, Freund Publishing House, England, 1988, p. 141.
[19] F. Jiménez-Cruz, L.A. Maldonado, R. Cetina, Tetrahedron Lett. 39 (1998) 2685.
[20] F. Jiménez-Cruz, L.A. Maldonado, R. Cetina, H. Rios-Olivares, Synth. Commun. 30 (2000) 3439.
[21] J. Jurkschat, C. Mügge, A. Tzschach, A. Zschunke, F.M. Larin, V.A. Pestunovich, M.G. Voronkov, J. Organomet. Chem. 139 (1977) 279.
[22] J. Otera, J. Organomet. Chem. 221 (1981) 57.
[23] J. Holecek, M. Nadvornik, K. Handlir, A. Lycka, J. Organomet. Chem. 315 (1986) 299.
[24] A. Lycka, J. Holecek, M. Nadvornik, Main Group Met. Chem. 12 (1989) 169.
[25] B. Wrackmeyer, in: G.A. Webb (Ed.), Ann. Rep. NMRSpectroscopy, vol. 16, Academic Press, New York, 1985, pp. 73–186.

PERGAMON

Polyhedron 21 (2002) 421–424

POLYHEDRON

www.elsevier.com/locate/poly

Syntheses and characterization of nickel thiolate complexes: X-ray structure of [Ni(SCH_2CH_2S)($PPh_2CH{=}CHPPh_2$)]

Maria Aparecida Castro Martins [a], Rosalice Mendonça Silva [a,*], John Curtis Huffman [b]

[a] *Departamento de Química, Universidade Federal de Minas Gerais, 31270-901 Belo Horizonte, MG, Brazil*
[b] *Department of Chemistry and Molecular Structure Center, Indiana University, Bloomington, IN 47405, USA*

Received 19 June 2001; accepted 26 November 2001

Abstract

The complexes [Ni(SCH_2CH_2S)(dppen)], dppen = $PPh_2CH{=}CHPPh_2$ (**1**) and [Ni($SCH_2CH_2CH_2S$)(dppen)] (**2**), have been prepared by reacting dried $NiCl_2$, the phosphine and the appropriate dithiolate compound, in a 1:1:1 molar ratio. For both complexes the ^{31}P NMR spectra confirmed that a chelate ring was formed around the metal, as the single resonance showed a downfield shift compared to the free phosphine. A less shielding effect was observed for the five-member ring formed in complex **1**. In the ^{13}C NMR could be observed a pseudo triplet for the resonance of the methylene carbons as a result of a different coupling to the phosphorus atoms. The crystal structure of complex **1** was determined by X-ray diffraction. Two molecules were found in the unit cell with square planar geometries, with one of them more distorted than the other. © 2002 Elsevier Science Ltd. All rights reserved.

Keywords: Nickel; Thiolate; *cis*-1,2-Bis(diphenylphosphino)ethene; X-ray structures

1. Introduction

Sulfoxides are chiral compounds and complexes that have them as ligands can be used to induce chirality in other compounds in asymmetric synthesis [1]. One way to obtain sulfoxides is from thiolates by oxidation [2]. Accordingly we decided to obtain nickel complexes containing thiolate ligands, to be used as precursors to sulfoxides. As has been observed by others, monomeric homoleptic thiolate complexes of nickel and platinum are not formed. In general what is obtained is a polymeric, insoluble, material [3]. In order to avoid this problem, we decided to use as an ancillary ligand, *cis*-1,2-bis(diphenylphosphine)ethene, dppen, as a strong chelating ligand is necessary to form monomers in this type of reaction. In this paper we wish to describe the synthesis of two nickel thiolate complexes, their characterization by spectroscopic methods and elemental analysis, as well as the solution of the X-ray structure of complex **1**.

2. Experimental

2.1. Methods and materials

All solvents were used without purification. $NiCl_2{\cdot}6H_2O$, ethanedithiol, from Aldrich and *cis*-1,2-bis(diphenylphosphine)ethene, dppen, from Strem, were used as received. Elemental analyses (C, H, N) were performed on a Perkin–Elmer model PE-2400 CHN instrument. IR spectra were recorded on a Perkin–Elmer 283B instrument. ^1H (200 MHz) and ^{13}C (50 MHz) NMR spectra were recorded on a Bruker Advance DPX200, using Me_4Si as an internal reference and ^{31}P NMR (161.97 MHz) on a Bruker Advance DPX400, using H_3PO_4 as internal reference and operating at room temperature (r.t.).

* Corresponding author. Tel.: +55-31-3499-5734; fax: +55-31-3499-5700.
E-mail address: rosalice@apolo.qui.ufmg.br (R.M. Silva).

0277-5387/02/$ - see front matter © 2002 Elsevier Science Ltd. All rights reserved.
PII: S0277-5387(01)01007-5

2.2. Syntheses

2.2.1. cis-1,2-Bis(diphenylphosphino)-etheneethanedithiolatenickel(II) (1)

This complex was prepared according to the procedure described in the literature, with small modifications [3]. Previously dried $NiCl_2 \cdot 6H_2O$ (0.150 g, 1.16 mmol) was dissolved in 3 ml of water, filtered and diluted with 40 ml of EtOH (95%). Dppen (0.459 g, 1.16 mmol) was added and the mixture was left under reflux for 20 min. On addition of 0.109 g (1.16 mmol) of ethanedithiol the solution darkened, and 0.50 ml of Et_3N was added. The mixture was left under stirring at r.t. for 12 h. A violet precipitate settled at the bottom of the flask after this time. The mixture was filtered and the solid was dissolved in CH_2Cl_2 followed by extraction with a saturated aq. solution of NaCl. The CH_2Cl_2 solution was separated and dried over $MgSO_4$. The solvent was removed under reduced pressure, giving complex **1** in 58% yield. *Anal.* Calc. for $C_{28}H_{26}NiP_2S_2 \cdot 1/2CH_2Cl_2$: C, 59.00; H, 4.74. Found: C, 58.25; H, 4.55%. Atomic absorption for Ni: 10.00. Found: 11.38. ^{1}H NMR (δ, $CDCl_3$): 7.94–7.44 (m, $4C_6H_5$), 7.03–6.70 (dd, 2H, CH=CH), 2.78 (s, CH_2CH_2); $^{13}C\{^1H\}$ NMR (δ, $CDCl_3$): 146.82 (t, CH=CH, $J_{C-P} = 36.7$ Hz), 133.19–125.83 (m, C_6H_5), 40.61 (t, CH_2CH_2). ^{31}P NMR (δ, $CDCl_3$): 67.34 (s). IR (CsI, cm^{-1}): $\nu_{Ni-S} = 295$ and 320, $\nu_{Ni-P} = 420$ and 440.

2.2.2. cis-1,2-Bis(diphenylphosphino)-etheneethanedithiolatenickel(II) (2)

This complex was prepared in a similar manner as described above for complex **1**. Complex **2** was obtained in 46% yield. *Anal.* Calc. for $C_{29}H_{28}NiP_2S_2 \cdot 1/2CH_2Cl_2$: C, 59.62; H, 4.96. Found: C, 59.33; H, 5.12%. Atomic absorption for Ni: 9.77. Found: 10.94. ^{1}H NMR (δ, $CDCl_3$): 7.79–7.35 (m, $4C_6H_5$, dd, 2H), 2.44 (q, $CH_2CH_2CH_2$), 2.0 (m, $CH_2CH_2CH_2$); $^{13}C\{^1H\}$ NMR (δ, $CDCl_3$): 146.82 (t, CH=CH, $J_{C-P} = 36.7$ Hz), 133.46–125.83 (m, C_6H_5), 30.97 (t, $CH_2CH_2CH_2$). ^{31}P NMR (δ, $CDCl_3$): 59.67 (s). IR (CsI, cm^{-1}): $\nu_{Ni-S} = 280$ and 325, $\nu_{Ni-P} = 420$ and 435.

Table 1
Crystallographic data for complex **1**

Empirical formula	$C_{28}H_{26}NiP_2S_2$
Formula weight	547.29
Temperature (°C)	−173
Space group	$P\bar{1}$
a (Å)	9.545(3)
b (Å)	16.381(5)
c (Å)	9.387(3)
α (°)	100.26(1)
β (°)	118.14(1)
γ (°)	84.74(1)
V (Å^{-3})	1273.53
Z	2
Radiation (Mo Kα)	0.71069
D_{calc} (g cm^{-3})	1.427
μ (cm^{-1})	10.668
$2\theta_{max}$ (°)	50
R, R_w	0.0460, 0.0321
Parameters refined	16
Reflections (collected/independent)	9114/8992
Goodness-of-fit	1.552

2.3. X-ray crystal structure elucidation of complex 1

General operating procedures and listings of programs have been given previously [4]. Data were collected using a standard moving crystal, moving detector technique with fixed background counts at each extreme of the scan. All data were corrected for Lp, and equivalent data were then averaged to yield a unique set of intensities. The sample consisted of transparent green needles of various morphologies and sizes up to several mm. A small, nearly equidimensional fragment was cleaved from one of the larger crystals and was affixed to a glass fiber. The crystal was then transferred to the goniostat where it was cooled to 100 K for characterization and data collection. A systematic search of reciprocal space located a set of diffraction maxima with no obvious symmetry or systematic absences. Subsequent solution and refinement confirmed a non-centrosymmetric triclinic space group $P\bar{1}$. Data were collected using a standard $\theta/2-\theta$ scan with fixed backgrounds at each extreme of the scan. The structure was solved using MULTAN-78 and Fourier techniques. Two independent molecules were present in the asymmetric cell. A difference Fourier located most of the hydrogen atoms. In the final cycles of refinement, all hydrogens were included as fixed isotropic contributors. No absorption correction was attempted. The absolute structure was confirmed by refinement of the two possible configurations. Details of crystallographic data collection, structure refinement and crystal data are given in Table 1. Complex **1** crystallizes in the space group $P\bar{1}$. Cell constants were obtained from the refinement of 16 reflections. A total of 9114 reflections were collected of which 8992 were independent and 6938 were flagged as observed ($F > 2.33\sigma(F)$).

3. Results and discussion

The compounds studied in the present work are shown in Fig. 1. The first step in the syntheses of the complexes consists on the formation of [Ni(Cl)$_2$(dppen)], in situ, that can contaminate the final products, if appropriate care is not taken to ensure complete reaction, as shown for the preparation of complex **1**.

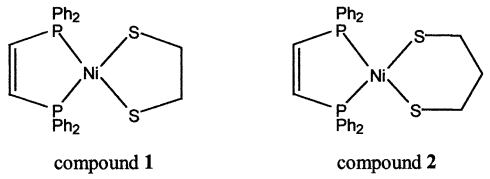


Fig. 1. Compounds studied in the present work.

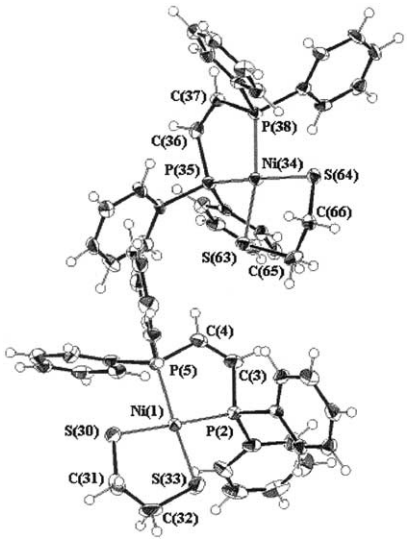
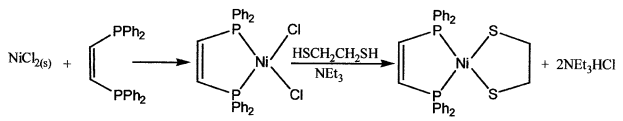


Fig. 2. ORTEP for complex **1** with ellipsoids at 30% probability.



The complexes were obtained as powdered red–maroon solids, stable in air, and soluble in common organic solvents. In both syntheses a small amount of CH_2Cl_2 was found in the products, as in the IR and ^1H NMR spectra could be found absorptions due to it, and this was confirmed by the elemental analyses. However, no solvent molecules were found upon resolution of the structure of complex **1**. In the ^{13}C NMR spectra of both complexes could be observed a pseudo triplet for the resonance of the methylene carbons, as a result of a different coupling to the phosphorus atoms. The compounds exhibit a single chemical shift in the ^{31}P NMR spectrum. The ^{31}P chemical shift values of δ 64.70 and 59.67 for complexes **1** and **2**, respectively, are characteristic of compounds that have chelating phosphines, as they are less shielded as compared to the free phosphine, δ −22.36. Also, the ^{31}P shift of the five membered chelate ring, in compound **1**, is less shielded than the six membered chelate ring in compound **2**, as observed previously for diphosphine complexes [5–9].

Crystals of good quality for a X-ray diffraction analysis were obtained from an ethanolic solution that was left under room temperature for several days. The structure consists of two crystallographically independent molecules (Fig. 2).

Table 2
Selected bond distances (Å) and angles (°) for complex **1**

Bond distances			
Ni(1)–P(2)	2.138(18)	Ni(34)–P(35)	2.131(17)
Ni(1)–P(5)	2.148(17)	Ni(34)–P(38)	2.130(16)
Ni(1)–S(30)	2.155(19)	C(36)–C(37)	1.315(7)
Ni(1)–S(33)	2.173(18)	C(65)–C(66)	1.510(7)
C(3)–C(4)	1.300(7)	P(2)–C(3)	1.819(5)
C(31)–C(32)	1.430(8)	P(5)–C(4)	1.819(6)
Ni(34)–S(63)	2.184(16)	P(35)–C(36)	1.832(5)
Ni(34)–S(64)	2.176(16)	P(38)–C(37)	1.828(5)
S(30)–C(31)	1.762(6)	S(33)–C(32)	1.745(7)
S(63)–C(65)	1.830(6)	S(64)–C(66)	1.812(5)
Bond angles			
S(30)–Ni(1)–S(33)	92.40(7)	S(63)–Ni(34)–S(64)	93.69(6)
P(5)–Ni(1)–P(2)	88.03(6)	P(35)–Ni(34)–P(38)	88.99(6)
S(33)–Ni(1)–P(5)	177.02(7)	S(63)–Ni(34)–P(35)	89.37(6)
S(30)–Ni(1)–P(2)	177.60(9)	S(64)–Ni(34)–P(35)	166.07(6)
S(30)–Ni(1)–P(5)	90.08(7)	S(63)–Ni(34)–P(38)	166.62(6)
S(33)–Ni(1)–P(2)	89.53(7)	S(64)–Ni(34)–P(38)	91.08(6)

Each nickel atom is four coordinated by two sulfur atoms and two phosphorus atoms in a square-planar arrangement. In Table 1 are given crystallographic data and structure refinement details.

In one of the molecules the nickel atom and its four neighbors deviate from a plane through the following atoms: Ni(34), 0.0064; S(64), −0.2429; S(63), 0.2432; P(38), 0.2565 and P(35), −0.2631. As a consequence the square-planar geometry of the nickel atom shows a larger distortion than in the other molecule, leading to S–Ni–P angles of 166.07(6)° and 166.62(6)°, Table 2.

The Ni, P and the carbons atoms that forms the double bond are almost coplanar: deviations are Ni(34), −0.0097; P(35), 0.0054; P(38), 0.0133; C(37), −0.0135; C(36), 0.0045. The angle between these two planes is 4.28°. Larger deviations are found in the ring formed by Ni, S and the methylene carbons: Ni(34), 0.0294; S(64), −0.1734; S(63), 0.1080, C(65), −0.3086; C(66), 0.3446. The Ni–P and Ni–S bond distances are nearly identical, 2.131(17), 2.130(16) and 2.184(16), 2.176(16) Å, respectively, Table 2. These values are shorter than the corresponding bond distances in the complex $[Ni(dipdtc)(PPh_3)_2]ClO_4{\cdot}CHCl_3$ [10]. The C=C bond distance in this molecule is 1.315(7) Å. In the other molecule, a least-squares planes through Ni, S and P gave the following results: Ni(1), −0.0018; S(33), 0.0294, S(30), −0.0284, P(2), −0.0299. The angles around the nickel atoms were more close to the ideal ones for a square-planar geometry. The Ni, P and C atoms that form the double bond were almost coplanar, but more disordered than the previous molecule: Ni(1), −0.0254; C(3), 0.0124; C(4), −0.0366; P(2), 0.0141; P(5), 0.0355. The angle between these two

planes is only 1.95°. As before, larger deviations were found in the plane formed by Ni, S and the methylene carbons: Ni(1), −0.0268; S(33), 0.0927; S(30), −0.0372, C(32), −0.1591; C(31), 0.1305. The Ni–P bond distances were Ni(1)–P(2) = 2.138(18), Ni(1)–P(5) = 2.148(17) Å, longer than the previous ones and the Ni–S bond distances were smaller: Ni(1)–S(30) = 2.146(19) and Ni(1)–S(33) = 2.173(18) Å. The C=C bond distance was 1.300(7) Å. Similar to complex **1**, double bond distance values of 1.316(5), 1.280(2) and 1.315(5) Å were found in complexes $[Ni(Cl)_2$(*cis*-dppen)] [8], $[Pt(Cl)_2$(*cis*-dppen)] [6] and $[Pt($*cis*-dppen$)_2[BPh_4]_2$ [8]. The Ni–P and Ni–S bond distances are relatively short as compared to the distances reported for $[Ni(dipdtc)(PPh_3)_2]ClO_4 \cdot CHCl_3$ [10] and $[Ni(S_2CO)$-(dippe)] [11].

In one of the molecules there is better coplanarity in the plane formed by Ni, P and C's of the double bond (rms deviation of 0.010) but less coplanarity in the plane formed by Ni, and the ethanedithiolate unit; the Ni–P bond distance is smaller, and the Ni–S and C=C bond distances are longer, Table 2. In the other molecule, where there is more distortion on the plane formed by Ni, P and C's of the double bond (rms deviation of 0.0268) but more coplanarity in the plane formed by Ni and the ethanedithiolate unit, the Ni–P bond distance is longer and the other ones are smaller.

It is known that crystal packing effects can lead to structural differences and variations in bond distances and angles parameters, for molecules belonging to the same unit cell as well for different crystalline forms of the same molecule. Recently, a study that compared geometric data for crystal structures, for which more than one molecule of complex is present per crystallographic asymmetric unit, was performed. This study allowed a quantification of the crystal packing effect on molecular structures. The determined metal–ligand bond distance deviations were found to be in the range 0.01–0.02 Å and for the bond angles the range was 1–2° (or 3°). Also, this study showed that there exists a flexibility of metal complexes in crystals [12].

In the present work the Ni–P and Ni–S bond distance differences (mean values) within the two molecules are 0.013 and 0.011 Å, respectively, and the P–Ni–P and S–Ni–S bond angle differences (mean values) are 1.29° and 0.96°, respectively, and according to the previously mentioned work these differences are due to crystal packing effects. However, the reduction of the double bond distance below the ideal value of 1.337(6) Å and an almost coplanarity in the plane formed by the metal, P and C=C atoms, is an indication, for some authors, of a π bonding interaction throughout the atoms [6–9].

4. Conclusion

Compounds **1** and **2** are described for the first time. Both the Ni–P and Ni–S bond distances of compound **1** are shorter as compared to related bond distances for similar compounds described in the literature [10,11]. Also, there is a reduction of the C=C bond distance below the ideal value, and the planes formed by the metal and the two rings showed small deviations from coplanarity. This data can indicate that for this complex a π backbonding is occurring for both phosphorus and sulfur, Ni ⇒ P and Ni ⇒ S. The unsaturated nature of the diphosphine can lead to an enhancement of this interaction.

5. Supplementary data

Crystallographic data for the structural analysis have been deposited with the Cambridge Crystallographic Data Center under deposition number 163995 for complex **1**. Copies of this information may be obtained free of charge from The Director, CCDC, 12 Union Road, Cambridge, CB2 1EZ, UK (fax: +44-1223-336033; e-mail: deposit@ccdc.cam.ac.uk or www: http://www.ccdc.cam.ac.uk).

Acknowledgements

To agencies Fapemig, for a grant support, and CNPq for a scholarship to M.A.C.M.

References

[1] D. Hesek, Y. Inoue, S.R.L. Everrit, M. Kunied, M.G.B. Drew, J. Chem. Soc., Dalton Trans. (1999) 3701.
[2] D.C. Goodman, R.M. Buonomo, P.J. Farmer, J.H. Reibenspies, M.Y. Darensbourg, Inorg. Chem. 35 (1996) 4029.
[3] T.B. Rauchfuss, D.M. Roundhill, J. Am. Chem. Soc. 97 (1975) 3386.
[4] M.H. Chisholm, K. Folting, J.C. Huffman, C.C. Kirkpatrick, Inorg. Chem. 23 (1984) 1021.
[5] A.K. Fazlur-Rahman, J.G. Verkade, Inorg. Chem. 31 (1992) 5331.
[6] W. Oberhauser, C. Bachmann, P. Brüggller, Inorg. Chim. Acta 238 (1995) 35.
[7] W. Oberhauser, C. Bachmann, T. Stamfl, P. Brüggller, Inorg. Chim. Acta 256 (1997) 223.
[8] W. Oberhauser, C. Bachmann, T. Stamfl, P. Brüggller, Polyhedron 16 (1997) 2827.
[9] W. Oberhauser, C. Bachmann, T. Stamfl, R. Haid, P. Brüggller, Inorg. Chim. Acta 274 (1998) 143.
[10] V. Venkatachalam, K. Ramalingam, Polyhedron 15 (1996) 1295.
[11] Z. Trávnícek, R. Pastorek, Z. Sindelár, R. Klicka, Transition Met. Chem. 21 (1996) 81.
[12] A. Martin, A.G. Orpen, J. Am. Chem. Soc. 118 (1996) 1464.

PERGAMON

Polyhedron 21 (2002) 425–433

POLYHEDRON

www.elsevier.com/locate/poly

Lanthanide(III) complexes of six-nitrogen-donor macrocyclic ligands with benzyl-type peripheral substituents, and crystal structure of $[La(NO_3)_2(H_2O)(C_{36}H_{38}N_6)](NO_3)(H_2O)$

Franco Benetollo [a], Gabriella Bombieri [b], Adedoyín M. Adeyga [c], Kathleen K. Fonda [c], William A. Gootee [c], Kristine M. Samaria [c], Lidia M. Vallarino [c,*]

[a] *I.C.T.M.A., C.N.R., Corso Stati Uniti 4, Padova 35127, Italy*
[b] *Istituto di Chimica Farmaceutica, Università di Milano Milano, Italy*
[c] *Department of Chemistry, Virginia Commonwealth University, Richmond, VA 23284-2006, USA*

Received 14 July 2001; accepted 26 November 2001

Abstract

Lanthanide(III) complexes of six-nitrogen-donor macrocyclic ligands carrying a benzyl-type group, $–CH_2–C_6H_4–X$ (X = –H, –OH, or $–NH_2$), at each di-imine side chain were synthesized by the metal-templated, cyclic Schiff-base condensation of 2,6-diacetylpyridine with substituted *S*- or *R*,*S*-1,2-diaminopropanes. The complexes were obtained as mixtures of constitutional isomers and stereoisomers, which were identified by ^{1}H NMR spectra and separated by fractional crystallization. The molecular structure of the 11-coordinate complex $[La(NO_3)_2(H_2O)(C_{36}H_{38}N_6)](NO_3)(H_2O)$ was established by X-ray crystallography. © 2002 Elsevier Science Ltd. All rights reserved.

Keywords: Lanthanide(III) complexes; Macrocyclic ligands; 2,6-Diacetylpyridine; 3-Substituted-1,2-diaminopropanes

1. Introduction

The potential usefulness of the lanthanide(III) ions as markers for histochemical techniques and immunoassays has focused attention on the complexes of these elements with macrocyclic ligands having functionalized peripheral substituents suitable for attachment to biosubstrates [1–5]. The symmetrically di-substituted complexes of this class (Fig. 1), synthesized by the metal-templated cyclic Schiff-base condensation of 2,6-diacetylpyridine with carbon-substituted 1,2-diaminopropanes, can exist as stereoisomers as well as constitutional isomers, depending on the chirality of the substituent-bearing carbon-3 of the parent diamine and on the relative positions of the R substituents at the di-imine side chains, $=N–CH_2–CH(R)–N=$, of the macrocycle moiety [6–8]. Previous studies on the simplest members of this series—the complexes in which the R substituents are methyl groups—have shown that, when a lanthanum(III) salt is used as template in the synthesis of the di-substituted macrocycles, constitutional isomers are indeed formed and can be distinguished on the basis of their different ^{1}H NMR spectra [6]. It was found that lanthanum(III) acetate provides high yields of macrocyclic complexes with useful solubilities, and that the temperature at which the synthesis

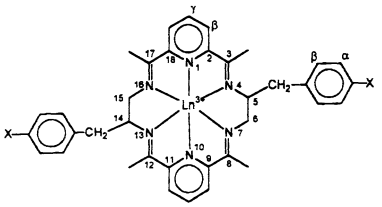


Fig. 1. Schematic formula of one of the two constitutional isomers of the cationic entity {LnL}, where Ln is a lanthanide(III) ion and L is a neutral six-nitrogen-donor macrocyclic ligand with identical substituents at the di-imine side chains. X = –H for L_A, –OH for L_B and $–NH_2$ for L_C. According to the conventional numbering scheme of the macrocycle cavity, this formula represents the 5,14 isomer. The absolute configurations of the 5 and 14 stereocenters are not specified.

* Corresponding author. Tel.: +1-804-828-7515; fax: +1-804-828-8599.
E-mail address: lvallar@atlas.vcu.edu (L.M. Vallarino).

0277-5387/02/$ - see front matter © 2002 Elsevier Science Ltd. All rights reserved.
PII: S0277-5387(01)01008-7

is carried out offers some degree of isomer selectivity. At room temperature, products obtained from *S*-1,2-diaminopropane were greatly enriched in the 5,14 isomer, whereas products obtained from the *R*,*S*-diamine consisted primarily of the (*R*,*S*)-5,15 isomer. It was also noted that in each case the more abundant isomer had the side-chain $-CH_3$ groups in the same hemisphere relative to the macrocycle [6].

The preceding results provided a general guideline for the synthesis and study of a series of lanthanide(III) complexes of macrocyclic ligands with benzyl-type substituents carrying hydroxo, amino, and isothiocyanato functionalities that offer the opportunity for covalent coupling to a variety of substrates. Examples of their applications have been reported [2–4]. The related complexes with non-functionalized benzyl substituents were also investigated as models, and the crystal structure of a La(III) derivative is reported as characteristic of this class.

2. Experimental

2.1. Materials and instrumental procedures

Metal salts (Aldrich Chem. Co.), *S*-phenylalanine amide, *S*-tyrosine amide, *S*- and *R*,*S*-(4-aminophenyl)alanine (all from Sigma Chem. Co.) were used as received. Solvents were of reagent or analytical grade and anhydrous. NMR spectra were obtained with a GE QE-300 spectrometer at ambient temperature (24–26 °C). Chemical shifts for ^1H spectra are reported as δ (ppm); coupling constants, *J*, are given in Hz; spectra were referenced to tetramethylsilane (TMS, 0.00) or to the residual proton signal of the solvent: $CHCl_3$, 7.26(1); CD_3OD, 3.30(5); deutero-dimethylsulfoxide, DMSO-d_6, 2.49(5). Abbreviations: s = singlet, d = doublet, dd = doublet of doublets, m = multiplet, br = broad, v = very. Infrared spectra were obtained on a Perkin–Elmer Model 1600 FT instrument (4000–500 cm^{-1}). Samples were examined as KBr pellets. Absorption frequencies are reported in cm^{-1}; abbreviations: s = strong, m = medium, w = weak, br = broad, v = very; asterisk indicates absorption only partly resolved from adjacent stronger peak. Microanalyses (C, H, N) were performed by Atlantic Microlab, Atlanta, GA; compounds had analyses corresponding to the given formulas.[1] Solvent content was confirmed by thermogravimetric analysis using a Perkin–Elmer TGS-2 instrument with helium flow. The complexes lost solvent completely between 50 and 110 °C; they decomposed without melting at 160–180 °C. Dried samples reabsorbed moisture when exposed to the atmosphere.

[1] Tables of analytical data, carbon-13 NMR spectra, and details of synthetic procedures are available upon request from the corresponding author.

2.2. Syntheses of amine precursors

The hydrochlorides of *S*-1,2-diamino-3-phenylpropane [9] and *S*-1,2-diamino-3-(4-hydroxyphenyl)-propane [10] were obtained from the commercially available amides by reduction with BH_3/thf [10]. The *S*- and *R*,*S*-1,2-diamino-3-(4-aminophenyl)propane were obtained from the corresponding *S*- and *R*,*S*-aminoacids according to the scheme:

$$NH_2–C_6H_4–CH(NH_2)–COOH$$
$$\rightarrow (NH_3^+Cl^-)–C_6H_4–CH(NH_3^+Cl^-)–COOCH_3$$
$$\rightarrow (NH_3^+Cl^-)–C_6H_4–CH(NH_3^+Cl^-)–CONH_2$$
$$\rightarrow NH_2–C_6H_4–CH(NH_2)–CONH_2$$
$$\rightarrow (NH_3^+Cl^-)–C_6H_4CH(NH_3^+Cl^-)–CH_2–NH_3^+Cl^-.$$

The first three steps were carried out by standard procedures; the amide was converted to the amine trihydrochloride as reported for the 4-hydroxyphenyl-analog [10].

2.2.1. S- and R,S-(4-aminophenyl)alanine methyl ester dihydrochloride

Colorless crystals. Diagnostic IR: 3424 m*, 2900 vs, br* and 2590* s, ν(OH) water and $\nu(NH_3^+)$; 1743 vs, ν(C=O) ester. ^1H NMR (DMSO-d_6/TMS): 3.12 dd, 1H and 3.20 dd, 1H (ABX pattern, $J_{AB} = 14.1$, $J_{AX} = 7.2$, $J_{BX} = 5.7$, $CH_{(A)}H_{(B)}$, with coupling to vicinal $CH_{(X)}$); 4.26 br, 1H (CH); 7.32 m, 4H (phenyl); 8.75 s 2H and 10.4 vbr, 2H (NH_3^+, deprotonated in DMSO).

2.2.2. S- and R,S-(4-aminophenyl)alanine amide hydrochloride

Colorless crystals. Diagnostic IR: 3500–2500 vs vbr, with partly resolved peaks, ν(OH) water and $\nu(NH_3^+)$; 1690 vs, ν(C=O) amide. ^1H NMR (D_2O/DSS): 3.07 dd, 1H and 3.15 dd, 1H (ABX pattern, $J_{AB} = 14.4$, $J_{AX} = 7.5$, $J_{BX} = 6.6$, $CH_{(A)}H_{(B)}$, with coupling to vicinal $CH_{(X)}$); 4.19 dd, 1H (CH); 6.85 d, 2H and 7.14 d, 2H ($J = 8.1$, phenyl); $CONH_2$ exchanged in D_2O, in DMSO-d_6: 8.08 s, 1H and 8.56 s, 1H; NH_3^+ exchanged in D_2O, in DMSO-d_6: 8.3 vbr, 3H.

2.2.3. S- and R,S-(4-aminophenyl)alanine amide

Cream-colored hygroscopic powder. Diagnostic IR: 3401 vs (sharp) and 3318 vs (sharp), $\nu(NH_2)$; 1675–1638 s, ν(C=O) amide. ^1H NMR (DMSO-d_6/TMS): 2.69 dd, 1H and 2.73 dd, 1H (ABX pattern, $J_{AB} = 13.4$, $J_{AX} = 8.3$, $J_{BX} = 5.0$, $CH_{(A)}H_{(B)}$, with coupling to vicinal $CH_{(X)}$); 3.19 dd, 1H (CH); 6.45 d, 2H and 6.83 d, 2H ($J = 8.1$, phenyl); 6.91 s, 1H and 7.24 s, 1H, $CONH_2$); 4.85 s, 4H (NH_2).

2.2.4. S- and R,S-1,2-diamino-3(4-aminophenyl)-propane trihydrochlorides

Colorless, hygroscopic microcrystals. IR: 3406 m–s, br, 2876 vs, br, and 2590 m–s, br, $\nu(NH_3^+)$; 1980 w br; 1579 m–w; 1511 vs; 1411 w; 1389 vvw; 1291 vw; 1245 m–s; 1190 w; 1121 w; 1054 w; 988 vvw; 934 vvw; 897 vvw; 860 w; 816 w; 642 vw; 549 vw; 495 w. ^{1}H NMR (DMSO-d_6/TMS): 2.9–3.1 two overlapping dd, 4H (CH_2–phenyl and CH_2–NH_3^+); 3.58 m, 1H (CH); 7.32 d, 2H and 7.41 d, 2H ($J = 8.4$, phenyl); 8.68 s br, 2H, 8.58 s, br, 2H and 10.3 s, br, 2H (NH_3^+, deprotonated in DMSO).

2.3. Macrocyclic complexes from metal-templated syntheses

The complexes were obtained from 2,6-diacetylpyridine, the appropriate diamine, and lanthanide(III) acetate (2:2:1 mole ratio), following the procedure described for the dimethyl-substituted analogs [6]. The products were washed with Et_2O and dissolved in $CHCl_3$ (for the dibenzyl-complexes) or in 9:1 $CHCl_3$–MeOH (for the dihydroxybenzyl- and diaminobenzyl-complex), discarding the undissolved inorganic salts. The solutions were diluted with Et_2O, and the solids that formed were isolated and dried in vacuo over Drierite. The IR spectra of the La(III), Eu(III) and Gd(III) complexes of each macrocyclic ligand were nearly identical, except for the intensity of the ν(OH) absorption of water; for the di-(4-aminophenyl)-macrocycles, no difference was observed between the IR spectra of complexes obtained from the *S*- and *R*,*S*-diamine. The ^{1}H NMR spectra of the products served to establish the original isomer composition.

2.3.1. (S,S)-{LaL_A}$(CH_3COO)_{2.5}Cl_{0.5}\cdot 6.5(H_2O)$, (S,S)-{$EuL_A$}$(CH_3COO)_2Cl\cdot 1.5(H_2O)$, and (S,S)-{$GdL_A$}$(CH_3COO)_2Cl\cdot 2.5(H_2O)$

Pale yellow powders, very soluble in $CHCl_3$, MeOH, EtOH, Me_2SO and DMF; moderately soluble in water; insoluble in Et_2O and hydrocarbons. Bulk recrystallization from MeOH–(charcoal)–Et_2O gave colorless microcrystals; IR: 3400 s vbr, ν(OH) water; 3060 vw; 3027 vw; 2926 vw; 1636 m, ν(C=N) imine; 1587 m, ν(C=N) pyridine; 1542 vs, ν_{asymm}(COO); 1496 w; 1435 vs ν_{symm}(COO); 1378 m–w; 1291 vw; 1248 m; 1199 m; 1152 w; 1130 vvw; 1082 w; 1004 m; 926 w; 817 m; 746 m; 706 m–w; 665 m, δ(COO); 636 w; 615 vw; 563 vw; 492 vw (the last several peaks overlaid on the broad absorption of lattice water at 650 cm^{-1}). The ^{1}H NMR ($CDCl_3$) spectrum of the bulk-purified La(III) complex showed the presence of two isomers: (*S*,*S*)-5,14 60% and (*S*,*S*)-5,15 40%. Repeated fractional crystallization from MeOH–Et_2O gave isomer-enriched fractions but complete separation was not achieved. ^{1}H NMR spectra: Table 1.

2.3.2. (S,S)-{LaL_B}$(CH_3COO)_{2.25}Cl_{0.25}\cdot 2.75(H_2O)$ and (S,S)-{EuL_B}$(CH_3COO)_2Cl\cdot 3(H_2O)$

Pale yellow powders, very soluble in MeOH, EtOH, Me_2SO and DMF; moderately soluble in water; insoluble in $CHCl_3$, Et_2O and hydrocarbons. Bulk recrystallization from 1:9 MeOH–$CHCl_3$(charcoal)–Et_2O gave colorless microcrystals. IR: 3409–2900 s, vbr (with shoulders and ill-resolved splitting), ν(OH) and ν(C–H); 1637 m, ν(C=N) imine; 1589 m, ν(C=N) pyridine; 1543 vs, ν_{asymm}(COO); 1516 s; 1435 vs. ν_{symm}(COO); 1378 m; 1248 m; 1187 m; 1066 w; 933 w; 813 m; 742 m; 669 m, δ(COO); 635 w; 617 w; 568 w. The ^{1}H NMR ($CDCl_3$) spectrum of the bulk-purified La(III) complex showed the presence of two isomers: (*S*,*S*)-5,14 60% and (*S*,*S*)-5,15 40%. Repeated fractional crystallization from MeOH–Et_2O gave isomer-enriched fractions but complete separation was not achieved. ^{1}H NMR spectra: Table 1.

2.3.3. (S,S)-{LaL_C}$(CH_3COO)_3\cdot 3.0(H_2O)$, (R,S)-{$LaL_C$}$(CH_3COO)_3\cdot 4.0(H_2O)$, (R,S)-{$EuL_C$}–$(CH_3COO)_3\cdot 3.5(H_2O)\cdot 1.5(CH_3OH)$, and (R,S)-{$GdL_C$}$(CH_3COO)_3\cdot 3.25(H_2O)$

Orange–brown glassy solids, moderately soluble in $CHCl_3$; very soluble in MeOH, EtOH, Me_2SO and DMF; insoluble in Et_2O, hydrocarbons and water. Bulk recrystallization from 9:1 $CHCl_3$–MeOH(charcoal)–Et_2O gave pale mustard–yellow powders, much less soluble in $CHCl_3$ than the original products. IR: 3420–3300 vs, vbr, ν(OH) water; 3220 m*, $\nu(NH_2)$; 3063 w; 3006 w; 2925 w; 2910 w; 1632 s, ν(C=N) imine; 1585 s, ν(C=N) pyridine; 1538 vs, ν_{asymm}(COO); 1515 vs; 1432 vs, ν_{symm}(COO); 1373 m–w; 1290 w; 1248 m–s; 1196 m–s; 1153 vw; 1125 vw; 1080 vw; 1004 m; 927 vw; 809 m; 739 w; 666 m–s. δ(COO); 635 w; 616 vw; 563 vw. The ^{1}H NMR ($CDCl_3$–CD_3OD 9:1) spectrum of the La(III) complex from the *S*-diamine showed the presence of two isomers, (*S*,*S*)-5,14 60% and (*S*,*S*)-5,15 40%. For the La(III) complex obtained from the *R*,*S*-diamine, the ^{1}H NMR spectrum ($CDCl_3$–CD_3OD 9:1) showed four isomers, of which three were identified: (*R*,*S*)-5,15 43%, (*S*,*S*)-5,14 18% and (*S*,*S*)-5,15 17%. A fourth set of signals in the –CH_3 (macrocycle) region was tentatively identified as arising from the (*R*,*S*)-5,14 isomer (22%), but the spectrum was not fully assigned. Repeated fractional crystallization from MeOH–Et_2O produced fractions enriched in the major isomer but complete separation was not achieved. ^{1}H NMR spectra: Table 1.

2.4. Macrocyclic complexes from anion metathesis

These were obtained by procedures similar to those described for the di-methyl-substituted analogs [6].

Table 1
Proton NMR spectra of lanthanum(III) complexes of di(benzyl)-, di(4-hydroxybenzyl)- and di(4-aminobenzyl)-substituted macrocyclic ligands [a]

Group	Complex, isomer, solvent						
	L_A trichloride [b], (*S*,*S*)-5,14, DMSO-d_6	L_A trichloride [b], (*S*,*S*)-5,15, DMSO-d_6	L_B triacetate [c], (*S*,*S*)-5,14, $CDCl_3$–CD_3OD 9:1	L_B triacetate [c], (*S*,*S*)-5,15, $CDCl_3$–CD_3OD 9:1	L_C triacetate [d], (*S*,*S*)-5,14, $CDCl_3$–CD_3OD 9:1	L_C triacetate [d], (*S*,*S*)-5,15, $CDCl_3$–CD_3OD 9:1	L_C triacetate [d], (*R*,*S*)-5,15, $CDCl_3$
CH_3 macrocycle	2.03 s, 6H 2.56 s, 6H	2.11 s, 6H 2.55 s, 6H	2.06 s, 6H 2.44 s, 6H	2.11 s, 6H 2.45 s, 6H	2.18 s, 6H 2.55 s, 6H	2,23 s, 6H 2.55 s, 6H	2.30 s 6H 2.44 s 6H
$C(H_A)(H_B)$ benzyl	H_A 3.02 dd [e] 2H H_B 3.08 dd [e] 2H J_{AB} 13.1 J_{AX} 8.7 J_{BX} 5.7	3.07 br [f] 4H	H_A 2.83 dd [e] 2H H_B 2.88 dd [e] 2H J_{AB} 13.5 J_{AX}, J_{BX} 7.5	2.74 d [g] *J* 7.5	H_A 2.93 dd [e] H_B 3.00 dd [e] J_{AB} 13.5 J_{BX} 4.5	2.80 d 4H [g] *J* 7.4	2.83 d 4H [h] *J* 7.5
$C(H_A)(H_B)$ macrocycle	H_A 4.08 d [i] 2H H_B 4.14 d [i] 2H J_{AB} 13.0	H_A 3.99 d [i] 2H H_B 4.09 d [i] 2H J_{AB} 14.1	H_A 3.94 d [i] 2H H_B 4.03 d [i] 2H J_{AB} 13.2	H_A 3.41 d [i] 2H H_B 4.02 d [i] 2H J_{AB} 14.7	[j]	[j]	3.96 s, br 4H [k]
CH_X	4.61 br [l] 2H	4.63 br [l] 2H	4.36–4.45 br [m] 2H	4.36–4.45 br [m] 2H	4.5 s, br 2H [n]	4.43 s, br 2H [n]	4.435 s, br, 2H [n]
Phenyl	7.25–7.39 m 10H	7.23–7.38 m 10H	α-H 6.68 d [o] 4H β-H 6.78 d [o] 4H $J_{\alpha\beta}$ 8.4	α-H 6.65 d [o] 4H β-H 6.78 d [o] 4H $J_{\alpha\beta}$ 8.4	α-H 6.63 d [o] 4H β-H 6.84 d [o] 4H $J_{\alpha\beta}$ 8.1	α-H 6.66 d [o] 4H β-H 6.84 d [o] 4H $J_{\alpha\beta}$ 8.1	α-H 6.63 d [o] 4H β-H 7.04 d [o] 4H $J_{\alpha\beta}$ 8.0
Pyridine	β-H 8.21 [p] 2H β-H′ 8.37 [p] 2H γ-H 8.41 [p] 2H $J_{\beta\gamma}$ 7.7 $J_{\beta'\gamma}$ 8.2 $J_{\beta\beta'}$ 1.2	*Pyridine 1* β-H 8.22 [q] 2H γ-H 8.33 [q] 1H $J_{\beta\gamma}$ 8.1 *Pyridine 2* β-H 8.41 [q] 2H γ-H 8.49 [q] 1H $J_{\beta'\gamma'}$ 7.6	β-H 7.93 2H [p] β-H′ 8.08 2H [p] γ-H 008.22 2H [p] $J_{\beta\gamma} = J_{\beta'\gamma}$ 8.1	*Pyridine 1* β-H 7.95 2H [q] γ-H 8.16 1H [q] $J_{\beta\gamma}$ 7.5 *Pyridine 2* β-H 8.11 2H [q] γ-H 8.26 1H [q] $J_{\beta\gamma}$ 7.5	β-H 8.05 [p] 2H β-H′ 8.19 [p] 2H γ-H 8.32 [p] 2H $J_{\beta\gamma} = J_{\beta'\gamma}$ 8.1	*Pyridine 1* β-H 8.08 [q] 2H γ-H 8.21 [q] 1H $J_{\beta\gamma}$ 7.8 *Pyridine 2* β-H 8.28 [q] 2H γ-H 8.36 [q] 1H $J_{\beta\gamma}$ 7.8	*Pyridine 1* β-H 8.03 [q] 2H γ-H 8.26 [q] 1H $J_{\beta\gamma}$ 7.8 *Pyridine 2* β-H 8.10 [q] 2H γ-H 8.35 [q] 1H $J_{\beta\gamma}$ 8.1
CH_3 acetate			1.67 s 9H	1.67 s 9H	1.74 s 9H	1.74 s 9H	1.65 s 6H

[a] Minor variations in chemical shifts were observed for samples with different moisture contents.
[b] Pure isomer.
[c] Enriched isomer mixture. The signal of the (phenyl)–OH group was not detected in $CDCl_3$–CD_3OD solution; in DMSO-d_6, the signal appeared as a broad singlet (2H) at approximately 9.3 ppm.
[d] Enriched isomer mixture. The signal of the (phenyl)–NH_2 group was not detected in $CDCl_3$ or $CDCl_3$–CD_3OH solution; in DMSO-d_6, the signal appeared as a broad singlet (4H) at 5.0 ppm.
[e] ABX spin pattern. Each component of the pattern was broadened with ill-resolved splitting (coupling to CH_2 of macrocycle, $J < 1.5$ Hz).
[f] Broad with ill-resolved splitting.
[g] Coupling to vicinal CH; each component of the doublet was broad with ill-resolved splitting (coupling to CH_2 of macrocycle).
[h] Coupling to vicinal CH. The higher-field component of the doublet was broad with ill-resolved splitting (coupling to CH_2 of macrocycle).
[i] AB spin pattern. Each component of the pattern was broadened with ill-defined splitting (coupling to vicinal CH and CH_2 of benzyl).
[j] Partly obscured by strong signal at 4.25 ppm (water of hydration in complex).
[k] With ill-resolved splitting (coupling to vicinal CH and CH_2 of benzyl).
[l] With ill-resolved splitting.
[m] Signals of isomers overlapped.
[n] With ill-resolved splitting (coupling to CH_2 of macrocycle and CH_2 of benzyl). Signals of isomers overlapped. AB spin pattern.
[o] Distorted toward AB spin pattern.
[p] ABC spin pattern.
[q] A_2B spin pattern.

2.4.1. $\{LaL_A\}Cl_3\cdot n(H_2O)$, (S,S)-5,14 and (S,S)-5,15 pure isomers

Fractional crystallization of the (*S*,*S*)-5,14/(*S*,*S*)-5,15 isomer mixture from MeOH–Et_2O gave small amounts of the pure isomers, having virtually identical IR spectra but different and structurally diagnostic ^{1}H NMR spectra. Colorless microcrystals, very soluble in polar organic solvents; slightly soluble in water; insoluble in Et_2O and hydrocarbons. IR: 3400 s, br, ν(OH) water; 3060 vw; 3025 vw; 2927 vw; 1638 s, ν(C=N) imine; 1590 s, ν(C=N) pyridine; 1449 m; 1372 m; 1254 m; 1199 m; 1153 vw; 1084 vw; 1004 m–w; 932 vw; 815 m–w; 745 m; 706 m; 671 m–s; 637 vw; 614 vw; 568 vw; 519 vw. ^{1}H NMR spectra: Table 1.

2.4.2. R,S-$\{LaL_C\}(NCS)_2(CH_3COO)\cdot CH_3OH$

Rosettes of opaque red–brown needles, slightly soluble in Me_2SO and DMF; insoluble or nearly insoluble in other common organic solvent. IR: 3423 m–s*, 3335 m–s* and 3290*m $\nu(NH_2)$; 3078 w; 3013 w; 2919 w; 2043 vvs, ν(C≡N) of SCN^-; 1628 s, ν(C=N) imine; 1587 s, ν(C=N) pyridine, 1538 m* ν_{asymm}(COO), 1515 s; 1438 m, ν_{symm}(COO); 1373 m; 1248 m; 1192 m; 1152 w; 1126 w; 1004 m–w;, 954 vw; 866 vw; 812 m–s, ν(C–S) of SCN^-; 738 w; 635 w; 553 vw; 511 w. The ^{1}H NMR spectrum (poorly resolved, DMSO-d_6) showed the presence of several isomers. Separation of the isomers by fractional crystallization was not attempted for lack of solubility in useful solvents.

2.4.3. R,S-$\{EuL_C\}(NCS)_3\cdot 0.25(H_2O)$

Dark red ill-formed prisms, nearly insoluble in most organic solvents and water. IR: 3423 m*, 3337 m* and 3216 m–s* $\nu(NH_2)$; 3013 w; 3007 w; 2924 w; 2017 w; 2048 vvs, ν(C≡N) of SCN^-; 1626 s, ν(C=N) imine; 1590 s, ν(C=N) pyridine, 1542 vw; 1517 s; 1439 m; 1376 m–w; 1360 m–w; 1290 m; 1260 m; 1243 m*; 1195 m; 1154 w; 958 w; 812 m, ν(C–S) of SCN^-; 739 m; 650 w; 600 vw; 553 vw; 513 vw.

2.4.4. $\{LaL_A\}(NO_3)_3\cdot 2(H_2O)$

A MeOH solution of $\{LaL_A\}$ acetate chloride (90% (*S*,*S*)-5,14-isomer) and lithium nitrate, filtered on a 0.45 μm pore-size syringe filter and refrigerated at 4 °C, gave crystals suitable for X-ray analysis (see later section).

2.5. Investigation of the inertness of the lanthanide-macrocycle moieties

2.5.1. ^{1}H NMR study of the interaction of $\{LaL_C\}(CH_3COO)_3$ with 2,4-pentanedione

The complex *R*,*S*-$\{LaL_C\}(CH_3COO)_3\cdot 4(H_2O)$ was dissolved in 9:1 $CDCl_3$–CD_3OD and a threefold molar amount of 2,4-pentanedione (acetylacetone) was added. The ^{1}H NMR spectrum of the solution gave the typical pattern of the *R*,*S*-$\{LaL_C\}$ macrocycle, together with the signals of acetate and acetylacetone–acetylacetonate, showing that no decomposition of the lanthanum-macrocycle moiety had occurred. The spectrum remained unchanged over time.

2.5.2. Attempted transmetallation between the $\{LaL_C\}$ macrocycle and 'free' Eu(III) ion

The complex *R*,*S*-$\{LaL_C\}(CH_3COO)_3\cdot 4(H_2O)$ was dissolved in CD_3OD and a twofold molar amount of Eu(III) acetate was added. The ^{1}H NMR spectrum of the resulting solution showed the typical pattern of the $\{LaL_C\}$macrocycle, with no change over time. In contrast, the presence of the paramagnetic Eu(III) ion caused the signal of the acetate $-CH_3$ to shift in a manner dependent on concentration, as previously observed for the unsubstituted macrocyclic complex [11].

2.6. Reactions of peripheral functional groups

2.6.1. Esterification of the hydroxo-phenyl groups with acetic anhydride

The reaction was carried out under dry nitrogen flow. The finely ground $\{LaL_B\}$ acetate–chloride complex (5.0 mmol, *S*,*S* isomer mixture) was dehydrated at 90 °C for 30 min in a dry nitrogen flow, dissolved in 5 ml of anhydrous DMF, and treated with acetic anhydride (5.0 ml, approximately 50 mmol) and 4-dimethylaminopyridine (0.40 ml, approximately 2.5 mmol). The mixture was refluxed for 12 h. Diethyl ether was added to the cooled solution and the solid that formed was isolated and taken up in $CHCl_3$. The undissolved residue was discarded and the solution was evaporated to dryness under reduced pressure. The residue was crystallized from MeOH–Et_2O. Cream-colored powder (yield, 40%) of composition $C_{46}H_{58}N_6O_{13.5}La$=La-$\{C_{22}H_{24}N_6(CH_2C_6H_4OCOCH_3)_2\}(CH_3COO)_3\cdot 3.5(H_2O)$. IR: 3425 s, ν(OH) water; 2919 w; 1755 s, ν(C=O) ester; 1637 s, ν(C=N) imine; 1587 s, br, ν(C=N) pyridine and ν_{asymm}(COO); 1559 w; 1542 s; 1508 s; 1436 s, ν_{symm}(COO); 1372 s; 1244 m; 1218 m; 1195 s; 1167 m; 1014 w; 1005 w; 913 w; 812 m; 741 w; 666w; 638 m, δ(COO); 556 w. ^{1}H NMR (DMSO-d_6/TMS): 1.48 s, 6H (CH_3 acetate); 2.18 s and 2.20 s, 6H total (CH_3 ester); 2.01 s, 2.06 s, 2.45 s, 2.48 s, 12H total (CH_3 macrocycle); 2.80–3.10 m, 4H (CH_2 benzyl); 3.75–4.15 m, 4H (CH_2 macrocycle); 4.60 br, 2H (CH); 6.93–7.05 m, 8H (phenyl); 8.09–8.33 m, 6H (pyridine).

2.6.2. Reaction of the amino-phenyl groups with thiophosgene

The reaction was carried out at room temperature, avoiding contact with atmospheric moisture. The $\{EuL_C\}$ triacetate complex (0.50 g, bulk-product from *R*,*S*-amine) was allowed to react for 24 h with thiophosgene (2.00 ml) and calcium carbonate (0.50 g) in $CHCl_3$ (250 ml). The resulting mixture was filtered,

Table 2
Selected bond lengths (Å) and angles (°) for $[La(NO_3)_2(H_2O)(C_{36}H_{38}N_6)](NO_3)(H_2O)$

Bond lengths			
La–N(1)	2.775(6)	La–N(2)	2.659(9)
La–N(3)	2.735(6)	La–N(4)	2.738(6)
La–N(5)	2.695(9)	La–N(6)	2.776(7)
La–O(1)	2.654(7)	La–O(2)	2.691(9)
La–O(4)	2.74(1)	La–O(5)	2.642(7)
La–O(7)	2.607(8)	N(1)–C(1)	1.33(1)
N(1)–C(5)	1.33(1)	N(2)–C(6)	1.29(1)
N(2)–C(8)	1.46(1)	N(3)–C(9)	1.49(1)
N(3)–C(10)	1.28(1)	N(4)–C(12)	1.36(1)
N(4)–C(16)	1.35(1)	N(5)–C(17)	1.27(1)
N(5)–C(19)	1.48(1)	N(6)–C(20)	1.47(1)
N(6)–C(21)	1.29(1)	N(7)–O(1)	1.28(1)
N(7)–O(2)	1.22(1)	N(7)–O(3)	1.21(1)
N(8)–O(4)	1.26(1)	N(8)–O(5)	1.26(1)
N(8)–O(6)	1.22(1)	N(9)–O(8)	1.26(2)
N(9)–O(9)	1.22(2)	N(9)–O(10)	1.24(2)
C(1)–C(21)	1.50(1)	C(5)–C(6)	1.50(1)
C(6)–C(7)	1.50(1)	C(8)–C(9)	1.51(1)
C(9)–C(30)	1.54(2)	C(10)–C(11)	1.52(1)
C(10)–C(12)	1.49(1)	C(16)–C(17)	1.49(1)
C(17)–C(18)	1.51(2)	C(19)–C(20)	1.52(1)
C(20)–C(23)	1.55(1)	C(21)–C(22)	1.50(1)
C(23)–C(24)	1.51(1)	C(24)–C(25)	1.38(2)
Bond angles			
O(5)–La–O(7)	71.1(2)	O(4)–La–O(7)	62.8(3)
O(4)–La–O(5)	46.9(2)	O(2)–La–O(7)	123.1(3)
O(1)–La–O(7)	156.0(2)	O(1)–La–O(2)	46.8(2)
N(1)–La–N(6)	58.5(2)	N(1)–La–N(2)	59.5(2)
N(3)–La–N(4)	59.9(2)	N(2)–La–N(3)	62.3(2)
N(5)–La–N(6)	62.8(2)	N(4)–La–N(5)	58.9(2)

discarding the solid, and the solution was evaporated to dryness under reduced pressure at 40 °C. Work up with Et_2O gave a brown solid (yield, 70%) of composition $C_{42}H_{44.5}N_8O_{0.75}S_2Cl_6Eu$=$\{EuL_D\}Cl_3\cdot(CHCl_3)\cdot0.75(C_4H_{10}O)$. IR: 3080 w; 2919 w; 2101 vs, ν(C≡N) of –NCS group; 1639 s, ν(C=N) imine; 1589 s, ν(C=N) pyridine; 1504 s; 1444 m–s; 1376 m; 1357* m–w; 1254 m–s; 1199 m–s; 1155 vw; 1111 w; 1078 vw; 1008 w; 929 w; 879 vw; 811 m–s; 744 w; 638 w; 511 vw.

2.6.3. Crystal data for $[La(NO_3)_2(H_2O)(C_{36}H_{38}N_6)](NO_3)(H_2O)$

Mr = 915.7 monoclinic, space group $P2_1$, a = 10.123(2), b = 16.943(3), c = 11.748(3) Å, β = 107.64(3)°, V = 1920.2(8) Å^3, Z = 2, Dx = 1.58 Mg m^{-3}, λ(Mo Kα) = 0.71069 Å, μ (Mo Kα) = 11.8 cm^{-1}, T = 293 K.

A prismatic white transparent crystal of dimensions 0.14 × 0.20 × 0.28 mm was centered on a four-circle Philips PW1100 (Febo System) [12] diffractometer operating in θ–2θ scan mode with graphite-monochromated Mo Kα radiation, following standard procedures. There were no significant fluctuations of intensities other than those expected from Poisson statistics. The intensity data were corrected for Lorentz-Polarization effects and for absorption, as described by North et al. [13]. No correction was made for extinction.

The structure was solved by heavy atom method. Refinement was carried out by full-matrix least-squares; the function minimized was $\Sigma w(F_o^2 - F_c^2)^2$, with weighting scheme $w = 1/[2(F_o^2) + 6.54P]$, where $P = \max(F_o^2 + 2F_c^2)/3$. All non-hydrogen atoms were refined with anisotropic thermal parameters. The H-atoms were placed in calculated positions with fixed, isotropic thermal parameters (1.2 Uequiv of the parent carbon atom). For a total of 519 parameters, $wR' = [\Sigma w(F_o^2 - F_c^2)^2/\Sigma w(F_o^2)^2]^{1/2} = 0.086$, $S = 1.131$, and conventional $R = 0.037$, based on the F values of 3272 reflections having $F_o^2 \geq 2.5\ \sigma(F_o^2)$.

The absolute configuration of the space group was assigned on the basis of Flack parameter [14]. Structure refinement and final geometrical calculations were carried out with SHELXL-93 [15] and PARST [16] programs, drawings were produced using ORTEP II [17]. Selected geometric parameters are reported in Table 2.

3. Results and discussion

3.1. Synthesis and characterization of the complexes

Complexes of La(III), Eu(III), and Gd(III) with the macrocyclic ligands $L_A = C_{22}H_{24}N_6(CH_2C_6H_5)_2$, $L_B = C_{22}H_{24}N_6(CH_2C_6H_4–OH)_2$ and $L_C = C_{22}H_{24}N_6$-$(CH_2C_6H_4–NH_2)_2$, in which the two benzyl-type substituents are attached to opposite di-imine side chains (Fig. 1), were synthesized by the condensation of 2,6-diacetylpyridine with the appropriate *S*- or *R*,*S*-diamine in the presence of a lanthanide acetate. The complexes from the (*S*)-diamines had general formula $\{LaL\}$-$(CH_3COO)_2Cl\cdot n(H_2O)$, where Ln = La(III), Eu(III), or Gd (III); L = L_A, L_B, or L_C; and n = 0.25–2.75; they were obtained as mixtures of the two possible isomers, containing, respectively the (*S*,*S*)-5,14- and (*S*,*S*)-5,15-di-substituted metal-macrocycle moieties. The complexes from (*R*,*S*)-(4-aminophenyl)-1,2-diaminopropane had formula $\{LnL_C\}(CH_3COO)_3\cdot nH_2O$, with Ln = La(III), Eu(III), Gd,(III) and n = 1.5–4.0; they were obtained as a mixture of species, three of which were identified as the (*R*,*R*/*S*,*S*)-5,14, (*R*,*R*/*S*,*S*)-5,15, and (*R*,*S*)-5,15 isomers. The L_A and L_B complexes formed colorless, crystalline solids, soluble in highly polar organic solvents, insoluble in diethyl ether, hydrocarbons and water; the L_A complexes were also soluble in chloroform and dichloromethane. The L_C complexes were obtained as yellow-tan amorphous solids, very soluble in highly polar organic solvents, moderately soluble in chloroform, insoluble in diethyl ether, hydrocarbons and water. In their thermal behavior, as in

other properties, all complexes resembled those of the corresponding non-substituted analogues [18–22]. In particular, the La-macrocycles moieties were found to be inert to decomposition by hydrogen chloride, metal exchange with competing metal ions, and metal release in the presence of strongly complexing ligands such as β-diketones [22]. The coordinated anions, however, were labile; complexes of formula $\{EuL_B\}(NCS)_2Cl\cdot 0.25(H_2O)$, $\{LaL_C\}(NCS)_2(CH_3COO)\cdot 3.5(H_2O)$, $\{LaL_C\}(NCS)_3\cdot 0.25(H_2O)$ and $\{LaL_A\}(NO_3)_3\cdot 2(H_2O)$ were easily obtained from the triacetates or acetate chlorides by exchange with sodium thiocyanate or lithium nitrate.

The infrared spectra of all complexes showed the characteristic macrocycle absorptions arising from the imine and pyridine C=N stretching modes at 1640–1637 and 1588–1584 cm^{-1}, respectively. The absorptions of the counterion-ligands appeared in their usual ranges and were structurally informative. The isothiocyanates had a very strong ν(C≡N) absorption at 2045–2030 cm^{-1}, consistent with the presence of *N*-coordinated SCN^- ligands [23,24]. The triacetates and diacetate chlorides had two strong ν(COO) absorptions at approximately 1540 and 1430 cm^{-1}, identical in each case to those of the non-substituted europium(III) analogues, $[Eu(CH_3COO)_2(C_{22}H_{26}N_6)]$–$(CH_3COO)\cdot 9H_2O$ [20] and $[Eu(CH_3COO)_2(C_{22}H_{26}N_6)]Cl\cdot 4H_2O$ [19], and suggesting similar structures with bidentate chelating carboxylate groups.

The nuclear magnetic resonance spectra of the La(III) complexes, examples of which are given in Table 1, showed that the signals of the protons belonging to the macrocycle moiety retain the typical pattern previously observed for the dimethyl-macrocycles [6]. Specifically, the $-CH_3$ groups of each isomer gave rise to two equal-intensity singlets, one for the two $-CH_3$ groups neighboring the benzyl-type substituents and one for the other two. Thus, the $-CH_3$ region of the spectrum (2.00–2.70 ppm) provided information on the number of isomers present in a sample as well as on their relative abundance. The macrocycle CH, CH_2 and pyridine signals also followed the patterns of the dimethyl-analogs, with the pyridine signals (8.0–8.5 ppm) sensitive to isomer structure. In the (*R*,*R*/*S*,*S*)-5,14 isomers, where the two pyridine moieties are identical and non-symmetrical, their signals appeared as a single ABC spin pattern. In contrast, both the (*R*,*R*/*S*,*S*)-5,15 and the (*R*,*S*)-5,15 isomers, in which the pyridine moieties are symmetrical but different from one another, produced two equal intensity A_2B patterns. Thus the pyridine sections of the spectra, which correlate univocally with the structures established by X-ray crystallography for the dimethyl-macrocycles [6] and for the dibenzyl-macrocycle $\{LaL_A\}(NO_3)_3\cdot 2(H_2O)$ described in the following section, provide a convenient general tool for the identification of constitutional isomers in macrocyclic complexes of this type. On the basis of these considerations, it was established that all complexes obtained from the (*S*)-diamines consist of two non-interconvertible species—the two possible constitutional isomers, (*S*,*S*)-5,14 and (*S*,*S*)-5,15—in the approximate ratio 6:4. In the products from the (*R*,*S*)-diamine, only three of the four possible isomers—the (*S*,*S*)-5,14, (*S*,*S*)-5,15 and (*R*,*S*)-5,15 species—were unambiguously identified, with the (*R*,*S*)-5,15 isomer being by far the most abundant.

3.2. Crystal structure of $[La(NO_3)_2(H_2O)(C_{36}H_{38}N_6)](NO_3)(H_2O)$

The complex consists of a mono-positive coordination entity associated with an ionic nitrate. In the cationic entity, the La(III) ion is linked to the six N-donor atoms of the uncharged macrocyclic ligand, to two bidentate chelating nitrates situated on opposite sides of the macrocycle, and to a water molecules on the convex side. An additional water molecule per complex unit is clathrated in the crystal lattice. An ORTEP view of the cationic coordination entity, with the atom numbering scheme, is shown in Fig. 2.

In the macrocyclic ligand, the two benzyl substituents are in *cis* position to each other with respect to the macrocycle and are attached to the ethylenic chain at the 5 and 14 positions (see Fig. 1 for conventional numbering of the cavity atoms). The complex is thereby identified as the 5*S*,14*S* isomer, according to the CIP rules [25]. A comparison of the structural features of this complex with those of related La(III) complexes containing the same six-nitrogen-donor macrocyclic moiety but less bulky methyl substituents reveals both

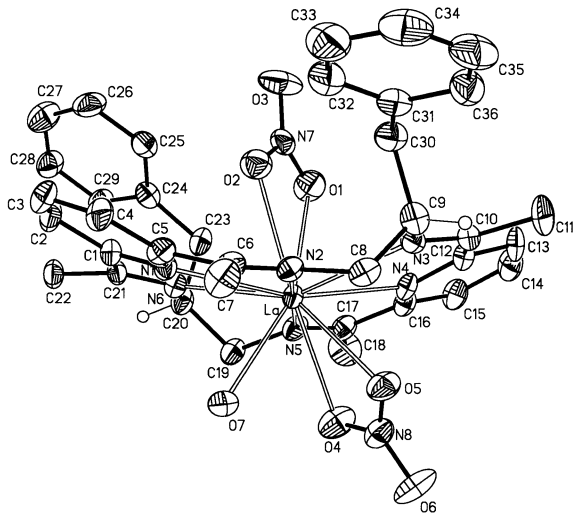


Fig. 2. ORTEP drawing of the cationic moiety $[La(NO_3)_2(H_2O)(C_{36}H_{38}N_6)]^+$ containing the (*S*,*S*)-5,14-dibenzyl-substituted macrocyclic ligand. Note that atoms C20 and C9 of the ORTEP drawing correspond to positions 5 and 14, respectively, of the macrocycle cavity shown in Fig. 1.

similarities and differences. In the dibenzyl-macrocycle, the conformation of the ethylenic side chains is characterized by the torsion angles, N(5)–C(19)–C(20)–N(6) $-61.1(9)°$ and N(2)–C(8)–C(9)–N(3) $-58.9(9)°$, that determine a rather puckered conformation for the entire macrocycle. The total puckering amplitude of the six-nitrogen ring is 0.742(9) Å, considerably greater than the value of 0.493(6) Å found in the 5*R*,15*S* (or 5*S*,15*R*) isomer of the dimethyl-substituted complex $[La(Me_2Mac)(NCS)_3(H_2O)]$, [6]. The interplanar angle between the two pyridine-containing section of the dibenzyl-macrocycle, 35.0(1)°, is also greater than the interplanar angle, 14.4(1)°, of the (5*R*,15*S*)-$[La(Me_2Mac)(NCS)_3(H_2O)]$ complex, but approaches the value of 38.3(3)° found in the nine-coordinated isomer (5*S*,15*S*)-$[La(Me_2Mac)(NCS)_3]$ [7]. In each case, the flexibility of the ethylenic side-chains allows the macrocycle moiety to assume the conformation that best accommodates the steric requirements of both the metal ion and the exocyclic anionic or neutral ligands.

The La–nitrogen bond distances in the dibenzyl-macrocycle are rather irregular. The $La–N_{(imine)}$ bonds range from 2.659(9) to 2.776(7) Å, while the two $La–N_{(pyridine)}$ are 2.738(6) and 2.775(6) Å, respectively. The two La–O bond distances of the chelated nitrate on the concave part of the macrocycle are fairly similar to one another (2.654(7) and 2.691(9) Å), but they differ significantly in the nitrate on the convex side (2.642(7) and 2.74(1) Å). The coordinated water molecule is more loosely bound in the dibenzyl-complex, with a La–O(7) distance of 2.607(6) Å, than in the dimethyl-complex $[La(Me_2Mac)(NCS)_3(H_2O)]$, [6] where the La–Ow distance is 2.536(6) Å. Since in both complexes the coordinated water molecule occupies the same hemisphere as one of the counterion ligands, the difference in La–water bond lengths is most likely due to the greater steric hindrance of the bidentate chelating nitrate relative to the monodentate and linear thiocyanate. The coordinated water molecule of the dibenzyl-complex is involved in hydrogen bonding with the clathrated water molecule ($O(11)_{water}\cdots O(7)'$ 2.76(1) Å) (′ at $1-x, 0.5+y, -z$); the latter is also hydrogen bonded to the 'free' nitrate ($O(11)_{water}\cdots O(8)$ 2.82(1) Å), contributing to the crystal packing (see Fig. 3).

The structure of the tri-nitrate dibenzyl-macrocycle complex reported here leads to another meaningful comparison. In the related tri-nitrate complex $[LaL(NO)_3]$ [26], where $L = C_{22}H_{26}N_6$ is the prototype six-nitrogen-donor macrocyclic ligand with unsubstituted ethylene side-chains, the three nitrates are all chelated to the La(III) ion, resulting in an uncharged coordination entity. In contrast, when the macrocyclic ligand contains two bulky benzyl substituents in the conformation observed here, one of the three nitrates remains ionic and is substituted within the coordination sphere by a less sterically demanding water molecule.

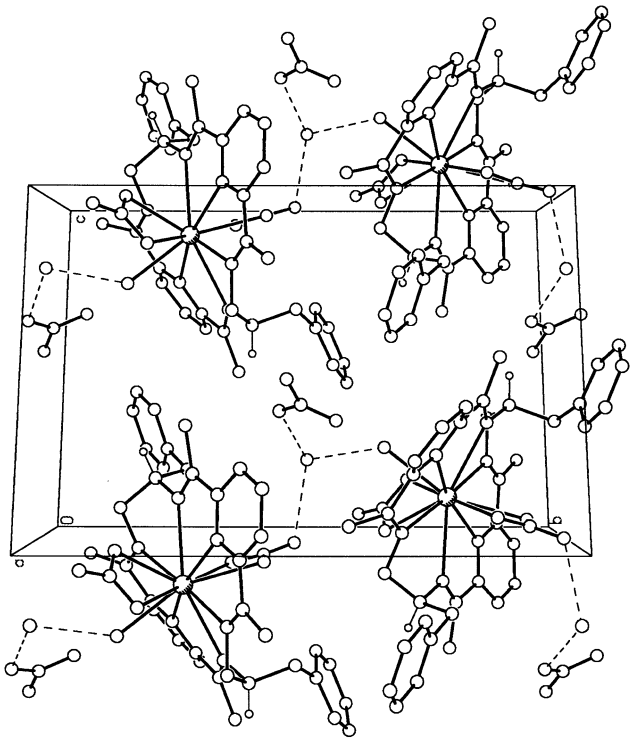


Fig. 3. Crystal packing of the $[La(NO_3)_2(H_2O)(C_{36}H_{38}N_6)](NO_3)(H_2O)$ complex, showing the hydrogen bonding interactions of the cationic moiety with the ionic nitrate and the clathrated water molecule.

These observations, as well as those previously reported for the dimethyl-substituted complexes, suggest that changing the substituents at the ethylenic chains of the macrocycle and/or the anions may allow to modulate the formation of neutral or cationic complexes with different coordinations and geometries.

4. Conclusions

A facile route has been developed for the synthesis of complexes of the lanthanide(III) ions with six-nitrogen-donor macrocyclic ligands containing peripheral hydroxo-benzyl or amino-benzyl groups. These complexes combine the characteristic properties of this type of lanthanide-macrocycles with the reactivities typical of the peripheral –OH and $–NH_2$ functionalities. Specifically, the lanthanide-macrocycle moieties are inert to metal release or exchange in the presence of competing ligands or competing metal ions, whereas the exocyclic anionic ligands are labile and can be easily exchanged. The hydroxo-benzyl group forms esters by reaction with acid anhydrides, and the primary amino-benzyl group reacts with thiophosgene to produce the corresponding isothiocyanate, which in turn combines with primary amines via a thiourea linkage [1,2]. These complexes are therefore suitable for coupling to a vari-

ety of substrates—biomolecules, polymers, functionalized glass surfaces—and the unique inertness of the lanthanide-macrocycle moieties ensures that the characteristic properties of the lanthanide ion, such as luminescence and paramagnetism, will remain incorporated in the substrate under conditions that would cause rapid degradation of complexes of the same metal ion with other ligands.

As a structural model, complexes with non-functionalized benzyl substituents were also synthesized. The characterization of $[La(NO_3)_2(H_2O)(C_{36}H_{38}N_6)](NO_3)\cdot(H_2O)$ by X-ray crystallography established unambiguously the S configuration of both stereocenters in the macrocycle, proving that no racemization or isomerization had occurred during the series of reactions by which the complex had been obtained from the *S*-phenylalanine amide as precusor. A similar retention of conformation was observed in the synthesis of dimethyl-substituted macrocycle complexes of La(III) [6,7].

For all complexes obtained in this work, the metal-templated synthesis presented the same isomer preferences previously observed for complexes containing the less sterically demanding methyl groups: in each case the more abundant isomer was that with the side-chain benzyl groups in '*cis*' positions relative to the metal macrocycle moiety. This preference may be related to the general tendency of the trivalent lanthanide ions to remain in contact with three mononegative anionic partners, two of which can be accommodated on one side of the macrocycle if the peripheral substituents are on the other side, still affording sufficient space for the third anion.

5. Supplementary material

Crystallographic data (excluding structure factors) for the structure in this paper have been deposited with the Cambridge Crystallographic Data Centre as supplementary publication no. CCDC 146221. Copies of the data can be obtained free of charge, on application to The Director, CCDC, 12 Union Road, Cambridge, CB2 1EZ, UK (fax: +44-1223-336033 or e-mail: deposit@ccdc.cam.ac.uk or www: http://www.ccdc.cam.ac.uk).

Acknowledgements

This work was supported in part by NIH/NCR STTR Grant 01-0218 to Newport Instruments, San Diego, CA, with VCU as academic contractor.

References

[1] L.M. Vallarino, J. Alloys Compounds 249 (1997) 69.
[2] L.M. Vallarino, R.C. Leif, US Patent 5,373,093 (1994).
[3] R.C. Leif, P.M. Harlow, L.M. Vallarino, Proc. of Advances in Fluorescence-Sensing Technology, J.R. Lakovicz, R.B. Thompson (Eds.), A. Katzir Progress in Biomedical Optics, SPIE Proc. Series, 1885, 1993, p. 376.
[4] R.C. Leif, L.M. Vallarino, P.M. Harlow, Progress in Biomedical Optics, R.F. Bonner, G.E. Cohn, T.M. Laue, V. Priezzhex (Eds.), SPIE Proc. Series, 2136, 1993, p. 255.
[5] R.C. Leif, L.M. Vallarino, ACS Symposium Series 464, Cell Separation Science and Technology, D.S. Kompala, P.W. Todd (Eds.), American Chemical Society, 1991, p. 41.
[6] F. Benetollo, G. Bombieri, W.A. Gootee, K.K. Fonda, K.M. Samaria, L.M. Vallarino, Polyhedron 17 (1998) 3633.
[7] F. Benetollo, G. Bombieri, K.M. Samaria, L.M. Vallarino, J. Chem. Crystall. 26 (1996) 9.
[8] W.A. Gootee, Doctoral Dissertation, Virginia Commonwealth University, Richmond, VA, 1989.
[9] H. Brunner, M. Schmidt, G. Unger, Eur. J. Med. Chem.—Chim. Ther. 20 (1985) 509.
[10] C.F. Meares, S.M. Yeh, D.G. Sherman, US Patent 4,622,420, 1986.
[11] K.K. Fonda, Doctoral Dissertation, Virginia Commonwealth University, Richmond, VA, 1990.
[12] D. Belletti, 'FEBO', A New Hardware and Software System for Controlling a Philips PW1100 Single CrystalDiffractometer. Internal Report 1/93. Centro di Studio per la Strutturistica Diffrattometrica del CNR, Parma.
[13] A.C.T. North, D.C. Philips, F.S. Mathews, Acta Crystallogr. 87 (1968) 902.
[14] H.D. Flack, Acta Crystallogr., Sect. A 39 (1983) 876.
[15] (a) G.M. Sheldrick, Acta Crystallogr., Sect. A 46 (1990) 467; (b) G.M. Sheldrick, Z. Dauter, K.S. Wilson, H. Hope, L.C. Sieker, Acta Crystallogr., Sect. D 49 (1993) 18.
[16] M. Nardelli, Computing Chem. 7 (1983) 95.
[17] C.K. Johnson 'ORTEP II' report ORNL-5138, Oak Ridge National Laboratory, Tennessee.
[18] L. De Cola, D.L. Smailes, L.M. Vallarino, Inorg. Chem. 25 (1986) 1729.
[19] F. Benetollo, A. Polo, G. Bombieri, K.K. Fonda, L.M. Vallarino, Polyhedron 9 (1990) 1411.
[20] K.K. Fonda, D.L. Smailes, L.M. Vallarino, G. Bombieri, F. Benetollo, A. Polo, L. De Cola, Polyhedron 11 (1993) 549.
[21] F. Benetollo, A. Polo, G. Bombieri, K.K. Fonda, L.M. Vallarino, Polyhedron 10 (1991) 1385.
[22] F. Benetollo, G. Bombieri, K.K. Fonda, L.M. Vallarino, Polyhedron 16 (1997) 1907.
[23] F. Benetollo, A. Polo, L. DeCola, W.T. Hawkins, G. Bombieri, L.M. Vallarino, Polyhedron 8 (1989) 2157.
[24] F. Benetollo, G. Bombieri, L.M. Vallarino, Acta Crystallogr., Sect. C 52 (1996) 1190.
[25] V. Prelog, Science 193 (1976) 17.
[26] J.D.J. Backer-Dirks, C.J. Gray, F.A. Hart, M.B. Hurthouse, B.C. Schoop, J. Chem. Soc., Chem. Com. (1979) 774.

PERGAMON

Polyhedron 21 (2002) 435–438

POLYHEDRON

www.elsevier.com/locate/poly

Conformation of adenosine-5′-triphosphate in the presence of Mg^{2+} at different pH

Ling Jiang, Xi-An Mao *

Laboratory of Magnetic Resonance and Atomic Molecular Physics, Wuhan Institute of Physics and Mathematics, The Chinese Academy of Sciences, P.O. Box 71010, Wuhan 430071, China

Received 7 August 2001; accepted 26 November 2001

Abstract

NOESY experiments have been performed on adenosine-5′-triphosphate (ATP) in the presence of 1:1 Mg^{2+} ($MgCl_2$) at different pH. The results show that H8–H1′ and H8–H2′ interproton NOE intensities change with pH, with nearly equal intensity at low pH (pH 1.9) and with H8–H2′ signal stronger than the H8–H1′ signal at higher pH (between 3.7 and 8.5). The H8–H1′ and H8–H2′ distances and the C4–N9–C1′–O4′ torsion angle (χ) have been measured from random structures of adenosine and ATP. It is concluded that the lower pH allows the formation of a P_γ–O–Mg^{2+}–N1 bridge and the torsion angle takes a *cis* conformation accordingly. © 2002 Elsevier Science Ltd. All rights reserved.

Keywords: Adenosine-5′-triphosphate (ATP); Mg(II); NOESY; Torsion angle (χ)

1. Introduction

It is well known that nucleic acid structures are strongly dependent on the conformation of individual nucleotide residues. A-form DNA differs from B-form DNA by different sugar puckering (C2′ endo for B-form DNA and C3′ endo for A-form DNA). In Z-form DNA, the glycosidic bond of guanosine takes a *syn* conformation, in contrast to the *anti* conformations in normal B- and A- form DNA [1]. Because the biological effects of nucleotides have a strong relation to their conformations, the conformational study of nucleotides, particularly in solutions, has attracted much attention. X-ray crystallography, NMR spectroscopy and CD (circular dichroism) have been widely used for this purpose [2–4]. The conformation of a nucleotide also influences the binding site when it binds to metal ions. It is believed that the glycosidic bond of most guanosines and adenosines takes the *anti* conformation and they bind to metal ions with N7 in the purine ring [5–7]. However, recent reports suggest that when pH is low, ATP (adenosine-5′-triphosphate) binds to metal ions with N1 and this would require the glycosidic bond to be in the *syn* conformation [8–10].

In order to see if the *syn* conformation of the glycosidic bond in ATP is natural, we performed NMR NOESY experiments on 1:1 ATP–Mg^{2+} solutions with varied pH. The results are reported in this paper and they show a rotation range from 20 to $-150°$ for the torsion angle C4–N9–C1′–O4′ (χ). This torsion angle range covers part of the *syn* conformation (defined by $\chi = 0 \pm 90°$ [11]) and part of the *anti* conformation ($\chi = 180 \pm 90°$). At very low pH (pH 1.9), the H8–H1′ and the H8–H2′ NOE cross peaks have nearly equal intensities, while at higher pH (pH $\geq$ 3.7), the H8–H2′ peak become stronger than the H8–H1′ peak. A quantitative relationship between the interproton distance and the base-to-sugar torsion angle is established with the help of molecular modelling, which shows that, in the presence of Mg^{2+}, at lower pH ATP takes a *syn* conformation, while at higher pH *anti* conformations predominate.

Conformations of nucleotides that are affected by pH have been well documented. Some new conformations of Pt complexes with nucleotides have been discovered in variable pH experiments [12–14]. Although the mechanism of the pH dependent conformation of nucleotides is not yet fully understood, the phenomenon

* Corresponding author.
E-mail address: xamao@email.unc.edu (X.-A. Mao).

0277-5387/02/$ - see front matter © 2002 Elsevier Science Ltd. All rights reserved.
PII: S0277-5387(01)01013-0

has been suggested to be very important in biological activity of the nucleotides [15]. Since the ATP–Mg^{2+} complex is of great importance in biology, the pH dependent conformation of ATP in the presence of Mg^{2+} reported in this paper would provide some insight to the pH dependent binding site of Mg^{2+} on ATP.

2. Experimental

The Na salt of ATP was used in this study, which was purchased from Boehringer Mannheim, GmbH, Germany and used directly without further purification. Other chemicals ($MgCl_2 \cdot 6H_2O$, NaOH and HCl) were of analytic purity from Shanghai Chemical Company, China. The pH values were determined by a Cole–Parmer pH meter equipped with a Cole–Parmer glass-body combination pH electrode (Chicago). Buffers of pH 4.01, 6.86 and 9.18 were used to calibrate the pH meter.

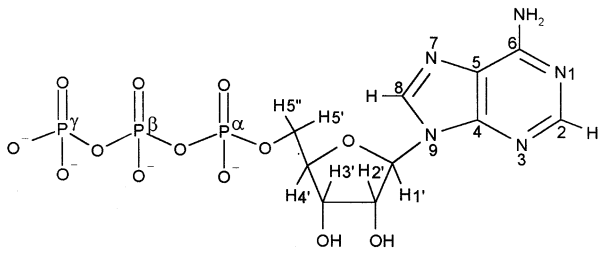


Fig. 1. The schematic structure of ATP.

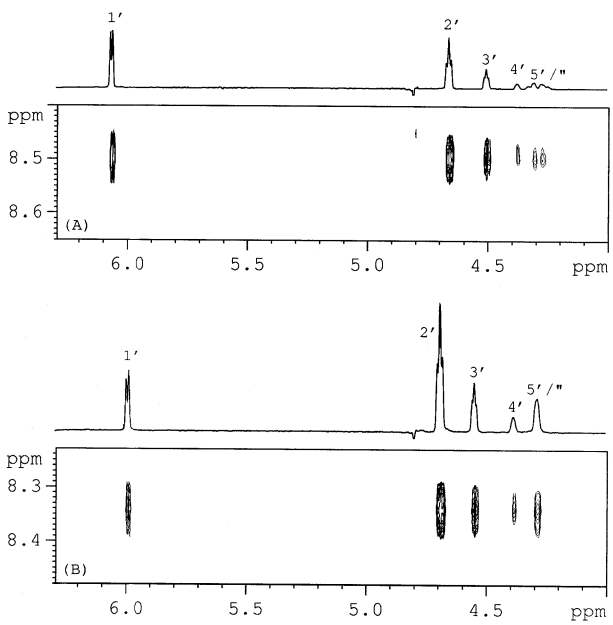


Fig. 2. Regional NOE spectrum of ATP in the presence of equimolar $MgCl_2$ at pH 1.9 (A) and pH 8.5 (B), showing the NOE correlation between H8 (8.51 ppm at pH 1.9 and 8.35 ppm at pH 8.5) and the sugar protons. The slices are shown at the top as projections.

ATP solutions, with and without equimolar $MgCl_2$, were prepared by quantitatively dissolving the chemical(s) in H_2O with 10% D_2O for field lock purpose. The pH values were adjusted by adding tiny drops of NaOH and HCl. The concentrations of ATP and $MgCl_2$ were all kept at 0.2 mol l^{-1}.

NMR experiments were performed on both ATP and ATP–Mg^{2+} samples on a Bruker ARX-500 spectrometer at 298.2 K. Two-dimensional phase-sensitive NOESY spectra were recorded with $2048(\omega 2) \times 256(\omega 1)$ data points and 16 scans per FID. The mixing time was set to 500 ms for all experiments. Water suppression was accomplished by low power, continuous wave presaturation. All 2D FID were apodized in both dimensions with a $\pi/2$ shifted, squared sine-bell function and zero filled to give a 2048×512 matrix before Fourier transformation. The water signal serves as the reference (4.8 ppm).

Molecular modelling was performed on a silica graphics workstation with the CNS version 1.0 (Crystallography and NMR System, http://cns.csb.yale.edu) software package. InsightII module was used for molecule display. In CNS, a single stranded DNA consisting of 63 adenine residues was generated. The 63 residues had random conformations, and their interproton distances and torsion angles were measured. In the meantime, molecular dynamics were performed on an ATP molecule using simulation annealing protocol. Sixty dynamics structures were sampled.

3. Results and discussion

For clarity we present the ATP structure in Fig. 1, with the atoms numbered. We have measured NOESY spectra of ATP in the presence of equimolar Mg^{2+} at four pH values (pH 1.9, 3.7, 5.0 and 8.5). Fig. 2 shows the H8 slices of the NOESY spectra for the ATP–Mg^{2+} system at pH 1.9 and 8.5, where H8 correlates mainly with H1′ (6.06 ppm at pH 1.9 and 5.99 ppm at pH 8.5) and H2′ (4.66 ppm at pH 1.9 and 4.69 ppm at pH 8.5). Since the other protons (H3′, 4.50–4.55 ppm; H4′, 4.38 ppm; H5′ and H5″, 4.26–4.32 ppm) are also in the proximity of H8 with the distance under 0.5 nm, the NOE peaks correlating with those protons also appear, partly due to a spin diffusion effect or a multiple-step NOE transfer effect during the long mixing time (500 ms). However, the nearly equal intensity of the H8–H1′ and H8–H2′ cross peaks implies that H8 has nearly equal distances to H1′ and to H2′. The cross peak intensities relative to the diagonal peak of H8 are listed in Table 1. For comparison, the NOE data for ATP solutions free of Mg^{2+} are also presented. The data in Table 1 suggest that the interproton distances are dependent on pH.

Table 1
Integration volumes of the H8–H1′ and H8–H2′ NOE peaks of ATP at different pH, referenced to the H8 diagonal peak in each spectrum

pH	With Mg^{2+}		Without Mg^{2+}	
	H8–H1′	H8–H2′	H8–H1′	H8–H2′
1.9	0.075	0.073	−0.003	−0.043
3.7	0.148	0.278	−0.000	−0.050
5.0	0.116	0.279	−0.010	−0.069
8.5	0.073	0.190	−0.014	−0.064

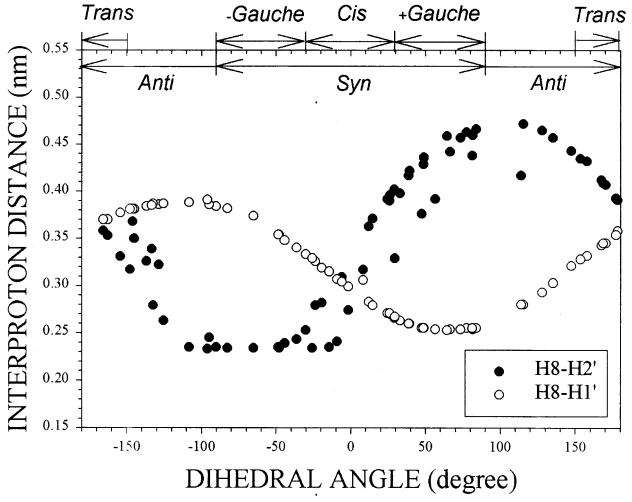


Fig. 3. Plot of H8–H1′ and H8–H2′ distances versus the torsion angle χ for adenine.

The relative intensities of the NOE peaks should be an indication of the relative distances of the involved spins. It is true that the mixing time in our experiments is rather long (500 ms), compared to those used in macrobiomolecules. But since ATP is a small molecule, the spin diffusion effect should not be too serious and stronger NOE peaks should correspond to shorter distances, although the spin diffusion effect probably has broken the r^{-6} rule for quantitative analysis. In solutions, the ATP molecule can take all possible conformations, but at a given pH, the molecule should have a certain average conformation, and this average conformation can be pH dependent, because pH can change the charge distribution of the molecule. As a result, the H8–H2′ and H8–H1′ distances are also pH dependent.

The curves presented in Fig. 3 are helpful to our understanding of the conformation-dependent interproton distances, where the H8–H1′ (open circles) and H8–H2′ distances (filled circles) are plotted versus the torsion angle χ, i.e. the dihedral angle C4–N9–C1′–O4′. The data were taken from 63 random CNS structures for adenosine. Similar curves have also been obtained from DISCOVER structures of ATP sampled in molecular dynamics calculations. The H8–H1′ curve is a perfect sine function, but the H8–H2′ curve is not so smooth as the H8–H1′ curve. In generating the CNS structures and in the molecular dynamics calculation, the ribose sugar can take random conformations or puckers (C3′ endo, C2′ endo, etc.). Since the H8–H1′ distance, or r(H8–H1′), is not affected by the sugar pucker, the curve is smooth, which shows a sine function of the torsion angle in a full rotation cycle (from -180 to 180°). As a contrast, the H8–H2′ distance, or r(H8–H2′), is strongly dependent on the sugar pucker, so at a given χ angle, the H8–H2′ distance can have two or more values. Even so, the H8–H2′ curve can still be approximated by a sine function. In biochemistry, a full rotation of the glycosidic bond can be described by *anti* and *syn* conformations which are defined by $\chi = 0 \pm 90°$ and $\chi = 180 \pm 90°$, respectively. In the meantime, another set of notations are also in current use: *cis* ($\chi = 0 \pm 30°$), *trans* ($\chi = 180 \pm 30°$), *+gauche* ($\chi = 60 \pm 30°$) and *−gauche* ($\chi = 300 \pm 30°$, or $\chi = -60 \pm 30°$) [11], but in this set of notations names are not given to $\chi = 120 \pm 30°$ and $\chi = 240 \pm 30°$ ($-120 \pm 30°$). For clarity, the two sets of notations are indicated in Fig. 3. When χ is close either to 0° (*cis* conformation) or to $\pm 180°$ (*trans* conformation), the two distances do not differ much. Their differences reach maxima when χ is close to $\pm 90°$. Fig. 3 indicates that when χ falls in the range from 0 to $-180°$, the r(H8–H1′) distance is longer, while when χ is between 0 and 180°, r(H8–H2′) is longer. Thus, NOE experiments can indicate, at least qualitatively, the conformation of the glycosidic bond in ATP.

The data in Table 1 show that at pH 1.9, the H8–H1′ and H8–H2′ NOE peaks have nearly equal intensities, with the implication that the torsion angle is around 0 or 180°. As pH is increased, the H8–H2′ signal becomes stronger than the H8–H1′ signal, corresponding mainly to the *−guache* conformation. We have shown that for solutions where ATP interacts with Mg^{2+}, Zn^{2+} and Fe^{3+}, N1 binds with the metal ions [8–10,15]. Therefore, it is reasonable to propose that, in the pH range we are studying in this paper, the torsion angle of ATP is in the range from 20 to $-150°$. The conformation of the ATP molecule changes from *cis* to *trans* through *−guache*, as the pH of the solution is increased. At lower pH, the ATP molecule are more likely to take the *cis* conformation, while at higher pH, the *trans* conformation is more stable, in full agreement with the ^{1}H–^{15}N HMBC experiments reported recently [15].

The data for the pure ATP solutions show a much narrower rotation range for the glycosidic bond, most probably in the *−gauche* conformation. The negative sign in the intensities for pure ATP shown in Table 1 is the indication of the fast motion limit. The much wider conformation range for ATP in the presence of Mg^{2+} than in the absence of Mg^{2-} suggests that the ATP–metal interaction is easily affected by pH. At lower pH, there is a binding competition between metal ion and

H^+. Since the charge of the metal ions (Mg^{2+}, Zn^{2+} and Fe^{3+}, etc.) is stronger than H^+, the metal ions usually win the competition. In the meantime, the γ-phosphate can become negatively charged even when pH is very low. A P_γ–O–M–N1 bridge is likely to form in the solution, where M denotes the metal ion. In this case the ATP molecule can easily take the *cis* conformation. When pH is increased from 1.9 to 5, the binding ability of the metal ion should be reduced, since the hydrated metal ion could form hydroxo species. As a result, N1 loses connection with the metal ion, leading to $-$*gauche* conformations, which are the most common structure for ATP and adenosine in DNA. In the absence of the metal ions, the hydrogen cannot build a bridge between P_γ and N1. So only the $-$*gauche* conformation can be found.

Our NMR experiments do not show any evidence for the existence of the $+$*gauche* conformation either in the presence or in the absence of the Mg^{2+} ion, although the CNS-generated structures can have all conformations. Intuitively, $+$*gauche* conformations have higher tension than $-$*gauche* conformations, since in $+$*gauche* conformations the six-member ring of the adenine is directly on the top of the sugar. It should be pointed out that not all *anti* conformations have the lowest energy; the torsion angle range between 30 and 90° (i.e. $+$*gauche* conformation) which is just in the *anti* conformation range, has not been found in our experiments, probably due to the very high tension. But since the structures generated by CNS and sampled in molecular simulation represent molecules in vacuum rather than in solutions, all structures have similar energy. In vacuum, the dissociation (or association) of the phosphate protons and the protonation (or deprotonation) of N1, N7 and the amine nitrogen (N6) are hardly taken into account.

From Fig. 3 it can be seen that both $r(\mathrm{H8–H2}') > r(\mathrm{H8–H1}')$ and $r(\mathrm{H8–H2}') < r(\mathrm{H8–H1}')$ can happen in *syn* conformation range as well as in *anti* conformations. Thus, it is better to use the *cis*, *trans* and $\pm$*gauche* notations to describe the conformation of ATP and adenosine when NOE intensity is involved, although the notations are not complete.

4. Conclusion

The change of the relative NOE intensities with pH, as has been observed in 1:1 ATP–Mg^{2+} solutions, suggests that, as the pH increased, the conformation of the torsion angle χ of ATP changes from *cis* to *trans* over $-$*gauche*. The *cis* conformation is probably due to a bridge between P_γ and N1 built by a Mg^{2+} ion. At higher pH such a bridge is broken, because hydration of metal ions is strengthened and $-$*gauche* conformations predominate.

Acknowledgements

This work has been supported by the National Natural Science Foundation of China under Grant No. 29725307.

References

[1] R.R. Sinden, DNA structure and function, Academic Press, San Diego, CA, 1994.
[2] A. Odani, R. Shimata, H. Masuda, O. Yamauchi, Inorg. Chem. 30 (1991) 2133.
[3] H. Sigel, Chem. Soc. Rev. (1993) 255.
[4] E.R. Jamieson, S.J. Lippard, Chem. Rev. 99 (1999) 2467.
[5] I. Somasundaram, M. Palaniandavar, J. Inorg. Biochem. 53 (1994) 95.
[6] H. Sigel, Eur. J. Biochem. 165 (1987) 65.
[7] B. Song, H. Sigel, Inorg. Chem. 37 (1998) 2066.
[8] F. Du, X.-A. Mao, D.F. Li, Z.R. Liao, Polyhedron 18 (1999) 2327.
[9] F. Du, X.-A. Mao, Spectrochim. Acta A 56 (2000) 2391.
[10] F. Du, X.-A. Mao, D.F. Li, Z.R. Liao, J. Inorg. Biochem. 83 (2001) 101.
[11] J.L. Markley, A. Bax, Y. Arata, C.W. Hilbers, R. Kaptein, B.D. Sykes, P.E. Wright, K. Wuthrich, J. Biomol. NMR 12 (1998) 1.
[12] U. Bierbach, J.D. Roberts, N. Farrell, Inorg. Chem. 37 (1998) 717.
[13] M.D. Reily, T.W. Hambley, L.G. Marzilli, J. Am. Chem. Soc. 110 (1988) 2999.
[14] S.O. Ano, F.P. Intini, G. Natile, L.G. Marzilli, Inorg. Chem. 38 (1999) 2989.
[15] L. Jiang, X.-A. Mao, Spectrochim. Acta A 57 (2001) 1711.

PERGAMON

Polyhedron 21 (2002) 439–444

POLYHEDRON

www.elsevier.com/locate/poly

Metal carbonyl complexes containing heterocyclic nitrogen ligands Part IX. $MnBr(CO)_3$(3,3′-R-2,2′-biquinoline) compounds

Sergio A. Moya [a,*], Juan Guerrero [a,*], Rubén Pastene [a], Ignacio Azócar-Guzmán [a], Alvaro J. Pardey [b]

[a] *Departamento de Química de los Materiales, Facultad de Química y Biología, Universidad de Santiago de Chile, Santiago, Chile*
[b] *Escuela de Química, Facultad de Ciencia, Universidad Central, Caracas 1020-A, Venezuela*

Received 15 August 2001; accepted 26 November 2001

Abstract

The *fac*-$MnBr(CO)_3$(3,3′-R-2,2′-biquinoline) (R = CH_3 and CH_3; H and H; $–CH_2–CH_2–$ or $–CH_2–CH_2–CH_2–$) compounds were synthesized and characterized. The *fac*-conformation for the carbonyl complexes was established by IR spectroscopy. Conformational effects were investigated by means of ^1H NMR and UV–Vis spectroscopical and electrochemical properties and these properties were compared with related rhenium compounds. © 2002 Published by Elsevier Science Ltd.

Keywords: Metallic carbonyl complexes; Manganese; Heterocyclic nitrogen ligands

1. Introduction

The ability of bidentate nitrogen donor ligands to modify chemical, catalytic and photochemical properties of Os(II), Ir(III), Re(I), Ru(II), and Mn(I) transition metal complexes has prompted numerous studies [1]. The goal of these studies has been to learn more about the chemistry of these systems and to apply such knowledge to develop better catalysts for reactions of practical interest [2]. Some of these compounds have been used as sensitizers in conversions from solar to chemical energy, as models of natural and artificial photosynthesis, in the preparation of molecular-level devices and in the manufacturing of drugs for medical applications [1]. Their applicability has recently been extended to potential antitumor agents [3].

The desirable properties of the complexes could be controlled by judicious steric and electronic modifications of the pyridine ligand. In addition, studies of photochemical and photophysical properties of these complexes provide information about the relation between the ligand structure, the energy gap and the properties of the ground and the excited states nonradiative decay [4]. Consequently, we have studied how changes in the π electronic density and in the structural conformation of the polypyridine ligands affect the properties of the tricarbonylrhenium complexes [5].

In the present paper, we report the synthesis of new complexes of the type $BrMn(CO)_3(L)$, where L corresponds to ligands derived from the annelated or substituted 2,2′-biquinoline in 3,3′ positions (Fig. 1). The preparation, as well as the spectroscopic and redox

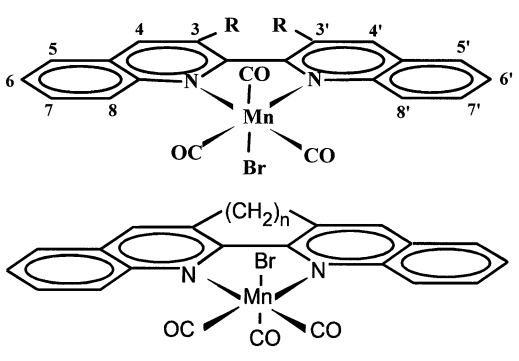


Fig. 1. Structure of *fac*-$BrMn(CO)_3(L)$ complexes with L being the biquinoline ligand derivatives used in this study.

* Corresponding authors. Present address: Departamento de Química Aplicada, Facultad de Química y Biología, Universidad de Santiago de Chile, Casilla 307-Correo 2, Santiago, Chile. Tel.: + 56-2-681-2575; fax: + 56-2-681-2108.
E-mail addresses: smoya@lauca.usach.cl (S.A. Moya), jguerrer@lauca.usach.cl (J. Guerrero).

0277-5387/02/$ - see front matter © 2002 Published by Elsevier Science Ltd.
PII: S0277-5387(01)01009-9

properties are described. The electronic effects provided by the aromatic rings and the steric and conformational effects caused by the annelation or the 3,3′-substitution of the ligand are investigated by comparison of our results with those found for analogous rhenium complexes.

2. Experimental

2.1. Physical measurements

IR spectra were measured on a Bruker IFS-66 V FTIR spectrophotometer in the solid state (KBr cell of 0.2 mm length) and $CHCl_3$ solution. Proton NMR spectra were recorded on a 250 MHz Bruker spectrometer. Absorption spectra were measured on a Shimadzu UV-160 spectrophotometer. Molar extinction coefficients were calculated from a least-square linear regression of absorbance data at different concentrations. Microanalyses were performed at the Departamento de Química Orgánica, Facultad de Química y Farmacia, Universidad de Chile. Molar conductivities were determined in $CHCl_3$ at 25 °C using a conductivity meter Cole-Parmer 01481. The X-ray fluorescence spectra were recorded on a Phillip EDAD PV-9500 (energy dispersion type) at 20 kV and 150 μA. Electrochemical data were acquired by cyclic voltammetry following the procedure already reported [1d]. Potentials were reported as $E_{1/2}$ values versus SCE and were determined from the following relationship: $E_{1/2} = 1/2(Ep_a + Ep_c)$, where Ep_a and Ep_c are the anodic and cathodic peak potentials, respectively. Ferrocene was used as an internal standard ($E_{1/2} = +0.418$ V in dimethylformamide vs. SCE). The cyclic voltammograms were recorded at a sweep rate of 200 mV s^{-1} for all the scans, at room temperature (r.t.) and in a nitrogen atmosphere. Coulometric measurements were carried out using a reticulated vitreous carbon (ERG) and a saturated calomel as working and reference electrodes, respectively. The platinum spiral wire counter electrode was separated by means of a salting bridge.

2.2. Chemicals

Solvents were purified, distilled from the appropriate drying agents and stored under dry N_2 over 3 Å molecular sieves [6]. 2,2′-Biquinoline (0,2N), 1,2-cyclohexanedione, 3,4-hexanedione, 1,2-nitrobenzaldehyde, and $BrMn(CO)_5$ were commercially available and used without further purification. The ligands 3,3′-dimethyl-2,2′-biquinoline, (Me,2N), 3,3′-dimethylene-2,2′-biquinoline, (2,2N), and 3,3′-trimethylene-2,2′-biquinoline, (3,2N), were prepared according to literature procedures [7].

2.3. General synthesis procedure for the complexes

The complexes were prepared by replacement of two carbonyl groups in $BrMn(CO)_5$ by the corresponding bidentate heterocyclic ligand. A stochiometric amount of heterocyclic nitrogen ligand in $C_6H_5CH_3$ was added to a solution of $BrMn(CO)_5$ in the same solvent. The mixture was refluxed in a dry N_2 atmosphere until formation of a red precipitate. The solid was collected by filtration, washed with $C_6H_5CH_3$ under dry N_2 and then it was dried under vacuum. Yields for all complexes were equal to or higher than 80%.

2.4. $MnBr(CO)_3(0,2N)$

Yield 85%. ν_{CO} (KBr disk) 2012, 1931, 1905 (broad) cm^{-1}, ($CHCl_3$ solution) 2026, 1948, 1918 cm^{-1}. Molar conductivity (CH_3CN) 0.03 S cm^2 mol^{-1}. m.p. (dec.) 185 °C. *Anal.* Calc.: C, 53.08; H, 2.54; N, 5.88. Found: C, 52.69; H, 2.47; N, 5.69%.

2.5. $MnBr(CO)_3(Me,2N)$

Yield 83%. ν_{CO} (KBr disk) 2020, 1940, 1920 cm^{-1}, ($CHCl_3$ solution) 2027, 1941, 1920 cm^{-1}. Molar conductivity (CH_3CN) 0.01 S cm^2 mol^{-1}. m.p. (dec.) 176 °C. *Anal.* Calc.: C, 54.89; H, 3.20; N, 5.56. Found: C, 54.02; H, 3.11; N, 5.32%.

2.6. $MnBr(CO)_3(2,2N)\cdot H_2O$

Yield 80%. ν_{CO} (KBr disk) 2014, 1912 (broad) cm^{-1}, ($CHCl_3$ solution) 2025, 1945, 1919 cm^{-1}. Molar conductivity (CH_3CN) 0.05 S cm^2 mol^{-1}. m.p. (dec.) 187 °C. *Anal.* Calc.: C, 53.22; H, 3.11; N, 5.39. Found: C, 52.11; H, 2.89; N, 5.23%.

2.7. $MnBr(CO)_3(3,2N)\cdot H_2O$

Yield 87%. ν_{CO} (KBr disk) 2014, 1918 (broad) cm^{-1}, ($CHCl_3$ solution) 2026, 1943, 1919 cm^{-1}. Molar conductivity (CH_3CN) 0.12 S cm^2 mol^{-1}. m.p. (dec.) 186 °C. *Anal.* Calc.: C, 54.06; H, 3.40; N, 5.25. Found: C, 53.41; H, 3.02; N, 5.24%.

3. Results and discussion

The complexes are sparingly soluble in most common organic solvents, e.g. methylenechloride, acetone, ethyl alcohol. Solutions of these complexes decompose in air after 20 min and a dark brown solid is formed. IR and UV–Vis spectra of the resulting solution were similar to those containing only the uncoordinated ligand. However, solutions kept under nitrogen were stable for periods equal to or longer than 15 days. The low

Table 1
^{1}H NMR spectral data for the $Mn(CO)_3(L)$ complexes and the free ligand [a]

Compound	Aromatic protons						Bridged protons		
	$H_{3,3'}$	$H_{4,4'}$	$H_{6,6'}$	$H_{8,8'}$	$H_{5,5'}$	$H_{7,7'}$	H_a	H_b	H_c
0,2N	8.85d	8.30s	7.58t	8.25d	7.86d	7.75t			
2,2N		8.03s	7.52t	8.43d	7.77d	7.68t		3.20s	
3,2N		8.00s	7.54t	8.35d	7.81d	7.69t	2.70t		2.20q
Me,2N		8.08s	7.52t	8.11d	7.80d	7.65t		2.30s	
$MnBr(CO)_3$(0,2N)	8.25	8.43	7.72	8.98	7.95	7.95			
$\delta_{complex}-\delta_{precursor}$	−0.16	+0.13	+0.14	+0.73	+0.09	+0.20			
$MnBr(CO)_3$(2,2N)		8.10	7.61	8.83	7.85	7.85	3.30		3.15
$\delta_{complex}-\delta_{precursor}$		+0.07	+0.09	+0.40	+0.05	+0.20			
$MnBr(CO)_3$(3,2N)		8.16	7.66	8.84	7.84	7.84	2.89	2.71	2.42
$\delta_{complex}-\delta_{precursor}$		+0.16	+0.12	+0.49	+0.07	+0.16			
$MnBr(CO)_3$(Me,2N)		8.25	7.75	9.15	7.88	7.88		2.50 [b]	
$\delta_{complex}-\delta_{precursor}$		+0.18	+0.23	+1.04	+0.07	+0.19		2.60 [b]	
		8.15		8.65					
		+0.08		+0.54					

[a] δ in ppm relative to internal $SiMe_4$ at 25 °C in $CDCl_3$.
[b] CH_3, protons signals.

solubility of the complexes limited the spectroscopic studies to a smaller range of solvents. The proposed $BrMn(CO)_3(L)$ formulation for the products is supported by the elemental analysis, conductivity measurements and X-ray fluorescence (that confirms the bromine and manganese presence). The spectroscopic studies are in accord with the proposed structures.

The solid state or solution infrared spectra of the manganese complexes do not show the effect of the metal–nitrogen coordination on the characteristic bands of the ligand. The ν_{CO} pattern of three equal intense bands for the complexes in solution is consistent with a facial arrangement of the carbonyl groups in a C_s molecular symmetry [8]. A similar ν_{CO} pattern is observed in the solid IR spectrum for both $MnBr(CO)_3$(Me,2N) and $MnBr(CO)_3$(0,2N) complexes. For the other complexes the presence of only two bands in the solid IR spectra can be due to the overlapping of the two smaller energy bands.

These complexes exhibited similar ν_{CO} frequency values in the IR spectra. It appears, therefore, that structure modifications on the biquinoline ligand were small enough to produce only negligible changes in the electronic density of the metal. The two smaller frequency bands appear to higher energies in the manganese compounds than those found for similar rhenium compounds already prepared [5g]. This experimental observation suggests a stronger interaction between the Mn and a π-orbital of the nitrogen than in homologous rhenium complexes [8c].

Proton NMR data for the manganese complexes are shown in Table 1. The low solubility of the complexes only allowed partial assignment of the resonances. Although it is impossible to make an accurate estimation of the coupling constants, the basic signal pattern of the polypyridine ligand is in good agreement with previously published NMR spectra of related rhenium complexes [5a,5b,5e] (Fig. 2). The spectra of the analogous Re compounds were used for the signal assignments of the Mn complexes.

Nearly all aromatic proton signals for the biquinoline ligand in the complex are shifted to lower field. This deshielding effect is a characteristic feature of quinoline coordinated to the metal. The shift to lower field of the $H_{8,8'}$ proton in the free ligand was assigned for a *peri* interaction with the nitrogen. The increasing shift of this proton should be the consequence of a great steric hinderance and the paramagnetic effect of the carbonyls in a facial configuration of the Mn complexes. The *syn* conformation of the 0,2N ligand affords a more protected environment around the $H_{3,3'}$ proton and explains well the observed shielding.

The double signal pattern observed in the spectrum of $MnBr(CO)_3$(Me,2N) (Table 1) is due to the presence of two conformers in solution. It is possible that the slow exchange rate between both mirror image isomers caused by the great distortion of the 3,3′-dimethyl 2,2′-biquinoline ligand in the complexes is responsible for the presence of these two conformers. Such a distortion was observed in the X-ray diffraction structure of the related $ReBr(CO)_3$(Me,2N) compound [9].

UV–Vis spectra of the $MnBr(CO)_3L$ complexes (Table 2) show most intense bands to highest energy corresponding to intraligand transitions ($\pi \rightarrow \pi^*$ biquinoline). The lowest energy band found around 400 nm is assigned to a metal to ligand charge transfer transition (MLCT $t_{2g} \rightarrow \pi^*$). This assignment is based on the band intensity, spectral response to solvent polarity and assignments previously reported for related complexes [4,5a]. The energy for the MLCT band

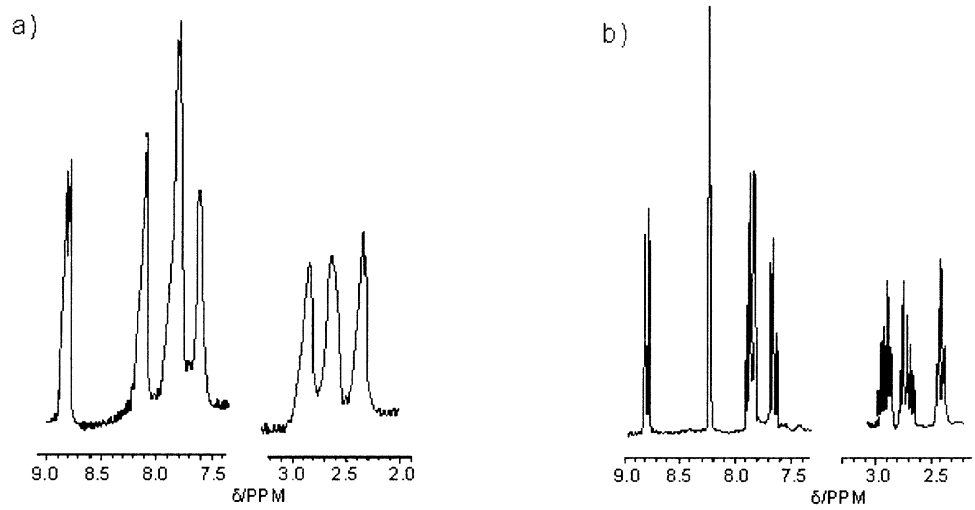


Fig. 2. Proton NMR spectra for: (a) $BrMn(CO)_3(3,2N)$; and (b) $BrRe(CO)_3(3,2N)$ complexes ($CDCl_3$ at 300 MHz).

Table 2
UV–Vis spectral data for $Mn(CO)_3(L)$ complexes at 25 °C

Compound	Solvent	λ_{abs} (nm) (10^{-3} ε, $dm^3\ mol^{-1}\ cm^{-1}$)			
		$(t_{2g} \rightarrow \pi^*_L)$		$(\pi \rightarrow \pi^*)$	
(0,2N)	$CHCl_3$		343(sh)	327(175.15)	258(475.79)
(2,2N)	$CHCl_3$		360(91.18)	345(81.25)	263(248.93)
(3,2N)	$CHCl_3$		319(98.84) [a]	255(48.35)	
(Me,2N)	$CHCl_3$		320(128.53)	307(108.00) 260(300.29)	
$MnBr(CO)_3(0,2N)$	$C_6H_6CH_3$	508(19.19)	372(130.51)	338(145.25)	
	$CHCl_3$	495(16.27)	373(134.94)	338(167.47)	261(498.19)
	C_3H_6O	482(21.38)	371(180.91)	337(141.10)	
$MnBr(CO)_3(2,2N)$	$C_6H_6CH_3$	517(7.77)	390(89.09)	371(81.08)	
	$CHCl_3$	497(20.41)	390(221.55)	370(168.42)	296(396.49)
	C_3H_6O	474(26.61)	387(251.77)	368(212.83)	
$MnBr(CO)_3(3,2N)$	$C_6H_6CH_3$	491(14.05)	361(102.67)	330(sh)	
	$CHCl_3$	477(21.24)	359(151.33)	269(365.71)	
	C_3H_6O	464(19.20)	367(134.05)		
$MnBr(CO)_3(Me,2N)$	$C_6H_6CH_3$	473(7.16)	363(25.18)		
	$CHCl_3$	452(18.76)	359(13.150)	269(322.83)	
	C_3H_6O	414(sh)	359(54.13)		

[a] Broad; ε, molar extinction coefficient.

increases in the order of (0,2N) > (2,2N) > (3,2N) > (Me,2N) showing a slight dependence of the MLTC absorption maximum with the deviation of the quinoline halves from planarity in the coordinated biquinoline ligand. The related rhenium complexes with these ligands exhibit a similar trend.

Potentials obtained from cyclic voltammograms for $BrMn(CO)_3(L)$ complexes in DMF are shown in Table 3. The potentials quoted are relative to SCE. Measurements in acetonitrile were not possible due to the fast chemical decomposition observed in the system.

Two successive reductions and one oxidation were the only observed waves with fresh solutions of the complexes (Fig. 3).

Two electrochemical reductions on the first scan occur in the $E_{1/2} = -0.82$ to -1.04 V range and $E_{1/2} = -1.27$ to -2.2 V range versus SCE for the complexes series. The first reduction is a quasi-reversible one-electron transfer process determined by using the method of comparative waves with the Fc^+–Fc couple under identical conditions. Coulometric measurements yield result supporting a one-electron process. Literature re-

Table 3
Electrochemical data of the manganese complexes [a]

Complex	Redox potential (V)				λ_{max} (eV)
	Reduction		Oxidation[b]		
$MnBr(CO)_3(0,2N)$	−2.09	−0.85	+1.13	+1.33	2.505
$MnBr(CO)_3(2,2N)$		−0.82	+1.11	+1.34	2.495
$MnBr(CO)_3(3,2N)$		−0.89	+1.12	+1.34	2.599
$MnBr(CO)_3(Me,2N)$	−2.20	−1.04	+1.06	+1.38	2.743

[a] Potentials are in volts versus SCE. Solution concentration for complexes was 5×10^{-4} mol dm^{-3}.
[b] Values represent anodic peak potentials.

ports on related polypyridine manganese(I) complexes do not provide reduction potentials [10]. In analogous rhenium(I) complexes, these waves correspond to quasi-reversible one-electron transfer processes, assigned to the reduction of the heterocyclic nitrogen ligand.

On the other hand, the electrochemistry in dichloromethane for identically formulated manganese(I) complexes containing a bidentate phosphine ligand has shown that the reduction is a two-electron process that releases the halogen atom to form the corresponding $Mn(CO)_3(dpm)$ species, (dpm = $Ph_2PCH_2PPh_2$). The $Mn(CO)_3(dpm)$ decomposes after a short time [10]. In our case, the observation of one-electron processes suggests that the reduction is located mainly on the biquinoline ligands similarly to those of the rhenium(I) complex, which is quite different from the reduction processes found in the manganese–phosphine complexes.

The first oxidation wave is irreversible and it is found in the +1.06–1.13 V range. This one-electron oxidation process can be assigned to the Mn(II)/Mn(I) pair in accord with the one observed with $MnX(CO)_3L$ (L = phosphines) and $[MnX(CO)_3L]^+$ complexes by Bond et al. [10]. The second irreversible oxidation wave is observed in the potential 1.33–1.38 V range and it is commonly observed with this type of compound. An additional one-electron oxidation is likely followed by decomposition of the product [10]. The irreversibility in both processes can be correlated with the chemical instability of these complexes.

An additional wave near to +0.75 V was observed during the second scan (Fig. 3b). This wave is related to the first oxidation process. Bond et al. have established that it is due to the oxidation of *mer*-$MnBr(CO)_3L$, i.e. a product of isomerization of the oxidized facial complex [10].

It was possible to establish a correlation between the position of the lower energy MLCT band and $E_{1/2}$ potentials of the first reduction wave (Fig. 4). This correlation assumes that reduction in those orbitals involved in the MLCT are the same involved in the oxidation and reduction processes [5,11]. The linear correlation:

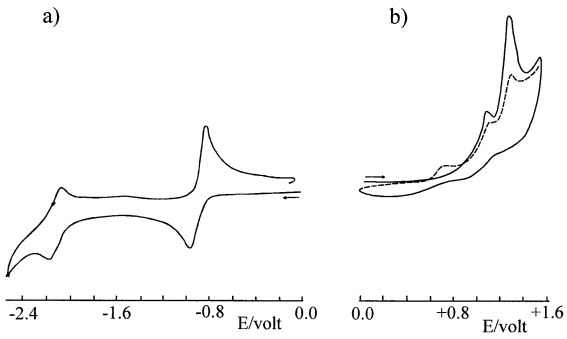


Fig. 3. Cyclic voltammogram of $BrMn(CO)_3(2,2N)$ complex.

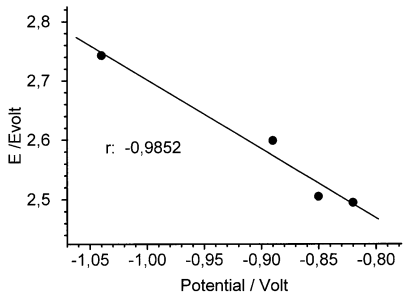


Fig. 4. MLCT energy versus $E_{1/2}$ reduction potential plot.

$$E_{abs} = -1.377E_{1/2}\,\text{red} + 0.537$$

with $r = 0.99$, supports the assignment of the process as a reduction centered on the biquinoline ligand.

4. Conclusions

The X-ray studies for rhenium complexes with the same biquinoline ligands revealed that the structure of the complexes deviate in various degrees from a perfect octahedron [5a,9b,9c]. Spectroscopic and electrochemical results already discussed are in accord with such deviations. Indeed, these deviations can be related to a decrease in the electronic repulsion between the d-metal orbital and the π-biquinoline orbitals when quinoline halves are removed from a perfect plane. Destabilization of the LUMO and stabilization of the HOMO will usually result from such increasing distortion.

Acknowledgements

We thank DICYT-USACH and FONDECYT-CHILE for their financial support. The authors wish to thank J.C.C. for his assistance in the coulometric measurements.

References

[1] (a) M. Grätzel, Energy Resources Through Photochemistry and Catalysis, Academic Press, New York, 1983;
(b) K. Kalyanasundaram, Coord. Chem. Rev. 46 (1982) 159;
(c) K. Kalyanasundaram, M. Grätzel, Photosensitization and Photocatalysis Using Inorganic Organometallic Compounds, Kluwer Academic Publishers, The Netherlands, 1993;
(d) S.A. Moya, R. Pastene, R Sariego, R. Sartori, P. Aguirre, H. Le Bozec, Polyhedron 15 (1996) 1823;
(e) M.R. Féliz, G. Ferraudi, J. Phys. Chem. 96 (1992) 3059;
(f) A. Juris, V. Balzani, F. Barigelletti, S. Campagna, P. Belser, A. von Zelewsky, Coord. Chem. Rev. 84 (1988) 85;
(g) J.R. Shoonover, G.F. Strouse, R.B. Dyer, W.D. Bates, P. Chen, T.J. Meyer, Inorg. Chem. 35 (1996) 273;
(h) J.A. Treadway, B. Loeb, R. Lopez, P. Anderson, F.R. Keene, T.J. Meyer, Inorg. Chem. 35 (1996) 2242;
(i) J. Guerrero, O.E. Piro, E. Wolcan, M.R. Féliz, G. Ferraudi, S.A. Moya, Organometallics 20 (2001) 2842;
(j) R.M. Carlos, M.G. Neuman, J. Photochem. Photobiol. A: Chem. 131 (2000) 67;
(k) M.J. Bermejo, J.Y. Ruiz, X. Solans, J. Vinaixa, Inorg. Chem. 27 (1988) 4385.

[2] (a) A. Terraza, J. Guerrero, R. Quijada, F.M. Rabagliati, S.A. Moya, Polym. Bull. 40 (1998) 27;
(b) A. Terraza, J. Guerrero, S.A. Moya, F.M. Rabagliati, Polym. Bull. 41 (1998) 669.

[3] R. Sartori, G. Rencoret, A. Mora, C. Pérez, R Sariego, E. Lissi, R. Pastene, S.A. Moya, Anticancer Drugs 7 (1996) 1.

[4] G. Ferraudi, M. Feliz, E. Wolcan, I. Hsu, S.A. Moya, J. Guerrero, J. Phys. Chem. 99 (1995) 4929.

[5] (a) S.A. Moya, J. Guerrero, R. Pastene, R. Sartori, R. Schmidt, R. Sariego, J. Sanz-Aparicio, I. Fonseca, M. Martínez-Ripoll, Inorg. Chem. 33 (1994) 2341;
(b) S.A. Moya, J. Guerrero, R. Pastene, A.J. Pardey, P. Baricelli, Polyhedron 17 (1998) 2289;
(c) S.A. Moya, R. Pastene, R. Schmidt, J. Guerrero, R. Sariego, R. Sartori, Bol. Sol. Chil. Quím. 37 (1992) 43;
(d) S.A. Moya, R. Pastene, R. Schmidt, J. Guerrero, R. Sartori, Polyhedron 11 (1992) 1665;
(e) S.A. Moya, J. Guerrero, R. Pastene, R. Sartori, R. Schmidt, R. Sariego, Bol. Soc. Chil. Quím. 37 (1992) 311;
(f) S.A. Moya, R. Pastene, A.J. Pardey, P. Baricelli, Bol. Soc. Chil. Quím. 41 (1996) 251;
(g) S.A. Moya, R. Pastene, R. Sartori, P. Dixneuf, H. Le Bozec, J. Braz, Chem. Soc. 6 (1995) 29.

[6] A.I. Gordon, R.A. Ford, The Chemist's Companion, John Wiley and Sons, New York, 1972.

[7] (a) J.W. Opie, C.T. Smith, Organic Syntheses, vol. III, Wiley, New York, 1965, p. 56 Collect;
(b) R.W. Vanderhear, R.C. Voter, C.V. Banks, J. Org. Chem. 14 (1949) 883;
(c) R.H. Reiman, E.J. Singleton, J. Organomet. Chem. 59 (1973) 309;
(d) W. Hieber, H.Z. Fuchs, Anorg. All. Chem. 248 (1941) 256;
(e) R.P. Thummel, F.J. Lefoulon, Org. Chem. 50 (1985) 666.

[8] (a) J.R. Wagner, D.G. Hendricker, J. Inorg. Nucl. Chem. 37 (1975) 1375;
(b) A.M. Bond, R. Colton, P. Panagiotidou, Organometallics 7 (1998) 1767;
(c) S. Van Wallendael, R.J. Shaver, P. Rillema, B.J. Yoblinski, M. Stathis, T.F. Guarr, Inorg. Chem. 27 (1988) 4007.

[9] (a) S.A. Moya, R. Pastene, R. Schmidt, R. Sartori, U. Müller, G. Frenzen, Organometallics 15 (1996) 3463;
(b) J. Guerrero, S.A. Moya, M.T. Garland, R.F. Baggio, Acta Crystallogr., Sect. C 54 (1998) 1592;
(c) J. Guerrero, S.A. Moya, M.T. Garland, R.F. Baggio, Acta Crystallogr., Sect. C 55 (1999) 932.

[10] (a) A.M. Bond, R. Colton, M.J. McCormick, Inorg. Chem. 16 (1997) 155;
(b) M. Krejcik, M. Danek, F. Hartl, J. Electroanal. Chem. Interfacial Electrochem. 317 (1991) 179;
(c) A.M. Bond, B.S. Grabaric, Z. Grabaric, Inorg. Chem. 17 (1978) 1013;
(d) R. Colton, M.J. McCormick, Aust. J. Chem. 29 (1976) 1657.

[11] (a) M.S. Wrighton, D.L. Morse, J. Am. Chem. Soc. 96 (1974) 998;
(b) P.J. Giordano, M.S. Wrighton, J. Am. Chem. Soc. 101 (1979) 2888;
(c) J.C. Luong, R.A. Faltynek, M.S. Wrighton, J. Am. Chem. Soc. 102 (1980) 7892;
(d) A.J. Juris, S. Campagna, I. Bidd, J.M. Lehn, R. Ziessel, Inorg. Chem. 27 (1988) 4007;
(e) S.A. Moya, R. Pastene, H. Le Bozec, A.J. Pardey, P. Baricelli, Bol. Soc. Chil. Quím. 44 (1999) 423;
(f) Infrared for rhenium complexes. $Re(CO)_3$(0,2N)Br: ν_{CO}(KBr): 2016, 1894 (broad); $Re(CO)_3$(Me,2N)Br: ν_{CO}(KBr): 2017, 1918; $Re(CO)_3$(2,2N)Br: ν_{CO}(KBr): 2016, 1898 (broad); $Re(CO)_3$(3,2N)Br: ν_{CO}(KBr): 2017, 1901 (broad).

PERGAMON

Polyhedron 21 (2002) 445–455

POLYHEDRON

www.elsevier.com/locate/poly

Yttrium halide complexes of phosphine- and arsine oxides: synthesis, multinuclear NMR and structural studies

Nicholas J. Hill, William Levason *, Michael C. Popham, Gillian Reid, Michael Webster

Department of Chemistry, University of Southampton, Southampton SO17 1BJ, UK

Received 12 November 2001; accepted 30 November 2001

Abstract

The reactions of $YCl_3{\cdot}6H_2O$, $YBr_3{\cdot}6H_2O$ and $YI_3{\cdot}8H_2O$ with Ph_3PO, Ph_3AsO, Ph_2MePO, Me_3PO, Me_3AsO, o-$C_6H_4\{P(O)Ph_2\}_2$ (ppO_2) and $Ph_2P(O)CH_2P(O)Ph_2$ ($dppmO_2$) have been examined in EtOH or Me_2CO solution. Complexes isolated in the solid state include $[YX_2(Ph_3PO)_4]Z$ (X = Cl, Br or I; Z = X or PF_6), $[YX_3(Ph_2MePO)_3]$, $[YCl_2(Ph_2MePO)_4]PF_6$, $[YCl(Ph_3PO)_5][SbCl_6]_2$, $[Y(Me_3PO)_6]X_3$, $[YX_2(Ph_3AsO)_4]X$, $[Y(Me_3AsO)_6]Cl_3$ and $[YCl_2(L{-}L)_2]Cl$ (L–L = ppO_2 or $dppmO_2$) which were characterised by analysis, IR and multinuclear (^1H, $^{31}P\{^1H\}$ and ^{89}Y) NMR spectroscopy and conductance measurements. The X-ray crystal structures of $[YCl_2(Ph_3PO)_4]Cl{\cdot}2.5EtOH{\cdot}H_2O$, $[YBr_2(Ph_3PO)_4]PF_6{\cdot}Et_2O$ and $[Y(Me_3PO)_6]Br_3$ are reported and discussed. The solution speciation (in CH_2Cl_2) in the various systems was examined by variable temperature multinuclear NMR spectroscopy. The ^{89}Y NMR chemical shifts show systematic trends with donor set which are described. No reaction between these ligands and $YF_3{\cdot}1/2H_2O$ was observed. © 2002 Elsevier Science Ltd. All rights reserved.

Keywords: Yttrium; Phosphine oxide; Arsine oxide; X-ray structures

1. Introduction

The chemistry of yttrium is the least studied of any 4d element, although interest has increased in recent years with applications in oxide materials [1], ethene and α-olefin polymerisation and ROMP catalysis [2–4], whilst complexes of the radioisotope ^{90}Y are used in radiotherapy [5]. The only oxidation state achieved in aqueous solution, Y(III) $[Kr]4d^05s^0$, is diamagnetic and colourless, and the high lability of many yttrium complexes, has seriously hindered studies. Potentially ^{89}Y NMR (^{89}Y = 100%, I = 1/2) spectroscopy could provide a valuable probe [6], but its poor sensitivity D_c (receptivity relative to ^{13}C) of 0.67, low resonance frequency Ξ = 4.92 MHz, and very long T_1's have restricted studies. We have recently reported [7,8] detailed studies of $Y(NO_3)_3$ complexes with R_3PO and R_3AsO ligands which exhibit a range of stoichiometries including nine-coordinate $[Y(R_3PO)_3(NO_3)_3]$, eight-coordinate $[Y(R_3PO)_4(NO_3)_2]^+$ and six-coordinate $[Y(Me_3AsO)_6]^{3+}$. Curiously little has been reported about yttrium halide complexes. Reviews [9,10] indicate that the lanthanides and yttrium form $M(Ph_3PO)_xCl_3$ complexes (x = 4 or 3), claimed as non-conductors in solution, indicating seven- and six-coordination, respectively. However, consultation of the original references often reveals incomplete studies of a few lanthanide examples which are taken as characteristic of the whole series (including Y) [11–13]. Specific information on yttrium compounds is sparse [14,15] and none have been structurally characterised or their solution behaviour explored. Here we report detailed studies of complexes of these ligands with yttrium halides $YX_3{\cdot}nH_2O$ (X = F, Cl, Br or I).

2. Results and discussion

2.1. Synthesis

Reactions of the hydrated yttrium halides (excluding fluoride) with Ph_3PO, Ph_3AsO, Ph_2MePO, Me_3PO and

* Corresponding author. Tel.: +44-2380-593-792; fax: +44-2380-593-781.

E-mail address: wxl@soton.ac.uk (W. Levason).

0277-5387/02/$ - see front matter © 2002 Elsevier Science Ltd. All rights reserved.
PII: S0277-5387(01)01011-7

Me_3AsO in ethanol, acetone or CH_2Cl_2 were carried out using a variety of molar ratios and reaction conditions (see Section 2.2). Isolated complexes were identified by a combination of analysis, IR, $^{31}P\{^1H\}$ and ^{89}Y NMR spectroscopy. X-ray structures were determined for three examples. The insoluble $YF_3 \cdot 1/2H_2O$ did not react with Ph_3PO or Me_3PO in refluxing ethanol or acetone even with extended reaction times.

2.2. $[Y(Me_3PO)_6]X_3$ (X = Cl, Br or I) and $[Y(Me_3AsO)_6]Cl_3$

The reaction of $YX_3 \cdot nH_2O$ with Me_3PO with a YX_3:Me_3PO ratio of 1:6 produced $[Y(Me_3PO)_6]X_3$. These complexes are insoluble in acetone, CH_2Cl_2 or cold ethanol, slightly soluble in $MeNO_2$, and decomposed by DMF or DMSO. The IR spectra of these complexes are superimposable, with a strong broad feature at 1110 cm^{-1} assigned as ν(PO), which compares with 1161 cm^{-1} in the 'free' ligand. In nitromethane solution all have conductivities in the range typical of 3:1 electrolytes, and the ^1H NMR spectra (d^3-$MeNO_2$) each show a doublet with $^2J(^{31}P–^1H) = 13$ Hz. The $^{31}P\{^1H\}$ NMR spectra in $MeNO_2$ at 295 K are singlets at $\delta \sim 55$, which on cooling to 248 K show doublet coupling to ^{89}Y of ~ 8 Hz. The poor solubility in $MeNO_2$ and the relatively high m.p. (244 K) made obtaining ^{89}Y NMR data very difficult. No ^{89}Y resonances were observed at ambient temperatures, but from $[Y(Me_3PO)_6]Cl_3$ in $MeNO_2$ at 245 K after very long accumulations, a weak multiplet pattern consistent with the central five lines of a binomial septet $^2J(^{89}Y–^{31}P)$ approximately 8 Hz, was observed at δ 133. The bromide and iodide salts were less soluble than the chloride and no ^{89}Y spectra were obtained from these. Confirmation of the composition was obtained from the X-ray crystal structure of $[Y(Me_3PO)_6]Br_3$ which shows the six trimethylphosphine oxide ligands octahedrally coordinating to the yttrium (Fig. 1). The yttrium is located on a centre of symmetry with the O–Y–O angles close to the idealized values (Table 1). There is little change in geometry among the three crystallographically independant phosphine oxides with the largest variation being in the Y–O–P angle (142°–159°). As noted before [7], these angles are smaller than those in complexes of the triphenyl derivative (see later).

The $[Y(Me_3AsO)_6]Cl_3$ was obtained from hydrated YCl_3 and Me_3AsO in ethanol, and has similar properties to those of $[Y(Me_3PO)_6]Cl_3$, including a broad ν(AsO) at 877 cm^{-1}, the conductance of a 3:1 electrolyte in 10^{-3} mol dm^{-3} $MeNO_2$, δ(Me) at 2.0(s) in the ^1H NMR spectrum and an ^{89}Y NMR resonance (in $EtNO_2$ at 185 K) at δ 135. The $[Y(Me_3AsO)_6](NO_3)_3$ previously characterised by an X-ray study [8], has ν(AsO) = 877 cm^{-1} and $\delta(^{89}Y)$ 133, and the presence of the same octahedral YO_6 cation in the present complex is therefore clear. It is notable that in the nitrate systems, $[Y(Me_3PO)_3(\eta^2\text{-}NO_3)_3]$ and $[Y(Me_3PO)_4(\eta^2\text{-}NO_3)_2]NO_3$ form, but not $[Y(Me_3PO)_6](NO_3)_3$, showing that the preference of the oxophilic Y(III) for nitrate is stronger than for halides. In the halide systems, reactions using a Y:Me_3PO ratio of $1: < 6$ resulted only in precipitation of $[Y(Me_3PO)_6]X_3$, albeit in poor yield.

2.3. $[YX_2(Ph_3PO)_4]Z$ (X = Cl, Br or I; Z = X or PF_6)

The reaction of $YCl_3 \cdot 6H_2O$, $YBr_3 \cdot 6H_2O$ or $YI_3 \cdot 8H_2O$ with Ph_3PO in ethanol in a 1:3–4 mol ratio produced white $[YX_2(Ph_3PO)_4]X$ (X = Cl or Br) or pale yellow $[YI_2(Ph_3PO)_4]I$. If the reactions are conducted in the

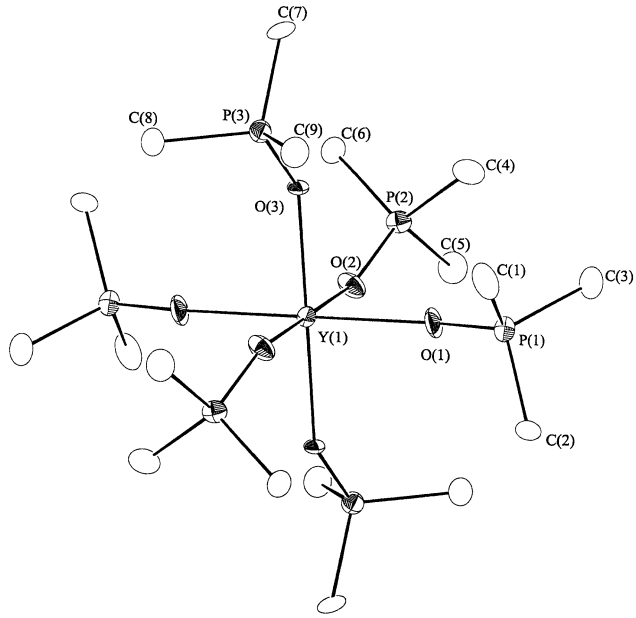


Fig. 1. Structure of the cation in $[Y(Me_3PO)_6]Br_3$ showing the atom numbering scheme. Thermal ellipsoids are drawn at the 40% probability level and H atoms omitted for clarity. The yttrium is located on a centre of symmetry.

Table 1
Selected bond lengths (Å) and angles (°) for $[Y(Me_3PO)_6]Br_3$

Bond lengths			
Y(1)–O(1)	2.214(5)	P(1)–O(1)	1.510(6)
Y(1)–O(2)	2.224(5)	P(2)–O(2)	1.514(5)
Y(1)–O(3)	2.233(5)	P(3)–O(3)	1.514(5)
P(1)–C	1.763(8)–1.772(8)	P(2)–C	1.758(8)–1.780(8)
P(3)–C	1.757(8)–1.778(8)		
Bond angles			
Y(1)–O(1)–P(1)	158.5(3)	Y(1)–O(2)–P(2)	142.5(3)
Y(1)–O(3)–P(3)	142.1(3)	O(1)–Y(1)–O(2)	89.6(2)
O(1)–Y(1)–O(3)	91.4(2)	O(2)–Y(1)–O(3)	90.8(2)
O(1)–P(1)–C	110.2(4)–112.6(4)	O(2)–P(2)–C	109.9(4)–111.9(4)
O(3)–P(3)–C	111.2(3)–111.7(4)		

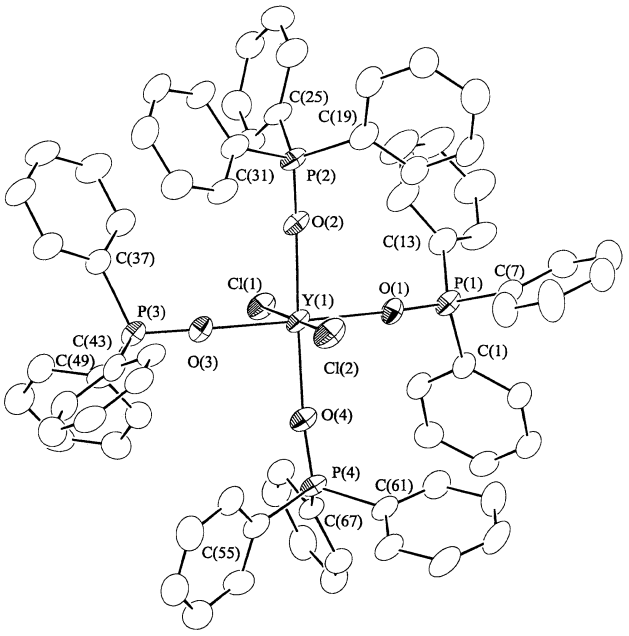


Fig. 2. Structure of the cation in $[YCl_2(Ph_3PO)_4]Cl{\cdot}2.5EtOH{\cdot}H_2O$ showing the atom numbering scheme. Thermal ellipsoids are drawn at the 40% probability level and H atoms omitted for clarity.

presence of NH_4PF_6, the products are $[YX_2(Ph_3PO)_4]$-PF_6, which apart from features due to PF_6^- anions are spectroscopically identical to the X^- salts. The isolated chloro- and bromo-complexes are air and moisture stable, the iodocomplexes darken slowly in the solid state and turn brown in a few hours in solution in chlorocarbon solvents due to liberation of diiodine, and this is accompanied by the appearance of new phosphine oxide resonances in the ^{31}P NMR spectra. The latter reaction does not occur in the absence of oxygen, and would appear to involve yttrium-promoted oxidation of the coordinated iodide ligands by oxygen.

The X-ray structures of $[YCl_2(Ph_3PO)_4]Cl{\cdot}2.5EtOH{\cdot}H_2O$ and $[YBr_2(Ph_3PO)_4]PF_6{\cdot}Et_2O$ (Figs. 2 and 3) reveal *trans*-octahedral cations with angles at Y close to the idealized values. The Y–O distances (Tables 2 and 3) are all very similar (approximately 2.2 Å) to the values found in the hexakis-trimethylphosphine oxide structure (Table 1). The difference in the Y–halogen distance closely reflects the difference in the ionic radii of the two halogens (0.14 Å). The complexed phosphine oxide geometry is unexceptional and shows Y–O–P angles of 167–174° (Cl) and 156–172° (Br) which are in general larger than the trimethyl derivative (Table 1). The IR spectra of the complexes each exhibit a very strong broad feature in the range 1150–1130 cm^{-1} assignable to ν(PO), which move to high frequency along the series $I \rightarrow Br \rightarrow Cl$. Uncomplexed Ph_3PO exhibits ν(PO) at 1195 cm^{-1} [7]. In CH_2Cl_2 solution the complexes are 1:1 electrolytes [7], and show $^{31}P\{^1H\}$ NMR resonances at room temperature which are doublets due to coupling to ^{89}Y with $^2J(^{89}Y–^{31}P)$ 10–12 Hz. The resonances shift to high frequency along the series $Cl \rightarrow Br \rightarrow I$, and are unchanged on cooling to 200 K. Dilute solutions of $[YX_2(Ph_3PO)_4]X$ (X = Cl, Br or I) show weak resonances ($\leq 5\%$ of the tetrakis signal) approximately 1 ppm to low frequency of the main peak, which on cooling the solutions show doublet ^{89}Y couplings. These resonances disappear on adding Ph_3PO to the solutions and are attributed to some dissociation into the tris $[YX_3(Ph_3PO)_3]$ complexes. A CH_2Cl_2 solution of $[YCl_2(Ph_3PO)_4]Cl$ boiled with $YCl_3{\cdot}6H_2O$ showed three ^{31}P NMR resonances with δ 36.0 (tetrakis), 27.0 (Ph_3PO) and 34.5 which is probably due to $[YCl_3(Ph_3PO)_3]$. The ^{89}Y NMR spectrum obtained from this solution showed two multiplets at δ 192 ($[YCl_2(Ph_3PO)_4]Cl$ below) and 242(quartet), the latter consistent with $[YCl_3(Ph_3PO)_3]$, although at-

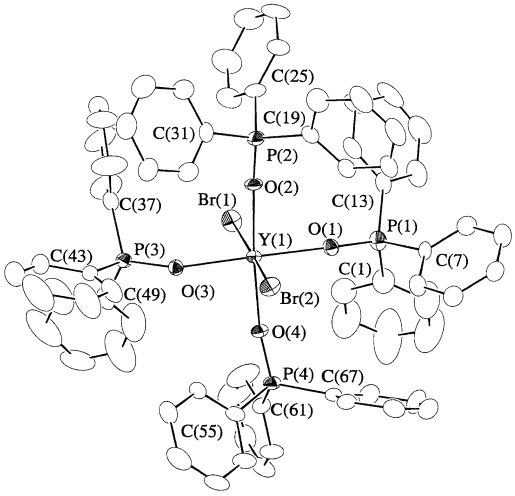


Fig. 3. Structure of the cation in $[YBr_2(Ph_3PO)_4]PF_6{\cdot}Et_2O$ showing the atom numbering scheme. Thermal ellipsoids are drawn at the 40% probability level and H atoms omitted for clarity.

Table 2
Selected bond lengths (Å) and angles (°) for $[YCl_2(Ph_3PO)_4]Cl{\cdot}2.5EtOH{\cdot}H_2O$

Bond lengths			
Y(1)–Cl(1)	2.625(1)	Y(1)–Cl(2)	2.613(2)
Y(1)–O(1)	2.231(3)	Y(1)–O(3)	2.233(3)
Y(1)–O(2)	2.226(3)	Y(1)–O(4)	2.223(3)
P(n)–O(n) (n = 1–4)	1.502(4)–1.507(4)	P–C	1.771(6)–1.799(5)
Bond angles			
Cl(1)–Y(1)–Cl(2)	177.14(4)	Cl(1)–Y(1)–O(1)	87.10(9)
Cl(1)–Y(1)–O(2)	90.18(9)	Cl(1)–Y(1)–O(3)	87.09(9)
Cl(1)–Y(1)–O(4)	91.49(9)	O(1)–Y(1)–O(2)	88.2(1)
O(1)–Y(1)–O(4)	90.1(1)	O(2)–Y(1)–O(3)	91.7(1)
O(3)–Y(1)–O(4)	90.2(1)	Y(1)–O(1)–P(1)	167.1(2)
Y(1)–O(2)–P(2)	172.2(2)	Y(1)–O(3)–P(3)	170.1(2)
Y(1)–O(4)–P(4)	173.8(2)	O–P–C	108.3(2)–112.5(2)

Table 3
Selected bond lengths (Å) and angles (°) for $[YBr_2(Ph_3PO)_4]PF_6 \cdot Et_2O$

Bond lengths			
Y(1)–Br(1)	2.775(1)	Y(1)–Br(2)	2.794(1)
Y(1)–O(1)	2.221(5)	Y(1)–O(3)	2.233(5)
Y(1)–O(2)	2.220(4)	Y(1)–O(4)	2.221(4)
P(*n*)–(*n*) ($n = 1$–4)	1.501(4)–1.506(5)	P–C	1.779(7)–1.811(8)
P–F	1.556(6)–1.606(5)		
Bond angles			
Br(1)–Y(1)–Br(2)	174.67(4)	Br(1)–Y(1)–O(1)	87.1(1)
Br(1)–Y(1)–O(2)	90.0(1)	Br(1)–Y(1)–O(3)	85.8(1)
Br(1)–Y(1)–O(4)	95.9(1)	O(1)–Y(1)–O(2)	89.2(2)
O(1)–Y(1)–O(4)	88.2(2)	O(2)–Y(1)–O(3)	95.0(2)
O(3)–Y(1)–O(4)	88.4(2)	Y(1)–O(1)–P(1)	166.7(3)
Y(1)–O(2)–P(2)	172.5(3)	Y(1)–O(3)–P(3)	155.9(3)
Y(1)–O(4)–P(4)	161.4(3)	O–P–C	108.5(3)–113.6(3)

tempts to isolate $[YCl_3(Ph_3PO)_3]$ as a solid have been unsuccessful. Solutions of $[YX_2(Ph_3PO)_4]PF_6$ containing 2 equiv. of Ph_3PO show weak features at δ 37.5 and 40.0 (X = Cl) or δ 37.0 and 38.0 (X = Br), which by comparison with data for $[YCl(Ph_3PO)_5][SbCl_6]_2$ may be identified as due to $[YX(Ph_3PO)_5]^{2+}$, suggesting a competitive equilibrium between X^- and Ph_3PO for the Y centre. In these cases insufficient of the second species was formed to permit its identification via ^{89}Y NMR. The iodide complexes differ in that mixtures of $[YI_2(Ph_3PO)_4]^+$ and 5 equiv. of Ph_3PO in CH_2Cl_2 at ambient temperatures show markedly broadened resonances indicating the onset of intermolecular exchange. At 180 K this solution shows strong resonances due to Ph_3PO, $[YI_2(Ph_3PO)_4]^+$, intense doublets at δ 37.5 and 38.0 (integral 4:1) attributable to formation of $[YI(Ph_3PO)_5]^{2+}$, and some weaker unassigned features. The greater proportion of $[YX(Ph_3PO)_5]^{2+}$ formed when X = I is consistent with easier displacement of the soft iodide from the oxophilic yttrium. Solutions of $[YX_2(Ph_3PO)_4]^+$ fail to exhibit ^{89}Y resonances at 300 K, but on cooling to 200 K a single resonance is present in each complex, which under high resolution appear as binomial quintets due to coupling to four equivalent R_3PO ligands (Table 4, Fig. 4).

2.4. $[YCl(Ph_3PO)_5][SbCl_6]_2$

The reaction of $[YCl_2(Ph_3PO)_4]^+$ with Ph_3PO in dry CH_2Cl_2 in the presence of 2 equiv. of the strong Lewis acid $SbCl_5$ results in chloride abstraction to form $[YCl(Ph_3PO)_5][SbCl_6]_2$. Excess $SbCl_5$ causes decomposition to form (among other products) $[SbCl_5(Ph_3PO)]$ [16] (δ (^{31}P) = 47) while $[Y(Ph_3PO)_6][SbCl_6]_3$ does not appear to form. The $[YCl(Ph_3PO)_5][SbCl_6]_2$ shows a $^{31}P\{^1H\}$ NMR spectrum containing two doublets at δ 37.5 and 40.0 (integral 4:1). The corresponding ^{89}Y NMR resonance is at δ 179 and approximates to a sextet pattern, although the outer lines were ill-defined. This is attributed to the very similar ^{89}Y–^{31}P couplings to the axial and equatorial phosphine oxides (10, 11 Hz). The ν(PO) frequency occurs at 1141 cm^{-1} for the dication, some 10 cm^{-1} lower than in $[YCl_2(Ph_3PO)_4]^+$ showing the effect of the increased positive charge. The presence of $[SbCl_6]^-$ is shown by a strong band at 347 cm^{-1} [17].

2.5. $[YX_2(Ph_3AsO)_4]X$

The corresponding reactions to those in Section 2.3, but replacing Ph_3PO with Ph_3AsO, produced $[YX_2(Ph_3AsO)_4]X$. The iodide systems are again sensitive to air and, as described in the Section 3, the polyiodide $[YI_2(Ph_3AsO)_4](I_5)$ has been characterised. Spectroscopically these complexes are very similar to their phosphine oxide analogues: 1:1 electrolytes in solution and showing a single broad ν(AsO) at approximately 890 cm^{-1}. The ^{89}Y NMR spectra from CH_2Cl_2 solutions at 200 K contain single sharp resonances (Table 4) attributable to the $[YX_2(Ph_3AsO)_4]^+$ cations, the resonances being slightly (≤ 10 ppm) to high frequency of those in $[YX_2(Ph_3PO)_4]X$ for constant X. An acetone solution of $[YCl_2(Ph_3AsO)_4]Cl$ containing 1 equiv. of YCl_3 showed (at 200 K) only a singlet ^{89}Y NMR resonance at δ 200 attributable to the tetrakis complex, with no evidence for formation of $[YCl_3(Ph_3AsO)_3]$ for which $\delta(^{89}Y)$ would be expected approximately δ 250–260. The poor sensitivity of ^{89}Y NMR means that minor species could easily escape detection, but this shows that the $[YCl_3(Ph_3AsO)_3]$ is not formed in substantial amounts.

2.6. $[YX_3(Ph_2MePO)_3]$

In marked contrast to the Ph_3PO systems, reaction of $YX_3 \cdot 6H_2O$ (X = Cl or Br) with Ph_2MePO in ethanol or acetone irrespective of the ratio gave solid $[YX_3(Ph_2MePO)_3]$ complexes. The complexes are non-conductors in solution, and the IR spectra show a very strong feature in the range 1150–1140 cm^{-1} attributable to ν(PO) (cf. 'free' Ph_2MePO 1172 cm^{-1} [7]). In solution each complex shows a single $^{31}P\{^1H\}$ NMR resonance which appear as singlets at ambient temperature, but show ill-defined doublet couplings to ^{89}Y on cooling. The ^{89}Y resonances are only observed at 200 K, and under high resolution are binomial quartets showing coupling to 3 equiv. phosphorus atoms, consistent with a *fac* geometry (Table 4, Fig. 4). On addition of Ph_2MePO to the solutions very broad ^{31}P NMR resonances δ approximately 29 and 40 were present at room temperature, showing intermolecular exchange is occurring. On cooling the resonances sharpen, but in addition to those of $[YX_3(Ph_2MePO)_3]$ and Ph_2MePO, a new feature is present δ approximately 41. In the

Table 4
^{89}Y and $^{31}P\{^1H\}$ NMR data [a]

	δ ^{89}Y	δ $^{31}P\{^1H\}$ [b]	$^2J(^{31}P–^{89}Y)$ (Hz)	Solvent	Temperature (K)
$[YCl_2(Ph_3PO)_4]Cl$	191 (quintet)	35.0 (d)	13	$CH_2Cl_2/CDCl_3$	200
$[YCl_2(Ph_3PO)_4]PF_6$	191 (quintet)	35.0 (d)	13	$CH_2Cl_2/CDCl_3$	200
$[YBr_2(Ph_3PO)_4]Br$	220 (quintet)	36.5 (d)	11	$CH_2Cl_2/CDCl_3$	200
$[YBr_2(Ph_3PO)_4]PF_6$	220 (quintet)	36.0 (d)	11	$CH_2Cl_2/CDCl_3$	200
$[YI_2(Ph_3PO)_4]I$	245 (quintet)	37.5 (d)	11	$CH_2Cl_2/CDCl_3$	200
$[YI_2(Ph_3PO)_4]PF_6$	245 (quintet)	37.0 (d)	11	$CH_2Cl_2/CDCl_3$	200
$[YCl_2(Ph_3AsO)_4]Cl$	198 (s)			$CH_2Cl_2/CDCl_3$	200
$[YBr_2(Ph_3AsO)_4]Br$	224 (s)			$CH_2Cl_2/CDCl_3$	200
$[YI_2(Ph_3AsO)_4]I$	254 (s)			$CH_2Cl_2/CDCl_3$	200
$[YCl(Ph_3PO)_5][SbCl_6]_2$	179 (m)	37.5 (d), 40.0 (d)	11, 10	$CH_2Cl_2/CDCl_3$	200
$[YCl_3(Ph_2MePO)_3]$	256 (quartet)	40.0 (d)	10	$CH_2Cl_2/CDCl_3$	200
$[YBr_3(Ph_2MePO)_3]$	299 (quartet)	40.0 (d)	11	$CH_2Cl_2/CDCl_3$	185
$[YI_3(Ph_2MePO)_3]$	354 [c]	41.5 (d)	14	$CH_2Cl_2/CDCl_3$	180
$[YCl_2(Ph_2MePO)_4]PF_6$	192 (quintet)	40.5 (d)	10	$CH_2Cl_2/CDCl_3$	185
$[Y(Me_3PO)_6]Cl_3$	133 (m) [c]	54.0 (d)	ca. 9	$MeNO_2$	245
$[Y(Me_3PO)_6]Br_3$		55.0 (d)	9	$MeNO_2$	245
$[Y(Me_3PO)_6]I_3$		55.0 (d)	9	$MeNO_2$	245
$[Y(Me_3AsO)_6]Cl_3$	135 (s)			$EtNO_2/d^6$-Me_2CO	200
$[YCl_2(ppO_2)_2]Cl$	210 (quintet)	36.0 (d)	7	$CH_2Cl_2/CDCl_3$	200
$[YCl_2(dppmO_2)_2]Cl$	213 (multiplet) [c]	32.0 [c]		$CH_2Cl_2/CDCl_3$	200
$[Y(NO_3)_3(Ph_3PO)_3]$ [d]	−37.7 (quartet)				
$[Y(NO_3)_2(Ph_3PO)_4]NO_3$ [d]	−2.0 (quintet)				
$[Y(NO_3)_3(Me_3PO)_3]$ [d]	−17.7 (quartet)				
$[Y(NO_3)_2(Me_3PO)_4]NO_3$ [d]	−0.3 (quintet)				
$[Y(NO_3)_2(Ph_3AsO)_4]NO_3$ [e]	21 (s)				
$[Y(Me_3AsO)_6](NO_3)_3$ [e]	133 (s)				

[a] The ^2J couplings are often not evident at higher temperatures, possibly due to exchange, although in some cases they are probably lost in the line widths.
[b] The PF_6^- resonances at approximately −145 (septet) are not listed; ^{31}P NMR shifts at 300 K are given in Section 3.
[c] Couplings not resolved or ill-defined.
[d] Data from Ref. [7].
[e] Data from Ref. [8].

presence of a large excess of ligand, ^{89}Y NMR spectra (200 K) showed quintet patterns near δ 190 (Cl) or 220 (Br) which by comparison with the Ph_3PO analogues can be attributed to the formation of $[YX_2(Ph_2MePO)_4]^+$, although only $[YX_3(Ph_2MePO)_3]$ were isolated from these solutions as solids. However, the reaction of $YCl_3{\cdot}6H_2O$, Ph_2MePO and NH_4PF_6 in ethanol in a 1:4:1 ratio produced white $[YCl_2(Ph_2MePO)_4]PF_6$, which showed a quintet ^{89}Y NMR resonance at δ 192 and $\delta(^{31}P)$ at 40.5. Low

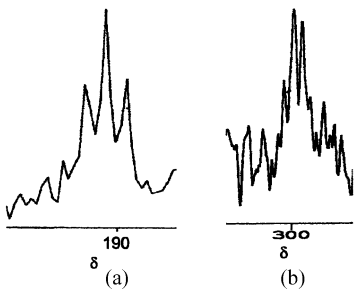
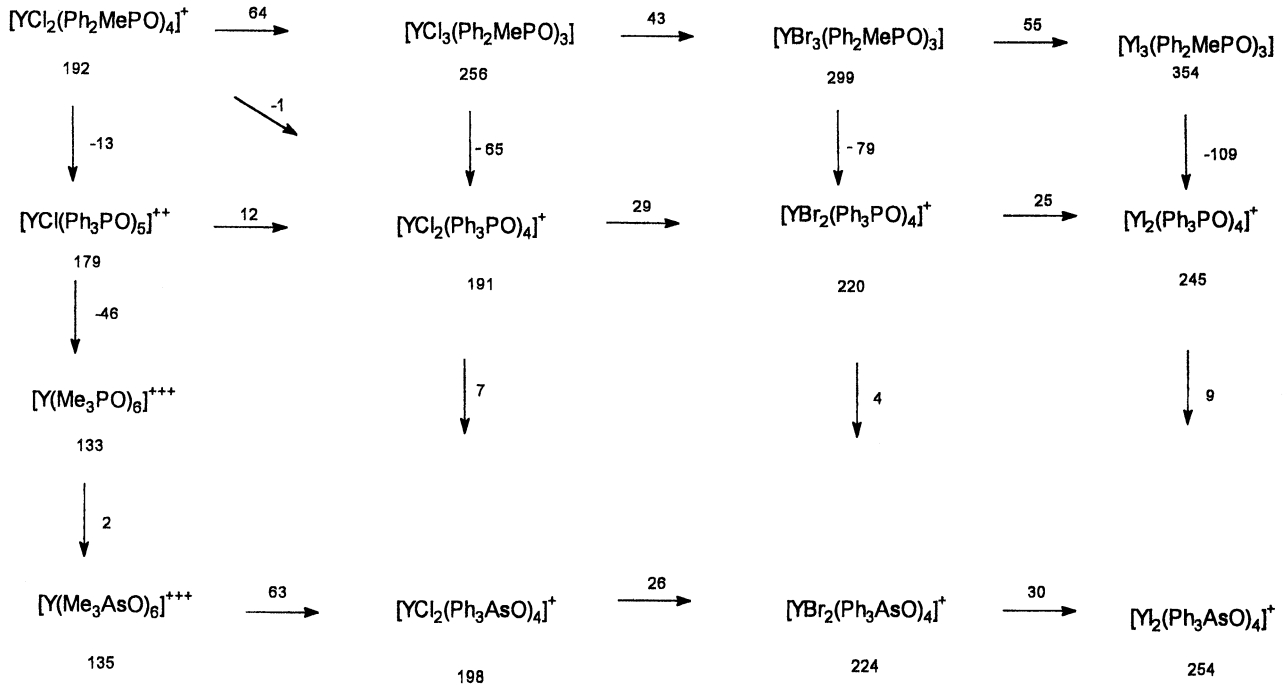


Fig. 4. ^{89}Y NMR spectra of: (a) $[YCl_2(Ph_3PO)_4]^+$; (b) $[YBr_3(Ph_2MePO)_3]$ in $CH_2Cl_2/CDCl_3$ at 200 K.

temperature ^{31}P NMR studies reveal the presence of some Ph_2MePO and $[YCl_3(Ph_2MePO)_3]$ in CH_2Cl_2 solutions of $[YCl_2(Ph_2MePO)_4]PF_6$, showing an equilibrium is present. The $[YBr_2(Ph_2MePO)_4]PF_6$ was not prepared.

The $YI_3{\cdot}8H_2O$–Ph_2MePO system is more labile and isolation of pure complexes proved difficult. A pale yellow $[YI_3(Ph_2MePO)_3]$ was isolated from ethanol solution containing a YI_3:Ph_2MePO of 1:2. At 180 K in CH_2Cl_2 solution this shows a rather broad ^{89}Y resonance at δ 354 which seems reasonable for an I_3O_3 donor set (see Table 4), but the coupling was not clearly resolved. The ^{31}P NMR spectrum has a very broad feature at δ 41.5 at 300 K which on cooling sharpens and at 190 K shows a doublet at 41.5 ($^2J(^{89}Y–^{31}P) = 14$ Hz) and some other weak features to higher frequency. In the $[YI_3(Ph_2MePO)_3]$ with excess Ph_2MePO, ligand exchange is fast on the ^{31}P NMR time scale down to low temperatures, and even at 190 K the lines are still broad, although separate resonances at 29.0 (Ph_2MePO), 41.5 (d) ($[YI_3(Ph_2MePO)_3]$) and 42.0 (d) ($[YI_2(Ph_2MePO)_4]^+$?) are resolved. The corresponding $YI_3/Ph_2MePO/PF_6^-$ system is complex and appears to



Scheme 1. ^{89}Y NMR chemical shifts of various yttrium complexes. Values below formulae represent chemical shifts and values alongside the arrows are the differences in chemical shift. For practical reasons (see text) the $[Y(Me_3EO)_6]^{3+}$ were recorded in $MeNO_2$ or $EtNO_2$, and the others in CH_2Cl_2. Although small solvent and temperature shifts may be present in the data, they are unlikely to alter the pattern of characteristic shifts with X, R_3EO, and X:R_3EO ratio, which are clear.

contain at least three yttrium species, but attempts to isolate pure solid complexes from this system failed.

2.7. Diphosphine dioxide complexes

The reaction of $YCl_3{\cdot}6H_2O$ with $Ph_2P(O)CH_2P(O)Ph_2$ (dppmO_2) or o-$C_6H_4\{P(O)Ph_2\}_2$ (ppO_2) in ethanol gave white $[YCl_2(L–L)_2]Cl$, which appear to be the first reported diphosphine dioxide complexes of yttrium. Both are 1:1 electrolytes in CH_2Cl_2 solution. The $[YCl_2(ppO_2)_2]Cl$ exhibits a single broad $^{31}P\{^1H\}$ NMR resonance at ambient temperatures and no ^{89}Y resonance is evident. However, at 200 K the ^{89}Y NMR spectrum shows a clearly resolved quintet at δ 210 ($^2J(^{89}Y–^{31}P) = 7$ Hz) showing it is the *trans* cation with a Cl_2O_4 donor set. The $[YCl_2(dppmO_2)_2]Cl$ is generally similar although its solubility in CH_2Cl_2 is poor.

2.8. ^{89}Y NMR studies

The identification of solution species as discussed in previous sections relied in most cases on the $^{31}P–^{89}Y$ coupling patterns. Here we compare chemical shifts in an attempt to correlate these with donor set. Data from our previous studies of the nitrate systems are also included. Scheme 1 shows the systematic changes observed as the nature and number of X and R_3EO ligands are varied. As expected the effect on the ^{89}Y chemical shift of changing R groups on the ligand is small, and changing R_3PO to R_3AsO produces a high frequency shift of ≤ 10 ppm. The homoleptic $[Y(Me_3EO)_6]^{3+}$ (E = P or As) have $\delta(^{89}Y)$ 133–135. Incorporating Cl in the coordination sphere in $[YCl(Ph_3PO)_5]^{2+}$, $[YCl_2(Ph_3PO)_4]^+$ and $[YCl_3(Ph_2MePO)_3]$ causes a stepwise high frequency shift. Similarly exchanging Cl for Br and then I causes progressive high frequency shifts (Scheme 1). Comparison with data on the nitrate systems (Table 4) shows that replacement of NO_3 by R_3EO results in a high frequency shift, although the trends are less regular, probably due to the varying coordination numbers in the nitrate systems. The $^{31}P\{^1H\}$ chemical shifts are much less useful in identifying complexes since they differ by approximately 1–2 ppm between $[YX_2(R_3PO)_4]^+$ and $[YX_3(R_3PO)_3]$.

3. Experimental

Multinuclear NMR spectra were obtained on a Bruker DPX400 at 161.9 MHz ($^{31}P\{^1H\}$) and referenced to external 85% H_3PO_4 or 19.60 MHz (^{89}Y) using a 2–4 s pulse delay and TEMPO as a relaxation agent and referenced to 1 mol dm^{-3} YCl_3 in water. Other physical measurements were made as before [7]. Ph_3PO, Ph_2MePO, Ph_3AsO, $YCl_3{\cdot}6H_2O$ (Aldrich) and Me_3PO (Alfa) were used as received. Me_3AsO was made by H_2O_2 oxidation of Me_3As in Et_2O and purified by

sublimation in vacuo [8]. $YF_3 \cdot 1/2H_2O$ was made by precipitation from aq. solutions of $Y(NO_3)_3$ and NaF, washed with H_2O and dried in vacuo. $YBr_3 \cdot 6H_2O$ was prepared by evaporating Y_2O_3 with 48% HBr, and recrystallising the product from H_2O. *Anal*. Found: Br, 54.8. Calc. for $YBr_3 \cdot 6H_2O$: Br, 54.9%. $YI_3 \cdot 8H_2O$ was made by metathesis of aq. solutions of yttrium sulfate and barium iodide, removal of the precipitated $BaSO_4$, and evaporation to dryness in vacuo. The fawn hygroscopic solid was stored in a desiccator. Yield: 92%. *Anal*. Found: I, 61.9. Calc. for $YI_3 \cdot 8H_2O$: I, 62.0%. Several attempts to prepare this compound from Y_2O_3 and aq. HI gave materials containing excess diiodine, which could not be removed.

3.1. $[YCl_2(Ph_3PO)_4]Cl$

$YCl_3 \cdot 6H_2O$ (0.20 g, 0.66 mmol) and Ph_3PO (1.11 g, 4.0 mmol) were dissolved separately in cold EtOH (2×5 cm^3) and the solutions mixed. Refrigeration overnight resulted in colourless crystals, which were filtered off and dried in vacuo. Yield: 0.56 g, 60%. *Anal*. Found: C, 65.7; H, 4.5. Calc. for $C_{72}H_{60}Cl_3O_4P_4Y$: C, 66.1; H, 4.6%. IR (cm^{-1}) (Nujol mull): 1310m, 1188w, 1150vs (PO), 1119s, 1087s, 1074m, 997w, 975w, 749s, 692s, 543s, 420w, 398w, 353w, 310m, 260m. ^{1}H NMR (300 K, $CDCl_3$): 7.1–7.9 (m). $^{31}P\{^1H\}$ NMR (300 K, $CH_2Cl_2/CDCl_3$): 35.0 (d) $^2J(^{31}P–^{89}Y) = 12$ Hz. Λ_M (10^{-3} mol dm^{-3} CH_2Cl_2) = 30 Ω^{-1} cm^2 mol^{-1}.

3.2. $[YCl_2(Ph_3PO)_4]PF_6$

To a solution of $YCl_3 \cdot 6H_2O$ (0.30 g, 1.0 mmol) in warm EtOH (10 cm^3) were added sequentially $[NH_4][PF_6]$ (0.16 g, 1.0 mmol) and Ph_3PO (1.1 g, 4.0 mmol) dissolved in EtOH (10 cm^3), resulting in a fine white precipitate. The solution was stirred for 1 h, the precipitate filtered off and dried in vacuo. Yield: 1.09 g, 75%. *Anal*. Found: C, 61.1; H, 4.4. Calc. for $C_{72}H_{60}Cl_2F_6O_4P_5Y$: C, 61.0; H, 4.3%. IR (cm^{-1}) (CsI disc): 3061w, 1439m, 1318m, 1192w, 1150vs (PO), 1122s, 1092s, 1028m, 999m, 839s, 750m, 725s, 693s, 559s, 543s, 459m, 446m, 421m, 305m, 267s. ^{1}H NMR (300 K, $CDCl_3$): 7.1–7.9 (m). $^{31}P\{^1H\}$ NMR (300 K, $CH_2Cl_2/CDCl_3$): 35.0 (d) $^2J(^{31}P–^{89}Y) = 13$ Hz, -145(septet) PF_6^-. Λ_M (10^{-3} mol dm^{-3} CH_2Cl_2) = 21 Ω^{-1} cm^2 mol^{-1}.

3.3. $[YBr_2(Ph_3PO)_4]Br$

Prepared similarly to $[YCl_2(Ph_3PO)_4]Cl$. Yield: 52%. *Anal*. Found: C, 59.6; H, 4.2. Calc. for $C_{72}H_{60}Br_3O_4P_4Y$: C, 59.9; H, 4.2%. IR (cm^{-1}) (CsI disc): 1307m, 1188w, 1140vs (PO), 1119s, 1087s, 1084m, 998w, 973w, 763m, 693s, 543s, 449m, 417w, 305m, 262m. ^{1}H NMR (300 K, $CDCl_3$): 7.2–7.9 (m). $^{31}P\{^1H\}$ NMR (300 K, $CH_2Cl_2/CDCl_3$): 36.0 (d) $^2J(^{31}P–^{89}Y) = 11$ Hz. Λ_M (10^{-3} mol dm^{-3} CH_2Cl_2) = 20 Ω^{-1} cm^2 mol^{-1}.

3.4. $[YBr_2(Ph_3PO)_4]PF_6$

Prepared similarly to $[YCl_2(Ph_3PO)_4]PF_6$. Yield: 90%. *Anal*. Found: C, 57.9; H, 4.2. Calc. for $C_{72}H_{60}Br_2F_6O_4P_5Y$: C, 57.4; H, 4.2%. IR (cm^{-1}) (CsI disc): 3061w, 1439m, 1359w, 1191w, 1147vs (PO), 1123s, 1089s, 1029m, 1000m, 839vs, 750m, 726s, 693s, 559sh, 543s, 449m, 417m, 305m, 250w. ^{1}H NMR (300 K, $CDCl_3$): 7.2–7.9 (m). $^{31}P\{^1H\}$ NMR (300 K, $CH_2Cl_2/CDCl_3$): 36.0 (d) $^2J(^{31}P–^{89}Y) = 11$ Hz, -145(septet) PF_6^-. Λ_M (10^{-3} mol dm^{-3} CH_2Cl_2) = 19 Ω^{-1} cm^2 mol^{-1}.

3.5. $[YI_2(Ph_3PO)_4]I$

Prepared similarly to $[YCl_2(Ph_3PO)_4]Cl$ as a pale yellow solid. Yield: 38%. *Anal*. Found: C, 54.2; H, 3.8. Calc. for $C_{72}H_{60}I_3O_4P_4Y$: C, 54.6; H, 3.8%. IR (cm^{-1}) (CsI disc): 1485w, 1438m, 1359m, 1188w, 1136vs (PO), 1121s, 1083s, 1027w, 1000w, 749m, 725s, 696s, 543s, 460m, 449m, 421w, 299m. ^{1}H NMR (300 K, $CDCl_3$): 7.1–7.6 (m). $^{31}P\{^1H\}$ NMR (300 K, $CH_2Cl_2/CDCl_3$): 37.2 (d) $^2J(^{31}P–^{89}Y) = 11$ Hz. Λ_M (10^{-3} mol dm^{-3} CH_2Cl_2) = 25 Ω^{-1} cm^2 mol^{-1}.

3.6. $[YI_2(Ph_3PO)_4]PF_6$

Prepared similarly to $[YCl_2(Ph_3PO)_4]PF_6$ as pale yellow powder. Yield: 39%. *Anal*. Found: C, 53.8; H, 3.7. Calc. for $C_{72}H_{60}F_6I_2O_4P_5Y$: C, 54.0; H, 3.8%. IR (cm^{-1}) (CsI disc): 1486w, 1439m, 1359w, 1183w, 1144vs (PO), 1122s, 1087s, 1029w, 999m, 842vs, 753m, 725s, 696s, 559sh, 542s, 460m, 445m, 424m, 304m. ^{1}H NMR (300 K, $CDCl_3$): 7.4–7.8 (m). $^{31}P\{^1H\}$ NMR (300 K, $CH_2Cl_2/CDCl_3$): 37.5 (d) $^2J(^{31}P–^{89}Y) = 11$ Hz, -145(septet) PF_6^-. Λ_M (10^{-3} mol dm^{-3} CH_2Cl_2) = 23 Ω^{-1} cm^2 mol^{-1}.

3.7. $[YCl(Ph_3PO)_5][SbCl_6]_2$

Under a nitrogen atmosphere antimony pentachloride (0.05 g, 0.17 mmol) was added dropwise to a solution of $[YCl_2(Ph_3PO)_4]Cl$ (0.11 g, 0.08 mmol) in anhydrous CH_2Cl_2 (5 cm^3). A solution of Ph_3PO (0.02 g, 0.08 mmol) in CH_2Cl_2 (5 cm^3) was added, resulting in a milky suspension. The solution was concentrated to 5 cm^3, the white powder filtered off and dried in vacuo. Yield: 0.12 g, 56%. *Anal*. Found: C, 49.6; H, 3.3. Calc. for $C_{90}H_{75}Cl_{13}O_5P_5Sb_2Y$: C, 49.4; H, 3.5%. IR (cm^{-1}) (CsI disc): 2975w, 1484w, 1437m, 1357m, 1191w, 1141s (PO), 1121s, 1090m, 1027w, 995m, 745s, 692s, 543s, 347s($SbCl_6^-$). ^{1}H NMR (300 K, $CDCl_3$): 7.2–7.7 (m).

Λ_M (10^{-3} mol dm^{-3} CH_2Cl_2) = 42 Ω^{-1} cm^2 mol^{-1}.

3.8. $[YCl_2(Ph_3AsO)_4]Cl$

$YCl_3 \cdot 6H_2O$ (0.30 g, 1.0 mmol) and Ph_3AsO (1.28 g, 4.0 mmol) were dissolved in boiling EtOH (10 cm^3). Cooling to room temperature (r.t.) followed by refrigeration overnight resulted in white crystals, which were filtered off and dried in vacuo. Yield: 0.32 g, 20%. *Anal.* Found: C, 57.7; H, 3.9. Calc. for $C_{72}H_{60}As_4Cl_3O_4Y$: C, 58.3; H, 4.1%. IR (cm^{-1}) (CsI disc): 1440m, 1359m, 1186w, 1089m, 1071w, 1026w, 999w, 894vs (AsO), 744s, 693s, 553w, 481s, 376m, 365s, 273m, 260s. ^{1}H NMR (300 K, $CDCl_3$): 7.3–7.8. Λ_M (10^{-3} mol dm^{-3} CH_2Cl_2) = 31 Ω^{-1} cm^2 mol^{-1}.

3.9. $[YBr_2(Ph_3AsO)_4]Br$

Made similarly to the above. Yield: 55%. *Anal.* Found: C, 53.0; H, 3.8. Calc. for $C_{72}H_{60}As_4Br_3O_4Y$: C, 53.4; H, 3.7%. IR (cm^{-1}) (CsI disc): 1440m, 1359m, 1089m, 1071w, 1025w, 999w, 893vs (AsO), 744s, 691s, 478s, 368s, 338sh, 272m, 243m. ^{1}H NMR (300 K, $CDCl_3$): 7.2–7.8. Λ_M (10^{-3} mol dm^{-3} CH_2Cl_2) = 23 Ω^{-1} cm^2 mol^{-1}.

3.10. $[YI_2(Ph_3AsO)_4]I_5$

Made similarly as dark brown crystals. Yield: 25%. *Anal.* Found: C, 38.2; H, 2.9. Calc. for $C_{72}H_{60}As_4I_7O_4Y$: C, 38.1; H, 2.7%. IR (cm^{-1}) (CsI disc): 1484m, 1440m, 1360w, 1186w, 1088s, 1025w, 999m, 893vs (AsO), 740s, 691s, 477s, 457m, 367m, 356m, 273w, 244w. ^{1}H NMR (300 K, $CDCl_3$): 7.2–7.8. Λ_M (10^{-3} mol dm^{-3} CH_2Cl_2) = 41 Ω^{-1} cm^2 mol^{-1}.

3.11. $[Y(Me_3PO)_6]Cl_3$

An ethanolic solution (10 cm^3) of $YCl_3 \cdot 6H_2O$ (0.15 g, 0.5 mmol) was added to Me_3PO (0.28 g, 3.0 mmol) in EtOH (10 cm^3) and the solutions stirred for 1 h. Refrigeration gave a white precipitate. Yield: 0.34 g, 90%. *Anal.* Found: C, 28.9; H, 7.6. Calc. for $C_{18}H_{54}Cl_3O_6P_6Y$: C, 28.9; H, 7.2%. IR (cm^{-1}) (CsI disc): 2960w, 1423w, 1358w, 1299w, 1111vs, br (PO), 960m, 872m, 762m, 396m, 364w, 332m. ^{1}H NMR (300 K, d^3-$MeNO_2$): 1.60 (d) $^2J(^{31}P–^1H)$ = 14 Hz. Λ_M (10^{-3} mol dm^{-3} $MeNO_2$) = 225 Ω^{-1} cm^2 mol^{-1}.

3.12. $[Y(Me_3PO)_6]Br_3$

Boiling EtOH solutions (2 × 10 cm^3) of $YBr_3 \cdot 6H_2O$ (0.44 g, 1.0 mmol) and Me_3PO (0.37 g, 4.0 mmol) were mixed, resulting in a white suspension, which redissolved on shaking. Refrigeration of the resulting solution overnight deposited white needles. Yield: 0.39 g, 66%. *Anal.* Found: C, 24.2; H, 6.2. Calc. for $C_{18}H_{54}Br_3O_6P_6Y$: C, 24.5; H, 6.1%. IR (cm^{-1}) (CsI disc): 2962w, 2896w, 1358m, 1299m, 1111s,br (PO), 959s, 872m, 761m, 395s, 364m, 330m. ^{1}H NMR (300 K, d^3-$MeNO_2$): 1.69 (d) $^2J(^{31}P–^1H)$ = 13 Hz. Λ_M (10^{-3} mol dm^{-3} $MeNO_2$) = 207 Ω^{-1} cm^2 mol^{-1}.

3.13. $[Y(Me_3PO)_6]I_3$

A boiling EtOH solution (10 cm^3) of $YI_3 \cdot 8H_2O$ (0.31 g, 0.5 mmol) was added to a solution of Me_3PO (0.18 g, 2.0 mmol) resulting in a yellow suspension. The mixture was refrigerated overnight, the solid filtered off and dried in vacuo. Yield: 0.21 g, 50%. *Anal.* Found: C, 20.9; H, 5.4. Calc. for $C_{18}H_{54}I_3O_6P_6Y$: C, 21.2; H, 5.3%. IR (cm^{-1}) (CsI disc): 2964w, 2897w, 1421w, 1358m, 1299m, 1110s, br (PO), 957s, 871m, 761m, 396s, 364m, 331m. ^{1}H NMR (300 K, d^3-$MeNO_2$): 1.73 (d) $^2J(^{31}P–^1H)$ = 13 Hz. Λ_M (10^{-3} mol dm^{-3} $MeNO_2$) = 228 Ω^{-1} cm^2 mol^{-1}.

3.14. $[YCl_3(Ph_2MePO)_3]$

A solution of $YCl_3 \cdot 6H_2O$ (0.30 g, 1.0 mmol) in boiling EtOH (10 cm^3) was added to a solution of Ph_2MePO (0.22 g, 1.0 mmol) in EtOH (5 cm^3) and the mixture stirred for 1 h, then concentrated to approximately 5 cm^3 and refrigerated overnight. The white solid was filtered off and dried in vacuo. Yield: 0.28 g, 88%. *Anal.* Found: C, 54.5; H, 4.1. Calc. for $C_{39}H_{39}Cl_3O_3P_3Y$: C, 55.5; H, 4.7%. IR (cm^{-1}) (CsI disc): 1709w, 1641m, 1439m, 1363w, 1225w, 1148vs (PO), 1127m, 1101m, 999w, 896m, 783w, 752m, 696m, 614m, 515s, 306w, 254s. ^{1}H NMR (300 K, $CDCl_3$): 2.29 (br), 7.4–7.7 (m). Λ_M (10^{-3} mol dm^{-3} CH_2Cl_2) = 2 Ω^{-1} cm^2 mol^{-1}.

3.15. $[YBr_3(Ph_2MePO)_3]$

Made similarly to the above from a 1:3 molar ratio of $YBr_3 \cdot 6H_2O$: Ph_2MePO. Yield: 46%. *Anal.* Found: C, 48.2; H, 4.1. Calc. for $C_{39}H_{39}Br_3O_3P_3Y$: C, 47.9; H, 4.0%. IR (cm^{-1}) (CsI disc): 1591w, 1439m, 1358w, 1178sh, 1144vs (PO), 1127sh, 1098s, 998m, 894s, 782w, 750s, 720m, 694m, 515s, 503sh, 392w, 312w. ^{1}H NMR (300 K, $CDCl_3$): 2.18 (br), 7.3–7.7 (m). Λ_M (10^{-3} mol dm^{-3} CH_2Cl_2) = 7 Ω^{-1} cm^2 mol^{-1}.

3.16. $[YI_3(Ph_2MePO)_3]$

Prepared similarly using $YI_3 \cdot 8H_2O$ and Ph_2MePO in a 1:2 molar ratio, as a yellow powder. Yield: 28%. *Anal.* Found: C, 42.5; H, 3.7. Calc. for $C_{39}H_{39}I_3O_3P_3Y$: C, 41.9; H, 3.5%. IR (cm^{-1}) (CsI disc): 2896w, 1592w, 1439m, 1359w, 1178sh, 1140vs (PO), 1125s, 1093s,

1071m, 1029m, 996m, 895s, 786w, 749s, 720m, 696m, 519s, 478m, 421m, 383w. ^{1}H NMR (300 K, $CDCl_3$): 2.0 (d), 7.2–7.7 (m). Λ_M (10^{-3} mol dm^{-3} CH_2Cl_2) = 5 Ω^{-1} cm^2 mol^{-1}.

3.17. $[YCl_2(Ph_2MePO)_4]PF_6$

To a solution of $YCl_3{\cdot}6H_2O$ (0.15 g, 0.5 mmol) in boiling EtOH (10 cm^3) was added solid NH_4PF_6 (0.082 g, 0.5 mmol), and the mixture allowed to cool to r.t. A solution of Ph_2MePO (0.43 g, 2.0 mmol) in EtOH (5 cm^3) was added resulting in an immediate precipitate. After some hours this was filtered off, and dried in vacuo. Yield: 0.28 g, 43%. *Anal*. Found: C, 53.0; H, 4.4. Calc. for $C_{52}H_{52}Cl_2F_6O_4P_5Y$: C, 53.4; H, 4.5%. IR (cm^{-1}) (CsI disc): 1591w, 1486w, 1440m, 1305w, 1165sh, 1151s (PO), 1126m, 1101w, 1075w, 1031w, 1000m, 903s, 840s, 782s, 756s, 748s, 720m, 698s, 559s, 511s, 498s, 455m, 418m, 387w, 312m, 264s. ^{1}H NMR (300 K, $CDCl_3$): 1.92 (br), 7.2–7.7 (m). Λ_M (10^{-3} mol dm^{-3} CH_2Cl_2) = 20 Ω^{-1} cm^2 mol^{-1}.

3.18. $[Y(Me_3AsO)_6]Cl_3$

$YCl_3{\cdot}6H_2O$ (0.15 g, 0.5 mmol) was dissolved in boiling EtOH (10 cm^3) and a solution of Me_3AsO (0.41 g, 3.0 mmol) in EtOH (10 cm^3) added. The solvent was removed in vacuo, the oil remaining dissolved in cold C_3H_6O which on standing produced a colourless powder. Yield: 0.22 g, 43%. *Anal*. Found: C, 21.0; H, 5.2. Calc. for $C_{18}H_{54}As_6Cl_3O_6Y$: C, 21.3; H, 5.4%. IR (cm^{-1}) (CsI disc): 2896w, 1418m, 1359s, 1269m, 1097w, 925w, 877s, 648s, 344s, 285m. ^{1}H NMR (300 K, $CDCl_3$): 2.0(s). Λ_M (10^{-3} mol dm^{-3} $MeNO_2$) = 224 Ω^{-1} cm^2 mol^{-1}.

3.19. $[YCl_2(dppmO_2)_2]Cl$

To a solution of $YCl_3{\cdot}6H_2O$ (0.076 g, 0.25 mmol) in boiling EtOH (5 cm^3) an ethanolic solution (10 cm^3) of $dppmO_2$ (0.10 g, 0.25 mmol) was added, resulting in an immediate white precipitate. The mixture was left to stand for 1 h, the precipitate filtered off and dried in vacuo. Yield: 0.06 g, 47%. *Anal*. Found: C, 57.9; H, 4.4. Calc. for $C_{50}H_{44}Cl_3P_4O_4Y$: C, 58.4; H, 4.3%. IR (cm^{-1}) (CsI disc): 3042w, 1437m, 1410s, 1368m, 1167s (PO), 1120m, 1071w, 997w, 843s, 790s, 742m, 692m, 572w. ^{1}H NMR (300 K, $CDCl_3$): 2.2 (s), 7.2–7.8 (m). Λ_M (10^{-3} mol dm^{-3} CH_2Cl_2) = 21 Ω^{-1} cm^2 mol^{-1}.

3.20. $[YCl_2(ppO_2)_2]Cl$

Was made similarly to the above. Yield: 55%. *Anal*. Found: C, 62.9; H, 4.3. Calc. for $C_{60}H_{48}Cl_3P_4O_4Y$: C, 62.6; H, 4.2%. IR (cm^{-1}) (CsI disc): 2960w, 1439m, 1410s, 1359m, 1171br, s (PO), 1121m, 1073w, 1005w, 844m, 750s, 730s, 694s, 562s, 549s, 534m. ^{1}H NMR (300 K, $CDCl_3$): 7.2–7.8 (m). Λ_M (10^{-3} mol dm^{-3} CH_2Cl_2) = 19 Ω^{-1} cm^2 mol^{-1}.

3.21. Crystallography

Crystals of the Ph_3PO complexes were obtained by vapour diffusion from CH_2Cl_2/Et_2O in a refrigerator. $[Y(Me_3PO)_6]Br_3$ was obtained directly from the synthesis. Crystallographic details are shown in Table 5; data were collected on a Nonius–Kappa CCD diffractometer fitted with Mo Kα radiation and graphite monochromator and the cell dimensions were taken from the diffractometer software recognizing that the e.s.d. values are unreasonably small [18]. Structure solution and refinement were routine [19–21] and data processing used the SORTAV absorption correction [22]. Phenyl and methyl H atoms were introduced in calculated positions. During the structure solution for two of the compounds, solvent molecules appeared in the difference electron density maps and these were modelled. One EtOH molecule was given a reduced s.o.f. (0.5) in order to obtain adp's similar to the other EtOH molecules.

4. Conclusions

This study has shown that yttrium halides (X = Cl, Br or I) form complexes with phosphine oxides in ratios varying from 1:6 through 1:3 (although not all types form with each ligand), and there are similar complexes with R_3AsO. Only certain of these complexes have been isolated in the solid state. Solution studies have shown that often a mixture of species is present in equilibrium, the relative amounts being easily varied by addition of R_3EO. In spite of this, it is usually possible to crystallise a single pure species from these solutions. Contrary to the literature reports [9–11,14] and in contrast to the nitrate systems [7,8] all the halide complexes contain six-coordinate *pseudo*-octahedral yttrium. Fluxionality in solution was observed in the nitrate systems [7], but the NMR spectra of $[YX(Ph_3PO)_5]^{2+}$ cations show these are not fluxional. Fluxionality is relatively rare in six-coordinate species (except metal hydrides) and although the symmetry is too high in the cases of the other complexes to provide evidence one way or the other, it seems likely that all the halide complexes are stereochemically rigid in solution.

5. Supplementary material

Crystallographic data for the structures have been deposited with the Cambridge Crystallographic Data

Table 5
Crystallographic details [a]

Compound	$[Y(Me_3PO)_6]Br_3$	$[YCl_2(Ph_3PO)_4]Cl\cdot 2.5EtOH\cdot H_2O$	$[YBr_2(Ph_3PO)_4]PF_6\cdot Et_2O$
Molecular formula	$C_{18}H_{54}Br_3O_6P_6Y$	$C_{72}H_{60}Cl_3O_4P_4Y + C_5H_{17}O_{3.5}$	$C_{72}H_{60}Br_2F_6O_4P_5Y + C_4H_{10}O$
M_r	881.08	1441.53	1580.96
Temperature (K)	100	150	150
Crystal system	monoclinic	monoclinic	triclinic
Space group	$C2/c$ (no. 15)	$P2_1/c$ (no. 14)	$P\bar{1}$ (no. 2)
a (Å)	17.5730(9)	14.3599(3)	13.1913(1)
b (Å)	16.9269(9)	17.5316(4)	14.9556(2)
c (Å)	12.5446(7)	29.1891(7)	18.1360(2)
α (°)			98.1110(4)
β (°)	95.304(3)	97.748(1)	94.1310(4)
γ (°)			96.2750(8)
U (Å^3)	3715.5(3)	7281.3(3)	3506.99(6)
Z	4	4	2
μ (cm^{-1})	50.81	10.52	21.57
S	0.99	1.02	2.09
$F(000)$/e	1776	2996	1608
Total no. of observations	18 530	54 736	49 343
No. of unique observations (R_{int})	3787 (0.166)	13067 (0.099)	14107 (0.087)
Max/min transmission	0.788/0.694	0.875/0.743	0.864/0.760
No. of data in refinement	3787	13067	9456 ($I > 2\sigma(I)$)
No. of parameters	156	847	856
Residual electron density (e Å^{-3})	−0.78–0.84	−0.58–0.57	−1.58–2.33
R [$F_o > 4\sigma(F_o)$]	0.062 (2098 reflections)	0.068 (6746 reflections)	0.079 (9456 reflections)
R (all data)	0.144	0.166	
wR_2 (all data)	0.152	0.175	
wR [$F_o > 4\sigma(F_o)$]			0.086

$[R = \Sigma \, ||F_o| - |F_c|| / \Sigma \, |F_o|;\ wR_2 = [\Sigma \, w(F_o^2 - F_c^2)^2 / \Sigma \, wF_o^4]^{1/2};\ wR = [\Sigma \, w(F_o - F_c)^2 / \Sigma \, wF_o^2]^{1/2}]$.
[a] Common data: Mo Kα ($\lambda = 0.71073$ Å).

Centre (CCDC) and given numbers 173577–79 for compounds $[YCl_2(Ph_3PO)_4]Cl$, $[YBr_2(Ph_3PO)_4]PF_6$, $[Y(Me_3PO)_6]Br_3$, respectively. Copies of the data may be obtained free of charge from The Director, CCDC, 12 Union Road, Cambridge, CB2 1EZ, UK (fax: +44-1223-336033; e-mail: deposit@ccdc.cam.ac.uk or www: http://www.ccdc.cam.ac.uk).

Acknowledgements

We thank EPSRC for support and Professor M.B. Hursthouse for access to the Nonius–Kappa CCD diffractometer.

References

[1] W.J. Evans, M.S. Sollberger, Inorg. Chem. 27 (1988) 4417.
[2] S. Bambirra, D. van Leusen, A. Meetsma, B. Hessen, J.H. Teuben, Chem. Commun. (2001) 637.
[3] W.J. Evans, J.L. Shreeve, R.J. Doedens, Inorg. Chem. 32 (1993) 245.
[4] E.B. Coughlin, J.E. Bercaw, J. Am. Chem. Soc. 114 (1992) 7606.
[5] (a) D. Parker, Chem. Soc. Rev. 19 (1990) 271; (b) Y.H. Jang, M. Blanco, S. Dasgupta, D.A. Keire, J.E. Shively, W.A. Goddard, J. Am. Chem. Soc. 121 (1999) 6142 and references therein.
[6] J. Mason (Ed.), Multinuclear NMR, Plenum, New York, 1987.
[7] L. Deakin, W. Levason, M.C. Popham, G. Reid, M. Webster, J. Chem. Soc., Dalton Trans. (2000) 2439.
[8] W. Levason, B. Patel, M.C. Popham, G. Reid, M. Webster, Polyhedron 20 (2001) 2711.
[9] T.S. Lobana, in: F.R. Hartley (Ed.), The Chemistry of Organophosphorus Compounds, vol. 2, Wiley, New York, 1992, p. 409.
[10] E. Giesbrecht, Pure Appl. Chem. 51 (1979) 925.
[11] D.R. Cousins, F.A. Hart, J. Inorg. Nucl. Chem. 30 (1968) 3009.
[12] H.-K. Wang, M.-J. Zhang, X.-Y. Jing, J.-T. Wang, R.-J. Wang, H.-G. Wang, Inorg. Chim. Acta 163 (1989) 19.
[13] J.V. Kingston, E.M. Krankovits, R.J. Magee, Inorg. Nucl. Chem. Lett. 5 (1969) 485.
[14] H. Gehrke Jr., R. De Jong, Proc. S. Dak. Acad. Sci. 47 (1968) 210 (Chem. Abs. 71 (1969) 108605f).
[15] An extreme case is Ref. [11] which although entitled 'Complexes of yttrium and lanthanide chlorides and thiocyanates with triphenylarsine oxide and triphenylphosphine oxide' contains no further mention of yttrium chloride complexes, only those of Sm and Nd.
[16] B. Neumüller, R.M. Köcker, K. Dehnicke, Z. Krystallogr. 209 (1994) 90.
[17] I.R. Beattie, T. Gilson, K. Livingston, V. Fawcett, G.A. Ozin, J. Chem. Soc. A (1967) 712.
[18] F.H. Herbstein, Acta Crystallogr., Sect. B 56 (2000) 547.

[19] P.T. Beurskens, G. Admiraal, G. Buerskens, W.P. Bosman, S. Garcia-Granda, R.O. Gould, J.M.M. Smits, C. Smykalla, The DIRDIF program system, University of Nijmegen, 1992.
[20] TEXSAN for Windows, Single crystal structure analysis software, version 1.06, Molecular Structure Corporation, The Woodlands, TX, 1997–9.
[21] G.M. Sheldrick, SHELXL-97, Program for crystal structure refinement, University of Göttingen, 1997.
[22] R.H. Blessing, Acta Crystallogr., Sect. A 51 (1995) 33.

PERGAMON

Polyhedron 21 (2002) 457–464

POLYHEDRON

www.elsevier.com/locate/poly

2-Anilinopyridinate of Cu(I) and adducts of 2-anilinopyridine and metal acetates. Crystal structure of $Cu_2(\mu\text{-}OAc)_4(PhNHpy)_2$

José M. Seco [a], María J. González Garmendia [a,*], Elena Pinilla [b,c], María R. Torres [b]

[a] *Grupo de Química Inorgánica, Facultad de Ciencias Químicas, Universidad del País Vasco, UPV/EHU, Apartado 1072, E-20080 San Sebastian, Spain*

[b] *Laboratorio de Difracción de Rayos-X, Facultad de Ciencias Químicas, Universidad Complutense, E-28040 Madrid, Spain*

[c] *Departamento de Química Inorgánica, Facultad de Ciencias Químicas, Universidad Complutense, E-28040 Madrid, Spain*

Received 17 July 2001; accepted 6 December 2001

Abstract

The adducts of $M(OAc)_2{\cdot}nH_2O$ (M = Cu, Co, Ni, Zn) with 2-anilinopyridine, $M(OAc)_2(PhNHpy)$, have been synthesized and characterized. The X-ray crystal structure of $Cu_2(\mu\text{-}OAc)_4(PhNHpy)_2$ shows the dimer structure of $Cu_2(\mu\text{-}OAc)_4(H_2O)_2$ with the PhNHpy ligand in the axial positions of the water molecules. It is antiferromagnetic ($2J = -286\ cm^{-1}$). Signals of the triplet state are observed in its EPR spectrum and the zero field splitting parameter ($D = 0.33\ cm^{-1}$) has been calculated. The electronic spectra and the strong antiferromagnetism of the cobalt ($2J = -324\ cm^{-1}$) and nickel ($2J = -382\ cm^{-1}$) compounds allow to propose also a dimeric structure for them. By excess of ligand, in the anionic form, the Cu(I) compound Cu(PhNpy) was obtained for which a dinuclear structure with a lineal coordination in Cu(I) is proposed. © 2002 Elsevier Science Ltd. All rights reserved.

Keywords: 2-Anilinopyridine; Crystal structures; Antiferromagnetic dimers; Dinuclear acetates; Copper(I)

1. Introduction

The dinuclear copper(II) acetate dihydrate $[Cu_2(\mu\text{-}OAc)_4(H_2O)_2]$, with four bridging acetate groups and the water molecules in the axial positions, is one of the most studied dinuclear compounds of Cu(II) in the structural and magnetic aspects [1,2]. Also the adducts $[Cu_2(\mu\text{-}OAc)_4L_2]$ and $[Cu_2(\mu\text{-}O_2CR)_4L_2]$ with different ligands in the axial positions [3–6].

The hydrated acetates of cobalt(II) and nickel(II), $M(OAc)_2{\cdot}4H_2O$, are monomers and isostructurals [7]. The acetate groups are monodentate and two of them are coordinated to each metal atom. The octahedral coordination is completed by four water molecules. Intermolecular hydrogen bonds between non-coordinated oxygen atoms of the acetate groups and hydrogen atoms of water are involved in a tridimensional net. They have normal magnetic moments at room temperature. Among the carboxylate complexes of Co(II) and Ni(II) the dimer structures as that of $[Cu_2(\mu\text{-}OAc)_4L_2]$ are infrequent. The X-ray diffraction has confirmed this structure in $[M_2(\mu\text{-}O_2CPh)_4(quin)_2]$, for quin = quinoline and M = Co(II) [8] and Ni(II) [9]. These complexes are antiferromagnetic, unlike other compounds with the same components but different structure, as $[Co_3(O_2CPh)_6(quin)_2]$ [10].

In $Zn(OAc)_2{\cdot}2H_2O$ two bidentate acetate anions and two water molecules are coordinated to the zinc atom [11]. The hydrogen bonds are established in a bidimensional net.

The 2-anilinopyridine, (*N*-phenyl-2-pyridinamine, PhNHpy), is an asymmetrical ligand, with two nitrogen atoms in the 1,3 positions, which can coordinate as monodentate or bidentate. As monodentate ligand the coordination is established through the pyridinic nitrogen and as anionic bidentate through both nitrogen atoms [12,13]. In previous papers we reported the reaction between $[Cu_2(NN)_2(\mu\text{-}OH)_2]X_2{\cdot}nH_2O$, where *NN* = 2,2′-bipyridyl or 1,10-phenanthroline and X^- =

* Corresponding author. Tel.: +34-943-018208; fax: +34-943-212236.

E-mail address: qppgogam@sq.ehu.es (M.J. González Garmendia).

0277-5387/02/$ - see front matter © 2002 Elsevier Science Ltd. All rights reserved.
PII: S0277-5387(01)01015-4

PF_6^- or CLO_4^-, and PhNHpy. For $X^- = PF_6^-$ [14] each PhNHpy molecule is coordinated to a copper atom through the pyridinic nitrogen and the hydrogen bonded to the anilinic nitrogen is involved in an hydrogen bond with the oxygen atom of a bridging OH group. When $X^- = ClO_4^-$ [15] the ligand interacts with the medium (methanol) and a methylene group is inserted between the anilinic nitrogen atom and the bridging oxygen. The corresponding magneto–structural correlations were established for the resulting dinuclear complexes.

In this paper we describe the interaction between PhNHpy and the $M(OAc)_2{\cdot}nH_2O$ acetates (M = Cu, Co, Ni, Zn). The scope of substitution of AcO^- by the anionic ligand $PhNpy^-$ was unsuccessful and the Cu(I) compound CuPhNpy was obtained. The other adducts of PhNHpy, $M(OAc)_2$(PhNHpy) were obtained. Crystal structure of Cu(II) compound has been determined. Electronic spectra and magnetic and EPR results are also described and allow to make a structural proposition.

2. Experimental

2.1. Synthesis

The anionic form of PhNHpy was prepared, in situ. The ligand was dissolved in the minimal volume of absolute EtOH and metallic Na, in stoichiometric proportion, was added. The mixture was allowed to stand 15 min before using it [16].

2.1.1. Cu(PhNpy) (**1**)

A solution of anionic PhNHpy (5 mmol) in absolute EtOH (10 ml) was added to a solution of $Cu(OAc)_2{\cdot}H_2O$ (1 mmol) in MeOH (30 ml). The mixture was refluxed for 3 h and cooled at room temperature (r.t.). A yellow precipitate was formed. It was filtered off, washed with MeOH and dried by air suction.

Yield: 83%. m.p. (dec.) 262 °C. *Anal.* Found: C, 56.6; H, 3.9; Cu, 27.6; N, 11.9. Calc. for $C_{11}H_9CuN_2$: C, 56.8; H, 3.9; Cu, 27.3; N, 12.0%. Soluble in C_6H_6 and CH_2Cl_2 under nitrogen and slightly soluble in dimethylformamide.

2.1.2. Cu(OAc)$_2$(PhNHpy) (**2**)

A solution of PhNHpy (0.34 g, 2 mmol) in THF (10 ml) was added to $Cu(OAc)_2{\cdot}H_2O$ (0.20 g, 1 mmol) in THF (40 ml). The solution was stirred during 2 h and a precipitate was formed. The blue green precipitate was filtered off, washed with THF and dried in vacuo over $CaCO_3$.

Yield: 80%. m.p. (dec.) 262 °C. *Anal.* Found: C, 51.7; H, 4.5; Cu, 17.9; N, 7.7. Calc. for $C_{15}H_{16}CuN_2O_4$: C, 51.2; H, 4.6; Cu, 18.0; N, 8.0%. Soluble in dimethylformamide, $C_6H_5NO_2$, nitromethane and partially soluble in $CHCl_3$ and MeOH.

2.1.3. M(OAc)$_2$(PhNHpy), M = Co (**3**), Ni (**4**), Zn (**5**)

These complexes were synthesized according to the method described by Brookes and Martin [17] for the reaction of NiOAc with azaindole. A solution of PhNHpy (0.68 g, 4 mmol) in MeOH (10 ml) was added to a solution of $M(OAc)_2{\cdot}nH_2O$ (2 mmol) in MeOH (40 ml). The solution was stirred during 5 min and was concentrated to dryness in the rotavapor. The product was of colour garnet for Co, green for Ni and white for Zn. It was dissolved in $C_6H_5CH_3$ and heated at 100 °C during 45 min (30 min for the Zn compound). The precipitate formed was filtered off, washed with $C_6H_5CH_3$ and dried by air suction.

Compound ***3****:* Dark green powder. Yield: 79%. m.p. (dec.) 215 °C. *Anal.* Found: C, 51.8; H, 4.4; N, 8.5. Calc. for $C_{15}H_{16}CoN_2O_4$: C, 51.9; H, 4.6; N, 8.1%. Soluble in $C_6H_5NO_2$. Soluble in dimethylformamide, MeOH, EtOH and C_3H_6O with colour change from green to garnet. Partially soluble in $CHCl_3$.

Compound ***4****:* Light green powder. Yield: 60%. m.p. (dec.) 209 °C. *Anal.* Found: C, 51.2; H, 4.5; N, 78.3; Ni, 17.3. Calc. for $C_{15}H_{16}N_2NiO_4$: C, 51.9; H, 4.6; N, 8.1; Ni, 16.7%. Soluble in dimethylformamide and $C_6H_5NO_2$ and partially soluble in MeOH, EtOH and $CHCl_3$.

Compound ***5****:* White powder. Yield: 87%. m.p. (dec.) 172 °C. *Anal.* Found: C, 50.5; H, 4.4; N, 7.6; Zn, 18.7. Calc. for $C_{15}H_{16}N_2O_4Zn$: C, 50.9; H, 4.6; N, 7.9; Zn, 18.4%. Soluble in dimethylformamide, $C_6H_5NO_2$, MeOH and $CHCl_3$ (partially).

2.2. Measurements

C, H and N were analysed in a Perkin–Elmer 240C Elemental Analyser. Copper, Ni and Zn were measured with an Atomic Absorption Spectrophotometer Perkin–Elmer 2380, $\lambda = 324.8$, 232.0 and 213.9 nm, respectively. Melting points were measured on an Electrothermal 9300. Conductivity measurements were made using a Metrhom E518 conductometer. IR spectra were recorded on a Nicolet FT-IR 510 spectrometer in the range 4000–400 cm^{-1} using KBr pellets and on a Nicolet 740 in 650–50 cm^{-1} range using nujol on a polyethylene film. Mass spectrum was obtained on an VG Autospec instrument with the liquid secondary ion mass spectra technique (LSISM), using nitrobenzyl alcohol as matrix with the addition of trifluoroacetic acid. Cs^+ cations at 30 Kv were used. Electronic spectra were recorded on a Shimadzu UV-265 FW spectrophotometer.

Magnetic measurements were carried out with a magnetometer Manics DSM-8 or a SQUID MPMSXL of

Quantum Design. Diamagnetic corrections have been applied [2]. The EPR spectra were recorded on a Bruker ESP 300 spectrometer with a Bruker ER 035 M gaussmeter, and HP 5325B frequency counter.

2.3. Crystal structure determination

Prismatic single crystals of $C_{30}H_{32}Cu_2N_4O_8$ (**2**) were grown by layering MeOH solution of copper(II) acetate dihydrate, MeOH and ether solution of 2-anilinopyridine. The X-ray diffraction data were collected, at 296 K, on a Bruker Smart CCD diffractometer, with graphite-monochromated Mo Kα radiation ($\lambda =$ 0.71073 Å), operating in the ω and φ scanning mode. A summary of the crystallographic data, conditions used for the data collection and some refinement data are listed in Table 1.

Data were collected over and hemisphere of the reciprocal space by combination of the three exposure sets. Each exposure of 20 s covered 0.3 in ω. The first 50 frames were collected at the end of the data collection to monitor crystal decay. No appreciable drop in the intensities of standard reflections was observed.

The structure was solved by Patterson (Cu atoms) and conventional Fourier techniques and refined by full-matrix least-squares on F^2 [18]. All atoms were refined anisotropically. Hydrogen atoms were included in calculated positions and refined riding on the respective carbon atoms, with some exceptions. H(2) has been located in a Fourier synthesis, included and riding on a N bonded atom.

Table 1
Crystallographic and structure refinement data for [$Cu_2(\mu$-$O_2CCH_3)_4(PhNHpy)_2$] (**2**)

Empirical formula	$C_{30}H_{32}Cu_2N_4O_8$
Formula weight	703.68
Temperature (K)	296(2)
Wavelength (Å)	0.71073
Crystal system	monoclinic
Space group	$P2_1/n$
Unit cell dimensions	
a (Å)	11.3622(12)
b (Å)	7.5900(8)
c (Å)	17.9726(19)
β (°)	101.093(2)
V (Å^3)	1521.0(3)
Z	2
D_{calc} (g cm^{-3})	1.536
Absorption coefficient, μ (mm^{-1})	1.455
F (000)	724
Crystal size (mm)	$0.20 \times 0.20 \times 0.40$
θ Range for data collection (°)	1.96–23.29
Index ranges	(−12, −8, −19) to (11, 7, 19)
Reflections collected	6446
Independent reflections	2188 ($R_{int} = 0.0448$)
Completeness to $\theta = 23.29°$ (%)	99.6
Absorption correction	None
Refinement method	full-matrix least-squares on F^2
Data/restraints/parameters	2188/0/209
Final R indices [$I > 2\sigma(I)$]	$R_1 = 0.0365$ (obs. 1545)
R indices (all data)	$wR_2 = 0.0893$
Goodness-of-fit on F^2	0.904
Maximum residual (e^{-3})	0.39

$R_1 = \Sigma(|F_o| - |F_c|)/\Sigma|F_o|$; $wR_2 = \{\Sigma[w(F_o^2 - F_c^2)^2]/\Sigma[w(F_o^2)^2]\}^{1/2}$.

Table 2
Mass spectra results for Cu(PhNpy) (**1**), (L = PhNpy)

m/z	Ion	Relative intensity (%)
465	Cu_2L_2+1	3
403	CuLLH+1	42
233	CuL+1	75
171	LH+1	100
78	py^{+1}	13
63	Cu^{+1}	8

3. Results and discussion

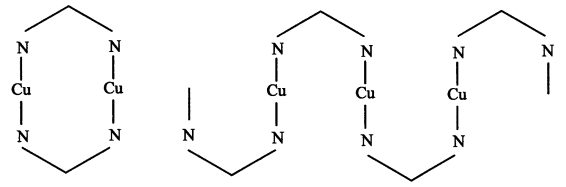
3.1. Characterization

The molar conductivity values for **1** in dimethylformamide and for **2**–**5** in methanol correspond to non-ionic compounds. The most significant band in the IR spectra is that assigned to the stretching ν(N–H) at approximately 3300 cm^{-1}. In compound **1** this band is not observed. This result confirms the presence of the anion $PhNpy^-$. In compounds **2**–**5** this band appears between 3274 and 3312 cm^{-1}, indicating the neutral form of the ligand.

In Table 2 are registered the mass spectra results for the Cu(I) compound. They agree with the dimeric structure of **1**. The most intense signals are those of LH + 1, CuL + 1 and CuLLH + 1, which can be generated in the matrix, from the dimer Cu_2L_2. The spectrum exhibits some signals for a mass higher than that of the dimer, but of very low intensity (< 1%). The corresponding cations can be due to molecular associations.

The electronic spectrum of **1** shows the ligand band at 280 nm and no d → d transition bands. The yellow colour is due to charge transfer. The compound is diamagnetic.

According to the coordination possibilities of the ligand and the ligand–metal ratio, the compound **1** may present a dimeric or a linear chain structure (Scheme 1). In both cases the Cu(I) cation adopts a linear coordination and the ligand, in the anionic form, acts as bridging bidentate through pyridine and aniline nitrogen atoms. The dimeric structure has been found in [$Cu_2(dab)_2$] (dab = diazoaminobenzene) [19], [$Cu_2(form)_2$] (form = *N*,*N*′-di-*p*-tolylformamidinato) [20] and [$Cu_2(hpp)_2$] (hppp = 1,3,4,6,7,8-hexahydro-2H-



Scheme 1. Dimer and linear chain disposition for Cu(PhNpy) (**1**).

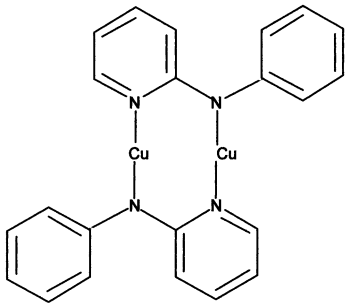


Fig. 1. Proposed structure for Cu(PhNpy) (**1**).

pyrimido[1,2-a]pyrimidinate) [21a]. In all three cases an eight members ring is formed, with a short Cu···Cu distance (2.45–2.50 Å) attributed to a combination of strong Cu–N bonding (1.86–1.94 Å) and very short bite distance for the ligands. In the ligand $PhNpy^-$ the relative position of the coordinating nitrogen atoms is the same that in the reported complexes and a similar dimeric structure is proposed (Fig. 1). The chain structure will be hindered by the steric effects between pyridine and phenyl groups of neighbouring ligands. The same dimeric structure has been proposed for $[Cu_2(MeNpy)_2]$ [21b].

3.2. Crystal structure of $[Cu_2(\mu\text{-}OOCCH_3)_4(PhNHpy)_2]$ (2)

Compound **2** consists of centrosymmetric dinuclear units, similar to other copper acetate derivates, in which four acetate groups are bridging the two copper atoms and a PhNHpy neutral ligand occupies the axial position of each copper atom, coordinated to them through the pyridine nitrogen atom. Fig. 2 shows an ORTEP view of the dimer geometry with 35% probability ellipsoids that includes the atom labelling. The hydrogen atoms have been omitted for clarity, only H(2) involved in an hydrogen bond is included. Selected interatomic distances and angles are listed in Table 3.

Each copper atom has a distorted square-planar pyramidal coordination, with four oxygen atoms in a plane, at an average distance of 1.971(3) Å; the fifth coordination position is occupied by the pyridine nitrogen, N(1), of a ligand molecule at 2.186(3) Å. The copper atom rises from the basal plane to the apical N(1) atom by 0.209(0.001) Å. The Cu···Cu separation is 2.6479(9) Å. The hydrogen atom, H(2), bonded to the anilinic nitrogen, N(2), is involved in an hydrogen bond to the oxygen, O(1), of an acetate group. Only two of the four acetate groups are involved in hydrogen bond.

The results are similar to those found for $[Cu_2(\mu\text{-}OAc)_4(H_2O)_2]$ [2] and other complexes, as the polymeric adduct of copper(II) acetate with 2-amonipyrimidine [22]. Hydrogen bonds of PhNHpy have been before described [12,14].

3.3. Electronic spectra

The dimethylformamide solution and diffuse reflectance spectral data are summarized in Table 4. The $\pi \rightarrow \pi^*$ band on the ligand, at 274 nm, which in the reflectance spectra presents a broad absorption in the 360–190 nm range, is reproduced in all the complexes.

For $[Cu_2(\mu\text{-}OAc)_4(PhNHpy)_2]$ in solution, the three expected bands are observed: (a) 700 nm for the $d \rightarrow d$ transitions; (b) 360 nm, characteristic of copper acetate dimer structure and which is not observed in analogue monomers; and (c) 300 nm for charge transfer [23,24].

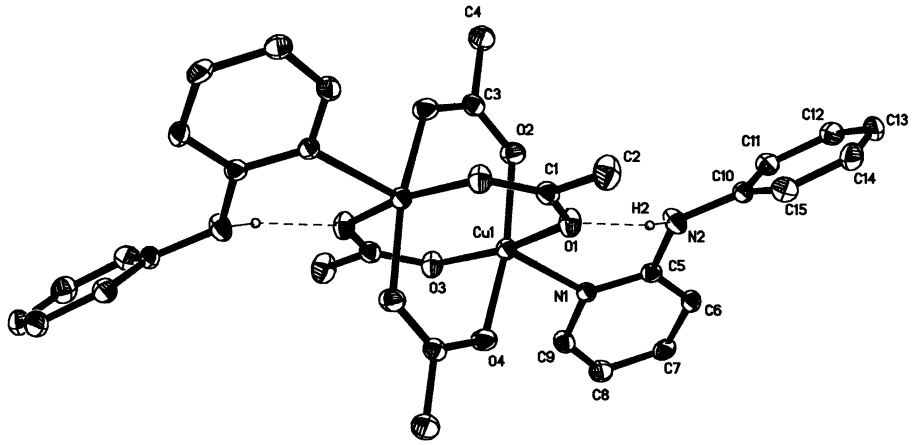


Fig. 2. ORTEP view of $[Cu_2(\mu\text{-}OAc)_4(PhNHpy)_2]$ (**2**).

Table 3
Selected interatomic distances (Å) and angles (°) for $[Cu_2(\mu\text{-}OOCCH_3)_4(PhNHpy)_2]$ (**2**)

Interatomic distances	
Cu(1)–O(2)	1.969(3)
Cu(1)–O(4)	1.964(3)
Cu(1)–O(3)	1.976(3)
Cu(1)–O(1)	1.974(3)
Cu(1)–N(1)	2.186(3)
Cu(1)···Cu(1)*	2.6479(9)
O(1)–C(1)	1.268(5)
N(1)–C(5)	1.349(5)
N(1)–C(9)	1.344(5)
C(1)–C(2)	1.499(6)
O(2)–C(3)	1.252(5)
N(2)–C(5)	1.385(5)
N(2)–C(10)	1.417(5)
C(3)–C(4)	1.505(6)
C(5)–C(6)	1.400(5)
C(6)–C(7)	1.371(6)
C(7)–C(8)	1.385(6)
C(8)–C(9)	1.359(6)
C(10)–C(11)	1.383(6)
C(10)–C(15)	1.392(6)
C(11)–C(12)	1.391(6)
C(12)–C(13)	1.376(6)
C(13)–C(14)	1.373(6)
C(14)–C(15)	1.376(6)
Bond angles	
O(2)–Cu(1)–O(4)	167.6(1)
O(2)–Cu(1)–O(3)	89.4(1)
O(4)–Cu(1)–O(3)	90.0(1)
O(2)–Cu(1)–O(1)	88.4(1)
O(4)–Cu(1)–O(1)	89.5(1)
O(3)–Cu(1)–O(1)	168.0(1)
O(2)–Cu(1)–N(1)	98.4(1)
O(4)–Cu(1)–N(1)	94.0(1)
O(3)–Cu(1)–N(1)	95.7(1)
O(1)–Cu(1)–N(1)	96.3(1)
O(2)–Cu(1)–Cu(1)*	84.24(8)
O(4)–Cu(1)–Cu(1)*	83.38(8)
O(3)–Cu(1)–Cu(1)*	83.97(8)
O(1)–Cu(1)–Cu(1)*	84.03(8)
Hydrogen bond	
N(2)–H(2)	0.95
H(2)···O(1)	1.99
N(2)···O(1)	2.912(4)
N(2)–H(2)–O(1)	162.7

Symmetry transformations used to generate equivalent atoms: *, $-x+2, -y+2, -z$.

The cobalt compound **3** changes colour from green (solid) to pink (solution). The solution spectrum may be explained in basis to an octahedral coordination. The absorption at 540 nm is assigned to the $^4T_{1g}(F) \rightarrow {}^4T_{1g}(P)$ transition. Of the three possible transitions for a d^7 high spin state: $^4T_{1g}(F) \rightarrow {}^4T_{2g}(F)$, $^4T_{1g}(F) \rightarrow {}^4A_{2g}(F)$ and $^4T_{1g}(F) \rightarrow {}^4T_{1g}(P)$, the first is of low energy and can be not observed and the second is a transition of two electrons (Scheme 2).

The diffuse reflectance spectrum corresponds to a d^7 high spin ion in a square-pyramidal (C_{4v}) environment [25]. The spectrum is similar to those described for the dimer $[Co_2(\mu\text{-}O_2CPh)_4(quin)_2]$ [10]. The transition $^4A_2 \rightarrow {}^4E$ ($^4T_{2g}$) can be of lower energy than the limit of the spectrophotometer (900 nm). The bands at 730, 585 and 440 nm are assigned to the transition to $^4B_1$, ^4E ($^4T_{1g}$) and $^4A_2$ ($^4T_{1g}$), respectively. The shoulders at 530 and 370 nm may be due to transitions to levels of the ^2G and ^2F free ion terms, respectively.

The reflectance spectrum of the nickel compound **4** is similar to those of $[Ni_2(\mu\text{-}O_2CPh)_4(quin)_2]$ [9]. Scheme 3 shows the splitting of the $T(O_h)$ levels for a d^8 ion, in a square-pyramidal symmetry (C_{4v}). The transitions to $^3E[^3T_{2g}(F)]$, $^3B_2[^3T_{2g}(F)]$, and $^3A_2[^3T_{1g}(F)]$ are of low energy. The band at 690 nm is assigned to the $^3B_1 \rightarrow {}^3E[^3T_{1g}(F)]$ transition and the band at 410 nm to the non-resolved transitions to $^3A_2$ and ^3E levels of $^3T_{1g}(P)$. The solution spectrum is similar. The shoulder at 740 nm can be assigned to the spin forbidden $^3A_{2g} \rightarrow {}^1E_g$ transition, which frequently is observed near the $^3A_{2g} \rightarrow {}^3T_{1g}(F)$ transition when Dq/B is close to one. In this case, the assumption of 687 and 400 nm as the $^3A_{2g} \rightarrow {}^3T_{1g}(F)$ and $^3A_{2g} \rightarrow {}^3T_{1g}(P)$ transitions, respectively, allows to estimate the values $Dq = 830\ cm^{-1}$ and $B = 850\ cm^{-1}$ ($Dq/B = 0.98$). The absorption at 300 nm is assigned to charge transfer between metal and acetates.

For the zinc compound **5** only the ligand band and the charge transfer between metal and acetates are observed.

3.4. Magnetic results

Compounds of Cu(I), (**1**), and Zn(II), (**5**), are diamagnetic. Other three compounds **2**, **3** and **4** are antiferromagnetic.

The plots of $\chi_M T$ versus temperature (T) for compound **2** are shown in Fig. 3. The data, between 14 and 300 K, were fitted to the Bleaney–Bowers equation for a dimer with $S_1 = S_2 = 1/2$, modified by the inclusion of the fraction of monomeric impurity [26]:

$$\chi_M = [Ce^x(1-\rho)/(1+3e^x)] + C\rho/4 + N\alpha$$

where $C = Ng^2\beta^2/kT$, $x = 2J/kT$, ρ is the fraction of monomeric impurity and $N\alpha$ is the temperature independent paramagnetism (TIP). The results of the best fit for $g = 2.16$ (EPR result) and $N\alpha = 60 \times 10^{-6}\ cm^3\ mol^{-1}$ are collected in Table 5. The $2J$ value, indicating a significant antiferromagnetic intradimer interaction, is similar to the values found in other adducts of copper acetate [27,28].

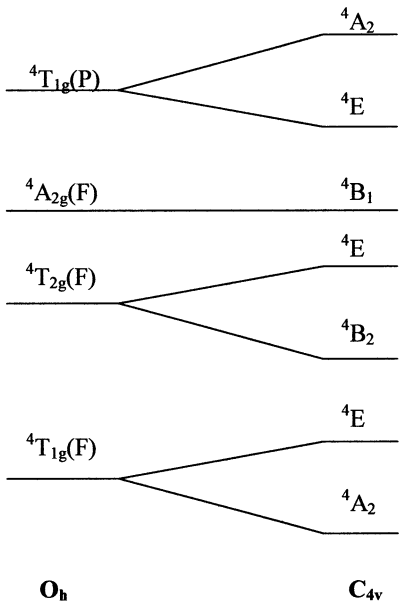
For Co(II) (**3**) and Ni(II) (**4**) complexes, a strong antiferromagnetic effect is observed. The magnetic moment decreases with decreasing temperature, from 3.03 (287 K) to 0.75 MB (4 K) for **3** and from 2.16 (293 K) to 1.24 MB (14 K) for **4**. This effect is still stronger than the found in other dimeric carboxylate complexes

Table 4
Electronic spectral data

Compound	λ_{max} (nm), in dimethylformamide	ε_{max} (l mol^{-1} cm^{-1})	λ (nm), diffuse reflectance
PhNHpy	274	25 900	360–190
2	700	193	725
	360	810	380
	300	10 030	310–190
	275	26 600	
3	540	39	730
	310	(sh)	585
	275	24 000	530(sh)
			440
			370(sh)
			360–190
			274
4	740	(sh)	690
	687	50	410
	400	230	310–190
	310	9440	
	274	24 000	
5	310	8000	380–190
	272	19 860	

sh, shoulder.

of Co(II) and Ni(II) [9,10,29]. These results are interpreted in basis to a dimeric structure, with an intramolecular interaction between the cations through the bridging acetate groups. The plots of $\chi_M T$ versus T (Fig. 4) have been fitted using the application of the Van Vleck equation to each case [30]. These are, with



Scheme 2. Level splitting for d^7, high spin configuration, in C_{4v} symmetry.

$C = Ng^2\beta^2/kT$, $x = 2J/kT$ and $\rho =$ fraction of monomeric impurity, for cobalt(II) dimer ($S_1 = S_2 = 3/2$):

$$\chi_M = C[e^x + 5e^{3x} + 14e^{6x}](1-\rho)/[1 + 3e^x + 5e^{3x} + 7e^{6x}] + 5C\rho/4 + N\alpha$$

for nickel(II) dimer ($S_1 = S_2 = 1$):

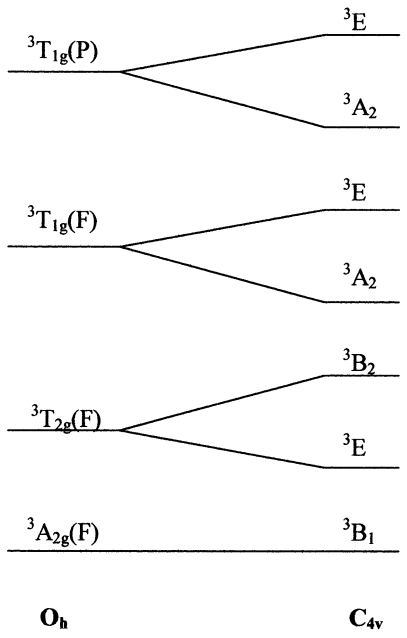
$$\chi_M = C[e^x + 5e^{3x}](1-\rho)/[1 + 3e^x + 5e^{3x}] + 2C\rho/3 + N\alpha$$

The results of these fittings in the range 50–300 K, with $N\alpha = 60 \times 10^{-6}$ and 100×10^{-6}, for **3** and **4**, respectively, are summarized in Table 5.

The magnetic behaviour below 50 K may be complicated by zero field splitting effects, especially in nickel compound, and other possible intermolecular interactions. The lack of knowledge of the crystal structure prevents us to make a more accurate interpretation. The conjunction of electronic spectra and magnetic results lets suppose a dimeric structure for the compounds **3** and **4**, $[M_2(\mu\text{-}OAc)_4(PhNHpy)_2]$, similar to one of Cu(II) compound.

3.5. EPR spectra

The powder EPR spectra of **2** in Q band, at room temperature, shows the typical signals of the triplet state ($S = 1$) for $D \neq 0$ and $E \approx 0$ (Fig. 5). The spectra were interpreted according to the Wasserman, Snyder and Yager equations [31,32], based on the Hamiltonian



Scheme 3. Level splitting for d^8 configuration in C_{4v} symmetry.

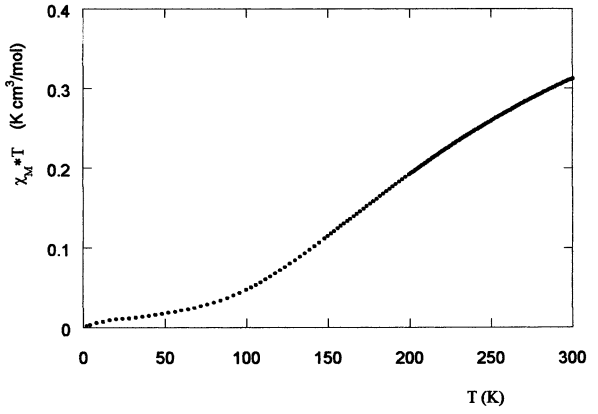


Fig. 3. Plot of χT versus T for **2**.

Table 5
Magnetic results

Compound	g	$2J$ (cm^{-1})	ρ	R^a
2	2.12	−286 [b]	0.0083	7.85×10^{-5}
3	4.27	−324 [c]	0.020	2.46×10^{-4}
4	2.78	−382 [d]	0.119	4.45×10^{-4}

[a] $R=\Sigma(\chi T_{iexp}-\chi T_{ical})^2/\Sigma(\chi T_{iexp})^2$.
[b] Calculated from $\chi_M=[Ce^x(1-\rho)/(1+3e^x)]+C\rho/4+N\alpha$.
[c] Calculated from $\chi_M=C[e^x+5e^{3x}+14e^{6x}]\ (1-\rho)/[1+3e^x+5e^{3x}+7e^{6x}]+5C\rho/4+N\alpha$.
[d] Calculated from $\chi_M=C[e^x+5e^{3x}]\ (1-\rho)/[1+3e^x+5e^{3x}]+2C\rho/3+N\alpha$.

$\mathcal{H}=gHS\beta+D[S_z^2-2/3]+E[S_x^2-S_y^2]$, with $D\neq0$ y $E=0$. For $\Delta M=\pm1$:

$$H_{\parallel}=(g_e/g_{\parallel})(H_o-D')$$

$$H_{\perp1}=(g_e/g_{\perp})[H_o(H_o-D')]^{1/2}$$

$$H_{\perp2}=(g_e/g_{\perp})[H_o(H_o+D')]^{1/2}$$

For $\Delta M=\pm2$:

$$H_{min}=(g_e/g_{min})[(H_o^2/4)-(D'^2/3)]^{1/2}$$
$$H_{dq}=(g_e/g_{av})[H_o^2-D'^2/3]^{1/2}$$

$$H_o=h\nu/g_e\beta;\ D'=D/g_e\beta$$

From the experimental values: $H_{min}=4896$; $H_{\parallel}=7262$; $H_{\perp1}=9755$; $H_{\perp2}=13\,317$ and $H_{dq}=11\,035$ G, the following parameters have been calculated: $g_{\parallel}=2.33$; $g_{\perp}=2.07$; $g_{av}=2.16$ and $D=0.33$ cm^{-1}. These results agree with the results found for analogue compounds [23,28].

4. Supplementary material

Crystallographic data for the structural analysis have been deposited with the Cambridge Crystallographic Data Centre, CCDC No. 167019 for compound **2**. Copies of this information may be obtained free of charge from The Director, CCDC, 12 Union Road,

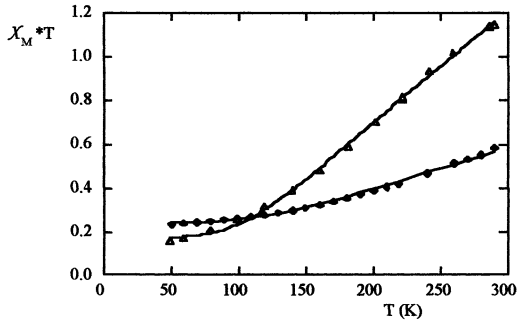


Fig. 4. Temperature dependence of χT for **3** (△) and **4** (◆).

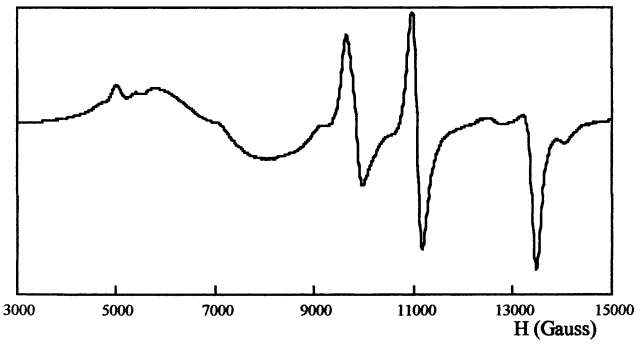


Fig. 5. EPR Q band spectrum of powdered $[Cu_2(\mu\text{-}OAc)_4(PhNHpy)_2]$ (**2**), at room temperature.

Cambridge, CB2 1EZ, UK (fax: +44-1223-336033; e-mail: deposit@ccdc.cam.ac.uk or www: http://www.ccdc.cam.ac.uk).

Acknowledgements

This work was supported by the 'Diputación Foral de Gipuzkoa'.

References

[1] P. De Meester, S.R. Fletcher, A.C. Skapski, J. Chem. Soc., Dalton Trans. (1973) 2575.
[2] R.L. Carlin, Magnetochemistry, Springer, Berlin Heidelberg, 1986.
[3] J. Catterick, P. Thornton, Adv. Inorg. Chem. Radiochem. 20 (1977) 291.
[4] R.J. Doedens, Progr. Inorg. Chem. 21 (1976) 209.
[5] V.M. Rao, D.N. Sathyanarayana, H. Manohar, J. Chem. Soc., Dalton Trans. (1983) 2167.
[6] M. Nakagawa, Y. Inomata, F.S. Howell, Inorg. Chim. Acta 295 (1999) 121.
[7] J.N. Van Niekerk, F.R.L. Schoening, Acta Crystallogr. 6 (1953) 609.
[8] J. Catterick, M.B. Hursthouse, P. Thornton, A.J. Welh, J. Chem. Soc., Dalton Trans. (1977) 223.
[9] A. Bencini, C. Benelli, D. Gatteschi, C. Zanchini, J. Am. Chem. Soc. 102 (1980) 5820.
[10] J. Catterick, P. Thornton, J. Chem. Soc., Dalton Trans. (1976) 1634.
[11] J.N. Van Niekerk, F.R.L. Schoening, Acta Crystallogr. 6 (1953) 720.
[12] A.R. Chakravarty, F.A. Cotton, Inorg. Chim. Acta 105 (1985) 19.
[13] D. Barr, W. Clegg, R.E. Mulvey, R. Snaith, J. Chem. Soc., Chem. Commun. (1984) 469.
[14] J.M. Seco, U. Amador, M.J. González Garmendia, Polyhedron 18 (1999) 3605.
[15] J.M. Seco, U. Amador, M.J. González Garmendia, Inorg. Chim. Acta 303 (2000) 256.
[16] D.A. Tocher, J.H. Tocher, Polyhedron 5 (1986) 1615.
[17] R.W. Brookes, R.L. Martin, Aust. J. Chem. 27 (1974) 1569.
[18] G.M. Sheldrick, 'SHELXL-97. A Program for Refinement of Crystal Structure', University of Göttingen. 1977.
[19] I.D. Brown, J.D. Dunitz, Acta Crystallogr. 14 (1961) 480.
[20] F.A. Cotton, X. Feng, M. Matusz, R. Poli, J. Am. Chem. Soc. 110 (1988) 7077.
[21] (a) F.A. Cotton, X. Feng, D.J. Timmons, Inorg. Chem. 37 (1998) 4066;
(b) H. Aghabozorg, H. Hosseini-Monfarred, Iran. J. Chem. Chem. Eng. 14 (1995) 6.
[22] G. Smith, C.H. Kennard, K.A. Byriel, Polyhedron 8 (1991) 873.
[23] F. Sapiña, M. Burgos, E. Escriva, J.V. Folgado, D. Beltrán, P. Gómez Romero, Inorg. Chim. Acta 216 (1994) 185.
[24] B.J. Edmonson, A.B.P. Lever, Inorg. Chem. 4 (1965) 1608.
[25] A.B.P. Lever, Inorganic Electronic Spectroscopy, 2nd ed., Elsevier, 1984.
[26] M. Nakashima, M. Mikuriya, Y. Muto, Bull. Chem. Soc. Jpn. 58 (1985) 968.
[27] M. Melník, Coord. Chem. Rev. 42 (1982) 259.
[28] J.S. Valentine, A.J. Silverstein, Z.G. Soos, J. Am. Chem. Soc. 96 (1974) 97.
[29] J. Catterick, P. Thornton, J. Chem. Soc., Dalton Trans. (1975) 233.
[30] C.J. O'Connor, Progr. Inorg. Chem. 29 (1982) 203.
[31] E. Wasserman, L.C. Snyder, W.A. Yager, J. Chem. Phys. 41 (1964) 1763.
[32] A. Bencini, D. Gatteschi, EPR of Exchange Coupled Systems, Springer, Berlin, 1990.

PERGAMON

Polyhedron 21 (2002) 465

POLYHEDRON

www.elsevier.com/locate/poly

Foreword

Polyhedron Symposia-in-Print, number 24
Subvalent and multiply bonded compounds of the p-block elements

Two of the more interesting areas of development in the chemistry of the p-block elements over recent years have been concerned with their subvalent and multiply bonded complexes. In particular, much emphasis has been given to the heavier elements due to the existence of the so-called 'classical double bond rule' which states that compounds featuring (p–p)π-bonds between the heavier main-group elements would not be stable, in contrast to the numerous examples that are known for the lighter elements, carbon, nitrogen and oxygen. Synthetic chemists have, however, faced the challenge presented by the 'classical double bond rule' and have been successful in isolating many novel species that exhibit multiple bonding between the heavier elements. Likewise, theoretical chemists have addressed the nature of the bonding in such complexes. The latter is an area that is not without controversy, clearly emphasizing the current interest in the topic. Subvalent complexes have a close relationship to multiply bonded derivatives in that they are frequently the synthetic precursors to multiply bonded complexes. The present Symposium-in-Print serves to provide a forum for discussing various aspects of the chemistry of these interesting subvalent and multiply bonded complexes and related derivatives metal–metal bonds.

G. Parkin
Department of Chemistry (Box 3115), Columbia University, New York, NY 10027, USA
E-mail: parkin@chem.columbia.edu

0277-5387/02/$ - see front matter © 2002 Published by Elsevier Science Ltd.
PII: S0277-5387(02)00862-8

PERGAMON

Polyhedron 21 (2002) 467–472

POLYHEDRON

www.elsevier.com/locate/poly

Multiple bonds to silicon: 20 years later

Robert West *

Organosilicon Research Center, Department of Chemistry, University of Wisconsin, Madison, WI 53706 USA

Received 15 May 2001; accepted 7 December 2001

Abstract

The discovery of stable compounds containing Si=C and Si=Si bonds in 1981 led to the overturning of the 'double bond rule', and paved the way for the recent explosive growth in multiple bond chemistry of the heavier elements. This paper traces the events leading up to the 1981 discoveries, summarizes some of the developments in multiply-bonded silicon chemistry since that date, and outlines challenges for further research in this area. © 2002 Elsevier Science Ltd. All rights reserved.

Keywords: Disilenes; Silenes; Silanones; Matrix isolation; Photolysis

1. Introduction

Silicon is the immediate congener to carbon, which forms multiple bonds in profusion. The search for multiply-bonded silicon therefore attracted the attention of chemists throughout the twentieth century. The pioneer organosilicon chemist, F.S. Kipping of the University of Nottingham, carried out extensive attempts to make compounds with Si=C, Si=O and Si=Si bonds. At one point, he believed he had synthesized a disilene, Ph(Et)Si=Si(Et)Ph [1]. However, later physical and chemical studies showed that not only this, but all of the compounds obtained in his studies were singly-bonded oligomers or polymers and not the sought for multiply-bonded compounds. Kipping eventually concluded that multiple bonds to silicon were not possible [2,3].

Similar negative results were obtained by other workers who attempted to make multiply-bonded compounds of elements outside the first row of the periodic table, including phosphorus, arsenic, antimony, and germanium [4]. Early theoretical papers by Pitzer [5] and Mulliken [6] rationalized these results, showing that π bonds between heavier elements should be weak. The combined experimental and theoretical results led to the consensus embodied in the 'double bond rule', which stated that elements with a principal quantum number greater than 2 do not form multiple bonds with themselves or with other elements [7]. This was the view expressed in most chemistry textbooks until the 1980s.

A major breakthrough came in 1981. At the 15th Organosilicon Symposium in Durham, NC, companion papers announcing stable compounds containing Si=C [8] and Si=Si [9] bonds were presented; and shortly thereafter Yoshifuji and coworkers reported the synthesis of a stable diphosphene, Mes*P=PMes* [10]. These findings led to decisive overturning of the double bond rule. The resulting paradigm shift paved the way for the remarkable flowering of multiple bond chemistry of the heavier elements which continues to the present day.

The first sections of this paper describe retrospectively the events leading up to the syntheses of stable silenes (Si=C) and disilenes (Si=Si). In later sections, some of the developments since 1981 in the multiple bond chemistry of silicon are recounted, and challenges for future researchers are presented.

Many useful reviews on multiply-bonded silicon compounds are available [11,12]. The early history is covered in some detail in a 1979 review by Gusel'nikov and Nametkin [12a].

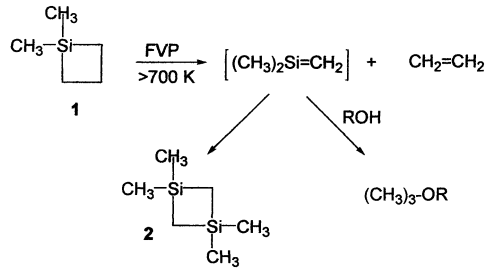
* Corresponding author. Tel.: +1-608-262-1873; fax: +1-608-262-6143.

E-mail address: west@chem.wisc.edu (R. West).

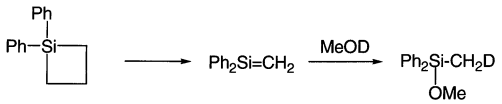
0277-5387/02/$ - see front matter © 2002 Elsevier Science Ltd. All rights reserved.
PII: S0277-5387(01)01017-8

2. The discovery of a stable silene

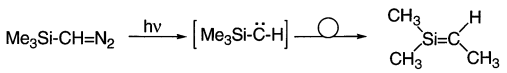
The synthesis of molecules with novel types of chemical bonding often follows a common progression. First, evidence is presented for the species as a transient intermediate in chemical reactions. Next, it may be isolated at very low temperatures, in a matrix, for example. Finally, with appropriate steric or electronic stabilization, a molecule stable at room temperature may be synthesized. Just such a sequence was followed in the discovery of stable silenes.



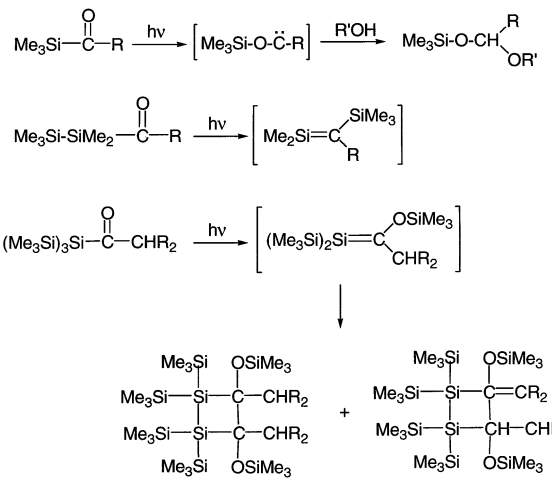
Scheme 1.



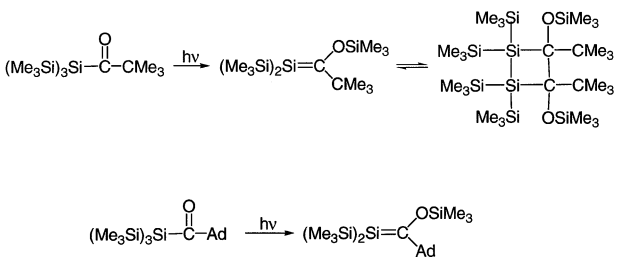
Scheme 2.



Scheme 3.



Scheme 4.



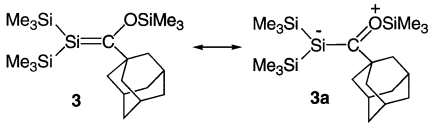
Scheme 5.

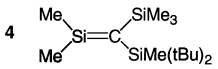
The first convincing evidence for silenes as reaction intermediates came in 1966 from studies of the gas-phase thermolysis of 1,1-dimethyl-1-silacyclobutane (**1**) by Gusel'nikov and coworkers [13]. At 700–1000 K and low pressures, **1** fragments cleanly. The products are ethane and 1,1,3,3-tetramethyl-1,3-disilacyclobutane (**2**), the latter arising from the dimerization of the intermediate silene (Scheme 1). The kinetics of the reaction are strikingly similar to those for the gas-phase thermolysis of dialkylcyclobutanes into alkenes [14]. Furthermore the intermediate silene could be intercepted by various trapping agents. For instance, as shown in Scheme 1, addition of alcohols to the pyrolysis stream produced the corresponding alkoxysilanes. Later, Boudjouk and Sommer showed that photolytic fragmentation of cyclobutanes could also produce transient silenes (Scheme 2) [15].

The next development was the isolation of unstable silylenes in an argon matrix, at 10–20 K. This was accomplished almost simultaneously by three different groups. Mal'tsev and coworkers employed the thermolysis of **1**, trapping the products by condensation in argon [16]. The two other groups both used the photolysis of trimethylsilyldiazomethane to generate a silyl carbene, which rearranged to the silene (Scheme 3) [17,18]. These experiments allowed the infrared spectrum of silenes to be determined, and a band near 1000 cm^{-1} was identified as the C=Si stretching mode.

We proceed now to the final step: the actual isolation of a stable silene. During the 1960s and 1970s, photolysis of acylsilanes (organosilyl ketones) was under investigation in Adrian Brook's laboratories at the University of Toronto. The usual reaction involved rapid reversible rearrangement of silicon from carbon to oxygen, producing a siloxycarbene, which could be intercepted by various trapping agents (Scheme 4) [19]. The question then arose: What would happen in the case of an acyldisilane? A 1,2 rearrangement would produce a disiloxycarbene, but a 1,3 rearrangement would lead to a silene, as shown in Scheme 4.

Experiments showed that the 1,3 rearrangement is favored. The next step was to carry out the photolysis with acylpolysilanes, $(Me_3Si)_3Si–CO–R$. When R is small, methyl, phenyl etc., the product observed is a linear or cyclic, head-to-head dimer of the silene [20]. When R is *t*-butyl, photolysis produced an equilibrium mixture of silene and cyclic dimer [21]. Finally, with R = 1-adamantyl, the stable, crystalline silene **3** is produced [22] (Scheme 5).





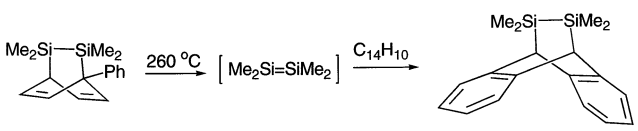
The X-ray crystal structure of **3** gave a value of 176.4 pm for the Si=C bond length, somewhat longer than the theoretically predicted value of ~170 pm. The bond lengthening arises from ylidic electron donation from the siloxy oxygen into the Si–C π bond, as illustrated by the resonance form **3a**. Subsequently the non-ylidic silene **4** was synthesized by Wiberg and his group, by a route involving lithium fluoride elimination, and shown to have a normal Si=C bond length of 170.2 ppm [23].

3. A stable disilene

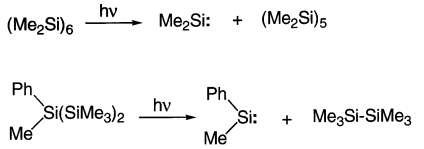
The pathway which actually led to the discovery of stable disilenes involved only the first antecedent step, the identification of disilenes as transient intermediates. A classic, convincing study was carried out by Peddle and Roark in 1972 [24]. Pyrolysis of a 7,8-disilabicycloocta-2,5-diene led to retrodiene fragmentation to give tetramethyldisilene, which could be trapped by naphthalene, anthracene or 1,4-diphenyl-1,3-butadiene. The reaction with anthracene is illustrated in Scheme 6.

Investigations in this area by our group at the University of Wisconsin began in a collaboration with Josef Michl, then at the University of Utah [25]. We thought of combining our experience with organosilicon compounds with his expertise in matrix isolation of unstable species, to obtain matrix-isolated disilenes. A graduate student, Tim Drahnak, traveled from Madison to Utah with the plan to solve this problem by isolating tetramethyldisilene, produced through metal-induced, flow dehalogenation of 1,2-dihalodisilanes, $Me_2SiX–SiXMe_2$. However, attempts to do this were dismally unsuccessful. If the desired disilene ever formed, it did not survive long enough to be captured on the cold surface.

Since this investigation gave no useful results, we turned our attention to diorganosilylenes, R_2Si:. Previously, Kumada and Ishikawa had shown that transient



Scheme 6.



Scheme 7.

silylenes were formed in the photolysis of cyclic or linear polysilanes, as shown in Scheme 7 [26], although they had not been detected. Drahnak carried out the photolysis of $(Me_2Si)_6$ in argon at ~10 K, which was immediately successful and provided the first direct observation of the important intermediate, Me_2Si:. This allowed studies of its electronic and IR spectra to be carried out [27].

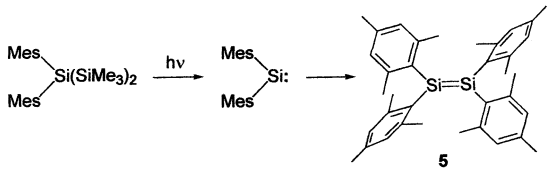
Eventually at Wisconsin silylenes were shown to be stable not only in inert gas matrices, but also in hydrocarbon glass (3-methylpentane) at liquid nitrogen temperature. This made investigations of silylenes much simpler, since a liquid helium cryostat was not required. We then began a study of substituent effects on the electronic spectra of silylenes, generated either from cyclic polysilanes or from aryltrisilanes, $Ar(R)Si(SiMe_3)_2$ (in the trisilanes, an aryl group proved necessary for absorption of UV light). Phenyl groups gave some side reactions, but with mesityl as the aryl group the results were clean.

Silylenes have strong visible absorption bands, resulting from an s–p electronic transition. Some of the silylenes made during these experiments and their absorption wavelengths are listed in Table 1 [28]. The electronic spectra are strongly influenced by the substituents. Either increasing the size of the R groups or substituting an aryl group leads to bathochromic shifts. These effects combine in the hindered species dimesitylsilylene, which is blue with absorption at 610 nm.

In some cases, as the 3-methylpentane matrix was melted, the color of the silylene gave way to a yellow solution, which persisted through part of the warm-up process. This, we now know, was due to disilenes, which had been formed by dimerization of the silylenes.

Table 1
Electronic absorption of silylenes in 3-methylpentane matrix

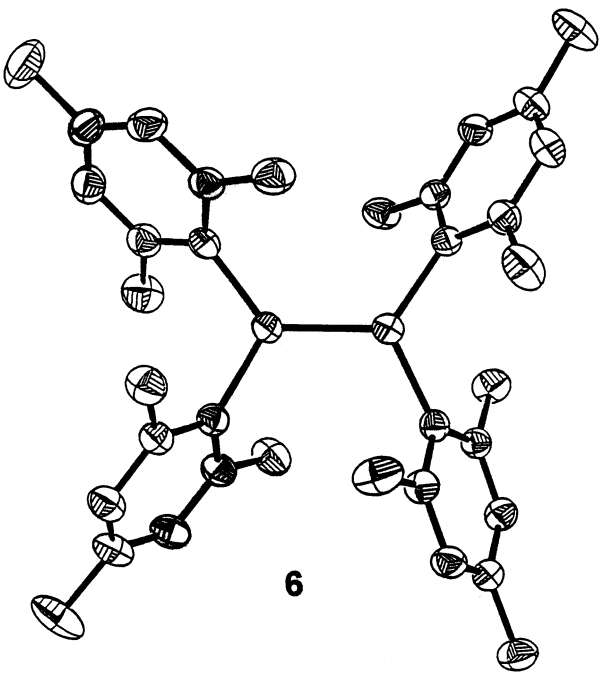
Silylene	λ_{max} (nm)	Color
Me_2Si	453	yellow
Et_2Si	460	yellow
$t\text{-}Bu_2Si$	480	orange
Ph(Me)Si	490	red
Ph_2Si	495	red
Mes(Me)Si	496	red
Mes(Ph)Si	530	purple
Mes_2Si	577	blue



Scheme 8.

With dimesitylsilylene, the yellow color was still present even after the solution was warmed to room temperature. Mark Fink carried out the crucial experiment in 1981, by evaporating the solvent, to yield bright yellow crystals of tetramesityldisilene (**5**) (Scheme 8) [29].

Complete characterization of **5**, including an X-ray crystal structure, was soon obtained. This prototypical compound, the best studied of disilenes, exhibits surprisingly complex behavior in the solid state. No less than four different conformational isomers have been isolated [30]. The structure of one form is shown as **6**.



4. Multiple bonds to silicon: 1981–2001

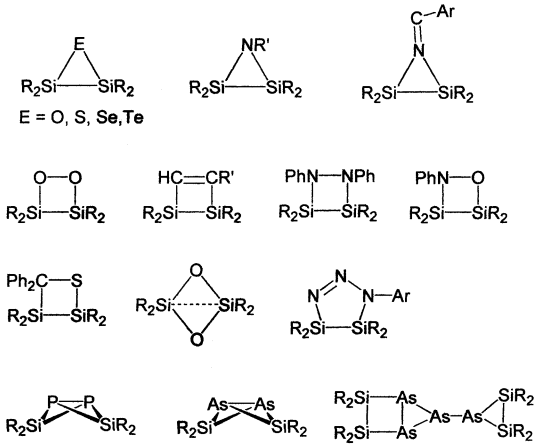
The 1981 discoveries opened the way for the synthesis of many new classes of multiply-bonded compounds of the heavier elements. The key proved to be steric protection of the multiple bond to provide kinetic stability, as employed in all three of the 1981 syntheses. The types of multiply-bonded silicon compounds isolated as stable compounds to date are listed in Table 2. In addition, many other kinds of stable multiply-bonded compounds have now been made, involving the elements Ge, Sn, Pb, As, Sb, Bi, B, Al, and Ga.

The chemistry of disilenes has evolved remarkably over the past 20 years. Only one tetraalkyldisilene, $[(Me_3Si)_2CH]_2Si{=}Si[CH(SiMe_3)_2]$, has been reported [41], but many tetraaryl and alkyl–aryl disilenes have been made, and tetra(organosilyl)disilenes have been synthesized and carefully studied by Kira and coworkers [42]. A 1996 review lists 38 different stable disilenes, including Z and E isomers [11], and perhaps a dozen more have been reported since. Reactions of stable disilenes, and of silenes, have led to the synthesis of a host of new structural types not available by other means. Some examples from disilene reactions are shown in Scheme 9 [11].

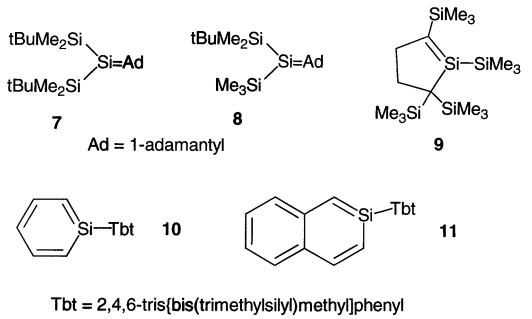
Significant developments have also taken place in the chemistry of silenes. Many reactions are now known for **3**, from studies in Brook's group [12e]. Important recent advances in Si=C double bond chemistry include the new synthesis of stable silenes **7** and **8** by Apeloig and coworkers via a sila-Peterson type reaction [43], and the synthesis of cyclic silene **9**, obtained by rearrangement of a silylene [44]. In addition, the first stable silaaromatic compounds, **10** and **11**, have been reported by Okazaki [45,46].

Table 2
The synthesis of stable multiply-bonded silicon compounds

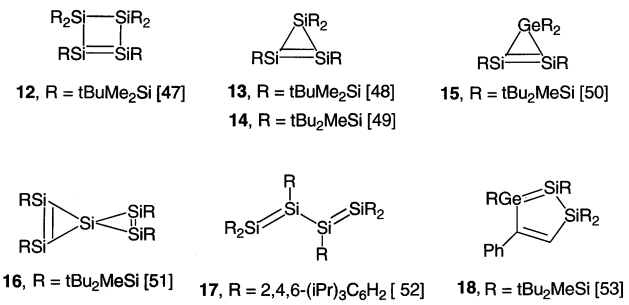
Bond	Year	Reference	Bond	Year	Reference
Si=C	1981	[22]	$[P\cdots Si\cdots P]^-$	1989	[35]
Si=Si	1981	[29]	$[N\cdots Si\cdots N]^-$	1990	[36]
Si=P	1984	[31]	Si=C=C	1993	[37]
Si=N	1985	[32]	Si=C=P	1999	[38]
Si=As	1992	[33]	Si=S	1994	[39]
Si=Ge	1992	[34]	Si=Se	1999	[40]
			Si=Te	1999	[40]



Scheme 9.



Several stable compounds containing Si=Si double bonds and having new and beautiful structures have recently been synthesized [47–51,53]. Examples are shown in structures **12**–**18**.



5. Future possibilities

In spite of the great progress in the chemistry of multiply-bonded silicon, a number of significant synthetic challenges remain. Silanones, $R_2Si{=}O$, are unknown as isolable compounds, although they have been identified in matrix and there is plenty of evidence that they are important reaction intermediates. The problem to be overcome is the very great energy of the Si–O single bond, which gives silanones a strong tendency to oligomerize to siloxanes [12i]. Yet it seems likely that this barrier will be overcome, allowing stable silanones to be isolated.

No stable triply-bonded silicon compound yet exists, although there is evidence for $CH_3Si{\equiv}SiCH_3$ [54] and PhSi≡N [55] as reaction intermediates, both HSi≡N [56] and PhSi≡N [57] have been trapped in low-temperature matrices, and HC≡SiF and HC≡SiCl have recently been identified in the gas phase by neutralization–reionization mass spectrometry [58]. Calculations suggest that highly hindered aryl ligands should stabilize the Si–Si triple bond against dimerization [59], but an attempt to synthesize a compound of this type led to insertion of the silicon atoms into C–C bonds [60]. In the future we can expect to see additional attempts, which may eventually be successful, to make stable compounds with Si≡Si, Si≡C, Si≡N and Si≡P triple bonds.

Although the synthesis of the first conjugated tetrasilabutadiene by Weidenbruch and coworkers represents a significant advance [52], a major challenge is to extend this π delocalization by synthesizing conjugated polymers, **19** and **20**, which may be expected to have highly unusual electronic properties.

Now that many reactions of silenes and disilenes are known, studies of reaction mechanisms are needed. Early results indicate that the reaction mechanisms for disilenes may be quite different from those for alkenes, and may involve unique pathways. Examples include the reaction of disilenes with dioxygen [61], and the addition of alcohols [62] and haloalkanes [63] to disilenes, all of which involve novel, unexpected reaction routes. Additional careful studies of silene and disilene reaction mechanisms will undoubtedly appear.

Acknowledgements

Research on multiply-bonded silicon compounds at the University of Wisconsin has been supported by grants from the National Science Foundation.

References

[1] F.S. Kipping, J.E. Sands, J. Chem. Soc. (Trans.) 119 (1921) 830, 848.
[2] F.S. Kipping, Proc. R. Soc. Ser. A 159 (1937) 139.
[3] The term "silicone", originally intended to mean a compound containing an Si=O bond (a "silicon ketone"), has however been carried over to refer to the actual products, siloxane polymers.
[4] A.J. Cowley, Polyhedron 3 (1984) 389.
[5] K.S. Pitzer, J. Am. Chem. Soc. 70 (1848) 2140.
[6] R.S. Mulliken, J. Am. Chem. Soc. 77 (1955) 884.
[7] P. Jutzi, Angew. Chem., Int. Ed. Engl. 14 (1975) 232 An exception was allowed for sulfur, since thioketones were known.
[8] A.G. Brook, F. Abdesaken, B. Gutekunst, G. Gutekunst, K.K. Kallury, Abstracts of papers, 15th Organosilicon Symposium, Durham, NC, March 27–28, 1981, p. 45.
[9] R. West, M.J. Fink, J. Michl, Abstracts of papers, 15th Organosilicon Symposium, Durham, NC, March 27–28, 1981, p. 46.
[10] M. Yoshifuji, I. Shima, N. Inamoto, K. Hirotsu, T. Higuchi, J. Am. Chem. Soc. 103 (1981) 4587 Mes* = 2,4,6-tri-*t*-butylphenyl.
[11] R. Okazaki, R. West, Adv. Organomet. Chem. 39 (1996) 232 disilenes.
[12] (a) L.E. Gusel'nikov, N.S. Nametkin, Chem. Rev. 79 (1979) 529;
(b) G. Raabe, J. Michl, Chem. Rev. 85 (1985) 419;
(c) G. Raabe, J. Michl, in: S. Patai, Z. Rappoport (Eds.), The Chemistry of Organic Silicon Compounds, Wiley, Chichester, 1989, pp. 1015–1142 Chapter 17;
(d) A.H. Cowley, Acc. Chem. Res. 17 (1984) 386;
(e) A.G. Brook, M.A. Brook, Adv. Organomet. Chem. 39 (1996) 71 silenes;
(f) I. Hemme, U. Klingebiel, Adv. Organomet. Chem. 39 (1996) 159 silaimines;
(g) M. Driess, Adv. Organomet. Chem. 39 (1996) 193 Si=P and Si=As compounds;
(h) T. Müller, W. Ziche, N. Auner, in: Z. Rappoport, Y. Apeloig (Eds.), The Chemistry of Organic Silicon, vol. 2, Wiley, Chichester, 1998 Chapter 16, Si=C and Si=N compounds;
(i) N. Tokitoh, R. Okazaki, in: Z. Rappoport, Y. Apeloig (Eds.),

The Chemistry of Organic Silicon, vol. 2, Wiley, Chichester, 1998, pp. 1063–1103 Chapter 17, Si=chalcogen compounds.
[13] N.S. Nametkin, L.E. Gusel'nikov, V.M. Vdovin, P.L. Grinberg, V.I. Zav'yalov, V.D. Oppengiem, Dokl. Akad. Nauk SSSR 171 (1966) 630.
[14] (a) L.E. Gusel'nikov, M.C. Flowers, Chem. Commun. (1967) 864;
(b) M.C. Flowers, L.E. Gusel'nikov, J. Chem. Soc. B 419 (1968) 1396.
[15] P. Boudjouk, L.E. Sommer, Chem. Commun. (1973) 54.
[16] A.K. Mal'tsev, V.N. Khabashesku, O.M. Nefedov, Izv. Akad. Nauk SSSR, Ser. Khim. (1976) 1193.
[17] M.R. Chedekel, M. Skoglund, R.L. Dreeger, H. Schechter, J. Am. Chem. Soc. 98 (1976) 7846.
[18] O.L. Chapman, C.-C. Chang, J. Kole, M.E. Jung, J.A. Lowe, T.J. Barton, M.L. Tumey, J. Am. Chem. Soc. 98 (1976) 7844.
[19] A.G. Brook, Adv. Organomet. Chem. 7 (1968) 95.
[20] A.G. Brook, J.W. Harris, J. Lennon, M. El Sheikh, J. Am. Chem. Soc. 101 (1979) 83.
[21] A.G. Brook, S.C. Nyburg, W.F. Reynolds, Y.C. Poon, Y.-M. Chang, J.-S. Lee, J.-P. Picard, J. Am. Chem. Soc. 101 (1979) 6750.
[22] A.G. Brook, S.C. Nyburg, F. Abdesaken, B. Gutekunst, G. Gutekunst, R.K. Kallury, Y.C. Poon, Y.M. Chang, W. Wong-Ng, J. Am. Chem. Soc. 104 (1982) 5667.
[23] N. Wiberg, G. Wagner, G. Müller, J. Reids, Angew. Chem., Int. Ed. Engl. 22 (1984) 381.
[24] D.N. Roark, G.J.D. Peddle, J. Am. Chem. Soc. 94 (1972) 5837.
[25] A more detailed account of the beginnings of this collaboration is given in [12b].
[26] M. Ishikawa, M. Kumada, Adv. Organomet. Chem. 19 (1981) 51.
[27] (a) T.J. Drahnak, J. Michl, R. West, J. Am. Chem. Soc. 101 (1979) 5427;
(b) C.A. Arrington, K.A. Klingensmith, R. West, J. Michl, J. Am. Chem. Soc. 106 (1984) 525.
[28] For a complete listing see table 3 in: P.P. Gaspar, R. West, in: Z. Rappoport, Y. Apeloig (Eds.), The Chemistry of Organic Silicon Compounds, vol. 2, Wiley, Chichester, 1998, pp. 2463–2568 Part 3, Chapter 43.
[29] R. West, M.J. Fink, J. Michl, Science (Washington, DC) 214 (1981) 2343.
[30] L.A. Leites, S.S. Bukalov, J.E. Mangette, T.A. Schmedake, R. West, Mendeleev Commun. (1998) 43.
[31] C.N. Smit, F.M. Look, F. Bickelhaupt, Tetrahedron Lett. 25 (1984) 3011.
[32] N. Wiberg, K. Schurz, G. Fischer, Angew. Chem., Int. Ed. Engl. 24 (1985) 1053.
[33] M. Driess, H. Pritzkow, Angew. Chem., Int. Ed. Engl. 31 (1992) 316.
[34] K.M. Baines, J.A. Cooke, Organometallics 11 (1992) 3487.
[35] E. Niecke, E. Klein, M. Nieger, Angew. Chem., Int. Ed. Engl. 28 (1989) 751.
[36] G. Undereiner, R. West, Angew. Chem., Int. Ed. Engl. 29 (1990) 529.
[37] G.E. Miracle, J.L. Ball, R. West, D.R. Powell, J. Am. Chem. Soc. 115 (1993) 11598.
[38] L. Rigon, H. Ranaivonjatovo, J. Escudié, A. Dubourg, J.-P. Declercq, Chem. Eur. J. 5 (1999) 774.
[39] H. Suzuki, N. Tokitoh, S. Nagase, R. Okazaki, J. Am. Chem. Soc. 116 (1994) 11978.
[40] N. Tokitoh, R. Okazaki, Acc. Chem. Res. 33 (2000) 625.
[41] S. Masamune, Y. Eriyama, T. Kawase, Angew. Chem., Int. Ed. Engl. 26 (1987) 584.
[42] M. Kira, T. Maruyama, C. Kabuto, K. Ebata, H. Sakurai, Angew. Chem., Int. Ed. Engl. 33 (1994) 1489.
[43] Y. Apeloig, M. Bendikov, M. Yuzefovich, M. Nakash, D. Bravo-Zhivotovskii, D. Blaser, R. Boese, J. Am. Chem. Soc. 118 (1996) 12228.
[44] M. Kira, S. Ishida, T. Iwamoto, C. Kabuto, J. Am. Chem. Soc. 121 (1999) 9722.
[45] K. Wakita, N. Tokitoh, R. Okazaki, S. Nagase, P. von Schleyer, H. Jiao, J. Am. Chem. Soc. 121 (1999) 11336.
[46] K. Wakita, N. Tokitoh, R. Okazaki, S. Nagase, Angew. Chem., Int. Ed. Engl. 39 (2000) 634.
[47] M. Kira, T. Iwamoto, J. Organomet. Chem. 611 (2000) 236.
[48] T. Iwamoto, C. Kabuto, M. Kira, J. Am. Chem. Soc. 121 (1999) 886.
[49] M. Ichinohe, T. Matsuno, A. Sekiguchi, Angew. Chem., Int. Ed. Engl. 38 (1999) 2194.
[50] V.Y. Lee, M. Ichinohe, A. Sekiguchi, N. Takagi, S. Nagase, J. Am. Chem. Soc. 122 (2000) 9034.
[51] T. Iwamoto, M. Tamura, C. Kabuto, M. Kira, Science (Washington, DC) 290 (2000) 504.
[52] M. Weidenbruch, S. Willms, W. Saak, G. Henkel, Angew. Chem., Int. Ed. Engl. 36 (1997) 1433.
[53] V.Y. Lee, M. Ichinohe, A. Sekiguchi, J. Am. Chem. Soc. 122 (2000) 12604.
[54] (a) A. Sekiguchi, S.S. Ziegler, R. West, J. Michl, J. Am. Chem. Soc. 108 (1986) 4241;
(b) B.S. Thies, R.S. Grev, H.F. Schaefer III, Chem. Phys. Lett. 140 (1987) 355/.
[55] J.G. Radziszewski, D. Littmann, V. Balaji, L. Fabry, G. Gross, J. Michl, Organometallics 12 (1993) 4816.
[56] G. Maier, J. Glathaar, Angew. Chem., Int. Ed. Engl. 33 (1994) 473.
[57] W. Kuhn, W. Sander, Organometallics 17 (1998) 4776.
[58] M. Karni, Y. Apeloig, D. Schröder, W. Zummack, R. Rabezzana, H. Schwartz, Angew. Chem., Int. Ed. Engl. 38 (1999) 332.
[59] K. Kobayashi, N. Takagi, S. Nagase, Organometallics 20 (2001) 234.
[60] R. Pietschnig, R. West, D.R. Powell, Organometallics 19 (2000) 2724.
[61] K.L. McKillop, G.L. Gillette, D.R. Powell, R. West, J. Am. Chem. Soc. 114 (1992) 5203.
[62] Y. Apeloig, M. Nakash, J. Am. Chem. Soc. 118 (1996) 9798.
[63] M. Kira, T. Ishima, T. Iwamoto, M. Ichinohe, J. Am. Chem. Soc. 123 (2001) 1676.

PERGAMON

Polyhedron 21 (2002) 473–488

POLYHEDRON

www.elsevier.com/locate/poly

Low valent and would-be multiply bonded derivatives of the Group 13 metals Al, Ga and In revealed through matrix isolation

Anthony J. Downs [a,*], Hans-Jörg Himmel [b], Laurent Manceron [c]

[a] *Inorganic Chemistry Laboratory, University of Oxford, South Parks Road, Oxford OX1 3QR, UK*
[b] *Institut für Anorganische Chemie der Universität Karlsruhe (TH), Engesserstrasse, 76128 Karlsruhe, Germany*
[c] *LADIR/Equipe de Spectrochimie Moléculaire, CNRS UMR, Université Pierre et Marie Curie, Case courrier 49, 4 Place Jussieu, 75252 Paris Cedex 05, France*

Received 28 September 2001; accepted 27 November 2001

Abstract

Two aspects of Group 13 metal chemistry are surveyed in the light of recent matrix-isolation and quantum chemical studies. The first concerns derivatives of the metals Al, Ga and In (M) in formal oxidation states less than +3: these include the M^0 derivatives ML_n, where L = CO, N_2, NH_3 or PH_3, and $n = 1$ or 2; the M^I derivatives MX, where X = H, CH_3 or NH_2, and M_2H_2; and the M^{II} derivatives HMX, where X = H, CH_3, NH_2 or PH_2. The second concerns derivatives in which there is the opportunity for the metal to engage in multiple bonding, as exemplified by the cases of M_2H_2 and H_2MNH_2. Experimental studies have involved thermally or photolytically excited reactions between M atoms, or sometimes M_2 molecules, and an appropriate substrate, e.g. H_2, CO, N_2, CH_4, NH_3 or PH_3. The reagents have been trapped in solid noble gas matrices, the IR spectra of which have been exploited to deduce the course of events and identities of the products. Confirmation of the identity and geometry of each of the products have been achieved primarily on the basis (i) of isotopic effects and (ii) of comparison of the measured spectrum with that anticipated by quantum chemical calculations. This liaison of experiments with theory has led to the characterisation not only of numerous simple molecules that are short-lived under normal conditions, but also of some of the reaction channels open to them, typically through photolytic activation. The structure, energies and reactivities of the compounds are reviewed. © 2002 Elsevier Science Ltd. All rights reserved.

Keywords: Low valent; Multiply bonded derivatives; Group 13 metals; Matrix isolation

"*Theory is a good thing, but a good experiment lasts forever.*"

P.L. Kapitsa, Experiment, Theory, Practice: Articles and Addresses of P.L. Kapitsa, Reidel, Boston, MA, 1980.

1. Introduction

For anyone filled, like the elephant's child, with 'satiable curiosity' [1], aluminium, gallium and indium have given good hunting in the past decade [2]. Surprising discoveries have emerged mainly through the search for new materials, or new ways of making known materials, with specific electrical, optical, thermal or chemical properties—ranging from films or nanocrystals through microporous or layered solids to discrete complexes having applications in nuclear medicine. At the same time, curiosity-led research has resulted in the synthesis and characterisation of two types of compound, which had hitherto attracted rather little attention. One type features the metal in a formal oxidation state less than +3, e.g. $[Et_3N{\cdot}AlBr]_4$, $Ga_5Cl_7(OEt_2)_5$, and $[GaSi(SiMe_3)_3]_4$ [2–5], the other invites the engagement of the metal in multiple bonding, e.g. $Na_2[Ar^*GaGaAr^*]$ [$Ar^* = 2,6\text{-}(2,4,6\text{-}Pr^i_3C_6H_2)_2C_6H_3$] and Me_2AlNH_2 [2,6]. This is molecular, rather than macromolecular territory, although compounds such as $[Ga_{84}\{N(SiMe_3)_2\}_{20}][Li(thf)_4]_2[Li_2Br(thf)_6]_2{\cdot}2$ toluene [7]

* Corresponding author. Tel.: +44-1865-272-673; fax: +44-1865-272-690.
E-mail address: tony.downs@chem.ox.ac.uk (A.J. Downs).

0277-5387/02/$ - see front matter © 2002 Elsevier Science Ltd. All rights reserved.
PII: S0277-5387(01)01036-1

and $[Al_{77}\{N(SiMe_3)_2\}_{20}][Li_2I(OEt_2)_5]_2 \cdot 2$ toluene [8] appear to prefigure the transition from molecular cluster to bulk metal. These are but two of some of the remarkable structures that have come to light, stimulating a lively debate about questions of bonding [2,6], while at the same time holding out tantalising prospects of new properties. It is with low-valent and would be multiply bonded hydride derivatives of the Group 13 metals that this article is concerned.

Simple subvalent molecules of the types MH and MH_2, where M = Al, Ga or In, are highly endoergic with respect to both decomposition to the elements in their standard states and to disproportionation into M atoms and MH_3 molecules. A degree of stabilisation can be achieved through aggregation to give oligomers, viz. $[MH]_n$ and $[MH_2]_n$, respectively, but not so as to produce a compound that is lastingly stable under normal conditions. The molecules AlH, GaH, InH and AlH_2 have each been sighted and characterised in some detail by high-resolution spectroscopic studies of discharges including H_2 and the appropriate metal atoms [3,9]. The lifetimes of such molecules can be extended up to a point by operating at low pressures and low temperatures, achieved for example by seeding a supersonic jet [10], but more or less indefinitely by matrix isolation, i.e. by entrapment at high dilution in a solid inert matrix at low temperatures [10,11]. Otherwise stabilisation of subvalent derivatives of the Group 13 metals other than thallium requires the replacement of hydrogen by a much bulkier substituent, e.g. C_5Me_5, $CH(SiMe_3)_2$, $Si(SiMe_3)_3$, or 2,6-(2,4,6-$Pr^i_3C_6H_2)_2C_6H_3$ [4,5,12]. Even then, aggregation takes place under normal conditions to give products with cores composed of two or more metal atoms. As a result M^{II} derivatives are isolated, for example, not as paramagnetic monomers but as diamagnetic M–M bonded dimers, e.g. $[(Me_3Si)_2(H)C]_2MM[C(H)(SiMe_3)_2]_2$ (M = Al, Ga or In) [4]. Electron delocalisation in some of these aggregates may then admit the possibility of partial oxidation or reduction so that the metal atoms take on other, fractional oxidation states, as in $[Al_6Bu^t_6]^{\bullet -}$ [5], or a mixture of different oxidation states, as in $Ga_5Cl_7(OEt)_5$ or the Al_{77} [8] and Ga_{84} [7] cluster compounds. While ligand bulk is undoubtedly the dominant influence, bonding electronic interactions between metal and ligand cannot be discounted, and stabilisation may also depend to a significant degree on coordination by a neutral base and, where the metal fragment is charged, on coulombic factors as well.

In the same vein, simple hydride species such as $[HMMH]^{2-}$, $[H_2MMH_2]^{2-}$, and H_2MNH_2, which afford the Group 13 metal atom M the opportunity for multiple bonding, may be fertile ground for the theoretician [2,6,13,14], but quite barren ground for the experimentalist working under normal conditions. Once again, aggregation or decomposition gains the upper hand to deny a sight of molecular units simple enough to be intelligible to both experiment and theory. Instead, lasting stability of what may be multiply bonded MM or MN units requires the mediation of highly encumbered ligands like 2,4,6-$Bu^t_3C_6H_2$ and 2,6-(2,4,6-$Pr^i_3C_6H_2)_2C_6H_3$ [2,6,12], but at the expense of theoretical tractability.

Here, we describe the results of studies carried out for the most part in our separate laboratories and in which attempts have been made to reconcile theory with experiment by investigating simple molecules of the type ML (L = CO, N_2, NH_3 or PH_3), MH, M_2H_2, HMX (X = H, CH_3, NH_2 or PH_2), and H_2MNH_2, where M = Al, Ga or In. All of these are amenable to detailed quantum chemical calculations at various levels of theory; they have been made experimental reality by carrying out thermally or photolytically induced reactions of the metal atoms, or sometimes their dimers M_2, with the appropriate reagent molecules, and trapping the products at high dilution in a solid noble gas matrix at temperatures of 4–20 K. Here the new molecules have been detected and interrogated by their IR spectra, their identities, geometries and vibrational properties being underwritten by the effects of isotopic change, and also by comparison with the vibrational properties forecast by theory. The resulting synergy between experiment and theory helps us to establish with confidence some physical and chemical characteristics of these low valent and/or would-be multiply bonded molecules. While the molecules remain high-energy species with no more than a fleeting existence outside a matrix at normal temperatures, they still hold important lessons for Group 13 metal chemistry at large.

2. Matrix isolation as a vehicle for chemical exploration

The general principles of matrix isolation are now familiar enough [10,11]. The trapped molecule is at once isolated and effectively immobilised in a rigid, inert matrix such as solid argon which is transparent to broad regions of electromagnetic radiation. Spectroscopic measurements can then be made at leisure and therefore in detail, and several different methods can be applied to the interrogation of a particular sample. In practice, IR spectroscopy has been the principal agent of detection, identification and characterisation. Critical features of such a matrix experiment are as follows [15].

- The structure of a molecule is unaffected by trapping, provided that there is no direct reaction with the solid matrix.
- The matrix environment provides for efficient quenching of any surplus energy the trapped molecule may possess as a result of the means of its

formation; excited electronic states do not enjoy lifetimes significantly different from those in the gas phase.

- Dynamic processes leading to the interconversion of different isomers or conformers are halted; at a matrix temperature of 10 K ($kT = 0.08$ kJ mol^{-1}) a barrier of only 5 kJ mol^{-1} cannot be overcome by thermal means.
- The rigidity of the matrix produces a marked *cage effect*. Only very small molecules or atoms are able to diffuse, and only the very smallest molecules, e.g. NH_3 or H_2O, to rotate in the matrix. As a result of this cage effect, photo-induced unimolecular reactions are arrested immediately after decomposition or rearrangement of the molecular precursor, and may even be reversed. The inability of the products to migrate from the matrix site at which they are formed contrasts with the freedom they enjoy in the fluid phases where they are often lost to facile reactions with other molecules. Just as atom–molecule or molecule–molecule pairs are entrained as the products of photodissociation, so similar pairs play an essential role as *precursors* to *bimolecular* changes, whether thermally or photolytically activated.
- The quenching of rotational motion combines with the relatively isotropic, weakly interacting matrix environment and low temperatures to produce sharp IR absorptions the positions of which can meaningfully be measured to ± 0.1 cm^{-1} in many cases. The linelike character of the vibrational transitions has a crucial part to play when it comes to investigating subtle isotopic effects.

Identification of an unfamiliar captive molecule on the basis of its IR spectrum is then typically achieved in the following steps.

- First, the number of distinct species present in the matrix has to be established on the evidence of a detailed investigation of how the spectrum responds to changes in the experimental conditions, e.g. concentrations, annealing, photolysis time and wavelength, etc.
- It is then necessary to assess the number, wavenmubers and relative intensities of all the absorptions associated with a given molecule before seeking to formulate its likely identity by drawing on the testimony of what may be distinctive features signalling the presence of specific groups, analogies with known compounds, or the vibrational selection rules expected to operate.
- Annealing or photolysis of the matrix may be instructive, particularly if it results in the conversion of the unknown molecule into a clearly identifiable product.
- Most revealing of all in purely experimental terms is likely to be the response of the spectrum to changes in the isotopic composition of the molecule. Hence it is possible, in principle, to establish the stoicheiometry, to test whether particular atoms are equivalent or inequivalent, and to assess the most plausible geometry for the molecule.
- In parallel with the experiments, quantum chemical calculations are carried out to determine possible equilibrium structures corresponding to a particular atomic composition, and to simulate their IR spectra. The final decision on the identity and geometry of the trapped molecule then rests on how closely theory matches experiment. There are few reporters more sensitive to the precise geometry and bonding of a molecule than its IR spectrum, and even small changes of bond distance or interbond angle are likely to translate into substantial changes of vibrational wavenumber and/or IR intensity. Accordingly, the ability to reproduce by calculation the wavenumber and intensity patterns of the observed spectrum constitutes an exacting test of molecular identity. Provided only that there are sufficient experimental data, the conclusions are quite compelling.

Fig. 1 illustrates schematically the matrix apparatus used in the experiments carried out at Oxford [16]. The metal is evaporated from a resistively heated Knudsen cell and the vapour codeposited with an excess of the matrix gas (usually argon) doped with the reagent on a CsI window cooled to approximately 12 K. The IR spectrum of the resulting deposit is then measured in transmission. The assemblies at both Karlsruhe [17] and Paris [18] differ only in matters of detail, for example, in that the matrix is condensed on a highly polished copper block, so that the IR spectrum can be measured in reflectance, thereby giving some advantage in sensitivity. In all cases the outer shroud of the apparatus carries a quartz window that enables the matrix deposit to be irradiated with light spanning an appropriate range of wavelengths. Only simple addition reactions of the precursor species opposed by little or no activation barrier are likely to occur spontaneously given the low thermal energy available under the conditions of the experiment. By contrast, a much higher price in activation will usually have to be paid for changes that involve bond dissociation, insertion into a bond, or isomerisation. Photons are then the only currency available to matrix-isolated species.

Quantum chemical calculations have been performed with the aid of the GAUSSIAN-98 [19] or Amsterdam Density Functional (ADF) [20] program systems. In most cases, these have involved the use of density functional theory (DFT) methods, but the scope of some calculations has been extended by drawing also on ab initio (MP2) methods. The B3LYP hybrid methodology has found the most general application, this having been shown previously to give satisfactory results for small aluminium and gallium compounds [21]. A 6-311g(d) basis set was chosen for Al and Ga, a

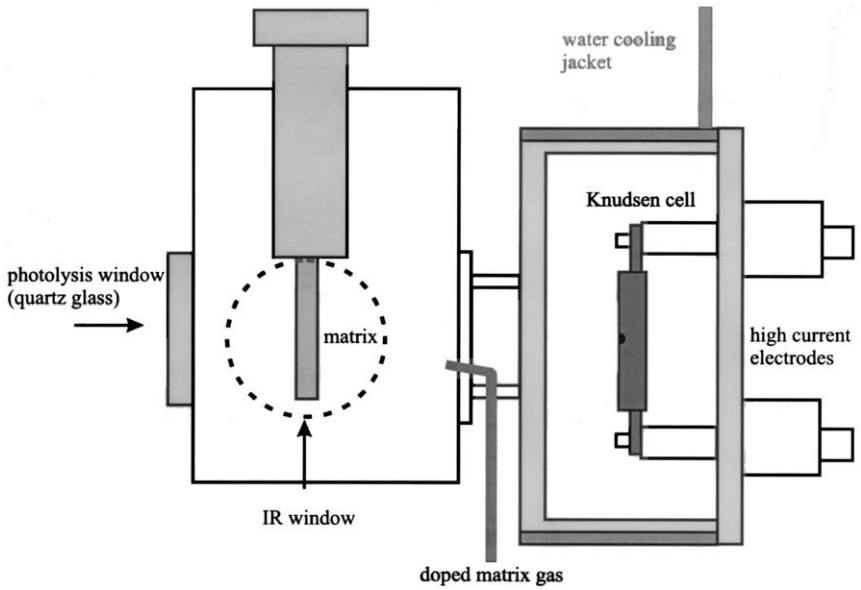


Fig. 1. Schematic picture of the matrix-isolation apparatus used in Oxford [16].

LANL2DZ basis set with additional d-polarisation functions (exponent 0.5) for In.

3. Oxidation state 0: metal atom complexes

3.1. Metal carbonyls

Main Group metals, unlike d-block metals, do not form lastingly stable derivatives with neutral molecules like CO, PF_3 or C_6H_6, so that the bulk metals are effectively the sole representatives of the oxidation state 0. The first sign that the Group 13 metal atoms are in fact capable of binding CO came in 1972 with the report [22] that the matrix formed by co-condensing Al atoms with an excess of krypton doped with CO at approximately 20 K displays new bands in the ν(CO) region of the IR spectrum that are red-shifted by approximately 150 cm^{-1} with respect to the corresponding band of free CO. These could be attributed to an aluminium dicarbonyl, $Al_x(CO)_2$. Subsequent studies involving different matrices and EPR [23] as well as IR [24,25] measurements have confirmed this first sighting and shown that $x = 1$. The most recent and detailed IR study, carried out in Paris [25], has explored systematically the effects of varying the metal and CO concentrations, and of annealing the resulting argon matrices, as well as extending the range of IR analysis down to 200 cm^{-1}. Typical results are illustrated in Fig. 2. Hence it has become clear that more than one product is formed, and examination of how the intensities of the different IR bands vary with the metal or CO concentrations has led, in addition, to the identification of AlCO and also the bimetallic species Al_2CO and $Al_2(CO)_4$. For example, the intensities of bands due to species containing more than one Al atom or CO molecule are found to increase more or less quadratically as a function of the concentration of that particular reagent.

In experimental terms, $Al(CO)_2$ is the most fully characterised of these products with no less than six IR bands attributable to vibrational fundamentals having been observed in the range 2000–200 cm^{-1}. Its signature includes two IR-active ν(CO) modes near 1995 and 1908 cm^{-1}, although the picture is complicated somewhat by the occupancy of more than one type of matrix site (see Fig. 2). Perhaps the clearest indication of stoicheiometry comes from experiments with an equimolar mixture of ^{12}CO and ^{13}CO which reveal 1:2:1 triplet patterns for each of the ν(CO) bands corresponding to the three distinct isotopomers $Al(^{12}CO)_2$, $Al(^{12}CO)(^{13}CO)$, and $Al(^{13}CO)_2$, respectively. The observation of two bands corresponding to the in-phase

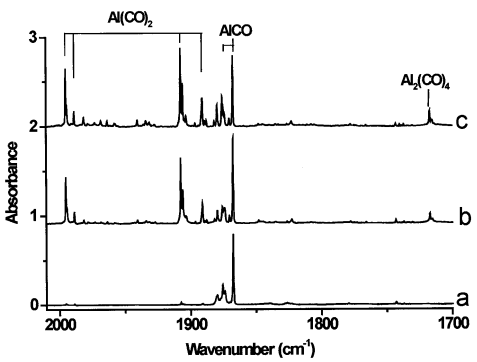


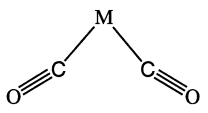
Fig. 2. IR spectrum of a solid Ar matrix showing the formation of AlCO and $Al(CO)_2$: (a) after deposition at 10 K; (b) after annealing at 32 K; and (c) after annealing at 38 K [25].

Table 1
Calculated and observed properties for mono- and dicarbonyls of the Group 13 metals [27]

Compound	Calculated structure		ν(CO) (cm^{-1})		Calculated energy (kJ mol^{-1})
	Distances [a]	Angles [a]	Calculated	Observed [b]	
AlCO	r(M–C) 2.146, r(C–O) 1.167	∠M–C–O 168	1890	1867.7 [c]	−81 [d]
GaCO	r(M–C) 2.254, r(C–O) 1.164	∠M–C–O 180	1898	1875.6	−61 [d]
InCO	r(M–C) 2.582, r(C–O) 1.159	∠M–C–O 180	1909	1920.8	−43 [d]
$Al(CO)_2$	r(M–C) 2.044	∠C–M–C 73.5	1953	1995.3, 1988.7 [b,c]	−176 [d]
	r(C–O) 1.162	∠M–C–O 165.4	1905	1907.6, 1891.0 [b,c]	
$Ga(CO)_2$	r(M–C) 2.169	∠C–M–C 72.6	1972	2016.8, 2011.8, 2009.2 [b]	−125 [d]
	r(C–O) 1.158	∠M–C–O 163.1	1911	1933.6, 1920.4, 1912.4 [b]	
$In(CO)_2$	r(M–C) 2.561	∠C–M–C 61.8	1971	2029.2	−85 [d]
	r(C–O) 1.155	∠M–C–O 174.0	1909	1985.0	

[a] Distances in Å, angles in °.
[b] Values are given for the molecule isolated in an Ar matrix; splitting observed in some cases is due to matrix site effects.
[c] [25].
[d] Energy with respect to CO and each M atom in its ^2P ground state.

and out-of-phase ν(CO) fundamentals then implies an angular skeleton. If the simplifying assumption is made that the bond moments can be added vectorially, it follows that the angle θ subtended by the two CO oscillators is given by the ratio of the intensities I_{sym}: $I_{asym} = \cot^2(\theta/2)$, whence a value of $\theta = 110° \pm 5°$ has been estimated. Ab initio and DFT calculations [26,27] suggest a value near 102° but, more strikingly, a tight C–Al–C angle of about 74°, so that the Al–C–O arms are bent slightly but significantly outwards (**1**) with the two carbon atoms appearing to be drawn towards each other. This may reflect simply the achievement of optimum overlap between the vacant np valence orbital of Al coincident with the twofold axis of the molecule and the π-orbitals of the CO ligands, but there are at least three alternative explanations, viz. (i) repulsive interaction between the metal ns^2 electrons and the 5σ donor pair on CO; (ii) the establishment of a C···C interaction between the two CO groups made admissible to the bonding scheme, say, through an O=C=C=O contribution to the ground-state wave function [25]; or (iii) coulombic repulsion between the O atoms which carry a small but significant negative charge and are otherwise brought unusually close together by the narrow C–Al–C angle.

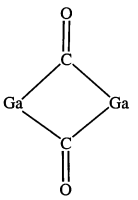


1

Similar experiments with gallium or indium in place of aluminium have revealed that the following molecules are formed on deposition: GaCO, InCO, Ga·GaCO, In·InCO, Ga(μ-CO)Ga, $Ga(CO)_2$, $In(CO)_2$ and $In(CO)_2$·In, the proportions of which vary markedly with the metal and CO concentrations [27]. The identification of binuclear products, both here and in the earlier experiments with aluminium [25], suggests that addition of CO occurs to the metal dimers M_2 (M = Al, Ga or In) which are also trapped when the metal vapours are co-condensed with an excess of a noble gas [28]. That these dimers have a chemistry of their own and do not merely shadow the parent atoms will soon be apparent when we come to consider the reactions with H_2 (see Section 5). The presence of products like Al(μ-CO)Al and Ga(μ-CO)Ga is signalled by the appreciably lower wavenumbers of the IR bands associated with the ν(CO) modes (1737 and 1828 cm^{-1}, respectively). DFT studies find that all three metals behave in a similar fashion in their response to coordination by CO. What is striking, though, is the magnitude of the estimated binding energies, ranging from 81 to 43 kJ mol^{-1} for AlCO, GaCO, and InCO, and from 176 to 85 kJ mol^{-1} for $Al(CO)_2$, $Ga(CO)_2$, and $In(CO)_2$ (see Table 1 for example). These, in common with the wavenumbers of the ν(CO) modes, signify M–CO bonds at least as strong as those formed by a late transition metal like Ni [27]. This must surely challenge conventional wisdom regarding the ability of CO to bind to a Main Group metal.

The known photolability of transition metal carbonyls [11,29] has prompted an investigation of the action of UV light on the matrix-isolated gallium and indium carbonyls [27]. Hence it is found that Ga(μ-CO)Ga can be induced to take up an additional CO molecule to produce the symmetrical $Ga(\mu\text{-}CO)_2Ga$ molecule, **2**, which is characterised by a ν(CO) IR band at 1774 cm^{-1}. DFT calculations suggest a potential minimum corresponding to a singlet planar structure with D_{2h} symmetry, with the following dimensions (distances in Å, angles in °): Ga···Ga 3.188; Ga–C 2.155; C–O 1.178; < Ga–C–Ga 95.4. The compound suffers

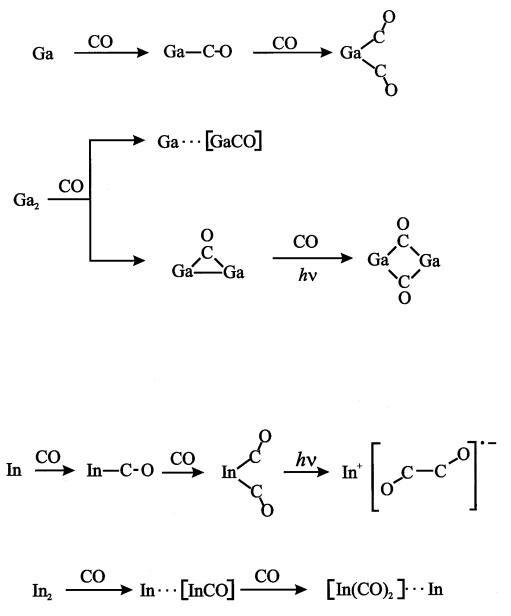
decomposition under the action of visible radiation. UV irradiation causes the decay of all the indium carbonyls formed on deposition but no new product is evident until the matrix is exposed to broad-band UV–Vis radiation. Then it appears that photoactivation of $In(CO)_2$ results in metal-to-ligand charge transfer with the coupling of the two CO molecules to produce the ion-pair $In^+[OCCO]^{\bullet -}$. Calculations show an increased electron density between the two carbon atoms in the first excited state of $In(CO)_2$, and so hint at the mechanism of this photoisomerisation. Scheme 1 contrasts the reaction pathways taken by Ga atoms and Ga_2 molecules in the presence of CO with those taken by In atoms and In_2 molecules under similar (matrix) conditions.



2

3.2. Other adducts of the metal atoms

Experiments along the same lines have also been carried out with Al, Ga or In atoms isolated in argon matrices doped with H_2 [30], N_2 [31], CH_4 [16], NH_3 [32] or PH_3 [33]. In the cases of H_2 and CH_4 it has not been possible to detect in the IR spectra of the deposits any new bands that can be ascribed to $M{\cdot}H_2$ or $M{\cdot}CH_4$ adducts, although the presence, at the very least, of contact pairs is implicit in the photochemical changes which can be induced in these matrices [16,30]. There are, however, signs that N_2 forms very loosely bound $M{\cdot}N_2$ pairs in that IR absorptions in the ν(NN) region are detectable, being red-shifted by approximately 16 cm^{-1} with respect to ν(NN) of free N_2 [31].



Scheme 1. Pathways for the thermally and photolytically activated matrix reactions of Ga, Ga_2, In and In_2 with CO [27].

Stronger interactions are apparent in the $M{\cdot}NH_3$ adducts formed on isolation of the metal atoms in argon matrices doped with 0.3–2% NH_3 [32]. The IR spectra recorded after deposition of these matrices include new bands identifiable with ν(N–H), $\delta_{asym}(NH_3)$ and $\delta_{sym}(NH_3)$ modes of a perturbed NH_3 molecule. Correlating with these features is a new band at approximately 440 nm in the visible spectrum. That the intensities of both the IR and visible absorptions should vary roughly in *direct* proportion to the matrix concentration of NH_3 argues strongly, moreover, for the formulation of each of these species as monoammines, viz. $M{\cdot}NH_3$. The IR properties of the adducts are then notable for the *blue* shifts of 108–157 cm^{-1} suffered by the $\delta_{sym}(NH_3)$ mode as compared with the corresponding mode of free NH_3. The implication of ligand-to-metal charge transfer is confirmed by DFT calculations which find a global minimum for an $M{\cdot}NH_3$ molecule with the geometry **3** deviating slightly from regular C_{3v} symmetry as a result of Jahn–Teller distortion [14,32,34,35]. The calculations reproduce well the general patterns presented by the IR spectra, with isotopic responses (D for H and ^{15}N for ^{14}N) wholly in line with those observed, and the direction of charge transfer, with a small negative charge on the metal, is also consistent with the results of very recent EPR studies [36] involving the $Al–NH_3$ system. Similar 1:1 metal ammines have been described previously in experiments involving severally the alkali metals [37], Fe [38], Ni [38], and Cu [38].



3 **4**

Experiments with PH_3-doped matrices give superficially similar results [33,34]. With each of the metals Al, Ga and In, new IR bands associated with the ν(P–H), $\delta_{asym}(PH_3)$ and $\delta_{sym}(PH_3)$ fundamentals of a perturbed PH_3 molecule can be discerned more or less clearly. Indeed, two families of bands can typically be recognised and distinguished by their dependence on the PH_3 concentration as arising from complexes of the types $M{\cdot}PH_3$ and $M(PH_3)_2$, respectively. Intriguingly, though, the most intense feature in each family, which corresponds to the $\delta_{sym}(PH_3)$ transition is not blue-shifted

Table 2
Calculated binding energies for neutral Group 13 metal atom complexes of the types M·L and M·L_2 [33,34]

Ligand, L	Metal atom, M	Binding energy (kJ mol^{-1}) [a]	
		M·L	M·L_2
N_2	Al	16.4	26.4
	Ga	8.4	17.1
	In	7.0	14.6
PH_3	Al	21.8	48.9
	Ga	22.1	45.0
	In	17.0	34.1
NH_3	Al	60.2	103.0
	Ga	51.8	86.1
	In	48.5	79.8
CO	Al	81	176
	Ga	61	125
	In	43	85

[a] Energy with respect to L and each M atom in its ^2P ground state.

but *red*-shifted by 20–30 cm^{-1} with respect to uncoordinated PH_3. It appears, therefore, not only that the degree of charge transfer is smaller than in the M–NH_3 adducts, but also that the transfer proceeds in the *opposite* sense to produce a slight positive charge on the metal atom, as indicated by recent independent theoretical studies on Al·PH_3 [39]. The vibrational properties are thus comparable with those displayed by PH_3 in the transition metal complexes $Cu(PH_3)_n$ ($n = 1–3$) [40a], $Ni(PH_3)_4$ [40a,b], and $H_3P{\cdot}TiCl_4$ [40c]. They are also replicated pleasingly well by DFT calculations [33,34], the 1:1 complexes resembling geometrically their ammonia counterparts and the 1:2 complexes conforming to C_{2v} symmetry, **4**, with P–M–P angles in the order of 80° and M···P distances about 0.06–0.08 Å shorter than in their 1:1 counterparts.

The calculated binding energies of the various neutral complexes of Al, Ga, and In atoms are listed in Table 2. Hence it emerges (i) that ligand–metal interactions increase in the orders In < Ga < Al and $N_2 < PH_3 < NH_3 < CO$, and (ii) that, with the exception of $Al(N_2)_2$, the 1:2 complexes each have a total binding energy similar to, or slightly greater than, twice the value associated with the corresponding 1:1 complex. The maximum bond energies thus range from 16 kJ mol^{-1} (for Al·N_2), through 24 and 60 kJ mol^{-1} [for $Al(PH_3)_2$ and Al·NH_3, respectively], to a remarkable 88 kJ mol^{-1} [for $Al(CO)_2$].

4. Oxidation state +2: metal hydrides of the type HMX (X = H, CH_3, NH_2 or PH_2)

Somewhat perversely, it might seem, we move next to the formal oxidation state +2, where paramagnetic behaviour is to be expected, at least in a mononuclear derivative of the Group 13 metal. As noted previously, compounds like AlH_2 are normally prey to rapid decomposition or disproportionation. It turns out, however, that they are also the *first* stage in the train of reactions typically induced by photoexcitation of the metal atom in a solid noble gas matrix that also includes as a prospective reagent H_2, CH_4, SiH_4, NH_3 or PH_3.

4.1. The hydrides MH_2

The earliest report of AlH_2, made by Herzberg [41], identified the molecule in a hydrogen discharge on the evidence of its emission spectrum. Matrix methods have been exploited subsequently to characterise the molecule by its IR [42] and EPR [43] spectra following its formation (i) by the reaction of photo-excited or laser-ablated Al atoms with H_2 [42]; or (ii) by a secondary reaction triggered by the photolysis of another divalent aluminium compound, HAlOH [43]. GaH_2 has been described as one of several photoproducts formed on broad-band photolysis of solid argon matrices including Ga atoms and H_2 [44]. However, the most detailed investigation of the dihydrides formed by all three metals Al, Ga, and In has been that carried out in Paris and published in 1994 [45]. Not only did this confirm how the molecules come to be formed from the metal atoms and H_2, it also made clear their photolytic fates.

When the Group 13 metal atoms (M) are condensed with H_2 molecules in solid argon, the IR spectrum observed directly after deposition displays no absorption attributable to M·H_2 or any other product. It requires irradiation of the matrix to induce any reaction, but only when the photolysing radiation coincides with the $^2S \leftarrow {}^2P$ or $^2D \leftarrow {}^2P$ transition of the M atoms (occurring in the wavelength range 290–340 nm) does the IR spectrum witness the appearance of new bands in the region 1500–1820 cm^{-1} suggestive of the formation of a metal hydride [45]. As illustrated in Fig. 3(a), each of the metals then gives a primary product characterised by three IR bands, two in the ν(M–H) region and one at 600–770 cm^{-1}. That this product is the angular triatomic molecule MH_2 is confirmed by experiments with D_2 and HD. In the case of the gallium compound, each of the two IR features attributable to stretching modes displays splitting due to the ^{69}Ga and ^{71}Ga isotopes present in natural abundance; this is best observed with GaD_2, where there is greater motion of the metal, with isotopic shifts of 0.75 and 0.22 cm^{-1} (see Fig. 3(b)). An interbond angle close to 120° is thus implied. Knowledge of the vibrational wavenumbers of the three isotopomers MH_2, MHD and MD_2 is sufficiently detailed to admit force field calculations which yield the following M–H stretching force constants (in

N m^{-1}): AlH_2 183, GaH_2 182, and InH_2 147. These trends, as well as the other spectroscopic characteristics, are exactly reproduced in the properties calculated by ab initio DFT and coupled cluster (CCSD) methods: the Al–H and Ga–H internuclear distances are thus estimated to be almost identical (1.609 and 1.615 Å, respectively) and approximately 0.2 Å shorter than the In–H distance [45].

In the past there have of course been numerous false starts with compounds professing by their formulae to be M^{II} derivatives [3], the most celebrated cases being those of $GaCl_2$ and Me_4NGaCl_3 which are in reality a mixed valence compound $Ga^{I}[Ga^{III}Cl_4]$ and metal–metal bonded compound $[Me_4N]_2[Cl_3GaGaCl_3]$, respectively. Another false impression is created by the paramagnetic compounds $M(dbab)_2$, where M = Al or Ga and dbab = $Bu^tNCHCHNBu^t$, but which actually contain the trivalent metal bound to one singly and one doubly reduced dbab ligand [3]. Any doubts about the credentials of the matrix-isolated MH_2 molecules have been set aside, however, by the EPR spectra displayed by AlH_2 [43] and GaH_2 [46].

Once formed, the MH_2 molecules themselves prove to be photolabile. Moving the photolysing radiation to shorter wavelengths (250–290 nm) results in the decay of the IR bands due to MH_2 with the simultaneous growth of a single new band at 1380–1600 cm^{-1} corresponding to the MH diatomic which has been well characterised previously in the gas phase [9]. This implies the existence of an excited electronic state of the MH_2 molecule about 4.5 eV above the ground state which is dissociative towards MH + H. Consistent with such a view are the findings of an ab initio study of the excited states of AlH_2 in that the first Rydberg state is calculated to have a linear geometry and a term value close to 4.75 eV [47]. Nor is this the end of the tale for the AlH photoproduct observed in the matrix experiments. Changing the character of the photolysing radiation yet again—and moving this time to longer wavelength (ca. 400 nm)—causes the AlH absorption to decay with the simultaneous growth of three new bands at 1883, 784, and 698 cm^{-1} identifiable, on the basis of deuteration experiments and of the results of parallel matrix studies [42b,48,49], with the planar AlH_3 molecule. The amount of AlH actually disappearing is found to be proportional to the H_2 concentration in the matrix, and it is evident, therefore, that both AlH and H_2 are needed to form AlH_3 in what must then be, overall, a three-photon process (Eq. (1)). The efficient wavelength range (365–410 nm) is indeed close to the first electronic transition ($A\ ^1\Pi \leftarrow X\ ^1\Sigma^+$) of AlH for which ν_{00} = 23470.93 cm^{-1} according to gas-phase studies [50]. This insertion into the H–H bond of electronically excited AlH does not appear to be matched by similar reactions on the part of GaH and InH, although analogous reactions *can* be engineered with photoexcited MCl molecules to give H_2MCl (M = Ga [51a] or In [51b]). To access GaH_3 and InH_3 it is necessary to introduce H atoms to the metal atoms; the IR spectra of the resulting matrices recorded immediately after deposition then attest the formation of all three hydrides MH, MH_2 and MH_3 for M = Al, Ga or In [49]. Although photostable, all the trihydride molecules are rapidly lost to either aggregation or decomposition under normal conditions. The vapour over solid gallane, $[GaH_3]_n$, at low temperatures (180–215 K) does contain in addition to the dimer $H_2Ga(\mu\text{-}H)_2GaH_2$ much lower partial pressures of GaH_3, so further matrix studies

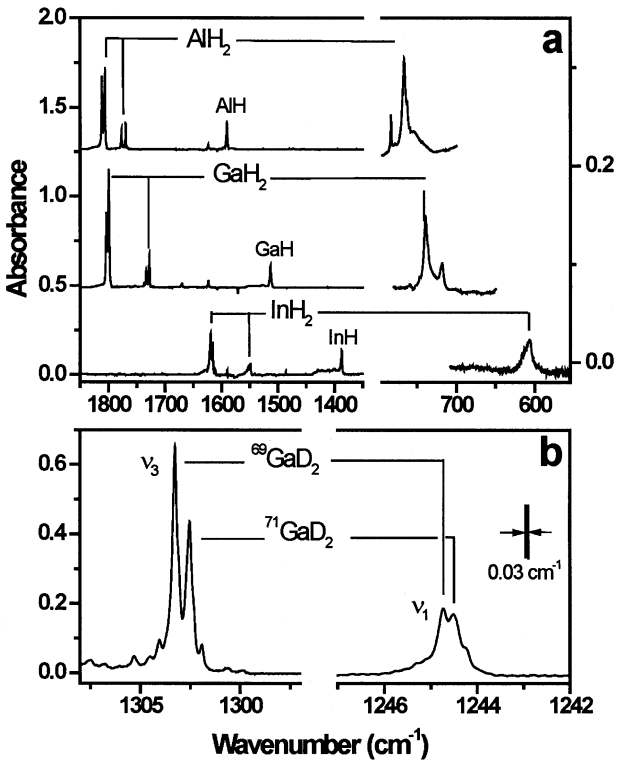
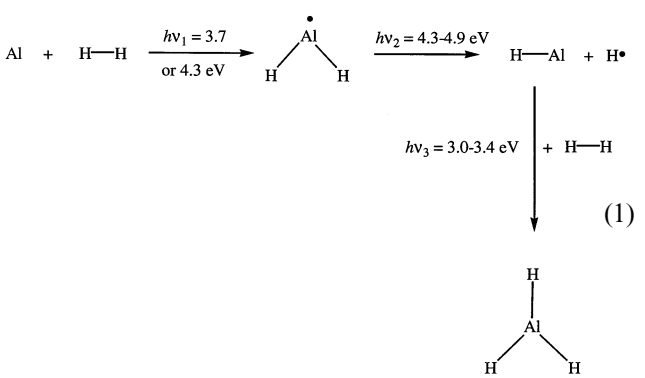


Fig. 3. (a) IR difference spectra showing the formation of simple Group 13 metal hydrides in solid Ar matrices at 10 K after irradiation at λ = approximately 334 nm (Ga) or 289 nm (Al and In). Other bands are due to traces of AlH_3 (top spectrum) and HMOH (M = Ga or In). (b) IR spectrum of $^{69}GaD_2$ and $^{71}GaD_2$ in the antisymmetric and symmetric ν(Ga–D) regions [45].



(1)

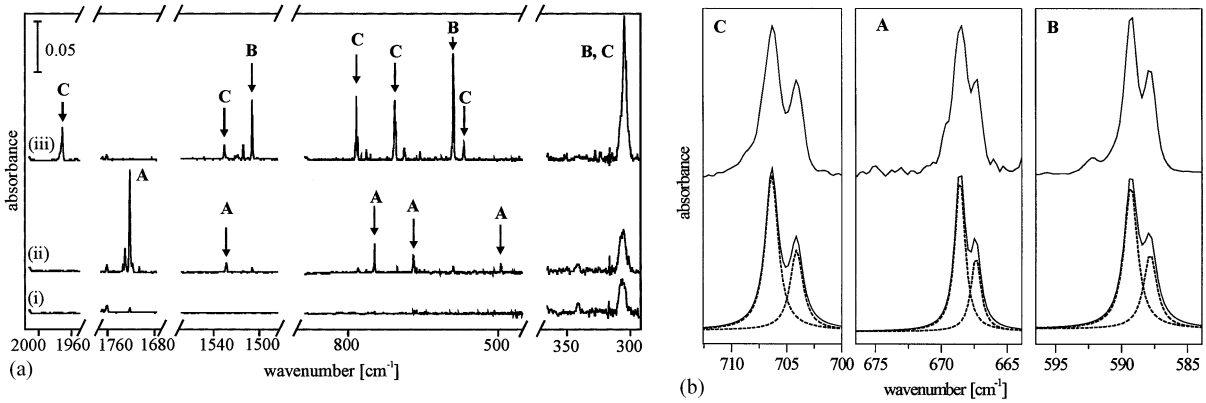
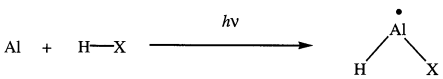


Fig. 4. IR spectra of an Ar matrix containing Ga and NH_3: (a) (i) following deposition; (ii) following UV photolysis ($\lambda = 200$–400 nm); and (iii) following broad-band UV–Vis photolysis ($\lambda = 200$–800 nm); (b) bands near 700 (**C**), 670 (**A**), and 590 cm^{-1} (**B**) showing $^{69}Ga/^{71}Ga$ splitting. **A** = $HGaNH_2$, **B** = $GaNH_2$, and **C** = H_2GaNH_2 [32].

suggest [52]. Otherwise we must depend largely on theory for our knowledge of MH_3 molecules.

4.2. Other hydrides of the type HMX

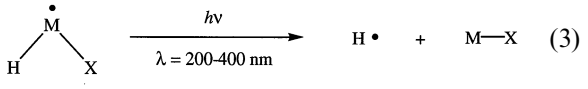
Insertion into the H–H bond is by no means the limit to the reactivity of a Group 13 metal atom once excited to its ^2S or ^2D electronic state. Indeed, replacement of H_2 by CH_4, SiH_4, NH_3 or PH_3 as a partner to the excited metal atom has been found under matrix conditions to give rise to a primary reaction analogous to the first stage of Eq. (1); breaching of a C–H, Si–H, N–H or P–H bond occurs with the formation of an angular hydride molecule of the type HMX, where X = CH_3 [16,53], SiH_3 [54], NH_2 [32] or PH_2 [33], respectively (Eq. (2)). The photolysis conditions vary somewhat according to the initial degree of interaction between M in its electronic ground state and the prospective reagent. Where there is little or no specific interaction—as with CH_4, for example—optimum conversion is achieved with radiation having wavelengths close to that of the $^2S \leftarrow {}^2P$ transition of the matrix-isolated M atom (ca. 340 nm or $h\nu = 3.7$ eV). Where specific interaction yields a recognisable adduct, however, there is a move to longer wavelengths. For example, the visible absorption near 440 nm ($h\nu$ = ca. 2.8 eV) associated with the formation of an M·NH_3 complex in an argon matrix is the ideal target for the photolysing radiation needed to promote insertion and so give what may be regarded as a tautomer of the original complex. Although it has not been possible to locate all the IR-active fundamentals, the effects of isotopic change and the ability of DFT calculations to match the observed spectra put beyond question the identities and structures of the HMX products. To judge by the EPR spectra recorded for CH_3AlH [53], CH_3GaH [46], and $HAlNH_2$ [36], moreover, we need be in no doubt that these too are authentic M^{II} derivatives. Only in the case of the M–PH_3 system does it appear that the M^{II} product $HMPH_2$ is accompanied by an M^{III} isomer, H_2MPH, where the unpaired electron is localised on the P rather than the M atom [33].



(2)

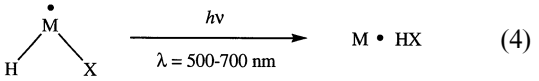
The HMX molecules share the photolability of the parent dihydrides, and indeed feature quite a rich photochemistry. The response of the dihydrides to UV photolysis is echoed by CH_3MH and $HMNH_2$; under the action of broad-band UV–Vis light, these suffer photodissociation of the M–H bond with the formation of the univalent products CH_3M [16] and MNH_2 [32], respectively (Eq. (3)). Given the unselective nature of the photolysis, it is not possible to decide whether the primary photochemical act is truly selective or whether both the M–H and the M–CH_3 or M–NH_2 bonds are ruptured and the matrix cage then filters the products by admitting the escape of the small, mobile $H^\bullet$ atoms while denying that of the larger $^\bullet CH_3$ or $^\bullet NH_2$ radicals [55]. In the case of the M–NH_3 system, broad-band photolysis also results in a significant yield of a secondary product, namely the M^{III} compound H_2MNH_2, so that the M^{II} precursor appears to have disproportionated into MNH_2 and H_2MNH_2 (see Fig. 4). A fuller discussion of this last product is deferred, however, to Section 6. But this is by no means the end of the photochemical channels that can be accessed by HMX molecules, for there is evidence—direct in some cases, less direct in others—that some at least are characterised by visible absorption in the range 500–700 nm. For example, $HAlPH_2$ displays an absorption near 550 nm. Irradiation at these wavelengths then opens up the possibility of a reversal of reaction 2, with the regeneration of the M·HX contact-pair or complex (Eq. (4)). This is certainly the case with HX = SiH_4 [54b] and with HX = PH_3, although there is competition in the second case from alternative decomposition channels

that afford, among other products, PH (when M = Ga or In) [33]. Earlier experiments suggest that matrix-isolated CH_3AlH and CH_3GaH are likewise susceptible to reversion to $CH_4{\cdot}M$ when exposed to light at wavelengths >450 nm [53].



(3)

$X = CH_3$ or NH_2



(4)

5. Oxidation state +1: mononuclear derivatives MX (X = H, CH_3 or NH_2) and dinuclear derivatives M_2H_2

5.1. Mononuclear derivatives

As noted in the preceding section, irradiation of matrix-formed HMX molecules with light at wavelengths in the range 200–400 nm affords a source of monomeric univalent MX molecules, where X = H [45], CH_3 [16], or NH_2 [32] (Eq. (3)). The monohydrides and CH_3Al have been detected in the gas phase, for example by their rotational spectra [3,9,56], but most of the knowledge about simple molecules of this type available hitherto has come from theoretical inquiries. With the new experimental results it is possible not only to check the fidelity of quantum chemical calculations, but also to compare the bonding in molecules of the type MX with that in HMX, MX_3 and H_2MNH_2 molecules, where X = H, CH_3 or NH_2. Bond distances, r(MX) (mostly estimated by theoretical methods) and stretching force constants, k(MX) (all determined by experiment), are set out in Table 3. For a given metal M, it is thus evident that the steady decrease in r(MX) in the order $M^I > M^{II} > M^{III}$ is matched by a steady *increase* in k(MX) as the M–X bond becomes less polar and the curvature at the foot of the potential well correspondingly steeper. There is also an intriguing change in the pattern of r(MX) and k(MX) as a function of the

Table 3
Calculated and observed bond distances and stretching force constants for some simple M^I, M^{II} and M^{III} molecular derivatives of the Group 13 metals

Molecule	M–H		M–CH_3		M–NH_2	
	r(M–H) (Å)	k(M–H) (N m^{-1})	r(M–C) (Å)	k(M–C) (N m^{-1})	r(M–N) (Å)	k(M–N) (N m^{-1})
AlH_3	1.593[49]	202[49]	–	–	–	–
GaH_3	1.586[49]	216[49]	–	–	–	–
InH_3	1.789[49]	181[49]	–	–	–	–
$Al(CH_3)_3$	–	–	1.957 [a]	247 [b]	–	–
$Ga(CH_3)_3$	–	–	1.967 [c]	241 [b]	–	–
$In(CH_3)_3$	–	–	2.161 [d]	193 [b]	–	–
H_2AlNH_2	1.581[34]	220.5[34]	–	–	1.779[34]	408[34]
H_2GaNH_2	1.562[34]	243[34]	–	–	1.821[34]	397[34]
H_2InNH_2	1.725[34]	192[34]	–	–	1.970[34]	315[34]
AlH_2	1.608[45]	183[45]	–	–	–	–
GaH_2	1.612[45]	182[45]	–	–	–	–
InH_2	1.816[45]	147[45]	–	–	–	–
CH_3AlH	1.598[53]	176[16]	1.981[53]	214[16]	–	–
CH_3GaH	1.612[16]	173[16]	2.014[16]	219[16]	–	–
CH_3InH	1.782[16]	141[16]	2.181[16]	160[16]	–	–
$HAlNH_2$	1.605[34]	180[34]	–	–	1.788[34]	364[34]
$HGaNH_2$	1.602[34]	174[34]	–	–	1.836[34]	344[34]
$HInNH_2$	1.768[34]	139[34]	–	–	1.993[34]	265[34]
AlH	1.645[9]	160[9]	–	–	–	–
GaH	1.662[9]	142[9]	–	–	–	–
InH	1.836[9]	120[9]	–	–	–	–
CH_3Al	–	–	1.994[56]	185[16]	–	–
CH_3Ga	–	–	2.044[16]	165[16]	–	–
CH_3In	–	–	2.226[16]	158[16]	–	–
$AlNH_2$	–	–	–	–	1.813[34]	313.5[34]
$GaNH_2$	–	–	–	–	1.884[34]	272[34]
$InNH_2$	–	–	–	–	2.039[34]	210[34]

[a] A. Almenningen, S. Halvorsen, A. Haaland, Acta Chem. Scand. 25 (1971) 1937.
[b] R.J. O'Brien, G.A. Ozin, J. Chem. Soc. A (1971) 1136.
[c] B. Beagley, D.G. Schmidling, I.A. Steer, J. Mol. Struct. 21 (1974) 437.
[d] T. Fjeldberg, A. Haaland, R. Seip, Q. Shen, J. Weidlein, Acta Chem. Scand. A36 (1982) 495.

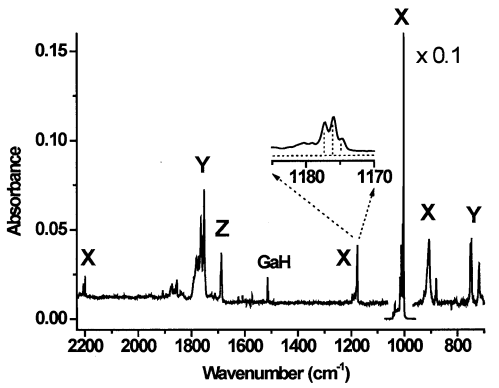
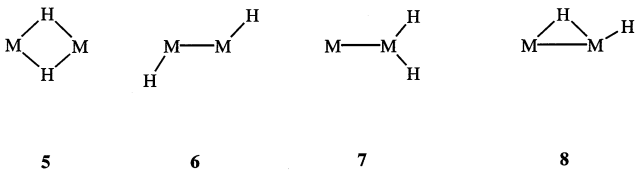


Fig. 5. IR spectrum in the region 2300–700 cm^{-1} for Ga vapour codeposited with H_2 in an excess of Ar ($Ga/H_2/Ar = 0.6/1/100$) at 14 K. The absorbance scale in the 1100–950 cm^{-1} region is divided by 10 for the sake of presentation. **X** = Ga(μ-H)$_2$Ga, **Y** = $GaGaH_2$, and **Z** = HGaGaH [30]. The inset presents an enlarged view of the $a_g + b_{1u}$ combination transition with a stick spectrum symbolising the intensity pattern expected for the natural isotopic composition of a symmetrical digallium species.

valence state of M according to whether M = Al, Ga or In. Univalent derivatives consistently comply with the sequence Al > Ga > In for k(MX) [with the reverse order for r(MX)], whereas the corresponding sequence for trivalent derivatives is Al ~ Ga > In in keeping with the extra stability of the 4s valence shell in Ga.

5.2. Binuclear derivatives M_2H_2

Subhydrides of the Group 13 metals of the type M_2H_2 have attracted the attention of theorists despite a dearth of hard experimental fact. Part of the concern has arisen from the question of what part multiple bonding between the M atoms might play. Diborene, B_2H_2, has been identified by its EPR and IR spectra in matrix-isolation experiments and the consensus of experiment and theory is that it has a linear triplet ground state with little or no B–B double-bonding [2,9,57,58]. By contrast, a bis(μ-hydrido) structure **5** with D_{2h} symmetry is calculated to be the most stable form for all the other Group 13 elements [2,9,58,59]. Instead of the linear form which is now only a transition state, a *trans*-bent isomer **6** (C_{2h}) appears as a second minimum on the PE surface, and there are two other possible isomers, namely the asymmetric M–MH_2, **7** (C_{2v}), and mono-H-bridged HM(μ-H)M, **8** (C_s), also giving minima at energies not far above the global minimum. None of these molecules offers the opportunity for significant M–M multiple bonding. Only with the addition of two extra electrons to give a species isoelectronic at the valence level with C_2H_2 does such bonding seem feasible, the lowest energy form assuming not a linear but a *trans*-bent configuration akin to **6** [2,13]. No simple hydride derivative of this sort has yet been sighted, but replacement of hydrogen by a very bulky ligand Ar* = 2,6-(2,4,6-$Pr^i_3C_6H_2$)$_2C_6H_3$ has led to the isolation of the deeply coloured compound Na_2[Ar*GaGaAr*] featuring a relatively short Ga–Ga bond and a non-linear C–Ga–Ga–C skeleton with C_{2h} symmetry [13,60].



5 **6** **7** **8**

The first experimental evidence of a neutral hydride of the type M_2H_2 came in 1993 when it was reported by Xiao et al. [44] that co-condensation of gallium vapour, produced by thermal evaporation, with H_2 in a noble gas matrix results in the formation of a molecule believed to be Ga(μ-H)$_2$Ga, i.e. with the structure **5**. Since it is known that a small proportion of the gallium is trapped as Ga_2 and larger clusters [28], the obvious inference is that the product is formed *spontaneously* by the reaction of Ga_2 with H_2. Furthermore, the IR spectra of argon matrices formed by condensing laser-ablated Al atoms with H_2 are found to include absorptions attributable on the evidence of their wavenumbers and isotopic responses and theoretical modelling to Al(μ-H)$_2$Al, **5**, and, more tentatively, to HAl(μ-H)Al, **8** [42b,61]. However, the high energy of the atoms produced in this way, including some that are in electronically excited states, and the potential for photolysis by the hard radiation emanating from the focussed laser plume at the metal target make it difficult to judge how these particular products come to be formed.

More recent studies carried out in Paris [30] confirm that a new product is indeed formed by the spontaneous reaction of Ga_2 with H_2 in solid argon matrices at approximately 12 K. Five bands traceable to the product occur at 2200, 1176, 1002, 906.5, and 880 cm^{-1}, with the third of these being the most intense by an order of magnitude (see Fig. 5). Particularly striking is the triplet pattern displayed by the weak band at 1176 cm^{-1}; the intensity pattern of the closely spaced components tallies closely with that expected (2.3:3:1) for naturally occurring ^{69}Ga and ^{71}Ga with the freedom to occupy two equivalent sites. On these grounds alone, models **7** and **8** would appear to be excluded. Arguing against model **6**, moreover, is the failure to find any bands in the region associated with the stretching of *terminal* Ga–H bonds (1500–2050 cm^{-1}) [9]. The most plausible interpretation of the results is that the compound is indeed the dihydrido-bridged molecule Ga(μ-H)$_2$Ga with the structure **5**. For a planar molecule of this sort with D_{2h} symmetry only three vibrational fundamentals are expected to be active in IR absorption and calculations in the optimised geometry anticipate that one of these, corresponding to the

ring-puckering mode, will occur at a wavenumber (ca. 200 cm^{-1}) and with an intensity (ca. 1% that of the strongest absorption) which will make it hard to locate in practice. On the other hand, the same calculations find no difficulty in identifying the intense band at 1002 cm^{-1} with the b_{1u} ring-stretching mode and its weaker neighbour at 906.5 cm^{-1} with the corresponding b_{2u} mode. The weak band at 880 cm^{-1} can then be ascribed to the b_{3g} ring-stretching mode made active by the reduced symmetry (C_{2v}) of the $^{69}Ga^{71}GaH_2$ isotopomer making up 48% of the product. With the aid of the vibrational properties calculated for the optimum geometry, the remaining bands can be attributed to combination tones each involving an IR-silent (a_g) fundamental. The net result is that all but one (b_{3u}) of the six fundamentals of the molecule ($2a_g + b_{3g} + b_{1u} + b_{2u} + b_{3u}$) have been located more or less certainly, the assignments being underwritten by the effects of isotopic change ($^{69}Ga/^{71}Ga$ and D for H) and by the properties forecast by theory. Experiments with mixtures of H_2 and D_2 give no hint of absorptions due to the mixed isotopomer Ga(μ-H)(μ-D)Ga (formed from HD) and so confirm the bimolecular nature of the reaction between Ga_2 and H_2. Intriguingly, though, the reaction shows a marked kinetic isotope effect, being much slower with D_2 than with H_2 or HD at 10–12 K, although it can be accelerated by exposure of the matrix to additional IR radiation.

In similar studies carried out partly in Oxford but mainly in Karlsruhe [30], replacement of gallium by indium gives matrices that tell a rather different tale. In this case, the IR spectra of the initial deposits give no sign of any reaction between In_2 and H_2. On the other hand, such a reaction can be induced by irradiation of the matrix with light having wavelengths near 365 nm. Hence the corresponding indium hydride In(μ-H)$_2$In is formed. The parallel with the gallium compound is at once announced by the IR spectrum which is dominated by an intense absorption at 955 cm^{-1}, accompanied by much weaker ones at 2021, 1079, 848 and 800 cm^{-1}. The interpretation of the spectrum follows closely that of the gallium compound, allowing five of the six fundamentals to be identified, with conclusions again endorsed both by the effects of deuteration and by the results of calculations at different levels of theory.

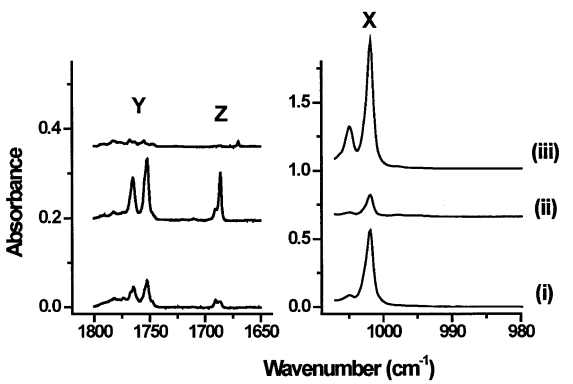
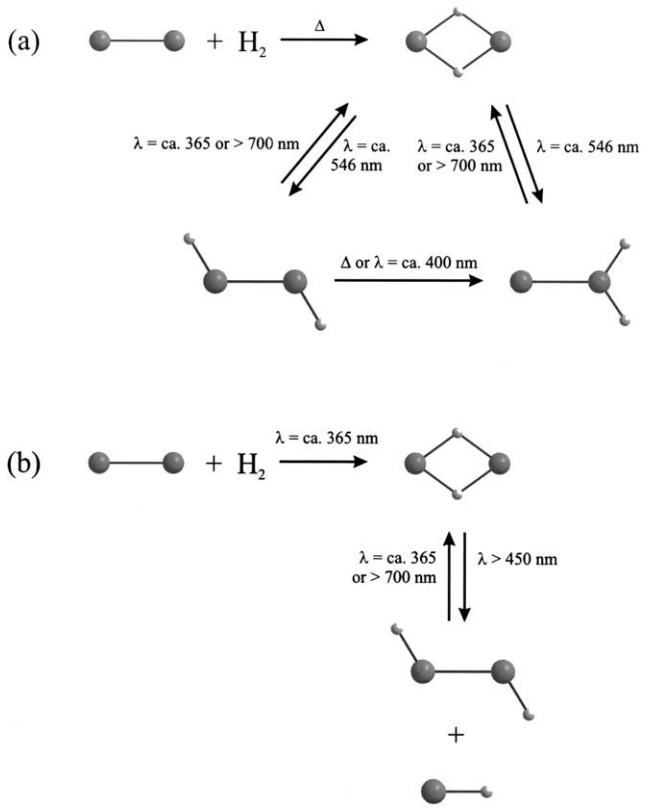


Fig. 6. IR spectrum of an Ar matrix containing Ga vapour and H_2 in the regions 1800–1650 and 1100–980 cm^{-1} (i) after deposition, (ii) after irradiation at λ = approximately 546 nm, and (iii) after irradiation at $\lambda = 600–800$ nm [30].

The contrasting reactivities of Ga_2 and In_2 in these reactions pose a teasing problem to which there is no obvious solution. It is generally agreed that the electronic ground state of each of the dimers is a *triplet*, although the first singlet state lies only approximately 50 kJ mol^{-1} higher in energy. The M(μ-H)$_2$M molecule, on the other hand, almost certainly possesses a *singlet* ground state. Calculations then suggest that the reaction of triplet ($^3\Pi_u$) M_2 molecules with H_2 to form singlet M(μ-H)$_2$M is mildly endothermic, whereas the corresponding reaction of singlet ($^1\Sigma_g^+$) M_2 molecules is strongly exothermic. A possible explanation is then that a fraction of the M_2 molecules entering the matrix populates the excited singlet state, and that the difference in reactivity depends on the lifetime of this state.

But that is by no means the end of the tale. For both Ga(μ-H)$_2$Ga and In(μ-H)$_2$In prove to be photolabile under visible light ($\lambda > 450$ nm) [30]. Exposure of the gallium compound to green light (λ = ca. 546 nm) results in its conversion to two distinct products **X** and **Y**, the first being marked by IR bands at 1765, 1752 and 752 cm^{-1}, the second by just one sharp band near 1686 cm^{-1} (see Fig. 6). **Y** can be distinguished from **X** and indeed converted into it by annealing the matrix at temperatures up to 30 K or by irradiation with near-UV light. Comparison with the spectra of other gallium hydrides and with the spectra simulated for different Ga_2H_2 isomers with the geometries **6**–**8**, allied to the response to deuteration, suggests that **X** is $GaGaH_2$ (**7**) and **Y**, HGaGaH (**6**). By contrast, irradiation of In(μ-H)$_2$In with visible light ($\lambda > 450$ nm) gives rise to only a single isomer, HInInH, together with InH. The isomerisation can be reversed by UV photolysis (λ = ca. 365 nm) of HMMH (M = Ga or In) and $GaGaH_2$, or by near-IR photolysis ($\lambda > 700$ nm) of HGaGaH and $GaGaH_2$. Of isomers of the type HM(μ-H)M, **8**, however, there is as yet no trace. Scheme 2 summarises the reactions variously activated by thermal or photolytic means and which have thus been charted by experiment.

All of this must be seen as a major triumph for the theoretical studies that foreshadowed subhydrides of the type M_2H_2 [58,59]. Yet experiment does more than vindicate theory, for 'nothing ever becomes real till it is experienced'.



Scheme 2. Pathways for the matrix reactions of Ga_2 and In_2 molecules with H_2 [30].

6. Trivalent metal hydrides with the potential for multiple bonding

There is no question but that π-type bonding to the heavier p-block elements is relatively weak and that compounds containing such bonds are ready prey to aggregation or electrophilic attack. On the other hand, the increase in coordination number at the p-block element in the transition state and often in the product means that this vulnerability can be countered by steric congestion. Accordingly, it has been found that encumbering the heavier elements of Groups 14 and 15 with sufficiently bulky ligands affords isolable mononuclear compounds featuring more or less well authenticated multiple bonding [62]. The same strategy has also been tried with more limited success with the Group 13 metals, but the bonding status of even the most promising products, e.g. Na_2[Ar*GaGaAr*], is still the subject of considerable debate [2,13,60]. As noted in the preceding section, neither quantum chemical calculations nor experiment find evidence for a stable M_2H_2 molecule that involves significant M–M π-type interactions. Here we consider not the wider issue but the special case of the heavier homologues of H_2BNH_2, viz. H_2MNH_2, where M = Al, Ga or In. Once again, matrix isolation brings practical substance to theoretical speculation.

Amido derivatives of Group 13 metals are normally oligomeric or polymeric, with a coordination number of 4 or greater at the metal [3]. Only with the introduction of bulky substituents at the metal and nitrogen centres can monomeric compounds with three-coordinated M and N atoms be sustained under normal conditions [63]. Despite the planar structures favoured by the skeletons of such compounds, however, it is difficult to assess the contributions made to the overall properties by bonding and non-bonding interactions associated with the ligands. The difficulty is minimised in a simple monomeric compound like H_2GaNH_2, but this aggregates under normal conditions as the trimer $[H_2GaNH_2]_3$, which decomposes on heating not to regenerate the monomer but to eliminate H_2 and form GaN [64]. Quantum chemical calculations on molecules of the type H_2MNH_2 [14,32,34,35] certainly indicate a planar, ethene-like structure **9** with C_{2v} symmetry for the equilibrium geometry. In this respect there is no difference from the structure deduced previously by both experiment and theory for the corresponding boron compound H_2BNH_2 [65].



9 **10**

The IR spectra of argon matrices containing initially M atoms and NH_3 signal that the first photoproduct $HMNH_2$ decomposes on exposure to broad-band UV–Vis light to give both the M^I derivatives MNH_2 and the M^{III} derivative H_2MNH_2 as the photostable end-products [32]. For example, photolysis of $HGaNH_2$ results, particularly in the later stages, in the growth of no less than nine bands which can be attributed to the formation of H_2GaNH_2 (see Fig. 4). There are several immediate clues to this identity: (i) absorptions at 1970.8 and 779.6 cm^{-1} are strongly suggestive of a terminal GaH_2 unit in a *trivalent* gallane derivative [cf. GaH_3 1923.2 and 758.7 cm^{-1} [49], and H_2GaCl 1978.1/1964.6 and 731.4 cm^{-1} [51a]; (ii) absorptions at 3510.7, 3413.4, 1530.4, 782.8, and 567.7 cm^{-1} bear all the hallmarks of an NH_2 group; and (iii) the doublet pattern of an absorption at 706.2/704.1 cm^{-1} implies $^{69}Ga/^{71}Ga$ splitting arising from the motion of a single Ga atom, most likely in a ν(Ga–N) vibration. Confirmation is provided both by the response of the IR signature to isotopic enrichment of the molecule in D or ^{15}N, and by the strikingly close agreement of the measured spectra with those simulated for the different isotopomers of the H_2GaNH_2 molecule by DFT calculations. The corresponding aluminium and indium compounds have been detected and characterised in a similar manner.

How well the calculations are able to reproduce the measured spectra is demonstrated by rms deviations of no more than 3.3 and 5.8% for the wavenumbers of the different isotopomers of H_2AlNH_2 and H_2GaNH_2, respectively. No less impressive are the ^{15}N shifts (all negative and in cm^{-1}) presented in parentheses in the order experimental/calculated for the following bands of H_2GaNH_2 (with wavenumbers also in cm^{-1}): 3510.7 (10.0/10.8), 3413.4 (7.5/4.9), 1970.8 (0.1/0.1), 1530.4 (6.1/5.4), 782.8 (4.5/4.7), 779.6 (4.4/3.5), 706.2/704.1 (14.0/13.1), 567.7 (0.3/0.0), and 304.9 (2.1/2.4). In addition, the observed $^{69}Ga/^{71}Ga$ splitting of 2.1 cm^{-1} characterising the band near 705 cm^{-1} matches admirably the calculated value of 1.9 cm^{-1} for what approximates demonstrably to the ν(Ga–N) mode.

How these products come to be formed is not immediately obvious. The knowledge that H_2 molecules undergo photoactivated addition to matrix-isolated GaCl [51a] or InCl [51b] to give the trivalent product H_2MCl (M = Ga or In) suggests one mechanism in which a similar reaction is induced between the univalent metal amide MNH_2 and H_2 (formed by recombination of the H atoms released on photodissociation of the M^{II} molecule $HMNH_2$ (Eq. (3)). There is another possibility, however, namely the direct addition of the H atoms released to the subvalent metal compounds MNH_2 and $HMNH_2$. Telling evidence that this is indeed the principal—possibly sole—means of access to H_2MNH_2 comes from experiments in which a matrix containing Ga atoms and NH_3 is additionally doped with D_2 [32,34]. Were D_2 addition the primary reaction, the main product would then be D_2GaNH_2 readily recognisable by strong IR absorptions near 1400 cm^{-1} due to its ν(Ga–D) modes. In the event, only weak absorptions are observed to build up hereabouts, whereas relatively strong bands develop near 1970 cm^{-1} [due to ν(Ga–H) modes]. It is also apparent that the yield of H_2GaNH_2 decreases almost to vanishing point when the matrix concentration of NH_3 is reduced by a factor of 10. There seems to be little doubt, then, that H atoms are the main precursors to the formation of H_2MNH_2 in a reaction sequence that plainly requires the activation of more than one NH_3 molecule.

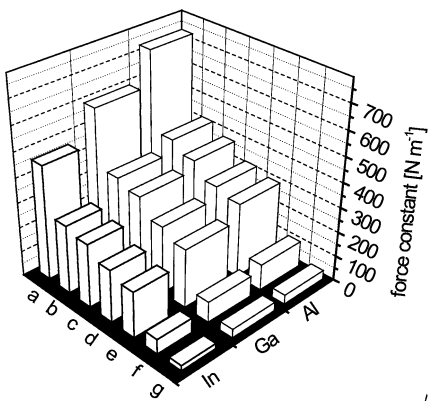


Fig. 7. Plot of the force constants k(MN) of compounds with the general formula H_mMNH_n (M = Al, Ga or In; m, $n = 0$–3): (a) HMNH; (b) H_2MNH_2; (c) $HMNH_2$; (d) MNH_2; (e) MN; (f) $H_3M{\cdot}NH_3$; (g) $M{\cdot}NH_3$ [34].

The calculated M–N distances in the H_2MNH_2 molecules—1.779, 1.821, and 1.970 Å for M = Al, Ga and In, respectively—are indeed short, being near or below the lower limits for the observed distances in three-coordinated amido derivatives of the relevant metal (Al 1.78 Å, Ga 1.818 Å, and In 2.049 Å) [34]. As shown in Fig. 7, the M–N stretching force constants determined by experiment are also larger than those of any other compound of the type H_mMNH_n (m, $n = 0$–3), with the sole exception of the hypothetical, high-energy species HMNH which has so far eluded the experimentalist. The planar geometry calculated for the H_2MNH_2 molecule contrasts with the *trans*-C_{2h} geometry of H_2SiSiH_2 [63a,66] and while it must imply some π-bonding, the barrier to inversion of NH_3 and its derivatives is so small that planarity is of itself no guarantor of a strong π-interaction.

To explore further the nature of the M–N bond, DFT methods have been used to optimise each H_2MNH_2 molecule in the conformation where the H_2M and NH_2 planes are orthogonal to each other [34]. The resulting twisted conformation is a transition state with two imaginary frequencies, one for the torsion back to the planar molecule and the other for pyramidalisation of the M–NH_2 unit. Calculation of the energy of the transition state relative to the equilibrium ground state of the molecule then gives an estimate of the barrier to rotation about the M–N bond, ΔE. Hence it has been estimated [34], in agreement with results reported elsewhere [14,67], that $\Delta E = 161.9$, 50.6, 65.7, and 51.5 kJ mol^{-1} for M = B, Al, Ga, and In, respectively. If ΔE is taken to be a lower limit to the π-bond strength, there are then just two conclusions to be drawn. Firstly, only in H_2BNH_2 does π-bonding add significantly to the strength of the M–N bond. Secondly, such bonding varies in strength in the order $B \gg Al < Ga > In$; that gallium should again be out of line with its neighbours is noteworthy but scarcely destined to stem the tide running against π-bonding as a major influence.

Of phosphorus analogues of H_2MNH_2 there is no obvious glimpse when matrix-isolated $HMPH_2$ molecules are similarly irradiated with broad-band UV–Vis light. DFT calculations lead us to expect that the hypothetical H_2MPH_2 molecules will assume non-planar geometries, **10**, with C_s symmetry and incorporating sharply pyramidal MPH_2 fragments [34]. Very similar results have been reported previously for H_2AlPH_2 and H_2GaPH_2 on the basis of SCF calculations which nevertheless encourage the belief that the non-planar skeletons are not necessarily incompatible with some M–P double-bond character [68]. In fact, the

different structures of H_2MNH_2 and H_2MPH_2 have more to do with the grossly different inversion barriers of the parent molecules NH_3 and PH_3 (24 vs. 148 kJ mol^{-1} according to one estimate [34]) than with π-bonding ability. Interestingly, the inversion barriers of H_2MPH_2 molecules are estimated to be 39–53 kJ mol^{-1}, i.e. only about one-third the values for free PH_3, suggesting that there is appreciable stabilisation of the planar transition state [34]. What is more, the barrier to rotation around the M–P bond of this state has been calculated to be 65.9, 80.1, and 65.3 kJ mol^{-1} for M = Al, Ga, and In, respectively [34]. M–P π-bonding is somewhat stronger than M–N π-bonding, so theory proposes: how real or significant this may be has yet to be tested by experiment.

Acknowledgements

The authors thank Dr T.M. Greene, Professor J.C. Green and Dr P. Pullumbi for their major contributions to the research described in this article, the EPSRC for support of the research in Oxford, the Deutsche Forschungsgemeinschaft for the award of grants to H.-J.H. in both Oxford and Karlsruhe, and the C.N.R.S. for support of the research in Paris.

References

[1] R. Kipling, Just So Stories for Little Children, Macmillan, London, 1902.
[2] A.J. Downs, Coord. Chem. Rev. 189 (1999) 59.
[3] M.J. Taylor, P.J. Brothers, in: A.J. Downs (Ed.), Chemistry of Aluminium, Gallium, Indium and Thallium, Blackie, Glasgow, 1993, p. 111.
[4] W. Uhl, Angew. Chem., Int. Ed. Engl. 32 (1993) 1386.
[5] C. Dohmeier, D. Loos, H. Schnöckel, Angew. Chem., Int. Ed. Engl. 35 (1996) 129.
[6] P.J. Brothers, P.P. Power, Adv. Organomet. Chem. 39 (1996) 1.
[7] A. Schnepf, H. Schnöckel, Angew. Chem., Int. Ed. Engl. 40 (2001) 712.
[8] A. Ecker, E. Weckert, H. Schnöckel, Nature 387 (1997) 379.
[9] S. Aldridge, A.J. Downs, Chem. Rev. 101 (2001) 3305.
[10] A.J. Downs, T.M. Greene, Adv. Inorg. Chem. 46 (1999) 101.
[11] (a) M.J. Almond, A.J. Downs, Adv. Spectrosc. 17 (1989) 1;
(b) L. Andrews, M. Moskovits (Eds.), Chemistry and Physics of Matrix-Isolated Species, North Holland, Amsterdam, 1989;
(c) I.R. Dunkin, Matrix-Isolation Techniques: A Practical Approach, Oxford University Press, Oxford, 1998.
[12] B. Twamley, S.T. Haubrich, P.P. Power, Adv. Organomet. Chem. 44 (1999) 1.
[13] Y. Xie, R.S. Grev, J. Gu, H.F. Schaefer III, P.v.R. Schleyer, J. Su, X.-W. Li, G.H. Robinson, J. Am. Chem. Soc. 120 (1998) 3773.
[14] (a) R.D. Davy, K.L. Jaffery, J. Phys. Chem. 98 (1994) 8930;
(b) T.P. Hamilton, A.W. Shaikh, Inorg. Chem. 36 (1997) 754.
[15] R.N. Perutz, in: R. Fausto (Ed.), Low Temperature Molecular Spectroscopy, NATO ASI Series, Series C: Mathematical and Physical Sciences, vol. 483, Kluwer Academic Publishers, Dordrecht, 1996, p. 95.
[16] H.-J. Himmel, A.J. Downs, T.M. Greene, L. Andrews, Organometallics 19 (2000) 1060.
[17] A. Zumbusch, H. Schnöckel, J. Chem. Phys. 108 (1998) 8092.
[18] L. Manceron, A. Loutellier, J.P. Perchard, Chem. Phys. 92 (1985) 75.
[19] M.J. Frisch, G.W. Trucks, H.B. Schlegel, G.E. Scuseria, M.A. Robb, J.R. Cheeseman, V.G. Zakrzewski, J.A. Montgomery, R.E. Stratmann, J.C. Burant, S. Dapprich, J.M. Millam, A.D. Daniels, K.N. Kudin, M.C. Strain, O. Farkas, J. Tomasi, V. Barone, M. Cossi, R. Cammi, B. Mennucci, C. Pomelli, C. Adamo, S. Clifford, J. Ochterski, G.A. Petersson, P.Y. Ayala, Q. Cui, K. Morokuma, D.K. Malick, A.D. Rabuck, K. Raghavachari, J.B. Foresman, J. Cioslowski, J.V. Ortiz, B.B. Stefanov, G. Lui, A. Liashenko, P. Piskorz, I. Komaromi, R. Gomperts, R.L. Martin, D.J. Fox, T. Keith, M.A. Al-Laham, C.Y. Peng, A. Nanayakkara, C. Gonzalez, M. Challacombe, P.M.W. Gill, B.G. Johnson, W. Chen, M.W. Wong, J.L. Andres, M. Head-Gordon, E.S. Replogle, J.A. Pople, GAUSSIAN-98, Revision A.3, Gaussian Inc., Pittsburgh, PA, 1998.
[20] (a) E.J. Baerends, A. Berces, C. Bo, P.M. Boerringter, L. Cavallo, L. Deng, R.M. Dickson, D.E. Ellis, L. Fan, T.H. Fischer, C. Fonseca Guerra, S.J. van Gisbergen, J.A. Groeneveld, O.V. Gritsenko, F.E. Harris, P. van den Hoek, H. Jacobsen, G. van Kessel, F. Kootstra, E. van Lenthe, V.P. Osinga, P.H.T. Philipsen, D. Post, C.C. Pye, W. Ravenek, P. Ros, P.R.T. Schipper, G. Schreckenbach, J.G. Snijders, M. Sola, D. Swerhone, G. Te Velde, P. Vernooijis, L. Versluis, O. Visser, E. van Wezenbeek, G. Wisenekker, S.K. Wolff, T.K. Woo, T. Ziegler, ADF Program System Release 2.3, 1997;
(b) C. Fonseca Guerra, J.G. Snijders, G. Te Velde, E.J. Baerends, Theor. Chim. Acta 99 (1998) 391.
[21] B.S. Jursic, J. Mol. Struct. (THEOCHEM) 428 (1998) 61.
[22] A.J. Hinchcliffe, J.S. Ogden, D.D. Oswald, J. Chem. Soc., Chem. Commun. (1972) 338.
[23] (a) P.H. Kasai, P.M. Jones, J. Am. Chem. Soc. 106 (1984) 8018;
(b) J.H.B. Chenier, C.A. Hampson, J.A. Howard, B. Mile, R. Sutcliffe, J. Phys. Chem. 90 (1986) 1524.
[24] (a) J.H.B. Chenier, C.A. Hampson, J.A. Howard, B. Mile, J. Chem. Soc., Chem. Commun. (1986) 730;
(b) G.V. Chertikhin, I.L. Rochanskii, L.V. Serebrennikov, V.F. Shevel'kov, Russ. J. Phys. Chem. (Engl. Transl.) 62 (1988) 1165.
[25] C. Xu, L. Manceron, J.P. Perchard, J. Chem. Soc., Faraday Trans. 89 (1993) 1291.
[26] (a) V. Balaji, K.K. Sunil, K.D. Jordan, Chem. Phys. Lett. 136 (1987) 309;
(b) P. Pullumbi, Y. Bouteiller, Chem. Phys. Lett. 234 (1995) 107;
(c) S.S. Wesolowski, T.D. Crawford, J.T. Fermann, H.F. Schaefer III, J. Chem. Phys. 104 (1996) 3672.
[27] H.-J. Himmel, A.J. Downs, J.C. Green, T.M. Greene, J. Phys. Chem. A 104 (2000) 3642.
[28] (a) M.A. Douglas, R.H. Hauge, J.L. Margrave, J. Phys. Chem. 87 (1983) 2945;
(b) F.W. Froben, W. Schulze, U. Kloss, Chem. Phys. Lett. 99 (1983) 500;
(c) K. Balasubramanian, J. Li, J. Chem. Phys. 88 (1988) 4979.
[29] See for example: (a) G.L. Geoffroy, M.S. Wrighton, Organometallic Photochemistry, Academic Press, New York, 1979, Chapter 2;
(b) R.B. Hitam, K.A. Mahmoud, A.J. Rest, Coord. Chem. Rev. 55 (1984) 1.
[30] H.-J. Himmel, L. Manceron, unpublished results.
[31] H.-J. Himmel, A.J. Downs, unpublished results.
[32] H.-J. Himmel, A.J. Downs, T.M. Greene, J. Am. Chem. Soc. 122 (2000) 9793.
[33] H.-J. Himmel, A.J. Downs, T.M. Greene, Inorg. Chem. 40 (2001) 396.
[34] H.-J. Himmel, A.J. Downs, J.C. Green, T.M. Greene, J. Chem. Soc., Dalton Trans. (2001) 535.

[35] S. Sakai, J. Phys. Chem. 96 (1992) 8369.
[36] B. Gaertner, H.-J. Himmel, P.H. Kasai, unpublished results.
[37] (a) S. Süzer, L. Andrews, J. Am. Chem. Soc. 109 (1987) 300; (b) A. Loutellier, L. Manceron, J.P. Perchard, Chem. Phys. 146 (1990) 179.
[38] (a) J.W. Kauffman, R.H. Hauge, J.L. Margrave, High Temp. Sci. 17 (1984) 237; (b) J. Szczepanski, M. Szczesniak, M. Vala, Chem. Phys. Lett. 162 (1989) 123; (c) D.W. Ball, R.H. Hauge, J.L. Margrave, High Temp. Sci. 25 (1988) 95.
[39] R.D. Davy, H.F. Schaefer III, J. Phys. Chem. A 101 (1997) 3135.
[40] (a) G.A. Bowmaker, Aust. J. Chem. 31 (1978) 2549; (b) M. Trabelsi, A. Loutellier, J. Mol. Struct. 43 (1978) 151; (c) J.B. Everhart, B.S. Ault, Inorg. Chem. 35 (1996) 4090.
[41] G. Herzberg, Molecular Spectra and Molecular Structure. III. Electronic Spectra and Electronic Structure of Polyatomic Molecules, van Nostrand, Princeton, NJ, 1966, p. 583.
[42] (a) J.M. Parnis, G.A. Ozin, J. Phys. Chem. 93 (1989) 1215; (b) G.V. Chertihin, L. Andrews, J. Phys. Chem. 97 (1993) 10295.
[43] L. Knight Jr., J.R. Woodward, T. Kink, C.A. Arrington, J. Phys. Chem. 97 (1993) 1304.
[44] Z.L. Xiao, R.H. Hauge, J.L. Margrave, Inorg. Chem. 32 (1993) 642.
[45] P. Pullumbi, C. Mijoule, L. Manceron, Y. Bouteiller, Chem. Phys. 185 (1994) 13.
[46] L.B. Knight Jr., J.J. Banisaukas III, R. Babb, E.R. Davidson, J. Chem. Phys. 105 (1996) 6607.
[47] J.-P. Gu, F. Kong, M.-B. Huang, J. Mol. Struct. (THEOCHEM) 228 (1991) 87.
[48] F.A. Kurth, R.A. Eberlein, H. Schnöckel, A.J. Downs, C.R. Pulham, J. Chem. Soc., Chem. Commun. (1993) 1302.
[49] P. Pullumbi, Y. Bouteiller, L. Manceron, C. Mijoule, Chem. Phys. 185 (1994) 25.
[50] K.P. Huber, G. Herzberg, Molecular Spectra and Molecular Structure. IV. Constants of Diatomic Molecules, van Nostrand Reinhold, New York, 1979.
[51] (a) R. Köppe, H. Schnöckel, J. Chem. Soc., Dalton Trans. (1992) 3393; (b) H.-J. Himmel, A.J. Downs, T.M. Greene, J. Am. Chem. Soc. 122 (2000) 922.
[52] (a) C.R. Pulham, A.J. Downs, M.J. Goode, D.W.H. Rankin, H.E. Robertson, J. Am. Chem. Soc. 113 (1991) 5149; (b) A.J. Downs, T.M. Greene, H.-J. Himmel, E. Johnsen, unpublished results.
[53] (a) J.M. Parnis, G.A. Ozin, J. Phys. Chem. 93 (1989) 1204, 1220; (b) R.D. Lafleur, J.M. Parnis, J. Phys. Chem. 96 (1992) 2429.
[54] (a) M.A. Lefcourt, G.A. Ozin, J. Am. Chem. Soc. 110 (1988) 6888; (b) B. Gaertner, H.-J. Himmel, unpublished results.
[55] V.E. Bondybey, M. Räsänen, A. Lammers, Annu. Rep. Prog. Chem., Sect. C 95 (1999) 331.
[56] J.S. Robinson, L.M. Ziurys, Astrophys. J. Lett. 472 (1996) L131.
[57] (a) L.B. Knight Jr., K. Kerr, P.K. Miller, C.A. Arrington, J. Phys. Chem. 99 (1995) 16842; (b) T.J. Tague Jr., L. Andrews, J. Am. Chem. Soc. 116 (1994) 4970.
[58] G. Treboux, J.-C. Barthelat, J. Am. Chem. Soc. 115 (1993) 4870.
[59] (a) Z. Palágyi, R.S. Grev, H.F. Schaefer III, J. Am. Chem. Soc. 115 (1993) 1936; (b) Z. Palágyi, H.F. Schaefer III, Chem. Phys. Lett. 203 (1993) 195; (c) Y. Yamaguchi, B.J. DeLeeuw, C.A. Richards Jr., H.F. Schaefer III, G. Frenking, J. Am. Chem. Soc. 116 (1994) 11922.
[60] (a) J. Su, X.-W. Li, R.C. Crittendon, G.H. Robinson, J. Am. Chem. Soc. 119 (1997) 5471; (b) G.H. Robinson, Acc. Chem. Res. 32 (1999) 773; (c) G.H. Robinson, Chem. Commun. (2000) 2175.
[61] J.C. Stephens, E.E. Bolton, H.F. Schaefer III, L. Andrews, J. Chem. Phys. 107 (1997) 119.
[62] F.G.A. Stone, R. West (Eds.), Advances in Organometallic Chemistry, vol. 39, Academic Press, San Diego, 1996.
[63] (a) P.P. Power, Chem. Rev. 99 (1999) 3463; (b) W.H. Fink, P.P. Power, T.L. Allen, Inorg. Chem. 36 (1997) 1431.
[64] J.P. Campbell, J.-W. Hwang, V.G. Young Jr., R.B. Von Dreele, C.J. Cramer, W.L. Gladfelter, J. Am. Chem. Soc. 120 (1998) 521.
[65] (a) J.D. Carpenter, B.S. Ault, J. Phys. Chem. 95 (1991) 3502; (b) J.D. Carpenter, B.S. Ault, Chem. Phys. Lett. 197 (1992) 171; (c) M. Sugie, H. Takeo, C. Matsumura, Chem. Phys. Lett. 64 (1979) 573; (d) M.L. McKee, J. Phys. Chem. 96 (1992) 5380.
[66] M.W. Schmidt, P.N. Truong, M.S. Gordon, J. Am. Chem. Soc. 109 (1987) 5217.
[67] C. Schade, P.v.R. Schleyer, J. Chem. Soc., Chem. Commun. (1987) 1399.
[68] T.J. Dudley, W.W. Brown, M.R. Hoffmann, J. Phys. Chem. A 103 (1999) 5152.

PERGAMON

Polyhedron 21 (2002) 489–501

POLYHEDRON

www.elsevier.com/locate/poly

Synthesis and structure of metalloid aluminum clusters —intermediates on the way to the elements

Hansgeorg Schnöckel *, Harald Köhnlein

Institut für Anorganische Chemie, Universität Karlsruhe (TH), Engesserstrasse, Geb. 30.45, 76128 Karlsruhe, Germany

Received 9 August 2001; accepted 27 November 2001

Abstract

Metastable Aluminum(I) halide solutions proved to have a high potential for the synthesis of novel subvalent Al compounds, such as Al_nX_m species (X = Cl, Br, I; $n < m$, average oxidation state of Al below $+3$ or $n > m$, average oxidation state of Al below $+1$) or Al_nR_m species (R = bulky ligand; $n > m$). There are two principal reaction types, which are essential for the formation of the compounds discussed herein. The disproportionation, which finally results in Al(III) halides and Al metal and the metathesis which leads to a substitution of X atoms against R groups. By this way the *metalloid* cluster compounds $[Al_7\{N(SiMe_3)_2\}_6]^-$, $[Al_{12}\{N(SiMe_3)_2\}_8]^{-\bullet}$, $[Al_{14}I_6\{N(SiMe_3)_2\}_6]^{2-}$, $[Al_{69}\{N(SiMe_3)_2\}_{18}]^{3-}$, and $[Al_{77}\{N(SiMe_3)_2\}_{20}]^{2-\bullet}$ could be isolated. The characteristic feature of these *metalloid* Al clusters is the number of Al–Al contacts being larger than the number of Al–ligand bonds, i.e. there are more 'naked' than ligand-bonded Al atoms. Furthermore, the topology of the closest packing in Al metal is already pre-formed in these compounds. © 2002 Elsevier Science Ltd. All rights reserved.

Keywords: Aluminum(I) halides; Metalloid clusters; Nanosized clusters; Intermediates; Metal lattice; X-ray structural analysis

1. Introduction

Recently we introduced the term of *metalloid* cluster [1] in order to limit the very broad definition of Cotton's *metal atom* cluster [2]. The fact that the core of a *metal atom* cluster can also contain non-metal atoms leads to the logical consequence of describing the large selenide and sulfide clusters—e.g. $Cu_{146}Se_{73}$ synthesized by Fenske and co-workers [3]—as *metal atom* clusters as well. In contrast, the definition *metalloid* was originally limited to the macroscopic properties of elements (e.g. germanium) and shall now also include the topology of atoms, i.e. *metalloid* clusters exhibit a similar topology of the atoms as in the metal itself. The suffix *-oid* from the Greek term ειδος means idea, prototype: i.e. the topology of a *metalloid* cluster contains the idea of the formation of metals. For elements occurring in various modifications (e.g. gallium) the term *elementoid* would be more comprehensive.

However, *metalloid* clusters do not necessarily have to be *metallic* clusters, as these—apart from the topology of atoms—should also possess other properties attributed to metals (e.g. electrical conductivity). However, *metallic* clusters of this type ought to be obtained only with far larger sized metal frames than the *metalloid* aluminum clusters described below. For instance, within the $[Al_{77}\{N(SiMe_3)_2\}_{20}]^{2-}$ cluster compound [4] there is a core of 57 'naked', no ligand-bearing metal atoms surrounded by 20 ligand bound metal atoms which results in the number of metal–ligand bonds being smaller than the number of metal–metal contacts.

Metalloid clusters might well be formed as intermediates during the reduction of metal compounds on the way to the metal, i.e. the oxidation state approximates 0. *Metalloid* precious metal clusters were firstly in the center of interest, as these precious metals which represent the final steps during the reduction process are known to be stable even under drastic chemical conditions (e.g. acid). In the last decades, a considerable number of results concerning such *metalloid* clusters, e.g. of gold, palladium and platinum, have been obtained and discussed in numerous monographs [5,6].

* Corresponding author. Tel.: +49-721-608-2981; fax: +49-721-608-4854.

E-mail address: hansgeorg.schnoeckel@chemie.uni-karlsruhe.de (H. Schnöckel).

0277-5387/02/$ - see front matter © 2002 Elsevier Science Ltd. All rights reserved.
PII: S0277-5387(01)01028-2

However, until recently only a few precious metal clusters with a larger number of 'naked' metal atoms were known and could be characterized unambiguously by X-ray structural analysis. For example, the $[Ni_{38}Pt_6(CO)_{48}H_{6-n}]^{n-}$ cluster [7] synthesized in 1985 contains only six 'naked' metal atoms, and the $Pd_{59}(CO)_{32}(PMe_3)_{21}$ cluster molecule [8] published in 1999 carries 11 of them. The most astonishing cluster compound of this type is a $Pd_{145}(CO)_{60}(PEt_3)_{30}$ cluster [9] with 55 'naked' Pd atoms. Therefore, the publication describing the $[Al_{77}R_{20}]^{2-}$ cluster in 1997 [4] came as a surprise in many respects:

1. It was the first molecular *metalloid* cluster of a non-precious metal to be structurally analyzed. The crystals of the $[Al_{77}R_{20}]^{2-}$ compound showed to be reactive, partly pyrophoric.
2. It was the largest *metalloid* cluster (57 'naked' Al atoms) ever to be structurally analyzed [10].

How unexpected the formation of such a cluster of non-precious metals had been can be seen in the fact that only 8 years before the first molecular compound with one Al–Al bond had been published [11].

For a better insight of the formation of *metalloid* Al clusters we start with a short survey of the historical development of their synthesis principle. This cluster chemistry of nanosized species has its origin in the spectroscopical characterization of biatomic high-temperature molecules AlX (X = Cl, Br, I), whose reactivity was examined by means of matrix isolation techniques in our group several years ago. For instance, in solid argon, molecular AlF was found to react with O atoms to give O=AlF, the first compound with an Al=O double bond [12]; another example is the reaction between HCl and AlCl in solid argon leading to the extraordinary $HAlCl_2$ molecule [13]. Evidently, the roots of *metalloid* clusters are to be found in the area of pure basic research of smallest molecules. Subsequently, we transferred the synthesis of AlX from matrix conditions (μg- to mg-scale) to the preparative scale (g-scale) [14–16] and thus obtained metastable AlX solutions, which are unstable towards disproportionation to give AlX_3 and solid aluminum. This behavior is plausible due to the high temperature equilibrium (Scheme 1):

Under mild conditions (in the range of -78 to $+50$ °C) this disproportionation reaction can be controlled in a way that intermediates, such as Al_2X_4 species, can be trapped on the way to AlX_3 and *metalloid* Al clusters on the way to metal (Al_nX_m with $n > m$, resp. Al_nR_m upon substituting the halogenide by larger ligands R). In this review we will show that by simple variation of the reaction conditions the number of Al atoms in these *metalloid* clusters can be altered and that actually the topology of the Al metal with closed packing of Al atoms is already pre-formed in small molecular units. If, however, a variation from the close packing of Al atoms is observed, these clusters may give an indication for hypothetical new modifications of Al (cf. Chapter 3b).

$$3\ AlX_{(g)} \rightleftharpoons 2\ Al_{(s)} + AlX_{3\,(g)}$$

Scheme 1.

$$2\ Al_{(l)} + AlX_{3\,(g)} \rightleftharpoons 3AlX_{(g)}$$

Scheme 2.

2. Technique for the synthesis of metastable AlX solutions

The synthesis of *metalloid* AlX solutions (X = Cl, Br, I) is based on the primary generation of molecular AlX, which unlike the disproportionation to solid Al and AlX_3 will be thermodynamically stable only at a temperature of about 1000 °C and a pressure of 10^{-3} mbar, i.e. in principle AlX is synthesized by comproportionation (Scheme 2).

AlX is generated by passing gaseous AlX_3 over liquid Al. Lower temperatures such as 500 °C or higher pressures will move the equilibrium to the $Al + AlX_3$ side. Due to the difficulties in handling of AlX_3 HX proved to be more suitable for our synthesis technique. Passing HX over liquid aluminum contained in a graphite oven [15,16] leads to the formation of either AlX_3 at lower temperatures (Scheme 3) or immediately to the formation of AlX in the hot zone (Scheme 4).

The AlX molecules emitted from the graphite oven are frozen on a surface which is cooled to -196 °C under high vacuum conditions (10^{-5} mbar) before any disproportionation can occur. Simultaneously a mixture of solvents such as toluene/ether is condensed, so that the AlX molecules are embedded in a solid matrix of the solvent. The solvent has to fulfil the following criteria:

1. it has to be vaporizable easily at room temperature,
2. it should have good solving properties with a melting point as low as possible (e.g. toluene at $T = -83$ °C),
3. it should contain a donor component such as Et_2O or NEt_3, which can contribute to stabilize the AlX molecules.

$$Al_{(l)} + 3\ HX_{(g)} \xrightarrow{500\ °C} AlX_{3\,(g)} + 3/2\ H_{2\,(g)}$$

Scheme 3.

$$Al_{(l)} + HX_{(g)} \xrightarrow{1000\ °C} AlX_{(g)} + 1/2\ H_{2\,(g)}$$

Scheme 4.

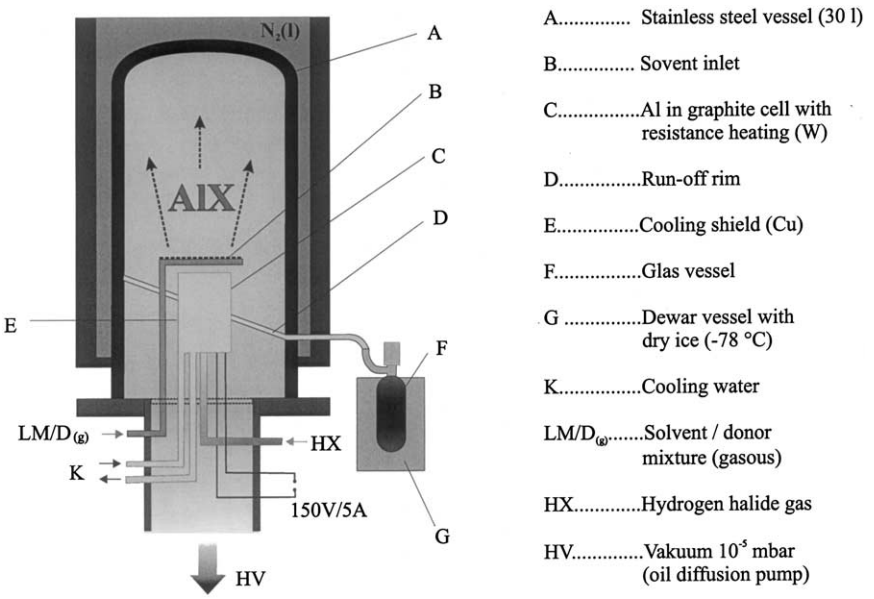


Fig. 1. Schematic illustration of the cocondensation apparatus for the generation of gaseous AlX high-temperature species.

For obvious reasons, H-acide solvents such as alcohol are omitted ($AlX + HOR \rightarrow HAlXOR$). Fig. 1 shows a sketch of the apparatus we used for this experiment. Upon removing the coolant a metastable AlX solution is obtained at a temperature of approximately -100 °C which is collected in a Schlenk vessel attached to the apparatus. This solution can be kept in a freezer (e.g. at -30 °C) without signs of disproportionation. These AlX solutions will be discussed with regard to the following questions.

1. Which species Al_nX_n are contained in the primary solution?
2. Which metathesis reactions to $(AlR)_n$ oligomers have been carried out?
3. Which Al_nX_m $(n > m)$ clusters are developed in the primary solution?
4. Which *metalloid* clusters will arise if both reactions—disproportionation and metathesis reaction—go off simultaneously?

For comprehensible reasons, we herein mainly focus on those *metalloid* clusters, which are listed under Section 3.4.

3. Subvalent Al compounds from AlX solutions

3.1. Al_nX_n species in the primary AlX solution

First of all, our special interest was focussed on the nature of the species existing in the primary AlX solutions. The detection and characterization of the dissolved species in AlX solutions proved to be difficult due to the lack of suitable analytical methods [17]. Thus, only crystalline products can be definitely characterized by X-ray structural analysis. We succeeded in synthesizing several crystalline $(AlX)_4$ tetramers which consist of a planar 4-membered ring of Al atoms stabilized by donor molecules: $Al_4X_4{\cdot}4D$ (X = Br, I; D = MeOPh, NEt_3, PEt_3) [18,19]. The molecular structure of $Al_4Br_4{\cdot}4NEt_3$ shown in Fig. 2 is representative for all these species.

As these compounds—in contrast to most other subvalent Al species—are soluble in toluene, they could be used as starting materials in substitution reactions with bulky ligands such as $Si(SiMe_3)_3$ or $N(SiMe_3)_2$ (cf. next chapters).

3.2. Metathesis reaction

An established strategy for the synthesis of subvalent aluminum compounds is the substitution of the halide by a ligand with great steric demand according to the metathesis in Scheme 5.

The driving force for the metathesis reaction is the formation of solid MX salt. So far, no monomeric AlR products [20], but several $(AlR)_4$ tetramers [21] are structurally characterized which implies that the metathesis of AlX species is accompanied by the forma-

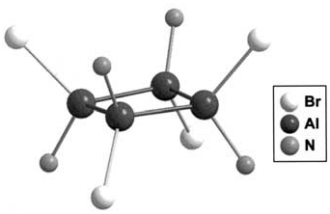


Fig. 2. Molecular structure of $Al_4Br_4{\cdot}4NEt_3$ (ethyl groups are omitted). The Al–Al bond length amounts to 2.653 Å.

$$AlX + MR \longrightarrow AlR + MX$$

(X = Cl, Br, I; M = Li, Na;

R = nonmetallic ligand, e.g. Cp = C_5H_5, Cp* = C_5Me_5)

Scheme 5.

tion of new Al–Al bonds. The ligand R must be able to (i) compensate partially the electron deficiency of the aluminum atoms, (ii) shield the 'metallic' skeleton from the insertion of further Al(I) species, and (iii) prevent reactions of O_2, e.g. via the formation of heterocuban-like $Al_4O_4R_4$ species [22].

3.2.1. $Al_4Cp^*_4$ (1)

Arenes with 6π electrons such as the substituted cyclopentadienyde anion $Cp^* = C_5Me_5$ are because of their sterical demand and their capability to act as electron donor well suited for stabilizing metals in low oxidation states. In 1986 Jutzi et al. synthesized the first monomeric Si(II) compound with a Cp* ligand. The analogous Al(I) compound, $Al_4Cp^*_4$ (**1**) (Fig. 3), prepared in our group 10 years ago [23], was the first example of a crystallographically characterized stable Al(I) compound at 300 K [24].

Compound **1** was prepared via a metathesis reaction between dissolved AlCl and $MgCp^*_2$ according to Scheme 6 [23,25].

The characteristic structural feature of **1** is the central Al_4 tetrahedron. The average Al–Al bond length amounts to 2.767 Å [23,26].

3.2.2. Al_4R_4

Other tetrameric Al(I) compounds could be stabilized by the ligands $R = Si^tBu_3$ (*supersilyl*), [22,27], $Si(SiMe_3)_3$ (*hypersilyl*) [26,28], $C(SiMe)_3$ (*trisyl*) [29]. The *supersilyl* and *hypersilyl* compounds exhibiting T_d symmetry are products of metathesis reactions of AlCl with LiR, the $Al_4\{C(SiMe)_3\}_4$ tetraedral species was synthesized by H.W. Roesky and co-workers by reductive elimination: $AlCl_2C(SiMe)_3$ is reduced by potassium while heating up to 100 °C [29]. Furthermore a new tetrahedral Al_4 species with two different substituents is known: $Al_4Cp^*_3N(SiMe_3)_2$ [30].

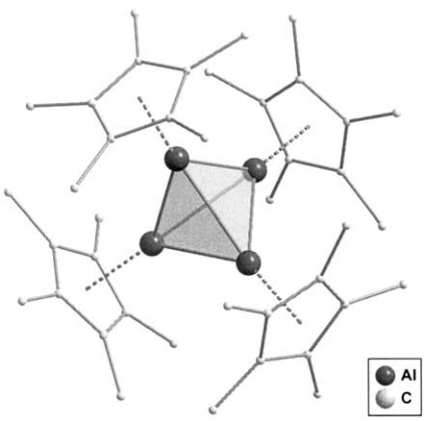


Fig. 3. Molecular structure of **1** (H atoms are excluded).

$$4\,AlCl + 4\,MgCp^*_2 \longrightarrow 2\,(MgCp^*Cl)_2 + Al_4Cp^*_4$$

Scheme 6.

3.3. Disproportionation

The disproportionation of Al^IX species finally results in the formation of Al(III) halides and aluminum metal. Upon warming a metastable AlX solution the disproportionation process is initiated which leads to intermediates Al_nX_m ($n > m$) with average oxidation states of the aluminum atoms between +1 and 0—in addition to species with oxidation states between +1 and +3 ($n < m$). Starting from Al^IX solutions we were able to trap the first aluminum subhalides with $n > m$ (oxidation state of Al below +1) and $n < m$ (oxidation state of Al below +3). In contrast to the other elements of the 13th Group, aluminum subhalides were not known before. Even M_2X_4 species, well-known for gallium (e.g. Ga_2Br_4 [31]) and boron (e.g. B_2Cl_4 [32]), have been obtained for the first time via the condensation technique described here: Al_2Br_4·2anisol which is shown in Fig. 4 [33].

3.3.1. Al_5Br_7·5THF (2)

By concentrating an AlBr·THF solution to half the volume at room temperature the solvent excess is removed. From this solution the mixed-valent compound $[Al_5Br_6{\cdot}6THF]^+[Al_5Br_8{\cdot}4THF]^-$ (**2a** and **2b**, respectively; Fig. 5 [34]) crystallized which represents the first salt-like subvalent Al species. The average oxidation state of the aluminum atoms is 1.4. Therefore, the disproportionation of AlBr has been stopped on the way to Al_2Br_4 and finally $AlBr_3$. Both ions consist of a central Al atom, which is tetrahedrally surrounded by four Al atoms. While the anion is coordinated by four $AlBr_2$·THF groups, in the cation two $AlBr_2$·THF and two AlBr·2THF units are arranged around the central Al atom.

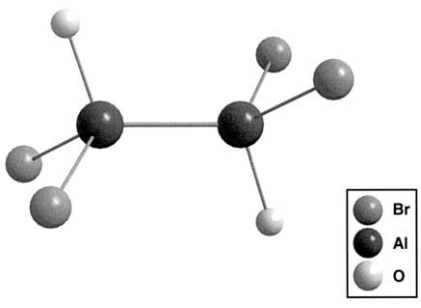


Fig. 4. Molecular structure of Al_2Br_4·2anisol.

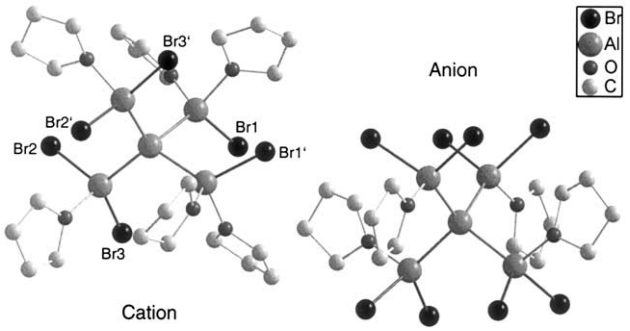


Fig. 5. Molecular structure of $[Al_5Br_6{\cdot}6THF]^+$ (**2a**; left) and $[Al_5Br_8{\cdot}4THF]^-$ (**2b**; right); without H atoms. Average bond lengths (Å): Al–Al: 2.532, Al–Br: 2.346, Al–Br2/Br2′: 2.380, Al–O: 1.884.

Starting from $GaCl{\cdot}Et_2O$ the analogous neutral compound, $Ga_5Cl_7{\cdot}5Et_2O$, with only one $GaCl{\cdot}2Et_2O$ unit and three $GaCl_2{\cdot}Et_2O$ units surrounding a central Ga atom can be synthesized [35].

A hypothetical mechanism for the formation of $E_5X_7{\cdot}5D$ (E = Al, Ga; X = Cl, Br; D = THF, Et_2O) species proceeds as follows. Starting from $E^{III}X_3{\cdot}D$ the comproportionation products $E_2X_4{\cdot}2D$ [36], $E_3X_5{\cdot}3D$ [37] and finally $E_5X_7{\cdot}5D$ can be formed by successive insertion of $E^{I}X{\cdot}D$ units [34].

3.3.2. $Al_{22}X_{20}{\cdot}12D$ [X = Br, D = THF (3a); X = Cl, D = THF (3b); X = Cl, D = THP (3c)]

Simultaneously with the synthesis of the halogen-rich oxidation product $Al_5Br_7{\cdot}5THF$ (**2**) we were able to isolate the halogen-deficient species $Al_{22}Br_{20}{\cdot}12THF$ (**3a**) as a product of a reduction [38]. From AlCl·D (D = THF, THP) solution the species $Al_{22}Cl_{20}{\cdot}12THF$ (**3b**) resp. $Al_{22}Br_{20}{\cdot}12THP$ (**3c**) could be isolated [39]. The $Al_{22}X_{20}{\cdot}12D$ molecules are the first polyhedral subvalent Al species with a novel type of structure in the chemistry of the 13th Group and, to the best of our knowledge, in the entire field of chemistry. Even for boron such types of molecule are not known, though solid boron exhibits B_{12} icosahedra that can be connected to further boron atoms. The result of the X-ray structural analysis of **3a** is shown in Fig. 6.

The common feature of **3** is a compressed icosahedral Al_{12} framework coordinated via Al–Al bonds by 10 $AlX_2{\cdot}D$ groups and two donor molecules for the stabilization of the 'naked' Al atoms at the top and the bottom. Therefore, the formula $Al_{12}[AlX_2{\cdot}L]_{10}{\cdot}2L$ is a more appropriate description for these compounds. The aluminum atoms' average oxidation state amounts to 0.91. The formal oxidation state of the 12 Al atoms of the icosahedral unit is 0, whereas the 10 halide bearing Al atoms have the oxidation state +2. Thus, the $Al_{22}X_{20}$ molecules can be considered as products of an *internal* disproportionation of 24 AlX units with formal elimination of Al_2Br_4.

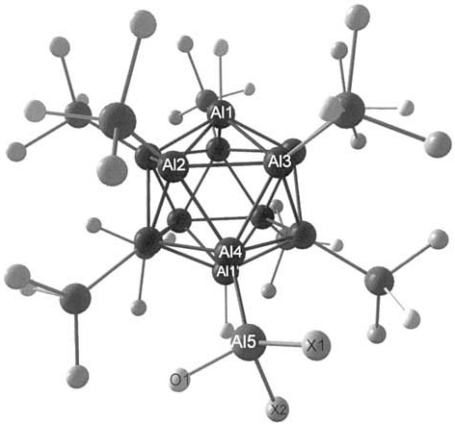


Fig. 6. Molecular structure of $Al_{22}Br_{20}{\cdot}12THF$ (**3a**). Only the O atoms of the donor molecules are illustrated. Selected Al–Al distances (Å): Al1–Al2: 2.650, Al2–Al3: 2.762, Al3–Al4: 2.692, Al4–Al5: 2.526.

The bonding situation can be described according to the Wade's rules: The 2 *para*-positioned Al atoms of the inner icosahedron can each contribute three electrons to the polyhedral framework, whereas the remaining 10 Al atoms, which bear AlX_2 groups, can only each provide two electrons. This 26 electron framework ($2n + 2$ with $n = 12$) corresponds to a *closo*-type molecule (icosahedron).

If we consider the icosahedral Al_{12} core as an intermediate on the way to the metal formation, the polyhedral coordination with the lack of a central atom doesn't fit with the *fcc* structure of aluminum metal. This arises the question if there might exist a second Al modification (β-Al) consisting of icosahedral Al_{12} entities—in contrast to the anticuboctahedral coordination pattern of *fcc* Al metal (α-Al). By means of ab inito full-potential calculations [39] we compared the *fcc* type and the hypothetical new modification which would be analogous to the β-rhombohedral boron. In order to minimize computing time we calculated the hypothetical β-Al type with the structure of α-B where B_{12} icosahedra are arranged as in a cubic close packing of spheres. The results principally show, that β-Al as the less compact allotrope (in comparison to *fcc* α-Al) is indeed energetically between **3** and Al metal (α-Al). By means of quantum chemical calculations it has been demonstrated that starting from AlCl about 80% of the disproportionation energy is gained by the formation of **3**. During the remaining energy drop the hypothetical β-Al, at first, and finally $AlCl_3$ and Al metal is formed as the bottom of the thermodynamical ladder. Thus, in principle it may be possible to reach this new Al allotrope via species like **3**.

In order to get a better insight in this novel type of clusters we performed some spectroscopic investigations.

In addition to the X-ray structural analysis, the different types of Al atoms in $Al_{22}Br_{20}{\cdot}12THF$ were validated by ^{27}Al MQMAS (Multiple Quantum Magic

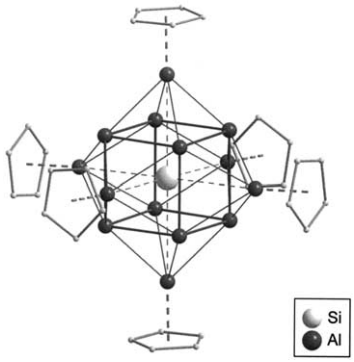


Fig. 7. Molecular structure of $SiAl_{14}Cp^*_6$ (**4**); methyl groups are excluded. Selected distances (Å): Al–Si: 2.49…2.51, Al_{cube}–Al_{cube}: 2.90, Al_{cube}–Al_{Cp^*} : 2.79…2.81.

Angle Spinning) spectroscopy and XPS. The three types of Al atoms—the exterior Al atoms which bear the AlX_2·THF groups, the 'naked' Al atoms and the THF coordinated—were found in the expected ratio of 10:10:2. The results of ^{27}Al MQMAS spectroscopy and XPS for **3a** and **3b** indicate that the 'quasi-naked' Al atoms, which are only coordinated by THF molecules are relatively close to those obtained for elemental aluminum. In contrast, the Al atoms in **3a** and **3b** which are neighbored to halide bearing Al atoms, in spite of their oxidation state of 0, behave differently. However, the two spectroscopic methods can distinguish between the Al atoms in their different chemical environments. Ab initio calculations lend further support for the experimental results. It was firstly demonstrated that XPS has the capacity to identify subvalent Al atoms by the measurement of the Al(I) compound $Al_4Cp^*_4$ [39].

Following the detailed quantum chemical calculations for **3** we tried to find a simple, general scheme to classify bonding in Al resp. Ga subhalides and partially substituted subhalides. We found, that in E_nX_{n+y} species there are $n-1/2y$ bonding MOs for E–E bonds [39,40]. Only for $y \leq 0$ there exist $2e^-$–2c bonds—e.g. Al_4X_4 [18,19]: four Al–Al bonds, Al_5X_7 [34]: four Al–Al bonds, $Al_5Cp^*_3I_6$ [41]: three Al–Al bonds, Al_2X_4 [33]: one Al–Al bond, AlX_3: no Al–Al bonds—while multiple center bonding is observed for $y < 0$ like in the species E_nX_{n-2}, e.g. $Al_{22}X_{20}$ [38,39]; E_nX_{n-4} ($\triangleq E_nX^{2-}_{n-2}$), e.g. $Al_{14}R_6I^{2-}_6$ [42] (cf. Chapter 4c); E_nX_{n-5}, e.g. $Al_{12}R_8^-$ [43] (cf. Chapter 4b). That means, a decreasing number of X ligands in comparison with the number of E atoms leads to an increasing quantity of multiple center bonds.

3.3.3. $SiAl_{14}Cp^*_6$ (4)

In this chapter the compound $SiAl_{14}Cp^*_6$ (**4**) is discussed together with the disproportionation products of halides because a precursor of **4** is (i) the $SiAl_4Cl_8$ halide [44] where a Si atom is tetrahedrally surrounded by four Al atoms and (ii) besides **4** Cl-containing species, e.g. $SiAl_{14}Cl_2Cp^*_6$, are generated [45] (cf. below). The species **4** is synthesized via two routs: (i) the reaction between $SiCp^*_2$ and AlCl and (ii) the reaction of $SiCl_4$ with AlCp*. The molecular structure of **4** is shown in Fig. 7.

$$Si(AlCl_2)_4 + 6\,AlCl \longrightarrow SiAl_8Cl_8 + 2\,AlCl_3$$

Scheme 7.

The main structural unit of **4** is a body-centered Al_8 cube with a Si atom in the center. The six faces of the cube are capped by six AlCp* groups.

Besides the X-ray characterization, the composition of the $SiAl_{14}$ cluster was validated by laser desorption mass spectroscopy. The existence of the molecular peak of **4** (M^+: 1217 m/e) in the mass spectrum demonstrated that **4** exhibits a relatively stable species which can be vaporized without decomposition [45].

Counting the electrons gave another hint of the stability of **4**. If the central Si atom contributes four electrons to the cluster core, each of the eight Al atoms of the $SiAl_8$ cube adds three electrons and the outer six Al atoms each contribute two electrons, then 40 electrons result for the whole cluster entity. Metal clusters with 40 electrons correspond to a stable *Jellium* state [46].

However, the X-ray structural determination indicated that besides **4** there exist a $SiAl_{14}Cl_2Cp^*_6$ (**4a**) species in the same crystal. Species like **4a** are plausible, since the above mentioned $SiAl_4Cl_8$ compound [44] may react with AlCl to generate $SiAl_8Cl_8$ which contains a cube of Al atoms in the first step (Scheme 7).

In a second step, the eight Cl atoms are removed by reacting with AlCl or AlCp* and the six AlCp* units are added to complete the formation of **4**. Thus, **4a** is an intermediate on this way to **4** [45] (Scheme 8) as shown by a DFT calculation.

The formula $SiAl_8(AlCp^*_6)$ emphasizes the different types of Al atoms: the six exohedral Al atoms have each a formal oxidation state of +1, i.e. **4** is formed via a disproportionation of Al(I) halides and, finally, a substitution with the help of the reductive capacity of AlCp*. In contrast, as the result of a disproportionation reaction, the oxidation state of the inner eight Al atoms is 0.

The structure of the inner $SiAl_8$ cube of **4** represents a cut-off from a *bcc* metal lattice—instead of the *fcc* lattice of metallic aluminum. In view of the Si atom in the center the $SiAl_8$ framework of **4** could be regarded

$$AlCp^* + SiAl_{14}Cl_2Cp^*_6\,(\mathbf{4a}) \longrightarrow SiAl_8(AlCp^*)_6\ (\mathbf{4}) + AlCp^*Cl_2$$

Scheme 8.

as a molecular Si–Al alloy. It seems to be promising if it would be possible to prepare more of similar clusters as molecular alloys perhaps even in the gas phase [47].

3.4. Metathesis and disproportionation reaction

The formation of the species discussed above is determined by one reaction type, i.e. metathesis ($AlX + MR \rightarrow AlR + MX$) [48] or disproportionation ($3AlX \rightarrow 2Al + AlX_3$) [49]. In this chapter we will describe the simultaneous process of both reactions. While the disproportionation reaction is controlling the growth of the cluster framework [50], the metathesis reaction is responsible for the structure of the ligand shell. When the ligand shell is completed, the cluster core is completely protected and, therefore, no further reaction can occur. Hence, disproportionation and metathesis reaction are competing and it depends on various parameters—like temperature, concentration of Al(I), AlX/MR ratio, solubility of the ligand compound MR, etc.—which one is finally predominant.

3.4.1. $[Al_7\{N(SiMe_3)_2\}_6]^-$ (5)

A mixture of $AlCl{\cdot}OEt_2$ solution and $LiN(SiMe_3)_2$ reacts to $[Al_7\{N(SiMe_3)_2\}_6]^-{\cdot}[Li(OEt_2)_3]^+$ [51] which precipitates while warming from -78 to 25 °C. Fig. 8a illustrates the molecular structure of **5**. The coordination of the central Al atom of **5** is similar to the cuboctahedral coordination of the Al atoms in the metallic *fcc* lattice (Fig. 8b).

The central 'naked' Al atom is quasi-octahedral coordinated by six AlR groups. The coordination may also be described as two Al_4R_3 tetrahedra which are vertices-bridged via the central Al atom, i.e. the *metalloid* cluster species **5** is an unique example for an element E to form E_4R_3 tetrahedra coordinated via a 'naked' E atom.

We performed SCF calculations on the ^{27}Al NMR shift of the Al atoms in **5**. The result for the central Al atom ($\delta^{27}Al = +652$) shows that the bonding situation is 'on the way' to the Al atoms in metallic aluminum ($\delta^{27}Al = +1640$). A description as a central Al^{3+} 'ion' sandwiched by two $Al_3R_3^{2-}$ [52] ligands could be excluded since such a central Al^{3+} species should exhibit a ^{27}Al NMR high field shift like $[AlCp^*_2]^+$ ($\delta^{27}Al = -84$) [53].

3.4.2. $[Al_{12}\{N(SiMe_3)_2\}_8]^{-\bullet}$ (6)

If a solution with the same starting materials employed for the synthesis of **5**, i.e. $AlCl{\cdot}OEt_2$ and $LiN(SiMe_3)_2$, is heated to 60 °C for 1 h, black crystals result which were identified by X-ray diffraction to be $[Al_{12}\{N(SiMe_3)_2\}_8]^-{\cdot}[Li(OEt_2)_3]^+$ (**6**; Fig. 9a) [43]. The coordination in this *metalloid* cluster—as in the case of **5**—is comparable with the topology of the Al atoms in metallic aluminum (Fig. 9b).

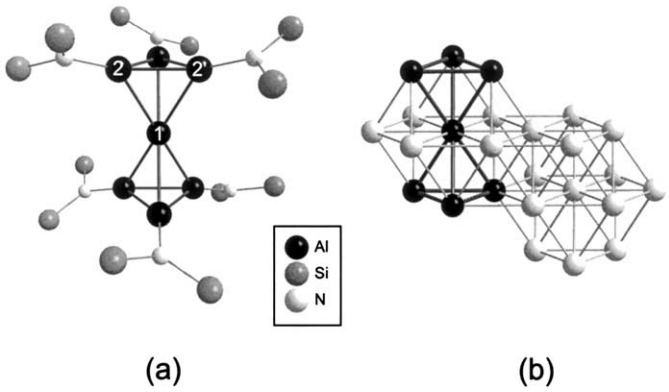


Fig. 8. (a) Molecular structure of $[Al_7\{N(SiMe_3)_2\}_6]^-$ (**5**); methyl groups are excluded. (b) Section of the cubic close packing of Al metal. The Al_7 unit is marked. Characteristic Al–Al distances (Å): Al1–Al2: 2.737, Al2–Al2′: 2.540.

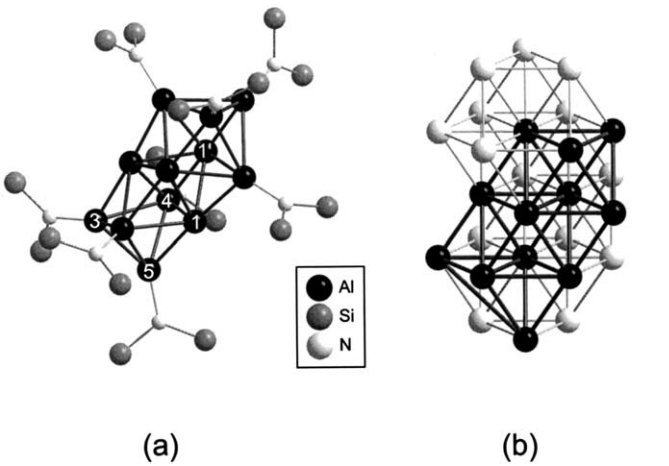


Fig. 9. (a) Molecular structure of $[Al_{12}\{N(SiMe_3)_2\}_8]^{-\bullet}$ (**6**); methyl groups are excluded. (b) Section of the cubic close packing of Al metal (the Al_{12} unit in black). Characteristic Al–Al distances (Å): Al1–Al5: 2.598, Al1–Al4: 2.788, Al3–Al5: 2.542, Al4–Al5: 2.818, Al1–Al1′: 2.629.

The odd number of electrons ($12 \times 3 + 1 = 37$) was confirmed by an ESR measurement.

Wiberg et al. synthesized a neutral $In_{12}R_8$ (**6a**; R = $Si'Bu_3$) cluster which contains a structurally identical metal framework like **6**, but the ligand sphere in **6a** is built up by the larger $Si'Bu_3$ instead of the $N(SiMe_3)_2$ ligand in **6** [54]. This result seems not to be unexpected, as the larger metal cluster framework of In_{12} can only be completely protected by ligands with a greater steric demand, i.e. the $Si'Bu_3$ group. In contrast, a similar Ga_{12} species has not been obtained so far. However, a $Ga_{12}R_{10}^{2-}$ species (R = $C_{13}H_9$, *fluorenyl*; $Ga_{12}R_8 + 2R^-$) formed an icosahedral framework [55]. This different behavior seems to be plausible since contrary to the metals aluminum and indium for gallium no *fcc*-like allotrope has been detected so far [56].

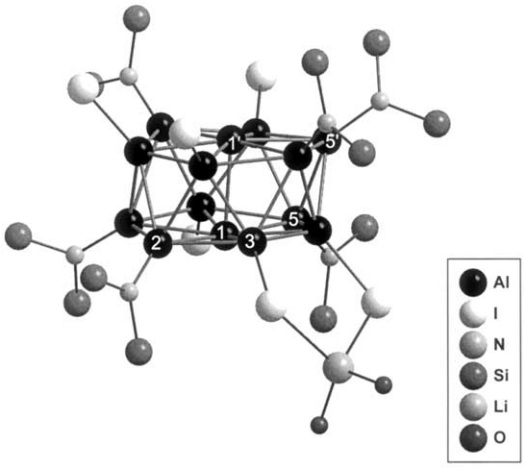


Fig. 10. Molecular structure of $[Al_{14}\{N(SiMe_3)_2\}_6I_6]^{2-}$ (**7**); methyl groups are excluded. Selected Al–Al distances (Å): Al1–Al3: 2.662, Al1–Al2: 2.690, Al1–Al1′: 2.728, Al1–Al3: 2.662, Al3–Al4: 2.597, Al5–Al5′: 2.910.

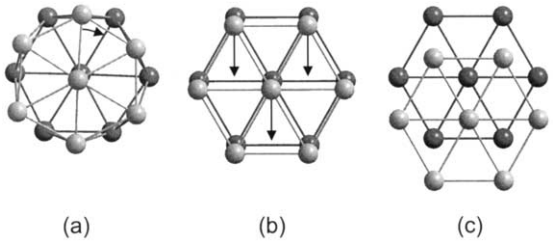


Fig. 11. Transformation of the arrangement of the Al atoms in **7** to that in the closest packing in Al metal: Rotation of the upper ring (a) by 30° leads to a structure (b) which can easily be transformed into a section of the closest packing of Al metal (c) by shifting in the layer of the page by (1/4, 1/4, 0).

3.4.3. $[Al_{14}I_6\{N(SiMe_3)_2\}_6]^{2-}$ (7)

If we use a mixture of Al(I) iodide instead of the Al(I) chloride with the same ligand and heat this solution several times shortly to 60 °C, black crystals grow after a few days at 7 °C. The X-ray structural analysis showed the compound to be $[Al_{14}\{N(SiMe_3)_2\}_6I_6Li(OEt_2)_2]^-\cdot[Li(OEt_2)_4]^+\cdot$toluene (**7**; Fig. 10) [42].

The main structural element of **7** is a twice capped hexagonal prism of Al atoms with a distorted D_{6h} symmetry, which resembles to the geometry of a wheel. There are two 'naked' Al atoms in the center of each Al_6 ring. The topology of the Al atoms in **7** may be regarded as a partially preformed metal structure. If we perform a rotation by 30° and a subsequent translation (Fig. 11), the closest packing of the Al metal structure results.

So far, the reactions of Al^IX with LiR ($R = N(SiMe_3)_2$) were characterized by a total substitution of the halide X against the $N(SiMe_3)_2$ group—cf. the products $[Al_7R_6]^-$ (**5**), $[Al_{12}R_8]^-$ (**6**) as well as $[Al_{69}R_{18}]^{3-}$ (**8**) and $[Al_{77}R_{20}]^{2-}$ (**9**) which will be presented in the following chapter. In contrast, $[Al_{14}I_6R_6]^{2-}$ (**7**) represents the first partially substituted *metalloid* aluminum halide cluster. Its formation seems to be plausible, as exclusively the less reactive AlI reacts in the way described above, while starting with AlCl a complete substitution results.

In **7** and **5** the average oxidation state of the Al atoms has the value of 0.71, i.e the disproportionation process of the primary monovalent Al species to aluminum metal is on the same stage for both compounds. Possibly, there could exist a common precursor like $Al_7R_3X_3^-$ that is quickly substituted for X = Cl to give the 'monomer' $Al_7R_6^-$ (**5**). For X = I the dimerization to $[Al_{14}I_6R_6]^{2-}$ (**7**) is obviously kinetically preferred.

In order to understand the bonding situation in **7**, we carried out DFT calculations on the model compounds $Al_7R_6^-$ (**5a**; $R = NH_2$), $Al_{14}R_{12}^{2-}$ (**7a**; $R = NH_2$) and an polyhedral isomer $Al_{14}R_{12}^{2-}$ (**7b**; $R = NH_2$), that arises by elongating the central Al atoms from the Al–Al distance 269.3 (**7a**) up to 490.3 pm (**7b**). According to these calculations the dimerization reaction **5a** → **7a** is exothermic (-275 kJ mol^{-1}). The species **7b** is calculated to be clearly destabilized with respect to **7a** ($+123$ kJ mol^{-1}). According to the Wade's rules, one expect a *precloso* or *nido* structure for $Al_{14}R_{12}^{2-}$. This doesn't match with **7a**, where neither a *precloso* nor a *nido* structure is realized. The higher stability of **7a** is accountable to the additional Al–Al bond between the central Al atoms.

In contrast, calculations on the similar $Ga_{14}R_{12}^{2-}$ compound [57] show that in this case a polyhedral species is energetically preferred compared with the 'wheel' structure of **7** [58]. This result demonstrates that for every element that structure among the *metalloid* clusters is preferred which exhibits similarities to the structure of the element and its possible allotropes. This is even true for elements with the same number of valence electrons since for *metalloid* clusters of B, Al and Ga containing the same number of metal atoms and ligands different structures of the metal core are obtained (cf. 3b: Al_{12} and In_{12} clusters).

3.4.4. $[Al_{69}\{N(SiMe_3)_2\}_{18}]^{3-}$ (8) and $[Al_{77}\{N(SiMe_3)_2\}_{20}]^{2-\bullet}$ (9)

By suitable variation of the reaction parameters in the system $AlX\cdot OEt_2$ (X = Cl, I)/LiR ($R = N(SiMe_3)_2$)/toluene we succeeded in synthesizing nanosized *metalloid* Al clusters with an oxidation state of the Al atoms close to that of the metal.

From the reaction of $LiN(SiMe_3)_2$ with $AlCl\cdot OEt_2$ the *metalloid* cluster compound $[Al_{69}\{N(SiMe_3)_2\}_{18}]^{3-}\cdot[Li(OEt_2)_3]_3^+\cdot$6toluene (**8**; Fig. 12a) [59] was isolated, and, 5 years ago, using the same starting materials—with the exception that iodide instead of chloride was used—the largest *metalloid* Al cluster, $[Al_{77}\{N(SiMe_3)_2\}_{20}]^{2-\bullet}\cdot[Li_2I(OEt_2)_5]_2\cdot$2toluene (**9**; Fig.

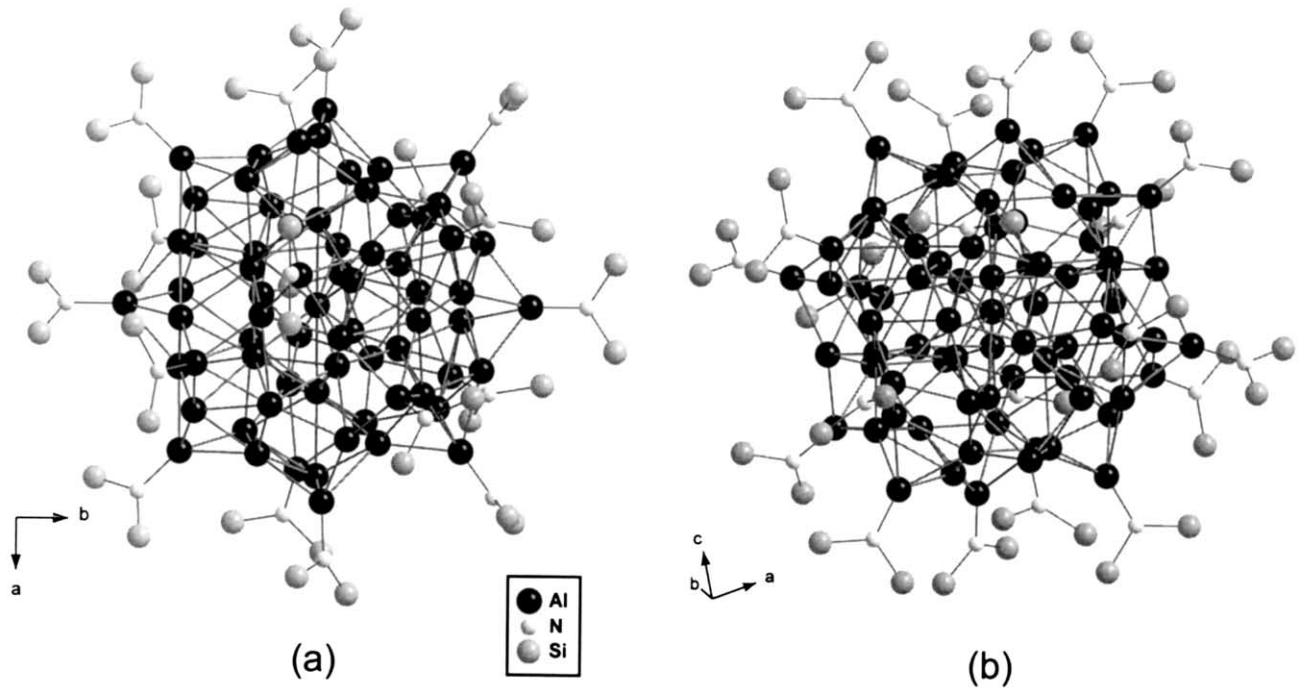


Fig. 12. Molecular structure of (a) $[Al_{69}\{N(SiMe_3)_2\}_{18}]^{3-}$ (**8**) and (b) $[Al_{77}\{N(SiMe_3)_2\}_{20}]^{2-\bullet}$ (**9**); methyl groups are excluded.

12b) [4] was formed. The synthesis of **8** and **9** proceeded under similar preparative conditions: The reaction mixture was heated for 1 h to 60 °C and subsequently cooled either to +25 or to +7 °C. After a few days black crystals precipitated.

The lack of an ESR signal is in agreement to the even electron number of the $Al_{69}R_{18}^{3-}$ cluster core ($51 \times 3 + 18 \times 2 + 3 = 192$). In contrast, we proved the $Al_{77}R_{20}^{2-}$ cluster anion (electron number: $57 \times 3 + 20 \times 2 + 2 = 213$) to be a radical species. After numerous runs of the cluster synthesis we collected enough crystalline material of **9** to perform a measurement of the magnetic moment (and with it the susceptibility) with a SQUID magnetometer (Superconduction Quantum Interference Device) which demonstrated the paramagnetic character of **9** [57].

The common characteristic of **8** and **9** is a 3-shell framework of Al atoms with the 3rd shell consisting of $AlN(SiMe_3)_2$ units, which are arranged so that a complete protection of the cluster core is achieved. To emphasize the number of 'naked' Al atoms, which have exclusively Al–Al contacts, we write the modified formula $[Al_{51}(AlR)_{18}]^{3-}$ (**8**) resp. $[Al_{57}(AlR)_{20}]^{2-}$ (**9**). Fig. 13 illustrates the shell-like structure of the Al frame of **8** and **9**.

The *metalloid* aluminum cluster anions **8** and **9** represent intermediate stages of the disproportionation of Al(I) compounds to aluminum metal and Al(III) compounds. Although **8** and **9** show similarities in the shell-like structure, the Al/R ratio (**8**: 3.83, **9**: 3.85) and, consequently, the oxidation state (**8**: +0.217, **9**: +0.234), there are significant differences in the particular topology as well as in the bonding relations.

The geometries of both clusters differ already in the inner shell: In each cluster the central Al atom is coordinated by 12 Al atoms. The first shell of **8** exhibits a distorted D_{5h} symmetry, while the inner shell of **9** can be described as a polyhedral icosahedron, which is distorted in direction of a cuboctahedron. The second shell of **8** consists of 38 Al atoms, that of **9** is built up by 44 Al atoms. The outer shell contains 18 Al atoms (**8**) resp. 20 Al atoms (**9**).

In Table 1 the average Al–Al distances for **8** within and between the shells are summarized, the analogous values of **9** are given in Table 2.

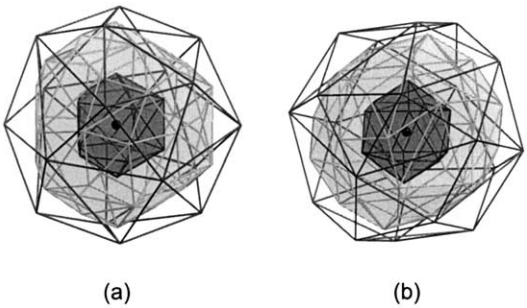


Fig. 13. (a) Al frame of **8** (from central atom to exterior); 1st shell: 12 Al atoms, 2nd shell: 38 Al atoms, 3rd shell: 18 Al atoms. (b) Al frame of **9** (from central atom to exterior): 1st shell: 12 Al atoms, 2nd shell: 44 Al atoms, 3rd shell: 20 Al atoms. Each illustration with the same orientation as in the corresponding comprehensive view (**8**: Fig. 12a, **9**: Fig. 12b) The Al–Al bonds between the shells are omitted for a better visualization of the shell-like structure.

Table 1
Al–Al distances within and between (e.g. 1 → 2) the Al_{69} cluster shells

Shell	Center	1	1 → 2	2	2 → 3	3
Atoms	1	12		38		18
c.n. [a]	12	9 [b]	4	7 [c]	2	(4) [d]
$d_{average}$ (Å)	2.783	2.782	2.783	2.797	2.683	(5.103)

[a] c.n., coordination number. Number of the next atoms surrounding the central atom and forming the 1st shell ('Center'; column 2), coordination of each of the atoms in the 1st shell by the atoms in the 2nd shell ('1 → 2'; column 4) etc. For the coordination within the 1st resp. 3rd shell (column 3 resp. 5) a total c.n. is given. All numbers represent average values (except for column 2).

[b] The total c.n. of an atom in the 1st resp. 2nd shell is the sum of the next atoms within the same shell and the next atoms of the neighboring shells. Total $c.n. = c.n._{1.shell \rightarrow central\ atom} + c.n._{1.shell} + c.n._{1 \rightarrow 2.\ shell} = 1+4+4 = 9$.

[c] Total $c.n. = c.n._{2 \rightarrow 1.shell} + c.n._{2.\ shell} + c.n._{2 \rightarrow 3.shell} = 1.5+3.5+2 = 7$.

[d] There is no significant bonding between the pairs of Al atoms within the 3rd shell.

Only atoms with a distance ranging from 2.5 to 3.0 Å from a particular atom were included and considered for the coordination number.

Table 2
Al–Al distances within and between (e.g. 1 → 2) the Al_{77} cluster shells

Shell	Center	1	1 → 2	2	2 → 3	3
Atoms	1	12		44		20
c.n.	12	9 [a]	4	7 [b]	2	(4) [c]
$d_{average}$ (Å)	2.762	2.795	2.818	2.756	2.688	(5.019)

[a] Total $c.n. = c.n._{1.shell \rightarrow central\ atom} + c.n._{1.shell} + c.n._{1 \rightarrow 2.shell} = 1+4+4 = 9$.

[b] Total $c.n. = c.n._{2 \rightarrow 1.shell} + c.n._{2.shell} + c.n._{2 \rightarrow 3.shell} = 1+4+2 = 7$.

[c] There is no significant bonding between the pairs of Al atoms within the 3rd shell.

Only atoms with a distance ranging from 2.5 to 3.0 Å from a particular atom were included and considered for the coordination number.

The distances within the 2nd shell (i.e. including the center and the 1st shell) are almost identical in **8**, but not in **9** where the distances slightly increase in the direction from the center to the 2nd shell. Both clusters have their shortest Al–Al bonds between the 2nd and the 3rd shell, which means that in the outer sphere the bonding situation becomes more similar to that of molecular bonded Al(I) compounds where the average oxidation number of the Al atoms is closer to +1 [60].

The most obvious difference between **8** and **9** can be found in the second shell (38 resp. 44 Al atoms). In the space-filling model (Fig. 14) two significant gaps in the second shell of **8** stand out, so that a closer look on the first shell is possible; in **9** the second shell encloses completely the inner 12-membered shell.

While according to the MACKAY closed-shell model an icosahedron is surrounded by a 42-membered regular shell this could not be expected to be the case for **8** and **9**, as their inner shells possess no I_h symmetry. The 1st shells may be described as a decahedron (**8**) or a distorted icosahedron (**9**). These significant changes of details within the topology of **8** and **9** could only be extracted from the X-ray structural analysis, since other methods normally used in nano-technology like AFM would not be able to give this information, which may be essential for the interpretation of other physical properties. The measurement of these properties (e.g. electrical conductivity) might be the next step in order to understand the intermediate character of bonding in **8** and **9**. However, handling of *metalloid* clusters like **8** and **9** is by far not trivial since they have pyrophoric properties in the presence of oxygen.

In order to get a feeling for the topology of the *metalloid* clusters **8** and **9** with respect to the final

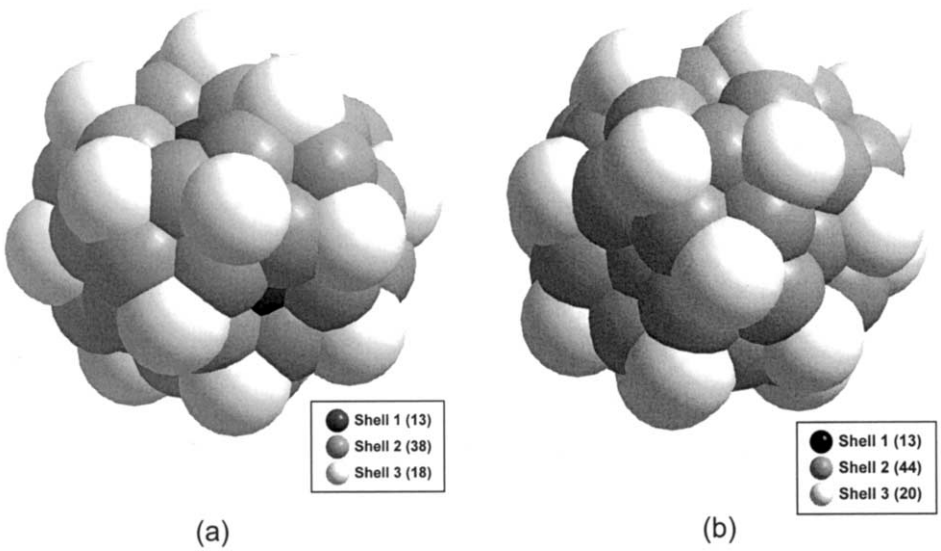


Fig. 14. Space-filling model of **8** (a) and **9** (b). Only Al atoms are shown.

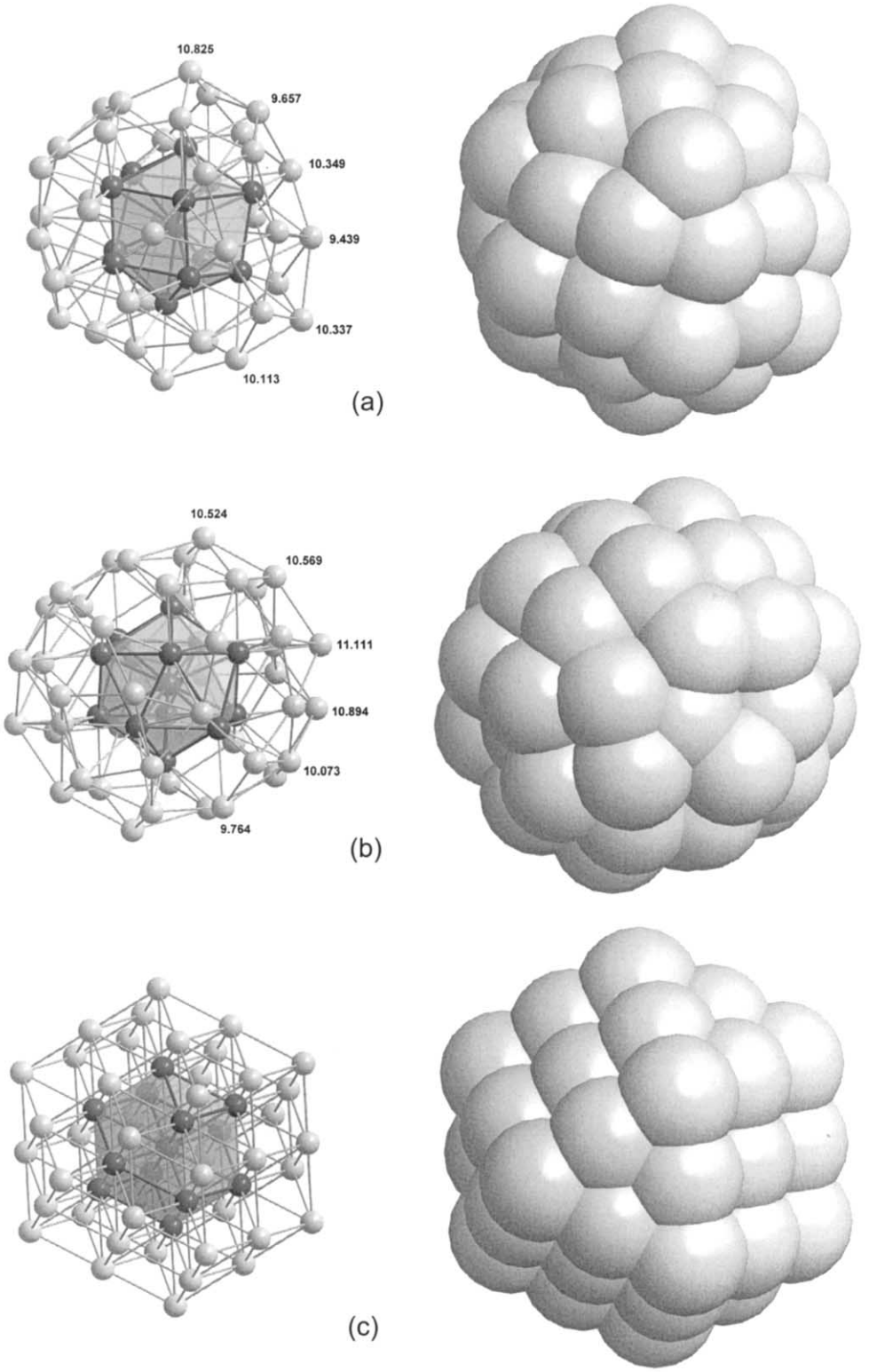


Fig. 15. Ball-and-stick models and space-filling models of the Al_n clusters. (a) shells $1 + 2$ of **8a**: Al_{51} ($1 + 12 + 38$ Al atoms); (b) shells $1 + 2$ of **9a**: Al_{57} ($1 + 12 + 44$ Al atoms); (c) hypothetical Al_{55} cluster section (**10**) from the *fcc* lattice of Al metal ($1 + 12 + 42$ Al atoms). For Al_{51} and Al_{57} the different diameters are shown in the illustration.

product Al metal, which is formed in every experiment, we calculated the atomic volume of the 'naked' Al atoms in **8** and **9** and compared it with the volume of a hypothetical molecular section of the *fcc* Al metal lattice [59]. For a better comparison the same charge of -3 was assumed for the 'naked' Al_{51} (**8a**; $1 + 12 + 38$

Al atoms from **8**; Fig. 15a) and Al_{57} (**9a**; 1 + 12 + 44 Al atoms from **9**; Fig. 15b) species and for a Al_{55} species (**10**; 1 + 12 + 42 Al from α-Al; Fig. 15c).

For **8a** and **9a** the topology within the experimentally determined structure of **8** and **9** was the basis for a singe point SCF calculation and for **10** the coordinates of Al metal. As a result, the atomic volume decreases in the order **8a** (29.61 Å), **9a** (29.51 Å^3) and **10** (29.21 Å^3). That means the driving force for the formation of the bulk metal is the energy gained by the most compact arrangement with the highest possible c.n. of 12 even if the distances are large. The intermediates **8a** and **9a** are less compact with smaller, more molecular distances and lower c.n. (cf. Tables 1 and 2).

4. Conclusions and outlook

On the way from metastable AlX solutions to the bulk metal only a small variation of the reaction parameters (e.g. temperature, concentration of the Al(I) species etc.) in the system $AlX{\cdot}OEt_2$ (X = Cl, I)/LiR (R = $N(SiMe_3)_2$)/toluene leads to the different crystalline *metalloid* aluminum clusters **5**, **6**, **7**, **8**, and **9** which all are protected by the $N(SiMe_3)_2$ ligand. Further examples with other ligands are necessary to understand the influence of the ligand type on the cluster size. Besides the topology of these *metalloid* clusters their physical properties (e.g. conductivity, UV–Vis spectra) will be important to understand the intermediate character on the way to the metal. Additional support comes from theoretical calculations, e.g. by means of band structure calculations, which recently have been performed for **9** [61]. Within further experimental and theoretical investigations there may be expected surprises such as the superconductivity of the $Ga_{84}R_{20}^{4-}$ compound [10,62] as the largest structurally characterized *metalloid* cluster with respect to the 'naked' metal atoms. Thus, studies starting with pure fundamental chemistry have opened a novel field in cluster chemistry, which may give essential impulses to applied science, e.g. in nano-technology.

Acknowledgements

We are grateful to Dr H.-J. Himmel for helpful discussions. We thank the Deutsche Forschungsgemeinschaft and the Fonds der Chemischen Industrie for financial support.

References

[1] A. Schnepf, G. Stößer, H. Schnöckel, J. Am. Chem. Soc. 122 (2000) 9178.
[2] F.A. Cotton, Q. Rev. Chem. Soc. (1966) 389.
[3] (a) H. Krautscheid, D. Fenske, G. Baum, M. Semmelmann, Angew. Chem. 105 (1993) 1364;
(b) H. Krautscheid, D. Fenske, G. Baum, M. Semmelmann, Angew. Chem., Int. Ed. 32 (2001) 1303.
[4] A. Ecker, E. Weckert, H. Schnöckel, Nature 387 (1997) 379.
[5] G. Schmidt (Ed.), Cluster and Colloids, Wiley-VCH, Weinheim, 1994.
[6] P. Braunstein, L.A. Oro, P.R. Raithby, Metal Clusters in Chemistry, Wiley-VCH, Weinheim, 1999.
[7] (a) A. Ceriotti, F. Demartin, G. Longoni, M. Manassero, M. Marchionna, G. Piva, M. Sansoni, Angew. Chem. 97 (1985) 708;
(b) A. Ceriotti, F. Demartin, G. Longoni, M. Manassero, M. Marchionna, G. Piva, M. Sansoni, Angew. Chem., Int. Ed. Engl. 24 (1985) 697.
[8] N.T. Tran, M. Kawano, D.R. Powell, L.F. Dahl, J. Am. Chem. Soc. 120 (1998) 10986.
[9] (a) N.T. Tran, D.R. Powell, L.F. Dahl, Angew. Chem. 112 (2000) 4287;
(b) N.T. Tran, D.R. Powell, L.F. Dahl, Angew. Chem., Int. Ed. Engl. 39 (2000) 4121.
[10] The $[Ga_{84}\{N(SiMe_3)_2\}_{20}]^{4-}$ cluster compound contains 64 'naked' Ga atoms. (a) A. Schnepf, H. Schnöckel, Angew. Chem. 113 (2001) 734.
(b) A. Schnepf, H. Schnöckel, Angew. Chem., Int. Ed. 40 (2001) 712.
[11] W. Uhl, Z. Naturforsch. 43B (1988) 1113.
[12] H. Schnöckel, J. Mol. Struct. 50 (1978) 275.
[13] H. Schnöckel, J. Mol. Struct. 50 (1978) 267.
[14] P.L. Timms, Adv. Inorg. Chem. Radiochem. 14 (1972) 142.
[15] (a) C. Dohmeier, D. Loos, H. Schnöckel, Angew. Chem. 108 (1996) 141;
(b) C. Dohmeier, D. Loos, H. Schnöckel, Angew. Chem., Int. Ed. Engl. 35 (1996) 129.
[16] M. Tacke, H. Schnöckel, Inorg. Chem. 28 (1989) 2895.
[17] However, some attempts have been performed in order to assign ^{27}Al NMR spectra to definite species. Reference: A. Ecker, R. Köppe, C. Üffing, H. Schnöckel, Z. Anorg. Allg. Chem. 624 (1998) 817.
[18] $Al_4Br_4{\cdot}4NEt_3$: (a) M. Mocker, C. Robl, H. Schnöckel, Angew. Chem. 106 (1994) 1860.
(b) M. Mocker, C. Robl, H. Schnöckel, Angew. Chem., Int. Ed. Engl. 33 (1994) 1754.
[19] $Al_4I_4{\cdot}4D$: A. Ecker, H. Schnöckel, Z. Anorg. Allg. Chem. 624 (1998) 813.
[20] Recently, H.W. Roesky succeeded in a classical synthesis of a monomeric AlR species. (a) C. Cui, H.W. Roesky, H.-G. Schmidt, M. Noltemeyer, H. Hao, F. Cimpaesu, Angew. Chem., Int. Ed. 112 (2000) 4444.
(b) C. Cui, H.W. Roesky, H.-G. Schmidt, M. Noltemeyer, H. Hao, F. Cimpaesu, Angew. Chem., Int. Ed. 39 (2000) 4274.
[21] In solution and in the gas phase sometimes there exists a dissoziation equilibrum to the monomers, e.g. AlCp*. Reference: [15].
[22] A. Purath, H. Schnöckel, J. Organomet. Chem. 579 (1999) 373.
[23] (a) C. Dohmeier, C. Robl, M. Tacke, H. Schnöckel, Angew. Chem. 103 (1991) 594;
(b) C. Dohmeier, C. Robl, M. Tacke, H. Schnöckel, Angew. Chem., Int. Ed. Engl. 30 (1991) 564.
[24] A classical synthesis of **1** by H.W. Roesky has been described later on. (a) S. Schulz, H.W. Roesky, H.J. Koch, G.M. Sheldrick, D. Stalke, A. Kuhn, Angew. Chem. 105 (1993) 1828
(b) S. Schulz, H.W. Roesky, H.J. Koch, G.M. Sheldrick, D. Stalke, A. Kuhn, Angew. Chem., Int. Ed. Engl. 32 (1993) 1729.
[25] C. Dohmeier, R. Köppe, C. Robl, H. Schnöckel, J. Organomet. Chem. 448 (1993) 5.

[26] Purath, A., Dissertation. Universität Karlsruhe, 1999.
[27] C. Dohmeier, T. Passler, H. Schnöckel, N. Wiberg, in: A.R. Bassindale, P.P. Gaspar (Eds.), Frontiers of Organosilicon Chemistry, RSC, Cambridge, 1991.
[28] A. Purath, C. Dohmeier, A. Ecker, H. Schnöckel, K. Amelunxen, T. Passler, N. Wiberg, Organometallics 17 (1998) 1894.
[29] (a) C. Schnitter, H.W. Roesky, C. Röpken, R. Herbst-Irmer, H.-G. Schmidt, M. Noltemeyer, Angew. Chem. 110 (1998) 2059; (b) C. Schnitter, H.W. Roesky, C. Röpken, R. Herbst-Irmer, H.-G. Schmidt, M. Noltemeyer, Angew. Chem., Int. Ed. Engl. 37 (1998) 1952.
[30] H. Sitzmann, M.F. Lappert, C. Dohmeier, C. Üffing, H. Schnöckel, J. Organomet. Chem. 561 (1998) 203.
[31] R.W.H. Small, I.J. Worrall, Acta Crystallogr. Sect. B 38 (1982) 250.
[32] H.J. Becher, H. Schnöckel, Z. Anorg. Allg. Chem. 379 (1970) 136.
[33] (a) M. Mocker, C. Robl, H. Schnöckel, Angew. Chem. 106 (1994) 946; (b) M. Mocker, C. Robl, H. Schnöckel, Angew. Chem., Int. Ed. Engl. 33 (1994) 862.
[34] (a) C. Klemp, G. Stößer, I. Krossing, H. Schnöckel, Angew. Chem. 112 (2000) 3834; (b) C. Klemp, G. Stößer, I. Krossing, H. Schnöckel, Angew. Chem., Int. Ed. 39 (2000) 3591.
[35] D. Loos, H. Schnöckel, D. Fenske, Angew. Chem., Int. Ed. Engl. 32 (1993) 1059.
[36] Based on the crystallographically characterized Al(II) halide $Al_2I_4{\cdot}2THF$.
[37] The compound $Ga_3I_5{\cdot}3PEt_3$ is known. Ref: A. Schnepf, C. Doriat, E. Möllhausen, H. Schnöckel, Chem. Commun. (1997) 2111.
[38] (a) C. Klemp, R. Köppe, E. Weckert, H. Schnöckel, Angew. Chem. 111 (1999) 1851; (b) C. Klemp, R. Köppe, E. Weckert, H. Schnöckel, Angew. Chem., Int. Ed. 38 (1999) 1739.
[39] C. Klemp, M. Bruns, J. Gauss, U. Häussermann, M. Jansen, G. Stößer, L. van Wüllen, H. Schnöckel, J. Am. Chem. Soc. 123 (2001) 9099.
[40] C. Klemp, Dissertation. Universität Karlsruhe, 2000.
[41] (a) C. Üffing, E. Baum, R. Köppe, H. Schnöckel, Angew. Chem. 110 (1998) 2488; (b) C. Üffing, E. Baum, R. Köppe, H. Schnöckel, Angew. Chem., Int. Ed. Engl. 37 (1998) 2397.
[42] (a) H. Köhnlein, G. Stößer, E. Baum, E. Möllhausen, U. Huniar, H. Schnöckel, Angew. Chem. 112 (2000) 828; (b) H. Köhnlein, G. Stößer, E. Baum, E. Möllhausen, U. Huniar, H. Schnöckel, Angew. Chem., Int. Ed. 39 (2000) 799.
[43] A. Purath, H. Schnöckel, Chem. Commun. (1999) 1933.
[44] A. Purath, C. Dohmeier, E. Baum, R. Köppe, H. Schnöckel, Z. Anorg. Allg. Chem. 625 (1999) 1.
[45] A. Purath, C. Dohmeier, A. Ecker, R. Köppe, H. Krautscheid, H. Schnöckel, R. Ahlrichs, C. Stoermer, J. Friedrich, P. Jutzi, J. Am. Chem. Soc. 122 (2000) 6955.
[46] The Jellium model implies that the high stability of clusters is corresponding to particular closed-shell electronic configurations. It describes the cluster electronic structure by considering only the valence electrons, which are assumed to move 'freely' in a smooth attractive spherical field potential. A crucial approximation is that the detailed positions of nuclei do not play a significant role. Ref: W.A. de Heer, W.D. Knight, M.Y. Chou, M.L. Cohen, Solid State Phys. 40 (1987) 93.
[47] K. Weiß, R. Köppe, H. Schnöckel, Intern. J, Mass Spectrom., in press.
[48] This reaction—if the disproportionation is excluded—may result in Al_nR_m $(n=m)$ species, for example $Al_4Cp^*_4$.
[49] The disproportionation may lead to Al_nX_m with $n<m$ (e.g. $Al_5Br_7{\cdot}5THF$) or with $n>m$ (e.g. $Al_{22}Br_{20}{\cdot}12THF$).
[50] This could proceed by insertion of AlX·D units in existing Al–Al bonds and subsequent elimination of, e.g. Al_2X_4 or AlX_3 units, from the sphere of the *metalloid* core.
[51] (a) A. Purath, R. Köppe, H. Schnöckel, Angew. Chem. 111 (1999) 3114; (b) A. Purath, R. Köppe, H. Schnöckel, Angew. Chem., Int. Ed. Engl. 38 (1999) 2926.
[52] Similar to cyclic $Ga_3R_3^{2-}$ species. References: (a) X.-W. Li, W.T. Pennington, G.H. Robinson, Am. Chem. Soc. J. 117 (1995) 7578. (b) W.-W. Li, Y. Xie, P.R. Schreiner, K.D. Gripper, R.C. Crittendon, C.F. Campana, H.F. Schaefer, G.H. Robinson, Organometallics 15 (1996) 3798.
[53] (a) C. Dohmeier, H. Schnöckel, C. Robl, U. Schneider, R. Ahlrichs, Angew. Chem. 105 (1993) 1714; (b) C. Dohmeier, H. Schnöckel, C. Robl, U. Schneider, R. Ahlrichs, Angew. Chem., Int. Ed. Engl. 32 (1993) 1655.
[54] (a) N. Wiberg, T. Blank, H. Nöth, W. Ponikwar, Angew. Chem. 111 (1999) 887; (b) N. Wiberg, T. Blank, H. Nöth, W. Ponikwar, Angew. Chem., Int. Ed. Engl. 38 (1999) 839.
[55] (a) A. Schnepf, G. Stößer, R. Köppe, H. Schöckel, Angew. Chem. 112 (2000) 1709; (b) A. Schnepf, G. Stößer, R. Köppe, H. Schöckel, Angew. Chem., Int. Ed. Engl. 39 (1999) 1637.
[56] H. Schnöckel, A. Schnepf, Adv. Organomet. Chem. 47 (2001) 235.
[57] H. Köhnlein, Dissertation. Universität Karlsruhe, 2001.
[58] The same structure is expected for a similar boron compound.
[59] H. Köhnlein, A. Purath, C. Klemp, E. Baum, I. Krossing, G. Stößer, H. Schnöckel, Inorg. Chem. 40 (2001) 4830.
[60] Compare the Al–Al distances (Å) in $[Al_7\{N(SiMe_3)_2\}_6]^-$ (**5**): 2.540 resp. 2.737, $[Al_{12}\{N(SiMe_3)_2\}_8]^-$ (**6**): 2.542…2.759, $Al_{12}(AlBr_2{\cdot}THF)_{10}{\cdot}2THF$ (**3a**): 2.526…2.762.
[61] X.G. Gong, D.Y. Sun, X.-Q. Wang, Phys. Rev. 62B (2000) 15413.
[62] J. Hagel, M.T. Kelemen, G. Fischer, B. Pilawa, J. Wosnitza, E. Dormann, H. v. Löhneysen, A. Schnepf, H. Schöckel, U. Neisel, J. Beck, Eur. Phys. Lett., submitted.

PERGAMON

Polyhedron 21 (2002) 503–509

POLYHEDRON

www.elsevier.com/locate/poly

Understanding the electron counts of aluminum metalloid clusters

Wai Han Lam, Zhenyang Lin *

Department of Chemistry, Hong Kong University of Science and Technology, Clear Water Bay, Kowloon, Hong Kong

Received 10 July 2001; accepted 27 November 2001

Abstract

The structures and bonding of several Al metalloid clusters have been analyzed with the aid of density functional theory calculations. These clusters include $[Al_7\{N(SiMe_3)_2\}_6]^-$ (**1**), $[Al_{12}\{N(SiMe_3)_2\}_8]^-$ (**2**), $[Al_{22}Br_{20}\cdot 12THF]$ (**3**) $[Al_{14}\{N(SiMe_3)_2\}_6I_6]^{2-}$ (**4**), $Al_{14}(\mu_8\text{-Si})Cp^*_6$ (**5**), $[(AlEt)_8(\mu_4\text{-}CCH_2Ph)_5(\mu_4\text{-H})]$ (**6**), $[(AlMe)_8(\mu_4\text{-}CCH_2Ph)_5(\mu_4\text{-}C{\equiv}CPh)]$ (**7**) and $[(AlMe)_7(\mu_4\text{-}CCH_2Me)_4(\mu_2\text{-H})_2]$ (**8**). In this paper, an attempt has been made to illustrate the relationship between the observed geometry and electron counts for these metalloid clusters. © 2002 Elsevier Science Ltd. All rights reserved.

Keywords: Electron counts; Aluminum; Metalloid clusters

1. Introduction

In recent years, the chemistry of the heavier group 13 elements has made rapid progress. Through the excellent work of Schnöckel, Uhl and their coworkers over the last decade, numerous high nuclearity aluminum and gallium clusters have been synthesized and structurally characterized [1–13]. Amazing examples include the most recently reported $[Al_{69}\{N(SiMe_3)_2\}_{18}]^{3-}$ [6], $[Al_{77}\{N(SiMe_3)_2\}_{20}]^{2-}$ [7] and $[Ga_{84}\{N(SiMe_3)_2\}_{20}]^{4-}$ [10]. These high nuclearity clusters are classified as metalloid clusters in which the number of metal–metal contacts far exceeds the number of metal–ligand interactions. Unlike the boron clusters, the majority of these group 13 metalloid clusters, which show much more versatile structural varieties, do not follow Wade's electron counting rules [14].

In view of the abundant knowledge on the synthetic routes to these clusters and structural data available [15], we still lack the understanding of their electronic structures. A general understanding of their electronic structures has not emerged although several theoretical calculations have been done [1–5,9a]. In an effort to establish relationships between the observed geometries and electron counts for these metalloid clusters, we attempt to analyze several recently reported high nuclearity aluminum clusters in this paper. These clusters include $[Al_7\{N(SiMe_3)_2\}_6]^-$ **(1)** [3], $[Al_{12}\{N(SiMe_3)_2\}_8]^-$ **(2)** [5], $[Al_{22}Br_{20}\cdot 12THF]$ **(3)** [4], $[Al_{14}\{N(SiMe_3)_2\}_6I_6]^{2-}$ **(4)** [2], $Al_{14}(\mu_8\text{-Si})Cp^*_6$ **(5)** [1], $[(AlEt)_8(\mu_4\text{-}CCH_2Ph)_5(\mu_4\text{-H})]$ **(6)** [9a], $[(AlMe)_8(\mu_4\text{-}CCH_2Ph)_5(\mu_4\text{-}C{\equiv}CPh)]$ **(7)** [9a] and $[(AlMe)_7(\mu_4\text{-}CCH_2Me)_4(\mu_2\text{-H})_2]$ **(8)** [9a] (see Fig. 1). With the aid of molecular orbital calculations, our approach is to analyze the electronic structures of these clusters one by one in terms of concepts of orbital interactions [16] and the knowledge we have had on the cluster bonding [17]. We hope that the discussion below will provide a better insight into our understanding of these clusters in a simple and understandable manner. We also hope that the analyses provided here will be used as a starting point to further understand the even more complicated and versatile clusters of the analogous gallium element. Because of their structural versatility and complicated electronic behavior, electron counts of gallium clusters can be very different when compared to these of aluminum clusters. Therefore, in this paper we limit our discussion to the clusters of aluminum except in Section 3.5 where some comments are given to $[Ga_{84}\{N(SiMe_3)_2\}_{20}]^{4-}$.

* Corresponding author. Fax: +852-2358-1594.
E-mail address: chzlin@ust.hk (Z. Lin).

0277-5387/02/$ - see front matter © 2002 Elsevier Science Ltd. All rights reserved.
PII: S0277-5387(01)01020-8

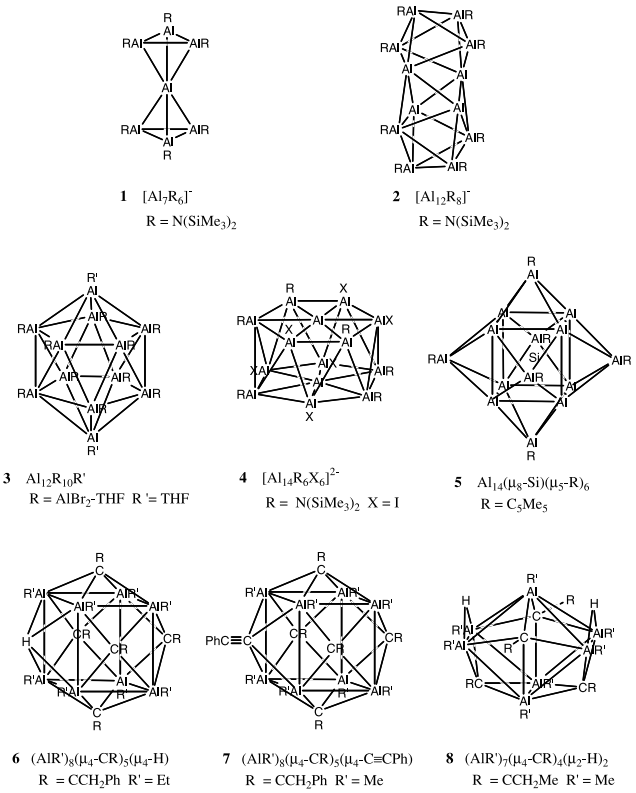


Fig. 1. Structures of various Al metalloid clusters.

2. Molecular orbital calculations

Density functional theory calculations at the Becke3LYP (B3LYP) level [18] have been performed to study the detailed electronic structures of various aluminum clusters. Geometry optimizations have been done for the following model clusters $[Al_7(N(H_2)_6]^-$ (**1a**), $[Al_{12}(NH_2)_8]^-$ (**2a**), $[Al_{14}(NH_2)_6I_6]^{2-}$ (**4a**), $Al_{14}(\mu_8\text{-Si})Cp_6$ (**5a**), $[(AlMe)_8(\mu_4\text{-}CCH_3)_5(\mu_4\text{-H})]$ (**6a**), $[(AlMe)_8(\mu_4\text{-}CCH_3)_5(\mu_4\text{-C}\equiv\text{CH})]$ (**7a**) and $[(AlMe)_7(\mu_4\text{-}CCH_3)_4(\mu_2\text{-H})_2]$ (**8a**). The effective core potentials (ECPs) of Hay and Wadt with double-ξ valence basis set (LanL2DZ) [19] were used to describe main group atoms of period three with polarization functions for Al ($\xi_d(Al) = 0.198$) and Si ($\xi_d(Si) = 0.262$) atoms [20], while the standard 6-31G basis set [21] was used for all other atoms. For model complex $Al_{14}(\mu_8\text{-Si})Cp_6$ (**5a**), the STO-3G basis [22] set was used for C and H of the Cp ligands. The size of the cluster together with the limited computational resource prevents us from using a better basis set. The use of the smaller basis set for **5a** does not affect our qualitative discussion in the text, which will be seen below.

All calculations were performed with the use of GAUSSIAN 98 [23] on Silicon Graphics Indigo^2 workstations and PC Pentium III computers. The electron density analysis was carried out with MOPLOT 2.4 [24] and the natural bond orbital (NBO) analysis was performed by using the NBO program [25] associated with the GAUSSIAN 98 package. The molecular orbitals obtained from the B3LYP calculations were plotted using the MOLDEN 3.7 program [26].

3. Results and discussion

3.1. $[Al_7\{N(SiMe_3)_2\}_6]^-$

In $[Al_7\{N(SiMe_3)_2\}_6]^-$ (**1**), the seven Al atoms form a vertex-shared bitetrahedral structure and the six $-N(SiMe_3)_2$ groups are bonded to the six non-shared Als (see Fig. 1). The bonding of this cluster has been described as follows [3]. An Al^{3+} center binds two $[Al_3\{N(SiMe_3)_2\}_3]^{2-}$ units in a ferrocene-type fashion. The approximately planar $[Al_3\{N(SiMe_3)_2\}_3]^{2-}$ structural unit conforms to the aromatic electronic structure having two π electrons in addition to three Al–Al σ bonds. Geometry optimization on the model complex $[Al_7(NH_2)_6]^-$ (**1a**) gives the Al–Al bond distances consistent with the experimental data (see Table 1). Fig. 2 shows the spatial plots of the molecular orbitals accommodating the eight pairs of metal electrons. These eight Al–Al bonding molecular orbitals correspond to the in-phase and out-of-phase combinations of orbitals derived from the two $[Al_3(NH_2)_3]^{2-}$ fragments. Each fragment contributes four orbitals, i.e. three Al–Al σ bonds and one delocalized π bond. The role of the central aluminum is to use its s and p orbitals to stabilize some of the eight Al–Al bonding molecular

Table 1
The calculated Al–Al bond distances and Wiberg bond indices for various model complexes

Model clusters		Al–Al bond distances (Å)	Wiberg bond indices (WBI)
$[Al_7(NH_2)_6]^-$	**1a**	2.554–2.806 (2.540–2.737)	0.59–0.89
$[Al_{12}(NH_2)_8]^-$	**2a**	2.532–2.785 (2.542–2.818)	0.37–0.76
$[Al_{14}(NH_2)_6I_6]^{2-}$	**4a**	2.671–2.818 (2.570–2.910)	0.37–0.60
$Al_{14}(\mu_8\text{-Si})(\mu_5\text{-Cp})_6$	**5a**	2.869–2.906 (2.786–2.912)	0.32–0.42
$(AlMe)_8(\mu_4\text{-}CCH_3)_5(\mu_4\text{-H})$	**6a**	2.606–2.845 (2.585–2.858)	0.08–0.09
$(AlMe)_8(\mu_4\text{-}CCH_3)_5(\mu_4\text{-C}\equiv\text{CH})$	**7a**	2.582–2.849 (2.603–2.913)	0.06–0.08
$(AlMe)_7(\mu_4\text{-}CCH_3)_4(\mu_2\text{-H})_2$	**8a**	2.608–2.881 (2.569–2.816)	0.07–0.11

For comparison, the corresponding experimental Al–Al bond distances are given in parentheses.

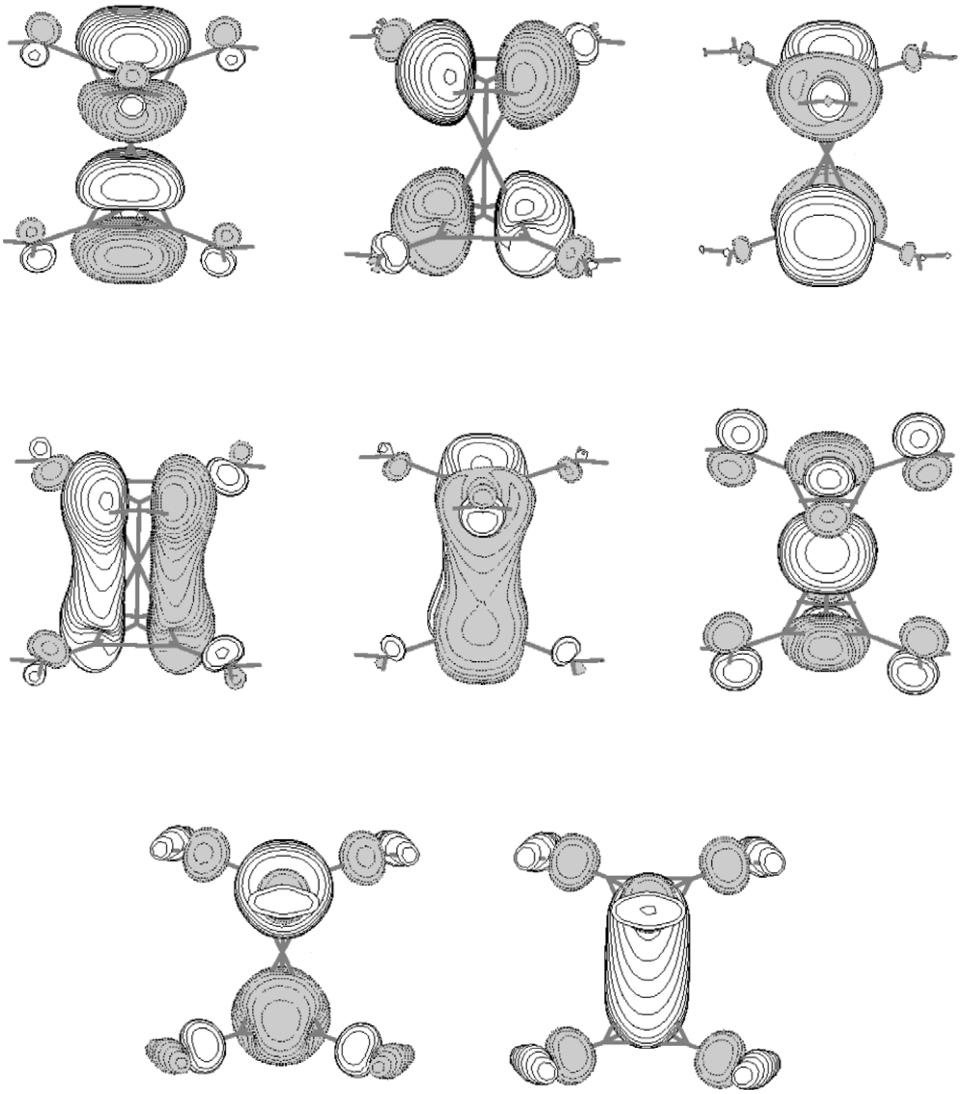


Fig. 2. Spatial plots of the eight skeletal Al–Al bonding molecular orbitals for model complex $[Al_7(NH_2)_6]^-$. The highest occupied molecular orbital is on the top of the left hand side. The orbital energies decrease from left to right and from top to bottom.

orbitals. These results support the qualitative bonding description given by Schnöckel and his coworkers [3].

3.2. $[Al_{12}\{N(SiMe_3)_2\}_8]^-$

Similar to $In_{12}(SiBu^t_3)_8$ [27], $[Al_{12}\{N(SiMe_3)_2\}_8]^-$ (**2**) [5] adopts a stretched ellipsoid structural shape among the 12 Al atoms. The structure can also be described as linking two distorted octahedral $Al_6\{N(SiMe_3)_2\}_4$ fragments in a staggered fashion (see Fig. 1). Each distorted octahedral fragment breaks an Al–Al bond. Geometry optimization was performed for the model cluster $[Al_{12}(NH_2)_8]^-$ (**2a**). Consistent with an early calculation [5], the calculated Al–Al distance together with the experimental data are shown in Table 1 and the calculated geometry reproduces its experimental structure quite well. To better understand the metal–metal interactions, it is more convenient if we consider the metal–metal molecular orbitals in terms of the two distorted octahedral fragments. Because of the mixing of N's p orbitals into the $[Al_{12}(NH_2)_8]^-$ skeletal molecular orbitals, we employ a simpler model $[Al_{12}H_8]^-$ here to illustrate the orbital interactions between the two distorted octahedral fragments. Fig. 3 shows such a qualitative orbital interaction diagram. The left and right columns in the figure give the fragment orbitals for the two distorted octahedral units arranged in a staggered fashion. Each fragment has nine orbitals shown in the figure. These nine fragment orbitals correspond to seven skeletal orbitals, commonly found for an octahedral cluster (e.g. $[B_6H_6]^{2-}$) [28], and two out-pointing orbitals based on the two Al atoms which do not have terminal H atoms. The central column represents the resulting MOs. In the central column of Fig. 3, the bottom ten MOs are simply the results of addition from the two fragments. The top eight MOs form the impor-

tant part derived from the orbital interactions between the two fragments. Among the top eight MOs, four are bonding and four antibonding. One can envisage the situation as follows. Each fragment uses the two out-pointing fragments' orbitals to interact/stabilize the two high-energy skeletal fragment orbitals from the other fragment. These mutual orbital stabilizing interactions between the two fragments give rise to four bonding and four antibonding MOs. The total number of the skeletal electrons is 28 for $Al_{12}H_8$ [or $[Al_{12}\{N(SiMe_3)_2\}_8]$ or $In_{12}(SiBu^t_3)_8$]. The electron count of 14 skeletal electron pairs represents the simple addition of electron counts from two octahedral clusters. In order to achieve this simple addition, the four metal atoms in the middle part of the cluster do not have a terminal R group. $[Al_{12}\{N(SiMe_3)_2\}_8]^-$ (**2**) represents a case when the lowest of the four antibonding orbitals is singly occupied. That there is no In analog anionic species implies the higher electronegativity of Al in comparison to In.

3.3. $[Al_{22}Br_{20}\cdot 12THF]$, $[Al_{14}\{N(SiMe_3)_2\}_6I_6]^{2-}$ and $Al_{14}(\mu_8\text{-}Si)Cp^*_6$

According to Schnöckel and his coworkers, $[Al_{22}Br_{20}\cdot 12THF]$ (**3**) (see Fig. 1) can be reformulated as $Al_{12}\{AlBr_2(THF)\}_{10}(THF)_2$ [4]. The central Al_{12} unit can be described as an icosahedral. The cluster is isoelectronic to $[Al_{12}Bu^i_{12}]^{2-}$ [29] and conforms to Wade's $n+1$ rule if the ten $AlBr_2(THF)$ moieties and the two THF solvent molecules are considered as ligands forming single bonds with the central Al_{12} structural unit. Each $AlBr_2(THF)$ moiety contributes one electron and each THF donates two electrons to the electron count of the cluster. The total electron count of 50 $(=10+4+3\times 12)$ can be derived, giving the $4n+2$ (here $n=12$) electrons. Therefore, the bonding of this cluster can be easily understood.

$[Al_{14}\{N(SiMe_3)_2\}_6I_6]^{2-}$ **4** has been described as two staggered, approximately Al-centered Al_6 rings (see Fig.

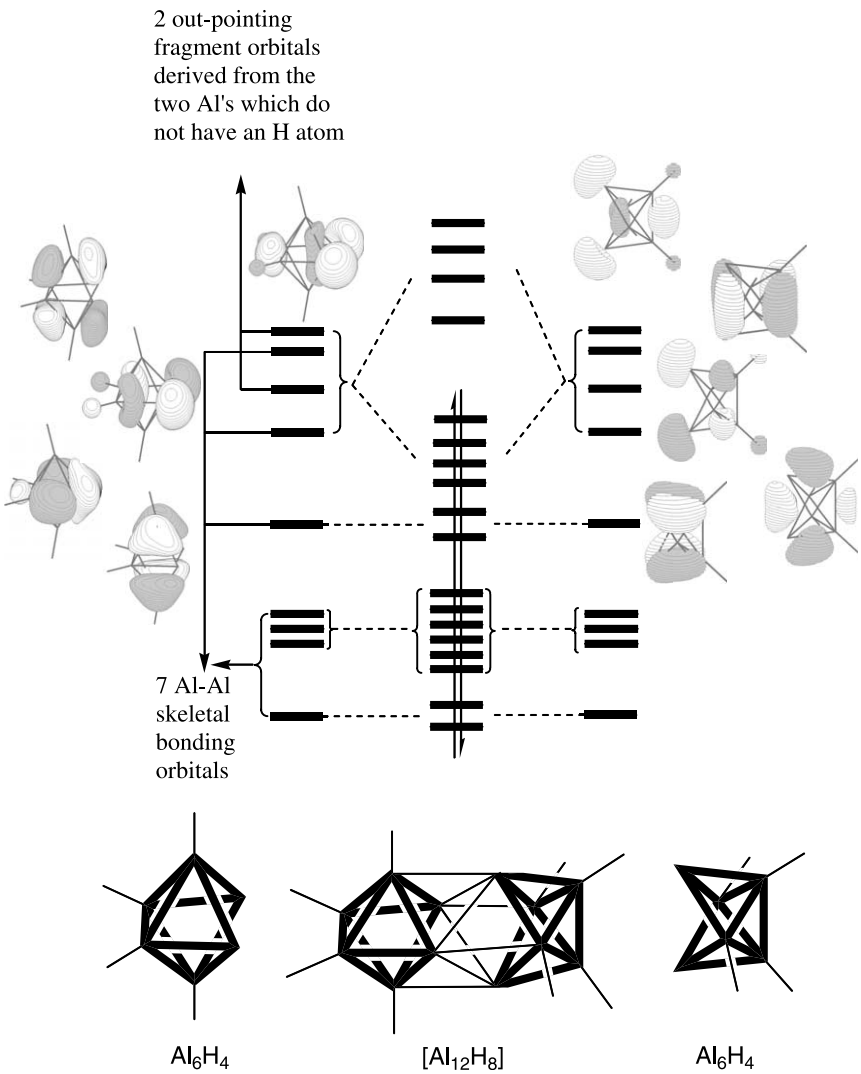


Fig. 3. A schematic diagram showing the orbital interactions between two perpendicular distorted octahedral Al_6H_4 fragments for $[Al_{12}H_8]$.

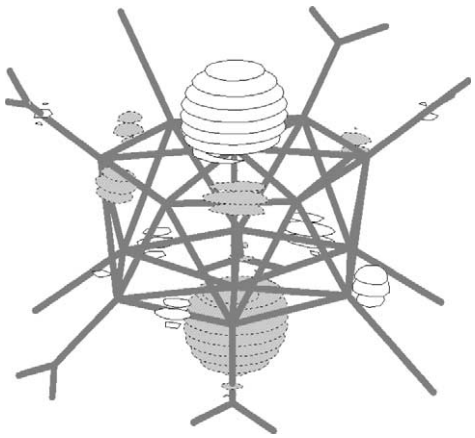


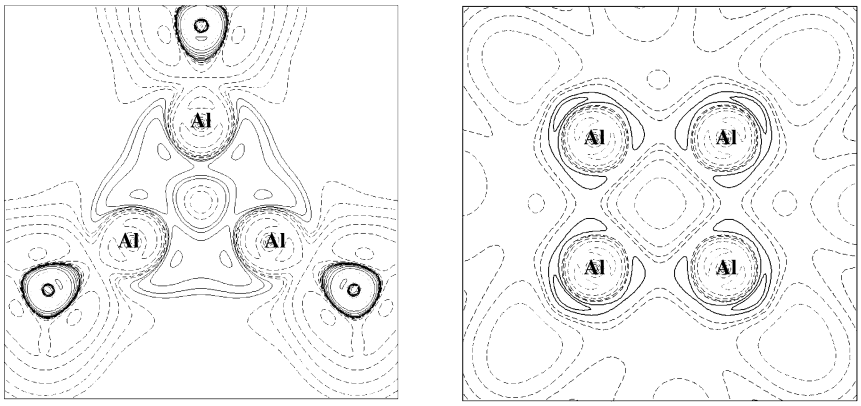
Fig. 4. Spatial plot of the lowest unoccupied molecular orbital (LUMO) for model complex $[Al(NH_2)_6I_6]^{2-}$.

1). The central Al atoms do not have ligands associated with them, while each of the remaining Al atoms is coordinated by either iodide or $N(SiMe_3)_2$ ligands. Geometry optimization on the model complex $[Al_{14}(NH_2)_6I_6]^{2-}$ (**4a**) gives the Al–Al bond distances consistent with the experimental data (see Table 1). The total electron count of the cluster is 56 ($=3\times14+6+6+2$). Instead of conforming to the $4n+2$ rule, the cluster has an electron count of $4n$. In the structural studies of neutral silicon clusters, it has been concluded that the spherical (deltahedral) geometries exhibited by boranes, characterized by $4n+2$ electrons, are not stable for Si_n which have $4n$ electrons. In order to achieve a stable electron configuration with a substantial HOMO–LUMO gap for these $4n$-electron clusters, two mechanisms have been proposed. One is oblate distortion from the spherical polyhedron to remove one axially antibonding orbital from the bonding region and the other is capping of a suitable spherical polyhedron [30]. Clearly, cluster $[Al_{14}\{N(SiMe_3)_2\}_6I_6]^{2-}$ (**4**) adopts the former mechanism by forming an oblate structure derived from a bicapped hexagonal antiprism. Due to the closer contact of two apical Al atoms in oblate structure, the out-of-phase combination MO from the two apical Al atoms in the bonding region will be pushed up. Indeed, this MO can be found in the LUMO region in model cluster $[Al_{14}\{NH_2)_6I_6]^{2-}$ (**4a**) (see Fig. 4). One may ask why a spherical polyhedron cannot be formed by adding two electrons or two R groups to the cluster framework. In order to form a spherical polyhedron, the two apical Al atoms have to move away from each other. Therefore, unfavorable Al–Al interactions would arise between the apical atoms and the hexagonal Als because of the long Al(apical)–Al(hexagonal) distances. The long distances are the result of moving the apical atom away from the center of a hexagon.

$Al_{14}(\mu_8\text{-Si})Cp^*_6$ **5** can be reformulated as $Al_8((\mu_8\text{-Si})(\mu_4\text{-AlCp})_6$ and described as a Si-centered Al_8 cube capped by six AlCp fragments. Based on the detailed analysis of the DFT molecular orbital calculations, Schnöckel and his coworkers [1] nicely invoked the simple Jellium model [31] to account for the 40 metal valence cluster electrons in the clusters by having a closed-shell electron configuration of $1s^21p^61d^{10}2s^21f^{14}2p^6$ (here 1s, 1p, … are the Jellium orbitals). Alternatively, the cluster can also be considered as having a regular electron count for a cubic structure. A cubic C_8R_8 molecule is actually having 40 valence electrons. Many analogous cubic $M_8(\mu_4\text{-E})_6L_8$ (M = Ni; E = S, Se, or PPh; L = phosphine or CO) transition metal clusters which have 120 cluster valence electrons can be found in the literature [32]. When M is a main group atom, the type of clusters should have 40 cluster valence electrons because the d orbitals of a main group atom normally do not play a role in increasing the number of bonding/non-bonding orbitals. In this alternative description, the cluster **5** formally has 12 metal–metal bonds and each Al atom in the cubic structural unit is expected to have an electron pair which shows out-pointing. These out-pointing orbitals accommodating the Al electron pairs also have significant contribution from the capping AlCp fragments. The capping AlCp fragments play important roles in stabilizing these electrons.

3.4. $[(AlEt)_8(\mu_4\text{-}CCH_2Ph)_5(\mu_4\text{-}H)]$, $[(AlMe)_8(\mu_4\text{-}CCH_2Ph)_5(\mu_4\text{-}C{\equiv}CPh)]$ and $[(AlMe)_7(\mu_4\text{-}CCH_2Me)_4(\mu_2\text{-}H)_2]$

In $[(AlEt)_8(\mu_4\text{-}CCH_2Ph)_5(\mu_4\text{-}H)]$ (**6**) and $[(AlMe)_8(\mu_4\text{-}CCH_2Ph)_5(\mu_4\text{-}C{\equiv}CPh)]$ (**7**) (see Fig. 1), the eight Al atoms of each cluster form a cubic arrangement in which each Al has a terminal R ligand. The structures can be also described as a hexa-capped cube. These two clusters are actually isoelectronic, each having an electron count of 48 [$=(3+1)\times8+5\times3+1$]. Unlike the cubic cluster $Al_{14}(\mu_8\text{-Si})Cp^*_6$ discussed above, these two clusters does not have the regular electron count of 40. Based on the quantum chemical calculations, Uhl and his coworkers [9a] concluded a delocalized multicenter bonding situation with only weak direct Al–Al interactions for these clusters. Interestingly, one can formally assign +3 to each Al center in these clusters including $[(AlMe)_7(\mu_4\text{-}CCH_2Me)_4(\mu_2\text{-}H)_2]$ (**8**) (see Fig. 1). In other words, one can envisage the bonding in these clusters as follows. The Al atoms in these clusters provide all their valence electrons to make sure that all bonded carbon atoms satisfy the octet rule and hydrogen atoms the 2-electron closed-shell electronic requirement. The multicenter bonding situation is realized through the bridging units. The electronic structures and bonding picture for these clusters are thus quite simple from such a



(a) (b)

Fig. 5. Laplacian plots of the electron density for model cluster $[Al_7(NH_2)_6]^-$ on a triangle plane formed by three non-shared Al atom (a) and for model cluster $[(AlMe)_8(\mu_4\text{-}CCH_3)_5(\mu_4\text{-}C \equiv CH)]$ on the plane of the square face opposite to square face capped by the μ_4-acetylenyl ligand (b). Solid lines represent local electron density concentration, and dashed lines represent local density depletion.

traditional view. Based on such a simple bonding picture, it is not difficult to understand that the direct Al–Al interactions are weak in these clusters. Geometry optimization were performed for the model cluster $[(AlMe)_8(\mu_4\text{-}CCH_3)_5(\mu_4\text{-}H)$ (**6a**), $[(AlMe)_8(\mu_4\text{-}CCH_3)_5(\mu_4\text{-}C{\equiv}CH)]$ (**7a**) and $[(AlMe)_7(\mu_4\text{-}CCH_2Me)_4(\mu_2\text{-}H)_2]$ (**8a**). The calculated geometries are in good agreement with the corresponding experimental complexes $[(AlEt)_8(\mu_4\text{-}CCH_2Ph)_5(\mu_4\text{-}H)]$ (**6**), $[(AlMe)_8(\mu_4\text{-}CCH_2Ph)_5(\mu_4\text{-}C{\equiv}CPh)]$ (**7**) and $[(AlMe)_7(\mu_4\text{-}CCH_2Me)_4(\mu_2\text{-}H)_2]$ (**8**). The Wiberg bond indices (WBI) of model clusters **6a**, **7a** and **8a** have been shown in Table 1. Consistent with the qualitative analyses above, these model clusters have relatively smaller WBI when compared with other types of Al clusters. Fig. 5 showed the Laplacian plots of model clusters $[(AlMe)_8(\mu_4\text{-}CCH_3)_5(\mu_4\text{-}C{\equiv}CH)]$ (**7a**) and $[Al_7(NH_2)_6]^-$ (**1a**). Significant electron density concentrations can be found along the Al–Al bonding path in **1a**, but not in **7a**. These results suggest that there is considerable Al–Al bonding in other types of Al clusters except **6**, **7** and **8** in which Al^{3+} can be formally assigned to each aluminum center of the clusters.

3.5. Comments on $[Al_{77}\{N(SiMe_3)_2\}_{20}]^{2-}$ and $[Ga_{84}\{N(SiMe_3)_2\}_{20}]^{4-}$

Recently, three remarkably large clusters, $[Al_{69}\{N(SiMe_3)_2\}_{18}]^{3-}$ [6], $[Al_{77}\{N(SiMe_3)_2\}_{20}]^{2-}$ [7] and $[Ga_{84}\{N(SiMe_3)_2\}_{20}]^{4-}$ [10], have been successfully synthesized and structurally characterized. All three clusters have a shell-like structural arrangement. For $[Al_{77}\{N(SiMe_3)_2\}_{20}]^{2-}$, successive shells contain 1, 12, 44 and 20 Al atoms while for $[Al_{69}\{N(SiMe_3)_2\}_{18}]^{3-}$ they are 1, 12, 38 and 18 Al atoms. For $[Ga_{84}\{N(SiMe_3)_2\}_{20}]^{4-}$, the successive shells have 2, 20, 42 and 20 Ga atoms. Detailed structural descriptions have been given by Schnöckel and his coworkers [6,7,10]. Apparently, there is no simple rule which can be used to appreciate the electron counts of these three large clusters. $[Al_{69}\{N(SiMe_3)_2\}_{18}]^{3-}$ has a total number of 192 metal electrons, having the $3n-15$ electron count for Al–Al bonding. $[Al_{77}\{N(SiMe_3)_2\}_{20}]^{2-}$ has a total number of 213 metal electrons, giving the $3n-18$ electron count for Al–Al bonding. $[Ga_{84}\{N(SiMe_3)_2\}_{20}]^{4-}$ has a total number of 236 metal electrons, leading to the $3n-16$ electron count for Ga–Ga bonding. $3n$ metal electrons are associated with metallic aluminum and gallium. Clearly, the electron counts given here for the three large clusters indicate that they are approaching the metallic character in terms of metal–metal interactions. A better understanding of their bonding requires further studies. It is only when more and more of these types of metalloid clusters become known that one will be in a position to establish the structure–electron count relationship.

4. Summary

The aluminum metalloid clusters provide much more versatile structural varieties which differ markedly from those of their lighter congener. Although these clusters do not simply follow Wade's electron counting rules, through the bonding analyses given in this paper, we demonstrate that the existing bonding knowledge on other types of clusters, e.g. boranes, hydrocarbons and metal–carbonyl clusters can still be used to understand the electron counts for the majority of these aluminum metalloid clusters. $[Al_{69}\{N(SiMe_3)_2\}_{18}]^{3-}$, $[Al_{77}\{N(SiMe_3)_2\}_{20}]^{2-}$ and $[Ga_{84}\{N(SiMe_3)_2\}_{20}]^{4-}$ are believed to possess more metallic characters.

Acknowledgements

This work is supported by the Research Grants Council of Hong Kong and the Hong Kong University of Science and Technology.

References

[1] A. Purath, C. Dohmeier, A. Ecker, R. Köppe, H. Krautscheid, H. Schnöckel, R. Ahlrichs, C. Stoermer, J. Friedrich, P. Jutzi, J. Am. Chem. Soc. 122 (2000) 6955.
[2] H. Köhnlein, G. Stösser, E. Baum, E. Möllhausen, U. Huniar, H. Schnöckel, Angew. Chem., Int. Ed. Engl. 39 (2000) 799.
[3] A. Purath, R. Köppe, H. Schnöckel, Angew. Chem., Int. Ed. Engl. 38 (1999) 2926.
[4] C. Klemp, R. Köppe, E. Weckert, H. Schnöckel, Angew. Chem., Int. Ed. Engl. 38 (1999) 1739.
[5] A. Purath, R. Köppe, H. Schnöckel, Chem. Commun. (1999) 1933.
[6] H. Köhnllein, A. Purath, C. Klemp, E. Baum, I. Krossing, G. Stösser, H. Schnöckel, Inorg. Chem. 40 (2001) 4830.
[7] A. Ecker, E. Weckert, H. Schnöckel, Nature 387 (1997) 379.
[8] (a) A. Purath, H. Schnöckel, J. Organomet. Chem. 579 (1999) 373;
(b) H. Sitzmann, M.F. Lappert, C. Dohmeier, C. Üffing, H. Schnöckel, J. Organomet. Chem. 561 (1998) 203;
(c) A. Purath, C. Dohmeier, A. Ecker, H. Schnöckel, K. Amelunxen, T. Passler, N. Wiberg, Organometallics 17 (1998) 1894;
(d) C. Dohmeier, C. Robl, M. Tacke, H. Schnöckel, Angew. Chem., Int. Ed. Engl. 30 (1991) 564.
[9] (a) W. Uhl, F. Breher, Organometallics 19 (2000) 4536;
(b) W. Uhl, F. Breher, A. Lützen, W. Saak, Angew. Chem., Int. Ed. Engl. 39 (2000) 406;
(c) W. Uhl, F. Breher, Angew. Chem., Int. Ed. Engl. 38 (1999) 1477.
[10] A. Schnepf, H. Schnöckel, Angew. Chem., Int. Ed. Engl. 40 (2001) 711.
[11] A. Schnepf, G. Stösser, H. Schnöckel, J. Am. Chem. Soc. 122 (2000) 9181.
[12] A. Schnepf, G. Stößer, R. Köppe, H. Schnöckel, Angew. Chem., Int. Ed. Engl. 39 (2000) 1637.
[13] A. Schnepf, E. Weckert, G. Linti, H. Schnöckel, Angew. Chem., Int. Ed. Engl. 38 (1999) 3381.
[14] K. Wade, Adv. Inorg. Radiochem. 18 (1976) 1.
[15] G. Linti, H. Schnöckel, Coord. Chem. Rev. 206/207 (2000) 285.
[16] T.A. Albright, J.K. Burdett, M.-H. Whangbo, Orbital Interactions in Chemistry, Wiley, New York, 1985.
[17] D.M.P. Mingos, D.J. Wales, Introduction to Cluster Chemistry, Prentice-Hall, New Jersey, 1990.
[18] (a) C. Lee, W. Yang, G. Parr, Phys. Rev. B 37 (1988) 785;
(b) B. Miehlich, A. Savin, H. Stoll, H. Preuss, Chem. Phys. Lett. 157 (1989) 200;
(c) A.D. Becke, J. Chem. Phys. 98 (1993) 5648.
[19] (a) P.J. Hay, W.R. Wadt, J. Chem. Phys. 82 (1985) 270;
(b) W.R. Wadt, P.J. Hay, J. Chem. Phys. 82 (1985) 284;
(c) P.J. Hay, W.R. Wadt, J. Chem. Phys. 82 (1985) 299.
[20] J. Andzelm, S. Huzinaga, Gaussian Basis Sets for Molecular Calculations, Elsevier, New York, 1984.
[21] P.C. Hariharan, J.A. Pople, Theor. Chim. Acta 28 (1973) 213.
[22] W.J. Hehre, R.F. Stewart, J.A. Pople, J. Chem. Phys. 51 (1969) 2657.
[23] M.J. Frisch, G.W. Trucks, H.B. Schlegel, G.E. Scuseria, M.A. Robb, J.R. Cheeseman, V.G. Zakrzewski, J.A. Montgomery, Jr., R.E. Stratmann, J.C. Burant, S. Dapprich, J.M. Millam, A.D. Daniels, K.N. Kudin, M.C. Strain, O. Farkas, J. Tomasi, V. Barone, M. Cossi, R. Cammi, B. Mennucci, C. Pomelli, C. Adamo, S. Clifford, J. Ochterski, G.A. Petersson, P.Y. Ayala, Q. Cui, K. Morokuma, D.K. Malick, A.D. Rabuck, K. Raghavachari, J.B. Foresman, J. Cioslowski, J.V. Ortiz, A.G. Baboul, B.B. Stefanov, G. Liu, A. Liashenko, P. Piskorz, I. Komaromi, R. Gomperts, R.L. Martin, D.J. Fox, T. Keith, M.A. Al-Laham, C.Y. Peng, A. Nanayakkara, M. Challacombe, P.M.W. Gill, B. Johnson, W. Chen, M.W. Wong, J.L. Andres, C. Gonzalez, M. Head-Gordon, E.S. Replogle, J.A. Pople, Gaussian 98 (Revision A.9), Gaussian, Inc., Pittsburgh, PA, 1998.
[24] Interactive MOPLOT: a package for the interactive display and analysis of molecular wave functions, incorporating the programs MOPLOT (D. Lichtenburger), PLOTDEN (R.F.W. Bader, D.J. Kenworthy, P.M. Beddal, G.R. Runtz, S.G. Anderson), SCHUSS (R.F.W. Bader, G.R. Runtz, S.G. Anderson, F.W. Biegler-Koenig), and EXTREM (R.F.W. Bader, F.W. Bieger-Koenig) by P. Sherwood, P.J. MacDougall, 1989.
[25] E.D. Glendening, A.E. Reed, J.E. Carpenter, F. Weinhold, NBO version 3.1.
[26] Schaftenaar, G. Molden v3.7, CAOS/CAMM Center Nijmegen, Toernooiveld, Nijmegen, Netherlands, 2001.
[27] N. Wiberg, T. Blank, H. Nöth, W. Ponikwar, Angew. Chem., Int. Ed. Engl. 38 (1999) 839.
[28] D.M.P. Mingos, T. Slee, Z. Lin, Chem. Rev. 90 (1990) 383.
[29] W. Hiller, K.-W. Klinkhammer, W. Uhl, J. Wagner, Angew. Chem., Int. Ed. Engl. 30 (1991) 179.
[30] T. Slee, Z. Lin, D.M.P. Mingos, Inorg. Chem. 28 (1989) 2256.
[31] W.D. Knight, K. Clemenger, W.A. de Heer, W. Saunders, M.Y. Chou, M.L. Cohen, Phys. Rev. Lett. 52 (1984) 2141.
[32] J.F. Halet, J.Y. Saillard, Structure Bonding 87 (1997) 81 and references therein.

PERGAMON

Polyhedron 21 (2002) 511–518

POLYHEDRON

www.elsevier.com/locate/poly

Molecular self-assembly controlled by gallium–gallium single bonds—facile syntheses of macrocyclic octagallium compounds

Werner Uhl *, Lars Cuypers, Malte Prött, Klaus Harms

Fachbereich Chemie der Philipps Universität Marburg, Hans-Meerwein-Straße, D-35032 Marburg, Germany

Received 3 July 2001; accepted 27 November 2001

Abstract

Treatment of the digallane(4) derivative $R_2Ga–GaR_2$ (**1**) [$R = CH(SiMe_3)_2$] with the dicarboxylic acid muconic acid or with squaric acid yielded macrocyclic compounds (**4** and **5**, respectively) by retention of the Ga–Ga single bonds and release of 2 equiv. of bis(trimethylsilyl)methane per formula unit of **1**. Both products contain four Ga–Ga single bonds connected by four dicarboxylato or diolato ligands. Large heterocycles resulted which contain 36 (**4**) and 20 atoms (**5**), respectively. The cavity of the macrocycle of **5** is filled by two *n*-pentane molecules. In contrast, two pentane molecules are located in hollows on the surface of the macrocycle of **4** in a supramolecular arrangement. They influence the molecular conformation significantly. The reaction with squaric acid gave a by-product (**6**) which also has eight gallium atoms in a heterocycle, but one Ga–Ga bond was cleaved by oxidation and probably by the release of elemental hydrogen. © 2002 Elsevier Science Ltd. All rights reserved.

Keywords: Gallium–gallium bonds; Macrocycles; Supramolecular chemistry

1. Introduction

The first known and well-characterized organoelement compounds containing Al–Al, Ga–Ga and In–In single bonds were obtained in our group about 10 years ago [1–3]. Their syntheses succeeded by reduction of the corresponding dialkylelement halides or by treatment of subhalides still containing element–element single bonds with alkyllithium derivatives. They need bulky substituents in order to prevent the thermodynamically favored disproportionation reaction and the formation of elemental aluminum, gallium or indium. We employed bis(trimethylsilyl)methyl groups for the stabilization of compounds of the type $R_2E–ER_2$ (E = Al, Ga, In). Later on, many further derivatives were published bearing bulky aryl [4] or silyl [5] substituents. These compounds showed a remarkable chemical reactivity and six different types of reaction were observed such as insertion reactions or the formation of radical anions possessing 1e–E–E π-bonds [6]. Substituent exchange by retention of the E–E bonds is another particularly important reaction. It succeeds only with the digallium derivative $R_2Ga–GaR_2$ (**1**) [$R = CH(SiMe_3)_2$] [2] and requires treatment of **1** with protic reagents containing chelating residues [7–10]. In contrast, the originally expected cleavage of the element–element single bonds by oxidation of the bivalent elements and the release of elemental hydrogen was observed in all cases when we employed the aluminum or indium derivatives under similar conditions [11]. Substituent exchange products derived from **1** were isolated in almost quantitative yield when we treated **1** with carboxylic acids such as acetic acid or benzoic acid (**2**, Scheme 1) [7], while a decrease of the acidic strength gave side reactions with the formation of mixtures of products and at least partial cleavage of Ga–Ga bonds [10]. Much more interesting are reactions with bifunctional dicarboxylic acids, because owing to the bridging capability of their residues they open the route to the synthesis of polymeric or macrocyclic organoelement compounds. Dimeric products, in which two Ga–Ga units were bridged by two dicarboxylato ligands, were obtained with those dicarboxylic acids which have a more flexible backbone such as phenylene diacetic acid (**3**, Scheme 1) [8]. In contrast, the rigid backbone of

* Corresponding author. Tel.: +49-6421-282-5751; fax: +49-6421-282-5653.

E-mail address: uhl@chemie.uni-marburg.de (W. Uhl).

0277-5387/02/$ - see front matter © 2002 Elsevier Science Ltd. All rights reserved.
PII: S0277-5387(01)01019-1

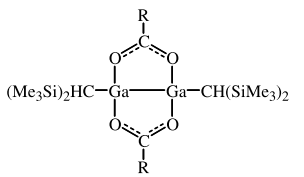
ferrocene dicarboxylic acid prevented the formation of a dimer, and a tetramer was formed with four Ga–Ga bonds and four dicarboxylato bridges [9]. We report here on further investigations into the syntheses of macrocyclic polygallium compounds by the treatment of **1** with bifunctional acidic reagents. One aspect of this chemistry is the approach to supramolecular interactions with the inclusion of solvent molecules into the cavity of the macrocycles, for instance.

2. Experimental

All procedures were carried out under purified argon. *n*-Pentane was dried over $LiAlH_4$; THF over Na/benzophenone; acetonitrile over P_4O_{10}. $Ga_2[CH(SiMe_3)_2]_4$ (**1**) was obtained according to a literature procedure [2]. Commercially available muconic acid (*trans–trans*-2,4-hexadienedioic acid, Aldrich) and squaric acid (3,4-dihydroxy-3-cyclobuten-1,2-dione, Merck) were employed without purification.

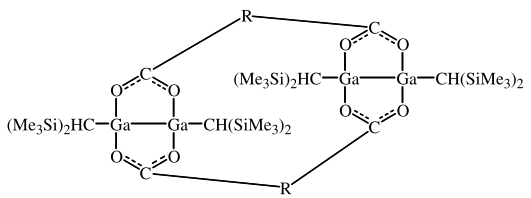
2.1. Synthesis of compound *4*

A cooled (0 °C) solution of 0.278 g (0.358 mmol) of **1** in 40 ml of THF was treated with solid *trans–trans*-muconic acid (0.051 g, 0.358 mmol). The mixture was warmed to room temperature and stirred for 22 h. The solvent was removed in vacuum, and the thoroughly evacuated residue was treated with *n*-pentane. After filtration and concentration, the product (**4**) crystallized upon cooling to − 30 °C. Yield: 0.133 g (62%), bright yellow crystals. Dec. (argon, sealed capillary): above 180 °C (see text). ^{1}H NMR (C_6D_6, 300 MHz): $\delta = 7.20$ (2 H, part of a AA′ spectrum, distances between the inner and outer lines 8 and 14 Hz, respectively, C=CH), 5.91 (2 H, second part of the AA′XX′ spectrum, distances between the inner and outer lines 8 and 14 Hz, respectively, C=C–H), 0.31 (36 H, s, $SiMe_3$), − 0.15 (2 H, s, GaCH). ^{13}C NMR (C_6D_6, 75.5 MHz): $\delta = 176.3$ (CO_2), 142.2 and 123.0 (C=C), 4.4 (GaC), 2.9 ($SiMe_3$). IR (CsBr plates, paraffin, cm^{-1}): 1615 w, 1532 m $\nu(CO_2)$; 1461 vs, 1378 vs paraffin; 1291 w, 1248 m δCH_3; 1013 w, 1003 w δCH; 968 sh, 943 w, 864 m, 844 s, 759 w, 723 w ρCH_3(Si); 675 vw ν_{as}(SiC); 629 vw ν_s(SiC); 601 vw, 514 vw, 466 vw ν(GaC), ν(GaO). UV–Vis (*n*-hexane): λ_{max} (nm) (log ε) = 210 (4.3), 270 (4.5), 280 (4.5), 290 (4.3), 330 (3.1).



2

R = -CH_3, -C_6H_5, -4-Br-C_6H_4, -3,5-$C_6H_3Me_2$, -CMe_3, -Adamantyl



3

R = 1,4-$(CH_2)_2C_6H_4$, 1,4-C_6H_{10}, $(CH_2)_6$, $(CH_2)_4$

Scheme 1.

2.2. Synthesis of compound *5*

A mixture of the digallium compound **1** (0.119 g, 0.153 mmol) and squaric acid (0.0175 g, 0.153 mmol) was treated with 25 ml of acetonitrile. The suspension was refluxed for 1 h. A clear solution resulted in the heat. After cooling to room temperature the solvent was removed in vacuum, and the residue was treated with *n*-pentane and filtered. The colorless product precipitated upon cooling of the solution to − 70 °C. Yield: 0.026 g (30%). Dec. (argon, sealed capillary): 284 °C. ^{1}H NMR (C_6D_6, 200 MHz): $\delta = 0.26$ (36 H, s, $SiMe_3$), − 0.13 (2 H, s, GaCH). ^{13}C NMR (C_6D_6, 75 MHz): $\delta = 196.6$ (CO), 10.4 (GaC), 3.6 ($SiMe_3$). IR (CsBr plates, paraffin, cm^{-1}): 1590 sh, 1539 vs, 1515 vs ν(CO), ν(CC); 1463 vs, 1377 vs paraffin; 1302 w, 1252 sh, 1248 s δCH_3; 1111 w, 1095 m ν(CC) (pentane); 1013 w δCH; 964 m, 851 sh, 843 s, 777 m, 759 m, 724 m ρCH_3(Si); 673 m ν_{as}(SiC); 625 w ν_s(SiC); 610 vw, 507 w, 447 w, 419 m ν(GaC), ν(GaO). UV–Vis (*n*-hexane): λ_{max} (nm) (log ε) = 210 (1.5), 270 (4.0).

2.3. Crystal structure determination of *4*

Single crystals of **4** by slow concentration of a solution in *n*-pentane at room temperature over several days; crystals grew above the surface of the solvent; they included two molecules of pentane per formula unit of **4**; $C_{90}H_{192}O_{16}Si_{16}Ga_8$, crystal size 0.60 × 0.12 × 0.07, STOE IPDS diffractometer, temperature 193 K, monoclinic, $P2_1/c$ (no. 14 [12]), $a = 1247.34(3)$, $b = 2712.1(1)$, $c = 2142.13(7)$ pm, $\beta = 105.179(3)°$, $V = 6993.7(4) \times 10^{-30}$ m^3, $D_{calc} = 1.205$ g cm^{-3}, $Z = 2$ (**4**) and 4 (*n*-pentane), μ(Mo Kα) = 1.70 mm^{-1}, numerical absorption correction, 2θ range $3.9 \leq 2\Theta \leq 52°$, index ranges $-13 \leq h \leq 13$, $-33 \leq k \leq 33$, $-26 \leq l \leq 25$, number of unique reflections 12 841, number of parameters 596, structure solution by direct methods,

programs SHELXTL-PLUS and SHELXL-97 [13], refinement by the full-matrix least-squares method based on F^2, R_1 (6891 reflections $I > 2\sigma(I)) = 0.041$, wR_2 (all data) = 0.128, max/min residual electron density = $0.678/-0.404 \times 10^{30}$ e m^{-3}. The molecules reside on crystallographic inversion centers. One $CH(SiMe_3)_2$ group (C3/Si5/Si6) was disordered, the carbon atoms of its methyl groups were refined isotropically on split positions.

2.4. Crystal structure determination of **5**

Single crystals of **5** by slow concentration of a solution in *n*-pentane at room temperature over several days; the crystals included two molecules of pentane per formula unit of **5**; $C_{82}H_{176}O_{16}Si_{16}Ga_8$, crystal size $0.36 \times 0.36 \times 0.09$, STOE IPDS diffractometer, temperature 193 K, triclinic, $P\bar{1}$ (no. 2 [12]), $a = 1868.25(9)$, $b = 1957.63(9)$, $c = 2191.6(1)$ pm, $\alpha = 95.494(6)$, $\beta = 107.960(6)$, $\gamma = 118.481(5)°$, $V = 6413.3(5) \times 10^{-30}$ m^3, $D_{calc} = 1.256$ g cm^{-3}, $Z = 2$, μ(Mo Kα) = 1.85 mm^{-1}, numerical absorption correction, 2θ range $3.8 \leq 2\Theta \leq 52°$, index ranges $-22 \leq h \leq 22$, $-23 \leq k \leq 23$, $-26 \leq l \leq 26$, number of unique reflections 23 273, number of parameters 1101, structure solution by direct methods, programs SHELXTL-PLUS and SHELXL-97 [13], refinement by the full-matrix least-squares method based on F^2, R_1 (16 425 reflections $I > 2\sigma(I)) = 0.043$, wR_2 (all data) = 0.117, max/min residual electron density = $1.293/-1.028 \times 10^{30}$ e m^{-3}; the molecules reside on crystallographic inversion centers, and two half molecules were found in each asymmetric unit.

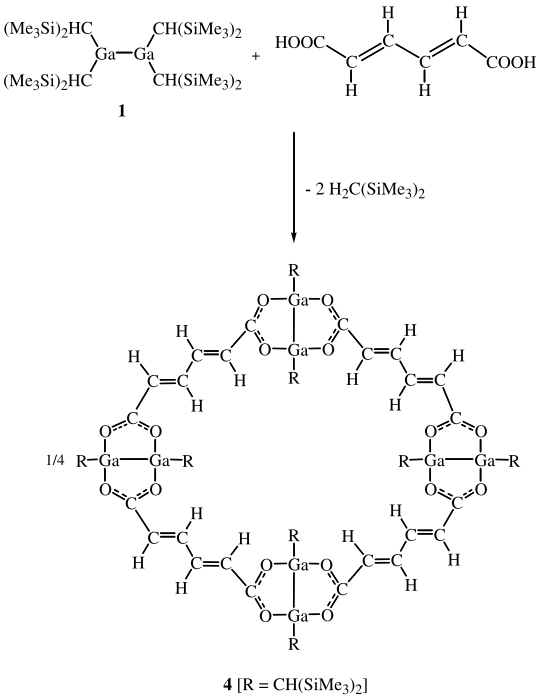
2.5. Crystal structure determination of **6**

Single crystals of **6** by slow concentration of a solution of an impure reaction product (see text) in *n*-pentane at room temperature over several days; $C_{86}H_{190}O_{16}Si_{20}Ga_8$, crystal size $0.24 \times 0.18 \times 0.15$, STOE IPDS diffractometer, temperature 193 K, triclinic, $P\bar{1}$ (no. 2 [12]), $a = 1654.5(1)$, $b = 1886.0(1)$, $c = 2476.9(2)$ pm, $\alpha = 72.542(6)$, $\beta = 86.456(6)$, $\gamma = 75.193(5)°$, $V = 7127.1(8) \times 10^{-30}$ m^3, $D_{calc} = 1.212$ g cm^{-3}, $Z = 2$, μ(Mo Kα) = 1.70 mm^{-1}, numerical absorption correction, 2θ range $2.5 \leq 2\Theta \leq 50.7°$, index ranges $-19 \leq h \leq 19$, $-22 \leq k \leq 22$, $-29 \leq l \leq 29$, number of unique reflections 25 896, number of parameters 1232, structure solution by direct methods, programs SHELXTL-PLUS and SHELXL-97,[13] refinement by the full-matrix least-squares method based on F^2, R_1 (12 911 reflections $I > 2\sigma(I)) = 0.045$, wR_2 (all data) = 0.116, max/min residual electron density = $1.607/-0.624 \times 10^{30}$ e m^{-3}.

3. Results and discussion

3.1. Reactions of **1** with muconic acid and squaric acid

A bright yellow solution was obtained upon treatment of digallane(4) **1** with muconic acid. A small quantity of a colorless solid precipitated, the constitution of which is unknown. Possibly a polymer had formed as a by-product which would be of particular interest in the context of this research project. Investigations concerning its composition are in progress. After filtration, evaporation and recrystallization, yellow crystals of the product **4** were isolated in 62% yield (Eq. (1)). Crystalline **4** was thermally stable up to 180 °C. Above that temperature it adopted an orange color and became black at about 305 °C. The ^{1}H and ^{13}C NMR resonances of the central hydrogen and carbon atoms of the bis(trimethylsilyl)methyl groups neighboring gallium are strongly shifted to a higher field compared to those of the starting compound **1** (**1**: $\delta = 1.11$ (^{1}H) and 25.9 (^{13}C); **4**: $\delta = -0.15$ and 4.4, respectively), which is characteristic of an enhancement of the coordination numbers of the gallium atoms from three in **1** to four in **4** [14]. An absorption at 1532 cm^{-1} was observed in the IR spectrum for the bridging carboxylato groups, which is in the very narrow range of related compounds (**2** and **3**, Scheme 1) [7–9].



(1)

Reaction of **1** with squaric acid in pentane afforded a mixture of compounds as was detected by several broad lines in the ^{1}H NMR spectrum of the crude product. One of these compounds could be isolated in a pure form in trace amounts; its crystal structure is discussed

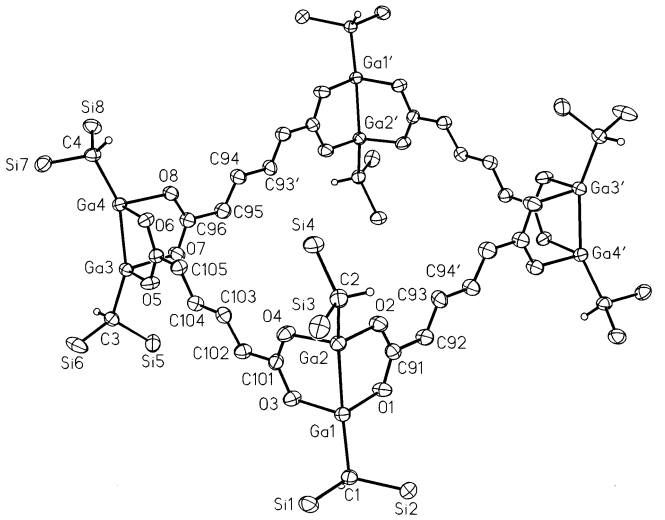


Fig. 1. Molecular structure of **4**. The thermal ellipsoids are drawn at the 40% probability level. Methyl groups and hydrogen atoms of the bridging ligands are omitted for clarity.

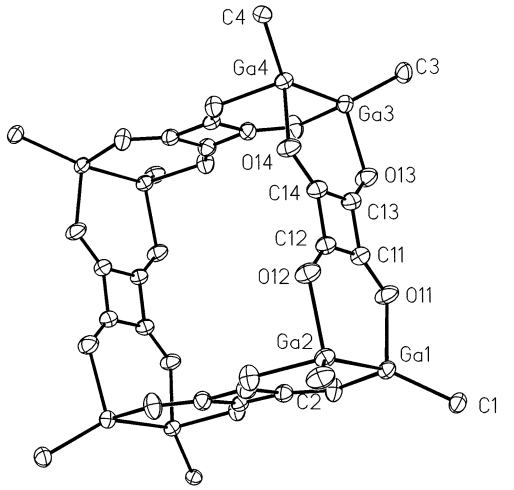
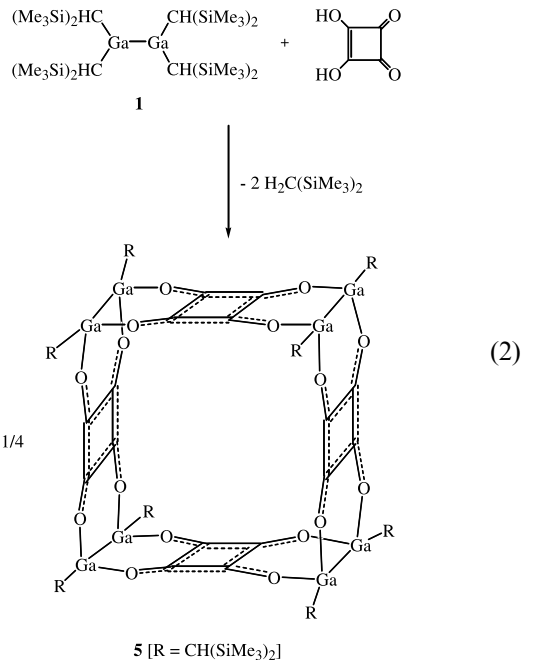


Fig. 2. Molecular structure of **5**. Only one of the two independent molecules is shown. The thermal ellipsoids are drawn at the 40% probability level. Trimethylsilyl groups and hydrogen atoms are omitted for clarity.

below. The spectra of the crude products became clearer when we employed solvents with increasing polarity, and finally an almost pure compound (**5**) with only one singlet of $SiMe_3$ groups was obtained in acetonitrile. Colorless crystals of **5** (Eq. (2)) were isolated after recrystallization from *n*-pentane. Similar to **4**, the inner hydrogen and carbon atoms of the bis(trimethylsilyl)methyl groups were shifted to a higher field ($\delta = -0.13$ and 10.4, respectively) compared to the starting compound **1**. Three absorptions (1590, 1539 and 1515 cm^{-1}) were observed in the IR spectrum for the C–C and C–O bonds of the C_4O_4 bridging ligand possessing a delocalized π-bonding system. Compound **5** is thermally quite stable and does not decompose before 284 °C.



(2)

3.2. Crystal structures

The molecular structure of **4** as determined by X-ray diffraction is depicted in Fig. 1, and a schematic drawing is given in Eq. (1). Compound **4** contains four Ga–Ga single bonds bridged by four dicarboxylato ligands. A large organometallic macrocycle results, consisting of 36 gallium, oxygen and carbon atoms. Each Ga–Ga bond is bridged by two carboxylato groups similar to all dicarboxylatodigallium derivatives reported before [7–9]. Each gallium atom is coordinated by two oxygen atoms of different chelating ligands, by a carbon atom of a bis(trimethylsilyl)methyl group and by the second gallium atom of the Ga–Ga bond. A similar structure was observed for the squaric acid derivative **5** (Fig. 2), which has two 20-membered heterocycles connected by four Ga–Ga and eight C–C bonds. Similar macrocyclic compounds, which contain four pairs of transition metal atoms bridged by four dicarboxylato groups, were published only recently [15].

Owing to the smaller bite of the bridging carboxylato group, the Ga–Ga bond lengths of **4** (238.3 pm on average, Table 1) are shorter than those of **5** (245.5 pm, Table 2). A similar lengthening compared to carboxylatodigallium compounds was observed for the five-atomic imidotetraphenyldiphosphinato ligand [16]. All distances are shorter than the Ga–Ga bond of the unsupported tetraalkyl compound **1** (254.0 pm) [2]. The bridging ligands of each Ga–Ga bond are almost ideally perpendicular to one another (angles O–Ga–O = 92.1° (**4**) and 91.0° (**5**) on average), and the Ga–Ga–C groups approach linearity (156.8°) for the carboxylato derivative **4** (139.7° for the less stressed squaric acid

Table 1
Selected bond lengths (pm) and angles (°) of compound **4**

Bond lengths			
Ga1–C1	195.2(5)	Ga2–C2	196.4(5)
Ga1–O1	200.6(3)	Ga2–O2	200.7(3)
Ga1–O3	202.7(3)	Ga2–O4	200.3(3)
Ga1–Ga2	237.75(8)		
Ga3–C3	195.8(5)	Ga4–C4	195.1(5)
Ga3–O5	199.5(4)	Ga4–O6	202.2(3)
Ga3–O7	201.7(3)	Ga4–O8	201.0(3)
Ga3–Ga4	238.77(8)		
Bond angles			
C1–Ga1–Ga2	156.5(2)	C2–Ga2–Ga1	155.5(2)
O1–Ga1–Ga2	88.2(1)	O2–Ga2–Ga1	88.1(1)
O3–Ga1–Ga2	88.2(1)	O4–Ga2–Ga1	88.2(1)
O1–Ga1–O3	90.8(2)	O2–Ga2–O4	93.5(2)
C3–Ga3–Ga4	158.8(2)	C4–Ga4–Ga3	156.6(2)
O5–Ga3–Ga4	88.1(1)	O6–Ga4–Ga3	87.8(1)
O7–Ga3–Ga4	87.6(1)	O8–Ga4–Ga3	88.4(1)
O5–Ga3–O7	92.7(2)	O6–Ga4–O8	91.4(2)

Table 2
Selected bond lengths (pm) and angles (°) of compound **5**

Bond lengths			
Ga1–C1	196.8(3)	Ga2–C2	195.2(3)
Ga1–O11	200.4(2)	Ga2–O12	200.8(2)
Ga1–O31	200.0(3)	Ga2–O32	203.2(3)
Ga1–Ga2	245.88(6)		
Ga3–C3	195.5(4)	Ga4–C4	196.4(3)
Ga3–O13	200.8(2)	Ga4–O14	199.9(2)
Ga3–O21	201.5(3)	Ga4–O22	199.0(3)
Ga3–Ga4	245.31(6)		
Ga5–C5	196.3(3)	Ga6–C6	195.9(4)
Ga5–O41	200.9(2)	Ga6–O42	201.8(2)
Ga5–O61	200.3(3)	Ga6–O62	200.5(2)
Ga5–Ga6	245.58(6)		
Ga7–C7	196.6(4)	Ga8–C8	196.4(3)
Ga7–O43	199.9(2)	Ga8–O44	200.1(2)
Ga7–O51	200.9(3)	Ga8–O52	200.7(2)
Ga7–Ga8	245.04(6)		
Bond angles			
Ga2–Ga1–C1	143.2(1)	Ga1–Ga2–C2	140.2(1)
Ga2–Ga1–O11	102.70(7)	Ga1–Ga2–O12	101.26(7)
Ga2–Ga1–O31	98.68(7)	Ga1–Ga2–O32	103.84(7)
O11–Ga1–O31	88.7(1)	O12–Ga2–O32	90.5(1)
Ga4–Ga3–C3	138.4(1)	Ga3–Ga4–C4	140.5(1)
Ga4–Ga3–O13	100.93(7)	Ga3–Ga4–O14	102.99(7)
Ga4–Ga3–O21	103.30(8)	Ga3–Ga4–O22	100.18(7)
O13–Ga3–O21	93.2(1)	O14–Ga4–O22	90.1(1)
Ga6–Ga5–C5	138.3(1)	Ga5–Ga6–C6	139.9(1)
Ga6–Ga5–O41	101.85(8)	Ga5–Ga6–O42	101.85(8)
Ga6–Ga5–O61	102.10(7)	Ga5–Ga6–O62	101.89(8)
O41–Ga5–O61	87.9(1)	O42–Ga6–O62	92.6(1)
Ga8–Ga7–C7	137.9(1)	Ga7–Ga8–C8	138.8(1)
Ga8–Ga7–O43	101.84(8)	Ga7–Ga8–O44	102.50(7)
Ga8–Ga7–O51	100.97(8)	Ga7–Ga8–O52	102.34(8)
O43–Ga7–O51	93.9(1)	O44–Ga8–O52	91.3(1)

derivative **5**). The particular bonding situation resulting from these structural parameters has been discussed extensively before [7]. The bond lengths and angles of the bridging anionic organic ligands are similar to those observed in other derivatives [17] and do not need a more detailed discussion. They verify alternating C–C single and double bonds (145.2 and 132.1 pm) in the case of *trans*,*trans*-muconic acid and a completely delocalized π-electronic system in the case of squaric acid (C–C 145.8 pm; C–O 125.6 pm).

The crystals of compound **5** enclose two molecules of *n*-pentane per formula unit. These solvent molecules approach the molecular center from both sides of the macrocycle and occupy its cavity in a supramolecular arrangement [18]. They are almost completely covered by the organic substituents of the octagallium compound. Both independent molecules of **5** differ with respect to the depth of penetration of the solvent molecules, which is most effective for that molecule containing the atoms Ga5–Ga8 (Fig. 3(b)). Here, the pentane molecules approach a narrow distance between their nearest terminal carbon atoms of only 341.7 pm, which is shorter than the intramolecular contact distances observed in crystalline alkanes (about 360 pm) [19]. These pentane molecules deviate only slightly from the ideal perpendicular position to the average plane of the gallium atoms (78.9°). They are more tilted for the second macrocycle comprising the atoms Ga1–Ga4 (angle between the average plane of the macrocycle and the pentane molecule = 63.3°) (Fig. 3(a)). In this case, the pentane molecules penetrate the cavity to a lesser extent, and the distance between the terminal carbon atoms is enlarged by more than 100 pm to 452.5 pm. Thus, interestingly, the pentane molecules stand more upright the more they approach the center of the macrocycle. Short contact distances are observed between the terminal carbon atoms of the pentane molecules and atoms of the squaric acid residue (372.6 pm to C51′, 374.0 pm to C52, 376.0 pm to C62, 378.4 pm to C44, 382.6 pm to C42; second molecule 357.7 pm to O13′, 365.4 pm to C13′). Also, the crystals of **4** enclose two solvent molecules per formula unit, but these do not reside in the cavity of the macrocycle. Instead, they are localized in opposite exocyclic positions between the bulky organoelement substituents of two Ga–Ga bonds and are parallel to two butadiene backbones of the muconic acid residues (Fig. 4). Several short intermolecular contact distances between carbon atoms of the pentane molecules and oxygen or carbon atoms of the macrocycle and trimethylsilyl groups of >385 pm indicate weak van der Waals interactions as expected for crystal solvents. However, these pentane molecules cause a distortion of the macrocycle so that those butadienyl bridges which are not covered by the solvent molecules (C92–C95′) form a concave line, while those neighboring pentane (C102–

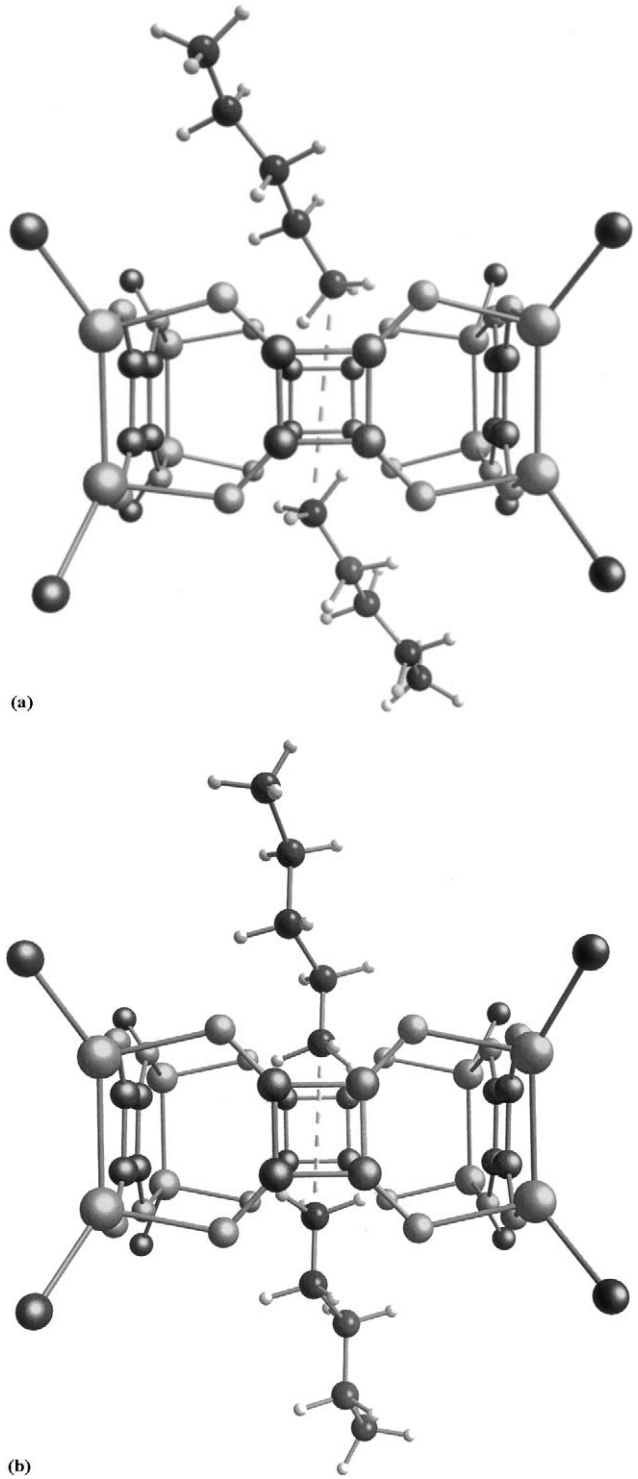


Fig. 3. Arrangement of *n*-pentane molecules in the molecular center of **5**. Only the inner carbon atoms of the bis(trimethylsilyl)methyl groups are shown, its hydrogen atoms and $SiMe_3$ groups are omitted. The pentane molecules are almost completely covered by the organic substituents.

C105) have a convex orientation. The shortest transannular distances between the inner carbon atoms of the opposite concave muconic acid residues (C93, C94) are 1021 pm on average compared to 1249 pm between C102 and C103 of the remaining bridging ligands. This particular conformation causes the tilting of the Ga_2R_2 groups. The hollows for the deposit of the pentane molecules become larger, and the contacts between butadienyl and pentane carbon atoms are closer. Thus, we observe a remarkable supramolecular influence on the structure of the macrocycle. The distances between two gallium atoms along the edges of the macrocycle of **4** are 1088–1186 pm and in a narrower range compared to the transannular C–C distances. The macrocycle of **5** is smaller. The Ga–Ga distances along the edges are 708.1–710.2 pm, and the transannular C–C contacts are only slightly lengthened (709–735 pm), indicating a weak deviation from an ideal planar arrangement of the atoms at one face of the molecule.

The reaction of **1** with squaric acid in non-polar solvents gave mixtures of products. In one case we isolated a few single crystals of one of these products (**6**) by very slow concentration of a solution in *n*-pentane under reduced pressure at room temperature over several days. Its molecular structure is depicted in Fig. 5, and Scheme 2 gives a schematic drawing. It is quite similar to compound **5**, but has three intact Ga–Ga bonds only. One bond was opened by oxidation of its two gallium atoms (Ga1, Ga2) from $+2$ to $+3$. These atoms are bridged by two squaric acid residues and

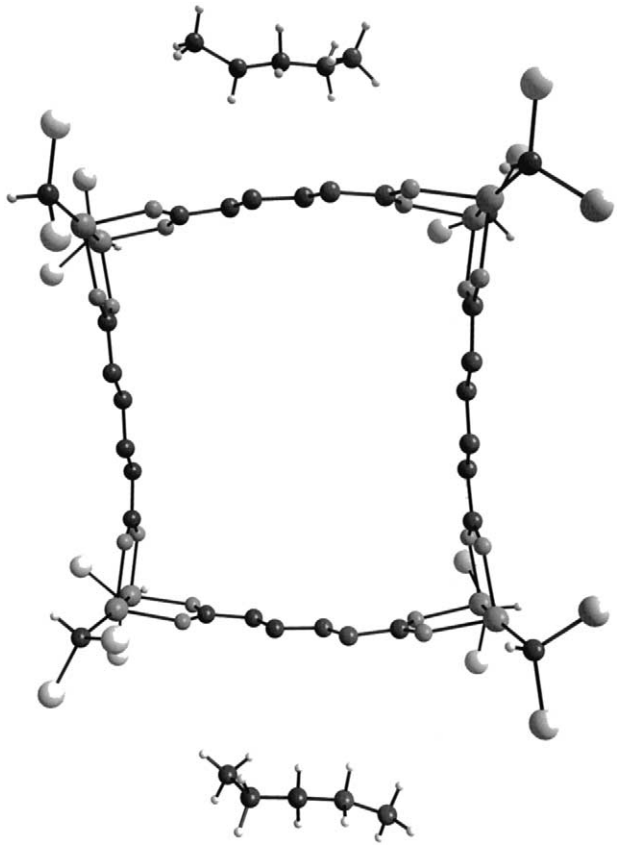


Fig. 4. Arrangement of *n*-pentane molecules at the heterocycle of **4**. Methyl groups are omitted.

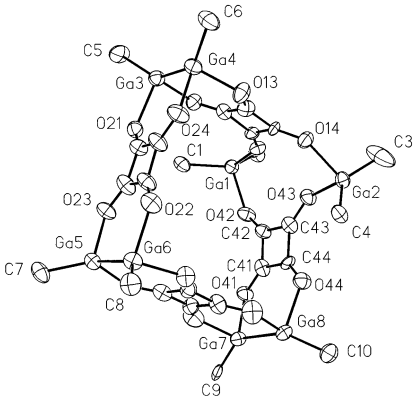
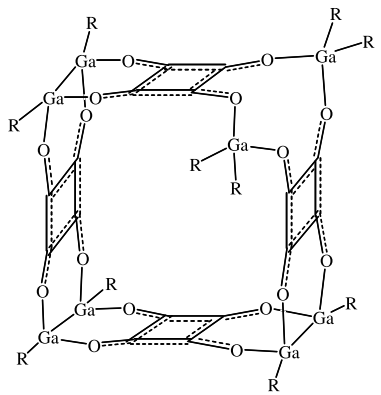


Fig. 5. Molecular structure of **6**. The thermal ellipsoids are drawn at the 40% probability level. Trimethylsilyl groups and hydrogen atoms are omitted for clarity.



6 [R = $CH(SiMe_3)_2$]

Scheme 2.

have a distorted tetrahedral coordination sphere, in which each gallium atom is coordinated by two oxygen atoms of squaric acid and two carbon atoms of two bis(trimethylsilyl)methyl substituents. The largest deviation from the ideal tetrahedral angle is observed between the bulky organoelement groups (130.2° and 136.5°, Table 3). The enhanced oxidation state of the gallium atoms has only a minor influence on the Ga–C or Ga–O bond lengths, and quite similar values are observed within the molecule (Ga–C = 195.9 pm for Ga1 and Ga2, 195.2 pm for the remaining gallium atoms; Ga–O = 198.8 pm and 200.1 pm, respectively). The Ga–Ga bond lengths (245.2 pm on average) correspond to those of compound **5**. As expected, the Ga1–Ga2 distance of the opened Ga–Ga bond (583.5 pm) is far outside the range of significant bonding interaction (sum of the van der Waals radii of Ga 380 pm [20]). The remaining structural parameters are quite similar to those of **5**. The squaric acid residues bridging one Ga–Ga bond are almost ideally perpendicular to one another, and even at the trivalent gallium atoms (Ga1, Ga2) the O–Ga–O angles approach 90°. The opening of Ga–Ga bonds was observed in our group several times before when we treated **1** with very weak protonic acids such as diphenyltriazene [10]. Also in the case of squaric acid, the acidic strength does not seem to be high enough to ensure the selective substitution reaction, and partial or complete opening of Ga–Ga bonds resulted. Thus, the mixture obtained by the reaction in non-polar solvents may comprise the whole series of products expected by the successive opening of Ga–Ga bonds including compound **5**, which was detected by NMR spectroscopy as a main component in all crude products. No further compound was obtained in a pure form, and **6** was isolated only in trace amounts so that with the exception of **5**, spectroscopic findings could not unambiguously be assigned to particular derivatives.

Table 3
Selected bond lengths (pm) and angles (°) of compound **6**

Bond lengths			
Ga1–C1	196.7(6)	Ga2–C3	194.3(7)
Ga1–C2	196.0(6)	Ga2–C4	196.4(5)
Ga1–O11	198.3(3)	Ga2–O14	197.8(4)
Ga1–O42	198.4(3)	Ga2–O43	200.5(3)
Ga3–C5	195.9(5)	Ga4–C6	194.9(6)
Ga3–O12	201.4(4)	Ga4–O13	197.2(4)
Ga3–O21	200.1(3)	Ga4–O24	201.6(4)
Ga3–Ga4	244.08(8)		
Ga5–C7	195.8(5)	Ga6–C8	194.4(5)
Ga5–O23	198.7(3)	Ga6–O22	201.6(4)
Ga5–O31	199.7(4)	Ga6–O34	199.7(4)
Ga5–Ga6	245.14(8)		
Ga7–C9	195.5(5)	Ga8–C10	194.6(5)
Ga7–O32	200.7(4)	Ga8–O33	200.6(4)
Ga7–O41	199.4(3)	Ga8–O44	200.2(4)
Ga7–Ga8	246.43(8)		
Bond angles			
C1–Ga1–C2	130.2(2)	C3–Ga2–C4	136.5(3)
C1–Ga1–O11	110.1(2)	C3–Ga2–O14	103.7(3)
C1–Ga1–O42	107.5(2)	C3–Ga2–O43	102.5(3)
C2–Ga1–O11	106.4(2)	C4–Ga2–O14	106.3(2)
C2–Ga1–O42	105.4(2)	C4–Ga2–O43	110.1(2)
O11–Ga1–O42	89.8(1)	O14–Ga2–O43	86.5(1)
Ga4–Ga3–C5	139.0(2)	Ga3–Ga4–C6	137.8(2)
Ga4–Ga3–O12	103.3(1)	Ga3–Ga4–O13	101.1(1)
Ga4–Ga3–O21	101.3(1)	Ga3–Ga4–O24	102.4(1)
O12–Ga3–O21	90.2(2)	O13–Ga4–O24	89.7(2)
Ga6–Ga5–C7	141.1(2)	Ga5–Ga6–C8	138.4(2)
Ga6–Ga5–O23	101.2(1)	Ga5–Ga6–O22	101.8(1)
Ga6–Ga5–O31	102.8(1)	Ga5–Ga6–O34	100.9(1)
O23–Ga5–O31	89.6(2)	O22–Ga6–O34	90.0(2)
Ga8–Ga7–C9	143.3(2)	Ga7–Ga8–C10	147.7(2)
Ga8–Ga7–O32	102.0(1)	Ga7–Ga8–O33	100.9(1)
Ga8–Ga7–O41	101.8(1)	Ga7–Ga8–O44	101.26(9)
O32–Ga7–O41	88.6(2)	O33–Ga8–O44	89.2(2)

4. Supplementary material

Further details of the crystal structure determinations have been deposited with the Cambridge Crystallographic Data Centre, CCDC Nos. 163401 (**4**), CCDC 163402 (**5**), and CCDC 163403 (**6**). Copies of this information may be obtained free of charge from The Director, CCDC, 12 Union Road, Cambridge, CB2 1EZ, UK (fax: +44-1223-336033; e-mail: deposit@ccdc.cam.ac.uk or www: http://www.ccdc.cam.ac.uk).

Acknowledgements

We are grateful to the Deutsche Forschungsgemeinschaft and the Fonds der Chemischen Industrie for generous financial support.

References

[1] W. Uhl, Z. Naturforsch. 343 (1988) 1113.
[2] W. Uhl, M. Layh, T. Hildenbrand, J. Organomet. Chem. 364 (1989) 289.
[3] W. Uhl, M. Layh, W. Hiller, J. Organomet. Chem. 368 (1989) 139.
[4] (a) X. He, R.A. Bartlett, M.M. Olmstead, K. Ruhlandt-Senge, B.E. Sturgeon, P.P. Power, Angew. Chem. 105 (1993) 761; Angew. Chem., Int. Ed. Engl. 32 (1993) 717;
(b) X.-W. Li, P. Wei, B.C. Beck, Y. Xie, H.F. Schaefer III, J. Su, G.H. Robinson, Chem. Commun. (2000) 453;
(c) A.H. Cowley, A. Decken, C.A. Olazábal, J. Organomet. Chem. 524 (1996) 271.
[5] (a) N. Wiberg, K. Amelunxen, H. Nöth, H. Schwenk, W. Kaim, A. Klein, T. Scheiring, Angew. Chem. 109 (1997) 1258; Angew. Chem., Int. Ed. Engl. 36 (1997) 1213;
(b) G. Linti, W. Köstler, Angew. Chem. 108 (1996) 593; Angew. Chem., Int. Ed. Engl. 35 (1996) 550;
(c) M. Kehrwald, W. Köstler, A. Rodig, G. Linti, T. Blank, N. Wiberg, Organometallics 20 (2001) 860.
[6] W. Uhl, Coord. Chem. Rev. 163 (1997) 1.
[7] (a) W. Uhl, I. Hahn, H. Reuter, Chem. Ber. 129 (1996) 1425;
(b) W. Uhl, T. Spies, R. Koch, J. Chem. Soc., Dalton Trans. (1999) 2385;
(c) W. Uhl, Chem. Soc. Rev. 29 (2000) 259.
[8] W. Uhl, T. Spies, W. Saak, Eur. J. Inorg. Chem. (1998) 1661.
[9] W. Uhl, T. Spies, D. Haase, R. Winter, W. Kaim, Organometallics 19 (2000) 1128.
[10] (a) W. Uhl, I. Hahn, R. Wartchow, Chem. Ber. 130 (1997) 417;
(b) W. Uhl, R. Graupner, I. Hahn, T. Spies, W. Frank, Eur. J. Inorg. Chem. (1998) 355.
[11] W. Uhl, R. Graupner, S. Pohl, W. Saak, W. Hiller, M. Neumayer, Z. Anorg. Allg. Chem. 623 (1997) 883.
[12] T. Hahn (Ed.), International Tables for Crystallography, Space Group Symmetry, vol. A, Kluwer Academic Publishers, Dordrecht, 1989.
[13] SHELXTL-PLUS, REL. 4.1, Siemens Analytical X-RAY Instruments Inc., Madison, WI, 1990; G.M. Sheldrick, SHELXL-97, Program for the Refinement of Structures; Universität Göttingen, Göttingen, Germany, 1997.
[14] (a) W. Uhl, L. Cuypers, K. Schüler, T. Spies, C. Strohmann, K. Lehmen, Z. Anorg. Allg. Chem. 626 (2000) 1526;
(b) W. Uhl, T. Spies, Z. Anorg. Allg. Chem. 626 (2000) 1059;
(c) W. Uhl, F. Hannemann, W. Saak, R. Wartchow, Eur. J. Inorg. Chem. (1999) 771;
(d) W. Uhl, F. Hannemann, Eur. J. Inorg. Chem. (1999) 201.
[15] F.A. Cotton, L.M. Daniels, C. Lin, C.A. Murillo, J. Am. Chem. Soc. 121 (1999) 4538.
[16] W. Uhl, T. Spies, W. Saak, Z. Anorg. Allg. Chem. 625 (1999) 2095.
[17] (a) J. Bernstein, L. Leiserowitz, Isr. J. Chem. 10 (1972) 601;
(b) S.E. Filippakis, L. Leiserowitz, G.M.J. Schmidt, J. Chem. Soc. B (1967) 290;
(c) D.S. Yufit, D.J. Price, J.A.K. Howard, S.O.H. Gutschke, A.K. Powell, P.T. Wood, Chem. Commun. (1999) 1561;
(d) C.-R. Lee, C.-C. Wang, Y. Wang, Acta Crystallogr., Sect. B 52 (1996) 966;
(e) C. Robl, A. Weiss, Z. Naturforsch. B41 (1986) 1490.
[18] J.-M. Lehn, Supramolecular Chemistry, VCH, Weinheim, Germany, 1995.
[19] R. Boese, H.-C. Weiß, D. Bläser, Angew. Chem. 111 (1999) 1042; Angew. Chem., Int. Ed. 38 (1999) 988.
[20] J.E. Huheey, E.A. Keiter, R.L. Keiter, Inorganic Chemistry, 4th ed., Harper Collins, New York, 1993.

PERGAMON

Polyhedron 21 (2002) 519–524

POLYHEDRON

www.elsevier.com/locate/poly

The nature of subvalent gallium and indium in aqueous media

Lars Kloo [a,*], Jan Rosdahl [a], Michael J. Taylor [b]

[a] *Inorganic Chemistry, Royal Institute of Technology, S-10044, Stockholm, Sweden*
[b] *Department of Chemistry, University of Auckland, Private Bag 92019, Auckland, New Zealand*

Received 13 August 2001; accepted 7 December 2001

Abstract

Subvalent gallium can exist in aqueous solutions as Ga–Ga bonded gallium(II) species stabilised by halide ligands in the form of the complex anions $Ga_2X_6^{2-}$ (X = Cl, Br or I) whose formation and reactivity are discussed. Gallium(I) compounds and mixed valence compounds of gallium react vigorously with water, converting any Ga^+ ions into Ga(III) products. Indium(I) is more tolerant of water, so that perchlorate and other non-complexing aqueous media can support In^+ ions at concentrations up to 10^{-3} mol l^{-1} before disproportionation to In(0) and In(III) occurs. Subvalent indium concentrations of approximately 10^{-1} mol l^{-1} are attained in halogen acid solution, particularly HBr which yields red, solid InBr upon dilution. Spectroscopic data suggest the precursor is an In(II)–In(II) bromide complex (probably $In_2Br_6^{2-}$) capable of breaking up into In(I) and In(III) products.
© 2002 Elsevier Science Ltd. All rights reserved.

Keywords: Subvalent indium and gallium; Gallium(II); Indium(I); Indium(II); Halide complexes; Raman spectra

1. Introduction

The Group 13 elements gallium, indium and thallium, the first group of the p-block, can attain the univalent state by the loss of an electron to form M^+ ions with the ns^2 configuration. The divalent state represented by M^{2+} with a single valence-shell electron is highly unstable, but when dimerised to $[M–M]^{4+}$ forms a stable nucleus which is chemically significant for gallium and, to a lesser extent, indium although practically unknown for thallium [1,2].

For gallium and indium, the subvalent states have pronounced roles. The Ga(I) and In(I) states have an important chemistry, while the M(II) state attained by virtue of direct Ga–Ga or In–In linkage also plays a part. Gallium and indium in subvalent states are liable to disproportionation and/or oxidation and hence function as reducing agents in aqueous conditions, however, the exact nature of the species remains subject to conjecture [3,4]. For thallium the Tl(I) state is usually more stable than Tl(III) and the stability of the Tl^+ ion in aqueous solution is a feature of the chemistry of this element [2].

This contribution reviews the occurrence in aqueous media of the subvalent forms of gallium and indium which can arise when these metals are attacked by acids or during electrolytic dissolution of a gallium or indium anode. Spectroscopic data are often the means of deducing the structures involved. Pertinent early work is re-examined and experiments on the indium bromide system, offering evidence of In(II) species in aqueous solution, are described and discussed.

2. Experimental

2.1. Preparative

Gallium, supplied in the form of pellets, was converted into a fine powder by melting the metal in water warmed to about 35 °C within a stoppered flask, then shaking the flask very vigorously while cooling took place. After decanting the water the powdered gallium was rinsed with acetone in order to dry it and shaken through a fine-mesh sieve to remove any larger pieces. Aqueous solutions of gallium in HCl, HBr or HI were prepared by allowing the powdered metal to dissolve in cold, concentrated acid, without stirring. Samples of the solution were withdrawn by pipette for investigation by

* Corresponding author.
E-mail address: larsa@inorg.kth.se (L. Kloo).

0277-5387/02/$ - see front matter © 2002 Elsevier Science Ltd. All rights reserved.
PII: S0277-5387(01)01030-0

Raman spectroscopy. In some experiments an equal volume of diethyl ether was added to form an upper solvent layer into which gallium solute species were extracted spontaneously from the acidic aqueous phase.

Solutions of gallium in the halogen acids were also prepared by electrolytic oxidation from the anode of a simple cell. This cell consisted of gallium cast around a platinum wire which dipped into the acid phase (HCl, HBr or HI of predetermined concentration) and was connected to a platinum plate cathode through an external circuit made up of a low-voltage DC power supply with a milliammeter to monitor the current.

Indium metal was cut into thin shavings for use. Indium chloride and bromide solutions were prepared by dissolving the metal in concentrated hydrochloric or hydrobromic acid, without heating. For electrochemical experiments a short length of indium rod was attached to platinum wire and suspended in the halogen acid electrolyte as the anode of a cell similar to that for gallium.

2.2. Spectroscopy

Raman spectra of aqueous solutions and solvent extracts, contained in thin glass tubes, were obtained with a Bio-Rad Fourier Transform Raman system which employed the 1024 nm radiation of an infrared laser and hence minimised any possible photochemical decomposition.

X-ray absorption (EXAFS) data were recorded at the Stanford Synchrotron Radiation Laboratory (SSRL), using beamline 4 at 3.0 GeV and 50–60 mA. Monochromatic radiation was obtained from a Si(220) double crystal monochromator. High-order harmonics were rejected by 50% detuning. Incident and transmitted X-rays were monitored with argon-filled ion chambers. Seven scans were made for the indium sample, internally referenced by the K-edge of the corresponding metal foil to 27.924 keV. The liquid sample was contained in a cell of 2 mm thickness with Kapton film as windows. The FEFF program was employed to calculate the In–Br and In–In phase shift and amplitude functions, which were used in the non-linear, least squares fit of the new EXAFS data [5]. Final data evaluation was made by least-squares fitting [6].

2.3. Calculations

All quantum chemical calculations were performed using GAUSSIAN-98 (rev. A7) [7] ECP-based basis sets were used for indium and bromine, employing the Stuttgart-group quasi-relativistic ECP's (36 and 28 core electrons, respectively) and non-contracted valence spaces; (8s6p7d) and (5s5p1d), respectively, [8,9]. Calculations were performed at Hartree–Fock (HF) and 2nd-order Møller–Plesset perturbation theory (MP2) level.

3. Results and discussion

3.1. Subvalent gallium in halogen acid solutions

During early work [10] the Raman spectrum of a freshly prepared solution of gallium in hydrochloric acid was recorded by chance while effervescence was taking place. Despite some marring of the spectrum by reflected primary radiation, the result showed extra bands, in addition to those characteristic of the $GaCl_4^-$ complex. The tetrachlorogallate ion can be removed from the acidic aqueous phase by solvent extraction as the ion pair $[H^+(aq)][GaCl_4^-]$. A further sample was prepared by dissolving gallium into concentrated HCl in contact with an ether phase in an effort to achieve separation of the Ga(III) complex from the low-valent material within the aqueous phase; however, both species were found to transfer efficiently to the organic layer. Subsequent investigations [11,12] established that the low-valent species were gallium(II) complex anions of the type $Ga_2X_6^{2-}$ (X = Cl, Br or I). These can be prepared selectively by anodic oxidation of gallium in a medium consisting of the concentrated acid HX plus acetonitrile [13].

Experiments aimed at characterising low-valent gallium species in HCl media (aqueous solutions and solvent extracts) have revealed only $Ga_2Cl_6^{2-}$. This complex is recognised by a very strong Raman band at 233 cm^{-1} due to the coupled Ga–Ga and Ga–Cl symmetric stretching mode. The predominant species extracted from aqueous 6 mol l^{-1} HBr is also of this form, i.e. $Ga_2Br_6^{2-}$ present in the ether phase as the complex acid $H_2Ga_2Br_6$. An intense Raman band at 162 cm^{-1} characterises this complex.

The $Ga_2Cl_6^{2-}$ and $Ga_2Br_6^{2-}$ complex ions persist at ambient temperature for several hours in aqueous halogen acid media and for some days in an ether phase. Bubbles of hydrogen gas are produced during this period while slow oxidation occurs by the reaction:

$$Ga_2X_6^{2-} + 2H^+ + 2X^- \rightleftharpoons 2GaX_4^- + H_2 \quad (1)$$

The aqueous solution contains a reserve of the excess HX required. After the complex acid $H_2Ga_2Cl_6$ has been transferred to an ether phase, no longer in contact with HCl, there is a deficit of halide ligand for this reaction. Two processes have then been observed, which appear to be in competition. The major one involves co-ordination of the solvent to produce the ether adduct of $GaCl_3$:

$$Ga_2Cl_6^{2-} + 2H^+ + 2Et_2O \rightleftharpoons 2GaCl_3{\cdot}Et_2O + H_2 \quad (2)$$

Clear evidence for this process is given by the Raman spectrum, where the known Ga–Cl symmetric stretching band of $GaCl_3{\cdot}Et_2O$ at 364 cm^{-1} shows up as the reaction proceeds. The second process leads to deposition of a white solid. Only small amounts were collected

and this material has not been identified, however, a reasonable hypothesis suggests that the solid is Ga_2Cl_4, i.e. removal of two ligands from a $Ga_2Cl_6^{2-}$ anion to furnish the chloride ions required by reaction (1) leaves a Ga_2Cl_4 molecule which then disproportionates to the familiar mixed-valence form of $Ga[GaCl_4]$. Another possibility is that the solid may be a hydrolysis product of the form $Ga_2Cl_{4-n}(OH)_n$.

These preparations can be duplicated with gallium as the anode of a cell and aqueous HCl or HBr as the electrolyte, An ether layer serves to collect the products. When the cell contains 6 mol l^{-1} HBr the main product is $Ga_2Br_6^{2-}$. Subsequent changes in the Raman spectrum of the ether phase monitor the disappearance of this gallium(II) complex. Instead there are bands at 210 and 230 cm^{-1} which identify $GaBr_4^-$ and $GaBr_3{\cdot}Et_2O$, respectively, which are the obvious gallium(III) end products following oxidation.

When less concentrated HBr is employed, there is evidence of different subvalent gallium species. Thus, if 3 or 4 mol l^{-1} HBr is used, new bands appear at 173 and 186 cm^{-1}. Separate species are responsible for these, because the latter band becomes more intense when the bromide concentration is depleted, namely the pair of gallium(II) complexes, $Ga_2Br_5(Et_2O)^-$ and $Ga_2Br_4(Et_2O)_2$. The quantities have been insufficient to obtain the complete spectra by which structures might be confirmed, however, they are related to $Ga_2Br_6^{2-}$ by substitution of diethyl ether molecules for either one or two of the bromide ligands. The Raman features are assignable to the in-phase Ga–Ga plus Ga–Br stretching modes: the 173 cm^{-1} band to $Ga_2Br_5(Et_2O)^-$ and the 186 cm^{-1} band to $Ga_2Br_4(Et_2O)_2$. The latter is a molecular complex analogous to the series $Ga_2X_4L_2$ (X = Cl, Br or I; L = dioxane or other O- or N-donor) obtained by interaction of the ligand L with the halides $Ga[GaX_4]$ [14].

Dissolving powdered gallium in cold, concentrated hydriodic acid has been shown to yield $Ga_2I_6^{2-}$ alongside GaI_4^- [11]. Unfortunately the electrochemical approach fails to yield gallium complexes in HI solution because the oxidation of iodide to iodine (as I_3^-) takes over from the anodic dissolution of the metal. In consequence this system is not as well understood as those of gallium with HCl and HBr.

3.2. Subvalent indium in halogen acid solutions

Freshly prepared solutions of indium chloride, made by dissolving shavings of indium metal in concentrated (12 mol l^{-1}) hydrochloric acid, show signs of the presence of low-valent species. These acidic solutions continue to evolve hydrogen after all visible trace of the metal has disappeared, and liberate a stream of bubbles if gently stirred. The bleaching of potassium permanganate solution confirms the presence of reducing species, and warming the HCl solution causes evolution of hydrogen gas (after which the reducing property is lost).

The Raman spectrum of such an indium chloride solution is dominated by a broad band at 275 cm^{-1} arising from the In–Cl stretching modes of various chloride complexes, believed to include $InCl_4^-$ and $InCl_5^{2-}$ in their aquated forms [15]. To investigate further, this solution was diluted with water, causing indium to be regenerated in the form of a black powder and confirming the presence of low-valent species which disproportionate. Previous workers have ascribed such behaviour to the instability of indium(I) species, relative to In(III) and the metal:

$$3In(I) \rightleftharpoons 2In(0) + In(III) \quad (3)$$

Failure to detect the errant material in the Raman spectrum may be because it is simply the bare In^+ cation, or be due to masking by indium(III) chloride species whose spectra would tend to overlay those of any low-valent indium chloride complexes.

The remainder of the hydrochloric acid solution was extracted with diethyl ether. The Raman spectrum of this extract shows the strong band at 321 cm^{-1} which is characteristic of $InCl_4^-$ [15] but reveals no other indium complexes. The spectrum of the aqueous phase following extraction contains only the In–Cl band (ca. 280 cm^{-1}) due to residual indium(III) chloro-complexes.

The behaviour of indium when attacked by concentrated HBr also shows that subvalent species are implicated. Work by Dronskowsky [16] has demonstrated that the quantity of indium taken into solution is substantially more than expected by formation of In(III). In particular, experiments to measure the excess solubility of indium in the acid HX give figures of 15% for HCl, 16% for HBr, 24% for HI. The resulting solutions appeared stable in an open beaker at ambient temperature, although if heated at 50 °C and stirred, hydrogen gas was evolved. The solution in 9 mol l^{-1} HBr was estimated to contain In(III) at 2.62 mol l^{-1} along with low-valent indium at 0.90 mol l^{-1} (calculated as In(I)). Dronskowski pointed out that such a high concentration of In^+ was far beyond the levels typical reported during indium anodisation studies using aqueous media (typically less than 10^{-3} mol l^{-1}).

We have now repeated these investigations of the indium bromide system, as follows. When an equal volume of water is added to the freshly prepared, colourless solution of indium in HBr, a bright red precipitate is produced. Dronskowski showed that this material corresponds to indium monobromide [17]. Extending the investigation of this system, we find that the red solid InBr redissolves in HBr, or in a concentrated aqueous solution of NaBr, only with immediate oxidation, which is signalled by hydrogen being evolved.

Dronskowski [16] suggested that the precursor of the InBr precipitate might be an indium(I) bromide complex, proposing In_2Br^+. If so, this (or some other In(I) complex) should be regenerated on dissolution of the solid in the presence of bromide ions, which is contrary to our observations.

We investigated the aqueous solutions of indium in HBr by Raman spectroscopy. A concentrated solution of indium in 6 mol l^{-1} HBr, after heating to complete the oxidation, gives an intense ν(In–Br) band at 197 cm^{-1} due to In(III) bromide complexes, as expected [18]. However, when a freshly prepared sample was examined we obtained the Raman spectrum in Fig. 1. This spectrum contains an additional feature at 139 cm^{-1}. Initially we supposed this band might belong to an indium(I) bromide complex. Plausible In(I) complexes are $InBr_2^-$ and $InBr_3^{2-}$. The latter has a Raman spectrum [19] with ν(In–Br) bands at 149 and 177 cm^{-1} and so can be eliminated. The triatomic species $InBr_2^-$, with its smaller co-ordination number and lower charge, should exhibit In–Br stretching modes at higher

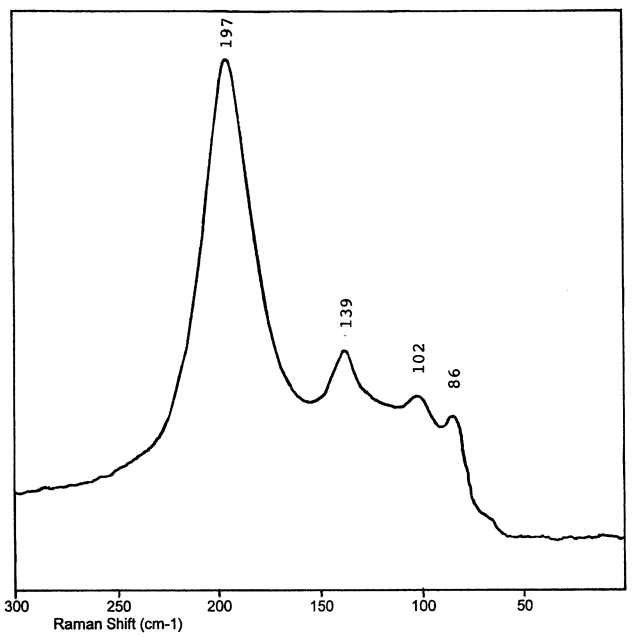


Fig. 1. Raman spectrum of a freshly prepared solution of indium in HBr with bands attributed to $InBr_4^-$ at 197 cm^{-1} and $In_2Br_6^{2-}$ at 139 cm^{-1}. The features at 86 and 102 cm^{-1} probably include bending modes.

Table 1
The calculational results for $In_2Br_6^{2-}$ of D_{3d} symmetry

Method	d_{In-Br} (Å)	d_{In-In} (Å)	Frequency (A_{1g}) (cm^{-1})
HF	2.633	2.847	136
MP2	2.614	2.808	133

The vibrational band of A_{1g} symmetry given above is dominated by stretching of the In–In bond.

frequencies than $InBr_3^{2-}$ and hence can also be discounted. Calculations made for the $InBr_2^-$ and $InBr_3^{2-}$ species indicate that the In–Br bond lengths are too long, at least 0.3 Å longer compared with $In_2Br_6^{2-}$, thus giving symmetrical In–Br stretch frequencies of potentially high Raman intensity that are about 100 cm^{-1} or less. The cation suggested earlier, namely In_2Br^+, is a possibility, although it seems unlikely that this would survive where potential ligands in the shape of bromide ions are present in large quantity.

Our alternative view is that the low-valent form co-existing with $InBr_4^-$ is an indium(II) complex of which the most probable is $In_2Br_6^{2-}$. This species, akin to $Ga_2Br_6^{2-}$, possesses an In–In bond and has been prepared and identified by Tuck who reported its vibrational spectrum [20]. The most intense Raman band (comprising the coupled In–In and In–Br symmetric stretch) appears at 139 cm^{-1} which fits the bill for the present species. Other Raman active modes of $In_2Br_6^{2-}$ are In–Br stretches at 202 and 244 cm^{-1}, however, both these are weak bands which would be hidden by those of $InBr_4^-$ at 197 and 239 cm^{-1}. The results of quantum chemical calculations given in Table 1 give good support to the proposed presence of $In_2Br_6^{2-}$. The Hessian show that the ground state configuration of $In_2Br_6^{2-}$ is the staggered (D_{3d} symmetry), whereas the eclipsed (D_{3h} symmetry) is only a transition state with respect to rotational transformation of the staggered conformer. Indium K-edge EXAFS measurements of a freshly prepared solution were also recorded. However, the results can very accurately be described in terms of tetrahedral $InBr_4^-$ complexes with an In–Br distance of 2.55 ± 0.01 Å as the only indium-containing species present. The fundamental problem is that if $In_2Br_6^{2-}$ is present as well at a reasonable but lower concentration, the very similar indium neighbourhood (three In–Br and one In–In contact at 2.6–2.8 Å) will make it extremely difficult to identify the In(II) in the presence of $InBr_4^-$. Despite this, it is possible to fit a somewhat rigid model of $In_2Br_6^{2-}$ to the EXAFS data, which is shown in Fig. 2(a) and (b). On the other hand, the EXAFS data give no indication for any significant amount of In(I) species with substantially longer In–Br distances (about 3 Å).

3.3. Mechanism of formation of InBr

It would be desirable to isolate the subvalent indium bromide complex for more complete identification, however, we were unable to prepare aqueous HBr solutions of indium, or ether extracts, other than those in which indium(III) bromide complexes are heavily predominant. We assume that the indium(II) state is stabilised in the form of $In_2Br_6^{2-}$ when bromide is in excess, but that this complex dissociates upon dilution and that the resulting product ($In_2Br_5^-$ or its solvated

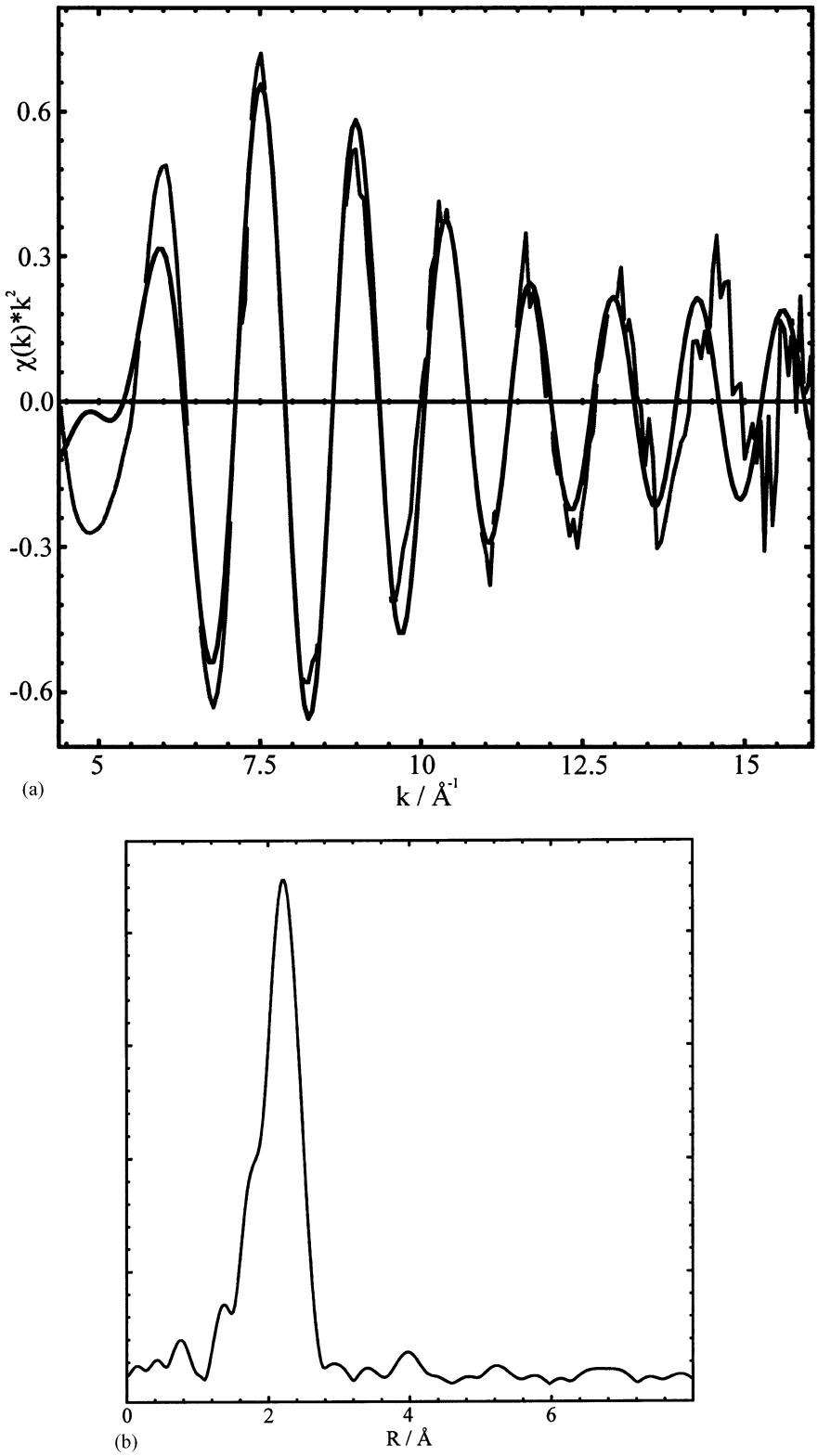


Fig. 2. (a) EXAFS data with a model of $In_2Br_6^{2-}$ included. The model has a In–In distance of 2.69 Å and a In–Br distance of 2.43 Å. (b) Fourier transform of the EXAFS data.

form $In_2Br_5(H_2O)^-$) then disproportionates to yield InBr.

$$In_2Br_6^{2-} \rightleftharpoons In_2Br_5^- + Br^- \quad (4)$$

$$In_2Br_5^- \rightleftharpoons InBr + InBr_4^- \quad (5)$$

In support of this mechanism we note that the second step parallels the reaction $In_2X_6^{2-} = InX_2^- + InX_4^-$

which has been proposed in prior studies of the stability of In–In bonded species relative to InX and InX_3 when these form an equilibrium system in suitable organic-ligand-based media [21].

The two-step mechanism proposed here accounts for the fact that InBr does not dissolve in bromide rich media (either HBr or NaBr) to regenerate a long-lived species. Instead, the solid reacts with the solution so that any indium(I) bromide complexes formed, e.g. $InBr_2^-$, will be promptly oxidised:

$$InBr_2^- + 2H^+ + 2Br^- \rightleftharpoons InBr_4^- + H_2 \quad (6)$$

Due to this reaction only a low level of indium(I) will remain in the aqueous solution.

3.4. Anodic oxidation of indium

Electrode reactions of indium provide ample evidence of the subvalent state. For indium, the value of n in the reaction $M = M^{n+} + ne^-$ (determined by measuring the weight loss of the metal anode for a given current and time) approaches unity in non-complexing media (whereas n never falls below two in the case of gallium). Thus, in acetonitrile, anodic oxidation of indium metal yields solutions with In^+ concentrations up to 0.1 mol l^{-1} [22] Similarly, anodic oxidation of indium or an indium/mercury amalgam in aqueous perchlorate media generates In^+ (presumably as the aquated cation), although the levels are much smaller than in acetonitrile, e.g. 3×10^{-4} mol l^{-1} in dilute $HClO_4$ [23]. The standard reduction potentials -0.126 V for $In^+ + e = In$ compared with -0.338 V for $In^{3+} + 3e = In$ [2] emphasise the slight stability the $+1$ state of indium relative to its $+3$ state. An aqueous solution of the hypovalent indium(I) state can be prepared as a useful reducing agent by treatment of In(Hg) with silver triflate in acetonitrile [24]. If iodide is present, a precipitate of indium monoiodide is produced during electrolysis [25] corresponding to the electrode reaction:

$$In + I^- \rightleftharpoons InI + e^- \quad (7)$$

Attempts to generate low-valent indium in HCl or HBr solutions electrolytically are beset by spontaneous disproportionation of the solute species. Such cells tend to deposit finely divided metal beneath the anode and indium(III) halide complexes dominate the resulting solution.

Acknowledgements

We are grateful for support from the Swedish Natural Science Research Council and the University of Auckland Research Committee. The SSRL is gratefully acknowledged for the allocation of beamtime.

References

[1] M.J. Taylor, Metal-to-metal Bonded States of the Main Group Elements, Academic Press, London, 1975.
[2] A.J. Downs (Ed.), Chemistry of Aluminium, Gallium, Indium and Thallium, Blackie, Glasgow, 1993.
[3] D.G. Tuck, Polyhedron 9 (1990) 377.
[4] D.G. Tuck, Chem. Soc. Rev. (1993) 269.
[5] A.L Ankoudinov, Ph.D. Thesis, Multiple Scattering Calculations of X ray Absorption Spectra, University of Washington, 1996.
[6] T. Ressler, J. Phys. IV Fr. 7 (1997) 269.
[7] M.J. Frisch, G.W. Trucks, H.B. Schlegel, G.E. Scuseria, M.A. Robb, J.R. Cheeseman, V.G. Zakrzewski, J.A. Montgomery, Jr., R.E. Stratmann, J.C. Burant, S. Dapprich, J.M. Millam, A.D. Daniels, K.N. Kudin, M.C. Strain, O. Farkas, J. Tomasi, V. Barone, M. Cossi, R. Cammi, B. Mennucci, C. Pomelli, C. Adamo, S. Clifford, J. Ochterski, G.A. Petersson, P.Y. Ayala, Q. Cui, K. Morokuma, D.K. Malick, A.D. Rabuck, K. Raghavachari, J.B. Foresman, J. Cioslowski, J.V. Ortiz, B.B. Stefanov, G. Liu,A. Liashenko, P. Piskorz, I. Komaromi, R. Gomperts, R.L. Martin, D.J. Fox, T. Keith, M.A. Al-Laham, C.Y. Peng, A. Nanayakkara, C. Gonzalez, M. Challacombe, P.M.W. Gill, B. Johnson, W. Chen, M.W. Wong, J.L. Andres, C. Gonzalez, M. Head-Gordon, E.S. Replogle, J.A. Pople, program GAUSSIAN-98, 1999.
[8] T. Leininger, A. Nicklass, H. Stoll, M. Dolg, P. Schwerdtfeger, J. Chem. Phys. 105 (1996) 1052.
[9] A. Bergner, M. Dolg, W. Küchle, H. Stoll, H. Preuss, Mol. Phys. 80 (1993) 1431.
[10] L.A. Woodward, M.J. Taylor, J. Inorg. Nucl. Chem. 27 (1965) 737.
[11] C.A. Evans, M.J. Taylor, Chem. Commun. (1969) 1201.
[12] C.A. Evans, K.H. Tan, S.P. Tapper, M.J. Taylor, J. Chem. Soc., Dalton Trans. (1973) 988.
[13] M.J. Taylor, D.G. Tuck, Inorg. Synth. 22 (1983) 135.
[14] J.C. Beamish, A. Boardman, R.W.H. Small, I.J. Worrall, Polyhedron 4 (1985) 983.
[15] L.A. Woodward, M.J. Taylor, J. Chem. Soc. (1960) 4473.
[16] R. Dronskowski, Inorg. Chem. 33 (1994) 5960.
[17] (a) T. Staffel, G. Meyer, Z. Anorg. Allg. Chem. 552 (1987) 113; (b) T. Staffel, G. Meyer, Z. Anorg. Allg. Chem. 563 (1988) 27.
[18] L.A. Woodward, P.T. Bill, J. Chem. Soc. (1955) 1699.
[19] J.G. Contreras, J.S. Poland, D.G Tuck, J. Chem. Soc., Dalton Trans. (1973) 992.
[20] B.H. Freeland, J.L. Hencher, D.G. Tuck, J.G. Contreras, Inorg. Chem. 15 (1976) 2144.
[21] C. Peppe, D.G. Tuck, Can. J. Chem. 62 (1984) 2793.
[22] J.B. Headridge, D. Pletcher, Inorg. Nucl. Chem. Lett. 3 (1967) 475.
[23] R.S. Taylor, A.G. Sykes, J. Chem. Soc. (A) (1969) 2419.
[24] S.K. Chandra, E.S. Gould, Inorg. Chem. 35 (1996) 3881.
[25] V.V. Losev, Electrochim. Acta 15 (1970) 1095.

PERGAMON

Polyhedron 21 (2002) 525–529

POLYHEDRON

www.elsevier.com/locate/poly

Reaction of $\{HC(CMeNAr)_2\}Li$ (Ar = 2,6-*i*-$Pr_2C_6H_3$) with indium monochloride to yield the In–In bonded dimer $[\{HC(CMeNAr)_2\}InCl]_2$ and the hydroxide $[\{HC(CMeNAr)_2\}InCl(\mu\text{-}OH)]_2$

Matthias Stender, Philip P. Power *

Department of Chemistry, University of California Davis, One Shields Avenue, Davis, CA 95616, USA

Received 17 August 2001; accepted 27 November 2001

Abstract

The reaction of the sterically encumbered lithium β-diketiminate $\{HC(CMeNAr)_2\}Li$ (Ar = 2,6-*i*-$Pr_2C_6H_3$) with InCl in THF at approximately −78 °C yielded In metal and $[\{HC(CMeNAr)_2\}InCl]_2$ (**1**) as well as minor amounts of the hydroxide $[\{HC(CMeNAr)_2\}In(Cl)(\mu\text{-}OH)]_2$, **2**. The compounds **1** and **2** were characterized by ^1H, ^{13}C NMR, IR spectroscopy and X-ray crystallography. The centrosymmetric structure of **1** features an In–In bond that is 2.8343(7) Å long which is well within the known range of In–In single bond distances. The metal β-diketiminate ring (i.e. C_3N_2In) is folded along the N···N vector and features an out of plane deviation by the indium of 0.8953 Å and a dihedral angle between the C_3N_2 and InN_2 arrays of 145.8°. This can be attributed to steric effects of the Ar groups on the β-diketiminiate ligand. The structure of the hydroxide derivative **2** is a dimer in which the indiums are bridged by hydroxides to afford a planar In_2O_2 core with an average In–O distance of 2.13(2) Å. Attempted reduction of the dihalide compounds $\{HC(CMeNAr)_2\}InX_2$ (X = Cl, I) with sodium or potassium led to the formation of metallic indium and the free β-aminoimine $(Ar)NC(Me_2)CHC(Me_2)N(Ar)H$ rather than the desired In(I) species, $\{HC(CMeNAr)_2\}In$:. © 2002 Elsevier Science Ltd. All rights reserved.

Keywords: β-Diketiminate; Low valent indium; Bulky ligands; Metal–metal bonds

1. Introduction

Recent years have witnessed an impressive revival of interest in bidentate, β-diketiminate ligands which have been known for more than four decades [1]. Much of the recent work has focused on more sterically encumbered derivatives that feature bulky substituents at the nitrogens. These ligands have proved to be very useful in a variety of rôles including the stabilization of low coordinate, low valent main Group 13 metal complexes [2–4]. Through the use of the ligand $[HC(CMeNAr)_2]^-$ (Ar = 2,6-*i*-$Pr_2C_6H_3$) the unusual, two-coordinate, monomeric M(I) species $[HC(CMeNAr)_2]M$: (M = Al [3], Ga [4]), which are analogous to carbenes, have been stabilized. The corresponding In(I) species are unknown, although there is widespread interest in In(I) compounds as evidenced by the growing number of organometallic [5–7] and related derivatives [7,8] of In(I) that have been synthesized. Almost all of the organoindium(I) compounds are associated in the solid state. However, the trispyrazolylborate complexes $HB(pz)_3In$ (pz = 3-phenylpyrazolyl [7], 3,5-di-*tert*-butylpyrazolyl [8a], 3-*tert*-butylpyrazolyl [8b], 3,5-$(CF_3)_2$-pyrazolyl [8b,8c]), in which the In atom is coordinated by three N donors, are monomeric in the solid state. There is only one example of a monomeric, organometallic In(I) species in the literature and this species involves the bulky *m*-terphenyl group $-C_6H_3$-2,6-$Trip_2$ (Trip = $-C_6H_2$-2,4,6-*i*-Pr_3) [9]. This ligand shows a steric resemblance to the bulkyl β-diketiminate $[HC(CMeNAr)_2]^-$ (Ar = 2,6-*i*-$Pr_2C_6H_3$) [10]. Due to the very rich chemistry already displayed by the monomeric M(I) species $[HC(CMeNAr)_2]M$: (M = Al, Ga) [11–14] it is of interest to synthesize the In ana-

* Corresponding author. Tel.: +1-530-752-6913; fax: +1-530-752-8995.

E-mail address: pppower@ucdavis.edu (P.P. Power).

0277-5387/02/$ - see front matter © 2002 Elsevier Science Ltd. All rights reserved.
PII: S0277-5387(01)01033-6

logue and explore its chemistry. We now report that the reaction of $\{HC(CMeNAr)_2\}Li$ with InCl leads not to the expected monomeric $\{HC(CMeNAr)_2\}In$ analogue but to disproportionation reactions that yield the unexpected In–In bonded species $[\{HC(CMeNAr)_2\}InCl]_2$ (**1**) and the hydroxo complex $[\{HC(CMeNAr)_2\}InCl(\mu\text{-}OH)]_2$ (**2**).

2. Experimental

2.1. Synthesis

2.1.1. General procedures

All manipulations were carried out using modified Schlenk techniques under an atmosphere of N_2 or in a Vacuum Atmospheres HE-43 drybox. All solvents were distilled from Na–K alloy and degassed three times before use. The compound $\{HC(CMeNAr)_2\}H$ (Ar = C_6H_3-2,6-*i*-Pr_2) was prepared as previously described [10]. InCl (99.99%) was purchased commercially and used as received.

2.2. $[\{HC(CMeNAr)_2\}InCl]_2$ (1) and $[\{HC(CMeNAr)_2\}InCl(\mu\text{-}OH)]_2$ (2)

A solution of $\{HC(CMeNAr)_2\}Li$ in THF (generated by reaction of 1.06 g of $\{HC(CMeNAr)_2\}H$ and 1.6 ml of 1.6 M *n*-BuLi in 20 ml of THF with cooling in an ice bath) was added dropwise to a suspension of InCl (0.42 g, 2.79 mol) in THF (30 ml) with rapid stirring and cooling in a dry ice acetone bath. The reaction mixture was stirred for 2 h and then allowed to come to approximately −10 °C (ice–NaCl bath). After stirring for an additional 1 h the solvents were removed under reduced pressure. The solid residue was extracted with cold hexane (40 ml, ca. −10 °C). The solution was allowed to come to ambient temperature where the dark precipitate which had formed (indium metal and lithium chloride) was allowed to settle. The amber supernatant solution was then filtered through celite. Concentration under reduced pressure produced a low yield of large colorless needles which were collected after ca. 8 h in a ca. 4 °C refrigerator. These were identified as the hydroxide derivative **2**. Yield: 0.05 g, 0.037 mmol, 15%, melting point (decomposition) m.p. (dec.) > 100 °C. ^{1}H NMR (400 MHz, C_6D_6): δ 7.2–7.1 (m, 12H, Ph), 4.63 (s, 2H, γ-CH), 3.31 (sept, 8H, $J = 6.8$ Hz, C*H*Me$_2$), 1.48 (s, 12H, Me), 1.25 (d, 24H, $J = 6.8$ Hz, CH*Me*$_2$), 1.10 (d, 24H, $J = 6.8$ Hz, CH*Me*$_2$), 0.93 (s, broad, 2H, O*H*); ^{13}C NMR (C_6D_6): δ (ppm) = 159.2 (CN), 142.7, 141.3, 125.8, 123.6 (Ph), 94.2 (γ-C), 28.6 (*C*HMe$_2$), 24.4 (CH*Me*$_2$), 23.4 (CH*Me*$_2$), 20.7 (Me); IR (Nujol): ν (cm^{-1}) = 3660 (νOH). The supernatant solution was decanted and concentrated under reduced pressure to incipient crystallization (ca. 30 ml). Storage for 30 h in a ca. 4 °C refrigerator yielded the product **1** as colorless crystals. Yield: 0.23 g, 0.20 mmol, 16%, m.p. 155–157 °C. ^{1}H NMR (400 MHz, C_6D_6): δ 7.2–7.0 (m, 12H, Ph), 4.73 (s, 2H, γ-CH), 3.33 (sept, 8H, $J = 6.8$ Hz, C*H*Me$_2$), 1.58 (s, 12H, Me), 1.35 (d, 24H, $J = 6.8$ Hz, CH*Me*$_2$), 1.21 (d, 24H, $J = 6.8$ Hz, CH*Me*$_2$); ^{13}C NMR (C_6D_6): δ (ppm) = 171.8 (CN), 144.5, 138.0, 124.8 (Ph), 98.1 (γ-C), 28.3 (*C*HMe$_2$), 25.8 (CH*Me*$_2$), 25.2 (CH*Me*$_2$), 24.6 (Me).

The attempted reduction of the dihalides $\{HC(CMeNAr)_2\}InX_2$ (X = Cl, I) with finely divided potassium in toluene resulted in the precipitation of In metal at room temperature (r.t.).

Table 1
Data collection parameters for **1** and **2**

	1·hexane	**2**·2PhMe
Formula	$C_{64}H_{96}Cl_2In_2N_4$	$C_{72}H_{100}Cl_2In_2N_4O_2$
Formula weight	1222.98	1354.13
Crystal system	monoclinic	monoclinic
Space group	$P2_1/c$	$P2_1/c$
β (°)	102.051(2)	101.440(2)
a (Å)	13.5411(10)	13.6314(17)
b (Å)	13.3095(10)	13.6336(17)
c (Å)	17.2363(13)	18.915(2)
V (Å^3)	3038.0(4)	3445.3(7)
Z	2	2
μ(Mo Kα) (mm^{-1})	0.888	0.792
T (K)	90(2)	90(2)
R_1	0.0650	0.0260
wR_2	0.1117	0.0648

$R_1 = \Sigma||F_0|-|F_c||/|F_0|$. $wR_2 = [\Sigma\omega(F_0^2-F_c^2)^2\Sigma[\omega(F_0^2]]^{1/2}$.

2.3. X-ray data collection

X-ray quality crystals of **1** or **2** were removed from the Schlenk tube and immediately covered with a layer of hydrocarbon oil. A suitable crystal was selected, attached to a glass fiber and placed in the cold temperature N_2-stream as previously described [15]. The data were collected near 90 K using a Bruker SMART 1000 diffractometer and Mo Kα ($\lambda = 0.71073$ Å) radiation. The SHELXTL version 5.03 program package was used for the structure solutions and refinements [16]. Absorption corrections were applied using the SADABS program [17]. The structures were solved by direct methods and refined by full matrix, least-squares procedures. All non-hydrogen atoms were refined anisotropically. Hydrogen atoms were included in the refinement at calculated positions using a riding model included in the SHELXTL program package. Some details of the data collection and refinement are given in Table 1. Selected bond distances and angles for **1** and **2** are provided in Table 2.

Table 2
Selected bond lengths (Å) and angles (°) for **1** and **2**

1		**2**	
Bond lengths			
In(1)–N(1)	2.169(4)	In(1)–N(1)	2.1654(12)
In(1)–N(2)	2.172(4)	In(1)–N(2)	2.1874(12)
In(1)–Cl(1)	2.4142(14)	In(1)–Cl(1)	2.3876(4)
In(1)–In(1A)	2.8342(7)	In(1)–O(1)	2.1148(11)
N(1)–C(1)	1.335(7)	In(1)–O(1A)	2.1534(11)
N(2)–C(3)	1.347(7)	N(1)–C(1)	1.3343(19)
C(1)–C(2)	1.389(7)	N(2)–C(3)	1.3325(19)
C(2)–C(3)	1.392(7)	C(1)–C(2)	1.407(2)
		C(2)–C(3)	1.401(2)
Bond angles			
N(1)–In(1)–N(2)	87.85(16)	N(1)–In(1)–N(2)	87.26(5)
N(1)–In(1)–Cl(1)	99.39(12)	N(1)–In(1)–Cl(1)	106.12(4)
N(2)–In(1)–Cl(1)	99.81(11)	N(2)–In(1)–Cl(2)	103.91(3)
N(1)–In(1)–In(1A)	126.60(11)	O(1)–In(1)–O(1A)	71.47(5)
N(2)–In(1)–In(1A)	126.75(11)	O(1)–In(1)–N(1)	145.70(5)
Cl(1)–In(1)–In(1A)	110.59(4)	O(1)–In(1)–N(2)	94.48(5)
N(1)–C(1)–C(2)	125.8(3)	In(1)–O(1)–In(1A)	108.53(5)
C(1)–C(2)–C(3)	128.5(5)	N(1)–C(1)–C(2)	124.66(13)
C(2)–C(3)–N(2)	125.9(5)	C(1)–C(2)–C(3)	129.27(14)
		C(2)–C(3)–N(2)	124.72(14)

3. Discussion

3.1. Synthesis

The compounds **1** and **2** were both obtained by the addition of $\{HC(CMeNAr)_2\}Li$, generated in THF, to a suspension of InCl in THF with cooling in an approximately −78 °C dry ice acetone bath. None of the expected product $\{HC(CMeNAr)_2\}In$: was isolated from the reaction under these conditions. This was to some extent surprising since the aluminum(I) and gallium(I) analogues of this putative indium species were already known [3,4]. Furthermore, the one coordinate indium derivative of the $-C_6H_3$-2,6-$Trip_2$ ($Trip = C_6H_2$-2,4,6-*i*-Pr_3) group, which bears a close steric resemblance to the $\{HC(CMeNAr)_2\}$ ligand, was already characterized [9]. Moreover 2,6-$Trip_2H_3C_6In$: was synthesized by the direct reaction of the lithiated terphenyl ligand with InCl in THF under almost identical conditions to those described in this paper. In view of the fact that indium metal, lithium chloride and free ligand were produced during the course of the attempted synthesis of $\{HC(CMeNAr)_2\}In$:, it seems probable that disproportionation and ligand redistribution reactions occur to give the observed product **1** in 16% yield. Small amounts of the hydroxo-bridged species **2** were also obtained in much lower yield. The latter species is probably the result of moisture contamination and it is possible to carry out the reaction to generate negligible amounts of **2** by using extremely strict anaerobic and anhydrous procedures. In spite of the unanticipated nature of the product **1**, it has been recently reported [18] that the reaction of the aza alkyl lithium compound $PhC\{(Me_3Si)_2C\}\{N(SiMe_3)\}Li$ with InBr afforded the In–In bonded dimer $[PhC\{C(SiMe_3)_2\}\{N(SiMe_3)_2\}InBr]_2$. This reaction is significant in that the uninegative, bidentate nature of this ligand is related to the β-diketiminate $\{HC(CMeNAr)_2\}^-$. Other examples of disproportionation reactions of various lithium amide ligands with indium(I) halides to afford In–In bonded products are also known [19,20].

3.2. Structures

The structure of **1** is illustrated in Fig. 1. Selected bond distances and angles are provided in Table 2. The structure possesses a center of symmetry at the midpoint of the In–In bond. The indiums are four-coordinate with a very distorted tetrahedral geometry at the metals. The In–In distance is 2.8334(7) Å which may be regarded as a typical one since it falls in the middle of the currently known range (2.696(2)–2.922(1) Å [21,22]) for neutral molecular In–In singly bonded species. The In–N distances, av. 2.171(2) Å, are marginally longer than the 2.111(3)–2.147(1) Å range observed in the $\{HC(CMeNAr)_2\}InX_2$ (X = Cl or I) [2], but they are shorter than the average distance of 2.197(4) Å in $\{HC(CMeNAr)_2\}InMe_2$ [2]. The variation in these distances illustrates the influence of coligands on the effective ionic radius of indium. More electronegative co-ligands contract the radius, whereas more electropositive ligands expand it; hence the longer In–N distances in $\{HC(CMeNAr)_2\}InMe_2$. The C_3N_2 ring fragment of the β-diketiminate ligand has planar geometry and the C–C and C–N distances are symmetric indicating delocalization of the negative charge. However, the C_3N_2In ring is folded along the N···N vector such that there is a dihedral angle of 145.8° between the InN_2 and C_3N_2 planes. The indium atom lies 0.895 Å from the extended C_3N_2 plane. This folding is similar to that reported in $\{HC(CMeNAr)_2\}InMe_2$ but it is higher than that seen in the halide derivatives. Another feature

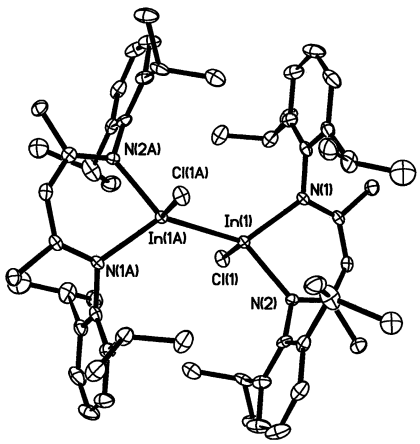


Fig. 1. Thermal ellipsoid plot (30%) of **1**. H atoms are not shown.

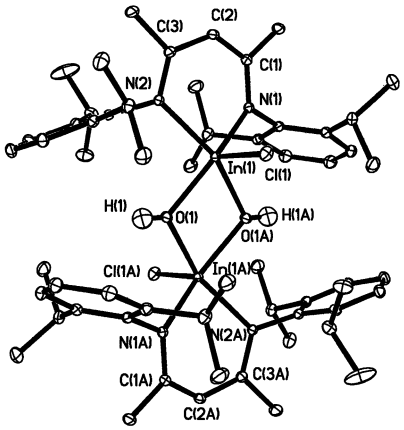


Fig. 2. Thermal ellipsoid plot (30%) of **2**. H atoms are not shown.

of the structure of **1** is the narrow N–In–N angle and this is similar to those reported for the halide and methyl derivatives [2] which all have N–In–N angles that are less than 90°. The In–Cl bond length is 2.4142(14) Å which is very similar to the 2.4174(9) Å in the tropoiminate complex $(Me_2ATI)_2InCl$ [23] and slightly longer than the average of 2.396(3) Å in $\{HC(CMeNAr)_2\}InCl_2$ [2] although the accuracy of the latter distance is reduced by the presence of bromine contaminant.

The structure of the hydroxide bridged dimer **2** is illustrated in Fig. 2. Like **1**, it is centrosymmetric with a crystallographically required planarity for the In_2O_2 core in this case. The core has diamond geometry with a difference of approximately 18° between the ring angles at indium and oxygen. The two In–O distances differ slightly and have an average value of 2.13(2) Å which is not significantly different from the average of 2.14(1) Å observed in bis(3-(2-pyridyl)pyrazolyl-1-yl)methane stabilized complex of the dimer $\{ClIn(\mu\text{-}OH)\}_2$ [24] or the average of 2.164(2) Å observed for $[\{(Me_3Si)_2CH\}_2In(\mu\text{-}OH)]_2$ [25]. The In–N bond lengths in **2** are essentially indistinguishable from those observed in **1** in spite of the increase in coordination number of the metal from four to five. As in **1**, the C_3N_2In ring is folded along the N···N vector. A dihedral angle of 150° is observed between the C_3N_2 and InN_2 planes and the indium lies 0.800 Å from the extended C_3N plane. The N–In–N angle is also less than 90° and within 0.6° of the value reported for **1**.

4. Conclusions

The attempted synthesis of $\{HC(CMeNAr)\}In$: has led to the disproportionation or hydrolysis products **1** or **2**. The reasons for the apparent lack of stability $\{HC(CMeNAr)_2\}In$: are not obvious, especially since the sterically related species $2,6\text{-}Trip_2H_3C_6In$: [9] is known to be stable. The existence of this compound and the aluminum and gallium species $\{HC(CMeNAr)\}M$: (M = Al [3] or Ga [4]) strongly suggest that $\{HC(CMeNAr)\}In$: should be obtainable under different reaction conditions.

5. Supplementary material

Crystallographic data for the structural analysis have been deposited with the Cambridge Crystallographic Data Center, CCDC nos. 169219 and 169220 for compounds **1** and **2**. Copies of this information may be obtained from The Director, CCDC, 12 Union Road, Cambridge, CB2 1EZ, UK (fax: +44-1233-336-033; e-mail: deposit@ccdc.cam.ac.uk or www: http://www.ccdc.cam.ac.uk).

Acknowledgements

We are grateful to the National Science Foundation and the Petroleum Research Fund administered by the American Chemical Society for financial support.

References

[1] R.H. Holm, M.J. O'Connor, Prog. Inorg. Chem. 14 (1971) 241.
[2] M. Stender, B.E. Eichler, N.J. Hardman, P.P. Power, J. Prust, M. Noltemeyer, H.W. Roesky, Inorg. Chem. 40 (2001) 2794.
[3] C. Cui, H.W. Roesky, H.-G. Schmidt, M. Noltemeyer, H. Hao, F. Cimpoesu, Angew. Chem., Int. Ed. 39 (2000) 4274.
[4] N.J. Hardman, B.E. Eichler, P.P. Power, Chem. Commun. (2000) 1491.
[5] (a) O.T. Beachley Jr., R. Blom, M.R. Churchill, J. Fettinger, J.C. Pazik, L. Victoriano, J. Am. Chem. Soc. 108 (1986) 4666;
(b) O.T. Beachley Jr., R. Blom, M.R. Churchill, K. Faegri Jr., J.C. Fettinger, J.C. Pazik, L. Victoriano, Organometallics 8 (1989) 346;
(c) O.T. Beachley Jr., J.C. Pazik, T.E. Glassman, M.R. Churchill, J.C. Fettinger, R. Blom, Organometallics 7 (1988) 1051;
(d) O.T. Beachley Jr., J.F. Lees, T.E. Glassman, M.R. Churchill, L.A. Buttrey, Organometallics 9 (1990) 2488;
(e) O.T. Beachley Jr., J.F. Lees, R.D. Rodgers, J. Organomet. Chem. 418 (1991) 165.
[6] H. Schumann, C. Janiak, F. Gorlitz, J. Loebel, A. Dietrich, J. Organomet. Chem. 418 (1991) 165.
[7] A. Frazer, B. Piggott, M.B. Hursthouse, M. Mazid, J. Am. Chem. Soc. 116 (1994) 4127.
[8] (a) M.C. Kuchta, H.V.R. Dias, S.G. Bott, G. Parkin, Inorg. Chem. 35 (1996) 943;
(b) H.V.R. Dias, L. Huai, W. Jin, S.G. Bott, Inorg. Chem. 34 (1995) 1973;
(c) H.V.R. Dias, W. Jin, Inorg. Chem. 35 (1996) 267;
(d) H.V.R. Dias, W. Jin, Inorg. Chem. 39 (2000) 815.
[9] S.T. Haubrich, P.P. Power, J. Am. Chem. Soc. 120 (1998) 2202.
[10] J. Feldman, S.J. McLain, A. Parthasarathy, W.J. Marshall, J.C. Calabrese, S.D. Arthur, Organometallics 16 (1997) 1514.
[11] C. Cui, H.W. Roesky, H.-G. Schmidt, M. Noltemeyer, Angew. Chem., Int. Ed. 30 (2001) 4351.

[12] N.J. Hardman, P.P. Power, Chem. Commun. (2001) 1184.
[13] N.J. Hardman, C. Cui, H.W. Roesky, W. Fink, P.P. Power, Angew. Chem., Int. Ed. 40 (2001) 2172.
[14] N.J. Hardman, P.P. Power, Inorg. Chem. 40 (2001) 2474.
[15] H. Hope, in: A.L. Wayda, M.Y. Darensbourg (Eds.), Experimental Organometallic Chemistry, ACS Symposium Series, vol. 357, American Chemical Society, Washington, DC, 1987 Chapter 10.
[16] SHELXTL Version 5.1, Bruker AXS, Madison, WI, 1998.
[17] SADABS an Empirical Absorption Correction Program Part of the SAINT PLUS NT Version 5.0 Package, Bruker AXS, Madison, WI, 1998.
[18] K. Klimek, C. Cui, H.W. Roesky, M. Noltemeyer, H.-G. Schmidt, Organometallics 19 (2000) 3085.
[19] K.W. Hellmann, L.H. Gade, A. Steiner, D. Stalke, F. Moller, Angew. Chem., Int. Ed. 36 (1997) 160.
[20] L. Grocholl, I. Schranz, L. Stahl, R.J. Stables, Inorg. Chem. 37 (1998) 2469.
[21] P.J. Brothers, K. Hubler, V. Hubler, B.C. Noll, M.M. Olmstead, P.P. Power, Angew. Chem., Int. Ed. 35 (1996) 2355.
[22] N. Wiberg, K. Amelunxen, H. Nöth, M. Schmidt, H. Schwenk, Angew. Chem., Int. Ed. 35 (1996) 65.
[23] I. Krossing, H. Nöth, H. Schwerk-Kircher, Eur. J. Inorg. Chem. (1998) 923.
[24] K.L.V. Mann, J.C. Jeffrey, J.A. McCleverty, P. Thornton, M.D. Ward, J. Chem. Soc., Dalton Trans. (1998) 89.
[25] M. Hausslein, H.-D. Hansen, K.W. Klinkhammer, J. Weidlein, K. Merz, Z. Anorg. Allg. Chem. 625 (1999) 1608.

PERGAMON

Polyhedron 21 (2002) 531–534

POLYHEDRON

www.elsevier.com/locate/poly

Synthesis and molecular structure of tris(pentamethylphenyl)gallium

Jason K. Vohs, L. Ellen Downs, Michael E. Barfield, Sonya D. Goodwin, Gregory H. Robinson *

Department of Chemistry, The University of Georgia, Athens, GA 30602-2556, USA

Received 20 August 2001; accepted 27 November 2001

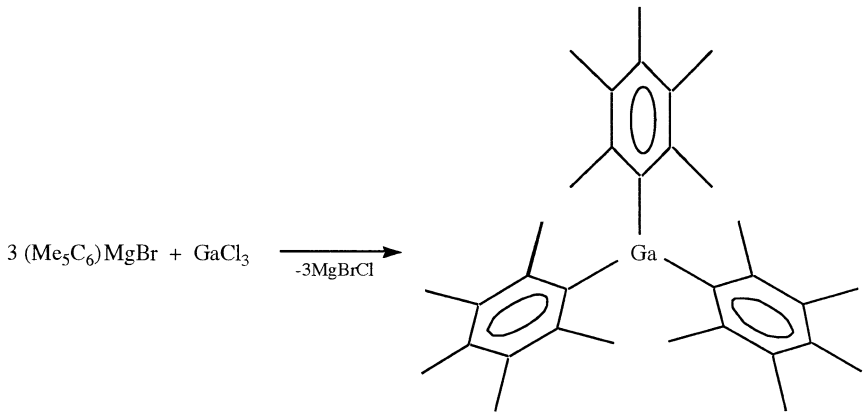
Abstract

Tris(pentamethylphenyl)gallium, $(Me_5C_6)_3Ga$, was prepared by reaction of pentamethylphenylmagnesium bromide with gallium(III) chloride in diethyl ether. The title compound, characterized by ^1H and ^{13}C NMR, elemental analyses, and single crystal X-ray diffraction, crystallizes in the $P\bar{1}$ (No. 2) space group with $a = 9.003(9)$ Å, $b = 10.713(1)$ Å, $c = 16.066(2)$ Å, $\alpha = 107.63\ (3)°$, $\beta = 97.63\ (3)°$, $\gamma = 90.08(3)°$, for $Z = 2$. Refinement converged at $R_1 = 0.050$, $wR_2 = 0.11$. The pentamethylphenyl ligands are configured about the gallium center in a propeller fashion at angles of 67.3°, 62.3°, and 60.9°. © 2002 Published by Elsevier Science Ltd.

Keywords: Tris(pentamethylphenyl)gallium; Pentamethylphenylmagnesium bromide; Elemental analyses; Single crystal X-ray diffraction

1. Introduction

The initial breakthrough in low-valent organogallium chemistry resulting in Ga–Ga bonds may be traced to the utilization of sterically demanding ligands [1]. Although, the phenyl ligand, $C_6H_5^-$, is not generally considered to possess significant steric bulk, it has served as the template upon which some notable sterically demanding ligands have been derived [2]. It is interesting that the methyl-saturated phenyl derivative, pentamethylphenyl, $Me_5C_6^-$, has not been examined in the organometallic chemistry of gallium (*vide infra*). Herein, we report the synthesis and molecular structure of tris(pentamethylphenyl)gallium. The title compound was isolated from reaction of the pentamethylphenylmagnesium bromide Grignard reagent with gallium(III) chloride (Eq. (1)).



(1)

* Corresponding author.
E-mail address: robinson@sunchem.chem.uga.edu (G.H. Robinson).

0277-5387/02/$ - see front matter © 2002 Published by Elsevier Science Ltd.
PII: S0277-5387(01)01034-8

2. Experimental

2.1. General comments

Standard Schlenk technique was employed in conjunction with an inert atmosphere dry-box (MBraun LabMaster 130). Diethyl ether was distilled over sodium/potassium benzophenone under an atmosphere of nitrogen prior to use. Bromopentamethylbenzene was purchased from Lancaster Synthesis, Inc. (Windham, NH) while gallium(III) chloride was obtained from Strem Chemical Co. (Newburyport, MA). All reagents were used without further purification. Pentamethylphenylmagnesium bromide was prepared by reaction of bromopentamethylbenzene with magnesium in diethyl ether. Elemental analyses were performed by E & R Microanalytical Laboratories (Parsipanny, NJ). Single crystal X-ray diffraction data were collected on a Bruker SMART™ CCD instrument.

2.2. Synthesis of $(Me_5C_6)_3Ga$

A reaction vessel was charged with diethyl ether and $GaCl_3$ (0.880 g; 5.00 mmol). Pentamethylphenylmagnesium bromide (3.86 g; 15.0 mmol) was added to this solution at -78 °C. This reaction mixture was allowed to stir overnight, slowly warming to room temperature (r.t.). The colorless solution was filtered leaving from a white precipitate (MgBrCl). Solvent reduction of the filtrate, coupled with subsequent cooling, afforded colorless, needle crystals of $(Me_5C_6)_3Ga$ (0.910 g, 31.0% yield): melting point (m.p.): 163 °C. Calc. (found) for $C_{33}H_{45}Ga$: C, 77.50 (77.42); H, 8.90 (8.67)%. ^1H NMR (400 MHz, 298 K, THF-d_8): $\delta = 1.82$ (s, 18H, m-CH_3), 1.90 (s, 9H, p-CH_3), 2.01 (s, 18H, o-CH_3); ^{13}C NMR (400 MHz, 298 K, $CDCl_8$): $\delta = 16.3$, 23.7, 25.4, 68.9, 131.8, 135.0, 137.6.

2.3. Structural solution and refinement for $(Me_5C_6)_3Ga$

A colorless needle crystal of $(Me_5C_6)_3Ga$ was mounted in a thin-walled glass capillary under an inert atmosphere of nitrogen. X-ray intensity data were measured at r.t. on a Bruker SMART™ CCD-based X-ray diffractometer system with graphite-monochromated Mo Kα radiation ($\lambda = 0.71073$ Å). The structure was solved by direct methods using the SHELXTL-6.1 [3] system of computer programs. The non-hydrogen atoms were refined anisotropically while hydrogen atoms were placed in idealized positions with their coordinates and thermal parameters riding on the attached carbon atoms. Crystallographic Data: triclinic, space group $P\bar{1}$ (No. 2), $a = 9.003(9)$ Å, $b = 10.713(1)$ Å, $c = 16.066(2)$ Å, $\alpha = 107.63$ (3)°, $\beta = 97.63$ (3)°, $\gamma = 90.08(3)$°, for $Z = 2$. Full-matrix least-squares F^2 refinement converged at $R_1 = 0.050$, $wR_2 = 0.11$ for 10 369 collected reflections.

3. Results and discussion

The first organogallium compound, triethylgallium, was reported by Dennis and Patnode [4] almost 70 years ago. Unlike its aluminum analog, triethylgallium is a trigonal planar-based monomer as opposed to a tetrahedral-based dimer containing electron deficient Al–C_{Et}–Al bridges. Decades later the molecular structure of triphenylgallium, Ph_3Ga, [5] would confirm the gallium center residing in a virtually idealized trigonal planar environment and a mean Ga–C bond distance of 1.957 Å. Again, the trigonal planar-based monomeric nature of triphenylgallium is easily contrasted with the dimeric structure of di-μ-phenyl-bis(diphenylaluminum), Ph_6Al_2 (i.e. the triphenylaluminum dimer), with tetrahedral aluminum centers and electron deficient three center-two electron Al–C_{Ph}–Al bridges [6,7]. However, careful examination of the structure of triphenylgallium reveals subtle factors at work contributing to this observed orientation. In particular, one of the phenyl rings of Ph_3Ga is co-planar with the GaC_3 basal plane while the remaining two phenyl rings were observed with dihedral angles of 13.2 and 31.6°. Moreover, while the immediate coordination about the gallium center in Ph_3Ga is certainly trigonal planar, an examination of the unit cell packing reveals weak intermolecular interactions (3.42 Å) between a gallium atom of one Ph_3Ga molecule and the phenyl π-electrons of a neighboring Ph_3Ga molecule. Thus, when taken in a larger context, the coordination of the gallium center in triphenylgallium approaches five-coordinate trigonal bipyramidal.

Almost two decades would pass before the synthesis and molecular structure of trimesitylgallium, Mes_3Ga (Mes = 1,3,5-$Me_3C_6H_2$),[8] would be reported. The sterically demanding Mes_3Ga molecule resides about a threefold crystallographic axis with approximate D_3 symmetry. While the Ga–C bond distance of 1.968 Å and the trigonal planar coordination about the gallium center in Mes_3Ga compares with the values obtained for Ph_3Ga (Ga–C: 1.957 Å), the dihedral angle of the mesityl rings relative to the GaC_3 plane is noteworthy. Each of the aromatic rings of the mesityl ligands reside in a propeller arrangement about the gallium atom at an angle of 55.9°. The gallium center is sufficiently protected to prevent diethyl ether coordination. Indeed, the orientation of the three mesityl ligands of trimesitylgallium preclude the weak secondary interactions present in triphenylgallium and the associated secondary trigonal bipyramidal coordination of the metal center. The molecular structure of trimesitylaluminum

was shown to be very similar to that of trimesitylgallium [9].

The pentamethylphenyl ligand has received considerably less attention than the mesityl derivative in Group 13 chemistry. This is due, perhaps in large measure, to the fact that it is not immediately obvious that adding steric bulk (in the form of methyl groups) in the *meta* positions of the of a phenyl-based ligand (compared with the mesityl ligand) would effect significant changes at the metal center. In an effort to ascertain what effects, if any, would result from this ligand (compared with other $(aryl)_3Ga$ compounds) we prepared the title compound from reaction of the Grignard reagent pentamethylphenylmagnesium bromide with gallium chloride. The crystal structure of $(Me_5C_6)_3Ga$ is given in Fig. 1. The coordination of the gallium atom is almost idealized trigonal planar with a mean C–Ga–C bond angle of 120.0(1)°. Similar to Mes_3Ga, $(Me_5C_6)_3Ga$ has approximate D_3 symmetry. The mean Ga–C bond distance of 1.981(5) Å in $(Me_5C_6)_3Ga$ is considerably longer than that observed for either Ph_3Ga (1.957 Å) or Mes_3Ga (1.968 Å). This is somewhat surprising considering that the additional two methyl groups on each ligand are not in close proximity to the metal bonding site (compared with the mesityl ligand). A factor contributing to the elongated Ga–C bond distance in the title compound perhaps involves an electronic component. It is plausible that the pentamethylphenyl ligand donates more electron density (as compared with the phenyl or mesityl ligands) into a Ga–C anti-bonding orbital (thereby resulting in a longer Ga–C bond).

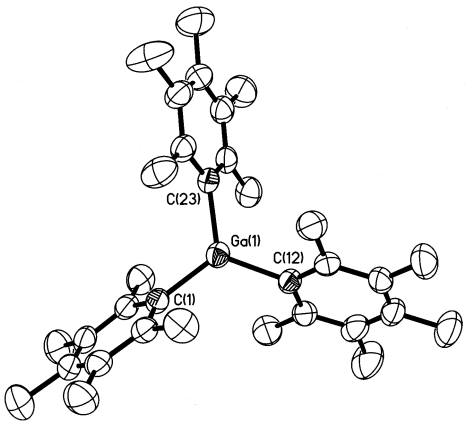


Fig. 1. A view of the $(Me_5C_6)_3Ga$ molecule showing the atom-labeling scheme. Thermal ellipsoids show 50% probability levels. Bond distances (Å): Ga–C(1): 1.974(3); Ga–C(12): 1.986(3); Ga–C(23): 1.984(3). Bond angles (°): C(1)–Ga–C(12) 121.9(1); C(1)–Ga–C(23): 120.4(1); C(12)–Ga–C(23): 117.7(1).

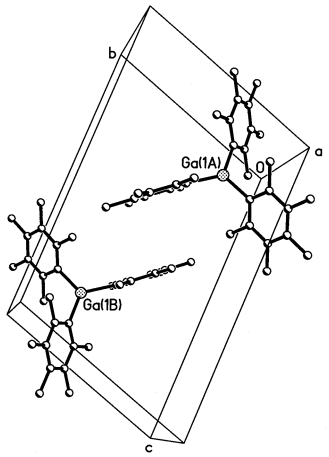


Fig. 2. A view of the unit cell of $(Me_5C_6)Ga$ showing the parallel nature of two pentamethylphenyl ligands (4.1 Å).

Also surprising about $(Me_5C_6)_3Ga$ is the dihedral angle of the pentamethylphenyl ligands with the GaC_3 basal plane. The dihedral planes were found to be 67.3°, 62.3°, and 60.9° for the C(1), C(12), and C(23) pentamethylphenyl planes, respectively. These angles are considerably greater than values obtained for Ph_3Ga (0°, 13.2° and 31.6°). Indeed, the dihedral angles observed in the title compound are significantly greater than the values obtained for Mes_3Ga (55.9°). As for possible causes for the dihedral plane angles observed in the title compound, one is drawn to the unit cell. In the unit cell of $(Me_5C_6)_3Ga$ it is shown that there is an aromatic–aromatic interaction, albeit a weak one at 4.1 Å, between parallel rings between two $(Me_5C_6)_3Ga$ molecules (Fig. 2). The only $(aryl)_3Ga$ derivative with dihedral bond angles greater that those observed for $(Me_5C_6)_3Ga$ is 2,6-dimesitylphenyldimesitylgallium, $(Mes_2C_6H_2)Mes_2Ga$, [10] with wherein the rings approach orthogonality values of 82.4°, 82.4°, and 86.3°.

Although, this laboratory has been interested in the organometallic chemistry of *m*-terphenyl-based ligands resulting in compounds containing sub-valent gallium species for some time [11–16], it is significant that simple ligands such as pentamethylphenyl can cause surprising structural effects about metal centers.

References

[1] W. Uhl, Angew. Chem., Int. Ed. Engl. 32 (1993) 1386.
[2] G.H. Robinson, Adv. Organomet. Chem. 47 (2001) 283.
[3] G.M. Sheldrick, SHELXTL-6.1, Crystallographic Computing System, Bruker Analytical X-Ray Systems, Madison, WI, 2000.
[4] L.M. Dennis, W. Patnode, J. Am. Chem. Soc. 54 (1932) 182.
[5] J.F. Malone, W.S. McDonald, J. Chem. Soc. (A) (1970) 3362.
[6] J.F. Malone, W.S. McDonald, Chem. Commun. (1967) 444.
[7] J.F. Malone W.S. McDonald, J. Chem. Soc., Dalton Trans. (1972) 2646.
[8] O.T. Beachley, M.R. Churchill, J.C. Pazik, J.W. Ziller, Organometallics 5 (1986) 1814.
[9] J.J. Jerius, J.M. Hahn, A.F.M.M. Rahman, O. Mols, W.H. Ilsley, J.P. Oliver, Organometallics 5 (1986) 1812.

[10] R.C. Crittendon, X.-W. Li, J. Su, G.H. Robinson, Organometallics 16 (1997) 2443.
[11] X.-W. Li, W.T. Pennington, G.H. Robinson, J. Am. Chem. Soc. 117 (1995) 7578.
[12] X.-W. Li, Y. Xie, P.R. Schreiner, K.D. Gripper, R.C. Crittendon, C.F. Campana, H.F. Schaefer, G.H. Robinson, Organometallics 15 (1996) 3798.
[13] J. Su, X.-W. Li, R.C. Crittendon, C.F. Campana, G.H. Robinson, Organometallics 16 (1997) 4511.
[14] J. Su, X.-W. Li, R.C. Crittendon, G.H. Robinson, J. Am. Chem. Soc. 119 (1997) 5471.
[15] G.H. Robinson, Acc. Chem. Res. 32 (1999) 773.
[16] G.H. Robinson, Chem. Commun. (2000) 2175.

PERGAMON

Polyhedron 21 (2002) 535–542

POLYHEDRON

www.elsevier.com/locate/poly

Synthesis, structure and bonding situation of [(dcpe)Pt(InCp*)$_2$] and {(dcpe)Pt[GaC(SiMe$_3$)$_3$]$_2$}—two novel examples of platinum complexes of low valent Group 13 metal species

Dana Weiß [a], Manuela Winter [a], Klaus, Merz [a], Annegret Knüfer [a], Roland A. Fischer [a,*], Nikolaus Fröhlich [b], Gernot Frenking [b,*]

[a] *Chemische Fakultät, Ruhr-Universität Bochum, Universitätsstraße 150, 44780 Bochum, Germany*
[b] *Fachbereich Chemie, Philipps-Universität Marburg, Hans-Meerwein-Straße, 35032 Marburg, Germany*

Received 8 August 2001; accepted 27 November 2001

Abstract

In analogy to the corresponding Cp*Al- and Cp*Ga-compounds two further bis(phosphine)platinum complexes [(dcpe)Pt(InCp*)$_2$] (**1(In)**) and {(dcpe)Pt[GaC(SiMe$_3$)$_3$]$_2$} (**2(Ga)**) containing monovalent Group 13 metal species as ligands are accessible by thermal activation of [(dcpe)Pt(H)(CH$_2$*t*-Bu)] (dcpe = bis(dicyclohexylphosphino)ethane) followed by the reaction with 2 equiv. of InCp* (Cp* = pentamethylcyclopentadienyl) or GaC(SiMe$_3$)$_3$. The crystal structure analysis reveals a distorted tetrahedral coordination of the platinum center for both compounds. The Pt–In distances in **1(In)** amount to 2.569(1) and 2.556(1) Å. The Pt–Ga distances in **2(Ga)** are exceptionally short and amount to 2.315(1) and 2.318(1) Å. Comparative theoretical investigations have been performed on this type of complexes and allow a deeper insight in the bonding situation. The NBO analysis reveals a significantly larger Pt → Ga π-back-donation for the model compound {(dhpe)Pt[GaC(SiH$_3$)$_3$]$_2$} (**2M(Ga)**) (0.44 e; dhpe = 1,2-diphosphinoethane) in comparison with the related model compound [(dhpe)Pt(GaCp)$_2$] (**1M(Ga)**) (0.29 e) bearing a strong π-donating organic ligand at the Ga center. A similar trend is observed for the Pt–Ga bond dissociation energies (D_e = 33.0 kcal mol^{-1} for **2M(Ga)**, D_e = 18.3 kcal mol^{-1} for **1M(Ga)**). For the model compound [(dhpe)Pt(InCp)$_2$] (**1M(In)**) a value of D_e = 19.1 kcal mol^{-1} has been calculated. © 2002 Elsevier Science Ltd. All rights reserved.

Keywords: Gallium; Indium; Platinum; Heterobimetallic complexes; X-ray structure analysis; Quantum chemical calculations

1. Introduction

The coordination chemistry of Group 13 elements in a low oxidation state is presently a topic of intensive research that has led to the successful synthesis of appealing new types of transition metal compounds [1]. Common synthetic routes to transition metal Group 13 metal compounds with the Group 13 metal in the formal oxidation state +I are the substitution of weakly bonded ligands like CO or olefins by ligands of the type ER (E = Al, Ga, In; R = e.g. Cp*, C(SiMe$_3$)$_3$, Si(*t*-Bu)$_3$ or sterically demanding aryl groups) as well as salt elimination and insertion reactions [2]. In a preliminary report we have shown that bis(phosphine)platinum complexes of the type [(dcpe)Pt(ECp*)$_2$] (E = Al (**1(Al)**), Ga (**1(Ga)**); dcpe = bis(dicyclohexylphosphino)ethane), carrying no additional π-acceptor ligands like CO, are readily accessible [3] by trapping the reactive intermediate [(dcpe)Pt], produced via reductive alkyl elimination from the platinum hydride compound [(dcpe)Pt(H)(CH$_2$*t*-Bu)], with the low valent aluminum and gallium species Cp*Al and Cp*Ga. Here we wish to describe two new compounds obtained by the same strategy, namely [(dcpe)Pt(InCp*)$_2$] (**1(In)**) and {(dcpe)Pt[GaC(SiMe$_3$)$_3$]$_2$} (**2(Ga)**). This latter compound is of particular interest in comparison with its close congener [(dcpe)Pt(GaCp*)$_2$] because of the ligand effects at the Ga center on the Pt–Ga bond.

* Corresponding authors. Tel.: +49-234-3224174; fax: +49-234-3214174 (R.A.F.); tel.: +49-6421-2825563; fax: +49-6421-2825566 (G.F.).

E-mail addresses: rfischer@aci.ruhr-uni-bochum.de (R.A. Fischer), frenking@chemie.uni-marburg.de (G. Frenking).

0277-5387/02/$ - see front matter © 2002 Elsevier Science Ltd. All rights reserved.
PII: S0277-5387(01)01027-0

2. Experimental

2.1. Reagents, solvents, and general procedures

All manipulations were carried out under purified Ar atmosphere using standard vacuum techniques. The solvents were distilled over sodium and stored over molecular sieves prior to use. Procedures described in the literature were followed for the preparation of [(dcpe)Pt(H)(CH_2t-Bu)] [4], $(InCp^*)_6$ [5] and [GaC($SiMe_3$)$_3$] [6]. Elemental analyses were performed by the Microanalytical Laboratory of the Ruhr-Universität Bochum. The NMR spectra were recorded in benzene-d_6 at 298 K using a Bruker Avance DPX-250 spectrometer (^{1}H, 250.1 MHz; ^{13}C, 62.9 MHz; ^{31}P, 101.3 MHz). Chemical shifts were referenced to the solvent resonances as internal standards and orthophosphoric acid as external standard, respectively. Infrared spectra were recorded as KBr pellets using a Perkin–Elmer 1720 X FT-IR spectrometer. Absorptions are described as follows: strong (s), medium (m), weak (w), and shoulder (sh).

2.2. Preparation of [(dcpe)Pt($InCp^*)_2$] (**1(In)**)

A sample of 100 mg (0.145 mmol) of [(dcpe)Pt(H)(CH_2t-Bu)] and 73 mg (0.048 mmol) of $(InCp^*)_6$ were combined and suspended in 0.4 ml of methylcyclohexane in an evacuated and sealed NMR tube. After the reaction mixture was heated 2 h at 60 °C the reaction was complete according to the ^{31}P NMR spectrum. The NMR tube was opened in the glove box, the content was transferred to a Schlenk tube and all volatile components were removed in vacuo, whereby the raw product could be obtained in quantitative yield. The resulting solid was recrystallized by slow evaporation of a solution of **1(In)** in toluene in the glove box to give ocre colored needle-shaped crystals. Yield of the isolated crystalline product: 106 mg (65%). The compound decomposes slowly at 108 °C. ^{1}H NMR: δ 2.40 (s, 30H, 10CH_3, Cp*), 2.00–0.95 (complex and broad superpositions, 48H, Cy_2P(CH_2)$_2$PCy_2). ^{13}C{^{1}H} NMR: δ 11.3 (10CH$_3$, Cp*), 26.8–38.0 (complex superpositions), 113.1 (10 ring C atoms, Cp*). ^{31}P NMR: δ 61.0 (s with ^{195}Pt satellites, $^1J_{(P-Pt)} = 5077$ Hz). IR: 2911 (s), 2845(s), 1443 (s), 1417 (m), 1377 (m), 1334(w), 1257 (s), 1172 (w), 1096 (s), 1022 (s), 883 (w) 847 (m), 802 (s), 733 (m), 638 (w), 587 (w), 521 (m), 459 (w). *Anal.* Calc. for $C_{46}H_{78}In_2P_2Pt$ (1117.79): C, 49.43; H, 7.03. Found: C, 49.16; H, 7.41%.

2.3. Preparation of [(dcpe)Pt{$GaC(SiMe_3)_3$}$_2$] (**2(Ga)**)

A sample of 100 mg (0.145 mmol) of [(dcpe)Pt(H)(CH_2t-Bu)] and 88 mg (0.073 mmol) of [GaC($SiMe_3$)$_3$]$_4$ were suspended in 0.4 ml of methylcyclohexane in an evacuated and sealed NMR tube. After the reaction mixture was heated 4 h at 70 °C the reaction was complete according to the ^{31}P NMR spectrum. The sample was treated following the procedure described for compound **1(In)** to give yellowish orange rhombic crystals. Yield of the isolated crystalline product: 87 mg (49%). The compound decomposes slowly at 80 °C. ^{1}H NMR: δ 0.69 (s, 54H, 18CH_3, 2C($SiMe_3$)$_3$), 2.20–0.97 (complex and broad superpositions, 48H, Cy_2P(CH_2)$_2$PCy_2). ^{13}C{^{1}H} NMR: δ 6.8 (18CH$_3$, C($SiMe_3$)$_3$), 23.3–35.8 (complex superpositions). ^{31}P NMR: δ 62.6 (s with ^{195}Pt satellites, $^1J_{(P-Pt)} = 3285$ Hz). IR: 2923 (vs), 2845 (s), 1448 (m), 1409 (w), 1342 (w), 1251 (s), 1173 (w), 1103 (m, b), 1004 (m, b), 846 (vs, b), 741 (w), 673 (m), 652 (m), 585 (m), 522 (w) 463 (w). *Anal.* Calc. for $C_{46}H_{102}Ga_2P_2PtSi_6$ (1220.30): C 45.28, H 8.42. Found: C 45.57, H 8.56%.

2.4. Crystal structure determination

Diffraction data from a ocre colored needle-shaped crystal (compound **1(In)**, crystal size $0.10 \times 0.20 \times 0.20$ mm^3) and a rhombic yellowish orange crystal (compound **2(Ga)**, crystal sizes $0.25 \times 0.20 \times 0.15$ mm^3), respectively, were collected on a Bruker-axs-SMART 1000 diffractometer (ω-scans). The structures were solved by direct methods using the SHELXS-97 program [7] and were refined by the full-matrix least square method on F^2 with the SHELXL-97 program. [8] Crystallographic data for **1(In)**: empirical formula $C_{46}H_{78}In_2P_2Pt$, $F_w = 1117.759$, monoclinic, space group $P2_1/c$, $a = 12.366(2)$, $b = 20.27(4)$, $c = 20.211(4)$ Å, $\beta = 106.629(5)°$, $V = 4796(2)$ Å^3, $Z = 4$, $\lambda = 0.71073$ Å, $T = 203$ K, reflections collected 20 642, 8424 independent reflections ($R_{int} = 0.0708$), reflections observed 6188, 460 parameters, completeness to $\theta = 25.68°$: 89.8%, final $R[I > 2\sigma(I)] = 0.0396$, $R_w[I > 2\sigma(I)] = 0.0821$, semi-empirical absorption correction, GOF = 0.958; crystallographic data for **2(Ga)**: empirical formula $C_{46}H_{102}Ga_2P_2PtSi_6$, $F_w = 1220.30$, triclinic, space group $P\bar{1}$, $a = 13.569(2)$, $b = 14.117(2)$, $c = 16.195$ Å, $\alpha = 103.872(3)$, $\beta = 94.823(3)$, $\gamma = 94.689(3)°$, $V = 2984.4(8)$ Å^3, $Z = 2$, $\lambda = 0.71073$ Å, $T = 203$ K, reflections collected 15 597, 10 398 independent reflections ($R_{int} = 0.1055$), reflections observed 7182, 572 parameters, completeness to $\theta = 25.13°$: 97.2%, final $R[I > 2\sigma(I)] = 0.0590$, $R_w[I > 2\sigma(I)] = 0.1461$, empirical absorption correction, GOF = 0.970, $R = [\Sigma(||F_o| - |F_c||)/\Sigma|F_o|]^{1/2}$, $R_w = [\Sigma w(F_o^2 - F_c^2)^2/\Sigma w(F_o^2)^2]^{1/2}$. Selected geometric parameters are listed in Tables 1 and 2. The trimethylsilyl groups of compound **2(Ga)** were disordered and have been calculated for two positions.

Table 1
Selected interatomic distances (Å) and angles (°) for the complexes **1(Al)**, **1(Ga)** (values for the second conformational Isomer have been omitted for reasons of a better overview; see also [3]) and **1(In)** and the model complexes **1M(Al)**, **1M(Ga)** and **1M(In)**

	[(dcpe)Pt(AlCp*)$_2$] (**1(Al)**) (E = Al)	[(dhpe)Pt(AlCp)$_2$] (**1M(Al)**) (E = Al)	[(dcpe)Pt(GaCp*)$_2$] (**1(Ga)**) (E = Ga)	[(dhpe)Pt(GaCp)$_2$] (**1M(Ga)**) (E = Ga)	[(dcpe)Pt(InCp*)$_2$] (**1(In)**) (E = In)	[(dhpe)Pt(InCp)$_2$] (**1M(In)**) (E = In)
Bond lengths						
Pt(1)–E(1)	2.327(2)	2.358	2.355(2)	2.439	2.569(1)	2.600
Pt(1)–E(2)	2.335(2)	2.358	2.367(2)	2.439	2.556(1)	2.600
E(1)···E(2)	3.502	3.659	3.538	3.680	3.666	3.916
Pt(1)–P(1)	2.291(2)	2.353	2.251(4)	2.326	2.247(2)	2.317
Pt(1)–P(2)	2.294(2)	2.353	2.256(5)	2.326	2.242(2)	2.317
E(1)–C(11)	2.313(6)	2.367	2.39(2)	2.445	2.582(6)	2.608
E(1)–C(12)	2.288(6)	2.356	2.33(2)	2.446	2.584(6)	2.613
E(1)–C(13)	2.284(6)	2.343	2.29(2)	2.442	2.589(6)	2.620
E(1)–C(14)	2.302(7)	2.345	2.37(2)	2.442	2.572(6)	2.620
E(1)–C(15)	2.322(6)	2.360	2.38(2)	2.444	2.567(6)	2.613
E(2)–C(21)	2.306(7)	2.367	2.40(2)	2.445	2.605(6)	2.608
E(2)–C(22)	2.291(6)	2.356	2.36(2)	2.446	2.581(6)	2.613
E(2)–C(23)	2.310(6)	2.343	2.32(2)	2.442	2.554(6)	2.620
E(2)–C(24)	2.332(6)	2.345	2.37(2)	2.442	2.557(6)	2.620
E(2)–C(25)	2.334(7)	2.360	2.44(2)	2.444	2.593(5)	2.613
$Cp^*_{centroid}$–E(1)	1.958	2.028	2.017	2.122	2.282	2.314
$Cp^*_{centroid}$–E(2)	1.975	2.028	2.058	2.122	2.280	2.314
Bond angles						
E(1)–Pt(1)–E(2)	97.37(8)	103.2	97.07(7)	99.9	91.34(2)	97.7
P(1)–Pt(1)–P(2)	90.38(7)	88.8	92.2(2)	90.5	93.22(6)	91.0
P(1)–Pt(1)–E(1)	115.27(6)	116.0	119.1(2)	116.8	117.71(4)	117.3
P(2)–Pt(1)–E(2)	117.50(7)	116.0	118.4(2)	116.8	116.76(4)	117.3
P(1)–Pt(1)–E(2)	119.40(7)	116.7	117.6(1)	117.2	120.16(4)	117.5
P(2)–Pt(1)–E(1)	118.76(6)	116.7	114.3(1)	117.2	120.15(4)	117.5

3. Results and discussion

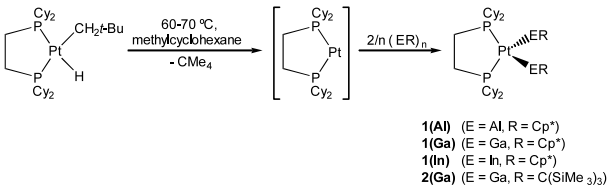
The previously reported compounds [(dcpe)Pt(ECp*)$_2$] (E = Al (**1(Al)**), Ga (**1(Ga)**)) and the related title compounds [(dcpe)Pt(InCp*)$_2$] **1(In)** and {(dcpe)Pt[GaC(SiMe$_3$)$_3$]$_2$} **2(Ga)** were obtained by the same synthetic pathway according to Scheme 1. When a suspension of [(dcpe)Pt(H)(CH$_2$*t*-Bu)] [4] in methylcyclohexane was treated with 2 equiv. of the respective Group 13-diyl compound [5,6] and heated to 60–70 °C for several hours in an evacuated and sealed NMR tube the quantitative conversion of the starting material was observed by in situ ^{31}P NMR spectroscopy. By slow evaporation of a solution of **1(In)** or **2(Ga)** in toluene the product complexes could be gathered in the form of ocre colored needles (**1(In)**) and yellowish orange rhombic crystals (**2(Ga)**), respectively. Complexes **1(In)** and **2(Ga)** have been characterized by means of ^{1}H, ^{13}C and ^{31}P NMR, as well as IR spectroscopy, elemental analysis and single crystal X-ray diffraction.

3.1. NMR spectra

The ^{1}H and ^{13}C NMR spectra are complex and provide only little information relevant to the discussion of the Pt–E bonding. Therefor, they will not be discussed in detail here. The ^{31}P NMR spectra in benzene show characteristic singlets with ^{195}Pt-satellites at 61.0 ppm ($^1J_{(P-Pt)} = 5077$ Hz; compound **1(In)**) and 62.6 ppm ($^1J_{(P-Pt)} = 3285$ Hz; compound **2(Ga)**) indicat-

Table 2
Selected interatomic distances (Å) and angles (°) for complex **2(Ga)** and the model complex **2M(Ga)**

	{(dcpe)Pt[GaC(SiMe$_3$)$_3$]$_2$} (**2(Ga)**)	{(dhpe)Pt[GaC(SiH$_3$)$_3$]$_2$} (**2M(Ga)**)
Bond lengths		
Pt(1)–Ga(1)	2.315(1)	2.360
Pt(1)–Ga(2)	2.318(1)	2.360
Ga(1)···Ga(2)	3.556	3.657
Pt(1)–P(1)	2.286(2)	2.348
Pt(1)–P(2)	2.285(3)	2.348
Ga(1)–C(3)	2.06(1)	2.060
Ga(2)–C(4)	2.060(9)	2.060
Bond angles		
Ga(1)–Pt(1)–Ga(2)	100.28(4)	101.5
P(1)–Pt(1)–P(2)	89.08(9)	87.6
C(3)–Ga(1)–Pt(1)	177.7(3)	175.8
C(4)–Ga(2)–Pt(1)	178.4(3)	175.8
P(1)–Pt(1)–Ga(1)	119.45(7)	115.0
P(2)–Pt(1)–Ga(2)	114.99(7)	115.0
P(1)–Pt(1)–Ga(2)	117.75(7)	119.4
P(2)–Pt(1)–Ga(1)	116.41(7)	119.4



Scheme 1.

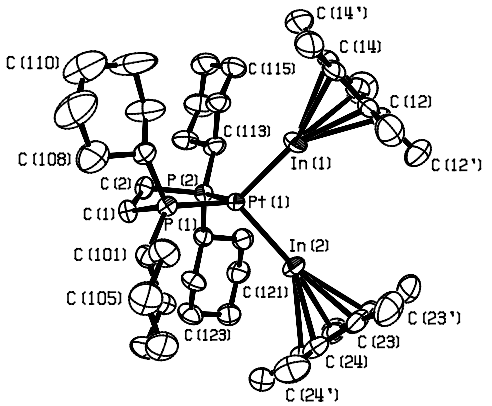


Fig. 1. Molecular structure of [(dcpe)Pt(InCp*)$_2$] (**1(In)**) (ORTEP plot).

ing an analogous chemical environment of the phosphorus atoms in each compound which is in accordance with the approximate C_2 symmetry of the complexes confirmed by X-ray analyses. The values for the chemical shifts are in a range comparable to the values of 52.5 and 53.6 ppm found for the signals of the homologous complexes [(dcpe)Pt(ECp*)$_2$] (E = Al, Ga). For compounds of the type [(dcpe)Pt(ECp*)$_2$] a steady increase of the coupling constant $^1J_{(P-Pt)}$, accompanied by a shortening of the interatomic P–Pt distances following the order E = Al ($^1J_{(P-Pt)} = 3482$ Hz, $d(P-Pt)_{average} = 2.286$ Å), Ga ($^1J_{(P-Pt)} = 4625$ Hz, $d(P-Pt)_{average} = 2.259$ Å), In ($^1J_{(P-Pt)} = 5077$ Hz, $d(P-Pt)_{average} = 2.245$ Å) has been observed. In none of the cases discussed a coupling $^2J_{(P-P)}$ was observed, possibly due to dynamic conformational effects in solution. Neither ^{195}Pt nor ^{71}Ga NMR resonances have been identified yet either, most likely because of extensive quadrupolar line broadening effects caused by the Ga and In nuclei.

3.2. Molecular structures of *1(In)* and *2(Ga)*

A single crystal X-ray diffraction study was performed, the results of which confirm the structural predictions based on analytical and spectroscopic data. The molecular structure of the title compound **1(In)** is outlined in Fig. 1.

Compound **1(In)** crystallizes in the monoclinic space group $P2_1/c$ ($Z = 4$). As is has been shown for the above mentioned congeners, the platinum center of **1(In)** is coordinated in a nearly tetrahedral mode by the two phosphorus atoms of the chelating ligand dcpe and the two η^5-Cp*In units. The Pt–In distances of 2.569(1) and 2.556(1) Å are distinctly longer in comparison with the Pt–In distances of 2.441(2) Å of the homoleptic compound {Pt[InC(SiMe$_3$)$_3$]$_4$}, reported by Uhl et al. [9], but slightly shortened compared with [(dcpe)Pt(InR$_2$)(R)] (R = CH$_2$SiMe$_3$), the only further example of a structurally characterized molecular compound with a direct, unsupported Pt–In bond (2.601(0) Å) [10]. Expectedly the Pt–In bonds are somewhat shorter than estimated from covalent single bond radii (2.80–2.89 Å). The shortest Pt–In distance described for binary alloys amounts to 2.534 Å [11]. For the In(1)–Pt(1)–In(2) angle a value of 91.34(2)° has been determined, distinctly narrowed in comparison to the corresponding E–Pt–E angles of the complexes [(dcpe)Pt(ECp*)$_2$] (E = Al, Ga) with values in a range of 95.21(7)°–100.02(7)°. This feature of the solid state structure of **1(In)** is presumably caused by the smaller cone angle of the Cp*In unit (98°) within compound **1(In)** in comparison to the cone angles of the Cp*Al (107°) and Cp*Ga units (102°) within the homologous Al–Pt and Ga–Pt complexes. The small angle also explains the somewhat larger extent of the deviation of the Cp*$_{centroid}$–In–Pt vectors from linearity (169.52° and 172.75°), in comparison to the Al and Ga complexes with average values for the Cp*$_{centroid}$–E–Pt angles of 176.10° and 175.01°. The Pt–P distances of **1(In)** are nearly identical and exhibit values of 2.247(2) and 2.242(2) Å. In comparison to the compounds [(dcpe)Pt(AlCp*)$_2$] and [(dcpe)Pt(GaCp*)$_2$] with average Pt–P distances of 2.286 and 2.259 Å a shortening of the Pt–P distances following the order E = Al, Ga, In and a corresponding increase of the ^{31}P coupling constants $^1J_{(P-Pt)}$ from 3482 to 4625 and 5071 Hz, respectively, was found. For the P(1)–Pt(1)–P(2) angle a value of 93.22(6)° has been determined, similar to the respective angles in the Al and Ga compounds of around 90.50° and 92.25° (average values for the two coexisting isomers, see [3]). Within the Cp*In fragments, the η^5-bonding mode of the Cp* ring is maintained, although small deviations from ideal η^5-bonding are observed. The Cp*$_{centroid}$–In distances amount to 2.282 and 2.280 Å. These values are close to the one found for the free ligand in the gas phase (2.288(4) Å) [5]. The Cp*$_{centroid}$–E distance is regarded as an indirect measure for the polarity of the Pt–E bond (E = Group 13 metal), a subject that has already been discussed extensively in the literature [2a,2c,3,12], so that the polarity of the Pt–In bond of compound **1(In)** seems to be low compared with [(CO)$_5$Cr–InCp*], the only known metal carbonyl complex of an Cp*In ligand and Cp*$_{centroid}$–In bond distance of 2.168(4) Å [13].

The complex {(dcpe)Pt[GaC(SiMe$_3$)$_3$]$_2$} (**2(Ga)**) crystallizes in the triclinic space group $P\bar{1}$ ($Z = 2$). The molecular structure in the crystal is depicted in Fig. 2.

The platinum center is coordinated by the phosphine ligand dcpe and two $(Me_3Si)_3Ga$ units in a distorted tetrahedral mode.

The Pt(1)–Ga(1) and Pt(1)–Ga(2) distances of 2.315(1) and 2.318(1) Å represent the shortest Pt–Ga bonds known so far. The Pt–Ga distances of the related complexes $[(dcpe)Pt(GaCp^*)_2]$ (2.355(2) to 2.382(2) Å for the two coexisting isomers) and $\{(dcpe)Pt[Ga(CH_2t\text{-}Bu)_2](CH_2t\text{-}Bu)\}$ [14] (2.438(1) Å) are distinctly longer. $[Pt_2(GaCp^*)_2(\mu_2\text{-}GaCp^*)_3]$ [15], the only homoleptic Pt–Ga complex, shows terminal Pt–Ga distances that are with an average value of 2.329 Å close to the respective values for **2(Ga)**. The Ga(1)–C(3) and Ga(2)–C(4) bond lengths of 2.06(1) and 2.060(9) Å ($Cp^*_{centroid}$–Ga distances of $[(dcpe)Pt(GaCp^*)_2]$: 2.017 to 2.067 Å) correspond to the value found for the free ligand $(Me_3Si)_3Ga$ (monomer, gas phase) of 2.06(2) Å

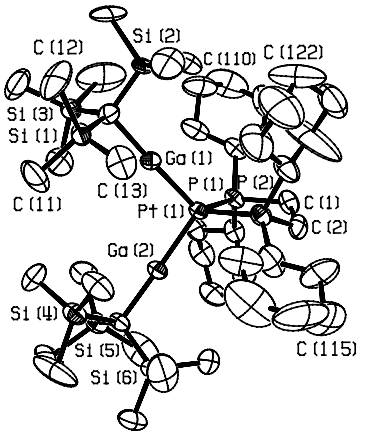


Fig. 2. Molecular structure of {(dcpe)Pt[GaC(SiMe3)3]2} (**2(Ga)**) (ORTEP plot).

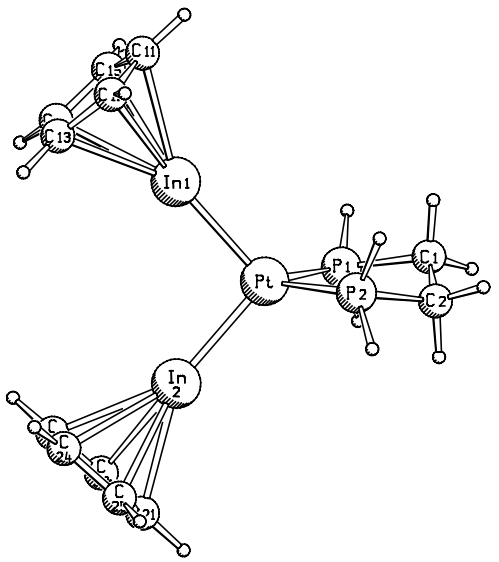


Fig. 3. Calculated structure of $[(dhpe)Pt(InCp)_2]$ (**1M(In)**) (SCHAKAL plot).

[16]. They differ clearly from the average Ga–C distances of 1.993 and 1.982 Å of the only $(Me_3Si)_3Ga$-substituted metal carbonyl complexes known so far, $\{Mn_2(CO)_8[\mu\text{-}GaC(SiMe_3)_3]_2\}$ and $\{Fe_3(CO)_9(\mu\text{-}CO)[\mu\text{-}GaC(SiMe_3)_3]_2\}$ [17], which should provide a higher polar character of the M–Ga bond. The Ga–C bond length of the only further complex with terminal coordinating $(Me_3Si)_3Ga$ units, $\{Ni[GaC(SiMe_3)_3]_4\}$ amounts to 2.014(4) Å [18]. The quantum-chemically calculated Ga–C distances of the homoleptic platinum model complex $[Pt(GaMe)_4]$ are 2.040 (BP86) and 2.028 Å (B3LYP), respectively. The Ga(1)–Pt(1)–Ga(2) angle of 100.28(4)° of compound **2(Ga)** is widened in comparison to the analogous angle of the complex $[(dcpe)Pt(GaCp^*)_2]$ with an average value of 96.14° for the two conformational isomers. The nonbonding Ga(1)···Ga(2) distance of 3.556 Å is comparable with the corresponding value in $[(dcpe)Pt(GaCp^*)_2]$ (3.510 and 3.538 Å for the two isomers). In contrast the solid state structure of tetrameric cluster compound $[(Me_3Si)_3Ga]_4$ shows Ga–Ga distances of 2.678(4) to 2.702(3) Å. The cone angle of $(Me_3Si)_3CGa$ within compound **2(Ga)** amounts to 73° (cone angle of Cp*Ga within $[(dcpe)Pt(GaCp^*)_2]$: 102°), so that steric reasons do not seem to predominate in the widening of the Ga(1)–Pt(1)–Ga(2) angle. The average Pt–P distances of compound **2(Ga)** (2.286 Å) are significantly elongated in comparison to the situation for $[(dcpe)Pt(GaCp^*)_2]$ (2.259 Å). This is presumably a consequence of a stronger Pt → Ga back-donation as predicted by quantum chemical calculations for M–ER bonds (M = transition metal, E = Group 13 element) with alkyl substituents R at the Group 13 element in contrast to the situation where R represents a π-donor ligand. This is discussed below.

4. Theoretical studies on model complexes

The structures of the model complexes $[(dhpe)Pt(InCp)_2]$ (**1M(In)**) and $\{(dhpe)Pt[GaC(SiH_3)_3]_2\}$ (**2M(Ga)**) (dhpe = 1,2-diphosphinoethane) have been optimized with the DFT functional BP86 and SVP basis sets and a relativistic pseudopotential for Pt (Figs. 3 and 4) [19–27]. The comparison of the calculated and experimental bond lengths and angles shows that the structural data of **1M(In)** and **2M(Ga)** are in good agreement with the observed values of **1(In)** and **2(Ga)** (Tables 1 and 2). The use of Cp instead of Cp* explains the somewhat longer E–C distances of the model compounds.

The calculated structures of the aluminum and gallium analogues **1M(Al)** and **1M(Ga)** of the model compound **1M(In)** have been reported by us in a previous investigation [3]. The data of **1M(Ga)** can now be compared with those of **2M(Ga).** In order to facilitate

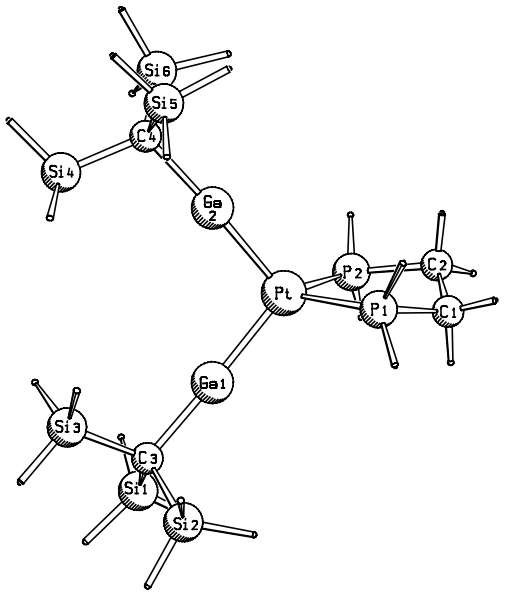


Fig. 4. Calculated structure of {(dhpe)Pt[GaC(SiH$_3$)$_3$]$_2$} (**2M(Ga)**) (SCHAKAL plot).

the comparison we give the most important bond lengths and angles in Table 1. Note that the Pt–Ga distance of **1M(Ga)** is longer than in **2M(Ga)** (Table 2) and that the latter complex has a longer Pt–P bond than the former. We analyzed the bonding situation in the model complexes with the NBO partitioning scheme [26] in order to see whether the shorter Pt–Ga bond of **2M(Ga)** correlates with stronger Pt → Ga back-donation. Tables 3 and 4 give the results of the NBO analysis of **1M(E)** (E = Al, Ga, In) and **2M(Ga)**.

The calculated atomic partial charges show that the platinum atom carries in all model compounds a negative charge between −0.2 and −0.3 e while the Group 13 elements have a large positive charge between +0.6 and +0.8. We want to point out that the atomic partial charges may be a deceptive indicator for the electrostatic forces between the atoms because they do not give information about the topographical distribution of the electronic charge. The calculated partial charges suggest that there is electrostatic attraction between the positively charged element E and the negatively charged Pt. However, the elements E in the ligands ER behave like a Lewis base because they have an electron lone pair as HOMO which donates electronic charge into the LUMO of the metal fragment. The latter species is a Lewis acid where the Pt atom is

Table 3
NBO analysis of [(dhpe)Pt(ECp)$_2$] (**1M(E)**) (E = Al, Ga, In) at the BP86/SVP level

E	q[(dhpe)Pt]	q(Pt)	q(E)	q(Cp)	p_x(E) [a]	p_y(E) [a]	p_z(E)	Δq(E) [c]	Δq_π(E) [c]	Δq_σ(E) [c]	Δq(Cp) [c]	P(Pt–E)
Al	−0.14	−0.28	0.68	−0.61	0.28	0.27	0.29	+0.04	−0.29	+0.33	+0.03	0.52
Ga	−0.03	−0.21	0.59	−0.58	0.25	0.27	0.23	−0.03	−0.22	+0.19	+0.04	0.42
In	−0.14	−0.32	0.77	−0.68	0.22	0.22	0.16	+0.10	−0.18	+0.29	+0.01	0.42
Free ligand ECp [b]												
Al			0.65	−0.65	0.13	0.13	0.21					
Ga			0.62	−0.62	0.15	0.15	0.15					
In			0.67	−0.67	0.13	0.13	0.13					

Partial charges q, p-orbital populations, charge difference Δq of the ECp moieties between the complex and the free ligand, Wiberg bond index P.

[a] p(π) AO of E.

[b] Values for the free ligand ECp, calculated in the geometry of the complexes.

[c] Negative values represent a higher electronic charge, and positive values represent a lower electronic charge in the complex relative to the free ligand. De\{[(dhpe)Pt(ECp)$_2$]\} = 29.6 (E = Al), 18.3 (E = Ga), 19.1 kcal mol^{-1} (E = In). The data for **1M(Al)** and **1M(Ga)** have been taken from reference [3].

Table 4
NBO analysis of {(dhpe)Pt[GaC(SiH$_3$)$_3$]$_2$} **2M(Ga)** at the BP86/SVP level

q[(dhpe)Pt]	q(Pt)	q(Ga)	q(R)	p_x(Ga) [a]	p_y(Ga) [a]	p_z(Ga)	Δq(Ga) [c]	Δq_π(Ga) [c]	Δq_σ(Ga) [c]	Δq(R) [c]	P(Pt–E)
0.04	−0.23	0.66	−0.68	0.25	0.23	0.34	−0.14	−0.44	+0.30	+0.12	0.57
Free ligand GaCSiH$_3$ [b]		0.80	−0.80	0.02	0.02	0.27					

Partial charges q, p-orbital populations, charge difference Δq of the EC(SiH$_3$)$_3$ moieties between the complex and the free ligand, Wiberg bond index P, R = C(SiH$_3$)$_3$.

[a] p(π) AO of E.

[b] Values for the free ligand GaC(SiH$_3$)$_3$, calculated in the geometry of the complexes.

[c] Negative values represent a higher electronic charge, and positive values represent a lower electronic charge in the complex relative to the free ligand. De({(dhpe)Pt[GaC(SiH$_3$)$_3$]$_2$}) = 33.0 kcal mol^{-1}.

the acceptor atom. We have recently shown in a detailed analysis of the metal–ER bonding in Group 13-diyl complexes that the *electrostatic attraction of the M–ER bond arises from the local negative charge concentration of the overall positively charged atom E with the locally charged depleted metal atom M which has an overall negative charge* [28]. The partial atomic charges give important information about the total charge flow between the atoms in a molecule but they do not tell where the charge is concentrated and where it is depleted within an atomic basin.

The ligands ECp become slightly positively charged in **1M(E)** while the ligand GaR ($R = C(SiH_3)_3$) receives a small negative charge in **2M(Ga)** (Tables 3 and 4). Note that the total charge of atom E changes only little upon formation of the Pt–ECp and Pt–GaR bonds (see the Δq(E) values in Tables 3 and 4) but the differences of the σ and π charges Δq_σ(E) and Δq_π(E) are much larger. The change in the π charges Δq_π(E) give directly the Pt → E π-back-donation. The data in Table 3 show that the Pt → E π-back-donation in **1M(E)** has the trend Al > Ga > In. The comparison of **1M(Ga)** with **2M(Ga)** shows clearly that the Pt → GaCp π-back-donation is significantly less than the Pt → GaR back-donation. This is in agreement with the results, which have been obtained for complexes $(CO)_4$Fe–ER [29]. The stronger Pt → GaR π-back-donation is in agreement with the higher bond dissociation energy (BDE) of **2M(Ga)**. The theoretically predicted BDE for dissociation of one GaR ligand is $D_e = 33.0$ kcal mol^{-1}, while the BDE of the Pt–GaCp bond of **1M(Ga)** is only $D_e = 18.3$ kcal mol^{-1}. The bond energies of the other ECp complexes are $D_e = 29.6$ kcal mol^{-1} for **1M(Al)** and $D_e = 19.1$ kcal mol^{-1} for **1M(In)**.

5. Conclusions

Recently the first examples of phosphine transition metal complexes with low valent Group 13 metal substituents, [(dcpe)Pt(ECp*)$_2$] (E = Al, Ga), have been reported by our group [3]. The row of this type of compounds has now been extended to the complexes [(dcpe)Pt(InCp*)$_2$] **1(In)** and {(dcpe)Pt[GaC(SiMe$_3$)$_3$]} **2(Ga)**, which have been fully characterized and analyzed quantum-chemically. Thus we have shown that bimetallic Pt–E (E = Al, Ga, In) compounds can be synthesized by trapping the reactive, low coordinated fragment [(dcpe)Pt] with Group 13-diyl species like ECp* (E = Al, Ga, In) or EC(SiMe$_3$)$_3$ (E = Ga). The current data suggest that the concept depicted in Scheme 1 is extendable to a variety of compounds of the type [(dcpe)Pt(ER)$_2$] which are now available with different homologues of the Group 13 metal E and organic groups R influencing the properties of the Pt–E bond. Besides, the spectator ligands at the transition metal fragment play also an important role concerning the polarity and characteristics of the Pt–E bond [3]. All complexes of the type [(dcpe)Pt(ER)$_2$] show a distorted tetrahedral coordination sphere at the platinum center. It has to be emphasized that **2(Ga)** possesses extraordinarily short Pt–Ga bonds of 2.315(1) and 2.318(1) Å. The calculated geometries of the model complexes [(dhpe)Pt(InCp)$_2$] **1M(In)** and {(dhpe)Pt-[GaC(SiH$_3$)$_3$]$_2$} **2M(Ga)** are in good agreement with the experimental values of **1(In)** and **2(Ga)**, respectively. In these bis(phosphine)platinum complexes the ER fragment functions as a two electron donor/acceptor ligand substitute in a terminal position. The NBO analysis shows that the Pt → GaC(SiH$_3$)$_3$ π-back-donation in **2M(Ga)** is significantly larger than the Pt → GaCp π-back-donation in [(dcpe)Pt(GaCp)$_2$] (**1M(Ga)**) as a result of the weaker π-donor properties of the organic ligand C(SiH$_3$)$_3$ in comparison with Cp. These accents are also reflected in the bond dissociation energies of **1M(Ga)** ($D_e = 18.3$ kcal mol^{-1}) and **2M(Ga)** ($D_e = 33.0$ kcal mol^{-1}). For **1M(In)** a value of $D_e = 19.1$ kcal mol^{-1}, comparable with the bond strength of the model compound **1M(Ga)** has been calculated.

6. Supplementary data

Supplementary data are available on request, quoting the deposition numbers CCDC 172598 and CCDC 172599 from The Director, CCDC, 12 Union Road, Cambridge, CB2 1EZ, UK (fax: +4-1223-336033; e-mail: deposit@ccdc.cam.ac.uk or www: http://www.ccdc.cam.ac.uk).

Acknowledgements

The support of this work by the Degussa AG and the W.C. Heraeus GmbH is gratefully acknowledged. We also thank the Deutsche Forschungsgemeinschaft and the Fonds der Chemischen Industrie for financial support.

References

[1] (a) W. Uhl, Angew. Chem. 105 (1993) 1449; Angew. Chem., Int. Ed. Engl. 32 (1993) 1386;
(b) C. Dohmeier, D. Loos, H. Schnöckel, Angew. Chem., Int. Ed. Engl. 108 (1996) 141; 35 (1996) 129;
(c) R.A. Fischer, J. Weiß, Angew. Chem., Int. Ed. Engl. 111 (1999) 3002; 38 (1999) 2830.

[2] (a) C. Üffing, A. Ecker, R. Köppe, H. Schnöckel, Organometallics 17 (1998) 2373;
(b) W. Uhl, M. Pohlmann, R. Wartchow, Angew. Chem. 110 (1998) 1007; Angew. Chem., Int. Ed. Engl. 37 (1998) 961;
(c) J. Weiß, D. Stetzkamp, B. Nuber, R.A. Fischer, C. Boehme, G. Frenking, Angew. Chem., Int. Ed. Engl. 109 (1997) 95; Angew. Chem., Int. Ed. Engl. 36 (1997) 70;

(d) P. Jutzi, B. Neumann, L.O. Schebaum, A. Stammler, H.-G. Stammler, Organometallics 19 (1999) 1445.
[3] D. Weiß, T. Steinke, M. Winter, R.A. Fischer, N. Fröhlich, J. Uddin, G. Frenking, Organometallics 19 (2000) 4583.
[4] (a) M. Hackett, J.A. Ibers, P. Jernakoff, G.M. Whitesides, J. Am. Chem. Soc. 108 (1986) 8094;
(b) M. Hackett, J.A. Ibers, G.M. Whitesides, J. Am. Chem. Soc. 110 (1988) 1436.
[5] O.T. Beachley Jr., R. Blom, M.R. Churchill, K. Faegri Jr., J.C. Fettinger, J.C. Pazik, L. Victoriano, Organometallics 8 (1989) 346.
[6] W. Uhl, A. Jantschak, J. Organomet. Chem. 555 (1998) 263.
[7] G.M. Sheldrick, SHELXS-97, Program for the Solution of Crystal Structures, University of Göttingen, Germany, 1997.
[8] G.M. Sheldrick, SHELXL-97, Program for the Refinement of Crystal Structures, University of Göttingen, Germany, 1997.
[9] (a) W. Uhl, M. Benter, S. Melle, W. Saak, Organometallics 18 (1999) 3778;
(b) W. Uhl, S. Melle, Z. Anorg. Allg. Chem. 626 (2000) 2043.
[10] R.A. Fischer, H.D. Kaesz, S.I. Khan, H.-J. Müller, Inorg. Chem. 29 (1990) 1601.
[11] M. Ellner, S. Bhan, K. Schubert, J. Less Common Met. 19 (1969) 245.
[12] C.L.B. Macdonald, A.H. Cowley, J. Am. Chem. Soc. 121 (1999) 12113.
[13] P. Jutzi, B. Neumann, G. Reumann, L.O. Schebaum, H.-G. Stammler, Organometallics 18 (1999) 2550.
[14] R.A. Fischer, H.D. Kaesz, S.I. Khan, H.-J. Müller, Inorg. Chem. 29 (1990) 1601.
[15] D. Weiß, M. Winter, R.A. Fischer, C. Yu, K. Wichmann, G. Frenking, Chem. Commun. 24 (2000) 2495.
[16] A. Haaland, K.-G. Martinsen, H.V. Volden, W. Kaim, E. Waldhör, W. Uhl, U. Schütz, Organometallics 15 (1996) 1146.
[17] W. Uhl, M. Benter, M. Prött, J. Chem. Soc., Dalton Trans. (2000) 643.
[18] (a) W. Uhl, M. Pohlmann, R. Wartchow, Angew. Chem. 110 (1998) 1007;
(b) W. Uhl, M. Pohlmann, R. Wartchow, Angew. Chem., Int. Ed. Engl. 37 (1998) 961.
[19] The DFT calculations were performed with the gradient-corrected exchange functional of Becke [20] and the correlation functional of Perdew [21] (BP86). The Ahlrichs SVP basis set was used throughout [22]. This basis set contains a quasi-relativistic pseudopotential for Pt [23] with a (7s6p5d) valence basis set in a [2111111/411/41] contraction especially optimized for the Ahlrichs SVP basis. Geometry optimizations were carried out using the RI approximation [24] as implemented in the Turbomole program package [25]. The NBO analysis [26] was carried out using GAUSSIAN-98 [27]. All stationary points were characterized as minima by full calculation of the Hessian matrix.
[20] A.D. Becke, Phys. Rev. A 38 (1988) 3098.
[21] J.P. Perdew, Phys. Rev. B 33 (1986) 8822.
[22] A. Schäfer, H. Horn, R. Ahlrichs, J. Chem. Phys. 97 (1992) 2571.
[23] D. Andrae, U. Häußermann, M. Dolg, H. Stoll, H. Preuß, Theor. Chim. Acta 77 (1990) 123.
[24] K. Eichkorn, O. Treutler, H. Öhm, M. Häser, R. Ahlrichs, Chem. Phys. Lett. 240 (1995) 283.
[25] (a) R. Ahlrichs, M. Bär, M. Häser, H. Horn, C. Kölmel, Chem. Phys. Lett. 162 (1989) 165;
(b) O. Treutler, R. Ahlrichs, J. Chem. Phys. 102 (1995) 346.
[26] A.E. Reed, L.A. Curtiss, F. Weinhold, Chem. Rev. 88 (1988) 899.
[27] GAUSSIAN-98 (Revision A.1): M.J. Frisch, G.W. Trucks, H.B. Schlegel, G.E. Scuseria, M.A. Robb, J.R. Cheeseman, V.G. Zakrzewski, J.A. Montgomery, R.E. Stratmann, J.C. Burant, S. Dapprich, J.M. Milliam, A.D. Daniels, K.N. Kudin, M.C. Strain, O. Farkas, J. Tomasi, V. Barone, M. Cossi, R. Cammi, B. Mennucci, C. Pomelli, C. Adamo, S. Clifford, J. Ochterski, G.A. Petersson, P.Y. Ayala, Q. Cui, K. Morokuma, D.K. Malick, A.D. Rabuck, K. Raghavachari, J.B. Foresman, J. Cioslowski, J.V. Ortiz, B.B. Stefanov, G. Liu, A. Liashenko, P. Piskorz, I. Komaromi, R. Gomberts, R.L. Martin, D.J. Fox, T.A. Keith, M.A. Al-Laham, C.Y. Peng, A. Nanayakkara, C. Gonzalez, M. Challacombe, P.M.W. Gill, B.G. Johnson, W. Chen, M.W. Wong, J.L. Andres, M. Head-Gordon, E.S. Replogle, J.A. Pople, Gaussian Inc., Pittsburgh, PA 1998.
[28] J. Uddin, G. Frenking, J. Am. Chem. Soc. 123 (2001) 1683.
[29] J. Uddin, C. Boehme, G. Frenking, Organometallics 19 (2000) 571.

PERGAMON

Polyhedron 21 (2002) 543–548

POLYHEDRON

www.elsevier.com/locate/poly

Studies on BCl and on the exchange reaction of BCl_3 with polyboron fluorides

Jennifer A.J. Pardoe, Nicholas C. Norman, Peter L. Timms *

School of Chemistry, University of Bristol, Bristol BS8 1TS, UK

Received 16 August 2001; accepted 7 December 2001

Abstract

Gaseous BCl has been prepared at low pressure by reaction of BCl_3 with boron at 2000 °C or by decomposition of B_2Cl_4 using either an electric discharge or using flash thermolysis at 1150 °C, and then condensed at −196 °C. Reasons are discussed why each method gives BCl capable of generating $(Cl_2B)_3BCO$ when the condensate at −196 °C is treated with CO, but B_4Cl_4 is only formed from BCl prepared from B_2Cl_4. The stepwise conversion of $(F_2B)_3BCO$ to $(Cl_2B)_3BCO$ by treatment with BCl_3 has been followed by ^{11}B NMR spectroscopy. Evidence from mass spectrometry and ^{11}B NMR spectroscopy suggests that reaction of polyboron fluorides, particularly B_8F_{12} and $B_{10}F_{12}$, with BCl_3 yields a new form of B_9Cl_9 of, as yet, unknown structure which converts slowly to *closo*-B_9Cl_9 or *closo*-B_8Cl_8 depending on the solvent. © 2002 Elsevier Science Ltd. All rights reserved.

Keywords: Boron monochloride; Halogen exchange; Polyboron halides

1. Introduction

Knowledge of the chemistry of the polyboron halides has been growing for about 50 years since the original discovery of B_4Cl_4 by Schlesinger [1]. The chemistry of polyboron chlorides and bromides was reviewed in 1991 [2] and there have been some developments since [3]. An earlier review also embraced the polyboron fluorides [4]. The work reported here concentrates on two aspects of this field, on the chemistry of BCl and on halogen exchange reactions by which polyboron fluorides are converted into chlorides.

2. Experimental

All boron compounds described in this work were handled under high vacuum conditions on diffusion pumped, glass vacuum lines equipped with Teflon stopcocks, with Viton O-ring joints (J. Young) and with efficient means of separating volatiles on a low temperature vacuum distillation column [5]. Pre-dried solvents were further dried over vacuum treated 3 Å molecular sieves just before use; dry CO was obtained by collecting liquid CO from a cylinder in a liquid nitrogen cooled Schlenk tube and allowing the liquid CO to evaporate only at very low temperatures; BCl_3 (Aldrich) was pumped on to remove HCl before use; B_2Cl_4 was prepared either by reaction of excess BCl_3 with B_2F_4 in the gas phase at room temperature or by reduction of BCl_3 with copper atoms [6]; $(F_2B)_3BCO$ was prepared by reaction of CO with B_8F_{12} which had been prepared from low temperature condensation of BF [7].

A 10–1000 amu Micromass quadrupole mass spectrometer integral to the vacuum lines permitted immediate analysis of products of sufficient volatility. Less volatile samples were put in capped vials under strictly oxygen free conditions and analysed using a VG Analytical Autospec mass spectrometer. All samples for ^{11}B NMR spectroscopy were fusion sealed in 5 mm Pyrex tubes; the spectra were run at 96 MHz on a JEOL 300 MHz Eclipse spectrometer.

* Corresponding author. Tel.: +44-117-9287654; fax: +44-117-9251295.

E-mail address: peter.timms@bristol.ac.uk (P.L. Timms).

0277-5387/02/$ - see front matter © 2002 Elsevier Science Ltd. All rights reserved.
PII: S0277-5387(01)01032-4

3. Results and discussion

3.1. Studies on BCl prepared by different methods

Boron monochloride is a well studied molecule because of its interest to spectroscopists [8,9], its importance in plasma chemistry of BCl_3 [10] and its involvement in the formation of B_2Cl_4 [11]. We have recently employed three routes to making BCl to use it as a chemical reagent. Using two procedures originally described 25 years ago [12,13], BCl has been prepared by passing the vapour of B_2Cl_4 at the rate of about 1 mmol min^{-1} and a pressure of a few mbar, either through a 2 kV, 50 Hz electrical discharge in a copper tube or through a short length of 2 mm bore quartz tubing heated to 1150 °C to allow flash thermolysis to occur. The off-gases from the discharge or flash thermolysis units were expanded into a vacuum at a pressure $< 10^{-3}$ mbar and were condensed rapidly on the liquid nitrogen cooled walls of the vacuum chamber. The discharge preparation is somewhat easier experimentally as in the flash thermolysis system there are two competing reactions shown in Eqs. (1) and (2):

$$B_2Cl_4(g) \rightarrow BCl(g) + BCl_3(g) \quad (1)$$

$$3B_2Cl_4 \rightarrow 2B(s) + 4BCl_3(g) \quad (2)$$

The reaction of Eq. (1) is less thermodynamically favoured than the reaction of Eq. (2) but the reaction of Eq. (1) can be kinetically favoured because there is a high activation energy for nucleation of solid boron in the homogeneous gas phase reaction of Eq. (2). Unfortunately, it is hard to suppress the formation of boron in a heterogeneous reaction with the tube walls and the flash thermolysis tube often blocked after only a few mmol of B_2Cl_4 had passed through.

The only molecular product of condensation of the off-gases from the discharge or flash thermolysis treatment of B_2Cl_4 was B_4Cl_4, characterised by ^{11}B NMR spectroscopy and by mass spectrometry [2]. This was formed together with a larger amount of a colourless, intractable solid. Maddren [13] was able to suppress B_4Cl_4 formation by condensation of the off-gases from the discharge with a large excess of ethyne (which gave $C_4H_4B_2Cl_2$, 1,4-diboracyclohexa-2,5-diene), showing that the B_4Cl_4 formed on the cold surface not in the discharge (or flash thermolysis) region. However, we have found that if the condensate from the discharge or flash thermolysis system is allowed to warm from −196 °C in the presence of approximately 0.5 atm pressure of CO, a new compound not found in the earlier work can be isolated in addition to B_4Cl_4. This solid was identified as $(Cl_2B)_3BCO$ from its ^{11}B NMR spectrum (peaks at 68.2 and −20.7 ppm), from its IR spectrum (showing a strong υ CO stretch at 2176 cm^{-1}) and from its crystal structure [14]. The original compound of this type, $(F_2B)_3BCO$, was prepared by reaction of CO with B_8F_{12} [7]. However, $(F_2B)_3BCO$ can also be made by reacting CO at low temperatures with $(F_2B)_2BF$, which disproportionates above −50 °C to B_8F_{12} and B_2F_4. The formation of $(Cl_2B)_3BCO$ strongly suggests that some $(Cl_2B)_2BCl$ was formed by insertion of BCl into the B–B bond or a B–Cl bond of B_2Cl_4 and that this reacted with CO as shown in Eq. (3):

$$2(Cl_2B)_2BCl + CO \rightarrow (Cl_2B)_3BCO + B_2Cl_4 \quad (3)$$

We have also recently prepared BCl by a new route, the reduction of BCl_3 by passing the gas over boron at approximately 2000 °C at low pressure. The apparatus used was similar to that previously used to prepare BF [7]. The BCl_3 was passed at a rate of 0.8 mmol min^{-1} and at pressure of < 2 mbar through a column of granular boron contained in an inductively heated graphite tube. The off-gases from the tube emerged into a vacuum at $< 10^{-4}$ mbar and passed directly to the walls of a stainless steel vessel, part immersed in liquid nitrogen. By measuring the loss of weight of boron and calculating using Eq. (4) below, about 12% of the BCl_3 seemed to be converted to BCl.

$$2B(s) + BCl_3(g) \rightarrow 3BCl(g) \quad (4)$$

On allowing the stainless steel reaction vessel to warm up, BCl_3 and B_2Cl_4 were pumped out below room temperature. With the vessel warmed to room temperature (22 °C), a mixture of green and yellow–brown solids could be pumped out slowly. Release of these solids was speeded up by warming the stainless steel vessel to approximately 40 °C. Studies of these solids by ^{11}B NMR and mass spectrometry showed the most volatile compound to be B_8Cl_8 while the less volatile solids were mainly B_9Cl_9 with some $B_{10}Cl_{10}$, $B_{11}Cl_{11}$ and $B_{12}Cl_{12}$. No B_4Cl_4 was detected. An insoluble, involatile but very air-sensitive solid was left on the walls of the reactor after exhaustive pumping to pressures $< 10^{-4}$ mbar. Repeating the experiment with addition of CO to the cold reactor after the condensate had collected, resulted in the formation of $(Cl_2B)_3BCO$, suggesting that some $(Cl_2B)_2BCl$ was among the products formed on the cold surface. The formation of $(Cl_2B)_2BCl$ and its decomposition at low temperatures may explain the formation of the observed poly-boron chlorides via the mechanism proposed by Davan and Morrison [15] in their studies of the thermal decomposition of B_2Cl_4.

The complete absence of B_4Cl_4 formation from BCl in the above experiments was a surprise but the result may give a clue as to the true mode of formation of B_4Cl_4. Earlier work has shown that B_4Cl_4 is not one of the products of decomposition of B_2Cl_4 even at temperatures up to 300 °C [15]. Apart from our work on flash thermolysis of B_2Cl_4, B_4Cl_4 has only been formed by the use of electrical discharges in BCl_3 or in B_2Cl_4. In

an electrical discharge, there is energy available to form BCl in its singlet ground state, X $^1\Sigma^+$, and also in its triplet excited state, a $^3\Pi_1$, which lies 242 kJ mol^{-1} above the ground state [9]. As suggested earlier [16], it could be that B_2Cl_4 arises from insertion of singlet BCl into the B–Cl bonds of BCl_3 while B_4Cl_4 arises from aggregation of triplet BCl. If both singlet and triplet BCl were condensed on a cold surface, polymerisation of the latter may be the source of the observed B_4Cl_4. The idea of forming a mixture of singlet and triplet forms of BCl seems less obvious in relation to the work on flash thermolysis. There would not appear to be sufficient energy available at 1150 °C to form BCl in its excited triplet state yet B_4Cl_4 is formed in amounts similar to that observed from the discharge route. The answer may lie in the mode of decomposition of B_2Cl_4 by the gas phase reaction of Eq. (1). As shown by McKee for the flash thermolysis of 1,2-$P_2B_4Cl_4$ [17], energy barriers to apparently simple modes of decomposition can be high, providing kinetic enhancement of thermodynamically less favourable pathways. So flash thermolysis of B_2Cl_4 could yield a mixture of the expected singlet BCl with some of the higher energy triplet form.

Preparing BCl at 2000 °C in a heterogeneous reaction from boron and BCl_3 is likely to be a route to the most thermodynamically favoured form, i.e. singlet, ground state BCl, and this on condensation gives no B_4Cl_4. All routes to BCl give some singlet BCl and it is believed that this is the form most suited to react efficiently with BCl_3 to give B_2Cl_4 or to react with B_2Cl_4 to give $(Cl_2B)_2BCl$ which is the precursor to $(Cl_2B)_3BCO$.

It is clear from this research that more theoretical work is needed to give a proper understanding of the mode of formation of B_4Cl_4 from BCl.

3.2. Conversion of $(F_2B)_3BCO$ to $(Cl_2B)_3BCO$ by reaction with BCl_3

The conversions of B_2F_4 to B_2Cl_4 and of B_2Cl_4 to B_2Br_4 by reaction with BCl_3 and BBr_3, respectively, have been known for many years [4]. We have found that halogen exchange also works well starting with $(F_2B)_3BCO$ and treating it with BCl_3.

Reaction of $(F_2B)_3BCO$ with BCl_3 in the vapour phase at room temperature gives a virtually quantitative conversion to $(Cl_2B)_3BCO$ in less than an hour with liberation of BF_3 [14]. This is by far the most convenient preparation of $(Cl_2B)_3BCO$ in our laboratories because $(F_2B)_3BCO$ can be made in gram quantities by allowing the products formed by condensing BF at −196 °C to warm to room temperature in the presence of CO gas. A similar reaction occurs between $(F_2B)_3BPF_3$ [18] and BCl_3 yielding $(Cl_2B)_3BPF_3$ (showing ^{11}B resonances at δ +65.9 and −17.1 ppm); no exchange of P–F for P–Cl was observed within the time scale needed to exchange B–F for B–Cl.

The stepwise nature of the above fluorine-for-chlorine exchange process was revealed by ^{11}B NMR spectroscopy. Liquid BCl_3 was allowed to interact with $(F_2B)_3BCO$ for 50 min at 0 °C, followed by cooling to −70 °C, pumping boron trihalides away and then dissolving the remaining solid in CD_2Cl_2. The ^{11}B–^{11}B COSY spectrum of the product is shown in Fig. 1. Progressive replacement of F by Cl as $(F_2B)_3BCO$ converts to $(Cl_2B)_3BCO$ can give a total of ten different compounds containing combinations of BF_2, BFCl and BCl_2 groups. The spectrum of Fig. 1 gives evidence for at least eight of these ten possible structures. Considering first the four-coordinate boron environments ranging in δ values from −50.6 ppm for $(F_2B)_3BCO$ to −20.7 ppm for $(Cl_2B)_3BCO$. There are seven different peaks corresponding to successive replacements of F by Cl in compounds of type $B_4F_{6-x}Cl_xCO$. The peaks at −45.0 and −24.4 ppm are directly assignable to $(F_2B)_2(FClB)BCO$ and to $(Cl_2B)_2(FClB)BCO$, respectively. Of the remaining three peaks, that at −29.0 ppm has an asymmetry indicating that both $(F_2B)(Cl_2B)_2BCO$ and $(Cl_2B)(FClB)_2BCO$ are present although the precise positions of their respective resonances cannot be resolved from the COSY spectrum. The COSY spectrum also suggests that both $(F_2B)(FClB)(Cl_2B)BCO$ and $(FClB)_3BCO$ and both $(F_2B)(Cl_2B)_2CO$ and $(FClB)_2(Cl_2B)BCO$ contribute to the peaks at −34.3 and −39.8 ppm, respectively. In addition, the spectrum shows three broad resonances corresponding to BF_2, BFCl and BCl_2 groups with chemical shifts at +32.4, +50.8 and +68.9 ppm, respectively. These values are similar to those previously reported for species of the type $B_2F_{4-x}Cl_x$ [19]; in pure $(BF_2)_3BCO$, the chemical shift for the BF_2 groups is +31.3. The COSY spectrum shows how the ^{11}B chemical shifts for these BF_2, BFCl and BCl_2 groups move slightly to higher field as the fluorine content of the molecules increases.

3.3. Reaction of polyboron fluorides with BCl_3

Boron trichloride has also been reacted with some of the polyboron fluorides originating from condensation of BF at −196 °C which contain eight or more boron atoms [4]. The reactions have yielded a new, unstable polyboron chloride, the detailed structure, of which can not yet be assigned from the available NMR data.

Some explanation of the nature of the starting boron fluoride materials is needed as single crystal X-ray structures have only recently been obtained for two of the polyboron fluorides, B_8F_{12} and $B_{10}F_{12}$ [20]. The structure of B_8F_{12} differs from the diborane-like structure $B_2(BF_2)_6$ proposed on the basis of its reactivity [7] mainly through the presence of a short, central B–B

bond, supported by bridging BF_2 groups and a folded rather than planar central $B_2(\mu\text{-}BF_2)_2$ unit. The existence of $B_{10}F_{12}$ was not apparent from previous studies of higher boron fluorides based largely on mass spectrometry [4], but it is now clear that this molecule with a central tetrahedral core of four boron atoms with four terminal and two bridging BF_2 groups having S_4 symmetry, is the most abundant component of the polyboron fluorides of lower volatility than B_8F_{12}.

The reaction of either B_8F_{12} or of higher polyboron fluorides rich in $B_{10}F_{12}$ with excess liquid BCl_3 follows the same pattern. Reaction begins below -30 °C with a darkening in colour, which intensifies slowly. Holding the temperature at 0 °C for several hours gives a red–brown solution and BF_3, BF_2Cl and $BFCl_2$ are formed by reaction with the BCl_3 in the vapour. If the temperature is then raised to 60 °C in the presence of BCl_3 vapour before all the highly volatile boron trihalides are pumped away, the residue is a dark brown–purple solid. Direct extraction of this solid with CD_2Cl_2 at room temperature gives a brown solution which initially exhibits a an ^{11}B NMR spectrum showing six main resonances, the chemical shifts and relative intensities of which are given in Fig. 2. Essentially the same spectrum can be obtained by heating the brown–purple solid to 40 °C and pumping out a solid by short-path distillation on to a cold finger, and dissolving the material on the cold finger in CD_2Cl_2 or C_6D_6. The colour of the sublimate can vary from run to run from almost colourless to yellow–brown. It seems likely that

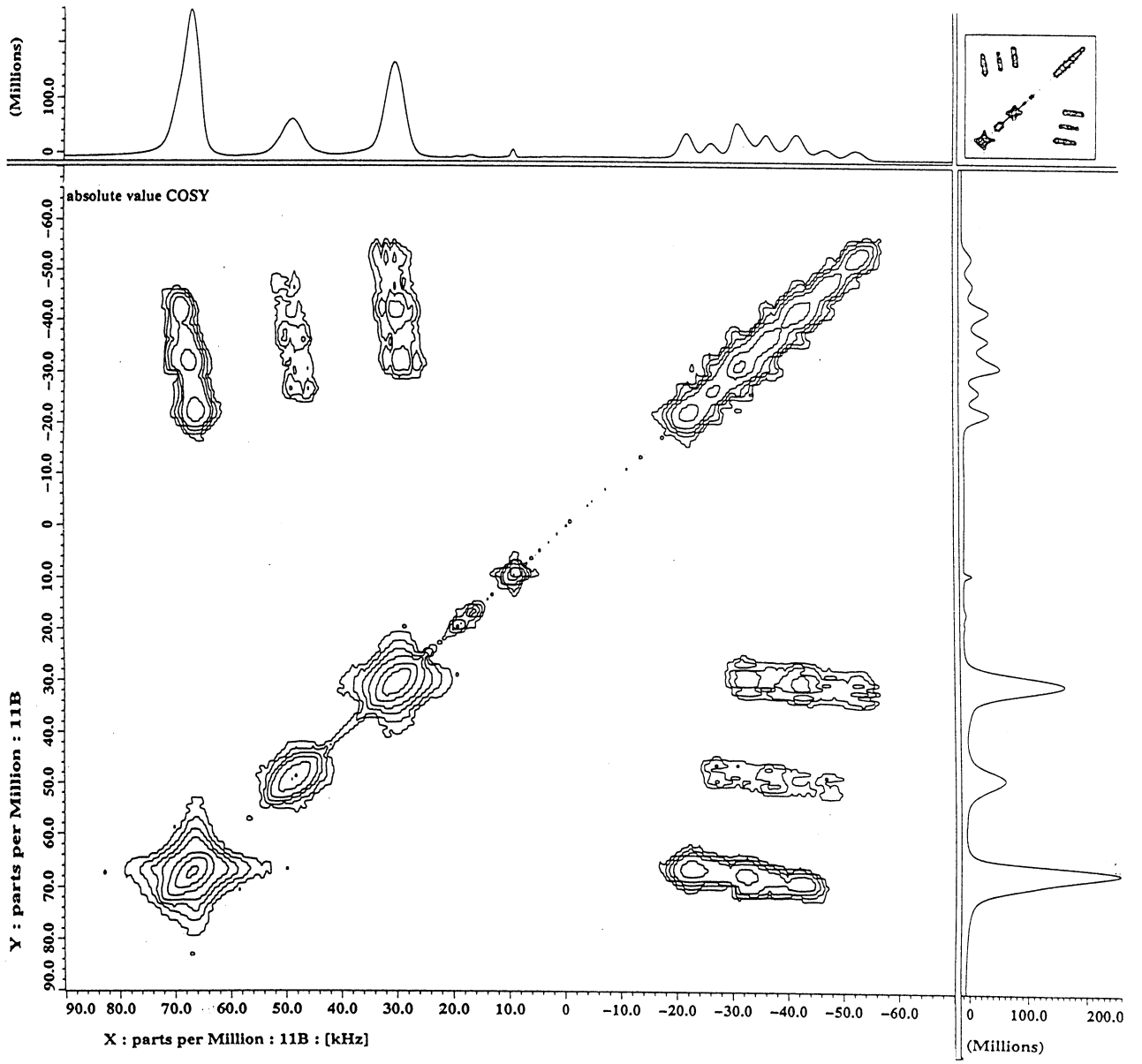


Fig. 1. ^{11}B–^{11}B COSY NMR spectrum of compounds of type $B_4F_{6-x}Cl_xCO$ prepared by reacting $(BF_2)_3BCO$ with BCl_3 (CD_2Cl_2 as solvent).

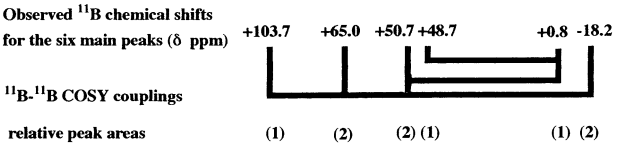


Fig. 2. ^{11}B NMR data for the dominant product formed by reacting polyboron fluorides rich in $B_{10}F_{12}$ with BCl_3 at 0 °C until chlorine for fluorine exchange was complete (CD_2Cl_2 as solvent).

the main component of the sublimate is colourless but that it is unstable and becomes contaminated to a varying extent by intensely coloured decomposition products.

The mass spectrum of the sublimate, run within a few minutes of dissolving the solid in C_6D_6, showed BCl_2^+ as the base peak, with $B_8Cl_6^+$ (m/z 293–307, centred at 299) as the dominant high mass peak, approximately 40 times more intense than the highest mass peak group at m/z 410–426, centred at 416, corresponding to $B_9Cl_9^+$. The mass spectrum of *closo*-B_9Cl_9 run under the same conditions shows a much lower ratio of the intensities of $B_8Cl_6^+$: $B_9Cl_9^+$ in line with that reported by Morrison [2]. The mass spectrum suggests that the main volatile component of the sample may have been B_9Cl_9 but an isomer of different structure to the known *closo*-B_9Cl_9, with a much greater tendency to eliminate BCl_3 to form $B_8Cl_6^+$.

In the ^{11}B NMR spectrum, the six peaks identified in Fig. 2 seem to belong to a single molecular species as they are always found in the same ratio and decline in intensity together as the sample decomposes over time. The exact position and relative intensity of the peak at +65 ppm is least certain as this region in the spectrum overlays a group of peaks associated with the *closo*-boranes and with BCl_2 groups from a variety of sources. It has been clearly demonstrated by ^{11}B and ^{19}F NMR spectra, that none of the six peaks is caused by any residual B–F containing species. The way the peaks are inter-related is shown in Fig. 2 from the ^{11}B–^{11}B COSY spectrum couplings. The peak at −18.2 ppm is coupled to peaks at +103.7, +65.0 and +50.7 ppm while the peak at +0.8 ppm is coupled to the peaks at +50.7 and +48.7 ppm. The wide range of ^{11}B chemical shifts within a single molecule points to a variety of chemical environments. The peaks at +0.8 and at −18.2 ppm may be from boron atoms without direct chlorine substituents {cf. the central boron of $(Cl_2B)_3BCO$}. The peaks at +65.0, +50.7 and +48.7 ppm are likely due to boron atoms with one or two chlorine substituents. The peak at +103.7 ppm seems to suggest a boron atom of a BCl group in a more highly strained environment than the boron atoms in B_4Cl_4 which resonate at +85.5 ppm [2].

The NMR data alone by no means proves the structure or composition of the compound giving the six resonances in the ^{11}B NMR. However, our results do strongly suggest the existence of a type of polyboron chloride never previously described. Morrison's proposals on the way in which B_2Cl_4 molecules react together to form *closo*-B_nCl_n structures with elimination of BCl_3 [2] hint at the existence of open structured intermediates but he has not reported an intermediate of this type stable enough to be sublimed. The relatively high stability of the polyboron chloride observed in our work may be due to the way it is formed from $B_{10}F_{12}$, i.e. it may not be possible to form such a species by decomposition of B_2Cl_4. Further support for the idea that the polyboron chloride giving the six ^{11}B NMR resonances may be accessible only from the reaction of BCl_3 with polyboron fluorides comes from the following observation. The product was not detected among the *closo*-B_nCl_n compounds generated under very mild conditions from the products obtained made by condensing at −196 °C, BCl made from boron and BCl_3 at 2000 °C.

The solutions obtained either by direct extraction or by sublimation followed by dissolution of the sublimate, which give the peaks at positions shown in Fig. 2, are not stable. When held at room temperature, the colour intensity increases and the ^{11}B NMR spectrum changes in a complex but fairly reproducible way. All six of the peaks of Fig. 2, decrease in intensity and become broader, but there is massive growth of one sharp resonance. For samples dissolved in C_6D_6, this occurs at δ +58.5 ppm corresponding to *closo*-B_9Cl_9. For one sample decomposing just in CD_2Cl_2, the single peak, which grew was at 65.2 ppm corresponding to *closo*-B_8Cl_8 [2]. Morrison has reported that the formation of *closo*-B_nCl_n species from B_2Cl_4 is solvent sensitive with *closo*-B_8Cl_8 favoured over B_9Cl_9 in CCl_4 as solvent [2]. In the ^{11}B NMR spectra of samples undergoing decomposition, there was some increase in the intensity of the resonance due to BCl_3, but not enough to indicate that BCl_3 was eliminated to a major extent by the transformation. If the product of reaction of BCl_3 with polyboron fluorides was left for a few days at room temperature under vacuum in the absence of a solvent and was then pumped on to remove very volatile products, the resulting intensely coloured product showed from its ^{11}B NMR and mass spectrum the presence of a mixture of the known *closo*-boranes from B_8Cl_8 to $B_{12}Cl_{12}$, with B_9Cl_9 as by far the major product.

The ^{11}B NMR spectra of the samples after treatment with BCl_3 always contain other small peaks than the six noted in Fig. 2, including a very sharp peak at +47.7 ppm due to BCl_3 which occurs in all the samples and is used as internal reference. However, the intensity ratios and chemical shifts vary appreciably from sample to sample unlike the six peaks discussed above. Their presence simply reinforces the idea that the reaction of

BCl_3 with the polyboron fluorides is an exceedingly complex process, generating a wide range of boron containing products.

The fact that the product which showed in its ^{11}B NMR spectrum the dominant six peaks of Fig. 2 could be obtained by reaction of excess BCl_3 with either B_8F_{12} or $B_{10}F_{12}$ at 0 °C can be explained by the following observation. When B_8F_{12} was treated with BCl_3 at -60 °C for a few minutes, mass spectrometry on the product showed that the B_8F_{12} had been largely converted to $B_{10}F_{12}$ and BF_3 with no evidence for chlorine-for-fluorine exchange in the polyboron fluorides. Thus, it can be assumed that conversion of B_8F_{12} to $B_{10}F_{12}$ was a rapid first step in the reaction with BCl_3 at 0 °C.

Investigations into the reaction of BCl_3 with polyboron fluorides are on-going. The primary objective will be to try to get a crystal structure of the key intermediate giving the six ^{11}B NMR resonances discussed. It may not be possible to crystallise this compound from solution because of its instability and low temperature laser techniques on the solid may also promote the transformation to a stable *closo*-B_nCl_n structure, making this a difficult problem.

Related experiments on the reaction of BBr_3 with higher boron fluorides have also been carried out. The end result is a series of known *closo*-B_nBr_n compounds but the intermediates are at least as complicated as those from the BCl_3 reaction.

4. Conclusions

The research has provided clear results relating to the synthesis of $(Cl_2B)_3BCO$ and the stepwise conversion of $(F_2B)_3BCO$ to $(Cl_2B)_3BCO$ by reaction with BCl_3. It has also provided some evidence for the existence of a new type of open-structured polyboron chloride, which can readily isomerise to the much more stable *closo*-B_nCl_n compounds. Full characterisation of this compound will be experimentally challenging. It has been shown that the formation of B_4Cl_4 from BCl is sensitive to the way the BCl is synthesised and this suggests that there is a need for theoretical work on the decomposition of B_2Cl_4 and on the mechanism by which B_4Cl_4 forms from BCl.

Acknowledgements

We thank Dr. Colin Western for helpful discussions about the electronic state of BCl and we are grateful to the Engineering and Physical Sciences Research Council for their support of this research and for a studentship to Jennifer A.J. Pardoe.

References

[1] G. Urry, T. Wartik, H.I. Schlesinger, J. Am. Chem. Soc. 74 (1952) 5809.
[2] J.A. Morrison, Chem. Rev. 91 (1991) 35.
[3] W. Hönle, Y. Grin, A. Burkhardt, U. Wedig, M. Schultheiss, H.G. von Schnering, R. Kellner, H. Binder, J. Solid State Chem. 133 (1997) 59.
[4] P.L. Timms, in: A.L. Rheingold (Ed.), Homoatomic Rings, Chains and Macromolecules of Main-Group Elements, Elsevier, Amsterdam, 1977, p. 151.
[5] D.F. Shriver, The Manipulation of Air-sensitive Compounds, McGraw-Hill, New York, 1969, p. 91.
[6] P.L. Timms, J. Chem. Soc., Dalton Trans. (1972) 830.
[7] P.L. Timms, J. Am. Chem. Soc. 89 (1967) 1629.
[8] K.K. Baeck, Y. Joo, Chem. Phys. Lett. 337 (2001) 190.
[9] K.K. Irikura, R.D. Johnson, J.W. Hudgens, J. Phys. Chem. A 104 (2000) 3800.
[10] G.A. Hebner, M.G. Blain, T.W. Hamilton, J. Vac. Sci. Technol. A 17 (1999) 3218.
[11] A.G. Briggs, A.G. Massey, M.S. Reason, P.J. Portal, Polyhedron 3 (1984) 369.
[12] P.L. Timms, in: M. Moskovits, G.A. Ozin (Eds.), Cryochemistry, Wiley, New York, 1976, p. 108.
[13] P.S. Maddren, Ph.D. Thesis, University of Bristol 1975.
[14] J.C. Jeffrey, N.C. Norman, J.A.J. Pardoe, P.L. Timms, Chem. Commun. (2000) 2367.
[15] T. Davan, J.A. Morrison, Inorg. Chem. 25 (1986) 2366.
[16] T. Davan, J.A. Morrison, Inorg. Chem. 18 (1979) 3194.
[17] M.L. McKee, J. Phys. Chem. 95 (1991) 9273.
[18] R.W. Kirk, D.L. Smith, W. Airey, P.L. Timms, J. Chem. Soc., Dalton Trans. (1972) 1392.
[19] D.A. Saulys, J. Castillo, J.A. Morrison, Inorg. Chem. 28 (1989) 1619.
[20] J.A.J. Pardoe, N.C. Norman, P.L. Timms, S. Parsons, I. Mackie, C.R. Pulham, D.W.H. Rankin, in preparation.

PERGAMON

Polyhedron 21 (2002) 549–552

POLYHEDRON

www.elsevier.com/locate/poly

Synthesis and X-ray structure of a complex containing the trisimido borate trianion—the imido analogue of the orthoborate trianion

John C. Jeffery, Angela P. Leedham, Christopher A. Russell *

School of Chemistry, University of Bristol, Cantock's Close, Bristol, BS8 1TS, UK

Received 31 July 2001; accepted 27 November 2001

Abstract

Reaction of BCl_3 with 2-methoxyaniline (1:6 equiv.) in toluene, and subsequent metallation with ^{n}BuLi (3 equiv.) produces $\{[Li_4B(NR)_3{\cdot}THF]^+[B^nBu_4]^-{\cdot}toluene\}_2$ (R = 2-methoxyphenyl), which contains the first example of a trisimido borate trianion—the imido analogue of the orthoborate trianion, $[BO_3]^{3-}$. © 2002 Elsevier Science Ltd. All rights reserved.

Keywords: Boron; Lithium; Imido; Complexes; X-ray

1. Introduction

Recently much of our chemistry has been focussed towards the preparation of p-block element imido $\{RN^{2-}\}$ complexes. We have synthesised these anions by amination of a main group element halide followed by metallation of the amide protons with an alkyllithium reagent. The application of this approach to the group 15 elements has led to the preparation of imido analogues of the orthophosphate anion, $[PO_4]^{3-}$ [1], the phosphite anion $[HPO_3]^{2-}$ [2], and the arsenate anion, $[AsO_3]^{3-}$ [3]. Related studies into imido analogues of the group 14, heavier group 15, and 16 anions have been extensively examined by the groups of Chivers, Stalke and Wright [4–8]. These studies have partial multiple E⋯N bonding for the lighter (period 3 elements) but predominantly single bonds for the heavy p-block elements. However, no corresponding compounds of the group 13 elements have been reported to date, despite the extensive body of data concerning boron–nitrogen linkages. Recent studies by Chivers et al. into the reactions of alkyllithium reagents (RLi) with the trisaminoborane, $B\{N(H)^tBu\}_3$ (3:1 equiv.), have shown the alkyllithium compounds acting as a base to remove two amide protons and as a nucleophile to substitute the third amide group to produce dilithio boraamidinate complexes $[Li_2\{RB(N^tBu\}_2\}]_x$ (R = ^{n}Bu, $x = 2$; R = Me, $x = 3$) [9]. We reasoned that use of more elaborate amines bearing side-arm donor substituents may stabilise the cations and lead to trisimido borate ions. Herein we report the synthesis and crystal structure of a complex which contains the first example of the trisimido borate trianion $[B(NR)_3]^{3-}$, which is an imido analogue of the $[BO_3]^{3-}$ anion.

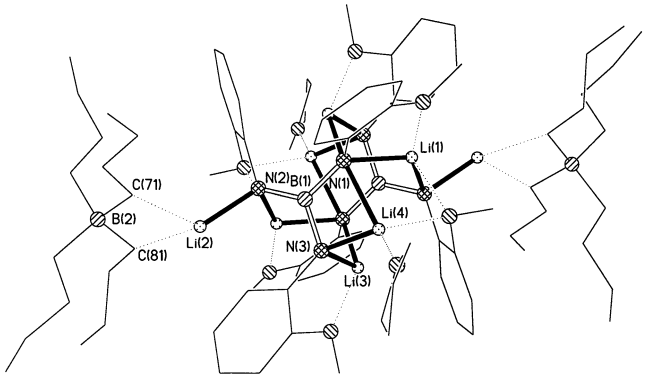


Fig. 1. Structure of $\{[Li_4B(NR)_3{\cdot}THF]^+[B^nBu_4]^-{\cdot}toluene\}_2$ (R = 2-methoxyphenyl, **1**) with the toluene molecules and all hydrogen atoms omitted for clarity. The suffix 'A' to an atom label indicates a symmetry equivalent atom.

* Corresponding author. Tel.: +44-117-928-7599; fax: +44-117-929-0509.

E-mail address: chris.russell@bristol.ac.uk (C.A. Russell).

0277-5387/02/$ - see front matter © 2002 Elsevier Science Ltd. All rights reserved.
PII: S0277-5387(01)01023-3

Table 1
Selected bond lengths (Å) and angles (°) for complex **1** (e.s.d.s in parentheses)

Bond lengths			
B(1)–N(1)	1.495(4)	Li(2)–N(2)	1.977(6)
B(1)–N(2)	1.440(4)	Li(3)–N(3)	2.038(6)
B(1)–N(3)	1.492(2)	Li(3)–N(1A)	2.056(6)
Li(1)–N(1)	2.032(6)	Li(4)–N(3)	1.962(6)
Li(1)–N(2A)	1.982(6)	Li(4)–N(1)	2.236(6)
Bond angles			
N(1)–B(1)–N(2)	123.6(3)	C(31)–N(3)–Li(3)	104.6(2)
N(2)–B(1)–N(3)	119.5(3)	B(1)–N(3)–Li(3)	108.4(2)
N(1)–B(1)–N(3)	115.7(3)	Li(4)–N(3)–Li(3)	100.21(13)
C(11)–N(1)–B(1)	120.7(3)	O(1)–Li(1)–N(2A)	153.15(13)
C(11)–N(1)–Li(1)	105.3(2)	O(1)–Li(1)–N(1)	84.02(12)
B(1)–N(1)–Li(1)	126.9(2)	N(2A)–Li(1)–N(1)	120.55(12)
C(11)–N(1)–Li(3A)	115.7(2)	O(1)–Li(1)–O(2A)	102.43(12)
Li(1)–N(1)–Li(4)	81.41(11)	N(2A)–Li(1)–O(2A)	84.27(11)
B(1)–N(1)–Li(3A)	99.7(2)	N(1)–Li(1)–O(2A)	101.31(12)
Li(1)–N(1)–Li(3A)	81.16(12)	N(2)–Li(2)–C(71)	125.24(13)
C(11)–N(1)–Li(4)	84.40(19)	N(2)–Li(2)–C(81)	129.24(15)
B(1)–N(1)–Li(4)	78.38(18)	C(71)–Li(2)–C(81)	75.98(14)
Li(3A)–N(1)–Li(4)	156.32(13)	O(3)–Li(3)–N(3)	86.08(12)
C(21)–N(2)–B(1)	122.0(3)	O(3)–Li(3)–N(1A)	127.53(13)
C(21)–N(2)–Li(2)	110.60(19)	N(3)–Li(3)–N(1A)	111.08(12)
B(1)–N(2)–Li(2)	115.9(2)	O(4)–Li(4)–N(3)	120.92(13)
C(21)–N(2)–Li(1A)	108.8(2)	O(4)–Li(4)–O(2A)	102.41(13)
B(1)–N(2)–Li(1A)	93.98(19)	N(3)–Li(4)–O(2A)	121.23(13)
Li(2)–N(2)–Li(1A)	101.71(13)	O(4)–Li(4)–N(1)	146.09(13)
C(31)–N(3)–B(1)	121.8(3)	N(3)–Li(4)–N(1)	72.42(11)
C(31)–N(3)–Li(4)	129.8(2)	O(2A)–Li(4)–N(1)	93.62(11)
B(1)–N(3)–Li(4)	89.35(19)		

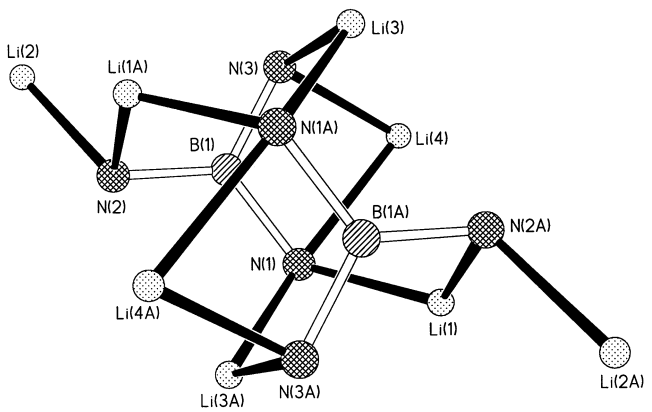


Fig. 2. Core of $[\{Li_4B(NR)_3{\cdot}THF\}_2]^{2+}$ (R = 2-methoxyphenyl) depicting just the B, N and Li centres.

2. Results and discussion

Reaction of BCl_3 with 6 equiv. of 2-methoxyaniline in toluene, followed by addition of 3 equiv. of ^{n}BuLi produces $\{[Li_4B(NR)_3{\cdot}THF]^+[B^nBu_4]^-{\cdot}toluene\}_2$ (R = 2-methoxyphenyl, **1**) in low but reproducible yield as moisture-sensitive yellow crystals. Complex **1** was characterised using ^{1}H and ^{11}B NMR spectroscopy, IR spectroscopy and elemental analyses. The lack of an N–H stretch in the IR spectrum showed that all these amido protons had been removed. The ^{11}B NMR spectrum revealed resonances at $\partial = 23.4$ (broad singlet) and -3.6 (sharp singlet), consistent with the presence of both three-coordinate and four-coordinate boron centres [10]. To confirm this assignment and to explore further features of this system we undertook a low-temperature single crystal X-ray diffraction study. This revealed that complex **1** crystallises as a dimer in the triclinic space group, $P\bar{1}$, with two $B^nBu_4^-$ anions loosely linked through Li···H and Li···C contacts to a cage that contains eight lithium cations and two trisimido borate trianions. In addition there are two molecules of toluene in the lattice for each dimeric $\{[Li_4B(NR)_3{\cdot}THF]^+[B^nBu_4]^-\}_2$ unit. The molecular structure of **1** is shown in Fig. 1 with key bond lengths and angles shown in Table 1.

The B^nBu_4 units are unremarkable, with the boron centres having distorted tetrahedral geometries {C–B–C angles range from 108.2(3)° to 110.6(3)°} and with slightly differing B–C bond distances {B–C(61) 1.652(5) Å, B–C(91) 1.642(5) Å, B–C(81) 1.676(5) Å, B–C(71) 1.679(6) Å}, presumably as a result of the contacts between two of the *n*-butyl groups and lithium centres of the central caged cation.

Within this caged cation, the core of which is illustrated in Fig. 2, two trigonal planar trisimido borate moieties are held together by four lithium centres {Li(1), Li(3), Li(1A) and Li(3A)}, with the remaining lithium centres binding on the periphery of the cage.

Of the four core lithium centres, Li(1) {and its symmetry equivalent Li(1A)} have distorted tetrahedral geometries, with contacts to a nitrogen centre from each trisimido borate moiety {Li(1)–N(1) 2.032(6), Li(1)–N(2A) 1.982(6) Å}, as well as two contacts to methoxy side arms of the 2-methoxyphenyl group moiety {Li(1)–O(1) 1.928(6), Li(1)–O(2A) 2.071(6) Å}. The remaining core lithium centres {Li(3) and the symmetry equivalent Li(3A)} have distorted pyramidal geometries, binding to an imido nitrogen centre from each trisimido borate moiety {Li(3)–N(3) 2.038(6), Li(3)–N(1A) 2.056(6) Å} with an additional contact to a methoxy side arm {Li(3)–O(3) 1.924(6) Å} from one of these imido units.

The remaining four lithium centres do not appear to play any direct role in binding the two halves of the dimer together in the solid state; Li(4) {and its symmetry equivalent Li(4A)} contact two nitrogen centres from the same trisimido borate moiety with a short contact to N(3) at 1.962(6) Å and a relatively long contact of 2.236(6) Å to N(1), in addition to being solvated by a methoxy sidearm of a methoxyphenyl group {Li(4)–O(2A) 2.114(6) Å} and a THF molecule {Li(4)–O(4) 1.887(6) Å}. By contrast, Li(2) {and its symmetry equivalent Li(2A)} contact only a single imido nitrogen centre {Li(2)–N(2) 1.977(6) Å} and has

additional Li···C and Li···H contacts to the butyl group of the $[B^nBu_4]^-$ anion {Li(2)···C(71) 2.229(6), Li(2)···C(81) 2.254(7) Å; Li(2)···H(71A) 1.910(6) Å, Li(2)···H(71B) 1.986(6) Å, Li(2)···H(81A) 1.974(6) Å, Li(2)···H(81B) 1.976(6) Å}.

Two of the nitrogen centres {N(2) and N(3)} possess distorted tetrahedral geometries, being bound to the boron centre, a carbon atom of a methoxyphenyl group and two lithium centres. The third nitrogen centre, N(1), is similarly bound to the boron centre and a carbon atom of a methoxyphenyl group but is bound to three lithium centres to give a distorted five coordinate geometry.

The pseudo trigonal planar boron atom coordinates three imido nitrogen centres (sum of NBN angles 358.8°). The B–N distances of 1.440(4), 1.448(4) and 1.492(4) Å are shorter than the commonly accepted literature values for single bonds (ca. 1.58 Å) but larger than for formal double bonds (ca. 1.40 Å) [11]. This is indicative of partial multiple bond character that would be expected as a consequence of lone pairs on the imido groups overlapping the vacant p orbital at the sp^2 boron centre. The fact that one B–N distance {B–N(1)} is considerably larger than the other two can be attributed to fact that larger coordination numbers lead to longer bonds, as has been observed in related studies of trisiimidosilanes [12,13].

Unlike the related $[E(NR)_3]^{2-}$ (E = S, Se, Te) [7,14,15], where the pyramidal trisimido chalcogenide dianions allow the formation of cages of molecular C_{2h} symmetry, which readily accommodate strong Li–N contacts in arrangements similar to those that are well known in lithium amide chemistry [16,17], the imposition of trigonal planar geometry at the boron centres in the central core of **1** does not facilitate comparable Li···N motifs. Perhaps this inability to readily accommodate the bonding requirements of the lithium centres accounts in part for the difficulty in synthesising the direct imido analogue of the orthoborate trianion.

The reaction to form **1** is evidently not as straightforward as we initially anticipated. We would suggest that the initial amination of the BCl_3 with 2-methoxyaniline is probably incomplete, leaving free BCl_3 present at the metallation step. Addition of ^{n}BuLi results in the production of LiB^nBu_4, that combines with the lithiation product of the proposed $B\{N(H)R\}_3$ intermediate to give a mixed anionic species with empirical formula $Li_4B(NR)_3B^nBu_4$ (i.e. the monomer of the observed product).

3. Conclusions

The synthesis of complex **1** illustrates that the transmetallation/metallation methodology that we have previously employed to synthesise group 15 imido anions may be employed to make corresponding group 13 imido anions. Taken with the recent results of Chivers et al. [9], it is probable that the precise nature of the product is heavily dependent on the nature of the amine used.

4. Experimental

All reagents and products were handled on a vacuum line (in an efficient fume cupboard) under dry/oxygen-free argon or dinitrogen using standard inert atmosphere techniques [18]. Toluene, THF, and hexane were dried over alumina, while a supported copper catalyst was used to remove trace oxygen from hydrocarbons prior to the reactions [19]. The products were isolated and characterised with the aid of an argon-filled Saffron Beta glove box. ^{1}H and ^{11}B NMR spectra were recorded on a JEOL Lambda 300MHz Multinuclear FT spectrometer in dry deuterated pyridine (using the solvent resonances as the internal reference standard for ^{1}H spectra and an external standard of $F_3B{\cdot}OEt_2$ for ^{11}B spectra). Infrared spectra were recorded as Nujol mulls using NaCl plates and were run on a Perkin–Elmer Spectrum One FTIR spectrophotometer. Elemental analyses were performed by first sealing the samples under argon in air-tight aluminium boats (1–2 mg) and C, H and N content was analysed using a Perkin–Elmer 240 Elemental Analyser.

4.1. Synthesis of *1*

Boron trichloride (1 ml, 1 M solution in heptane, 1 mmol) was reacted with 6 equiv. of 2-methoxyaniline (0.68 ml, 6 mmol) in toluene (20 ml). This solution was stirred for 6 h at room temperature before being filtered (porosity 3 sinter with Celite) and metallated with 3 equiv. of ^{n}BuLi (1.88 ml, 1.6 M solution in hexanes, 3 mmol). This left a yellow solution containing a small amount of residual solid that was redissolved with approximately 1 ml THF. The resulting yellow solution was left for 72 h at 5 °C, which yielded pale yellow blocks of **1**.

Yield: 0.11 g (14% based on BCl_3). IR (cm^{-1}): no distinguishing absorptions. ^{1}H NMR (+25 °C, 300 MHz, [D$_5$]-pyridine): $\delta = 7.3$–7.1 (collection of overlapping m, 17H, –NC$_6H_4$OMe and C$_6H_5$Me), 3.65 (m, 4H, THF), 3.55 (s, 9H, –OCH_3), 2.20 (s, 3H, C$_6$H$_5$CH_3), 1.98 (broad collection of m, 8H, –CH_2CH$_2$CH$_2$CH$_3$), 1.77 (broad collection of m, 8H, –CH$_2$CH$_2$CH_2CH$_3$), 1.59 (m, 4H, THF), 1.13 (t, 12H, –CH$_2$CH$_2$CH$_2$CH_3), 0.85 (broad collection of m, 8H, –CH$_2$CH_2CH$_2$CH$_3$). ^{11}B NMR (+25 °C, 96.23 MHz, [D$_5$]-pyridine): $\delta =$ 23.4 (broad singlet, $[B(NR)_3]^{3-}$), −3.6 (singlet, $[B^nBu_4]^-$). *Anal.* Found: C, 71.01; H, 8.91; N, 5.40. Calc. for $C_{74}H_{114}B_4Li_8N_6O_6{\cdot}(C_4H_8O)_2{\cdot}(C_7H_8)_2$ requires C, 71.55; H, 9.07; N, 5.22%.

4.2. X-ray crystallography

Data were collected on a Siemens SMART CCD area-detector diffractometer with Mo Kα radiation ($\lambda = 0.71073$ Å) [20] using a crystal mounted on a glass fibre in a rapidly cooled perfluoropolyether [21]. Details of the data collection, refinement and crystal data are listed below. The structure was solved by direct methods and refined by least squares on F^2 values for all reflections [22]. Absorption corrections were applied, based on multiple and symmetry equivalent measurements [23]. All hydrogen atoms were constrained to ideal geometries and refined with fixed isotropic displacement parameters.

$C_{96}H_{146}B_4Li_8N_6O_8$, $M = 1610.94$, triclinic, space group $P\bar{1}$, $a = 13.6351(19)$, $b = 13.9809(19)$, $c = 16.450(2)$ Å, $\alpha = 88.828(3)°$, $\beta = 65.990(2)°$, $\gamma = 61.734(2)°$, $V = 2464.4(6)$ Å^3, $Z = 1$, $T = 173$ K, crystal size $0.2 \times 0.2 \times 0.1$ mm. 25 719 reflections were collected of which 11 166 were independent (R_{int} 0.0767) to give $R_1[I > 2\sigma(I)] = 0.0767$, $wR_2[I > 2\sigma(I)] = 0.1969$ and R_1 (all data) $= 0.2020$, wR_2 (all data) $= 0.2513$.

5. Supplementary data

Crystallographic data (excluding structure factors) for the structures in this paper have been deposited with the Cambridge Crystallographic Data Centre, CCDC No. 167979. Copies of these data may be obtained free of charge from The Director, CCDC, 12 Union Road, Cambridge, CB2 1EZ, UK (fax: +44-1223-336033; e-mail: deposit@ccdc.cam.ac.uk or www: http://www.ccdc.cam.ac.uk).

Acknowledgements

We gratefully acknowledge The Royal Society (University Research Fellowship for C.A.R.), The University of Bristol (Scholarship for A.P.L.) for financial support. One of the authors (J.C.J.) thanks the EPSRC for supporting diffractometer facilities. We would also like to thank Mr Jon Moore for running ^{11}B NMR experiments and Dr Nick Norman for helpful discussions during preparation of this manuscript.

References

[1] P.R. Raithby, C.A. Russell, A. Steiner, D.S. Wright, Angew. Chem. 109 (1997) 670; Angew. Chem., Int. Ed. Engl. 36 (1997) 649.
[2] L.T. Burke, E. Hevia-Freire, R. Holland, J.C. Jeffery, C.A. Russell, A.P. Leedham, A. Steiner, A. Zagorski, Chem. Commun. (2000) 1769.
[3] L.T. Burke, J.C. Jeffery, A.P. Leedham, C.A. Russell, J. Chem. Soc., Dalton Trans. (2001) 423.
[4] M.A. Beswick, D.S. Wright, Coord. Chem. Rev. 176 (1998) 373.
[5] T. Chivers, M. Parvez, G. Schatte, G.P.A. Yap, Inorg. Chem. 38 (1999) 1380.
[6] J. Brask, T. Chivers, B. McGarvey, G. Schatte, R. Sung, R. Boere, Inorg. Chem. 37 (1998) 4633.
[7] R. Fleischer, D. Stalke, Coord. Chem. Rev. 176 (1998) 431.
[8] J.K. Brask, T. Chivers, M. Parvez, Inorg. Chem. 39 (2000) 2508.
[9] J.K. Brask, T. Chivers, G. Schatte, Chem. Commun. (2000) 1805.
[10] H. Nöth, B. Wrackmeyer, in: Nuclear Magnetic Resonance Studies of Boron Compounds, Berlin, 1978, p. 74.
[11] N.N. Greenwood, A. Earnshaw, Chemistry of the Elements, Oxford, 1997, p. 210.
[12] D. Brauer, H. Bürger, G.R. Lienwald, J. Wilke, J. Organomet. Chem. 287 (1985) 305.
[13] D. Brauer, H. Bürger, G.R. Lienwald, J. Organomet. Chem. 308 (1986) 119.
[14] T. Chivers, X. Gao, M. Parvez, Angew. Chem. 107 (1995) 2756. Angew. Chem., Int. Ed. Engl. 34 (1995) 2459.
[15] T. Chivers, M. Parvez, G. Schatte, Inorg. Chem. 35 (1995) 4094.
[16] R.E. Mulvey, Chem. Soc. Rev. 20 (1991) 167.
[17] K. Gregory, R. Snaith, P.v.R. Schleyer, Adv. Inorg. Chem. 37 (1991) 47.
[18] D.F. Shriver, M.A. Drezdzon, The Manipulation of Air-Sensitive Compounds, Wiley, 1986.
[19] A.B. Pangborn, M.A. Giardello, R.H. Grubbs, R.K. Rosen, F.J. Timmers, Organometallics 15 (1996) 1518.
[20] SMART Software, Siemens Analytical X-ray Instruments Inc., Madison, WI, 1994.
[21] T. Kottke, D. Stalke, J. Appl. Crystallogr. 26 (1993) 615.
[22] SHELXTL, Siemens Analytical X-ray Instruments Inc., Madison, WI, 1995.
[23] SADABS absorption correction software, Siemens Analytical X-ray Instruments Inc., Madison, WI, 1994.

PERGAMON

Polyhedron 21 (2002) 553–562

POLYHEDRON

www.elsevier.com/locate/poly

Thallium(I) complexes with modified poly(pyrazolyl)borate ligands—metal-ligand coordination and crystal packing

Emma Craven [1], Esra Mutlu, Daniel Lundberg [2], Savaş Temizdemir, Sebastian Dechert, Horst Brombacher, Christoph Janiak *

Institut für Anorganische und Analytische Chemie, Universität Freiburg, Albertstrasse 21, D-79104 Freiburg, Germany

Received 2 August 2001; accepted 27 November 2001

Abstract

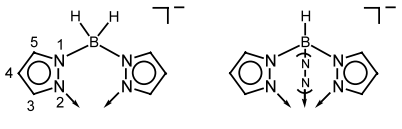
The structures of the thallium(I) complexes with hydrotris(pyrazolyl)borate (TpTl, **2**-Tl), and the modified Bp and Tp ligands dihydrobis(1,2,4-triazolyl)borate (**3**-Tl), hydrotris(imidazolyl)borate (**6**-Tl), dihydrobis(indazolyl)borate (**7**-Tl), and hydrotris(indazolyl)borate (**8**-Tl) are reported and discussed in terms of their (molecular) metal–ligand arrangement and their crystal packing. Compounds **2**-Tl and **7**-Tl feature molecular TpTl and Bp′Tl units with pronounced Tl···π_{azolyl} interactions between neighboring molecules. In **8**-Tl the molecular units are arranged in pairs through indazolyl π···π stacking. Complexes **3**-Tl and **6**-Tl form extended 3D and 1D structures, respectively, through the bridging action of the poly(azolyl)borate ligand between three symmetry related thallium centers. Compounds **2**-Tl, **3**-Tl, and **8**-Tl crystallize in the chiral space groups $P2_1$, $P2_12_12_1$, and $C2$, respectively.
© 2002 Elsevier Science Ltd. All rights reserved.

Keywords: Thallium(I) complexes; Scorpionate ligands; Crystal packing; π-Stacking; Cation–π interaction

1. Introduction

Thallium(I) is formally a low-valence p-block metal with a closed sub-shell (s^2). Yet its structural chemistry can feature unusual patterns of aggregation in the solid state [1–8] through what could be attractive metal–metal interactions [9–13]

Poly(pyrazolyl)borate ligands (scorpionates) are versatile ligands in physio-chemical, bio-inorganic and structurally oriented coordination chemistry [14–20]. The parent compounds are dihydrobis(pyrazolyl)borate (Bp, **1**) and hydrotris(pyrazolyl)borate (Tp, **2**).



Bp, **1** Tp, **2**

-(N-N)- denotes the third pyrazolyl ring which is oriented to the rear

Thallium(I) derivatives of poly(pyrazolyl)borato ligands are important (i) as a means of isolation and characterization of new scorpionate ligands and (ii) as a mild (less reducing) and often more stable ligand transfer reagent in place of alkali metal salts of scorpionate ligands [21].

In recent years we, and others, have been interested in metal complexes with modified poly(pyrazolyl)borate ligands and in their supramolecular architecture. These modified scorpionate ligands are bis- and tris(1,2,4-triazolyl)borate (**3** and **4**) [22–27], bis(tetrazolyl)borate (**5**) [28–30], bis- and tris(imidazolyl)borate (**6**) [31–33] or bis-and tris(indazolyl)borate (**7** and **8**) [34,35]. Examples of modified poly(pyrazolyl)borate ligands studied by others are fluorinated tris(pyrazolyl)borate [36] and tris(mercaptoimidazolyl)borate [37–40].

We report here the structures of the thallium(I) complexes with **2**, **3**, **6**, **7**, and **8**, with special consideration to their supramolecular assembly. Thallium(I) complexes are also used by others to investigate supramolecular metal–ligand structures [41]. The structural investigations of **2**, **6**, and **8** have already been communicated as short notes [42,43].

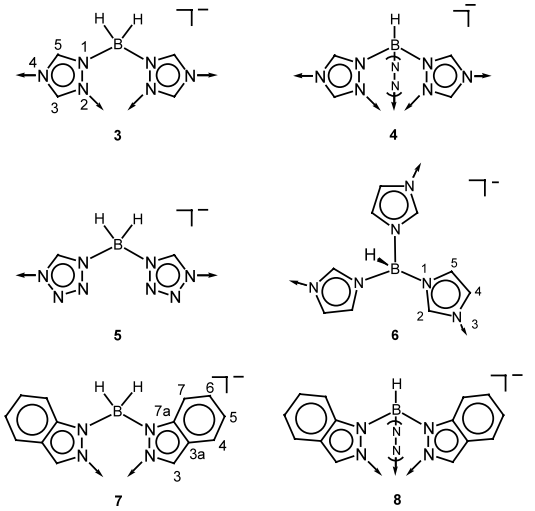
* Corresponding author. Tel.: +49-761-203-6127; fax: +49-761-203-6147.

E-mail address: janiak@uni-freiburg.de (C. Janiak).

[1] Exchange student from the University of Western Australia, Perth, Australia.

[2] Eramus fellow from Uppsala University, Uppsala, Sweden.

0277-5387/02/$ - see front matter © 2002 Elsevier Science Ltd. All rights reserved.
PII: S0277-5387(01)01026-9



2. Experimental

NMR spectra were collected on a Bruker ARX200 (200.1 MHz for ^{1}H, 50.3 MHz for ^{13}C) or ARX400 (**8**-Tl) and calibrated against the solvent signal ($CDCl_3$ ^{1}H NMR 7.26 ppm, ^{13}C NMR 77.0 ppm; d_6-DMSO ^{1}H NMR 2.53 ppm, ^{13}C NMR 39.5 ppm). Mass spectra were obtained on a Varian MAT 311A/AMD in solid-probe at an ionization energy of 70 eV. CHN analysis: Perkin–Elmer 2400 Series II CHNS/O-Analyzer and Analyzer E240 C. IR: Nicolet–Magna Spectrometer 750 or Bruker IFS 25 spectrometer, using KBr disks (only major peaks are listed).

The potassium salts of **2** [44], **3** [24], **6** [31], and **8** [34,43] were obtained as described in the literature. The synthesis of the potassium salt of **7** is given below. CH_3OH for the preparation of **7**-Tl, was dried with CaO by heating under reflux for 4 h under an inert gas, followed by distillation.

2.1. Syntheses

2.1.1. Hydrotris(pyrazolyl)boratothallium(I) (*2*-Tl)

A solution of $TlNO_3$ (530 mg, 1.99 mmol) in a mixture of 5 ml of methanol and 5 ml of water was overlayered with a solution of potassium hydrotris(pyrazolyl)borate (500 mg, 1.98 mmol) in 10 ml of methanol. Slow diffusion of the solutions together with evaporation of the solvent to half the initial volume led to crystal growth. The crystals were collected after 1 week (yield 450 mg, 54%). The melting point of 155 °C and the ^{1}H NMR and mass spectrometric characterizations agree with literature values [45]. ^{13}C NMR ($CDCl_3$): δ (ppm) = 104.11, 135.60, 139.14. IR: $\tilde{\nu}$ (cm^{-1}) = 3112w (νCH), 2443m, 2400w, 2369w (νBH), 1501m, 1422m, 1394m,1382m, 1295s, 1210s, 1185m, 1114s, 1078m, 1048s, 1038s, 970s, 774m, 754s, 737m, 722s, 665 m, 627m, 619m.

$C_9H_{10}BN_6Tl$ (417.41): Calc. C, 25.90; H, 2.41; N, 20.13; Tl, 48.96%; Found: C, 26.09; H, 1.93; N, 20.68; Tl, 48.52%. The absence of K in the crystals was confirmed by AAS.

2.1.2. Dihydrobis(1,2,4-triazolyl)boratothallium(I) (*3*-Tl)

A solution of potassium dihydrobis(triazolyl)borate (0.19 g, 1.00 mmol) in methanol (5 ml) was added to a solution of 266 mg (1.00 mmol) of $TlNO_3$ in a 1:1 mixture of H_2O–MeOH (6 ml). The cloudy solution was filtered and left to stand, partially open to air, for 3 weeks. Filtering the clear solution, now half volume, yielded large, clear crystals within 2 days, in a reproducible process (crystal yield 41 mg, 12%). IR: $\tilde{\nu}$ (cm^{-1}) = 3114w (νCH), 2405s, 2270w (νBH), 1498s (νCH), 1306w, 1264m, 1158vs, 1129s, 1016w, 966m, 874w, 669s. $C_4H_6BN_6Tl$ (353.33): Calc. C, 13.60; H, 1.71; N 23.79. Found: C, 13.60; H, 1.85; N, 23.51%.

2.1.3. Hydrotris(imidazolyl)boratothallium(I) (*6*-Tl)

A solution of $TlNO_3$ (530 mg, 1.99 mmol) in methanol (5 ml) and water (5 ml) was overlayered with a solution of potassium hydrotris(imidazolyl)borate (500 mg, 1.98 mmol) in methanol (10 ml). Slow diffusion of the solutions together with evaporation of the solvent to half of the initial volume led to crystal growth. The colorless needle-shaped crystals were collected after 1 week (yield 520 mg, 63%). Melting point (m.p.) 268–270 °C. ^{1}H NMR (d_6-DMSO): δ (ppm) = 6.80 (s, 2H, H-4 and H-5), 7.24 (s, 1H, H-2). ^{13}C NMR (d_6-DMSO): δ (ppm) = 120.60 (C-4), 127.98 (C-5), 139.65 (C-2). IR: $\tilde{\nu}$ (cm^{-1}) = 2430m, 2412m (νBH), 1477s, 1207s, 1119s, 1073s, 924s. $C_9H_{10}BN_6Tl$ (417.41): Calc. C, 25.90; H, 2.41; N, 20.13. Found: C, 25.96; H, 2.40; N, 20.07%.

2.1.4. Dihydrobis(indazolyl)boratopotassium(I) (*7*-K)

KBH_4 (2.41 g, 44.6 mmol) was added to indazole (20.75 g, 178.6 mmol) and the mixture heated for 2 h at 170 °C under nitrogen. The mixture melted, with evolution of hydrogen, and was cooled down after the theoretical amount (2.2 l by wet-test-meter) of hydrogen had evolved. The excess indazole was sublimed out (120 °C, 5×10^{-2} mbar). To ensure complete sublimation, the unsublimed residue was crushed and sublimation continued. At this stage, the product may be sufficiently pure in a yield usually above 95%. If the NMR of the unsublimed residue still indicates impurities of indazole, the impure product can be dissolved in a minimum amount of boiling toluene, filtered and cooled. Precipitation/crystallization of the product may have to be induced by overlayering with petroleum

ether (30/50). Recrystallization from toluene gives relatively pure products but results in a considerably decreased yield (30–45%). The potassium salt of **7** can also be purified by conversion to the thallium salt (see below). ^{1}H NMR (d_6-DMSO): δ (ppm) = 6.85 (dtd, 4H, H-5 and H-6), 7.15 (dt, 2H, H-4), 7.58 (dt, 2H, H-7), 7.85 (d, 2H, H-3) (see drawing **7** for the NMR labeling). IR: $\tilde{\nu}$ (cm^{-1}) = 2359m (νBH), 1615s, 1495s, 1476m, 1459s, 1258s, 1201s, 978m, 944m, 912s, 864m, 697m, 658m, 647m, 595m, 474m, 427m. Calc. for $C_{14}H_{12}BN_4K$ (286.19) C, 58.76; H, 4.23; N, 19.58. Found: C, 56.14; H, 4.25; N, 18.61%. The potassium salt of **7** is water sensitive. Dissolution in methanol and water yields indazole.

2.1.5. Dihydrobis(indazolyl)boratothallium(I) (7-Tl)

$TlNO_3$ (2.55 g, 9.57 mmol) was dissolved in dried methanol (200 ml) with heating and ultrasonication. The solution was added to **7**-K (2.74 g, 9.57 mmol) in methanol (50 ml). The product forms almost instantly upon mixing. The immediate product yield (2.51 g, 58%) can be enhanced by cooling of or slow solvent evaporation from the mother liquor. Crystals were grown by slow solvent evaporation of either the mother liquor or a methanol solution of **7**-Tl. ^{1}H NMR ($CDCl_3$): δ (ppm) = 7.06 (td, 2H, H-6), 7.38 (td, 2H, H-5), 7.63 (dt, 2H, H-4), 8.04 (d, 2H, H-3), 8.10 (dd, 2H, H-7) (see drawing **7** for the NMR labeling). IR: $\tilde{\nu}$ (cm^{-1}) = 2360m (νBH), 1614s, 1497s, 1459s, 1399m, 1337m, 1259m, 1211m, 1185m, 1132s, 1111s, 1008m, 986m, 912s, 837m, 820m, 757s, 746s, 691m, 656m, 638m, 596m, 433m. Calc. for $C_{14}H_{12}BN_4Tl$ (451.47) C, 37.25; H, 2.68; N, 12.41. Found: C, 36.63; H, 2.55; N, 13.06%.

2.1.6. Hydrotris(indazolyl)boratothallium(I) (8-Tl)

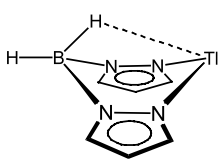
$TlNO_3$ (0.53 g, 2.0 mmol) in CH_3OH (10 ml) reacts with the potassium salt of **8** (0.80 g, 2.0 mmol), forming a white precipitate. This precipitate was filtered off and crystallized from dioxane through overlayering with petroleum ether (30/50). The product formed as colorless crystals (yield 0.67 mg, 59%). ^{1}H NMR (d_6-DMSO): δ = 7.00 (ddd, 3H, H-5, $J_{5,4}$ = 8.07 Hz, $J_{5,6}$ = 6.77 Hz, $J_{5,7}$ = 0.92 Hz), 7.26 (ddd, 3H, H-6, $J_{6,7}$ = 8.58 Hz, $J_{6,5}$ = 6.77 Hz, $J_{6,4}$ = 1.10 Hz), 7.67 ('dt', 3H, H-4, $J_{4,5}$ = 8.07 Hz, $J_{4,6}$ = 1.10 Hz, $J_{4,7}$ = 0.98 Hz), 7.89 ('dq', 3H, H-7, $J_{7,6}$ = 8.58 Hz, $J_{7,4}$ = 0.98 Hz, $J_{7,3}$ = 0.93 Hz, $J_{7,5}$ = 0.92 Hz), 8.15 (d, 3H, H-3, $J_{3,7}$ = 0.93 Hz) (see drawing **7** for the NMR labeling). MS (230 °C): 568 (26%, $[M]^+$). Calc. for $C_{21}H_{16}BN_6Tl$ (567.59) C, 44.44; H, 2.84; N, 14.81; Tl, 36.00. Found: C, 43.67; H, 2.56; N, 14.51; Tl, 35.70%.

2.2. X-ray structure determinations

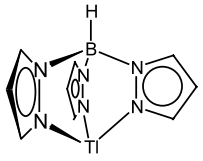
Data were collected using the ω-scan method with Mo Kα radiation (λ = 0.71073) and a graphite monochromator on a Syntex $P2_1$ four-circle diffractometer (**2**-Tl) or a Bruker AXS CCD diffractometer. All crystals were colorless. Structure solution was done using direct methods (SHELXS-97 [46]); refinement was done by full-matrix least squares on F^2, again using SHELXL-97 [46]. All non-hydrogen atoms were found and refined anisotropically. The hydrogen atoms on boron were found and refined in **3**-Tl and **6**-Tl, and calculated for **2**-Tl, **8**-Tl (AFIX 13) and **7**-Tl (AFIX 23) with U(H) = 0.08. The hydrogen atoms on carbons were placed at calculated positions with bond lengths free to refine (HFIX 44 for **6**-Tl) or with d_{C-H} = 0.94 Å, using appropriate riding models (HFIX 43) and isotropic temperature factors of U(H) = 0.08 (**2**-Tl, **7**-Tl, **8**-Tl) or U(H) = 1.2 Ueq(C, N) (**3**-Tl) or U(H) = 1.5 Ueq(C, N) (**6**-Tl). The growth of good quality crystals for **2**-Tl was difficult and hence its X-ray structure is not without problems (see Table 1 and Fig. 1). Crystal data are given in Table 1. Graphics were obtained with ORTEP3 for Windows [47] with displacement ellipsoids shown at the 50% probability level and H atoms shown as spheres of arbitrary radii.

3. Results and discussion

The basic metal-ligand motif of most BpTl [4] and TpTl complexes [21] is as depicted in compound **9** and **10**, respectively. The bonding of the bidentate Bp is supplemented by a weak agostic B–H···Tl interaction [48–50].



BpTl, **9**



TpTl, **10**

Otherwise there is little variation in the bis- and tris-chelating mode of the two scorpionate ligands towards thallium. A few structures show additional Tl···Tl contacts below 4.0 Å, namely BpTl [4], $Bp^{bipy}Tl$ (bipy = 6-2,2′-bipyridine) [51], $Tp^{cyclopropyl}Tl$ [52], and $Tp^{p\text{-tolyl}}Tl$ [53]. The abbreviation Bp^{XR} and Tp^{XR} follows the suggested nomenclature by Trofimenko [14,15] to indicate a substituent R in the X position on the pyrazolyl ring.

Exceptions to the common C_3-trigonal motif for TpTl complexes only occur when the hydrogen atom on boron is replaced by a more sterically demanding group. Known compounds are $PhTp^{tBu}Tl$ [54], FcTpTl (Fc = ferrocenyl) [55], and $MeTp^{Me2}Tl$ [56]. Probably due to steric effects, one of the pyrazolyl rings rotates

Table 1
Crystal data for the thallium complexes of **2**, **3**, **6**, **7**, and **8**

Compound	**2**-Tl [a]	**3**-Tl	**6**-Tl	**7**-Tl	**8**-Tl
Formula	$C_9H_{10}BN_6Tl$	$C_4H_6BN_6Tl$	$C_9H_{10}BN_6Tl$	$C_{14}H_{12}BN_4Tl$	$C_{21}H_{16}BN_6Tl$
M (g mol^{-1})	417.41	353.34	417.41	451.46	567.58
Crystal size (mm)	$0.2\times0.2\times0.15$	$0.45\times0.29\times0.23$	$0.24\times0.05\times0.05$	$0.62\times0.25\times0.08$	$0.48\times0.21\times0.08$
T (K)	298(2)	207(2)	298(2)	173(2)	173(2)
2θ Range (°)	2.4–55.0	5.7–56.5	5.2–50.0	3.7–55.0	4.0–55.0
h; k; l Range	0, 10; 0, 12; −22, 22	−9, 9; −22, 23; −7, 8	−10, 10; −10, 8; −18, 15	−12, 17; −6, 7; −22, 22	−34, 26; −9, 9; −14, 14
Crystal system	monoclinic	orthorhombic	monoclinic	monoclinic	monoclinic
Space group	$P2_1$	$P2_12_12_1$	$P2_1/n$	$P2_1/n$	$C2$
a (Å)	7.928(6)	7.721(2)	8.706(2)	13.2472(6)	26.6043(4)
b (Å)	9.306(4)	17.793(4)	9.192(2)	5.8224(2)	7.1280(2)
c (Å)	17.16(2)	6.029(1)	15.261(4)	17.5104(8)	11.0435(4)
β (°)	92.06(8)	90.00	94.740(9)	94.681(3)	111.179(3)
V (Å^3)	1265(2)	828.2(2)	1217.0(3)	1346.1(1)	1952.79(5)
Z	4	4	4	4	4
D_{calc} (g cm^{-3})	2.191	2.834	2.278	2.228	1.931
μ (cm^{-1})	127.5	194.5	132.6	119.9	82.9
F(000)	768	632	768	840	1080
Absorption correlation	none [b]	SADABS	SADABS	SADABS	SADABS [60]
Max; min transmission		1.000; 0.3015	1.0000; 0.408	1.000; 0.508	1.000; 0.321
Measured reflection	3330	7350	6084	9883	7635
Unique reflection (R_{int})	3083 (0.0878)	1939 (0.0555)	2136 (0.0645)	3083 (0.0456)	4265 (0.0549)
Observed reflection [$I>2\sigma(I)$]	1637	1756	1618	2645	3583
Parameters refined	310	116	167	181	263
Max; min $\Delta\rho$ (eÅ^{-3}) [c]	1.042; −1.834 [d]	2.115; −1.660 [d]	0.969; −1.361 [d]	0.738; −1.152 [d]	1.918; −2.548 [d]
R_1; wR_2 [$I>2\sigma(I)$]	0.0692; 0.1256	0.0287; 0.0600	0.0345; 0.0730	0.0259; 0.0535	0.0496; 0.1101
R_1; wR_2 all reflection	0.1556; 0.1611	0.0304; 0.0602	0.0489; 0.0771	0.0358; 0.0558	0.0622; 0.1151
Extinction coefficient	0.00810(13)	0.0109(4)	not refined	not refined	not refined
GOF on F^2 [e]	1.081	0.963	0.923	1.026	1.006
Weighting scheme w [f] a; b	0.0607; 0.000	0.023; 0.0000	0.0426; 0.0000	0.0165; 0.0000	0.0548; 0.0000
Absolute structure parameter (Flack value)[61]	−0.02(4)	0.01(2)	–	–	0.14(2)

[a] Two independent molecules in the unit cell.
[b] An empirical absorption correction (DIFABS) for **2**-Tl was carried out but did not lead to a significant improvement and, therefore, was not included in the final refinement.
[c] Residual electron density, largest difference peak and hole.
[d] In the vicinity of the thallium atom.
[e] GOF, goodness of fit.
[f] $w = 1/[\sigma^2(F_o^2)+(a\cdot P)^2+b\cdot P]$ where $P = (\max(F_o^2 \text{ or } 0)+2\cdot F_c^2)/3$.

around the B–N bond and either coordinates with N1 to thallium, as in PhTp^{tBu}Tl, or with N2 to a thallium atom of another molecule. The latter is the case in FcTpTl and MeTp^{Me2}Tl, which exhibit polymeric structures due to the bridging nature of the ligand.

The molecular and crystal structures of the complexes reported here will be discussed in the following. Unremarkable distances and angles are not discussed in detail but are listed in the figure captions and are summarized in Table 2. Unless otherwise noted, the Tl–N distances fall in the normal range of 2.50–2.73 Å [1,21] found for Tl–N contacts in BpTl and TpTl structures.

A notable feature of most of the structures reported here is that they crystallize in chiral space groups. This is the case for **2**-Tl ($P2_1$), **3**-Tl ($P2_12_12_1$) and **8**-Tl ($C2$). The structures of **2**-Tl and **3**-Tl were refined as pure enantiomers. For **8**-Tl the crystal structure was refined as a twin with an enantiomer ratio of 86(2) to 14(2)%

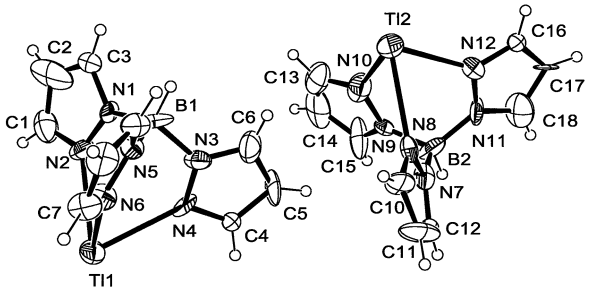


Fig. 1. The two independent molecular moieties in **2**-Tl. Selected distances (Å) and angles (°): Tl1–N2 2.665(6), Tl1–N4 2.575(7), Tl1–N6 2.730(7), Tl2–N8 2.651(7), Tl2–N10 2.547(7), Tl2–N12 2.590(8) Å, N–Tl–N 69.6(2)°–73.6°.

Table 2
Range of bond distances (Å) and angles (°) in the thallium complexes of **2**, **3**, **6**, **7**, and **8**

Compound	**2**-Tl [a]	**3**-Tl	**6**-Tl	**7**-Tl	**8**-Tl
Tl–N range	2.547(7)–2.730(7)	2.674(7)–2.803(7)	2.633(7)–2.663(7)	2.565(3)–2.652(4)	2.584(8)–2.747(8)
B–H	calculated	1.05(9), 1.14(9)	1.04(9)	calculated	calculated
N–Tl–N range	69.6(2)–73.6(2)	76.1(2)–83.7(2)	77.4(2)–86.3(2)	75.6(1)	68.4(3)–74.6(3)
Shortest Tl···π contacts					
Tl···N	3.557, 3.638	3.360, 3.762	3.767, 3.829	3.280, 3.340	3.672, 3.711
Tl···C	3.654, 3.683	3.854, 4.402	3.723, 3.755	3.479, 3.579	3.968, 4.010
Tl···ring centroid	3.500, 3.555	3.834	3.643, 3.695	3.267	3.894, 3.926

[a] Two independent molecules in the unit cell.

for the selected crystal. The crystallization of these poly(azolyl)borate thallium structures in non-centrosymmetric space groups cannot be dismissed as accidental but instead may be a more general phenomena in poly(azolyl)borate complexes with univalent metals. Unresolved chiral materials usually crystallize as a racemate and the frequency of spontaneous resolution is unusual here. A non-centrosymmetric space group ($Pna2_1$) is also found for hydrotris(1,2,4-triazolyl)boratosilver(I) [25]. In addition, the same chiral space group ($P2_12_12_1$) was determined for both dihydrobis(1,2,4-triazolyl)boratopotassium [57] and the thallium analog **3**-Tl.

The chirality is due to the solid-state packing in these structures. The ligands (or metal centers) by themselves are achiral. In **2**-Tl the chirality may be traced to the formation of 2_1-helical strands. In **3**-Tl it is due to the pyramidal or pseudo-tetrahedral coordination (taking into account the space of the presumed lone-pair) of the thallium centers by three (four) different ligands which creates the asymmetric centers. The structure of **8**-Tl features pairs of molecules where the two halves are related through a C_2 symmetry operation. Each pair represents a chiral entity.

The molecular structure of the prototypical hydrotris(pyrazolyl)thallium, **2**-Tl shows the usual pyramidal geometry of the thallium atom (Fig. 1). The packing of **2**-Tl reveals kinked, chain-type arrangements of the metal-ligand moieties (Fig. 2), with two different chain types present in the unit cell for the two crystallographically different Tl centers. The packing is most likely dictated by electrostatic interactions between the thallium and pyrazolyl π-manifolds from neighboring molecules. These non-bonded Tl···C and Tl···N distances are in the range of 3.683–3.781 Å (ring N1b·C3b) and 3.668–4.162 Å (ring C7b·C9b) for Tl1, and 3.557–3.884 Å (ring N7b·N12b) and 3.638–4.036 Å (ring N11b·C18b) for Tl2. These, along with the Tl···C/N contacts in the other structures, are included in Table 2. It can be seen that the distances in **2**-Tl are among the shortest (see also the Tl···centroid distances) and hence, are more significant. Resulting Tl···Tl′ contacts of 4.80 and 5.12 Å are too long for any metal–metal interaction. There is a Tl1–N bond length variation from 2.575(7) to 2.665(6) and 2.730(7) Å. For Tl2–N the variation is from 2.547(7) to 2.651(7) Å. The longer Tl–N bonds are to those pyrazolyl rings which are engaged in Tl···π interactions. There is a reciprocal correlation between the length of the Tl′···N contacts and the Tl–N bonds.

The building blocks of the extended 3D-structure of dihydrobis(1,2,4-triazolyl)boratothallium, **3**-Tl, are illustrated in Figs. 3 and 4. The essentially threefold nitrogen coordination in a pyramidal geometry around thallium is constructed from three different, albeit symmetry related ligands. A fourth nitrogen interaction is present at a considerably greater distance of 3.132 Å.

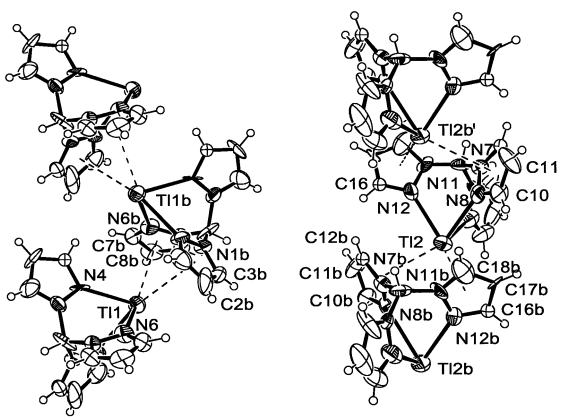


Fig. 2. Section of the strands formed in **2**-Tl. The left strand contains the Tl1-, the right strand the Tl2-molecular units. The strands run along *b*. Pyrazolyl π contacts to thallium between neighboring molecules are indicated. Shortest Tl···C/N distances (Å): Tl1···N2b 3.685, Tl1···C1b 3.683, Tl1···centroid (N1b–C3b) 3.555, Tl1···N6b 3.668, Tl1···C7b 3.817, Tl1···centroid (N5b–C8b) 3.748, Tl2···N7b 3.557, Tl2···C12b 3.654, Tl2···centroid (N7b·C12b) 3.500, Tl2···N11b 3.638, Tl2···C18b 3.760, Tl2···centroid (N11b·C18b) 3.665. Symmetry relation for Tl1: $b = -x+2,\ y+1/2,\ -z$; for Tl2: $b = -x+1,\ y+1/2,\ -z+1,\ b' = -x+1,\ y-1/2,\ -z+1$.

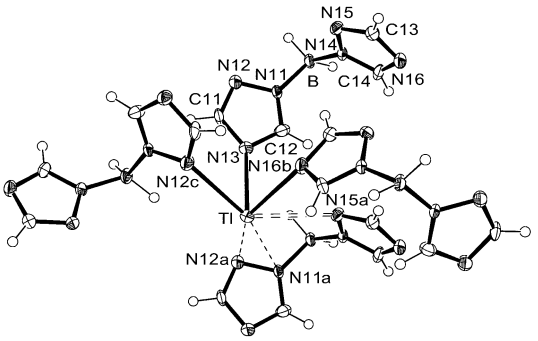


Fig. 3. Coordination environment around thallium in **3**-Tl. Selected distances (Å) and angles (°): Tl–N12c 2.767(7), Tl–N13 2.674(7), Tl–N16b 2.803(7), Tl···N15a 3.132(7), Tl···N12a 3.360(7), Tl···N11a 3.762(7), N12c–Tl–N13 76.1(2), N12–Tl–N16b 77.4(2), N13–Tl–N16b 83.7(2). Symmetry relation $a = x, y, z+1$; $b = -x+1/2, -y, z+1/2$; $c = x+1/2, -y+1/2, -z+2$.

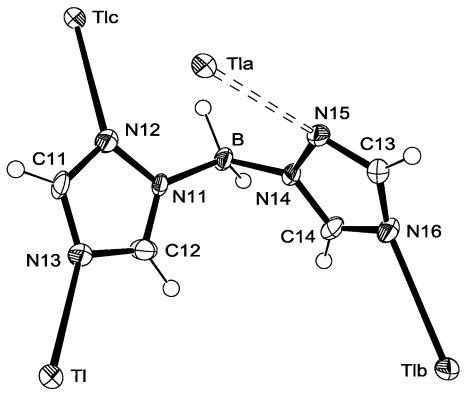


Fig. 4. Bridging action of the ligand in **3**-Tl. For distances see the caption to Fig. 3. Symmetry relation $a = x, y, z-1$; $b = -x+1/2, -y, z-1/2$; $c = x-1/2, -y+1/2, -z+2$.

There are two different donor atoms in the 1,2,4-triazolyl ring, with both the endo-(2-N) and the exo-dentate (4-N) nitrogen atoms acting as donor atoms. Thus, each ligand bridges three thallium atoms (Fig. 4), leaving one of the endo-dentate nitrogen atoms (N15) with only a weak thallium coordination. Similar bridging actions of poly(triazolyl)borate ligands between transition-metal centers have been observed previously [22,23,25,26]. In **3**-Tl, the bridging leads to an extended, three-dimensional (3D) structure (Fig. 5). Electrostatic interactions between thallium and triazolyl rings from neighboring molecules can also be seen (see Fig. 3).

Unlike **2**, the isomeric hydrotris(imidazolyl)borate ligand **6** cannot chelate a metal center but instead bridges metal ions. The formation of coordination polymers is then expected. In the structure of hydrotris(imidazolyl)boratothallium(I), **6**-Tl, each of the three imidazolyl rings coordinates to a different (albeit symmetry related) metal center, as shown in Fig. 6. Two adjacent ligands bridge two neighboring thallium ions. From this a one-dimensional (1D) ladder-like strand is formed. A two- or even three-dimensional framework, as in **3**-Tl, may be another possibility for the metal-ligand assembly. The packing of adjacent strands in **6**-Tl is probably dictated by electrostatic interactions between the thallium ion and imidazolyl π manifolds as in **2**-Tl. These non-bonding Tl···C and Tl···N interactions appear less significant than in the structures of **1**-Tl and **7**-Tl (see Table 2). Tl···centroid contacts start at 3.69 Å and Tl···C/N distances are above 3.723/3.767 Å. At the same time, the packing of neighboring strands is such that there are no close Tl···Tl distances (> 4.69 Å). The bridging action of **6** is again reminiscent of the bridge formation of the related poly(1,2,4-triazolyl)borate [22,23,25,26] and dihydrobis(tetrazolyl)borate ligand [28,30], which also possess nitrogen donors in a 1,3-position to the B–N bond.

In a first approximation the crystal structure of dihydrobis(indazolyl)boratothallium(I), **7**-Tl consists of monomeric units (Fig. 7). Yet these monomeric unit are arranged in centrosymmetric pairs, apparently through thallium–π interactions, as indicated in Fig. 8. The indazolyl moiety from N21 to C27 which is engaged in the Tl–π interaction has a longer Tl–N(22) bond [2.652(4) Å] than the other [Tl–N12, 2.565(3) Å]. The Tl–π contact may relieve the need for an agostic B–H···Tl interaction. The B···Tl and (B-)H···Tl distances are 3.52 and 3.16 Å, respectively, which is considerably greater than the B···Tl distance of 3.2–3.3 Å observed in most $Bp^{RR'}Tl$ compounds [4]. Additional packing in the crystal structure of **7**-Tl is controlled by intermolecular C–H···π interactions [34,58], as may be seen in Fig. 9. Shortest C–H···C/N contacts are between C11–H of the five-membered ring to N11d (2.81 Å), N12d (2.72 Å) and C11d (2.80 Å) of a neighboring five-membered ring (symmetry relation $d = 3/2-x, -1/2+y, 3/2-z$) The dihedral angle between these two five-membered rings is 53.3°. C–H···C contacts between the six-membered rings of the indazolyl moiety are above 2.93 Å. The shortest Tl···Tl distances of 4.156 Å in **7**-Tl are not within the Tl···π pairs but are to a neighboring molecule with symmetry relation $-x+1, -y, -z+1$.

The molecular structure of hydrotris(indazolyl)boratothallium(I), **8**-Tl, is depicted in Fig. 10. At first sight, the molecule appears to show the typical C_{3v} symmetrical metal-ligand motif. However, there is a considerable Tl–N bond length variation; from 2.584(8) Å for Tl–N12 and 2.590(9) Å for Tl–N22 to 2.747(8) Å for Tl–N32. The cause of this variation becomes apparent from the molecular packing: in the crystal structure these molecules are arranged in pairs. These pairs are obviously held together by slipped face-to-face π-stacking [59] of two indenyl moieties as shown in Fig. 11. The π-stacking is such that the two thallium centers are pointing in the same direction. The molecular units of

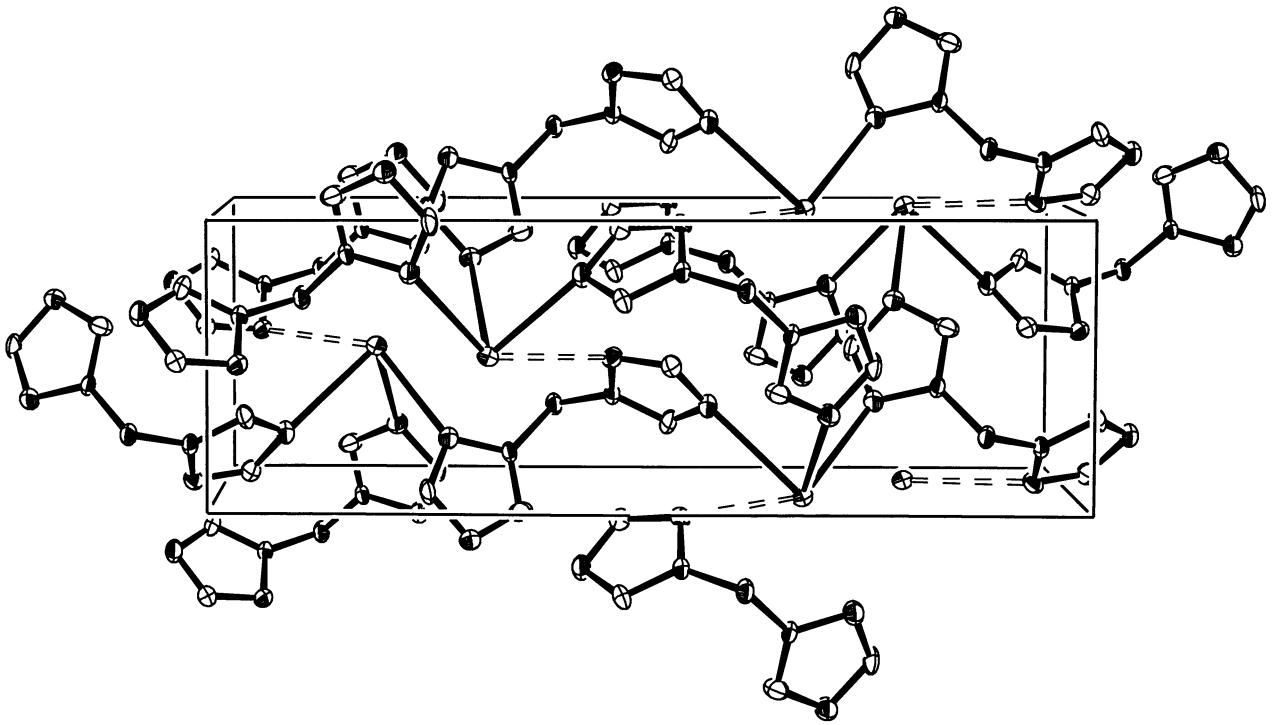


Fig. 5. Packing diagram of **3**-Tl, illustrating the extended 3D framework; view along a. Hydrogen atoms have been omitted for clarity. The weak Tl···N15 interactions are shown as dashed lines. Tl···Tl distances are 4.564 Å.

each pair are related through a C_2-symmetry operation, with no mirror plane or center of inversion. Hence each pair represents a chiral entity. As pointed out above, the single crystal did not show a 50:50 mixture of *R*- and *S*-pairs. Structure solution and refinement was only successful in the non-centrosymmetric space group *C*2. The crystal structure was refined as a (racemic) twin with an enantiomer ratio of 86(2) to 14(2)% for the selected crystal.

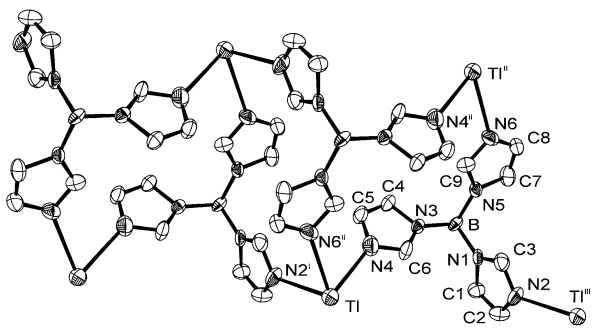


Fig. 6. Section of the one-dimensional polymeric structure of **6**-Tl. Hydrogen atoms have been omitted for clarity. The chains run along the crystallographic a direction. Selected distances (Å) and angles (°): Tl–N4 2.663(7), Tl–N2′ 2.656(6), Tl–N6″ 2.633(7), N6″–Tl–N2′ 80.8(2), N6″–Tl–N4 77.4(2), N2′–Tl–N4 86.3(2). Angles between the imidazolyl ring planes: ring N1·N2–N3·N4 89.8(5)°, ring N3·N4–N5·N6 72.4(5)°, ring N1·N2–N5·N6 79.4(5)°. Symmetry relations: $' = x-1,\ y,\ z$; $'' = 1-x,\ 1-y,\ 1-z$; $''' = x+1,\ y,\ z$.

Non-bonded Tl···C and Tl···N distances are again less significant than in the structures of **1**-Tl and **7**-Tl (see Table 2). Tl···centroid contacts start at 3.89 Å and Tl···C/N distances are above 3.968/3.672 Å, respectively. There are no close Tl···Tl distances (> 4.45 Å). Further packing interactions are dictated by C–H···π interactions between the indazolyl groups [34].

The Tl–N bond to the π-interacting indazolyl ring is longer than the other two Tl–N bonds. The solution NMR spectra of **8**-Tl shows that all three rings are equivalent due to loose or solvent-separated cation–anion contacts and to the absence of neighboring π-interactions, respectively.

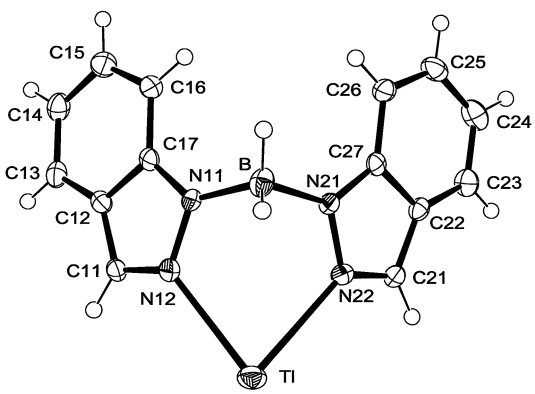


Fig. 7. Monomeric unit in **7**-Tl. Selected distances (Å) and angles (°): Tl–N12 2.565(3), Tl–N22 2.652(4), N21–Tl–N22 75.6(1).

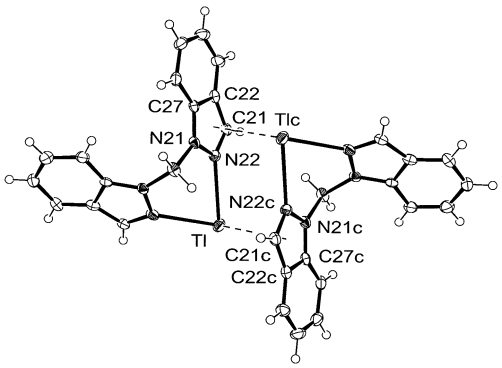


Fig. 8. Arrangement of centrosymmetric pairs in the structure of **7**-Tl. Selected Tl-π distances (Å): Tl···N21c 3.340(4), Tl···N22c 3.280(4), Tl···C21c 3.479(4), Tl···C22c 3.690(4), Tl···C27c 3.579(4), Tl···centroid (N21c·C27c) 3.267(4), Tl···Tlc 4.654(4). Symmetry relation $c = -x+1, -y+1, -z+1$.

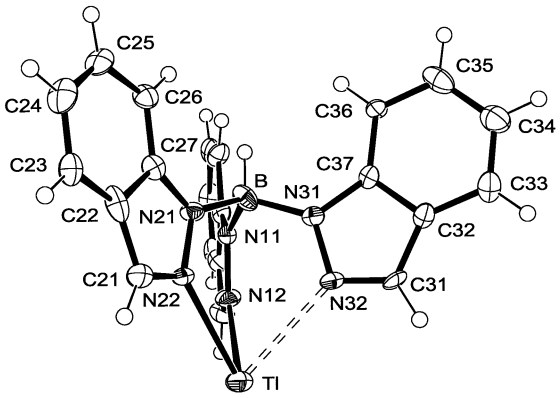


Fig. 10. Monomeric unit in **8**-Tl. The indazolyl ring with N11 and N12 could not be fully labeled for obvious reasons, yet the numbering scheme follows that of the other two rings. Selected distances (Å) and angles (°): Tl–N12 2.590(9), Tl–N22 2.584(8), Tl–N32 2.747(8), N22–Tl–N12 74.6(3), N22–Tl–N32 70.2(3), N12–Tl–N32 68.4(3).

4. Conclusions

Thallium complexes of modified poly(pyrazolyl)-borate ligands offer a great variability in their metal-ligand and crystal packing arrangement. Additional donor atoms in the azolyl ring or a 1,3- (cf. 1,2-) position of the nitrogen atoms in the ring gives rise to extended structures with bridging borate ligands. Electrostatic Tl···π_{azolyl} interactions can be quite prominent in the crystal packing of the molecular

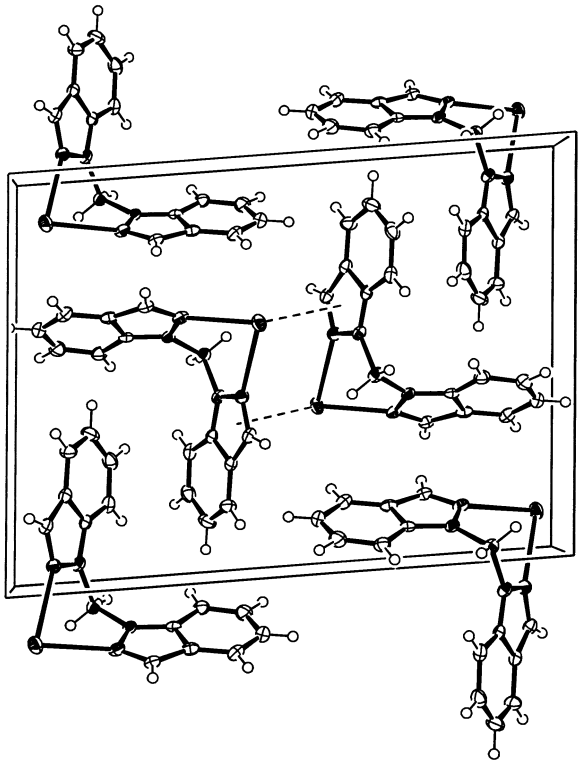


Fig. 9. Packing diagram for **7**-Tl; view along *b*.

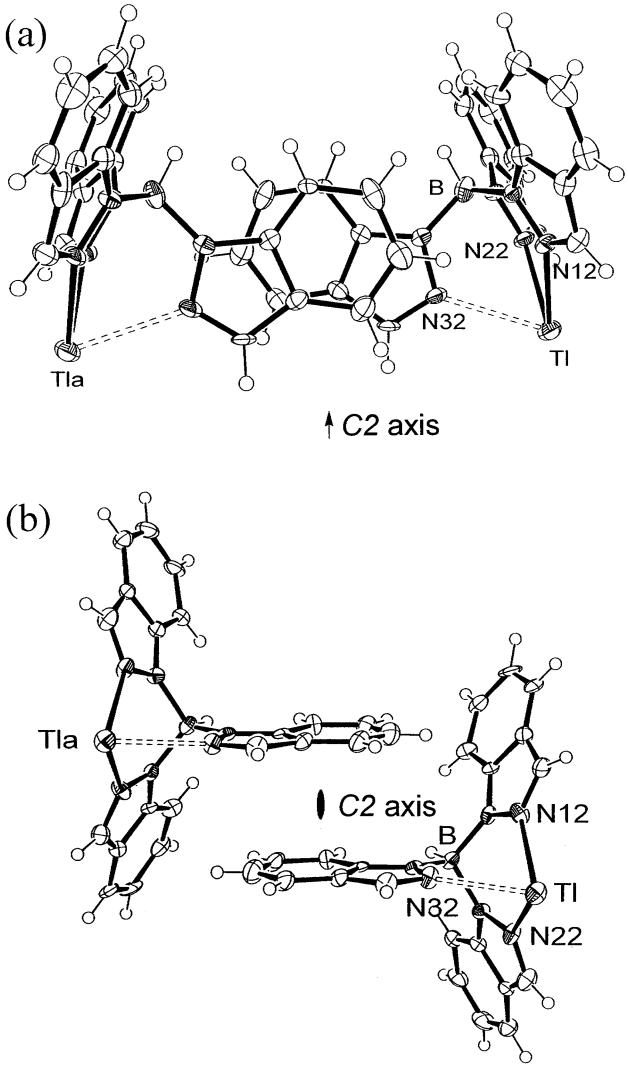


Fig. 11. π–π-stacked pairs of molecular units of **8**-Tl in the solid state, (a) top view, (b) front view. The π···π separation is 3.58 Å. Symmetry relation $a = 1-x, y, 1-z$.

thallium-ligand chelate complexes. For azolyl rings with extended π-systems, such as indazolyl, an offset $(\pi\text{–}\pi)_{\text{indazolyl}}$ stacking can also be significant. These solid-state packing effects are seen as the origin of the frequent crystallization of thallium(I) or in general metal(I) poly(azolyl)borate complexes in chiral space groups. The azolyl rings which are engaged in these type of π interactions show an increase in their Tl–N bond. There appears to be a reciprocal correlation between the strength of the π interactions and the Tl–N bonds.

5. Supplementary material

Crystallographic data (excluding structure factors) have been deposited with the Cambridge Crystallographic Data Centre as Supplementary Publication No. CCDC-101006 (**2**-Tl), -168036 (**3**-Tl), -135180 (**6**-Tl), -168037 (**7**-Tl), -141090 (**8**-Tl). Copies of the data can be obtained free of charge on application to CCDC, 12 Union Road, Cambridge CB2 1EZ, UK (fax: +44-1223-336033; email: deposit@ccdc.cam.ac.uk or www: http://www.ccdc.cam.ac.uk).

Acknowledgements

This work is supported by the Deutsche Forschungsgemeinschaft (Grant Ja466/11-1) and the Fonds der Chemischen Industrie.

References

[1] C. Janiak, Coord. Chem. Rev. 183 (1997) 107.
[2] H. Schumann, C. Janiak, J. Pickardt, U. Börner, Angew. Chem., Int. Ed. Engl. 26 (1987) 789.
[3] H. Schumann, C. Janiak, in: B. Krebs (Ed.), Unkonventionelle Wechselwirkungen in der Chemie metallischer Elemente, VCH, Weinheim, 1991, p. 185.
[4] P. Ghosh, A.L. Rheingold, G. Parkin, Inorg. Chem. 38 (1999) 5464.
[5] C.H. Galka, L.H. Gade, Chem. Commun. (2001) 899.
[6] C.J. Galka, L.H. Gade, Inorg. Chem. 38 (1999) 1038.
[7] G.B. Deacon, E.E. Delbridge, C.M. Forsyth, B.W. Skelton, A.H. White, J. Chem. Soc., Dalton Trans. (2000) 745.
[8] O.W. Howarth, J. Nelson, V. McKee, Chem. Commun. (2000) 21.
[9] C. Janiak, R. Hoffmann, J. Am. Chem. Soc. 112 (1990) 5924.
[10] C. Janiak, R. Hoffmann, in: B. Krebs (Ed.), Unkonventionelle Wechselwirkungen in der Chemie metallischer Elemente, VCH, Weinheim, 1991, p. 45.
[11] P.H.M. Budzelaar, J. Boersma, Recl. Trav. Chim. Pays-Bas. 109 (1990) 187.
[12] C. Janiak, R. Hoffmann, Angew Chem., Int. Ed. Engl. 28 (1989) 1688.
[13] P. Schwerdtfeger, Inorg. Chem. 30 (1991) 1660.
[14] S. Trofimenko, Scorpionates—Polypyrazolylborate Ligands and Their Coordination Chemistry, Imperial College Press, 1999.
[15] S. Trofimenko, Chem. Rev. 93 (1993) 943.
[16] P.K. Byers, A.J. Canty, R.T. Honeyman, Adv. Organomet. Chem. 34 (1992) 1.
[17] N. Kitajima, W.B. Tolman, Prog. Inorg. Chem. 43 (1995) 419.
[18] G. Parkin, Adv. Inorg. Chem. 42 (1995) 291.
[19] D.L. Reger, Coord. Chem. Rev. 147 (1996) 571.
[20] M. Etienne, Coord. Chem. Rev. 156 (1997) 201.
[21] C. Janiak, Main Group Met. Chem. 21 (1998) 33.
[22] C. Janiak, T.G. Scharmann, W. Günther, F. Girgsdies, H. Hemling, W. Hinrichs, D. Lentz, Chem. Eur. J. 1 (1995) 637.
[23] C. Janiak, H. Hemling, J. Chem. Soc., Dalton Trans. (1994) 2947.
[24] C. Janiak, T.G. Scharmann, H. Hemling, D. Lentz, J. Pickardt, Chem. Ber. 128 (1995) 235.
[25] C. Janiak, T.G. Scharmann, P. Albrecht, F. Marlow, R. Macdonald, J. Am. Chem. Soc. 118 (1996) 6307.
[26] C. Janiak, T.G. Scharmann, W. Günther, W. Hinrichs, D. Lentz, Chem. Ber. 129 (1996) 991.
[27] C. Janiak, S. Temizdemir, T.G. Scharmann, A. Schmalstieg, J. Demtschuk, Z. Anorg. Allg. Chem. 626 (2000) 2053.
[28] C. Janiak, Chem. Commun. (1994) 545.
[29] C. Janiak, L. Esser, Z. Naturforsch. B 48 (1993) 394.
[30] C. Janiak, T.G. Scharmann, K.-W. Brzezinka, P. Reich, Chem. Ber. 128 (1995) 323.
[31] C. Janiak, S. Temizdemir, C. Röhr, Z. Anorg. Allg. Chem. 626 (2000) 1265.
[32] Effendy, G.G. Lobbia, M. Pellei, C. Pettinari, C. Santini, B.W. Skelton, A.H. White, J. Chem. Soc., Dalton Trans. (2001) 528.
[33] K. Fujita, S. Hikichi, M. Akita, Y. Moro-oka, J. Chem. Soc., Dalton Trans. (2000) 117.
[34] C. Janiak, S. Temizdemir, S. Dechert, W. Deck, F. Girgsdies, J. Heinze, M.J. Kolm, T.G. Scharmann, O.M. Zipffel, Eur. J. Inorg. Chem. (2000) 1229.
[35] A.L. Rheingold, B.S. Haggerty, G.P.A. Yap, S. Trofimenko, Inorg. Chem. 36 (1997) 5097.
[36] H.V. Rasika Dias, W. Jin, Inorg. Chem. 39 (2000) 815.
[37] B.M. Bridgewater, G. Parkin, J. Am. Chem. Soc. 122 (2000) 7140.
[38] C. Kimblin, B.M. Bridgewater, T. Hascall, G. Parkin, J. Chem. Soc., Dalton Trans. (2000) 1267.
[39] C. Kimblin, B.M. Bridgewater, D.G. Churchill, G. Parkin, Chem. Commun. (1999) 2301.
[40] J. Reglinski, M. Garner, I.D. Cassidy, P.A. Slavin, M.D. Spicer, D.R. Armstrong, J. Chem. Soc., Dalton Trans. (1999) 2119.
[41] S. Bhandari, M.F. Mahon, K.C. Molloy, J.S. Palmer, S.F. Sayers, J. Chem. Soc., Dalton Trans. (2000) 1053.
[42] C. Janiak, S. Temizdemir, T.G. Scharmann, Z. Anorg. Allg. Chem. 624 (2000) 755.
[43] C. Janiak, S. Temizdemir, S. Dechert, Inorg. Chem. Commun. 3 (2000) 271.
[44] S. Trofimenko, Inorg. Synth. 12 (1970) 99.
[45] G. Bruno, E. Ciliberto, I. Fragalá, G. Granozzi, Inorg. Chim. Acta 48 (1981) 61.
[46] G.M. Sheldrick, SHELXS 97, SHELXL 97, Programs for Crystal Structure Analysis, University of Göttingen, Germany, 1997.
[47] (a) M.N. Burnett, C.K. Johnson, ORTEP-III: Oak Ridge Thermal Ellipsoid Plot Program for Crystal Structure Illustrations, Oak Ridge National Laboratory Report ORNL-6895, 1996;
(b) L.J. Farrugia, ORTEP3 for windows, version 1.0.1β, University of Glasgow, 1997;
(c) L.J. Farrugia, J. Appl. Crystallogr. 30 (1997) 565.
[48] T. Fillebeen, T. Hascall, G. Parkin, Inorg. Chem. 36 (1997) 3787.
[49] P. Ghosh, T. Hascall, C. Dowling, G. Parkin, J. Chem. Soc., Dalton Trans. (1998) 3355.
[50] C. Dowling, P. Ghosh, G. Parkin, Polyhedron 16 (1997) 3469.
[51] J.S. Fleming, E. Psillakis, S.M. Couchman, J.C. Jeffery, J.A. McCleverty, M.D. Ward, J. Chem. Soc., Dalton Trans. (1998) 537.

[52] A.L. Rheingold, L.M. Liable-Sands, S. Trofimenko, Chem. Commun. (1997) 1691.
[53] C. Ferguson, M.C. Jennings, F.J. Lalor, C. Shanahan, Acta. Crystallogr., Sect. C. 47 (1991) 2079.
[54] J.L. Kisko, T. Hascall, C. Kimblin, G. Parkin, J. Chem. Soc., Dalton Trans. (1999) 1929.
[55] F. Jäkle, K. Polborn, M. Wagner, Chem. Ber. 129 (1996) 603.
[56] C. Janiak, L. Braun, F. Girgsdies, J. Chem. Soc., Dalton Trans. (1999) 3133.
[57] C. Janiak, T.G. Scharmann, unpublished results.
[58] M. Nishio, M. Hiroto, Y. Umezawa, The CH/π Interaction, Wiley-VCH, New York, 1998.
[59] C. Janiak, J. Chem. Soc., Dalton Trans. (2000) 3885.
[60] G. Sheldrick, Program SADABS: Area-Detector Absorption Correction, University of Göttingen, Germany, 1996.
[61] H.D. Flack, Acta. Crystallogr., Sect. A 39 (1983) 876.

PERGAMON

Polyhedron 21 (2002) 563–577

POLYHEDRON

www.elsevier.com/locate/poly

Synthesis and characterization of an extremely hindered tetraaryl-substituted digermene and its unique properties in the solid state and in solution

Norihiro Tokitoh [a,b,*], Kuniyuki Kishikawa [b], Renji Okazaki [b,c], Takahiro Sasamori [a], Norio Nakata [a], Nobuhiro Takeda [a]

[a] *Institute for Chemical Research, Kyoto University, Gokasho, Uji, Kyoto 611-0011, Japan*

[b] *Department of Chemistry, Graduate School of Science, The University of Tokyo, 7-3-1 Hongo, Bunkyo-ku, Tokyo 113, Japan*

[c] *Department of Chemical and Biological Sciences, Faculty of Science, Japan Women's University, 2-8-1 Mejirodai, Bunkyo-ku, Tokyo 112-8681, Japan*

Received 4 September 2001; accepted 27 November 2001

Abstract

An extremely hindered digermene (*E*)-Tbt(Mes)Ge=Ge(Mes)Tbt (**1**; Tbt = 2,4,6-tris[bis(trimethylsilyl)methyl]phenyl; Mes = mesityl) was synthesized. X-ray crystallographic analysis of the hexane solvated single crystal [**1**·0.5hexane] revealed that **1** has an extremely long germanium–germanium double bond [2.416(2) Å] as that of a carbon-substituted digermene. The temperature-dependent change of UV–Vis absorption of digermene **1** in solution indicated the quantitative interconversion between **1** and the corresponding germylene Tbt(Mes)Ge: (**3**). The thermodynamic parameters ($\Delta H = 14.7 \pm 0.2$ kcal mol^{-1} and $\Delta S = 42.4 \pm 0.8$ cal mol^{-1} deg^{-1}) for the dissociation of digermene **1** to germylene **3** were obtained from temperature dependence of the absorption of **1**. Since the reactivity of germylene **3** is much higher than that of digermene **1**, almost all the intermolecular reactions of **1** in solution proceeded via dissociated **3**. For instance, the reaction of **1** with oxygen in solution resulted in a non-stereospecific formation of the *cis*- and *trans*-1,3,2,4-dioxadigermetanes **11** and **7** via the initial formation of germanone **12** derived from oxygenation of the dissociated germylene **3**. In case of the oxidation in the solid state, however, digermene **1** reacted with O_2 without dissociation to give the corresponding *trans*-substituted 1,3,2,4-dioxadigermetane stereospecifically. The reaction of digermene **1** with $W(CO)_5$(THF) was also examined to give the corresponding terminal tungsten complex of the dissociated germylene **3**, i.e. Tbt(Mes)Ge=$W(CO)_5$ (**23**), as a marginally stable orange yellow paste. © 2002 Published by Elsevier Science Ltd.

Keywords: Digermene; Germylene; X-ray crystallographic analysis; Dissociation; Equilibrium; Bond dissociation energy; Dioxadigermetane; Terminal tungsten complexes

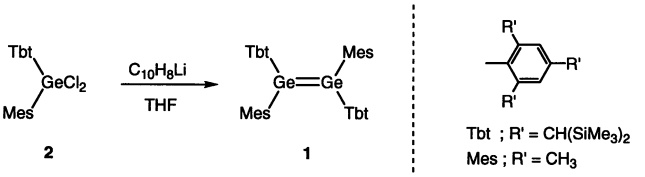
1. Introduction

During the last two decades remarkable progress has been made in the chemistry of low-coordinate compounds of heavier group 14 elements, especially in those of dimetallenes and metallylenes because of their unique structures and reactivities [1]. Since the first isolation of a stable disilene by West et al. in 1981 [2], a number of stable dimetallenes (disilene [1c–e], digermene [1b,d,f], and distannene [1b,d,f]) have been synthesized and the intrinsic nature of the metal–metal double bonds in those dimetallenes has been elucidated to a considerable extent. For example, the thermal dissociation of a disilene into silylenes [3] and that of a distannene into stannylenes [4] in solution have been experimentally demonstrated on the basis of their reactivities and spectroscopic properties, and energetics for their dissociation processes have been estimated. As for digermenes, a unique 1,2-migration of the mesityl group has been reported in the thermolysis of tetramesityldigermene ($Mes_2Ge=GeMes_2$) leading to the formation of mesityl(trimesitylgermyl)germylene [5], while the thermolysis of more hindered tetraaryldigermenes (*E*)- and (*Z*)-Mes(Tip)Ge=Ge(Tip)Mes (Tip = 2,4,6-triisopropyl-

* Corresponding author. Tel.: +81-774-38-3200; fax: +81-774-38-3209.

E-mail address: tokitoh@boc.kuicr.kyoto-u.ac.jp (N. Tokitoh).

0277-5387/02/$ - see front matter © 2002 Published by Elsevier Science Ltd.
PII: S0277-5387(01)01035-X



Scheme 1.

lphenyl) resulted in the rotational isomerization between these two stereoisomers [6]. Furthermore, tetrakis(2,6-diethylphenyl)digermene ($Dep_2Ge{=}GeDep_2$; Dep = 2,6-diethylphenyl) was reportedly converted into the corresponding cyclotrigermane on heating, probably via dissociation into the germylene $(Dep)_2Ge$: followed by its cyclotrimerization [1c]. Such thermal dissociation into the corresponding germylenes has also been postulated in the thermolysis of $[(Me_3Si)_2CH]_2Ge{=}Ge[CH(SiMe_3)_2]_2$ [7] and $(2\text{-}t\text{Bu-}4,5,6\text{-}Me_3C_6H)_2Ge{=}Ge(2\text{-}t\text{Bu-}4,5,6\text{-}Me_3C_6H)_2$ [8], but the evidence for the dissociation was provided only by trapping reactions of the germylenes [9]. To the best of our knowledge, no experimental estimation for the bond dissociation energy of a Ge=Ge double bond has been reported so far.

In view of these situations, we became interested in the properties of a digermene, Tbt(Mes)Ge=Ge(Mes)Tbt (**1**; Tbt = 2,4,6-tris[bis(trimethylsilyl)methyl]-phenyl [10], Mes = mesityl), the silicon analogue of which showed a quite unique structure and reactivity. Here, we present the synthesis and characterization of this extremely hindered digermene **1**, which led us to the first spectroscopic observation of an equilibrium between a digermene and germylenes. Digermene **1** provided us with a good opportunity to perform the first measurement of a bond dissociation energy for the germanium–germanium double bond.

2. Results and discussion

2.1. Synthesis and structure

Reaction of dichlorogermane [Tbt(Mes)$GeCl_2$, **2**] with lithium naphthalenide in THF at −78 °C gave a dark-brown solution. The solvent exchange from THF to hexane followed by filtration of inorganic salts and sublimation of naphthalene in vacuo afforded the corresponding (*E*)-substituted digermene **1** exclusively as orange crystals (Scheme 1). Although digermene **1** is stable at room temperature under inert atmosphere, it undergoes decomposition at 92 °C in the solid state.

The molecular structure of **1** was determined by X-ray crystallographic analysis of the hexane solvated single crystal [**1**·0.5hexane], the ORTEP drawing of which is shown in Fig. 1 along with the selected bond lengths and angles.

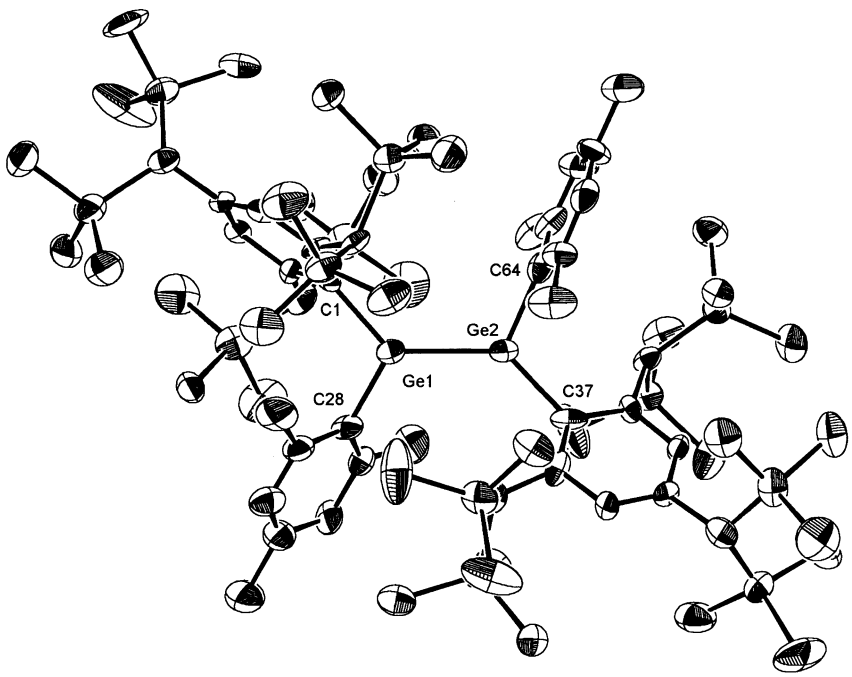


Fig. 1. ORTEP drawing of (*E*)-Tbt(Mes)Ge=Ge(Mes)Tbt·0.5hexane (**1**·0.5hexane) with thermal ellipsoid plots (30% probability). The fragment of solvated hexane is omitted for clarity. Selected bond lengths (Å) and angles (°): Ge(1)–Ge(2) 2.416(2), Ge(1)–C(1) 2.017(12), Ge(1)–C(28) 1.960(14), Ge(2)–C(37) 2.045(13), Ge(2)–C(64) 1.996(14), C(1)–Ge(1)–C(28) 108.0(5), C(1)–Ge(1)–Ge(2) 130.5(3), C(28)–Ge(1)–Ge(2) 118.1(4), C(37)–Ge(2)–C(64) 109.1(5), C(37)–Ge(2)–Ge(1) 132.7(4), C(64)–Ge(2)–Ge(1) 113.5(3).

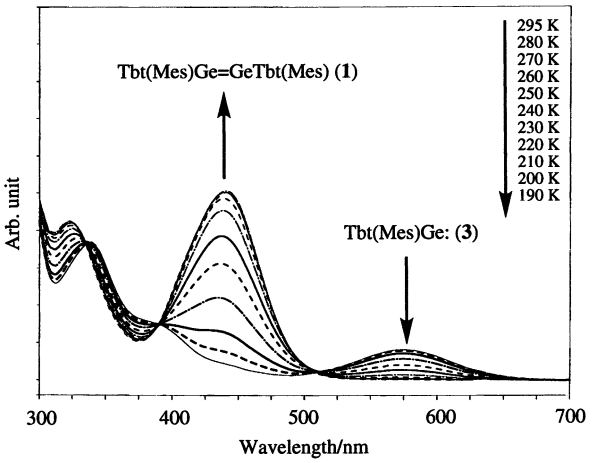
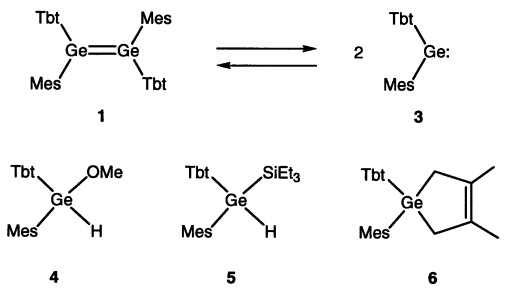


Fig. 2. Temperature-dependent UV–Vis spectra of **1** in hexane (3.7×10^{-4} M).



Scheme 2.

The Ge(1)–Ge(2) bond length [2.416(2) Å] of digermene **1** is remarkably longer than the germanium–germanium double bond lengths of previously reported digermenes bearing carbon substituents [2.21–2.35 Å] [6–8,11] and close to the germanium–germanium single bond length [2.465 Å in $(Ph_2Ge)_4$ or 2.463 and 2.457 Å in $(Ph_2Ge)_6$] [12], reflecting the large steric repulsion between Tbt and Mes groups. Weidenbruch et al. have already reported that strongly twisted (*E*)-1,2-diamino-1,2-disilyldigermenes having a unique skeleton have extremely elongated Ge=Ge double bonds [2.453–2.460 Å] [13]. The sums of the bond angles around Ge(1) and Ge(2) of **1** are 356.6° and 355.3°, respectively. The twist angles along the germanium–germanium bond axis are 16.5(8)° and 34.6(7)°. These structural features of **1** indicate that **1** still retains sp^2 hybridized germanium centers even though its Ge=Ge double bond is weak and elongated.

2.2. Behavior in solution

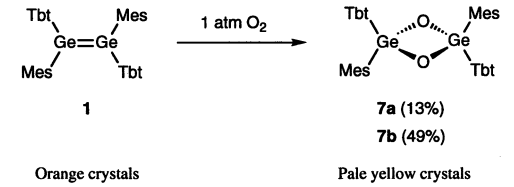
Interestingly, a hexane solution of **1** showed a reversible thermochromism; the hexane solution of **1** (3.7×10^{-4} M) was blue ($\lambda_{max} = 575$ nm) at room temperature, but it turned orange yellow ($\lambda_{max} = 439$ nm) at low temperature [14]. The change in UV–Vis absorption shown in Fig. 2 clearly indicates that **1** dissociates into the corresponding germylenes **3** at room temperature, while it does not at low temperature (Scheme 2), because tetraaryldigermenes and diarylgermylenes reportedly have their λ_{max} in the range of 408–440 nm [1f,8] and 466–581nm [15], respectively.

The absorptions observed at 190 K ($\lambda_{max} = 439$ nm, ε 2.0×10^4) and 295 K ($\lambda_{max} = 575$ nm, ε 1.6×10^3) are assignable to the π–π^* transition of digermene **1** and the n–p transition of germylene **3**, respectively. The isosbestic points observed at 335, 390 and 509 nm indicate the quantitative interconversion between **1** and **3**. The structure of digermene **1** in solution is reasonably assumed to be the (*E*)-isomer as in the solid state, since the (*Z*)-isomer has obviously much severer steric repulsion between two extremely bulky substituents (Tbt groups) facing each other.

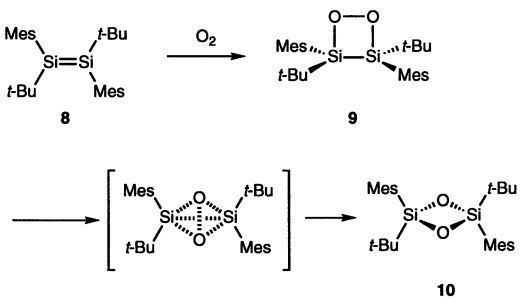
The thermodynamic parameters ($\Delta H = 14.7 \pm 0.2$ kcal mol^{-1} and $\Delta S = 42.4 \pm 0.8$ cal mol^{-1} deg^{-1}) for the dissociation of digermene **1** to germylene **3** were obtained from the temperature dependence of the absorptions shown in Fig. 2. This bond dissociation energy (14.7 kcal mol^{-1}) of digermene **1** into germylene **3** is much smaller than the calculated value (30–45 kcal mol^{-1}) for the parent system ($H_2Ge{=}GeH_2$) [7a,16], indicating that the germanium–germanium double bond in **1** is considerably weakened due to the severe steric repulsion between the bulky substituents. In this connection, it is intriguing that Tbt(Tip)Ge: (Tip = 2,4,6-triisopropylphenyl) [15c,15d] and Tip(Mes)Ge: [6], which are more and less sterically demanding than **3**, have been shown to exist only as a monomer and a dimer, respectively, in solution. These observations point to the subtle effect of the size of substituents on the equilibrium between a digermene and germylenes. It is interesting that disilene Tbt(Mes)Si=Si(Mes)Tbt bearing the same substituents as **1** exists essentially as a dimer (i.e. disilene) [3,17]. The bis(trimethylsilyl)methyl-substituted disilene–digermene pair, $[(Me_3Si)_2CH]_2M{=}M[CH(SiMe_3)_2]_2$, (M = Si, Ge), is known to show a similar phenomenon [7,18]. In these systems, the disilene does not undergo any thermal dissociation in solution, but the digermene is reportedly isolable only in the solid state and readily dissociates in solution into the corresponding germylenes at room temperature [7,18]. It should be noted that the interconversion between **1** and **3** is the first example of an experimentally observed equilibrium between a digermene and germylenes [19].

2.3. Reactions in solution

In order to investigate the reactivity of digermene **1** having an extremely elongated Ge=Ge double bond, a solution of digermene **1** was treated at -100 °C with methanol which is known to add readily across a



Scheme 3.



Scheme 4.

Ge=Ge double bond [1f,11a], but the orange–yellow color of the solution due to **1** did not disappear after the solution was kept for 6 h at the same temperature. Upon warming up to room temperature the solution became colorless to give a methoxygermane **4** (44%), the insertion product of germylene **3** into the O–H bond of methanol (Scheme 2). These facts show that the Ge=Ge double bond in **1** is so effectively protected by the surrounding four bulky aryl groups as revealed by X-ray crystallographic analysis that **1** is incapable of reacting with methanol at low temperatures. At elevated temperatures, however, digermene **1** dissociates into the corresponding germylene **3**, which readily reacts with methanol to give the methoxygermane **4**. Germylene **3** generated by dissociation of digermene **1** also reacted with Et_3SiH and 2,3-dimethyl-1,3-butadiene at room temperature to afford the corresponding adducts **5** (70%) and **6** (62%), respectively (Scheme 2).

2.4. Oxidation reactions

Since the reaction with oxygen can be performed either in the solid state or in solution, we made a careful investigation of the oxidation reactions of the extremely hindered digermene **1** to elucidate the intrinsic reactivity.

2.4.1. Reaction of *1* with oxygen in the solid state

At first, the oxidation of digermene **1** was examined in the solid state. When a finely powdered orange sample of **1** was exposed to oxygen for 3 days in the dark, the color changed into pale yellow and two conformational isomers of *trans*-1,3,2,4-dioxadigermetanes **7a** (13%) and **7b** (49%) were obtained after usual chromatographic separation (Scheme 3).

In this reaction *cis*-1,3,2,4-dioxadigermetane was not obtained. These facts show that the reaction of the digermene with oxygen proceeds stereospecifically. Although the oxidation of disilenes is known to take place stereospecifically in solution or in the solid state [20], there have been very few reports on the stereochemistry of the oxidation of a digermene. As for the case of (*Z*)-1,2-diamino-1,2-disilyldigermene, Weidenbruch et al. have reported the stereospecific oxidation reaction with molecular oxygen leading to the formation of the corresponding *cis*-1,3,2,4-dioxadigermetane.

The mechanistic studies of the oxidation of (*E*)-Mes(*t*-Bu)Si=Si(*t*-Bu)Mes (**8**) in solution have revealed that the reaction of **8** with oxygen first gives the [2 + 2]cycloadducts, (*E*)-1,2,3,4-dioxadisiletane (**9**), stereospecifically, which then undergoes rearrangement to afford *trans*-1,3,2,4-dioxadisiletane **10** [20d]. In the solid state, (*E*)-1,2,3,4-dioxadisiletane (**9**) rearranged stereospecifically to afford *trans*-1,3,2,4-dioxadisiletane **10** (Scheme 4) [20d]. These facts suggest that the oxidation of (*E*)-digermene **1** might take place in two steps via 1,2,3,4-dioxadigermetane intermediate with retention of the stereochemistry although the observation of the intermediate was not successful in this case.

The structures of the two conformational isomers of the *trans*-1,3,2,4-dioxadigermetanes **7a** and **7b** were determined by the X-ray crystallographic analysis as shown in Figs. 3 and 4. Single crystals of *trans*-1,3,2,4-dioxadigermetane **7a** were obtained as those solvated with hexane and have been revealed to have two non-identical *trans*-1,3,2,4-dioxadigermetane molecules in the unit cell, while no solvation with hexane was observed for the conformational isomer **7b**. In Fig. 3 are shown the ORTEP drawings of [**7a**·hexane] (fragments 1 and 2, respectively). Fig. 4 shows the ORTEP drawing of another *trans*-1,3,2,4-dioxadigermetane **7b**.

Figs. 5 and 6 show the selected bond lengths and angles of the central dioxadigermetane rings of **7a** and **7b**. The dioxadigermetane rings of the fragment 1 and fragment 2 of **7a** and that of **7b** are almost planar with the sum of the interior bond angles being 360.0°, 359.9°, and 360.0°, respectively. The germanium–germanium distances of fragments 1 and 2 of **7a** and that of **7b** [2.653(2), 2.660(2), and 2.691(4) Å, respectively] are much longer than a typical Ge–Ge single bond length (2.457–2.463 Å) [12]. Dihedral angles of **7a** and **7b** formed by two O–Ge–O planes are 2.5°, 3.9°, and 1.9°, respectively, as shown in Figs. 7 and 8. There is

Fig. 3. ORTEP drawings of *trans*-1,3,2,4-dioxadigermetane [**7a**·hexane] with thermal ellipsoid plots (30% probability). (a) Fragment 1; and (b) fragment 2 for the independent molecules in the unit cell. The fragment of solvated hexane is omitted for clarity.

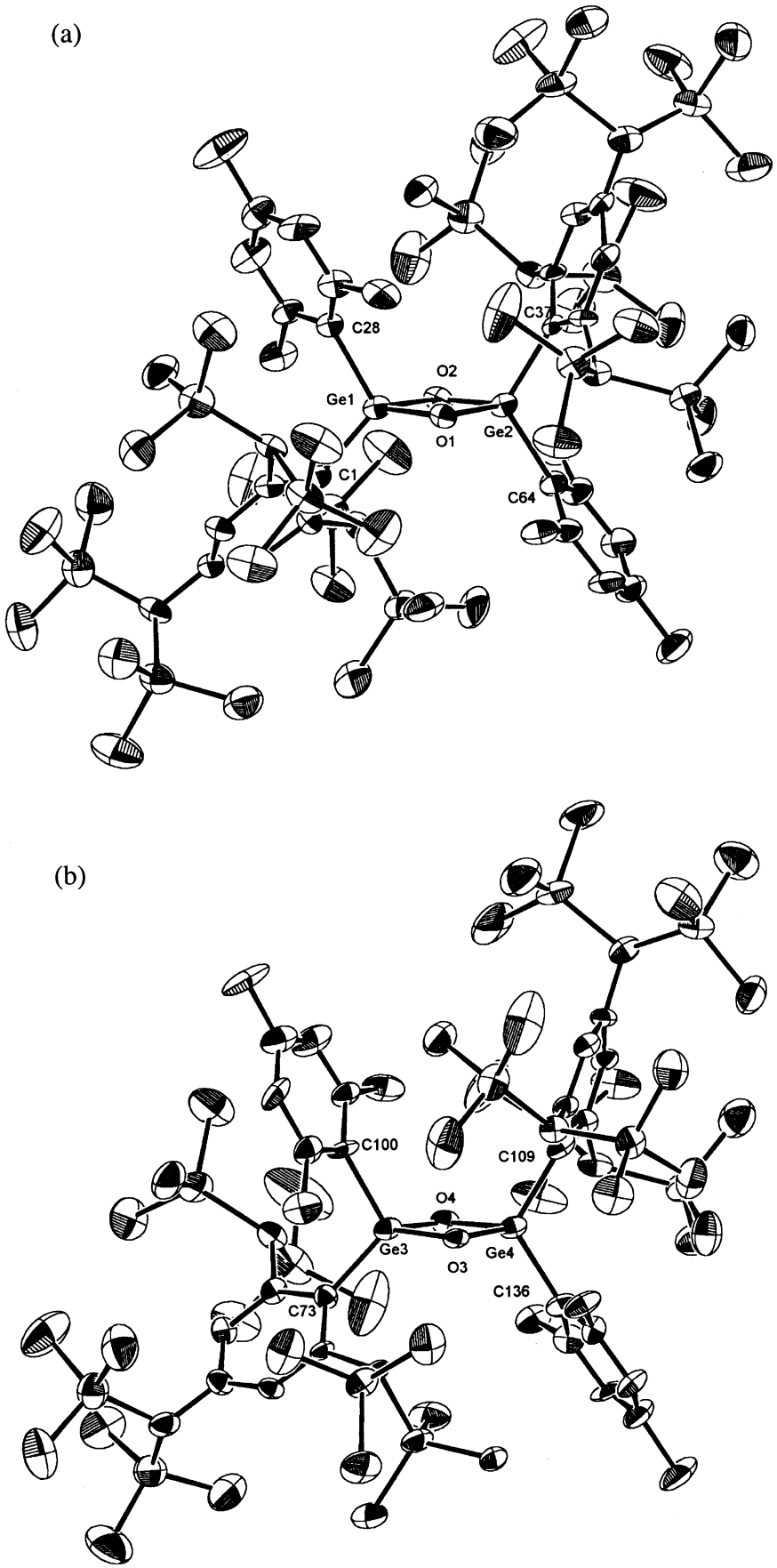


Fig. 3.

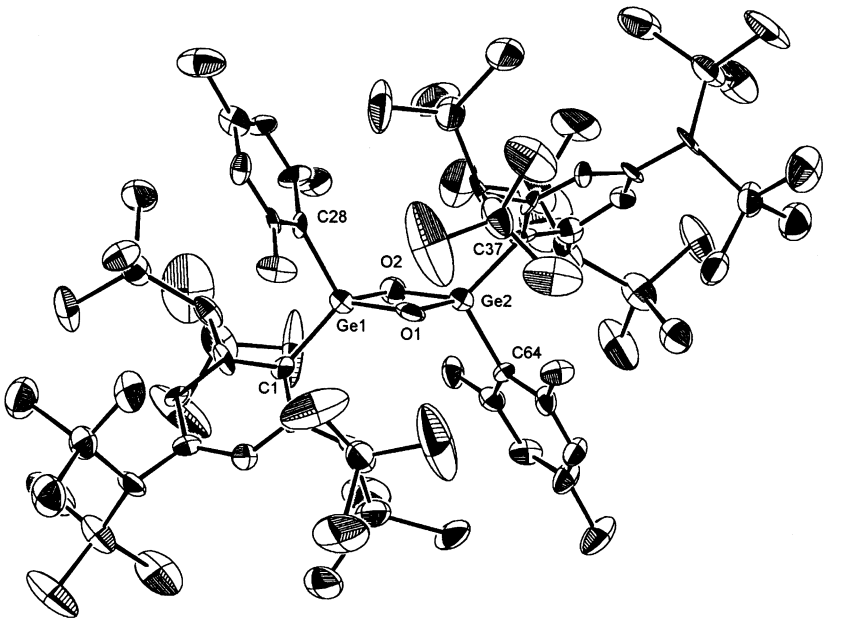


Fig. 4. ORTEP drawing of *trans*-1,3,2,4-dioxadigermetane **7b** with thermal ellipsoid plots (30% probability).

little difference in the geometries of the four-membered rings of **7a** between the two fragments as shown in Figs. 5 and 7.

The molecular structure of **7a** is different from that of **7b** in dihedral angles between the central four-membered ring and Tbt, Mes aromatic ring planes (compound **7b**: 44.8° and 41.9° for the Tbt rings and 61.0° and 61.2° for the Mes rings; fragment 1: 49.6° and 72.3° for the Tbt rings and 67.1° and 56.6° for the Mes rings; fragment 2: 48.2° and 74.6° for the Tbt rings and 68.5° and 57.4° for the Mes rings).

Although we cannot understand at present why the conformational isomers are isolated as stable compounds, it is probably due to hindered rotation of the aromatic rings with regard to the four-membered ring in the case of **7b**. Since ^{1}H NMR spectrum of **7a** shows two signals in the aromatic region, each of two Tbt and Mes groups are equivalent and hence they rotate with regard to the four-membered ring. In contrast, ^{1}H NMR spectrum of **7b** shows four signals in the aromatic region, suggesting that the Tbt and Mes groups do not rotate. Furthermore, compound **7b** exhibits a very complicated ^{1}H NMR spectrum in other regions, suggesting greater steric congestion around Tbt and Mes groups than its isomer **7a**. Consequently, the germanium–germanium distance of **7b** is slightly longer than that of **7a** and the angles of Ge–O–Ge and O–Ge–O are larger and smaller than those of **7a**, respectively.

The structures of the four-membered rings of **7a** and **7b** are similar to that of the previously reported tetrakis(2,6-diethylphenyl)-1,3,2,4-dioxadigermetane [21], although its dihedral angle between two O–Ge–O planes (8.4°) is slightly larger in **7a** and **7b**. In this connection, there have been some interesting reports on the structural properties of dioxadisiletanes. Although the 1,3,2,4-dioxadisiletane rings are generally nearly

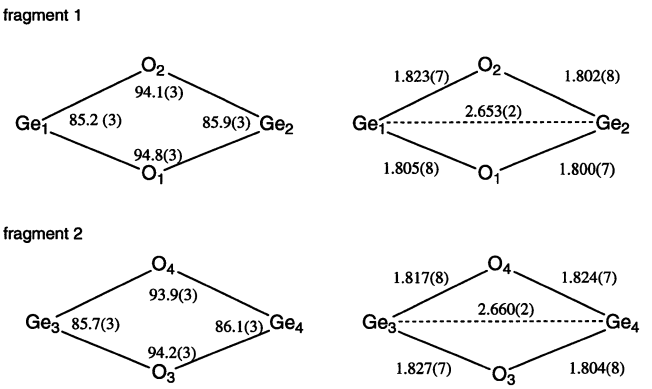


Fig. 5. Selected bond lengths (Å) and angles (°) for **7a** (fragments 1 and 2).

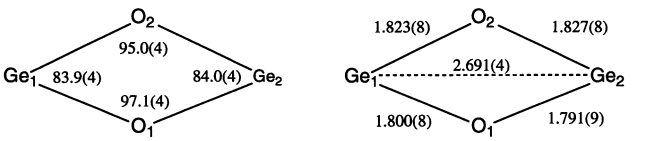


Fig. 6. Selected bond lengths (Å) and angles (°) for **7b**.

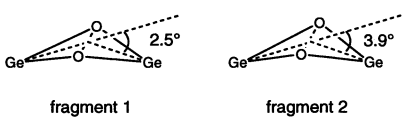


Fig. 7. Dihedral angles of **7a** (fragments 1 and 2).

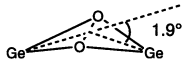


Fig. 8. A dihedral angle of **7b**.

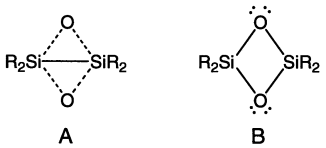
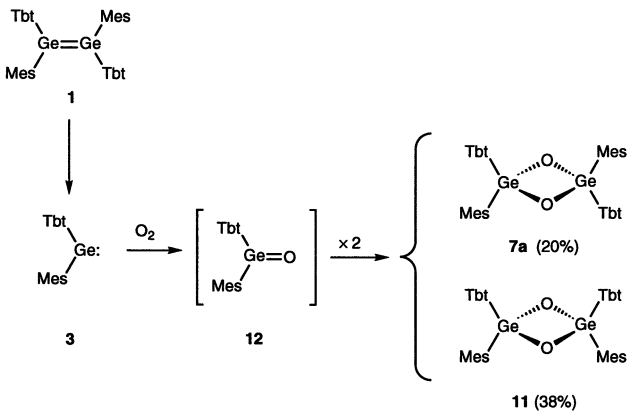


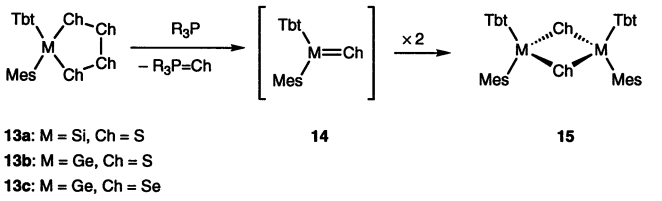
Fig. 9. Schematic representation for the core ring structure of 1,3,2,4-dioxadisiletanes.



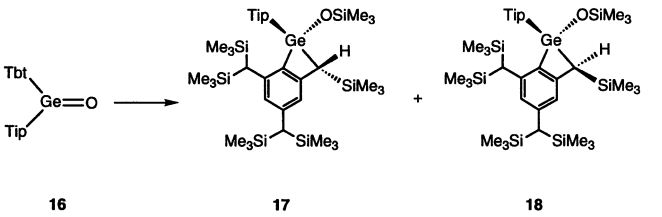
Scheme 5.

planar as in the case of the dioxadigermetane rings, the silicon–silicon distances are as long as, or even shorter than a typical Si–Si single bond lengths [22]. Two extreme qualitative explanations have been postulated for these structures (Fig. 9): (1) there is a σ bond between the two silicon atoms, and the Si–O bonds are necessarily electron deficient (structure A) and (2) the strong repulsion between the oxygen atoms causes the silicon atom to be close together, but there is no bonding between them (structure B). NMR studies confirmed the view that there is no σ bonding between the silicons [23].

The structural difference between the 1,3,2,4-dioxadisiletane and their germanium analogues is explained as follows; the Si–O bond lengths are too short to release the repulsion between the oxygen atoms. As a result, the silicon–silicon distances are close to a Si–Si single bond length, whereas the Ge–O bond lengths are



Scheme 7.



Scheme 8.

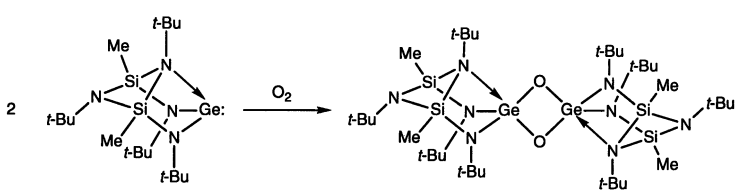
long enough to release the repulsion between the oxygen atoms.

2.4.2. Reaction of *1* with oxygen in solution

The reaction of digermene **1** with oxygen in solution gave *trans*-1,3,2,4,-dioxadigermetane **7a** (20%) and *cis*-1,3,2,4,-dioxadigermetane **11** (38%) as shown in Scheme 5, although the reaction of **1** with oxygen in the solid state gave only the *trans*-1,3,2,4-dioxadigermetanes **7a** and **7b** stereospecifically (vide supra). The most plausible reaction mechanism is that digermene **1** dissociates into the corresponding germylene **3** in solution and **3** readily reacts with molecular oxygen to give the germanium–oxygen double-bond species (germanone) **12**, which might dimerize to afford *trans*- and *cis*-1,3,2,4,-dioxadigermetanes as in the case of the previously reported germylene (Scheme 6) [24].

It is noteworthy that Tbt- and Mes-substituted metallanethiones (**14a** and **14b**) and metallaneselone **14c** derived from the dechalcogenation of 1,2,3,4,5-tetrachalcogenamatallolanes **13** dimerized to give only the *cis*-substituted 1,3,2,4-dichalcogenadimetalletanes **15** (Scheme 7) [25].

The lack of stereoselectivity in the dimerization of germanone **12** is explicable in terms of its high reactivity. It has already been reported that the germanone Tbt(Tip)Ge=O (**16**) readily underwent intramolecular C–Si insertion to give **17** and **18** in solution (Scheme 8),



Scheme 6.

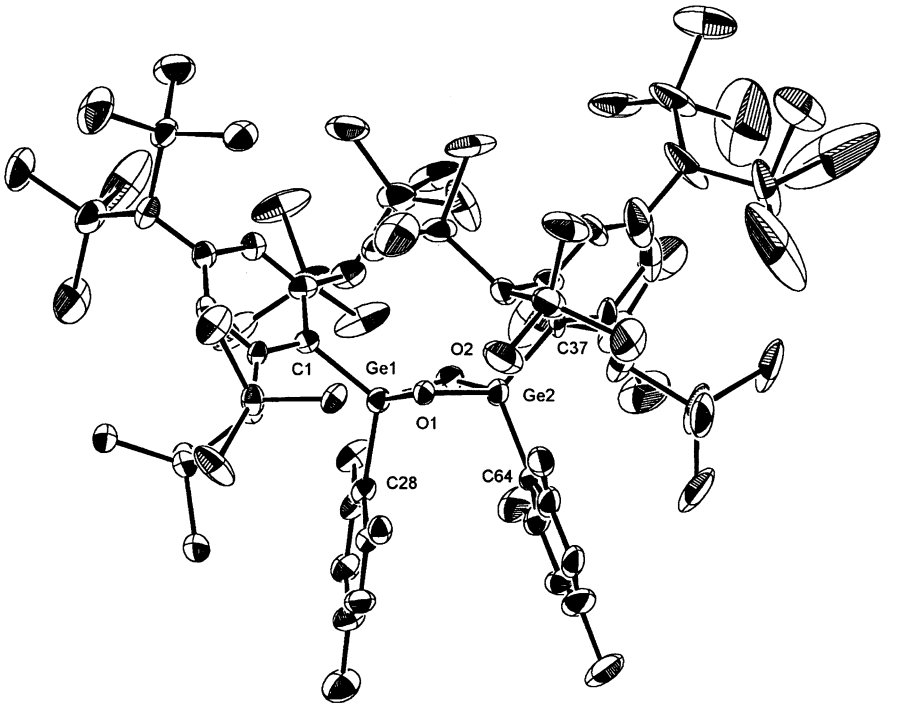


Fig. 10. ORTEP drawing of *cis*-1,3,2,4-dioxadigermetane **11** with thermal ellipsoid plots (30% probability).

although Tbt(Tip)Ge=S (**19**) and Tbt(Tip)Ge=Se (**20**) were stable in solution [25,26]. The fact that germanone **16** shows quite a different reactivity from germanethione **19** and germaneselone **20** is probably due to the difference in the polarity of Ge=X (X = O, S, and Se) [25,26]. The high polarity of the Ge=O has been predicted by ab initio calculation for dimethylgermanone [27].

The molecular geometry of the *cis*-1,3,2,4-dioxadigermetane **11** was also determined by X-ray crystallographic analysis. In Fig. 10 is shown the ORTEP drawing of **11**, and some selected structural parameters for **11** are schematically illustrated in Fig. 11. Fig. 11(a) shows selected bond lengths and angles for the central dioxadigermetane ring in **11**. Fig. 11(b) shows that the dihedral angle formed by two O–Ge–O planes is 19.4°. In the case of *trans*-1,3,2,4-dioxadigermetanes **7a** (fragment 1 and fragment 2) and **7b**, the dihedral angles of the central ring are 2.5°, 3.9°, and 1.9°, respectively. These facts show that the steric repulsion between two Tbt groups facing each other may be released by folding the four-membered ring in the *cis*-1,3,2,4-dioxadigermetane **11**. The large folding angles have also been observed in the Tbt- and Mes-substituted *cis*-1,3,2,4-dichalcogenadimetalletane derivatives [25].

2.4.3. Stability of the oxidation products

In the oxidation of digermene **1** in the solid state, two conformational isomers (**7a** and **7b**) of a 1,3,2,4-dioxadigermetane were obtained as oxidation products. In order to investigate the possible interconversion between them, the thermolysis of **7a** and **7b** was monitored by ^{1}H NMR spectroscopy. Although no change was observed for compound **7a** at 85 °C, compound **7b** decomposed to afford the *trans*-1,3,2,4-dioxadigermetane **7a** (34%) under the same conditions (Scheme 9). When a mixture of **7b** and methanol or mesitonitrile oxide, which are useful trapping reagents for a germanone [26], was heated at 85 °C, the corresponding trapping product of germanone **12**, i.e. methoxygermanol **21** (56%) or dioxazagermole **22** (33%), was obtained together with the isomerized *trans*-1,3,2,4-dioxadigermetane **7a** (Scheme 9) [26]. On the other hand, **7a** did not give any methanolysis products in the presence of methanol under the same conditions. These

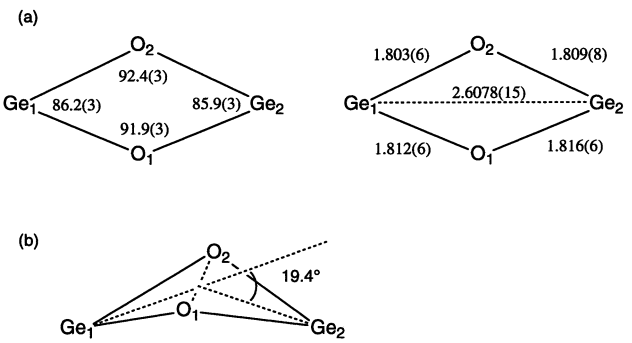
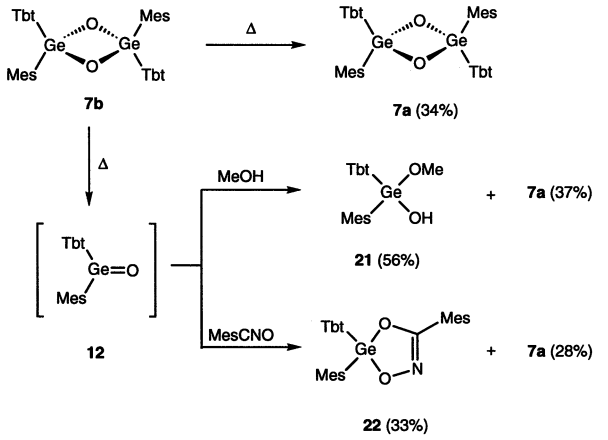
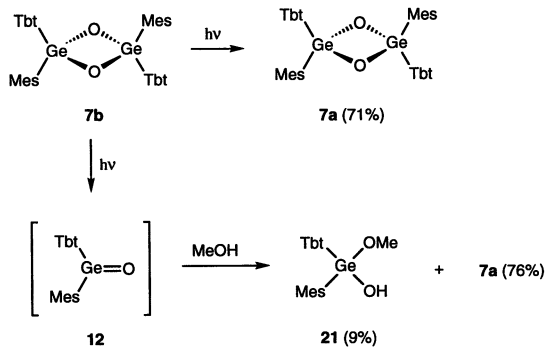


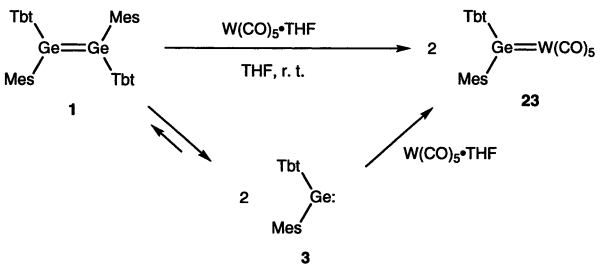
Fig. 11. (a) Selected bond lengths (Å) and angles (°) for **11**. (b) A dihedral angle between planes O(1)–Ge(1)–O(2) and O(1)–Ge(2)–O(2).



Scheme 9.



Scheme 10.



Scheme 11.

facts show that germanone **12** is generated in the thermolysis of **7b** and then **12** reacts with methanol or mesitonitrile oxide to give the methoxygermanol **21** or [3 + 2]cycloadduct **22**, respectively.

Since the 1,3,2,4-dioxadigermetane **7b** was found to dissociate thermally into the germanone **12**, we next examined the photolysis of **7a** and **7b**. Upon photolysis **7b** gave another *trans*-1,3,2,4-dioxadigermetane **7a** (71%). Dioxadigermetane **7b** was irradiated in the presence of methanol to afford **7a** (76%) and methoxygermanol **21** (9%) (Scheme 10). On the other hand, photolysis of **7a** in the presence of methanol under the same conditions did not give any photoreaction products but resulted in the complete recovery of **7a**. These results show that germanone **12** is only generated by the photolysis of the more hindered conformational isomer **7b** of the two *trans*-1,3,2,4-dioxadigermetanes.

*2.4.4. Reaction of germylene **3** derived from digermene **1** with $W(CO)_5$·THF*

In order to verify the ability of steric protection afforded by the combination of Tbt and Mes groups, we have examined the reaction of the diarylgermylene, Tbt(Mes)Ge: (**3**), generated by the dissociation of the corresponding digermene **1** in solution, with tungsten pentacarbonyl tetrahydrofuran complex.

When digermene **1** was treated with $W(CO)_5$·THF in THF at room temperature, the color of the solution changed from blue to orange suggesting the formation of the expected terminal tungsten complex of germylene, Tbt(Mes)Ge=$W(CO)_5$ (**23**) (Scheme 11). Although the tungsten complex **23** was separated from the reaction mixture by silica gel column chromatography, the further purification by GPLC resulted in the decomposition probably due to the reaction with moisture or oxygen even if toluene was used as an eluent. This marginal stability of **23** is in sharp contrast to that of the more crowded germylene–tungsten complex, Tbt(Tip)Ge=$W(CO)_5$ [15c], which is quite stable in solution or in the solid state and can be purified by GPLC and silica gel column chromatography without any decomposition. These results suggest that at least the steric protection afforded by the combination of Tbt and Tip groups is indispensable to isolate the germylene-transition metal complexes as stable compounds.

3. Conclusion

An extremely hindered digermene (*E*)-Tbt(Mes)Ge=Ge(Mes)Tbt (**1**) was synthesized, and its X-ray crystallographic analysis revealed a remarkable elongation of the Ge=Ge double bond of **1**. The temperature-dependent change in the electronic spectra of **1** indicated the quantitative interconversion between **1** and the corresponding germylene Tbt(Mes)Ge: (**3**) in solution. Since the reactivity of germylene **3** is much higher than that of digermene **1**, almost all the intermolecular reactions of **1** in solution proceeded via dissociated **3**. For example, the reaction of **1** with oxygen in solution resulted in a non-stereospecific formation of the *cis*- and *trans*-1,3,2,4-dioxadigermetanes **11** and **7** via the initial formation of germanone **12** derived from oxygenation of the dissociated germylene **3**. In case of the oxidation of **1** in the solid state, however, digermene **1** reacted with O_2 molecule as a Ge=Ge double bond compound to give the corresponding *trans*-1,3,2,4-dioxadigermetanes (**7a** and **7b**; isolable and separable conformational isomers) stereospecifically. In addition, it was revealed that an extremely

hindered tetraaryl-substituted *trans*-1,3,2,4-dioxadigermetane **7b** decomposes to generate the corresponding germanone **12** by both thermolysis and photolysis.

Further investigation of physical and chemical properties of the newly obtained, overcrowded digermene **1** and dioxadigermetanes **7** and **11** is currently in progress.

4. Experimental

All experiments were performed under argon atmosphere otherwise noted. THF was purified by distillation from sodium benzophenone ketyl before use. All solvents used in the reactions were purified by the reported method. The ^{1}H (500 MHz), ^{13}C (126 MHz) NMR spectra were measured in $CDCl_3$ and C_6D_6 with a Bruker AM-500, JEOL α-500, or JEOL AL-300 spectrometer with $CHCl_3$ and C_6D_5H as internal standard. Preparative gel permeation liquid chromatography (GPLC) was performed on LC-908 (JAI gel 1H and 2H columns) with chloroform as an eluent. Preparative thin-layer chromatography (PTLC) and dry column chromatography (DCC) were performed with Merck Kieselgel 60 PF 254 (Art. No. 7747) and ISN silica DCC 60A. Electronic spectra were recorded on a JASCO Ubest-50 UV–Vis spectrometer. All melting points (m.p.) were determined on a Yanaco micro melting point apparatus and are uncorrected. Elemental analyses were carried out at the Microanalytical Laboratory of Department of Chemistry, Faculty of Science, The University of Tokyo.

4.1. Preparation of (E)-1,2-dimesityl-1,2-bis{2,4,6-tris[bis(trimethylsilyl)methyl]phenyl}digermene (1)

To a solution of dichlorogermane **2** [28] (1.36 g, 1.67 mmol) in THF (70 ml) was added lithium naphthalenide (0.54 M, 3.6 mmol) at −78 °C, and the mixture was warmed up to room temperature (r.t.). After removal of the solvent, hexane was added to the residue to precipitate inorganic salts. The filtrate was subjected to sublimation in vacuo for 3 h at 60 °C. Then the residue was washed with hexane several times to afford digermene **1** (288 mg, 0.19 mmol, 23%).

1: Orange crystals (hexane), m.p. (dec.) 92 °C; ^{1}H NMR (500 MHz, C_6D_6, 300 K) δ 0.19 (s, 18H), 0.21 (s, 18H), 0.23 (s, 18H), 1.52 (s, 1H), 2.15 (s, 2H), 2.17 (s, 3H), 2.59 (brs, 6H), 6.55 (s, 1H), 6.67 (s, 1H), 6.77 (s, 2H).

4.2. Observation of an equilibrium between digermene 1 and germylene 3 and estimation of the thermodynamic parameters (ΔH, ΔS) for the dissociation of 1 to 3

In a quartz UV cell was placed a hexane solution (5 ml) of digermene **1** (3.2 mg). After two freeze–pump–thaw cycles, the cell was evacuated and sealed. The absorbance of the solution was observed at each temperature (Fig. 2) on a variable temperature liquid nitrogen cryostat DN1704 (Oxford Instruments Limited) and the temperature was monitored by a temperature controller model ITC (Oxford Instruments Limited) with the calibration error being ±0.2 °C.

The thermodynamic parameters (ΔH, ΔS) for dissociation of digermene **1** to germylene **3** were calculated by the equation below.

$$\ln(A_B^2/A_A) = -\Delta H/RT + (\Delta S/R - \ln(\varepsilon_A/\varepsilon_B^2)) \quad (1)$$

$$A_B = -(2\varepsilon_B/\varepsilon_A)A_A + C \quad (2)$$

A_A and ε_A are the absorbance and the molar absorption coefficient of **1**, respectively, and A_B and ε_B are that of **3**. C is a constant. The absorbances of digermene **1** and germylene **3** were obtained at 439 nm for **1** and at 575 nm for **3**. The ε_B was determined by a separate experiment for a hexane solution which was prepared by adding hexane (6 ml) to a hexane solution (3 ml) of **1** (2.0 mg, 0.0013 mmol). Their statistical errors were calculated by a standard method.

$\Delta H = 14.7 \pm 0.2$ kcal mol^{-1} and

$\Delta S = 42.4 \pm 0.8$ cal mol^{-1} K^{-1}

($\lambda_{max} = 439$ nm, ε_B 2.0×10^4)

($\lambda_{max} = 575$ nm, ε_A 1.6×10^3)

4.3. Reaction of digermene 1 with methanol

To an orange–yellow solution of **1** (65.5 mg, 0.044 mmol) in THF (5 ml) was added methanol (50 μl, 1.23 mmol) at −100 °C. The orange–yellow color due to **1** did not disappear after 6 h at same temperature, but the solution became colorless on warming up to r.t. After removal of the solvent, the reaction residue was chromatographed over GPLC and PTLC (SiO_2 with hexane) to afford methoxygermene **4** (30.2 mg, 0.039 mmol, 44%).

4: White crystals, m.p. 174–176 °C; ^{1}H NMR (500 MHz, $CDCl_3$, 300 K) δ −0.15 (s, 9H), −0.08 (s, 9H), 0.048 (s, 18H), 0.051 (s, 18H), 1.11 (s, 1H), 2.18 (s, 1H), 2.26 (s, 3H), 2.47 (s, 6H), 2.57 (s, 1H), 3.39 (s, 3H), 6.24 (s, 1H), 6.40 (s, 1H), 6.45 (s, 1H), 6.82 (s, 2H); ^{13}C NMR (126 MHz, $CDCl_3$, 300 K) δ 0.33 (q), 0.63 (q), 0.74 (q), 0.81 (q), 0.95 (q), 1.31 (q), 21.08 (q), 23.75 (q), 26.68 (d), 26.78 (d), 30.34 (d), 53.70 (q), 122.77 (d), 127.40 (d), 128.21 (s), 128.79 (d), 133.10 (s), 139.38 (s), 143.38 (s), 144.37 (s), 150.20 (s), 150.82 (s). *Anal.* Calc. for $C_{37}H_{74}OGeSi_6$: C, 57.26; H, 9.61. Found: C, 56.88; H, 9.45%.

4.4. Reaction of **1** with Et_3SiH

To a solution of **1** (63.7 mg, 0.043 mmol) in THF (3 ml) was added Et_3SiH (100 μl, 0.63 mmol) at r.t. The solution was stirred for overnight. After removal of the solvent, the reaction residue was chromatographed over GPLC and WCC (SiO_2 with hexane) to afford silylgermane **5** (51.5 mg, 0.060 mmol, 70%).

5: White crystals, m.p. (dec.) 168–170 °C; ^{1}H NMR (500 MHz, $CDCl_3$, 300 K) δ −0.20 (s, 9H), −0.14 (s, 9H), 0.02 (s, 9H), 0.03 (s, 9H), 0.09 (s, 9H), 0.10 (s, 9H), 0.77 (q, $J = 7.8$ Hz, 6H), 0.89 (t, $J = 7.8$ Hz, 9H), 1.26 (s, 1H), 1.96 (brs, 3H), 1.98 (s, 1H), 2.05 (s, 1H), 2.19 (s, 3H), 2.50 (brs, 3H), 5.09 (s, 1H), 6.29 (s, 1H), 6.41 (s, 1H), 6.63 (s, 1H), 6.78 (s, 1H); ^{13}C NMR (126 MHz, $CDCl_3$, 300 K) δ 0.91 (q), 1.01 (q), 1.05 (q), 1.17 (q), 1.68 (q), 1.78 (q), 5.21 (t), 8.12 (q), 20.96 (q), 25.48 (q), 26.52 (q), 29.10 (d), 29.55 (d), 30.13 (q), 122.78 (d), 128.04 (d), 128.46 (dx2), 133.60 (s), 136.86 (s), 137.36 (s), 141.94 (s), 142.49 (s), 143.47 (s), 149.30 (s), 149.90 (s). *Anal.* Calc. for $C_{42}H_{86}GeSi_7 \cdot H_2O$: C, 57.43; H, 10.10. Found: C, 57.79; H, 9.63%.

4.5. Reaction of **1** with 2,3-dimethyl-1,3-butadiene

To a solution of **1** (59.5 mg, 0.040 mmol) in THF (5 ml) was added 2,3-dimethyl-1,3-butadiene (90 μl, 0.80 mmol) at r.t. The solution was stirred for overnight. After removal of the solvent, the reaction residue was chromatographed over GPLC and PTLC (SiO_2 with hexane) to afford germacyclopentene **6** (40.7 mg, 0.049 mmol, 62%).

6: White crystals, m.p. (dec.) 190–192 °C; ^{1}H NMR (500 MHz, $CDCl_3$, 300 K) δ −0.08 (s, 36H), 0.02 (s, 18H), 1.24 (s, 1H), 1.69 (s, 6H), 1.90 (s, 1H), 2.01 (s, 1H), 2.03 (ABq, $J_{AB} = 16$ Hz, $\nu_{AB} = 130$ Hz, 4H), 2.20 (s, 3H), 2.35 (s, 6H), 6.24 (s, 1H), 6.36 (s, 1H), 6.75 (s, 2H); ^{13}C NMR (126 MHz, $CDCl_3$, 300 K) δ 0.83 (q), 1.04 (q), 1.28 (q), 19.31 (q), 20.79 (q), 25.68 (q), 27.48 (d), 27.61 (d), 30.05 (d), 34.56 (t), 122.54 (d), 127.71 (d), 129.01 (d), 130.76 (s), 132.32 (s), 137.67 (s), 141.13 (s), 142.35 (s), 142.73 (s), 150.40 (s), 150.64 (s). *Anal.* Calc. for $C_{42}H_{80}GeSi_6$: C, 61.06; H, 9.76. Found: C, 60.77; H, 9.48%.

4.6. Reaction of digermene **1** with oxygen in the solid state

Finely powdered orange crystals of digermene **1** (47.5 mg, 0.0319 mmol) were exposed to oxygen in the dark for 3 days, during which time the color changed into pale yellow. The crystals were chromatographed over GPLC and PTLC (SiO_2 with hexane) to give two conformational isomers of *trans*-2,4-dimesityl-2,4-bis{2,4,6-tris[bis(trimethylsilyl)methyl]phenyl}-1,3,2,4-dioxadigermetanes (**7a**) (6.3 mg, 0.0041 mmol, 13%) and **7b** (23.9 mg, 0.0199 mmol, 49%).

7a: White crystals ($CHCl_3$–EtOH), m.p. >300 °C; ^{1}H NMR (500 MHz, C_6D_6, 350 K) δ −0.04 (s, 72H), 0.00 (s, 36H), 1.51 (s, 2H), 2.13 (s, 6H), 2.85 (brs, 12H), 3.09 (s, 2H), 6.57 (s, 4H), 6.73 (s, 4H) (the peak assignable to methine protons of *o*-bis(trimethylsilyl)methyl groups of Tbt group was not observed); HRMS (FAB) m/z 1519.6611 ($[M+H]^+$), calc. for $C_{72}H_{140}O_2{}^{72}Ge^{74}GeSi_{12}$ 1519.6595. *Anal.* Calc. for $C_{72}H_{140}O_2Ge_2Si_{12}$: C, 56.88; H, 9.28. Found: C, 56.10; H, 8.76%.

7b: White crystals ($CHCl_3$–EtOH), m.p. (dec.) 153–155 °C; ^{1}H NMR (500 MHz, C_6D_6, 350 K) δ −0.07 (s, 36H), 0.19 (s, 18H), 0.23 (s, 18H), 0.32 (s, 18H), 0.48 (s, 18H), 1.53 (s, 2H), 1.87 (s, 2H), 2.16 (s, 6H), 2.26 (s, 6H), 2.94 (s, 6H), 3.40 (s, 2H), 6.63 (s, 2H), 6.69 (s, 2H), 6.74 (s, 2H), 6.78 (s, 2H); *Anal.* Calc. for $C_{72}H_{140}O_2Ge_2Si_{14}$: C, 56.88; H, 9.28. Found: C, 56.08; H, 9.01%.

4.7. Reaction of digermene **1** with oxygen in solution

To a solution of **1** (67.0 mg, 0.045 mmol) in THF (5 ml) was bubbled oxygen dried by passing through sulfuric acid and Sicapent® at r.t. The solution was stirred overnight. After removal of the solvent, the reaction residue was chromatographed over GPLC and PTLC (SiO_2 with hexane) to afford *trans*-1,3,2,4-dioxadigermetane **7a** (13.7 mg, 0.009 mmol, 20%) and *cis*-2,4-dimesityl-2,4-bis{2,4,6-tris[bis(trimethylsilyl)-methyl]phenyl}-1,3,2,4-dioxadigermetane (**11**) (25.8 mg, 0.017 mmol, 38%).

11: White crystals ($CHCl_3$–EtOH), m.p. >300 °C; ^{1}H NMR (500 MHz, C_6D_6, 350 K) δ 0.19 (s, 18H), 0.25 (s, 36H), 0.38 (s, 18H), 0.40 (s, 18H), 0.51 (s, 18H), 1.57 (s, 2H), 2.07 (s, 2H), 2.12 (s, 6H), 2.45 (s, 6H), 2.75 (brs, 6H), 3.25 (s, 2H), 6.38 (s, 2H), 6.65 (s, 4H), 6.69 (s, 2H); HRMS (FAB) m/z 1519.6611 ($[M+H]^+$), calc. for $C_{72}H_{140}O_2{}^{72}Ge^{74}GeSi_{12}$ 1519.6595. *Anal.* Calc. for $C_{72}H_{140}O_2Ge_2Si_{12}$: C, 56.88; H, 9.28. Found: C, 56.80; H, 8.99%.

4.8. Thermolysis of 1,3,2,4-dioxadigermetane **7b**

In a 5 mm NMR tube was placed a C_6D_6 solution (0.6 ml) of **7b** (12.8 mg, 0.0084 mmol). After three freeze–pump–thaw cycles, the tube was evacuated and sealed. When the solution was heated at 85 °C for 18.5 h, the ^{1}H NMR spectrum of the reaction mixture showed the absence of starting material **7b**. After removal of the solvent, the residue was separated by PTLC (SiO_2 with hexane) to afford **7a** (4.3 mg, 0.0028 mmol, 34%).

4.9. Thermolysis of 1,3,2,4-dioxadigermetane **7a**

In a 5 mm NMR tube was placed a C_6D_6 solution (0.6 ml) of **7a** (13.2 mg, 0.0087 mmol). After three freeze–pump–thaw cycles, the tube was evacuated and sealed. When the solution was heated at 85 °C for 21 h, no change was observed in the ^{1}H NMR spectrum.

4.10. Thermal reaction of **7b** with methanol

In a 5 mm NMR tube was placed a $CDCl_3$ solution (0.6 ml) of **7b** (13.0 mg, 0.0086 mmol) and methanol (50 μl, 1.24 mmol). After three freeze–pump–thaw cycles, the tube was evacuated and sealed. When the solution was heated at 85 °C for 18.5 h, the ^{1}H NMR spectrum of the reaction mixture showed the absence of starting material **7b**. After removal of the solvent the residue was separated by PTLC (SiO_2 with hexane) to afford **7a** (4.9 mg, 0.0032 mmol, 37%) and (hydroxyl)mesityl-(methoxy){2,4,6-tris[bis(trimethylsilyl)methyl]-phenyl}-germane (**21**) (7.5 mg, 0.0097 mmol, 56%).

21: ^{1}H NMR (500 MHz, $CDCl_3$, 300 K) δ −0.18 (s, 9H), −0.11 (s, 9H), 0.028 (s, 18H), 0.032 (s, 18H), 1.30 (s, 1H), 1.41 (s, 1H), 2.25 (s, 3H), 2.50 (s, 6H + 1H), 2.81 (s, 1H), 3.35 (s, 3H), 6.25 (s, 1H), 6.39 (s, 1H), 6.81 (s, 2H); ^{13}C NMR (126 MHz, $CDCl_3$, 300 K) δ 0.37 (q), 0.70 (q), 0.82 (q), 1.13 (q), 1.43 (q), 21.00 (q), 23.96 (q), 26.91 (d × 2), 30.50 (d), 50.34 (q), 122.90 (d), 127.63 (d), 129.29 (d), 129.59 (s), 131.96 (s), 139.83 (s), 143.67 (s), 145.28 (s), 150.58 (s), 150.90 (s).

4.11. Thermal reaction of **7b** with mesitonitrile oxide

In a 5 mm NMR tube was placed a $CDCl_3$ solution (0.6 ml) of **7b** (14.4 mg, 0.0093 mmol) and mesitonitrile oxide (79.8 mg, 0.50 mmol). After three freeze–pump–thaw cycles, the tube was evacuated and sealed. When the solution was heated at 85 °C for 32 h, the ^{1}H NMR spectrum of the reaction mixture showed the absence of starting material **7b**. After removal of the solvent, the residue was separated by GPLC and PTLC (SiO_2 with hexane) to afford **7a** (4.0 mg, 0.0026 mmol, 28%), and the second fraction was again separated by PTLC (SiO_2 with $CHCl_3$–hexane 1/1) to afford 2-mesityl-2-{2,4,6-tris[bis(trimethylsilyl)methyl]phenyl}-4-mesityl-1,3,5,2-dioxazagermole (**22**) (5.8 mg, 0.0063 mmol, 34%).

22: ^{1}H NMR (500 MHz, $CDCl_3$, 300 K) δ −0.07 (s, 18H), 0.00 (s, 9H), 0.03 (s, 9H), 0.05 (s, 9H), 0.06 (s, 9H), 1.38 (s, 1H), 2.07 (s, 6H), 2.10 (s, 1H), 2.22 (s, 1H), 2.23 (s, 6H), 2.52 (s, 6H), 6.36 (s, 1H), 6.49 (s, 1H), 6.775 (s, 2H), 6.782 (s, 2H); HRMS (FAB) m/z 922.4185 ($[M+H]^+$), calc. for $C_{46}H_{82}O_2N^{74}GeSi_6$ 922.4173.

4.12. Thermal reaction of **7a** with methanol

In a 5 mm NMR tube was placed a $CDCl_3$ solution (0.6 ml) of **7a** (13.0 mg, 0.0086 mmol) and methanol (50 μl, 1.24 mmol). After three freeze–pump–thaw cycles, the tube was evacuated and sealed. When the solution was heated at 85 °C for 21 h, no change was observed in the ^{1}H NMR spectrum.

4.13. Photolysis of **7b**

In a 5 mm NMR tube was placed a $CDCl_3$ solution (0.6 ml) of **7b** (12.5 mg, 0.0082 mmol). After five freeze–pump–thaw cycles, the tube was evacuated and sealed. The solution was irradiated with a 400 W high pressure Hg lamp approximately −45 °C for 14 min. After removal of the solvent, the residue was separated by PTLC (SiO_2 with hexane) to afford **7a** (8.8 mg, 0.0058 mmol, 71%).

4.14. Photolysis of **7b** in the presence of methanol

In a 5 mm NMR tube was placed a $CDCl_3$ solution (0.6 ml) of **7b** (12.5 mg, 0.0082 mmol) and methanol (50 μl, 1.2 mmol). After three freeze–pump–thaw cycles, the tube was evacuated and sealed. When the solution was irradiated with a 400 W high-pressure Hg lamp at approximately −45 °C for 16 min. After removal of the solvent, the residue was separated by PTLC (SiO_2 with hexane) to afford **7a** (9.5 mg, 0.063 mmol, 76%) and hydroxy(methoxy)germane **21** (1.2 mg, 0.0015 mmol, 9%).

4.15. Photolysis of **7a** in the presence of methanol

In a 5 mm NMR tube was placed a $CDCl_3$ solution (0.6 ml) of **7a** (11.8 mg, 0.0078 mmol) and methanol (60 μl, 1.4 mmol). After three freeze–pump–thaw cycles, the tube was evacuated and sealed. The solution was irradiated with a 400 W high pressure Hg lamp at approximately −45 °C for 20 min. The ^{1}H NMR spectrum of the reaction mixture showed no signal of **21**.

4.16. [{2,4,6-Tris[bis(trimethylsilyl)methyl]phenyl}-(2,4,6-trimethylphenyl)germylidene]pentacarbonyltungsten(0) (**23**)

To a THF solution (2 ml) of digermene **1** (0.279 g, 0.187 mmol) was added an excess of $W(CO)_5$(THF), which was prepared by the photolysis of $W(CO)_6$ (0.173 g, 0.491 mmol) in 15 ml of THF using a 100 W high pressure mercury lamp [29]. After stirring for 12 h at r.t., the reaction mixture was evaporated to give an

orange–yellow paste. The orange–yellow paste was purified by flush column chromatography (SiO_2–hexane) to give the pentacarbonyltungsten(0) complex **23** (0.124 g, ca. 31%) as an orange solid. Complete purification of **23** was failed due to its instability in the open air. **23**: ^{1}H NMR ($CDCl_3$, 300 MHz) δ −0.04 (s, 9H), 0.04 (s, 9H), 0.05 (s, 27H), 0.10 (s, 9H), 1.37 (s, 1H), 2.21 (s, 6H), 2.24 (s, 3H), 2.45 (s, 1H), 2.48 (s, 1H), 6.37 (br s, 1H), 6.44 (br s, 1H), 6.75 (s, 2H). IR(KBr) 1943,1949, 2068 cm^{-1}. UV–Vis(CH_2Cl_2) 432 nm (ε, 14 000).

4.17. X-ray data collection for [1·0.5hexane], [7a·hexane], 7b, and 11

Single crystals of [**1**·0.5hexane], [**7a**·hexane], **7b**, and **11** were grown by the slow evaporation of the saturated solution of each compounds in hexane at r.t. All measurements were made on a Rigaku AFC7R diffractometer (for [**1**·0.5hexane], [**7a**·hexane], and **7b)** with graphite monochromated Mo Kα radiation (λ = 0.71069 Å) and a rotating anode generator and on a Rigaku/MSC Mercury CCD for **11** with graphite monochromated Mo Kα radiation (λ = 0.71070 Å). An orange prismatic crystal of [**1**·0.5hexane] was mounted in a glass capillary, while the other crystals of [**7a**·hexane], **7b**, and **11** were subjected to data collection without sealing. The structure was solved by direct methods (SHELXS-97) and refined by full-matrix least-squares procedures on F^2 for all reflections (SHELXL-97) [30]. In all cases non-hydrogen atoms were refined anisotropically, while all hydrogens except for those of solvated hexane were placed using AFIX instructions. As for the solvated hexane for [**1**·0.5hexane] and [**7a**·hexane], all non-hydrogen atoms were refined isotropically, and the intramolecular C–C bond lengths and angles are restrained to be ideal lengths using DFIX instruction.

Crystal data for [**1**·0.5hexane]: $C_{72}H_{140}Ge_2Si_{12}\cdot 0.5C_6H_{14}$, FW = 1531.19, crystal dimensions 0.30 × 0.20 × 0.15 mm, monoclinic, space group $P2_1/c$ (# 14), a = 18.779(7), b = 18.375(7), c = 28.495(16) Å, β = 96.53(4)°, V = 9769(7) Å^3, Z = 4, D_{calc} = 1.041 g cm^{-3}, μ(Mo Kα) = 7.96 cm^{-1}, $2\theta_{max}$ = 50°, T = 173(2) K, R_1 = 0.1177 [$I > 2\sigma(I)$], wR_2 = 0.2991 (all data), GOF = 0.841. The largest difference peak and hole were 0.816 and −0.605 e Å^{-3}. The final cycle of full-matrix least-squares refinement was based on 17158 reflections and 799 variable parameters with nine restraints.

Crystal data for **7a**·hexane: $C_{72}H_{140}Ge_2O_2Si_{12}\cdot C_6H_{14}$, FW = 1606.27, crystal dimensions 0.60 × 0.55 × 0.05 mm, triclinic, space group $P\bar{1}$ (# 2), a = 23.735(7), b = 30.169(11), c = 13.533(3) Å, α = 95.60(3)°, β = 90.47(2)°, γ = 88.16(3)°, V = 9639(5) Å^3, Z = 4, D_{calc} = 1.107 g cm^{-3}, μ(Mo Kα) = 8.11 cm^{-1}, $2\theta_{max}$ = 50°, T = 296(2) K, R_1 = 0.0945 [$I > 2\sigma(I)$] and wR_2 = 0.2651 (all data), GOF = 0.928. The largest difference peak and hole were 0.849 and −1.266 e Å^{-3}. The final cycle of full-matrix least-squares refinement was based on 25212 reflections and 1631 variable parameters with 20 restraints.

Crystal data for **7b**: $C_{72}H_{140}Ge_2O_2Si_{12}$, FW = 1520.10, crystal dimensions 0.20 × 0.10 × 0.05 mm, triclinic, space group $P\bar{1}$ (# 2), a = 21.28(2), b = 16.103(13), c = 16.105(14) Å, α = 84.36(7)°, β = 109.00(7)°, γ = 71.01(7)°, V = 4804(8) Å^3, Z = 2, D_{calc} = 1.051 g cm^{-3}, μ(Mo Kα) = 8.10 cm^{-1}, $2\theta_{max}$ = 45°, T = 296(2) K, R_1 = 0.1013 [$I > 2\sigma(I)$] and wR_2 = 0.1735 (all data), GOF = 0.807. The largest difference peak and hole were 0.371 and −0.664 e Å^{-3}. The final cycle of full-matrix least-squares refinement was based on 12566 reflections and 784 variable parameters with two restraints. The rigid-bond restraint to U_{ij}-values of two bonded atoms using DELU construction were applied to the *ortho*- and *para*- C–C bonds of one Tbt group (C40–C44 and C42–C45).

Crystal data for **11**: $C_{72}H_{140}Ge_2O_2Si_{12}$, FW = 1520.10, crystal dimensions 0.60 × 0.55 × 0.10 mm, orthorhombic, space group $Pna2_1$ (# 33), a = 22.135(6), b = 30.788(8), c = 13.214(4) Å, $\alpha = \beta = \gamma$ = 90°, V = 9005(4) Å^3, Z = 4, D_{calc} = 1.121 g cm^{-3}, μ(Mo Kα) = 8.64 cm^{-1}, $2\theta_{max}$ = 50°, T = 103(2) K, R_1 = 0.1049 [$I > 2\sigma(I)$] and wR_2 = 0.2495 (all data), GOF = 1.079. The largest difference peak and hole were 0.864 and −0.989 e Å^{-3}. The final cycle of full-matrix least-squares refinement was based on 14179 reflections and 793 variable parameters with eight restraints. One of the carbon atoms of the trimethylsilyl group at *para*-position of a Tbt group was restrained to be approximately isotropic (C56).

5. Supplementary material

All the crystallographic data (excluding structure factors) of [**1**·0.5hexane], [**7a**·hexane], **7b**, and **11** have already been deposited at the Cambridge Crystallographic Data Centre as supplementary publication numbers CCDC 169633, 169634, 169635, and 169636, respectively. Copies of the data can be obtained free of charge on application to CCDC, 12 Union Road, Cambridge CB21EZ, UK (fax: +44-1233-336-033, e-mail: deposit@ccdc.cam.ac.uk).

Acknowledgements

This work was partially supported by Grants-in-Aid for Scientific Research from the Ministry of Education,

Culture, Sports, Science and Technology, Japan. We are also grateful to Shin-etsu Chemical Co., Ltd., and Tosoh Akzo Co., Ltd., for the generous gift of chlorosilanes and alkyllithiums, respectively. T. S. thanks Research Fellowships of the Japan Society for the Promotion of Science for Young Scientists.

References

[1] For recent reviews, see: (a) G. Raabe, J. Michl, Chem. Rev. 85 (1985) 419;
(b) J. Barrau, J. Escudié, J. Satgé, Chem. Rev. 90 (1990) 283;
(c) T. Tsumuraya, S.A. Batcheller, S. Masamune, Angew. Chem., Int. Ed. Engl. 30 (1991) 902;
(d) M. Driess, H. Grützmacher, Angew. Chem., Int. Ed. Engl. 35 (1996) 828;
(e) R. Okazaki, R. West, R. Adv. Organomet. Chem. 39 (1996) 232;
(f) K.M. Baines, W.G. Stibbs, Adv. Organomet. Chem. 39 (1996) 275.

[2] R. West, M.J. Fink, J. Michl, Science (Washington DC) 214 (1981) 1343.

[3] (a) N. Tokitoh, H. Suzuki, R. Okazaki, K. Ogawa, J. Am. Chem. Soc. 115 (1993) 10428;
(b) H. Suzuki, N. Tokitoh, R. Okazaki, Bull. Chem. Soc. Jpn. 68 (1995) 2471.

[4] (a) T. Fjeldberg, A. Haaland, M.F. Lappert, B.E.R. Schilling, R. Seip, A.J. Thorne, J. Chem. Soc., Chem. Commun. (1982) 1407;
(b) J.D. Cotton, P.J. Davidson, M.F. Lappert, J. Chem. Soc., Dalton. Trans. (1976) 2275;
(c) K.W. Zilm, G.A. Lawless, R.M. Merrill, J.M. Millar, G.G. Webb, J. Am. Chem. Soc. 109 (1987) 7236.

[5] K.M. Baines, J.A. Cooke, C.E. Dixon, H.W. Liu, M.R. Netherton, Organometallics 13 (1994) 631.

[6] S.A. Batcheller, T. Tsumuraya, O. Tempkin, W.M. Davis, S. Masamune, J. Am. Chem. Soc. 112 (1990) 9394.

[7] (a) D.E. Goldberg, P.B. Hitchcock, M.F. Lappert, K.M. Thomas, A.J. Thorne, T. Fieldberg, A. Haaland, B.E.R. Schilling, J. Chem. Soc., Dalton Trans. (1986) 2387;
(b) P.B. Hitchcock, M.F. Lappert, S.J. Miles, A.J. Thorne, J. Chem. Soc., Chem. Commun. (1984) 480.

[8] M. Weidenbruch, M. Stürmann, H. Kilian, S. Pohl, W. Saak, Chem. Ber. 130 (1997) 735.

[9] Weidenbruch et al. reported [8] that (2-*t*-Bu-4,5,6-$Me_3C_6H)_2$Ge=Ge(2-*t*-Bu-4,5,6-$Me_3C_6H)_2$ was found to exist as the corresponding monomer, germylene, in solution by cryoscopic molecular weight measurement, but no experimental details are described. Furthermore, the electronic spectra did not show the presence of the monomer in solution.

[10] We have recently succeeded in the synthesis of highly reactive species containing heavier main group elements by taking advantage of the effective protection group, Tbt. For example, see; (a) N. Tokitoh, K. Wakita, R. Okazaki, S. Nagase, P.v.R. Schleyer, H. Jiao, J. Am. Chem. Soc. 119 (1997) 6951;
(b) N. Tokitoh, Y. Arai, R. Okazaki, S. Nagase, Science 277 (1997) 78;
(c) N. Takeda, H. Suzuki, N. Tokitoh, R. Okazaki, S. Nagase, J. Am. Chem. Soc. 119 (1997) 1456;
(d) N. Tokitoh, Pure & Appl. Chem. 71 (1999) 495;
(e) K. Wakita, N. Tokitoh, R. Okazaki, N. Takagi, S. Nagase, J. Am. Chem. Soc. 122 (2000) 5648, and references cited therein.

[11] (a) J.T. Snow, S. Murakami, S. Masamune, D.J. Williams, Tetrahedron Lett. 25 (1984) 4191;
(b) A. Sekiguchi, H. Yamazaki, C. Kabuto, H. Sakurai, J. Am. Chem. Soc. 117 (1995) 8025;
(c) M. Kira, T. Iwamoto, T. Maruyama, C. Kabuto, H. Sakurai, Organometallics 15 (1996) 3767.

[12] (a) L. Ross, M. Dräger, J. Organomet. Chem. 199 (1980) 195;
(b) M. Dräger, L. Ross, Z. Anorg. Allg. Chem. 476 (1981) 95.

[13] (a) A. Schäfer, W. Saak, M. Weidenbruch, Z. Anorg. Allg. Chem. 624 (1998) 1405;
(b) A. Schäfer, W. Saak, M. Weidenbruch, H. Marsmann, G. Henkel, Chem. Ber. 130 (1997) 1733.

[14] Recently, a remarkable temperature dependent thermochromism was observed for a solution of persilylated digermenes. The authors suggested that the thermochromism originated from an equilibrium between two different structures around the Ge=Ge bond. See Ref. [11c].

[15] (a) W. Ando, T. Tsumuraya, A. Sekiguchi, Chem. Lett. (1987) 317;
(b) W. Ando, H. Itoh, T. Tsumuraya, Organometallics 8 (1989) 2759;
(c) N. Tokitoh, K. Manmaru, R. Okazaki, Organometallics 13 (1994) 167;
(d) N. Tokitoh, K. Kishikawa, T. Matsumoto, R. Okazaki, Chem. Lett. (1995) 827.

[16] (a) G. Trinquier, J.-P. Malrieu, P. Rivière, J. Am. Chem. Soc. 104 (1982) 4529;
(b) R.S. Grev, H.F. Schaefer III, K.M. Baines, J. Am. Chem. Soc. 112 (1990) 9458.

[17] H. Suzuki, N. Tokitoh, R. Okazaki, J. Harada, K. Ogawa, S. Tomoda, M. Goto, Organometallics 14 (1995) 1016.

[18] S. Masamune, Y. Eriyama, T. Kawase, Angew. Chem., Int. Ed. Engl. 26 (1987) 584.

[19] K. Kishikawa, N. Tokitoh, R. Okazaki, Chem. Lett. (1998) 239.

[20] (a) M.J. Fink, K.J. Haller, R. West, J. Michl, J. Am. Chem. Soc. 106 (1984) 822;
(b) M.J. Michalczyk, R. West, J. Michl, J. Chem. Soc., Chem. Commun. (1984) 1525;
(c) M.J. Michalczyk, M.J. Fink, K.J. Haller, R. West, J. Michl, Organometallics 5 (1986) 531;
(d) A.J. Millevolte, D.R. Powell, S.G. Johnson, R. West, Organometallics 11 (1992) 1091;
(e) K.L. McKillop, G.R. Gillette, D.R. Powell, R. West, J. Am. Chem. Soc. 114 (1992) 5203.

[21] S. Masamune, S.A. Batcheller, J. Park, W.M. Davis, J. Am. Chem. Soc. 111 (1989) 1888.

[22] H. Sohn, R.P. Tan, D.R. Powell, R. West, Organometallics 13 (1994) 1390 and references cited therein.

[23] H.B. Yokelson, A.J. Millevolte, B.R. Adam, R. West, J. Am. Chem. Soc. 109 (1987) 4116.

[24] M. Veith, S. Becker, V. Huch, Angew. Chem., Int. Ed. Engl. 28 (1989) 1237.

[25] (a) N. Tokitoh, T. Matsumoto, H. Ichida, R. Okazaki, Tetrahedron Lett. 32 (1991) 6877;
(b) H. Suzuki, N. Tokitoh, R. Okazaki, S. Nagase, M. Goto, J. Am. Chem. Soc. 120 (1998) 11096;
(c) T. Matsumoto, N. Tokitoh, R. Okazaki, J. Am. Chem. Soc. 121 (1999) 8811;
(d) N. Tokitoh, T. Matsumoto, R. Okazaki, Bull. Chem. Soc. Jpn. 72 (1999) 1665;
(e) R. Okazaki, N. Tokitoh, Acc. Chem. Res. 33 (2000) 625;
(f) N. Tokitoh, R. Okazaki, Adv. Organomet. Chem. 47 (2001) 121.

[26] (a) N. Tokitoh, T. Matsumoto, R. Okazaki, Chem. Lett. (1995) 1087;
(b) T. Matsumoto, N. Tokitoh, R. Okazaki, Chem. Commun. (1997) 1553.

[27] (a) G. Trinquier, J.C. Barthelat, J. Satgé, J. Am. Chem. Soc. 104 (1982) 5931;
(b) G. Trinquier, M. Pelissier, B. Saint-Roch, H. Lavayssiere, J. Organomet. Chem. 214 (1981) 169.
[28] R. Okazaki, N. Tokitoh, T. Matsumoto, in: W.A. Herrmann (Ed.), Synthetic Methods of Organometallic and Inorganic Chemistry, in: N. Auner, U. Klingebiel (Eds.), vol. 2, Thieme, New York, 1996, pp. 260–269.
[29] W. Strohmeier, F.J. Müller, Chem. Ber. 102 (1969) 3608.
[30] G.M. Sheldrick, SHELXL-97: Program for Crystal Structure Analysis (Release 97-2), University of Göttingen, Göttingen, Germany, 1998.

PERGAMON

Polyhedron 21 (2002) 579–585

POLYHEDRON

www.elsevier.com/locate/poly

Relative stability of multiple bonds between germanium and arsenic. A theoretical study

Chin-Hung Lai [a], Ming-Der Su [b,*], San-Yan Chu [a,*]

[a] *Department of Chemistry, National Tsing Hua University, Hsinchu 30043, Taiwan, ROC*
[b] *School of Chemistry, Kaohsiung Medical University, Kaohsiung 80708, Taiwan, ROC*

Received 17 July 2001; accepted 7 December 2001

Abstract

Substituent effects on the potential energy surface of XGeAs (X = H, Li, Na, BeH, MgH, BH_2, AlH_2, CH_3, SiH_3, NH_2, PH_2, OH, SH, F, and Cl) were investigated by using B3LYP and CCSD(T) methods. The isomers include structures with formal double (Ge=AsX) and triple (XGe≡As) bonds to germanium–arsenic, so a direct comparison of these types of species is possible. Our model calculations indicate that electropositively substituted Ge=AsX species are thermodynamically and kinetically more stable than their isomeric XGe≡As molecules. Moreover, the theoretical findings suggest that F, OH, NH_2, and CH_3 substitution prefer to shift the double bond (Ge=AsX) by forming a triple bond (XGe≡As). © 2002 Elsevier Science Ltd. All rights reserved.

Keywords: B3LYP; CCSD(T); Germanium; Arsenic

1. Introduction

The chemistry of multiple-bond compounds between Group 14 elements and heavier pnicogen atoms has continued to occupy the attention of chemists in various fields [1]. For instance, since HC≡P was characterized spectroscopically by Gier in 1961 [2], phosphorus compounds with low coordination have been studied extensively both experimentally and theoretically [3]. In comparison with this, the area of respective molecules containing multiple bonds to arsenic is rather poorly explored. Although, there have been some successful examples of arsaethene (C=As) [4], arsaethyne (C≡As) [5], and arsasilene (Si=As) [6] stabilized by taking advantage of steric protection groups, neither arsagermene (Ge=As) nor arsagermyne (Ge≡As) have been studied experimentally as yet. This is not very surprising since compounds possessing a germanium–arsenic multiple bond (such as arsagermenes and arsagermynes) are less stable than the corresponding carbon and silicon derivatives. From a synthetic point of view, while steric effects should definitely play an important role in stabilizing the germanium–arsenic multiple bonds, the contribution of electronic effects, which may be even more significant, is still unknown. Knowledge of substituent effects is of great importance in selecting new Ge–As multiple bonded molecules as possible candidates for synthesis or for understanding the nature of the germanium–arsenic bonding.

It is, therefore, worthwhile to investigate the structures and energetics of a series of substituted XGeAs species to gain some insight into the relative stability and instability among these molecules. The substituents X that were chosen from elements of the second and third rows of the periodic table, i.e. X = H, Li, Na, BeH, MgH, BH_2, AlH_2, CH_3, SiH_3, NH_2, PH_2, OH, SH, F, and Cl, exhibit a wide range of electronic properties [7,8] and make the resulting XGeAs species be isovalent. Substitution at both the germanium (X–Ge≡As) and the arsenic (Ge=As–X) ends of the multiple bonds are examined and the effect of substituents on the thermodynamic and the kinetic stability of these isomers is discussed. Our study gives the trends for the geometries, vibrational frequencies and energetics for the ground states of the XGe≡As and Ge=AsX species. All of these isomers have not yet been reported in the literature and the calculated molecular properties presented in this work should be useful when these molecules become experimentally accessible.

* Corresponding authors. Fax: +886-7-312-5339.
E-mail address: midesu@cc.kmu.edu.tw (M.-D. Su).

0277-5387/02/$ - see front matter © 2002 Elsevier Science Ltd. All rights reserved.
PII: S0277-5387(01)01021-X

2. Methodology

The geometries and energetics of the stationary points on the potential energy surface of Eq. (1) (see Table 1) have been calculated with density functional theory (DFT), i.e. the B3LYP methods [9], in conjunction with the 6-311 + + G(d,p) basis set [10]. Only the singlet surface was considered throughout this work. All the stationary points have been positively identified as equilibrium structures (the number of imaginary frequency (NIMAG = 0)) or transition states (NIMAG = 1). Additionally, the vibrational zero-point energy (ZPE) corrections determined at the B3LYP/6-311 + + G(d,p) level are also included, i.e. B3LYP/6-311 + + G(d,p) + ZPE (B3LYP/6-311 + + G(d,p)) (hereafter designated B3LYP). For better energetics, single-point calculations with B3LYP/6-311 + + G(d,p) geometries were carried out at a higher level of theory: coupled cluster singles and doubles including a perturbational estimate of the triples [CCSD(T)] [11]. Unless otherwise noted, relative energies given in the text and in the figures are those determined at CCSD(T)/6-311 + + G(3df,3pd)//B3LYP/6-311 + + G(d,p) + ZPE (B3LYP/6-311 + + G(d,p)) (hereafter designed CCSD(T)). All calculations were carried out using the GAUSSIAN 98 series of program [12].

3. Results and discussion

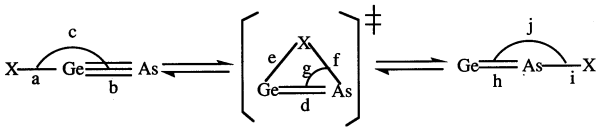
Table 1 shows molecular parameters of the XGe≡As and Ge=AsX species, calculated at the B3LYP level of theory, while their predicted vibrational frequencies, dipole moments, rotational constants, and net atomic charges are furnished in Table 2. The corresponding reaction profiles for the XGeAs intramolecular isomerizations at B3LYP and CCSD(T) levels of theory are outlined in Scheme 1.

One of the interesting structural features of the XGeAs species are the Ge≡As and Ge=As bond lengths. In the parent HGe≡As and Ge=AsH molecules, their germanium–arsenic internuclear distance is 2.111 Å (Ge≡As) and 2.251 Å (Ge=As), respectively, at B3LYP/6-311 + + G(d,p) level of theory. The data in Table 1 show that the Ge≡As bond lengths which fall in the range of 2.117–2.148 Å change quite substantially upon substitution. As expected, Ge=As double bonds are considerably longer, being in the range of 2.210–2.360 Å. It is worth noting that, based on the present study, highly electropositive substitutions at the arsenic (i.e. Ge=As–X) shortens the Ge=As bond relative to Ge=AsH (except for X = AlH_2), while electronegative substitution at arsenic causes elongation. An especially large elongation is observed in the Ge=AsPH_2 (2.360 Å). In any event, the bond-length differences between these isomers may be substantial and large enough to be observed experimentally.

The effect of the substituents on the Ge=As double bond length may be understood in terms of bond polarity. The Ge=As bond in Ge=AsH is polarized so that the germanium atom is positively charged and the arsenic is negatively charged, i.e. $Ge^{\delta+}$=$As^{\delta-}$–H. Substituents that increase this polarization and thus the degree of ionicity of the Ge=As bond are expected to

Table 1
Geometrical parameters of structures for Eq. (1) at the B3LYP/6-311 + + G(d,p) level of theory (distance in Å, angles in °)

(1)



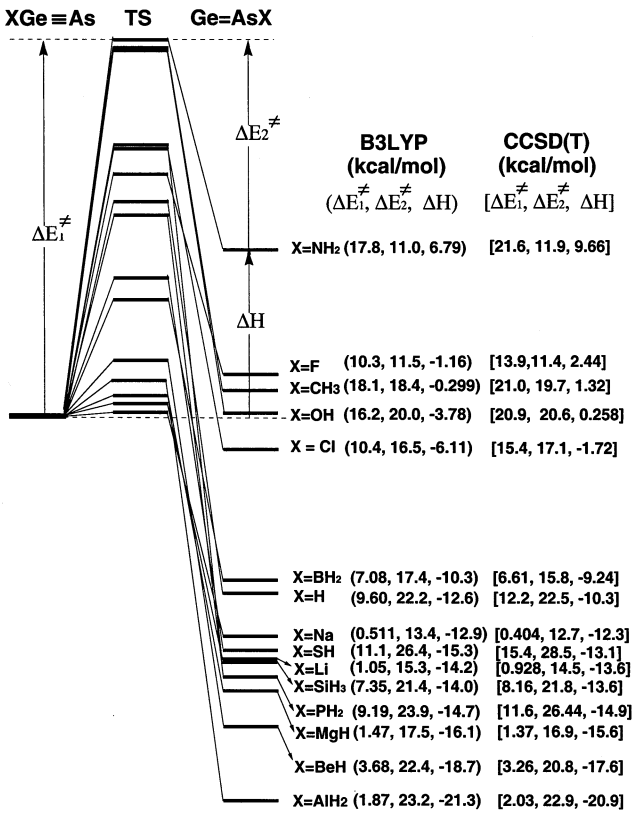
X	a	b	c	d	e	f	g	h	i	j
H	1.529	2.111	180.0	2.230	1.585	2.740	35.35	2.251	1.593	61.75
Li	2.415	2.145	180.0	2.156	2.411	4.155	26.01	2.210	2.409	76.99
Na	2.732	2.148	179.9	2.157	2.727	4.559	23.76	2.210	2.754	76.77
BeH	2.156	2.128	180.0	2.159	2.165	3.632	32.90	2.239	2.109	82.56
MgH	2.561	2.135	180.0	2.153	2.559	4.224	28.87	2.225	2.539	83.08
BH_2	2.014	2.132	180.0	2.203	2.105	2.776	48.34	2.237	1.998	105.3
AlH_2	2.460	2.132	179.9	2.158	2.460	4.013	31.85	2.387	2.311	69.40
CH_3	1.966	2.117	180.0	2.246	2.115	3.075	43.44	2.260	2.071	77.45
SiH_3	2.394	2.121	179.9	2.195	2.457	3.583	42.38	2.298	2.350	72.91
NH_2	1.823	2.124	175.1	2.344	1.914	3.054	38.79	2.304	1.887	108.9
PH_2	2.339	2.123	172.1	2.225	2.441	3.548	42.82	2.360	2.293	62.92
OH	1.779	2.126	175.0	2.383	1.867	3.040	37.89	2.301	2.044	58.00
SH	2.223	2.125	175.6	2.286	2.330	3.407	42.95	2.310	2.379	65.14
F	1.753	2.128	179.9	2.395	1.824	3.091	36.08	2.305	2.027	57.95
Cl	2.150	2.126	180.0	2.322	2.261	3.459	40.34	2.310	2.400	65.21

Table 2
Calculated harmonic vibrational frequencies, rotational constants, dipole moments, Mulliken charges and zero-point energy of the species in XGeAs isomerization reactions at the B3LYP/6-311++G(d,p) level of theory

Species	Frequencies (cm^{-1})	Rotational constants (MHz)	Dipole Moments (Debye)	q(Ge)	q(As)	q(X)	ZPE (kcal mol^{-1})
HGeAs	2129, 423, 269	A 2927.86	1.844	0.0668	−0.0787	0.0119	4.032
HGeAs–TS	1901, 340, 498i						3.204
GeAsH	1829, 502, 351	A 256 610.98 B 2678.89 C 2651.22	1.216	0.2549	−0.2288	−0.0261	3.835
LiGeAs	462, 369, 54	A 1996.77	10.02	−0.3827	−0.4177	0.8004	1.265
LiGeAs–TS	445, 374, 71i						1.171
GeAsLi	424, 366, 121	A 13 885.21 B 2743.04 C 2290.54	6.235	−0.0850	−0.4521	0.5371	1.302
HbeGeAs	2191, 555, 481, 481, 390, 70	A 1831.04	1.756	0.0066	0.0368	0.1135(Be) −0.1569(H)	5.957
HbeGeAs–TS	2177, 527, 479, 467, 384, 89i						5.766
GeAsBeH	2157, 554, 519, 491, 349, 125	A 10 985.86 B 2592.12 C 2097.27	1.185	0.1368	−0.1817	0.2108(Be) −0.1658(H)	5.996
H_2BgeAs	2724, 2610, 1129, 851, 627, 568, 382, 87, 68	A 230 532.15 B 1740.15 C 1727.11	1.710	0.0502	−0.0480	0.0170(B) −0.0096(H)	12.93
H_2BgeAs–TS	2715, 2593, 1116, 833, 595, 464, 365, 257, 226i						12.78
$GeAsBH_2$	2694, 2588, 1147, 902, 660, 573, 339, 88, 38	A 12 016.36 B 2189.22 C 1881.85	1.275	0.2550	−0.2504	0.0293(B) −0.0169(H)	12.91
H_3CgeAs	3142, 3142, 3047, 1450, 1450, 1257, 791, 791, 591, 381, 82, 82	A 157 272.77 B 1684.80	3.546	0.2251	−0.1593	−0.5343(C) 0.1562(H)	23.17
H_3CgeAs–TS	3158, 3151, 3052, 1461, 1443, 1194, 758, 721, 435, 323, 121, 187i						22.61
$GeAsCH_3$	3158, 3090, 2921, 1466, 1437, 1280, 819, 807, 482, 341, 251, 123	A 8504.38 B 2505.72 C 1959.89	1.196	0.2114	−0.1070	−0.5682(C) 0.1546(H)	23.12
H_2NgeAs	3631, 3529, 1561, 847, 713, 423, 376, 102, 76	A 296 801.76 B 1718.47 C 1712.02	4.121	0.3385	−0.1614	−0.7529(N) 0.2879(H)	16.10
H_2NgeAs–TS	3612, 3502, 1567, 776, 610, 430, 317, 240, 286i						15.80
$GeAsNH_2$	3616, 3516, 1584, 933, 694, 489, 299, 176, 99	A 14 227.52 B 3728.71 C 2965.63	1.755	0.1828	−0.0148	−0.6632(N) 0.2476(H)	16.30
HOGeAs	3821, 852, 688, 370, 91, 80	A 648 369.60 B 1717.81 C 1713.27	2.225	0.2433	−0.1117	−0.4028(O) 0.2712(H)	8.440
HOGeAs–TS	3818, 737, 550, 251, 165, 217i						7.892
GeAsOH	3821, 853, 721, 493, 330, 238	A 10 521.23.47 B 2554.09 C 2066.86	1.567	0.3099	−0.1274	−0.4745(O) 0.2920(H)	9.230
FgeAs	684, 361, 73	A 7 798 419423.87 B 1668.44	0.6288	0.3997	−0.1490	−0.2506	1.599

Table 2 (*Continued*)

Species	Frequencies (cm^{-1})	Rotational constants (MHz)	Dipole Moments (Debye)	q(Ge)	q(As)	q(X)	ZPE (kcal mol^{-1})
FGeAs–TS	569, 236, 147i						1.151
GeAsF	474, 331, 169	A 10 166.33 B 2554.93 C 2041.80	2.530	0.3619	−0.0598	−0.3021	1.393
NaGeAs	417, 204, 31	A 7 733 624 967.11 B 1095.93	11.43	−0.1261	−0.3993	0.5254	0.9328
NaGeAs–TS	405, 209, 39i						0.8780
GeAsNa	366, 219, 80	A 3839.00 B 2558.80 C 1535.41	7.618	−0.1140	−0.4432	0.5571	0.9508
HmgGeAs	1655, 438, 303, 265, 257, 39	A 1084.73	3.172	−0.1224	−0.1664	0.5207(Mg) −0.2320(H)	4.229
HmgGeAs–TS	1651, 413, 305, 303, 270, 51i						4.206
GeAsMgH	1640, 360, 318, 308, 294, 78	A 4190.74 B 2260.74 C 1468.53	0.5637	0.0769	−0.3612	0.5217(Mg) −0.2374(H)	4.285
$H_2AlGeAs$	1982, 1956, 748, 539, 445, 411, 269, 50, 39	A 128 476.30 B 1049.22 C 1040.72	2.822	−0.1787	−0.0988	0.6191(Al) −0.1708(H)	9.204
$H_2AlGeAs$–TS	1974, 1947, 742, 541, 409, 392, 290, 130, 48i						9.184
$GeAsAlH_2$	1983, 1390, 1086, 500, 415, 411, 369, 269, 251	A 4306.92 B 2290.01 C 1495.07	1.428	0.1922	−0.2882	0.4368(Al) −0.1703(H)	9.538
$H_3SiGeAs$	2252, 2252, 2231, 941, 941, 867, 508, 507, 461, 279, 52, 52	A 84 381.18 B 1038.83	3.080	−0.1198	−0.0757	0.4903(Si) −0.0982(H)	16.22
$H_3SiGeAs$–TS	2245, 2237, 2220, 957, 940, 869, 519, 491, 369, 289, 57, 89i						16.00
$GeAsSiH_3$	2234, 2222, 1885, 973, 942, 877, 547, 485, 366, 333, 278, 141	A 3870.04 B. 2347.49 C 1487.03	1.070	0.1935	−0.3267	0.4494(Si) −0.1054(H)	16.13
H_2PgeAs	2388, 2379, 1101, 671, 647, 456, 277, 59, 59	A 110 377.25 B 1045.96 C 1045.44	2.926	0.0425	−0.0870	0.1006(P) −0.0281(H)	11.49
H_2PgeAs–TS	2381, 2370, 1113, 632, 598, 337, 275, 142, 125i						11.22
$GeAsPH_2$	2434, 2422, 1127, 637, 502, 459, 378, 289,217	A 4174.13 B 2392.47 C 1543.31	1.329	0.1500	−0.2406	0.1305(P) −0.0200(H)	12.10
HSGeAs	2654, 713, 474, 306, 73, 51	A 261 740.41 B 1096.59 C 1092.02	2.059	0.0190	−0.0506	−0.0321(S) 0.0636(H)	6.11
HSGeAs–TS	2622, 677, 317, 289, 184, 114i						5.844
GeAsSH	2600, 724, 529, 353, 297, 202	A 3958.43 B 2503.26 C 1549.49	1.292	0.1612	−0.2010	−0.0382(S) 0.0780(H)	6.728
ClGeAs	486, 309, 57	A 1094.42	0.3541	0.1327	−0.0393	−0.0935	1.218
ClGeAs–TS	342, 255, 127i						0.8532
GeAsCl	342, 297, 147	A 3792.95 B 2524.66 C 1515.75	2.035	0.2438	−0.1553	−0.0885	1.125



Scheme 1.

shorten this bond. Consequently, electron-donating substituents (e.g. Li and Na) increase the negative charge at arsenic (see Table 2) and, in turn, the degree of bond ionicity. As a result, the Ge=As double bond shortens. On the other hand, electronegative substituents decrease the negative charge at arsenic (see Table 2), the bond ionicity decreases, and thus the Ge=As bond lengthens. Nevertheless, in the case of XGe≡As, its Ge≡As triple bond length is always elongated relative to the parent HGe≡As, regardless of the substituents. Indeed, some electropositive substituents donate sufficient electron density to the germanium center, so that the sign of density on Ge is no longer positive. A strictly ionic contribution would then lead to repulsion and presumably bond elongation rather than shortening. However, this simple ionicity explanation cannot apply to the XGe≡As systems with electronegative substituents.

Besides these, our B3LYP calculations indicate that XGe≡As exist as stable linear species, but their Ge=AsX isomers are strongly bent in their singlet states, as shown in Table 1. Additionally, in the present study, all linear Ge=AsX molecules were found to be second-order transition structures. The reason for the double-bonded Ge=AsX species prefers a bent rather than linear structure may be due to the phenomenon of orbital nonhybridization. That is to say, the arsenic atom may be reluctant to take part in hybridization. Thus, it tends to form a nonbonding orbital acquiring mainly s-character, while the remaining p-electrons are used up to form bonds with the neighboring atom. As a result, the formation of a sp-hybrid orbital is disfavored and bent Ge=AsX (**1a**) becomes considerably more stable than its linear structure (**1b**). Of course, to obtain a better understanding of the nature of such a chemical bonding requires further computational studies, as well as experiments. Such studies, however, are beyond the scope of the present work. In any event, from our DFT calculations on the model compound Ge=AsX, it is concluded that the bent structure (**1a**) is the best representation of its conformation.



1a **1b**

From Scheme 1, it is worth noting that the B3LYP and CCSD(T) energy differences are roughly similar, suggesting that the less expensive B3LYP level can be used with some confidence for larger germanium–arsenic systems for which more elaborate calculations are not practical. Furthermore, it is clear from Scheme 1 that the electropositively substituted arsagermenes (Ge=AsX) are generally more stable than the isomeric arsagermynes (XGe≡As). That is, our best estimate (at CCSD(T)) places XGe≡As 9.2–21 kcal mol^{-1} above its more stable isomer Ge=AsX for the electropositively substituted species. On the other hand, our CCSD(T) results suggest that the highly electronegative substituents can reverse the order of the relative stabilities of the double-bonded and triple-bonded XGeAs systems, although the energy difference (ΔH) between them is quite small. For instance, FGe≡As, HOGe≡As, $H_2NGe{\equiv}As$, and $H_3CGe{\equiv}As$ are calculated to be more stable than Ge=AsF, Ge=AsOH, $Ge{=}AsNH_2$, and $Ge{=}AsCH_3$ only by 2.4, 0.26, 9.7, and 1.3 kcal mol^{-1}, respectively. This strongly implies that substituents which are more electropositive than germanium as well as arsenic increase the energy difference ΔH between XGe≡As and Ge=AsX (relative to X = H), whereas more electronegative substituents decrease this energy gap. In particular, as mentioned above, when the substituent X is highly electronegative (such as X = F and OH), the XGe≡As and Ge=AsX isomers are predicted to be nearly degenerate in energy, with an energy gap of less than 3.0 kcal mol^{-1}. In other words, our model calculations suggest that germanium and arsenic are less reluctant to form Ge=As double-bonded than Ge≡As triple-bonded molecules.

The generally higher stabilities of Ge=AsX compared with XGe≡As primarily reflect the differences in the bond energies of Ge–X versus As–X. If the Ge–X bond

is stronger than the As–X bond, then XGe≡As is expected to be more stable than Ge=AsX. According to some available experimental bond dissociation energies (in kcal mol^{-1}) [13]: Ge–F (116), As–F (98.0); Ge–O (158), As–O (115); Ge–H (≤ 76.9), As–H (65.5); and Ge–Cl (103), As–Cl (107), one may easily predict the relative stabilities of arsagermenes and arsagermynes. Thus, the preference of XGe≡As over Ge=AsX is found for X = F and OH because the Ge–F and Ge–O bonds are substantially stronger than the corresponding As–X bonds. Accordingly, the change in Ge–X and As–X bonding should be parallel to the order of the relative stabilities of XGe≡As and Ge=AsX.

However, it would seem, from a practical point of view, that the potential barrier between XGe≡As and Ge=AsX is also as important as their relative energy. The transition structures for the intramolecular isomerization reaction, (i.e. XGe≡As → Ge=AsX) were determined at the B3LYP level of theory, which were shown in Scheme 1and Tables 1 and 2. As seen in Tables 1 and 2, it is evident that those transition states, which are all at the first-order saddle point as determined by the frequency calculation at the B3LYP level, proceed in a three-center pattern involving germanium, arsenic, and substituent elements.

As one can see in Table 1, our B3LYP results indicate that the longer the Ge–As bond, the more product-like the transition state structure. For instance, the Ge–As bonds stretched in the transition structures are 5.6% (HGeAs–TS), 0.51% (LiGeAs–TS), 0.42% (NaGeAs–TS), 1.5% (HBeGeAs–TS), 0.84% (HMgGeAs–TS), 3.3% (H_2BGeAs–TS), 1.2% (H_2AlGeAs–TS), 3.5% (H_3SiGeAs–TS), 6.1% (H_3CGeAS–TS), 4.8% (H_2PGeAs–TS), 10% (H_2NGeAs–TS), 7.6% (HSGeAs–TS), 12% (HOGeAs–TS), 9.2% (ClGeAs–TS), and 13% (FGeAs–TS) which are longer than those in the corresponding XGe≡As species. According to the Hammond's postulate [14], the above data strongly imply that the XGe≡As species with electropositive substituents (e.g. Li, Na, BeH, MgH, BH_2, AlH_2 and SiH_3) should arrive at the transition state relatively early, while the arsagermynes with electronegative substituents (e.g. F, OH, NH_2 and CH_3) should reach the transition state relatively late. Thus, one may anticipate a smaller activation barrier, as well as a larger exothermicity for the former than for the latter, which is confirmed by our CCSD(T) calculations. For example, the barrier heights for the isomerization reactions of electropositive-substituted arsagermynes (i.e. $\Delta E_1^{\ddagger}$; from left to right in Eq. (1)) are within the range of 0.40–8.2 kcal mol^{-1}, which are much smaller than those for electronegative-substituted arsagermynes with activation barriers of 14–22 kcal mol^{-1}). Additionally, the reaction enthalpies (ΔH) for the isomerizations of electronegative-substituted XGe≡As fall in the range of 0.26–9.7 kcal mol^{-1}, which are larger than those for the electropositive-substituted XGe≡As (i.e. -9.2–-21 kcal mol^{-1}). Furthermore, as the reaction proceeds in the reverse direction, the intramolecular rearrangement Ge=AsX → XGe≡As is much more difficult to achieve for electropositively substituted Ge=AsX systems, with energy barriers (i.e. $\Delta E_2^{\ddagger}$) of 13–29 kcal mol^{-1}. Similarly, as seen in Scheme 1, it is apparent that electronegative-substituted Ge=AsX species are also separated from the triple-bonded XGe≡As isomer by large potential barriers (at least >12 kcal mol^{-1} at CCSD(T) for X=F, OH, NH_2, and CH_3). Again, from the above results, it is found that electropositive substitution can thermodynamically and kinetically stabilize the double-bonded Ge=AsX species relative to the isomeric XGe≡As, while electronegative substitution can cause the XGe≡As and Ge=AsX isomers to be nearly thermoneutral.

4. Conclusions

The conclusions, which may be drawn from this work, are as follows:

1. Our theoretical calculations show that the reluctance of the arsenic atom in forming GeAs triple bond in singlet ground state.
2. Although germanium and arsenic are two elements that are notoriously reluctant to form p–π multiple bonds, electronegative substitution on germanium preferentially stabilizes formal triple bonds (XGe≡As) relative to double bonds (Ge=AsX).
3. Electropositively substituted Ge=AsX molecules are thermodynamically and kinetically more stable than the isomeric XGe≡As species.
4. The second-row substituents with high electronegativity (such as F, OH, NH_2 and CH_3) can stabilize the XGe≡As triply bonded species in a kinetic sense, although germanium and arsenic are less reluctant to form Ge=As doubly bonded than Ge≡As triply bonded compounds.

As a consequence, the detection of such molecules as a monomer should be achieved in either the low-pressure gas phase (e.g. as low as 10^{-4} torr) or the low-temperature inert matrix. Moreover, the above conclusions of substituent effects on germanium–arsenic multiple bonding provide some interesting clues for designing molecules with either a Ge=As double-bond or a Ge≡As triple-bond.

We encourage experimentalists to carry out further experiments to confirm our predictions.

Acknowledgements

We would like to thank the National Center for High-Performance Computing of Taiwan for generous

amounts of computing time. We also thank the National Science Council of Taiwan for their financial support. We are grateful to the referees for their critical comments and helpful corrections of the manuscript.

References

[1] (a) J. Barrau, J. Esoudié, J. Satgé, Chem. Rev. 90 (1990) 283;
(b) R.S. Grev, Adv. Organomet. Chem. 33 (1991) 125;
(c) J. Esoudié, C. Couret, H. Ranaivonjatovo, J. Satgé, Coord. Chem. Rev. 130 (1994) 427;
(d) J. Barrau, G. Rima, Coord. Chem. Rev. 178 (1998) 593;
(e) J. Esoudié, C. Couret, H. Ranaivonjatovo, Coord. Chem. Rev. 178 (1998) 565;
(f) N. Tokitoh, T. Matsumoto, R. Okazaki, Bull. Chem. Soc. Jpn. 72 (1999) 1665;
(g) P.P. Power, Chem. Rev. 99 (1999) 3463;
(h) W.J. Leigh, Pure Appl. Chem. 71 (1999) 453;
(i) N. Tokitoh, Pure Appl. Chem. 71 (1999) 495.

[2] T.E. Gier, J. Am. Chem. Soc. 83 (1961) 1769.

[3] For a series of reviews, see: (a) M. Regitz, O.J. Scherer, (Eds.) Multiple Bonds and Low coordination in Phosphorus Chemistry, Thieme, Struttgart, 1990;
(b) J.F. Nixon, Chem. Rev. 88 (1988) 1327;
(c) R. Appel, F. Knoll, Adv. Inorg. Chem. 33 (1989) 259;
(d) M. Regitz, Chem. Rev. 90 (1990) 191;
(e) N.C. Norman, Polyhedron 12 (1993) 2431;
(f) H.M. Schmidt, H. Stoll, H. Preuss, G. Becker, O. Mundt, J. Mol. Struct. (Theochem) 262 (1992) 171.

[4] (a) L. Weber, Chem. Ber. 129 (1996) 367 and references cited therein;
(b) L. Weber, O. Kaminski, H.G. Stammler, B. Neumann, Chem. Ber. 129 (1996) 223.

[5] (a) G. Märkl, H. Sejpka, Angew. Chem., Int. Ed. Engl. 25 (1986) 264;
(b) P.B. Hitchcock, C. Jones, J.F. Nixon, J. Chem. Soc., Chem. Commun. (1994) 2061;
(c) J.-C. Guillemin, L. Lassalle, P. Drêan, G. Wlodarczak, J. Demaison, J. Am. Chem. Soc. 116 (1994) 8930.

[6] M. Driess, Coord. Chem. Rev. 145 (1995) 1.

[7] A. Pross, L. Radom, Prog. Phys. Org. Chem. 13 (1981) 1.

[8] (a) C.-H. Lai, M.-D. Su, S.-Y. Chu, Chem. Commun. (2001) 1120;
(b) C.-L. Lin, M.-D. Su, S.-Y. Chu, J. Phys. Chem. A 104 (2000) 9250;
(c) C.-L. Lin, M.-D. Su, S.-Y. Chu, Chem. Phys. Lett. 339 (2001) 147;
(d) H.-Y. Liao, M.-D. Su, S.-Y. Chu, Chem. Phys. Lett. 341 (2001) 122;
(e) H.-Y. Liao, M.-D. Su, S.-Y. Chu, J. Phys. Chem. B 105 (2001) 9239.

[9] (a) A.D. Becke, J. Chem. Phys. 98 (1993) 5648;
(b) C. Lee, W. Yang, R.G. Parr, Phys. Rev. B37 (1988) 785.

[10] R.A. Kendall, T.H. Dunning Jr., R.J. Harrison, J. Chem. Phys. 96 (1992) 6796.

[11] (a) J.A. Pople, M. Head-Gordon, K. Raghavachari, J. Chem. Phys. 87 (1987) 5968;
(b) K. Raghavachari, G.W. Trucks, J.A. Pople, M. Head-Gordon, Chem. Phys. Lett. 157 (1989) 479;
(c) R.J. Rico, M. Head-Gordon, Chem. Phys. Lett. 213 (1993) 224;
(d) T.J. Lee, G. Scuseria, in: S.F. Langoff (Ed.), Quantum Mechanical Electronic Structure Calculations with Chemical Accuracy, Kluwer Academic, New York, 1995.

[12] GAUSSIAN 98: M.J. Frisch, G.W. Trucks, H.B.P. Schlegel, M.W. Gill, B.G. Johnson, M.A. Robb, J.R. Cheeseman, T. Keith, G.A. Petersson, J.A. Montgomery, K. Raghavachari, M.A. Al-Laham, V.G. Zakrzewski, J.V. Ortiz, J.B. Foresman, J. Cioslowski, B.B. Stefanov, A. Nanayakkara, M. Challacombe, C.Y. Peng, P.Y. Ayala, W. Chen, M.W. Wong, J.L. Andres, E.S. Replogle, R. Gomperts, R.L. Martin, D.J. Fox, J.S. Binkley, D.J. Defrees, J. Baker, J.P. Stewart, M. Head-Gordon, C. Gonzalez, J.A. Pople, Gaussian, Inc., Pittsburgh PA, 1995.

[13] D.R. Lide, H.P.R. Frederikse, CRC Handbook of Chemistry and Physics, CRC, New York, 1998, pp. 9–51.

[14] G.S. Hammond, J. Am. Chem. Soc. 77 (1954) 334.

PERGAMON

Polyhedron 21 (2002) 587–598

POLYHEDRON

www.elsevier.com/locate/poly

Dihypersilylstannylene and dihypersilylplumbylene —two Lewis-amphoteric carbene homologues☆

K. Klinkhammer

Universitat Stuttgart, Stuttgart, Germany

Received 10 August 2001; accepted 27 November 2001

Dedicated to Professor Hans Bürger on the occasion of his 65th birthday

Abstract

Dihypersilylstannylene $[(Me_3Si)_3Si]_2Sn$ (**1**) and dihypersilylplumbylene $[(Me_3Si)_3Si]_2Pb$ (**2**) are Lewis-amphoteric compounds, i.e. they may behave as Lewis-acid and/or as Lewis-base. Quantum-chemical calculations indicate that their Lewis-acidity is strongly enhanced compared with their diorganyl substituted relatives by the electropositive silyl substituents present. Furthermore silyl substituents are expected to migrate more easily than organyl groups, due to relatively weak E–Si bonds formed to the heavier Group 14 congeners (tetrels) leading to different reaction patterns. Here I will give a brief report about our recent investigations on the chemical behavior of the title compounds towards other Lewis-acidic or Lewis-basic or Lewis-amphoteric species. © 2002 Elsevier Science Ltd. All rights reserved.

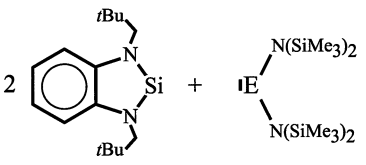
Keywords: Stannylenes; Plumbylenes; Distannenes; Diplumbenes; Lewis-amphoteric behavior

1. Introduction

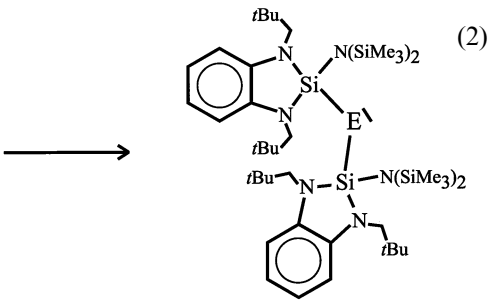
In 1995, we reported the synthesis of the title compounds, dihypersilylstannylene (**1**) and dihypersilylplumbylene (**2**). They are obtained by simple metathesis reactions of the appropriate bis[bis(trimethylsilyl)amino]-substituted tetrylene with unsolvated alkali metal hypersilanides under homogenous conditions in inert hydrocarbon solvents at −60 °C (Eq. (1)) [1] and are easily separated from the sparingly soluble alkali metal amide by filtration at −30 °C. At this time **1** and **2** were the first bis(silyl) substituted stannylene and plumbylene ever isolated. In the meantime few further *heteroleptic* species, bearing one silyl and one aryl group could be synthesized, partially via ligand exchange reactions of **1** and **2** with other tetrylenes or aryl copper derivatives (see below) [2]. The only examples with two silyl groups other than hypersilyl

$$E[N(SiMe_3)_2]_2 + M^{I}Si(SiMe_3)_3 \quad (E = Sn, Pb;\ M^{I} = Na\cdots Cs)$$

$$\xrightarrow[-60°C]{<n\text{-pentane}>} M^{I}N(SiMe_3)_2 + E[Si(SiMe_3)_3]_2 \quad \mathbf{1, 2} \qquad (1)$$



4



(2)

3a (E = Sn), **3b** (E = Pb)

☆ Hypersilyl: tris(trimethylsilyl)silyl, $[(H_3C)_3Si]_3Si$. Since there is no common name for the elements E of Group 14 (E = C, Si, Ge, Sn and Pb), the terms tetrels—as suggested by the IUPAC—and tetrylene are used for the elements E and their divalent two-coordinate derivatives R_2E, respectively.

E-mail address: kw@iac.uni-stuttgart.de (K. Klinkhammer).

0277-5387/02/$ - see front matter © 2002 Elsevier Science Ltd. All rights reserved.
PII: S0277-5387(01)01029-4

attached to the low valent tetrel atom were reported by Gehrhus and Lappert in 1997 [3]. These particular compounds (**3a**, **b**) were obtained by the insertion of the bisaminosilylene **4** into the Sn–N and Pb–N bonds of bis[bis(trimethylsilyl)amino]stannylene and plumbylene, respectively (Eq. (2)); other related insertion reactions involving Sn–C or Sn–N bonds led to heteroleptic species, however [2h].

In the following, we will briefly review our investigations—partially performed in fruitful cooperation with other groups—on the Lewis-acids/Lewis-base behavior of dihypersilylstannylene (**1**) and dihypersilylplumbylene (**2**). Some of the reported results are still unpublished and have been reported only during my lecture on the occasion of the Pacific Basin Conference in Honolulu (Hawaii) in December 2000.

Before going into experimental details some substantial remarks will be made concerning the electronic structures of stannylenes and plumbylenes for a better understanding of their reactivity. Stannylenes and plumbylenes as other carbene homologous species comprise both, an energetically high-lying HOMO predominantly constituted by a lone-pair on the tetrel atom of high s-character and a low-lying LUMO having high contributions of the empty valence p-orbital of the two-valent tetrel atom. Thus all stannylenes and plumbylenes are Lewis-amphoteric compounds, i.e. are expected to show both, Lewis-acidic and Lewis-basic behavior. But, in contrast to many other compounds, the amphoteric behavior is located at the *same* atom, i.e. at the two-valent tetrel center. The energy difference between the frontier orbitals is however decreasing going up Group 14 (Table 1) [4]. For most simple carbenes, finally, both orbitals are of nearly the same energy and same radial expansion such leading to a triplet ground-state or at least to a very low lying triplet state. Thus carbenes usually are extremely reactive high-energy compounds not only showing strong Lewis-acid/Lewis-base behavior, but also giving reactions typical for radicals. Dimerization of carbenes lead to alkenes as the 'natural' dimerization produc0t of two triplet species forming a σ- and a π-bond. They exhibit the typical structural, spectroscopic and chemical features attributed to doubly-bonded species. Already in the case of silylenes things markedly change. As shown by Kutzelnigg both, the difference in energy and the radial expansion of s- and p-valence orbitals strongly increase down Group 14, thus leading to a low hybridization tendency and resulting in non-radical singlet species for all heavier carbene congeners [5]. Therefore, many reactions of these species can be described in terms of simple Lewis-acid/Lewis-base reactions, not only the addition of external Lewis-acids or Lewis-bases, but also insertion reactions, and the dimerization of heavier tetrylenes to *formal* alkene homologues. The bonding within latter compounds, their structural features as well as their spectroscopic and chemical behavior was a topic of controversial discussions in the last decade, but is now well understood and widely accepted as a more or less strong double donor–acceptor bond (double dative bond) between the two constituting Lewis-amphoteric tetrylenes [4,6,7]. Going down Group 14 the energy difference between the interacting orbitals strongly increase and thus—as generally found for dative bonds—the interaction energy decreases. Due to a strong relativistic contraction of the valence s-orbital on lead the s–p gap is very large for this case (about 150 kJ mol^{-1}) resulting in no or very week double donor–acceptor bonds within plumbylene dimers (diplumbenes) and in general leading to a very weak donor ability of plumbylenes.

A simple theoretical model—the CGMT-model—which emerged during the last decade allows for a more detailed prediction of the bonding in alkene homologues and for the prediction of their structures [7]. This model addresses the relation between the HOMO–LUMO gap of the constituting tetrylene moieties (better: the singlet–triplet gap $\Sigma\Delta E_{ST}$) and the dimerization energy of the respective hypothetical triplet species: $E_{\sigma+\pi}$.

Classical double bonded systems ($\sigma+\pi$ bond; local D_{2h} symmetry) are expected if $\Sigma\Delta E_{ST} < 1/2E_{\sigma+\pi}$ (this holds for all alkenes and some disilenes). Double-dative bonds (*trans*-bent structures; local C_{2h} symmetry) are expected if $1/2E_{\sigma+\pi} < \Sigma\Delta E_{ST} < E_{\sigma+\pi}$. If $\Sigma\Delta E_{ST} > E_{\sigma+\pi}$, i.e. if the preparation energy for the triplet fragments is finally larger than the total expected E–E bond energy (see Table 1) no dimer is expected to form.

Table 1
Calculated sum of singlet–triplet gaps ($\Sigma\Delta E_{ST}$) in hydrides EH_2 (E = C–Pb), dimerization energies for the triplet species ($E_{\sigma+\pi}$) (kJ mol^{-1}) and expected structures of the dimers $H_2E{=}EH_2$ [4]

EH_2	$\Sigma\Delta E_{ST}$	$1/2E_{\sigma+\pi}$	$E_{\sigma+\pi}$	Expected structure
CH_2	−65	397	794	planar D_{2h}
SiH_2	160	214	427	planar
GeH_2	192	188	377	*trans*-bent C_{2h}
SnH_2	194	156	311	*trans*-bent
PbH_2	286	131	262	no dimer

2. Dihypersilyltetrylenes as Lewis-base—the formation of heteroleptic monomers and dimers

Lewis-acid–Lewis-base adducts between two same or two different stannylenes have been previously observed yielding dimers with double donor–acceptor or single donor–acceptor bonds [8], depending on the nature of the employed compounds. No such reaction, however, could be verified for plumbylenes until our own recent work, since bulky groups had been utilized

Table 2
Calculated dissociation energies (ΔE_{Diss}) of Lewis-base adducts of $Pb(CH_3)_2$ and $Pb(SiH_3)_2$ (kJ mol^{-1}) as well as bond lengths of the respective dative D→Pb bond (pm)

D	$Pb(CH_3)_2$	$Pb(SiH_3)_2$	*D*	$Pb(CH_3)_2$	$Pb(SiH_3)_2$
H_2O→			H_2S→		
ΔE_{Diss}	55	69	ΔE_{Diss}	25	40
Pb–O	264.1	260.8	Pb–S	319.8	311.0
H_3N→			H_3P→		
ΔE_{Diss}	69	89	ΔE_{Diss}	25	48
Pb–N	262.7	259.9	Pb–P	308.1	292.8
P_4→			O≡C→		
ΔE_{Diss}	4	15	ΔE_{Diss}	19	37
Pb–P	342.8	307.8	Pb–C	278.4	255.1
HN≡C→			HC≡N→		
ΔE_{Diss}	38	64	ΔE_{Diss}	29	43
Pb–C	266.8	251.3	Pb–N	277.0	265.8
Dimer (Pb→)					
ΔE_{Diss}	46	102			
Pb–Pb	302.1	288.5			

Method: B3LYP [19]; H, C, N, O, P, S: all electrons, cc-pvdz (Dunning) basis-sets [19]; Pb: quasirelativistic pseudopotentials (Stuttgart group) and appropriate double-zeta (d) basis [20]. No counterpoise correction.

for obtaining kinetically stable plumbylenes, which in the light of the very small expected dimerization energy prevented dimerization for sterical reasons.

Some years ago calculations by Apeloig and others indicated that electropositive substituents should generally lead to a diminished HOMO–LUMO gap for tetrylenes and therefore should enhance their tendency to form Lewis-acid–Lewis-base adducts and thus strengthen the bonds within the respective dimers [9]. Our own calculations on the simple model compounds $E(CH_3)_2$ and $E(SiH_3)_2$ and their dimers $(H_3C)_2E$=$E(CH_3)_2$ and $(H_3Si)_2E$=$E(SiH_3)_2$ on DFT (and MP2) level clearly show that the substitution of CH_3 for the more electropositive SiH_3 group dramatically increases (in the case of E = Pb more than doubles) the dimerization energies (last row in Table 2). Therefore, bis(silyl)stannylenes and bis(silyl)plumbylenes are expected to exhibit a much higher tendency to dimerize giving the respective distannenes and diplumbenes than the related diorganyl substituted species. Nevertheless cryoscopic measurements and its crystal structure showed dihypersilylplumbylene (**2**) to be strictly monomeric even in the solid state (Fig. 1). A closer inspection of the structural details revealed that an extreme sterical congestion is present in **2**: (a) the Si–Pb–Si angle with about 114° is much larger than in the bis(silyl)plumbylene **3a** and other less congested plumbylenes; (b) severe distortions from tetrahedral geometry is found around the silicon atoms of the hypersilyl ligands (Pb–Si–Si: 98.3–129.2°). Thus, inspite of a high electronic tendency to dimerize, dimerization is obviously prevented by sterical congestion. Dihypersilylstannylene (**1**) showing a monomer–dimer equilibrium already in solution—other than its lead analog **2**—does form a dimer in the solid state (Fig. 2). Although an even stronger sterical congestion is present for stannylene **1** than for the plumbylene **2**, since Sn is smaller than Pb, (Sn–Si–Si: 99.8–131.9°) the tendency to dimerize is such high that a distannene $(\mathbf{1})_2$ with a severely distorted Sn_2Si_4 skeleton is formed; a very pronounced torsion about the Sn–Sn bond of about 62.7° with respect to the expected undistorted *trans*-bent structure and a markedly elongated Sn–Sn bond of 282.5 pm is observed. The very large Si–Sn–Si angle at the two stannylene moieties of about 120.5° indicates a notable involvement of the former lone-pairs in the Sn–Sn-bond [10].

It should be noted that there is also spectroscopic evidence for a very small HOMO–LUMO gap in plumbylene **2**. The UV-spectra of diluted *n*-pentane

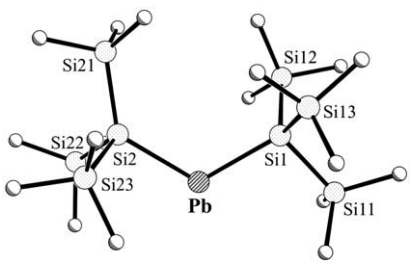


Fig. 1. Molecular structure of dihypersilylplumbylene (**2**) in the crystal. Selected bond lengths (pm) angles and torsion angles (°) of one of the four independent molecules: Pb–Si1 270.0(3), Pb–Si2 270.4(4), Si1–Pb–Si2 113.55(10), Pb–Si1–Si11 99.6(2), Pb–Si1–Si12 104.8(2), Pb–Si1–Si13 125.0(2), Pb–Si2–Si21 129.2(2), Pb–Si–Si22 98.3(2), Pb–Si–Si23 101.6(2); Si11–Si1–Pb–Si2 176.8(2), Si21–Si2–Pb–Si1 26.1(2).

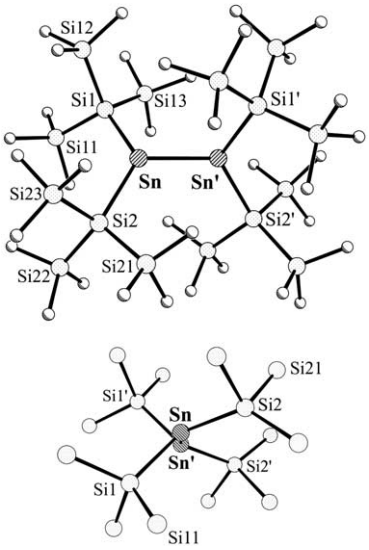


Fig. 2. Molecular structure of tetrahypersilyldistannene ($(\mathbf{1})_2$) in the crystal (top: whole molecule only hydrogens omitted, bottom: Sn_2Si_4 skeleton). Selected bond lengths (pm) angles and torsion angles (°): Sn–Sn′ 282.47(6), Sn–Si1 266.67(11), Sn–Si2 267.81(11), Si1–Sn–Si2 120.46(4), Sn–Si1–Si11 112.06(5), Sn–Si1–Si12 115.51(5), Sn–Si1–Si13 112.35(5), Sn–Si2–Si21 106.19(5), Sn–Si–Si22 131.88(6), Sn–Si–Si23 99.78(5); Si11–Si1–Sn–Si2 −21.0, Si21–Si2–Sn–Si1 176.9.

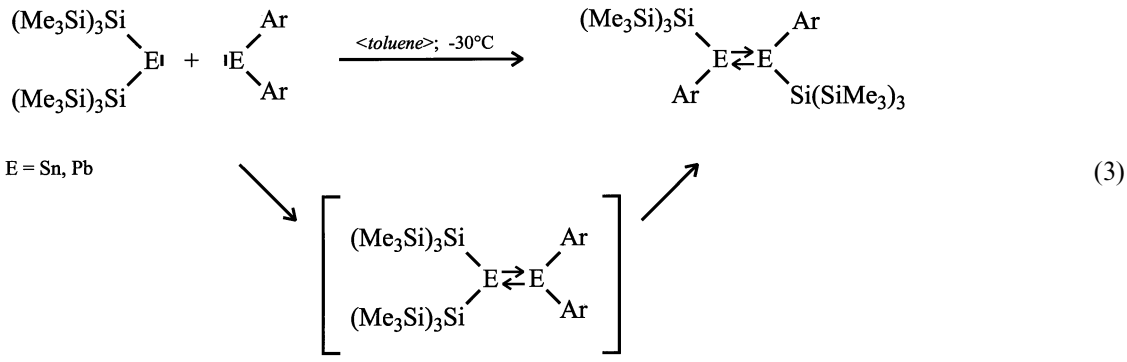
Table 3
E–E bond lengths (pm) determined for heteroleptic dihypersilyl(diorganyl)ditetrenes Hyp(R)E=E(R)Hyp and for respective homoleptic tetraorganylditetrenes $R_2E{=}ER_2$ [2,21,22]

R	E	Hyp(R)E=E(R)Hyp	$R_2E{=}ER_2$
Ar^F	Sn	283.3	363.9
Ar^F	Pb	353.7 (**6**)	monomer
Bmp	Sn	279.1	291.0
Bmp	Pb	337.0 (**5**)	monomer
Trip	Pb	299.0	305.2
Mes	Sn	270.2	oligomer
Mes	Pb	290.3 (**8**)	unknown [a]

[a] A $MgBr_2(THF)_4$ adduct is known however with Pb–Pb 335.5 pm [2f].

solutions of **2** show two bands of low to medium intensity in the visible and near IR region which we according to CIS calculations on the model compounds $Pb(SiH_3)_2$ and $Pb[Si(SiH_3)_3]_2$ assign to the $S_0 \rightarrow S_1$ and $S_0 \rightarrow T_0$ transitions, respectively. The low energy band (putatively $S_0 \rightarrow T_0$) is experimentally found at 1056 nm, implying a ΔE_{ST}-value of 113 kJ mol^{-1} only, thus significantly lower than calculated for the parent PbH_2 (143 kJ mol^{-1}; Table 1).

From the CGMT model (see above) it can be followed that the tendency to dimerize is dependent on the *sum* of the HOMO–LUMO gaps (ΣE_{ST}) of the constituting monomers. Therefore, our simple presumption was that one could perhaps obtain stable *mixed* dimers, i.e. distannenes, stannaplumbenes or diplumbenes, by mixing the sterically congested dihypersilyltetrylenes **1** and **2**—which have high electronical tendency to dimerize (small ΔE_{ST})—with much less congested diorganyltetrylenes—which have low or even no tendency to dimerize (large ΔE_{ST}). In cooperation with the groups of Grützmacher and Weidenbruch several diaryltetrylenes R_2E' (E = Sn, Pb, R = Ar) were reacted with stannylene **1** and plumbylene **2**—and indeed quantitatively yielded *dimers* in the solid state for all investigated cases [2]. The crystal structure analyses revealed, however, that not the expected homoleptic hetero-dimers $R_2E' = EHyp_2$ (homoleptic with respect to each tetrylene moiety) were isolated, but instead a rearrangement (Eq. (3)) had taken place and homo-dimers of the heteroleptic tetrylenes were obtained: R(Hyp)E = E(Hyp)R and R(Hyp)E′ = E′(Hyp)R, respectively. In those cases where stannylenes were mixed with plumbylenes both homo-dimers were formed and could be easily separated by fractionating crystallization (the distannenes are less soluble than the diplumbenes). Despite two very bulky hypersilyl substituents present, all distannenes and diplumbenes have markedly shorter E–E bonds than the dimers of the parent tetraorganylditetrenes (Table 3) thus verifying the CGMT-model. Moreover *all* heteroleptic dimers synthesized so far exhibit an undistorted *trans*-bent structure with the expected C_i symmetry (E-isomer). Especially for E = Pb the observed Pb–Pb distance was found to be very sensitive to the organyl substituent employed. Depending on its bulkiness, its electron-withdrawing or electron-releasing power and functional groups present, the Pb–Pb distance varied from 299.0 in **5** (R = 2,4,6-^{i}Pr$_3$-C$_6$H$_2$) [2f] to 353.7 pm in **6** (R = 2,4,6-



(3)

F_3C-C_6H_2) [2a]. Very recently Weidenbruch showed that silyl groups are not mandatory for the existence of diplumbenes: a *homoleptic* aryl substituted species has been obtained using the modestly bulky 2,4,6-^{i}Pr$_3$-C_6H_2 groups [11]. Nevertheless, the Pb–Pb bond in this homoleptic diplumbene is markedly longer (305.2 pm) and putatively weaker than in the respective heteroleptic species **5**—again showing the validity of the CGMT-model.

A diplumbene with an even shorter Pb–Pb bond was formed from the reaction of dihypersilylplumbylene with mesitylcopper—one of the few reactions we investigated so far where plumbylene **2** reacts purely as a Lewis-base [2d]. The putatively formed primary

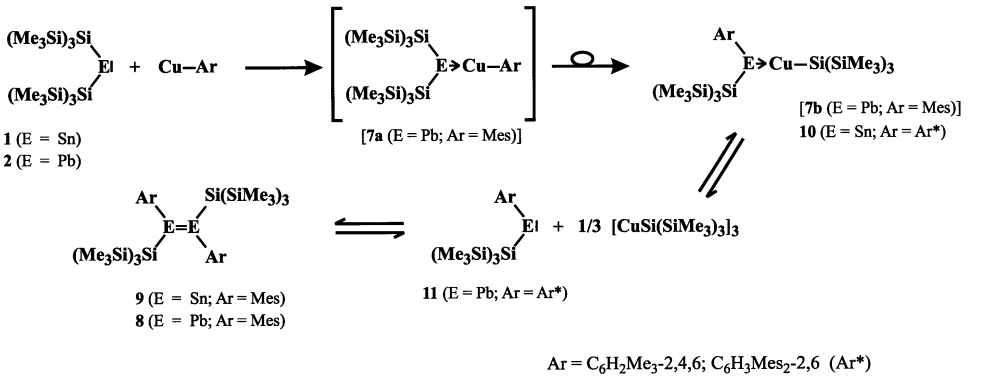
Table 4
Summary of crystal structure data [a] for compounds **8**, **9**, **12a**, **12b**, **13a**, **18** and **21a** [23]

	8	**9**	**12a** [b]	**12b** [b]	**13a**	**18**	**21a**
Empirical formula	$C_{36}H_{76}Pb_2Si_8$	$C_{36}H_{76}Sn_2Si_8$	$C_{23}H_{63}NSi_8Sn$	$C_{23}H_{63}NSi_8Pb$	$C_{25}H_{65}NSi_8Sn$	$C_{28}H_{62}N_3PbSi_8\cdot 0.5C_5H_{12}$	$C_{31}H_{79}Cs_2NSi_{10}Sn\cdot 0.75C_5H_{12}$
Formula weight	1148.06	971.07	697.15	785.65	723.19	914.84	592.74
Crystal system	triclinic	triclinic	monoclinic	monoclinic	monoclinic	triclinic	triclinic
Space group	$P\bar{1}$	$P\bar{1}$	Cc	Cc	$P2_1/c$	$P\bar{1}$	$P\bar{1}$
Z	1	1	4	4	4	2	4
a (Å)	9.087(2)	9.142(2)	14.495(3)	14.475(3)	21.260(3)	9.375(3)	13.751(3)
b (Å)	11.767(2)	11.861(2)	12.911(3)	13.016(3)	10.2992(14)	12.820(3)	19.749(2)
c (Å)	13.688(2)	13.478(2)	21.896(4)	22.076(6)	19.142(5)	21.422(6)	23.184(3)
α (°)	77.340(13)	76.32(3)	90	90	90	101.25(2)	88.95(2)
β (°)	73.778(12)	72.80(3)	90.27(3)	90.47(3)	90.153(19)	94.08(2)	76.35(2)
γ (°)	67.943(15)	67.86(3)	90	90	90	105.19(2)	78.73(2)
V (Å^3)	1291.6(4)	1280.2(5)	4098(2)	4159(2)	4191.3(14)	2416.5(12)	5998(2)
μ (Mo Kα) (mm^{-1})	6.716	1.184	0.870	4.299	0.853	3.711	1.844
2θ Range	3.1–46	3.7–56	3.7–56	3.7–54	4.3–48	3.4–50	3.1–42
Reflections collected	4894	5974	6015	8915	6686	9057	13 273
Unique/observed reflections	4031/4027	5629/5629	5533/5531	6799/6764	6462/6462	8486/8485	12 600/12 004
R_{int}	0.0516	0.0200	0.0433	0.0720	0.0820	0.0483	0.0580
R_1 ($I>2\sigma(I)$) [c]	0.0476	0.0257	0.0504	0.0546	0.0538	0.0632	0.0554
wR_2 (all data) [c]	0.1831	0.0655	0.1356	0.1573	0.1212	0.1043	0.1467
Weighting factors a; b [c]	0.0184; 0	0.0352; 0.47	0.0757; 2.84	0.0712; 28.87	0.022; 0	0; 5.96	0.0471; 0
Goodness-of-fit [c]	0.799	1.044	1.086	1.048	0.708	1.132	0.912
Residual density (min./max.)	−1.046/1.363	−0.230/0.664	−1.198/2.107	−2.599/2.507	−0.550/0.686	−1.103/1.767	−0.584/1.115

[a] All data were collected on four-circle diffractometers at 173 K using monochromatic Mo Kα radiation ($\lambda = 0.71073$ Å).

[b] The individuals used for data collection were treated as inversion twins; the fraction of inverted domains present for **8** and **9** had been determined to be 0.443(10) and 0.10(4), respectively.

[c] $R_1 = \Sigma||F_o|-|F_c||/\Sigma|F_o|$; $wR_2 = [\Sigma w(F_o^2-F_c^2)^2/\Sigma F_o^4]^{0.5}$; $w = \{[\sigma^2F_o^2]-(aP)^2-b\}^{-1}$, $P = (F_o^2-2F_c^2)/3$; goodness-of-fit = $\{\Sigma[w(F_o^2-F_c^2)^2]/(N_o-N_p)\}$.



Scheme 1.

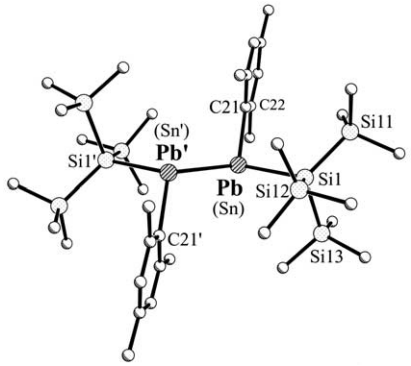


Fig. 3. Molecular structure of the heteroleptic diplumbene **8**. Selected bond lengths (pm), angles and torsion angles (°): Pb–Pb 290.31(11), Pb–Si1 268.1(3), Pb–C21 231.4(10), Si1–Pb–C21 102.5(3), Pb–Si1–Si11 113.66(13), Pb–Si1–Si12 110.42(13), Pb–Si–Si13 101.75(14), C21–Pb–Si1–Si11 −10.3, Si1–Pb–C21–C22 105.6. Selected parameters of the isostructural distannene **9**: Sn–Sn 270.23(8), Sn–Si1 260.18(10), Sn–C21 218.1(2), Si1–Sn–C21 105.46(6), Sn–Si1–Si11 112.48(4), Sn–Si1–Si12 104.63(4), Sn–Si–Si13 110.89(3), C21–Sn–Si1–Si11 −7.6, Si1–Sn–C21–C22 102.7.

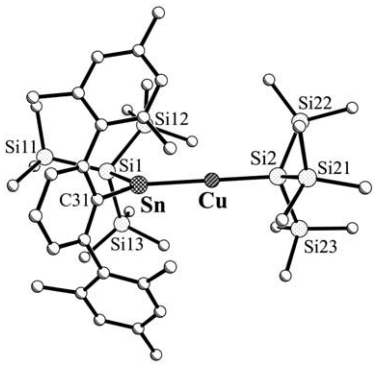


Fig. 4. Molecular structure of the hypersilyl copper adduct **10**. Selected bond lengths (pm), angles and torsion angles (°): Cu–Sn 249.92(6), Sn–Si1 259.65(12), Sn–C31 216.6(4), Cu–Si2 227.28(12), Sn–Cu–Si2 179.36(4), Si1–Cu–C31 114.51(10), Cu–Sn–Si1 116.90(3), Cu–Sn–C31 128.59(10), Si1–Sn–C31–C32 89.1, C31–Sn–Si1–Si11 18.1.

product **7a** (Scheme 1), the adduct of dihypersilylplumbylene (**2**) with mesitylcopper could neither be isolated nor could be detected spectroscopically. It immediately undergoes a rearrangement to form the adduct of the heteroleptic plumbylene Mes(Hyp)Pb with hypersilylcopper **7b** which then dissociated to finally form trimeric hypersilylcopper and the diplumbene Mes(Hyp)Pb=Pb(Hyp)Mes (**8**) with the shortest Pb=Pb bond (290.3 pm) detected so far (Fig. 3, Table 4). The respective reaction with dihypersilylstannylene (**1**) yielded the appropriate distannene **9** again comprising a very short Sn=Sn bond (270.2 pm). To date only few red (**8**) and red-lilac (**9**) crystals ($< 10\%$ yield) of these compounds could be isolated since during the time needed for crystallization (ca. 12 h) most of the initially formed products (ca. 30%) underwent subsequent reactions which could not be elucidated so far.

The reaction path postulated is very probable, however, since in co-operation with Niemeyer we could show that the extremely congested 2,6-dimesityl-phenylcopper reacts in a clean manner with stannylene **1** and plumbylene **2**, respectively, giving either the adduct of the appropriate heteroleptic stannylene with hypersilylcopper (**10**) (Fig. 4) or a mixture of the heteroleptic plumbylene (**11**) and trimeric hypersilylcopper in good yields [2d]. Thus, we finally propose a reaction scheme (Scheme 1) for reactions of copper aryls with dihypersilyltetrylenes, which must be of course still verified to have general validity. Further investigations of this reaction and of related ones with other coordinatively unsaturated metal derivatives such as diorganylzinc, diorganylmercury and triorganylboron derivatives are in our hands.

At first we were surprised about the ease with which the mentioned rearrangements of putatively formed intermediates with two hypersilyl groups still residing at the tetrel atom to the final heteroleptic products took place. The overall reactions were usually finished within a few seconds, even at −30 °C, and no intermediates could be detected by NMR-experiments so far. Preliminary ab initio calculations for the ligand exchange processes for silyl substituted distannenes $H(H_3Si)Sn{=}Sn(SiH_3)H$ and $H(H_3C)Sn{=}Sn(SiH_3)H$ revealed, however, that energetically very low lying transition-states ($E^{\#} < 40$ kJ mol^{-1}; CCSD(T) level of theory) and intermediates may be involved, which are related to the various isomers of very similar energy found on the hypersurface of the parent compound $H_2Sn{=}SnH_2$ [4,6,7]. These results imply that stannylenes and plumbylenes—at least silyl substituted ones—exhibit probably fluctional behavior in solution at ambient temperature and below, and thus allow for easy rearrangement to energetically favorable and less sterically strained products. The release of sterical strain seems to be indeed the major driving force in the formation of the rearranged products, since the angle at Sn or Pb unusually large within the tetrylenes **1** [10] and **2** is markedly less obtuse in most heteroleptic compounds. This may also be true for the rearrangements observed in other Lewis-acid–base reactions discussed in details in the next section.

3. Dihypersilyltetrylenes as Lewis-acid

The smaller HOMO–LUMO gap calculated and experimentally found for bis(silyl)stannylenes and plumbylenes compared with species bearing more electronegative substituents implies either a stronger basicity or a stronger acidity of former or both. Intuitively, one would think that the introduction of electron-re-

leasing groups such as hypersilyl groups should enhance the basicity and diminish the acidity of the divalent tetrel center. DFT calculations on several simple adducts of Lewis-bases and acids with $Pb(CH_3)_2$ on one hand and with $Pb(SiH_3)_2$ on the other hand show, however, that the opposite seems to be true. As can be seen from the calculated dissociation energies of several adducts given in Table 2, adducts of Lewis-bases with disilylplumbylene are by far more stable than respective adducts with dimethylplumbylene. Additionally, the length of the new formed dative bond is markedly shorter for adducts with $Pb(SiH_3)_2$ than for $Pb(CH_3)_2$. Even the very week donor P_4 (note that the lone-pairs on P_4 are only weakly basic, having predominantly s-character in contrast to those in phosphanes PR_3) is calculated to be substantially bonded to $Pb(SiH_3)_2$ only, but not to $Pb(CH_3)_2$.

As can be seen in the following, the dihypersilyltetrylenes **1** and **2** are indeed remarkably strong Lewis-acids compared with related species bearing more electronegative substituents.

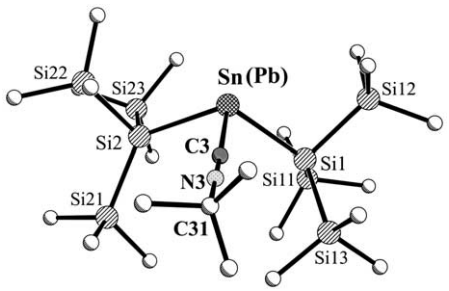


Fig. 5. Molecular structure of the *tert*-butylisonitrile adduct **12a** to dihypersilylstannylene (**1**). Selected bond lengths (pm), angles and torsion angles (°): Sn–C3 228.3(8), Sn–Si1 267.9(2), Sn–Si2 265.0(2), C3–N3 115.8(10), N3–C31 147.2(10), Si1–Sn–Si2 115.42(7), Si1–Sn–C3 91.7(2), Si2–Sn–C3 90.6(2), Si2–Sn–Si1–Si12 160.3; Si1–Sn–Si2–Si22 172.0. Selected parameters of the isostructural adduct **13a** to dihypersilylplumbylene (**2**): Pb–C3 249.5(14), Pb–Si1 275.4(3), Pb–Si2 272.8(3), C3–N3 114(2), N3–C31 147.9(14), Si1–Pb–Si2 114.00(11), Si1–Pb–C3 90.8(3), Si2–Pb–C3 89.8(3), Si2–Pb–Si1–Si12 162.3; Si1–Pb–Si2–Si22 169.9.

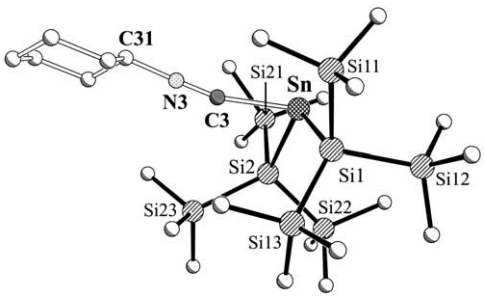
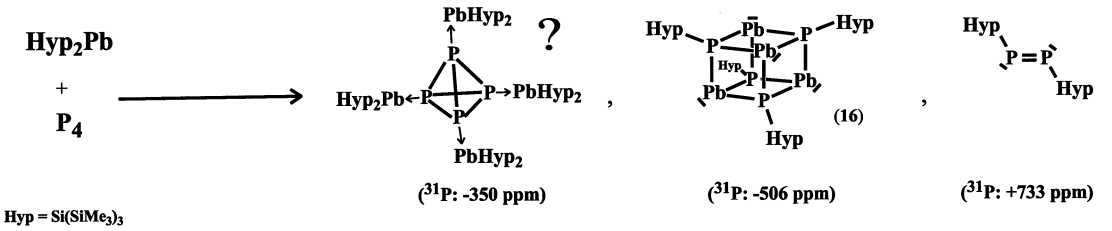


Fig. 6. Molecular structure of the cyclohexylisonitrile adduct **12b** to dihypersilylstannylene (**1**). Selected bond lengths (pm), angles and torsion angles (°): Sn–C3 226.0(12), Sn–Si1 265.2(2), Sn–Si2 267.8(3), C3–N3 118.3(14), N3–C31 146.5(14), Si1–Sn–Si2 114.95(8), Si1–Sn–C3 94.6(6), Si2–Sn–C3 89.6(10), Si2–Sn–Si1–Si11 162.3; Si1–Sn–Si2–Si21 169.8.

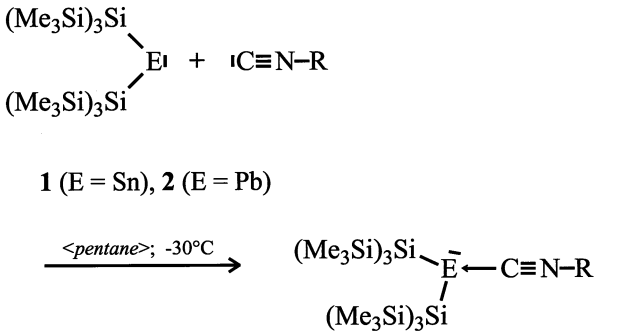
4. Reactions with isonitriles

Both dihypersilyltetrylenes, **1** and **2**, were reacted with two different dialkylisonitriles at −30 °C: *tert*-butyl isonitrile [12] and cyclohexyl isonitrile [13]. The immediate color change from brown to yellow and blue to red, respectively, indicated a fast and complete reaction. Indeed, the expected isonitrile adducts **12a**, **b** and **13a**, **b** were obtained in nearly quantitative yields as orange–yellow and red crystalline compounds, respectively (Eq. (4)). All adducts are fairly stable in *n*-pentane solution at room temperature as far as light is excluded. The lead derivatives **13a**, **b** in solution slowly decompose cleanly to Pb, Hyp–Hyp and the appropriate isonitrile when stored under ambient light, the tin derivatives are indefinitely stable, however. In contrast to the only known isonitrile–stannylene adduct $MesN{\equiv}C \rightarrow SnAr^F_2$ **14**, prepared by Grützmacher several years ago by reaction of an diarylstannylene $SnAr^F_2$ with two strongly electron-withdrawing 2,4,6-$(F_3C)_3C_6H_2$ (Ar^F) groups [14a], there is no experimental evidence for re-dissociation of the adducts **12a**, **b** and **13a**, **b** in solution or under reduced pressure. The molecular structures of **12a**, **b** and **13a** could be determined by X-ray crystallography (Figs. 5 and 6, Table 4) and indeed show shorter C→E bonds than found for other dative C→E(II) bonds, for instant in the isonitrile adduct **14** (240 pm), or in related adduct of nucleophilic carbenes to stannylenes or plumbylenes bearing hydrocarbyl or other more electronegative ligands [15]. Recently, Weidenbruch et al. reported the molecular structure of an adduct of a heteroleptic aryl(hypersilyl)stannylene with a nucleophilic krypto-carbene [16]. Here, due to a significant double bond character of the Sn–C bond a much shorter SnC bond (203 pm) is observed as in compounds with pure donor-carbenes [17]. A significant contribution of the possible mesomeric form $RN{=}C{=}EHyp_2$ for the isonitrile adducts **12a**, **b** and **13a**, **b**, postulated by Grützmacher [14] for **14** can be ruled out by the structural data, the IR-data and from the results of NBO-analyses on model compounds. The results of X-ray diffraction showed that the NC vector is nearly perpendicular orientated to the Si–E–Si plane, thus only very weak bent σ-type interaction may be possible from the lone-pair on E to the π*(N=C)-orbital. Such interactions should however lead to a bathochromic shift of the ν(CN) band (reducing the triple-bond character of the NC bond). The opposite is true, however, the respective bands are shifted by about 30 cm^{-1} to higher energies, going from the pure isonitrile to the adducts **12a**, **b** and **13a**, **b**. Further evidence for no or at least negligible



Scheme 2.

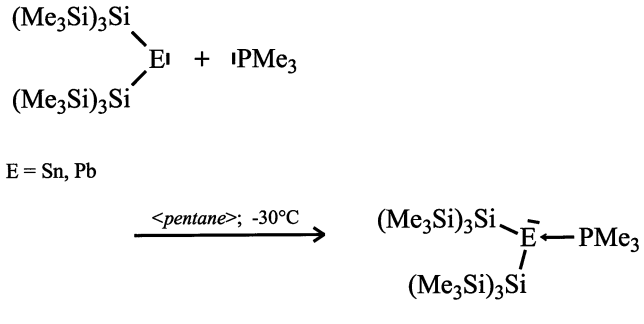
double bond character to C→E(II) bonds in isonitrile adducts was given by the detailed spectroscopic investigations by Okazaki et al. of related isonitrile adducts to a silylene, Tbt(Mes)Si←CNR (R = Tip, Tbt, Mes*; Tbt = $C_6H_2[CH(SiMe_3)_2]_3$-2,4,6; Tip = $C_6H_2^iPr_3$-2,4,6; Mes* = $C_6H_2^tBu$-2,4,6), synthesized by the reaction of the isonitriles with the appropriate sterically extremely hindered disilene Tbt(Mes)Si = Si(Mes)Tbt [14b].



(4)

5. Reaction with trimethylphosphane

To the best of our knowledge no simple stable triorganylphosphane adduct to stannylenes or plumbylenes has ever been isolated. But, when the dihypersilyltetrylenes **1** and **2** are reacted with PMe_3 in *n*-pentane or toluene again an immediate color change is observed and stable crystalline adducts with similar colors like those of the appropriate isonitrile adducts **12**



(5)

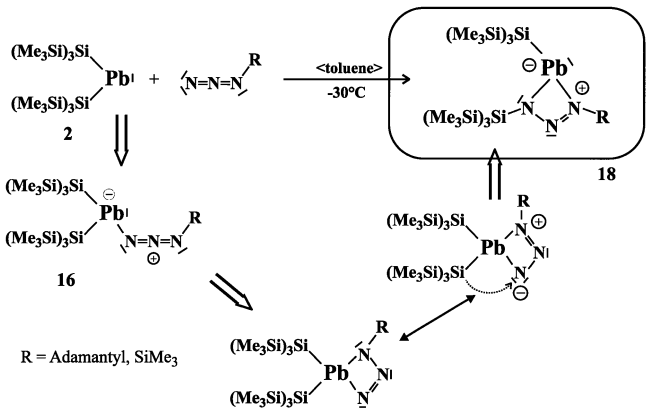
and **13** are isolated, again in quantitative yields [13b]. Not only the stability against heat and light is virtually the same as found for the isonitrile adducts, but also no re-dissociation is detectable in solution or under reduced pressure. Unfortunately, no structural data are available to date, since all crystals obtained from *n*-pentane solution were twinned, but all NMR-spectroscopic and analytical data are in accordance with the formulated simple 1:1 adducts (Eq. (5)).

6. Reaction with white phosphorus

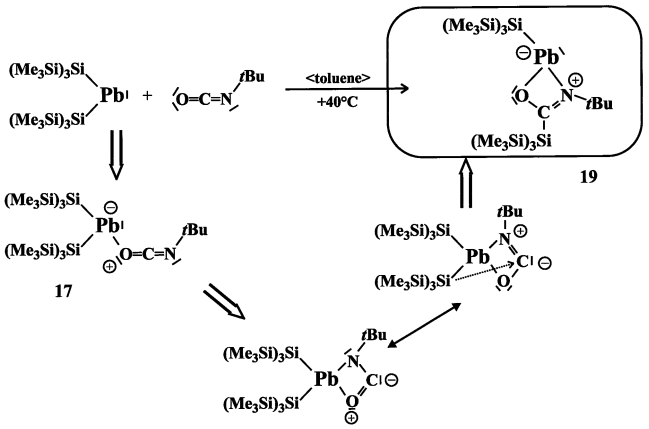
According to personal communication from Weidenbruch, white phosphorus does not react with several diaryl stannylenes and plumbylenes. Nevertheless, when brought in contact with dihypersilyltetrylenes **1** and **2** at −30 °C in toluene P_4 within several minutes gives a reaction, again indicated by a color change from brown or blue to violet [13b]. The reaction of plumbylene **2** is clean, i.e. giving only few products under these conditions, the ^{31}P NMR spectra of the reaction mixture showing only three dominant signals in varying ratios. The extreme low field signal at +733 pm could be unambiguously attributed to dihypersilyldiphosphene HypP=PHyp. The extreme high field signal, according to the observed high order spectrum of its ^{207}Pb satellites and its ^{1}H and ^{29}Si resonances derives from the heterocubane **16** (Scheme 2) which during the refereeing of this paper could be proofed by X-ray crystallography. Both are thermally stable at room temperature. The third compound, however, is thermally unstable, quickly decomposing at room temperature giving P_4, Pb and Hyp–Hyp. We think it to be the simple 1:4 adduct of P_4 with **2** (Scheme 2), since the ^{207}Pb satellites in the ^{31}P NMR spectrum exhibit intensities consistent with four Pb-atoms which are equivalent on the NMR time scale and show no fine structure, indicating a rapid exchange process. Further spectroscopic work has to be done, however, to verify the identity of this product. Nevertheless, a Lewis-acid–base adduct between P_4 and **2** is a very probable intermediate for all possibly following reactions, since it allows at least for a low energy approach of both reactants.

7. Reactions with ambident Lewis-bases

A second outcome of the calculations (Table 2) is worth mentioning: the harder bases H_2O and NH_3 are calculated to form stronger bonded complexes to the soft bis(silyl)tetrylenes than their heavier softer congeners H_2S and PH_3. Nevertheless, one has to keep in mind that the former species are harder, indeed, but also much stronger bases than the latter.



Scheme 3.



Scheme 4.

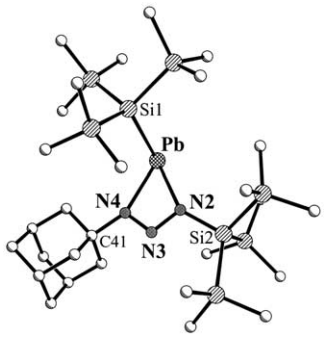


Fig. 7. Molecular structure of the hypersilylleadtriazenide **18**. Selected bond lengths (pm), angles and torsion angles (°): Pb–Si1 273.7(2), Pb–N2 237.2(6), Pb–N4 234.4(7), N2–Si2 178.0(7), N4–C41 152.4(10), Si1–Pb–N2 105.8(2), Si1–Pb–N4 100.1(2), N2–N3–N4 109.3(6), N3–N2–Si2 114.1(5), N3–N4–C41 112.6(6), N2–N3–N4–C41 −179.2, N4–N3–N2–Si2 −163.7.

However, no simple adduct could be isolated so far with simple ethers or amines, but promisingly, (complicated) reactions take place when bubbling ammonia or wet argon through pentane solutions of **1** or **2**, thus further investigations are in our hand.

Isolable products are however obtained in good yields when ambident nitrogen/oxygen bases such as azides or isocyanates are reacted with plumbylene **2** in toluene [13a]. Again simple Lewis-adducts **16** and **17** may be formulated as initial intermediate, but for all investigated cases rearrangements took place: one hypersilyl group migrates from Pb to a heteroatom bearing a formal negative charge thus leading to a heteroleptic formal Pb(II) derivative (Schemes 3 and 4). For the reaction with adamantylazide the product could unambiguously identified by X-ray diffraction to be the red monomeric Pb(II) triazenide complex **18** with one hypersilyl and one chelating 1-adamantyl-3-hypersilylazenide present (Fig. 7, Table 4). The proposed reaction path is given in Scheme 3. We have spectroscopic evidence that trimethylsilylazide Me_3SiN_3 gives the respective violet–red 1-trimethylsilyl-3-hypersilylazenide complex, but no crystals of sufficient quality for X-ray diffraction could be obtained so far. The reaction of plumbylene **2** with *tert*-butylisocyanate produces an extraordinary air and moisture sensitive dark blue–violet compound which for its NMR and analytical data most probably is the imidato complex **19** (Scheme 4). But again no suitable crystals could be obtained and more spectroscopic work has to be done to verify this assumption. No evolution of N_2 or CO has been observed during these reaction, thus the formation of iminoplumbanes RN=PbHyp can be excluded. During attempted reactions of azides with dihypersilylstannylene (**1**), the evolution of nitrogen is observed however, but according to the ^{1}H NMR spectra of the oily residues only complex mixtures of products were obtained so far.

8. Reactions with other bases

Some attempts have been made to react lithium organyls and alkali metal silanides with the dihypersilyltetrylenes **1** and **2**. However, only few clean reactions were found so far. Thus the reaction of sodium hypersilanide with stannylene **1** quantitatively yields the yellow toluene solvate of sodium tris(hypersilyl)stannanide (**20**) (Fig. 8) [18], a very promising reagent providing an extremely bulky substituent for the synthesis of other low coordinated compounds. In contrast to this finding, plumbylene **2** is a much weaker Lewis-acid than its lighter homologue **1** and does not react with alkali

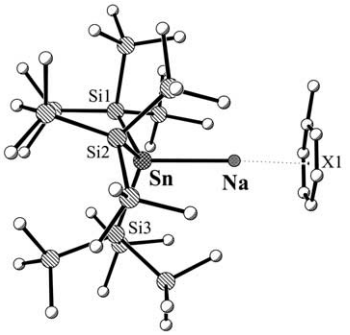
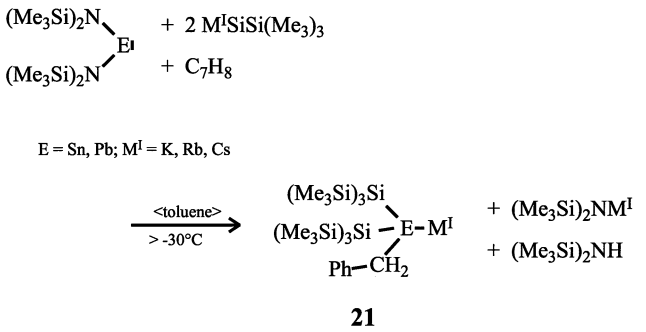


Fig. 8. Molecular structure of the sodium trihypersilylstannanide **20**. Selected bond lengths (pm) and angles (°): Na–Sn 307.0(5), Sn–Si1 270.7(3), Sn–Si2 270.2(3), Sn–Si3 270.4(3), Si1–Sn–Si2 110.14(9), Si1–Sn–Si3 110.49(9), Si2–Sn–Si3 109.15(10), Na–Sn–Si1 109.58(14), Na–Sn–Si2 108.8(2), Na–Sn–Si3 108.7(2), Na···C 282(5)–292(4), Na–X1 260. (X1: centroid of arene ring).

metal hypersilanides, or at least does not form any isolable product. Different very bulky stannanides and even plumbanides are formed, however, in reasonable yields when toluene instead of *n*-pentane is used as a non-innocent solvent for the (attempted) synthesis of the tetrylenes **1** and **2** with potassium, rubidium or cesium hypersilanides at temperatures above −30 °C. Virtually no tetrylene is obtained under these conditions. Instead the formal adducts of the appropriate alkali metal phenylmethanide, **21**, with **1** and **2** are isolated as orange–yellow or red crystalline materials, respectively (Eq. (6)). The molecular structure of the cesium stannanide **21a** could be determined for a mixed salt with cesium bis(trimethylsilyl)amide as the second product of the metathesis [12]. The mixed dimers found in the solid-state structure (Fig. 9(a), Table 4) are extensively linked by π-coordination of the phenyl groups of the phenylmethanide anions to the cesium cations (Fig. 9(b)).



(6)

The reactions of simple lithium organyls such as ^{n}BuLi, ^{t}BuLi or ^{i}PrLi in non-coordinating solvents did not lead to any isolable product so far, but to mixtures of mostly unidentified products (for **1**) or a rapid decomposition of the tetrylene (for **2**). In all reaction mixtures only lithium hypersilanide $LiSi(SiMe_3)_3$ could be unambiguously identified spectroscopically, thus

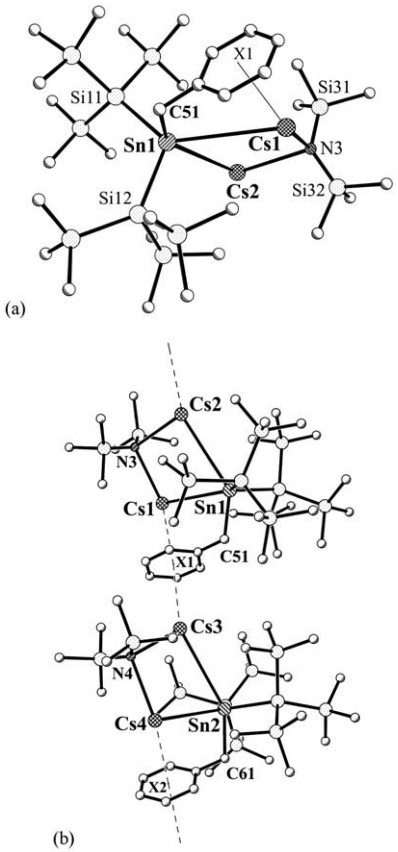
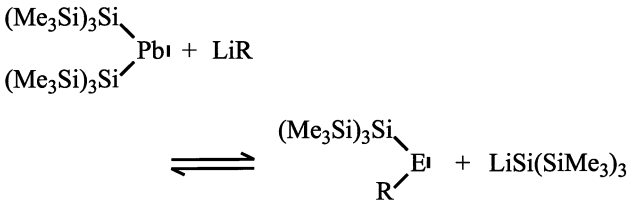


Fig. 9. Molecular structure of the cesium benzyldihypersilylstannanide **21a** (a: dimer; b: coordination polymer). Selected bond lengths (pm) and angles (°) in one of the two independent dimers: Cs1–Sn1 403.9(2), Cs2–Sn1 428.22(15), Cs1–N3 300.5(10), Cs2–N3 303(11), Sn1–Si11 268.3(4), Sn1–Si12 268.4(4), Sn1–Cs1–N3 100.2(2), Sn1–Cs2–N3 95.1(2), Cs1–Sn1–Cs2 66.05(2), Cs1–N3–Cs2 98.2(3), Si11–Sn1–Si12 114.47(13), Si11–Sn1–C51 93.7(4), Si12–Sn1–C51 97.1(4), Si31–N3–Si32 130.3(7), Cs···C (intramolecular) 344.4–367.5, Cs···C (intermolecular) 358.7.8–371.0, Cs1–X1 331, Cs3–X1 338, Cs4–X2 327, Cs2–X2′ 333. (X1; X2: centroids of arene rings)

probably again ligand exchange reactions took place yielding heteroleptic alkyl(hypersilyl) stannylenes and plumbylenes (Eq. (7)) which are not stable under these conditions. Further investigations in the absence and presence of coordinating solvents are in our hand.



(7)

9. Summary

Dihypersilylstannylene (**1**) and dihypersilylplumbylene (**2**) react as Lewis-amphoteric carbene ho-

mologues with several Lewis-acids and Lewis-bases. Their acidity seems to be higher than for other tetrylenes with more electronegative substituents as was proposed on the base of quantum chemical calculations on Lewis-base adducts of simple suitable model compounds and verified for some bases such as isonitriles, phosphanes and white phosphorous. But still the experimental evidence is scarce and must be extended in the future. All reactions where the tetrylenes act as a Lewis-base did not yield the expected adduct, but in each investigated case led to rearrangement reactions, and after migration of one hypersilyl group from Sn or Pb to a hetero atom finally giving derivatives of heteroleptic stannylenes or plumbylenes. Reactions of this particular type also led to the first plumbylene dimers (diplumbenes) with Pb–Pb distances indicating medium to weak double-dative bonds.

10. Supplementary material

All crystallographic data (excluding structure factors) for the so far unpublished structures reported in this paper have been deposited with the Cambridge Crystallographic Data Center as supplementary publication no. 173102 (**8**), 173103 (**9**), 173104 (**13a**), 173105 (**18**), 100901 (**21a**), 100905 (**12b**) and 100907 (**12a**). Copies of the data can be obtained free of charge on application to CCDC, 12 Union Road, Cambridge CB2 1EZ, UK (fax: +44-1223-336033; e-mail: deposit@ccdc.cam.ac.uk or www: http://www.ccdc.cam.ac.uk).

Acknowledgements

I would like to thank my coworkers Jan Klett, Shenglai Yao and Yun Xiong for their enthusiasm and my colleagues, Professor Hansjörg Grützmacher, Professor Manfred Weidenbruch and Dr. Konstantin Karaghiosoff for fruitful cooperations and discussions. The work has been financially supported by the 'Fonds der Chemischen Industrie'.

References

[1] K.W. Klinkhammer, W. Schwarz, Angew. Chem., Int. Ed. Engl. 34 (1995) 1334.
[2] (a) K.W. Klinkhammer, T.F. Fässler, H. Grützmacher, Angew. Chem., Int. Ed. Engl. 37 (1998) 124;
(b) C.J. Cardin, D.J. Cardin, S.P. Constantine, A.K. Todd, S.J. Teat, S. Coles, Organometallics 17 (1998) 2144;
(c) S. Benet, C.J. Cardin, D.J. Cardin, S.P. Constantine, P. Heath, H. Rashid, S. Teixeira, J.H. Thorpe, A.K. Todd, Organometallics 18 (1999) 389;
(d) K.W. Klinkhammer, M. Niemeyer, J. Klett, Chem. Eur. J. 5 (1999) 2531;
(e) M. Stürmann, W. Saak, K.W. Klinkhammer, M. Weidenbruch, Z. Anorg. Allg. Chem. 625 (1999) 1955;
(f) M. Stürmann, W. Saak, M. Weidenbruch, K.W. Klinkhammer, Eur. J. Inorg. Chem. (1999) 579;
(g) M. Stürmann, M. Weidenbruch, K.W. Klinkhammer, F. Lissner, H. Marsmann, Organometallics 17 (1998) 4425;
(h) C. Drost, B. Gehrhus, P.B. Hitchcock, M.F. Lappert, Chem. Commun. (1997) 1845.
[3] B. Gehrhus, P.B. Hitchcock, M.F. Lappert, Angew. Chem., Int. Ed. Engl. 36 (1997) 2514.
[4] H. Jacobsen, T. Ziegler, J. Am. Chem. Soc. 116 (1994) 3667.
[5] W. Kutzelnigg, Angew. Chem., Int. Ed. Engl. 23 (1984) 272.
[6] (a) G. Trinquier, J.-P. Malrieu, J. Am. Chem. Soc. 112 (1990) 2130;
(b) T.L. Windus, M.S. Gordon, J. Am. Chem. Soc. 114 (1992) 9559;
(c) M. Driess, H. Grützmacher, Angew. Chem., Int. Ed. Engl. 35 (1996) 827;
(d) K.W. Klinkhammer, Angew. Chem., Int. Ed. Engl. 36 (1997) 2320;
(e) P.P. Power, Chem. Rev. 99 (1999) 3463;
(f) H. Grützmacher, T.F. Fässler, Chem. Eur. J. 6 (2000) 2317.
[7] (a) E.A. Carter, W.A. Goddard, J. Phys. Chem. 90 (1986) 998;
(b) G. Trinquier, J.-P. Malrieu, J. Am. Chem. Soc. 109 (1987) 5303;
(c) G. Trinquier, J.-P. Malrieu, J. Am. Chem. Soc. 111 (1989) 5916;
(d) G. Trinquier, J.-P. Malrieu, in: S. Patai (Ed.), The Chemistry of Double Bonded Functional Groups, vol. 2, Wiley, Chichester, 1989, p. 1 Part 1.
[8] See for example: (a) W.P. Leung, W.-H. Kwok, F. Xue, T.C.W. Mak, J. Am. Chem. Soc. 119 (1997) 1145;
(b) C. Drost, P.B. Hitchcock, M.F. Lappert, Angew. Chem., Int. Ed. Engl. 38 (1999) 1113
(c) W.-P. Leung, H. Cheng, R.-B. Huang, Q.-C. Yang, T.C.W. Mak, J. Chem. Soc., Chem. Commun. (2000) 451.
[9] (a) Y. Apeloig, M. Karni, J. Chem. Soc., Chem. Commun. (1985) 1048;
(b) S.G. Bott, P. Marshall, P.E. Wagenseller, Y. Wong, R.T. Conlin, J. Organomet. Chem. 499 (1995) 11.
[10] The Si–Sn–Si angle in monomeric stannylene 1 which can not be determined directly because of the dimer formation in the solid-state, may be estimated from the respective value in its isonitrile adducts, since this value should not be influenced by a coordinated slim base. The Si–Sn–Si angle in both structurally characterized isonitrile adducts with 115.0 and 115.4° is hardly larger than the Si–Pb–Si angle in dihypersilylplumbylene 1 (113.6–114.5°) and its *tert*-butyl isonitrile adduct (114.0°). Thus the dimerization of the stannylene **1** obviously leads to rehybridization at Sn—pronounced involvement of the s-orbital in bonding—and to a larger Si–Sn–Si angle of 120.5°.
[11] M. Stürmann, W. Saak, H. Marsmann, M. Weidenbruch, Angew. Chem., Int. Ed. Engl. 38 (1999) 187.
[12] K.W. Klinkhammer, in: Silylderivate der schweren Alkalimetalle in der Synthese niedervalenter Hauptgruppenelementverbindungen (Habilitation Thesis in German), U. Grauer, Stuttgart, 1998.
[13] (a) M. Haag, K.W. Klinkhammer, N. Schöne, unpublished results;
(b) S. Yao, K.W. Klinkhammer, unpublished results.
[14] (a) H. Grützmacher, S. Freitag, R. Herbst-Irmer, G.S. Sheldrick, Angew. Chem., Int. Ed. Engl. 31 (1992) 437;
(b) N. Takeda, H. Suzuki, N. Tokitoh, R. Okazaki, J. Am. Chem. Soc. 119 (1997) 1456.
[15] (a) H. Schumann, M. Glanz, F. Girgsdies, F.E. Hahn, M. Tamm, A. Grzegorzewski, Angew. Chem., Int. Ed. Engl. 36 (1997) 2232;
(b) A. Schäfer, M. Weidenbruch, W. Saak, S. Pohl, J. Chem. Soc., Chem. Commun. (1995) 1157;

(c) N. Kuhn, T. Kratz, D. Bläser, R. Boese, Chem. Ber. 128 (1995) 245;
(d) F. Stabenow, W. Saak, M. Weidenbruch, J. Chem. Soc., Chem. Commun. (1999) 1131.

[16] M. Stürmann, W. Saak, M. Weidenbruch, A. Berndt, D. Sclesclkewitz, Heteroatom Chem. 10 (1999) 554.

[17] (a) H. Meyer, G. Baum, W. Massa, S. Berger, A. Berndt, Angew. Chem., Int. Ed. Engl. 26 (1997) 5546;
(b) M. Weidenbruch, H. Kilian, M. Stürmann, S. Pohl, W. Saak, H. Marsmann, D. Steiner, A. Berndt, J. Organomet. Chem. 530 (1997) 255.

[18] K.W. Klinkhammer, Chem. Eur. J. 3 (1997) 1418.

[19] GAUSSIAN 98, Revision A.7, M.J. Frisch, G.W. Trucks, H.B. Schlegel, G.E. Scuseria, M.A. Robb, J.R. Cheeseman, V.G. Zakrzewski, J.A. Montgomery, Jr., R.E. Stratmann, J.C. Burant, S. Dapprich, J.M. Millam, A.D. Daniels, K.N. Kudin, M.C. Strain, O. Farkas, J. Tomasi, V. Barone, M. Cossi, R. Cammi, B. Mennucci, C. Pomelli, C. Adamo, S. Clifford, J. Ochterski, G.A. Petersson, P.Y. Ayala, Q. Cui, K. Morokuma, D.K. Malick, A.D. Rabuck, K. Raghavachari, J.B. Foresman, J. Cioslowski, J.V. Ortiz, A.G. Baboul, B.B. Stefanov, G. Liu, A. Liashenko, P. Piskorz, I. Komaromi, R. Gomperts, R.L. Martin, D.J. Fox, T. Keith, M.A. Al-Laham, C.Y. Peng, A. Nanayakkara, C. Gonzalez, M. Challacombe, P.M.W. Gill, B. Johnson, W. Chen, M.W. Wong, J.L. Andres, C. Gonzalez, M. Head-Gordon, E.S. Replogle, and J.A. Pople, Gaussian, Inc., Pittsburgh, PA, 1998.

[20] (a) A. Bergner, M. Dolg, W. Kuechle, H. Stoll, H. Preuss, Mol. Phys. 80 (1993) 1431;
(b) T. Leininger, A. Nicklass, W. Küchle, H. Stoll, M. Dolg, A. Bergner, Chem. Phys. Lett. 255 (1996) 274;
(c) W. Kuechle, M. Dolg, H. Stoll, H. Preuss, Mol. Phys. 74 (1991) 1245.

[21] U. Lay, H. Pritzkow, H. Grützmacher, J. Chem. Soc., Chem. Commun. (1992) 260.

[22] M. Weidenbruch, H. Kilian, K. Peters, H.G. von Schnering, H. Marsmann, Chem. Ber. 128 (1995) 983.

[23] Crystals had been covered with a layer of viscous hydrocarbon oil (Paratone N, Exxon). A suitable crystal was selected, attached to a glass fiber, and instantly placed in a low-temperature N_2-stream [12]. All data were collected on Siemens four-circle diffractometers ($P2_1$ or P4) at 173 K using monochromatic Mo Kα radiation ($\lambda = 0.71073$ Å). Selected data collection parameters and other crystallographic data are summarized in Table 4. Calculations were carried out with the SHELXTL PC 5.03 program system installed on a local PC. The phase problem was solved by direct methods for all cases, and the structures were refined on F_o^2 by full-matrix least-squares refinement. Absorption corrections were applied to all data, using semiempirical ψ-scans.

PERGAMON

Polyhedron 21 (2002) 599–609

POLYHEDRON

www.elsevier.com/locate/poly

$\tilde{X}\ ^3\Sigma^-$ and $\tilde{A}\ ^3\Pi$ electronic states of linear disilaketenylidene (SiSiO): analysis of the Renner effect in the $\tilde{A}\ ^3\Pi$ state. Comparison with the analogous multiple bonded systems SiCO, CSiO, and CCO

Shawn T. Brown [a], Nicholas D.K. Petraco [b], Yukio Yamaguchi [b], Henry F. Schaefer III [b,*]

[a] *Q-Chem Inc., Export, PA 15632, USA*

[b] *Center for Computational Quantum Chemistry, University of Georgia, Athens, GA 30602, USA*

Received 26 May 2001; accepted 21 December 2001

Abstract

Ab initio electronic structure theory has been employed to investigate systematically the $\tilde{X}\ ^3\Sigma^-$ and $\tilde{A}\ ^3\Pi$ electronic states of linear disilaketenylidene (SiSiO). The ground state displays a SiSi double bond while the excited $\tilde{A}\ ^3\Pi$ state may be assigned a SiSi bond order of 5/2. The ground ($\tilde{X}\ ^3\Sigma^-$) state of SiSiO possesses a real degenerate bending vibrational frequency, while the first excited triplet ($\tilde{A}\ ^3\Pi$) state is subject to the Renner–Teller interaction, resulting in two distinct real vibrational frequencies along the bending coordinate. The total energies and physical properties including equilibrium geometries, dipole moments, harmonic vibrational frequencies, and associated infrared (IR) intensities of the two lowest-lying triplet states were predicted using the SCF, CISD, CCSD, and CCSD(T) levels of theory with a wide range of basis sets. The $\tilde{A}\ ^3\Pi$ state was also studied using the equation-of-motion CCSD (EOM-CCSD) technique in order to avoid a possible variational collapse to the lower-lying state. With the cc-pVTZ EOM-CCSD method, the Renner parameter and average harmonic bending vibrational frequency for the $\tilde{A}\ ^3\Pi$ state were determined to be $\varepsilon = -0.078$ and $\omega_2 = 219\ \mathrm{cm}^{-1}$, respectively. With our most reliable method, cc-pVQZ CCSD(T), the $\tilde{X}$–$\tilde{A}$ splitting (T_e value) of SiSiO was predicted to be 55.7 kcal mol^{-1} (2.41 eV, 19 500 cm^{-1}) and the splitting including zero-point vibrational energy correction (T_0 value) to be 56.1 kcal mol^{-1} (2.43 eV, 19 600 cm^{-1}). The bond energy for Si–SiO was determined to be $D_e = 26.1$ ($D_0 = 25.2$) kcal mol^{-1} indicating considerable thermodynamic stability for the ground state of SiSiO against the dissociation reaction SiSiO ($\tilde{X}\ ^3\Sigma^-$) $\rightarrow$ Si (^3P_g) + SiO ($\tilde{X}\ ^1\Sigma^+$). © 2002 Published by Elsevier Science Ltd.

Keywords: Electronic states; Linear disilaketenylidene (SiSiO); Renner effect; Analogous multiple bonded systems

1. Introduction

Disilaketenylidene (SiSiO) is the fully silicon substituted analogue of the ketenylidene (CCO) molecule. While CCO has received a great deal of experimental and theoretical attention in the past (see Ref. [1]), there is only fleeting evidence for the existence of SiSiO. The first evidence of its existence was given in 1987 by van Zee, Ferrante, and Weltner [2]. They reported the electron spin resonance (ESR) spectra of the $C_2^{17}O$, $SiC^{17}O$, and $^{29}Si_2O$ molecules. Although the ESR spectra of isomers of C_2O and SiCO were reported previously [3–5], SiSiO ($\tilde{X}\ ^3\Sigma^-$) was thought to be detected for the first time, but the assignment of the spectra was made on circumstantial evidence. Based on the fact that the feature assigned to Si_2O had a doublet structure and almost all of the spin-density is on one silicon atom, the asymmetric isomer (SiSiO) was chosen as the likely molecule over the symmetric isomer (SiOSi).

Shortly after, in 1989, DeKock, Yates, and one of us attempted to answer the question as to the relative stability of the $\tilde{X}\ ^3\Sigma^-$ state of linear SiOSi to SiSiO using SCF, CISD, and CASSCF ab initio methods [6], and it was found that the SiOSi isomer was more stable by about 10 kcal mol^{-1}. In 1993 Boldyrev and Simons

* Corresponding author.

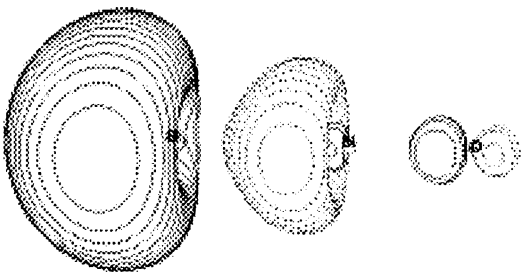
E-mail address: hfsiii@arches.uga.edu (H.F. Schaefer, III).

0277-5387/02/$ - see front matter © 2002 Published by Elsevier Science Ltd.

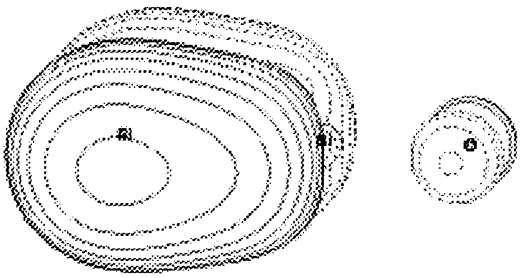
PII: S0277-5387(02)00830-6

extended the search for the most stable isomer to bent isomers with singlet or triplet multiplicities in their investigation of Si_2O and Si_3O [7]. They reported structures and vibrational frequencies with MP4STDQ/6–311 + G(2df and QCISD(T)/6–311 + G(2df) methods and the bent singlet C_{2v} ($^1A_1$) Si_2O structure was found to be the global minima of the Si_2O system. The bent triplet C_{2v} ($^3B_1$) Si_2O, linear triplet ($^3\Sigma_g^-$) SiOSi, and linear triplet ($^3\Sigma^-$) SiSiO structures were predicted to lie above the global minimum C_{2v} ($^1A_1$) structure by 17.5, 20.7, and 27.0 kcal mol^{-1}, respectively, at the QCISD(T)/6–311 + G*(2df) level. Then Iraqi, Goldberg, and Schwarz sought to further confirm this conclusion from the results of their neutralization–reionization mass spectrometry experiments [8]. By subjecting the gas-phase Si_2O clusters to collisional activation with helium, they observed strong evidence that the molecule should have an Si–Si bond and, therefore, ruling out any linear SiOSi structures. In the following year (in 1994) Boldyrev, Simons, Zakrzewski, and von Niessen presented vertical and adiabatic ionization energies and electron affinities of the new Si_nC and Si_nO ($n = 1$–3) molecules [9].

While the relative stabilities of these isomers are interesting, they are not the focus of this research, for we shall concentrate on the ground and first excited state of only one of these possibilities. Recently, we



(a) 11σ



(b) 4π

Fig. 1. The 11σ and 4π molecular orbitals for the $\tilde{X}\,^3\Sigma^-$ ground state of SiSiO determined at the TZ3P(2f) SCF level of theory.

reported theoretical studies of the $\tilde{X}\,^3\Sigma^-$ and $\tilde{A}\,^3\Pi$ and states of CCO [1], SiCO [10], and CSiO [11] radicals. We have presented highly reliable CCSD(T) results for energetics, harmonic vibrational frequencies and geometric parameters for these radicals. The Renner–Teller effect [12–20] in the $\tilde{A}\,^3\Pi$ states for this series were also discussed. The $\tilde{X}\,^3\Sigma^-$ states of these three radicals posses degenerate bending vibrational frequencies, while the states $\tilde{A}\,^3\Pi$ present two distinct frequencies along the bending coordinates. The Renner parameters and average harmonic bending frequencies have been predicted for the $\tilde{A}\,^3\Pi$ states employing the equation-of-motion CCSD (EOM-CCSD) technique. The EOM-CCSD wave function does not suffer from the orbital instability problem (vide infra) because the excited-state energies are determined as higher roots of the reference CCSD wave function in the same symmetry. The present study on the SiSiO radical is a logical extension of our previous investigations on the linear ketenylidene type radicals with 14 valence electrons. The physical properties and energetics of the two lowest-lying states of linear SiSiO will be compared with those of its carbon analogues.

2. Electronic structure considerations

The ground electronic state of the linear SiSiO radical has the electronic configuration:

$$[\text{core}](8\sigma)^2(9\sigma)^2(10\sigma)^2(3\pi)^4(11\sigma)^2(4\pi_i)(4\pi_o) \quad \tilde{X}^3\Sigma^- \tag{1}$$

where [core] abbreviates the 11 core (Si:1s-, 2s-, 2p-like and O:1s-like) orbitals and π_i and π_o indicate the in-plane and out-of-plane π orbitals, which are degenerate in the ground state. The 8σ molecular orbital (MO) mainly represents the Si–O σ bond, while the 9σ MO describes the Si–Si σ bond. The 10σ and 11σ MOs are the lone pair orbitals on the O atom and the Si atom, respectively. The 3π MO components describe the Si–O π bonds, whereas the 4π MO components are attributed to the Si–Si π bond. The 11σ and $4\pi_o$ MOs for the $\tilde{X}\,^3\Sigma^-$ state of SiSiO are depicted in Fig. 1. The first excited triplet state of SiSiO corresponds to a single electron excitation

$$(11\sigma)^2(4\pi)^2 \rightarrow (11\sigma)(4\pi)^3 \tag{2}$$

and has the electronic configuration

$$[\text{core}](8\sigma)^2(9\sigma)^2(10\sigma)^2(3\pi)^4(11\sigma)(4\pi)^3 \quad \tilde{A}^3\Pi \tag{3}$$

The $\tilde{X}\,^3\Sigma^-$ state possesses a real degenerate bending vibrational frequency, whereas the $\tilde{A}\,^3\Pi$ state presents the two distinct real vibrational frequencies along the SiSiO bending coordinate. Therefore, the $\tilde{A}\,^3\Pi$ state is a type A Renner molecule as classified by Lee, Fox, Schaefer, and Pitzer for linear triatomic molecules [18].

At this point, it is useful to analyze the MO Hessian [21] of the reference self-consistent-field (SCF) wave functions. The MO Hessian is defined as the second derivatives of the SCF electronic energy with respect to MO rotations at a given geometry. For the $\tilde{X}\ ^3\Sigma^-$ state the MO Hessian possesses all positive eigenvalues at the linear equilibrium configuration, confirming that the SCF wave function for the ground state of SiSiO is *stable*. On the other hand, the $\tilde{A}\ ^3\Pi$ state of SiSiO has one zero and one negative eigenvalue of the MO Hessian. The eigenvector corresponding to the zero eigenvalue refers to the $4\pi_i$–$4\pi_o$ MO rotation, indicating that the SCF energy is not altered by such a MO rotation. The eigenvector of the negative eigenvalue is associated with the 11σ–4π MO rotation and, therefore, the SCF wave function of the $\tilde{A}\ ^3\Pi$ state of SiSiO is *unstable* with respect to a lower-lying state at this equilibrium geometry. The lower-lying state in this case is the $\tilde{X}\ ^3\Sigma^-$ state, and it may be obtained by exchanging the 11σ and 4π orbitals. Physical properties involving the 11σ–4π MO rotation should be interpreted cautiously for the $\tilde{A}\ ^3\Pi$ state of SiSiO (in this case, the ω_2^- bending frequency, see below). By the same token, the magnitudes of the eigenvalues for the MO Hessian also provide information as to the degree of stability for the SCF wave function [21–23].

3. Renner effects

Following Herzberg's exposition [15], the Renner parameter (ε) and average harmonic bending frequency (ω_2) are described in the following manner. The potential function of a linear molecule possessing a degenerate electronic state splits into two components upon bending, because in the bent conformation degeneracy no longer exists. For the Π and Δ states the 'upper' (inner) potential function is denoted V^+, while the 'lower' (outer) one V^-. The parity of the potential refers to its symmetry with respect to the plane of the bent molecule [24]. The zero-order bending potential function may be written

$$V^0 = aq^2 + bq^4 + \ldots \tag{4}$$

and the splitting of the potential function in Π, Δ, … states must also have the same form

$$V^+ - V^- = \alpha q^2 + \beta q^4 + \ldots \tag{5}$$

where a and α are quadratic force constants, b and β are quartic force constants, and q is a bending displacement coordinate. The Renner parameter (ε) is defined neglecting anharmonicity terms by

$$\varepsilon = \frac{\alpha}{2a} \tag{6}$$

It may be shown that Eq. 6 is equivalent to

$$\varepsilon = \frac{f^+ - f^-}{f^+ + f^-} = \frac{(\omega^+)^2 - (\omega^-)^2}{(\omega^+)^2 + (\omega^-)^2} \tag{7}$$

where f^+ and f^- are the force constants while ω^+ and ω^- are the harmonic vibrational frequencies associated with the 'upper' and 'lower' bending potentials. Denoting μ to be the kinetic energy contribution to the bending motion, the average harmonic bending frequency (ω_2) may be determined using the equation

$$\omega_2 = \frac{1}{2\pi c}\sqrt{\frac{a}{\mu}} = \frac{1}{2\pi c}\sqrt{\frac{f^+ + f^-}{2\mu}} \tag{8}$$

which may be rewritten as

$$\omega_2 = \sqrt{\frac{1}{2}((\omega^+)^2 + (\omega^-)^2)} \tag{9}$$

The experimentally observable values, ε and ω_2, may be compared with the corresponding theoretical values determined independently through the use of eqn. 4–9.

4. Theoretical procedures

Six triple-ζ (TZ) plus quality basis sets were employed in this research. The TZ basis set for O is obtained from Dunning's triple-ζ contraction [25] of Huzinaga's primitive Gaussian set [26] and is designated (10s6p/5s3p). The TZ basis set for Si is derived from McLean and Chandler's contraction [27] of Huzinaga's primitive Gaussian set [28] and is designated (12s9p/6s5p). The orbital exponents of the polarization functions are: $\alpha_d(O) = 1.70$ and 0.425, and $\alpha_d(Si) = 1.00$ and 0.25 for double polarization (TZ2P); and $\alpha_d(O) =$ 3.40, 0.85, 0.2125, and $\alpha_d(Si) = 2.00$, 0.50, 0.125 for triple polarization (TZ3P). The orbital exponents of the higher angular momentum functions are: $\alpha_f(O) = 1.40$, and $\alpha_f(Si) = 0.32$ for one set of higher angular momentum functions [TZ2P(f)]; and $\alpha_f(O) = 2.80$, 0.70, and $\alpha_f(Si) = 0.64$, 0.16, for two sets of higher angular momentum functions [TZ3P(2f)]. The orbital exponents of the diffuse functions are: $\alpha_p(O) = 0.05840$ and $\alpha_s(O) =$ 0.08993, and $\alpha_p(Si) = 0.02354$ and $\alpha_s(Si) = 0.02567$, for one set of diffuse functions [TZ2P + diff and TZ2P(f) + diff]. Pure angular momentum d and f functions were used throughout. The largest TZ plus basis set, TZ3P(2f), comprises 143 contracted Gaussian functions for SiSiO with a contraction scheme of O (10s6p3d2f/5s3p3d2f) and Si (12s9p3d2f/6s5p3d2f). Finally, two correlation consistent basis sets, cc-pVTZ and cc-pVQZ, developed by Dunning and coworker [29,30] have also been used. The cc-pVQZ basis set consists of 173 contracted Gaussian functions with a contraction scheme of O (12s6p3d2f1g/5s4p3d2f1g) and Si (16s11p3d2f1g/6s5p3d2f1g).

The zeroth-order descriptions for the $\tilde{X}\ ^3\Sigma^-$ and $\tilde{A}\ ^3\Pi$ states of SiSiO were obtained using single-configuration SCF (restricted open-shell Hartree–Fock) wave

Table 1
Optimized structures for the $\tilde{X}\ ^3\Sigma^-$ and $\tilde{A}\ ^3\Pi$ states of the SiSiO molecule

Electronic state	$\tilde{X}\ ^3\Sigma^-$ state		$\tilde{A}\ ^3\Pi$ state	
	r_e(SiSi)	r_e(SiO)	r_e(SiSi)	r_e(SiO)
Level of theory				
TZ2P CISD	2.2957	1.5046	2.0685	1.5125
TZ2P+diff CISD	2.2949	1.5049	2.0696	1.5128
TZ3P CISD	2.2930	1.5023	2.0638	1.5097
TZ2P(f) CISD	2.2703	1.5022	2.0608	1.5096
TZ2P(f)+diff CISD	2.2697	1.5027	2.0613	1.5102
TZ3P(2f) CISD	2.2623	1.4984	2.0536	1.5050
cc-pVTZ CISD	2.2721	1.5055	2.0641	1.5130
cc-pVQZ CISD	2.2602	1.4995	2.0554	1.5062
TZ2P EOM-CCSD			2.1002	1.5272
TZ2P+diff EOM-CCSD			2.1020	1.5275
TZ3P EOM-CCSD			2.0959	1.5239
TZ2P(f) EOM-CCSD			2.0890	1.5243
TZ2P(f)+diff EOM-CCSD			2.0899	1.5249
TZ3P(2f) EOM-CCSD			2.0820	1.5189
cc-pVTZ EOM-CCSD			2.0924	1.5274
TZ2P CCSD	2.3094	1.5163	2.0901	1.5264
TZ2P+diff CCSD	2.3093	1.5167	2.0917	1.5267
TZ3P CCSD	2.3080	1.5138	2.0856	1.5231
TZ2P(f) CCSD	2.2791	1.5140	2.0803	1.5235
TZ2P(f)+diff CCSD	2.2789	1.5146	2.0811	1.5240
TZ3P(2f) CCSD	2.2729	1.5097	2.0733	1.5181
cc-pVTZ CCSD	2.2810	1.5169	2.0837	1.5265
cc-pVQZ CCSD	2.2694	1.5107	2.0747	1.5192
TZ2P CCSD(T)	2.3139	1.5289	2.1037	1.5408
TZ2P+diff CCSD(T)	2.3146	1.5293	2.1055	1.5412
TZ3P CCSD(T)	2.3141	1.5263	2.0994	1.5374
TZ2P(f) CCSD(T)	2.2848	1.5266	2.0933	1.5379
TZ2P(f)+diff CCSD(T)	2.2851	1.5271	2.0943	1.5384
TZ3P(2f) CCSD(T)	2.2797	1.5220	2.0861	1.5321
cc-pVTZ CCSD(T)	2.2871	1.5293	2.0970	1.5407
cc-pVQZ CCSD(T)	2.2762	1.5231	2.0876	1.5333

Bond distances are in Å.

functions. Correlation effects were included using configuration interaction with single and double excitations (CISD), coupled cluster including singles and doubles (CCSD) [31,32], and CCSD with perturbative triples correction [CCSD(T)] [33,34] levels of theory. The EOM-CCSD wave function [35–38] was also employed for the study of the $\tilde{A}\ ^3\Pi$ state. In correlated procedures with the TZ basis sets a frozen core approximation for the 11 core (Si:1s-, 2s-, 2p-like and O:1s-like) orbitals was employed, and the three highest-lying virtual (Si,O:1s*-like) orbitals were excluded from correlation. Only the frozen core approximation was used for the correlation consistent basis sets. With the cc-pVQZ basis set, the numbers of configuration state functions (CSFs) in the CISD procedures in the Hartree–Fock interacting space [39,40] are 190 782 for the $\tilde{X}\ ^3\Sigma^-$ state of SiSiO in C_{2v} symmetry and 375 642 in C_s symmetry, 190 586 for the $\tilde{A}\ ^3\Pi$ state of SiSiO in C_{2v} symmetry and 375 151 in C_s symmetry, respectively.

The geometrical structures of the two lowest-lying triplet states of SiSiO were optimized at the SCF and CISD levels of theory using analytic derivative methods [41–43], while all coupled-cluster optimizations were performed via five point numerical differentiation of total energies [44]. Harmonic vibrational frequencies at the SCF level were evaluated analytically, while at the CISD, CCSD, EOM-CCSD, and CCSD(T) levels of theory they were obtained by finite differences of analytic gradients and/or energies [44]. All computations were carried out using the PSI 2.0.8 program package [45] except the EOM-CCSD wave functions which were performed with the ACES II package[46] on IBM RS/6000 workstations.

5. Results and discussion

5.1. Geometries

The optimized geometric parameters for the $\tilde{X}\ ^3\Sigma^-$ and $\tilde{A}\ ^3\Pi$ states of SiSiO at the SCF, CISD, CCSD, and CCSD(T) levels of theory with all basis sets employed in this work are presented in Table 1. EOM-CCSD results are provided for only the $\tilde{A}\ ^3\Pi$ state since EOM-CCSD is an excited state method. Figs. 2 and 3 show optimized geometries for only the largest basis sets for each level of correlation. These representations of the theoretical predictions illustrate a number of interesting points.

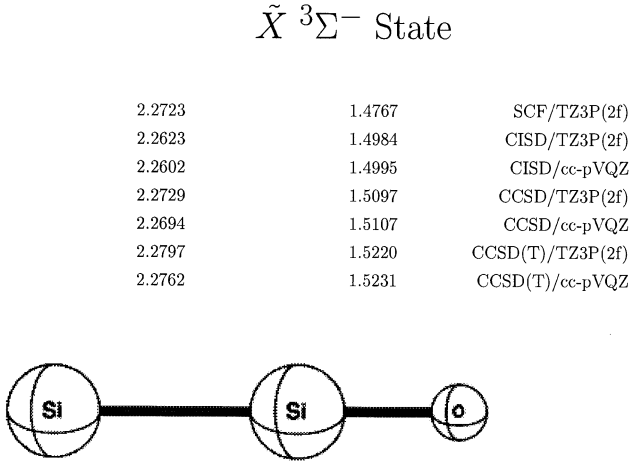


Fig. 2. Optimized geometries for $\tilde{X}\ ^3\Sigma^-$ SiSiO determined by various theoretical methods employed in this research. Bond distances are in angstroms.

$\tilde{A}\ ^3\Pi$ State

2.0479	1.4821	SCF/TZ3P(2f)
2.0536	1.5050	CISD/TZ3P(2f)
2.0554	1.5062	CISD/cc-pVQZ
2.0820	1.5189	EOM-CCSD/TZ3P(2f)
2.0924	1.5274	EOM-CCSD/cc-pVTZ
2.0733	1.5181	CCSD/TZ3P(2f)
2.0747	1.5192	CCSD/cc-pVQZ
2.0861	1.5321	CCSD(T)/TZ3P(2f)
2.0876	1.5333	CCSD(T)/cc-pVQZ

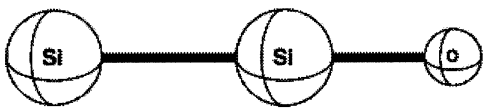


Fig. 3. Optimized geometries for $\tilde{A}\ ^3\Pi$ SiSiO determined by various theoretical methods employed in this research. Bond distances are in angstroms.

Upon excitation, the SiSi bond length significantly shortens (approximately 0.2 Å) and the SiO bond distance slightly lengthens (by approximately 0.01–0.02 Å). This can easily be explained by the nature of the MO's involved in the excitation.The 11σ MO of SiSiO in Eq. 1 (in Fig. 1(a)) is the non-bonding orbital on the Si atom, whereas the 4π MO (in Fig. 1(b)) possesses strong Si–Si π bonding and weak Si–O anti-π bonding character. Thus, a single electron excitation from the 11σ to the 4π MO distinctly shortens the Si–Si bond and marginally lengthens the Si–O bond. From Table 1, it can be seen that, as expected, the bond distances are generally contracting with basis set size, and from Figs. 2 and 3 the bond distances generally elongate with improvement of the treatment of correlation effects. Similar geometrical features have been recognized for the corresponding two triplet states of the isovalent CCO [1], SiCO [10], and CSiO [11] molecules.

It is interesting to note that, the SiO bond length changes very little upon excitation (1.5231 Å for the $\tilde{X}\ ^3\Sigma^-$ state 1.5333 Å for the $\tilde{A}\ ^3\Pi$ state at the cc-pVQZ CCSD(T) level of theory). Both of these parameters are close to the cc-pVQZ CCSD(T) equilibrium bond distance for diatomic $\tilde{X}\ ^3\Sigma^-$ SiO of 1.5201 Å. This is an implication of the strength of the SiO bond and the relatively poor ability of the Si atom to pull electrons away from the very strong SiO bond [6]. This is in contrast to CCO, where the CO bond distance is greatly affected by the addition of the terminal carbon as a consequence of the greater tendency of first-row atoms to hybridize [1,47,48]. Similar concerns will be addressed later for all of the ketenylidene analogues.

Table 2
Theoretical predictions of the total energy (in hartrees), dipole moment (in debye), harmonic vibrational frequencies (in cm^{-1}), infrared (IR) intensities (in parentheses in km mol^{-1}), and zero-point vibrational energy (ZPVE in kcal mol^{-1}) for the $\tilde{X}\ ^3\Sigma^-$ state of the SiSiO molecule[a]

Level of theory	Energy	μ_e	$\omega_1(\sigma)$ SiO str.	$\omega_2(\pi)$ Bend	$\omega_3(\sigma)$ SiSi str.	ZPVE
TZ2P CISD	−653.045037	2.855	1298(152.5)	143(46.2)	357(0.2)	2.78
TZ2P+diff CISD	−653.047112	3.015	1296(158.3)	141(40.9)	359(0.1)	2.77
TZ3P CISD	−653.052365	3.024	1308(147.7)	154(42.1)	354(0.0)	2.82
TZ2P(f) CISD	−653.080660	2.835	1308(154.3)	151(49.1)	387(0.1)	2.86
TZ2P(f)+diff CISD	−653.082456	3.008	1306(160.2)	143(43.5)	388(0.0)	2.83
TZ3P(2f) CISD	−653.095016	3.039	1323(151.3)	163(44.9)	389(0.0)	2.91
cc-pVTZ CISD	−653.090984	2.790	1318(138.3)	158(44.0)	390(0.0)	2.89
cc-pVQZ CISD	−653.127639		1325	161	398	2.92
TZ2P CCSD	−653.090441		1250	127	348	2.65
TZ2P+diff CCSD	−653.092683		1249	124	349	2.64
TZ3P CCSD	−653.098302		1262	138	342	2.69
TZ2P(f) CCSD	−653.130375		1260	136	381	2.74
TZ2P(f)+diff CCSD	−653.132300		1258	127	382	2.71
TZ3P(2f) CCSD	−653.145710		1276	149	380	2.79
cc-pVTZ CCSD	−653.141519		1271	143	384	2.78
cc-pVQZ CCSD	−653.180699		1278	146	391	2.80
TZ2P CCSD(T)	−653.111995		1196	123	354	2.57
TZ2P+diff CCSD(T)	−653.114351		1195	117	354	2.55
TZ3P CCSD(T)	−653.120620		1208	132	345	2.60
TZ2P(f) CCSD(T)	−653.154854		1206	133	384	2.65
TZ2P(f)+diff CCSD(T)	−653.156847		1205	120	384	2.61
TZ3P(2f) CCSD(T)	−653.171369		1223	142	380	2.70
cc-pVTZ CCSD(T)	−653.166759		1217	137	386	2.68
cc-pVQZ CCSD(T)	−653.208268		1224	139	392	2.71

[a] IR intensities of the degenerate ω_2 mode were doubled.

Table 3
Theoretical predictions of the total energy (in hartree), dipole moment (in debye), harmonic vibrational frequencies (in cm^{-1}), and infrared (IR) intensities (in parentheses in km mol^{-1}) for the $\tilde{A}\ ^3\Pi$ state of the SiSiO molecule

Level of theory	Energy	μ_e	$\omega_1(\sigma)$ SiO str.	$\omega_2(\pi_i, {}^3A'')$ bend	$\omega_2(\pi_o, {}^3A'')$ bend	$\omega_3(\sigma)$ SiSi str.
TZ2P CISD	−652.948902	3.981	1278(163.1)		224(45.2)	585(5.0)
TZ2P+diff CISD	−652.950582	4.125	1276(169.2)		220(41.0)	584(4.7)
TZ3P CISD	−652.956002	4.112	1290(162.3)		219(37.1)	584(4.9)
TZ2P(f) CISD	−652.987559	3.970	1290(165.7)		227(48.3)	596(5.4)
TZ2P(f)+diff CISD	−652.988998	4.122	1288(172.4)		222(43.3)	595(4.9)
TZ3P(2f) CISD	−653.002307	4.128	1307(169.3)		229(39.4)	599(5.2)
cc-pVTZ CISD	−652.996715	3.886	1299(151.7)		228(39.5)	596(4.9)
cc-pVQZ CISD	−653.035226		1308		229	601
TZ2P EOM-CCSD	−652.996331		1214	219	205	535
TZ2P+diff EOM-CCSD	−652.998219		1212	210	200	533
TZ3P EOM-CCSD	−653.003964		1227	213	200	532
TZ2P(f)EOM-CCSD	−653.039782		1227	228	209	553
TZ2P(f)+diff EOM-CCSD	−653.041384		1225	217	204	552
TZ3P(2f) EOM-CCSD	−653.055442		1246	233	212	552
cc-pVTZ EOM-CCSD	−653.050120		1236	227	210	552
TZ2P CCSD	−652.995442		1221		207	551
TZ2P+diff CCSD	−652.997318		1218		202	549
TZ3P CCSD	−653.003229		1233		202	548
TZ2P(f) CCSD	−653.038850		1233		210	565
TZ2P(f)+diff CCSD	−653.040452		1231		205	563
TZ3P(2f) CCSD	−653.054751		1252		214	565
cc-pVTZ CCSD	−653.049097		1242		212	564
cc-pVQZ CCSD	−653.090182		1253		213	569
TZ2P CCSD(T)	−653.018824		1166		193	528
TZ2P+diff CCSD(T)	−653.020818		1164		187	526
TZ3P CCSD(T)	−653.027481		1179		187	526
TZ2P(f) CCSD(T)	−653.065021		1178		196	543
TZ2P(f)+diff CCSD(T)	−653.066705		1176		190	541
TZ3P(2f) CCSD(T)	−653.082229		1197		199	543
cc-pVTZ CCSD(T)	−653.076229		1187		197	542
cc-pVQZ CCSD(T)	−653.119538		1198			547

5.2. Dipole moments

The dipole moments in debye for the $\tilde{X}\ ^3\Sigma^-$ and $\tilde{A}\ ^3\Pi$ states of SiSiO are given in Tables 2 and 3 along with the total energies. With the TZ3P(2f) CISD method the dipole moments of the two states of SiSiO are predicted to be $\mu_e\ (^+SiSiO^-) = 3.04$ ($\tilde{X}\ ^3\Sigma^-$) and $\mu_e\ (^+SiSiO^-) = 4.13$ ($\tilde{A}\ ^3\Pi$) debye, where the signs indicate the direction of the dipole moments. Immediately we see that the first excited triplet state is more polar than the ground state. One of the 11σ lone pair electrons on the terminal Si atom (in Fig. 1(a)) is promoted to the 4π orbital (in Fig. 1(b)), causing a shift in electron density to toward the oxygen atom, and the character of the orbitals involved in excitation may be attributed as the cause for the change in dipole moments between the two states. Given a basis set, correlation effects decrease the dipole moments of the $\tilde{X}$ and $\tilde{A}$ states. The dipole moments of the $\tilde{X}\ ^3\Sigma^-$ and $\tilde{A}\ ^3\Pi$ states of CCO were predicted to be 1.42 ($\tilde{X}\ ^3\Sigma^-$) and 1.47 ($\tilde{A}\ ^3\Pi$) debye [1]. According to Pauling [49] the electronegativities for the three relevant atoms are C(2.5), Si(1.8), and O(3.5). The smaller electronegativity of Si and the larger difference in electronegativities between Si–O than between C–O may be the main reason for the larger dipole moments of SiSiO compared with those of CCO. The theoretically predicted dipole moment of the diatomic SiO ($\tilde{X}\ ^1\Sigma^+$) is $\mu_e\ (^+SiO^-) = 3.28$ debye with the TZ3P(2f) CISD method, while the experimental value is $\mu_e = 3.098$ debye [50], which once again shows the terminal Si atom interacts very little with the strong SiO bond. The dipole moment for the ground state SiSiO is close to that for the diatomic SiO ($\tilde{X}\ ^1\Sigma^+$). Since the dipole moment of SiSiO is reasonably large, microwave spectroscopic investigation may be feasible.

5.3. Harmonic vibrational frequencies

Harmonic vibrational frequencies for the $\tilde{X}\ ^3\Sigma^-$ and $\tilde{A}\ ^3\Pi$ states are given in Tables 2 and 3, respectively. The Si–Si stretching (ω_3) frequency of SiSiO is significantly higher for the $\tilde{A}\ ^3\Pi$ state than for the $\tilde{X}\ ^3\Sigma^-$ state, in accordance with the shortening of the bond length of the $\tilde{A}\ ^3\Pi$ state. On the contrary, the Si–O stretching frequency (ω_1) is slightly higher for the $\tilde{X}$

$^3\Sigma^-$ state than for the $\tilde{A}\ ^3\Pi$ state. The SiO stretching frequencies of the two states generally decrease with advanced treatments of correlation effects, probably owing to elongated bond distances. Upon bending, the $^3A''$ component of the $\tilde{A}\ ^3\Pi$ state may suffer from a variational collapse to the lower lying $^3A''$ state originating from the $\tilde{X}\ ^3\Sigma^-$ state. In Table 4 the $^3A'$ component of the bending frequency is reported for the CISD, CCSD and CCSD(T) methods. The $\omega_2^-(^3A'')$ bending frequencies from the EOM-CCSD technique is more reliable in a physical and mathematical sense, since the EOM-CCSD wave function is not subjected to the variational collapse, as mentioned in Section 1. With the cc-pVQZ CCSD(T) method, the harmonic vibrational frequency of the diatomic SiO ($\tilde{X}\ ^1\Sigma^+$) is predicted to be 1235 cm^{-1}, whereas the experimental value is 1241.6 cm^{-1} [50]. The SiO stretching fundamental, 1224 cm^{-1} ($\tilde{X}\ ^3\Sigma^-$) for the ground state of SiSiO, has a slightly lower frequency than the diatomic SiO ($\tilde{X}\ ^1\Sigma^+$). The bending (ω_2) frequency is higher for the first excited state compared with that for the ground state, owing to the more contracted structure of the $\tilde{A}\ ^3\Pi$ state as mentioned above.

5.4. Infrared (IR) intensities

The IR intensities (shown in Tables 2 and 3) of the SiO stretching mode are the largest for both the $\tilde{X}\ ^3\Sigma^-$ and $\tilde{A}\ ^3\Pi$ states, due to the polar nature of the SiO bond. The SiSi stretching mode has a small vanishing IR intensity for the $\tilde{X}\ ^3\Sigma^-$ state and a marginal intensity for the $\tilde{A}\ ^3\Pi$ state. The bending modes of the two states present considerably strong intensities. It is found that the IR intensities of the SiO stretching mode of the ground and first excited triplet state of linear SiSiO are significantly larger than that of the isolated SiO ($\tilde{X}\ ^3\Sigma^+$) molecule [62.4 km mol^{-1} at the TZ3P(2f) CISD level of theory]. A similar tendency has been observed for the IR intensities of the CO stretching mode of SiCO and CO [10]. IR spectroscopic investigation of the SiSiO radical may be possible, because some of the IR intensities are relatively large.

Table 4
The predicted Renner parameter (ε) and harmonic bending vibrational frequency (ω_2) in cm^{-1} for the $\tilde{A}\ ^3\Pi$ state of SiSiO, neglecting anharmonicity

Level of theory	$\omega_2^-(^3A'')$	$\omega_2^+(^3A')$	ε	$\omega_2(\pi)$
TZ2P EOM-CCSD	219	205	−0.0678	212
TZ2P+diff EOM-CCSD	210	200	−0.0460	205
TZ3P EOM-CCSD	213	200	−0.0659	207
TZ2P(f) EOM-CCSD	228	209	−0.0859	219
TZ2P(f)+diff EOM-CCSD	217	204	−0.0627	217
TZ3P(2f) EOM-CCSD	235	212	−0.0923	223
cc-pVTZ EOM-CCSD	227	210	−0.0780	219

5.5. Renner effects

Predicted Renner parameters (ε) and average harmonic bending vibrational frequencies (ω_2) for the $\tilde{A}\ ^3\Pi$ state are presented in Table 4. These values were obtained using the equations described in Section 3. Following the symmetry of the EOM-CCSD wave functions, ω^+ is assigned to the bending motion producing the $^3A'$ state and ω^- to the $^3A''$ state. The theoretical Renner parameters and ω_2 frequencies are reasonably consistent among the seven basis sets. As expected, the sign of the Renner parameter is negative, as were the cases for CCO [1], SiCO [10], and CSiO [11] indicating the potential surface corresponding to a bending motion that is antisymmetric with respect to the plane of the bent molecule lies above the symmetric, and the magnitude of ε for SiSiO is the smallest among the four ketenylidene type radicals.

5.6. Energetics

The excitation energies for the $\tilde{A}\ ^3\Pi$ state relative to the $\tilde{X}\ ^3\Sigma^-$ state are presented in Table 5. With the TZ3P(2f) basis set, the classical energy separation (T_e value) [51] is predicted to be 58.0 (SCF), 58.2 (CISD), 56.6 (EOM-CCSD), 57.1 (CCSD), and 55.9 kcal mol^{-1} [CCSD(T)], respectively. The $\tilde{X}$–$\tilde{A}$ splitting gradually decreases with the correlation level and basis set size. The upper state, with a higher silicon bond order, seems to be stabilized preferentially with the correlation effects; however, this stabilization by correlation effects for the SiSiO system appear less evident compared with that for the CCO system [1]. At the most reliable level of theory employed in this study, cc-pVQZ CCSD(T), the T_e value is predicted to be 55.7 kcal mol^{-1} (2.41 eV, 19 500 cm^{-1}). Employing the three cc-pVQZ CCSD(T) harmonic vibrational frequencies for the $\tilde{X}\ ^3\Sigma^-$ state and the two cc-pVQZ CCSD(T) harmonic stretching frequencies while doubling the TZ3P(2f) EOM-CCSD ω_2 frequency for the $\tilde{A}\ ^3\Pi$ state, the zero-point vibrational energy (ZPVE) correction is predicted to be 136 cm^{-1}. Consequently, the quantum mechanical excitation energy (T_0 value) for the $\tilde{A}\ ^3\Pi$ state is determined to be 56.1 kcal mol^{-1} (2.43 eV, 19 600 cm^{-1}).

5.7. Bond energy

The Si–SiO bond energy was evaluated from the dissociation energy of the reaction

$$SiSiO(\tilde{X}\ ^3\Sigma^-) \rightarrow Si(^3P) + SiO(\tilde{X}\ ^1\Sigma^+) \quad (10)$$

Table 5
Adiabatic excitation energies (T_e) to the $\tilde{A}\ ^3\Pi$ state of SiSiO

Level of theory	ΔE		
	kcal mol^{-1}	eV	cm^{-1}
TZ2P CISD	60.33	2.616	21 100
TZ2P+diff CISD	60.57	2.627	21 190
TZ3P CISD	60.47	2.622	21 150
TZ2P(f) CISD	58.42	2.533	20 430
TZ2P(f)+diff CISD	58.65	2.543	20 510
TZ3P(2f) CISD	58.18	2.523	20 350
cc-pVTZ CISD	59.15	2.565	20 690
cc-pVQZ CISD	57.99	2.515	20 280
TZ2P EOM-CCSD	59.05	2.561	20 655
TZ2P+diff EOM-CCSD	59.28	2.570	20 732
TZ3P EOM-CCSD	59.20	2.567	20 705
TZ2P(f) EOM-CCSD	56.85	2.465	19 883
TZ2P(f)+diff EOM-CCSD	57.05	2.474	19 954
TZ3P(2f) EOM-CCSD	56.64	2.456	19 812
cc-pVTZ EOM-CCSD	57.35	2.487	20 060
TZ2P CCSD	59.61	2.585	20 850
TZ2P+diff CCSD	59.84	2.595	20 930
TZ3P CCSD	59.66	2.587	20 870
TZ2P(f) CCSD	57.43	2.491	20 090
TZ2P(f)+diff CCSD	57.64	2.499	20 160
TZ3P(2f) CCSD	57.08	2.475	19 960
cc-pVTZ CCSD	58.00	2.515	20 280
cc-pVQZ CCSD	56.80	2.463	19 870
TZ2P CCSD(T)	58.47	2.535	20 450
TZ2P+diff CCSD(T)	58.69	2.545	20 530
TZ3P CCSD(T)	58.45	2.534	20 440
TZ2P(f) CCSD(T)	56.37	2.444	19 720
TZ2P(f)+diff CCSD(T)	56.57	2.453	19 780
TZ3P(2f) CCSD(T)	55.94	2.426	19 560
cc-pVTZ CCSD(T)	56.81	2.463	19 870
cc-pVQZ CCSD(T)	55.68	2.414	19 470

The bond dissociation energies at the SCF, CCSD, CCSD(T) levels of theory are presented in Table 6. It should be noted that these three methods are size-consistent. The dissociation energy is more sensitive to the level of correlation and basis set size than the excitation energy discussed above. The SCF dissociation energy is not reliable compared with the dissociation energies from the more sophisticated CCSD and CCSD(T) methods. At the highest level of theory, cc-pVQZ CCSD(T), the Si–SiO bond energy is predicted to be $D_e = 26.1$ kcal mol^{-1} (1.13 eV) and $D_0 = 25.2$ kcal mol^{-1} (1.09 eV). This is about 10 kcal mol^{-1} higher than DeKock et al.'s CISD/TZ + 2P result [6], but it is still the lowest of all the carbon/silicon ketenylidene analogues.

5.8. Comparisons among CCO, SiCO, CSiO, and SiSiO

In Table 7 the structural characteristics and energetics are compared for the four ketenylidene type radicals, XYO (X, Y = C, Si). It is first important to mention some discussion given by Kutzelnigg in reference to the character of first and second row atoms [47,48]. The s and p valence atomic orbitals (AOs) of first row atoms are localized in roughly the same region of space, whereas for second row atoms or higher they are much more extended into space. Consequently, single bonds between first row elements are weak and multiple bonds are strong, and vice versa for second row elements. Also, ideal hybridization is realized if the s and p valence AOs are localized in the same region of space and hence have comparable bonding and overlapping capabilities. Only the first row elements possess this property, and this is particularly the case for carbon. In second row elements or higher, the actual valence configurations are somewhere in between the ground configuration and the ideal valence, differing considerably from ideal hybridization. This argument, for our purposes, explains many of the trends that we see amongst these analogues. For instance the trend in the XY bond distance is given as

$$\mathrm{SiSiO} > \mathrm{CSiO} > \mathrm{SiCO} > \mathrm{CCO} \quad (11)$$

and it is apparent that the CO bond lengths deviate from the free diatomic bond length relative to the change in the SiO bond lengths, indicating more interaction with the terminal atom in the CO case. Also the trend in the bond dissociation energy opposes the above sequence (Eq. (11)), which is consistent with the above analysis.

Table 6
Bond dissociation [Si–SiO → Si(^3P_g) + SiO($^1\Sigma^+$)] energies, D_e, (D_0 value in parentheses) for the $\tilde{X}\ ^3\Sigma^-$ state of SiSiO

Level of theory	In kcal mol^{-1}	In eV
TZ2P SCF	9.28(8.32)	0.402(0.361)
TZ2P+diff SCF	9.58(8.62)	0.415(0.374)
TZ3P SCF	10.43(9.43)	0.452(0.409)
TZ2P(f) SCF	10.38(9.41)	0.450(0.408)
TZ2P(f)+diff SCF	10.51(9.55)	0.456(0.414)
TZ3P(2f) SCF	11.81(10.79)	0.512(0.468)
TZ2P CCSD	15.27(14.42)	0.662(0.625)
TZ2P+diff CCSD	15.53(14.69)	0.673(0.637)
TZ3P CCSD	15.93(15.06)	0.691(0.653)
TZ2P(f) CCSD	20.60(19.68)	0.893(0.853)
TZ2P(f)+diff CCSD	20.70(19.81)	0.898(0.859)
TZ3P(2f) CCSD	21.70(20.75)	0.941(0.900)
cc-pVTZ CCSD	21.35(20.40)	0.926(0.885)
cc-pVQZ CCSD	22.96(22.00)	0.996(0.954)
TZ2P CCSD(T)	17.94(17.10)	0.778(0.742)
TZ2P+diff CCSD(T)	18.16(17.33)	0.787(0.752)
TZ3P CCSD(T)	18.57(17.71)	0.805(0.768)
TZ2P(f) CCSD(T)	23.60(22.69)	1.023(0.984)
TZ2P(f)+diff CCSD(T)	23.64(22.77)	1.025(0.987)
TZ3P(2f) CCSD(T)	24.68(23.74)	1.070(1.029)
cc-pVTZ CCSD(T)	24.30(23.37)	1.054(1.013)
cc-pVQZ CCSD(T)	26.12(25.18)	1.133(1.092)

Table 7
Comparison of the ketenylidene XYO (X, Y = C, Si) type radicals

Physical properties	State	CCO [a]	SiCO [b]	CSiO [c]	SiSiO [d]
Renner–Teller type [e]	$\tilde{A}\ ^3\Pi$	A	A	A	A
XY distance [f]	$\tilde{X}\ ^3\Sigma^-$	1.370	1.825	1.854	2.280
	$\tilde{A}\ ^3\Pi$	1.274	1.706	1.662	2.086
$\tilde{X}-\tilde{A}$ % Difference		(−7.0%)	(−6.5%)	(−10.4%)	(−8.5%)
YO distance [f]	$\tilde{X}\ ^3\Sigma^-$	1.163	1.159	1.520	1.522
	$\tilde{A}\ ^3\Pi$	1.186	1.176	1.525	1.532
$\tilde{X}-\tilde{A}$ % difference		(+2.0%)	(+1.5%)	(+0.3%)	(+0.7%)
XO distance [f]	$\tilde{X}\ ^3\Sigma^-$	2.533	2.984	3.373	3.802
	$\tilde{A}\ ^3\Pi$	2.460	2.882	3.187	3.618
$\tilde{X}-\tilde{A}$ % difference		(−2.9%)	(−3.4%)	(−5.5%)	(−4.8%)
Renner parameter (ε) [g]	$\tilde{A}\ ^3\Pi$	−0.153	−0.103	−0.253	−0.092
Bending frequency (ω_2) (cm^{-1})	$\tilde{A}\ ^3\Pi$	627	447	337	223
Dipole moment [h]	$\tilde{X}\ ^3\Sigma^-$	−1.42	0.29	0.67	3.04
	$\tilde{A}\ ^3\Pi$	1.47	2.49	1.77	4.13
$\tilde{X}-\tilde{A}$ splitting [i]		33.1	68.5	29.8	55.7
XYO ($\tilde{X}\ ^3\Sigma^-$) → X (^3P_g) + YO ($\tilde{X}\ ^1\Sigma^+$) [i]		52.9	31.5	32.6	26.1
ZPVE corrected		(50.3)	(30.0)	(31.4)	(25.2)

[a] From ref. [1].
[b] From ref. [10].
[c] From ref. [11].
[d] From this study.
[e] See text and ref. [18].
[f] Bond distances are in Å with the TZ3P(2f) CCSD(T) method.
[g] The Renner parameter is dimensionless.
[h] Dipole moments are in debye with the TZ3P(2f) CISD method. Values are given in chemists' notation where the polarity (+/−) yields a positive value.
[i] Energetics are in kcal mol^{-1} with the cc-pVQZ CCSD(T) method.

Now let us turn to the dipole moments in these analogues, for there is something very interesting that occurs upon excitation. In all cases, the electron density of the molecule shifts toward the oxygen atom upon excitation from the non-bonding lone pair σ orbital to the π orbital. This can be seen visually in Fig. 1 for the SiSiO case and is analogous for all of these molecules. The 11σ orbital extends well past the terminal Si atom and upon excitation to the 4π orbital, which is a SiSi π bonding orbital, the electron migrates closer to the O atom causing the above mentioned shift in electron density. In the case of CCO the migration is great enough to cause the polarity to change sign. A well-known and similar change in polarity is experienced in the diatomic CO molecule [52,53]. The $X\ ^1\Sigma^+$ state of CO has small dipole moment with the surprising polarity of $^-CO^+$. Excitation to the $a\ ^3\Pi$ state involves excitation from a non-bonding lone pair σ orbital from the carbon to a π orbital [54] which in turn shifts polarity to the oxygen causing a flip in the overall polarity of the molecule to $^+CO^-$. Although less pronounced in SiCO, CSiO, and SiSiO, there is definitely an electron density shift toward the oxygen atom, causing the excited state to be more polar. The percent of atomic orbital character for these MOs is presented in Table 9, and it can clearly be seen that the above analysis is correct. Therefore, the trend in this shift is

$$CCO > SiCO > CSiO > SiSiO \quad (12)$$

and the results of Table 9 provide adequate explanation for the this trend follows the p_x character contribution from the O atom to the π involved in excitations (CSiO and SiSiO have nearly the same contribution and dipole moment shift).

The polarities of the ground states of the four radicals are in order of (expressed in chemists notation where the polarity (+/−) is positive)

$$SiSiO > CSiO > SiCO > CCO \quad (13)$$

Recall that the dipole moment for the SiSiO is close to that of diatomic SiO, so this trend is once again an indication of Kutzelnigg's argument for the greater tendency of the carbon atom to hybridize. The trend in the dipole moments for the first excited triplet states follows

$$SiSiO > SiCO > CSiO > CCO \quad (14)$$

The $\tilde{A}\ ^3\Pi$ states of the four radicals are classified as type A Renner–Teller molecules. Upon the $\tilde{A} \leftarrow \tilde{X}$ excitation, the XY distances are shortened, the YO distances are elongated, and the molecular sizes (XO distances) are contracted for all four radicals.

The magnitudes of the Renner–Teller effect for the $\tilde{A}\ ^3\Pi$ states are given by the quantity $\varepsilon\omega$ [20] and are in the order of

Table 8
Orbital energy difference in hartrees between the non-bonding σ orbital and the 4π orbital of XYO

XYO (X, Y = C, Si)	Adiabatic [a]
CSiO	0.0583
CCO	0.0985
SiSiO	0.1064
SiCO	0.1494

[a] Adiabatic refers to the difference between the ground state 11σ orbital energy computed at the optimized TZ2P CISD ground state geometry and the excited state 4π orbital energy computed at the optimized TZ2P CISD excited state geometry.

$$CCO > CSiO > SiCO > SiSiO \quad (15)$$

while the trend in the absolute value of the Renner parameter, ε is

$$CSiO > CCO > SiCO > SiSiO \quad (16)$$

And the trend in the ω_2 bending frequency yields an expected ordering of

$$CCO > SiCO > CSiO > SiSiO \quad (17)$$

Since the trend in the bending frequency seems correct, it would appear that the trend in the Renner parameter is an electronic effect. This characteristic of the Renner parameter was attributed by John Brown to the tendency of the parameter to show the same proportionality to the inverse square root reduced mass of the bending coordinate ($\mu^{-1/2}$) [20]. A literature search for reported trends in the Renner–Teller splitting in a series of molecules produced only a single reference, to the work of Adachi, Kosugi, Shigemasa, and Yagishita [55]. Their work involved studying the R–T splitting in states arising from C $1s \rightarrow \pi^*$ transitions in the molecules CO_2, CSO, and CS_2. They observed the following trend:

$$CO_2 > OCS > CS_2 \quad (18)$$

Although not completely analogous, it would appear to suggest that the substitution of second-row atoms decreases the magnitude of the R–T splitting, which agrees with the trend in $\varepsilon\omega$ above.

The $\tilde{X}$–$\tilde{A}$ splittings of the four species are in the order

$$SiCO > SiSiO > CCO > CSiO \quad (19)$$

This trend can be understood by looking at the orbital energy difference in the non-bonding σ orbital from the ground state and the relaxed π orbital that is occupied after excitation. At the CISD TZ2P geometry, the orbital energy difference in these SCF reference orbitals is given in Table 8. The so-called adiabatic orbital energy difference indicates the splitting allowing for the excited state orbitals to 'relax' after excitation and follows the trend in excitation energies.

6. Concluding remarks

The ground ($\tilde{X}\ ^3\Sigma^-$) and first excited triplet ($\tilde{A}\ ^3\Pi$) electronic states of linear disilaketenylidene (SiSiO) have been studied using ab initio SCF, CISD, EOM-CCSD, CCSD, and CCSD(T) levels of theory. The $\tilde{A}\ ^3\Pi$ state of SiSiO is subject to a Renner–Teller interaction. The two distinct bending vibrational frequencies associated with the $\tilde{A}\ ^3\Pi$ state have been investigated with the EOM-CCSD technique. The $\tilde{A}\ ^3\Pi$ state of SiSiO presents the smallest Renner parameter among the four ketenylidene radicals with 14 valence electrons; however, it has the largest dipole moment. At the highest level of theory employed in this research, cc-pVQZ CCSD(T), the classical $\tilde{X}$–$\tilde{A}$ splitting is determined to be 55.7 kcal mol^{-1} (2.41 eV, 19 500) and the separation including ZPVE is 56.1 kcal mol^{-1} (2.43 eV, 19 600). The Si–SiO bond dissociation energy is predicted to be $D_e = 26.1$ kcal mol^{-1} (1.13 eV) and $D_0 =$ 25.2 kcal mol^{-1} (1.09 eV).

Table 9
Percent of atomic orbital character of selected orbitals for the $\tilde{X}\ ^3\Sigma^-$ state of the ketenylidene XYO (X, Y = C, Si) type radicals at the CISD/TZ3P(2f) optimized geometry

Molecule		X			Y			O		
		%s	%p_x	%p_z	%s	%p_x	%p_z	%s	%p_x	%p_z
CCO	7σ	45.9		10.0	8.4		5.8	1.5		2.5
	$2\pi_x$ [a]		43.7			20.5			21.9	
CSiO	9σ	26.0		15.3	19.5		11.8	0.8		9.4
	$3\pi_x$		49.6			20.3			12.0	
SiCO	9σ	40.7		11.1	21.1		8.0	3.5		5.3
	$3\pi_x$		49.6			18.2			18.7	
SiSiO	10σ	27.9		16.5	15.4		12.7	2.7		7.4
	$4\pi_x$		45.9			22.0			13.6	

[a] Only the π_x orbital results are presented because by symmetry, the π_y will have the same percent decomposition except with py atomic orbitals.

Acknowledgements

The authors would like to thank Dr. Wesley D. Allen for his many helpful discussions. This research was supported by the US National Science Foundation grant number CHE-9815397.

References

[1] S.T. Brown, Y. Yamaguchi, H.F. Schaefer, J. Phys. Chem. A 104 (2000) 3603.
[2] R.J. van Zee, R.F. Ferrante, W. Weltner, Chem. Phys. Lett. 139 (1987) 426.
[3] R.L. DeKock, W. Weltner, J. Am. Chem. Soc. 93 (1971) 7106.
[4] G.R. Smith, W. Weltner, J. Chem. Phys. 62 (1975) 416.
[5] R.R. Lembke, R.F. Ferrante, W. Weltner, J. Am. Chem. Soc. 28 (1977) 416.
[6] R.L. DeKock, B.F. Yates, H.F. Schaefer, Inorg. Chem. 97 (1989) 5875.
[7] A.I. Boldyrev, J. Simons, J. Phys. Chem. 97 (1993) 5875.
[8] M. Iraqi, N. Goldberg, H. Schwarz, J. Phys. Chem. 97 (1993) 11371.
[9] A.I. Boldyrev, J. Simons, V.G. Zakrzewski, W. von Niessen, J. Phys. Chem. 98 (1994) 1427.
[10] N.D.K. Petraco, S.T. Brown, Y. Yamaguchi, H.F. Schaefer, J. Chem. Phys. 112 (2000) 3201.
[11] N.D.K. Petraco, S.T. Brown, Y. Yamaguchi, H.F. Schaefer, J. Phys. Chem. A 104 (2000) 10165.
[12] G. Herzberg, E. Teller, Z. Phys. Chem. Abt. B 21 (1933) 410.
[13] R. Renner, Z. Phys. 92 (1934) 172.
[14] J.T. Hougen, J. Chem. Phys. 36 (1962) 1874.
[15] G. Herzberg, Molecular Spectra and Molecular Structure III. Electronic Spectra and Electronic Structure of Polyatomic Molecules, Krieger, Malabara, FL, 1991.
[16] C. Jungen, A.J. Merer, in: K.N. Rao (Ed.), Molecular Spectroscopy: Modern Research, vol. 2, Academic Press, New York, 1976, p. 127.
[17] J.M. Brown, F. Jørgenson, Adv. Chem. Phys. 52 (1983) 117.
[18] T.J. Lee, D.J. Fox, H.F. Schaefer, R.M. Pitzer, J. Chem. Phys. 81 (1984) 356.
[19] P.R. Bunker, P. Jensen, Molecular Symmetry and Spectroscopy, 2nd ed., NRC Research Press, Ottawa, Canada, 1998.
[20] J.M. Brown, in: P.R. Bunker, P. Jensen (Eds.), Computational Molecular Spectroscopy, Wiley, West Sussex, UK, 2000 Chapter 16.
[21] Y. Yamaguchi, I.L. Alberts, J.D. Goddard, H.F. Schaefer, Chem. Phys. 147 (1990) 309.
[22] N.A. Burton, Y. Yamaguchi, I.L. Alberts, H.F. Schaefer, J. Chem. Phys. 95 (1991) 7466.
[23] T.D. Crawford, J.F. Stanton, W.D. Allen, H.F. Schaefer, J. Chem. Phys. 107 (1997) 10626.
[24] R.N. Dixon, Phil. Trans. Roy. Soc. London A 252 (1960) 1007.
[25] T.H. Dunning, J. Chem. Phys. 55 (1971) 716.
[26] S. Huzinaga, J. Chem. Phys. 42 (1965) 1293.
[27] A.D. McLean, G. Chandler, J. Chem. Phys. 72 (1980) 5639.
[28] S. Huzinaga, Technical report, Department of Chemistry, University of Alberta, Edmonton, Alta., Canada, unpublished.
[29] T.H. Dunning, J. Chem. Phys. 90 (1989) 1007.
[30] D.E. Woon, T.H. Dunning, J. Chem. Phys. 98 (1993) 1358.
[31] G.D. Purvis, R.J. Bartlett, J. Chem. Phys. 76 (1910) 1982.
[32] M. Rittby, R.J. Bartlett, J. Phys. Chem. 92 (1988) 3033.
[33] K. Raghavachari, G.W. Trucks, J.A. Pople, M. Head-Gordon, Chem. Phys. Lett. 157 (1989) 479.
[34] G.E. Scuseria, Chem. Phys. Lett. 176 (1991) 27.
[35] H.J. Monkhorst, Int. J. Quantum Chem. S11 (1977) 421.
[36] H. Koch, P. Jørgensen, J. Chem. Phys. 93 (1990) 3333.
[37] H. Koch, H.J.A. Jensen, P. Jørgensen, T. Helgaker, J. Chem. Phys. 93 (1990) 33.
[38] J.F. Stanton, R.J. Bartlett, J. Chem. Phys. 98 (1993) 7029.
[39] A. Bunge, J. Chem. Phys. 53 (1970) 20.
[40] C.F. Bender, H.F. Schaefer, J. Chem. Phys. 55 (1971) 4789.
[41] P. Pulay, Mol. Phys. 17 (1969) 197.
[42] P. Pulay, in: H.F. Schaefer (Ed.), Modern Theoretical Chemistry, vol. 4, Plenum Press, New York, 1977, pp. 153–185.
[43] Y. Yamaguchi, Y. Osamura, J.D. Goddard, H.F. Schaefer, A New Dimension to Quantum Chemistry: Analytic Derivative Methods in Ab Initio Molecular Electronic Structure Theory, Oxford University Press, New York, 1994.
[44] M. Abramowitz, I.A. Stegun, Handbook of Mathematical Functions, Dover Publications, New York, NY, 1972.
[45] C.L. Janssen, E.T. Seidl, G.E. Scuseria, T.P. Hamilton, Y. Yamaguchi, R.B. Remington, Y. Xie, G. Vacek, C.D. Sherrill, T.D. Crawford, J.T. Fermann, W.D. Allen, B.R. Brooks, G.B. Fitzgerald, D.J. Fox, J.F. Gaw, N.C. Handy, W.D. Laidig, T.J. Lee, R.M. Pitzer, J.E. Rice, P. Saxe, A.C. Scheiner, H.F. Schaefer, PSI 2.0.8, PSITECH, Inc., Watkinsville, GA 30677, USA, 1995.
[46] ACES II is a program product of the Quantum Theory Project, University of Florida. Authors: J.F. Stanton, J. Gauss, J.D. Watts, M. Nooijen, N. Oliphant, S.A. Perera, P.G. Szalay, W.J. Lauderdale, S.R. Gwaltney, S. Beck, A. Balková D.E. Bernholdt, K.-K Baeck, P. Rozyczko, H. Sekino, C. Hober, R.J. Bartlett, Integral packages included are VMOL (J. Almlöf and P.R. Taylor); VPROPS (P. Taylor) ABACUS; (T. Helgaker, H.J. Aa Jensen, P. Jørgensen, J. Olsen, P.R. Taylor).
[47] W. Kutzelnigg, J. Mol. Struct. 169 (1988) 403.
[48] W. Kutzelnigg, Angew. Chem., Int. Ed. Engl. 22 (1984) 272.
[49] L. Pauling, The Nature of the Chemical Bond, 3rd ed., Cornell University Press, New York, 1960.
[50] K.P. Huber, G. Herzberg, Constants of Diatomic Molecules, van Nostrand Reinhold, New York, 1979.
[51] The classical energy separation is defined as the splitting that does not include the zero-point vibrational energy (ZPVE) correction. The quantum mechanical splitting is the ZPVE corrected value.
[52] B.G. Wicke, R.W. Field, W. Klemperer, J. Chem. Phys. 56 (1972) 5758.
[53] J. Muenter, J. Mol. Spect. 55 (1975) 490.
[54] W. Hou, J. Chem. Phys. 43 (1965) 624.
[55] J. Adachi, N. Kosugi, E. Shigemasa, A. Yagishita, J. Chem. Phys. 107 (1997) 4919.

PERGAMON

Polyhedron 21 (2002) 611–618

POLYHEDRON

www.elsevier.com/locate/poly

Reactions of divalent group 14 compounds containing an azide functionality: synthesis and characterization of $[HB(3,5\text{-}(CF_3)_2Pz)_3]AgGe(N_3)[(n\text{-}Pr)_2ATI]$ and $[HB(3,5\text{-}(CF_3)_2Pz)_3]AgSn(N_3)[(n\text{-}Pr)_2ATI]$

H.V. Rasika Dias *, Ashley E. Ayers

Department of Chemistry and Biochemistry, The University of Texas at Arlington, Box 19065, Arlington, TX 76019-0065, USA

Received 27 July 2001; accepted 27 November 2001

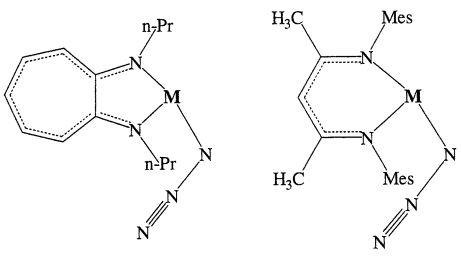
Abstract

A mixture of $[HB(3,5\text{-}(CF_3)_2Pz)_3]Ag(\eta^2\text{-toluene})$ and $[(n\text{-}Pr)_2ATI]GeN_3$ or $[(n\text{-}Pr)_2ATI]SnN_3$ in CH_2Cl_2, rather than undergoing metathesis or nitrogen elimination or silver ion coordination to the nitrogen atoms of the azide moiety, formed 1:1 adducts $[HB(3,5\text{-}(CF_3)_2Pz)_3]AgM(N_3)[(n\text{-}Pr)_2ATI]$ (**1**, M = Ge and **2**, M = Sn) featuring unsupported silver–germanium and silver–tin bonds (where $[HB(3,5\text{-}(CF_3)_2Pz)_3]$ = hydrotris(3,5-bis(trifluoromethyl)pyrazolyl)borate; $[(n\text{-}Pr)_2ATI]$ = N-(*n*-propyl)-2-(*n*-propylamino)troponiminate). Compounds $[HB(3,5\text{-}(CF_3)_2Pz)_3]AgGe(N_3)[(n\text{-}Pr)_2ATI]$ and $[HB(3,5\text{-}(CF_3)_2Pz)_3]AgSn(N_3)[(n\text{-}Pr)_2ATI]$ were characterized by X-ray crystallography. The Ag–Ge and Ag–Sn bond distances of **1** and **2** are 2.4146(7) and 2.5943(6) Å, respectively. The azide moieties are linear. The azide group of the germanium adduct adopts a *trans* orientation relative to the GeN_2C_7 ring system upon silver ion coordination whereas the azido moiety of the tin adduct occupies a site above the SnN_2C_7 ring (*cis*). IR spectra of **1** and **2** display $\nu_{asym}(N_3)$ bands at 2083 and 2070 cm^{-1}, respectively. The ^{119}Sn NMR spectrum of **2** shows a broad signal at 90 ppm ($^1J(^{119}Sn-^{107/109}Ag)$ = 4866 Hz). These adducts show unusually high thermal stability. © 2002 Elsevier Science Ltd. All rights reserved.

Keywords: Azide; Germanium; Tin; Silver; Tris(pyrazolyl)borate; Aminotroponimine

1. Introduction

Azido derivatives of carbon represent the most widely studied group among covalent azides [1–3]. They are excellent starting materials for the preparation of a variety of organic and inorganic compounds [1,2,4–7]. Related azides of heavier group 14 members such as those of silicon(IV) and tin(IV) are also fairly well known [3,8]. Some of these are commercially available as well. In contrast, very little is known about the azide derivatives of low valent group 14 elements [9–12]. One of the difficulties in isolating such species is their tendency to decompose with the elimination of nitrogen. The lead(II) azide $Pb(N_3)_2$, for example, is widely used as a primary explosive [3,13–15]. We described the isolation of several azides of germanium(II) and tin(II) using aminotroponiminate (ATI) and diazapentadienyl (DAP) ligands (Fig. 1) [9,10]. These azides ($[(n\text{-}Pr)_2ATI]MN_3$ and $[(Mes)_2DAP]MN_3$ where M = Ge(II) or Sn(II)) show very good thermal stability.



$[(n\text{-}Pr)_2ATI]MN_3$ $[(Mes)_2DAP]MN_3$

M = Ge or Sn

Fig. 1. Azide derivatives of germanium(II) and tin(II).

* Corresponding author. Tel.: +1-817-272-3813; fax: +1-817-272-3808.

E-mail address: dias@uta.edu (H.V.R. Dias).

0277-5387/02/$ - see front matter © 2002 Elsevier Science Ltd. All rights reserved.
PII: S0277-5387(01)01022-1

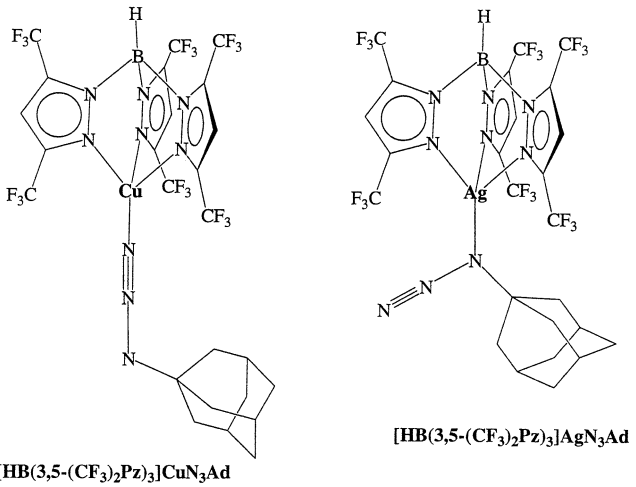


Fig. 2. Thermally stable metal organo azide complexes of copper(I) and silver(I).

There are only a very few other structurally characterized examples of this type known. Those include $Pb(N_3)_2$, $[HB(3,5\text{-}(CH_3)_2Pz)_3]GeN_3$ and $[(C_5H_5)Co\{P(O)(OEt)_2\}_3]GeN_3$ [11,12,14].

There are many transformations of organo azides mediated by transition metal ions [1,2]. It is commonly believed that such processes involve organoazido metal complexes as intermediates [16–22]. However, the isolation and characterization of such species are difficult mainly due to the rapid loss of nitrogen [17,18]. $[HB(3,5\text{-}(CF_3)_2Pz)_3]CuNNN(1\text{-}Ad)$ and $[HB(3,5\text{-}(CF_3)_2Pz)_3]AgN(1\text{-}Ad)NN$ (where 1-Ad = 1-adamantyl) represent two examples of organoazido metal adducts that can be isolated as thermally stable solids (Fig. 2) [23]. As illustrated in Fig. 2, they show different bonding modes, but the azido group remains linear. There are others that show significant distortions to the azido functionality upon metal coordination [19–21,24].

Overall, despite their importance, stable metal complexes containing organo azide ligands are extremely rare [23,25], and those involving divalent main group 14 elements are unknown. Therefore, it would be worthwhile to explore the chemistry between azides such as $[(n\text{-}Pr)_2ATI]MN_3$ or $[(Mes)_2DAP]MN_3$ (where M = Ge or Sn) and transition metal ions. As indicated earlier, metal ions may promote nitrogen elimination, or form isolable adducts with these azides. If adducts are formed, the site of coordination is also of interest because, in contrast to organo azides (e.g. $1\text{-}AdN_3$) where metals coordinate exclusively to azide nitrogen atoms, the azides of divalent group 14 compounds have one additional site (the group 14 lone pair) for metal ion coordination.

In this paper, we report the synthesis of the first transition metal complexes of divalent germanium and tin azides from a reaction between $[(n\text{-}Pr)_2ATI]MN_3$ (where M = Ge or Sn) and a silver(I) derivative of a fluorinated tris(pyrazolyl)borate. The solid state structural data of $[HB(3,5\text{-}(CF_3)_2Pz)_3]AgGe(N_3)[(n\text{-}Pr)_2ATI]$ and $[HB(3,5\text{-}(CF_3)_2Pz)_3]AgSn(N_3)[(n\text{-}Pr)_2ATI]$ are also reported.

2. Experimental

2.1. General procedures

All manipulations were carried out under an atmosphere of purified nitrogen using either standard Schlenk techniques or in a Vacuum Atmospheres single station drybox equipped with a −25 °C refrigerator. Solvents were purchased from commercial sources and distilled from conventional drying agents prior to use. Glassware was oven-dried at 150 °C overnight. The NMR spectra were recorded at room temperature on a JEOL Eclipse 500 (^1H, 500.16 MHz; ^{19}F, 470.62 MHz; ^{13}C, 125.78 MHz; ^{119}Sn, 186.5 MHz). Proton and carbon chemical shifts are reported in parts per million versus Me_4Si. ^{19}F and ^{119}Sn NMR chemical shifts were referenced to external $CFCl_3$ and Me_4Sn standards, respectively. Melting points were obtained on a Mel-Temp II apparatus. Elemental analyses were performed at the University of Texas at Arlington using a Perkin–Elmer Model 2400 CHN analyzer. $[(n\text{-}Pr)_2ATI]GeN_3$, $[(n\text{-}Pr)_2ATI]SnN_3$ and $[HB(3,5\text{-}(CF_3)_2Pz)_3]Ag(\eta^2\text{-toluene})$ were prepared using published procedures [10,26].

2.2. $[HB(3,5\text{-}(CF_3)_2Pz)_3]AgGe(N_3)[(n\text{-}Pr)_2ATI]$ (1)

$[(n\text{-}Pr)_2ATI]GeN_3$ (39 mg, 0.12 mmol) and $[HB(3,5\text{-}(CF_3)_2Pz)_3]Ag(\eta^2\text{-toluene})$ (100 mg, 0.12 mmol) were mixed in dichloromethane (10 mL) at room temperature. Upon mixing, the solution turned bright yellow. After the solution was stirred for 2 h, the solvent was removed under vacuum and the resulting solid was dissolved in toluene. Filtration through Celite and removal of the toluene under vacuum gave $[HB(3,5\text{-}(CF_3)_2Pz)_3]AgGe(N_3)[(n\text{-}Pr)_2ATI]$ as a yellow solid (120 mg, 94%). X-ray quality crystals were grown from hexane at room temperature. M.p.: turns brown around 120 °C and melts 146–148 °C. ^1H NMR ($CDCl_3$): δ 1.04 (t, 6H, $J = 7.5$ Hz, $CH_3CH_2CH_2$), 1.82 (m, 4H, $CH_3CH_2CH_2$), 3.70 (m, 4H, $CH_3CH_2CH_2$), 6.90 (s, 3H, Pz-CH), 6.94 (t, 1H, $J = 9.5$ Hz, H_5), 6.99 (d, 2H, $J = 11.3$ Hz, $H_{3,7}$), 7.48 (m, 2H, $H_{4,6}$); ^{19}F NMR ($CDCl_3$): δ −58.6 (d, $^5J(F,H) = 2.2$ Hz), −60.7 (s); $^{13}C\{^1H\}$ NMR ($CDCl_3$): δ 11.2 ($CH_3CH_2CH_2$), 21.6 ($CH_3CH_2CH_2$), 47.3 ($CH_3CH_2CH_2$), 106.3 (CH), 116.0 (C_5), 119.3 (q, $^1J(C,F) = 271$ Hz, CF_3), 120.4 (q, $^1J(C,F) = 270$ Hz, CF_3), 125.2 ($C_{3,7}$), 138.4 ($C_{4,6}$), 140.1 (q, $^2J(C,F) = 40$ Hz, CCF_3), 143.5 (q, $^2J(C,F) = 38$ Hz, CCF_3), 159.1 ($C_{2,8}$); IR (KBr, cm^{-1}): 3338 (w), 3144

(w), 2974 (m), 2606 (w, B-H), 2083 (s, asym N_3), 1598 (m), 1558 (w), 1523 (m), 1447 (m), 1423 (m), 1397 (m), 1361 (w), 1270 (s), 1145 (s), 1082 (w), 1039 (s), 987 (m), 886 (w), 830 (m), 783 (m), 736 (m), 708 (w), 665 (w), 612 (w), 485 (w), 419 (m); *Anal.* Calc. for $C_{28}H_{23}AgBF_{18}GeN_{11}$: C, 32.13; H, 2.21; N, 14.72. Found: C, 32.04; H, 2.24; N, 14.39%.

2.3. [HB(3,5-$(CF_3)_2Pz)_3$]AgSn(N_3)[(n-Pr)$_2$ATI] (2)

[(n-Pr)$_2$ATI]SnN_3 (44 mg, 0.12 mmol) and [HB(3,5-$(CF_3)_2Pz)_3$]Ag(η^2-toluene) (100 mg, 0.12 mmol) were mixed in dichloromethane (10 mL) at room temperature. Upon mixing, the solution turned bright yellow in color. After the solution was stirred for 2 h, the solvent was removed under vacuum and the resulting solid was dissolved in toluene. Filtration through Celite and removal of the toluene under vacuum gave [HB(3,5-$(CF_3)_2Pz)_3$]AgSn(N_3)[(n-Pr)$_2$ATI] as a yellow solid (120 mg, 91%). X-ray quality crystals were grown from toluene–hexane at room temperature. M.p.: turned dark red and decomposed around 135–140 °C. ^{1}H NMR ($CDCl_3$): δ 1.09 (t, 6H, $J = 7.3$ Hz, $CH_3CH_2CH_2$), 1.97 (m, 4H, $CH_3CH_2CH_2$), 3.70 (m, 4H, $CH_3CH_2CH_2$), 6.88 (t, 1H, $J = 9.3$ Hz, H_5), 6.92 (s, 3H, Pz-CH), 6.99 (d, 2H, $J = 11.5$ Hz, $H_{3,7}$), 7.44 (m, 2H, $H_{4,6}$); ^{19}F NMR ($CDCl_3$): δ −58.7 (d, ^5J(F,H) = 3.3 Hz), −60.6 (s); ^{13}C{^{1}H} NMR ($CDCl_3$): δ 11.5 ($CH_3CH_2CH_2$), 23.6 ($CH_3CH_2CH_2$), 50.3 ($CH_3CH_2CH_2$), 106.4 (CH), 116.5 (C_5), 119.2 (q, ^1J(C,F) = 271 Hz, CF_3), 120.4 (q, ^1J(C,F) = 270 Hz, CF_3), 124.4 ($C_{3,7}$), 137.4 ($C_{4,6}$), 140.3 (q, ^2J(C,F) = 40 Hz, CCF_3), 143.5 (q, ^2J(C,F) = 38 Hz, CCF_3), 161.7 ($C_{2,8}$); ^{119}Sn-{^{1}H} NMR ($CDCl_3$): δ 90 (d, $^1J(^{119}Sn-^{109/107}Ag)$ = 4866 Hz); IR (KBr, cm^{-1}): 3138 (w), 2973 (w), 2940 (w), 2884 (w), 2632 (w, B-H), 2070 (s, asym N_3), 1597 (m), 1558 (m), 1514 (m), 1440 (w), 1421 (m), 1391 (m), 1364 (m), 1274 (s), 1248 (w), 1174 (s), 1078 (m), 1041 (s), 991 (m), 886 (w), 856 (w), 831 (m), 778 (w), 735 (m), 696 (w), 612 (w), 565 (w), 483 (w); *Anal.* Calc. for $C_{28}H_{23}AgBF_{18}N_{11}Sn$: C, 30.77; H, 2.12; N, 14.10. Found: C, 30.65; H, 2.10; N, 13.97%.

2.4. X-ray structure determination

A suitable crystal covered with a layer of hydrocarbon oil was selected and attached to a glass fiber and immediately placed in the low-temperature nitrogen stream [27]. Data collections were carried out at low temperature on a Siemens P4 diffractometer equipped with a LT-2A device for low-temperature work and graphite monochromated Mo Kα radiation ($\lambda = 0.710$ 73 Å). The unit cell parameters of [HB(3,5-$(CF_3)_2Pz)_3$]-AgGe(N_3)[(n-Pr)$_2$ATI] and [HB(3,5-$(CF_3)_2Pz)_3$]AgSn-(N_3)[(n-Pr)$_2$ATI] were determined by least-squares refinement of 39 and 46 reflections, respectively. Three standard reflections were measured at every 97 data points to check for crystal deterioration and/or misalignment. No significant deterioration in intensity was observed. Data were corrected for Lorentz, polarization, and absorption (using ψ scans) effects. Structures were solved by direct methods followed by successive cycles of full-matrix least-squares refinement on F^2 and difference Fourier analysis. All the non-hydrogen atoms were refined anisotropically. Hydrogen atoms on boron were located from the difference map. The remaining hydrogen atoms were included at calculated positions. Software programs and the sources of scattering factors are contained in the Bruker SHELXTL 5.1 software package [28] provided by Bruker Analytical X-ray Instruments, Inc.

Cell dimensions and structure refinement data for [HB(3,5-$(CF_3)_2Pz)_3$]AgGe(N_3)[(n-Pr)$_2$ATI] and [HB(3,5-$(CF_3)_2Pz)_3$]AgSn(N_3)[(n-Pr)$_2$ATI] are listed in Table 1. Selected bond lengths and angles are given in Tables 2 and 3.

3. Results and discussion

Reaction of [HB(3,5-$(CF_3)_2Pz)_3$]Ag(η^2-toluene) and [(n-Pr)$_2$ATI]MN_3 (where M = Ge or Sn) in dichloromethane produces the very interesting adduct compounds [HB(3,5-$(CF_3)_2Pz)_3$]AgGe(N_3)[(n-Pr)$_2$ATI] (**1**) and [HB(3,5-$(CF_3)_2Pz)_3$]AgSn(N_3)[(n-Pr)$_2$ATI] (**2**) in high yield (Scheme 1). The essentially quantitative formation of a single product is particularly noteworthy considering the potential for several possible outcomes

Table 1
Crystal data and summary of data collection and refinement for [HB(3,5-$(CF_3)_2Pz)_3$]AgGe(N_3)[(n-Pr)$_2$ATI] (**1**) and [HB(3,5-$(CF_3)_2Pz)_3$]AgSn(N_3)[(n-Pr)$_2$ATI] (**2**)

	1	**2**
Empirical formula	$C_{28}H_{23}AgBF_{18}GeN_{11}$	$C_{28}H_{23}AgBF_{18}SnN_{11}$
Formula weight	1046.84	1092.94
Space group	$P2_1/c$	$P\bar{1}$
Temperature (K)	208(2)	208(2)
λ (Å)	0.71073	0.71073
a (Å)	11.7723(18)	8.255(2)
b (Å)	18.236(3)	14.812(2)
c (Å)	18.351(4)	17.552(3)
α (°)	90	113.808(8)
β (°)	104.991(18)	96.137(16)
γ (°)	90	96.418(15)
V (Å^3)	3805.4(11)	1923.7(7)
Z	4	2
ρ_{calc} (g cm^{-3})	1.827	1.887
μ (mm^{-1})	1.432	1.285
R_1, wR_2 [$I > 2\sigma(I)$] [a]	0.0394, 0.1015	0.0263, 0.0653
R_1, wR_2 (all data) [a]	0.0456, 0.1063	0.0302, 0.0676

[a] $R_1 = \Sigma||F_o|-|F_c||/\Sigma|F_o|$ and $wR_2 = [\Sigma[w(F_o^2-F_c^2)^2]/\Sigma[w(F_o^2)^2]]^{1/2}$.

Table 2
Selected bond lengths (Å) and angles (°) for [HB(3,5-$(CF_3)_2Pz)_3$]AgGe(N_3)[$(n$-Pr$)_2$ATI]

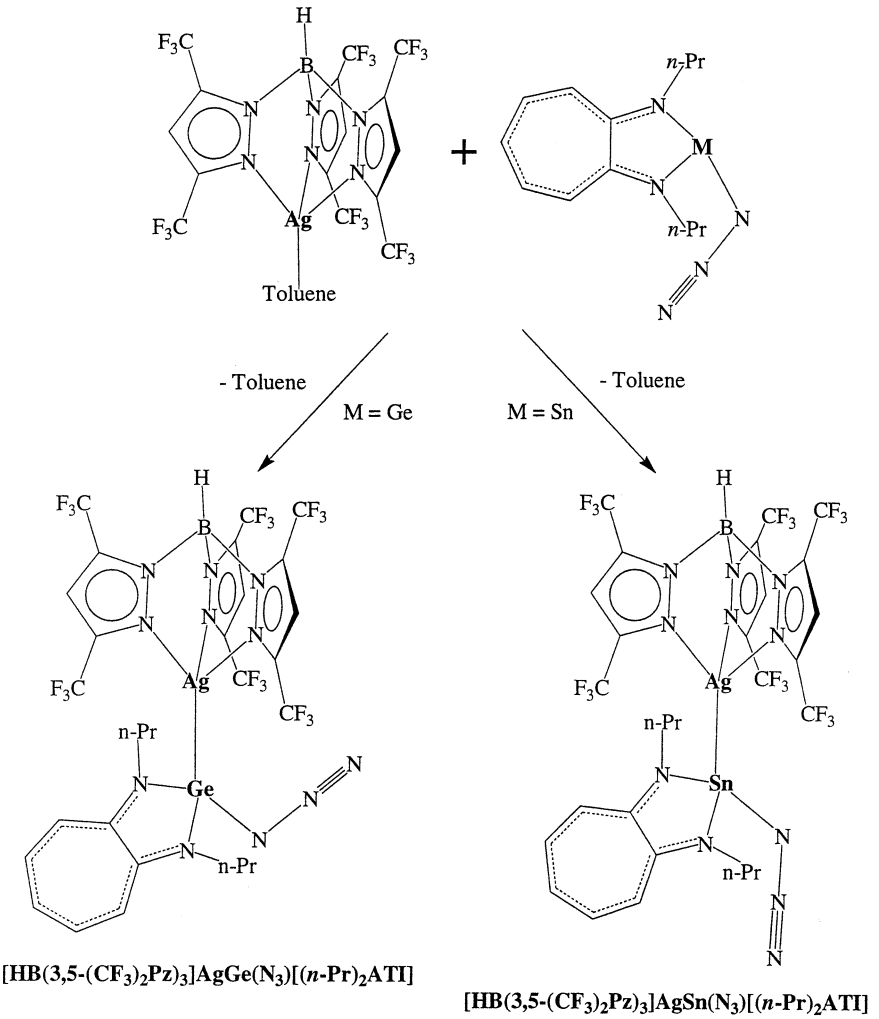
Bond lengths	
Ag–N(12)	2.396(4)
Ag–N(32)	2.405(4)
Ag–Ge	2.4146(7)
Ag–N(22)	2.432(4)
Ge–N(1)	1.882(4)
Ge–N(9)	1.884(4)
Ge–N(2)	1.916(4)
N(2)–N(3)	1.221(6)
N(3)–N(4)	1.138(7)
N(1)–C(2)	1.337(6)
N(9)–C(8)	1.340(6)
N(11)–N(12)	1.363(5)
N(11)–B	1.544(6)
N(21)–N(22)	1.367(5)
N(21)–B	1.540(6)
N(31)–N(32)	1.351(5)
N(31)–B	1.547(6)
Bond angles	
N(12)–Ag–N(32)	82.93(12)
N(12)–Ag–Ge	133.60(9)
N(32)–Ag–Ge	133.23(9)
N(12)–Ag–N(22)	81.02(12)
N(32)–Ag–N(22)	79.55(12)
Ge–Ag–N(22)	126.49(9)
N(1)–Ge–N(9)	82.66(17)
N(1)–Ge–N(2)	100.0(2)
N(9)–Ge–N(2)	97.24(17)
N(1)–Ge–Ag	124.87(13)
N(9)–Ge–Ag	129.38(12)
N(2)–Ge–Ag	115.05(13)
N(3)–N(2)–Ge	118.9(3)
N(4)–N(3)–N(2)	175.8(5)
C(2)–N(1)–C(10)	123.1(4)
C(2)–N(1)–Ge	116.2(3)
C(10)–N(1)–Ge	118.6(3)
C(8)–N(9)–C(13′)	123.6(4)
C(8)–N(9)–Ge	115.8(3)
C(13′)–N(9)–Ge	120.5(3)
N(11)–N(12)–Ag	113.3(2)
N(21)–N(22)–Ag	112.8(2)
N(31)–N(32)–Ag	112.9(3)
N(21)–B–N(11)	108.8(4)
N(21)–B–N(31)	109.5(4)
N(11)–B–N(31)	110.5(4)

from such a reactant combination. For instance, metal catalyzed decomposition reactions of [$(n$-Pr$)_2$ATI]MN_3 are possible. However, we did not observe the elimination of nitrogen gas, which is a common sign of azide decomposition. Silver halide metathesis is also a facile process [29,30]. Thus, when [HB(3,5-$(CF_3)_2Pz)_3$]Ag is treated with a pseudo-halide like [$(n$-Pr$)_2$ATI]MN_3, a metathesis process leading to [$(n$-Pr$)_2$ATI]M[HB(3,5-$(CF_3)_2Pz)_3$] adducts and AgN_3 is also a possibility. Interestingly, this did not occur either. This is not totally surprising since the chloride in [$(n$-Pr$)_2$ATI]MCl is inert to abstraction with [HB(3,5-$(CF_3)_2Pz)_3$]Ag [31]. Other possibilities include silver ion coordination to the azide moiety, via either the terminal nitrogen or the substituted nitrogen atom, or to the lone pair on the Ge(II) or Sn(II) atom.

Compounds [HB(3,5-$(CF_3)_2Pz)_3$]AgGe(N_3)[$(n$-Pr$)_2$ATI] and [HB(3,5-$(CF_3)_2Pz)_3$]AgSn(N_3)[$(n$-Pr$)_2$ATI] exhibit higher melting temperatures (>120 °C) and better air stability than their silver free counterparts [$(n$-Pr$)_2$ATI]MN_3 (where M = Ge or Sn) [10]. Indeed, [HB(3,5-$(CF_3)_2Pz)_3$]AgGe(N_3)[$(n$-Pr$)_2$ATI] and [HB(3,5-$(CF_3)_2Pz)_3$]AgSn(N_3)[$(n$-Pr$)_2$ATI] may be handled for a

Table 3
Selected bond lengths (Å) and angles (°) for [HB(3,5-$(CF_3)_2Pz)_3$]AgSn(N_3)[$(n$-Pr$)_2$ATI]

Bond lengths	
Ag–N(12)	2.349(3)
Ag–N(22)	2.401(3)
Ag–N(32)	2.405(3)
Ag–Sn	2.5943(6)
Sn–N(1)	2.096(3)
Sn–N(9)	2.097(3)
Sn–N(2)	2.157(4)
N(2)–N(3)	1.116(5)
N(3)–N(4)	1.186(6)
N(1)–C(2)	1.340(5)
N(1)–C(10)	1.468(5)
N(9)–C(8)	1.340(5)
N(11)–N(12)	1.349(4)
N(11)–B	1.559(5)
N(21)–N(22)	1.360(4)
N(21)–B	1.551(5)
N(31)–N(32)	1.356(4)
N(31)–B	1.550(5)
Bond angles	
N(12)–Ag–N(22)	81.23(10)
N(12)–Ag–N(32)	77.19(10)
N(22)–Ag–N(32)	79.31(10)
N(12)–Ag–Sn	129.31(7)
N(22)–Ag–Sn	123.50(7)
N(32)–Ag–Sn	144.08(7)
N(1)–Sn–N(9)	76.21(11)
N(1)–Sn–N(2)	96.71(13)
N(9)–Sn–N(2)	94.51(13)
N(1)–Sn–Ag	123.06(9)
N(9)–Sn–Ag	139.75(8)
N(2)–Sn–Ag	115.12(10)
N(3)–N(2)–Sn	120.9(3)
N(2)–N(3)–N(4)	177.3(5)
C(2)–N(1)–Sn	117.4(2)
C(10)–N(1)–Sn	120.2(2)
C(8)–N(9)–Sn	117.0(2)
C(13′)–N(9)–Sn	122.8(2)
N(12)–N(11)–B	120.8(3)
N(11)–N(12)–Ag	121.5(2)
N(22)–N(21)–B	120.8(3)
N(21)–N(22)–Ag	120.1(2)
N(32)–N(31)–B	122.3(3)
N(31)–N(32)–Ag	118.9(2)
N(31)–B–N(21)	109.6(3)
N(31)–B–N(11)	109.5(3)
N(21)–B–N(11)	110.6(3)



Scheme 1.

longer time in air before decomposing. They show good solubility in solvents such as dichloromethane and toluene, and moderate solubility in hexanes.

IR spectra of $[HB(3,5\text{-}(CF_3)_2Pz)_3]AgGe(N_3)[(n\text{-}Pr)_2ATI]$ and $[HB(3,5\text{-}(CF_3)_2Pz)_3]AgSn(N_3)[(n\text{-}Pr)_2ATI]$ in KBr display strong absorption bands at 2083 and 2070 cm^{-1}, respectively. These bands can be assigned to the N_3 asymmetric stretching vibrations [1,8]. The $\nu_{asym}(N_3)$ bands for compounds **1** and **2** both appear at a slightly higher frequency compared to those of $[(n\text{-}Pr)_2ATI]GeN_3$ (2048 cm^{-1}) and $[(n\text{-}Pr)_2ATI]SnN_3$ (2039 cm^{-1}) [10]. It is difficult to predict whether the products show any direct interaction between the silver ion and azide moiety solely on $\nu_{asym}(N_3)$ data. For example, the $\nu_{asym}(N_3)$ band does not change much upon 1-AdN_3 ($\nu_{asym}(N_3) = 2110$ cm^{-1}) coordination to silver(I) ion as in $[HB(3,5\text{-}(CF_3)_2Pz)_3]AgN(1\text{-}Ad)NN$ ($\nu_{asym}(N_3) = 2120$ cm^{-1}) [23].

The room temperature NMR (^1H, ^{13}C, ^{19}F) spectra of $[HB(3,5\text{-}(CF_3)_2Pz)_3]AgGe(N_3)[(n\text{-}Pr)_2ATI]$ and $[HB(3,5\text{-}(CF_3)_2Pz)_3]AgSn(N_3)[(n\text{-}Pr)_2ATI]$ display resonances for three equivalent pyrazolyl rings. Chemical shift values corresponding to the tris(pyrazolyl)borate moiety are very similar to those observed for various $[HB(3,5\text{-}(CF_3)_2Pz)_3]^-$ adducts [23,26,32–39]. The ^{119}Sn NMR spectroscopic data of $[HB(3,5\text{-}(CF_3)_2Pz)_3]AgSn(N_3)[(n\text{-}Pr)_2ATI]$ clearly suggest a strong interaction between the silver ion and the tin center in solution. It shows a broad doublet centered at 90 ppm. The $^1J(^{119}Sn-^{109/107}Ag)$ of 4866 Hz ($^{109/107}Ag$ not resolved) is in the range observed for other structurally characterized compounds featuring a direct Ag–Sn bond. For example, $[HB(3,5\text{-}(CF_3)_2Pz)_3]AgSn(Cl)[(n\text{-}Pr)_2ATI]$ and $[(THF)Ag(\mu\text{-}SCN)Sn\{CH(SiMe_3)_2\}_2]_2$ show broad signals at 117 ppm ($^1J(^{119}Sn-^{109/107}Ag) = 5234$ Hz) and 250 ppm ($^1J(^{119}Sn-^{109}Ag) = 4632$, $^1J(^{119}Sn-^{107}Ag) = 4063$ Hz) in their ^{119}Sn NMR spectra, respectively [40,41]. The silver free $[(n\text{-}Pr)_2ATI]SnN_3$ displays a broad singlet at a higher frequency (-122 ppm) [10].

The X-ray crystallographic data for these compounds reveal a Ag–Ge bond for **1** and a Ag–Sn bond for **2** (Figs. 3 and 4). Neither compound shows bonding

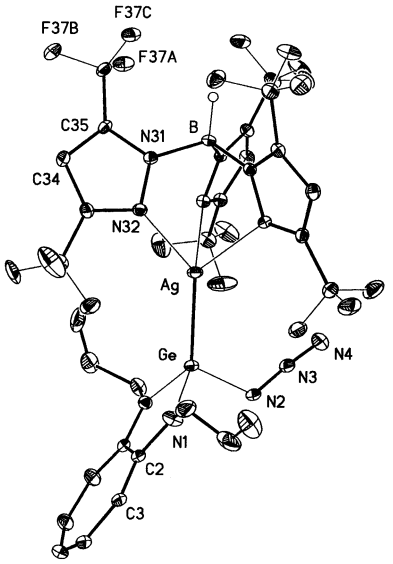


Fig. 3. Molecular structure of $[HB(3,5\text{-}(CF_3)_2Pz)_3]AgGe(N_3)[(n\text{-}Pr)_2ATI]$ (**1**), hydrogen atoms except the one on boron have been omitted for clarity.

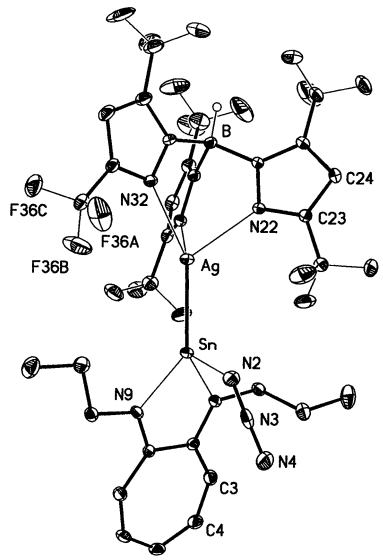


Fig. 4. Molecular structure of $[HB(3,5\text{-}(CF_3)_2Pz)_3]AgSn(N_3)[(n\text{-}Pr)_2ATI]$ (**2**), hydrogen atoms except the one on boron have been omitted for clarity.

between one of the azide nitrogens and the silver atom, as has been observed in organoazide compounds. The lone pairs on the germanium and tin atoms appear to be more favorable for bonding with silver than the lone pairs on any of the nitrogen atoms of the azide moiety [42]. The silver–germanium bond distance of **1** is 2.4146(7) Å, while the silver–tin bond distance of **2** is 2.5943(6) Å. A longer distance for the Ag–Sn bond is expected based on the larger atomic radius of tin. Compounds **1** and **2** belong to a rare class of structurally characterized molecules with unsupported silver–germanium and silver–tin bonds [31,41,43].

The silver and germanium atoms of **1** show tetrahedral coordination geometry. The heterobicyclic C_7N_2Ge ring system is planar. The Ag–Ge distance in **1** may be compared to those of $[HB(3,5\text{-}(CF_3)_2Pz)_3]AgGe(Cl)[(Me)_2ATI]$ (2.4215(9) Å) and $[HB(3,5\text{-}(CF_3)_2Pz)_3]AgGe(OSO_2CF_3)[(Me)_2ATI]$ (2.4116(10) Å) [31]. The $Ge–N_{ring}$ distances are slightly shorter and $N_{ring}–Ge–N_{ring}$ angle is slightly larger in the silver adduct **1** compared to the corresponding distances and angle of the silver free species $[(n\text{-}Pr)_2ATI]GeN_3$ (Table 4) [10]. The $Ge–N_{azide}$ distance also shows a similar trend. This is probably a result of an increased *s*-character of the Ge–N bond due to silver ion coordination to the germanium atom [31,44]. An alternative explanation for the shortening of M–N is that coordination of the Lewis acid silver ion to Ge and Sn causes them to become more like M(IV) species (with increased formal positive charge) leading to a decrease in M–N bond length [45].

The azide moiety of $[HB(3,5\text{-}(CF_3)_2Pz)_3]AgGe(N_3)[(n\text{-}Pr)_2ATI]$ and $[HB(3,5\text{-}(CF_3)_2Pz)_3]AgSn(N_3)[(n\text{-}Pr)_2ATI]$ is essentially linear. Interestingly, the X-ray crystal structure of $[HB(3,5\text{-}(CF_3)_2Pz)_3]AgGe(N_3)[(n\text{-}Pr)_2ATI]$ reveals an azide moiety turned away from the C_7N_2Ge ring plane while structural data for $[(n\text{-}Pr)_2ATI]GeN_3$ show an azide group in the *cis* orientation with the ring system. DFT calculations have shown the *trans* arrangement to be very slightly less stable by 0.2 kcal mol^{-1} for the related $[(Me)_2ATI]GeN_3$ system [10].

The azide moieties in both $[HB(3,5\text{-}(CF_3)_2Pz)_3]AgSn(N_3)[(n\text{-}Pr)_2ATI]$ and $[(n\text{-}Pr)_2ATI]SnN_3$ are in the *cis* arrangement. Compound **2** features a $Sn–N_{azide}$ bond distance of 2.157(4) Å that is slightly shorter than the average $Sn–N_{azide}$ bond distance of 2.242(5) Å for $[(n\text{-}Pr)_2ATI]SnN_3$ ($[(n\text{-}Pr)_2ATI]SnN_3$ crystallizes with two molecules in the asymmetric unit) [10]. Thus, coordination to the silver ion results in a shortening of the $Sn–N_{azide}$ bond. The azide moiety is linear as evident from the NNN bond angle of 177.3(5)°. The heterobicyclic C_7N_2Sn ring system is planar.

Overall, results from this study show that it is possible to isolate thermally stable transition metal adducts of divalent group 14 azides. The silver ion preferentially coordinates to the germanium and tin atom even in the presence of donor sites of the azide moiety. The theory of Hard and Soft Acids and Bases may explain this tendency [42]. Compounds $[HB(3,5\text{-}(CF_3)_2Pz)_3]AgGe(N_3)[(n\text{-}Pr)_2ATI]$ and $[HB(3,5\text{-}(CF_3)_2Pz)_3]AgSn(N_3)[(n\text{-}Pr)_2ATI]$ also belong to a rare group of structurally characterized compounds with unsupported Ag–Ge and Ag–Sn bonds. These adducts may also be considered as models for intermediates related to the silver salt metathesis process [29–31,46,47].

Table 4
Selected bond lengths (Å) and angles (°) and IR spectroscopic data (cm^{-1}) and ^{119}Sn NMR spectroscopic data (ppm) for $[(n\text{-Pr})_2ATI]MN_3$ (where M = Ge or Sn), $[HB(3,5\text{-}(CF_3)_2Pz)_3]AgGe(N_3)[(n\text{-Pr})_2ATI]$ (**1**) and $[HB(3,5\text{-}(CF_3)_2Pz)_3]AgSn(N_3)[(n\text{-Pr})_2ATI]$ (**2**)

	$[(n\text{-Pr})_2ATI]GeN_3$	$[(n\text{-Pr})_2ATI]SnN_3$ Molecule 1, Molecule 2	**1**	**2**
$M–N_{azide}$	2.047(2)	2.230(5), 2.253(4)	1.916(4)	2.157(4)
$M–N_{ring}$	1.945(2)	2.156(3), 2.166(3)	1.882(4)	2.096(3)
	1.945(2)	2.190(3), 2.173(3)	1.884(4)	2.097(3)
N(2)–N(3)	1.197(3)	1.105(6), 1.188(5)	1.221(6)	1.116(5)
N(3)–N(4)	1.144(4)	1.177(6), 1.156(6)	1.138(7)	1.186(6)
M–N(2)–N(3)	115.3(2)	119.1(3), 117.5(3)	118.9(3)	120.9(3)
N(2)–N(3)–N(4)	177.5(3)	179.5(5), 177.3(4)	175.8(5)	177.3(5)
$N_{ring}–M–N_{ring}$	79.68(8)	73.0(1), 73.7(1)	82.66(17)	76.21(11)
Ag–M			2.4146(7)	2.5943(6)
$\nu_{asym}(N_3)$	2048	2039	2083	2070
^{119}Sn NMR		−122		90

4. Supplementary material

Crystallographic data for $[HB(3,5\text{-}(CF_3)_2Pz)_3]AgGe(N_3)[(n\text{-Pr})_2ATI]$ and $[HB(3,5\text{-}(CF_3)_2Pz)_3]AgSn(N_3)[(n\text{-Pr})_2ATI]$ have been deposited with the Cambridge Crystallographic Data Centre, CCDC Nos. 167859 and 167860, respectively. Copies of this information may be obtained free of charge from The Director, CCDC, 12 Union Road, Cambridge, CB2 1EZ, UK (fax: +44-1223-336033; e-mail: deposit@ccdc.cam.ac.uk or www: http://www.ccdc.cam.ac.uk).

Acknowledgements

We thank The Robert A. Welch Foundation (grant: Y-1289) for support of this work. We also thank the National Science Foundation (CHE-9601771) for providing funds to purchase the 500 MHz NMR spectrometer.

References

[1] S. Patai (Ed.), The Chemistry of the Azido Group, Interscience, New York, 1971.
[2] E.F.V. Scriven (Ed.), Azides and Nitrenes: Reactivity and Utility, Academic, New York, 1984.
[3] I.C. Tornieporth-Oetting, T.M. Klapötke, Angew. Chem., Int. Ed. Engl. 34 (1995) 511.
[4] W. Lwowski, Nitrenes, Interscience, New York, 1970.
[5] W.A. Nugent, B.L. Haymore, Coord. Chem. Rev. 31 (1980) 123.
[6] W.A. Nugent, J.M. Mayer, Metal–Ligand Multiple Bonds, Wiley, New York, 1988.
[7] D.E. Wigley, Prog. Inorg. Chem. 42 (1994) 239.
[8] J.S. Thayer, Organomet. Chem. Rev. 1 (1966) 157.
[9] A.E. Ayers, T.M. Klapötke, H.V.R. Dias, Inorg. Chem. 39 (2001) 1000.
[10] A.E. Ayers, D.S. Marynick, H.V.R. Dias, Inorg. Chem. 39 (2000) 4147.
[11] A.C. Filippou, P. Portius, G. Kociok-Köhn, Chem. Commun. (1998) 2327 and references therein.
[12] A.C. Filippou, P. Portius, G. Kociok-Köhn, V. Albrecht, J. Chem. Soc., Dalton Trans. (2000) 1759.
[13] S. Budavari (Ed.), The Merck Index, 11th ed., Merck and Co., Inc., New Jersey, 1989, p. 5274 and references therein.
[14] C.S. Choi, E. Prince, W.L. Garrett, Acta Crystallogr., Sect. B 33 (1977) 3536.
[15] N.N. Greenwood, A. Earnshaw, Chemistry of the Elements, 2nd ed., Butterworth-Heinemann, Woburn, MA, 1998, p. 417.
[16] G.L. Hillhouse, B.L. Haymore, J. Am. Chem. Soc. 104 (1982) 1537.
[17] S. Gambarotta, A. Chiesi-Villa, C. Guastini, J. Organomet. Chem. 270 (1984) C49.
[18] D.M. Antonelli, W.P. Schaefer, G. Parkin, J.E. Bercaw, J. Organomet. Chem. 462 (1993) 213.
[19] G. Proulx, R.G. Bergman, Organometallics 15 (1996) 684.
[20] G. Proulx, R.G. Bergman, J. Am. Chem. Soc. 117 (1995) 6382.
[21] M.G. Fickes, W.M. Davis, C.C. Cummins, J. Am. Chem. Soc. 117 (1995) 6384.
[22] D. Margosian, P. Kovacic, J. Org. Chem. 46 (1981) 877.
[23] H.V.R. Dias, S.A. Polach, S.-K. Goh, E.F. Archibong, D.S. Marynick, Inorg. Chem. 39 (2000) 3894.
[24] T.A. Hanna, A.M. Baranger, R.G. Bergman, Angew. Chem., Int. Ed. Engl. 35 (1996) 653.
[25] M. Barz, E. Herdtweck, W.R. Thiel, Angew. Chem., Int. Ed. Engl. 37 (1998) 2262.
[26] H.V.R. Dias, W. Jin, Z. Wang, Inorg. Chem. 36 (1997) 6205.
[27] H. Hope, in: A.L. Wayda, M.Y. Darensbourg (Eds.), Experimental Organometallic Chemistry; ACS Symposium Series, No. 357, American Chemical Society, Washington, DC, 1987, p. 257.
[28] Siemens SHELXTL (PC version 5.0), Siemens Industrial Automation, Inc., Madison, WI, USA, 1994.
[29] N.J. Patmore, A.S. Weller, J.W. Steed, Chem. Commun. (2000) 1055.
[30] D.J. Liston, Y.J. Lee, W.R. Scheidt, C.A. Reed, J. Am. Chem. Soc. 111 (1989) 6643.
[31] H.V.R. Dias, Z. Wang, Inorg. Chem. 39 (2000) 3890.
[32] H.V.R. Dias, H.-L. Lu, R.E. Ratcliff, S.G. Bott, Inorg. Chem. 34 (1995) 1975.
[33] H.V.R. Dias, H.-L. Lu, Inorg. Chem. 34 (1995) 5380.
[34] H.V.R. Dias, W. Jin, J. Am. Chem. Soc. 117 (1995) 11381.
[35] H.V.R. Dias, W. Jin, Inorg. Chem. 35 (1996) 267.
[36] H.V.R. Dias, W. Jin, H.-J. Kim, H.-L. Lu, Inorg. Chem. 35 (1996) 2317.

[37] H.V.R. Dias, H.-L. Lu, J.D. Gorden, W. Jin, Inorg. Chem. 35 (1996) 2149.
[38] H.V.R. Dias, H.-J. Kim, H.-L. Lu, K. Rajeshwar, N.R. Tacconi, A. Derecskei-Kovacs, D.S. Marynick, Organometallics 15 (1996) 2994.
[39] H.V.R. Dias, W. Jin, Inorg. Chem. 35 (1996) 3687.
[40] H.V.R. Dias, A. Ayers, unpublished work.
[41] P.B. Hitchcock, M.F. Lappert, L.J.-M. Pierssens, Organometallics 17 (1998) 2686.
[42] G.L. Miessler, D.M. Tarr, Inorganic Chemistry, 2nd ed., Prentice-Hall, Englewood Cliffs, NJ, 1999, p. 173.
[43] B. Findeis, L.H. Gade, I.J. Scowen, M. McPartlin, Inorg. Chem. 36 (1997) 960.
[44] For examples of M–N bond shortening in low valent group 13 compounds, see: J.G. Green, J.L. Suter, J. Chem. Soc., Dalton Trans. (1999) 4087.
[45] Authors thank one of the reviewers for providing this explanation.
[46] Z. Xie, T. Jelinek, R. Bau, C.A. Reed, J. Am. Chem. Soc. 116 (1994) 1907.
[47] C.A. Reed, Acc. Chem. Res. 31 (1998) 133.

PERGAMON

Polyhedron 21 (2002) 619–627

POLYHEDRON

www.elsevier.com/locate/poly

Synthesis and structural characterization of the first trialkylguanidinate and hexahydropyramidopyramidinate complexes of tin

Stephen R. Foley, Glenn P.A. Yap, Darrin S. Richeson *

Department of Chemistry, University of Ottawa, Ottawa, Ont., Canada K1N 6N5

Received 28 June 2001; accepted 7 December 2001

Abstract

The first guanidinate complexes of tin have been prepared using *N*,*N*′,*N*″-trialkylguanidinates ($[(RN)_2C(NRH)]^-$; R = cyclohexyl; isopropyl) and 1,3,4,6,7,8-hexahydro-2*H*-pyramido[1,2-*a*]pyramidinate (hpp^-) as ligands. The direct reaction between triisopropylguanidine and $SnCl_4$ provided the complex $\{[^iPrN]_2C[NH^iPr]\}SnCl_3$ (**1**) along with concomitant formation of the guanidinium salt $\{C[NH^iPr]_3\}^+[SnCl_5(THF)]^-$ (**2**). The Sn(II) guanidinate complexes $\{(C_6H_{11}N)_2C[NH(C_6H_{11})]\}_2Sn$ (**3**) and $\{CN[N(CH_2)_3]_2\}_2Sn$ (**4**) were prepared through metathesis reactions between 0.5 equiv. $SnCl_2$ and $(C_6H_{11}N)_2C[NH(C_6H_{11})]Li$ or hppLi, respectively. Complex **4** is the first reported mononuclear complex of this ligand. In contrast, the reaction of hppLi with 1 equiv. $SnCl_2$ afforded a bridging dinuclear species, $\{CN[N(CH_2)_3]_2SnCl\}_2$ (**5**). A second mononuclear complex of the hpp^- ligand, $\{CN[N(CH_2)_3]_2\}_2SnCl_2$ (**6**), was the product obtained from the reaction of 2 equiv. of hppLi with $SnCl_4$. The full structural details of compounds **1** and **3**–**6** are reported. In the case of compounds **1** and **3** these results revealed a distinctly unsymmetrical bonding mode for the bidentate guanidinate ligand and suggest variable degrees of π delocalization with the ligand. The geometries of the Sn centers in **3**, **4** are derived from distorted trigonal bipyramidal coordination with a stereochemically active lone pair occupying one coordination site. In contrast, complex **5** displayed a geometry derived from a tetrahedral ligand array with one vertex occupied by a lone pair of electrons. Complex **6** is six coordinate and possesses 2 equiv. chelating bidentate hpp^- ligands and two *cis*-chloro groups. © 2002 Elsevier Science Ltd. All rights reserved.

Keywords: Guanidinate; 1,3,4,6,7,8-Hexahydro-2*H*-pyramido[1,2-*a*]pyramidinate; Tin; Mononuclear; Dinuclear

1. Introduction

Amidinates are versatile ligands that have been used to stabilize fundamentally interesting and catalytically active complexes of tin and germanium. For example, the terminal chalcogenido complexes, $(CyNC(^tBu)NCy)_2Sn{=}S$ and $(CyNC(^tBu)NCy)_2Ge{=}E$ ($Cy = C_6H_{11}$; E = S, Se), were prepared by oxidative addition of styrene sulfide or elemental selenium to the corresponding M(II) precursors, $(CyNC(^tBu)NCy)_2M$ (M = Ge, Sn) [1,2]. An unusual cyclotetrasulfido complex, $[CyNC(Me)NCy]Sn[N(SiMe_3)_2]S_4$, was prepared with an amidinate supporting ligand [3]. Many of these complexes function as excellent catalysts for the rapid and selective cyclotrimerization of aryl isocyanates to yield isocyanurates [3,4]. Additional variation of the central N–C–N ligand framework can be achieved by employing guanidinate ligands (Chart 1). Guanidinate ligands should offer all of the coordination flexibility of amidinates and may provide added steric and electronic variability. For example, the presence of a third nitrogen center in these species allows for variation of the substitution pattern to give di-, tri-, or tetrasubstituted ligands. The main resonance contributions for

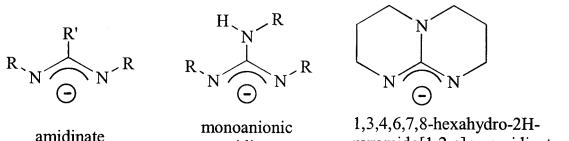
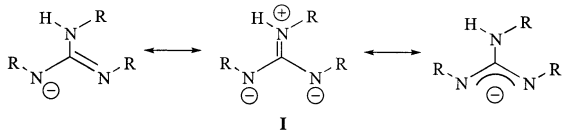


Chart 1.

* Corresponding author.
E-mail address: darrin@science.uottawa.ca (D.S. Richeson).

0277-5387/02/$ - see front matter © 2002 Elsevier Science Ltd. All rights reserved.
PII: S0277-5387(01)01018-X



I

Chart 2.

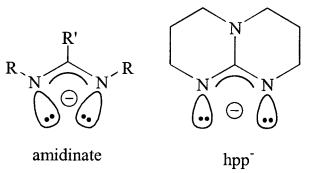


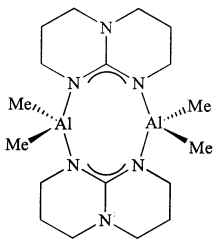
Chart 3.

N,*N*′,*N*″-trisubstituted guanidinate anions are summarized in Chart 2. The zwitterionic structure **I** does not have an analogy for amidinate ligands.

Guanidinates have received relatively limited attention as ligands in comparison with amidinates, with only three reports for main group metal complexes of *N*,*N*′,*N*″-trisubstituted guanidinate anions appearing in the literature. These consist of the lithium salts $Li_2(C(NPh)_3)$ [5], $Li_2(C(N^tBu)_3)$ [6], $Li(C(N^tBu)_2(N(H)^tBu))$ [6] and the only p-block element complex, $[(^iPrN)_2C(NH^iPr)][(^iPrN)_2C(N^iPr)]Sb$ [7].

An interesting variation on the guanidinate framework, in tetrasubstituted form, is provided by the anion of 1,3,4,6,7,8-hexahydro-2*H*-pyramido[1,2-*a*]pyramidine (hpp^-) (Chart 1). The steric bulk as well as the orientation of the N lone pairs of this heterobicyclic system is substantially restricted by the tethering of the N centers. For example, it has been suggested that the tying back of the N–R groups and the resultant projection of the σ donor orbitals in a parallel direction (Chart 3) is a critical difference between this species and the amidinate anion and is one of the reasons that hpp^- promotes the formation of bridged dinuclear transition metal complexes [8]. The restrictions of the bicyclic framework should enhance the correct orientation for π-overlap of the central C center with all three N centers and may stabilize resonance structure **I** and Y-conjugation within the ligand.

The only reported main group metal complex of hpp^- is $[(\mu\text{-hpp})AlMe_2]_2$ (**II**) [9]. As with all of the reported transition metal complexes, this aluminum complex adopts a dimeric structure in which the hpp^- ligands bridge two $AlMe_2$ moieties.



II

Given the general lack of guanidinate complexes of main group metals and of tin in particular, application of these ligands to group 14 metals is warranted and we now report the first Sn(II) and Sn(IV) complexes with guanidinate ligands employing both monoanionic *N*,*N*′,*N*″-trialkylguanidinates and the pyramidinate anion (hpp^-). These include the first examples of mononuclear complexes displaying chelating hpp^- ligand.

2. Experimental

2.1. General procedure

All manipulations were carried out in either a Vacuum Atmospheres drybox or under nitrogen using standard Schlenk-line techniques. Diethyl ether, toluene and THF were sparged with nitrogen then dried by passage through column of activated alumina using an apparatus purchased from Anhydrous Engineering. CH_2Cl_2 and $CDCl_3$ were distilled under nitrogen from CaH_2. Deuterated benzene was distilled under nitrogen from Na/K alloy. 1,3,4,6,7,8-Hexahydro-2*H*-pyrimido[1,2-*a*]pyrimidine (Hhpp), $SnCl_2$, $SnCl_4$ and MeLi (1.4 M in diethyl ether) were purchased from Aldrich and used without further purification.

NMR spectra were recorded on a Varian Gemini 200 MHz spectrometer with deuterated benzene or $CDCl_3$ as a solvent and internal standard. All elemental analyses were run on a Perkin–Elmer PE CHN 4000 elemental analysis system. All melting points were determined on a Gallenkamp Melting Point Apparatus in sealed capillary tubes.

2.2. Preparation of $\{[(CH_3)_2CHN]_2C[NHCH(CH_3)_2]\}SnCl_3$ (1) and $\{[(CH_3)_2CHNH]_3C\}SnCl_5(THF)$ (2)

To a solution of 0.500 g *N*,*N*′,*N*″-triisopropylguanidine (2.70 mmol) in toluene (50 ml) was added 1 equiv. $SnCl_4$ (0.703 g, 2.70 mmol). The reaction mixture was stirred for 12 h and then was filtered to remove complex **2** as an insoluble solid. Complex **1** was isolated by removal of the reaction solvent under vacuum. White crystals of **1** were obtained from diethyl ether at −34 °C (0.54 g, 49% yield). ^1H NMR (C_6D_6, ppm): 3.20, (br, overlapping signals CH, 3H); 3.19 (br, NH, 1H); 1.20 (d, $J_{HH} = 6.6$ Hz, CH_3, 12H); 0.62 (d, $J_{HH} = 6.0$ Hz, CH_3, 6H). ^{13}C NMR (C_6D_6, ppm): 160.1 (s, N*C*N); 48.2 (s, $C(CH_3)_2$); 46.4 (s, $C(CH_3)_2$); 23.4 (s, CH_3); 23.2 (s, CH_3). ^{119}Sn NMR (C_6D_6, ppm vs. $SnMe_4$): −356.9. *Anal.* Found: C, 29.76; H, 5.55; N, 9.81. Calc. for $C_{10}H_{22}Cl_3N_3Sn$: C, 29.34; H, 5.42; N, 10.26%. m.p. 54–56 °C.

Solid **2** that was isolated from the above filtration was washed with toluene (3 × 5 ml) and dried. White crystals of **2** were obtained from CH_2Cl_2 at −34 °C (0.46 g, 35% yield). ^{1}H NMR ($CDCl_3$, ppm): 5.18 (d, $J_{NH} = 7.8$ Hz, NH, 3H); 4.37 (br, THF, 4H); 3.88 (br, CH, 3H); 2.01 (br, THF, 4H); 1.33 (d, $J_{HH} = 6.4$ Hz, CH_3, 18H). ^{13}C NMR ($CDCl_3$, ppm): 152.1 (s, N*C*N); 45.3 (s, $C(CH_3)_2$); 22.7 (s, CH_3). *Anal.* Found: C, 30.62; H, 5.85; N, 7.51. Calc. for $C_{10}H_{24}Cl_5N_3SnTHF$: C, 30.44; H, 5.47; N, 7.61%. m.p. 133–134 °C.

2.3. Preparation of {[(C$_6$H$_{11}$)N)$_2$C[NHC(C$_6$H$_{11}$)]}$_2$Sn (3)

To a solution of 0.500 g *N*,*N*′,*N*″-tricyclohexylguanidine (1.64 mmol) in diethyl ether (40 ml) was added 1 equiv. MeLi (1.17 ml, 1.4 M, 1.64 mmol). The solution was stirred for 30 min followed by addition of 0.5 equiv. $SnCl_2$ (0.155 g, 0.82 mmol). The reaction mixture was stirred for an additional 12 h, filtered to remove the LiCl precipitate and the solvent was removed under vacuum. Crystals of **3** were obtained from diethyl ether at −34 °C (0.47 g, 78% yield). ^{1}H NMR (C_6D_6, ppm): 3.95, (br, C_6H_{11}, 2H); 3.40 (br d, $J_{NH} = 11$ Hz, NH, 2H); 3.10 (br, C_6H_{11}, 2H); 2.90 (br, C_6H_{11}, 2H); 2.19–0.74 (m, C_6H_{11}, 60H). ^{13}C NMR (C_6D_6, ppm): 148.4 (s, N*C*N); 55.0, 52.0, 49.2, 35.9, 34.7, 34.0, 26.8, 26.6, 25.9, 25.6, 25.3 (11s, C_6H_{11}, intensity ratio:1:1:1:2:2:2:1:1:1:4:2). *Anal.* Found: C, 62.29; H, 9.56; N, 11.11. Calc. for $C_{38}H_{68}N_6Sn$: C, 62.72; H, 9.42; N, 11.55%. m.p. 163–164 °C.

Table 1
Crystal data and structure refinement for {[^{i}PrN]$_2$C[NH^{i}Pr]}SnCl$_3$ (**1**) and {[CyN)$_2$C[NHCy]}$_2$Sn (**3**)

	1	**3**
Empirical formula	$C_{10}H_{22}Cl_3N_3Sn$	$C_{38}H_{68}N_6Sn$
Formula weight	409.35	719.61
Temperature (K)	203(2) K	298(2) K
λ (Å)	0.71073	0.71073
Space group	$P2_1/c$	$C2/c$
a (Å)	13.980(1)	17.542(7)
b (Å)	10.501(1)	12.284(7)
c (Å)	11.828(1)	18.584(9)
α (°)	90	90
β (°)	97.041(2)	93.36(1)
γ (°)	90	90
V (Å^3)	1723.2(3)	3998(3)
Z	4	4
D_{calc} (g cm^{-3})	1.578	1.196
μ (mm^{-1})	1.934	0.671
R_1	0.0307	0.0626
wR_2	0.0605	0.1185

$R_1 = \Sigma||F_o|-|F_c||/\Sigma|F_o|$. $wR_2 = (\Sigma w(|F_o|-|F_c|)^2/\Sigma w|F_o|^2)^{1/2}$.

2.4. Preparation of {CN[N(CH$_2$)$_3$]$_2$}$_2$Sn (4)

To a solution of 0.300 g Hhpp (2.16 mmol) in THF (35 ml) was added 1.54 ml of MeLi (1.4 M, 2.16 mmol). Gas evolution was observed during the addition. The solution was stirred for 2 h then 0.5 equiv. $SnCl_2$ (0.204 g, 1.08 mmol) was added. The solution was stirred for an additional 24 h, filtered to remove LiCl and the solvent removed under vacuum. White crystals of **4** were obtained from THF at −34 °C (0.31 g, 73% yield). ^{1}H NMR ($CDCl_3$, ppm): 3.25, (br, CH_2, 16H); 1.85 (br, CH_2, 8H). The low solubility of **4** prevented us from obtaining a ^{13}C NMR spectrum. *Anal.* Found: C, 42.01; H, 6.10; N, 20.85. Calc. for $C_{14}H_{24}N_6Sn$: C, 42.56; H, 6.12; N, 21.27%. m.p. 154–156 °C.

2.5. Preparation of {CN[N(CH$_2$)$_3$]$_2$SnCl}$_2$ (5)

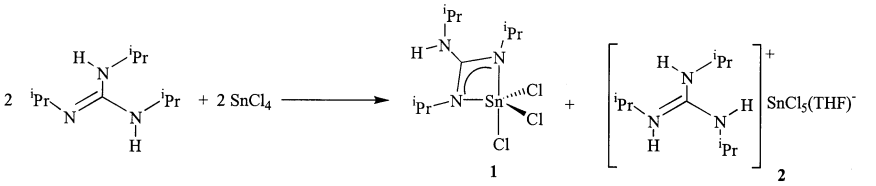
Dropwise addition of 1.54 ml of MeLi (1.4 M, 2.16 mmol) to a THF (35 ml) solution of 0.300 g Hhpp (2.16 mmol) resulted in gas evolution and formation of a pale yellow solution. This solution was stirred for 2 h then 1 equiv. $SnCl_2$ (0.408 g, 2.15 mmol) was added. The reaction mixture was stirred for an additional 24 h, filtered to remove LiCl and the solvent removed under vacuum. White crystals of **5** were obtained from CH_2Cl_2 at −34 °C (0.40 g, 63% yield). ^{1}H NMR ($CDCl_3$, ppm): 3.40, (br, CH_2, 8H); 3.20 (br, CH_2, 8H); 1.94 (br, CH_2, 8H). ^{13}C NMR ($CDCl_3$, ppm): 144.9 (s, N*C*N); 47.4 (s, CH_2); 40.9 (br, CH_2); 23.6 (br, CH_2). *Anal.* Found: C, 27.02; H, 4.23; N, 12.58. Calc. for $C_{14}H_{24}Cl_2N_6Sn_2(CH_2Cl_2)$: C, 26.91; H, 3.91; N, 12.55%. m.p. 175 °C (dec.).

2.6. Preparation of {CN[N(CH$_2$)$_3$]$_2$}$_2$SnCl$_2$ (6)

Dropwise addition of 2.56 ml of MeLi (1.4 M, 3.58 mmol) to a THF (50 ml) solution of 0.500 g Hhpp (3.59 mmol) resulted in gas evolution and formation of a pale yellow solution. This solution was stirred for 30 min then 0.5 equiv. $SnCl_4$ (0.470 g, 1.80 mmol) was added. The reaction mixture was stirred for an additional 24 h, filtered to remove LiCl and the solvent removed under vacuum. White crystals of **6** were obtained from THF at −34 °C (0.40 g, 48% yield). ^{1}H NMR ($CDCl_3$, ppm): 3.22, (br, CH_2, 8H); 3.10 (br, CH_2, 8H); 1.91 (br, CH_2, 8H). ^{13}C NMR ($CDCl_3$, ppm): 155.4 (s, N*C*N); 46.2 (s, CH_2); 40.4 (br, CH_2); 23.7 (br, CH_2). *Anal.* Found: C, 36.50; H, 5.56; N, 17.74. Calc. for $C_{14}H_{24}Cl_2N_6Sn$: C, 36.08; H, 5.19; N, 18.03%.

2.7. Structural determinations for 1, 3, 4, 5 and 6

Single crystals were mounted on thin glass fibers using viscous oil and then cooled to the data collection temperature. Crystal data and details of the measure-



Scheme 1.

ments are summarized in Tables 1 and 4. Data were collected on a Bruker AX SMART 1k CCD diffractometer using 0.3° ω-scans at 0°, 90°, and 180° in ϕ. Unit-cell parameters were determined from 60 data frames collected at different sections of the Ewald sphere. Semi-empirical absorption corrections based on equivalent reflections were applied. The structures were solved by direct methods, completed with difference Fourier syntheses and refined with full-matrix least-squares procedures based on F^2. All non-hydrogen atoms were refined with anisotropic displacement parameters. All hydrogen atoms were treated as idealized contributions. All scattering factors and anomalous dispersion factors are contained in the SHELXTL 5.1 program library.

3. Results and discussion

3.1. *N,N′,N″*-Trialkylguanidinate complexes of tin

The reaction of *N,N′,N″*-triisopropylguanidine with $SnCl_4$ proceeded smoothly at room temperature as depicted in Scheme 1 to give complexes **1** and **2**. In this case, we envisage the parent guanidine functioning as the base to generate the guanidinate anion bonded to **1** and the guanidinium cation of compound **2** [10]. The two products of this reaction were easily separated due to their differences in solubility and we were able to propose formula for each species on the basis of NMR spectroscopic and microanalytical characterization. The ^{1}H and ^{13}C NMR spectra of complex **1** show two sets of isopropyl resonances in a ratio of 2:1 consistent with formation of a monoanionic ligand with rapid rotation of the N(H)^{i}Pr group at room temperature. The most obvious change in the ^{13}C NMR for the guanidine upon deprotonation and coordination is a shift for the central sp^2 carbon, CN_3, from 148 to 160 ppm. This is in accord with the formulation for **1** as a monoanionic guanidinate complex [11]. Complex **1** was stable in solution at temperatures up to 125 °C.

Complex **2**, $[(^i\mathrm{PrNH})_3C^+][SnCl_5(THF)^-]$, is apparently derived from the reaction of guanidinium hydrochloride, the byproduct in the formation of **1**, with $SnCl_4$. The ^{1}H and ^{13}C NMR spectra of **2** are consistent with formation of guanidinium cation and clearly show only one set of resonances for the equivalent ^{i}Pr groups of this species [12].

Further confirmation of the connectivity of **1** comes from a single crystal X-ray diffraction study (Table 1). The resultant structure with atom labeling scheme is shown in Fig. 1 and corresponding values for bond distances and angles are given in Table 2. These results confirm the pseudotrigonal bipyramidal coordination environment for the Sn(IV) center consisting of one chelating bidentate guanidinate ligand spanning axial/equatorial sites and three chloride ligands. The pseudo-equatorial plane is defined by N(1) of the guanidinate ligand and Cl(1) and Cl(2) (Σ angles = 357°). The pseudo-axial vector defined by Cl(3)–Sn–N(2) exhibits an angle of 159.76(7)°.

While the sum of the angles around the central carbon, C(7), and N(2) of the NCN framework indicate planarity, the sum of angles around N(1) is only 349°, possibly indicating that it retains some sp^3 character. As a result, the ligand does not yield a planar four-membered ring with the Sn center. Further asymmetry is observed in the ligand with the N(1)–C(7) distance (1.361(4) Å) being slightly longer than the N(2)–C(7) distance (1.341(3) Å). The third guanidinate nitrogen, N(3), lies in the plane of the ligand (Sn–C(7)–N(3) 179.1(2)°) and the C(8)–N(3)–C(7) angle of 127.3(3)° suggests sp^2 hybridization about N(3). The short N(3)–C(7) distance of 1.339(4) Å indicates a degree of multiple bonding between these centers. For conjugation of the p orbital of an sp^2 N(3) with the π system of

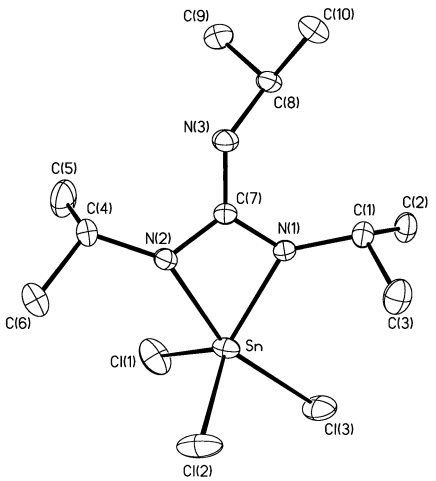
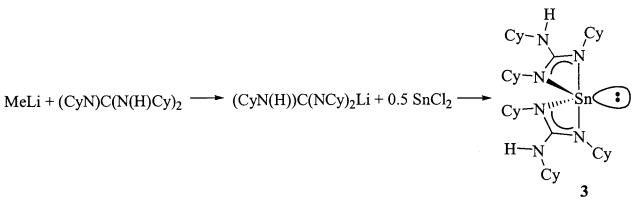


Fig. 1. Molecular structure and atom numbering scheme for $\{[^i\mathrm{PrN}]_2C[\mathrm{NH}^i\mathrm{Pr}]\}SnCl_3$ (**1**). Hydrogen atoms have been omitted for clarity.

Table 2
Selected bond distances (Å) and angles (°) for complex **1**

Bond distances			
Sn–N(1)	2.091(2)	N(2)–C(4)	1.474(4)
Sn–N(2)	2.137(2)	N(3)–C(7)	1.339(4)
Sn–Cl(1)	2.3188(9)	N(3)–C(8)	1.465(4)
Sn–Cl(2)	2.3221(9)	C(1)–C(2)	1.515(4)
Sn–Cl(3)	2.3897(9)	C(1)–C(3)	1.525(4)
Sn–C(7)	2.564(3)	C(4)–C(6)	1.512(4)
N(1)–C(7)	1.361(4)	C(4)–C(5)	1.523(5)
N(1)–C(1)	1.485(4)	C(8)–C(9)	1.524(5)
N(2)–C(7)	1.341(3)	C(8)–C(10)	1.531(5)
Bond angles			
N(1)–Sn–N(2)	63.48(9)	C(7)–N(2)–Sn	92.11(17)
N(1)–Sn–Cl(1)	121.87(7)	C(4)–N(2)–Sn	140.87(19)
N(2)–Sn–Cl(1)	96.13(7)	C(7)–N(3)–C(8)	127.3(3)
N(1)–Sn–Cl(2)	124.81(7)	N(1)–C(1)–C(2)	110.9(3)
N(2)–Sn–Cl(2)	97.18(7)	N(1)–C(1)–C(3)	111.1(3)
Cl(1)–Sn–Cl(2)	110.74(4)	C(2)–C(1)–C(3)	111.1(3)
N(1)–Sn–Cl(3)	96.34(7)	N(2)–C(4)–C(6)	108.4(3)
N(2)–Sn–Cl(3)	159.76(7)	N(2)–C(4)–C(5)	112.1(3)
Cl(1)–Sn–Cl(3)	93.47(4)	C(6)–C(4)–C(5)	111.9(3)
Cl(2)–Sn–Cl(3)	96.01(4)	N(3)–C(7)–N(2)	124.2(3)
N(1)–Sn–C(7)	31.98(9)	N(3)–C(7)–N(1)	124.9(3)
N(2)–Sn–C(7)	31.51(8)	N(2)–C(7)–N(1)	110.8(3)
Cl(1)–Sn–C(7)	111.18(7)	N(3)–C(7)–Sn	179.1(2)
Cl(2)–Sn–C(7)	114.65(7)	N(2)–C(7)–Sn	56.38(15)
Cl(3)–Sn–C(7)	128.27(7)	N(1)–C(7)–Sn	54.49(14)
C(7)–N(1)–C(1)	122.4(2)	N(3)–C(8)–C(9)	109.5(3)
C(7)–N(1)–Sn	93.53(17)	N(3)–C(8)–C(10)	110.2(3)
C(1)–N(1)–Sn	132.95(18)	C(9)–C(8)–C(10)	110.6(3)
C(7)–N(2)–C(4)	123.8(2)		



Scheme 2.

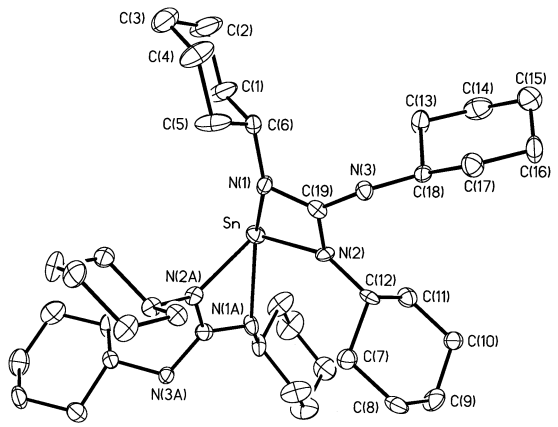
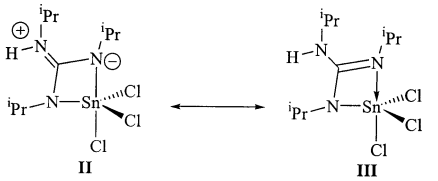


Fig. 2. Molecular structure and atom numbering scheme for $\{[CyN)_2C[NHCy]\}_2Sn$ (**3**). Hydrogen atoms have been omitted for clarity.

the N(1)–C(7)–N(2) group, the plane defined by C(8)–N(3)–C(7) should be coincident with the plane defined by N(1)–C(7)–N(2). The observed angle between these two planes of 32.9° allows some degree of π bonding between N(3) and C(7). On the basis of these results it appears that all three C(7)–N bonds of the guanidinate have some degree of double bond character with resonance contributors **II** and **III** being particularly important in a bonding description for **1**.



In contrast to the above reaction of $SnCl_4$, direct reaction of guanidine and $SnCl_2$ was not a successful method for generating a guanidinate complex of Sn(II). We attribute this to the reduced acidity of Sn(II) relative to Sn(IV). Therefore, an alternative metathetical route for introduction of guanidinate anions was investigated that employed the lithium salt of *N*,*N*′,*N*″-tricyclohexylguanidinate in reaction with $SnCl_2$. Following the pathway shown in Scheme 2, $[(CyN)_2C(HNCy)]_2Sn$ (**3**) ($Cy = C_6H_{11}$) was isolated in 78% yield. When the reaction is performed with an equimolar ratio of guanidinate and $SnCl_2$, in an attempt to generate a monoguanidinato tin(II) chloride species, only complex **3** and unreacted $SnCl_2$ were isolated.

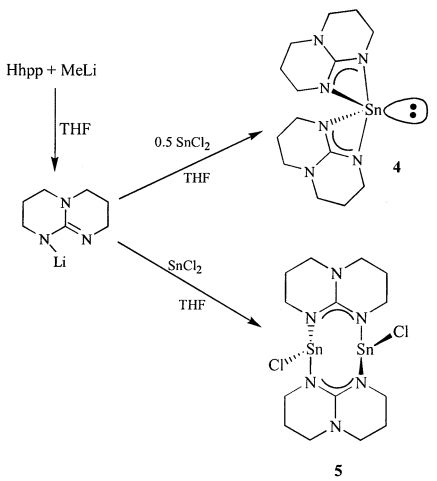
The ^1H and ^{13}C NMR spectra of **3** displayed three independent cyclohexyl groups of equal intensity and are consistent with a rigid geometry derived from a trigonal bipyramid with an equatorial site occupied by a lone pair of electrons. One signal arises from a pair of unique NCy groups which occupy a pseudoequatorial position, another from the pair that resides in the pseudoaxial position, and the two noncoordinated N(H)Cy groups provide a third resonance.

In order to confirm the geometry of **3** and clarify the structural details for the guanidinate ligand, an X-ray diffraction study was performed (Table 1). From Fig. 2, it is clear that the environment about the Sn(II) center consists of two chelating bidentate guanidinate anions and that the geometry of **3** is consistent with the spectroscopic data. The two ligands are made equivalent by a crystallographic C_2 axis. Selected bond distances and angles for **3** are provided in Table 3.

The pseudoaxial vector for **3** is defined by N(1)–Sn–N(1A), with an angle of 140.4(3)° is heavily distorted from linearity due to the restricted bite angle (58.1(2)°) of the ligands. This bite angle is typical of both amidinates and guanidinates [1,11,13]. Like complex **1**, the guanidinate ligands in **3** are non-planar; while the sum of the angles around N(2) is 360°, the angles around N(1) only sum to 344°. The N(1)–C(19)

Table 3
Selected bond distances (Å) and angles (°) for complex **3**

Bond distances			
Sn–N(2)	2.152(6)	N(1)–C(6)	1.453(8)
Sn–N(2A)	2.152(6)	N(2)–C(19)	1.344(8)
Sn–N(1)	2.424(6)	N(2)–C(12)	1.429(8)
Sn–N(1A)	2.424(6)	N(3)–C(19)	1.435(9)
N(1)–C(19)	1.306(9)	N(3)–C(18)	1.473(9)
Bond angles			
N(2)–Sn–N(2A)	99.4(3)	C(19)–N(1)–Sn	86.3(5)
N(2)–Sn–N(1)	58.1(2)	C(6)–N(1)–Sn	136.1(5)
N(2A)–Sn–N(1)	95.1(2)	C(19)–N(2)–C(12)	122.8(7)
N(2)–Sn–N(1A)	95.1(2)	C(19)–N(2)–Sn	97.4(5)
N(2A)–Sn–N(1A)	58.1(2)	C(12)–N(2)–Sn	139.8(5)
N(1)–Sn–N(1A)	140.4(3)	C(19)–N(3)–C(18)	118.2(6)
C(19)–N(1)–C(6)	121.8(6)		



Scheme 3.

Table 4
Crystal data and structure refinement for $\{CN[N(CH_2)_3]_2\}_2Sn$ (**4**), $\{CN[N(CH_2)_3]_2SnCl\}_2$ (**5**) and $\{CN[N(CH_2)_3]_2\}_2SnCl_2$ (**6**)

	4	**5**	**6**
Empirical formula	$C_{14}H_{24}N_6Sn$	$\{(C_7H_{12}ClN_3Sn)\cdot(CH_2Cl_2)\}_2$	$C_{14}H_{24}Cl_2N_6Sn\cdot(THF)$
Formula weight	395.08	754.52	538.09
Temperature (K)	203(2)	238(2)	238(2)
λ (Å)	0.71073	0.71073	0.71073
Space group	*Pbca*	*C*2/*c*	*C*2/*c*
a (Å)	8.282(3)	17.270(2)	12.354(3)
b (Å)	16.129(6)	13.821(1)	13.778(3)
c (Å)	23.783(8)	23.395(2)	14.123(4)
α (°)	90	90	90
β (°)	90	105.361(2)	110.900(3)
γ (°)	90	90	90
V (Å^3)	3177(2)	5385(1)	2246(1)
Z	8	8	4
D_{calc} (g cm^{-3})	1.652	1.861	1.591
μ (mm^{-1})	1.613	2.467	1.397
R_1	0.0496	0.0428	0.0316
wR_2	0.0981	0.1006	0.0731

$R_1 = \Sigma||F_o|-|F_c||/\Sigma|F_o|$. $wR_2 = (\Sigma w(|F_o|-|F_c|)^2/\Sigma w|F_o|^2)^{1/2}$.

distance (1.306(9) Å) is shorter than that of N(2)–C(19) (1.344(8) Å), suggesting a degree of localization of the π bond between N(1) and C(19). While the noncoordinated guanidinate nitrogen, N(3), lies in the plane of the ligand and the C(8)–N(3)–C(7) angle of 118.3(6)° suggests sp^2 hybridization for N(3), the N(3)–C(19) distance of 1.435(9) Å indicates little π interaction between these centers. Consistent with this is the observed angle of 57.3° between the plane defined by C(18)–N(3)–C(19) and that defined by N(1)–C(19)–N(2).

3.2. Hexahydro-2H-pyramido[1,2-a]pyramidinate complexes of tin

The lithium salt of hpp$^-$ was readily prepared by reaction of Hhpp with 1 equiv. MeLi. Subsequent reaction with $SnCl_2$ follows one of two paths depending on the reaction stoichiometry (Scheme 3). Addition of 0.5 equiv. $SnCl_2$ resulted in the formation of a mononuclear complex $(hpp)_2Sn$ (**4**) in 73% yield while a stoichiometric ratio of 1:1 produced complex **5** in 63% yield.

Proton NMR spectra of **4** and **5** showed only broad signals which were of little help in assigning the structural features of this species. The presence of single quaternary signal at 144.9 ppm for the central C of the hpp$^-$ ligand in the ^{13}C NMR spectrum of **5** as well as observation of only three signals for the CH_2 groups is indicative of equivalent environments for the two ligands of **5**. In order to determine the structural details of these species, single crystals of **4** and **5** were subjected to an X-ray diffraction study (Table 4). The molecular structures of these two complexes are shown in Figs. 3 and 4 with corresponding values for selected bond distances and angles provided in Tables 5 and 6.

Contrary to all previously reported structures involving the hpp$^-$ anion, the Sn(II) complex **4** is mononuclear with two chelating bidentate ligands. The geometry of the Sn center in **4** is similar to that of **3** and can be derived from a distorted trigonal bipyramidal geometry with an equatorial site occupied by a lone pair of electrons [1]. Again, we attribute the distortion of the pseudoaxial angle (N(7)–Sn–N(17) = 129.6(3)°) to the restricted bite angle of the ligand (N(2)–Sn–N(1) = 58.1(2)°).

The sum of angles around all three nitrogen centers of the ligand varies only slightly over a range of 356–358°, suggesting sp^2 character for these atoms. The three C(central, sp^2)–N bond distances on each ligand vary from 1.30–1.37 Å. These features indicate that all three nitrogen atoms of the ligand participate to some degree in π bonding to the central carbon [C(6) or C(16)] and suggest, in comparison with **3**, that the tethering of the N centers has increased the degree of π delocalization within the ligand.

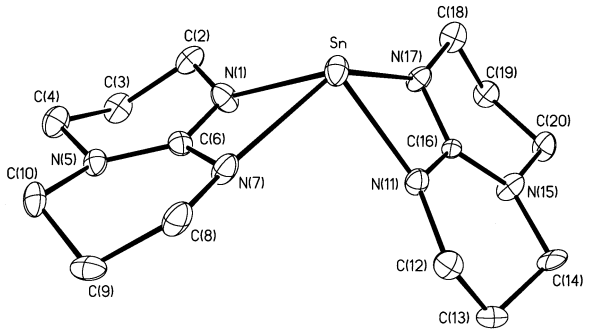


Fig. 3. Molecular structure and atom numbering scheme for $\{CN[N(CH_2)_3]_2\}_2Sn$ (**4**). Hydrogen atoms have been omitted for clarity.

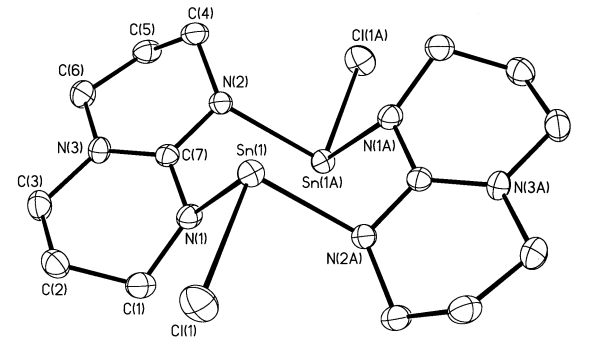


Fig. 4. Molecular structure and atom numbering scheme for one of the unique molecules of $\{CN[N(CH_2)_3]_2SnCl\}_2$ (**5**) in the unit cell. Hydrogen atoms have been omitted for clarity.

In contrast to the mononuclear complex **4**, complex **5** displayed a dinuclear structure with two hpp^- ligands bridging the two Sn atoms (Fig. 4). Two independent molecules, each lying on a crystallographic inversion center, were found in the unit cell with only marginal differences in their bond lengths and angles. Within each molecule the three N–C(central, sp^2) distances are equivalent (1.34–1.35 Å) within experimental error and correspond to a degree of NC π bonding. The Sn–N distances are equivalent at 2.21 Å. In this case the Sn(II) centers have pyramidal geometries derived from a distorted tetrahedron in which one vertex is occupied by a stereochemically active lone pair of electrons. The lone pairs on the Sn centers appear to be oriented in orthogonal directions, thus precluding any interaction between them.

A similar metathetical route can be used to prepare a Sn(IV) complex of the hpp^- ligand. Addition of 2 equiv. of in situ prepared hppLi to $SnCl_4$ in THF gave a new complex that was formulated as the mononuclear Sn(IV) complex $(hpp)_2SnCl_2$ (**6**) (Scheme 4) on the basis of what appeared to be a single ligand environment in the ^1H and ^{13}C NMR spectra and on our previous experience with similar formamidinate/amidinate complexes [13].

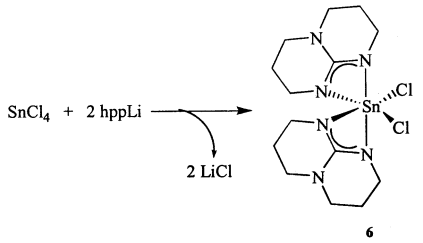
A single crystal X-ray diffraction analysis confirmed the structural features of **6** (Table 4). As seen in Fig. 5, complex **6** is a mononuclear Sn(IV) species with a coordination environment consisting of two chelating bidentate hpp^- ligands along with two chloride ligands. Values for selected bond distances and angles are pro-

Table 5
Selected bond distances (Å) and angles (°) for complex **4**

Bond distances			
Sn–N(11)	2.171(8)	C(4)–N(5)	1.458(12)
Sn–N(1)	2.204(7)	N(5)–C(10)	1.456(12)
Sn–N(7)	2.327(8)	C(6)–N(7)	1.331(12)
Sn–N(17)	2.394(7)	N(11)–C(16)	1.350(11)
N(1)–C(6)	1.302(12)	N(15)–C(16)	1.343(12)
N(1)–C(2)	1.462(12)	C(16)–N(17)	1.324(11)
N(5)–C(6)	1.373(11)		
Bond angles			
N(11)–Sn–N(1)	102.2(3)	C(6)–N(7)–C(8)	120.6(9)
N(11)–Sn–N(7)	88.8(3)	C(6)–N(7)–Sn	89.9(6)
N(1)–Sn–N(7)	58.2(3)	C(8)–N(7)–Sn	144.7(7)
N(11)–Sn–N(17)	57.9(3)	C(16)–N(11)–C(12)	121.0(9)
N(1)–Sn–N(17)	90.5(3)	C(16)–N(11)–Sn	99.0(7)
N(7)–Sn–N(17)	129.6(3)	C(12)–N(11)–Sn	138.2(7)
C(6)–N(1)–C(2)	123.7(8)	C(16)–N(15)–C(14)	120.8(9)
C(6)–N(1)–Sn	96.5(6)	C(16)–N(15)–C(20)	118.3(9)
C(2)–N(1)–Sn	135.6(6)	C(14)–N(15)–C(20)	118.8(8)
C(6)–N(5)–C(10)	120.3(9)	N(17)–C(16)–N(11)	112.2(11)
C(6)–N(5)–C(4)	119.0(9)	N(17)–C(16)–N(15)	125.5(10)
C(10)–N(5)–C(4)	116.9(8)	N(11)–C(16)–N(15)	122.2(10)
N(1)–C(6)–N(7)	113.9(9)	C(16)–N(17)–C(18)	119.7(9)
N(1)–C(6)–N(5)	122.9(9)	C(16)–N(17)–Sn	89.8(7)
N(7)–C(6)–N(5)	123.2(10)	C(18)–N(17)–Sn	147.0(7)

Table 6
Selected bond distances (Å) and angles (°) for complex **5**

Bond distances			
Sn(1)–N(1)	2.208(4)	N(2)–C(7)	1.352(6)
Sn(1)–N(2) # 1	2.213(4)	N(2)–Sn(1) # 1	2.213(4)
Sn(1)–Cl(1)	2.5293(15)	N(3)–C(7)	1.344(6)
Sn(2)–N(4)	2.214(4)	N(4)–C(14)	1.341(6)
Sn(2)–N(5) # 2	2.217(4)	N(5)–C(14)	1.344(6)
Sn(2)–Cl(2)	2.5316(14)	N(5)–Sn(2) # 2	2.217(4)
N(1)–C(7)	1.350(6)	N(6)–C(14)	1.347(6)
Bond angles			
N(1)–Sn(1)–N(2) # 1	92.50(14)	C(14)–N(4)–C(8)	117.0(4)
N(1)–Sn(1)–Cl(1)	91.71(11)	C(14)–N(4)–Sn(2)	106.7(3)
N(2) # 1–Sn(1)–Cl(1)	91.96(11)	C(8)–N(4)–Sn(2)	127.5(3)
N(4)–Sn(2)–N(5) # 2	92.84(14)	C(14)–N(5)–C(11)	114.3(4)
N(4)–Sn(2)–Cl(2)	89.27(11)	C(14)–N(5)–Sn(2) # 2	111.0(3)
N(5) # 2–Sn(2)–Cl(2)	92.01(10)	C(11)–N(5)–Sn(2) # 2	122.4(3)
C(7)–N(1)–C(1)	116.2(4)	C(14)–N(6)–C(10)	123.1(4)
C(7)–N(1)–Sn(1)	108.1(3)	C(14)–N(6)–C(13)	122.3(4)
C(1)–N(1)–Sn(1)	126.0(3)	C(10)–N(6)–C(13)	114.6(4)
C(7)–N(2)–C(4)	116.0(4)	N(3)–C(7)–N(1)	122.4(4)
C(7)–N(2)–Sn(1) # 1	107.3(3)	N(3)–C(7)–N(2)	122.8(4)
C(4)–N(2)–Sn(1) # 1	127.5(3)	N(1)–C(7)–N(2)	114.8(4)
C(7)–N(3)–C(3)	122.5(4)	N(4)–C(14)–N(5)	115.2(4)
C(7)–N(3)–C(6)	122.4(4)	N(4)–C(14)–N(6)	121.8(4)
C(3)–N(3)–C(6)	114.9(4)	N(5)–C(14)–N(6)	123.0(4)



Scheme 4.

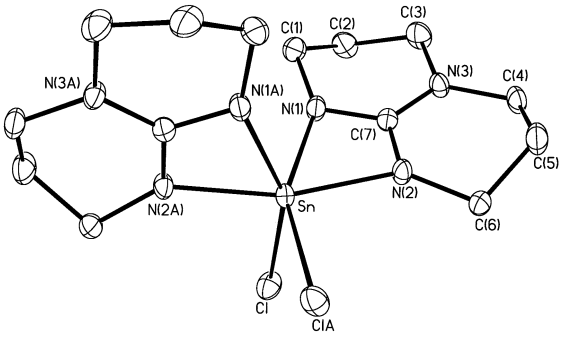


Fig. 5. Molecular structure and atom numbering scheme for $\{CN[N(CH_2)_3]_2\}_2SnCl_2$ (**6**). Hydrogen atoms have been omitted for clarity.

vided in Table 7. The geometry of **6** is based on a *cis*-dichloro distorted octahedron with a crystallographic C_2 bisecting the Cl–Sn–Cl angle making the two hpp^- ligands equivalent. Complex **6** is reminiscent of bis(amidinate) Sn(IV) dichloride species [13].

In **6** the hpp^- ligand is bonded to Sn(IV) through nitrogen atoms N(1) and N(2). The N–C(7) bond distances for N(1) and N(2) are the same at 1.326(6) Å. The sum of the angles around these two atoms is 359° and 358°, suggestive of sp^2 character. The sum of angles around N(3) is 360° and the N(3)–C(7) distance is 1.344(6) Å. As with complex **4**, this indicates that all three nitrogen atoms within the ligand participate to some degree in π bonding to C(7) and further suggests that tethering of the N centers promotes π delocalization between all three nitrogen atoms and the central carbon.

In conclusion, we have demonstrated the utility of guanidinate monoanions as ligands for complexes of tin by reporting the first examples of Sn(II) and Sn(IV) compounds of *N*,*N*′,*N*″-trialkylguanidinates ($[(RN)_2C(NRH)]^-$; R = cyclohexyl; isopropyl) and 1,3,4,6,7,8-hexahydro-2*H*-pyramido[1,2-*a*]pyramidinate (hpp^-). In the case of the trialkylguanidinate complexes, structural analysis revealed a distinctly unsymmetrical bonding mode for the bidentate ligand and suggests a degree of π localization with the ligand. We are investigating the role of this feature in the reactivity of these species. The bis(hpp) complexes of Sn(II) (**4**) and Sn(IV) (**6**) are mononuclear with chelating bidentate ligands thus representing the first reported mononuclear complexes of this ligand. Reducing the coordination number and steric bulk about tin by preparing a mono(hpp) Sn(II) complex resulted in the formation of a dinuclear species with bridging hpp^- ligands, $\{CN[N(CH_2)_3]_2SnCl\}_2$ (**5**). Structural characterization of the hpp^- complexes suggests that the tethering of the N centers may favor π delocalization within the ligand. We are further investigating the reactivity of the reported complexes and related species.

Table 7
Selected bond distances (Å) and angles (°) for complex **6**

Bond distances			
Sn–N(2)	2.104(4)	N(1)–C(7)	1.326(6)
Sn–N(2A)	2.104(4)	N(1)–C(1)	1.448(6)
Sn–N(1)	2.191(4)	N(2)–C(7)	1.326(6)
Sn–N(1A)	2.191(4)	N(2)–C(6)	1.456(6)
Sn–Cl	2.4202(14)	N(3)–C(7)	1.344(6)
Sn–ClA	2.4202(14)	N(3)–C(3)	1.455(7)
Sn–C(7)	2.582(5)	N(3)–C(4)	1.453(6)
Sn–C(7A)	2.582(5)		
Bond angles			
N(2)–Sn–N(2A)	164.1(2)	N(2)–Sn–C(7A)	136.64(16)
N(2)–Sn–N(1)	61.64(15)	N(2A)–Sn–C(7A)	30.76(15)
N(2A)–Sn–N(1)	106.43(16)	N(1)–Sn–C(7A)	101.35(15)
N(2)–Sn–N(1A)	106.43(16)	N(1A)–Sn–C(7A)	30.89(15)
N(2A)–Sn–N(1A)	61.64(15)	Cl–Sn–C(7A)	122.62(12)
N(1)–Sn–N(1A)	92.2(2)	ClA–Sn–C(7A)	96.80(11)
N(2)–Sn–Cl	99.11(12)	C(7)–Sn–C(7A)	123.0(2)
N(2A)–Sn–Cl	91.87(12)	C(7)–N(1)–C(1)	119.1(4)
N(1)–Sn–Cl	93.50(12)	C(7)–N(1)–Sn	91.1(3)
N(1A)–Sn–Cl	153.42(11)	C(1)–N(1)–Sn	148.8(3)
N(2)–Sn–ClA	91.87(12)	C(7)–N(2)–C(6)	119.6(4)
N(2A)–Sn–ClA	99.11(12)	C(7)–N(2)–Sn	95.0(3)
N(1)–Sn–ClA	153.42(11)	C(6)–N(2)–Sn	143.2(3)
N(1A)–Sn–ClA	93.50(12)	C(7)–N(3)–C(3)	120.8(4)
Cl–Sn–ClA	92.88(7)	C(7)–N(3)–C(4)	120.3(4)
N(2)–Sn–C(7)	30.76(15)	C(3)–N(3)–C(4)	118.9(4)
N(2A)–Sn–C(7)	136.64(16)	N(2)–C(7)–N(1)	112.3(4)
N(1)–Sn–C(7)	30.89(15)	N(2)–C(7)–N(3)	123.6(4)
N(1A)–Sn–C(7)	101.35(15)	N(1)–C(7)–N(3)	124.1(5)
Cl–Sn–C(7)	96.80(11)	N(2)–C(7)–Sn	54.3(2)
ClA–Sn–C(7)	122.62(12)	N(1)–C(7)–Sn	58.0(2)
N(3)–C(7)–Sn	177.6(4)		

4. Supplementary material

Crystallographic data for the structural analysis have been deposited with the Cambridge Crystallographic Data Centre, CCDC Nos. 166027 (**1**), 166026 (**3**), 166028 (**4**), 166029 (**5**), and 166030 (**6**). Copies of this information may be obtained free of charge from The Director, CCDC, 12 Union Road, Cambridge, CB2 1EZ, UK (fax: +44-1223-336033; e-mail: deposit@ccdc.cam.ac.uk or www: http://www.ccdc.cam.ac.uk).

5. Note added in proof

An example of the chelating coordination mode for the hpp anion appeared prior to publication of this manuscript [14].

Acknowledgements

This work was supported by the Natural Sciences and Engineering Research Council of Canada.

References

[1] Y. Zhou, D.S. Richeson, J. Am. Chem. Soc. 118 (1996) 10850.
[2] S.R. Foley, C. Bensimon, D.S. Richeson, J. Am. Chem. Soc. 119 (1997) 10359.
[3] S.R. Foley, G.P. Yap, D.S. Richeson, Organometallics 18 (1999) 4700.
[4] S.R. Foley, Y. Zhou, G.P.A. Yap, D.S. Richeson, Inorg. Chem. 39 (2000) 924.
[5] P.J. Bailey, A.J. Blake, M. Kryszczuk, S. Parsons, D. Reed, J. Chem. Soc., Chem. Commun. (1995) 1647.
[6] T. Chivers, M. Parvez, G.J. Schatte, Organomet. Chem. 550 (1998) 213.
[7] P.J. Bailey, R.O. Gould, C.N. Harmer, S. Pace, A. Steiner, D.S. Wright, Chem. Commun. (1997) 1161.
[8] For examples, see: (a) J.L. Bear, Y. Li, B. Hen, K.M. Kadish, Inorg. Chem. 35 (1996) 1395;
(b) F.A. Cotton, J.H. Matonic, C.A. Murillo, J. Am. Chem. Soc. 119 (1997) 7889;
(c) F.A. Cotton, L.M. Daniels, C.A. Murillo, D.J. Timmons, J. Chem. Soc., Chem. Commun. (1997) 1449;
(d) F.A. Cotton, X. Feng, D.J. Timons, Inorg. Chem. 37 (1998) 4066;
(e) F.A. Cotton, D.J. Timmons, Polyhedron 17 (1998) 179. (f) F.A. Cotton, C.A. Murillo, D.J. Timmons, J. Chem. Soc., Chem. Commun. (1999) 1427.
[9] S.L. Aeilts, M.P. Coles, D.G. Swenson, R.F. Jordan, V.G. Young, Organometallics 17 (1998) 3265.
[10] Alternative synthetic routes to **1**, including reactions between lithium guanidinate and $SnCl_4$ or use of trialkylamines as a base, have been explored. Thus far all such attempts have led to complex reaction mixtures from which **1** cannot be cleanly separated.
[11] (a) N. Thirupathi, G.P.A. Yap, D.S. Richeson, Organometallics 19 (2000) 2573;
(b) M.K.T. Tin, N. Thirupathi, G.P.A. Yap, D.S. Richeson, J Chem. Soc., Dalton Trans. (1999) 2947.
[12] A preliminary crystal structure was obtained for **2** and confirmed the proposed connectivity. S.F. Foley, G.P.A. Yap, D.S. Richeson, unpublished results.
[13] Y. Zhou, D.S. Richeson, Inorg. Chem. 36 (1997) 501.
[14] M.P. Cole, P.B. Hitchcock, J. Chem. Soc., Dalton Trans (2001) 1169.

PERGAMON

Polyhedron 21 (2002) 629–633

POLYHEDRON

www.elsevier.com/locate/poly

A C_3-chiral lithium triamidostannate(II) containing a Sn–Li bond

Isabelle Haller, Patrick Renner, Lutz H. Gade *

Laboratoire de Chimie Organométallique et de Catalyse (UMR 7513), Institut Le Bel, Université Louis Pasteur, 4, rue Blaise Pascal, F-67070 Strasbourg, France

Received 15 August 2001; accepted 27 November 2001

Abstract

Reaction of the trisilylmethane derivative $HC(SiMe_2Br)_3$ with three molar equivalents of (*S*)-1-(1-naphthyl)ethylamine gave the corresponding triamine $HC\{SiMe_2NH[(S)\text{-}1\text{-}(1\text{-naphthyl})ethyl]\}_3$ (**1**) which in solution undergoes partial dissociation to give $HC\{SiMe_2NH((S)\text{-}1\text{-}(1\text{-naphthyl})ethyl)\}\{(SiMe_2)_2N((S)\text{-}1\text{-}(1\text{-naphthyl})ethyl)\}$ (**2**). Lithiation and subsequent reaction with $SnCl_2$ yielded the solvated lithium triamidostannate $[HC\{SiMe_2N[(S)\text{-}1\text{-}(1\text{-naphthyl})ethyl]\}_3Sn\text{–}Li(thf)_3]$ (**4**). An X-ray diffraction (XRD) study established the molecular structure of the C_3-chiral triamidostannate and a direct Sn–Li contact of 3.06(2) Å. © 2002 Elsevier Science Ltd. All rights reserved.

Keywords: C_3-chiral triamidostannate; Amides; Tin; Lithium

1. Introduction

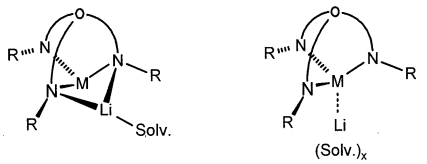
During the past 15 years a number of metallated tin compounds of the general type R_3SnM (R = alkyl, aryl, alkoxy, imido; M = alkali metal) have been structurally characterized [1,2]. In spite of their utility in synthetic organic chemistry [3], the isolated pure compounds are highly reactive and frequently thermally labile. To overcome these difficulties the use of polydentate ligand systems, which offer the stabilizing effect of chelation along with the partial shielding of the low valent metal center was found to be an efficient approach. We first employed tripodal amido ligands for the synthesis of highly rigid anionic triamidometallate cages, such as **A**, containing divalent Group 14 metals [4–8]. More recently, a related approach using tripodal amides of greater flexibility (**B**) has been published by Veith et al. [9].



A **B**

M = group 14 metal

An interesting aspect of the structural chemistry of the lithium triamidometallates in solution and in the solid state is the type of interaction between the anionic cage and the counter-cation (in most cases solvated Li^+). Both solvent-separated salts and contact ions have been found [4]. In the latter, the alkali metal ion is either attached to the amido-N atoms in a bridging coordination mode (**I**), thus breaking the overall threefold symmetry of the system or directly bound to the Group 14 metal (**II**) in what is thought to be a primarily ionic interaction.



I **II**

Apart from the stabilization by integration within a molecular cage, the use of the electronegative N-substituents at the divalent Group 14 metal centers effects their stabilization towards oxidation. The triamido metallates were thus found to be excellent anionic 'ligands' for oxidizing transition metal centers such as Ag(I) [5], Au(I–III) [6] or the tetravalent Group 4

* Corresponding author. Fax: +33-388-415-363.
E-mail address: gade@chimie.u-strasbg.fr (L.H. Gade).

0277-5387/02/$ - see front matter © 2002 Elsevier Science Ltd. All rights reserved.
PII: S0277-5387(01)01031-2

metals [7]. This capacity to act as ligands (which are isoelectronic to phosphines) has been the motivation behind the synthesis of enantiomerically pure, chiral derivatives [10]. In this paper we report the synthesis and structural characterization of such a C_3-chiral triamido metallate.

2. Results and discussion

Reaction of the previously characterized trisilylmethane derivative $HC(SiMe_2Br)_3$ [11] with three molar equivalents of (*S*)-1-(1-naphthyl)ethylamine in the presence of an excess of triethylamine as auxiliary base, after work up, cleanly gave the corresponding triamine $HC\{SiMe_2NH[(S)\text{-}1\text{-}(1\text{-naphthyl})ethyl]\}_3$ (**1**) in good yield (Scheme 1). The ^1H, ^{13}C and ^{29}Si NMR spectra of **1** are consistent with a threefold molecular symmetry on the time scale of the experiment. The ^1H NMR spectroscopic shift of the apical CH proton in the trisilylmethane backbone is characteristically at high field (δ −0.76 recorded in C_6D_6). As a consequence of the chiral ligand periphery, the methyl groups of the $SiMe_2$ units are diastereotopic and their resonances are observed at δ 0.14 and 0.27.

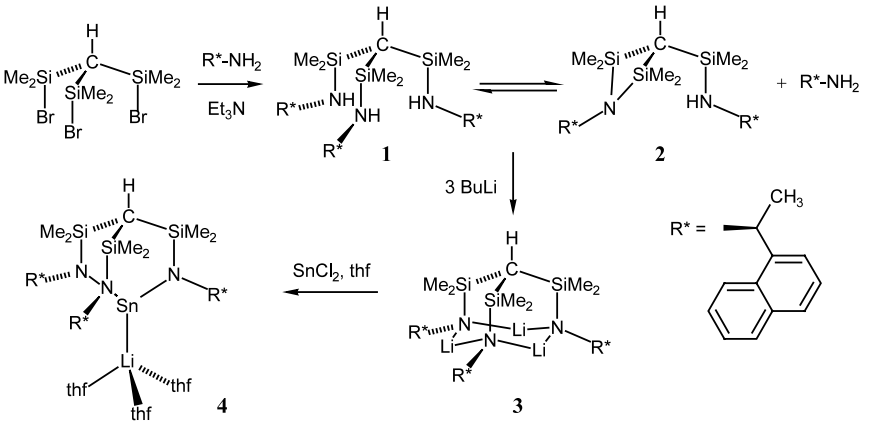
^1H and ^{13}C NMR spectroscopy of solutions of **1** established an equilibrium between the triamine **1** and the cyclic diamine **2** which is generated by elimination of one molecule of (*S*)-1-(1-naphthyl)ethylamine (Scheme 1) [12]. We previously reported the isolation and characterization of a similar azadisilacyclobutane species, $PhC\{(SiMe_2)_2N\textit{t}\text{-}Bu\}\{SiMe_2NH\textit{t}\text{-}Bu\}$ [11].

The triamine was converted to the corresponding trilithium triamide $[HC\{SiMe_2N(Li)[(S)\text{-}1\text{-}(1\text{-naphthyl})ethyl]\}_3]$ (**3**) by reaction with 3 equiv. of *n*-BuLi. It is notable that the result of this metalation is the same whether the reaction is carried out with the essentially pure tripodal amine **1** or a mixture of the triamine and the cyclic product **2** in the presence of the dissociated primary amine.

Reaction of the isolated lithium amide **3** with one molar equivalent of $SnCl_2$ at 0 °C in diethyl ether/thf gave the lithium triamidostannte $[HC\{SiMe_2N[(S)\text{-}1\text{-}(1\text{-naphthyl})ethyl]\}_3Sn\text{–}Li(thf)_3]$ (**4**). Pale yellow crystals of **4** were obtained by cooling a pentane–thf (20:1) solution of the complex after separation of the lithium chloride by centrifugation. Since, the ^1H and ^{13}C NMR spectra of the compound were consistent with a threefold molecular symmetry in solution (even at 200 K) a coordination of the lithium ion to the amido N-atoms could be ruled out. In order to establish the details of the molecular structure of the compound and, in particular relate it to the previously studied triamidostannates(II) [4–7] and triamidostannanes [13], a single crystal X-ray structure analysis was carried out. The molecular structure of **4** is displayed in Fig. 1 along with the principal bond lengths and interbond angles.

As in the previously studied tripodal triamidotin compounds, the structural center piece is the [2,2,2]bicyclooctane-related cage comprising the trisilylmethane unit and the triamidotin unit. The three N-bonded 1-naphthyl groups are turned away from the Sn atom to give the C_3-symmetrical 'propeller' arrangement which is apparent in the view along the molecular threefold axis displayed in Fig. 1(b). The most interesting structural feature is the Li–Sn contact of 3.06(2) Å, which is somewhat longer than the Li–Sn bond lengths in [Ph_3Sn–Li(pmdeta)] [2.871(7) Å] reported by Wright et al. [2a] and in [$\{HC(SiMe_2NpTol)_3\}SnLi(thf)_3$] [2.93(5) Å] studied previously in our group [4b]. The lithium cation is solvated by three thf molecules, which is a structural arrangement frequently observed in solvated lithium salts [14].

Compound **4** is the second chiral triamidodistannate to be structurally characterized [10] and the first to contain an Sn–Li bonding interaction. The $<$(N–Sn–N) angles in the triamidostannate(II) **4** (94.6–95.0°) are close to 90° indicating little or no sp hybridization at the tin atoms. These angles are gener-



Scheme 1. Synthesis of compounds **1**–**4**.

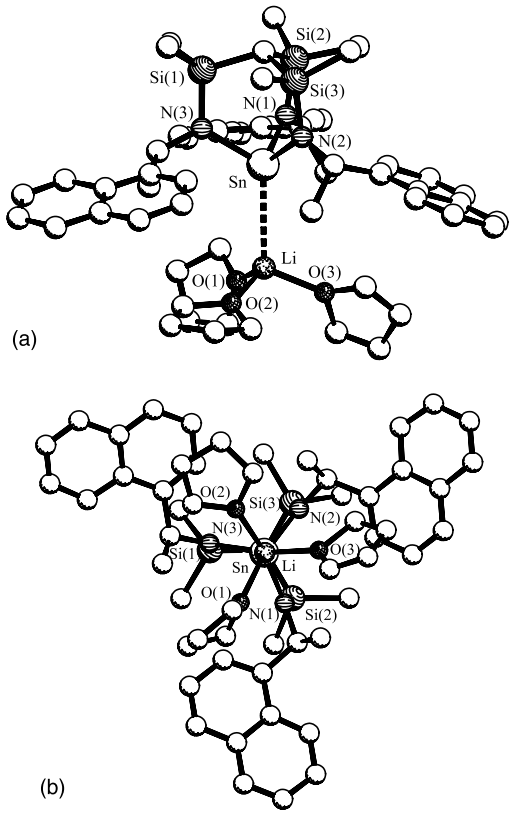


Fig. 1. (a) Molecular structure of the lithium stannate **4**. Principal bond lengths (Å) and interbond angles (°):Sn–N(1) 2.125(6), Sn–N(2) 2.125(7), Sn–N(3) 2.132(7), Sn–Li 3.06(2), N(1)–Si(2) 1.718(6) N(3)–Si(1) 1.705(7), N(2)–Si(3) 1.714(7), Li–O(1) 1.95(2), Li–O(2) 1.89(2), Li–O(3) 1.90(2), N(1)–Sn–N(2) 94.6(3), N(1)–Sn–N(3) 94.9(3), N(1)–Sn–Li 122.6(4), N(2)–Sn–N(3) 95.0(3), N(2)–Sn–Li 120.3(4), N(3)–Sn–Li 122.3(4), N(1)–Sn–N(2) 94.6(3), N(1)–Sn–N(3) 94.9(3), N(1)–Sn–Li 122.6(4), N(2)–Sn–N(3) 95.0(3), N(2)–Sn–Li 120.3(4), N(3)–Sn–Li 122.3(4). (b) View of **4** along the Li–Sn axis illustrating the approximate C_3-symmetry of the system.

ally increased in the Sn–M-heterobimetallics and triamidostannanes(IV) to values between 100° and 102°. The Sn–N bond lengths [Sn–N(1) 2.125(6), Sn–N(2) 2.125(7), Sn–N(3) 2.132(7) Å] lie in the usual range for divalent amido-tin compounds.

3. Conclusion

We have synthesized and structurally characterized a novel chiral triamido stannate(II) possessing a rare Li–Sn contact in its crystal structure. In view of the previously established suitability of such tripodal triamido stannates as ligands in transition metal coordination chemistry and the fact that compound **4** represents a chiral derivative with a very large cone angle, the application of such compounds in stereoselective transition metal-induced transformations is currently being studied.

4. Experimental

All manipulations were performed under an inert-gas atmosphere of dried argon in standard (Schlenk) glassware, which was flame-dried with a Bunsen burner prior to use. Solvents were dried according to standard procedures and saturated with Ar or N_2. The deuterated solvents used for the NMR spectroscopic measurements were degassed by three successive 'freeze-pump-thaw' cycles and dried over 4 Å molecular sieves.

The ^1H, ^{13}C, and ^{29}Si NMR spectra were recorded on Bruker AC 200, AC 300 and AMX 400 spectrometers equipped with a B-VT-2000 variable temperature unit (at 200.13, 50.32 and 39.76 MHz, respectively) with tetramethylsilane as reference.

Elemental analyses were carried out in the microanalytical laboratories of the chemistry departments at Würzburg and Strasbourg. The compound $HC(SiMe_2Br)_3$ was prepared as reported previously [11]. All other chemicals used as starting materials were obtained commercially and used without further purification.

4.1. Preparation of the compounds

4.1.1. Preparation of $HC\{SiMe_2NH[(S)\text{-}1\text{-}(1\text{-naphthyl})ethyl]\}_3$ (1)

To a stirred solution of (*S*)-1-(1-naphthyl)ethylamine (2.27 ml, 14.0 mmol) and triethylamine (2.10 ml, 15.2 mmol) in diethylether (30 ml) a solution of $HC(SiMe_2Br)_3$ (2.00 g, 4.68 mmol) in diethylether (20 ml) was added at 0 °C. After stirring for 14 h at room temperature (r.t.), the triethylammoniumbromide was separated by centrifugation and the precipitate was washed with diethylether (40 ml). The solvent of the combined ether solutions and the excess of triethylamine were removed in vacuo. Upon storing at 4 °C in diethylether for 24 h, compound **1** was obtained as a colorless, highly crystalline solid. Yield: 2.78 g, 3.98 mmol (86%). ^1H NMR (200.13 MHz, C_6D_6, 295 K): $\delta = -0.76$ (s, 1 H, $HC(Si\ldots)_3$), 0.14, 0.27 (s, 2×9 H, $Si(CH_3)_2$), 1.35 (d, 9 H, $^3J_{HH} = 6.6$ Hz, $HCCH_3$), 2.06 (d, 3 H, $^3J_{H(N)H(C)} = 9.8$ Hz, N*H*), 4.89 (dq, 3 H, $HCCH_3$), 7.22–8.07 (m, 21 H, naphthyl). $\{^1H\}^{13}C$ NMR (50.32 MHz, C_6D_6, 295 K): $\delta = 4.0$, 4.4 ($Si(CH_3)_2$), 6.2 ($HC(Si\ldots)_3$), 28.0 ($HCCH_3$), 47.9 ($HCCH_3$), 123.3, 123.5, 125.7, 125.8, 126.1, 127.6, 129.6 (C^{4-8} of 1-naphthyl), 131.2, 134.7, 145.6 ($C^{4a,8a,1}$ of 1-naphthyl); $\{^1H\}^{29}Si$ NMR (39.76 MHz, C_6D_6, 295 K): $\delta = 1.4$; $C_{43}H_{55}N_3Si_3$ (698.19): *Anal.* Calc.: C, 73.97; H, 7.94; N, 6.02. Found: C, 73.78; H, 7.93; N, 5.91.

4.1.2. Spectroscopic characterization of $HC\{SiMe_2NH\text{-}((S)\text{-}1\text{-phenylethyl})\}\{(SiMe_2)_2N((S)\text{-}1\text{-phenylethyl})\}$ (2)

Upon storing a solution of **1** in benzene for 24 h at r.t. formation of the equilibrium of **1** and

$HC\{SiMe_2NH((S)\text{-}1\text{-}(1\text{-naphthyl})ethyl)\}\{(SiMe_2)_2N\text{-}((S)\text{-}1\text{-}(1\text{-naphthyl})ethyl)\}$ (**2**) and (*S*)-1-napthylethylamine was observed. At 330 K only compound **2** and the primary amine were detected in the ^1H NMR experiment. Spectroscopic data of **2**: ^1H NMR (200.13 MHz, C_6D_6, 330 K): $\delta = -0.10$ (s, 1 H, $HC(SiMe_2)_3$), -0.02, 0.00, 0.06, 0.08, 0.10, 0.25 ($6 \times$ s, 6×3 H, $Si(CH_3)_2$), 1.44, 1.50 (d, 2×3 H, $^3J_{HH} = 6.6$ Hz, $HCCH_3$), 4.89 (m, 2 H, $HCCH_3$), 4.91 (q, 1H, $^3J_{HH} = 6.6$ Hz, $HCCH_3$), 7.22–8.20 (m, 14 H, naphthyl); $\{^1H\}^{13}C$ NMR (50.32 MHz, C_6D_6, 330 K): $\delta = 2.7$, 2.9, 3.3, 3.6, 4.7, 5.0 ($Si(CH_3)_2$), 6.8 ($HC(Si\ldots)_3$), 24.9, 28.1 ($HCCH_3$), 48.1, 49.2 ($HCCH_3$), 122.9, 123.4, 123.6, 124.2, 125.3, 125.5, 125.6, 125.7, 127.2, 127.8, 129.1, 129.2, (C^{2-8} of naphthyl), 131.0, 132.1, 134.4, 134.5, 142.6, 145.4 ($C^{4a,8a,1}$ of naphthyl); $\{^1H\}^{29}Si$ NMR (39.76 MHz, C_6D_6, 330 K): $\delta = -0.2$ ($SiMe_2N(H)(\ldots)$), 5.9, 6.0 ($(SiMe_2)_2N(\ldots)$).

4.2. Preparation of $HC\{SiMe_2NLi[(S)\text{-}1\text{-}(1\text{-naphthyl})ethyl]\}_3$ (3)

To a stirred solution of **1** (3.06 g, 4.38 mmol) in *n*-pentane (40 ml) a 2.5 M solution of *n*-BuLi in *n*-hexane (5.26 ml, 13.1 mmol) was added at -78 °C. After stirring for 1 h at r.t. and concentrating to 20 ml the white precipitate was separated by centrifugation. Upon storing at 4 °C in *n*-pentane for 24 h the product was obtained as a colorless, highly crystalline solid. Yield: 2.56 g (82%). ^1H NMR (400.14 MHz, C_6D_6, 295 K): $\delta = -1.00$ (s, 1 H, $HC(Si\ldots)_3$), 0.35, 0.50 ($2 \times$ s, 2×9 H, $Si(CH_3)_2$), 0.67 (d, 9 H, $^3J_{HH} = 6.2$ Hz, $HCCH_3$), 4.71 (q, 3 H, $HCCH_3$), 6.06 (m, 3 H), 7.09 (dd, 3H, $^3J_{HH} = 7.5$ Hz), 7.25 (ddd, 3H, $^3J_{HH} = 8.2$ Hz, $^4J_{HH} = 1.0$ Hz), 7.36 (dd, 3 H, $^3J_{HH} = 7.5$ Hz), 7.49 (d, 3 H, $^3J_{HH} = 8.2$ Hz), 7.67 (dd, 3 H, $^3J_{HH} = 8.2$ Hz, $^4J_{HH} = 1.0$ Hz), 8.22, (m, 3 H, all naphthyl); $\{^1H\}^{13}C$ NMR (100.62 MHz, C_6D_6, 295 K): $\delta = 5.3$, 10.0 ($Si(CH_3)_2$), 11.9 ($HC(Si\ldots)_3$), 26.4 ($HCCH_3$), 49.7 ($HCCH_3$), 119.4, 121.8, 126.3, 126.7, 127.2, 128.4, 130.1 (C^{2-8} naphthyl), 129.0, 135.3, 149.4 ($C^{4a,8a,1}$ of naphthyl);); $\{^1H\}^{29}Si$ NMR (39.76 MHz, C_6D_6, 295 K): $\delta = -3.2$; $\{^1H\}^7Li$ NMR (155.51 MHz, C_6D_6, 295 K): $\delta = 1.4$; $C_{43}H_{52}Li_3N_3Si_3$ (715.99): *Anal.* Calc.: C, 72.13; H, 7.32; N, 5.87. Found: C, 71.86; H, 7.28; N, 5.59.

4.3. Preparation of $[HC\{SiMe_2N[(S)\text{-}1\text{-}(1\text{-naphthyl})ethyl]\}_3Sn–Li(thf)_3]$ (4)

Solid $SnCl_2$ (0.29 g, 1.53 mmol) was added to a stirred solution of the lithium amide **3** (1.00 g, 1.53 mmol) in 20 ml of diethylether which was cooled at 0 °C. After warming to r.t. and stirring for 1 h the solvent was evaporated in vacuo. The solid residue was extracted with pentane (15 ml), the extract centrifugated and the organic phase concentrated to approximately 8 ml. Storing of this solution at -30 °C gave the lithium stannate **4** as a pale yellow crystalline solid. Yield 43%. ^1H NMR (400.14 MHz, C_6D_6, 295 K): $\delta = -0.72$ (s, 1 H, $HC(Si\ldots)_3$), 0.14, 0.27 ($2 \times$ s, 2×9 H, $Si(CH_3)_2$), 1.37 (d, 9 H, $^3J_{HH} = 6.6$ Hz, $HCCH_3$), 7.24–8.10 (m, 21 H, naphthyl); $\{^1H\}^{13}C$ NMR (100.62 MHz, C_6D_6, 295 K): $\delta = 3.8$, 4.2 ($Si(CH_3)_2$), 6.2 ($HC(Si\ldots)_3$), 27.8 ($HCCH_3$), 42.7 ($HCCH_3$), 123.1, 123.3, 125.6, 125.9, 126.1, 127.4, 129.4, (C^{2-8} naphthyl), 129.4, 134.6, 145.4 ($C^{4a,8a,1}$ of naphthyl); due to the instability of this compound to loss of thf a correct elemental analysis could not be obtained.

4.4. X-ray diffraction study of $[HC\{SiMe_2N[(S)\text{-}1\text{-}(1\text{-naphthyl})ethyl]\}_3Sn–Li(thf)_3]$ (4)

4.4.1. Crystal data

$C_{55}H_{76}LiN_3O_3Si_3Sn \cdot C_6H_6$, M: 1115.24, trigonal, space group: $P3_2$, $a = 14.7874(2)$, $c = 23.4637(5)$ Å, $U = 4443.4(1)$ Å^3, $Z = 3$, $D_{calc} = 1.25$ g cm^{-3}, $F(000) = 1764$, μ (Mo Kα) $= 0.537$ mm^{-1}.

4.4.2. Data collection

X-ray intensity data were collected at 173 K from a pale yellow block-shaped crystal of **4** ($0.16 \times 0.10 \times 0.08$ mm) in the θ-range 2.50–27.48° ($-19 < h < 19$, $-15 < k < 16$, $-30 < l < 20$) using an Nonius Kappa CCD diffractometer using graphite monochromatized Mo Kα radiation ($\lambda = 0.71073$ Å). A total of 9656 independent reflections were collected with 4367 having an intensity greater than 3 $\sigma(I)$.

4.4.3. Structure solution and refinement

The structure was solved using direct methods and refined against *F*. H-Atoms were introduced as fixed contributors. The Flack parameter of $-0.03(3)$ confirmed the assignment of the absolute configuration $R_1 = 0.043$; $wR = 0.061$. For all computations, the *Enraf-Nonius* OpenMolN Package was used (OpenMolN, interactive Structure Solution, Nonius B.V., Delft, The Netherlands, 1997).

5. Supplementary material

Crystallographic data (excluding structure factors) for compound **4** have been deposited with the Cambridge Crystallographic Data Centre. Copies of this data may be obtained free of charge from The Director, 12 Union Road, Cambridge CB2 1EZ (Fax: +44-1223-336-033; e-mail: deposit@ccdc.cam.ac.uk or www: http://www.ccdc.cam.ac.uk).

Acknowledgements

We thank the CNRS (France), the Institut Universitaire de France and the Deutsche Forschungsgemein

schaft (SFB 347) for funding. We are grateful to Dr. André De Cian and N. Gruber for the X-ray diffraction study.

References

[1] A.G. Davies, in: E.W. Abel, F.G.A. Stone, G. Wilkinson (Eds.), Comprehensive Organometallic Chemistry, vol. 2, 2nd ed., Pergamon, Oxford, 1995, p. 217.

[2] Early examples include: (a) D. Reed, D. Stalke, D.S. Wright, Angew. Chem., Int. Ed. Engl. 30 (1991) 1459;
(b) M. Veith, C. Ruloff, V. Huch, F. Töllner, Angew. Chem., Int. Ed. Engl. 27 (1988) 1381;
(c) P.B. Hitchcock, M.F. Lappert, G.A. Lawless, B. Royo, J. Chem. Soc., Chem. Commun. (1993) 554;
(d) A. Steiner, D. Stalke, J. Chem. Soc., Chem. Commun. (1993) 1702;
(e) A.J. Edwards, M.A. Paver, P.R. Raithby, C.A. Russell, A. Steiner, D. Stalke, D.S. Wright, J. Chem. Soc., Dalton Trans. (1993), 1465;
(e) G.D. Smith, P.E. Fanwick, I.P. Rothwell, Inorg. Chem. 28 (1989) 618;
(f) M. Veith, R.Z. Rösler, Naturforsch., Teil B. 41 (1986) 1071;
(g) M.J. McGeary, R.H. Cayton, K. Folting, J.C. Huffman, K.G. Caulton, Polyhedron 11 (1992) 1369;
(h) A. Steiner, D. Stalke, Inorg. Chem. 34 (1995) 4846.

[3] (a) J.A. Marshall, Chem. Rev. 96 (1996) 31;
(b) M. Fieser, Reagents for Organic Synthesis, vol. 15, Wiley-Interscience, New York, 1990;
(c) M. Pereyre, J.-P. Quintard, A. Rahm, Tin in Organic Synthesis, Butterworth, London, 1987;
(d) Y. Yamamoto (Ed.), Organotin Compounds in Organic Synthesis: Tetrahedron, 45 (1989) 909;
(e) I. Omae, Organotin Chemistry, Elsevier, Amsterdam, 1989;
(f) P.G. Harrison, Chemistry of Tin, Chapman and Hall, New York, 1989;
(g) H. Nozaki, in: M. Schlosser (Ed.), Organometallics in Synthesis—A Manual, Wiley, New York, 1994, p. 535.

[4] (a) K.W. Hellmann, P. Steinert, L.H. Gade, Inorg. Chem. 33 (1994) 3859;
(b) K.W. Hellmann, L.H. Gade, O. Gevert, P. Steinert, J.W. Lauher, Inorg. Chem. 34 (1995) 4069.

[5] B. Findeis, L.H. Gade, I.J. Scowen, M. McPartlin, Inorg. Chem. 36 (1997) 960.

[6] (a) M. Contel, K.W. Hellmann, L.H. Gade, I.J. Scowen, M. McPartlin, M. Laguna, Inorg. Chem. 35 (1996) 3713;
(b) B. Findeis, M. Contel, L.H. Gade, M. Laguna, M.C. Gimeno, I.J. Scowen, M. McPartlin, Inorg. Chem. 36 (1997) 2386.

[7] M. Lutz, B. Findeis, M. Haukka, T.A. Pakkanen, L.H. Gade, Organometallics 20 (2001) 2505.

[8] (a) K.W. Hellmann, S. Friedrich, L.H. Gade, W.-S. Li, M. McPartlin, Chem. Ber. 128 (1995) 29;
(b) M. Lutz, B. Findeis, M. Haukka, T.A. Pakkanen, L.H. Gade, Eur. J. Inorg. Chem. (2001) 3155.

[9] (a) M. Veith, O. Schütt, V.Z. Huch, Anorg. Allg. Chem. 625 (1999) 1155;
(b) M. Veith, O. Schütt, V. Huch, Angew. Chem., Int. Ed. 39 (2000) 601.

[10] H. Memmler, U. Kauper, L.H. Gade, D. Stalke, J.W. Lauher, Organometallics 15 (1996) 3637.

[11] L.H. Gade, C. Becker, J.W. Lauher, Inorg. Chem. 32 (1993) 2308.

[12] L.H. Gade, P. Renner, H. Memmler, F. Fecher, C.H. Galka, M. Laubender, S. Radojevic, M. McPartlin, J.W. Lauher, Chem. Eur. J. 7 (2001) 2563.

[13] K.W. Hellmann, C. Bott, L.H. Gade, I.J. Scowen, M. McPartlin, Polyhedron 17 (1998) 737.

[14] See for example: A. Heine, R. Herbst-Irmer, G.M. Sheldrick, D. Stalke, Inorg. Chem. 32 (1993) 2694 and references cited therein.

PERGAMON

Polyhedron 21 (2002) 635–640

POLYHEDRON

www.elsevier.com/locate/poly

Some 2,6-bis(dimethylamino)phenyl–mercury(II) and –boron complexes

David Cornu, Peter B. Hitchcock, Michael F. Lappert *, Patrick G.H. Uiterweerd

The Chemistry Laboratory, School of Chemistry, Physics and Environmental Science, University of Sussex, Falmer, East Sussex, Brighton BN1 9QJ, UK

Received 28 September 2001; accepted 27 November 2001

Abstract

As a continuation of our studies on the 2,6-bis(dimethylamino)phenyl ligand (R^-), we report on the synthesis and characterisation, including the X-ray structures, of HgR_2 and BCl(Ph)R. © 2002 Elsevier Science Ltd. All rights reserved.

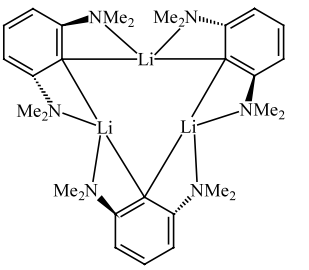
Keywords: Arylmetal complexes; Mercury(II); Boron; The 2,6-bis(dimethylamino)phenyl ligand

1. Introduction

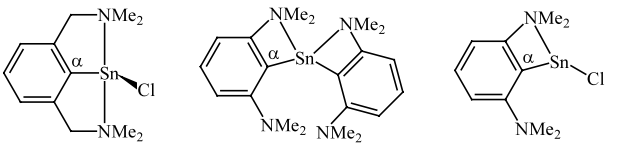
In 1997, we drew attention to the potential of the 2,6-bis(dimethylamino)phenyl ligand $^-C_6H_3(NMe_2)_2$-2,6 (≡ R^-); it was suggested that R^- might find a useful role in organometallic chemistry by virtue of facile on/off co-ordination of a pendant NMe_2 group [1], especially in catalytic systems. The ligand R^- differs from the more widely studied $^-C_6H_3(CH_2NMe_2)_2$-2,6 (≡ R′) [2], in that in their metal complexes intramolecular N → M ligation is largely strain-free for (M–R′)-, but not (M–R)-, containing derivatives. This is clearly illustrated when comparing solid state and solution structures of Sn(Cl)R′ (**I**) [3], SnR_2 (**II**) [1] and Sn(Cl)R (**III**) [1,4]. In the crystalline complexes the angle α at the *ipso*-carbon is close to the sp^2 value in **I** [3], but in **II** it has an average value of 104° [1], while in **III** it is 112.1(4)° [4]. Furthermore, whereas in toluene-d_8 solution, ^{1}H NMR VT spectra showed that in **II** and **III** there was a rapid exchange process:

$$2\text{-}Me_2N \rightarrow Sn \rightleftharpoons 6\text{-}Me_2N \rightarrow Sn$$

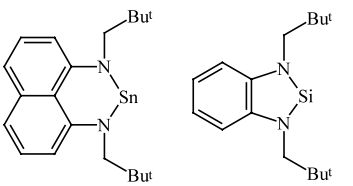
at ambient temperature [1] (as also proved to be the rule for the Group 14 metal(II) complexes listed in Table 1), this was not the case for **I** [3].



1



I **II** **III**



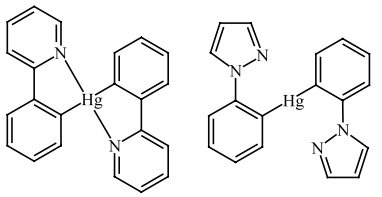
IV **V**

The conjugate acid RH of the ligand R^- was first prepared in 1970 from 1,3-diaminobenzene and trimethyl phosphate [5]. Almost 20 years later, LiR (**1**)

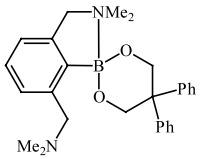
* Corresponding author.
E-mail address: kafj5@sussex.ac.uk (M.F. Lappert).

0277-5387/02/$ - see front matter © 2002 Elsevier Science Ltd. All rights reserved.
PII: S0277-5387(01)01037-3

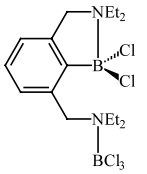
was obtained by direct lithiation of RH and shown to have a trinuclear structure in the crystal; this was retained in benzene or toluene solution, but in THF there was a monomer ⇆ trimer equilibrium [2].



VI VII



VIII



IX

We have used the ligand R^- to prepare the 12 crystalline germanium(II), tin(II) and lead(II) complexes listed in Table 1 [1,4,6–8]. For **1** [2] and eight others X-ray data are available; the principal point of interest in the present context and highlighted in Table 1 is that each R^- ligand has a single N···M intramolecular close contact in every case except in $GeR_2(BH_3)$ [6]. The germanium atom in the latter compound is four-coordinate, whereas in $SnR_2(BH_3)$ the tin atom is five-coordinate. In both, the MR_2 moiety behaves as a Lewis acid, as is also the case when SnX_2 (**IV**) [7] rather than BH_3 [6] is the electron pair acceptor. By contrast, with SnR_2 or $Sn[N(SiMe_3)_2]R$ as reagent, treatment with the thermally stable silylene **V** [abbreviated as Si(NN)] led to its product of insertion into the Sn–R or Sn–$N(SiMe_3)_2$ bond, respectively [8].

Table 1
Previously reported metal (M) crystalline complexes containing the 2,6-bis(dimethylamino)phenyl ligand (R^-)

Complex	Coordination number of M	Reference
$[Li(\mu\text{-}R)]_3$ (**1**)	2+2N	[2]
GeR_2	2+2N	[1]
SnR_2 (**II**)	2+2N	[1]
PbR_2	2+2N	[1]
$GeR_2(BH_3)$	3+1N	[6]
$SnR_2(BH_3)$	3+2N	[6]
Sn(Cl)R	2+1N	[1,4]
$Sn\{N(SiMe_3)_2\}R$	[a]	[1]
$Sn\{CH(SiMe_3)_2\}R$	[a]	[1]
$GeR_2(SnX_2)$ [b]	[a]	[7]
$SnR_2(SnX_2)$ [b]	3+2N	[7]
Sn{Si(NN)R}R [c]	2+2N	[8]
$Sn\{Si(NN)N(SiMe_3)_2\}R$ [c]	[a]	[8]

[a] Not determined.
[b] SnX_2 has the structure **IV**.
[c] Si(NN) is an abbreviation for **V**.

2. Experimental

All manipulations were carried out in flame-dried glassware under argon, using standard Schlenk techniques. Solvents were distilled from drying agents and degassed. Elemental analyses were carried out by Medac Ltd, Uxbridge. Melting points were determined in sealed capillaries under an argon atmosphere on an electrothermal apparatus and are uncorrected. The NMR spectra were recorded in benzene-d_6 at 298 K using a Bruker DPX 300 (^{1}H, 300.1; ^{13}C, 75.4 MHz) or AMX 500 (^{11}B, 160.4; ^{199}Hg, 89.1 MHz) instrument; the solvent resonances were used as internal references for ^{1}H and ^{13}C, while $^{11}BF_3(OEt_2)$ and $^{199}HgMe_2$ were the external references for the ^{11}B and ^{199}Hg NMR spectra, respectively. Electron-impact mass spectra (70 eV) were recorded using a Kratos MS 80 RF instrument. The compound $[Li(\mu\text{-}R)]_3$ (**1**) was prepared as described in the literature [2]. The other chemicals used were commercial samples (Aldrich).

2.1. Preparation of HgR_2 (2)

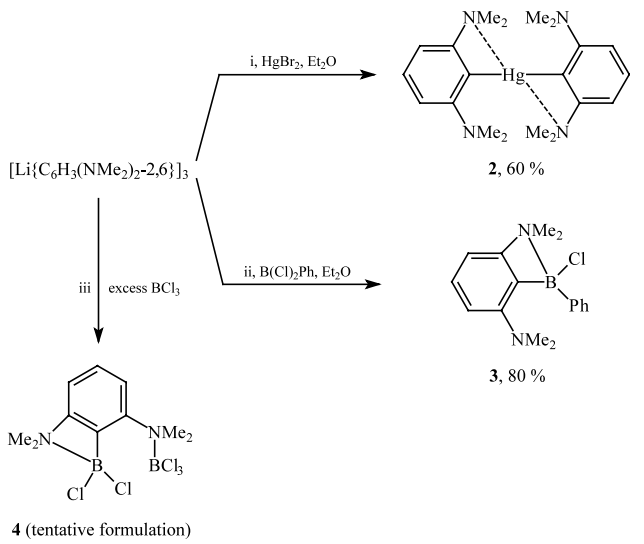
Solid $HgBr_2$ (0.63 g, 1.75 mmol) was added in small portions to a solution of LiR (0.60 g, 3.53 mmol) in Et_2O (30 cm^3) at room temperature. The reaction mixture was stirred for 20 h; the volatiles were then removed in vacuo. The residue was extracted with pentane (20 cm^3), the filtrate was concentrated in vacuo and stored at −25 °C, yielding compound **2** (0.55 g, 60%), as colourless plate-shaped crystals. *Anal.* Found: C, 45.6; H, 5.71; N, 10.5. Required for $C_{20}H_{30}HgN_4$: C, 45.6; H, 5.74; N, 10.6%. M.p. 63.0–64.0 °C. Mass spectrum [m/z (%)]: 528 (35, $[M+1]^+$), 163 (100, $[R]^+$), 147 (59, $[R\text{–}Me-1]^+$), 120 (24, $[R\text{–}NMe_2+1]^+$), 77 (19, $[C_6H_5]^+$). ^{1}H NMR: δ 2.71 (s, 12H, NMe_2), 6.92 (d, 2H, *m*-H in R), 7.23 (t, 1H, *p*-H in R). $^{13}C\{^1H\}$ NMR: δ 45.90 (s, NMe_2), 113.78 (s, *m*-C in R), 129.24 (s, *p*-C in R), 160.45 (s, *o*-C in R), 161.32 (s, *ipso*-C in R). $^{199}Hg\{^1H\}$ NMR: δ −642.0 (s).

2.2. Preparation of BCl(Ph)R (3)

Dichloro(phenyl)borane (1.25 cm^3, 9.63 mmol) was added dropwise at −78 °C to a stirred solution of LiR (1.61 g, 9.46 mmol) in Et_2O (75 cm^3). The resulting

Table 2
Crystal data and structure refinement for HgR_2 (**2**) and BCl(Ph)R (**3**) [R = $C_6H_3(NMe_2)_2$-2,6]

	2	**3**
Formula	$C_{20}H_{30}HgN_4$	$C_{16}H_{20}BClN_2$
M	527.1	286.6
T (K)	173(2)	173(2)
Crystal system	orthorhombic	monoclinic
Space group	*Pbca* (no. 61)	$P2_1/n$ (no. 14)
a (Å)	13.311(6)	9.213(2)
b (Å)	19.253(9)	12.193(4)
c (Å)	8.012(3)	14.389(4)
β (°)	90	108.60(2)
U (Å^3)	2053(2)	1531.9(7)
Z	4	4
Total reflections	1803	3885
Independent reflections	1803	3676 [$R_{int} = 0.08$]
Reflections with $I > 2\sigma(I)$	953	2037
Data/restraints/parameters	1803/0/115	3676/0/181
R_1 [$I > 2\sigma(I)$]	0.033	0.066
wR_2 (all data)	0.094	0.167



Scheme 1.

viscous white suspension was allowed to warm to room temperature, stirred for 4 h and filtered. The filtrate was concentrated in vacuo and stored at −25 °C, then filtered; the residue was washed with pentane (2 × 10 cm^3) and dried in vacuo, yielding compound **3** (2.18 g, 80%) as a cream solid. *Anal*. Found: C, 66.8; H, 6.97; N, 9.63. Required for $C_{16}H_{20}BClN_2$: C, 67.1; H, 7.03; N, 9.77%. M.p. 104–106 °C. Mass spectrum [*m*/*z* (%)]: 286 (100, $[M-1]^+$), 251 (32, $[M–Cl]^+$), 209 (73, $[M–Ph-1]^+$), 163 (49, $[R]^+$), 147 (13, $[R–Me-1]^+$). ^{1}H NMR: *δ* 2.42 (s, 12H, NMe_2), 6.23 (d, 2H, *m*-H in R), 7.12–7.28 (m, 4H, R/Ph), 7.83 (d, 2H, *m*-H in Ph). $^{11}B\{^1H\}$ NMR: *δ* 14.7 (br s, $w_{1/2} = 200$ Hz). $^{13}C\{^1H\}$ NMR: *δ* 43.85 (s, NMe_2), 106.33 (s, *m*-C in R), 126.76 (s, R/Ph), 127.77 (s, R/Ph), 128.26 (s, R/Ph), 130.86 (s, R/Ph), 134.61 (s, *ipso*-C in Ph), 144.21 (s, *ipso*-C in R), 153.70 (s, *o*-C in R).

2.3. Crystal data and refinement details for **2** and **3**

Suitable single crystals of HgR_2 (**2**) and BCl(Ph)R (**3**) were obtained from a concentrated diethyl ether (**2**) or THF–hexane (**3**) solution at −25 °C. Data were collected on an Enraf–Nonius CAD4 diffractometer using monochromated Mo Kα radiation, *λ* 0.71073 Å, with the crystals under a stream of cold nitrogen gas. Intensities were measured by an $\omega - 2\theta$ scan. Corrections were made for absorption using psi-scan measurements. The programs used for structure solutions and refinement (full-matrix on all F^2) were SHELXS-97 [9] and SHELXL-97 [10], respectively. Further details are in Table 2.

3. Results and discussion

The objectives of the present study were to prepare 2,6-bis(dimethylamino)phenyl–mercury(II) and –boron compounds.

The mercury(II) aryl HgR_2 (**2**) was sought as a potentially useful R^- or $R^\bullet$ transfer agent. A particular target was $^\bullet SnR_3$; crystalline, mononuclear tin(III) compounds are unknown, although earlier researches had revealed that in toluene solution $^\bullet Sn[CH(SiMe_3)_2]_3$ [11] and nitrogen analogues such as $^\bullet Sn[N(SiMe_3)_2]_3$ [11,12] were indefinitely stable at ambient temperature. In the event, there was no reaction between SnR_2 [1] and HgR_2. [Alternative strategies, based on $Sn(Br)R_3$ as a precursor, failed since this tin(IV) bromide proved to be inaccessible]. An added interest in HgR_2 was as a possible source of RHg–HgR {such mercury(I) organic compounds are unknown, an exception being XHg–HgX, X = $Si[Si(Me)_2SiMe_3]_3$ [13]}; but this also proved to be disappointing, as attempted reduction of **2** invariably yielded elemental mercury.

The compound $B(Cl)R_2$ appeared to be an attractive source of the crystalline $^\bullet BR_2$ radical or cation $[BR_2]^+$, both of which would be highly novel. However, we were unable unambiguously to displace a second chloride ion from BCl_3 using an excess of LiR, perhaps for steric reasons. An alternative strategy led us to the less hindered compound BCl(Ph)R (**3**).

Treatment of $HgBr_2$ with 2 equiv. of LiR in diethyl ether at ambient temperature yielded (step i of Scheme 1) HgR_2 (**2**) in 60% yield after crystallisation from pentane. The reaction between $B(Cl)_2Ph$ and an equivalent portion of LiR in diethyl ether at −78 °C afforded (step ii of Scheme 1) crystalline BCl(Ph)R (**3**) in high yield.

Each of the crystalline colourless **2** or cream **3** compounds was characterised by satisfactory elemental

analysis, melting point (63–64 °C, **2**; 104–106 °C, **3**), multinuclear NMR and mass (molecular ions ± 1 mass units) spectra, and single crystal X-ray diffraction (see-below). The mercury compound **2** was light-sensitive both in the solid state and in solution, a feature well documented for compounds containing Hg(II)–C bonds [14]. Substantial decomposition was significant in benzene solution only after approximately 3 weeks at ambient temperature.

The $^{199}Hg\{^1H\}$ NMR spectrum of **2** in benzene-d_6 showed a singlet at δ −642. This value is at higher frequency than the recorded values for $HgPh_2$, which range from δ −808 (acetone-d_6) to −742 (CD_2Cl_2) [15]; but is close to the δ −689 (in $CDCl_3$) reported for **VI**, for which intramolecular N···Hg interaction was inferred [16]. A further comparison is available with compound **VII**, having δ −778 in $CDCl_3$, in which such a close N···Hg contact was excluded [17].

The $^{11}B\{^1H\}$ NMR spectrum of BCl(Ph)R (**3**) in benzene-d_6 showed a singlet at δ 14.7, consistent with the solution of **3** containing a single tetrahedrally co-ordinated boron compound [18] and having a strong N→B bond [19]. This chemical shift is close to the δ 14.4 for **VIII** [19].

Attempts were made to reduce compound **3** with potassium or potassium–graphite in order to obtain either the radical $^{\bullet}$B(Ph)R or its boron–boron bonded dimer. Although in each experiment the colour of the reaction mixture changed from colourless to fluorescent green, the ^1H NMR spectra showed only signals attributable to **3**. Likewise, efforts to generate the salts $[B(Ph)R][BX_4]$, by treating **3** with $NaBPh_4$ or $[NEt_3H][B(C_6F_5)_4]$, were unsuccessful; no evidence was found for a reaction having taken place.

Treatment of BCl_3 with 2 equiv. of LiR in diethyl ether or toluene gave a white, sparingly soluble powder and unreacted LiR. This suggests that it was not possible to introduce two R^- ligands onto the boron atom, which may have a steric explanation. When an excess of boron trichloride was added to a solution of LiR, a complicated reaction mixture was obtained, from which a compound having somewhat greater solubility was eventually isolated. The $^{11}B\{^1H\}$ NMR spectrum showed two signals of approximately equal intensity at δ 11.4 and 17.5. A plausible formulation would be that shown in **4** (Scheme 1), by analogy with the crystallographically authenticated compound **IX**, for which ^{11}B spectral data were not recorded [20].

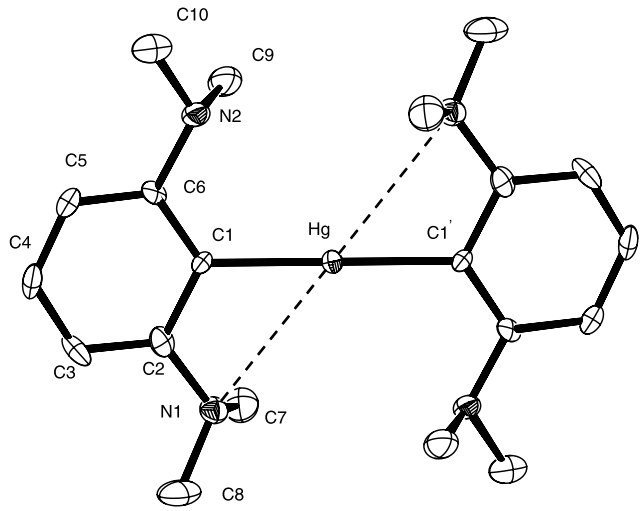


Fig. 1. The X-ray crystal structure of complex **2**.

Table 3
Selected bond distances (Å) and angles (°) for **2**

Bond distances		Bond angles	
Hg–C(1)	2.081(8)	C(1)–Hg–C(1′)	180
Hg···N(1)	3.077(8)	C(1)–C(2)–N(1)	116.7(7)
Hg···N(2)	3.247(8)	C(1)–C(6)–N(2)	117.6(7)
		Hg–C(1)–C(2)	117.0(5)
		Hg–C(1)–C(6)	123.3(6)
		Hg–C(1)···C(4)	168.7(6)

Symmetry element ′ is $-x, -y, -z$.

3.1. The molecular structure of HgR_2 (2)

The molecular structure of crystalline HgR_2 (**2**) is illustrated in Fig. 1; selected bond distances and bond angles are in Table 3.

Crystalline **2** is a centrosymmetric monomer, with a linear C(1)–Hg–C(1)′ vector. This structure is thus unexceptional. The Hg···N(1) and Hg···N(2) contacts of 3.077(8) and 3.247(8) Å are somewhat longer than those found in $Hg(C_6H_4CH_2NMe_2\text{-}2)_2$ (**X**) [2.89(1) Å] [21] or the 2-pyridylphenyl complex **VI** [2.798(7) Å] [16], but still fall well within the sum of the van der Waals radii for nitrogen (1.55 Å) [22] and a reasonable value of 1.73 Å for mercury [23]. Hence we suggest that there is a single weak Hg···N bonding interaction in **2** involving each of the R^- ligands. This is consistent with (i) the slight deviation from the sp^2 value in the angles C(1)–C(2)–N(1) and C(1)–C(6)–N(2) and (ii) magnitudes of the Hg–C(1)–C(2/6) angles which demonstrate that the fragment incorporating N(1) is slightly bent towards the mercury atom. The Hg–C(1) bond length of 2.081(8) Å in **2** is close to the 2.085(7) Å in $HgPh_2$ [24], the 2.10(2) Å in **X** [20] and the 2.098(8) Å in **VI** [16]. The mercury atom in **2** is 0.41 Å out of the C_6 aromatic mean plane, a situation similar to that in $HgPh_2$ in which, however, the deviation is only 0.1 Å [24]. The Hg–C(1)···C(4) angle in **2** is 168.7(6)°, the molecule being slightly bent at the C(1) atom. The phenyl planes are parallel to one another.

3.2. The molecular structure of BCl(Ph)R (3)

The molecular structure of crystalline BCl(Ph)R (**3**) is illustrated in Fig. 2; selected bond distances and bond angles are in Table 4.

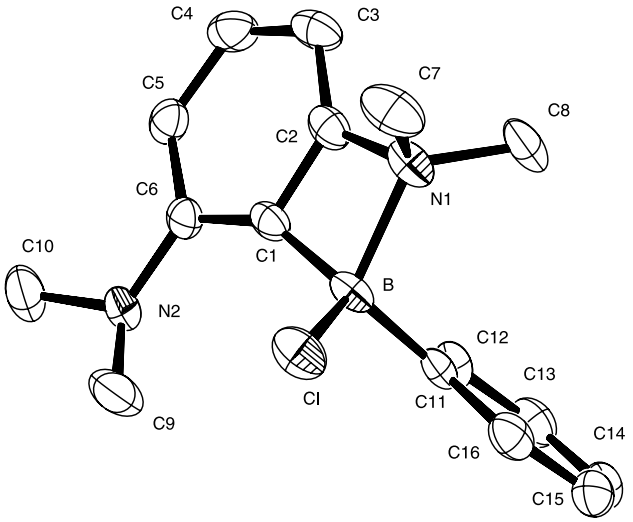


Fig. 2. The X-ray crystal structure of complex **3**.

Table 4
Selected bond distances (Å) and angles (°) for **3**

Bond distances		Bond angles	
B–C(1)	1.599(5)	C(1)–C(2)–N(1)	101.1(3)
B–C(11)	1.591(5)	B–C(1)–C(2)	92.4(3)
B–Cl	1.865(4)	C(1)–B–N(1)	82.3(2)
B···N(1)	1.740(4)	B–N(1)–C(2)	83.5(2)

Crystalline **3** is a monomer, with the boron atom in a four-coordinate, distorted tetrahedral environment. This distortion is evidently caused by the chelating R^- ligand, as reflected in the significantly narrower than the sp^2 value of the endocyclic angles at C(1) and C(2). The latter is also much narrower than in, for example, SnR_2 (**II**), 113.6(4)° [1], which is attributed to the relative sizes of the boron and tin atoms, B ≪ Sn. The B–N(1)–C(2)–C(1) ring is planar, the sum of the endocyclic bond angles being 359.3°.

The B–Cl bond in **3**, 1.865(4) Å, is significantly longer than in the three-coordinate boron chloride $B(C_6F_5)_2Cl$, 1.746(5) Å [25], but is similar to those in the four-coordinated chloroboranes $B(Cl)Ph_2(THF)$, 1.893(2) Å [26], **IX** (av. 1.86 Å) [27], and the pyridine adduct of 1-chloro-1-borafluorene **XI**, 1.898(2) Å [28].

The mean B–C distance in **3** of 1.59 Å is slightly longer than in $B(C_6F_5)_2Cl$, 1.56 Å [25], but similar to that in the four-coordinated boron chlorides **IX**, 1.60 Å [27], or **XI**, 1.61 Å [28]. The B···N(1) distance in **3** is significantly longer than in $B(Br)_2(\kappa^2\text{-}C,N\text{–}C_6H_4CH_2\text{-}NMe_2\text{-}2)$, 1.625(1) Å [29] or **IX**, 1.649(5) Å [27]. Evidently the methylene group in the latter two complexes facilitates the $R'_2N \rightarrow B$ coordination (R′ = Me or Et), whereas this effect in **3** is subject to greater strain. The B···N separation in the spiro compound $B(C_6H_4CH_2\text{-}NMe_2\text{-}2)\{\kappa^2\text{-}O,O'\text{–}OCH_2C(Ph)_2O\}$ of 1.754(4) Å [30] is similar to that in **3**.

4. Supplementary material

Crystallographic data for the structural analysis have been deposited with the Cambridge Crystallographic Centre, CCDC Nos. 170829 for **2** and **3**. Copies of this information may be obtained free of charge from The Director, CCDC 12 Union Road, Cambridge CB2 1EZ, UK (fax: +44-1223-366-033; e-mail: deposit@ccdc.cam.ac.uk or www: http://www.ccdc.cam.ac.uk).

Acknowledgements

We thank the European Commission for providing a TMR Category 20 studentship to P.G.H.U. and the University of Lyon II for granting a period of study leave to D.C.

References

[1] C. Drost, P.B. Hitchcock, M.F. Lappert, L.J.-M. Pierssens, Chem. Commun. (1997) 1141.
[2] S. Harder, J. Boersma, L. Brandsma, J.A. Kanters, W. Bauer, P.v.R. Schleyer, Organometallics 8 (1989) 1696.
[3] J.T.B.H. Jastrzebski, P.A. van der Schaaf, J. Boersma, G. van Koten, M.C. Zoutberg, D. Heijdenrijk, Organometallics 8 (1989) 1373.
[4] (a) P.B. Hitchcock, M.F. Lappert, P.G.H. Uiterweerd, in preparation;
(b) P.G.H. Uiterweerd, D.Phil. Thesis, University of Sussex, 2001.
[5] G. Friedmann, M. Brini, P. Ederle, J. Gasser, P.-J. Holderith, M. Vernois, J.-M. Widmaier, Bull. Soc. Chim. Fr. (1970) 706.
[6] C. Drost, P.B. Hitchcock, M.F. Lappert, Organometallics 17 (1998) 3838.
[7] C. Drost, P.B. Hitchcock, M.F. Lappert, Angew. Chem., Int. Ed. Engl. 38 (1999) 1113.
[8] C. Drost, B. Gehrhus, P.B. Hitchcock, M.F. Lappert, Chem. Commun. (1997) 1845.
[9] G.M. Sheldrick, SHELXS-97, Program for the Solution of Crystal Structures, University of Göttingen, 1997.
[10] G.M. Sheldrick, SHELXL-97, Program for Crystal Structure Refinement, University of Göttingen, 1997.
[11] A. Hudson, M.F. Lappert, P.W. Lednor, J. Chem. Soc., Dalton Trans. (1976) 2369.
[12] M.J.S. Gynane, D.H. Harris, M.F. Lappert, P.P. Power, P. Rivière, M. Rivière-Baudet, J. Chem. Soc., Dalton Trans. (1977) 2004.
[13] D. Bravo-Zhivotovskii, M. Yuzefovich, M Bendikov, K. Klinkhammer, Y. Apeloig, Angew. Chem., Int. Ed. Engl. 38 (1999) 1100.
[14] *Cf.* A.G. Davies, J.L. Wardell, Comprehensive Organometallic Chemistry, In: E.W. Abel, F.G.A. Stone, G. Wilkinson (Eds.), 2nd ed., vol. 3 (J.L. Wardell, ed.), Pergamon, Oxford, 1995.
[15] *Cf.* B. Wrackmeyer, R. Contreras, Ann. Rep. NMR Spectrosc. 24 (1992) 267.

[16] D.St.C. Black, G.B. Deacon, G.L. Edwards, B.M. Gatehouse, Aust. J. Chem. 46 (1993) 1323.
[17] A.J. Canty, P. Barron, P.C. Healey, J. Organomet. Chem. 179 (1979) 447.
[18] S. Toyota, T. Futakawa, H. Ikeda, M. Ōki, J. Chem. Soc., Chem. Commun. (1995) 2499.
[19] M. Lauer, G. Wulff, J. Organomet. Chem. 256 (1983) 1.
[20] R. Schlengermann, J. Sieler, S. Jelonek, E. Hey-Hawkins, Chem. Commun. (1997) 197.
[21] J.L. Atwood, D.E. Berry, S.R. Stobart, M.J. Zaworotko, Inorg. Chem. 22 (1983) 3480.
[22] A. Bondi, J. Phys. Chem. 68 (1964) 441.
[23] A.J. Canty, G.B. Deacon, Inorg. Chim. Acta 45 (1980) L225.
[24] D. Grdenić, B. Kamenar, A. Nagl, Acta Crystallogr., Sect. B 33 (1977) 587.
[25] W.E. Piers, R.E.v.H. Spence, L.R. MacGillivray, M.J. Zaworotko, Acta Crystallogr., Sect. C 51 (1995) 1688.
[26] W.I. Cross, M.P. Lightfoot, F.S. Mair, R.G. Pritchard, Inorg. Chem. 39 (2000) 2690.
[27] R. Schlengermann, J. Sieler, E. Hey-Hawkins, Main Group Chem. 2 (1997) 141.
[28] C.K. Narula, H. Nöth, Inorg. Chem. 24 (1985) 2532.
[29] D.S. Brown, C.J. Carmalt, A.H. Cowley, A. Decken, H.S. Isom, Heteroatom Chem. 9 (1998) 79.
[30] S. Toyota, M. Ōki, Bull. Chem. Soc. Jpn. 65 (1992) 1832.

PERGAMON

Polyhedron 21 (2002) 641–649

POLYHEDRON

www.elsevier.com/locate/poly

Isolated deltahedral clusters of lead in the solid state: synthesis and characterization of Rb_4Pb_9 and $Cs_{10}K_6Pb_{36}$ with Pb_9^{4-}, and $A_3A'Pb_4$ (A = Cs, Rb, K; A′ = Na, Li) with Pb_4^{4-}

Svilen Bobev, Slavi C. Sevov *

Department of Chemistry and Biochemistry, University of Notre Dame, Notre Dame, IN 46556, USA

Received 8 May 2001; accepted 27 November 2001

Abstract

The title compounds were synthesized by direct fusion of the corresponding elements in appropriate atomic ratios at 700 °C, and the structures were determined by single-crystal X-ray diffraction. They contain isolated deltahedral clusters of lead with charge of 4−. The clusters in Rb_4Pb_9 and $Cs_{10}K_6Pb_{36}$ are Pb_9^{4-}. They are *nido* according to their charge, but their shapes do not always correspond to the classical *nido* geometry, a monocapped square antiprism. Some are differently distorted tricapped trigonal prisms. The relationship between these different geometries is discussed, and new classification for such clusters is proposed. The $A_3A'Pb_4$ compounds are isostructural and contain isolated tetrahedra of Pb_4^{4-}. © 2002 Elsevier Science Ltd. All rights reserved.

Keywords: Clusters; Crystal structures; Intermetallic compounds; Lead; Zintl phases

1. Introduction

The growing tendency for miniaturizing semiconducting devices has developed, in recent years, into research on synthesis, characterization and properties of 'quantum-size' particles, i.e. small enough particles that exhibit novel quantum effects [1,2]. Such nanoparticles consist of anywhere between a few atoms to a few hundred atoms of metals or semiconductors. The limited number of atoms in the particle leads to a physical phenomenon known as 'quantum confinement' where the properties of the system fall into the transition region between bulk material and molecules [3]. This leads to different thermodynamic properties such as melting point, phase transitions, and different electronic and optical behavior [4,5].

Large, negatively-charged deltahedral clusters of main-group elements also belong to this group. Such isolated and naked clusters are usually found in compounds containing alkali metals as countercations [6]. Recently, numbers of such species were discovered in 'neat solids' [6,7]. Many of them were previously characterized only in compounds crystallized from liquid ammonia or ethylenediamine solutions of various precursors [8,9]. Such clusters, when in solutions, can react with other molecules, can form polymers, or can oligomerize into larger nanoparticles. They are also fascinating with the aesthetics of their topologies, and better understanding of their unusual bonding will bring knowledge that is otherwise inaccessible [6].

We have undertaken a systematic and thorough search for homoatomic deltahedral clusters of the heavier elements of the carbon group in the solid state. This has resulted in the discovery of the first large deltahedral cluster of group 14, a monocapped square antiprism of Ge_9^{4-} in the binary solid Cs_4Ge_9 [10]. Similar nine-atom clusters of Si, Sn and Pb were later found in Zintl compounds with general stoichiometries A_4Tt_9 and $A_{12}Tt_{17}$ where A = alkali metal and Tt = Tetrel is an element of group 14 (except carbon) [11–14]. Some of these clusters are identical with the Zintl ions crystallized from solutions, and thus establish the relationship between Zintl phases and Zintl ions [10].

* Corresponding author. Tel.: +1-219-631-5891; fax: +1-219-631-6652.

E-mail address: ssevov@nd.edu (S.C. Sevov).

0277-5387/02/$ - see front matter © 2002 Elsevier Science Ltd. All rights reserved.
PII: S0277-5387(01)01016-6

The exploration for clusters in the solid state was later extended into pseudo-binary systems with two different alkali–metal countercations. This has produced several unprecedented compounds with novel features. For example, the first isolated *arachno*-clusters of group 14, square antiprisms of Sn_8^{6-}, were discovered in two Li-containing Zintl phases with stoichiometry of $A_4Li_2Sn_8$ (A = K, Rb) [15]. Similarly, mixed alkali metals and Ge provide the largest, so far, isolated clusters of group 14, giant truncated tetrahedra of Ge_{12}^{12-} in the compound $RbLi_7Ge_8$ [16]. In addition to these compounds with isolated clusters, extended structures are also feasible. Thus, appropriate mixtures of Na/Rb or Na/Cs with Si, Ge and Sn, yielded the first stoichiometric clathrates of type II, $A_8Na_{16}Si_{136}$ and $A_8Na_{16}Ge_{136}$ (A = Rb, Cs) [17,18], the first intermetallic clathrate–III compound, $Cs_{30}Na_{(1.33x-10)}Sn_{(172-x)}$ [19], and a layered clathrate derivative $A_3Na_{10}Sn_{23}$ (A = K, Rb, Cs) with clathrate-II layers 'stuffed' with the Zintl phase A_4Sn_4 [20]. Here, we report on the extension of these studies into the heaviest homologue of the carbon group, lead, and the interesting cluster chemistry of the systems of mixed alkali metals and lead.

Table 1
Selected data collection and refinement parameters for Rb_4Pb_9, $Cs_{10}K_6Pb_{36}$ and Cs_3NaPb_4

Empirical formula	Rb_4Pb_9	$Cs_{10}K_6Pb_{36}$	Cs_3NaPb_4
Formula weight	2206.59	9022.54	1250.48
Temperature (K)	293(2)	293(2)	293(2)
Wavelength (Å), Mo Kα	0.71073	0.71073	0.71073
Crystal system	monoclinic	triclinic	orthorhombic
Space group	$P2_1/m$	$P\bar{1}$	*Cmcm*
Unit cell dimensions			
a (Å)	9.888(1)	9.843(2)	7.267(1)
b (Å)	13.393(4)	15.155(2)	17.282(1)
c (Å)	16.224(3)	15.289(3)	11.074(1)
α (°)		104.51(2)	
β (°)	102.987(8)	97.63(2)	
γ (°)		99.55(1)	
V (Å^3)	2093.7(8)	2149.8(7)	1390.7(2)
Z	4	1	4
D_{calc} (g cm^{-3})	7.000	6.998	5.972
Absorption coefficient (cm^{-1})	812.91	749.49	559.86
Data/parameters	3860/131	7842/439	703/27
Goodness-of-fit on F^2	1.155	0.999	1.034
R_1/wR_2 [a] [$I>2\sigma_I$] (%)	9.12/23.01	11.81/26.34	4.73/11.77

[a] $R_1 = [\Sigma||F_o|-|F_c||]/\Sigma|F_o|$; $wR_2 = \{[\Sigma w[(F_o)^2-(F_c)^2]^2]/[\Sigma w(F_o^2)^2]\}^{1/2}$; $w = [\sigma^2(F_o)^2+(AP)^2+BP]^{-1}$, where $P = [(F_o)^2+2(F_c)^2]/3$.

2. Experimental

2.1. Synthesis

All manipulations were handled in an inert atmosphere glove box or under vacuum. Mixtures of the elements in appropriate atomic ratios (all from Alfa–Aesar or Acros, > 99.9% pure) were loaded in niobium containers. Details on the procedures and the containers can be found elsewhere [21]. Initially mixtures with compositions $(A_{1-x}A'_x)_4Pb_9$ were heated at 700 °C for 1 week and were then slowly cooled to room temperature at a rate of 3° h^{-1}. Phase analysis of the products was carried out with powder X-ray diffraction (Enraf–Nonius Guinier camera with Cu $K\alpha_1$ radiation). For some of them the results were quite ambiguous, and therefore, more reactions with the same atomic ratios were carried out at different temperature regimes. Nevertheless, this did not improve the phase purity of the products, which often contained traces of elemental lead. Later, reactions were loaded with a slight excess of lead intended to serve as a flux for more facile crystal growth. These were carried out at lower temperatures and for prolonged periods of time of about 4 weeks. They produced crystals of better quality that were suitable for data collection.

2.2. Structure determination

A few crystals of each sample were selected in the glove box, sealed in glass capillaries, checked for singularity on a Enraf–Nonius CAD4 single crystal diffractometer with Mo Kα radiation, and data were collected for the best of them at room temperature ($\omega-2\theta$ scans, $2\theta_{max} = 50°$). The following are more details of the data collections: (a) a quarter of a sphere of data was collected of a black, bar-like crystal of Rb_4Pb_9 with dimensions $0.18 \times 0.12 \times 0.10$ mm; (b) a hemisphere of data was collected of a black, very brittle and irregular crystal of $Cs_{10}K_6Pb_{36}$ with dimensions $0.20 \times 0.12 \times 0.10$ mm; (c) an octant of a sphere of data was collected of a dark, bar-like crystal of Cs_3NaPb_4 with dimensions $0.20 \times 0.10 \times 0.06$ mm. The data were corrected for Lorentz and polarization effects, and for absorption with the aid of the XABS program [22a]. The structures were solved by direct methods and refined by full-matrix least-squares on F^2 using the SHELXTL V5.1 package [22b]. Further details of the data collection and structure refinements are given in Table 1. Cs_3LiPb_4, Rb_3LiPb_4 and K_3LiPb_4 are isostructural with Cs_3NaPb_4, and only their lattice parameters are reported (Table 2). Important Pb–Pb distances for Rb_4Pb_9 and $Cs_{10}K_6Pb_{36}$ are given in Tables 3 and 4, respectively.

Table 2
Lattice parameters for other lead compounds with Pb_4^{4-} tetrahedra [a]

Compound	Space group	a (Å)	b (Å)	c (Å)	V (Å^3)
Cs_3NaPb_4 [b]	*Cmcm*	7.267(1)	17.282(1)	11.074(1)	1390.7(2)
Cs_3LiPb_4	*Cmcm*	7.274(1)	16.74(1)	10.75(1)	1309(2)
Rb_3LiPb_4	*Cmcm*	7.133(1)	16.276(2)	10.534(1)	1223.0(3)
K_3LiPb_4	*Cmcm*	6.932(1)	16.09(1)	10.508(2)	1172(3)

[a] Determined from powder diffraction patterns taken at room temperature on an Enraf–Nonius Guinier camera with vacuum chamber, Cu Kα radiation ($\lambda = 1.540562$ Å) and NBS (NIST) silicon as an internal standard.
[b] Determined from 25 reflections at high θ-angles on a CAD4 single crystal diffractometer.

Table 3
Important distances (Å) within the two Pb_9^{4-} clusters in Rb_4Pb_9

	Cluster A			Cluster B	
Pb1A	Pb2A	3.065(6)	Pb1B	Pb3B	3.067(4)
	Pb4A	3.066(6)		Pb4B	3.094(4)
	Pb3A	3.110(4)		Pb5B	3.126(4)
	Pb5A	3.110(4)		Pb2B	3.165(4)
Pb2A	Pb1A	3.065(6)	Pb2B	Pb1B	3.165(4)
	Pb6A	3.142(4)		Pb7B	3.165(4)
	Pb7A	3.142(4)		Pb5B	3.210(4)
	Pb3A	3.397(4)		Pb6B	3.210(4)
	Pb5A	3.397(4)		Pb3B	3.426(6)
Pb3A	Pb8A	3.101(4)	Pb3B	Pb1B	3.067(4)
	Pb1A	3.110(4)		Pb7B	3.067(4)
	Pb7A	3.142(4)		Pb4B	3.317(5)
	Pb2A	3.397(4)		Pb8B	3.317(5)
	Pb4A	3.533(5)		Pb2B	3.426(6)
Pb4A	Pb1A	3.066(6)	Pb4B	Pb1B	3.094(4)
	Pb8A	3.118(5)		Pb9B	3.108(5)
	Pb9A	3.118(5)		Pb8B	3.119(7)
	Pb3A	3.533(5)		Pb3B	3.317(5)
	Pb5A	3.533(5)		Pb5B	3.866(5)
Pb5A	Pb1A	3.110(4)	Pb5B	Pb9B	3.074(4)
	Pb9A	3.131(7)		Pb6B	3.088(7)
	Pb6A	3.142(4)		Pb1B	3.126(4)
	Pb2A	3.397(4)		Pb2B	3.210(4)
	Pb4A	3.533(5)		Pb4B	3.866(5)
Pb6A	Pb9A	3.059(4)	Pb6B	Pb9B	3.074(4)
	Pb7A	3.111(8)		Pb5B	3.088(7)
	Pb2A	3.142(4)		Pb7B	3.126(4)
	Pb5A	3.142(4)		Pb2B	3.210(4)
	Pb8A	4.370(4)		Pb8B	3.866(5)
Pb7A	Pb8A	3.059(4)	Pb7B	Pb3B	3.067(4)
	Pb6A	3.111(8)		Pb8B	3.094(4)
	Pb2A	3.142(4)		Pb6B	3.126(4)
	Pb3A	3.142(4)		Pb2B	3.165(4)
Pb8A	Pb7A	3.059(4)	Pb8B	Pb7B	3.094(4)
	Pb3A	3.101(4)		Pb9B	3.108(5)
	Pb4A	3.118(5)		Pb4B	3.119(7)
	Pb9A	3.131(7)		Pb3B	3.317(5)
	Pb6A	4.370(4)		Pb6B	3.866(5)
Pb9A	Pb6A	3.059(4)	Pb9B	Pb5B	3.074(4)
	Pb4A	3.111(8)		Pb6B	3.074(4)
	Pb5A	3.131(7)		Pb4B	3.108(5)
	Pb8A	3.131(7)		Pb8B	3.108(5)
Average Pb–Pb distance 3.180 Å			Average Pb–Pb distance 3.158 Å		

Table 4
Important distances (Å) within the four Pb_9^{4-} clusters in $Cs_{10}K_6Pb_{36}$

	Cluster C			Cluster D	
Pb1C	Pb5C	3.05(2)	Pb1D	Pb2D	3.03(2)
	Pb2C	3.08(2)		Pb5D	3.05(2)
	Pb4C	3.14(2)		Pb4D	3.07(2)
	Pb3C	3.14(2)		Pb3D	3.08(2)
Pb2C	Pb1C	3.08(2)	Pb2D	Pb1D	3.03(2)
	Pb7C	3.09(3)		Pb7D	3.11(2)
	Pb6C	3.24(2)		Pb5D	3.17(2)
	Pb5C	3.26(2)		Pb6D	3.24(2)
	Pb3C	3.30(2)		Pb3D	3.34(2)
Pb3C	Pb7C	3.05(3)	Pb3D	Pb1D	3.08(2)
	Pb1C	3.14(2)		Pb7D	3.12(2)
	Pb4C	3.15(2)		Pb8D	3.23(2)
	Pb8C	3.29(2)		Pb4D	3.31(2)
	Pb2C	3.30(2)		Pb2D	3.34(2)
Pb4C	Pb8C	3.06(2)	Pb4D	Pb1D	3.07(2)
	Pb9C	3.12(2)		Pb8D	3.11(2)
	Pb1C	3.14(2)		Pb9D	3.16(2)
	Pb3C	3.15(2)		Pb3D	3.31(2)
	Pb5C	3.95(2)		Pb5D	3.72(2)
Pb5C	Pb1C	3.05(2)	Pb5D	Pb1D	3.05(2)
	Pb6C	3.11(2)		Pb6D	3.11(2)
	Pb9C	3.16(2)		Pb9D	3.11(2)
	Pb2C	3.26(2)		Pb2D	3.17(2)
	Pb4C	3.95(2)		Pb4D	3.72(2)
Pb6C	Pb5C	3.11(2)	Pb6D	Pb9D	3.07(2)
	Pb7C	3.11(2)		Pb7D	3.10(2)
	Pb9C	3.14(2)		Pb5D	3.11(2)
	Pb2C	3.24(2)		Pb2D	3.24(2)
	Pb8C	3.91(2)		Pb8D	4.09(2)
Pb7C	Pb3C	3.05(3)	Pb7D	Pb8D	3.07(2)
	Pb2C	3.09(2)		Pb6D	3.10(2)
	Pb6C	3.11(2)		Pb2D	3.11(2)
	Pb8C	3.12(2)		Pb3D	3.12(2)
Pb8C	Pb4C	3.06(2)	Pb8D	Pb7D	3.07(2)
	Pb7C	3.12(2)		Pb9D	3.09(2)
	Pb9C	3.14(2)		Pb4D	3.11(2)
	Pb3C	3.29(2)		Pb3D	3.23(2)
	Pb6C	3.91(2)		Pb6D	4.09(2)
Pb9C	Pb4C	3.12(2)	Pb9D	Pb6D	3.07(2)
	Pb6C	3.14(2)		Pb8D	3.09(2)
	Pb8C	3.14(2)		Pb5D	3.11(2)
	Pb5C	3.16(2)		Pb4D	3.16(2)
Average Pb–Pb distance 3.14 Å			Average Pb–Pb distance 3.13 Å		
	Cluster E			Cluster F	
Pb1E	Pb5E	3.03(2)	Pb1F	Pb5F	3.06(2)
	Pb3E	3.07(3)		Pb4F	3.08(2)
	Pb4E	3.11(2)		Pb2F	3.16(2)
	Pb2E	3.13(3)		Pb3F	3.18(2)
Pb2E	Pb1E	3.13(3)	Pb2F	Pb6F	3.13(2)
	Pb7E	3.18(2)		Pb7F	3.15(2)
	Pb5E	3.21(2)		Pb1F	3.16(2)
	Pb6E	3.27(2)		Pb5F	3.23(2)
	Pb3E	3.38(2)		Pb3F	3.43(2)
Pb3E	Pb1E	3.07(3)	Pb3F	Pb7F	3.15(2)
	Pb8E	3.14(2)		Pb4F	3.17(2)
	Pb7E	3.15(3)		Pb1F	3.18(2)
	Pb4E	3.28(2)		Pb8F	3.26(2)
	Pb2E	3.38(2)		Pb2F	3.43(2)
Pb4E	Pb8E	3.08(2)	Pb4F	Pb9F	3.07(2)
	Pb9E	3.11(2)		Pb1F	3.08(2)
	Pb1E	3.11(2)		Pb8F	3.14(2)
	Pb3E	3.28(2)		Pb3F	3.17(2)
	Pb5E	3.90(2)		Pb5F	3.70(2)

Table 4
Important distances (Å) within the four Pb_9^{4-} clusters in $Cs_{10}K_6Pb_{36}$

Pb5E	Pb1E	3.03(2)	Pb5F	Pb1F	3.06(2)
	Pb6E	3.07(2)		Pb6F	3.07(2)
	Pb9E	3.07(2)		Pb9F	3.11(2)
	Pb2E	3.21(2)		Pb2F	3.23(2)
	Pb4E	3.90(2)		Pb4F	3.70(2)
Pb6E	Pb5E	3.07(2)	Pb6F	Pb5F	3.07(2)
	Pb7E	3.07(2)		Pb7F	3.07(2)
	Pb9E	3.13(2)		Pb2F	3.13(2)
	Pb2E	3.27(2)		Pb9F	3.13(2)
	Pb8E	3.96(2)		Pb8F	4.08(2)
Pb7E	Pb6E	3.07(2)	Pb7F	Pb8F	3.06(2)
	Pb8E	3.09(2)		Pb6F	3.07(2)
	Pb3E	3.15(3)		Pb2F	3.15(2)
	Pb2E	3.18(2)		Pb3F	3.15(2)
Pb8E	Pb4E	3.08(2)	Pb8F	Pb7F	3.06(2)
	Pb7E	3.09(2)		Pb9F	3.13(2)
	Pb9E	3.10(2)		Pb4F	3.14(2)
	Pb3E	3.14(2)		Pb3F	3.26(2)
	Pb6E	3.96(2)		Pb6F	4.08(2)
Pb9E	Pb5E	3.07(2)	Pb9F	Pb4F	3.07(2)
	Pb8E	3.10(2)		Pb5F	3.11(2)
	Pb4E	3.11(2)		Pb6F	3.13(2)
	Pb6E	3.13(2)		Pb8F	3.13(2)
Average Pb–Pb distance 3.14 Å			Average Pb–Pb distance 3.15 Å		

2.3. Magnetic measurements

The magnetizations of the compounds were measured on a Quantum Design MPMS-SQUID magnetometer at a field of 3 T in the temperature range of 10–300 K. Typically 20–40 mg of sample are packed in a special holder designed for air-sensitive compounds [21]. They all showed temperature-independent and negative magnetizations (-3.0×10^{-4}, -3.7×10^{-4}, and -7.2×10^{-4} emu for 37 mg of Rb_4Pb_9, 24 mg of $Cs_{10}K_6Pb_{36}$, and 33 mg of Cs_3NaPb_4, respectively) consistent with electronically-balanced compounds.

2.4. Electronic structure

Extended-Hückel band and MO calculations were carried out within the tight binding approximation with only the lead atoms included (H_{ii} and ζ_1 for Pb 6s: -15.70 eV and 2.35, for Pb 6p: -8.00 eV and 2.06).

3. Results and discussion

3.1. Rb_4Pb_9

This compound is isostructural with K_4Pb_9 [12]. The structure is built of isolated nine-atom clusters of lead, Pb_9^{4-}, that are surrounded by rubidium cations. There are two different clusters in the structure, clusters **A** and **B** (Fig. 1). The geometry of clusters **A** is clearly close to a monocapped square antiprism (Fig. 1(a)), while that of type **B** is closer to a tricapped trigonal prism with two elongated vertical edges (Fig. 1(b)). The way cluster **A** is shown in Fig. 1(a) is somewhat unconventional since the monocapped square antiprism is shown lying on its side. The square of atoms 2–3–4–5 is capped by 1, while square 6–7–8–9 is open. The distances within the clusters range from 3.059(4) to 3.533(5) Å for **A** and from 3.067(4) to 3.426(6) Å for **B** (Table 4). The rubidium cations cap faces, edges, and vertices with the shortest Rb–Pb distances of 3.68(1) Å. There are some relatively short intercluster contacts of 3.767(5) Å between atoms Pb7A and Pb8A of clusters **A** (Fig. 1), and suggest some intercluster interactions. This distance is even shorter in the isostructural K_4Pb_9,

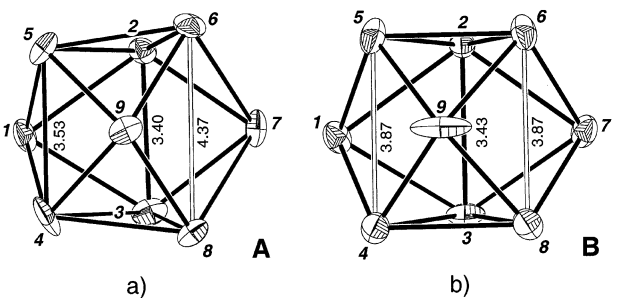


Fig. 1. The two different clusters in Rb_4Pb_9, (a) **A** and (b) **B**. Cluster **A** is a monocapped square antiprisms shown lying on its side (atom 1 caps the square face of atoms 2–3–4–5 while the square face 6–7–8–9 is open). The geometry of cluster **B** is closer to a tricapped (atoms 1, 7, 9) trigonal prism (triangular bases of atoms 2–5–6 and 3–4–8) with two elongated vertical edges (edges 4–5 and 6–8). The thermal ellipsoids are drawn at 50% probability level.

3.669(3) Å, obviously due to the larger size of the rubidium. Nonetheless, it has been proven for the potassium compound that the clusters are not bonded at all [12]. However, the 'short' intercluster contacts affect the density of states by broadening the valence *p*-band more than usual, to a width of about 5 eV. This, in turn, results in a narrow band gap of only about 0.30 eV.

3.2. $Cs_{10}K_6Pb_{36}$

This compound with mixed cations crystallizes in a novel structure type. The triclinic structure (space group *P*1), shown in Fig. 2, contains four crystallographically different clusters of Pb_9^{4-}, labeled **C**, **D**, **E** and **F** (Fig. 3). Interestingly, the corresponding binaries $K_{16}Pb_{36}$ and $Cs_{16}Pb_{36}$ are also known and both contain isolated Pb_9^{4-} [12,13], and yet the mixed cation system provides a new compound with the same overall composition $(Cs_{10}K_6)Pb_{36}$ and the same type of clusters but with a different structure. The shortest intercluster distances in this compound are very similar to those in Rb_4Pb_9, 3.70(2) Å, and similarly are not associated with any intercluster bonding interactions. The clusters are ordered in layers parallel to the (*a*, *b*)-plane (horizontal in Fig. 2). Their positions in each layer correspond to the positions of close-packed spheres, and the layers are stacked on top of each other as in hexagonal close-packed structures, i.e. they follow the order ABAB.

All four clusters in $Cs_{10}K_6Pb_{36}$ have two open square faces (Fig. 3) which clearly excludes classification as monocapped square antiprisms which have only one such face. All four geometries are somewhat closer to tricapped trigonal prisms with two elongated heights.

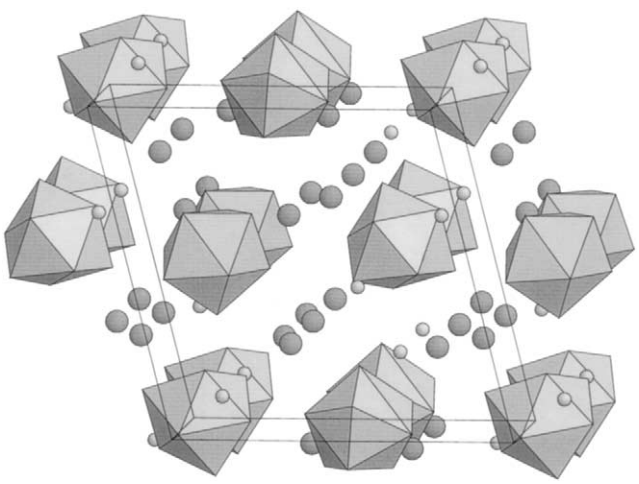


Fig. 2. A polyhedral view of the structure of $Cs_{10}K_6Pb_{36}$ along the *a* axis (*b* is horizontal) with the triclinic cell outlined. The isolated clusters of Pb_9^{4-} form nearly close-packed layers parallel to the (*a*,*b*)-plane, and these layers are stacked in a hexagonal close-packing fashion, i.e. ABAB. There are four clusters per unit cell and all are crystallographically different. The large and small isolated circles are Cs and K, respectively.

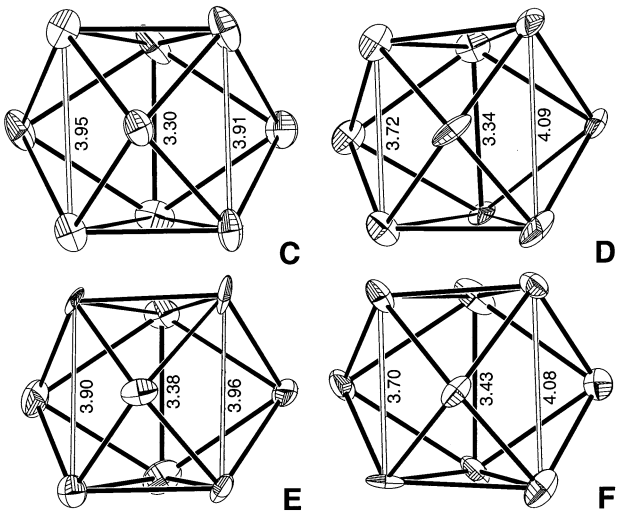


Fig. 3. The four clusters in $Cs_{10}K_6Pb_{36}$ labeled **C**, **D**, **E** and **F**. The atom numbering is the same as in Fig. 1. The thermal ellipsoids are drawn at 50% probability level.

Despite the 'deviations' from the classical *nido* shape, however, each of these clusters carries a charge typical for *nido*-clusters, 4−, according to the formula $Cs_{10}K_6(Pb_9)_4$. Thus, in this compound as well as in Rb_4Pb_9, we find clusters that do not conform to the *nido*-shape but need the same number of electrons for bonding as the *nido*-clusters. This needs more detailed investigation, and this is presented in the following section.

3.3. Nine-atom clusters

There have been quite extensive discussions in the literature about the geometry of nine-atom clusters and their classification into two classes according to their shapes, monocapped square antiprisms or tricapped trigonal prisms (usually elongated), and accordingly into *nido*- or *closo*-types, respectively [23–25]. However, this classification into two very strict classes is quite an ambiguous process since the clusters are almost never perfect, and it is impossible to draw a line between the two geometries. This is usually done based on a multitude of dihedral angles and edge ratios like those presented in Table 5. Thus, it can be seen from this table that the open square face of cluster **A** (face of atoms 6–7–8–9, Fig. 1) is perfectly planar with a 0° dihedral angle and is also nearly rectangular (Table 3) as expected for a monocapped square antiprism. Also typical for that geometry are the dihedral angles of atoms 5–9–4–1 and 2–1–3–7, 32.1(5) and 33.1(5)°, respectively. In the way the cluster is shown in Fig. 1(a), these angles are also dihedral angles within the waist of a trigonal prism of atoms 5–2–6 (upper triangular base) and 4–3–8 (bottom base) that is tricapped by atoms 1, 9, and 7. Thus, the monocapped square antiprism can be viewed as a tricapped trigonal prism

Table 5
Selected edge ratios and dihedral angles in some nine-atom lead clusters [a]

Cluster	Edge ratios		Dihedral angles			Ref.
	(6–8):(2–3)	(4–5):(2–3)	(6–7–8)/(6–8–9)	(5–9–4)/(1–4–5)	(1–2–3)/(2–3–7)	
Pb_9^{3-}	1.057(1)	1.003(1)	14	20	21	[25]
Pb_9^{4-}	1.305(1)	1.024(1)	0.7(4)	28.8(4)	30.5(4)	[23]
Pb_9^{4-}	1.277(2)	1.047(2)	5.3(2)	22.6(2)	30.6(1)	[13]
Pb_9^{4-}	1.283(1)	1.036(1)	0	32.4(4)	32.9(4)	[12]
Pb_9^{4-}	1.128(1)	1.128(1)	13.0(5)	13.0(5)	28.3(4)	[12]
Pb_9^{4-} (A)	1.286(2)	1.040(2)	0	33.1(5)	32.1(5)	[b]
Pb_9^{4-} (B)	1.128(2)	1.128(2)	13.1(5)	13.1(5)	28.4(4)	[b]
Pb_9^{4-} (C)	1.185(9)	1.197(9)	17.3(7)	9.5(6)	25.3(6)	[b]
Pb_9^{4-} (D)	1.225(9)	1.114(7)	11.5(7)	17.0(6)	25.5(6)	[b]
Pb_9^{4-} (E)	1.172(9)	1.154(8)	9.8(6)	12.7(6)	27.0(7)	[b]
Pb_9^{4-} (F)	1.189(9)	1.079(8)	12.2(6)	13.1(5)	24.9(5)	[b]

[a] The numbering system is from Fig. 1.
[b] This work.

with two normal edges, edges 4–5 and 3–2, and one elongated edge, the 8–6 edge. This is also indicated by the ratios between the three edges (Table 5), a number larger than one for the ratio (6–8): (2–3), 1.286(2), and a number close to one for the ratio of (5–4): (2–3), 1.040(2). The geometry with two short and one long edges is typical for a monocapped square antiprism, and is also the reason for the two large and one zero dihedral angles when considered as a tricapped trigonal prism. These dihedral angles and edge ratios of **A** also compare very well with known lead clusters that have already been 'classified' in the class of monocapped square antiprisms (Table 5).

The corresponding dihedral angles and edge ratios look quite different for the remaining five clusters, **B** through **F**. There are two small and one large deltahedral angles as well as two long and one short edges for the trigonal prism. Such clusters would be classified as distorted tricapped trigonal prisms with two elongated edges. A non-distorted prism, i.e. with three normal edges, would be expected to be a *closo*-cluster with a charge of 2− ($2n+2=20$ bonding electrons for a 9-atom cluster) according to Wade's rules [26]. However, obviously this is not the case for these clusters according to the stoichiometry of the compounds for which the clusters carry charges of 4− ($2n+4=22$ bonding electrons). This is also in agreement with the results from the extended-Hückel molecular orbital calculations performed for these clusters which show large HOMO–LUMO gaps of more than 3 eV for a total of 40 electrons (22 bonding electrons and $9\times 2=18$ lone pair electrons on 9 vertices), and correspondingly charges of 4−. Other examples of tricapped trigonal prisms distorted similarly to a different degree also carry $2n+4$ bonding electrons. Such are the cluster of Bi_9^{5+} in $BiBi_9(HfCl_6)_3$ and $Bi_9(Bi_3Cl_{14})$ [27], the heteroatomic clusters $[In_4Bi_5]^{3-}$ in (K-crypt)$_6$[In_4Bi_5]-[In_4Bi_5]·1.5en·0.5tol [28], Sn_9^{4-} in K(K-crown)$_3$[Sn_9]·en [24], and E_9^{3-} for E = Sn or Pb in (K-crypt)$_6E_9E_9$·1.5en·0.5tol where 'crypt' and 'crown' stand for 4,7,13,16,21,24-hexaoxa-1,10-diazabicyclo-[8,8,8]-hexacosane) and 1,4,7,10,13,16-hexaoxacyclooctadecane, respectively [25].

Introduced here is a new approach towards the shapes of the nine-atom deltahedral clusters. It is based on the general overall MO schemes for these clusters. In essence, it abolishes the classification into the two classes of monocapped square antiprisms and tricapped trigonal prisms, and uses only the class of the tricapped trigonal prisms but with different numbers of elongated edges. Shown in Fig. 4(a, b, c, and d) are four tricapped trigonal prisms with zero, one, two and three elongated

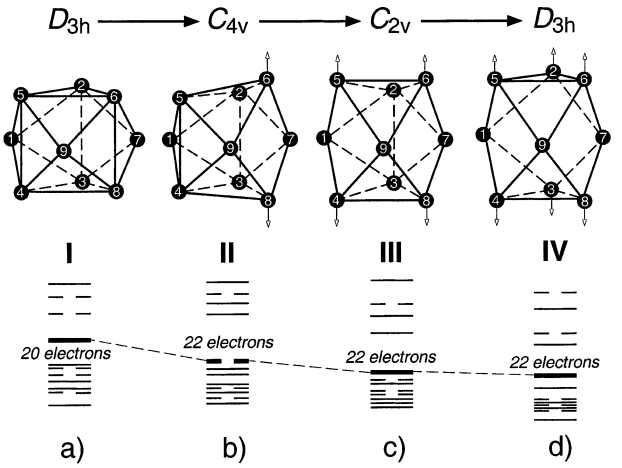


Fig. 4. A schematic representation of the consecutive opening of the three vertical edges of a tricapped trigonal prism (D_{3h}), cluster **I** in (a), along with the corresponding schematic MO diagrams. (b) The elongation of the 6–8 edge leads to a cluster, cluster **II**, with one open square face (C_{4v}) which also happens to be a monocapped square antiprism (shown lying on its side). (c) The elongation of the edge 4–5 of cluster **II** leads to cluster **III** with two open faces (C_{2v}). (d) The elongation of the edge 2–3 of cluster **III** results in an elongated tricapped trigonal prism, cluster **IV**, with three open faces (D_{3h}).

edges, respectively, and the corresponding schematic molecular orbital diagrams. Cluster **I** (Fig. 4(a)) is an ideal tricapped trigonal prism with D_{3h} symmetry and 'normal' (bonding) vertical edges (can be called 'three short' referring to the three vertical edges). The HOMO here is at $2n+2=20$ skeletal electrons but for this particular geometry there is also a relatively large gap above the LUMO a_2'' (shown with a thicker line). This would make the LUMO quite 'attractive' for additional electrons if lowered only a little more, and this can happen as a result of the distortions described below. This a_2' orbital, as it has been discussed before [29], is bonding within the triangular bases of the trigonal prism, i.e. triangles 2–5–6 and 3–4–8, but is antibonding between them (the capping atoms 1, 7, and 9, do not participate). This particular character of the orbital makes it very sensitive to changes in the heights of the prism, and this, combined with its position in the middle of a big gap (Fig. 4(a)), makes it the decisive orbital for the electron count of the cluster.

The cluster shown in Fig. 4(b), cluster **II**, is derived from cluster **I** by elongation of one vertical edge, the edge 6–8. As a result of just this relatively small distortion, the antibonding interactions in what was a_2' LUMO in cluster **I** are relieved, it drops down in energy, becomes occupied as a result of this, and now it is a part of a doubly degenerate HOMO for $2n+4$ electrons. The degeneracy is the result of the C_{4v} symmetry for this cluster which besides being a tricapped trigonal prism with one elongated edge ('two short and one long'), is also the classical monocapped square antiprism as already discussed above (compare with cluster **A** in Fig. 1(a)). This is also the classical shape for a *nido*-deltahedron, i.e. a deltahedron with one missing vertex and a charge of $4-$.

Elongation of a second edge of cluster **II**, the edge 4–5, leads to cluster **III** (Fig. 4(c)). The net character of the orbital in question is even more bonding since the antibonding interactions are reduced even more due to elongation of two instead of one edges. The HOMO–LUMO gap is still at $2n+4$ since nothing else changes significantly in the MO diagram. This cluster of C_{2v} symmetry has two long and one normal edges ('two long and one short') and, therefore, two open square faces. It resembles clusters **B** through **F** (Figs. 1 and 3). Usually the degree of elongation for each edge in a type **III** cluster with two long edges is smaller than that in a type **II** clusters with only one elongated edge. Thus, the edge 6–8 in cluster **A** (type **II**) is 4.370(4) Å while the two edges 4–5 and 6–8 in cluster **B** (type **III**) are 3.866(5) Å (Fig. 1). The same is true for the two long edges in clusters **C** through **F** which are of type **III**; they are all significantly shorter than 4.370(4) Å (Table 4).

Finally, elongation of the remaining third vertical edge of cluster **III** brings back a cluster of D_{3h} symmetry, cluster **IV** (Fig. 4(d)), which is again a tricapped trigonal prism like cluster **I** but is elongated along the threefold axis. The molecular diagram of this cluster ('three long') does not change much from that of cluster **III** and the HOMO–LUMO gap is at the same position. A well known example of this geometry is Bi_9^{5+} in $Bi[Bi_9](HfCl_6)_3$ with three long edges of 3.737 Å [27a].

As already mentioned above, the discussion of the type of a particular nine-atom cluster is often reduced to its classification as a tricapped trigonal prism or a monocapped square antiprism. Fig. 4 clearly shows that such a classification does not unambiguously define the electronic state of the cluster. Thus, clusters **I** and **IV** are both tricapped trigonal prisms but have different electronic requirements due to the relative position of the a_2' orbital. Clusters **II**, **III**, and **IV**, on the other hand, look quite different but have the same numbers of electrons. A very good illustration of this are the clusters **A** through **F**. Therefore, the usual classification of nine-atom clusters into the two classes is an oversimplification since, after all, the monocapped square antiprism is just one component of the series of distorted tricapped trigonal prisms: that with one elongated edge. Table 5 presents a good example of the difficulties when comparing edge ratios and dihedral angles since there are too many of them per cluster and it is impossible to define a cut-off line between the two categories. It is, perhaps, better to use two much more general categories such as 'normal' tricapped trigonal prism and elongated tricapped trigonal prism since these two shapes encompass all observed shapes and also differ in their electron counts. Ultimately, of course, each particular cluster can be discussed in the context of the particular stoichiometry, possible charges based on it, specifics of the shape, measured physical properties, along with careful consideration of the corresponding molecular orbital diagram.

3.4. $A_3A'Pb_4$

The four compounds Cs_3NaPb_4, Cs_3LiPb_4, Rb_3LiPb_4, and K_3LiPb_4 are isostructural with the known Cs_3LiSi_4 [30], and crystallize in the C-centered centrosymmetric space group *Cmcm*. They contain isolated tetrahedral anions of Pb_4^{4-} isoelectronic with the P_4 molecule. The four alkali metal cations provide the four extra electrons and surround the clusters in a very similar way as in the binary APb ($=A_4Pb_4$). However, the much smaller size of Na and Li and their high polarizing power and high electronegativity provide for different interactions in such compounds. For example, the structure of Cs_3NaPb_4 can also be viewed as made of isolated polymeric chains of $_\infty^1[Na(Pb)_4]^{3-}$ (Fig. 5)

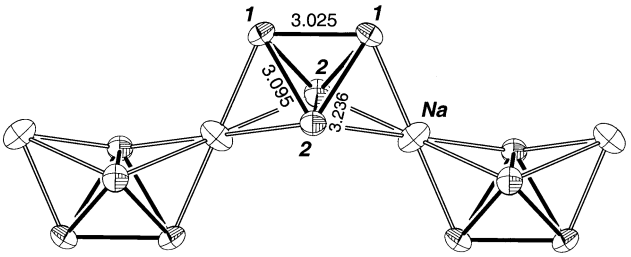


Fig. 5. The isolated polymeric chains of $_{\infty}^{1}[Na(Pb)_4]^{3-}$ running parallel to the c axis in the structure of the mixed-cation compound Cs_3NaPb_4. Lead and sodium are shown as full and crossed ellipsoids, respectively. All thermal ellipsoids are drawn at 80% probability level.

where the sodium cations act as μ_3-ligands coordinated to the staggered faces of two Pb_4^{4-} tetrahedra. The large alkali–metal cations, on the other hand, provide more complete charge transfer and simply separate and screen the chains from each other. Good evidence for the degree of covalency of the Na–Pb interactions is provided by the very different distances in the Pb_4^{4-} cluster. Thus, the edges coordinated to sodium, 1–2 and 2–2, are distinctly longer with distances of 3.095(2) and 3.236(3) Å, respectively, than the edge that is not, 1–1 with a distance of 3.025(2) Å. Furthermore, the edge that is coordinated to two sodium atoms is quite longer than the edges that are coordinated to only one such atom. Semi-covalent interactions of sodium and lithium are quite extensive in other known compounds. It should be pointed out that the 1–1 edge is not completely noncoordinated since it is capped by larger alkali–metal cations, but since the interactions there are almost purely ionic it does not experience elongation. Such combinations of very different alkali metals have been exploited extensively before and account for a large number of novel compounds with unique structures that form only with mixed cations [15–20,31].

4. Conclusions

The isolated nine-atom clusters of lead in the new compounds Rb_4Pb_9 and $Cs_{10}K_6Pb_{36}$ are best described as tricapped trigonal prisms with one or two elongated edges. They carry charges of $4-$, which is consistent with these shapes, and according to the charge they are all *nido* species with $2n+4$ bonding electrons. The commonly used classification of nine-atom clusters into two geometrical classes is not sufficient for accurate description of the electron counts for the clusters.

5. Supplementary material

A combined CIF file for the three structures has been deposited. Further details of the crystal structure determinations can be ordered from Fachinformationszentrum Karlsruhe, D-76344 Eggenstein-Leopoldsshafen, Germany (fax: +49-7247-808-666; e-mail: crysdata@fiz-karlsruhe.de), on quoting the depository CSD-numbers 411891 (Rb_4Pb_9), 411892 ($Cs_{10}K_6Pb_{36}$) and 411893 (Cs_3NaPb_4).

Acknowledgements

We thank the Petroleum Research Fund, administered by the ACS, for the financial support of this research.

References

[1] Special Section in Science, 254 (1991) 1300.
[2] V.L. Colvin, M.C. Schlamp, A.P. Alivisatos, Nature 370 (1994) 354.
[3] L.E. Brus, Appl. Phys. A 53 (1991) 465.
[4] H. Weller, Angew. Chem., Int. Ed. Engl. 32 (1993) 41.
[5] A.P. Alivisatos, Science 271 (1996) 933.
[6] J.D. Corbett, Angew. Chem., Int. Ed. 39 (2000) 670.
[7] The use of 'neat' here (after J.D. Corbett in Ref. [8]) is to distinguish solids made by solid-state reactions from 'molecular' solids crystallized from solution.
[8] J.D. Corbett, Chem. Rev. 85 (1985) 383.
[9] J.D. Corbett, Structure Bonding 87 (1997) 157.
[10] V. Quenéau, S.C. Sevov, Angew. Chem., Int. Ed. Engl. 36 (1997) 1754.
[11] V. Quenéau, E. Todorov, S.C. Sevov, J. Am. Chem. Soc. 120 (1998) 3263.
[12] V. Quenéau, S.C. Sevov, Inorg. Chem. 37 (1998) 1358.
[13] E. Todorov, S.C. Sevov, Inorg. Chem. 37 (1998) 3889.
[14] H.-G. v. Schnering, M. Baitinger, U. Bolle, W. Carrilo-Cabrera, J. Curda, Y. Grin, F. Heinemann, J. Llanos, K. Peters, A. Schmeding, M. Somer, Z. Anorg. Allg. Chem. 623 (1997) 1037.
[15] S. Bobev, S.C. Sevov, Angew. Chem., Int. Ed. 39 (2000) 4108.
[16] S. Bobev, S.C. Sevov, Angew. Chem., Int. Ed. 40 (2001) 1507.
[17] S. Bobev, S.C. Sevov, J. Am. Chem. Soc. 121 (1999) 3795.
[18] S. Bobev, S.C. Sevov, J. Solid State Chem. 153 (2000) 92.
[19] S. Bobev, S.C. Sevov, J. Am. Chem. Soc. 123 (2001) 3389.
[20] S. Bobev, S.C. Sevov, Inorg. Chem. 39 (2000) 5930.
[21] S. Bobev, S.C. Sevov, Inorg. Chem. 38 (1999) 2672.
[22] (a) N. Walker, D. Stuart, Acta Crystallogr., Sect. A 39 (1983) 158; (b) SHELXTL, Version 5.1: Bruker AXS, Madison, WI, 1998.
[23] J. Campbell, D.A. Dixon, H.P.A. Mercier, G.J. Schrobilgen, Inorg. Chem. 34 (1995) 5798.
[24] T.F. Fässler, R. Hoffmann, Angew. Chem., Int. Ed. Engl. 38 (1999) 543.
[25] (a) T.F. Fässler, M. Hunziker, Inorg. Chem. 33 (1994) 5380; (b) T.F. Fässler, M. Hunziker, Z. Anorg. Allg. Chem. 622 (1996) 837.
[26] K. Wade, Adv. Inorg. Chem. Radiochem. 18 (1976) 1.
[27] (a) R.M. Friedman, J.D. Corbett, Inorg. Chem. 12 (1973) 1134; (b) A. Hershaft, J.D. Corbett, Inorg. Chem. 2 (1963) 979.
[28] L. Xu, S.C. Sevov, Inorg. Chem. 39 (2000) 5383.
[29] J.D. Corbett, R.E. Rundle, Inorg. Chem. 3 (1964) 1408.
[30] H.-G. v. Schnering, M. Schwarz, R. Nesper, Angew. Chem., Int. Ed. Engl. 25 (1986) 566.
[31] (a) H.-G. v. Schnering, M. Schwarz, R. Nesper, J. Less-Common Metals 137 (1988) 297; (b) R. Nesper, Angew. Chem., Int. Ed. Engl. 30 (1991) 789 and references therein.

PERGAMON

Polyhedron 21 (2002) 651–656

POLYHEDRON

www.elsevier.com/locate/poly

Stabilization of homonuclear Bi_5^{+} and Bi_6^{2+} polycations by cluster anions in the crystal structures of $Bi_{12-x}IrCl_{13-x}$, $Bi_{12-x}RhCl_{13-x}$ and $Bi_{12-x}RhBr_{13-x}$

Michael Ruck *, Silke Hampel

Institut für Anorganische Chemie, Technische Universität Dresden, D-01062 Dresden, Germany

Received 30 July 2001; accepted 27 November 2001

Abstract

The melting reaction of Bi with Rh or Ir and $BiCl_3$ or $BiBr_3$ yields black, metallic lustrous, air insensitive crystals of the subhalides $Bi_{12-x}MX_{13-x}$ (M = Rh, Ir; X = Cl, Br; $x < 1$). The compounds have the same structural principle as the previously reported subbromide $Bi_{34}Ir_3Br_{37}$. The structures can be subdivided in four types of complex ionic groups: cuboctahedral $[MBi_6X_{12}]^{-}$ clusters, $[MBi_6X_{13}]^{2-}$ clusters with an additional halide ion, Bi_5^{+} square pyramids and distorted Bi_6^{2+} octahedra. The range of homogeneity is due to variable contributions of the different clusters. $Bi_{12-x}IrCl_{13-x}$ is a semiconductor with an extended extrinsic regime below 200 K and a band gap of about 0.4 eV at room temperature. The subchlorides are diamagnetic at room temperature though a paramagnetic contribution appears towards lower temperature. Below 40 K, both compounds pass through a magnetic ordering that shows a hysteresis curve in the magnetization. © 2002 Elsevier Science Ltd. All rights reserved.

Keywords: Polycations; Cluster compounds; Crystal structures; Bismuth; Iridium; Rhodium

1. Introduction

The usual way to stabilize bismuth polycations in solids is the reaction of metal-rich melts of bismuth chlorides with Lewis acids like $AlCl_3$, $GaCl_3$, $HfCl_4$ or even $BiCl_3$ itself. The solids that crystallize from the melts always consist of chloro-metallate anions—$AlCl_4^{-}$ or $GaCl_4^{-}$ tetrahedra, $HfCl_6^{2-}$ octahedra or $^2_\infty[Bi_3Cl_{14}^{5-}]$ layers—combined with the objects of interest namely the well-known homonuclear bismuth polycations Bi_5^{3+} (a trigonal bipyramid [1]), Bi_8^{2+} (a square antiprism [2]), Bi_9^{5+} (a tricapped trigonal prism [3]), or the brand new heteronuclear polycation $[Bi_4Te_4]^{4+}$ (a heterocubane [4]).

Recently we introduced a new alternative for the stabilization of homonuclear bismuth polycations: the reaction of bismuth metal and bismuth halides with a moderately electron-rich transition metal (M = Rh or Ir) results in the formation of anionic $[MBi_6X_{12}]^{n-}$ clusters and polycations like Bi_5^{+} [5,6], Bi_6^{2+} [6] and $[Bi_8Si_2]^{3+}$ [7]. Here the transition metal acts as a Lewis acid by trying to achieve a favorable 16 or 18 valence electron count.

With this method a variety of ternary subhalides of bismuth have been synthesized [8]. Even within one ternary system several metal-rich compounds with diverse structural principles are formed when the reaction conditions are modified. For example, from the system Bi/Rh/Br, which comprises one of the title compounds, the subbromides $Bi_{12}Rh_3Br_2$, a slightly oxidized intermetallic phase [9], $Bi_9Rh_2Br_3$, a quasi one-dimensional metal [10] and Bi_7RhBr_8, a molecular cluster compound [11], are also accessible.

Here we present the synthesis and the crystal structures of the ternary subchlorides $Bi_{12-x}MCl_{13-x}$ (M = Rh, Ir) and of the subbromide $Bi_{12-x}RhBr_{13-x}$. In addition, the electrical conductivity and the magnetic properties of the two bismuth subclorides are described.

* Corresponding author. Tel.: +49-351-463-3244; fax: +49-351-463-7287.

E-mail address: michael.ruck@chemie.tu-dresden.de (M. Ruck).

0277-5387/02/$ - see front matter © 2002 Elsevier Science Ltd. All rights reserved.
PII: S0277-5387(01)01025-7

2. Experimental

2.1. Synthesis

Bismuth powder (chemical pure, Riedel de Haën) was reduced with hydrogen at 220 °C prior to use in synthesis. $BiCl_3$ (>98%, Alpha) and $BiBr_3$ (synthesized from the elements) were sublimed twice at 10^{-3} mbar in a temperature gradient of 200–100 °C. Rhodium powder (>99.9%, Merck) and iridium powder (>99.9%, Merck) were used without further treatment. The use of $RhCl_3$ and $RhBr_3$ in synthesis proved to be less favorable.

The starting materials were mixed together in molar relations of $Bi:BiX_3:M = 7.21:4.11:1$ (corresponding to the composition $Bi_{34}M_3X_{37}$) and sealed in evacuated quartz ampoules (inner diameter 13 mm; volume about 18 cm^3). The mixture was heated to 1000 °C in a tube furnace and subsequently cooled to room temperature (r.t.) within a period of several days. The products are fine-crystalline powders of $Bi_{12-x}MX_{13-x}$ in high yields.

Faster cooling of the melt with about 100 K h^{-1} provided single crystals suitable for X-ray structure determination. The by-products of the rapid cooling process—$BiCl_3$ (colorless) or $BiBr_3$ (yellow) and Bi_6Cl_7 or Bi_6Br_7 (needle like, black crystals)—were removed by sublimation in a temperature gradient of 300–100 °C. A slightly higher proportion of rhodium or iridium reduces the competing formation of the binary bismuth subhalides.

$Bi_{12-x}IrCl_{13-x}$, $Bi_{12-x}RhCl_{13-x}$, and $Bi_{12-x}RhBr_{13-x}$ form black, metallic lustrous crystals. The crystals have typical morphologies like steps-pyramids or u-shaped open channels. All compounds are brittle, insensitive to air and chemically resistant to diluted acids (hydrochloric acid, nitric acid, acetic acid) and to organic solvents. Upon heating the rhodium compounds decompose to Bi_4Rh [12], which is the intermetallic phase with the highest bismuth content in the Bi/Rh system, bismuth and bismuth halides.

2.2. Crystal structure determination

Powders samples and several single crystals of $Bi_{12-x}IrCl_{13-x}$, $Bi_{12-x}RhCl_{13-x}$, and $Bi_{12-x}RhBr_{13-x}$ from various preparations were characterized by X-ray diffraction methods. Precession photographs showed rhombohedral patterns for all crystals. Due to the symmetry of the low trigonal Laue group $\bar{3}$ and the absence of zonal reflection conditions the space groups $R\bar{3}$ or $R3$ were assigned. Measurements with different types of single crystal diffractometers (imaging plate system, CCD system and four-circle goniometer) confirmed these crystallographic observations; neither additional Bragg reflections nor diffuse scattering were observed. Special care was taken to avoid and correct absorption effects (Ag radiation, ψ-positions with maximum transmission [13], optimized numerical absorption correction [14,15]). The crystallographic data and experimental details of the crystal structure determinations are summarized in Tables 1 and 2.

The structures of the investigated crystals $Bi_{12-x}IrCl_{13-x}$ ($x \approx 0.77$), $Bi_{12-x}RhCl_{13-x}$ ($x \approx 0.30$) and $Bi_{12-x}RhBr_{13-x}$ ($x \approx 0.72$) have a close relationship to the previously described compound $Bi_{34}Ir_3Br_{37}$, which corresponds to $Bi_{12-x}IrBr_{13-x}$ with $x = 2/3$ [6]. The unit cell (hexagonal setting) of $Bi_{34}Ir_3Br_{37}$ contains one Bi_6^{2+} and two Bi_5^+ polycations as well as one $[IrBi_6Br_{13}]^{2-}$ and two $[IrBi_6Br_{12}]^-$ cluster anions in an ordered arrangement. Accordingly, the rhombohedral symmetry proved to only be a pseudo-symmetry with multiple twinning of triclinic structural domains [17].

Unfortunately, in the present cases it was not possible to attain fully ordered models of the crystal structures by reducing the symmetry below $R3$ because of the 'arbitrary' non-stoichiometry of the compounds and the disorder in the crystals (probably very small twin and anti-phase domains). The refinements under the symmetry of the space group $R3$ still allow to quote approximate compositions, i.e. proportions of the four cluster types, for the investigated single crystals of $Bi_{12-x}MX_{13-x}$.

2.3. Measurements of electrical conductivity and magnetic properties

The electrical resistance of a pressed pellet of $Bi_{12-x}IrCl_{13-x}$ was measured between r.t. and 12 K using the van der Pauw method. To attain low temperature a two-steps Gifford–McMahon-Refrigerator was used.

Variable-temperature susceptibility measurements (zero-field cooled) were carried out in the temperature range 1.5–300 K using an AC susceptometer (Oxford Instruments) for $Bi_{12-x}IrCl_{13-x}$ and $Bi_{12-x}RhCl_{13-x}$. Isothermal magnetization measurements were performed as a function of the external magnetic field from -1 to 1 T at 5 K. The powdered samples were introduced into a holder that consists of an inert polymer folded into a very small packet.

3. Discussion

$Bi_{12-x}IrCl_{13-x}$ and $Bi_{12-x}RhCl_{13-x}$ are the first ternary subchlorides of bismuth that not merely bismuth chloro-metallates but have the chloride ions bound to bismuth atoms in the low oxidation state +II. Like $Bi_{12-x}RhBr_{13-x}$ and the previously described $Bi_{12-x}IrBr_{13-x}$ [6] they crystallize in a unique although apparently favored structure type. The principle arrangement is similar to the CsCl type apart from

the fact that the ions are complex units, explicitly $[MBi_6X_{12}]^-$ and $[MBi_6X_{13}]^{2-}$ cluster anions along with Bi_5^+ and Bi_6^{2+} polycations Fig. 1). Allusions to the cubic symmetry of the CsCl type are the angles of the primitive rhombohedral cell, which are close to 90° (Table 1). All subhalides $Bi_{12-x}MX_{13-x}$ (M = Rh, Ir; X = Cl, Br) show a range of homogeneity ($x < 1$) that is due to changes of the relative proportions of single and double charged ions.

Within the cuboctahedral $[MBi_6X_{12}]^-$ clusters, six Bi atoms coordinate the central M atom octahedrally (Fig. 2); halide ions bridge all twelve edges of the octahedron. Whilst the short Bi–M contacts can be described as mainly covalent single bonds, the edge-lengths of the octahedra preclude any significant interaction between the Bi atoms (Table 3). Corresponding to previously reported considerations [5–8] the $[MBi_6X_{12}]^-$ cluster can be formally subdivided in a neutral $(Bi^{II}X_2)_6$ shell and an internal M atom with a −I oxidation state. Together with the six Bi–M bonds a total of 16 valence electrons on the central atom results.

The addition of a thirteenth halide ion to the $[MBi_6X_{12}]^-$ unit leads to the $[MBi_6X_{13}]^{2-}$ anion and reduces the point symmetry of the cluster from O_h to

Table 1
Crystallographic data and details of the crystal structure determinations

Empirical formula	$Bi_{12-x}IrCl_{13-x}$ ($x = 0.77(1)$)	$Bi_{12-x}RhCl_{13-x}$ ($x = 0.30(2)$)	$Bi_{12-x}RhBr_{13-x}$ ($x = 0.72(1)$)
Crystal system	rhombohedral	rhombohedral	rhombohedral
Space group	$R\bar{3}$	$R\bar{3}$	$R\bar{3}$
Lattice parameters			
Hexagonal			
a_h (Å)	12.666(2)	12.612(1)	12.961(7)
c_h (Å)	15.860(3)	15.917(2)	16.416(8)
Rhombohedral			
a_r (Å)	9.024(1)	9.009(1)	9.294(1)
α_r (°)	89.14(1)	88.85(1)	88.65(1)
Cell volume V_h (Å^3)	2203.5(5)	2192.6(5)	2388(3)
Z	3	3	3
Crystal size (mm)	$0.07 \times 0.04 \times 0.02$	$0.14 \times 0.14 \times 0.02$	$0.17 \times 0.08 \times 0.02$
Color	black	black	black
Diffractometer	imaging plate diffraction system IPDS (Stoe)	CCD diffractometer SMART (Siemens)	four-circle-diffractometer AED 2 (Siemens/Stoe)
Radiation (Å)	λ(Ag Kα) = 0.56087	λ(Mo Kα) = 0.71073	λ(Mo Kα) = 0.71073
Temperature (K)	293(2)	293(2)	255(2)
2θ Range (°)	$3 \le 2\theta \le 51$	$3 \le 2\theta \le 58$	$3 \le 2\theta \le 50$
Range of indices	$-19 \le h$, $k \le 19$; $-24 \le l \le 24$	$-16 \le h$, $k \le 16$; $-20 \le l \le 21$	$-15 \le h$, $k \le 15$; $-17 \le l \le 19$
Measurement	$0° \le \phi \le 180°$; $\Delta\phi = 0.8°$		ω-scan; ψ-position optimized for maximum transmission [13]
Corrections	background; Lorentz factor; polarization factor	background; Lorentz factor; polarization factor	background; Lorentz factor; polarization factor
Absorption correction	numerical [14] with optimized crystal description [15]	numerical [14] with optimized crystal description [15]	numerical [14] with optimized crystal description [15]
Absorption coefficient, μ (cm^{-1})	μ (Ag Kα) = 397	μ (Mo Kα) = 718	μ (Mo Kα) = 780
Transmission factors	$t_{max} = 0.541$; $t_{min} = 0.142$	$t_{max} = 0.257$; $t_{min} = 0.008$	$t_{max} = 0.152$; $t_{min} = 0.015$
Number of reflections			
Measured	8822	6128	3702
Unique	3748	2348	1733
R indices of merging	$R_{int} = 0.052$; $R_\sigma = 0.079$	$R_{int} = 0.053$; $R_\sigma = 0.047$	$R_{int} = 0.081$; $R_\sigma = 0.091$
Structure refinement	least squares method; full matrix; inversion twins [16]	least squares method; full matrix; inversion twins [16]	least squares method; full matrix; inversion twins [16]
Twin ratio	1:1	3:2	2:1
Number of parameters	89	82	89
Extinction correction	$x = 2.3(2) \times 10^{-5}$	$x = 2.6(2) \times 10^{-5}$	$x = 3.8(2) \times 10^{-5}$
Difference electron density (e Å^{-3})	+1.6/−1.8	+1.9/−1.9	+1.8/−1.7
R indices of refinement	R_1 (2443 $F_o > 4\sigma(F_o)$) = 0.030, $R_1 = 0.073$, $wR_2 = 0.030$	R_1 (2112 $F_o > 4\sigma(F_o)$) = 0.037, $R_1 = 0.043$, $wR_2 = 0.048$	R_1 (1137 $F_o > 4\sigma(F_o)$) = 0.038, $R_1 = 0.091$, $wR_2 = 0.050$

Table 2
Wyckoff positions (W.p.), atomic coordinates, occupation factors (k) and equivalent coefficients U_{eq} (Å^2) of the anisotropic displacement factors for $Bi_{12-x}IrCl_{13-x}$ (first lines), $Bi_{12-x}RhCl_{13-x}$ (second) and $Bi_{12-x}RhBr_{13-x}$ (third)

Atom	W.p.	x	y	z	k	U_{eq}
Bi(1)	9 *b*	0.19383(9)	0.13884(9)	0.1004(1)	1	144(2)
		0.19366(7)	0.13847(7)	0.0982(2)	1	178(2)
		0.1886(3)	0.1359(3)	0.0971(8)	1	212(8)
Bi(2)	9 *b*	−0.1927(1)	−0.1393(1)	−0.0980(1)	1	210(2)
		−0.19042(7)	−0.13858(8)	−0.1003(2)	1	203(2)
		−0.1893(3)	−0.1369(3)	−0.0946(8)	1	178(8)
Bi(3)	9 *b*	0.1516(2)	0.1226(2)	0.5862(1)	0.745(5)	381(3)
		0.1598(1)	0.1238(1)	0.5829(2)	0.951(4)	327(3)
		0.1540(3)	0.1318(3)	0.5791(8)	0.762(4)	328(8)
Bi(4)	9 *b*	−0.1607(1)	−0.1299(2)	−0.5733(1)	1	548(4)
		−0.1545(1)	−0.1363(1)	−0.5774(2)	0.947(5)	340(3)
		−0.1484(4)	−0.1289(4)	−0.5749(8)	1	740(10)
M	3 *a*	0	0	0	1	88(1)
		0	0	0	1	108(3)
		0	0	0	1	120(5)
X(1)	9 *b*	0.3425(6)	0.0652(5)	0.0129(4)	1	210(10)
		0.3458(5)	0.0712(6)	0.0101(4)	1	290(10)
		0.3516(7)	0.0803(7)	0.0064(9)	1	310(20)
X(2)	9 *b*	−0.3498(6)	−0.0903(6)	–0.0005(4)	1	280(10)
		−0.3497(5)	−0.0912(6)	0.0002(4)	1	300(10)
		−0.3529(7)	−0.0832(8)	−0.0055(9)	1	340(20)
X(3)	9 *b*	0.1415(7)	−0.0534(7)	0.2140(4)	1	410(20)
		0.1441(4)	−0.0581(4)	0.2057(3)	1	310(10)
		0.1496(9)	−0.0605(9)	0.205(1)	1	560(30)
X(4a)	9 *b*	−0.1573(7)	0.0643(7)	−0.1939(5)	0.77(1)	180(20)
		−0.177(2)	0.080(2)	−0.188(2)	0.30(2)	320(50)
		−0.1538(9)	0.0601(9)	−0.206(1)	0.72(1)	310(30)
X(4b)	9 *b*	−0.180(1)	0.092(1)	−0.171(1)	0.23(1)	210(30)
		−0.1944(7)	0.0881(7)	−0.1654(6)	0.70(2)	310(20)
		−0.1954(9)	0.092(1)	−0.171(1)	0.28(1)	320(40)
X(5)	3 *a*	0	0	−0.225(1)	0.23(1)	150(50)
		0	0	−0.2352(6)	0.70(2)	280(30)
		0	0	−0.237(1)	0.28(1)	290(50)

e.s.d. values are given in parentheses.

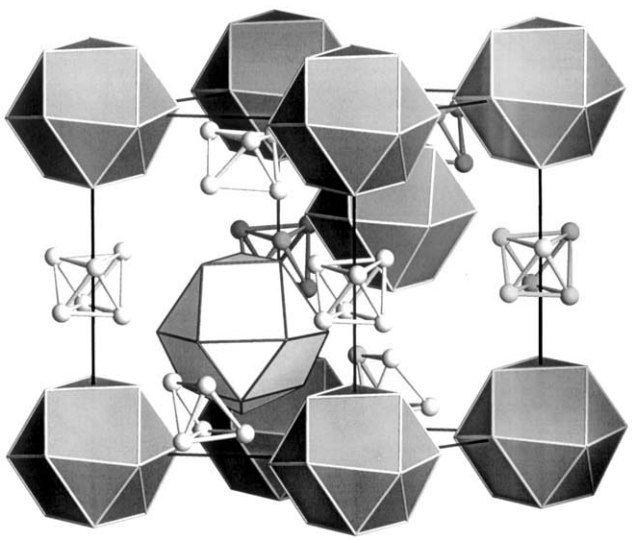


Fig. 1. A potential ordered arrangement of the four cluster types in the pseudo-rhombohedral unit cell of $Bi_{12-x}MX_{13-x}$ for $x = 2/3$ [6,18].

C_3. The fact that both types of anions have at least the symmetry of a threefold rotational axis as well as their spatial arrangement in the motif of a body centered cubic packing dominate the entire crystal structure and is responsible for the rhombohedral pseudo-symmetry.

The voids in the packing are filled with squarely pyramidal Bi_5^+ and distorted octahedral Bi_6^{2+} polycations (Fig. 3). Their bond lengths and angles are known from a (fortunately) ordered triclinic crystal of

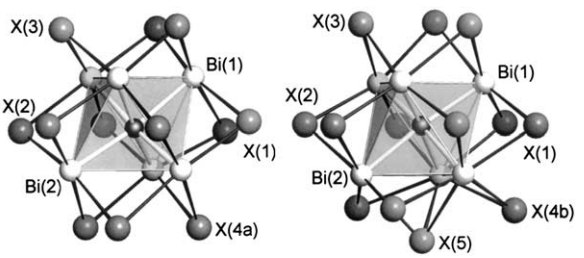


Fig. 2. $[MBi_6X_{12}]^-$ and $[MBi_6X_{13}]^{2-}$ clusters in $Bi_{12-x}MX_{13-x}$ [18].

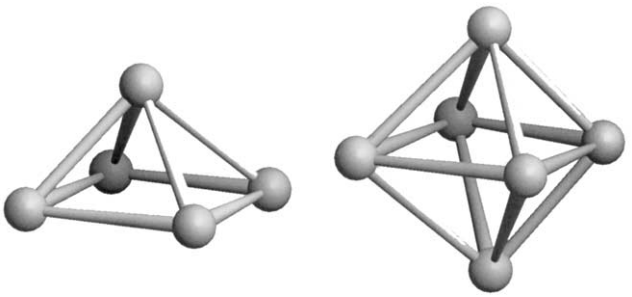


Fig. 3. The polycations Bi_5^+ (square pyramid) and Bi_6^{2+} (distorted octahedron) in $Bi_{12-x}MX_{13-x}$ [6,18].

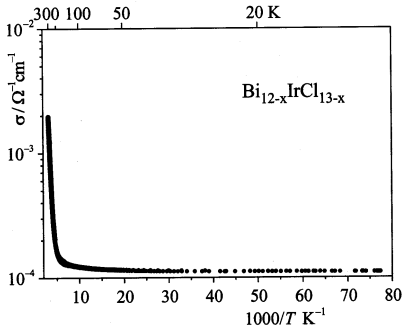


Fig. 4. Electrical conductivity of $Bi_{12-x}IrCl_{13-x}$ in the temperature range 12–310 K.

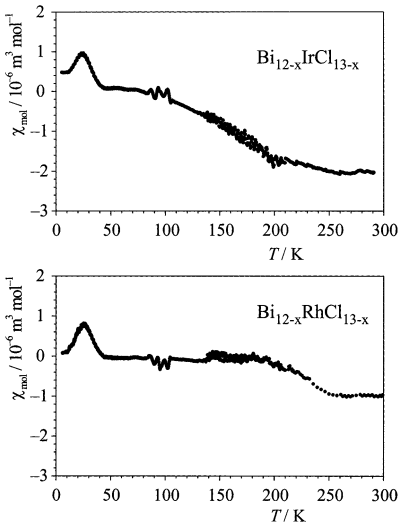


Fig. 5. Molar magnetic susceptibility of $Bi_{12-x}IrCl_{13-x}$ and $Bi_{12-x}RhCl_{13-x}$ in the temperature range 1.5–300 K (zero-field cooled).

$Bi_{34}Ir_3Br_{37}$, i.e. $Bi_{12-x}IrBr_{13-x}$ with $x = 2/3$ [6]. From the present structure determinations the precise shapes of the polycations cannot be derived because of the structural disorder and the overlying non-matching threefold pseudo-symmetry.

Whilst the square-based pyramidal Bi_5^+ cation with 14 framework electrons (only 6p electrons are counted) can easily be classified as a *nido*-cluster, with the distorted 'octahedral' Bi_6^{2+} cation things are not so simple. The seeming contradiction between the 16 framework electrons, which suggest a *nido*-cluster, and the apparently closed cage is resolved on closer examination: the shape of the Bi_6^{2+} cation deviates significantly from that of a regular octahedron so that it is as if a seventh atom has been removed from a hypothetical *closo*-cluster.

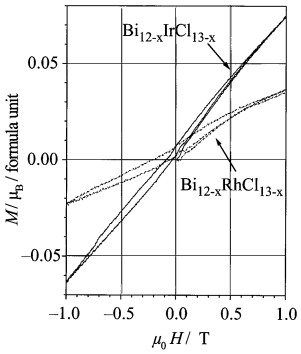


Fig. 6. Magnetization of $Bi_{12-x}IrCl_{13-x}$ and $Bi_{12-x}RhCl_{13-x}$ at 5 K in an external magnetic field from -1 to 1 T.

Table 3
Interatomic distances (Å) in the cuboctahedral $[MBi_6X_{12}]^-$ clusters

	$[IrBi_6Cl_{12}]^-$	$[RhBi_6Cl_{12}]^-$	$[RhBi_6Br_{12}]^-$
M–Bi(1)	2.708(2)	2.682(2)	2.704(8)
M–Bi(2)	2.679(2)	2.679(2)	2.688(8)
Bi(1)–Bi(1)	3.796(2)	3.775(1)	3.784(6)
Bi(1)–Bi(2)	3.823(1)	3.817(1)	3.830(4)
	3.839(1)	3.846(1)	3.836(3)
Bi(2)–Bi(2)	3.781(2)	3.725(1)	3.801(6)
Bi–X(av.)	2.83	2.86	2.97

e.s.d. values are given in parentheses.

$Bi_{12-x}IrCl_{13-x}$, as well as the other cluster salts of the type $Bi_{12-x}MX_{13-x}$, is a semiconductor with a considerable electric resistance. The black color of the compounds indicates that the band gaps must lie below the energy of visible light. There are two regimes in the electrical conductivity (Fig. 4). Below 150 K the extrinsic conductivity that arises from the inherent impurity level in the non-stoichiometric compound is dominant, the temperature dependence is small. Above 150 K the charge carrier density is determined mainly by the thermal excitation of electrons directly from the valence to the conduction band, and therefore, the conductivity shows a strong temperature dependence. From the slope of the curve in the Arrhenius plot between 280 and 330 K the band gap at room temperature is calculated to about 0.4 eV.

Under ambient conditions the subchlorides $Bi_{12-x}IrCl_{13-x}$ and $Bi_{12-x}RhCl_{13-x}$ are very weak magnetic, diamagnetism prevails (Fig. 5). However, the molar magnetic susceptibility increases with decreasing

temperature revealing paramagnetic contributions. Probably, the paramagnetic part arises from two unpaired electrons in the HOMO (non-bonding t_{2g} orbitals of the M atom with 16 valence electrons [7]) of the cluster anion. At higher temperature the substantial diamagnetism of 1294 or 1262 electrons per formula unit $Bi_{12}IrCl_{13}$ or $Bi_{12}RhCl_{13}$ dominates.

For both compounds the susceptibility passes through a local maximum at almost the same temperature of 25 K. The hysteresis in the magnetization curves at 5 K (Fig. 6) indicate a magnetic ordering process. Whether it is only a matter of local, uncorrelated interactions of either ferromagnetic or antiferromagnetic order transformation cannot be decided at the current point of our investigations.

4. Supplementary material

Further details of the crystal structure determinations are available from the Fachinformationszentrum Karlsruhe, D-76344 Eggenstein-Leopoldshafen (Germany), e-mail: crysdata@fiz-karlsruhe.de, on quoting the depository numbers CSD-412014 for $Bi_{12-x}IrCl_{13-x}$ ($x = 0.77(1)$), CSD-412015 for $Bi_{12-x}RhCl_{13-x}$ ($x = 0.30(2)$) and CSD-412016 for $Bi_{12-x}RhBr_{13-x}$ ($x = 0.72(1)$).

Acknowledgements

We are grateful to the Fonds der Chemischen Industrie for financial support and Professor Dr J. Sieler, Dr H. Borrmann and Dr T. Doerr for experimental assistance.

References

[1] (a) J.D. Corbett, Inorg. Chem. 7 (1967) 198;
(b) B. Krebs, M. Mummert, C. Brendel, J. Less-Common Met. 116 (1986) 159;
(c) S. Ulvenlund, K. Ståhl, L. Bengtsson-Kloo, Inorg. Chem. 35 (1996) 223.

[2] (a) B. Krebs, M. Hucke, C.J. Brendel, Angew. Chem. 94 (1982) 453;
(b) B. Krebs, M. Hucke, C.J. Brendel, Angew. Chem., Int. Ed. Engl. 21 (1982) 445.

[3] (a) A. Hershaft, J.D. Corbett, Inorg. Chem. 2 (1963) 979;
(b) R.M. Friedman, J.D. Corbett, Inorg. Chim. Acta 7 (1973) 525;
(c) J. Beck, C.J. Brendel, L. Bengtsson-Kloo, B. Krebs, M. Mummert, A. Stankowski, S. Ulvenlund, Chem. Ber. 129 (1996) 1219;
(d) H. von Benda, A. Simon, W. Bauhofer, Z. Anorg. Allg. Chem. 438 (1978) 53;
(e) R.M. Friedman, J.D. Corbett, Inorg. Chem. 12 (1973) 1134;
(f) A.N. Kuznetsov, A.V. Shevel'kov, S.I. Troyanov, B.A. Popovkin, Zh. Neorg. Khim. 41 (1996) 958; Russ. J. Inorg. Chem. 41 (1996) 920;
(g) A.N. Kuznetsov, A.V. Shevel'kov, B.A. Popovkin, Koord. Khim. 24 (1998) 919;
(h) A.N. Kuznetsov, A.V. Shevel'kov, B.A. Popovkin, Russ. J. Coord. Chem. 24 (1998) 861.

[4] (a) J. Beck, M. Dolg, S. Schlüter, Angew. Chem. 113 (2001) 2347;
(b) J. Beck, M. Dolg, S. Schlüter, Angew. Chem., Int. Ed. 40 (2001) 2287.

[5] M. Ruck, Z. Anorg. Allg. Chem. 623 (1997) 1591.

[6] M. Ruck, Z. Anorg. Allg. Chem. 624 (1998) 521.

[7] M. Ruck, Z. Anorg. Allg. Chem. 626 (2000) 14.

[8] (a) M. Ruck, Angew. Chem. 113 (2001) 1222;
(b) M. Ruck, Angew. Chem., Int. Ed. 40 (2001) 1182.

[9] M. Ruck, Solid State Sci. 3 (2001) 369.

[10] M. Ruck, R.M. Heich, Z. Anorg. Allg. Chem. 626 (2000) 2449.

[11] (a) M. Ruck, Angew. Chem. 109 (1997) 2059;
(b) M. Ruck, Angew. Chem., Int. Ed. Engl. 36 (1997) 1971.

[12] (a) V.P. Glagoleva, G.S. Zhdanov, Sov. Phys. JETP (Engl. Transl.) 3 (1956) 155;
(b) Y. Grin, U. Wedig, H.G. von Schnering, Angew. Chem. 107 (1995) 1318;
(c) Y. Grin, U. Wedig, H.G. von Schnering, Angew. Chem., Int. Ed. Engl. 34 (1995) 1204.

[13] W. Herrendorf, Program MESSOPT for the calculation of ψ-angles with maximum transmission, University of Karlsruhe, 1993.

[14] N.W. Alcock, P.J. Marks, K.-G. Adams, Modified version of the program ABSPSI (by N.W. Alcock, P.J. Marks) for absorption correction of single crystal data, University of Karlsruhe, 1995.

[15] W. Herrendorf, Program HABITUS for the optimization of the crystal description for numerical absorption correction using ψ-scans, University of Karlsruhe, 1993.

[16] G.M. Sheldrick, Program SHELXL-97 for crystal structure determination, University of Göttingen, Germany, 1997.

[17] M. Ruck, Z. Kristallogr. 215 (2000) 148–156.

[18] K. Brandenburg, G. Bergerhoff, Program DIAMOND, visual information system for crystal structures, Crystal Impact GbR, Bonn, 1999.

PERGAMON

Polyhedron 21 (2002) 657–665

POLYHEDRON

www.elsevier.com/locate/poly

Cycloaddition reactions of an iminophosphorane bearing the Martin ligand with some double-bond compounds: syntheses, structures and thermolyses of a 1,3,2λ^5-oxazaphosphetidine and a 1,3,2λ^5-diazaphosphetidine-4-thione

Naokazu Kano, Jia-Hua Xing, Seiji Kawa, Takayuki Kawashima *

Department of Chemistry, Graduate School of Science, The University of Tokyo, 7-3-1 Hongo, Bunkyo-ku, Tokyo 113-0033, Japan

Received 30 July 2001; accepted 27 November 2001

Abstract

Reactions of an iminophosphorane bearing the Martin ligand (2,4,6-$Pr^i_3C_6H_2$)(–C_6H_4-2-$C(CF_3)_2O$–)P=NPh **1** with carbonyl compounds and phenyl isothiocyanate gave the corresponding [2 + 2]-cycloadducts, 1,3,2λ^5-oxazaphosphetidine **2a** and 1,3,2λ^5-diazaphosphetidine-4-thione **8a**, respectively, whose structures were characterized by X-ray crystallographic analyses. Thermolysis of cycloadduct **2a**, which is considered as an intermediate of the aza-Wittig reaction, showed two reactivities giving cyclic phosphinate **4** and imine **5** as well as **1** and ketone **3**, respectively. Thermolysis of **8a** afforded not only **1** and phenyl isothiocyanate **7a**, but also cyclic thiophosphinate **10** and diphenylcarbodiimide **11a**. The formation of **10** and **11a** suggests the bond recombination around phosphorus atom of **8a**. © 2002 Elsevier Science Ltd. All rights reserved.

Keywords: Iminophosphorane; Cycloaddition; Four-membered ring compounds; Thermolysis; Aza-Wittig reaction; X-ray analysis

1. Introduction

There has been much interest in the chemistry of four-membered ring compounds with two or more main group elements in the ring due to their characteristic structures and unique reactivities [1]. In the course of our study on the heteracyclobutanes bearing a highly coordinate main group element at the position adjacent to the heteroatom [1b,2], we have achieved the synthesis of 1,2λ^5-oxaphosphetanes [3] and 1,2λ^5-azaphosphetidines [4], i.e. the intermediates of Wittig reactions, by taking advantage of the Martin ligand [5]. On the other hand, iminophosphoranes have been explored in connection with phosphonium ylides [6], providing aza-Wittig reactions, which have been utilized as effective methods for the synthesis of nitrogen-containing heterocycles [7]. For the elucidation of the mechanism of aza-Wittig reactions, it is valuable to isolate their intermediates, i.e. 1,3,2λ^5-oxazaphosphetidines, because it can provide a direct evidence on its mechanism. Furthermore, taking into consideration the polarized electronic structure of an iminophosphorane, it is expected to be a useful building block of small-membered ring compounds. In the course of our study on the reactivities of an iminophosphorane bearing the Martin ligand, we preliminary reported the formation of 1,3,2λ^5-oxazaphosphetidine **2**, which is the first example of dioxyazaphosphorane [10-P-5(C_2O_2N)] with an 1,3,2-oxazaphosphetidine ring, by the reaction of iminophosphorane **1** with carbonyl compounds [8]. The thermolysis of the four-membered ring compound **2a** revealed the formation of the Wittig-type products and the existence of the equilibrium with the starting materials. These results encouraged us to study the synthesis and reactivities of the four-membered ring compounds derived from iminophosphorane **1**. We report here the details of the synthesis and reactions of 1,3,2λ^5-oxazaphosphetidine **2a**, which is an intermediate of the aza-Wittig reaction, as well as 1,3,2λ^5-diazaphosphetidine-4-thione. In this paper, we used the Martin ligand and

* Corresponding author. Tel./fax: +81-3-5800-6899.
E-mail address: takayuki@chem.s.u-tokyo.ac.jp (T. Kawashima).

0277-5387/02/$ - see front matter © 2002 Elsevier Science Ltd. All rights reserved.
PII: S0277-5387(01)01024-5

a bulky 2,4,6-triisopropylphenyl (denoted as Tip hereafter) group for the stabilization of the cycloadducts.

2. Experimental

2.1. General procedures

All reactions were performed under degassed and sealed tube unless otherwise noted. Solvents were dried by standard methods and freshly distilled prior to use. Iminophosphorane **1** was prepared according to the literature procedure [9]. The amount of **1** was estimated based on the integral of ^{19}F NMR spectra. Preparative gel permeation liquid chromatography (GPLC) was performed by LC-908 with JAIGEL 1H and 2H columns (Japan Analytical Industry) with toluene as solvent. Preparative thin layer chromatography (PTLC) was carried out with Merck Kieselgel 60 PF254. The melting point was determined on a Yanaco micro melting point apparatus and was uncorrected. ^1H (500 MHz) and ^{13}C (126 MHz) NMR spectra were recorded on a JEOL A500 spectrometer using tetramethylsilane as an internal standard. ^{19}F (254 MHz) and ^{31}P (109 MHz) NMR spectra were recorded on a JEOL EXcalibur270 spectrometer using Fleon® and 85% H_3PO_4 as external standards, respectively. Mass spectral data were recorded on a JEOL SX-102 mass spectrometer. Elemental analysis was carried out at the Microanalytical Laboratory of Department of Chemistry, Faculty of Science, The University of Tokyo.

2.2. Synthesis of 1,3,2λ^5-oxazaphosphetidine (2a)

Iminophosphorane **1** (21.9 g, 38.6 mmol) derived from hexafluorocumyl alcohol [9] in THF (200 ml) was allowed to react with hexafluoroacetone (denoted as HFA hereafter) gas **3**, which was generated by treatment of HFA·$3H_2O$ (16.2 ml, 116 mmol) with concentrated H_2SO_4 at 140 °C, in a three-necked flask at room temperature (r.t.) for 2.5 h under nitrogen atmosphere afforded 1,3,2λ^5-oxazaphosphetidine **2a** which could be purified by GPLC and recrystallization from CH_2Cl_2–ethanol giving colorless crystals (7.31 g, 26%). Compound **2a**, colorless crystals; melting point (m.p.) 178–181 °C (dec.); ^1H NMR (500 MHz, $CDCl_3$) δ 0.27 (d, $^3J_{HH} = 6.6$ Hz, 3H), 1.06 (d, $^3J_{HH} = 6.6$ Hz, 3H), 1.11 (d, $^3J_{HH} = 6.6$ Hz, 3H), 1.13 (d, $^3J_{HH} = 6.9$ Hz, 6H), 1.33 (d, $^3J_{HH} = 6.6$ Hz, 3H), 2.76 (sept, $^3J_{HH} = 6.9$ Hz, 1H), 3.54 (sept, $^3J_{HH} = 6.6$ Hz, 1H), 3.72 (sept, $^3J_{HH} = 6.6$ Hz, 1H), 6.77 (d, $^4J_{PH} = 7.2$ Hz, 1H), 7.03 (d, $^4J_{PH} = 7.2$ Hz, 1H), 7.12 (d, $^3J_{HH} = 7.6$ Hz, 2H), 7.22–7.29 (m, 3H), 7.58 (brs, 1H), 7.67 (t, $^3J_{HH} = 7.6$ Hz, 1H), 7.73 (dd, $^3J_{HH} = 7.6$ Hz, $^4J_{HP} = 9.4$ Hz, 1H), 8.52 (dd, $^3J_{HH} = 7.6$ Hz, $^3J_{HP} = 11.4$ Hz, 1H); $^{13}C\{^1H\}$ NMR (126 MHz, $CDCl_3$) δ 23.0 (s), 23.5 (s), 23.6 (s), 24.5 (s), 26.3 (s), 30.2 (d, $^3J_{CF} = 31$ Hz), 31.2 (d, $^3J_{CF} = 31$ Hz), 33.9 (s), 83.4 (sept, $^2J_{CF} = 31$ Hz), 85.3 (sept, $^2J_{CF} = 31$ Hz), 121.4 (q, $^1J_{CF} = 290$ Hz), 121.6 (q, $^1J_{CF} = 290$ Hz), 121.7 (q, $^1J_{CF} = 290$ Hz), 121.8 (q, $^1J_{CF} = 288$ Hz), 122.0 (d, $J_{CP} = 18$ Hz), 123.5 (d, $J_{CP} = 16$ Hz), 124.6 (d, $J_{CP} = 14$ Hz), 128.4 (s), 129.0 (s), 130.9 (d, $J_{CP} = 14$ Hz), 131.6 (s), 132.9 (d, $1J_{CP} = 176$ Hz), 133.4 (d, $J_{CP} = 3$ Hz), 133.7 (d, $^1J_{CP} = 147$ Hz), 134.7 (d, $J_{CP} = 3$ Hz), 136.5 (d, $J_{CP} = 12$ Hz), 137.4 (d, $J_{CP} = 22$ Hz), 148.7 (d, $J_{CP} = 21$ Hz), 150.6 (d, $J_{CP} = 4$ Hz), 150.8 (d, $J_{CP} = 12$ Hz); ^{19}F NMR (254 MHz, $CDCl_3$) δ −76.53 (q, $^4J_{FF} = 9.8$ Hz, 3F), −74.99 (q, $^4J_{FF} = 9.8$ Hz, 3F), −72.71 (q, $^4J_{FF} = 9.8$ Hz, 3F), −72.35 (q, $^4J_{FF} = 9.8$ Hz, 3F); ^{31}P NMR (109 MHz, $CDCl_3$) δ −18.6 (s); FAB MS; m/z 734 ($[M+H]^+$). *Anal.* Calc. for $C_{33}H_{32}F_{12}NO_2P$: C, 53.80; H, 4.46; N, 2.09. Found: C, 54.03; H, 4.40; N, 1.91%.

2.3. Reaction of iminophosphorane 1 with benzaldehyde

A C_6D_6 (0.8 ml) solution of iminophosphorane **1** (135 mg, 0.238 mmol) and benzaldehyde (24 μl, 0.24 mmol) in a degassed and sealed glass tube was heated at 60 °C for 16 h. Monitoring of the reaction solution by ^{19}F and ^{31}P NMR spectroscopy showed the disappearance of **1** and the formation of new peaks assignable to a mixture of two diastereomers of 1,3,2λ^5-oxazaphosphetidine **2b** (**2b**; isomer A:isomer B = 1:3 as determined by the integral of ^{19}F NMR spectrum). Separation of the crude oil involving **2b** using with GPLC and PTLC quantitatively afforded a hydrolyzed product, cyclic phosphinate **4** as a sole identifiable compound bearing the Martin ligand and a phosphorus atom because of instability of **2b**. **2b** (isomer A): ^{19}F NMR (254 MHz, C_6D_6) δ −73.39 (A_3B_3, $^4J_{FF} = 9.7$ Hz, 3F), −74.33 (A_3B_3, $^4J_{FF} = 9.7$ Hz, 3F); ^{31}P NMR (109 MHz, C_6D_6) δ −26.3. **2b** (isomer B): ^{19}F NMR (254 MHz, C_6D_6) δ −73.24 (A_3B_3, $^4J_{FF} = 9.7$ Hz, 3F), −73.36 (A_3B_3, $^4J_{FF} = 9.7$ Hz, 3F); ^{31}P NMR (109 MHz, C_6D_6) δ −27.8. **4**: colorless crystals, m.p. 136.9–139.0 °C; ^1H NMR (500 MHz, $CDCl_3$) δ 1.01 (d, $^3J_{HH} = 6.6$ Hz, 6H), 1.21 (d, $^3J_{HH} = 6.8$ Hz, 6H), 1.27 (d, $^3J_{HH} = 6.7$ Hz, 6H), 2.86 (sept, $^3J_{HH} = 6.8$ Hz, 1H), 3.60 (d, $^3J_{HH} = 6.6$ Hz, 2H), 7.08 (d, $^4J_{PH} = 6.6$ Hz, 2H), 7.72–7.76 (m, 3H), 8.14–8.19 (m, 1H); $^{13}C\{^1H\}$ NMR (126 MHz, $CDCl_3$) δ 23.4 (s), 23.5 (s), 24.5 (d, $^4J_{PC} = 4.3$ Hz), 32.4 (d, $^3J_{PC} = 5.5$ Hz), 32.4(s), 84.7 (sept, $^2J_{FC} = 33.1$ Hz, $C(CF_3)_2$), 121.1 (q, $^1J_{FC} = 286.5$ Hz, CF_3), 121.4 (q, $^1J_{FC} = 290.9$ Hz, CF_3), 122.6 (d, $^3J_{PC} = 14.0$ Hz), 124.6 (d, $^2J_{PC} = 11.5$ Hz), 125.7 (d, $^1J_{PC} = 142.0$ Hz), 130.4 (d, $^2J_{PC} = 11.6$ Hz), 131.9 (d, $^3J_{PC} = 11.9$ Hz), 133.4 (s), 134.3 (d, $^1J_{PC} = 134.0$ Hz), 134.0 (d, $^2J_{PC} = 17.6$ Hz), 151.4 (d, $^2J_{PC} = 13.0$ Hz), 153.0 (d, $^4J_{PC} = 2.8$ Hz), ^{19}F NMR (254 MHz, $CDCl_3$) δ −75.10 (q, $^4J_{FF} = 8.9$ Hz, 3F), −75.72 (q, $^4J_{FF} = 8.9$ Hz, 3F); $^{31}P\{^1H\}$ NMR (109 MHz, $CDCl_3$) δ 56.2 (s);

Anal. Calc. for $C_{24}H_{27}F_6O_2P$: C, 58.54; H, 5.53. Found: C, 58.38; H, 5.62%.

2.4. Reaction of iminophosphorane **1** with trifluoroacetophenone

Similarly, the reaction of iminophosphorane **1** (113 mg, 0.201 mmol) with trifluoroacetophenone (31 μl, 0.21 mmol) in C_6D_6 (1.2 ml) at 70 °C for 12 h gave a mixture of two diastereomers of 1,3,2λ^5-oxazaphosphetidine **2c** (**2c**; isomer A:isomer B = 1:3 as determined by the integral of ^{19}F NMR spectrum), which decomposed during separation by GPLC and PTLC due to its instability. **2c** (isomer A): ^{19}F NMR (254 MHz, C_6D_6) δ −72.22 (A_3B_3, $^4J_{FF}$ = 10.2 Hz, 3F), −72.69 (A_3B_3, $^4J_{FF}$ = 10.2 Hz, 3F), −78.37 (s); ^{31}P NMR (109 MHz, C_6D_6) δ −23.0 (s). **2c** (isomer B): ^{19}F NMR (254 MHz, C_6D_6) δ −72.69 (A_3B_3, $^4J_{FF}$ = 10.2 Hz, 3F), −73.26 (A_3B_3, $^4J_{FF}$ = 10.2 Hz, 3F), −75.66 (s); ^{31}P NMR (109 MHz, C_6D_6) δ −25.1 (s).

2.5. Thermolysis of 1,3,2λ^5-oxazaphosphetidine (**2a**)

A solution of **2a** (10 mg, 0.014 mmol) in toluene-d_8 (0.6 ml) was heated at 130 °C for 135 h in a degassed and sealed tube. Monitoring of the reaction solution by ^{1}H, ^{13}C, ^{19}F and ^{31}P NMR spectra showed the formation of cyclic phosphinate **4** (100%) and imine **5** (90%). The yields of the products were determined by the integral of ^{19}F NMR spectrum.

2.6. Thermolysis of 1,3,2λ^5-oxazaphosphetidine (**2a**) in the presence of water

Similarly, the reaction of a mixture of **2a** (10 mg, 0.014 mmol) and water (24 μl) in toluene-d_8 (0.5 ml) at 140 °C for 3 h gave HFA **3** (96%), cyclic phosphinate **4** (100%), imine **5** (4%), and aniline (89%).

2.7. Attempted hydrolysis of imine **5**

Similarly, imine **5** (0.10 ml) and water (0.10 ml) in toluene-d_8 (0.6 ml) was heated at 140 °C for 24 h. Monitoring of the reaction mixture by ^{1}H and ^{19}F NMR spectra showed no change.

2.8. Thermolysis of 1,3,2λ^5-oxazaphosphetidine (**2a**) in the presence of methanol

Similarly, the reaction of a mixture of **2a** (10 mg, 0.014 mmol) and methanol (35 μl, 1.4 mmol) in toluene-d_8 (0.5 ml) at 140 °C for 50 min gave HFA **3** (1%), cyclic phosphinate **4** (22%), imine **5** (1%), aniline, and methoxyphosphorane **6** (75%). The yields of the products were determined by the integral of ^{19}F NMR spectrum. On exposure to open air, compound **6** was hydrolyzed to give cyclic phosphinate **4**. **6**: ^{19}F NMR (254 MHz, toluene-d_8) δ −78.01 (brs, 3F), −79.32 (brs, 3F); ^{31}P NMR (109 MHz, toluene-d_8) δ −15.0 (s); FAB MS: m/z 599 (M^+).

2.9. Synthesis of 1,3,2λ^5-diazaphosphetidine-4-thione (**8**)

Similarly, the reaction of iminophosphorane **1** (455 mg, 0.800 mmol) and phenyl isothiocyanate **7a** (0.40 ml, 3.3 mmol) in benzene (5 ml) at 50 °C for 15 h gave 1,3,2λ^5-diazaphosphetidine-4-thione **8a**. Purification with GPLC and PTLC and recrystallization from hexane–CH_2Cl_2 afforded colorless crystals of **8a** (73.0 mg, 13%). **8a**: colorless crystals; m.p. 120.5–122.0 °C (dec.); ^{1}H NMR (500 MHz, $CDCl_3$) δ −0.08 (d, $^3J_{HH}$ = 6.5 Hz, 3H), −0.07 (d, $^3J_{HH}$ = 6.5 Hz, 3H), 1.21 (d, $^3J_{HH}$ = 6.5 Hz, 3H), 1.21 (d, $^3J_{HH}$ = 6.5 Hz, 3H), 1.52 (d, $^3J_{HH}$ = 7.0 Hz, 3H), 1.56 (d, $^3J_{HH}$ = 7.0 Hz, 3H), 2.58 (sept, $^3J_{HH}$ = 6.4 Hz, 1H), 2.85 (sept, $^3J_{HH}$ = 6.9 Hz, 1H), 4.75 (sept, $^3J_{HH}$ = 6.6 Hz, 1H), 6.62 (d, $^4J_{PH}$ = 8.5 Hz, 1H), 6.81 (brs, 2H), 7.20–7.30 (m, 9 H), 7.63 (brs, 1H), 7.78 (brs, 1H), 7.89 (brs, 1H), 8.85 (dd, $^3J_{HH}$ = 9.0 Hz, $^3J_{PH}$ = 12.5 Hz, 1H); ^{13}C{^{1}H} NMR (126 MHz, $CDCl_3$) δ 21.8 (s), 23.2 (s), 23.3 (s), 23.5 (s), 23.7 (s), 26.4 (s), 32.0 (d, $^3J_{CP}$ = 6 Hz), 32.2 (d, $^3J_{CP}$ = 5 Hz), 36.0 (s) 82.6 (sept, $^2J_{CF}$ = 31 Hz), 120.9 (q, $^1J_{CF}$ = 288 Hz), 121.8 (d, J_{CP} = 20 Hz), 121.9 (q, $^1J_{CP}$ = 290 Hz), 123.7 (d, J_{CP} = 15 Hz), 125.5 (d, J_{CP} = 14 Hz), 127.5 (s), 128.2 (d, J_{CP} = 3 Hz), 128.7 (s), 128.8 (d, $^1J_{CP}$ = 163 Hz), 128.9 (s), 129.3 (s), 131.1 (d, $^1J_{CP}$ = 134 Hz), 131.8 (d, J_{CP} = 13 Hz), 133.9 (d, J_{CP} = 11 Hz), 134.6 (d, J_{CP} = 3 Hz), 136.8 (s), 138.2 (d, J_{CP} = 21 Hz), 141.8 (d, J_{CP} = 4 Hz), 147.1 (d, J_{CP} = 21 Hz), 149.1 (d, J_{CP} = 10 Hz), 151.4 (d, J_{CP} = 4 Hz), 190.0 (d, J_{CP} = 6 Hz); ^{19}F NMR (254 MHz, $CDCl_3$) δ −73.17 (A_3B_3, J = 10.3 Hz, 3F), −74.78 (A_3B_3, J = 10.3 Hz, 3F); ^{31}P NMR (109 MHz, $CDCl_3$) δ −18.9 (s); FAB MS: m/z 703 ($[M+H]^+$), 568 ($[M+H–PhNCS]^+$), 194 ($[PhN{=}C{=}NPh]^+$); *Anal.* Calc. for $C_{37}H_{37}F_6N_2O$: C, 63.24; H, 5.31; N, 3.99; S, 4.56. Found: C, 63.06; H, 5.36; N, 3.99; S, 4.42%.

2.10. Reaction of cyclic phosphinate **4** with phenyl isothiocyanate

Heating of **4** (10 mg, 0.020 mmol) with phenyl isothiocyanate (2.4 μl, 0.020 mmol) in C_6D_6 (0.5 ml) at 100 °C for 1 day resulted in no change in ^{1}H, ^{19}F and ^{31}P NMR spectra.

2.11. Reaction of cyclic thiophosphinate **10** with phenyl isothiocyanate

Heating of **10** (10 mg, 0.020 mmol) with phenyl isothiocyanate (2.4 μl, 0.020 mmol) in C_6D_6 (0.5 ml) at

100 °C for 1 day resulted in no change in ^{1}H, ^{19}F and ^{31}P NMR spectra.

2.12. Thermolysis of 1,3,2λ^5-diazaphosphetidine-4-thione (8a)

Similarly, heating of a C_6D_6 (0.6 ml) solution of **8a** (8.0 mg, 0.011 mmol) at 50 °C for 4 h gave iminophosphorane **1** (29%), cyclic phosphinate **4** (54%) and cyclic thiophosphinate **10** (17%). The yields of the products were determined by the integral of ^{19}F NMR spectra. After exposure of the reaction mixture to open air, phenyl isothiocyanate **7a**, aniline and diphenylcarbodiimide **11a** were detected by GC-MS spectra. Compound **10**: colorless crystals; m.p. 152.0–153.5 °C; ^{1}H NMR (500 MHz, $CDCl_3$) δ −0.59 (brs, 6H), 1.21 (d, $^{3}J_{HH}$ = 6.8 Hz, 6H), 1.33 (brs, 6H), 2.85 (sept, $^{3}J_{HH}$ = 6.8 Hz, 1H), 3.39 (brs, 1H), 4.34 (brs, 1H), 7.07 (brs, 2H), 7.62–7.81 (m, 3H), 8.22–8.26 (m, 1H); $^{13}C\{^{1}H\}$ NMR (126 MHz, $CDCl_3$) δ 23.5 (s), 23.6 (s), 24.2 (brs), 32.7 (brs), 34.1 (s), 85.6 (sept, $^{2}J_{CF}$ = 29.8 Hz), 121.2 (q, $^{1}J_{CF}$ = 285.6 Hz), 121.3 (q, $^{1}J_{CF}$ = 287.1 Hz), 121.4 (brs), 124.2 (d, $^{2}J_{CP}$ = 11.1 Hz), 124.3 (brs), 131.8 (d, $^{3}J_{CP}$ = 12.2 Hz), 132.0 (d, $^{1}J_{CP}$ = 113.3 Hz), 132.2 (d, $^{3}J_{CP}$ = 12.1 Hz), 132.9 (s), 133.2 (d, J = 16.5 Hz), 138.3 (d, $^{1}J_{CP}$ = 94.5 Hz), 146.7 (brs), 152.2 (d, J_{CP} = 2.8 Hz); ^{19}F NMR (254 MHz, $CDCl_3$) δ −74.65 (q, $^{4}J_{FF}$ = 9.4 Hz, 3F), −75.52 (q, $^{4}J_{FF}$ = 9.4 Hz, 3F); ^{31}P NMR (109 MHz, $CDCl_3$) δ 106.6 (s); *Anal.* Calc. for $C_{24}H_{27}F_6OPS$: C, 56.69; H, 5.35; S, 6.31. Found: C, 56.47; H, 5.35; S, 6.29%.

2.13. Reaction of iminophosphorane 1 with p-tolyl isothiocyanate

Similarly, the reaction of **1** (42 mg, 0.062 mmol) with *p*-tolyl isothiocyanate **7b** (0.10 ml, 0.74 mmol) in C_6D_6 (0.5 ml) at 60 °C for 5 h, at r.t. for 2 days, and 60 °C for 10 h gave cyclic thiophosphinate **10**, other 1,3,2λ^5-diazaphosphetidine-4-thiones **8b**, **8c**, and **8d** (**8b**:**8c**:**8d** = 1:1:1), phenyl(*p*-tolyl)carbodiimide **11b**, di(*p*-tolyl)carbodiimide **11c** (**11b**:**11c** = 6:1), and iminophosphorane **12**. The ratio of **8b**, **8c**, and **8d** was determined by the integral of ^{19}F NMR spectra. The ratio of **11b** and **11c** was determined by GC-MS spectra. After exposure of the reaction mixture to open air, it was separated by GPLC and PTLC to give **8d**, **11b**, **11c**, and a mixture of **8b** and **8c** (**8b**:**8c** = 1:1). A mixture of **8b** and **8c** could not be separated. Diastereomeric mixture of **8b** and **8c**: ^{19}F NMR (254 MHz, $CDCl_3$) δ −74.80 (q, $^{4}J_{FF}$ = 10.2 Hz), −74.62 (q, $^{4}J_{FF}$ = 10.2 Hz), −73.20 (q, $^{4}J_{FF}$ = 10.2 Hz), −73.17 (q, $^{4}J_{FF}$ = 10.2 Hz); ^{31}P NMR (109 MHz, $CDCl_3$) δ −18.73 (s), −19.23 (s). Compound **8d**: ^{19}F NMR (254 MHz, $CDCl_3$) δ −74.63 (A_3B_3, $^{4}J_{FF}$ = 10.4 Hz, 3F), −73.20 (A_3B_3, $^{4}J_{FF}$ = 10.4 Hz, 3F); ^{31}P NMR (109 MHz, $CDCl_3$) δ −19.06 (s). **12**: ^{31}P NMR (109 MHz, C_6D_6) δ −25.46 (s).

2.14. X-ray crystallographic studies of 2a and 8a

The intensity data of **2a** and **8a** were collected at 298 K using a Rigaku AFC7R diffractometer with graphite monochromated Mo Kα radiation (λ = 0.71069 Å) and a rotating anode generator. The structure was solved by direct methods and refined by the full matrix least squares procedures on *F*. All non-hydrogen atoms were refined anisotropically. Hydrogen atoms were included but not refined. Some details of the data collection and refinement are given in Table 1.

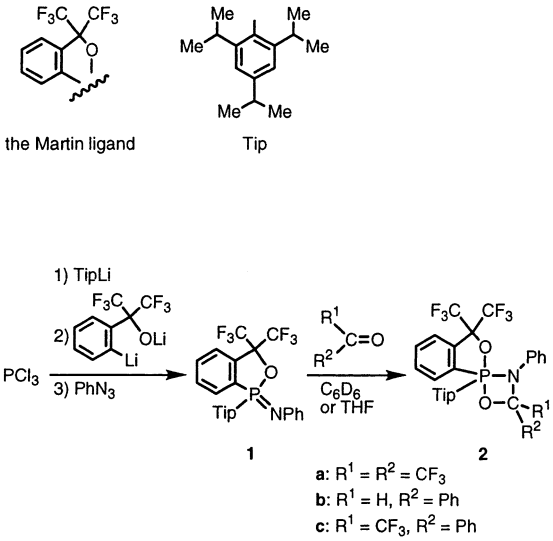
3. Results and discussion

3.1. Synthesis and structure of 1,3,2λ^5-oxazaphosphetidines

Iminophosphorane **1** was prepared in situ according to the literature which we previously reported [9]. Since **1** is sensitive to the moisture, it was used without further purification as such for the following reactions. Iminophosphorane **1** was allowed to react with HFA at r.t. to give the corresponding 1,3,2λ^5-oxazaphosphetidine **2a**. Compound **2a** was obtained as colorless crystals after chromatographic separation in 26% yield from hexafluorocumyl alcohol (Scheme 1). ^{31}P NMR spectra showed the quantitative conversion from **1** to **2a**. Formation of the 1,3,2λ^5-oxazaphosphetidine **2a** was confirmed by the up-field shift in ^{31}P NMR spectra of the crude products compared with **1** (from δ_P 25.6 in C_6D_6 for **1** to δ_P −18.6 for **2a** in $CDCl_3$), indicating

Table 1
Crystal and experimental data for **2a** and **8a**

	2a	**8a**
Empirical formula	$C_{33}H_{32}F_{12}NO_2P$	$C_{37}H_{37}F_6N_2OPS$
Formula weight	733.58	702.74
Crystal system	monoclinic	monoclinic
Space group	$P2_1/c$	$P2_1/c$
Unit cell dimensions		
a (Å)	10.437(2)	10.503(8)
b (Å)	18.668(3)	10.51(1)
c (Å)	17.753(3)	65.007(7)
β (°)	105.29(1)	90.96(4)
V (Å^3)	3336.5(9)	7179(7)
Z	4	8
D_{calc} (g cm^{-3})	1.460	1.300
μ (cm^{-1})	1.81	1.97
Variable parameters	570	865
Reflections observed [$I > 3\sigma(I)$]	4629	4459
R	0.043	0.059
R_w	0.023	0.042



Scheme 1.

the pentacoordinate phosphorane structure of **2a** [3,4]. The molecular structure of **2a** was established by X-ray crystallographic analysis, the result of which has already been reported in a preliminary communication [8]. The crystal data and structural parameters of **2a** are shown in Tables 1 and 2, respectively. Compound **2a** was shown to have the distorted trigonal-bipyramidal (TBP) structure at phosphorus atom with two oxygen atoms at the apical positions and two carbon and nitrogen atoms at the equatorial positions. It is noteworthy that **2a** was obtained from the iminophosphorane, which was generated from the corresponding phosphine and azide as reported for the general aza-Wittig reactions. In contrast to the formation of **2a**, the previously reported 1,3,2λ^5-oxazaphosphetidines were not synthesized from the corresponding iminophosphoranes, but from the aminophosphines [10]. The reactions of iminophosphorane **1** with benzaldehyde and trifluoroacetophenone at 60 and 70 °C, respectively, also afforded 1,3,2λ^5-oxazaphosphetidines **2b** and **2c**, respectively, as the diastereomeric mixtures. Formation of **2b** and **2c** was confirmed by up-filed shifts in ^{31}P NMR spectra, (δ_P −26.3, −27.8 for **2b** and δ_P −23.0, −25.1 for **2c** in C_6D_6, respectively), compared with that (δ_P −25.6) of **1**. Unfortunately, oxazaphosphetidines **2b** and **2c** could not be purified, because they were easily hydrolysed on silica gel. Therefore, the yields of **2b** and **2c** could not be determined. On the other hand, no reaction took place upon heating of a C_6D_6 solution of **1** and benzophenone in a sealed tube even at 120 °C due to its low reactivity and steric congestion.

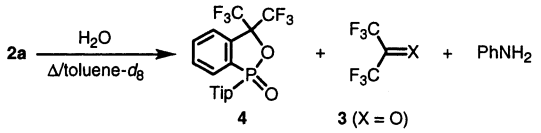
3.2. Reactions of a 1,3,2λ^5-oxazaphosphetidine

Oxazaphosphetidine **2a** did not dissociate into iminophosphorane **1** and HFA in $CDCl_3$ solution at r.t. in contrast to Schmidpeter's 1,3,2λ^5-oxazaphosphetidines [11]. *N*-apical pseudorotamer of **2a** was not detected by variable temperature NMR spectra between 27 and 107 °C, although *N*-equatorial pseudorotamers which violate the apicophilicity rule were observed at r.t. for azaphosphetidines [4]. This is interesting because difference in electronegativity between oxygen and nitrogen atoms for **2a** is almost same as that between carbon and nitrogen atoms for the azaphosphetidines.

Thermolysis of **2a** was performed at 140 °C in toluene-d_8. The formation of cyclic phosphinate **4** (100%) and imine **5** (90%) in the reaction mixture was confirmed by ^{1}H, ^{19}F, and ^{31}P NMR spectra (Scheme 2). The products were identified by comparing their spectral data of GC-MS and NMR spectra with those of the authentic samples. The ratio of these products was determined based on the integral of ^{19}F NMR spectra of the reaction solution. Furthermore, the oxazaphosphetidine is expected to exhibit another reactivity on the thermolysis, i.e. the formation of the iminophosphorane as in the cases of azaphosphetidines. Since this process must be reversible, thermolysis of **2a** in the presence of water was performed to offer an evidence for the existence of **1**. In fact, thermolysis of **2a** with excess amount (20 equiv.) of water at 140 °C for 3 h gave

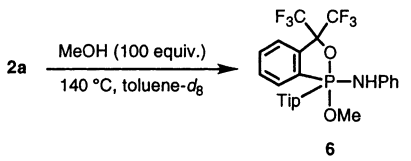
Table 2
Selected bond lengths (Å) and angles (°) for **2a** and **8a**

2a		**8a**		
			Molecule A	Molecule B
Bond lengths				
P(1)–O(1)	1.786(5)	P(1)–O(1)	1.727(5)	1.732(5)
P(1)–N(1)	1.688(2)	P(1)–N(1)	1.901(6)	1.911(6)
P(1)–C(3)	1.844(2)	P(1)–N(2)	1.716(6)	1.692(6)
C(1)–O(1)	1.379 (2)	P(1)–C(2)	1.806(7)	1.812(8)
P(1)–O(2)	1.719(1)	P(1)–C(3)	1.829(7)	1.824(7)
P(1)–C(2)	1.815(2)	C(1)–N(1)	1.329(9)	1.338(8)
C(1)–N(1)	1.443(2)	C(1)–N(2)	1.418(8)	1.421(9)
		S(1)–C(1)	1.647(8)	1.619(8)
Bond angles				
O(1)–P(1)–O(2)	167.29(7)	O(1)–P(1)–N(1)	162.7(3)	162.8(3)
O(1)–P(1)–N(1)	74.84(7)	O(1)–P(1)–N(2)	91.3(3)	92.2(3)
O(1)–P(1)–C(2)	94.57(9)	O(1)–P(1)–C(2)	88.7(3)	88.7(3)
O(1)–P(1)–C(3)	95.78(8)	O(1)–P(1)–C(3)	93.5(3)	94.8(3)
O(2)–P(1)–N(1)	93.05(8)	N(1)–P(1)–N(2)	71.4(3)	70.7(3)
O(2)–P(1)–C(2)	88.45(9)	N(1)–P(1)–C(2)	99.1(3)	98.5(3)
O(2)–P(1)–C(3)	93.98(8)	N(1)–P(1)–C(3)	96.3(3)	95.3(3)
N(1)–P(1)–C(3)	122.31(9)	N(2)–P(1)–C(2)	117.6(3)	117.5(3)
N(1)–P(1)–C(2)	121.50(9)	N(2)–P(1)–C(3)	123.9(3)	123.0(4)
C(2)–P(1)–C(3)	115.87(10)	C(2)–P(1)–C(3)	118.3(4)	119.1(4)
P(1)–N(1)–C(1)	95.1(1)	N(1)–C(1)–N(2)	100.6(6)	98.5(6)
P(1)–O(1)–C(1)	93.2(1)	P(1)–N(1)–C(1)	91.5(4)	91.8(5)
N(1)–C(1)–O(1)	96.9(2)	P(1)–N(2)–C(1)	96.4(5)	98.7(5)
		S(1)–C(1)–N(1)	132.7(6)	132.7(7)
		S(1)–C(1)–N(2)	126.6(6)	128.8(6)



	yields/%			
H_2O/equiv.	3	4	5	$PhNH_2$
0	0	100	90	0
20	96	100	4	89

Scheme 2.

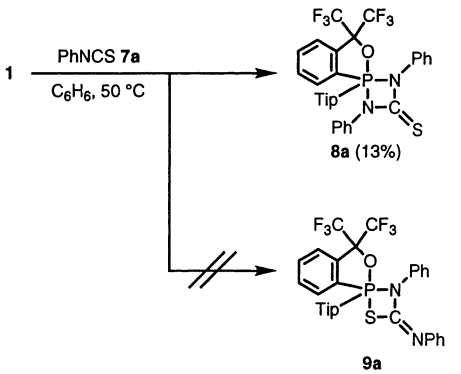


Scheme 3.

HFA **3** (96%), **4** (100%) and aniline (89%) as main products with a small amount of imine **5** (4%). It was confirmed by the control experiment that aniline is not derived from imine **5** but iminophosphorane **1**. Since aniline and **4** are hydrolysis products of **1**, thermolysis process of **2a** giving **1** and HFA was evidenced by their formation. In the experiment in the presence of water, the possible product **1** was irreversibly removed from its system by its hydrolysis. Furthermore, thermolysis of **2a** in the presence of methanol (100 equiv.) at 140 °C afforded methoxyphosphorane **6** (75%), which seems to be formed by alcoholysis of **1** formed (Scheme 3). Unfortunately, compound **6** could not be purified because of its instability to the moisture, its formation was confirmed by ^{19}F and ^{31}P NMR spectra and FAB MS spectra of the reaction solution. These results indicate two reaction pathways for the thermolysis of **2a**: one is formation of the aza-Wittig reaction products, cyclic phosphinate **4** and imine **5**, and another is regeneration of iminophosphorane **1** and HFA **3**. Since the former path is the second step of the aza-Wittig reaction, 1,3,2λ^5-oxazaphosphetidines **2a** can be regarded as an intermediate of the aza-Wittig reaction.

3.3. Synthesis and structure of a 1,3,2λ^5-diazaphosphetidine-4-thione

There has been only one report on the X-ray crystallographic analysis of a 1,3,2λ^5-thiazaphosphetidine ring to date [12]. The formation and isolation of 1,3,2λ^5-oxazaphosphetidine **2a** bearing the Martin ligand as an isolable solid encouraged us to study the cycloaddition reactions with carbon–sulfur double-bond compounds in anticipation of the formation of the 1,3,2λ^5-thiazaphosphetidines [13]. An attempted reaction of iminophosphorane **1** with thiobenzophenone resulted in



Scheme 4.

no reaction, while monitoring the reaction of **1** with carbon disulfide in C_6D_6 at 60 °C afforded the cyclic thiophosphinate **10** without an observable intermediate. On the other hand, the reaction of compound **1** with phenyl isothiocyanate **7a** in benzene at 50 °C gave the corresponding adduct **8a** (Scheme 4). Monitoring of the reaction solution by ^{31}P NMR spectra showed the appearance of a new peak at δ_P −20.7 assignable to a pentacoordinate phosphorus atom of **8a**. In the ^1H NMR spectrum of **8a**, the ortho proton of the Martin ligand resonated at low field (δ 8.85), which is a typical feature of compounds with a TBP structure bearing a polar apical bond [14]. Further heating resulted in the decrease of **8a** and the increase of cyclic thiophosphinate **10**. Compound **8a** could be easily purified by chromatographic separation and recrystallization. X-ray crystallographic study revealed that compound **8a** is not 1,3,2λ^5-thiazaphosphetidine **9a**, but 1,3,2λ^5-diazaphosphetidine-4-thione **8a**. The unit cell of the crystal of **8a** contains two almost identical molecules. One of the crystal structures of **8a** was illustrated by the thermal ellipsoid plots in Fig. 1. Selected bond lengths and angles are listed in Table 2. The sum of three equatorial bond angles around phosphorus atom [359.8°] indicates that the phosphorus atom is placed on the equatorial plane. The bond angle between two apical bonds [162.7(3)°] indicates the distortion from the linearity. Thus, it can be clearly seen that **8a** is a distorted TBP structure at P1 atom with an oxygen and a nitrogen atoms at apical positions and other three atoms at equatorial positions, respectively, (%TBP→SP, 14%) [15]. It makes contrast to the nearly square pyramidal structure of the previously reported pentacoordinate 1,2-diazaphosphetidine-4-thione [16]. The apical P1–N1 bond length of **8a** are longer than that of equatorial P1–N2 bond. Similar characteristic feature is also shown in the cases of other phosphoranes exhibiting TBP geometry [3,4]. It is interesting that the reaction of iminophosphorane **1** with phenyl isothiocyantate gave the corresponding [2 + 2]-cycloadducts, while that of the phosphorus ylide bearing the Martin ligand af-

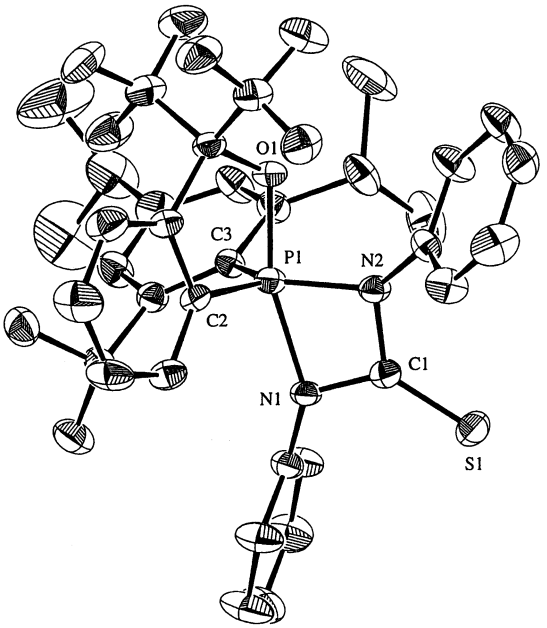
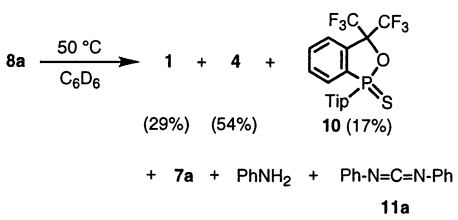


Fig. 1. ORTEP drawing of **8a** (30% probability). Hydrogen atoms are omitted for clarity.

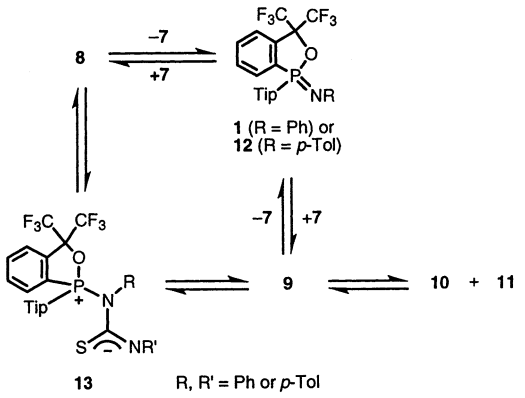
forded another type of product, a 1,2λ^5-thiaphosphetene [17]. Although compound **8a** can be handled in open air without special care in the solid state for a while, about 10% was decomposed even in the solid state after 1 week.

3.4. Reactions of 1,3,2λ^5-diazaphosphetidine-4-thiones

1,3,2λ^5-Diazaphosphetidine-4-thione **8a** was subjected to thermolysis in C_6D_6 at 50 °C (Scheme 5). Monitoring of the reaction solution by ^{19}F and ^{31}P NMR spectra revealed the disappearance of **8a** and formation of iminophosphorane **1** (29%), cyclic phosphinate **4** (54%), and cyclic thiophosphinate **10** (17%). Further heating of the reaction mixture caused no change as confirmed by NMR spectra. After exposure of the reaction mixture to open air, the formation of phenyl isothiocyanate **7a**, carbodiimide **11a**, and aniline was confirmed by GC-MS spectra. The formation of carbodiimide **11a** is most likely explained as shown in Scheme 6. Upon heating, 1,3,2λ^5-diazaphosphetidine-4-thione **8a** is firstly expected to undergo the cycloreversion giving **1** and phenyl isothiocyanate **7a**. The



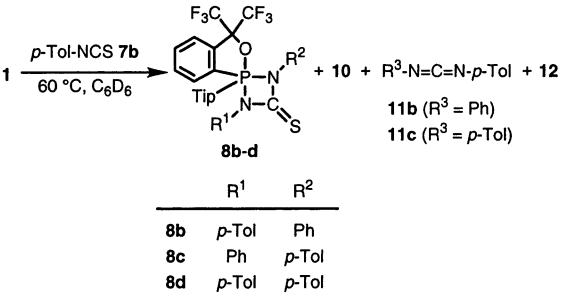
Scheme 5.



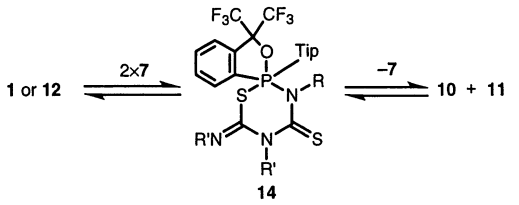
Scheme 6.

sequential [2 + 2]-cycloaddition of the P=N unit of **1** with C=S unit of the isothiocyanate gives the intermediary 1,3,2λ^5-thiazaphosphetidine **9a**, which affords cyclic thiophosphinate **10** and carbodiimide **11a** due to its thermal instability. For the formation of **9a**, the P–N bond dissociation of **8a** followed by intramolecular P–S bond formation of thus obtained zwitterion **13** is also considered as another mechanism. Since four-membered ring compounds with a P–S apical bond are suspected to be labile as indicated by the study on the pentacoordinate 1,2λ^5-thiaphosphetane, bond dissociation would take place in the transient 1,3,2λ^5-thiazaphosphetidine under such reaction conditions [18]. Although compounds $ZP(MeNCH_2CH_2)_3N$ (Z = O, S) can selectively catalyze the transformation of isocyanates to carbodiimides, the control experiments revealed that neither cyclic phosphinate **4** nor thiophosphinate **10**, which were formed in the thermolysis of **8a**, catalyzes such a transformation [19].

To reveal the formation mechanism of cyclic thiophosphinate **10** and carbodiimide **11a**, reaction of **1** with excess amount of *p*-tolyl isothiocyanate **7b** was performed in C_6D_6 at 60 °C (Scheme 7). Monitoring of the reaction solution by ^{31}P NMR spectra showed the formation of two new signals at δ_P −20.6 and −21.0 assignable to two diastereomers of 1,3,2λ^5-diazaphosphetidine-4-thiones **8b** and **8c** bearing both *N*-Ph and *N*-*p*-tolyl groups after heating 5 h, and additionally new peak at δ_P −20.8 assignable to **8d** with two *N*-*p*-tolyl groups after further standing at r.t. for 2 days. The formation of cyclic thiophosphinate **10** and iminophosphorane **12** (δ_P 25.46) bearing a *p*-tolyl group instead of a phenyl group of **1** was also observed. Further heating at 60 °C for 10 h reduced the ratio of first two peaks compared with that of the new peak. Formation of three 1,3,2λ^5-diazaphosphetidines **8b**–**d**, two carbodiimides **11b** and **11c**, and cyclic thiophosphinate **10** was confirmed by GC-MS and/or ^{31}P NMR spectra after exposure of the reaction mixture to open air and successive separation with chromatography. Three 1,3,2λ^5-diazaphosphetidine-4-thiones **8b**–**d** could



Scheme 7.



Scheme 8.

not be separated from one another due to the structural similarity. The formation of **8d** is consistent with the existence of iminophosphorane **12**. Cycloreversion of 1,3,2λ^5-diazaphosphetidine-4-thiones **8b** and **8c** gives iminophosphoranes **1** and **12**, which undergo cycloaddition with *p*-tolyl isothiocyanate to give the starting mixture and **8d**, respectively. Two following mechanisms are possible for the formation of carbodiimides **11**. In the mechanism as shown in Scheme 8, each iminophosphorane **1** and **12** reacts with two molecules of an isothiocyanate to give a six-membered ring compound **14**, which undergoes ring opening to afford its carbodiimide **11** together with cyclic thiophosphinate **10** and the isothiocyanate **7**. The other mechanism involves P–N bond dissociation of **8**, formation of 1,3,2λ^5-thiazaphosphetidine **9a**, and Wittig-type ring opening reaction similarly to the thermolysis of **8a** (Scheme 6). The experimental result that phenyl(*p*-tolyl)carbodiimide **11b** was formed in higher yield than di(*p*-tolyl)carbodiimide **11c** (**11b**:**11c** = 6:1) can exclude the mechanism shown in Scheme 8, because **11c** should predominantly be formed for that mechanism. The present formation of cyclic thiophosphinate **10** and carbodiimide **11** from 1,3,2λ^5-thiazaphosphetidine **8** is considered to proceed via P–N bond dissociation in marked contrast to the reactivity of Schmidpeter's 1,3,2λ^5-diazaphosphetidine-4-thiones, which rearrange intramolecularly but do not give the corresponding P=S and carbodiimide units [20].

In summary, we have shown that the reactions of an iminophosphorane **1** bearing the Martin ligand with HFA and phenyl isothiocyanate gave the corresponding cycloadducts **2a** and **8**. It was found that 1,3,2λ^5-oxazaphosphetidine **2a** has two reactivities on its thermolysis giving imine **5** and ketone **3**, respectively. The former reactivity exhibits that **2a** is an intermediate of the aza-Wittig reaction. Thermolysis of **8** revealed two reaction pathways, that is, regeneration of **1** and the isothiocyanate **7**, and formation of cyclic thiophosphinate **10** and carbodiimide **11** via **9**. The formation of the iminophosphorane is found to be a characteristic reactivity of not only a 1,2λ^5-azaphosphetidine but also a 1,3,2λ^5-oxazaphosphetidine and a 1,3,2λ^5-diazaphosphetidine-4-thione, respectively.

4. Supplementary material

Crystallographic data for the structural analysis have been deposited with the Cambridge Crystallographic Data Centre, CCDC Nos. 167822 and 167823 for compounds **2a** and **8a**. Copies of this information may be obtained from The Director, CCDC, 12 Union Road, Cambridge, CB2 1EZ, UK (fax: +44-1233-336033; e-mail: deposit@ccdc.cam.ac.uk or www: http://www.ccdc.cam.ac.uk).

Acknowledgements

This work was partially supported by Grants-in-Aid for Scientific Research from the Ministry of Education, Culture, Sports, Science, and Technology of Japan. We are grateful to Central Glass and Tosoh Finechem Corporation for the gifts of organofluorine compounds and alkyllithiums, respectively.

References

[1] (a) E. Lukevics, O. Pudova, in: A.R. Katritzky, C.W. Rees, E.F.V. Scriven (Eds.), Comprehensive Heterocyclic Chemistry II, vol. 1B, Pergamon, Oxford, UK, 1996, pp. 1189–1213;
(b) T. Kawashima, R. Okazaki, in: B. Halton (Ed.), Advances in Strained and Interesting Organic Molecules, vol. 7, JAI Press Inc, Stamford, CT, 1999, pp. 1–41.
[2] T. Kawashima, R. Okazaki, Synlett (1996) 600–608 and references therein.
[3] (a) T. Kawashima, K. Kato, R. Okazaki, J. Am. Chem. Soc. 114 (1992) 4008;
(b) T. Kawashima, K. Kato, R. Okazaki, Angew. Chem., Int. Ed. Engl. 32 (1993) 869.
[4] T. Kawashima, T. Soda, R. Okazaki, Angew. Chem., Int. Ed. Engl. 35 (1996) 1096.
[5] A bidentate ligand, –$C_6H_4C(CF_3)_2O$–, developed by Martin for stabilizing hypervalent species, see: E.F. Perozzi, R.S. Michalak, G.D. Figuly, W.H. Stevenson III, D.B. Dess, M.R. Ross, J.C. Martin, J. Org. Chem. 46 (1981) 1049.
[6] (a) J. Koketsu, Y. Ninomiya, Y. Suzuki, N. Koga, Inorg. Chem. 36 (1997) 694;
(b) W.C. Lu, C.B. Liu, C.C. Sun, J. Phys. Chem. A 103 (1999) 1078.
[7] (a) Y.G. Gololobov, L.F. Kasukhin, Tetrahedron 48 (1992) 1353;
(b) P. Molina, M.J. Vilaplana, Synthesis (1994) 1197.

[8] N. Kano, X.J. Hua, S. Kawa, T. Kawashima, Tetrahedron Lett. 41 (2000) 5237.
[9] N. Kano, J.-H. Xing, A. Kikuchi, T. Kawashima, Heteroatom. Chem. 12 (2001) 282.
[10] (a) R. Francke, D. Dakternieks, R.W. Gable, B.F. Hoskins, G.-V. Röschenthaler, Chem. Ber. 118 (1985) 922;
(b) W. Storzer, G.-V. Röschenthaler, R. Schmutzler, W.S. Sheldrick, Chem. Ber. 114 (1981) 3609.
[11] W.S. Sheldrick, D. Schomburg, A. Schmidpeter, T. von Criegern, Chem. Ber. 113 (1980) 55.
[12] M. Fulde, W. Ried, J.W. Bats, Helv. Chim. Acta 72 (1989) 139.
[13] U. Dressler, E. Niecke, S. Pohl, W. Saak, W.W. Schoeller, H.-G. Schäfer, J. Chem. Soc., Chem. Commun. (1986) 1086.
[14] I. Granoth, J.C. Martin, J. Am. Chem. Soc. 101 (1979) 4618.
[15] R.R. Holmes, J.A. Deiters, J. Am. Chem. Soc. 99 (1977) 3318.
[16] V. Novomestska, J. Marek, J. Prihoda. Polyhedron 18 (1999) 2723.
[17] T. Kawashima, T. Iijima, H. Kikuchi, R. Okazaki, Phosphorus, Sulfur, Silicon Relat. Elem. 146 (1999) 149.
[18] (a) S. Wilker, C. Lauren, C. Sarter, C. Puke, G. Erker, J. Am. Chem. Soc. 117 (1995) 7293;
(b) C. Puke, G. Erker, N.C. Aust, E.U. Wurthwein, R. Frohlich, J. Am. Chem. Soc. 120 (1998) 4863;
(c) C. Puke, G. Erker, B. Wibbeling, R. Frohlich, Eur. J. Org. Chem. (1999) 1831.
[19] J. Tang, T. Mohan, J.G. Verkade, J. Org. Chem. 59 (1994) 4931.
[20] A. Schmidpeter, T. von Criegern, Angew. Chem., Int. Ed. Engl. 17 (1978) 443.

PERGAMON

Polyhedron 21 (2002) 667–674

POLYHEDRON

www.elsevier.com/locate/poly

N-[2-(4-Methoxyphenyltelluro)ethyl]benzamide ($\mathbf{L}^1$) and *N*-[2-(4-methoxyphenyl telluro)propyl]phthalimide ($\mathbf{L}^2$): synthesis and ligation with palladium(II), platinum(II) and ruthenium(II). Crystal structures of $\mathbf{L}^1$ and $\mathbf{L}^2$, the latter as a mixed crystal with $\mathbf{L}^2\mathbf{H}_2$

Ajai K. Singh [a,*], J. Sooriyakumar [a], M. Kadarkaraisamy [a], John E. Drake [b], Michael B. Hursthouse [c], Mark E. Light [c], Raymond J. Butcher [d]

[a] *Department of Chemistry, Indian Institute of Technology, New Delhi 110016, India*
[b] *Department of Chemistry and Biochemistry, University of Windsor, Windsor, Ont., Canada N9B 3P4*
[c] *Department of Chemistry, University of Southampton, Southampton SO17 1BJ, UK*
[d] *Department of Chemistry, Howard University, Washington, DC 20059, USA*

Received 7 June 2001; accepted 3 January 2002

Abstract

The reactions of *N*-(2-chloroethyl)benzamide and *N*-[3-bromopropyl]phthalimide with $ArTe^-$ Na^+ generated in situ by borohydride reduction of Ar_2Te_2, have resulted in *N*-[2-(4-methoxyphenyltelluro)ethyl]benzamide ($\mathbf{L}^1$) and *N*-[2-(4-methoxyphenyltelluro)propyl] phthalimide ($\mathbf{L}^2$) respectively. The $\mathbf{L}^1$ and $\mathbf{L}^2$ both exhibit characteristic ^1H and ^{13}C NMR spectra. The single crystal structures of $\mathbf{L}^1$ and $\mathbf{L}^2$, the latter as a mixed crystal with $\mathbf{L}^2\mathbf{H}_2$ are determined by X-ray diffraction (XRD). The Te–C(alkyl) bond length is 2.140(8)/2.149(4) Å and longer than Te–C(aryl), 2.107(8)/2.123(5) Å. The complexes having stoichiometries $[PdCl_2(\mathbf{L}^1)]$ (**1**), $[PtCl_2(\mathbf{L}^1)]$(**2**), $[(Phen)Pd(\mathbf{L}^1)](ClO_4)_2$ (**3**), $[(DPPE)Pd(\mathbf{L}^1)](ClO_4)_2$ (**4**) and $[RuCl_2(\mathbf{L}^2)_2]$ (**5**) were synthesized and characterized by elemental analyses, conductance and molecular weight measurements, NMR (^1H and ^{13}C) and FT-IR spectra. The deshielding of CH_2Te ($\sim$0.2 ppm in ^1H NMR and up to 22 ppm in $^{13}C\{^1H\}$ NMR) and NH signals (upto 0.8 ppm in ^1H NMR) of **1**–**4**, with respect to those of free $\mathbf{L}^1$ indicates that $\mathbf{L}^1$ coordinates with Pd–Pt(II) as a (Te, N) ligand. The CH_2Te/CH_2N signals in ^1H and ^{13}C NMR spectra of **5** appear deshielded (0.8/0.14 and 20/8 ppm, respectively), when compared with those of free $\mathbf{L}^2$, indicating ligation of $\mathbf{L}^2$ via Te and N. © 2002 Elsevier Science Ltd. All rights reserved.

Keywords: *N*-[2-(4-Methoxyphenyltelluro)ethyl]benzamide; *N*-[2-(4-Methoxyphenyl telluro)propyl]phthalimide; Palladium(II); Platinum(II); Ruthenium(II); Complexes; Crystal structures

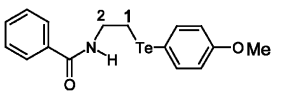
1. Introduction

The current interest in the chemistry of hybrid organotellurium ligands (having other donor sites along with Te) [1–7] is due to their obvious importance in understanding further the ligation of heaviest metalloid tellurium vis a vis other well known donors. The designing of (Te_x, N_y) type of hybrid organotellurium ligands has been carried out by tellurating aliphatic amines [1,2,8,9] and pyridine derivatives [10]. However, ligand chemistry of hybrid organotellurium donor containing amide functionality is unknown so far [2–4]. Similarly the telluration of imide derivatives has been reported [4] scantly. It was, therefore, thought worthwhile to design *N*-[2-(4-methoxyphenyltelluro)ethyl]-benzamide ($\mathbf{L}^1$) and *N*-[2-(4-methoxyphenyltelluro)-propyl] phthalimide ($\mathbf{L}^2$) and investigate their ligand chemistry. The results of these investigations are reported in this paper. Both the ligands are structurally characterized. However, for $\mathbf{L}^2$, the crystal used was found to be a mixed crystal of $\mathbf{L}^2$ and $\mathbf{L}^2\mathbf{H}_2$, with

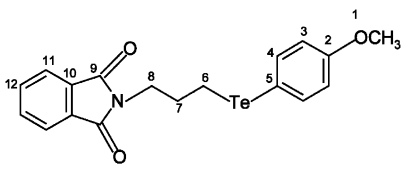
* Corresponding author. Fax: +91-11-6862037.
E-mail address: aksingh@chemistry.iitd.ernet.in (A.K. Singh).

0277-5387/02/$ - see front matter © 2002 Elsevier Science Ltd. All rights reserved.
PII: S0277-5387(02)00831-8

occupancies of 40 and 60%, respectively. None of the complexes could be structurally characterized due to poor quality of their crystals. However, using their spectroscopic (NMR and IR) data it can be readily inferred that $\mathbf{L}^1$ and $\mathbf{L}^2$ both ligate as a (Te, N) donor in all the complexes **1**–**5**.



$\mathbf{L}^1$



$\mathbf{L}^2$

Table 1
Crystal data and structure refinement for $\mathbf{L}^1$ and '$\mathbf{L}^2$'

	$\mathbf{L}^1$	'$\mathbf{L}^2$'
Empirical formula	$C_{16}H_{17}NO_2Te$	$C_{18}H_{18.2}NO_3Te$ $[(C_{18}H_{17}NO_3Te)_{0.4}$-$(C_{18}\ H_{18.2}NO_3\ Te)_{0.6}]$
Formula weight	382.91	424.14
Temperature (K)	293(2)	150(2)
Wavelength (Å)	0.71073	0.71073
Crystal system	Orthorhombic	Orthorhombic
Space group	$P2_12_12_1$	*Pbca*
Unit cell dimensions	$a = 5.410(4)$ (Å)	14.646(3) (Å)
	$b = 9.915(4)$ (Å)	5.9656(12) (Å)
	$c = 28.760(3)$ (Å)	38. 213(8) (Å)
Volume, (Å^3)	1542.6(15)	3338.7(12)
Z	4	8
D_{calc} (Mg m^{-3})	1.649	1.688
Absorption coefficient (mm^{-1})	1.929	1.796
$F(000)$	752	1674
Crystal size (mm)	$0.1 \times 1.00 \times 0.1$	$0.15 \times 0.10 \times 0.02$
θ Range for data collection (°)	2.17–25.00	2.98–27.47
Reflections collected	1630	10791
Independent reflections	1630 $[R_{int} = 0.000]$	3627 $[R_{int} = 0.0684]$
Refinement method	full-matrix least-squares on F^2	full-matrix least-squares on F^2
Data/restraints/parameters	1630/0/201	3627/0/214
Goodness-of-fit on F^2	1.047	0.895
Final R indices $[F^2 > 2/4\sigma(F^2)]$	$R_1 = 0.0382$, $wR_2 = 0.0791$	$R_1 = 0.0394$, $wR_2 = 0.0688$
R indices (all data)	$R_1 = 0.0572$, $wR_2 = 0.0873$	$R_1 = 0.1211$, $wR_2 = 0.0864$
Largest diff. peak and hole (e Å^{-3})	0.432 and −0.389	0.494 and −0.542

2. Experimental

The C and H analyses were carried out with a Perkin–Elmer elemental analyzer 240 C. Tellurium was estimated volumetrically [4]. The ^{1}H and ^{13}C{^{1}H} NMR spectra were recorded on a Bruker Spectrospin DPX-300 NMR spectrometer at 300.13 and 75.47 MHz, respectively. IR spectra in the range 4000–250 cm^{-1} were recorded on a Nicolet Protége 460 FT-IR spectrometer as KBr and CsI pellets. The conductance measurements were made in acetonitrile (concentration ~ 1 mM) using an ORION conductivity meter model 162. The molecular weights (concentration ~ 5 mM) in chloroform were determined with a Knauer vapour pressure osmometer model A0280. The melting points (m.p.) determined in open capillary are reported as such. *N*-(2-Chloroethyl)benzamide and *N*-[3-bromopropyl]phthalimide obtained from Aldrich (USA) were used as received. The reported methods were used to synthesize $[(Phen)PdCl_2]$ [11,11a] and $[(DPPE)PdCl_2]$ [11b].

2.1. X-ray diffraction analysis

The Bruker P4S X-ray diffractometer was used for the data collection on $\mathbf{L}^1$, employing ω–2θ technique. The unit cell was determined from 25 randomly selected reflections using automatic search, index and least square routines. Empirical absorption correction was applied using SHELXA programme [12,12a]. The structure was solved by routine heavy atom/Fourier methods (using SHELXL 93 [12b]/SHELX 86 [12c]) and refined by full-matrix least-squares on F^2. The crystal and refinement data of $\mathbf{L}^1$ are given in Table 1. For structure determination of '$\mathbf{L}^2$' (mixed crystal of $\mathbf{L}^2$ and $\mathbf{L}^2\mathbf{H}_2$, which are colourless plates) a suitable specimen was mounted on a glass fibre and cell dimensions and intensity data were recorded on an Enraf Nonius KCCD diffractometer, with ϕ and ω scans chosen to give a complete asymmetric unit. The data collection and cell refinement [13] gave cell constants corresponding to an orthorhombic cell whose dimensions are given in Table 1 along with other experimental parameters An absorption correction was applied [14], which resulted in transmission factors ranging from 0.9650 to 0.7744. The structures were solved by direct methods [15]. All of the non-hydrogen atoms were treated anisotropically. During the course of the refinement, it was found that oxygen O(2) was split over two positions. This was interpreted as resulting from the use of a mixed crystal of $\mathbf{L}^2$ and $\mathbf{L}^2\mathbf{H}_2$. The rigidity of the phthalimide system is apparently such that all atoms are in identical positions in $\mathbf{L}^2$ and $\mathbf{L}^2\mathbf{H}_2$ with the exception of the terminal oxygen, >C(11)–O(2B) in $\mathbf{L}^2$ and the hydroxyl oxygen, >C(11)H–O(2A)H in $\mathbf{L}^2\mathbf{H}_2$. The effect is an apparent disorder of this oxygen atom

with the occupancy of O(2B):O(2A) of 0.4:0.6. Hydrogen atoms were included in idealized positions with isotropic thermal parameters set at 1.2 times that of the carbon and oxygen atom to which they were attached. The parameters for final cycle of full-matrix least-squares refinement of mixed crystal, '$\mathbf{L}^2$' [16] are also given in Table 1. The ORTEP diagram of $\mathbf{L}^2$ is displayed in Fig. 3(a) and that of $\mathbf{L}^2H_2$ in Fig. 3(b).

2.2. Synthesis of *N*-[2-(4-methoxyphenyltelluro)ethyl]benzamide ($\mathbf{L}^1$)

The solution of bis(4-methoxyphenyl)ditelluride (1.87 g, 4 mmol) made in 50 cm^3 of ethanol was refluxed under oxygen free nitrogen atmosphere. Sodium borohydride (0.5 g dissolved in 10 cm^3 of 10% aqueous NaOH) was added to it drop wise till it became colourless. *N*-(2-Chloroethyl)benzamide (1.46 g, 8 mmol) dissolved in 10 cm^3 of ethanol, was added drop wise to the refluxing colourless solution. The reaction mixture was further refluxed for 1–2 h, cooled to 25 °C and poured into ice cold water (200 cm^3). $\mathbf{L}^1$ was extracted from it into dichloromethane (100 cm^3). The extract was washed with water, dried over sodium sulfate and evaporated on a rotary evaporator, resulting in a yellowish oil, which was dissolved in a 1:2 mixture of dichloromethane and petroleum ether (40–60 °C). The solution was kept at 0–5 °C for 24 h. The fibrous white crystals of $\mathbf{L}^1$ were filtered and dried in vacuo. Yield: 70%; m.p. 68–70 °C Λ_M (Ω^{-1} cm^2 mol^{-1}) 5.3. *Anal.* Calc. for $C_{16}H_{17}O_2NTe$: C, 50.19; H, 4.44; N, 3.66; Te, 32.50. Found: C, 49.81; H, 4.58; N, 3.17; Te, 32.70%. Mol. wt.: 375 (Calc. 382). ^1H NMR ($CDCl_3$, 25 °C) (δ vs. TMS) 3.00–3.04 (t, 2H, H_1), 3.76–3.82 (m, 5H, H_2 and OMe), 6.52 (bs, 1H, NH), 6.72–6.75 (d, 2H, ArH *m* to Te), 7.35–7.49 (m, 3H, ArH *p* and *m* to CO), 7.62–7.64 (d, 2H, ArH *o* to CO), 7.69–7.72 (d, 2H, ArH *o* to Te). $^{13}C\{^1H\}$ NMR ($CDCl_3$, 25 °C) (δ vs. TMS): 8.1 (C_1), 41.5 (C_2), 54.9 (OCH_3), 99.3 (ArC–Te), 115.2 (ArC *m* to Te), 126.8 (ArC *m* to CO), 128.2 (ArC *p* to CO), 131.7 (ArC *o* to CO), 134.1 (ArC–CO), 140.8 (ArC *o* to Te), 160.9 (ArC *p* to Te), 167.1 (CO).

2.3. Synthesis of [$PdCl_2(\mathbf{L}^1)$] (**1**)

The [$(C_6H_5CN)_2PdCl_2$] (0.49 g, 1 mmol) dissolved in 20 cm^3 of dichloromethane was mixed with a solution of ligand $\mathbf{L}^1$ (0.38 g, 1 mmol) made in 10 cm^3 of dichloromethane with vigorous stirring. The mixture was further stirred for 2 h at room temperature (r.t.), concentrated to 7–8 cm^3 on a rotary evaporator and mixed with hexane (5 cm^3). The resulting brown precipitate of **1** was filtered, washed with diethylether, recrystallized from chloroform–hexane (1:2) mixture and dried in vacuo. Yield: 85%; m.p. 84–85 °C (d) Λ_M (Ω^{-1} cm^2 mol^{-1}) 30 *Anal.* Calc. for $C_{16}H_{17}O_2NTePdCl_2$: C, 34.29; H, 3.03; N, 2.50; Te, 22.86. Found: C, 34.35; H, 3.10; N, 2.84; Te, 21.93%. Mol. wt.: 550 (Calc. 560). ^1H NMR ($CDCl_3$, 25 °C) (δ vs. TMS): 3.37 (bs, 2H, H_1), 3.77 (s, 3H, OMe), 3.87 (bs, 2H, H_2), 6.84–6.86 (d, 2H, ArH *m* to Te), 7.08 (bs, 1H, NH), 7.34–7.48 (m, 3H, ArH *p* and *m* to CO), 7.77–7.80 (d, 2H, ArH *o* to CO), 7.82–7.85 (d, 2H, ArH *o* to Te). $^{13}C\{^1H\}$ NMR ($CDCl_3$, 25 °C) (δ vs. TMS): 22.9 (C_1), 38.1 (C_2), 55.3 (OCH_3), 105.1 (ArC–Te), 115.9 (ArC *m* to Te), 127.3 (ArC *m* to CO), 128.5 (ArC *p* to CO), 131.7 (ArC *o* to CO), 133.5 (ArC–CO), 137.8 (ArC *o* to Te), 161.5 (ArC *p* to Te), 167.8 (CO).

2.4. Synthesis of [$PtCl_2(\mathbf{L}^1)$](**2**)

To a solution of $K_2[PtCl_4]$ (0.17 g, 0.4 mmol) made in 10 cm^3 of water, ligand $\mathbf{L}^1$ (0.15 g 0.4 mmol) dissolved in 10 cm^3 of acetone was added. The resulting mixture was stirred for 1 h at r.t. and poured into 100 cm^3 of water. The complex **2** was extracted into chloroform (100 cm^3). The extract was dried over anhydrous sodium sulphate, concentrated to $\sim$10 cm^3 on a rotary evaporator and mixed with hexane (15 cm^3). The resulting precipitate of **2** was filtered, washed with hexane and recrystallized from hexane–dichloromethane (1:1) mixture. The yellow colored compound was separated, filtered and dried in vacuo. Yield: 80%; m.p. 112–113 °C (d) Λ_M (Ω^{-1} cm^2 mol^{-1}) 36. *Anal.* Calc. for $C_{16}H_{17}O_2NTePtCl_2$: C, 29.54; H, 2.61; N, 2.16 Te, 18.97. Found: C, 30.05; H, 2.84; N, 1.94; Te, 18.97%. Mol. wt.: 641 (Calc. 649.3). ^1H NMR ($CDCl_3$, 25 °C) (δ vs. TMS): 3.39 (bs, 2H, H_1), 3.74 (s, 3H, OMe), 3.86 (bs, 2H, H_2), 6.83–6.86 (d, 2H, ArH *m* to Te), 7.01 (bs, 1H, NH), 7.36–7.47 (m, 3H, ArH *p* and *m* to CO), 7.78–7.84 (m, 4H, ArH *o* to CO and *o* to Te). $^{13}C\{^1H\}$ NMR ($CDCl_3$, 25 °C) (δ vs. TMS): 29.7 (C_1), 39.6 (C_2), 55.5(OCH_3), 104.8 (ArC–Te), 115.9 (ArC *m* to Te), 127.3 (ArC *m* to CO), 128.5 (ArC *p* to CO), 131.7 (ArC *o* to CO), 133.5 (ArC–CO), 137.8 (ArC *o* to Te), 161.5 (ArC *p* to Te), 167.8 (CO).

2.5. Synthesis of [(Phen)$Pd(\mathbf{L}^1)$]$(ClO_4)_2$ (**3**)

Solution of $AgClO_4$ (0.08 g, 0.4 mmol) made in methanol (10 cm^3) was mixed with the slurry of [(Phen)$PdCl_2$] (0.07 g, 0.2 mmol) prepared in chloroform (10 cm^3). The resulting mixture was stirred for 30 min at r.t., mixed with a solution of ligand $\mathbf{L}^1$ (1.52 g, 0.4 mmol) made in chloroform (10 cm^3) and stirred further for 2 h. The white precipitate of AgCl was filtered off. The filtrate was concentrated to 10 cm^3 on a rotary evaporator and mixed with hexane (10 cm^3). The resulting precipitate of **3** was filtered, washed with hexane–chloroform (5:1) mixture, recrystallized from acetonitrile and dried in vacuo. Yield: 68%; m.p. 114–115 °C (d) Λ_M (Ω^{-1} cm^2 mol^{-1}) 250. *Anal.* Calc. for

$C_{30}H_{25}N_3TePdCl_2O_{10}$: C, 38.66; H, 2.87; N, 4.84; Te, 14.70. Found: C, 38.88; H, 2.36; N, 4.79; Te, 14.10%. Mol. wt.: 286 (Calc. 868). ^{1}H NMR ($CDCl_3$, 25 °C) (δ vs. TMS): 3.42 (bs, 2H, H_1), 3.77–3.81 (m, 5H, H_2 and OMe), 6.66–6.62 (d, 2H, ArH *m* to Te), 6.95 (bs, 1H, NH), 7.33–7.46 (m, 3H, ArH *p* and *m* to CO), 7.62–7.80 (m, 8H, ArH *o* to CO, *o* to Te, H_a and H_b of phen), 8.46–8.49 (m, 2H, H_c of phen), 9.17–9.19 (m, 2H, H_d of phen).^{13}C{^{1}H} NMR ($CDCl_3$, 25 °C) (δ vs. TMS): 19.3 (C_1), 39.2 (C_2), 55.1 (OCH_3), 104.0 (ArC–Te), 115.9 (ArC *m* to Te), 127–138(ArC of phen + ArC *o* to Te + ArC of benzamide), 160.5 (ArC *p* to Te), 168.1 (CO).

2.6. Synthesis of [(DPPE)Pd(**L**^{1})](ClO$_4$)$_2$ (**4**)

Solution of [(DPPE)$PdCl_2$] (0.12 g, 0.2 mmol) in chloroform (10 cm^3) was mixed with $AgClO_4$ (0.08 g, 0.4 mmol) dissolved in 5 cm^3 of methanol. The mixture was stirred for 30 min. The AgCl was filtered off. The $\mathbf{L}^1$ (0.76 g, 0.2 mmol) dissolved in chloroform (10 cm^3) was added to the filtrate. The mixture was stirred for 2 h at r.t., concentrated on a rotary evaporator to 10 cm^3 and mixed with hexane (20 cm^3). The resulting precipitate of **4** was filtered, recrystallized from chloroform–diethylether mixture and dried in vacuo. Yield: 70%; m.p. 96–97 °C (d) Λ_M (Ω^{-1} cm^2 mol^{-1}) 246 *Anal.* Calc. for $C_{42}H_{41}O_{10}NP_2TePdCl_2$: C, 46.34; H, 3.77; N, 1.28; Te, 11.77. Found: C, 46.04; H, 4.09; N, 1.53; Te, 11.60%. Mol. wt.: 359 (Calc. 1087.5). ^{1}H NMR ($CDCl_3$, 25 °C) (δ vs. TMS): 2.76–2.94 (m, 4H,CH_2–P), 3.55 (m, 2H, H_1), 3.67 (s, 3H, OMe), 3.81–3.83 (m, 2H, H_2), 6.49–6.52 (d, 2H, ArH *m* to Te), 7.02–7.82 (m, 28H, NH, ArH of DPPE, ArH *o* to Te, ArH of benzamide). ^{13}C{^{1}H} NMR ($CDCl_3$, 25 °C) (δ vs. TMS): 16.1 (C_1), 24.0 (CH_2–P), 38.5 (C_2), 57.3 (OCH_3), 103.8 (ArC–Te), 115.4 (ArC *m* to Te), 127.3–138.0 (ArC of DPPE + ArC *o* to Te + ArC of benzamide), 161.5 (ArC *p* to Te), 167.6 (CO).

2.7. Synthesis of **L**^{2}

The solution of *N*-[3-bromopropyl]phthalimide (1.44 g, 4.2 mmol) made in 10 ml of THF was added to a refluxing colourless solution of $ArTe^-Na^+$ generated in situ by the procedure given in Section 2.2. The mixture was refluxed further for 1 h, cooled to r.t. and poured into 100 cm^3 of water. $\mathbf{L}^2$ was extracted from it into 50 cm^3 of CH_2Cl_2. The extract was dried over Na_2SO_4, concentrated to 5 cm^3 on a rotary evaporator and mixed with petroleum ether (40–60 °C). The resulting white crystalline solid $\mathbf{L}^2$ was filtered, washed with petroleum ether (40–60 °C) and dried in vacuo. The single crystals of $\mathbf{L}^2$ were grown from a mixture (8:2) of dichloromethane and petroleum ether (40–60 °C). Yield: 80%; m.p. 102–103 °C (d) Λ_M 0.8 (Ω^{-1} cm^2 mol^{-1}) *Anal.* Calc. for $C_{18}H_{17}O_3NTe$: C, 51.13; H, 4.02; N, 3.31; Te 30.18. Found: C, 50.60; H, 4.41; N, 3.53; Te, 30.77%. Mol. wt.: (Calc.). ^{1}H NMR ($CDCl_3$, 25 °C) (δ vs. TMS): 2.06–2.15 (q, 2H, H_2–C_7); 2.74–2.80 (t, 2H, H_2C–Te); 3.72–3.75 (t, 2H, H_2C–N); 3.76 (s, 3H, OCH_3); 6.73–6.76 (d, 2H, ArH *m* to Te); 7.67–7.73 (m, 4H, ArH of phthalimide ring); 7.82–7.84 (d, 2H, ArH, *o* to Te). ^{13}C{^{1}H} NMR ($CDCl_3$, 25 °C) (δ vs. TMS): 4.5 (C_6), 30.6 (C_7), 39.7 (C_8), 55.1 (C_1); 100.2 (C_5), 115.2 (C_3), 123.2 (C_{11}), 132.2 (C_{10}), 133.5 (C_{12}), 141.3 (C_4), 159.8 (C_2), 168.3 (C_9).

2.8. Synthesis of [RuCl$_2$(**L**^{2})$_2$] (**5**)

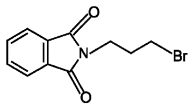
Solution of $RuCl_3 \cdot xH_2O$ (0.21 g, 1 mmol) in 20 cm^3 of methanol was mixed with $\mathbf{L}^2$ (0.86 g, 2 mmol) dissolved in 20 cm^3 of dichloromethane. The mixture was stirred for 3 h at r.t., filtered and concentrated to a solid residue on a rotary evaporator. The residue was dissolved in acetonitrile (10 cm^3) and resulting solution filtered. The filtrate was layered with 20 cm^3 of diethyl ether and kept at 0 °C for 48 h. The pale brown needle shaped crystals were separated and dried under vacuo. Yield: 55%; m.p. 168–169 °C. Λ_M 29.8 (Ω^{-1} cm^2 mol^{-1}) *Anal.* Calc. for $C_{36}H_{34}O_6N_2Te_2RuCl_2$: C, 42.49; H, 3.34; N, 2.76; Te 25.08. Found: C, 43.10; H, 2.42; N, 2.56; Te, 25.58%. Mol. wt.: 988.4 (Calc. 1017.5). ^{1}H NMR ($CDCl_3$, 25 °C) (δ vs. TMS): 2.52–2.62 (q, 2H, H_2–C_7); 3.62–3.69 (t, 2H, H_2C–Te); 3.86–3.93 (t, 2H, H_2C–N + OCH_3); 7.03–7.06 (d, 2H, ArH *m* to Te); 7.77–7.88 (m, 4H, ArH of phthalimide ring); 8.03–8.08 (d, 2H, ArH, *o* to Te). ^{13}C{^{1}H} NMR ($CDCl_3$, 25 °C) (δ vs. TMS): 25.0 (C_6), 38.3 (C_7), 47.5 (C_8), 55.6 (C_1), 115.7 (C_3), 123.5 (C_{11}), 131.9 (C_{10}), 134.2 (C_{12}), 135.0 (C_3), 162.3 (C_2), 168.3 (C_9).

3. Results and discussion

The ligands $\mathbf{L}^1$ and $\mathbf{L}^2$ and their complexes were prepared according to the reaction given in Eqs. (1)–(6)

$$ArTeNa + C_6H_5CONHCH_2CH_2Cl \rightarrow \mathbf{L}^1 \text{ or } \mathbf{L}^2 + NaCl \quad (1)$$

or



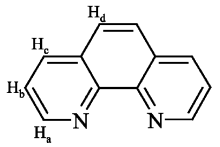
$$(C_6H_5CN)_2PdCl_2 + \mathbf{L}^1 \rightarrow [PdCl_2(\mathbf{L}^1)](\mathbf{1}) + 2C_6H_5CN \quad (2)$$

$$K_2PtCl_4 + \mathbf{L}^1 \rightarrow [PtCl_2(\mathbf{L}^1)](\mathbf{2}) + 2KCl \quad (3)$$

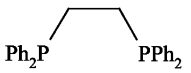
$$[(\text{Phen})PdCl_2] + 2AgClO_4 + \mathbf{L}^1 \rightarrow [(\text{Phen})Pd(\mathbf{L}^1)](ClO_4)_2(\mathbf{3}) + 2AgCl^- \downarrow \quad (4)$$

$$[(\text{DPPE})PdCl_2] + 2AgClO_4 + \mathbf{L}^1 \rightarrow [(\text{DPPE})Pd(\mathbf{L}^1)](ClO_4)_2(\mathbf{4}) + 2AgCl^- \downarrow \quad (5)$$

$$RuCl_3 \cdot xH_2O + 2\mathbf{L}^2 \rightarrow [RuCl_2 \cdot (\mathbf{L}^2)_2](\mathbf{5}) \quad (6)$$

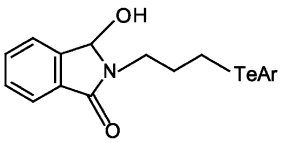


Phen



DPPE

Since BH_4^- was taken in slight excess to avoid oxidation of $ArTe^-$ back to Ar_2Te_2, it probably reduced one >C=O group resulting in $\mathbf{L}^2H_2$, which formed with $\mathbf{L}^2$ a mixed crystal, '$\mathbf{L}^2$' (with occupancies 60 and 40%, respectively), selected by chance for X-ray data collection. However, the percentage of $\mathbf{L}^2H_2$ in the sample of $\mathbf{L}^2$ was below the detection limit of ^1H NMR spectra.



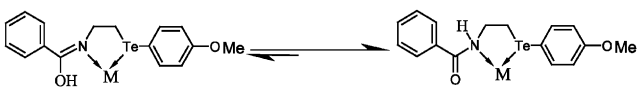
$\mathbf{L}^2H_2$

The ligands $\mathbf{L}^1$ and $\mathbf{L}^2$ and complexes **1**–**5** are soluble in common organic solvents. The complex **5** shows the sign of decay after 1 week even in nitrogen atmosphere. All other compounds were found stable under ambient conditions. The stoichiometries of the complexes have been authenticated by their elemental analyses. The molar conductance values (in acetonitrile at ~1 mM concentration level) and molecular weights of **3** and **4** (~one third of calculated values) suggest that they are 1:2 electrolytes [17]. For **1**, **2** and **5** the molar conductance values (Λ_M) have been found to be much lower than that of a 1:1 electrolyte [17]. Their observed molecular weights were found to be very close to the calculated ones.

3.1. Spectral data

IR spectrum of $\mathbf{L}^1$ has bands at 1641 and 3384 cm^{-1} due to CO and NH vibrations, respectively. The band appearing at 441 cm^{-1} [Te–C (aliphatic) vibrations] in IR of $\mathbf{L}^1$ shifts to ~419 cm^{-1} on the formation of **1**–**4**, indicating that $\mathbf{L}^1$ coordinates through Te. In IR spectra of **1**–**4**, NH band also shows a red shift of ~30 cm^{-1} with respect to that of free ligand $\mathbf{L}^1$, suggesting that ligation of $\mathbf{L}^1$ is through nitrogen also. However, in the spectra of **1**–**4**, the band having major contribution from CO was found almost unchanged with respect to that of $\mathbf{L}^1$, indicating that CO is not involved in coordination. In IR spectra of **3** and **4** perchlorate bands appear around 1100 (anti-symmetric stretching) and 620 cm^{-1} (anti-symmetric bending) suggesting that perchlorate ions are not coordinated. In the IR spectrum of $\mathbf{L}^2$ ν(CO) appearing at 1696 cm^{-1} remains unchanged on the formation of **5**.

In ^1H NMR spectrum of $\mathbf{L}^1$, the broad NH signal appearing at 6.52 ppm disappears with a D_2O shake. It shows a downfield shift (~0.2–0.8 ppm) in the spectra of **1**–**4** (relative to free $\mathbf{L}^1$) indicating that $\mathbf{L}^1$ ligates with Pd–Pt(II) through N. The signals of CH_2Te and aryl protons (*o* and *m* to Te) are observed deshielded (~ upto 0.2 ppm) in ^1H NMR of **1**–**4**, with respect to those of free $\mathbf{L}^1$, supporting the ligation of $\mathbf{L}^1$ through Te. However, signals of CH_2N in ^1H NMR spectra of **1**–**4** appear virtually unaffected when compared with those of free $\mathbf{L}^1$. This suggests that probably a N···Te secondary interaction exists in $\mathbf{L}^1$ and on coordination with Pd–Pt it is replaced by N→M bond. The broadness of signals of aliphatic protons in the spectra of **1**–**4** may be attributed to the coexistence of tautomers given below.



In $^{13}C\{^1H\}$ NMR spectra of **1**–**4**, the signals of C_1 and aryl C *ipso* to Te were found deshielded (upto ~22 and 6 ppm, respectively) with respect to those of free $\mathbf{L}^1$. However, signal of C_2 is found unaffected or marginally shielded (with respect to that of $\mathbf{L}^1$), supporting the existence of N···Te secondary interaction in $\mathbf{L}^1$. The signal of –CONH– is found unshifted in $^{13}C\{^1H\}$ NMR of **1**–**4**. The ^1H and $^{13}C\{^1H\}$ NMR spectra of $\mathbf{L}^2$ are characteristic and their assignments are supported by HETCOR spectrum shown in Fig. 1. In ^1H NMR spectrum of **5** the signals of CH_2Te, middle CH_2 and $N–CH_2$ appear deshielded (~0.80, 0.46 and 0.14 ppm, respectively) with respect to those of $\mathbf{L}^2$, indicating in **5** ligation of $\mathbf{L}^2$ is as a (Te, N) donor, which is corroborated by deshielding of C_6, C_7 and C_8 signals (~20, 7.5 and 8 ppm, respectively) in ^{13}C NMR spectrum of **5**, with respect to those of free $\mathbf{L}^2$. The crystals suitable for X-ray diffraction (XRD) could not be grown for **1**–**5**.

3.2. Crystal structures of $\mathbf{L}^1$ and $\mathbf{L}^2$

The molecular structure of $\mathbf{L}^1$ is shown in Fig. 2. The selected bond lengths and angles are given in Table 2. The Te–C(1) (2.107(8) Å) is shorter than Te–C(8) (2.140(8) Å), as is generally reported [18–20] for Te–C(aryl) in comparison to Te–C(alkyl). The

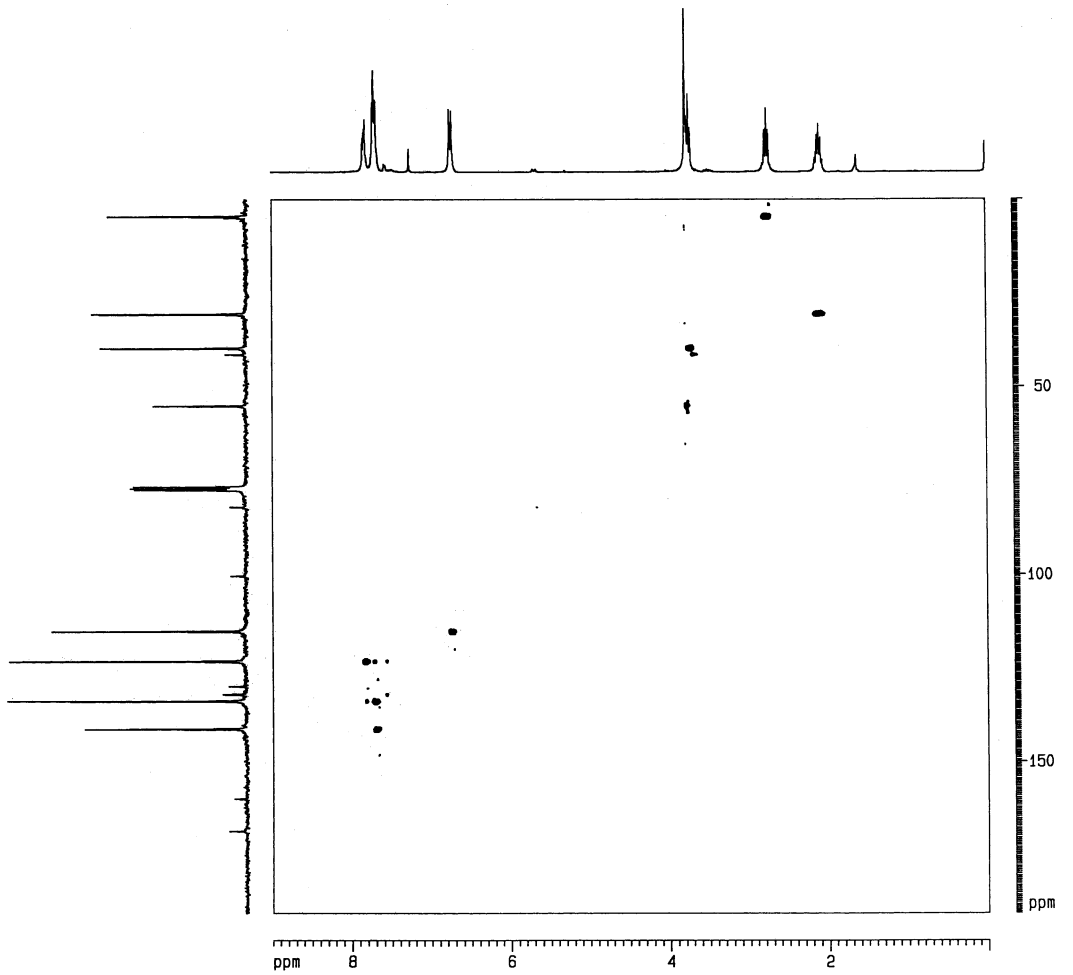


Fig. 1. HETCOR spectrum of $\mathbf{L}^2$.

C(1)–Te–C(8) angle (98.8(3)°) is consistent with the literature reports on alkyl aryl tellurides [18–20]. The C–C bond lengths and C–C–C bond angles of aryl groups are normal (average values 1.372(4)–1.377(4) Å and 119.96(1)°, respectively). The molecular structure of $\mathbf{L}^2$ is shown in Fig. 3(a) and $\mathbf{L}^2\mathbf{H}_2$ in Fig. 3(b). The selected bond lengths and angles for $\mathbf{L}^2$ are given in Table 3. The Te–C(alkyl) bond length is longer than Te–C(aryl) in this case also as observed for $\mathbf{L}^1$. The C(1)–Te(1)–C(8) angle is 94.96(14)° and consistent with the value observed for $\mathbf{L}^1$. The average C–C bond lengths and C–C–C bond angles of substituted phenyl groups are normal (1.384(1) Å and 120.0(1)°). The defining features for the two molecules $\mathbf{L}^2$ and $\mathbf{L}^2\mathbf{H}_2$ present in the mixed crystal ['$\mathbf{L}^2$'] are the angles about C(11) and the C(11)–O(2) bond distances. In spite of the site mixing at C(11)–O(2), resulting from the use of a co-crystal, the geometric parameters for C(11)–O(2) as a carbonyl in the $\mathbf{L}^2$ compound are in very good agreement with expected values. Thus, in $\mathbf{L}^2$ the C(11)=O(2B) bond length is 1.221(4) Å compared with 1.223(4) Å for C(18)=O(3) and the sum of the angles O(2B)–C(11)–N(1), O(2B)–C(11)–C(12), and N(1)–C(11)–C(12) is 356.7° compared with the sum for the corresponding angles around C(18) of 360.1°, as expected for planar sp^2 carbon. In $\mathbf{L}^2\mathbf{H}_2$, the C(11)–O(2A)H bond length is 1.298(6) Å as expected

Table 2
Selected bond lengths (Å) and angles (°) for $\mathbf{L}^1$

Bond lengths			
Te–C(1)	2.107(8)	Te–C(8)	2.140(8)
O(1)–C(4)	1.369(9)	O(1)–C(5)	1.416(13)
O(2)–C(10)	1.215(9)	N–C(10)	1.345(10)
C(10)–C(11)	1.507(10)	C(8)–C(9)	1.490(12)
N–C(9)	1.451(10)		
Bond angles			
C(1)–Te–C(8)	98.8(3)	C(4)–O(1)–C(5)	118.9(8)
C(10)–N–C(9)	122.1(8)	C(6)–C(4)–O(1)	124.4(8)
C(2)–C(1)–Te	118.2(6)	C(7)–C(1)–Te	123.5(6)
O(1)–C(4)–C(3)	116.1(8)	C(9)–C(8)–Te	114.0(7)
N–C(9)–C(8)	111.4(8)	O(2)–C(10)–N	124.4(7)
O(2)–C(10)–C(11)	121.0(7)	N–C(10)–C(11)	114.7(7)
C(16)–C(11)–C(10)	118.2(8)	C(12)–C(11)–C(10)	123.5(7)

Table 3
Selected bond lengths (Å) and angles (°) for $\mathbf{L}^2$

Bond lengths			
Te(1)–C(1)	2.123(4)	Te(1)–C(8)	2.149(4)
O(1)–C(4)	1.367(5)	O(1)–C(7)	1.425(4)
O(3)–C(18)	1.223(4)	O(2B)–C(11)	1.221(4)
N(1)–C(10	1.469(4)	N(1)–C(18)	1.372(4)
C(8)–C(9)	1.521(5)	N(1)–C(11)	1.442(5)
C(11)–C(12)	1.504(6)	C(9)–C(10)	1.499(5)
C(12)–C(13)	1.381(5)	C(12)–C(17)	1.386(5)
C(14)–C(15)	1.402(6)	C(13)–C(14)	1.390(5)
C(16)–C(17)	1.373(5)	C(15)–C(16)	1.378(5)
C(17)–C(18)	1.479(5)		
Te(1)–O(3)	3.700(4)	Te(1)–O(2B)	6.321(4)
Bond angles			
C(1)–Te(1)–C(8)	94.96(14)	C(4)–O(1)–C(7)	117.7(3)
C(2)–C(1)–Te(1)	120.3(3)	C(6)–C(1)–Te(1)	121.1(3)
O(1)–C(4)–C(3)	115.5(4)	O(1)–C(4)–C(5)	124.4(4)
C(9)–C(8)–Te(1)	114.1(3)	C(10)–C(9)–C(8)	113.5(3)
O(2B)–C(11)–N(1)	131.0(5)	O(2B)–C(11)–C(12)	123.1(5)
O(3)–C(18)–N(1)	125.3(4)	O(3)–C(18)–C(17)	128.5(4)
C(18)–N(1)–C(10)	122.8(3)	C(18)–N(1)–C(11)	113.6(3)
C(11)–N(1)–C(10)	123.4(3)	N(1)–C(10)–C(9)	113.4(3)
N(1)–C(11)–C(12)	102.3(3)	N(1)–C(18)–C(17)	106.3(3)
C(17)–C(12)–C(13)	120.3(4)	C(16)–C(15)–C(14)	121.0(4)
C(17)–C(12)–C(11)	109.7(4)	C(17)–C(16)–C(15)	118.0(4)
C(13)–C(12)–C(11)	129.9(4)	C(16)–C(17)–C(12)	122.0(4)
C(12)–C(13)–C(14)	118.5(4)	C(16)–C(17)–C(18)	129.9(4)
C(13)–C(14)–C(15)	120.2(4)	C(12)–C(17)–C(18)	108.1(4)

In $\mathbf{L}^2H_2$, O(2A)–C(11) 1.298(6) Å, O(2A)–C(11)–N(1) 114.7(4)°, O(2A)–C(11)–C(12) 121.8(5)°.

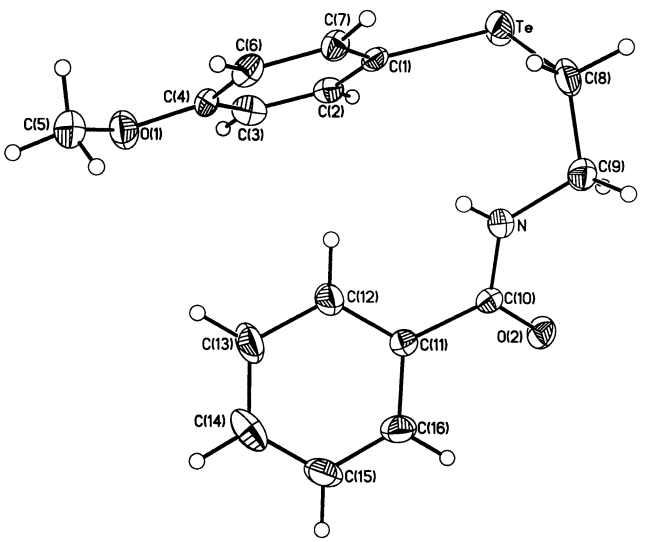


Fig. 2. Molecular structure of $\mathbf{L}^1$.

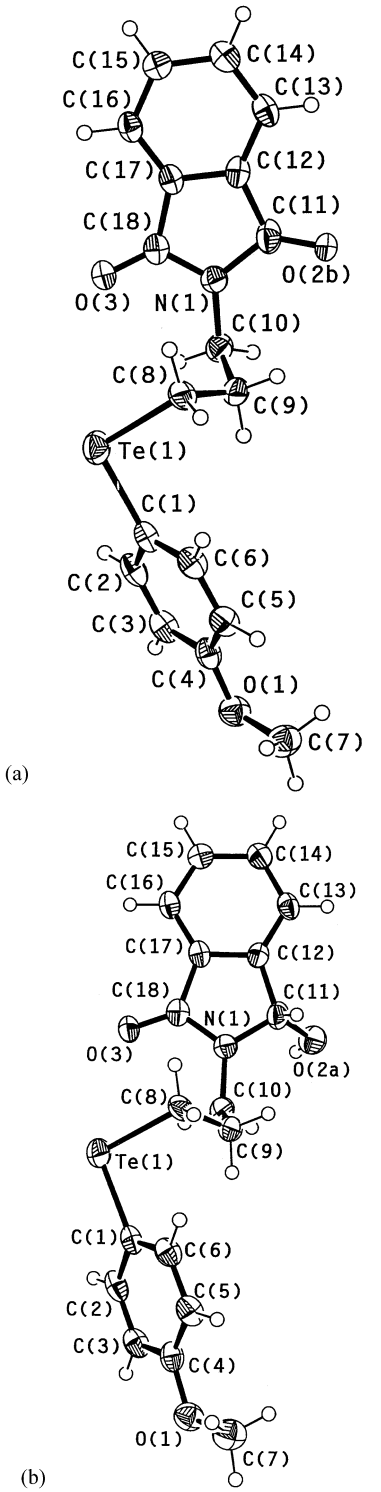


Fig. 3. (a) Molecular structure of $\mathbf{L}^2$. (b) Molecular structure of $\mathbf{L}^2H_2$.

for a C–O single bond, and the sum of the angles O(2A)–C(11)–N(1), O(2A)–C(11)–C(12), and N(1)–C(11)–C(12) is 338.8°, consistent with tetrahedral sp^3 carbon. The possibility of coordinating as a (Te, N) donor is apparent for $\mathbf{L}^1$ and $\mathbf{L}^2$ (Figs. 2 and 3). They may also act as a (Te, N, O) donor in bimetallic complexes.

4. Conclusion

Two new hybrid organotellurium ligands *N*-[2-(4-methoxyphenyltelluro)ethyl]benzamide ($\mathbf{L}^1$) and *N*-[2-(4-methoxyphenyltelluro)propyl]phthalimide($\mathbf{L}^2$) have been synthesized and characterized structurally. The

Te–C(alkyl) bond length is 2.140(8)/2.149(4) Å and longer than Te–C(aryl) 2.107(8)/2.123(5) Å. Both of them coordinate as a (Te, N) donor with Pd(II), Pt(II) or Ru(II).

5. Supplementary material

Crystallographic data for the structural analysis have been deposited with the Cambridge Crystallographic Data Centre, CCDC 151396 for $\mathbf{L}^1$ and 151397 for $\mathbf{L}^2$. Copies of this information may be obtained free of charge from: The Director, CCDC, 12 Union Road, Cambridge CB2 1EZ, UK (fax: +44-1223-336-033; e-mail: deposit@ccdc.cam.ac.uk or www: http://www.ccdc.cam.ac.uk).

Acknowledgements

J.E. Drake wishes to thank the Natural Sciences and Engineering Research Council, Canada. Ajai K. Singh, J. Sooriyakumar and M. Kadarkaraisamy thank Department of Science and Technology (India) for financial support.

References

[1] (a) A.K. Singh, V. Srivastava, J. Coord. Chem. 27 (1992) 237; (b) E.G. Hope, W. Levason, Coord. Chem. Rev. 122 (1993) 109.
[2] A.K. Singh, S. Sharma, Coord. Chem. Rev. 209 (2000) 49.
[3] (a) A. Khalid, A.K. Singh, Polyhedron 16 (1997) 33; (b) R. Batheja, A.K. Singh, Polyhedron 16 (1997) 2509.
[4] (a) V. Srivastava, R. Batheja, A.K. Singh, J. Organomet. Chem. 484 (1994) 93; (b) R. Batheja, S.K. Dhingra, A.K. Singh, J. Organomet. Chem. 487 (1995) 173; (c) A.K. Singh, M. Kadarkaraisamy, G.S. Murthy, J. Srinivas, B. Varghese, R.J. Butcher, J. Organomet. Chem. 605 (2000) 39; (d) A.K. Singh, J. Sooriyakumar, M. Kadarkaraisamy J.E. Drake, M.B.Hursthouse, M.E. Light, R.J. Butcher, J. Chem. Res. (S) (2001) 339.
[5] W.F. Liaw, C.H. Lai, S.J. Chiou, Y.C. Horng, C.C. Chou, M.C. Liaw, G.H. Lee, S.M. Peng, Inorg. Chem. 34 (1995) 3755 and references therein.
[6] (a) W. Levason, S.D. Orchard, G. Reid, Organometallics 18 (1999) 1275; (b) W. Levason, S.D. Orchard, G. Reid, J. Chem. Soc., Dalton Trans. (1999) 823; (c) J.R. Black, N.R. Champness, W. Levason, G. Reid, Inorg. Chem. 35 (1996) 1820; (d) W. Levason, S.D. Orchard, G. Reid, V.-A. Tolhurst, J. Chem. Soc., Dalton Trans. (1999) 2071.
[7] (a) M. Misra, A.K. Singh, Phosphorus Sulfur Silicon 134/135 (1998) 537; (b) M. Misra, A.K. Singh, J. Coord. Chem. 48 (1999) 43; (c) A.K. Singh, C.V. Amburose, M. Misra, R.J. Butcher, J. Chem. Res. (S) (1999) 716.
[8] (a) A.K. Singh, V. Srivastava, Phosphorus Sulfur Silicon 47 (1990) 471; (b) A.K. Singh, V. Srivastava, B.L. Khandelwal, Polyhedron 9 (1990) 495; (c) V. Srivastava, R. Batheja, A.K. Singh, J. Organomet. Chem. 484 (1994) 93.
[9] (a) V.K. Jain, S. Chaudhury, R. Bohra, Polyhedron 12 (1993) 2377; (b) A.K. Singh, V. Srivastava, J. Coord. Chem. 21 (1990) 39; (c) A.K. Singh, J. Sooriyakumar, S. Husebye, K.W. Tornroos, J. Organomet. Chem. 612 (2000) 46.
[10] A. Khalid, A.K. Singh, Polyhedron 16 (1997) 33.
[11] (a) K.D. Hodges, J.V. Rund, Inorg. Chem. 14 (1975) 525; (b) T.B. Rauchfuff, J.S. Shu, D.M. Roundhill, Inorg. Chem. 15 (1976) 2096.
[12] (a) G.M. Sheldrick, SHELXA: Program for Empirical Absorption Correction, University of Göttingen, Göttingen, Germany, 1993; (b) G.M. Sheldrick, SHELXA: Program for Refinement of Crystal Structure, University of Göttingen, Göttingen, Germany, 1993; (c) G.M. Sheldrick, SHELXA: Program for Solution of Crystal Structure, University of Göttingen, Göttingen, Germany, 1986.
[13] Denzo (Z. Otwinowski, W. Minor, Methods in enzymology, in: C.W. Carter Jr., R.M. Sweet, (Eds.), Macromolecular Crystallography, Part A, vol. 276, Academic Press, 1997 pp. 307).
[14] SORTAV (R.H. Blessing, Acta Crystallogr. A51 (1995) 33; R.H. Blessing, J. Appl. Cryst. 30 (1997) 421.
[15] G.M. Sheldrick, Acta Crystallogr. A46 (1990) 467.
[16] G.M. Sheldrick, SHELXL97, University of Göttingen, Germany, 1997.
[17] W.J. Geary, Coord. Chem. Rev. 7 (1971) 81.
[18] J.E. Drake, J. Yang, A. Khalid, V. Srivastava, A.K. Singh, Inorg. Chim. Acta 254 (1997) 57.
[19] J.E. Drake, J.H.E. Bailey, A.K. Singh, V. Srivastava, Acta Crystallogr. C49 (1993) 684.
[20] A.K. Singh, V. Srivastava, S.K. Dhingra, J.E. Drake, J.H.E. Bailey, Acta Crystallogr. C48 (1992) 655.

PERGAMON

Polyhedron 21 (2002) 675–676

POLYHEDRON

www.elsevier.com/locate/poly

Author Index of Symposia-In-Print number 24

Ayers, A.E., see Dias, H.V.R., 611

Barfield, M.E., see Vohs, J.K., 531
Bobev, S. and Sevov, S.C., Isolated deltahedral clusters of lead in the solid state: synthesis and characterization of Rb_4Pb_9 and $Cs_{10}K_6Pb_{36}$ with Pb_9^{4-}, and $A_3A'Pb_4$ (A = Cs, Rb, K; A′ = Na, Li) with Pb_4^{4-}, 641
Brombacher, H., see Craven, E., 553
Brown, S.T., Petraco, N.D.K., Yamaguchi, Y. and Schaefer, H.F., III, $\tilde{X}\ ^3\Sigma^-$ and $\tilde{A}\ ^3\Pi$ electronic states of linear disilaketenylidene (SiSiO): analysis of the Renner effect in the $\tilde{A}\ ^3\Pi$ state. Comparison with the analogous multiple bonded systems SiCO, CSiO, and CCO, 599
Butcher, R.J., see Singh, A.K., 667

Chu, S.-Y., see Lai, C.-H., 579
Cornu, D., Hitchcock, P.B., Lappert, M.F. and Uiterweerd, P.G.H., Some 2,6-bis(dimethylamino)phenyl–mercury(II) and –boron complexes, 635
Craven, E., Mutlu, E., Lundberg, D., Temizdemir, S., Dechert, S., Brombacher, H. and Janiak, C., Thallium(I) complexes with modified poly(pyrazolyl)borate ligands—metal-ligand coordination and crystal packing, 553
Cuypers, L., see Uhl, W., 511

Dechert, S., see Craven, E., 553
Dias, H.V.R. and Ayers, A.E., Reactions of divalent group 14 compounds containing an azide functionality: synthesis and characterization of $[HB(3,5\text{-}(CF_3)_2Pz)_3]AgGe(N_3)[(n\text{-}Pr)_2ATI]$ and $[HB(3,5\text{-}(CF_3)_2Pz)_3]AgSn(N_3)[(n\text{-}Pr)_2ATI]$, 611
Downs, A.J., Himmel, H.-J. and Manceron, L., Low valent and would-be multiply bonded derivatives of the Group 13 metals Al, Ga and In revealed through matrix isolation, 473
Downs, L.E., see Vohs, J.K., 531
Drake, J.E., see Singh, A.K., 667

Fischer, R.A., see Weiß, D., 535
Foley, S.R., Yap, G.P.A. and Richeson, D.S., Synthesis and structural characterization of the first trialkylguanidinate and hexahydropyramidopyramidinate complexes of tin, 619
Frenking, G., see Weiß, D., 535
Fröhlich, N., see Weiß, D., 535

Gade, L.H., see Haller, I., 629
Goodwin, S.D., see Vohs, J.K., 531

Haller, I., Renner, P. and Gade, L.H., A C_3-chiral lithium triamidostannate(II) containing a Sn–Li bond, 629
Hampel, S., see Ruck, M., 651
Harms, K., see Uhl, W., 511
Himmel, H.-J., see Downs, A.J., 473
Hitchcock, P.B., see Cornu, D., 635
Hursthouse, M.B., see Singh, A.K., 667

Janiak, C., see Craven, E., 553
Jeffery, J.C., Leedham, A.P. and Russell, C.A., Synthesis and X-ray structure of a complex containing the trisimido borate trianion—the imido analogue of the orthoborate trianion, 549

Kadarkaraisamy, M., see Singh, A.K., 667
Kano, N., Xing, J.-H., Kawa, S. and Kawashima, T., Cycloaddition reactions of an iminophosphorane bearing the Martin ligand with some double-bond compounds: syntheses, structures and thermolyses of a 1,3,2λ^5-oxazaphosphetidine and a 1,3,2λ^5-diazaphosphetidine-4-thione, 657
Kawashima, T., see Kano, N., 657
Kawa, S., see Kano, N., 657
Kishikawa, K., see Tokitoh, N., 563
Klinkhammer, K., Dihypersilylstannylene and dihypersilylplumbylene—two Lewis-amphoteric carbene homologues, 587
Kloo, L., Rosdahl, J. and Taylor, M.J., The nature of subvalent gallium and indium in aqueous media, 519
Knüfer, A., see Weiß, D., 535
Köhnlein, H., see Schnöckel, H., 489

Lai, C.-H., Su, M.-D. and Chu, S.-Y., Relative stability of multiple bonds between germanium and arsenic. A theoretical study, 579
Lam, W.H. and Lin, Z., Understanding the electron counts of aluminum metalloid clusters, 503
Lappert, M.F., see Cornu, D., 635
Leedham, A.P., see Jeffery, J.C., 549
Light, M.E., see Singh, A.K., 667
Lin, Z., see Lam, W.H., 503
Lundberg, D., see Craven, E., 553

Manceron, L., see Downs, A.J., 473
Merz, K., see Weiß, D., 535
Mutlu, E., see Craven, E., 553

Nakata, N., see Tokitoh, N., 563
Norman, N.C., see Pardoe, J.A.J., 543

Okazaki, R., see Tokitoh, N., 563

Pardoe, J.A.J., Norman, N.C. and Timms, P.L., Studies on BCl and on the exchange reaction of BCl_3 with polyboron fluorides, 543
Parkin, G., Polyhedron Symposa-in-Print, number 24: Subvalent and multiply bonded compounds of the p-block elements, 465
Petraco, N.D.K., see Brown, S.T., 599
Power, P.P., see Stender, M., 525
Prött, M., see Uhl, W., 511

Renner, P., see Haller, I., 629
Richeson, D.S., see Foley, S.R., 619

PII: S0277-5387(02)00890-2

Robinson, G.H., see Vohs, J.K., 531
Rosdahl, J., see Kloo, L., 519
Ruck, M. and Hampel, S., Stabilization of homonuclear Bi_5^{+} and Bi_6^{2+} polycations by cluster anions in the crystal structures of $Bi_{12-x}IrCl_{13-x}$, $Bi_{12-x}RhCl_{13-x}$ and $Bi_{12-x}RhBr_{13-x}$, 651
Russell, C.A., see Jeffery, J.C., 549

Sasamori, T., see Tokitoh, N., 563
Schaefer, H.F., III, see Brown, S.T., 599
Schnöckel, H. and Köhnlein, H., Synthesis and structure of metalloid aluminum clusters—intermediates on the way to the elements, 489
Sevov, S.C., see Bobev, S., 641
Singh, A.K., Sooriyakumar, J., Kadarkaraisamy, M., Drake, J.E., Hursthouse, M.B., Light, M.E. and Butcher, R.J., *N*-[2-(4-Methoxyphenyltelluro)ethyl]benzamide ($\mathbf{L}^1$) and *N*-[2-(4-methoxyphenyl telluro)propyl]phthalimide ($\mathbf{L}^2$): synthesis and ligation with palladium(II), platinum(II) and ruthenium(II). Crystal structures of $\mathbf{L}^1$ and $\mathbf{L}^2$, the latter as a mixed crystal with $\mathbf{L}^2H_2$, 667
Sooriyakumar, J., see Singh, A.K., 667
Stender, M. and Power, P.P., Reaction of $\{HC(CMeNAr)_2\}Li$ (Ar = 2,6-*i*-$Pr_2C_6H_3$) with indium monochloride to yield the In–In bonded dimer $[\{HC(CMeNAr)_2\}InCl]_2$ and the hydroxide $[\{HC(CMeNAr)_2\}InCl(\mu\text{-}OH)]_2$, 525
Su, M.-D., see Lai, C.-H., 579

Takeda, N., see Tokitoh, N., 563
Taylor, M.J., see Kloo, L., 519
Temizdemir, S., see Craven, E., 553
Timms, P.L., see Pardoe, J.A.J., 543
Tokitoh, N., Kishikawa, K., Okazaki, R., Sasamori, T., Nakata, N. and Takeda, N., Synthesis and characterization of an extremely hindered tetraaryl-substituted digermene and its unique properties in the solid state and in solution, 563

Uhl, W., Cuypers, L., Prött, M. and Harms, K., Molecular self-assembly controlled by gallium–gallium single bonds—facile syntheses of macrocyclic octagallium compounds, 511
Uiterweerd, P.G.H., see Cornu, D., 635

Vohs, J.K., Downs, L.E., Barfield, M.E., Goodwin, S.D. and Robinson, G.H., Synthesis and molecular structure of tris(pentamethylphenyl)gallium, 531

Weiß, D., Winter, M., Merz, K., Knüfer, A., Fischer, R.A., Fröhlich, N. and Frenking, G., Synthesis, structure and bonding situation of $[(dcpe)Pt(InCp^*)_2]$ and $\{(dcpe)Pt[GaC(SiMe_3)_3]_2\}$—two novel examples of platinum complexes of low valent Group 13 metal species, 535
West, R., Multiple bonds to silicon: 20 years later, 467
Winter, M., see Weiß, D., 535

Xing, J.-H., see Kano, N., 657

Yamaguchi, Y., see Brown, S.T., 599
Yap, G.P.A., see Foley, S.R., 619

PERGAMON

Polyhedron 21 (2002) 677–681

POLYHEDRON

www.elsevier.com/locate/poly

Investigation of phthalocyanine crystals exposed to NO_2 ambient gas

Rudolf Słota *, Gabriela Dyrda, Witold Wacławek

Institute of Chemistry, University of Opole, ul. Oleska 48, 45-095 Opole, Poland

Received 3 August 2001; accepted 31 October 2001

Abstract

Crystals of free base phthalocyanine (H_2pc) and its unsubstituted metal derivatives Mpc (where M = Ni, Cu, Zn, Pb, and pc = $C_{32}H_{16}N_8^{2-}$ = phthalocyanine ligand) were examined after being exposed to NO_2 ambient gas. Scanning electron microscopy (SEM) supported by X-ray microprobe analysis (EDAX), UV–Vis and FTIR spectroscopy as well as X-ray powder diffractometry (XRD) were applied to study the crystals chemistry and surface morphology. The NO_2 molecules were found to penetrate the crystal unit which led to the breakdown of the phthalocyanine macrocycle. The surface of the doped crystals has been scaled and covered by a layer composed predominantly of phthalimide. Despite vacuum desorption, it has been proved some free NO_2 to be still adsorbed by the studied material. © 2002 Published by Elsevier Science Ltd.

Keywords: Phthalocyanines; Nitrogen dioxide; Scanning electron microscopy; X-ray microprobe; UV–Vis and FTIR spectroscopy; X-ray powder diffractometry

1. Introduction

Metal complexes of phthalocyanine (H_2pc) along with a number of its derivatives are considered for many electronic and opto-electronic applications, one of the most promising to be gas sensors [1,2]. High thermal stability of the molecules, semi-conductivity (or even metallic features) and interesting optical properties have placed phthalocyanine based materials among the top attractive ones for modern technologies. It is obvious, that quality demands also include a considerable durability of those materials towards chemicals and radiation, which might have affected the molecular structure and thus alter its properties. This is of particular importance when phthalocyanine based devices are designed to operate under oxidising conditions, e.g. in the presence of nitrogen oxides, halogens, air oxygen etc.

The phthalocyanines represent a family of quite well recognised macrocyclic compounds characterised by a variety of molecular structures [3]. However, regardless of the structural modification, the chemistry of these species has been dominated by the nature of the phthalocyanine ligand. This may be addressed to the strength of the overall molecular set-up, as well.

In a phthalocyanine moiety, the four coupled benzopyrole units forming the characteristic macrocycle produce a quite stable bonding system, the properties of which is determined by the conjugated π electron system of the whole molecule. This arrangement becomes more stable when a metal atom is complexed by the four inner nitrogen atoms.

Under oxidising conditions the molecules stability has proved to be considerably reduced, particularly when in solution. In the studied cases, the system was found completely chemically altered by the action of oxidants like NO_2 [4–6]. However, as far as the solid phthalocyanine material is concerned, there is some discussion in the literature as to the extent the phthalocyanine molecules are being affected. Although there is enough evidence for a structural breakdown (e.g. [6,7]) which is reflected in the reaction products of the phthalocyanine–NO_2 interaction, such as phthalimide, however, at lower concentrations of NO_2 that interaction is also considered in terms of reversible chemisorption [5,8].

It seems that the surface processes occurring at a phthalocyanine grain during the adsorption of NO_2 still need to be given a detailed research. The morphology of

* Corresponding author. Tel.: +48-77-454-5841x2554; fax: +48-77-441-0740.

E-mail address: rslota@uni.opole.pl (R. Słota).

0277-5387/02/$ - see front matter © 2002 Published by Elsevier Science Ltd.
PII: S0277-5387(02)00832-X

Table 1
Effect of NO_2 molecules, not removed by vacuum desorption, upon the kinetics of H_2pc and Pbpc decomposition in concentrated H_2SO_4

Sample	H_2pc				Pbpc
	Reference [a]	1 h desorption	24 h desorption	No desorption	1 h desorption
k_e (min^{-1})	0.0018	0.0027	0.0025	0.0041	0.0028

$X_{NO_2} \sim 5 \times 10^{-5}$, $T = 298$ K, 10 min exposure time; k_e, effective reaction rate constant. ($H_2pc \rightarrow^{k_e}$ products; $-dc/dt = k_e c$, according to [17]).
[a] Sample not exposed to NO_2.

phthalocyanine thin solid films used for NO_2 detection was discussed, e.g. in [9] and [10] but merely for the non doped material. However, results of a SEM investigation presented in [11] have supplied evidence for the phthalocyanine ligand decay due to the action of NO_2. One may suppose then that most of the calibration problems reported for phthalocyanine-based gas sensors (e.g. [9,10]) may result from a molecular degradation rather than from different reasons related to physical changes only in the phthalocyanine layer exposed to the ambient gas.

The research carried out by our group was designed to supplement the existing data concerning the influence of oxidising radical chemicals upon the phthalocyanine compounds. In particular, it was focused on the chemistry of the crystal surface during and after gas doping. Unlike others, in our study we have used predominantly single crystals of the phthalocyanine material, first of all in order to minimise the effect of a large specific surface area displayed by the polycrystalline solid films or powders. Electronic absorption spectra were registered predominantly in concentrated sulfuric acid, which is believed to be the best phthalocyanine solvent and allows also to explore the UV range. Thus, we could follow not only the changes of the phthalocyanine moiety, represented by a set of bands in the Vis range but also trace the formation of the phthalocyanine decay products, which absorb exclusively in the UV range.

2. Experimental

The phthalocyanines used were synthesised and purified in our laboratory. Well developed needle-like crystals approximately 0.2 mm thick and 3–10 mm long of H_2pc and Mpc (where M = Ni, Cu, Zn) as well as the prismatic crystals of Pbpc (ca. 0.3 mm thick and 4 mm long) were obtained by vacuum sublimation. For comparison, fine polycrystalline powders of these compounds were used, as well.

Vacuum dried samples (0.005 g) of the phthtalocyanine material were exposed to NO_2 in a 2 l round-bottomed glass flask at 298 K for 10 min. Afterwards the system was evacuated at the same temperature for 1 h ($p \approx 10$ Pa) and the samples were stored in a desiccator over silica gel. Gas concentrations, expressed by the molar fraction of NO_2 in the ambient (X_{NO_2}), were approximately 1×10^{-6}, 1×10^{-5} and 5×10^{-5}. Higher temperatures (up to 473 K) as well as longer exposure and evacuation (desorption) times were also applied.

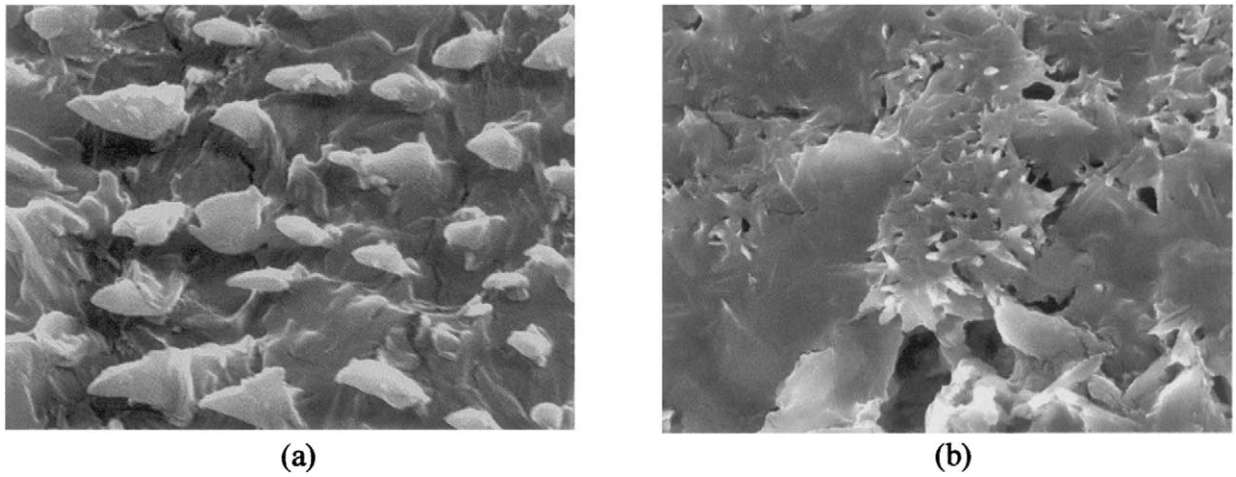


Fig. 1. SEM micrographs of the surface of phthalocyanine crystals after exposure to NO_2 at 298 K. (a) H_2pc, $X_{NO_2} \sim 10^{-6}$ (10 000 ×); (b) Cupc, $X_{NO_2} \sim 10^{-5}$ (2000 ×). A crystalline copper reaction product (centre).

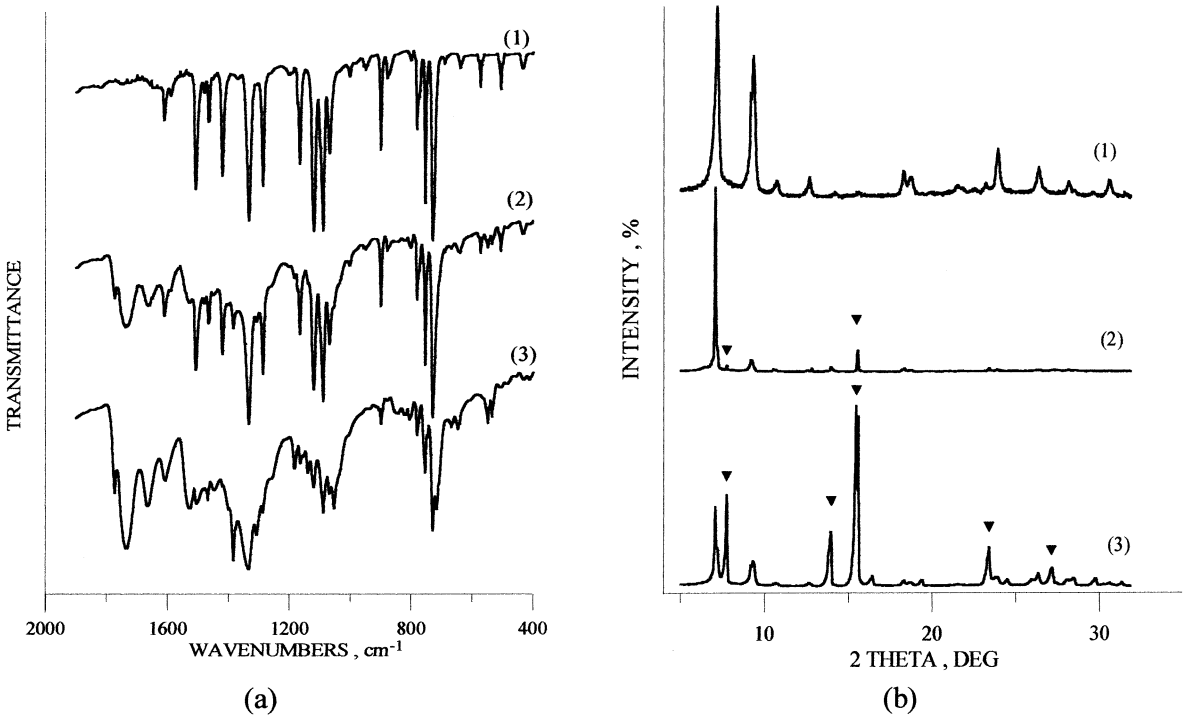


Fig. 2. Effect of NO_2 upon Cupc crystals expressed by FTIR spectra (a) and X-ray powder diffraction patterns (b). $X_{NO_2} \sim 5 \times 10^{-5}$, exposure time 10 min, desorption time 1 h. (1) Pure β-Cupc (Ref. [13]), (2) Cupc+NO_2 at 298 K, (3) Cupc+NO_2 at 473 K. ▼-phthalimide (Ref. [13]).

For the SEM investigations a JEOL JSM-5400 scanning electron microscope equipped with an energy dispersive X-ray analyser (EDAX) was used and all specimens were gold coated. The chemistry of the studied material was followed by UV–Vis (Unicam UV-300) and FTIR (Philips FTIR PU 9800) spectroscopy as well as X-ray powder diffractometry (XRD) (Philips PW 3710). Higher gas concentrations ($X_{NO_2} \approx 5 \times 10^{-5}$) were used only to emphasise the effect of NO_2 in the IR spectra and powder diffraction patterns as well as in the UV–Vis quantitative and kinetic studies.

The electronic absorption spectra were registered in concentrated sulfuric acid (95.5%) and in the case of Znpc and Pbpc also in dimethylformamide. IR spectra were collected for samples in KBr pellets.

3. Results and discussion

As it may be learned from Fig. 1, the morphology of the primarily smooth and clean phthalocyanine crystals has been dramatically changed after being exposed to NO_2. The surface is scaled and reaction products could be seen spread over it. Surface line-scans performed by the X-ray microprobe have revealed perforations of approximately 1–5 μm which indicate for a quite deep penetration of the crystal unit by NO_2 even at 298 K. Elemental EDAX analyses performed at the materials surface have shown particular high concentrations of the oxygen atoms, in contrast to the pure (undoped) phthalocyanine crystals. This confirms the reaction products to be oxidised fragments of the phthalocyanine ring. Crystalline metal compounds including both N and O elements have also been found, presumably nitrates of the complexed metals (Fig. 1(b)). IR spectroscopic studies (Fig. 2(a)) have proved the fragmentation of the macrocycle and the formation of phthalimide, featured by a characteristic set up of bands including a very strong one at 1745 cm^{-1} with a *satellite* at 1753 cm^{-1} [12]. This is also reflected in the X-ray powder diffractograms presented in Fig. 2b, registered for the doped material, which show a pattern of peaks corresponding to phthalimide [13]. At elevated temperatures the penetration of the crystals by NO_2 and thus the macrocycle degradation is yet more pronounced (Fig. 2). Similar effects one may expect not only at higher NO_2 concentrations but also at a longer exposure time, as it has been proved in our tests. The reaction progress has been noticeably increased when the phthalocyanine material used in our experiments was a powder instead of single crystals.

There is also some evidence both in the IR spectra and X-ray patterns for other intermediate and/or by-products being formed. Changes observed exclusively in the X-ray patterns of metal phthalocyanines, as shown in Fig. 2b, are similar to those reported in [14] and may suggest the formation of a phthalocyanine derivative with axially co-ordinated NO_2 ligand(s), as shown in

[15,16]. However, attempts to isolate or identify other reaction products but phthalimide have failed.

Spectra registered in the UV–VIS range also proved the cleavage of the phthalocyanine macrocycle by NO_2, reflected by a decrease in absorbance (Q band) of about 5% when and $X_{NO_2} \approx 1 \times 10-5$ and 13–15% when $X_{NO_2} \approx 5 \times 10^{-5}$ (exposure for 10 min at $T = 298$ K). Moreover, there is also a new distinct band to be seen at $\lambda = 227$ nm in the spectra registered in sulphuric acid, which we have proved to be characteristic of phthalimide. We have found no peculiar relation to the complexed metal, as far as the strength of the phthalocyanine macrocycle towards NO_2 is concerned. However, studies performed in concentrated sulphuric acid have revealed some differences in the chemistry of H_2pc and the studied metal phthalocyanines after being exposed to NO_2. Both H_2pc and Mpc' s treated with NO_2, on evacuation release the previously adsorbed gas molecules, which have not yet reacted with the solid material. Kinetic studies of such after-desorption samples dissolved in the acid have revealed a progressive decrease in the compounds concentration but only in the cases of H_2pc and Pbpc. Although it is typical for H_2pc to decompose in concentrated sulphuric acid [17], nevertheless the reaction rate has been considerably increased in comparison with samples not exposed to NO_2, as shown in Table 1. The labile Pbpc complex is being immediately converted into H_2pc when dissolved in sulphuric acid [4], thus the observed kinetic effects in the both cases were similar. Extending of the desorption time up to 24 h in the case of H_2pc resulted in a little change only in the reaction rate. Opposite to H_2pc and Pbpc, solutions of Nipc, Cupc and Znpc remained stable. However, samples which were not subject to desorption gradually decomposed in sulphuric acid solutions regardless of the complexed metal.

This observation has provided evidence that after a low pressure desorption there is some free NO_2 left in the system, still adsorbed by the material, probably under the layer of the reaction products covering the crystals surface. These gas molecules may have a little chance to escape due to difficulties in diffusion. After dissolving in sulphuric acid, due to the presence of NO_2, the oxidising potential of the obtained solution is being increased and consequently the decay of the phthalocyanine macrocycle is accelerated, as we have found for H_2pc (and Pbpc). It is not quite clear why this was not observed in the case of Nipc, Cupc and Znpc. One reason could be a less compact structure of the bulk layer of reaction products which would enhance the diffusion of NO_2 molecules out of the system during desorption. One may expect the metal nitrates (identified in the SEM studies, see Fig. 1b) to contribute in the formation of a more loose bulk structure than that of phthalimide being the only solid product formed in the case of H_2pc exposed to NO_2. Another explanation may result from the formation (besides phthalimide and metal nitrates) also of axially NO_2-substituted metal phthalocyanines of the kind shown in [15,16]. The gas molecules entrapped at the crystals surface could be used to produce such a complex, whereas in the case of the metal free phthalocyanine, H_2pc, it would not be possible. However, such a complex of Pbpc, due to the labile metal–ligand (Pb^{2+}–pc^{2-}) bond should rapidly decompose in the sulfuric acid to produce H_2pc and give off the NO_2 molecules. This may explain the different behaviour of Pbpc in comparison with the other metal phthalocyanines.

In conclusion of our work, it has to be emphasised that the cleavage of the phthalocyanine macrocycle by NO_2 is an irreversible process. Formation of phthalimide as the principal reaction product clearly indicates the attack of NO_2 molecules has been focused first of all at the bridging nitrogen atoms, thought to be the weakest site of the phthalocyanine ring [18]. Since that, it seems not possible to stabilise the macrocycle towards NO_2 neither by changing the co-ordinated metal nor axial or peripheral substitution of the phthalocyanine molecule. The extent of the macrocycle decay is strongly related to the concentration of NO_2 in the ambient and the chemistry at the surface of the doped compound. Our SEM investigations have confirmed the reaction to occur even at $X_{NO_2} \approx 10^{-6}$. Therefore, the question, if there is a possible reversible chemisorption at much lower (e.g. sub-ppm) concentrations of NO_2 seems to be still open and needs to be given a reasonable explanation.

References

[1] N.R. Armstrong, J. Porphyrins Phthalocyanines 4 (2000) 414.
[2] A.W. Snow, W.R. Barger, in: C.C. Leznoff, A.B.P. Lever (Eds.), Phthalocyanines Properties and Applications, vol. 1, VCH Publishers, New York, 1989.
[3] C. Ercolani, J. Porphyrins Phthalocyanines 4 (2000) 340.
[4] A.B.P. Lever, Adv. Inorg. Radiochem. 7 (1965) 86.
[5] J. Souto, J.A. de Saja, M.I. Gobernado-Mitre, M.L. Rodriguez, R. Aroca, Sens. Actuat. B 15–16 (1993) 306.
[6] R. Słota, Ph.D. Thesis, Warsaw Polytechnical University, Warsaw, Poland, 1995.
[7] C.L. Honeybourne, R.J. Ewen, J. Phys. Chem. Solids 44 (1983) 215.
[8] D.G. Zhu, M.C. Petty, M. Harris, Sens. Actuat. B 2 (1990) 265.
[9] M. Trometer, R. Even, J. Simon, A. Dubon, J.-Y. Laval, J.P. Germain, C. Maleysson, A. Pauly, H. Robert, Sens. Actuat. B 8 (1992) 129.
[10] Y. Sadaoka, T.A. Jones, W. Gopel, Sens. Actuat. B 1 (1990) 148.
[11] M.S. Nieuwenhuizen, A.J. Nederlof, A.W. Barendsz, Anal. Chem. 60 (1988) 230.
[12] Hummel and Scholl Atlas of Polymer and Plastic Analysis, vol. 2Part a/II, No. 4249 (Phthalimide), Carl Hanser Verlag, Munich, 1990.
[13] X-ray Powder Diffraction Files, PC-APD Diffraction software, β-H_2pc (ref. No. 37-1844), β-Cupc (ref No. 39-1881), phthalimide (ref. No. 11-0924).

[14] R. Kubiak, J. Janczak, K. Ejsmont, Chem. Phys. Lett. 245 (1995) 249.
[15] H. Homborg, H. Huckstadt, Z. Naturforsch., Teil. B 52 (1997) 1003.
[16] S. Sieversten, et al., J. Porphirines Phthalocyanines 1 (1997) 379.
[17] B.D. Berezin, Coordination Compounds of Porphyrins and Phthalocyanines, Wiley, New York, 1981.
[18] J.D. Wright, Mat. Sci. 13 (1987) 295.

PERGAMON

Polyhedron 21 (2002) 683–687

POLYHEDRON

www.elsevier.com/locate/poly

The thermodynamic studies of the molecular interactions of dimethyltin(IV) dichloride with free base *meso*-tetraarylporphyrins

Mozaffar Asadi [a,*], Abedien Zabardasti [a], Jahanbakhsh Ghasemi [b]

[a] *Chemistry Department, College of Sciences, Shiraz University, Shiraz, Islamic Republic of Iran*
[b] *Chemistry Department, College of Sciences, Razi University, Kermanshah, Islamic Republic of Iran*

Received 7 September 2001; accepted 28 November 2001

Abstract

The interactions of Me_2SnCl_2 with *para*-substituted *meso*-tetraphenylporphyrins ($H_2T(4\text{-}X)PP$; X = OCH_3, CH_3, H and Cl) have been studied by the UV–Vis method. Equilibrium constants, K_1 and K_2, have been calculated by using UV–Vis titration spectra and data refinement was carried out with the computer SQUAD program. Adducts of composition 1:1 and 2:1 of Me_2SnCl_2 to porphyrins, [$(Me_2SnCl_2)(H_2T(4\text{-}X)PP)$] and [$(Me_2SnCl_2)_2(H_2T(4\text{-}X)PP)$], coexist in the solution. Thermodynamic parameters for adduct formation are also determined. Adduct stability constants decrease with decreasing electron donation of the free base porphyrins in the order: $H_2TpAP > H_2TpTP > H_2TPP > H_2TpCP$. © 2002 Published by Elsevier Science Ltd.

Keywords: Adduct formation; Thermodynamics; Tin compounds; Porphyrins; Equilibrium constant; Spectral method

1. Introduction

Molecular interactions of organotin(IV) halides with a variety of uni- and bidentate nitrogen donor ligands have been studied [1–4]. Organotin(IV) halides are very important because of their antitumor properties [5]. Therefore their interactions with biological systems have been the subject of a lot of investigations [6–8]. Studies of compounds of the type R_2SnX_2L, where L is a bidentate N-donor ligand showed that increasing stability is thought to reduce activity by hindering the dissociation of the ligand which is necessary for binding between tin and DNA [9]. In view of these encouraging results, this led us to investigate the solution equilibria of organotin(IV) halide complexes with a number of free base *para*-substituted *meso*-tetraphenylporphyrins. The molecular interactions of tetraarylporphyrins with π-acceptor molecules such as nitroaromatic systems [10,11], tetracyanoethylene [12] and 2,3-dichloro-5,6-dicyanobenzoquinone have been studied [13]. Here we believe that tetraarylporphyrins act as bidentate bridging ligands toward dimethyltin(IV) dichloride. This work is specified to the studies of the thermodynamics of the adduct formation of Me_2SnCl_2 with H_2TPP (*meso*-tetraphenylporphyrin), H_2TpCP (*meso-tetrakis*-(*para*-chlorophenyl)porphyrin), H_2TpTP (*meso*-tetra-*para*-tolylporphyrin) and H_2TpAP(*meso*-tetra-*para*-anisylporphyrin).

2. Experimental

2.1. Chemicals

Benzaldehyde and *para*-substituted benzaldehydes (Merck and Fluka) were used as received. Pyrrole (Fluka) was distilled before use. Propionic acid and chloroform (Merck) employed for the synthesis and the purification of free base porphyrins were used as received. Chloroform solvent for UV–Vis measurements was distilled over K_2CO_3 before use.

2.2. Instrumental

UV–Vis measurements were carried out in a JASCO V-530 UV–Vis spectrometer equipped with a LAUDA ecoline RE 104 thermostat.

* Corresponding author. Tel.: +98-711-228-4822; fax: +98-711-228-0926.
E-mail address: asadi@chem.susc.ac.ir (M. Asadi).

0277-5387/02/$ - see front matter © 2002 Published by Elsevier Science Ltd.
PII: S0277-5387(02)00850-1

2.3. Preparations

Dimethyltin(IV) dichloride was prepared by the reaction between Me_4Sn and anhydrous $SnCl_4$ and purified by sublimation [14]. H_2TPP, H_2TpCP, H_2TpTP and H_2TpAP were prepared by a general procedure for the synthesis of *meso*-tetraarylporphyrins [15], and purified by chromatography on a neutral alumina column.

2.3.1. General procedure for the synthesis of meso-tetraarylporphyrins

meso-Tetra(4-methoxyphenyl)porphyrin: 4-methoxybenzaldehyde (10 mmoles) was mixed with propionic acid (35 ml) and nitrobenzene (15 ml). Pyrrole (10 mmoles) was added and the mixture was kept at 120° C for 1 h. On cooling, the porphyrin precipitated directly from the reaction mixture and was isolated by filtration.

2.4. Spectroscopic measurements

UV–Vis measurements were carried out by the titration method at 5.0, 10.0, 15.0, 20.0, and 25.0 ± 0.1 °C. In a typical measurement, 2.5 ml solution of H_2TPP (1×10^{-5} M) in chloroform was titrated with Me_2SnCl_2 (0.0125 M). UV–Vis spectra were recorded in range 396–710 nm about 15 min after each addition. In this range of spectra about 30–40 wavelengths which had suitable variations of absorbance upon addition of Lewis acid were selected and the equilibrium constants and other thermodynamic parameters of adduct formation were calculated. Equilibrium constants were calculated by the SQUAD program [16,17].

SQUAD is a program with the capability of refining the stability constants of a general complex $M_mM_lH_kL_nL_q$, where $m,l,n,q > 0$ and k is positive for protons, negative for hydroxide ions or zero, employing a non-linear least-squares approach. The data fed to SQUAD are absorption spectra, chemical composition (total concentrations of M, M′, L, L′, and pH) and a chemical model to describe the system. The residual sum (U) is calculated from the following equation:

$$U = \sum_{\mathrm{I}}^{\mathrm{I}} \sum_{\mathrm{I}}^{\mathrm{NW}} (A_{i,k}^{\mathrm{calc}} - A_{i,k}^{\mathrm{obs}})^2$$

where the $A_{i,k}$ is the absorbance value of the ith solution at the kth wavelength, given a total of I solutions and a grand total of NW wavelengths.

3. Results and discussion

On addition of excess of Me_2SnCl_2 to a solution of free base porphyrin in chloroform its purple color changes to green, change in color is due to the interactions of Me_2SnCl_2 with free base porphyrin. By addition of *n*-hexane to these green solutions, slowly, green powdery products were obtained; attempts for further purification and recrystallization of these crude products were unsuccessful. This product can also be obtained by dissolving H_2TPP and excess Me_2SnCl_2 in $CHCl_3$ or CH_2Cl_2 followed by evaporation of the solvent at room temperature. Elemental analysis of these products (Table 1) have good agreement with adducts of composition 2:1 Me_2SnCl_2 to $H_2T(4\text{-}X)PP$. On the basis of these results we suggest that free base porphyrins as bidentate bridging ligands make a bridge between two molecules of the Lewis acid. It is probable that two neighboring nitrogen atoms of the porphyrin bound to one of the Me_2SnCl_2 molecules which is positioned above of the porphyrin plane and other two nitrogen atoms bound to the second Me_2SnCl_2 molecule from below this plane (Fig. 1). Therefore we have a structure relatively similar to that suggested by Smith et al. for XHg–TPP–HgX; $X=Cl^-$, CH_3COO^- [18]. Interactions of Me_2SnCl_2 with $H_2T(4\text{-}X)PP$ are very sensitive to temperature (Fig. 2). By increasing the temperature, the green color of the product solution changes to brown and returns to the primary color of free base porphyrin solution, eventually. Adduct forma-

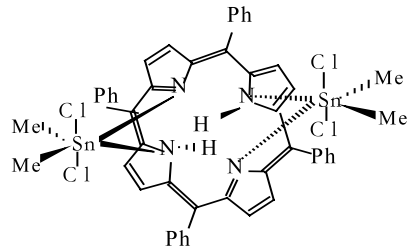


Fig. 1. The schematic illustration of bonding interactions for $(Me_2SnCl_2)_2H_2TPP$ adducts.

Table 1
Elemental microanalysis of Me_2SnCl_2–$H_2T(4\text{-}X)PP$ adducts

	Found (%)			Calculated (%)		
	C	H	N	C	H	N
$(Me_2SnCl_2)_2H_2TpCP$	49.16	3.25	4.95	48.30	3.18	4.69
$(Me_2SnCl_2)_2H_2TPP$	52.15	3.89	4.98	54.60	3.98	5.30
$(Me_2SnCl_2)_2H_2TpTP$	59.10	4.72	5.30	56.87	4.50	5.04
$(Me_2SnCl_2)_2H_2TpAP$	51.13	4.46	4.50	53.40	4.25	4.77

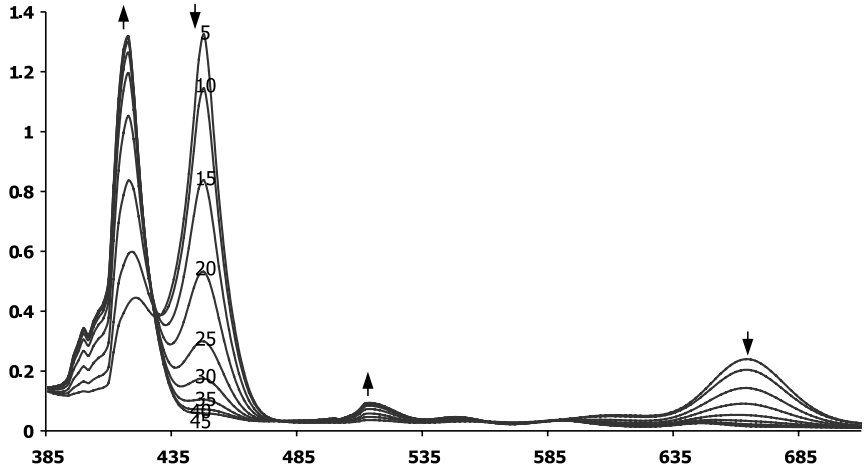


Fig. 2. Thermal dissociation spectra of Me_2SnCl_2–H_2TpCP adduct: by addition of Me_2SnCl_2 (0.0125 M, 0.5 ml) to the solution of H_2TpCP (5×10^{-6} M, 2.5 ml) in chloroform in an UV–Vis cell at 5° C, the Me_2SnCl_2–H_2TpCP adducts were recently formed. The composition of the cell remained constant and the temperature was raised to 45° C stepwise, isosbestic point at 428 nm. This spectrum is similar to that reported for acidic dissociation of the ClHg–TPP–HgCl complex, [21] in which ClHg–TPP–HgCl returned to H_2TPP and $HgCl_2$.

tions are not observed in ligating solvents such as CH_3CN and DMSO under these conditions. Interactions of dimethyltin(IV) dichloride with free base porphyrins were studied spectrometrically by the UV–Vis method.

3.1. UV–Vis analysis

By interaction of $H_2T(4\text{-X})PP$ with Me_2SnCl_2, the original peaks of free base tetraarylporphyrins slowly vanished and two new peaks appeared (Table 2). For example, by addition of Me_2SnCl_2 to H_2TpCP the original peaks (418, 514, 550, 589, 645 nm) vanished and new peaks appeared at 447 and 664 nm with a clear isosbestic point at 428 nm (Fig. 3).

3.2. Thermodynamic studies

The thermodynamic parameters are useful tools for studying these interactions and understanding the relative stability of adducts. The equilibrium constants were determined at several temperatures by analyzing the concentration and temperature dependence of UV–Vis absorptions by the SQUAD program. These absorptions were analyzed by using the following mole ratios of the acid to base as models of interaction between Me_2SnCl_2 and the typical $H_2T(4\text{-X})PP$: (1) formation of the 1:1 adduct, (2) formation of the 2:1 adduct and (3) simultaneous formation of the 1:1 and 2:1 adducts. The fit of the model to the experimental data, 15 points, is measured by the sum of the squares of the deviations of the experimental points from the point calculated by the model. For the proposed models, the simultaneous formation of 1:1 and 2:1 adducts of acid to base has the best fitting and the produced error sum of squares was between 10^{-2} and 10^{-3}. Van't Hoff plots of these formation constants, K_1 and K_2, and the overall formation constant β_2 led to the other thermodynamic parameters ΔH° and ΔS° (Tables 3–5).

Table 2
UV–Vis peaks λ ($CHCl_3$, nm) of the free base $H_2T(4\text{-X})PP$ and $H_2T(4\text{-X})PP$ adducts with Me_2SnCl_2

H_2TPP	417	514	549	589	646
H_2TPP (adduct)	445			660	
H_2TpCP	418	514	550	589	645
H_2TpCP (adduct)	447			664	
H_2TpTP	419	516	552	591	647
H_2TpTP (adduct)	448				672
H_2TpAP	421	518	555	593	650
H_2TpAP (adduct)	453				690

The data of Table 3 show that the equilibrium constant of adducts undergo a regular increase from H_2TpCP, H_2TPP, H_2TpTP, to H_2TpAP. For example, at 5° C we have the following order of formation constants:

$$Me_2SnCl_2\text{–}H_2TpCP < Me_2SnCl_2\text{–}H_2TPP < Me_2SnCl_2\text{–}H_2TpTP < Me_2SnCl_2\text{–}H_2TpAP$$

$$\log K_1 \quad 2.15 < 3.56 < 4.84 < 4.90$$

$$\log K_2 \quad 3.95 < 4.05 < 5.22 < 5.35$$

Tables 4 and 5 show the thermodynamic parameters obtained for the interactions of Me_2SnCl_2 with $H_2T(4\text{-X})PP$ in chloroform.

The results in Tables 3 and 4 show that the kind of substituent (X) on the phenyl rings of $H_2T(4\text{-X})PP$ significantly influences the interactions of the corresponding free base porphyrin with Me_2SnCl_2. Both the free energy and the enthalpies of adduct formation become more negative through the series H_2TpCP, H_2TPP, H_2TpTP to H_2TpAP, considerably, which

Table 3
The formation constants log K_1 and log K_2 for Me_2SnCl_2–$H_2T(4\text{-X})PP$ adducts in $CHCl_3$ solvent

		Temperature (°C)				
		5	10	15	20	25
H_2TpCP	log K_1	2.15±0.01	2.00±0.01	1.73±0.01	1.45±0.01	
	log K_2	3.95±0.01	3.66±0.01	3.41±0.01	3.19±0.01	
H_2TPP	log K_1	3.56±0.01	3.20±0.01	2.96±0.01	2.80±0.01	2.42±0.01
	log K_2	4.05±0.02	3.75±0.01	3.50±0.01	3.01±0.01	2.63±0.01
H_2TpTP	log K_1	4.84±0.01	4.50±0.01	4.10±0.01	3.68±0.01	3.37±0.01
	log K_2	5.22±0.01	4.80±0.01	4.36±0.01	4.13±0.01	3.62±0.01
H_2TpAP	log K_1	4.90±0.01	4.60±0.01	4.15±0.01	3.76±0.01	3.50±0.01
	log K_2	5.35±0.01	4.83±0.01	4.54±0.01	4.20±0.01	3.70±0.01

Table 4
The thermodynamic parameters for interaction of Me_2SnCl_2 with $H_2T(4\text{-X})PP$ in chloroform [a]

	ΔH_1°	ΔH_2°	ΔS_1°	ΔS_2°	ΔG_1° [b]	ΔG_2° [b]
Me_2SnCl_2–H_2TpCP	−69 (±4)	−83 (±5)	−207 (±15)	−223 (±19)	−11 (±4)	−21 (±5)
Me_2SnCl_2–H_2TPP	−80 (±5)	−107 (±8)	−228 (±16)	−306 (±27)	−17 (±5)	−22 (±8)
Me_2SnCl_2–H_2TpTP	−112 (±5)	−116 (±5)	−311 (±17)	−317 (±18)	−25 (±5)	−29 (±5)
Me_2SnCl_2–H_2TpAP	−112 (±6)	−121 (±6)	−310 (±21)	−336 (±21)	−26 (±6)	−28 (±6)

[a] ΔH° (kJ mol^{-1}) and ΔS° (J K^{-1} mol^{-1}).
[b] ΔG° at 5 °C (kJ mol^{-1}).

indicates the stronger interaction along this sequence. The successive adducts $(Me_2SnCl_2)(H_2T(4\text{-X})PP)$ and $(Me_2SnCl_2)_2(H_2T(4\text{-X})PP)$ have negative values of ΔH° and ΔS°.

Our results are in agreement with the pre-equilibrium step demonstrated by previous studies on the kinetics of incorporation of some divalent metal ions into the free base porphyrins. Tanaka and coworkers [19] investigated the reaction of transition metal ions with H_2TPP in DMF. They suggested pre-complexes (M–H_2TPP, M=Cu(II), Zn(II)) with a formation constant K of 1.6×10^4 for Cu(II) and 7.2×10^2 for Zn(II). Similar results have been obtained by Robinson and Hambright [20] on the kinetics of catalyzed and uncatalyzed incorporation of Zn(II) into free base porphyrins (H_2P) in DMF. They suggested that metal ions and porphyrins formed an intermediate with composition [M–H_2P; M=Zn(II), Cd(II), Cu(II)] [18,19] in which coordination of H_2P with the metal ion causes a deformation of the porphyrin plane in such a manner that a second metal ion would more readily be able to be incorporated into this bent porphyrin structure on the opposite side. This lead to the formation of M–H_2P–Zn followed by dropping the Zn(II) ion into the porphyrin cavity [20,21]. But here dealing with stable adducts, because of our bulky Lewis acids, Me_2SnCl_2 could not drop into the free base porphyrin cavity under these conditions. We think that primarily 1:1 adduct formation, [(Me_2SnCl_2) $H_2T(4\text{-X})PP$], induces a distortion in the porphyrin plane; this deformation enhances the coordinating ability of the nitrogen lone pairs by directing them away from the central porphyrin cavity. Therefore the distorted porphyrin readily accepts the second Me_2SnCl_2 molecule on the opposite side and eventually favors the formation of the 2:1 adduct [($Me_2SnCl_2)_2$ $H_2T(4\text{-X})PP$]. Adducts have negative va-

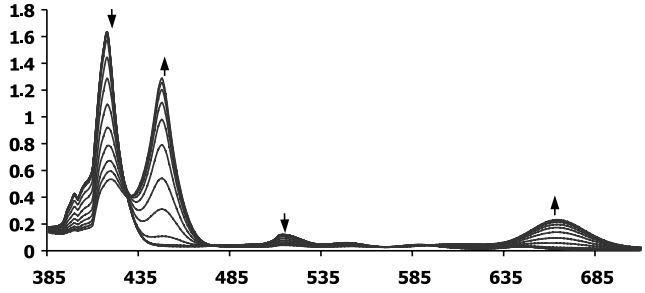


Fig. 3. Typical titration spectra for titration of H_2TpCP with Me_2SnCl_2 in chloroform. Bands appeared at 447 and 664 nm are related to the adduct, isosbestic point at 428 nm.

Table 5
The overall thermodynamic parameters ΔH°, ΔS° and ΔG° for interaction of Me_2SnCl_2 with $H_2T(4\text{-X})PP$ in chloroform [a]

	ΔH°	ΔS°	ΔG° [b]
Me_2SnCl_2–H_2TpCP	155 (±5)	−442 (±19)	−32 (±5)
Me_2SnCl_2–H_2TPP	−187 (±7)	−529 (±21)	−40 (±7)
Me_2SnCl_2–H_2TpTP	−228 (±5)	−628 (±17)	−53 (±5)
Me_2SnCl_2–H_2TpAP	−234 (±7)	−644 (±23)	−55 (±7)

[a] ΔH° (kJ mol^{-1}) and ΔS° (J K^{-1} mol^{-1}).
[b] ΔG° at 5 °C (kJ mol^{-1}).

lues of ΔH°, ΔS° and ΔG°. Generally, the negative values of ΔS° refer to association between donor and acceptor molecules. The most negative values of ΔH° and ΔG° for the Me_2SnCl_2–H_2TpAP system indicate the strongest interactions in this system relative to the other members of the series. These results show that the interactions of $H_2T(4\text{-X})PP$ toward Me_2SnCl_2 vary in the order:

$$H_2TpAP > H_2TpTP > H_2TPP > H_2TpCP$$

This trend is in accordance with the electron donation of the free base porphyrins.

Acknowledgements

We are grateful to Shiraz University Research Council for their financial support.

References

[1] B. Alberte, A.S. Gonzalez, E. Garcia, J.S. Casas, J. Sordo, E.E. Castellano, J. Organomet. Chem. 338 (1988) 187.
[2] C.H. Yoder, D. Mokrynka, J.N. Spencer, S.M. Coley, J.C. Otter, R.E. Haines, A. Grushow, L.J. Ansel, J.W. Horick, J. Mikus, M.A. Shermak, Organometallics 6 (1987) 1679.
[3] H. Fujiwara, F. Sakai, Y. Mikawa, Y. Sakai, Bull. Chem. Soc. Jpn. 58 (1985) 1741.
[4] Y. Farhagi, D.P. Garddon, J. Organomet. Chem. 87 (1975) 67.
[5] A.J. Crowe, Drugs future 2 (1987) 255.
[6] M.M. Shoukry, Talanta 43 (1996) 177.
[7] J. McManus, D. Cunningham, M.J. Hynes, J. Organomet. Chem. 468 (1994) 87.
[8] R. Barbieri, A. Silvestri, A.M. Giuliani, V. Piro, F. Di Simone, G. Madonia, J. Chem. Soc., Dalton Trans. (1992) 585.
[9] A.J. Crowe, P.J. Smith, C.J. Cordin, H.E. Parge, F.E. Smith, Cancer Lett. 24 (1984) 45.
[10] K. Kano, T. Hayakawa, S. Hashimoto, Bull. Chem. Soc. Jpn. 64 (1991) 778.
[11] L. Guilleux, P. Krausz, L. Nadjo, R. Uzan, C. Giannotti, J. Chem. Soc., Perkin Trans. II (1984) 475.
[12] D. Mohajer, H. Dehghani, Bull. Chem. Soc. Jpn. 73 (2000) 1477.
[13] D. Mohajer, H. Dehghani, J. Chem. Soc., Perkin Trans. II (2000) 199.
[14] A.C. Smith, Jr., E.G. Rochow, J. Am. Chem. Soc. 75 (1953) 4103.
[15] d'A.R.A.M. Gonsalves, J.M.T.B. Vare Jao, M.M. Pereira, J. Heterocycl. Chem. 28 (1991) 635.
[16] D.J. Leggett, Computational Methods for the Determination of Formation Constant, Plenum press, New York, 1985.
[17] D.J. Leggett, S.L. Kelly, L.R. Shiue, Y.T. Wu, Talanta 30 (1983) 579.
[18] M.F. Hudson, K.M. Smith, Tetrahedron 32 (1976) 597.
[19] S. Funahashi, Y. Yamaguchi, M. Tanaka, Bull. Chem. Soc. Jpn. 57 (1984) 204.
[20] L.R. Robinson, P. Hambright, Inorg. Chim. Acta 185 (1991) 17.
[21] B. Shah, B. Shears, P. Hambright, Inorg. Chem. 10 (1971) 1828.

ELSEVIER

Polyhedron 21 (2002) 689–695

POLYHEDRON

www.elsevier.com/locate/poly

Assembly via H-bonds and Ag–Ag attractions of one-dimensional silver(I) complexes of nicotinamide and nicotinic acid with sulfonate counter-anions

Cai-Hong Chen, Jiwen Cai *, Xiao-Long Feng, Xiao-Ming Chen *

School of Chemistry and Chemical Engineering & Instrumentation Analysis and Research Center, Zhongshan University, Guangzhou 510275, People's Republic of China

Received 13 August 2001; accepted 30 November 2001

Abstract

Three silver(I) complexes containing pyridine derivatives have been synthesized and structurally characterized by X-ray single crystal diffraction, in order to evaluate the effect of counter anions upon the assembly process of complex cations via intermolecular hydrogen bonds. $[Ag(nia)_2]_2(bpds)\cdot 2H_2O$ (**1**) and $[Ag(nia)_2](asa)$ (**2**) (nia = nicotinamide, bpds = 4,4′-biphenyldisulfonate, asa = aminosulfonate) contain cationic complexes comprised of two nicotinamide ligands coordinated with the pyridine nitrogen atoms to a silver(I) ion in a linear fashion. The linear unit is connected to another one by a weak Ag–Ag interaction leading to an H-shaped dimeric unit. The dimeric units are linked through hydrogen bonds formed between amide groups in a head-to-head mode, creating one-dimensional cationic ribbons. In **1**, the ribbons are extended into two-dimensional network via hydrogen bonds formed by the amide groups. The cationic complex cations in $[Ag(niac)_2]_2(1,5nds)\cdot 2H_2O$ (**3**) (niac = nicotinic acid, 1,5nds = 1,5-disulfonate) are also connected to each other through Ag–Ag interactions, leading to H-shaped dimeric units. The dimeric units are propagated via C–H···O hydrogen bonds between the aromatic hydrogen atom and the carbonyl oxygen. A database search shows that the unique Ag–Ag interaction between the discrete silver(I) coordinated linearly just by two pyridine nitrogen atoms is only observed in salts containing sulfonate or sulfate as counter anions. © 2002 Published by Elsevier Science Ltd.

Keywords: Silver(I); Nicotinamide; Nicotinic acid; Sulfonate; Hydrogen bond; Ag–Ag interaction; Assembly chemistry

1. Introduction

Crystal engineering of metal–organic complexes represents an important and rapidly growing area of research [1]. Coordinate covalent bonds have been extensively exploited to create coordination polymers [2]. Meanwhile, the ability to design and control the assembly of coordination networks through both coordination and H-bonding interactions has been of great interest in recent years [3–5]. This strategy is realized by employing organic ligands with H-bonding functionalities combined with coordination sites for a transition metal. Yet systems sustained by soft connections, such as hydrogen bonds, π–π stacking and weak metal–metal interactions, are more flexible and sensitive to the chemical environment, and consequently are less designable and possess abundant assembly chemistry that remains to be further investigated. Especially when the building blocks are complex cations or anions, the nature of counter ions and solvent molecules play crucial roles in determining the final assembly architectures.

Due to the inherent coordination and hydrogen-bonding donor/acceptor functionalities, both nicotinamide (nia) and nicotinic acid (niac) were used in crystal engineering to construct extended frameworks sustained by both coordination and hydrogen bonds [6,7]. Herein, in order to exam the effect of counter anions upon the intermolecular interactions and assembly process of the bis(nicotinamide-*N*)silver(I) ion [6], we report the crystal and packing structures of $[Ag(nia)_2]_2(bpds)\cdot 2H_2O$ (**1**) and $[Ag(nia)_2](asa)$ (**2**) (bpds = 4,4′-biphenyldisulfonate, asa = aminosulfonate). Their nicotinic acid analogue,

* Corresponding authors. Tel.: +86-20-84110782; fax: +86-20-84038784.

E-mail address: puscjw@zsu.edu.cn (J. Cai).

0277-5387/02/$ - see front matter © 2002 Published by Elsevier Science Ltd.
PII: S0277-5387(02)00851-3

$[Ag(niac)_2]_2(1,5nds)\cdot 2H_2O$ (**3**) (1,5nds = 1,5-disulfonate) was also synthesized and structurally characterized. The results show that, by changing the counter anions, the assembling architectures of the $[Ag(nia)_2]^+$ ion through non-covalent interactions can be modified dramatically and highly ordered extended networks can be constructed.

2. Experimental

2.1. Material and methods

All materials were commercially available and used as received. elemental analyses were carried out with an elementar Vario EL elemental analyzer. FTIR spectra were obtained on a Bruker EQUINOX 55 FTIR spectrometer with KBr pellets. TGA was performed using a Netzsch TG 209 analyzer in flowing nitrogen.

2.2. Syntheses and characterization

2.2.1. $[Ag(nia)_2]_2(bpds)\cdot 2H_2O$ (*1*)

An aqueous solution (20 ml) of 4,4′-biphenyldisulfonate acid (0.32 g, 1 mmol) was added to Ag_2O (0.24 g, 1 mmol) with constant stirring until all of the solids dissolved. Nicotinamide (0.25 g, 2 mmol) was added to this solution. Colorless crystals of **1** were collected after 6 days (54% yield based on Ag). $C_{36}H_{36}O_{12}N_8S_2Ag_2$ (**1**) Required: C 41.08, H 3.45, N 10.65; Found: C 41.03, H 3.34, N 10.76%. IR data (cm^{-1}, KBr): 3400s, 3308s, 3171s, 3094s, 2825m, 2787m, 1694s, 1635s, 1596s, 1574m, 1429s, 1399s, 1199s, 1129s, 1037s, 998s, 818m, 783m, 722s, 694m, 655m, 617s.

2.2.2. $[Ag(nia)_2](asa)$ (*2*)

The same procedure as that for **1** was used to obtain **2** (56% yield based on Ag). $C_{12}H_{14}O_5N_5SAg$ (**2**) Required: C 32.16, H 3.15, N 15.63; Found: C 32.15, H 2.895, N 15.92%. IR data (cm^{-1}, KBr): 3396s, 3318s, 3270s, 3173s, 3094s, 2831m, 2776m, 1695s, 1631s, 1596s, 1574m, 1428s, 1398s, 1231s, 1184s, 1121s, 1053s, 965m, 785s, 690s, 651s.

2.2.3. $[Ag(niac)_2]_2(1,5nds)\cdot 2H_2O$ (*3*)

An aqueous solution (20 ml) for hexaqua 1,5-naphthalenedisulfonic acid (0.36 g, 1 mmol) was added to Ag_2O (0.24 g, 1 mmol) with constant stirring until all of the solids dissolved. Nicotinic acid (0.25 g, 2 mmol) and acetonitrile (20 ml) were added to this solution. Colorless crystals of **3** were collected after 3 days (30% yield based on Ag). $C_{34}H_{30}O_{16}N_4S_2Ag_2$ (**3**) Required: C 39.63, H 2.93, N 5.44; Found: C 39.46, H 2.90, N 5.64%.

2.3. X-ray crystallography

Experimental details of the X-ray analyses are provided in Table 1. All diffraction data were collected on a Bruker Smart 1000 CCD diffractometer with graphite monochromated Mo Kα radiation ($\lambda = 0.71073$ Å) at room temperature using the program SMART [8] and processed by SAINT+ [9]. Absorption corrections were applied by SADABS [10]. Space groups of these compounds were determined from systematic absences and further justified by the results of refinement. In all cases, the structures were solved by direct methods and refined using full-matrix least-squares/difference Fourier techniques using SHELXTL [11,12]. All non-hydrogen atoms were refined with anisotropic displacement parameters. After that, all hydrogen atoms of the ligands were placed at idealized positions and refined as riding atoms with the relative isotropic parameters of the heavy atoms to which they are attached. Hydrogen atoms of water were located from the difference Fourier map at the finale state of refinement. Selected bond distances, angles and hydrogen bonds are shown in Tables 2–4, respectively.

3. Results and discussion

3.1. Spectral characterization and thermal analyses

The IR spectra showed that both compounds **1** and **2** have absorptions at 3000–3400 cm^{-1}, corresponding to the N–H stretching vibrations of the amide group. The C=O stretching frequency of **1** and **2** was recorded at 1694 and 1695 cm^{-1}, respectively. The aromatic C–H stretching extends through the region 2770–2840 cm^{-1}. The well-resolved frequencies of the aromatic rings span over 600–1000 cm^{-1} and 1240–1600 cm^{-1}. Those frequencies characteristic of the fundamental and split ν_3 S–O stretching modes are observed in the range 1000–1240 cm^{-1}.

TGA analyses indicated that complex **1** releases water molecules at 89.3–131.1 °C, and nicotinamide at 249.2–391.2 °C. Complex **2** is stable until release of nicotinamide at 212.9–273.5 °C.

3.2. Description of the structures

Both $[Ag(nia)_2]_2(bpds)\cdot 2H_2O$ (**1**) and $[Ag(nia)_2](asa)$ (**2**) contain cationic complexes comprised of two nicotinamide ligands coordinated through the pyridine nitrogen atoms to a silver(I) ion in a linear fashion. The amide moieties are arranged *trans* with respect to each other. The coordination geometry of the silver(I) ion, as shown in Fig. 1(a) and Fig. 2(a), is similar to that observed in the bis(nicotinamide-*N*)silver(I) triflate [6], except that in the triflate, the amide moieties are

Table 1
Crystallographic data for compounds **1**–**3**

Compound	**1**	**2**	**3**
Formula	$C_{18}H_{16}AgN_4O_6S$	$C_{12}H_{14}AgN_5O_5S$	$C_{34}H_{30}Ag_2N_4O_{16}S_2$
Formula weight	524.28	448.21	1030.48
Crystal system	triclinic	triclinic	monoclinic
Space group	$P\bar{1}$	$P\bar{1}$	$C2/c$
a (Å)	7.8716(11)	7.3424(11)	19.842(3)
b (Å)	8.6746(12)	8.6314(13)	14.061(2)
c (Å)	14.730(2)	13.0994(19)	13.507(2)
α (°)	83.786(2)	95.508(3)	90
β (°)	81.569(2)	100.207(3)	97.467(3)
γ (°)	88.202(3)	108.172(3)	90
V (Å^3)	988.9(2)	766.1(2)	3736.4(9)
Z	2	2	4
D (calc.) (g cm^{-3})	1.761	1.943	1.832
Absorption coefficient (mm^{-1})	1.169	1.488	1.241
θ Range for data collection (°)	4.08–29.99	2.76–29.99	4.20–30.01
Reflections collected/unique	7954/5467	6312/4125	12 745/5308
Observed reflections ($I > 2\sigma(I)$)	3830	3020	4135
Transmission factors	0.7431–0.9438	0.7166–0.9709	0.6849–0.8454
Goodness of fit	0.939	0.956	1.005
$R(F)$; $R_W(F)$ ($I > 2\sigma(I)$)	0.0360; 0.0900	0.0394; 0.0918	0.0308;0.0823

Table 2
Selected bond distance (Å) for compounds **1**–**3**

*[Ag(nia)$_2$]$_2$(bpds)·2H$_2$O (**1**)*			
Ag(1)–Ag(1) [a]	3.3731(6)	S(1)–O(3)	1.448(2)
Ag(1)–N(1)	2.174(2)	S(1)–O(4)	1.4424(19)
Ag(1)–N(2)	2.190(2)	S(1)–O(5)	1.445(2)
S(1)–C(13)	1.775(2)		
*[Ag(nia)$_2$](asa) (**2**)*			
Ag(1)–Ag(1) [b]	3.3776(7)	S(1)–O(3)	1.451(2)
Ag(1)–N(1)	2.171(2)	S(1)–O(4)	1.448(2)
Ag(1)–N(3)	2.168(2)	S(1)–O(5)	1.452(2)
S(1)–N(5)	1.644(3)		
*[Ag(niac)$_2$]$_2$(1,5nds)·2H$_2$O (**3**)*			
Ag(1)–Ag(1) [c]	3.1978(6)	S(1)–O(1)	1.4464(16)
Ag(1)–N(1)	2.1687(18)	S(1)–O(2)	1.4493(15)
Ag(1)–N(2)	2.1672(16)	S(1)–O(3)	1.4484(17)
S(1)–C(2)	1.7782(18)		

[a] Symmetry for compound **1**: [i] $-x, -y+2, -z+1$.
[b] Symmetry for compound **2**: [i] $-x+1, -y+2, -z+1$.
[c] Symmetry for compound **3**: [i] $-x+1, y, -z+1/2$.

Table 3
Selected bond angles (°) for compounds **1**–**3**

*[Ag(nia)$_2$]$_2$(bpds)·2H$_2$O (**1**)*			
N(1)–Ag(1)–N(2)	174.28(7)	C(5)–N(1)–Ag(1)	120.87(16)
N(1)–Ag(1)–Ag(1) [a]	78.21(6)	C(7)–N(2)–Ag(1)	119.87(17)
N(2)–Ag(1)–Ag(1) [a]	105.75(6)	C(11)–N(2)–Ag(1)	122.31(17)
C(1)–N(1)–Ag(1)	120.99(17)		
*[Ag(nia)$_2$](asa) (**2**)*			
N(1)–Ag(1)–Ag(1) [b]	80.09(7)	C(5)–N(1)–Ag(1)	118.84(19)
N(3)–Ag(1)–N(1)	172.56(9)	C(7)–N(3)–Ag(1)	123.9(2)
N(3)–Ag(1)–Ag(1) [b]	106.70(7)	C(11)–N(3)–Ag(1)	118.19(19)
C(1)–N(1)–Ag(1)	123.25(19)		
*[Ag(niac)$_2$]$_2$(1,5nds)·2H$_2$O (**3**)*			
N(1)–Ag(1)–Ag(1) [c]	92.95(4)	C(8)–N(1)–Ag(1)	122.32(13)
N(2)–Ag(1)–N(1)	168.65(7)	C(12)–N(2)–Ag(1)	119.96(14)
N(2)–Ag(1)–Ag(1) [c]	93.73(5)	C(16)–N(2)–Ag(1)	121.96(13)
C(6)–N(1)–Ag(1)	119.77(14)		

[a] Symmetry for compound **1**: [i] $-x, -y+2, -z+1$.
[b] Symmetry for compound **2**: [i] $-x+1, -y+2, -z+1$.
[c] Symmetry for compound **3**: [i] $-x+1, y, -z+1/2$.

arranged *cis* with respect to each other [6]. The Ag–N bond length and N–Ag–N bond angle are 2.174(2), 2.190(2) Å and 174.28(7)° in **1**, 2.168(2), 2.171(2) Å and 172.56(9)° in **2**, respectively. The linear unit is connected to another one, generated by an inversion center, through Ag–Ag interactions, with Ag–Ag = 3.373(6) (**1**) and 3.3776(7) Å (**2**). Consequently, H-shaped dimeric units are generated. The pyridine rings on the same side of the Ag–Ag bond are almost co-planar, forming dihedral angles of 16.5° (**1**) and 3.4° (**2**) with the distance between the two coordinated *N* atoms being 3.527 (**1**) and 3.631 Å (**2**). As shown in Fig. 1(b) and Fig. 2(b), these H-shaped cationic fragments are propagated through two head-to-head intermolecular hydrogen bonds designated as $R_2^2(8)$ [13], formed by the amide groups (N···O = 2.916(3) and 3.013(3) Å, N–H···O = 171.5° and 170.3° in **1**; N···O = 2.946 and 2.925 Å, N–H···O = 172.19° and 174.33° in **2**). The resulting ribbon-like structures sustained by hydrogen bonds are similar to that observed in the coordination polymers of silver(I) bipyridyl [14].

In **1**, the adjacent cationic ladders are further linked by $R_4^4(8)$ hydrogen bonds between another amine hydrogen and the carbonyl oxygen of a nitotinamide from an adjacent ladder (N···O = 2.960(3) Å, N–H···O = 145.9°), resulting in an infinite two-dimensional

Table 4
Selected hydrogen bond interactions (Å, °) for compounds **1**–**3**

D–H···A	d(D–H)	d(H···A)	d(D···A)	<(DHA)
*[Ag(nia)$_2$]$_2$(bpds)·2H$_2$O (**1**)*				
N(3)–H(3B)···O(2)^{i}	0.86	2.06	2.916(3)	171.5
N(3)–H(3C)···O(5)^{ii}	0.86	2.08	2.924(3)	165.1
N(4)–H(4B)···O(1)^{iii}	0.86	2.16	3.013(3)	170.3
N(4)–H(4C)···O(1)^{iv}	0.86	2.21	2.960(3)	145.9
*[Ag(nia)$_2$](asa) (**2**)*				
N(2)–H(2A)···O(2)^{ii}	0.86	2.09	2.948(3)	172.2
N(2)–H(2B)···O(3)^{i}	0.86	2.24	3.071(3)	163.1
N(4)–H(4A)···O(1)^{iii}	0.86	2.07	2.926(3)	174.4
N(4)–H(4B)···O(4)^{iv}	0.86	2.28	3.031(3)	145.4
N(5)–H(5A)···O(4)^{v}	0.81(4)	2.22(4)	3.025(4)	178(3)
N(5)–H(5B)···O(3)^{vi}	0.88(4)	2.23(4)	3.082(4)	163(3)
*[Ag(niac)$_2$]$_2$(1,5nds)·2H$_2$O (**3**)*				
O(2)–H(2W)···O(5)^{i}	0.86(5)	1.79(5)	2.628(3)	165(5)
N(2)–H(2A)···O(4)^{ii}	0.90	2.04	2.903(3)	160.5

Symmetry for compound **1**: ^{i} $x, y, z+1$; ^{ii} $x-1, y+1, z$; ^{iii} $x, y, z-1$; ^{iv} $-x+1, -y+2, -z+1$; Symmetry for compound **2**: ^{i} $-x+1, -y+2, -z+1$; ^{ii} $x, y+1, z+1$; ^{iii} $x, y-1, z-1$; ^{iv} $x+1, y, z$; ^{v} $-x, -y+1, -z+1$; ^{vi} $-x+1, -y+1, -z+1$; Symmetry for compound **3**: ^{i} $-x+2, -y, -z$; ^{ii} $x, -y-1/2, z+1/2$.

network, as illustrated in Fig. 1(b). The bpds anions are sandwiched between two cationic sheets and anchored by hydrogen bonds formed by the SO_3^- oxygen and amino hydrogen of the amide groups. Meanwhile, water molecules are intercalated in the void space constructed by the cationic sheets and counter-anions, as illustrated in Fig. 1(c). The overall crystal packing displays alternating cationic sheets and anionic pillars. While in **2**, there are no further hydrogen bonding interactions between the adjacent cationic ladders, the anions also forms a complementary $R_2^2(8)$ motif hydrogen bonding ribbon through amino hydrogen atoms and sulfonate oxygen atoms, as shown in Fig. 2(b). The cationic chains are connected by the anionic chains through hydrogen bonds between the remaining amide hydrogen atoms and the sulfonate oxygen atoms (N···O = 3.070 Å, N–H···O = 163.10°), as shown in Fig. 2(c).

Finally, in [Ag(niac)$_2$]$_2$(1,5nds)·2H$_2$O (**3**), a near-linear cationic complex comprised of two nicotinic acid ligands coordinated through the pyridine nitrogen atoms to a silver(I) ion is present. The carboxylate moieties are arranged *trans* with respect to each other. The coordination geometry of the silver(I) ion, as shown in Fig. 3(a), is similar to that observed in **1** and **2**. The Ag–N bond length is 2.1672(16) and 2.1687(18) Å, while the N–Ag–N bond angle is 168.65(7)°. The linear unit is connected to another one through a screw axis operation (symmetric operator $-x+1, y, -z+1/2$), with Ag–Ag = 3.1978(6) Å, also resulting in a H-shaped dimeric unit. Interestingly, unlike in **1** and **2** where one-dimensional structures are constructed by strong inter-amide hydrogen bonds, in **3** the dimeric units are propagated via C–H···O hydrogen bonds between the aromatic hydrogen atom and the carbonyl oxygen (C···O = 3.178 Å, C–H···O = 133.6°), as shown in Fig. 3(a). This hydrogen bonding mode formed by two nicotinic acids is quite unusual, in comparison with the more common and stable $R_2^2(8)$ pattern we observed in another series of nicotinic acids-coordinated compounds [15]. The other two carboxylate groups are involved in strong hydrogen bonds with the water molecules, forming a pattern described as $R_4^4(12)$ (OO 2.543(2) and 2.800(3) Å, O–H···O = 172.4° and 166.7°), as illustrated in Fig. 3(b). The 1,5nds anions occupy the void space formed by the dimeric silver(I) units and water-carboxylate cluster.

3.3. Other interesting structural aspects

Due to the torsional freedom of the Ag–Ag bond, the Ag–N bond, and the C–C bond between the pyridine ring and the amide/carboxylate group, the H-shaped fragment reveals some flexibilities which can accommodate different chemical environments, as typically represented by different counter anions and water of hydration, and still retains the same double $R_2^2(8)$ intermolecular hydrogen bonding capability. There are two possible conformations for the H-shaped unit generated by the linear Ag(I) complex with the functional groups in *trans* positions, as illustrated in Scheme 1. The different orientations of the four functional groups determine the pattern of inter-units interactions.

The packing arrangements of compounds **1** and **2** do not resemble any of the reported bis(nicotinamide-*N*)silver(I) analogues with different counter anions [6]. Remarkably, the linear cationic building blocks have the same coordination environment, however, there are no Ag–Ag interactions reported for the known structures [6]. Hence, we searched the Cambridge Structure Database [16] for discrete silver(I) complexes coordinated linearly only by two pyridine nitrogen atoms (polymeric Ag(I) compounds were excluded), and identified a total of 15 entries [6,17–24]. Among them, we found two entries, namely bis(nicotinamide-*N*)silver(I) triflate [6] and bis(4-4(4-methoxystyryl)pyridinato)-silver(I) octylsulfate hemihydrate [18], containing complexes with Ag–Ag interactions (Ag–Ag = 3.307 and 3.194/3.209 Å, respectively). Most significantly, in both of these complexes and also in the three title complexes, sulfonates or sulfate are employed as counter anions. This sulfonate/sulfate-related Ag–Ag interaction is best demonstrated by the structures of bis(nicotinamide-*N*)silver(I) triflate, tetrafluoroborate and hexafluorophosphate [6]. Ag–Ag interactions are observed in the SO_3^--containing triflate but not in the last two complexes. Nevertheless, whether the Ag–Ag interaction observed in the linear pyridine-coordinated silver(I) complex is uniquely sulfonate/sulfate-promoted remains for further investigation.

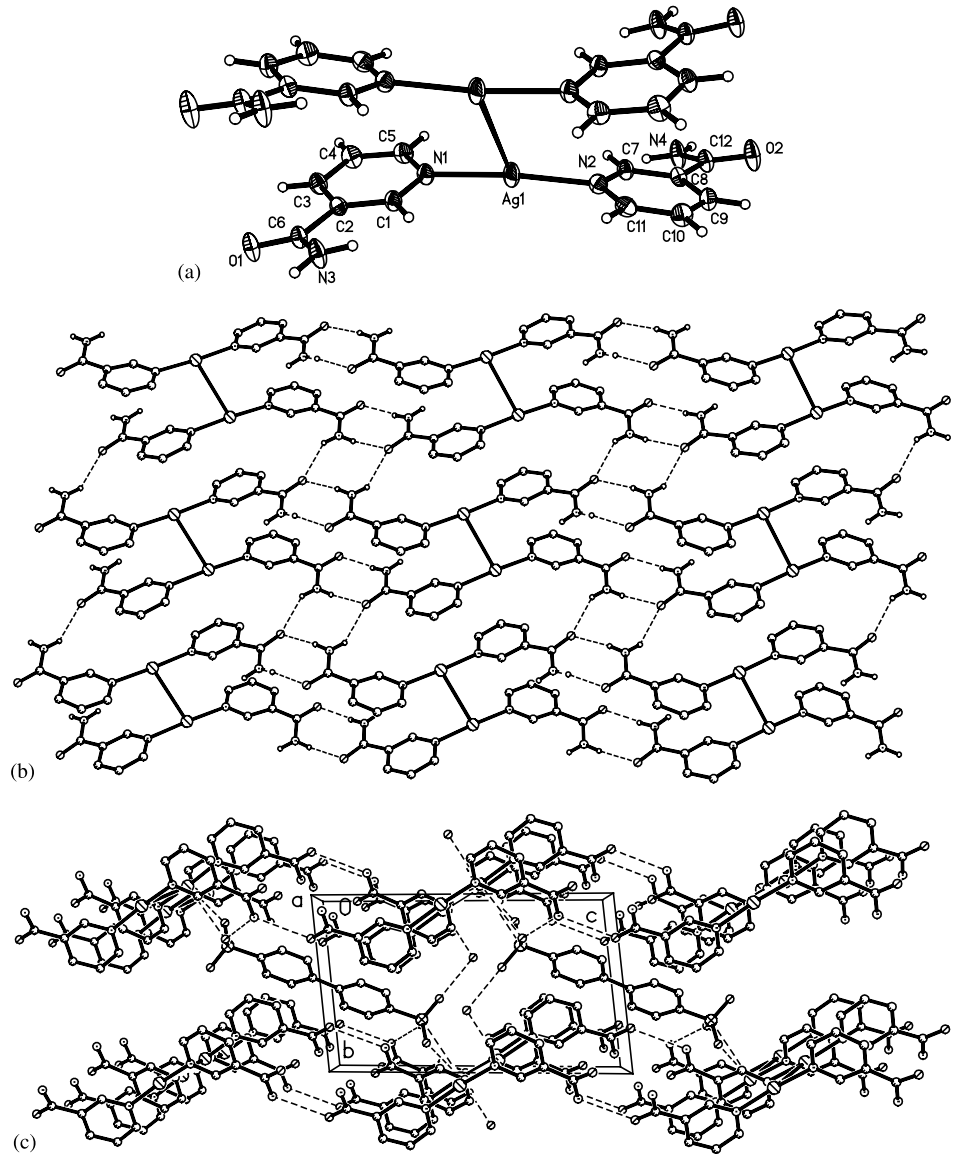


Fig. 1. (a) The dimeric cationic complex in **1**; (b) The two-dimensional cationic sheet in **1**; (c) The alternating cationic sheets and anionic pillars.

4. Supplementary material

Crystallographic data for the structural analyses have been deposited with the Cambridge Crystallographic Data Centre, CCDC Nos. 168155–168157 for compounds **1**–**3**, respectively. Copies of this information can be obtained free of charge from The Director, CCDC, 12 Union Road, Cambridge, CB2 1EZ, UK (fax: +44-1223-336033; e-mail: deposit@ccdc.cam.ac.uk or www:http//www.ccdc.cam.ac.uk).

Acknowledgements

We thank the National Natural Science Foundation of China for their financial support (Grant No. 29801006).

References

[1] M. Fujita, Y.J. Kwon, S. Washizu, K. Ogura, J. Am. Chem. Soc. 116 (1994) 1151.
[2] S. Subramanian, M.J. Zaworotko, Angew. Chem., Int. Ed. Engl. 34 (1995) 2127.
[3] D. Braga, F. Grepioni, G.R. Desiraju, Acc. Chem. Res. 33 (2000) 601.
[4] D. Braga, F. Grepioni, Chem. Rev. 98 (1998) 1375.
[5] (a) J.C. MacDonald, P.C. Dorrestein, M.M. Oilley, M.M. Foote, J.L. Lundburg, R.W. Henning, A.J. Schultz, J.L. Manson, J. Am. Chem. Soc. 122 (2000) 11692;
(b) M. Munakata, L.P. Wu, M. Yamamoto, T. Kuroda-Sowa, M. Maekawa, J. Am. Chem. Soc. 118 (1996) 3117;
(c) A.D. Burrows, D.M.P. Mingos, A.J.P. White, D.J. Williams, Chem. Commun. (1996) 97.;
(d) J.C.M. Rivas, L. Brammer, New J. Chem. 22 (1998) 1315.
[6] C.B. Aakeröy, A.M. Beatty, Chem. Commun. (1998) 1067.

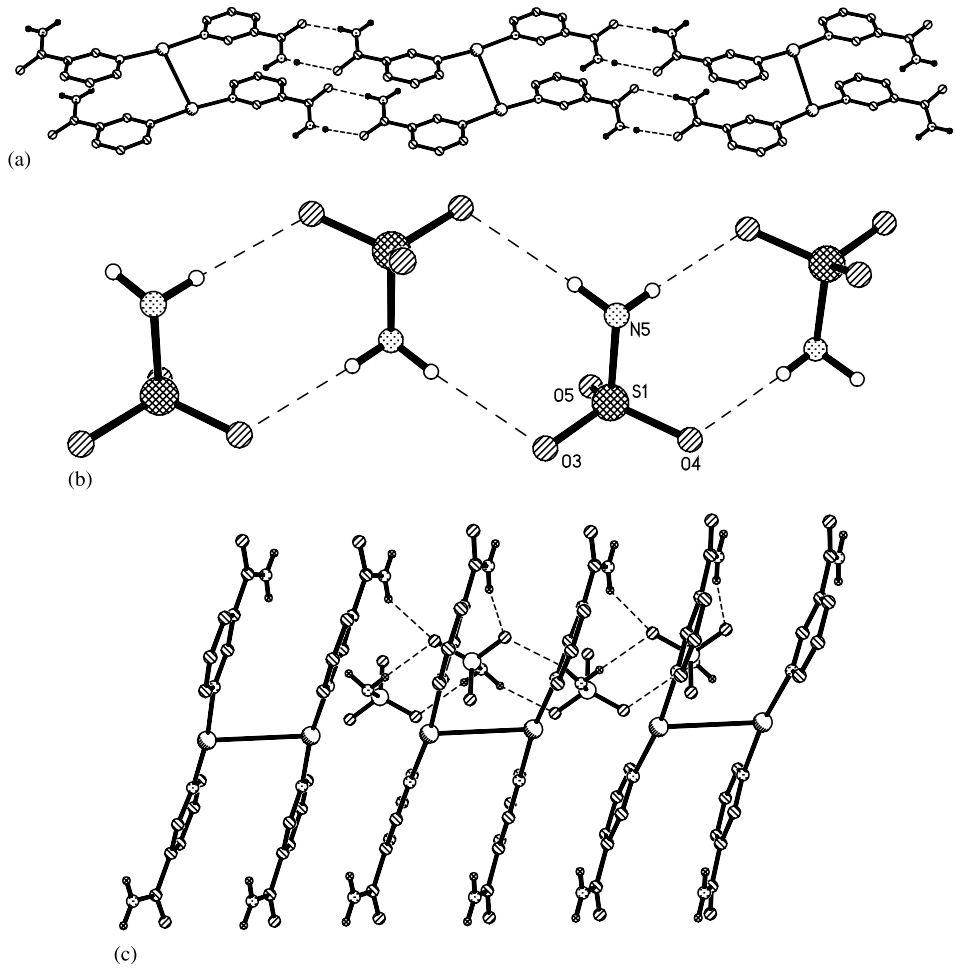


Fig. 2. (a) The one-dimensional ladder-like cationic ribbons in **2**; (b) The anionic ribbon in **2**; (c) The cationic dimers interact with anionic ribbons via hydrogen bonds.

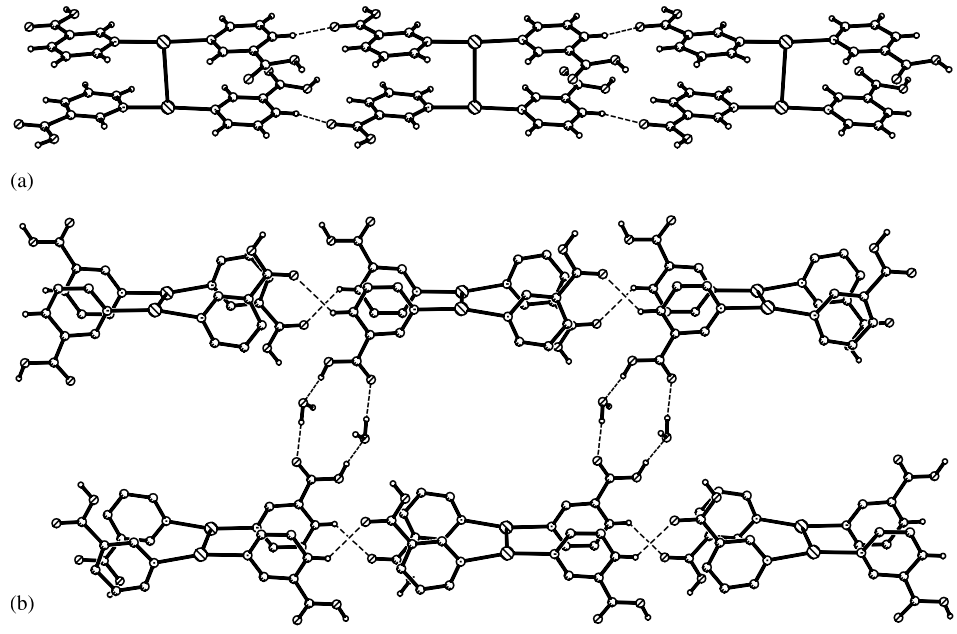
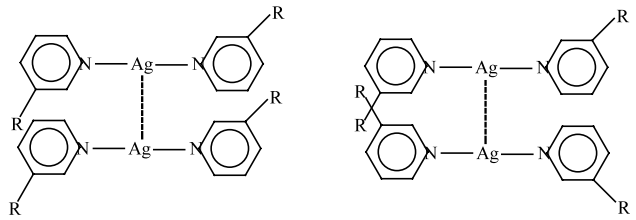


Fig. 3. (a) The one-dimensional ribbon in **3**; (b) The extended network featuring the hydrogen bonds between the carboxylate groups and the water molecules.



Scheme 1. Schematic representation of the two possible conformations adopted by the linear silver(I) complexes (a) is that observed in **1** and **2**, with R = amide group. (b) is that observed in **3**, with R = carboxylate group. Note that (a) carries an inversion center between the two silver atoms, and (b) a twofold axis.

[7] (a) J.C.M. Rivas, L. Brammer, New J. Chem. (1998) 1315.;
(b) L. Brammer, J.C.M. Rivas, R. Atencio, S. Fang, F.C. Pigge, J. Chem. Soc., Dalton Trans. (2000) 3855.
[8] A.X.S. Bruker, SMART, Version 5.0, Bruker AXS, Madison, WI, USA, 1998.
[9] A.X.S. Bruker, SAINT+, Version 6.0, Bruker AXS, Madison, WI, USA, 1999.
[10] R. Blessing, Acta Crystallogr., Sect. A 51 (1995) 33.
[11] A.X.S. Bruker, SHELXTL, Version 5.1, Bruker AXS, Madison, WI, USA, 1998.
[12] G.M. Sheldrick, SHELX-97, Program for X-ray Crystal Structure Solution and Refinement, Göttingen University, Germany, 1997.
[13] (a) M.C. Etter, Acc. Chem. Res. 23 (1990) 120;
(b) J. Bernstein, R.E. Davis, L. Shimoni, N.-L. Chang, Angew. Chem., Int. Ed. Engl. 34 (1995) 1555.
[14] A.J. Blake, N.R. Champness, P. Hubberstey, W.-S. Li, M.A. Withersby, M. Schröder, Coord. Chem. Rev. 183 (1999) 117.
[15] G. Yang, H.-G. Zhu, B.-H. Liang, X.-M. Chen., J. Chem., Soc., Dalton Trans. (2001) 580.
[16] CSD database released on October, 2000. F.H. Allen, O. Kennard, Chemical Design Automation News 8 (1993) 31.
[17] C.B. Aakeroy, A.M. Beatty, D.S. Leinen, J. Am. Chem. Soc. 120 (1998) 7383.
[18] H. Adams, N.A. Bailey, D.W. Bruce, S.C. Davis, D.A. Dunmur, P.D. Hempstead, S.A. Hudson, S. Thorpe, J. Mater. Chem. 2 (1992) 395.
[19] S. Menchetti, G. Rossi, V. Tazzoli, Rend. Ist Lomb. Acc. Sci. Lett. A 104 (1970) 309.
[20] O. Kristiansson, Acta Crystallogr., Sect. C C56 (2000) 165.
[21] L.M. Engelhardt, C. Pakawatchai, A.H. White, P.C. Healy, J. Chem. Soc., Dalton Trans. (1985) 17.
[22] J.C. Dyason, P.C. Healy, L.M. Engelhardt, A.H. White, Aust. J. Chem. 38 (1985) 1325.
[23] S. Gotsis, A.H. White, Aust. J. Chem. 40 (1987) 1603.
[24] F. Jaber, F. Charbonnier, R. Faure, M. Petit-Ramel, Z. Kristallogr. 209 (1994) 536.

PERGAMON

Polyhedron 21 (2002) 697–704

POLYHEDRON

www.elsevier.com/locate/poly

The interconversion of dichlorobis(*N*-*n*-propylsalicylaldimine)zinc(II) and bis(*N*-*n*-propylsalicylaldiminato)zinc(II)

Michele A. Torzilli, Shalton Colquhoun, Danielle Doucet, Robert H. Beer *

Department of Chemistry, Fordham University, Bronx, NY 10458, USA

Received 1 August 2001; accepted 3 December 2001

Abstract

The interconversion of the zinc(II) complex of the neutral ligand adduct of *N*-*n*-propylsalicylaldimine $Zn(L^{pr}H)_2Cl_2$ and its salicylaldiminato counterpart $Zn(L^{pr})_2$ is investigated. The compound $Zn(L^{pr}H)_2Cl_2$ is prepared by the reaction of anhydrous $ZnCl_2$ with 2 equiv. of *N*-*n*-propylsalicylaldimine ($L^{pr}H$) in benzene. A crystallographic study of the distorted tetrahedral $Zn(L^{pr}H)_2Cl_2$ adduct reveals that the oxygen atom of the ligand is deprotonated and bound to the zinc atom while the nitrogen is protonated and non-coordinating. An infrared spectrum of $Zn(L^{pr}H)_2Cl_2$ exhibits a C=N stretch at a higher energy (1658 cm^{-1}) than the free ligand (1632 cm^{-1}) consistent with the presence of the iminium moiety. In contrast, the deprotonated ligand of the crystallographically characterized salicylaldiminato complex $Zn(L^{pr})_2$ coordinates to zinc in its prototypical bidentate monoanionic coordination mode. Deprotonation of $Zn(L^{pr}H)_2Cl_2$ with Et_3N or NaOH forms $Zn(L^{pr})_2$. The reverse reaction, protonation of $Zn(L^{pr})_2$ with anhydrous HCl, produces $Zn(L^{pr}H)_2Cl_2$. These reactions demonstrate the interrelationship between the zinc salicylaldimine adduct and its corresponding salicylaldiminato complex. © 2002 Elsevier Science Ltd. All rights reserved.

Keywords: Schiff bases; Salicylaldimine adducts; Interconversion; X-ray crystal structures; Zinc complexes; Zwitterion

1. Introduction

The salicylaldimine ligand forms the basis of an extensive class of chelating ligands that has enjoyed popular use in the coordination chemistry of transition and main group elements [1–3]. The reaction of the neutral phenol-imine form of the salicylaldimine ligand with a suitable metal starting material in the presence of base is a simple and direct means of preparing metal salicylaldiminato complexes (Scheme 1). In these complexes, the deprotonated phenolate-imine form of the ligand acts as a bidentate monoanionic N/O donor.

Despite the frequent use of this preparative method, comparatively few of the putative precursors or intermediates involved in this reaction prior to deprotonation of the ligand have been structurally characterized [1,2,4–11] and, similarly, the precursors formed by the reverse reaction are not isolated typically [12,13]. We report here an example of the interconversion of a structurally characterized precursor and its corresponding deprotonated salicylaldiminato complex using the zinc(II) dichloride adduct of *N*-*n*-propylsalicylaldimine ($L^{pr}H$). These reactions corroborate the role of neutral salicylaldimine adducts in the formation of salicylaldiminato complexes.

2. Experimental

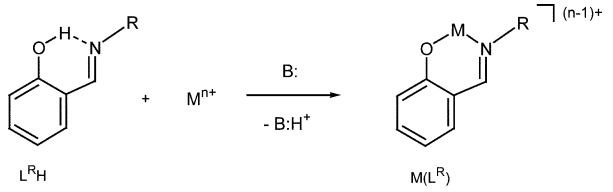
2.1. Materials and methods

Reagents and solvents were used as received from commercial sources. The ligand *N*-*n*-propylsalicylaldimine ($L^{pr}H$) and the protonated ligand ($L^{pr}H_2$)(CF_3SO_3) were synthesized by generally accepted methods [1,14] and $Zn(L^{pr})_2$ by modification of related literature procedures [15,16]. Infrared and electronic spectroscopic data were collected on a Mattson Satellite FTIR and Perkin–Elmer Lambda 6 instrument, respectively. The ^1H NMR spectroscopic data were obtained on a Bruker AVANCE 300 NMR spectrometer at

* Corresponding author. Tel.: +1-718-817-4430; fax: +1-718-817-4432.

E-mail address: beer@fordham.edu (R.H. Beer).

0277-5387/02/$ - see front matter © 2002 Elsevier Science Ltd. All rights reserved.
PII: S0277-5387(02)00839-2



Scheme 1.

ambient room temperature. Chemical shifts are referenced as ppm downfield of tetramethylsilane. A conventional numbering scheme was adopted for ligand aromatic hydrogen atoms attached to carbons for ^{1}H NMR assignments in which the imine moiety was attached to ring C1, the OH to ring C2 and so on. Robertson Microlit Laboratories (Madison, NJ) and Quantitative Technologies Inc. (Whitehouse, NJ) performed the elemental analyses.

2.2. X-ray crystallographic structure determination of $Zn(L^{pr})_2$ and $Zn(LH)_2Cl_2$

Data collection, solution and refinement details are given in Table 1 and bond lengths and distances in Figs. 1 and 2 captions and Table 2. Complete crystallographic information is available as supplementary material. Rhomb-shaped single crystals of $Zn(L^{pr}H)_2Cl_2$ suitable for X-ray crystallographic studies could be obtained from slowly evaporating methanol or acetonitrile solutions in air. X-ray quality single crystals of $Zn(L^{pr})_2$ were grown by evaporating the compound dissolved in toluene over a period of 1 week. The crystals were glued to a glass fiber with epoxy and mounted on a Bruker P4 (formerly Siemens) diffractometer equipped with a SMART CCD and the data collected at low temperature under a dinitrogen cold stream.

Data collection, solution and refinement for both compounds were obtained by routine methods using SHELXTL [17] (see Table 1). A data set was collected by obtaining an initial set of cell constants calculated from reflections harvested from three sets of 20 frames. These initial sets of frames were oriented such that orthogonal wedges of reciprocal space were surveyed. The unit cell was further refined by the inclusion of reflections from the data set and the program SAINT (Bruker AXS). The structure was solved by direct methods and all non-hydrogen atoms were refined anisotropically by full-matrix least-squares on F^2. All hydrogen atom parameters, with the exception of the iminium hydrogens

Table 1
Crystal data, data collection, structure solution and refinement for $Zn(L^{pr}H)_2Cl_2$ and $Zn(L^{pr})_2$

	$Zn(L^{pr}H)_2Cl_2$	$Zn(L^{pr})_2$
Crystal data		
Empirical formula	$C_{20}H_{26}Cl_2N_2O_2Zn$	$C_{20}H_{24}N_2O_2Zn$
Crystal system	monoclinic	orthorhombic
Space group	$P2_1/c$	$Fdd2$
a (Å)	10.0551(5)	18.172(6)
b (Å)	25.080(1)	39.16(1)
c (Å)	9.1355(5)	5.171(2)
β (°)	109.058(1)	
V (Å^3)	2177.5(2)	3680(2)
Z	4	8
Formula weight	462.70	389.78
D_{calc} (Mg m^{-3})	1.411	1.407
Absorption coefficient (mm^{-1})	1.390	1.350
$F(000)$	960	1632
Data collection		
Wavelength (Å)	0.71073	0.71073
Temperature (K)	213(2)	228(2)
θ Range for data collection (°)	1.62–28.33	2.08–28.28
Index ranges	$-13 \le h \le 7$, $-31 \le k \le 27$, $-11 \le l \le 11$	$-24 \le h \le 16$, $-44 \le k \le 50$, $-6 \le l \le 6$
Reflections collected	16 161	6419
Independent reflections	5027 ($R_{int} = 0.0161$)	2057 ($R_{int} = 0.0440$)
Solution and refinement		
Solution	Direct methods	Direct methods
Refinement method	Full-matrix least-squares F^2	Full-matrix least-squares F^2
Absorption correction	SADABS	SADABS
Max. and min. transmission	0.8735 and 0.6805	0.7740 and 0.6143
Data/restraints/ parameters	5027/0/253	2057/1/117
Final R indices ($I > 2\sigma(I)$]	$R_1 = 0.0229$, $wR_2 = 0.0604$	$R_1 = 0.0423$, $wR_2 = 0.0929$
R indices (all data)	$R_1 = 0.0269$, $wR_2 = 0.0625$	$R_1 = 0.0517$, $wR_2 = 0.0957$
Goodness-of-fit on F^2	1.028	1.115
Largest difference peak and hole (e Å^{-3})	0.37 and -0.295	0.440 and -0.584

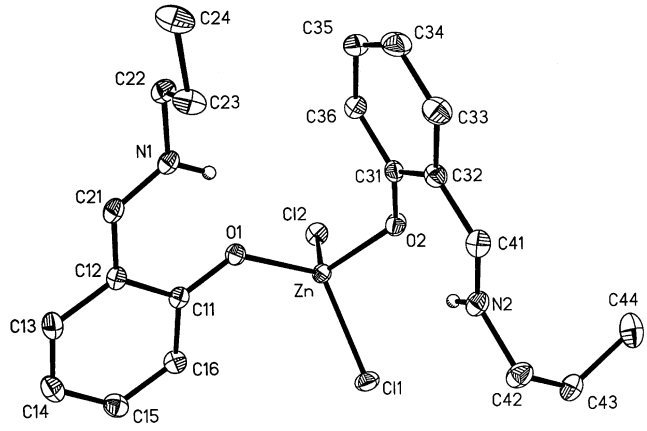


Fig. 1. Molecular structure of $Zn(L^{pr}H)_2Cl_2$. Bond distances (Å): Zn–O(1), 1.9535(9), Zn–O(2), 1.974(1), Zn–Cl(2), 2.2317(4), Zn–Cl(1), 2.2478(4), O(1)–C(11), 1.313(2), O(2)–C(31), 1.3083(17), N(1)–C(21), 1.292(2), N(1)–C(22), 1.467(2), N(2)–C(41), 1.289(2), N(2)–C(42), 1.462(2), C(12)–C(21), 1.422(2), C(22)–C(23), 1.508(2), C(23)–C(24), 1.531(2), C(32)–C(41), 1.428(2), C(42)–C(43), 1.508(2), C(43)–C(44), 1.505(3), average C(ring)–C(ring), 1.398(2), N(1)–H(1), 0.84(2), N(2)–H(2), 0.80(2), O(1)···N(1), 2.674(2), O(2)···N(2), 2.617(2), N(1)···Cl(2), 5.704(2), N(2)···Cl(1), 3.562(2). Bond angles (°): O(1)–Zn–O(2), 102.89(4), O(1)–Zn–Cl(2), 112.31(3), O(2)–Zn–Cl(2), 111.83(4), O(1)–Zn–Cl(1), 116.83(3), O(2)–Zn–Cl(1), 96.30(3), Cl(2)–Zn–Cl(1), 114.73(2), C(11)–O(1)–Zn, 127.01(9), C(31)–O(2)–Zn, 131.69(9), C(21)–N(1)–C(22), 122.6(1), C(41)–N(2)–C(42), 125.8(2), O(1)–C(11)–C(16), 123.4(1), O(1)–C(11)–C(12), 119.6(1), C(21)–C(12)–C(11), 122.3(1), C(13)–C(12)–C(21), 117.6(1), O(2)–C(31)–C(36), 122.4(1), O(2)–C(31)–C(32), 119.7(1), N(1)–C(21)–C(12), 126.0(1), N(1)–C(22)–C(23), 112.3(1), C(22)–C(23)–C(24), 110.7(2), N(2)–C(41)–C(32), 124.4(2), N(2)–C(42)–C(43), 111.6(1), C(44)–C(43)–C(42), 113.7(2), C(33)–C(32)–C(41), 118.9(2), C(31)–C(32)–C(41), 121.6(1), average C(ring)–C(ring)–C(ring), 120.0(2), N(1)–H(1)···O(1), 132(2), N(2)–H(2)···O(2), 134(2), N(2)–H(2)···Cl(1), 143(2).

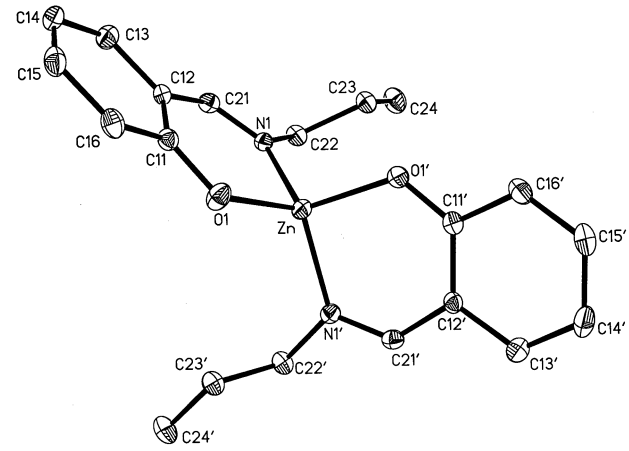


Fig. 2. Molecular structure of $Zn(L^{pr})_2$. Bond distances (Å): Zn–O(1)′, 1.928(2), Zn–N(1)′, 1.998(3), Zn–N(1), 1.998(3), O(1)–C(11), 1.307(4), N(1)–C(21), 1.276(5), N(1)–C(22), 1.483(4), C(12)–C(21), 1.438(5), C(22)–C(23), 1.518(5), C(23)–C(24), 1.524(6), average C(ring)–C(ring), 1.396(6). Bond angles (°): O(1)′–Zn–O(1), 111.26(19), O(1)′–Zn–N(1)′, 95.76(11), O(1)–Zn–N(1)′, 113.34(11), O(1)′–Zn–N(1), 113.34(11), O(1)–Zn–N(1), 95.76 (11), N(1)′–Zn–N(1), 127. 83(16), C(11)–O(1)–Zn, 125.1(2), C(21)–N(1)–C(22), 117.4(3), C(21)–N(1)–Zn, 120.4(2), C(22)–N(1)–Zn, 122.2(2), O(1)–C(11)–C(16), 119.3(3), O(1)–C(11)–C(12), 123.3(3), C(13)–C(12)–C(21), 116.5(3), C(11)–C(12)–C(21), 124.5(3), N(1)–C(21)–C(12), 128.8(3), N(1)–C(22)–C(23), 111.3(3), C(22)–C(23)–C(24), 110.9(4), average C(ring)–C(ring), 120.0(4).

Table 2
Comparative selected crystallographic data for $Zn(L^{pr}H)_2Cl_2$ and $Zn(L^{pr})_2$

$Zn(L^{pr}H)_2Cl_2$		$Zn(L^{pr})_2$	
Bond distances (Å)			
Zn–O(1)	1.9535(9)	Zn–O(1)	1.928(2)
Zn–O(2)	1.974(1)	Zn–N(1)	1.998(3)
Zn–Cl(1)	2.2478(4)		
Zn–Cl(2)	2.2317(4)		
N(1)–C(21)	1.292(2)	N(1)–C(21)	1.276(5)
N(2)–C(41)	1.289(2)		
O(1)–C(11)	1.313(2)	O(1)–C(11)	1.307(4)
O(2)–C(31)	1.308(2)		
Bond angles (°)			
O(1)–Zn–O(2)	102.89(4)	O(1)–Zn–O(1)′	111.3(2)
Cl1–Zn–Cl2	114.73(2)	N(1)–Zn–N(1)′	127.8(2)
O1–Zn–Cl1	116.83(3)	O(1)–Zn–N(1)′	113.3(1)
O2–Zn–Cl1	96.30(3)	O(1)–Zn–N(1)	95.8(1)
O1–Zn–Cl2	112.31(3)		
O2–Zn–Cl2	111.83(4)		
Zn–O1–C11	127.01(9)	Zn–O(1)–C(11)	125.1(2)
Zn–O2–C31	131.69(9)	Zn–N(1)–C(22)	122.2(2)

H(1) and H(2) in $Zn(LH)_2Cl_2$, were placed in ideal positions and refined as riding atoms with individual (or group if appropriate) isotropic displacement. The atoms H(1) and H(2) were found in the difference map and refined to convergence with isotropic displacement parameters.

2.3. Preparation of compounds

2.3.1. N-n-Propylsalicyaldimine ($L^{pr}H$)

A solution of salicylaldehyde (6.106 g, 0.05 mol) in 50 ml of benzene was added to a 100 ml round bottom flask fitted with a Dean–Stark trap and a condenser. To this solution, 2.956 g (0.05 mmol) of *n*-propylamine was added slowly with stirring since the reaction was slightly exothermic and then refluxed for 1 h. After cooling, the reaction mixture was dried over anhydrous magnesium sulfate and gravity filtered. The filtrate was evaporated to yield 7.057 g (78%) of a yellow–brown oil that could be used without further purification. *Anal.* Found: C, 73.30; H, 8.04; N, 8.73. Calc. for $C_{10}H_{13}NO$: C, 73.59; H, 8.03; N, 8.58%. FTIR (neat) 3061(w), 2963(s), 2931(s), 2874(s), 2738(w), 2660(w), 1664(m), 1632(vs), 1582(s), 1497(s), 1461(s), 1416(m), 1382(w), 1338(w), 1279(s), 12059(m), 1150(m), 1115(w), 1054(w), 1031(w), 1013(w), 977(m), 882(m), 850(m, br), 755(s), 640, 553, 463 cm^{-1}. ^1H NMR ($CDCl_3$) δ 13.60 (1H, s br, OH),

8.23 (1H, s, NCH), 7.20 (1H, t, H5), 7.14 (1H, d, H6), 6.87 (1H, d, H3), 6.77 (1H, t, H4), 3.46 (2H, t, NCH_2), 1.63 (2H, m, NCH_2CH_2), 0.89 (3H, t, CH_3) ppm.

2.3.2. $(L^{pr}H)(CF_3SO_3)$

In a 100 ml Schlenk tube, 0.429 g (2.63 mmol) of *N-n*-propylsalicylaldimine was added to 20 ml of anhydrous diethyl ether under argon. To this solution, 0.760 ml (0.448 g, 2.99 mmol) of trifluoromethanesulfonic acid was added in drops with vigorous stirring. The resulting cloudy, slightly pink suspension was stirred for 5 min, then filtered and washed with anhydrous diethyl ether to yield 0.780 g of a white solid after drying under vacuum (95% yield). The compound could be recrystallized from hot chloroform. *Anal*. Found: C, 42.16; H, 4.46; N, 4.45; F, 18.31. Calc. for $C_{11}H_{14}F_3NOS$: C, 42.17; H, 4.50; N, 4.47; F, 18.19%. IR (KBr): 3214(s), 3140(m, br), 3006(m), 2973(m), 2885(w), 1674(m), 1611(m), 1502(w), 1459(w), 1381(w), 1360(w), 1280(vs), 1245(vs), 1223(s), 1151(m), 1061(w), 1031(s), 1000(w), 903(w), 882(w), 758(m), 645(m), 574(w), 517(w), 447(w) cm^{-1}.

2.3.3. $Zn(L^{pr}H)_2Cl_2$

In a 100 ml Schlenk tube, 1.10 g (6.74 mmol) of *N-n*-propylsalicylaldimine was dissolved in 12 ml of dry benzene (distilled over $LiAlH_4$) under Ar. A 3.3 ml solution of 1.0 M $ZnCl_2$ (3.3 mmol) in diethyl ether (Aldrich) was then added via syringe in drops forming a thick orange oil. With vigorous manual agitation the oil slowly changed to a yellow solid after approximately 0.5 h. The reaction mixture was allowed to stir for an additional 1.5 h. The solid was filtered and washed in air with 5 ml of benzene and diethyl ether (3×5 ml) to yield 1.493 g of a yellow powder after drying under vacuum (98% yield). *Anal.* Found: C, 51.57; H, 5.58; N, 6.00; Cl, 14.93. Calc. for $C_{20}H_{26}Cl_2N_2O_2Zn$: C, 51.91; H, 5.66; N, 6.05; Cl, 15.32%. m.p. 151–154 °C. Electronic spectrum ($CHCl_3$, ε M^{-1} cm^{-1}): 316 (7300), 390 (2300) nm. FTIR (KBr): 3060(m, br), 2977(sh), 2957(m), 2935(m), 2877(w), 1658 (vs), 1607(s), 1542(s), 1490(s), 1459(w), 1344(w), 1302(m), 1288(m), 1232(m), 1202(m), 1141(m), 1027(m), 989(w), 911(w), 894(w), 8649w), 787(w), 759(s), 7349(w), 583(m), 514(w), 490(w), 450(w) 434(w), 4169(w) cm^{-1}. ^1H NMR ($CDCl_3$) δ 13.6 (1H, s br, OH), 8.16 (1H, s, NCH), 7.37 (1H, t, H5), 7.23 (1H, d, H6), 7.11 (1H, d, H3), 6.74 (1H, t, H4), 3.61 (2H, t, NCH_2), 1.79 (2H, m, NCH_2CH_2), 0.99 (3H, t, CH_3) ppm.

2.3.4. $Zn(L^{pr})_2$

To a solution of 1.50 g (9.19 mmol) of *N-n*-propylsalicylaldimine in 20 ml of ethanol, 1.01 g (4.60 mmol) of $Zn(O_2CCH_3)_2 \cdot 2H_2O$ was added with stirring. A pale yellow precipitate formed after several minutes and was stirred for an additional 45 min. The precipitate was filtered and dried under vacuum to yield 0.98 g of a light yellow powder (55%). This compound could be recrystallized from acetone and water to obtain a colorless microcrystalline product. *Anal*. Found: C, 61.59; H, 6.08; N, 7.05. Calc. for $C_{20}H_{24}N_2O_2Zn$: C, 61.62; H, 6.21; N, 7.19%. Electronic spectrum ($CHCl_3$, ε M^{-1} cm^{-1}): 316 (6200), 369 (3100) nm FTIR (KBr): 3083(w), 3048(w), 3025(w), 2974(w), 2956(w), 2933(m), 2908(m, br), 2864(m), 1626(vs), 1600(m), 1535(s), 1470(s), 1447(s), 1407(m), 1348(m), 1329(m), 1240(w), 1189(m), 1148(m), 1125(w), 1052(m), 1031(w), 1017(w), 982(w), 922(w), 887(m), 850(w), 795(w), 752(m), 741(m), 654(w), 600(w), 562(w), 512(w), 464(m) cm^{-1}. ^1H NMR ($CDCl_3$) δ 8.17 (1H, s, NCH), 7.29 (1H, t, H5), 7.11 (1H, d, H6), 6.85 (1H, d, H3), 6.60 (1H, t, H4), 3.51 (2H, t, NCH_2), 1.64 (2H, m, NCH_2CH_2), 0.88 (3H, t, CH_3) ppm.

2.3.5. $Zn(L^{pr})_2$ prepared from $Zn(L^{pr}H)_2Cl_2$

In a 125 ml Erlenmeyer flask, 0.179 g (0.387 mmol) of $Zn(L^{pr}H)_2Cl_2$ was added followed by 16.8 ml (0.769 mmol) of aqueous 0.0458 M NaOH with stirring. The solution initially became a light yellow suspension followed by the formation of a white precipitate. After 2 h the product was filtered and dried under vacuum to yield 0.136 g of an off-white solid (90%). Alternatively, solid $Zn(L^{pr}H)_2Cl_2$ (0.110 g, 0.238 mmol) was dissolved in 15 ml of chloroform with stirring in a 25 ml round bottom flask. The slightly cloudy yellow solution became clear and pale yellow after 0.0485 g (0.479 mmol) of Et_3N was added by syringe. The chloroform solution was evaporated on a rotoevaporator and the resulting solid was triturated with deionized water until chloride free (by testing with $AgNO_3$(aq)). The solid was then dried under vacuum to yield 0.083 g of off-white product (89%). This material was judged to be pure based on ^1H NMR and IR spectroscopic measurements.

2.3.6. $Zn(L^{pr}H)_2Cl_2$ prepared from $Zn(L^{pr})_2$

A 2.1 ml (2.1 mmol) aliquot of a 1.0 M solution of HCl in diethyl ether (Aldrich) was added via syringe in drops to a rapidly stirring solution of 0.391 g (1 mmol) of $Zn(L^{pr})_2$ in 20 ml of benzene in a Schlenk tube under argon. The reaction mixture immediately became cloudy and yellow. After several minutes of stirring, a thick orange oil formed. Continued stirring yielded a yellow solid after 1 h. The solvent was decanted and the remaining solid was washed with 5 ml of benzene followed by 3×10 ml of diethyl ether and dried to yield 0.428 g of product (92%). Both preparations yielded material that was pure based on ^1H NMR and IR spectroscopic measurements.

3. Results and discussion

3.1. Synthesis and interconversion reactions

In accord with syntheses of zinc(II) adducts of salicylaldimine ligands [6,18], the reaction of 1 equiv. of anhydrous $ZnCl_2$ in diethyl ether with 2 equiv. of *N*-*n*-propylsalicylaldimine in benzene forms $Zn(L^{pr}H)_2Cl_2$ in a nearly quantitative 98% yield. In the presence of 2 equiv. of NaOH(aq) or Et_3N in chloroform, this compound readily forms $Zn(L^{pr})_2$ in excellent yield upon work-up (Eq. (1)). The zinc salicylaldiminato complex prepared in this manner is identical to the commonly reported method that employs $Zn(O_2CCH_3)_2\cdot 2H_2O$ with *N*-alkylsalicylaldimines [15,16,19–21]. The isolated 89–90% yield of $Zn(L^{pr})_2$ from the precursor $Zn(L^{pr}H)_2Cl_2$ is significantly greater than the 55% yield of the reaction by the more conventional preparative method, which is often problematic [22].

$$Zn(L^{pr}H)_2Cl_2 \underset{2HCl}{\overset{2Et_3N:\ or\ 2NaOH}{\rightleftarrows}} Zn(L^{pr})_2 \quad (1)$$

Conversely, the $Zn(L^{pr}H)_2Cl_2$ precursor can be prepared from $Zn(L^{pr})_2$ and 2 equiv. of HCl in benzene/diethyl ether in 92% yield indicating the ready, clean interconversion between the salicylaldimine adduct and its salicylaldiminato counterpart (Eq. (1)). Despite the presence of two nascent equivalents of HCl, this ''reverse'' reaction in the absence of base does not occur. Attempts to affect the elimination of HCl from this complex by heating the neat solid $Zn(L^{pr}H)_2Cl_2$ at 100 °C under vacuum for several days resulted in no reaction. Heating the evidently robust solid to a melt at 155 °C under vacuum or in DMSO under a N_2 purge resulted in no change after 5 h. After prolonged heating over several days, only partial decomposition to the free ligand and unidentifiable products by ^1H NMR and IR spectroscopy was observed.

3.2. Structural characterization

The X-ray crystal structures of $Zn(L^{pr}H)_2Cl_2$ and $Zn(L^{pr})_2$ allow a direct comparison between both compounds of the neutral and deprotonated *N*-*n*-propylsalicylaldimine ligand. The structure of $Zn(L^{pr}H)_2Cl_2$ shown in Fig. 1 reveals a tetrahedral zinc(II) atom bound to two chlorides and two neutral salicylaldimine ligands in their phenolate-iminium (zwitterion) form. Only the phenolate oxygen atom of the potentially bidentate mixed N/O donor ligand binds to zinc in this complex, a rare example of a mononuclear zinc complex with terminal phenolate ligands [23–25]. Notably, the imine nitrogen is non-coordinating and protonated, i.e. an iminium $\{HC{=}NH\}^+$ group. The structure is similar, overall, to the previously reported structure of zinc(II) salicylaldimine adduct $Zn(L^{ipr}H)I_2$ [26], with the exception that $Zn(L^{pr}H)Cl_2$ possesses approximate C_2 symmetry with the phenyl rings of the ligand disposed *trans* to one another rather than *cis* with respect to the normal of the X–Zn–X ($X = Cl^-$ or I^-) plane. In spite of its relative anonymity, this coordination mode has appeared in various reports of Schiff base complexes or adducts [27]. Since the coordinated salicylaldimine zwitterion was first definitively structurally characterized [28], it has appeared in novel compounds [29,30] or useful starting materials for heterobimetallic complexes of multidentate macrocyclic complexes [7–10].

The coordination mode of the monodentate zwitterion salicylaldimine in $Zn(L^{pr}H)_2Cl_2$ is in marked contrast to that of the salicylaldiminato ligand in the structure of the $Zn(L^{pr})_2$ shown in Fig. 2. In this structure, the ligand in its phenolate-imine form uses both N/O donors to bind to tetrahedral zinc(II) in its ubiquitous bidentate monoanionic coordination mode (Scheme 1). The structure of $Zn(L^{pr})_2$ is comparable to analogous bis(salicylaldiminato)zinc (II) complexes [15,16,21,26].

The ligands in both complexes impose a distorted tetrahedral coordination geometry with angles about the zinc atom ranging from 96.30(3)° to 116.83(3)° in $Zn(L^{pr}H)_2Cl_2$ and 95.8(1)° to 127.8(2)° in $Zn(L^{pr})_2$ (see Table 2). The Zn–O bond distances of the coordinated neutral ligand in $Zn(L^{pr}H)_2Cl_2$ (1.9535(9), 1.9742(1) Å) are slightly longer than the 1.928(2) Å distance in the corresponding salicylaldiminato complex $Zn(L^{pr})_2$, but in good agreement with the mean Zn–O distance of 1.955 Å for the reported structure of $Zn(L^{ipr}H)_2I_2$ [26]. The Zn–O–C angles (127.01(9)°, 131.69(9)°) in $Zn(L^{pr}H)_2Cl_2$ are within the range (118°–137°) of limited available data for zinc(II) complexes with terminal phenolate ligands [18,23–26,31]. The Zn–Cl bond lengths (2.2478(4), 2.2312(4) Å) of $Zn(L^{pr}H)_2Cl_2$ are comparable to related zinc dichloride adducts [18,31,32] and between those of $ZnCl_4^-$ (range 2.263–2.273 Å) [33] and $Zn(py)_2Cl_2$ (2.215, 2.228 Å) [34].

Despite the obvious difference in coordination mode, the metrical parameters of the zwitterion salicylaldimine ligand in $Zn(L^{pr}H)_2Cl_2$ are crystallographically equivalent to its bidentate anionic counterpart in $Zn(L^{pr})_2$ (see Table 2) and other coordinated salicylaldiminato ligands in general [1,2]. The C–O bond distances in both $Zn(L^{pr}H)_2Cl_2$ (1.308(2), 1.313(2) Å) and $Zn(L^{pr})_2$ (1.307(4) Å) are normal for deprotonated phenols bound to zinc [15,16,18,21–26,31]. The C–N bond distances of the protonated imine in $Zn(L^{pr}H)_2Cl_2$ (1.289(2), 1.292(2) Å) as well as the C–N–C angles (122.6(1)°, 125.8(2)°) compare favorably with the corresponding distances and angles for the imine moiety in $Zn(L^{pr})_2$ of 1.276(5) Å and 117.4(3)° consistent with a sp^2 hybridized nitrogen in a C–N double bond [35].

Of particular relevance to the interconversion of salicylaldimine and salicyclaldiminato complexes is the iminium proton in $Zn(L^{pr}H)_2Cl_2$ shown in Fig. 1. The coordinates of the hydrogen atom attached to nitrogen in the structure of $Zn(L^{pr}H)_2Cl_2$ converge upon refinement to yield N–H bond distances of 0.84(2) (N(1)–H(1)) and 0.80(2) Å (N(2)–H(2)) and positions located well within the ligand plane (the atoms in the $L^{pr}H$ fragment are co-planar with a maximum deviation of 0.05 Å). The N···O distances (2.674(2), 2.619(2) Å) and N–H···O angles (132(2), 134(2)°) in $Zn(L^{pr}H)_2Cl_2$ are consistent with an intraligand hydrogen bond between a protonated nitrogen and a phenolate oxygen [18,26,31]. In addition, the N(2)···Cl(1) distance of 3.562(2) Å and the N(2)–H(2)···Cl(1) angle of 143(2)° approach those of weak hydrogen bonds between N–H and chloride, e.g. $(CH_3NH_3)_2[ZnCl_4]$ (3.210–3.546 Å) [33]. The data suggest that H(2) participates in a three-center hydrogen bond [36] with O(2) and Cl(1).

The protonation of the iminium hydrogen in $Zn(L^{pr}H)_2Cl_2$ results from the reaction of the strong Lewis acid zinc dichloride with the oxygen atom of the phenol-imine form (Scheme 1) of the ligand. This stable hydrogen bonded form of the free ligand, seemingly, converts to the zwitterion form by intermolecular proton transfer from the metalated phenol-imine, {Zn–OH···N}, to form a hydrogen bonded phenolate-iminium species, {Zn–O···H:N}. The iminium proton participates in a moderate strength hydrogen bond [36] to the coordinated phenolate oxygen atom stabilizing this otherwise high-energy zwitterion form (in non-aqueous solvents) of the neutral ligand [2]. An alternative monodentate coordination mode, in which the zinc atom is bound to the imine and the proton resides on the phenol, e.g. {OH···Zn–N}, would lack the O–H···N hydrogen bond and is presumably less stable.

3.3. Spectroscopic characterization

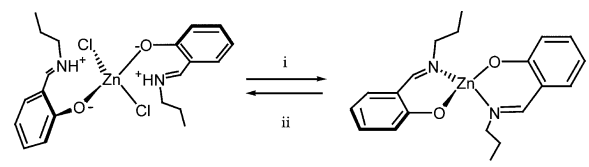
The solid-state infrared spectrum of $Zn(L^{pr}H)_2Cl_2$ displays a distinctive, intense C=N stretch at 1658 cm^{-1}. The C=N stretch occurs at a considerably higher energy than the corresponding frequency in the ligand $L^{pr}H$ (1632 cm^{-1}) or the salicylaldiminato complex $Zn(L^{pr})_2$ (1626 cm^{-1}). A similar positive shift was obtained for the iminium triflate salt $L^{pr}H_2(O_3SCF_3)$ (1674 cm^{-1}) prepared from *N*-*n*-propylsalicylaldimine and trifluorosulfonic acid. This high energy stretch is a well-established characteristic of the iminium ion [14] and substantiates that the salicylaldimine ligand in $Zn(L^{pr}H)_2Cl_2$ coordinates to zinc in its zwitterion form. Infrared spectra of $Zn(L^{pr}H)_2Cl_2$ obtained in chloroform indicate the retention of the iminium C=N stretch at a slightly lower energy (1651 cm^{-1}) in solution. The electronic spectra of the complex substantiate the solution IR data. In chloroform, the lowest energy electronic absorption of $Zn(L^{pr})_2$ shifts from 369 to 390 nm in $Zn(L^{pr}H)_2Cl_2$. This absorption, assigned to a π to π* transition in *N*-alkylsalicylaldimines, is known to shift to lower energy upon formation of the iminium-phenolate form of the free ligand [37].

The iminium proton can also be observed directly as a broad exchangeable resonance at 13.6 ppm in the ^1H NMR spectrum of $Zn(L^{pr}H)_2Cl_2$ in deuterated chloroform. Previously reported NMR spectra of zinc halide salicylaldimine adducts in dimethylsulfoxide were unstable with respect to the salicylaldiminato complexes [6]. We observe, however, we observed no evidence for this in our experiments. Otherwise, the ^1H NMR spectra of $Zn(L^{pr}H)_2Cl_2$ and $Zn(L^{pr})_2$ are alike, with aromatic and propyl protons of the adduct exhibiting small discernible downfield chemical shifts.

3.4. Rationale for interconversion

The presence of the iminium proton in $Zn(L^{pr}H)_2Cl_2$ helps explain how the interconversion reaction occurs (Eq. (1) and Scheme 2). Loss of the iminium proton from $Zn(L^{pr}H)_2Cl_2$ in the form of HCl or deprotonation in the presence of comparatively weak bases to form the salicylaldiminato complex $Zn(L^{pr})_2$ is a reasonable outcome since the iminium proton is fairly acidic ($pK_a \sim 5$) [38,39]. The zwitterion form of the ligand in the adduct, furthermore, provides an explanation for why many salicylaldiminato complexes can be prepared readily from simple metal salts in the absence of base or with bases [1] which are incapable of deprotonating the salicylaldimine ligand ($pK_a \sim 10$–12) [39,40].

The reverse reaction, the protonation of $Zn(L^{pr})_2$ to $Zn(L^{pr}H)_2Cl_2$, can be considered in a similar fashion. In this reaction, the imine nitrogen of the coordinated salicyclaldiminato ligand in $Zn(L^{pr})_2$ is protonated; predictably, this nitrogen is fairly basic given that it is in resonance with the anionic nitrogen of the keto-eneamido form of the ligand [2]. Following protonation of the nitrogen, heterolytic cleavage of the zinc nitrogen bond and formation of the O···H–N hydrogen bond could occur. Under the conditions used here, addition of HCl to $Zn(L^{pr}H)_2Cl_2$, both protonation of the nitrogen and ligand substitution of chloride for imine could take place. The structure of $Zn(L^{pr}H)_2Cl_2$ (Fig. 1) hints at what the intermediate of the addition reaction might look like since it depicts the N(2)–H(2), Zn–O(2) and



i = 2 NaOH, -2 H_2O, -2NaCl or 2 Et_3N, -2 Et_3NHCl
ii = 2 HCl

Scheme 2.

Zn–Cl(1) moieties in close proximity (taking part in a three center hydrogen bond).

The formation/scission of the Zn–N bond would also affect a geometric reorganization of the complex as the ligand changes from a bidentate to a monodentate coordination mode. Examination of the structures of $Zn(L^{pr}H)_2Cl_2$ in Fig. 1 and the representations shown in Scheme 2 indicate that the zinc atom in $Zn(L^{pr})_2$ would have to move out of the same approximate plane as the ligand atoms. This could be accomplished by the rotation of the acute torsion angles in $Zn(L^{pr})_2$ (Zn–O(1)–C(11)–N(1), 16.2°) to the more obtuse corresponding angles about the C–O bond in the adduct (Zn–O(2)–C(31)–C(32), 131.4° and Zn–O(1)–C1(1)–C(12), 174.2°). Inspection of models of the complexes suggests that these rotations as well as other requisite geometric changes are feasible.

4. Supplementary material

Crystallographic data for $Zn(L^{pr}H)_2Cl_2$ and $Zn(L^{pr})_2$ have been deposited with the Cambridge Crystallographic Data Centre, CCDC Nos. 167224 and 167225. Copies of this information may be obtained free of charge from The Director, CCDC, 12 Union Road, Cambridge, CB2 1EZ, UK (fax: +44-1223-336033; e-mail: deposit@ccdc.cam.ac.uk or www: http://www.ccdc.cam.ac.uk).

Acknowledgements

The authors acknowledge the financial support of Fordham University and the Camille and Henry Dreyfus Foundation Award of Research Corporation (to R.H.B. and S.C., Award #HS0558) and the NSF Division of Undergraduate Education Grant DUE#9650684 for the NMR spectrometer at Fordham. The authors also thank Mr. Scott Bisso and Professor Massud Shoja (Fordham University), and Dr. Brian Bridgewater and Professor Gerard Parkin (Columbia University) for crystallographic assistance.

References

[1] R.H. Holm, G.W. Everett, Jr., A. Chakavorty, Prog. Inorg. Chem. 7 (1966) 83.
[2] M. Calligaris, L. Randaccio, in: G. Wilkinson, R.D. Gillard, J.A. McCleverty (Eds.), Comprehensive Coordination Chemistry, vol. 2, Pergamon Press, Oxford, 1987, p. 715.
[3] E.N. Jacobsen, in: E.W. Abel, F.G.A. Stone, G. Wilkinson (Eds.), Comprehensive Organometallic Chemistry, vol. 12, Elsevier, New York, 1995.
[4] (a) P. Bamfield, J. Chem. Soc., A (1967) 804;
(b) A. Van den Bergen, K.S. Murray, M.J. O'Connor, N. Rehak, B.O. West, Aust. J. Chem. 21 (1968) 1505.
[5] F.L. Bowden, D. Ferguson, J. Chem. Soc., Dalton Trans. (1974) 460.
[6] F.A. Bottino, P. Finocchiaro, E.J. Libertini, Coord. Chem. 16 (1988) 341.
[7] D.G. McCollum, L. Hall, C. White, R. Ostrander, A.L. Rheingold, J. Whelan, B. Bosnich, Inorg. Chem. 33 (1994) 924.
[8] M.G.B. Drew, O.W. Howarth, G.G. Morgan, J. Nelson, J. Chem. Soc., Dalton Trans. (1994) 3149.
[9] E.V. Rybak-Akimova, N.W. Alcock, D.H. Busch, Inorg. Chem. 37 (1998) 1563.
[10] P.E. Kruger, F. Launay, V. McKee, Chem. Commun. (1999) 639.
[11] J. Strauch, T.H. Warren, G. Erker, R. Frohlich, P. Saarenketo, Inorg. Chim. Acta 300 (2000) 810.
[12] R.S. McQuate, D.L. Leussing, J. Am. Chem. Soc. 97 (1975) 5117.
[13] R. Knoch, H. Elias, H. Paulis, Inorg. Chem. 34 (1995) 4032.
[14] H. Böhme, H.G. Viehe (Eds.) Iminium Salts in Organic Chemistry, Part 1, Wiley, New York, 1976, pp. 23 and 108.
[15] M. Dreher, H. Elias, Z. Naturforsch., Teil B 42 (1987) 707.
[16] L. Tatar, D. Ulku, O. Atatkol, Acta Crystallogr., Sect. C 55 (1999) 508.
[17] G.M. Sheldrick, SHELXTL, An Integrated System for Solving, Refining, and Displaying Crystal Structures from Diffraction Data, University of Göttingen, Göttingen, Germany, 1981; SHELXTL PC Bruker.
[18] V.S. Sergienko, A.E. Mistryukov, V.V. Livinov, M.I. Knyazhanskii, A.D. Garnovskii, M.A. Porai-Koshits, Koord. Khim. 16 (1990) 168.
[19] P.L. Orioli, M. Di Vaira, L. Sacconi, Inorg. Chem. 3 (1966) 400.
[20] G.E. Batley, D.P. Graddon, Aust. J. Chem. 20 (1967) 877.
[21] H. Sakiyama, H. Okawa, N. Matsumoto, S. Kida, J. Chem. Soc., Dalton Trans. (1990) 2935.
[22] G.A. Morris, H. Zhou, C.L. Stern, S.T. Nguyen, Inorg. Chem. 40 (2001) 3222.
[23] R.L. Geerts, J.C. Huffman, K.G. Caulton, Inorg. Chem. 25 (1986) 1803.
[24] R. Walz, K. Weis, M. Ruf, H. Vahrenkamp, Chem. Ber. 130 (1997) 975.
[25] D.J. Darensburg, M.W. Holtcam, G.E. Struck, M.S. Zimmer, S.A. Niezgoda, P. Rainey, J.B. Robertson, J.D. Draper, J.H. Reibenspies, J. Am. Chem. Soc. 121 (1999) 107.
[26] F.A. Bottino, P. Finocchiaro, E. Libertini, G. Mattern, Z. Kristallogr. 187 (1989) 72.
[27] Seventy-five examples of the salicylaldimine moiety as a monodentate oxygen atom donor (primarily to main group metals) are documented in the Cambridge Structural Database (CSD Version 5.2; F.H. Allen, O. Kennard, Chemical Design Automation News 8 (1993) pp. 1 and 31–37) compared to over 2400 in the phenolate-imine bidentate coordination mode.
[28] J.I. Bullock, M.F.C. Ladd, D.C. Povey, H.-A. Tajmir-Riahi, Acta Crystallogr., Sect. B 35 (1979) 2013.
[29] F.L. Lee, E.G. Gabe, L.E. Khoo, G. Eng, F.E. Smith, Polyhedron 9 (1990) 653.
[30] N. Bag, S.B. Chouhury, A. Pramanik, G.K. Lahiri, A. Chakavorty, Inorg. Chem. 29 (1990) 5014.
[31] $ZnLCl_2$ (where L = 2,6-(bisdialkylaminomethyl)-4-alkylphenol): N. Habbadi, M. Dartiguenave, L. Lamande, M. Sanchez, M. Simard, A.L. Beauchamp, A. Souiri, New J. Chem. 22 (1998) 983.
[32] W. Hoffmuller, K. Polborn, W. Beck, Z. Naturforsch., Teil B 54 (1999) 734.
[33] B. Morosin, K. Emerson, Acta Crystallogr., Sect. B 32 (1976) 294.
[34] W.L. Steffen, G. Palenik, Acta Crystallogr., Sect. B 32 (1976) 298.
[35] J. March, Advanced Organic Chemistry, Wiley, New York, 1985, p. 19.

[36] G.A. Jeffrey, An Introduction to Hydrogen Bonding (Chapter 4), Oxford University Press, New York, 1997.
[37] D.L. Leussing, K.S. Bai, Anal. Chem. 40 (1968) 575.
[38] pK_a values of imines are difficult to determine due to their hydrolytic instability: J.W. Smith, in: S. Patai (Ed.), The Chemistry of Carbon–Nitrogen Double Bond, Wiley, New York, 1970, p. 236.
[39] Approximate range of tabulated protonation equilibrium constants of the salicylaldimine ligands: D.D. Perrin, Stability Constants of Metal-Ion Complexes (Part B), Pergamon Press, Oxford, 1979.
[40] C.E. Metzler, A. Cahill, D.E. Metzler, J. Am. Chem. Soc. 102 (1980) 6075.

PERGAMON

Polyhedron 21 (2002) 705–713

POLYHEDRON

www.elsevier.com/locate/poly

Structural and ^{1}H NMR spectroscopic characterization of bis(*N*-isopropylsalicylaldiminato)iron(II)

Michele A. Torzilli, Shalton Colquhoun, Jin Kim, Robert H. Beer *

Department of Chemistry, Fordham University, Bronx, NY 10458, USA

Received 23 August 2001; accepted 3 December 2001

Abstract

Coordinatively unsaturated iron(II) species form reactive organometallic and coordination complexes and are integral to the reactivity of non-heme iron proteins and their synthetic analogues. Iron(II) Schiff base complexes have proven to be easily prepared and useful starting materials for such compounds. Here we report a detailed preparative procedure and the solid-state structure of the iron(II) complex of *N*-isopropylsalicylaldimine ($L^{ipr}H$) based on the compounds first synthesized by Larkworthy (J. Chem. Soc., A (1968) 1048). The title compound is prepared by adding 2 equiv. of salicylaldehyde (salH) to $Fe(O_2CCH_3)_2$ in $KOH–CH_3OH$ to produce a precursor formulated as $Fe(sal)_2$ which is reacted subsequently with isopropylamine in THF to form $Fe(L^{ipr})_2$ in 34% isolated yield. A single crystal X-ray crystallographic study of $Fe(L^{ipr})_2$ reveals a mononuclear complex with two bidentate salicylaldiminate ligands bound to an iron(II) atom in a tetrahedral coordination geometry. The ^{1}H NMR spectrum of $Fe(L^{ipr})_2$ in benzene-d_6 exhibits six paramagnetically shifted ligand resonances ranging from +195 to −31 ppm that are consistent with a mononuclear high spin ($S = 2$) iron(II) complex in solution. Upon exposure to air, $Fe(L^{ipr})_2$ forms the oxo-bridged dinuclear iron(III) complex $[(L^{ipr})_2Fe]_2O$ as shown by ^{1}H NMR spectroscopy. © 2002 Elsevier Science Ltd. All rights reserved.

Keywords: Iron(II); Zinc(II); Schiff base; X-ray crystal structures; ^{1}H NMR spectroscopy; Dioxygen reactivity

1. Introduction

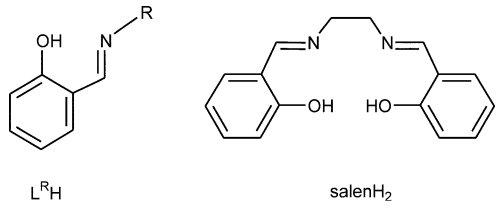
The salicylaldimine ligands shown in Scheme 1 are easy to prepare and synthetically versatile and, accordingly, have been popular ligands for the synthesis of transition metal complexes [1–4]. Among metal salicylaldimine compounds, the iron complexes have been prepared extensively to investigate various aspects of their magnetic and spectroscopic properties and wide-ranging bioinorganic, organometallic, and catalytic chemistry [2,5]. A common approach to prepare these compounds takes advantage of the reactivity of an iron(II) salicylaldimine complex, notably Fe(salen), in concert with the complex being coordinatively unsaturated. By virtue of its ability to be reduced or oxidized as well as to expand its coordination number, Fe(salen) has been employed historically to introduce iron nitrosyl [6], alkyl [7], halide [7], quinone [8], and bridging oxo [9], sulfido [10], peroxo [11] and imido [12] bonds into iron salicylaldimine compounds. Similarly, widespread recent interest in iron(II) species that possess low coordination numbers has led to unusual coordination or organometallic compounds [13–25]. These compounds frequently exhibit desirable reactions with small molecules, e.g. the activation of dioxygen by non-heme iron(II) proteins and their model complexes [26–28].

Iron complexes of the L^RH and salen ligands shown in Scheme 1 figured early in studies of the magnetic, electronic and Mössbauer properties of iron(II) [5,6,29–31]. The bis(salicylaldiminato)iron(II) complexes, formulated as $Fe(L^R)_2$ (R = alkyl or aryl), were first prepared reliably by Larkworthy [6,29]. The compounds were determined to be high spin ($S = 2$), but their structure was not confirmed. In fact, a four coordinate iron(II) complex of salicylaldimine or a related Schiff base ligand with a N_2O_2 donor set has yet to be characterized by single crystal X-ray crystallography or solution NMR spectroscopy. Herein we describe explicit details of the synthesis of the iron(II) complex of *N*-isopropylsalicylaldimine ($L^{ipr}H$) based on a modifi-

* Corresponding author. Tel.: +1-718-817-4430; fax: +1-718-817-4432.

E-mail address: beer@fordham.edu (R.H. Beer).

0277-5387/02/$ - see front matter © 2002 Elsevier Science Ltd. All rights reserved.
PII: S0277-5387(02)00837-9



L^RH salenH_2

Scheme 1.

cation of the general procedure by Larkworthy [29] and show that this complex is a soluble discrete mononuclear complex in the solid state and solution. We also demonstrate that Fe(L^{ipr})$_2$ reacts readily with air to form the corresponding oxo-bridged dinuclear iron(III) complex indicating that it is a useful material for synthetic strategies involving low coordinate iron(II) salicylaldimine compounds.

2. Experimental

2.1. Materials and methods

All reagents were used as received from commercial suppliers. Benzene and tetrahydrofuran were distilled under pre-purified dinitrogen from sodium benzophenone ketyl and stored under dinitrogen. Methanol was dried and distilled over activated molecular sieves under dinitrogen and stored under dinitrogen. The preparation and manipulation of bis(*N*-isopropylsalicylaldiminato)iron(II) was carried out under argon in a glove box and on a vacuum line using standard inert atmosphere methods [32]. Care must be taken to ensure all equipment is fully dried and solvents are de-gassed to successfully prepare bis(*N*-isopropylsalicylaldiminato)iron(II).

Elemental analysis of bis(*N*-isopropylsalicylaldiminato)iron(II) was performed by Desert Analytics (Tuscon, AZ). Elemental analysis of *N*-isopropylsalicyaldimine and bis(*N*-isopropylsalicylaldiminato)zinc(II) were carried out by QTI (Whitehouse, NJ). Infrared spectra were recorded on a Mattson Satellite FTIR. The NMR spectroscopic data were obtained on a Bruker AVANCE 300 spectrometer at 23 °C and are reported as positive shifts upfield of tetramethylsilane. The numbering scheme for the aromatic ring protons for the salicylaldimine anion moiety is given in Fig. 2.

2.2. X-ray crystallography of bis(*N*-isopropylsalicylaldiminato)iron(II)

Single crystals suitable for X-ray crystallographic studies were obtained by dissolving bis(*N*-isopropylsalicylaldiminato)iron(II) in tetrahydrofuran under argon in a Schlenk tube and cooling to −20 °C in a freezer for several days. The data collection, solution and refinement of bis(*N*-isopropyisalicyl-aldiminato)iron(II) summarized in Table 1 were carried out by routine methods using the SHELXTL suite of programs [33]. The ORTEP diagram and selected bond distances and angles are given in Fig. 1 and Table 2, respectively. Full crystallographic details are available as supplementary material.

Table 1
Crystal data, data collection, and solution and refinement for Fe(L^{ipr})$_2$

Crystal data	
Empirical formula	$C_{20}H_{24}FeN_2O_2$
Crystal habit, color	plate, orange
Crystal size (mm)	0.35 × 0.30 × 0.05
Crystal system	orthorhombic
Space group	*Pbca*
a (Å)	15.0650(6)
b (Å)	13.2631(6)
c (Å)	19.3374(9)
V (Å^3)	3863.8(3)
Z	8
Formula weight	380.26
D_{calc} (Mg m^{-3})	1.307
Absorption coefficient (mm^{-1})	0.795
F(000)	1600
Data collection	
Wavelength (Å)	0.71073
Temperature (K)	173(2)
θ Range for data collection (°)	2.11–25.04
Index ranges	$-17 \le h \le 17$, $-15 \le k \le 11$, $-22 \le l \le 22$
Reflections collected	17 845
Independent reflections	3395 ($R_{int} = 0.0763$)
Solution and refinement	
Solution	direct methods
Refinement method	full-matrix least-squares on F^2
Weighting scheme	$w = [\sigma^2(F_o^2)+(AP)^2+(BP)]^{-1}$, where $P = (F_o^2+2F_c^2)/3$, $A = 0.0001$, and $B = 5.2692$
Absorption correction	semi-empirical
Max/min transmission	0.58808 and 0.53736
Data/restraints/parameters	3395/0/254
Final *R* indices ($I > 2\sigma(I)$]	$R_1 = 0.0645$, $wR_2 = 0.0854$
R indices (all data)	$R_1 = 0.0875$, $wR_2 = 0.0914$
Goodness-of-fit on F^2	1.248
Largest difference peak and hole (e Å^{-3})	0.229 and −0.269

A crystal of bis(*N*-isopropylsalicylaldiminato)iron(II) was attached to a glass fiber and mounted on the Siemens SMART CCD platform diffractometer system for a data collection at 173(2) K. An initial set of cell constants was calculated from reflections harvested from three sets of 20 frames. These initial sets of frames were oriented such that orthogonal wedges of reciprocal space were surveyed. This produced orientation matrices determined from 45 reflections. Final cell constants were calculated from a set of 6495 reflections from the actual

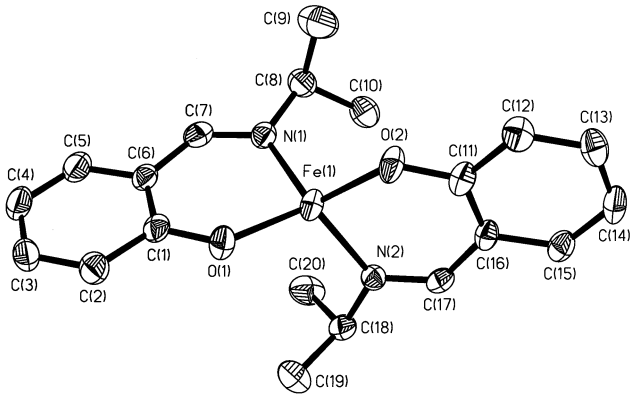


Fig. 1. Molecular structure of $Fe(L^{ipr})_2$ shown with 50% probability level thermal ellipsoids.

Table 2
Selected bond distances (Å) and angles (°) for $Fe(L^{ipr})_2$

Coordination sphere			
Fe(1)–O(2)	1.912(2)	Fe(1)–N(1)	2.040(3)
Fe(1)–O(1)	1.916(2)	Fe(1)–N(2)	2.053(3)
O(1)–Fe(1)–N(1)	93.4 (1)	O(1)–Fe(1)–N(2)	114.3(1)
O(2)–Fe(1)–N(2)	93.0(1)	O(2)–Fe(1)–N(1)	113.3(1)
O(2)–Fe(1)–O(1)	125.8(1)	ϕ [a]	82.7
N(1)–Fe(1)–N(2)	119.5(1)	θ [b]	6.1, 6.9
Ligand geometry			
Ligand 1		Ligand 2	
O(1)–C(1)	1.317(4)	O(2)–C(11)	1.312(4)
C(1)–O(1)–Fe(1)	128.5(2)	C(11)–O(2)–Fe(1)	129.4(2)
N(1)–C(7)	1.293(4)	N(2)–C(17)	1.296(4)
N(1)–C(8)	1.486(4)	N(2)–C(18)	1.483(4)
C(7)–N(1)–Fe(1)	122.0(2)	C(17)–N(2)–Fe(1)	122.1(2)
C(7)–N(1)–C(8)	116.4(3)	C(17)–N(2)–C(18)	117.1(3)
C(8)–N(1)–Fe(1)	121.5(2)	C(18)–N(2)–Fe(1)	120.8(2)
C(6)–C(7)	1.444(5)	C(16)–C(17)	1.442(5)
C(8)–C(9)	1.526(5)	C(18)–C(19)	1.520(5)
C(8)–C(10)	1.522(5)	C(18)–C(20)	1.526(5)
$C–C(ring)_{avg}$	1.396(6)	$C–C(ring)_{avg}$	1.398(5)
$C–C–C(ring)_{avg}$	120.0(4)	$C–C–C(ring)_{avg}$	120.0(4)

[a] The dihedral angle between the mean planes formed by the atoms O(1)–Fe(1)–N(1) and O(2)–Fe(1)–N(2).

[b] The two dihedral angles between the mean plane formed by carbon atoms of the aromatic ring of ligand 1 (C1–C6) and O(1)–Fe(1)–N(1) and the carbon atoms of ligand 2 (C11–C16) and the mean plane formed by O(2)–Fe(1)–N(2).

data collection. A semi-empirical absorption correction was carried out using the SHELXTL XPREP absorption routine. The space group *Pbca* was determined based on systematic absences and intensity statistics. A successful direct-methods solution was calculated which provided most non-hydrogen atoms from the E-map. Several full-matrix least-squares/difference Fourier cycles were performed which located the remainder of the non-hydrogen atoms. All non-hydrogen atoms were refined with anisotropic displacement parameters. All hydrogen atoms were placed in ideal positions and refined as riding atoms with individual (or group if appropriate) isotropic displacement parameters. A weak intermolecular hydrogen bond was observed between H(15) and O(2) equal to 2.484 Å.

2.3. Preparation of compounds

2.3.1. *N*-iso-propylsalicyaldimine ($L^{ipr}H$)

This compound was synthesized by a generally accepted method for the preparation of salicylaldimine ligands [2]. A solution of 16.69 g (0.137 mol) of salicylaldehyde in 150 ml of benzene was added to a 250 ml round bottom flask fitted with a Dean–Stark trap and condenser. To this solution, 12 ml (8.3 g, 0.14 mol) of isopropylamine was added slowly with stirring and then refluxed for 1 h. After cooling, the reaction mixture was dried over anhydrous magnesium sulfate and gravity filtered. The filtrate was rotoevaporated and dried under vacuum to yield 16.8 g (75%) of a yellow–brown oil that could be used without further purification. *Anal*. Calc. for $C_{10}H_{13}NO$: C, 73.59; H, 8.03; N, 8.58. Found: C, 73.39; H, 7.84; N, 8.44%. FTIR (neat): 3060, 2969, 2869, 1679, 1631(s), 1582, 1499, 1460, 1420, 1385, 1322, 1279, 1210, 1150, 1032, 977, 951, 905, 846, 755, 738, 632 cm^{-1}. ^1H NMR ($CDCl_3$) δ 13.72 (1H, s, OH), 8.35 (1H, s, N=CH), 7.26 (2H, m, H3, H4), 6.95 (1H, d, H6), 6.86 (1H, t, H5), 3.52 (1H, septet, $NCH(CH_3)_2$, 1.29 (6H, d, $NCH(CH_3)_2$) ppm.

2.3.2. Bis(*N*-isopropylsalicylaldiminato)iron(II) $Fe(L^{ipr})_2$

This synthetic procedure is a modification of the preparation by Larkworthy [29]. A solution of 4.21 g (34.5 mmol) of salicylaldehyde (salH) dissolved in 20 ml of a 0.14 M KOH methanol solution was added to 3.00 g (17.2 mmol) of $Fe(O_2CCH_3)_2$ (Aldrich) in 100 ml of methanol with stirring. A dark red solid formed. The solvent was decanted after 10 min. The solid product was dried to yield 2.99 g of a red-purple powder of the iron(II) salicylaldehyde compound 'Fe(sal)$_2$'. To 0.474 g (1.78 mmol) of $Fe(sal)_2$ dissolved in 50 ml of tetrahydrofuran, 0.378 g (6.40 mmol) of isopropylamine was added under argon. The opaque solution became dark orange and was allowed to stir for 3 h. The solvent was evaporated under vacuum and the crude product was dissolved in 300 ml of pentane. A small amount of product crystallized immediately as orange flakes along with a substantial amount of a red precipitate, a presumed hydrolysis product. The solution, which is extremely sensitive to moisture and dioxygen, was filtered and cooled in a freezer (−20 °C) for 2 days. The crystalline product was filtered and dried under vacuum to yield 0.23 g of orange flakes (34%). The solid product is comparatively stable when exposed briefly to air. *Anal*. Calc. for $C_{20}H_{24}N_2O_2Fe$: C, 63.17; H, 6.36; N, 7.37. Found: C, 62.97; H, 6.24; N, 7.24%. FTIR (KBr): 3447 (br), 3050, 2964, 2924, 2889, 1617, 1599 (s), 1537, 1467, 1442, 1402, 1367, 1331, 1315, 1195, 1143, 1122,

1031, 976, 919, 855, 786, 763, 756, 740, 612, 578, 493 cm^{-1}. ^1H NMR (C_6D_6, 300 MHz, 23 °C) δ 195.4 (1H, s, NCH(CH$_3$)$_2$), 67.7 (1H, s, H4), 62.0 (1H, s, H6), −15.9 (1H, s, H5), −21.8 (1H, s, H3), −30.5 (6H, s, NCH(CH$_3$)$_2$) ppm.

2.3.3. Bis(N-isopropylsalicylaldiminato)zinc(II) $Zn(L^{ipr})_2$

To a rapidly stirring suspension of 4.17 g (25.6 mmol) of *N*-isopropylsalicylaldimine in 15 ml of deionized water, 1.74 g of $ZnCl_2$ (12.8 mmol) was added slowly. A 10 ml solution of 1.02 g (24.3 mmol) of NaOH dissolved in deionized water was then added slowly to the slightly yellow solution to produce a white solid. The heterogeneous reaction mixture was stirred for an additional 10 min and filtered. The precipitate was washed with deionized water (3 × 5 ml) followed by pentane (3 × 5 ml) to remove any unreacted ligand. The product was dried under vacuum to yield 4.12 g of a white powder (83%). The product can be recrystallized from acetone–water. *Anal*. Calc. for $C_{20}H_{24}N_2O_2Zn$: C, 61.62; H, 6.21; N, 7.19. Found: C, 61.95; H, 6.10; N, 7.00%. FTIR (KBr): 3051, 2966, 2926, 2901, 1616 (s), 1537, 1466, 1445, 1408, 1333, 1316, 1191, 1145, 1123, 1032, 999, 959, 918, 857, 759, 603, 505, 449 cm^{-1}. ^1H NMR ($CDCl_3$) δ 8.35 (1H, s, N=CH), 7.29 (1H, t, H4), 7.09 (1H, d, H3), 6.85 (1H, d, H6), 6.59 (1H, t, H5), 3.63 (1H, m, NCH(CH$_3$)$_2$), 1.33 (3H, d, NCH(CH$_3$)$_2$); 1.21 (3H, d, NCH(CH$_3$)$_2$) [note: the NCH(CH$_3$)$_2$ methyl groups are diastereotopic] ppm.

3. Results and discussion

3.1. Synthesis

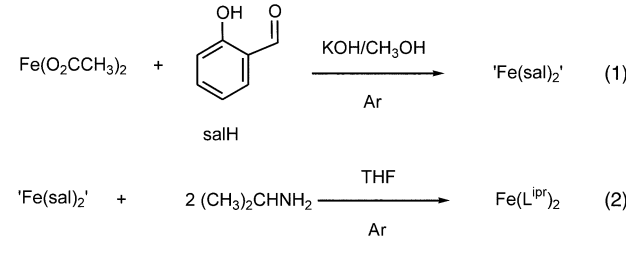
A general method for the reliable synthesis of bis(salicylaldiminato)iron(II) complexes has been described by Larkworthy [6,29]; these compounds had been prepared prior to this study, but because of their acute air sensitivity the complexes frequently yielded impure oxidized products. As indicated by Larkworthy [29], the optimal procedure for the preparation of bis(salicylaldiminato)iron(II) complexes was the formation of a precursor from salicylaldehyde and iron(II) acetate in the presence of a strong base followed by the addition of a primary amine in alcohol solvents [34]. No preparative details, e.g. amounts of material, yields, etc., however, are given in Larkworthy's or subsequent papers [6,12,29–31]. We have re-examined this synthetic method to render a more detailed experimental procedure for the preparation of the *N*-isopropylsalicylaldimine derivative, $Fe(L^{ipr})_2$.

The reaction of the *N*-isopropylsalicylaldimine with iron(II) acetate in tetrahydrofuran failed to produce pure product as indicated by ^1H NMR spectroscopy. We find, as previously determined, that the reaction of the primary amine with the pre-formed iron salicylaldehyde complex forms the desired pure product in an acceptable yield. Two equiv. of salicylaldehyde (salH) are deprotonated in a methanol solution of potassium hydroxide and added to 1 equiv. of iron(II) acetate as shown in Scheme 2, Eq. (1). A precipitate forms, presumed to be bis(salicyaldehydato)iron(II) 'Fe(sal)$_2$', which is dried under vacuum to yield a purple solid.

The ^1H NMR spectrum of Fe(sal)$_2$ in CD_3CN exhibits four broad markedly shifted resonances for the ligand aromatic ring protons ranging from +45 to −16 ppm. This shift range is expected since iron(II) complexes with phenolate oxygen donors ordinarily display large upfield and downfield shifts [25,35–37]. The shifts are a consequence of the alternating sign of delocalized unpaired electron spin density from partially filled iron(II) d π symmetry orbitals into ligand π orbitals [38–41]. As a result, alternating upfield and downfield ^1H NMR shifts are observed for one proton attached to a ring carbon atom to the next. On this basis and by analogy to the assignments of other iron(II) phenolate complexes, the ^1H NMR resonances of Fe(sal)$_2$ can be assigned to 6H(+44.8), 4H(+35.3), 5H(−10.4) and 3H(−16.0) in accord with the ring proton numbering scheme for salicylaldimine given in Fig. 2.

Early magnetic studies of Fe(sal)$_2$ suggest it is a high spin iron(II) ($S = 2$) complex [29], otherwise very little is known about this compound. The most closely related crystallographically characterized salicylaldehyde metal complex is the dinuclear manganese(II) compound, $Mn_2(sal)_4(CH_3OH)_2$ [42], in which phenolate oxygen atoms from two of the salicylaldehyde anions bridge the manganese centers. Our ^1H NMR studies suggest that 'Fe(sal)$_2$' is mononuclear in solution (though perhaps solvated) since only one set of ring proton resonances is observed for what we presume to be terminally coordinated salicylaldehydato ligands.

The condensation of excess isopropylamine with the coordinated aldehyde moiety in the complex 'Fe(sal)$_2$' in tetrahydrofuran produced a dark orange solution from which orange microcrystalline $Fe(L^{ipr})_2$ could be isolated in 34% yield (Eq. (2)). While solutions of $Fe(L^{ipr})_2$ are very susceptible to decomposition in air, the solid compound could be handled briefly in air. The com-



Scheme 2.

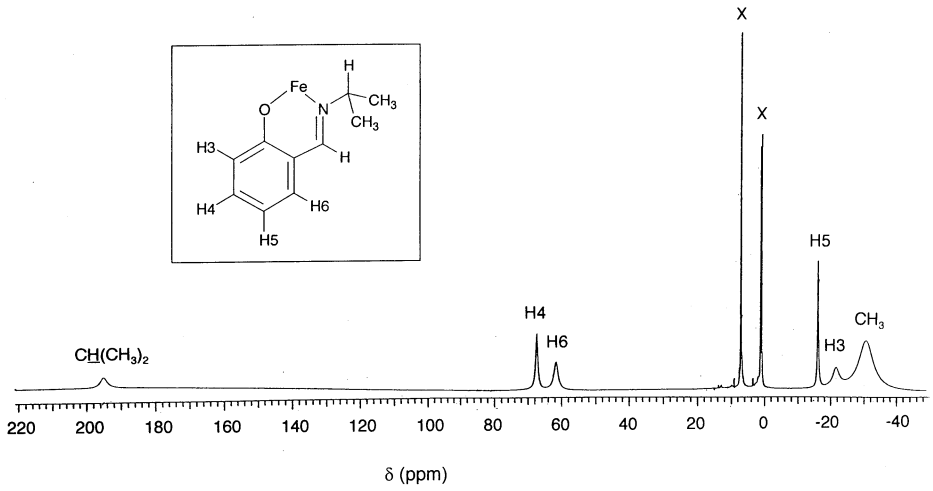


Fig. 2. The ^{1}H NMR spectrum of Fe(L^{ipr})$_2$ in benzene-d_6 at 23 °C. Chemical shift (δ) in ppm downfield of tetramethylsilane. The schematic indicates the proton assignments (inset). The symbol (×) indicates solvent or residual solvent impurity.

pound is very soluble in non-polar solvents. The solubility behavior is in marked contrast to its closest analogue, Fe(salen), which requires donor solvents to dissolve due to its assumed polymeric structure [35,43].

For comparative purposes the Zn(L^{ipr})$_2$ analog, a discrete mononuclear tetrahedral complex [45–47], was also prepared. This straightforward synthesis employed $ZnCl_2$, *N*-isopropylsalicylaldimine and sodium hydroxide, a general preparative method for zinc(II) *N*-alkylsalicylaldimines that generally gives good yields in our hands [44]. Both compounds, M(L^{irp})$_2$ (M = Fe, Zn) have very similar solubility characteristics and solid-state infrared spectra, indicative of an analogous structure. The most intense infrared stretch, assigned typically to the imine C=N bond, is found at 1599 (Fe) and 1616 (Zn) cm^{-1}. The value for the energy of the stretch in the iron complex is in excellent agreement with the C=N stretch (1603 cm^{-1}) reported for the tetrahedral iron(II) complex of the nitrogen analogue *t*-BuN=C(H)$C_6H_4NH^-$ of the salicylaldiminate ligand [18].

3.2. Structure determination by X-ray crystallography

The structure of Fe(L^{ipr})$_2$ shown in Fig. 1 displays a four coordinate iron atom coordinated to two bidentate *N*-isopropylsalicylaldimine anions. The bond distances and angles provided in Table 2 reveal relatively short Fe–O (1.912(2), 1.916(2) Å) and Fe–N (2.040(3), 2.053(3) Å) bond distances and a distorted tetrahedral coordination geometry most likely due to the acute O–Fe–N bite angles (93.4(1)°, 93.0(1)°). Metrical parameters of the ligand, also given in Table 2, indicate that the ligand is coordinated to iron in its characteristic phenolate-imine form [2]. Overall ligand geometry is very similar to generally accepted norms for salicylaldimine ligands in this coordination mode [1,2].

Though no four coordinate iron(II) salicylaldimine complex has been structurally characterized previously, the structure of Fe(L^{ipr})$_2$ and the Zn analog [46,47] are most comparable while those of the other first row d block analogs Co, Ni, and Cu deviate somewhat more significantly [48]. No simple trend is obvious and their differences are likely due to the both the nature of the metal–ligand bonding, the electronic structure of the metal atoms and the structural requirements of the ligand. The average Zn–O (1.913 Å) and Fe–O (1.914 Å) bond lengths are indistinguishable compared with the Co–O (1.905 Å), Ni–O (1.896 Å) and Cu–O (1.805 Å) bond distances. The Zn–N (2.009 Å) bond distance is only slightly shorter than the corresponding Fe–N (2.047 Å) distance while those of Co (1.992 Å), Ni (1.970 Å), and Cu (1.979 Å) are considerably shorter. The average ligand bite angles (O–M–N) for Fe (93.2°), Co (96.4°), Ni (94.4°), Cu (94.9°) and Zn (96.7°) are largely invariant due to the constraints of the ligand. Likewise, the corresponding interligand angles (N–M–O_{avg}, N–M–N, O–M–O) of the Fe complex (113.8°, 119.5°, 125.8°), Co (112.3°, 122.6°, 118.5°), Ni (112.4°, 120.9°, 125.1°), and Zn complex (112.6°, 117.2°, 122.9°) diverge only slightly, while the Cu angles (100.3°, 137.9°, 137.2°) are markedly different because of its very large distortion from tetrahedral geometry. Overall tetrahedral geometry as determined by the dihedral angle, ϕ, between the planes formed by the metal atom and corresponding ligand donor atoms, e.g. N(1)–Fe(1)–O(1), as well as a measure of the deviation of these atoms from the plane formed by ligand aromatic ring (dihedral angle θ), are most similar for the Fe (ϕ = 82.7°, θ_{avg} = 6.5°) and Zn (ϕ = 84.2°, θ_{avg} = 3.9°) complexes, whereas Co, Ni (ϕ = 94°), and Cu (ϕ = 60°) are, again, less comparable.

The most closely related structurally characterized tetrahedral iron(II) complex is that of the salicylaldi-

mine nitrogen analogue, t-BuN=C(H)$C_6H_4NH^-$ [18]. The average iron imine nitrogen distance of 2.061 Å in this complex is nearly equivalent to the corresponding distance in $Fe(L^{ipr})_2$. The remaining structural parameters of its coordination sphere, while not as similar to $Fe(L^{ipr})_2$ as $Zn(L^{ipr})_2$, are characteristic of a bidentate monoanionic ligand bound to iron(II) in a tetrahedral coordination geometry. Other similar iron nitrogen imine distances include those of tetrahedral amidinato $FeCl_2$ adducts (2.100 Å) [24] and the tropocoronand N4 macrocycle (2.020 Å) [16].

An obvious comparison, that of Fe–O bond distances of low coordinate mononuclear complexes (ranging from three to five) with terminal phenolate ligands is more problematic. The number of these complexes is limited and typically have shorter Fe–O bond distances than observed in $Fe(L^{ipr})_2$, for example, the three coordinate homoleptic phenoxide $[Fe\{O(2,4,6\text{-}t\text{-}BuC_6H_2)\}_2]_2$ (1.822 Å) [25], four coordinate trispyrazolylborate phenoxide $HB\{(3,5\text{-}i\text{pr})pz\}_3Fe(OC_6F_5)$ (1.876 Å) [49], and a five coordinate iron calixarene adduct of THF (1.895 Å) [17].

One can examine the iron ligand bond distances of the four coordinate $Fe(L^{irp})_2$ complex reported here and corresponding examples of five and six coordinate neutral high spin iron(II) salicylaldimine complexes, i.e. 'salen type' ligands with additional donors, N,N'-(3,3′-dipropylmethylamine)bis-(salicylideneimine) (a pentadentate ligand that incorporates one amine donor) [50] and 1,10-bis(5-nitrosalicylaldehyde)-1,4,7,10-tetraazadecane (a hexadentate ligand with two supplementary amines) [51]. The average iron donor bond distances (Fe–N, Fe–O) in this series from coordination number six to four are (2.127, 2.093), (2.045, 2.041), (1.953, 1.914) Å, respectively. Neglecting the differences between the ligands, the change in iron(II)-donor bond distance follows the predictable trend of decreasing bond length with decreasing coordination number.

Early studies of bis(salicylaldiminato)iron(II) or related complexes, which included electronic and Mössbauer spectroscopic measurements as well as magnetic measurements, suggested that the compound was either polymeric or monomeric with a coordination number ranging from four to six [6,29–31,52]. These conclusions are reasonable given the tendency for coordinatively unsaturated Schiff base complexes to add donors as well as undergo bridging with the oxygen atom donor portion of the ligand. For example, Fe(salen) is presumably a polymer in the solid state, but readily coordinates to good donor solvents to form soluble species or exogenous anionic ligands to form five coordinate mononuclear species in solution [35]. Likewise, a more soluble Fe(salen) analogue, Fe(acen), is dinuclear in the solid state and mononuclear in benzene [43]. Here, in contrast, we have shown that $Fe(L^{ipr})_2$ is mononuclear and tetrahedral in the solid state.

3.3. Characterization by ^1H NMR spectroscopy

The ^1H NMR spectrum of $Fe(L^{ipr})_2$ shown in Fig. 2 exhibits broad ligand resonances that experience large upfield and downfield shifts ranging from +195 to −31 ppm resulting from the paramagnetism of the complex [29]. The observed peaks and their assignment are given in Table 3. The shifts and linewidths of the peaks at 67.7, 62.0, −15.9 and −21.8 ppm in Fig. 2 are similar to those observed previously for high spin iron(II) complexes $[Fe(salen)X]^-$ (X = anion) [35] and are assigned accordingly to the aromatic ring protons H4, H6, H5, and H3. The observation of one set of ligand resonances for the ring protons in $Fe(L^{ipr})_2$ suggests that, like $Fe(sal)_2$, there is a single static ligand environment consistent with a mononuclear complex (however, we cannot exclude that a rapidly averaged environment is present in either complex).

The large peak observed at −30.5 ppm in Fig. 2 is assigned to the isopropyl methyl protons based on its 6:1 relative intensity compared with each of the aromatic ring protons. The methyl protons, which are diastereotopic in our ^1H NMR spectrum of $Zn(L^{ipr})_2$ [45,53] (see Scheme 3), are either not resolved in the spectrum of $Fe(L^{ipr})_2$ or its chirality is lost due ligand exchange or inversion through a square planar intermediate [54]. The anomalously large linewidth (700 Hz) may indicate the former explanation.

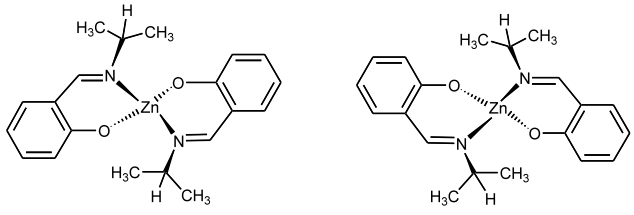
The remaining resonance at 195.4 ppm is assigned tentatively to the tertiary hydrogen of the isopropyl group. Hydrogen atoms attached to carbon atoms adjacent to tertiary amines bound to iron(II) have been observed to experience shifts greater than 100 ppm, i.e. in $[FeM(BPMP)(L)_2]^+$ (M = Fe, Zn, Ga, BPMP = 2,6-bis[[bis(2-pyridylmethylamino]methyl]-4-methylphenol anion; $L = O_2CR^-$ or $O_2P(OR)_2^-$) [37] and $(TMEDA)Fe(CH_2Ph)_2$ (TMEDA = N,N,N',N'-tetramethyl-ethylenediamine) [23]. The imine hydrogen, HC=N, resonance has not been reported previously in ^1H NMR studies of iron(II) Schiff base compounds [35,36], so its absence is predictable. Since the proton of interest is two bonds away from the iron atom in the delocalized, conjugated imine moiety of the salicylaldiminate ligand, a large proportion of electron spin density would presumably broaden this resonance beyond detection.

The observation that the linewidths (in Hz) of the ring protons H3(254), H6(200), H4(125) and H5(55) for $Fe(L^{ipr})_2$ become progressively smaller the farther the proton is from the iron center, i.e. H3(4.5 Å), H6(5.3 Å), H4(6.3 Å) and H5(6.6 Å), is consistent with their assignment. The nature of the shifts of the isopropyl protons is more difficult to discern. The fact that the proton attached to the tertiary carbon apparently shifts upfield while the methyl group attached to the same carbon shifts downfield implies a contact spin delocali-

Table 3
Tabulated ^{1}H NMR spectral data of Fe(L^{ipr})$_2$

Assignment [a]	Chemical shift [b] (δ_{obs}, ppm)	Linewidth [c] (Hz)	Integration (number of H's)	Isotropic shift [d] (δ, ppm)
H3	−21.8	254	1	−28.9
H4	67.7	125	1	60.4
H5	−15.9	55	1	−22.5
H6	62.0	200	1	55.2
C$\underline{H}$(CH$_3$)$_2$	195.4 [e]	400	1	191.8
CH(C$\underline{H}_3$)$_2$	−30.5	700	6	−31.8

Concentrated sample in C_6D_6 at 23 °C at 300 MHz.
[a] Ligand schematic is shown in Fig. 2.
[b] Chemical shift positive upfield of tetramethylsilane.
[c] Measured at half-height.
[d] $(\Delta v/v_0)^{iso} = \delta_{Fe} - \delta_{Zn}$.
[e] Tentative assignment.



Scheme 3.

zation mechanism similar to the shifts observed for methylene protons adjacent to a coordinated tertiary amine in $[Fe_2(BPMP)(O_2P(OPh)_2)_2]^+$ [37]. Since tetrahedral iron(II) has an anisotropic ground state (^{5}E), it generally experiences a significant dipolar contribution to the isotropic shift which depends on the relative orientation and distance of proton to the iron atom [39–41]. The isopropyl group protons in Fe(L^{ipr})$_2$ are likely to be very susceptible to dipolar interactions since they can experience close contacts with the iron atom (as close as 2.8 Å estimated from the X-ray structure and model building) as the isopropyl group rotates freely.

3.4. Reactivity

When a solution of Fe(L^{ipr})$_2$ in benzene-d_6 is exposed briefly to air (<1 min), the ^{1}H NMR resonances due to the iron(II) complex disappear and less shifted resonances ranging from 28.8 to 1.2 ppm are observed in the spectrum accompanied by peaks due to a small amount of free ligand ($<10\%$ by integration). The five broad resonances are consistent with the formation of the oxo-bridged dinuclear iron(III) species [Fe(L^{ipr})$_2$]$_2$O from Fe(L^{ipr})$_2$ and air (Eq. (3)). The observed ^{1}H NMR shifts found at 28.8 (very broad), 13.1, 10.1, 2.3 (overlapping), and 1.2 ppm in an approximate 1:1:1:6:1 ratio can be assigned to the (CH$_3$)$_2$C$\underline{H}$, 4H, 6H, 5H and (C$\underline{H}_3$)$_2$CH (overlapping) and 3H protons, respectively, based on comparison with published spectra of [Fe(L^R)$_2$]$_2$O [55] and Fe(salen)$_2$O [38,56] and their integration. A near identical spectrum was

$$2Fe(L^{ipr})_2 \xrightarrow[C_6D_6]{air} [Fe(L^{ipr})_2]_2O \quad (3)$$

obtained from [Fe(L^{ipr})$_2$]$_2$O prepared independently by the literature method [57]. The small exclusively upfield shifts are characteristic of oxo-bridged diiron(III) complexes with strong antiferromagnetic coupling ($J > 100$ cm^{-1}) between high-spin ($S = 5/2$) iron(III) centers mediated by an oxo bridge [38]. Since high spin iron(III) has a symmetrical electronic environment ($^6A_{1g}$), the shifts are primarily contact in origin and, therefore, proportional to the magnetic susceptibility of the complex [39–41]. The relatively small magnetic moment (~ 1.9 BM) of [Fe(L^R)$_2$]$_2$O complexes [55] results in a marked attenuation of their isotropic shift compared with Fe(L^{ipr})$_2$. With the exception of a small amount of ligand, due possibly to ligand dissociation or protonolysis, the reaction did not result in an observable precipitate or any other apparent iron species as monitored by ^{1}H NMR.

Oxo-bridged diiron(III) species have been observed previously from the reaction of air or dioxygen with mononuclear iron(II) porphyrin [58,59], salen [9], or acen [43] complexes. In contrast to Fe(salen), the reaction with Fe(L^{ipr})$_2$ can be carried out in non-polar, non-coordinating solvents in which both Fe(L^{ipr})$_2$ and [Fe(L^{ipr})$_2$]$_2$O are soluble and where Fe(L^{ipr})$_2$ is, plausibly, a discrete mononuclear species. As emphasized previously for Fe(acen) [43], these attributes are essential for studying the reactions of low coordinate iron(II) compounds. A case in point is the reaction of iron(II) porphyrins and dioxygen in toluene to detect the diiron(III) peroxo intermediate by ^{1}H NMR at low temperature [59].

In addition, tetradentate ligands like acen, salen or porphyrins enforce typically a square planar geometry about the iron center. While this allows for an often critical available coordination site, it may be of interest to probe iron(II) reactions with ligands such as L^{ipr}H that allow access to coordination geometries other than those based on square planar, e.g. as observed in the

active sites of iron(II) centers in non-heme iron proteins [28].

4. Supporting information

Full crystallographic information for $Fe(L^{ipr})_2$ is available as deposit number 168259 from the Cambridge Crystallographic Database Center (12 Union Road, Cambridge, CB2 1EZ, UK or on the web at www: http://www.ccdc.cam.ac.uk).

Acknowledgements

The authors gratefully acknowledge financial support from Fordham University, the Camille and Henry Dreyfus Foundation Award of Research Corporation Award #H50558 (to R.H.B. and S.C.), and a NSF Division of Undergraduate Education Grant DUE #9650684 for the NMR spectrometer at Frodham. The authors also thank Dr. Jennifer L. Kisko for preliminary experiments and Dr. Victor G. Young, Jr. at the X-ray Crystallographic Laboratory at the University of Minnesota for crystallographic studies on $Fe(L^{ipr})_2$.

References

[1] R.H. Holm, G.W. Everett, Jr., A. Chakavorty, Prog. Inorg. Chem. 7 (1966) 83.
[2] M. Calligaris, L. Randaccio, in: G. Wilkinson, R.D. Gillard, J.A. McCleverty (Eds.), Comprehensive Coordination Chemistry, vol. 2, Pergamon Press, Oxford, 1987.
[3] E.N. Jacobsen, in: E.W. Abel, F.G.A. Stone, G. Wilkinson (Eds.), Compreshensive Organometallic Chemistry, vol. 12, Elsevier, New York, 1995.
[4] The salicylaldimine ligands, prepared by condensation of the salicylaldehyde and primary amines, are also termed salicylideneamines or salicylideneimines and belong to a greater class of ligands generally referred to as Schiff bases.
[5] G. Wilkinson, R.D. Gillard, J.A. McCleverty (Eds.), Comprehensive Coordination Chemistry, vol. 4, Pergamon Press, Oxford, 1987.
[6] A. Earnshaw, E.A. King, L.F. Larkworthy, J. Chem. Soc., A (1969) 2459.
[7] C. Floriani, F. Calderazzo, J. Chem. Soc., A (1971) 3655.
[8] S.L. Kessel, D.N. Hendrickson, Inorg. Chem. 17 (1978) 2630.
[9] F. Calderazzo, C. Floriani, R. Henzi, F. L'Eplattier, J. Chem. Soc., A (1969) 1378.
[10] (a) C. Floriani, G. Fachinetti, Gazz. Chim. Ital. 103 (1973) 1317; (b) P.C.H. Mitchell, D.A. Parker, J. Chem. Soc., Dalton Trans. (1976) 1821.
[11] L.M. Proniewicz, T. Isobe, K. Nakamoto, Inorg. Chim. Acta 155 (1989) 91.
[12] P.J. Nichols, G.D. Fallon, K.S. Murray, B.O. West, Inorg. Chem. 27 (1988) 2795.
[13] S. Kiani, A. Tapper, R.J. Staples, P. Stavropoulos, J. Am. Chem. Soc. 122 (2000) 7503.
[14] C.E. MacBeth, A.P. Golombek, V.G. Young, Jr., C. Yang, K. Kuczera, M.P. Hendrich, A.S. Borovik, Science 289 (2000) 938.
[15] A.K. Verma, S.C. Lee, J. Am. Chem. Soc. 121 (1999) 10838.
[16] K.J. Franz, S.J. Lippard, J. Am. Chem. Soc. 121 (1999) 10504.
[17] M. Giusti, E. Solari, L. Giannini, C. Floriani, A. Chiesa-Villa, Organometallics 16 (1997) 5610.
[18] G. Weymann, A.A. Danopulos, G. Wilkinson, T.K.N. Sweet, M.B. Hursthouse, Polyhedron 15 (1996) 3605.
[19] S.L. Stokes, W.M. Davis, A.L. Odom, C.C. Cummins, Organometallics 16 (1996) 4521.
[20] W.-P. Leung, H.K. Lee, L.-H. Weng, B.-S. Luo, Z.-Y. Zhou, T.C.W. Mak, Organometallics 15 (1996) 1785.
[21] H. Müller, W. Seidal, H. Görls, Angew. Chem., Int. Ed. Engl. 34 (1995) 325.
[22] A. Kose, E. Solari, C. Floriani, A. Chiesi-Villa, C. Rizzoli, N. Re, J. Am. Chem. Soc. 116 (1994) 9123.
[23] D.H. Hill, M.A. Parvez, A. Sen, J. Am. Chem. Soc. 116 (1994) 2889.
[24] F.A. Cotton, L.M. Daniels, D.J. Maloney, J.H. Matonic, C.A. Murillo, Polyhedron 5 (1994) 815.
[25] R.A. Bartlett, J.J. Ellison, P.P. Power, S.C. Shoner, Inorg. Chem. 30 (1991) 2888.
[26] N. Kitajima, N. Tamura, H. Amagai, H. Fukui, Y. Moro-oka, Y. Mizutani, T. Kitagawa, R. Mathur, K. Heerwegh, C.A. Reed, C.R. Randall, L. Que, Jr., K. Tatsumi, J. Am. Chem. Soc. 116 (1994) 9071.
[27] (a) D. Lee, S.J. Lippard, J. Am. Chem. Soc. 120 (1998) 12153; (b) J.R. Hagdorn, L. Que, Jr., W.B. Tolman, J. Am. Chem. Soc. 120 (1998) 13531.
[28] (a) L. Que, Jr., R.Y.N. Ho, Chem. Rev. 96 (1996) 2607; (b) E.I. Solomon, T.C. Brunold, M.I. Davis, J.N. Kemsley, S.-K. Lee, N. Lehnert, F. Neesse, A.J. Skulkun, Y.-S. Yang, J. Zhou, Chem. Rev. 100 (2000) 235.
[29] A. Earnshaw, E.A. King, L.F. Larkworthy, J. Chem. Soc., A (1968) 1048.
[30] B.W. Fitzsimmons, A.W. Smith, L.F. Larkworthy, K.A. Rodgers, J. Chem. Soc., Dalton Trans. (1973) 676.
[31] J.L.K.F. de Vries, J.M. Trooster, E. de Boer, J. Chem. Soc., Dalton Trans. (1974) 1771.
[32] (a) D.F. Shriver, The Manipulation of Air-Sensitive Compounds, Wiley, New York, NY, 1986; (b) J.P. McNally, V.S. Leong, N.J. Cooper, ACS Symp. Ser. 357 (1987) 6.
[33] G.M. Sheldrick, SHELXTL, An Integrated System for Solving, Refining, and Displaying Crystal Structures from Diffraction Data, University of Göttingen, Göttingen, Federal Republic of Germany, 1981.
[34] A well-accepted 'template' method for the preparation of salicylaldimine complexes is described in reference [1].
[35] R.N. Mukherjee, A.J. Abrahamson, G.S. Patterson, T.D.P. Stack, R.H. Holm, Inorg. Chem. 27 (1988) 2137.
[36] B.S. Synder, G.S. Patterson, A.J. Abrahamson, R.H. Holm, J. Am. Chem. Soc. 111 (1989) 5214.
[37] (a) A.S. Borovik, M.P. Hendrich, T.R. Tolman, E. Münck, V. Papaefthymiou, L. Que, Jr., J. Am. Chem. Soc. 112 (1990) 6031; (b) L.-J. Ming, H.G. Jang, L. Que, Jr., Inorg. Chem. 31 (1992) 359.
[38] G.N. La Mar, G.R. Eaton, R.H. Holm, F. Ann Walker, J. Am. Chem. Soc. 95 (1973) 63.
[39] G.N. La Mar, W.D. Horrocks, Jr., R.H. Holm (Eds.), NMR of Paramagnetic Molecules, Academic Press, New York, NY, 1973.
[40] I. Bertini, C. Luchinat, NMR of Paramagnetic Molecules in Biological Systems, Benjamin/Cummings, Menlo Park, CA, 1986.
[41] L.-J. Ming, in: L. Que, Jr. (Ed.), Physical Methods in Bioinorganic Chemistry (Chapter 8), University Science Books, Sausalito, CA, 2000.

[42] S.-B. Yu, C.-P. Wang, E.P. Day, R.H. Holm, Inorg. Chem. 30 (1991) 4067.
[43] F. Corazza, C. Floriani, M. Zehnder, J. Chem. Soc., Dalton Trans. (1987) 709.
[44] M.A. Torzilli, S. Colquhoun, D. Doucet, R.H. Beer, Alternative syntheses employ *N*-alkylsalicyaldimine and $Zn(O_2CCH_3)_2 \cdot 2H_2O$ as described in reference [45], Polyhedron, in press.
[45] (a) F.A. Bottino, P. Finocchiaro, E.J. Libertini, Coord. Chem. 16 (1988) 341;
(b) A. Recca, F.A. Bottino, P. Finocchiaro, J. Inorg. Nucl. Chem. 42 (1980) 479.
[46] F.A. Bottino, P. Finocchiaro, E. Libertini, G. Mattern, Z. Kristallogr. 187 (1989) 72.
[47] M. Dreher, H. Elias, Z. Naturforsch. 42, Teil B (1987) 707.
[48] (a) [Co] Y. Elerman, M. Kabat, M. Nawaz Tahir, Acta Crystallogr., Sect. C 52 (1996) 2434.;
(b) [Ni] M.R. Fox, P.L. Orioli, E.C. Lingafelter, L. Sacconi, Acta Crystallogr. 17 (1964) 1159.;
(c) [Cu] R.J. Butcher, E. Sinn, Inorg. Chem. 15 (1976) 1604.
[49] M. Ito, H. Amaigai, H. Fukui, N. Kitajima, Y. Moro-oka, Bull. Chem. Soc. Jpn. 69 (1996) 1937.
[50] R. Cini, Inorg. Chim. Acta 73 (1983) 147.
[51] D. Boinnard, A. Bousseksou, A. Dworkin, J.-M. Savariault, F. Varret, J.-P. Tuchagues, Inorg. Chem. 33 (1994) 271.
[52] D.H. Gerlach, R.H. Holm, Inorg. Chem. 9 (1970) 588.
[53] The methyl resonances of $Zn(L^{i\,pr})_2$ were reported previously as only being resolved at low temperature in $CDCl_3$ (reference [45]). The reported spectrum, however, was recorded at a lower field at which the chemical shift difference between the diastereotopic protons may not have been resolved—a complication noted in M.J. O'Connor, R.E. Ernst, J.E. Shoenborn, R.H. Holm, J. Am. Chem. Soc. 90 (1968) 1744.
[54] R.H. Holm, M.J. O'Connor, A. Chakavorty, Prog. Inorg. Chem. 14 (1971) 241.
[55] P.D.W. Boyd, K.S. Murray, J. Chem. Soc. (A) (1971) 2711.
[56] J.R. Dorfman, J.-J. Girerd, E.D. Simhon, T.D.P. Stack, R.H. Holm, Inorg. Chem. 23 (1984) 4407.
[57] A. Van den Bergen, K.S. Murray, M.J. O'Connor, N. Rehak, B.O. West, Aust. J. Chem. 21 (1968) 1505.
[58] (a) J.P. Collman, T.R. Halbert, K.S. Suslick, in: T.G. Spiro (Ed.), Metal Ion Activation of Dioxygen, Wiley, New York, NY, 1980, pp. 1–70;
(b) L. Que, Jr., Y. Watanabe, Science 292 (2001) 5517.
[59] D.-H. Chin, G.N. La Mar, A.L. Balch, J. Am. Chem. Soc. 102 (1980) 4344.

ELSEVIER

Polyhedron 21 (2002) 715–719

POLYHEDRON

www.elsevier.com/locate/poly

Cocrystallization of a dinuclear platinum complex as a monomer and a one-dimensional polymer

Jeongsoo Yoo [a,b,*], Young-Kyu Han [b], Yoon Sup Lee [b], Youngkyu Do [b,*]

[a] *Division of Radiological Sciences, Washington University School of Medicine, Box 8225, Mallinckrodt Institute of Radiology, 510 South Kingshighway, St. Louis, MO 63110, USA*

[b] *Department of Chemistry, School of Molecular Science-BK21 and Center for Molecular Design and Synthesis, Korea Advanced Institute of Science and Technology, Daejeon 305-701, Republic of Korea*

Received 30 June 2001; accepted 3 December 2001

Abstract

The reaction of $Pt(DMB)Cl_2$ (DMB = 3,3′-dihydroxymethyl-2,2′-bipyridine) with AgF_3CSO_3 in H_2O yielded a dimeric platinum complex, $[\{Pt(DMB)(\mu\text{-}OH)\}_2](F_3CSO_3)_4\cdot 2H_2O$. X-ray structure reveals that two conformational isomers are self-assembled by different hydrogen bonding motifs in one crystal, resulting in a new type of co-crystal of monomer and its polymer. One conformer is self-assembled into the one-dimensional polymeric chain by strong hydrogen bonds, while the other conformer of which possible hydrogen bond donors/acceptors are blocked by two triflate anions exists as an isolated molecule itself. DFT calculations show that the strong hydrogen bonds and crystal packing force might compensate for the energy gap of ~ 14 kcal mol^{-1} between two conformers and the conformational energetics are dominated by the energies of the coordinated ligands rather than those of hydroxo-bridged platinum cores. © 2002 Published by Elsevier Science Ltd.

Keywords: Cocrystallization; Dinuclear platinum complexes; One-dimensional polymers

1. Introduction

Molecular self-assembly employing hydrogen bonding and its significance in crystal engineering are of considerable interest [1]. Hydrogen bonding is known to play an important role in governing the crystal packing of molecules due to its moderately strong interaction and high degree of directionality [2]. Recently, the incorporation of transition metal into supramolecular chemistry triggered the development of new molecular architecture, and several elegant examples for the combination of coordination and hydrogen bonding in self-assembly are published [3].

Some coordination or organometallic complexes which possess conformational flexibility or possible hydrogen bond donor/acceptor, could crystallize in two or more different crystal systems containing each conformational isomer or differently self-assembled molecule, respectively, by tuning crystallization conditions precisely, i.e. co-crystallization with other molecules [4] or different solvent pairs [5]. To the best of our knowledge, we are not aware, however, of any previous examples in which two differently self-assembled conformational isomers co-crystallize in one asymmetric unit.

Herein, we report a new example of the self-assembly of a platinum dinuclear complex $[\{Pt(DMB)(\mu\text{-}OH)\}_2](F_3CSO_3)_4\cdot 2H_2O$ into a co-crystal containing a dinuclear monomer and a hydrogen-bonded one-dimensional chain of the dinuclear monomer.

2. Experimental

2.1. General procedures

K_2PtCl_4 was purchased from Strem. All other reagents were purchased from Aldrich and used without further purification. Solvents were of reagent grade and

* Corresponding authors. Tel.: +1-314-362-8636; fax: +1-314-362-9940 (J.Y.); tel.: +82-42-869-2829; fax: +82-42-869-2810 (Y.D.).

E-mail addresses: yooj@mir.wustl.edu (J. Yoo), ykdo@kaist.ac.kr (Y. Do).

0277-5387/02/$ - see front matter © 2002 Published by Elsevier Science Ltd.
PII: S0277-5387(02)00838-0

were dried by standard methods. Pt(DMB)Cl_2 (DMB = 3,3′-dihydroxymethyl-2,2′-bipyridine) was prepared according to the published procedure [6].

^{1}H and ^{13}C{^{1}H} NMR spectra were measured on a Bruker AM 300 spectrometer and were referenced to internal solvent peaks. IR spectra were recorded in KBr discs on a Bruker Equinox 55 FT–IR spectrometer. C, H and N elemental analyses were carried out at the Seoul Branch Analytical Laboratory, Korea Basic Science Institute, on an Elementar Analysensysteme GmbH Vario EL elemental analyzer.

2.2. Synthesis of [{Pt(DMB)(μ-OH)}$_2$]$_2$-(F_3CSO_3)$_4$·2H_2O (1)

To a water solution (30 ml) of Pt(DMB)Cl_2 (190 mg, 0.40 mmol) was added a twofold amount of solid AgF_3CSO_3 (210 mg, 0.80 mmol). The reaction mixture was warmed to 55 °C and was allowed to stir for 20 h in the absence of light. The precipitated AgCl was filtered off by a membrane filter. The slow evaporation of the solvent from the yellow filtrate at room temperature gave yellow crystalline product **1**, which was collected over glass frit, washed with a small amount of cold water and dried in air (120 mg, 52%). *Anal*. Found: C, 26.85; H, 2.42; N, 4.77. Calc. for $C_{52}H_{56}F_{12}N_8O_{26}Pt_4S_4$: C, 26.63; H, 2.41; N, 4.78%. ^{1}H NMR (300 MHz, DMF-d_7, 273 K): δ 8.73 (dd, $J = 5.5$, 1.2 Hz, 4H), 8.67 (dd, $J = 8.0$, 1.2 Hz, 4H), 8.13 (dd, $J = 8.0$, 5.5 Hz, 4H), 6.00 (t, $J = 5.8$ Hz, 4H), 5.92 (s, 2H), 4.74 (d, $J = 5.8$ Hz, 8H). ^{13}C{^{1}H} NMR (75 MHz, DMF-d_7, 297 K): δ 155.0, 148.1, 143.5, 143.3, 127.2, 61.5. IR (KBr, cm^{-1}): 3425 (br m, OH stretch), 1029 (s, OH bend), 575 (m, PtO stretch).

2.3. X-ray structure determination

Yellow crystals of **1** suitable for X-ray diffraction study were grown by slow evaporation of solvent from an aqueous solution. A crystal was mounted on a glass fiber tip. Crystal data were collected on an Enraf–Nonius CAD4 diffractometer equipped with graphite monochromated Mo Kα radiation. Cell dimensions and orientation matrix for data collection were obtained from least-squares refinement, using the setting angles of 25 centered reflections. Intensity data were collected in the $\omega-\theta$ scan mode to a maximum 2θ of 50°. Data were corrected for Lorentz and polarization effects, and an empirical absorption correction was applied.

The structure was solved by using the SHELXS-86 system [7] and refined by full-matrix least-squares on F^2 (SHELXL-93) [8]. The non-hydrogen atoms were refined anisotropically and all hydrogen atom positions, except those of μ-OH hydrogen, were initially calculated and then refined using a riding model. Geometrical restraint was applied for four triflates using SADI in SHELXL-93. The detailed crystallographic data are listed in Table 1.

Table 1
Crystallographic data for **1**

Empirical formula	$C_{52}H_{56}N_8O_{26}F_{12}S_4Pt_4$
Formula weight	2345.7
Crystal system	triclinic
Space group	$P\bar{1}$ (No. 2)
Unit cell dimensions	
a (Å)	15.692(3)
b (Å)	15.758(3)
c (Å)	17.953(6)
α (°)	64.17(3)
β (°)	65.58(2)
γ (°)	62.83(2)
V (Å^3)	3424.8(16)
Z	2
D_{calc} (g cm^{-3})	2.275
Absorption coefficient (mm^{-1})	8.385
Radiation (Å)	0.71073
Temperature (K)	293
R_1 [$I \geq 2\sigma(I)$] [a]	0.0432
wR_2 [$I \geq 2\sigma(I)$] [b]	0.1166

[a] $R_1 = \Sigma||F_o|-|F_c||/\Sigma|F_o|$.
[b] $wR_2 = [\Sigma[w(F_o^2-F_c^2)^2]/\Sigma[w(F_o^2)^2]]^{1/2}$.

2.4. Computational method

The B3LYP calculations [9] were carried out with GAUSSIAN98 program [10]. Single point energy evaluations were performed using the experimental geometries. A pseudopotential was used to replace 60 core electrons while a (8s7p6d)/[6s5p3d] basis set was used to describe the valence orbitals of Pt [11]. The 6-31G** basis set was used for the other elements. The 6-31++G* and 6-311++G** basis sets were also applied for the calculation of four residues, but there was no noticeable discrepancy between energy values.

3. Results and discussion

3.1. Crystal structure of 1

ORTEP representation of **1** is shown in Fig. 1 and selected bond distances and angles are summarized in Table 2. X-ray structure determination of **1** has revealed that the asymmetric unit contains two independent conformational isomers, **1a** and **1b**, of a dinuclear $[Pt(DMB)(\mu\text{-}OH)]_2^{2+}$ unit. The crystal and molecular structures with the numbering schemes of the conformers **1a** and **1b** are shown in Figs. 2 and 3, respectively.

The conformer **1a** is a dinuclear monomer and has the expected hydroxymethyl conformation in which two hydroxymethyl substituents are oriented as far as possible to minimize steric interaction between themselves as seen in the structure of Pt(DMB)Cl_2 [6]. The

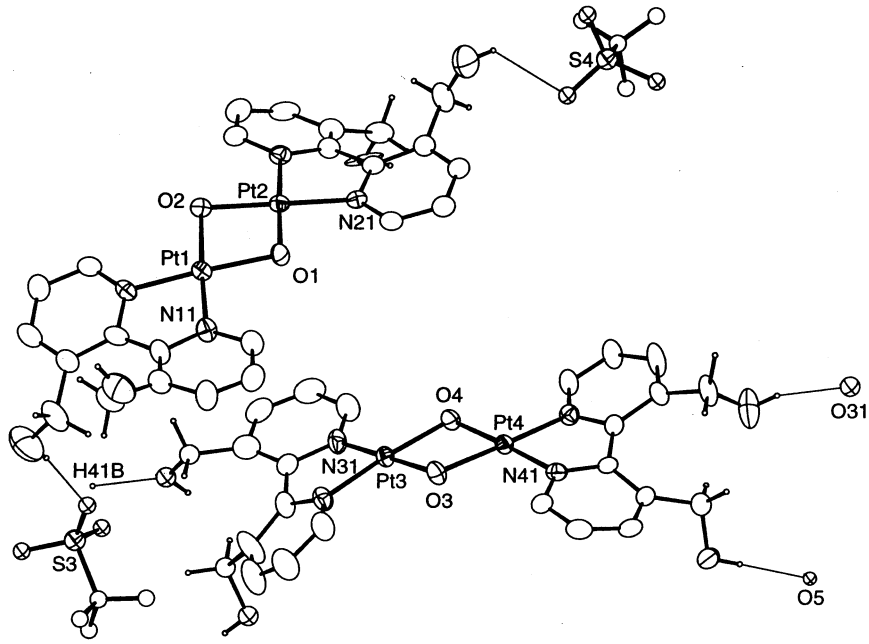


Fig. 1. ORTEP drawing of **1** showing the atom numbering scheme. Two triflates and one solvated water, which show no intermolecular interaction with two $[\{Pt(DMB)(\mu\text{-}OH)\}_2]_2$ complexes, are omitted for clarity.

Table 2
Selected bond distances (Å) and angles (°) for **1**

Bond lengths			
Pt(1)–Pt(2)	3.1283(14)	Pt(1)–N(11)	1.997(8)
Pt(1)–N(11′)	1.977(9)	Pt(1)–O(1)	2.038(6)
Pt(1)–O(2)	2.063(7)	Pt(2)–N(21)	1.970(8)
Pt(2)–N(21′)	1.991(8)	Pt(2)–O(1)	2.048(6)
Pt(2)–O(2)	2.042(7)	O(11)···O(312^{i})	2.759(7)
O(21)···O(411^{ii})	2.840(6)	Pt(3)–Pt(4)	3.1275(12)
Pt(3)–N(31)	1.974(9)	Pt(3)–N(31′)	2.013(9)
Pt(3)–O(3)	2.050(7)	Pt(3)–O(4)	2.023(6)
Pt(4)–N(41)	1.979(8)	Pt(4)–N(41′)	1.970(8)
Pt(4)–O(3)	2.032(6)	Pt(4)–O(4)	2.033(6)
O(41)···O(5^{iv})	2.649(5)	O(41′)···O(31^{ii})	2.689(3)
Bond angles			
N(11′)–Pt(1)–N(11)	80.5(4)	O(1)–Pt(1)–O(2)	79.0(2)
N(21)–Pt(2)–N(21′)	80.8(3)	O(2)–Pt(2)–O(1)	79.2(3)
Pt(1)–O(1)–Pt(2)	99.9(3)	Pt(2)–O(2)–Pt(1)	99.3(3)
O(11)–H(11A)···O(312^{i})	167.1(5)	O(21)–H(21A)···O(411^{ii})	107.7(2)
N(31)–Pt(3)–N(31′)	81.7(4)	O(4)–Pt(3)–O(3)	79.0(3)
N(41′)–Pt(4)–N(41)	80.2(3)	O(3)–Pt(4)–O(4)	79.1(3)
Pt(4)–O(3)–Pt(3)	100.0(3)	Pt(3)–O(4)–Pt(4)	100.9(3)
O(41)–H(41A)···O(5^{iv})	158.5(8)	O(41′)–H(41B)···O(31^{ii})	160.8(2)

two OH groups in *trans* position (relative to the plane which contains two Pt atoms and is perpendicular to the Pt_2O_2 plane) is hydrogen bonded to the oxygen atom of two triflates, which prevents the approach of other molecules for further hydrogen bonding. The O···O distances in hydrogen-bonded OH···O are 2.76 and 2.84 Å and the O–H···O angles are 167° and 108°. The

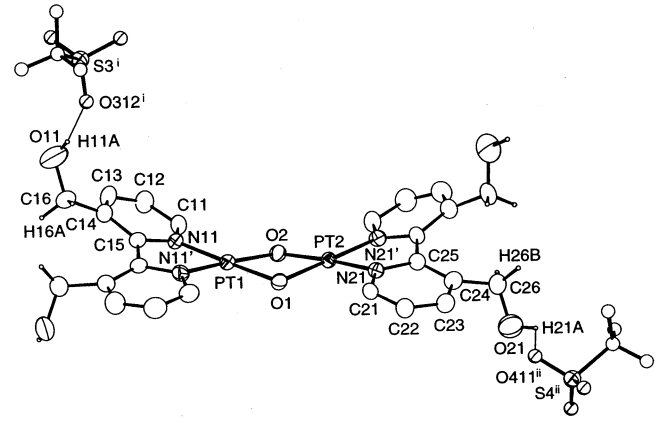


Fig. 2. Crystal and molecular structure of the conformer **1a**. Hydrogen atoms of hydroxymethyl group are only seen for clarity. Symmetry operation: (i) $x, y, -1+z$; (ii) $1-x, 1-y, 1-z$.

extreme disparity of the hydrogen bond angle from 180° may be attributed to the effect of crystal packing force [12].

In contrast to **1a**, the conformer **1b** exists as a hydrogen-bonded one-dimensional chain of the dinuclear unit and has a completely different pattern of crystal packing. The orientations of the oxygen atoms of hydroxymethyl groups are directed toward the same direction, resulting in the unfavorable interactions of C(36′)···O(31) [3.07 Å] and C(46)···O(41′) [3.08 Å]. Furthermore, the conformer **1b** self-assembles to form a one-dimensional linear polymer through the formation of intermolecular hydrogen bonding between the two hydroxymethyl OH groups of neighboring monomers. Two OH groups in **1b** involved in the connection of

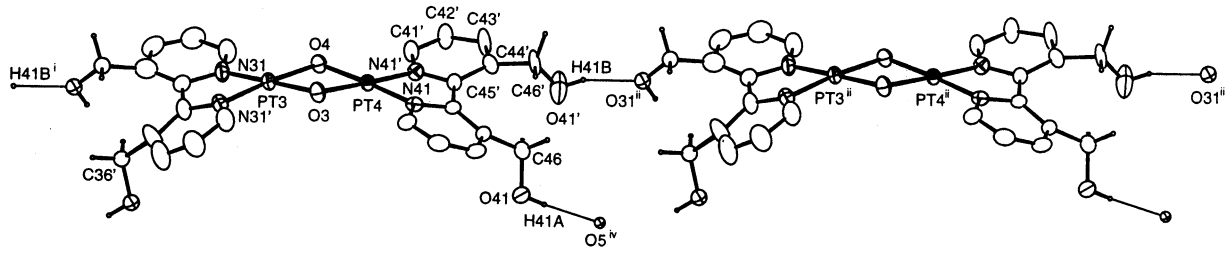


Fig. 3. Crystal and molecular structure of conformer **1b**. Hydrogen bonds are represented by thin lines. Symmetry operation: (i) $x, y, 1+z$; (ii) $x, y, -1+z$; (iii) $x, y, -2+z$; (iv) $1-x, 1-y, -z$.

building blocks are situated in *cis* position. The intermolecular O(41′)···O(31) distance of 2.69 Å and O(41′)–H(41B)···O(31) angle of 161° shows that the hydrogen bond between donor OH and acceptor O is reasonably strong [13]. One OH hydrogen atom (H41A) of the two remaining hydroxymethyl groups in **1b** is also strongly hydrogen-bonded to a crystal water [O(41)···O(5) 2.65 Å].

Perspective view of **1** clearly shows the different orientations of hydroxymethyl groups of ligands (Fig. 1). Two hydroxymethyl oxygen atoms in DMB residues of **1a** are directed to the opposite side, up and down, but those of **1b** are all oriented to the lower direction. The structures around the platinum cores of the two conformers are of close similarity. The coordination geometries of the two platinum centers are approximately square planar. Two least-squares planes of N_2PtO_2 in **1a** and **1b** are not coplanar but tilted by 15.5° and 12.2°, respectively.

3.2. Calculations

The B3LYP calculations, summarized in Table 3, indicate that the conformer **1a** is more stable than **1b**, as expected, by 13.8 kcal mol^{-1}. The stability of two conformers was further analyzed by carrying out calculations on four coordinated DMB residues using the same method. The residue *n* refers to DMB coordinated to Pt*n* ($n = 1$–4). Surprisingly, the residue 4 is more stable than the residues 1, 2 and 3 by +1.6, +2.0, and +15.6 kcal mol^{-1}, respectively. These somewhat unexpected results could be rationalized by close examination of dihedral angle between the average pyridyl planes of DMB units and torsional angles in each residue (Table 4). The dihedral angle of two least-squares pyridine planes in residue 4 is 24.1° that is smaller than 28.1° for residue 3, indicating that the residue 4 is expected to be more stable because the better π-conjugation between the two pyridyl rings can be achieved as the dihedral angle decreases [14]. The dihedral angle of 24.9° in the residue 1 is comparable with that of the residue 4 and there is no close interaction between two hydroxymethyl groups. However, torsional angles of C13–C14–C16–O11 (35.7°) and C13′–C14′–C16′–O11′ (43.7°) for the residue 1 are far from 60° of the ideal *gauche* conformation, which makes the residue 1 unstable due to torsional strain. No steric repulsion between two substituents and the favorable torsional angles of C23–C24–C26–O21 (46.8°) and C23′–C24′–C26′–O21′ (50.0°) in the residue 2 compensate less overlap of π-conjugation between the two pyridyl rings (dihedral angle: 28.2°). The energy difference of 13.6 kcal mol^{-1} [*E*(residue 3 and 4)−*E*(residue 1 and 2)] is comparable to 13.8 kcal mol^{-1} derived from intact **1a** and **1b**. This implies that the conformational energetics of **1a** and **1b** are dominated by the energies of the coordinated ligands, residue 1–4 rather than those of two hydroxo-bridged platinum cores, $N_2PtO_2PtN_2$.

Table 3
Summary of B3LYP calculations with 6-31G** basis set on the relative stability of the conformational isomers, **1a** and **1b** and DMB residues

Entries	Energy (a.u.)	Relative difference [a] (kcal mol^{-1})
1a	−1838.81907657	0.0
1b	−1838.79703584	13.8
Residue 1	−724.1657956	1.6
Residue 2	−724.1651554	2.0
Residue 3	−724.1435419	15.6
Residue 4	−724.1683875	0.0

[a] Unit conversion: a.u. × 627.51 = kcal mol^{-1}. Relative differences are referenced to **1a** and the residue 4 for the comparison of the conformers and the residues, respectively.

Table 4
Dihedral angles (°) of the two least-squares pyridine planes and selected torsional angles (°) for **1**

Residue 1	24.91 (0.53)	Residue 2	28.19 (0.53)
Residue 3	28.14 (0.36)	Residue 4	24.08 (0.52)
C13–C14–C16–O11	−35.7	C13′–C14′–C16′–O11′	−43.7
C23–C24–C26–O21	46.8	C23′–C24′–C26′–O21′	50.0
C33–C34–C36–O31	69.6	C33′–C34′–C36′–O31′	−56.6
C43–C44–C46–O41	49.7	C43′–C44′–C46′–O41′	−68.3

4. Conclusions

Two different hydrogen bonding patterns involving *cis*- and *trans*-positioned OH groups stabilize each conformational isomer, yielding a new co-crystal of the dinuclear monomer terminated by two triflates (**1a**) and the self-assembled infinite one-dimensional polymer (**1b**). This work provides a new type of co-crystal containing two differently self-assembled conformational isomers in one crystal system. This is also a good example of the important role of hydrogen bonding in self-assembly and of the usefulness of flexible molecule in studying the nature of forces controlling the molecular structure in the crystal. The strong hydrogen bonds and crystal force seem to compensate for ~ 14 kcal mol^{-1} of energy gap between two conformers.

5. Supplementary material

Crystallographic data for the structural analysis have been deposited with the Cambridge Crystallographic Data Centre, CCDC No. 166378 for compound **1**. Copies of this information may be obtained free of charge from The Director, CCDC, 12 Union Road, Cambridge, CB2 1EZ, UK (fax: +44-1223-336033; e-mail: deposit@ccdc.cam.ac.uk or www: http://www.ccdc.cam.ac.uk).

Acknowledgements

We gratefully acknowledge the financial support provided by Non-Directed Research Fund, Korea Research Foundation, 1998. We also thank the KISTI Supercomputing center for the use of CRAY C90.

References

[1] (a) J.L. Atwood, J.E.D. Davies, D.D. MacNicol, F. Vögtle, Comprehensive Supramolecular Chemistry, Pergamon, Oxford, 1996;
(b) D. Braga, F. Grepioni, G.R. Desiraju, Chem. Rev. 98 (1998) 1375.

[2] (a) R. Taylor, O. Kennard, Acc. Chem. Res. 17 (1984) 320;
(b) D. Braga, F. Grepioni, P. Sabatino, Organometallics 13 (1994) 3532.

[3] (a) J.A.R. Navarro, B. Lippert, Coord. Chem. Rev. 185 (1999) 653;
(b) M.-C. Tse, K.-K. Cheung, M.C.-W. Chan, C.-M. Che, Chem. Commun. (1998) 2295;
(c) V.Y. KuKushkin, T. Nishioka, D. Tudela, K. Isobe, I. Kinoshita, Inorg. Chem. 36 (1997) 6157;
(d) D. Walther, T. Klettke, A. Schmidt, Organometallics 15 (1996) 2314;
(e) P.J. Davies, N. Veldman, D.M. Grove, A.L. Spek, B.T.G. Lutz, G. van Koten, Angew. Chem., Int. Ed. Engl. 35 (1996) 1959;
(f) S.L. James, G. Verspui, A.L. Spek, G. van Koten, Chem. Commun. (1996) 1309;
(g) M.M. Chowdhry, D.M.P. Mingos, A.J.P. White, D.J. Williams, Chem. Commun. (1996) 899;
(h) A.D. Burrows, D.M.P. Mingos, A.J.P. White, D.J. Williams, J. Chem. Soc., Dalton Trans. (1996) 149;
(i) S.B. Copp, K.T. Holman, J.O.S. Sangster, S. Subramanian, M.J. Zaworotko, J. Chem. Soc., Dalton Trans. (1995) 2233.

[4] (a) F. Cervantes-Lee, H.K. Sharma, K.H. Pannell, A. Derecskei-Kovacs, D.S. Marynick, Organometallics 17 (1998) 3701;
(b) D. Braga, F. Grepioni, C.M. Martin, E. Parisini, Organometallics 13 (1994) 2170.

[5] (a) D. Braga, F. Grepioni, Acc. Chem. Res. 27 (1994) 51;
(b) Z. Qin, H.A. Jenkins, S.J. Coles, K.W. Muir, R.J. Puddephatt, Can. J. Chem. 77 (1999) 155;
(c) T. Ishida, R. Manabe, Y. In, H. Takashima, K. Kitamura, A. Wakahara, Bull. Chem. Soc. Jpn. 72 (1999) 947;
(d) S.B. Sembiring, S.B. Colbran, R. Bishop, D.C. Craig, A.D. Rae, Inorg. Chim. Acta 228 (1995) 109.

[6] J. Yoo, J.-H. Kim, Y.S. Shon, Y. Do, Inorg. Chim. Acta 263 (1997) 53.

[7] G.M. Sheldrick, SHELXS 86. Program for Crystal Structure Determination, University of Göttingen, Göttingen, Germany, 1986.

[8] G.M. Sheldrick, SHELXL 93. Program for Crystal Structure Refinement, University of Göttingen, Göttingen, Germany, 1993.

[9] (a) A.D. Becke, J. Chem. Phys. 98 (1993) 5648;
(b) C. Lee, W. Yang, R.G. Parr, Phys. Rev. B 37 (1988) 785.

[10] M.J. Frisch, G.W. Trucks, H.B. Schlegel, G.E. Scuseria, M.A. Robb, J.R. Cheeseman, V.G. Zakrzewski, J.A. Montgomery, R.E. Stratmann, J.C. Burant, S. Dapprich, J.M. Millam, A.D. Daniels, K.N. Kudin, M.C. Strain, O. Farkas, J. Tomasi, V. Barone, M. Cossi, R. Cammi, B. Mennucci, C. Pomelli, C. Adamo, S. Clifford, J. Ochterski, G.A. Petersson, P.Y. Ayala, Q. Cui, K. Morokuma, D.K. Malick, A.D. Rabuck, K. Raghavachari, J.B. Foresman, J. Cioslowski, J.V. Ortiz, B.B. Stefanov, G. Liu, A. Liashenko, P. Piskorz, I. Komaromi, R. Gomperts, R.L. Martin, D.J. Fox, T. Keith, M.A. Al-Laham, C.Y. Peng, A. Nanayakkara, C. Gonzalez, M. Challacombe, P.M.W. Gill, B.G. Johnson, W. Chen, M.W. Wong, J.L. Andres, M. Head-Gordon, E.S. Replogle, J.A. Pople, Gaussian 98 (Revision A.7), Gaussian, Inc., Pittsburgh, PA, 1998.

[11] P. Schwerdtfeger, M. Dolg, W.H.E. Schwarz, G.A. Bowmaker, P.D.W. Boyd, J. Chem. Phys. 91 (1989) 1762.

[12] P. Dauber, A.T. Hagler, Acc. Chem. Res. 13 (1980) 105.

[13] (a) P. Gilli, V. Bertolasi, V. Ferretti, G. Gilli, J. Am. Chem. Soc. 116 (1994) 909;
(b) G.M. Kapteijn, P.J. Baesjou, P.L. Alsters, D.M. Grove, W.J.J. Smeets, H. Kooijman, A.L. Spek, G. van Koten, Chem. Ber. 130 (1997) 35.

[14] V.M. Miskowski, V.H. Houlding, C.-M. Che, Y. Wang, Inorg. Chem. 32 (1993) 2518.

ELSEVIER

Polyhedron 21 (2002) 721–728

POLYHEDRON

www.elsevier.com/locate/poly

Assembly chemistry of a cadmium(II) complex with cyanometalate anions $[Fe(CN)_5NO]^{2-}$, $[Pd(CN)_4]^{2-}$ and $[Pt(CN)_6]^{2-}$

Hao Zhang [a], Jiwen Cai [a,b,*], Xiao-Long Feng [b], Hai-Yu Sang [a], Jian-Zhong Liu [c], Xiao-Yuan Li [d,*], Liang-Nian Ji [a,*]

[a] *State Key Laboratory of Ultrafast Laser Spectroscopy, School of Chemistry and Chemical Engineering, Zhongshan University, Guangzhou 510275, People's Republic of China*

[b] *Instrumentation Analysis and Research Center, Zhongshan University, Guangzhou 510275, People's Republic of China*

[c] *Key Laboratory of Gene Engineering of Ministry of Education, Zhongshan University, Guangzhou 510275, People's Republic of China*

[d] *Department of Chemistry, The Hong Kong University of Science and Technology, Clear Water Bay, Kowloon, Hong Kong, People's Republic of China*

Received 15 August 2001; accepted 3 December 2001

Abstract

Three complexes, namely [Cd(tren)][$Fe(CN)_5NO$] (**2**), [Cd(tren)][$Pd(CN)_4$] (**3**) and [Cd(tren)][$Pt(CN)_6$] (**4**), were prepared via direct reactions of $Na_2[Fe(CN)_5NO]$, $K_2[Pd(CN)_4]$ and $K_2[Pt(CN)_6]$, respectively, with cadmium acetate and tris(2-aminoethyl)amine (tren) in aqueous solution. X-ray structural analysis shows that **2** features a shelf-like structure formed by stacking of the quasi-square building block. Compound **3** is a battlement-like polymer constructed from cyanometalate building blocks and compound **4** represents the first example of a cyano-bridged trinuclear hexacyanoplatinate(IV) complex. © 2002 Elsevier Science Ltd. All rights reserved.

Keywords: Cyanometalate; Coordination polymers; Crystal structures; Cadmium(II) complexes

1. Introduction

Interest in the construction of multinuclear or polymeric metal cyanides has been driven by application-oriented subjects, such as design and synthesis of molecular magnets, light-emitting devices and zeolite-like materials, and also by the advantages of using cyanometalates as building blocks [1–6]. The cyanide system based on Prussian Blue and its analogs has been fully studied by the reaction of metal (especially copper and nickel) amine complexes with $[Fe(CN)_6]^{4-}$ or $[M(CN)_6]^{3-}$ (M = Fe, Mn, Co or Cr) [2]. Systematic attempts employing complementary bridging or chelating ligands have been made to modify the supramolecular architectures, in combination with octahedral, square-planar, tetrahedral and linear cyanometalate anions [3–5]. Additionally, series of crystal structures have also been reported for the organotin-cyanometalate family of coordination polymers [6].

In the binuclear or multinuclear polymeric complexes using $[M_x(CN)_y]$ as building blocks, the two most common coordination modes of the cyanide group are either the terminal C-bound mode or the linear-bridged arrangement (μ_2-κC:κN), which are based on the well-known fact that the cyanide ion owns a donor electron pair at both its C and N terminals. In our preceding communication, we reported a rare coordination mode of μ_3-κN:κN:κC in the two-dimensional (2D) coordination polymer $[Cd(tren)]_2[Fe(CN)_6]$ (**1**), where tren = tris(2-aminoethyl)amine [7]. This unusual μ_3 mode of cyanide was also observed in $[Cu(dmen)]_2[Fe(CN)_6]$, where dmen = 2-dimethylaminoethylamine [8]. As an extension to our studies on this class of cyanometalates, we report herein the results of investigations into the assembly of $[Cd(tren)]^{2+}$ with anions $[Fe(CN)_5NO]^{2-}$ (**2**), $[Pd(CN)_4]^{2-}$ (**3**), and $[Pt(CN)_6]^{2-}$ (**4**).

* Corresponding authors. Tel.: +852-20-8411-0782; fax: +852-20-8403-8784 (J.C.).

E-mail address: puscjw@zsu.edu.cn (J. Cai).

0277-5387/02/$ - see front matter © 2002 Elsevier Science Ltd. All rights reserved.
PII: S0277-5387(02)00846-X

2. Experimental

2.1. Materials and methods

All reagents were commercially available and used as received. Elemental analysis was performed on a Perkin–Elmer 240 elemental analyzer. All infrared spectra were recorded on a Nicolet 5DX FT-IR spectrophotometer with KBr disks in the region of 4000–400 cm^{-1}.

2.2. Syntheses

2.2.1. $[Cd(tren)]_2[Fe(CN)_6]\cdot 3H_2O$ (1)

In our previous communication [7], compound **1** was obtained by diffusion in the opposite directions of a U-tube with aqueous solutions of $K_4[Fe(CN)_6]$, $Cd(NO_3)_2$ and tren ligand. Alternatively, compound **1** can be prepared by the following procedure: tren (0.668 mmol, 0.10 ml) was added to a 15 ml aqueous solution of cadmium acetate (0.668 mmol). The resulting colorless solution was added dropwise to a 10 ml aqueous solution of $K_3[Fe(CN)_6]$ (0.668 mmol) at room temperature. A brown precipitate was formed immediately and filtered out. Plate-like single crystals were obtained from the resulting brown solution after one week. Crystal structure analysis revealed that it had the same structure as the reported compound **1**.

2.2.2. $[Cd(tren)][Fe(CN)_5NO]$ (2)

Tren (0.668 mmol, 0.10 ml) was added to a 15 ml aqueous solution of cadmium acetate (0.668 mmol). The resulting colorless solution was then added dropwise to a 10 ml aqueous solution of $Na_2[Fe(CN)_5NO]$ (0.668 mmol) at 50–60 °C. Brown crystals formed immediately (ca. 76%). Prismatic crystals suitable for X-ray structural determination were obtained by recrystallization. *Anal.* Calc. for $C_{11}H_{18}CdFeN_{10}O$: C, 27.84; H, 3.82; N, 29.51. Found: C, 27.84; H, 3.89; N, 29.47%. Main IR (cm^{-1}): 3328s, 3272m, 3165m, 2164m, 2142 s, 1921vs and 1604m.

2.2.3. $[Cd(tren)][Pd(CN)_4]$ (3)

The same procedure used for **2** was performed for $Cd(Ac)_2$ (0.668 mmol), tren (0.668 mmol, 0.10 ml) and $K_2[Pd(CN)_4]$ (0.668 mmol) at 50–60 °C, affording colorless prismatic crystals by slowly diffusing diethyl ether into the DMF solution (ca. 74%). *Anal.* Calc. for $C_{10}H_{18}CdN_8Pd$: C, 25.60; H, 3.87; N, 23.89. Found: C, 25.57; H, 3.84; N, 23.85%. Main IR (cm^{-1}): 3329s, 3286s, 3253m, 3165m, 2153s, 1664m and 1596s.

2.2.4. $[Cd(tren)][Pt(CN)_6]$ (4)

The same procedure used for **2** was performed for $Cd(Ac)_2$ (0.668 mmol), tren (0.668 mmol, 0.10 ml) and $K_2[Pt(CN)_6]$ (0.668 mmol) at 50–60 °C, affording colorless prismatic crystals by recrystallization (ca. 67%). *Anal.* Calc. for $C_{12}H_{18}CdN_{10}Pt$: C, 23.64; H, 2.98; N, 22.97. Found: C, 23.65; H, 3.03; N, 22.92%. Main IR (cm^{-1}): 3352s, 3313s, 3273s, 3184m, 2218m, 2190s, 2177m, 1613m and 1586m.

2.3. X-ray crystallography

X-ray data were collected on a Bruker SMART 1000 CCD diffractometer at 293 K. Absorption correction was applied with the SADABS program [9]. The structure solution and full-matrix least-squares refinement based on F^2 were performed using SHELXTL-97 [10]. Non-hydrogen atoms were refined anisotropically. All hydrogen atoms were placed in idealized positions. Crystallographic data for structures **2**, **3** and **4** are shown in Table 1. Selected bond distances and angles are given in Table 2.

3. Results and discussion

3.1. Synthesis

As reported previously, Cd^{2+}, $[Fe(CN)_6]^{4-}$ and tren are self-assembled from silica in a U-tube to build up a μ_3-cyano-bridged heterotrimetallic 2D coordination polymer $[Cd(tren)]_2[Fe(CN)_6]\cdot 3H_2O$ (**1**) constructed by rectangular grids [7]. Interestingly, **1** was also obtained

Table 1
Crystal data and structure refinement parameters for compounds **2**, **3** and **4**

	2	**3**	**4**
Empirical formula	$C_{11}H_{18}CdFeN_{10}O$	$C_{10}H_{18}CdN_8Pd$	$C_{12}H_{18}CdN_{10}Pt$
Formula weight	474.58	469.12	609.75
Crystal system	monoclinic	orthorhombic	monoclinic
Space group	$P2_1/n$	$P2_12_12_1$	$P2_1/c$
Unit cell dimensions			
a (Å)	6.8171(13)	10.1704(12)	8.1903(9)
b (Å)	22.535(4)	10.8931(13)	14.8562(17)
c (Å)	11.320(2)	14.4707(17)	16.2353(18)
α (°)	90	90	90
β (°)	92.777(4)	90	98.059(2)
γ (°)	90	90	90
V (Å^3)	1736.9(6)	1603.2(3)	1955.9(4)
Z	2	4	4
μ (Mo Kα) (cm^{-1})	2.081	2.451	8.247
Number of data collected	12 242	11 469	13 825
Goodness-of-fit value	1.058	1.052	1.011
R_1 ($I > 2\sigma$)	0.0298	0.0201	0.0269
wR_2 (all data)	0.0751	0.0480	0.0768

Table 2
Selected bond lengths (Å) and bond angles (°) for compounds **2**, **3** and **4**

*[Cd(tren)][Fe(CN)$_5$NO] (**2**)*							
Bond lengths							
Cd–N(1)	2.339(2)	Cd–N(2)#1	2.333(2)	Cd–N(3)	2.343(3)	Cd–N(4)	2.421(2)
Cd–N(5)	2.367(3)	Cd–N(6)	2.416(3)	Fe–C(7)	1.941(3)	Fe–C(8)	1.948(3)
Fe–C(9)	1.933(3)	Fe–C(10)	1.944(3)	Fe–C(11)	1.946(3)	Fe–N(10)	1.662(3)
C(7)–N(5)#2	1.145(4)	C(8)–N(6)	1.149(4)	C(9)–N(7)	1.153(4)	C(10)–N(8)	1.140(4)
C(11)–N(9)	1.132(4)	N(10)–O(1)	1.126(4)				
N(1)···N(8)#1	3.098(4)	N(1)···N(7)#4	3.178(4)				
N(3)···N(7)#4	3.351(4)	N(3)···N(9)#5	3.087(4)	N(2)···N(8)	3.294(4)		
Bond angles							
N(2)#1–Cd–N(1)	97.55(9)	N(5)–Cd–N(6)	91.54(10)	N(5)#2–C(7)–Fe	175.0(3)		
N(8)–C(10)–Fe	179.5(3)	C(7)#2–N(5)–Cd	159.6(3)	C(8)–N(6)–Cd	151.6(2)		
O(1)–N(10)–Fe	176.5(3)						
*[Cd(tren)][Pd(CN)$_4$] (**3**)*							
Bond lengths							
Cd–N(1)	2.299(2)	Cd–N(2)	2.458(2)	Cd–N(3)	2.307(2)	Cd-N(4)	2.397(3)
Cd–N(5)	2.268(2)	Cd–N(6)#1	2.493(3)	Pd(1)–C(7)	1.988(3)	Pd(1)–C(8)	1.990(3)
Pd(1)–C(9)	2.000(3)	Pd(1)–C(10)	1.994(3)	C(7)–N(5)	1.146(3)	C(8)–N(6)	1.145(4)
C(9)–N(8)	1.137(4)	C(10)–N(7)	1.146(4)	N(1)···N(8)#3	3.112(4)	N(1)···N(7)#4	3.108(3)
N(3)···N(8)#5	3.224(5)	N(3)···N(7)#6	3.273(4)				
Bond angles							
N(6)–C(8)–Pd(1)	177.2(2)	C(8)–N(6)–Cd#2	138.0(2)	C(7)–Pd(1)–C(8)	93.84(10)		
N(5)–C(7)–Pd(1)	172.8(3)	C(7)–N(5)–Cd	159.7(2)				
*[Cd(tren)][Pt(CN)$_6$] (**4**)*							
Bond lengths							
Cd(1)–N(1)	2.268(4)	Cd(1)–N(2)	2.391(3)	Cd(1)–N(3)	2.272(3)	Cd(1)–N(4)	2.283(4)
Cd(1)–N(5)	2.260(4)	Pt(1)–C(7)	1.999(4)	Pt(1)–C(8)	2.025(4)	Pt(1)–C(9)	2.007(5)
Pt(2)–C(10)	2.025(4)	Pt(2)–C(11)	2.020(4)	Pt(2)–C(12)	2.014(4)	C(7)–N(5)	1.133(5)
C(8)–N(6)	1.129(5)	C(9)–N(7)	1.147(6)	C(10)–N(8)	1.135(5)	C(11)–N(9)	1.136(5)
C(12)–N(10)	1.131(5)	N(1)···N(8)#3	3.158(5)	N(1)···N(7)#4	3.358(6)	N(1)···N(10)#4	3.061(5)
N(3)···N(6)#5	3.337(6)	N(4)···N(9)#6	3.201(6)	N(4)···N(7)#5	3.361(6)		
Bond angles							
C(7)–N(5)–Cd(1)	167.7(4)	N(5)–C(7)–Pt(1)	179.6(4)	C(7)#1–Pt(1)–C(7)	180.0		

Symmetry codes: For **2**, #1 $x+1, y, z$; #2 $-x+1, -y, -z$; #3 $x-1, y, z$; #4 $x+1/2, -y+1/2, z+1/2$; #5 $x+1, y, z+1$. For **3**, #1 $-x+1, y-1/2, -z+1/2$; #2 $-x+1, y+1/2, -z+1/2$; #3 $x+1/2, -y+1/2, -z+1$; #4 $-x+1/2, -y+1, z+1/2$; #5 $-x, y-1/2, -z+1/2$; #6 $x, y-1, z$. For **4**, #1 $-x+1, -y+1, -z$; #2 $-x+1, -y, -z$; #3 $x, y+1, z$; #4 $-x+1, y+1/2, -z+1/2$; #5 $x+1, y, z$; #6 $-x+2, y+1/2, -z+1/2$.

from aqueous solution when $[Fe(CN)_6]^{3-}$ was used instead of $[Fe(CN)_6]^{4-}$. The reduction mechanism of the iron cation ($Fe^{3+} \rightarrow Fe^{2+}$) is not clear.

Quantitative syntheses of **2**, **3** and **4** were achieved via direct reactions of $Na_2[Fe(CN)_5NO]$, $K_2[Pd(CN)_4]$ and $K_2[Pt(CN)_6]$, respectively, with $Cd(Ac)_2$ and tren in aqueous solution. Single crystals of **2** and **4** were obtained by recrystallization, while crystals of **3** suitable for X-ray diffraction were produced by slow diffusion of diethyl ether into its DMF solution.

3.2. Crystal structure of *[Cd(tren)][Fe(CN)$_5$NO] (**2**)*

Complex **2** features a shelf-like structure formed by stacking of the quasi-square building block, namely $[Cd(tren)]_2[Fe(CN)_5NO]_2$. As illustrated in Fig. 1(a), the Cd atom is coordinated by four nitrogen atoms from two tren ligands and two nitrogen atoms from two $[Fe(CN)_5NO]^{2-}$ anions. The Cd–N (2.333(2)–2.421(2) Å) distances are consistent with that of complex **1**, and the bond lengths of Fe–C (1.933(3)–1.948(3) Å), Fe–N (1.662(3) Å), C–N (1.132(4)–1.153(4) Å) and N–O (1.126(4) Å) in the $[Fe(CN)_5NO]^{2-}$ moiety are also comparable to the reported analogs [11]. Two *cis*-$[Fe(CN)_5NO]^{2-}$ fragments and two $[Cd(tren)]^{2+}$ moieties are held together by CN^- bridges, and result in distorted square tetra-nuclear building blocks with slightly bent edges (Cd···Fe 5.345 Å, Cd···Fe# 5.351 Å; N(5)–Cd–N(6) 91.54(10)°, C(7)–Fe–C(8) 88.16(11)°, C(7#)–N(5)–Cd 159.6(3)°, C(8)–N(6)–Cd 151.6(3)°). These square moieties are linked to each other by two tren ligands to build up the shelf-like 1D column (Fig. 1(b) and (c)). The ligation mode of tren has been observed only in a few compounds [12].

Compound **2** is structurally reminiscent of the 1D 'ladder' coordination polymer with simple, linear *N*,*N*′-donor spacers such as 4,4′-bipyridine pyrazine, and other related species [13]. In the realm of molecular

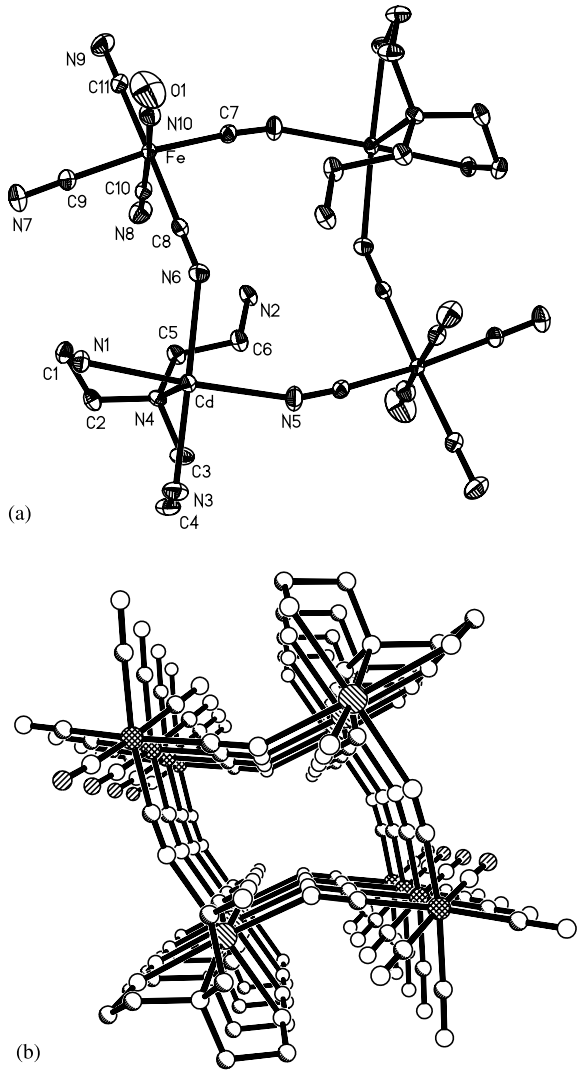


Fig. 1. (a) Perspective view of the square building block of complex **2**, with 30% probability displacement ellipsoids. Hydrogen atoms are omitted for clarity. (b) Top views showing the shelf-like column in **2**. (c) Side views showing the shelf-like column in **2**. (d) Packing diagram along *b* axis featuring the inter-column hydrogen bonds.

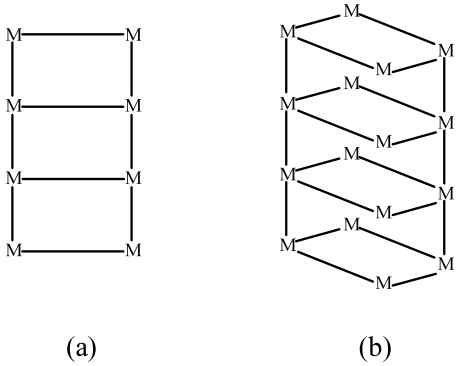


Chart 1. Comparison between two types of 1D coordination polymers: (a) molecular ladder; (b) molecular shelf.

ladders, most of inner rungs are made up of single rod-like spacers (Chart 1(a)). In contrast, square rings instead of inner rungs are assembled in **2**. Therefore, compound **2** represents a new topology of 1D coordination polymers (Chart 1(b)).

The shelf-like columns are further extended into a 3D network by inter-column hydrogen bonds (Fig. 1(d)), which are formed between the amino hydrogens of tren ligands and the N-end of terminal cyanides, with the distances of donor and acceptor ranging from 3.087(4) to 3.351(4) Å.

3.3. Crystal structure of [Cd(tren)][Pd(CN)$_4$] (**3**)

Compound **3** crystallizes in the chiral space group $P2_12_12_1$, providing a battlement-like, 1D coordination polymer as shown in Fig. 2. The infinite chain is formed by the alternate arrangement of $[Cd(tren)]^{2+}$ and $[Pd(CN)_4]^{2-}$ which are bridged by CN^- in a *cis*

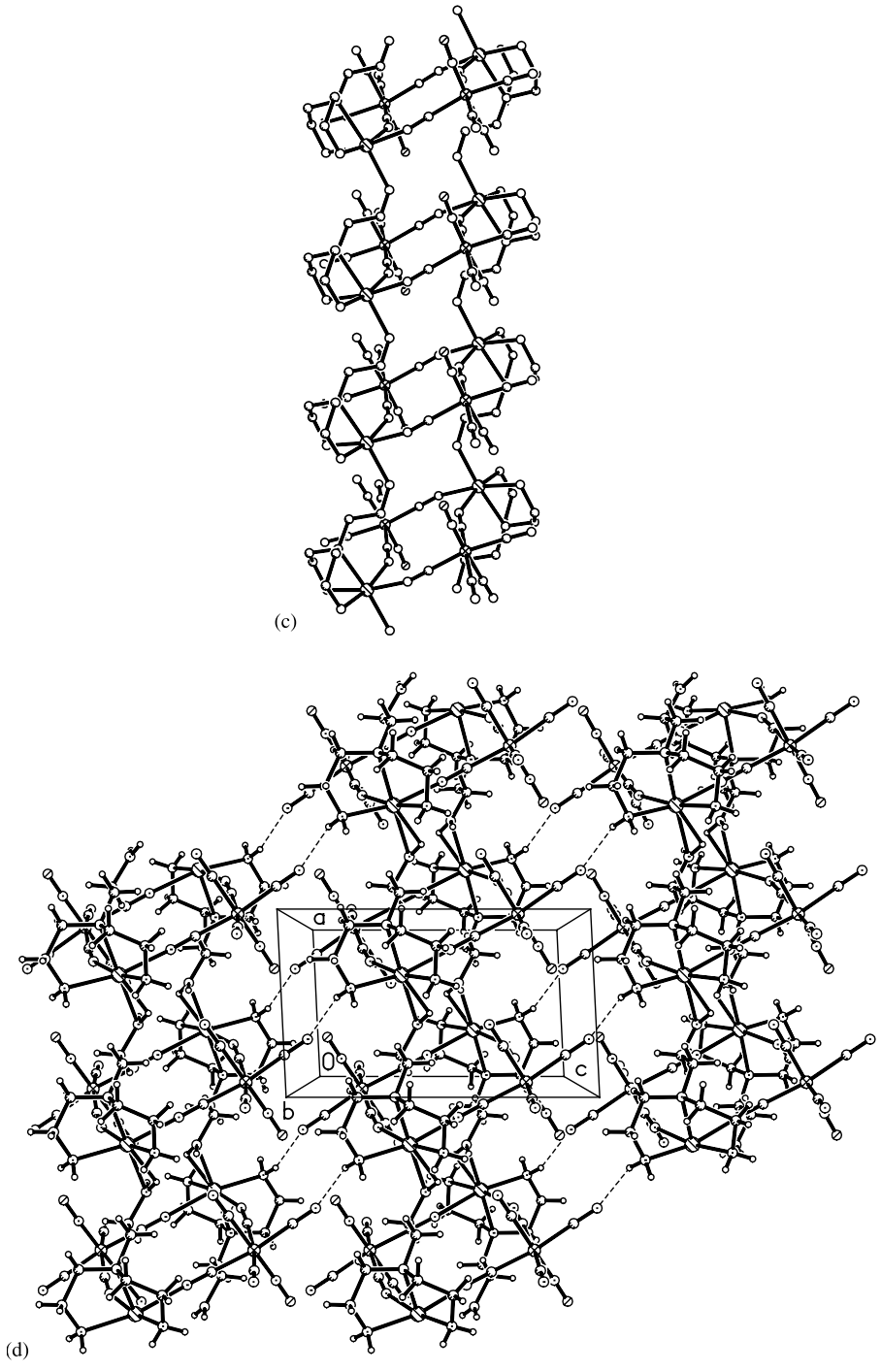


Fig. 1 (*Continued*)

fashion. The Cd atom has a distorted octahedral coordination configuration with six N atoms, four of them from one tren ligand and two from different $[Pd(CN)_4]^{2-}$ units. The Cd–N distances range from 2.299(2) to 2.493(3) Å. The $[Pd(CN)_4]^{2-}$ ion assumes four-coordination square geometry with normal Pd–C bonds (1.988(3)–2.000(3) Å) and C–N bonds (1.137(4)–1.146(4) Å), comparable to those found in the other tetracyanopalladate complexes [14]. The Cd–N(5)–C(7) and Cd#–N(6)–C(8) angles are bent significantly at the N atoms (159.7(2)° and 138.0(2)°, respectively).

In most of the cyanide-bridged species, the common theme is that cyanometallate anions, such as linear $[Ag(CN)_2]^-$, square $[Pd(CN)_4]^{2-}$, and octahedral $[Fe(CN)_6]^{3-}$ bridge metal ions in a *cis* or *trans* fashion, and create various mutinuclear 1D, 2D and 3D poly-

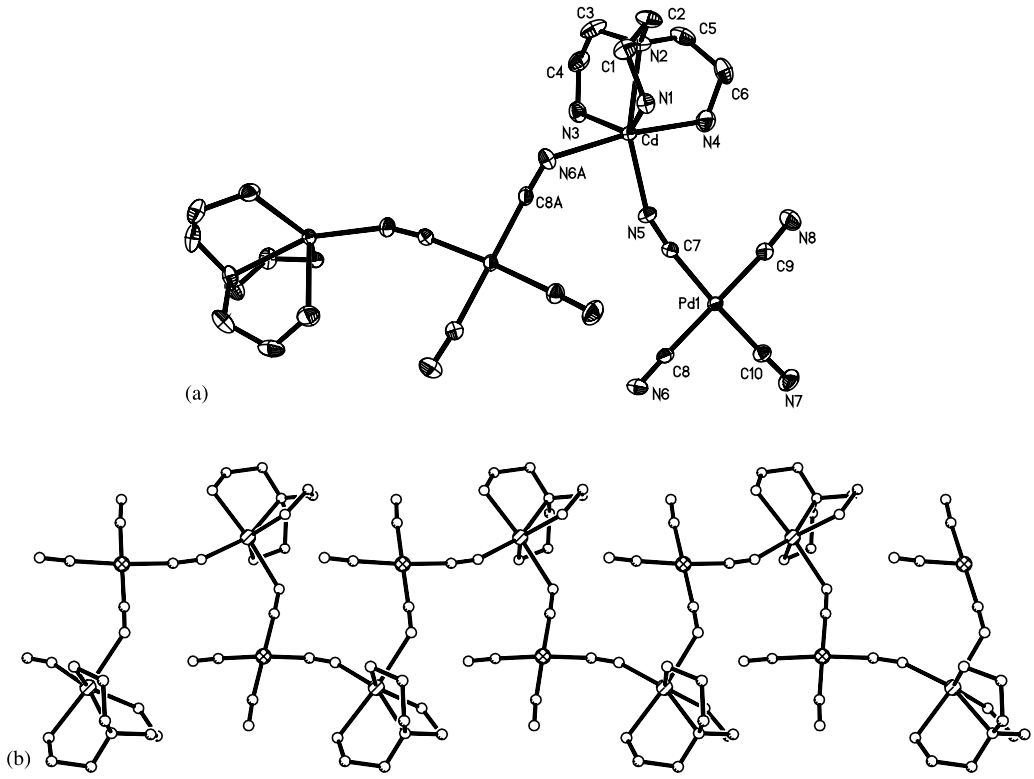


Fig. 2. (a) Perspective view of complex **3** showing the building block, with 30% probability displacement ellipsoids. (b) The 1D battlement-like string constructed in **3**. Hydrogen atoms are omitted for clarity.

meric complexes. The family of 1D cyano-bridged coordination polymers described to date is summarized in Chart 2(a)–(e) [14,15]. However, to the best of our knowledge, the battlement-like motif revealed in **3** is unprecedented (Chart 2(f)).

Hydrogen bonds are also presented in **3** between the terminal CN^- in the *cis*-$[Pd(CN)_4]^{2-}$ and the amino hydrogens of the tren ligand, with distances of D···A ranging from 3.108(3) to 3.273(4) Å. Thus the 1D coordination polymers are extended into a 3D network.

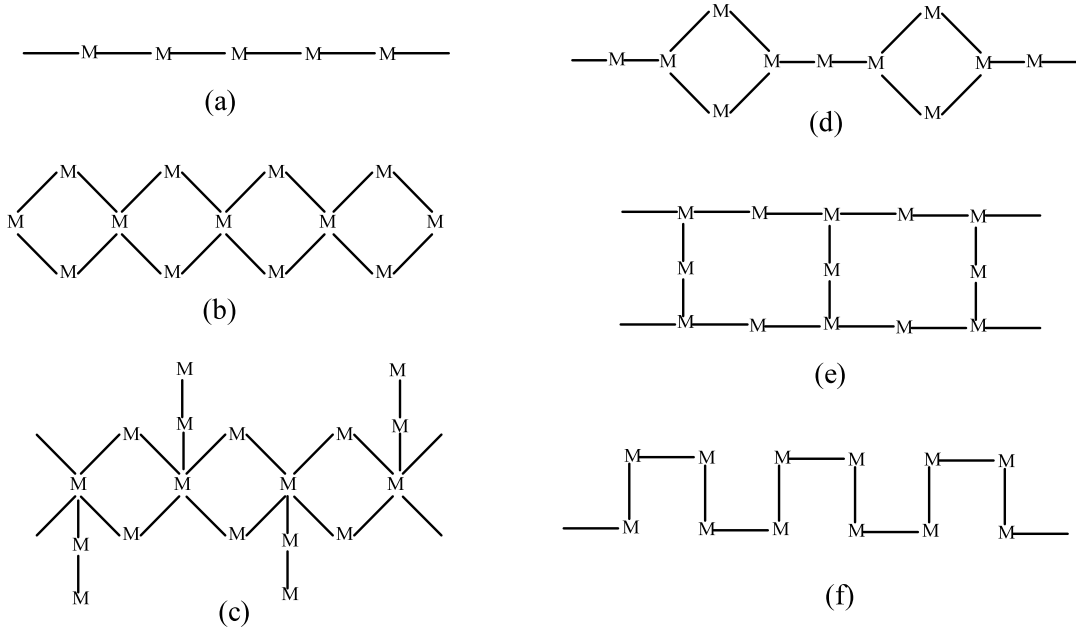


Chart 2. Possible structural types of 1D coordination polymer constructed from cyanometalate building blocks.

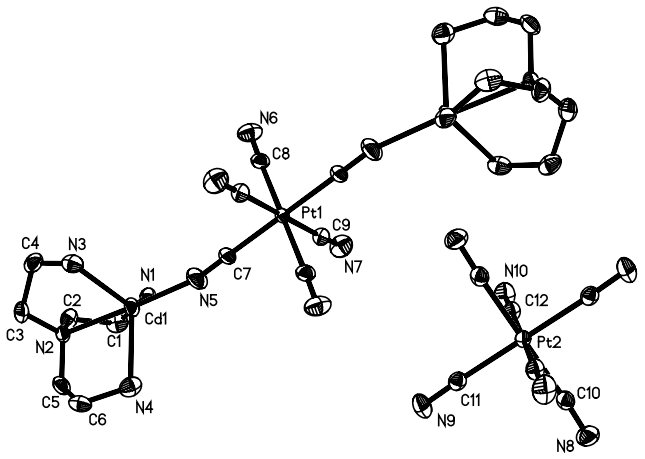


Fig. 3. Perspective view of complex **4** with 30% probability displacement ellipsoids. Hydrogen atoms are omitted for clarity.

3.4. Crystal structure of $[Cd(tren)][Pt(CN)_6]$ (4)

Different from polymeric complexes **1**, **2** and **3**, compound **4** consists of discrete trinuclear $[\{Cd(tren)\}_2Pt(CN)_6]^{2+}$ cations and $[Pt(CN)_6]^{2-}$ anions. As shown in Fig. 3, the trinuclear Cd_2Pt unit is constructed from two $[Cd(tren)]^{2+}$ complex cations spanned by an hexacyanoplatinate(IV) anion via *trans* cyanide bridges. In the discrete and bridging $[Pt(CN)_6]^{2-}$ anion, each platinum atom is bound to six cyanide ions, with Pt–C and C–N bond length ranges of 1.999(4)–2.025(4) and 1.129(5)–1.147(6) Å, respectively. In light of the Pt–C and C–N bond lengths, there is no significant difference between $[Pt(CN)_6]^{2-}$ in **4** and $[Pt(CN)_4]^{2-}$ anions in the previous cyano-bridged trinuclear complex [16]. As far as we know, no trinuclear hexacyanoplatinate(IV) complex is characterized structurally. Therefore, compound **4** represents the first structural characterization of cyano-bridged trinuclear hexacyanoplatinate(IV) complex. Additionally, a 3D hydrogen-bonding network is formed, similar to that observed in **2** and **3**.

4. Concluding remarks

Two heterometallic coordination polymers (**2** and **3**) and one trinuclear complex (**4**) containing different cyanometalate anions have been prepared and characterized. The shelf-like column of **2** represents a new topology of 1D coordination polymers. Meanwhile, compound **3** provides the first example of a battlement-like polymer constructed from cyanometalate building blocks, and compound **4** is the first case of a cyano-bridged trinuclear hexacyanoplatinate(IV) complex. It is interesting to observe the different assembly chemistry of $[Cd(tren)]^{2+}$ with the closely related complex anions of $[Fe(CN)_6]^{4-}$ (**1**), $[Fe(CN)_5NO]^{2-}$ (**2**), $[Pd(CN)_4]^{2-}$ (**3**) and $[Pt(CN)_6]^{2-}$ (**4**).

5. Supplementary material

Crystallographic data for the structural analysis have been deposited with the Cambridge Crystallographic Data Centre, CCDC Nos. 156516–156518 for compounds **1**–**3**, respectively. Copies of this information may be obtained free of charge from The Director, CCDC, 12 Union Road, Cambridge, CB2 1EZ, UK (fax: +44-1223-336033; e-mail: deposit@ccdc.cam.ac.uk or www: http://www.ccdc.cam.ac.uk).

Acknowledgements

This work was supported by the National Natural Science Foundation of People's Republic of China, State Key Laboratory of Coordination Chemistry in Nanjing University, and State Key Laboratory of Bio-organic and Natural Products Chemistry of Shanghai Institute of Organic Chemistry.

References

[1] (a) Z. Stasicka, E. Wasielewska, Coord. Chem. Rev. 159 (1997) 271;
(b) H. Vahrenkamp, A. Geiß, G.N. Richardson, J. Chem. Soc., Dalton Trans. (1997) 3643.
[2] (a) H.-Z. Kou, S. Gao, B.-Q. Ma, D.-Z. Liao, Chem. Commun. (2000) 1309;
(b) A. Yuan, J. Zou, B. Li, Z. Zha, C. Duan, Y. Liu, Z. Xu, S. Keizer, Chem. Commun. (2000) 1297;
(c) J.A. Smith, J.-R. Galán-Mascarós, R. Clérac, K.R. Dunbar, Chem. Commun. (2000) 1077;
(d) S.-W. Zhang, D.-G. Fu, W.-Y. Sun, Z. Hu, K.-B. Yu, W.-X. Tang, Inorg. Chem. 39 (2000) 1142;
(e) W.E. Buschmann, J.S. Miller, Inorg. Chem. 39 (2000) 2411;
(f) L.G. Beauvais, M.P. Shores, J.R. Long, J. Am. Chem. Soc. 122 (2000) 2763;
(g) Z.J. Zhong, H. Seino, Y. Mizobe, M. Hidai, A. Fujishima, S. Ohkoshi, K. Hashimoto, J. Am. Chem. Soc. 122 (2000) 2952;
(h) A. Bleuzen, C. Lomenech, V. Escax, F. Villain, F. Varret, C.C. dit Moulin, M. Verdaguer, J. Am. Chem. Soc. 122 (2000) 6648.
[3] H. Yuge, Y. Noda, T. Iwamoto, Inorg. Chem. 35 (1996) 1842.
[4] T. Kitazawa, Chem. Commun. (1999) 891.
[5] (a) T. Soma, T. Iwamoto, Chem. Lett. (1994) 821;
(b) T. Soma, H. Yuge, T. Iwamoto, Angew. Chem., Int. Ed. 33 (1994) 1665;
(c) T. Soma, T. Iwamoto, Inorg. Chem. 35 (1996) 1849.
[6] (a) T. Niu, J. Lu, X. Wang, J.D. Korp, A.J. Jacobson, Inorg. Chem. 37 (1998) 5324;
(b) T. Niu, A.J. Jacobson, Inorg. Chem. 38 (1999) 5346.
[7] H. Zhang, J. Cai, X.-L. Feng, B.-H. Ye, X.-Y. Li, L.-N. Ji, J. Chem. Soc., Dalton Trans. (2000) 1687.
[8] N. Mondal, M.K. Saha, B. Bag, S. Mitra, V. Gramlich, J. Ribas, M.S.E. Fallah, J. Chem. Soc., Dalton Trans. (2000) 1601.
[9] R. Blessing, Acta Crystallogr., Sect. A 51 (1995) 33.

[10] (a) G.M. Sheldrick, SHELXL-97: Program for X-ray Crystal Structure Solution, University of Göttingen, Göttingen, Germany, 1997.;
(b) G.M. Sheldrick, SHELXL-97: Program for X-ray Crystal Structure Refinement, University of Göttingen, Göttingen, Germany, 1997.
[11] S. Zhan, X. Chen, A. Vij, D. Guo, Q. Meng, Inorg. Chim. Acta 292 (1999) 157.
[12] E.C. Plappert, D.M.P. Mingos, S.E. Lawrence, D.J. Williams, J. Chem. Soc., Dalton Trans. (1997) 2119.
[13] M.-L. Tong, H.-J. Chen, X.-M. Chen, Inorg. Chem. 39 (2000) 2235(and references therein).
[14] (a) D.W. Knoeppel, S.G. Shore, Inorg. Chem. 35 (1996) 1747;
(b) D.W. Knoeppel, J. Liu, E.A. Meyers, S.G. Shore, Inorg. Chem. 37 (1998) 4828.
[15] (a) A. Marvilliers, S. Parsons, E. Rivière, J.-P. Audière, T. Mallah, Chem. Commun. (1999) 2217;
(b) H.-Z. Kou, D.-Z. Liao, P. Cheng, Z.H. Jiang, S.-P. Yan, G.-L. Wang, X.-K. Yao, H.-G. Wang, J. Chem. Soc., Dalton Trans. (1997) 1503;
(c) M. Ohba, N. Fukita, H. Okawa, J. Chem. Soc., Dalton Trans. (1997) 1733;
(d) N. Re, E. Gallo, C. Floriani, H. Miyasaka, N. Matsumoto, Inorg. Chem. 35 (1996) 6004;
(e) D.G. Fu, J. Chen, X.S. Tan, L.J. Jiang, S.W. Zhang, P.J. Zheng, W.X. Tang, Inorg. Chem. 36 (1997) 220.
[16] G.N. Richardson, U. Brand, H. Vahrenkamp, Inorg. Chem. 38 (1999) 3070.

ELSEVIER

Polyhedron 21 (2002) 729–737

POLYHEDRON

www.elsevier.com/locate/poly

Structural studies of metal complexes of 2-pyridineformamide N(4)-methylthiosemicarbazone

Isabel García [a], Elena Bermejo [a], Ayman K. El Sawaf [b], Alfonso Castiñeiras [a,*], Douglas X. West [c]

[a] *Departamento de Química Inorgánica, Facultad de Farmacia, Universidad de Santiago de Compostela, E-15706 Santiago de Compostela, Spain*
[b] *Department of Chemistry, Faculty of Science, El Menoufia University, Shebin El-Kom, Egypt*
[c] *Department of Chemistry, 351700, University of Washington, Seattle, WA 98195-1700, USA*

Received 20 August 2001; accepted 4 December 2001

Abstract

Reduction of 2-cyanopyridine by sodium in dry methanol in the presence of N(4)-methylthiosemicarbazide produces 2-pyridineformamide N(4)-methylthiosemicarbazone, HAm4M. In the crystals of $[Ni(HAm4M)_2](ClO_4)_2\cdot 2H_2O$, $[Zn(Am4M)OAc]_2$ and $[Cd(HAm4M)Cl_2]\cdot DMSO$ the major ligand coordinates via its pyridyl nitrogen, imine nitrogen and sulfur atoms, the last of which forms a thione in the neutral ligand HAm4M and a thiolato group in $(Am4M)^-$. Both the acetato ligands in $[Zn(Am4M)OAc]_2$ are bis-monodentate bridges, which is unique among acetato-bridged binuclear complexes of thiosemicarbazones of this type. As in the complexes of other 2-pyridineformamide thiosemicarbazones, hydrogen bonds play an important role in these compounds. As well as by X-ray diffractometry, the new compounds were characterized by elemental analysis, FAB mass spectrometry and IR spectroscopy; in the case of the nickel(II) complex, by electronic spectroscopy and by molar conductivity and magnetic susceptibility measurements; and in the case of the zinc(II) and cadmium(II) complexes, by NMR spectroscopy (^1H, ^{13}C and, for Cd(II), ^{113}Cd). © 2002 Published by Elsevier Science Ltd.

Keywords: 2-Pyridineformamide; Thiosemicarbazone; Nickel(II); Zinc(II); Cadmium(II); Crystal structures

1. Introduction

The structures of a number of crystalline metal complexes of 2-pyridineformamide thiosemicarbazone (HAm4DH) have recently been studied [1–4], as have those of iron(III), cobalt(II) and nickel(II) complexes of 2-pyridineformamide N(4)-methylthiosemicarbazone, HAm4M [6] (Scheme 1). Spectra of copper(II) complexes of HAm4M have also been reported [5]. Having now obtained diffraction quality crystals of the binuclear zinc(II) complex $[Zn(Am4M)OAc]_2$, the cadmium(II) complex $[Cd(HAm4M)Cl_2]\cdot DMSO$ and the nickel(II) complex $[Ni(HAm4M)_2](ClO_4)_2\cdot 2H_2O$, we here compare their structures with those of the analogous compounds of HAm4DH and the previously reported metal complexes of HAm4M [6].

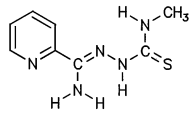
2. Experimental

2.1. Materials and instruments

All solvents used were reagent grade. $Ni(ClO_4)\cdot 6H_2O$ (Shering-Kalbaum), $Zn(CH_3COO)_2\cdot 2H_2O$ (ABCR), $CdCl_2\cdot H_2O$ (Aldrich), 2-cyanopyridine (Aldrich) and 4-methyl-3-thiosemicarbazide (Aldrich) were used with no further purification. HAm4M was prepared from 2-cyanopyridine as described previously [6]. Elemental analyses for C, H, N and S were performed on a Carlo Erba EA model 1108 elemental analyser. Melting points were determined in open tubes with a Büchi apparatus and are uncorrected. IR spectra were obtained in the 4000–400 cm^{-1} region using KBr pellets in a Mattson Cygnus 100 spectrometer, and in the 500–100 cm^{-1} region using polyethylene-sandwiched Nujol mulls in a Bruker IFS 66V spectrometer. ^1H and ^{13}C NMR spectra in DMSO-d_6 were run in Bruker AMX 300 and WM 300 instruments, respectively, using TMS as internal refer-

* Corresponding author. Tel.: +34-981-594-636; fax: +34-981-547-163.
E-mail address: qiac01@usc.es (A. Castiñeiras).

0277-5387/02/$ - see front matter © 2002 Published by Elsevier Science Ltd.
PII: S0277-5387(02)00835-5



Scheme 1.

ence. The ^{113}Cd NMR spectrum of the cadmium(II) complex was run on a Bruker AMX 500 apparatus in dimethylformamide with D_2O as reference and is expressed relative to 0.1 M $Cd(ClO_4)_2$. Mass spectra (FAB, 3-nitrobenzyl alcohol, Xe, 8 kV) were obtained in a Kratos MS 50 apparatus equipped with a DS-90 data acquisition system. Solid state electronic absorption (diffuse reflectance) spectra were recorded over the 900–350 nm region in a Shimadzu UV–Vis/NIR UV-3101PC spectrophotometer. Magnetic susceptibility measurements were performed at 25 °C using a Johnson Matthey Alfa MSB-MK1 Gouy balance; the data were corrected for diamagnetic susceptibilities. Molar conductivities of 10^{-3} M solutions were measured with a WTW LF-3 conductivity meter.

2.2. Synthesis and crystallization of the complexes

The complexes were prepared by the following procedure. A solution of HAm4M (0.25 g, 1.19 mmol) in ethanol (20 ml) was added to a solution of zinc(II) acetate (0.26 g, 1.19 mmol), cadmium(II) chloride (0.22 g, 1.19 mmol) or nickel(II) perchlorate (0.22 g, 0.60 mmol; **caution, perchlorates are potentially explosive and should be handled carefully**) in 20 ml of 96% ethyl alcohol, and the mixture was stirred for several days. The resulting solids were filtered off, washed thoroughly with cold ethanol and dried over $CaCl_2$.

2.2.1. $[Ni(HAm4M)_2](ClO_4)_2\cdot H_2O$

Green; 0.265 g, 63.7%; m.p. 250 °C. MS (FAB): $m/z = 477$ $[Ni(HAm4M)_2]^+$, 443 $[Ni_4(HAm4M)]^+$, 385 $[Ni_3(HAm4M)]^+$, 268 $[Ni(HAm4M)]^+$. *Anal.* Found: C, 27.90; H, 3.30; N, 19.94; S, 9.65%. Calc. for $C_{16}H_{24}Cl_2N_{10}NiO_9S_2$ (694.18): C, 27.68; H, 3.48; N, 20.07; S, 9.24%. IR (KBr, ν/cm^{-1}): 3420, 3353, 3313, 3181 (N–H); 1679, 1573, 1483 [(C=N)+(C=C)]; 1133–1089 (ν_3, ClO_4); 1030 (N–N); 940–929 (ν_4, ClO_4); 790 (C=S); 636 (py). Far-IR (Nujol, ν/cm^{-1}): 417 (py); 339 (Ni–S); 243, 225 (Ni–N). UV–Vis (ν/cm^{-1}): 28 735, 26 525, 15 611, 11 337.

2.2.2. $[Ni(HAm4M)_2](ClO_4)_2\cdot 2H_2O$

Single crystals of $[Ni(HAm4M)_2](ClO_4)_2\cdot 2H_2O$ suitable for analysis by X-ray diffractometry were obtained by slow evaporation of the mother liquor in air at room temperature. *Anal.* Found: C, 26.96; H, 3.77; N, 19.66; S, 8.99. Calc. for $C_{16}H_{26}Cl_2N_{10}NiO_{10}S_2$ (712.20): C, 26.98; H, 3.68; N, 19.67; S, 9.00%.

2.2.3. $[Zn(Am4M)(OAc)]_2\cdot H_2O$

Yellow; 0.336 g, 82.6%; m.p. 225 °C. MS (FAB): $m/z = 332$ $[Zn(HAm4M)(OAc)]^+$, 273 $[Zn(HAm4M)]^+$. *Anal.* Found: C, 35.18; H, 4.14; N, 20.49; S, 9.48%. Calc. for $C_{20}H_{28}N_{10}O_5S_2Zn_2$ (683.38): C, 35.15; H, 4.13; N, 20.50; S, 9.38%. IR (KBr, ν/cm^{-1}): 3432, 3314 (N–H); 1644, 1582 (ν_{as}, CO_2); 1564, 1514, 1469 [(C=N)+(C=C)]; 1385 (ν_s, CO_2); 1014 (N–N); 791 (C=S); 638 (py). Far-IR (Nujol, ν/cm^{-1}): 410 (py); 321 (Zn–S); 288 (Zn–O); 254 (Zn–N). ^1H NMR (DMSO-d_6, δ/ppm): 2.82 (s, 3H, C8H); 6.35 (s,a, 1H, N4H); 6.89 (s, 2H, N5H); 7.57, 8.06, 8.47 (4H, py). ^{13}C NMR (DMSO-d_6, δ/ppm): 29.6 (C8), 119.9 (C2), 125.3 (C4), 39.6 (C3), 144.9 (C6), 146.2 (C5), 147.1 (C1), 175.3 (C7).

2.2.4. $[Zn(Am4M)(OAc)]_2$

Single crystals of $[Zn(Am4M)(OAc)]_2$ suitable for analysis by X-ray diffractometry were obtained by slow evaporation of the mother liquor in air at room temperature. *Anal.* Found: C, 35.98; H, 3.74; N, 21.49; S, 9.68. Calc. for $C_{20}H_{26}N_{10}O_4S_2Zn_2$ (665.37): C, 36.10; H, 3.94; N, 21.06; S, 9.64%.

2.2.5. $[Cd(HAm4M)Cl_2]\cdot H_2O$

Yellow; 0.324 g, 66.3%; m.p. 234 °C. MS (FAB): $m/z = 531$ $[Cd(HAm4M)_2]^+$, 357 $[Cd(HAm4M)Cl]^+$. *Anal.* Found: C, 23.69; H, 2.86; N, 16.99; S, 8.75. Calc. for $C_8H_{13}CdCl_2N_5OS$ (410.59): C, 23.40; H, 3.19; N, 17.06; S, 7.81%. IR (KBr, ν/cm^{-1}): 3473, 3343, 3209 (N–H); 1665, 1631, 1565, 1441 [(C=N)+(C=C)]; 1016 (N–N); 794 (C=S); 640 (py). Far-IR (Nujol, ν/cm^{-1}): 404 (py); 322 (Cd–S); 252 (Cd–N); 219, 182 (Cd–Cl). ^1H NMR (DMSO-d_6, δ/ppm): 2.95 (s, 3H, C8H); 6.91 (s, 2H, N5H); 7.62 N (s,a, 1H, N4H); 7.43, 7.76, 8.44, 8.55 (4H, py); 10.06 (s, 1H, N3H). ^{13}C NMR (DMSO-d_6, δ/ppm): 30.1 (C8), 121.1 (C2), 126.4 (C4), 138.2 (C3), 140.6 (C6), 146.0 (C5), 149.0 (C1), 176.5 (C7).

2.2.6. $[Cd(HAm4M)Cl_2]\cdot DMSO$

Single crystals of $[Cd(HAm4M)Cl_2]\cdot DMSO$ suitable for analysis by X-ray diffractometry were obtained by slow evaporation of a DMSO solution in air at room temperature. *Anal.* Found: C, 25.45; H, 3.61; N, 14.85; S, 13.59. Calc. for $C_{10}H_{17}CdCl_2N_5OS_2$ (470.71): C, 25.52; H, 3.64; N, 14.88; S, 13.26%.

2.3. Crystal structure determination

Data were collected from selected crystals mounted on glass fibres. The data for $[Ni(HAm4M)_2](ClO_4)_2\cdot 2H_2O$ were processed with SAINT [7] and corrected for absorption using SADABS (transmission factors: 1.000–0.732) [8]. For $[Zn(Am4M)OAc]_2$ and $[Cd(HAm4M)Cl_2]\cdot$DMSO, cell constants and orientation matrices for data collection were obtained by least-squares refine-

ment of the diffraction data from 25 reflections in the ranges $21.95^\circ < \theta < 45.72^\circ$ and $6.55^\circ < \theta < 10.81^\circ$, respectively, and semi-empirical absorption corrections were made (ψ-scans) [9]. The structures were solved by direct methods using the program SHELXS-97, and were refined by full-matrix least-squares techniques on F^2 using anisotropic displacement parameters [10]. Hydrogen atoms were placed at the calculated positions. Idealized H atoms were refined with isotropic displacement parameters set to 1.2 (1.5 for methyl groups) times the equivalent isotropic U values of the parent atom. Atom scattering factors were taken from the International Tables for X-ray Crystallography [11] and molecular graphics were produced using SCHAKAL [12].

3. Discussion

3.1. Synthesis and physicochemical properties

Reaction of the stated quantities of $Ni(ClO_4)\cdot 6H_2O$, $Zn(CH_3COO)_2\cdot 2H_2O$ and $CdCl_2\cdot H_2O$ with HAm4M in ethanol gave products of compositions $[Ni(HAm4M)_2](ClO_4)_2\cdot H_2O$, $[Zn(Am4M)OAc]_2\cdot H_2O$ and $[Cd(HAm4M)Cl_2]\cdot H_2O$, as shown by microanalytical. All three complexes are stable in air and are highly soluble in DMF and DMSO, less soluble in H_2O, MeOH, EtOH, MeCN and Me_2CO, and insoluble in $HCCl_3$ and toluene.

The mass spectra of the complexes all show peaks attributable to the species $[Ni(HAm4M)_2]^+$, $[Cd(HAm4M)_2]^+$ or $[Zn(Am4M)(OAc)]^+$ and, at lower m/z, to $[Ni(HAm4M)]^+$, $[Zn(Am4M)]^+$ or $[Cd(HAm4M)Cl]^+$; these species are common in the mass spectra of compounds of the form $[ML_n]X_m$ in which monovalent anions coordinate metals in oxidation states II or III [13]. The spectra also all contain peaks due to oligomeric species or ligand fragmentation (not listed), and the spectrum of the nickel compound shows peaks corresponding to multinuclear single-ligand species.

The IR spectrum of HAm4M has five strong bands in the range 4000–3000 cm^{-1}. Those at 3366 and 3234 cm^{-1} are due to the stretching modes $\nu_a(NH_2)$ and $\nu_s(NH_2)$, respectively; that at 3183 cm^{-1} to the hydrazinic NH; and the other two probably to thioamide NH stretching. The IR spectra of the nickel(II) and cadmium(II) complexes exhibit shoulders at 3420 and 3473 cm^{-1}, respectively, and broad bands at 3353–3313 and 3181 cm^{-1} (in the nickel complex) or 3343 and 3208 cm^{-1} (in the cadmium complex); all these bands probably arise from both the ν(OH) modes of the lattice water and the ν(NH) modes of the ligand. In the spectrum of the zinc(II) complex ν(NH) vibrations appear at 3431 and 3313 cm^{-1}, but there is no band corresponding to stretching of the hydrazinic NH, which is consistent with deprotonation of HAm4M. Neither does this spectrum show bands characteristic of thioamide or imino groups, which suggests that the ligand is coordinated in thiolato form, an interpretation that is further supported by the presence of a new band near 1514 cm^{-1} that seems to be due to the stretching mode of the conjugated >C=N–N=C< group (as in azines [14]) and hence implies that the sulfur is thiolic. The shift of the thiocarbonyl stretching mode from 797 cm^{-1} in HAm4M to lower frequencies in all the complexes is in keeping with coordination through sulfur [15], and the parallel shift of ν(C=N) from 1591 cm^{-1} to 1564–1578 cm^{-1} likewise corroborates coordination of the azomethine nitrogen [16]. Coordination of the pyridine nitrogen atom is less easily inferred from the pyridine bands, since the 1600–1400 cm^{-1} region is complicated by the presence of thioamide bands, but is clearly shown by the shift to higher frequencies of the deformation mode bands that appear near 625 and 405 cm^{-1} in the spectrum of HAm4M [17]. In the 400–100 cm^{-1} region the IR spectra of the complexes show bands that are not observed in that of the free ligand: a weak band in the range 340–320 cm^{-1} is attributable to ν(MS), bands in the range 260–220 cm^{-1} to ν(MN) vibrations [18], a band at 288 cm^{-1} in the spectrum of the zinc complex to ν(ZnO) [19], and two strong bands at 219 and 182 cm^{-1} in the spectrum of the cadmium complex to ν(CdCl) [20].

The molar conductivity of freshly prepared 10^{-3} M solutions of the nickel(II) compound in DMF, 166.9 S cm^2 mol^{-1}, corresponds to a 1:2 electrolyte [21]. The effective magnetic moment determined at room temperature is 3.18 MB, which is typical of high-spin octahedral complexes [22]. The diffuse reflectance spectrum is typical of hexacoordinate compounds of nickel(II) [22]. In the visible and near-IR regions, a low-energy band at 11 340 cm^{-1} can be assigned to the $^3A_{2g}(F) \rightarrow {}^3T_{2g}(F)$ transition (ν_1), and the band at 16610 cm^{-1} to the $^3A_{2g}(F) \rightarrow {}^3T_{1g}(F)$ transition (ν_2); the ν_3 band, which corresponds to the transition $^3A_{2g}(F) \rightarrow {}^3T_{1g}(P)$, is masked by the high-intensity charge transfer bands at 26 525 and 28 735 cm^{-1}. The first CT band probably reflects a metal–ligand CT transition, whereas the second is probably the result of an intraligand transition.

In the ^1H NMR spectrum of the zinc complex the nonappearance of the N3H signal (at 10.03 ppm in the free ligand) shows that the ligand is deprotonated in DMSO solution. The deshielding of N4H is probably due to withdrawal of charge from N4 as the result of an increase in charge delocalization upon complexation through the thiocarbonyl sulfur atom; the shielding of the N4 methyl protons is attributable to the same mechanism. In the cadmium complex the persistence of the N3H signal shows that this proton is retained in DMSO solution; the downfield shifts of the N3H and

N4H signals are attributable to coordination through the azomethine nitrogen atom and thiocarbonyl sulfur atom, respectively, and/or to the formation of hydrogen bonds between N3H (and to a much lesser extent N4H) and solvent.

In the ^{13}C NMR spectra of the zinc and cadmium complexes the shielding of C7 and C8 is attributable to a combination of the inductive effect of the metal and the move towards the thiol form induced by deprotonation (in the zinc complex) or coordination through the sulfur atom (in the cadmium complex). The shift of the C6 signal to higher field in the cadmium complex is in consonance with coordination through the azomethine nitrogen atom, but in the zinc complex an increase in electronic delocalization in the thiosemicarbazone moiety moves this signal to lower field. Coordination through the pyridine nitrogen atom is pointed to by the shielding of the pyridine C5 signals [15].

The ^{113}Cd NMR spectrum shows a single signal at 385.5 ppm. The fact that the metal atom is less deshielded than in $CdCl_2$ in DMSO [23] is consistent with data for other complexes of cadmium(II) chloride with thiosemicarbazones, and is compatible with pentacoordination of the metal [2].

3.2. Crystal structures

Table 1 summarizes crystal data and data collection details for the complexes $[Ni(HAm4M)_2](ClO_4)_2\cdot 2H_2O$, $[Zn(Am4M)OAc]_2$ and $[Cd(HAm4M)Cl_2]\cdot DMSO$. Selected bond lengths are listed in Table 2, and bond angles in Table 3. Perspective views of $[Ni(HAm4M)_2](ClO_4)_2$, $[Zn(Am4M)OAc]_2$ and $[Cd(HAm4M)Cl_2]$ are shown in Figs. 1–3, respectively. Intermolecular hydrogen bonding parameters are compiled in Table 4, and least-squares mean-plane data in Table 5.

3.2.1. Structure of $[Ni(HAm4M)_2](ClO_4)_2\cdot 2H_2O$ (1)

The crystal structure of planar, tetracoordinate $[Ni(Am4M)(OAc)]\cdot H_2O$, in which HAm4M has lost its N3 hydrogen, was described previously [6]. The structure of $[Ni(HAm4DH)_2](NO_3)_2$, where HAm4DH is 2-pyridineformamide thiosemicarbazone, has also been solved, and $[Ni(HAm4DH)(Am4DH)]ClO_4$ has been synthesized by reaction of HAm4DH with nickel(II) perchlorate [3]. We are therefore able to compare the coordination of neutral HAm4M with that of anionic Am4M and with similar complexes of HAm4DH.

In $[Ni(HAm4M)_2](ClO_4)_2\cdot 2H_2O$ the two ligands coordinate in the expected meridional conformation via the pyridine nitrogen, imine nitrogen and sulfur atoms. The N12–Ni1–N22 angle involving the imine nitrogens of the two ligands is 173.1(3)°, showing less distortion from octahedral symmetry than in $[Ni(HAm4DH)_2](NO_3)_2$, in which this angle is 169.6(2)° [3]. The other two *trans* angles, each of which involves the terminal donors of one of the tridentate ligands, are approximately 159.5°.

As in all 2-pyridyl thiosemicarbazones, the $Ni–N_{im}$, $Ni–N_{py}$ and Ni–S bonds increase in length in that order. The differences between the two ligands as regards these bond lengths are within twice their combined esds. Coordination does not significantly affect the imine C=N bond length, and the C=S bond is shortened only very slightly, from an average 1.699(5) Å to an average 1.680(9) Å (probably due to the loss of intermolecular hydrogen bonds present in HAm4M [6]). The other bonds of the coordinated thiosemicarbazone moiety are also similar in length to those found in HAm4M. The bond angles of the thiosemicarbazone moiety are altered somewhat upon coordination; the largest change affects N13–C17–S1 and N23–C27–S2, which average 122.5(2)° in $[Ni(HAm4M)_2](ClO_4)_2$ as against 120.0(4)° in HAm4M [6].

All of the coordinating bonds are, as expected, longer than in [Ni(Am4M)(OAc)] [6], which is tetracoordinate. The C17–S1 and N13–C17 bonds are significantly shorter than in [Ni(Am4M)(OAc)], but the C16–N12 bonds of the two compounds have the same length. As expected, there are significant differences between the bond angles of coordinated HAm4M and the coordinated N3-deprotonated anion [6].

The extensive hydrogen bonding in $[Ni(HAm4M)_2](ClO_4)_2\cdot 2H_2O$ involves the perchlorate ions, the water molecules, and all the uncoordinated nitrogens (Table 4). N14–H14 binds two oxygens belonging to the same perchlorate ion (one more strongly than the other), and ligand 1 binds the O1#1 water molecule via two different NH groups (N13–H13 and N15–H15A), but ligand 2 only forms hydrogen bonds with perchlorate oxygen.

The angle between the least-squares planes of the pyridine ring and the thiosemicarbazide moiety in $[Ni(HAm4M)_2](ClO_4)_2$ averages 5.5(4)° {cf. 11.0(2)° in $[Ni(HAm4DH)_2](NO_3)_2$ [3]}. The angle between the planes of the two thiosemicarbazone moieties is 87.3(1)°, but the Ni(II) ion lies 0.058(6) Å from one plane and 0.022(7) Å from the other. The angles between the planes of the thiosemicarbazone moieties in $[Ni(HAm4DH)_2](NO_3)_2$ and $[Ni(HAm4DH)(Am4DH)]ClO_4$ are 88.6(2)° and 84.9(2)°, respectively [3].

3.2.2. Structure of $[Zn(Am4M)(OAc)]_2$ (2)

$[Zn(Am4M)(OAc)]_2$ crystallizes as a centrosymmetric binuclear molecule with the two acetato bridging ligands in a *syn–syn* arrangement and with a Zn–Zn distance of 3.6942(7) Å. By contrast, $[Zn(Am4DH)(OAc)]_2$ has two different kinds of acetato bridge: one is *syn–syn* but the other involves just a single oxygen, as in $[Zn(Ac4E)(OAc)]_2$, where Ac4E is the anion of 2-acetylpyridine N(4)-ethylthiosemicarbazone [24]. The two Zn–O distances of $[Zn(Am4M)(OAc)]_2$, which are slightly

Table 1
Crystal and structure refinement data for, $[Ni(HAm4M)_2](ClO_4)_2\cdot 2H_2O$, $[Zn(Am4M)(OAc)]_2$ and $[Cd(HAm4M)Cl_2]\cdot DMSO$

Empirical formula	$C_{16}H_{25}Cl_2N_{10}NiO_{10}S_2$	$C_{20}H_{26}N_{10}O_4S_2Zn$	$C_{10}H_{17}CdCl_2N_5OS_2$
Colour; habit	red–brown, prism	yellow, plate	yellow, prism
Formula weight	711.19	665.37	470.71
Temperature (K)	293(2)	293(2)	293(2)
Crystal size (mm)	$0.23 \times 0.18 \times 0.11$	$0.25 \times 0.25 \times 0.10$	$0.20 \times 0.16 \times 0.08$
Diffractometer	Bruker Smart CCD 1000	Nonius CAD4	Nonius MACH3
Radiation, (λ, Å)	Mo Kα (0.71073)	Cu Kα (1.54184)	Mo Kα (0.71073)
Crystal system	monoclinic	monoclinic	triclinic
Space group	$P2_1/n$ (No. 14)	$C2/c$ (No. 15)	$P\bar{1}$ (No. 2)
Unit cell dimensions			
a (Å)	12.721(2)	26.713(3)	9.148(3)
b (Å)	16.171(2)	8.183(1)	9.856(2)
c (Å)	14.155(2)	19.568(2)	11.849(2)
a (°)	90.0	90.0	108.56(2)
β (°)	97.711(3)	131.727(6)	93.63(2)
γ (°)	90.0	90.0	112.46(1)
V (Å^3)	2885.5(6)	3192.5(5)	915.0(3)
Z	4	4	2
Density (Mg m^{-3})	1.637	1.384	1.709
Absorption coefficient (mm^{-1})	1.069	3.418	1.717
θ Range for data collection (°)	1.92–28.03	4.44–75.92	2.41–23.68
Index ranges	$-16 \le h \le 13$	$-24 \le h \le 33$	$-10 \le h \le 0$
	$-19 \le k \le 21$	$-10 \le k \le 0$	$-10 \le k \le 11$
	$-18 \le l \le 18$	$-24 \le l \le 0$	$-13 \le l \le 13$
Reflections collected	37 720	3340	2965
Independent reflections	6898 $\{R_{int} = 0.117\}$	3326 $\{R_{int} = 0.029\}$	2765 $\{R_{int} = 0.204\}$
Data/parameters	6898/382	3326/173	2765/190
Final R indices [$I > 2\sigma(I)$]	$R_1 = 0.095$, $wR_2 = 0.217$	$R_1 = 0.044$, $wR_2 = 0.121$	$R_1 = 0.059$, $wR_2 = 0.074$
R indices (all data)	$R_1 = 0.219$, $wR_2 = 0.277$	$R_1 = 0.049$, $wR_2 = 0.126$	$R_1 = 0.356$, $wR_2 = 0.109$
Goodness-of-fit	1.022	1.057	0.905
Largest difference peak and hole (e Å^{-3})	1.248 and -0.775	0.694 and -0.829	0.670 and -1.350

different, are the shortest of the five coordinating bond lengths. As in other 2-pyridyl thiosemicarbazones, the Zn–N_{im}, Zn–N_{py} and Zn–S bond lengths increase in that order. In the anionic Am4M ligand the C7–S1 bond is longer than in free HAm4M [1.750(3) Å as against 1.699(5) Å], and the N3–C7 bond (formally a double bond following loss of the proton from N3) is shorter [1.307(4) Å as against 1.358(6) Å] [6]. The other

Table 2
Selected bond lengths (Å) in $[Ni(HAm4M)_2](ClO_4)_2\cdot 2H_2O$ (**1**), $[Zn(Am4M)(OAc)]_2$ (**2**), and $[Cd(HAm4M)Cl_2]\cdot DMSO$ (**3**)

Bond	**1**	Bond	**2**	Bond	**3**
Ni1–N12	2.007(6)	Zn1–N2	2.050(2)	Cd1–N2	2.335(9)
Ni1–N22	2.005(6)	Zn1–N1	2.227(2)	Cd1–N1	2.365(10)
Ni1–N11	2.099(6)	Zn1–S1	2.370(1)	Cd1–S1	2.597(4)
Ni1–N21	2.117(6)	Zn1–O11 [a]	1.988(2)	Cd1–Cl1	2.493(4)
Ni1–S1	2.420(2)	Zn1–O12	2.020(2)	Cd1–Cl2	2.447(3)
Ni1–S2	2.416(2)				
S1–C17	1.691(9)	S1–C7	1.750(3)	S1–C7	1.692(12)
C16–N12	1.292(10)	C6–N2	1.296(3)	C6–N2	1.282(14)
N12–N13	1.396(8)	N2–N3	1.387(3)	N2–N3	1.379(11)
N13–C17	1.341(10)	N3–C7	1.307(4)	N3–C7	1.319(13)
C17–N14	1.328(9)	C7–N4	1.337(4)	C7–N4	1.328(14)
C16–N15	1.350(11)	C6–N5	1.339(3)	C6–N5	1.346(13)
S2–C27	1.670(8)				
C26–N22	1.288(9)	C11–O11	1.251(3)		
N22–N23	1.364(8)	C11–O12	1.264(3)		
N23–C27	1.386(9)				
C27–N24	1.337(10)				
C26–N25	1.349(11)				

[a] Symmetry transformation used to generate equivalent atoms: $-x, +1/2, -y+1/2, -z+1$.

Table 3
Selected bond angles (°) for $[Ni(HAm4M)_2](ClO_4)_2\cdot 2H_2O$ (**1**), $[Zn(Am4M)(OAc)]_2$ (**2**), and $[Cd(HAm4M)Cl_2]\cdot DMSO$ (**3**)

Angle	**1**			Angle	**2**	Angle	**3**
S1–Ni–N22	101.2(2)			S1–Zn1–N1	156.58(6)	S1–Cd1–N1	142.4(3)
S1–Ni–N12	82.0(2)			S1–Zn1–N2	81.87(6)	S1–Cd1–N2	75.1(3)
S1–Ni–N11	159.5(2)			S1–Zn1–Ol1 [a]	105.64(7)	S1–Cd1–Cl1	106.0(1)
S1–Ni–N21	93.5(2)			S1–Zn1–O12	102.78(6)	S1–Cd1–Cl2	107.2 (1)
S1–Ni–S2	92.8(1)			N1–Zn1–N2	74.77(8)	N1–Cd1–N2	67.4(4)
S2–Ni–N22	82.3(2)			N1–Zn1–Ol1 [a]	88.69(8)	N1–Cd1–Cl1	94.0(3)
S2–Ni1–N12	103.7(2)			N1–Zn1–O12	86.26(8)	N1–Cd1–Cl2	94.6(3)
S2–Ni1–N11	92.4(2)			N2–Zn1–Ol1 [a]	122.80(9)	N2–Cd1–Cl1	117.6(3)
S2–Ni1–N21	159.6(2)			N2–Zn1–Ol2	115.89(8)	N2–Cd1–Cl2	129.2(3)
N11–Ni1–N22	99.1(2)			Ol1 [a]–Zn1–O12	117.12(9)	Cl1–Cd1–Cl2	110.4(1)
N11–Ni1–N12	77.5(2)			O11–C11–O12	124.7(2)		
N11–Ni1–N21	88.5(2)			O11–C11–C12	117.7(3)		
N21–Ni1–N22	77.5(2)			O12–C11–C12	117.5(2)		
N21–Ni1–N12	96.3(2)			Zn1–O11 [a]–C11 [a]	130.1(2)		
N12–Ni1–N22	173.1(3)			Zn1–O12–C11	125.0(2)		
Ni1–S1–C17	96.0(3)	Ni–S2–C27	96.5(3)	Zn1–S1–C7	95.1(1)	Cd1–S1–C7	99.6(5)
Ni1–N12–C16	118.9(5)	Ni–N22–C26	120.1(5)	Zn1–N2–C6	121.4(2)	Cd1–N2–C6	120.9(9)
Ni1–N12–N13	120.7(5)	Ni–N22–N23	120.8(4)	Zn1–N2–N3	122.9(2)	Cd1–N2–N3	118.9(7)
N15–C16–N12	127.9(8)	N25–C26–N22	126.0(8)	N5–C6–N2	123.3(3)	N5–C6–N2	125.6(13)
C15–C16–N12	113.3(7)	C25–C26–N22	114.5(7)	C5–C6–N2	115.5(2)	C5–C6–N2	117.9(12)
C16–N12–N13	118.9(5)	C26–N22–N23	119.1(6)	C6–N2–N3	115.6(2)	C6–N2–N3	119.1(11)
N12–N13–C17	117.9(6)	N22–N23–C27	118.2(6)	N2–N3–C7	113.6(2)	N2–N3–C7	121.4(11)
N13–C17–N14	114.7(7)	N23–C27–N24	113.8(7)	N3–C7–N4	117.1(3)	N3–C7–N4	114.0(12)
N13–C17–S1	123.0(6)	N23–C27–S2	122.0(6)	N3–C7–S1	126.5(2)	N3–C7–S1	124.8(11)
N14–C17–S1	122.3(7)	N24–C27–S2	124.2(6)	N4–C7–S1	116.4(2)	N4–C7–S1	121.2(11)

[a] Symmetry transformation used to generate equivalent atoms: $-x,+1/2,\ -y+1/2,\ -z+1$.

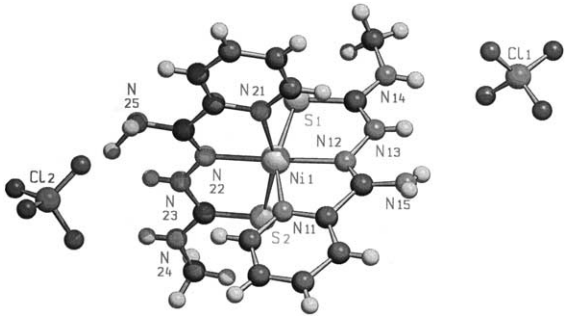


Fig. 1. Drawing of $[Ni(HAm4M)_2](ClO_4)_2$.

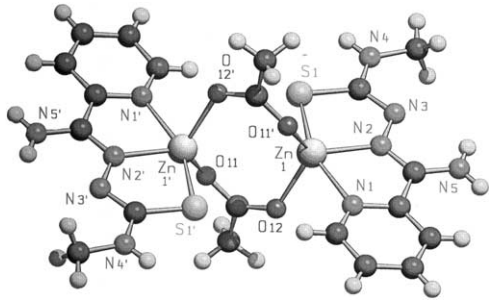


Fig. 2. Drawing of $[Zn(Am4M)(OAc)]_2$.

bond lengths in the thiosemicarbazone moiety do not differ significantly from those of HAm4M. The lengths of the two C–O bonds of the acetato groups are slightly

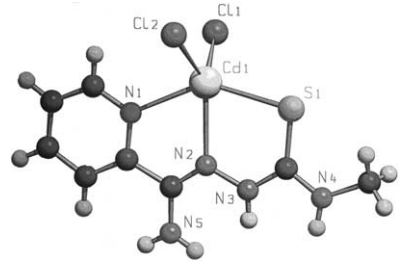


Fig. 3. Drawing of $[Cd(HAm4M)Cl_2]$.

different, in keeping with the different Zn–O distances. Compared to $[Zn(Am4DH)(OAc)]_2$, $[Zn(Am4M)(OAc)]_2$ has a significantly longer $Zn–N_{im}$ bond [2.227(2) Å as against an average 2.161(2) Å] and slightly shorter Zn–S and Zn–O distances, but the $Zn–N_{py}$ distance is the same in both compounds.

The identical ZnN_2O_2S kernels of $[Zn(Am4M)(OAc)]_2$ have N1–Zn–S angles of 156.58(6)° {cf. 150.44(5)° and 157.27(6)° for $[Zn(Am4DH)(OAc)]_2$}. With N1–Zn–S assigned as β and N1–Zn–O11′ as α, $\tau = 0.56$ [25], indicating that the arrangement about Zn is very slightly closer to a trigonal bipyramid (with N1 and S axial, and N2, O11′ and O12 equatorial) than to a square pyramid. By contrast, in $[Zn(Am4DH)(OAc)]_2$ both centres are more nearly square pyramids ($\tau = 0.20$ and 0.0), as in another recently studied binuclear zinc complex with dissimilar acetato bridges, [Zn(Ampip)-

Table 4
Hydrogen bond parameters (Å and °) in $[Ni(HAm4M)_2](ClO_4)_2\cdot 2H_2O$ (**1**), $[Zn(Am4M)(OAc)]_2$ (**2**) and $[Cd(HAm4M)Cl_2]\cdot DMSO$ (**3**)

Compound	D–H···A	d(D–H)	d(H···A)	d(D···A)	∠ (DHA)
1 [a]	N13–H13···O1#1	0.86	2.19	3.05(1)	172.1
	N14–H14···O11	0.86	2.29	3.06(1)	149.1
	N14–H14···O13	0.86	2.66	3.29(2)	131.7
	N15–H15A···O1#1	0.69	2.21	2.89(1)	165.0
	N15–H15B···O12#2	0.90	2.18	3.08(1)	174.0
	N23–H23···O22	0.86	2.12	2.97(1)	168.5
	N24–H24···O24	0.86	2.13	2.99(2)	171.5
	N25–H25A···O22	1.18	2.17	3.15(1)	137.0
	N25–25B···O14#3	0.78	2.75	3.26(2)	127.0
2 [b]	N4–H4···S1#1	0.86	2.67	3.47(3)	154.3
	N5–H5B···O12#2	0.86	2.20	2.97(3)	149.7
3 [c]	N3–H3···O2#1	0.86	1.91	2.76(1)	170.4
	N4–H4···Cl2#1	0.86	2.68	3.37(1)	137.6
	N5–H5A···O2#1	0.86	2.05	2.90(1)	171.7
	N5–H5B···Cl1#2	0.86	2.52	3.32(1)	154.1

Symmetry transformations used to generate equivalent atoms:
[a] #1: $-x+1/2$, $y+1/2$, $-z+3/2$; #2: $x-1/2$, $-y+3/2$, $z-1/2$; #3: x, y, $z-1$.
[b] #1: $-x$, y, $-z+1/2$; #2 $-x+1/2$; $y+1/2$, $-z+1/2$.
[c] #1: $-x+1$, $-y+1$, $-z+1$; #2: $-x$, $-y$, $-z+1$.

$(OAc)]_2$ (where Ampip is the anion of 2-pyridineformamide 3-piperidylthiosemicarbazone), for which $\tau = 0.04$ and 0.25 [26]. The difference between the two acetato ligands both being bis-monodentate (as in $[Zn(Am4M)(OAc)]_2$) and their one of them being bis-monodentate and the other bridging only through one oxygen (as in $[Zn(Am4DH)(OAc)]_2$ and $[Zn(Ampip)(OAc)]_2$) thus has a significant effect on the coordination polyhedra of both the zinc atoms.

There is less intermolecular hydrogen bonding in $[Zn(Am4M)(OAc)]_2$ than in other complexes of 2-pyridineformamide thiosemicarbazones because of the absence of solvate molecules. However, N4H4 interacts with a non-bonding pair of electrons on a coordinated thiolato sulfur, the N4H4···S1#1 distance and angle [3.446(3) Å and 154.3°] being similar to those found in uncomplexed N–(2-pyridyl)–N′–arylthiourea molecules [27]; and an N5 hydrogen interacts with a lone pair of electrons on a coordinated acetato oxygen atom, with a N···O distance, 2.973(3) Å, that is slightly shorter than that between an analogous nitrogen and the oxygen of a solvating water molecule in $[Zn(Am4DH)(OAc)]_2\cdot H_2O$, 3.018(3) Å [4]. As in other complexes of Am4M, the mean plane of the coordinated thiosemicarbazide moiety is just slightly inclined to that of the pyridine ring, with which it makes an angle of 3.8(2)° (Table 5).

3.2.3. Structure of $[Cd(HAm4M)Cl_2]\cdot DMSO$ (3)

A number of $[Cd(NNS)X_2]$ compounds have been reported recently (NNS being a neutral 2-pyridyl thiosemicarbazone and X being Cl, Br or I). They include $[Cd(HAm4DH)Cl_2]$ [4] and $[Cd(HAc4M)Cl_2]$ [15], where HAc4M is 2-acetylpyridine N(4)-methylthiosemicarbazone. In **3** the major ligand coordinates via its pyridine nitrogen, imine nitrogen and sulfur atoms, and the coordinating bonds between Cd and the HAm4M and chloro ligands are very similar in length to those of $[Cd(HAm4DH)Cl_2]$ [4]. The Cd–N1 and Cd–S distances are also very similar to those found in

Table 5
Characteristics of least-squares planes in $[Ni(HAm4M)_2](ClO_4)_2\cdot 2H_2O$ (**1**), $[Zn(Am4M)(OAc)]_2$, (**2**) and $[Cd(HAm4M)Cl_2]\cdot DMSO$ (**3**)

Compound	Plane	Rms dev. (Å)	Largest dev. (Å)	Angle with previous plane (°)
1	N11–C11–C12–C13–C14–15	0.0088	C14, 0.014(6)	
	C16–N12–N13–C17–S1–N14	0.0488	N12, 0.097(5)	7.1(4)
	C26–N22–N23–C27–S2–N24	0.0396	N23, 0.069(6)	87.3(1)
	N21–C21–C22–C23–C24–25	0.0053	C21, 0.008(6)	3.8(4)
2	C6–N2–N3–C7–N4–S1	0.0202	N2, 0.032(2)	
	N1–C1–C2–C3–C4–C5	0.0045	N1, 0.008(2)	3.8(2)
	N1–N2–S1	0.0000		4.4(2)
	O11–O12–C12	0.0000		89.8(2)
3	C6–N2–N3–C7–N4–S1	0.0422	N2, 0.085(9)	
	N1–C1–C2–C3–C4–C5	0.0061	C4, 0.010(9)	8.6(4)

Table 6
Distortion from square pyramidal geometry in $[Cd(NNS)Cl_2]$ complexes

Compound	β(N1–Cd1–S1)	α(N2–Cd1–Cl)	$\beta-\alpha$	$\tau=(\beta-\alpha)/60$	Ref.
$[Cd(HAm4DH)Cl_2]$ [a]	142.8	138.4	4.4	0.07	[4]
$[Cd(HAm4M)Cl_2]$	142.4	129.2	13.2	0.22	this work
$[Cd(HAmpip)Cl_2]$ [b]	134.6	137.9	3.3	0.06	[26]
$[Cd(HAc4DH)Cl_2]$ [c]	141.5	137.7	3.8	0.06	[28]
$[Cd(HAc4M)Cl_2]$ [d]	139.8	136.7	3.1	0.05	[15]
$[Cd(HAc4DM)Cl_2]$ [e]	145.2	135.5	9.7	0.16	[29]

[a] HAm4DH = 2-pyridineformamide thiosemicarbazone.
[b] HAmpip = 2-pyridineformamide 3-piperidylthiosemicarbazone.
[c] HAc4DH = 2-acetylpyridine thiosemicarbazone.
[d] HAc4M = 2-acetylpyridine N(4)-methylthiosemicarbazone.
[e] HAc4DM = 2-acetylpyridine N(4)-dimethylthiosemicarbazone.

$[Cd(HAc4M)Cl_2]$ [15], but the Cd–N2 distance is significantly shorter than in the latter [2.365(10) Å as against 2.432(2) Å], showing that electron donation by the formamide NH_2 is significantly greater than that of the acetyl CH_3. This difference is probably responsible for the Cd–Cl bond being somewhat longer in $[Cd(HAm4M)Cl_2]$. Like all other $[Cd(NNS)Cl_2]$ compounds, $[Cd(HAm4M)Cl_2]$ has a square pyramidal coordination polyhedron, but it also exhibits greater distortion towards trigonal bipyramidal stereochemistry than any other known compound of this type (Table 6).

In the thiosemicarbazone moiety the only bond of $[Cd(HAm4M)Cl_2]$ to differ significantly in length from the corresponding bonds of $[Cd(HAm4DH)Cl_2]$ [4] and $[Cd(HAc4M)Cl_2]$ [15] is N3–C7 {1.319(13) Å in $[Cd(HAm4M)Cl_2]$, 1.358(6) Å in $[Cd(HAm4DH)Cl_2]$ and 1.370 Å in $[Cd(HAc4M)Cl_2]$}. The mean planes of the pyridine ring and the thiosemicarbazide chain make an angle of 8.6(4)° {cf. 2.0(2)° in $[Cd(HAm4DH)Cl_2]$}.

2-Pyridineformamide thiosemicarbazones have more possibilities of hydrogen bonding than 2-formyl-, 2-acetyl- and 2-benzoylpyridine thiosemicarbazones because of the presence of the formamide NH_2 group. In the present case, the four hydrogen bonds of $[Cd(HAm4M)Cl_2]\cdot DMSO$ (N3H3 and N5H5A with the oxygen of a neighbouring DMSO, N4H4 with the corresponding Cl2, and N5H5B with Cl1 of another neighbouring molecule; see Table 4) may be compared with the two of $[Cd(HAc4M)Cl_2]\cdot 2DMSO$, in which it is N3H3 and N4H4 that both interact with the same DMSO oxygen.

4. Supplementary material

Crystallographic data for the structures reported in this paper (excluding structure factors) have been deposited with the Cambridge Crystallographic Data Centre, CCDC Nos. 168861 (for $[Ni(HAm4M)_2](ClO_4)_2\cdot 2H_2O$), 168862 (for $[Zn(Am4M)(OAc)]_2$) and 168863 (for $[Cd(HAm4M)Cl_2]\cdot DMSO$). Copies of this information may be obtained free of charge from The Director, CCDC, 12 Union Road, Cambridge, CB2 1EZ, UK (fax: +44-1223-336033; e-mail: deposit@ccdc.cam.ac.uk or www: http://www.ccdc.cam.ac.uk).

References

[1] A. Castiñeiras, I. Garcia, E. Bermejo, D.X. West, Z. Naturforsch., Teil B 55 (2000) 511.
[2] A. Castiñeiras, I. Garcia, E. Bermejo, D.X. West, Polyhedron 19 (2000) 1873.
[3] A. Castiñeiras, I. Garcia, E. Bermejo, K.A. Ketcham, D.X. West, manuscript in preparation.
[4] A. Castiñeiras, I. Garcia, E. Bermejo, D.X. West, manuscript in preparation.
[5] D.X. West, J.K. Swearingen, A.K. El-Sawaf, Transition Met. Chem. 25 (2000) 87.
[6] D.X. West, J.K. Swearingen, J. Valdés-Martínez, S. Hernández-Ortega, A.K. El-Sawaf, F. van Meurs, A. Castiñeiras, I. Garcia, E. Bermejo, Polyhedron 18 (1999) 2919.
[7] Bruker, SMART and SAINT. Area Detector Control and Integration Software, Bruker Analytical X-ray Instruments Inc., Madison, WI, USA, 1997.
[8] G.M. Sheldrick, SADABS. Program for Empirical Absorption Correction of Area Detector Data. University of Göttingen, Göttingen, Germany, 1997.
[9] A.C.T. North, D.C. Phillips, F.S. Mathews, Acta Crystallogr., Sect. A 24 (1968) 351.
[10] G.M. Sheldrick, SHELXL-97. Program for the Refinement of Crystal Structures, University of Göttingen, Göttingen, Germany, 1997.
[11] International Tables for X-ray Crystallography, Vol. C, Kluwer Academic Publishers, Dordrecht, The Netherlands, 1995.
[12] E. Keller, SCHAKAL97. A computer program for the graphic representation of molecular and crystallographic models, University of Freiburg, Germany, 1997.
[13] G. Bojesen, Org. Mass. Spectrom. 20 (1985) 413.
[14] M.F. Iskander, L. El-Sayed, M.A. Lasheem, Inorg. Chim. Acta 16 (1976) 147.
[15] E. Bermejo, R. Carballo, A. Castiñeiras, R. Domínguez, A.E. Liberta, C. Maichle-Mössmer, M.M. Salberg, D.X. West, Eur. J. Inorg. Chem. (1999) 965.
[16] M.B.elicchi Ferrari, S. Capacchi, F. Bisceglie, G. Pelosi, P. Tarasconi, Inorg. Chim. Acta 32 (2001) 81.
[17] D.K. Rastoh, K.C. Sharma, J. Inorg. Nucl. Chem. 36 (1974) 2219.

[18] (a) K. Nakamoto, Infrared and Raman Spectra of Inorganic and Coordination Compounds, Wiley, New York, 1986;
(b) J. Weidlein, U. Müller, K. Dehnicke, Schwingungsfrequenzen II, Thieme Verlag, Stuttgart, 1986.
[19] H. Ackermann, F. Weller, B. Neumüller, K. Dehnicke, Z. Anorg. Allg. Chem. 625 (1999) 147.
[20] A. Castiñeiras, R. Carballo, T. Perez, Polyhedron 20 (2001) 441.
[21] W.J. Geary, Coord. Chem. Rev. 7 (1971) 81.
[22] A.B.P. Lever, Inorganic Electronic Spectroscopy, Elsevier, New York, 1984.
[23] T. Drakenberg, N.-O. Björk, R. Portanova, J. Phys. Chem. 82 (1978) 2423.
[24] L. Bresolin, R.A. Burrow, M. Hörner, E. Bermejo, A. Castiñeiras, Polyhedron 16 (1997) 3947.
[25] A.W. Addison, T.N. Rao, J. Reedijt, J. van Rijn, G.C. Verschoor, J. Chem. Soc., Dalton Trans. (1984) 1349.
[26] A. Castiñeiras, I. Garcia, E. Bermejo, K.A. Ketcham, A.K. El-Sawaf, D.X. West, unpublished results.
[27] (a) J. Valdés-Martínez, S. Hernández-Ortega, D.X. West, L.J. Ackerman, J.K. Swearingen, A.K. Hermetet, J. Mol. Struct. 478 (1999) 219;
(b) D.X. West, J.K. Swearingen, A.K. Hermetet, L.J. Ackerman, C. Presto, J. Mol. Struct. 522 (2000) 27;
(c) J. Valdés-Martínez, S. Hernández-Ortega, L.J. Ackerman, D.T. Le, J.K. Swearingen, D.X. West, J. Mol. Struct. 524 (2000) 51.
[28] J.S. Casas, M.V. Castaño, M.S. Garcia-Tasende, I. Martínez-Santamarta, J. Sordo, E.E. Castellano, J. Zuckerman-Schpector, J. Chem. Res. (S) (1992) 324; (M) (1992) 2626.
[29] E. Bermejo, R. Carballo, A. Castiñeiras, R. Domínquez, C. Maichle-Mössmer, A.E. Liberta, D.X. West, Z. Naturforsch., Teil B 54 (1999) 777.

PERGAMON

Polyhedron 21 (2002) 739–744

POLYHEDRON

www.elsevier.com/locate/poly

Crystal and molecular structures of cadmium(II) nitrate complexes with triamines: 1,5-diamino-3-azapentane, 1,6-diamino-3-azahexane and 1,7-diamino-4-azaheptane

Elzbieta Bartoszak-Adamska, Romualda Bregier-Jarzebowska, Lechoslaw Lomozik *

Faculty of Chemistry, A. Mickiewicz University, Grunwaldzka 6, 60-780 Poznan, Poland

Received 12 September 2001; accepted 5 December 2001

Abstract

The following new complexes of Cd(II) nitrate with triamines have been prepared and characterized: $[Cd(NH_2(CH_2)_2NH(CH_2)_2NH_2)_2](NO_3)_2$ (**1**), $[Cd(NH_2(CH_2)_2NH(CH_2)_3NH_2)_2](NO_3)_2$ (**2**) and $[Cd(NH_2(CH_2)_3NH(CH_2)_3NH_2)_2](NO_3)_2$ (**3**). Their structures have been determined by a single-crystal X-ray diffraction method. Because of the instability of the crystals **2** and **3** at room temperature, all complexes were examined at 100 K. In the complexes investigated all nitrogen atoms of the triamines coordinate the Cd(II) atom. All data sets showed {N6}-coordinated complexes. The stoichiometry of the complexes in the solid state is always 1:2, although the crystals were grown from solutions with different concentration ratios of the components (Cd–triamine: 1:1, 1:2 or 1:3). The Cd(II) atom of complex **1** is sandwiched between two triamines related by a twofold axis. Complexes **2** and **3** are characterized by a distorted octahedral coordination. The conclusions obtained correspond to the solution structures obtained from NMR, IR as well as equilibrium studies. © 2002 Elsevier Science Ltd. All rights reserved.

Keywords: Cadmium(II) complexes; Polyamines; X-ray structures

1. Introduction

As has been observed for a number of systems, polyamines form molecular complexes with fragments of molecular acids and the metal ions present in the systems influence the character of non-covalent interactions [1–9]. Biogenic amines change the conformation of nucleic acids and directly affect the processes of genetic information transfer [10–13]. Putrescine, spermidine and spermine occur practically in all kinds of living cells and because of their high basicity in the physiological environment they are protonated and act as positive interaction centres. Often in analysis of interactions only the magnitude of the charge is taken into account, which is an oversimplification preventing the explanation of the specificity of a number of processes, and the character of interactions is also significantly affected by the structural factor. The length of the chain and the kind of chelate ring also influence the properties of coordination complexes of polyamines with metal ions. It has been recently found that Cu(II) in systems with polyamines tend to assume a coordination type {N4} or {N5}, with one or two vacant axial positions of the ML_2 type of complex [14,15]. In contrast to copper, cadmium(II) shows a tendency to bind polyamines exhausting all accessible donor atoms of the bioligand [16]. Analysis of biosystems with cadmium ions becomes a problem of particular importance in view of the established toxic influence of this metal, associated with Hg and Pb to the group of the most toxic environmental pollutants [17–20]. Recently, an increase in the concentration of the metals in living organisms has been observed [21–24]. Cadmium is accumulated in kidneys, liver and blood where it can destroy erythrocytes, also being detrimental to bones [19,20,25]. This metal competes with Zn and blocks active sites of metal–enzymes and as a relatively soft acid it can dislodge Zn(II) in cysteine-coordinated zinc compounds

* Corresponding author. Tel.: +48-61-829-1358; fax: +48-61-865-8008.

E-mail addresses: ela@krystal.amu.edu.pl (E. Bartoszak-Adamska), bregier@main.amu.edu.pl (R. Bregier-Jarzebowska), lomozik@main.amu.edu.pl (L. Lomozik).

0277-5387/02/$ - see front matter © 2002 Elsevier Science Ltd. All rights reserved.
PII: S0277-5387(02)00848-3

or Ca(II) ions in bone cells [26,27]. This paper describes the synthesis and structure of three new complexes of Cd(II) nitrate with 1,5-diamino-3-azapentane (dien), 1,6-diamino-3-azahexane (2,3-tri) and 1,7-diamino-4-azaheptane (3,3-tri).

2. Experimental

$Cd(NO_3)_2 \cdot 4H_2O$, 99% was purchased from Merck; the polyamines: diethylenetriamine (dien), NH_2–$(CH_2)_2$–NH–$(CH_2)_2$–NH_2, 99%; 1,6-diamino-3-azahexane (2,3-tri), NH_2–$(CH_2)_2$–NH–$(CH_2)_3$–NH_2, 97% and 1,7-diamino-4-azaheptane (3,3-tri), NH_2–$(CH_2)_3$–NH–$(CH_2)_3$–NH_2, 98%, were purchased from Aldrich. The reagents were used without further purification.

2.1. Synthesis of complexes

Compounds: $Cd(dien)_2(NO_3)_2$ (**1**), $Cd(2,3\text{-tri})_2(NO_3)_2$ (**2**) and $Cd(3,3\text{-tri})_2(NO_3)_2$ (**3**) were obtained by mixing a solution containing 0.5 mM $Cd(NO_3)_2 \cdot 4H_2O$ in 2.5 cm^3 of methanol with a solution of 1.0 mM dien, 10.0 mM 2,3-tri or 1.0 mM 3,3-tri, respectively, in 2.5 cm^3 of methanol at room temperature (solutions for compounds **1** and **3** were evaporated to about three-fourth of the initial volume). Single crystals of all compounds appeared after a few days. They were filtered off, washed with methanol and diethyl ether and dried in the air. Elemental analysis of compounds **1** and **3** was performed using a Perkin Elmer CHN 2400 analyser and compound **2** on a Euro-Vector EA 3000 analyser.

Compound ***1***: Yield ~30%; *Anal*. Calc.: for $C_8H_{26}N_8O_6Cd$ ($M = 442.76$ g mol^{-1}): C, 21.70; H, 5.92; N, 25.31. Found: C, 21.82; H, 5.88; N, 25.26%; *Compound* ***2***: Yield ~35%. *Anal*. Calc. for $C_{10}H_{30}N_8O_6Cd$ ($M = 470.81$ g mol^{-1}): C, 25.51; H, 6.42; N, 23.80. Found: C, 25.85; H, 6.36; N, 23.54%. *Compound* ***3***: Yield ~30%. *Anal*. Calc. for $C_{12}H_{34}N_8O_6Cd$ ($M = 498.86$ g mol^{-1}): C, 28.90; H, 6.87; N, 22.46. Found: C, 29.06; H, 6.82; N, 22.38%.

2.2. Spectral studies

IR spectra were taken in a Brucker FT-IR spectrometer model IFS 113v and Nicolet Magna 760 instrument, in the range 4000–200 cm^{-1}, for the solid complexes in tablets with CsBr and for free polyamine in a film. NMR measurements (in D_2O) were performed using NMR Gemini-300VT Varian and NMR Varian Unity 300.

2.3. X-ray measurements

X-ray data collection at 100 K was performed in a KM4-CCD κ-geometry diffractometer equipped with an Oxford Cryosystem [28] and using graphite-monochromated Mo Kα radiation. The integrated intensities and direction cosines were obtained using the CRYSALIS program [29]. The data were corrected for Lorentz, polarization and absorption effects. Semi-empirical absorption correction was made using the raw data for absorption curve determination. The structure was solved by the heavy atom Patterson superposition method using SHELXS [30] and refined by full-matrix least-squares techniques using anisotropic displacement parameters for non-hydrogen atoms and isotropic ones for H atoms. C–H and N–H hydrogen atoms were generated geometrically and included into the refinement process. The refinement (in SHELX-97 [31]) was based on all F^2 data and included an empirical extinction parameter x, used to correct F_c according to $F_c^* = kF_c(1+0.01xF_c^2/\sin 2\theta)^{1/4}$. The highest peaks and holes in the final $\Delta\rho$ map were all located near Cd atoms (for crystals **1** and **3**) or near the N(2) atom (for crystal **2**). Crystal data and experimental details are listed in Table 1. Atomic scattering factors were taken from International Tables for X-ray Crystallography [32]. Molecular graphics were obtained using programs from XP package [33,34].

3. Results and discussion

As it has been found earlier, in complexes of cadmium with triamines $Cd(PA)_x$ in solution, a tendency has been observed to involve all donor nitrogen atoms of polyamines in the coordination [16]. Changes in all ^{13}C NMR signals assigned to carbon atoms from polyamines were observed both in Cd(PA) as well as in $Cd(PA)_2$ complexes. For example, at pH of about 10, i.e. in the range of $Cd(2,3\text{-tri})_2$ complex domination, the chemical shift values testify to participation of six nitrogen atoms of the 2,3-tri ligand in the metallation. Changes in the signals coming from C(1), C(2), C(3), C(4) and C(5) atoms (in relation to free amine) are: 0.432, 1.175, 0.157, 1.732 and 0.084 ppm, respectively (NMR signals were assigned to particular atoms on the basis of literature data [35]). Moreover, taking into consideration steric limitations, a greater difference in the stability constants for ML_1 and ML_2 complexes of triamines when compared to diamine compounds ($\log \beta_{Cd(dien)} = 7.68$, $\log \beta_{Cd(dien)_2} = 13.34$; $\log \beta_{Cd(en)} = 5.31$, $\log \beta_{Cd(en)_2} = 9.66$), also suggests the involvement of all donor atoms from each ligand in metallation. Although a comparison of the modes of coordination of analogous complexes in solid state and in solution may be risky, the results of studies in both phases are complementary. It should be added that the number of donor atoms, in particular, those more weakly bonded in the axial positions, plays an essential role in the

Table 1
Crystal data and structure refinement parameters for compounds **1**–**3**

Compound	**1**	**2**	**3**
Empirical formula	$C_8H_{26}N_8O_6Cd$	$C_{10}H_{30}N_8O_6Cd$	$C_{12}H_{34}N_8O_6Cd$
Formula weight	442.77	470.82	498.87
Temperature (K)	100	100	100
Wavelength (Å)	0.71073	0.71073	0.71073
Crystal system	tetragonal	monoclinic	monoclinic
Space group	$I4_1/acd$	$P2_1/c$	$P2_1/c$
Unit cell dimensions			
a (Å)	14.625(2)	11.491(2)	11.648(2)
b (Å)		12.428(2)	12.267(2)
c (Å)	30.996(6)	13.469(3)	14.255(3)
β (°)		91.68(3)	90.60(3)
Volume (Å^3)	6629.8(18)	1922.7(6)	2036.7(6)
Z	16	4	4
D_{calc} (g cm^{-3})	1.774	1.627	1.627
Absorption coefficient (mm^{-1})	1.361	1.179	1.118
$F(000)$	3616	968	1032
Crystal size (mm)	0.34 × 0.28 × 0.28	0.18 × 0.25 × 0.30	0.4 × 0.4 × 0.6
θ Range for data collection (°)	3.69–29.30	3.44–29.96	3.31–29.31
Index ranges	$-19 \le h \le 12$, $-18 \le k \le 20$, $-42 \le l \le 42$	$-15 \le h \le 15$, $-16 \le k \le 13$, $-17 \le l \le 18$	$-15 \le h \le 15$, $-12 \le k \le 16$, $-18 \le l \le 19$
Reflections collected	21 136	18 217	12 265
Reflections unique	2195	5055	5126
R_{int}	0.0292	0.0329	0.0418
Refinement method	full-matrix least-squares on F^2	full-matrix least-squares on F^2	full-matrix least-squares on F^2
Data/restrains/parameters	2195/0/158	5055/0/238	5126/8/288
Goodness-of-fit on F^2	1.249	1.076	1.086
Final R indices [$I > 2\sigma(I)$] (R_1, R_2)	0.0260, 0.0482	0.0578, 0.1391	0.0472, 0.1156
R indices (all data) (R_1, wR_2)	0.0275, 0.0487	0.0684, 0.1471	0.0567, 0.1237
Extinction coefficient	0.00015(2)	0.0011(7)	0.0002(6)
Largest difference peak and hole (e Å^{-3})	0.875 and −0.424	2.36 and −1.055	2.15 and −1.361

reactions of enzymatic catalysis involving metal complexes.

3.1. X-ray crystallography

For atomic coordinates, equivalent isotropic displacement parameters, anisotropic displacement parameters for non-hydrogen atoms, hydrogen atoms coordinates with isotropic temperature factors and full geometry of the **1**–**3** complexes see supplementary material. Table 2 lists the Cd–N distances and the geometry of compound **1** and the geometry of complexes **2** and **3**. Torsion angles of the triamines are presented in Table 3.

3.1.1. Compound *1*

The Cd^{2+} cation occupies Wyckoff position 16 e.2. in the $I4_1/acd$ space group with the origin on a centre of symmetry. An asymmetric unit cell consists of half of a Cd^{2+} cation, one triamine and one nitrate anion. The second triamine and NO_3^- anion are related by a twofold axis. Therefore, the Cd atom is coordinated by six nitrogen atoms and all N atoms of the polyamine are engaged in forming the complex. The C_2-symmetric polyhedron is presented in Fig. 1. The Cd(II) atom is sandwiched between two triamines. As a consequence of the crystallographic C_2-symmetry of the $[Cd(NH_2(CH_2)_2NH(CH_2)_2NH_2)_2]^{2+}$ complex, both triamines adopt exactly the same $g^+g^+tg^+$ conformation (Table 3(a)). The nitrogen atoms of the primary amines of the ligand form shorter Cd(1)–N distances (Cd(1)–N(1) and Cd(1)–N(3) bond lengths are 2.340(2) and 2.336(2) Å, respectively) than the N atom of the secondary amine (Cd(1)–N(2) is 2.431(2) Å). The NO_3^- anions do not play an important role in the coordination system as ligands.

3.1.2. Compound *2*

An asymmetric unit cell consists of a Cd^{2+} cation, two 2,3-triamines and two nitrate anions. The {N6}-coordinated complex is formed (Fig. 2). Conformations of the ligands bonded to the Cd(II) atom are characterized by similar torsion angles but with the opposite sign (Table 3(b)). The Cd–N distances range from 2.326(4) to 2.413(6) Å for Cd(1)–N(1') and Cd(1)–N(2), respectively. In contrast to compound **1**, the present complex does not form a sandwiched structure but it is characterized by a distorted octahedral coordination with the four equatorial nitrogen atoms (N1, N1′, N3 and N3′) and two (N2 and N2′) axial atoms (Fig. 2).

Table 2
Selected bond lengths (Å) and bond angles (°) for compounds **1**–**3**

(a) *Compound* **1**	
Bond lengths	
Cd(1)–N(1)	2.340(2)
Cd(1)–N(2)	2.431(2)
Cd(1)–N(3)	2.336(2)
Bond angles	
N(1)–Cd(1)–N(2)	74.42(6)
N(1)–Cd(1)–N(2)#1	149.52(6)
N(1)–Cd(1)–N(3)	120.09(7)
N(1)–Cd(1)–N(3)#1	90.29(6)
N(1)–Cd(1)–N(1)#1	92.61(9)
N(2)–Cd(1)–N(3)	73.73(6)
N(2)–Cd(1)–N(3)#1	88.02(6)
N(2)–Cd(1)–N(2)#1	129.15(8)
N(3)–Cd(1)–N(3)#1	137.00(9)
Bond lengths	
N(1)–C(1)	1.465(3)
C(1)–C(2)	1.520(3)
C(2)–N(2)	1.466(3)
N(2)–C(3)	1.466(2)
C(3)–C(4)	1.514(3)
C(4)–N(3)	1.469(2)
Bond angles	
N(1)–C(1)–C(2)	111.0(2)
C(1)–C(2)–N(2)	110.8(2)
C(2)–N(2)–C(3)	115.1(2)
N(2)–C(3)–C(4)	109.5(2)
N(3)–C(4)–C(3)	110.0(2)
Bond lengths	
N(4)–O(1)	1.239(2)
N(4)–O(2)	1.252(2)
N(4)–O(3)	1.249(2)
Bond angles	
O(1)–N(4)–O(3)	120.3(2)
O(1)–N(4)–O(2)	121.2(2)
O(3)–N(4)–O(2)	118.5(2)
(b) *Compound* ***2***	
Bond lengths	
Cd(1)–N(1′)	2.326(4)
Cd(1)–N(1)	2.352(4)
Cd(1)–N(3)	2.359(4)
Cd(1)–N(3′)	2.390(4)
Cd(1)–N(2′)	2.398(5)
Cd(1)–N(2)	2.413(6)
Bond angles	
N(1′)–Cd(1)–N(1)	97.32(16)
N(1′)–Cd(1)–N(3)	90.55(18)
N(1)–Cd(1)–N(3)	155.91(16)
N(1′)–Cd(1)–N(3′)	156.80(18)
N(1)–Cd(1)–N(3′)	93.09(15)
N(3)–Cd(1)–N(3′)	88.27(16)
N(1′)–Cd(1)–N(2′)	84.9(2)
N(1)–Cd(1)–N(2′)	92.45(15)
N(3)–Cd(1)–N(2′)	110.97(17)
N(3′)–Cd(1)–N(2′)	74.0(2)
N(1′)–Cd(1)–N(2)	110.0(2)
N(1)–Cd(1)–N(2)	81.07(18)
N(3)–Cd(1)–N(2)	74.85(19)
N(3′)–Cd(1)–N(2)	92.1(2)
N(2′)–Cd(1)–N(2)	164.3(2)
(c) *Compound* ***3***	
Bond lengths	
Cd(1)–N(1)	2.349(3)
Cd(1)–N(1′)	2.352(4)
Cd(1)–N(2)	2.413(3)
Cd(1)–N(2′)	2.374(4)
Cd(1)–N(3)	2.390(3)
Cd(1)–N(3′)	2.379(3)
Bond angles	
N(1)–Cd(1)–N(1′)	96.9(1)
N(1)–Cd(1)–N(2′)	90.2(2)
N(1′)–Cd(1)–N(2′)	88.5(2)
N(1)–Cd(1)–N(3′)	95.3(1)
N(1′)–Cd(1)–N(3′)	165.6(1)
N(2′)–Cd(1)–N(3′)	83.9(1)
N(1)–Cd(1)–N(3)	167.1(1)
N(1′)–Cd(1)–N(3)	85.2(1)
N(2′)–Cd(1)–N(3)	102.7(2)
N(3′)–Cd(1)–N(3)	84.6(1)
N(1)–Cd(1)–N(2)	80.8(1)
N(1′)–Cd(1)–N(2)	96.6(1)
N(2′)–Cd(1)–N(2)	170.1(2)
N(3′)–Cd(1)–N(2)	92.8(1)
N(3)–Cd(1)–N(2)	86.2(1)

Symmetry transformations used to generate equivalent atoms: #1 x,

Table 3
Selected torsion angles (°) for compounds **1**–**3**

(a) *Compound* ***1***	
N(1)–C(1)–C(2)–N(2)	57.9(2)
C(1)–C(2)–N(2)–C(3)	78.5(2)
C(2)–N(2)–C(3)–C(4)	−166.81(17)
N(2)–C(3)–C(4)–N(3)	60.0(2)
(b) *Compound* ***2***	
N(1)–C(1)–C(2)–C(3)	−71.7(8)
C(1)–C(2)–C(3)–N(2)	73.3(8)
C(2)–C(3)–N(2)–C(4)	166.9(7)
C(3)–N(2)–C(4)–C(5)	165.4(6)
N(2)–C(4)–C(5)–N(3)	−53.7(8)
N(1′)–C(1′)–C(2′)–C(3′)	72.9(11)
C(1′)–C(2′)–C(3′)–N(2′)	−72.6(9)
C(2′)–C(3′)–N(2′)–C(4′)	−175.5(6)
C(3′)–N(2′)–C(4′)–C(5′)	−169.9(6)
N(2′)–C(4′)–C(5′)–N(3′)	62.1(7)
(c) *Compound* ***3*** (the disordered amine is omitted)	
N(1)–C(1)–C(2)–C(3)	68.5(5)
C(1)–C(2)–C(3)–N(2)	−73.1(5)
C(2)–C(3)–N(2)–C(4)	−164.9(3)
C(3)–N(2)–C(4)–C(5)	173.2(3)
N(2)–C(4)–C(5)–C(6)	95.5(4)
C(4)–C(5)–C(6)–N(3)	−50.9(5)

3.1.3. Compound 3

Compound **3** crystallizes in the $P2_1/c$ space group with a and b parameters very similar to the previous structure and with a longer c parameter ($\sim$0.78 Å). The isostructurality of compounds **2** and **3** is reflected in the same behaviour of the crystals and a very similar 'morphology'. At room temperature both crystals are unstable, faces are not well defined, edges are not sharp

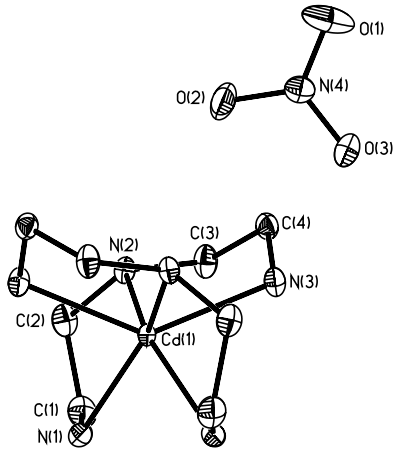


Fig. 1. Cadmium(II) nitrate complex with 1,5-diamino-3-azapentane. Twofold axis is in the plane of the drawing. Hydrogen atoms have been omitted for clarity. Ellipsoids are drawn at the 50% probability level.

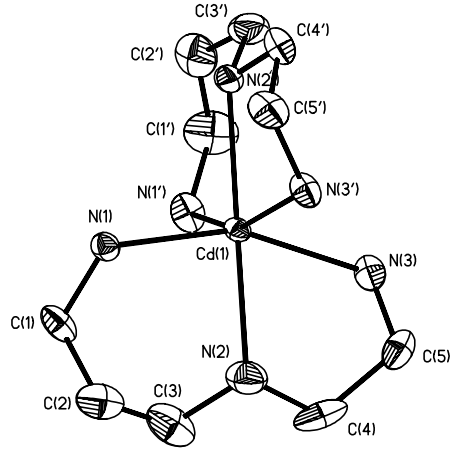


Fig. 2. Cadmium(II) nitrate complex with 1,6-diamino-3-azahexane. Hydrogen atoms are omitted. Ellipsoids are drawn at the 30% probability level.

and the molecular structure revealed large displacement parameters of the carbon atoms of both amines in complex **2** and one amine in complex **3**. In the present structure the unprimed amine is ordered and the primed one is affected by a disorder, especially the C(2′) and C(5′) atoms. The Cd(II) atom is coordinated by six nitrogen atoms from two polyamines (Fig. 3). Both 3,3-triamines

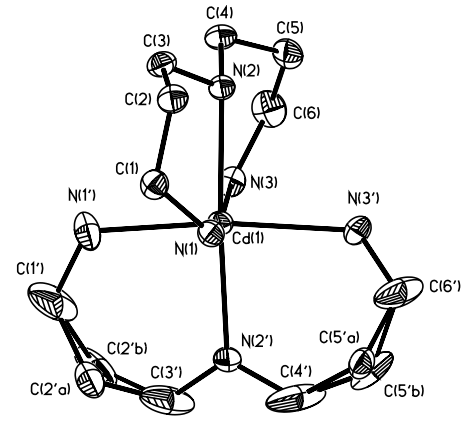


Fig. 3. Cadmium(II) nitrate complex with 1,7-diamino-4-azaheptane. Hydrogen atoms are omitted. Ellipsoids are drawn at the 50% probability level. The alternative positions A and B of the C(2′) and C(5′) atoms are shown. The split atoms positions are occupied in a 3:2 ratio (A:B).

form almost perpendicular folded sheets. The lengthening of the carbon chain causes the relief of the molecular strains and a less-distorted octahedral geometry is observed on comparing to complex **2** (Table 2(c)). The rule that nitrogen atoms of primary amines form shorter Cd–N coordination bonds than N atoms of secondary amines is fulfilled in the present structure by all equatorial (N1, N1′, N3, N3′) atoms and one axial N atom. Because of the disorder of the primed amine, the second axial N atom of the complex forms a shorter Cd–N bond than the N(2) atom of the unprimed ligand (Table 2(c)).

Results of the supplementary IR study are consistent with the conclusions of the investigations presented above. As illustrated by the data in Table 4, the metallation of triamines leads to changes in the stretching vibrations of the amine groups in the range 3400–3100 cm^{-1} and in the scissor vibrations of amine groups, occurring at about 1600 cm^{-1} in the spectra of free amines. The disappearance of a wide and intense band at $\sim$890–830 cm^{-1} (in the spectra of the complexes) assigned to deformation vibrations of $-NH_2$ groups, typical for uncoordinated amines, indicates the involvement of all nitrogen donor atoms in metallation.

The shift of the stretching vibration bands of –C–N– groups from triamines and the appearance of additional

Table 4
Infrared spectral data of triamines and their complexes with Cd(II) (cm^{-1})

Compounds	$-NH_2$	ν C–N	ν NO_3^- ion	ν M–N
dien	ν 3351, 3276, 3178; δ 1597; γ 841, 906	1129, 1064		
$[Cd(dien)_2](NO_3)_2$ (**1**)	ν 3298, 3266, 3225, 3150; δ 1585	1137, 1122, 1102, 1065, 1034	1368, 834	496
2,3-tri	ν 3357, 3280; δ 1599; γ 832	1128, 1076		
$[Cd(2,3\text{-tri})_2](NO_3)_2$ (**2**)	ν 3311, 3266, 3175; δ 1601	1155, 1126, 1089, 1058	1368, 828	485
3,3-tri	ν 3353, 3271; δ 1597; γ 891, 860	1122, 1065		
$[Cd(3,3\text{-tri})_2](NO_3)_2$ (**3**)	ν 3303, 3232, 3189, 3151; δ 1582	1144, 1104, 1060	1359, 833	492

peaks can be explained as a result of the electron drainage from the nitrogen atom on account of its coordination to the metal ion. The positions of the bands for free amines have been taken from the literature [36–39].

In the spectra of compounds **1**–**3** there are very strong high-symmetry (D_{3h}) broad bands (at about 1360 and about 830 cm^{-1}) assigned to a nitrate anions; the assignment of the bands corresponding to uncoordinated NO_3^- ions has been made on the basis of literature [40–42].

The characteristic bands appearing at about 490 cm^{-1} in the spectra of the complexes studied are a result of the formation of cadmium–nitrogen bonds in the complexes $Cd(PA)_2$. The analogous band has been observed earlier in the spectrum of a solid Cd(II) complex with dien [43].

4. Supplementary material

Crystallographic data for the structural analysis have been deposited with the Cambridge Crystallographic Data Centre, CCDC Nos. 168183, 169666 and 169825 for compounds **1**–**3**, respectively. Copies of this information may be obtained free of charge from The Director, CCDC, 12 Union Road, Cambridge, CB2 1EZ, UK (fax: +44-1223-336033; e-mail: deposit@ccdc.cam.ac.uk or www: http://www.ccdc.cam.ac.uk).

Acknowledgements

This work was supported by the Grant No. 3 T09A 151 19 of the Polish State Committee for Scientific Research.

References

[1] S. Bunce, E.S.W. Kong, Biophys. Chem. 8 (1978) 357.
[2] L. Lomozik, A. Odani, O. Yamauchi, Inorg. Chim. Acta 219 (1994) 107.
[3] L. Lomozik, A. Gasowska, L. Bolewski, J. Chem. Soc., Perkin Trans. II (1997) 1161.
[4] L. Lomozik, A. Gasowska, L. Bolewski, J. Inorg. Biochem. 63 (1996) 191.
[5] L. Lomozik, A. Gasowska, J. Inorg. Biochem. 72 (1998) 37.
[6] A. Gasowska, L. Lomozik, R. Bregier-Jarzebowska, Pol. J. Chem. 73 (1999) 909.
[7] A. Gasowska, L. Lomozik, R. Jastrzab, J. Inorg. Biochem. 78 (2000) 139.
[8] M.L. Antonelii, B. Balzamo, V. Carunchio, E. Cernia, R. Purrello, J. Inorg. Biochem. 32 (1988) 153.
[9] M.L. Antonelli, V. Carunchio, E. Cernia, R. Purrello, J. Inorg. Biochem. 37 (1989) 201.
[10] C.W. Tabor, H. Tabor, Annu. Rev. Biochem. 53 (1984) 749.
[11] J. Janne, L. Alhonen, P. Leinonen, Ann. Med. 23 (1991) 241.
[12] A. Raina, J. Janne, Med. Biol. 53 (1975) 121.
[13] M.D. Bratek-Wiewiórowska, M. Alejska, M. Figlerowicz, J. Barciszewski, M. Wiewiórowski, M. Jaskólski, W. Zielenkiewicz, A. Zielenkiewicz, M. Kaminski, Pure Appl. Chem. 59 (1987) 407.
[14] L. Lomozik, L. Bolewski, R. Bregier-Jarzebowska, Pol. J. Chem. 69 (1995) 197.
[15] L. Lomozik, L. Bolewski, R. Dworczak, J. Coord. Chem. 41 (1997) 261.
[16] L. Lomozik, R. Bregier-Jarzebowska, Pol. J. Chem. 73 (1999) 927.
[17] G. De Munno, S. Mauro, T. Pizzino, D. Viterbo, J. Chem. Soc., Dalton Trans. (1993) 1113.
[18] Y. Katono, Y. Inoue, R. Chújô, Polym. J. 9 (1977) 471.
[19] H.P. Srivastava, D. Tiwari, J. Indian Chem. Soc. 70 (1993) 499.
[20] M.D. Walker, D.R. Williams, J. Chem. Soc., Dalton Trans. (1974) 1186.
[21] M.L.S. Simoes Gonçalves, M.M. Correia dos Santos, J. Electroanal. Chem. 187 (1985) 333.
[22] N. Bunce, Environmental Chemistry (Chap. 10), Wuerz Publishing Ltd, Winnipeg, 1991.
[23] M. Branica, I. Pižeta, G. Branica-Jurkovic, M. Zelic, Mar. Chem. 28 (1989) 227.
[24] E. Merian (Ed.), Metals and their Compounds in the Environment, VCH, Weinheim, 1991.
[25] I. Bodek, W.L. Lyman, W.F. Reehl, D.H. Rosenblatt (Eds.), Environmental Inorganic Chemistry. Properties, Processes and Estimation Methods (Chap. 7), Pergamon Press, New York, 1988.
[26] W. Kaim, B. Schwederski, Bioinorganic Chemistry: Inorganic Elements in Chemistry of Life, Wiley, New York, 1994.
[27] W.G. Petropavlovski, I.P. Starovoitova, Medicina truda i promyslennaja ekologija 3 (1996) 28.
[28] J. Cosier, A.M. Glazer, J. Appl. Crystallogr. 19 (1986) 105 (Operating Manual for the Cryostream Cooler, October 1992, version 3.1A).
[29] CRYSALIS Data Reduction, version 1.162, release 26, Kuma Diffraction, Wroclaw, Poland, November, 1999.
[30] G.M. Sheldrick, SHELX-86, Program for the Solution of Structures, University of Göttingen, Göttingen, Germany, 1986.
[31] G.M. Sheldrick, SHELX-97, Program for the Refinement of Crystal Structures, University of Göttingen, Göttingen, Germany, 1997.
[32] International Tables for X-ray Crystallography, vol. IV, Kynoch Press, Birmingham, 1974.
[33] G.K. Johnson, ORTEPII, Report ORNL-5138, Oak Ridge National Laboratory, Oak Ridge, TN, 1976.
[34] Stereochemical Workstation Operation Manual, Release 3.4, Siemens Analytical X-ray Instruments Inc., Madison, WI, 1989.
[35] S.P. Dagnall, D.N. Hague, M.E. McAdam, J. Chem. Soc., Perkin Trans. II (1984) 435.
[36] F. Cariati, G. Ciani, L. Menabue, G.C. Pellacani, G. Rassu, A. Sironi, Inorg. Chem. 22 (1983) 1897.
[37] J.R. Dyer, Application of Absorption Spectroscopy of Organic Compounds, Prentice-Hall, Englewood Cliffs, NJ, 1965.
[38] J.G. Grasselli, W.M. Ritchey (Eds.), Atlas of Spectral Data and Physical Constants for Organic Compounds, CRC Press, Cleveland, OH, 1975.
[39] L.A. Kazicina, N.B. Kupletska, Primenenie UV, IR i NMR spektroskopii v organiceskoj khimii, Vyssaja Skola, Moscow, 1971.
[40] J.C.G. Bünzli, in: K.A. Gschneidner, Jr., L. Eyring (Eds.), Handbook of the Physics and Chemistry of Rare Earths, Elsevier Science, Amsterdam, 1987, p. 352.
[41] C.C. Addison, N. Logan, S.C. Wallwork, C.D. Garner, Q. Rev. 25 (1971) 289.
[42] P.H. Merrell, E.C. Alyea, L. Ecott, Inorg. Chim. Acta 59 (1982) 25.
[43] D.B. Pawell, N. Sheppard, J. Chem. Soc. (1961) 1112.

PERGAMON

Polyhedron 21 (2002) 745–751

POLYHEDRON

www.elsevier.com/locate/poly

Spectroscopic and potentiometric investigation of the solution structure and stability of Ni(II) and Co(II) complexes with adenosine 5′-monophosphate and 1,12-diamino-4,9-diazadodecane (spermine) or 1,11-diamino-4,8-diazaundecane

Anna Gasowska, Lechoslaw Lomozik *

Faculty of Chemistry, A. Mickiewicz University, Grunwaldzka 6, 60-780 Poznan, Poland

Received 17 October 2001; accepted 7 December 2001

Abstract

The solution structures of nickel(II) and cobalt(II) mixed-ligand complexes with adenosine 5′-monophosphate and tetramines have been found. The nickel(II) ions were proved to coordinate the nitrogen atoms N(1) and N(7) from the nucleotide forming chromophore {N1} in the molecular complexes of type ML·····L′ and chromophore {N3} in the protonated complexes. In the mixed-ligand complexes with nickel(II) ions, a coordination dichotomy N1/N7 was observed. In the mixed complexes with cobalt(II) ions, the presence of a chromophore {N1,O}, with N(7) nitrogen atom and oxygen atoms from the AMP phosphate group, was found. On the other hand, in molecular complexes the non-covalent interactions between the totally protonated polyamine and nucleotide atoms of high electron density were established. The presence of interligand non-covalent interactions, additionally stabilising the complex, was discovered in the species Ni(AMP)H_2(Spm). Results of the equilibrium study for the species Ni(AMP)H_2(3,3,3-tet) indicated that only one nitrogen atom from the polyamine was involved in the coordination. © 2002 Elsevier Science Ltd. All rights reserved.

Keywords: Ni(II); Co(II); Tetramines; Adenosine 5′-monophosphate; Mixed-ligand complexes

1. Introduction

The reactions of complexation of metal ions with nucleic acids and their constituents (nucleotides, nucleosides) determine the character of many chemical processes taking place in living organisms and hence are important from biological and clinical points of view [1,2]. The results of a recent study proved the formation of molecular complexes including fragments of nucleic acids and biogenic amines (putrescine, spermidine, spermine and their analogues) present practically in all living cells [3–6]. The contents of polyamines (PA) in cells depend on the kind and age of the tissue, and according to the collected evidence, these biomolecules affect such processes as cell differentiation and proliferation, enzyme activity, DNA replication, synthesis of proteins and stabilisation of membranes [7–13]. The biogenic amines stabilise nucleic acids and prevent their thermal denaturation [14] or enzymatic degradation [15]. The interactions of polyamines are also essential for DNA packing into phage heads [16] and in condensation of native DNA [17,18]. It has been noted that such diseases as cancer, psoriasis and sickle cell anaemia are accompanied by an increase of polyamine concentration in cells [19–22]. Unfortunately, the functions of polyamines, mechanisms of their interactions and role in genetic information transfer, including development of neoplasmic diseases, have not been fully recognised yet [6,7]. The hypothesis claiming that the main factor determining the character of interactions is the charge of the protonated polyamine [23] does not explain the specificity of a number of reactions. Of course, the charge is one of the most important factors determining the character of the reaction in which a given polyamine is involved, but many data seem to indicate a significant

* Corresponding author. Tel.: +48-61-829-1358; fax: +48-61-865-8008.

E-mail address: lomozik@main.amu.edu.pl (L. Lomozik).

0277-5387/02/$ - see front matter © 2002 Elsevier Science Ltd. All rights reserved.
PII: S0277-5387(02)00849-5

role of the structural factor [3–5,8,24–26]. Investigation of the intermolecular interactions in living organisms should be performed taking into regard the fact that the reaction centres usually are the donor atoms of biomolecules which are also the sites of metal ion binding. Therefore, the metal ions should be treated as interfering agents. To gain more information on the biological significance of the reactions and the role of metal ions, studies of model systems have been undertaken. This paper reports results of investigation of model systems containing metal ions, adenosine 5′-monophosphate and polyamines.

2. Experimental

Adenosine 5′-monophosphate (AMP) (disodium salt), spermine hydrochloride (Spm·4HCl) and 1,11-diamino-4,8-diazaundecane (3,3,3-tet) were purchased from Sigma. The tetrachloride of 1,11-diamino-4,8-diazaundecane (3,3,3-tet·4HCl) was obtained by mixing one chemical equivalent of the amine suspended in methanol with four chemical equivalents of a water–methanol solution of HCl. The salt obtained was dried over P_4O_{10}. Results of the elemental analysis were consistent with the theoretical results ($\pm 0.5\%$). Nickel(II) and cobalt(II) nitrates (from POCh, Poland) were purified by twice repeated crystallisation from water solution. The concentrations of nickel and cobalt ions in parent solutions were determined by complexometry [27]. The potentiometric titration was performed using an instrument made by Methrom (713 pH Meter, 725 Dosimat, electrode 6.0233.100, after calibration [28]). All potentiometric measurements were carried out at 20 ± 1 °C, at a constant ionic strength of 0.1 M (KNO_3), in a neutral gas atmosphere (helium) and at a metal:AMP:-polyamine ratio varied from 1:2:2 to 1:3.5:3.5 (the concentrations of AMP and polyamine were varied from 0.001 to 0.003 M). The titrant was a CO_2-free solution of NaOH. The composition and stability constants of the complexes forming in the systems studied were determined on the basis of a computer analysis of the results of potentiometric titration with the use of the program SUPERQUAD [29]. The species distributions were found with the use of the program HALTAFALL [30]. Measurements of ^{13}C and ^{31}P NMR were performed in D_2O, while pD values of the solutions were corrected according to the formula pD = pH reading +0.40 [31]. The ligand concentration in the samples for NMR study varied from 0.05 to 0.1 M at a metal:ligand ratio from 1:50 to 1:90. NMR measurements were carried out on a Gemini 300 Varian and Unity 300 Varian spectrometer with dioxane as internal standard for ^{13}C NMR and H_3PO_4 as internal standard for ^{31}P NMR. The concentrations of the components in samples for VIS study (H_2O solutions) were the same as used in the potentiometric measurements. The VIS spectra were recorded on a UV 160 Shimadzu spectrometer.

3. Results and discussion

3.1. Ni(II)/AMP/Spm system

In the Ni(II)/AMP/Spm system, the presence of Ni(AMP)H_4(Spm) and Ni(AMP)H_2(Spm) mixed-ligand complexes was detected (Table 1).

The complex Ni(AMP)H_4(Spm) starts forming from a pH of about 5 and at pH 8 it binds the maximum number of nickel ions, ~80% (Fig. 1).

The composition of this compound, in which all donor nitrogen atoms are fully protonated and blocked for metallation, and the pH range of its occurrence suggest that this is a molecular complex of type ML·····L′, formed as a result of a non-covalent intermolecular interaction. This supposition is confirmed by the value of the equilibrium constant of Ni(AMP)H_4(Spm) formation ($\log K_e = 4.23$, Table 2) which is much smaller than that for the anchoring complex NiSpm ($\log K_e = 7.42$), in which metal ions are bonded by four spermine atoms. The positions of the d–d bands at pH 8 are: $\lambda_{max} = 385$ and 626 nm (Table 3), and they point to coordination of the nickel ion by one nitrogen atom (chromophore {N1}) [27].

Table 1
Overall stability constants ($\log \beta$) of H^+ and Ni(II) complexes with AMP and polyamines (Spm and 3,3,3-tet)

System	Species	$\log \beta$
AMP	HAMP	6.43(2) [a]
	H_2AMP	10.45(2) [a]
Spm	HSpm	10.91(1) [b]
	H_2Spm	21.28(3) [b]
	H_3Spm	30.39(2) [b]
	H_4Spm	38.67(2) [b]
3,3,3-tet	H(3,3,3-tet)	10.36(2) [b]
	H_2(3,3,3-tet)	20.38(3) [b]
	H_3(3,3,3-tet)	29.01(3) [b]
	H_4(3,3,3-tet)	36.39(2) [b]
Ni(II)/AMP	NiH(AMP)	11.26(4)
	NiH_2(AMP)	16.50(8)
	Ni(AMP)	3.07(14) [a]
Ni(II)/AMP/Spm	NiH_3(Spm)	33.19(8)
	NiH_2(Spm)	24.77(9)
	Ni(Spm)	7.42 (6)
	$Ni(Spm)_2$	10.87(11)
Ni(II)/3,3,3-tet	NiH_2(3,3,3-tet)	27.83(14)
Ni(II)/AMP/Spm	Ni(AMP)H_4(Spm)	45.97(5)
	Ni(AMP)H_2(Spm)	28.66(8)
Ni(II)/AMP/3,3,3-tet	Ni(AMP)H_4(3,3,3-tet)	44.87(6)
	Ni(AMP)H_2(3,3,3-tet)	27.95(7)

[a] Ref. [27].
[b] Ref. [32].

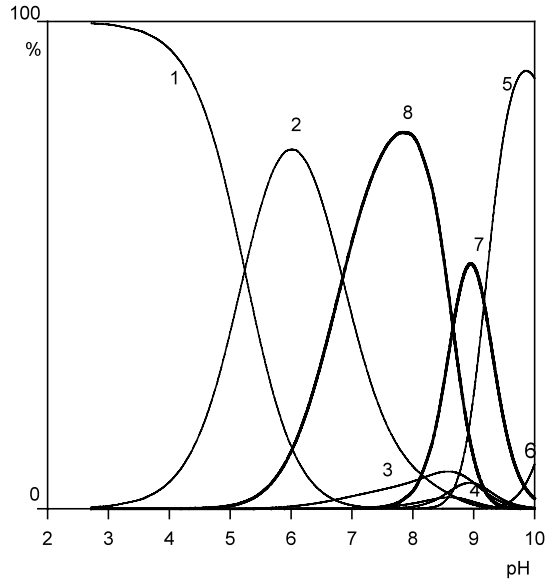


Fig. 1. Distribution diagrams for the Ni(II)/AMP/Spm system: (1) NiH_2(AMP); (2) NiH(AMP); (3) Ni(AMP); (4) NiH_2(Spm); (5) Ni(Spm); (6) $Ni(Spm)_2$; (7) Ni(AMP)H_2(Spm); and (8) Ni(AMP)H_4(Spm). $C_{AMP} = C_{Spm} = 0.001$ M; $C_{Ni} = 0.0005$ M.

Table 2
Equilibrium constants (log K_e) of complex formation in Ni(II) or Co(II) with AMP and poliamine (Spm, 3,3,3-tet) systems

Reactions	log K_e
$Ni + Spm \rightleftharpoons Ni(Spm)$	7.42
$Ni + H_2Spm \rightleftharpoons NiH_2(Spm)$	3.49
$Ni(AMP) + H_2Spm \rightleftharpoons Ni(AMP)H_2(Spm)$	4.31
$Ni(AMP) + H_4Spm \rightleftharpoons Ni(AMP)H_2(Spm)$	4.23
$Ni + H_2(3,3,3\text{-tet}) \rightleftharpoons NiH_2(3,3,3\text{-tet})$	7.45
$Ni(AMP) + H_2(3,3,3\text{-tet}) \rightleftharpoons Ni(AMP)H_2(3,3,3\text{-tet})$	4.50
$Ni(AMP) + H_4(3,3,3\text{-tet}) \rightleftharpoons Ni(AMP)H_4(3,3,3\text{-tet})$	5.41
$Co + Spm \rightleftharpoons Co(Spm)$	7.36
$Co(AMP) + H_4Spm \rightleftharpoons Co(AMP)H_4(Spm)$	4.65
$Co + 3,3,3\text{-tet} \rightleftharpoons Co(3,3,3\text{-tet})$	7.36
$Co(AMP) + H_4(3,3,3\text{-tet}) \rightleftharpoons Co(AMP)H_4(3,3,3\text{-tet})$	5.01

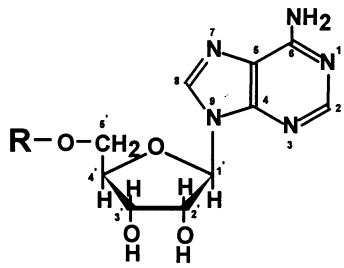
As a consequence of the interactions related to the formation of the species, in its ^{13}C NMR spectrum (pH 8) the signals assigned to the nucleotide carbon atoms neighbouring the N(1), N(7) donor atoms and phosphate group are changed [C(6), C(2), C(8), C(5) and C(5′) are shifted with respect to their positions in the free ligand spectrum by 0.055, 0.126, 0.033, 0.045 and 0.132 ppm]. Moreover, in the ^{31}P NMR spectrum at pH 8, a shift of the phosphorus atom signal by 0.182 ppm is observed. The signal assigned to C(4), the atom which does not neighbour any donor centres of the nucleotide, is shifted only by 0.014 ppm. Also the signals attributed to all carbon atoms of the polyamine C(1), C(2), C(3), C(4) and C(5) are shifted by 0.246, 0.158, 0.233, 0.416 and 0.194 ppm, respectively (numeric positions of particular atoms of the ligands are given in Scheme 1;

Table 3
Absorption spectral data for Ni(II) and Co(II) complexes with AMP and polyamines (Spm, 3,3,3-tet)

Complexes	λ_{max} (nm)	ε_{max} ($dm^3\ mol^{-1}\ cm^{-1}$)	Chromophore	pH
Ni(AMP)	386, 628	27.4	{N1}	8.0
Ni(AMP)H_4(Spm)	385, 626	24.3	{N1}	8.0
NiH_2(Spm)	377, 627	19.6	{N2}	7.0
Ni(AMP)H_2(Spm)	363, 624	18.1	{N3}	9.0
Ni(AMP)H_4(3,3,3-tet)	383, 624	22.5	{N1}	7.0
Ni(3,3,3-tet)	350, 627	16.3	{N4}	7.0
Co(AMP)	511, 820	23.7	{N1,O}	7.0
Co(AMP)H_4(Spm)	506, 822	22.3	{N1,O}	8.0
Co(AMP)H_4(3,3,3-tet)	502, 818	20.1	{N1,O}	8.0

NMR signals have been assigned on the basis of literature data [33–35]). Thus, bearing in mind the full protonation of all nitrogen atoms of the amine, the pattern of the changes indicates that the metallation and {N1} chromophore formation involve the N(1) and N(7) atoms from the purine ring (the coordination dichotomy—N1/N7) while spermine, involved in non-covalent interactions with the phosphate group of the nucleotide, remains outside the inner coordination sphere of the metal ion. The conclusions from the NMR study are in full agreement with the results of the equilibrium and VIS study, which confirm the possibility of the critical application of nuclear resonance as a supplementary method in analysis of systems with paramagnetic ions as suggested earlier [24,35–38].

Ni(AMP)H_2(Spm) starts forming from pH ~ 7.5, and is dominant in the system at pH 9, binding about 50% of nickel(II) ions (Fig. 1). The equilibrium constant of the reaction of H_2Spm binding to Ni(AMP) is log $K_e = 4.31$. This value is 0.82 log K_e units higher than that of NiH_2Spm complex formation, corresponding to the attraction of H_2Spm to Ni ions (Table 2), which suggests the presence of intramolecular nucleotide–polyamine interactions in the species Ni(AMP)H_2(Spm), additionally stabilising the complex. The positions of the d–d bands at pH 9, when the species Ni(AMP)H_2(Spm) dominates, are 363 and 624 nm, which points to the occurrence of the chromophore {N3} (Table 3) [39]. The shifts of signals in the ^{13}C NMR spectrum indicate the N(1) or N(7) (coordination dichotomy) atoms from AMP and two deprotonated nitrogen atoms of the polyamine as the coordination centres in Ni(AMP)H_2(Spm) [the shifts of the signals of C(6), C(2), C(8) and C(5) from AMP are 0.112, 0.093, 0.101 and 0.079 ppm, respectively, and the shifts for all the



AMP R = H_2PO_3

NH_2-CH_2-CH_2-CH_2-NH-CH_2-CH_2-CH_2-NH-CH_2-CH_2-CH_2-NH_2 3,3,3-tet

NH_2-CH_2-CH_2-CH_2-NH-CH_2-CH_2-CH_2-CH_2-NH-CH_2-CH_2-CH_2-NH_2 Spm

Scheme 1.

carbon atoms from spermine C(1), C(2), C(3), C(4) and C(5) are 0.193, 0.087, 0.203. 0.159 and 0.091 ppm, respectively]. The change in the positions of the C(5′) atom and P atom by 0.134 and 0.157 ppm, suggests that the phosphate group of AMP is involved in the intramolecular interaction additionally stabilising the complex. The proposed model of interactions clarifies the problems related to the mode of Ni(II) coordination in the systems containing both donor nitrogen atoms and oxygen atoms as potential reaction sites [23,40–45].

3.2. The system Co(II)/AMP/Spm

In this system a mixed complex—$Co(AMP)H_4(Spm)$ is formed in the pH range from ~5.5 to 9.5, and at pH ~8 it binds 75% of cobalt ions (Fig. 2). The same reasoning as above, based on the pH range of formation as well as stoichiometric composition of the compound, indicates that it is a molecular complex.

The equilibrium constant of $Co(AMP)H_4(Spm)$ formation is 4.65 (Table 2) and is smaller than that of CoSpm formation (log $K = 7.36$, Table 4), which confirms the molecular character of $Co(AMP)H_4(Spm)$.

The positions of the d–d absorption bands in the spectrum of Co/AMP/Spm at pH 8, where the molecular complex dominates, found at 506 and 822 nm (Table 3) are the same as for the complex CoAMP and it proves that chromophore {N1,O} is formed [27] including N(7) atom and oxygen atoms of the phosphate group (for steric reasons the chelation involving the phosphate group and N(1) atom should be excluded, as shown in Refs. [46–48]), and the fully protonated polyamine is involved in non-covalent interactions mainly with the N(1) atom from the nucleotide. This pattern of interactions is confirmed by analysis of the ^{13}C and ^{31}P NMR

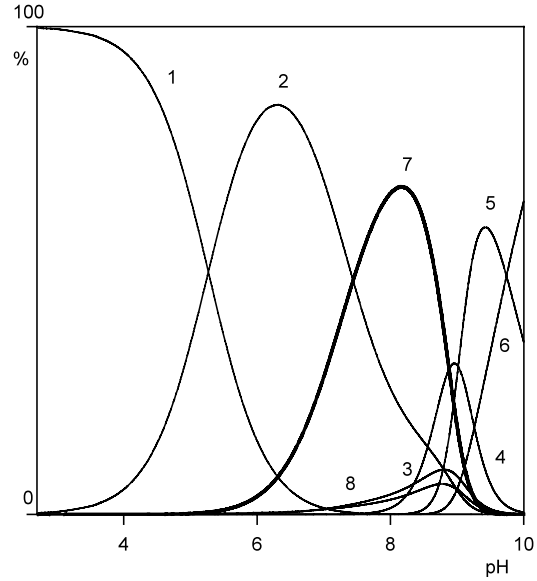


Fig. 2. Distribution diagrams for the Co(II)/AMP/Spm system: (1) $CoH_2(AMP)$; (2) CoH(AMP); (3) Co(AMP); (4) $CoH_2(Spm)$; (5) Co(Spm); (6) Co(Spm)(OH); and (7) $Co(AMP)H_4(Spm)$. $C_{AMP} = C_{Spm} = 0.001$ M; $C_{Co} = 0.0005$ M.

spectra (an explanation of application of NMR investigation of coordination mode with paramagnetic ions was discussed earlier [24]). In the $Co(AMP)H_4(Spm)$ complex at pH 8, changes in signal positions assigned to carbon atoms in the neighbourhood of N(1) and N(7) and the signal from C(5′) as well as from P atom are observed [0.073, 0.067, 0.057, 0.097, 0.063 and 0.121 ppm for C(6), C(2), C(8), C(5), C(5′) and P, respectively]. Moreover, the signals from all carbon atoms of the polyamine C(1), C(2), C(3), C(4), C(5) are shifted by 0.107, 0.131, 0.174, 0.115, 0.127 ppm, respectively.

Table 4
Overall stability constants (log β) of Co(II) complexes with AMP and polyamines (Spm and 3,3,3-tet)

Systems	Species	log β
Co(II)/AMP	CoH(AMP)	11.87(7)
	CoH_2(AMP)	17.14(9)
	Co(AMP)	2.72 (9) [a]
Co(II)/Spm	CoH_2(Spm)	25.39(11)
	Co(Spm)	7.36 (5)
	Co(Spm)(OH)	−2.38(11)
Co(II)/3,3,3-tet	Co(3,3,3-tet)	7.88(4))
Co(II)/AMP/Spm	Co(AMP)H_4(Spm)	46.04(4)
Co(II)/AMP/3,3,3-tet	Co(AMP)H_4(3,3,3-tet)	44.12(7)

[a] Ref. [27].

3.3. Ni(II)/AMP/(3,3,3-tet) system

In the system Ni(II)/AMP/(3,3,3-tet), the complex Ni(AMP)H_4(3,3,3-tet) forms starting from pH ~ 4 and it binds a maximum number of 95% of nickel ions at pH about 7.5, Fig. 3.

The equilibrium constant of its formation (log K_e = 5.41, Table 2), which is smaller than that of the NiH_2(3,3,3-tet) complex (Table 2), the stoichiometry of the compound and the pH range of its occurrence indicate that it is also a molecular complex. In the pH range of its domination the positions of the d–d bands are 383 and 624 nm (Table 3), which corresponds to the formation of the chromphore {N1} [27]. As follows from the analysis of ^{13}C and ^{31}P NMR spectra, analogously as for the species with Spm, the N(1) or N(7) atoms from AMP (coordination dichotomy) take part in the coordination, while the protonated polyamine is involved in non-covalent interactions with the phosphate group of the nucleotide remaining in the outer coordination sphere. The NMR signals assigned to the carbon atoms in the vicinity of N(1), and N(7): C(6), C(2), C(8), C(5), C(5′) are shifted by 0.087, 0.079, 0.091, 0.088, 0.107 ppm, and the signal from the P atom of the nucleotide is shifted by 0.127 ppm. The signals corresponding to the carbon atoms of the polyamine C(1), C(2), C(3), C(4) and C(5) are shifted by 0.057, 0.068, 0.097, 0.059 and 0.077 ppm, respectively.

Another mixed complex Ni(AMP)H_2(3,3,3-tet) forms together with the molecular complex and the coordination compound Ni(3,3,3-tet), which makes it impossible to obtain its spectral data (Fig. 3). The equilibrium constant of Ni(AMP)H_2(3,3,3-tet) formation is 4.50 (species Ni(AMP) is an anchoring complex), while the value of log K_e for NiH_2(3,3,3-tet), in which two deprotonated nitrogen atoms from the polyamine take part in the coordination, is 7.45 (Table 2). The lower value of log K_e for the mixed complex suggests the presence of only one nitrogen atom of the polyamine in the inner sphere of coordination (besides the donor atoms from AMP).

3.4. Co(II)/AMP/(3,3,3-tet) system

In this system the complex Co(AMP)H_4(3,3,3-tet) forms starting from pH ~ 5 and dominates from pH ~ 7.5 binding a maximum 60% of cobalt ions (Fig. 4).

As indicated by the composition of Co(AMP)-H_4(3,3,3-tet) and the pH range of its occurrence, this is a molecular complex of type ML·····L′. The d–d

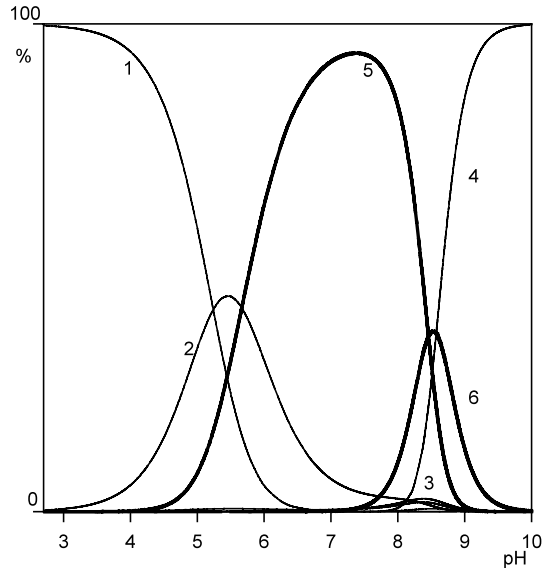


Fig. 3. Distribution diagrams for the Ni(II)/AMP/3,3,3-tet system: (1) NiH_2(AMP); (2) NiH(AMP); (3) Ni(AMP); (4) Ni(3,3,3-tet); (5) Ni(AMP)H_4(3,3,3-tet); and (6) Ni(AMP)H_2(3,3,3-tet). $C_{AMP} = C_{3,3,3tet} = 0.001$ M; $C_{Ni} = 0.0005$ M.

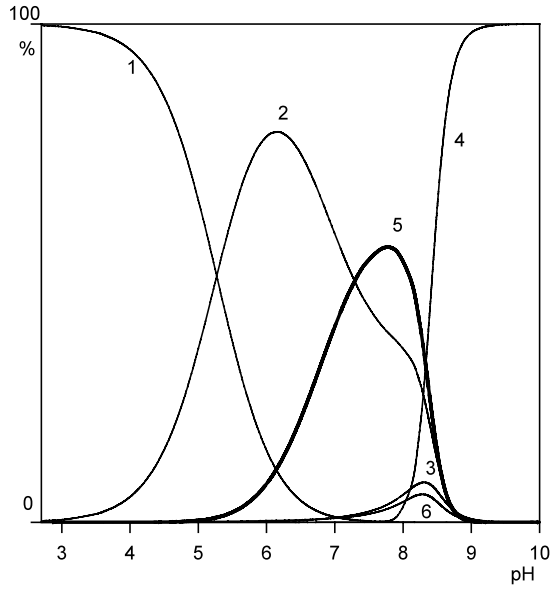


Fig. 4. Distribution diagrams for the Co(II)/AMP/3,3,3-tet system: (1) CoH_2(AMP); (2) CoH(AMP); (3) Co(AMP); (4) Co(3,3,3-tet); (5) Co(AMP)H_4(3,3,3-tet); and (6) Co^{2+}. $C_{AMP} = C_{3,3,3tet} = 0.001$ M; $C_{Co} = 0.0005$ M.

absorption bands in the conditions of Co(AMP)-H_4(3,3,3-tet) domination (pH 8) appear at 502 and 818 nm, so their positions are practically the same as for CoAMP [27]. As follows from the analysis of ^{13}C and ^{31}P NMR spectra, the N(7) atom, the phosphate group from AMP, the N(1) atom from the nucleotide as well as all the protonated nitrogen atoms from the polyamine are involved in this molecular complex formation. The signals assigned to the AMP carbon atoms C(6), C(2), C(8), C(5), C(5′) at pH 8 are shifted by 0.082, 0.099, 0.077, 0.105, 0.179 ppm, respectively, the signal ascribed to the phosphorus atom is shifted by 0.154 ppm, and the signals from the polyamine carbon atoms C(1), C(2), C(3), C(4) and C(5) are shifted by 0.081, 0.085, 0.073, 0.050, 0.073 ppm, respectively. The position of the signal assigned to the C(4) atom, which is not located close to any of the donor atoms, is changed only by 0.011 ppm. The presented pattern of changes in the spectra of the studied system proves that Co(II) in Co(AMP)H_4(3,3,3-tet) binds N(7) and the oxygen atoms from the AMP phosphate group (chromophore {N1,O}), while the fully protonated polyamine is involved in non-covalent interactions mainly with the N(1) atom and remains in the outer coordination sphere.

The above-discussed evidence proves the formation of molecular complexes of type ML$\cdots\cdots$L′, e.g. M(AMP)-H_4(PA) but with different modes of coordination in all systems considered. The nickel ions prefer the coordination with donor nitrogen atoms from AMP (coordination dichotomy was found), whereas the cobalt ions bind the N(7) atom and the phosphate group from the nucleotide. Differences also appear in the character of the non-covalent interactions between the fully protonated polyamine and the nucleotide (PA remains in the outer sphere of coordination). In the nickel(II) complexes, the main centre of non-covalent interactions is the phosphate group, while in the cobalt(II) compounds such a centre is the N(1) atom.

In the diprotonated complexes Ni(AMP)H_2(Spm) and Ni(AMP)H_2(3,3,3-tet), significant differences were found in the character of interactions of the two polyamines with the anchoring Ni(AMP) species. In Ni(AMP)H_2(Spm) two nitrogen atoms from the polyamine take part in the coordination of the nickel ion and the complex is additionally stabilised by the interaction of the two protonated nitrogen atoms from spermine with the phosphate group of the nucleotide. In Ni(AMP)H_2(3,3,3-tet), according to the results of the equilibrium study, only one nitrogen atom from the polyamine takes part in the coordination of the nickel(II) ion.

Moreover, as follows from our results, besides the charge value of protonated PA, the structure (length) of PA is also an essential factor in the types of interaction observed and the polyamine cations should not be considered as point charges as it has been sometimes suggested in the studies of model systems.

Acknowledgements

This work was supported by the Grant No. 3 T09A 151 19 of the Polish State Committee for Scientific Research.

References

[1] P. Köpf Maier, H. Köpf, Chem. Rev. 87 (1987) 1137.
[2] S.E. Sherman, S.J. Lippard, Chem. Rev. 87 (1987) 1153.
[3] L. Łomozik, A. Gąsowska, J. Inorg. Biochem. 62 (1996) 103.
[4] L. Łomozik, A. Gąsowska, L. Bolewski, J. Inorg. Biochem. 63 (1996) 191.
[5] L. Łomozik, A. Gąsowska, L. Bolewski, J. Chem. Soc. Perkin Trans. 2 (1997) 1161.
[6] M.L. Antonelli, S. Balzamo, V. Carunchio, E. Cernia, R. Purrello, J. Inorg. Biochem. 32 (1988) 153.
[7] C.W. Tabor, H. Tabor, Annu. Rev. Biochem. 45 (1976) 285.
[8] D. Esposito, P. Del Vecchio, G. Barone, J. Am. Chem. Soc. 119 (1997) 2606.
[9] S.S. Cohen, Proc. Fed. Am. Soc. Exp. Biol. 41 (1982) 3061.
[10] W.C Russel, B. Precious, S.R. Martin, P.M. Baylej, EMBO J. 2 (1983) 1647.
[11] A.E. Pegg, Cancer Res. 48 (1988) 759.
[12] V. Zappia, A.E. Pegg (Eds.), Progress in Polyamine Research, Plenum Press, New York, 1988.
[13] O. Heby, L. Persson, Trends Biochem. Sci. 15 (1990) 153.
[14] P.M. Vertino, R.J. Bergeron, P.F. Camanaugh, Jr., C. Porter, Biopolymers 26 (1987) 691.
[15] U. Bachrach, G. Eilon, Biochim. Biophys. Acta 179 (1969) 494.
[16] S.S. Cohen, M.L. Greenberg, Proc. Natl. Acad. Sci. USA 78 (1981) 5470.
[17] S.A. Allison, J.C. Herr, J.M. Schurr, Biopolymers 20 (1981) 469.
[18] J.A. Schellman, N. Parthasarathy, J. Mol. Biol. 175 (1984) 313.
[19] C.W. Porter, L. Herrera-Ornelas, P. Pera, N.F. Petrelli, A. Mittelman, Cancer 60 (1987) 1275.
[20] S. Sarhan, N. Seiler, Biol. Chem. Hoppe-Seyler 370 (1989) 1279.
[21] R.W. Davis, D.R. Morris, P. Coffino, Microbiol. Rev. 56 (1992) 280.
[22] B.G. Feuerstein, J. Szolli, H.S. Basu, L.J. Marton, Cancer Res. 52 (1992) 6782.
[23] C. De Stefano, O. Giuffrè, S. Sammartano, J. Chem. Soc., Faraday Trans. 94 (1998) 1091.
[24] A Gasowska, L. Lomozik, R. Jastrzab, J. Inorg. Biochem. 78 (2000) 139.
[25] Y. Huse, Y. Mitsui, Y. Iitaca, K. Miyaki, J. Mol. Biol. 122 (1978) 43.
[26] E.E. Minyat, V.I. Ivanov, A.M. Kritzyn, L.E. Minchenk, A.K. Schyolkina, J. Mol. Biol. 128 (1978) 397.
[27] A. Gasowska, L. Lomozik, Pol. J. Chem. 73 (1999) 465.
[28] M.H. Irving, M.G. Miles, L.D. Pettit, Anal. Chim. Acta 38 (1967) 475.
[29] P. Gans, A. Sabatini, A. Vacca, J. Chem. Soc., Dalton Trans. (1985) 1195.
[30] N. Ingri, W. Kakolowicz, L.G. Sillen, B. Warqvist, Talanta 14 (1967) 1261.
[31] P.K. Glasoe, F.A. Long, J. Phys. Chem. 64 (1960) 188.
[32] A. Wojciechowska, L. Bolewski, L. Lomozik, Monatsh. Chem. 122 (1991) 131.

[33] S. Bunce, E.S.W. Kong, Biophys. Chem. 8 (1978) 357.
[34] S.P. Dagnall, D.N. Hague, M.E. McAdam, J. Chem. Soc., Perkin Trans. 2 (1984) 435.
[35] A.J. Jones, D.M. Grant, M.W. Winkley, R.K. Robins, J. Am. Chem. Soc. 92 (1970) 4079.
[36] H.A. Azab, A. Hassan, A.M. El-Nady, R.S.A. Azkal, Monatsh. Chem. 124 (1993) 267.
[37] G. Kotowicz, O. Suzuki, Biochemistry 12 (1973) 5325.
[38] U. Weser, G.J. Strobel, H. Rupp, W. Voelter, Eur. J. Biochem. 50 (1974) 91.
[39] L. Lomozik, A. Gasowska, L. Bolewski, unpublished data.
[40] M.M. Taqui Khan, A.E. Martell, J. Am. Chem. Soc. 84 (1962) 3037.
[41] H. Sternlicht, D.E. Jones, K. Kustin, J. Am. Chem. Soc. 90 (1968) 7110.
[42] T.A. Glassman, C. Cooper, L.W. Harrison, T.J. Swift, Biochemistry 10 (1971) 843.
[43] M. Cohn, T.R. Hughes, J. Biol. Chem. 237 (1962) 176.
[44] M.J. Hynes, H. Diebler, Biophys. Chem. 16 (1982) 79.
[45] T. Pawłowski, J. Swiatek, K. Gasiorowski, Inorg. Chim. Acta 136 (1987) 185.
[46] P.W. Schneider, H. Brintzinger, H. Erlenmeyer, Helv. Chim. Acta 47 (1964) 992.
[47] R.B. Martin, Y.H. Mariam, Met. Ions Biol. Syst. 8 (1979) 57.
[48] K.H. Scheller, F. Hofstetter, R.P. Mitchell, B. Prijs, H. Sigel, J. Am. Chem. Soc. 103 (1981) 247.

PERGAMON

Polyhedron 21 (2002) 753–762

POLYHEDRON

www.elsevier.com/locate/poly

Osmium–azopyrimidine chemistry. Part VII: synthesis, structural characterisation and electrochemistry☆

S. Senapoti [a], U.S. Ray [a], P.K. Santra [a], C. Sinha [a,*], Alexandra M.Z. Slawin [b], J. Derek Woollins [b]

[a] *Department of Chemistry, The University of Burdwan, Burdwan 713104, India*
[b] *Department of Chemistry, University of St Andrews, St Andrews KY16 9ST, UK*

Received 14 June 2001; accepted 10 December 2001

Abstract

Reaction of 2-(arylazo)pyrimidines ($R-C_6H_4-N=N-C_4H_3N_2$, abbreviated aapm; R = H (papm), *o*-Me (*o*-tapm), *m*-Me (*m*-tapm), *p*-Me (*p*-tapm), *p*-Cl (*p*-Clpapm)) with $(NH_4)_2[OsCl_6]$ in 2-methoxyethanol gives two isomers of composition $OsCl_2(aapm)_2$. They are structurally characterised by ^1H NMR spectra and established as the *cis–trans–cis* (*ctc*) and *cis–cis–cis* (*ccc*) isomer. With reference to the coordination pairs of Cl; N(pyrimidine) (N) and N(azo) (N′), the structure of *ctc*-$OsCl_2(p\text{-tapm})_2$ is confirmed by an X-ray diffraction study. The complexes exhibit multiple MLCT transitions in the visible to near-IR region. Redox studies show an Os(III)/Os(II) couple at 1.2–1.3 V and Os(IV)/Os(III) couple at ~2 V versus SCE. EHMO calculations and comparison with analogous ruthenium(II) complexes explain the spectral and redox properties of the complexes. © 2002 Published by Elsevier Science Ltd.

Keywords: Arylazopyrimidines; Osmium(II) complexes; Geometrical isomers; X-ray structures; MLCT transitions; Redox property

1. Introduction

The coordination complexes of heterocycles continues to be of attraction and their applications encompass catalysis, organic synthesis and bioinorganic chemistry [1,2]. Incorporation of an arylazo group into the heterocycle backbone gives arylazoheterocycles [3–33]. They have been used to stabilise low-valent metal redox states [3–20]; oxo-metal complexes [21–23], for the purpose of colouring and dyeing agents [24,25], metallo-chromic indicators in analytical chemistry [26–28] and some of them exhibit novel electrochemistry or non-linear optical properties [4,10,29,30]. The heterocycle moiety may be hooked to polymeric bed by an azo group and has been used in micro scale solid-phase extraction process [31,32]. Electronic property and π-acidity of arylazoheterocycles have largely been dependent on the nature and number of heteroatoms, ring size and the substituent type in the rings [34,35]. With this background, we have initiated a programme to study the chemistry of the azoimine function in the pyrimidine heterocycle [16–19]. It is chosen because of its higher π-acidity than conventional widely used pyridine bases [34,35] and its biochemical importance [1,36,37]. The ruthenium chemistry of arylazopyrimidines has already been developed by our group [17]. In this report we describe the synthesis, spectral studies, redox property and single-crystal X-ray structure of one of the isomers of osmium(II) complexes of 2-(arylazo)pyrimidines (aapm). The electronic properties of osmium(II) complexes are different from that of ruthenium(II)–arylazopyrimidine [17] complexes and have been interpreted from theoretical calculations using EHMO approximation.

☆ For Part VI, see Ref. [33].

* Corresponding author. Tel.: +91-342-557-683; fax: +91-342-564-452.
E-mail address: c_r_sinha@yahoo.com (C. Sinha).

0277-5387/02/$ - see front matter © 2002 Published by Elsevier Science Ltd.
PII: S0277-5387(02)00833-1

2. Experimental

2.1. Materials

Osmium tetroxide was purchased from Johnson Matthey. $(NH_4)_2[OsCl_6]$ and 2-(arylazo)pyrimidine were prepared following the literature procedures [6,38]. All other chemicals, solvents, their purification process used for different measurements, etc. were described in Ref. [17].

2.2. Preparation of complexes: ctc and ccc-dichloro-bis-[2-(phenylazo)pyrimidine]osmium(II), $OsCl_2(papm)_2$ (blue–violet ctc (**2a**); red–violet ccc (**3a**))

To brown–red solution of $(NH_4)_2[OsCl_6]$ (0.5 g, 1.14 mmol) in 2-methoxyethanol (50 cm^3) nitrogen gas was bubbled continuously and refluxed on an oil-bath for 20 min. 2-(Phenylazo)pyrimidine (0.44 g, 2.4 mmol) in ethanol (10 cm^3) was added in drops to this refluxing solution over another half-an hour. The mixture was refluxed under nitrogen with magnetic stirring for 24 h. During this period, the solution turned brown–violet to blue–violet. This was concentrated to about 20 cm^3 by slow bubbling of N_2 gas. The solution was cooled to room temperature and kept in refrigerator overnight. The shining dark coloured crystalline precipitate was collected by filtration and washed with ethanol–water (1:1, v/v) and dried over P_4O_{10}. The dried product was dissolved in a small volume of CH_2Cl_2 and was chromatographed on an alumina (neutral) column. A small portion of orange–red band was eluted with benzene and rejected. Blue–violet band was eluted using 4:1 (v/v) benzene–acetonitrile. Red–violet band was eluted by acetonitrile. The solutions were collected separately and evaporated slowly in air. The crystals so obtained were dried over P_4O_{10}. The yields were of blue–violet *ctc*-$OsCl_2(papm)_2$ (**2a**), 38% and red-violet, *ccc*-$OsCl_2(papm)_2$ (**3a**), 11%.

All other complexes were prepared by following the identical procedure and the yields were varied between 30–50% for the blue–violet isomers and 10–15% for the red–violet isomers.

2.3. X-ray crystallography

Crystal that was suitable for X-ray diffraction study of *ctc*-$OsCl_2(p\text{-tapm})_2$ (**2d**) was grown by slow diffusion of hexane into a dichloromethane solution at 298 K (crystal size (mm): $0.2 \times 0.2 \times 0.1$). Data were collected on a Siemens SMART CCD diffractometer with graphite monochromatised Mo Kα radiation ($\lambda = 0.71073$ Å) at 293 K. Crystal data and collection parameters are listed in Table 1. The data were corrected for absorption effects by empirical method using azimuthal scan data. Systematic absences led to the identification of space group $P\bar{1}$. Of 7753 collected reflections 3530 with $I > 2\sigma(I)$ were used for the structure solution. The structure was solved by the conventional heavy-atom method and was refined by the full-matrix least-squares method on all F_o^2 data using SHELXTL 5.03 package on silicon Graphics Indigo-R4000 computers. Hydrogen atoms were included in calculated positions and refined with isotropic thermal parameters which were 1.2 aromatic (H) times the equivalent isotropic thermal parameters of their parent carbon atoms.

Table 1
Crystal data and structure refinement parameters for *ctc*-$Os(p\text{-tapm})_2Cl_2$ (**2d**)

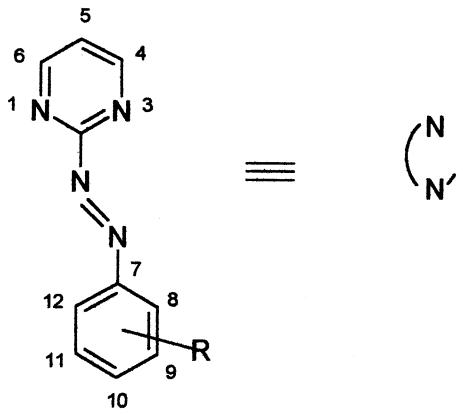
Empirical formula	$C_{22}H_{20}Cl_2N_8Os$
Formula weight	657.56
Crystal system	triclinic
Temperature	293 (2)
Space group	$P\bar{1}$
Unit cell dimensions	
a (Å)	10.0300(4)
b (Å)	10.2587(4)
c (Å)	12.2855(4)
α (°)	96.387(2)
β (°)	101.029(2)
γ (°)	90.522(2)
V (Å^3)	1232.47(8)
λ (Å)	0.71073
D_{calc} (g cm^{-3})	1.77
Z	2
μ (mm^{-1})	5.417
R [a]	0.0434
wR [b]	0.0977
Goodness-of-fit [c]	0.878

[a] $R = \Sigma|F_o - F_c|/\Sigma F_o$.
[b] $wR = [\Sigma w(F_o^2 - F_c^2)/\Sigma wF_o^4]^{1/2}$, $w = 1/[\sigma^2(F_o^2) + (0.0604P)^2]$, $P = (F_o^2 + 2F_c^2)/3$.
[c] Goodness-of-fit is defined as $[w(F_o - F_c)/(n_o - n_v)]^{1/2}$ where n_o and n_v denote the number of data and variables, respectively.

3. Results and discussion

3.1. Synthesis and assignment of isomers

2-(Arylazo)pyrimidines (aapm, **1**) possess the azoimine, –N=N–C=N–, functional group and the donor centres are N(pyrimidine), N and N′. Analogues that have been used in this work are 2-(phenylazo)pyrimidine (papm, R = H, **1a**), 2-(*o*-tolylazo)pyrimidine (*o*-tapm, R = 8-Me, **1b**), 2-(*m*-tolylazo)pyrimidine (*m*-tapm, R = 9-Me, **1c**), 2-(*p*-tolylazo)pyrimidine (*p*-tapm, R = 10-Me, **1d**), 2-(*p*-chlorophenylazo)pyrimidine (*p*-Clpapm, R = 10-Cl, **1e**).



aapm

1

The reaction of aapm with $(NH_4)_2[OsCl_6]$ in 2-methoxyethanol–ethanol proceeds shortly under refluxing condition and upon concentrating dark-coloured crystals of composition $OsCl_2(aapm)_2$ (**2/3**) were isolated (Eq. (1)).

$$OsCl_6^{2-} + 2aapm \rightarrow OsCl_2(aapm)_2 + 4Cl^- \quad (1)$$

The product was purified by chromatographic separation on alumina (neutral) bed to give blue–violet (isomer A) and red–violet (isomer B) complexes. The alcoholic solvent may be responsible [6] for the reduction of Os(IV) to Os(II) in Eq. (1). Microanalytical (Table 3) data support the composition of the complexes $OsCl_2(aapm)_2$. Blue–violet and red–violet isomers are assigned to **2** and **3**, respectively. The complexes are diamagnetic in the crystalline state and are non-electrolytic in nitromethane and acetonitrile. Isomers are soluble in common organic solvents to give blue–violet (for **2**) and red–violet (for **3**) solution. The blue–violet isomer ($OsCl_2(p$-tapm$)_2$ (**2d**)) has been characterised by X-ray crystallographic method.

3.2. Structure of blue–violet $OsCl_2(p$-tapm$)_2$ (**2d**)

A view of the molecule is shown in Fig. 1. The coordination around osmium is approximately octahedral. The atomic arrangement involves sequentially *cis*-chlorine, *trans*-N(pyrimidine) and *cis*-N(azo) and is abbreviated *cis–trans–cis* (*ctc*) configuration (C_2-symmetry). Selected bond parameters are listed in Table 2.

Two atomic groups Os, Cl(1), N(22), N(27), N(2) and Os, Cl(2), N(22), N(7), N(2) constitute two planes (mean deviation < 0.04 Å) and are orthogonal (dihedral angle 91.87°). The atomic groups Os, Cl(1), Cl(2), N(7), N(27) do not constitute a good plane and is deviated by ~ 0.16 Å. The distortion from octahedral geometry is due to acute chelate bite angle 76.4(3)°. The azo nitrogens, N(7) (deviation, 0.16 Å) and N(27) (deviation, -0.15 Å) are

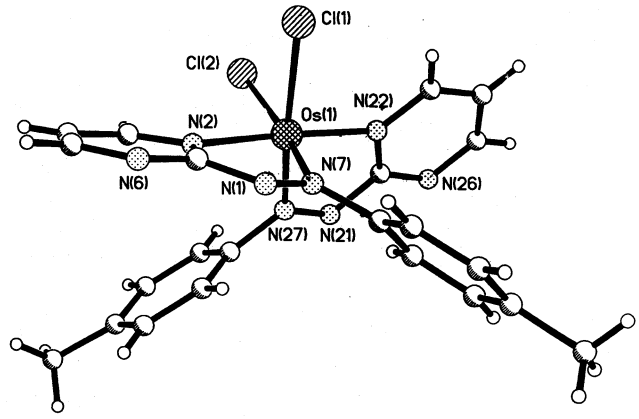


Fig. 1. Crystal structure and atom labelling scheme for *ctc*-$OsCl_2(p$-tapm$)_2$ (**2d**).

Table 2
Selected bond lengths (Å) and bond angles (°) for compound *ctc*-$OsCl_2(p$-tapm$)_2$ **2d**

Bond length (Å)		Bond angles (°)	
Os–N(2)	2.029(7)	N(2)–Os–N(7)	76.4(3)
Os–N(22)	2.030(8)	N(22)–Os–N(27)	76.4(3)
Os–N(7)	1.974(7)	Cl(1)–Os–Cl(2)	88.48(9)
Os–N(27)	1.967(8)	N(2)–Os–N(22)	177.1(3)
Os–Cl(1)	2.389(2)	N(7)–Os–N(27)	100.7(3)
Os–Cl(2)	2.393(2)	N(2)–Os–Cl(1)	86.0(2)
N(1)–N(7)	1.320(10)	N(2)–Os–Cl(2)	94.1(2)
N(21)–N(27)	1.329(11)	N(22)–Os–Cl(1)	96.1(2)
C(1)–N(2)	1.368(11)	N(27)–Os–Cl(2)	84.9(2)
C(1)–N(6)	1.328(12)	N(7)–Os–Cl(1)	86.9(2)
C(21)–N(22)	1.350(12)	N(7)–Os–Cl(2)	169.7(2)
C(21)–N(26)	1.348(13)	N(27)–Os–Cl(1)	170.2(2)
		N(27)–Os–N(2)	101.7(3)
		N(7)–Os–N(22)	101.6(3)
		N(22)–Os–Cl(2)	88.0(2)

associated with this distortion. Each chelate ring constitutes a good plane and no atom deviating by more than 0.04 Å. The dihedral angle between the chelate rings is 105.83°. The pendant *p*-tolyl ring is twisted by 36–54° from the respective chelate ring plane.

The Os–N(pyrimidine) [Os–N(2) = 2.029(7), Os–N(22) = 2.030(8) Å] bond distance is longer than Os–N(azo) [Os–N(7) = 1.974(7), Os–N(27) = 1.967(8) Å] bond distance (Table 2). The N=N distances are 1.32–1.33 Å elongated by 0.07 Å compared to free azo distance (1.26 Å) [6,39]. The coordination can lead to a decrease in the N–N bond order due to both σ-donor and π-acceptor characters of the ligand. The elongation of the N–N distance and shortening of Os–N(azo) bond length are thus an indication of the existence of considerable Os–aapm π-bonding with major involvement of the azo group.

Comparison of bond distances between ruthenium(II) [17] and osmium(II) complexes (Fig. 2) reveals that the

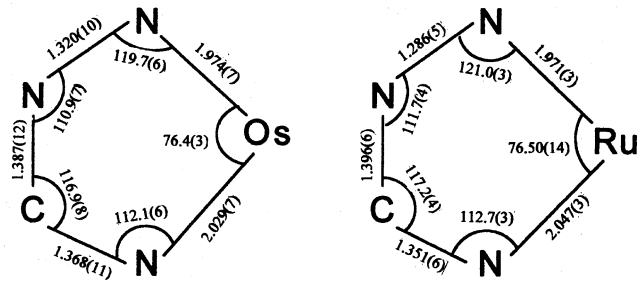


Fig. 2. Dimensions of chelate rings with e.s.d. of: (a) *ctc*-$OsCl_2$(*p*-tapm)$_2$ (**2d**) and (b) *ccc*-$OsCl_2$(*p*-tapm)$_2$ (**3d**).

N–N distance is elongated by 0.03 Å in the latter complex, the C–N distances vary only slightly. The systematic shortening of M–N(azo) distance compared to M–N(pyrimidine) distance in Ru(II) and Os(II) complexes is a further indication of the presence of stronger M–azo π-bonding. The Os–N(pyrimidine) bond distance is shortened by 0.02 Å compared to Ru–N(pyrimidine) bond distance suggesting the π-interaction order Os > Ru.

3.3. Spectral studies

The infrared spectra of the isomers differ significantly in the region 4000–200 cm^{-1}. All the complexes exhibit intense bands at 1530–1560 and 1340–1370 cm^{-1}, corresponding to C=N and N=N stretching, respectively. It is observed that endocyclic C=N is shifted to lower frequency region by 60–90 cm^{-1} and ν(N=N) is reduced by 140–150 cm^{-1} [6,17]. This supports the *N*,*N*′-chelation to osmium(II). The spectra are in agreement with the π-bonding scheme in the order Os–N(azo) > Os–N(pyrimidine) (vide supra). The N=N frequency of $OsCl_2(aapm)_2$ are systematically lowered (by 30–60 cm^{-1}) more than that of $RuCl_2(aapm)_2$ [17]. The spectra exhibit two medium intense bands at 300–310 and 320–330 cm^{-1} corresponding to two Os–Cl bonds. This supports the *cis*-$OsCl_2$ configuration in the complexes.

The vibrational spectra of isomer A, $OsCl_2(aapm)_2$ and *ctc*-$RuCl_2(aapm)_2$ are nearly superimposable in the above region [17] except for frequency shifting of N=N and C=N stretching bonds to the lower frequency region. Isomer B is similar to the spectrum of *ccc*-$RuCl_2(aapm)_2$. These observations suggest that the isomer A (blue–violet compound) has the *cis–trans–cis* (**2**) and isomer B (red–violet compound) has the *cis–cis–cis* (**3**) configuration.

The solution electronic spectra of the complexes in $CHCl_3$ exhibit multiple bands and shoulder in the region 250–1200 nm (Table 3). The absorption below 400 nm is due to intraligand charge transfer transitions ($n \rightarrow \pi^*$, $\pi \rightarrow \pi^*$) and are not considered further. High intense absorptions ($\varepsilon \sim 10^4$) are observed in the range 410–430, 510–530, 560–640 nm along with two weak shoulders ($\varepsilon \sim 10^3$) at longer wavelength region 700–730 and 900–1030 nm. Main absorption bands are assigned to $t_2 \rightarrow \pi^*$charge transfer transitions where the π*orbital has a large azo character [6,35]. The spectral comparison (Fig. 3) show that the profile pattern is comparable and the bands are blue shifted by 10–100 nm on going from *ctc*-$OsCl_2(aapm)_2$ to *ccc*-$OsCl_2(aapm)_2$ complexes. In d^6-metal complexes, multiple $t_2(Os) \rightarrow \pi^*$ charge-transfer transition [6,38] can occur from low symmetry splitting of the metal level from the presence of more than one interacting ligands (each contributing π* orbital(s)) and from mixing of singlet and triplet configuration in the excited state via spin–orbit coupling. Comparison of the electronic spectra of the present series of complexes and those of $RuCl_2(aapm)_2$ reveal that the transitions are blue shifted by 30–150 nm on going from ruthenium(II) to osmium(II) complexes. The spectral behaviour of $OsCl_2(aapm)_2$ is comparable to that of $OsCl_2(aap)_2$ [aap = 2-(arylazo)pyridine]; the absorption positions are red shifted by 20–35 nm on going from $OsCl_2(aap)_2$ to $OsCl_2(aapm)_2$. This is in agreement with the π-acidity order, arylazopyridine > arylazopyrimidine [34,35].

The ^{1}H NMR spectra of the complexes were recorded in $CDCl_3$ and were compared with the spectra of free ligands and analogous ruthenium(II) complexes. The proton-numbering patterns are shown in aapm (**1**) and are assigned on the basis of spin–spin interaction and the effect on substitution therein. Protons in two-aapm units of $OsCl_2(aapm)$ are separately assigned as H and H^1. The spectral data are summarised in Table 4. The Ar–Me signal has been particularly useful in determining isomer configuration. *ctc*-$OsCl_2(tapm)_2$ (**2b–2d**) have C_2-symmetry and are expected to exhibit a single Ar–Me signal while the *ccc*-$OsCl_2(tapm)_2$ (**3b–3d**) are C_1-symmetric and are expected to exhibit two –Me signals of equal intensities. This is indeed observed (Fig. 4). The pyrimidine protons (4–6-H) [16] appear at higher frequency region (7.4–9.3 ppm) and the signals at 6.6–7.4 ppm are due to azoaryl protons (8–12-H). The doublet at approximately 9.3 ppm refers to 4-H because of the closest position to the metal centre followed by the 6-H (ca. 8.8 ppm) and 5-H shows multiplet at approximately 7.4 ppm. Aryl protons (8–12-H) in the present complexes have been perturbed in a peculiar manner. Usually 8,12-H appears at lower frequency side compared to 9–11-H signals because of the closest position of the electron withdrawing azo group. Besides, the substitution 10-R perturbs 9 and 11-H more profoundly than 8,12-H. The electron donating substituent (–Me group in *p*-tapm) shifts 9- and 11-H to lower frequency region while the electron withdrawing group (–Cl group in *p*-Clpapm) shifts them to higher frequency side relative to phenyl-H. This has been observed in the free ligand, aapm [16] and complexes of ruthenium(II) [17] and palladium(II) [18]. It is

Table 3
Elemental analyses [a], UV–Vis spectral [b] and cyclic voltammetric data [c]

Compound	Elemental analyses [a] (%)			λ_{max} (nm) (10^{-3} ε, M^{-1} cm^{-1})	Os(III)/Os(II) $E^1_{1/2}$ (V) (ΔE, mV)	Os(IV)/Os(III) $E^2_{1/2}$ (V) (ΔE, mV)	Ligand reductions E^L (V) (ΔE, mV)
	C	H	N				
ctc-$OsCl_2(papm)_2$ (**2a**)	38.25 (38.14)	2.46 (2.54)	17.74 (17.80)	1016 (1.137) [d], 719 (1.119) [d], 572 (7.496), 521 (11.033), 414 (9.774)	1.224 (80)	2.41 (140)	−0.24 (90), −0.63 (100), −1.259 [e], −1.582 [e]
ccc-$OsCl_2(papm)_2$ (**3a**)	38.19 (38.14)	2.62 (2.54)	17.76 (17.80)	907 (1.007) [d], 604 (3.922), 513 (9.815), 414 (11.367)	1.198 (80)	1.996 (160)	−0.318 (80), −0.678 (90), −1.303 [e], −1.644 [e]
ctc-$Os(o\text{-tapm})_2Cl_2$ (**2b**)	40.09 (40.17)	3.00 (3.04)	17.11 (17.04)	1005 (0.876) [d], 676 (4.183), 578 (8.660), 538 (10.321), 492 (8.041), 408 (5.490)	1.182 (80)	1.987 (160)	−0.319 (90), −0.704 (100), −1.468 [e], −1.809 [e]
ccc-$OsCl_2(o\text{-tapm})_2$ (**3b**)	40.25 (40.17)	2.98 (3.04)	17.00 (17.04)	890 (0.674) [d], 662 (4.783), 560 (7.883), 405 (6.709)	1.158 (70)	1.903 (170)	−0.584 (100), −0.860 (120), −1.612 [e], −1.864 [e]
ctc-$OsCl_2(m\text{-tapm})_2$ (**2c**)	40.23 (40.17)	3.10 (3.04)	16.97 (17.04)	1020 (0.986) [d], 708 (1.286) [d], 570 (6.486), 522 (9.038), 414 (9.715)	1.185 (80)	1.978 (170)	−0.311 (80), −0.696 (100), −1.455 [e], −1.721 [e]
ccc-$OsCl_2(m\text{-tapm})_2$ (**3c**)	40.12 (40.17)	2.96 (3.04)	17.11 (17.04)	886 (0.710) [d], 687 (0.854) [d], 518 (6.128), 414 (7.270)	1.152 (80)	1.888 (160)	−0.577 (100), −0.844 (110), −1.598 [e], −1.818 [e]
ctc-$OsCl_2(p\text{-tapm})_2$ (**2d**)	40.08 (40.17)	2.96 (3.04)	17.11 (17.04)	1011 (1.035) [d], 722 (0.988) [d], 635 (3.204), 586 (5.655), 522 (8.817), 415 (12.966)	1.189 (70)	2.008 (140)	−0.308 (100), −0.648 (120), 1.418 [e], −1.725 [e]
ccc-$OsCl_2(p\text{-tapm})_2$ (**3d**)	40.23 (40.17)	2.96 (3.04)	16.95 (17.04)	903 (0.720) [d], 719 (1.135) [d], 610 (3.60), 514 (6.154), 429 (10.067)	1.170 (70)	1.964 (160)	−0.588 (100), −0.813 (120), −1.558 [e], −1.805 [e]
ctc-$OsCl_2(p\text{-Clpapm})_2$ (**2e**)	34.44 (34.37)	2.08 (2.01)	16.14 (16.04)	1023 (1.061) [d], 736 (0.984) [d], 525 (9.344), 414 (12.242)	1.290 (80)	2.106 (180)	−0.212 (90), −0.603 (120), −1.164 [e], −1.523 [e]
ccc-$OsCl_2(p\text{-Clpapm})_2$ (**3e**)	34.42 (34.37)	2.06 (2.01)	16.10 (16.04)	782 (1.872) [d], 702 (3.744), 561 (8.186), 425 (7.924)	1.257 (78)	2.000 (170)	−0.284 (100), −0.674 (110), −1.157 [e], −1.592 [e]

[a] Calculated values are in parentheses.
[b] In $CHCl_3$.
[c] Solvent, CH_3CN; supporting electrolyte, $[NBu_4][ClO_4]$ (0.01 M), solute concentration, 10^{-3} M, scan rate, 0.05 V s^{-1}.
[d] Shoulder.
[e] Cathodic peak potential, E_{pc}, V.

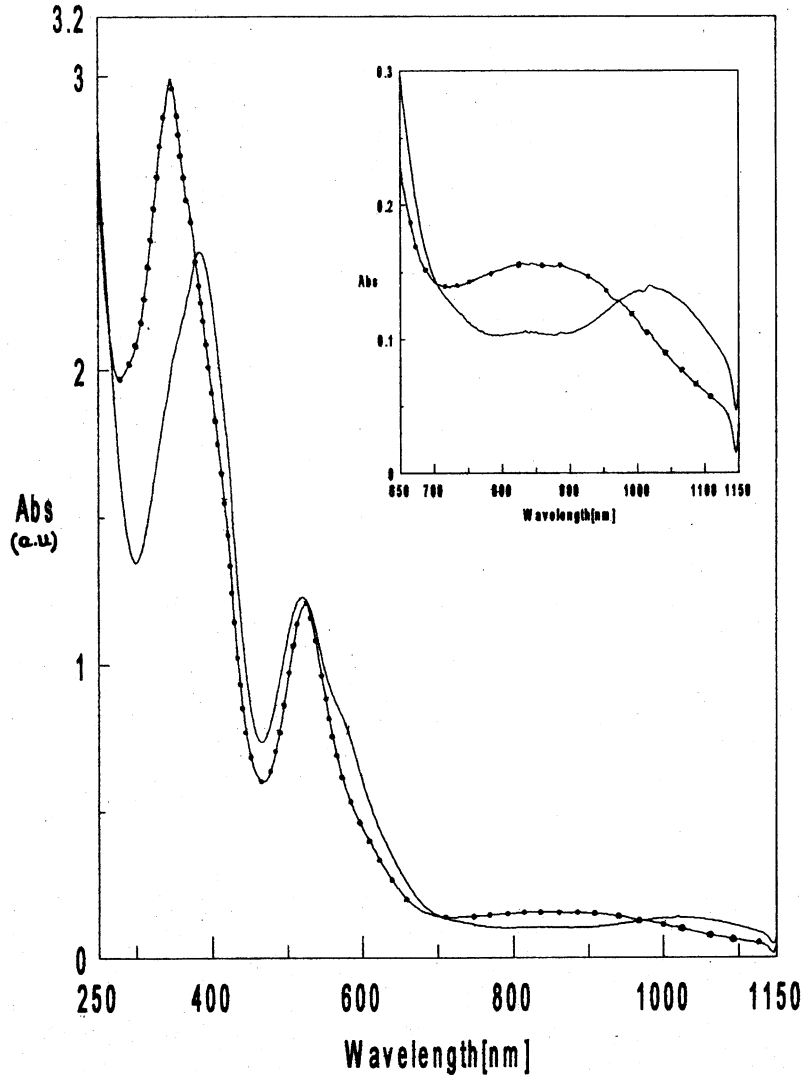


Fig. 3. Electronic spectra of *ctc*-$OsCl_2$(*p*-clpapm)$_2$ (**2e**) (—) and *ccc*-$OsCl_2$(*p*-clpapm)$_2$ (**3e**) (- - -) in $CHCl_3$ at 298 K.

observed that a doublet (2H) appears at lowest frequency side in the *ctc*-$OsCl_2$(*p*-Raapm)$_2$ (av. 6.6 ppm) which feels little perturbation on substitution at aryl ring (*p*-R) and second doublet perturbes significantly. The former doublet has been assigned to 8,12-H and the second doublet refers to the signal corresponding to 9,11-H. In $OsCl_2$(*o*-tapm)$_2$ (**2b/3b**) and $OsCl_2$(*m*-tapm)$_2$ (**2c/3c**) aryl-H are unsymmetrical. In $OsCl_2$(*m*-tapm)$_2$(**2c/3c**) a singlet (1H) resonance is observed at 6.55 ppm that is unambiguously assigned to 8-H and is followed by a doublet (6.60 ppm) for 12-H. This unusual proton movement may be concluded on considering the charge delocalisation, $t_2(Os) \rightarrow \pi^*$ orbitals. Thus, 8-H and 12-H protons are affected first and feel severe perturbation. This observation mismatches with our experience on isoelectronic ruthenium(II) complexes [17]. Because of the relativistic effect [40], 5d orbitals in Os(II) have been perturbed more effectively than that of 4d-orbitals of Ru(II) by the π acidic ligands and hence the reverse swings of charge densities.

3.4. Electrochemistry

The electrochemical properties of the complexes have been examined by cyclic volammetry on a platinum milli working electrode in super dry MeCN using $[Bu_4N][ClO_4]$ (0.1 M) as supporting electrolyte. Electrochemical data are given in Table 3 and a representative voltammogram is shown in Fig. 5. In the potential range +0.5 to +2.4 V at a scan rate 50 mV s^{-1} a nearly reversible osmium(III)–osmium(II) couple (2) is observed with peak-to-peak separation of 70–80 mV.

$$OsCl_2(aapm)_2^+ + e \rightleftharpoons OsCl_2(aapm)_2 \quad (2)$$

The formal potential, E^0_{298}, lies close to 1.2 V and is the highest potential amongst the known complexes of

Table 4
^{1}H NMR data of $OsCl_2(aapm)_2$ in $CDCl_3$

Compound	δ (ppm)/J (Hz) [a]								
	4-H [b] [4′-H]	5-H [b] [5′-H]	6-H [b] [6′-H]	8-H [b] [8′-H]	9-H [9′-H]	10-H [10′-H]	11-H [11′-H]	12-H [b] [12′-H]	Me [Me′]
2a	9.25 (6.0)	7.38 (6.0)	8.84 (6.0)	6.65 (7.5)	7.12 [c] (6.0)	7.30 [c] (7.0)	7.12 [c] (6.0)	6.65 (7.5)	
3a	9.46 (6.0)	7.82 (6.0)	8.86 (6.0)	7.72 (7.0)	7.16 (6.0)	7.38 (7.0)	7.16 (6.0)	7.72 (7.0)	
	[8.91 (6.6)]	[7.41 (6.0)]	[8.30 (6.0)]	[7.40 (7.0)]	[6.59 (6.0)]	[7.23 (7.0)]	[6.59 (6.0)]	[7.40 (7.0)]	
2b	9.30 (6.0)	7.37 (6.0)	8.81 (6.0)		6.81 [b] (6.0)	7.09 [c] (7.0)	7.09 [c] (7.0)	6.61 (6.0)	2.44
3b	9.44 (6.0)	7.78 (6.0)	8.80 (6.0)		7.09 (6.0)	7.24 (7.0)	7.24 (7.0)	6.95 (6.0)	2.66 [2.45]
	[8.83 (6.0)]	[7.39 (6.0)]	[8.25 (6.0)]		[6.64 (6.0)]	[6.88 (7.0)]	[6.88 (7.0)]	[6.42 (6.0)]	
2c	9.32 (6.0)	7.38 (6.0)	8.82 (6.0)	6.55 [d]		7.00 [b] (7.0)	7.05 [c] (7.0)	6.60 (6.5)	2.30
3c	9.30 (6.0)	7.75 (6.0)	8.75 (6.0)	6.83 [d] (6.34 [d])		7.31 (7.0)	7.40 (7.0)	6.94 (7.0)	2.61 [2.40]
	[8.81 (6.0)]	[7.42 (6.0)]	[8.23 (6.0)]			[6.69 (7.0)]	[6.77 (7.0)]	[6.49 (7.0)]	
2d	9.32 (6.0)	7.40 (6.0)	8.83 (6.0)	6.56 [b] (6.5)	6.87 [b] (6.0)		6.87 [b] (6.0)	6.56 (6.5)	2.23
3d	9.42 (6.0)	7.77 (6.0)	8.79 (6.0)	7.72 (9.0)	6.97 (6.0)		6.97 (6.0)	7.72 (9.0)	2.40 [2.24]
	[8.86 (6.0)]	[7.07 (6.0)]	[8.24 (6.0)]	[7.17 (9.0)]	[6.55 (6.0)]		[6.55 (6.0)]	[7.71 (9.0)]	
2e	9.28 (6.0)	7.46 (6.0)	8.89 (5.5)	6.59 [c] (7.5)	7.09 [c] (6.0)		7.09 [b] (6.0)	6.59 (7.5)	
3e	9.41 [e] [8.91 [e]]	7.80 (6.0)	8.86 [e] [8.28 [e]]	7.77 (7.0)	7.18 (6.0)		7.18 (6.0)	7.77 (7.0)	
		[7.10 (6.0)]		[7.37 (7.0)]	[6.76 (6.0)]		[6.76 (6.0)]	[7.37 (7.0)]	

[a] For *ccc*-$Os(aapm)_2Cl_2$ respective protons of two aapm are distinguished as H and H′.
[b] Doublet.
[c] Triplet.
[d] Singlet.
[e] Broad.

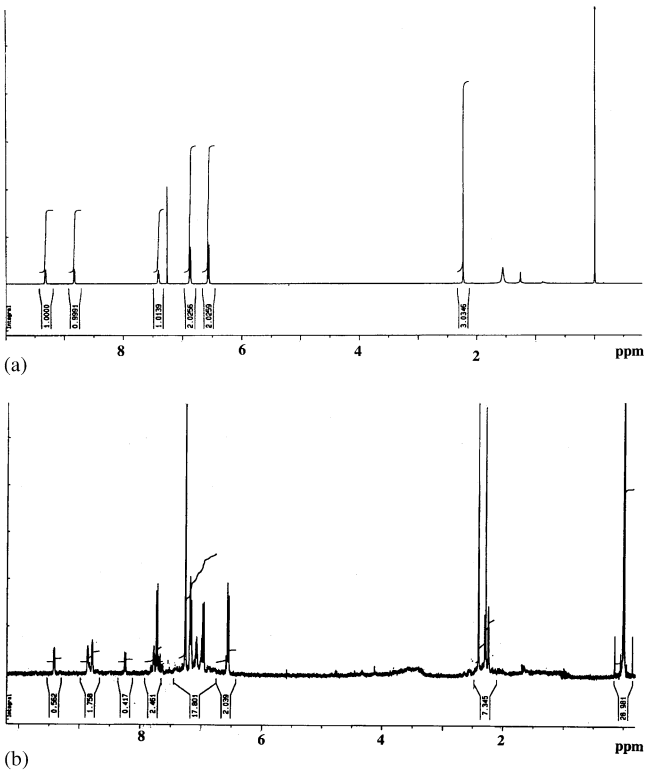


Fig. 4. ^{1}H NMR spectra of: (a) *ctc*-$OsCl_2(p\text{-tapm})_2$ (**2d**) and (b) *ccc*-$OsCl_2(p\text{-tapm})_2$ in $CDCl_3$ at 298 K.

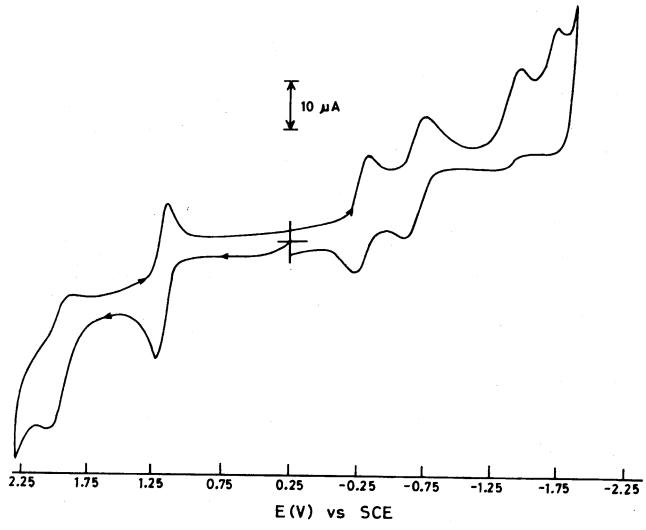


Fig. 5. Cyclic voltammogram of *ctc*-$OsCl_2(p\text{-tapm})_2$ in MeCN using Pt-disc working electrode. The solute concentration and scan rate are 10^{-3} M and 50 mV s^{-1}, respectively.

the azoimine system. A second one-electron response observed at approximately 2 V (close to solvent cutoff limit) is quasireversible ($\Delta E_p = 140$–180 mV) in nature. This is assigned to the osmium(IV)–osmium(III) redox couple [6]. The data reveal that between the two isomers the order of E^0_{298} is $tc > cc$. The one-electron stoichiometry of the first couple was established by controlled potential coulometry of one complex *ctc*-$OsCl_2(papm)_2$ at potential 1.4 V versus SCE using Pt-net working electrode. The solution colour changes from blue–violet to brown–red. Reported potentials are higher than those of osmium(II)–arylazopyridines which may be due to π-acidity order of pyrimidine > pyridine [34,35]. The azopyridine ligands thus stabilise (with respect to oxidation) osmium(II) better than the azopyridines. Reductions are observed in the potential range 0 to −2.0 V using glassy-carbon working electrode. Four successive redox couples are observed (Table 3); the first two couples are quasi-reversible ($\Delta E_p = 100$–140 mV) in nature. The remaining two responses at negative to SCE do not exhibit reasonable anodic peaks on scan reversal. These reductions are believed to be the successive electron addition into two azoimine functions [4,6,17].

3.5. EHMO calculation

Approximate composition studies of the frontier orbitals in osmium(II) complexes of 2-(arylazo)pyrimidine were performed by the extended Hückel calculation on a model complex of *ctc*-$OsCl_2(p\text{-tapm})_2$. Similar calculation has also been carried out to ruthenium(II) analogues. Since crystallographic data for *ctc*-$RuCl_2(p\text{-tapm})_2$ are not available with us; herein, we are using crystal data of *ccc*-$RuCl_2(papm)_2$ [17] for gross comparison of spectral and electrochemical properties with osmium(II) complexes. The calculated molecular orbitals, have been used in order to assess the solution spectra and redox properties of the osmium(II) complexes and their comparison with ruthenium(II) complexes. The HOMO and LUMO of the complexes are depicted in Fig. 6. In osmium(II) complex, the HOMO ($E_{HOMO} = -11.152$ eV) is constituted by 81% metal d-orbitals and the LUMO ($E_{LUMO} = -10.768$ eV) is composed of 68% ligand orbitals. The azoimine function contributes 42% to the LUMO.

In *ccc*-$RuCl_2(p\text{apm})_2$, the HOMO ($E'_{HOMO} = -11.316$ eV) is composed of 77% d(Ru) and the LUMO ($E'_{LUMO} = -10.510$ eV) is 59% ligand orbitals. In ruthenium complex the HOMO is laying 0.164 eV below than the HOMO of osmium complex and the LUMO is stabilised by 0.258 eV in osmium complex compared to ruthenium complex. Thus, the energy difference between HOMO and LUMO is higher in $RuCl_2(aapm)_2$ than $OsCl_2(aapm)_2$. This is also observed in the ordering of MLCT transitions.

The EHMO results suggest that the HOMO, HOMO-1, HOMO-2, etc. are predominantly metal character and LUMO, LUMO+1, LUMO+2 are basically π*-ligand character. So, multiple charge transfer transitions may be observed. This is indeed observed. Energy difference determines the MLCT transitions and explains the shorter wavelength absorption of osmium complexes

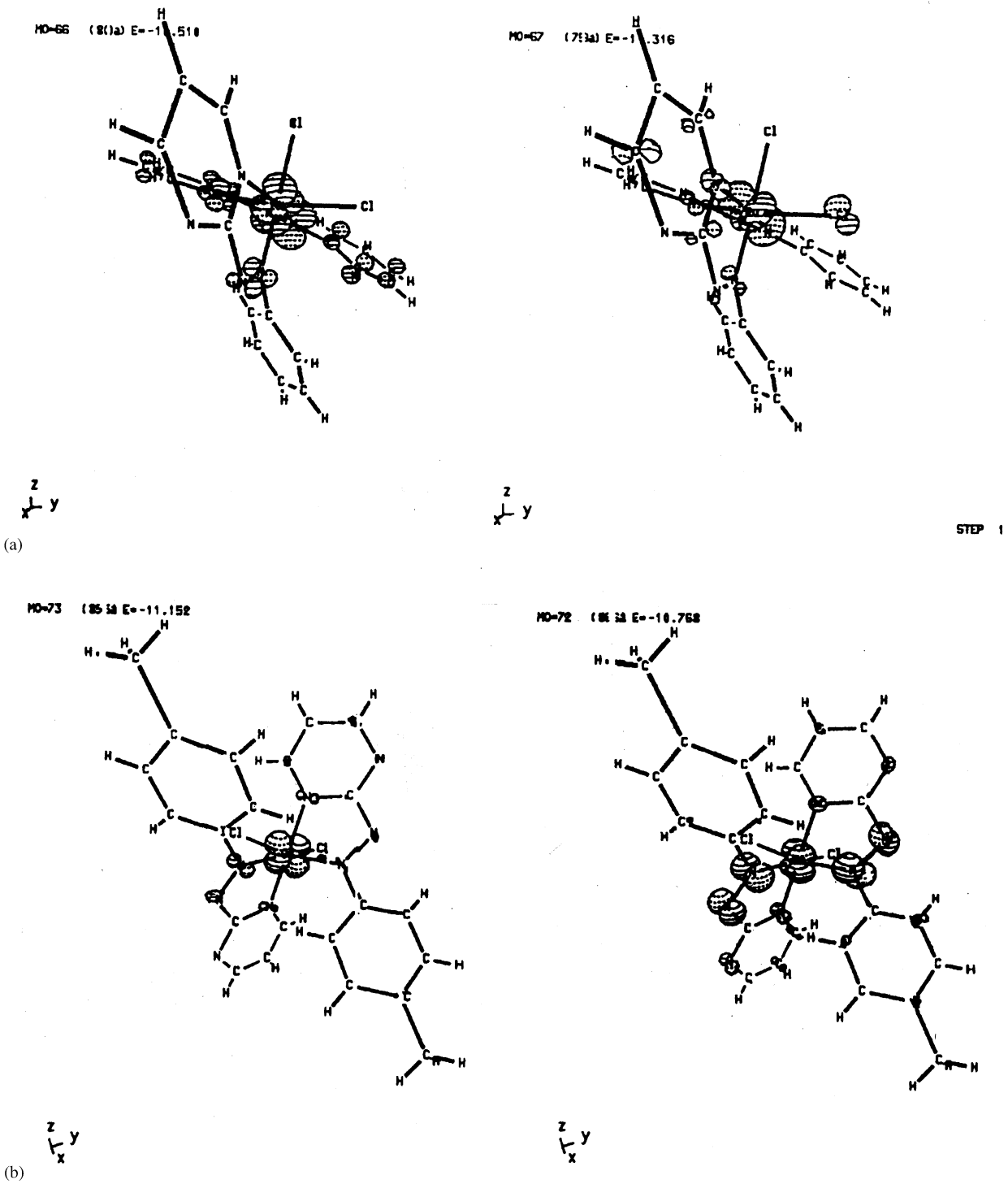


Fig. 6. Frontier orbitals, HOMO and LUMO of: (a) *ctc*-$OsCl_2(p\text{-tapm})_2$ and (b) *ccc*-$RuCl_2(p\text{-papm})_2$.

than that of ruthenium complexes. In cyclic voltammetric experiment the complexes exhibit both metal oxidations and ligand reductions. The oxidation involves electron extraction from HOMO which is metal orbital dominated and the reduction involves electron accommodation at LUMOs. Because of higher energy of HOMO of osmium complex (−11.152 eV) compared to ruthenium complex (−11.316 eV) the Os(III)/Os(II) and Os(IV)/Os(III) couples appear at higher potentials than that of Ru(III)/Ru(II) and Ru(IV)/Ru(III) complexes, respectively. The energy of LUMO of osmium complex is lower than that of ruthenium complex. Thus reduction of ligand is observed at lower potential in osmium complexes than ruthenium complexes (Table 3).

4. Supplementary material

Crystallographic data for the structural analysis have been deposited with the Cambridge Crystallographic Data Centre, CCDC No. 168654 for compound **2d**. Copies of this information may be obtained free of charge from The Director, CCDC, 12 Union Road, Cambridge, CB2 1EZ, UK (fax: +44-1223-336033; e-mail: deposit@ccdc.cam.ac.uk or www: http://www.ccdc.cam.ac.uk).

Acknowledgements

Financial assistance from the University Grants Commission, and Department of Science & Technology, New Delhi is gratefully acknowledged.

References

[1] D.J. Brown, in: Comprehensive Heterocyclic Chemistry, A.R. Katritzky, C.W. Rees, A.J. Boulton, A. McKillop (Eds.), vol. 3, 1984, p. 57.
[2] J. Reedijk, in: Comprehensive Coordination Chemistry, G. Wilkinson, R.D. Gillard, J.A. McCleverty (Eds.), vol. 2, Pergamon Press, Oxford, 1987, p. 73.
[3] D. Datta, A. Chakravorty, Inorg. Chem. 22 (1983) 1085.
[4] B.K. Ghosh, A. Chakravorty, Coord. Chem. Rev. 95 (1989) 239.
[5] S. Goswami, A.R. Chakravarty, A. Chakravorty, Inorg. Chem. 20 (1981) 2246.
[6] B.K. Ghosh, A. Mukhopadhyay, S. Goswami, S. Ray, A. Chakravorty, Inorg. Chem. 23 (1984) 4633.
[7] S. Ganguly, S. Karmakar, C.K. Pal, A. Chakravorty, Inorg. Chem. 38 (1999) 598.
[8] A. Bharath, B.K. Santra, P. Munshi, G.K. Lahiri, J. Chem. Soc., Dalton Trans. (1998) 2643.
[9] M. Heilmann, F. Baumann, W. Kaim, J. Fiedler, J. Chem. Soc., Faraday Trans. 92 (1996) 4227.
[10] K. Pramanik, M. Shivakumar, P. Ghosh, A. Chakravorty, Inorg. Chem. 39 (2000) 195.
[11] R. Samanta, P. Munshi, B.K. Santra, N.K. Loknath, M.A. Sridhar, J.S. Prasad, G.K. Lahiri, J. Organomet. Chem. 31 (1999) 579.
[12] B.K. Santra, P. Munshi, G. Das, P. Bharadwaj, G.K. Lahiri, Polyhedron 18 (1999) 617.
[13] A.K. Ghosh, P. Majumder, L.R. Falvello, G. Mostafa, S. Goswami, Organometallics 18 (1999) 5086.
[14] V.W.W. Yam, V.C.Y. Lan, L.X. Wu, J. Chem. Soc., Dalton Trans. (1998) 1461.
[15] T.K. Misra, D. Das, C. Sinha, Polyhedron 16 (1997) 4163.
[16] P.K. Santra, D. Das, T.K. Misra, R. Roy, C. Sinha, S.-M. Peng, Polyhedron 18 (1999) 1909.
[17] P.K. Santra, T.K. Misra, D. Das, C. Sinha, A.M.Z. Slawin, J.D. Woollins, Polyhedron 18 (1999) 2869.
[18] P.K. Santra, R. Roy, C. Sinha, Proc. Indian Acad. Sci. (Chem. Sci.) 112 (2000) 523.
[19] P.K. Santra, C. Sinha, W.-J. Sheen, F.-L. Liao, T.-H. Lu, Polyhedron 20 (2001) 599.
[20] T.K. Misra, D. Das, C. Sinha, P.K. Ghosh, C.K. Pal, Inorg. Chem. 37 (1998) 1672.
[21] K.S.Y. Leung, Y. Li, Inorg. Chem. Commun. 2 (1999) 599.
[22] N.C. Pramanik, S. Bhattacharya, Transition Met. Chem. 22 (1997) 524.
[23] S. Banerjee, S. Bhattacharyya, B.K. Dirghangi, M. Menon, A. Chakravorty, Inorg. Chem. 39 (2000) 6.
[24] S. Goswami, A.R. Chakravarty, A. Chakravorty, J. Chem. Soc., Chem. Commun. (1982) 1288.
[25] N. Ertan, Dyes Pigments 44 (1999) 41.
[26] T.G. Deligeorgiev, D. Simov, Dyes Pigments 38 (1998) 115.
[27] I. Sing, R. Saini, Anal. Chim. 85 (1995) 193.
[28] T.C.B. Saldanha, M.C.U. de Araujo, B.B. Neto, H.C. Chame, Anal. Lett. 33 (2000) 1187.
[29] G.A. Kochelaeva, V.M. Ivanov, G.V. Prochorova, J. Anal. Chem. 55 (2000) 14.
[30] G.B. Luo, T.T. Liu, L.M. Ying, X.S. Zhao, Y.Y. Huang, D.G. Nu, C.H. Huang, Langmuir 16 (2000) 3657.
[31] P. Chattopadhyay, C. Sinha, D.K. Pal, Fresenius' J. Anal. Chem. 357 (1997) 368.
[32] (a) D. Das, A.K. Das, C. Sinha, Talanta 48 (1999) 1013;
(b) D. Das, A.K. Das, C. Sinha, Anal. Lett. 32 (1999) 567.
[33] P.K. Santra, U.S. Ray, S.N. Pal, C. Sinha, Inorg. Chem. Commun. 4 (2001) 269.
[34] E.C. Constable, Coord. Chem. Rev. 93 (1989) 205.
[35] F. Casalboni, Q.G. Mulazzani, C.D. Clark, M.Z. Hoffman, P.L. Orizondo, M.W. Perkovic, D.P. Rillema, Inorg. Chem. 36 (1997) 2252.
[36] F. Jolibois, J. Cadet, A. Grand, R. Subra, N. Raga, V. Barone, J. Am. Chem. Soc. 120 (1998) 1864.
[37] M. Louloudi, Y. Deligiannakis, J.-P. Tuchagues, B. Donnadieu, N. Hadjiliadis, Inorg. Chem. 36 (1997) 6335.
[38] S. Pal, T.K. Misra, P. Chattopadhyay, C. Sinha, Proc. Indian Acad. Sci. (Chem. Sci.) 111 (1999) 687.
[39] D. Das, PhD Thesis, Burdwan University, Burdwan, India, 1998.
[40] F.A. Cotton, G. Wilkinson, Advanced Inorganic Chemistry, Wiley, New York, 1972.

ELSEVIER

Polyhedron 21 (2002) 763–768

POLYHEDRON

www.elsevier.com/locate/poly

Lower rim substituted *tert*-butylcalix[4]arenes (II). Complexing ability of 5,11,17,23-tetra-*tert*-butyl-25,26,27,28-tetrakis-*O*-(piperidinylcarbonyl)methylenecalix[4]arene. The crystal structures of the ligand and its sodium complex☆

Maria Bocheńska [a], Anna Zielińska [a], Victor Ch. Kravtsov [b], Maria Gdaniec [c], Emilia Luks [c], Wanda Radecka-Paryzek [c,*]

[a] *Department of Chemical Technology, Technical University of Gdańsk, 80-952 Gdańsk, Poland*
[b] *Institute of Applied Physics, Academy of Science of Moldova, MD2028 Chişinau, Moldova*
[c] *Faculty of Chemistry, Adam Mickiewicz University, 60-780 Poznań, Poland*

Received 28 August 2001; accepted 10 December 2001

Abstract

The sodium(I) chloride and yttrium(III), lanthanum(III), samarium(III) and gadolinium(III) nitrate complexes of 5,11,17,23-tetra-*tert*-butyl-25,26,27,28-tetrakis(piperidinylcarbonyl)methylene)calix[4]arene were prepared in direct reaction of the ligand and appriopriate metal salts and characterized by spectral data (IR, UV–Vis, ^{1}H NMR, FAB MS), and elemental analysis. The transmetallation reactions of the sodium complex by the lanthanide ions was also achieved. The crystal structures of the ligand and its sodium complex were determinated by single X-ray analysis. © 2002 Published by Elsevier Science Ltd.

Keywords: *tert*-Butylcalix[4]arenes; Amide; Sodium complexes; Yttrium(III) complexes; Lanthanide(III) complexes; X-ray structures

1. Introduction

Calixarenes have been widely used in the last 15 years in supramolecular chemistry. The high preorganization and complementarity with the guests make these macrocycles hosts a rich source for molecular receptors [1–3]. Functionalization at the lower rim may lead to the design and synthesis of the ligands suitable for various metal complexation. We have recently reported on the synthesis of new series of lower rim substituted *tert*-butylcalix[4]arenes and their complexing properties in ion-selective PVC membrane electrodes [4]. In this paper we present the preparation and characterization of 5,11,17,23-tetra-*tert*-butyl-25,26,27,28-tetrakis-O(piperidinylcarbonyl)methylene)calix[4]arene (**L**) complexes with the hard cations as sodium and rare earth ions. The crystal structure of the ligand and its complex with sodium ion is also described.

2. Experimental

5,11,17,23-tetra-*tert*-Butyl-25,26,27,28-trakis(piperidinylcarbonyl)methylene)calix[4]arene (**L**) was prepared according to the procedure published earlier [4]. The hydrated yttrium and lanthanide(III) nitrates were prepared by dissolving the 99.99% oxides (Fluka) in a slight excess of nitric acid. The solutions were evaporated and precipitates recrystallized from methanol.

2.1. Preparation of the complexes

2.1.1. Sodium(I) chloride complex of *L*

To *p*-*tert*-butylcalix[4]arene (1 mmol) in 30 cm^3 of the of dried tetrahydrofuran (THF) and dimethylformamide (DMF) (5:1) 10 mmoles of sodium hydride (55% in oil) was added followed by addition of piperidide of α-

☆ For Part I see [J. Incl. Phenom. Macroc. Chem. 39 (2001) 219].

* Corresponding author. Fax: +48-61-8658-008.
E-mail address: wrp@main.amu.edu.pl (W. Radecka-Paryzek).

0277-5387/02/$ - see front matter © 2002 Published by Elsevier Science Ltd.
PII: S0277-5387(02)00834-3

chloroacetic acid in twofold excess (8 mmol). The mixture was heated and stirred at 80 °C for 20 h. The solvent was removed by evaporation, the residue was quenched with 20 ml of water and extracted twice with methylene chloride (2 × 25 ml). The combined organic layers were washed with water, dried with $MgSO_4$ and after removing the solvent under reduced pressure the product as sodium complex was obtained with 82% yield; melting point (m.p.) 245–50 °C.

2.1.2. Crystallization

The complex Na**L**Cl (0.05 mmol) was dissolved in 10 cm^3 of refluxing methanol and left at room temperature. After 2 days crystals suitable for X-ray analysis precipitated; m.p. 248–51.

2.1.3. Na**L**Cl (**2**)

IR (cm^{-1}): 1655 s, ν(C=O), 293 m (Cl); FAB MS: $m/z = 1172.5$ $(Na\mathbf{L})^+$. ^1H NMR ($CDCl_3$, ppm): δ 1.15 (s, 36H, *t*-but), 1.67 (br, s, 24H, $(CH_2)_3$), 3.22 (br, s, 8H, NCH_2), 3.32 (d, $J = 12.5$ Hz, 4H, $ArCH_2,H_{eq}$), 3.62 (br, s, 8H, NCH_2), 4.48 (d, $J = 12.5$ Hz, 4H, $ArCH_2,H_{ax}$), 4.6 (s, 8H, $OCH_2C{=}O$), 7.12 (s, 8H, H_{arom}).

2.1.4. Yttrium(III), lanthanum(III), samarium(III) and gadolinium(III) nitrate complexes of **L**

2.1.4.1. Direct complexation reaction. All complexes were performed under similar conditions. To a solution of metal nitrate (0.005 mmol) in methanol (1 cm^3) the ligand L (0.005 mmol) in methanol (1 cm^3) was added dropwise with stirring. The reaction was carried out for 3 days. The solution volume was then reduced to 0.3 cm^3 by roto-evaporation and yellow precipitate formed on addition of a small amount of diethyl ether. This was filtered off, washed with ether, and dried in vacuo.

2.1.4.2. Transmetallation reaction. To a methanolic solution (1 cm^3) of Na**L**Cl (0.005 mmol), appropriate nitrate salt (0.005 mmol) in methanol (1 cm^3) was added dropwise with stirring. The reaction was carried out for 3–7 days until the solution turned yellow. The solvent was then partially removed by roto-evaporation. The yellow precipitate obtained by the addition of diethyl ether was collected by filtration, washed with ether, and dried in vacuo. The presence of chloride anions in the filtrate was confirmed by the reaction with $AgNO_3$.

2.1.5. $YL(NO_3)_3{\cdot}3H_2O$ ($L = C_{72}H_{100}N_4O_8$)

Found: C, 58.0, H, 7.1; N, 6.5. Calc.: C, 58.4, H, 7.2, N, 6.6%; IR (cm^{-1}): 3397 m,br, ν(OH), 1649 s, ν(C=O), 1384 br, s, 815 m (NO_3); FAB MS: $m/z = 1444.4$ $(Y\mathbf{L}(NO_3)_3{\cdot}H_2O)^+$, 1426.2 $(Y\mathbf{L}(NO_3)_3)^+$.

2.1.6. $LaL(NO_3)_3{\cdot}7H_2O$ ($L = C_{72}H_{100}N_4O_8$)

Found: C, 52.7, H, 7.2; N, 5.9. Calc.: C, 54.0, H, 7.2, N, 6.1%; IR (cm^{-1}): 3409 m, br, ν(OH), 1647 s,ν(C=O), 1363 br, s, 817 m (NO_3); ^1H NMR ($CDCl_3$,ppm): ^1H NMR ($CDCl_3$, ppm): δ 1.15 (s, 36H, *t*-but), 1.73 (br, s, 24H, $(CH_2)_3$), 3.21 (br, s, 8H, NCH_2), 3.32 (d, $J =$ 11.5Hz, 4H, $ArCH_2,H_{eq}$), 3.62 (br, s, 8H, NCH_2), 4.47 (d, $J = 11.3$Hz, 4H, $ArCH_2,H_{ax}$), 4.6 (s, 8H, $OCH_2C{=}O$), 7.27 (s, 8H, H_{arom}). FAB MS: $m/z = 1512.3$ $(La\mathbf{L}(NO_3)_3{\cdot}2H_2O)^+$, 1387.4 $(La\mathbf{L}(NO_3){\cdot}2H_2O)^+$, 1412.4 $(La\mathbf{L}(NO_3)_3{\cdot}2H_2O)^+$.

2.1.7. $SmL(NO_3)_3{\cdot}7H_2O$ ($L = C_{72}H_{100}N_4O_8$)

Found: C, 53.6, H, 6.8; N, 6.1. Calc.: C, 53.6, H, 7.1, N, 6.1%; IR (cm^{-1}): 3355 m,br, ν(OH), 1648 s, ν(C=O), 1384 br, s, 810 m (NO_3); FAB MS: $m/z = 1576.0$ $(Sm\mathbf{L}(NO_3)_3{\cdot}5H_2O)^+$, 1381.0 $(Sm\mathbf{L}(NO_3){\cdot}2H_2O)^+$, 1151.2 $\mathbf{L}^+$.

2.1.8. $GdL(NO_3)_3{\cdot}2H_2O$ ($L = C_{72}H_{100}N_4O_8$)

Found: C, 57.1, H, 6.7; N, 6.5. Calc.: C, 56.6, H, 6.8, N, 6.4%; IR (cm^{-1}): 3383 m,br, ν(OH), 1655 s, ν(C=O), 1758 w, 1734 w, 1384 br, s, 815 m (NO_3); FAB MS: $m/z = 1510.24$ $(Gd\mathbf{L}(NO_3)_3{\cdot}H_2O)^+$, 1408.1 $(Gd\mathbf{L}(NO_3)_2{\cdot}2H_2O)^+$.

2.2. Measurements

IR spectra were recorded using CsI pellets in the range 4000–200 cm^{-1} on a IR Spectrometer, Magna 760, FT-Raman, Nicolet. Electronic spectra were measured on a V-550 (JASCO) spectrophotometer. ^1H NMR spectra were run in DMSO-d_6 on a Varian Gemini 300 spectrometer using TMS as an internal reference. FAB-mass spectra were obtained on a AMD-604 mass spectrometer with 3-nitrobenzyl alcohol as matrix. All data reported refer to isolated materials judged to be homogenous by thin layer chromatography performed on precoated silica gel plates (0.2 mm 60 F-254 E. Merck) and visualized by UV light.

2.3. X-ray crystal structure analysis

2.3.1. Collection of X-ray diffraction data; solution and refinement of the structures

Experimental data for **1** and **2** were collected on a KUMA KM4CCD *k*-axis diffractomiter with graphite monochromated Mo Kα radiation. The data were processed using the KUMA Diffraction (Wroclaw, Poland) program. Summaries of crystal data and details data collection together with structure refinement are given in Table 1. The available colorless transparent prism habit crystals of compound **1** have a small size and are very poorly diffracted at room temperature (r.t.). The colorless crystals of **2** were unstable under ambient conditions. These were the reasons to collect

Table 1
Crystal data and summary of data collection for **1** and **2**

Compound	**L** CH_2Cl_2 (**1**)	[**L** Na](Cl) $2(CH_2Cl_2)$ $2(CH_3OH)$ (**2**)
Empirical formula	$C_{73}H_{102}Cl_2N_4O_8$	$C_{76}H_{112}Cl_5\ N_4NaO_{10}$
Crystal system	monoclinic	tetragonal
Space group	$P2_1/c$	$P4/ncc$
a (Å)	25.937(2)	17.000(2)
b (Å)	14.947(1)	17.000(2)
c (Å)	17.0870(1)	28.123(6)
β (°)	100.626(6)	90
Molecules/unit cell, Z	4	4
Crystal size (mm)	$0.10 \times 0.10 \times 0.05$	$0.20 \times 0.20 \times 0.10$
θ-Range for data collection (°)	3.37–22.56	3.69–25.05
Reflections collected/unique	26 104/8529	76 953/3549
Reflections observed, $[I > 2\sigma(I)]$	2499	3028
Completeness	99.5% to θ 22.56°	98.2% to θ 25.05
Data/restraints/parameters	8529/33/824	3549/18/273
Goodness-of-fit on F^2	0.675	1.023
Final R indices $[I > 2\sigma(I)]$	$R_1 = 0.0575$, $wR_2 = 0.0700$	$R_1 = 0.0992$, $wR_2 = 0.2779$
R indices (all data)	$R_1 = 0.2291$, $wR_2 = 0.0878$	$R_1 = 0.1080$, $wR_2 = 0.2873$
Largest difference peak and hole (e Å^{-3})	0.337 and −0.216	0.510 and −0.631

diffraction data at low 100 K temperature for both compounds and we were able to obtain sufficient data to determine the structure details unequivocally. The fresh moist crystal of **2** was used for experiment. An initial structure models of **1** and **2** were obtained by direct methods and most of the non-hydrogen atoms were refined with anisotropic thermal parameters by full-matrix least-squares procedure based on F^2. Calculations were carried out using the SHELX-97 system of computer programs [5].

A partial occupancy dichloromethane solvent molecules were found to be disordered over three sites with 25.1, 16.3 and 9.1% probability in the structure of compound **1**. The structure of compound **2** was successfully refined with dichloromethane molecules and chlorine anions being alternate and occupied the close sites with the 50% probability. The *tert*-butyl group and methanol solvent molecules are also disordered over two (87 and 13%) and four position (0.25%), respectively, in the structure of **2**. Restraints were applied to make chemically equivalent bonds approximately equal in the disordered fragments. The carbon atoms and chlorine atoms of minor occupancy in the disordered fragments were refined isotropically.

The hydrogen atoms were placed in calculated positions and were refined as constrained to bonding atoms. All H atoms were included in model of structure with isotropic U values fixed at 1.5 times U_{eq} of C atoms for CH_3 groups and 1.2 U_{eq} for others.

3. Results and discussion

The sodium(I) chloride and yttrium(III), lanthanum(III), samarium(III) and gadolinium(III) nitrate complexes of 5,11,17,23-tetra-*tert*-butyl-25,26,27,28-tetrakis-*O*(piperidinylcarbonyl)methylene)calix[4]arene (**L**) were prepared by direct reaction of the metal salt with ligand in methanol and identified (see Experimental) by spectral data (IR, UV–Vis, ^{1}H NMR, FAB MS), and elemental analysis. The structure of the ligand and its sodium complex was established by X-ray analysis. The transmetallation reactions of the sodium complex by the yttrium(III), lanthanum(III), samarium(III) and gadolinium(III) nitrates give rise to corresponding complexes which appear to be identical with those prepared in the direct synthesis. The complexes are air stable, soluble in common organic solvents.

The infrared spectra of these complexes taken in the region 4000–200 cm^{-1} are all very similar except for anion vibrational modes and provide some information regarding the bonding in the complexes. The most significant variations between the free ligand and complexes concern the ν(C=O) vibrations. The C=O absorption band observed in the IR spectrum of **L** at 1664 cm^{-1} is shifted by 9, 15, 17, 16 and 9 cm^{-1} to lower wavennumbers upon complexation with Na(I), Y(III), La(III), Sm(III) and Gd(III) ions, respectively, as a result of the decrease in the bond order of the C=O groups, owing to a donation of electron density towards the metal cation. The rare earth ion complexes show the broad diffuse band centered at 3409–3355 cm^{-1} region due to the stretching and bending modes of lattice and coordinated water. The broadening of the bands at 1384 cm^{-1} along with medium bands at 817–810 cm^{-1} observed in the spectra of rare earth nitrate complexes suggests that the nitrate counterions are partially involved in the coordination sphere of the metal ion [6]. However, the ligand modes also fall in this region.

The electronic spectra of the ligand and its complexes in chloroform show similar features containing the intense and medium absorption bands with maxima at 233 and 276.5 nm (ligand), 230.5 nm and 275 nm (La^{3+} complex), 230.5 nm and 274.5 nm (Sm^{3+} complex), 231 nm and 274.5 nm (Gd^{3+} complex), which may be assigned to the $\pi \rightarrow \pi^*$ transitions within the ligand.

The FAB mass spectra serve an important role in confirming the formation of the complexes with ligand **L**. The observed stepwise loss of the nitrate counterions and water molecules appears to be a common route of fragmentation and supports the presence of these species in the coordination sphere of the rare earth complexes [7].

The ^{1}H NMR spectra of $CDCl_2$ solution of the sodium and diamagnetic lanthanum complexes afford further evidence for the coordination ability of the ligand **L** towards these cations. Coordination of the

oxygen atoms to metal ion is confirmed by the upfield shift of the $OCH_2C{=}O$ protons from δ 5.0 in the free ligand to 4.6 in the complexes. The multiplet at δ 3.38–3.58 assigned to the CH_2 protons adjacent to the nitrogen in the ligand piperidide moiety split to two signals in the ratio 1:1 at δ 3.2 and 3.6 in the complexes. The remaining CH_2 protons upshield from δ 1.45 to 1.7. The significant downfield shift of the aromatic protons is found in the spectra of the complexes (δ 7.1 for Na^+ complex and 7.3 for La^{3+} complex) compared with the free ligand (δ 6.8). The chemical shift of the *tert*-butyl protons (from δ 1.09 to 1.15) is, as expected, only slightly affected by coordination due to the greater distance from the donor sites. The two dublets arising from equatorial and axial protons of $ArCH_2$ groups undergo shift from δ 3.2 and 5.1 in the ligand to δ 3.3 and 4.5 in the complexes. These data suggest that the coordination influences the conformation of calixarene ligand which adopt the more rigid structure upon complexation.

It should be noted here that attempts to obtain the complexes of **L** with dioxouranium ion were unsuccessful. The remarkably high stability and selectivity for the dioxouranium(VI) demonstrated by calixarenes makes these chelators potential 'uranophiles' [8]. However, the linear geometry of UO_2^{2+} limits the coordination structure to quasi-planar equatorial one [9]. Thus, the arrangement of potential donor atoms in this lower rim substituted calix[4]arene, on the contrary to unsubstituted ones, appears to be not appropriately designed to accommodate dioxouranium(VI) ion.

In order to establish the structure of the ligand and its complex an X-ray analysis of 5,11,17,23-tetra-*tert*-butyl-25,26,27,28-tetrakis-*O*(piperidinylcarbonyl)methylene)calix[4] arene and its sodium complex was performed.

3.1. Description of the crystal structures of **L** CH_2Cl_2 (**1**) and [**L** Na](Cl)·2(CH_2Cl_2)·2(CH_3OH) (**2**)

Details for the diffraction experiments are given in Section 1 and Table 1.

The crystals of **1** have been obtained by slow crystallization from methanol–methylene chloride; suitable for X-ray study crystals of complex **2** were obtained by recrystallization from methanol. m.p. 267–270 °C

The calixarene molecular structure of **1** reveals the slightly distorted open *cone* conformation in the solid state and creates a cavity which is large enough to accommodate a solvent molecules and this is what we observe, Fig. 1a. A partial occupancy (50.5%) dichloromethane molecule disordered over three positions is enclatrate within this cavity forming the solvent inclusion complex. Apparently the position of the CH_2Cl_2 guest molecule is determined by the interplay of rather weak forces and steric fit.

The calix conformation is defined by the dihedral angles which the aromatic rings make with the plane through the carbon atoms of the methylene groups which link them, viz. 62.7(1)° (A), 62.9(1)° (B), 58.6(1)° (C), and 71.9(1)° (D), all rings being tilted so that their *tert*-butyl groups are pitched away from the open cavity, Fig. 1b. The methylene bridge carbon atoms show out-of-plane distances less than 0.008 Å. The regularity of the cone may be also characterized by a set of torsion angles, φ and χ^i [10] about the methylene bonds at the calixarene macrocycle. These are listed in Table 2. Despite the relatively regular arrangement of the aromatic rings the mutual positions of lower rim amide substitutients are essentially asymmetrical. Three amide branches on A, B and D rings have a similar conformation with the ethereal and carbonyl oxygen in the *cis*-position in respect of singular C–C bond while in the fourth on C-ring the corresponding oxygen atoms are *gauche*, Table 2.

The piperidine moiety of the amide branches on A, B and D rings forms a pseudo-cavity in which enters the piperidine moiety of the amide branches on C ring and hydrophobic binding of piperidine moieties is the reason for this. The observed conformation of calixarene molecule could be also such due to the formation of three intramolecular C–H···O hydrogen bonds between amide methylene groups and the carbonyl oxygen atoms, excluding the O(6) carbonyl oxygen atom of C-amide branch, Table 3.

The calixarene sodium complex **2**, [**L** Na](Cl)·2(CH_2Cl_2)·2(CH_3OH) in the crystal structure has fourfold symmetry and adopts a relatively open *cone* conformation with the sodium on the fourfold axis (Fig. 2). The coordination polyhedron around Na^+ is a regular square antiprism, which is formed by four ether and four carbonyl oxygen atoms from four amide subunits with Na1–O1 and Na1–O2 distances 2.503(2) and 2.470(3) Å, respectively. The position of sodium is such that it is 1.140(3) Å from the plane of the four etheral oxygen atoms and 1.180(3) Å from the plane of the four carbonyl oxygen atoms. The cavity conformation of the complexed calixarene is rather similar to that of metal free analogue in **1**. The dihedral angles made by the aromatic rings with the plane through the carbon atoms of the methylene linking groups, all 65.17(7)° and close to that found in the structure of **1,** where the average value of such dihedral angles equal 64.03°. The torsion angles, φ and χ about the methylene bonds in **1** and **2** are also similar, Table 2. In the structures of related lower rim substituted calix amide and its sodium complex [11] the same manner of Na coordination have been found but in contrast to **1** and **2** the conformation of metal free and complexed calixarene macrocycles are essentially different. So one can conclude that the ligand **L** is better preorganized for sodium complexation. The extraction studies may provide evidence for this sugges-

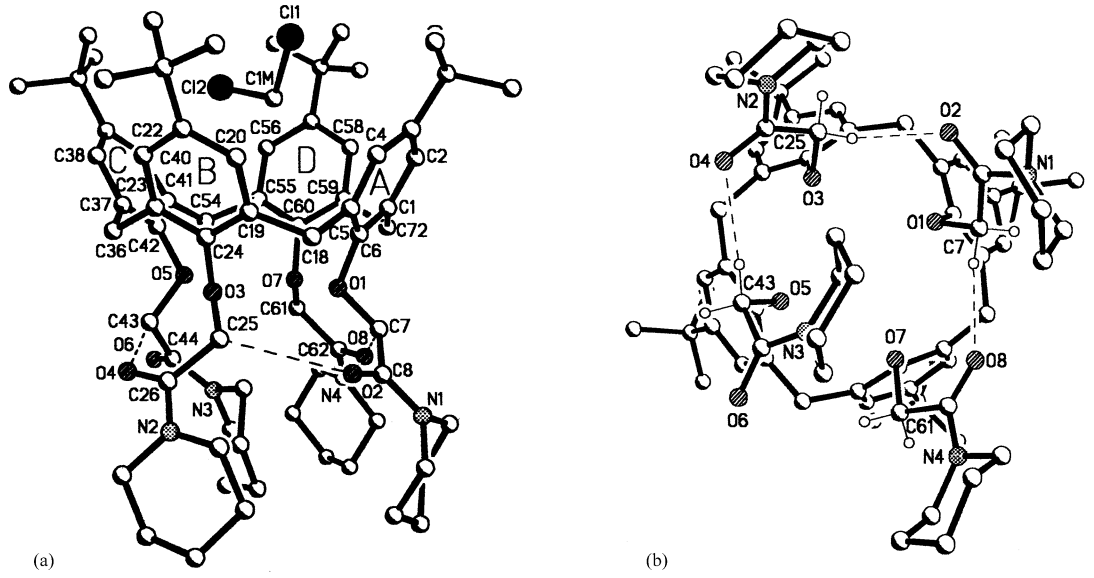


Fig. 1. (a), A general view of $\mathbf{L}\cdot CH_2CL_2$. The only highest occupancy position of disordered dichloromethane molecule is shown within the calixarene cavity. H-atoms are omitted for sake of clarity; (b), Lower rim view of the calixarene molecule illustrates the *self*-inclusion phenomena. The piperidine moiety enters a pseudo-cavity formed by three other amide branches. The hydrogen atoms involved in hydrogen bonds are shown.

Table 2
Selected torsion angles (°)

		1	2
C(4)–C(5)–C(18)–C(19)	φ_1	83.0(6)	
C(4)–C(5)–C(18)–C(1)#1			79.1(3)
C(5)–C(18)–C(19)–C(20)	χ_1	−81.7(6)	
C(5)–C(18)–C(1)#1–C(2)#1			−79.3(3)
C(22)–C(23)–C(36)–C(37)	φ_2	83.9(6)	
C(23)–C(36)–C(37)–C(38)	χ_2	−86.8(6)	
C(40)–C(41)–C(54)–C(55)	φ_3	86.8(6)	
C(41)–C(54)–C(55)–C(56)	χ_3	−73.2(6)	
C(58)–C(59)–C(72)–C(1)	φ_4	72.4(6)	
C(59)–C(72)–C(1)–C(2)	χ_4	−82.0(6)	
C(1)–C(6)–O(1)–C(7)		63.2(6)	97.8(3)
C(6)–O(1)–C(7)–C(8)	A	111.4(5)	−152.5(3)
O(1)–C(7)–C(8)–O(2)		−0.6(7)	3.8(5)
C(19)–C(24)–O(3)–C(25)		61.8(6)	
C(24)–O(3)–C(25)–C(26)	B	114.2(5)	
O(3)–C(25)–C(26)–O(4)		−2.5(8)	
C(37)–C(42)–O(5)–C(43)		73.6(6)	
C(42)–O(5)–C(43)–C(44)	C	127.1(5)	
O(5)–C(43)–C(44)–O(6)		−102.2(6)	
C(55)–C(60)–O(7)–C(61)		70.0(6)	
C(60)–O(7)–C(61)–C(62)	D	126.7(5)	
O(7)–C(61)–C(62)–O(8)		0.8(8)	

Symmetry transformations used to generate equivalent atoms: #1 $-y+1/2, x, z$.

Table 3
Intramolecular hydrogen bonds for **1** (Å and °)

D–H···A	d(D–H)	d(H···A)	d(D···A)	<(DHA)
C(7)–H···O(8)	0.99	2.18	3.120(7)	158.0
C(25)–H···O(2)	0.99	2.24	3.148(6)	152.7
C(43)–H···O(4)	0.99	2.36	3.333(7)	167.0

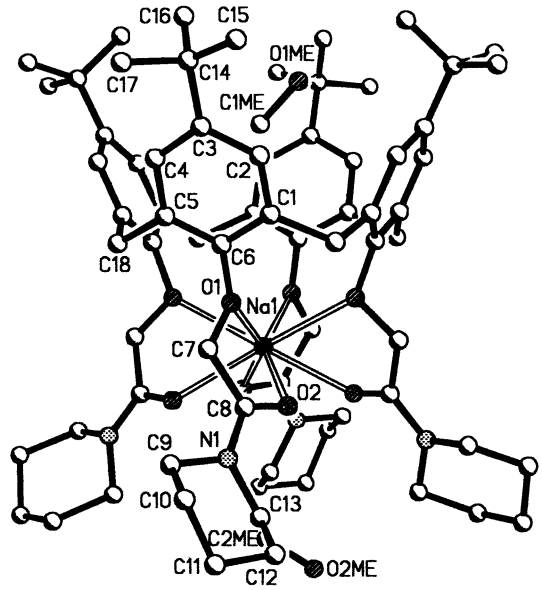


Fig. 2. A view of the Na-calixarene complex **2.** The methanol molecules (C1ME–O1ME and C1ME–O1ME) are disordered about the fourfold axis passing through C1ME, Na1 and C2ME atoms. Only one position of disordered solvent molecules and *tert*-butyl groups are shown.

tion and we are pursuing that line of investigation. Methanol molecule is enclatrated within calix cavity with the carbon atom residing on the fourfold axis and the oxygen disordered over four sites about the fourfold axis. There is also a second methanol molecule residing

on the fourfold axis like a 'saucer' of the four piperidine groups (Fig. 2). Similar to the calixarene–amide copper(II) complex [12] in the crystal structure of **2** the calixarene complexes are packing in head-to-tail manner along fourfold axis so that the methanol molecules may be involved in hydrogen bonding. The O1ME···O2ME spacing for four disordered positions are 2.68(3), 2.92(3), 3.19 (3) and 3.39(3) Å and at least two of them suitable for O–H···O hydrogen bonds. These methanol pairs enclose the calixarene cavity and a 'saucer' for the four piperidine groups, which result in total encapsulating of Na^+ cation and extend the calixarene complexes as one-dimensional chain along *c* axis of the crystal. The disordered chlorine anions reside on twofold-axes and well separated in the structure from the Na^+ cations. This feature of the crystal structures according to the principals reported in [13] is favorable for membrane electrode response, considering **L** as Na^+ ion carrier.

On the basis of available evidence it can be concluded that the sodium, yttrium and lanthanide ions, contrary to dioxouranium(VI) ion, are suitable guests for 5,11,17,23-tetra-*tert*-butyl-25,26,27,28-tetrakis-*O*(piperidinylcarbonyl)methylene)calix[4]arene host. The effectiveness of transmetallation reaction and the failure of this system to undergo the complexation reaction with dioxouranium ion reveals that the lower rim substituted *tert*-butyl calix[4]arenes may be regarded as interesting ligands towards the rare earth ions, either for extraction purposes, or for other potential application involving the biomedical diagnostics, fluorescence labels and photonic supramolecular devices.

4. Supplementary material

Suplementary data are available from the Cambridge Crystallographic Data Centre (CCDC), 12 Union Road, Cambridge CB2 1EZ, UK on request quoting the deposition numbers CCDC 168643 (**1**), CCDC 168644) (**2**).

References

[1] A. Casnati, Gaz. Chim. Ital. (1997) 127, 637 and refs therein.
[2] C. Jeunesse, C. Dieleman, S. Steyer, D. Matt, J. Chem. Soc., Dalton Trans. (2001) 881.
[3] F. Arnaud-Neu, S. Cremin, S. Harris, A. McKervey, M.-J. Schwig-Wiell, P. Schwinté, A. Walker, J. Chem. Soc., Dalton Trans. (1997) 329.
[4] M. Bocheńska, R. Banach, A. Zielinska, V.C. Kravtsov, J. Incl. Phenom. Macroc. Chem. 39 (2001) 219.
[5] G.M. Sheldrick, SHELX-97: Programs for the Solution and Refinement of the Crystal Structures, University of Göttingen, Germany, 1997.
[6] W. Radecka-Paryzek, V. Patroniak-Krzyminiewska, H. Litkowska, Polyhedron 17 (1998) 1477.
[7] W. Radecka-Paryzek, M. Kaczmarek, V. Patroniak, I. Pospieszna-Markiewicz, J. Alloys Comp. 323–324 (2001) 173.
[8] J. Harrowfield, Gaz. Chim. Ital. (1997) 127, 663 and refs therein.
[9] P. Thuéry, M. Nierlich, B. Masci, Z. Asfari, J. Vicens, J. Chem. Soc., Dalton Trans. (1999) 3151.
[10] F Ugozzoli, G. Andreetti, J. Inclusion Phenom. Mol. Recognit. Chem. 13 (1992) 337.
[11] L. Frkanec, A. Visnjevac, B. Kojic-Prodic, M. Zinic, Chem. Eur. J. 6 (2000) 442.
[12] F. Arnaud-Neu, G. Barret, D. Corry, S. Cremin, G. Ferguson, J.F. Gallagher, S.J. Harris, M.A. McKervey, M.-J. Schwing-Weill, J. Chem. Soc., Perkin Trans. 2 (1997) 575.
[13] E. Luboch, J.F. Biernat, Y.A. Simonov, V.C. Kravtsov, V.K. Bel'ski, Supramolecular Chem. 11 (1999) 109.

PERGAMON

Polyhedron 21 (2002) 769–777

POLYHEDRON

www.elsevier.com/locate/poly

Complexation of 3-(2-pyridyl)substituted *N*-methyl isoxazolidine with Pd(II), Zn(II) and Cu(II): stereochemistry of co-ordination compounds in solution and solid-state

Andrey B. Lysenko [a], Konstantin V. Domasevitch [a], Emma Peralta-Pérez [b], Fernando López-Ortiz [b], Jonathan W. Steed [c], Rostislav D. Lampeka [a,*]

[a] *Department of Chemistry, Kiev National University, Vladimirskaja Str. 64, 01033 Kiev, Ukraine*
[b] *Área de Química Orgánica, Universidad de Almería, Carretera Sacramento s/n, 04120 Almería, Spain*
[c] *Department of Chemistry, King's College London, Strand, London, WC2 R2LS, UK*

Received 3 August 2001; accepted 13 December 2001

Abstract

2-Methyl-3-(2-pyridyl)isoxazolidine (**L**) and its Pd(II), Zn(II) and Cu(II) complexes have been prepared and characterized by IR, ^{1}H, ^{13}C 1D and HMBC, NOESY 2D NMR spectroscopies. The stereochemistry of the 'free' and co-ordinated ligand has been assigned by nuclear Overhauser effect (NOE). The molecular structures of [Zn(*cis*-**L**)Cl_2]·0.5$CHCl_3$ (**2a**), [Zn(*cis*-/*trans*-**L**)Cl_2] (**2a**–**b**) and [Cu(*cis*-/*trans*-**L**)Cl_2]$_2$ (**4a**–**b**) have been established by means of X-ray crystallography. The crystal structure of **2a** consists of a racemic mixture of *cis*-**L** (3*SR*,5*RS*), while the crystal structure of **2b** comprises a racemate of *cis*- and *trans*-isomeric forms. For both complexes the zinc atoms adopt nearly tetrahedral co-ordination with two chlorine atoms and *N*,*N*-bidentate co-ordinated **L**. The crystal structure of **4a**–**b** consists of dinuclear [Cu(*cis*-/*trans*-**L**)Cl_2]$_2$ moieties with *N*,*N*-bidentate co-ordinated ligands. The square pyramidal co-ordination spheres of copper ions are completed by a bridging chloride ligand at the apex (Cu–Cl 2.79, 2.82 Å).
© 2002 Elsevier Science Ltd. All rights reserved.

Keywords: Isoxazolidines; Pd-, Zn-, Cu-complexes; Syntheses; X-ray; NMR

1. Introduction

Isoxazolidine systems are important in bioscience as intermediates for organic synthesis of a number of natural compounds: 1,3-aminoalcohols, alkaloids and amino sugars [1–4]. Their pharmacological properties [5–9] have stimulated interest on the control of diastereo- and enantioselectivity in 1,3-nitrone-olefine dipolar cycloaddition as the isoxazolidine preparation method. The last decade has revealed a great deal of research on improving methods for stereoselective synthesis of isoxazolidines [10–18]. Thus, nitrone-tricarbonyl(η^6-arene)chromium(0) adducts undergo cycloaddition reactions in a highly stereoselective manner yielding *cis*-3,5-disubstituted isoxazolidines [19,20]. Very recently, Cu(II)- and Zn(II)-bisoxazoline [21] as well as (BINOL)–AlMe complexes (BINOL = 2,2′-dihidroxy-1,1′-binaphthyl) [22] have been utilized as catalysts in the enantioselective synthesis of isoxazolidines through 1,3-dipolar cycloadditions of nitrones to electron-rich olefins. The stereochemistry of the products has been explained by assuming the formation of a complex between the nitrone and the catalysts.

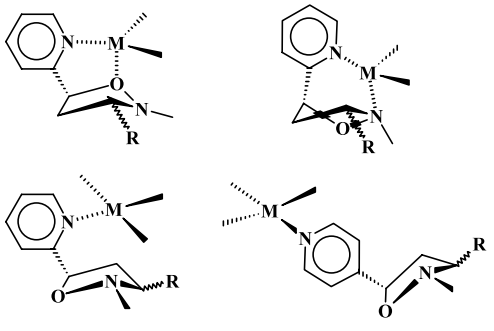
Our interest is focused on co-ordination chemistry of the isoxazolidine systems concerning possible application of the metal complexes for the asymmetric 1,3-dipolar cycloaddition reactions between alkenes and acyclic nitrones [23,24]. Elaboration of this approach is closely related with investigation of isoxazolidine co-ordination compounds themselves because it may give significant information for understanding the importance of inherent structure of the co-ordination compounds for 1,3-dipolar cycloaddition and processes of purification and separation of isomeric isoxazolidines.

* Corresponding author. Fax: +380-44-463-6417.
E-mail address: r.lampeka@clariant.com.ua (R.D. Lampeka).

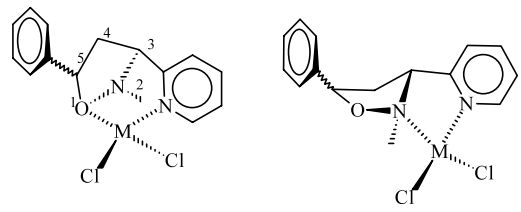
0277-5387/02/$ - see front matter © 2002 Elsevier Science Ltd. All rights reserved.
PII: S0277-5387(02)00840-9

Recently, we have shown that the pyridyl substituted *N*-methyl isoxazolidines readily give co-ordination compounds with d-metal ions [23,25]. The 5-(2-pyridyl)substituted isoxazolidine core may act either as monodentate ligand through the nitrogen atom of the pyridyl substituent or as bidentate ligand (*N*,*N* for Pd, Pt; *N*,*O* for Zn). In each case, the metal co-ordinates the pyridyl nitrogen atom and one of the heteroatoms of the isoxazolidine ring (Scheme 1).

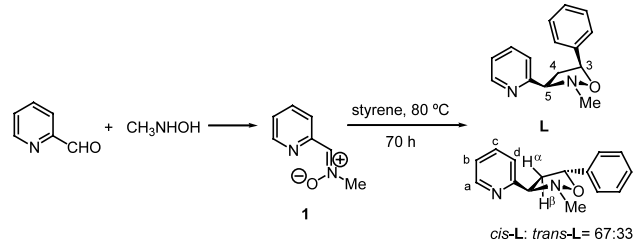
Herein we present our results on the synthesis of isomeric *cis*-/*trans*-2-methyl-3-(2-pyridyl)-5-phenylisoxazolidine (**L**) and the study of its co-ordination behavior with Pd, Zn and Cu metal ions. The presence of one co-ordinatively active substituent on the isoxazolidine ring may give rise to different co-ordination modes to the metals (Scheme 2).



Scheme 1. Co-ordination features of 5-pyridyl substituted isoxazolidines.



Scheme 2. The possible modes of chelate complexation for 2-methyl-3-(2-pyridyl)-5-phenylisoxazolidine.



Scheme 3. NOE correlations of **L**.

2. Results and discussion

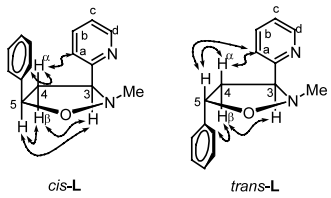
2.1. Synthesis and structural identification of *L*

The organic ligand **L** was obtained through the [3+2] dipolar cycloaddition of *N*-methyl-*C*-(2-pyridyl)nitrone (**1**) to freshly distilled styrene in refluxing toluene–benzene (1:1, v/v) (Scheme 3). Analysis of the crude reaction showed the presence of two products in an approximate ratio 67:33 which were identified, respectively, as the *cis*- and *trans*-stereoisomers of 2-methyl-3-(2-pyridyl)-5-phenylisoxazolidine, i.e. a single regioisomer was observed. Column chromatography on silicagel (acetone–hexane 1:1) of the crude product afforded pure *cis*-/*trans*-**L** without altering the relative ratio of isomers.

The IR spectrum of **L** is similar to the related 5-(2-pyridyl)isoxazolidine [23] and shows characteristic strong absorptions at 2990–3090 (ν(C–H) ph, py), 1490–1590 (ν(C=C) ph, py), 2780–2960, 1335–1475 cm^{-1} (ν(C–H) and δ(C–H) of the aliphatic groups).

The ^{1}H NMR spectrum of **L** suggests the presence of two diastereomers. The analysis of the coupling constants in combination with nuclear Overhauser effects (NOEs) (Scheme 3) allows facile determination of both the configurations for 3,5-disubstituted isoxazolidine systems.

The ^{1}H NMR spectrum measured in DMSO-d_6 showed separate signals for the most significant protons of both stereoisomers (overlap occurred for the phenyl protons and H(c) of the 2-pyridyl group). The HMQC and HMBC correlation spectra allowed the straightforward assignment of the ^{1}H and ^{13}C NMR spectra. The use of $CDCl_3$ as solvent produced only minor changes in the chemical shifts of the signals (see Section 4). In principle, the relative stereochemistry of the stereogenic centers of **L** could be established from the observed coupling constants for the proton at C(5) as it has been shown for several 3,5-disubstituted isoxazolidines [26] (H(5) proton appeared as a double doublet ($^3J_{HH}$ 3–6 Hz) for the *cis* isomer, and a doublet for the *trans* derivative ($^3J_{HH}$ $\sim$5 Hz). Unfortunately, in our case both isomers produced the same multiplicity pattern for H(5), a triplet, with the same vicinal couplings ($^3J_{HH}$ 7.7 Hz), precluding to draw any stereochemical conclusion of the configuration of the isoxazolidine moiety. The 2D NOESY spectrum of the *cis*-, *trans*-**L** mixture allowed to solve the ambiguity. The major isomer is assigned the *cis* stereochemistry based on the intense correlation observed between H(3) (δ 4.19) and H(5) (δ 5.32). Additionally, the methylene proton at δ 2.46 (H(4α), dt, $^2J_{HH}$ 12.3, $^3J_{H4\alpha H3} = {}^3J_{H4\alpha H5}$ 6.9 Hz) shows the expected cross peaks with both the 2-pyridyl (δ(H^d) 7.58, see Scheme 2 for labeling) and the phenyl (δ(H^o) 7.3) substituents corresponding to their *syn* orientation. Consequently, the double triplet at δ 3.23 ($^2J_{HH}$ 12.3, $^3J_{H4\beta H3} = {}^3J_{H4\beta H5}$ 7.7 Hz) is assigned to the other methylene proton H(4β) (Scheme 4).



Scheme 4. H(α) defines the proton *syn* to the 2-pyridyl ring.

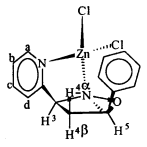
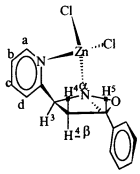
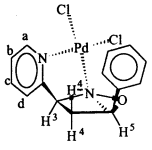
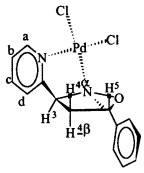
Therefore, the minor component of the mixture is the *trans* isomer. This assignment is supported by the NOE correlation between H(3) (δ 4.04, dd, $^3J_{H4\alpha H3}$ 6.5, $^3J_{H4\beta H3}$ 7.7 Hz) and the *ortho* protons (δ 7.42, m) of the phenyl ring linked to C(5) (δ 5.07, t, $^3J_{HH}$ 7.7 Hz). Again, the methylene protons are assigned from the respective correlations with H(3) and H(5) (see Section 4).

2.2. Synthesis and structural identification of complexes 2–4

Complexation of the isomeric mixture of isoxazolidines **L** with Pd(II), Zn(II) and Cu(II) metal ions was carried out by heating an alcoholic solution of the ligand with the corresponding zinc and copper chloride, or with the $Na_2[PdCl_4]$ complex for palladium. Cooling the reaction mixture to room temperature afforded a precipitate which was separated, washed with alcohol (methanol or 2-propanol) and dried, yielding the metal complexes [Zn(*cis*-/*trans*-**L**)Cl_2] (**2a**–**b**), [Pd(*cis*-/*trans*-**L**)Cl_2] (**3a**–**b**), and compound [Cu(*cis*-/*trans*-**L**)$Cl_2]_2$ (**4a**–**b**). All the compounds are air stable both as solids and in solution. They are readily soluble in acetonitrile, *N*,*N*-dimethylformamide, dimethyl sulfoxide and almost insoluble in hexane.

The ^{1}H and ^{13}C NMR data of compounds **2**–**4** acquired in DMSO-d_6 are given in Table 1. The assignment of the proton and carbon atom signals was easily made based on the analysis of the 1D (^{1}H, APT) and 2D (HMQC, HMBC) spectra. The NMR spectra of the complexes showed two sets of signals derived from the co-ordinated isomeric *cis*- and *trans*-isoxazolidines. The ratio of isomers was similar to that of the free ligand **L** (average *cis*–*trans* ratio of 65:35). As for the free ligand, the relative stereochemistry of the two carbon stereogenic centers was unambiguously deduced from the NOE correlations observed in the corresponding NOESY spectra. In all cases H(3) and H(5) exhibited a strong dipolar correlation for the *cis* isomers, while for the *trans* derivatives a correlation of low intensity was

Table 1
^{1}H and ^{13}C NMR data of complexes **2**–**3**

Compound		^{1}H NMR (δ, ppm; *J* Hz)		Assignment	^{13}C NMR (δ, ppm)		Assignment
2a	**2b**	**2a**	**2b**		**2a**	**2b**	
		2.79 (s, 3H)	2.71 (s, 3H)	CH_3	44.63	44.38	C-4
		2.45 (m, 1H)	2.61 (m, 1H)	$H^{4\alpha}$	44.71	44.94	CH_3
		3.29 (m, 1H)	2.89 (m, 1H)	$H^{4\beta}$	72.70	73.11	C-3
		4.33 (m, 1H)	4.16 (m, 1H)	H^3	78.25	79.28	C-5
		5.36 (t, ^3J 7.6, 1H)	5.03 (dd, ^3J 7.2, 1H)	H^5	122.19	122.59	C^d
		7.1-7.3 (m, 3H)	7.1-7.3 (m, 3H)	*m,p*-Ph,	123.22	123.48	C^b
		7.24 (m, 2H)	7.48 (m, 2H)	*o*-Ph	126.95	127.09	*o*-Ph
		7.38 (m, 1H)	7.4 (m, 1H)	H^b	127.98	128.22	*p*-Ph
		7.6 (m, 1H)	7.6 (m, 1H)	H^d	128.67	128.82	*m*-Ph
		7.85 (m, 1H)	7.87 (m, 1H)	H^c	137.92	137.92	C^c
		8.54 (m, 1H)	8.57 (m, 1H)	H^a	141.35	140.85	*Ipso*-Ph
					149.00	149.23	C^a
					160.01	159.0	*Ipso*-Py
3a	**3b**	**3a**	**3b**		**3a**	**3b**	
		3.42 (s, 3H)	3.37 (s, 3H)	CH_3	45.16	43.82	C-4
		2.77 (dt, ^3J 8.4, ^2J 12.7, 1H)	3.07 (ddd, ^3J 6.8, 7.8, ^2J 12.7 1H)	$H^{4\alpha}$	53.35	52.09	CH_3
		3.42 (m, 1H)	2.96 (ddd, ^3J 7.8, 10.0, ^2J 12.7, 1H)	$H^{4\beta}$	81.60	81.37	C-3
		5.32 (dd, ^3J 7.4, 8.4, 1H)	5.12 (dd, ^3J 7.1, 10.0, 1H)	H^3	81.73	82.12	C-5
		5.58 (dd, ^3J 6.3, 8.4, 1H)	5.92 (t, ^3J 7.8, 1H)	H^5	123.74	123.34	C^d
		7.35 (m, 2H)	7.35 (m, 2H)	*m*-Ph	125.23	125.49	C^b
		7.42 (m, 1H)	7.42 (m, 1H)	*p*-Ph	127.21	127.75	*o*-Ph
		7.53 (m, 1H)	7.52 (m, 2H)	*o*-Ph	128.97	129.09	*m*-Ph
		7.61 (ddd, ^4J 1.4, ^3J 6.0, 7.9, 1H)	7.67 (ddd, ^4J 1.2, ^3J 6.0, 7.8, 1H)	H^b	129.03	129.38	*p*-Ph
		7.71 (dd, ^4J 1.4, ^3J 7.9, 1H)	7.77 (dd, ^4J 1.2, ^3J 7.8, 1H)	H^d	137.48	137.01	*Ipso*-Ph
		8.15 (dt, ^4J 1.8, ^3J 7.9, 1H)	8.21 (dt, ^4J 1.4, ^3J 7.8, 1H)	H^c	141.10	141.31	C^c
		8.88 (dd, ^4J 1.8, ^3J 6.0, 1H)	8.89 (dd, ^4J 1.4, ^3J 6.0, 1H)	H^a	149.23	149.63	C^a
					162.16	161.42	*Ipso*-Py

detected between H(5) and the *ortho* protons of the phenyl substituent on C(3). The methylene protons H(4) were again assigned through their respective correlations with the vicinal protons H(3)/H(5).

The complexation of both ligands is evidenced by the variations of the proton chemical shifts compared with the free isoxazolidines. In compounds **2a**–**b**, the co-ordination of **L** to Zn(II) produce a broadening of all proton signals and a partial overlap of the aromatic protons corresponding to both stereoisomers. Clearly, for **2a**–**b** co-ordination occurred in the proximity of H(3). This is the only proton of the isoxazolidine moiety showing a significant deshielding effect due to the complexation ($\Delta\delta$H(3)^{cis} (**2a**–**L**) = 0.14 ppm; $\Delta\delta$H(3)^{trans} (**2b**–**L**) = 0.12 ppm). Variations on H(4) and H(5) are lower than 0.05 ppm. In principle, the effect on H(3) is compatible with **L** acting either as a *N*-monodentate or *N*,*N*-bidentate ligand. Co-ordination through the nitrogen of the pyridine is supported by the deshielding observed for the protons H(b) ($\Delta\delta$H(b)^{cis} (**2a**–**L**) = 0.07 ppm; $\Delta\delta$H(b)^{trans} (**2b**–**L**) = 0.05 ppm) and H(c) ($\Delta\delta$H(c)^{cis} (**2a**–**L**) = 0.16 ppm; $\Delta\delta$H(c)^{trans} (**2b**–**L**) = 0.17 ppm) of the heterocycle. On the other hand, co-ordination to the nitrogen of the isoxazolidine would prevent rapid inversion of the heteroatom, originating a new stereogenic center which relative configuration could be identified in the NOESY spectrum. Indeed, the methyl protons of *cis*-**L** in **2a**–**b** (δ 2.74) showed a dipolar correlation with H(3) and H(5), while for *trans*-**L** only the correlation of the methyl protons at δ 2.67 with H(3) was detected. These evidences indicate that in complex **2a**–**b** the ligand is bonded to the metal in a *N*,*N*-bidentate mode.

The same trends have been observed in the proton spectrum of the mixture of isomers **3a**–**b**. In this case, co-ordination of **L** to palladium produced a much stronger effect on the proton spectrum of isoxazolidine and all signals appeared deshielded compared to the free ligand. The low field shift ranged from $\Delta\delta$(**3a**–**b**–**L**) = 0.19–0.85 ppm for H(4), H(5) and the methyl protons. Even though, the shifts for H(3) exceeded 1 ppm ($\Delta\delta$H(3)^{cis} (**3**–**L**) = 1.13 ppm; $\Delta\delta$H(3)^{trans} (**3**–**L**) = 1.08 ppm). Again, the deshielding of the pyridine protons (see Table 1) and the NOEs measured for the methyl protons are consistent with **L** being doubly co-ordinated to the metal through the nitrogen atoms.

The differences in line-broadening and range of chemical shifts variations promoted by Zn versus Pd co-ordination to **L** suggest that in DMSO the solvent is competing with the ligand **L** for binding to the zinc ion and therefore, the proton spectrum of **2a**–**b** corresponds to the average situation derived from the exchange between free and complexed ligand which is rapid on the NMR time scale.

2.3. Crystal structures of [Zn(*cis*-**L**)Cl_2]·0.5$CHCl_3$ (**2a**), [Zn(*cis*-/*trans*-**L**)Cl_2] (**2a**–**b**) and [Cu(*cis*-/*trans*-**L**)Cl_2]$_2$ (**4**)

The NMR results described above indicated that compounds **2**–**4** are mixtures of stereoisomers. Recrystallization of the crude products obtained opens up different possibilities for these systems: resolution of racemic *cis*-/*trans*-isomers, self-resolution of enantiomers and co-crystallization of *cis*- and *trans*-isomers. In all cases, further insight into the structural characteristic of the co-ordination complexes could be gained through the analysis of the solid state structure (Fig. 1).

Recrystallization of **2** by slow diffusion of 2-propanol into a chloroform solution of the metal complex afforded two products suitable for X-ray analysis. One of them, [Zn(*cis*-**L**)Cl_2]·0.5$CHCl_3$ (**2a**) consists of racemic mixture of *cis*-**L** (3*SR*,5*RS*), while another one [Zn(*cis*-/*trans*-**L**)Cl_2] (**2a**–**b**) is a racemate including both *cis*- and *trans*-forms. These structures are built up from molecular [Zn(**L**)Cl_2] species, but are dramatically different in the spatial arrangement of the molecules (Figs. 2 and 3). There is a lack of strong intermolecular interactions such as co-ordination or hydrogen bonding. However, the packing pattern for the compounds is determined by stacking interactions between two aromatic functions of the ligand. Complex **2a** consists of dimers sustained by π–π, or face-to-face, stacking between pyridine groups. These weak but commonly encountered interactions contribute to crystal structures of aromatic species [27] and may be loosely regarded as a kind of 'supramolecular synthon' [28]. Two pyridine rings are parallel and the distance between their planes is approximately 3.28 Å. Two molecular complexes being paired in such a way (Py–Py) evidently generates a center of inversion in the triclinic crystal, and the lattice comprises a racemic mixture.

Stacking interactions are also present in the packing pattern of complex **2a**–**b** but between different functions, the pyridyl and phenyl groups. They also appear to be parallel with interplanar separation at approximately 3.45 Å. From this point of view, structures **2a** and **2a**–**b** may be regarded as supramolecular isomers (see Fig. 3). For complex **2a**–**b**, face-to-face stacking interactions connect the molecules into 1D chain and unsymmetric pairing results in the absence of a center of inversion. Nevertheless, the crystal also comprises both enantiomers that are related by a glide plane.

Another important feature of the structure **2a**–**b** is disordering of the C(3)–Ph fragment. This disorder has a clear chemical significance as two components correspond to *cis*- and *trans*-isomeric forms of the ligand. Refinement of partial occupancies suggested contributions of *cis*- (72%) and *trans*- (28%) isomers similar to that found in the crude product mixture (67 and 33%). Both isomers have actually the same size, shape and

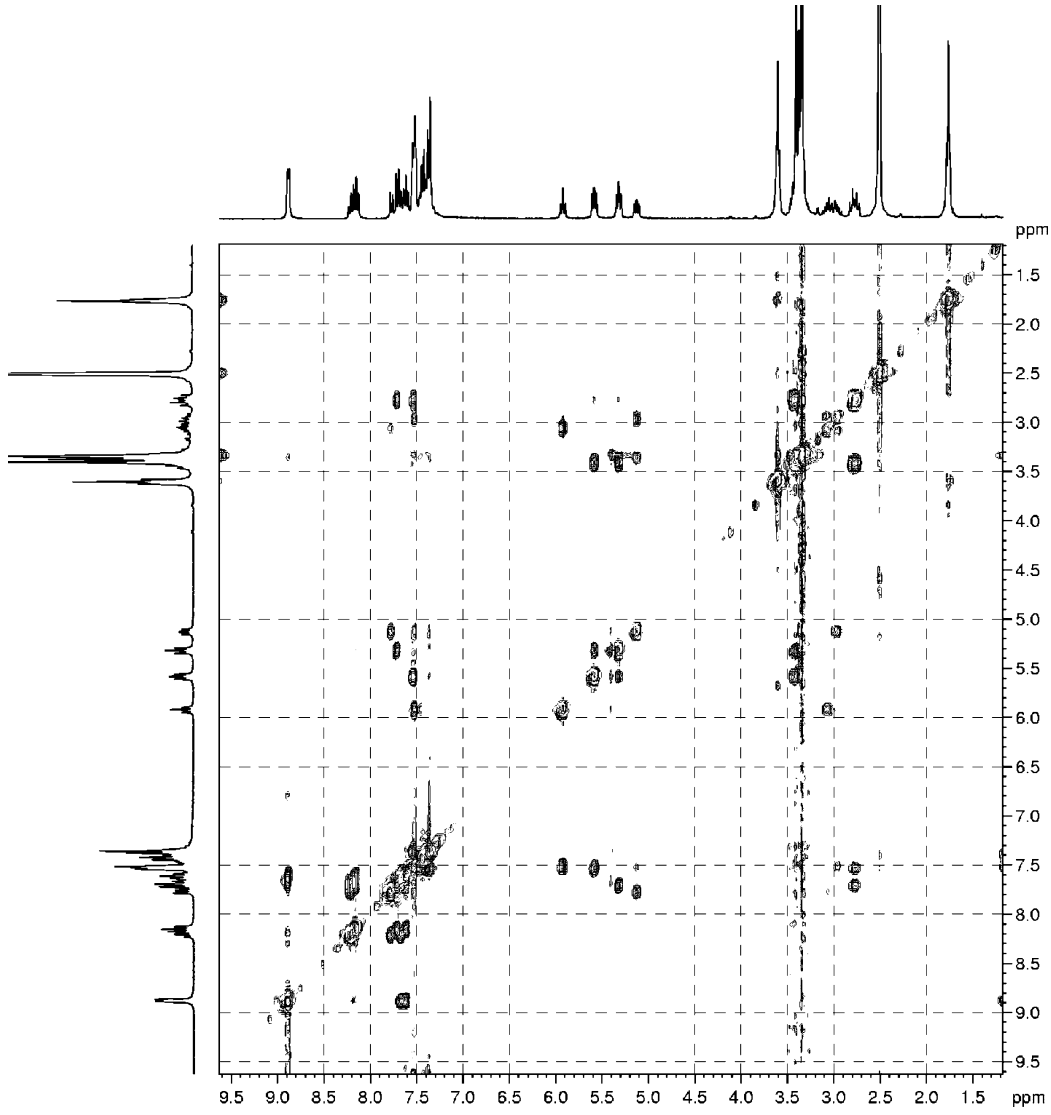


Fig. 1. The 2D NOESY spectrum of [Pd(*cis*-/*trans*-**L**)Cl_2] (300 MHz, DMSO-d_6/THF-d_8).

orientation of functional groups and (Fig. 2) therefore statistically occupy positions in the crystal. The resulting structure may be described as a solid-state solution of isomeric complexes. The existence of such phases may preclude the possibility of separation of isomeric isoxazolidines and their metal complexes by crystallization.

The zinc atoms in **2a**–**b** adopt a nearly tetrahedral co-ordination polyhedron with two chloride ligands and one *N*,*N*-bidentate co-ordinated **L**. In contrast to the X-ray data for a related structure of the palladium complex with *trans*-2-methyl-5-(2-pyridyl)-3-phenylisoxazolidine, the structure of **2a** possesses a Zn–N(1) bond (2.134(4) Å) longer than Zn–N(2) 2.049(4) Å) [23]. The five-membered chelate ring in both structures of zinc complex is almost planar. The atoms Zn(1) and N(1) deviate by −0.12 and 0.18 Å, respectively, from the mean plane of the other atoms this cycle. The isoxazolidine ring in the structures possesses an envelope conformation. In structure **2a**, the methyl group has an axial orientation to the isoxazolidine ring, while the phenyl and pyridine substituents are situated in an equatorial manner (C(6)–C(7)–C(8)–C(9) 159.5(4)°) (Table 2). In structure **2a**–**b**, the phenyl group and pyridyl ring are situated in an equatorial manner at the isoxazolidine cycle (C(10)–C(3)–C(2)–C(1) 153.7°) while the methyl group is located in an axial position (C(4)–N(1)–O(1)–C(3) −93.4°) (Table 3). The structure of copper complex **4a**–**b** (Fig. 4) consists of a neutral dimers [Cu(*cis*-/*trans*-**L**)Cl_2]$_2$. The copper atoms are co-ordinated in a distorted square pyramid comprising two nitrogen and two chlorine atoms in an equatorial plane (Cu–Cl 2.244(2)–2.262(2) Å) and an additional chloride ligand is situated in the apex (Cu–Cl 2.795(2), 2.818(2) Å). Thus two bridging chlorine atoms

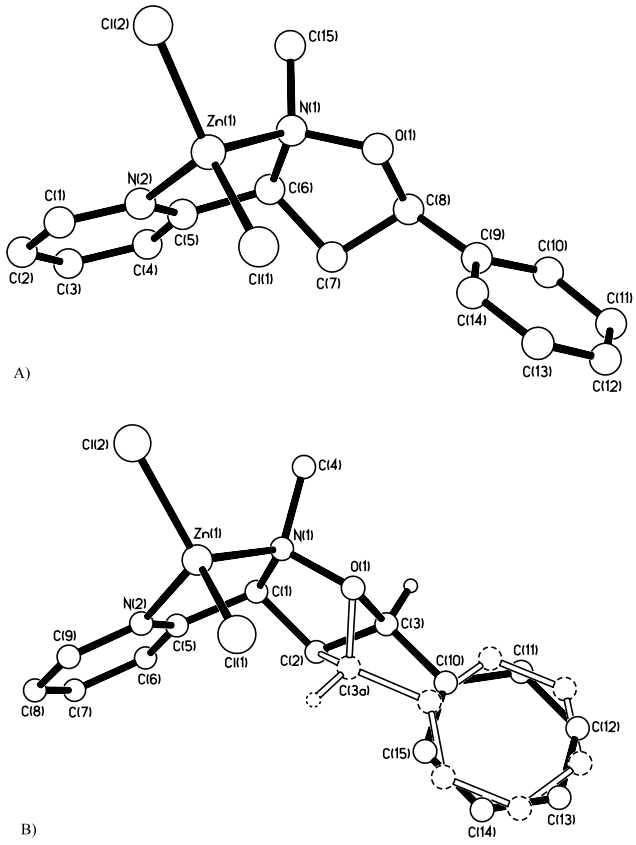


Fig. 2. Molecular structure of [Zn(**L**)Cl_2]: (A) *cis*-isomeric form of the ligand in structure **1a**. Selected bond length, Å: Zn(1)–N(2) 2.049(4); Zn(1)–N(1) 2.134(4); Zn(1)–Cl(2) 2.208(1); Zn(1)–Cl(1) 2.209(1); (B) disordering scheme for C–C_6H_5 fragment in structure **1b** suggests presence of *cis*- and *trans*-isomeric forms that possess the same shape and form mixed crystal. Selected bond length, Å: Zn(1)–N(2) 2.038(3); Zn(1)–N(1) 2.109(4); Zn(1)–Cl(1) 2.202(1); Zn(1)–Cl(2) 2.211(1).

connects molecular units [Cu(**L**)Cl_2] into the dimer (Table 4). The latter one is actually centrosymmetric, and all three pairs of isoxazolidine asymmetric atoms within the dimer frame possess opposite chirality. N-co-ordination of the isoxazolidine to the metal atom also makes impossible pyramidal inversion at the nitrogen atom, and the co-ordinated isoxazolidine core possesses three chiral centers simultaneously. Nevertheless, systematic absences suggest the chiral space group $P2_12_12_1$. The structure also shows high parameters for thermal motion of the isoxazolidine C–Ph fragment (U_{iso} 0.1–0.2 $Å^2$) that may be ascribed to co-crystallization of *cis*- and *trans*-isomeric forms, by analogy with **2a**–**b**. Both five-membered chelate rings formed are almost planar. The isoxazolidine ring has an envelope conformation and the methyl group possesses the axial position in the isoxazolidine ring (C(1A)–N(1A)–C(4A)–C(3A) 115.0°), whereas the pyridyl substituted is located in an *anticlinal* arrangement with the C(2)–C(3) bond.

3. Conclusions

2-Methyl-3-(2-pyridyl)-5-phenylisoxazolidine has been regioselectively synthetized as a 67:33 *cis*–*trans* mixture by reaction of *N*-methyl-*C*-(2-pyridyl)nitrone with styrene. The new ligand readily forms co-ordination compounds with Zn(II), Cu(II) and Pd(II) chlorides which solution structure has been assigned through 1D and 2D NMR spectroscopy. The organic ligand in the complexes is co-ordinated in a *N*,*N*-bidentate chelating mode, in contrast to isomeric 5-(2-pyridyl)substituted *N*-methyl isoxazolidine. The configuration and conformation of the isoxazolidine ring have been determined by NOE NMR experiments and confirmed by means of the X-ray diffraction data for zinc and copper chloride complexes. The crystal structure of [Zn(*cis*-/*trans*-**L**)Cl_2] (**2a**–**b**) and [Cu(*cis*-/*trans*-**L**)Cl_2] (**4a**–**b**) revealed the co-crystallization of *cis*- and *trans*-isomers of the ligand. For the zinc complex it has been also possible to isolate and characterize the co-ordination compound derived from the *cis*-isoxazolidine [Zn(*cis*-**L**)Cl_2]·0.5$CHCl_3$ (**2a**).

4. Experimental

4.1. Synthesis

All solvents were used as supplied or distilled using standard methods. The starting materials for the synthesis of organic ligands and complexes were commercial products of reagent grade (Fluka, Aldrich). The *N*-methyl-*C*-(2-pyridyl)nitrone (**1**) was prepared as previously described [24].

4.1.1. 2-Methyl-3-(2-pyridyl)-5-phenylisoxazolidine (**L**)

Freshly distilled styrene (20.2 ml, 18.36 g, 176.54 mmol) was added to a $C_6H_5CH_3$–C_6H_6 solution (1:1 v/v, 30 ml) of *N*-methyl-*C*-(2-pyridyl)nitrone (3.00 g, 22.06 mmol). The reaction mixture was stirred at reflux for 70 h and then concentrated in vacuo. Undesired side products were removed by means of column chromatography on silica gel with C_3H_6O–C_6H_{14} (1:1) as an eluent. The yield of **L** (yellow oil, mixture of *cis*–*trans* isomers in a ratio 67:33) was 3.18 g ($\sim$60%).

IR (film between KBr discs, cm^{-1}): 3085, 3065, 3035, 3010, 2990, 2960, 2960, 2915, 2875, 2850, 2780, 1670, 1590, 1570, 1495, 1475, 1450, 1440, 1400.

cis-**L**, ^1H NMR spectrum ($CDCl_3$): δ 2.54 (dt, 1H, ^3J 7.9, ^2J 12.7, H(4α)), 2.84 (s, 3H, NCH_3), 3.24 (dt, 1H, ^3J 7.9, ^2J 12.7, H(4β)), 4.17 (t, 1H, ^3J 7.9, H(3)), 5.33 (t, 1H, ^3J 7.9, H(5)), 7.15 (m, 1H, H^b), 7.25 (m, 1H, H^p–Ph), 7.31 (m, 2H, H^m–Ph), 7.36 (m, 2H, H^o–Ph), 7.58 (dt, 1H, ^4J 1.0, ^3J 7.9, H^d), 7.66 (dt, 1H, ^4J 1.9, ^3J 7.7, H^c), 8.51 (ddd, 1H, ^4J 1.0, 1.9, ^3J 5, H^a). ^{13}C NMR ($CDCl_3$): δ 44.61 (Me), 45.61 (C(4), 74.28 (C(3)), 78.49 (C(5)), 121.35 (C(d)), 122.46 (C(b)), 126.41 (C^o–Ph),

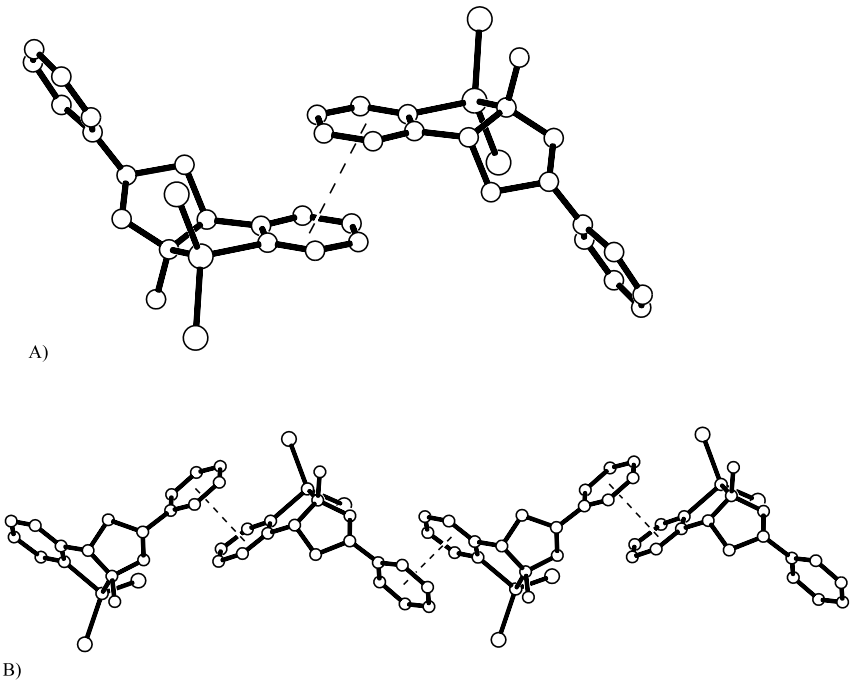


Fig. 3. Intermolecular interactions in the structures of $[Zn(\mathbf{L})Cl_2]$ complex and nature of its supramolecular isomerism: (A) dimeric centrosymmetric ensemble sustained by $\pi\cdots\pi$ stacking interaction between pyridine functions in **1a**; (B) polar chain formed by $\pi\cdots\pi$ stacking between pyridine and phenyl groups in structure **1b**.

Table 2
Selected angles (°) for structure of **2a** ($[Zn(cis\text{-}\mathbf{L})Cl_2]\cdot 0.5CHCl_3$)

Bond angles			
N(2)–Zn(1)–N(1)	81.43(16)	N(1)–C(6)–C(5)	110.8(4)
Cl(2)–Zn(1)–Cl(1)	119.97(5)	N(1)–C(6)–C(7)	102.3(4)
C(8)–O(1)–N(1)	109.5(3)	N(2)–Zn(1)–N(1)–C(6)	−21.5(3)
O(1)–N(1)–C(15)	106.9(4)	N(1)–Zn(1)–N(2)–C(1)	−164.7(4)
O(1)–N(1)–C(6)	106.3(3)	N(1)–Zn(1)–N(2)–C(5)	12.9(3)
C(15)–N(1)–C(6)	111.2(4)	O(1)–N(1)–C(6)–C(5)	145.1(4)
C(8)–C(7)–C(6)	101.9(4)	Zn(1)–N(1)–C(6)–C(5)	26.4(4)
O(1)–C(8)–C(7)	101.4(4)	O(1)–N(1)–C(6)–C(7)	20.5(5)
C(6)–N(1)–Zn(1)	108.1(3)	C(15)–N(1)–C(6)–C(7)	136.5(4)
C(5)–N(2)–Zn(1)	114.8(3)	C(8)–O(1)–N(1)–C(15)	−112.5(4)
N(2)–C(5)–C(6)	118.4(4)	C(6)–C(7)–C(8)–C(9)	159.5(4)

Table 3
Selected angles (°) for structure of **2a**–**b**

Bond angles			
N(2)–Zn(1)–N(1)	81.98(16)	C(4)–N(1)–C(1)	112.0(4)
Cl(1)–Zn(1)–Cl(2)	115.82(7)	N(1)–C(1)–C(2)	105.1(3)
C(3)–O(1)–N(1)	106.8(4)	O(1)–C(3)–C(2)	102.0(5)
O(1)–N(1)–C(4)	106.8(3)	C(1)–N(1)–Zn(1)	111.2(3)
O(1)–N(1)–C(1)	106.6(3)	C(5)–N(2)–Zn(1)	116.7(3)
C(3A)–O(1)–N(1)	106.3(5)	O(1)–C(3A)–C(2)	101.6(9)

127.6 (C^p–Ph), 128.44 (C^m–Ph), 136.95 (C(c)), 141.4 (C^{ipso}–Ph), 149.08 (C(a)), 160.29 (C^{ipso}–Py).

trans-**L**, ^{1}H NMR ($CDCl_3$): δ 2.71 (ddd, 1H, ^3J 7.2, 7.9, ^2J 12.7, H(4α)), 2.80 (s, 3H, NCH_3), 2.88 (dt, 1H, ^3J 7.9, ^2J 12.7, H(4β)), 4.03 (dt, 1H, ^3J 7.2, 7.9 H(3)), 5.22 (t, 1H, ^3J 7.9, H(5)), 7.21 (m, 1H, H^b), 7.25 (m, 1H, H^p–Ph), 7.35 (m, 2H, H^m–Ph), 7.43 (m, 2H, H^o–Ph), 7.56 (dt, 1H, ^4J 1.0, ^3J 7.9, H^d), 7.69 (dt, 1H, ^4J 1.9, ^3J 7.7, H^c), 8.57 (ddd, 1H, ^4J 1.0, 1.9, ^3J 5, H^a). ^{13}C NMR ($CDCl_3$): δ 44.25 (C(4)), 46.26 (Me), 74.28 (C(3)), 79.31 (C(5)), 121.94 (C(d)), 122.73 (C(b)), 126.68 (C^o–Ph), 127.93 (C^p–Ph), 128.52 (C^m–Ph), 136.95 (C(c)), 140.49 (C^{ipso}–Ph), 149.40 (C(a)), 159.47 (C^{ipso}–Py).

cis-**L**, ^{1}H NMR (DMSO-d_6): δ 2.46 (dt, 1H, ^3J 6.9, ^2J 12.3, H(4α)), 2.74 (s, 3H, NCH_3), 3.23 (dt, 1H, ^3J 7.7, ^2J 12.3, H(4β)), 4.19 (t, 1H, ^3J 6.9, H(3)), 5.32 (t, 1H, ^3J 7.7, H(5)), 7.19–7.36 (m, 3H, H^m–, H^p–Ph), 7.22 (m, 1H, H^b), 7.3 (m, 2H, H^o–Ph), 7.58 (dt, 1H, ^4J 1.0, ^3J 7.9, H^d), 7.78 (dt, 1H, ^4J 1.9, ^3J 7.7, H^c), 8.51 (ddd, 1H, ^4J 1.0, 1.9, ^3J 5, H^a). ^{13}C NMR (DMSO-d_6): δ 45.0 (C(4)), 44.57 (Me), 73.37 (C(3)), 77.95 (C(5)), 121.69 (C(d)), 122.83 (C(b)), 126.90 (C^o–Ph), 127.81 (C^p–Ph), 128.62 (C^m–Ph), 137.23 (C(c)), 142.02 (C^{ipso}–Ph), 149.27 (C(a)), 160.78 (C^{ipso}–Py).

trans-**L**, ^{1}H NMR (DMSO-d_6): δ 2.56 (ddd, 1H, ^3J 7.7, 8.5, ^2J 12.3, H(4β)), 2.67 (s, 3H, NCH_3), 2.88 (ddd, 1H, ^3J 6.5, 7.7, ^2J 12.3, H(4α)), 4.04 (dd, 1H, ^3J 6.5, 8.5, H(3)), 5.07 (t, 1H, ^3J 7.7, H(5)), 7.19–7.36 (m, 3H, H^m–, H^p–Ph), 7.33 (m, 1H, H^b), 7.42 (m, 2H, H^o–Ph), 7.58 (dt, 1H, ^4J 1.0, ^3J 7.9, H^d), 7.82 (dt, 1H, ^4J 1.9, ^3J 7.7, H^c), 8.55 (ddd, 1H, ^4J 1.0, 1.9, ^3J 5, H^a). ^{13}C NMR (DMSO-d_6): δ 44.71 (C(4)), 44.57 (Me), 73.65 (C(3)), 78.99 (C(5)), 122.37 (C(d)), 123.19 (C(b)), 127.07 (C^o–Ph), 128.13 (C^p–Ph), 128.77 (C^m–Ph), 137.34 (C(c)), 141.15 (C^{ipso}–Ph), 149.40 (C(a)), 159.59 (C^{ipso}–Py).

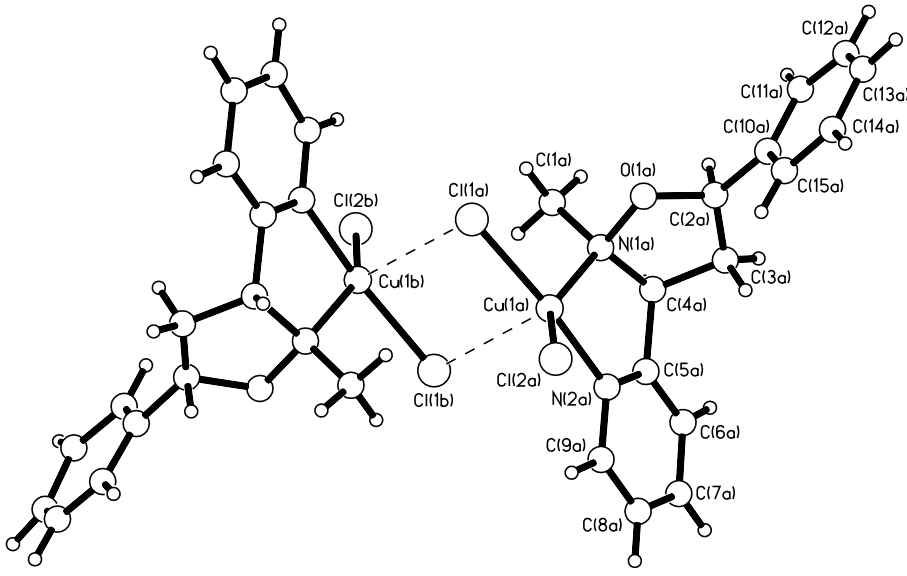


Fig. 4. Structure of the dimeric $[Cu(\mathbf{L})Cl_2]_2$ complex. Selected bond lengths, Å: Cu(1A)–N(2A) 1.996(7); Cu(1A)–N(1A) 2.077(7); Cu(1A)–Cl(2A) 2.245(3); Cu(1A)–Cl(1B) 2.795(2).

Table 4
Selected angles (°) for structure of **4a**–**b**

Bond angles			
N(2A)–Cu(1A)–N(1A)	80.6(3)	C(2A)–O(1A)–N(1A)	105.5(7)
Cl(2A)–Cu(1A)–Cl(1A)	94.33(10)	C(4A)–N(1A)–O(1A)	106.3(6)
N(2A)–Cu(1A)–Cl(2A)	94.4(2)	O(1A)–N(1A)–C(1A)	105.5(7)
N(1A)–Cu(1A)–Cl(2A)	148.1(2)	C(4A)–N(1A)–C(1A)	111.8(8)
N(2A)–Cu(1A)–Cl(1A)	168.9(2)	C(3A)–C(2A)–O(1A)	107.7(12)
N(1A)–Cu(1A)–Cl(1A)	95.4(2)	O(1A)–N(1A)–Cu(1A)	102.1(4)
C(2A)–C(3A)–C(4A)	107.6(10)	C(1A)–N(1A)–Cu(1A)	116.3(6)
N(1A)–C(4A)–C(3A)	105.1(8)		

4.1.2. *[Zn(cis-/trans-**L**)Cl$_2$] (**2a**–**b**)*

A warm mixture 2-propanol–C_3H_6O solution (8/4 ml) of **L** (0.090 g, 0.375 mmol) was added to 2-propanol (5 ml) containing $ZnCl_2$ (0.051 g, 0.375 mmol). The red precipitate was formed immediately. After cooling to room temperature (r.t.), the precipitate of **1** was separated, washed with cold 2-propanol and dried in vacuum. Yield: 0.086 g (61%). *Anal*. Found: C, 48.4; H, 4.3; N, 7.4. Calc. for $C_{15}H_{16}Cl_2N_2OZn$: C, 47.84; H, 4.28; N, 7.44%. Recrystallization from 2-propanol–$CHCl_3$ afforded single crystals of **1a** (orange) and **1b** (white).

4.1.3. *[Pd(cis-/trans-**L**)Cl$_2$] (**3a**–**b**)*

A warm methanolic solution (5 ml) of **L** (0.156 g, 0.65 mmol) was added to a warm MeOH (5 ml) containing $Na_2[PdCl_4]$ (0.191 g, 0.65 mmol). A yellow precipitate was formed at once. The reaction mixture was cooled to r.t., the precipitate of **3a**–**b** was filtered, washed with cold MeOH and dried. Yield: 0.185 g (65%). *Anal*. Found: C, 43.2; H, 3.8; N, 6.6. Calc. for $C_{15}H_{16}Cl_2N_2OPt$: C, 43.62; H, 3.93; N, 6.60%.

4.1.4. *[Cu(cis-/trans-**L**)Cl$_2$]$_2$ (**4a**–**b**)*

A sample of **L** (0.065 g, 0.27 mmol) in warm 2-propanol (5 ml) was added to a $C_5H_{11}O$ solution (10 ml) of $CuCl_2 \cdot 2H_2O$ (0.046 g, 0.27 mmol). A light-green precipitate was formed at once. After cooling to r.t., the precipitate was separated, washed with cold 2-propanol and dried in vacuo to afford a solid 0.062 g (74%). *Anal*. Found: C, 48.0; H, 4.1; N, 7.4. Calc. for $C_{15}H_{16}Cl_2CuN_2O$: C, 47.94; H, 4.29; N, 7.46%. Crystals of the complex, green platelets, were grown by the slow liquid diffusion in next mixtures $CHCl_3$–2-propanol–C_6H_{14} and 2-propanol–DMF as well as an isothermal evaporation of $CHCl_3$ solution.

Table 5
Crystal data and structure refinement for compounds **2a**, **2a**–**b** and **4a**–**b**

Compound	**2a**	**2a**–**b**	**4a**–**b**
Temperature (K)	100(2)	223(2)	293(2)
Crystal system	triclinic	orthorhombic	orthorhombic
Space group	$P\bar{1}$	$Pna2_1$	$P2_12_12_1$
a (Å)	8.5986(4)	16.9776(11)	8.9215(11)
b (Å)	9.9688(4)	7.3273(5)	14.9093(18)
c (Å)	23.1035(12)	13.1536(9)	25.089(3)
α (°)	80.410(3)	90.00	90.00
β (°)	80.170(3)	90.00	90.00
γ (°)	65.075(3)	90.00	90.00
U (Å^3)	1759.61(14)	1636.3(2)	3337.1(7)
Z	4	4	8
D_{calc} (Mg m^{-3})	1.647	1.529	1.492
μ (mm^{-1})	1.931	1.826	1.628
Reflections collected	10 601	8322	15 181
Reflections unique	6840	2667	4761
R_{int}	0.0807	0.0622	0.1013
R_1	0.0582	0.0371	0.0569
wR_2	0.1757	0.0885	0.1325

4.2. Measurements

The IR spectrum of liquid **L** was recorded on a UR-10 (Carl Zeiss, Jena) spectrometer (film between KBr discs; 400–4000 cm^{-1}).

^{1}H (300 MHz), ^{13}C (75.5 MHz) NMR spectra were recorded at r.t. on a Bruker Avance DPX300 spectrometer equipped with a 5 mm QNP-Z probe (^{1}H, ^{13}C, ^{15}N, ^{31}P). The solvents were $CDCl_3$, C_3H_6O-d_6 and DMSO-d_6–THF-d_8 mixture (internal standard—TMS). Standard Bruker software and microprograms were applied for all NMR experiments. The sweep width covered was 3000 Hz for ^{1}H, digitalized in 16 K, and 15 000 Hz for ^{13}C, digitalized in 64 K.

Crystallographic measurements were made using a Siemens SMART CCD area-detector three-circle diffractometer (KappaCCD for **2a**). Graphite monochromated Mo Kα radiation ($\lambda = 0.71073$ Å) was employed. The data frames were integrated using SAINT [29] and empirical absorption corrections (SADABS) [29] were employed. The essential experimental conditions and resulting crystal data are given in Table 5. All structures were solved by direct methods using the SHELXTL-PLUS set of programs [30], and refined by full-matrix least-squares methods. Positions of the hydrogen atoms were idealized.

The $CHCl_3$ of crystallization in structure **2a** have no close contacts with other atoms and fill up emptiness of the crystal. These solvate molecules are disordered over two closely situated positions with partial site occupancy factors at 0.7 and 0.3.

In structure **2a**–**b** high anisotropy of thermal motion for C(3)–C_6H_5 carbon atoms suggested that this fragment of the molecule is disordered. The disorder was resolved under constraining the standard geometry of the phenyl rings and refinement of partial occupancies led to values of 0.72 and 0.28. Refinement of the disorder proceeded smoothly and therefore it was possible to refine all atoms of the major component anisotropically, while atoms of the minor component were left isotropic and the hydrogen atoms of phenyl cycle were not included. Actually the same problem was observed for copper complex **4**. In this case, all attempts to divide the oscillatory movement of C–C_6H_5 between two positions with different partial occupancies were not successful.

5. Supplementary material

Crystallographic data for the structural analysis have been deposited with the Cambridge Crystallographic Data Centre, CCDC No. 164044–164046 for compounds **2a**, **2a**–**b** and **4**. Copies of this information may be obtained free of charge from The Director, CCDC, 12 Union Road, Cambridge, CB2 1EZ, UK (fax: +44-1223-336033; e-mail: deposit@ccdc.cam.ac.uk or www: http://www.ccdc.cam.ac.uk).

References

[1] K.B.G. Torssell, Nitrile Oxides, Nitrones, and Nitronates in Organic Synthesis Novel Strategies in Synthesis, VCH Publishers, Inc, New York, 1988.
[2] P. DeShong, W. Li, J.W. Kennington, J.L. Ammon, H.L. Ammon, J. Org. Chem. 56 (1991) 1364.
[3] H.G. Aurich, M. Geiger, C. Gentes, K. Harms, H. Koster, Tetrahedron 54 (1998) 3181.
[4] P. DeShong, M.C. Dicken, J.M. Leginus, R.R. Whittle, J. Am. Chem. Soc. 106 (1984) 5598.
[5] M. Ito, Ch. Kibayashi, Tetrahedron 47 (1991) 9329.
[6] M. Maeda, F. Okazaki, M. Murayama, Y. Tachibana, Y. Aoyagi, A. Ohta, Chem. Pharm. Bull. 45 (1997) 962.
[7] P. Marino, S. Franco, N. Garces, F.L. Merchan, T. Tejero, Chem. Commun. (1998) 493.
[8] E. Colacino, A. Converso, A. De Nino, A. Leggio, A. Liguori, L. Maiulo, A. Napoli, A. Procopio, C. Siciliano, G. Sindona, Nucleosides Nucleotides 18 (1990) 581.
[9] P.N. Canfalone, F. Jin, S.A. Mousa, Bioorg. Med. Chem. Lett. 9 (1999) 55.
[10] G. Broggini, F. Folcio, M. Sardone, G. Zecchi, Tetrahedron 52 (1996) 11849.
[11] P. Bravo, L. Bruche, A. Farina, G. Fronza, S.V. Meille, A Merli, Tetrahedron: Asymmetry 4 (1993) 2131.
[12] P.C.B. Page, M. Purdie, D. Lathbury, Tetrahedron 53 (1997) 7365.
[13] B. Carboni, M. Ollivault, F. Le Bouguenec, R. Carrie, M. Jazouli, Tetrahedron Lett. 38 (1997) 6665.
[14] T. Geffault, U. Bauer, K. Airola, A.M.P. Koskinen, Tetrahedron: Asymmetry 7 (1996) 3099.
[15] K.V. Gothelf, R.G. Hazell, K.A. Jørgensen, J. Org. Chem. 61 (1996) 346.
[16] R.C. Bernotas, J.S. Jeffrey, I. Sing, D. Friedrich, Synlett (1999) 653.
[17] K.B. Simonsen, K.A. Jorgensen, Q.-S. Hu, L. Pu, Chem. Commun. (1999) 811.
[18] T. Ishikawa, T. Kudo, K. Shigemori, S. Saito, J. Am. Chem. Soc. 122 (2000) 7633.
[19] C. Mukai, I.J. Kim, W.J. Cho, M. Kido, M. Hanaoka, J. Chem. Soc., Perkin Trans. 1 (1993) 2495.
[20] C. Baldoli, P.D. Buttero, E. Licandro, S. Maiorana, A. Papagni, A. Aibinati, A. Papagni, Tetrahedron: Asymmetry 5 (1994) 809.
[21] K.B. Jensen, R.G. Hazell, K.A. Jorgensen, J. Org. Chem. 64 (1999) 2353.
[22] K.B. Simonsen, P. Bayon, R.G. Hazell, K.V. Gothelf, K.A. Jorgensen, J. Am. Chem. Soc. 121 (1999) 3845.
[23] A.B. Lysenko, O.V. Shishkin, R.D. Lampeka, Z. Naturforsch. 55b (2000) 373.
[24] R.D. Lampeka, A.B. Lysenko, Zh. Obshchei Khim. 70 (2000) 1900.
[25] A.B. Lysenko, S.V. Shishkina, O.V. Shishkin, E. Peralta-Pérez, F. López-Ortiz, R.D. Lampeka, Polyhedron 20 (2001) 957.
[26] P. DeShong, C.M. Dicken, R.R. Staib, A.J. Freyer, S.M. Weinreb, J. Org. Chem. 47 (1982) 4397.
[27] C. Janiak, J. Chem. Soc., Dalton Trans. (2000) 3885.
[28] G.R. Desiraju, Crystal Engineering: The Design of Organic Solids, Elsevier, New York, 1989.
[29] Siemens X-Ray Instruments, Madison, WI, 1995.
[30] G.M. Sheldrick, SHELXTL PLUS. PC Version. A system of computer programs for the determination of crystal structure from X-ray diffraction data, Review 5-02-1994.

PERGAMON

Polyhedron 21 (2002) 779–785

POLYHEDRON

www.elsevier.com/locate/poly

Synthesis and spectroscopic studies of cobalt(III) complexes with 5-methyl-3-formylpyrazole-N(4)-diethylthiosemicarbazone (HMP_zNEt_2): X-ray crystallography of $[Co(MP_zNEt_2)_2]ClO_4\cdot 2H_2O$ (**I**) and $[Co(MP_zNEt_2)_2]BF_4\cdot 2H_2O$ (**II**)

Nitis Chandra Saha [a], Ray J. Butcher [b], Siddhartha Chaudhuri [c], Nityananda Saha [a,*]

[a] *Department of Chemistry, University of Calcutta, 92 Acharya Prafulla Chandra Road, Kolkata 700009, India*
[b] *Department of Chemistry, Howard University, Washington, DC, USA*
[c] *R.S.I.C., Bose Institute, Kolkata 700009, India*

Received 17 August 2001; accepted 13 December 2001

Abstract

The co-ordination mode of the title ligand, HMP_zNEt_2 (synthesised for the first time and characterised by elemental analyses, mass, IR and ^1H NMR spectral parameters), is reported by solid state isolation and physico-chemical identification of cobalt(III) complexes, $[Co(MP_zNEt_2)_2]X\cdot 2H_2O$ (X = Cl, Br, ClO_4, BF_4 and NO_3). Electronic spectral features of these diamagnetic Co(III) species classify them as six co-ordinate distorted octahedral ones. IR spectra (4000–200 cm^{-1}) indicate that the Co(III) complexes have monoanionic tridentate NNS co-ordination of the title ligand through the pyrazolyl (tertiary) ring nitrogen, azomethine nitrogen and thiolato sulfur atoms. ^1H NMR data (in $CDCl_3$ at 300 MHz) for the uncomplexed ligand and those of its Co(III) complexes are commensurate with the NNS function of the monodeprotonated HMP_zNEt_2, as ascertained from downfield shift of the relevant protons adjacent to the bonding sites. X-ray crystallographic data of **I** and **II** (both $P\bar{1}$, triclinic) have authenticated a CoN_4S_2 octahedral co-ordination in both the complex ions. © 2002 Elsevier Science Ltd. All rights reserved.

Keywords: Cobalt(III); Pyrazolylthiosemicarbazone; ^1H NMR; X-ray crystallography

1. Introduction

Heterocyclic thiosemicarbazones (TSCs) have attracted much interest in chemistry and biology due to their antibacterial, antimalarial, antitumour and antiviral activities and represent an important series of compounds because of potentially beneficial biological activities [1,2]. In several instances, the highest in vivo activity is associated with a metal ion complex rather than the parent TSC [3]. The last decade has recorded substantial research on transition metal ion complexes of pyridyl thiosemicarbazones [4,5]. Pyrazole derivatives with potential binding sites have long been the focal point of attention [6–8] for co-ordination chemists because of their well-acclaimed pharmacological values [9]. As a part of our comprehensive effort towards establishing a correlation between the structural nature of transition metal ion complexes of pyrazolyl thiosemicarbazones and their wide spectrum therapeutic applications, and in continuation of our earlier work [10–12], the present communication reports the synthesis and spectroscopic identification of cobalt(III) complexes with 5-methyl-3-formylpyrazole-N(4)-diethylthiosemicarbazone (HMP_zNEt_2) together with X-ray crystallographic studies of $[Co(MP_zNEt_2)_2]ClO_4\cdot 2H_2O$ (**I**) and $[Co(MP_zNEt_2)_2]BF_4\cdot 2H_2O$ (**II**).

* Corresponding author. Present address: University of Kalyani, Kalyani 741235, India. Tel.: +91-33-582-8690; fax: +91-33-582-8282.
E-mail address: n.saha@cucc.ernet.in (N. Saha).

0277-5387/02/$ - see front matter © 2002 Elsevier Science Ltd. All rights reserved.
PII: S0277-5387(02)00847-1

2. Experimental

All reagents were of AR grade and were obtained from commercial sources and used without further purification. Spectrograde solvents were used for spectral and conductance measurements, and $CDCl_3$ (Sigma) was used for recording ^1H NMR spectral data.

2.1. Preparation of HMP_zNEt_2

The title ligand, HMP_zNEt_2 (Fig. 1) has been synthesised for the first time by a method similar to that reported earlier [13], but appropriately modified, followed by the final transamination [14] of the *S*-methyldithiocarbazate of 5-methyl-3-formylpyrazole (HMP_zSMe) with diethylamine. The white crystallised product (from ethanol) melted at 160–162 °C. Yield ~ 60%. *Anal*. Found: C, 50.3; H, 7.1; N, 29.5. Calc. for $C_{10}H_{17}N_5S$: C, 50.2; H, 7.1; N, 29.3%. *m/z* 239 (M^+, 86%).

2.2. Preparation of the complexes $[Co(MP_zNEt_2)_2]X\cdot 2H_2O$ ($X = Cl$, Br, ClO_4, BF_4 and NO_3)

The reported Co(III) complexes have been prepared by refluxing ethanolic solution of the ligand (0.00105 mole) and corresponding hydrated Co(II) salts (0.000525 mole) in a water bath for 1 h. On slow evaporation of the dark brown solutions, the desired Co(III) complexes have been obtained. The reddish brown solids were filtered off, washed with cold ethanol, and were dried over anhydrous $CaCl_2$. The yield has been recorded to be 75–80% in each case. Dark red brown crystals of **I** and **II** were found to be suitable for X-ray diffraction.

It is pertinent to note that the ligand, HMP_zNEt_2 favours Co(II) → Co(III) transformation inducing oxidation as is known with similar ligands [15].

2.3. Physical measurements

Elemental analyses (C, H and N) were done at the Indian Association for the Cultivation of Science (IACS), Kolkata, with a Perkin–Elmer 2400 CHNS/O analyser and the cobalt contents of the complexes were determined gravimetrically as anhydrous $CoSO_4$. The molar conductances of the complexes in methanolic solution were measured with a Systronics 304 digital conductivity meter. The electronic spectra of the complexes in methanolic solution and the diffuse reflectance spectra were recorded on a Hitachi U-3501 spectrophotometer. IR spectra (4000–200 cm^{-1}) were recorded on JASCO FT/IR-420 spectrophotometer with KBr pellets at Burdwan University, West Bengal. Magnetic measurements were made in the polycrystalline state on a PAR 155 sample vibrating magnetometer at IACS, Kolkata. ^1H NMR spectra were recorded in $CDCl_3$ with Bruker AM300L (300 MHz) superconducting FT NMR. Mass spectrum of the ligand was done at Central Drug Research Institute, Lucknow, with JEOL JMS-D300 mass spectrometer.

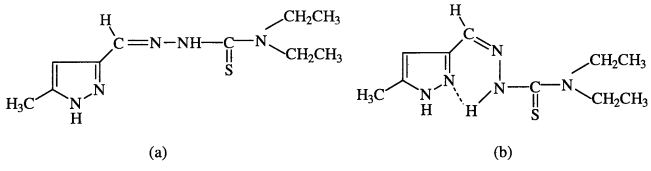


Fig. 1. Schematic diagram of HMP_zNEt_2.

2.4. Structure determination

X-ray diffraction data of the complexes were collected on a Bruker P4 diffractometer using Mo Kα radiation. The data were corrected for Lorentz and polarisation effects and for absorption by using ψ-scans.

The structures were solved by direct methods using SHELXS [16] and refined by full-matrix least-squares based on $|F_{obs}|^2$ using SHELXL [16]. The non-hydrogen atoms were refined anisotropically. The hydrogen atoms, either located from difference electron density maps or generated using idealised geometry, were made to "ride" on their parent atoms and used in the structure factor calculations. Neutral atom scattering factors were taken from Cromer and Weber [17] and anomalous dispersion effects were included in F_{calc} [18]. The crystallographic data are summarised in Table 4 and the final positional and thermal parameters are available as supplementary material.

3. Results and discussion

3.1. Spectroscopic characterisation of HMP_zNEt_2

The ligand, HMP_zNEt_2, has been characterised by elemental analyses (C, H and N), IR, ^1H NMR and mass spectra. The characteristic IR bands (cm^{-1}) at 3290–3200 (ν_{NH}), 1620 ($\nu_{CH=N}$), 1510 ($\nu_{CH=N}$), 1030 ($\nu_{N-N}P_z$), 865 ($\nu_{C=S}$), are in good agreement with the structure in Fig. 1(a). The ligand molecule has a proton adjacent to the thiocarbonyl group and consequently can exhibit thione–thiol tautomerism. The IR spectrum of the free ligand does not show any (ν_{SH}) band in the region 2600–2200 cm^{-1}, indicating that the thiol tautomer is absent in the solid state [19,20], but exhibits (ν_{NH}) bands in the region 3290–3200 cm^{-1} indicating the existence of only thioketo tautomer Fig. 1(a). The ^1H NMR spectrum of the free ligand in $CDCl_3$ gives singlets at δ 2.29 (3H), δ 6.22 (1H) assigned to C_5–CH_3 and C_4–H of the pyrazole ring, respectively. The one proton singlet at δ 7.39 is ascribed to –CH=N–. The

Table 1
Analytical data and other pertinent physico-chemical properties of the complexes

Complex (colour)	Elemental analyses, Found (Calc.)				Conductivity at 30 °C in MeOH (Ω^{-1} cm^2 mol^{-1})
	%C	%H	%N	%Co	
$[Co(MP_zNEt_2)_2]Cl\cdot 2H_2O$ (red brown)	39.6 (39.6)	5.9 (5.9)	23.1 (23.1)	9.8 (9.7)	85
$[Co(MP_zNEt_2)_2]Br\cdot 2H_2O$ (red brown)	36.8 (36.9)	5.5 (5.5)	21.6 (21.5)	9.1 (9.1)	97
$[Co(MP_zNEt_2)_2]ClO_4\cdot 2H_2O$ (dark red brown)	35.7 (35.8)	5.4 (5.4)	20.9 (20.9)	8.9 (8.8)	110
$[Co(MP_zNEt_2)_2]BF_4\cdot 2H_2O$ (red brown)	36.5 (36.5)	5.5 (5.5)	21.3 (21.3)	8.9 (8.9)	105
$[Co(MP_zNEt_2)_2]NO_3\cdot 2H_2O$ (dark red brown)	37.6 (37.9)	5.7 (5.7)	24.4 (24.3)	9.4 (9.3)	92

spectrum shows a signal at δ 13.40, indicating the presence of a hydrogen-bonded proton coming from the hydrazinic hydrogen (of the thiosemicarbazone part) [21]. This is shown in Fig. 1(b) as the hydrogen-bonded stabilised form of the ligand. The thione–thiol tautomerism of the ligand in solution is also indicated by another low field signal, $\delta = 12.89$ due to the formation of the S–H bond [22]. Another singlet at $\delta = 10.71$ is due to hydrazinic proton (–NH–). The mass fragmentation data are compatible with the proposed molecular formula $C_{10}H_{17}N_5S$. The strongest molecular ion peak appears at *m/z* 239 (86%).

3.2. Characterisation of the Co(III) complexes

All these Co(III) complexes give satisfactory C, H, N and Co analyses and conform to the general composition of the complexes as $[Co(MP_zNEt_2)_2]X\cdot 2H_2O$ (X = Cl, Br, ClO_4, BF_4 and NO_3). The molar conductance values in MeOH (30 °C) classify them as 1:1 electrolytes [23] (Table 1) and the complexes are diamagnetic (at 27 °C) as expected for a low spin d^6 ion.

3.2.1. Spectroscopy

The diffuse reflectance spectra of all the reported Co(III) complexes are similar in nature and show three bands in the regions 15105–15455 cm^{-1} ($^1A_{1g} \rightarrow {}^3T_{2g}$), 21097–21645 cm^{-1} ($^1A_{1g} \rightarrow {}^1T_{1g}$), and 23364–23866 cm^{-1} ($^1A_{1g} \rightarrow {}^1T_{2g}$), consistent with an overall octahedral symmetry. Since the observed lower energy bands are not split to a large extent, the reported Co(III) complexes are indicated not to be *trans* isomers [24]. The electronic spectra of the methanolic solutions of the complexes exhibit two bands in the region 43859–44286 cm^{-1} (log $\varepsilon = 4.56$–4.59 lit cm^{-1} mol^{-1}) and 30959–31055 cm^{-1} (log $\varepsilon = 4.52$–4.55 lit cm^{-1} mol^{-1}) attributable to intraligand charge transfer bands ($\pi \rightarrow \pi^*$ and $n \rightarrow \pi^*$, respectively). The spectra also show a shoulder at 25706–26315 cm^{-1} (log $\varepsilon = 4.02$–4.07 lit cm^{-1} mol^{-1}) which may arise due to S→Co(III) charge transfer (LMCT) bands. The absence of any d→d

Table 2
IR assignments (cm^{-1}) for the ligand (HMP_zNEt_2) and its Co(III) complexes

Compound	$\nu_{(CH=N)}$ (azomethine)	$\nu_{(C=N)}$ (pyrazole)	$\nu_{(C=S)}$	$\nu_{(Co-N)}$ (azomethine)	$\nu_{(Co-N)}$ (pyrazole)	$\nu_{(Co-S)}$
HMP_zNEt_2	1620	1510	865			
$[Co(MP_zNEt_2)_2]Cl\cdot 2H_2O$	1597	1520	795	472	275	355
$[Co(MP_zNEt_2)_2]Br\cdot 2H_2O$	1592	1532	775	470	285	360
$[Co(MP_zNEt_2)_2]ClO_4\cdot 2H_2O$	1594	1535	790	465	272	372
$[Co(MP_zNEt_2)_2]BF_4\cdot 2H_2O$	1598	1525	795	468	280	380
$[Co(MP_zNEt_2)_2]NO_3\cdot 2H_2O$	1592	1530	797	475	273	375

Table 3
^{1}H NMR data for the ligand (HMP_zNEt_2) and its Co(III) complexes (in δ ppm) relative to TMS

Compound	N*H* imino	Azomethine –C–*H*	Ring(P_z) N^1–*H*	Ring(P_z) C_5–C*H*$_3$	Ring(P_z) C_4–*H*	N(C*H*$_2$–C)$_2$	N(C–C*H*$_3$)$_2$
HMP_zNEt_2	12.89 10.71	7.39	13.10	2.29	6.22	3.80	1.28
$[Co(MP_zNEt_2)_2]Cl\cdot 2H_2O$		8.21	13.85	2.43	6.27	3.95	1.31
$[Co(MP_zNEt_2)_2]Br\cdot 2H_2O$		8.20	14.08	2.41	6.33	3.92	1.39
$[Co(MP_zNEt_2)_2]ClO_4\cdot 2H_2O$		8.27	14.10	2.42	6.28	3.90	1.38
$[Co(MP_zNEt_2)_2]BF_4\cdot 2H_2O$		8.25	13.97	2.32	6.29	3.89	1.31
$[Co(MP_zNEt_2)_2]NO_3\cdot 2H_2O$		8.20	14.05	2.33	6.31	3.87	1.37

Table 4
Crystal data

	$[Co(MP_zNEt_2)_2]^+ ClO_4^- \cdot 2H_2O$ (**I**)	$[Co(MP_zNEt_2)_2]^+ BF_4^- \cdot 2H_2O$ (**II**)
Empirical formula	$C_{20}H_{36}ClCoN_{10}O_6S_2$	$C_{20}H_{36}BCoF_4N_{10}O_2S_2$
Crystal colour	dark red brown	red brown
Temperature (K)	293(2)	293(2)
Wavelength (Å)	0.71073	0.71073
Crystal system	triclinic	triclinic
Space group	$P\bar{1}$	$P\bar{1}$
Unit cell dimensions		
a (Å)	9.553(3)	9.546(2)
b (Å)	12.395(3)	12.265(2)
c (Å)	13.961(4)	14.057(2)
α (°)	76.88(2)	76.82(1)
β (°)	71.93(2)	71.74(1)
γ (°)	86.85(3)	86.97(1)
V (Å^3)	1530.4(7)	1521.5(5)
Z	2	2
Crystal size (mm)	$0.16 \times 0.74 \times 0.46$	$0.10 \times 0.74 \times 0.26$
θ Range for data collection (°)	2.04–27.50	2.04–24.99
Index ranges	$0 \le h \le 12$, $-15 \le k \le 15$, $-17 \le l \le 18$	$0 \le h \le 11$, $-14 \le k \le 14$, $-15 \le l \le 16$
Reflections collected	7422	5691
Independent reflections	7003 ($R_{int} = 0.0382$)	5344 ($R_{int} = 0.0390$)
Absorption correction	empirical	empirical
Max/min transmission	0.6081 and 0.5088	0.6007 and 0.5497
Refinement method	full-matrix least-squares on F^2	full-matrix least-squares on F^2
Observed reflections	3965	3171
Number of parameters	443	459
Number of restraints	24	20
Goodness-of-fit on F^2	1.010	1.008
Final R indices [a] $[F_o > 4\sigma(F_o)]$	$R_1 = 0.0592$, $wR_2 = 0.1436$	$R_1 = 0.0587$, $wR_2 = 0.1156$
Final R indices (all data)	$R_1 = 0.1158$, $wR_2 = 0.1705$	$R_1 = 0.1180$, $wR_2 = 0.1376$
Largest difference peak and hole (e Å^{-3})	0.687 and −0.365	0.364 and −0.330

[a] $R_1 = \Sigma||F_o| - |F_c||/\Sigma|F_o|$. $wR_2 = \{\Sigma[(F_o^2 - F_c^2)^2]/\Sigma[w(F_o^2)^2]\}^{1/2}$; $w = 1/[\sigma^2(F_o^2) + (aP)^2 + bP]$, where $a = 0.0793$ and $b = 0.0000$ for **I**, and $a = 0.0487$ and $b = 0.1060$ for **II**, and $P = [\max(F_o^2, 0) + 2F_c^2]/3$.

transition bands may be due to the masking of d→d bands by strong CT bands.

The characteristic IR bands (4000–200 cm^{-1}) for the free ligand HMP_zNEt_2 when compared with those of its Co(III) complexes provide meaningful information regarding the bonding sites of the primary ligand molecule (Table 2). A negative shift in $\nu_{(CH=N)}$ band ($\sim$1620 cm^{-1}) in the spectrum of the free ligand to lower value (1592–1598 cm^{-1}) in its complexes is consistent with co-ordination of the azomethine nitrogen to the central Co(III) ion, the IR bands at 465–475 cm^{-1} in the complexes are then assignable to $\nu_{(Co-N)}$ [23]. An intense band at 865 cm^{-1} in the free ligand spectrum, assigned to $\nu_{(C=S)}$, has been found to shift to lower frequency regions (775–797 cm^{-1}) in the complexes, indicating the co-ordination of the thiol sulfur to Co(III); moreover, the appearance of a new band in the region (355–380 cm^{-1}) in the complexes is assignable to $\nu_{(Co-S)}$ [10]. IR bands at 1510 cm^{-1} and 615 cm^{-1} in the free ligand spectrum, assignable to $\nu_{(C=N)}$ (pyrazole ring) and the in-plane deformation of the pyrazole ring, have been shifted to the higher frequency region, indicating that the tertiary ring nitrogen atom (^{2}N) is a possible bonding site [12,25,26]. The presence of bands around 272–285 cm^{-1} in the complexes are clearly assignable to $\nu_{(Co-N)}$ (pyrazole ring) [10].

^{1}H NMR spectral data of the complexes (Table 3) when compared to that of free ligand (HMP_zNEt_2), the following features are notable:

(i) The peaks $\delta = 12.89$ and 10.71 due to imino ^{2}NH (at the thiosemicarbazone part) in the free ligand disappear after complexation. The data indicate that during complexation, the ligand undergoes deproto-

Table 5
Bond distances (Å) and angles (°) involving the Co(III) ions

	Complex **I**	Complex **II**
Bond distances		
Co–N(1A)	1.951(3)	1.964(4)
Co–N(1B)	1.967(3)	1.950(4)
Co–N(3A)	1.908(3)	1.906(4)
Co–N(3B)	1.904(3)	1.916(4)
Co–S(1A)	2.2159(14)	2.2224(14)
Co–S(1B)	2.2201(14)	2.2175(14)
Bond angles		
N(3A)–Co–N(3B)	178.07(14)	177.94(16)
N(3A)–Co–N(1B)	99.70(14)	96.59(16)
N(3B)–Co–N(1B)	81.61(14)	81.59(16)
N(3A)–Co–N(1A)	81.54(14)	81.47(16)
N(3B)–Co–N(1A)	97.08(14)	99.45(15)
N(1A)–Co–N(1B)	89.58(14)	89.81(15)
N(3A)–Co–S(1B)	93.75(10)	96.65(12)
N(3B)–Co–S(1B)	84.90(11)	85.18(12)
N(1B)–Co–S(1B)	166.40(10)	166.74(12)
N(1A)–Co–S(1B)	90.43(11)	91.58(11)
N(3A)–Co–S(1A)	85.24(11)	84.94(12)
N(3B)–Co–S(1A)	96.15(11)	94.09(11)
N(1B)–Co–S(1A)	91.95(10)	90.49(12)
N(1A)–Co–S(1A)	166.76(10)	166.35(11)
S(1A)–Co–S(1B)	91.15(5)	91.25(6)

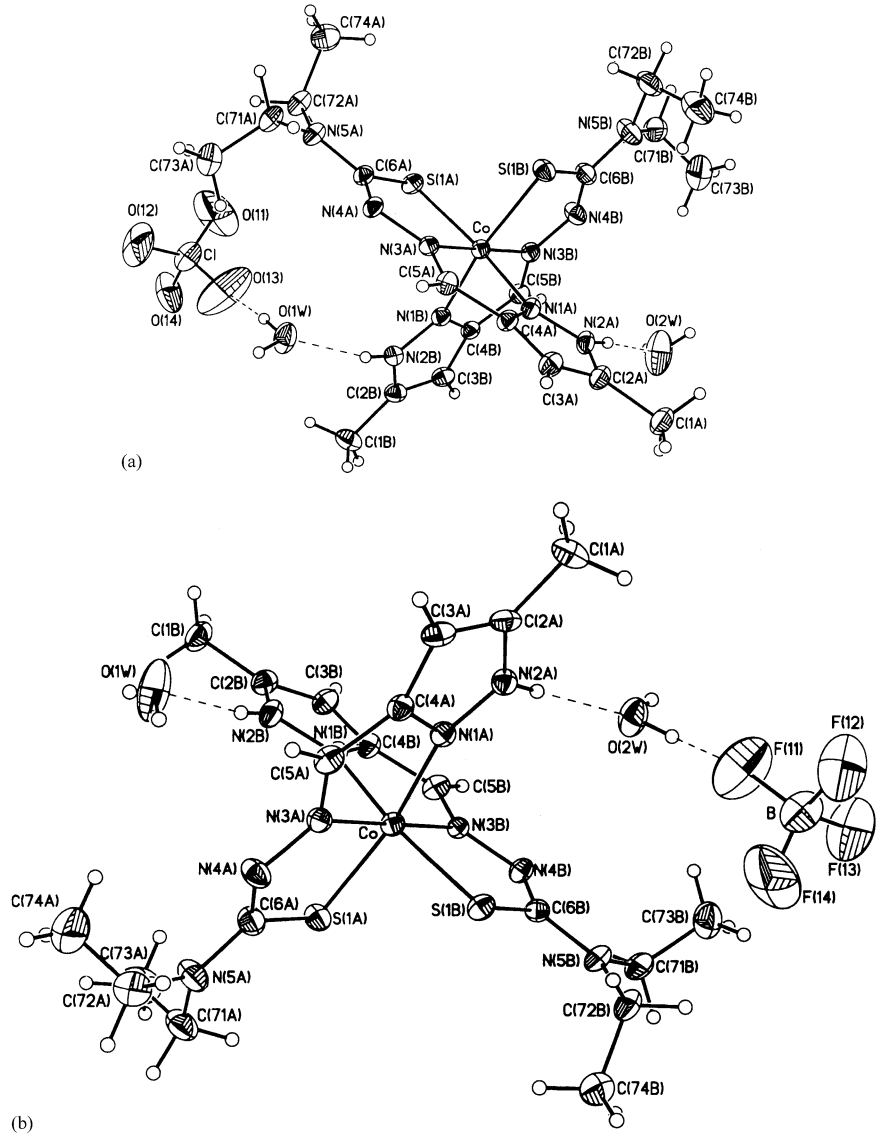


Fig. 2. (a) ORTEP diagram of complex **I**; (b) complex **II**.

nation followed by co-ordination to the Co(III) ion through the thiolato sulfur atom.

(ii) Terminal N(n-Et_2)$_2$ peaks showing slightly downfield shifts are ascribed to the co-ordination of the thiol sulfur to the Co(III) ion resulting in reduction of electron density at the terminal N-atom of N(n-Et_2)$_2$.

(iii) Azomethine CH proton peaks at $\delta = 7.39$ in the free ligand, and suffers maximum downfield shift in the complexes ($\delta = 8.20$–8.27) as expected due to the co-ordination of the azomethine nitrogen to the central Co(III) ion.

The shifting of ^{4}CH (pyrazole ring) from $\delta = 6.22$ (free ligand) to $\delta = 6.27$–6.33 in the complexes is consistent with the fact that the pyrazole ring ^{2}N(tertiary) co-ordinates to the Co(III) ion. ^{1}H NMR spectra, thus, provide support for the bonding characteristics of the primary ligand system (HMP_zNEt_2) in forming complexes with Co(III) through pyrazolyl ring nitrogen ^{2}N(tertiary), azomethine nitrogen and thiolato sulfur atom [10,21] as also envisaged by IR data.

3.3. Crystal structures of $[Co(MP_zNEt_2)_2]ClO_4 \cdot 2H_2O$ (*I*) and $[Co(MP_zNEt_2)_2]BF_4 \cdot 2H_2O$ (*II*)

Fig. 2(a) and (b) show ORTEP [27] diagrams of the complexes together with the atom numbering schemes. Cobalt(III) has a distorted octahedral co-ordination in both the complexes. In either complex, a pair of monodeprotonated ligands ($MP_zNEt_2^-$) co-ordinate to the Co(III) ion through the thiolato sulfur [S(1A), S(1B)], the pyrazolyl (tertiary) ring nitrogen [N(1A), N(1B)], and the hydrazinic chain nitrogen [N(3A), N(3B)]. The crystallographic asymmetric unit in complex **I** consists of a $[Co(MP_zNEt_2)_2]^+$ cation, a ClO_4^-

Table 6
Hydrogen bonding distances (Å) and angles (°)

D–H···A	D–H	D···A	H···A	∠ D–H···A
Complex ***I***				
N(2A)–H(11A)···O(2W)	0.860(4)	2.701(7)	1.848(6)	171.6(3)
N(2B)–H(21A)···O(1W)	0.860(4)	2.742(6)	1.929(4)	157.3(3)
O(1W)–H(1W2)···N(4A)^{i}	0.945(4)	3.008(6)	2.076(4)	168.8(3)
Complex ***II***				
N(2A)–H(2A)···O(2W)	0.874(5)	2.750(8)	1.924(7)	157.0(3)
N(2B)–H(2B)···O(1W)	0.770(5)	2.701(12)	1.943(10)	168.3(5)
O(2W)–H(2W1)···N(4B)^{ii}	0.726(7)	3.019(8)	2.305(4)	168.0 (5)

Symmetry equivalents: (i) $-x+2$, $-y+1$, $-z+1$; (ii) $-x+1$, $-y$, $-z$.

anion and two molecules of water of crystallisation. The crystallographic asymmetric unit in complex **II** is similar to that in complex **I** except that the anion is BF_4^-. The anions in both the structures are disordered.

Table 5 lists the bond distances and angles involving the Co(III) ions. In either complex, two molecules (A and B) of the tridentate 5-methyl-3-formylpyrazole-N(4)-diethylthiosemicarbazone ligand co-ordinate to the Co(III) ions to form four five-membered chelate rings [Co–S(1A)–C(6A)–N(4A)–N(3A), Co–S(1B)–C(6B)–N(4B)–N(3B), Co–N(1A)–C(4A)–C(5A)–N(3A) and Co–N(1B)–C(4B)–C(5B)–N(3B)].

The geometry about the Co(III) ions in both the complexes compare well with those reported for other similar structures [28–30]. The shortening of the Co–N distance involving the azomethine nitrogen atoms relative to that of the pyrazolyl ring nitrogen atoms may be attributed to the fact that the azomethine nitrogen is a stronger base compared to the pyrazolyl nitrogen. The two azomethine nitrogen atoms [N(3A) and N(3B)] are *trans* to each other while the pyrazolyl ring nitrogen atoms [N(1A) and N(1B)] and the thiolato sulfurs [S(1A) and S(1B)] are in the *cis* positions.

The tridentate ligands ($MP_zNEt_2^-$) in both the complexes are practically planar. In complex **I**, C(2A) and C(4A) in ligand A, and C(3B) and N(4B) in ligand B, have the largest deviations in opposite directions [C(2A): +0.060(5) Å, C(4A): −0.055(5) Å, C(3B): +0.115(4) Å, and N(4B): −0.110(4) Å] from the least-squares mean planes through Co–S(1)–C(6)–N(4)–N(3)–C(5)–C(4)–C(3)–C(2)–N(2)–N(1). The corresponding deviations in complex **II** are N(4A): +0.103(4) Å, C(3A): −0.144(5) Å, C(4B): +0.042(5) Å, and C(2B): −0.073(6) Å. In both the complexes, the co-ordinating ligands A and B are orthogonal to each other; the dihedral angle between ligand A and ligand B is 89.37(3)° in complex **I** and 89.38(3)° in complex **II**. In both the structures, the three individual rings, namely, the pyrazole and the two five-membered chelate rings, are individually almost planar with small dihedral angles between them. In complex **I**, the maximum dihedral angle of 6.0(1)° is between the pyrazole ring N(1B)–N(2B)–C(2B)–C(3B)–C(4B) and the chelate ring Co–S(1B)–C(6B)–N(4B)–N(3B); in complex **II**, the rings N(1A)–N(2A)–C(2A)–C(3A)–C(4A) and Co–S(1A)–C(6A)–N(4A)–N(3A) have the maximum dihedral angle of 6.7(2)°.

Table 6 gives the details of the hydrogen bonding contacts excluding those involving the disordered atoms.

4. Supplementary material

Crystallographic data for the structures reported here have been deposited with the Cambridge Crystallographic Data Centre, CCDC Nos. 150099 and 150100. Copies of this information may be obtained free of charge from The Director, CCDC, 12 Union Road, Cambridge, CB2 1EZ, UK (fax: +44-1223-336033; e-mail: deposit@ccdc.cam.ac.uk or www: http://www.ccdc.cam.ac.uk).

Acknowledgements

One of the authors (N.C.S.) is thankful to the University of Calcutta for providing the state-funded research fellowship during the tenure of this work

References

[1] A.E. Liberta, D.X. West, Biometals 5 (1992) 121.
[2] F.A. French, E. Blanz, Jr., J. Med. Chem. 13 (1970) 1117.
[3] L.A. Saryan, K. Mailer, C. Krishnamurti, W. Antholini, D.H. Petering, Biochem. Pharm. 30 (1981) 1595.
[4] (a) D.X. West, S.B. Padhye, P.B. Sonawane, Struct. Bonding 76 (1991) 1;
(b) D.X. West, A.E. Liberta, S.B. Padhye, R.C. Chikate, P.B. Sonawane, A.S. Kumbhar, R.G. Yerande, Coord. Chem. Rev. 123 (1993) 49.
[5] (a) D. Kovala-Demertzi, A. Domopoulou, M.A. Demertzis, A. Papageorgiou, D.X. West, Polyhedron 16 (1997) 3625;
(b) D. Kovala-Demertzi, M.A. Demertzis, A. Castiñeiras, D.X. West, Polyhedron 17 (1998) 3739.
[6] S. Trofimenko, Chem. Rev. 72 (1972) 479.
[7] S. Trofimenko, Progr. Inorg. Chem. 34 (1986) 117.
[8] S. Trofimenko, Chem. Rev. 93 (1993) 943.
[9] R.C. Elderfield (Ed.), Heterocyclic Compounds, Wiley, New York, 1959, p. 565.
[10] A. Mitra, T. Banerjee, P. Roychowdhury, S. Chaudhuri, P. Bera, N. Saha, Polyhedron 16 (1997) 3735.
[11] P. Bera, R.J. Butcher, N. Saha, Chem. Lett. (1998) 559.
[12] P. Bera, N. Saha, S. Kumar, D. Banerjee, R. Bhattacharyya, Transition Met. Chem. 24 (1999) 425.
[13] N. Saha, N. Mukherjee, Polyhedron 3 (1984) 1135.
[14] J.P. Scovill, Phosphorus Sulfur Silicon 60 (1991) 15.
[15] A.V. Ablov, N.I. Belichuk, Russ. J. Inorg. Chem. 14 (1969) 93.
[16] G.M. Sheldrick, SHELX97, Program for the Refinement of Crystal Structure, University of Göttingen, Göttingen, Germany, 1997.

[17] D.T. Cromer, J.T. Weber, International Tables for X-ray Crystallography, table 2.2A, Vol. IV, The Kynoch Press, Birmingham, England, 1994.
[18] J.A. Ibers, W.C. Hamilton, Acta Crystallogr. 17 (1964) 781.
[19] M.A. Ali, M. Tarafder, J. Inorg. Nucl. Chem. 39 (1977) 1785.
[20] M.M. Mostafa, A. Hamid, A.M. Shallaby, A.A. El-Asmay, Transition Met. Chem. 6 (1981) 303.
[21] D.X. West, B.L. Mokijewski, H. Gebremedhin, T.J. Romack, Transition Met. Chem. 17 (1992) 384.
[22] D.X. West, C.S. Carlson, K.J. Bouck, A.E. Liberta, Transition Met. Chem. 16 (1991) 271.
[23] W.J. Geary, Coord. Chem. Rev. 7 (1971) 81.
[24] A.B.P. Lever, Inorganic Electronic Spectroscopy, Elsevier, New York, 1984, p. 463.
[25] R.C. Agarwal, T.R. Rao, J. Inorg. Nucl. Chem. 40 (1978) 1177.
[26] J.R. Ferraro, Appl. Spectrosc. 23 (1969) 60.
[27] L.J. Farrugia, J. Appl. Crystallogr. 30 (1997) 565.
[28] M.B. Ferrari, G.G. Fava, M. Lanfranchi, C. Pelizzi, P. Tarasconi, J. Chem. Soc., Dalton Trans. (1991) 1951.
[29] A. Castiñeiras, D.X. West, H. Gebremedhin, T.J. Romack, Inorg. Chim. Acta 216 (1994) 229.
[30] M.B. Ferrari, G.G. Fava, G. Pelosi, M.C. Rodriguez-Argüelles, P. Tarasconi, J. Chem. Soc., Dalton Trans. (1995) 3035.

PERGAMON

Polyhedron 21 (2002) 787–790

POLYHEDRON

www.elsevier.com/locate/poly

Monomeric and polymeric nickel complexes of malate: X-ray crystal structure of polymeric homochiral *S*-malato nickel(II), [Δ-Ni(*S*-Hmal)$(H_2O)_2]_n \cdot nH_2O$

Zhao-Hui Zhou *, Jian-Jun Ye, Yuan-Fu Deng, Geng Wang, Jing-Xing Gao, Hui-Lin Wan

Department of Chemistry and State Key Laboratory for Physical Chemistry of Solid Surface, Xiamen University, Xiamen 361005, People's Republic of China

Received 10 September 2001; accepted 13 December 2001

Abstract

Polymeric *S*-malate nickel(II) [Δ-Ni(*S*-Hmal)$(H_2O)_2]_n \cdot nH_2O$ (**1**) was prepared from the reaction of nickel chloride and malate salt. By prolonging the reaction time and heating, the kinetic monomeric product *cis*-[Ni(*S*-H_2mal)$_2(H_2O)_2]\cdot 2H_2O$ (**2**) can be converted into the thermodynamic polymeric product **1**. The coordination polymer is linked strongly by the tetradentate malate ligand, forming an homochiral zigzag chain. It is proposed that the chiral metal center of the complex may also be involved in the enantioselective synthesis as well as the chiral ligand. © 2002 Published by Elsevier Science Ltd.

Keywords: Nickel; Malic acid; Malate; Coordination polymer; Asymmetric catalysis; Crystal structures; Electroplating

1. Introduction

Up until now, only a few heterogeneous asymmetric catalytic systems have been investigated in some detail. One of these is the enantioselective hydrogenation of activated carbonyl compounds over an α-hydroxy acid modified Raney nickel catalyst [1]. On the basis of systematic studies it has been proposed that a modifier like tartaric acid is adsorbed and forms a binuclear Ni tartrato complex [Ni(*R*,*R*-tart)$_2$] on the surface [2]. However, the possible interactions and the resultant coordinated species between the modifier and metal are not known exactly and require further attention. Direct investigation of the interaction between the modifier and Raney nickel is not yet possible. Any indirect evidence for the adsorption mode is therefore of importance for a better understanding of reactions like malic acid on a Ni surface [3].

Complex formation between nickel and malate has been reported as a negatively charged malate complex in several nickel-accumulating plants like *Dichapetalum gelonioides* subsp. *tuberculatum* and *Psychotria douarrei* of New Caledonian species [4]. It is also found as a cationic or neutral complex in electroplating baths for various Ni alloys [5]. The role of malic acid is to complex the free metal ion thus preventing precipitation of metal hydroxide species in solution and the concomitant spontaneous decomposition of the plating solution. Moreover, the malic acid-aided process serves in the preparation of well-defined and high surface area particles at low temperature [6]. The only nickel(II) malate complex with a well-characterized crystal structure was reported as monomeric bidentated dimalato diaquonickel(II) and considered as a weak coordinated complex [7]. In the present work, the reaction behavior of malate with nickel salt and the X-ray crystal structure of chiral polymeric neutral nickel malate [Δ-Ni(*S*-Hmal)$(H_2O)_2]_n \cdot nH_2O$ (**1**) (malic acid = H_3mal), which contains the tetradentate coordinated carboxylate/hydroxy moiety, are reported.

* Corresponding author. Tel.: +86-592-218-4531; fax: +86-592-218-3047.

E-mail address: zhzhou@xmu.edu.cn (Z.-H. Zhou).

0277-5387/02/$ - see front matter © 2002 Published by Elsevier Science Ltd.
PII: S0277-5387(02)00845-8

2. Experimental

2.1. Preparation of $[\Delta$-Ni(S-Hmal)$(H_2O)_2]_n \cdot nH_2O$ (1)

In a typical reaction, nickel chloride hexahydrate (10 mmol, 2.38 g) was added to a solution of potassium hydrogen malate (0.5 M, 20 cm^3) prepared from the reaction of *S*-malic acid and potassium hydroxide (1:2). The mixture (pH 3.5) was heated in a water bath at 70 °C for 8 h. The precipitate was collected and washed with ethanol to give a light green solid **1** (1.9 g, 78%). Electronic spectrum of **1**: λ_{max} (nm, ε, M^{-1} cm^{-1}): 389 (12.9); $[\alpha]_D^{20}$ −20° (water, *c* 0.1); IR (KBr, cm^{-1}): ν_{as}(CO) 1642 s, ν_s(CO) 1429m, 1386s, 1348m. *Anal.* Calc. for $C_4H_{10}O_8Ni_1$: C, 19.6; H, 4.1. Found: C, 19.2; H, 4.2%.

2.2. Preparation of Δ/Λ-cis-$[Ni(S\text{-}H_2mal)_2(H_2O)_2]\cdot 2H_2O$ (2) [7]

The monomeric malato complex Δ/Λ-*cis*-[Ni(*S*-H_2mal)$_2$(H_2O)$_2$]·2H_2O (**2**) was prepared from the reaction of nickel chloride hexahydrate (7.5 mmol, 1.8 g), malic acid (1.0 M, 5 cm^3) and potassium dihydrogen malate (1.0 M, 10 cm^3) in a 3:2:4 ratio. The potassium dihydrogen malate was prepared from the reaction of *S*-malic acid and potassium hydroxide in an equimolar ratio [7]. The reaction mixture (pH 2.6) was reacted for 1 h and cooled in a refrigerator for several days. The resultant crystals were collected and washed with ethanol to give a light green solid **2** (1.3 g, 44%). Electronic spectrum of **2**: λ_{max} (nm, ε, M^{-1} cm^{-1}): 389 (8.6); $[\alpha]_D^{20}$ −18° (water, *c* 1.0); IR (KBr, cm^{-1}): 1716s, 1624s, ν_s(CO) 1438m, 1397s, 1332m. *Anal.* Calc. for $C_8H_{18}O_{14}Ni_1$: C, 24.2; H, 4.6. Found: C, 23.9; H, 4.6%.

2.3. Conversion of cis-$[Ni(S\text{-}H_2mal)_2(H_2O)_2]\cdot 2H_2O$ (2) to $[\Delta$-Ni(S-Hmal)$(H_2O)_2]_n \cdot nH_2O$ (1)

A solution of monomeric nickel malate **2** (1.0 g, 2.5 mmol) was heated in a water bath at 70 °C for one day. The green precipitate was separated, washed with water and ethanol and gave [Δ-Ni(*S*-Hmal)$(H_2O)_2]_n \cdot n$$H_2O$ (**1**) in 82% yield (0.5 g).

Crystals of suitable quality for the subsequent X-ray diffraction studies were obtained as transparent light green rhomboids from the heating of the reaction mixture, which is controlled by programmed-temperature apparatus. The crystals were mounted in a capillary for X-ray analysis.

2.4. Physical measurements

Electronic spectra were recorded on a Shimadzu UV 2501 spectrometer. Infrared spectra were recorded as Nujol mulls between KBr plates on a Nicolet 370 FT-IR spectrometer. Elemental analysis was performed on EA 1110 elemental analyzers.

2.5. X-ray data collection, structure solution and refinement

Crystallographic data for the polymeric malato nickel complex **1** are summarized in Table 1. Diffraction data were collected on an Enraf–Nonius CAD-4 diffractometer with graphite monochromated Mo Kα radiation at 297 K. Lp factor, anisotropic decay and empirical absorption corrections were applied. The primary structure was solved by WINGX package [8] and refined by full-matrix least-squares procedures with anisotropic thermal parameters for all the non-hydrogen atoms. Hydrogen atoms were located from difference Fourier maps and were not refined. Final calculations were performed on a PC using MOLEN software package [9]. Selected atomic distances and bond angles are given in Table 2.

3. Results and discussion

The preparation of the malato nickel(II) complex depends mainly on the reaction temperature. The effects

Table 1
Crystal data and structure refinement parameters for [Δ-Ni(*S*-Hmal)$(H_2O)_2]_n \cdot n$$H_2O$ (**1**)

Empirical formula	$C_4H_{10}NiO_8$
Formula weight	244.81
Crystal color, habit	light green, rhombic
Crystal system	monoclinic
Space group	$P2_1$
Unit cell dimensions	
a (Å)	5.7574(9)
b (Å)	8.990(2)
c (Å)	8.396(2)
β (°)	105.54(2)
V (Å^3)	418.7(3)
Formula units/unit cell	2
D_{calc} (g cm^{-3})	1.942
μ (Mo Kα) (mm^{-1})	2.33
$F(000)$	252
Crystal size (mm)	0.15 × 0.15 × 0.20
Decay of standards (%)	4.2
2θ Range (°)	2–56
Reflections used for unit cell determination (2θ range in °)	25 (15.0–17.0)
Reflections measured	1170
Reflections observed ($F_o \leq 3\sigma(F_o)$]	1026
Parameters varied	119
Weight (w^{-1})	$\sigma(F_o)^2+0.0004(F_o)^2+1$
Goodness-of-fit	0.80
$R = \Sigma(\|F_o\|-\|F_c\|)/\Sigma\|F_o\|$	0.035
R_w	0.042
Largest feature final difference map (e Å^{-3})	0.62

Table 2
Selected bond lengths (Å) and bond angles (°) for [Δ-Ni(*S*-Hmal)$(H_2O)_2]_n \cdot nH_2O$ (**1**)

Bond lengths			
Ni(1)–O(1)	2.082(5)	Ni(1)–O(2)	2.021(4)
Ni(1)–O(3)	2.044(4)	Ni(1)–O(4a)	2.039(4)
Ni(1)–O(5)	2.049(4)	Ni(1)–O(6)	2.059(4)
Bond angles			
O(1)–Ni(1)–O(2)	78.8(2)	O(1)–Ni(1)–O(3)	86.4(2)
O(1)–Ni(1)–O(4a)	168.5(2)	O(1)–Ni(1)–O(5)	94.2(2)
O(1)–Ni(1)–O(6)	95.9(2)	O(2)–Ni(1)–O(3)	90.2(2)
O(2)–Ni(1)–O(4a)	97.8(2)	O(2)–Ni(1)–O(5)	172.4(2)
O(2)–Ni(1)–O(6)	90.3(2)	O(3)–Ni(1)–O(4a)	82.7(2)
O(3)–Ni(1)–O(5)	92.3(2)	O(3)–Ni(1)–O(6)	177.7(2)
O(4a)–Ni(1)–O(5)	89.6(2)	O(4a)–Ni(1)–O(6)	95.0(2)
O(5)–Ni(1)–O(6)	87.5(2)		
Hydrogen bonding			
O(3)···O(5)	2.953(6)	O(2)···O(5c)	2.642(6)
O(4)···O(5d)	2.880(6)	O(5)···O(8f)	2.918(6)
O(1)···O(7b)	2.688(6)	O(3)···O(6d)	2.732(6)
O(4)···O(8e)	2.910(7)	O(6)···O(7g)	2.732(6)

a $(1-x, 1/2+y, 2-z)$; b $(1+x, y, z)$; c $(-1+x, y, z)$; d $(1-x, -1/2+y, 2-z)$; e $(x, -1+y, z)$; f $(2-x, -1/2+y, 2-z)$; g $(-x, 1/2+y, 1-z)$.

of pH variation seemed not so crucial for the two neutral products. Instead of the protonated mononuclear malato nickel complex **2**, solid separation from the reaction of nickel chloride with malic acid and potassium dihydrogen malate or potassium hydrogen malate resulted only in the main product **1** after heating or prolonged standing. The polymeric product **1** is the most stable species over the pH range 2.0–5.0. This implies a special stability of the superstructure. There is no direct evidence of the other crystalline phase of the ionic malato nickel(II) complex in pH range 2.0–5.0, although solution studies have suggested the existence of cationic and anionic malato nickel species [10]. It is undoubted that two malato nickel species form neutral complexes. This is not only the result from charge balance in the complex, but also the result from measurements of the small molar electrical conductivities (3.8×10^{-3} S m^2 mol^{-1} for **1** and 2.5×10^{-3} S m^2 mol^{-1} for **2**) [11]. Further attempts to separate the other products using nickel sulfate or other nickel salts only resulted in the isolation of a mixed salt without coordination of the malate ligand.

X-ray analysis reveals that **1** possesses an infinite chain structure (Fig. 1). It is interesting that monomeric **2** can be converted easily into **1** after heating. The reaction of nickel chloride and potassium malate yields the mononuclear complex **2** after a relatively short reaction time at room temperature, whereas the coordination polymer **1** is obtained after a prolonged reaction time or heating.

$$NiCl_2 + KH_2mal \xrightarrow{\text{r.t.}} cis-[Ni(S-H_2mal)_2 \cdot 2H_2O \xrightarrow{\Delta} [Ni(S-Hmal)(H_2O)_2]_n \cdot nH_2O$$

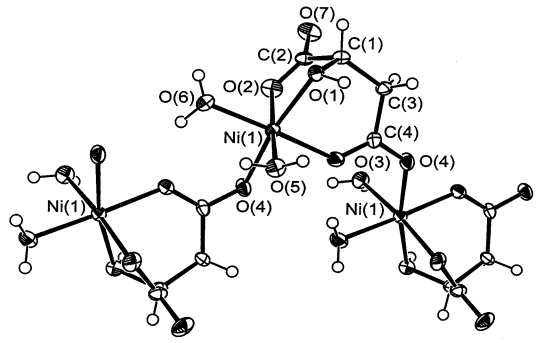


Fig. 1. Perspective view of the polymeric structure of [Δ-Ni(*S*-Hmal)$(H_2O)_2]_n \cdot nH_2O$, showing f50% thermal ellipsoids.

$$NiCl_2 + K_2Hmal \xrightarrow{\text{pH } 2-5/\Delta} [Ni(S-Hmal)(H_2O)_2]_n \cdot nH_2O$$

At high temperature one of the coordinated malates in **1** is replaced by a β-carboxylate of the other malate, inducing the formation of an infinite chain. The present results indicate that the mononuclear nickel(II) is a kinetic product formed reversibly from the components, which progressively converts into the thermodynamic product **2**. The high stability of **2** might be attributed to several factors, such as chelate effect and strain in the bound ligand and/or at the coordinate centers, hydrogen bond and enthalpic contribution.

The crystals were insoluble in most solvents and only slightly soluble in water. The structure of **1** comprises of discrete neutral chiral polymeric nickel *S*-malate and water molecules. The chiral configuration of the metal center is determined by the chiral ligand and the noncentrosymmetric space group [12]. Fig. 1 is the plot of the chiral polymeric structure of **1**, which shows nickel(II) centers bridged by *S*-malate groups. The smallest structural subunit appears to be the monomeric entity Δ-Ni(*S*-Hmal)$(H_2O)_2$. Nickel atoms are *quasi*-octahedrally coordinated by two water molecules and two different malate ligands. The malate ion acts as a tridentate ligand via its hydroxyl, α-carboxyl and β-carboxyl groups in *fac*-mode, while the β-carboxyl group further coordinates monodentately to the other nickel atom in the *trans*-position of the hydroxyl group, forming a catenarian zigzag coordination polymer. Tetradentate coordination of malate through its hydroxyl, α-carboxyl and β-carboxyl group is different from its mononuclear reactant [7]. It is a much more stable species than that of mononuclear malato nickel(II).

In some chiral coordination polymers, the chiral metal center is vague like in the *S*-lactato zinc(II) complex $[Zn(S\text{-lact})_2]_n$ for *trans*-coordination. Note that the *R*-configuration is improperly assigned in the final product [13]. As shown in Fig. 2, there are six possible diastereoisomers of the coordination polymer, which result from the geometric and asymmetric octahedral coordination environment around nickel. The

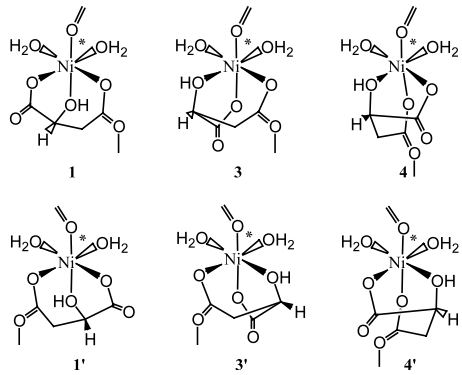


Fig. 2. Possible diastereoisomers of $[Ni(S\text{-Hmal})(H_2O)_2]_n$.

present product **1** is one of the diastereoisomers (**1** and **1′**) separated from the reaction. The bridged monodentate O(4) atom is occupied by the hydroxyl O(1) atom, which is similar to the dinuclear citrato molybdate(VI) and tungstate complex [14,15]. Usually, a chiral modifier like *S*-malic acid is involved directly in heterogeneous enantioselective catalysis [3]. It is proposed that the chiral metal center of the complex may also be involved in the enantioselective synthesis.

As shown in Table 2, the Ni–O malato nickel distances lie between 2.021(4) and 2.082(5) Å. The Ni–O (hydroxy) bonds are slightly longer [2.082(5) Å], indicating a protonated hydroxyl group in the malate anion, which is different from the alkoxy group coordination in other metal malate complexes such as vanadium, molybdenum and tungsten [16–18]. The Ni–O (water) bonds [2.049(4) and 2.059(4) Å] are slightly longer than those of Ni–O (β-carboxyl) [2.044(4) and 2.039(4) Å], and those to the α-carboxyl group are the shortest [2.021(4) Å].

4. Supplementary material

Crystallographic data for the structural analysis have been deposited with the Cambridge Crystallographic Data Centre, CCDC No. 156031 for compound **1**. Copies of this information are may be obtained free of charge from The Director, CCDC, 12 Union Road, Cambridge, CB2 1EZ, UK (fax: +44-1223-336033; e-mail: deposit@ccdc.cam.ac.uk or www: http://www.ccdc.cam.ac.uk).

Acknowledgements

We thank the National Science Foundation of China (No. 29973032) and the Foundation for University Key Teacher by the MOE for supporting this work.

References

[1] (a) Y. Izumi, Adv. Catal. 32 (1983) 215;
(b) A. Tai, T. Harada, in: Y. Iwasawa (Ed.), Tailored Metal Catalysts, D. Reidel, Dordrecht, 1986, p. 265;
(c) G. Webb, P.B. Wells, Catal. Today 12 (1992) 319;
(d) A. Baiker, H.U. Blaser, in: G. Ertl, H. Knözinger, J. Veitkamp (Eds.), Handbook of Heterogeneous Catalysis, vol. 5, Wiley-VCH, New York, 1997, p. 2422.
[2] A. Hoek, W.M.H. Sachtler, J. Catal. 58 (1979) 276.
[3] (a) T. Osawa, T. Harada, A. Tai, Catal. Today 37 (1997) 465;
(b) T. Osawa, T. Marada, J. Catal. 121 (1990) 7;
(c) T. Inoue, K. Kojima, R. Shimozawa, Bull. Chem. Soc. Jpn. 59 (1986) 1683;
(d) M. Yokozeki, K. Shimokoshi, E. Miyazaki, Bull. Chem. Soc. Jpn. 59 (1986) 2969.
[4] (a) X.E. Yang, V.C. Baligar, J.C. Foster, D.C. Martens, Plant Soil 196 (1997) 271;
(b) F.A. Homer, R.D. Reeves, R.R. Brooks, A.M. Baker, Photochemistry 30 (1991) 2141;
(c) W.J. Kersten, R.R. Brooks, R.D. Reeves, T. Jaffré, Photochemistry 19 (1980) 1963.
[5] N.M. Martyak, Trans. Inst. Metal Finish. 78 (2000) 71.
[6] (a) M.E. Baydi, S.K. Tiwari, R.N. Singh, J.L. Rehspringer, P. Chartier, J.F. Koenig, G. Poillerat, J. Solid State Chem. 116 (1995) 157;
(b) S.K. Tiwari, P. Chartier, R.N. Singh, J. Electrochem. Soc. 142 (1995) 148;
(c) S. Yasodhai, S. Govindarajan, Indian J. Chem., Sect. A 38 (1999) 1244.
[7] W. Van Havere, A.T.H. Lenstra, Bull. Soc. Chim. Belg. 89 (1980) 427.
[8] L.J. Farrugia, J. Appl. Crystallogr. 32 (1999) 837.
[9] MOLEN: An Interactive Intelligent System for Crystal Analysis, Enraf–Nonius, Delft, The Netherlands, 1990.
[10] (a) R. Gajerski, S. Labus, A. Malecki, B. Prochowska-Klisch, Bull. Pol. Acad. Sci. Chem. 41 (1993) 17;
(b) H. Hoffmann, U. Nickel, Ber. Bunsen-Ges. Phys. Chem. 72 (1968) 1096.
[11] R.J. Angelici, Synth. Tech. Inorg. Chem. (1977) 13.
[12] U. Knof, A. von Zelewsky, Angew. Chem., Int. Ed. 38 (1999) 302.
[13] Z.F. Chen, J. Zhang, R.G. Xiong, X.Z. You, Inorg. Chem. Commun. 3 (2000) 493.
[14] (a) Z.H. Zhou, H.L. Wan, K.R. Tsai, Polyhedron 16 (1997) 75;
(b) Y.H. Xing, J.Q. Xu, H.R. Sun, D.M. Li, R.Z. Wang, T.G. Wang, W.M. Bu, L. Ye, G.D. Yang, Y.G. Fan, Acta Crystallogr., Sect. C 54 (1998) 1615;
(c) J.J. Cruywagen, E.A. Rohwer, G.F.S. Wessels, Polyhedron 14 (1995) 3481.
[15] (a) J.J. Cruywagen, L.J. Saayman, M.L. Niven, J. Crystallogr. Spectrosc. Res. 22 (1992) 737;
(b) E. Llopis, J.A. Ramirez, A. Doménec, A. Cervilla, J. Chem. Soc., Dalton Trans. (1993) 1121.
[16] C. Djordjevic, M. Leerenslo, E. Sinn, Inorg. Chim. Acta 233 (1995) 97.
[17] C.B. Knobler, A.J. Wilson, R.N. Hider, I.W. Jensen, B.R. Penfold, W.T. Robinson, C.J. Wilkins, J. Chem. Soc., Dalton Trans. (1983) 1299.
[18] Z.H. Zhou, G.F. Wang, S.Y. Hou, H.L. Wan, K.R. Tsai, Inorg. Chim. Acta 314 (2001) 184.

PERGAMON

Polyhedron 21 (2002) 791–795

POLYHEDRON

www.elsevier.com/locate/poly

Thermal reactions of dimanganese decacarbonyl with tetraalkyldiphosphine disulfides (R = Me, Et, Pr^n, Bu^n) and crystal structure of $[Mn_2(CO)_8(\mu\text{-}PBu^n_2)_2]$

Graeme Hogarth [a,*], Fadime Sarýkahya [b], Ozan Sanlý Þentürk [a,b]

[a] *Chemistry Department, University College London, 20 Gordon Street, London, WC1H 0AJ, UK*
[b] *Ege University, Faculty of Science, Department of Chemistry, Bornova, 35100, Ýzmir, Turkey*

Received 7 September 2001; accepted 8 January 2002

Abstract

Reaction of $Mn_2(CO)_{10}$ with $R_2P(S)P(S)R_2$ (R = Me, Et, Pr^n, Bu^n) in toluene at 120 °C yields binuclear $[Mn_2(CO)_8(\mu\text{-}PR_2)_2]$ and trinuclear $[Mn(CO)_3(\mu\text{-}S{=}PR_2)]_3$ complexes. Both result from phosphorus–phosphorus bond scission, while in the former sulfur abstraction has also occurred. An X-ray diffraction study of $[Mn_2(CO)_8(\mu\text{-}PBu^n_2)_2]$ confirms that the manganese adopts a distorted octahedral geometry with local C_{2v} symmetry. © 2002 Elsevier Science Ltd. All rights reserved.

Keywords: Diphosphine disulfide; Dimanganese decacarbonyl; Phosphido; Phosphidosulfide

1. Introduction

Dimanganese decacarbonyl contrasts strongly with most other metal carbonyls in that only a relatively limited number of simple substitution derivatives have been prepared; by way of comparison, the Group VI carbonyls form literally hundreds of simple substitution products [1]. The tendency of the parent carbonyl to undergo valence disproportionation instead of substitution and the intractability of substitution products once formed are among the most important factors in the scarcity of substitution products of dimanganese decacarbonyl [2].

Since the preparation of the first tetraalkyldiphosphine disulfides complexes in 1965 [3–5], such compounds have continued to attract attention, in part because of the different possible coordination geometries which the ligand may adopt. We have recently discovered a photochemical reaction of $M(CO)_6$ (M = Mo, W) with $R_2P(S)P(S)R_2$ to give the chelate complexes $[M(CO)_4\{\mu\text{-}R_2P(S)P(S)R_2\}]$ [6], where the ligand is presumed to adopt the expected *cis*-chelate bidentate coordination. However, in certain cases, the ligand bridges between two metals affording $[M_2(CO)_{10}\{\mu\text{-}R_2P(S)P(S)R_2\}]$ [7] as secondary products.

Both product types detailed above are characterised by the tetraalkyldiphosphine disulfides remaining intact. This is not always the case and in certain reactions fragmentation has been observed. For example, the formation of, inter alia, $[Me_2PS_2]$ ions has been reported upon reaction of OH^- with $Me_2P(S)P(S)Me_2$ in the chemical ionization source of a mass spectrometer [8]. Reaction of $Co_2(CO)_8$ and $Me_2P(S)P(S)Me_2$ was first described in 1972 and two clusters were reported [9], while later the X-ray crystal structure of one of these, namely $[Co_4(CO)_9(\mu_3\text{-}S)(\mu\text{-}PMe_2)]$ confirmed that both phosphorus–sulfur and phosphorus–phosphorus scission had occurred [10].

Gelmini and Stephan [11] have reported that upon reaction with $Cp_2Ti(CO)_2$ under UV irradiation, diphosphine disulfides extrude a PR_2 unit yielding titanium(III) complexes $Cp_2Ti(\eta^2\text{-}S_2PR_2)$. We have recently shown that under similar *photochemical* conditions, $Mn_2(CO)_{10}$ also reacts with $Me_2P(S)P(S)Me_2$ to give $[Mn(CO)_4(\eta^2\text{-}S_2PMe_2)]$ as a result of PMe_2 extrusion [12]. Herein we show that the outcome of this reaction is dependent upon the conditions such that under *thermal*

* Corresponding author. Tel.: +44-20-7679-4664; fax: +44-20-7380-7463.
E-mail addresses: g.hogarth@ucl.ac.uk (G. Hogarth), sanli@sci.ege.edu.tr (O.S. Þentürk).

0277-5387/02/$ - see front matter © 2002 Elsevier Science Ltd. All rights reserved.
PII: S0277-5387(02)00843-4

conditions two different products result, namely: binuclear phosphido-bridged $[Mn_2(CO)_8(\mu\text{-}PR_2)_2]$ and trinuclear phosphido-sulfido-bridged $[Mn(CO)_3(\mu\text{-}S{=}PR_2)]_3$.

2. Experimental

2.1. General

Reactions were carried out under dry nitrogen by using Schlenk techniques. All solvents were dried and degassed prior to use. Elemental analyses were carried out using a Carlo Erba Strummentaione Model 1106 by Technical and Scientific Research Council of Turkey, Tubıtak. FTIR spectra were recorded on samples in hexane at the Ege University on a Mattson 1000 FT spectrophotometer. ^{31}P NMR spectra were recorded in $CDCl_3/CH_2Cl_2$ at UCL on a Varian VXR400 spectrometer. FAB mass spectra were recorded at UCL. $Mn_2(CO)_{10}$ (Aldrich) was used as supplied and tetraalkyldiphosphine disulfides $R_2P(S)P(S)R_2$ were prepared by literature methods [33,34].

2.2. Synthesis

Complexes, **1a**–**d** and **2a**–**d** were prepared by the thermal reactions of $Mn_2(CO)_{10}$ with $R_2P(S)P(S)R_2$ (R = Me, Et, Pr^n, Bu^n) and obtained in 20–40% yield. A typical preparation is given. $Mn_2(CO)_{10}$ (2 mmol) and $Me_2P(S)P(S)Me_2$ (2 mmol) were dissolved in toluene (20 cm^3) and the mixture refluxed under nitrogen overnight. At the end of the reaction, unreacted $Mn_2(CO)_{10}$ was not detected by FTIR. The solution was evaporated to dryness in vacuo producing a dark yellow–orange mixture. Work up procedures were performed in air. The reaction mixture was dissolved in CH_2C1_2 (2 cm^3) and preparative thin-layer chromatography (TLC) was carried out on commercial Merck plates coated with a 0.25 mm layer of silica, using light petroleum as an eluent. At the end of the chromatographic separation, two major different bands were obtained. The first band is pale yellow, **1a** (30%); the second band is dark yellow, **2a** (20%).

1a: Found C, 31.1; H, 2.2; Calc. C, 31.5; H, 2.6%. **1b**: Found C, 37.4; H, 3.7; Calc. C, 37.5; H, 3.9%. **1c**: Found C, 42.0; H, 4.6; Calc. C, 42.2; H, 4.8%. **1d**: Found C, 46.1; H, 5.8; Calc. C, 46.1; H, 5.7%. **2a**: Found C, 28.4; H, 2.2; Calc. C, 28.8; H, 2.5%. **2b**: Found C, 32.0; H, 3.7; Calc. C, 32.3; H, 3.8%. **2c**: Found C, 37.5; H, 4.9; Calc. C, 37.7; H, 4.7%. **2d**: Found C, 41.8; H, 5.7; Calc. C, 41.7; H, 5.6%.

1a: ν(CO) 2046(vs), 2016(vs), 1984(vs), 1962(s); δ_P: 106.0 ppm. **1b**: ν(CO) 2044(vs), 1985(vs), 1969(vs), 1960; δ_P: 105.8 ppm. **1c**: ν(CO) 2041(vs), 1977(vs), 1962(s), 1958(vs); δ_P: 105.6 ppm. **1d**: ν(CO) 2041 (s), 1977(vs), 1966(m), 1958(vs); δ_P: 105.6 ppm. **2a**: ν(CO) 2018(s), 2002(vs), 1989(m), 1946(s), 1943(sh), 1934(m), 1930(sh), 1922(s), 1913(s); δ_P: 90.783 ppm. **2b**: ν(CO) 2016(vs), 2003(m), 1984(vs), 1943(s), 1933(vs), 1928(vs), 1910(vs), 1913(s); δ_P: 69.3 ppm. **2c**: ν(CO) 2019(s), 2007(s), 1992(vs), 1982(m), 1943(s), 1932(vs), 1928(vs), 191 1(vs), 1900(s); δ_P: 62 ppm. **2d**: ν(CO) 2018(vs), 2007(m), 1990(vs), 1979(sh), 1942(vs), 1932(vs), 1928(s), 1912(vs), 1900(s); δ_P: 64.0 ppm.

m/z **1a** (M.W. = 456): 456 (5) $[M^+]$; **1b** (M.W. = 512); 5 12 (15) $[M^+]$; **1c** (M.W. = 568): 568 (10) $[M^+]$; **1d** (M.W. = 624): 624 (10) $[M^+]$; **2a** (M.W. = 696): 586 (5) $[M^+ - S + P + 3Me]$; **2b**: (M.W = 780): 780 (5) $[M^+]$; **2c** (M.W. = 864): 864 (5) $[M^+]$; **2d** (M.W. = 948): 891 (5) $[M^+ - Bu]$.

2.3. Crystallography

A single crystal of **1d** was mounted on a glass fibre and all geometric and intensity data were taken from this sample using an automated four-circle diffractometer (Nicolet R3mV) equipped with Mo Kα radiation ($\lambda = 0.71073$ Å). Important crystallographic parameters are summarised in Table 1. The lattice parameters were identified by application of the automatic indexing

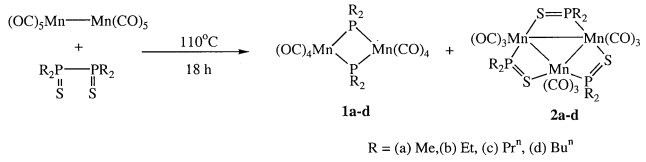
Table 1
Crystal data and structure refinement of **1d**

Empirical formula	$C_{12}H_{18}MnO_4P$
Formula weight	312.17
Temperature (K)	293(2)
Wavelength (Å)	0.71073
Crystal system	triclinic
Space group	$P\bar{1}$
Unit cell dimensions	
a (Å)	8.656(2)
b (Å)	8.698(2)
c (Å)	11.072(2)
α (°)	99.40(3)
β (°)	97.39(3)
γ (°)	104.64(3)
V (Å^3)	783.0(3)
Z	2
Density (Mg m^{-3})	1.324
Absorption coefficient (mm^{-1})	0.947
F(000)	324
Crystal size (mm)	0.96 × 0.84 × 0.84
θ Range for data collection (°)	2.79–25.09
Index ranges	$0 < h < 10$, $-10 < k < 10$, $-13 < l < 13$
Reflections collected	2961
Independent reflections	2767 [$R_{int} = 0.0510$]
Absorption correction	none
Refinement method	full-matrix least-squares on F^2
Data/restraints/parameters	2761/0/163
Goodness-of-fit on F^2	1.113
Final R indices [$I > 2\sigma(I)$]	$R_1 = 0.0362$, $wR_2 = 0.0945$
R indices (all data)	$R_1 = 0.0378$, $wR_2 = 0.1028$
Largest difference peak and hole (e Å^{-3})	0.400 and −0.584

routine of the diffractometer to the positions of a number of reflections taken from a rotation photograph and centred by the diffractometer. The $\omega-2\theta$ technique was used to measure reflections in the range $5^\circ < 2\theta < 50^\circ$. Three standard reflections (remeasured every 97 scans) showed no significant loss in intensity during data collection. The data was corrected for Lorentz and polarisation effects. The unique data with $I > 2\sigma(I)$ were used to solve and refine the structure. The structure was solved by direct methods and developed by alternating cycles of least-squares refinement and difference Fourier synthesis. All non-hydrogen atoms were refined anisotropically. Hydrogens were located from difference maps but were refined isotropically with a common isotropic thermal parameter ($U = 0.08$ Å^2) Final difference Fourier maps were featureless and contained no peaks greater than 1.00 e Å^{-3}. Structure solution used the SHELXTL program on an IBM PC [35].

3. Results and discussion

Heating toluene solutions of $Mn_2(CO)_{10}$ and $R_2P(S)P(S)PR_2$ (R = Me, Et, Pr^n, Bu^n) for 18 h produced dark yellow–orange solutions from which pale yellow $[Mn_2(CO)_8(\mu\text{-}PR_2)_2]$ **1a–d** (25–30%) and dark yellow $[Mn(CO)_3(\mu\text{-}S{=}PR_2)]_3$ **2a–d** (20–25%) were isolated after chromatography. Characterisation was made on the basis of IR, NMR, mass spectral and analytical data.



R = (a) Me,(b) Et, (c) Pr^n, (d) Bu^n

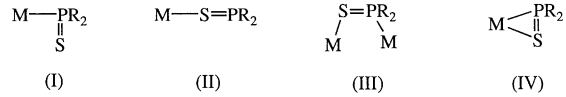
Phosphido-bridged complexes $[Mn_2(CO)_8(\mu\text{-}PR_2)_2]$ **1a–d** result from loss of sulfur and phosphorus–phosphorus bond scission. Such complexes are well known [13–22] and indeed the first such complex reported (R = Ph) [13] was prepared upon phosphorus–phosphorus cleavage of Ph_2PPPh_2 when refluxed with $Mn_2(CO)_{10}$. Characterisation was straightforward, with all showing molecular ions in the mass spectra. The carbonyl region of the IR spectra show four strong bands associated with the local C_{2v}, symmetry at manganese while the equivalence of the phosphorus nuclei was shown by the observation of a singlet (δ 106.0–105.6) in the ^{31}P NMR spectra. Single crystals of $[Mn_2(CO)_8(\mu\text{-}PBu^n_2)_2]$ (**1d**) were grown upon slow evaporation of a saturated dichloromethane solution and the results of the X-ray diffraction study are shown in Table 2 and Fig. 1.

The molecule is centrosymmetric and consists of two approximately octahedral manganese centres being bridged by the butylphosphido ligands which occupy equatorial sites. The phosphorus ligands subtend an angle of 77.23(3)° at the metal centre while the Mn–P–Mn angle is 102.77(3)°. These values are within experimental error the same as those found in the dimethylphosphido-bridged complex $[Mn_2(CO)_8(\mu\text{-}PMe_2)_2]$ (**1a**) [76.9(1)°; 103.1(1)°] which is also centrosymmetric [18]. The Mn–P bond lengths [**1a**: 2.345(4), 2.348(2) Å; **1d**: 2.3949(9), 2.4017(11) Å] do differ slightly between the two structures; values in **1d** being similar to those in the diphenylphosphido-bridged complex $[Mn_2(CO)_8(\mu\text{-}PPh_2)_2]$ [Mn–P: 2.383(2)–2.394(2) Å] [19]. A number of other complexes of this type have also been crystallographically characterised and structural features do not vary significantly between them [18–22].

Table 2
Selected bond lengths (Å) and angles (°) for **1d**

Bond lengths			
Mn–C(2)	1.847(3)	Mn–P	2.4017(11)
Mn–C(4)	1.849(3)	C(l)–O(l)	1.147(3)
Mn–C(3)	1.848(3)	C(2)–O(2)	1.150(3)
Mn–C(1)	1.857(3)	C(3)–O(3)	1.150(3)
Mn–P# 1	2.3949(9)	C(4)–O(4)	1.153(3)
Bond angles			
C(2)–Mn–C(4)	93.98(11)	C(3)–Mn–P	86.94(8)
C(2)–Mn–C(3)	93.76(12)	C(1)–Mn–P	88.39(8)
C(4)–Mn–C(3)	93.15(11)	P#1–Mn–P	77.23(3)
C(2)–Mn–C(1)	90.35(11)	Mn#1–P–Mn	102.77(3)
C(4)–Mn–C(1)	90.58(11)	O(l)–C(l)–Mn	178.0(2)
C(3)–Mn–C(1)	174.24(10)	O(2)–C(2)–Mn	178.2(2)
C(2)–Mn–P	171.22(8)	O(3)–C(3)–Mn	178.8(2)
C(4)–Mn–P	94.72(8)	O(4)–C(4)–Mn	178.4(2)

Identification of the second product as trinuclear dialkylphosphidosulfide complexes $[Mn(CO)_3(\mu\text{-}S{=}PR_2)]_3$ (**2a–d**) is based primarily on mass spectral data. Thus, while IR and analytical data are consistent with a $[Mn(CO)_3(SPR_2)]$ formulation, it is only the latter that provides insight into the nuclearity. Complexes **2b–c** both show a molecular ion in the mass spectrum consistent with a trinuclear unit, while **2d** shows the expected ion after loss of a butyl group. In the ^{31}P NMR spectrum all show a singlet, the chemical shift of which (δ 90.8–62.0 ppm) suggests that the sulfur–phosphorus bond remains intact. Phosphidosulfide ligands are known to bind to metal centres in four different ways (I–IV) as shown below [23].



(I) (II) (III) (IV)

In the absence of crystallographic data it is known that assigning specific binding modes to phosphidosulfide complexes is difficult, as spectroscopic properties depend also on both the metal centre(s) and associated other ligands [23]. Precedence strongly favours the

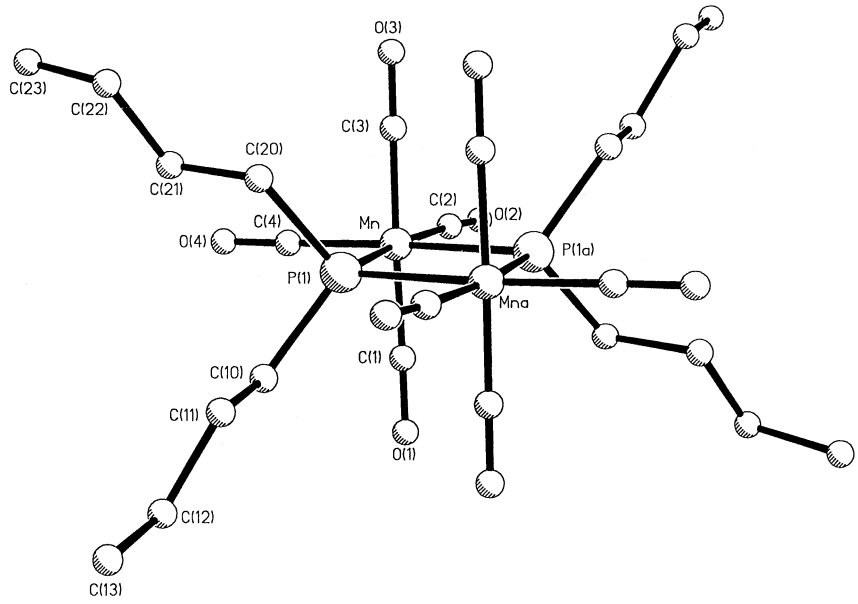


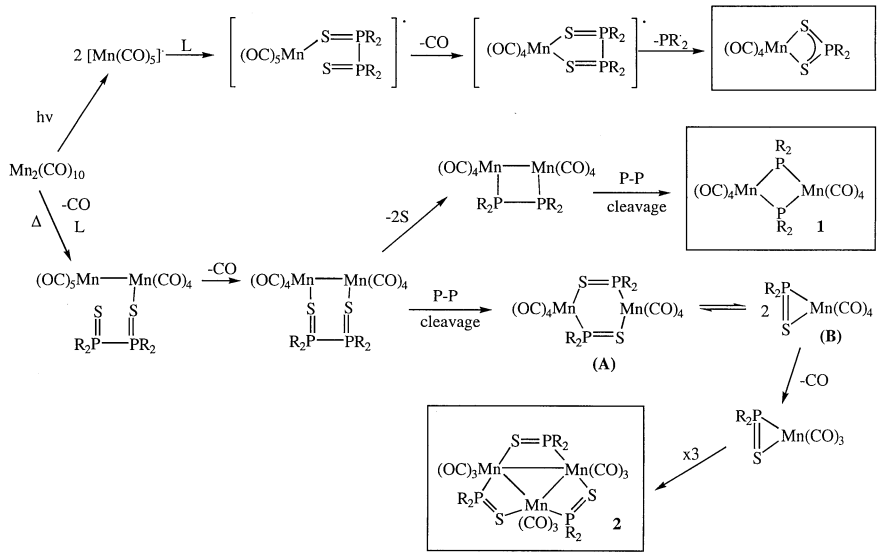
Fig. 1. Molecular structure of $[Mn_2(CO)_8(\mu\text{-}PBu^n_2)_2]$ **1d**.

doubly bridging mode (III) in **2** as, while binding mode (I) is most frequently seen, mode (III) is adopted in *all* bi- or polynuclear complexes containing this ligand reported to date [23,24]. We thus assign the structure of **2** as shown. The observation of nine bands in the carbonyl region of the IR spectrum further supports a local C_{3v} symmetric structure. As each dialkylphosphine sulfide ligand acts as a three-electron donor ligand, a total cluster electron count of 48 suggests that there are three metal–metal bonds. The observation of a single phosphorus resonance is also consistent with the proposed structure, while when in a chelate mode (IV) chemical shifts are normally upfield of H_3PO_4 (i.e. negative). We note here a report that suggests that $Fe(CO)_5$ reacts with $Me_2P(S)P(S)Me_2$ under UV irradiation to give $[Fe_2(CO)_6(\mu\text{-}SPMe_2)_2]$ as the major product, in which the ligand is bound only through sulfur (II) [25]. In light of more recent results this formulation is probably incorrect and we are currently reinvestigating this chemistry.

The condition dependence of the reaction of diphosphine disulfides with $Mn_2(CO)_{10}$ are worthy of further note and a plausible explanation and mechanistic route is shown in Scheme 1. The reactivity of $Mn_2(CO)_{10}$ is known to be condition dependent, such that photolysis favours Mn–Mn bond homolysis while under thermal conditions carbonyl loss dominates. *Photochemical* conditions leads to PR_2 extrusion [12] and probably proceeds via reaction of diphosphine disulfides with the 17-electron $[Mn(CO)_5]^\bullet$ radical. Such species are known to undergo facile substitution reactions after which PR_2 extrusion is competitive with reformation of the Mn–Mn bond. An intermediate in the process may be the 19-electron species $[(CO)_4Mn\{\eta^2\text{-}S{=}P(R_2)P(R_2){=}S)]^\cdot$, and in support of this postulation we have recently prepared analogous 18-electron molybdenum complexes [6]. *Thermal* conditions favour CO loss and formation of a bridged species $[\{Mn(CO)_4\}_2(\mu\text{-}S{=}P(R_2)P(R_2){=}S)]$ can be envisaged. Again, support for this comes from our recent preparation of the analogous dimolybdenum complexes $[\{Mo(CO)_5(\mu\text{-}S{=}P(R_2)P(R_2){=}S)]$ [7]. Cleavage of the phosphorus–phosphorus bond at this stage via oxidative-addition to the binuclear centre would afford the known complexes $[\{Mn(CO)_4(\mu\text{-}S{=}PR_2\}_2]$ (**A**) [26–29]. Such complexes are known and have been shown to be in equilibrium in solution with monomers (**B**) [30–32]. Loss of CO from the latter would result in formation of a reactive 16-electron species, trimerisation of which affords **2**. In a second pathway, disulfur extrusion from the diphosphine disulfide bridged intermediate would give diphosphine-bridged $[\{Mn(CO)_4\}_2(\mu\text{-}R_2P\text{-}PR_2)]$, oxidative addition of the phosphorus–phosphorus bond affording **1**.

4. Supplementary material

A complete list of bond lengths and angles and tables of atomic coordinates and thermal parameters have been deposited with the Cambridge Crystallographic Data Centre, CCDC No. 173950. Copies of this information may be obtained free of charge from The Director, CCDC, 12 Union Road, Cambridge, CB2 1EZ, UK (fax: +44-1223-336033; e-mail: deposit@ccdc.cam.ac.uk or www: http://www.ccdc.cam.ac.uk).



Scheme 1.

Acknowledgements

We thank the Technical and Scientific Research Council of Turkey, TUBI'TAK and the Research Foundation of Ege University for funds. We thank the Royal Society for financial support allowing O.S.Þ. to visit University College London.

References

[1] G. Wilkinson, F.G.A. Stone, E.W. Abel, Comp. Organomet. Chem. 4 (1982) 103.
[2] G. Wilkinson, F.G.A. Stone, E.W. Abel, Comp. Organomet. Chem. 6 (1995) 1.
[3] K. Baker, G.W.A. Fowles, J. Less. Common Met. 8 (1965) 45.
[4] H. Teichmann, Angew. Chem., Int. Ed. Engl. 4 (1965) 785.
[5] D.W. Meek, P. Nicpon, J. Am. Chem. Soc. 87 (1965) 4651.
[6] M.J. Almond, F. Sarýkahya, O.S. Þentürk, Polyhedron 16 (1997) 1101.
[7] F. Sarýkahya, O.S. Þentürk, Synth. React. Inorg. Met.-Org. Chem. 31 (2001) 1843.
[8] R.A.J. O'Hair, J.C. Sheldon, H.H. Bowie, J. Chem. Soc., Dalton Trans. (1988) 2837.
[9] G. Natile, S. Pignataro, G. Jnnorta, G. Bor, J. Organomet. Chem. 40 (1972) 955.
[10] (a) G. Geraviso, F. Musso, S. Vastag, G. Bor, G. Szalantai, L. Marko, J. Cluster Sci. 5 (1994) 401;
(b) F. Sarýkahya, O.S. Þentürk, I. Topaloglu, Synth. React. Inorg. Met.-Org. Chem. 30 (2000) 1697.
[11] L. Gelmini, D.W. Stephan, Organometallics 6 (1987) 1515.
[12] M.J. Almond, M.G.B. Drew, F. Sarýkahya, O.S. Þentürk, Polyhedron 14 (1995) 1433.
[13] R.G. Hayter, J. Am. Chem. Soc. 86 (1964) 823.
[14] R.J. Doedens, W.T. Robinson, J.A. Ibers, J. Am. Chem. Soc. 89 (1967) 4323.
[15] E.W. Abel, I.H. Sahberwal, J. Organomet. Chem. 10 (1967) 491.
[16] R. Demuth, J. Grobe, J. Fluorine Chem. 2 (1973) 299.
[17] H. Vahrenkamp, Chem. Ber. 111 (1978) 3472.
[18] M. Masuda, T. Taga, K. Machida, T. Kawamura, J. Organomet. Chem. 331 (1987) 239.
[19] B. Deppisch, H. Schafer, D. Binder, W. Leske, Z. Anorg. Allg. Chem. 519 (1984) 53.
[20] (a) U. Florke, H.J. Haupt, Acta Crystallogr., Sect. C 49 (1993) 374;
(b) U. Florke, H.J. Haupt, Acta Crystallogr., Sect. C 49 (1993) 533.
[21] (a) H. Schafer, J. Zipfel, B. Gutekunst, Y. Lemmert, Z. Anorg. Allg. Chem. 529 (1985) 157;
(b) H. Schafer, J. Zipfel, B. Migula, D. Binder, Z. Anorg. Allg. Chem. 501 (1983) 111.
[22] M.P. Brown, J. Buckett, M.M. Harding, R.M. Lynden-Bell, M.J. Mays, K.W. Woulfe, J. Chem. Soc., Dalton Trans. (1991) 3097.
[23] B. Walther, Coord. Chem. Rev. 60 (1984) 67.
[24] L. Gelmini, D.W. Stephan, Can. J. Chem. 66 (1988) 2647 (and references therein).
[25] G.J. Kruger, S. Lotz, L. Linford, M. Van Dyk, H.G. Raubenheimer, J. Organomet. Chem. 280 (1985) 241.
[26] E. Lindner, H. Dreher, J. Organomet. Chem. 105 (1976) 85.
[27] E. Lindner, B. Schilling, Chem. Ber. 110 (1977) 3889.
[28] V.K. Ullmer, H. Vahrenkamp, Chem. Ber. 110 (1977) 237.
[29] E. Lindner, C.-P. Kreig, S. Hoehne, A. Rau, Z. Naturforsch., Teil B 36 (1981) 1487.
[30] E. Lindner, V. Kass, Chem. Ber. 122 (1989) 2269.
[31] E. Lindner, V. Kass, R. Fawzi, Angew. Chem., Int. Ed. Engl. 28 (1989) 448.
[32] E. Lindner, V. Kass, H.A. Mayer, Chem. Ber. 123 (1990) 783.
[33] (a) T. Moeller, H.J. Birch, N.C. Nielson, Inorg. Synth. 4 (1953) 71;
(b) S.A. Butter, J. Chatt, Inorg. Synth. 15 (1974) 186;
(c) A.I. Vogel, Text-book of Practical Organic Chemistry, 3rd ed., Longman, London,, 1977, pp. 139–145, 163–179, 193 and 280–288.;
(d) H. Nierbergall, B. Langenfeld, Chem. Ber. 95 (1962) 64.
[34] P.J. Christen, L.M. Van der Linde, F.N. Hooge, Rec. Trav. Chim. 78 (1959) 161.
[35] G.M. Sheldrick, SHELXTL-93, Program package for structure solution and refinement, Siemens Analytical Instruments Inc., Madison, WI, 1993.

PERGAMON

Polyhedron 21 (2002) 797–804

POLYHEDRON

www.elsevier.com/locate/poly

Mononuclear coordination compounds based on a novel chelating triazole ligand: 1-vinyl-3-acetylamino-1,2,4-triazole

Mark B. Bushuev [a], Alexander V. Virovets [a], Yann Garcia [b], Christine Gieck [b], Lilia A. Sheludyakova [a], Vladimir N. Ikorskii [a], Wolfgang Tremel [a], Philipp Gütlich [b], Ludmila G. Lavrenova [a,*]

[a] *Institute of Inorganic Chemistry SD RAS, Prospekt Lavrent'ev 3, 630090 Novosibirsk, Russia*
[b] *Institut für Anorganische Chemie und Analytische Chemie, Universität Mainz, Staudingerweg 9, 55099 Mainz, Germany*

Received 20 August 2001; accepted 3 December 2001

Abstract

The synthesis, X-ray structure, magnetic and spectroscopic properties of new Co(II), Ni(II) and Cu(II) complexes with 1-vinyl-3-acetylamino-1,2,4-triazole (vaat) are reported. The crystal structures of $[Ni(vaat)_2(H_2O)_2](NO_3)_2$ and $[Cu(vaat)_2(H_2O)_2]Cl_2$ have been determined by X-ray diffraction. In these mononuclear complexes, the metal ion is surrounded by two water molecules in axial positions and two oxygen and two nitrogen ($N4$) atoms coming from two *trans*-oriented chelating vaat molecules. Anions are noncoordinated and are involved in a hydrogen bonding network. The complex cations of $[Cu(vaat)_2(H_2O)_2]Cl_2$ are aligned within chains. In the structure of $[Ni(vaat)_2(H_2O)_2](NO_3)_2$ the nitrate anions establish a bridge in the plane by hydrogen bonding giving a 2-D character for this compound. In addition, a colour change from pink to blue upon heating has been observed for $[Co(vaat)_2(H_2O)_2]Cl_2$, which is due to the removal of the two coordinated water molecules and the subsequent molecular reorganisation of the molecular structure. © 2002 Elsevier Science Ltd. All rights reserved.

Keywords: Mononuclear complexes; Triazole derivatives; Crystal structures

1. Introduction

1,2,4-Triazoles derivatives represent an interesting class of heterocycles. Their versatility as ligands is determined by the number and the arrangement of the nitrogen atoms in the aromatic cycle as well as by the nature of their substituents. Transition metal complexes with these ligands have a great interest from both theoretical and practical viewpoints since they can be subject to spin crossover or magnetic exchange studies [1–17]. Various applications in bioinorganic chemistry are well known [18,19]. They are also used as precursors of photographic materials and some of them demonstrate anticorrosion properties [20,21]. With the absence of a donor atom in the substituent, triazoles are coordinated to metal ions mainly as bridging ligands forming polynuclear complexes [1–15]. The 3-acetylamino-1,2,4-triazole (hereafter abbreviated Haat) and its derivatives are some of the most interesting ligands as they demonstrate possibilities of both chelating and bridging coordination modes and can form various types of complexes [22–28]. In addition, coordination abilities of these ligands increase with their deprotonation. Indeed, it should be mentioned, that the Haat molecule can loose acidic protons of the triazole ring and of the NH group of its substituent. Thus, variation of the synthetic conditions, i.e. the molar metal:ligand ratio, the acidity of the solution, the nature of the solvent and so forth, can result in the formation of different complex species.

Numerous papers dealing with the synthesis of Co(II), Ni(II) and Cu(II) Haat coordination compounds have been published in the last decade. Fascinating triangular trinuclear Cu(II) compounds with deprotonated forms of Haat and its 5-amino derivative, involving a pyramidal $Cu_3(\mu_3\text{-}O(H))$ core were obtained [26,29,30]. The first crystal structure of this type was found for a Cu(II)

* Corresponding author. Tel.: +7-383-2-391143; fax: +7-383-2-344489.
E-mail address: ludm@che.nsk.su (L.G. Lavrenova).

0277-5387/02/$ - see front matter © 2002 Elsevier Science Ltd. All rights reserved.
PII: S0277-5387(02)00844-6

complex with 3,5-dimethyl-4-amino-1,2,4-triazole (L). Two structural formulae, namely $(H_3O)[(\mu_3\text{-}OH)(\mu,\eta^2\text{-}L)_3Cu_3Cl_6]$ and $[(\mu_3\text{-}OH)(\mu,\eta^2\text{-}L)_2(\mu_2,\eta^2\text{-}LH)Cu_3Cl_6]$, were, however, proposed for this compound as hydrogen atoms could not be properly localised [30]. Other complexes of the same type with the following composition $[Cu_3(\mu_3\text{-}OH)(aat)_3A(H_2O)_2]A\cdot nH_2O$ ($A = NO_3^-$, $CF_3SO_3^-$, ClO_4^-, $n = 0$, 2) [26] and $[Cu_3(\mu_3\text{-}OH)(aaat)_3(H_2O)_3](NO_3)_2\cdot H_2O$ [29] where aat and aaat are the deprotonated forms of 3-acetylamino-1,2,4-triazole and 3-acetylamino-5-amino-1,2,4-triazole, have also been obtained. All of them contain a triangular Cu_3 skeleton with μ_3-bridging OH-groups. The copper atoms are linked by *N*1*N*2 atoms of three peripheral bridging triazoles.

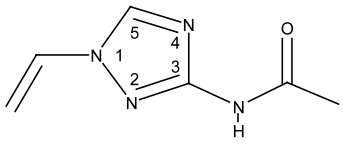
Mononuclear complexes with Haat such as $[M(Haat)_2(H_2O)_2]A\cdot nH_2O$ (M = Co(II), Ni(II), Cu(II); $A = Cl^-$, Br^-, SO_4^{2-}, NO_3^-, $n = 0$, 2, 5), $[Cu(Haat)_2(NO_3)_2]$ and two linkage isomers of $[Cu(Haat)_2(NCS)_2]$ have been synthesised and investigated [22–25,27,28]. In these compounds Haat is coordinated to the metal as a chelating ligand. Such diversity in the structure of these compounds requires further research on this topic. This is why we have synthesised complexes with a new ligand related to Haat: 1-vinyl-3-acetylamino-1,2,4-triazole, hereafter abbreviated as vaat (see Scheme 1). A vinyl group has been introduced in 1-position of the triazole ring, thus modifying the electronic distribution of the triazole ring.

This present contribution deals with the synthesis, X-ray structures, magnetic and spectroscopic properties of new coordination compounds with this ligand, i.e. $[M(vaat)_2(H_2O)_2](NO_3)_2$ (M = Co(II), Ni(II), Cu(II) (**1**, **2**, **3**)), $[M(vaat)_2(H_2O)_2]Cl_2$ (M = Co(II), Ni(II) (**4**, **5**)) and $[Cu(vaat)_2(H_2O)_2]A_2$ ($A = Cl^-$, Br^- (**6**, **7**)).

2. Experimental

2.1. General

Infrared spectra were obtained with Specord 75IR and Specord M-80 spectrophotometers in the region 200–3600 cm^{-1}. Ligand field spectra were recorded in the region 350–2200 nm on a Unicam 700A spectrophotometer by using the diffuse-reflectance technique with MgO as a reference. Thermogravimetric measurements were carried out with a "Paulik–Paulic–Erdey" apparatus in the temperature range 300–450 K with a heating rate of 2.5 K min^{-1} under ambient atmosphere. Gravimetric measurements were carried out at 420 K under ambient atmosphere according to the following technique. The sample was heated and thermostated at a certain constant temperature. Then it was cooled in a closed dessiccator over $Mg(ClO_4)_2$ and its mass was measured. X-ray powder diffraction experiments were carried out on a Philips diffractometer (Cu Kα-irradiation, Ni filter). Magnetic susceptibilities of polycrystalline samples were measured by the Faraday's method at room temperature (**1**, **2**, **4**, **5**, **7**) and in the temperature range 78–300 K for compounds **3** and **6**. Values of effective magnetic moments μ_{eff} were calculated according to the equation $\mu_{eff} = [8\chi T]^{1/2}$, where χ is the molar susceptibility corrected for diamagnetic contributions.



Scheme 1. 1-Vinyl-3-acetylamino-1,2,4-triazole.

2.2. Synthesis

Commercially available salts were used without further purification. The vaat ligand was synthesised and kindly provided by Professor L.I. Vereshchagin (Irkutsk State University).

2.2.1. $[M(vaat)_2(H_2O)_2](NO_3)_2$ (M = Co(II), Ni(II), Cu(II) (**1**, **2**, **3**))

A hot aqueous solution of vaat (3 mmol, 0.46 g) was rapidly added to a solution containing 1.5 mmol of metal salt (0.44 g $Co(NO_3)_2\cdot 6H_2O$, 0.44 g $Ni(NO_3)_2\cdot 6H_2O$, 0.36 g $Cu(NO_3)_2\cdot 3H_2O$) dissolved in 5 ml of hot water. A precipitate was obtained after evaporation and cooling of the resulting solution. It was subsequently filtered, washed with water and dried in ambient air.

$[Co(vaat)_2(H_2O)_2](NO_3)_2$: *Anal*. for $C_{12}H_{20}CoN_{10}O_{10}$: Calc. (found): C, 27.5 (26.8); H, 3.9 (4.3); N, 26.8 (27.0); Co, 11.3 (11.1). Yield: 15%.

$[Ni(vaat)_2(H_2O)_2](NO_3)_2$: *Anal*. for $C_{12}H_{20}N_{10}NiO_{10}$: Calc. (found): C, 27.6 (27.1); H, 3.9 (4.2); N, 26.8 (26.8); Ni, 11.2 (11.3). Yield: 30%.

$[Cu(vaat)_2(H_2O)_2](NO_3)_2$: *Anal*. for $C_{12}H_{20}CuN_{10}O_{10}$: Calc. (found): C, 27.3 (26.2); H, 3.8 (4.0); N, 26.5 (26.8); Cu, 12.0 (11.8). Yield: 40%.

2.2.2. $[M(vaat)_2(H_2O)_2]Cl_2$ (M = Co(II), Ni(II) (**4**, **5**))

An aqueous solution of 1.5 mmol (0.36 g) of $CoCl_2\cdot 6H_2O$ or 2 mmol (0.48 g) of $NiCl_2\cdot 6H_2O$ was mixed with a solution of vaat (3 mmol, 0.46 g (**4**) or 4 mmol, 0.61g (**5**)). Evaporation and cooling of the resulting solution led to the formation of a precipitate.

$[Co(vaat)_2(H_2O)_2]Cl_2$: *Anal*. for $C_{12}H_{20}Cl_2CoN_8O_4$: Calc. (found): C, 30.7 (30.4); H, 4.3 (5.0); N, 23.8 (23.9); Co, 12.5 (11.7). Yield: 45%.

$[Ni(vaat)_2(H_2O)_2]Cl_2$: *Anal*. for $C_{12}H_{20}Cl_2N_8NiO_4$: Calc. (found): C, 30.7 (29.9); H, 4.3 (4.6); N, 23.8 (23.5); Ni, 12.5 (12.0). Yield: 50%.

2.2.3. $[Cu(vaat)_2(H_2O)_2]A_2$ ($A = Cl^-$, Br^- (**6**, **7**))

A solution of 1.5 mmol of the corresponding metal salt (0.26 g $CuCl_2 \cdot 2H_2O$; 0.34 g $CuBr_2$) in 5 ml of water and a solution of 4.5 mmol (0.68 g) of vaat were mixed and then evaporated. The evaporation was followed by cooling the reaction mixture and by filtering the formed precipitate.

$[Cu(vaat)_2(H_2O)_2]Cl_2$: *Anal*. for $C_{12}H_{20}Cl_2CuN_8O_4$: Calc. (found): C, 30.4 (29.9); H, 4.2 (4.0); N, 23.6 (24.1); Cu, 13.4 (13.1). Yield: 30%.

$[Cu(vaat)_2(H_2O)_2]Br_2$: *Anal*. for $C_{12}H_{20}Br_2CuN_8O_4$: Calc. (found): C, 25.6 (24.7); H, 3.6 (3.6); N, 19.9 (19.5); Cu, 11.3 (11.1). Yield: 60%.

The metal content was determined by trilonometric analysis after decomposition of the samples in a mixture of $H_2SO_{4(c)}$ and $HClO_{4(c)}$. C, H and N determinations were performed by the Laboratory of Microanalysis, Novosibirsk Institute of Organic Chemistry.

Suitable crystals of $[Ni(vaat)_2(H_2O)_2](NO_3)_2$ for X-ray analysis were obtained by slow evaporation of a solution of the compound in a mixture of ethanol, DMFA and benzene (1:1:1) after 2 months. Single crystals of $[Cu(vaat)_2(H_2O)_2]Cl_2$ were obtained from an aqueous solution of this complex after 1 month.

2.3. X-ray structure determination

Crystallographic data and details of diffraction experiments are given in Table 1. Data were collected with a Siemens (Bruker) SMART platform with a CCD detector using monochromatized Mo Kα radiation ($\lambda = 0.71073$ Å) over more than a hemisphere of reciprocal space ($2\theta < 55^\circ$) for compound **2** at room temperature. The SMART software was used for data acquisition and the SAINT software for data extraction [34a]. Absorption corrections were done using SADABS [34a], and the structure was solved and refined using the SHELXS-86 [34b] and SHELXTL program systems [34c]. Selected bond distances and angles for **2** are given in Table 2.

Compound **6** was studied by X-ray analysis at room temperature using an automatic four-cycle Enraf-Nonius CAD4 diffractometer (radiation Mo Kα, graphite monochromator, standard technique, θ–2θ scan with variable speed). The structure was solved by direct methods and refined by full-matrix least-squares methods using the SHELX97 program set [35]. Hydrogen atoms were located geometrically and refined in a rigid body approximation. Selected bond distances and angles for compound **6** are given in Table 3.

Table 1
Crystal data and details of the structure refinement for compounds **2** and **6**

	2	**6**
Empirical formula	$C_{12}H_{20}O_{10}NiN_{10}$	$C_{12}H_{20}Cl_2O_4CuN_8$
Formula weight	523.09	474.80
Colour	blue	blue
Crystal size (mm)	$2.6 \times 1.3 \times 3.3$	$1.30 \times 0.55 \times 0.25$
Crystal system	triclinic	triclinic
Space group	$P\bar{1}$ (no. 2)	$P\bar{1}$ (no. 2)
a (Å)	7.2846(6)	7.602(1)
b (Å)	8.1376(7)	8.217(1)
c (Å)	9.6436(8)	8.5139(9)
α (°)	78.266(10)	73.63(1)
β (°)	72.398(10)	71.4666(9)
γ (°)	82.429(10)	77.03(1)
V (Å^3)	532.00(8)	478.5(1)
Z	1	1
ρ_{calc} (g cm^{-3})	1.633	1.648
Device	SMART CCD	CAD4
λ (Å), Mo Kα	0.71073	0.71073
μ (mm^{-1})	0.985	1.457
Collected reflections	5612	1786
Observed unique reflections	2576	1649
R_{int}	0.0179	0.0145
Parameters	160	165
$R(F)$ [a]	0.0358	0.0374
$wR(F)^2$ [a]	0.0989	0.0995
Goodness-of-fit on F^2	1.084	1.101

[a] $R(F) = \Sigma||F_o|-|F_c||/\Sigma|F_o|$ for $F_o > 4\sigma(F_o)$, $wR(F_2) = [\Sigma w(F_o^2 - F_c^2)^2/\Sigma wF_o^2]^{1/2}$, $w = 1/\sigma^2(F_o^2) + 0.035F^2)$.

Table 2
Selected bond lengths (Å) and angles (°) for compound **2**

Bond lengths			
Ni1–O1w	2.0778(16)	C3–N4	1.351(2)
Ni1–N4	2.0173(15)	C3–N5	1.387(2)
Ni1–O1	2.0447(14)	N4–C5	1.325(2)
N1–N2	1.369(2)	N5–C6	1.359(2)
N1–C5	1.327(2)	C6–O1	1.229(2)
N1–C8	1.426(2)	C6–C7	1.497(3)
N2–C3	1.325(2)	C8–C9	1.303(3)
Bond angles			
N4#1–Ni1–O1w	89.18(7)	N2–C3–N4	115.05(16)
N4–Ni1–O1w	90.82(7)	N2–C3–N5	120.37(17)
N4–Ni1–O1w#1	89.18(7)	N4–C3–N5	124.57(16)
N4#1–Ni1–O1	93.36(6)	C3–N4–Ni1	126.52(13)
N4–Ni1–O1	86.64(6)	C5–N4–Ni1	130.24(13)
N4–Ni1–O1#1	93.36(6)	C5–N4–C3	103.11(15)
O1–Ni1–O1w	88.63(7)	N1–C5–N4	109.89(17)
O1#1–Ni1–O1w	91.37(7)	C6–N5–C3	126.22(17)
O1–Ni1–O1w#1	91.37(7)	N5–C6–C7	115.71(17)
N2–N1–C8	122.39(16)	O1–C6–N5	123.9(18)
C5–N1–N2	110.52(15)	O1–C6–C7	120.37(17)
C5–N1–C8	127.04(18)	C6–O1–Ni1	131.79(13)
C3–N2–N1	101.42(15)	C9–C8–N1	123.1(2)

Estimated standard deviations are given in parentheses. Symmetry transformations used to generate equivalent atoms: #1: $-x$, $-y+1$, $-z+1$.

Table 3
Selected bond lengths (Å) and angles (°) for compound **6**

Bond lengths			
Cu1–O1w	2.433(2)	C3–N4	1.358(3)
Cu1–N4	1.937(2)	C3–N5	1.379(3)
Cu1–O1	2.008(2)	N4–C5	1.330(3)
N1–N2	1.370(3)	N5–C6	1.334(3)
N1–C5	1.328(3)	C6–O1	1.239(3)
N1–C8	1.415(3)	C6–C7	1.499(3)
N2–C3	1.313(3)	C8–C9	1.301(4)
Bond angles			
N4#1–Cu1–O1w	87.06(7)	N2–C3–N4	114.9(2)
N4–Cu1–O1w	92.94(7)	N2–C3–N5	121.1(2)
N4–Cu1–O1w#1	87.06(7)	N4–C3–N5	124.0(2)
N4#1–Cu1–O1	91.71(7)	C3–N4–Cu1	126.9(2)
N4–Cu1–O1	88.29(7)	C5–N4–Cu1	129.7(2)
N4–Cu1–O1#1	91.71(7)	C5–N4–C3	103.3(2)
O1–Cu1–O1w	85.77(7)	N1–C5–N4	109.3(2)
O1#1–Cu1–O1w	94.23(7)	C6–N5–C3	126.1(2)
O1–Cu1–O1w#1	94.23(7)	N5–C6–C7	115.8(2)
N2–N1–C8	121.8(2)	O1–C6–N5	124.1(2)
C5–N1–N2	110.7(2)	O1–C6–C7	120.1(2)
C5–N1–C8	127.5(2)	C6–O1–Cu1	130.2(2)
C3–N2–N1	101.8(2)	C9–C8–N1	123.4(2)

Estimated standard deviations are given in parentheses. Symmetry transformations used to generate equivalent atoms: #1: $-x+1$, $-y$, $-z$.

3. Results and discussion

3.1. Synthetic aspects

The coordination compounds of Co(II), Ni(II) and Cu(II) were synthesised by mixing hot aqueous solutions of the corresponding metal salts and the ligand. Precipitates were obtained after evaporation and cooling of the resulting solutions. The small yields are due to the relatively high solubility of the complexes in water. Further evaporation of mother liquors increases the yields. For the synthesis of compounds **1**–**5**, metal:ligand molar ratios of 1:1 and 1:2 were used. Complexes of the same composition were obtained by adopting such synthetic conditions. The synthesis of complexes **6** and **7** were carried out with a metal:ligand ratio of 1:3, as a metal:ligand ratio of 1:2 did not lead to the formation of compounds having a 1:2 stoichiometry. All compounds are soluble in water and organic solvents (ethanol, isopropanol, acetone, DMFA, DMSO, and in their mixtures with benzene and toluene).

Complexes **2** and **4** were recrystallised from water. The results of elemental analysis of the recrystallised phases were not different from the data of the parent compounds.

3.2. Description of the crystal structures

The molecular structure of compound **2** is shown in Fig. 1. The Ni(II) ion exhibits a slightly distorted

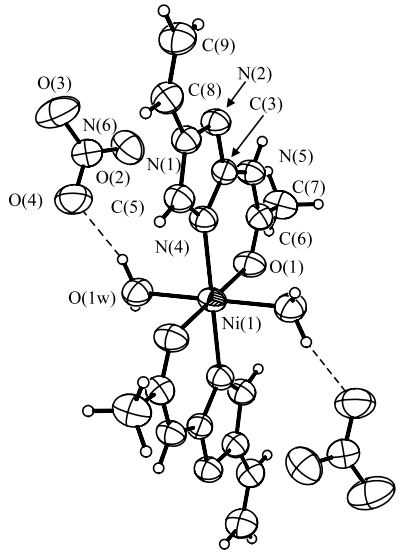


Fig. 1. View of the crystal structure of $[Ni(vaat)_2(H_2O)_2](NO_3)_2$ (**2**) (50% probability ellipsoids).

octahedral coordination geometry with two water molecules in axial positions and two nitrogen and oxygen atoms coming from two coplanar vaat ligands situated in the equatorial plane (Table 2). The nitrate anions are not involved in the coordination sphere in contrast to $[CuL_2(NO_3)_2]$ with L = 3-acetylamino-1,2,4-triazole [25]. Fig. 2 shows a view of the crystal packing on the (ab) plane. The nitrate anions appear to be involved in an extensive hydrogen bonding network involving the water molecules coordinated to the nickel ions and the amido groups attached to the triazole ligands. This

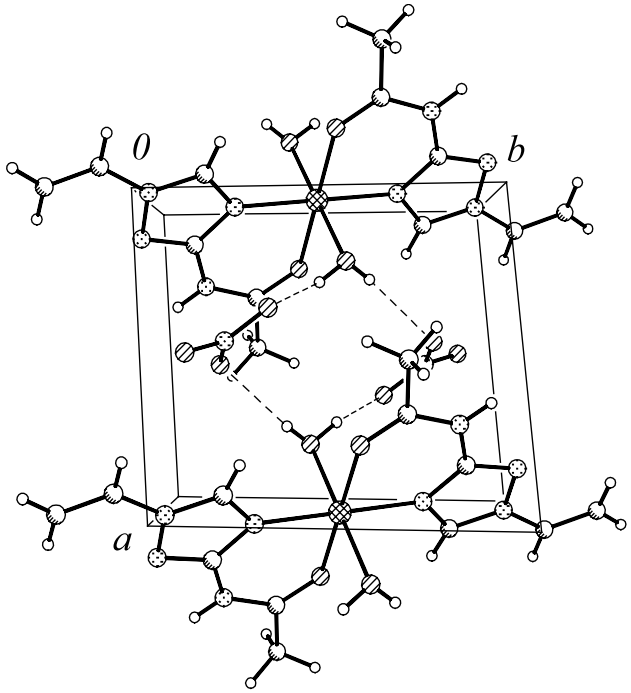


Fig. 2. View of the crystal packing of compound **2** on the (ab) plane.

allows a link to be established between the mononuclear complexes in the *a* and *b* directions, the Ni···Ni distance being equal to 7.285 Å.

The cationic unit $[Cu(vaat)_2(H_2O)_2]^{2+}$ of **6** is shown in Fig. 3. As usual in Cu(II) complexes, the coordination polyhedron of the metal ion is an elongated square bipyramid with two bidentate triazole ligands in equatorial positions and two water molecules in axial positions. The Cu–N and Cu–O bond distances have their typical values. The triazole ligand is practically planar, the deviations of N(1), N(2), C(3), N(4) and C(5) atoms from the common least-squares plane are less than 0.004 Å. The aceto-group and the copper atom also lie very close to this plane, the deviations are within 0.07 Å. This means that π–π aromatic coupling is possible in the ligand. This is also confirmed by analysis of the bond distances in the triazole ring. Indeed, the "single" bonds N(1)–N(2), N(1)–C(5) and C(3)–N(4) are only slightly longer than the "double" bonds N(2)–C(3) and N(4)–C(5) (Table 3). The crystal packing of **6** is shown in Fig. 4. There are short Cl(1)···H–N(5) and Cl(1)···H–O(1w) non-bonding contacts with Cl–N and Cl–O distances of 3.13 and 3.14 Å, respectively, which can be considered as intermolecular hydrogen bonds. In this way the chlorine anions link the complex cations into chains running along the *b* axis (Fig. 4).

Relevant interatomic distances and angles for the hydrogen bonding interactions in **2** and **6** are given in Tables 4 and 5, respectively.

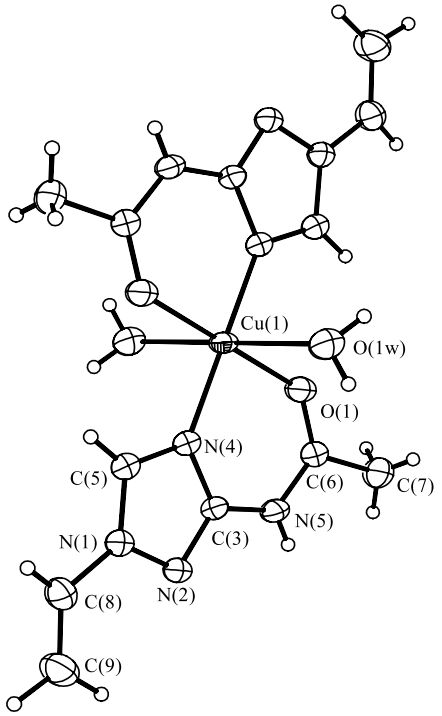


Fig. 3. View of the cationic unit $[Cu(vaat)_2(H_2O)_2]^{2+}$ of **6** (50% probability ellipsoids).

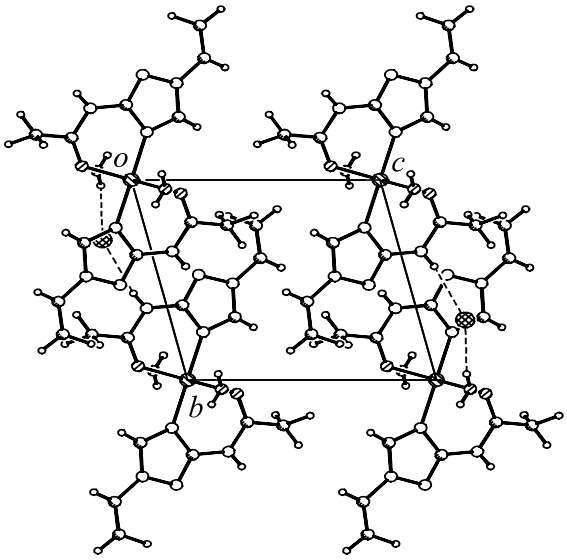


Fig. 4. View of the crystal packing of compound **6**. The $Cl^{-}\cdots H$ contacts are shown as dashed lines.

Table 4
Relevant interatomic distances and angles of the hydrogen bonding interactions in compound **2**

D–H···A	D–H	H···A	D···A	D–H···A
O1W–H1A···O4 [a]	0.87	1.88	2.716	159
O1W–H1B···O2	0.70	2.16	2.858	173
N5–H5A···O2 [b]	0.86	2.12	2.956	163
C8–H8···O3 [c]	0.93	2.51	3.342	149
C9–H9A···O1W [b]	0.93	2.59	3.453	154

Atoms marked with a letter are generated by symmetry operations: (a) $1-x, 1-y, 1-z$; (b) $x, -1+y, z$; (c) $-1+x, -1+y, 1+z$.

Table 5
Relevant interatomic distances and angles of the hydrogen bonding interactions in compound **6**

D–H···A	D–H	H···A	D···A	D–H···A
O1W–H1W···Cl1	0.77	2.39	3.144	166
N5–H5N···Cl1 [a]	0.77	2.38	3.134	168
C5–H5C···O1 [b]	0.88	2.65	3.012	106

Atoms marked with a letter are generated by symmetry operations: (a) $-x, 1-y, -z$; (b) $1-x, -y, -z$.

3.3. Colour change of $[Co(vaat)_2(H_2O)_2]Cl_2$

Upon heating, complex **4** does show a pronounced colour change from pink to blue. Thermogravimetric analysis shows that this compound loses part of its mass in the temperature range 383–423 K. A more precise determination was obtained gravimetrically. It corresponds to the removal of (2.4 ± 0.1) water molecules per complex molecule. Additional increase of this value in comparison with the expected one (two water molecules per complex) can be due to the presence of non-

coordinating water molecules in the crystal lattice (0.4 per complex). The reversibility of the process has been checked. If the blue compound is placed in a closed dessiccator with a relative high humidity, the pink colour is recovered after 12 h. This reversible colour change has been confirmed by electronic and IR spectroscopy. Hereafter the anhydrous compound will be assigned as **4′**. A similar phenomenon was observed by us earlier for $[Co(trba\cdot HCl)]Cl_2\cdot 4H_2O$, where trba = *N*-(1,2,4-triazol-5-yl)benzamidine [31].

3.4. Spectroscopic characterisation

3.4.1. Infrared spectra

The most significant bands are summarised in Table 6. Changes observed in the spectra of the complexes (shifts of ν(CO) and ν(CN)+δ(NH) bands) with respect to the free vaat ligand show that the ligand is coordinated to M(II) through the nitrogen atom of the triazole ring and oxygen atom of the acetylamino-group in agreement with the results of the X-ray diffraction study. The ν(C=C) bands are practically not shifted in the spectra of the complexes with respect to the spectra of the free ligand. This indicates that the vinyl group of vaat is non-coordinated. The $\nu(H_2O)$ frequences were not assigned due to their possible mixing with ν(NH) bands.

Complexes were recrystallised from D_2O. It allowed us to reveal the $\nu(H_2O)$ frequencies at 3400–3000 cm^{-1}, because in the spectra of deuterated compounds these bands are displaced to lower frequencies with a coefficient of 1.34–1.38. The shifts of $\gamma(H_2O)$ and the ν(M–O) bands were also indicated by deuteration. The ν(M–N) vibrations appear at frequencies characteristic for metal complexes with triazoles and tetrazoles [32]. Thus, a comparative analysis of the spectra of the deuterated complexes with respect to their parent ones allows conclusions to be drawn about the presence of coordinated water molecules in the title compounds.

It should be pointed out that the spectrum of the blue complex **4′** changed dramatically in comparison to the one of **4** as the $\nu(H_2O)$ and $\gamma(H_2O)$ vibrations are no longer observed. This indicates that the coordination environment of Co(II) in the blue compound **4′** is changed in comparison to that of compound **4**.

3.4.2. Diffuse reflectance spectra

Table 7 lists the electronic spectra bands. The values of the maxima and the number of bands observed are in accordance with an octahedral environment for M(II) (M = Co, Ni) and allows us to propose a tetragonal geometry for the Cu(II) ion. Values of Δ (= 10 Dq) for Co(II) complexes **1** and **4**, which were calculated with the equation $\nu_1 = 0.88\Delta$ given in Ref. [33], fit with those obtained for the related mononuclear complexes $[Co(Haat)_2(H_2O)_2]Cl_2$ and $[Co(Haat)_2(H_2O)_2](NO_3)_2$, where Haat is 3-acetylamino-1,2,4-triazole [28]. For the Ni(II) complexes, **2** and **5**, the Δ parameters are larger than those of the similar complexes $[Ni(Haat)_2(H_2O)_2]Cl_2$ and $[Ni(Haat)_2(H_2O)_2](NO_3)_2\cdot 2H_2O$ [28]. One might expect that the difference is due to some change in the bonding character, but in the latter probably due to the introduction of a vinyl group in the composition of the ligand.

The spectrum of **4′** is typical for tetrahedral Co(II) complexes. An interesting feature of this spectrum,

Table 6
Selected IR bands (cm^{-1}) for vaat and its corresponding complexes

	ν(CO)	ν(C=C)	ν(CN)+δ(NH)	$\gamma(H_2O)$	ν(MO)	ν(MN)
vaat	1703	1653	1598, 1550			
Complexes **1**–**7**	1670–1660	1653–1650	(1605–1625), (1530–1545)	530–470	400–450	270–340

Table 7
Electronic spectra maxima and magnetic moments for compounds **1**–**7** and **4′**

Compound	λ_{max} (cm^{-1})	$\Delta\cdot 10^{-3}$ (cm^{-1})	μ_{eff} (BM)
1	21300s [a](ν_3), 8700(ν_1)	9.9	4.74 [b]
2	28110s(ν_3), 16900s(ν_2), 10900b(ν_1)	10.9	3.18 [b]
3	14705s, 12600sh		1.89 [c]
4	20600s(ν_3), 8330(ν_1)	9.5	4.89 [b]
5	28110s(ν_3), 16800s(ν_2), 10800b(ν_1)	10.8	3.19 [b]
6	14705s, 12400sh		1.91 [c]
7	14085s, 11340sh		1.86 [b]
4'	18310sh, 15100s(ν_3), 8050b, 6115w(ν_2), 5435w(ν_1), 4695w	5.4	

[a] b = broad band with a maximum not well defined, s = strong, sh = shoulder, w = weak.
[b] At 293 K.
[c] In the temperature range 78–300 K.

however, is the presence of relatively intense spin-forbidden bands.

3.5. Magnetic measurements

Magnetic moments (Table 7) correspond to high-spin d^7 and d^8 configurations of cobalt(II) and nickel(II) complexes, respectively, and d^9 configuration of copper(II) complexes. The magnetic moments of **3** and **6** do not show any temperature dependence (78–300 K).

4. Conclusion

In this paper we have prepared and characterised new coordination compounds containing the new 1-vinyl-3-acetylamino-1,2,4-triazole ligand. This ligand acts as a chelating ligand and leads to mononuclear complexes comparable to those reported with the non-deprotonated 3-acetylamino-1,2,4-triazole ligand [22–25,27,28]. Triazole molecules are nearly planar and π–π aromatic coupling is possible in the ligand. Thus, addition of a vinyl group in position 1 of 3-acetylamino-1,2,4-triazole does not change the coordination mode of the ligand. Furthermore, coordination of the vinyl group, which could have been expected, has not been observed. The interest of these materials resides in their ability to form an extensive hydrogen bonding network giving rise to chains for compound **6** or to a 2-D character for compound **2**. Such diversity in the structures of these compounds is indeed correlated to the nature of the counteranions. The nitrate anion for instance has three oxygen atoms which lie in the same plane and can be involved by hydrogen bonding in several directions thus establishing a link between the molecules.

Another interesting aspect of this work concerns the astonishing reversible colour change observed for $[Co(vaat)_2(H_2O)_2]Cl_2$ upon heating. It has been convincingly demonstrated on the basis of spectroscopic measurements as well as gravimetric studies that this phenomenon is actually connected to the removal and addition of water molecules giving rise to a reversible octahedron–tetrahedron transition according to the following reaction:

$$\underset{\mathbf{4}}{[Co(vaat)_2(H_2O)_2]Cl_2 \cdot 0.4H_2O} \Leftrightarrow \underset{\mathbf{4'}}{[Co(vaat)_2]Cl_2} + 2.4\ H_2O$$

The microscopic phenomenon which is present can be termed chemochromism as a chemical change at heating and cooling is involved during the above mentioned transformation.

5. Supplementary material

Crystallographic data have been deposited at the Cambridge Crystallographic Data Centre, CCDC No. 162493 for compound **2** and CCDC No. 162444 for compound **6**. Copies of this information may be obtained free of charge from The Director, CCDC, 12 Union Road, Cambridge, CB2 1EZ, UK (fax: +44-1223-336033; e-mail: deposit@ccdc.cam.ac.uk or www: http://www.ccdc.cam.ac.uk).

Acknowledgements

We thank Professor L.I. Vereshchagin, Yu.I. Mironov and S. Stauf. The European Science Foundation, the Deutsche Forschungsgemeinschaft, the TMR Research Network ERB-FMRX-CT98-0199 (TOSS), the Fonds der Chemischen Industrie and the Materialwissenschaftliches Forschungszentrum der Universität Mainz are also thanked for funding.

References

[1] L.G. Lavrenova, V.N. Ikorskii, V.A. Varnek, I.M. Oglezneva, S.V. Larionov, Koord. Khim. 12 (1986) 207.
[2] L.G. Lavrenova, V.N. Ikorskii, V.A. Varnek, I.M. Oglezneva, S.V. Larionov, Koord. Khim. 16 (1990) 654.
[3] L.G. Lavrenova, V.N. Ikorskii, V.A. Varnek, I.M. Oglezneva, S.V. Larionov, J. Struct. Chem. 34 (1993) 960.
[4] L.G. Lavrenova, N.G. Yudina, V.N. Ikorskii, V.A. Varnek, I.M. Oglezneva, S.V. Larionov, Polyhedron 14 (1995) 1333.
[5] (a) O. Kahn, E. Codjovi, Y. Garcia, P.J. van Koningsbruggen, R. Lapouyade, L. Sommier, ACS Symp. Series 644 (1996) 298; (b) O. Kahn, C. Jay-Martinez, Science 279 (1998) 44.
[6] Y. Garcia, P.J. van Koningsbruggen, E. Codjovi, R. Lapouyade, O. Kahn, L. Rabardel, J. Mater. Chem. 7 (1997) 857.
[7] P.J. van Koningsbruggen, Y. Garcia, E. Codjovi, R. Lapouyade, O. Kahn, L. Fournes, L. Rabardel, J. Mater. Chem. 7 (1997) 2069.
[8] Y. Garcia, P.J. van Koningsbruggen, G. Bravic, P. Guionneau, D. Chasseau, G.L. Cascarano, J. Moscovici, K. Lambert, A. Michalowicz, O. Kahn, Inorg. Chem. 36 (1997) 6357.
[9] Y. Garcia, P.J. van Koningsbruggen, R. Lapouyade, L. Rabardel, O. Kahn, M. Wierczorek, R. Bronisz, Z. Ciunik, M.F. Rudolf, C.R. Acad. Sci. Paris, IIc (1998) 523.
[10] Y. Garcia, P.J. van Koningsbruggen, R. Lapouyade, L. Fournès, L. Rabardel, O. Kahn, V. Ksenofontov, G. Levchenko, P. Gütlich, Chem. Mater. 10 (1998) 2426.
[11] Y. Garcia, O. Kahn, L. Rabardel, B. Chansou, L. Salmon, J.-P. Tuchagues, Inorg. Chem. 38 (1999) 4663.
[12] Y. Garcia, P.J. van Koningsbruggen, H. Kooijman, A.L. Spek, J.G. Haasnoot, O. Kahn, Eur. J. Inorg. Chem. (2000) 307 and 507.
[13] Y. Garcia, P. Guionneau, G. Bravic, D. Chasseau, J.A.K. Howard, O. Kahn, V. Ksenofontov, S. Reiman, P. Gütlich, Eur. J. Inorg. Chem. (2000) 1531.
[14] Y. Garcia, V. Ksenofontov, G. Levchenko, P. Gütlich, J. Mater. Chem. 10 (2000) 2274.
[15] J.G. Haasnoot, Coord. Chem. Rev. 200-202 (2000) 131.

[16] R. Prins, P.J.M.W.L. Birker, J.G. Haasnoot, G.C. Verschoor, J. Reedijk, Inorg. Chem. 24 (1985) 4128.
[17] P.J. van Koningsbruggen, J.G. Haasnoot, R.A.G. de Graaf, J. Reedijk, S. Singerland, Acta Crystallogr., Sect. C 48 (1992) 1923.
[18] R. Bohm, C. Karow, Pharmazie 4 (1981) 243.
[19] S.C. Bahel, B.L. Dubey, N. Nath, J.K. Srivastava, Inorg. Chim. Acta L43 (1984) 91.
[20] D.J. Cash, A.N. Ferguson, J. Photogr. Sci. 28 (1980) 121.
[21] D.L. Smith, H.L. Luss, Photogr. Sci. Eng. 20 (1976) 184.
[22] M.B. Cingi, A.M. Manotti Lanfredi, A. Tiripicchio, J.G. Haasnoot, J. Reedijk, Acta Crystallogr., Sect. C 45 (1989) 601.
[23] M. Biagini Cingi, M. Lanfranchi, A.M. Manotti Lanfredi, S. Ferrer, J.G. Haasnoot, J. Reedijk, Inorg. Chim. Acta 209 (1993) 219.
[24] S. Ferrer, J.G. Haasnoot, J. Reedijk, E. Muller, M. Biagini Cingi, A.M. Manotti Lanfredi, F. Ugozzoli, C. Foglia, J. Chem. Soc., Dalton Trans. (1999) 3029.
[25] A.V. Virovets, D.Yu. Naumov, L.G. Lavrenova, M.B. Bushuev, Acta Crystallogr., Sect. C45 (1999) IUC9900059.
[26] S. Ferrer, J.G. Haasnoot, J. Reedijk, E. Muller, M. Biagini Cingi, M. Lanfranchi, A.M. Manotti Lanfredi, J. Ribas, Inorg. Chem. 39 (2000) 1859.
[27] A.V. Virovets, M.B. Bushuev, L.G. Lavrenova, J. Struct. Chem. 41 (2000) 871.
[28] L.G. Lavrenova, M.B. Bushuev, A.V. Vrovets, D.Yu. Naumov, L.A. Sheludyakova, Yu.G. Shvedenkov, J. Neorg. Chem. 45 (2000) 1658.
[29] M. Liu-Gonzalez, F. Sanz-Ruiz, XVIII IUG Congress General Assembly (1999) 429.
[30] A.V. Virovets, N.V. Podberezskaya, L.G. Lavrenova, J. Struct. Chem. 38 (1997) 441.
[31] L.G. Lavrenova, A.R. Amamchan, S.V. Larionov, V.A. Dorohov, Izv. Acad. Nauk., Ser. Khim. 10 (1992) 2311.
[32] L.A. Sheludyakova, L.G. Lavrenova, J. Struct. Chem. 38 (1997) 853.
[33] C.J. Ballhausen, Introduction to Ligand Field Theory, Moscow, 1964.
[34] (a) SMART, SAINT V-4, SADABS Programs; Bruker Analytical X-ray Systems Inc.: Madison, WI, 1996.;
(b) G.M. Sheldrick, SHELXS-86: Programme for crystal structure solution, University of Göttingen, Göttingen, Germany, 1986.;
(c) G.M. Sheldrick, SHELXL-97: Programme for crystal structure refinement, University of Göttingen, Göttingen, Germany, 1997.
[35] SHELX 97 Release 97-2. G.M. Sheldrick, University of Göttingen, Göttingen, Germany, 1998.

PERGAMON

Polyhedron 21 (2002) 805–810

POLYHEDRON

www.elsevier.com/locate/poly

Stability constants of inner- and outer-sphere complexes of hydrated tris(1-(2-thienyl)-4,4,4-trifluoro-1,3-butanedionato) lanthanide(III) with tris(2,4-pentanedionato) cobalt(III)

Naohiro Kameta [a], Hisanori Imura [a,*], Kousaburo Ohashi [a], Takashi Aoyama [b]

[a] *Department of Environmental Sciences, Faculty of Science, Ibaraki University, Mito 310-8512, Japan*
[b] *MCR Center, Hitachi Research Laboratory, Hitachi Ltd., Hitachi 319-11, Japan*

Received 8 August 2001; accepted 19 December 2001

Abstract

Binuclear complexation between hydrated tris(1-(2-thienyl)-4,4,4-trifluoro-1,3-butanedionato)lanthanide(III) ($Ln(tta)_3$) and tris(2,4-pentanedionato)cobalt(III) ($Co(acac)_3$) in benzene has been studied by a liquid–liquid distribution method and spectroscopic methods such as electronic absorption for d–d transition, IR for OH vibration of coordinated water molecules, and ^{59}Co NMR. The stability constants of a binuclear complex ($\beta_{s,1}$) across the lanthanide series were determined by both distribution and spectrophotometric methods. The $\beta_{s,1}$ values for La to Nd were close to each other and much higher than those for Er to Lu, which were almost constant. As a result, there was the large difference in $\beta_{s,1}$ between the light and the heavy Ln. The spectrochemical studies by IR and ^{59}Co NMR suggested that the binuclear complex has two different structures with inner- and outer-sphere coordination. In the former $Co(acac)_3$ displaces the coordinated water molecules in the Ln chelate and directly coordinates to the central Ln ion through the coordinating oxygen atoms of the acac ligands. In the latter hydrogen-bonding is formed between the coordinating oxygen atoms in $Co(acac)_3$ and hydrogen atoms of coordinated water molecules in the Ln chelate. Both binuclear complexes coexist in the solution of light Ln, while the outer sphere type mostly exist in heavy Ln. © 2002 Elsevier Science Ltd. All rights reserved.

Keywords: Lanthanide(III) chelate; Cobalt(III) chelate; Binuclear complexes; Inner-sphere coordination; Outer-sphere coordination; Stability constant

1. Introduction

In our recent studies on the liquid–liquid distribution of tris(1-(2-thienyl)-4,4,4-trifluoro-1,3-butanedionato)lanthanide(III) ($Ln(tta)_3$), the La, Eu and Lu chelates have been found to form binuclear complexes with inert cobalt(III) chelates such as tris(2,4-pentanedionato)cobalt(III) ($Co(acac)_3$) [1] and tris(8-quinolinolato)cobalt(III) ($Co(q)_3$) [2] in an organic phase. This phenomenon was explained by the reaction between $Ln(tta)_3$ as a Lewis acid and the cobalt(III) chelates as a Lewis base or a complex ligand in the organic phase.

In the above short paper dealing with $Co(acac)_3$ [1], we have pointed out the existence of two types of the binuclear complexes on the basis of the result of ^{59}Co NMR, i.e. the slow chemical-exchange species between free and complexed $Co(acac)_3$ on the NMR time scale in the La case, the fast exchange species in Lu, and both in Eu. However, the structure of the binuclear complexes and the effect of the central Ln metals could not be elucidated.

Since $Ln(tta)_3$ has residual coordinated water molecules even in the organic phase, some water molecules must be released from the inner coordination sphere of Ln when the binuclear complex is formed by the direct coordination of $Co(acac)_3$ to the Ln ion. Therefore, it is very important to study the behavior of the coordinated water molecules in the binuclear complexation.

In this paper, the stability constants of the binuclear complexes composed of $Ln(tta)_3$ and $Co(acac)_3$ are

* Corresponding author. Tel.: +81-29-228-8364; fax: +81-29-228-8403.
E-mail address: imura@mito.ipc.ibaraki.ac.jp (H. Imura).

0277-5387/02/$ - see front matter © 2002 Elsevier Science Ltd. All rights reserved.
PII: S0277-5387(02)00858-6

determined over the Ln series by both distribution method and spectrophotometry. The effect of the central Ln ions and the role of water on the stability of the binuclear complexes are clarified. Furthermore, the bonding and the structure of the binuclear complex are investigated by means of spectrochemical methods such as IR and ^{59}Co NMR spectroscopy. In particular, IR spectroscopy for the coordinated water molecules has been successfully used to differentiate the inner- and the outer-sphere coordination in the binuclear complexes.

2. Experimental

2.1. Reagents

Ln stock solutions were prepared by the same manner as in the previous paper [1]. Trioctylphosphine oxide (TOPO) was obtained from Dojindo Lab. and used without further purification. Htta, $Co(acac)_3$, and other reagents were the same as those used previously [1].

$Eu(tta)_3(H_2O)_3$ was synthesized according to the literature [3] and stored in a vacuum desiccator. Yield 53%. Melting point (m.p.) 132–140 °C. *Anal*. Calc. for $C_{24}H_{18}EuF_9S_3O_9$: C, 33.15; H, 2.17. Found: C, 33.31; H, 2.10%. The number of coordinated water molecules was also confirmed to be three by IR spectrophotometry in the benzene solution as described later.

2.2. Distribution method

The procedure for the liquid–liquid distribution of Ln was carried out in the same manner as reported previously [1]. The distribution ratio (D) of Ln was determined from the Ln concentrations in both phases.

2.3. Sample preparations and spectroscopic measurements

Sample preparations and measurements of the electronic absorption and ^{59}Co NMR were performed by the same manner reported previously [1].

The sample solutions for the IR measurements were prepared by mixing the $Ln(tta)_3$ solution obtained by the solvent extraction of 1.0×10^{-2} M Ln with 3.0×10^{-2} M Htta in benzene at pH 5.7–6.3. The concentration of the remaining Htta in the organic phase was less than 9×10^{-4} M. The water content in the sample solutions was kept constant at 2.0×10^{-2} M using anhydrous and water-saturated benzene. In the IR experiment, synthesized $Eu(tta)_3(H_2O)_3$ was also used in anhydrous benzene. IR spectra of free water and the coordinated water of 6.0×10^{-3} M $Ln(tta)_3$ in benzene were measured in the presence of varying concentrations of $Co(acac)_3$ or TOPO at 3000–4000 cm^{-1} with a Shimadzu-8200A FT IR spectrophotometer at 25 °C. A demountable liquid cell with calcium fluoride windows was used and the path length was adjusted to 1 mm.

3. Results and discussion

3.1. Determination of stability constant by the distribution method

Lanthanide(III) is extracted with Htta in nonpolar solvents as a hydrated neutral chelate, $Ln(tta)_3(H_2O)_n$. The distribution ratio (D_o) of Ln between an organic (org) and an aqueous (aq.) phase is expressed as follows:

$$D_o = \frac{[Ln(tta)_3]_{org}}{[Ln^{3+}]_{aq} + \sum[Ln(tta)_n^{(3-n)+}]_{aq}}, \quad (1)$$

where the coordinated water molecules of Ln^{3+} and $Ln(tta)_3$ were omitted to simplify. Eq. (1) can be rewritten using the equilibrium constants, $K_D\beta_3 = [Ln(tta)_3]_{org}/[Ln^{3+}]_{aq}[tta^-]_{aq}^3$, where K_D and β_3 are the distribution constant of $Ln(tta)_3$ between two phases and the stability constant of $Ln(tta)_n^{(3-n)+}$ in the aqueous phase, respectively, that is:

$$D_o = \frac{K_D\beta_3[tta^-]_{aq}^3}{1 + \sum \beta_n[tta^-]_{aq}^n} \quad (2)$$

where $[tta^-]_{aq}$ denotes the concentration of an anion of Htta in the aqueous phase. $[tta^-]_{aq}$ is readily calculated from total concentration (C_{HA}) of Htta and pH using the following equation:

$$[tta^-]_{aq} = \frac{C_{HA}}{1 + (K_{D,HA} + 1)[H^+]_{aq}/K_{HA}}, \quad (3)$$

where K_{HA} and $K_{D,HA}$ are the acid-dissociation constant of Htta in the aqueous phase and the distribution constant of Htta between two phases, respectively. In this paper, the literature values, $\log K_{HA} = -6.23$ [4] and $\log K_{D,HA} = 1.62$ [5], were adopted. The extraction of Dy, Ho, Tm, and Yb with 1.0×10^{-2} M Htta at pH 3.7–4.9 was carried out. The plots of $\log D$ versus $\log[tta^-]_{aq}$ based on Eq. (2) for those Ln indicated straight lines with a slope of 3.0 at $[tta^-] = 10^{-6.2}$–$10^{-5.0}$. Therefore, the existence of $Ln(tta)_3^{(3-n)+}$ in the aqueous phase can be neglected under the given conditions and then Eq. (2) can be rewritten as follows:

$$D_o = K_D\beta_3[tta^-]_{aq}^3 \quad (4)$$

The logarithmic values of $K_D\beta_3$ for each Ln were determined from the plots of $\log D$ versus $\log[tta^-]_{aq}$ as follows: 16.37 (Dy), 16.61 (Ho), 16.79 (Tm) and 16.96 (Yb). The $K_D\beta_3$ of La, Eu and Lu was expressed as K_e in our previous paper [1], and the logarithmic values were calculated to be 13.41 (La), 15.91 (Eu) and 16.89 (Lu) using the data shown there. The $\log K_D\beta_3$ values for

other Ln were calculated from the extraction constant reported previously on the basis of the relation of $K_{ex} = [Ln(tta)_3]_{org}[H^+]^3_{aq}/[Ln^{3+}]_{aq}[Htta]^3_{org} = K_D\beta_3 \times K^3_{HA}/K^3_{D,HA}$, and were as follows: 14.36 (Ce), 14.56 (Pr), 15.03 (Nd), 15.85 (Sm), 15.93 (Gd), 16.34 (Tb) and 16.66 (Er) [6]. Consequently, the D_o values at a certain $[tta^-]_{aq}$ can be calculated by Eq. (4).

If $Ln(tta)_3$ forms a binuclear complex with $Co(acac)_3$ in the organic phase, the distribution ratio (D) of Ln is expressed as follows:

$$D = \frac{[Ln(tta)_3]_{org} + [Ln(tta)_3(Co(acac)_3)]_{org}}{[Ln^{3+}]_{aq} + \sum[Ln(tta)_n^{(3-n)+}]_{aq}} \quad (5)$$

Since the existence of $Ln(tta)_3^{(3-n)+}$ in the aqueous phase can be neglected under the given conditions as described above, Eq. (5) can be rewritten as follows:

$$D = K_D\beta_3[tta^-]^3_{aq}(1 + \beta_{s,1}[Co(acac)_3]_{org}), \quad (6)$$

where $\beta_{s,1}$ is the stability constant of a binuclear complex and is defined by:

$$\beta_{s,1} = \frac{[Ln(tta)_3(Co(acac)_3)]_{org}}{[Ln(tta)_3]_{org}[Co(acac)_3]_{org}} \quad (7)$$

When $[tta^-]_{aq}$ in both Eqs. (4) and (6) is equal, the following equation is derived:

$$D/D_o = 1 + \beta_{s,1}[Co(acac)_3]_{org}. \quad (8)$$

Fig. 1 shows the plot of $\log(D/D_o)$ versus $\log[Co(acac)_3]_{org}$ based on Eq. (8). The plots for light Ln, for Ce to Nd, show straight lines with a slope of 1.0 over the wide concentration range of $Co(acac)_3$. For middle and heavy Ln, the plots approach to straight lines with a slope of unity in the higher concentration region of $Co(acac)_3$. These results indicate the formation of a binuclear complex in the organic phase and are in agreement with the results of La, Eu and Lu reported previously [1]. The $\beta_{s,1}$ values are determined by applying a nonlinear least-squares method to those plots based on Eq. (8), and are listed in Table 1 together with those of La, Eu and Lu.

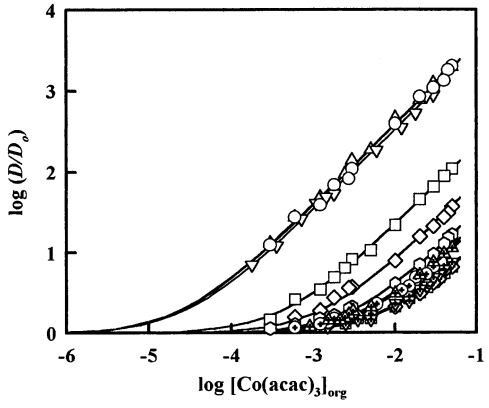


Fig. 1. $\text{Log}(D/D_o)$ of Ln as a function of the $Co(acac)_3$ concentration in benzene. 1.0×10^{-2} M Htta, pH 3.8–5.1. △, Ce; ○, Pr; ▽, Nd; □, Sm; ◇, Gd; ⬡, Tb; ⧋, Dy; ⊙, Ho; ⧩, Er; ⊞, Tm; ◈, Yb.

Table 1
Stability constant of the binuclear complexes in benzene at 25 °C

Ln(III)	Distribution	Spectrophotometry
La	4.64±0.01 [a]	4.70±0.36 [b]
Ce	4.60±0.01	
Pr	4.59±0.02	4.69±0.34
Nd	4.53±0.02	4.60±0.31
Sm	3.34±0.01	3.39±0.18
Eu	2.95±0.01 [a]	3.21±0.01[b]
Gd	2.87±0.02	3.03±0.10
Tb	2.50±0.01	2.56±0.01
Dy	2.35±0.01	
Ho	2.31±0.01	
Er	2.09±0.01	2.17±0.17
Tm	2.05±0.01	
Yb	2.07±0.01	
Lu	2.07±0.02 [a]	2.21±0.21 [b]

Numerical values after ± show the standard error.
[a] Ref. [1].
[b] Calculated using the data in Ref. [1].

3.2. Determination of stability constant by spectrophotometry

In a previous paper [1], it has been shown that the molar absorptivity for the d–d ($^1T_{1g} \leftarrow {}^1A_{1g}$) transition of $Co(acac)_3$ increases on complexation with $Ln(tta)_3$ (Ln:La, Eu, and Lu). A similar increase in the molar absorptivity of $Co(acac)_3$ was also observed with Pr, Nd, Sm, Gd, Tb and Er. Fig. 2 shows the relationship between the apparent molar absorptivity of $Co(acac)_3$ at 595 nm corresponding to the d–d transition and the molar ratio of $Ln(tta)_3$ to $Co(acac)_3$ in the solution. The plot of Pr or Nd well fits with two straight lines having an intersection at $[Ln(tta)_3]_{total}/[Co(acac)_3]_{total} = 1$, which corresponds to a 1:1 stoichiometry as expected

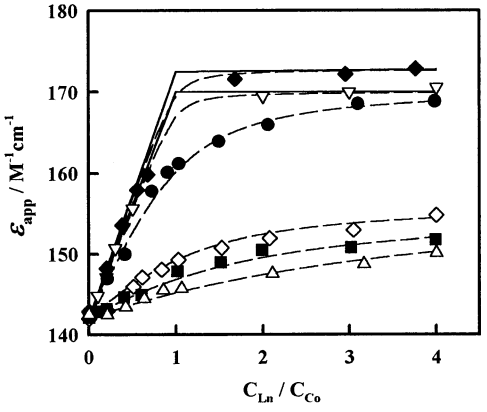


Fig. 2. Relationship between the apparent molar absorptivity of $Co(acac)_3$ at 595 nm and the molar ratio of $Ln(tta)_3$ to $Co(acac)_3$. C_{Co}, 2.0×10^{-3} M; C_{Ln}, 2.0×10^{-4}–8.0×10^{-3} M. ◆, Pr; ▽, Nd; ●,Sm; ◇,Gd; ■,Tb; △,Er.

from the result of the distribution method. To determine $\beta_{s,1}$ of the binuclear complex, the following equation was derived with respect to the apparent absorbance (A_{app}) of $Co(acac)_3$:

$$A_{app} = \varepsilon_{BNC}[Ln(tta)_3(Co(acac)_3)]_{org} + \varepsilon[Co(acac)_3]_{org}$$

$$D = (\varepsilon_{BNC} - \varepsilon)\frac{(\beta_{s,1}C_{Ln} + \beta_{s,1}C_{Co} + 1) - \sqrt{(\beta_{s,1}C_{Ln} + \beta_{s,1}C_{Co} + 1)^2 - 4\beta_{s,1}^2 C_{Ln}C_{Co}}}{2\beta_{s,1}} + \varepsilon C_{Co} \quad (9)$$

where ε_{BNC} and ε denote the molar absorptivity of complexed $Co(acac)_3$ in the binuclear complex and free $Co(acac)_3$, respectively, and C_{Co} and C_{Ln}, the total concentration of $Co(acac)_3$ and $Ln(tta)_3$, respectively. The $\beta_{s,1}$ values were calculated by a least-squares fitting for the plots in Fig. 2 on the basis of Eq. (9). The broken lines in Fig. 2 indicate the values calculated by using Eq. (9) and the $\beta_{s,1}$ values obtained, and are in good agreement with the experimental plots for all the Ln.

The $\beta_{s,1}$ values are listed in Table 1 along with those obtained by the distribution method. The values determined by both methods are reasonably consistent with each other, although, the values obtained by spectrophotometry are slightly higher than those by the distribution method. Such a little difference in $\beta_{s,1}$ is probably due to the difference in the water content of the benzene solution in both methods, i.e., 2.0×10^{-2} M H_2O in the spectrophotometry method compared with 3.1×10^{-2} M in the distribution method. In fact, it has been confirmed that the binuclear complexation between $Ln(tta)_3$ and tris(8-quinolinolato)cobalt(III) was dependent on the water content in benzene [2].

Fig. 3 shows the variation of log $\beta_{s,1}$ across the Ln series. The log $\beta_{s,1}$ values decrease with increasing the atomic number of Ln, showing a steep decrease between Nd and Sm. As a result, there are very large differences in $\beta_{s,1}$ between the light Ln (La to Nd) and the heavy Ln (Er to Lu).

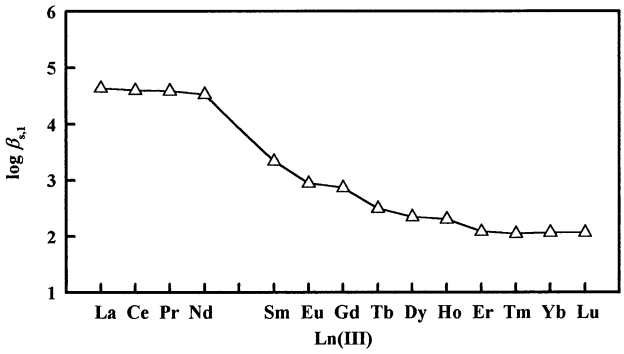


Fig. 3. Variation of the stability constant for $Ln(tta)_3(Co(acac)_3)$ across the lanthanide series.

3.3. IR spectroscopy

In an IR absorption spectrum of water in benzene, there were two intense peaks at 3600 and 3680 cm^{-1} which are assigned to the symmetric and asymmetric O–H stretching vibration of free water, respectively.

An IR absorption spectrum of $Eu(tta)_3(H_2O)_3$ in anhydrous benzene is shown in Fig. 4. The hydrated Eu chelate has two narrow absorption bands at 3552 and 3649 cm^{-1} and a broad band at 3335 cm^{-1}, which are significantly different from those of free water. To assign these absorption bands, the effect of TOPO was utilized. The absorbance of these three bands decreases with increase in the TOPO concentration in the sample solution, and alternately the two intense peaks corresponding to free water appear and gradually increase. After the addition of an equivalent quantity of TOPO to the Eu chelate, the three bands initially observed disappear, and the absorbance of free water becomes almost constant. These observations completely agree with those expected from the previous luminescence study in which the Eu–tta chelate becomes anhydrous by the formation of a 1:1 adduct of $Eu(tta)_3$TOPO [7].

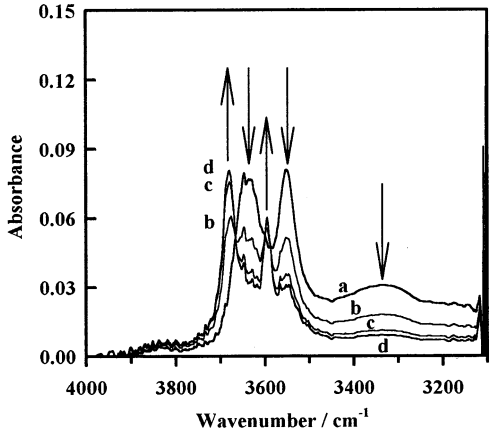


Fig. 4. IR spectra of 6.0×10^{-3} M $Eu(tta)_3(H_2O)_3$ in the presence or absence of 3.0×10^{-3}–2.3×10^{-2} M $Co(acac)_3$ in benzene. (a) Free $Eu(tta)_3(H_2O)_3$; (b) $[Co(acac)_3]_{total}/[Eu(tta)_3(H_2O)_3]_{total} = 0.5$; (c) $[Co(acac)_3]_{total}/[Eu(tta)_3(H_2O)_3]_{total} = 1.0$; (d) $[Co(acac)_3]_{total}/[Eu(tta)_3(H_2O)_3]_{total} = 3.8$.

The total number of water molecules released from the hydrated Eu chelate was determined to be 2.9 by IR spectrophotometry, which agrees with the water content in the crystal.

Therefore, the three absorption bands observed in $Eu(tta)_3(H_2O)_3$ are assigned to the O–H stretching vibration of the coordinated water molecules. The broad band in the lower wavenumber region suggests the existence of hydrogen-bonded O–H caused by the intramolecular hydrogen-bonding between hydrogen atoms of coordinated water and oxygen atoms of the ligands in the chelate. Such an hydrogen bond has been observed by IR spectra of a solid crystal of monohydrated tris(2,4-pentanedionato)RE(III) (RE: La, Pr, Nd, Sm, Gd, Dy, Ho, Er, and Y) [8].

The effect of $Co(acac)_3$ on the IR spectrum of $Eu(tta)_3(H_2O)_3$ is also shown in Fig. 4. The variation of the spectra observed by the addition of increasing concentration of $Co(acac)_3$ is similar to that in the TOPO case, i.e. the decrease in coordinated water but the increase in free water. This is indicative of the inner sphere (direct) coordination of $Co(acac)_3$ to the Eu chelate. Compared with TOPO, however, the coordinated water is not completely removed from the inner sphere of Eu even after almost all the Eu chelate becomes the binuclear complex with $Co(acac)_3$. This will be described later as a topic of the middle Ln.

The present IR method was applied to the Nd, Gd, Er, and Lu chelates which were prepared by the distribution method. The addition of TOPO gave almost the same results as in the Eu case, although, an excess of free water (2.0×10^{-2} M) existed in benzene. Fig. 5 shows the IR spectra of a hydrated Er chelate in the presence or absence of $Co(acac)_3$. Compared with Eu, the reverse trend of the variation of the broad absorption band corresponding to the hydrogen-bonded water

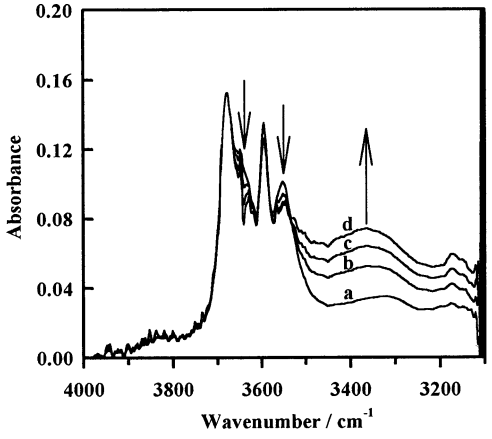


Fig. 5. IR spectra of 6.0×10^{-3} M $Er(tta)_3(H_2O)_n$ in the presence or absence of 3.0×10^{-3}–2.0×10^{-2} M $Co(acac)_3$ in benzene containing 2×10^{-2} M H_2O. (a) Hydrated $Er(tta)_3$; (b) $[Co(acac)_3]_{total}/[Er(tta)_3(H_2O)_n]_{total} = 0.5$; (c) $[Co(acac)_3]_{total}/[Er(tta)_3(H_2O)_n]_{total} = 1.0$; (d) $[Co(acac)_3]_{total}/[Er(tta)_3(H_2O)_n]_{total} = 3.3$.

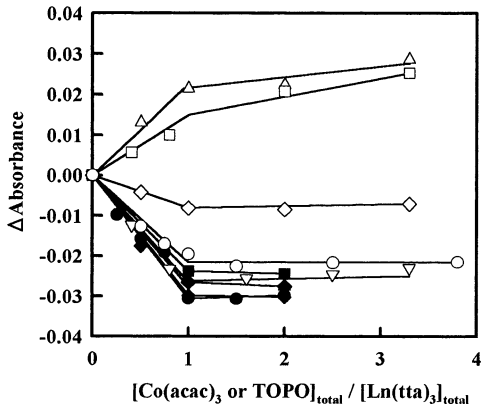


Fig. 6. Relationship between the variation of absorbance for the coordinated water of $Ln(tta)_3(H_2O)_n$ at 3320 cm^{-1} and the molar ratio of $Co(acac)_3$ or TOPO to $Ln(tta)_3$. Open symbols, $Ln(tta)_3$–$Co(acac)_3$; Closed symbols, $Ln(tta)_3$–TOPO. ▽ ▼, Nd; ○ ●, Eu; ◇ ◆, Gd; △ ▲, Er; □ ■, Lu.

is observed. The absorbance increases with increase in the $Co(acac)_3$ concentration. Furthermore, the amount of free water in benzene scarcely increases in the Er case. This fact strongly suggests the formation of hydrogen bonding between the coordinated water molecules and $Co(acac)_3$.

Relationship between the variation of the absorbance of $Ln(tta)_3$ at 3320 cm^{-1} (broad absorption band) and the molar ratio of $Co(acac)_3$ or TOPO to $Ln(tta)_3$ is shown in Fig. 6. All these plots have the intersection at $[Co(acac)_3 \text{ or } TOPO]_{total}/[Ln(tta)_3]_{total} = 1$ as expected from the results described above. The plot for the binuclear complex of Nd is very close to those of the TOPO adducts, supporting that the inner sphere coordination of $Co(acac)_3$ to the central Ln ions mainly occurs. On the other hand, the Er and the Lu complex show the increase in the absorbance, which is ascribed to the formation of hydrogen-bonding between coordinated water molecules of $Ln(tta)_3$ and $Co(acac)_3$. Consequently, the hydrogen-bonded complex or the outer-sphere binuclear complex is formed in the heavy Ln. In the middle Ln, especially Gd, however, the variation of the absorbance was much smaller than that of other Ln. This indicates that the fraction of the outer-sphere binuclear complex is higher than that of the light Ln.

3.4. ^{59}Co NMR spectroscopy

^{59}Co NMR spectra of $Co(acac)_3$ were measured in the presence or absence of $Ln(tta)_3$ (Ln: Pr, Nd, Sm, Gd, Tb and Er). When the resonance of $Co(acac)_3$ in $CDCl_3$ was set as a reference (0 ppm) on the spectra, the resonance of free $Co(acac)_3$ in benzene was observed at 112 ppm lower magnetic field. In the presence of the tta chelate of Pr, Nd and Sm, two separate resonances were observed as found in Eu [1]. Higher-field resonances appeared at

−345, −342 and −291 ppm for Pr, Nd and Sm, respectively, and were independent of the concentration of $Ln(tta)_3$. On the other hand, lower-field resonances were observed at 58, 59 and 49 ppm for Pr, Nd and Sm, respectively, at $[Ln(tta)_3]_{total}/[Co(acac)_3]_{total} = 3$ and were gradually shifted to the higher-field with increase in the $Ln(tta)_3$ concentration. Consequently, as discussed in the previous paper [1], the binuclear complex with the higher-field resonance has slow chemical exchange of $Co(acac)_3$ on the NMR time scale, while that with the lower-field resonance has rapid exchange. In the Gd, Tb and Er case, only the lower-field resonances were observed at 53, 53 and 54 ppm, respectively, and they were affected by the $Ln(tta)_3$ concentration. Therefore, there are two different kinds of binuclear complexes with slow and rapid chemical exchange of $Co(acac)_3$.

Fig. 7 shows the change in the chemical shift of ^{59}Co NMR ($\Delta\delta = \delta_{Co,BNC} - \delta_{Co}$) across the lanthanide series, where δ_{Co} and $\delta_{Co,BNC}$ express the chemical shift of free $Co(acac)_3$ and complexed $Co(acac)_3$ in the binuclear complex, respectively. The values of $\delta_{Co,BNC}$ for the rapid exchange species were corrected using the ratio of the complexed $Co(acac)_3$ and free $Co(acac)_3$, which were calculated using $\beta_{s,1}$, since the resonance appears at the averaged position. The chemical shift for the slow exchange complexes was clearly dependent on the Ln ion, whereas that for the rapid exchange complexes was almost independent of the Ln ion. The $\Delta\delta$ values observed for the slow exchange complexes of La to Eu are quite similar to those for the binuclear complexes of anhydrous tris(6,6,7,7,8,8,8-heptafluoro-2,2-dimethyl-3,5-octanedionato)lanthanide(III) ($Ln(fod)_3$, Ln:La to Eu) with $Co(acac)_3$ [9].

The large difference in $\Delta\delta$ observed between the diamagnetic ions La and Lu demonstrates the strong interaction of $Co(acac)_3$ with the former but the weak interaction with the latter. On the basis of this result, the binuclear complexes of La through Eu with slow chemical exchange should be of inner-sphere coordination. The $\Delta\delta$ values of those complexes are strongly affected by the number of f-electrons of Ln, because, the proximity of the paramagnetic Ln ions to the cobalt(III) ion brings about the contact or the pseudo-contact shift. On the other hand, the rapid exchange complexes of Pr through Lu are of outer-sphere coordination since the $\Delta\delta$ values are small and almost independent of the Ln ions. The Ln–Co distance in the outer-sphere complexes is expected to be long enough to be free from the contact or pseudo-contact shift. In previous studies performed by Lindoy et al. [10–12], only inner-sphere complexes of $Eu(fod)_3$ with tris(β-diketonato)cobalt(III) were found, because, anhydrous Eu chelate was entirely used in anhydrous solvents.

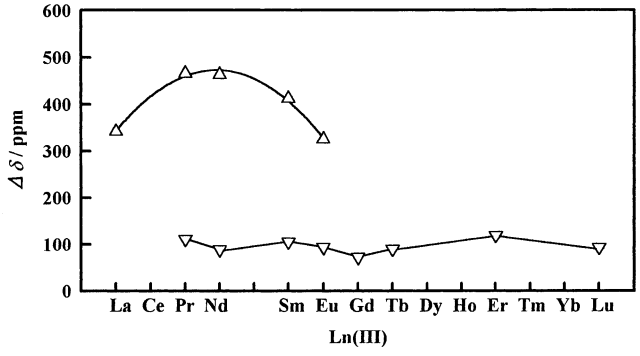


Fig. 7. Variation of the ^{59}Co NMR chemical shifts of complexed $Co(acac)_3$ in binuclear complexes across the lanthanide series. The data of La, Eu, and Lu were cited from Ref. [1]. △, slow exchange complexes; ▽, rapid exchange complexes.

4. Conclusion

Hydrated lanthanide–tta chelates form stable binuclear complexes with $Co(acac)_3$ in benzene. Since $Co(acac)_3$ has three coordinating oxygen atoms on an open octahedral face, it is expected to act as a terdentate ligand. In the light Ln of which the coordination number (CN) is usually nine in solution, the inner-sphere binuclear complex with the terdentate $Co(acac)_3$ exists along with the outer-sphere hydrogen-bonded complex as an equilibrium mixture. The inner-sphere complex has a more stable structure and an higher stability constant. In the heavy Ln which has a CN of eight and a small ionic radius, only the outer-sphere complex is formed, because, the $Co(acac)_3$ molecule cannot enter the inner-coordination sphere of $Ln(tta)_3$. The stability of the outer-sphere complex formed by the hydrogen bonding is much lower than that of the inner sphere complex.

References

[1] N. Kameta, H. Imura, K. Ohashi, T. Aoyama, Inorg. Chem. Commun. 2 (1999) 124.
[2] H. Imura, N. Kameta, M. Osada, K. Ohashi, T. Kimura, Z. Yoshida, Solv. Extr. Ion Exch. 17 (1999) 585.
[3] R.G. Charles, R.C. Ohlmann, J. Inorg. Nucl. Chem. 27 (1965) 255.
[4] J.C. Reid, M. Calvin, J. Am. Chem. Soc. 72 (1950) 2948.
[5] T. Wakabayashi, S. Oki, T. Omori, N. Suzuki, J. Inorg. Nucl. Chem. 26 (1964) 2255.
[6] N. Kameta, H. Imura, Bull. Chem. Soc. Jpn. 74 (2001) 1641.
[7] S. Lis, J.N. Mathur, G.R. Choppin, Solv. Extr. Ion Exch. 9 (1991) 637.
[8] M.F. Richardson, W.F. Wagner, D.E. Sands, Inorg. Chem. 7 (1968) 2495.
[9] M. Hirayama, Y. Kawamata, Y. Fujii, Y. Nakano, Bull. Chem. Soc. Jpn. 55 (1982) 1798.
[10] L.F. Lindoy, H.C. Lip, H.W. Louie, M.G.B. Drew, M.J. Hudson, J. Chem. Soc., Chem. Commun. (1977) 778.
[11] L.F. Lindoy, H.W. Louie, J. Am. Chem. Soc. 101 (1979) 841.
[12] D.P. Graddon, L. Muir, L.F. Lindoy, H.W. Louie, J. Chem. Soc., Dalton Trans. (1981) 2596.

PERGAMON

Polyhedron 21 (2002) 811–816

POLYHEDRON

www.elsevier.com/locate/poly

Chiral macrocyclic La(III), Ce(III), Pr(III) and Eu(III) complexes with chloride anions

Jerzy Lisowski *, Jarosław Mazurek

Department of Chemistry, University of Wrocław, 14 F. Joliot-Curie, 50-383 Wrocław, Poland

Received 8 August 2001; accepted 20 December 2001

Abstract

The new enantiopure macrocyclic complexes $[LnL]Cl_3 \cdot nH_2O$ or their racemic mixtures $[Lnrac\,L]Cl_3 \cdot nH_2O$ ($Ln = La^{+3}$, Ce^{+3}, Pr^{+3} and Eu^{+3}) have been synthesised in a template condensation of *trans*-1,2-diaminocyclohexane and 2,6-diformylpyridine. The complexes have been studied by ^1H and ^{13}C NMR spectroscopy. The signal assignment was based on the COSY, NOESY and HMQC measurements. The X-ray crystal structure of $[Larac\,L]Cl_3$ complex has been determined. The lanthanum ion in this complex is coordinated by six nitrogen atoms of the macrocyclic ligand and three chloride anions. The macrocycle exhibits a twist–bent conformation of approximate C_2 symmetry. On the other hand, NMR spectra of the investigated compounds in methanol–chloroform solution indicate effective D_2-symmetry that results from the fast dynamic exchange of chloride anions. © 2002 Elsevier Science Ltd. All rights reserved.

Keywords: Macrocycles; Lanthanide complexes; Crystal structures; Chiral complexes; NMR of paramagnetic compounds

1. Introduction

The Schiff bases obtained in a template 2+2 condensation of diamines and 2,6-diformylpyridine or 2,6-diacetylpyridine are particularly suitable for the coordination of relatively large metal ions [1]. The complexes of these hexaazamacrocyles with lanthanide(III) ions have attracted attention as efficient catalysts for the cleavage of the phosphate ester bond [2]. The Gd(III) complexes have also been studied as potential MRI contrast agents [3].

When the chiral precursor *R*,*R*′-1,2-diaminocyclohexane is used in the above template reaction, chiral lanthanide(III) complexes (Fig. 1) $[LnL](NO_3)_3 \cdot nH_2O$ (where Ln is the lanthanide(III) ion and L = 4(*R*),9(*R*),19(*R*),24(*R*)-3,10,18,25,31,35-hexaazapentacyclo[25.3.1.1^{12,24}.0^{4,9}.0^{19,24}]-dotriaconta-1(31),2,10,12,14,16(32),17,25,27,29-decaene) are formed [4,5]. The coordination of the lanthanide(III) ion in a chiral macrocyclic environment leads to interesting properties of these compounds. Thus the $[TbL](NO_3)_3$ and $[EuL](NO_3)_3$ complexes have been shown to exhibit circularly polarised luminescence [4] and the paramagnetic $[EuL](NO_3)_3$ and $[YbL](NO_3)_3$ complexes have been shown to form diastereoisomeric complexes with D- and L-aminoacids [5].

Here we present the study of new lanthanide complexes of the ligand L with chloride counteranions. These complexes have been synthesised as racemic mixtures $[Lnrac\,L]Cl_3 \cdot nH_2O$ or as enatiopure compounds $[LnL]Cl_3 \cdot nH_2O$ using either racemic *trans*-1,2-diaminocyclohexane or *trans*-*R*,*R*′-1,2-diaminocyclohexane, respectively. We have previously shown that the nitrate derivatives $[LnL](NO_3)_3 \cdot nH_2O$ exhibit D_2 symmetry both in solution and in the solid state [5,6]. This symmetry arises from the presence of a helically twisted macrocycle and symmetric coordination of nitrate anions above and below the macrocycle. In contrast, the X-ray crystal structure of $[Lnrac\,L]Cl_3$, presented here, shows lower symmetry of the complex due to unsymmetrical coordination of chloride anions above and below the macrocycle plane.

* Corresponding author. Tel.: +48-71-3757-252; fax: +48-71-3282-348.

E-mail address: jurekl@wchuwr.chem.uni.wroc.pl (J. Lisowski).

0277-5387/02/$ - see front matter © 2002 Elsevier Science Ltd. All rights reserved.
PII: S0277-5387(02)00854-9

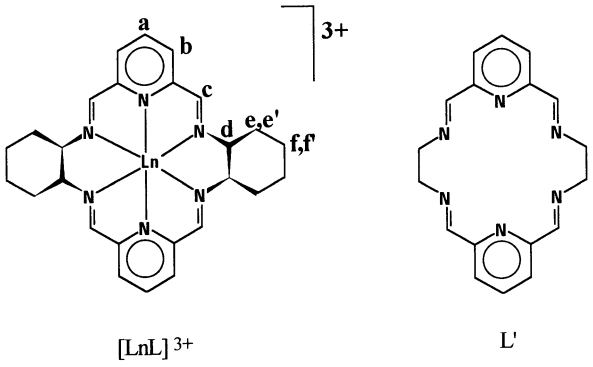


Fig. 1. The general structure and labelling scheme of the lanthanide complexes of the macrocycle L (coordinated anions and/or solvent molecules are omitted); the structure of the macrocycle L′.

2. Experimental

2.1. Synthesis

The [La*rac*L]$Cl_3\cdot 3H_2O$, [Ce*rac*L]$Cl_3\cdot 3H_2O$ and [Pr*rac*L]$Cl_3\cdot 2H_2O$ complexes have been prepared in the same way as the respective Gd(III) complex [7] in 61, 66 and 40% yields, respectively. The enantiomericaly pure complex [EuL]$Cl_3\cdot 2H_2O$ has been obtained in a similar manner in a template condensation. Thus 1 mmol (114.2 mg) of *R*,*R*-1,2-diaminocyclohexane, 1 mmol (135.1 mg) of 2,6-diformylpyridine and 0.5 mmol (167.9 mg) of europium(III) chloride hydrate were refluxed for 4 h in 15 ml of methanol. The solution was filtered and evaporated to dryness. The crude product was recrystallised from methanol–acetonitrile and dried in vacuum to give 177 mg of the desired complex in 49% yield. [PrL]$Cl_3\cdot 2H_2O$ has been synthesised similarly in 65% yield. The [PrL]$(NO_3)_3\cdot H_2O$ complex has been prepared in the same way as other nitrate derivatives [4,5]. All compounds gave satisfactory C, H and N analyses.

2.2. Methods

The NMR spectra were taken on Bruker Avance 500 and AMX 300 spectrometers. The chemical shifts were referenced to the residual solvent signal or TMS. The magnitude COSY spectra were acquired using 512 data points in both dimensions. The data were processed by using a square sine bell window in both dimensions and zero filled to $1K\times 1K$ matrix. The phase-sensitive (TPPI) NOESY spectra were recorded using mixing times varying from 25 to 600 ms and shifted square sine function. HMQC spectra were recorded using the BIRD preparation period and 512×512 data points. A square sine function was used for apodisation in both dimensions. T_2 relaxation times were evaluated from the linewidths. Elemental analyses were obtained from elemental analyses facility in this department.

2.3. X-ray data collection

The crystals of [La*rac*L]Cl_3 were grown by slow diffusion of diethyl ether into a chloroform–methanol solution of the complex. A crystal of approximate $0.4\times 0.4\times 0.3$ mm was mounted on a Kuma KM4 diffractometer equipped with an CCD counter and an Oxford Cryosystem low-temperature device. The measurement was performed at 100 K. The structure was solved with direct methods using SHELXS-97 [8] and least-squares full-matrix refinement were performed using SHELXL-97 [8]. The absorption correction was applied based on face indexing with SHELX-76 [9]. All of the hydrogen atoms were included geometrically and their positions were constrained to the relevant C atoms, while their temperature factors were set at 1.2 times the trace of C atoms. Peaks ~ 2 e $Å^{-3}$ were found in the Fourier difference map and presumably result from disordered solvent. Details of the data collection are listed in the Table 1. Publication and validation data were created using the WINGX program [10].

Table 1
Crystal data

Empirical formula	$C_{26}H_{30}Cl_3LaN_6$
Formula weight	671.82
Temperature (K)	100(2)
Wavelength (Å)	0.71073
Crystal system	monoclinic
Space group	*C*2/*c*
Unit cell dimensions	
a (Å)	16.690(3)
b (Å)	16.677(3)
c (Å)	13.103(3)
β (°)	119.49(4)
V ($Å^3$)	3174.6(11)
Z	4
Density (calculated) (Mg m^{-3})	1.406
Absorption coefficient (mm^{-1})	1.622
F(000)	1344
Crystal size (mm)	$0.40\times 0.40\times 0.30$
θ Range for data collection (°)	3–25
Limiting indices	$-19\leq h\leq 17$, $-19\leq k\leq 19$, $-15\leq l\leq 15$
Reflections collected/unique	8516/2773 [$R_{int}=0.0305$]
Absorption correction	analytical (SHELX-76)
Max. and min. transmission	0.6419 and 0.5632
Refinement method	Full-matrix least-squares on F^2
Data/restraints/parameters	2773/0/164
Goodness-of-fit on F^2	1.221
Final *R* indices [$I>2\sigma(I)$]	$R_1=0.0361$, $wR_2=0.0940$
R indices (all data)	$R_1=0.0391$, $wR_2=0.0955$
Largest difference peak and hole (e $Å^{-3}$)	1.820 and −0.594

3. Results and discussion

3.1. X-ray crystal structure

The structure of [La*rac*L]Cl_3 is composed of a macrocyclic complex and chloride anions connected to the central lanthanum(III) cation. The lanthanum cation has a characteristic nine-coordinate geometry (Fig. 2) that is very similar to that of [Gd*rac*L$(H_2O)_3$]$Cl_3\cdot 3H_2O$ [7]—the difference is that in [La*rac*L]Cl_3 the chloride anions instead of water molecules are placed in the coordination sphere. The coordination environment is composed of six nitrogen atoms belonging to the macrocycle (La–N distances in the range 2.732(3)–2.810(4) Å) and three chloride anions (La–Cl distances equal to 2.816(2) and 2.872(2) Å). The selected bond lengths and angles are listed in Table 2. Two chloride anions are placed above and one below the mean plane of the macrocyclic ligand. The angles Cl(1)–La–Cl(2) and Cl(2)–La–Cl(2)^i are 141.5(1)° and 80.0(1)°, respectively. The macrocyclic ligand is twisted in similar range as it was observed for analogue nitrate complexes [NdL]$(NO_3)_3\cdot CH_3OH$ and [TmL]$(NO_3)_3\cdot CH_3OH$ [6]: the angle between pyridine rings (N2 C2 C3 C4 C5 C6 and N2^i, C2^i, C3^i, C4^i, C5^i, C6^i) is 24.8(1)°. The angle between the least-squares mean planes of the cyclohexyl fragments (C8, C9, C10, C11, C12, C13 and C8^i, C9^i, C10^i, C11^i, C12^i, C13^i) is 56.7°. The Cremer and Pope ring puckering parameters [11] calculated with the PARST program [12,13] are $Q = 0.578(5)$ and $\theta = 173.9(5)°$, which means that the cyclohexyl rings display a fairly good chair conformation. The crystal structure is held together by van der Waals interactions although several relatively short intermolecular distances between aromatic or imine C–H groups and the chloride anions are present.

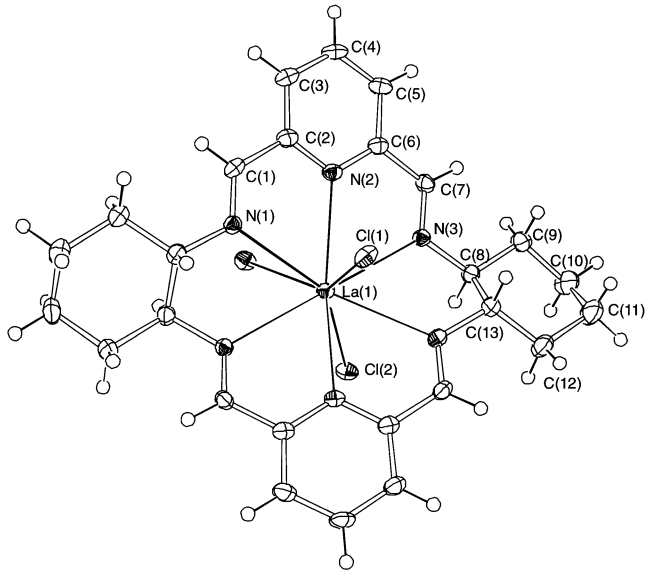


Fig. 2. View of the [La*rac*L]Cl_3 complex.

Table 2
Selected geometrical parameters (Å, °)

Bond lengths			
N(1)–La(1)	2.781(4)	Cl(1)–La(1)	2.816(2)
N(2)–La(1)	2.732(4)	Cl(2)–La(1)	2.872(2)
N(3)–La(1)	2.810(4)		
Bond angles			
N(2)^i–La(1)–Cl(1)	77.99(7)	N(1)^i–La(1)–Cl(1)	74.37(6)
N(1)–La(1)–Cl(1)	74.37(6)	N(3)–La(1)–Cl(1)	90.94(6)
N(3)^i–La(1)–Cl(1)	90.94(6)	N(2)–La(1)–Cl(2)	126.67(7)
N(2)^i–La(1)–Cl(2)	74.25(7)	N(1)^i–La(1)–Cl(2)	69.41(7)
N(1)–La(1)–Cl(2)	140.67(7)	N(3)–La(1)–Cl(2)	81.50(7)
N(3)^i–La(1)–Cl(2)	97.02(7)	Cl(1)–La(1)–Cl(2)	141.52(2)
N(2)–La(1)–Cl(2)^i	74.25(7)	N(2)^i–La(1)–Cl(2)^i	126.67(7)
N(1)^i–La(1)–Cl(2)^i	140.67(7)	N(1)–La(1)–Cl(2)^i	69.41(7)
N(3)–La(1)–Cl(2)^i	97.02(7)	N(3)^i–La(1)–Cl(2)^i	81.50(7)
Cl(1)–La(1)–Cl(2)^i	141.52(2)	Cl(2)–La(1)–Cl(2)^i	76.95(4)

Symmetry code: (i) $-x+1, y, -z+3/2$.

The twist–bent conformation of the ligand in the discussed complex is similar to that of [Gd*rac*L$(H_2O)_3$]$Cl_3\cdot 3H_2O$ [7]. This type of conformation is characteristic for complexes of hexaaza tetraimine macrocycles [1] and for the saturated tetraamine analogue [14] of L. The angle between two planar sections defined by nine atoms from C8 through N2 to C13^i and the symmetry related nine atoms from C8^i through N2^i to C13 is 18.0(1)°, and this is smaller than the value of 42.8° observed for [Gd*rac*L$(H_2O)_3$]$Cl_3\cdot 3H_2O$ [7]. The value of this angle for [La*rac*L]Cl_3 is similar to that for [NdL]$(NO_3)_3\cdot CH_3OH$ and [TmL]$(NO_3)_3\cdot CH_3OH$ [6].

The macrocycle in [La*rac*L]Cl_3 is considerably bent, in contrast to what is observed in the case of [NdL]$(NO_3)_3\cdot CH_3OH$ and [TmL]$(NO_3)_3\cdot CH_3OH$ complexes [6]. This bending can be measured by the angle determined by the pyridine nitrogen atoms and the lanthanide ion. This fragment is practically linear [6] in the nitrate Nd(III) complex (178.5)°, while the value of this angle is 160.0(1)° in the chloride La(III) complex. The bent conformation of the macrocycle in the [La*rac*L]Cl_3 complex can be explained by the different steric requirements of axial ligands positioned above and below the macrocycle plane. In the case of the [NdL]$(NO_3)_3\cdot CH_3OH$ and [TmL]$(NO_3)_3\cdot CH_3OH$ complexes, the symmetrical coordination of axial ligands favours a more symmetrical conformation of the macrocycle. Thus the different axial ligation of the lanthanide(III) ions brings about the change in conformation of the coordinated macrocycle L. The above observations are not obvious, since in the case of lanthanide(III) complexes of the related macrocycle L′ (Fig. 1), containing more flexible ethylene lateral chains, the bending of the macrocycle tends to increase with

decreasing metal ion radius [1] and is observed even for complexes with symmetrical axial coordination [1,15].

3.2. NMR spectroscopy

The investigated compounds give rise to eight signals in their ^{1}H NMR spectra and seven signals in ^{13}C NMR spectra, which is consistent with the presence of diastereotopic cyclohexane protons and indicates the effective D_2 symmetry of the $[LnL]Cl_3$ complexes in the investigated solutions. The same symmetry was observed for solutions of the nitrate derivatives $[LnL](NO_3)_3$ [5]. In the case of the latter complexes this symmetry is in accord with the helical twist conformation of the macrocyclic ligand observed in the solid state [6]. On the other hand the X-ray crystal structure of [Ln*rac*L]Cl_3, discussed above, shows a lower symmetry of the complex due to unsymmetrical coordination of chloride anions above and below the macrocycle plane accompanied by bending of the macrocycle. This structure, of approximately C_2 symmetry, should give rise to 15 ^{1}H NMR signals and 13 ^{13}C NMR signals. The discrepancy between the number of expected and observed signals can be explained by dynamic exchange of chloride anions, e.g. in a dissociative process depicted in Fig. 3. When such a process is fast on the NMR time scale, averaged signals are observed for respective pairs of protons that would give different signals for the static structure. For instance, the non-equivalent pyridine protons $\mathbf{b}^1$ and $\mathbf{b}^2$ give rise to an averaged signal **b** (Figs. 3 and 4). In other words the top and the bottom of the macrocycle become equivalent giving rise to effective D_2 symmetry.

The ^{1}H and ^{13}C NMR spectra of the diamagnetic [La*rac*L]Cl_3 can be assigned (Table 3) on the basis of chemical shift values as well as similarity to the spectra of the analogous nitrate complex, $[LaL](NO_3)_3$ [5]. This assignment is confirmed by COSY, HMQC and HMBC spectra. On the other hand, the values of chemical shifts of paramagnetic $[LnL]Cl_3$ complexes are difficult to predict and assignment of their spectra based on these values is not possible. The paramagnetic metal ions strongly influence the chemical shifts of the nearby protons by introducing an additional chemical shift called isotropic shift, δ_{iso}. This shift arises from interaction of the nuclear and electronic spins and can be separated into through-space (i.e. dipolar or pseudo-contact) and through bonds (i.e. contact) contributions [16–20].

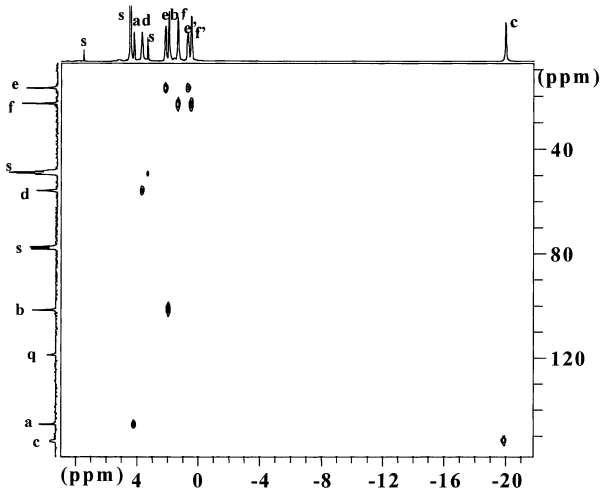


Fig. 4. The HMQC spectrum of $[EuL]Cl_3 \cdot 2H_2O$ (CD_3OD–$CDCl_3$ 1:2 v/v solution, 294 K), s-solvent and HDO signals.

The ^{1}H NMR spectra of the paramagnetic Ce(III), Pr(III) and Eu(III) complexes in question can be assigned (Table 3) using 2D NMR techniques in the following way. The HMQC spectra of the solutions of the investigated complexes in $CD_3OD/CDCl_3$ 1:2 v/v identify resonances of two pairs of geminal protons correlated to one carbon signal each (see Fig. 4 for example). As expected, the geminal protons are also COSY correlated (see Fig. 5 for example). One of the geminal protons exhibits an additional COSY crosspeak that has to correspond to a correlation between protons **d** and **e**′ (see the labelling scheme, Fig. 1). Thus the cyclohexane positions **d**, **e**, **e**′, **f** and **f**′ are identified. The COSY correlated signals of protons **a** and **b** can be easily identified on the basis of integration of signal **a** (intensity 2H, in contrast to signals of intensity 4H for other positions). The remaining signal has to correspond to the azomethine proton **c**. The above assignment is confirmed by NOESY spectra that show a sequence of NOE connectivities starting from the easily identified signal of proton **a**. Thus NOESY crosspeaks corresponding to pairs of protons **a** and **b**, **b** and **c**, **c** and **e**, **c** and **e**′, **d** and **e**, **d** and **e**′, **e** and **e**′, **e** and **f** as well as **f** and **f**′ can be observed.

The HMQC spectra of the investigated complexes allow correlation of the ^{13}C signals with the assigned

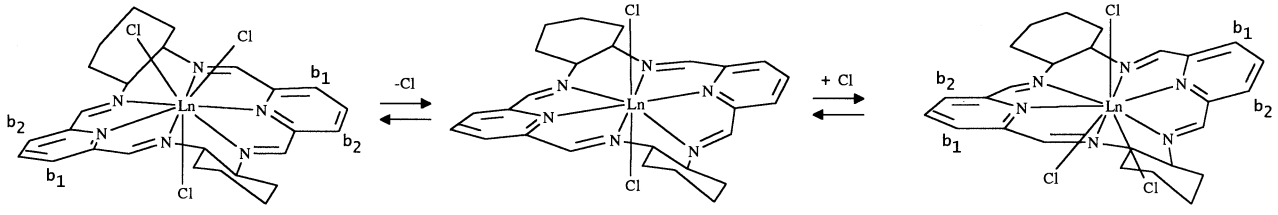


Fig. 3. The dynamic axial ligand exchange in $[LnL]Cl_3$ complexes

Table 3
^{1}H NMR and ^{13}C NMR chemical shifts of the [LnL]X_3 complexes at 298 K

Complex	A	b	c	d	e	e′	f	f′
^{1}H NMR								
[La*rac* L]$Cl_3\cdot 3H_2O$ [a]	8.31	8.03	8.74	3.88	2.51	1.71	2.07	1.48
[Ce*rac* L]$Cl_3\cdot 3H_2O$ [a]	11.86	12.32	16.19	−0.69	2.46	2.03	1.94	0.76
[PrL]$Cl_3\cdot 2H_2O$ [a]	14.93	16.46	25.47	−3.95	2.61	2.46	2.12	0.29
[PrL]$Cl_3\cdot 2H_2O$ [b]	13.55	15.23	27.26	7.14	5.97	5.43	4.00	2.94
[PrL]$(NO_3)_3\cdot H_2O$ [a]	12.15	13.33	24.63	6.90	4.79	4.45	3.68	2.61
[PrL]$(NO_3)_3\cdot H_2O$ [b]	13.59	15.23	27.23	6.95	5.88	5.40	3.97	2.89
[EuL]$Cl_3\cdot 2H_2O$ [a]	4.19	1.93	−19.96	3.68	2.15	0.68	1.33	0.46
								C_{quat}
^{13}C NMR								
[La*rac* L]$Cl_3\cdot 3H_2O$ [a]	142.62	130.42	163.41	68.58	30.59		24.83	153.62
[Ce*rac* L]$Cl_3\cdot 3H_2O$ [a]	147.82	139.23	169.92	65.06	31.65		24.12	172.84
[PrL]$Cl_3\cdot 2H_2O$ [a]	150.98	150.55	176.05	64.89	35.59		24.19	187.97
[PrL]$(NO_3)_3\cdot H_2O$ [a]	146.85	144.95	173.23	77.02	39.75		26.44	174.45
[EuL]$Cl_3\cdot 2H_2O$ [a]	145.32	101.66	151.89	55.85	17.02		22.86	118.84

[a] CD_3OD–$CDCl_3$ 1:2 v/v.
[b] D_2O.

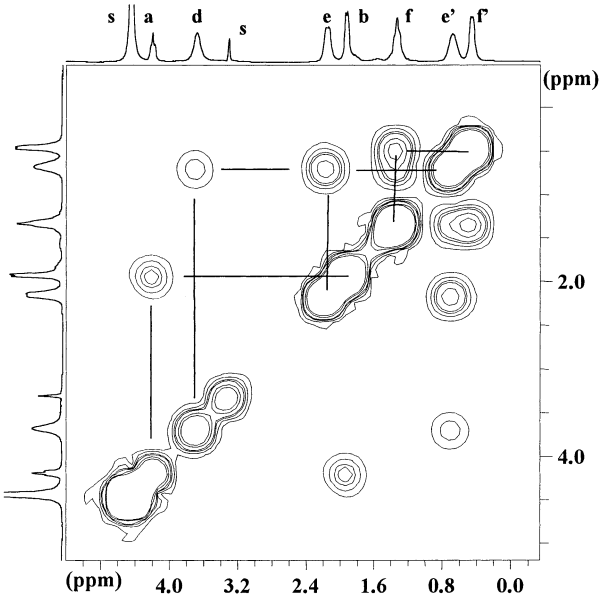


Fig. 5. The COSY spectrum of [EuL]$Cl_3\cdot 2H_2O$ (CD_3OD–$CDCl_3$ 1:2 v/v solution, 294 K), s-solvent and HDO signals.

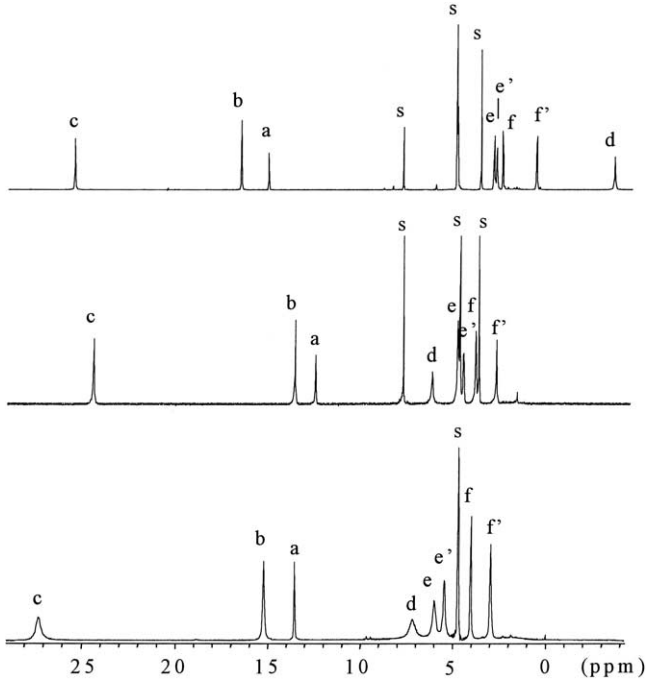


Fig. 6. ^{1}H NMR spectra of: top [PrL]$Cl_3\cdot 2H_2O$ (CD_3OD–$CDCl_3$ 1:2 v/v solution, 298 K), middle [PrL]$(NO_3)_3\cdot H_2O$ (CD_3OD–$CDCl_3$ 1:2 v/v solution, 298 K) and bottom [PrL]$Cl_3\cdot 2H_2O$ (D_2O solution, 298 K).

signals of the connected protons (Fig. 4). Thus the ^{13}C NMR spectra can be fully assigned (Table 3) since the molecule contains only one quaternary carbon atom that corresponds to ^{13}C NMR signal without HMQC correlation.

The NMR spectra of the investigated paramagnetic [LnL]Cl_3 complexes differ markedly from the spectra of the corresponding [LnL]$(NO_3)_3$ complexes [5], as illustrated for Pr(III) complexes in Fig. 6. Such differences can be caused by different conformations of the macrocycle, leading to different dipolar and/or contact shifts for a given position. Moreover, it was shown [5,21,22] that NMR spectra of macrocyclic lanthanide complexes can be very sensitive to axial ligation even when the conformation of the macrocycle remains essentially unchanged.

The differences of the shift values between the series of chloride and nitrate derivatives indicate that chloride anions are bound to the lanthanide(III) ions not only in the solid state, but also in the investigated chloroform–methanol solutions. As mentioned above, the X-ray crystal structure of the Gd(III) chloride derivative,

$[GdL(H_2O)_3]Cl_3 \cdot 3H_2O$, shows that the water molecules, and not chloride anions, are bound to the lanthanide(III) ion [7]. This rises the question whether chloride versus water coordination depends on the size of Ln(III) ion (and it changes along the lanthanide ions series), or is it a matter of relative amounts of water present? To answer this question, the ^1H NMR spectra of deuterated water solutions of the investigated complexes were recorded. In the case of paramagnetic complexes the spectra of water solutions were very different to those of chloroform–methanol solutions (Fig. 6, Table 3). Moreover, the NMR spectra of water solutions of nitrate and chloride complexes of the same lanthanide ion are practically identical (Table 3). This result shows that in water solution both nitrate and chloride anions dissociate and the axial positions are occupied by water molecules. Hence the difference in the coordination spheres of the La(III) and Gd(III) complexes of the ligand L, observed in the solid state, arise most likely from the different crystallisation conditions.

4. Supplementary material

Supplementary data for the $[Ln\textit{rac}L]Cl_3$ structure are available from the Cambridge Crystallographic Data Centre, 12 Union Road, Cambridge CB2 1EZ, UK (fax: +44-1223-336033; e-mail: deposit@ccdc.cam.ac.uk) on request, quoting the deposition number CCDC 165711.

Acknowledgements

We thank Katarzyna Wiglusz for synthetic assistance. This work was supported by KBN grant 3 T09A 11519.

References

[1] V. Alexander, Chem. Rev. 95 (1995) 273.
[2] R.W. Hay, N. Govan, Polyhedron 24 (1997) 4233.
[3] P.H. Smith, J.R. Brainard, D.E. Morris, G.D. Jarvinen, R.R. Ryan, J. Am. Chem. Soc. 111 (1989) 7437.
[4] T. Tsubomura, K. Yasaku, T. Sato, M. Morita, Inorg. Chem. 31 (1992) 447.
[5] J. Lisowski, Magn. Reson. Chem. 37 (1999) 287.
[6] J. Lisowski, P. Starynowicz, Polyhedron 19 (2000) 465.
[7] S.W.A. Bligh, N. Choi, W.J. Cummins, E.G. Evagorou, J.D. Kelly, M. McPartlin, J. Chem. Soc., Dalton Trans. (1994) 3369.
[8] SHELX97—Programs for Crystal Structure Analysis (Release 97-2). G.M. Sheldrick, Institüt für Anorganische Chemie der Universität, Tammanstrasse 4, D-3400 Göttingen, Germany, (1998).
[9] SHELX76—Program for Crystal Structure Refinement. G.M. Sheldrick, Institüt für Anorganische Chemie der Universität, Tammanstrasse 4, D-3400 Göttingen, Germany, (1976).
[10] L.J. Farrugia, J. Appl. Crystallogr. 32 (1999) 837.
[11] D. Cremer, J.A. Pople, J. Am. Chem. Soc. 97 (1975) 1354.
[12] M. Nardelli, Comput. Chem. 7 (1983) 95.
[13] M. Nardelli, J. Appl. Crystallogr. 28 (1995) 659.
[14] S.W.A. Bligh, N. Choi, E.G. Evagorou, W.-S. Li, M. McPartlin, J. Chem. Soc., Chem. Commun. (1994) 2399.
[15] F. Benetollo, A. Polo, G. Bombieri, K.K. Fonda, L.M. Vallarino, Polyhedron 9 (1990) 1411.
[16] G.N. La Mar, W.D. Horrocks, Jr., R.H. Holm (Eds.), NMR of Paramagnetic Molecules, Academic Press, New York, 1973.
[17] I. Bertini, C. Luchinat, NMR of Paramagnetic Molecules in Biological Systems, Benjamin/Cummings, Menlo Park, CA, 1986.
[18] I. Bertini, P. Turano, A.J. Vila, Chem. Rev. 93 (1993) 2833.
[19] I. Bertini, C. Luchinat, Coord. Chem. Rev. 150 (1996) 1.
[20] A.D. Sherry, C.F.G.C. Geraldes, in: J.-C.G. Bunzli (Ed.), Lanthanide Probes in Life, Chemical and Earth Sciences. Theory and Practice (Chapter 4), Elsevier, Amsterdam, 1989.
[21] J. Lisowski, J.L. Sessler, V. Lynch, T.D. Mody, J. Am. Chem. Soc. 117 (1995) 2273.
[22] J. Lisowski, J.L. Sessler, T.D. Mody, Inorg. Chem. 34 (1995) 4336.

PERGAMON

Polyhedron 21 (2002) 817–823

POLYHEDRON

www.elsevier.com/locate/poly

Nickel(II) complexes of amino acids in comparison with the cobalt(III) analogues: interesting structural aspects relative to intermolecular hydrogen bonds and chiral recognition

Jiwen Cai [a,*], Xiaopeng Hu [a], Ivan Bernal [b], Liang-Nian Ji [a]

[a] School of Chemistry and Chemical Engineering, Zhongshan University, Guangzhou 510275, People's Republic of China
[b] Department of Chemistry, University of Houston, Houston, TX 77204, USA

Received 21 August 2001; accepted 20 December 2001

Abstract

The crystal and packing structures of three racemic compounds with the formula, [Ni(tren)(DL-aminoacidato)]Cl·nH$_2$O have been investigated, aiming to compare the homochiral–heterochiral assembly process of the nickel(II) chiral complex cations with their well-studied cobalt(III) analogues. Due to the inherent hydrogen bonding donors–acceptors carried by the complex cations, infinite 1-dimensional (1-D) chains are generated by complementary inter-cationic H- bonds in both the Ni(II) and Co(III) analogues, but with different H- bond patterns. In all the Co(III) analogues studied by this group, the cations are linked together via the same pattern and strength of H- bonds which are designated as C6[$R_2^1(6)$]. They are homochiral, irrespective of the nature of the amino acidato ligands. In the Ni(II) analogues, the cations are linked by H- bonds described as $C_2^1(6)[R_2^2(12)]$. However, when the side chain of the amino acid is bulkier, the homochiral assembly of the cations becomes ambiguous due to the observed disorder of the asymmetric carbon. Additionally, it is interesting to note that the deprotonated carboxylic group of the amino acid coordinates with Ni(II) and Co(III) in different modes, as a delocalized and localized anion, respectively. © 2002 Elsevier Science Ltd. All rights reserved.

Keywords: Nickel(II); Amino acid; Coordination chemistry; Hydrogen bond; Chiral recognition

1. Introduction

The conglomerate crystallization behavior adopted by racemic coordination compounds has been our long-term research interest [1,2]. When a racemic compound crystallizes in an enantiomorphic space group as a conglomerate, the process is one of enantioselective aggregation [3]. Species of the same chirality aggregate together during the nucleation and growth of a molecular crystal. This process is the most impressive example of chiral recognition in the solid state. Assisted by X-ray crystallography, the recognition pattern can be easily revealed by characterization of the intermolecular, or noncovalent forces involved in the supramolecular assemblies. Unfortunately, there are only a few examples of systematic investigations concerning the crystallization behavior of racemic coordination compounds [1,4–6], with helical chirality (designated as Δ and Λ) imposed by the asymmetric screw arrangement of multidentate ligands around the metal centers. The series of compounds $[M(bpy)_3](PF_6)_2$ ($M = Ni^{2+}$, Zn^{2+}, Ru^{2+}) [4] reveal that minor modification in molecular size and shape, induced by varying central metal atoms, can alter the crystallization pathway; i.e. racemic versus conglomerate, adopted by these compounds. In the structures of copper(II) complexes with $[Cu(H_2L)](ClO_4)_2$ formula (L = pentadentate Schiff-base ligands) [5], the double-faced H- bonding recognition motif carried by the Schiff-based ligand is considered as the directing force for the homochiral-assembly of the complex cations into …ΔΔΔ… and …ΛΛΛ…1-D chains. However, none of these copper(II) complexes crystallizes as a true conglomerate since the crystals contain heterochiral chains. Recently, the same research group reported the conglomerate

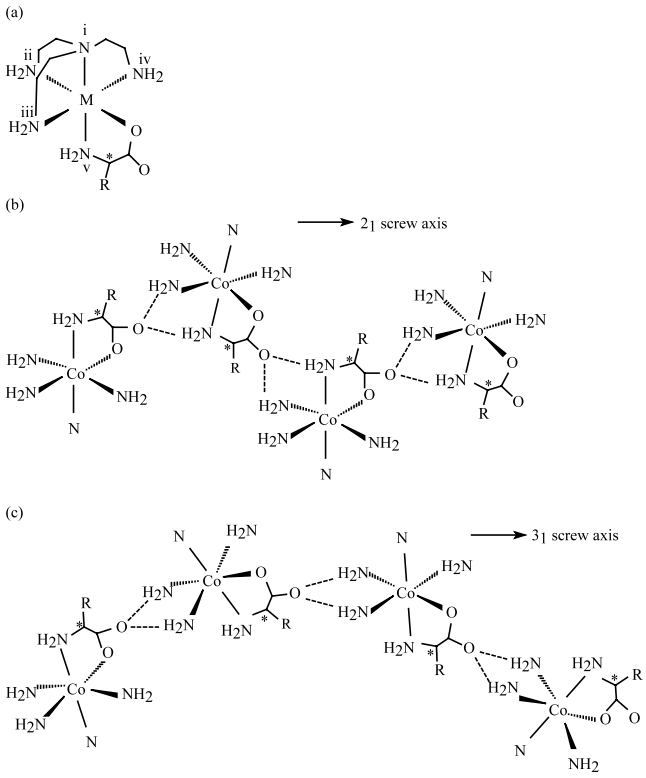
* Corresponding author. Tel.: +86-20-8411-0782.
E-mail address: puscjw@zsu.edu.cn (J. Cai).

0277-5387/02/$ - see front matter © 2002 Elsevier Science Ltd. All rights reserved.
PII: S0277-5387(02)00856-2

crystallization behavior of nickel(II) complexes with a formula $[Ni(H_3L)]X_2 \cdot MeOH$ (L = a tripod Schiff-base ligand) when $X = NO_3^-$, ClO_4^-. When $X = C_6H_5COO^-$, it crystallizes as a racemate [6]. The complex cations do not form a multidimensional network through H-bonds, and it is obvious that counter-anions play a crucial role in determining the crystallization pathway of the complex cation in this case. Finally, Bernal's group has been conducting systematically structural analyses of racemic cobalt(III) compounds with the formula $[Co(L1)_a(L2)_b]^{n+}$ (L1 = bidentate or one tetradentate amino ligands, $L2 = NO_2^-$ or $C_2O_4^{2-}$ ligands) [1]. These cobalt(III) complexes also contain the double-faced H-bonding motif carried by different ligands with H-bonding donor and acceptor functional groups. Effects of steric substitution and counter-ions were discussed. It was concluded that, in these systems, most of the conglomerates are formed by fragments which are capable of forming extended 1D chains through inter-molecular interactions, while the final aggregation of homochiral chains is effected by the so-called 'stitching agent(s)'; i.e. counter-ions and water of crystallization.

Therefore, at the moment it is not practical to rationalize the overall structural factors that will produce conglomerate crystallization, since this will raise the same issue as 'are crystal structures predictable?' [7]. In a typical molecular coordination complex, the final crystallization pathway is the result of a delicate balance between inter-molecular interactions and topological complements [4]. Thus, the structural factors controlling this supramolecular assembly process are encoded in the nature of metal atom and ligands, the coordination geometries and the counter-ions [4]. In spite of these problems, a systematic investigation of the crystallization behavior of racemic coordination compounds, especially conglomerates, is still valuable from both perspectives of chiral recognition in the solid state and in inorganic crystal engineering, a new branch of crystal engineering coined recently as a natural bridge between the two primary classes; i.e. the organic and covalent (coordination polymer) crystal engineering [8,9].

In our preceding papers, based upon our investigation about the packing arrangement of chiral $[Co(tren)(L\text{-aminoacidato})]^{2+}$ complexes, we predicted [10] and documented [2] that racemic $[Co(tren)(DL\text{-aminoacidato})]^{2+}$ complexes tend to favor conglomerate crystallization. Most significantly, in both enantiomorphic and racemic crystals, there is one dominant hydrogen bonding pattern designated as $C(6)[R_2^1(6)]$ [11], formed by the carboxylic oxygen of the amino acidato ligand and amino hydrogen atoms of the tren or amino acidato ligands. These H- bonds connect cations containing the same enantiomorphic amino acidato ligand into chiral helixes, as illustrated in Scheme 1. We refer to this pattern as the 'chiral recognition motif' of this system [2,10]. In order to compare the homo-



Scheme 1. (a) Schematic representation of the $[M(tren)(aminoacidato)]^{n+}$ complex cation; (b) schematic representation of the chiral helical chain with 2_1 symmetry generated by $[Co(tren)(aminoacidato)]^{2+}$ complex cations; (c) schematic representation of the chiral helical chain with 3_1 symmetry generated by $[Co(tren)(aminoacidato)]^{2+}$ complex cations. Amino acids, Val; Leu; Ile; Phe.

chiral–heterochiral assembly process of the nickel(II) chiral complex cations with their cobalt(III) analogues, as well as to evaluate the role played by metal atom upon the chiral recognition process, we report herein the syntheses and crystal structures of the *trans*(*N*, *t*-*N*) isomer of $[Ni(tren)(DL\text{-valinato})]Cl \cdot 2H_2O$ (**1**), $[Ni(tren)(DL\text{-phenylalaninato})]Cl \cdot 3H_2O$ (**2**) and $[Ni(tren)(DL\text{-leucinato})]Cl \cdot 2H_2O$ (**3**) (tren = tris(2-aminoethyl)amine).

2. Experimental

2.1. Syntheses

All reagents were commercially available and used as received. Elemental analysis was carried out with a Perkin–Elmer 240 elemental analyzer.

Compounds **1**–**3** were prepared as follows, to an aqueous solution of tren (0.30 g 3 mmol), an equal molar amount of amino acid and freshly prepared 10% NaOH solution was added. An aqueous solution of $NiCl_2 \cdot 6H_2O$ (0.48 g 3 mmol) was added under stirring. The color of the solution slowly changed to blue while

the solution was kept at 60 °C for several hours in a water bath. During the heating, water was added to keep the volume constant. The solution was cooled to room temperature (r.t.) and filtered. Crystals suitable for X-ray diffraction (XRD) were obtained by slow evaporation of the result solution at ambient temperature. Compound **1**: $C_{11}H_{32}ClN_5NiO_4$ required: C, 33.66; H, 8.22; N, 17.84. Found: C, 33.26; H, 7.82; N, 17.24%. Compound **2**: $C_{15}H_{34}ClN_5NiO_5$ required: C, 39.29; H 7.47; N, 15.27. Found: C, 39.41; H, 7.07; N, 14.96%. Compound **3**: $C_{12}H_{35}ClN_5NiO_{4.5}$ required: C, 34.68; H, 8.49; N, 16.85. Found: C, 34.82; H, 8.01; N 16.66%.

2.2. X-ray crystallography

All diffraction data were collected on a Bruker SMART 1000 CCD diffractometer with graphite monochromated Mo Kα radiation ($\lambda = 0.71073$ Å) at r.t. [12]. Absorption corrections were applied with the Bruker Area Detector absorption program [13,14]. Space groups of these complexes were determined from systematic absences and further justified by the results of refinement. In all cases, structures were solved by direct methods and refined using full-matrix least-squares/difference Fourier techniques [15,16]. All non-hydrogen atoms were refined with anisotropic displacement parameters. After that, all hydrogen atoms were placed in idealized positions and refined as riding atoms with the relative isotropic parameters.

In compounds **2** and **3**, disorders of the asymmetric carbon atom of the amino acidato ligand (in **2**) and its adjacent atom (in **3**) were observed. All the disordered atoms were refined over two sites, labeled as A and B. The $|E^*E-1|$ values (0.926 and 0.931 for **2**, and **3**, respectively) unambiguously point to centrosymmetric space groups. Compound **3** was also solved and refined in space group $P1$, in order to investigate the possibility that an incorrectly assigned space group imposed the disorders. The results show that in both $P1$ and $P\bar{1}$ space group, the same magnitude of disordered was observed.

Crystal data are listed in Table 1. Selective bond lengths and distances are listed in Table 2. The coordinates, anisotropic thermal parameters, bond distances, angles and torsion angles for these complexes are submitted as supplementary materials in CIF format.

3. Results and discussion

3.1. Structural descriptions

Interestingly, in contrast with the crystal structures of [Co(tren)(aminoacidato)]X_2 which have been well-investigated [2,10,17,18], there are no crystal structures reported for either the Ni(II) tren analogues, nor any other material with the general formula $[Ni(N_4)(aminoacidato)]^+$ (N_4 = amine or ammonium ligands), according to a Cambridge Structural Database search [19,20]. As illustrated in Fig. 1, compounds **1**–**3** adopt the *trans*(*N*, *t*-*N*) geometry in which the tertiary N-atom of the tren ligand is in the *trans* position to the N-atom of the amino acidato ligand. The Ni–N bond distances are in the ranges 2.0737(12)–2.1446(13), 2.0737(12)–2.1446(13), 2.070(4)–2.169(4) Å, and those of Ni–O are 2.0742(11), 2.1027(16), 2.067(3)/2.083(3) Å in **1**, **2** and **3**, respectively. The most striking difference between the Ni(II) and Co(III) analogues resides in the deprotonated carboxylic group of the amino acidato ligands. In the Ni(II) compounds, the average distances of the two carboxylic C–O distances is 1.256 Å for the coordinated O-atoms and 1.245 Å for the unbound O-atom, indicative of conjugate bonds. In the Co(III) analogue, for instance, in [Co(tren)(DL-leucinato)]$(ClO_4)_2$ [2], the C–O distance is 1.296(6) Å for the coordinated O-atoms and 1.187(6) Å for the unbound O-atom, indicative of single and double bonds. Therefore, the carboxylic group coordinates to Ni(II) as a delocalized carboxylate anion and to Co(III) as a more localized anion. This coordination mode is valid for all the amino acidato Co(III) complexes studied by our group [2,10,17].

As shown in Fig. 1(b and c), in complexes **2** and **3**, the asymmetric carbon or/and the carbon atom next to it are disordered and were refined over two positions. Consequently, the absolute configurations of the asymmetric carbons are different in these two sites. Such disorder is indicative of the fact that D- and L-amino acids occupy the same lattice site in complexes **2** and **3**. The same phenomenon has been observed and documented previously in related Co(III) analogues [2,18]. The name conglomeratic solid was then coined [18] to describe this phenomenon since the racemic material crystallizes in an enantiomorphic space group. However, the circumstances are different here, complexes **2** and **3** crystallize in the centrosymmetric space groups $P2_1/n$ and $P\bar{1}$. In other words, they are real racemates in the crystalline lattice.

3.2. Packing descriptions

As shown in Figs. 2 and 3, the cations of **1** and **2** are assembled into 1-D chains by the same pattern of intermolecular H- bonds. The unbound carboxylic oxygen is H- bonded divergently to two amino H-atoms of the tren ligands belonging to two different adjacent cations (N···O = 3.1533(18), 3.175(2) Å and N–H···O = 142.3, 142° in **1**. N···O = 3.279(3), 3.320(3) Å and N–H···O = 129.3°, 147.6° in **2**), resulting in a ribbon-like arrangement of the cations along the *b* axis. The extended notation for the H- bond pattern can be described as $C_2^1(6)[R_2^2(12)]$ [11]. The amino H-atoms of the amino acidato ligand are not involved in any inter-

Table 1
Crystallographic data

Compound	1	2	3
Empirical formula	$C_{11}H_{32}ClN_5NiO_4$	$C_{15}H_{34}ClN_5NiO_5$	$C_{12}H_{34}ClN_5NiO_4$
Formula weight	392.58	458.63	406.60
Crystal system	monoclinic	monoclinic	triclinic
Space group	$P2_1/n$	$P2_1/n$	$P\bar{1}$
Unit cell dimensions			
a (Å)	13.385(2)	14.189(3)	12.578(2)
b (Å)	8.4566(14)	8.7596(17)	13.431(2)
c (Å)	16.553(3)	17.303(3)	14.785(3)
α (°)	90	90	67.687(3)
β (°)	92.667(3)	90.535(4)	70.507(3)
γ (°)	90	90	63.859(3)
V (Å^3)	1871.6(5)	2150.6(7)	2032.3(6)
Z	4	4	4
Absorption coefficient (mm^{-1})	1.202	1.061	1.109
Θ Range of data collection (°)	4.03–30.04	2.61–29.97	1.76–30.00
Total reflections collected	13096	13874	14629
Independent/observed reflections($I > 2\sigma(I)$)	5418/4233	5689/4172	9560/5973
Data/restraints/parameters	5418/0/215	5689/0/261	10551/0/447
Goodness-of-fit on F^2	1.034 $R_1 = 0.0293$	0.993 $R_1 = 0.0398$	0.980 $R_1 = 0.0601$
Final R indices ($I > 2\sigma(I)$)	$wR_2 = 0.0775$	$wR_2 = 0.1113$	$wR_2 = 0.1845$

Table 2
Selected bond lengths (Å) and angles (°) for the Ni^{2+} complexes

	1	2	3(Ni)	3(Ni′)
Bond lengths				
Ni–N(1)	2.0874(13)	2.0973(19)	2.086(3)	2.112(3)
Ni–N(2)	2.1389(14)	2.157(2)	2.120(3)	2.123(3)
Ni–N(3)	2.0996(13)	2.0906(19)	2.118(3)	2.100(3)
Ni–N(4)	2.1446(13)	2.138(2)	2.149(3)	2.169(4)
Ni–N(5)	2.0737(12)	2.0833(19)	2.071(3)	2.070(4)
Ni–O(1)	2.0742(11)	2.1027(16)	2.085(3)	2.067(3)
Bond angles				
N(1)–Ni–N(2)	83.40(5)	81.96(8)	82.69(13)	83.14(14)
N(1)–Ni–N(3)	83.50(5)	83.36(8)	83.31(13)	82.69(14)
N(4)–Ni–N(1)	82.33(5)	82.48(8)	82.62(13)	81.73(15)
N(5)–Ni–N(1)	174.68(5)	179.05(9)	174.30(12)	177.95(14)
N(3)–Ni–N(2)	92.46(5)	92.30(9)	90.93(13)	92.59(14)
N(4)–Ni–N(2)	164.80(5)	162.13(9)	164.34(14)	161.85(15)
N(5)–Ni–N(2)	98.43(6)	98.98(9)	97.18(14)	96.20(17)
N(4)–Ni–N(3)	91.10(5)	94.57(9)	92.71(14)	95.36(15)
N(5)–Ni–N(3)	101.36(5)	96.48(7)	102.39(13)	99.28(15)
N(5)–Ni–N(4)	95.34(5)	96.61(9)	96.90(14)	98.58(17)
O(1)–Ni–N(1)	94.12(5)	99.93(7)	93.90(11)	96.77(12)
O(1)–Ni–N(2)	85.99(5)	86.48(8)	89.84(12)	88.29(12)
O(1)–Ni–N(3)	177.31(5)	176.28(7)	176.99(12)	178.91(14)
N(4)–Ni–O(1)	89.84(5)	87.62(8)	85.78(12)	83.62(13)
N(5)–Ni–O(1)	81.06(4)	80.27(7)	80.40(11)	81.26(13)

cationic H- bonds. Instead, they are so engaged by the counter anions and waters of crystallization. Interestingly in complex **1**, the cations which are H- bonded together are generated by 2_1 operations and align along the screw axis, i.e. the b axis. Therefore, they are homochiral. In contrast, cations in **2** adopt the same packing arrangement along the b axis, connected by the same pattern of H- bonds with weaker strength. The fact that D- and L- isomers occupy the equivalent lattice places makes it ambiguous to determine the chiralities of the H- bonded cations.

In **3**, there are two complex cations in the asymmetric unit. As shown in Fig. 4, the cations are also linked into 1-D chains by intermolecular H- bonds. Each complex cation forms two H- bonds with the same cation of the next unit, generating pairs of Ni–Ni and Ni′–Ni′ with the same H- bond pattern as that observed in **1** and **2** (N···O = 3.202(5), 2.919(4) Å; N–H···O = 151.4°, 164.9°), with the notation for the H- bond pattern described as $R_2^2(12)$ [11], and there is only one H- bond connecting the pairs together (N···O = 2.940(4) Å and N–H···O = 145.1°). Nevertheless, the ribbon-like arrangement of the cations is very similar to that observed in **1** and **2**. The observed disorder also suggests that the chiralities of the cations that are linked together cannot be determined.

The purpose of this investigation is to compare the inter-cationic H- bonding patterns between the Ni(II) and Co(III) analogues. Therefore, H- bonds formed by the Cl^- anion and water of hydration are not discussed in detail here. However, it should be pointed out that counter anions and water molecules play important roles in determining the overall crystallization pathway, as we concluded in our previous papers [1].

3.3. Effect of the metal atom on the inter-molecular H-bond pattern

Metal atoms play a unique role that distinguishes inorganic crystal engineering from its organic counter-

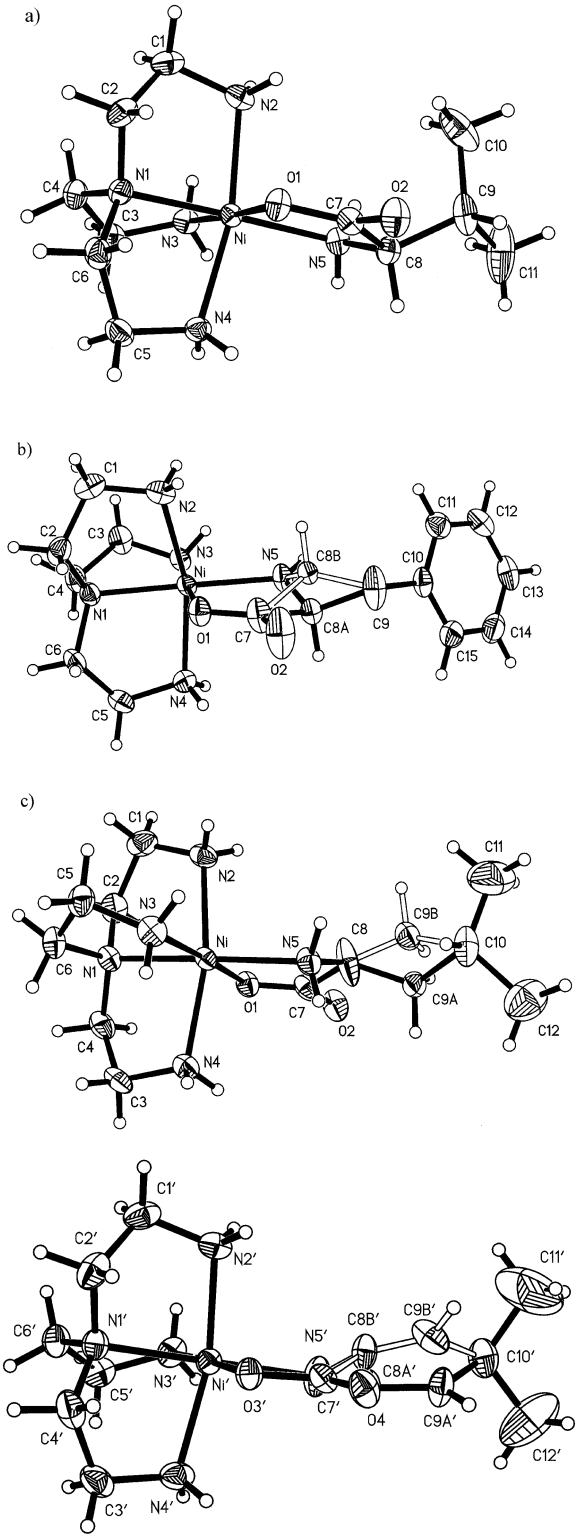


Fig. 1. (a)–(c) Atomic numbering scheme of the complex cations in **1**–**3**, respectively, with 30% probability displacement ellipsoids. Note that the asymmetric carbon atom or/and the one next to it, namely C8 **2**, C9 in **3** (cation 1), and C8′, C9′ in **3** (cation 2) are disordered and refined over two positions. These result in different absolute configurations for the two portions.

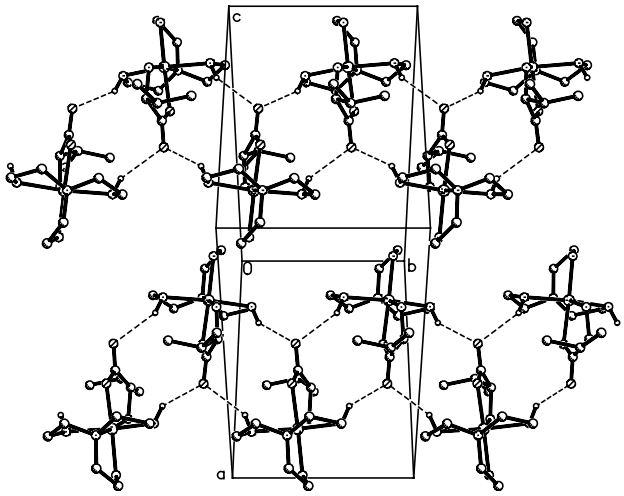


Fig. 2. Packing arrangement of the complex cations in **1.** Note that the complex cations are related to each other by the 2_1 operation and align along the *b* axis.

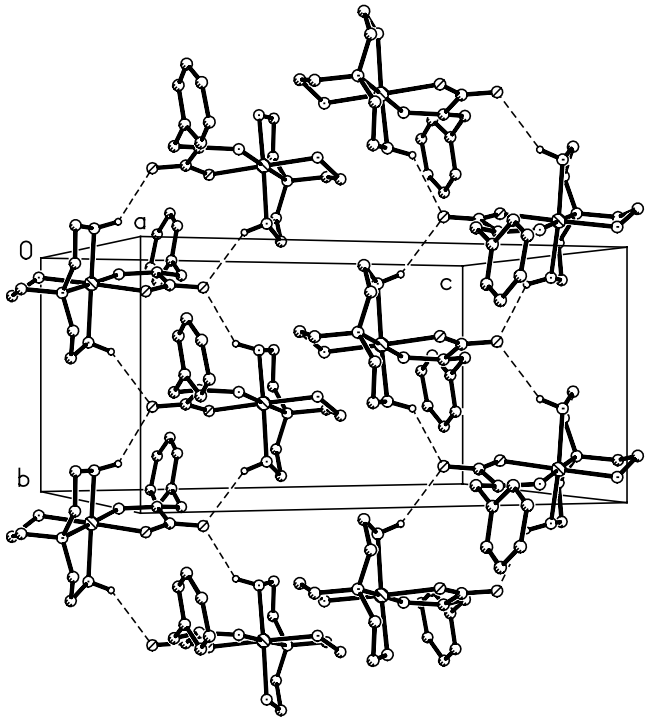


Fig. 3. Packing arrangement of the complex cations in **2**. Note that the complex cations are related to each other by the 2_1 operation and align along the *b* axis. One portion of the disordered fragments is omitted for clarity.

part. The properties, including crystal packing, of metal-containing materials depend on the electronic nature of the metals as well as on the characteristics of the ligands [8]. It was pointed out that in organo-metallic or coordination compounds, the metal centers are mostly situated in the molecular cores and well-shielded from neighboring molecules [9], and the peripheral portion of the molecules, i.e. the organic ligands, are crucial in

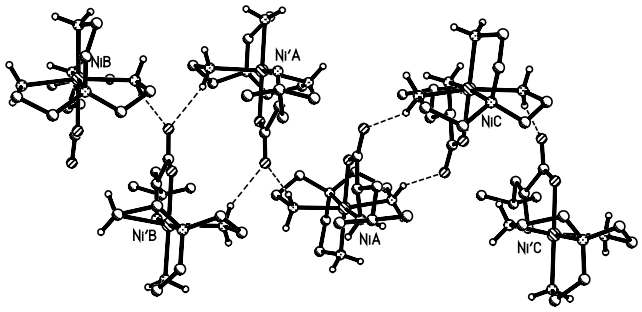
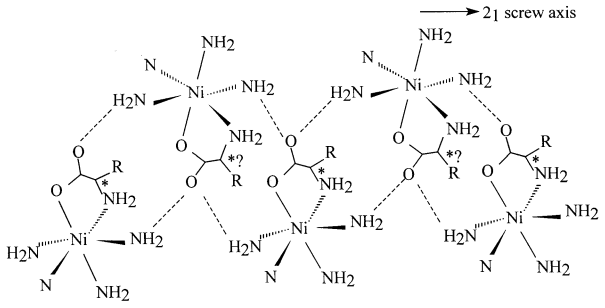


Fig. 4. Packing arrangement of the complex cations in **3**. Note that the complex cations are arranged into a 1-D chain in a similar fashion as that observed in **1** and **2**. One portion of the disordered fragments is omitted for clarity.

determining the crystal structures since they are directly involved in inter-molecular, noncovalent interactions. This is indeed what was observed for the bis(imidazolium 2,6-pyridinedicarboxylate)M(II) trihydrate complexes, where M = Mn^{2+}, Co^{2+}, Ni^{2+}, Cu^{2+} or Zn^{2+} [21]. Packing in these solids is dominated by H- bonding between imidazolium cations and carboxylate anions. All of the metal complexes crystallize in the same space group with similar unit cell parameters. However, in the structure of a 14-membered polyazamacrocyclic copper(II) complex, appended by the heterocyclic melamine, it was predicted that the metal ions play a minor role in the formation of the supramolecular array [22]. Both systems share the common feature that the metal atoms are buried by the outer portion of the molecules and the metal-bonded atoms are not involved in any inter-molecular interaction. By contrast, in the series of $[M(tren)(aminoacidato)]^{n+}$ compounds, H- bonding interactions are formed directly between the complex cations which comprise the 1-D backbone [2,10]. As illustrated in Schemes 1 and 2, atoms that are involved in the inter-cationic H- bonds as donors, i.e. the amino groups, are coordinated with the metal atoms. Therefore, the nature of the metal centers adjusts the acidity of the donors. While for the acceptor, which is the carboxylic oxygen, as mentioned above the carboxylate anions coordinate in a different mode, as a delocalized



Scheme 2. Schematic representation of the homochiral–heterochiral helical chain with 2_1 symmetry generated by $[Ni(tren)(aminoacidato)]^+$ complex cations.

and localized anion to Ni(II) and Co(III), respectively. Therefore, the basicities of the free O-atoms of the carboxylic group are different in the Ni(II) and Co(III) analogues. The tuning of the acidity–basicity of the donor–acceptor in the organic ligands by the metal atoms shows a response in their H- bonding capacity, and alters the pattern and strength of inter-molecular interactions as illustrated in Schemes 1 and 2.

3.4. Intermolecular H- bonding interactions, packing forces and chiral recognition

In our previous report [2], we demonstrated that for most of the racemic $[Co(N4)(aminoacidato)]^{2+}$ complexes, inter-cationic H- bonding interactions generally exist which bring cations with the same chirality together into helical chains. The helical chain arrangement remains the same in both racemic and enantiomorphic crystals. The only difference is that in the former adjacent helices are of opposite handedness, while in the latter only one handedness of the helical array is observed. Since the H- bonding pattern observed in racemic crystals is the same as that observed in the enantiomeric form, we refer to it as the 'chiral recognition motif' of these systems. For the $[Co(tren)(aminoacidato)]^{2+}$ series, the inter-cationic H-bond pattern is characterized as $C(6)[R_2^1(6)]$ and illustrated in Scheme 1, with an average strength of N···O = 2.875/2.965 Å, N–H···O = 15···5.3/133.2°. However, the complex cations generally align along the crystallographic screw axis. This observation raises a query, i.e. is this homochiral assembly/chiral recognition process forced by the packing forces? How to evaluate the roles played by the inter-molecular interactions and the packing forces during the homochiral assembly/chiral recognition process? This doubt is resolved by the comparison of the crystal structures of Ni(II) complexes **1** and **2**. They crystallize in the same space group with similar packing arrangements. However, homochiral arrangements are observed in **1**, and cannot be determined in **2**. The fact that D- and L- isomers occupy the same crystalline lattice in **2** indicates the possibility that inter-molecular interactions in **2** are not capable of discriminating the heterochiral fragment from the homochiral one. **3** Crystallizes in a space group devoid of any screw axis operation, but the fragments are still arranged as 1-D chains connected by H- bonds. This reveals another important feature of this crystal structure, i.e. it is the double inter-molecular H- bonds, not the packing forces, that controls the assembly of the complex cations into the 1-D helix. These observations sustain our previous conclusion that the inter-molecular interactions between $[Co(N4)(aminoacidato)]^{2+}$, which combine both strength and directionality, is the 'chiral recognition motif' which drives the homochiral assembly.

4. Concluding remarks

The origin of handedness in biological molecules is one of nature's mysteries. Recently, an elegant work has been performed to demonstrate that chiroselectivity in peptide self-replication is a direct result of complementary *non-covalent interactions* that pass on both binding and stereochemical information simultaneously [23]. Herein and in our previous papers [2,10], we have illustrated a simple molecular coordination system whose chiral recognition capability is realized by non-covalent intermolecular interactions. This series of compounds can serve as a unique model to evaluate the roles played by the nature of the metal center, as well as the steric effects of the side chain of an amino acid, during the homochiral–heterochiral assembly process.

5. Supplementary material

Crystallographic data for the structural analysis have been deposited with the Cambridge Crystallographic Data Center, CCDC Nos. 164478–164480 for compounds **1**–**3**, respectively. Copies of this information can be obtained free of charge from The Director, CCDC, 12 Union Road, Cambridge, CB2 1EZ, UK (fax: +44-1223-336033; e-mail: deposit@ccdc.cam.ac.uk or www: http//www.ccdc.cam.ac.uk).

Acknowledgements

This work is supported by the National Natural Science Foundation of China (Grand No. 29801006) and by the Robert A. Welch Foundation (to IB; No. 592).

References

[1] (a) J. Cai, J. Myrczek, I. Bernal, J. Chem. Soc., Dalton Trans. (1995) 611.;
(b) I. Bernal, J. Cetrullo, J. Cai, Transition Met. Chem. 19 (1994) 221;
(c) I. Bernal, J. Cetrullo, J. Cai, R.A. Geanangel, J.H. Worrell, J. Chem. Soc., Dalton Trans. (1995) 99.;
(d) I. Bernal, J. Myrczek, J. Cai, Polyhedron 12 (1993) 1149;
(e) I. Bernal, J. Cai, F. Somoza, J. Coord. Chem. 42 (1997) 33;
(f) I. Bernal, J. Cetrullo, J. Myrczek, J. Cai, W.T. Jordan, J. Chem. Soc., Dalton Trans. (1993) 1771.
[2] X.-P. Hu, J. Cai, C.-H. Chen, X.-M. Chen, L.-N. Ji, Crystal Eng. 4 (2001) 141.
[3] J. Jacques, A. Collet, S.H. Wilen, Enantiomers, Racemates, and Resolutions, Wiley, New York, 1981.
[4] J. Breu, H. Domel, A. Stoll, Eur. J. Inorg. Chem. (2000) 2401.
[5] (a) Y. Shii, Y. Motoda, T. Matsuo, F. Kai, T. Nakashima, J.-P. Tuchagues, N. Matsumoto, Inorg. Chem. 38 (1999) 3513;
(b) H. Miyasaka, S. Okamura, T. Nakashima, N. Matsumoto, Inorg. Chem. 36 (1997) 4329.
[6] I. Katsuki, N. Matsumoto, M. Kojima, Inorg. Chem. 39 (2000) 3350.
[7] A. Gavezzotti, Acc. Chem. Res. 27 (1994) 309.
[8] D. Braga, F. Grepioni, G.R. Desiraju, Acc. Chem. Res. 33 (2000) 601.
[9] D. Braga, F. Grepioni, Chem. Rev. 98 (1998) 1375.
[10] J. Cai, X.-P. Hu, X.-L. Feng, W.-Y. Shao, L.-N. Ji, I. Bernal, Eur. J. Inorg. Chem. (2000) 2199.
[11] (a) M.C. Etter, Acc. Chem. Res. 23 (1990) 120;
(b) J. Bernstein, R.E. Davis, L. Shimoni, N.-L. Chang, Angew. Chem., Int. Ed. Engl. 34 (1995) 1555.
[12] Bruker AXS, SMART, Version 5.0, Bruker AXS, Madison, WI, USA, (1998).
[13] Bruker AXS, SAINT+, Version 6.0, Bruker AXS, Madison, WI, USA, (1999).
[14] R. Blessing, Acta Crystallogr. A51 (1995) 33.
[15] Bruker AXS, SHELXTL, Version 5.1, Bruker AXS, Madison, WI, USA, (1998).
[16] G.M. Sheldrick, SHELXL-97, Program for X-ray Crystal Structure Solution and Refinement, Göttingen University, Germany, 1997.
[17] J. Cai, X.-P. Hu, X.-L. Feng, L.-N. Ji, I. Bernal, Acta Cryst. Sect. B 57 (2001) 45.
[18] (a) K. Yamanari, A. Fuyuhiro, Chem. Lett. (1991) 1551.;
(b) K. Yamanari, A. Fuyuhiro, Bull. Chem. Soc. Jpn. 68 (1995) 2543;
(c) K. Yamanari, A. Fuyuhiro, Bull. Chem. Soc. Jpn. 69 (1996) 1289.
[19] F.H. Allen, O. Kennard, Chem. Des. Automation News 8 (1993) 31.
[20] I.J. Bruno, J.C. Cole, J.P.M. Lommerse, R.S. Rowland, R. Taylor, M. Verdonk, J. Computer-aided Mol. Des. 11-6 (1997) 525.
[21] J.C. MacDonald, P.C. Dorrestein, M.M. Oilley, M.M. Foote, J.L. Lundburg, R.W. Henning, A.J. Schultz, J.L. Manson, J. Am. Chem. Soc. 122 (2000) 11692.
[22] P.V. Bernhardt, Inorg. Chem. 38 (1999) 3481.
[23] A. Saghatelian, Y. Yokobayashi, K. Soltani, M.R. Ghadiri, Nature 409 (2001) 797.

PERGAMON

Polyhedron 21 (2002) 825–834

POLYHEDRON

www.elsevier.com/locate/poly

Synthesis, spectroscopy and redox properties of a novel (*E*–*E*) *vic*-dioxime and its mono-, di- and trinuclear complexes bearing an 18-membered $N_2O_2S_2$ macrocyle

Mehmet Kandaz [a,*], İsmail Yılmaz [b,*], Semra Keskin [a], Atıf Koca [c]

[a] *Department of Chemistry, Sakarya University, 54100 Serdivan, Sakarya, Turkey*
[b] *Department of Chemistry, Technical University of Istanbul, 80626 Maslak, Istanbul, Turkey*
[c] *Chemical Engineering Department, Engineering Faculty, Marmara University, 81040, Kadıköy, Istanbul, Turkey*

Received 17 July 2001; accepted 21 December 2001

Abstract

A new 18-membered ligand, 2,3-dibromo-6,7,13,14,15,16,22,23-octahydro 14, 15-bis(hydroxyimino)-tribenzo [e,k,q] [1,4,10,13,7,16] diazadioxadithiacyclooctadecine (LH_4) containing three different heteroatoms (N–, O–, S–) has been prepared from 1,2-bis (2′-amino phenylsulfanylethoxy)-4,5-dibromobenzene and cyanogen di-*N*-oxide. Mononuclear $(LH_3)_2M$, where M = Ni(II), Cu(II), Co(II), Fe(II) binuclear $(LH)_2(UO_2)_2(OH)_2$ and trinuclear $(LH)_2M_3$, where M = Cu (II), Co (II) complexes of LH_4 have been obtained with a metal:ligand ratio 1:2, 2:2 and 3:2, respectively, through *N*,*N*-coordinating or N, N, S, S-coordinating in the presence of a base, as do most of the *vic*-dioximes. ^{1}H NMR, IR, UV–Vis and MS data are presented. The cyclic voltammetric (CV) measurements of the newly synthesized compounds were measured. Voltammetric results showed that oxime-containing ligands stabilize Ni(III), Fe(III), Co(III) and Cu(III). The Fe(II) complex displayed a different behavior with respect to other complexes. This indicated that both Fe(III) and Fe(I) species are stable while oxime containing ligands tend to stabilize only one of the oxidized forms of the metal center of the complexes. Differently, ligand based reduction was recorded only with the Ni(II) complex. © 2002 Elsevier Science Ltd. All rights reserved.

Keywords: *vic*-Dioxime; Nickel(II), Cobalt(II), Copper(II), Iron(II), Uranyl(IV), Electrochemistry; LH_4; $N_2O_2S_2$ macrocyle

1. Introduction

Oximes and their metal complexes are of current interest for their rich physicochemical properties, reactivity patterns and potential applications in many important chemical processes in the areas of medicine [1–4], bioorganic systems [5,6], catalysis [7,8], electrochemical and electrooptical sensors [9–12]. The high stability of the complexes prepared with *vic*-dioxime ligands has been extensively used for various purposes including model compounds for vitamin B_{12} or trace metal analysis [13,14]. The successful design and synthesis of ligands capable of forming heteronuclear complexes have been receiving world-wide attention for obtaining special effects in magnetic, optical and electrical properties [15–20]. Examples of heteronucleating ligands that could serve as polytopic receptor molecules for the binding or cobinding of metal ions and molecular substrates include molecules that contain various functionalities appended to porphyrins, phthalocyanines, salen centers and macrocyclic tetraammines [21–23]. The investigations of the redox properties of these types of complexes are also of great interest in terms of their various technological applications [24–28]

Incorporation of a *vic*-dioxime moiety on the macrocycle provides an efficient binding site for transition metal ions by formation of an MN_4 core with two additional hydrogen bridges [29]. The presence of weakly acidic hydroxyl groups and slightly basic nitrogen atoms make vicinal dioxime amphoteric ligands which form corrin-type square-planar, square-pyramidal and octahedral complexes with transition metals, such as nickel(II), copper(II), palladium(II) and cobalt(II) as central atoms [30]. When starting compounds

* Corresponding authors. Fax: +90-264-276-2059.
E-mail address: mkandaz@sau.edu.tr (M. Kandaz).

0277-5387/02/$ - see front matter © 2002 Elsevier Science Ltd. All rights reserved.
PII: S0277-5387(02)00860-4

with macrocyclic groups were used, *vic*-dioximes incorporating macrocyclic groups capable of binding transition and alkali metal ions simultaneously have been achieved [15,29–31].

The ability of oxime-containing ligands to stabilize reduced and oxidized forms of metal ions has a vital importance in their role in the areas of technological applications. However, the literature dealing with the electrochemistry of metal-oximes especially in organic solvents is scarce [32–34]. In the present work, we have prepared a 18-membered macrocyclic *vic*-dioxime ligand, which contains two oxygen, two nitrogen and two sulfur binding sites. The mono- di- and tri-nuclear complexes of this ligand with various transition metals have been synthesized. Also, electrochemistry of the mono- and dinuclear complexes have been investigated.

2. Experimental

Routine IR spectra were recorded on a Mattison 1000 Spectrophotometer using KBr pallets, and electronic spectra on an unicam UV2 spectrophotometer. Elemental analysis was performed by the Instrument Analysis Laboratory of TUBITAK Marmara Research Centre. Proton NMR spectra were recorded on a Bruker 250 MHz spectrometer using $SiMe_4$ as reference and MS:EI on a VG Zabspec GS-MS spectrometer. The metal contents of the complexes were determined with a Hitachi 180-80 atomic absorption spectrophotometer in conc. $HClO_4$ and conc. HNO_3 solution followed by digestion in conc. HCl solution. The homogeneity of **2** and **3** were tested in each step by TLC (SiO_2, EtOH). 1,2-Di iodo-(2′-etoxyphenoxy)-4,5-dibromobenzene and *anti*-dichloroglyoxime were synthesized according to the published methods [35–40].

Cyclic voltammetric (CV) and controlled potential coulometric (CPC) measurements were carried out with an instrument (Princeton Applied Research Model 273 potentiostat controlled by an external PC, using the computer program, HEADSTRT) utilizing a three electrode configuration at 25 °C. ORIGIN 5.0 graph program was used to evaluate HEADSTRT data, to draw voltammograms and analyze them. A platinum wire served as the counter electrode. A saturated calomel electrode (SCE) was employed as the reference electrode and was separated from the bulk of the solution by a glass bridge. The working electrode was a platinum plate with an area of 1.0 cm^2. The surface of the working electrode was polished with a water suspension of Al_2O_3 before each run. Tetrabutylammoniumperchlorate (0.1 mol dm^{-3}) (TBAP) in extra pure DMSO was employed as the supporting electrolyte. High purity nitrogen was used for deaeration and to maintain an nitrogen blanket for at least 15 min prior to each run. For CPC studies, a Pt gauze working electrode (10.5 cm^2 surface area), a platinum wire counter electrode separated by a glass bridge, a saturated calomel reference electrode, and a model 377/12 Synchronous stirrer were used. With CPC studies of the complexes, complete electrolysis of the solution at the working electrode at constant potential (E_{pc} of redox couple) was done and as a result time integration of the electrolysis current was recorded. The electroactive species in the solution was depleted during the electrolysis and the accumulated current time integral, the charge Q at the end of electrolysis, was calculated by using the current–time response of the solution. Faraday's Law was used to calculate the number of electrons transferred for electron transfer reactions.

2.1. 1,2-Bis (2′-aminophenylsulfanylethoxy)-4,5-dibromobenzene (2)

2-Aminothiophenol (2.50 g, 20.0 mmol) was dissolved in 30.0 cm^3 ethanol under nitrogen. Then 2.00 cm^3 40% NaOH solution was added and the mixture was stirred and heated at reflux for 10 min. To this solution, 1,2-di iodo-(2′-etoxyphenoxy)-4,5-dibromobenzene (5.76 g, 10.0 mmol) in 20.0 cm^3 hot ethanol was added dropwise over a period of 1 h. After the reaction mixture had been refluxed for 2 h, the solvent was distilled off. The yellow residue was dissolved in 50.0 cm^3 diethylether and the solution was filtered. The filtrate was washed firstly with Na_2CO_3 (5%) and then with water (3×30.0 cm^3) to separate any inorganic residues, dried with sodium sulphate and finally filtered. When the hydrochloric acid gas was passed through the filtrate, white amine salt was separated. The solid was washed with diethylether and dichloromethane. The precipitate was dissolved in absolute ethanol. The pH of the solution was adjusted to 8 with 1.00 N KOH solution in methanol and free amine was separated as white crystals. It was filtered and washed with cold ethanol. Yield: 3.21 g (56.3%). This compound is soluble in chloroform, dichloromethane, diethylether, THF and slightly hot ethanol. m.p.: 96 °C. IR (KBr, cm^{-1}) ν: 3460–3350 (NH_2), 3080, 3030 (Ar-H), 2950, 2870 (Aliph-H), 1590 (w), 1515–1450 (Ar-skelt.vib.), 1270–1250 (C–O–C), 640 (C–Br). ^{1}H NMR (250 MHz, DMSO-d_6) δ:7.34 (s, 2H, Ar-H), 7.27(dd, $^3J = 7.5$ Hz, $^4J = 1.7$ Hz, 2H, Phenyl-H3), 7.01 (dt, $^3J = 7.5$ Hz, $^4J = 1.5$ Hz, 2H, Phenyl-H5), 6.67 (dt, $^3J = 7.8$ Hz, $^4J = 1.7$ Hz, 2H, Phenyl-H4), 6.50 (dd, $^3J = 7.8$ Hz, $^4J = 1.5$ Hz, 2H, Phenyl-H6), 5.38 (s, br, 4H, $-NH_2$), 4.01 (t, $^3J = 6.2$ Hz, 4H, O–CH_2CH_2) and 2.89 (t, $^3J = 6.2$ Hz, 4H, S–CH_2CH_2). MS (EI): $m/z = 570.2$ (20%) [M^+].

2.2. Synthesis of 5,6, 17,18-dibenzo-11,12-dibromobenzo, 2,3-bis(hydroxyimino)-1,4-diaza, 7, 16-dithia-10,13dioza-2,3,8,9,14,15-hexahydrocyclodecine (Diazadithiadioxa Macrocycle) (LH_4) (**3**)

Compound **1** (2.85 g, 5.00 mmol) was dissolved in 200 cm^3 dichloromethane and cooled to −20 °C with stirring. To this solution, a solution of cyanogen di N-oxide in 70.0 cm^3 dicholoromethane, which was prepared from *anti*-dichloroglyoxime (0.790 g, 5.00 mmol) and aqueous 1.00 N Na_2CO_3 solution, was added dropwise. The reaction was continued at this temperature for 6 h with stirring and then the yellow compound was separated by filtration, washed with dichloromethane, ethanol and diethylether and dried in vacuo. Yield: 0.820 g, (25.1%); m.p. 142 °C. This compound is soluble in THF, Dioxane, DMF and DMSO and slightly soluble in MeOH. IR (KBr, cm^{-1}) ν: 3350 (NH), 3220 (br, OH), 3070, 3020 (Ar-H), 2985–2850 (Aliph-H), 1640 (C=N), 1580–1420 (Ar-skel. Vib.), 1270–1230 (C–O–C), 1010 (N–O), 700, 650 (C–Br), 560. ^{1}H NMR (250 MHz, DMSO-d_6) δ: 10.72 (s, 2H, =N–OH, D-exchangeable), 8.65 (s, 2H, –NH, D-exchangeable), 7.48 (s, 2H, Ar–H), 7.23 (dd, $^3J = 7.2$ Hz, $^4J = 1.7$ Hz, 2H, Phenyl-H3), 7.04 (dt, $^3J = 7.1$ Hz, $^4J = 1.6$ Hz, 2H, Phenyl-H5), 6.73 (dt, $^3J = 7.8$ Hz, $^4J = 1.7$ Hz, 2H, Phenyl-H4), 6.50 (dd, $^3J = 7.1$ Hz, $^4J = 1.5$ Hz, 2H, Phenyl-H6), 4.24 (t, $^3J = 6.1$ Hz 4H, O–CH_2CH_2), 3.01 (t, $^3J = 6.1$ Hz 4H, S–CH_2CH_2). UV–Vis (in DMSO) λ_{max}, nm (ε, $dm^3\ mol^{-1}\ cm^{-1}$): 320 (6100), 307 (9840) (sh), 290 (12 500), MS (positive FAB, solution in DMSO, Magnet BpI: 3582): $m/z = 655(35)$ $[M^+ + 1]$.

2.3. Mononuclear complexes

2.3.1. (LH_3)$_2$Ni (**4**)

$Ni(NO_3)_2 \cdot 6H_2O$ (0.0360 g, 0.120 mmol in 10.0 cm^3 THF) solution was slowly added with stirring to **3** (0.160 g, 0.250 mmol in 20.0 cm^3 THF). The color of the solution turned immediately into red–orange. A decrease in pH was observed. So the pH of the mixture was raised to about 7.0 by addition of $(C_2H_5)_3N$. The reaction mixture was kept at 60 °C with stirring until the precipitation was completed. Then it was brought to room temperature (r.t.) and the orange crystalline complex precipitated. The product was filtered, washed with water, ethanol, THF and diethylether and finally dried in vacuo. This compound is soluble in DMF and DMSO. Yield: 0.080 g (50%); m.p.: > 200 °C. IR (KBr, cm^{-1}): ν: 3410 (–NH), 3050 (Ar-H), 2975–2840 (Aliph-H), 1700 (O–H...O), 1620 (–CN), 1590, 1590–1460 (Ar-skel.), 1260–1240 (Ar-O-Aliph, Aliph-O-Ar), 1010 (N–O), 695, 660 (C–Br), 550. ^{1}H NMR (250 MHz, DMSO-d_6) δ:16.70 (s, 2H, O–H...O, D-exchangeable), 8.64 (s, 4H, –NH, D-exchangeable), 7.70 (s, 2H, Ar-H), 7.19 (d, $^3J = 7.8$ Hz, 4H, Phenyl-H3), 7.05 (dt, $^3J = 7.6$ Hz, $^4J = 1.7$ Hz, 4H, Phenyl-H5), 6.84 (dt, $^3J = 7.8$ Hz, $^4J = 1.5$ Hz, 4H, Phenyl-H4), 6.52 (d, $^3J = 7.2$ Hz, 4H, Phenyl-H6), 4.07 (t, $^3J = 6.2$ Hz, 8H, O–CH_2CH_2), 3.01 (t, $^3J = 6.2$ Hz, 8H, S–CH_2CH_2). UV–Vis (in DMSO) λ_{max}, nm (ε, $dm^3\ mol^{-1}\ cm^{-1}$): 350 (6700), 321 (11 090), 303 (13030). MS (positive FAB, solution in DMSO): m/z 1365 (15%) $[M^+]$

2.3.2. (LH_3)$_2$Cu (**5**)

To a solution of **3** (0.160 g, 0.250 mmol) in 20.0 cm^3 THF, with stirring a solution of (0.0360 g, 0.120 mmol) $Cu(NO_3)_2 \cdot 6H_2O$ in 20.0 cm^3 THF was added dropwise at r.t. The color of the solution turned into dark brown. The pH of the mixture was adjusted to about 7.0 by adding $(C_2H_5)_3N$. Then the mixture was heated on a water bath until the precipitation was completed. It was brought to r.t., then the product was filtered, washed with water, ethanol, THF and diethylether and dried in vacuo. This compound is soluble in DMF, DMSO and slightly soluble in pyridine. Yield 0.07 g (41.76%). m.p.: > 200 °C. IR (KBr, cm^{-1}) ν: 3420 (NH), 3070 (Ar-H), 2950, 2845 (Aliph-H), 1710 (w), 1650 (CN), 1590 (N–H bending), 1510–1460 (Ar-skel.), 1250 (C–O–C), 1015 (N–O), 690, 640 (C–Br), 560. UV–Vis (in DMSO) λ_{max}, nm (ε, $dm^3\ mol^{-1}\ cm^{-1}$): 348 (2240) (sh), 303 (10 500). MS (positive FAB, solution in DMSO): 1370.5 (12%) $[M^+ + 1]$.

2.3.3. (LH_3)$_2$Co (**6**)

These pale brown complexes were prepared by following the same procedure as described for the preparation of $(LH_3)_2Cu$, starting from **3** (0.160 g, 0.250 mmol) and $Co(NO_3)_2 \cdot 6H_2O$ (0.0360 g, 0.120 mmol).

Yield: 0.0640 g (37.6%); m.p.: > 200 °C. IR (KBr, cm^{-1}) ν: 3420 (NH), 3030 (Ar-H), 2920, 2860–2830 (Aliph-H), 1710, 1630 (CN), 1590, 1505–1450, 1270, 1240 (C–O–C), 1020 (N–O), 700, 650 (C–Br), 555. UV–Vis (in DMSO) λ_{max}, nm (ε, $dm^3\ mol^{-1}\ cm^{-1}$): 350 (1550) (sh), 305 (4670).

2.3.4. (LH_3)$_2$ Fe (**7**)

To a solution of **3** (0.160 g 0.250 mmol) in 20.0 cm^3 THF, with stirring, $Fe(NO_3)_2 \cdot 9H_2O$ solution (0.041 g, 0.12 mmol in 20.0 cm^3 THF) was slowly added at r.t. When the mixture was neutralized by adding $(C_2H_5)_3N$ and heated for 2 h at 60 °C, the precipitation was completed. The reaction mixture was brought to r.t., then the product was filtrated, washed with water and ethanol and then dried in vacuo. This compound is soluble in DMF, DMSO and slightly in pyridine.

Yield: 0.0540 g (31.7%); m.p. > 200 °C. IR (KBr, cm^{-1}) ν: 3420 (NH), 3060, 3030 (Ar-H), 2930, 2840 (Aliph-H), 1700 (H–O...H), 1630 (CN), 1590 (w), 1515–1440, 1250 (C–O–C), 1020 (N–O), 680, 660 (C–Br), 550. UV–Vis (in DMSO) λ_{max}, nm (ε, $dm^3\ mol^{-1}$

cm^{-1}): 319 (1460), 307 (9100). MS (positive FAB, solution in DMSO): 1362.5 (7%) [M^+].

2.4. Binuclear uranyl complex: $(LH)_2(UO_2)_2(NO_3)\cdot 6(OH)_2$ (**8**)

To a solution of **3** (0.160 g, 0.250 mmol in 20.0 cm^3 THF), a solution of $UO_2(NO_3)_2\cdot 6H_2O$ (0.172 g, 0.0980 mmol) in 10.0 cm^3 THF was slowly added with stirring. The pH of the mixture was adjusted to about 7.0 by adding $(C_2H_5)_3N$. The mixture was heated for 3 h at 60 °C, then it was brought to r.t. and the crystalline complex precipitated completely. The product was filtered, washed with water, ethanol and diethylether and dried in vacuo. Yield: 0.070 g (29.8%). m.p. > 200 °C. The binuclear uranyl complex is soluble in DMF and DMSO. IR (KBr, cm^{-1}): $\nu = 3370$ (N–H), 3250 (–OH), 3060, 3040 (Ar-H), 2930–2840 (CH-Aliph), 1630 (C=N), 1500–1450 (Ar-Skel.), 1260, (Ar-O–C), 1000 (N–O), 900 (O=U=O), 700, 640 (C–Br), 540. ^{1}H NMR (250 MHz, DMSO-d_6) δ:10.90 (s, 1H, N–OH, D-exchangeable), 10.45 (s, 1H, N–OH, D-exchangeable), 8.50 (s, weak, 2H, –NH, D-exchangeable), 8.30 (s, 2H, –NH, D-exchangeable), 7.60 (s, 2H, Ar-H), 7.53 (d, $^3J = 7.8$ Hz, 4H, Ar-H3), 7.45 (dt, $^3J = 7.5$ Hz, $^4J = 1.7$ Hz, 4H, Phenyl-H5), 7.08 (dt, $^3J = 7.8$ Hz, $^4J = 1.7$ Hz, 4H, Phenyl-H4), 6.73 (d, $^3J = 7.2$ Hz, 4H, Phenyl-H6), 4.28 (t, $^3J = 12.0$ Hz, 8H, O–CH_2CH_2), 2.86 (t, $^3J = 12.0$ Hz, 8H, S–CH_2CH_2). UV–Vis (in DMSO) λ_{max}, nm (ε, dm^3 mol^{-1} cm^{-1}): 405 (sh), (4350), 321(8900), 303 (11 300).

2.5. Trinuclear complexes $(LH)_2Ni_3$ (**9**) and $(LH)_2Cu_3$ (**10**)

Complex **4** (0.0500 g, 0.0360 mmol) was dissolved in 15.0 cm^3 of DMF with heating and stirring. A solution of $Ni(NO_3)_2\cdot 6H_2O$ (0.0160 g, 0.0540 mmol in 10 cm^3 of DMF) was added dropwise to the hot solution of **4** with stirring. After the mixture was stirred for 3 h at 40 °C, the pH of the solution decreased, so it was raised to 6.85 by the addition of triethylamine. After the solvent of the solution was removed under reduced pressure to nearly dryness, the precipitate was filtrated off, washed with ethanol and ether and finally dried in vacuo. This compound is slightly soluble in DMF, DMSO and pyridine.

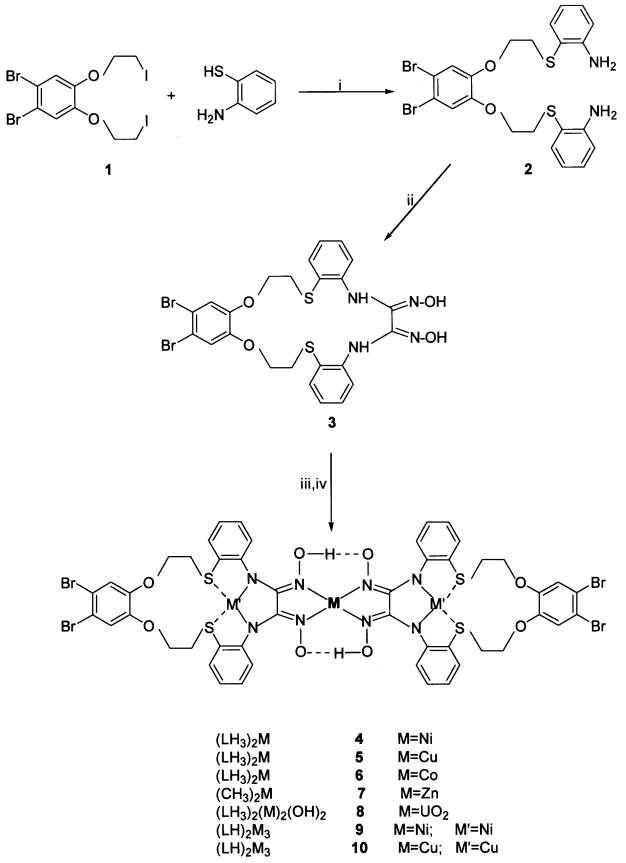
$(LH)_2Ni_3$ (**9**): Yield: 0.02 g (18.75%), m.p. > 200 °C. IR (KBr, cm^{-1})ν: 3040 (Ar-H), 2925–2850 (Aliph-H), 1700 (w, O–H–O), 1640 (C=N), 1510–1440 (Ar-skel.), 1250(C–O–C), 990(N–O), 660, 640 (C–Br), 540. UV–Vis (in DMSO) λ_{max}, nm (ε, dm^3 mol^{-1} cm^{-1}): 375 (1940), 310 (8820). MS (positive FAB, solution in DMSO):1479.0 (10%) [M^+].

The same procedure as described for the preparation of $(LH)_2Ni_3$ (**9**) starting from **5** (0.0490 g, 0.0360 mmol) and $Cu(NO_3)_2\cdot 6H_2O$ (0.0160 g, 0.0540 mmol) was used to prepare $(LH)_2Cu_3$ (**10**).

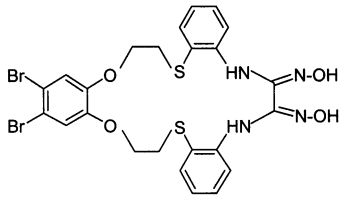
$(LH)_2Cu_3$ (**10**): Yield: 0.023 g (20.41%); m.p. > 200 °C. The complex is slightly soluble in DMF, DMSO and pyridine. IR (KBr, cm^{-1}): ν:3060, (Ar-H), 2925, 2870 (Aliph-H), 1705 (O–H...O), 1635, 1280, 1230 (Ar-O-Aliph, Aliph-O-Ar), 990 (N–O), 675, 650 (C–Br), 550. UV–Vis (in DMSO) λ_{max}, nm (ε, dm^3 mol^{-1} cm^{-1}): 390 (2400), 350 (6700), 302 (12 350). MS (positive FAB, solution in DMSO): 1493.7 (7%) [$M+1$]$^+$.

3. Results and discussion

The routes for the synthesis of **3** are given in Scheme 1. The first step is the synthesis of **2** starting from 2-aminothiophenol and 1,2-bis (2′-iodoethoxy)-4,5-dibromobenzene [35–38]. Compound **3**, shown in Fig. 1, was prepared by the reaction of **2** with dicyan di-*N*-oxide [33–35] which was prepared by treating a suspension of *anti*-dichloroglyoxime in CH_2Cl_2 with 1 N aqueous Na_2CO_3 at −20 °C.



Scheme 1. (i) 40% NaOH, EtOH (ii) Cyanogen di *N*-oxide, CH_2Cl_2, −40 °C; (iii) THF, $ML_2\,6H_2O$ (L = NO_3, M = Ni, Cu, Co, Fe, UO_2), Et_3N; (iv), dmf, $(LH_3)_2Ni$, $(LH_3)_2Cu$, $ML_2\,6H_2O$ (L = NO_3, M = Ni, Cu)Et_3N, 40 °C.

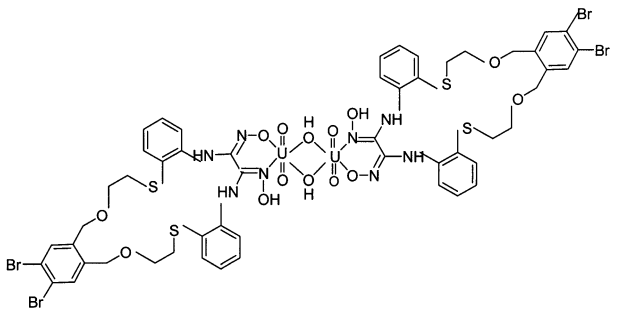


LH_4 (3)

Fig. 1. LH_4, **3**: diazadithiadioxa macrocycle.

The ligand **3** has two nitrogen, two oxygen, and two sulfur atoms in the macrocyclic ring, in addition to two oxime groups. Consequently, this *vic*-dioxime is capable of forming mono-, di- and tri-nuclear complexes [13,14,31]. While the mono and di-nuclear complexes have been synthesized from **3** with nitrates of Ni(II), Cu(II), Co(II), Fe(II) and UO_2(VI), tri-nuclear complexes have been obtained by using the relevant mononuclear complexes. Ni(II), Cu(II), Fe(II) and Co(II) mononuclear complexes have a metal:ligand ratio of 1:2 and the ligand is coordinated only by the *N*, *N*′ atoms of the *vic*-dioxime. The metal–ligand ratio was 2:2 in the dinuclear uranyl complex (**8**) having the N, O atoms of the *vic*-dioximes coordinating as shown in Fig. 2. The elemental analysis of **8** also indicated a metal:ligand ratio of 2:2. On the other hand, in trinucleating complexes (**9**, **10**), two metal ions are coordinated to the two aza and two sulfur atoms of each macrocycle, while the third metal ion is coordinated by the *N*, *N*′ atoms of each oxime group in the two ligand molecules with a ratio of 3:2. The colors and elemental analyses of **2**, **3** and the metal derivatives are listed in Table 1.

The $-NH_2$ stretching vibrations at 3460–3350 cm^{-1} and the aromatic C–Br bending vibration at 640 cm^{-1} are the most dominant ones showing the formation of **2** in the IR spectrum. In the IR spectrum of **3**, the OH stretching absorption is observed at 3220 cm^{-1} as a slightly broad band in addition to C=N, N–O and C–Br stretching absorptions at 1640, 1010 and 640 cm^{-1}, respectively. These values are in harmony with the



8 $(LH_3)_2(UO_2)_2(OH)_2$

Fig. 2. Binuclear uranyl complex: $(LH)_2(UO_2)_2(NO_3)\cdot 6(OH)_2$ **(8).**

previously reported diaminoglyoxime derivatives [15,20,31].

While weak (O–H...O) deformations of all mono- and tri-nuclear complexes are observed at around 1700 cm^{-1}, these vibrations are not involved in the IR spectra of the di-nuclear uranyl complex due to the coordination of the uranyl complex. Moreover, the vibration at 1000 cm^{-1} (N–O), 900 cm^{-1} (O=U=O) and 3370 cm^{-1} (N–H) are characteristics for **8** [15,20,31]. The –NH stretching vibrations at around 3410 and 3420 cm^{-1} observed for **4** and **5** have disappeared in the IR spectrum of **9** and **10** indicating the formation of these tri-nuclear complexes[31,40–42]. The aromatic, aliphatic, (C=N), (N–O) and (C–Br) stretching and bending vibrations of the $(LH)_2M_3$ complexes are very close to **4** and **5**. The S–C vibrations of the macrocycle in **4** and **5**, which appear as split bands at 695, 550 and 690, 560 cm^{-1}, shift to 660, 540 and 675, 550 cm^{-1}, respectively, in the IR spectra of **9** and **10** suggesting the bending of nickel or copper ions to the macrocycle sulfur atoms. The rest of the spectra of **9** and **10** are very similar to **4** and **5** with small differences in chemical shift. According to these data, in **9** and **10** the two Ni(II) or Cu(II) ions are coordinated to two aza and thia atoms of the each ligand, whereas the third Ni(II) or Cu(II) ion is coordinated by the *N*,*N*′-atoms in the complex.

In the ^{1}H NMR spectrum of **2**, the primary aromatic amine protons are observed at 5.38 ppm (s, br, 4H, NH_2, D-exchangeable) as a singlet, which is also easily identified by deuterium exchange. In addition to this resonance, there are triplets at 4.01 and 2.89 ppm, which correspond to the methylene protons. In the ^{1}H NMR spectrum of **3**, a singlet, which belongs to the NH_2 protons in **2,** disappears upon macrocyclization of **2** with cyanogens di N-oxide and a new chemical shift at 8.65 ppm is observed which can be assigned to –NH protons in the neighbourhood of the oxime groups. The deuterium-exchangeable protons of the –N–OH groups show a chemical shift at 10.72 ppm as a singlet indicating the amphi form for the oxime groups [18,23,28,29]. The signals belonging to the aromatic and methylene protons in **3** are observed at 7.48, 7.23, 7.04, 6.73, 6.50 and 4.24, 3.01 ppm, respectively. These signals indicate the (E, E) structure of the *vic*-dioxime (Scheme 1). The singlets, which belong to NH and OH, disappear after addition of D_2O. The chemical shifts of the aromatic and methylene protons of **3** are in accord with those of the macrocyclic compounds given in references [15,20,31]. The ^{1}H NMR spectrum of the diamagnetic complex **4** in DMSO-d_6 shows the disappearance of –OH at $\delta = 10.72$ ppm belonging to the neighboring oxime group. The existence of intra-molecular H-bridge protons is observed by a new signal at lower field, $\delta = 16.70$ ppm, in addition to NH protons at 8.64 ppm very near to oxime group. NH protons and

Table 1
Elemental analysis data for LH_4 and its mono-, di- and tri- complexes

Compounds	Color	Calc. (Found)%			
		C	H	N	M′
2	Yellow–brown	46.32 (46.23)	3.86 (3.78)	4.91 (4.77)	
LH_4 (**3**)	Light–yellow	44.04 (43.90)	3.36 (3.25)	8.56 (8.19)	
$(LH_3)_2Ni$ (**4**)	Reddish–brown	42.20 (41.96)	3.08 (3.10)	8.21 (8.02)	4.30 (4.28)
$(LH_3)_2Cu$ (**5**)	Brown–black	42.06 (41.93)	3.07 (3.00)	8.18 (7.87)	4.64 (4.55)
$(LH_3)_2Fe$ (**6**)	Dark–brown	42.29 (41.96)	3.08 (3.04)	8.22 (7.89)	4.11 (4.01)
$(LH_3)_2Co$ (**7**)	Dark–brown	42.16 (41.95)	3.07 (3.08)	8.19 (7.75)	4.31 (4.24)
$(LH_3)_2(UO_2)_2(OH)_2$ (**8**)	Orange	30.63 (30.11)	2.34 (2.33)	5.96 (5.87)	
$(LH)_2Ni_3$ (**9**)	Dark–brown	38.99 (38.43)	2.57 (2.50)	7.58 (7.23)	11.98 (11.66)
$(LH)_2Cu_3$ (**10**)	Black	38.59 (38.22)	2.54 (2.45)	7.50 (7.17)	12.76 (12.51)

Required values are given in parentheses.

intra-molecular binding H–O. . .H protons in **4** observed at 8.64 and 16.70 ppm disappear after addition of the D_2O. The signals for methylene protons in **4** are similar with those of **3** with small differences. As expected for a d_8 configuration in a square-planar field, **4** is diamagnetic, as confirmed by the NMR spectrum. The NMR spectrum of the complex contains two peaks for N–OH protons at 10.90 and 10.45 ppm, and peaks for NH protons at 8.50 and 8.30 ppm, which can be attributed to the magnetic anisotropy of the uranyl ion, as discussed in relation to some carboxylate and amine complexes in previous works in the Bekaroğlu group [15,20,31]. It is known that uranyl ions enhance the chemical shift difference between non-equivalent protons [15,31,41,42].

The mass spectra of **2** and **3** (EI electron impact technique) show the molecular ion peaks at $m/z = 570.2$ $[M^+]$ and $m/z = 655[M^+ + 1]$ (Fig. 1) which confirm the proposed structure and obey the rules of amino and oxime compounds formed in addition to major fragments. The mass spectrometry studies by the FAB (*p*-nitrobenzylalcohol) technique on the newly synthesized metal complexes (**4**, **5**, **7**, **9** and **10**) gave molecular ion species for metal complexes. The masses of the parent molecular ions show good agreement with the calculated values for **4** ($[M^+]$ m/z:1365), **5** ($[M^+ + 1]$ m/z:1370.5), **7** ($[M^+]$ m/z:1362.5), **9** ($[M^+]$ m/z:1479) and **10** ($[M+1]^+$ m/z:1493.7) as well as various fragments with good intensities formed from these parent ions.

The UV–Vis spectral data of **3** exhibited the characteristic n–π^* absorption of the oxime group. The weak d–d transitions of all complexes could not be observed, so they do not identify the complexes. In the electronic spectrum of **8**, a strong absorption at around 400 nm, which is assigned to a charge transfer from the π orbitals of the donor atoms to the 5f and 6d orbitals of uranium, appears as reported previously for similar compounds [19,31]. The IR spectrum of **8** is also consistent with the di-nuclear structure. A strong band around 900 cm^{-1} is characteristic of ν(O=U=O) vibrations. In the UV–Vis spectra of **9**, charge-transfer bands and characteristic $n \rightarrow \pi^*$ transitions due to (C=N) groups are also observed.

The electrochemical properties of **4**–**8** were investigated using voltammetric techniques and the results are summarized in Table 2. The number of electrons transferred was determined by the CPC technique and indicated that all electron transfer processes involved one-electron except for the two-electron R-II peak of **4**.

In the CV measurements, upon scanning cathodically **4** displayed two reduction peaks at −0.350 and −1.50 V versus SCE without the corresponding anodic waves on the reverse scan (Fig. 3). The R-I peak is assigned to Ni(II)/Ni(I) processes while R-II is due to the oxime moieties, because in highly polar solvent. DMSO polarization of the hydroxy groups of the oxime moieties occurs and this causes an increase in the negative charge in the coordinated oxime moieties. Thus the ligand-based reduction in **4** occurs at more negative potentials. The variation of the R-I peak potential with scan rate ($E_p/\log v = 0.052$ V) suggests that the charge transfer step is not totally irreversible. The absence of the anodic signal should be indicative of a fast chemical reaction following the charge transfer step and instability of the electrochemically generated Ni(I) species. The oxime reduction peak is totally irreversible with the absence of an anodic wave and considerably high $E_p/\log v$ value (0.143 V). The cyclic voltammetry of the Ni(II) complex also showed an anodic redox couple, which describes a net one-electron oxidation and is clearly attributable to Ni(II)/Ni(III). The peak separation (ΔE_p) of this couple is 0.068 V at 0.010 V s^{-1} and increases with scan rate, but remains in the usual range for quasi-reversible systems ($\Delta E_p =$ 0.250 mV at 1.0 V s^{-1}). The approximately unit value of the cathodic to anodic peak current ratio ($i_{p,c}/i_{p,a}$) for this couple within the range of 0.010–1.000 V s^{-1} scan rates indicates the absence of subsequent chemical reactions and stability of the electrochemically generated Ni(III) species (Fig. 4).

Table 2
Cyclic voltammetric parameters of complexes versus SCE

Complexes	$E_{1/2}$ (V) [a]			$\partial E_p/\partial \log v$ (V) [b]			ΔE_p (V) [c]		
	R-I	R-II	O-I	R-I	R-II	O-I	R-I	R-II	O-I
$(LH_3)_2Ni$ (**4**)	−0.350	−1.500	0.885	0.052	0.140	0.054			0.068
$(LH_3)_2Cu$ (**5**)	−0.867		0.200	0.143		0.037			0.057
$(LH_3)_2Fe$ (**6**)	−0.990		0.235	0.054		0.030	0.061		0.080
$(LH_3)_2Co$ (**7**)	−1.088		0.125	0.075		0.044			0.061
$(LH_3)_2(UO_2)_2(OH)_2$ (**8**)	−0.750			0.045			0.065		

[a] $E_{1/2} = (E_{pa} + E_{pc})/2$ for redox couple; E_{pc} for irreversible peaks at 0.010 V s^{-1} scan rate.
[b] E_{pc} for reduction, E_{pa} for oxidation.
[c] $\Delta E_p = E_{pa} - E_{pc}$ at 0.010 V s^{-1} scan rate.

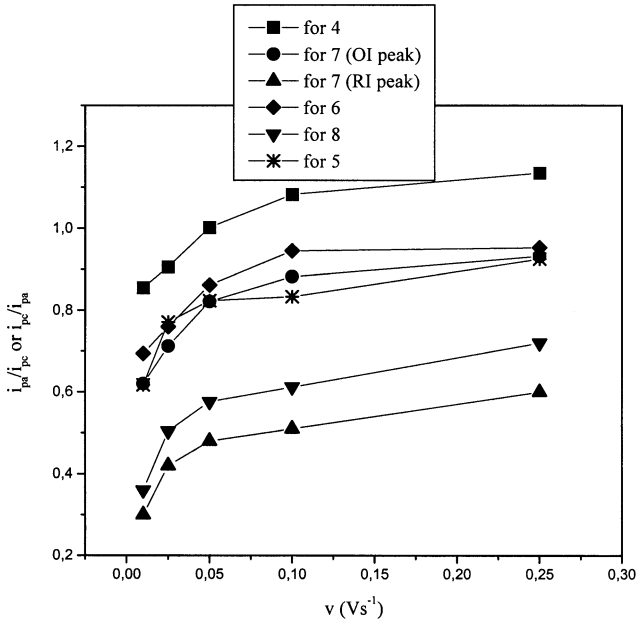


Fig. 4. Graph of peak current ratio ($i_{p,a}/i_{p,c}$ for reduction, $i_{p,c}/i_{p,a}$ for oxidation) vs. scan rate (v) for the redox couples of all complexes.

Fig. 5 represents the cyclic voltammograms of complex **6.** As shown in Fig. 5, a reduction and an oxidation couple were recorded. Analysis of the reduction peak indicated that it has a reversible peak character at very low scan rates ($\Delta E_p = 0.061$ V at 0.010 V s^{-1} scan rate) and approaches quasi-reversible behaviors with increasing scan rate. The $i_{p,a}/i_{p,c}$ values at slow scan rates are slightly lower than unity but increase towards unity with increasing scan rates. This is a characteristic response of a slow chemical reaction succeeding the electron transfer reaction [43]. The oxidation peak of **6** also has a quasi-reversible character with an ΔE_p value of 0.080 mV at 0.010 V s^{-1} scan rate and it approaches to an irreversible case at higher scan rates. Variation of $i_{p,c}/i_{p,a}$ with scan rate indicated the existence of an irreversible chemical reaction following $O-I$ electron transfer reaction of **6**.

As shown in Fig. 6, **7** gave a one-electron reduction peak without the corresponding anodic signal during the reverse scan. The absence of an anodic signal even at very high scan rates is attributed to the instability of the Co(I) species and fast chemical reaction succeeding the

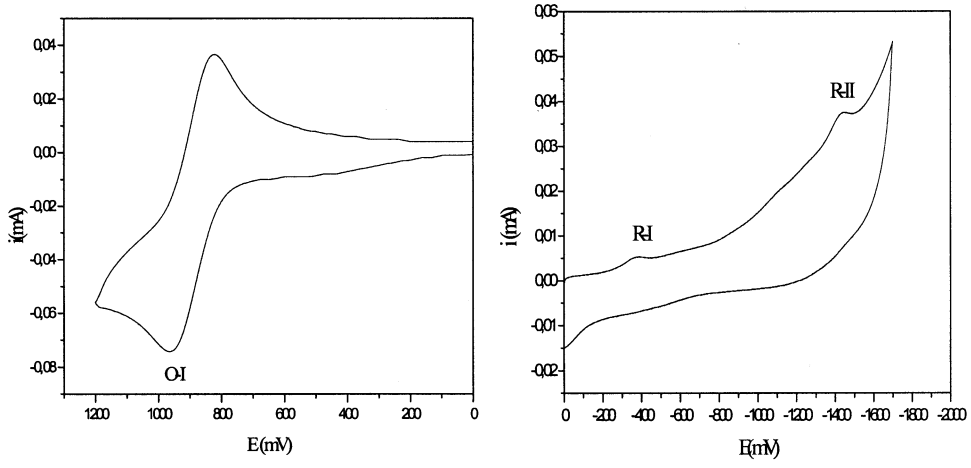


Fig. 3. Cyclic voltammogram of 1.0×10^{-4} M of **4** in DMSO/(0.1 M TBAP) at 0.100 V s^{-1} scan rate.

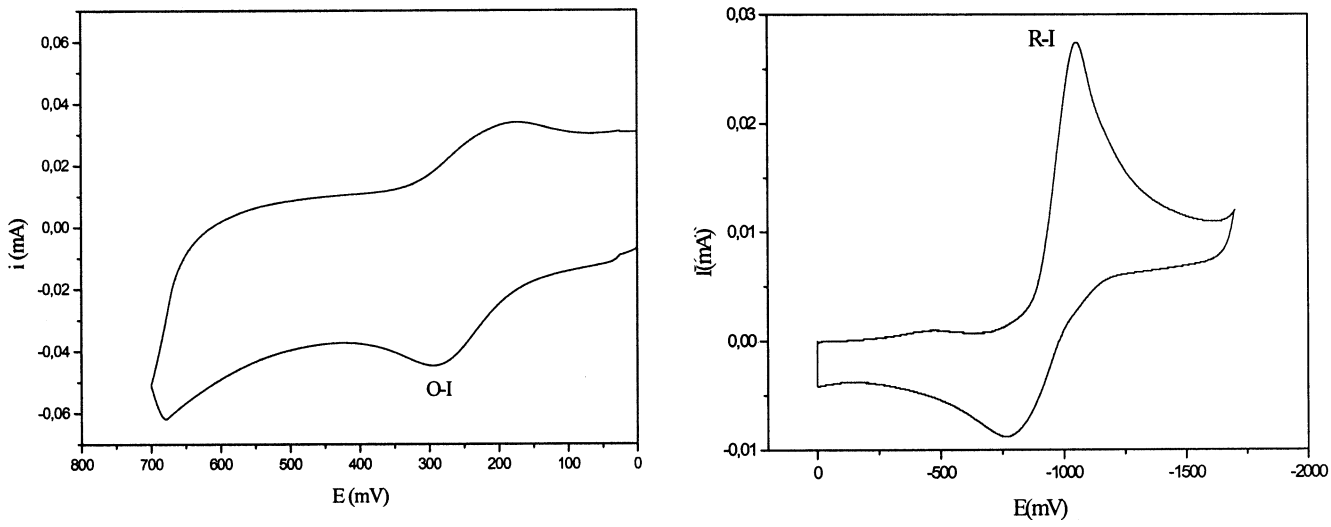


Fig. 5. Cyclic voltammogram of 1.0×10^{-4} M of **7** in DMSO/(0.1 M TBAP) at 0.100 V s^{-1} scan rate.

electrochemical reaction. The slope of $E_{p,c}$ versus log v (0.075 V) indicates the quasi-reversible character of this couple. **7** also displayed a one-electron oxidation couple, which corresponds to the Co(II)/Co(III) couple. The peak separation value of this couple is 0.061 V at 0.010 V $s^{-1}$and increases with scan rate. This behavior shows that the heterogeneous electron transfer rate is relatively slow, so that ΔE_p varies with scan rate slowly. Variation of the $i_{p,c}/i_{p,a}$ ratio with scan rate for oxidation of the Co(II) complex is also presented in Fig. 4. The shape of the curve obtained for this couple signals the existence of slow chemical reaction succeeding electrochemical reaction.

Compound **5** showed a one-electron oxidation peak with the corresponding signal during the return scan (Fig. 7). This peak corresponds to the Cu(II)/Cu(III) couple. The peak separation of this couple is approximately 0.057 V at 0.010 mV s^{-1} and changes very slowly with scan rate. This indicates the reversible characters of the redox couple. As shown in Fig. 4, the $i_{p,c}/i_{p,a}$ value indicated that this redox couple was followed by a chemical reaction. Compound **5** also gave a reduction peak without a corresponding anodic wave. The slope of $E_{p,a}$ versus log v for this peak is around 0.140 V, which indicates the irreversible nature of the peak.

Over the scan width of the voltammograms there was only one pair of peaks for **8** (Fig. 8), which can be assigned to UO_2(II)/UO_2(I). Peak separation of this couple is approximately 0.065 V at 0.010 mV s^{-1} and changes slowly with scan rate, indicating the quasi-reversible character of the redox couple. The deviation of $i_{p,a}/i_{p,c}$ from unity and the increase in this ratio with scan rate should be a consequence of the fact that the charge transfer processes for **8** is followed by slow

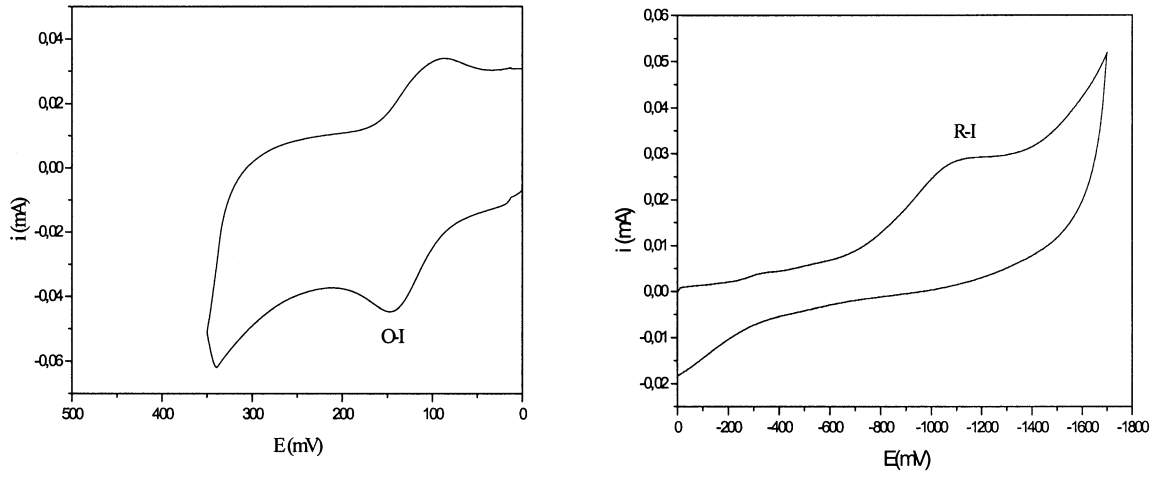


Fig. 6. Cyclic voltammogram of 1.0×10^{-4} M of **6** in DMSO/(0.1 M TBAP) at 0.100 V s^{-1} scan rate.

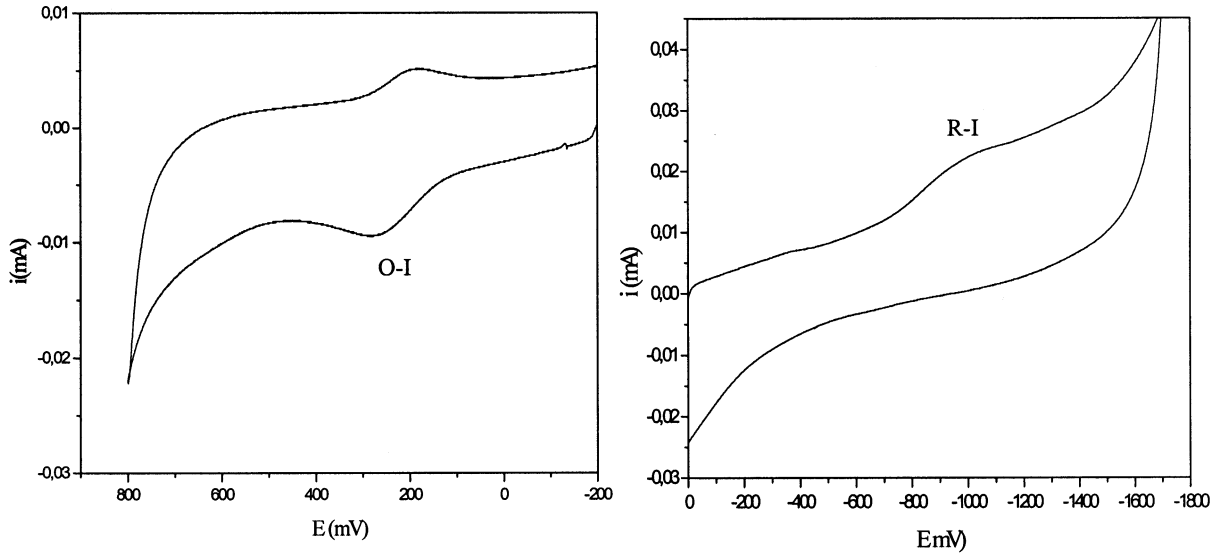


Fig. 7. Cyclic voltammogram of 1.0×10^{-4} M of **5** in DMSO/(0.1 M TBAP) at 0.100 V s^{-1} scan rate.

chemical reactions. Before and during the reverse scan electrochemically generated $U(V)O_2$ species around the electrode surface should decompose slowly.

4. Conclusion

In the present work, we have prepared and characterized a new oxime ligand in which a higher member macrocycle has been peripherally substituted. The synthesis of new hexadentate '$N_2S_2O_2$' macrocyclic oxime ligands is significant in that they provide coordination not only within but also outside the macrocycles. Therefore, complexations of both the oxime groups and the cavities of the macrocycle with transition metals, exhibiting two electron-rich centers were achieved. Mononuclear complexes have a metal:ligand ratio of 1:2 and the ligand is coordinated only by the *N*, *N′* atoms of the *vic*-dioxime. In contrast to the mononuclear complexes, in trinuclear complexes, two metal ions are coordinated to the two aza and two sulfur atoms of each macrocycle, while the third metal ion is coordinated by the *N*, *N′* atoms of each oxime group in the two ligand molecules.

This work clearly shows the prediction of the binding sites' reactivity of oximes and macrocycles and frames synthetic strategies for the preparation of interesting mixed ligand complexes. The goal of increasing electron density at the center of the macrocyles by replacing O by S donors in hexadentate diazadithiadioxa oxime ligand could be reached. This donor replacing process also increased the reactivity of complexation of the macrocyles ligand with a relatively high acidic aromatic NH near the oxime group in trinuclear complexes.

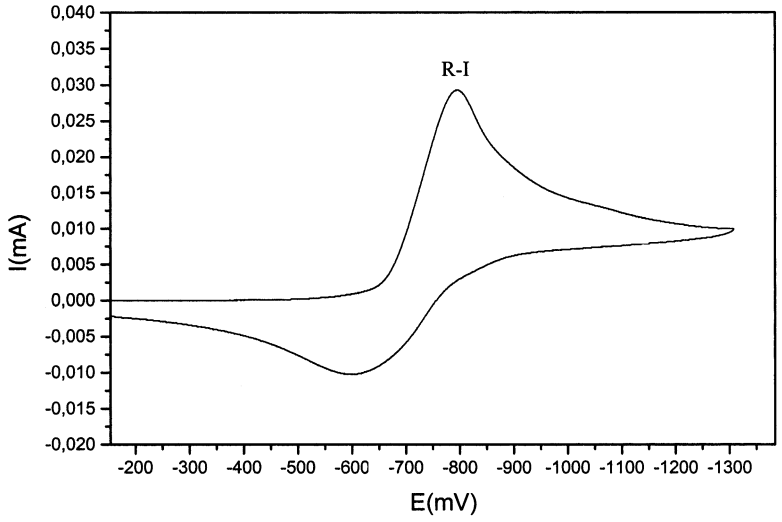


Fig. 8. Cyclic voltammogram of 1.0×10^{-4} M of **8** in DMSO/(0.1 M TBAP) at 0.100 V s^{-1} scan rate.

Voltammetric results obtained in this study showed that oxime-containing ligands stabilize Ni(III), Fe(III), Co(III) and Cu(III) since the oxidation peaks with the corresponding cathodic signals were observed for the complexes of these metals. Higher oxidation states of the complexes appeared to be accessible in systems with oximato-nitrogen donors, probably as a results of the coulombic influence of the negative charge on the HOMO [44] and of σ-donation effects [40]. Compound **7** displayed a different behavior with respect to other complexes. A reduction peak with the corresponding signal during the return scan was observed only with **7**. This indicated that both Fe(III) and Fe(I) species are stable while oxime containing ligands tend to stabilize only one of the oxidized forms of the metal center of the complexes. The stabilization of both M(I) and M(III) by the same ligand is quite uncommon. It is generally observed that a larger number of imino oxime nitrogen donors stabilize the formation of Ni(III), Fe(III), Co(III) and Cu(III) whereas thioether containing groups may stabilize Fe(I). Thus, the observed data showed that π-acceptor capability of the ligand is dominant with iron and stabilizes Fe(I) species.

Ligand based reduction was recorded with only the Ni(II) complex. In oxime containing complexes metal to ligand charge-transfer (MLCT), d(metal) to π*(N–N) and ligand to metal charge transfer (LMCT) transitions in **4** shift to less energy compared with the other complexes [45]. Metal–ligand interactions and coordination of the complexes affect the charge transfer properties of the ligand and metal. Thus both reduction and oxidation processes were recorded at a more positive potential. As a result of this, ligand based reduction was observed at the end of the solvent window (−1.50 V).

Acknowledgements

We thank the Research Fund of Sakarya University and Technical University of Istanbul for financial support.

References

[1] (a) G.A. Melson, Co-ordination Chemistry of Macrocyclic Compounds (Ch. 2), Plenum Press, New York, 1979;
(b) J.J. Christensen, J.J. Eatough, R.M. Izatt, Chem. Rev. 74 (1974) 351.
[2] J.R. Dilworth, S.J. Parrott, Chem. Soc. Rev. 27 (1998) 43.
[3] P.J. Blower, Transition Met. Chem. (Weinheim) 23 (1998) 109.
[4] S.S. Jurisson, J.D. Lydon, Chem. Rev. 99 (1999) 2205.
[5] W.A. Wolkert, T.J. Hoffman, Chem. Rev. 99 (1999) 2269.
[6] K. Ohta, R. Higashi, M. Ikejima, I. Yamamoto, N. Kobayashi, J. Mater. Chem. 8 (1998) 1979.
[7] P. Mitchell, Science 206 (1979) 1148.
[8] B.G. Malmstrom, Acc. Chem. Res. 26 (1993) 332.
[9] M.C.M. Laranleira, R.A. Marusak, A.G. Lappin, Inorg. Chim. Acta 186 (2000) 300.
[10] M. Bakir, J. Electroanal. Chem. 466 (1999) 60.
[11] M. Bakir, J.A.M. McKenzie, J. Electroanal. Chem. 425 (1997) 621.
[12] M. Bakir, J.A.M. McKenzie, J. Chem. Soc., Dalton Trans. (1997) 3571.
[13] S. Kurse, S. Motomizu, K. Toei, Anal. Chim. Acta 70 (1974) 65.
[14] D. Dolphin, B12, vol. 1 and 2, Wiley, New York, 1982.
[15] A. Gül, Ö. Bekaroğlu, J. Chem. Soc., Dalton Trans. (1983) 2537.
[16] E.C. Constable, C. Sacht, G. Pato, D.A. Tocher, M.R. Truter, J. Chem. Soc., Dalton. Trans. (1993) 1307.
[17] M. Kandaz, Ö. Bekaroğlu, Chem. Ber. 130 (1997) 1833.
[18] I. Yilmaz, Ö. Bekaroğlu, Chem. Ber. 129 (1996) 967.
[19] M. Kandaz, I. Yilmaz, S.Z. Coruhlu, A.R. Özkaya, Transition Met. Chem., in press.
[20] A. Gül, A.I. Okur, A. Cihan, N. Tan, Ö. Bekaroğlu, Synth. React. Inorg. Met-Org. Chem. 16 (1986) 971.
[21] A. Chakravorty, Coord. Chem. Rev. 13 (1974) 12.
[22] M. Kandaz, Ö. Bekaroğlu, J. Porphyrins Phthalocyanines 3 (1999) 339.
[23] M. Kandaz, I. Yilmaz, Ö. Bekaroğlu, Polyhedron 19 (2000) 115.
[24] A.R. Özkaya, A.I. Okur, A. Gül, Ö. Bekaroğlu, J. Coord. Chem. 33 (1994) 311.
[25] A.R. Özkaya, E. Musluoglu, A. Gül, Ö. Bekaroğlu, J. Chem. Res. 450(S) (1995) 2721(M).
[26] A.R. Özkaya, A. Gürek, A. Gül, Ö. Bekaroğlu, Polyhedron 16 (1997) 1877.
[27] A.R. Özkaya, I. Yilmaz, Ö. Bekaroğlu, J. Porphyrins Phthalocyanines 2 (1998) 483.
[28] A.R. Özkaya, E. Hamuryudan, Z. Altuntaş Bayır, Ö. Bekaroğlu, J. Porphyrins Phthalocyanines 4 (2000) 689.
[29] G.N. Schrauzer, J. Kohnle, Chem. Ber. 97 (1964) 3056.
[30] M. Ertaş, V. Ahsen, A. Gul, Ö. Bekaroğlu, J. Organomet. Chem. 335 (1987) 105.
[31] E. Hamuryudan, Ö. Bekaroğlu, Chem. Ber. 127 (1994) 2483.
[32] P.S. Reddy, K.H. Reddy, Polyhedron 19 (2000) 1687.
[33] M.J. Prushan, A.W. Addison, R.J. Butcher, Inorg. Chim. Acta 300-302 (2000) 992.
[34] A.J. Román, J.M. Sevilla, T. Pineda, M. Blázquez, J. Electroanal. Chem. 1-6 (2000) 485.
[35] D. Landin, F. Montanari, F. Rolla, Synthesis (1978) 223.
[36] O.A. Gansow, A.R. Kansar, B. Triplett, J. Heterocyclic Chem. 18 (1981) 297.
[37] F. Cornelus, V. Nostrum, S.J. Picken, A. Jan Schuten, R.J.M. Nolte, J. Am. Chem. Soc. 117 (1995) 9957.
[38] J. Martin, J. Dale, Acta Chem. Scand. 36 (1982) 241.
[39] G. Panzio, F. Baldrocca, Gazz. Chim. Ital. 60 (1930) 415.
[40] H. Brintzinger, R. Titman, Chem. Ber. 85 (1952) 344.
[41] A. Gül, A.I. Okur, A. Cihan, N. Tan, Ö. Bekaroğlu., J. Chem. Res. (S) (1986) 90–91; T(M) (1986) 881.
[42] I. Gürol, V. Ahsen, Ö. Bekaroglu, J. Chem. Soc., Dalton Trans. (1992) 2283.
[43] M. Kandaz, A.R. Özkaya, Ö. Bekaroğlu, Monatsh. Chem. 132 (2001) 1013.
[44] K.K. Nanda, A.W. Addison, N. Paterson, E. Sinn, L.K. Thompson, U. Sakuguchi, Inorg. Chem. 37 (1988) 1028.
[45] A.N. Singh, R.P. Singh, J.G. Mohanty, A. Chakravorty, Inorg. Chem. 16 (1997) 2597.

PERGAMON

Polyhedron 21 (2002) 835–841

POLYHEDRON

www.elsevier.com/locate/poly

Preparation, crystal structures and spectroscopic properties of chloro(pentane-2,4-dionato){1,1,1-tris(dimethylphosphinomethyl)ethane}chromium(III), –cobalt(III) and –rhodium(III) hexafluorophosphate: comparison of the M–P, M–Cl and M–O (M = Cr, Co and Rh) bond lengths among the three M^{III} complexes

Takayoshi Suzuki [a,*], Takeshi Imamura [a], Sumio Kaizaki [a], Kazuo Kashiwabara [b]

[a] *Department of Chemistry, Graduate School of Science, Osaka University, Toyonaka 560-0043, Japan*
[b] *Department of Chemistry, Graduate School of Science, Nagoya University, Chikusa, Nagoya 464-8602, Japan*

Received 5 September 2001; accepted 8 January 2002

Abstract

Three metal(III)-tripodal tridentate phosphine complexes of the formula $[MCl(acac)(tdmme)]PF_6$, where M = Cr, Co or Rh; acac = pentane-2,4-dionate; tdmme = 1,1,1-tris(dimethylphosphinomethyl)ethane, were prepared and their molecular and crystal structures and spectroscopic properties examined. All the complexes crystallized in an isomorphous space group $P2_12_12_1$, which is indicative of spontaneous resolution of the enantiomeric pair. The Cr–P bond lengths in $[CrCl(acac)(tdmme)]PF_6$ (average 2.437 Å) are remarkably longer than the corresponding Co–P (average 2.201 Å) and Rh–P (average 2.252 Å) ones. The longer and therefore the weaker Cr–P bonds may explain the relatively weak *trans* influence of the $-PMe_2$ group in $[CrCl(acac)(tdmme)]PF_6$; among the three M^{III} complexes, the elongation of M–O bond lengths in $[MCl(acac)(tdmme)]PF_6$ from those in $[M(acac)_3]$ has been found to be Cr^{III} (0.016 Å) < Co^{III} (0.059 Å) < Rh^{III} (0.096 Å), indicating a much weaker *trans* influence of the $-PMe_2$ group in the Cr^{III} complex than in the Co^{III} and Rh^{III} complexes. The first d–d transition band of $[CrCl(acac)(tdmme)]^+$ was observed at 18590 cm^{-1}. This is appreciably smaller than the corresponding band of the Co^{III} complex at 20960 cm^{-1}, suggesting the ligand-field strength of tdmme is fairly weak in the Cr^{III} complex. The ligand-field strength Δ and the Racah's *B* parameters of $[CrCl(acac)(tdmme)]^+$ were also discussed. © 2002 Elsevier Science Ltd. All rights reserved.

Keywords: *Trans* influence; Crystal structures; Ligand-field strength; Tripodal tridentate phosphine; Acetylacetonate complexes; Chromium(III) complexes

1. Introduction

We have prepared various complexes of 1,1,1-tris(dimethylphosphinomethyl)ethane (tdmme) with cobalt(II or III), rhodium(III), iron(II), molybdenum(0), tungsten(0) and chromium(0 or III) [1–8]. Compared with a large number of metal complexes of 1,1,1-tris(diphenylphosphinomethyl)ethane (tdpme) [9], which is commercially available, tdmme has been used much less frequently to prepare its metal complexes [10–12], probably, because of the difficulty in synthesizing tdmme [13]. In particular, chromium(III)–tdmme complexes are rather rare [8,10,11], which is mainly due to the inherently weak coordinate bonds between Cr^{III}, a typical hard Lewis acid, and phosphines, typical soft Lewis bases, in addition to the above-mentioned difficulty. However, it is interesting to examine tdmme metal complexes more extensively since tdmme has the following advantages over tdpme in preparing various mixed-ligand complexes: (1) a lesser steric requirement around a central metal ion to incorporate with a larger ligand; (2) a higher electron density on the P atom to give a stronger σ-donicity and *trans* influence making the

* Corresponding author. Tel.: +81-6-6850-5410; fax: +81-6-6850-5408.
E-mail address: suzuki@chem.sci.osaka-u.ac.jp (T. Suzuki).

0277-5387/02/$ - see front matter © 2002 Elsevier Science Ltd. All rights reserved.
PII: S0277-5387(02)00859-8

trans-positioned ligand labile; and (3) a higher solubility of the mixed-ligand complexes in polar organic solvents.

In our previous studies on cobalt(III) and rhodium(III)–phosphine complexes it has been shown that phosphine ligands, especially with dimethylphosphino donor groups, unequivocally exhibited a strong *trans* influence with significant elongation of the *trans*-positioned metal(Co^{III} or Rh^{III})–ligand bond [1,2,5,14,15]. For the chromium(III)–phosphine complexes, however, there has been no report mentioning that the phosphines induce the elongation of the *trans*-positioned Cr^{III}–ligand bond; e.g. there is no difference in the lengths between the Cr–Cl bonds *trans* to P and the mutually *trans* Cr–Cl ones in $(NPr^n_4)[CrCl_4(cis\text{-}Ph_2PCH{=}CHPPh_2)]$ [16] and *mer*-$[CrCl_3\{P(CH_2CH_2PPh_2)_3\text{-}\kappa^3P\}]$ [17]. For the better understanding of the specific interactions between Cr^{III} and phosphines, it seems essential to accumulate more examples of Cr^{III} complexes with phosphines containing dimethylphosphino donor groups which is expected to be a better σ-donor compared with the well studied diphenylphosphino ones as in tdpme.

In this study, we describe the preparation, structures and spectroscopic properties of the pentane-2,4-dionato (acac) complexes with the tdmme ligand, $[MCl(acac)(tdmme)]PF_6$ (M = Cr, Co or Rh), prepared by the ligand substitution reaction of $[MCl_3(tdmme)]$ by $acac^-$. Since it has been found that all three M^{III} complexes of $[MCl(acac)(tdmme)]PF_6$ crystallize in an isomorphous space group $P2_12_12_1$, likewise the series of $[M(acac)_3]$ complexes in $P2_1/c$ [18–20], these complexes are most suitable for a comparison of the *trans* influence of the $-PMe_2$ group by probing the M–O bond lengths.

2. Experimental

2.1. Materials and measurements

The complexes, $[MCl_3(tdmme)]$ (M = Cr [10], Co [1] and Rh [5]), were prepared by the literature methods. Lithium pentane-2,4-dionate and ammonium hexafluorophosphate were used as purchased from Aldrich Co. Ltd. and Wako Chemicals, respectively. All solvents (Wako reagent grade for preparation of complexes) were used without further purification. UV–Vis spectra in acetonitrile (DOTITE, spectrosol) were measured on a Perkin–Elmer Lambda 19 spectrophotometer at room temperature (r.t.). NMR spectra in acetonitrile-d_3 (Aldrich, 99.8 atom% D) were recorded on a JEOL EX-270 or GSX-400 spectrometer at 27 °C; chemical shifts are given in δ scale relative to TMS (^1H and ^{13}C) or 85% H_3PO_4 (^{31}P).

2.2. [CrCl(acac)(tdmme)]PF_6

To a methanol solution (100 cm^3) of $[CrCl_3(tdmme)]$ (522 mg, 1.27 mmol) was added Li(acac) (150 mg, 1.42 mmol) and the mixture was refluxed for 5 h. The red solution was cooled to r.t. and filtered. A methanol solution (10 cm^3) of NH_4PF_6 (221 mg, 1.53 mmol) was added to the filtrate and the mixture was allowed to stand in the open air for 2 days to evaporate the solvent slowly, depositing red purple columnar crystals. Yield: 379 mg (51%). *Anal*. Found: C, 32.6; H, 5.8. Calc. for $C_{16}H_{34}ClCrF_6O_2P_4$: C, 32.9; H, 5.9%. UV–Vis: 538 nm ($\varepsilon = 494$ dm^3 mol^{-1} cm^{-1}), 404 (358), 361^{sh} (2390), 338^{sh} (3960), 320 (5530), 256 (19300), 213^{sh} (17800).

2.3. [CoCl(acac)(tdmme)]PF_6 and its Rh^{III} analogue

To a suspension of $[CoCl_3(tdmme)]$ (1.00 g, 2.39 mmol) in methanol (25 cm^3) was added Li(acac) (254 mg, 2.40 mmol) with stirring, and the mixture was stirred for 1 h at r.t. The resulting red solution was evaporated to approximately 10 cm^3 under reduced pressure and a methanol solution (10 cm^3) of NH_4PF_6 (1.23 g, 7.55 mmol) was added to the concentrate to afford an orange red precipitate. The crude product was collected by filtration and recrystallized from CH_3CN–Et_2O, affording red columnar or prismatic crystals. Yield: 1.23 g (87%). *Anal*. Found: C, 32.7; H, 5.8. Calc. for $C_{16}H_{34}ClCoF_6O_2P_4$: C, 32.5; H, 5.8%. ^1H NMR (TMS): δ 1.263 (qr, $J = 3.0$ Hz, CCH_3 (tdmme), 3H); 1.346 (d, $J = 12.2$ Hz, PCH_3, 6H); 1.58–1.97 (m, PCH_3 and PCH_2C, 18H); 2.003(s, CCH_3 (acac), 6H); 5.487(s, =CH–, 1H). $^{13}C\{^1H\}$ NMR (TMS): δ 11.97(t, $J = 16$ Hz); 13.64(d, $J = 32$ Hz); 17.39(t, $J = 18$ Hz); 27.85(t, $J = 4$ Hz); 33.35(t, $J < 4$ Hz); 33.71(td, $J = 15$ and 5 Hz); 34.70(qr, $J = 11$ Hz); 38.85(s); 99.50(s); 188.91(s). UV–Vis: 646^{sh} nm ($\varepsilon = 3.5$ dm^3 mol^{-1} cm^{-1}), 477(1060), 333^{sh}(2700), 258(23600), 226(14200).

The Rh^{III} analogue, $[RhCl(acac)(tdmme)]PF_6$, was prepared similarly by mixing $[RhCl_3(tdmme)]$ and Li(acac). Colorless columnar crystals were obtained by recrystallization from CH_3CN–Et_2O. Yield: 92%. *Anal*. Found: C, 30.3; H, 5.4. Calc. for $C_{16}H_{34}ClF_6O_2P_4Rh$: C, 30.3; H, 5.4%. ^1H NMR (TMS): δ 1.291(qr, $J = 3.3$ Hz, CCH_3 (tdmme), 3H); 1.446(d, $J = 12.9$ Hz, PCH_3, 6H); 1.713(filled-in d, PCH_3, 6H); 1.79–1.85(m, PCH_3 and PCH_2C, 12H); 2.000(s, CCH_3(acac), 6H); 5.459(s, =CH–, 1H). $^{13}C\{^1H\}$ NMR (TMS): δ 12.08(t, $J = 18$ Hz); 13.60(d, $J = 37$ Hz); 16.77(t, $J = 21$ Hz); 28.28(t, $J = 4$ Hz); 32.94(t, $J < 4$ Hz); 33.56(td, $J = 20$ and 6 Hz); 35.21(qr, $J = 11$ Hz); 41.29(d, $J < 2$ Hz); 100.36(s); 188.37(s). $^{31}P\{^1H\}$ NMR (85% H_3PO_4): δ 22.50 (dd, $^1J_{Rh-P} = 102.6$ Hz, $^2J_{P-P} = 32.4$ Hz); 25.85(dt, $^1J_{Rh-P} = 104.9$ Hz). UV–Vis: 322 nm($\varepsilon = 4180$ dm^3 mol^{-1} cm^{-1}), 313(4070), 296^{sh}(3580), 218(37 500).

2.4. Crystal structure determination

The X-ray intensities were measured at 23(2) °C on a Rigaku AFC-7R four-circle diffractometer (graphite-monochromated Mo Kα radiation ($\lambda = 0.71073$ Å), the $2\theta-\omega$ scan mode, $2\theta_{max} = 60°$, three standard reflections monitored every 150 reflections with no serious decomposition ($\leq 0.18\%$)). Final lattice parameters were determined by the least-squares treatment using setting angles of 25 reflections in the range of $25° < 2\theta < 30°$. The intensities were corrected for Lp factors and for absorption effects either by the numerical integration method [21] or by an empirical method based on a set of Ψ-scans [22]. The space group was uniquely determined by systematic absences as $P2_12_12_1$. The structures were solved by the direct method using SHELXS86 program [23] and refined by SHELXL97 program [24] (on F^2, full-matrix, complex neutral-atom scattering factors, anisotropic thermal parameters for all non-H atoms, calculated H atoms with riding models). The absolute structures were determined by the Flack's method [25]. All calculations were carried out using a TEXSAN software package [26].

Crystallographic data are summarized in Table 1 and selected structural parameters are collected in Table 2. The perspective drawings of the complex cations in $[MCl(acac)(tdmme)]PF_6$ (M = Cr, Co and Rh) are shown in Fig. 1(a–c), respectively.

Table 2
Selected structural parameters (Å), (°)

M =	Cr	Co	Rh
Bond lengths			
M–Cl	2.316(2)	2.317(3)	2.430(2)
M–P(1)	2.439(2)	2.201(3)	2.258(2)
M–P(2)	2.436(1)	2.200(3)	2.249(2)
M–P(3)	2.436(2)	2.201(3)	2.249(2)
M–O(1)	1.954(4)	1.942(6)	2.078(4)
M–O(2)	1.977(4)	1.951(6)	2.097(4)
Bond angles			
P(1)–M–P(2)	84.09(5)	89.95(10)	89.26(6)
P(1)–M–P(3)	84.11(5)	89.88(10)	89.41(6)
P(2)–M–P(3)	84.51(5)	89.08(10)	88.84(6)
O(1)–M–O(2)	91.2(2)	93.7(3)	90.2(2)
P(1)–M–Cl	173.67(6)	174.6(1)	175.29(7)
P(2)–M–O(1)	173.1(1)	174.3(2)	176.3(2)
P(3)–M–O(2)	170.8(1)	176.3(2)	177.0(2)
Torsion angles			
M–P(1)–C(3)–C(2)	23.1(4)	−26.2(8)	−23.5(5)
M–P(2)–C(4)–C(2)	25.3(4)	−28.3(8)	−25.1(6)
M–P(3)–C(5)–C(2)	22.8(5)	−23.3(8)	−21.8(6)
ϕ [a]	4.8(1)	9.3(3)	5.8(2)
D [b]	0.124(2)	0.007(3)	0.002(2)

[a] Dihedral angle between the least-squares equatorial coordination plane [defined by P(2), P(3), O(1) and O(2)] and the mean acac plane [defined by O(1), O(2), C(13), C(14) and C(15)].

[b] Displacement of M atom from the least-squares equatorial coordination plane.

Table 1
Crystallographic data for $[MCl(acac)(tdmme)]PF_6$

M =	Cr	Co	Rh
Chemical formula	$C_{16}H_{34}ClCrO_2P_3 \cdot PF_6$	$C_{16}H_{34}ClCoO_2P_3 \cdot PF_6$	$C_{16}H_{34}ClO_2P_3Rh \cdot PF_6$
Colour and habit	red purple, column	red, prism	colorless, column
Crystal size (mm)	0.38 × 0.20 × 0.20	0.32 × 0.23 × 0.17	0.24 × 0.18 × 0.12
Crystal system	orthorhombic	orthorhombic	orthorhombic
Unit cell dimension			
a (Å)	15.882(5)	15.809(5)	15.796(3)
b (Å)	18.702(4)	18.361(4)	18.502(4)
c (Å)	8.767(2)	8.651(3)	8.717(2)
U (Å^3)	2604(1)	2511(1)	2547.6(9)
Space group	$P2_12_12_1$	$P2_12_12_1$	$P2_12_12_1$
Z	4	4	4
Number of reflection measured	4702	4525	4210
Number of independent reflection	4378	4213	4201
R_{int}	0.0187	0.0335	0.0191
Number of reflection observed [a]	2952	1884	3068
Transmission factors	0.816–0.857	0.710–0.829	0.824–0.877
Number of parameters	280	280	280
$R_1(F^2{:}F^2 > 2\sigma(F^2))$	0.046	0.051	0.040
$WR_2(F^2$: all data)	0.152	0.193	0.120
Weighting parameter, A, B [b]	0.0936, 0.0674	0.0975, 0.0	0.0623, 0.8406
Goodness-of-fit	1.042	1.003	1.033
Flack's parameter	0.02(4)	0.00(4)	−0.01(5)

[a] Cut-off criteria: $I > 2\sigma(I)$.

[b] $w^{-1} = \sigma^2(F_o^2) + (AP)^2 + BP$, where $P = (F_o^2 + 2F_c^2)/3$.

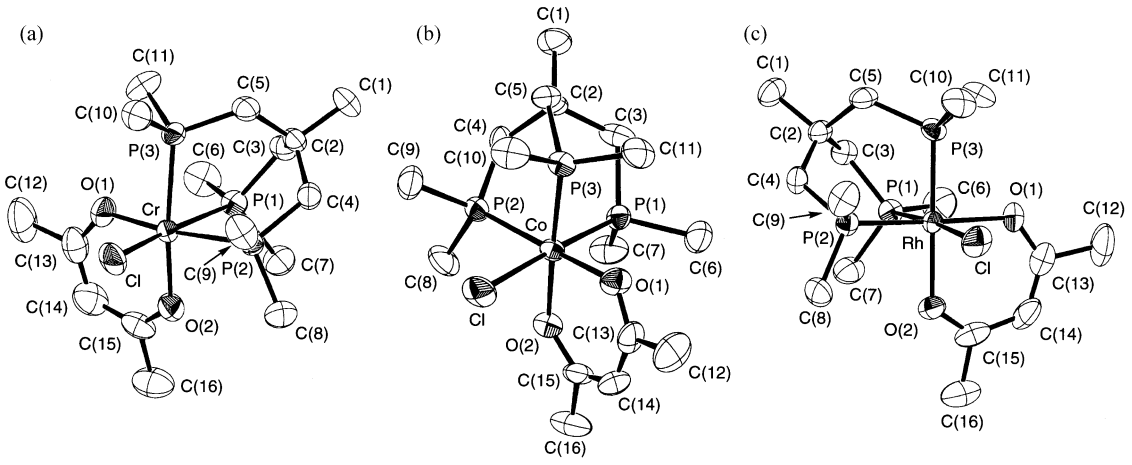


Fig. 1. Perspective drawings (50% probability level) of the cationic parts of $[MCl(acac)(tdmme)]PF_6$ {M = Cr (a), Co (b) and Rh (c)}. Hydrogen atoms are omitted for clarity.

3. Results and discussion

3.1. Preparation and chemical behaviors of $[MCl(acac)(tdmme)]PF_6$

The reaction of $[MCl_3(tdmme)]$ (M = Co or Rh) and Li(acac) in methanol proceeded smoothly to yield $[MCl(acac)(tdmme)]^+$, which was isolated as a PF_6^- salt in a nearly quantitative yield. However, a similar procedure afforded the corresponding Cr^{III} complex in merely a 50% yield. Such a low yield seems to be caused by the partial dissociation of tdmme from $[CrCl_3(tdmme)]$ in methanol; a characteristic odor of free phosphine was detected. However, once the acac complex is formed, it is stable in the solid state and in solution. As seen in the next section, the single-crystal X-ray analysis of $[CrCl(acac)(tdmme)]PF_6$ shows that the Cr–P bond lengths (average 2.437 Å) are shorter than those in $[CrCl_3(tdmme)]$ (average 2.456 Å [10]), indicating that the Cr–P bonds are stronger in the former complex.

The Co^{III} and Rh^{III} complexes of $[MCl(acac)(tdmme)]PF_6$ could be converted quantitatively into the acetonitrile complexes, $[M(acac)(tdmme)(CH_3CN)](PF_6)_2$, by a reaction with $AgPF_6$. The acetonitrile complexes thus produced were successfully used to prepare $[M(acac)(tdmme)L]^{2+}$-type complexes (L = pyridine or its derivatives) [3]. On the other hand, $[CrCl(acac)(tdmme)]PF_6$ did not give any characterizable products by the same procedures.

3.2. Crystal structures

The single-crystal X-ray analyses revealed that all the compounds of $[MCl(acac)(tdmme)]PF_6$ (M = Cr, Co and Rh) crystallize in an isomorphous space group $P2_12_12_1$, which is indicative of the spontaneous resolution of the enantiomeric pair. The complex cations $[MCl(acac)(tdmme)]^+$ are chiral owing to the synchronous twist of the three arms of tdmme (Fig. 2). The absolute structures of the complex cations analyzed in this study are assigned as Δ for the Cr and Λ for the Co and Rh complexes based on the twist of tdmme. The torsion angles of M–P(n)–C(2+n)–C(2) (n = 1, 2, 3) are in the range of ±21°–29° (+ for the Δ and − for the Λ isomers), which are comparable to those found in $[MCl_3(tdmme)]$ [2,5,10] or $[M(CN)_3(tdmme)]$ [2,8]. The acac plane (defined by O(1), O(2), C(13), C(14) and C(15)) is not strictly co-planar to the equatorial coordination plane defined by P(2), P(3), O(1) and O(2), as indicated by the dihedral angle between these two planes: 4.8(1)°, 9.3(3)° and 5.8(2)° for the Cr, Co and Rh complexes, respectively. This order of Cr < Rh < Co for the dihedral angle is opposite to that of the M–P(1) bond length (Cr: 2.439(2) > Rh: 2.258(2) > Co: 2.201(3) Å), suggesting that a steric interaction with the axial $-PMe_2$ group exists to some extent to bend the acac plane away from the equatorial coordination plane. Another intriguing difference between the three complex cations is the deviation of the central M atom from the least-squares equatorial coordination plane. The dis-

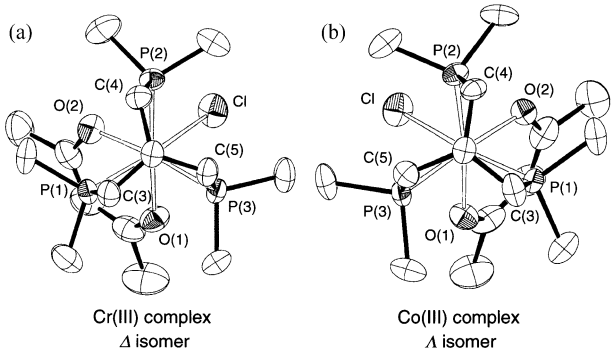


Fig. 2. Top views (along the C(1)–C(2)···M direction) of $[MCl(acac)(tdmme)]^+$ {M = Cr (a) and Co (b)}, showing the enantiomeric isomerism of the complexes.

tance, d, of the Cr atom from the equatorial coordination plane is 0.124(2) Å, while the Co or Rh atom is located on the plane (Table 2). This would result from the smaller bite angle of tdmme in [CrCl(acac)(tdmme)]PF_6 (average 84.24°) than those close to a right angle in the Co^{III} and Rh^{III} complexes.

The metrical difference between two chemically inequivalent M–P bond lengths (M–P(1) vs. M–P(2), M–P(3)) in [MCl(acac)(tdmme)]PF_6 is negligibly small for all three M^{III} complexes (Table 2). As seen in Table 3, the Co–P and Rh–P bond lengths in [MCl(acac)(tdmme)]PF_6 are comparable to those in [MCl_3(tdmme)], while the Cr–P bonds in [CrCl(acac)(tdmme)]PF_6 are shorter by approximately 0.02 Å than those in [$CrCl_3$(tdmme)]. Such a difference in the Cr^{III}–P bond lengths may be related to the higher stability of the acac complex than the trichloro complex. It should also be noted that the Cr–P bonds in Cr^{III} complexes such as [CrCl(acac)(tdmme)]PF_6, [$CrCl_3$(tdmme)] [10] and *trans*-$[CrCl_2(dmpe)_2]^+$ (dmpe = 1,2-bis(dimethylphosphino)ethane) [27] are longer by 0.2–0.25 Å than the Co–P bonds in the corresponding Co^{III} complexes [2,14], and are also longer by 0.1–0.2 Å than the Rh–P bonds in the corresponding Rh^{III} complexes [5,28]. On the other hand, the Cr–Cl bond lengths in *trans*-$[CrCl_2(dmpe)_2]^+$ and the Cr–O ones in [$Cr(acac)_3$] are longer than the corresponding Co–Cl and Co–O bond lengths, but are shorter than the corresponding Rh–Cl and Rh–O bond lengths. It seems that the ionic radii of Cr^{3+} (0.62 Å), Co^{3+} (low-spin: 0.55 Å) and Rh^{3+} (0.67 Å) [29] account satisfactorily for the differences in the M–Cl bond lengths of *trans*-$[MCl_2(dmpe)_2]^+$ and the M–O bond lengths of [$M(acac)_3$], but not for the difference in the M–P bond lengths in the phosphine complexes. Therefore, the extremely long Cr–P bonds are attributed to the inherently weak coordinate bond between Cr^{III} and P.

Table 3
Comparisons of the structural parameters (Å), (°) among Cr(III), Co(III) and Rh(III) complexes

Structural parameter complex	M		
	Cr	Co	Rh
M–P			
[MCl_3(tdmme)]	2.456[10]	2.203[2]	2.253[5]
$[MCl(acac)(tdmme)]^+$	2.437	2.201	2.252
trans-$[MCl_2(dmpe)_2]^+$	2.445[27]	2.259[14]	2.337[28]
M–Cl			
[MCl_3(tdmme)]	2.322[10]	2.323[2]	2.444[5]
$[MCl(acac)(tdmme)]^+$	2.316(2)	2.317(3)	2.430(2)
trans-$[MCl_2(dmpe)_2]^+$	2.293(4)[27]	2.260(1)[14]	2.358[28]
M–O			
$[MCl(acac)(tdmme)]^+$	1.965	1.947	2.088
[$M(acac)_3$]	1.951[18]	1.888[19]	1.992[20]
P–M–P (bite angle of tdmme)			
[MCl_3(tdmme)]	83.48[10]	89.5[2]	89.1[5]
$[MCl(acac)(tdmme)]^+$	84.24	89.64	89.17
O–M–O (bite angle of acac)			
[$M(acac)_3$]	90.1[18]	96.5[19]	95.3[20]
$[MCl(acac)(tdmme)]^+$	91.2(2)	93.7(2)	90.2(2)

The value without e.s.d. is the average one. The figures in square brackets (superscript) are the reference numbers.

It is also seen from Table 3 that the difference in the Cr–P bond lengths between *trans*-$[CrCl_2(dmpe)_2]^+$ and [CrCl(acac)(tdmme)]PF_6 is only 0.008 Å, while the mutually *trans* Co–P and Rh–P bonds in *trans*-$[MCl_2(dmpe)_2]^+$ are longer by 0.058 and 0.085 Å, respectively, than the bonds *trans* to Cl or O in $[MCl(acac)(tdmme)]^+$; i.e.

$$\Delta(\text{M–P}) = l(\text{M–P}) \text{ in } \textit{trans}\text{-}[MCl_2(dmpe)_2]^+ - l(\text{M–P}) \text{ in } \textit{trans}\text{-}[MCl(acac)(tdmme)]^+$$

$$\Delta(\text{Cr–P}) = 0.008 < \Delta(\text{Co–P}) = 0.058 < \Delta(\text{Rh–P}) = 0.085 \text{ Å} \quad (1).$$

The M–Cl bonds *trans* to the P donor in $[MCl(acac)(tdmme)]^+$ are longer than the mutually *trans* M–Cl bonds in *trans*-$[MCl_2(dmpe)_2]^+$ as follows:

$$\Delta(\text{M–Cl}) = l(\text{M–Cl}) \text{ in } \textit{trans}\text{-}[MCl(dmpe)]^+ - l(\text{M–Cl}) \text{ in } \textit{trans}\text{-}[MCl_2(dmpe)_2]^+$$

$$\Delta(\text{Cr–Cl}) = 0.023 < \Delta(\text{Co–Cl}) = 0.057 < \Delta(\text{Rh–Cl}) = 0.062 \text{ Å} \quad (2).$$

Furthermore, the elongation of the M–O bonds in $[MCl(acac)(tdmme)]^+$ from those in [$M(acac)_3$] are:

$$\Delta(\text{M–O}) = l(\text{M–O}) \text{ in } \textit{trans}\text{-}[MCl(acac)(tdmme)]^+ - l(\text{M–O}) \text{ in } [M(acac)_3]^+$$

$$\Delta(\text{Cr–O}) = 0.014 < \Delta(\text{Co–O}) = 0.057 < \Delta(\text{Rh–Cl}) = 0.096 \text{ Å} \quad (3).$$

Such elongations of the M–L (L = P, Cl and O) bond lengths may be related to the *trans* influence of the $-PMe_2$ group in tdmme (or dmpe), and the magnitude of Δ(M–L) for different M reflects the difference in the strength of the *trans* influence for specific M^{III} complexes. In particular, the comparison of M–O bond lengths in (3) would be valid, because each set of three M^{III} compounds, [MCl(acac)(tdmme)]PF_6 and [$M(acac)_3$], crystallize in an isomorphous space group and the packing effects to deviate the coordinate bond lengths would, therefore, be identical to one another. In conclusion, the strength of the *trans* influence of the $-PMe_2$ group in tdmme increases in the order of $Cr^{III} < Co^{III} < Rh^{III}$. The negligibly weak *trans* influence of $-PMe_2$ group in the Cr^{III} complex is attributed to the extremely long (and therefore weak) coordinate bonds between Cr^{III} and phosphorus.

3.3. Structures in solution and spectroscopic properties

The NMR spectra of the Co^{III} and Rh^{III} complexes of $[MCl(acac)(tdmme)]PF_6$ in CD_3CN (see Section 2) reflect the molecular C_s-symmetry of the complexes; the cations are not chiral in solution due to the fluxionality of the synchronous twist of three arms of tdmme. The $^{31}P\{^1H\}$ NMR spectrum of the Rh^{III} complex gave two resonances, a doublet-of-doublets and doublet-of-triplets with an intensity ratio of 2:1. The observed coupling constants, $^1J_{Rh-P}$ (102.6 and 104.9 Hz) and $^2J_{P-P}$ (32.4 Hz), parallel those observed for $[RhCl(tdmme)(H_2O)_2]^{2+}$ ($^1J_{Rh-P} = 106.7$ and 101.3, $^2J_{P-P} = 31.1$ Hz) [5].

In the UV–Vis absorption spectrum (Fig. 3) of the Co^{III} complex, a medium intensity band ($\varepsilon = 1060$ dm^3 mol^{-1} cm^{-1}) assignable to the first d–d ($^1A_1 \rightarrow {}^1T_1$: O_h) transition is observed at 20960 cm^{-1} (477 nm), but the explicit band-splitting expected for the lowering of the molecular symmetry is not observed. A very weak shoulder ($\varepsilon \approx 3.5$ dm^3 mol^{-1} cm^{-1}) observed around 15 500 cm^{-1} (645 nm) would be assignable to the spin-forbidden d–d transition ($^1A_1 \rightarrow {}^3T_2$: O_h) band.

In the spectrum of the Cr^{III} complex, two bands are observed at 18 590 cm^{-1} (538 nm, $\varepsilon = 494$ dm^3 mol^{-1} cm^{-1}) and 24 750 cm^{-1} (404 nm, $\varepsilon = 358$ dm^3 mol^{-1} cm^{-1}). Provided that these bands are the first ($^4A_2 \rightarrow {}^4T_2$: O_h) and the second ($^4A_2 \rightarrow {}^4T_1$: O_h) d–d transition bands, the ligand-field strength Δ and the Racah's B parameter of $[CrCl(acac)(tdmme)]^+$ are estimated as 18 590 and 513 cm^{-1}, respectively. The Δ value coincides closely with the expected value (18 610 cm^{-1}) from $\Delta_{Cl} = 13\,180$ cm^{-1}, $\Delta_{tdmme} = 20\,920$ cm^{-1} (estimated from the spectral data of $[CrCl_3(tdmme)]$ with $\Delta_{Cl} = 13\,180$ cm^{-1}) [8] and $\Delta_{acac} = 17\,860$ cm^{-1} [30]. Such a coincidence indicates that the ligand-field perturbation energies of Cl, tdmme and acac in $[CrCl(acac)(tdmme)]^+$ are almost identical to those in $[CrCl_3(tdmme)]$ and $[Cr(acac)_3]$, which is inferred from the crystallographic observation that the Cr^{III}–L bond lengths differ only slightly in these three complexes. In contrast, the B parameter of $[CrCl(acac)(tdmme)]^+$ (513 cm^{-1}) is much larger than that of $[CrCl_3(tdmme)]$ (354 cm^{-1}). In a previous paper [8], we have shown that the extremely small B value (< 360 cm^{-1}) is limited to the $[Cr(Cl\text{ or }Br)_3(tdmme)]$ complexes and the B parameters for $[CrCl_2(PMe_3)(tdmme)]^+$ (500 cm^{-1}) and $[CrCl_2(dmpp)_2]^+$ (dmpe = 1,3-bis(dimethylphosphino)-propane, 539 cm^{-1}) are large similarly to those of the di- or triamine complexes. This study also indicates that the substitution of $acac^-$ for two Cl^- induces large interelectronic repulsion by approximately 150 cm^{-1}.

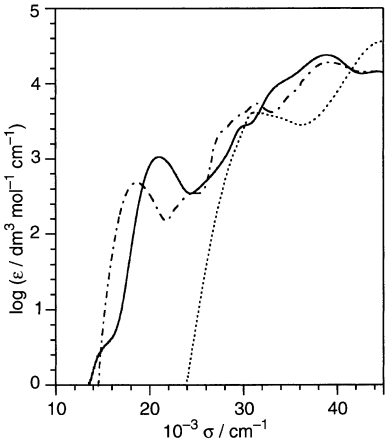


Fig. 3. UV–Vis absorption spectra of $[MCl(acac)(tdmme)]PF_6$ (M = Cr (—·—), Co (—) and Rh (·····)) in CH_3CN at room temperature.

4. Supplementary material

Supplementary data are available from the CCDC,12 Union Road, Cambridge, CB2 1EZ, UK on request, quoting the deposition numbers CCDC 169342–169344.

References

[1] T. Ando, M. Kita, K. Kashiwabara, J. Fujita, S. Kurachi, S. Ohba, Bull. Chem. Soc. Jpn. 65 (1992) 2748.
[2] K. Kashiwabara, M. Kita, J. Fujita, S. Kurachi, S. Ohba, Bull. Chem. Soc. Jpn. 67 (1994) 2145.
[3] M. Ogita, Y. Yamamoto, T. Suzuki, S. Kaizaki, Eur. J. Inorg. Chem. 2002, in press.
[4] (a) S. Iwatsuki, H. Kato, K. Obeyama, S. Funahashi, N. Koshino, K. Kashiwabara, T. Suzuki, H.D. Takagi, Inorg. Chem. Commun. 3 (2000) 501;
(b) S. Iwatsuki, K. Obeyama, N. Koshino, S. Funahashi, K. Kashiwabara, T. Suzuki, H.D. Takagi, Can. J. Chem. 79 (2000) 1344.
[5] T. Suzuki, K. Isobe, K. Kashiwabara, J. Fujita, S. Kaizaki, J. Chem. Soc., Dalton Trans. (1996) 3779.
[6] K. Kashiwabara, Y. Ozeki, M. Kita, J. Fujita, K. Nakajima, Bull. Chem. Soc. Jpn. 68 (1995) 3453.
[7] T. Suzuki, T. Imamura, S. Kaizaki, Acta Crystallogr. Sect. C 55 (1998) 184.
[8] T. Suzuki, K. Kashiwabara, T. Usami, T. Imamura, M. Kiki, J. Fujita, S. Kaizaki, Bull. Chem. Soc. Jpn. 74 (2001) 1055.
[9] (a) H.A. Mayer, W.C. Kaska, Chem. Rev. 94 (1994) 1239;
(b) V. Körner, G. Huttner, S. Vogel, A. Barth, L. Zsolnai, Chem. Ber. Recueil. 130 (1997) 489;
(c) C. Bianchini, A. Meli, J. Chem. Soc., Dalton Trans. (1996) 801; references therein.
[10] A.M. Arif, J.G. Hefner, R.A. Jones, B.R. Whittlesey, Inorg. Chem. 25 (1986) 1080.
[11] E.G. Thaler, K. Folting, J.C. Huffman, K.G. Caulton, J. Organomet. Chem. 376 (1989) 343.
[12] (a) A. Pastor, A. Galindo, J. Chem. Soc., Dalton Trans. (1997) 3749.;
(b) J. Scherer, G. Huttner, O. Walter, B.C. Janssen, L. Zsolnai, Chem. Ber. 129 (1996) 1603;
(c) References [24–29] cited in [5].
[13] G.M. Whitesides, C.P. Casey, J.K. Krieger, J. Am. Chem. Soc. 93 (1971) 1379.

[14] M. Kita, K. Kashiwabara, J. Fujita, H. Tanaka, S. Ohba, Bull. Chem. Soc. Jpn. 67 (1994) 2457.
[15] (a) T. Suzuki, M. Rude, K.P. Simonsen, M. Morooka, H. Tanaka, S. Ohba, F. Galsbøl, J. Fujita, Bull. Chem. Soc. Jpn. 67 (1994) 1013;
(b) T. Suzuki, S. Kaizaki, K. Kashiwabara, Inorg. Chim. Acta 298 (2000) 131;
(c) T. Suzuki, K. Kashiwabara, M. Kita, J. Fujita, S. Kaizaki, Inorg. Chim. Acta 281 (1998) 77.
[16] L.R. Gray, A.L. Hale, W. Levason, F.P. McCullough, M. Webster, J. Chem. Soc., Dalton Trans. (1983) 2573.
[17] L.R. Gray, A.L. Hale, W. Levason, F.P. McCullough, M. Webster, J. Chem. Soc., Dalton Trans. (1984) 47.
[18] B. Morosin, Acta Crystallogr. 19 (1965) 131.
[19] G.J. Kruger, E.C. Reynhardt, Acta Crystallogr. Sect. B 30 (1974) 822.
[20] J.C. Morrow, E.B. Parker, Jr., Acta Crystallogr. Sect. B 29 (1973) 1145.
[21] P. Coppens, L. Leiserowitz, D. Rabinovich, Acta Crystallogr. 18 (1965) 1035.
[22] A.C.T. North, D.C. Phillips, F.S. Mathews, Acta Crystallogr. Sect. A 24 (1968) 351.
[23] G.M. Sheldrick, Acta Crystallogr. Sect. A 46 (1990) 467.
[24] G.M. Sheldrick, SHELXL97, Univesity of Göttingen, Germany, 1997.
[25] H.D. Flack, Acta Crystallogr. Sect. A 39 (1983) 876.
[26] K. Chau, TEXSAN, Single Crystal Structure Analysis Software Package, Ver. 1.11, Molecular Structure Corporation, The Woodlands, TX, USA, 2000.
[27] J.E. Salt, G. Wilkinson, M. Motevalli, M.B. Hursthouse, J. Chem. Soc., Dalton Trans. (1986) 1141.
[28] K.P. Simonsen, N. Suzuki, M. Hamada, M. Kojima, S. Ohba, Y. Saito, J. Fujita, Bull. Chem. Soc. Jpn. 62 (1989) 3791.
[29] (a) R.D. Shannon, Acta Crystallogr. Sect. A 32 (1976) 751;
(b) U. Müller, Inorganic Structural Chemistry, Wiley, Chichester, UK, 1993, p. 36.
[30] A.B.P. Lever, Inorganic Electronic Spectroscopy, Elsevier, Amsterdam, 1984.

PERGAMON

Polyhedron 21 (2002) 843–848

POLYHEDRON

www.elsevier.com/locate/poly

Synthesis and crystal structures of palladium(II) complexes containing benzyl 8-quinolyl sulfide and phenethyl 8-quinolyl sulfide

Masakazu Kita [a,*], Shin-ichi Abiko [a], Akira Fuyuhiro [b], Kazuaki Yamanari [b], Katsuo Murata [a], Shinsuke Yamashita [a]

[a] *Chemistry Department, Naruto University of Education, Takashima, Naruto 772-8502, Japan*
[b] *Department of Chemistry, Graduate School of Science, Osaka University, Toyonaka, Osaka 560-0043, Japan*

Received 14 September 2001; accepted 8 January 2002

Abstract

Four palladium(II) complexes $[PdX_2(L\text{-}N,S)]$ (X = Cl, Br; L: BzSq = benzyl 8-quinolyl sulfide, PheneSq = phenethyl 8-quinolyl sulfide) were prepared. The crystal structure of $[PdCl_2(BzSq\text{-}N,S)]$ revealed the presence of an intraligand stacking between the phenyl and quinolyl groups of BzSq. This stacking interaction was confirmed even in Me_2SO, MeCN and $MeNO_2$. On the other hand, $[PdCl_2(PheneSq\text{-}N,S)]$ did not show such an intraligand stacking both in the solid and in solutions. © 2002 Published by Elsevier Science Ltd.

Keywords: Palladium(II) complexes; Benzyl 8-quinolyl sulfide; Phenethyl 8-quinolyl; Crystal structures

1. Introduction

Aromatic interactions such as face-to-face π–π, face-to-edge π–π, and CH-π play an important role in molecular recognition [1]. Such interactions have been found in many coordination compounds. For example, there is a face-to-face interligand stacking between a phenyl group of 1,2-bis(diphenylphosphino)ethane (dppe) and an acetylacetonato (acac) ring in *cis*-$[Co(CN)_2(acac)(dppe)]$ in the solid [2]. This stacking mode is confirmed in $CHCl_3$ by its ^1H NMR spectrum. Similar π–π stacking phenomena in the solid have been reported in [Cu(bpy)(L-tyr)(ClO_4-*O*)] (bpy = 2,2′-bipyridine and L-tyr = L-tyrosine) [3], $[Pd(bpy)(L\text{-}tyr\cdot gly)]\cdot 3H_2O$ (L-tyr·gly = L-tyrosylglycine) [4], [Cu(bpy)(L-trp)]ClO_4 (L-trp = L-tryptophan) [5].

Here we report the synthesis of four palladium(II) complexes $[PdX_2(L\text{-}N,S)]$ (X = Cl, Br; L: BzSq = benzyl 8-quinolyl sulfide, PheneSq = phenethyl 8-quinolyl sulfide) and examine whether there are any intra- and/or interligand stacking interactions for these complexes both in solid and in several solvents.

2. Experimental

2.1. BzSq

An ethanol solution (30 cm^3) containing 1.0 g of 8-quinolinethiol (5.1 mmol) and 0.64 g of benzyl chloride (5.1 mmol) was refluxed for 24 h, until the initial yellow color disappeared. After cooling, white needlelike crystals were obtained by addition of 100 cm^3 of water. Yield: 1.1 g (86%). Found: C, 75.75; H, 5.24; N, 5.51%. Calc. for $C_{16}H_{13}NS$: C, 75.85; H, 5.94; N, 5.53%. NMR: δ_H (*J* (Hz), d_6-DMSO) 8.89(dd, $J_{2-3} = 4.1$, $J_{2-4} = 1.4$; 1H, H(2)), 8.35(dd, $J_{3-4} = 8.3$, $J_{2-4} = 1.4$; 1H, H(4)), 7.72(d, $J_{5-6} = 8.0$; 1H, H(5)), 7.63(d, $J_{6-7} = 7.3$; 1H, H(7)), 7.58(q, $J_{2-3} = 4.1$, $J_{3-4} = 8.3$; 1H, H(3)), 7.52(t, $J_{5-6} = 8.0$, $J_{6-7} = 7.3$; 1H, H(6)), 7.49(d, $J_{12-13} = 7.9$; 2H, H(12) and H(16)), 7.34(t, $J_{12-13} = 7.9$, $J_{13-14} = 8.1$; 2H, H(13) and H(15)), 7.29(t, $J_{13-14} = 8.1$, $J_{14-15} = 8.1$; 1H, H(14)), 4.34(s; 2H, H(21)); δ_C(d_6-DMSO) 149.2(C(2)), 144.5(C(10)), 138.2(C(9)), 137.0(C(11)), 136.3(C(4)), 128.8(C(12) and C(16)), 128.4(C(13) and

* Corresponding author. Tel.: +81-886-87-1311; fax: +81-886-87-1090.
E-mail address: kitam@naruto-u.ac.jp (M. Kita).

0277-5387/02/$ - see front matter © 2002 Published by Elsevier Science Ltd.
PII: S0277-5387(02)00864-1

(C(15)), 127.7(C(8)), 127.0(C(14)), 126.6(C(6)), 124.0(C(7)), 123.9(C(5)), 121.9(C(3)), 34.3(C(21)).

2.2. PheneSq

To an ethanol solution (30 cm^3) containing 1.0 g of 8-quinolinethiol (5.1 mmol) and 0.71 g of 2-chloroethylbenzene (5.1 mmol) was added a solution of sodium hydroxide (0.45 g, 10.2 mmol) in 50 cm^3 of water. The mixture was refluxed for 24 h and 100 cm^3 of diethyl ether was added to it. The diethyl ether extract was evaporated to remove diethyl ether. The crude oily residue, which showed a desirable ^1H NMR spectrum, was used for the preparations without further purification. Yield: 1.1 g (82%).

Table 1
Crystallographic data

Complex	$[PdCl_2(BzSq)]$	$[PdCl_2(PheneSq)]\cdot CH_2Cl_2$
Formula	$C_{16}H_{13}NSCl_2Pd$	$C_{18}H_{17}NSCl_4Pd$
Crystal system	triclinic	triclinic
Space group	$P\bar{1}$ (#2)	$P\bar{1}$ (#2)
a (Å)	15.601(2)	10.638(1)
b (Å)	13.316(3)	11.156(1)
c (Å)	9.160(2)	9.999(1)
α (°)	70.08(2)	114.980(7)
β (°)	83.19(1)	107.346(8)
γ (°)	66.68(1)	75.454(8)
Z	4	2
V (Å)^3	1642.7(6)	1016.0(2)
D_{calc} (g cm^{-3})	1.733	1.725
μ (Mo Kα) (cm^{-1})	15.73	15.43
Transmission factor	0.776–1.000	0.85–1.00
Crystal color	pale yellow	yellow–orange
Crystal habit	prismatic	prismatic
Crystal size (mm)	0.20 × 0.12 × 0.25	0.25 × 0.25 × 0.40
Scan type	ω–2θ	ω–2θ
2θ max (°)	60	60
Reflections measured	$\pm h, \pm k, +l$	$-h, \pm k, \pm l$
Number of reflections measured	7890	6205
Number of reflections observed $[\|F_o\| > 6s(\|F_o\|)]$	4900	4942
R	0.032	0.041
R_w	0.039	0.057
W	$1/\sigma^2(\|F_o\|)^2$	$1/\sigma^2(\|F_o\|)^2$

3. Preparation of complexes

3.1. $[PdX_2(BzSq)]$ (X = Cl and Br)

To a solution of $Na_2[PdCl_4]\cdot H_2O$ (0.52 g, 1.7 mmol) in 50 cm^3 of ethanol was added a solution of BzSq (0.43 g, 1.7 mmol) in 50 cm^3 of ethanol. After stirring at room temperature (r.t.), the resulting orange precipitate was filtered and recrystallized from CH_2Cl_2. Yield: 0.31 g (43%). Found: C, 45.08; H, 2.95; N, 3.25%. Calc. for $[PdCl_2(BzSq)] = C_{16}H_{13}Cl_2PdNS$: C, 44.83; H, 3.06; N, 3.27%. Its NMR data is shown in Table 3. The corresponding dibromo complex was prepared from $K_2[PdBr_4]$ in a similar way. Yield: 0.18 g (88%). Found: C,36.51; H, 2.53; N, 2.47%. Calc. for $[PdBr_2(BzSq)] = C_{16}H_{13}Br_2PdNS$: C, 37.13; H, 2.53; N, 2.71%. NMR: $\delta_H(J$ (Hz), d_6-DMSO) 9.62(d, $J_{2-3} = 5.0$; 1H, H(2)), 8.75(d, $J_{3-4} = 8.3$; 1H, H(4)), 8.32(d, $J_{6-7} = 7.5$; 1H, H(7)), 8.27(d, $J_{5-6} = 7.7$; 1H, H(5)), 7.92(t, $J_{5-6} = 7.7$, $J_{6-7} = 7.5$; 1H, H(6)), 7.74(t, $J_{2-3} = 5.0$, $J_{3-4} = 8.3$; 1H, H(3)), 7.21(t, $J_{12-13} = 6.8$; 2H, H(12) and H(16)), 7.09–6.98 (m; 3H, H(13)–H(15)), 4.76(d, $J = 12.9$; 1H, H(21a)), 4.59(d, $J = 12.9$; 1H, H(21b)); $\delta_C(d_6$-DMSO) 155.8(C(2)), 130.9(C(9)), 130.6(C(12) and C(16)),

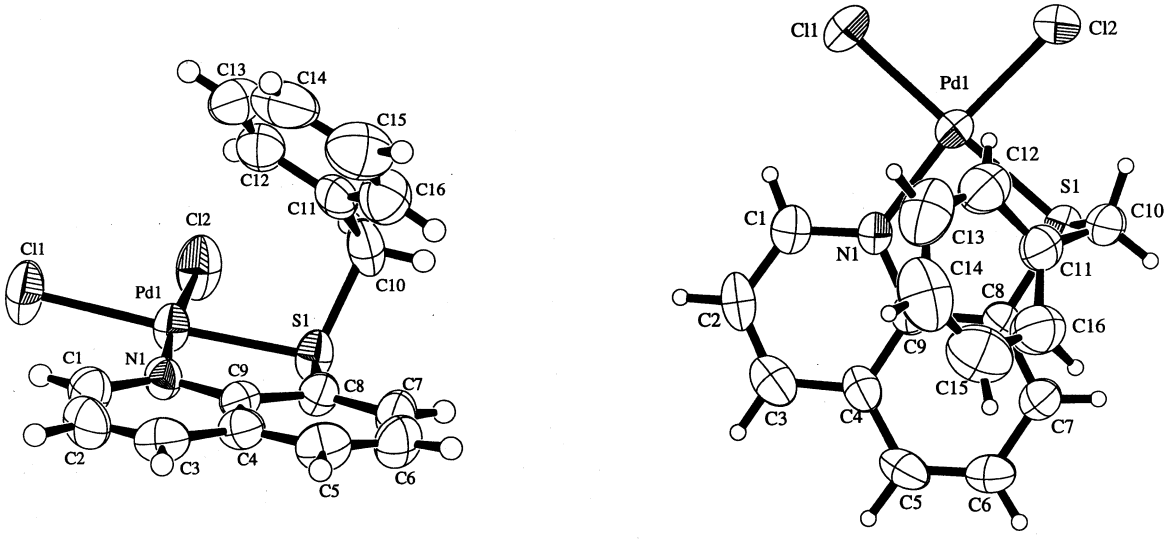


Fig. 1. ORTEP [8] drawings of $[PdCl_2(BzSq)]$ and its intraligand stacking.

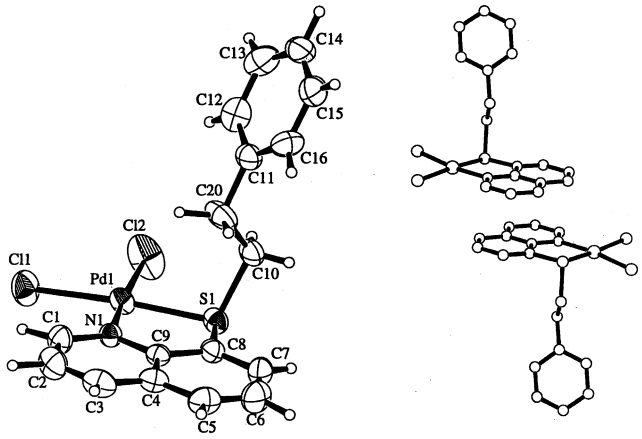
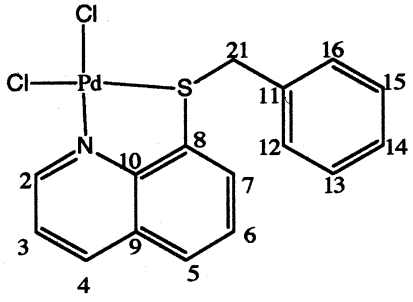


Fig. 2. ORTEP [8] drawings of $[PdCl_2(PheneSq)]$ and its interligand stacking.

Table 2
Selected bond distances (Å) and bond angles (°) for $[PdCl_2(BzSq$ or PheneSq)]

$[PdCl_2(BzSq)]$			
Bond lengths			
Pd(1)–Cl(1)	2.315	Pd(2)–Cl(21)	2.311(1)
Pd(1)–Cl(2)	2.293(1)	Pd(2)–Cl(22)	2.283(1)
Pd(1)–S(1)	2.248(1)	Pd(2)–S(2)	2.237(1)
Pd(1)–N(1)	2.046(3)	Pd(2)–N(2)	2.036(4)
S(1)–C(8)	1.780(4)	S(2)–C(28)	1.752(7)
S(1)–C(10)	1.848(5)	S(2)–C(30)	1.832(5)
C(10)–C(11)	1.489(7)	C(30)–C(31)	1.489(7)
Bond angles			
Cl(1)–Pd(1)–Cl(2)	91.07(4)	Cl(21)–Pd(2)–Cl(22)	91.28(5)
Cl(1)–Pd(1)–S(1)	177.45(5)	Cl(21)–Pd(2)–S(2)	177.63(5)
Cl(1)–Pd(1)–N(1)	95.65(9)	Cl(21)–Pd(2)–N(2)	95.6(1)
Cl(2)–Pd(1)–S(1)	87.18(4)	Cl(22)–Pd(2)–S(2)	86.69(5)
Cl(2)–Pd(1)–N(1)	172.74(9)	Cl(22)–Pd(2)–N(2)	173.1(1)
S(1)–Pd(1)–N(1)	86.01(9)	S(2)–Pd(2)–N(2)	86.5(1)
Pd(1)–S(1)–C(8)	99.1(1)	Pd(2)–S(2)–C(28)	99.0(2)
Pd(1)–S(1)–C(10)	104.5(2)	Pd(2)–S(2)–C(30)	107.9(2)
C(8)–S(1)–C(10)	100.3(2)	C(28)–S(2)–C(30)	101.6(2)
S(1)–C(10)–C(11)	115.3(3)	S(2)–C(30)–C(31)	115.3(3)
$[PdCl_2(pheneSq)]$			
Bond lengths			
Pd(1)–Cl(1)	2.315(1)		
Pd(1)–Cl(2)	2.287(1)		
Pd(1)–S(1)	2.2530(9)		
Pd(1)–N(1)	2.036(3)		
S(1)–C(8)	1.775(4)		
S(1)–C(10)	1.828(4)		
C(10)–C(20)	1.507(6)		
C(20)–C(11)	1.519(2)		
Bond angles			
Cl(1)–Pd(1)–Cl(2)	91.60(4)		
Cl(1)–Pd(1)–S(1)	174.96(4)		
Cl(1)–Pd(1)–N(1)	94.52(8)		
Cl(2)–Pd(1)–S(1)	87.96(4)		
Cl(2)–Pd(1)–N(1)	172.42(8)		
S(1)–Pd(1)–N(1)	86.33(8)		
Pd(1)–S(1)–C(8)	98.9(1)		
Pd(1)–S(1)–C(10)	106.7(1)		
C(8)–S(1)–C(10)	102.4(2)		
S(1)–C(10)–C(20)	113.5(2)		
C(10)–C(20)–C(11)	111.4(3)		

Table 3
NMR data of $[PdCl_2(BzSq)]$ in d_6-DMSO



^{1}H NMR		^{13}C NMR	
Position	δ (J/Hz)	Position	δ
2	9.42(d, $J_{2-3}=5.2$; 1H)	2	153.6
4	8.74(d, $J_{3-4}=8.2$; 1H)	10	150.5
7	8.32(d, $J_{6-7}=7.4$; 1H)	4	1470.7
5	8.27(d, $J_{5-6}=8.0$; 1H)	7	136.9
6	7.92(t, $J_{5-6}=8.0$, $J_{6-7}=7.4$; 1H)	11	133.4
3	7.74(t, $J_{2-3}=5.2$, $J_{3-4}=8.2$; 1H)	5	131.6
12,16	7.27(t, $J_{12-13}=6.1$; 2H)	9	130.2
13,14,15	7.08–7.00(m; 3H)	12,16	130.1
21a	4.69(d, $J=12.9$; 1H)	6	128.6
21b	4.51(d, $J=12.9$; 1H)	14	128.4
		13,15	127.9
		8	126.1
		3	123.2
		21	47.2

129.3(C(6)), 129.0(C(14)), 128.5(C(13) and C(15)), 127.9(C(8)), 124.1(C(3)), 48.3(C(21)).

3.2. $[PdX_2(PheneSq)]$ (X = Cl and Br)

To a solution of $Na_2[PdCl_4]\cdot H_2O$ (0.24 g, 0.8 mmol) in 50 cm^3 of ethanol was added a solution of PheneSq (0.21 g, 0.8 mmol) in 50 cm^3 of ethanol. After stirring at r.t., the resulting orange precipitate was filtered and recrystallized from CH_2Cl_2. Yield: 0.30 g (85%). Found: C, 40.88; H, 3.19; N, 2.70%. Calc. for $[PdCl_2(PheneSq)] = C_{17}H_{15}Cl_2PdNS$: C, 40.97; H, 3.25; N, 2.65%. Its NMR data is shown in Table 4. The corresponding dibromo complex was prepared from $K_2[PdBr_4]$ in a similar way. Yield: 0.38 g (88%). Found: C,36.92; H, 2.77; N, 2.38%. Calc. for $[PdBr_2(PheneSq)] = C_{17}H_{15}Br_2PdNS$: C, 38.41; H, 2.84; N, 2.64%. NMR: δ_H(J (Hz), d_6-DMSO) 10.14 (d, $J_{2-3}=5.3$; 1H, H(2)), 8.48 (d, $J_{3-4}=8.2$; 1H, H(4)), 8.04(d, $J_{5-6}=7.5$, $J_{6-7}=7.2$; 2H, H(7) and H(5)), 7.76(t, $J_{5-6}=7.2$, $J_{6-7}=7.2$; 1H, H(6)), 7.67(q, $J_{2-3}=5.3$, $J_{3-4}=8.2$; 1H, H(3)), 7.07(d, $J=3.9$; 5H, H(12)–H(16)), 3.83(d, $J=11.9$; 1H, H(22)), 3.58(s; 2H, H(22)), 3.01(d, $J=11.9$; 1H, H(21b)); δ_C(d_6-DMSO) 156.9(C(2)), 150.4(C(10)),140.4(C(4)), 137.5(C(7)), 135.7(C(11)), 131.7(C(5)), 130.2(C(8)), 129.2(C(6)),

129.1(C(12) and C(16)), 128.8(C(13) and C(15)), 127.3(C(14)), 124.2(C(3)), 45.4(C(21)), 36.5(C(22)).

4. Crystallography

Single crystals of $[PdCl_2(BzSq)]$ ($0.25 \times 0.20 \times 0.12$ mm) and $[PdCl_2(PheneSq)]$ ($0.40 \times 0.25 \times 0.25$ mm) were fixed on the end of a glass fiber with epoxy resin. They were mounted on a Rigaku AFC-7R diffractometer and the diffraction data were collected at 298 K with graphite-monochromated Mo Kα radiation ($\lambda = 0.71069$ Å) using $\omega-2\theta$ scan mode. Cell dimensions were determined by least-squares refinement of the angular positions of 25 independent reflections in the range $28 < 2\theta < 39^\circ$ for each sample. Crystallographic data and experimental details are listed in Table 1. The position of the palladium was determined by direct methods (SHELXS-86 [6]) for each complex and the remaining non-hydrogen atoms were located by subsequent Fourier syntheses. The structure was refined on F by full-matrix least-square techniques with anisotropic thermal parameters for non-hydrogen atoms. Hydrogen atoms were located at positions determined by Fourier-difference syntheses or by calculations. All calculations were carried out with the TEXAN [7] software.

5. Measurement

UV–Vis absorption spectra were recorded on an Hitachi U-3400 spectrophotometer, ^1H and ^{13}C NMR spectra with a Bruker ARX300 spectrometer. X-Ray crystal analysis was made at the X-ray Diffraction Service of the Department of Chemistry of Osaka University.

6. Results and discussion

Neutral complexes $[PdX_2(L)]$ ($X = Cl^-$ or Br^-; L = BzSq or PheneSq) were obtained in high yields by the

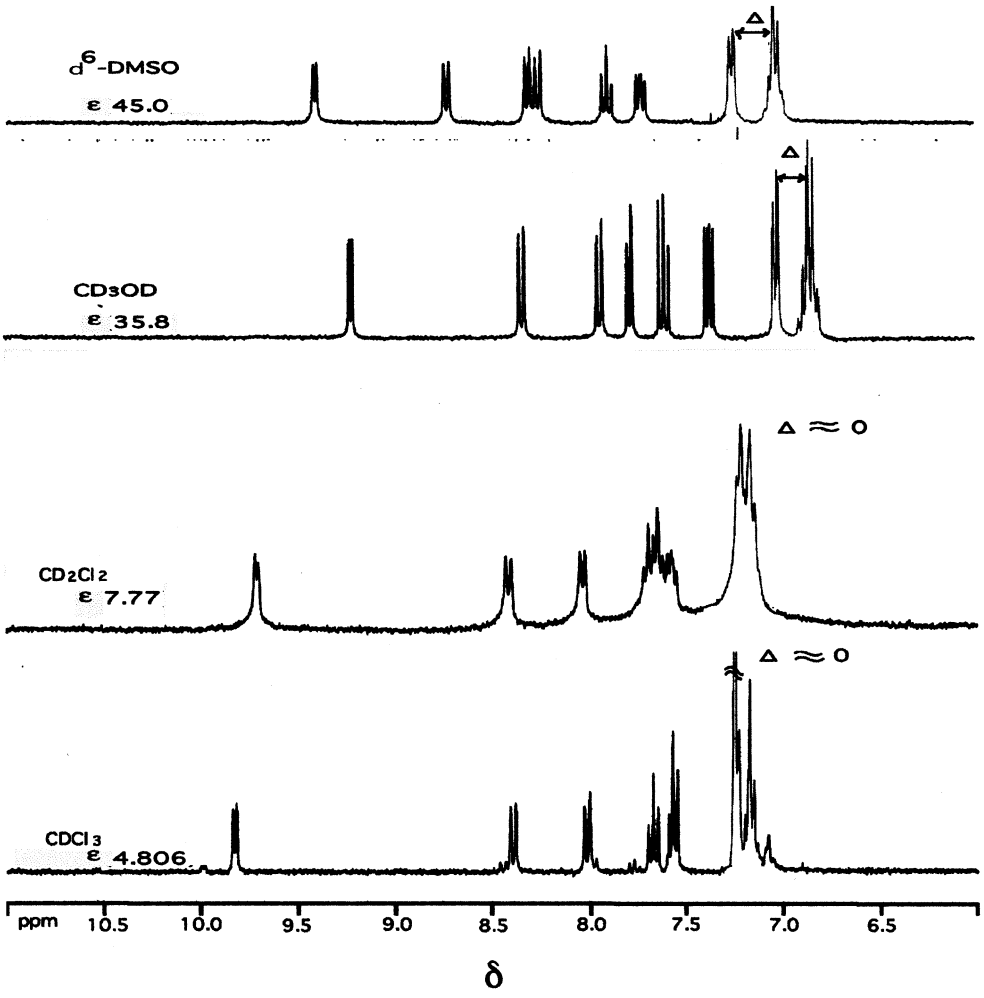
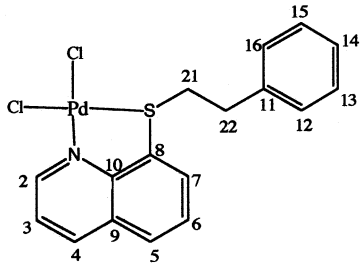


Fig. 3. Proton NMR spectra of $[PdCl_2(BzSq)]$ in several solvents. Δ is the magnitude of the splitting of phenyl protons and ε is the dielectric constant of solvent.

Table 4
NMR data of [$PdCl_2$(pheneSq)] in DMSO



^{1}H NMR		^{13}C NMR	
Position	δ (J/Hz)	Position	δ
2	9.90(d, $J_{2-3}=5.3$, $J_{2-4}=1.5$; 1H)	2	155.3
4	8.48(d, $J_{3-4}=8.3$, $J_{2-4}=1.5$; 1H)	10	150.4
7,5	8.03(d, $J_{3-6}=7.8$, $J_{6-7}=7.8$; 2H)	4	140.6
6	7.78(t, $J_{5-6}=7.8$, $J_{6-7}=7.8$; 1H)	7	137.5
3	7.68(q, $J_{2-3}=5.3$, $J_{3-4}=8.3$; 1H)	11	135.5
12,13	7.11–7.03(m; 5H)	5	131.7
14	3.77–3.46(m; 3H)	9	131.3
15,16	3.11–3.02(m; 1H)	6	129.2
		12,16	129.1
		8	128.9
		13,15	128.8
		14	127.4
		3	124.0
		21	45.1
		22	36.3

reaction of $[PdX_4]^{2-}$ with sulfide ligands. They were characterized by NMR spectroscopy and elemental analysis.

X-ray crystal structures were determined for [$PdCl_2$(BzSq)] and [$PdCl_2$(PheneSq)]. ORTEP [8] drawings of the present complexes are shown in Figs. 1 and 2. Selected bond distances and angles are listed in Table 2. Though there are two similar but independent molecules in [$PdCl_2$(BzSq)], we describe only the structure of Pd(1) hereafter.

The BzSq ligand coordinates bidentately through the N,S donors. The Pd–Cl bond distance *trans* to the sulfur in [$PdCl_2$(BzSq-*N*,*S*)] is 2.315(1) Å, which is longer by 0.022(1) Å than the Pd–Cl one *trans* to imine. A similar lengthening of the Pd–Cl bond [0.028(1) Å] was also observed in [$PdCl_2$(PheneSq-*N*,*S*)]. This bond weakening is known as *trans* influence [9]. The ligand bite angles [BzSq = 86.01(9)° and PheneSq = 86.33(8)°] are normal and typical values. A remarkable feature is the presence of an intraligand stacking interaction between the phenyl group and the quinolyl of BzSq (see Fig. 1(a) (left)). The angle between the phenyl plane and the quinolyl is 46.6°. The top view indicates clearly the superimposition between the phenyl group and the quinolyl (Fig. 1(b) (right)). The C(8)–S–C(10) angle of 100.3(2)° is considerably less than a tetrahedral angle of 109.5°, which is reasonably ascribed to the intraligand stacking interaction of BzSq. The dihedral angle C(8)–S–C(10)–C(11) is 43.9(4)°. The distance between C(11) and C(9) is 3.60(1) Å, which is the standard value for a π–π distance. This stacking conformation generates the repulsive interactions of Pd–Cl(2)···H–C(10) 3.41(2) Å and Pd···H–C(12) 2.99(2) Å [11]. Interligand stacking interactions between a phenyl group and another ligand (for example, bpy) in a given complex have been often reported [2–5] but intraligand stacking in the same ligand described here seems to be quite rare. There is no intermolecular stacking interaction between aromatic rings in the present complex.

On the other hand, [$PdCl_2$(PheneSq-*N*,*S*)] does not show such an intraligand stacking mode (Fig. 2(a) (left)). In general, a long alkyl chain is apt to adopt an *anti* conformation, that is, *trans* conformation, due to the repulsion between adjacent methylene protons. The C(8)-S-C(10)–C(11) dihedral angle is 56.3(4)° and the S–C(10)–C(20)–C(11) one is 173.4(3)°. The S–CH_2–CH_2–C sequence takes an *anti* conformation, so that the phenyl group becomes apart from the quinolyl. This is the reason why the PheneSq complex does not have an intraligand stacking mode. Instead there is an intermolecular stacking interaction between two quinolyl groups of adjacent molecules as shown in Fig. 2(b) (right). The distance between the quinolyl planes 3.40(1) Å is considerably shorter than the standard value (3.60 Å) for a π–π distance. Since the crystallographic inversion is located at the center of the intermolecular quinolyl stacking, the angle between two quinolyl planes becomes 0°.

The assignments of ^{1}H and ^{13}C NMR signals were carried out by proton homo-decoupling, ^{1}H-detected multiple quantum coherence (HMQC), and ^{1}H-detected multiple bondquantum coherence (HMBC) spectra. The results are listed in Tables 3 and 4.

In the ^{1}H NMR spectrum of [$PdCl_2$(BzSq-*N*,*S*)] an interesting splitting was observed: the phenyl proton signals are split into two groups, the group of H(12) and H(16) (δ 7.21) and one of H(13), H(14) and H(15) (δ 7.09–6.98), in d_6-Me_2SO as shown in Fig. 3. The free BzSq in d_6-Me_2SO shows the phenyl protons at δ7.49 (H(12) and H(16)), δ 7.34 (H(13) and H(15)), and δ 7.29 (H(14)). The changes of chemical shifts on complexation can be related to the ring current effect [10] of π-electrons of the quinolyl group by the aromatic intraligand interaction in d_6-Me_2SO. Similar changes were observed in CD_3OD (7.02 and 6.84) (Fig. 3). On the other hand, the signals of H(13), H(14), H(15) appear at relatively low magnetic field and the chemical shift separations are negligible in CD_2Cl_2 (δ 7.2) or $CDCl_3$ (δ 7.2) with low dielectric constants. This result suggests that the aromatic intraligand interaction is recognized in high dielectric solvents and does not occur in low dielectric solvents.

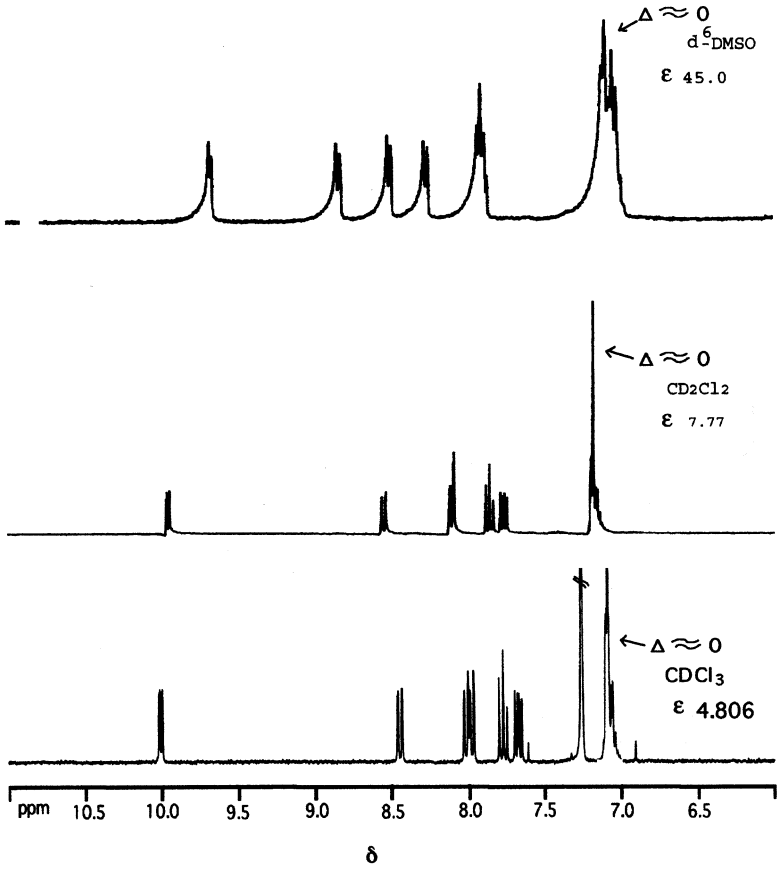


Fig. 4. Proton NMR spectra of [$PdCl_2$(PheneSq)] in several solvents. Δ is the magnitude of the splitting of phenyl protons and ε is the dielectric constant of solvent.

Similar ^{1}H NMR measurements were carried out for [$PdCl_2$(pheneSq-*N*,*S*)]. However, this complex did not show any splitting of the phenyl proton signals as shown in Fig. 4. Thus, the aromatic intraligand interaction could not be observed in the crystal and in solvents.

Each dibromo complex [$PdBr_2$(BzSq)] or [$PdBr_2$(PheneSq)] showed the same results as the corresponding dichloro complex. Hence we conclude that [$PdBr_2$(BzSq)] also has a similar noble intraligand stacking interaction as [$PdCl_2$(BzSq)] does in solid and in solvents with high dielectric constants.

7. Supplementary material

Crystallographic data have been deposited with the CCDC, 12 Union Road, Cambridge, CB2 1EZ, UK (fax: +44-1223-366033; e-mail: deposit@ccdc.cam.ac.uk or www: http://www.ccdc.cam.ac.uk) and are available on request quoting the deposition numbers 169087 for [$PdCl_2$(BzSq)] and 169088 for [$PdCl_2$(pheneSq)].

References

[1] (a) C.A. Hunter, Chem. Soc. Rev. (1994), 101, and references therein.;
(b) M. Mishio, M. Hirota, Y. Umezawa, The CH–π Interaction, Wiley-VCH, 1998;
(c) A. Magistrato, M. Merlin, O.S. Pregosin, U. Rothlisberger, Organometallics 19 (2000) 3591.
[2] M. Kita, K. Kashiwabara, J. Fujita, Bull. Chem. Soc. Jpn. 61 (1988) 3187.
[3] H. Masuda, T. Sugimori, A. Odani, O. Yamauchi, Inorg. Chim. Acta 180 (1991) 73.
[4] T. Sugimori, K. Shibakawa, H. Masuda, A. Odani, O. Yamauchi, Inorg. Chem. 32 (1993) 4951.
[5] O. Yamauchi, A. Odani, H. Masuda, Inorg. Chim. Acta 198–200 (1992) 749.
[6] G.M. Sheldrick, SHELXS-86, Program for Crystal Structure Determination, University of Göttingen, 1986.
[7] TEXSAN, Crystal Structure Analysis Package, Molecular Structure Corporation, 1985 and 1992.
[8] C.K. Johnson, ORTEP-II. Report ORNL-5138, Oak Ridge National Laboratory, Oak Ridge, TN, 1976.
[9] M. Kita, K. Kashiwabara, Polyhedron 16 (1997) 2771.
[10] A. Odani, S. Deguchi, O. Yamauchi, Inorg. Chem. 25 (1986) 62.
[11] Such repulsive interactions within 3.60 Å are absent in [$PdCl_2$(pheneSq)].

PERGAMON

Polyhedron 21 (2002) 849–857

POLYHEDRON

www.elsevier.com/locate/poly

Synthesis, electrochemistry and spectroelectrochemistry of hydrazido(2-) bridged bimetallic molybdenum species, and the X-ray crystal structure of [Mo{HB(3,5-Me_2pz)$_3$}(NO)Cl]$_2$(μ-NHNH) in solid solution

Stephen M. Charsley [a], Christopher J. Jones [b], Brian D. Neaves [a], Roman A. Kresiński [c,*], Sean L.W. McWhinnie [c], Jon A. McCleverty [d], Lesley J. Yellowlees [e]

[a] School of Chemistry, The University of Birmingham, Edgbaston, Birmingham, B15 2TT, UK
[b] School of Chemical Sciences, The University of Birmingham, Edgbaston, Birmingham, B15 2TT, UK
[c] Materials Research Group, Kingston University, Penrhyn Road, Kingston-upon-Thames, KT1 2EE, UK
[d] Department of Inorganic Chemistry, The University of Bristol, Cantock's Close, Bristol, BS8 1TS, UK
[e] Department of Chemistry, University of Edinburgh, Kings Buildings, West Mains Road, Edinburgh, EH9 3JJ, UK

Received 24 September 2001; accepted 8 January 2002

Abstract

The species [Mo{HB(3,5-Me_2pz)$_3$}(NO)Cl]$_2$(μ-NHNH) (**1**) (3,5-Me_2pz = 3,5-dimethylpyrazol-1-yl) and [Mo{HB(3,5-Me_2pz)$_3$}(NO)I]$_2$(μ-NHNH) have been synthesised. Electrochemical reduction of **1** results in a species with a near-infrared spectral band which shows no solvent dependence. Reoxidation results in the formation of another species which undergoes reversible reduction resulting in the development of another near-infrared spectral band which also is insensitive to solvent. These observations suggest that, in both cases, the mixed-valence species are class III. Additionally, **1** has been characterised structurally as a component of a solid solution also containing its chlorinated analogues; this determination shows that all components of the solution contain a near-planar Mo–NH–NH–Mo array and that Cl replacement is isomorphous. © 2002 Published by Elsevier Science Ltd.

Keywords: Nitrogenase; Hydrazido(2-); Molybdenum; Crystal structures; Spectroelectrochemistry

1. Introduction

Bimetallic complexes of redox active metal centres are of considerable interest since those containing bridging polyatomic ligands, such as pyrazine or 4,4′-bipyridyl, raise a number of theoretical challenges [1] with regard to describing the general nature of electronic interactions between metal centres. Bimetallic complexes incorporating small bridges such as O^{2-} and N_2 are clearly also of interest [2], these species often being best described by a delocalised bonding system akin to a metal–metal bond [3,4]. We have previously reported that [Mo{HB(3,5-Me_2pz)$_3$}(NO)I_2] and [W{HB(3,5-Me_2pz)$_3$}(NO)Br_2] react with various substituted hydrazines, H_2NNRR', to produce monodentate hydrazido(1-) complexes [5]. In addition, the complexes [Mo{HB(3,5-Me_2pz)$_3$}(NO)I($NHNH_2$)] and [W{HB(3,5-Me_2pz)$_3$}(NO)Br($NHNH_2$)] have been reported [5], and it is thought that these probably incorporate monodentate hydrazido(1-) ligands.

In order to further our studies of the {Mo{HB(3,5-Me_2pz)$_3$}(NO)X} (X = Cl, I) metal fragment bridged by small ligands [6–9], bimetallic species were synthesised incorporating $NHNH^{2-}$ as a bridge. [Mo{HB(3,5-Me_2pz)$_3$}(NO)I]$_2$(μ-O) has been shown to undergo a one-electron reduction, the product of which appears to be valence-trapped on the ESR timescale [10], and we were interested to establish if other bimetallic species with the metals in close proximity might display similar

* Corresponding author. Tel.: +44-208-547-7461; fax: +44-208-547-7562.
E-mail address: r.kresinski@king.ac.uk (R.A. Kresiński).

0277-5387/02/$ - see front matter © 2002 Published by Elsevier Science Ltd.
PII: S0277-5387(02)00841-0

properties. Furthermore, it was of interest to us to investigate the relevance of this system as a possible model for some of the chemical intermediates postulated in the past for the process of nitrogen fixation [11]. The fixation by nitrogenase is thought to occur via a process of reduction and concomitant protonation of dinitrogen coordinated to a transition metal, with one of the intermediate products in this process being a hydrazido moiety [12]. Whilst it is now thought more likely that the binding of nitrogen occurs at iron atoms [13,14], the possibility of binding occurring at molybdenum is still accepted by some [15]. Bimetallic molybdenum species are of considerable interest as reductive nitrogen-activating systems in their own right, and the Mo(III) complex $[Mo(N\{3,5\text{-}Me_2C_6H_3\}\{CCH_3(CD_3)_2\})_3]$ binds dinitrogen to form bimetallic species which can be cleaved thermally to afford the corresponding Mo(VI) nitrido-complexes [16]. Examples are known of bimetallic molybdenum complexes bridged by hydrazine [17–29], including some remarkable Fe–S–Mo clusters structurally reminiscent of the nitrogenase active site itself [28,29]. There is one example of a (μ_3-η^1,η^2-NH_2NH) ligand [30] and a few examples of bimetallic transition metal complexes containing the M-(η^1,η^1-NHNH)-M array have been structurally characterised [31], but none of these contain molybdenum. The N–N bond distances in these range from 1.23 to 1.41 Å and the nature of the bridge is thought to vary between the diazene-type [26,31–36] M–NH=NH–M for the shorter distances and the hydrazide(2-)-type [37] M–NH–NH–M for the longer. The 'side-on' bridging η^2,η^2-hydrazide ligand is also known [18].

2. Results and discussion

2.1. Synthetic studies

The compound $[Mo\{HB(3,5\text{-}Me_2pz)_3\}(NO)Cl]_2(\mu\text{-}NHNH)$ (**1**) was obtained in 42% yield from the reaction between hydrazine hydrate and $[Mo\{HB(3,5\text{-}Me_2pz)_3\}(NO)Cl_2]$ in toluene. Further reactions were carried out to investigate the formation of diastereomers, but changes in conditions failed to provide any conclusive evidence for the formation of a second isomer of $[Mo\{HB(3,5\text{-}Me_2pz)_3\}(NO)Cl]_2(\mu\text{-}NHNH)$, although a species tentatively identified as $[Mo\{HB(3,5\text{-}Me_2pz)_3\}(NO)Cl(NHNH_2)]$ was isolated in low yield. $[Mo\{HB(3,5\text{-}Me_2pz)_3\}(NO)I]_2(\mu\text{-}NHNH)$ (**2**) was synthesised in a similar manner to $[Mo\{HB(3,5\text{-}Me_2pz)_3\}(NO)Cl]_2(\mu\text{-}NHNH)$, but a shorter reaction time was required.

2.2. Spectroscopic studies

^1H NMR spectra were obtained for both **1** and **2**. As with [10] $[Mo\{HB(3,5\text{-}Me_2pz)_3\}(NO)Cl]_2(\mu\text{-}O)$, the spectra showed that the two metals are nonequivalent. Additionally, the methyl resonances are spread over a range of 1.69 and 1.68 ppm for **1** and **2**, respectively, a consequence of ring currents due to the interleaving of pyrazole rings. This range is less than that observed [10] for $[Mo\{HB(3,5\text{-}Me_2pz)_3\}(NO)Cl]_2(\mu\text{-}O)$, of 2.15 ppm, and may reflect the presence of a slightly longer bridge. AB patterns are observed for the NH protons in both bridges as a consequence of the molecular asymmetry, which persists in the solution state. The observation of sharp signals likely results from the hydrazine protons undergoing slow exchange, and because ^{14}N in a low symmetry environment will undergo very fast relaxation and so effectively decouple from the NH protons. Compounds **1** and **2** display two nitrosyl stretching frequencies at 1665 and 1635 cm^{-1} for **1** and 1670 and 1640 cm^{-1} for **2**. These frequencies are lower than those observed for $[Mo\{HB(3,5\text{-}Me_2pz)_3\}(NO)Cl]_2(\mu\text{-}O)$ and are in accord with greater π-donation from the NHNH bridging system. A Raman spectrum (Fig. 1) was obtained for **1**. This spectrum is unusual in that three vibrations are very intense in comparison with the remainder of the spectrum. The intensity of these vibrations cannot be due to resonance enhancement since the electronic absorption spectrum of **1** is transparent at the energy corresponding to the laser. Such high intensities will likely only occur if the Mo–N–N–Mo bonding system is delocalised and therefore polarisable, which explanation would be in accord with the spectroelectrochemical and crystallographic studies discussed below.

2.3. Electrochemical studies

Cyclic voltammetry of **1** in dichloromethane revealed one reduction process with a half wave potential of -0.480 ± 0.005 V. Further studies of digitised data using CONDECON software [38] indicated that the electron transfer involved one electron and was slightly slower than diffusion controlled and that some decomposition of the reduced product occurred [38–40]. The mechanism for the process is EC_{irrev}. Electrochemical studies of **2** were carried out in tetrahydrofuran and in acetonitrile, and in both cases two reduction processes were observed. A reversible one-electron process was observed with $E_{1/2} = -0.420 \pm 0.005$ V ($\Delta E = 80 \pm 10$ mV) in tetrahydrofuran and $E_{1/2} = -0.395 \pm 0.005$ V ($\Delta E = 60 \pm 10$ mV) in acetonitrile. Additionally an irreversible process, with E_p values of -1.970 ± 0.010 and -2.030 ± 0.005 V in tetrahydrofuran and acetonitrile respectively, was observed. In the case of **1** the absence of a second reduction process within the ranges attainable in these solvents, and the large potential difference between the

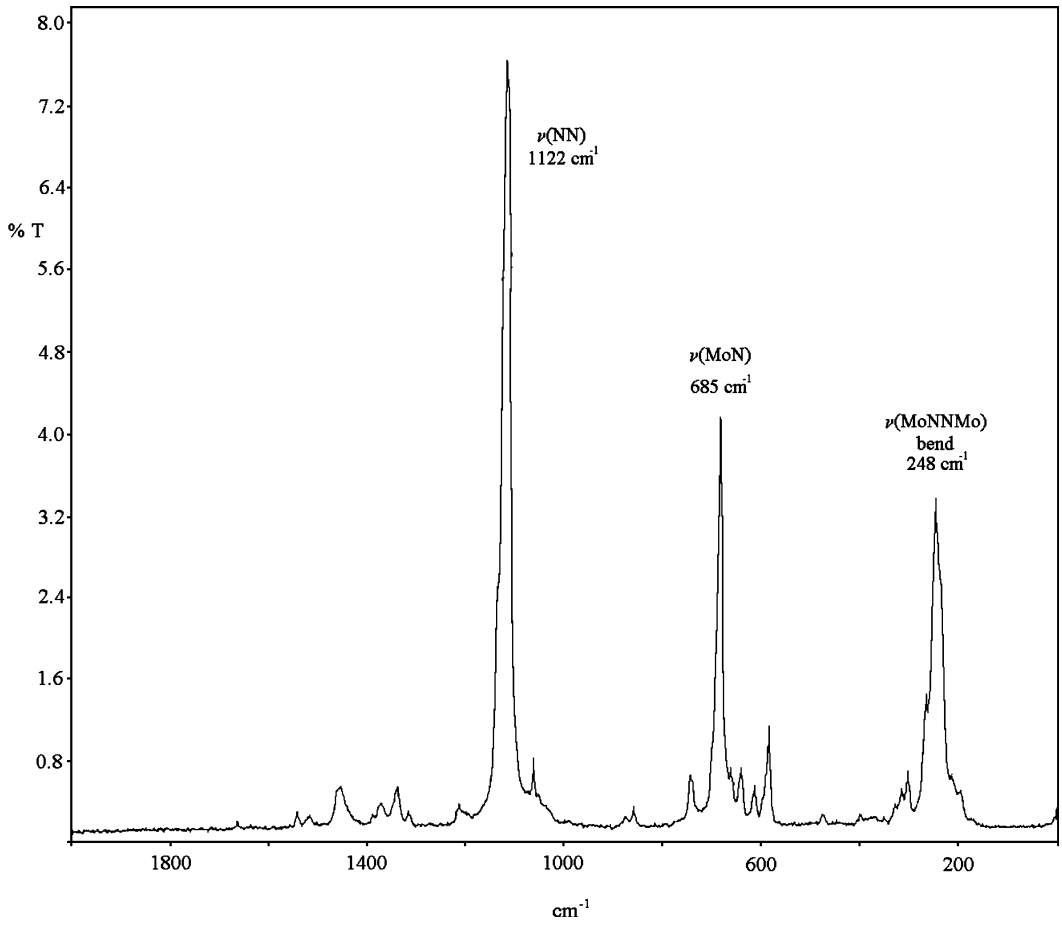


Fig. 1. Raman spectrum of $[Mo\{HB(3,5\text{-}Me_2pz)_3\}(NO)Cl]_2(\mu\text{-}NHNH)$.

first and second reduction processes in **2**, suggest that both species have strongly interacting metal centres.

2.4. Spectroelectrochemical studies

Reductive electrolysis of **1** was carried out in various solvents at 0 °C while monitoring the UV–Vis–NIR spectrum of the reaction mixture. The results are shown in Table 1. When electrolysis of **1** was carried out in chloroform, dichloromethane, or acetone the reduction process proved to be irreversible. Oxidation of the reduced product, $\mathbf{1}^-$, was also an irreversible process and afforded a compound **3** with a different absorption spectrum from that of the starting material. However, **3**

Table 1
Spectroelectrochemical data for $[Mo\{HB(3,5\text{-}Me_2pz)_3\}(NO)Cl]_2(\mu\text{-}NHNH)$ and its electrolytic products

Solvent		ν_{max} (cm^{-1}) (ε $dm^3\ mol^{-1}\ cm^{-1}$)			
$CHCl_3$	starting material (**1**)		19320(24652)	31170(84200)	
	after 1st reduction (to $\mathbf{1}^-$)	9135(4810)	22810(10500)	27750(21560)	
	after reoxidation (to **3**)		19280(8160)	32470(14780)	
	after 2nd reduction (to $\mathbf{3}^-$)	8680(85)	22180(8160)		
CH_2Cl_2	**1**		19230(18300)	30980(5910)	
	$\mathbf{1}^-$	9190(18300)	22220(14680)	27470(10368)	35920(12010)
	3		19260(6330)	31810(5420)	37090(10440)
	$\mathbf{3}^-$	8650(115)	22090(7840)		
CH_3COCH_3	**1**		19290(26180)		
	$\mathbf{1}^-$	9170(3920)	22300(19390)	27530(17990)	
	3		19610(2930)		
	$\mathbf{3}^-$	8540(90)	22140(4930)		
CH_3CN	**1**		19320(14820)	31260(5300)	
	3	8700(430)	22180(26130)		

could be reduced reversibly, the spectrum of $\mathbf{3}^-$ differing from that of $\mathbf{1}^-$.

In acetonitrile a reversible electrolytic process was observed, but the reduction product appeared to be that which was obtained upon the *second* reduction cycle of **1** (i.e. $\mathbf{3}^-$) in the other three solvents. Attempts were made to generate **3** in bulk, with a view to its chemical characterisation. Electrochemical reduction of **1** in dichloromethane followed by electrochemical or aerial reoxidation yielded a material with identical UV–Vis spectral characteristics to that of **3**. However, after passing this down a silica gel column, **1** was once again obtained, as evidenced by UV–Vis and ^{1}H NMR spectra, with recoveries of 50–80%. Attempts were made to avoid the reversion to **1** by measuring the ^{1}H NMR spectrum of the reduction–reoxidation product without chromatography. Once again the spectrum was identical to that of **1**. It is not yet clear why the transformation to **3** should occur upon oxidation of $\mathbf{1}^-$, nor why the electrochemical behaviour of **1** in acetonitrile is different. An additional bulk electrolysis was carried out upon **1** in order to generate the electrolytic product for cyclic voltammetry. The electrolysis was carried out at room temperature in CH_2Cl_2 containing 0.2 M Bu_4NBF_4 as supporting electrolyte. Following reduction of 20 mg of **1** in 10 cm^3 of solvent at -1.0 V and reoxidation at $+0.1$ V relative to a SCE, 5 cm^3 of the product solution was transferred to a nitrogen filled electrochemical cell. Cyclic voltammetry revealed a broad wave ($\Delta E_p = 230$ mV) which appeared to represent a reversible process characterised by $E_{1/2} = -0.550 \pm 0.020$ V. The broad nature of the wave probably indicates slow electron transfer which contrasts with the behaviour exhibited by **1** and the $E_{\frac{1}{2}}$ data indeed shows that **1** is 70 ± 40 mV easier to reduce than its electrolysis product **3**. The UV–Vis bands of **3** are also shown in Table 1. The similarity between the electronic spectra of the two species, and the facile transformation of **3** back into **1**, suggest that they are closely related.

It is difficult to come to any conclusion about the nature of the bands in any of the species observed. The spectra are dominated by charge transfer bands and these show varying amounts of solvent dependence. Figs. 2–4 show the progress of an experiment involving the electrolysis of, respectively, **1**–$\mathbf{1}^-$, $\mathbf{1}^-$–**3**, and **3**–$\mathbf{3}^-$ in $CHCl_3$. It should be noted that the absence of clean isosbestic points indicates the presence of more than two species in solution, which may indicate that some decomposition accompanies these redox processes.

Whereas many models describing mixed-valence behaviour are currently vying for acceptance, that developed by Hush [41] remains the easiest to apply. This model relates the energy of any intervalence charge transfer (IVCT) band, E_{op}, to spectroscopically measurable properties of the molecule under consideration and

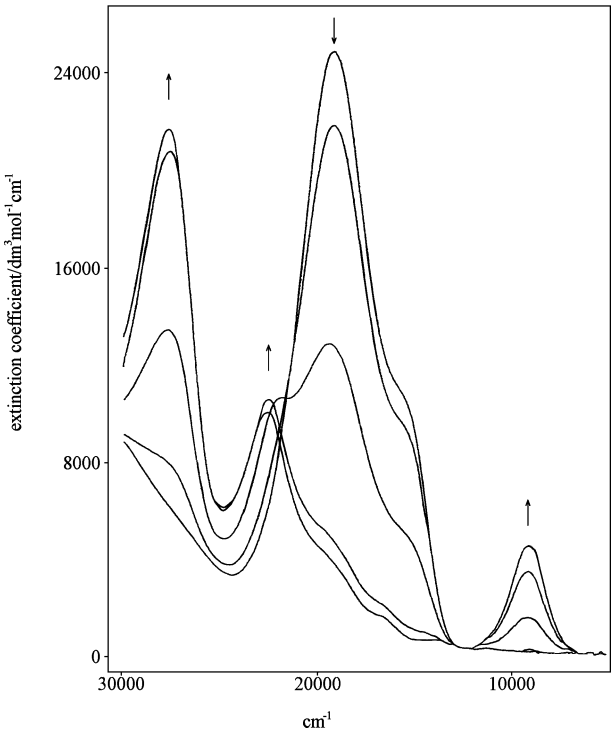


Fig. 2. Plots showing the changes in the electronic spectrum of $[Mo\{HB(3,5\text{-}Me_2pz)_3\}(NO)Cl]_2(\mu\text{-}NHNH)$ (**1**) upon electrolytic reduction to $\mathbf{1}^-$ in chloroform at 0 °C.

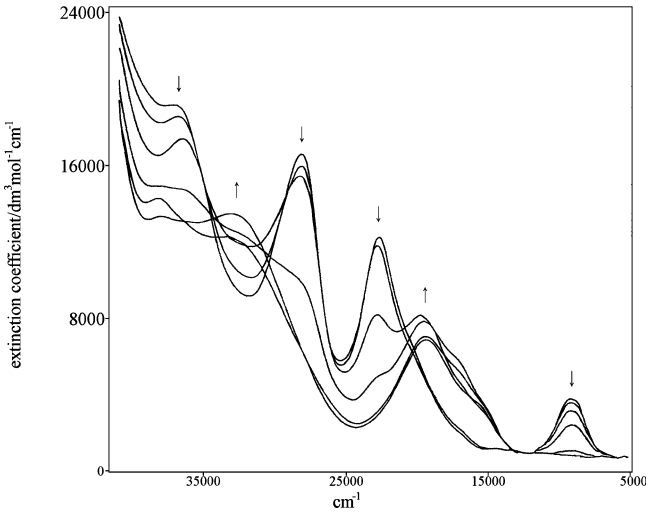


Fig. 3. Plots showing the changes in the electronic spectrum of $\mathbf{1}^-$ upon electrolytic reoxidation to **3** in chloroform at 0 °C.

to solvent properties. Amongst the many predictions of the model is that E_{op} is dependent upon $(1/D_{op} - 1/D_s)$, where D_{op} and D_s are the optical and static dielectric constants of the solvents. However, plots of E_{op} against $(1/D_{op} - 1/D_s)$ for the NIR bands observed for $\mathbf{1}^-$ show no solvent dependence; this and the comparatively high intensity of the bands suggest that $\mathbf{1}^-$ is a delocalised species.

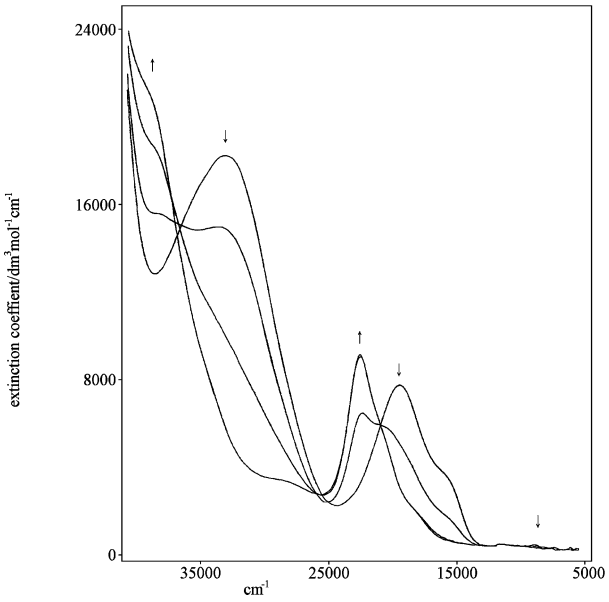


Fig. 4. Plots showing the changes in the electronic spectrum of **3** upon electrolytic reduction to $\mathbf{3}^-$ in chloroform at 0 °C.

2.5. Structural studies

Repeated attempts to grow single crystals of pure **1** suitable for analysis by X-ray diffraction failed. However, we found that crystals could be grown from a dichloromethane solution of a sample which dated from a period when, in our studies, we found it difficult to prepare the precursor [Mo{HB(3,5-Me_2pz)$_3$}(NO)Cl_2] reproducibly due to some degree of pyrazolyl ring chlorination [42]. On the basis of the ^{1}H NMR spectrum of the resulting crystalline matrix **7**, it appears to be a solid solution of four components, namely **1**, the chloro-derivative [Mo(HB(3,5-Me_2pz)$_2$(4-Cl-3,5-Me_2pz)}(NO)Cl](μ-NHNH)[Mo{HB(3,5-Me_2pz)$_3$}(NO)Cl] (two isomers, **4** and **5**), and the dichloro-derivative [Mo{HB(3,5-Me_2pz)$_2$(4-C1-3,5-Me_2pz)}(NO)Cl]$_2$(μ-NHNH) (**6**). The latter three components presumably originate from ring chlorination during the synthesis of [Mo{HB(3,5-Me_2pz)$_3$}(NO)Cl_2], rather than rearrangement or decomposition at a later stage [42]. Integrations of the signals originating from the hydrazido and pyrazolyl 4-position protons are consistent with a **1**:**4**:**5**:**6** ratio of 41.0:34.0:15.5:9.5, which corresponds to 43.5% chlorine substitution at one site and 25.0% at the other giving an overall average of 34.3% chlorine substitution in the sample as a whole.

A representation [43] of the model of **1** in **7** is shown in Fig. 5. Table 2 contains selected bond distances and angles. The structure is clearly binuclear, containing two {Mo{HB(3,5-Me_2pz)$_3$}(NO)Cl} moieties possessing different degrees of chlorine occupancy at the 4-position of the pyrazolyl ring *trans*- to the nitrosyl ligand. These two groups are linked by a (μ-NHNH) bridge. Final, refined, chlorine occupancies for the two 4-pyrazolyl

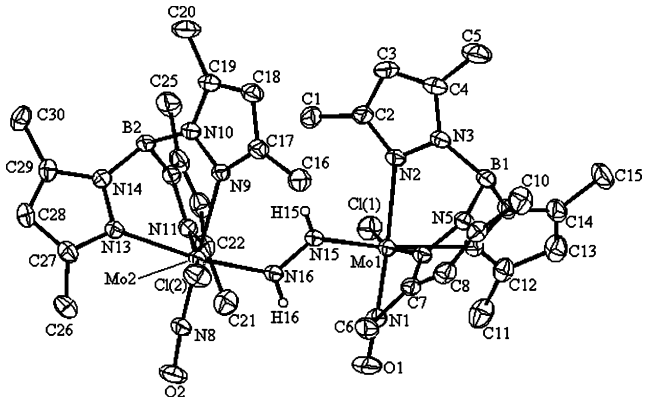


Fig. 5. A representation 43 of **1** within the matrix **7**. All hydrogens, apart from H15 and H16, have been omitted for clarity. Thermal ellipsoids are depicted at the 30% probalitity level.

Table 2
Selected bond lengths (Å) and angles (°) for **1** within the matrix **7**

Bond lengths (Å)			
Mo1–N1	1.756(3)	Mo2–N8	1.761(3)
Mo1–N2	2.241(3)	Mo2–N9	2.249(3)
Mo1–N4	2.181(3)	Mo2–N11	2.180(3)
Mo1–N6	2.200(3)	Mo2–N13	2.171(3)
Mo1–N15	1.950(3)	Mo2–N16	1.969(3)
Mo1–Cl(1)	2.400(1)	Mo2–Cl(2)	2.399(1)
N1–O1	1.198(4)	N8–O2	1.196(4)
N15–H15	0.75(4)	N16–H16	0.82(4)
N15–N16	1.362(4)		
Bond angles (°)			
N1–Mo1–N2	176.82(14)	N8–Mo2–N9	177.82(13)
N1–Mo1–N4	96.00(14)	N8–Mo2–N11	96.53(14)
N1–Mo1–N6	97.75(14)	N8–Mo2–N13	96.03(13)
N1–Mo1–N15	91.87(15)	N8–Mo2–N16	89.66(14)
N1–Mo1–Cl(1)	92.45(12)	N8–Mo2–Cl(2)	92.04(11)
N2–Mo1–N4	84.63(11)	N9–Mo2–N11	85.19(11)
N2–Mo1–N6	85.43(12)	N9–Mo2–N13	85.58(11)
N2–Mo1–N15	84.99(12)	N9–Mo2–N16	89.11(12)
N2–Mo1–Cl(1)	87.59(9)	N9–Mo2–Cl(2)	86.46(8)
N4–Mo1–N6	79.73(11)	N11–Mo2–N13	80.05(12)
N4–Mo1–N15	92.15(12)	N11–Mo2–N16	86.46(12)
N4–Mo1–Cl(1)	165.41(8)	N11–Mo2–Cl(2)	167.96(9)
N6–Mo1–N15	167.98(13)	N13–Mo2–N16	165.86(12)
N6–Mo1–Cl(1)	87.36(9)	N13–Mo2–Cl(2)	90.67(9)
N15–Mo1–Cl(1)	99.46(10)	N16–Mo2–Cl(2)	102.09(10)
O1–N1–Mo1	176.9(3)	O2–N8–Mo2	175.4(3)
H15–N15–N16	105.0(3)	H16–N16–N15	105.0(3)
H15–N15–Mo1	121.0(3)	H16–N16–Mo2	122.0(3)
N16–N15–Mo1	133.3(3)	N15–N16–Mo2	129.9(3)

positions were 48.0% for Cl(3) and 20.3% Cl(4), meaning the average chlorine 4-position occupancy, as estimated by crystallographic means, is 33.6%, which figure is in very close agreement with that obtained from NMR experiments. The two Mo centres are crystallographically distinct, as they are in solution also. Both nitrosyls point in the same direction away from the metal centres and thus the overall conformation of the molecule can be contrasted with that of [Mo{HB(3,5-

$Me_2pz)_3\}(NO)I]_2(\mu\text{-}O)$, which has nitrosyls at a relative torsion [10] of approximately 90°, or $[Mo\{HB(3,5\text{-}Me_2pz)_3\}(NO)I]_2(\mu\text{-}SS)$, in which the nitrosyls are inclined [6] at 180°.

The coordination environment around the Mo atoms is distorted octahedral, as is typical of complexes of this sort [42,44–50]. The trispyrazolylborate ligand, which occupies three *fac*- sites of the octahedron, is held by Mo–N bonds of average distance 2.207[1] Å. This compares with a mean distance of 2.221[2] Å ($[\ ] = \{\Sigma_{i=1}^{i=n}(\sigma_i^2)\}^{1/2}/n$) obtained from a survey of 10 other $\{Mo^{II}\{HB(3,5\text{-}Me_2pz)_3\}(NO)X\}$ (X = Cl, I)—containing structures for which bond error data is published [5,51–57]. It might be expected that the steric crowding which causes the nonequivalence of the metals might also result in greater Mo–(N)pyrazolyl distances but, on the contrary, the above comparison indicates that the trispyrazolylborate ligands are held closely to the metal. The low N–O bond order indicated by the low infrared stretching frequency of the nitrosyl ligand appears also to be detectable in the crystal structure. The N–O distances of 1.195(3) and 1.193(3) Å are significantly longer than the mean of 1.169(5) Å from the above survey group; despite the possibility that the implied electron richness of the Mo centre originates from some degree of pπ–dπ electron donation from ligand to metal, the Mo–N(hydrazido) bond distances of 1.948(2) and 1.968(2) Å do not appear to be especially short, as compared with Mo–N(amido) distances of 1.945(19) and 1.935(20) Å in $[Mo\{HB(3,5\text{-}Me_2pz)_3\}(NO)(NHBu)_2]$, for example [46].

The bridge is the most interesting aspect of the molecular structure. Overall, it is almost planar, deviations from the best plane through Mo1–N15–N16–Mo2 being 0.065(1), −0.073(1), −0.054(1), 0.061(1), −0.24(3) and 0.17(3) Å for Mo1, N15, N16, Mo2, H15 and H16, respectively. Mo1 and Mo2 are in mutual *trans*- positions across the planar bridge, the Mo–N–N–Mo torsion angle being 169.9(1)°. The N15–N16 bond length in the (NHNH) bridge is 1.362(3) Å and as such is only 0.05 Å shorter than that observed in $[W(\eta^5\text{-}C_5Me_4(^tBu))(CCMe_3)I](\mu\text{-NHNH})$ (1.410(9) Å) [37], but is 0.11 Å longer than that found in $[Cr(CO)_5]_2(\mu\text{-NHNH})$ [32] (1.250 Å), which would indicate that the (NHNH) bridge is more akin to the $(NH–NH)^{2-}$ hydrazido(2-) type than the (HN=NH) diazene type. The angles at the bridge nitrogens do not seem to be diagnostic of the nature of the bridge, all the (μ-NHNH) complexes which have been crystallographically characterised displaying similar M–N–N angles. In the present study the angles are 133.5(2)° and 130.2(2)°, in the case of $[W(\eta^5\text{-}C_5Me_4(^tBu))(CCMe_3)I]_2(\mu\text{-NHNH})$ the angle [37] is 131.7(5)°, whilst in $[Cr(CO)_5]_2(\mu\text{-NHNH})$ the angle is 130.5°. Additionally, the two complexes $[Ru(PPh_3)(L)]_2(\mu\text{-NHNH})$ (where H_2L is [35] $\{HS(C_6H_4\text{-}2)SCH_2\}_2$ or [36] $\{HS(C_6H_2(3,5\text{-}CMe_3)\text{-}2)SCH_2\}_2$, display N–N distances of 1.301(14) and 1.279(14) Å and Ru–N–N angles of 129.3(9)° and 131.9(8)°, respectively. An sp^2 hybridisation appears to be the norm for any N ligand attached to the $\{Mo\{HB(3,5\text{-}Me_2pz)_3\}(NO)\}$ fragment [47], and the bridge hydrogens were easily located and refined to positions consistent with this in the present study. The N–H vectors do not quite bisect the complements of the Mo–N–N angles, the hydrogens being inclined away from the Mo atoms by 5°–8°.

The variation in N–N bond length in μ-NHNH bridges suggests that a balance exists between donation of the nitrogen 2p electron density to empty metal orbitals and population of a N–N bond of π-symmetry. A qualitative bonding scheme for the M–N–N–M fragment is shown in Fig. 6, which is applicable to any of the systems discussed above. The exact nature of the NHNH bridge will be affected by the relative coefficients of the metal and nitrogen orbitals. Fig. 6 also provides an explanation for the spectral changes upon reduction of **1**. In the neutral form the 1a and 1b levels will be filled and reduction will result in an electron occupying the 2a level. The unpaired electron may then undergo low energy transitions to the 2b level.

3. Conclusion

$[Mo\{HB(3,5\text{-}Me_2pz)_3\}(NO)Cl]_2(\mu\text{-NHNH})$ (**1**) and $[Mo\{HB(3,5\text{-}Me_2pz)_3\}(NO)I]_2(\mu\text{-NHNH})$ (**2**) were synthesised. Species **1** is electrochemically reducible to $\mathbf{1}^-$ which, on reoxidation, affords the structurally uncharacterised **3**, whose electrochemical behaviour is different from **1** in that it undergoes reversible reduction. All attempts to isolate **3** resulted in reversion to **1**, implying that **1** and **3** are closely related structurally. Investigation of **1** by Raman spectroscopy and of the reduction products of **1** by spectroelectrochemistry suggest that both **1** and $\mathbf{1}^-$ are electronically delocalised, and that $\mathbf{1}^-$ and $\mathbf{3}^-$ are class III mixed-valence species.

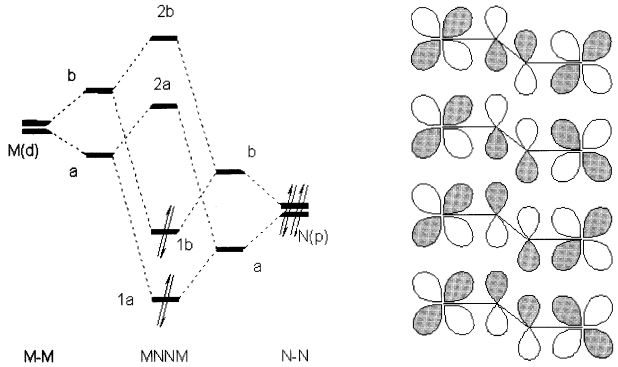


Fig. 6. Qualitative Mo diagram of an M–NH–NH–M bridge treated in C_2 symmetry, assuming sp^2 hybridisation of the nitrogens.

The molecular structure of the solid solution **7** confirms the presence of a (μ-NHNH) ligand for all its constituents. The structure also supports the suggestion that the nitrogens in the bridge are sp^2-hybridised. Consideration of other structural data in the literature suggests that the (NHNH) bridge in the present study displays some double bond character, but rather less than some similar compounds. It is appropriate, then, that the bridging ligand in $[Mo\{HB(3,5\text{-}Me_2pz)_3\}(NO)Cl]_2(\mu\text{-}NHNH)$ be considered a hydrazide(2-) moiety, albeit with sp^2 nitrogens which allow donation of electron density into empty metal orbitals.

4. Experimental

4.1. Materials

All reactions were carried out under dry nitrogen and $C_6H_5CH_3$ was distilled from Na and benzophenone prior to use. The complexes $[Mo\{HB(3,5\text{-}Me_2pz)_3\}(NO)X_2]$ (X = Cl or I) were prepared as described in the literature [42,44,45]. Column chromatography was carried out using silica gel as the stationary phase (Merck 60, 70–230 mesh).

4.2. Physical measurements

Infrared, electronic, mass, 300 and 400 MHz NMR spectra were recorded respectively, on Perkin–Elmer 297, Perkin–Elmer Lambda 9, Kratos MS 90, Bruker WH300 and Bruker WH400 instruments. Raman spectra were obtained on a Perkin–Elmer FT-Raman 1700X spectrometer using a Nd:YAG laser (1064 nm) and an InGaAs detector cooled to 77 K. Spectra were obtained from solids as powders pressed into a cup sample holder. Elemental analysis was performed by the Microanalytical Laboratory, University of Birmingham. Cyclic voltammetry studies were carried out in 0.2 M Bu_4NBF_4 CH_2Cl_2 solution, the CH_2Cl_2 having been stored over K_2CO_3 and redistilled from CaH_2, in a three-electrode cell comprising a Pt bead working electrode, a Pt wire secondary electrode and a calomel reference electrode. Ferrocene (Fc) was added as an internal reference (Fc/Fc^+: $E_{\frac{1}{2}} = 0.550$ V). Initial studies were carried out using a PAR 174A potentiostat with built-in waveform generator with a Philips X–Y pen recorder. Data were also acquired using a PAR 360 potentiostat interfaced with an Amstrad PC1512 computer via an EG&G analogue–digital convertor and processed using EG&G CONDECON [38] 300 software. Spectroelectrochemistry was carried out using a Perkin–Elmer Lambda 9 spectrometer whilst samples were electrolysed in an optically transparent thin layer electrochemistry (OTTLE) cell using a Metrohm potentiostat. The temperature was held at 0 °C. Samples were dissolved in 0.4 M Bu_4NBF_4 of the requisite solvent and an Ag–AgCl reference electrode was employed. Reductive electrolysis was carried out at potentials between −1.0 and −1.3 V relative to a Ag–AgCl electrode.

4.3. Synthesis of $[Mo\{HB(3,5\text{-}Me_2pz)_3\}(NO)Cl]_2(\mu\text{-}NHNH)$

A solution of $[Mo\{HB(3,5\text{-}Me_2pz)_3\}(NO)Cl_2]$ (0.50 g, 1.01 mmol) and hydrazine hydrate (0.04 g, 0.80 mmol) in $C_6H_5CH_3$ (100 cm^3) was heated to reflux for 3 days. The resulting purple solution was cooled, filtered and the filtrate was evaporated to dryness in vacuo. The solid obtained was purified by column chromatography using CH_2Cl_2 as eluant. The main purple fraction was collected. Recrystallisation from CH_2Cl_2–n-C_5H_{12} gave purple microcrystals (0.2 g, 42%). IR cm^{-1} (KBr): 3310, 3260 ν(NH), 2550 ν(BH), 1665, 1635 ν(NO). ^{1}H NMR ($CDCl_3$): δ *AB* system, $A = 14.85$, $B = 13.63$ (2H, $J_{AB} = 13.6$ Hz), 5.95 (1H, s), 5.88 (1H, s), 5.83 (1H, s), 5.81 (1H, s), 5.47 (1H, s), 5.42 (1H, s) ($C–H_{pyrazolyl}$), 2.68 (3H, s), 2.63 (3H, s), 2.54 (3H, s), 2.52 (3H, s), 2.36 (3H, s), 2.34 (6H, s), 2.33 (6H, s), 2.31 (3H, s), 1.39 (3H, s), 0.99 (3H, s) ($C–H_{methyl}$). *Anal*. Found: $C_{30}H_{46}B_2Cl_2Mo_2N_{16}O_2$: C, 42.2; H, 5.8; N, 21.6. *Anal*. Calc. C, 39.4; H, 5.1; N, 24.5%.

4.4. Synthesis of $[Mo\{HB(3,5\text{-}Me_2pz)_3\}(NO)I]_2(\mu\text{-}NHNH)$

$[Mo\{HB(3,5\text{-}Me_2pz)_3\}(NO)I_2]$ (2.0 g, 2.95 mmol) was dissolved in CH_2Cl_2 (100 cm^3). Hydrazine hydrate (0.221 g, 4.43 mmol) was added to the stirred solution. The colour changed immediately to yellow. Upon stirring overnight the solution became blue. The solvent was removed in vacuo and the residue was redissolved in CH_2Cl_2 (10 cm^3). The solution was purified by column chromatography using CH_2Cl_2 as eluant. The second blue fraction was collected, the solvent removed in vacuo and the residue triturated with n-C_6H_{14}. The resulting blue product was filtered and dried (0.2 g, 10%). IR cm^{-1} (KBr): 3300, 3265 (ν_{NH}), 2545 (ν_{BH}), 1670, 1640 (ν_{NO}). ^{1}H NMR ($CDCl_3$): δ *AB* system, $A = 12.32$, $B = 11.80$ (2H, $J_{AB} = 9.0$ Hz), 5.89 (1H, s), 5.85 (1H, s), 5.80 (2H, s), 5.54 (1H, s), 5.48 (1H, s) ($C–H_{pyrazolyl}$), 2.72 (3H, s), 2.64 (3H, s), 2.57 (3H, s), 2.54 (3H, s), 2.45 (3H, s), 2.43 (3H, s), 2.38 (6H, s), 2.35 (6H, s), 1.38 (3H, s), 1.14 (3H, s) ($C–H_{methyl}$). *Anal*. Found: $C_{30}H_{46}B_2I_2Mo_2N_{16}O_2$: C, 32.2; H, 4.2; N, 19.6. Calc. C, 31.9; H, 3.9; N, 19.7%.

4.5. Crystallographic analysis of solid solution 7

$C_{30}H_{45.33}B_2Cl_{2.67}Mo_2N_{16}O_2$, $M = 970.4$, $P2_1/n$, $a = 11.3563(14)$ Å, $b = 22.3570(22)$ Å, $c = 16.5725(18)$ Å, $\beta = 97.430(11)°$, $V = 4172$ Å^3, and $Z = 4$, D_c, = 1.545 g

cm^{-3}, Mo Kα ($\lambda = 0.71069$ Å), $\mu = 0.822$ mm^{-1}, $T = 293$ K. A rhomboidal purple–black crystal of **7**, measuring approximately $0.6 \times 0.6 \times 0.2$ mm^3, was glued atop a glass fibre and mounted on an Enraf-Nonius CAD-4 diffractometer. The unit cell was determined using 14 randomly located reflections, and finally refined using 25 reflections selected from the data set. Intensities were measured with an ω–2θ bisecting geometry method using variable scan rate and angle $(1.00+0.35 \tan\theta)^\circ$. Nine thousand two hundred and sixty data were measured with $2^\circ < 2\theta < 50^\circ$, $-1 \leq h \leq 13$, $-1 \leq k \leq 26$, $-19 \leq l \leq 19$, during which two standard reflections were measured every hour, with little variation. Data were corrected for Lp and slight standard decay. Equivalent reflections were merged to give 7340 unique data. The Mo atoms were located using direct methods [58] and other non-H atoms located from subsequent difference Fourier syntheses [59]. Non-H atoms were refined [59] anisotropically, the two crystallographically distinct pyrazolyl Cl atoms being assigned individual refined site occupancies. Free positional refinement proved unstable, so the pyrazolyl Cl atoms were moved by hand, every few refinement cycles, onto theoretical positions with C–Cl distances of 1.715 Å. This resulted in satisfactory convergence. One aberrant reflection with $F_o \ll F_c$ was deleted from the dataset. Hydrogen atoms were placed in idealised positions on their parent atoms ($C–H_{pyrazolyl}$, 0.93 Å; $C–H_{methyl}$, 0.96 Å; B–H, 0.98 Å) and refined isotropically. An absorption correction [60] was applied, based on a converged model including anisotropic non-H and all hydrogen atoms. On reconvergence using the above procedure, the hydrogens' refined, type-specific isotropic thermal parameters were B–H, $C–H_{pyrazolyl}$ 0.058 $Å^2$, $C–H_{methyl}$ 0.102 $Å^2$ except for the hydrogens of the hydrazide bridge, which were successfully found and refined ($U_{iso} = 0.034$ Å). The final weighting scheme was $w^{-1} = (\sigma^2 F_o^2 + (0.0556\ P)^2 + 4.19\ P)$ where $3P = F_o^2 + 2F_c^2$. All atoms refined satisfactorily, with no indication of significant disorder, throughout the process, with the exception of Cl(4) (a pyrazolyl chlorine) whose thermal ellipsoid seems elongated roughly in the direction perpendicular to the pyrazolyl ring. Final figures of merit were $wR_2 = 11.01\%$ and equivalent $[I > 2\sigma(I)]$ $R_1 = 3.81\%$. The largest peak in the difference map was 1.70 e $Å^{-3}$, 1.07 Å from Cl(4).

5. Supplementary material

Crystallographic data for structural analysis have been deposited with the Cambridge Crystallographic Data Center, CCDC No. 170971 for compound **1**. Copies of this information may be obtained free of charge from The Director, CCDC, 12 Union Road, Cambridge, CB2 1EZ, UK (fax: +44-1223-336033; e-mail: deposit@ccdc.cam.ac.uk or www: http://www.ccdc.cam.ac.uk).

Acknowledgements

We would like to thank Terry Green for technical assistance and the EPSRC NMR service based at Warwick University for 400 MHz NMR spectra. We wish to acknowledge the use of the EPSRC's Chemical Database Service at Daresbury.

References

[1] D.E. Richardson, H. Taube, Coord. Chem. Rev. 60 (1984) 107.
[2] T.J. Meyer, Ann. N.Y. Acad. Sci. 313 (1978) 496.
[3] J.E. Early, T. Fealey, Inorg. Chem. 12 (1973) 323.
[4] C.K. Jorgensen, L.E. Orgel, Mol. Phys. 4 (1961) 215.
[5] J.A. McCleverty, A.E. Rae, I. Wolochowicz, N.A. Bailey, J.M.A. Smith, J. Chem. Soc., Dalton Trans. (1983) 71.
[6] S.L.W. McWhinnie, C.J. Jones, J.A. McCleverty, T.A. Hamor, J.-D.F. Foulon, Polyhedron 12 (1993) 37.
[7] H. Adams, N.A. Bailey, G. Denti, J.A. McCleverty, J.M.A. Smith, A. Wlodarczyk, Chem. Commun. (1981) 348.
[8] H. Adams, N.A. Bailey, G. Denti, J.A. McCleverty, J.M.A. Smith, A. Wlodarczyk, J. Chem. Soc., Dalton Trans. (1983) 2287.
[9] S.L.W. McWhinnie, S.M. Charsley, C.J. Jones, J.A. McCleverty, L.J. Yellowlees, J. Chem. Soc., Dalton Trans. (1993) 413.
[10] A. Wlodarczyk, J.P. Maher, S. Coles, D.E. Hibbs, M.H.B. Hursthouse, K.M.A. Malik, J. Chem. Soc., Dalton Trans. (1997) 2597.
[11] J. Chatt, G. Leigh, Chem. Soc. Rev. 1 (1972) 121.
[12] R.A. Henderson, I. Leigh, C.J. Pickett, Adv. Inorg. Chem. Radiochem. 27 (1983) 197.
[13] P.D. Christie, H.-I. Lee, L.M. Cameron, B.J. Hales, W.H. Orme-Johnson, B.M. Hoffman, J. Am. Chem. Soc. 118 (1996) 8707.
[14] S.D. Conradson, B.K. Burgess, S.A. Vaughn, A.L. Roe, B. Hedman, K.O. Hodgson, R.H. Holm, J. Biol. Chem. 264 (1989) 15967.
[15] K.L.C. Grönberg, C.A. Gormal, M.C. Durrant, B.E. Smith, R.A. Henderson, J. Am. Chem. Soc. 120 (1998) 10613.
[16] C.E. Laplaza, M.J.A. Johnson, J.C. Peters, A.L. Odom, E. Kim, C.C. Cummins, G.N. George, I.J. Pickering, J. Am. Chem. Soc. 118 (1996) 8623.
[17] S. Du, N. Zhu, X. Wu, J. Lu, Inorg. Chem. 31 (1992) 2847.
[18] L. Blum, I.D. Williams, R.R. Schrock, J. Am. Chem. Soc. 106 (1984) 8316.
[19] T. Furuhashi, M. Kawano, Y. Koide, R. Somazawa, K. Matsumoto, Inorg. Chem. 38 (1999) 109.
[20] M. Jahncke, A. Neels, H. Stoeckli-Evans, G. Suss-Fink, J. Organomet. Chem. 565 (1998) 97.
[21] L.-L. Nguyen, J. Kozelka, C. Bois, Inorg. Chim. Acta 190 (1991) 217.
[22] D. Sellmann, P. Kreutzer, G. Huttner, A. Frank, Z. Naturforsch., Teil. B 33 (1978) 1341.
[23] G. Barrado, D. Miguel, V. Riera, S. Garcia-Granda, J. Organomet. Chem. 489 (1995) 129.
[24] M. Kawano, C. Hoshino, K. Matsumoto, Inorg. Chem. 31 (1992) 5158.
[25] N. Zhu, S. Du, X. Wu, J. Lu, Angew. Chem. Int. Ed. Engl. 31 (1992) 87.
[26] D. Sellmann, K. Engl, F.W. Heinemann, J. Sieler, Eur. J. Inorg. Chem. (2000) 1079.

[27] K. Mashima, H. Kaneyoshi, S. Kaneko, K. Tani, A. Nakamura, Chem. Lett. (1997) 569.
[28] P.R. Challen, S.-M. Koo, C.G. Kim, W.R. Dunham, D. Coucouvanis, J. Am. Chem. Soc. 112 (1990) 8606.
[29] P.E. Mosier, C.G. Kim, D. Coucouvanis, Inorg. Chem. 32 (1993) 2620.
[30] T. Jenke, H. Stoeckli-Evans, G. Suss-Fink, J. Organomet. Chem. 391 (1990) 395.
[31] G. Huttner, W. Gartzke, K. Allinger, J. Organomet. Chem. 91 (1975) 47.
[32] G. Huttner, W. Gartzke, K. Allinger, Angew. Chem., Int. Ed. Engl. 13 (1974) 822.
[33] D. Sellmann, W. Soglowek, F. Knoch, M. Moll, Angew. Chem., Int. Ed. Engl. 28 (1989) 1271.
[34] D. Sellmann, H. Friedrich, F. Knoch, M. Moll, Z. Naturforsch., Teil. B 48 (1994) 76.
[35] D. Sellmann, E. Bohlen, M. Waeber, G. Huttner, L. Zsolnai, Angew. Chem., Int. Ed. Engl. 24 (1985) 981.
[36] D. Sellmann, J. Kappler, M. Moll, F. Knoch, Inorg. Chem. 32 (1993) 960.
[37] M.R. Churchhill, Y.-L. Li, L. Blum, R.R. Schrock, Organometallics 3 (1984) 109.
[38] Convolution techniques in electrochemistry using the CONDECON system, EG&G Instruments, Wokingham, Berkshire, UK.
[39] L. Nadjo, J.M. Saveant, Electroanal. Interf. Chem. 48 (1973) 113.
[40] J.C. Imbeau, J.M. Saveant, Electroanal. Interf. Chem. 44 (1973) 169.
[41] N.S. Hush, Prog. Inorg. Chem. 8 (1967) 391.
[42] J.A. McCleverty, D. Seddon, N.A. Bailey, N.W. Walker, J. Chem. Soc., Dalton Trams. (1976) 898.
[43] K. Davies, SNOOPI, Molecular Plotting Programme, University of Oxford, 1983.
[44] S. Trofimenko, J. Am. Chem. Soc. 89 (1967) 3904.
[45] S.J. Reynolds, C.F. Smith, C.J. Jones, J.A. McCleverty, Inorg. Synth. 23 (1985) 144.
[46] N. Al-Obaidi, T.A. Hamor, C.J. Jones, J.A. McCleverty, K. Paxton, J. Chem. Soc., Dalton Trans. (1986) 1525.
[47] D.A. Fletcher, R.F. McMeeking, D. Parkin, J. Chem. Inf. Comput. Sci. 36 (1996) 746.
[48] J.A. McCleverty, A.E. Rae, I. Wolochowicz, N.A. Bailey, J.M.A. Smith, J. Chem. Soc., Dalton Trans. (1982) 951.
[49] C.J. Jones, J.A. McCleverty, B.D. Neaves, S.J. Reynolds, H. Adams, N.A. Bailey, G. Denti, J. Chem. Soc., Dalton Trans. (1986) 733.
[50] S.A. Roberts, J.H. Enemark, Acta Crystallogr., Sect. C 45 (1989) 1292.
[51] J.A. McCleverty, G. Denti, S.J. Reynolds, A.S. Drane, N. El Murr, N.A. Bailey, H. Adams, J.M.A. Smith, J. Chem. Soc., Dalton Trans. (1983) 81.
[52] N. Al-Obaidi, T.A. Hamor, C.J. Jones, J.A. McCleverty, K. Paxton, A.J. Howes, M.J. Hursthouse, Polyhedron 7 (1988) 1931.
[53] A. Wlodarczyk, S.S. Kurek, J.-D.F. Foulon, T.A. Hamor, J.A. McCleverty, Polyhedron 11 (1992) 217.
[54] J.A. McCleverty, A.E. Rae, I. Wolochowicz, N.A. Bailey, J.M.A. Smith, J. Chem. Soc., Dalton Trans. (1982) 429.
[55] N. Al-Obaidi, S.L.W. McWhinnie, T.A. Hamor, C.J. Jones, J.A. McCleverty, J. Chem. Soc., Dalton Trans. (1992) 3299.
[56] N. Al-Obaidi, T.A. Hamor, C.J. Jones, J.A. McCleverty, K. Paxton, J. Chem. Soc., Dalton Trans. (1986) 2653.
[57] N.M. Rowley, S.S. Kurek, P.R. Ashton, T.A. Hamor, C.J. Jones, N. Spencer, J.A. McCleverty, G.S. Beddard, T.M. Feehan, N.T.H. White, E.J.L. McInnes, N.N. Payne, L.J. Yellowlees, Inorg. Chem. 35 (1996) 7526.
[58] G.M. Sheldrick, SHELXS-86, Program for the Solution of Crystal Structures, University of Göttingen, Germany, 1986.
[59] G.M. Sheldrick, SHELXL-93, Program for the Refinement of Crystal Structures, University of Göttingen, Germany, 1993.
[60] N. Walker, D. Stuart, Acta Crystallogr., Sect. A 39 (1983) 158.

PERGAMON

Polyhedron 21 (2002) 859–865

POLYHEDRON

www.elsevier.com/locate/poly

Spectral studies and X-ray crystal structures of three nickel(II) complexes of 2-pyridineformamide 3-piperidylthiosemicarbazone

Karen A. Ketcham [a], Isabel Garcia [b], John K. Swearingen [a], Ayman K. El-Sawaf [c], Elena Bermejo [b], Alfonso Castiñeiras [b], Douglas X. West [d,*]

[a] *Department of Chemistry, Illinois State University, Normal, IL 61790-4160, USA*
[b] *Departamento de Química Inorgánica, Universidad de Santiago de Compostela, E-15706 Santiago de Compostela, Spain*
[c] *Department of Chemistry, Faculty of Science, El Menoufia University, Shebin El-Kom, Egypt*
[d] *Department of Chemistry, 351700, University of Washington, Seattle, WA 98195-1700, USA*

Received 17 December 2000; accepted 8 January 2002

Abstract

Reduction of 2-cyanopyridine by sodium in dry methanol in the presence of 3-piperidylthiosemicarbazide produces 2-pyridineformamide 3-piperidylthiosemicarbazone, HAmpip. Complexes with nickel(II) have been prepared and characterized by magnetic susceptibility and spectroscopic techniques. The crystal structures of [Ni(Ampip)$_2$], [Ni(Ampip)OAc], and [Ni(HAmpip)Cl]Cl have been solved. Coordination of the anionic and neutral ligand is via the pyridyl nitrogen, imine nitrogen, and thiolato–thione sulfur. [Ni(Ampip)$_2$] is an approximately octahedral NiN_4S_2 center with the tridentate ligands in a meridonal arrangement. [Ni(Ampip)OAc] is essentially planar except for the acetato ligand, which is $>80^\circ$ out of the coordination plane, and the ionic [Ni(HAmpip)Cl]Cl involves the neutral thiosemicarbazone ligand. © 2002 Published by Elsevier Science Ltd.

Keywords: Crystal structures; 3-Piperidine; Thiosemicarbazone; 2-Pyridineformamide; Nickel(II); Spectra

1. Introduction

A new series of N(4)-substituted thiosemicarbazones has been prepared in which the thiosemicarbazone moiety is attached to an amide carbon rather than an aldehyde or ketone carbon in an attempt to enhance water solubility. 2-Formyl-, 2-acetyl-, and 2-benzoylpyridine N(4)-substituted thiosemicarbazones [1–3] possess substantial in vitro activity against various human tumor lines [4]. However, due to a lack of solubility in aqueous solutions, these thiosemicarbazones and their complexes show less promising in vivo activity. We have communicated our studies of metal complexes of 2-pyridineformamide thiosemicarbazone [5,6] and N(4)-methylthiosemicarbazone [7,8]. We report here spectral and structural properties of three nickel(II) complexes of 2-pyridineformamide 3-piperidylthiosemicarbazone, HAmpip, which is depicted in Fig. 1. Its structure is discussed in a communication with iron(II), cobalt(II,III), and copper(II) complexes [9].

2. Experimental

2.1. Synthetic methods

2-Cyanopyridine was purchased from Aldrich and used as received and 3-piperidylthiosemicarbazide was prepared as described by Scovill [10]. Following the literature procedure for the reduction of 2-cyanopyridine [11], sodium (0.092 g, 4 mmol) was added to 25 ml of MeOH, which had been dried over $CaSO_4$ (i.e. Drierite), and the solution stirred until complete dissolution occurred. 2-Cyanopyridine (2.6 g, 25 mmol) was then added, and the mixture stirred for 1/2 h, and 3-piperidylthiosemicarbazide (3.9 g, 25 mmol) was added in small portions over a period of 1/2 h. After addition of 15 ml of MeOH the mixture was gently refluxed for a minimum of 4 h. Slow evaporation of MeOH produced the yellow HAmpip, NMR ($CDCl_3$): N–*H* at $\delta =$

* Corresponding author. Fax: +1-206-685-8665.
E-mail address: westdx@chem.washington.edu (D.X. West).

0277-5387/02/$ - see front matter © 2002 Published by Elsevier Science Ltd.
PII: S0277-5387(02)00853-7

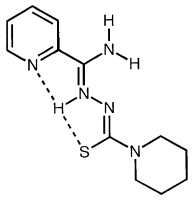


Fig. 1. Depiction of 2-pyridineformamide 3-piperidylthiosemicarbone, HAmpip.

13.186; C–*H* (Py) at $\delta = 7.995$, 7.835 and 7.422; NH_2 at $\delta = 6.4$ ppm; m.p., 154–156 °C.

The nickel(II) complexes were prepared as follows, nickel(II) chloride or acetate (0.002 mol) in EtOH (30 ml) was mixed with a solution of HAmpip (0.002 or 0.004 mol for [Ni(Ampip)$_2$]) in EtOH (30 ml), and the resulting mixture was stirred under reflux for 2 h or longer. The resulting solids were filtered, washed with anhydrous ether to apparent dryness, and placed on a warm plate at 35 °C until required for characterization. %Calc.(Found) for red brown [Ni(HAmpip)Cl]Cl·EtOH: C, 38.3(38.2); H, 4.8(5.3); N, 16.0(16.0); for brown [Ni(Ampip)OAc]: C, 44.3(44.3); H, 5.2(5.1); N, 18.2(18.5); for yellow brown [Ni(Ampip)$_2$]·H_2O: C, 48.2(47.9); H, 4.8(5.7); N, 22.9(23.3). The magnetic susceptibilities are as follows: [Ni(HAmpip)Cl]Cl·EtOH, 2.6 B.M., [Ni(Ampip)OAc], 0.0 B.M. and [Ni(Ampip)$_2$]·H_2O, 3.2 B.M.

2.2. Physical and spectroscopic methods

National Chemical Consulting, Inc. of Tenafly, NJ performed partial elemental analyses for two of the complexes and a Carlos Erba 1108 microanalyser at the Universidad de Santiago de Compostela analyzed [Ni(Ampip)OAc]. The magnetic susceptibilities were measured with a Johnson Matthey magnetic susceptibility balance. NMR spectra were obtained with a Varian 300 MHz Gemini spectrometer using $CDCl_3$ as the solvent; the chemical shifts are reported in parts per million downfield from tetramethylsilane. Infrared spectra were recorded with Nicolet 5SXC and Magna 850 FT-IR spectrometers using Nujol mulls between CsI plates; electronic spectra were acquired as Nujol mulls impregnated on filter paper with a Cary 5E spectrometer.

2.3. X-ray data collection, structure solution and refinement

Crystals of [Ni(HAmpip)Cl]Cl and [Ni(Ampip)$_2$] were grown from ethanol and crystals of [Ni(Ampip)OAc]

Table 1
Crystal data for [Ni(HAmpip)Cl]Cl, [Ni(Ampip)OAc], and [Ni(Ampip)$_2$]

Compound	[Ni(HAmpip)Cl]Cl	[Ni(Ampip)OAc]	[Ni(Ampip)$_2$]
Empirical formula	$C_{12}H_{17}Cl_2N_5NiS$	$C_{14}H_{19}N_5NiO_2S$	$C_{24}H_{32}N_{10}NiS_2$
Color; habit	brown, prism	brown, plate	brown, prism
Crystal size (mm)	$0.32 \times 0.08 \times 0.05$	$0.20 \times 0.20 \times 0.05$	$0.25 \times 0.15 \times 0.10$
Crystal system	orthorhombic	triclinic	monoclinic
Space group	*Pbca* (# 61)	$P\bar{1}$ (#2)	$P2_1/c$ (#14)
Unit cell dimensions			
a (Å)	8.471(2)	8.967(2)	14.762(3)
b (Å)	21.103(6)	9.263(3)	13.075(4)
c (Å)	18.057(3)	11.525(4)	15.427(5)
α (°)	90.00	69.07(3)	90.00
β (°)	90.00	68.37(2)	111.71(2)
γ (°)	90.00	84.87(2)	90.00
Volume (Å^3)	3227.9(1)	830.3(4)	2766.3(1)
Z	8	2	4
Formula weight	392.98	380.11	583.43
D_{calc} (Mg m^{-3})	1.617	1.520	1.401
Absorption coefficient (mm^{-1})	1.662	1.310	0.886
θ range for data collection (°)	1.93–27.46	2.36–28.45	1.48–27.48
Index ranges	$0 \le h \le 10$	$-12 \le h \le 11$	$0 \le h \le 19$
	$0 \le k \le 27$	$-12 \le k \le 0$	$0 \le k \le 16$
	$-23 \le l \le 0$	$-15 \le l \le 14$	$-20 \le l \le 20$
Max/min transmission	0.923/0.618	0.963/0.844	0.917/0.809
Reflections collected	3684	4419	6564
Independent reflection	2523	4170	6325
Final R indices [$I > 3\sigma(I)$]	$R_1 = 0.041$ $wR_2 = 0.119$	$R_1 = 0.056$ $wR_2 = 0.105$	$R_1 = 0.0320$ $wR_2 = 0.0789$
R indices (all data)	$R_1 = 0.072$ $wR_2 = 0.157$	$R_1 = 0.071$ $wR_2 = 0.145$	$R_1 = 0.0542$ $wR_2 = 0.0874$
Goodness-of-fit	1.049	0.937	1.025
Largest difference peak and hole (e Å^{-3})	0.512 and −0.600	0.412 and −0.443	0.374 and −0.340

from acetonitrile, mounted on glass fibers, and used for data collection at room temperature (r.t.) with a Nonius MACH3 diffractometer, Mo Kα, $\lambda = 0.71073$ Å. A semi-empirical absorption correction, ψ-scan, was applied. The structures were solved by direct methods [12], which revealed the position of all non-hydrogen atoms, and refined by a full-matrix least-squares procedure using anisotropic displacement parameters [13]. The C19, C110 and C111 (and C29, C210 and C211) atoms of the piperidine rings of [Ni(Ampip)$_2$] are disordered over two positions; the occupancy factor for each was refined resulting in a value of 0.793(6) for C19A, C110A and C111A. The hydrogens attached to nitrogens were located from difference Fourier maps and refined isotropically. The remaining hydrogens were located in their calculated positions (C–H 0.93–0.97 Å) and refined using a riding model. Atomic scattering factors are from 'International Tables for Crystallography' [14] and molecular graphics are from PLATON98 [15]. Relevant crystallographic information is summarized in Table 1.

3. Results and discussion

The bond distances for the nickel(II) complexes are given in Table 2 and their bond angles in Table 3. Table 4 shows the mean plane data and angles between planes and Table 5 lists the hydrogen bonding interactions. Figs. 2–4 show the ORTEP drawings of [Ni(HAmpip)Cl]Cl, [Ni(Ampip)OAc], and [Ni(Ampip)$_2$], respectively.

3.1. Crystal structure of [Ni(HAmpip)Cl]Cl

In [Ni(HAmpip)Cl]Cl, Fig. 2, coordination of tridentate HAmpip is via the pyridyl nitrogen, imine nitrogen and thione sulfur. As is most often the case with this type of NNS tridentate ligand [16–18], the imine nitrogen coordinates with a shorter Ni–N distance than the ring nitrogen and both are shorter than the Ni–S distance, Table 2. The two *trans* angles, S1–Ni1–N11 and Cl1–Ni1–N12, are $>170°$, Table 3, the *cis* angles range from 83.49(12)° to 96.82(9)° and the N11–N12–S1–Cl1 has minimal deviation from a plane, Table 4, all of which indicate an approximately square arrangement of the four donor atoms. The thiosemicarbazone moiety is nearly co-planar with the coordinate plane.

Coordination of neutral HAmpip does not cause large changes in its bond distances since the uncoordinated HAmpip is in the bifurcated *E′* form, Fig. 1, in which the hydrogen is located on the imine nitrogen [9], the same position as nickel(II) in [Ni(Ampip)Cl]Cl. For example, the S1–C17 bond distance is unchanged and C16–N12 is 1.320(4) Å compared with 1.300(3) in HAmpip. Among the other bonds of the thiosemicarbazone moiety the largest change is exhibited by C17–N14, 1.358(3) in HAmpip to 1.320(5) Å) in [Ni(Ampip)Cl]Cl. The angle N13–C17–N14 shows the largest difference on coordination, 115.2(2)° in HAmpip and 120.0(3)° in [Ni(Ampip)Cl]Cl, but all other angles except C16–N12–N13, which is unchanged, increase or decrease by as much as 3°–4°. H13A and H15B interact with a Cl2 ion (Table 5); the two N···Cl non-bonding distances and the N–H···Cl angles are similar. The

Table 2
Selected bond distances (Å) for [Ni(HAmpip)Cl]Cl, [Ni(Ampip)(OAc)], and [Ni(Ampip)$_2$]

Bond	[Ni(HAmpip)Cl]Cl	[Ni(Ampip)(OAc)]	[Ni(Ampip)$_2$] [a]
Ni1–S1	2.143(1)	2.153 (2)	2.4332(10)
			2.4142(7)
Ni1–N11	1.920(3)	1.916(4)	2.1436(18)
			2.1384(17)
Ni1–N12	1.845(3)	1.829(4)	2.0070(17)
			2.0058(17)
Ni1–X [b]	2.164(1)	1.871(3)	
S1–C17	1.735(4)	1.764(5)	1.739(2) 1.755(2)
C16–N12	1.320(4)	1.311(6)	1.303(3) 1.306(2)
N12–N13	1.398(4)	1.385(5)	1.384(2) 1.383(2)
N13–C17	1.347(4)	1.298(6)	1.323(3) 1.323(3)
C17–N14	1.320(5)	1.351(7)	1.373(3) 1.366(3)
C16–N15	1.318(5)	1.343(6)	1.358(3) 1.345(3)

[a] The second entries are for the S2 ligand.
[b] X = Cl1 for [Ni(HAmpip)Cl]Cl and O11 for [Ni(Ampip)OAc].

Table 3
Selected bond angles (°) for [Ni(HAmpip)Cl]Cl, [Ni(Ampip)(OAc)], and [Ni(Ampip)$_2$]

Angle	[Ni(HAmpip)-Cl]Cl	[Ni(Ampip)-(OAc)]	[Ni(Ampip)$_2$] [a]
S1–Ni1–X [b]	92.27(4)	93.97(12)	95.33(3)
S1–Ni1–N11	170.91(9)	168.82(14)	157.72(5) 158.35(5)
X [a]–Ni1–N11	96.82(9)	96.75(17)	93.47(5) 90.25(5)
S1–Ni1–N12	87.43(9)	85.83(14)	80.44(5) 80.50(5)
X [a]–Ni1–N12	178.2(1)	179.36(19)	105.52(6) 108.34(5)
N11–Ni1–N12	83.5(1)	83.50(19)	77.49(7) 77.89(7)
N11–Ni1–N21			89.05(7)
N11–Ni1–N22			93.27(7)
N12–Ni1–N21			96.03(7)
N12–Ni1–N22			169.13(7)
Ni1–S1–C17	98.4(1)	95.7(2)	94.76(7) 95.29(8)
Ni1–N12–C16	118.1(2)	116.7(4)	119.15(14) 117.99(13)
Ni1–N12–N13	121.1(2)	126.1(3)	125.71(12) 126.17(12)
Ni1–O11–C20		121.4(3)	
N15–C16–N12	126.0(3)	122.3(5)	123.6(2) 123.9(2)
C15–C16–N12	111.9(3)	114.4(5)	115.48(17) 115.30(17)
C16–N12–N13	120.5(3)	116.9(4)	115.08(16) 115.09(16)
N12–N13–C17	115.3(3)	109.9(4)	113.30(16) 113.01(16)
N13–C17–N14	120.0(3)	118.8(5)	114.96(18) 116.04(18)
N13–C17–S1	117.7(3)	122.4(4)	125.55(15) 124.82(15)
N14–C17–S1	122.2(3)	118.7(4)	119.49(15) 119.14(15)

[a] The second numbers are for the analogous angles for the S2 ligand.

Table 4
Mean planes, atoms with the largest deviations (Å) and angles (°) between planes for [Ni(HAmpip)Cl]Cl, [Ni(Ampip)(OAc)], and [Ni(Ampip)$_2$]

Plane	RMS deviations	Largest deviations	Angle [a]
[Ni(HAmpip)Cl]Cl			
N11–N12–S1–Cl1	0.0168	N12, 0.093(13)	
C16–N12–N13–C17–S1–N14	0.0347	C16, 0.0501(19)	2.77(13)
N11–C11–C12–C13–C14–C15	0.0056	C15, 0.0084(5)	3.75(19)
[Ni(Ampip)(Oac)]			
N11–N12–S1–O11	0.0336	N12, 0.0372(21)	
C16–N12–N13–C17–S1–N14	0.0231	C16, 0.0343(29)	2.85(26)
N11–C11–C12–C13–C14–C15	0.0081	N11, 0.0116(35)	6.02(34)
[Ni(Ampip)$_2$]			
N11–N12–S1–N22	0.0117	N12, 0.0140(10)	
C16–N12–N13–C17–S1–N14	0.0270	N12, 0.0543(15)	2.53(9)
N11–C11–C12–C13–C14–C15	0.0038	C15, 0.0054(15)	6.73(11)
N21–C21–C22–C23–C24–C25	0.0073	C24, 0.0111(18)	84.16(7)
C26–N22–N23–C27–S2–N24	0.0318	N22, 0.0647(15)	12.64(13)
N21–N22–S2–N12	0.0740	N22, 0.0884(9)	6.24(8)

[a] Angle with previously listed plane.

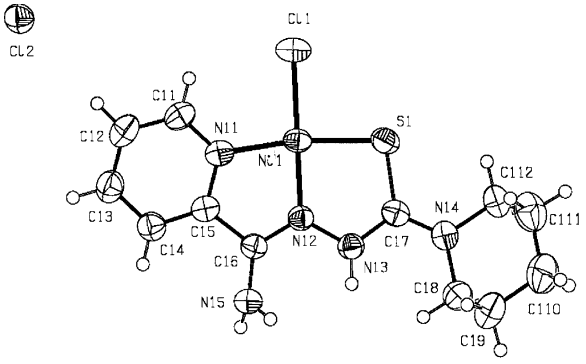


Fig. 2. ORTEP plot of [Ni(HAmpip)Cl]Cl at 50% probability.

other NH_2 hydrogen, H15A, hydrogen bonds to a different Cl2 ion with similar parameters to the above two interactions.

3.2. Crystal structure of [Ni(Ampip)OAc]

The crystal structure, Fig. 3, shows Ampip coordinated in the expected NNS tridentate fashion (i.e. the thiosemicarbazone moiety becomes conjugated) and a monodentate acetato ligand, which is the same stoichiometry found for [Ni(Am4M)OAc], where Am4M is the anion of 2-pyridineformamide N(4)-methylthiosemicarbazone [8]. The Ni1–O11 bond distance in [Ni(Ampi-

Table 5
Hydrogen bonding interactions for [Ni(HAmpip)Cl]Cl, [Ni(Ampip)(OAc)], and [Ni(Ampip)$_2$]

D–H···A	d(D–H) (Å)	d(H···A) (Å)	d(D···A) (Å)	∠ (DHA) (°)
[Ni(HAmpip)Cl]Cl				
N13H13A···Cl2^1	0.94(4)	2.30(4)	3.243(3)	175(3)
N15H15A···Cl2^2	0.84(6)	2.39(6)	3.217(4)	166(5)
N15-H15B···Cl2^1	0.83(6)	2.33(6)	3.159(4)	170(5)
Symmetry transformations, (1) $-x$, $y+1/2$, $-z+1/2$; (2) x, $-y+1/2$, $z-1/2$				
[Ni(Ampip)(OAc)]				
N15H15A···N13	0.86	2.35	2.658(6)	101.4
N15H15B···O12^1	0.86	2.03	2.836(5)	155.7
Symmetry transformations, (1) $-x$, $-y$, $-z+1$				
[Ni(Ampip)$_2$]				
N15H15A···N13	0.77(3)	2.29(3)	2.643(3)	109(2)
N25H25A···N23	0.83(3)	2.33(3)	2.646(3)	103(2)
N15H15B···S2^1	0.87(3)	2.71(3)	3.579(2)	174(3)
N25H25B···S1^2	0.83(3)	2.68(3)	3.477(2)	162(3)
Symmetry transformations,(1) $-x+1$, $-y+1$, $-z+1$; (2) x, $-y+1/2$, $z+1/2$				

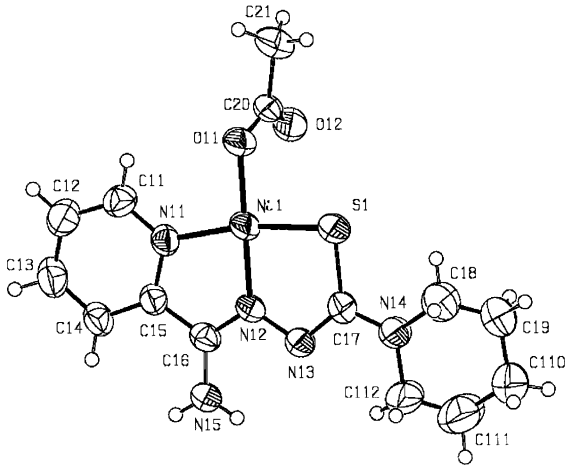


Fig. 3. ORTEP plot of [Ni(Ampip)OAc] at 50% probability.

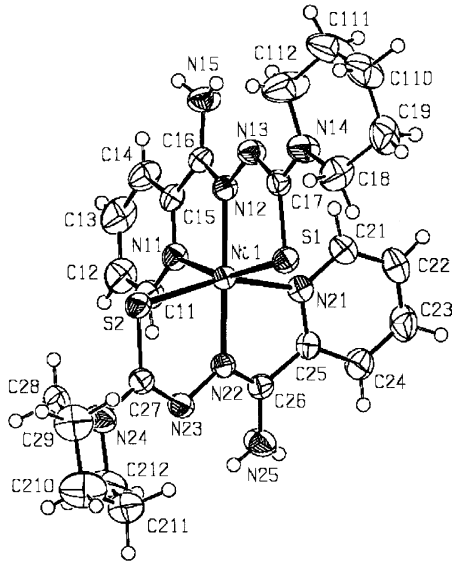


Fig. 4. ORTEP plot of [Ni(Ampip)$_2$] at 50% probability.

p)OAc], 1.871(3) Å, is marginally shorter than 1.888(3) Å for [Ni(Am4M)OAc]. The remaining metal–ligand bonds in the two complexes, as well as their thiosemicarbazone moieties, are within twice their combined e.s.d. values, and most are even more similar. Interestingly, N13–C17 is shorter than C16–N12 in [Ni(Ampip)OAc], but in [Ni(Am4M)OAc] N13–C17 is marginally longer than C16–N12. This difference is the likely cause of confusion in the thiosemicarbazone literature concerning the infrared assignment of ν(C=N) in metal complexes in which a shift to both higher and lower frequencies compared with the uncomplexed thiosemicarbazone has often been reported. Since crystal structures of a number of uncomplexed thiosemicarbazones and their metal complexes have recently been reported [19], it is now known that the C16=N12 bond distance is often somewhat longer or unchanged in the complexes. This suggests that a band in the spectrum of a complex at higher energy than in the uncomplexed thiosemicarbazone is more likely due to ν(N13=C17). Compared with HAmpip [9] [Ni(Ampip)OAc] has a longer S1–C17 bond, N13–C17 is $>0.040(6)$ Å shorter and C16–N12 is only marginally longer.

The anionic Ampip ligand in [Ni(Ampip)OAc] has a N11–Ni1–S1 *trans* angle of 168.82(14)° compared with 170.91(9)° for the neutral ligand in [Ni(HAmpip)Cl]Cl. The other angles about the nickel(II) ions in these complexes show smaller differences, but Ni1–S1–C17 and Ni1–N12–N13 are quite different for the two complexes, Table 2. A comparison of the neutral thiosemicarbazone ligand in [Ni(HAmpip)Cl]Cl to the anionic thiosemicarbazone ligand [Ni(Ampip)OAc] shows that the following angles C16–N12–N13, N12–N13–C17 and N13–C17–S1 are most different. The four donor atoms, N11–N12–S1–O11, in [Ni(Ampip)OAc] are nearly planar and nickel(II) is 0.0237(21) Å below the mean plane which is nearly twice the distance of 0.143(16) Å [Ni(Am4M)OAc] [8]. As is common for coordinated heterocyclic thiosemicarbazone ligands [1–3], the thiosemicarbazone moiety and pyridine ring are nearly co-planar with N11–N12–S1–O11, but the mean plane of the acetato ligand is 80.44(18)° out of the coordination plane. The distances and angles are listed in Table 5 for the hydrogen bonding interaction N15–H15A···N13, an intraligand hydrogen bond which is not found in HAmpip [9] or in complexes of HAmpip with other metal ions [9]. However, N15–H15A···N13 and the intermolecular N15–H15B···O12′ interaction are very similar to the interactions found for [Ni(Am4M)OAc] [8].

3.3. Crystal structure of [Ni(Ampip)$_2$]

The ORTEP plot for the approximately octahedral [Ni(Ampip)$_2$] is shown in Fig. 4. The coordination of the two ligands is meridonal due to the strong tendency toward planarity by heterocyclic thiosemicarbazones. As expected for a six-coordinate complex compared with four-coordinate complex, the donor atom bond distances to nickel(II) are all significantly longer than found for [Ni(Ampip)OAc]. The distortion from octahedral symmetry is indicated by the *trans* N11–Ni1–S1 and N21–Ni–S2 angles of approximately 158°, Table 3.

The hydrogen bonding interactions of the two ligands in [Ni(Ampip)$_2$] have similar parameters. The N15–H15B···N13 and N25–H25A···N23 intraligand interactions are identical to that discussed for [Ni(Ampip)OAc]. The other NH_2 hydrogen for each ligand has an intermolecular hydrogen bond to a thiolato sulfur of the other ligand on an adjacent molecule (Table 5). The mean planes of the coordinated thiosemicarbazones have small deviations from planarity although the imine nitrogens are substantially out of the plane. Table 4 shows deviations from planarity for the coordination

planes, N11–N12–S1–N22 and N21–N22–S2–N12, and for each plane the imine nitrogens, N22 and N12, respectively, show the greatest deviation from planarity.

3.4. Spectral and physical properties

The magnetic susceptibilities are consistent with monomeric complexes and suggest a distorted octahedral structure for [Ni(Ampip)$_2$], a planar structure for [Ni(Ampip)OAc] and a tetrahedrally distorted planar structure for [Ni(HAmpip)Cl]Cl. The latter complex could be a mixture of [Ni(HAmpip)Cl]Cl and five-coordinate [Ni(HAmpip)Cl$_2$].

The infrared bands most useful for determining the mode of coordination by HAmpip (and Ampip) are shown in Table 6. The ν(C=N) band of HAmpip at 1577 cm^{-1} undergoes shifts to lower frequencies in the spectra of the nickel complexes indicating coordination of the imine nitrogen [20]. A second band, assignable to ν(N=C) on loss of the hydrazinic hydrogen, is often observed in the 1585 cm^{-1} region of the complexes' spectra on coordination of an anionic thiosemicarbazone. Additional evidence for coordination of the imine nitrogen is the presence of ν(Ni–N) bands in the 425–455 cm^{-1} range [21]. The spectrum of HAmpip shows the thioamide IV band, which possesses considerable contribution from ν(C–S), at 823 cm^{-1}, and is found at lower energy (>60 cm^{-1}) on coordination of Ampip, but to a lesser extent for [Ni(HAmpip)Cl]Cl. The ν(Ni–S) bands are in the 355 cm^{-1} region [22]. Coordination of the pyridyl nitrogen is indicated by a 10–24 cm^{-1} shift to higher wave number for the ring in-plane deformation, ρ(py), which is at 594 cm^{-1} in the spectrum of HAmpip. The ν(M–N) bands for the pyridyl nitrogen are assigned in the 230 cm^{-1} region, ν(Ni–Cl) at 322 cm^{-1} for [Ni(HAmpip)Cl]Cl and ν(Ni–O) at 482 cm^{-1} for [Ni(Ampip)OAc].

The absorption maxima of the electronic spectra of the three nickel(II) complexes and HAmpip are shown in Table 7. The higher energy $\pi\rightarrow\pi^*$ bands are omitted because their energy is unaffected by complexation. Since HAmpip is primarily the bifurcated *E′* isomer (other isomeric forms present in small amounts are *Z* and *E* with respect to the imine bond) [9], we assign the band at 32340 cm^{-1} to $n\rightarrow\pi^*$ transitions for both the pyridine ring and imine function of the thiosemicarbazone moiety. The two lower energy bands result from $n\rightarrow\pi^*$ transitions associated with the thioamide portion of the thiosemicarbazone moiety. The broad band at 31 350 cm^{-1} in the spectrum of [Ni(HAmpip)Cl]Cl includes the Cl$\rightarrow$Ni(II) charge transfer band [23] and the thioamide $n\rightarrow\pi^*$ intraligand bands are not shifted to as high an energy on coordination of the thione sulfur. Bands in the 20 000–23 000 cm^{-1} are due to S$\rightarrow$Ni(II) charge transfer transitions and are primarily responsible for the brown color of these nickel(II) complexes. The S$\rightarrow$Ni(II) transition at 22 920 cm^{-1} in the spectrum of [Ni(Ampip)$_2$] masks the $^3A_{2g}\rightarrow{}^3T_{1g}$(P) transition.

The crystal structure of [Ni(Ampip)$_2$] shows distortion from octahedral symmetry {i.e. the angle between the imine nitrogens is 169.12(7)°}. However, calculation of ligand field parameters [24] by assigning the band at 7830 cm^{-1} to $^3A_{1g}\rightarrow{}^3T_{2g}$ and 11 330 cm^{-1} as $^3A_{1g}\rightarrow{}^3T_{1g}$(F) yields 17 640 cm^{-1} (presumably obscured by the charge transfer band at 22 920 cm^{-1}) for $^3A_{1g}\rightarrow{}^3T_{1g}$(P), Dq = 783 cm^{-1} and B = 365 cm^{-1}. The Dq and B values are higher and lower, respectively, than found for bis(ligand)nickel(II) complexes prepared with 2-formylpyridine and 2-acetylpyridine thiosemicarbazones [25]. The crystal structure of [Ni(HAmpip)Cl]Cl showed it to be a nearly planar arrangement of the four donor atoms about Ni(II), Table 4. However, the NIR spectrum shows bands below 10 000 cm^{-1}, which are not consistent with a planar structure, and suggests that this solid is a mixture of [Ni(HAmpip)Cl]Cl and five-coordinate [Ni(HAmpip)Cl$_2$]. The number of absorption

Table 7
Solid state electronic spectra (cm^{-1}) for a HAmpip and its nickel(II) complexes

Compound	Intraligand and charge transfer	d$\rightarrow$d
HAmpip	32340 24360 22360	–
[Ni(HAmpip)Cl]Cl	31350 26940 25640 23560 22020	20380 16950 11570 6710
[Ni(Ampip)(OAc)]	31560 28570 23150	20833 16920
[Ni(Ampip)$_2$]	34400 29290 22920	11330 7830

Table 6
IR assignments (cm^{-1}) for HAmpip and its nickel(II) complexes

Compound	νCN	νCS	ρpy	νMN	νMS	νMN(py)	νMX
Hampip	1577s	823m	594w	–	–	–	–
[Ni(HAmpip)Cl]Cl	1560m	792m	604w	454w	354m	232m	322m
[Ni(Ampip)(OAc)] [a]	1564m	856m	639m	470m	372m	246m	482m
[Ni(Ampip)$_2$]	1558sh	753sh	618w	429m	355m	225m	–

[a] Acetato ligand, ν_a(COO$^-$) = 1643s, ν_s(COO$^-$) = 1421m; X=O.

bands in the NIR region as well as the visible region is consistent with the presence of the latter.

The versatility of the heterocyclic thiosemicarbazones in forming a number of complexes having different coordination numbers and stereochemistry with the same metal ion has again been demonstrated. The present nickel(II) complexes involve coordination of the neutral HAmpip and anionic Ampip to produce five- and six-coordinate (and very likely five-coordinate) complexes.

4. Supplementary material

Crystallographic data (excluding structure factors) for the structures reported in this paper have been deposited with the Cambridge Crystallographic Data Center as CCDC-153294 for [Ni(HAmpip)Cl]Cl, CCDC-153295 for [Ni(Ampip)(OAc)] and CCDC-153296 for [Ni(Ampip)$_2$]. Copies of available material can be obtained, free of charge, on application to the Director, CCDC, 12 Union Road, Cambridge CB21EZ, UK, (fax: +44-1223-336033 or e-mail: deposit@ccdc.cam.ac.uk).

Acknowledgements

We thank the Donors of the Petroleum Research Fund, administered by the American Chemical Society for the partial support of this research.

References

[1] D.X. West, C.E. Ooms, J.S. Saleda, H. Gebremedhin, A.E. Liberta, Transition Met. Chem. 19 (1994) 553 and references therein.
[2] D.X. West, H. Gebremedhin, R.J. Butcher, J.P. Jasinski, A.E. Liberta, Polyhedron 12 (1993) 2489 and references therein.
[3] D.X. West, J.S. Ives, J. Krejci, M.M. Salberg, T.L. Zumbahlen, G.A. Bain, A.E. Liberta, J. Valdés-Martínez, S. Hernández-Ortega, R.A. Toscano, Polyhedron 14 (1995) 2189.
[4] (a) M.C. Miller, C.N. Stineman, J.R. Vance, D.X. West, I.H. Hall, Anticancer Res. 18 (1998) 4131;
(b) M.C. Miller, C.N. Stineman, J.R. Vance, D.X. West, I.H. Hall, Appl. Organomet. Chem. 13 (1999) 9.
[5] A. Castiñeiras, I. Garcia, E. Bermejo, D.X. West, Z. Naturforsch. Teil B 55 (2000) 511.
[6] A. Castiñeiras, I. Garcia, E. Bermejo, D.X. West, Polyhedron 19 (2000) 1873.
[7] D.X. West, J.K. Swearingen, A.K. El-Sawaf, Transition Met. Chem. 25 (2000) 87.
[8] D.X. West, J.K. Swearingen, J. Valdés-Martínez, S. Hernández-Ortega, A.K. El-Sawaf, F. van Meurs, A. Castiñeiras, I. Garcia, E. Bermejo, Polyhedron 18 (1999) 2919.
[9] K.A. Ketcham, J.K. Swearingen, A.K. El-Sawaf, A. Castiñeiras, I. Garcia, E. Bermejo, D.X. West, Polyhedron 20 (2001) 3565.
[10] J.P. Scovill, Phosphorus Sulfur Silicon Relat. Elem. 60 (1991) 15.
[11] J. van Koningsbruggen, J.G. Haasnoot, R.A.G. De Graaff, J. Reedijk, Inorg. Chim. Acta 234 (1995) 87.
[12] G.M. Sheldrick, Acta Crystallogr. A 46 (1990) 467.
[13] G.M. Sheldrick, SHELX-97. Program for the Refinement of Crystal Structures, University of Göttingen, Germany, 1997.
[14] International Tables for Crystallography, vol. C, Kluwer Academic Publishers, Dordrecht, The Netherlands, 1995.
[15] A.L. Spek, PLATON. A Multipurpose Crystallographic Tool, Utrecht University, Utrecht, The Netherlands, 1998.
[16] D.X. West, M.A. Lockwood, H. Gebremedhin, A. Castiñeiras, A.E. Liberta, Polyhedron 12 (1993) 1887.
[17] A. Castiñeiras, D.X. West, H. Gebremedhin, T.J. Romack, Inorg. Chim. Acta 216 (1994) 229.
[18] C. Maichle, A. Castiñeiras, R. Carballo, D.X. West, H. Gebremedhin, M.A. Lockwood, C.E. Ooms, T.J. Romack, Transition Met. Chem. 20 (1995) 228.
[19] (a) e.g., D.X. West, A. Castiñeiras, E. Bermejo, J. Mol. Struct. 520 (2000) 103;
(b) E. Labisbal, A. Sousa, A. Castiñeiras, J.A. García-Vázquez, J. Romero, G.A. Bain, D.X. West, Z. Naturforsch., B55 (2000) 162;
(c) D. Kovala-Demertzi, N. Kourkoumelis, M.A. Demertzis, J.R. Miller, C.S. Frampton, J.K. Swearingen, D.X. West, European J. Inorg. Chem. (2000) 727;
(d) N.T. Akinchan, U. Abram, Acta Crystallogr. C56 (2000) 549;
(e) E. Bermejo, A. Castiñeiras, R. Dominguez, R. Carballo, C. Maichle-Mössmer, J. Strähle, A.E. Liberta, D.X. West, Z. Anorg. Allg. Chem. 626 (2000) 878;
(f) G.F. de Sousa, D.X. West, C.A. Brown, J.K. Swearingen, J. Valdés-Martínez, R.A. Toscano, S. Hernández-Ortega, M. Hörner A.J. Bortoluzzi, Polyhedron 19 (2000) 841;
(g) E. Labisbal, A. Sousa, A. Castiñeiras, J.A. Garcia-Vásquez, J. Romero D.X. West, Polyhedron 19 (2000) 1255.
[20] (a) P. Sousa, J.A. Garcia-Vazquez, J.A. Masaquer, Transition Met. Chem. 9 (1984) 318;
(b) S.K. Agrawal, D.R. Tuflani, R. Gupta, S.K. Hajela, Inorg. Chim. Acta 129 (1987) 257;
(c) N. Saha, S. Sinha, Indian J. Chem. 29A (1990) 292.
[21] (a) S.K. Nag, D.S. Joarder, Can. J. Chem. 54 (1976) 2827;
(b) S.K. Sengupta, S.K. Sahni, R.N. Kapoor, Acta Chim. Acad. Sci. Hungary 104 (1990) 89;
(c) R. Roy, M. Chaudhury, S.K. Mondal, K. Nag, J. Chem. Soc., Dalton Trans., (1984) 1681;
(d) A.Z. El-Sonbati, E.M. Mabrouk, H.E. Megahed, Transition Met. Chem. 16 (1991) 280.
[22] G. DeVoto, M. Massacesi, R. Pinna, G. Ponticelli, Spectrochim. Acta, Part A 38 (1982) 725.
[23] (a) M. Suzuki, H. Kanatomi, H. Koyama, I. Murase, Bull. Chem. Soc. Japan 53 (1980) 1961;
(b) D. Kovala-Demertzi, J.M. Tsangaris, H. Hadjiliadis, Transition Met. Chem. 8 (1983) 140;
(c) M. Suzuki, H. Kanatomi, Y. Demura, I. Murase, Bull. Chem. Soc. Japan 57 (1984) 1003.
[24] A.B.P. Lever, Inorganic Electronic Spectroscopy, Elsevier, New York, 1968, p. 307.
[25] (a) D.X. West, C.S. Carlson, C.P. Galloway, A.E. Liberta, C.R. Daniel, Transition Met. Chem. 15 (1990) 91;
(b) D.X. West, C.S. Carlson, A.E. Liberta, J.N. Albert, C.R. Daniel, Transition Met. Chem. 15 (1990) 341;
(c) D.X. West, D.L. Huffman, J.S. Saleda, A.E. Liberta, Transition Met. Chem. 16 (1991) 565.

PERGAMON

Polyhedron 21 (2002) 867–872

POLYHEDRON

www.elsevier.com/locate/poly

Synthesis, crystal structure and catalysis for polyethylene of a paramagnetic chromium complex $[(\eta^5\text{-}Cp^{Si})Cr(\mu\text{-}Cl)Cl]_2$ $[Cp^{Si} = (C_5H_4)Si(CH_3)_2(C_6H_5)]$

Ying-Kai Xu [a,b,*], Ying Mu [b], Hui Sun [b], Zheng-Wang Qu [a], Fan Zhang [b], Yue-Tao Zhang [b], Yang Liu [a]

[a] *State Key Laboratory for Structural Chemistry of Unstable and Stable Species, Institute of Chemistry, Center for Molecular Science, the Chinese Academy of Sciences, North 1st Street No. 2, Zhongguancun, Beijing 100080, People's Republic of China*

[b] *Department of Chemistry, Jilin University, Changchun 130023, People's Republic of China*

Received 5 September 2001; accepted 9 January 2002

Abstract

The synthesis of the substituted silyl cyclopentadiene ligand $(C_5H_5)Si(CH_3)_2(C_6H_5)$ ($Cp^{Si}H$) (**1**) is described. Deprotonation of (**1**) gives ($Cp^{Si}Li$) (**2**) which reacts with $CrCl_3$ to produce the chloro-bridged complex $[(\eta^5\text{-}Cp^{Si})Cr(\mu\text{-}Cl)Cl]_2$ (**3**). Single-crystal X-ray structure analysis reveals that a centrosymmetric dimer exists in the solid state. When activated with methylaluminoxane (MAO), complex (**3**) exhibits several interesting features as a catalyst for ethylene polymerization. With the help of a semi-empirical MO calculation, a cationic sandwich intermediate structure in the catalytic process was proposed. © 2002 Elsevier Science Ltd. All rights reserved.

Keywords: Chromium; Crystal structures; Homogeneous catalyst; Electron spin resonance; Polyethylene

1. Introduction

The area of homogeneous metallocene-catalyzed olefin polymerization recently has received much attention, in part because ligand modification is an effective means of optimizing catalyst activity as well as polymer properties such as molecular weight, stereoregularity and microstructure, etc. [1–7]. Our most recent efforts were in this area [8,9].

Chromium has played a prominent role among the transition metals that catalyze the polymerization of olefins [10–12]. Recently, a class of chromium-based homogeneous catalysts has been synthesized [13–15], and some of them are cationic species, which are somewhat similar to the cationic Group 4 zirconocene complexes [16]. In some cationic zirconocene complexes, evidence for the coordination of a phenyl group to the zirconium center via agostic C–H–M interaction was obtained by NMR spectroscopy [17]. It is also noticeable that the active centers in homogeneous Kaminsky catalyst systems are cationic [18–20], and chromium proved easy to coordinate phenyl [21,22]. Therefore, we prepared a novel chromium-based paramagnetic homogeneous catalyst that bears a phenyl ring bound to the Cp group via a silicon bridge in the hope that the cation produced by methylaluminoxane (MAO) might give higher activity of polyethylene, which could be regarded as evidence for phenyl–chromium interactions.

2. Results and discussion

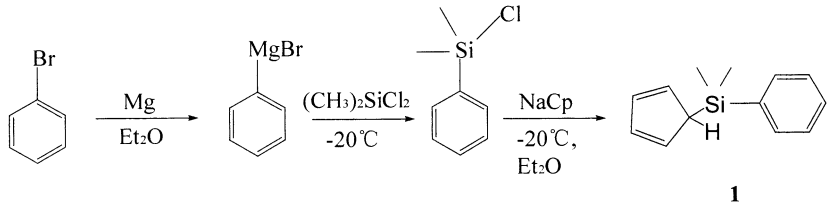
2.1. Ligand synthesis

Grignard reaction of Mg with bromobenzene in Et_2O followed by addition to $(CH_3)_2SiCl_2$ gives $(CH_3)_2SiCl(C_6H_5)$ as a light yellow oil in near quantitative yield (Scheme 1). Its isolation is possible, but not necessary since in situ addition of either NaCp or LiCp in Et_2O produces a yellow solution. This yellow solution

* Corresponding author. Tel.: +86-10-6257-1074; fax: +86-10-6255-9373.

E-mail address: xuyingkai@yahoo.com (Y.-K. Xu).

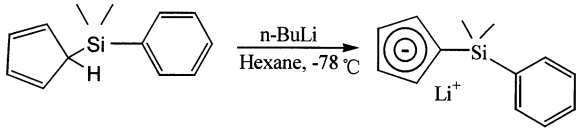
0277-5387/02/$ - see front matter © 2002 Elsevier Science Ltd. All rights reserved.
PII: S0277-5387(02)00866-5



Scheme 1.

was hydrolyzed, extracted by Et_2O, and then purified by column chromatography. The major yellow oil is the desired substituted cyclopentadiene $(C_5H_5)Si(CH_3)_2(C_6H_5)$ ($Cp^{Si}H$) (**1**) as identified by ^1H NMR, IR spectra and MS (Scheme 1).

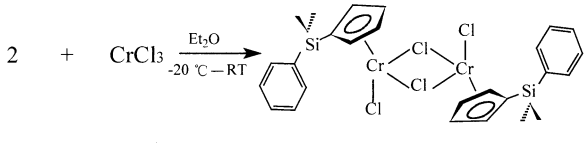
The ^1H NMR of (**1**) displays two broadened Cp ring resonances and we attribute this to rapid sigmatropic shifts of either the methine proton, the silyl group or both. Sigmatropic rearrangements are well known in related silyl substituted cyclopentadienyl systems [23,24]. Compound (**1**) is readily deprotonated by ^{n}BuLi in hexane to give the base-free lithium salt $Li(C_5H_4)Si(CH_3)_2(C_6H_5)$ (**2**) ($Cp^{Si}Li$) in good yield as an air sensitive white solid that is insoluble in aliphatic and aromatic hydrocarbons and soluble in ethers (Eq. (1)). Exposure of (**2**) to moisture produces (**1**) as observed by ^1H NMR.



(1)

2.2. Chromium complex synthesis

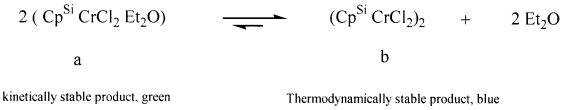
The reaction of 1 equiv. of (**2**) with 1 equiv. of $CrCl_3$ in Et_2O produces $[(\eta^5\text{-}Cp^{Si})Cr(\mu\text{-}Cl)Cl]_2$ (**3**) which is extracted and recrystallized in CH_2Cl_2 with high yield as an air sensitive dark blue crystal that is soluble in most common organic solvents (Eq. (2)). Complex (**3**) was identified by IR spectra, elemental analysis, MS, ESR and single-crystal X-ray analysis. Since complex (**3**) is paramagnetic, it cannot be identified by ^1H NMR.



3

(2)

In the process of the above reaction, we observed that the solution is firstly dark green, then gradually turns to green-blue, and finally becomes blue. Only this blue solution gives the dark blue crystals that can be identified as dimeric by X-ray diffraction. We also tried to isolate the green intermediate product, but it was easily lost Et_2O in vacuum so that it could not be obtained. A similar process was described by S. K. Noh [25], so we speculate that the following equilibrium may exist (Eq. (3)).



(3)

This hypothesis is further supported by the observation that if in the reaction there are other coordinatively stronger reagents such as PPh_3 or pyridine, the solution color is always green and we cannot obtain the dark blue crystals for X-ray diffraction.

2.3. Study of electron spin resonance

The ESR spectrum of (**3**) displayed in Fig. 1 shows that complex (**3**) has unpaired electrons and reveals that Cr (III) is located at a highly symmetric site.

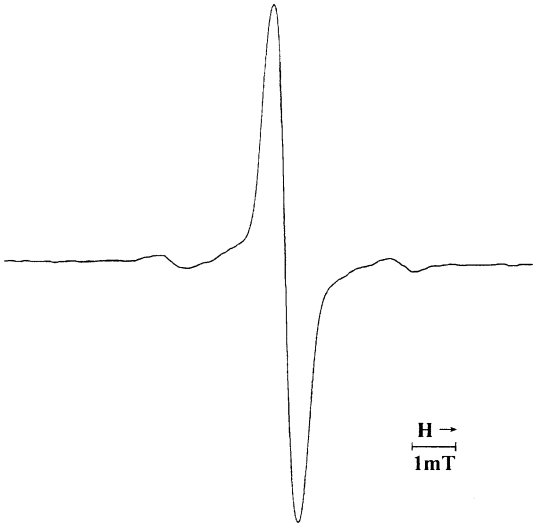


Fig. 1. ESR spectrum of complex (**3**) in toluene solution at room temperature; $g = 1.986$; microwave frequency: 9.77 GHz; microwave power: 20 dB, 2 mW; cavity: TE 104.

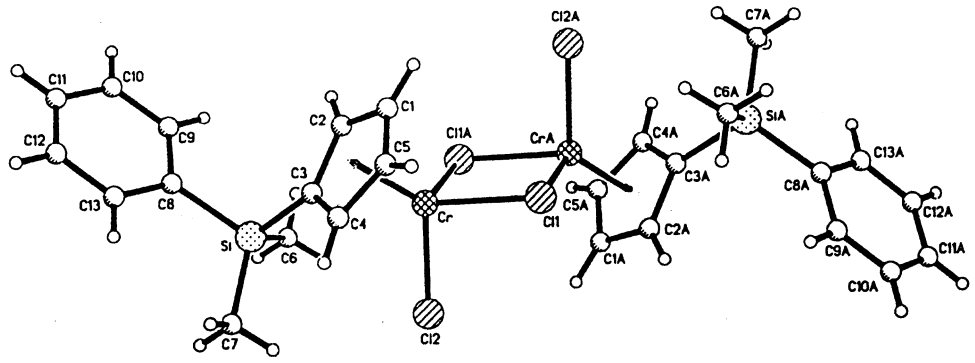


Fig. 2. Molecular structure of (**3**) with the atom-numbering scheme.

2.4. X-ray crystal structure analysis

The molecular structure of (**3**) is shown in Fig. 2. Selected bond distances and angles are given in Table 1. The complex (**3**) is a dimer located at a crystallographic inversion center. Each chromium atom is bonded to one Cp^{Si} ligand, one terminal chlorine atom and two bridging chlorine atoms, thus completing the familiar pseudooctahedral coordination environment of a three-legged piano stool. The Cp ring is bonded to the Cr atom in the η^5 manner and can be thought of as a tridentate ligand occupying one of the trigonal faces of the octahedron. This view is certainly consistent with its ESR behavior. Each chromium center has a 15-electron configuration, so it is slightly electronic unsaturated. The Cr–Cr (1A) distance of 3.336 Å is too long to form a metal–metal bond [25–27]. There are no short intermolecular contacts between dimers. The distance from the chromium to the Cp ring center is 1.861 Å. The angle between the Cp ring plane and the phenyl ring plane is 78.7°

2.5. Polymerization

In order to further our understanding of the structure of complex (**3**), it was tested for catalytic activity in ethylene polymerization. Upon activation with MAO, (**3**) shows moderate catalytic activity. The polymerization results are summarized in Table 2. As can be seen from the results, (**3**) shows several interesting features as a catalyst for ethylene polymerization. First, a low Al:Cr ratio (500:1) is needed to obtain full activity in contrast to the value of approximately 10^4:1 (Al:Zr) reported for the MAO-activated ansa-zirconocene catalysts, and this is similar to the amino-substituted cyclopentadienyl chromium catalyst [28]. Second, the catalytic activity of (**3**) does not decrease very much when the Al: Cr ratio changes from 500 to 1000. Third, the catalytic activity of (**3**) and the molecular weights of polyethylene are much higher than the reported chromium-based cationic half-sandwich catalysts [13]. It is obvious that these observed features could be explained on the basis of phenyl–chromium interactions, which could weaken the interaction between the cationic chromium center and the anionic cocatalyst and, therefore, efficiently prevent the active catalyst from bimolecular deactivation. On the other hand, this interaction could effectively lower the rate of chain termination by β-H elimination. So less MAO is required to keep the catalyst in an active state and a relatively long polyethylene chain can be formed. As a result, the catalytic activity and lifetime of the catalyst increase, and the

Table 1
Selected bond lengths (Å) and angles (°) for complex (**3**)

Bond lenghts			
Cr–C (4)	2.209(3)	Cr–C (2)	2.222(3)
Cr–C (3)	2.212(3)	Cr–Cl (2)	2.273(1)
Cr–C (1)	2.217(3)	Cr–Cl (1)	2.3679(9)
Cr–C (5)	2.218(3)	Si–C (8)	1.871(3)
Si–C (7)	1.852(3)	Si–C (3)	1.881(3)
Si–C (6)	1.851(3)		
Bond angles			
Cl (2)–Cr–Cl (1A)	96.56(4)	Cl (1A)–Cr–Cl (1)	90.40(4)
Cl (2)–Cr–Cl (1)	95.79(4)	C (7)–Si–C (6)	111.3(2)
C (7)–Si–C (8)	111.2(2)	C (8)–Si–C (6)	110.5(2)
C (8)–Si–C (3)	105.19(13)	C (7)–Si–C (3)	108.93(14)
C (6)–Si–C (3)	109.56(14)		

Table 2
Ethylene polymerization results obtained with complex (**3**) activated by MAO [a]

Number	Al:Cr	Activity [b] $\times 10^{-5}$	M_η [c] $\times 10^{-5}$	T_m (°C) [d]
1	80:1	0.279	0.66	133.77
2	300:1	0.976	1.4	134.32
3	500:1	3.81	1.47	134.03
4	1000:1	3.40	0.93	134.43
5	2000:1	1.11	0.699	132.77

[a] Polymerization conditions: 50 ml of toluene, catalyst 1.5 μmol, time 2 h, temp. 16 °C, $P_i(C_2H_4) = 1.5$ atm. MAO: methylaluminoxane.

[b] g PE (mol Cr)$^{-1}$ h^{-1}.

[c] Measured in decahydronaphthalene at 135 °C.

[d] Determined with DSC at a heating rate of 10 °C min^{-1}.

molecular weight of polyethylene increases correspondingly. In a word, there must be a sterically crowded environment around the metal center [8,9].

For understanding the catalytic process we calculated the cationic intermediate structure by a semi-empirical ZINDO/1 MO method. Two stable structures were obtained by geometry optimization (Fig. 3). The energy of the sandwich structure was 80.4 kcal mol^{-1} lower than that of the half-sandwich structure, which means the sandwich is so stable that it is the only possible structure in the catalytic process.

So we speculate that in the process of polymerization the dimer (**3**) first depolymerizes and then loses a chlorine to form a cationic sandwich complex in which the phenyl coordinates to the Cr(III) in the presence of MAO. This proposed structure is consistent with the experimental results. This process is illustrated in Scheme 2.

3. Experimental

3.1. General procedures and material

All reactions with moisture- and air-sensitive compounds were carried out under dry argon atmosphere (ultra-high purity) using standard Schlenk techniques. All reagents are commercially available and were used as received unless otherwise stated.

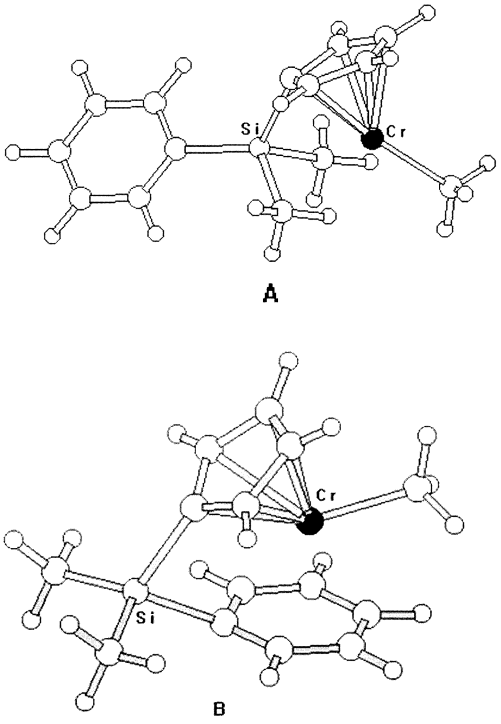


Fig. 3. Geometrically optimized structures of the cationic intermediate in the catalytic process by semi-empirical ZINDO/1 MO method. A: half-sandwich structure; B: sandwich structure.

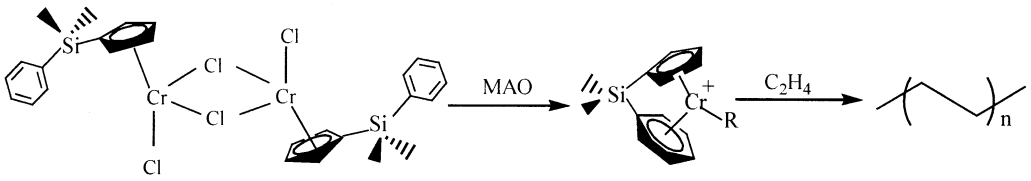
Tetrahydrofuran (THF), diethyl ether (Et_2O) and toluene were refluxed over sodium benzophenone ketyl and distilled before use under nitrogen. Hexane and dichloromethane (CH_2Cl_2) were refluxed and distilled from CaH_2 under nitrogen. $CrCl_3$ was prepared according to a published route [29,30]. Polymerization grade ethylene was further purified by passage through columns of 10 Å molecular sieves and MnO. Methylaluminoxane (MAO, 10 wt.% solution in toluene, M_n = 800 g mol^{-1}, Al = 5.3 wt.%) was purchased from Witco. ^{n}BuLi (1.6 M in hexanes) was purchased from Aldrich. Elemental analyses were performed on American PE-240 C elemental analyzer at the Center of Analysis and Test of Jilin University. The MS was obtained by Finningan GC–MS–DS MAT4510. The ESR spectrum was acquired by Bruker ER2000 EPR. NMR spectra were recorded on a Varian Unity-400 spectrometer and the X-ray structure on a Siemens P4 diffractometer. Viscosity-average molecular weights of the polyethylene were determined in decahydronaphthalene at 135 °C using a Schott Gerate model AVS/T2 Ubbelohde viscosimeter. Melting transition temperatures (T_m) of the polyethylene were determined by DSC (Du Pont 910 differential scanning calorimeter) at a heating rate of 10 °C min^{-1}.

3.2. Synthesis of $Cp^{Si}H$ (*1*)

To a solution of Me_2SiCl_2 (8ml, 66.33 mmol) in Et_2O (40 ml) was added dropwise a solution of PhMgBr (50 ml, 1.00 N, 50.03 mmol) in Et_2O (10 ml) at −50 °C and stirred for 1 h at room temperature (r.t.). Then solvent and excess Me_2SiCl_2 were removed in vacuo. The residue was redissolved in Et_2O (40 ml), and CpNa (26 ml, 1.1919 N, 49.9 mmol) in THF was added dropwise slowly to the above solution at −78 °C over 40 min, and stirred at r.t. for 5–6 h to give a pale yellow solution. The reaction was hydrolyzed and was extracted with Et_2O. The Et_2O layer was dried with $MgSO_4$. After filtration, the solvent was evaporated under vacuum and left behind a yellow oil. The product was purified by column chromatogram over silica gel (hexane-CH_2Cl_2, 3:1). Yield 83%. ^{1}H NMR ($CDCl_3$): δ 0.255 (s, 6H, Si $(CH_3)_2$); 3.135(s, 1/3H, methine); 3.676(br, 2/3H, methine); 6.580–6.696(br, 4H, Cp ring); 7.425–7.645(m, 5H, phenyl). IR (KBr): 3070.12(m), 2960.20(m), 1625.70(m), 1427.07(w), 1253.50(s), 1114.65(m), 1062.59(w), 975.80(m), 9530.85(m), 829.24(s), 802.24(s), 732.82(s), 700.03(s). Mass spectrum (*m/e*): 400.6[$(Me_2PhSiCpH)_2^+$], 200.3(M^+).

3.3. Synthesis of $Cp^{Si}Li$(*2*)

^{n}BuLi (14.5 ml) (1.6 M, 23.2 mmol) was injected slowly into a solution of $Cp^{Si}H$ (4.5043 g, 22.48 mmol)



Scheme 2.

in hexane (30 ml) at −78 °C. The reaction was allowed to warm to r.t. and left stirring for 5 h. A white precipitate was observed. The precipitate was cannula filtered, washed with 2 × 30 ml of hexane and dried under vacuum. Yield 70%.

3.4. Synthesis of $[(\eta^5\text{-}Cp^{Si})Cr(\mu\text{-}Cl)Cl]_2$ (3)

$Cp^{Si}Li$ powder (0.6367 g, 3.1 mmol), $CrCl_3$ powder (0.4946 g, 3.1 mmol) and 30 ml Et_2O was added to a dry 100 ml Schlenk flask under argon. The suspension was stirred at r.t. for 15 days. In this process the colorless solution gradually turns into green, then green–blue, and finally blue. The precipitate was filtered off and the solvent was removed in vacuo. The residue was extracted three times with CH_2Cl_2. The combined fractions were filtered and the solution was concentrated in vacuo. Recrystallization at −10 °C afforded (**3**) as a dark blue crystal. Yield 67.4%. IR: 3093.26(w), 3014.19(w), 2960.20(w), 2915.84(w), 1635.34(m), 1425.14(w), 1402.00(w), 1249.65(m), 1172.51(m), 1110.80(m), 1014.37(m), 833.10(s), 784.89(m), 736.67(m), 700.03(m). MS (*m/e*): 644.5(M^+). *Anal*. Calc. for $(Me_2PhSiCpCrCl_2)_2$: C, 48.46; H, 4.69; Found: C, 45.01; H, 4.42%.

3.5. X-ray structure determination

Data of (**3**) were collected on a Siemens P4 diffractometer with a graphite monochromator using Mo Kα radiation. The structure was solved by direct methods and refined by full-matrix least-squares methods on F^2. All calculations were performed using SHELX-93 [31]. Hydrogen atoms were treated as idealized contributions. Crystallographic data and parameters are summarized in Table 3.

Table 3
Crystal data and structure refinement for complex (**3**)

Empirical formula	$C_{13}H_{15}Cl_2CrSi$
Formula weight	322.24
Temperature (K)	293(2)
Wavelength (Å)	0.71073
Crystal system	monoclinic
Space group	$P2_1/c$
a (Å)	12.242(2)
b (Å)	9.621(2)
c (Å)	12.811(3)
β (°)	101.60(3)
V (Å^3)	1478.1(5)
Z	4
Absorption coefficient (mm^{-1})	1.192
Crystal size (mm)	0.50 × 0.42 × 0.28
θ Range for data collection (°)	2.67 to 25.01
Scan type	$\omega-2\theta$
Reflections collected	3481
Independent reflections	2594 ($R_{int} = 0.0238$)
Max./min. transmission	0.35464, 0.24856
Data/restraints/parameters	2594/0/154
Goodness-of-fit on F^2	0.705
Final *R* indices [$I > 2\sigma(I)$]	$R_1 = 0.0369$, $wR_2 = 0.0949$
R indices (all data)	$R_1 = 0.0504$, $wR_2 = 0.1023$
Largest difference peak and hole (e Å^{-3})	0.396 and −0.646

3.6. Polymerizations

A dry 250 ml steel reactor equipped with a magnetic stirrer was evacuated and pressurized with ethylene to 1.5 atm. Toluene and an appropriate amount of MAO were added to reactor through a septum port via syringe. After the solution was saturated with ethylene for 30 min, a solution of catalyst (1.5 μmol) in toluene was injected (total volume of the polymerization solution is 50 ml after the addition of catalyst). The vessel was repressurized to the required pressure with ethylene as soon as the catalyst was injected and the pressure was maintained by continuously feeding monomer. After the mixture was stirred for the desired reaction time, the reactor was vented and the polymerization was terminated by injecting acidified methanol [HCl (3 M)–methanol = 1:1]. The polymer was stirred in acidified methanol overnight, washed with water and methanol, dried in vacuo at 60 °C.

3.7. Semi-empirical MO calculation

The cationic intermediate structure in the catalytic process was calculated by a semi-empirical ZINDO/1 MO method of the HYPERCHEM 6.0 program [32]. The parameters are the following, Total charge: 1; spin multiplicity: 4; convergence limit: 0.01; RMS gradient of: 0.01 kcal mol^{-1}.

4. Supplementary material

Crystallographic data (excluding structure factors) for the structure reported in this paper have been deposited with the Cambridge Crystallographic Data Centre, CCDC No. 163491. Copies of the data can be obtained free of charge from The Director, CCDC, 12 Union Road, Cambridge, CB2 1EZ, UK (fax: +44-1223-336033; e-mail: deposit@ccdc.cam.ac.uk or www: http://www.ccdc.cam.ac.uk).

Acknowledgements

This work was supported by the National Natural Science Foundation of China (No. 29734143 and No. 29672013) and the Sinopec.

References

[1] N. Schneider, M.E. Huttenloch, U. Stehling, R. Kirsten, F. Schaper, H.H. Brintzinger, Organometallics 16 (1997) 3413.
[2] Y. Mu, W.E. Piers, L.R. MacGillivray, M.J. Zaworotko, Polyhedron 14 (1995) 1.
[3] W. Spaleck, M. Antberg, J. Rohrmann, A. Winter, B. Bachmann, P. Kiprof, J. Behm, W.A. Herrmann, Angew. Chem., Int. Ed. Engl. 31 (1992) 1347.
[4] W. Spaleck, F. Küber, A. Winter, J. Rohrmann, B. Bachmann, M. Antberg, V. Dolle, E.F. Paulus, Organometallics 13 (1994) 954.
[5] E.J. Thomas, J.C.W. Chien, M.D. Rausch, Organometallics 18 (1999) 1439.
[6] W. Kaminsky, Macromol. Chem. Phys. 197 (1996) 3907.
[7] Y. Mu, W.E. Piers, L.R. MacGillivray, M.J. Zaworotko, Organometallics 15 (1996) 2720.
[8] F. Zhang, Y. Mu, J. Wang, Z. Shi, W. Bu, S. Hu, Y. Zhang, S. Feng, Polyhedron 19 (2000) 1941.
[9] F. Zhang, Y. Mu, L. Zhao, Y. Zhang, W. Bu, C. Chen, H. Zhai, H. Hong, J. Organomet. Chem. 613 (2000) 68.
[10] F.J. Karol, Catal. Rev. Sci. Eng. 26 (1984) 557.
[11] H. Sinn, W. Kaminsky, Adv. Organomet. Chem. 18 (1980) 99.
[12] A. Clark, Catal. Rev. 3 (1969) 145.
[13] B.J. Thomas, S.K. Noh, G.K. Schulte, S.C. Sendlinger, K.H. Theopold, J. Am. Chem. Soc. 113 (1991) 893.
[14] G. Bhandari, Y. Kim, J.M. McFarland, A.L. Rheingold, K.H. Theopold, Organometallics 14 (1995) 738.
[15] K.H. Theopold, Eur. J. Inorg. Chem. (1998) 15.
[16] M. Bochmann, J. Chem. Soc., Dalton Trans. (1996) 255–257.
[17] L.H. Doerrer, M.L.H. Green, D. Häußinger, J. Saßmannshausen, J. Chem. Soc., Dalton Trans. (1999) 2111–2118.
[18] W. Kaminsky, M. Arndt, Adv. Polym. Sci. 127 (1995) 144.
[19] H.-H. Brintzinger, D. Fischer, R. Mühlhaupt, B. Rieger, R. Waymouth, Angew. Chem., Int. Ed. Engl. 34 (1995) 1143.
[20] G.L. Rempel, J. Huang, Prog. Polym. Sci. 20 (1995) 459.
[21] C. Elschenbroich, J. Hurley, B. Metz, W. Massa, G. Baum, Organometallics 9 (1990) 889–897.
[22] D.S. Richeson, J.F. Mitchell, K.H. Theopold, Organometallics 8 (1989) 2570–2577.
[23] P. Jutzi, Chem. Rev. 86 (1986) 983.
[24] F.A. Shafiq, D.E. Richardson, J.M. Boncella, J. Organomet. Chem. 555 (1998) 1.
[25] S.K. Noh, S.C. Sendlinger, C. Janiak, K.H. Theopold, J. Am. Chem. Soc. 111 (1989) 9127.
[26] L.B. Handy, J.K. Ruff, L.F. Dahl, J. Am. Chem. Soc. 92 (1970) 7312.
[27] H. Vahrenkamp, Chem. Ber. 111 (1978) 3472.
[28] Rainer emrich, Oliver Heinemann, Peter W. Jolly, Carl Kruger, Glenn P.J. Verhovnik, Organometallics, 16 (8) (1997).
[29] H. Hecht, Z. Anorg. Chem. 254 (1947) 37.
[30] G.B. Heisig, B. Fawkes, R. Hedin, Inorg. Synth. 2 (1946) 193.
[31] (a) G.M. Sheldrick, SHELXTL-PLUS, Structure Determination Software Programs, Siemens Analytical X-ray Instruments Inc., Madison, WI, USA, 1990;
(b) G.M. Sheldrick, SHELXL-93. Program for the Refinement of Crystal Structures, University of Göttingen, Germany, 1993.
[32] HYPERCHEM, Release 6.0; Hypercube Inc., Waterloo, Ont., 1999.

PERGAMON

Polyhedron 21 (2002) 873–878

POLYHEDRON

www.elsevier.com/locate/poly

Synthesis and characterization of bidentate organotin Lewis acid derivatives containing bis(pyrazol-1-yl)alkanes: X-ray crystal structure of $PhBr_2(L)SnCH_2SnPhBr_2$ (L = bis(4-chloropyrazol-1-yl)methane)

Zhi-Hong Wang [a,1], Liang-Fu Tang [a,*], Wen-Li Jia [a], Ji-Tao Wang [b], Hong-Gen Wang [c]

[a] *Department of Chemistry, Nankai University, Tianjin 300071, People's Republic of China*
[b] *State Key Laboratory of Elemento-Organic Chemistry, Nankai University, Tianjin 300071, People's Republic of China*
[c] *Central Laboratory of Nankai University, Tianjin 300071, People's Republic of China*

Received 31 October 2001; accepted 9 January 2002

Abstract

The reaction between bis(dibromophenylstannyl)methane, $[CH_2(SnPhBr_2)_2]$, with bis(pyrazol-1-yl)alkanes, $[(CH_2)_nPz_2]$ ($n = 1$ or 2; Pz = substituted pyrazole) in a 1:1 or 1:2 ratio yields only 1:1 adducts of $PhBr_2[(CH_2)_nPz_2]SnCH_2SnPhBr_2$, which have been confirmed by elemental analysis, ^1H NMR and IR spectroscopy. The electronic and steric characteristics of substituents on the pyrazole rings markedly influence the donating ability of bis(pyrazol-1-yl)alkanes to the bidentate organotin Lewis acid acceptor. The investigations on the reaction of the adducts with DMSO and NMR spectra of the adducts show the weak interactions between ligands and the bidentate organotin Lewis acid acceptor. X-Ray analysis of $PhBr_2(CH_2(4\text{-}ClPz)_2)SnCH_2SnPhBr_2$ showed that bis(4-chloropyrazol-1-yl)methane acts as a chelating bidentate ligand to only one tin atom. © 2002 Elsevier Science Ltd. All rights reserved.

Keywords: Bis(pyrazol-1-yl)alkane; Organotin(IV); X-ray structures

1. Introduction

The coordination behavior of organotin(IV) toward poly(pyrazol-1-yl)borate [1] ligands has been extensively investigated in recent years owing to the antitumor activity of some related organotin derivatives containing N-donor ligands. A number of organotin(IV) complexes containing poly(pyrazol-1-yl)borate ligands have been synthesized and characterized [2–8]. In these complexes, the coordinate geometry around the central tin atom depends on the steric and electronic properties of poly(pyrazol-1-yl)borate ligands, which can be easily controlled by changing the substituents on the pyrazole ring [1]. Some organotin(IV) complexes containing poly(pyrazol-1-yl)borate ligands have also shown interesting structural characteristics and reactivities [9–11]. Poly(pyrazol-1-yl)alkanes, a kind of isoelectronic and isosteric ligands with poly(pyrazol-1-yl)borate, have also been found to act as good donors to tin and organotin(IV) acceptors. The interactions between poly(pyrazol-1-yl)alkanes and tin or organotin(IV) acceptors have also been investigated in recent years [12–18]. However, in these known organotin(IV) derivatives with scorpionate ligands only one monodentate Lewis acid center acts as the acceptor.

At the present time, we have become interested in the coordination chemistry of multidentate Lewis acids, such as multidentate organotin(IV) compounds, in which Lewis acid tin centers are separated by the methylene spacer. These compounds have been found to be good acceptor molecules to heteroatom ligands [19–22]. Some different coordination behaviors have been observed in these complexes formed by multidentate organotin(IV) Lewis acids with nitrogen hetero-

* Corresponding author. Fax: +86-22-2350-2458.
E-mail address: tanglf@eyou.com (L.-F. Tang).
[1] Present address: Department of Chemistry, Texas A&M University, College Station, TX 77843, USA.

0277-5387/02/$ - see front matter © 2002 Elsevier Science Ltd. All rights reserved.
PII: S0277-5387(02)00863-X

cyclic ligands, such as pyridine, pyrazole and pyridazine [23]. But, there is no report on the interactions of multidentate organotin Lewis acids with the popular multidentate scorpionate ligands. In the present paper, we report the results of the reactions between the bidentate organotin Lewis acid with bis(pyrazol-1-yl)alkanes.

2. Experimental

All solvents were dried by standard methods and distilled prior to use, and all reactions related to organotin complexes were carried out under moisture-free conditions. Melting points were measured with a PHMK melting-point apparatus and were uncorrected. NMR spectra were recorded on a Bruker AC-P-200 spectrometer. The chemical shifts were reported in ppm with respect to the references. IR spectral data were obtained from a Nicolet FT-IR 170SX spectrometer using KBr discs. Elemental analyses were carried out on a Perkin–Elmer 240C analyser. Bis(dibromophenylstannyl)methane, $CH_2(SnPhBr_2)_2$ [24], bis(pyrazol-1-yl)-methane, CH_2Pz_2 [25], bis(4-halopyrazol-1-yl)methanes, $CH_2(4\text{-}XPz)_2$ and bis(3,5-dimethyl-4-chloropyrazol-1-yl)methanes, $CH_2(3,5\text{-}Me_2\text{-}4\text{-}XPz)_2$ [26], bis(3,4,5-trimethylpyrazol-1-yl)methane, $CH_2(3,4,5\text{-}Me_3Pz)_2$ [27], bis(3,5-dimethylpyrazol-1-yl)methane, $CH_2(3,5\text{-}Me_2Pz)_2$ and bis(3,5-dimethylpyrazol-1-yl)ethane, $(CH_2)_2(3,5\text{-}Me_2Pz)_2$ [28], bis(4-nitropyrazol-1-yl)methane, $CH_2(4\text{-}NO_2Pz)_2$ [29] and 3,5-dimethyl-4-benzylpyrazole [30] were prepared according to the literature methods.

2.1. Preparation of bis(3,5-dimethyl-4-benzylpyrazole)methane, $CH_2(3,5\text{-}Me_2\text{-}4\text{-}BzPz)_2$

This ligand was obtained by the similar method used for bis(pyrazol-1-yl)methane [25]. Yield: 75%; m.p. 174–175 °C. ν_{max} (cm^{-1}): 1576.3 s (pyrazole ring). ^1H NMR ($CDCl_3$), δ: 2.08 (6H, s, CH_3), 2.35 (6H, s, CH_3), 3.67 (4H, s, $PhCH_2$), 6.19 (2H, S, CH_2Pz), 7.02–7.20 (10H, m, C_6H_5). *Anal*. Calc. for $C_{25}H_{28}N_4$: C, 78.13; H, 7.29; N, 14.58. Found: C, 78.23; H, 7.15; N, 14.65%.

2.2. Preparation of $PhBr_2(CH_2Pz_2)SnCH_2SnBr_2Ph$ (**1**)

A solution of $CH_2(SnPhBr_2)_2$ (0.2 mmol) in 10 ml ether was added to a stirred solution of CH_2Pz_2 (0.2 mmol) in 5 ml CH_2Cl_2. The reaction mixture was continuously stirred for 2 h at room temperature (r.t.), and then the solvent was removed under a reduced pressure. The residue was recrystallized in CH_2Cl_2–hexane at −18 °C to yield white crystals of **1**. Yield: 70%; m.p. 185–187 °C. ν_{max} (cm^{-1}): 1516.0 s (pyrazole ring) and 454.1 m (Sn–C). ^1H NMR (CD_3COCD_3): δ 7.93–7.90 (m, 4H, H^3 and H^5 of pyrazole), 7.51–7.38 (m, 10H, C_6H_5), 6.41 (s, 2H, H^4 of pyrazole), 6.28 (s, 2H, CH_2Pz), 3.17 (s, 2H, CH_2Sn). *Anal*. Calc. for $C_{20}H_{20}Br_4N_4Sn_2\cdot 1/2CH_2Cl_2$: C, 26.84; H, 2.29; N, 6.11. Found: C, 26.73; H, 2.45; N, 6.11%. The same product was obtained when $CH_2(SnPhBr_2)_2$ was reacted with CH_2Pz_2 in a 1: 2 ratio.

2.3. Preparation of $PhBr_2(CH_2(4\text{-}ClPz)_2)SnCH_2SnPhBr_2$ (**2**)

This compound was obtained similarly using $CH_2(SnPhBr_2)_2$ and $CH_2(4\text{-}ClPz)_2$ as described above for **1**. Yield: 62%; m.p. 133–135 °C. ν_{max} (cm^{-1}): 1571.6 s (pyrazole ring) and 452.8 m (Sn–C). ^1H NMR ($CDCl_3$): δ 7.63–7.46 (m, 14H, H^3 and H^5 of pyrazole and C_6H_5), 6.17 (s, 2H, CH_2Pz), 2.32 (s, 2H, CH_2Sn). *Anal*. Calc. for $C_{20}H_{18}Br_4Cl_2N_4Sn_2$: C, 25.45; H, 1.91; N, 5.94. Found: C, 25.14; H, 1.79; N, 5.80%.

2.4. Preparation of $PhBr_2(CH_2(4\text{-}BrPz)_2)SnCH_2SnPhBr_2$ (**3**)

This compound was obtained similarly using $CH_2(SnPhBr_2)_2$ and $CH_2(4\text{-}BrPz)_2$ as described above for **1**. Yield: 54%; m.p. 135–136 °C. ν_{max} (cm^{-1}): 1569.6 s (pyrazole ring) and 451.8 m (Sn–C). ^1H NMR ($CDCl_3$): δ 7.64, 7.49 (m, m, 6H, 8H, H^3 and H^5 of pyrazole and C_6H_5), 6.18 (s, 2H, CH_2Pz), 2.32 (s, 2H, CH_2Sn). *Anal*. Calc. for $C_{20}H_{18}Br_6N_4Sn_2$: C, 23.26; H, 1.74; N, 5.43. Found: C, 23.12; H, 1.99; N, 5.29%.

2.5. Preparation of $PhBr_2(CH_2(3,5\text{-}Me_2Pz)_2)SnCH_2SnPhBr_2$ (**4**)

This compound was obtained similarly using $CH_2(SnPhBr_2)_2$ and $CH_2(3,5\text{-}Me_2Pz)_2$ as described above for **1**. Yield: 60%; m.p. 46–48 °C. ν_{max} (cm^{-1}): 1557.7 s (pyrazole ring) and 450.3 m (Sn–C). ^1H NMR ($CDCl_3$): δ 7.65, 7.49 (m, m, 4H, 6H, C_6H_5), 6.04 (s, 2H, CH_2Pz), 5.78 (s, 2H, H^4 of pyrazole), 2.42 (s, 2H, CH_2Sn), 2.39, 2.17 (s, s, 6H, 6H, CH_3). *Anal*. Calc. for $C_{24}H_{28}Br_4N_4Sn_2$: C, 30.97; H, 3.01; N, 6.02. Found: C, 31.36; H, 2.69; N, 6.25%.

This compound was also prepared in petroleum ether (60–90 °C). A solution of $CH_2(3,5\text{-}Me_2Pz)_2$ (0.5 mmol) in 40 ml petroleum ether (60–90 °C) was added dropwise to a stirred solution of $CH_2(SnPhBr_2)_2$ (0.25 mmol) in 40 ml petroleum ether (60–90 °C). A white solid began to precipitate when half of the solution of $CH_2(3,5\text{-}Me_2Pz)_2$ was added. After the addition completed, the mixture was stirred for 2 h to complete the reaction. The white precipitate was filtered off and washed, which was confirmed to be 1:1 adduct of **4** by its ^1H NMR spectrum.

2.6. Preparation of $PhBr_2(CH_2(3,4,5\text{-}Me_3Pz)_2)SnCH_2SnPhBr_2$ (5)

A solution of $CH_2(SnPhBr_2)_2$ (0.2 mmol) in 10 ml ether was added to a stirred solution of $CH_2(3,4,5\text{-}Me_3Pz)_2$ (0.2 mmol) in 5 ml CH_2Cl_2. White solids precipitated out immediately. After continuously stirring for 2 h at r.t., the precipitate was filtered off, washed with cold ether and recrystallized in CH_2Cl_2–hexane to yield white crystals of **5**. Yield: 55%; m.p. 132–134 °C. ν_{max} (cm^{-1}): 1570.5 s (pyrazole ring) and 451.6 m (Sn–C). ^1H NMR ($CDCl_3$): δ 7.67, 7.45 (m, m, 4H, 6H, C_6H_5), 6.14 (s, 2H, CH_2Pz), 2.45 (s, 2H, CH_2Sn), 2.34, 2.12, 1.84 (s, s, s, 6H, 6H, 6H, CH_3). ^{119}Sn NMR (CD_3COCD_3): δ −210.3. *Anal*. Calc. for $C_{26}H_{32}Br_4N_4Sn_2$: C, 32.57; H, 3.34; N, 5.85. Found: C, 32.26; H, 3.41; N, 5.52%.

2.7. Preparation of $PhBr_2[(CH_2)_2(3,5\text{-}Me_2Pz)_2]SnCH_2SnPhBr_2$ (6)

This compound was obtained similarly using $CH_2(SnPhBr_2)_2$ and $(CH_2)_2(3,5\text{-}Me_2Pz)_2$ as described above for **5**. Yield: 50%; m.p. 183–185 °C. ν_{max} (cm^{-1}): 1586.0 s (pyrazole ring) and 451.4 m (Sn–C). ^1H NMR (CD_3COCD_3): δ 7.99, 7.35 (m, m, 4H, 6H, C_6H_5), 5.92 (s, 2H, H^4 of pyrazole), 4.50 (s, 4H, CH_2CH_2), 2.23 (s, 2H, CH_2Sn), 2.21, 1.91 (s, s, 6H, 6H, CH_3). *Anal*. Calc. for $C_{25}H_{30}Br_4N_4Sn_2$: C, 31.78; H, 3.18; N, 5.93. Found: C, 31.46; H, 2.96; N, 5.64%.

2.8. Reaction of $CH_2(3,5\text{-}Me_2\text{-}4\text{-}BrPz)_2$, $CH_2(3,5\text{-}Me_2\text{-}4\text{-}ClPz)_2$, $CH_2(4\text{-}NO_2Pz)_2$ or $CH_2(3,5\text{-}Me_2\text{-}4\text{-}BzPz)_2$ with $CH_2(SnPhBr_2)_2$

The reaction was carried out as described in the preparation of **1**. The residue was recrystallized in CH_2Cl_2–hexane to yield white crystals, which were confirmed to be the ligands by ^1H NMR spectra.

2.9. Reaction of 1 or 2 with DMSO

A twofold amount of DMSO was added to the stirred solution of **1** (0.2 mmol) or **2** dissolved in 3 ml $CHCl_3$ at r.t., a white oil appeared immediately. After 2 h, the solvent was removed under a reduced pressure, and the residue was recrystallized from CH_2Cl_2 at −20 °C to yield white crystals, which were identified to be $CH_2(SnPhBr_2)_2$.2DMSO by ^1H NMR, elemental analyses and comparison of its IR and ^1H NMR spectra with the literature data [31].

2.10. Structure determination of 2

Crystals of **2** suitable for X-ray analysis were obtained by slow diffusion of hexane into a CH_2Cl_2 solution of **2** at r.t. All intensity data were collected on an Enraf–Nonius CAD4 diffractometer using graphite monochromated Mo Kα radiation ($\lambda = 0.71073$ Å). A total of 4298 independent reflections was collected in the range of $2^\circ \leq \theta \leq 25^\circ$ with an ω–2θ scan technique. The correction for empirical absorption was applied to intensity data, and the structure was solved by direct methods and refined by full-matrix least-squares on F^2. All non-hydrogen atoms were refined anisotropically. All calculations were performed on a PDP11/44 computer using SDP-PLUS program system. A summary of the fundamental crystal data is listed in Table 1.

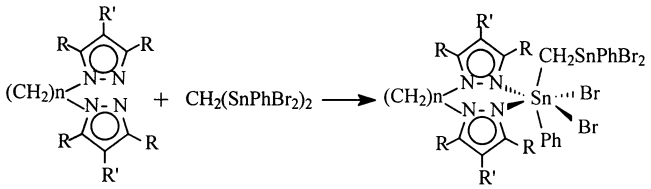
3. Results and discussion

3.1. Synthesis and properties

The reaction between bis(dibromophenylstannyl)-methane with bis(pyrazol-1-yl)methane, bis(4-chloropyrazol-1-yl)methane, bis(4-bromopyrazol-1-yl)-methane, bis(3,5-dimethylpyrazol-1-yl)methane, bis-(3,4,5-trimethylpyrazol-1-yl)methane or bis(3,5-dimethylpyrazol-1-yl)ethane in a 1:1 or 1:2 ratio yielded only 1:1 adducts (Scheme 1), according to the results of elemental analyses and ^1H NMR data. However, reactions of bis(dibromophenylstannyl)methane with bis(3,5-dimethyl-4-chloropyrazol-1-yl)methane, bis(3,5-dimethyl-4-bromopyrazol-1-yl)methane, bis(4-nitropyrazol-1-yl)methane and bis(3,5-dimethyl-4-benzylpyrazol-1-yl)methane did not take place. We think that the steric and electronic characteristics of the substituents on the pyrazole rings should be responsible for this result. The methyl and benzyl groups increase the steric

Table 1
Crystal data for **2**

Formula	$C_{20}H_{18}Br_4Cl_2N_4Sn_2$
Formula weight	942.32
Crystal size (mm)	0.30 × 0.40 × 0.40
Crystal class	monoclinic
Space group	$P2_1/n$
Cell parameters	
a (Å)	9.996(2)
b (Å)	22.614(5)
c (Å)	12.271(2)
β (°)	98.72(3)
V (Å^3)	2742(1)
Z	4
T (K)	299(2)
$D_{calc.}$ (Mg m^{-3})	2.283
$F(000)$	1760
λ(Mo Kα) (Å)	0.71073
μ (mm^{-1})	7.8195
Number of reflections measured	5202
Number of reflections observed [$I \geq 3\sigma(I)$]	2704
Number of parameters	289
Residuals R, R_w	0.042, 0.049



Scheme 1. $n = 1$, R = R′ = H (**1**); $n = 1$, R = H, R′ = Cl (**2**); $n = 1$, R = H, R′ = Br (**3**); $n = 1$, R = CH_3, R′ = H (**4**); $n = 1$, R = R′ = CH_3 (**5**); $n = 2$ R = CH_3, R′ = H (**6**).

hindrance of these ligands, and the electron-withdrawing bromine and nitro groups decrease the donating ability of the ligands to the organotin acceptor. All new complexes are insoluble in petroleum ether, slightly soluble in ether, moderately soluble in polar organic solvents such as CH_2Cl_2 and acetone, and they are stable in air.

When **1** or **2** was treated with DMSO, the bis(pyrazol-1-yl)alkane ligand was easily substituted by DMSO, indicating that bis(pyrazol-1-yl)alkane is a weaker donor to bis(dibromophenylstannyl)methane than DMSO.

The ^{1}H NMR spectra of complexes are consistent with the formulation of 1:1 adducts, which exhibit the expected proton signals for 2 equiv. pyrazole rings. The chemical shifts of protons for the ligands in complexes are similar to those of free ligands, being only slightly shifted downfield. Although 2 nonequiv. tin atoms exist in the solid (one case shown in Fig. 1), the ^{119}Sn NMR spectrum of **5** (CD_3COCD_3) determined at r.t. shows only one ^{119}Sn signal, which occurs at −210.3 ppm. This value is comparable to those of reported monodentate organotin Lewis acid derivatives of poly(pyrazol-1-yl)alkanes [12,15], indicating that extensive dissociation of these complexes in solution may exist. In addition, fast-exchanging ligands on the NMR time scale between two tin atoms by dissociation should be responsible for the observation of only one ^{119}Sn signal.

3.2. Crystal structure of 2

Selected bond distances and angles for **2** are listed in Table 2. The molecular structure of complex **2** is shown in Fig. 1, which clearly shows that the two tin atoms are in nonequivalent environments. Bis(4-chloropyrazol-1-yl)methane acts as a chelating bidentate ligand toward the Sn(1) atom, which is six-coordinate with a distorted octahedral geometry, containing a *cis* arrangement of the bromine atoms and a *trans* arrangement of the phenyl and methylene groups, whereas Sn(2) is four-coordinate with a slightly distorted tetrahedral geometry. The six-membered Sn–N–N–C–N–N metallacycle adopts a slightly distorted boat conformation, which is similar to that in the reported monodentate organotin Lewis acid derivatives of bis(pyrazol-1-yl)alkanes [12]. The average Sn(1)–N distance in complex **2** is 2.424 Å, which is within the range for the reported organotin complexes containing scorpionate ligands [2,15]. The average Sn(1)–Br distance (2.639 Å) is considerably longer than the average Sn(2)–Br distance (2.493 Å), the higher coordinate number of Sn(1) atom being accountable for this result. The angles ∠ Br–Sn(1)–Br and ∠

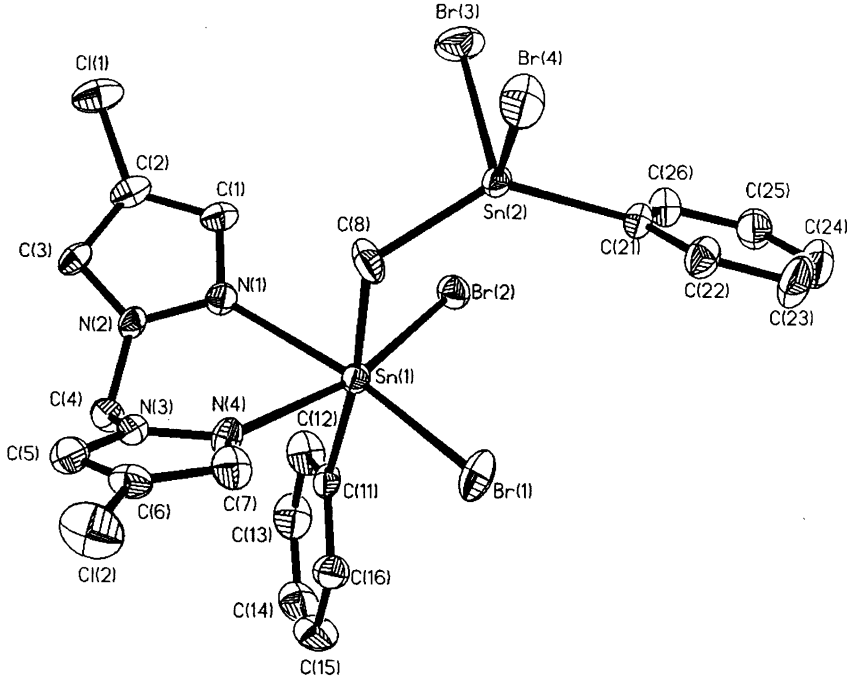


Fig. 1. Molecular structure of complex **2**. The thermal ellipsoids are drawn at the 30% probability level.

Table 2
Selected bond lengths (Å) and angles (°) for **2**

Bond lengths			
Sn(1)–Br(1)	2.596(2)	Sn(2)–Br(4)	2.505(2)
Sn(1)–Br(2)	2.681(2)	Sn(2)–C(8)	2.16(1)
Sn(1)–N(1)	2.445(9)	Sn(2)–C(21)	2.13(1)
Sn(1)–N(4)	2.40(1)	Cl(1)–C(2)	1.69(1)
Sn(1)–C(8)	2.10(1)	Cl(2)–C(6)	1.72(1)
Sn(1)–C(11)	2.13(1)	N(2)–C(4)	1.45(1)
Sn(2)–Br(3)	2.481(2)	N(3)–C(4)	1.46(1)
Bond angles			
Br(1)–Sn(1)–Br(2)	105.1(1)	N(1)–Sn(1)–C(11)	87.1(4)
Br(1)–Sn(1)–N(1)	165.0(2)	N(4)–Sn(1)–C(11)	90.0(4)
Br(2)–Sn(1)–N(1)	89.0(2)	C(8)–Sn(1)–C(11)	172.0(5)
Br(1)–Sn(1)–N(4)	88.6(2)	Br(3)–Sn(2)–Br(4)	101.8(1)
Br(2)–Sn(1)–N(4)	166.0(2)	Sn(1)–C(8)–Sn(2)	116.7(7)
N(1)–Sn(1)–N(4)	77.1(3)	N(1)–N(2)–C(4)	120.2(8)
Br(1)–Sn(1)–C(8)	90.0(4)	C(3)–N(2)–C(4)	127.0(10)
Br(2)–Sn(1)–C(8)	89.7(4)	N(4)–N(3)-C(4)	119.5(9)
N(1)–Sn(1)–C(8)	85.0(5)	N(4)-N(3)–C(5)	111.8(9)
N(4)–Sn(1)–C(8)	87.2(5)	C(4)–N(3)–C(5)	127.9(10)
Br(1)–Sn(1)–C(11)	97.4(3)	N(2)–C(4)–N(3)	110.5(9)
Br(2)–Sn(1)–C(11)	91.2(4)	C(8)–Sn(2)–C(21)	133.4(5)
Br(3)–Sn(2)–C(8)	107.7(4)	Br(3)–Sn(2)–C(21)	106.8(3)
Br(4)–Sn(2)–C(8)	101.2(4)	Br(4)–Sn(2)–C(21)	101.4(3)

C–Sn(1)–C in complex **2** ($\angle$ Br(1)–Sn(1)–Br(2) = 105.1(1)°, $\angle$ C(11)–Sn(1)–C(8) = 172.0(5)°), are larger than those in CH_2(3-iPrPz)$_2SnPh_2Br_2$ ($\angle$ Br–Sn–Br = 100.3(1)°, $\angle$ C–Sn–C = 168.2(5)°), and CH_2(3-iPrPz-5′-iPrPz)$SnPh_2Br_2$ ($\angle$ Br–Sn–Br = 94.68(2)°, $\angle$ C–Sn–C = 165.8(2)°) [12], possibly owing to the smaller repulsion of the CH_2(4-ClPz)$_2$ ligand with the other groups around the six coordinated tin atom in **2**, originating from the absence of substituents in the 3-position of pyrazole rings. The angle $\angle$ N–Sn–N of 77.1(3)° in complex **2** is similar to that in CH_2(3-iPrPz)$_2SnPh_2Br_2$ (77.6(3)°), CH_2(3-iPrPz-5′-iPrPz)-$SnPh_2Br_2$ (77.9(10)°) and CH_2(4-MePz)$_2SnMe_2Cl_2$ (76.4(3)°) [15].

4. Conclusion

The reaction between bis(dibromophenylstannyl)methane with bis(pyrazol-1-yl)alkanes yielded only 1:1 adducts, in which the organic ligands act in a chelating bidentate mode, and four- and six-coordinate tin atoms co-exist in the solid. The electronic and steric characteristics of substituents on the pyrazole rings markedly affect the donating ability of bis(pyrazol-1-yl)alkanes to the bidentate organotin Lewis acid acceptor. The investigations on the reaction of the adducts with DMSO and the NMR spectra of the adducts show the weak interactions between the ligands and the bidentate organotin Lewis acid acceptor.

5. Supplementary material

Atomic coordinates, thermal parameters and bond lengths and angles for complex **2** have been deposited at the Cambridge Crystallographic Data Centre (CCDC), 12 Union Road, Cambridge CB2 1EZ, UK (fax: +44-1223-336033; e-mail: deposit@ccdc.cam.ac.uk). Any request to the CCDC for this material should quote the full literature citation and the reference numbers CCDC168634.

Acknowledgements

This work is supported by the National Natural Science Foundation of China (No. 29902002), the Visiting Scholar Foundation of Key Lab. in University.

References

[1] S. Trofimenko, Chem. Rev. 93 (1993) 943.
[2] G.G. Lobbia, G. Valle, S. Calogero, P. Cecchi, C. Santini, F. Marchetti, J. Chem. Chem., Dalton Trans. (1996) 2475.
[3] G.G. Lobbia, P. Cecchi, R. Spagna, M. Colapietro, A. Pifferi, C. Pettinari, J. Organomet. Chem. 485 (1995) 45.
[4] G.G. Lobbia, P. Cecchi, S. Calogero, G. Valle, M. Chiarini, L. Stievano, J. Organomet. Chem. 503 (1995) 297.
[5] S. Calogero, G. Valle, G.G. Lobbia, C. Santini, P. Cecchi, L. Stievano, J. Organomet. Chem. 526 (1996) 269.
[6] S. Calogero, L. Stievano, G.G. Lobbia, A. Cingolani, P. Cecchi, G. Valle, Polyhedron 14 (1995) 1731.
[7] G.G. Lobbia, P. Cecchi, C. Santini, S. Calogero, G. Valle, F.E. Wagner, J. Organomet. Chem. 513 (1996) 139.
[8] G.G. Lobbia, P. Cecchi, G. Valle, S. Calogero, C. Santini, Main Group Met. Chem. 19 (1996) 571.
[9] D.K. Dey, M.K. Das, R.K. Bansal, J. Organomet. Chem. 535 (1997) 7.
[10] K. Mashima, T. Oshiki, K. Tani, Organometallics 16 (1997) 2760.
[11] T. Oshiki, K. Mashima, S. Kawamura, K. Tani, K. Kitaura, Bull. Chem. Soc. Jpn. 73 (2000) 1735.
[12] L.F. Tang, Z.H. Wang, W.L. Jia, Y.M. Xu, J.T. Wang, Polyhedron 19 (2000) 381.
[13] C. Pettinari, M. Pellei, A. Cingolani, D. Martini, A. Drozdov, S. Troyanov, W. Panzeri, A. Mele, Inorg. Chem. 38 (1999) 5777.
[14] C. Pettinari, A. Cingolani, B. Bovio, Polyhedron 15 (1996) 115.
[15] C. Pettinari, A. Lorenzotti, G. Sclavi, A. Cingolani, E. Rivarola, M. Colapietro, A. Cassetta, J. Organomet. Chem. 496 (1995) 69.
[16] G.G. Lobbia, F. Bonati, A. Cingolani, D. Leonesi, A. Lorenzotti, J. Organomet. Chem. 359 (1989) 21.
[17] G.G. Lobbia, A. Cingolani, D. Leonesi, A. Lorenzotti, F. Bonati, Inorg. Chim. Acta 130 (1987) 203.
[18] R. Visalakshi, V.K. Jain, S.K. Kulshreshtha, G.S. Rao, Inorg. Chim. Acta 118 (1986) 119.
[19] K. Jurkschat, F. Hesselbarth, M. Dargatz, J. Lehmann, E. Kleinpeter, A. Tzschach, J. Meunier-Piret, J. Organomet. Chem. 388 (1990) 259.
[20] M. Gielen, K. Jurkschat, J. Meunier-Piret, M. Van Meerssche, Bull. Soc. Chim. Belg. 93 (1984) 379.
[21] K. Jurkschat, M. Gielen, Bull. Soc. Chim. Belg. 91 (1982) 803.
[22] T.J. Karol, J.P. Hutchinson, J.R. Hyde, H.G. Kuivila, J.A. Zubieta, Organometallics 2 (1983) 106.

[23] M. Austin, K. Gebreyes, H.G. Kuivila, K. Swami, J.A. Zubieta, Organometallics 6 (1987) 834.
[24] M. Gielen, K. Jurkschat, J. Organomet. Chem. 273 (1984) 303.
[25] L.F. Tang, Z.H. Wang, Y.M. Xu, J.T. Wang, H.G. Wang, X.K. Yao, Polyhedron 17 (1998) 3765.
[26] L.F. Tang, Z.H. Wang, Y.M. Xu, J.T. Wang, H.G. Wang, X.K. Yao, Polyhedron 18 (1999) 2383.
[27] L.F. Tang, Z.H. Wang, W.L. Jia, Y.M. Xu, J.T. Wang, Chem. J. Chin. Univ. 20 (1999) 1720.
[28] L.F. Zhang, Q.Z. Jiang, F.L. Ye, T. Hao, G.N. Li, Youji Huaxue 11 (1991) 283.
[29] R.M. Claramunt, H. Hernandez, J. Elguero, S. Julia. Bull. Chem. Soc. Fr. (1983) 115.
[30] J.C. Jeffery, S.S. Kurek, J.A. McCleverty, E. Pasillakis, R.M. Richardson, M.D. Ward, A. Wlodarczyk. J. Chem. Soc., Dalton Trans. (1994) 2559.
[31] L.F. Tang, Z.H. Wang, W.L. Jia, J.F. Chai, J.T. Wang, Jiegou Huaxue 20 (2001) 56.

PERGAMON

Polyhedron 21 (2002) 879–884

POLYHEDRON

www.elsevier.com/locate/poly

Heteroleptic platinum(II) complexes with crown thioether and phosphine ligands: the crystal structures of $[Pt(9S3)(PPh_3)Cl](PF_6)\cdot CH_3NO_2$ and $[Pt(10S3)(PPh_3)Cl](PF_6)$☆

Gregory J. Grant [a,*], David F. Galas [a], Donald G. VanDerveer [b]

[a] *Department of Chemistry, Dept. 2252, The University of Tennessee at Chattanooga, 615 McCallie Avenue, Chattanooga, TN 37403-2598, USA*
[b] *School of Chemistry and Biochemistry, Georgia Institute of Technology, Atlanta, GA 30332, USA*

Received 16 November 2001; accepted 14 January 2002

Abstract

We wish to report the synthesis, spectroscopic properties, and crystal structures of two Pt(II) heteroleptic complexes with triphenylphosphine (PPh_3), chloride, and the crown trithioethers 9S3 (1,4,7-trithiacyclononane) or 10S3 (1,4,7-trithiacyclodecane). Both complexes have the general formula $[Pt(L)(PPh_3)Cl](PF_6)$ (L = 9S3 or 10S3) and form similar structures in which the Pt(II) center is surrounded by a *cis* arrangement of the chloride, the P donor from the phosphine, and two sulfur atoms from the 9S3 ligand. The third sulfur in each structure forms a longer interaction with the platinum resulting in an elongated square pyramidal structure. The ^{195}Pt NMR chemical shifts for both complexes show a value near −4100 ppm, consistent with a *cis*-PtS_2PCl coordination sphere. The trithioethers in both complexes are fluxional, resulting in relatively simple ^{13}C NMR spectra for them (9S3, one line; 10S3, four lines). Although the fluxional behavior of the 9S3 ligand in platinum group metal complexes is well-documented, our NMR and structural data confirm definite fluxional behavior of the 10S3 ligand for the first time. © 2002 Elsevier Science Ltd. All rights reserved.

Keywords: Thioether complexes; Platinum complexes; Trithiacyclononane; Platinum nuclear magnetic resonance; Phosphine complexes; Crown thioethers

1. Introduction

The past 15 years have seen remarkable activity in the study of the coordination chemistry of crown thioether ligands, such as 1,4,7-trithiacyclononane (9S3), in a number of areas including transition metal complexes, main group compounds, and organometallic complexes [2–7]. One of the most commonly studied metal ions with thioethers is platinum(II) due to the unusual properties exhibited by its complexes [8–13]. Structurally, the complexes form elongated square pyramids [S_4+S_1] coordination [8] or elongated octahedra [S_4+S_2] [10,12], a consequence of long distance Pt–S interactions involving the axial sulfur atoms present in the coordinated thioether crown. These long distance interactions result in unusual spectroscopic (d–d electronic transitions near 435 nm) and electrochemical properties (a reversible Pt(II)–Pt(III) couple observed near +0.35 V versus $Fc-Fc^+$ in cyclic voltammetry) properties [13]. The platinum–axial sulfur interactions are of considerable theoretical interest as they represent an intermediate case between bonding and non-bonding interactions [14]. Another key feature of the complexes is the fluxional behavior of the 9S3 ligand which appears to correlate with the axial interactions. Indeed, fluxional behavior of the 9S3 ligand has been observed in virtually every one of its Pd(II) or Pt(II) complexes [15–17]. In addition, Pt(II) complexes with 9S3 have been proposed as models for ligand substitution reactions which proceed by associative mechanisms in four coordinate complexes [18]. Several recent reports have focused on heteroleptic crown thioether complexes with phosphine ligands [19,20]. The current work extends that avenue of research to incorporate three different types of ligands

☆ For Part II, see [1].

* Corresponding author. Tel.: +1-423-755-4143; fax: +1-423-755-5234.
E-mail address: greg-grant@utc.edu (G.J. Grant).

0277-5387/02/$ - see front matter © 2002 Elsevier Science Ltd. All rights reserved.
PII: S0277-5387(02)00870-7

(thioether, phosphine, and chloride) bound to the Pt center in the complex [Pt(9S3)(PPh_3)Cl](PF_6). Few platinum(II) complexes containing these three types of ligands have been structurally characterized [22]. Lastly, we were also interested in the fluxional behavior of the related crown trithioether, 1,4,7-trithiacyclodecane, 10S3. In contrast to the 9S3 complexes, the fluxionality of this ligand had not yet been verified, so we have prepared the analogous complex, [Pt(10S3)(PPh_3)Cl]-(PF_6), for study in that regard.

2. Experimental

2.1. Materials

All solvents and reagents were purchased from Aldrich Chemical Company and used as received. The starting complex [Pt(9S3)Cl_2] was prepared by the published method [17].

2.2. Measurements

Analyses were performed by Atlantic Microlab, Inc., of Atlanta, Georgia. Fourier transform infrared spectra were obtained using a Galaxy FT-IR 5000 spectrophotometer and UV–Vis spectra were obtained on a Varian DMS 200 UV–Vis spectrophotometer. ^{13}C and proton NMR spectra were recorded on a Varian Gemini 300 NMR spectrometer using CD_3NO_2 for both the deuterium lock and reference. Carbon connectivity was confirmed via DEPT (Distortionless Enhancement by Polarization Transfer) experiments. Platinum-195 NMR spectra were recorded at 64.208 MHz using aqueous solutions of $[PtCl_6]^{2-}$ (0 ppm) as an external reference and delay time of 0.01 s. Referencing was verified versus authentic samples of $[PtCl_4]^{2-}$ which was found to have a chemical shift at −1626 ppm, in agreement with the reported value of −1624 ppm [23]. Phosphorus-31 NMR was measured at 121.470 MHz, and referencing was done using phosphoric acid (0 ppm) as an external standard.

2.3. Preparation of [Pt(9S3)(PPh_3)Cl]PF_6

A slurry of [Pt(9S3)Cl_2] (80.0 mg, 0.179 mmol) in 250 ml of 3:1 CH_3CN:CH_2Cl_2 was stirred and warmed slightly. Small portions of triphenylphosphine, PPh_3, (47.0 mg, 0.179 mmol) were added forming a clear yellow solution. Next excess NH_4PF_6 (0.300 g, 1.84 mmol) was added to form a white precipitate of NH_4Cl, and the precipitate was removed from the warm solution by filtration. The solution was then concentrated to 2/3 of its original volume, and ether was slowly added to precipitate [Pt(9S3)(PPh_3)Cl]PF_6 as yellow crystals (0.102 g, 69.6% yield). *Anal*. Calc. for $C_{25}H_{30}ClF_6NO_2P_2PtS_3$: C, 35.23; H, 3.32; S, 11.76; Cl, 4.33. Found: C, 35.00; H, 3.40; S, 11.71; Cl, 4.07%. The electronic absorption spectrum measured in acetonitrile showed a single λ_{max} at 258 nm ($\varepsilon = 23\,000$). FT-IR (KBr, cm^{-1}): 3065, 3061, 3057, 2973, 2951, 1437, 1097, 839 (s, PF_6^-), 732, 508. ^1H NMR (CD_3NO_2) δ: 7.82, 7.52 (m, PPh_3, 15 H), broad, complex multiplet centered at 3.07 (9S3, 12 H). $^{13}C\{^1H\}$ NMR(CD_3NO_2) δ: 136.1 (m, 6 C, PPh_3), 133.5 (s, 3 C, PPh_3), 130.2 (m, 6 C, PPh_3), 128.7 (d, 3 C, PPh_3, $^1J_{C-P} = 61$ Hz), 37.3 (s, 9S3, 6 C). $^{195}Pt\{^1H\}$ NMR (CD_3NO_2) δ ($\nu_{1/2}$): doublet at −4052 (70 Hz) and −4107 (70 Hz) ($^1J_{PtP} = 3399$ Hz). $^{31}P\{^1H\}$ NMR (CD_3NO_2) δ: 16.09 (s, $^1J_{PtP} = 3387$ Hz).

2.4. Preparation of [Pt(10S3)(PPh_3)Cl]PF_6

The complex is prepared by using the above procedure starting with [Pt(10S3)Cl_2] (0.0920 g, 0.200 mmol) and triphenylphosphine (0.0525 g, 0.200 mmol). These are mixed in 250 ml of 3:1 CH_3CN:CH_2Cl_2 with stirring and mild heating. Addition of excess NH_4PF_6 (0.300 g, 1.84 mmol), filtration of NH_4Cl, concentration of the solution to 2/3 of its original volume, and the slow addition of ether formed yellow crystals of [Pt(10S3)(PPh_3)Cl]PF_6 (0.130 g, 78.0% yield). *Anal.* Calc. for $C_{25}H_{29}ClF_6P_2PtS_3$: C, 36.08; H. 3.51; S, 11.56; Cl, 4.26. Found: C, 36.07; H, 3.45; S, 11.67; Cl, 4.35%. The electronic absorption spectrum measured in acetonitrile showed two λ_{max} at 260 nm ($\varepsilon = 24\,000$) and 234 nm ($\varepsilon = 35\,000$). FT-IR (KBr, cm^{-1}): 3090, 3045, 3030, 2983, 2923, 1437, 1105, 839 (s, PF_6^-), 810, 793, and 705. ^1H NMR (CD_3NO_2) δ: 7.95, 7.63 (m, PPh_3, 15 H), complex, overlapping peaks 3.35–2.75 (m, 10S3, α-methylene, 12 H), and 2.25–2.18 (m, 10S3, β-methylene, 2 H). $^{13}C\{^1H\}$ NMR(CD_3NO_2) δ: 136.3 (m, 6 C, PPh_3), 133.7 (s, 3 C, PPh_3), 130.5 (m, 6 C, PPh_3), 128.8 (d, 3 C, PPh_3, $^1J_{C-P} = 62$ Hz), 36.6, 36.2, 33.7 (s, 10S3, α-methylene, 6 C) 26.6 (s, 10S3, β-methylene, 1 C). $^{195}Pt\{^1H\}$ NMR (CD_3NO_2) δ ($\nu_{1/2}$): doublet at −4101 (73 Hz) and −4154 ppm (78 Hz) ($^1J_{PtP} = 3442$ Hz). $^{31}P\{^1H\}$ NMR (CD_3NO_2) δ: 14.20 (s, $^1J_{PtP} = 3438$ Hz).

2.5. Data collection and processing

Suitable crystals of both complexes were grown by slow diffusion of ether into a nitromethane solution. A summary of key crystallographic details for both structures is presented in Table 1. For both structures, intensity data were collected on a Siemens SMART 1K CCD diffractometer [24,25]. Both structures were solved using direct methods [24]. For the 9S3 complex, the h, k, l ranges used during its structure solution and refinement were −10/12, −25/26, −18/21. For 18 950 measured reflections 7140 were unique. The merging R-values on intensities were 0.0351. The structure was refined by a full-matrix least squares on F^2 using 7140

Table 1
Crystallographic data for $[Pt(9S3)(PPh_3)(Cl)]PF_6 \cdot CH_3NO_2$ (**1**) and $[Pt(10S3)(PPh_3)(Cl)]PF_6$ (**2**)

	(1)	(2)
Empirical formula	$C_{25}H_{30}ClF_6NO_2P_2Pt\ S_3$	$C_{25}H_{29}ClF_6P_2Pt\ S_3$
Formula weight, amu	879.16	832.14
Lattice	monoclinic	orthorhombic
Space group	$P2_1/n$	$P2_12_12_1$
a (Å)	9.5445(16)	8.61300(10)
b (Å)	19.529(3)	18.5002(3)
c (Å)	16.647(3)	18.6171(3)
α (°)	90	90
β (°)	96.532(3)	90
γ (°)	90	90
V (Å^3)	3082.7(9)	2966.48(8)
Z	4	4
Radiation (λ, Å)	0.71073	0.71073
ρ_{calc} (g cm^{-3})	1.894	1.863
μ (mm^{-1})	5.008	5.192
T (K)	198(2)	300(2)
R [a]	0.0241	0.0348
R_w [b]	0.0557	0.0475

[a] $R = \Sigma||F_o| - |F_c|/\Sigma|F_o|$.
[b] $R_w = [\Sigma\ w(|F_o| - |F_c|)^2/\Sigma\ w(F_o)^2]^{1/2}$.

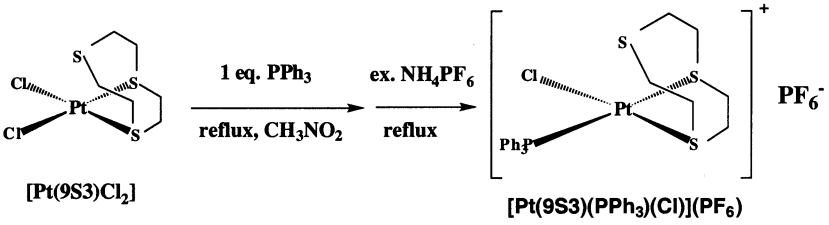
unique reflections and 430 parameters. The residuals were as follows, for reflections having $I > 2\sigma(I)$ $R = 0.0241$, $R_w = 0.0557$ and goodness of fit = 1.030; for all reflections $R = 0.0313$, $R_w = 0.0576$. The maximum shift/σ ratio was 0.002. In the last D-map, the deepest hole was −0.831 e Å^{-3} and the highest peak was 1.1410 e Å^{-3}. The secondary extinction coefficient was 0.00194(9) μ.

For the 10S3 complex, the h, k, l ranges used during the structure solution and refinement were −10/10, −22/20, −13/22. For 15 655 measured reflections 5223 were unique. The merging R-values on intensities were 0.0441. An absorption correction was performed using SADABS [25]. The structure was refined by a full-matrix least squares on F^2 using 5223 unique reflections and 417 parameters. The residuals were as follows: for reflections having $I > 2\sigma(I)$ $R = 0.0348$, $R_w = 0.05857$ and goodness of fit = 1.018; for all reflections $R = 0.0475$, $R_w = 0.0990$. The maximum shift/σ ratio was 0.002. In the last D-map, the deepest hole was −0.629 e Å^{-3} and the highest peak was 1.178 e Å^{-3}. The secondary extinction coefficient was 0.0072(3) microns. The structure of the 10S3 complex contains disorder in two carbons (C8, C9) of the propylene linkage within the thioether ring. The disorder model contains two orientations of this linkage in equal amounts.

3. Results and discussion

3.1. Synthesis and spectra

The two complexes are readily prepared by the reaction of the appropriate trithioether platinum dihalide salt with 1 equiv. of triphenylphosphine and isolated as the hexafluorophosphate salt as show below. Their composition is confirmed using a variety of spectroscopic techniques and elemental analysis. The proton NMR spectrum shows resonances for all phenyl and methylene protons in the appropriate ratios and splittings. In contrast to other phosphine complexes, the lower symmetry of both complexes results in a complicated pattern for the methylene protons of the thioether ligands [19,20]. In addition, ^{13}C DEPT experiments confirm all carbon connectivity in both complexes. As expected, the 9S3 ligand is fluxional in solution resulting in a single ^{13}C NMR resonance for the thioether ligand, showing all six carbon atoms to be equivalent. The fluxionality has been proposed to occur via rapid intramolecular exchanges of sulfur atoms (1,4-metallotropic shift) [15,17]. In combination with its crystal structure (see below), the ^{13}C NMR spectrum of the 10S3 ligand in $[Pt(10S3)(PPh_3)Cl](PF_6)$ does demonstrate that this ligand also undergoes an exchange process in its platinum complexes. Note that a four-line ^{13}C NMR spectrum cannot unambiguously determine if the complex is fluxional in solution since the symmetrical linkage isomer of the 10S3 would show this relatively simple spectrum. However, the linkage isomer of lower symmetry which is obtained in the crystal structure would yield a 7-line spectrum, indicating that a ligand exchange process is indeed occurring in solution. We have not been able to observe a slow trithioether exchange in the ^{13}C NMR spectrum of either complex down to −40 °C [21].



The ^{195}Pt NMR spectra for both complexes show the anticipated doublet splitting pattern centered at −4080 ppm for the 9S3 complex and −4127 ppm for the 10S3. These two values lie intermediate between the ones reported for $[Pt(9S3)Cl_2]$ at −3605 ppm and for $[Pt(9S3)(PPh_3)_2]2+$ at −4399 ppm, showing an average ligand field effect in the chemical shift [17]. The downfield shift of the platinum resonance upon the addition of the anionic chloride ligands is anticipated. The ^{31}P NMR spectra for each complex show a single resonance and a doublet of ^{195}Pt satellites. The values of $^1J(^{195}Pt-^{31}P)$ coupling constants of the two complexes occur at 3387 and 3438 Hz, respectively, and these values are relatively large compared with other thioether–phosphine complexes [1,20]. In addition, we observe the effects of coupling between the *ortho* and *meta* phenyl carbons and the phosphorus while the *para* carbon shows no coupling. We have previously observed similar coupling patterns in related thioether–phosphine complexes.

3.2. Structures

The complex $[Pt(9S3)(PPh_3)Cl](PF_6)\cdot CH_3NO_2$ crystallizes in the space group $P2_1/n$. An ORTEP perspective of the complex cation is shown in Fig. 1, and selected bond lengths are given in Table 2. A nitromethane solvent molecule is also incorporated into the crystal lattice. The complex forms an elongated square pyramidal structure which is common for heteroleptic crown thioether complexes of Pt(II) and Pd(II) [19,20]. The square plane is comprised of the Cl^- donor, the P donor from the PPh_3, and two sulfur donors from the 9S3. The third sulfur shows the elongated interaction to complete the square pyramidal structure. The Pt(II) ion is raised slightly (by 0.1172(4) Å) above the mean square plane and directed towards the axial sulfur donor. The four atoms in the equatorial plane have an average displacement of 0.0576 Å.

Table 2
Selected bond distances (Å) and angles (°) for $[Pt(9S3)(PPh_3)(Cl)]PF_6\cdot CH_3NO_2$ (**1**) and $[Pt(10S3)(PPh_3)(Cl)]PF_6$ (**2**)

	(1)	(2)
Distances (Å)		
$Pt-S_{axial}$	3.0778(8)	2.938(2)
$Pt-S_{eq}$	2.3365(8), 2.2609(9)	2.252(3), 2.350(2)
Pt–P	2.2838(8)	2.285(2)
Pt–Cl	2.3434(8)	2.332(3)
Angles (°)		
$S_{eq}-Pt-S_{eq}$	88.94(3)	87.80(9)
P–Pt–Cl	89.99(3)	88.95(9)
S(4)–Pt–Cl	86.98(1)	87.20(9)
S(7)–Pt–P	93.64(3)	95.41(9)
$S_{eq}-Pt-S_{ax}$	82.70(3), 110.55(3)	80.807(9), 94.971(9)

Of particular note is the distance between the axial sulfur donor and the platinum, as this distance is quite sensitive to the nature of the ancillary ligand(s). The structure reported here represents an intermediate case between the reported dichloro and bis(triphenylphosphine) Pt(9S3) complexes, and the three complexes follow the trend in Pt–Saxial distance: 2.638(3) Å < 3.0778(9) Å < 3.260(3) Å for the $(PPh_3)_2$, (PPh_3, Cl), (Cl_2) complexes, respectively, [17,20]. Although longer than the Pt–S bond distances, nevertheless, they are considerably shorter than 3.5 Å, the van der Waals distance for a platinum–sulfur interaction [26]. The relative π donor–acceptor characteristics of the chloride and the phosphine ligands have been proposed as being responsible for this trend. [19,20] The better π accepting phosphine ligand reduces electron density on the metal center, enhancing the positive charge and drawing the sulfur closer. In contrast, the better π donating chloride increases the electron density on the platinum, and a longer axial sulfur distance is observed. The Pt–P distance is slightly shorter than observed the one

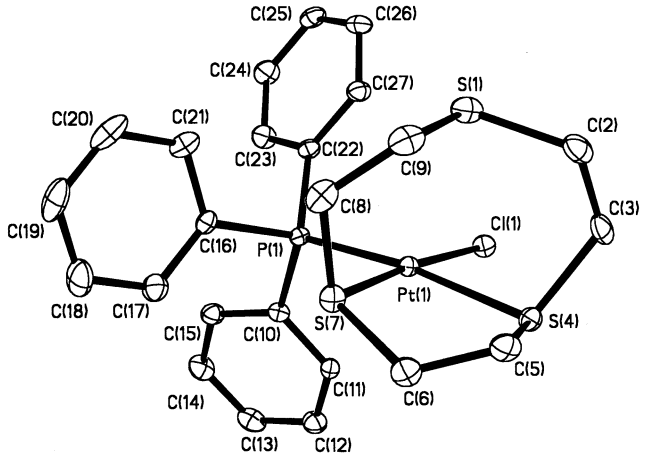


Fig. 1. ORTEP perspective of cation in $[Pt(9S3)(PPh_3)Cl](PF_6)\cdot CH_3NO_2$.

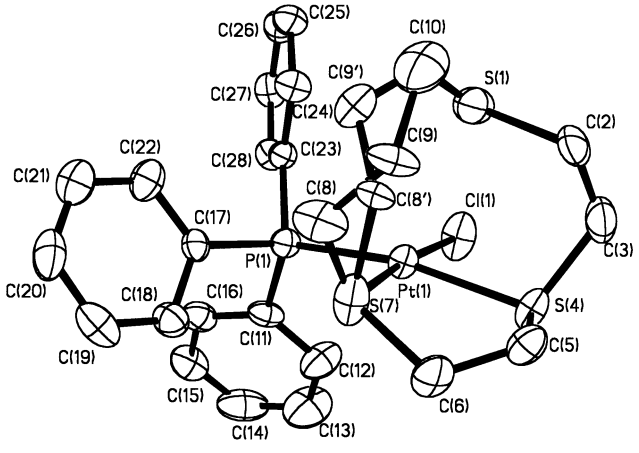


Fig. 2. ORTEP perspective of cation in $[Pt(10S3)(PPh_3)Cl](PF_6)$.

observed in $[Pt(9S3)(PPh_3)_2]^{2+}$ while the Pt–Cl distance is slightly longer than observed in $[Pt(9S3)Cl_2]$. Other structural features in the 9S3 complex including the Pt–S equatorial bond distances and the S–Pt–S bond angles lie intermediate between the values found in the two previously reported structures.

The complex $[Pt(10S3)(PPh_3)Cl](PF_6)$ crystallizes in the orthorhombic space group $P2_12_12_1$. An ORTEP perspective of the complex cation is shown in Fig. 2 and selected bond lengths are given in Table 2. This structure, too, is an elongated square pyramidal structure with the square plane comprised of the Cl^- donor, the P donor from the PPh_3, and two sulfur donors from the crown thioether. The third sulfur shows the elongated interaction with the Pt center at 2.928(9) Å to complete the square pyramidal structure. The space group is a chiral one, and the chirality arises from the single enantiomeric form of the complex that was obtained in the crystal [27]. Note that the propylene chelate ring links the axial sulfur (S1) with one of the equatorial sulfurs (S7). Its enantiomer would link S1 with the other equatorial sulfur donor, S4. The alternative *meso* diastereoisomer is the one that has this propylene chelate ring linking the two equatorial sulfur donors and would show a four line ^{13}C NMR spectrum for the 10S3 ligand. However, the exchange process of the 10S3 ligand interconverts the three stereoisomers in solution, resulting in the loss of chirality and accounting for the number of observed ^{13}C NMR signals.

As was true for the 9S3 complex, this axial Pt–S distance has shortened from those found in the dichloro analog $[Pt(10S3)Cl_2]$ (3.125(5), 3.121(5) Å) and lengthened relative to the reported value in a 10S3/diphosphine complex (2.6505(4) Å) [28,29]. In all analogous 10S3 complexes, the axial Pt–S distances are smaller than those found in the 9S3 complexes, possibly due to the greater conformational flexibility of the 10S3. In the structure the Pt(II) ion is again raised slightly (by 0.1228(12) Å) above the mean square plane and directed towards the axial sulfur donor. The four atoms in the equatorial plane have an average displacement of 0.1036 Å. In both structures, the shorter equatorial Pt–S bond lies *trans* to the Pt–Cl bond, a reflection of the relative *trans* directing strength between chloride and phosphine ligands.

4. Conclusions

One equiv. of the phosphine ligand, PPh_3, readily reacts with $[Pt(9S3)Cl_2]$ or $[Pt(10S3)Cl_2]$ forming unusual heteroleptic thioether–phosphine–chloride complexes with elongated square pyramidal structures $[S_2PCl+S_1]$ in the solid state. Increasing positive charge on the platinum center results in shorter axial Pt–S distances and an upfield ^{195}Pt NMR chemical shift. Both trithioethers are fluxional in solution, the first confirmation of fluxionality for the 10S3 ligand in platinum group complexes.

5. Supplementary material

Crystallographic data for the two structures reported in this paper have been deposited with the Cambridge Crystallographic Data Center as CCDC 172660 & 172661. Copies of the data can be obtained free of charge upon application to CCDC, 12 Union Road, Cambridge, CB2 1 EZ UK (fax: +44-1223 336 033); e-mail: deposit@ccdc.cam.ac.uk.

Acknowledgements

This research was generously supported by grants from the Petroleum Research Fund, administered by the American Chemical Society, the Research Corporation, and the William L. Wheeler Center for Odor Research at the University of Tennessee at Chattanooga.

References

[1] Heteroleptic Platinum(II) Complexes with Crown Thioether and Phosphine Ligands III; for Part II see G.J. Grant, S.M. Carter, A.L. Russell, I.M. Poullaos, D.G. VanDerveer, J. Organomet. Chem. 637–639 (2001) 683.
[2] A.J. Blake, M. Schröder, in: A.G. Sykes (Ed.), Advances in Inorganic Chemistry, vol. 35, Academic Press, New York, 1990, p. 2.
[3] S.R. Cooper, Acc. Chem. Res. 21 (1988) 141.
[4] S.R. Cooper, S.C. Rawle, Struct. Bonding (Berlin) 72 (1990) 1.
[5] M. Schröder, Pure Appl. Chem. 60 (1988) 517.
[6] W.N. Setzer, E.L. Cacioppo, Q. Guo, G.J. Grant, D.D. Kim, J.L. Hubbard, D.G. VanDerveer, Inorg. Chem. 29 (1990) 2672.
[7] R.D. Adams, S.B. Falloon, K.T. McBride, J.H. Yamamoto, Organometallics 14 (1995) 1739.
[8] A.J. Blake, R.O. Gould, A.J. Holder, T.I. Hyde, A.J. Lavery, M.O. Odulate, M. Schröder, J. Chem. Soc., Chem. Commun. (1987) 118.
[9] A.J. Blake, A.J. Holder, G. Reid, M. Schröder, J. Chem. Soc., Dalton Trans. (1994) 627.
[10] A.J. Blake, R.O. Gould, A.J. Lavery, M. Schröder, Angew. Chem., Int. Ed. Engl. 25 (1986) 274.
[11] S.J. Loeb, J.R. Mansfield, Can. J. Chem. 74 (1996) 1377.
[12] A.J. Blake, R.D. Crofts, M. Schröder, J. Chem. Soc., Dalton Trans. (1993) 2259.
[13] G.J. Grant, N.S. Spangler, W.N. Setzer, D.G. VanDerveer, Inorg. Chim. Acta 246 (1996) 41.
[14] T.W. Hambley, Inorg. Chem. 37 (1998) 3767.
[15] E.W. Abel, P.D. Beer, I. Moss, K.G. Orrell, V. Sik, P.A. Bates, M.B. Hurthouse, J. Chem. Soc., Chem. Commun. (1987) 978.
[16] M.A. Bennett, J.K. Felixberger, A.C. Willis, Gazz. Chim. Ital. 123 (1993) 405.
[17] G.J. Grant, C.G. Brandow, D.F. Galas, J.P. Davis, W.P. Pennington, J.D. Zubkowski, E.J. Valente, Polyhedron 20 (2001) 3333. The simplicity of the NMR spectrum of the complex

[Pt(10S3)Cl_2] implied that it too was functional in solution as is now confirmed in this report.

[18] H. Nikol, H.-B. Bürgi, K.I. Hardcastle, H.B. Gray, Inorg. Chem. 34 (1995) 6319.

[19] A.J. Blake, Y.V. Roberts, M. Schröder, J. Chem. Soc., Dalton Trans. (1996) 1885.

[20] G.J. Grant, I.M. Poullaos, D.F. Galas, D.G. VanDerveer, J.D. Zubkowski, E.J. Valente, Inorg. Chem. 40 (2001) 564.

[21] We also have studied both complexes in CD_3CN which enables variable temperature NMR experiments to be carried out at near -40°. We still, however, cannot observe a slow exchange of the ligand in the ^{13}C NMR spectrum. This is consistent with our previous observations on Pt(II) complexes containing trithioethers such as 9S3. Bürgi (Reference [18]) notes that the observed activation free energy for the 9S3 exchange is near the lower limit of detectable NMR fluxional processes.

[22] For other examples, see: L.V. Andreasen, O. Simonsen, O. Wernberg, Inorg. Chim. Acta 295 (1999) 153.
P. Kapoor, K. Luvqvist, A. Oskarsson, J. Mol. Struct. 470 (1998) 39.
A.R. Sanger, Can. J. Chem. 61 (1983) 2214.

[23] P.S. Pregosin, in: P.S. Pregosin, (Ed.), Transition Metal Nuclear Magnetic Resonance, Elsevier, New York, 1991 pp. 251, and references cited therein.

[24] The programs used for data collection, solution and refinement of this structure were: SMART 5.054, SAINT$^+$ 6.01, SHELXTL 5.1, 1998–1999, Bruker AXS, Madison, WI, USA.

[25] SADABS, R.H. Blessing, Acta Crystallogr., Sect. A 51 (1995) 33.

[26] The sum of the van der Waals radii for platinum and sulfur is 3.50 Å.J.E. Huheey, E.A. Keiter, R.L. Keiter, Inorganic Chemistry, fourth ed., Harper Collins, New York, 1993, pp. 292.

[27] The absolute configuration is confirmed through the Flack parameter. It is zero ($\pm$) for the correct absolute configuration (as it appears in the cif files of the structure).

[28] G.-H. Lee, Acta Crystallogr. C 54 (1998) 906.

[29] G.J. Grant, D.F. Galas, I.M. Poullaos, D.G. VanDerveer J. Chem. Soc., Chem. Dalton Trans. (2002), submitted for publication.

PERGAMON

Polyhedron 21 (2002) 885–892

POLYHEDRON

www.elsevier.com/locate/poly

Triosmium and triruthenium clusters containing deprotonated 2-mercapto-1-methylimidazole ligand: X-ray structures of $[(\mu\text{-H})Os_3(CO)_{10}\{\mu\text{-SC=NCH=CHN(CH}_3)\}]$, $[(\mu\text{-H})Ru_3(CO)_9\{(\mu_3\text{-}\eta^2\text{-SC=NCH=CHN(CH}_3)\}]$ and $[(\mu\text{-H})Os_3(CO)_8\{\mu\text{-SC=NCH=CHN(CH}_3)\}(\mu\text{-dppm})]$

Kazi A. Azam [a], Khandakar M. Hanif [a], Amaresh C. Ghosh [a], Shariff E. Kabir [a,*], Shafali R. Karmakar [a], K.M. Abdul Malik [b,*], Salina Parvin [a], Edward Rosenberg [c]

[a] *Department of Chemistry, Jahangirnagar University, Savar, Dhaka 1342, Bangladesh*
[b] *Department of Chemistry, Cardiff University, PO Box 912, Park Place, Cardiff CF10 3TB, UK*
[c] *Department of Chemistry, The University of Montana, Missoula, MT 59812, USA*

Received 5 December 2001; accepted 22 January 2002

Abstract

The reactions of $[Os_3(CO)_{10}(MeCN)_2]$, $[Ru_3(CO)_{12}]$, $[(\mu\text{-H})Os_3(CO)_8\{Ph_2PCH_2P(Ph)C_6H_4\}]$, $[Os_3(CO)_{10}(\mu\text{-dppm})]$ and $[Ru_3(CO)_{10}(\mu\text{-dppm})]$ with 2-mercapto-1-methylimidazole are reported. The labile cluster $[Os_3(CO)_{10}(MeCN)_2]$ reacts with 2-mercapto-1-methylimidazole at 25 °C to give $[(\mu\text{-H})Os_3(CO)_{10}\{\mu\text{-SC=NCH=CHN(CH}_3)\}]$ (**1**) whereas the corresponding reaction of $[Ru_3(CO)_{12}]$ with the ligand at 68 °C gives $[(\mu\text{-H})Ru_3(CO)_9\{\mu_3\text{-}\eta^2\text{-SC=NCH=CHN(CH}_3)\}]$ (**2**). Both $[(\mu\text{-H})Os_3(CO)_8\{Ph_2PCH_2P(Ph)C_6H_4\}]$ and $[Os_3(CO)_{10}(\mu\text{-dppm})]$ react with 2-mercapto-1-methylimidazole at 25 and 110 °C, respectively, to give $[(\mu\text{-H})Os_3(CO)_8\{\mu\text{-SC=NCH=CHN(CH}_3)(\mu\text{-dppm})]$ (**3**). In contrast $[Ru_3(CO)_{10}(\mu\text{-dppm})]$ reacts with 2-mercapto-1-methylimidazole at 68 °C to yield the known compound $[Ru_3(CO)_7(\mu_3\text{-CO})(\mu_3\text{-S})(\mu\text{-dppm})]$ (**4**). The structures of **1**–**3** have been determined by X-ray crystallography. © 2002 Elsevier Science Ltd. All rights reserved.

Keywords: Heterocyclic thioamides; Osmium; Ruthenium; 2-Mercapto-1-methylimidazole; X-ray structures

1. Introduction

The reactions of heterocyclic thioamides with trimetallic clusters of osmium, ruthenium and iron have been investigated [1–6]. It has been demonstrated that some reactions proceed with retention of the cluster nuclearity while in other cases fragmentation into dinuclear species as well as ring opening of the ligand takes place. For example, the reaction of $[Ru_3(CO)_{12}]$ with thiomorpholine gives the triruthenium cluster $[(\mu\text{-H})Ru_3(CO)_9(\mu_3\text{-}\eta^2\text{-SCH}_2\text{CH}_2\text{NH}_2)]$ by a ring opening reaction of thiomorpholine (C_4H_9NS) followed by elimination of a C_2 fragment whereas thiazolidine (C_3H_7NS) under identical condition gives the dinuclear compound $[Ru_2(CO)_6(\mu\text{-}\eta^3\text{-SCH}_2\text{CH}_2\text{–NHCH}_2)]$ formed by cluster fragmentation and ring opening cleavage of the C–S bond of the ligand [5]. On the other hand, benzothiazoline-2-thione reacts with $[Ru_3(CO)_{12}]$ to give both tri- and dinuclear complexes $[(\mu\text{-H})Ru_3(CO)_9(C_7H_4NS_2)]$ and $[Ru_2(CO)_6(C_7H_4NS_2)]$ containing deprotonated thioamide ligand [2,3] whereas with $[Fe_3(CO)_{12}]$ it yields $[Fe_3(CO)_9S_2]$ by desulfurization of the ligand [4]. As an extension of our studies on the reactions of trimetallic clusters with N- and S-heterocyclic ligands such as 4-methylthiazole [7], thiazole [8,9], thiomorpholine [5], thiazolidine [5], benzothiazole [6] and pyrimidine-2-thione [6], we investigated the reactions of 2-mercapto-1-methylimidazole with a series of trimetallic clusters such as $[Os_3(CO)_{10}(MeCN)_2]$, $[Ru_3(CO)_{12}]$, $[(\mu$-

* Corresponding authors. Tel.: +44-29-2087-4950; fax: +44-29-2087-4705.
E-mail address: malikka@cardiff.ac.uk (K.M. Abdul Malik).

0277-5387/02/$ - see front matter © 2002 Elsevier Science Ltd. All rights reserved.
PII: S0277-5387(02)00869-0

H)$Os_3(CO)_8${$Ph_2PCH_2P(Ph)C_6H_4$}], [$Os_3(CO)_{10}$(μ-dppm)] and [$Ru_3(CO)_{10}$(μ-dppm)]. The results of this study are reported herein.

2. Results and discussion

The reaction of [$Os_3(CO)_{10}(MeCN)_2$] with 2-mercapto-1-methylimidazole at 25 °C gave [(μ-H)$Os_3(CO)_{10}${μ-SC=NCH=CHN(CH_3)}] (**1**) (Scheme 1). This compound was characterised by spectroscopic data and by an X-ray structure determination. The infrared spectrum of **1** in the carbonyl stretching region is very similar to that of [(μ-H)$Os_3(CO)_{10}$(μ-dmpymt)] [10] (dmpymt = 4,6-dimethylpyrimidine-2-thiol) and [(μ-H)$Os_3(CO)_{10}$(SC=NCH_2CH_2S)] [1] indicating that they have very similar distribution of the carbonyl ligands. Besides the characteristic resonances for the heterocyclic ligand, the ^{1}H NMR contains a singlet at δ −16.76 due to the bridging hydride. The mass spectrum shows the molecular ion peak at *m*/*z* 964 and fragment ions formed by the loss of ten carbonyl ligands.

The X-ray structure of **1** is depicted in Fig. 1 and selected bond distances and angles are listed in Table 1. The molecule has a crystallographic mirror plane and consists of an isosceles triangle of osmium atoms with ten terminal carbonyl ligands, four bonded to Os(2) and three to each of Os(1) and Os(1′). The 2-mercapto-1-methylimidazole ligand symmetrically bridges the Os(1)–Os(1′) edge of the cluster via the exocyclic sulfur atom. The hydride ligand also bridges the same Os–Os edge. This doubly bridged Os–Os edge is only marginally longer than the other two edges {Os(1)–Os(1′) = 2.8569(10) Å vs. Os(1)–Os(2) = Os(2)–Os(1′) = 2.8439(8) Å}. The unique Os–S bond distance {2.415(3) Å} is similar to those found in other sulfur bridged triosmium clusters, e.g. 2.405(4) Å in [(μ-H)$Os_3(CO)_{10}$(μ-dmpymt)] [10], and 2.416(11) and 2.419(8) Å in [(μ-H)$Os_3(CO)_{10}$(μ-SC=NCH_2CH_2S)] [1]. The plane defined by Os(1), Os(1′) and S(1) is almost perpendicular to the Os_3 triangle {dihedral angle = 77.2(6)°}. The heterocyclic ligand is exactly planar and within it the exocyclic C(7)–S(1) bond at 1.75(2) Å is as expected for a single bond [11]. The C(7)–N(2) bond distance of 1.29(2) Å indicates a double bond character while the C(7)–N(1) bond at 1.37(2) Å is as expected for a C–N single bond [11].

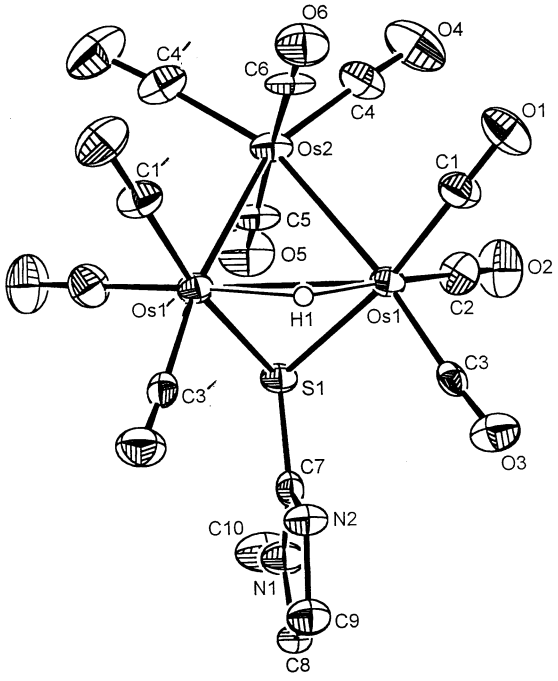
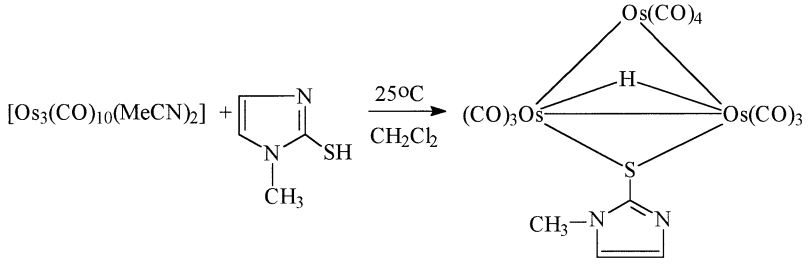


Fig. 1. X-ray structure of [(μ-H)$Os_3(CO)_{10}${μ-η^2-SC=NCH=CHN(CH_3)}] (**1**) showing the atom labelling scheme. The primed atoms, generated by the symmetry (*x*, 0.5−*y*, *z*) are related to the unprimed ones by a mirror plane. Thermal ellipsoids are drawn at 35% probability level. The ring hydrogen atoms are omitted for clarity.

In contrast, the reaction of [$Ru_3(CO)_{12}$] with 2-mercapto-1-methylimidazole at 68 °C gives [(μ-H)$Ru_3(CO)_9${μ_3-η^2-SC=NCH=CHN(CH_3)}] (**2**) (Scheme 2). The compound **2** has been characterised by spectroscopic data and single crystal X-ray diffraction studies. The infrared spectrum of **2** in the carbonyl region is similar to that of [(μ-H)$Ru_3(CO)_9${μ_3-η^2-$SN_2C_4H_3$}] [6], [(μ-H)$Ru_3(CO)_9${μ_3-η^2-$S_2NC_7H_4$}] [3] and [(μ-H)$Ru_3(CO)_9$(μ_3-η^2-pyS)] [12] in both the appearance and position of the bands indicating structural similarities. The mass spectrum shows the molecular ion peak at *m*/*z* 670 and fragment ions formed by the



1

Scheme 1.

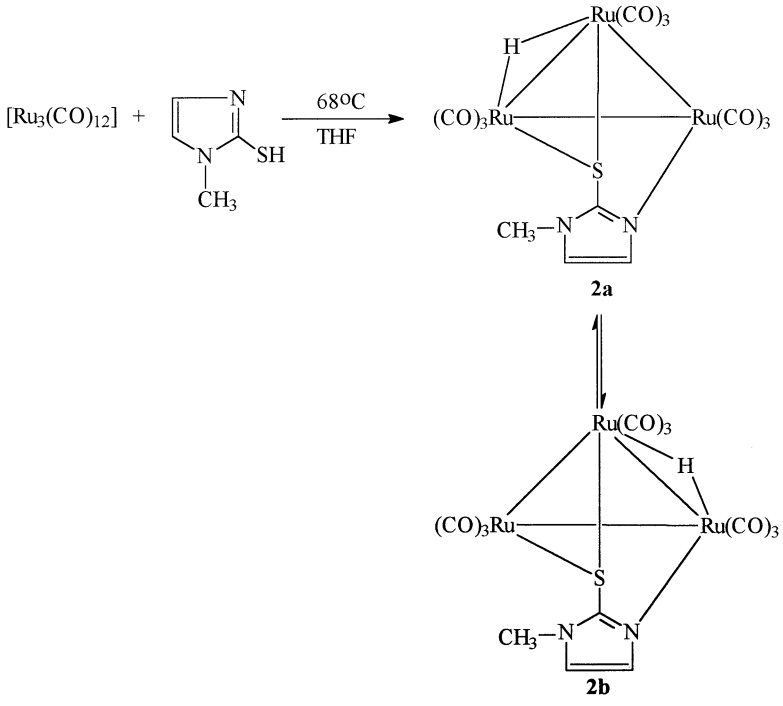
Table 1
Selected bond lengths (Å) and angles (°) for **1**

Bond lengths			
Os(1)–Os(2)	2.8439(8)	Os(1)–Os(1′) [a]	2.8569(10)
Os(1)–S(1)	2.415(3)	Os(1)–H(1)	1.70 [b]
S(1)–C(7)	1.75(2)	N(1)–C(7)	1.37(2)
N(1)–C(8)	1.39(2)	N(1)–C(10)	1.52(3)
N(2)–C(7)	1.29(2)	N(2)–C(9)	1.41(2)
C(8)–C(9)	1.32(3)	Os–C (CO)	1.91(2) [c]
C–O (CO)	1.15(3) [c]		
Bond angles			
C(1)–Os(1)–C(2)	89.2(6)	C(1)–Os(1)–C(3)	91.7(5)
C(2)–Os(1)–C(3)	99.3(6)	C(1)–Os(1)–S(1)	170.7(5)
C(2)–Os(1)–S(1)	94.4(5)	C(3)–Os(1)–S(1)	96.2(3)
C(1)–Os(1)–Os(2)	89.5(4)	C(2)–Os(1)–Os(2)	91.1(5)
C(3)–Os(1)–Os(2)	169.5(3)	S(1)–Os(1)–Os(2)	81.83(9)
C(1)–Os(1)–Os(1′) [a]	118.7(5)	C(2)–Os(1)–Os(1′) [a]	137.2(5)
C(3)–Os(1)–Os(1′) [a]	110.7(3)	S(1)–Os(1)–Os(1′) [a]	53.74(6)
C(5)–Os(2)–C(4)	90.8(6)	C(4)–Os(2)–C(4′) [a]	105.3(10)
C(5)–Os(2)–C(6)	174.0(8)	C(4)–Os(2)–C(6)	92.8(6)
C(4)–Os(2)–Os(1′)	157.4(5)	C(5)–Os(2)–Os(1)	90.7(5)
C(4)–Os(2)–Os(1)	97.2(5)	C(6)–Os(2)–Os(1)	84.2(5)
C(7)–S(1)–Os(1)	109.3(4)	Os(1)–S(1)–Os(1′)	72.53(12)
Os–C–O	177.0(2) [c]		

[a] The primed atoms are generated by the symmetry: $(x, 0.5-y, z)$.
[b] Approximate value.

sequential loss of nine CO groups. In addition to singlet resonances at δ 6.65, 6.57 and 3.62 for the heterocyclic ligand, the hydride region of the ^{1}H NMR spectrum of **2** at room temperature contains a broad singlet at δ −13.17 which on cooling to −60 °C resolves into two singlets at δ −13.25 and −13.05 in a relative intensity 4:1, pointing to the presence of two interconverting isomers at room temperature. This observation is consistent with the hydride ligand migration across two edges of the ruthenium triangle, which at lower temperature is frozen out giving two forms, the symmetric form (**2a**) and the asymmetric form (**2b**). Similar edge hopping of the bridging hydride ligand has been reported for the related trimetallic clusters [1].

The X-ray structure of **2** is shown in Fig. 2 and selected bond distances and angles are given in Table 2. There are two independent molecules in the asymmetric unit. Each molecule consists of a Ru_3 triangle with three different metal–metal bonds and nine terminal carbonyl ligands, three bonded to each ruthenium atom. The molecules differ in the relative location of the hydride ligand in the cluster. In molecule 1 (Fig. 2), it bridges the Ru(1)–Ru(2) edge and is consistent with the observation that this edge is significantly elongated {2.9948(1) Å} compared with the other two metal–metal bonds {Ru(1)–Ru(2) = 2.8341(10), Ru(2)–Ru(3) = 2.7041(10) Å}. However, in molecule 2 (Fig. 2) the hydride ligand bridges the Ru(2)–Ru(3) edge which is also consistent with this bond being elongated {Ru(2)–Ru(3) = 2.8376(10) Å} compared with the other two Ru–Ru distances {Ru(1)–Ru(2) = 2.8027(11), Ru(1)–Ru(3) = 2.8155(10) Å}. The overall structure of molecule 2 is symmetrical, and is similar to that reported for [(μ-H)Ru_3(CO)$_9${μ_3-η^2-$SN_2C_4H_3$)] [6] in which the hydride ligand bridges the same metal–metal edge as the exocyclic S-atom of the heterocyclic ligand. The Ru–S bond distances in both the molecules {Ru(2)–S(1) =



Scheme 2.

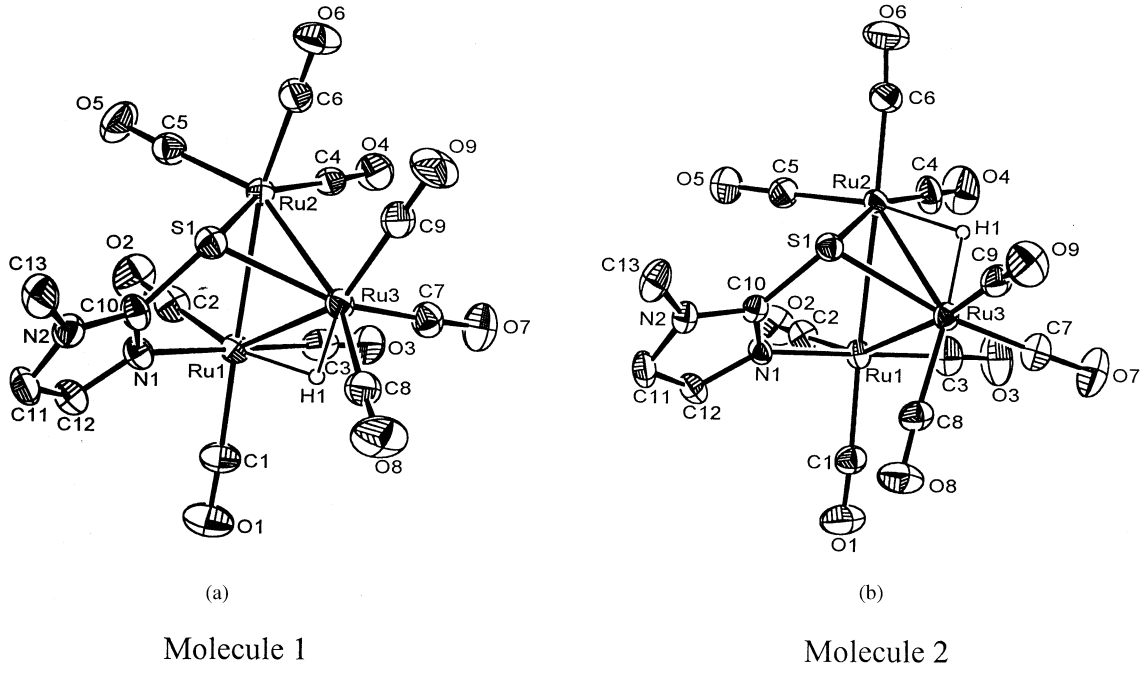


Fig. 2. X-ray structures of molecule 1 and molecule 2 of $[(\mu\text{-H})Ru_3(CO)_9\{\mu_3\text{-}\eta^2\text{-SC=NCH=CHN(CH}_3)\}]$ (**2**) showing the atom labelling scheme. Thermal ellipsoids are drawn at 35% probability level. The ring hydrogen atoms are omitted for clarity.

2.390(2), Ru(3)–S(1) = 2.422(2) Å in molecule 1 and Ru(3)–S(1) = 2.413(2), Ru(2)–S(1) = 2.422(3) Å in molecule 2} are comparable to those observed in **1** and other μ-SR triosmium and triruthenium clusters [1,6,10]. The dimensions of the 2-mercapto-1-methylimidazole ligands in both molecules are similar. Thus the S(1)–C(10), C(10)–N(1), C(10)–N(2) bond distances in molecule 1 are 1.742(9), 1.343(10) and 1.328(11) Å, respectively, while the corresponding distances in molecule 2 are 1.743(9), 1.320(10) and 1.346(10) Å, respectively.

Treatment of $[(\mu\text{-H})Os_3(CO)_8\{Ph_2PCH_2P(Ph)C_6H_4\}]$ with 2-mercapto-1-methylimidazole at room temperature yields $[(\mu\text{-H})Os_3(CO)_8\{\mu\text{-SC=NCH=CHN(CH}_3)(\mu\text{-dppm})]$ (**3**) (Scheme 3). The structure of **3** as obtained from an X-ray study, is shown in Fig. 3 and selected bond distances and bond angles are listed in Table 3. The structure consists of an Os_3 triangle with three different metal–metal bonds {Os(1)–Os(3) = 2.8453(6), Os(1)–Os(2) = 2.8661(6), Os(1)–Os(3) = 2.8581(6) Å}. The overall structural features of **3** are similar to $[(\mu\text{-H})Os_3(CO)_8(\mu\text{-SC}_2H_5)(\mu\text{-dppm})]$ [13]. The 2-mercapto-1-methylimidazole ligand bridges Os(2) and Os(3) via the exocyclic S(1) atom. The Os(2)–Os(3) edge is also bridged by the hydride ligand. The Os–S bridge is symmetrical as indicated by the nearly equal Os–S distances {2.420(2) Å} and these values compare well those {2.402(6)–2.426(4) Å} found in $[(\mu\text{-H})Os_3(CO)_8(\mu\text{-SC}_2H_5)(\mu\text{-dppm})]$ and other related complexes [1,6,10]. The Os–P bond lengths {average 2.33(2) Å} are comparable to those found in $[(\mu\text{-H})Os_3(CO)_8(\mu\text{-SC}_2H_5)(\mu\text{-dppm})]$ {2.324(4) Å} [13] and $[Os_3(CO)_{10}(\mu\text{-dppm})]$ {2.331(3) Å} [14]. Within the heterocyclic ligand, the exocyclic C(9)–S(1) bond length at 1.769(7) Å is similar in length to that of a C–S single bond and the imino C(9)–N(1) bond length of 1.314(8) Å indicates appreciable double bond character while the C(9)–N(2) bond distance of 1.379(8) Å is as expected for a C–N single bond [11]. These values are also comparable with the corresponding values in **1**.

The spectroscopic data of **3** are consistent with the solid-state structure. The infrared spectrum in the carbonyl region is very similar to that of $[(\mu\text{-H})Os_3(CO)_8(\mu\text{-SC}_2H_5)(\mu\text{-dppm})]$ [13] indicating that they are structurally similar. The mass spectrum shows the molecular ion peak at *m/z* 1293 and fragment ions formed by the sequential loss of eight carbonyl groups. In addition to the well separated signals for the heterocyclic and dppm ligands, the ^1H NMR spectrum of **3** in the hydride region contains a doublet at δ −15.49 because of its coupling to one of the ^{31}P nuclei. The $^{31}P\{^1H\}$ NMR spectrum contains two doublets at δ 24.8 and 25.4 indicating non-equivalent ^{31}P nuclei.

In view of our previous studies [15] on the reactivity of $[Os_3(CO)_{10}(\mu\text{-dppm})]$ with PhSH, we believed that the reaction of $[Os_3(CO)_{10}(\mu\text{-dppm})]$ with 2-mercapto-1-methylimidazole would lead to the S–H oxidative addition product **3**. As expected, the reaction of $[Os_3(CO)_{10}(\mu\text{-dppm})]$ with 2-mercapto-1-methylimidazole at 110 °C gave **3** (Scheme 3).

To compare the reactivity of $[Ru_3(CO)_{10}(\mu\text{-dppm})]$ with that of $[Os_3(CO)_{10}(\mu\text{-dppm})]$, we investigated the

Table 2
Selected bond lengths (Å) and angles (°) for **2**

	Molecule 1	molecule 2
Bond lengths		
Ru(1)–Ru(2)	2.8341(10)	2.8027(11)
Ru(1)–Ru(3)	2.9948(11)	2.8155(10)
Ru(2)–Ru(3)	2.7041(10)	2.8376(10)
Ru(2)–S(1)	2.390(2)	2.422(3)
Ru(3)–S(1)	2.422(2)	2.413(2)
Ru(1)–N(1)	2.118(7)	2.135(7)
Ru(1)/Ru(2)–H(1)	1.79 [a]	1.86 [a]
Ru(3)–H(1)	1.81 [a]	1.64 [a]
S(1)–C(10)	1.742(9)	1.743(9)
N(1)–C(10)	1.343(10)	1.320(10)
N(1)–C(12)	1.365(11)	1.357(11)
N(2)–C(10)	1.328(11)	1.346(11)
N(2)–C(11)	1.385(11)	1.386(11)
N(2)–C(13)	1.467(11)	1.461(11)
Ru–C (CO)	1.91(2) [b]	1.90(2) [b]
C–O (CO)	1.14(2) [b]	1.14(2) [b]
Bond angles		
Ru(2)–Ru(1)–Ru(3)	55.20(2)	60.67(3)
Ru(1)–Ru(2)–Ru(3)	65.42(3)	59.89(3)
Ru(1)–Ru(3)–Ru(2)	59.38(2)	59.44(3)
C(1)–Ru(1)–Ru(3)	116.3(3)	106.8(3)
C(3)–Ru(1)–Ru(3)	91.2(3)	86.9(3)
C(8)–Ru(3)–Ru(1)	116.4(3)	79.2(3)
C(4)–Ru(2)–Ru(3)	100.4(3)	109.6(3)
C(6)–Ru(2)–Ru(3)	99.7(3)	118.5(3)
C(10)–S(1)–Ru(2)	106.2(3)	102.4(3)
C(10)–S(1)–Ru(3)	107.4(3)	105.1(3)
Ru(2)–S(1)–Ru(3)	68.38(7)	71.87(7)
N(1)–Ru(1)–Ru(2)	86.8(2)	85.7(2)
N(1)–Ru(1)–Ru(3)	87.5(2)	88.2(2)
Ru–C–O	178.0(2) [b]	176.0(2) [b]

[a] Approximate value.

reaction of $[Ru_3(CO)_{10}(\mu\text{-dppm})]$ with 2-mercapto-1-methylimidazole. Instead of the expected S–H oxidative addition product, the reaction of $[Ru_3(CO)_{10}(\mu\text{-dppm})]$ with 2-mercapto-1-methylimidazole at 68 °C gave $[Ru_3(\mu_3\text{-CO})(CO)_7(\mu_3\text{-S})(\mu\text{-dppm})]$ (**4**) (Scheme 4). The compound was previously reported by Bonnet et al. [16] from C–S bond cleavage reaction of $[(\mu\text{-H})Ru_3(\mu\text{-SPh})(CO)_8(\mu\text{-dppm})]$ at 95 °C. We believe that most probably compound **4** proceeds via the intermediate

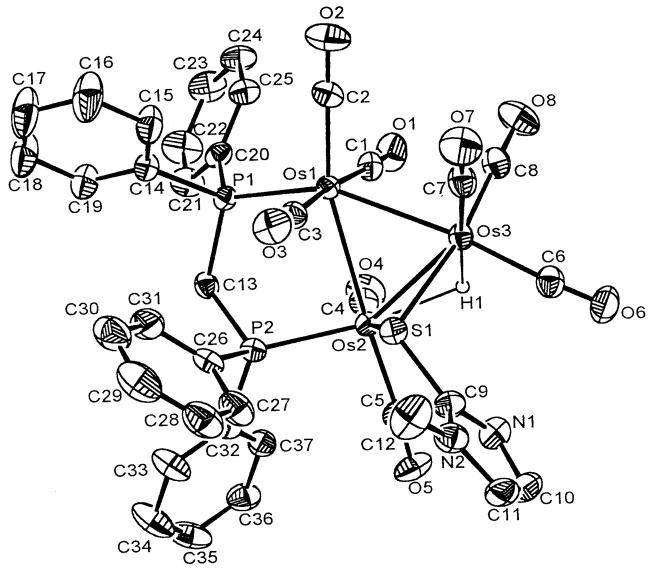
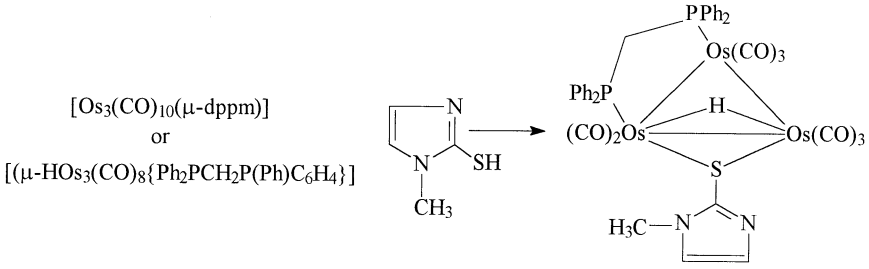


Fig. 3. X-ray structure of $[(\mu\text{-H})Os_3(CO)_8\{\mu\text{-SC=NCH=CHN(CH}_3)\}(\mu\text{-dppm})]$ (**3**) showing the atom labelling scheme. Thermal ellipsoids are drawn at 35% probability level. The ring hydrogen atoms are omitted for clarity.

formation of $[(\mu\text{-H})Ru_3(CO)_8\{\mu\text{-SC=NCH=CHN-(CH}_3\}(\mu\text{-dppm})]$, the ruthenium analogue of **3**, followed by a C–S bond cleavage reaction.

3. Experimental

All the reactions were performed out under a pre-purified nitrogen atmosphere by using standard Schlenk techniques. Reagent grade solvents were freshly distilled from appropriate drying agents. Infrared spectra were recorded on a Schimadzu FT IR 8101 spectrophotometer. NMR spectra were recorded on a Varian Unity Plus 400 spectrometer. $[Ru_3(CO)_{12}]$ was purchased from Strem Chemicals Inc. and used without further purification. $[Os_3(CO)_{10}(MeCN)_2]$ [17], $[(\mu\text{-H})Os_3(CO)_8\{Ph_2PCH_2P(Ph)C_6H_4\}]$ [18], $[Os_3(CO)_{10}(\mu\text{-dppm})]$ [18] and $[Ru_3(CO)_{10}(\mu\text{-dppm})]$ [19] were prepared according to the known methods.



3

Scheme 3.

Table 3
Selected bond lengths (Å) and angles (°) for **3**

Bond lengths			
Os(1)–Os(3)	2.8453(6)	Os(1)–Os(2)	2.8661(6)
Os(2)–Os(3)	2.8581(6)	Os(1)–P(1)	2.333(2)
Os(2)–P(2)	2.320(2)	Os(2)–S(1)	2.420(2)
Os(3)–S(1)	2.420(2)	Os(2)–H(1)	1.86 [a]
Os(3)–H(1)	1.79 [a]	S(1)–C(9)	1.769(7)
N(1)–C(9)	1.314(8)	N(1)–C(10)	1.357(9)
N(2)–C(11)	1.373(9)	N(2)–C(9)	1.379(8)
N(2)–C(12)	1.451(9)	C(10)–C(11)	1.352(10)
Os–C (CO)	1.91(1) [b]	C–O	1.14(1) [b]
P–C	1.83(1) [b]		
Bond angles			
C(2)–Os(1)–C(3)	89.2(3)	C(2)–Os(1)–C(1)	93.4(3)
C(3)–Os(1)–C(1)	173.3(3)	C(2)–Os(1)–P(1)	103.0(2)
C(3)–Os(1)–P(1)	95.46(19)	C(1)–Os(1)–P(1)	89.9(2)
C(2)–Os(1)–Os(3)	103.7(2)	C(3)–Os(1)–Os(3)	88.05(18)
C(1)–Os(1)–Os(3)	85.4(2)	P(1)–Os(1)–Os(3)	153.05(4)
C(2)–Os(1)–Os(2)	163.7(2)	C(3)–Os(1)–Os(2)	91.54(19)
C(1)–Os(1)–Os(2)	84.2(2)	P(1)–Os(1)–Os(2)	93.09(4)
C(4)–Os(2)–C(5)	92.6(3)	C(4)–Os(2)–P(2)	92.5(2)
C(5)–Os(2)–P(2)	96.7(2)	C(4)–Os(2)–S(1)	165.7(2)
C(5)–Os(2)–S(1)	94.4(2)	P(2)–Os(2)–S(1)	99.08(6)
C(4)–Os(2)–Os(3)	111.9(2)	C(5)–Os(2)–Os(3)	116.1(2)
P(2)–Os(2)–Os(3)	136.93(4)	S(1)–Os(2)–Os(3)	53.80(4)
C(4)–Os(2)–Os(1)	90.9(2)	C(5)–Os(2)–Os(1)	175.4(2)
P(2)–Os(2)–Os(1)	86.26(4)	S(1)–Os(2)–Os(1)	81.61(4)
C(7)–Os(3)–C(8)	90.9(3)	C(7)–Os(3)–C(6)	99.4(3)
C(8)–Os(3)–C(6)	93.8(3)	C(7)–Os(3)–S(1)	93.8(2)
C(8)–Os(3)–S(1)	168.4(2)	C(6)–Os(3)–S(1)	95.9(2)
C(7)–Os(3)–Os(1)	90.9(2)	C(8)–Os(3)–Os(1)	87.3(2)
C(6)–Os(3)–Os(1)	169.6(2)	S(1)–Os(3)–Os(1)	82.04(4)
C(7)–Os(3)–Os(2)	137.0(2)	C(8)–Os(3)–Os(2)	116.5(2)
C(6)–Os(3)–Os(2)	110.3(2)	S(1)–Os(3)–Os(2)	53.80(4)
Os(3)–S(1)–Os(2)	72.40(5)	C(9)–S(1)–Os(3)	109.0(2)
Os–C–O	176.0(2) [b]		

[a] Approximate values.
[b] Average values.

3.1. Reaction of $[Os_3(CO)_{10}(MeCN)_2]$ with 2-mercapto-1-methylimidazole

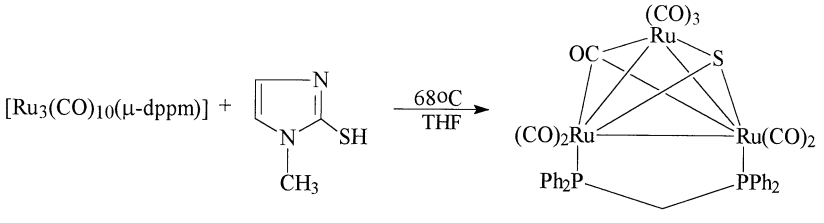
A CH_2Cl_2 solution (30 ml) of $[Os_3(CO)_{10}(MeCN)_2]$ (0.200 g, 0.214 mmol) and 2-mercapto-1-methylimidazole (0.048 g, 0.420 mmol) was stirred at room temperature (r.t.) for 50 min. The solvent was removed under reduced pressure and the residue chromatographed by TLC on silica gel. Elution with hexane–CH_2Cl_2 (7:3; v/v) gave one major band which afforded $[(\mu\text{-H})Os_3(CO)_{10}\{\mu\text{-SC=N–CH=CHN(CH}_3)\}]$ (**1**) (0.149 g, 72%). Yellow crystals were obtained after recrystallisation from hexane–CH_2Cl_2 at −20 °C. IR (ν(CO), hexane): 2109m, 2074s, 2063s, 2024vs, 2014vs, 1987m, cm^{-1}; ^1H NMR ($CDCl_3$): δ 6.92 (d, 1H, $J = 0.8$ Hz), 6.90 (d, 1H, $J = 0.8$ Hz), 3.78 (s, 3H), −16.76 (s, 1H). MS (*m*/*z*): 964 (M^+). *Anal*. Calc. for $C_{14}H_6N_2O_{10}Os_3S$: C, 17.43; H, 0.63; N, 2.90. Found: C, 17.65; H, 0.82; N, 2.98%.

3.2. Reaction of $[Ru_3(CO)_{12}]$ with 2- mercapto-1-methylimidazole

A THF solution (80 ml) of $[Ru_3(CO)_{12}]$ (0.400 g, 0.626 mmol) and 2-mercapto-1-methylimidazole (0.145 g, 1.27 mmol) was heated to reflux for 3 h. The solvent was removed under reduced pressure and the residue was chromatographed by TLC on silica gel. Elution with hexane–CH_2Cl_2 (9:1, v/v) gave one major band which yielded $[(\mu\text{-H})Ru_3(CO)_9\{\mu_3\text{-}\eta^2\text{-SC=NCH=CHN(CH}_3)\}]$ (**2**) (0.126 g, 30%) as yellow crystals after recrystallisation from hexane–CH_2Cl_2 at −20 °C. IR (ν(CO) hexane): 2086m, 2053s, 2007m, 1995w, 1974w cm^{-1}; ^1H NMR ($CDCl_3$): δ 6.65 (s, 1H), 6.57 (s, 1H), 3.62 (s, 3H), −13.17 (s, 1H); MS (*m*/*z*): 670 (M^+). *Anal*. Calc. for $C_{13}H_6N_2O_9Ru_3S$: C, 23.32; H, 0.91; N, 4.18. Found: C, 23.55; H, 1.15; N, 4.28%.

3.3. Reaction of $[(\mu\text{-H})Os_3(CO)_8\{Ph_2PCH_2P(Ph)\text{-}C_6H_4\}]$ with 2-mercapto-1-methylimidazole

A CH_2Cl_2 solution (20 ml) of $[(\mu\text{-H})Os_3(CO)_8\text{-}\{Ph_2PCH_2P(Ph)C_6H_4\}]$ (0.028 g, 0.024 mmol) and 2-mercapto-1-methylimidazole (0.007 g, 0.061 mmol) was stirred at r.t. for 10 days during which time the colour changed from green to yellow. The solvent was removed under reduced pressure and the residue chromatographed by TLC on silica gel. Elution with hexane–CH_2Cl_2 (10:3, v/v) afforded $[(\mu\text{-H})Os_3(CO)_8\{(\mu\text{-SC=NCH=CHN(CH}_3)\}(\mu\text{-dppm})]$ (**3**) (0.015 g, 48%) as yellow crystals from acetone–ethanol (0.015 g, 48%). IR (ν(CO), CH_2Cl_2): 2071vs, 2025m, 2000vs, 1990w, 1955w cm^{-1}; ^1H NMR ($CDCl_3$): δ 7.74 (d, 1H, $J = 0.8$ Hz), 7.62 (m, 2H), 7.44 (m, 9H), 7.27 (m, 5H), 7.16 (m,



4

Scheme 4.

2H), 7.08 (m, 2H), 6.91 (d, 1H, $J = 0.8$ Hz), 5.55 (m, 1H), 4.65 (m, 1H), 3.42 (s, 3H), −15.49 (d, 1H, $J = 25.2$ Hz); $^{31}P\{^{1}H\}$ NMR ($CDCl_3$): δ 24.8 (d, $J = 41.9$ Hz), 25.4 (d, $J = 41.9$ Hz); MS (m/z): 1293 (M^+). *Anal*. Calc. for $C_{37}H_{28}N_2O_8Os_3P_2S$: C, 34.36; H, 2.19; N, 2.17. Found: C, 34.58; H, 2. 32; N, 2.28%.

3.4. Reaction of $[Os_3(CO)_{10}(\mu\text{-dppm})]$ with 2-mercapto-1-methylimidazole

A toluene solution (15 ml) of $[Os_3(CO)_{10}(\mu\text{-dppm})]$ (0.083 g, 0.067 mmol) and 2-mercapto-1-methylimidazole (0.015 g, 0.131 mmol) was refluxed for 1 h. The solvent was removed under reduced pressure and the residue chromatographed by TLC on silica gel. A similar chromatographic separation to that above gave **3** (0.028 g, 32%).

3.5. Reaction of $[Ru_3(CO)_{10}(\mu\text{-dppm})]$ with 2-mercapto-1-methylimidazole

To a THF solution (30 ml) of $[Ru_3(CO)_{10}(\mu\text{-dppm})]$ (0.202 g, 0.209 mmol) was added 2-mercapto-1-methylimidazole (0.119 g, 1.04 mmol) and the reaction mixture was heated to reflux for 1 h. The solvent was removed under reduced pressure and the residue chromatographed by TLC on silica gel. Elution with hexane–CH_2Cl_2 (7:3, v/v) developed two bands. The faster moving band afforded unreacted $[Ru_3(CO)_{10}(\mu\text{-dppm})]$ (0.008 g) while the second band gave $[Ru_3(CO)_7(\mu_3\text{-}CO)(\mu_3\text{-}S)(\mu\text{-dppm})]$ (**4**) (0.069 g, 35%) as orange microcrystals.

3.6. X-ray crystallography

Crystallographic data for **1** and **3** were recorded on an CAD4 diffractometer and those for **2** on a FAST TV area detector using monochromatised Mo Kα radiation ($\lambda = 0.71073$ Å). All data sets were corrected for absorption effects by using DIFABS [20]. The structures were solved by direct methods (SHELXS-86) [21] and refined on F^2 by full-matrix least-squares (SHELXL-96) [22] using all unique data with intensities greater than 0. In all cases, the non-hydrogen atoms were anisotropic, with an ISOR = 0.01 constraint being applied for one oxygen atom [O(5)] in **1**. The bridging hydrides in all the structures were located from difference maps but not refined; all other hydrogen atoms were included in calculated positions (riding model). The crystallographic data are summarised in Table 4.

4. Supplementary data

Crystallographic data for the structure analysis have been deposited with the Cambridge Crystallographic

Table 4
Crystal data and details of data collection and structure refinement for **1**–**3**

	1	**2**	**3**
Chemical formula	$C_{14}H_6N_2O_{10}Os_3S$	$C_{13}H_6N_2O_9Ru_3S$	$C_{37}H_{28}N_2O_8Os_3P_2S$
Molecular weight	964.87	669.47	1293.21
Crystal system	orthorhombic	triclinic	triclinic
a (Å)	13.197(2)	10.5717(13)	11.279(2)
b (Å)	11.259(2)	13.575(2)	11.621(2)
c (Å)	13.980(2)	15.249(2)	15.595(3)
α (°)	90	110.811(7)	100.010(90
β (°)	90	99.22(2)	98.900(11)
γ (°)	90	96.404(12)	91.402(14)
V (Å^3)	2077.1(5)	1985.3(5)	1986.0(7)
Space group	*Pnma*	$P\bar{1}$	$P\bar{1}$
Z	4	4	2
Crystal size (mm)	0.35 × 0.12 × 0.08	0.25 × 0.20 × 0.15	0.35 × 0.35 × 0.15
Shape	rod-like	prism	parallelepiped
Colour	yellow	yellow	yellow
θ Range (°)	2.12–26.28	1.98–25.02	1.34–25.17
Reflection collected	2416	7532	7615
Total unique	2217	5344	7139
R_{int}	0.0243	0.0597	0.0219
Data/parameters in the refinement	2217/155	5344/507	7139/431
Goodness-of-fit on F^2	1.103	0.947	1.026
Final R_1/wR_2 indices [$I > 2\sigma(I)$] [a]	0.0504/0.1372	0.0400/0.1073	0.0277/0.0678
R_1/wR_2 indices (all data)	0.0627/0.1422	0.0477/0.1094	0.436/0.0708
Largest difference Peak and hole (e Å^{-3})	1.993 and −2.749	0.702 and −0.738	1.164 and −1.135

All measurements were done at 293 K.
[a] $R_1 = \Sigma(F_o^2 - F_c^2)/\Sigma(F_o)$; $wR_2 = (\Sigma[w(F_o^2 - F_c^2)^2]/\Sigma[w(F_o^2)^2])^{1/2}$.

Data Centre, CCDC reference numbers 175206 (**1**), 175206 (**2**) and 175207 (**3**). Copies of this information may be obtained free of charge from: The Director, CCDC, 2 Union Road, Cambridge CB2 IEZ, UK (fax: +44-1223-336033: e-mail: deposit@ccdc.cam.ac.uk or www: http://www.ccdc.cam.ac.uk).

Acknowledgements

The support of this research by the Ministry of Science and Technology, Government of Bangladesh, is gratefully acknowledged. We also acknowledge the EPSRC support of the X-ray Crystallography Service at Cardiff.

References

[1] A.M. Brodie, H.D. Holden, J. Lewis, M.J. Taylor, J. Chem. Soc., Dalton Trans. (1986) 633.
[2] S. Jeannin, Y. Jeannin, G. Lavigne, Transition Met. Chem. 1 (1976) 186.
[3] S. Jeannin, Y. Jeannin, G. Lavigne, Inorg. Chem. 17 (1978) 2103.
[4] R. Havlin, G.R. Knox, J. Organomet. Chem. 4 (1965) 247.
[5] K.M. Hanif, M.B. Hursthouse, S.E. Kabir, K.M.A. Malik, E. Rosenberg, J. Organomet. Chem. 580 (1999) 60.
[6] R. Dilshad, K.M. Hanif, M.B. Hursthouse, S.E. Kabir, K.M.A. Malik, E. Rosenberg, J. Organomet. Chem. 585 (1999) 100.
[7] K.A. Azam, R. Dilshad, S.E. Kabir, L. Nessa, K. Khatoon, M.M. Rahman, E. Rosenberg, M.B. Hursthouse, K.M.A. Malik, A.J. Deeming, J. Chem. Soc., Dalton Trans. (1996) 1731.
[8] K.A. Azam, M.B. Hursthouse, S.A. Hussain, S.E. Kabir, M.M. Rahman, K.M.A. Malik, E. Rosenberg, J. Organomet. Chem. 559 (1998) 81.
[9] K.A. Azam, M.B. Hursthouse, S.E. Kabir, K.M.A. Malik, M. Tesmer, H. Vahrenkamp, Inorg. Chem. Commun. 1 (1998) 402.
[10] Y.-K. Au, K.-K. Cheung, W.-T. Wong, Inorg. Chim. Acta 228 (1995) 267.
[11] J. Zabicky (Ed.), The Chemistry of Amides, Interscience, London, 1970, p. 388.
[12] A.J. Deeming, K.I. Hardcastle, M. Karim, Inorg. Chem. 31 (1992) 4792.
[13] S.M.T. Abedin, K.A. Azam, M.B. Hursthouse, S.E. Kabir, K.M.A. Malik, M.A. Mottalib, E. Rosenberg, J. Cluster Sci. 12 (2001) 5.
[14] K.A. Azam, M.B. Hursthouse, S.E. Kabir, K.M.A. Malik, M.A. Mottalib, J. Chem. Crystallogr. 29 (1999) 813.
[15] K.A. Azam, S.E. Kabir, A. Miah, M.W. Day, K.I. Hardcastle, E. Rosenberg, A.J. Deeming, J. Organomet. Chem. 435 (1992) 157.
[16] P. Fompeyrine, G. Lavigne; J.-J. Bonnet, J. Chem. Soc., Dalton Trans. (1987) 91.
[17] B.F.G. Johnson, J. Lewis, D.A. Pippard, J. Chem. Soc., Dalton Trans (1981) 407.
[18] J.A. Clucas, D.F. Foster, M.M. Harding, A.K. Smith, J. Chem. Soc., Chem. Commun. (1984) 949.
[19] M.I. Bruce, B.K. Nicholson, M.L. Williams, Inorg. Synth. 28 (1990) 225.
[20] N.P.C. Walker, D. Stuart, Acta Crystallogr., Sect. A 39 (1983) 158.
[21] G.M. Sheldrick, Acta Crystallogr., Sect. A 46 (1990) 467.
[22] G.M. Sheldrick, SHELXL-96 program for crystal structure refinement, University of Göttingen, Germany, 1996.

PERGAMON

Polyhedron 21 (2002) 893–898

POLYHEDRON

www.elsevier.com/locate/poly

Syntheses and crystal structures of cadmium(II) coordination polymers with end-to-end dicyanamide bridges

Jun-Hua Luo, Mao-Chun Hong *, Rong Cao, Yu-Cang Liang, Ying-Jun Zhao, Rui-Hu Wang, Jia-Bao Weng

State Key Laboratory of Structural Chemistry, Fujian Institute of Research on the Structure of Matter, Chinese Academy of Sciences, Fuzhou, Fujian, 350002, People's Republic of China

Received 15 August 2001; accepted 25 January 2002

Abstract

Two new derivatives of cadmium(II) dicyanamide (dicyanamide = $[N(CN)_2]^-$, dca), $[Cd(N(CN)_2)_2(phen)]_n$ (**1**) and $[Cd(N(CN)_2)_2(2,2'\text{-bipy})]_n$ (**2**), have been synthesized and structurally characterized. The cadmium(II) centers in **1** are connected through single or double end-to-end dca bridging ligand to form a 2-D layer structure, which furthermore condense into a 3-D structure through the π–π interaction between aromatic rings of adjacent layers. In **2**, the cadmium(II) coordination sphere is a distorted octahedron, bound to four dca ligands and one chelate 2,2′-bipy ligand, and the adjacent cadmium(II) centers are bridged by the double end-to-end $\mu_{1,5}$-N≡C–N–C≡N to form an extended structure with a zigzag 1-D chain, and a 2-D layer structure results from the π–π interactions of the adjacent chains. Crown Copyright © 2002 Published by Elsevier Science Ltd. All rights reserved.

Keywords: Cadmium complexes; Dca ligand; Double end-to-end; Zigzag chain; π–π interaction

1. Introduction

Metal-organic frameworks are widely regarded as promising materials for application in catalysis, separation and molecular recognition [1]. There have been numerous reports in which N-donor bridging ligands are used to form infinite metal-organic polymeric frameworks [2]. Dicyanamide, $[N(CN)_2]^-$, was selected due to its coordination versatility ranging from being monodentate to μ_4- coordination, and thus provides a suitable 'building block' for assembling novel inorganic/organic hybrid materials. Monodentate (terminal) coordination occurs in $[Cu(II)(o\text{-phen})_2\{N(CN)_2\}][C(CN)_3]$ [3,3a], $[Cu(II)(o\text{-phen})_2\{N(CN)_2\}_2]$ (o-phen = o-phenanthroline) [3b] and $[Zn_3(OAc)_4(4,4'\text{-bipy})_3\{N(CN)_2\}_2]$ [3c]. Bidentate coordination has often been observed and was reported for $Me_2Sn[N(CN)_2]_2$ [3d], $Me_3Sn[N(CN)_2]$ [3d], two polymorphs of $Ag[N(CN)_2]$ [3e,3f], and $Mn[N(CN)_2]_2(pyz)$ (pyz = pyrazine) [3g,3h]. Tri-coordinate μ_3-$[N(CN)_2]^-$ is observed in the rutile-type class of molecule-based magnets, $M(II)[N(CN)_2]_2$ (M = Co or Ni) [3i]. Unusual μ_4 coordination [1e] is also known and was found in the structures of $Me_2Tl[N(CN)_2]$ [3j]. Structures reported recently include $M(dca)_2L_2$ chains, (4,4) sheets, diamond-like works, interpenetrating networks, molecular tubes and self-penetrating works [4]. In these materials, σ-bond formation occurs through lone pair donation of the nitrile N atoms to an octahedral metal center. Our goal was to prepare and characterize new low-dimensional solids consisting of divalent transition metal complexes with the dicyanamide ligand. Herein, we report the syntheses, crystal structures, and vibrational properties of $[Cd(N(CN)_2)_2(phen)]_n$ (**1**) and $[Cd(N(CN)_2)_2(2,2'\text{-bipy})]_n$ (**2**), the first structurally characterized cadmium(II) dicyanamide complexes.

* Corresponding author. Tel.: +86-591-379-2460; fax: +86-591-371-4946.

E-mail address: hmc@ms.fjirsm.ac.cn (M.-C. Hong).

0277-5387/02/$ - see front matter Crown Copyright © 2002 Published by Elsevier Science Ltd. All rights reserved.
PII: S0277-5387(02)00868-9

2. Experimental

2.1. Materials and physical measures

Elemental analyses were determined on an Elementar Vario ELIII analyzer. IR spectra were measured as KBr pellets on a Nicolet Magna 750 FT IR spectrometer in the range of 200–4000 cm^{-1}. All reagents were commercially available and used as received.

2.2. Synthesis of the complexes

2.2.1. $[Cd(N(CN)_2)_2(phen)]_n$ (1)

To an aqueous solution (20 ml) of $Cd(NO_3)_2\cdot 4H_2O$ (0.155 g, 0.5 mmol), sodium dicyanamide (0.09 g, 1 mmol) was added. After stirring the mixture for about 30 min, the dmf solution (10 ml) of phen was added into it. The above mixture was stirred and heated for 1 h, then filtered when it was still hot. Well shaped crystals of $[Cd(N(CN)_2)_2(phen)]_n$ were obtained from the mother liquor by slow evaporation at room temperature (r.t.) for several days. They were filtered off, washed with a small mount of water, and dried in air. Yield 78%. Calc. for $C_{16}H_8CdN_8$: C, 45.21; H, 1.88; N, 26.37. Found: C, 44.89; H, 2.01; N, 27.68%.

2.2.2. $[Cd(N(CN)_2)_2(2,2'\text{-bipy})]_n$ (2)

The compound was synthesized as **1** except 2,2′-bipy instead of phen. Yield 78%. Calc. for $C_{14}H_8CdN_8$: C, 41.93; H, 2.00; N, 27.95. Found: C, 41.67; H, 1.85; N, 29.21%.

2.3. X-ray crystallography

Single crystals with approximate dimensions $0.52 \times 0.48 \times 0.40$ mm for **1** and $0.42 \times 0.30 \times 0.25$ mm for **2** were selected and coated with epoxy glue. Data collections was carried out on a Siemens Smart CCD diffractometer equipped with graphite-monochromated Mo Kα radiation ($\lambda = 0.71073$ Å) at 298 K. Intensities of both **1** and **2** were corrected for empirical absorption based on SADABS scan technique [5]. Their structures were solved by direct methods and all calculations were performed using the SHELXL-PC program [6]. The positions of H atoms were generated geometrically (C–H bond fixed at 0.96 Å), assigned isotropic thermal parameters. The structure was refined by full-matrix least-squares minimization of $\Sigma(F_o - F_c)^2$ with anisotropic thermal parameters for all atoms except the H atoms. Table 1 gives a structure determination summary and Table 2 and Table 3 list the selected bond lengths and angles.

Table 1
Crystallographic data for the title two complexes

	1	2
Empirical formula	$C_{16}H_8CdN_8$	$C_{14}H_8CdN_8$
Formula weight	424.70	400.34
Temperature (K)	293(2)	293(2)
Wavelength (Å)	0.71073	0.71073
Crystal system	monoclinic	monoclinic
Space group	$P2(1)/c$	$C2/c$
Unit cell dimensions	3D	2D
a (Å)	10.1502(3)	6.6849(10)
b (Å)	10.9815(4)	17.476(2)
c (Å)	14.5839(4)	13.231(2)
α (°)	90	90
β (°)	99.609(1)	91.142(3)
γ (°)	90	90
V (Å^3)	1602.78(9)	1545.4(4)
Z	4	4
D_{calc} (Mg m^{-3})	1.760	1.722
Absorption coefficient (mm^{-1})	1.379	1.424
$F(000)$	832	784
Crystal size (mm)	$0.30 \times 0.25 \times 0.15$	$0.27 \times 0.21 \times 0.15$
θ Range for data collection (°)	2.03–25.06	2.33–25.03
Index ranges	$-12 \le h \le 6$, $-13 \le k \le 12$, $16 \le l \le 17$	$-6 \le h \le 7$, $-20 \le k \le 10$, $-12 \le l \le 15$
Reflections collected	5804	3086
Refinement method	Full-matrix least-squares on F^2	Full-matrix least-squares on F^2
Data $[I > 2\sigma(I)]$/parameters	2832/226	1354/105
Goodness-of-fit on F^2	1.074	1.005
R_1 indices ($I > 2\sigma(I)$)	0.0328	0.0739
Wr_2 indices (all data)	0.779	0.1818
Largest difference peak and hole (e Å^{-3})	0.513 and −0.471	0.44 and −0.734

Table 2
Selected bond lengths (Å) and angles (°) for $[Cd(N(CN)_2)_2(phen)]_n$ (1)

Bond lengths			
Cd–N(4)	2.246(4)	Cd–N(1)	2.279(4)
Cd–N(3A)	2.291(4)	Cd–N(8)	2.322(3)
Cd–N(7)	2.342(3)	Cd–N(6B)	2.481(4)
C(1)–N(1)	1.143(5)	C(1)–N(2)	1.291(5)
C(2)–N(3)	1.134(5)	C(2)–N(2)	1.298(5)
C(3)–N(4)	1.123(5)	C(3)–N(5)	1.291(6)
C(4)–N(6)	1.136(5)	C(4)–N(5)	1.284(6)
Bond angles			
N(4)–Cd–N(1)	94.30(16)	N(4)–Cd–N(3A)	93.10(15)
N(1)–Cd–N(3A)	96.48(14)	N(4)–Cd–N(8)	165.83(15)
N(1)–Cd–N(8)	98.04(13)	N(3A)–Cd–N(8)	92.40(12)
N(4)–Cd–N(7)	94.58(14)	N(1)–Cd–N(7)	162.10(12)
N(3A)–Cd–N(7)	98.51(12)	N(8)–Cd–N(7)	71.68(11)
N(4)–Cd–N(6B)	89.17(16)	N(1)–Cd–N(6B)	83.01(13)
N(3A)–Cd–N(6B)	177.70(13)	N(8)–Cd–N(6B)	85.46(13)
N(7)–Cd–N(6B)	81.62(12)		

Symmetry transformations used to generate equivalent atoms: (A) x, $-y+1/2$, $z-1/2$; (B) $-x+1$, $-y$, $-z+2$; (C) x, $-y+1/2$, $z+1/2$ for complex **1**.

Table 3
Selected bond lengths (Å) and angles (°) for $[Cd(N(CN)_2)_2(2,2'\text{-bipy})]_n$ (**2**)

Bond lengths			
Cd–N(2A)	2.304(12)	Cd–N(2)	2.304(12)
Cd–N(1)	2.322(9)	Cd–N(1A)	2.322(9)
Cd–N(4B)	2.346(13)	Cd–N(4C)	2.346(13)
N(2)–C(6)	1.108(14)	C(6)–N(3)	1.237(16)
N(3)–C(7)	1.252(16)	C(7)–N(4)	1.099(16)
Bond angles			
N(2A)–Cd–N(2)	103.7(5)	N(2A)–Cd–N(1)	162.6(4)
N(2)–Cd–N(1)	93.2(4)	N(2A)–Cd–N(1A)	93.2(4)
N(2)–Cd–N(1A)	162.6(4)	N(1)–Cd–N(1A)	70.4(5)
N(2A)–Cd–N(4B)	89.8(4)	N(2)–Cd–N(4B)	86.7(4)
N(1)–Cd–N(4B)	95.5(4)	N(1A)–Cd–N(4B)	89.2(4)
N(2A)–Cd–N(4C)	86.7(4)	N(2)–Cd–N(4C)	89.8(4)
N(1)–Cd–N(4C)	89.2(4)	N(1A)–Cd–N(4C)	95.5(4)
N(4B)–Cd–N(4C)	174.3(6)		

Symmetry transformations used to generate equivalent atoms: (A) $-x, y, -z+1/2$; (B) $-x, -y, -z$; (C) $x, -y, z+1/2$.

3. Results and discussion

3.1. IR spectroscopic study

At room temperature, the solid state infrared spectrum depicts several ν_{CN} bands at 2301m, 2260(sh), 2216s, 2177s, 2156s cm^{-1} in complex **1** and 2303m, 2206(sh), 2229s, 2156s cm^{-1} in complex **2**, which are attributed to $\nu_{sym}+\nu_{asym}(C\equiv N)$, $\nu_{asym}(C\equiv N)$ and $\nu_{sym}(C\equiv N)$ modes, and are comparable to those of related compounds in Table 4. These bands differ significantly from those of $Na[N(CN)_2]$, which are at 2129, 2232 and 2286 cm^{-1} [7]. The bands at 1365m, 916m in **1** and 1344m, 916m in **2** are assigned to $\nu_{asym}(C–N)$ and $\nu_{sym}(C–N)$, respectively.

Table 4
Comparison of ν_{CN} absorption of selected $M(II)[N(CN)_2]_2L_n$ ($n=1$ or 2) complexes

Complexes	$\nu_{asym}^{-}+\nu_{sym}^{-}(C\equiv N)$	$\nu_{asym}(C\equiv N)$	$\nu_{asym}(C\equiv N)$	Reference
$Mn[N(CN)_2]_2(py)$	2295s	2234m	2167s	[3g]
$Fe[N(CN)_2]_2(MeOH)_2$	2306(sh), 2274m	2254s	2178s,2154m	[9]
$Co[N(CN)_2]_2\{iz\}_2$	2281s	2246s	2185vs	[10]
$Ni[N(CN)_2]_2(tetramepz)_2$	2285vs	2235(sh)	2212vs,2165vs	[11]
$Co[N(CN)_2]_2(2\text{-meiz})_2$	2279s	2250s	2180vs,2150w	[10]
$Pd[N(CN)_2]_2\{P(C_6H_5)_3\}_2$	2310m	2240s	2180vs	[12]
$Cu[N(CN)_2]_2(iz)_2$	2292s	2250m	2190s	[13]
$[Cd(N(CN)_2)_2(phen)]_n$	2301m,2260(sh)	2216s	2177s,2156s	this work
$[Cd(N(CN)_2)_2(2,2'\text{-bipy})]_n$	2303m	2229s	2156s	this work

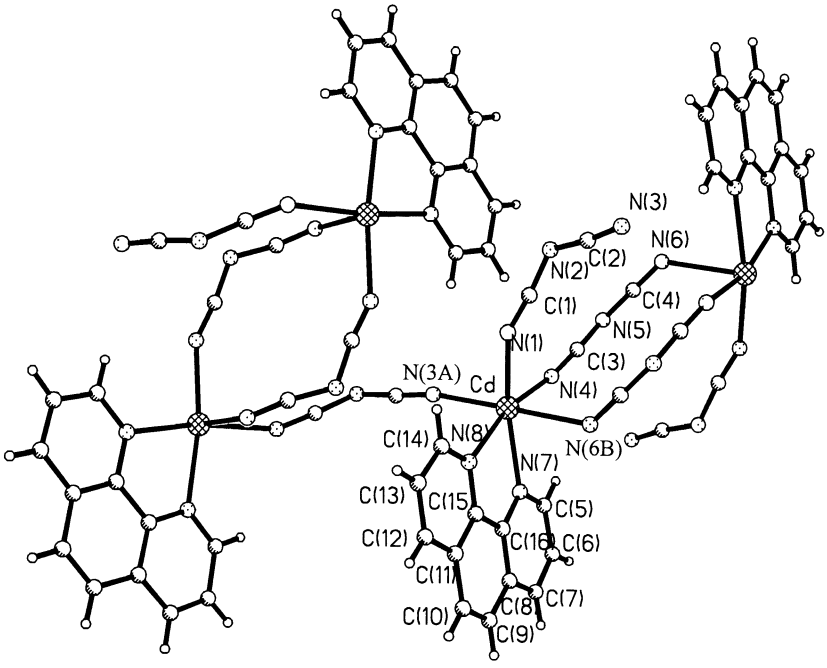


Fig. 1. An ORTEP drawing of $[Cd(N(CN)_2)_2(phen)]_n$ (**1**) with atomic numbering scheme.

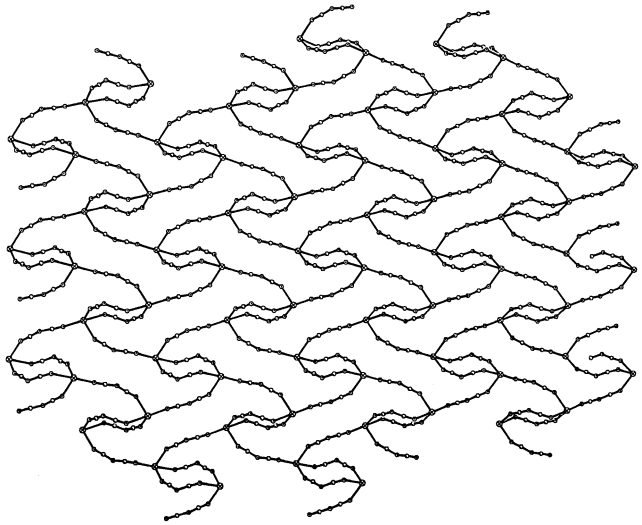


Fig. 2. The 2-D layer structure of $[Cd(N(CN)_2)_2(phen)]_n$ (**1**) (the terminal ligand Phen is omitted for clarity)

3.2. Crystal structure analysis

3.2.1. Crystal structure of complex *1*

Fig. 1 shows an ORTEP [8] diagram of the coordination sphere of the Cd(II) ion and atom labeling in $[Cd(N(CN)_2)_2(phen)]_n$ (**1**). Each cadmium(II) atom lies on an inversion center, and is connected to three other cadmium(II) centers through four dca ligands, one double end-to-end dca bridge to one cadmium(II) atom and two single end-to-end dca bridges to another two cadmium(II) atoms. Thus, all cadmium atoms form a 2-D layer structure through both the double end-to-end dca bridges and single end-to-end dca bridges as in Fig. 2, and furthermore generate a 3-D structure through the weak π–π interaction between aromatic rings of adjacent layers with distances 3.584 Å, as shown in Fig. 3. Each cadmium(II) center is six-coordinated and display a distorted octahedral coordination, with two terminal N atoms of two different dca ligands [Cd–N(1), 2.279(4); Cd–N(4), 2,246 Å] and two N atoms of the phen ligand [Cd–N(7), 2.342 (3); Cd–N(8), 2.322(3) Å] in the equatorial plane, while the other two N atoms of two dca ligands [Cd–N(3A), 2.291(4); Cd–N(6B), 2.481(4) Å] occupy the axial positions. Two kinds of bond angles may be found in the equatorial plane: the lower of 71.68° corresponding to the N(phen)–Cd–N(phen) bond angle and three greater N(phen)–Cd–N(dca) bond angles [N(1)–Cd–N(8), 98.04(13)°; N(4)–Cd–N(7), 94.58(14)°] and N(dca)–Cd–N(dca) bond angles [N(4)–Cd–N(1), 94.30(16)°]. The four equatorial donor atoms and the central cadmium(II) atom determine a plane with maximum deviation for Cd of −0.1628(5) Å. Approximate C_{2v} symmetry is observed for the dca ligand with C(2)–N(3), C(1)–N(1), C(4)–N(6) and C(3)–N(4) bond distances of 1.134(5), 1.143(5), 1.136(5) and 1.123(5) Å, respectively. The lack of significant electron density near the amide nitrogen N2 and N5 results in longer C(1)–N(2), C(2)–N(2), C(3)–N(5) and C(4)–N(5) bond distances, which average 1.291 Å, suggesting a small degree of π conjugation within the $[N(CN)_2]^-$ backbone [9].

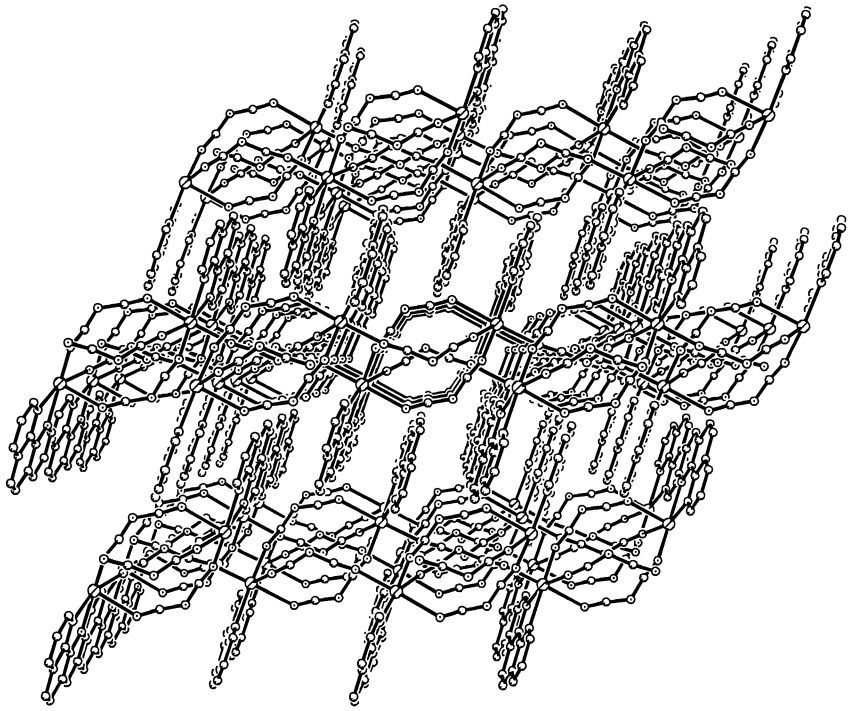


Fig. 3. The 3-D structure of $[Cd(N(CN)_2)_2(phen)]_n$ (**1**) through the weak π–π interaction between adjacent layers

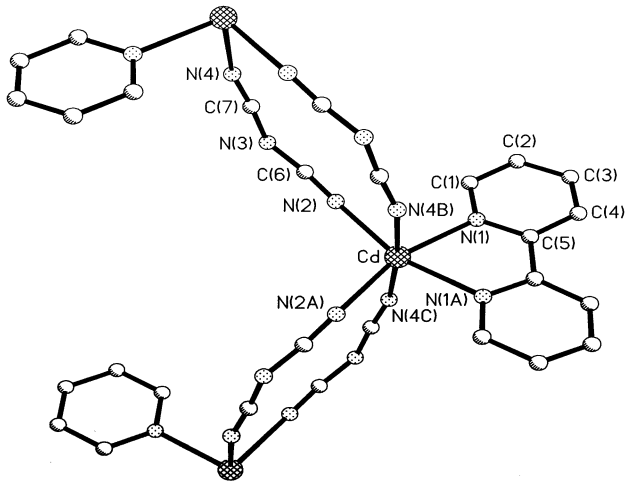


Fig. 4. An ORTEP drawing of $[Cd(N(CN)_2)_2(2,2'\text{-bipy})]_n$ (**2**) with atomic numbering scheme.

3.2.2. Crystal structure of complex *2*

In complex **2**, $[Cd(N(CN)_2)_2](2,2'\text{-bipy})]$, the adjacent cadmium(II) centers are bridged by the double end-to-end $\mu_{1,5}$-N≡C–N–C≡N to form an extended structure with a zigzag 1-D chain (Fig. 5). The cadmium(II) centers are bound to four dca ligands and one chelate 2,2′-bipy ligand (Fig. 4), the cadmium(II) coordination sphere is a distorted octahedron with two N atoms of two dca [Cd–N(2), 2.304 Å; Cd–N(2A), 2.304 Å] and two N atoms of the 2,2′-bipy ligand [Cd–N(1), 2.322(9) Å; Cd–N(1A), 2.322(9) Å] in the equatorial plane, and two N atoms of two other dca ligands [Cd–N(4B), 2.346(13) Å; Cd–N(4C), 2.346(13) Å] occupy the axial plane. The effect of the distortion is readily seen in *cis*-N–Cd–N′ bond angles, which vary from 70.4(5)° to 103.(5)° for N(1)–Cd–N(1A), N(1)–Cd–N(2) and N(2)–Cd–N(2A), respectively. $[N(CN)_2]^-$ bridging li-

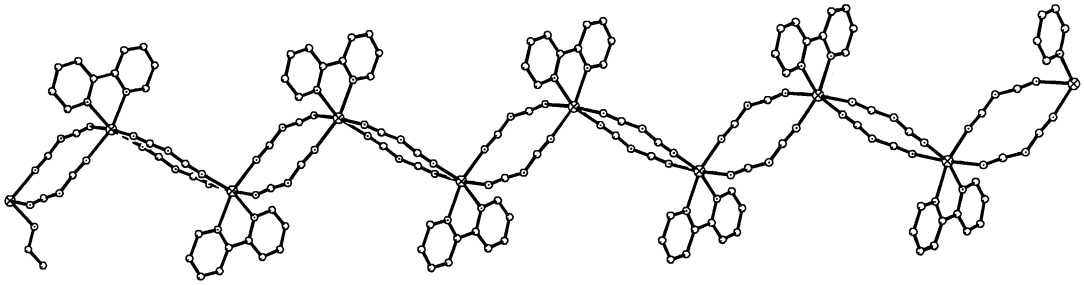


Fig. 5. The chain structure of $[Cd(N(CN)_2)_2(2,2'\text{-bipy})]_n$ (**2**).

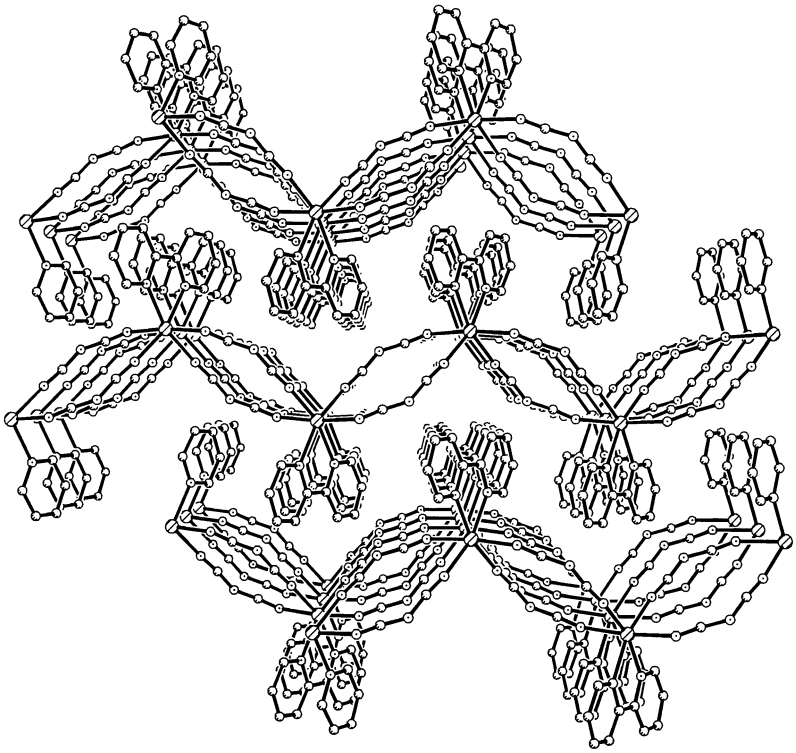


Fig. 6. The 2-D structure of $[Cd(N(CN)_2)_2(2,2'\text{-bipy})]_n$ (**2**) through the weak π–π interaction between adjacent chains.

gands retain approximate C_{2v} symmetry with C(7)–N(4) and C(6)–N(2) bond distances of 1.099(16) and 1.108(14) Å, respectively. Weak π–π interactions are evident, with the shortest distance between the pyridine rings of adjacent chains being 3.641 Å, thus forming a 2-D sheets as in Fig. 6.

4. Supplementary material

Atomic coordinates, thermal parameters and bond lengths and angles for compounds **1** and **2** have been deposited at the Cambridge Crystallographic Center (CCDC). Any request to the CCDC for this material should quote the full literature citation and the reference numbers CCDC 162756 and 162757. Copies of this information may be obtained free of charge from The Director, CCDC, 12 Union Road, Cambridge, CB2 1EZ, UK (fax: +44-1223-336033; e-mail: deposit@ccdc.cam.ac.uk or www:http://www.ccdc.cam.ac.uk).

Acknowledgements

The authors are grateful to the National Nature Science Foundation of China and the Key Project of Chinese Academy of Science for financial support.

References

[1] (a) O.M. Yaghi, H. Li, C. Davis, D. Richardson, T.L. Groy, Acc. Chem. Res. 31 (1998) 474;
(b) T.M. Reineke, M. Eddaoudi, M. O'Keeffe, O.M. Yaghi, Angew. Chem., Int. Ed. 38 (1999) 2590;
(c) H. Li, M. Eddaoudi, M. O'Keeffe, O.M. Yaghi, Nature (London) 402 (1999) 276;
(d) O.R. Evans, Z. Wang, R.-G. Xiong, B.M. Foxman, W. Lin, Inorg. Chem. 38 (1999) 2969;
(e) L. Pan, X. Huang, J. Li, Y. Wu, N. Zheng, Angew. Chem., Int. Ed. 39 (2000) 527.

[2] (a) P.J. Stang, B. Olenyuk, Acc. Chem. Res. 30 (1997) 502;
(b) P.J. Hagrman, D. Hagrman, J. Zubieta, Angew. Chem., Int. Ed. 38 (1999) 2639;
(c) M.-L. Tong, H.K. Lee, X.-M. Chen, R.-B. Huang, T.C.W. Mak, J. Chem. Soc., Dalton Trans. (1999) 3657;
(d) M.-L. Tong, H.-J. Chen, X.-M. Chen, Inorg. Chem. 39 (2000) 2235;
(e) P. Lightfoot, A. Snedden, J. Chem. Soc., Dalton Trans. (1999) 3549;
(f) L. Carlucci, G. Ciani, D.M. Proserpio, A. Sironi, Angew. Chem., Int. Ed. Engl. 34 (1995) 1895;
(g) L. Carlucci, G. Ciani, D.M. Proserpio, A. Sironi, J. Am. Chem. Soc. 117 (1995) 4562;
(h) M.-L. Tong, S.-L. Zheng, X.-M. Chen, Polyhedron 19 (2000) 1809;
(i) S. Noro, M. Kondo, T. Ishii, S. Kitagawa, H. Matsuzaka, J. Chem. Soc., Dalton Trans. (1999) 1569;
(j) A.J. Blake, N.R. Champness, S.S.M. Chung, M. Schröder, Chem. Commun. (1997) 1675;
(k) L. Carlucci, G. Ciani, P. Macchi, D.M. Proserpio, Chem. Commun. (1998), 1837;
(l) L. Carlucci, G. Ciani, D.W. v. Gudenberg, D.M. Proserpio, Inorg. Chem. 36 (1997) 3812.

[3] (a) I. Potocnák, M. Dunaj-Jurco, D. Miklos, L. Jäger, Acta Crystallogr., Sect. C 52 (1996) 1653;
(b) I. Potocnák, M. Dunaj-Jurco, D. Miklos, M. Kabesová, Acta Crystallogr., Sect. C 51 (1995) 600;
(c) B.-W. Sun, S. Gao, Z.-M. Wang, Chem. Lett. 1 (2001) 2;
(d) Y.M. Chow, Inorg. Chem. 10 (1971) 1938;
(e) Y.M. Chow, D. Britton, Acta Crystallogr., Sect. B 33 (1977) 697;
(f) D. Britton, Acta Crystallogr., Sect. C 46 (1990) 2297;
(g) J.L. Manson, C.D. Incarvito, A.L. Rheingold, J.S. Miller, J. Chem. Soc., Dalton Trans. (1998) 3705.;
(h) J.L. Manson, Q.-Z. Huang, J.W. Lynn, H.-J. Koo, M.-H. Whangbo, R. Bateman, T. Otsuka, N. Wada, D.N. Argyriou, J.S. Miller, J. Am. Chem. Soc. 123 (2001) 162;
(i) J.L. Manson, C.R. Kmety, Q. Huang, J.W. Lynn, G. Bendele, S. Pagola, P.W. Stephens, A.J. Epstein, J.S. Miller, Chem. Mater. 10 (1998) 2552;
(j) Y.M. Chow, D. Britton, Acta Crystallogr., Sect. B 31 (1975) 1934.

[4] (a) R. Batten. P. Jensen, B. Moubaraki, K.S. Murray, R. Robson, Chem. Commun. (1998) 439;
(b) K.S. Murray, S.R. Batten, B. Moubaraki, D.J. Price, R. Robson, Mol. Cryst. Liq. Cryst. 335 (1999) 313;
(c) J.L. Manson, C.R. Kmety, A.J. Epstein, J.S. Miller, Inorg. Chem. 38 (1999) 2552;
(d) P. Jensen, S.R. Batten, B. Moubaraki, K.S. Murray, Chem. Commun. (2000) 793;
(e) I. Dasna, S. Golhen, L. Ouahab, O. Pena, J. Guillevlc, M. Fettouhi. J. Chem. Soc., Dalton Trans. (2000) 129;
(f) T. Kusaka, T. Ishida, D. Hashizume, F. Iwasaki, T. Nogami, Chem. Lett. 7 (2000) 1146;
(g) A. Claramut-Escuer, F.A. Mautner, N. Sanz, R. Vicente, J. Chem. Soc., Dalton Trans. (2000) 2627

[5] G.M. Sheldrick, SADABS, A Program for Empirical Absorption Correction. Göttingen, Germany, 1998.

[6] SHELXTL PLUS, XS, Program for Crystal Structure Solution, XL, Program for Crystal Structure Determination, XP, Interactive Molecular Graphics, Siemens Analytical X-ray Institute Inc., 1990.

[7] H. Köhler, A. Kolbe, G. Lux, Z. Anorg. Allg. Chem. 428 (1977) 103.

[8] ORTEP3 for Windows, L.J. Farrugia, J. Appl. Crystallogr. 30 (1997) 565.

[9] J.L. Manson, A.M. Arif, J.S. Miller, J. Mater. Chem. 9 (1999) 979.

[10] M. Hvastijová, J. Kozisek, J. Kohout, L. Jäger, H. Fuess, Transition Met. Chem. 11 (1986) 481.

[11] M. Hvastijová, J. Kohout, H. Köhler, G. Ondrejovic, Z. Anorg. Allg. Chem. 566 (1988) 111.

[12] H. Köhler, H. Wusterhausen, M. Jeschke, A. Kolbe, Z. Anorg. Allg. Chem. 547 (1987) 69.

[13] H. Köhler, H. Hartung, B. Seifert, Z. Anorg. Allg. Chem. 347 (1966) 30.

PERGAMON

Polyhedron 21 (2002) 899–904

POLYHEDRON

www.elsevier.com/locate/poly

Synthesis and structure of pyridine-2-thiolato ruthenium aryls bearing a pendant imine–phenol function

Bikash Kumar Panda [a], Swarup Chattopadhyay [a], Kaushik Ghosh [a], Animesh Chakravorty [a,b,*]

[a] *Department of Inorganic Chemistry, Indian Association for the Cultivation of Science, Kolkata 700 032, India*
[b] *Jawaharlal Nehru Centre for Advanced Scientific Research, Bangalore 560 064, India*

Received 12 September 2001; accepted 25 January 2002

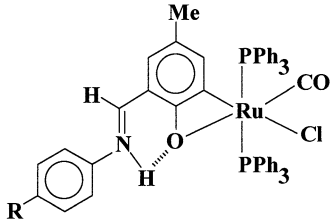
Abstract

The reaction of Ru(η^2-RL)(PPh_3)$_2$(CO)Cl (**1**) with sodium pyridine-2-thiolate (Napyt) has afforded the complexes of the type Ru(η^1-RL)(PPh_3)$_2$(CO)(pyt) (**3**) in excellent yield (η^2-RL is C_6H_2O-2-CHNC_6H_4R(*p*)-3-Me-5, η^1-RL is C_6H_2OH-2-CHNC_6H_4R(*p*)-3-Me-5 and R is Me, MeO, Cl). The reaction is irreversible and is believed to proceed via *cis* attack by pyt$^-$ on an octahedral face. The type **3** species are thermodynamically more stable than the corresponding carboxylates, nitrites and nitrates. Structure determination of the solvate, **3**(R = Cl)·C_6H_6·0.5C_6H_{14} has revealed a distorted octahedral RuC_2P_2NS coordination sphere with the pairs (P, P), (C(aryl), N) and (C(carbonyl), S) defining the three *trans* directions. The η^1-ClL ligand metallated *ortho* to the phenolic oxygen occurs in the imine–phenol tautomeric form (N···O, 2.639(8) Å) which is consistent with IR and ^{1}H NMR data. The transformation **1** → **3** is associated with changes in tautomeric form, hapticity and conformation (in relation to CO) of RL. The Ru(η^1-ClL) fragment excluding the pendant C_6H_4Cl(*p*) group is nearly coplanar (dihedral angle 6.1°) with the Ru(pyt) plane. The Ru–S distance, 2.524(1) Å, is longer than usual due to steric reasons. The type **3** complexes display a quasi-reversible Ru(III)/Ru(II) couple near 0.6 V versus SCE. © 2002 Elsevier Science Ltd. All rights reserved.

Keywords: Ruthenium aryls; Pyridine-2-thiolates of ruthenium; Imine–phenol function

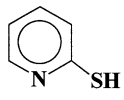
1. Introduction

Ruthenium organometallics of type Ru(η^2-RL)(PPh_3)$_2$(CO)Cl (**1**) were discovered in this laboratory a few years ago as products of decarbonylative metallation of 4-methyl-2,6-diformylphenol by $Ru(PPh_3)_3Cl_2$ in the presence of primary amines (RNH_2) [1–3]. We are scrutinising the reactivity of these compounds. Thus alkynes have been found to undergo facile insertion into the Ru–C(aryl) bond of **1** [4–7]. The chloride ligand has been found to be susceptible to displacement by anions such as carboxylates, nitrites and nitrates affording new organometallics [8–10].



Ru(η^2-RL)(PPh_3)$_2$(CO)(Cl)

1



Hpyt

2

In the present work we have explored for the first time the feasibility of introducing a sulfur donor site into the organometallic frame via chloride displacement using pyridine-2-thiol (Hpyt), **2** as the incoming ligand. This ligand choice was based on the documented affinity of pyt$^-$ for ruthenium [11–15]. The reaction of **1** with Napyt has indeed afforded a new family of S,N-chelated organometallics, the structure and properties of which are described in this work. Changes in the coordination mode, tautomeric state and rotameric conformation of the Schiff base ligand accompany the synthetic reaction.

* Corresponding author. Tel.: +91-33-472-4436; fax: +91-33-473-2805.
E-mail address: icac@mahendra.iacs.res.in (A. Chakravorty).

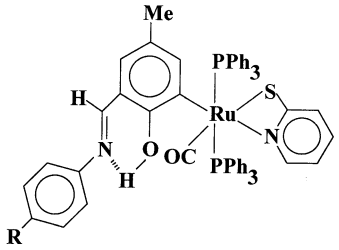
0277-5387/02/$ - see front matter © 2002 Elsevier Science Ltd. All rights reserved.
PII: S0277-5387(02)00867-7

2. Results and discussion

2.1. Synthesis and characterisation

Upon treating **1** in dichloromethane–acetone solution with a sevenfold excess of aqueous Napyt, a yellow solution was afforded from which Ru(η^1-RL)$(PPh_3)_2$-(CO)(pyt) (**3**) was obtained in excellent yield. The synthetic reaction is given in Eq. (1).

The η^1-RL



Ru(η^1-RL)$(PPh_3)_2$(CO)(pyt)

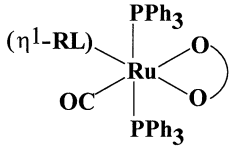
3

ligand in **3** is a tautomer of the η^2-RL ligand in **1** and they bind the metal in monodentate

$$\mathbf{1} + \text{Napyt} \rightarrow \mathbf{3} + \text{NaCl} \quad (1)$$

and bidentate modes, respectively, vide infra. Three R groups have been used in this work: Me, MeO, Cl. The organometallics of type **3** are non-electrolytic in solution and are uniformly diamagnetic consistent with the metal oxidation state of +2.

A note on the thermodynamic stability of **3** compared with related systems is in order. The reaction of Eq. (1) is irreversible and addition of an excess soluble chloride like Et_4NCl into the reaction medium fails to regenerate **1**. It was demonstrated earlier that **1** reacts with carboxylates, nitrates and nitrites affording O,O-chelated species of type **4** [8,9]. This reaction is reversible and is pushed backward upon addition of excess Et_4NCl to the solution. We have now observed that **4** reacts smoothly with Napyt



4

to furnish **3** in excellent yield via displacement of the (O,O) ligand. This conversion which has been quantitated in case of the acetate, Eq. (2), is also irreversible and no

$$\text{Ru}(\eta^1\text{MeL})(PPh_3)_2(CO)(O_2CMe) + \text{Napyt} \rightarrow \mathbf{3}(\text{R=Me}) + \text{NaO}_2\text{CMe} \quad (2)$$

backward reconversion is observed upon addition of an excess acetate to the reaction medium. Thus the Ru(N,S) ring in **3** is thermodynamically much more stable than the Ru(O,O) ring in **4**.

In dichloromethane solution, the complexes display two characteristic allowed bands in the regions 400–410 and 330–350 nm, the later being more intense. The carbon monoxide stretch is seen as a sharp band near 1935 cm^{-1}.

In the ^1H NMR spectrum of **3**, the four pyt protons occur as well-resolved doublets and triplets in the region 6.1–6.7 ppm. The high field shifts of these protons is due to the ring currents of the phosphine phenyl rings. The average ring current shifts estimated from the crystallographic data (see below) and isoshielding $\rho - z$ plots [16,17] is ~0.55 ppm. The PPh_3 and Schiff base aromatic protons form a complex multiplet in the region 7.1–7.6 ppm and the azomethine singlet occurs near 8.5 ppm.

In dichloromethane solution, **3** displays a quasi-reversible one-electron cyclic voltammetric response near 0.6 V versus SCE corresponding to the Ru(III)/Ru(II) couple. As R is varied, the $E_{1/2}$ values increase in the Hammett order OMe < Me < Cl. The reduction potentials are systematically lower than those of the type **1** precursors [3] by ~100 mV indicating better stabilisation of the trivalent state in **3** compared with **1**.

2.2. Crystal structure

The X-ray structure of Ru(η^1-ClL)$(PPh_3)_2$(CO)(pyt)·C_6H_6·0.5C_6H_{14}, **3**(R = Cl)·C_6H_6·0.5C_6H_{14} has been determined authenticating the binding mode shown in **3**. A molecular view excluding solvent of crystallisation is shown in Fig. 1 and selected bond parameters are listed in Table 1. The hexane molecule lies on a crystallographic centre of inversion, ~3.44 Å away

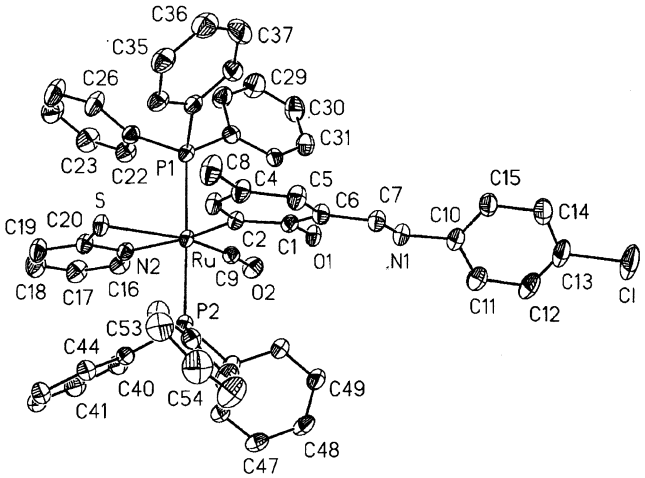


Fig. 1. ORTEP plot (30% probability ellipsoids) and atom-labelling scheme for **3**(R = Cl)·C_6H_6·0.5C_6H_{14} (excluding the solvent of crystallisation).

Table 1
Selected bond distances (Å) and angles (°) for **3**(R = Cl)·C_6H_6·0.5C_6H_{14}

Bond distances			
Ru–P1	2.394(1)	C9–O2	1.153(5)
Ru–P2	2.396(1)	C7–N1	1.280(5)
Ru–C2	2.114(4)	C1–O1	1.376(4)
Ru–C9	1.833(4)	C20–S	1.728(4)
Ru–S	2.524(1)	N1···O1	2.639(8)
Ru–N2	2.144(3)		
Bond angles			
P1–Ru–P2	174.43(4)	P2–Ru–C2	88.32(11)
P1–Ru–S	88.01(4)	Ru–C9–O2	169.9(4)
P1–Ru–N2	90.60(9)	C2–Ru–N2	165.56(13)
P1–Ru–C9	94.65(13)	C9–Ru–S	160.44(13)
P1–Ru–C2	88.45(11)	S–Ru–N2	65.50(9)
P2–Ru–S	88.09(4)	S–Ru–C2	100.07(10)
P2–Ru–N2	91.39(9)	C9–Ru–N2	95.1(2)
P2–Ru–C9	90.35(13)		

from the periphery of two PPh_3 ligands of two symmetry related molecules. The benzene of crystallisation lies in a zone near the pyt and PPh_3 aryl rings. This interesting packing situation viewed down *b* axis is highlighted in Fig. 2.

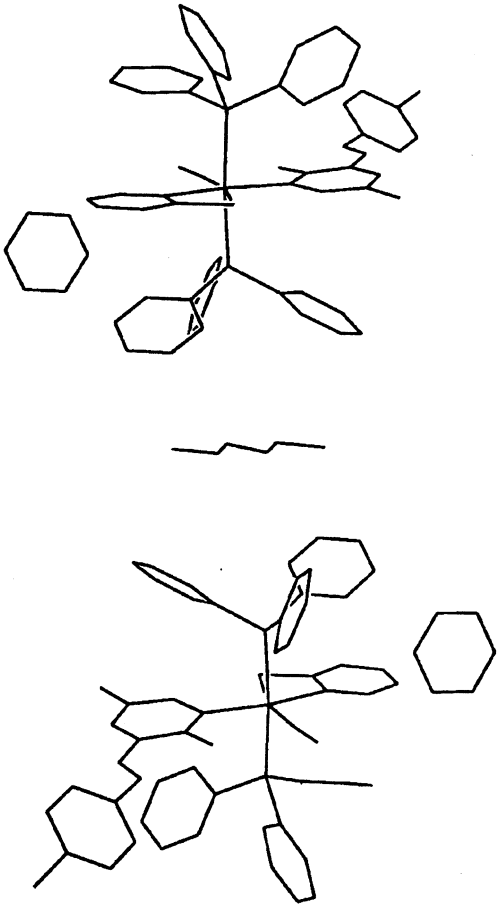


Fig. 2. Portion of packing diagram of **3**(R = Cl)·C_6H_6·0.5C_6H_{14} viewed down *b*-axis.

The RuC_2P_2NS coordination sphere has distorted octahedral geometry. The Ru, S, N2, C9 and C2 atoms define a good equatorial plane (mean deviation 0.019 Å) and the *trans* P1–Ru–P2 fragment is approximately linear. The η^1-ClL ligand is monodentate being coordinated to the metal only at the C2 atom. The phenolic oxygen atom (O1) is too far away for metal binding (Ru···O1, 3.439(3) Å).

The metallated aldimine ring (Ru, C1–C8, O1, N1) constitutes a satisfactory plane (plane A) of mean deviation 0.044 Å with which the pendant chlorophenyl ring makes a dihedral angle of 37.2°. The Ru(pyt) fragment along with carbon monoxide and the C2 atom also constitute a satisfactory plane of mean deviation 0.033 Å (plane B). The dihedral angle between planes A and B is 4.6°.

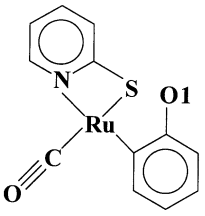
The Ru–S length, 2.524(1) Å, is significantly longer than the corresponding distances, 2.39–2.45 Å, in other structurally characterised Ru(II)(pyt) species [11–15]. This is attributed to S···C3 repulsion. The observed distance between these two non-bonded atoms is 3.420(4) Å which still falls slightly below the sum of the van der Waals radii (3.50 Å) of the carbon and sulphur atoms [18]. The interaction is thus repulsive but the repulsion would have been much more if the Ru–S bond length were shorter.

2.3. Prototropic shift and conformational change

The uncoordinated salicylaldimine fragment in **3** is in the imine–phenol tautomeric form, the N···O distance in **3**(R = Cl)·C_6H_6·0.5C_6H_{14} being 2.639(8) Å. In the precursor complex **1**, the metal is coordinated to the phenolato function and the Schiff base fragment occurs in the iminium–phenolato tautometic form [1]. The reaction of Eq. (1) is thus attended with tautomerization of the salicylaldimine function, corresponding to iminium–phenolato → imine–phenol prototropic shift. The process is a distant parallel of the imine-iminium tautomerization observed in rhodopsins [19].

The observed prototropic change is consistent with certain IR and ^{1}H NMR features. Thus the C=N stretching frequency in **3** ($\sim$1580 cm^{-1}) is expectedly [19,20] lower than that in **1** ($\sim$1620 cm^{-1}) [3]. In ^{1}H NMR, the phenolic proton of **3** occurs as a relatively sharp singlet near 13 ppm. In contrast, the iminium resonance of **1** is much broadened by the quadrupole moment of nitrogen [3].

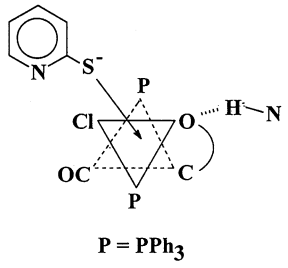
In both **1** and **3**, the carbon monoxide ligand lies *cis* to the metallated carbon atom. It is, however, located *cis* and *trans* to the phenolato oxygen in **3** and **1**, respectively.



5

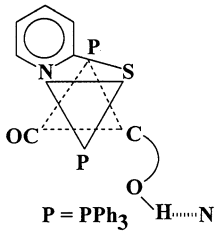
Thus the Schiff base fragment rotates by $\sim 180^\circ$ around the metal–carbon bond in course of the reaction of Eq. (1). Model studies have revealed that the transformation is driven by the large steric hindrance that would otherwise arise as depicted in **5** where the estimated O1···S distance is 2.39 Å, falling far short of the sum of van der Waals radii (3.30 Å) of sulphur and oxygen atoms. After rotation as in **3**(R = Cl)·C_6H_6·0.5C_6H_{14} the O1···S distance is 5.673(6) Å.

A plausible mechanism [21,8] for the displacement of chloride in **1** consists of *cis* attack by pyt^- is shown in **6**. The anchored ligand displaces the phenolato oxygen and halide atoms achieving pyt chelation with concomitant prototropic shift and conformational reorganisation as in **7**.



P = PPh_3

6



P = PPh_3

7

3. Experimental

3.1. Materials

The starting complexes $Ru(PPh_3)_3Cl_2$ [22] and $Ru(\eta^2$-RL)$(PPh_3)_2$(CO)Cl [3] were prepared by reported methods. The purification of dichloromethane and the preparation of tetraethylammonium perchlorate (TEAP) for electrochemical work were done as described in previous work [23]. Pyridine-2-thiol was obtained from Aldrich. All other chemicals and solvents were of analytical grade and were used as received.

3.2. Physical measurements

Electronic and IR spectra were recorded with a Shimadzu UV-1601PC spectrophotometer (thermostated cell compartment) and Perkin–Elmer 783 IR Spectrophotometer. ^{1}H NMR spectra were obtained using a Bruker 300 MHz FT NMR spectrometer (tetramethylsilane internal standard). The numbering scheme used for ^{1}H NMR is the same as in crystallography. Spin–spin structures are abbreviated as: s, singlet; d, doublet; t, triplet; m, multiplet. Microanalyses (C, H, N) were done using a Perkin–Elmer 240C elemental analyser. All electrochemical measurements were performed under nitrogen atmosphere using a PAR 370-4 electrochemistry system. The reported potentials are referenced to the saturated calomel electrode (SCE) without junction correction.

3.3. Preparation of Napyt

NaOH (0.864 g, 21.6 mmol) was taken in a beaker. Then 60 ml of distilled water was added to it. The solution was then stirred and to this stirred solution 2 g (18 mmol) of pyridine-2-thiol was added slowly. The mixture was then stirred for 30 min and then evaporated to deposit the salt. It was then filtered and dried in vacuo. Yield: 1.65 g (69%).

3.4. Synthesis of the complexes

The pyridine-2-thiolato complexes $Ru(\eta^1$-RL)-$(PPh_3)_2$(CO)(pyt) were synthesised by reacting $Ru(\eta^2$-RL)$(PPh_3)_2$(CO)Cl with Napyt. Details of a representative case are given below. The other compounds were prepared analogously.

3.4.1. [$Ru(\eta^1$-MeL)$(PPh_3)_2(CO)(pyt)$] (**3**) (R = Me)

To a vigorously stirred violet solution of $Ru(\eta^2$-MeL)$(PPh_3)_2$(CO)Cl (50 mg, 0.055 mmol) in a mixture of dichloromethane (20 ml) and acetone (20 ml) was added dropwise an aqueous solution of Napyt (51 mg, 0.38 mmol). The mixture was stirred for 3 h when the original violet colour became clear yellow. The solvent was then removed under reduced pressure leaving an aqueous suspension of a yellow residue, which was isolated by filtration, washed repeatedly with water, and dried in vacuo. Yield: 45 mg (83%). *Anal*. Found: C, 69.21; H, 4.95; N, 2.87. Calc. for $C_{57}H_{48}N_2O_2SP_2Ru$: C, 69.29; H, 4.90; N, 2.84%. UV–Vis [λ_{max}, nm (ε, dm^3 mol^{-1} cm^{-1})]: 410 (3820) and 342 (14 640). IR (KBr, cm^{-1}): 1577 (ν_{CN}) and 1934 (ν_{CO}). ^{1}H NMR ($CDCl_3$, δ): 8.47 (s, 1H, H(7)), 13.06 (s, 1H, O–H), 7.12–7.56 (m, 36H, $2PPh_3$, H(3), H(5), H(11), H(12), H(14), H(15)), 2.25 and 2.31 (2s, 6H, $2CH_3$), 6.67 (d, 1H, H(16), J_{HH} 8.1), 6.17 (t, 1H, H(17), J_{HH} 6.3), 6.57 (t, 1H, H(18), J_{HH} 6.3), 6.34 (d, 1H, H(19), J_{HH} 8.4). $E_{1/2}$ (vs. SCE, CH_2Cl_2, scan rate, 50 mV s^{-1}): 0.59 V (ΔE_P = 120 mV).

3.4.2. [Ru(η¹-MeOL)(PPh₃)₂(CO)(pyt)] (3) (R = MeO)

Ru(η²-MeOL)(PPh₃)₂(CO)Cl (50 mg, 0.054 mmol) and Napyt (51 mg, 0.38 mmol) were employed. Yield: 47 mg (87%). *Anal*. Found: C, 68.22; H, 4.77; N, 2.73. Calc. for $C_{57}H_{48}N_2O_3SP_2Ru$: C, 68.18; H, 4.82; N, 2.79%. UV–Vis [λ_{max}, nm (ε, dm^3 mol^{-1} cm^{-1})]: 408 (3270) and 348 (11 250). IR (KBr, cm^{-1}): 1579 (ν_{CN}) and 1935 (ν_{CO}). ^{1}H NMR ($CDCl_3$, δ): 8.49 (s, 1H, H(7)), 13.10 (s, 1H, O–H), 7.15–7.57 (m, 36H, 2PPh$_3$, H(3), H(5), H(11), H(12), H(14), H(15)), 2.24 (s, 3H, CH_3), 3.77 (s, 3H, OCH_3), 6.68 (d, 1H, H(16), J_{HH} 8.1), 6.19 (t, 1H, H(17), J_{HH} 6.3), 6.58 (t, 1H, H(18), J_{HH} 6.1), 6.36 (d, 1H, H(19), J_{HH} 8.1). $E_{1/2}$ (vs. SCE, CH_2Cl_2, scan rate, 50 mV s^{-1}): 0.58 V ($\Delta E_P = 180$ mV).

3.4.3. [Ru(η¹-ClL)(PPh₃)₂(CO)(pyt)] (3) (R = Cl)

Ru(η²-ClL)(PPh$_3$)$_2$(CO)Cl (50 mg, 0.054 mmol) and Napyt (51 mg, 0.38 mmol) were used. Yield: 46 mg (85%). *Anal*. Found: C, 66.62; H, 4.54; N, 2.72. Calc. for $C_{56}H_{45}N_2O_2SP_2ClRu$: C, 66.69; H, 4.50; N, 2.78%. UV–Vis [λ_{max}, nm (ε, dm^3 mol^{-1} cm^{-1})]: 415 (4160) and 333 (18 640). IR (KBr, cm^{-1}): 1580 (ν_{CN}) and 1936 (ν_{CO}). ^{1}H NMR ($CDCl_3$, δ): 8.50 (s, 1H, H(7)), 13.07 (s, 1H, O–H), 7.19–7.60 (m, 36H, 2PPh$_3$, H(3), H(5), H(11), H(12), H(14), H(15)), 2.25 (1s, 3H, CH_3), 6.68 (d, 1H, H(16), J_{HH} 8.0), 6.20 (t, 1H, H(17), J_{HH} 6.0), 6.58 (t, 1H, H(18), J_{HH} 6.0), 6.35 (d, 1H, H(19), J_{HH} 8.1). $E_{1/2}$ (vs. SCE, CH_2Cl_2, scan rate, 50 mV s^{-1}): 0.67 V ($\Delta E_P = 170$ mV).

3.5. Conversion of [Ru(η¹-MeL)(PPh₃)₂(CO)(O₂CMe)] to 3 (R = Me)

To a vigorously stirred yellow solution of [Ru(η^1-MeL)(PPh$_3$)$_2$(CO)(O$_2$CMe)] (50 mg, 0.053 mmol) in dichloromethane (20 ml) and acetone (20 ml) was added dropwise an aqueous solution of Napyt (71 mg, 0.53 mmol). After further stirring for 3 h, the organic solvent was removed under reduced pressure. The yellow residue was collected by filtration, washed thoroughly with water and dried in vacuo. Yield: 78%.

3.6. X-ray crystallography

A single crystal ($0.55 \times 0.4 \times 0.4$ mm) of [Ru(η^1-ClL)(PPh$_3$)$_2$(CO)(pyt)]·C$_6$H$_6$·0.5C$_6$H$_{14}$, grown by slow diffusion of hexane into benzene solution followed by evaporation, was used. Cell parameters were determined by a least-squares fit of 30 machine-centred reflections ($2\theta = 14°$–$28°$). Data were collected with the ω-scan technique in the range $3° \le 2\theta \le 47°$ on a Siemens R3m/V four-circle diffractometer with graphite-monochromated Mo Kα radiation ($\lambda = 0.71073$ Å). Two check reflections measured after every 198 reflections showed no significant intensity reduction in any case. All data were corrected for Lorentz polarisation effects and an empirical absorption correction [24] was done on the basis of azimuthal scan of six reflections for the crystal.

The metal atom was located from Patterson maps and the rest of the non-hydrogen atoms emerged from successive Fourier syntheses. The structure was refined by a full-matrix least-squares procedure on F^2. All non-hydrogen atoms were refined anisotropically. Hydrogen atoms were included at calculated positions. Calculations were performed using the SHELXTL, Version 5.03 [25] programme package. Significant crystal data are listed in Table 2.

3.7. Computer generation of motif 5

The relative positions of CO and the pyt chelate were retained as in the structure of Ru(η^1-ClL)(PPh$_3$)$_2$(CO)-(pyt)·C$_6$H$_6$·0.5C$_6$H$_{14}$ but the phenolic oxygen (O1) (the phenolic C–O length was set at 1.363 Å) was shifted so as to correspond to the relative position in **1** (R = Me). The O1···S distance is then found to be 2.39 Å.

3.8. Computation of chemical shifts due to PPh₃ ring currents

The crystallographic data of [Ru(η^1-ClL)(PPh$_3$)$_2$-(CO)(pyt)]·C$_6$H$_6$·0.5C$_6$H$_{14}$ were used. The cylindrical coordinates (ρ and z) [26] of the protons with respect to the centroids (G) of the PPh$_3$ phenyl rings were determined from: (i) the distance of the proton from the centroid (G) of each PPh$_3$ phenyl ring and (ii) the angle between the distance vector and the normal to the plane of the ring at G. These calculated ρ and z values were expressed in units of the radius of the benzene hexagon and the shifts were estimated with the help of the available isoshielding ρ versus z plots [16]. The net shift of a proton was obtained by summing the individual contributions from all the rings.

Table 2
Crystal data for **3**(R = Cl)·C$_6$H$_6$·0.5C$_6$H$_{14}$

Formula	$C_{65}H_{58}ClN_2O_2P_2RuS$
M	1129.65
Crystal system	triclinic
Space group	$P\bar{1}$
a (Å)	11.797(2)
b (Å)	12.935(3)
c (Å)	19.241(5)
α (°)	82.24(2)
β (°)	75.14(2)
γ (°)	78.88(2)
V (Å^3)	2773.4(10)
Z	2
μ (Mo Kα) (mm^{-1})	0.473
Total reflections	8302
Independent reflections (R_{int})	8161(0.0403)
R_1, wR_2 [$I > 2\sigma(I)$] (all data)	0.0436, 0.1071; 0.0587, 0.1388

4. Conclusions

The scope of synthesis of new ruthenium aryls via chloride displacement from **1** has been augmented to sulphur donor ligands using pyridine-2-thiolate as the incoming chelator affording species of type **3**. These are found to be thermodynamically more stable than carboxylates, nitrates and nitrites.

Rational changes in tautomeric form, hapticity and conformation of RL occur in going from **1**→**3** as revealed by structural and spectroscopic data. The presence of significant crowding is reflected in both non-bonded (C···S) as well as bonded (Ru–S) distances.

5. Supplementary material

Supplementary data are available from the Cambridge Crystallographic Data Centre, 12 Union Road, Cambridge CB2 1EZ, UK (fax: +44-1223-336033; e-mail: deposit@ccdc.cam.ac.uk) on request quoting the deposition number, CCDC 171587.

Acknowledgements

We thank the Department of Science and Technology, the Council of Scientific and Industrial Research, New Delhi, India, for financial support.

References

[1] N. Bag, S.B. Choudhury, A. Pramanik, G.K. Lahiri, A. Chakravorty, Inorg. Chem. 29 (1990) 5013.
[2] N. Bag, S.B. Choudhury, G.K. Lahiri, A. Chakravorty, J. Chem. Soc., Chem. Commun. (1990) 1626.
[3] P. Ghosh, N. Bag, A. Chakravorty, Organometallics 15 (1996) 3042.
[4] K. Ghosh, S. Pattanayak, A. Chakravorty, Organometallics 17 (1998) 1956.
[5] K. Ghosh, S. Chattopadhyay, S. Pattanayak, A. Chakravorty, Organometallics 20 (2001) 1419.
[6] S. Chattopadhyay, K. Ghosh, S. Pattanayak, A. Chakravorty, J. Chem. Soc., Dalton Trans. (2001) 1259.
[7] S. Chattopadhyay, K. Ghosh, S. Pattanayak, A. Chakravorty, Indian J. Chem. 40A (2001) 1.
[8] P. Ghosh, A. Pramanik, A. Chakravorty, Organometallics 15 (1996) 4147.
[9] P. Ghosh, A. Chakravorty, Inorg. Chem. 36 (1997) 64.
[10] K. Pramanik, P. Ghosh, A. Chakravorty, J. Chem. Soc., Dalton Trans. (1997) 3553.
[11] S.R. Fletcher, A.C. Skapski, J. Chem. Soc., Dalton Trans. (1972) 635.
[12] P. Mura, B.G. Olby, S.D. Robinson, J. Chem. Soc., Dalton Trans. (1985) 2101.
[13] E.C. Constable, P.R. Raithby, Inorg. Chim. Acta 183 (1991) 21.
[14] A.J. Deeming, K.I. Hardcastle, M. Karim, Inorg. Chem. 31 (1992) 4792.
[15] B.K. Santra, M. Menon, C.K. Pal, G.K. Lahiri, J. Chem. Soc., Dalton Trans. (1997) 1387.
[16] C.E. Johnson, Jr., F.A. Bovey, J. Chem. Phys. 29 (1958) 1012.
[17] P. Ghosh, Polyhedron 16 (1997) 1343.
[18] J.E. Huheey, E.A. Keiter, R.L. Keiter, Inorganic Chemistry: Principles of Structure and Reactivity, Harper Collins College Publishers, New York, 1993, p. 292.
[19] C. Sandorfy, D. Vocelle, Mol. Phys. Chem. Biol. 4 (1989) 195.
[20] H. Bohme, M. Haake, in: H. Bohme, H.G. Viehe (Eds.), Advances in Organic Chemistry, Part 1, vol. 9, Interscience Publication, New York, 1976, p. 1.
[21] N. Serpone, D.G. Bickley, Inorg. Chem. 17 (1972) 391.
[22] T.A. Stephenson, G. Wilkinson, J. Inorg. Nucl. Chem. 28 (1966) 945.
[23] P. Ghosh, A. Pramanik, N. Bag, G.K. Lahiri, A. Chakravorty, J. Organomet. Chem. 454 (1993) 237.
[24] A.C.T. North, D.C. Phillips, F.A. Mathews, Acta Crystallogr., Sect. A 24 (1968) 351.
[25] G.M. Sheldrick, SHELXTL, Version 5.03; Siemens Analytical X-ray System: Madison, WI, 1994.
[26] H. Margenau, G.M. Murphy, The Mathematics of Physics and Chemistry, D. van Nostrand, Princeton, NJ, 1956.

PERGAMON

Polyhedron 21 (2002) 905–907

POLYHEDRON

www.elsevier.com/locate/poly

Professor Achim Müller awarded 2001 Sir Geoffrey Wilkinson Prize



It is a great pleasure to announce that the 2001 *Sir Geoffrey Wilkinson Prize* has been awarded to Professor Achim Müller from the University of Bielefeld, Germany.

Professor Müller is regarded as one of today's leading international scholars on the subject of soluble metal oxides and sulfides. Being an immensely creative and highly successful inorganic chemist with extremely broad interests, his work includes the synthesis of the first discrete pure metal–sulfur clusters (e.g. $Mo_3S_{13}^{2-}$) as well as of the first isopolythioanions ($W_3S_9^{2-}$); the introduction of the unusual thiometalate ligands in the field of complex chemistry; template directed organisation of metal–oxide cluster shells; new aspects of inorganic host–guest chemistry; and contributions to the development of supramolecular magneto chemistry.

One of his most remarkable achievements is the discovery of the 'Bielefeld giant wheel' polyoxomolybdate. The largest molecular cluster structurally characterised at the time, it caused a worldwide sensation. Professor Müller and his co-workers have developed novel concepts for handling highly complex molecular nanostructures, which are amongst the most fascinating problems of contemporary inorganic chemistry.

The 2001 *Sir Geoffrey Wilkinson Prize* will be presented to Professor Müller by Professor Barry Lever, on July 22nd 2002 during the XXXVth International Conference on Coordination Chemistry in Heidelberg,

0277-5387/02/$ - see front matter © 2002 Published by Elsevier Science Ltd.
PII: S0277-5387(02)00918-X

Germany. The presentation will be followed by a Prize Lecture.

The *Sir Geoffrey Wilkinson Prize*, previously designated as the *Polyhedron Prize*, was renamed after the late Professor Geoffrey Wilkinson, the Prize's first recipient in 1989. As one of Elsevier's most prestigious awards, it has been designed to pay tribute to creativity in the field of inorganic and organometallic chemistry. The winner receives from Elsevier Science a commemorative medal accompanied by a cheque for US$ 10,000. The selection committee for the 2001 Prize consisted of Professor F. Albert Cotton, Professor Akio Yamamoto and Professor Lord Jack Lewis. Past winners include: Professor Richard H. Holm (1991), Professor M. Frederick Hawthorne (1993), Professor F. Albert Cotton (1995), Professor Lord Lewis (1997) and Professor Herbert Roesky (1999).

1. Biographical sketch of Professor Achim Müller

Achim Müller studied chemistry and physics at the Georg-August University in Göttingen, where he received his PhD degree under the supervision of Oskar Glemser with a thesis about experimental thermochemistry in 1965 (his subject included theoretical physics) and only 2 years later, in 1967, his habilitation with a thesis in the field of vibrational spectroscopy.

In 1971 Achim Müller became Associate Professor at the University of Dortmund and thereafter, in 1977, accepted the Chair of Inorganic Chemistry I at the University of Bielefeld, where he has since remained although he was offered an honorable professorship at the University of Saarbrücken as successor to Professor F. Seel.

As regards research Achim Müller's interests and achievements are extremely broad and range from (synthetic) transition metal chemistry, supramolecular chemistry, through inorganic structural chemistry, electronic structure of transition metal complexes and clusters, vibrational spectroscopy (matrix isolation, band-contour analysis, resonance Raman effect), molecular physics (theory of heavy atom substitution on molecular constants), heterogeneous catalysis (desulfurization of crude oils), to bioinorganic chemistry (biological nitrogen fixation, including microbiological and biochemical investigations). Recently he even extended his knowledge to the realm of natural philosophy and public understanding of science where he has already published his first papers.

The results of his widespread chemistry investigations have been recorded in more than 700 publications and received extreme resonance in the scientific community. An exceptional aspect is that the papers were published in ca. 70 different journals specific to the above-mentioned fields. In addition, he is the author of more than 40 reviews and editor/co-editor of ten books, again dealing with all the above-mentioned fields. One of his reviews was commented by a referee as '...a beautifully idiosyncratic approach and a joy to read. Would that more chemists dared to approach their work with such panache and breadth of vision!'

Indications of the international scientific reputation of his research work can also be inferred from the fact that about 50 postdoctoral fellows and guest professors from many different countries came to Göttingen (the first in fact prior to his Habilitation), Dortmund, and Bielefeld. Documentary proof supporting this statement can be furnished by the fact that Achim Müller has for many years been one of the most cited authors in science worldwide (science citation index of ISI). In the course of his entire scientific career he has maintained a remarkable collaboration, also on an interdisciplinary level, with many groups in very different parts of the world. The scientific results were also presented in more than 60 invited, plenary (including opening), and named lectures at international conferences.

Regarding his research topics—focussed here only on inorganic chemistry—he can be considered as one of the internationally leading figures on the subject of soluble metal oxides and sulfides with many essential impulses coming from him. The following key points furnish proof for this statement: the synthesis of the first discrete pure metal–sulfur cluster (e.g. $Mo_3S_{13}^{2-}$ besides $Mo_2S_{12}^{2-}$) and the first polythioanion ($W_3S_9^{2-}$), the discovery of the most simple ferredoxin model ($[Fe_4S_4(SH)_4]^{2-}$), the introduction of unusual thiometalate ligands like MS_4^{2-} (M = Mo, W) into the field of complex chemistry in connection with the discovery of their important ability to show internal redox processes, the unprecedented use of template-directed organisation of metal–oxide cluster shells, the development of new principles of inorganic host–guest chemistry, contributions to supramolecular magneto chemistry (some of his clusters became favorable objects of investigations in magneto chemistry and in the physics of magnetism), and in more recent years the spectacular discovery of the 'Bielefeld giant wheel' polyoxomolybdate—at that time with 154 metal atoms the largest molecular cluster (his record now being 264) structurally characterized. The species was isolated from a molybdenum blue solution which chemists had been probing for more than 200 years since the time of Scheele and Berzelius. In this context Professor Achim Müller and his coworkers have developed novel concepts for handling highly complex metal oxide based molecular nanostructures to perform well defined reactions at well defined sites of structurally well defined nanoobjects/clusters, thus dealing with one of the most fascinating problems of contemporary Inorganic Chemistry. In this sense not only the discovery of chemical reactions, i.e. nucleation processes, inside the cavity of spherical and ring-shaped nanoclus-

ters but also of the possibility to link or cross-link these in distinct predefined ways even in room temperature solid state reactions (crystal-engineering) are highlights.

An important step was clearly to form and to use pentagonal building units. In agreement with the paradigm of Buckminster Fuller, this allowed the synthesis of sizable (!) spherical nanoclusters with icosahedral symmetry (inorganic fullerenes, or so-called keplerates), for instance those with 132 and 102 metal atoms. The planned (!) synthesis of a new type of supramolecular species with host–guest topology (a quantum-dot within a magneto-dot) with an encapsulated cluster (Keggin-ion), which fits exactly into an unusual spherical nanocluster (the largest molecular paramagnet with 30 Fe^{III} centers), was commented by a referee as follows: '...the readership will likely experience the same type of progression that I did upon reading it: initial surprise ('Surely this cannot be!') then curiosity, subsequent admiration, and finally lingering thought-provoking reflection'.

Achim Müller's achievements have been recognized worldwide. His work has been highlighted in *Nature*, *Science* as well as by global newspapers and magazines, not just because of the mere beauty of the molecular entities he produced, but also because of the perspectives.

On account of his extremely wide range of scientific activities and indeed his conception of science in general, he has been acknowledged with Doctor honoris causa and Honorary Professor degrees, Honorary Memberships of science institutions as well as other important awards (Alfred-Stock-Gedächtnispreis (GDCh), Prix Gay-Lussac/Humboldt of the Ministère de la Recherche, Paris). He became a member of editorial boards of many international renowned journals and is elected member of several academies (e.g. Polish Academy of Sciences, Deutsche Akademie der Naturforscher Leopoldina, and Academia Europaea, among others).

Professor Achim Müller is a most deserved winner of the 2001 *Sir Geoffrey Wilkinson Award* and we extend our congratulations to him on this important occasion.

Sandra Migchielsen,
Publishing Editor Inorganic Chemistry
E-mail: a.migchielsen@elsevier.com

PERGAMON

Polyhedron 21 (2002) 909–915

POLYHEDRON

www.elsevier.com/locate/poly

Transition metal containing dendrimers based on cyclophosphazene units

Carlos Díaz *, M.L. Valenzuela

Departamento de Química, Facultad de Ciencias, Universidad de Chile, Las Palmeras 3425, Casilla 653, Santiago, Chile

Received 2 April 2001; accepted 8 January 2002

Abstract

The series of complexes $[N_3P_3(OC_6H_5)_5OC_6H_4CH_2CN\cdot MCl_n]PF_6$, $N_3P_3(OC_6H_4CH_2CN)_6\cdot(MCl_n)_6](PF_6)_6$, $[N_3P_3(OC_6H_5)_5OC_6H_4CH_2CN\cdot MCl_{n-1}]Cl$ and $[N_3P_3(OC_6H_4CH_2CN)_6\cdot(MCl_{n-1})_6]Cl_6$, $MCl_n = MnCl_2$, $FeCl_3$, $CoCl_2$, $NiCl_2$, $CuCl_2$ have been synthesized by reaction of the corresponding cyclophosphazene ligands: $N_3P_3(OC_6H_5)_5OC_6H_4CH_2CN$ (L_1) and $N_3P_3(OC_6H_4CH_2CN)_6$ (L_2) with the respective salts MCl_n in CH_3OH as solvent and in presence or absence of NH_4PF_6. The new compounds were characterized by elemental analysis and IR, UV–Vis and EPR spectroscopy as well as electrochemical methods. The reaction of $CuCl_2$ with the ligand L_1 affords the copper (I) complex. $[N_3P_3(OC_6H_5)_5OC_6H_4CH_2CN\cdot Cu]PF_6$ instead the expected Cu(II) complex, which was characterized by multinuclear NMR. For comparison, the complex $[N_3P_3(OC_6H_5)_5OC_6H_4CH_2CN\cdot ZnCl]PF_6$ was also prepared. The hexametalladendrimers of iron exhibits a six-electron reduction while that the correspondent monometalladendrimers exhibit a single one-electron reduction. Upon coordination νCN increase in a similar way to crystal field effects dependence with the metal. © 2002 Published by Elsevier Science Ltd.

Keywords: Dendrimers; Cyclophosphazene; Metal–nitrile complexes

1. Introduction

Dendrimers chemistry is a rapid developing field of research [1]. Dendrimers offer the prospect of novel material with advantageous properties allowing them to serve, as soluble catalysts [2], dendritic boxes [3], and other supramolecular dendritic arrangements. Since the initial report on this class of molecules by Vögtle in 1978, [4], and many different structural classes of dendritic macromolecules have been reported. Two main classes of dendrimers can be distinguished: the classical organic dendrimers [1] and the emergent inorganic dendrimers [5].

The incorporation of transition-metal complexes in both organic and inorganic dendrimers lead to new and interesting material with specific properties such as the capability to absorb visible light, to give luminescence and to undergo reversible multielectron redox processes [6]. Such species; in fact could find applications as component in molecular electronic and as a photochemical molecular devices for solar energy conversion and information storage [6]. Metal-containing dendrimers can be classified in to three categories, see Fig. 1:

A) Dendrimers with coordination centers at the core.
B) Dendrimers with coordination centers through all layers.
C) Dendrimers with coordination centers on the periphery.

Although dendrimers with coordination centers on the periphery have been reported [1,2,6] for those with the dendrimer, core being organic, few examples of inorganic dendrimers with metal derivatives on the surface have been reported [5–8]. This communication reports the synthesis and characterization of new inorganic dendrimers based on cyclophosphazene containing single metal complexes on the surface. We have recently reported some organometallic derivatives of partially branched cyclophosphazene derivatives [9,10].

* Corresponding author. Tel.: +56-2-678-7396; fax: +56-2-271-3888.

E-mail address: cdiaz@uchile.cl (C. Díaz).

0277-5387/02/$ - see front matter © 2002 Published by Elsevier Science Ltd.
PII: S0277-5387(02)00852-5

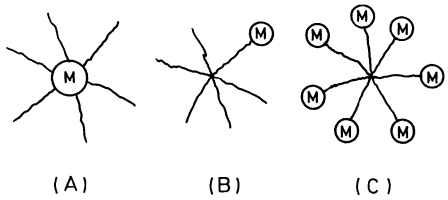


Fig. 1. Schematic representation of three classes of metallodendrimers.

2. Results and discussion

2.1. Synthesis

The synthesized complexes are showed in Table 1. As expected the synthesis of the dendrimers L_1 and L_2 was made by the divergent strategy [1], by reaction of $N_3P_3Cl_6$ with $HO–C_6H_4CH_2CN$ in acetone and in presence of the K_2CO_3 [9,10]. The metallic derivatives **1**–**17** were obtained by reaction of the respective dendrimer ligands with MCl_n in methanol as solvent (see Table 1). NH_4PF_6 as halide abstractor was used for preparation of complexes **1**–**11**. Compounds were characterized by elemental analyses, IR, UV–Vis and EPR spectroscopy as well cyclic voltammetry. The paramagnetism of the complexes precludes a NMR characterization, except diamagnetic complexes **5** and **11** which were characterized by multinuclear NMR spectroscopy. Some complexes are highly hygroscopic as revealed by its elemental analyses as well as their IR spectrum (see Section 4).

Table 1
Formulas of the complexes **1**–**17**

Complex	Metal	*n*
$[N_3P_3(OC_6H_5)_5OC_6H_4CH_2CN{\cdot}MCl_n]PF_6$		
1	Mn	1
2	Fe	2
3	Co	1
4	Ni	1
5	Cu	1
$[N_3P_3(OC_6H_4CH_2CN)_6{\cdot}(MCl_n)_6](PF_6)_6$		
6	Mn	1
7	Fe	2
8	Co	1
9	Ni	1
10	Cu	0
11	Zn	1
$[N_3P_3(OC_6H_5)_5OC_6H_4CH_2CN{\cdot}MCl_n]Cl$		
12	Mn	1
13	Fe	2
14	Co	1
15	Ni	1
16	Cu	1
$[N_3P_3(OC_6H_4CH_2CN){\cdot}(MCl_2)_6](Cl)_6$		
17	Fe	2

2.2. IR and crystal field correlations

The IR spectra of complexes **1**–**16** exhibit the expected bands due to ν(N=P) and ν(CN) modes of the ligand [11] as well as the $\nu(PF_6)$ band [9,10] for complexes **1**–**11**. Characteristic splitting of the ν(N=P) bands due to coordination was observed in all the series of complexes. This splitting pattern appears to be typical of metal coordination [9,10], as shown in Fig. 2, for ligand L_2 in their Fe and Zn complexes. Two intense and broad bands around 3479 and 3159 cm^{-1} corresponding to $\nu(OH_2)_{as}$ and $\nu(OH_2)_s$, respectively, as well as a medium intensity band around 1658 cm^{-1} corresponding to $\delta(OH_2)$ are consistent with the presence of a high degree of hydration for almost all the complexes. The IR spectra are collected in Table 2. Coordination of metal to ligands L_1 and L_2 produce an enhancing of the νCN band which suggest a considerable $\sigma(RCN) \rightarrow \sigma$(metal) contribution to the N···metal bond. Similar tendency has been observed for organometallic derivatives of ligands L_1 and L_2 [9,10]. The strengthening of the CN

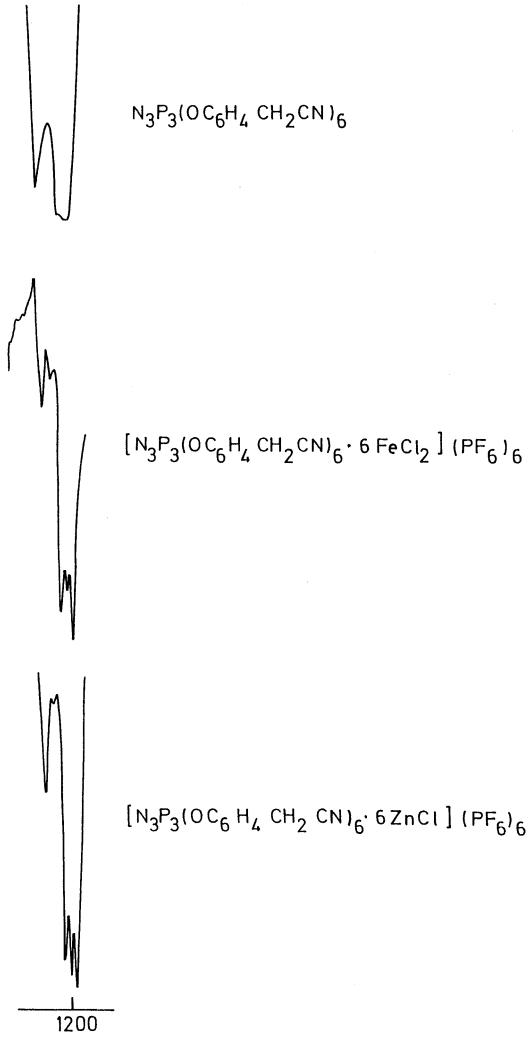


Fig. 2. IR spectra of ligand L_2 and their complexes of Fe and Zn.

Table 2
Selected IR data for complexes **1**–**17**

Complexes	ν(CN)	ν(P=N)	ν(PF6)
1	2362	11798	832
2	2345	1174	841
3	2294	1178	841
4	2305	1179	839
5	2345	1178	835
6	2264	1174	841
7	2345	1160	851
8	2296	1112	850
9	2303	1179	834
10	2381	1166	848
11	2252	1166	847
12	2247	1178	[b]
13	2264	1178	[b]
14	2210	1178	[b]
15	2246	1178	[b]
16	2245	1178	[b]
17	2293	1076	[b]

[a] in KBr pellet, in cm^{-1}.
[b] Cl is the counterion.

bond upon coordination can be due to the shift of electron density from the antibonding HOMO of the cyanide ligand to the orbitals of metal. Thus we have found that the difference ν_{CN} complex $-\nu_{CN}$ ligand follow a dependence typical of crystal field stabilization energies effects (understood as covalency effects across the 3d series) [12,13].

2.3. Cyclic voltammetry studies

There are few reports of electrochemical studies on any cyclophosphazene metal complexes [8b,8c]. Cyclic voltammetry provides some insight into the origin of the very different oxidation state distribution in the complexes. Only the complexes **2**, **5**, **7** and **10** were electrochemically active. Complexes **12**–**17** were not measured owing their oily nature. Data are shown in Table 3. As observed for other [RCN][ML_n] complexes [14a] with M = Mn,Co and Ni, it shows any wave in their voltammogramm in the studied range. The cyclic voltammogram recorded for complexes **2** and **7** are shown in Fig. 3. Analysis of the cyclic voltammetric responses for these complexes with scan rate varying from 50 to 200 mV s^{-1} showed an irreversible one-electron transfer for the Fe(III)/Fe(II) couple which is located around 0.50 and 0.44 V for complexes **2** and **7**, respectively. These data are consistent with the one reduction wave at 0.47 V for the complex [$Cl_3Fe(\mu$-NC)Mn(CO)(dppm)$_2$] [14a]. $N_3P_3(OC_6H_5)_6$ and $N_3P_3Cl(OC_6H_5)_5$ does not exhibit redox process in the range of potentials $-2.0 \rightarrow +2.0$ V [8b]. Similar substituted phosphazenes with CN groups also exhibit redox reduction activity below -1.8 V [8b].

The presence of a single reduction peak (although irreversible) indicates that the six irons are reduced to the same potential which suggests that the six redox iron

Table 3
Electrochemical, UV–Vis and EPR data for complexes **1**–**17**

Complexes	Electrochemical [a] E° (V) ΔEp	UV–Vis [b]	EPR giso [c]
1	[d]	872	2.01
2	0.50(i)	410(2300); 366(4300); 248(9900)	2.05
3	[d]	[f]	[i]
4	[d]	[f]	[i]
5	−0.48(i)	[g]	[h]
6	[d]	[f]	2.00
7	0.47(i)	405(3000); 314(8900); 233(2250)	2.01
8	[d]	592; 522	[i]
9	[d]	584(102); 798(21)	2.07
10	0.28(0.229); −0.025(i); −0.05(i); −0.30(0.66)	586(202)	2.18, 2.03
11	[d]	[f]	[h]
12	[e]	[g]	[e]
13	[e]		[e]
14	[e]	525	[e]
15	[e]	408; 673	[e]
16	[e]	750	2.04
17	[e]		2.02

[a] In methanol solution.
[b] In methanol solution at room temperature; in nm.
[c] In solid state.
[d] Electrochemically inactive, see text.
[e] Not measured.
[f] Not detected. Absorption above 400 nm.
[g] Absorption continue without a maximal.
[h] Diamagnetic sample.
[i] EPR silent sample in the measured conditions.

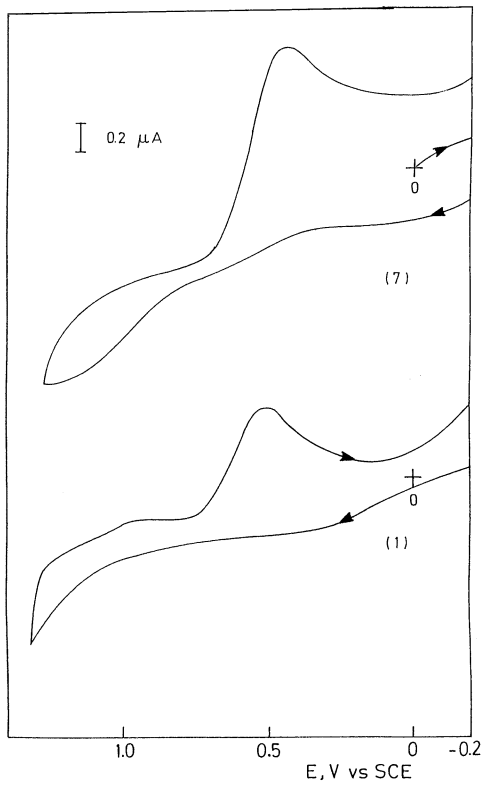


Fig. 3. Cyclic voltammogram of complexes **1** and **7**.

centers are non-interacting. Considering that the solutions have a concentration of 1.04×10^{-3} M for **2** and 7.76×10^{-4} M for **7** and assuming that the complex **2** is a monomeric unit, and the complex **7** can be considered as their polymer ($n = 6$), containing six non-interacting redox unit, then the electron number transferred in the reduction of **7** with respect to the electron transferred in **2** (one electron) can be estimated by the equation [14b]:

$$n_p = \frac{i_p/C_p}{i_m/C_m}\left[\frac{M_p}{M_m}\right]^{0.272} \quad (1)$$

where i_p and i_m are the current intensity for the polymers and the monomer, respectively, M_p and M_m are the molecular weight. Eq. (1) gives a value $n_p \approx 6$ for complex **7**.

On the other hand the cyclic voltammogram of the copper complex **10** exhibits a rather complex pattern of signals. Observed waves (see Fig. 4) can be interpreted tentatively as redox processes occurring on a copper(II) atom similar for the six position of the ligand instead of redox processes affecting each one of the Cu(II) centers. In this latter case a communication between the copper centers should cause the oxidation–reduction to occur at slightly different potentials observing several near waves [14b]. In the first cycle of the scan a single one wave at 0.28 V versus SCE was observed. Comparing with literature data for similar system [8] this wave can be tentatively assigned to the Cu(II)/Cu(III) couple.

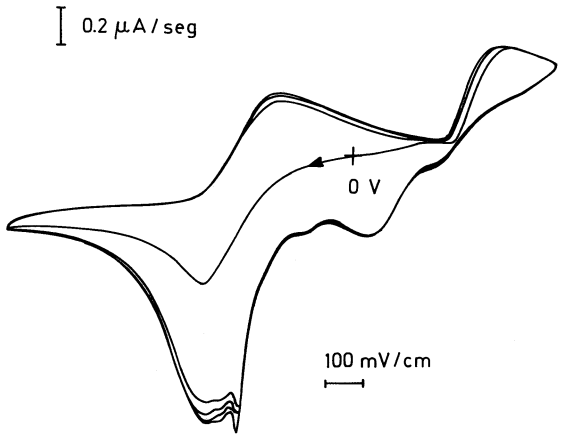


Fig. 4. Cyclic voltammogram of complex **11**.

Second and subsequent scans lead to an enhancing of the oxidation peak and the appearance of another reduction and three additional oxidation peaks. Simultaneously with this a strong characteristic stripping peak appeared which is probably due to the reoxidation of an unknown Cu(II)/Cu(III) electrodeposited planar species. According to literature data [8], the irreversible wave at 0.025, −0.05 and −0.30 V can be assigned tentatively to a Cu(I)/Cu(0), Cu(II)/Cu(0), and Cu(II)/Cu(I) processes, respectively.

2.4. UV–Vis

As found for $FeCl_3$ and other iron-chloride derivatives [13]; the UV–Vis spectra of the complexes **2** and **7** exhibit intense ligand–metal charge transfer bands around 360 and 400 nm, which obscure completely the very weak spin-forbidden d–d bands. The complexes do not exhibit absorption above 500 nm. Data are shown in Table 3. Intensity and position for the charge transfer transition are similar to those found for similar chloro–iron complexes [12,13]. The other complexes exhibit the expected d–d transition for the respective octahedral ions [12,13]. Absorption for the Mn and Co complexes are very weak; those for Cu(II) are broad probably due to a tetragonal distortion [13a].

2.5. EPR spectra

Complexes **1**, **2**, **6**, **7**, **9**, **10**, **13** and **17** exhibits intense signals both in solid as well as in dichloromethane solution. Data are displayed in Table 3. Complexes **3**, **4**, **8**, **14** and **15** are EPR silent in the measured conditions. On the other hand, the diamagnetic complexes **5** and **11** as expected, does not exhibit EPR signal. The paramagnetic complexes **2** and **7** exhibit the typical EPR signal of Fe(III) complexes [13]. The Fe(III) ion is a ground state ^6S (^6A_1g in the complexes) and is not split within an octahedral or even a lower symmetry ligand

field [15]. In addition, there can been no splitting by spin–orbital interaction. Then a single isotropic resonance line at $g = 2$ should be always observed. Hyperfine interaction of the unpaired electron with the ^{14}N nucleus ($I = 1$) of the cyanide group was not observed, although the broad, signal in solid state could contain some unresolved splitting. On the other hands, the g values (Table 3) near 2 for complexes **2** and **7** and this corresponds to high spin Fe(III) complexes, because low spin Fe(III) complexes exhibit higher g values [16–18]. The EPR spectrum of complex **10** exhibits the signal splitting typical of a tetragonal distortion of the copper complex. As observed for other similar complexes [13], compounds **3**, **4** and **8** are EPR silent.

2.6. Reaction of L_1 with $CuCl_2$ in presence of NH_4PF_6

Reaction of L_1 with $CuCl_2$ in MeOH and in presence of NH_4PF_6 affords the Cu(I) complex $[N_3P_3(O\text{-}C_6H_5)_5OC_6H_5CH_2CNCu][PF_6]$ instead of the expected Cu(II) complex. The diamagnetic white complex was characterized by elemental analysis, multinuclear NMR as well as cyclic voltammetric methods. The complex **5** exhibits the expected ^{31}P signal for the N_3P_3 ring namely a singlet at 11.64 ppm. The PF_6 anion was observed as a septuplet at −142 ppm. The ^{13}C NMR spectrum of complex exhibit among other, the typical signal of CN at 121.13 ppm. Full data are displayed in Section 4. Thus, these data compare well with the NMR multinuclear data for the diamagnetic complex $[N_3P_3(OC_6H_5)_5OC_6H_5CH_2CN\cdot ZnCl][PF_6]$ as well as with organometallic derivatives [9,10]. The single oxidation peak observed at −0.48 V can be tentatively assigned to the Cu(I)/Cu(II) processes.

2.7. Preparation of $[N_3P_3(OC_6H_5)_5OC_6H_4CH_2CN\cdot ZnCl][PF_6]$

For comparison purpose we have also prepared the complex $[N_3P_3(OC_6H_5)_5OC_6H_5CH_2CNZnCl][PF_6]$ which was characterized by multinuclear NMR. The ^{31}P NMR spectra exhibits the N_3P_3 signal at 15.4 ppm, a value at slightly high field than the Cu(I) complex due to the most low π-back-bonding Zn→ligand with respect to that of the Cu→ligand. Consistent with this, the ^{13}C NMR signal of the CN group in the Zn complex also appears at highest field with respect to the Cu(I) complex. Other data are observed normally, see Section 4.

3. Conclusions

The dendrimers L_1 and L_2 can coordinate one and six transition atoms, respectively, at the periphery. Formations of metallodendrimers 1–17 open interesting possible applications to solubilize conventionally insoluble inorganic compounds (as MX_n salts) in organic solvents. Although the redox properties of the complexes **7** and **10** are irreversible, they are reduced or oxidized at the same potential which suggest a possible application as molecular battery. Experiments to coordinate other transition metals with possible reversible redox properties are in progress. To our knowledge complexes **2** and **7** are the first iron(III) containing cyclophosphazene dendrimers [19].

4. Experimental

Experimental procedures and IR, UV–Vis, ESR and electrochemical measurements were performed as previously reported [9,10]. The ligands $N_3P_3(O\text{-}C_6H_5)_5OC_6H_4CH_2CN$ and $N_3P_3(OC_6H_4CH_2CN)_6$ were prepared as described previously [9,10]. $MnCl_2\cdot 4H_2O$, $FeCl_3\cdot 6H_2O$, $CoCl_2\cdot 6H_2O$, $NiCl_2\cdot 6H_2O$, $CuCl_2\cdot 2H_2O$ and NH_4PF_6 were used as received. Solvents were dried and purified by standard procedures.

4.1. Preparation of the complexes

4.1.1. $[MCl_n(L_1)]PF_6$

The ligand $N_3P_3(OC_6H_5)_5OC_6H_4CH_2CN$ (**1**) 0.2 g (0.27 mmol) and $MnCl_2$ 0.07 g (0.35 mmol) were stirred in a Schlenk in CH_3OH (20 ml) and in presence of the NH_4PF_6 0.12 g (0.74 mmol), for 24 h at room temperature (r.t.). From the slight pink solution the solvent was removed by rotary evaporation. The pale pink solid was dissolved in CH_2Cl_2 and filtered through celite. The solvent was removed under vacuum and the solid was washed several times with a *n*-hexano–diethylether mixture. The resulting cream solid was vacuum dried. Analysis, Found: C 31.97; H 6.27; N 4.19. Calc. for $C_{38}H_{31}F_6O_6N_4P_4Cl_2$: $Mn\cdot CH_2Cl_2$, C 32.17; H 6.27; N 3.9%.

The ligand $N_3P_3(OC_6H_5)_5OC_6H_4CH_2CN$ (**2**) 0.13 g (0.1775 mmol) and $FeCl_3$ 0.0617 g (0.2282 mmol) were stirred in a Schlenk in CH_3OH (15 ml) and in presence of the NH_4PF_6 0.072 g (0.44 mmol), for 24 h at r.t. From the orange solution, the solvent was removed by rotary evaporation. The orange solid was dissolved in CH_2Cl_2 and filtered though celite. The solvent was removed under vacuum and the oily solid was broken by washing several times with a *n*-hexano–diethylether mixture. The resulting orange solid was vacuum dried. Analysis, Found: C 43.52; H 3.50; N 3.80. Calc. for $C_{38}H_{31}F_6O_6N_4P_4Cl_2Fe\cdot CH_2Cl_2$, C 42.98; H 3.03; N 5.1%.

The ligand $N_3P_3(OC_6H_5)_5OC_6H_4CH_2CN$ (**3**) 0.15 g (0.21 mmol) and $CoCl_2$ 0.06 g (0.25 mmol) were stirred together with NH_4PF_6 0.08 g (0.49 mmol) in CH_3OH (15 ml) at r.t. for 24 h. Similar procedure as **1** affords a

cream solid. Yield: 0.32 g, 62%. Analysis, Found: C 49.50; H 4.15; N 4.14. Calc. for $C_{38}H_{31}F_6O_6N_4P_4Cl_2Co$, C 48.35; H 3.93; N 4.02%.

The ligand $N_3P_3(OC_6H_5)_5OC_6H_4CH_2CN$ (**4**) 0.16 g (0.22 mmol) and $NiCl_2$ 0.07 g (0.29 mmol) were stirred in a Schlenk in CH_3OH (15 ml) and in presence of the NH_4PF_6 0.08 g (0.49 mmol), for 24 h at r.t. From the pale green solution the solvent was removed by rotary evaporation. The pale green solid was dissolved in a CH_2Cl_2–methanol mixture and filtered through celite. The solvent was removed under vacuum and the paste/oil solid was broken by washing several times with dichloromethane and vacuum dried. Undetermined amounts of water preclude good analysis.

The ligand $N_3P_3(OC_6H_5)_5OC_6H_4CH_2CN$ (**5**) 0.12 g (0.16 mmol) and $CuCl_2$ 0.03 g (0.18 mmol) were stirred in a Schlenk in CH_3OH (15 ml) and in presence of the NH_4PF_6 0.06 g (0.37 mmol), for 24 h at r.t. From the pale yellow solution the solvent was removed by rotary evaporation. The solid was dissolved in CH_2Cl_2 and filtered through celite. From the clear solution, the solvent was removed under vacuum and the white solid was washed several times with a *n*-hexano–diethylether mixture and vacuum dried. Yield: 0.32 g, 62%. Analysis, Found: C 51.62; H 9.23; N 4.18. Calc. for $C_{38}H_{31}F_6O_6N_4P_4ClCu\cdot CH_2Cl_2$, C 51.53; H 4.39; N 5.46%.

^{1}H NMR(CD_2Cl_2, δ ppm) 7.3–6.8(m), aromatic, 3.6(s), CH_2. ^{31}P NMR (CD_2Cl_2, δ ppm) 11.64(s) N_3P_3, −142(h) PF_6. ^{13}C NMR (CD_2Cl_2, δ ppm) 129.94, 129.68, 125.48, 116.35. 35(m) aromatic, 121.13(s) CN, 24.21(s) CH_2.

4.1.2. $[(MCl_n)_6(L_2)][PF_6]_6$

The ligand $N_3P_3(OC_6H_4CH_2CN)_6$ (**6**) 0.14 g (0.15 mmol) and $MnCl_2$ 0.18 g (0.91 mmol) were stirred in a Schlenk in CH_3OH (20 ml) and in presence of the NH_4PF_6 0.3 g (1.84 mmol), for 24 h at r.t. Similar procedure as **2** affords a white solid. Yield: 0.32 g, 62%. Analysis, Found: C 24.03; H 4.41; N 4.41. Calc. for $C_{48}H_{36}F_{36}O_6N_9P_9Cl_6Mn_6$, C 24.51; H 1.53; N 5.36%.

The ligand $N_3P_3(OC_6H_4CH_2CN)_6$ (**7**) 0.14 g (0.15 mmol) and $FeCl_3$ 0.25 g (0.91 mmol) were stirred in a Schlenk in CH_3OH (20 ml) and in presence of the NH_4PF_6 0.3 g (1.81 mmol), for 24 h at r.t. From the orange solution, the solvent was removed by rotary evaporation. The orange solid was dissolved in 30 ml methanol–CH_2Cl_2 (1:2) mixture and filtered through celite. The solvent was removed under vacuum and the oily solid was broken by washing several times with a 10 ml *n*-hexano–diethylether (1:2) mixture. The resulting orange solid was vacuum dried. Yield: 0.32 g, 62%. Analysis, Found: C 14.35; H 3.39; N 4.48. Calc. for $C_{48}H_{36}F_{36}O_6N_9P_9Cl_{12}Fe_6$, C 15.24; H 4.65; N 3.33%.

The ligand $N_3P_3(OC_6H_4CH_2CN)_6$ (**8**) 0.15 g (0.16 mmol) and $CoCl_2$ 0.23 g (0.97 mmol) were stirred in a Schlenk in CH_3OH (20 ml) and in presence of the NH_4PF_6 0.31 g (1.90 mmol), for 24 h at r.t. From the pink solution, the solvent was removed by rotary evaporation. Similar procedure as **7** affords a blue solid. Yield: 0.32 g, 62%. Analysis, Found: C 24.05; H 4.24; N 6.33. Calc. for $C_{48}H_{36}F_{36}O_6N_9P_9Cl_6Co_6$, C 24.27; H 1.51; N 5.30%.

The ligand $N_3P_3(OC_6H_4CH_2CN)_6$ (**9**) 0.18 g (0.19 mmol) and $NiCl_2$ 0.28 g (1.18 mmol) were stirred in a Schlenk in CH_3OH (20 ml) and in presence of the NH_4PF_6 0.38 g (2.33 mmol), for 24 h at r.t. Similar procedures as **8** affords a green solid. Yield: 0.32 g, 62%. Analysis, Found: C 25.71; H 4.50; N 3.59. Calc. for $C_{48}H_{36}F_{36}O_6N_9P_9Cl_6Ni_6$, C 25.35; H 1.78; N 5.21%.

The ligand $N_3P_3(OC_6H_4CH_2CN)_6$ (**10**) 0.16 g (0.17 mmol) and $CuCl_2$ 0.25 g (0.91 mmol) were stirred in a Schlenk in CH_3OH (20 ml) and in presence of the NH_4PF_6 0.34 g (2.07 mmol), for 24 h at r.t. The green solution was treated similar to **9** to give a green solid. Yield: 0.32 g, 62%. Analysis, Found: C 15.65; H 3.26; N 4.71. Calc. for $C_{48}H_{36}F_{36}O_6N_9P_9Cl_6Cu_6$, C 15.99; H 3.01; N 4.41%.

The ligand $N_3P_3(OC_6H_4CH_2CN)_6$ (**11**) 0.1 g (0.11 mmol) and $ZnCl_2$ 0.09 g (0.66 mmol) were stirred in a Schlenk in CH_3OH (20 ml) and in presence of the NH_4PF_6 0.21 g (1.29 mmol), for 24 h at r.t. From the white solution the solvent was removed by rotary evaporation. The white solid was dissolved in 30 ml methanol–CH_2Cl_2 (1:2) mixture and filtered through celite. The solvent was removed under vacuum and the oil solid was broken by washing several times with a 10 ml *n*-hexano–diethylether (1:2) mixture. The resulting white solid was vacuum dried. Yield: 0.32 g, 62%. Analysis, Found: C 33.50; H 5.80; N 6.63. Calc. for $C_{48}H_{36}F_{36}O_6N_9P_9Cl_6Zn_6$, C 33.05; H 3.72; N 4.45%.

^{31}P NMR (CD_2Cl_2, δ ppm) 15.41(s), N_3P_3, −138(h) PF_6. ^{13}C NMR (CD_2Cl_2, δ ppm) 130.29, 128.73, 122.26(s) aromatic, 120.7(s) CN, 24.53(s) CH_2.

4.1.3. $[(MCl_{n-1})(L_1)][Cl]$

The ligand $N_3P_3(OC_6H_5)_5OC_6H_4CH_2CN$ (**12**) 0.17 g (0.23 mmol) and $MnCl_2$ 0.07 g (0.35 mmol) were stirred in a Schlenk in CH_3OH (10 ml) for 24 h at r.t. From the brown solution the solvent was removed by rotary evaporation. The brown oil was dissolved in 30 ml CH_2Cl_2 and filtered through celite. The solvent was removed under vacuum and the oil was washed with a 10 ml *n*-hexano–diethylether (1:2) mixture. The resulting green oil was vacuum dried.

The ligand $N_3P_3(OC_6H_5)_5OC_6H_4CH_2CN$ (**13**) 0.17 g (0.23 mmol) and $FeCl_3$ 0.08 g (0.30 mmol) were stirred in a Schlenk in CH_3OH (15 ml) for 24 h at r.t. The orange solution was treated similar to **12** to give an orange oil.

The ligand $N_3P_3(OC_6H_5)_5OC_6H_4CH_2CN$ (**14**) 0.17 g (0.23 mmol) and $CoCl_2$ 0.08 g (0.35 mmol) were stirred

in a Schlenk in CH_3OH (10 ml) for 24 h at r.t. From the pink solution, the solvent was removed by rotary evaporation. The blue oil was dissolved in 30 ml CH_2Cl_2 and filtered through celite. The solvent was removed under vacuum and the oil solid was washed with a 10 ml *n*-hexano–diethylether (1:1) mixture. The resulting blue oil was vacuum dried. Analysis, Found: C 51.82; H 6.3; N 4.7. Calc. for $C_{38}H_{31}O_6N_4P_3Cl_2Co$, C 52.0; H 4.2; N 3.7%.

The ligand $N_3P_3(OC_6H_5)_5OC_6H_4CH_2CN$ (**15**) 0.10 g (0.14 mmol) and $NiCl_2$ 0.04 g (0.17 mmol) were stirred in a Schlenk in CH_3OH (10 ml) for 24 h at r.t. The green solution was treated similar to **14** to give a green oily.

The ligand $N_3P_3(OC_6H_5)_5OC_6H_4CH_2CN$ (**16**) 0.14 g (0.82 mmol) and $CuCl_2$ 0.05 g (0.29 mmol) were stirred in a Schlenk in CH_3OH (10 ml), for 24 h at r.t. From the brown solution and using a similar procedure as **15**, a brown oil was obtained. Analysis, Found: C 46.50; H 3.89; N 5.43. Calc. for $C_{38}H_{31}O_6N_4P_3Cl_2Cu$, C 46.59; H 3.39; N 3.83%.

4.1.4. $[(MCl_{n-1})_6(L_2)][Cl]_6$

The ligand $N_3P_3(OC_6H_4CH_2CN)_6$ (**17**) 0.13 g (0.14 mmol) and $FeCl_3$ 0.23 g (0.85 mmol) were stirred in a Schlenk in CH_3OH (15 ml) for 24 h at r.t. From the orange solution and using a similar procedure as **16**, an orange oil solid was obtained. Analysis, Found: C 29.66; H 4.6; N 1.87. Calc. for $C_{48}H_{36}O_6N_4P_3Cl_{18}Fe_6$, C 30.15; H 6.5; N 1.88%.

Acknowledgements

Financial support from FONDECYT, project 1000672 is gratefully acknowledged.

References

[1] (a) G.R. Newkome, E. He, C.H. Moorefield, Chem. Rev. 99 (1999) 1689;
(b) F. Zeng, S.C. Zimmerman, Chem. Rev. 97 (1999) 1681.
[2] M.T. Reetz, G. Lohmer, R. Schwickardi, Angew. Chem. 109 (1997) 1559.
[3] F.G.A. Jansen, E.M.M. de Brabander-van den Berg, E.W. Meiser, Recl. Trav. Chim; Pays-Bas 114 (1995) 225.
[4] E. Buhleier, W. Wehnen, F. Vögtle, Synthesis (1978) 155.
[5] I.P. Majoral, A.M. Caminade, Chem. Rev. 99 (1999) 845.
[6] V. Balzani, S. Campagna, G. Denti, A. Juris, S. Serroni, M. Venturi, Acc. Chem. Res. 31 (1998) 26.
[7] G.J. Mccubbin, F.J. Stoddart, T. Welton, A.J.P. White, D.J. Williams, Inorg. Chem. 37 (1998) 3753.
[8] (a) R. Schneider, C. Köllner, I. Welbey, A. Togni, J. Chem. Soc., Chem. Commun. (1999) 2415;
(b) M. Gleria, R. Bertani, G. Facchim, F. Noe, R.A. Michelin, M. Mazzon, A.J.L. Pombeiro, M.F.C.G. Da Silva, I.L.F. Machado, J. Inorg. Organomet. Polym. 6 (1996) 145;
(c) K.R.J. Thomas, V. Parthasarathy Pal, S.R. Scott, R. Haldford, A.W. Cordes, Inorg. Chem. 32 (1993) 606.
[9] (a) C. Díaz, I. Izquierdo, Polyhedron 18 (1999) 1479;
(b) C. Díaz, Bol. Soc. Quim 44 (1999) 315.
[10] (a) C. Díaz, I. Izquierdo, F. Mendizabal, N. Yutronic, Inorg. Chim. Acta 294 (1999) 20;
(b) C. Díaz, unpublished results
[11] (a) For IR data and discussion of IR spectra of $N_3P_3X_6$ and $N_3P_3(OR)_6$ compound see: S.S. Khishnamurthy, C. Sau, Adv. Inorg. Chem. Radiochem. 21 (1978) 41;
(b) H.R. Allcock, L.J. Wagner, M.L. Levin, J. Am. Chem. Soc. 105 (1983) 1321;
(c) G.A. Carriedo, F.J.G. Alonso, P.A. Gonzalez, J.R. Menendez, J. Raman Spectroscopy 29 (1998) 327.
[12] (a) F.A. Cotton, G. Wilkinson, Advanced Inorganic Chemistry, Wiley, New York, 1980, p. 666;
(b) T.C. Bailar, H.J. Emeleus, R. Nyholm, A.F. Trotman-Dickenson (Eds.), Comprehensive Inorganic Chemistry (Chapter 40), Pergamon Press, Oxford, 1979, p. 1049.
[13] (a) B.N. Figgis, Introduction to Ligand Fields (chapter 11), Interscience Publishers, New York, 1996;
(b) H.A.O. Hill, P. Day, Physical Methods in Advanced Inorganic Chemistry (chapter 7), Interscience Publishers, Wiley, New York, 1968, p. 346.
[14] (a) N.G. Connelly, O.M. Hicks, G.R. Lewis, A. Guy Orpen, A.J. Wood, J. Chem. Soc., Chem. Commun. (1998) 517;
(b) D. Astruc, Electron Transfer and Radical Processes in Transition Metal Chemistry (Chapter 2), Wiley, New York, 1995, p. 116.
[15] E.A. Korner Von Gustorf, F.W. Grevals, I. Fischer (Eds.), The Organic Chemistry of Iron, vol. 1, Academic Press, New York, 1978, p. 257.
[16] A.S. Marlin, M.M. Olmstead, P.K. Mascharak, Inorg. Chem. 38 (1999) 3258.
[17] M.F. Reynald, D. Shelver, R.L. Kerby, R.B. Park, G.P. Roberts, J.N. Burstyn, J. Am. Chem. Soc. 120 (1998) 908.
[18] C. Díaz, Bol. Soc. Chil. Quim. 44 (1999) 315.
[19] (a) For reviews on the metal complexes of the cyclophophazene ligands see: V. Chandrasekhar, K.R. Justin Thomas, Applied Organometallic Chemistry 7 (1993) 1;
(b) H.R. Allcock, I.L. Desorcie, D.A. Riding, Polyhedron 6 (1987) 119, See also refs. [9] and [10].

PERGAMON

Polyhedron 21 (2002) 917–923

POLYHEDRON

www.elsevier.com/locate/poly

Synthesis of 14-π nickel(II) complexes with disubstituted benzoN_4 macrocycles and electrochemical studies of 14-π nickel(II) complexes with monosubstituted benzoN_4 macrocycles

H.G. Na [a], D.C. Lee [b], J.W. Lim [b], J.H. Choi [c], J.C. Byun [d], Y.C. Park [b,*]

[a] *Department of Chemistry, Daejin University, Pocheon 487-800, South Korea*
[b] *Department of Chemistry, Kyungpook National University, Taegu 702-701, South Korea*
[c] *Department of Chemistry, Andong National University, Andong 760-749, South Korea*
[d] *Department of Chemistry, Cheju National University, Cheju 690-756, South Korea*

Received 20 June 2001; accepted 25 January 2002

Abstract

The template reaction of a 1:1 mixture of 4,5-disubstituted(2CH_3 or 2Cl)-1,2-phenylenediamine and alkylenediamine [NH_2-$(CH_2)_n$-NH_2; $n = 2$ or 3] with 2,4-pentanedione in the presence of a nickel(II) salt gave a series of asymmetric 14-π nickel(II) complexes with disubstituted tetraazaannulene, [Ni(Me_4-X_2bzotetraaza[Y]ene)] (X = CH_3 and Cl, $Y = 14$ and 15), which were characterized by mass, infrared, ^{1}H and ^{13}C NMR spectra. The electronic effects of the disubstituent groups on the phenyl ring significantly affected the spectral properties of the complexes. The electrochemical behaviors of the nickel(II) complexes with monosubstituted benzoN_4 macrocycles, [Ni(Me_4-Xbzotetraaza[Y]ene)] (X = H, NO_3, CH_3 and Cl, $Y = 14$ and 15) exhibited cyclic voltammograms characterized by, two irreversible, one electron, waves due to oxidation of the macrocycle (Mc); $Mc \rightarrow Mc^{\bullet +}$ in the ranges of +0.06 – +0.28 V for 14-X and +0.01 – +0.29 V for 15-X, and $Mc^{\bullet +} \rightarrow Mc^{2+}$ in the ranges of +0.58 to +0.81 V for 14-X and +0.36 to +0.79 V for 15-X versus Ag/Ag^+ (0.01 M $AgNO_3$ in 0.1 M tetraethylammonium perchlorate (TEAP) acetonitrile solution). In the reduction area only one reversible wave Ni^{2+}/Ni^+ was detected at $E_{1/2} = -1.65$ to -2.65 V in DMSO. The relationships between the oxidation potentials (E_{ap}) and σ_p were linear with a slopes of 0.23 V for 14-X and 0.18 or 0.23 V for 15-X (correlation coefficients of 0.99). The catalytic reduction of dioxygen by the electropolymerized glassy carbon electrodes (GCE) occurred at about 400 mV more positive than by the bared one. The catalytic reduction using 14-X occurred at potentials somewhat more positive than using 15-X. © 2002 Published by Elsevier Science Ltd.

Keywords: Synthesis and electrochemistry; Asymmetric 14-π nickel(II) tetraazaannulene; Hammett plot; Electrocatalysis

1. Introduction

The transition metal complexes of tetraaza[14]annulene and tetraaza[15]annulene have attracted much attention for their similarity with porphyrins and corrins in biological system or their utilities as model compounds [1–4]. The potential of these macrocyclic complexes as catalysts has also fostered some interest and is efficient [5–7]. The complexes are also efficient as electrode modifiers for anodic oxidation or cathodic reduction [8,9]. Electropolymerization is an effective way for modification of the electrode surface by deposits of redox entities such as metallic complexes. Such a modification of an electrode by symmetric nickel(II) tetraazaannulene was first investigated by Bereman and coworkers [10]. It has been shown that the electropolymerization of the nickel(II) tetraazaannulene is possible even when the ligand has a large variety of substituents on the carbon atoms of the tetraaza macrocycle as well as the two benzene rings [11]. However, most of the tetraazaannulene complexes used to study electrocatalytic reactions have a symmetric structure, such as nickel(II)-5,7,12,14-tetramethyldibenzo[b,i][1,4,8,11]tetraaza[14] annulene which could be deposited on the electrode surface by oxidative electropolymerization. The synthesis of asymmetric complexes and their

* Corresponding author. Tel.: +82-53-950-5333; fax: +82-53-950-6330.
E-mail address: ychpark@knu.ac.kr (Y.C. Park).

0277-5387/02/$ - see front matter © 2002 Published by Elsevier Science Ltd.
PII: S0277-5387(02)00908-7

electrochemical studies are rarely carried out. We have synthesized several asymmetric nickel(II) complexes of tetraaza[14]annulene and tetraaza[15]annulene in previous papers [12,13]. It is expected that the electrochemical characteristics of such asymmetric complexes will be similar to those of the symmetric ones.

In this paper, we attempted to monitor the electrochemical behaviors of the asymmetric nickel(II) complexes with monosubstituted monobenzotetraazaannulene and considered the electrocatalytic properties of the glassy carbon electrodes (GCEs) electropolymerized by the complexes. The GCEs modified by such a process were applied for the electrocatalytic reduction of dioxygen. We also synthesized and characterized several asymmetric nickel(II) complexes with disubstituted monobenzotetraaza[14]annulene (or monobenzotetraaza[15]annulene) for future use in order to further understand the properties and the catalytic reactions of asymmetric tetraazaannulene macrocycles.

2. Experiments

2.1. Materials and instruments

All reagents used were of analytical grade. Dimethylsulfoxide and acetonitrile as solvents were distilled according to the published method [14]. Tetraethylammonium perchlorate (TEAP) as supporting electrolyte was prepared and purified by the method described by Kolthoff and Coetzee [15].

Elemental analyses (C, H, N) of the complexes synthesized were carried out on a Carlo–Ebra, EA 1108 analyzer. Electronic spectra were recorded in chloroform solution on a JASCO V 550 UV–Vis. spectrophotometer at r.t. ^{1}H (300 MHz) and ^{13}C (75.5 MHz) NMR spectra were recorded on a Bruker instrument in $CDCl_3$ at r.t. and the chemical shifts were given in ppm relative to tetramethylsilane as an internal reference standard. EI mass spectra were measured with a JEOL MS-DX 300 gas chromatograph mass spectrometer at 70 eV using a direct inlet system. Cyclic voltammetry was performed using a Bioanalytical System (BAS) CV-50W electrochemical analyzer and C2 cell stand at 25 ± 0.2 °C. The three electrode system for the electrochemical measurements was composed of the GCE as a working electrode, Ag/Ag^{+} (0.01 M $AgNO_3$ in 0.1 M TEAP acetonitrile solution) as a reference electrode, and platinum wire as an auxiliary electrode.

2.2. Synthesis of nickel(II) complexes with disubstituted tetraazaannulene macrocycles

2,4,9,11-Tetramethyl-15,16-dimethylbenzo-1,5,8,12-tetraaza[14]cyclotetradecinato(2-)-nickel(II) (14-2Me). Under nitrogen atmosphere, 2,4-pentanedione (0.06 mol) was added to a methanol (80 cm^3) solution of nickel(II) acetate tetrahydrate (0.03 mol). 4,5-Dimethyl-1,2-phenylenediamine (0.03 mol) and ethylenediamine (0.03 mol) were added to the hot mixture. The solution was refluxed for about 3 h until precipitation of the product was complete. The hot solution was filtered, washed with methanol, and then air-dried. The product was recrystallized from dichloromethane-methanol (1:1). Yield: 65%. *Anal*. Calc. for $NiC_{20}H_{26}N_4$: C, 63.03; H, 6.68; N, 14.70. Found: C, 62.30; H, 7.23; N, 14.72%. IR (KBr disc, cm^{-1}): ν(C=C), 1,534; ν(C=N), 1473 and 1410; ν(aromatic), 737. UV–Vis: λ_{max} (nm) and ε_{max} (M^{-1} cm^{-1}) in $CHCl_3$ 377 and 551, and 24 030 and 2630. ^{1}H NMR ($CDCl_3$, 300 MHz): δ 2.17 and 2.38 (s, MeH), 2.05 (s, ArMeH), 3.34 (s, ethyleneH), 4.98 (s, methineH), 6.95 (s, ArH). ^{13}C NMR ($CDCl_3$, 75.5 MHz): δ 20.28 23.18, 19.75, 52.60, 103.28 (methine), 121, 127.37, 120.70, 154.61, 157.49. EI MS: m/z 380 $[M]^{+}$.

2,4,9,11-Tetramethyl-15,16-dichlorobenzo-1,5,8,12-tetraaza[14]cyclotetradecinato(2-)-nickel(II) (14-2Cl) was prepared from 2,4-pentanedione (0.06 mol), nickel(II) acetate tetrahydrate (0.03 mol), 4,5-dichloro-1,2-phenylenediamine (0.03 mol) and ethylenediamine (0.03 mol) according to the procedure as described above. The product of fine dark violet was obtained by recrystallizing in chloroform. Yield: 54%. *Anal*. Calc. for $NiC_{18}H_{20}N_4Cl_2$: C, 51.23; H, 4.78; N, 13.88. Found: C, 51.26; H, 4.92; N, 14.11%. IR (KBr disc, cm^{-1}): ν(C=C), 1533; ν(C=N), 1483 and 1411; ν(aromatic), 733. UV–Vis: λ_{max} (nm) and ε_{max} (M^{-1} cm^{-1}) in $CHCl_3$ 381 and 542, and 22 440 and 2720. ^{1}H NMR ($CDCl_3$, 300 MHz): δ 2.07 and 2.35 (s, MeH), 3.37 (s, ethyleneH), 5.07 (s, methineH), 7.18 (s, ArH). ^{13}C NMR ($CDCl_3$, 75.5 MHz): δ 20.51 22.90, 52.75, 104.84 (methine), 119.93, 121.27, 144.65, 154.24, 158.77. EI MS: m/z 420 $[M]^{+}$.

2,4,9,11-Tetramethyl-16,17-dimethylbenzo-1,5,8,12-tetraaza[15]cyclotetradecinato(2-) -nickel(II) (15-2Me) was prepared from 2,4-pentanedione (0.06 mol), nickel(II) acetate tetrahydrate (0.03 mol), 4,5-dimethyl-1,2-phenylenediamine (0.03 mol) and propylenediamine (0.03 mol), following the above-mentioned procedures. Yield: 33%. *Anal*. Calc. for $NiC_{21}H_{28}N_4$: C, 63.83; H, 7.14; N, 14.18. Found: C, 64.02; H, 7.13; N, 14.06%. IR (KBr disc, cm^{-1}): ν(C=C), 1,525; ν(C=N), 1470 and 1410; ν(aromatic), 748. UV–Vis: λ_{max} (nm) and ε_{max} (M^{-1} cm^{-1}) in $CHCl_3$ 397 and 583, and 13 380 and 1810. ^{1}H NMR ($CDCl_3$, 300 MHz): δ 2.09 and 2.13 (s, MeH), 1.90 (s, ArMeH), 2.30 (m) and 2.79 (t) (propyleneH), 4.86 (s, methineH), 6.63 (s, ArH). ^{13}C NMR ($CDCl_3$, 75.5 MHz): δ 21.01, 21.22, 19.60, 31.90, 50.86, 103.48, 127.83 (methineC), 121.66, 160.46, 146.10, 154.61, 154.83. EI MS: m/z 394 $[M]^{+}$, 379 $[M\text{-}CH_3]^{+}$.

2,4,9,11-Tetramethyl-16,17-dichlorobenzo-1,5,8,12-tetraaza[15]cyclotetradecinato(2-)-nickel(II) (15-2Cl) was synthesized from 2,4-pentanedione (0.06 mol), nickel(II) acetate tetrahydrate (0.03 mol), 4,5-dichloro-1,2-phenylenediamine (0.03 mol) and propylenediamine (0.03 mol) by following the above procedure. Yield: 51%. *Anal*. Calc. for $NiC_{19}H_{22}N_4Cl_2$: C, 52.34; H, 5.09; N, 12.85. Found: C, 52.06; H, 5.15; N, 13.05%. IR (KBr disc, cm^{-1}): ν(C=C), 1,527; ν(C=N), 1,474 and 1,420; ν(aromatic), 748. UV–Vis: λ_{max} (nm) and ε_{max} (M^{-1} cm^{-1}) in $CHCl_3$ 388 and 565, and 19 310 and 1480. ^1H NMR ($CDCl_3$, 300 MHz): δ 1.92 and 2.07 (s, MeH), 2.34 (m) and 2.82 (s) (propyleneH), 4.91 (s, methineH), 6.84 (s, ArH). ^{13}C NMR ($CDCl_3$, 75.5 MHz): δ 20.78, 21.45, 31.66, 50.96, 104.85 (methineC), 120.73, 121.84, 145.68, 154.40, 161.38. EI MS: *m/z* 434 $[M]^+$, 419 $[M\text{-}CH_3]^+$.

The asymmetric nickel(II) complexes with monosubstituted tetraazaannulene macrocycles, 2,4,9,11-tetramethyl-Xbenzo-1,5,8,12-tetraaza[14]cyclotetradecinato(2-)- nickel(II) and 2,4,9,11-tetramethyl-Xbenzo-1,5,8,12-tetraaza[15]cyclotetradecinato(2-)nickel(II), wherein X = H (14-H and 15-H), X = Cl (14-Cl and 15-Cl), X = CH_3 (14-Me and 15-Me) and X = NO_2 (14-NO_2 and 15-NO_2), were prepared as reported previously [12,13].

2.3. Electropolymerization of the complexes on GCE

Before GCE (GC-2OS Tokai Carbon, $\phi = 5$ mm) modification, it was polished with alumina slurry (1.0, 0.3 and 0.05 μm) on carborundum papers, washed with deionized water, and then dried. After polishing, any residual material was removed by sonication (Branson co. Model 1210) for 1 min, and then it was dried. The electrochemical behavior of the modified electrode was greatly influenced by the solvent used. The reproducibility and stability of a given GCE surface was examined using a $K_2Fe(CN)_6$ solution which was accomplished by scanning the respective CV curve, briefly stirring the solution and rescanning the CV curve. Preliminary voltammetric evaluation indicated acceptable electrode behaviors. The repeated scanning (in a dioxygen saturated solution) between +1.0 and −2.0 V versus Ag/Ag^+ (0.01 M $AgNO_3$ in 0.1 or 0.05 M TEAP acetonitrile solution) caused a relative standard deviation of only 3% of the peak currents of ferri/ferro at the scan rates 100 mV s^{-1} for ten cycles. The oxidation potential had a deviation of about 0.005 V for four to ten scans, which were within the precision of the experimental measurement. Electropolymerization of the complexes as electrode modifiers was mostly carried out by cycling the potential between +0.5 and −2.5 V at 200 mV s^{-1} in freshly distilled acetonitrile solutions containing 1×10^{-4} M complexes and 5×10^{-2} M TEAP under a nitrogen atmosphere. After ten cycles, the electrode was removed from the solution, rinsed with water and dried in air.

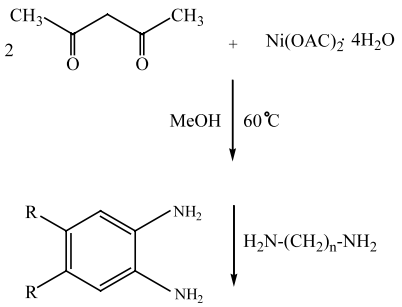
3. Results and discussion

The complexes 14-2Cl, 14-2Me, 15-2Cl and 15-2Me were prepared by the synthetic procedure as illustrated in Scheme 1. Template condensation of a (1:1) mixture of 4,5-disubstituted(2Cl or 2CH3)-1,2-diaminobenzene and ethylenediamine (or propylenediamine) with 2,4-pentanedione in the presence of nickel(II) ion gave the disubstituted complexes of the 14-2X and 15-2X series with a range of yields from 33% to 65%. Elemental analyses of these new complexes collected in the experimental part were consistent with their formulations.

3.1. Spectral properties of complexes with disubstituents

The EI mass spectra for 14-2Cl, 14-2Me and 15-2Me exhibited the presence of a molecular ion M^+ at *m/z* 420 (^{35}Cl, ^{58}Ni), 380 (^{58}Ni) and 394 (^{58}Ni), respectively, which are the base peaks in each mass spectrum. The 15-2Cl showed a molecular ion M^+ at *m/z* 434 (^{35}Cl, ^{58}Ni) that is not a base peak. The IR spectra of the new complexes exhibited bands at around 1530 cm^{-1} due to the vibrations of C=C and 1475 and 1410 cm^{-1} due to C=N modes but no N–H absorption at around 3200 cm^{-1}. The aromatic band occurred at around 750 cm^{-1}. These observations reflect the formation of C=N and C=C bonds, and the disappearance of N–H groups, and the formation of a conjugated six membered chelate ring in the reaction [16].

The electronic absorption spectra of these asymmetric complexes were examined over the 370–700 nm range. The bands in the near UV regions (375–390 nm) with molar absorptivities (ε_{max}) ranging from 10 000 to 25 000 M^{-1} cm^{-1} for each of the new complexes could be attributed to the $\pi \rightarrow \pi^*$ transitions of the macrocycles and are almost independent of the macrocycle rings (14- or 15-membered). The bands in the visible region had



Scheme 1.

energies between 500 and 550 nm ($\varepsilon_{max} = 2660–3220$ M^{-1} cm^{-1}) which are attributed to charge transfer (CT) transitions from the highest occupied ligand molecular orbital to the lowest empty d-orbital of the nickel. Their values of ε_{max} are much larger than those commonly assigned to ligand field transitions. This behaviour is comparable to that observed for D_{4h} nickel(II) complexes with four nitrogen donors [10,12,13]. The spectra of the 15-2X series showed shifts of λ_{max} to longer wavelengths compared with 14-2X ones. This observation is attributed to the different ring size between the 14-membered and 15-membered macrocycles, which is in agreement with other tetraazaannulene complexes [12,13]. Another feature of the electronic spectra is the variation of the band maximum according to the substituents of the phenyl ring on the macrocycle. The spectra of 14-2Me and 15-2Me with an electron-donating group showed 5 and 13 nm shifts of λ_{max} to longer wavelengths compared with 14-2H and 15-2H, respectively, while those of 14-2Cl and 15-2Cl with an electron-withdrawing group did relatively hypsochromic shifts. Such an electronic effect of the substituent group is supported by similar observations with nickel(II) tetraazaN_4 macrocycles [12,13,17,18].

The 14-2X and 15-2X complexes gave well-resolved ^1H and ^{13}C NMR spectra. The assignments of the chemical shifts were made mostly characterized by comparisons of the data with those of other nickel(II) macrocyclic complexes reported earlier [5,12,13]. The carbon sites of the diaminate framework of nickel(II)-tetraazaannulene complexes have been found to be a reactive nucleophilic centre named a methine site [13,19,20]. Thus, the resonance energies of the methine sites for the new complexes and the effects of macrocyclic rings are worth special mentioning. The methine proton peaks for 14-2Me and 15-2Me with two methyl substituents and those for 14-2Cl and 15-2Cl with two chloro substituents on the phenyl rings were equivalent and showed one singlet. The proton peaks of 14-2Me and 15-2Me, and 14-2Cl and 15-2Cl were shifted by about 0.05 and 0.02 ppm upfield, and 0.04 and 0.03 ppm downfield relative to 14-2H and 15-2H, respectively. The ^{13}C NMR peaks of 14-2Me and 15-2Me, and 14-2Cl and 15-2Cl were shifted by about 0.58 and 0.49 ppm upfield, and 0.98 and 0.88 ppm downfield relative to 14-2H and 15-2H, respectively. Such results are attributed to the shielding and deshielding effects of the substituents of the phenyl group on the macrocycle rings. The ^{13}C data was mostly in agreement with the corresponding ^1H NMR behaviour.

3.2. Electrochemical studies of complexes with a monosubstituent

Redox potentials of the monosubstituted nickel(II) complexes measured using cyclic voltammetry are given in Table 1. The cyclic voltammograms of 14-NO_2 and free base ligand, for example, are illustrated in Fig. 1 and exhibited cyclic voltammetric behaviors characterized by, two appreciably irreversible one electron waves corresponding to oxidation of the macrocycle (Mc), $Mc \rightarrow Mc^{\bullet +}$ and $Mc^{\bullet +} \rightarrow Mc^{2+}$, and only one regular and reversible wave ($Ni^{2+} \rightarrow Ni^{+}$). The number of electrons involved in each redox reaction could be determined by electrolyzing the complex relating to the more positive potential by 0.2 V more than that of each wave according to the method reported.[26] As listed in Table 1, the 1st and 2nd ligand based oxidations were detected at in the ranges of $+0.01–+0.30$ V and $+0.36–+0.81$ V versus Ag/Ag^+ (0.01 M $AgNO_3$ in 0.1 M TEAP acetonitrile solution), and the reduction of metal at $E_{1/2} = -1.65$ to -2.65 V in DMSO solution. The waves were of similar pattern to those exhibited by the symmetric nickel(II) tetraazaannulene, [10] indicating that diffusion coefficients of nickel(II) tetraazaannulene macrocycles do not appreciably differ with respect to symmetric or asymmetric complexes. The complexes, 14-X and 15-X contain macrocycles with various electron donor and withdrawing groups (X) that have different σ values [21]. As pointed out elegantly by Kadish et al. in ref. [21], the exact choice of Hammett parameters to use, i.e. σ_p, σ^+, σ^-, etc., is not clear. We have chosen σ_p ($\sigma_p = -0.17$ for CH_3, 0.00 for H, 0.23 for Cl and 0.78 for NO_3) because the correlation between redox potentials and σ_p are linear and it offers comparisons to the widest range of literature data. Totally the substituents effect on the reduction potential of the complexes was not large, but clearly appeared. The correlation between the substituent effect and the redox potentials of the complexes was examined by means of a Hammett plot. As shown in Fig. 2, the relationships between the 1st oxidation potentials (E_{ap1}) and σ_p were linear with a slopes of 0.23 V for both 14-X and 15-X series (correlation coefficients of 0.99), reflecting the similarity of structures of the 14-X and 15-X series. Interestingly, these slopes are similar to those of the oxidation potentials for metalloporphyrins with substituents located on the pyrrole residues of the porphyrin ligand [22,23].

The modification of a GCE could be carried out by scanning repeatedly in the range of a given potential and the modified electrodes were relatively stable even in air or solution. For example, the asymmetric complexes 14-H were electropolymerized by cycling from $+1.0$ to -2.0 V versus Ag/Ag^+ (0.01 M $AgNO_3$ in a 0.1 M TEAP acetonitrile solution) giving thin films on the GCE (Fig. 3). The nickel(II) complexes of tetraazaannulenes with benzoyl groups at the methine sites of the macrocycle are not electropolymerized on the GCE by cyclic voltammetry [24] supporting directly that the electropolymerization of nickel(II)-tetraazaannulene [25,26] occurs at the methine site on macrocycle. According to

Table 1
Redox potentials of 14-CH_3, 14-H, 14-Cl, 14-NO_2, 15-CH_3, 15-H, 15-Cl and 15-NO_2 vs. Ag/Ag^+ (0.01 M $AgNO_3$ in a 0.1 M TEAP [a] and in a 0.05 M TEAP [b] acetonitrile solution) at 25 °C

M	Composition	$E_{p(1)}$ (mV)	$E_{p(2)}$ (mV)	$E_{1/2}$ (V)	σ_p [c]
Ni	14-CH_3	56	582	−2.65 [d]	−0.17
	14-H	96	620	−2.65 [d]	0.00
	14-Cl	152	683	−2.65 [d]	0.23
	14-NO_2	282	805	−1.55	0.78
				−1.65 [d]	
H_2	14-H	238	614	-	0.00
Ni	15-CH_3	5 [d]	360 [d]	−2.45 [d]	−0.17
	15-H	107	645	−2.45 [d]	0.00
	15-Cl	174	705	-	0.23
	15-NO_2	287	787	−1.56	0.78
				−1.65 [d]	
H_2	15-H	194	606	-	0.00

[a] All 14-X data were measured from 1×10^{-4} M complexes in 0.1 M TEAP–acetonitrile solutions vs. Ag/Ag^+ (0.01 M $AgNO_3$ in acetonitrile) at 25 °C.
[b] All 15-X data were measured from 1×10^{-4} M complexes in 0.05 M TEAP–acetonitrile solutions vs. Ag/Ag^+ (0.01 M $AgNO_3$ in acetonitrile) at 25 °C and sweep rates 200 mV s^{-1}.
[c] The σ_p values are from, Swain, C.G., Lupton, E.C., J. Am. Chem. Soc., 1968, 90, 4328.
[d] Data from 1×10^{-3} M complexes in 0.1 M TEAP–DMSO solutions vs. Ag/Ag^+ (0.01 M) at 25 °C and sweep rates 200 mV s^{-1}.

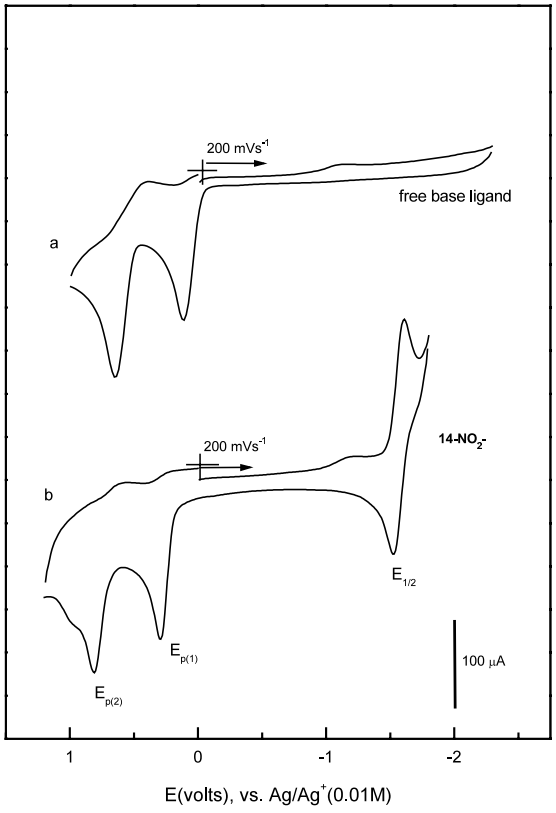


Fig. 1. Cyclic voltammograms of the free base ligand (a) and its complex, 14-NO_2 (b) in a 0.1 M TEAP acetonitrile solution at 25 °C and 200 mV s^{-1}.

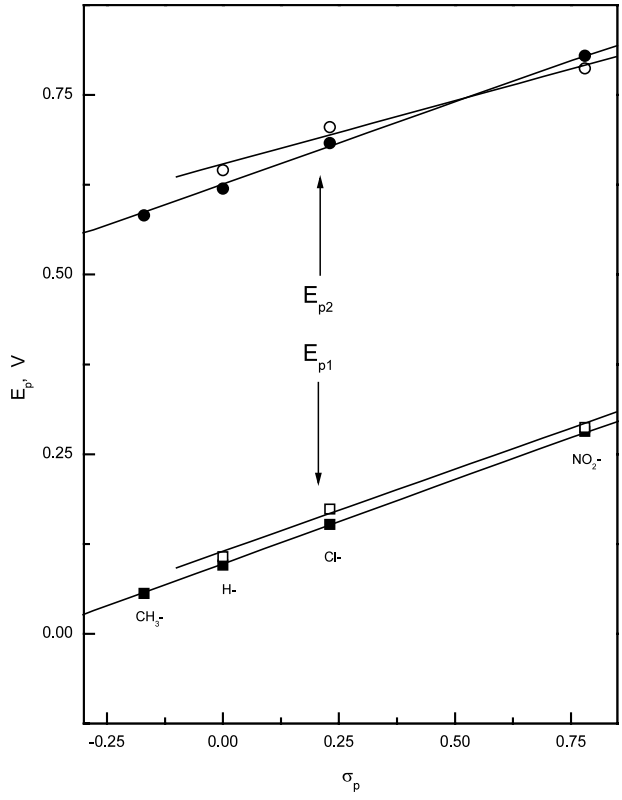


Fig. 2. Hammett plots of the first and second oxidation potentials (E_{p1} and E_{p2}) of the 14-X (■ and ●) and 15-X (□ and ○) series against the substituent constants (σ_p).

the pattern of electropolymerization and the electron number observed in each oxidation step and the results reported, we concluded that the polymer is formed at the electrode surface via a radical cation and dication. That is the mechanism for the electropolymerization of the asymmetric complex is thought to be similar to that of the symmetric one. The cyclic voltammograms of the modified electrode in neat 0.1 M TEAP acetonitrile exhibited both the $Mc/Mc^{\bullet +}$ and $Mc^{\bullet +}/Mc^{2+}$ irrever-

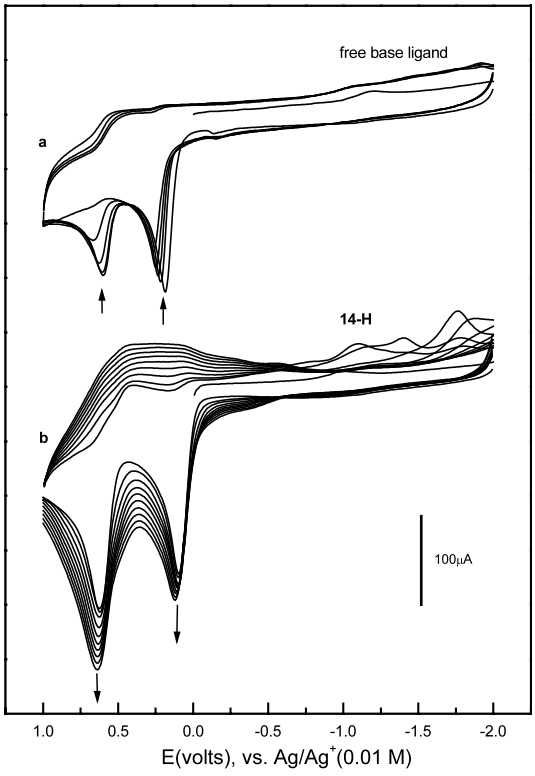


Fig. 3. Cyclic voltammetric behaviours of the free base ligand (a) and its complex, 14-H (b) cycling from +1.0 to −2.0 V vs. Ag/Ag^+ (0.01 M $AgNO_3$ in a 0.1 M TEAP acetontrile) at 25 °C and 200 mV s^{-1}.

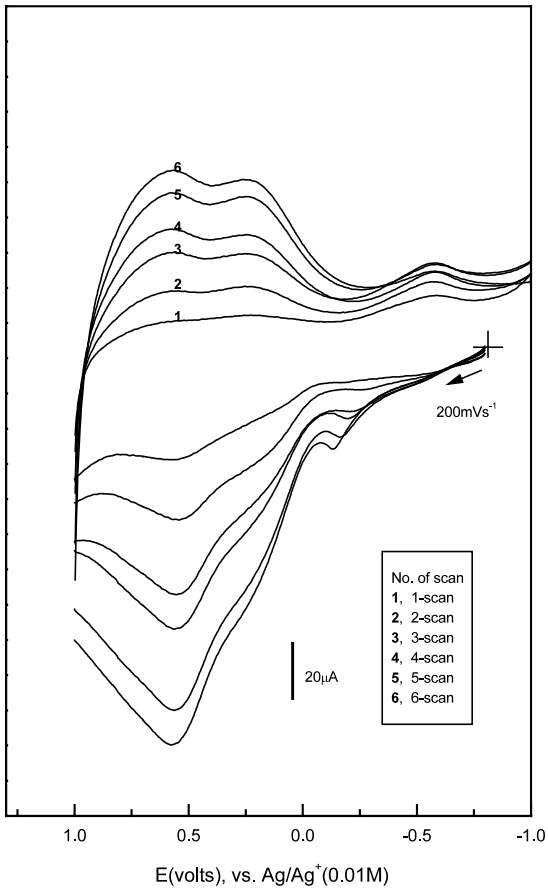


Fig. 4. Cyclic votammograms of the GCE electropolymerized by the 14-H in a neat 0.1 M TEAP acetonitrile solutions at 25 °C and 200 mV s^{-1}.

sible waves at around +0.10 and +0.60 V, respectively, as shown in Fig. 4. The first and second oxidation waves (Fig. 4) of the GCE electropolymerized by 14-H showed at almost the same potentials as those of the complex 14-H (Fig. 3), while no other chemical reaction following the electropolymerization on GCE could be found.

The applications of the GCEs modified by 14-H, 14-NO_2 and 15-NO_2 for dioxygen electroreduction were illustrated in Fig. 5. The traces a, b and c indicate the cyclic voltammograms for the GCEs electropolymerized by 14-H, 14-NO_2 and 15-NO_2 in an oxygen-saturated acetonitrile solution, respectively, while trace d is for the bare GCE in the same solution. The potential difference between the modified and bare electrodes was often used to evaluate the catalytic activity of the modifier. On comparing the voltammograms, the reduction potentials of dioxygen by the modified GCEs were reduced by about 400 mV compared with the bare one. In the case of the 14-X series, the catalytic reduction of dioxygen occurred at potentials somewhat more positive than in the 15-X series. Based upon the results herein (Fig. 5), it was shown that the electropolymerized electrodes using 14-H, 14-NO_2 and 15-NO_2 have good catalytic activities for use in electrocatalytic reduction of dioxygen. On the other hand, the same modified electrodes showed scarcely any catalytic activity in the electrooxidation of L-ascorbate [27].

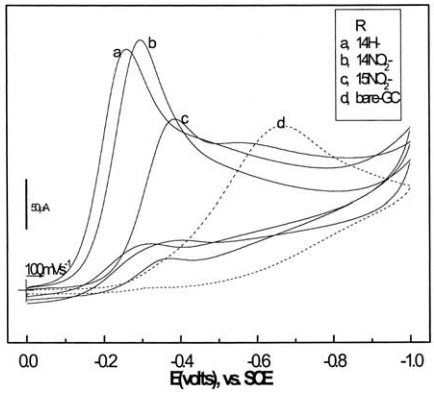


Fig. 5. Cyclic voltammograms of catalytic dioxygen reduction by the electropolymerized and bare GCEs in a 0.1 M phosphate buffer (pH 7.0) at 25 °C and 100 mV s^{-1}: (a), 14-H; (b), 14-NO_2; (c), 15- NO_2; (d), bare GCE.

Acknowledgements

This work was financially supported by the Korea Research Foundation Grant (KRF-2000-DP-0217) and partially by the Brain Korea 21 project.

References

[1] K. Sakata, M. Shimoda, M. Hashimoto, J. Heterocyclic Chem. 33 (1996) 1593.
[2] D. Mandon, J.M. Giraudon, L. Toupet, J. Sala-Pala, J.E. Gurechais, J. Am. Chem. Soc. 109 (1987) 3490.
[3] P.J. Hochgesang, R.D. Bereman, Inorg. Chim. Acta 162 (1989) 91.
[4] E.V. Caemelbecke, W. Kuntner, K.M. Kadish, Inorg. Chem. 32 (1993) 438.
[5] C.L. Bailey, R.D. Bereman, D.P. Rillema, R. Nowak, Inorg. Chim. Acta 116 (1986) 245.
[6] A. Gangi, R.R. Durand, Jr., J. Chem. Soc., Chem. Commun. (1986), 697.
[7] J. Eilemes, Polyhedron 10 (1991) 1779.
[8] K.M. Abraham, K. Pitts, W.P. Kilroy, J. Electrochem. Soc. 132 (1985) 2301.
[9] W.P. Kilroy, M. Alamgir, S.J. Perroti, K.M. Abraham, Proc. Electrochem. Soc. 86 (1988) 291.
[10] C.L. Bailey, R.D. Bereman, D.P. Rillema, R. Nowak, Inorg. Chem. 23 (1984) 3956.
[11] C. Miry, D.L. Brun, J.-M. Kerbaol, M. L'Her, J. Electroanal. Chem. 494 (2000) 53 (and references therein).
[12] Y.C. Park, Z.U. Bae, S.S. Kim, S.K. Baek, Bull. Korean Chem. Soc. 16 (1995) 287.
[13] Y.C. Park, S.S. Kim, D.C. Lee, C.H. An, Polyhedron 16 (1997) 253.
[14] J.F. Coetzee, Anal. Chem. 34 (1962) 1139.
[15] I.M. Kolthoff, J.F. Coetzee, J. Am. Chem. Soc. 79 (1957) 1852.
[16] J.G. Martin, S.C. Cummings, Inorg. Chem. 12 (1973) 1477.
[17] As pointed by Busch et al. in ref. [18], there is no conclusion about how the electronic effects might be transmitted (inductive vs. resonance) warranted from these data.
[18] J.A. Steehy, D.G. Pillsbury, D.H. Busch, Inorg. Chem. 19 (1980) 3148.
[19] A.L. Cutler, C.S. Alleyne, D. Dolphin, Inorg. Chem. 24 (1985) 2281 (and references therein).
[20] K. Sakata, H. Tagami, M.J. Hashimoto, J. Heterocyclic Chem. 26 (1989) 805.
[21] T. Malinshi, D. Chang, L.A. Bottomley, K.M. Kadish, Inorg. Chem. 121 (1982) 4248.
[22] A. Giraudeau, H. Callot, M. Gross, Inorg. Chem. 18 (1979) 201.
[23] A. Giraudeau, H. Callot, J. Jordon, I. Ezhar, M. Gross, J. Am. Chem. Soc. 101 (1979) 385.
[24] S.S. Kim, E.H. Kim, J.C. Byun, C.H. Choi, H.G. Na,Y.C. Park, J. Coord. Chem., in press.
[25] P.J. Hochgesang, Ph.D. Dissertation, North Carolina State University, Raleigh, USA, 1987.
[26] Z.U. Bae, Y.C. Park, Bull. Korean Chem. Soc. 21 (2000) 749.
[27] Private communication. For the GCEs electropolymerized by 14-H and 15-H, the oxidation potentials of L-ascorbic acid were lowered to about 100 mV in comparison with those of the unmodified GCE.

PERGAMON

Polyhedron 21 (2002) 925–933

POLYHEDRON

www.elsevier.com/locate/poly

Synthesis and structural characterization of complexes from the NOS ligating Schiff base of dfp: structurally different molecules in the unit cell of the manganese complex

N. Mangayarkarasi, M. Prabhakar, P.S. Zacharias *

School of Chemistry, University of Hyderabad, Hyderabad 500 046, India

Received 21 August 2001; accepted 9 January 2002

Abstract

Zinc, manganese, copper and nickel complexes (**1**–**4**) were synthesized by the template condensation of 2,6-diformyl-4-methylphenol (**dfp**) and 2-(methylmercapto)aniline with metal perchlorate salts in presence of pyrazole and triethylamine. These complexes are characterized by analytical, spectral, magnetic and electrochemical techniques. Based on these experimental data, the molecular composition of the complexes is found to be $[M_2L_2](ClO_4)_2$ instead of the pyrazole bridged binuclear complex. This is confirmed by X-ray crystal structures of zinc, **1** and manganese, **2** complexes. The geometry around the zinc atoms is pseudo octahedral with $N_2O_2S_2$ coordination. The asymmetric unit of manganese complex **2** consists of two crystallographically independent half molecules (**2A** and **2B**), two perchlorate anions and water molecules. Manganese atoms in **2A** have distorted pentagonal bipyramidal geometry and in **2B** they have irregular geometry. © 2002 Published by Elsevier Science Ltd.

Keywords: Acyclic; Binuclear; Pyrazole bridged; Asymmetric unit; Pentagonal bipyramidal

1. Introduction

Thio ligands are employed to generate model complexes for a number of metallobiosites [1] where sulfur atoms are coordinated to iron [2], nickel [3], copper [4] and zinc [5] atoms in mono-, bi- or tridentate fashion. First row transition metal Schiff base complexes of 2,6-diformyl-4-methylphenol (**dfp**) with N_2O_2, NON and NOO coordination sites are well characterized [6]. Though many thio bridged acyclic and macrocyclic complexes of 2,6-diformyl-4-methylthiophenol (**dftp**) are known [6,7], complexes with NOS coordination from **dfp** are rare [8]. Acyclic Schiff base complexes of **dfp** either with two different bridging groups (**Type a**) or with two same bridging groups (**Type b**) can be synthesized as shown in Scheme 1. In the former case, the endogenous phenoxo bridge of **dfp** remains constant and the exogenous bridge can be formed by groups such as hydroxide, alkoxide, halide, pseudohalide, carboxylate and pyrazolate [9]. These complexes provide an opportunity to study the effect of various bridging groups on spectral, magnetic and electrochemical properties [9]. Our attempts to synthesize **Type a** complexes of sulfur ligating **dfp** derivatives with a pyrazole bridge yielded only **Type b** complexes.

This paper deals with the synthesis and structural characterization of acyclic Schiff base binuclear complexes of Zn, Mn, Cu and Ni with NOS coordination obtained by the condensation of **dfp** and 2-(methylmercapto)aniline with the respective metal perchlorate salts and triethylamine in presence of pyrazole (Hpyz). X-ray structural characterization of zinc and manganese complexes reveals interesting structural features.

2. Experimental

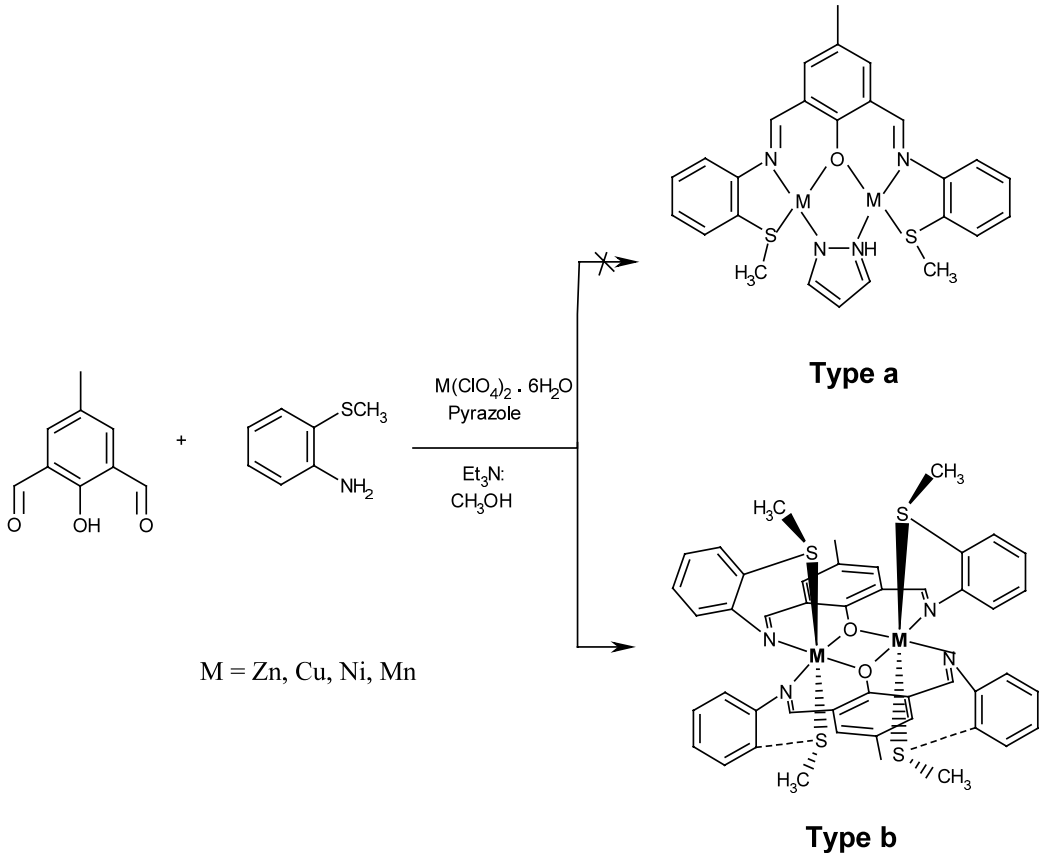
2.1. Chemicals and reagents

2,6-Diformyl-4-methylphenol was synthesized according to the literature procedure [10]. 2-(Methylmercapto)aniline was distilled prior to use. Other starting

* Corresponding author. Tel.: +91-40-301-1007; fax: +91-40-301-2460.

E-mail address: pszsc@uohyd.ernet.in (P.S. Zacharias).

0277-5387/02/$ - see front matter © 2002 Published by Elsevier Science Ltd.
PII: S0277-5387(02)00874-4



Scheme 1. The schematic representation of the product formation.

materials were used without further purification. Solvents were purified and dried by the usual methods [11,12].

2.2. Physical measurements

Elemental analyses were carried out on a Perkin–Elmer 240C CHN analyzer. IR spectra were recorded on a JASCO model FT/IR-5300 spectrophotometer in the range 4000–400 cm^{-1} as KBr pellets, electronic spectra on a JASCO model 7800 UV–Vis spectrophotometer (solution concentrations 1×10^{-3} mol dm^{-3} for the visible region and 1×10^{-5} mol dm^{-3} for the UV region) and ^1H NMR spectra on a Bruker ACF-200 spectrometer at 200 MHz with TMS as internal standard. The room temperature (r.t.) magnetic susceptibility experiments were carried out on a SHERWOOD SCIENTIFIC magnetic susceptibility balance. Diamagnetic corrections were made using Pascal's constants. Cyclic voltammograms were recorded on a Cypress System model CS-1090/CS-1087 computer controlled electroanalytical system. All experiments were performed in dry solvents under dry nitrogen atmosphere. 1×10^{-3} M solutions were used with 0.1 M tetrabutylammonium perchlorate (TBAP) as supporting electrolyte, using either glassy carbon (GC) or platinum (Pt) working electrodes, Ag–AgCl as the reference electrode and platinum wire as an auxiliary electrode. The ferrocene–ferrocenium couple was used as the redox standard.

2.3. Synthesis of complexes

The complexes **1**–**4** were synthesized from **dfp**, 2-(methylmercapto)aniline, metal perchlorate salt, pyrazole and triethylamine in 1:2:2.5:1.25:1 ratio. Representative details are given for the zinc complex, **1**. **Caution**: all perchlorate salts are prone to explosion and must be handled with care.

2.3.1. $[Zn_2L_2](ClO_4)_2$, *1*

To a methanolic solution (75 ml) of 2,6-diformyl-4-methylphenol (0.164 g, 1 mmol), 2-(methylmercapto)aniline (0.280 g, 2 mmol) in methanol (25 ml) was added and stirred at r.t. for 30 min. To the orange solution, $Zn(ClO_4)_2 \cdot 6H_2O$ (0.930 g, 2.5 mmol) and pyrazole (0.085 g, 1.25 mmol) were added successively. On slow addition of triethylamine (0.100 g 1 mmol) in methanol (5 cm^3), the reddish orange solution changed into golden yellow. The resulting solution was stirred at r.t. for 6 h, then filtered and kept for crystallization. Yellow crystals suitable for X-ray structure determination were ob-

tained from the reaction mixture on slow evaporation. Yield: 90%.

2.4. Spectral and analytical data of complexes *1*–*4*

2.4.1. $[Zn_2L_2](ClO_4)_2$ (*1*)

ν_{max}/cm^{-1} 1622, 1605, 1545, 1084, 622. δ_H (200 MHz, CD_3CN) 8.77 (4H, s, H–C=N), 7.97 (4H, s, Ar–H), 7.57 (4H, d, Ar–H), 7.45 (4H, t, Ar–H), 7.30 (4H, t, Ar–H), 7.00 (4H, d, Ar–H), 2.57 (6H, s, H_3C–Ar), 2.37 (12H, s, SCH_3). Found: C, 47.99; H, 3.68; N, 4.61; Calc. for $C_{46}H_{42}N_4O_{10}S_4Cl_2Zn_2$: C, 48.43; H, 3.71; N, 4.91%. λ_{max}/nm (ε/mol^{-1} dm^3 cm^{-1}) 390 (20870).

2.4.2. $[Mn_2L_2](ClO_4)_2 \cdot 2H_2O$ (*2*)

Yield: 60%; ν_{max}/cm^{-1} 3335, 1618, 1605, 1542, 1080, 622. Found: C, 47.52; H, 4.03; N, 4.88; Calc. for $C_{46}H_{46}N_4O_{12}S_4Cl_2Mn_2$: C, 47.79; H, 4.01; N, 4.84%.

2.4.3. $[Cu_2L_2](ClO_4)_2$ (*3*)

Yield: 90%; ν_{max}/cm^{-1} 1620, 1601, 1539, 1086, 621. Found: C, 48.48; H, 3.68; N, 4.61; Calc. for $C_{46}H_{42}N_4O_{10}S_4Cl_2Cu_2$: C, 48.59; H, 3.72; N, 4.93%. λ_{max}/nm (ε/mol^{-1} dm^3 cm^{-1}) 630 (229), 441 (20816).

2.4.4. $[Ni_2L_2](ClO_4)_2$ (*4*)

Yield: 90%; ν_{max}/cm^{-1} 1626, 1603, 1535, 1087, 623. Found: C, 48.98; H, 3.58; N, 4.84; Calc. for $C_{46}H_{42}N_4O_{10}S_4Cl_2Ni_2$: C, 49.01; H, 3.76; N, 4.97%. λ_{max}/nm (ε/mol^{-1} dm^3 cm^{-1}) 479 (34636).

Due to the insolubility of the manganese complex **2**, the electronic spectrum and cyclic voltammetric studies were not done.

3. X-ray crystal structure analysis

The yellow rectangular crystals of complex **1** and the reddish orange plate like crystals of **2** were grown by slow evaporation of the methanolic solution (the reaction mixture). The crystals of **3** (green) and **4** (orange) were thin plates and due to the poor diffraction quality, the data were not collected further. The crystals of complex **1** lose the solvent molecule spontaneously on removal from the mother liquor. So, a suitable single yellow crystal of complex **1** was mounted in the glass capillary along with the mother solution. Crystal data were collected on a Nonius Enraf MACH3 diffractometer for complex **1** and on a BRUKER SMART CCD area diffractometer for complex **2** equipped with graphite monochromated Mo Kα radiation ($\lambda = 0.71073$ Å). Twenty five carefully centered reflections were used to determine cell parameters. Using the ω scan technique, unique reflections were collected to a maximum 2θ value. The programs used for the data reduction were XTAL 3.5 [13] version and BRUKER SMART and SAINT [14] for control and integration software for complex **1** and **2**, respectively. The solution and refinement were carried out using SHELX-97 [15]. The locations of zinc and manganese atoms were determined by direct methods. The remaining non-hydrogen atoms were located through successive least-squares refinements on the difference Fourier map using SHELXL [15]. All the non-hydrogen atoms were made anisotropic. The hydrogen atoms for the molecular cations were fixed at calculated positions and were refined using the riding model and they were neither fixed nor located for the solvent molecules.

4. Results and discussion

Synthetic details of complexes **1**–**4** are given in Section 2. Pyrazole was added to promote the formation of binuclear metal complexes of **Type a** with the endogenous phenolic bridging oxygen and the exogenous pyrazole bridge as shown in Scheme 1.

The complexes show IR bands at around 1618–1626 cm^{-1} for C=N stretching vibrations. Absence of an aldehydic C=O stretch of **dfp** at 1680 cm^{-1} confirms the formation of both side condensed acyclic Schiff base complexes. The CHN analytical data of the complexes did not match with the expected molecular composition $[M_2L(pyz)](ClO_4)_2$ (**Type a**) but matched with the binuclear composition $[M_2L_2](ClO_4)_2$ (**Type b**). Since it is reported that the amount of pyrazole is an important factor governing the formation of the required complexes [16,17], the composition of substrates was also varied. Even then only binuclear complexes of **Type b** were obtained.

4.1. Binuclear zinc complex (*1*)

The zinc complex was synthesized by the procedure given in the Section 2. The IR spectrum of complex **1** shows stretching bands at around 1622 and 1545 cm^{-1} corresponding to the C=N and the oxo bridged phenolic C–O groups [18]. The bands at 1084 and 622 cm^{-1} indicate the presence of uncoordinated perchlorate ion. The ^1H NMR spectrum of the complex shows one singlet (4H) at 7.97 ppm due to the aromatic protons of **dfp** moieties in addition to a singlet (4H) at 8.77 ppm due to azomethine protons. The aromatic protons of the amine moieties appear as two doublets at 7.57 and 7.00 ppm and as two triplets at 7.45 and 7.30 ppm corresponding to four protons each. The methyl protons of **dfp** and $-SCH_3$ moieties appear at 2.57 and 2.37 ppm. No signal due to pyrazole protons is observed. The CHN analytical data agree with the binuclear composition $[Zn_2L_2](ClO_4)_2$ and confirms the presence of two perchlorate ions. The molecular structure of the complex is established by X-ray crystal structure.

The electronic spectrum of the complex in *N*,*N*-dimethylformamide (DMF) shows a band at 390 nm due to the charge transfer transitions.

4.1.1. X-ray structure determination of **1** $[Zn_2L_2](ClO_4)_2\cdot 2CO$

The zinc complex crystallizes in triclinic $P\bar{1}$ space group. The crystallographic parameters, interatomic distances and angles relevant to the coordination spheres are given in Tables 1 and 2. The asymmetric unit consists of a discrete binuclear cation $[Zn_2L_2]^{2+}$, two perchlorate anions and two methanol solvates. An ORTEP [19] diagram of the cation with the atom numbering scheme is shown in Fig. 1. The Zn(1) and Zn(2) atoms are coordinated by two azomethine nitrogen atoms, two bridging phenoxide oxygen atoms and two sulfur atoms of the thiomethyl groups of Schiff base moieties.

Each N_2O_2 coordination plane of the metal centers exhibits slight distortion from planarity. The coordination plane of Zn(1) displays the largest distortion (0.3408 Å). The plane of Zn(2) is at the normal angle of 85.01° with that of the plane of Zn(1). The in-plane distances to the phenoxide bridge Zn(1)–O(1), Zn(1)–O(2), Zn(2)–O(1), Zn(2)–O(2) are 2.001(4), 2.016(5), 2.013(5) and 2.002(4) Å.

Table 1
Crystallographic parameters of the binuclear zinc (**1**) and manganese (**2**) complexes

Compound	$[Zn_2L_2](ClO_4)_2\cdot 2CO$, **1**	$[Mn_2L_2(H_2O)_2](ClO_4)_2\cdot 6.5O$, **2**
Empirical formula	$C_{48}H_{42}N_4O_{12}S_4Cl_2Zn_2$	$C_{46}H_{46}N_4O_{18.5}S_4Cl_2Mn_2$
Formula weight	1196.82	1259.91
Temperature (K)	298(2)	293(2)
Wavelength (Å)	0.71073	0.71073
Crystal system	Triclinic	monoclinic
Space group	$P\bar{1}$	$C2/c$
a (Å)	12.915(2)	22.943(2)
b (Å)	13.957(2)	21.315(2)
c (Å)	16.85(2)	23.272(2)
α (°)	68.889(13)	90.0
β (°)	84.346(12)	92.095(2)
γ (°)	68.701(11)	90.0
U (Å^3)	2639(3)	11373.2(18)
Z	2	14
D_{calc} (Mg m^{-3})	1.677	1.467
Absorption coefficient (mm^{-1})	1.06	0.757
$F(000)$	1348	5136
θ Range (°)	1.30 to 27.47	1.30 to 28.38
Limiting indices	$0 \le h \le 16$, $-16 \le k \le 18$, $-21 \le l \le 21$	$-30 \le h \le 30$, $-19 \le k \le 28$, $-26 \le l \le 31$
Reflections collected	12 076	36 064
Reflections observed $[I > 2\sigma(I)]$	4807	13 629
Data, parameters	4807, 710	6497, 690
Goodness-of-fit on F^2	1.067	1.021
Final R indices $[I > 2\sigma(I)]$	$R_1 = 0.0635$, $wR_2 = 0.1472$	$R_1 = 0.1062$, $wR_2 = 0.2832$
R indices (all data)	$R_1 = 0.1781$, $wR_2 = 0.2151$	$R_1 = 0.1965$, $wR_2 = 0.3477$

$R_1 = \Sigma[|F_0| - |F_c|]/\Sigma|F_0|$; $wR_2 = \{\Sigma[w(F_0^2 - F_c^2)^2]/\Sigma[w(F_0^2)^2]\}^{1/2}$.

Table 2
Selected bond lengths (Å) and bond angles (°) of complex **1**

Bond lengths			
Zn(1)–O(1)	2.001(4)	Zn(1)–Zn(2)	3.137(3)
Zn(1)–N(3)	2.004(5)	Zn(2)–O(2)	2.002(4)
Zn(1)–O(2)	2.016(5)	Zn(2)–O(1)	2.013(5)
Zn(1)–N(1)	2.033(5)	Zn(2)–N(2)	2.019(5)
Zn(1)–S(1)	2.792(2)	Zn(2)–N(4)	2.023(6)
Zn(1)–S(3)	2.794(2)	Zn(2)–S(4)	2.675(2)
Bond angles			
O(1)–Zn(1)–N(3)	151.6(2)	S(1)–Zn(1)–Zn(2)	104.79(5)
O(1)–Zn(1)–O(2)	77.21(17)	S(3)–Zn(1)–Zn(2)	112.06(7)
N(3)–Zn(1)–O(2)	89.76(18)	O(2)–Zn(2)–O(1)	77.23(17)
O(1)–Zn(1)–N(1)	88.84(19)	O(2)–Zn(2)–N(2)	151.2(2)
N(3)–Zn(1)–N(1)	113.4(2)	O(1)–Zn(2)–N(2)	88.36(19)
O(2)–Zn(1)–N(1)	149.2(2)	O(2)–Zn(2)–N(4)	88.5(2)
O(1)–Zn(1)–S(1)	114.46(15)	O(1)–Zn(2)–N(4)	155.0(2)
N(3)–Zn(1)–S(1)	90.63(16)	N(2)–Zn(2)–N(4)	112.7(2)
O(2)–Zn(1)–S(1)	91.16(14)	O(2)–Zn(2)–S(4)	116.76(15)
N(1)–Zn(1)–S(1)	69.62(16)	O(1)–Zn(2)–S(4)	91.68(15)
O(1)–Zn(1)–S(3)	93.26(15)	N(2)–Zn(2)–S(4)	88.03(17)
N(3)–Zn(1)–S(3)	71.26(15)	N(4)–Zn(2)–S(4)	76.48(16)
O(2)–Zn(1)–S(3)	119.77(15)	O(2)–Zn(2)–Zn(1)	38.82(12)
N(1)–Zn(1)–S(3)	87.94(17)	O(1)–Zn(2)–Zn(1)	38.45(12)
S(1)–Zn(1)–S(3)	143.01(7)	N(2)–Zn(2)–Zn(1)	123.40(16)
O(1)–Zn(1)–Zn(2)	38.74(12)	N(4)–Zn(2)–Zn(1)	123.84(16)
N(3)–Zn(1)–Zn(2)	124.67(15)	S(4)–Zn(2)–Zn(1)	106.51(6)
O(2)–Zn(1)–Zn(2)	38.51(12)	Zn(2)–O(2)–Zn(1)	102.68(19)
Zn(1)–O(1)–Zn(2)	102.81(19)		

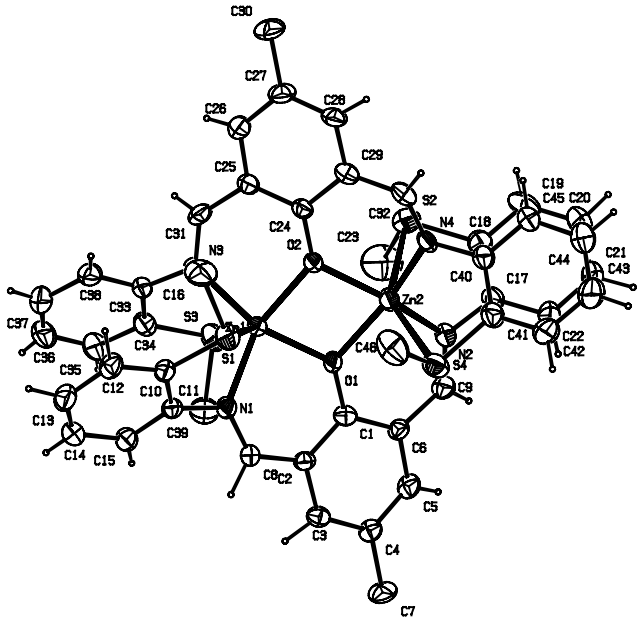


Fig. 1. ORTEP diagram of $[Zn_2L_2]^{2+}$, **1** (thermal ellipsoids at 20% probability level).

The metal-azomethine nitrogen Zn(1)–N(1), Zn(1)–N(3), Zn(2)–N(2), Zn(2)–N(4) distances are 2.033(5), 2.004(5), 2.019(5) and 2.023(6) Å, respectively. These values are similar to those of the chemically equivalent bonds in other structures [20]. However, the average distance between the zinc and axially coordinated sulfur atoms is 2.793 Å which is significantly longer than the sum of the covalent radii (2.33 Å) but shorter than the van der Waals radii (3.27 Å) indicative of weak bonding interactions. Although there are no chemically equivalent analogues of Zn–S bonds of Schiff base complexes with $-SCH_3$ groups, many Zn–S bonds with the distances in the range of 2.6–2.8 Å are reported [21].

The zinc···zinc separation is 3.137 Å. The phenoxide bridging angles Zn(1)–O(1)–Zn(2), Zn(1)–O(2)–Zn(2) are 102.81(19) and 102.68(19)°. They are larger than that of the analogous reported Schiff base complexes of **dfp** [20,22]. The geometry around the zinc atoms can be described as pseudo octahedral geometry.

The X-ray crystal structure of complex **1** confirms the formation a of binuclear complex of **type b** (Scheme 1).

4.2. Binuclear manganese complex (2)

The manganese complex was synthesized by the procedure given in Section 2. The IR spectrum of the complex shows a C=N stretching band at 1618 cm^{-1}, the characteristic bands of oxo bridged phenolic C–O groups and uncoordinated perchlorate ions at 1542, 1080 and 622 cm^{-1}. The CHN analysis of the complex supports the binuclear molecular composition, $[Mn_2L_2](ClO_4)_2\cdot 2H_2O$. The structure was confirmed by X-ray analysis. The room temperature magnetic moment value of 6.10 B.M. per manganese atom suggests the presence of high spin manganese(II) centers.

4.2.1. X-ray structure determination of 2, $[Mn_2L_2(H_2O)_2](ClO_4)_2\cdot 6.5O$

The complex crystallizes in monoclinic $C2_1/c$ space group. Due to weak diffraction intensity the refinements converged at a final $R = 10.62\%$. Crystallographic parameters are given in Table 1. The asymmetric unit consists of two crystallographically independent half molecules, two perchlorate anions and water molecules. The ORTEP diagrams of the two molecular cations (**2A** and **2B**) with atom numbering scheme are given in Figs. 2 and 3. Selected bond lengths and bond angles are given in Table 3.

In molecule **2A**, the average Mn–O(phenoxo), Mn–N(imino) bond distances are 2.131 and 2.265 Å, respectively. These distances fall within the range commonly found for bivalent manganese complexes [23] and are significantly longer than the equivalent bonds in the binuclear zinc(II) complex **1**. The Mn–O(water) bond length is 2.295(9) Å. The average Mn–S bond lengths are 2.803 Å (reported Mn–S bond distances are 2.6–2.9 Å) [24].

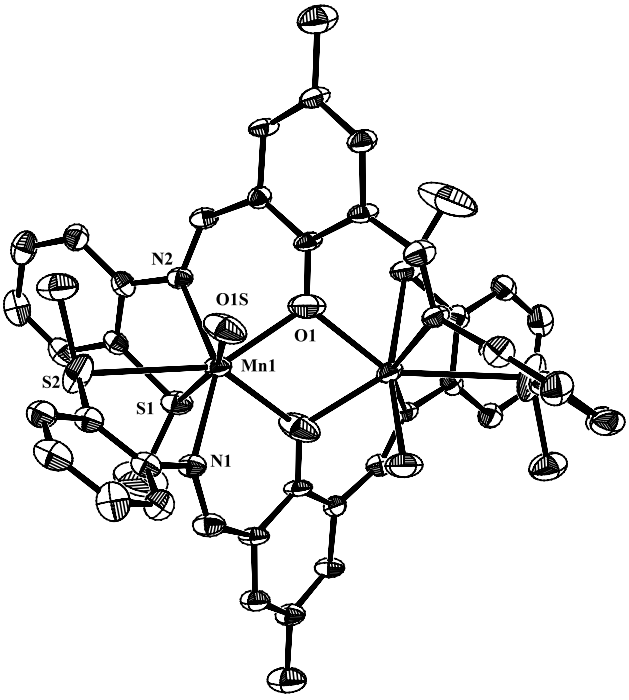


Fig. 2. ORTEP diagram of molecular cation of **2A** (thermal ellipsoids are at 30% probability level).

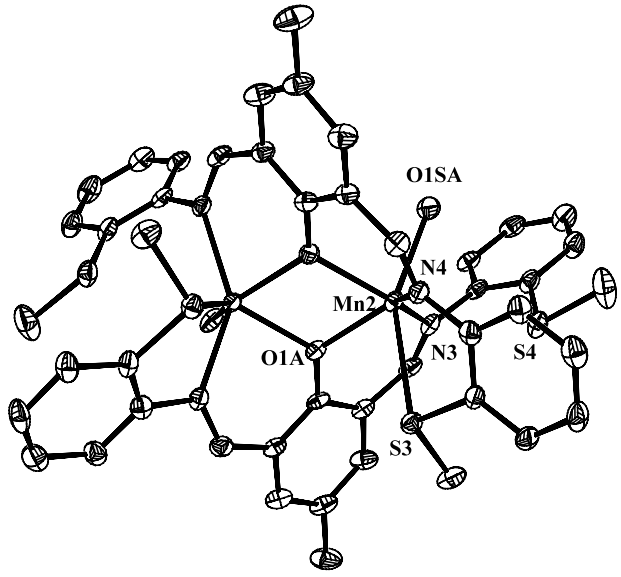


Fig. 3. ORTEP diagram of the molecular cation of **2B** (thermal ellipsoids are at 30% probability level).

The average bond angle between the metal and the axial groups O(1S)–Mn(1)–S(1) and O(1S)#1–Mn(1)#1–S(1)#1 is 165.0(4) Å. The angle between the basal pentagonal plane and the MnOS plane is 88.50°, i.e. nearly perpendicular. From the bond angles the coordination geometry around the manganese atoms

Table 3
Selected bond lengths (Å) and bond angles (°) of complex **2**

Bond lengths			
Mn(1)–O(1)#1	2.121(5)	Mn(2)–O(1A)	2.137(5)
Mn(1)–O(1)	2.140(5)	Mn(2)–O(1SA)	2.183(5)
Mn(1)–N(1)	2.256(6)	Mn(2)–N(4)	2.239(6)
Mn(1)–N(2)	2.274(6)	Mn(2)–N(3)	2.242(6)
Mn(1)–O(1S)	2.295(9)	Mn(2)–S(3)	2.830(2)
Mn(1)–S(2)	2.790(3)	O(1)–Mn(1)#1	2.121(5)
Mn(1)–S(1)	2.827(2)	O(1A)–Mn(2)#2	2.125(5)
Mn(2)–O(1A)#2	2.125(5)		
Bond angles			
O(1)#1–Mn(1)–O(1)	72.7(2)	O(1S)–Mn(1)–S(1)	165.0(4)
O(1)#1–Mn(1)–N(1)	131.3(2)	S(2)–Mn(1)–S(1)	84.94(9)
O(1)–Mn(1)–N(1)	79.5(2)	O(1A)#2–Mn(2)–O(1A)	71.7(2)
O(1)#1–Mn(1)–N(2)	80.85(19)	O(1A)#2–Mn(2)–O(1SA)	83.80(18)
O(1)–Mn(1)–N(2)	123.2(2)	O(1A)–Mn(2)–O(1SA)	131.9(2)
N(1)–Mn(1)–N(2)	147.2(2)	O(1A)#2–Mn(2)–N(4)	82.3(2)
O(1)#1–Mn(1)–O(1S)	76.1(3)	O(1A)–Mn(2)–N(4)	124.5(2)
O(1)–Mn(1)–O(1S)	116.5(5)	O(1SA)–Mn(2)–N(4)	90.9(2)
N(1)–Mn(1)–O(1S)	82.0(3)	O(1A)#2–Mn(2)–N(3)	132.0(2)
N(2)–Mn(1)–O(1S)	103.9(4)	O(1A)–Mn(2)–N(3)	80.9(2)
O(1)#1–Mn(1)–S(2)	145.53(16)	O(1SA)–Mn(2)–N(3)	86.5(2)
O(1)–Mn(1)–S(2)	141.38(15)	N(4)–Mn(2)–N(3)	144.8(2)
N(1)–Mn(1)–S(2)	68.56(16)	O(1A)#2–Mn(2)–S(3)	114.66(14)
N(2)–Mn(1)–S(2)	80.45(15)	O(1A)–Mn(2)–S(3)	78.52(13)
O(1S)–Mn(1)–S(2)	80.7(4)	O(1SA)–Mn(2)–S(3)	149.34(16)
O(1)#1–Mn(1)–S(1)	114.71(17)	N(4)–Mn(2)–S(3)	69.10(16)
O(1)–Mn(1)–S(1)	77.69(16)	N(3)–Mn(2)–S(3)	96.74(16)
N(1)–Mn(1)–S(1)	96.75(16)	Mn(1)#1–O(1)–Mn(1)	106.73(19)
N(2)–Mn(1)–S(1)	69.26(14)	Mn(2)#2–O(1A)–Mn(2)	108.3(2)

can be regarded as distorted pentagonal bipyramidal with the phenoxo oxygens, imino nitrogen and one sulfur atom in the basal plane and with the other sulfur and the oxygen of the water molecule at the apices. The phenoxide bridging angle Mn–O–Mn is 106.73(19)° and the Mn_2O_2 ring is nearly planar with a mean deviation of 0.07 Å from the plane. The Mn···Mn distance is 3.421 Å and is within the range reported for acyclic binuclear manganese complexes (3.324–3.584 Å) [23]. The basal plane of Mn(1) and Mn(1)#1 displays the greatest distortion and the plane of Mn(1)#1 has a normal angle of 76.17° with that of the plane of Mn(1). The aromatic rings with $-SCH_3$ groups are inclined by 33.70° and 81.47° relative to the Mn_2O_2 mean plane, while the phenolic aromatic rings are inclined by 42.27° relative to the Mn_2O_2 mean plane. The plane of the aromatic ring of one ligand has the normal angle of 73.09° with that of the plane of the aromatic ring of the other ligand and vice versa.

In molecule **2B**, the average Mn–O(phenolic), Mn–N(imino) and Mn–O(water) bond lengths are 2.132, 2.241 and 2.183(5) Å, respectively. The Mn–O(phenolic) bond length is similar that in molecule **2A** and Mn–N(imino) bond lengths are slightly different. The Mn–O(water) bond length is shorter than in **2A** and one sulfur atom remains uncoordinated. Its bond length is 3.124 Å which is slightly shorter than the van der Waals radii of the two atoms. The phenoxide bridging angle Mn(2)#2–O(1A)–Mn(2) is 108.3(2)° which is larger than in **2A**. The Mn···Mn distance is 3.452 Å. From the bond angles the geometry around the metal atom can better be described as irregular geometry and a few manganese(II) complexes with irregular geometries are known in literature [25].

In **2B**, the aromatic rings with $-SCH_3$ are inclined more towards the Mn_2O_2 mean plane (34.16° and 88.81°) and the $-SCH_3$ moiety is away form the Mn_2O_2 plane. On the other hand the phenolic aromatic rings are inclined by 41.12° relative to the Mn_2O_2 mean plane. The plane of the aromatic ring of one ligand has the normal angle of 68.95° with that of the plane of the aromatic ring of the other ligand and vice versa. The bridging Mn–O–Mn angle is also greater than in **2A**. It is apparent that there is a subtle structural difference in the molecules **2A** and **2B**.

The delicate balance between the ligand field effects, the non-planarity and the flexibility of the ligand and the stability of the seven coordination allows the d^5 Mn(II) ion to have pentagonal bipyramidal geometry in **2A**. It is known that the d^5 ion achieves slightly greater stability with seven coordination.

4.3. Binuclear copper complex (3)

The copper complex was synthesized as described in the Section 2. The IR spectrum of the complex shows C=N stretching at 1620 cm^{-1}, the characteristic oxo bridged phenolic C–O group at 1539 cm^{-1} and the bands due to uncoordinated perchlorate ions at 1086 and 621 cm^{-1}. The CHN analysis of the complex support the binuclear molecular composition of $[Cu_2L_2](ClO_4)_2$.

The electronic spectrum of the complex in DMF exhibits a strong band at 441 nm due to the metal to ligand charge transfer transition and a broad band at 630 nm due to a *d*–*d* electronic transition. The position of the *d*–*d* band of complex **3** indicates distorted octahedral geometry at the copper(II) centers with $N_2O_2S_2$ coordination [26]. The room temperature magnetic moment of 0.98 B.M. per copper atom indicates a strong antiferromagnetic interaction between the two copper centers. Based on the experimental data and a comparison with the zinc complex **1**, a structure similar to that of complex **1** is proposed for the copper complex.

The copper complex exhibits two irreversible one electron reduction peaks of the Cu(II) centers at −0.017 and −0.119 V in DMF with a GC electrode. As the number of scans increases, the peak height decreases which indicates the adsorption of metals on the electrode. In the positive region it shows two oxidation peaks at +0.685 and +1.082 V. With a Pt electrode, the reduction peaks are at +0.260 and +0.060 V and the oxidation peaks at +0.865 and +1.165 V.

4.4. Binuclear nickel complex (4)

The synthetic procedure is given in Section 2. The IR spectrum of the complex shows C=N and oxo bridged phenolic C–O stretching bands at 1626 and 1535 cm^{-1}. The bands at 1087 and 623 cm^{-1} show the presence of uncoordinated perchlorate ions. The CHN analysis of the complex supports the binuclear composition $[Ni_2L_2](ClO_4)_2$.

The electronic spectrum of the complex in DMF in the range 250–1100 nm exhibits a very high intensity absorption band at around 479 nm corresponding to the metal to ligand charge transfer transition. No other bands are observed in the visible region. It might probably be due to the masking of the high energy *d*–*d* bands by the metal to ligand charge transfer band [27]. The magnetic moment of the complex is 2.64 B.M per nickel atom at room temperature and suggests the presence of antiferromagentism between the high spin nickel(II) centers.

The nickel(II) complex shows two stepwise one electron reduction peaks in the negative potential at −1.068 and −1.230 V in DMF with a GC electrode. A similar cyclic voltammogram is observed for a macrocyclic binuclear nickel complex [28]. The peak height of the first electron reduction is lower than the second one and indicates the stability of the reduced species. In the positive range, a quasi reversible oxidation peak at +1.135 V and an irreversible peak at +1.359 V are observed. Variation in the scan rate gave a slight shift in the peaks towards negative potentials. An increase in the number of scans did not affect the profile. With a Pt electrode two stepwise one electron reduction peaks (−1.015, −1.375) and one reversible oxidation peak at $E_{1/2}$ +1.030 ($\Delta E = 78$) are also observed. The first reduction peak is irreversible and the second one is quasi reversible in nature.

5. Conclusions

The analytical, spectral, magnetic, electrochemical properties and X-ray structure determination of the complexes show the formation of binuclear **Type b** complexes of composition $[M_2L_2](ClO_4)_2$ in contrast to the expected pyrazole bridged **Type a** complexes. In spite of the steric hindrance due to the presence of a bulky aromatic side chain containing the weak bonding –SCH_3 group in the ligand, **Type b** complexes of $N_2O_2S_2$ coordination is formed. This preference can be the result of a possible N_2O_2 coordination core in **Type b** complexes. Crystallographic identification of molecules with two different geometries in the case of the manganese complex (**2A** and **2B**) is interesting from a structural point of view.

6. Supplementary material

Crystallographic data for the structural analyses have been deposited with the Cambridge Crystallograpahic Data Centre, CCDC no. 169459 and 169460. Copies of this information may be obtained free of charge from The Director, CCDC, 12 Union Road, Cambridge, CB2 1EZ, UK (fax: +44-1223-336033; e-mail: deposit @ccdc.cam.ac.uk or www: http://www.ccdc.cam.ac.uk).

Acknowledgements

N.M. and M.P. thank the Department of Science and Technology (DST), India for the financial support. We acknowledge the National Single Crystal Diffractometer Facility at the School of Chemistry and Professor D.E. Fenton of the Department of Chemistry, University of Sheffield, for data collection.

References

[1] (a) D.E. Fenton, Biocoordination Chemistry, Oxford Science Publications, Oxford, 1995;
(b) K.D. Karlin, Z. Tyeklar, Adv. Inorg. Biochem. 9 (1994) 123;
(c) W. Kaim, B. Schwederski, Bioinorganic Chemistry: Inorganic Elements in the Chemistry of Life, Wiley, Chichester, 1995;
(d) F.L. Urbach, in: H. Siegel (Ed.), Metal Ions in Biological Systems, vol. 13, Marcel Dekker, New York, 1981, p. 73;
(e) D.R. Winge, C.T. Dameron, G.N. George, I.J. Pickering, I.G. Dance, in: K.D. Karlin, Z. Tyelkar (Eds.), Bioinorganic Chemistry of Copper, Chapman & Hall, New York, 1993.

[2] (a) W. Lovenberg (Ed.), Iron–Sulfur Proteins, Academic Press, New York, 1973, p. 1977;
(b) S.J. Lippard, Angew. Chem., Int. Ed. Engl. 27 (1988) 344;
(c) E.-I. Ochiai, Bioinorganic Chemistry—An introduction, Allyn and Bacon, Boston, 1977;
(d) R.H. Holm, S. Ciurli, J.A. Weigel, in: S.J. Lippard (Ed.), Progress in Inorganic Chemistry: Bioinorganic Chemistry, vol. 38, Wiley-Interscience, New York, 1990, p. 1.

[3] (a) R. Cammack, in: J.R. Lancaster, Jr. (Ed.), The Bioinorganic Chemistry of Nickel (Chapter 8), VCH, New York, 1988;
(b) S.W. Ragsdale, H.G. Wood, J.A. Morton, L.G. Ljungdahl, D.V. Der Vartanian, in: J.R. Lancaster, Jr. (Ed.), The Bioinorganic Chemistry of Nickel (Chapter 14), VCH, New York, 1988;
(c) A. Volbeda, E. Garcin, C. Piras, A.L. De Lacey, V.M. Fernandez, E.C. Hatchikian, M. Frey, J.C. Fontecilla-Camps, J. Am. Chem. Soc. 118 (1996) 2989;
(d) A.F. Kolodziej, Prog. Inorg. Chem. 41 (1994) 493;
(e) M.A. Halcrow, G. Christou, Chem. Rev. 94 (1994) 2421.

[4] (a) T. Tsukihara, H. Aoyama, E. Yamshita, T. Tomizaki, H. Yamaguchi, K. Shinzawa-Itoh, R. Nakshima, R. Yaono, S. Yoshikawa, Science 272 (1996) 1136;
(b) S. Iwata, C. Ostermier, B. Ludwig, H. Michel, Nature 376 (1995) 660;
(c) H. Bertagnolli, W. Kaim, Angew. Chem., Int. Ed. Eng. 34 (1995) 771.

[5] (a) B.L. Vallee, D.S. Auld, Acc. Chem. Res. 26 (1993) 543;
(b) J.M. Berg, Science, 271 (1996) 271, 1081;
(c) D.T. Corwin, Jr., E.S. Gruff, S.A. Koch, Inorg. Chim. Acta 5 (1988) 151 (and references cited therein).

[6] (a) P. Guerriero, S. Tamburini, P.A. Vigato, Coord. Chem. Rev. 139 (1995) 17;
(b) P. Zanello, S. Tamburini, P.A. Vigato, G.A. Mazzocchin, Coord. Chem. Rev. 77 (1987) 165;
(c) S. Kita, H. Furutachi, H. Okawa, Inorg. Chem. 38 (1999) 4038;
(d) H. Furutachi, A. Ishida, H. Miyasaka, N. Fukita, M. Ohba, H. Okawa, M. Koikawa, J. Chem. Soc., Dalton Trans. (1999) 2441;
(e) S. Ryan, H. Adams, D.E. Fenton, M. Becker, S. Schindler, Inorg. Chem. 37 (1998) 2134;
(f) S.K. Dutta, J. Ensling, R. Werner, U. Florke, W. Hasse, P. Gutlich, K. Nag, Angew. Chem., Int. Ed. Engl. 36 (1997) 152;
(g) S.S. Tandon, L.K. Thompson, J.N. Bridson, C. Benelli, Inorg. Chem. 34 (1995) 5507;
(h) H. Okawa, S. Kida, Bull. Chem. Soc. Jpn. 45 (1972) 1759;
(i) D. Das, C.P. Cheng, J. Chem. Soc., Dalton Trans. (2000) 1081;
(j) S.R. Korupoju, P.S. Zacharias, Chem. Commun. (1998) 1267;
(k) S.R. Korupoju, N. Mangayarkarasi, S. Ameerunisha, E.J. Valente, P.S. Zacharias, J. Chem. Soc., Dalton Trans. (2000) 2845.

[7] (a) C.A. Goddard, Polyhedron 16 (1997) 4273;
(b) B.F. Hoskins, C.J. McKenzie, I.A.S. MacDonald, R. Robson, J. Chem. Soc., Dalton Trans. (1996) 2227;
(c) S. Brooker, T. Davidson, Chem. Commun. (1997) 2007;
(d) A.J. Atkins, A.J. Blake M. Schroder, J. Chem. Soc., Chem. Commun. (1993) 1662;
(e) S. Brooker, P.D. Croucher, F.M. Roxburgh, J. Chem. Soc., Dalton Trans. (1996) 3031;
(f) S. Brooker, P.D. Croucher, J. Chem. Soc., Chem. Commun. (1995) 1493;
(g) P.E. Kruger, V. McKee, Chem. Commun. (1997) 1341.

[8] R.S. Drago, M.J. Desmond, B.B. Corden, K.A. Miller, J. Am. Chem. Soc. 105 (1983) 2287.

[9] (a) C.J. O'Connor, D. Firmin, A.K. Pant, B.R. Babu, E.D. Stevens, Inorg. Chem. 25 (1986) 2300;
(b) T. Mallah, M.-L. Boillot, O. Kahn, J. Gouteron, S. Jeannin, Y. Jeannin, Inorg. Chem. 25 (1986) 3058;
(c) T. Mallah, O. Kahn, J. Gouteron, S. Jeannin, Y. Jeannin, C.J. O'Connor, Inorg. Chem. 26 (1987) 1375;
(d) M. Maekawa, S. Kitagawa, M. Munakata, H. Masuda, Inorg. Chem. 28 (1989) 1904;
(e) O.J. Gelling, A. Meetsma, B.L. Feringa, Inorg. Chem. 29 (1990) 2816;
(f) M.T. Rispens, O.J. Gelling, A.H.M. De Vries, A. Meetsma, F.V. Bolhuis, B.L. Feringa, Polyhedron 52 (1996) 3521;
(g) A. Asokan, B. Varghese, P.T. Manoharan, Inorg. Chem. 38 (1999) 4393;
(h) P. Dapporoto, M. Formica, V. Fusi, M. Micheloni, P. Paoli, R. Pontellini, P. Rossi, Inorg. Chem. 39 (2000) 4663;
(i) A. Erxleben, J. Hermann, J. Chem. Soc., Dalton Trans. (2000) 569;
(j) S. Torelli, C. Belle, I. Gautier-Luneau, J.L. Pierre, Inorg. Chem. 39 (2000) 3526.

[10] R.R. Gagne, C.L. Spiro, T.J. Smith, C.A. Hamann, W.R. Thies, A.K. Shiemke, J. Am. Chem. Soc. 103 (1981) 4073.

[11] A.I. Vogel, Textbook of Practical Organic Chemistry, 4th ed., ELBS and Longman, 1978.

[12] D.D. Perrin, W.L.F. Armarego, D.R. Perrin, Purification of Laboratory Chemicals, Pergamon, London, 1966.

[13] S.R. Hall, G.S.D. King, J.M. Stewart (Eds.), XTAL 3.5, Users Manual, University of Western Australia, Perth, 1995.

[14] SMART Version 5.10. SAINT Version 6.0. Bruker AXS Ltd., Madison, WI.

[15] (a) G.M. Sheldrick, SHELXS-86. SHELXL-93. Program for Crystal Structure Solution and Refinement, University of Göttingen, 1993;
(b) G.M. Sheldrick, SHELX-97. Program for Crystal Structure Solution and Refinement, University of Göttingen, 1997.

[16] (a) M. Mikuriya, K. Nakadera, T. Kotera, Bull. Chem. Soc. Jpn. 69 (1996) 399 (and references cited therein);
(b) R.R. Gagne, R.P. Kreh, J.A. Dodge, J. Am. Chem. Soc. 101 (1979) 6917;
(c) A.M. Bond, M.-A. Haga, I.S. Creece, R. Robson, J.C. Wilson, Inorg. Chem. 28 (1989) 559.

[17] P. Starynowicz, J. Lisowski, Chem. Commun. (1999) 769.

[18] (a) H.C. Aspinall, J. Black, I. Dodd, M.M. Harding, S.J. Winkly, J. Chem. Soc., Dalton Trans. (1993) 709;
(b) S.K. Mandal, K. Nag, J. Chem. Soc., Dalton Trans. (1983) 2429.

[19] C.K. Jhonson, ORTEP II, Report ORNL-5138, Oak Ridge National Laboratory, Oak Ridge, TN, 1976.

[20] (a) H. Adams, N.A. Bailey, P. Bertrand, C.O. Rodriguez de Barbarin, D.E. Fenton, S. Gou, J. Chem. Soc., Dalton Trans. (1995) 275;
(b) A. Erxleben, J. Hermann, J. Chem. Soc., Dalton Trans. (2000) 569.

[21] (a) R. Baggio, M. Perec, M.T. Garland, Acta Crystallogr. C52 (1996) 2457;
(b) M.L. Duran, J. Romero, J.A. Garcia-Vazquez, R. Castro, A. Castineiras, A. Sousa, Polyhedron 10 (1991) 197;
(c) J.I. Bruce, T.M. Donlevy, L.R. Gahan, C.H.L. Kennard, K.A.

Byriel, Polyhedron 15 (1996) 49;
(d) E. Bouwman, P. Evans, R.A.G. de Graaff, H. Kooijman, R. Poinsot, P. Rabu, J. Reedijk, A.L. Spek, Inorg. Chem. 34 (1995) 6302;
(e) D.C. Liles, M. McPartlin, P.A. Tasker, J. Chem. Soc., Dalton Trans. (1987) 1631.
[22] E. Asato, H. Furutachi, T. Kawahashi, M. Mikuria, J. Chem. Soc., Dalton Trans. (1995) 3897.
[23] (a) D. Luneau, J.-M. Savariault, P. Cassoux, J.-P. Tuchagues, J. Chem. Soc., Dalton Trans. (1988) 1225;
(b) A.J. Downard, V. McKee, S.S. Tandon, Inorg. Chim. Acta 173 (1990) 181.
[24] (a) A.H. Othman, K.-L. Lee, H.-K. Fun, B.-C. Yip, Acta Crystallogr. C52 (1996) 602;
(b) S. Karmakar, S.B. Choudhury, A. Chakravorty, Inorg. Chem. 33 (1994) 6148;
(c) P.K. Chakraborty, S.K. Chandra, A. Chakravorty, Inorg. Chem. 32 (1993) 5349;
(d) D.K. Towle, C.A. Botsford, D.J. Hodgson, Inorg. Chim. Acta 141 (1988) 167.
[25] (a) S. Brooker, R.J. Kelly, J. Chem. Soc., Dalton Trans. (1996) 2117 and references cited therein;
(b) J.E. Andrew, A.B. Blake, L.R. Fraser, J. Chem. Soc., Dalton Trans. (1975) 100.
[26] (a) B.J. Hathaway, A.A.G. Tomlinson, Coord. Chem. Rev. 5 (1970) 1;
(b) B.J. Hathaway, D.E. Billig, Coord. Chem. Rev. 5 (1970) 143;
(c) B.J. Hathaway, Struc. Bonding (Berlin) 57 (1984) 55.
[27] W.D. McFadyen, R. Robson, H. Schaap, Inorg. Chem. 11 (1972) 1777.
[28] K.G. Raghunathan, P.K. Bhardwaj, J. Chem. Soc., Dalton Trans. (1992) 2417.

PERGAMON

Polyhedron 21 (2002) 935–941

POLYHEDRON

www.elsevier.com/locate/poly

Cadmium complexation by aspartate. NMR studies and crystal structure of polymeric $Cd(AspH)NO_3$

Laura Gasque [a,*], Sylvain Bernès [b], Rosana Ferrari [a], Guillermo Mendoza-Díaz [c]

[a] *Departamento de Química Inorgánica, Facultad de Química, Universidad Nacional, Autónoma de México, Ciudad Universitaria, C.P. Mexico, D.F. 04510, Mexico*

[b] *Centro de Química, Instituto de Ciencias, B. Universidad Autónoma de Puebla, Apartado Postal 1613, Puebla, Pue., Mexico*

[c] *Facultad de Química, Universidad de Guanajuato, Noria Alta s/n, Guanajuato, Gto. 36050, Mexico*

Received 10 September 2001; accepted 24 January 2002

Abstract

Two cadmium compounds containing the aspartate ligand are described, with compositions $Cd(AspH)NO_3$ and Cd(Asp). The crystal structure of the first shows it is a two dimensional polymer in which each cadmium is coordinated to seven oxygen atoms, four from carboxylates and three from the nitrate moiety which acts both as a chelate and as a bridging ligand. For Cd(Asp), ^{111}Cd NMR studies suggests the presence of $Cd-NH_2$ interaction. © 2002 Published by Elsevier Science Ltd.

Keywords: Cadmium(II); Aspartate; Structures; ^{111}Cd NMR

1. Introduction

Though not as widely known to the general public as lead's, cadmium's toxicity is considerably larger [1]. As is the case with lead, the specific chemical interactions responsible for cadmium's toxicity are mostly unknown, although there has been some evidence that it mainly interferes in Zn^{2+} and Ca^{2+} sites and metabolism. The Cd uptake level is influenced by the calcium concentrations in the diet in a similar way as Lead, i.e. decreased by the increase of Ca intake [2]. The affinity that Cd^{2+} ion shows toward calcium binding sites, which are rich in aspartyl and glutamyl residues, has led to its use as a tool in studies of calcium binding sites in many systems as calbindin D_{9K} [3].

Similarities between cadmium and lead have been pointed out before, as one of several pairs of elements related by a knight's movement in the periodic table [4]. And just like lead's, classification of cadmium in the HSAB scheme has given problems, with some authors placing it among the soft acids, in agreement with Pearson's original papers [5] while others consider it borderline [6].

The behaviour of cadmium towards aminoacids has been studied both in solution and in the solid state. Stability constants for the 1:1 complexes are found to be consistently lower than for the corresponding lead complexes, usually for a little less than a logarithmic unit [7]. Several crystal structures of Cadmium–aminoacid complexes have been described [8]. The diversity of complexation modes is remarkable; from simple molecular structures with chelating aminoacid moieties, to polymeric structures where one or more of the donor groups are not coordinated to the metal.

In a recent paper, we reported two different lead complexes with aspartate, Pb(Asp) and $Pb(AspH)NO_3$ [9]. The X-ray structure of the latter showed it forms a three dimensional polymeric network in which each lead atom is coordinated only to oxygen atoms, from both carboxyl groups and the nitrate ion, while spectroscopic studies suggested amine group coordination in the former. Here, we present two cadmium–aspartate complexes with equivalent composition to those of lead, and discuss comparatively their structures.

* Corresponding author. Tel.: +52-5-622-3811; fax: +52-5-622-3724.

E-mail address: gasquel@servidor.unam.mx (L. Gasque).

0277-5387/02/$ - see front matter © 2002 Published by Elsevier Science Ltd.
PII: S0277-5387(02)00871-9

2. Experimental

Cadmium nitrate tetrahydrate and cadmium oxide were purchased from Aldrich; L-aspartic acid and L-aspartic acid monosodium salt hydrate from Sigma Chemical Co. Elemental analysis were carried out by Desert Analytics, Tucson, AZ.

2.1. Preparation of Cd(AspH)(NO$_3$) (I)

To 5 mmol of $Cd(NO_3)_2 \cdot 4H_2O$ dissolved in 25 ml of water, 5 mmol of NaAspH in 25 ml of water were added and pH adjusted to 4.3 with 1 M NaOH. The solution was left to stand and colourless prismatic crystals were collected after a few weeks. *Anal*. Calc. for $Cd(C_4H_6N_2O_7)$: C, 15.68; H, 1.96; N, 9.15. Found: C, 15.63; H, 2.08; N, 8.89%.

2.2. Preparation of Cd(Asp) (II)

Five mmol $AspH_2$ were dissolved in 150 ml of warm water and to this solution 2.5 mmol finely ground CdO were added in small portions, allowing for the solid CdO to dissolve after each addition. The clear solution was evaporated with the formation of a glassy material which analysed for $Cd(Asp) \cdot 1.5H_2O$. *Anal*. Calc. for $CdC_4H_6O_{5.5}N$: C, 17.76; H, 2.96; N, 5.18. Found: C, 17.32; H, 2.81; N, 5.02%.

2.3. Crystallography

Single-crystal X-ray diffraction data for **1** were measured at 298 K on a Bruker P4 diffractometer using common procedures [10] and a correction for absorption effect was applied based on 50 ψ-scans with χ close to 90°. The structure was solved and refined using standard procedures [11], without restraints nor constraints. H atoms were placed on idealised positions and refined using a riding model with fixed isotropic U. The refinement of a Flack parameter [12] confirmed the absolute configuration of the enantiopure amino acid AspH to be C3-*S*. Pertinent crystal data are collected in Table 1 and complete crystallographic information is deposited as a CIF file.

2.4. NMR spectroscopy

The ^{111}Cd CP-MAS NMR were recorded on a VARIAN Unity-Plus 300 MHz spectrometer operating at 63.602 MHz with a 7.5 μσ pulse. A 7 mm diameter silicon nitride rotor with kel-F caps was used. The rotor spin rate was kept between 3.5 and 5 KHz for all experiments, with a delay time between 5 and 10 s and between 500 and 10 000 transients were accumulated, 1–2.5 ms of contact time for cross polarisation was used, 0.05 s of acquisition time. $CdCO_3$ was used as external reference (−30 ppm). Spectra were recorded using total side band suppression when side bands were not well removed by spinning. Processing was made using a 20–40.11 Hz of line broadening, with the exception of the compound (II) spectra, where a 530 Hz line broadening was used. ^{13}C-CP-MAS NMR were recorded on the same spectrometer operating at 75.430 MHz, acquisition time 0.05 s. Typical contact times employed were of 1.25 ms; pulse width of 8.5 μS, and delay time of 4 s. Processing was made with zero filling and a line broadening of 20.33 Hz.

Solution ^{1}H NMR was made at 299.950 MHz with a VT-Switchable broad band probe; acquisition time 2.503 s, pulse of 45° (7.5 μs). Processing was made with zero filling and a line broadening apodisation of 1 Hz. In a typical experiment 32 transients were collected. D_2O was used as a solvent and pD was fixed with either DCl or NaOD.

Table 1
Crystal data

Empirical formula	$C_4H_6CdN_2O_7$
Formula weight	306.51
Crystal system	orthorhombic
Colour, habit	colourless, regular prism
Crystal size (mm)	$0.28 \times 0.22 \times 0.14$
Space group	$P2_12_12_1$
Unit cell dimensions	
a (Å)	7.1577(3)
b (Å)	7.2892(5)
c (Å)	14.9510(10)
Z	4
Absorption coefficient (mm^{-1})	2.819
Radiation	Mo Kα ($\lambda = 0.71073$ Å)
2θ Range (°)	5.44–59.98
Reflections collected	2675
Independent reflections [a]	2276 ($R_{int} = 2.15\%$)
Transmission factors (min, max)	0.257, 0.281
Final R indices [2156 $I > 2\sigma(I)$] (%) [a]	$R_1 = 2.61$, $wR_2 = 6.74$
Final R indices [all data] (%) [a]	$R_1 = 2.81$, $wR_2 = 6.88$
Goodness-of-fit, S [a]	1.042
Data-to-parameters ratio	2276/128

[a] R_{int}, R_1, wR_2 and S are defined as follows:

$$R_{int} = \frac{\sum |F_o^2 - \langle F_o^2 \rangle|}{\sum F_o^2}, \quad R_1 = \frac{\sum ||F_o| - |F_c||}{\sum |F_o|},$$

$$wR_2 = \sqrt{\frac{\sum w(F_o^2 - F_c^2)^2}{\sum w(F_o^2)^2}}, \quad S = \sqrt{\frac{\sum w(F_o^2 - F_c^2)^2}{m - n}}.$$

3. Results and discussion

3.1. Crystal structure

Relevant bond distances and angles for complex **1** are displayed in Table 2. The asymmetric unit contains one metal centre, one aspartate ligand and one nitrate ion,

Table 2
Selected bond lengths (Å) and angles (°) for complex **1**

Bond lengths			
Cd(1)–O(1)	2.213(3)	Cd(1)–O(4)#1	2.242(2)
Cd(1)–O(2)#2	2.258(2)	Cd(1)–O(3)#3	2.273(2)
Cd(1)–O(12)	2.464(3)	Cd(1)–O(11)	2.529(3)
Cd(1)–O(11)#4	2.600(3)	C(1)–O(1)	1.254(4)
C(1)–O(2)	1.273(4)	C(4)–O(3)	1.250(4)
C(4)–O(4)	1.248(4)	N(11)–O(13)	1.219(4)
N(11)–O(12)	1.258(4)	N(11)–O(11)	1.272(4)
Bond angles			
O(1)–Cd(1)–O(4)#1	87.15(10)	O(1)–Cd(1)–O(2)#2	171.03(9)
O(4)#1–Cd(1)–O(2)#2	101.38(10)	O(1)–Cd(1)–O(3)#3	91.27(10)
O(4)#1–Cd(1)–O(3)#3	149.38(10)	O(2)#2–Cd(1)–O(3)#3	82.81(10)
O(1)–Cd(1)–O(12)	85.36(10)	O(4)#1–Cd(1)–O(12)	127.67(9)
O(2)#2–Cd(1)–O(12)	87.19(10)	O(3)#3–Cd(1)–O(12)	82.56(10)
O(1)–Cd(1)–O(11)	85.49(10)	O(4)#1–Cd(1)–O(11)	76.80(9)
O(2)#2–Cd(1)–O(11)	93.70(9)	O(3)#3–Cd(1)–O(11)	133.58(10)
O(12)–Cd(1)–O(11)	51.02(9)	O(1)–Cd(1)–O(11)#4	105.87(10)
O(4)#1–Cd(1)–O(11)#4	72.22(9)	O(2)#2–Cd(1)–O(11)#4	79.67(9)
O(3)#3–Cd(1)–O(11)#4	78.87(10)	O(12)–Cd(1)–O(11)#4	158.40(9)
O(11)–Cd(1)–O(11)#4	146.20(6)	O(1)–C(1)–O(2)	125.5(3)
O(1)–C(1)–C(2)	115.8(3)	O(2)–C(1)–C(2)	118.6(3)
O(3)–C(4)–O(4)	128.5(3)	O(3)–C(4)–C(3)	117.6(3)
O(4)–C(4)–C(3)	113.8(3)		

Symmetry transformations used to generate equivalent atoms: #1, $-x+1, y+1/2, -z+1/2$; #2, $-x, y+1/2, -z+1/2$; #3, $x-1, y, z$; #4, $-x, y-1/2, -z+1/2$.

yielding a formula similar to that of $Pb(AspH)(NO_3)$ [9]. Nevertheless, the coordination geometry and the polymeric arrangement are different when substituting Pb(II) by Cd(II). As expected from the conditions of synthesis, the aspartate moiety presents two carboxylate groups while the amine function is protonated. The metal centre is seven-coordinated, with a geometry that can be described as distorted octahedral, where the sixth position is doubly occupied by two O atoms from the bidentating nitrate ion. Remaining coordination sites are occupied by one O atom from an crystallographic equivalent nitrate ion *trans* to the first one and four O atoms from 4 equiv. aspartate ligands *cis* to the nitrate moieties, as described in Fig. 1. Coordination distances span a range common for Cd(II) complexes [13], 2.213(3)–2.600(3) Å. The distortion from an ideal octahedral geometry is obvious, for example, from *trans* angles $O1–Cd1–O2' = 171.03(9)°$, $O3–Cd1–O4 = 149.38(10)°$ and from the bite *cis* angle formed by the nitrate ligand, $O11–Cd1–O12 = 51.02(9)°$, while remaining angles are in the range 72.22(9)°–133.58(10)°.

The complex is assembled in an original bi-dimensional polymeric network composed of perpendicularly connected chains (see Fig. 2). The main chains, running along the crystallographic *b* axis, result from the bridging character of the nitrate ion: O11 bridges 2 equiv. metallic centres, O12 is coordinated to one Cd atom and O13 is coordination-free. The different behaviour of each of these O atoms is clearly reflected in the N–O bond lengths (see Table 2), which can be compared with the N–O bond length of the free nitrate ion, 1.21 Å [14]. The 2D-polymer is formed by the connection of these chains through the α and β groups of the aspartate ligands along the *a* axis of the orthorhombic cell: O1 and O2 atoms from an aspartate ligand bridge two neighbouring Cd atoms of the previously described chain (running along the *b* axis) and the O3 and O4 atoms of the same ligand bridge two neighbouring Cd atoms of an other chain. In contrast to the iso-formula Pb complex [9], C–O bond lengths of the α and β carboxylic groups in **1** fall in a small range, 1.248(4)–1.273(4) Å. An other structural difference between $Pb(AspH)(NO_3)$ and $Cd(AspH)(NO_3)$ is that the polymeric connection of first one generates 18-membered rings containing three Pb ions and three AspH ligands, while for the last one the polymer includes 14-membered rings based on two Cd ions and two AspH ligands.

Moderate to weak hydrogen bonds sustain the cohesion between the 2D layers stacked along the *c* axis. The three H atoms of the ammonium group give short contacts with the three O atoms of the nitrate anion, with N–H···O separations ranging from 2.31 to 2.64 Å and angle from 118.0° to 148.3°. The carboxylic groups also participate as donor atoms in this network, with contacts N1–H1C···O2 (2.57 Å, 128.0°) and N1–H1B···O3 (2.56 Å, 158.2°). Finally, weak contacts are directed approximately along the *c* axis, using the aliphatic groups of the asp ligand as acceptor (C2 and C3) and O atoms as donors (O1, O12 and O13). C–H···O distances and angles ranges are characteristic of weak bonds: 2.48–2.58 Å and 136.7°–171.0°. (Table 3). These interactions are illustrated in Fig. 3.

3.2. NMR spectra

3.2.1. ^{111}Cd CP-MAS NMR spectra

Usually, ^{113}Cd is preferred since it has a slightly higher receptivity, but ^{111}Cd can also be used without an appreciable receptivity loss. As there is no primary isotope effect, results obtained on both isotopes can be directly compared [15]. As a tool for elucidating the coordination environment on the cadmium atom, a general observed trend for the Cd nuclei chemical shifts has been described [16,17]: shielding on a Cd atom is: (1) decreased when it is bonded to nitrogen (low field shift); (2) increased when bonded to oxygen (high field shift), but (3) decreased when it is part of a chelate ring. In the Cd CP-MAS spectra, distortions from octahedral symmetry are sufficient to produce large chemical shift anisotropies [18].

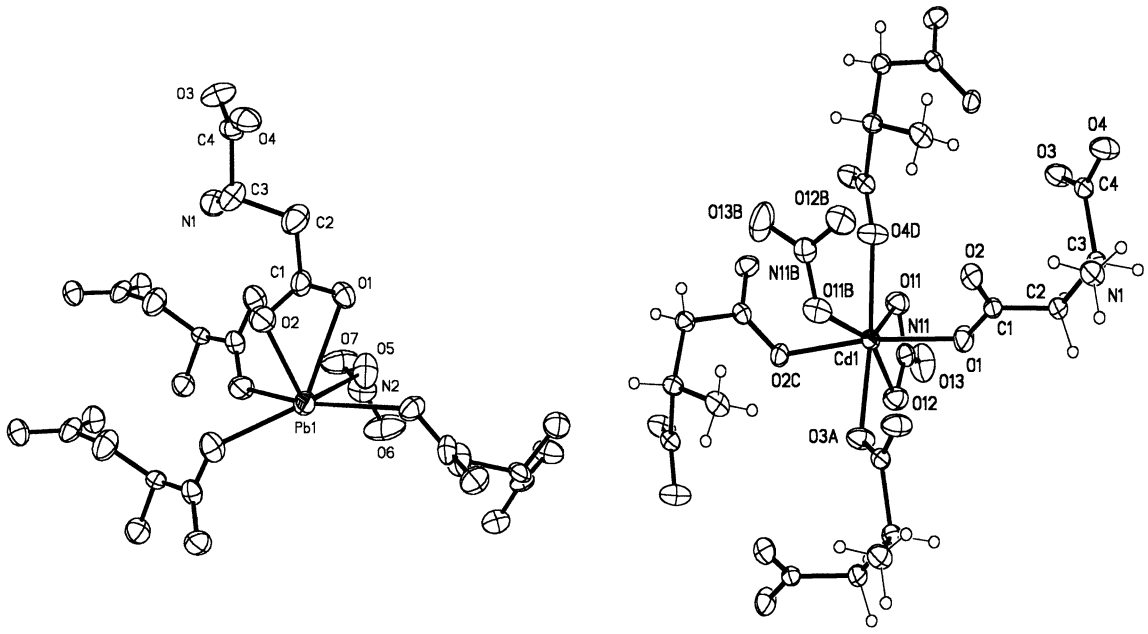


Fig. 1. The coordination environment for Cd atoms in **1** (right side) compared with the observed coordination environment in the isoformular Pb complex [9] (left side). Note that the metal centre is seven-coordinated in **1** and six-coordinated in Pb(AspH)(NO_3), leaving a large space available for a lone pair in the latter case. Thermal ellipsoids for **1** are at 50% probability level and symmetry codes used to generate equivalent atoms are the following: (A) $x-1$, y, z; (B) $-x$, $y-1/2$, $-z+1/2$, (C) $-x$, $y+1/2$, $-z+1/2$; (D) $-x+1$, $y+1/2$; $-z+1/2$.

In Cd(AspH)NO_3 (**I**), where there are seven oxygen atoms coordinated to each cadmium, an isotropic chemical shift of -78.6 ppm relative to $[Cd(H_2O)_6](ClO_4)_2$, was observed. In the latter each

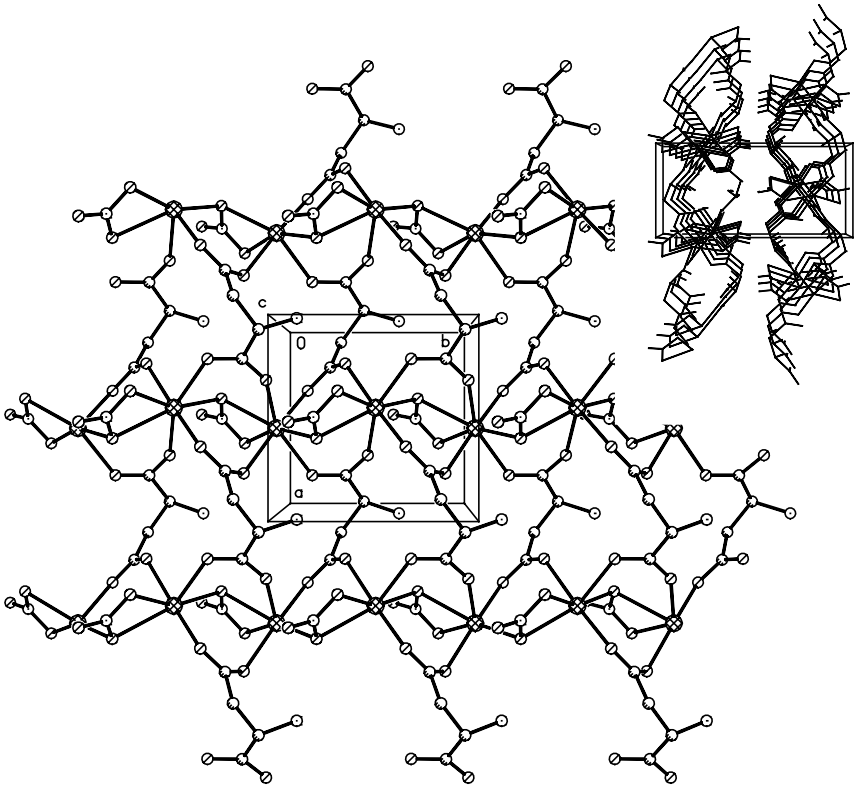


Fig. 2. The 2D polymeric layers of **1** viewed along the [001] axis. The inset shows a stick representation of two layers in a view normal to the [010] axis, i.e. as observed rotating the main figure around [100] by an angle of 90°. Note that no inter-layers contacts are observed, justifying the description of the polymer as an actual 2D framework. In both figures, H atoms are omitted for clarity.

Table 3
Hydrogen-bonds (Å and °), H···A < r (Å)+2.000 Å and D–H···A > 110°

D	H	A	Symmetry for A	D–H	H···A	D···A	D–H···A
N1	H1A	O11	$x, y-1, z$	0.890	2.462	2.985	117.96
N1	H1A	O13	$x+1/2, -y+3/2, -z$	0.890	2.561	3.139	123.24
N1	H1A	O12	$x+1/2, -y+3/2, -z$	0.890	2.637	3.320	134.26
N1	H1B	O2		0.890	2.259	2.838	122.48
N1	H1B	O3	$-x+1, y-1/2, -z+1/2$	0.890	2.559	3.401	158.19
N1	H1C	O12	$x+1, y-1, z$	0.890	2.310	3.103	148.31
N1	H1C	O2	$-x+1, y-1/2, -z+1/2$	0.890	2.568	3.193	127.95

D, donor atom; A, acceptor atom.

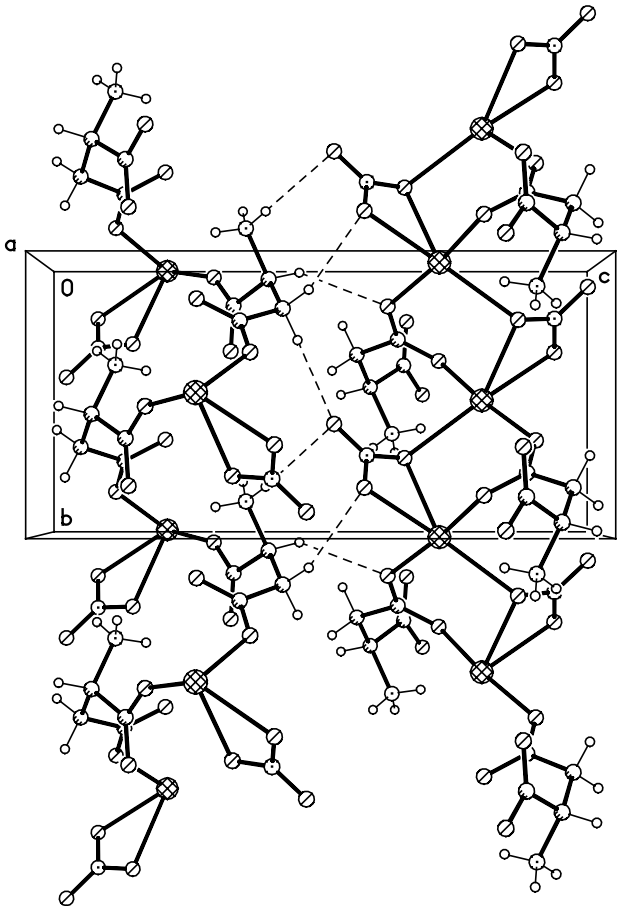


Fig. 3. Hydrogen bonding network.

Cd atom is coordinated octahedrally to six oxygen atoms from water molecules [19,20] i.e. a high field shifting is observed, as expected from the general trends mentioned above.

Nitrate chelation may be the cause of the apparent second order coupling between ^{111}Cd and ^{14}N in complex **I** as it can be seen in Fig. 4(b), together with the deconvoluted spectrum from which it is possible to see a 1:2:1 pattern, that displays a coupling constant of 125 Hz. As far as we know, there are no reported values for this second order coupling. This splitting includes the second order coupling constant and the residual splitting due to the residual dipolar interaction between ^{111}Cd and ^{14}N [21,22].

On the other hand, the spectrum for compound **II** has a very irregular, broad signal centred on 70 ppm with the highest peak in 36 ppm. This positive chemical shift is indicative of a coordination to one or more nitrogen atoms. Unfortunately, it is not possible to observe the coupling pattern between ^{111}Cd and ^{14}N. There are examples in the literature [22–26] of Cd–N environments that do not show noticeable coupling. In these cases, the observed line widths have been greater than the coupling. In complex **II**, the cadmium atom seems to be immersed in very asymmetrical site, and therefore, in spite of the spin rate used to obtain the spectrum, anisotropy could not be removed.

3.2.2. ^{13}C CP-MAS NMR spectra

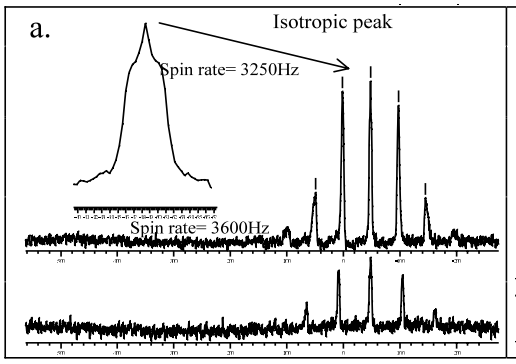
^{13}C NMR chemical shifts (ppm) are shown in Table 4. Compound **II** presents only one signal for carboxylic carbon atoms; indicating that in this compound the chemical environment for both carboxylates is quite similar. In compound **I**, however, even though both carboxylate groups are coordinated to cadmium nuclei, COOβ is involved in the strongest H-bond present in the crystal (H···O2 = 2.259 Å; N···O2 = 2.838 Å) with a H atom from the NH_3^+ group; besides, the other oxygen atom (O1) in COOβ has the strongest interaction with Cd^{2+} (shortest bond distance). Both interactions can cause a downfield shift for the COOβ carbon atom.

For compound **II**, not only the carboxylate carbon atoms show a sensible shift, but also the aliphatic ones. This could suggest the formation of a six membered chelate ring by the coordination of the amino group and the COOβ, in agreement with the observed Cd-CP-MAS data.

3.2.3. ^{1}H NMR versus pH

At a pH value close to the one used for crystallisation, the aminoacid, in presence of Cd^{2+}, develops a pattern of an ABC [27] spin system in the α-H signal (Fig. 5).

Considering the protonation state of the amine, a possible interpretation would be the formation of a chelate ring by the bonding of both carboxylate groups



c. Fit values:		
Freq(Hz)	**δ(ppm)**	**Integral**
-3210.22	-76.6	10283
-3085.50	-78.6	26435
-2960.02	-80.5	10900

Fig. 4. ^{111}Cd NMR spectrum.

Table 4
^{13}C NMR chemical shifts (ppm)

Nucleus	$AspH_2$	NaAspH	$Cd(AspH)NO_3$ (**I**)	Cd(Asp) (**II**)
COOα	176.32	174.24	174.56	180.67
CH	54.11	48.9	55.16	52.23
CH_2	38.26	34.85	34.76	40.50
COOβ	175.25	174.24	182.75	180.67

(α and β) to cadmium. By doing so, both β hydrogen atoms would become distinguishable turning into a BC spin system rather than B_2.

When the amine group deprotonates, at a higher pH value, a different chelate ring is feasible due to the coordination of the amino group and the α carboxylate oxygen atom, releasing the β carboxylate and therefore, both hydrogen atoms on the CH_2 moiety become again indistinguishable, causing the system to return to an AB_2 pattern. As it has been discussed, the compound as is isolated near pH 4, has no chelate rings formed by the two carboxylates and formation of a 3D polymer is preferred.

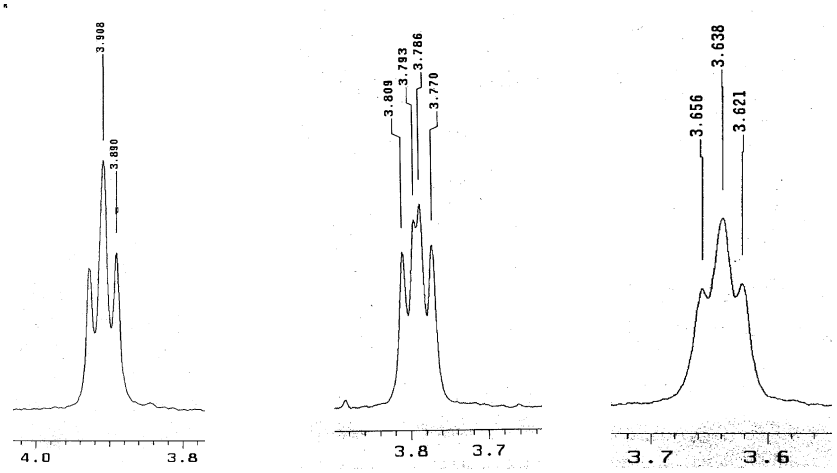
The accumulation of information on structural details of cadmium aqueous coordination chemistry—which is currently scarce—will hopefully contribute to a better understanding of this metal ion's interaction with biological molecules.

4. Supplementary material

Crystallographic data have been deposited with the CCDC. Copies of this information may be obtained free of charge from The Director, CCDC, 12 Union Road, Cambridge, CB2 1EZ, UK (fax: +44-1223-336033; e-mail: deposit@ccdc.cam.ac.uk or www: http://www.ccdc.cam.ac.uk) quoting the deposition number CCDC 169070.

Acknowledgements

S.B. is grateful to CONACyT for financial support (programa de retención, 000027).



Cd + Asp, pH=3.1 spin system AB_2 | Cd + Asp, pH=4.2 spin system ABC | Cd + Asp, pH=6.6

Fig. 5. ^{1}H NMR signal for $^{\alpha}$C–H at different pH values (Fig. 1).

References

[1] W. Kaim, B. Schwederski, Bioinorganic Chemistry: Inorganic Elements in the Chemistry of Life, Wiley, Chichester, UK, 1991.

[2] (a) P. Washko, R.J. Cousins, J. Nutr. 107 (1977) 920;
(b) P. Washko, R.J. Cousins, J. Toxicol. Environ. Health 1 (1976) 1055;
(c) A.A. Van Barneveld, C.J. Van der Hamer, Toxicol. Appl. Pharmacol. 79 (1985) 1.

[3] (a) S. Linse, W.J. Chazin, Protein Sci. 4 (1995) 1038;
(b) W. Chazin, T.D. Veenstra, Rapid Commun. Mass Spectrom. 13 (1999) 548;
(c) M. Akke, N. Skelton, J. Kordel, A.G. Palmer, W.J. Chazin, Biochemistry 32 (1993) 9832;
(d) N. Skelton, J. Koerdel, M. Akke, W.J. Chazin, J. Mol. Biol. 227 (1992) 1100;
(e) M. Akke, S. Forsén, W.J. Chazin, J. Mol. Biol. 252 (1995) 102;
(f) J. Matysik, A. Alia, G. Nachtegaal, H.J. van Gorkom, A.J. Hoff, H.J. de Groot, Biochemistry 39 (2000) 6751.

[4] M. Laing, South Afr. J. Sci. 87 (1991) 285.

[5] (a) R.G. Pearson, J. Chem. Ed. 45 (1968) 581;
(b) J.E. Huheey, E.A. Keiter, R.L. Keiter, Inorganic Chemistry Principles of Structure and Reactivity, fourth ed., Harper Collins, New York, 1993.

[6] (a) R.B. Martin, in: Seiler, Sigel, Sigel (Eds.), Handbook on Toxicity of Inorganic Compounds, Marcel Dekker, New York, 1988;
(b) G. Wulfsberg, Inorganic Chemistry, University Science Books, Sausalito, CA, 2000;
(c) G. Rayner-Canham, Descriptive Inorganic Chemistry, Freeman, New York, NY, 1996.

[7] A.E. Martell, R.M. Smith, Critical Stability Constants, vol. 1, Plenum, New York, 1977.

[8] (a) Y. Yukawa, Y. Inomata, T. Takeuchi, M. Simio, A. Ouchi, Bull. Chem. Soc. Jpn. 55 (1982) 335;
(b) A. Demaret, F. Abraham, Acta Crystallogr., Sect. C 43 (1987) 2067;
(c) M.Q. Ehsan, K.M.A. Malik, S.Z. Haider, J. Bangladesh Acad. Sci. 20 (1987) 175;
(d) P.J. Barrie, A. Gyani, M. Monteualli, P. O'Brian, Inorg. Chem. 32 (1993) 5262;
(e) H. Fuess, H. Bartunik, Acta Crystallogr., Sect. B 32 (1976) 2803;
(f) R.J. Flook, H.C. Freeman, C.J. Moore, M.L. Scudder, Chem. Commun. (1973) 753;
(g) D.W. Tomlin, T.M. Cooper, S.M. Cline, J.M. Hughees, W.W. Adams, Acta Crystallogr., Sect. C 53 (1997) 1815;
(h) A. Demaret, L. Abello, M. Fourati, G. Lapluye, J. Chem. Res. 354 (1978) 4339;
(i) R. Thulasidhass, J.K. Mohanarao, Curr. Sci. 49 (1980) 349;
(j) P. DeMester, D.J. Hodgson, J. Am. Chem. Soc. 99 (1977) 6884;
(k) H. Soylu, Eur. Cryst. Meeting 5 (1977) 313;
(l) I. Schaffers, D.A. Keszler, Acta Crystallogr., Sect. C 491 (1993) 156.

[9] L. Gasque, S. Bernès, R. Ferrari, C. Barbarín, M.J. Gutiérrez, G. Mendoza-Díaz, Polyhedron 19 (2000) 649.

[10] XSCANS Users Manual, Siemens Analytical X-ray Instruments Inc., Madison, WI, USA, 1996.

[11] G.M. Sheldrick, SHELXTL-PLUS, release 5.10, Siemens Analytical X-ray Instruments Inc., Madison, WI, USA, 1998; G.M. Sheldrick, SHELX-97 Users Manual, University of Göttingen, Germany, 1997.

[12] H.D. Flack, Acta Crystallogr., Sect. A 39 (1983) 876.

[13] G. Wilkinson, Comprehensive Co-ordination Chemistry, vol. 5, Pergamon, Oxford, UK, 1987.

[14] P. Pascal, Noveau Traité de Chimie Minérale. Tome X. Massun ET C^{ie} Editeurs, Paris, 1956.

[15] P. Grauger, Groups 11 and 12, Copper to Mercury; in P.S. Pergostin (Ed.), Transition Metal Nuclear Magnetic Resonance, 1st ed., 293, 1991.

[16] P.G. Mennitt, M.P. Shatlock, V.J. Bartuska, G.E. Maciel, J. Phys. Chem. 85 (1981) 2087.

[17] T. Takayama, S. Ohuchida, Y. Koike, M. Watanabe, D. Hashizume, Y. Ohashi, Bull. Chem. Soc. Jpn. 69 (1996) 1579.

[18] R.S. Honkonen, P.S. Marchetti, P.D. Ellis, J. Am. Chem. Soc. 108 (1986) 912.

[19] M.F. Summers, Coord. Chem. Rev. 86 (1988) 43.

[20] B. King, Enciclopedia of Inorganic Chemistry, vol. 1, Wiley, Chichester, UK, 1995.

[21] K. Eichele, R. Wasylishen, Inorg. Chem. 33 (1994) 2766.

[22] P.J. Barrie, A. Gyanu, M. Motevalli, P. O'Brien, Inorg. Chem. 32 (1993) 3862.

[23] O.F.Z. Khan, P. O'Brien, Polyhedron 10 (1991) 325.

[24] P.S. Marchetti, S. Bank, T.W. Bell, M.A. Kennedy, P.D.J. Ellis, J. Am. Chem. Soc. 111 (1989) 2063.

[25] M.A. Kennedy, J.L. Sessler, T. Murrai, P.D. Ellis, Inorg. Chem. 29 (1990) 1050.

[26] P. DuBois Murphy, W.C. Stevens, T.T.P. Cheung, S. Lacelle, B.C. Gerstein, D.M. Kurtz, Jr., J. Am. Chem. Soc. 103 (1981) 4400.

[27] R.J. Abraham, The Analysis of High Resolution NMR Spectra, Elsevier, Amsterdam, 1971, pp. 46–83.

PERGAMON

Polyhedron 21 (2002) 943–950

POLYHEDRON

www.elsevier.com/locate/poly

The coordination chemistry of dinitrato-di-2-pyridylamine copper(II). Crystal structures of *catena*-poly[[(di-2-pyridylamine)(nitrato-*O*,*O*′)copper(II)]-μ-nitrato-*O*:*O*′] and bis(nitrato-*O*,*O*′)(di-2-pyridylamine)copper(II) dihydrate

Sujittra Youngme [a,*], Narongsak Chaichit [b], Kannikar Damnatara [a]

[a] *Department of Chemistry, Faculty of Science, Khon Kaen University, Khon Kaen 40002, Thailand*
[b] *Department of Physics, Faculty of Science and Technology, Thammasart University Rangsit, Pathumthani 12121, Thailand*

Received 24 September 2001; accepted 10 January 2002

Abstract

The preparation, characterization and crystal structures of the mono(dpyam) copper(II)nitrato complexes $[Cu(dpyam)(O_2NO)_2]$ **(1)** and $[Cu(dpyam)(O_2NO)_2]\cdot 2H_2O$ **(2)** (dpyam = di-2-pyridylamine) have been investigated. Compound **1** consists of two crystallographically independent $[Cu(dpyam)(O_2NO)_2]$ neutral molecules. These molecules are linked into infinite chains by the bridging bidentate nitrate groups in the long-bonded tetragonal positions giving an elongated rhombic octahedral stereochemistry. The structure of **2** is composed of a couple of crystallographically independent $[Cu(dpyam)(O_2NO)_2]$ neutral molecules and four water molecules in the lattice. Each copper atom exhibits a tetrahedrally distorted square base of the N_2O_2 plane, with the second oxygen atoms of the monodentate nitrato groups weakly bound in nearly axial positions giving an extremely distorted octahedral coordination geometry. © 2002 Elsevier Science Ltd. All rights reserved.

Keywords: Crystal structures; Copper complexes; Nitrate complexes, Di-2-pyridylamine complexes

1. Introduction

The local molecular structures of the [Cu(chelate)$(OXO)_2$] or [Cu(chelate)(OXO)(OYO)] complexes, where chelate is ethylenediamine (en), *N*,*N*,*N*′,*N*′-tetramethylenediamine (tmen), 2-(2-dimethylaminoethyl)pyridine (DMAEP), 2,2′-bipyridyl (bpy) or di-2-pyridylamine (dpyam); and OXO and OYO are oxyanions, have been characterized [1–13]. Mononuclear complexes with a tetrahedrally distorted elongated octahedral geometry [2–9], dinuclear complexes with a square-pyramidal environment [8,10] and polynuclear complexes with an elongated rhombic (or tetragonal) octahedral stereochemistry [11–13], have been found by X-ray crystallography with respect to different coordinating and bridging roles of perchlorate, formate, nitrate and nitrite oxyanions. As a part of the investigation on the coordinating and bridging roles of oxyanions for this type of complexes, the compounds [Cu(dpyam)$(NO_3)_2$] **(1)** and $[Cu(dpyam)(NO_3)_2]\cdot 2H_2O$ **(2)** were prepared and their spectroscopic properties characterized. According to the differences in electronic spectra, the crystal structures of both complexes have been determined and compared with those of the above relevant complexes.

2. Experimental

All reagents were commercial grade materials and were used without further purification. Elemental analyses (C, H, N) were performed by the Microanalytical Service of Science and Technological Research Equipment Centre, Chulalongkorn University on Perkin–Elmer PE2400 CHNS/O Analyzer. Copper content was determined on atomic absorption spectrophotometer. The infrared spectra were recorded on a Biorad FTS-7/PC FTIR spectrophotometer as KBr pellets in the

* Corresponding author. Fax: +66-43-243-338.
E-mail address: sujittra@kku.ac.th (S. Youngme).

0277-5387/02/$ - see front matter © 2002 Elsevier Science Ltd. All rights reserved.
PII: S0277-5387(02)00857-4

4000–450 cm^{-1} region. Solid-state (diffuse reflectance) electronic spectra were recorded as polycrystalline samples on a Perkin–Elmer Lambda2S spectrophotometer over the range 8000–18 000 cm^{-1}. The X-band ESR spectra were recorded on polycrystalline samples at room temperature (r.t.) with a JEOL ESR JES-RE2X spectrometer (operating at the X-band) by the service of Scientific and Technological Research Equipment Centre, Chulalongkorn University. The complexes $[Cu(dpyam)(O_2CCH_3)_2]\cdot 2H_2O$ [6], $[Cu(dpyam)(O_2CCH_3)(NO_2)]\cdot H_2O$ [7], $[Cu(dpyam)(NO_2)_2]$ [7] and $[Cu(dpyam)(O_2CCH_2CH_3)(NO_3)]$ [13] were also prepared as the methods previously described in order to record their e.s.r. and electronic spectra for spectral comparison (Table 5).

2.1. Syntheses

2.1.1. Synthesis of [Cu(dpyam)(NO3)2] (1)

2.1.1.1. Method a. A boiling solution containing $CuCO_3\cdot Cu(OH)_2\cdot H_2O$ (0.22 g, 1.0 mmol) in water (10 ml) and 1.0 N nitric acid (2 ml) was added to a warm solution of dpyam (0.34 g, 2.0 mmol) in methanol (20 ml). The solution was stirred and solid $NaNO_3$ (0.17 g, 2.0 mmol) was added. The mixture was warmed and stirred for few minutes. On slow evaporation, green crystals of **1** (Table 5) were obtained. They were filtered off, washed with mother liquor and were dried in air. Yield approximately 84%. Found: C, 33.41; H, 2.48; Cu, 17.66; N, 19.56%. Calc. for $C_{10}H_9N_5CuO_6$: C, 33.48; H, 2.53; Cu, 17.71; N, 19.52%. IR (KBr pellet, cm^{-1}): 1380s $(\nu NO_3)_{asym}$, 1320s $(\nu NO_3)_{sym}$ and 650m (δNO_3).

2.1.1.2. Method b. Complex **1** was also prepared directly, by adding a boiling solution of $Cu(NO_3)_2\cdot 2.5H_2O$ (0.23 g, 1.0 mmol) in 20 ml acetone to a warm solution of dpyam (0.17 g, 1.0 mmol) in 10 ml methanol after which a hot solution of $CH_3COONa\cdot 3H_2O$ (0.27 g, 2.0 mmol) in 10 ml water was added. The mixture was warmed and stirred for 5 min. On slow evaporation, **1** was deposited as green crystals. Yield approximately 82%.

2.1.2. Synthesis of [Cu(dpyam)(NO3)2]·2H2O (2)

A boiling solution containing $CuCO_3\cdot Cu(OH)_2\cdot H_2O$ (0.22 g, 1.0 mmol) in water (30 ml) and 1.0 N nitric acid (2 ml) was added to a warm solution of dpyam (0.34 g, 2.0 mmol) in methanol (20 ml). The solution was stirred and solid $NaNO_3$ (0.17 g, 2.0 mmol) was added. On slow evaporation, compound **2** was obtained as greenish–blue crystals (Table 5). Yield approximately 75%. Found: C, 30.48; H, 3.28; Cu, 16.05; N, 17.70%. Calc. for $C_{10}H_{13}N_5CuO_8$: C, 30.42; H, 3.32; Cu, 16.10; N, 17.74%. IR (KBr pellet, cm^{-1}): 1380s $(\nu NO_3)_{asym}$, 1310s $(\nu NO_3)_{sym}$ and 650m (δNO_3).

2.2. Crystallography

Reflection data for complexes **1** and **2** were collected at 293 K on a 1K Bruker SMART CCD area-detector diffractometer using graphite monochromated Mo Kα radiation ($\lambda = 0.71073$ Å) at a detector distance of 4.5 cm and swing angle of -35°. A hemisphere of the reciprocal space was covered by combination of three sets of exposures; each set had a different ϕ angle (0, 88, 180°) and each exposure of 35 s for **1** and 15 s for **2** covered 0.3° in ω. Data reduction and cell refinements were performed using the program SAINT [14]. An empirical absorption correction by using the SADABS [15] program was applied, which resulted in transmission coefficients ranging from 0.705 to 1.000 for **1** and 0.759 to 1.000 for **2**. The structures were solved by direct methods and refined by full-matrix least-squares method on F^2_{obs} with anisotropic thermal parameters for all non-hydrogen atoms using the SHELXTL-PC V 5.03 [16] software package. All hydrogen atoms in **1** and **2** were located by difference synthesis and refined isotropically, except H(1), H(6), H(10) and H(15) in **2** which were geometrically fixed and allowed to ride on attached atoms and also two water hydrogen atoms were unable to locate. The O(3) in A; and O(10) and O(12) in B for complex **1** showed disorder with occupancies of 0.47 and 0.53; 0.58 and 0.42; and 0.50 and 0.50, respectively, for both conformers. The molecular graphics were created by using SHELXTL-PC. The crystal and refinement details for complexes **1** and **2** are listed in Table 1. Selected bond lengths and angles are given in Table 2 and Table 4. Fig. 1 illustrates the structure of **1**, Fig. 3 the structure of **2**, and the atom numbering scheme used.

3. Result and discussion

3.1. Structure of [Cu(dpyam)(O2NO)2] (1)

The asymmetric unit of **1** (Fig. 1) consists of a couple of similar and crystallographically independent $[Cu(dpyam)(O_2NO)_2]$ neutral molecules (A and B), self-assembled together by the week C–H···O intermolecular interactions involving the dpyam C–H group from A and one nitrato O atom from B and vice versa. The crystal structure is further stabilized by N–H···O hydrogen bonds. Both molecules (A and B) involve the six-coordinate $CuN_2O_2O_2'$ chromophore, with an elongated rhombic octahedral stereochemistry. The octahedra of both molecules are linked into infinite chains by the bridging bidentate nitrate group [17,18], Fig. 2(a). Two nitrogen atoms of the dpyam and two oxygen atoms of the bidentate chelate nitrate groups bond almost symmetrically in the basal CuN_2O_2 planes. The two oxygen atoms, O(4) and O(6′) in A; and O(10) and O(12′) in B, from the asymmetrically-bridging nitrate

Table 1
Crystal and refinement data for complexes **1** and **2**

Complex	**1**	**2**
Molecular formula	2[Cu(dpyam)-$(ONO_2)_2$]	2[Cu(dpyam)-$(ONO_2)_2$].$4H_2O$
Molecular weight	717.51	789.57
Temperature (K)	293(2)	293(2)
Crystal system	orthorhombic	triclinic
Space group	$Pca2_1$	P_1
a (Å)	20.6997(2)	7.33743(3)
b (Å)	9.8938(2)	10.9569(4)
C (Å)	13.7080(2)	11.2385(4)
α (°)	90	83.46(2)
β (°)	90	76.76(2)
γ (°)	90	73.35(2)
V (Å^3)	2807.38(8)	841.48(5)
Z	4	1
D_{calc} (g cm^{-3})	1.698	1.554
μ (mm^{-1})	1.594	1.345
$F(000)$	1448	400
Crystal size (mm)	0.43 × 0.38 × 0.30	0.15 × 0.55 × 0.08
θ Range (°)	1.97–29.99	1.86–30.43
$h/k/l$	−28,27/−13,13/−16,18	−10,10/−15,13/−15,10
Number of reflection collected	19 390	6263
Number of unique reflections	6911	5325
Number of observed reflections	5971	4299
Absorption correction	semi-empirical	semi-empirical
$T_{max.}$ and $T_{min.}$	1.0000, 0.7053	1.0000, 0.7594
Data/restraints/parameter	6911/1/449	5325/3/509
GOF	1.078	1.046
Final R indices [$I > 2\sigma(I)$]	$R_1 = 0.0446$, $wR_2 = 0.1105$	$R_1 = 0.0418$, $wR_2 = 0.1024$
R indices (all data)	$R_1 = 0.0537$, $wR_2 = 0.1168$	$R_1 = 0.0579$, $wR_2 = 0.1152$
Largest difference peak and hole (e Å^{-3})	1.523, −0.461	0.369, −0.568

Table 2
Selected bond lengths (Å) and angles (°) with e.s.d's in parentheses of [Cu(dpyam)$(ONO_2)_2$] (**1**)

A		B	
Bond lengths			
Cu(1)–N(1)	1.966(3)	Cu(2)–N(7)	1.974(3)
Cu(1)–N(2)	1.988(3)	Cu(2)–N(6)	1.987(3)
Cu(1)–O(1)	2.023(3)	Cu(2)–O(7)	2.041(3)
Cu(1)–O(2)	2.110(3)	Cu(2)–O(8)	2.080(3)
Cu(1)–O(4)	2.386(4)	Cu(2)–O(10)	2.422(6)
Cu(1)–O(6′)	2.522(4)	Cu(2)–O(10A)	2.433(8)
N(4)–O(1)	1.304(4)	Cu(2)–O(12′)	2.510(4)
N(4)–O(2)	1.295(5)	Cu(2)–O(12A′)	2.522(4)
N(4)–O(3)	1.247(8)	N(9)–O(7)	1.292(4)
N(4)–O(3A)	1.251(7)	N(9)–O(8)	1.298(5)
N(5)–O(4)	1.275(6)	N(9)–O(9)	1.215(4)
N(5)–O(5)	1.212(5)	N(10)–O(10)	1.310(7)
N(5)–O(6)	1.254(6)	N(10)–O(10A)	1.256(10)
		N(10)–O(11)	1.239(5)
		N(10)–O(12)	1.297(9)
		N(10)–O(12A)	1.262(9)
Bond angles			
N(1)–Cu(1)–N(2)	95.8(2)	N(7)–Cu(2)–N(6)	95.8(2)
N(1)–Cu(1)–O(1)	165.2(3)	N(7)–Cu(2)–O(7)	163.7(2)
N(1)–Cu(1)–O(2)	101.9(2)	N(6)–Cu(2)–O(7)	100.1(2)
N(2)–Cu(1)–O(1)	98.9(2)	N(7)–Cu(2)–O(8)	100.7(2)
N(2)–Cu(1)–O(2)	161.0(2)	O(12A′)–Cu(2)–O(10)	160.9(4)
O(1)–Cu(1)–O(2)	63.3(2)	N(7)–Cu(2)–O(10A)	106.6(3)
N(1)–Cu(1)–O(4)	83.6(2)	N(6)–Cu(2)–O(10A)	93.2(3)
N(2)–Cu(1)–O(4)	105.2(2)	O(7)–Cu(2)–O(10A)	76.4(2)
O(1)–Cu(1)–O(4)	93.5(2)	O(8)–Cu(2)–O(10A)	84.3(3)
O(2)–Cu(1)–O(4)	83.6(2)	O(2)–N(4)–O(1)	113.2(3)
O(6′)–Cu(1)–O(1)	84.2(2)	O(12A′)–Cu(2)–O(10A)	165.9(3)
O(6′)–Cu(1)–O(2)	91.1(2)	O(12′)–Cu(2)–O(7)	85.0(2)
O(6′)–Cu(1)–O(4)	165.9(4)	O(12′)–Cu(2)–O(8)	93.0(2)
O(6′)–Cu(1)–N(1)	95.6(2)	O(12′)–Cu(2)–N(6)	83.5(2)
O(6′)–Cu(1)–N(2)	83.5(2)	O(12′)–Cu(2)–N(7)	93.0(2)
O(5)–N(5)–O(6)	123.3(5)	O(12A′)–Cu(2)–O(7)	91.1(2)
O(5)–N(5)–O(4)	123.4(5)	O(12A′)–Cu(2)–O(8)	84.2(2)
O(6)–N(5)–O(4)	113.2(3)	O(12A′)–Cu(2)–N(6)	95.6(2)
O(3)–N(4)–O(2)	122.2(4)	O(12A′)–Cu(2)–N(7)	83.5(2)
O(3)–N(4)–O(1)	121.8(5)	O(7)–N(9)–O(8)	113.5(3)
O(3A)–N(4)–O(2)	122.1(4)	O(12′)–Cu(2)–O(10A)	160.3(3)
O(3A)–N(4)–O(1)	122.9(4)	O(9)–N(9)–O(7)	123.7(4)
		O(9)–N(9)–O(8)	122.8(4)
		O(10A)–N(10)–O(12A)	107.5(5)
		O(10A)–N(10)–O(12)	119.3(6)
		O(10A)–N(10)–O(11)	117.4(6)
		O(10)–N(10)–O(11)	123.6(5)
		O(10)–N(10)–O(12)	109.2(5)
		O(10)–N(10)–O(12A)	112.7(5)
		O(11)–N(10)–O(12)	122.9(5)
		O(11)–N(10)–O(12A)	123.2(6)

groups occupy axial positions above and below the CuN_2O_2 planes, with Cu–O distances of 2.386(4) and 2.522(4) Å in A; and 2.422(6) and 2.510(4) Å in B. These distances are consistent with 'semi-coordination' of the bridging nitrate groups [19]. The tetragonalities (T = the mean in-plane bond length/the mean out-of-plane bond length) of molecules A and B are 0.824 and 0.817, respectively. The N–O distances involving the coordinated O atoms of the nitrate group are significantly longer compared with those of free nitrate (N–O = 1.255 Å) and non-coordinated O atoms [20]. In addition, the non-coordinated O atoms exhibit a shorter N–O bond distance than does free nitrate. Four atoms of the square-planes are essentially coplanar with a slight tetrahedral twist (dihedral angles between the CuN_2 and CuO_2 planes = 7.0(2)° in A and 3.8(2)° in B). The dihedral angles of 71.9(4)° and 87.6(4)° between two nitrate groups for each chromophore are nearly 90°. The planar pyridine rings make a dihedral angles of 10.0(2)° and 6.1(2)° with each other for A and B, respectively.

An important feature of the structure of **1** is the two-coordinate bridging coordination of the nitrate anion in the tetragonal positions, which involves an unsymmetrical bonding to the copper atom in the elongated rhombic octahedral configuration. The bond lengths and angles in **1** are comparable with those observed in the closely related complexes [Cu(dpyam)(CH_3CH_2-CO_2)(NO_3)] (**3**), $T = 0.753$ [13], [Cu(dpyam)(CH_3-CO_2)(NO_3)] (**4**), $T = 0.785$ [12] and [Cu(dpyam)(CH_3-

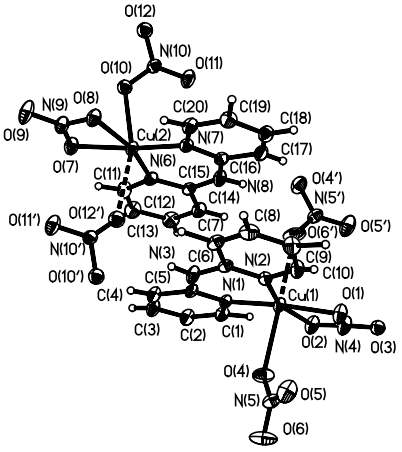


Fig. 1. The complex unit of $[Cu(dpyam)(ONO_2)_2]$ (**1**).

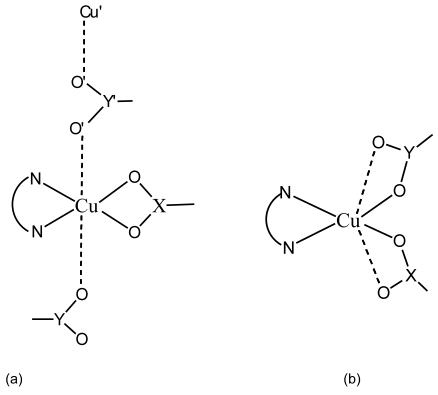


Fig. 2. Possible stereochemistries for [Cu(chelate)(OXO)(OYO)] complexes.

$CO_2)(ClO_4)]\cdot H_2O$ (**5**), $T = 0.765$ [11] but with the less elongation in the axial positions (Table 3) ($T = 0.824$ and 0.817 for A and B in **1**). Their local molecular geometries of the $CuN_2O_2O_2'$ chromophore are closely related, as in these three cases the in-plane coordinating atoms are the pyridine nitrogen atoms of the dpyam and two acetate or propionate oxygen atoms. In complex **5** the out-of-plane coordination sites are occupied by the oxygen atoms of the bridging perchlorate groups rather than the oxygen atoms of the bridging nitrate as in complexes **1**, **3** and **4**. To the best of our knowledge, complex **1** represents the first structurally characterized example of the [Cu(II)(chelate)$(OXO)_2$] derivative, exhibiting the polymeric chain with the two-coordinate bridging coordination of the nitrate anion in the tetragonal positions.

The complexes **1** and **3**–**5** are also compared with some other related complexes in Table 3. The elongated rhombic octahedral $CuN_2O_2O_2'$ chromophores of **1** and **3**–**5** are significantly different from those of the irregular rhombic octahedral CuN_4O_2 chromophore in $[Cu(bpy)_2(O_2ClO_2)](ClO_4)$ [21] or the CuN_4F_2 chromophore in $[Cu(bpy)_2(F_2BF_2)](BF_4)$ [21b] and the regular CuN_4O_2 chromophores in $[Cu(bpy)_2(S_4O_6)]$ [22] and $[Cu(bpy)_2(S_3O_6)]$ [22,23]. The in-plane CuN_4 chromophores of the remaining complexes have a marked tetrahedral distortion, with dihedral angles of approximately 37–57° (Table 3). This arises due to the steric interference of the two 2,9-hydrogen atoms of the dpyam ligand preventing these two rings from lying coplanar [21]. The unsymmetrical bonding role of the bridging nitrate group in **1** and **4** and bridging perchlorate group in **5** are comparable to that of $[Cu(bpy)_2(F_2BF_2)](BF_4)$ (Table 3) with the ΔO_{axial} of approximately 0.08–0.149 Å, but contrasts with those of the thionate complexes which involve more regular elongated rhombic octahedral chromophores. Furthermore **1** has the least out-of-plane distortion compared with those of the remaining complexes, denoted by the significantly larger tetragonalities, 0.824 and 0.817.

The one-coordinate bidentate mode of coordination is the predominating mode of the coordination of the nitrate group, involving both symmetric and asymmetric chelate nitrato coordination as in $[Cu(bpy)_2(O_2NO)](NO_3)$ [24]. The unsymmetrical bridging role of the nitrate group, which coordinates to the copper atom in the two coordinate manner as in **1**, **3** and **4** is unusual in Cu(II) chemistry. It is known to occur in an anhydrous $Cu(NO_3)_2$ [25] but with the near symmetric bridging bidentate coordination whose structure is described as distorted octahedral $(4+1+1')$. The related bpy complex $[Cu(bpy)(O_2NO)_2]$ is monomeric with an extremely distorted octahedron and both nitrate groups are bidentately bound to the copper atom [9]. In contrast, its silver analog forms a polymeric chain having the nitrate anion bridging between two Ag atoms, thereby achieving six-coordination [26].

3.2. Structure of $[Cu(dpyam)(O_2NO)_2]\cdot 2H_2O$ (**2**)

The asymmetric unit of **2** (Fig. 3) is made up of a couple of similar and crystallographically independent $[Cu(dpyam)(O_2NO)_2]$ neutral molecules (A and B) and four water molecules in the lattice. Molecules A and B are self-assembled by cooperative $O(NO_3)\cdots O(H_2O)$ in A and $O(NO_3)\cdots H(H_2O)$ in B. The crystallography structure is further stabilized by $O(NO_3)\cdots H(H_2O)$ and $N-H\cdots O(H_2O)$ hydrogen bonds via another water molecules. The Cu atoms of both molecules exhibit an irregular (4+2) coordination of the $CuN_2O_2O_2'$ chromophore. The coordination around each copper atom consists of two dpyam nitrogen atoms and two oxygen atoms from each nitrate group, forming a tetrahedral distorted square base. These equatorial planes of both molecules are markedly tetrahedrally twisted, as it is evident from the dihedral angles of 34.6(2)° and 33.0(3)°, respectively, at which the N–Cu–N and O–Cu–O planes cross. The second oxygen atoms from each nitrate group of both units then occupy the approxi-

Table 3
Structural data for some elongated octahedral copper(II) complexes with bridging semi-coordinate anions

Complex	Chromophore	Cu–O(apical) (Å)	Dihedral angle (°)	Tetragonality (T)	ΔO_{axial} (Å)	Reference
[Cu(dpyam)(O_2NO)(O_2NO)] (**1**)	$CuN_2O_2O'_2$	2.386, 2.522 & 2.422, 2.510		0.824, 0.817	0.136, 0.088	This work
[Cu(dpyam)($O_2CCH_2CH_3$)(O_2NO)] (**3**)	$CuN_2O_2O'_2$	2.411, 2.848		0.753	0.437	[13]
[Cu(dpyam)(O_2CCH_3)(O_2NO)] (**4**)	$CuN_2O_2O'_2$	2.454, 2.603		0.785	0.149	[12]
[Cu(dpyam)(O_2CCH_3)(O_2ClO_2)]·H_2O (**5**)	$CuN_2O_2O'_2$	2.541, 2.638		0.765	0.097	[11]
[Cu(bpy)$_2$(O_2ClO_2)][ClO_4] [a]	CuN_4O_2	2.45, 2.73	37	0.77	0.280	[21a]
[Cu(bpy)$_2$(O_2ClO_2)][ClO_4]	CuN_4O_2	2.512, 2.746	46.7	0.757	0.234	[21b]
[Cu(bpy)$_2$(F_2BF_2)][BF_4]	CuN_4F_2	2.560, 2.656	44.6	0.763	0.096	[21b]
[Cu(bpy)$_2$(S_4O_6)]	CuN_4O_2	2.627, 2.627	56.3	0.76	0.000	[22]
[Cu(bpy)$_2$(S_3O_6)]	CuN_4O_2	2.82, 2.82		0.704	0.000	[22,23]

[a] Original crystal structure.

Table 4
Selected bond lengths (Å) and angles (°) with e.s.d's in parentheses of [Cu(dpyam)(ONO_2)$_2$]·$2H_2O$ (**2**)

A		B	
Bond lengths			
Cu(1)–O(4)	1.978(7)	Cu(2)–N(6)	1.990(8)
Cu(1)–O(1)	1.979(6)	Cu(2)–N(7)	1.953(8)
Cu(1)–N(1)	2.001(8)	Cu(2)–O(7)	1.976(8)
Cu(1)–N(2)	2.007(9)	Cu(2)–O(8)	2.499(9)
Cu(1)–O(2)	2.696(8)	Cu(2)–O(10)	1.960(7)
Cu(1)–O(5)	2.475(8)	Cu(2)–O(11)	2.707(7)
N(4)–O(1)	1.236(11)	N(9)–O(7)	1.160(20)
N(4)–O(2)	1.274(10)	N(9)–O(8)	1.362(14)
N(4)–O(3)	1.512(9)	N(9)–O(9)	1.730(20)
N(5)–O(4)	1.302(8)	N(10)–O(10)	1.311(9)
N(5)–O(5)	1.211(10)	N(10)–O(11)	1.224(11)
N(5)–O(6)	1.502(7)	N(10)–O(12)	1.700(20)
Bond angles			
O(4)–Cu(1)–O(1)	88.4(3)	O(7)–Cu(2)–O(8)	58.3(3)
O(4)–Cu(1)–N(1)	95.1(3)	O(7)–Cu(2)–N(6)	93.7(4)
O(4)–Cu(1)–N(2)	154.7(3)	O(7)–Cu(2)–N(7)	155.4(3)
O(4)–Cu(1)–O(5)	57.8(3)	O(7)–Cu(2)–O(10)	89.8(3)
O(4)–Cu(1)–O(2)	114.5(3)	O(7)–Cu(2)–O(11)	114.5(3)
O(1)–Cu(1)–N(1)	156.6(3)	O(10)–Cu(2)–O(11)	53.3(3)
O(1)–Cu(1)–N(2)	94.7(3)	O(10)–Cu(2)–N(7)	93.2(3)
O(1)–Cu(1)–O(2)	54.1(3)	O(10)–Cu(2)–N(6)	157.7(3)
O(1)–Cu(1)–O(5)	93.9(3)	O(10)–Cu(2)–O(8)	95.5(3)
O(2)–Cu(1)–N(1)	104.0(3)	O(8)–Cu(2)–N(6)	105.1(3)
O(2)–Cu(1)–N(2)	87.1(3)	O(8)–Cu(2)–N(7)	97.1(3)
O(2)–Cu(1)–O(5)	148.0(3)	O(8)–Cu(2)–O(11)	148.8(3)
O(5)–Cu(1)–N(1)	107.5(3)	O(11)–Cu(2)–N(6)	105.8(3)
O(5)–Cu(1)–N(2)	96.9(3)	O(11)–Cu(2)–N(7)	86.4(3)
N(1)–Cu(1)–N(2)	92.0(3)	N(7)–Cu(2)–N(6)	92.8(3)
O(1)–N(4)–O(3)	118.2(6)	O(7)–N(9)–O(9)	127.2(13)
O(1)–N(4)–O(2)	124.3(7)	O(7)–N(9)–O(8)	124.0(13)
O(2)–N(4)–O(3)	117.4(8)	O(8)–N(9)–O(9)	108.6(15)
O(5)–N(5)–O(4)	121.8(6)	O(10)–N(10)–O(12)	115.5(10)
O(5)–N(5)–O(6)	123.4(5)	O(11)–N(10)–O(10)	120.1(8)
O(4)–N(5)–O(6)	114.7(6)	O(11)–N(10)–O(12)	124.3(10)

mately tetragonal (axial) positions above and below the CuN_2O_2 basal planes at longer distances of 2.699(8) and 2.472(8) Å in A; and 2.502(9) and 2.703(7) Å in B giving the extremely distorted octahedron, Fig. 2(b). However,

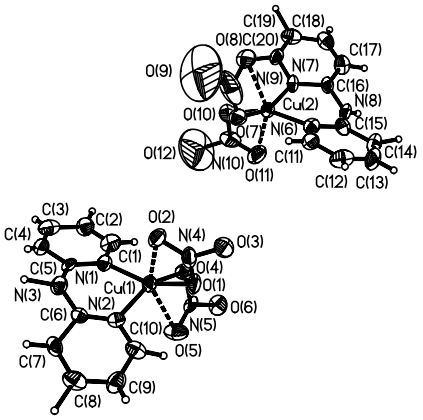


Fig. 3. The molecular structure of [Cu(dpyam)(ONO_2)$_2$]·$2H_2O$ (**2**).

both nitrate groups in A and B are bent towards the Cu atom to complete the fifth and sixth coordination sites in the axial positions with the O(2)–Cu–O(5) angle of 148.0(3)° in A and the O(8)–Cu–O(11) angle of 148.8(3)° in B which are markedly less than 180°. The dihedral angles between the individual dpyam pyridyl rings are 26.2(4)° and 25.7(4)° in A and B, respectively.

Both nitrate groups in A and B are planar and the planes of these two groups in each unit are almost perpendicular to each other [75.4(4)° in A and 72.8(6)° in B]. The coordination N–O distances [1.211(10)–1.302(8) Å in A and 1.224(11)–1.362(14) Å in B, and the subtended O–N–O angles of 124.3(7)° and 121.8(6)° in A; and 120.1(8)° and 124.0(13)° in B are consistent with an asymmetric bidentate coordination [9] compared with those of the symmetric bidentate coordination of the nitrate groups in **1** [subtended O–N–O angles = 113.2(3)° in A and 113.5(3)° in B]. However, there are some unreasonable N–O bond distances [N(4)–O(3), 1.512 Å and N(5)–O(6), 1.502 Å in A, and N(9)–O(7), 1.160 Å; N(9)–O(9), 1.730 Å and N(10)–O(12), 1.700 Å in B] with high temperature factors of some atoms [O(12), 0.192 and O(9), 0.392]. Hence, attempts were made to model and refine these

relevant atoms which were unsuccessful. There are the hydrogen bonds involved between water molecules and each of the nitrate groups in **2**. These bondings may be responsible for the evident distortion of these nitrate groups [the O–N–O angles vary from 108.6(15)° to 124.3(7)°] compared with those for the monodentate nitrate ligand (119.3°–120.6°) [10,13]. The close approach to the copper atoms of the second oxygen atoms from each nitrate group would indicate that the coordination mode of these oxygen atoms to the copper is intermediate between the purely monodentate nitrato-coordination [10,13] and the fully bidentate nitrato-coordination [27] as in **1**.

The coordination around the copper atoms of the molecules A and B is comparable to those observed in the related complexes $[Cu(bpy)(NO_2)_2]$ [4], $[Cu(bpy)(NO_3)_2]$ [9], $[Cu(tmen)(NO_3)_2]$ [2], $[Cu(DMAEP)(NO_3)_2]$ [3] and the corresponding dpyam complexes $[Cu(dpyam)(NO_2)_2]$ (**6**) [7], $[Cu(dpyam)(O_2CCH_3)(NO_2)]\cdot H_2O$ (**7**) [7], $[Cu(dpyam)(O_2CCH_3)_2]\cdot 2H_2O$ (**8**) [6], $[Cu(dpyam)(O_2CCH_3)(NO_2)]$ (**9**) [8] and $[Cu(dpyam)(O_2CCH_3)_2]\cdot H_2O$ (**10**) [5] and $[Cu(dpyam)(NO_2)_2]_2\cdot 2CH_3CN$ [8]. These complexes involve the tetrahedrally distorted elongated tetragonal-octahedral geometry with the long off-the-z-axis coordination of the second oxygen atoms from each OXO^- ligand in the axial positions. The latter complex exhibits the dinuclear complex containing both monodentate and O-bridging nitrite ligands. The most similarity in the $CuN_2O_2O'O'$ chromophore to that of **2** is observed in **8** and **10** exhibiting the similar axial distances of 2.5 and 2.7 Å and dihedral angles of 26.8° and 34.4° for both complexes, respectively, and the axial O–Cu–O angle of 148.2° for **8**. However, the coordination around the copper atoms in **2** differs from the arrangement observed in the related formato dinuclear derivative $[Cu(dpyam)(HCO_2)_2(H_2O)_{0.5}]_2\cdot H_2O$ [10], involving both monodentate and O,O′-bridging formato ligands. Each copper atom of this formate dimer is in a distorted square-pyramidal coordination environment.

3.3. Spectroscopic properties

3.3.1. ESR spectra

The polycrystalline e.s.r. spectrum of **1** is clearly axial ($g_{//} \gg g_\perp > 2.0$) with $g_{//} = 2.307$ and $g_\perp = 2.074$, suggesting a $d_{x^2-y^2}$ ground state which is consistent with an elongated rhombic-octahedral $CuN_2O_2O'_2$ chromophore of **1**. This type of polycrystalline e.s.r. spectrum is similar to that of **2** which also involves the axial type with $g_{//} = 2.225$ and $g_\perp = 2.086$, consistent with the tetrahedrally distorted elongated tetragonal-octahedral geometry with the off-the-z-axis coordination in the axial positions of **2**. The e.s.r. spectra of both **1** and **2** are compared (Table 5) with those of some relevant complexes.

3.3.2. Electronic spectra

The electronic reflectance spectrum of **1** has a broad peak centered at 14 340 cm^{-1}, with a poorly resolved shoulder to low energy at approximately 10 840 cm^{-1}, corresponding to the elongated rhombic-octahedral geometry [1,12]. This suggests the assignment [28] of the bands as the d_{xz}, $d_{yz} \rightarrow d_{x^2-y^2}$ and $d_{z^2} \rightarrow d_{x^2-y^2}$ transitions, respectively, with the position of the $d_{xy} \rightarrow d_{x^2-y^2}$ transition uncertain. The electronic spectrum of **1** are comparable to those found in the related complexes $[Cu(dpyam)(O_2CCH_3)(NO_3)]$, 15 000 and approximately 10 000 (sh) cm^{-1} and $[Cu(dpyam)(O_2CCH_3)(ClO_4)]\cdot H_2O$, 15 800 and approximately 10 000 (sh) cm^{-1} (Table 5). The higher energies in electronic spectra of the latter two complexes correspond to the more elongation in the axial distances with the less tetragonalities of 0.785 and 0.765, respectively. That of **2** (tetrahedral twist, 33.80° (av.)) involves a single broad peak at a lower energy of approximately 13 580 cm^{-1}. The observed single band in **2** is comparable to that of the single band in the related complexes $[Cu(dpyam)(NO_2)_2]$ (**6**) [7] (13 890 cm^{-1}; tetrahedral twist, 31.16°), $[Cu(dpyam)(O_2CCH_3)(NO_2)]\cdot H_2O$ (**7**) [7] (13 880 cm^{-1}; tetrahedral twist, 32.69°) and $[Cu(dpyam)(O_2CCH_3)_2]\cdot 2H_2O$ (**8**) [6] (13 510 cm^{-1}; tetrahedral twist, 34.38°) (Table 5). These spectra are consistent with an elongated rhombic-octahedral stereochemistry. All four d–d transitions (d_{z^2}, d_{xy}, d_{xz} and $d_{yz} \rightarrow d_{x^2-y^2}$) are assigned to lie within the band envelope at approximately 11 000–15 500 cm^{-1} for **2** and the similar assignment can be made for the other relevant complexes. This has been found that the higher tetrahedral twist in the basal planes, the lower energies in electronic spectra. Hence, the presence of higher energies in electronic spectra of **1** and its closely related complexes compared with those of **2** and **6**–**8**, is due to the essentially square-planar arrangement in the basal planes.

3.3.3. IR spectra

The most relevant feature of the infrared spectra in **1** and **2** is the evidence for the chelating and bridging bidentate coordination of the nitrate anions. As the nitrate ion [27,29,30] has characteristic absorption frequencies at approximately 1390 (ν_3), 1050 (ν_1), 831 (ν_2) and 720 (ν_4) cm^{-1} for D_{3h} symmetry and there is no nitrate ion in these complexes; the strong bands at 1380 and 1320 cm^{-1} for **1** and 1380 and 1310 cm^{-1} for **2**, and a medium band at 650 cm^{-1} for both complexes are involved in bidentate chelating and bridging modes of coordination. It is impossible to distinguish between mono- and bidentate ligands as the nitrate ion (D_{3h}) coordination to one or two oxygen atoms lowers the symmetry to that of C_{2v}.

Table 5
Electronic data for some elongated octahedral copper(II) complexes at room temperature

Complex	Tetragonality	Tetrahedral twist (°)	Band maxima (kK [a])	Polycrystalline e.s.r. spectrum			References
				g_1	g_2	g_3	
[Cu(dpyam)(O_2NO)$_2$] (**1**)	0.824, 0.817		14.34 (~ 10.85sh)	2.074		2.307	This work
[Cu(dpyam)($O_2CCH_2CH_3$)(O_2NO)] (**3**)	0.753		14.79 (~ 10 sh)	[b]	[b]	[b]	This work [e], [13]
[Cu(dpyam)(O_2CCH_3)(O_2NO)] (**4**)	0.785		15.0 (~ 10.20sh)	2.073		2.299	[12]
[Cu(dpyam)(O_2CCH_3)(O_2ClO_2)·H_2O (**5**)	0.765		15.8 (~ 10.0sh)	2.053 [c]	2.065 [c]	2.273 [c]	[11]
[Cu(dpyam)(O_2NO)$_2$]·2H_2O (**2**)	0.770, 0.757	33.80	13.58	2.086		2.225	This work
[Cu(dpyam)(O_2N)$_2$] (**6**)	0.813	31.16	13.89 (14.00) [d]	2.075		2.170	This work [e], [7]
[Cu(dpyam)(O_2CCH_3)(O_2N)]·H_2O (**7**)	0.810	32.69	13.88	2.058		2.263	This work [e], [7a]
[Cu(dpyam)(O_2CCH_3)$_2$]·2H_2O (**8**)	0.764	34.38	13.51	2.060		2.290	This work [e], [6]

[a] kK = 1000 cm^{-1}.
[b] $g_i = 2.062$.
[c] Single crystal e.s.r. values.
[d] From ref. [7].
[e] e.s.r. and electronic spectra recorded in the present work.

4. Supplementary material

Crystallographic data for the structures in this paper have been deposited with the Cambridge Crystallographic Data Centre as supplementary publication no. CCDC-168988, 168989 for structures **1** and **2**, respectively. Copies of the data can be obtained free of charge on application to CCDC, 12 Union Road, Cambridge CB2 1EZ, UK (fax: +44-1223-336033; e-mail: deposit@ccdc.cam.ac.uk).

Acknowledgements

The authors would like to thank the National Research Council of Thailand and Khon Kaen University for research grant. Support of the Postgraduate Education and Research Program in Chemistry is also gratefully acknowledged.

References

[1] I.M. Procter, B.J. Hathaway, P.G. Hodgson, Inorg. Nucl. Chem. 34 (1972) 3689.
[2] S.F. Pavkovic, D. Miller, Acta Crystallogr., Sect. B 33 (1977) 2894.
[3] D.L. Lewis, D.J. Hodgson, Inorg. Chem. 12 (1973) 2935.
[4] F.S. Stephens, J. Chem. Soc. A (1969) 2081.
[5] M.C. Munoz, J.M. Lazaro, J. Faus, M. Julve, Acta Crystallogr., Sect. C 49 (1993) 1756.
[6] S. Youngme, C. Pakawatchai, H.K. Fun, K. Chinnakali, Acta Crystallogr., Sect. C 54 (1998) 1586.
[7] (a) S. Youngme, S. Tonpho, K. Chinnakali, S. Chantrapromma, H.K. Fun, Polyhedron 18 (1999) 851;
(b) S. Youngme, N. Chaichit, C. Pakawatchai, S. Booncoon, Polyhedron (2002), in press.
[8] A. Camus, N. Marsich, A.M.M. Lanfredi, F. Ugozzoli, C. Massera, Inorg. Chim. Acta 309 (2000) 1.
[9] A. Tadsanaprasittipol, H.B. Kraatz, G.D. Enright, Inorg. Chim. Acta 278 (1998) 143.
[10] S. Youngme, W. Somjitsripunya, K. Chinnakali, S. Chantrapromma, H.K. Fun, Polyhedron 18 (1999) 857.
[11] N. Ray, S. Tyagi, B.J. Hathaway, Acta Crystallogr., Sect. B 38 (1982) 1574.
[12] S. Aduldecha, B.J. Hathaway, Acta Crystallogr., Sect. C 47 (1991) 84.
[13] S. Youngme, C. Pakawatchai, H.K. Fun, Acta Crystallogr., Sect. C 54 (1998) 451.
[14] Siemens. SAINT, Version4, Software Reference Manual, Siemens Analytical X- Ray Systems, Inc., Madison, WI, USA, 1996.
[15] G.M. Sheldrick, SADABS, Program for Empirical Absorption correction of Area Detector Data, University of Göttingen, Germany, 1996.
[16] Siemens. SHELXTL, Version 5, Reference Manual, Siemens Analytical X-ray Systems, Inc., Madison, Wisconsin, USA, 1996.
[17] C.C. Addison, N. Logan, S.C. Wallwork, C.D. Garner, Q. Rev. Chem. Soc. 25 (1971) 289.
[18] B.J. Hathaway, Comprehensive Coordination Chemistry. The Synthesis, Reaction, Properties & Applications of Coordination Compounds, Section 15.5, vol. 2, Pergamon, Oxford, 1987.
[19] I.M. Procter, B.J. Hathaway, P. Nicholls, J. Chem. Soc. A (1968) 1678.
[20] (a) C.C. Addison, S.C. Wallwork, C.D. Garner, Q. Rev. Chem. Soc. 25 (1971) 289;
(b) C.D. Garner, S.C. Wallwork, J. Chem. Soc., Chem. Commun. (1969) 108;
(c) P. Gallezot, D. Weigel, M. Prettre, Acta Crystallogr. 22 (1967) 699.
[21] (a) H. Nakai, Bull. Chem. Soc. Jpn. 44 (1971) 2412;
(b) J. Foley, D. Kennefick, D. Phelan, S. Tyagi, B.J. Hathaway, J. Chem. Soc., Dalton Trans. (1983) 2333.
[22] W.D. Harrison, B.J. Hathaway, Acta Crystallogr., Sect. B 34 (1978) 2843.
[23] M.B. Ferrari, G.G. Fava, C. Pelizzi, J. Chem. Soc., Chem. Commun. (1977) 8.
[24] R.J. Fereday, P. Hodgson, S. Tyagi, B.J. Hathaway, J. Chem. Soc., Dalton Trans. (1981) 2070.
[25] S.C. Wallwork, W.E. Addison, J. Chem. Soc. (1965) 2925.

[26] G.W. Bushnell, M.A. Khan, Can. J. Chem. 50 (1972) 315.
[27] K. Nakamoto, Infrared and Raman Spectra of Inorganic and Coordination Compounds, fourth ed., Wiley, New York, 1986.
[28] B.J. Hathaway, D.E. Billing, Coord. Chem. Rev. 5 (1970) 143.
[29] B.J. Hathaway, D.G. Holah, M. Hudson, J. Chem. Soc. (1963) 4586.
[30] D.L. Lewis, K.T. McGregor, W.E. Hatfield, D.J. Hodgson, Inorg. Chem. 11 (1972) 2216.

PERGAMON

Polyhedron 21 (2002) 951–957

POLYHEDRON

www.elsevier.com/locate/poly

Interaction of sulfur dioxide with zinc(II) tetrasulfo phthalocyanine in aqueous medium: steady state fluorescence quenching studies

N. Rajendiran, J. Santhanalakshmi *

Department of Physical Chemistry, University of Madras, Guindy Campus, Chennai 600 025, India

Received 4 October 2001; accepted 20 December 2001

Abstract

A sensitive fluorimetric method of determination of SO_2 dissolved in solvents using the steady state fluorescence of tetrasulfonated zinc(II) phthalocyanine and SO_2 in the concentration range (0.1–1.0 mM) was carried out. Effects of various solvents, pH, and salt on the interaction properties of ZnPcTs–SO_2 are determined, based on the quenchings by SO_2. Linear and non-linear Stern–Volmer plots have been analysed. Modified non-linear Stern–Volmer analysis produced best fits for a 1:2 stoichiometry. The association constant values of the ZnPcTs–SO_2 complex in various environments have been determined adopting single stage and two step equilibria processes. Stern–Volmer deviations are attributed to solvent extraplanar coordinations, a 20% DMSO–water mixture seems to produce a stability constant value higher than the other effects. A cyclic voltammogram in DMSO–water medium shows significantly suppressed redox processes of the central Zinc metal ion in ZnPcTs in the presence of SO_2 (1×10^{-3} M). Axial coordination leading to the formation of bis sulfonato ZnPcTs is envisaged. © 2002 Elsevier Science Ltd. All rights reserved.

Keywords: Zinc(II)tetrasulfophthalocyanine; Sulfur dioxide; Fluorescence quenching; Association constants

1. Introduction

There has been considerable interest in the detection and control of sulphur dioxide (SO_2) gas in aquatic environments since these constitute the fundamental aspects in the global natural sulphur cycle and in various chemical transformations of corrosion inducing pollutants [1,2]. Autoxidations of SO_2 in aquated conditions are catalysed by many catalysts and among these, transition metal(II) phthalocyanine (MPc) complexes outstand in catalytic behaviour [3–5]. Cobalt(II) tetrasulfonated phthalocyanine complex is reported to catalyse the autoxidation of SO_2 in aqueous medium with a well defined kinetic and mechanistic pathway [6]. However, study of photoassisted reactions of aquated SO_2 by MPc will be required from the economical and commercial stand points [7,8].

Sulfonation of MPc renders water solubility. Zinc(II)4,4′,4″,4‴-tetra sulfophthalocyanine (ZnPcTs) is a photo active, water soluble fluorophore showing S_1–S_0 emission fluorescence around 600–700 nm upon excitation with 390 nm wavelength light [9,10]. Many organic and other compounds act as quenchers of ZnPcTs fluorescence in aqueous homogeneous and microheterogeneous media [11–14]. Presence of SO_2 in aqueous medium has been found to quench the steady state fluorescence of ZnPcTs quantitatively with the extent of quenching being proportional to the amount of SO_2 present in water. In order to investigate the interaction of SO_2 and ZnPcTs in aqueous medium, steady state fluorescence quenching experiments are carried out in view to optimise the medium effects for maximum quenching and to deduce the quantitative results on the aspects of complexation pathway through interaction constants and stoichiometry parameters. Effects of pH, salt (NaCl) and solvent media such as DMSO, DMF, THF and MeOH as aqueous mixtures on the quenching of ZnPcTS fluorescence by SO_2 are attempted.

* Corresponding author. Tel.: +91-44-620-3507; fax: +91-44-635-6033.

E-mail address: jaysune@eth.net (J. Santhanalakshmi).

0277-5387/02/$ - see front matter © 2002 Elsevier Science Ltd. All rights reserved.
PII: S0277-5387(02)00861-6

ZnPcTs exists mostly as dimers in water at concentrations exceeding 1×10^{-7} M [15,16]. In the presence of solvents like DMSO, DMF, THF, MeOH etc, dimers of ZnPcTs exist as monomers which may be due to the solvent binding to the square-planar ZnPcTs complex at the axial sites and also by the solvent polarity effects [17]. Analysis of non-linear Stern–Volmer plots is attempted on the fluorescence quenching of ZnPcTs and a 1:2 stoichiometry of the ZnPcTs–SO_2 complex have been detected in certain cases. Solvent effect studies also show similar results as these. The association constant values of ZnPcTs–SO_2 complexes are determined for both 1:1 and 1:2 stoichiometries wherever possible. Single step and two stage equilibria pathways are proposed for the solvent, pH and electrolyte effect studies. From the best fitted modified Stern–Volmer plots, the association parameters are determined. The effectiveness of the SO_2 association process with ZnPcTs is revealed from the significant fluorescence quenching by smaller differences in the SO_2 concentrations ($\Delta c = 1 \times 10^{-4}$ M) in the DMSO–water mixture (20% w/v).

2. Experimental

2.1. Materials

ZnPcTs complex was prepared by using a modified synthesis method of Weber–Busch [18] and the solid sample was twice recrystallised from a water–ethanol mixture solvent. The sample purity was ensured by UV–Vis spectrophotometry and 99.9% pure sample was used. Hydrated SO_2 (AR grade, 99.0%) supplied by Loba-Chemi India was used as such and the concentration of SO_2 was estimated by $BaSO_4$ gravimetry as outlined in Vogel's text book [19]. Spectrosol grade solvents such as DMSO, THF, DMF and MeOH dried over 4A molecular sieves were used. Triple distilled water was always used. Various pH conditions were maintained using Tris–HCl buffer mixture. Analytical grade, Loba-Chemi NaCl salt was used.

2.2. Fluorimetric methods

Steady state fluorescence measurements were made on a Perkin–Elmer model LS-53 spectro fluorimeter fitted with 450 W Xenon arc lamp with 1 nm resolution. The fluorescence signal was detected perpendicular to the incident 390 nm excitation beam. The emission intensities are corrected for background and detector wavelength sensitivity. Electronic absorption spectra were recorded with UV–Vis Perkin–Elmer spectrometer with 1 nm resolution. Instrumental procedures are according to the manual instructions.

2.3. Cyclic voltammetry

Cyclic voltammograms were obtained from a BAS model No100A voltammetric analyser using a disk type glassy carbon working electrode (2 mm dia) (GCE) and platinum wire as the auxiliary electrode. The supporting electrolyte was tetraethyl ammonium perchlorate (TEAP) in 20% wt DMSO–water medium. The reference electrodes were silver wire dipped in 0.01 M $AgNO_3$ containing 0.1 M TEAP in 20% DMSO–water solvent and Ag/AgCl in 3 M KCl in aqueous solutions, respectively. GCE was polished with alumina, soaking in dilute nitric acid and rinsing repeatedly in water, acetone and DMSO–water solvent.

3. Results and discussion

3.1. Spectral studies

Fig. 1 represents the electronic absorption spectra of ZnPcTs in water and in various water solvent mixtures. The pronounced solvent effects are seen only in the Q band region while the S band region is unaffected. In water for ZnPcTs, the 636 nm peak corresponds to the dimer and the 673 nm peak corresponds to monomer forms [20,21]. At 1×10^{-5} M concentration, a considerable amount of dimers are present in the solution. Upon changing the solvent-nature, the monomer peak intensity seems to increase with a concomitant decrease in the dimer peak. The maximum in the monomer absorbance is seen for THF–water solvent mixture. The monomer molecules are stabilised through axial coordination of the solvent molecules to the square-planar ZnPcTs. The isosbestic point at 650 nm, detected from the solvent effect, ensures the existence of an equilibrium between the monomer and dimer species. The lowering of the band intensity also indicates the presence of lower

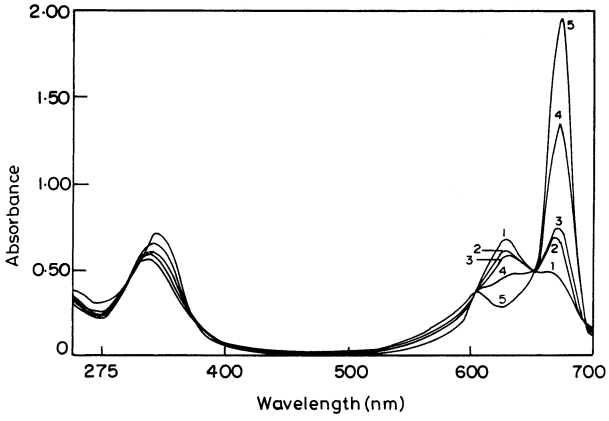


Fig. 1. Electronic absorption spectral changes on addition of various solvent–water mixtures (20% w/v), of ZnPcTs (1×10^{-5} M), (1) Water; (2) DMSO–water; (3) DMF–water; (4) MeOH–water; (5) THF–water.

amounts of dimer forms in THF. Addition of SO_2 as aqueous solution in the concentration range chosen (1×10^{-4}–1×10^{-3} M) bring in only minor changes in the visible region while almost no changes are detected in the S band region. This is possible because the sulfonate groups on the phthalocyanine do not interact with sulfur dioxide added externally. Also the absorbance spectra of metal free phthalocyanine (H_2PCTs^{4-}) taken in pyridine solvent possess strong bands at 650 and 700 nm [22,23] which are not affected by the addition of sulfur dioxide. This observation goes in hand with the reported one that tetrasulfonated phthalocyanines have satisfactory stability towards oxidation and reduction both in presence and absence of air. Alternatively, quenchings on the fluorescence spectra of ZnPcTs seem sensitive to the presence of SO_2 additions. Mostly, fluorescence intensities of ZnPcTs are lowered due to existence of dimers [24,10]. Hence, for a constant composition of ZnPcTs the fluorescence intensity is observed to be minimum in water and maximum in the presence of THF. Generally, dilution effects increase the composition of the monomer. For quenching studies involving aquated SO_2, conditions for the existence of monomeric forms are chosen. The 720–800 nm weak emission fluorescence corresponding to ZnPcTs dimers has not been considered in this study.

3.2. Fluorescence quenching studies

The fluorescence spectra of ZnPcTs show a strong florescence band in the red region (690–700 nm) when the excitation wavelength is 390 nm. The red fluorescence is mainly a radiative transition from the first excited singlet state S_1 while S_2–S_1 is a rapid process [9]. In aqueous solution even in the micromolar concentrations low intensity fluorescence exists. In DMSO solvent there is a sharp increase in the relative intensity due to ZnPcTs existing mostly as a monomer. It is thus of interest to study the fluorescence quenching of monomeric ZnPcTs, which actively interact with SO_2 in an aqueous environment and also in organic solvent such as DMSO. In Fig. 2 the stacked fluorescence quenching plots in DMSO–water (20%) are shown including other effects in solutions.

The addition of SO_2 brings about quenching of ZnPcTs fluorescence with yields $1-I_0/I$ reaching 0.5 at a quencher concentration of 9.5 mM, where I and I_0 stand for fluorescence intensity in the presence and in the absence of quencher, respectively. The corresponding conventional Stern–Volmer plot is shown in Fig. 3 [25]. The plot appears non-linear in certain systems although the quencher concentration is maintained low. The non-linearity increases towards higher quencher concentration and may be attributed to an interaction between ZnPcTs—quencher with a higher stoichiometry than 1:1. The association complex (one or more) formed

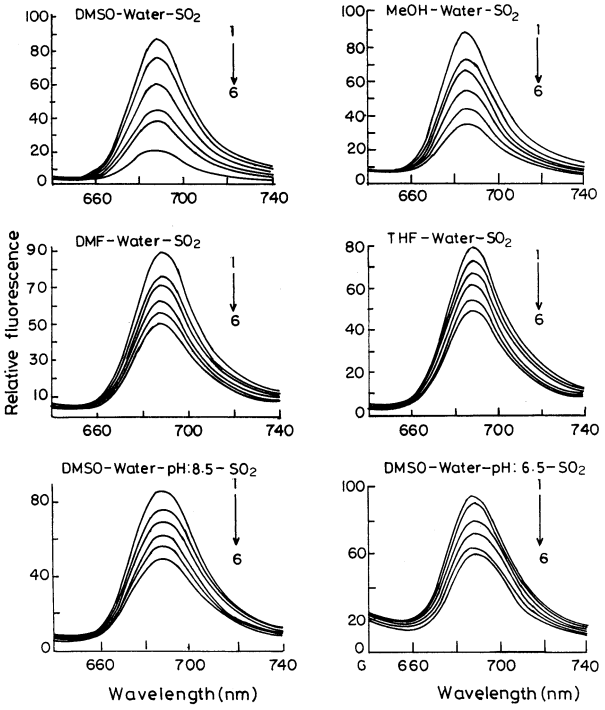


Fig. 2. Steady state fluorescence stacked spectra of ZnPcTs (1×10^{-5} M) in absence (no.1) and in presence of (nos. 2–6) $SO_2 \cdot H_2O$ [2×10^{-4}; 4×10^{-4}; 6×10^{-4}; 8×10^{-4}; 1×10^{-3}] at 25 °C and at various solvent–water mixtures and pH.

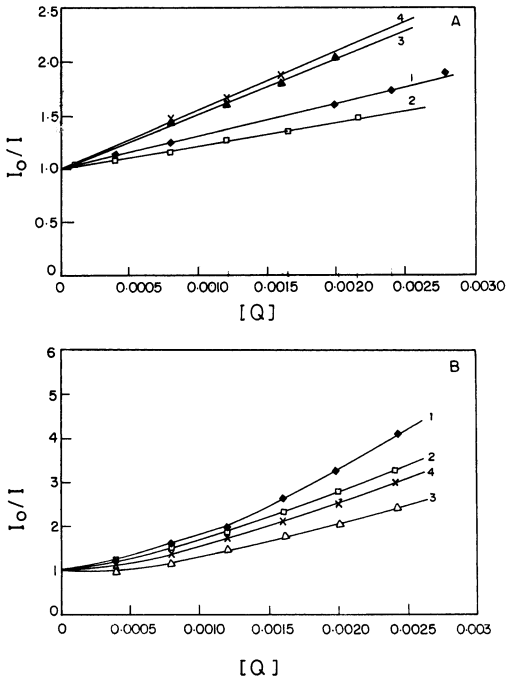


Fig. 3. Stern–Volmer plots of ZnPcTs (1×10^{-5} M) fluorescence quenching by $SO_2 \cdot H_2O$ with linear dependence (A) and non-linear dependence (B) at 25 °C. (A) (1) pH 10.5; (2) pH 8.5; (3) DMF–water (20% w/v) medium and (4) THF–water (20% w/v) medium. (B) (1) DMSO–water (20% w/v) medium; (2) MeOH–water (20% w/v) medium; (3) pH 6.5; (4) in 0.001 M NaCl.

by the quencher (ZnPcTs–nSO$_2$) are found to be non-fluorescent. There is ample evidence that SO_2 behaves as a relatively good ligand for axial site coordination to the central metal ion in ZnPcTs. Conversion of dimers to monomers seem to increase the relative fluorescence intensity in 600–700 nm region and in this region the dimer may be considered to be non-fluorescent. In the presence of various solvents like DMSO, DMF, THF and MeOH either in the pure form or in aqueous mixture, monomeric forms are increased and this is evident from the UV–Vis spectra as shown in Fig. 1. The dimer $\lambda_{max} = 630$ nm in water has been reduced considerably while there is a concomitant increase in the monomer absorbance at $\lambda_{max} = 666.5$ nm with no shifts even in presence of SO_2.

The interaction of ZnPcTs with SO_2 in aquated form is studied in presence of 20% DMSO–water mixture (when the monomeric forms show maximum absorbance due to better stability) including salt and pH effects. Also, this medium helps for carrying out selective quenching of SO_2.

In Fig. 2, stacked plots of fluorescence emission in a DMSO–water mixture with various effects are shown. From the Stern–Volmer analysis of I_0/I versus [Q] plots, it is seen that the ZnPcTs–SO_2 interaction obeys a Stern–Volmer type analysis forming 1:1 stoichiometric association in THF, and DMF-aqueous solvents at pH 10.5 and 8.5 maintained in a DMSO–water mixture, respectively. Fig. 3(A) depicts the Stern–Volmer plots based on the relation $I_0/I = 1 + K_D[Q]$, where K_D is the interaction constant for 1:1 stoichiometry. The non-linear dependances (upward deviation) of I_0/I versus [Q] are noticed in systems of DMSO and MeOH–water mixtures, in NaCl and at pH 6.5. Fig. 3(B) shows the predominate condition of the static quenching at high quencher concentration. This means that the quencher is able to bind presumably to the axial coordination sites of the central metal ion resulting in a 1:2 stoichiometry with each one of the 1:1 and 1:2 complexes formed stepwise being non-fluorescent. This observation is similar to the reported fluorescence quenching of AlPcTs [26]. In such a case, the formation of 1:2 association of ZnPcTs–SO_2 may be considered to occur via [case (i)] a stepwise equilibria as shown in Eqs. (1) and (2) or [case (ii)] in a single equilibrium step as in Eq. (3).

The products shown in Eqs. (1)–(3) are non-fluorescent

$$\mathrm{ZnPcTs} + \mathrm{SO_2} + \mathrm{S} \overset{K_1}{\rightleftharpoons} \mathrm{ZnPcTs \cdot SO_2 \cdot S} \quad (1)$$

$$\mathrm{ZnPcTs \cdot SO_2 \cdot S} + \mathrm{SO_2} \overset{K_2}{\rightleftharpoons} \mathrm{ZnPcTs(SO_2)_2} + \mathrm{S} \quad (2)$$

$$\mathrm{ZnPcTs} + 2\mathrm{SO_2} \overset{K_2}{\rightleftharpoons} \mathrm{ZnPcTs(SO_2)_2} \quad (3)$$

$\mathrm{S} = \text{Solvent molecule} \quad K_1 = K_D$

Case (i), at any instant of quenching, the total ZnPcTs concentration may be expressed as in Eq. (4) (assuming Z = ZnPcTs and Q = SO_2),

$$Z_0 = \mathrm{Ze} + \mathrm{Z \cdot Q} + \mathrm{Z \cdot Q_2} \quad (4)$$

where Z_0 and Ze are the total and free complex concentration and from Eqs. (1) and (2)

$$[\mathrm{Z \cdot Q}] = K_1[\mathrm{Z}][\mathrm{Q}] \text{ and } [\mathrm{Z \cdot Q_2}] = K_2K_1[\mathrm{Z}][\mathrm{Q}]^2$$

Substituting these in Eq. (4) and rearranging

$$[(Z_0/Z) - 1]/[\mathrm{Q}] = K_1 + K_1K_2[\mathrm{Q}] \quad (5)$$

In the above Eq. (5), $[(Z_0/Z) - 1]/[Q]$ equals $[(I_0/I) - 1]/[Q]$ where I_0 and I are the steady state fluorescence intensities observed in the absence and presence of a quencher. If linear regression analysis of Eq. (5) such as $[(I_0/I) - 1]/[Q]$ versus [Q] data shows linear plots, then the values of intercept = K_1 and slope/intercept = K_2.

Case (ii), considering single step equilibrium (Eq. (3)) to occur, then

$$K_T = [\mathrm{ZnQ_2}]/[\mathrm{Z}]\,[\mathrm{Q}]^2 \text{ and } [\mathrm{ZnQ_2}] = [Z_0] - [\mathrm{Z}]$$

Then $I_0/I = 1 + K_T[Q]^2$ and if linear regression applied on (I_0/I) versus $[Q]^2$ data shows linear plots, this produces values of slope = K_T and intercept = 1.

The fluorescence quenching measurements carried out with effects of solvents, salt and pH are subjected to Stern–Volmer (1:1 stoichiometry) and cases (i) and (ii) (1:2 stoichiometry) analyses by adopting a modified form of Stern–Volmer relation.

3.3. Solvent effect

When steady state fluorescence intensity of ZnPcTs at constant composition was measured in various percentage compositions of DMSO–water mixture, in 20% DMSO–water solvent mixture higher intensity fluorescence was detected. Hence, for comparative studies and for the use of aquated SO_2, in other studies 20% w/v of MeOH, THF and DMF–water mixtures were used. The extent of quenching at constant solvent conditions falls in the trend MeOH > DMF > DMSO > THF. In the water–solvent mixture conditions, and also at high SO_2 compositions the trend in the extent of quenching by SO_2 observed is DMSO > MeOH > DMF > THF. Higher extents of fluorescence quenchings are seen in solvents where 1:2 stoichiometry is favoured due to the higher order of association of SO_2 with ZnPcTs, and greater quenchings results. In the case of aqueous DMF and THF solvent mixtures linear Stern–Volmer plots are observed and 1:1 stoichiometry of ZnPcTs–SO_2 association complex produces best fits (Fig. 3(A)). This is because the solvent molecules concomitantly bind at the axial position of ZnPcTs. The K_1 values are 47.8 and 37.7 M^{-1} for DMF and THF, respectively. Thus, a DMF presence induces greater stability of the ZnPcTs–

SO_2 association complex than THF. Considering Stern–Volmer non-linear plots, application of case (ii) for a single step formation of the 1:2 stoichiometric association complex ZnPcTs·$(SO)_2$ produces linear fits (Fig. 3B, Fig. 4) and the K_T values of the complex are 57.14×10^4 and 35.30×10^4 M^{-1} for the DMSO and MeOH system (Table 1). The upward deviation in the Stern–Volmer plot for DMSO and MeOH may be due to the onset of 1:2 stoichiometry [27,28]. That is, the solvent effect on the ZnPcTs–SO_2 association seems peculiar and solvent specific (Fig. 5). DMSO solvent presence induces better association between ZnPcTs and SO_2, at the higher concentration range.

3.4. Salt effect

The fluorescence of a blank solution of ZnPcTs decreased slightly on addition of NaCl and with subsequent addition of SO_2 significant fluorescence quenching was noticed. In the presence of 0.001 M NaCl, SO_2 quenching measurements indicate a non-linear Stern–Volmer plot. Consideration of a stepwise, 1:2 stoichiometric [case (i)] formation of a ZnPcTs–$(SO)_2$ association complex seems to produce the best fit. The values of stepwise association constants K_1 and K_2 are found to be 1.5×10^2 and 2.00×10^3 M^{-1}, respectively. The total association constant value is: $K_T = K_1 \cdot K_2 = 30.00 \times 10^4$ M^{-2}. This indicates that 1:1 complex formation in step (i) is comparatively less stable

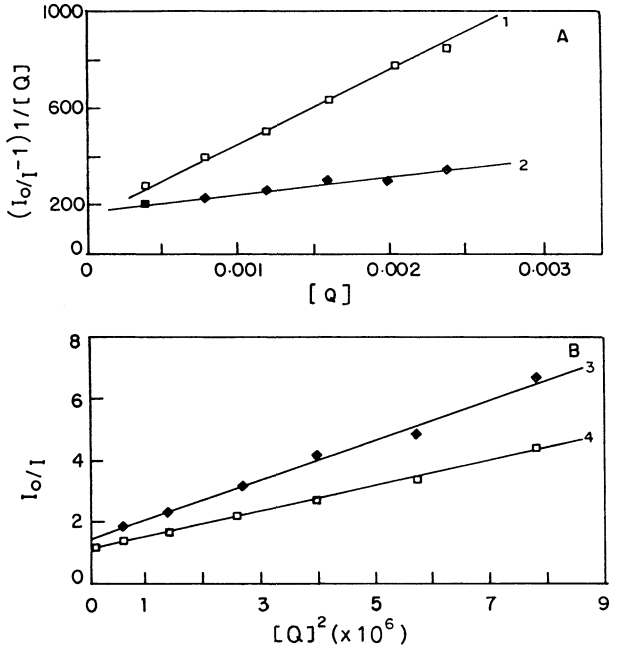


Fig. 4. Modified plots of Stern–Volmer relation on ZnPcTs fluorescence SO_2–H_2O for 1:2 stoichoimetry association via case (i)-Stepwise formations. (4-A) and case (ii)-Single step formation (4-B) at 25 °C. (A) (1) In 0.001 M NaCl; (2) in pH 6.5. (B) (3) In DMSO–water DMF–water (20% w/v) medium and (4) MeOH–water (20% w/v).

due to weak association forces that forms a driving force for the formation of a 1:2 complex with good stability which may be attributed to axial ligations. In presence of an electrolyte medium, solvation of SO_2 by water molecules are affected and due to a solvent structural effect, SO_2 coordination at the two axial positions on ZnPcTs becomes favoured [29]. This is reflected in Stern–Volmer plots corresponding to 1:2 stoichiometry (Fig. 5).

3.5. pH effects

Alkaline pH (10.5 and 8.5) conditions seem to direct the SO_2 quenching via 1:1 stoichiometry association with ZnPcTs and linear Stern–Volmer plots are obtained (Fig. 3(A)) for the two pH conditions. The K_D values are 9.10×10^2 and 3.75×10^2 M^{-1} at pH 8.5 and 10.5, respectively. The 1:1 association of ZnPcTs and SO_2 arises due to the binding of SO_2 and OH^- ions at the two axial sites instead of two SO_2 molecules binding at each axial site. Under neutral conditions linear Stern–Volmer plots corresponding to 1:1 stoichiometry and $K_D = 1.13 \times 10^2$ M^{-1} are obtained. Here SO_2 and H_2O bind as the axial ligands. At acidic pH 6.5, 1:2 stoichiometry via stepwise formation obeying case (i) pathway is observed, with K_1 and K_2 values of 1.8×10^2 and 6.94×10^2 M^{-1}, respectively and $K_T = K_1 \cdot K_2 = 12.5 \times 10^4$ M^{-2}. The values indicate more stability to the ZnPcTs$(SO)_2$ associations under acidic conditions than the 1:1 associations under basic conditions. In neutral pH weaker associations than in the acidic and basic media [30,31] are seen. The scheme presented in Fig. 5 represents the overall complexation processes involving SO_2.

3.6. Electrochemical studies

According to the scheme, sulfur dioxide coordination to the central zinc ion occurs through coordination at the axial positions and as a consequence, ring reduction through electron transfer may be possible. The electronic absorption spectral changes are negligible and hence fluorescence quenching effects are measured. Analogously Sn(IV) phthalocyanine exhibits ring reduction through electron transfer [22] and these processes are photo-assisted. Axial ligation can be monitored electrochemically in case of ZnPcTs when spectral differences are negligible [32]. The electrochemical response of ZnPcTs in the cathodic scan of the cyclic voltammogram is significant (Fig. 6) and the cathodic peak potential occurs at −0.097 V versus the silver–silver chloride reference electrode at r.t. in air and in 20% DMSO–H_2O medium containing 0.01 M tetraethyl ammonium perchlorate (TEAP) as the supporting electrolyte. Upon addition of sulfur dioxide the cathodic peak characteristic of the central metal ion completely

Table 1
Association constant and stoichiometry values of ZnPcTs–$(SO_2)_n$ complex in various solvents–aqueous (20% w/v) mixtures, pH and salt at 25 °C (S–V = Stern–Volmer plot)

Medium type	Stoichiometry	Analysis	Association constants (±0.005)
DMSO–water	1:2	S–V non-linear (single step)	$K_T = 57.14 \times 10^4\ M^{-2}$
MeOH–water	1:2	S–V non-linear (single step)	$K_T = 35.30 \times 10^4\ M^{-2}$
DMF–water	1:1	S–V linear	$K_D = 3.33 \times 10^2\ M^{-1}$
THF–water	1:1	S–V linear	$K_D = 3.00 \times 10^2\ M^{-1}$
pH 10.5	1:1	S–V linear	$K_D = 3.75 \times 10^2\ M^{-1}$
pH 8.5	1:1	S–V linear	$K_D = 9.10 \times 10^2\ M^{-1}$
pH 7.0	1:1	S–V (neutral) linear	$K_D = 1.13 \times 10^2\ M^{-1}$
pH 6.5	1:2	S–V non-linear (stepwise)	$K_1 = 1.80 \times 10^2\ M^{-1}$; $K_2 = 6.94 \times 10^2\ M^{-1}$; $K_T^{\dagger} = 12.50 \times 10^4\ M^{-2}$
0.001 M NaCl	1:2	S–V non-linear (stepwise)	$K_1 = 1.50 \times 10^2\ M^{-1}$; $K_2 = 2.00 \times 10^3\ M^{-1}$; $K_T^{\dagger} = 30.00 \times 10^4\ M^{-2}$

$K_{T\dagger}$ = total association constant = $K_1 \cdot K_2$.

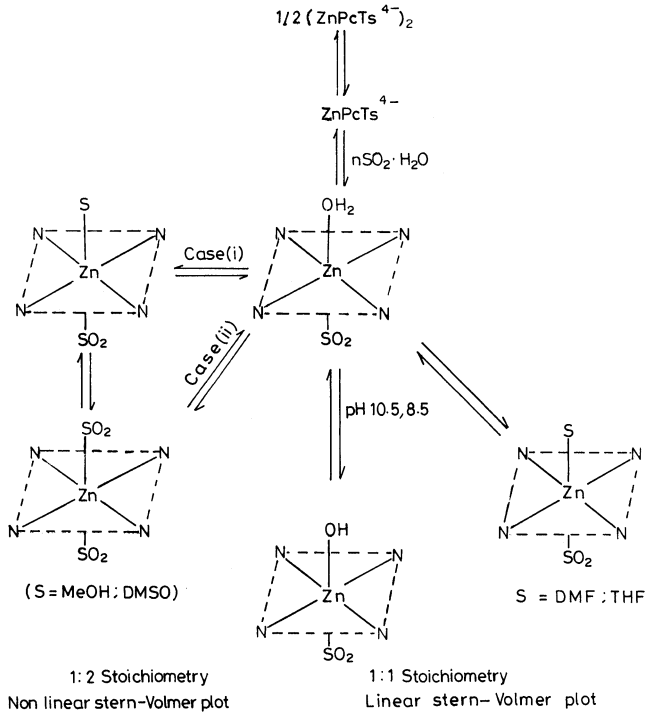


Fig. 5. Schematic representation of the proposed uni- and bi-substrate (SO_2) interaction of ZnPcTs in aqueous medium.

vanishes indicating the complete coordination at the axial sites of the square-planar ZnPcTs complex. The reducing effects of sulfur dioxide via electron transfer to the complex may be possible at the ring sites. The electrochemical evidence is a standby resource when electronic absorption spectral data prove ambiguous.

4. Conclusion

The results obtained in this work reveal that ZnPcTs can serve as an efficient fluorescent substrate to detect aquated SO_2 presence at low concentrations ($\sim 1 \times 10^{-4}$ M) in the lab and in effluent conditions. In DMSO–water (20%) solvent mixture, SO_2 association

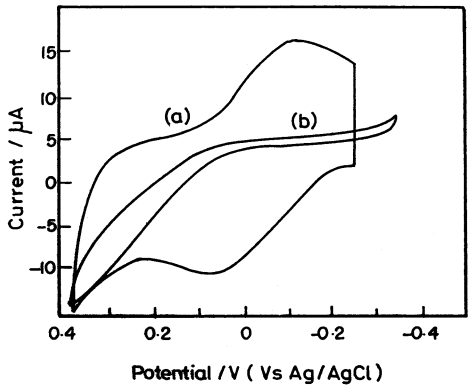


Fig. 6. Cyclic voltammograms of ZnPcTs (4×10^{-5} M) in 20% DMSO–water medium in the absence (a) and in the presence (b) of SO_2 at 25 °C in air. Supporting electrolyte is 0.1 mol dm^{-3} TEAP and scan rate 50 mV s^{-1}.

is stronger than under other conditions. Although MeOH medium shows higher extents of quenching, the DMSO–water solvent mixture (20%) is chosen since in the presence of NaCl and pH effects significant quenchings are detected. A stable 1:2 stoichiometry ZnPcTs–$(SO_2)_2$ complex has been found under acidic pH, NaCl, DMSO–water and MeOH–water conditions. The two axial ligations of sulfur dioxide at the central position of the ZnPcTs is well brought out from the CV results taken in air with and without SO_2 addition. In the oxidation reaction of SO_2 and molecular oxygen involving ZnPcTs as the catalyst, preliminary results such as these on the association characteristics at various conditions may prove vital.

Acknowledgements

The authors thank the director, National Centre for Ultrafast Process, Department of Inorganic Chemistry, University of Madras, Guindy Campus, Chennai-600 025 for the fluorescence measurements and N.R. thanks CSIR-India for the CSIR-SRF.

References

[1] D.B. Botkin, E.A. Keller, Environmental Science. Earth as a Living Planet, third ed. (Ch. 22), Wiley, New York, 2000, p. 466.
[2] J.H. Zagal, Coord. Chem. Rev. 119 (1992) 89.
[3] W. Pasiuk Bronikowska, M. Krajewska, I. Fliskabulska, Polyhedron 18 (1998) 561.
[4] M.R. Hoffmann, Environ. Sci. Technol. 14 (1980) 1061.
[5] A.B.P. Lever, M.R. Hempstead, C.C. Leznoff, W. Liu, M. Melnik, W.A. Nevin, P. Seymour, Pure Appl. Chem. 58 (1986) 1467.
[6] S.D. Boyce, M.R. Hoffmann, P. Andrew Hong, M. Moberly, Environ. Sci. Technol. 17 (1983) 602.
[7] J. Mack, S. Kirby, E.A. Ough, M.J. Stillman, Inorg. Chem. 31 (1992) 1717.
[8] J. Zakrzewski, C. Giannotti, Inorg. Chem. Acta 232 (1995) 63.
[9] L. Howe, J.Z. Zhang, J. Phys. Chem. A 101 (1997) 3207.
[10] R. Bonnstt, Chem. Soc. Rev. 24 (1995) 19.
[11] M.E. Daraio, P.F. Aramendia, E.S. Roman, Chem. Phys. Lett. 204 (1993) 415.
[12] M. Graetzel, Heterogeneous Photochemical Electron Transfer, CRC Press, Boca Raton, FL, 1989.
[13] J.D. Spikes, J.E. Van Lier, J.C. Bommer, J. Photochem. Photobiol. A 91 (1995) 193.
[14] A. Harriman, M. Claude Richoux, J. Chem. Soc. Faraday Trans. II 76 (1980) 1618.
[15] A.B.P. Lever, E.R. Milaeva, G. Speier, in: C.C. Leznoff, A.B.P. Lever (Eds.), Phthalocyanines: Properties and Applications, vol. 3, VCH, New York, 1993.
[16] Y. Kaneko, Y. Nishimura, T. Arai, H. Sakuragi, K. Tokumaru, D. Matsunaga, J. Photochem. Photobiol. A 89 (1995) 37.
[17] J.H. Weber, D.H. Busch, Inorg. Chem. 4 (1965) 472.
[18] J.H. Weber, D.H. Busch, Inorg. Chem. 4 (1965) 469.
[19] J. Bassett, R.C. Denney, G.H. Jeffery, J. Mendham, Vogel's Textbook of Quantitative Inorganic analysis, Longman, New York, 1981.
[20] P.C. Martin, M. Gouterman, B.V. Pepich, G.E. Renzoni, D.C. Schindele, Inorg. Chem. 30 (1991) 3305.
[21] N. Brasseu, H. Ali, R. Langlois, J.R. Wagner, J. Rousseau, J.E. Vanlier, J. Photochem. Photobiol. 45 (1987) 581.
[22] N.yokong Tebello, J. Chem. Soc., Chem. Commun. 17 (1994) 1983.
[23] S.E. Sheppard, A.L. Gedddes, J.Am. Chem. Soc. 66 (1944) 1995.
[24] J.A. Delaire, J.F. Delouis, J. Zakrzewski, J. Photochem. Photobiol. A: Chem. 141 (2001) 169.
[25] K. Kalyanasundaram, Photochemistry in Microheterogeneous Systems (Ch. 2), Academic Press, New York, 1987, p. 70.
[26] C. XiaoLan, L. DongHui, Y. HuangHao, Z. Qing Zhi, Z. Hong, X. Jin Gou, The Analyst 126 (2001) 523.
[27] T.L. Nemzek, W.R. Ware, J. Chem. Phys. 62 (1975) 477.
[28] W.R. Ware, T.L. Nemzek, Chem. Phys. Lett. 23 (1973) 557.
[29] Dong-Hai Li, Xian-Lan Chen,Ying Fang, Jin-Gou Xu, The Analyst 126 (2001) 581.
[30] R.B. Thompson, Topics in Fluorescence Spectroscopy, vol. 4, Plenum, New York, 1994, p. 151.
[31] P.R. Haugland, Handbook of Fluorescent Probes and Research Chemicals Molecular Probes, sixth ed., Eugene, OR, 1998, p. 144.
[32] N. Kobayashi, H. Lam, W.A. Nevin, P. Jandda, A.B.P. Lever, Inorg. Chem. 29 (1990) 3415.

PERGAMON

Polyhedron 21 (2002) 959–962

POLYHEDRON

www.elsevier.com/locate/poly

Rational synthesis and X-ray structure of $[Mn^{II}_4(H_2O)_2(As^{V}W_9O_{34})_2]^{10-}$ from $[As^{III}_4W_{40}O_{140}]^{28-}$, MnO_4^- and Mn^{2+}

Cristina Rosu [a,*], Debbie C. Crans [b,*], Timothy J.R. Weakley [c]

[a] Department of Inorganic Chemistry, Babes-Bolyai University, Cluj-Napoca, Romania
[b] Department of Chemistry, Colorado State University, Fort Collins, CO 80523-1872, USA
[c] Department of Chemistry, University of Oregon, Eugene, OR 97403, USA

Received 15 October 2001; accepted 25 January 2002

Abstract

The rational synthesis of an arsenic(V) oxopolymetalate cluster from an arsenic(III) oxopolymetalate cluster has been accomplished by a redox reaction. The sandwich Mn-complex of $As^{V}W_9O_{34}^{9-}$ ($Na_9K[Mn^{II}_4(H_2O)_2(As^{V}W_9O_{34})_2]\cdot 35H_2O$ (**1**) was prepared from a tetrameric complex $[As_4W_{40}O_{140}]^{28-}$ containing $As^{III}W_9O_{33}^{9-}$ units using both Mn^{VII} and Mn^{II} salts as reagents. Structures of **1** and $Na_{27}K[As_4W_{40}O_{140}]\cdot 56H_2O$ (**2**), are reported. © 2002 Elsevier Science Ltd. All rights reserved.

Keywords: Heteropolyoxometalate; Arsenic; Tungstate; Lacunary; Synthesis; Redox chemistry

1. Introduction

The synthesis of large and giant oxomolybdates and oxotungstates requires access to good starting materials and synthetic routes.[1,2] Specifically, a large heteroxotungstate of composition $As^{III}_{12}Ce^{III}_{16}(H_2O)_{36}W_{148}O_{524}]^{76-}$ has been reported [2] and can be described as originating from building blocks of lacunary anions such as $As^{III}W_9O_{33}^{9-}$ [2–9]. Building blocks such as $As^{V}W_9O_{34}^{9-}$ [10–12] has been used when forming oxometalates containing As in oxidation state V. In this paper we show that As^{III}–As^{V} oxometalates can be linked through redox chemistry and synthetic strategy.

The first precursor, $AsW_9O_{33}^{9-}$ was initially prepared by Tourné et al. from As_2O_3, Na_2WO_4 and HCl [6]. At this time dimeric [3,4,10], trimeric [5,6] and tetrameric structures [2,7–9] have all been reported. Tetrameric structures, containing four units of $AsW_9O_{33}^{9-}$, are linked through WO_2^{2+} groups and are also bonded to Na [2], Co [8], or Mn [9]. The sandwich anions consist of two $As^{III}W_9O_{33}^{9-}$ units linked by three metal atoms and have been reported with Cu, Mn, Co, and V [3,4]. The As^{V} sandwich compounds are linked by four metal ions, and those containing Zn, Co, Cu and Mn have been structurally characterized [10–12].

This paper describes the synthesis and structure of the mixed sodium-potassium salts of the Mn-sandwich $As^{V}W_9O_{34}^{9-}$complex ($Na_9K[Mn^{II}_4(H_2O)_2(As^{V}W_9O_{34})_2]\cdot 35H_2O$) and the tetrameric condensation product of $As^{III}W_9O_{33}^{9-}$ (Fig. 1, $Na_{27}K[As_4W_{40}O_{140}]\cdot 56H_2O$)). This work supplements structural findings [7,12] that were published while this work was in progress. More importantly, the synthetic approaches to these materials were previously limited by the starting materials heteroatom oxidation state. The concept of using a redox agent as part of the synthetic strategy is illustrated and thus allows application of a greater number of precursors for oxometalate synthesis. In this work we show by employing redox chemistry in the synthetic strategy, that an oxotungstate in the As^{III} class of compounds can be converted to an oxometalate in the As^{V} class of compounds.

* Corresponding author. Tel.: +1-970-491-7635; fax: +1-970-491-1801.
E-mail addresses: crisrosu@yahoo.com (C. Rosu), crans@lamar.colostate.edu (D.C. Crans).

0277-5387/02/$ - see front matter © 2002 Elsevier Science Ltd. All rights reserved.
PII: S0277-5387(02)00915-4

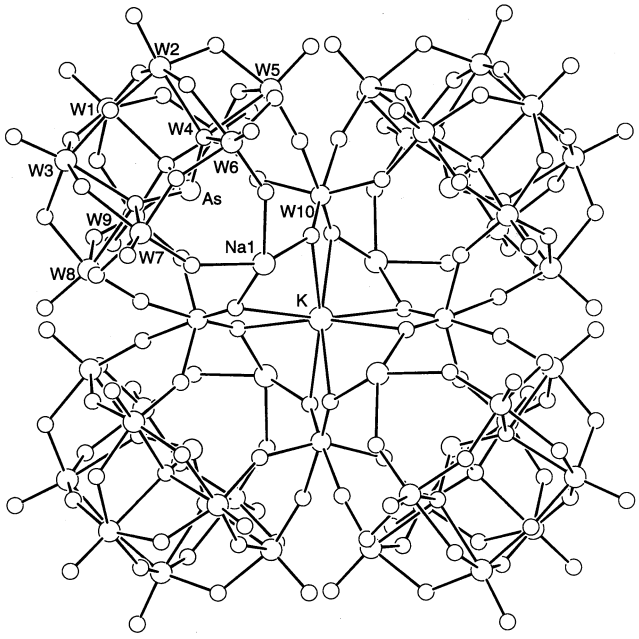


Fig. 1. The structure of the anion in $Na_{27}K[As_4W_{40}O_{140}]\cdot 56H_2O$.

2. Experimental

2.1. Reagents, solvents and procedures

The reagents were obtained from Merck and used without further purification. Elemental analyses were carried out by the microanalysis laboratories of 'Babes-Bolyai' University, Cluj-Napoca, Romania. Tungsten, manganese, sodium, potassium and arsenic were determinated by ICP. Water was determined by thermogravimetric analyses (TGA). Thermogravimetric studies (20–300 °C) were carried out with a MOM-OD 102 Paulik Erday thermoanalyser, at a heating rate of 10 °C min^{-1} and 250 mg sample.

2.2. Preparation of $Na_{27}K[As_4^{III}W_{40}O_{140}]\cdot 56H_2O$

The synthesis described in the literature was modified slightly [7]. An aqueous solution of $Na_2WO_4\cdot 2H_2O$ (33 g, 100 mmol) in 100 ml water was adjusted to pH 4.5 with glacial acetic acid and maintained at this pH for 5 min. The solution was heated to the boiling point and As_2O_3 (0.99 g, 5 mmol) in 11 M HNO_3 (1.3 ml) was added slowly under vigorous stirring. For stabilization and crystallization of the compound 0.211 g (2.68 mmol) KCl was added. The resultant clear, pale-yellow solution was heated under reflux for 1 h. In the event insoluble impurities formed, these were removed by filtration while the solution was hot. After 4–5 days of slow evaporation at ambient temperature prismatic colorless crystals were formed. The yield was 24.6 g (2.13 mmol, 85%). Recrystallization from hot water generated more uniform crystals. IR(cm^{-1}): 1640(m), 950(sh), 862(w), 750(sh), 690(m), 580(m), 510(w). ^{183}W NMR (D_2O–H_2O; Na_2WO_4 (0 ppm) −100, −110, −119, −138, −191 and −200 ppm. Elemental Analyses (%): Found: W, 63.53; As, 2.31; Na, 5.35; K, 0.35; H_2O, 8.75. Calc.: W, 63.60; As, 2.59; Na, 5.37; K, 0.34; H_2O, 8.72%.

2.3. Preparation of $Na_9K[Mn_4^{II}(H_2O)_2(As^VW_9O_{34})_2]\cdot 35H_2O$

$Na_7KAs_4W_{40}O_{140}\cdot 56H_2O$ (2.89 g, 0.251 mmol) was dissolved in 25 ml of water. Solutions of 0.143 g (0.633 mmol) of $KMnO_4$ in 5 ml of water and 0.431 g (1.76 mmol) of $Mn(OAc)_2\cdot 4H_2O$ in 5 ml of water were added drop-wise in an alternating fashion. The reaction mixture was then stirred for 30 min at 70 °C. Insoluble impurities were filtered off while the solution was hot, and the solution was left at ambient temperature. Yellow–orange crystalline plates of $Na_9K[Mn_4^{II}(H_2O)_2(As^VW_9O_{34})_2]\cdot 35H_2O$ were obtained after 10 days. The yield was 2.1 g (0.37 mmol, 74%). IR(cm^{-1}): 1642(m), 945(sh), 904(m), 858(w), 748(sh), 575(m), 510(w). Elemental Analyses(%): Found: W, 58.30; As, 2.55; Mn, 3.88; Na, 3.70; K, 0.65; H_2O, 11.75. Calc.: W, 58.27; As, 2.64; Mn, 3.87; Na, 3.64, K, 0.68; H_2O, 11.72%.

2.4. Crystal structure analyses

Data were collected by use of a Nonius CAD4 serial diffractometer. Table 1 contains a summary of crystal data and the final residuals for each compound. A more extensive table including particulars of data collection and structure refinement is provided in the supplementary material. The orientation parameters and cell dimensions were obtained from the diffractometer setting angles for 25 centered reflections. Data were corrected for absorption on the basis of azimuthal (ψ) scans. A SIR-92 E-map [13] showed all non-oxygen atoms of each polyoxoanion and many oxygen and sodium atoms. The TEXSAN program suite [14] was used in all calculations. Hydrogen atoms were not located or included in the refined model.

2.4.1. $Na_{27}K[As_4^{III}W_{40}O_{140}]\cdot 56H_2O$

A crystal of dimensions $0.11\times 0.14\times 0.25$ mm was mounted on a fiber and protected with a coating of epoxy. The $4/m$ Laue symmetry, lack of systematic absences other than those due to the I-centering, and acentric distribution of intensities indicated the space-group $I\bar{4}$. An atom clearly present at the $\bar{4}$ site at the center of the tetramer was identified as K on the basis of distances from O atoms, though its rather high refined thermal parameter may imply that the site is also partly occupied by a water molecule. Four of the seven independent Na atoms appeared to require fractional occupancy factors [Na(4–7), identified from bond lengths to oxygen]; altogether 22 Na were located per

Table 1
Crystallographic data for compounds $Na_{27}K[As_4W_{40}O_{140}]\cdot 56H_2O$ and $Na_9K[Mn_4^{II}(H_2O)_2(As^VW_9O_{34})_2]\cdot 35H_2O$

Composition	$Na_{27}K[As_4W_{40}O_{140}]\cdot 56H_2O$
Formula weight	11562.3
Space-group	$I\bar{4}$
a, b (Å)	19.491(2)
c (Å)	25.783(3)
V (Å^3)	9795(2)
Z	2
D_{calc} (g cm^{-3})	3.920
T (°C)	23
λ (Å)	0.71073
μ (cm^{-1})	242
Relative transmission coefficient	0.571–1.000 (ψ)
Observed reflections	3831 [$I \geq \sigma(I)$]
Total independent reflections	4687
$R(F)$, $wR(F)$ (observed)	0.050, 0.052
$R(F^2)$, $wR(F^2)$ (total)	0.091, 0.108
Composition	$Na_9K[Mn_4As_2W_{18}O_{70}H_4]\cdot 35H_2O$
Formula weight	5679.4
Space-group	$P\bar{1}$
a (Å)	11.6368(12)
b (Å)	14.2113(16)
c (Å)	17.6343(20)
α (Å)	98.876(9)
β (°)	105.682(9)
γ (°)	113.290(9)
V (Å^3)	2463.9(7)
Z	1
D_{calc}	3.824
T (°C)	22
λ	0.71073
μ (cm^{-1})	223.0
Relative transmission coefficient	0.322–1.000 (ψ)
Observed reflections	5812 [$I \geq \sigma(I)$]
Total independent reflections	7160
$R(F)$, $wR(F)$ (observed)	0.038, 0.042
$R(F^2)$, $wR(F^2)$ (total)	0.059, 0.081

$R(F) = \Sigma||F_o| - |F_c||/\Sigma|F_o|$, $wR(F^2) = [\Sigma w(|F_o|^2 - |F_c|^2)^2/\Sigma w|F_o|^4]^{1/2}$.

tetramer, it is likely that others are present but disordered. The As and W atoms and Na(1,2,3) were refined anisotropically. Anisotropic refinement of anion oxygen atoms led to many non-positive-definite ellipsoids, and the results given here are for isotropically-refined oxygens and illustrated in Fig. 1.

2.4.2. $Na_9K[Mn_4^{II}(H_2O)_2(As^VW_9O_{34})_2]\cdot 35H_2O$

A yellow plate of dimensions $0.07 \times 0.22 \times 0.41$ mm was secured by a trace of glue in a capillary containing mother-liquor. The triclinic symmetry together with the centric distribution of intensities indicated the space-group $P\bar{1}$. A total of five independent Na atoms were located, but one required a site occupancy factor of 0.5 for a satisfactory refinement. Five of the 20 independent water oxygens also appeared to be on half-occupied sites. The K atom whose presence was implied by the elemental analysis could not be located, and may be disordered over the sites of non-ligand water molecules. All atoms except oxygen atoms of water molecules were refined anisotropically.

3. Results and discussion

3.1. Synthesis of As^{III}–oxotungstate tetramer

The synthetic strategy for formation of the tetrameric condensation product illustrated in 1 was modified slightly from that reported by Leyrie and Herve [9]. The precursor sodium arsenite was replaced by As_2O_3, which was dissolved in 11 M HNO_3. Also the HCl was replaced by glacial acetic acid and HNO_3. This procedure was found to generate X-ray quality crystals directly from the reaction solution, although recrystallization from water resulted in a preparation with uniform crystal size.

$$40Na_2WO_4 + 2As_2O_3 + 52HOAc + KCl \rightarrow Na_{27}K[As_4W_{40}O_{140}] + NaCl + 52NaOAc + 26H_2O \quad (1)$$

3.2. Synthesis of As^V–oxotungstate sandwich compound

Attempts to modify the As^{III} in the tetrameric condensation product to form the As^V series compounds were explored using an oxidation reagent that is mild but yet sufficient to accomplish the oxidation. MnO_4^- is commonly used to oxidize As^{III} to As^V and was tried initially, but proved to be an unsuitable reagent. Furthermore, when treating solutions of tetramer with MnO_4^-, no change in color could be observed over several days. In the synthesis of complex oxometalates in molybdenum chemistry it is common to use reagents which involved two different oxidation states of the metal ion in order to achieve the desired redox potential in the reaction solutions. This approach was adapted in this system. Thus, the addition of both MnO_4^- and $Mn(OAc)_2$ did prove to be successful and the resulting reaction is shown in Eq. (2). The colorless solution turns violet upon addition of MnO_4^- which followed by addition of $Mn(OAc)_2$ changes the violet solution brown; the color continues to change for 5 h after which time the solution is deep orange. Although some flexibility exists with regard to the exact ratio of components, best yields were obtained when 1 equiv. of tetramer was treated with a threefold excess of MnO_4^- and a sevenfold excess of Mn^{2+} salt. When $Mn(OAc)_2$ was added to solutions of tetramer the color changed to yellow indicating a replacement of cations, however, only very small light yellow crystals were obtained. We conclude, that both redox states of the reagent were necessary to achieve the conversion of the

As^{III} oxometalate to the As^{V} oxometalate. In addition to providing an example of linking these two classes of compounds, this method significantly improves the yield of the synthesis of this type of material [7].

$$2Na_{27}K[As_4W_{40}O_{140}] + 4KMnO_4 + 14Mn(OAc)_2 + 12H_2O \rightarrow 4Na_9K[Mn_4(H_2O)_2(AsW_9O_{34})_2] + 8WO_3 + 2MnO_2 + 2KOAc + 18NaOAc + 8HOAc \quad (2)$$

3.3. Structure of $Na_{27}K[As_4^{III}W_{40}O_{140}]\cdot 56H_2O$

The tetrameric anion $[As_4W_{40}O_{140}]^{28-}$ consists of four α-B-$As^{III}W_9O_{33}$ units sharing octahedron corners with four linking WO_6 groups [W(10)]. It generally resembles the anion in $Na_{28}[(\alpha\text{-B-}AsO_3W_9O_{30})_4(WO_2)_4]\cdot 2NaCl\cdot 55H_2O$ that was reported while this work was in progress [7]. The structure differs from that of the anion in $(NH_4)_{28}Co_2As_4W_{40}O_{140}\cdot 20–22H_2O$ [8] in the following details. The point symmetry of the anion is exactly, rather than approximately $\bar{4}$. The site designated [8] S1 at the center of the tetramer is occupied by K^+ instead of by NH_4^+, bonded to the two *cis* O atoms of each bridging WO_6 group that are not involved in W–O–W linkages. The four S2 sites [8] are all occupied by Na^+ cations [Na(1)] instead of by two Co^{2+} and two NH_4^+. The four oxygens of the anion bonded to Na(1) define an approximate square which is planar to within one standard deviation (0.03 Å), and Na(1) lies 0.63(1) Å from the plane on the side away from the As atom with a possible weak bond [2.82(2) Å] to a water oxygen atom [O(43)] in an apical position. The As···Na(1) distance [3.26(1) Å] is to be contrasted with the short (2.65 Å) As···Co distance [8] in the other anion, where the Co is effectively six-coordinate. The differences from the anion in $Na_{28}[(\alpha\text{-B-}AsO_3W_9O_{30})_4(WO_2)_4]\cdot 2NaCl\cdot 55H_2O$ include the potassium, rather than sodium, central cation and the higher ($\bar{4}$) crystallographic point symmetry.

3.4. Structure of $Na_9K[Mn_4^{II}(H_2O)_2(As^{V}W_9O_{34})_2]\cdot 35H_2O$

The product of reaction (2) is $[Mn_4^{II}(H_2O)_2(As^{V}W_9O_{34})_2]^{10-}$. The assumed degree of hydration of the salt is based on the X-ray analysis. The anion lies on a crystallographic center of symmetry, with approximate point symmetry 2/*m* (C_{2h}) and contains a planar set of four Mn^{2+} ions separating two α-B-$AsW_9O_{34}^{9-}$ groups. Two Mn atoms each carry one water ligand. The anion is isostructural with the $[Co_4^{II}(H_2O)_2(P^{V}W_9O_{34})_2]^{10-}$ [15], $[Mn_4^{II}(H_2O)_2(P^{V}W_9O_{34})_2]^{10-}$ [15], and $[Co_4^{II}(H_2O)_2(As^{V}W_9O_{34})_2]^{10-}$ anions [10,11], with similar corresponding dimensions. The all-potassium salt $K_{10}[Mn_4^{II}(H_2O)_2(As^{V}W_9O_{34})_2]\cdot 18H_2O$, was reported while this work was in progress [12].

4. Supplemental material

Supplementary data are available from Fachinformationszentium Karlsruhe (FIZ) for $Na_{27}K[As_4^{III}W_{40}O_{140}]\cdot 56H_2O$ the number is 412184 and for $Na_9K[Mn_4^{II}(H_2O)_2(As^{V}W_9O_{34})_2]\cdot 35H_2O$ the number is 412183.

Acknowledgements

C.R. and D.C.C. thank the Humboldt Foundation for a Fellowship and Research Award, respectively. D.C.C. also thanks The Institute of General Medicine of the National Institutes of Health for funding. We thank Dr. Tiberiu Frentiu for the microanalyses at the Analytical Laboratory of the Department of Chemistry of 'Babes-Bolyai' University, Cluj-Napoca, Romania. We also thank Dr. Christopher D. Rithner and Dr. Jason Smee for recording the ^{183}W NMR spectra for us.

References

[1] A. Müller, F. Peters, M.T. Pope, D. Gatteschi, Chem. Rev. 98 (1998) 239.
[2] K. Wasserman, M.H. Dickman, M.T. Pope, Angew. Chem., Int. Ed. Engl. 36 (1997) 1445.
[3] F. Robert, M. Leyrie, G. Hervé, Acta Crystallogr., Sect. B 38 (1982) 358.
[4] P. Mialane, J. Marrot, E. Riviere, J. Nebout, G. Hervé, Inorg. Chem. 40 (2001) 44.
[5] K.-C. Kim, M.T. Pope, J. Chem. Soc., Dalton Trans. (2001) 986.
[6] C. Tourné, A. Revel, G. Tourné, M. Vendrell, CR Acad. Sci. Paris Ser. C 277 (1973) 643.
[7] K. Wasserman, M.T. Pope, Inorg. Chem. 40 (2001) 2763.
[8] F. Robert, M. Leyrie, G. Hervé, A. Tézé, Y. Jeannin, Inorg. Chem. 19 (1980) 1746.
[9] M. Leyrie, G. Hervé, Nouveau J. Chem. 2 (1978) 233.
[10] T.J.R. Weakley, Acta Crystallogr., Sect. C, (1997), 53, IUC9700025.
[11] H.T. Evans Jr., C. Tourné, G. Tourné, T.J.R. Weakley, J. Chem. Soc., Dalton Trans. (1986) 2699.
[12] L.-H. Bi, R.-D. Huang, J. Peng, E.-B. Wang, Y.-H. Wang, C.-W. Hu, J. Chem. Soc., Dalton Trans. (2001) 121.
[13] A. Altomare, G. Cascarano, C. Giacovazzo, A. Guagliardi, M.C. Burla, G. Polidori, N. Camalli, J. Appl. Crystallogr. 27 (1994) 435.
[14] Molecular Structures Corporation, 3200A Research Forest Drive, The Woodlands, TX 77381, USA. TEXSAN Software for Single-Crystal Structure Analysis, version 1.7, 1997.
[15] C.J. Gómez-García, E. Coronado, P. Gómez-Romero, N. Casañ-Pastor, Inorg. Chem. 32 (1993) 3378.

PERGAMON

Polyhedron 21 (2002) 963–967

POLYHEDRON

www.elsevier.com/locate/poly

Novel tetranuclear cubane-like Co(II) complexes involving chelate phosphoramide ligands

Kateryna E. Gubina [a,*], Vladimir A. Ovchynnikov [a], Jolanta Swiatek-Kozlowska [b], Vladimir M. Amirkhanov [a], Tatyana Yu. Sliva [a], Konstantin V. Domasevitch [a]

[a] *Department of Inorganic Chemistry, Kiev University, Vladimirskaya St. 64, Kiev 01033, Ukraine*
[b] *Department of Basic Medical Sciences, Medical Academy, Kochanowskiego 14, 51601 Wroclaw, Poland*

Received 31 October 2001; accepted 10 December 2001

Abstract

Interaction of cobalt(II) ions and sodium carbacylamidophosphates Na(L) (HL = PhC(O)NHP(O)$(NR_2)_2$; where NR_2 are morpholyl, HL^1; NMe_2, HL^2; NEt_2, HL^3) in methanol solution afforded polynuclear alkoxo complexes $[Co_4\{L^1\}_3(OCH_3)_4(OH)(H_2O)_5\cdot 3H_2O]$ **1** and $[Co_4\{L\}_4(OCH_3)_4(CH_3OH)_4]$ (L = L^2 **2**, L^3 **3**). Data of spectral and TGA studies are presented. Coordination compounds **1** and **3** have been characterized by means of X-ray diffraction. Both the structures consist of tetranuclear cubane alkoxo clusters with methoxide ions bridging three metal centers (Co–O 2.068(3)–2.093(4) Å) and phosphorylic ligands coordinated in a bidentatechelate fashion via the carbonyl oxygen atoms (Co–O **1**: 2.050(2); **3**: 2.031(4) Å) and the phosphoryl groups (2.093(2) and 2.106(4) Å). Isolation of these cubane alkoxo complexes is an important proof for close resemblance in behavior of carbacylamidophosphate systems and β-diketonates towards transition metal ions. © 2002 Elsevier Science Ltd. All rights reserved.

Keywords: Cobalt(II); Cubane complexes; Carbacylamidophosphates; X-ray data

1. Introduction

The cubane-like structure of tetranuclear metal complexes is a characteristic motif in coordination chemistry of different metal ions. It may dominate assembly of relatively simple compounds like thallium alkoxides [1] as well as of complicated molecular and supramolecular architectures [2]. This structural motif with close spatial alignment of metal centers is important also in the chemistry of transition metals where it may have an essential impact considering possible magnetic and catalytical properties of the compounds [3,4]. The structural and magnetochemical features of numerous Co(II) and Co(III) based cubane molecules have been reported [5–7]. Forming the complete or incomplete cubane complexes in solution is competitive for Co(II) complexes just as for Co(III).The cubane structure is also common in the realm of metal diketonates, recent examples include series of cobalt(II) and nickel (II) compounds [8–11]. We were interested in the generation of the cubane structure for new transition metal derivatives involving structural analogs of β-diketones. Such species may allow further functionalization of the metal-organic core, and phosphazo analogs of β-diketones are of special interest in this context: these *N*-acylated phosphoramides bear a close structural resemblance to the β-diketone frame, they usually act as effective chelating groups, and stoichiometry, structure and properties of coordination compounds thereof may be clearly related with known types of metal diketonates.

In this contribution we report on the engineering of a tetrameric cubane structure involving Co(II) ions and three chelating phosphoramide ligands.

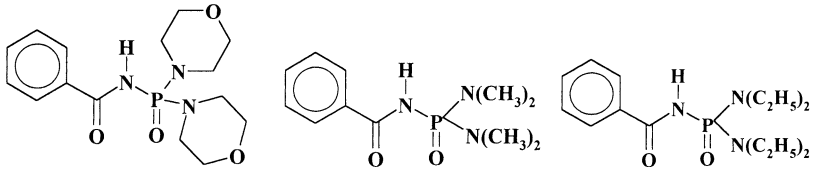
* Corresponding author. Tel.: +380-4422-10292; fax: +380-5031-07112.
E-mail address: katlig@mail.univ.kiev.ua (K.E. Gubina).

0277-5387/02/$ - see front matter © 2002 Elsevier Science Ltd. All rights reserved.
PII: S0277-5387(02)00895-1

2. Experimental

2.1. Preparation of $Co_4L_{4-n}(\mu_3\text{-}OCH3)_4(OH)_n \cdot mSolv$ ($Solv = H_2O$ or CH_3OH)

Dimorpholido-*N*-benzoylamidophosphate HL^1, *N*,*N*′-tetramethyl-*N*″-benzoyltriamido-phosphate HL^2 *N*,*N*′-tetraethyl-*N*″-benzoyltriamidophosphate HL^3 and their sodium salts were obtained and identified according to [12,13].



HL^1 HL^2 HL^3

Coordination compounds of cobalt(II) were synthesized reacting the metal chloride and sodium salts of the ligands in methanol solution:

$$4CoCl_2 \cdot 6H_2O + 8NaL \xrightarrow[-NaCl]{CH_3OH} Co_4L_{4-n}(\mu_3OCH_3)_4(OH)_n \cdot mSolv + 4HL$$

where $L^- = (L^1)^-, (L^2)^-, (L^3)^-$.

In a typical synthesis, $CoCl_2 \cdot 6H_2O$ (0.238 g, 1 mmol) was dissolved in methanol (15 ml) and combined with the solution of NaL^1 (0.722 g, 2 mmol) in 10 ml methanol. The mixture was allowed to stand in a vacuum desiccator over $CaCl_2$. After a while the pink-violet crystals of the complex $[Co_4\{L^1\}_3(OCH_3)_4(OH)(H_2O)_5 \cdot 3H_2O]$ **1** precipitated from the solution in the mixture along with neutral ligand HL^1. The latter was separated out by washing the product with methanol and identified according to IR spectra. Crystals of the complex were additionally washed with cool acetone, and dried over $CaCl_2$ (yield: 0.248 g, 65.6%). Complexes $[Co_4\{L\}_4(OCH_3)_4(CH_3OH)_4]$ (L = L^2 **2**, L^3 **3**) were prepared in the same manner. Single crystals of **1** and **3** were prepared by slow crystallization from acetone-methanol mixture.

The complexes are unstable in air and decompose under long-term storage. They were soluble in nonpolar aprotic solvents, less soluble in acetone, isopropanol and ethyl alcohol.

The compositions of the compounds were established on the basis of the elemental analysis. *Anal.* for **1**. Found: C 37.53, H 5.56, N 7.75. Calc. for $C_{49}H_{92}N_9Co_4O_{28}P_3$: C 38.32, H 5.8, N 8.2%. *Anal.* for **2**. Found: C 41.67, H 6.78, N 10.01. Calc. for $C_{52}H_{96}N_{12}Co_4O_{16}P_4$: C 41.40, H 6.38, N 11.16%. *Anal.* for 3. Found: C 47.01, H 8.6, N 9.3. Calc. for $C_{68}H_{128}N_{12}Co_4O_{16}P_4$: C 47.23, H 8.1, N 9.7%.

2.2. Methods

IR spectra of the compounds were recorded on an UR-10 spectrometer in the range 400–4000 cm^{-1} (samples as KBr pellets). Differential thermal analyses were carried out in the temperature range 20–500 °C using a Q-1500 'Quasi' thermoanalyzer at a heating rate of 5 °C min^{-1}. Electronic diffuse reflectance spectra were recorded on a SPECORD M-40 (Carl Zeiss, Jena) UV–Vis spectrometer.

X-ray diffraction data for **1** were collected using an Enraf-Nonius CAD-4 diffractometer. For **3** crystallographic measurements were made using a SMART CCD area-detector diffractometer (Siemens). Table 2 lists the cell parameters and details of data acquisition and structure refinement. Selected geometrical parameters of **1** and **3** are listed in Table 3. The structures were solved by direct methods and refined by full-matrix least-square methods using programs SHELXS-86 and SHELXL-93 [14,15]. All the non-hydrogen atoms were refined anisotropically. The hydrogen atoms were localized by difference Fourier techniques without further refinement.

Table 1
Main IR absorption bands and their assignments for carbacylamidophosphate compounds, cm^{-1}

Compound	ν(NH)	ν(C=O)	ν(C–N)	ν(P=O)
HL^1	3100	1685	1440	1200
NaL^1		1545	1385	1115
$[Co_4\{L^1\}_3(OCH_3)_4(OH)(H_2O)_5 \cdot 3H_2O]$		1530	1380	1110
HL^2	3070	1680	1460	1280
NaL^2		1595	1380	1130
$[Co_4\{L^2\}_4(OCH_3)_4(CH_3OH)_4]$		1535	1380	1085
HL^3	3070	1675	1450	1280
NaL^3		1535	1380	1120
$[Co_4\{L^3\}_4(OCH_3)_4(CH_3OH)_4]$		1530	1380	1090

Table 2
Crystal data and structure refinement for **1** and **3**

	1	**3**
Empirical formula	$C_{49}H_{92}Co_4N_9O_{25}P_3$	$C_{68}H_{128}Co_4N_{12}O_{16}P_4$
Temperature (K)	293	223
Wavelength (Å)	0.71073	0.71073
Crystal system	rhombohedral	tetragonal
Space group	$R\bar{3}$	$P\bar{4}2_1c$
Unit cell dimensions		
a (Å)	21.604(3)	16.921(2)
c (Å)	26.014(5)	15.404(3)
V (Å^3)	10515(3)	4410.5(11)
Z	6	2
Crystal size (mm)	0.25 × 0.25 × 0.30	0.2 × 0.2 × 0.25
$2\theta_{max}$ (°)	50.1	51.4
Reflections collected	5178	16341
Independent reflections	3449	4059
Reflections observed ($>2\sigma$)	2488	2490
Data used/parameters refined	3449/271	4059/266
Goodness-of-fit on F^2	0.998	1.050
R_1, wR_2 (observed)	0.037, 0.090	0.057, 0.106
R_1, wR_2 (all data)	0.068, 0.101	0.121, 0.142
Largest difference peak and hole (e Å^{-3})	0.52, −0.39	0.48, −0.43

3. Results and discussion

3.1. Spectroscopy

The IR spectra of the coordination compounds have a number of common features (Table 1). The IR bands in the region 3070–3100 cm^{-1}, observed in spectra of the neutral carbacylamidophosphates, may be ascribed to ν(NH) vibrations of the amide protons. These bands are absent in the spectra of the sodium and cobalt(II) carbacylamidophosphates **1**–**3**, which is evidence for ligand coordination in the deprotonated form. The spectra reveal significantly lower frequencies of ν(PO) as may be compared with those for the sodium salts ($\Delta\nu$(PO) = 45 and 30 cm^{-1} for compounds **2** and **3**, respectively), reflecting coordination via the phosphoryl oxygen atom [8,9]. In the case of compound **1**, the position of the ν(PO) band could not be related identically. The ν(CO) values in spectra of the complexes are shifted to lower frequencies ($\Delta\nu$(CO) = 5–60 cm^{-1}). These facts suggest a bidentate chelate coordination of the anionic ligands L^- via the oxygen atoms of phosphoryl and carbonyl groups.

UV–Vis absorption spectra reflect the octahedral environment the cobalt(II) ions in **1**–**3** [16]. The bands related to the electron transition $^4T_{1g}(P) \rightarrow {}^4T_{1g}$ are observed at 18 000, 19 000 and 21 000 cm^{-1} for **1**, **2** and **3**, respectively. The transition $^4A_{2g} \rightarrow {}^4T_{1g}$ is very weak and appears as a shoulder.

Table 3
Selected bond lengths (Å) and angles (°) for **1** and **3**

1		**3**	
Bond lengths			
Co(1)–O(2)	2.050(2)	Co(1)–O(2)	2.031(4)
Co(1)–O(7)^a	2.083(2)	Co(1)–O(3)^a	2.068(3)
Co(1)–O(6)	2.086(2)	Co(1)–O(3)^b	2.084(3)
Co(1)–O(7)	2.092(2)	Co(1)–O(3)	2.091(4)
Co(1)–O(l)	2.093(2)	Co(1)–O(1)	2.106(4)
Co(1)–O(5)	2.161(2)	Co(1)–O(4)	2.204(4)
Bond angles			
P(1)–O(l)	1.509(2)	P(1)–O(1)	1.523(4)
P(1)–N(1)	1.617(3)	P(1)–N(1)	1.625(5)
O(2)–C(1)	1.266(4)	O(2)–C(1)	1.264(7)
N(1)–C(1)	1.314(5)	N(1)–C(1)	1.294(7)
O(2)–Co(1)–O(7)^a	90.47(8)	O(2)–Co(1)–O(3)^a	176.23(14)
O(7)^a–Co(1)–O(6)	83.16(9)	O(2)–Co(1)–O(3)^b	93.55(14)
O(2)–Co(1)–O(7)	93.00(8)	O(2)–Co(1)–O(3)	98.1(2)
O(2)–Co(1)–O(1)	91.55(9)	O(3)^a–Co(1)–O(3)	82.73(14)
O(7)^a–Co(1)–O(1)	173.61(8)	O(2)–Co(1)–O(1)	89.9(2)
O(7)^a–Co(1)–O(5)	89.13(8)	O(3)^a–Co(1)–O(1)	93.76(15)
O(1)–Co(1)–O(5)	96.80(8)	O(3)^b–Co(1)–O(1)	175.09(13)
O(1)–P(1)–N(1)	118.37(14)	O(3)–Co(1)–O(1)	94.06(14)
C(1)–N(1)–P(1)	127.7(2)	O(2)–Co(1)–O(4)	93.1(2)
Co(1)^b–O(7)–Co(1)	96.46(9)	O(3)^a–Co(1)–O(4)	85.58(14)
		O(3)–Co(1)–O(4)	166.36(13)
		O(1)–Co(1)–O(4)	93.70(15)
		O(1)–P(1)–N(1)	118.7(2)
		C(1)–N(1)–P(1)	124.7(4)
		Co(1)^c–O(3)–Co(1)^b	96.74(14)
		Co(1)^c–O(3)–Co(1)	96.52(14)
		Co(1)^b–O(3)–Co(1)	97.7(2)

Symmetry transformations used to generate equivalent atoms for **1**: (a) $1-x+y, 1-x, z$; (b) $1-y, x-y, z$; for **3**: (a) $1-y, x, -z$; (b) $1-x, 1-y, z$; (c) $-y, 1-x, -z$.

3.2. Thermogravimetry

The thermal behavior of the cobalt complexes **2** and **3** is very similar. According to the TGA data, these complexes are stable up to 100 °C. In the temperature range 100 °C–290 °C, the thermoanalytical curves indicate two endothermic effects. The first of them (115 °C) is connected with the elimination of four molecules of methanol. This relatively elevated temperature of the methanol molecule removal indirectly indicates their disposition in the internal coordination sphere of the metal ions. The other endothermic stage corresponds to the beginning of the decomposition of the complex. It takes place at the same temperature for the both compounds, namely 265 °C. Full decomposition of the complex is accompanied by its vigorous exothermic oxidation at 285 °C. It is necessary to note that a difference in the temperatures of the maximal onset of the processes is not essential and it is equal to within 20 °C. This fact shows the important role of the methanol molecules in the formation of the crystal lattice of the cobalt complexes **2** and **3**. The similar character of the decomposition of these compounds and

the same temperature interval of thermal effects may suggest a similarity of their structures.

In the case of complex **1**, the TGA results are rather different. The thermoanalytical curves also reflect two endothermic effects at 130 and 200 °C, and an exothermic one at 335 °C. The first effect is connected with the elimination of three water molecules from the external sphere of the complex. The compound decomposes at 200 °C. The fact that the further dehydration of **1** is accompanied by its decomposition is evidence of the involvement of the other five water molecules in the internal coordination sphere and their strong bonding with the central atoms. The full exothermic decomposition of the complex takes place at 335 °C.

3.3. Description of the structures

We succeeded in confirming the conclusions about the structure of the obtained compounds based on IR and UV–Vis spectroscopy data by the results of full X-ray analysis of compounds **1** and **3**.

The solid-state structure of **3** contains discrete tetrameric molecules. $[Co_4\{L^3\}_4(\mu_3\text{-}OCH_3)_4(CH_3OH)_4]$, each octahedral Co(II) ion being bound to three μ_3-OMe^- ligands, one chelating carbacylphosphortriamide ligand (L^3), and one terminal MeOH ligand. Concerning the composition of the compound and the results of spectral and TGA studies, the same structure may also be ascribed for compound **2**. The molecule occupies a special position on an inversion fourfold axis and has virtual D_{2d} symmetry.

For both structures, the tetrameric skeletons are formed by four cobalt atoms and four oxygen atoms of methoxy groups. The octahedral environment for each cobalt atom in **3** and for three of four cobalt atoms in **1** comprises three oxygen atoms of methoxy groups, carbonylic and phosphoryl oxygen atoms of the chelate anionic ligands and an oxygen atom of an alcohol molecule in structure **3** (Fig. 1). The fourth cobalt atom in structure **1** is situated on a threefold axis and is connected with three oxygen atoms of methoxy groups, oxygen atoms of two water molecules and one OH^- group. These hydro and hydroxo ligands are structurally equivalent and all are related by a threefold axis.

The cubane-like frameworks in the present cases are slightly distorted, the angles O–Co–O are about 5° smaller than 90°, while the angles Co–O–Co are approximately 97°. The Co–O(2) bond with the carbonyl oxygen atom is the shortest in the cobalt environment in both structures (**1**: 2.050(2) and **3**: 2.031(4) Å). The Co–O(CH_3) bond lengths are typical for μ_2- and μ_3-OMe groups [17] and are in the range of 2.068(3)–2.093(4) Å for both structures. The distances to the phosphoryl oxygen atoms, Co–O(l) in **1** and **3**, are 2.093 (2), and 2.106(4) Å, respectively. The Co–O(4) bond with a coordinated water molecule (2.161(2) Å) for **1** and the Co–O bond with a coordinated methanol oxygen atom (2.204(4) Å) in the case of compound **3** are the longest.

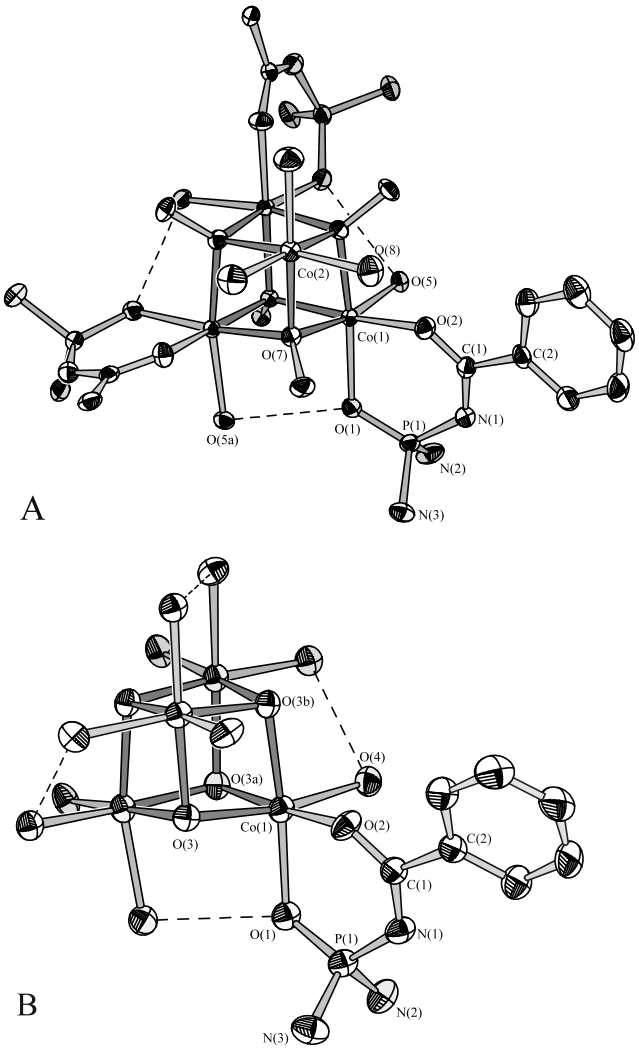
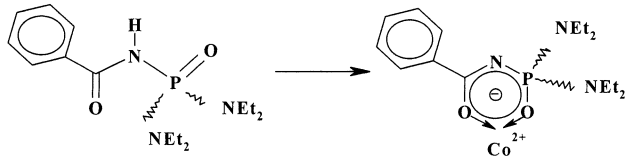


Fig. 1. Molecular structure of the cobalt cubane alkoxo complexes: A-$Co_4\{L^1\}_3(OCH_3)_4(OH)(H_2O)_5\cdot 3H_2O$ **1**, hydrogen atoms oxamethylene linkage of morpholine cycles and two of the three phenyl groups are omitted; B-$Co_4\{L^3\}_4(OCH_3)_4(CH_3OH)_4$ **3**, hydrogen atoms, ethyl and methyl fragments of the phosphorylic, metoxy and methoxo ligands are omitted for clarity, and only one of the four chelate frames is shown. Thermal ellipsoids are at 40% probability level and possible hydrogen bonding is shown as dotted lines.

The ligand deprotonation leads to the appearance of π-conjugation in the chelate ring of the compounds, which may be illustrated by the changes of the bond lengths. Thus the distances P=O (1: 1.509; 3: 1.523 Å) and C=O (1: 1.266; 3: 1.264 Å) both appeared slightly longer with respect to those for the non-coordinated molecules HL^1 and HL^3 [12,18]. The increase of the bond order for P–N and C–N caused by the increase of the π-bonding leads to the 0.05–0.09 Å shortening of these bond lengths in the complexes with respect to that observed for HL^1 and HL^3. The OPNCO chelate

fragment in both structures are planar to within 0.1 Å and the deviation of the metal atoms from these planes does not exceed 0.5 Å.



The phosphorus atoms have a distorted tetrahedral environment. The atoms forming the angles O(1)–P(1)–N(1) (118.37°, 118.7°) for both cases have the largest deviations because they are involved in the π-conjugation. All the other angles in the **3** are nearly tetrahedral.

For each type of the cubane molecules the OH and O counterparts are involved in extensive intramolecular hydrogen bonding. Thus, in **3** each MeOH hydroxy group forms an hydrogen bond with the phosphoryl oxygen atom of carbacylphosporamide ligand coordinated to a neighboring Co ion (O···O 2.78 Å). A similar pattern of intramolecular hydrogen bonding has also been observed in other alkoxides cubane complexes containing Co(II), Co(III) and Ni(II) and coordinated alcohol molecules [7,19].

4. Conclusions

Isolation of cobalt(II) tetranuclear cubane alkoxo complexes with carbacylamidophosphates is an important proof for close resemblance of behaviour of these ligand systems and β-diketonates towards transition metal ions. In the present case, the remarkable stability of $(Co\{L\})_4(OCH_3)_4$ or $(Co\{L\})_3(CoOH)(OCH_3)_4$ cores dominates the pathways of interaction in the system $M^{2+} - L^-$ and corresponding cubane molecules appear to be a most stable and common product. This effective stabilization of a cubane metal–alkoxide cluster with a carbacylamidophosphate anion may allow the preparation of novel functionalized condensed metal–alkoxide complexes.

5. Supplementary material

Crystallographic data for the structural analysis have been deposited at the Cambridge Crystallographic Data Center, CCDC numbers CSD-142056 (**1**) and CSD-166804 (**3**). Copies of this information may be obtained free of charge from the Director CCDC, 12 Union Road, Cambridge, CB2 1EZ, UK (fax: +44-1223-336033; e-mail: deposit@ccdc.cam.ac.uk or www: http://www.ccdc.cam.ac.uk).

References

[1] A.F. Wells, Structural Inorganic Chemistry, 5th ed., Clarendon, Oxford, 1986.
[2] M.D. Clark, M.I. Zaworotko, Chem. Commun. (1991) 1607.
[3] M.A. Banares, L. Dauphin, V. Calvo-Perez, T.P. Fehlner, E.E. Wolf, J. Catal. 152 (1995) 396.
[4] B.C. Gates, Catalytic Chemistry, Wiley-Interscience, New York, 1992.
[5] K. Dimitrou, J.-S. Sun, K. Folting, G.I. Christou, Inorg. Chem. 34 (1995) 4160.
[6] R.D. Kohn, M. Haufe, G. Kociok-Kohn, A. Filippou, Inorg. Chem. 36 (1997) 6064.
[7] T. Ama, M.d.M. Rashid, T. Yonemura, H. Kawaguchi, T. Yasui, Coord. Chem. Rev. 198 (2000) 101.
[8] V.A. Ovchynnikov, V.M. Amirkhanov, A.A. Kapshuk, T.Y.u. Sliva, T. Glowiak, H. Kozlowski, Z. Naturforsch., Teil. B 53 (1998) 836.
[9] E.A. Bundya, V.M. Amirkhanov, V.A. Ovchynnikov, V.A. Trush, K.V. Domasevitch, J. Sieler, V.V. Skopenko, Z. Naturforsch., Teil. B 54 (1999) 1033.
[10] Q.L. Tuan, J.D. Woollins, Coord. Chem. Rev. 176 (1998) 469.
[11] A.L. Kon'kin, V.G. Shtyrlin, N.G. Zabirov, I.A. Litvinov, A.T. Gubaidullin, R.R. Garipov, A.V. Aganov, A.V. Zacharov, Phosphorus, Sulfur Silicon 147 (1999) 449.
[12] K.E. Gubina, V.A. Ovchynnikov, V.M. Amirkhanov, V.V. Skopenko, O.V. Shishkin, Z. Naturforsch., Teil. B 55 (2000) 495.
[13] G.I. Derkach, V.V. Kruzement-Prichodko, A.V. Kirsanov, Zhurn. Neorg. Khimii (Russ.) 31 (1961) 2391.
[14] G.M. Sheldrick, SHELXS-86, Acta Crystallogr., Sect. A 46 (1990) 467.
[15] G.M. Sheldrick, SHELXL-93, In: Program for the Refinment of Crystal Structures, University of Göttingen, Göttingen, Germany, 1993.
[16] J. Reedijk, W.L. Driessen, W.L. Groeneveld, Rec. Trav. Chim. Pays-Bas. 88 (1969) 1095.
[17] C. Goh, B.M. Segal, J. Huang, J.R. Long, R.H. Holm, J. Am. Chem. Soc. 118 (1996) 11844.
[18] V.M. Amirkhanov, V.A. Ovchynnikov, T. Glowiak, H.Z. Kozlowski, Z. Naturforsch., Teil. B 52 (1997) 1331.
[19] M. Halcrow, J.S. Sun, J.C. Huffman, G. Christou, Inorg. Chem. 34 (1995) 4167.

PERGAMON

Polyhedron 21 (2002) 969–973

POLYHEDRON

www.elsevier.com/locate/poly

Syntheses and characterization of di- and mono-thiocyanato germanium (IV) complexes with 5,14-dihydro-6,8,15,17-tetramethyldibenzo[*b*,*i*][1,4,8,11]tetraazacyclotetradecine

Xuan Shen, Kazunori Sakata *, Mamoru Hashimoto

Department of Applied Chemistry, Faculty of Engineering, Kyushu Institute of Technology, Tobata-ku, Kitakyushu 804-8550, Japan

Received 31 October 2001; accepted 6 February 2002

Abstract

By controlling the molar ratio of Ge(tmtaa)Cl_2 and NH_4SCN at 1:2 and 1:1 in CH_3OH (H_2tmtaa = 5,14-dihydro-6,8,15,17-tetramethyldibenzo[*b*,*i*] [1,4,8,11]tetraazacyclotetradecine), two kinds of germanium(IV) complexes, Ge(tmtaa)$(NCS)_2$ (**1**) and Ge(tmtaa)(Cl)(NCS) (**2**), were prepared and characterized by IR, UV, mass and NMR spectra as well as DSC measurements. In the IR spectrum of **1**, two C≡N stretching bands of NCS groups were observed at 2073 and 2043 cm^{-1}, while in the IR spectrum of **2**, only one C≡N stretching band of a NCS group appeared at 2110 cm^{-1}. The crystal structure of a *trans* six-coordinate tmtaa complex of germanium in the +IV oxidation state is reported. X-ray single crystal analysis of **1** reveals that it adopts a six-coordinate geometry in which two NCS groups are in *trans* positions. The bond lengths of Ge–N between the central germanium and NCS groups are 1.996(6) and 2.031(6) Å. They are longer than those between the central metal and nitrogen atoms of tmtaa (1.926 Å). © 2002 Elsevier Science Ltd. All rights reserved.

Keywords: Macrocycles; Germanium(IV) tmtaa complexes; Crystal structures; Six-coordinate geometry; *Trans*-positions

1. Introduction

The chemistry of transition metal complexes of 5,14-dihydro-6,8,15,17-tetramethyldibenzo[*b*,*i*] [1,4,8,11] tetraazacyclotetradecine (H_2tmtaa, Fig. 1) spans nearly 30 years and comprises the majority of the research activity for this ligand [1,2]. Rare earth metal complexes containing tmtaa have attracted considerable renewed attention over the last decade [3–5]. However, the chemistry of main group elements with tmtaa has not been extensively developed and only several examples of Group 13 and 14 complexes of tmtaa have been reported [6–10]. Four- and five-coordinate tmtaa complexes of germanium in the +II oxidation state were synthesized and characterized by X-ray single crystal diffraction [6,7]. Furthermore, a tmtaa complex of germanium in the +IV oxidation state was synthesized [9], but its structure was not determined.

Metal-thiocyanato chemistry has had a considerable history of investigation [11–14]. We now present the syntheses, crystal structure and spectral properties of *trans* six-coordinate di- and mono-thiocyanato tmtaa complexes containing the Group 14 element germanium in the +IV oxidation state.

2. Experimental

2.1. Reagents and physical measurements

All solvents were distilled and all chemicals were of reagent grade. Ge(tmtaa)Cl_2 was prepared according to the literature [9]. Elemental analyses were performed on a Yanaco CHN corder MT-3. IR spectra (4000–400 cm^{-1}) were recorded on a JASCO FT/IR-400 spectrophotometer in KBr pellets at room temperature (r.t.). FAB^+ mass spectra were carried out with a JEOL JMS-SX102A gas chromatograph-mass spectrometer in a 2-nitrophenyl octyl ether matrix. Ultraviolet and visible spectra were recorded on a Shimadzu UV-200S double

* Corresponding author. Tel.: +81-93-884-3307; fax: +81-93-884-3300.

E-mail address: sakata@che.kyutech.ac.jp (K. Sakata).

0277-5387/02/$ - see front matter © 2002 Elsevier Science Ltd. All rights reserved.
PII: S0277-5387(02)00917-8

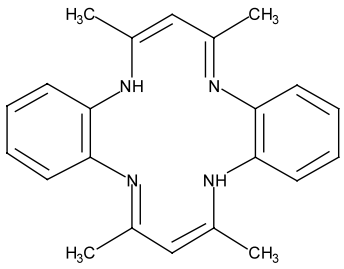


Fig. 1. Suggested structure of H_2tmtaa.

beam spectrophotometer in chloroform at r.t. DSC data were obtained using a Shimadzu DSC-50 differential calorimeter. ^{1}H NMR measurements were taken on a BRUKER AVANCE-400 in chloroform-*d* and dimethylsulfoxide (DMSO)-d_6, and chemical shifts were given in ppm relative to tetramethylsilane as an internal reference standard.

2.2. Preparation of Ge(tmtaa)(NCS)$_2$ (1)

A solution of NH_4SCN (0.045 g, 0.6 mmol) in CH_3OH (5 ml) was added dropwise to a solution of Ge(tmtaa)Cl_2 (0.146 g, 0.3 mmol) in CH_3OH (20 ml) under nitrogen atmosphere. After being heated at 50 °C for 20 h, a product precipitated as a red microcrystalline solid. The product was collected by filtration and washed with CH_3OH, and then was recrystallized from THF–acetonitrile (1:1 v/v) to give orange needles. Yield: 0.109 g (68%). *Anal*. Found: C, 54.16; H, 4.46; N, 16.01. Calc. for $C_{24}H_{22}N_6S_2Ge$: C, 54.27; H, 4.17; N, 15.83%. Melting point (m.p.) 333–336 °C (DSC). UV ($CHCl_3$, λ_{max}, nm): 378, 406, 424. IR (KBr, cm^{-1}): ν(C=C, C=N) 1581, 1541, 1470, 1412; ν(C≡N) 2073, 2043. FAB MS: $m/z = 474$ (M-NCS), 416 (M-2NCS). ^{1}H NMR ($CDCl_3$, ppm): δ 2.52 (s, 12H, CH_3), δ 5.37 (s, 2H, H (7,16-positions)), δ 7.19 (s, 8H, C_6H_4 (aromatic)).

2.3. Preparation of Ge(tmtaa)(Cl)(NCS) (2)

Changing the molar rate of NH_4SCN and Ge(tmtaa)Cl_2 from 2:1 to 1:1, the reaction was carried out in a similar method as outlined above. The orange powder was collected by filtration and washed with CH_3OH. Yield: 0.116 g (76%). *Anal*. Found: C, 53.95; H, 4.49; N, 13.69. Calc. for $C_{23}ClH_{22}N_5SGe$: C, 54.22; H, 4.36; N, 13.75%. M.p. 340–343 °C (DSC). UV ($CHCl_3$, λ_{max}, nm): 378, 408, 424. IR (KBr, cm^{-1}): ν(C=C, C=N) 1578, 1541, 1470, 1411; ν(C≡N) 2110. FAB MS: $m/z =$ 474 (M–Cl), 451 (M–NCS), 416 (M–NCS–Cl). ^{1}H NMR ($CDCl_3$, ppm): δ 2.51 (s, 12H, CH_3), δ 5.39 (s, 2H, H (7,16-positions)), δ 7.19, 7.21 (m, m, 4H, 4H, C_6H_4 (aromatic)).

3. Results and discussion

3.1. Synthesis

Due to the +IV oxidation state of germanium and a *trans* six-coordinate geometry, Ge(tmtaa)Cl_2 shows great reactivity at the axial positions. Di- and monothiocyanato tmtaa germanium(IV) complexes, **1** and **2**, were synthesized from substitution reactions of Ge(tmtaa)Cl_2 and NH_4NCS in exact 1:2 and 1:1 molar ratio under mild conditions (in a nitrogen atmosphere, 50 °C). Since **1** and **2** hardly dissolve in reaction solvent (methanol) and are air- and moisture-stable, subsequent isolation and purification procedures were carried out in air. Crystals of **1**, which were suitable for X-ray structure analysis, were grown in a THF–acetonitrile (1:1 v/v) solution at r.t. On the other hand, crystals suitable for X-ray analysis of **2** were not obtained.

3.2. IR spectrometry

The IR spectrum of **1** shows two strong peaks at 2073 and 2043 cm^{-1}, which are assigned to ν_{as} (C≡N) stretching vibrations. This suggests the presence of two thiocyanato ligands with different C≡N bond lengths and angles. **1** adopts a *trans* six-coordinate configuration and the two NCS ligands show different stretching frequencies after they coordinate to the central germanium. On the other hand, the IR spectrum of **2** gives one intense absorption band of a ν_{as} (C≡N) stretching vibration at 2110 cm^{-1}, which perhaps suggests the presence of one thiocyanato ligand. The similarity of the spectroscopic data of **1** and **2** suggests that **2** also adopts a six-coordinate geometry in which Cl and NCS groups are in *trans* positions.

3.3. Mass spectrometry

The FAB$^+$ mass spectrum of **1** shows major fragments at *m*/*z* 474 corresponding to [M-NCS]$^+$ and *m*/*z* 416 corresponding to [M-2NCS]$^+$. The FAB$^+$ mass spectrum of **2** shows the major fragments at *m*/*z* 474 corresponding to [M-Cl]$^+$, *m*/*z* 451 corresponding to [M-NCS]$^+$ and *m*/*z* 416 corresponding to [M-NCS–Cl]$^+$. No molecular ion peak was observed. These suggest **1** and **2** have the same geometry and the substituents in *trans* positions may be easily cleaved in FAB$^+$ mass measurements.

3.4. NMR spectrometry

It is well known that thiocyanato is often used in synthesizing metal polymers [15–17] and polynuclear complexes [18–21]. We had a hunch that **2** may be a polynuclear complex or a polymer. However, not only UV spectra, IR spectra, mass spectra and DSC mea-

surements, but also ^{1}H NMR spectra prove that **2** has the same *trans* six-coordinate configuration as **1**. ^{1}H NMR spectra of **1** and **2** measured in chloroform-*d* were described in Section 2. Furthermore, ^{1}H NMR spectra of **1**, **2** and Ge(tmtaa)Cl_2 measured in DMSO-d_6, are also described and compared. This proves that **2** has the same six-coordinate *trans* configuration as **1**.

Fig. 2 indicates the benzenoid ring signals of **1**, **2** and Ge(tmtaa)Cl_2 in DMSO-d_6. The DMSO solvent coordinates to the complexes and the signals split into several groups. We consider the following species to exist in solution.

Ge(tmtaa)$(NCS)_2$ (**1**, a) + DMSO
⇌Ge(tmtaa)(NCS)(DMSO) (d)
+Ge(tmtaa)$(DMSO)_2$(f)

Ge(tmtaa)(Cl)(NCS) (**2**, b) + DMSO
⇌Ge(tmtaa)(NCS)(DMSO) (d)
+Ge(tmtaa)(Cl)(DMSO) (e) + Ge(tmtaa)
× $(DMSO)_2$ (f)

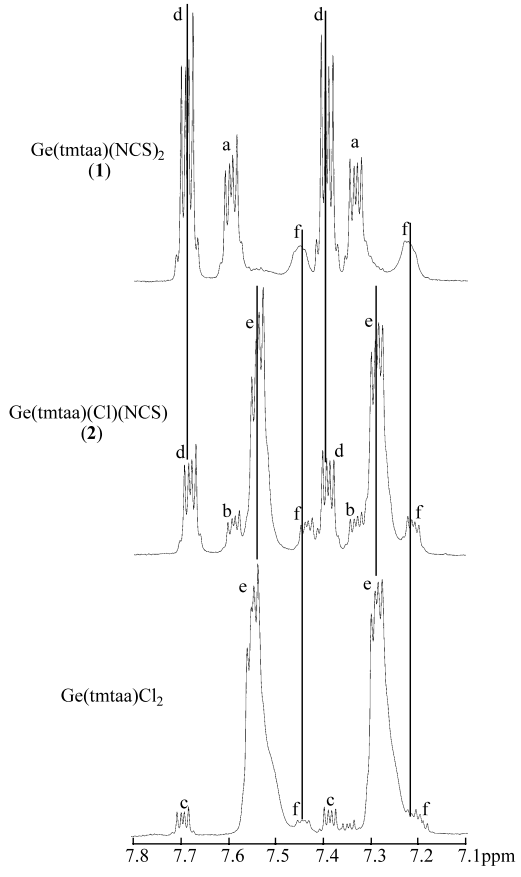


Fig. 2. NMR spectra of Ge(tmtaa)$(NCS)_2$ (**1**), Ge(tmtaa)(Cl)(NCS) (**2**) and Ge(tmtaa)Cl_2. (Section of benzenoid rings, in DMSO-d_6. (a) Ge(tmtaa)$(NCS)_2$ (**1**); (b) Ge(tmtaa)(Cl)(NCS) (**2**); (c) Ge(tmtaa)Cl_2; (d) Ge(tmtaa)(NCS)(DMSO); (e) Ge(tmtaa)(Cl)(DMSO); (f) Ge(tmtaa)$(DMSO)_2$.

Ge(tmtaa)Cl_2 (c) + DMSO
⇌Ge(tmtaa)(Cl)(DMSO) (e)
+Ge(tmtaa)$(DMSO)_2$ (f)

What signals a to f represent are stated in the next list.

a) Ge(tmtaa)$(NCS)_2$ (**1**).
b) Ge(tmtaa)(Cl)(NCS) (**2**).
c) Ge(tmtaa)Cl_2.
d) Ge(tmtaa)(NCS)(DMSO).
e) Ge(tmtaa)(Cl)(DMSO).
f) Ge(tmtaa)$(DMSO)_2$.

In Fig. 2, the signals of Ge(tmtaa)$(DMSO)_2$ (f) were observed in all three spectra. The signals of Ge(tmtaa)$(NCS)_2$ (a) and Ge(tmtaa)(NCS)(DMSO) (d) were observed in the spectrum of **1**. The signals of Ge(tmtaa)Cl_2 (c) and Ge(tmtaa)(Cl)(DMSO) (e) were observed in the spectrum of Ge(tmtaa)Cl_2. It may prove that **1** and Ge(tmtaa)Cl_2 have the same configuration. However, not only the signals of Ge(tmtaa)(Cl)(NCS) (b), but also the signals of Ge(tmtaa)(NCS)(DMSO) (d) and Ge(tmtaa)(Cl)(DMSO) (e) were observed in the spectrum of **2**. This may prove that **2** is also a six-coordinate complex with NCS and Cl groups in *trans* positions and it is not a polymer containing bridged-thiocyanato groups.

3.5. Description of the structure

An orange needle of **1** having approximate dimensions of 0.20 × 0.10 × 0.02 mm was measured at room temperature on a Rigaku AFC7R diffractometer equipped with a rotating anode generator using monochromatized Mo Kα radiation ($\lambda = 0.71069$ Å). Crystal data and details associated with the data collection are summarized in Table 1. Selected bond lengths and bond angles are listed in Table 2.

Notable features of the structural chemistry of tmtaa complexes are non-planar, saddle-shaped conformation and smaller N_4 coordination cavity 'hole size' than that of porphyrins and phthalocyanines. The ORTEP drawing of **1** is shown in Fig. 3. The structure determination of **1** reveals that it adopts a *trans* six-coordinate configuration similar to tmtaa tin(IV) complexes [9]. On the other hand, it does not behave like Group 4 (Ti, Zr or Hf) tmtaa complexes, which exhibit a *cis* six-coordinate configuration [21–25]. The saddle shape of the ligand is almost retained. The mean Ge–N bond distance in the N_4 plane is 1.926 Å. It is shorter than that of Ge–N bond of four- and five-coordinate tmtaa Ge(II) complexes (2.107 and 2.021 Å, respectively) [6,7]. The germanium atom is displaced from the N_4 plane towards the benzenoid face of the ligand by only 0.03 Å and is obviously shorter than that of the four-coordinate

Table 1
Crystal data, data collection and refinement parameters for **1**

Empirical formula	$C_{24}H_{22}N_6Ge_1S_2$
Formula weight	531.19
Crystal color, Habit	red, needle
Temperature (°C)	20.0
Crystal dimensions (mm)	0.20 × 0.10 × 0.02
Crystal system	monoclinic
Space group	$P2_1/a$ (#14)
Lattice parameters	
a (Å)	8.635(7)
b (Å)	24.560(8)
c (Å)	11.422(6)
α (°)	90.00
β (°)	103.22(5)
γ (°)	90.00
V(Å^3)	2358(2)
Z value	4
D_{calc} (g cm^{-3})	1.496
F(000)	1088.00
μ (Mo Kα) (cm^{-1})	15.01
$2\theta_{max}$ (°)	55.0
Number of reflections measured	5907
Number of observations ($I > -10.00\sigma(I)$)	5412
Number of variables	382
Goodness-of-fit indicator	1.04
R	0.058
wR	0.165

Table 2
Selected bond lengths (Å) and bond angles (°) of **1**

Bond lengths			
Ge(1)–N(1)	1.934(6)	Ge(1)–N(6)	1.996(6)
Ge(1)–N(2)	1.916(6)	N(5)–C(23)	1.176(9)
Ge(1)–N(3)	1.941(6)	N(6)–C(24)	1.164(8)
Ge(1)–N(4)	1.913(6)	C(23)–S(1)	1.597(8)
Ge(1)–N(5)	2.031(6)	C(24)–S(2)	1.592(8)
Ge(1)···N4 least-squares plane 0.03			
Bond angles			
N(5)–Ge(1)–N(6)	179.5(3)	N(5)–Ge(1)–N(3)	90.5(2)
Ge(1)–N(5)–C(23)	157.7(6)	N(5)–Ge(1)–N(4)	88.7(3)
Ge(1)–N(6)–C(24)	150.4(6)	N(6)–Ge(1)–N(1)	91.4(3)
N(5)–C(23)–S(1)	176.7(7)	N(6)–Ge(1)–N(2)	91.9(2)
N(6)–C(24)–S(2)	177.7(7)	N(6)–Ge(1)–N(3)	89.2(2)
N(1)–Ge(1)–N(3)	179.1(3)	N(6)–Ge(1)–N(4)	91.0(3)
N(2)–Ge(1)–N(4)	177.2(3)	N(1)–Ge(1)–N(2)	95.5(3)
N(5)–Ge(1)–N(1)	88.9(2)	N(2)–Ge(1)–N(3)	85.2(2)
N(5)–Ge(1)–N(2)	88.5(3)	N(3)–Ge(1)–N(4)	94.6(2)
		N(4)–Ge(1)–N(1)	84.7(3)

Ge(II) complex (0.909 Å) [6]. The small displacement may be a consequence of the *trans* geometry.

The two nitrogen atoms of NCS ligands and the central germanium are almost in the same line and the N(5)–Ge(1)–N(6) bond angle is 179.5(3)°. These two *trans* axial nitrogen atoms are almost vertical to the N_4 plane of the tmtaa ligand. The two NCS ligands keep their linearity. N–C–S bond angles are 177.7(7) and 176.7(7)°, whereas the Ge(1)–N(6)–C(24) and Ge(1)–N(5)–C(23) linkages are slightly bent (150.4(6) and 157.7(6)°).

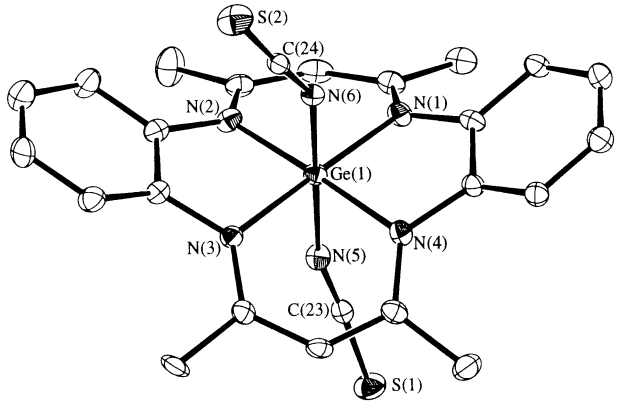


Fig. 3. ORTEP diagram of Ge(tmtaa)(NCS)$_2$ (**1**) with atom labelling scheme showing 50% probability thermal ellipsoids for all non-hydrogen atoms.

Each NCS ligand adopts the most stereochemically favorable orientation with respect to the saddle-shaped macrocycle. The bond length of N(6)–C(24) (1.164(8) Å) is about 0.012 Å shorter than that of N(5)–C(23). In addition, the bond length of Ge(1)–N(6), which is towards the benzenoid face of the ligand, is 1.996(6) Å, and the bond length of Ge(1)–N(5), which is away from the benzenoid face of the ligand, is 2.031(6) Å. It is the saddle-shaped macrocycle that leads to the structure characterization described above.

4. Supplementary material

Crystallographic data for the structural analysis have been deposited with the Cambridge Crystallographic Data Center, CCDC No. 164070 for complex **1**. Copies of this information may be obtained free of charge from: The Director, CCDC, 12 Union Road, Cambridge, CB2 1EZ, UK (fax: +44-1233-336033; e-mail: deposit@ccdc.cam.ac.uk or www: http://www.ccdc.cam.ac.uk).

Acknowledgements

We are grateful to the Center for Instrumental Analysis, Kyushu Institute of Technology for NMR spectra, mass spectra and elemental analyses. We also thank Mr. D. Hirayama in our laboratory for X-ray structure determination.

References

[1] F.A. Cotton, J. Czuchajowska, Polyhedron 9 (1990) 2553.

[2] P. Mountford, Chem. Soc. Rev. 27 (1998) 105.
[3] J. Magull, A. Simon, Z. Anorg. Chem. 615 (1992) 81.
[4] Z. Wang, K. Sakate, M. Hashimoto, Polyhedron 17 (1998) 4451.
[5] Z. Wang, N. Hu, K. Sakata, M. Hashimoto, J. Chem. Soc., Dalton Trans. (1999) 1695.
[6] D.A. Atwood, V.O. Atwood, A.H. Cowley, J.L. Atwood, E. Roman, Inorg. Chem. 31 (1992) 3871.
[7] D.A. Atwood, V.O. Atwood, A.H. Cowley, H.R. Gobran, J.L. Atwood, Inorg. Chem. 32 (1993) 4671.
[8] G.R. Willey, M.D. Rudd, Polyhedron 11 (1992) 2805.
[9] W.J. Belcher, P.J. Brothers, M.V. Land, C.E.F. Rickard, D.C. Ware, J. Chem. Soc., Dalton Trans. (1993) 2101.
[10] W.J. Belcher, P.J. Brothers, A.P. Meredith, C.E.F. Rickard, D.C. Ware, J. Chem. Soc., Dalton Trans. (1999) 2833.
[11] M. Kabesova, R. Boca, M. Melnick, D. Valigura, M. Dunaj-Jurco, Coord. Chem. Rev. 140 (1995) 115.
[12] K.K. Narang, J.P. Pandey, Synth. React. Inorg. Met.-Org. Chem. 24 (1994) 73.
[13] A.H. Norbury, Adv. Inorg. Chem. Radiochem. 17 (1975) 231.
[14] R.A. Bailey, S.L. Kozak, T.W. Michelsen, W.N. Mills, Coord. Chem. Rev. 6 (1971) 407.
[15] H. Krautscheid, N. Emig, N. Klaassen, P. Seringer, J. Chem. Soc., Dalton Trans. (1998) 3071.
[16] T.K. Maji, I.R. Laskar, G. Mostafa, A.J. Welch, P.S. Mukherjee, N.R. Chaudhuri, Polyhedron 20 (2001) 651.
[17] H. Zhang, X. Wang, K. Zhang, B.K. Teo, Inorg. Chem. 37 (1998) 3490.
[18] J. Ribas, C. Diaz, R. Costa, J. Tercero, X. Solans, M. Font-Bardia, H. Stoeckli-Evans, Inorg. Chem. 37 (1998) 233.
[19] L.A. Kovbasyuk, O.Y. Vassilyeva, V.N. Kokozay, W. Linert, J. Reedijk, B.W. Skelton, A.G. Oliver, J. Chem. Soc., Dalton Trans. (1998) 2735.
[20] C.A. White, G.P.A. Yap, N.P. Raju, J.E. Greedan, R.J. Crutchley, Inorg. Chem. 38 (1999) 2548.
[21] D.M. Roundhill, H.B. Gray, C.M. Che, Acc. Chem. Res. 22 (1989) 55.
[22] S.F. Rice, S.J. Milder, H.B. Gray, R.A. Goldbeck, D.S. Kliger, Coord. Chem. Rev. 43 (1982) 349.
[23] W.R. Mason, J. Am. Chem. Soc. 98 (1976) 5182.
[24] S.K. Chastain, W.R. Mason, Inorg. Chem. 21 (1982) 3717.
[25] M.M. Savas, W.R. Mason, Inorg. Chem. 26 (1987) 301.

PERGAMON

Polyhedron 21 (2002) 975–986

POLYHEDRON

www.elsevier.com/locate/poly

Synthesis of functionalized cobaltacarboranes based on the *closo*-[(1,2-$C_2B_9H_{11}$)$_2$-3,3′-Co]$^-$ ion bearing polydentate ligands for separation of M^{3+} cations from nuclear waste solutions. Electrochemical and liquid–liquid extraction study of selective transfer of M^{3+} metal cations to an organic phase. Molecular structure of the *closo*-[(8-(2-CH_3O–C_6H_4–O)-(CH_2CH_2O)$_2$-1,2-$C_2B_9H_{10}$)-(1′,2′-$C_2B_9H_{11}$)-3,3′-Co]Na determined by X-ray diffraction analysis

Jaromír Plešek [a], Bohumír Grüner [a,*], Stanislav Heřmánek [a], Jiří Báča [a], Vladimír Mareček [b], Jana Jänchenová [b], Alexandr Lhotský [b], Karel Holub [b], Pavel Selucký [c], Jiří Rais [c], Ivana Císařová [d], Josef Čáslavský [e]

[a] *Institute of Inorganic Chemistry, Academy of Sciences of the Czech Republic, 250 68 Řež near Prague, Czech Republic*
[b] *J. Heyrovský Institute of Physical Chemistry, Academy of Sciences of the Czech Republic, Dolejškova, 3, 182 23 Prague 8, Czech Republic*
[c] *Nuclear Research Institute plc., 250 68 Řež near, Prague, Czech Republic*
[d] *Department of Chemistry, Faculty of Natural Sciences of the Charles University, Hlavova 2030, Prague 2, Czech Republic*
[e] *Institute of Analytical Chemistry, Academy of Sciences of the Czech Republic, Veveří 97, 61142 Brno, Czech Republic*

Received 31 October 2001; accepted 9 January 2002

Abstract

A new series of the boron substituted cobalt bis(dicarbollide)(1-) ion (**1**) derivatives of the general formula *closo*-[(8-X-(CH_2–CH_2O)$_2$-1,2-$C_2B_9H_{10}$)(1′,2′-$C_2B_9H_{11}$)-3,3′-Co]$^-$ (X = 1-O-2-CH_3O–C_6H_4 (**3**), 1-O-2-$C_6H_5CH_2$–C_6H_4 (**4**), 1-O-4-t-C_8H_{17}–C_6H_4 (**5**), –P(O)(OC_4H_9)$_2$ (**6**) and –P(O)(OC_4H_9)(OH) (**7**) was prepared by ring cleavage of 8-dioxane-**1** derivative (**2**). The compounds were synthesized with the aim to develop a new class of extraction agents effective for liquid–liquid extraction of polyvalent cations, i.e. lanthanides and actinides from high level activity nuclear waste. All compounds were characterized by a combination of ^{11}B NMR, ^{1}H high field NMR methods, mass spectrometry with electrospray ionization, HPLC and other techniques. The molecular structure of the sodium salt of anion **3** was determined by single crystal X-ray diffraction analysis. Crystallographic results proved the sodium atom is tightly coordinated to five oxygen atoms of the spacer chain, the guaiacolyl terminal group X and one water molecule, and from the opposite side of the ligand plane the short B(8′)-H–Na contact (2.26(3) Å) was found to be within bonding distance. The sodium cation is enveloped with an hydrophobic outer sphere composed of hydrophobic CH_2 and CH groups of the organic substituent and B–H groups of cobalt bis(dicarbollide)(1-) cage. The complexation ability of all new anionic ligands for target metal cations was tested by means of cyclic voltammetry at the interface between two immiscible electrolyte solutions. The measurements confirmed stoichiometry of 1:3 (cation:ligand) for the Eu^{3+} complex. Liquid–liquid extraction tests proved the extraction efficiency of anionic species for M^{3+} cations, most of them being able to extract Eu^{3+} only from slightly acidic solutions up to pH 2. The compounds allowed the use of low polar, less environmentally dangerous solvents, e.g. toluene in the liquid–liquid extraction process. Encouraging results were obtained for compound **7**, for which the extraction coefficients from 1 M HNO_3 were found to be sufficiently high even in respect of possible technological applications. © 2002 Elsevier Science Ltd. All rights reserved.

Keywords: Carboranes; Carba metallaboranes; Dicarbollides; Cyclic voltammetry; Liquid–liquid extraction; Lanthanide and actinide extaction

* Corresponding author. Fax: +4202-209-40157.
E-mail address: gruner@iic.cas.cz (B. Grüner).

0277-5387/02/$ - see front matter © 2002 Elsevier Science Ltd. All rights reserved.
PII: S0277-5387(02)00865-3

1. Introduction

Derivatives of the cobalta bis(dicarbollide)(**1**-) ion, *closo*-[(1,2-$C_2B_9H_{11})_2$-3,3′-Co]$^-$ (**1**) [1,2] (Fig. 1), present a specific group of single-charged anionic species [1–3] particularly suitable for the extraction of ^{137}Cs from highly acidic solutions [4–11]. Based on the original Czechoslovak patent [5], a reliable, robust and efficient liquid–liquid extraction separation process for the separation of ^{137}Cs and ^{90}Sr had been developed about 25 years ago under cooperation of the I.I.C. and the Nuclear Research Institute, Řez, Czech Republic with the Radium Institute, Leningrad in the former Soviet Union. The acidic form of the hexachloroderivative of cobalt(III) bis(dicarbollide)(1-) ion *closo*-[(1,2-$C_2B_9H_8Cl_3)_2$-3,3′-Co]$^-H_3O^+$ in nitrobenzene or halogenated hydrocarbons are used as the extractant in this procedure. A slightly modified process has been recently successfully employed on an industrial scale at the Mayak complex, Ozersk, Russia for treatment of a large amount of high level activity liquid waste (HLW) [12,13].

The recent investigations were focused on a search for more powerful anion **1** based extractants for Cs^+ and Sr^{2+} with the main aim to minimize environmental risks, i.e. the extraction process had to meet the E.E.C. ecological requirements especially in respect of the solvents nocivity. A series of the new extractants for Cs^+ and Sr^{2+} based on various 8, 8′- arylene bridged and 4, 8′, 4′, 8 bis bridged (R = phenyl, tolyl, xylyl, biphenylene, tetraline, etc.) derivatives of **1** was developed and tested [14,15]. The substitution of the cluster anion with aromatic rings led to a pronounced hydrophobic behavior of the respective species and their enhanced solubility in aromatic hydrocarbons.

The main target of the current investigations is to develop an effective separation method for M(3+) lanthanides and minor actinides, i.e. long-lived nuclides from highly acidic solutions of HLW remaining after removal of Cs^+ and Sr^{2+}.

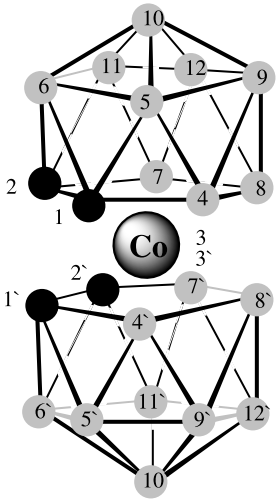


Fig. 1. Schematic structure of the parent anion [*closo*-*commo*-(1,2-$C_2B_9H_{11})_2$-3,3′-Co]$^-$ (**1**) with the cage numbering. For clarity, terminal hydrogen atoms (one on each unsubstituted skeletal vertex) are omitted.

A logical way, how to transfer the lanthanide and actinide M^{n+} cation from aqueous solution into a low polar organic phase proceeds through tight complex formation. In well known schemes employing organic ligands, the metal is surrounded with electron donor atoms of the uncharged ligands like crown ethers, malonamides, phosphine oxides, CMPO like or modified calixarenes [16–21], able to form a low polar, but still $n(+)$ charged complex. In this case, hydrated nitrate anions have to be transferred across the interface together with the target cation.

According to our considerations and the recent positive results in extraction properties of carbon substituted **1** derivatives gained by another group [22], cation transfer would be facilitated, provided that both chelating and hydrophobic anionic particles form inherent parts of the same molecule. The polyhapto-substituent/s, would allow for strong bonding of the target cation and displacement of water molecules in its primary coordination sphere. The cationic $n(+)$ charge of one M^{n+} metal ion would be compensated by the minus charge of n hydrophobic univalent anions on a short distance. Consequently, the resulting molecular assembly comprising of an inner polar cavity enveloped with an hydrophobic outer core (composed of cluster anions and organic hydrophobic groups) would tend to leave the water phase and enter the low-polar organic solvent. This principle is schematically depicted in Fig. 2.

The new compounds *closo*-[(8-X-$(CH_2–CH_2O)_2$-1,2-$C_2B_9H_{10})$(1′,2′-$C_2B_9H_{11}$)-3,3′-Co]$^-$ (**3**–**7**) prepared to test the above idea and described in this article, amalgamate in one molecule the strongly hydrophobic hydroborate anion with delocalised (1-) charge together with polyhapto-substituents bonded to boron atom $B_{(8)}$, allowing for selective bonding of the target cation. In these compounds, boron atom substitution brings an advantage in the direct blocking of the most reactive skeletal site $B_{(8)}$ of the molecule. Also some protection of the second one ($B_{(8')}$–H) bond by steric hindrance can be assumed. This causes an enhanced stability in strongly acidic HLW solutions.

The synthetic, electrochemical and extraction results described in this article bring evidence about viability and validity of the above concept.

2. Experimental

2.1. General

All reactions were carried out with use of standard vacuum or inert-atmosphere techniques as described by

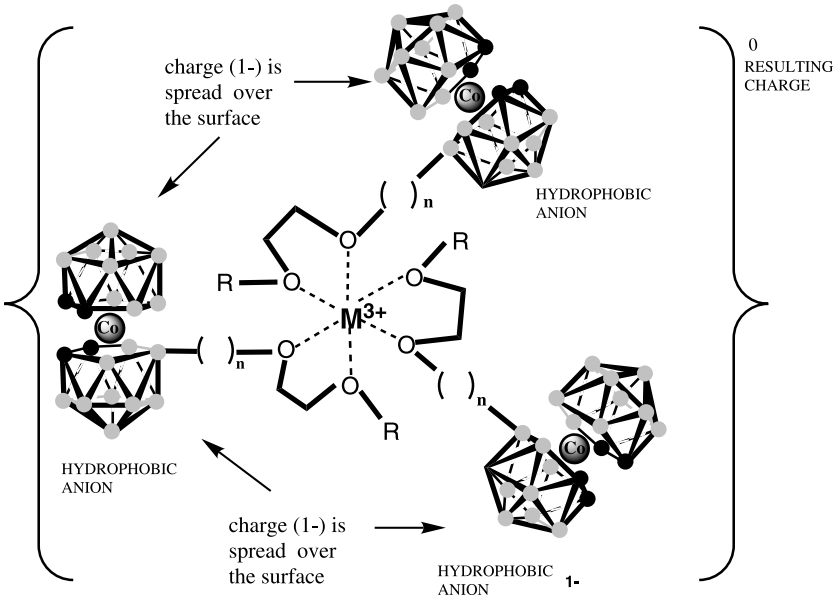


Fig. 2. Schematic drawing of the complex formation around M^{3+} cation with the ligating species of the general formula $[(8\text{-}X\text{-}(CH_2CH_2O)_2\text{-}1,2\text{-}C_2B_9H_{10}(1,2\text{-}C_2B_9H_{11})\text{-}3,3'\text{-}Co]^-$. The bonding via oxygen atoms in the spacer is just an example. Nevertheless, it can be considered as well for coordination *via* other donating atoms (O,P) in the selective terminal moiety.

Shriver [23], although some operations, such as column chromatography, were carried out in air. The starting dioxane of the anion **1**, *closo*-[(8-($\underline{CH_2CH_2–O}$–CH_2–CH_2O)-1,2-$C_2B_9H_{10}$)(1′,2′-$C_2B_9H_{11}$)-3,3′-Co]^0 (**2**) was prepared from commercially available anion **1** (Katchem Ltd., Prague, Czech Rep.) according to the literature procedure [24]. Toluene (Lachema, Brno, Czech Rep.) was dried over Na metal, THF (Aldrich) with sodium diphenylketyl and freshly distilled before use. High surface sodium hydride made at I.I.C. was used with a BET surface area of about 1 $m^2\ g^{-1}$. The commercially available dibutylphosphite (Aldrich) was used for introduction of the dibutylphosphite terminal moieties. Other chemicals were reagent or analytical grade and were used as purchased. Column chromatography was carried out on silica gel (Aldrich, 200–400 mesh) and the purity of the individual chromatographic fractions was monitored by analytical TLC on Silufol (silica gel on aluminium foil; yellow–orange spots, eventually detected by diiodine vapors followed by 2% aqueous $AgNO_3$ spray) and HPLC.

2.2. Physical measurements

2.2.1. NMR and mass spectrometry

Proton (^1H) and boron (^{11}B) NMR spectroscopy were performed at 11.75 T on Varian Unity-500 instruments. The procedure for [^{11}B–^{11}B]-COSY [25,26] and ^1H–{$^{11}B_{(selective)}$} [27] NMR experiments were essentially as described in other papers from our laboratories [28]. NMR chemical shifts are given in ppm to high-frequency (low field) of} = 160.380 MHz (nominally $F_3B{\cdot}OEt_2$ in $CDCl_3$) for ^{11}B (quoted ±0.5 ppm.) and} = 500 MHz ($SiMe_4$) for ^1H (quoted ±0.05 ppm.)} being defined as in the literature [25,26]. Residual solvent ^1H resonances were used as internal secondary standards. Coupling constants $^1J(^{11}B–^1H)$ are taken from resolution-enhanced ^{11}B spectra with a digital resolution of 2 Hz and are given in Hz. Peaks in ^{31}P spectra are referenced to H_3PO_4 as the external standard.

Mass Spectrometry measurements were performed on a Bruker Esquire-LC Ion Trap instrument using Electrospray Ionization. Negative ions were detected. Samples dissolved in acetonitrile (concentrations 1 ng μl^{-1}) were introduced to the ion source by infusion of 3 µl min^{-1}, drying temperature was 300 °C, drying gas flow 5 l min^{-1}, nebulising gas pressure 10 psi.

2.2.2. Analytical HPLC

Chromatographic procedure: The Ion-Pair RP chromatographic method for separation of hydrophobic borate anions with DAD detection was used [29] based on results described earlier in the literature [30] by authors from this laboratory. Column: RP Separon C8 7 µm (silica with chemically bonded octyl groups) Tessek Ltd., Prague. Chromatographic conditions: Mobile phase: 3 mmol hexylamine acetate in 58% aqueous acetonitrile, Flow rate 1 ml min^{-1}, detection DAD, fixed wavelengths 280, 295, 312 and 325 nm, Sensitivity range: 0.2 A.U.F.S, samples of concentration approximately 1 mg ml^{-1}, injection volume 5 µl.

2.2.3. X-ray crystallography

The orange crystal of compound **3** of dimensions 0.3 × 0.25 × 0.2 mm was mounted on a glass fiber with

glue and measured on four-circle diffractometer κ CCD with CCD area detector at 150(2) K with (graphite monochromated) Mo Kα radiation. The crystallographic details are summarized in Table 1. The structure was solved by the direct method (SIR-92) and refined by a full-matrix least-squares procedure based on F^2 (SHELXL-97) [31]. The absorption was neglected. Hydrogen atoms were localized on a difference Fourier map and refined isotropically except those of the methyl moiety, which were recalculated into idealized positions and refined with a temperature factor restricted to $1.2[U_{eq}(C)]$. A water molecule is disordered into two positions, one oxygen with higher occupancy was refined anisotropically, the second isotropically, because of the vicinity of disordered atoms, the positions of the hydrogen atoms of the water molecule could not be determined. Scattering factors were those implemented in the SHELX programs.

2.2.4. Electrochemical measurements

The details of the experimental arrangement have been described in the previously published article [32].

2.2.5. Extraction tests

All extraction experiments were performed in glass test-tubes with polyethylene stoppers at laboratory temperature (23 ± 1 °C). The phase volume ratio was 1:1 (2 ml of each phase). The samples were shaken for 1 h (10 min was sufficient for attaining extraction equilibrium) on a horizontal shaker. After shaking, the test-tubes were centrifuged and 1 ml samples of each phase were taken for radioactivity measurement. All reagents and solvents used were of A.R. quality. The distribution of Eu was investigated using carrier-free ^{152,154}Eu (radiochemical purity). The radioactivity of samples was measured using single-channel analyzer with NaI (Tl) well detector.

2.3. General synthetic procedure for the preparation of 8-L-functionalized derivatives by closo-[(8-(CH_2CH_2–O–CH_2–CH_2O)-1,2-$C_2B_9H_{10}$)(1′,2′-$C_2B_9H_{11}$)-3,3′-Co]^0 (2) ring opening

The respective phenol or dibutylphosphite reagent (10 mmol) dissolved in toluene (30 ml) was added dropwise under stirring to the high surface solid NaH (12 mmol) overlayed with toluene (20 ml) and the resulting slurry was stirred at room temperature for 1 h. Then a slurry of the starting compound **2** (2 g, 4.9 mmol) in toluene-THF solvent mixture (30 and 10 ml) was added and the reaction mixture was gently refluxed for approximately 2 h. The reaction course was monitored by TLC and the heating was stopped when the spot of the starting zwitterionic species **2** disappeared on TLC ($R_F = 0.47$, CH_2Cl_2). After cooling down, ethanol (10 ml) was carefully added followed by water (20 ml).

The solvents were evaporated almost to dryness, water (30 ml) was added and the products were extracted into diethylether (three times 25 ml). Water (10 ml) was added to the combined ether extracts and the solvents were evaporated. The residue was dissolved in chloroform-acetonitrile solvent mixture (3:1) and the products were purified by flash chromatography on a silica gel column using the same mobile phase for elution. After evaporation of the respective fractions to dryness orange powders resulted. For the respective yields, TLC R_F values, HPLC k', NMR data and other properties see Tables 1–3. Crystals of the $Na^+\mathbf{3}^-$ salt were obtained by crystallization upon slow cooling down of its hot aqueous-ethanolic solution.

2.4. Hydrolysis of the 8-$(BuO)_2PO$-$(CH_2CH_2O)_2$-cobalt bis(dicarbollide) (6) to the respective monobutylester 7

The sodium salt of compound **6** functionalized with dibutylester of the phosphonic acid (2 g, 3.2 mmol) was dissolved in 2.5 M sodium hydroxide solution in 60%

Table 1
Yields, m/z, TLC R_F and HPLC k' values of the functionalized cobalt bis(dicarbollide) of the of the general formula [(8-X-$(CH_2CH_2O)_2$)-1,2-$C_2B_9H_{10}$) (1′,2′-$C_2B_9H_{11}$)-3,3′-Co]Na

Terminal group X	Number	Yield (%)	m/z	TLC R_F [a]	HPLC k' [b]	Melting point (°C)
2-CH_3O-phenoxide-	3	82	537.2 534.3(100%)	0.54	6.11	125–128
2-Benzylphenoxide-	4	84	597.3 594.4(100%)	0.43	13.53	114–116
4-*t*-Octylphenoxide-	5	79	619.4 616.4(100%)	0.45	31.8	185–188
$[(BuO)_2P{=}O]^-$	6	58	607.2 604.4(100%)	0.38	6.96	202–204
$[(HO)[(BuO)P{=}O]^-$	7	74	551.3 548.3(100%)	0.17	0.94	152–155 [c]

[a] $CHCl_3$:CH_3CN 3:1.
[b] $k' = 3.18$ for parent cobalt bis(dicarbollide) ion **1** under these chromatographic conditions.
[c] Ca^{2+} salt.

Table 2
^{11}B and and ^{1}H (B–H) chemical shifts r $\delta(^{11}B)$, $^{1}J(^{11}B-^{1}H)$ in parentheses, for the functionalized cobalt bis(dicarbollide) series of the general formula [(8-X-$(CH_2CH_2O)_2$-1,2-$C_2B_9H_{10}$) (1′,2′-$C_2B_9H_{11}$)-3,3′-Co]Na, measured in deuterioacetone at 294–297 K

Terminal group X	Nunber	$\delta(^{11}B)$ [ppm], $^{1}J(^{11}B-^{1}H)$ (Hz)
2-CH_3O-phenoxide-	3	23.8s (B8), 5.2 (B8′) (131), 0.5 (B10′) (135), −2.5 (B10) (139), −4.6 (B4′,7′) (142), −7.0d, −7.5d (B9, 12, 9′,12′) (overlap), −8.7 (B4, 7) (176), −17.2 (B5′, 11′) (150), −20.3 (B5, 11) (150), −22.1d (B6′) (overlap), −28.5 (B6) (135).
2-Benzylphenoxide-	4	22.9s (B8), 3.9 (B8′) (135), 0.4 (B10′) (139), −2.4 (B10) (142), −4.3 (B4′,7′)(146), −7.4 (B9′,12′) (139), −8.2 (B 4, 7, 9, 12) (139), −17.3 (B5′, 11′) (154), −20.4 (B5, 11) (154), −22.0 (B6′) (overlap), −28.5 (B6)(150.1).
4-*t*-Octylphenoxide-	5	23.0s (B8), 4.0(B8′) (135), 0.5 (B10′) (139), −2.4 (B10) (143), −4.3 (B4′,7′) (142), −7.3 (B9′,12′) (135), −8.2 (B4, 7, 9, 12) (139), −17.3 (B5′, 11′) (154), −20.4 (B5, 11) (158), −22.0 (B6′) (overlap), −28.4 (B6) (142).
$[(BuO)_2P{=}O]^-$	6	23.4s (B8), 4.7 (B8′) (135), 0.5 (B10′) (139), −2.5 (B10) (142), −4.1 (B4′,7′)(139), −7.1 (B9′,12′)(127), −7.8d (B9, 12) (overlap), −8.4d (B4, 7) (overlap), −17.3 (B5′, 11′) (150), −20.4 (B5, 11) (150), −22.1 (B6′) (overlap), −28.5 (B6) (142).
$[(BuO)(HO)P{=}O]^-$	7	23.9s (B8), 6.6 (B8′) (135), 0.9 (B10′) (130), −2.3 (B10) (139), −4.9 (B4′,7′)(139), −6.5 (B 9,12, 9′,12′) (overlap), −9.0 d (B4, 7) (overlap), −17.1 (B5′, 11′) (119), −20.3 (B5, 11) (131), −22.1 (B6′) (overlap), −28.2 (B6) (145).

aqueous ethanol (30 ml). The solution was gently refluxed for a period of 1 h. After cooling down, the ethanol was stripped off in vacuum. The resulting aqueous slurry was acidified with HCl (4 M, 100 ml) and the species was extracted with three portions of ether (20 ml). A small volume of water (25 ml) was added to the combined ether extracts and the organic solvent was evaporated. Calcium chloride in water (1.6 mmol) was added. Then ethanol was added in small portions to the resulting slurry under gentle reflux until the product dissolved. After cooling down, the product was filtered off and dried. A second crop was obtained after partial evaporation of ethanol. Orange powder, yield 74%.

2.5. Conversion of the compounds (*3*–*7*) to the form of tetrabutylammonium salts used in electrochemical measurements

The respective sodium or calcium salt (0.5 g) (compound **6**) was dissolved in 50% aqueous ethanol (15 ml) and an excess of Bu_4NBr in water (10 ml) was added causing precipitation of a fluffy or oily precipitate. This was separated by decantation, stirred four times with

Table 3
^{1}H Chemical shifts $\delta(^{1}H)$, $\delta(^{1}H)$ for $^{1}H-\{^{11}B(selective)\}$ experiments in square brackets for the series of functionalized anions of the general formula formula [(8-X-$(CH_2CH_2O)_2$-1,2-$C_2B_9H_{10}$) (1′,2′-$C_2B_9H_{11}$)-3,3′-Co]Na, measured in deuterioacetone at 294–297 K

Terminal group X	Number	^{1}H Chemical shifts (ppm)
2-CH_3O-phenoxide	3	7,17 m (2H, Ar), 6,92 m (2H, Ar), 4,19 m (2H, CH_2–O), 4.18s (2H, H_2O), 4,14 s (2H, 2 CH_{carb}), 3,89 m (2H, CH_2–O), 3,87s (3H, CH_3O–), 3,73m (2H, CH_2–O), 3,66 m (2H, CH_2–O), 3,01 s (2H, $2CH_{carb.}$), [2.93] (H10′), [2.75] (H8′), [2.73] (H4′,7′), [2.70] (H10), [2.06, 1.84] (H 9, 12, 9′,12′), [1.86] (H 6′), [1.84] (H 4, 7), [1.63] (H 5′, 11′), [1.55] (H5, 11), [1.46] (H6).
2-Benzylphenoxide	4	7.29–6.854m (9H, Ar), 4.30 s (2H, H_2O), 4.27 (2H, CH_{carb}), 4.11m (2H, CH_2–O), 3.97s (2H, CH_2), 3.81 (2H, CH_2–O), 3.64–3.59 m (4H, $2CH_2$–O), 3.10s (2H, $2CH_{carb}$), [2.95] (H10′), [2.79] (H4′,7′), [2.72] (H10), [2.48] (H8′), [2.06] (H9′,12′), [2.06, 1.81] (H4, 7, 9, 12), [1.73] (H6′), [1.68] (H5′, 11′), [1.59] (H5, 11), [1.49] (H6).
4-*t*-Octylphenoxide-	5	7.31d (2H, Ar), 6.87 d (2H, Ar), 4.28s (2H, CH_{carb}), 4.11m (2H, CH_2O), 3.81 (2H, CH_2O), 3.63–3.59m (4H, $2CH_2O$), 2.95s (2H, $2CH_{carb}$), [2.92] (H10′), [2.77] (H4′,7′), [2.70] (H10), [2.48] (H8′), [2.01, 1.81] (H9′,12′), [2.01, 1.75] (H4, 7, 9, 12), 1.75s (2H, CH_2, t-octyl), [1.67] (H5′, 11′), [1.57] (H5, 11), [1.71] (H6′), [1.48] (H6), 1.34s (6H, CH_3, t-octyl), 0.72s (9H, CH_3, t-octyl).
$[(BuO)_2P{=}O]^-$	6	4.20s (4H, CH_{carb}), 4.05m (4H, 2 CH_2–O), 3.71, 3.67m (4H, $2CH_2$–O), 3.54m (2H, CH_2–O), 2,94s (6H, $3H_2O$), [2.85] (H10′), [2.70] (H4′,7′), [2.73] (H10), [2.69] (H8′), 2.10 m (2H, CH_2–P), [2.02, 1.83] (H9, 9′, 12, 12′), [2.02] (H4, 7), [1.70] (H6′), 1.65m (4H, 2 CH_2, C_4H_9), [1.63] (H5′, 11′), [1.55] (H5, 11), [1.46] (B6), 1.42 m (4H, 2 CH_2, C_4H_9), 0.94t (6H, 2 CH_3, C_4H_9).
$[(BuO)(HO)P{=}O]^-$	7	4.80br s (1H, OH), 4.13 m (2H, CH_2, C_4H_9), 4.06 (2H, CH_{carb}), 3.86m (2H, CH_2–O), 3.81s (2H, CH_{carb}), 3.62m (2H, CH_2–O), [3.13] (H8′), [2.949] (H4, 7), [2.72] (H10), [2.71] (H10′), [2.11] (H4′,7′), [2.11, 1.90] (H9, 12, 9′,12′), 2.23 m (2H, CH_2–P), [1.68] (H6′), 1.67 m (2H, CH_2, C_4H_9), [1.62] (H 5′, 11′), [1.53] (H5, 11), [1.52] (B6), 1.43 m (2H, CH_2, C_4H_9), 0.93t (3H, CH_3, C_4H_9)

20% aqueous ethanol (15 ml), decanted and dried in vacuum. Most of the products resulted as a sticky dark orange mass.

3. Results and discussion

3.1. Synthesis and properties of substituted cobalt bis(dicarbollide)anions

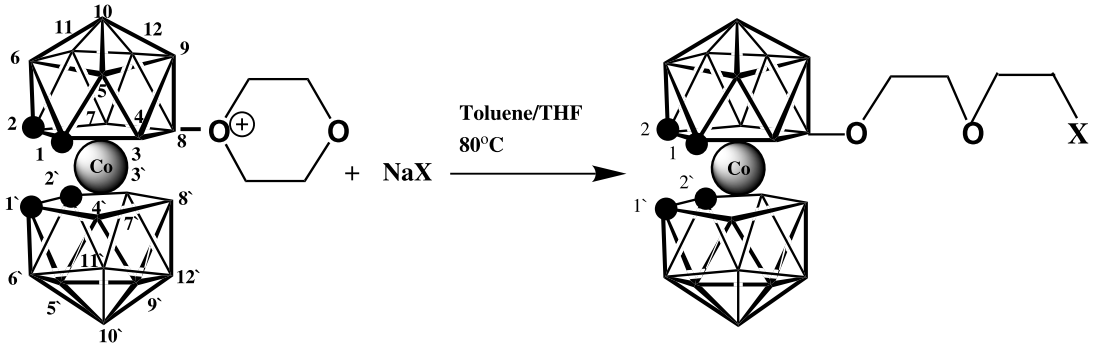
A reliable reaction path was found, producing boron substituted compounds at position $B_{(8)}$ in high yields. Resulting species differ only in the character of the sequestering end groups. This allowed for deeper comparison of effects of the combination of the selective group covalently bonded to cobalt bis(dicarbollide) anion on the metal extraction properties across the whole series. The possibility to modify the properties of the end-group R and whole substituent/s including steric strain of the chain, apparently also able to participate in metal bonding, was studied.

The synthetic method in this study is based on a simple, one step reaction, i.e. dioxane-ring cleavage of the 8-dioxane derivative of anion **1** (bi-polar species **2**). This compound became available on a larger scale only recently (based on results made recently by the I.I.C. Group) [24] and proved to be a versatile synthon in the present study. The dioxane ring of this compound, containing an oxonium oxygen atom, can be easily opened by almost any base $\mathbf{X}^-$ of choice (phenolate, dialkyl- or diaryl- phosphite, etc) producing the respective functionalized anionic species. For reaction paths see Scheme 1.

Parts of the molecule **X** were selected from a broad range of possible candidates with the aims of reaching a wide diversity in the solubility and bonding properties of the resulting extraction agents. In the compound **3**, 2-MeO-phenoxide (Guaiacol) with an extended system of the (–O–Ph–O–) groups was introduced, 2-benzylphenoxide in compound **4** provided a more hydrophobic and mobile benzyl group. The branched *p*–*t*-octylphenoxide moiety in compound **5** was selected as a relatively rigid end-group with increased basicity of the phenoxy-oxygen and providing expected enhancement in the solubility in organic solvents. In compound **6**, $[(BuO)_2P{=}O]^-$ with known powerful sequestering properties represented another kind of end-group attached to anion **1**. The resulting product with terminal ester functionalities was later hydrolyzed to the $[(BuO)(HO)P{=}O]^-$ monoester end group in compound **7**, in order to incorporate another acidic center into the molecule. The subsequent alkaline hydrolysis of this ester did not proceed even under forced conditions and prolonged reflux. On the other hand, further partial hydrolysis apparently occurs upon contact with concentrated nitric acid as can be seen from stability tests described in the extraction part (see below). As can be seen from extraction tests, presence of $[(BuO)(HO)P{=}O]^-$ monoester functionality, as another acidic center in the molecule, proved to increase the transfer of the cations to the organic phase from highly acidic waste solutions substantially.

The reactions were smooth and quantitative in the first four cases, whereas in the synthesis of compound **6** two species in the ratio approximately 2:1 resulted. Only one species contained the desired C–P bond, whereas the minor product, not fully characterized, probably containing a $-C-O-P(O)(O-Bu)_2$ arrangement, was useless for extraction. With the exception of compound **7**, which was purified as its calcium salt, all other species were isolated as sodium salts. Samples in this form were submitted for extraction tests, and after conversion to the Bu_4N^+ salts were submitted for electrochemical measurements. The molecular structure of compound **3** was determined by X-ray diffraction, for details see text below. For physical properties and NMR data of the new compounds see Tables 1–3.

It should be pointed out that the solubility of Na^+ salts of all species in low polar solvents (toluene, xylene, cumene, etc.) was substantialy enhanced compared with



Scheme 1. General synthetic method leading to anionic species bearing polydentate ligands based on ring cleavage of compound **2**.

the cobaltacarborane parent species **1** and its chlorinated derivatives. This fact seems to be a crucial point in the possible application of compounds of this class as selective extractants.

3.1.1. NMR and X-ray diffraction results

In the ^{11}B NMR spectra of all anions **3**–**7** (Table 2), a significant downfield (to higher frequency) shift of the substituted boron –O–$B_{(8)}$ signal (singlet) could be observed in comparison to the unsubstituted parent species **1** (6.4 ppm). The ^{11}B NMR spectral pattern of all compounds **3**–**7** in the series is very similar. As in the recently reported spectrum of 8-OH substituted anion **1**, boron signals of the unsubstituted and substituted dicarbollide ligands are mutually shifted and could be distinguished from ^{11}B–^{11}B-COSY NMR experiments. Each of two dicarbollide ligands exhibits six peaks of relative intensities 1:1:2:2:2:1, for signal assignment see Table 2. An interesting feature found in the spectra of compounds **3**–**6** is that the resonance corresponding to $B_{(8')}$ atoms of the unsubstituted dicarbollide ligand in compounds **4**–**6** are significantly shifted upfield in comparison with signals of the recently reported mono-hydroxy derivative of anion **1** (8-OH-**1**) (6.9 ppm) [33] and the parent zwitterion **2** (6.4 ppm) [24]. The magnitude of these effects seems larger than could be expected considering simple solvatation or long-range electronic effects caused by substituents. Such a difference in $B_{(8')}$ chemical shifts can probably be ascribed either to diethyleneglycol chain strain due to bonding of the cation close to the cage or to possible involvement of the B–H→M$^+$ contact in the cation bonding, or combination of both effects. Surprisingly, the $B_{(8')}$ signals and all spectral patterns of compound **3**, in which solid state structure was found to contain a short B–H–Na contact (see below), and anion **7** with the strongest metal binding properties closely resemble that of 8-OH-**1**. Again, the chemical shifts of the proton $B_{(8')}$-H resonance in ^{1}H-{^{11}B(selective)} NMR spectra of compounds **3** and **7** are the closest to the values found in 8-OH-**1** anion (3.10 ppm) [33]. Respective signals of compounds **4**–**6** are shifted by approximataly 0.5 ppm.

The signals in ^{1}H NMR spectra of all compounds in the series could be assigned, despite the spectra complexity. The spectral patterns and intensities correspond to the presence of one particular selective group per cage. For peak assignment see Table 2. Compounds **6** and **7** exhibit each one peak in ^{31}P{^{1}H} spectra at 30.74 and 28.75 ppm, respectively.

Also, the mass spectrometry results are in clear agreement with the composition of all compounds under study. Cut off peaks corresponding to molecular mass of all particular compounds were found using an electrospray ionization technique (see Table 1).

The molecular structure of the Na$^+$ complex of anion **3** (see Fig. 3 and Tables 4 and 5) proved the position of the sodium atoms being in the plane formed by the oxygen atoms of guaiacol moiety (distance of Na1 from the least-square plane defined by O1, O2, O3 and O4 is 0.248(1) Å. The unsubstituted part of the carborane cage with the shortest contact H8′-Na1 2.26(3) Å, is situated on one side of this plane, one molecule of water is located on the other side. This distance belongs to the shortest Na...H–B contacts among those found in the Cambridge Structural Database [34] (minimum at 2.169 Å being found in sodium triethylhydroborate [35]). In (7,8-(1,13-dithia-4,7,10-trioxatridecane-1,13-diyl)-7,8-dicarba-nido-undecaborane)-sodium [36], the compound considered as the most suitable for comparison, two symmetrically related intermolecular contacts Na···H(4) equal to 2.31 Å can be found. However, this particular hydrogen shows very unusual bond angles, since the interval H(4)–B(4)–B has limits 87.7–146.7°, unfortunately this effect has not been discussed by the authors in [36]. In the structure presented in this article, on effect of similar magnitude does not occur, the bond angles for H8′ are within 112–128° with an average estimation equal to 1.5°. In our knowledge, this sodium complex represents the first known example where the B–H–Na$^+$ bond was formed by crystallization under aqueous conditions. Apparently tight metal bonding of the Na$^+$ cation inside the polar cavity formed by oxygen atoms and water repulsion due to steric effects of BH and CH_2 groups forming the hydrophobic outer shell may account for this kind of bonding. Other geometric parameters of the cobalt bis(dicarbollide) cluster of compound **3** fall within the usual range including cobalt coordination (see Table 2). Only the substituted boron atom B(8) is moved slightly further from metal atom.

3.2. Electrochemical results

The ability of the synthesized anionic ligands to form a complex with metal cations was tested by means of cyclic voltammetry at the interface between two immiscible electrolyte solutions [37]. In the presence of ligand L in the organic phase (o), the transfer of cation M from the aqueous phase (w) is facilitated by complexation at the interface [38]:

$$M^{z+}(w) + sL^-(o) \leftrightarrows ML_s^{(z-s)}(o) \quad (1)$$

which results in a negative potential shift of the ion transfer reaction. This potential shift is related to the stability constant K_{MLs} of the complex in the organic phase by:

$$K_{MLs} = (c_{Mz+(w)})^{-1}(c_{L(o)})^{1-s}e^{(zF/RT)\Delta E1/2} \quad (2)$$

where c is the concentration and $\Delta E_{1/2}$ is the difference between the half-wave potential of the simple (in the absence of ligand L) and the facilitated ion transfer.

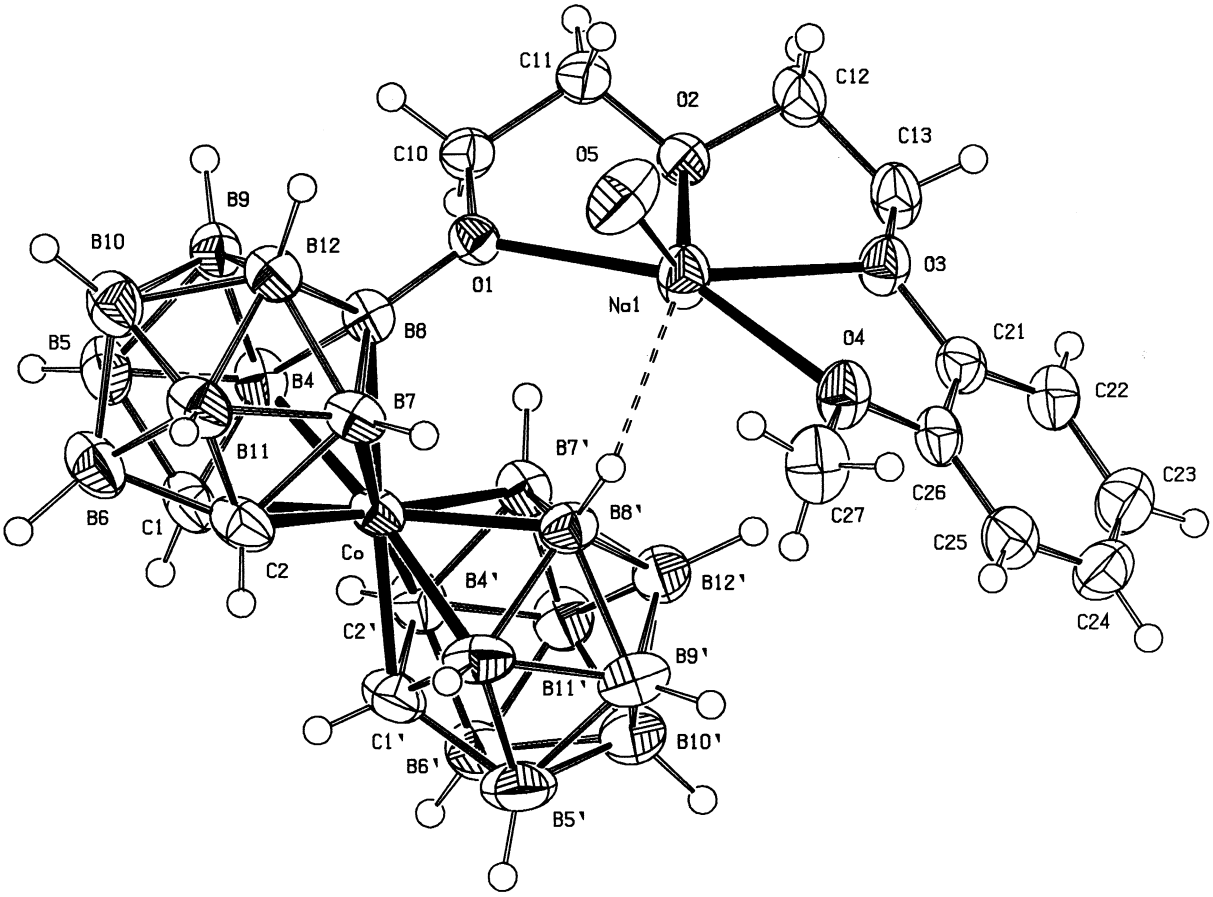


Fig. 3. Molecular structure with atom numbering scheme for **3**. Second position of water molecule (at 1.3 Å from O5) is omitted for clarity. Thermal ellipsoids are drawn at 50% probability level.

It has been shown [39] that if the transferred ion is present in excess with respect to the ligand, the peak potential difference of the cyclic voltammogram for the diffusion controlled charge transfer process is $0.059/z$, $0.087/z$ or $0.112/z$ for the stoichiometry of 1:1, 1:2 or 1:3 (cation:ligand), respectively.

Cyclic voltammograms of the facilitated transfer of Eu^{3+}, Cs^{+} and Na^{+} in the presence of ligand **3** in the organic phase are shown in Fig. 4. The peak potential difference for Cs^{+} and Na^{+} transfer is 0.06 V which corresponds to the stoichiometry of the complex of 1:1 (cation:ligand). The transfer of Cs^{+} is shifted to less positive potentials as compared with the transfer of Na^{+} and Eu^{3+}. This suggests that Cs^{+} would be extracted more easily from an equimolar solution in the aqueous phase, even when the stability constant of Cs^{+} is lower than that of Na^{+} and Eu^{3+} (Table 6). The peak potential difference of 0.04 V with Eu^{3+} is in agreement with the theoretical value $\Delta E_p = 0.112/3 = 0.037$ V, calculated for the stoichiometry of 1:3 (cation:ligand) of the complex. The same peak potential difference $\Delta E_p = 0.04$ V was also found for the transfer of La^{3+} and Ce^{3+} facilitated by the other ligands (Table 6), which indicates formation of a complex with the same stoichiometry. The peak potential difference $\Delta E_p = 0.045$–0.05 V of the facilitated Sr^{2+} transfer corresponds to the stoichiometry of the complexes of 1:2 (cation:ligand) (Table 6).

The half-wave potentials $E_{1/2}$ of the facilitated transfer of the studied ions by ligands **3**–**7** are shown in Fig. 5. Ligands 4 and 5 exhibit a similar behavior to ligand **3**. The apparent selectivity of these ligands for Cs^{+}, i.e. the lowest $E_{1/2}$ as compared with the other ions, points to a lower value of the formal potential of Cs^{+} transfer rather than to the value of the stability constant (Table 6). Ligand 7 exhibits the opposite behavior. In this case the lowest half-wave potential of the facilitated ion transfer is obtained for Eu^{3+}, La^{3+} and Ce^{3+}, which indicates that ligand **7** will be efficient in their extraction from aqueous solution.

Parameters of the facilitated ion transfer reaction of the studied ions derived from cyclic voltammograms are displayed in Table 6. Stability constants of the complexes of anionic ligands **3**–**7** with Cs^{+} and Na^{+} were calculated using the half-wave potential $E_{1/2}$ of the simple ion transfer, 0.56 V [40] and 0.788 V [41], respectively. The value of $E_{1/2} = 0.729$ V for Eu^{3+} was estimated from the cyclic voltammograms of the base

Table 4
Crystal data and structure refinement for **3**

Empirical formula	$C_{15}H_{38}B_{18}CoNaO_5$
M	574.95
Crystal system	monoclinic
Space group	$P2_1/c$
a (Å)	11.3923(3)
b (Å)	26.0256(4)
c (Å)	10.2345(2)
β (°)	105.610(1)
V (Å^3)	2922.5(1)
Z	4
μ (mm^{-1})	0.630
$D_{calc.}$ (Mg m^{-3})	1.307
Wavelength (Å)	0.71073
$F(000)$	1184
θ Range (°)	3.0–27.0
Scan mode	ϕ and ω
h, k, l collected	$-14 \le h \ge 14$, $-33 \le k \ge 33$, $-13 \le l \ge 12$
Number of reflections measured	22 780
Number of unique reflections	6235
Number of parameters	498
Goodness-of-fit all data [a]	1.022
Final R indices $[I > 2\sigma(I)]$ [a]	$R_1 = 0.047$, $wR_2 = 0.109$
R indices (all data) [a]	$R_1 = 0.084$, $wR_2 = 0.129$
w_1/w_2 [b]	0.0573/2.2152
$\Delta\rho$, max, min (e Å^{-3})	0.483 and −0.452

[a] Definitions: $R(F) = \Sigma\ ||F_o| - |F_c||/\Sigma\ |F_o|$, $wR_2 = [\Sigma\ (w(F_o^2 - F_c^2)^2)/\Sigma\ (w(F_o^2)^2)]^{1/2}$, goodness-of-fit $= [\Sigma\ (w(F_o^2 - F_c^2)^2)/(N_{reflns} - N_{params})]^{1/2}$.
[b] Weighting scheme $w = [\sigma^2(F_o^2) + (w_1P) + w_2P]^{-1}$; $P = [\max(F_o^2, 0) + 2F_c^2]/3$.

Table 5
Selected bond lengths (Å) and angles (°) for **3**

Bond lengths	
Co–C(2)	2.023(3)
Co–C(1)	2.034(3)
Co–C(2′)	2.044(3)
Co–C(1′)	2.051(3)
Co–B(7′)	2.086(3)
Co–B(7)	2.093(3)
Co–B(4′)	2.097(3)
Co–B(4)	2.099(3)
Co–B(8′)	2.101(3)
Co–B(8)	2.145(3)
Na(1)–O(5)	2.344(4)
Na(1)–O(2)	2.385(2)
Na(1)–O(1)	2.3938(19)
Na(1)–O(3)	2.403(2)
Na(1)–O(4)	2.425(2)
Na(1)–H(8′)	2.23(3)
Bond angles	
O(5)–Na(1)–O(2)	124.12(12)
O(5)–Na(1)–O(1)	84.98(11)
O(2)–Na(1)–O(1)	71.17(6)
O(5)–Na(1)–O(3)	127.85(13)
O(2)–Na(1)–O(3)	67.80(7)
O(1)–Na(1)–O(3)	137.44(8)
O(5)–Na(1)–O(4)	89.67(11)
O(2)–Na(1)–O(4)	131.76(8)
O(1)–Na(1)–O(4)	153.11(8)
O(3)–Na(1)–O(4)	64.13(7)
O(5)–Na(1)–H(8′)	96.0(7)
O(2)–Na(1)–H(8′)	127.9(7)
O(1)–Na(1)–H(8′)	82.3(7)
O(3)–Na(1)–H(8′)	114.9(7)
O(4)–Na(1)–H(8′)	72.1(7)

electrolytes with different concentration of $EuCl_3$ in the aqueous phase and 0.01 M tetrabutylammonium tetrakis(4-chlorophenyl)borate (TBATPBCl) in 1,2-dichloroethane. In all other measurements 0.01 M aqueous solution of MCl_z was used. The facilitated transfer of cations was measured in the presence of 0.5 mM of the ligand in 1,2-dichloroethane containing 0.01 M TBATPBCl or 0.01 M tetrabutylammonium dicarbollylcobaltate (TBADCC) as the base electrolyte. The potential E of the electrochemical cell was related to the formal potential difference for tetrabutylammonium ion $\Delta_o^w\phi^0_{TBA+} = -0.226$ V [42].

3.3. Extraction tests

It should be noted, Cs^+ extraction (not shown here) of all compounds was negligible, therefore Eu^{3+}/Cs^+ selectivity was quite high. Europium extraction results obtained with the above polydentate extractants are summarized in Table 7(a–d). All anionic species **3**–**7** were tested for Eu^{3+} extraction from acidic media. As can be seen from Table 7(a), with one exception, all compounds under study extract europium fairly well from media of slight acitidity up to 0.01 M HNO_3. However, with increasing acidity Eu distribution ratios strongly decrease, so that with the exception of extractant **7** no extraction of Eu can be observed from 1 M HNO_3 (Table 7(a)). Poor extraction properties of

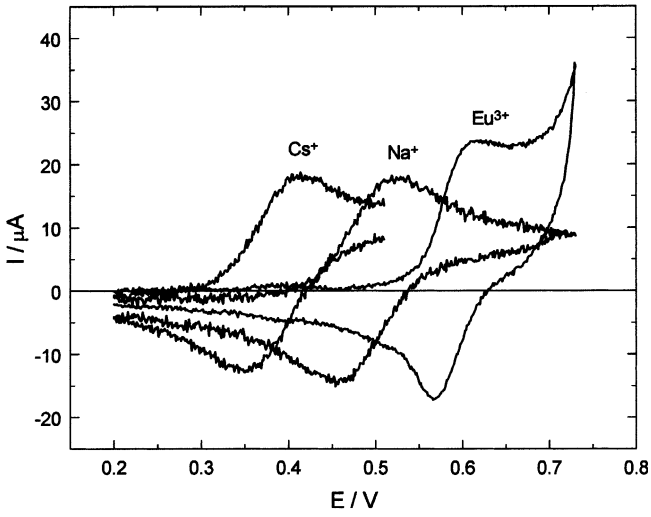


Fig. 4. Cyclic voltammograms of the transfer of Eu^{3+}, Cs^+ and Na^+ facilitated by anionic ligand 3. Aqueous phase: 0.01 M MCl_z. Organic phase: 0.01 M TBATPBCl and 0.5 mM ligand **1** in 1,2-dichloroethane. Area of the interface 26 mm^2. Polarization rate 0.05 V s^{-1}.

Table 6
Parameters of the facilitated ion transfer reaction of the studied ions derived from cyclic voltammograms

		L3	L4	L5	L6	L7
Eu^{3+}	$E_{1/2}/V$	0.61	0.67	0.66	0.45	0.24
	$\Delta E_p/V$	0.04	0.04	0.04	0.04	0.04
	log K_s	16.9	13.6	14.3	25.0	35.7
La^{3+}	$E_{1/2}/V$	0.60	0.67	0.66	0.45	0.24
	$\Delta E_p/V$	0.04	0.04	0.04	0.04	0.04
Ce^{3+}	$E_{1/2}/V$	0.60	0.67	0.66	0.46	0.24
	$\Delta E_p/V$	0.04	0.04	0.04	0.05	0.04
Sr^{2+}	$E_{1/2}/V$	0.58	0.68	0.66	0.48	0.38
	$\Delta E_p/V$	0.05	0.05	0.05	0.05	0.05
Cs^{+}	$E_{1/2}/V$	0.39	0.46	0.46	0.43	0.42
	$\Delta E_p/V$	0.06	0.06	0.07	0.06	0.06
	log K_s	5.5	4.2	4.2	4.7	4.8
Na^{+}	$E_{1/2}/V$	0.49	0.66	0.61	0.42	0.38
	$\Delta E_p/V$	0.06	0.07	0.06	0.06	0.06
	log K_s	7.6	4.7	5.5	8.3	9.4

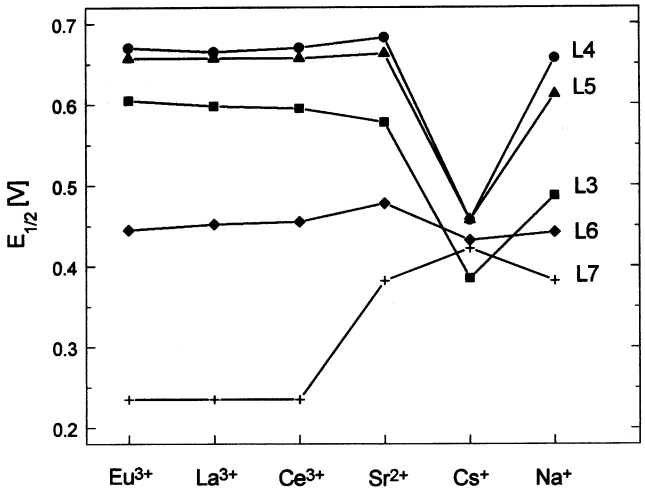


Fig. 5. Half-wave potentials of $E_{1/2}$ of the facilitated transfer of studied cations by anionic ligands **3**–**7**.

extractant **6** can be explained by complete esterification of the phosphate end group and steric hindrance of butyl groups. The same steric hindrance probably plays a role in the extraction mechanism of extractants **3** and **5**, however, the effect of protonization of oxygen atoms on the connecting link cannot be excluded. From this series, only compound **7** seems to be a potentially interesting effective extractant for treatment of highly acidic HLW. The dependence of extraction efficiency of extractant **7** on acidity is given in Table 7(b).

It can be seen that in the order of increasing acidities, the extraction of Eu starts to steeply increase then passes through maximum at approximately 0.1 M nitric acid and then steeply decreases in the media of high acidity. Nonetheless, the extraction from 1 M nitric acid is still sufficiently high for possible technological applications. The existence of a maximum can probably be explained by competition of protonized species for the extractant molecule. Interesting results were obtained with extractant **7** in the extraction—back-extraction cycle. The enormous increase of distribution ratio indicates the further hydrolysis of ester groups on the phosphate end group and increase of extraction efficiency (Table 7(c)).

Similar results were obtained during the tests of chemical stability (Table 7(d)) of extractant **7**. The continuous increase of distribution ratio of europium with time of contact again indicates the progress of a possible extractant hydrolysis. These two series of experiments seemed to indicate that hydrolysis of ester groups by 1 M nitric acid may be a convenient route to obtain the extractant with $(HO)_2(O)P$-end group. On the other hand, the ^{11}B and ^{1}H spectra of the sample dissolved in toluene and stirred for 1 month with 1 M HNO_3 proved that the unchanged butylester **7** was still present as the main component.

4. Conclusions

The first screening study is presented herein, showing a wide potential of the compound **2** dioxane ring cleavage reaction for the attachment of a variety of metal ligating groups. Reactions have proven to be smooth, reliable and of high yield for bonding oxygen donor atoms containing selective groups, as well as phosphorus comprising moieties. The first members of the novel class of the M^{3+} selective extractants were prepared, enabling transfer from acidic aqueous phase to aromatic solvents. The flexible podant chain apparently enables the selective groups to be appropriately oriented for the tight metal complexation and provides additional metal binding sites. The X-ray crystallography results obtained on the sodium complex of anion **3** indicate tight cation bonding inside the inner polar cavity enveloped by an outer hydrophobic sphere. The electrochemical study confirming 3: 1 stoichiometry of the complex, formed in the course of the M^{3+} cation transfer to the organic phase, brought basic evidence for the validity of the simple mechanistic model for metal transfer depicted in Fig. 2. Extraction results are in sound agreement with the above results and assumptions. They indicate that the cobalt bis(dicarbollide) derivatives combining polydentate ligands and hydrophobic anions in one molecule can serve as efficient selective extraction agents for M^{3+} cations. Indeed, results described in this study exemplify that such compounds, especially those with a phosphorus containing moiety, can serve for effective extraction of lanthanide M^{3+} cations from HLW into aromatic solvents without adding any synergic agent or other additive into the extraction system.

To our knowledge, compounds **6** and **7** represent the first combination of anion **1** with phosphorus contain-

Table 7

Extractant	3	4	5	6	7				
(*a*) *Eu^{3+} extraction results obtained with synthesized polydentate extractants* **1**–**6** [a]									
C_{HNO_3} (M)	D_{Eu}								
0.01	25.4	592/1061*	161	0.174	327				
0.10	0.36	0.143/1.01*	0.08	0.004	2759				
1.00	0.008	–	0.005	0.001	2.33				
(*b*) *The dependence of extraction efficiency of extractant 7 on acidity* [b]									
c_{HNO_3}	0.001	0.01	0.05	0.07	0.10	0.20	0.30	1.00	3.00
D_{Eu}	5.89	327	5569	11520	2759	718	166	2.33	0.046
(*c*) *Extraction-back-extraction cycle obtained with extractant 7* [c]									
	1. extraction	1. back-extraction	2. extraction						
D_{Eu}	2.33	0.029	2745						
(*d*) *Chemical stability of extractant 7* [d]									
Time of contact (h)	0	72	144	240					
D_{Eu}	4.28	258	745	1239					

[a] Na^+ salts (0.05 M) of reagents **3**, **5**–**7** in toluene, extractant **2** in nitrobenzene, *, distribution ratio for extractant **2**—0.1 M solution, extractant **7** was used in the form of the calcium salt, so anion concentration is doubled.
[b] Calcium salt (0.05 M) of extractant **6** in toluene.
[c] Extraction from 1 M HNO_3, back-extraction into 3 M HNO_3, 0.10 M extractant **7** in toluene.
[d] Extractant (0.05 M) in toluene in contact with 1 M HNO_3, Eu extraction from 1 M HNO_3.

ing moieties. Further improvements in the acidity dependence of the M^{3+} extraction coefficients are anticipated from the use of the above described reaction scheme for bonding of other potent phosphorus based sequestering groups like phopsphine oxide or CMPO (*N*,*N*-dialkyl carbamoylmethyl dialkyl phosphine oxides). This study is currently under progress.

5. Supplementary material

Crystallographic data for the structural analysis has been deposited with the Cambridge Crystallographic Data Center for compound **3**, deposition number CCDC no. 172419. Copies of this information may be obtained free of charge from: The Director, CCDC, 12 Union Road, Cambridge CB2 1EZ, UK (fax: +44-1223-336-033; e-mail: deposit@ccdc.cam.ac.uk or www: http://www.ccdc.cam.ac.uk).

Acknowledgements

The authors gratefully acknowledge Dr. Jiří Fusek from the Institute of Inorganic chemistry for NMR measurements. The partial support from the Grant Agency of the Czech Republic (Grants 104/ 99/1096, 104/01/0142 and 203/99/M037, later for purchase of the KappaCCD), the EEC Project IC CT 155 221 and the support of The Ministry of Education of Czech Republic (Projects LN 000A028 and LB98233) for the laboratory and NMR equipment and NMR network are highly appreciated.

References

[1] M.F. Hawthorne, T.D. Andrews, J. Chem. Soc., Chem. Commun. (1965) 443.
[2] M.F. Hawthorne, D.C. Young, P.A. Wegner, J. Am. Chem. Soc. 87 (1965) 1818.
[3] For review, see I.B. Sivaev, I. Bregadze, Collect. Czech. Chem. Commun. 64 (1999) 783, and references therein.
[4] J. Plešek Chem. Rev. 92 (1992) 269 and references therein.
[5] M. Kyrš, S. Heřmánek, J. Rais, J. Plešek, Czechoslovak Patent, 182 913 (11.2.1972).
[6] P. Selucký, K. Baše, J. Plešek, S. Heřmánek, J.Rais, Czechoslovak Patent, 215282 (1.8.1981).
[7] J. Rais, P. Selucký, M. Kyrš, J. Inorg. Nucl. Chem. 38 (1976) 1742.
[8] M. Štefek, M. Kyrš, J. Rais, Zh. Anal. Khim. 31 (1976) 1364.
[9] J. Rais, P. Selucký, M. Kyrš, J. Inorg. Nucl. Chem. 38 (1976) 1376.
[10] J. Plešek, S. Heřmánek, Czechoslovak, Patent No. 188587 (4.11.1981).
[11] L.N. Lazarev, R.I. Lyubtsev, B. Ya. Galkin, V.N. Romanovskii, D.N. Shishkin, M. Kyrš, P. Selucký, J. Rais, S. Heřmánek, J. Plešek, USSR Patent No. 1031088 (6.6.1981).
[12] D.L. Illman, Chem. Eng. News 71 (1993) 9.
[13] V.N. Romanovski, in: Proceedings of the Fifth International Information Exchange Meeting on Actinide and Fission Product Partitioning and Transmutation, Mol, Belgium, November 25–27, 1998, pp. 77–85.
[14] J. Plešek, S. Heřmánek, Collect. Czech. Chem. Commun. 60 (1995) 1297.
[15] F. Teixidor, B. Čásenský, J.F. Dozol, S. Heřmánek, H. Mongeot, J. Rais, Final report Contract New trends in the separation of ^{137}Cs and ^{90}Sr and transplutonium elements from radioactive HLW by borane and heteroborane anions. Final report EC-INCO-Copernicus, Contract CIPA-CT 93-1333, European Comission, Nuclear Science and Technology, 1998.
[16] J.F. Dozol, M.J. Schwing-Weill, F. Arnaud-Neu, V. Böhmer, R. Ungaro, F.C. van Veggel, G. Wipff, A. Costero, J.F. Desreux, J. de Mendoza: Extraction and Selective Separation of Long-Lived

Radionuclides by Functionalised Macrocycles, Report EC, EUR 19605, European Commission, Brussels, 2000.
[17] E.P. Horwitz, D.G. Kalina, H. Diamond, G. Vandergrift, W.W. Schultz, Solvent Extr. Ion Exch. 3 (1985) 75.
[18] J.D. Law, K.N. Brewer, R.S. Herbst, T.A. Todd, D.J. Wood, Waste Manage. 19 (1999) 27.
[19] C. Madic, M.J. Hudson, J.O. Liljenzin, J.P.Glatz, R. Nannicini, A. Facchini, Z. Kolarik, R. Odoj, New Partition Techniques for Minor Actinides, Report of EC Project EUR 19149 EN, European Commission, Brussels, 2000.
[20] A. Arduini, V. Bohmer, L. Delmau, J.F. Desreux, J.F. Dozol, M.A.G. Carrera, B. Lambert, B.C. Musigmann, A. Pochini, A. Shivanyuk, F. Ugozzoli, Chem. Eur. J. 6 (2000) 2135 (and references therein).
[21] P. Beudaert, V. Lamare, J.F. Dozol, L. Troxler, G. Wipff, J. Chem. Soc., Perkin Trans. 2 (1999) 2515.
[22] C. Vinas, S. Gomez, J. Bertran, F. Teixidor, J.F. Dozol, H. Rouquette, J. Chem. Soc., Chem. Commun. (1998) 191.
[23] D.F. Shriver, M.A. Drezdon, Manipulation of Air Sensitive Compounds, 2nd ed., 2nd ed., Wiley, New York, 1986.
[24] J. Plešek, S. Heřmánek, A. Franken, I. Císařová, C. Nachtigal, Coll. Czech. Chem. Communn. 62 (1997) 47.
[25] See, for example: J. Schraml, J.M. Bellama, Two-Dimensional NMR Spectroscopy, Wiley, New York, 1982, and references therein.
[26] W.C. Hutton, T.L. Venable, R.N. Grimes, J. Am. Chem. Soc. 106 (1984) 29.
[27] X.L.R. Fontaine, J.D. Kennedy, J. Chem. Soc., Dalton Trans. (1987) 1573.
[28] See, for example: J. Plešek, B. Štíbr, X.L.R. Fontaine, J.D. Kennedy, S. Heřmánek, T. Jelínek, Collect. Czech. Chem. Commun. 56 (1991) 1618.
[29] Z. Plzák, J. Plešek, B. Štíbr, J. Chromatogr. 212 (1981) 283.
[30] B. Grüner, Z. Plzák, J. Chromatogr. A 789 (1997) 497.
[31] G.M. Sheldrick, SHELX-97, Program for Crystal Structure Refinement from Diffraction Data, University of Göttingen, Germany, 1997.
[32] V. Mareček, Z. Samec, J. Electroanal. Chem. 195 (1985) 263.
[33] J. Plešek, B. Grüner, J. Báča, J. Fusek, I. Císařová, J. Organomet. Chem., submitted for publication.
[34] F.H. Allen, O. Kennard, Chem. Des. Autom. News 8 (1) (1993) 31.
[35] F.A. Cotton, J.H. Matonic, C.A. Murillo, J. Am. Chem. Soc. 120 (1998) 6047.
[36] F. Teixidor, C. Viñas, J. Rius, C. Miravitlles, J. Casabo, Inorg. Chem. 29 (1990) 149.
[37] J. Koryta, Electrochim. Acta 24 (1979) 293.
[38] D. Homolka, V. Mareček, Z. Samec, O. Ryba, J. Petránek, J. Electroanal. Chem. 125 (1981) 243.
[39] D. Homolka, K. Holub, V. Mareček, J. Electroanal. Chem. 138 (1982) 29.
[40] M.H. Abraham, A.F. Danil de Namor, J. Chem. Soc., Faraday Trans. 1 (72) (1976) 955.
[41] Z. Samec, V. Mareček, M.P. Colombini, J. Electroanal. Chem. 257 (1988) 147.
[42] A. Sabela, V. Mareček, Z. Samec, R. Fuocco, Electrochim. Acta 37 (1992) 231.

PERGAMON

Polyhedron 21 (2002) 987–996

POLYHEDRON

www.elsevier.com/locate/poly

Physical characteristics, vibrational spectroscopy and normal-coordinate analysis of 2-aminophenol and 2-phenylenediamine complexes

Khaled Bahgat [a,*], Adel S. Orabi [b]

[a] Chemistry Department, Faculty of Petroleum and Mining Engineering, Suez Canal University, Suez, Egypt
[b] Chemistry Department, Faculty of Science, Suez Canal University, Ismailia, Egypt

Received 8 November 2001; accepted 24 January 2002

Abstract

Hg(II) and Cd(II) complexes with 2-aminophenol (**Amph**) and 2-phenylenediamine (**Phda**) as ligands were prepared and characterized by elemental analysis, electrical conductivity, thermogravimetric analysis (DTA/TG), X-rays, FT-IR and FT-Raman spectra. The complexes formed can be formulated as $[M(L)_2 \cdot n H_2O] \cdot m H_2O$. The electrical conductivity of 0.001 M DMSO solutions revealed the non-electrolytic behavior of the **Amph** complexes while **Phda** complexes behave as a 1:2 electrolyte. DTA analysis reveals the presence of two types of water coordinating as aligned and as water of crystallization. ΔE_a of the stepwise decomposition was evaluated. X-ray powder diffraction studies on the ligands and their complexes are described. The fundamental frequencies of these complexes have been assigned on the basis of normal coordinate calculations, carried out using a generalized valence force field (GVFF). The proposed assignments are discussed in relation to the group frequencies in structurally related molecules and in terms of the computed potential-energy distributions among the symmetry coordinates. © 2002 Elsevier Science Ltd. All rights reserved.

Keywords: Cd(II) and Hg(II) complexes; Spectroscopic properties; Normal coordinate; Force constant; 2-Phenylenediamine; 2-Aminophenol

1. Introduction

The nature of metal–oxygen and metal–nitrogen bonds in metal chelate compounds has been a subject of considerable interest, and the studies of the vibrational spectra of metal chelates of 2-aminophenol and 2-phenylenediamine themselves are interesting from the viewpoint of molecular spectroscopy. So far, no normal coordinate treatment has been made on such a chelate ring system, where the M–O and M–N modes are of particular interest.

Kincaid and Nakamoto [1] first assigned both M–O and M–N stretching modes based on normal coordinate analysis of bis(glycino) complexes of Ni(II), Cu(II) and Co(II). However, their assignments were different from those of previous investigations. Loethr and Thomas [2] assigned the M–O and M–N stretching bands from an approximate normal coordinate analysis of bis(biuretato) and bis(oxamido) complexes. The study of Hg(II) and Cd(II) complexes of 2-aminophenol and 2-phenylenediamine is a subject of considerable interest due to their structural and spectroscopic properties in addition to their being potential models for a number of important biological and ecological systems [3,4]. The main purpose of this investigation is to provide a complete band assignment of 2-aminophenol and 2-phenylenediamine Cd(II) and Hg(II) complexes based on normal coordinate analysis for 1:1 complexes, taking into consideration the puckering of the six and five-membered rings. XRD combined with DTA/TG were additionally used to elucidate the structure of the complexes.

* Corresponding author. Fax: +20-64-370-197.
E-mail addresses: khabahgat1@hotmail.com (K. Bahgat), orabiadel@hotmail.com (A.S. Orabi).

0277-5387/02/$ - see front matter © 2002 Elsevier Science Ltd. All rights reserved.
PII: S0277-5387(02)00910-5

2. Experimental

2.1. Chemical

All chemicals used in the present study were reagent grade.

2.2. Preparation of the complexes

The complexes were prepared by mixing stoichiometric amounts of the ligand and metal ions (Cd(II), Hg(II)) in a 2:1 ratio in ethanolic solution. The mixture was refluxed for 2 h. The solid complexes formed after a few minutes when the temperature of the contents reached room temperature. $HgCl_2$ and $CdCl_2$ were used as the source of metal ions. The formed precipitates were washed and recrystallized from hot ethanol.

2.3. Instrumentation and analysis

Elemental analyses were carried out using an Heraeus C, H, N Rapid Analyzer. The conductance measurements of 0.001 M solutions of the complexes in DMSO were performed using a WTW model LF-42 conductivity bridge fitted with a LTA-100 conductivity cell. Thermal analysis of the complexes was carried out on a Perkin–Elmer DTA-7 differential thermal analyzer with a TAC 7/DX controller instrument using a platinum cell under nitrogen atmosphere at a heating rate of 10 °C min^{-1}. X-ray data were measured using Simens D 5000 XRD with scanning range $2\theta = 5–70°$. The infrared spectra were recorded with a Nicolet Magna 750 FT-IR spectrometer equipped with a room-temperature DTGS detector. The spectra of the solid (in the 4000–400 cm^{-1} spectral region) were recorded in the form of KBr pellets at 4 cm^{-1} spectral resolution accumulating 128 scans. The Raman spectra were measured with a Nicolet 950 FT-Raman spectrometer equipped with a liquid nitrogen cooled Ge detector, a 1064 nm Nd:YAG laser was used for excitation at 30–150 mW output power.

3. Results and discussion

Analytical data (Table 1) of the complexes show that Cd(II) complexes have the composition $[Cd(Amph)_2 \cdot 2H_2O] \cdot 2H_2O$ and $[Cd(Phda)_2 \cdot 2H_2O] \cdot 2H_2O \cdot 2Cl$. The Hg(II) complexes occur as $[Hg(Amph)_2] \cdot 2H_2O$ and $[Hg(Phda)_2] \cdot 2H_2O \cdot 2Cl$. The purity of the prepared complexes were confirmed by chemical analysis, melting point and TLC (silica gel GF 254 type 60, mesh size 50–250, eluted with H_2O–ethanol). The synthesized complexes were found to be grey or brown colored, non-hygroscopic powders.

3.1. Conductivity

The conductance of the complexes in DMSO (0.001 M) (Table 1) indicates that **Phda** complexes act as 2:1 electrolytes, consequently, two free Cl^- ions are present outside the coordination sphere of the Cd(II) and Hg(II) complexes [5]. The **Amph** complexes have non-electrolytic behavior.

3.2. Thermal gravimetric analysis (DTA/TG)

The application of TGA to evaluate solid-state reactions involving weight loss (or gain) has been studied by a number of workers [6–9]. The measurements were carried out in the temperature range 25–600 °C. The thermal gravimetric diagrams of the complexes (see Figs. 1–5) (Table 2) gave rise to the following observation:

1) Hg(II) complexes (**III** and **IV**) gave endothermic peaks in DTA, centered at 95 °C for complex **III** and 92 °C for **IV**, while at this temperature there is no weight loss in the TG diagrams. Consequently, these peaks could be assigned as phase transitions [9].
2) Cd(II) complexes (**I** and **II**) have endothermic peaks centered at 94 and 96 °C for complexes **I** and **II**, respectively. The Hg(II) complexes gave bands at 113 and 114 °C of the same nature for complexes **III** and **IV**, respectively. All the endothermic peaks were accompanied by weight loss in the TG diagram, which denote the liberation of water of crystallization; the % weight loss denotes liberation of two molecules of water [10,11].
3) Cd(II) complexes gave endothermic peaks centered at 151 and 171 °C for complexes **I** and **II** respectively, with % weight loss equivalent to losing two H_2O molecules, which may be assigned to water of coordination [10,11].
4) The decomposition of the ligand appeared as exothermic peaks for complexes **I** and **II** at 214 and 261 °C respectively; complex **III** gave an endothermic peak at 225 °C.
5) The endothermic peaks which appeared at 278 and 276 °C for complexes **III** and **IV**, gave no change in the TG diagrams and so could be assigned to phase transitions [7].
6) The activation energies of the thermal decomposition steps were calculated using the Piloyan method [12] (see Table 2), which can be summarized as follows:
   a) E_a of the liberation of water of crystallization has the following trend: **II** > **IV** > **I** > **III**.
   b) The liberation of water of coordination has the following sequence: **II** > **I**.

Table 1
Analytical and physical data of the synthesized complexes

Number	Complex	Molecular weight	Color	Melting point (m.p.)	Elemental analysis										Conductivity
					C%		H%		N%		M%		H_2O%		
					C.	F.	C.	F.	C.	F.	C.	F.	C.	F.	
I	$[Cd(C_6H_6NO)_2 \cdot 2H_2O] \cdot 2H_2O$	400.706	brown	> 300	35.97	36.21	5.03	4.92	6.99	6.73	28.05	28.51	17.98	18.03	7
II	$[Cd(C_6H_8N_2)_2 \cdot 2H_2O] \cdot 2Cl \cdot 2H_2O$	471.668	brown	180	30.56	30.82	5.13	5.26	11.88	11.52	23.83	24.15	15.30	15.43	143
III	$[Hg(C_6H_6NO)_2] \cdot 2H_2O$	452.854	grey	200	31.83	31.51	3.56	3.37	6.19	6.41	44.30	44.33	7.96	8.22	12
IV	$[Hg(C_6H_8N_2)_2] \cdot 2Cl \cdot 2H_2O$	523.816	grey	130	27.51	27.42	3.85	3.79	10.70	10.43	38.29	38.61	6.88	6.94	151

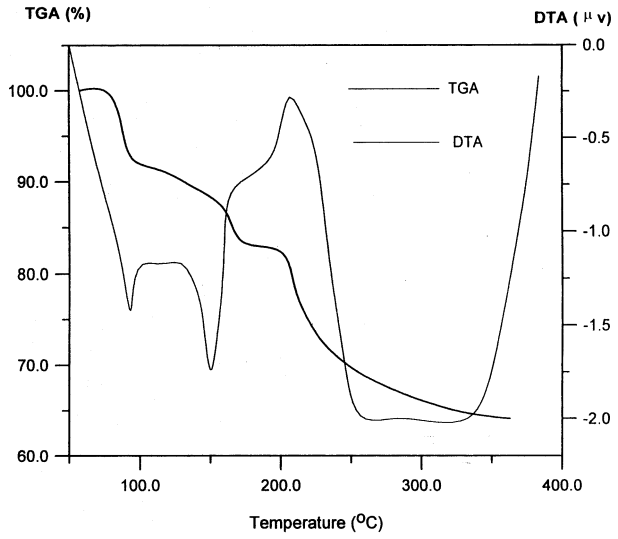


Fig. 1. Cd–aminophenol complex.

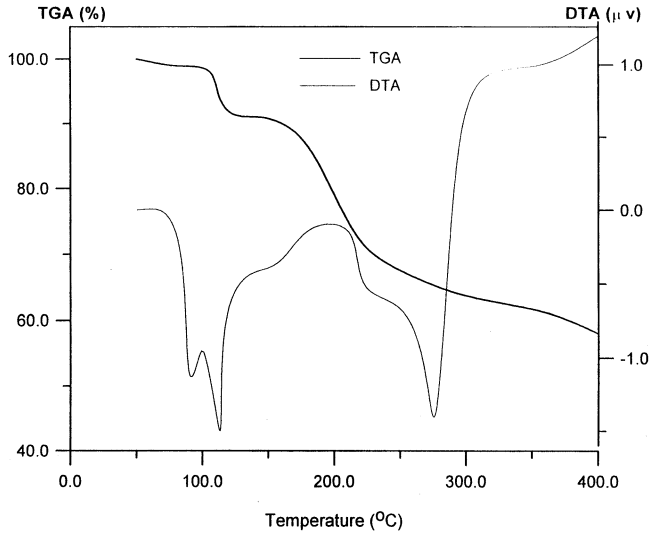


Fig. 3. Hg–aminophenol complex.

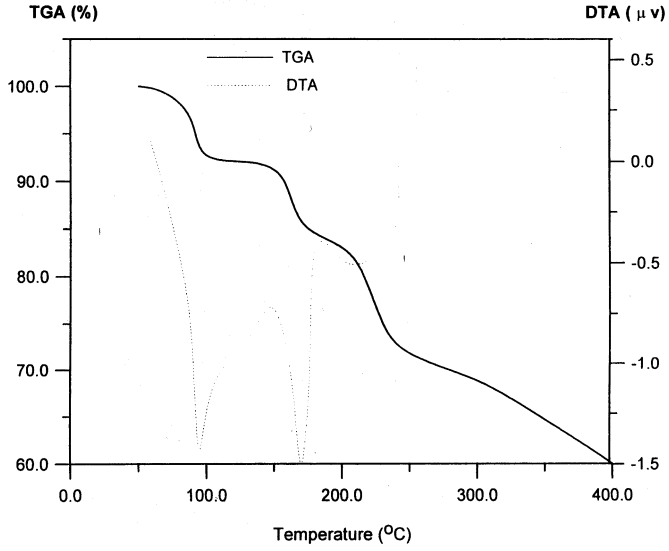


Fig. 2. Cd–phenylenediamin complex.

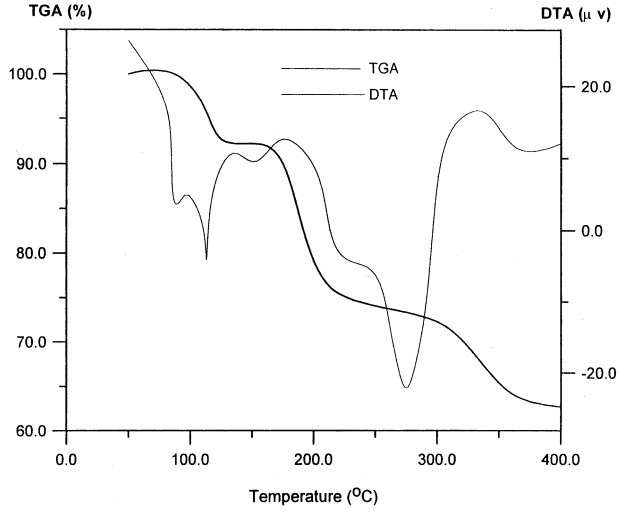


Fig. 4. Hg–phenylenediamin complex.

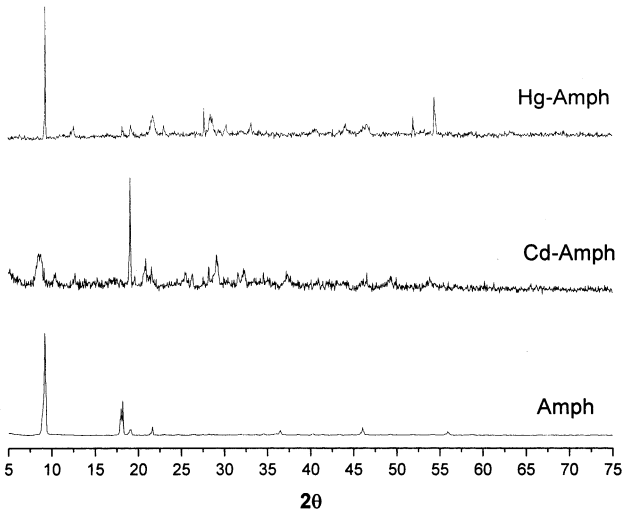
c) From the previous results, we can write the general thermal properties of the prepared complexes (**I**–**IV**): (1) water of crystallization for Cd(II) complexes has a greater stability than Hg(II) complexes. (2) The **Phda** complexes are generally more stable than **Amph** complexes. The stability of the **Phda** complexes may be due to the crystallinity structure of these complexes, which consequently require higher activation energies for decomposition.

3.3. X-ray for powder diffraction

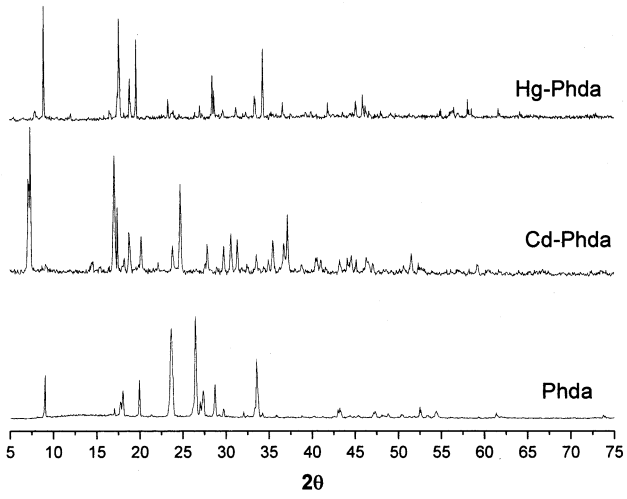
X-ray patterns of the prepared solid **Phda** and **Amph** complexes were taken over the range of $2\theta = 5–75°$. The principal 'd' lines and their intensities are represented in Table 3 and shown in Fig. 5. Generally the prepared complexes have a high degree of crystallinity when compared with the parent ligands. Cd(II) complexes have crystallinity higher than Hg(II) complexes. The complexes of **Phda** have crystallinity higher than **Amph** complexes. High symmetry, large unit cells size and various degrees of crystallinity, are characteristics of all crystalline compounds [13]. The results obtained confirmed the results obtained previously by using thermal gravimetric analysis.

3.4. FT-IR, FT-Raman and normal coordinates

In order to study the metal–oxygen and the metal–nitrogen vibrations of 2-aminophenol (**Amph**) and 2-phenylenediamine (**Phda**), a normal coordinate treatment has been made on a chelate ring using a 1:1



X-ray powder diffraction of the Amph ligand and its complexes



X-ray powder diffraction of the Phda ligand and its complexes

Fig. 5. X-ray powder diffraction analysis.

Table 3
X-ray powder diffraction of Cd(II) and Hg(II) complexes with **Amph** and **Phda** ligands

Amph		Cd–**Amph**		Hg–**Amph**	
D	*I*	*d*	*I*	*d*	*I*
9.591	100	10.20	45	9.475	100
4.932	30	4.644	100	4.420	28
4.871	35	4.225	35	3.214	27
		4.122	28	3.133	27
		3.158	30	1.759	20
		3.051	45	1.684	45
Phda		Cd–**Phda**		Hg–**Phda**	
D	*I*	*d*	*I*	*d*	*I*
9.829	50	12.26	80	9.907	85
4.924	30	11.94	100	5.029	100
4.449	45	5.195	95	4.707	40
3.760	100	5.078	40	4.523	75
3.364	100	4.721	35	3.135	50
3.255	30	4.397	30	3.108	28
3.104	35	3.733	25	2.681	28
2.669	65	3.598	65	2.611	62
		3.200	25		
		2.999	25		
		2.920	30		
		2.852	27		
		2.529	27		
		2.444	25		
		2.418	42		

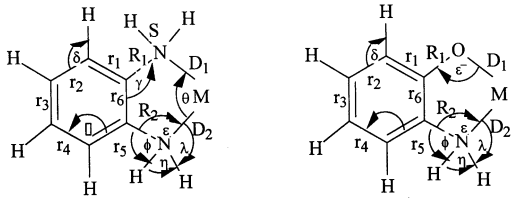


Fig. 6. Internal valence coordinates.

Table 2
Thermal analysis data

Number	Complex	Temperature peak	Peak type	Weight loss (%)		ΔE_a (kJ mol^{-1})	Assignment
				C.	F.		
I	$[Cd(C_6H_6NO)_2\cdot 2H_2O]\cdot 2H_2O$	94	endo	8.99	9.12	25.501	H_2O of cryst.
		151	endo	8.99	8.91	30.097	H_2O-coord.
		214	exo		15.96	−46.216	lig.-decomp.
II	$[Cd(C_6H_8N_2)_2\cdot 2H_2O]\cdot 2Cl\cdot 2H_2O$	96	endo	7.65	7.81	85.433	H_2O of cryst.
		170	endo	7.65	7.62	47.792	H_2O-coord.
		261	exo			−27.423	lig.-decomp.
III	$[Hg(C_6H_6NO)_2]\cdot 2H_2O$	95	endo			34.501	phase trans.
		113	endo	7.96	8.21	22.365	H_2O of cryst.
		225	endo		18.81		lig.-decomp.
		278	endo			136.696	phase trans.
IV	$[Hg(C_6H_8N_2)_2]\cdot 2Cl\cdot 2H_2O$	92	endo			37.293	phase trans.
		114	endo	6.88	6.94	41.966	H_2O of cryst.
		276	endo			273.313	phase trans.

Table 4
Symmetry coordinates for 2-phenylendiamine complexes

Symmetry coordinate (unnormalized)	Symbol	Description
Species A_1		
$S_1 = r_1+r_5+r_6+r_2+r_4+r_3$	ν_sCC	symmetric CC ring stretch
$S_2 = -r_1-r_5+2r_6-r_2-r_4+2r_3$	ν_{as}CC	asymmetric CC ring stretch
$S_3 = -r_1-r_5+2r_6+r_2+r_4-2r_3$	ν_{as}CC	asymmetric CC ring stretch
$S_4 = r_1+r_5-r_6-r_2-r_4+r_3$	ν_{as}CC	asymmetric CC ring stretch
$S_5 = P_1+P_4+P_2+P_3$	ν_sCH	symmetric CH stretch
$S_6 = P_1+P_4-P_2-P_3$	ν_{as}CH	asymmetric CH stretch
$S_7 = R_1+R_2$	ν_sCN	symmetric CN stretch
$S_8 = R_3+R_4$	ν_sNM	symmetric MN stretch
$S_9 = R_5+R_6+R_7+R_8$	ν_sNH	symmetric NH stretch
$S_{10} = -\infty_1-\infty_3+2\infty_2-\infty_4-\infty_6+2\infty_5$	δ_{as}CC	asymmetric CC aromatic deformation
$S_{11} = \delta_1-\delta_2+\delta_3-\delta_4-\delta_5+\delta_6-\delta_7+\delta_8$	δCH	in-plane CH deformation
$S_{12} = \delta_1-\delta_2-\delta_3+\delta_4+\delta_5-\delta_6-\delta_7+\delta_8$	δCH	in-plane CH deformation
$S_{13} = \beta(\gamma_1+\gamma_2)+\alpha(\varepsilon_1+\varepsilon_2)+\theta$	$\delta_5$ring	five-member ring deformation
$S_{14} = (\phi_1-\lambda_1)+(\phi_2-\lambda_2)+(\phi_3-\lambda_3)+(\phi_4-\lambda_4)$	δNH$_2$	out-of-plane NH$_2$ deformation
$S_{15} = (4\eta_1-\phi_1-\lambda_1-\phi_2-\lambda_2)+(4\eta_2-\phi_3-\lambda_3-\phi_4-\lambda_4)$	δ_{sc}NH$_2$	in-plane NH$_2$ scissoring
Species A_2		
$S_{16} = S_1-S_2-S_3+S_4$	ν_{as}NH	asymmetric NH stretch
$S_{17} = (\phi_1-\lambda_1)-(\phi_2-\lambda_2)-(\phi_3-\lambda_3)+(\phi_4-\lambda_4)$	δ_rNH$_2$	out-of-plane NH$_2$ rock
$S_{18} = (\phi_1+\lambda_1)-(\phi_2+\lambda_2)-(\phi_3+\lambda_3)+(\phi_4+\lambda_4)$	δ_rNH$_2$	out-of-plane NH$_2$ rock
$S_{19} = \omega_1+\omega_2-\omega_3-\omega_4$	ωCH	CH out-of-plane wagging
$S_{20} = \omega_1-\omega_2+\omega_3-\omega_4$	ωCH	CH out-of-plane wagging
$S_{21} = \tau_1-\tau_2+\tau_3-\tau_4+\tau_5-\tau_6$	τCC	aromatic ring torsion
$S_{22} = -\tau_1-\tau_2+2\tau_3-\tau_4-\tau_5+2\tau_6$	τCC	aromatic ring torsion
$S_{23} = \beta(\tau_7+\tau_{11})+\alpha(\tau_8+\tau_{10})+\tau_9$	τ5ring	five-member ring torsion
Species B_1		
$S_{24} = S_1-S_2+S_3-S_4$	ν_{as}NH	asymmetric NH stretch
$S_{25} = (\phi_1-\lambda_1)-(\phi_2-\lambda_2)+(\phi_3-\lambda_3)-(\phi_4-\lambda_4)$	δ_rNH$_2$	in-plane NH$_2$ rock
$S_{26} = (\phi_1+\lambda_1)-(\phi_2+\lambda_2)-(\phi_3+\lambda_3)-(\phi_4+\lambda_4)$	δ_rNH$_2$	in-plane NH$_2$ rock
$S_{27} = \omega_1+\omega_2+\omega_3+\omega_4$	ωCH	CH out-of-plane wagging
$S_{28} = \omega_1-\omega_2-\omega_3+\omega_4$	ωCH	CH out-of-plane wagging
$S_{29} = \tau_1-\tau_2+\tau_4-\tau_5$	τCC	aromatic ring torsion
$S_{30} = (1-\alpha)(\tau_{11}-\tau_7)+(\alpha-\beta)(\tau_{10}-\tau_8)+\tau_9$	τ5ring	five-member ring torsion
$S_{31} = \pi_1-\pi_2$	π2rings	out-of-plane bend of two rings
Species B_2		
$S_{32} = r_1-r_5+r_2-r_4$	ν_{as}CC	asymmetric CC ring stretch
$S_{33} = r_1-r_5-r_2+r_4$	ν_{as}CC	asymmetric CC ring stretch
$S_{34} = P_1-P_4+P_2-P_3$	ν_{as}CH	asymmetric CH stretch
$S_{35} = P_1-P_4-P_2+P_3$	ν_{as}CH	asymmetric CH stretch
$S_{36} = R_1-R_2$	ν_{as}CN	asymmetric CN stretch
$S_{37} = D_1-D_2$	ν_{as}MN	asymmetric MN stretch
$S_{38} = S_1+S_2-S_3-S_4$	ν_{as}NH	asymmetric NH stretch
$S_{39} = \infty_1-\infty_2+\infty_3-\infty_4+\infty_5-\infty_6$	δ_{as}CC	asymmetric CC ring deformation
$S_{40} = \infty_1-\infty_3+\infty_4-\infty_6$	δ_{as}CC	asymmetric CC ring deformation
$S_{41} = \delta_1-\delta_2+\delta_3-\delta_4+\delta_5-\delta_6+\delta_7-\delta_8$	δCH	in-plane CH deformation
$S_{42} = \delta_1-\delta_2-\delta_3+\delta_4-\delta_5+\delta_6+\delta_7-\delta_8$	δCH	in-plane CH deformation
$S_{43} = (1-\alpha)(\gamma_1-\gamma_2)+(\alpha-\beta)(\varepsilon_1-\varepsilon_2)$	$\delta_5$ring	five-member ring deformation
$S_{44} = (\phi_1-\lambda_1)+(\phi_2-\lambda_2)-(\phi_3-\lambda_3)-(\phi_4-\lambda_4)$	δ_rNH$_2$	out-of-plane NH$_2$ rock
$S_{45} = (4\eta_1-\phi_1-\lambda_1-\phi_2-\lambda_2)-(4\eta_2-\phi_3-\lambda_3-\phi_4-\lambda_4)$	δ_{sc}NH$_2$	out-plane NH$_2$ scissoring

$\alpha = \cos 72^\circ = 0.309017$, $\beta = \cos 144^\circ = -0.809107$.

complex model as shown in Fig. 6. Both models can be consider planar, **Amph** belongs to the C_s point group, where 39 fundamental vibrations are distributed as $29A'+10A''$, all i.r. and Raman active. **Phda** has C_2v symmetry, where 45 vibrations are grouped into four classes. Furthermore, the in-plane vibrations ($15A_1+14B_2$) are vibrationally separate from the out-of-plane vibrations ($8A_2+8B_1$). Inspection of the spectra for all the complexes reveals more i.r. than Raman features. This can probably be accounted for by a poor scattering ability of the complexes. The structure parameters were transferred from the X-ray data on the metals complexes

[14]. The bond length and bond angles are: C–C = 1.39 Å, C–N = 1.32 Å, C–H = 1.09 Å, C–O = 1.46 Å, N–H = 1.012 Å, N–M = 1.63 Å, O–M = 1.92 Å; CCC = 120°, CCH = 120°, CCN = 124°, CCO = 116°, CNM = 112.718°, COM = 109°, NMN = 90°, NMO = 90°.

The vibrational problem was set up in internal valance coordinate as given in Fig. 6. For the six and five-membered rings deformation and torsion local symmetry coordinates were constructed, which were defined in terms of the internal valance coordinates, following the IUPAC recommendation [15,16] and given in Table 4. Wilson's GF method [17] was applied to compute the normal frequencies. Before solving the secular equations the G and F matrices were transformed to the symmetry coordinates. For the in-plane vibrational frequencies of both planar complexes, the force constants used for the aromatic ring were transferred from the force field of nitrobenzene [18] substituting the values of γ and R from the force constant set of 6-amino-*m*-cresol [19] and *p*-dimethylaminobenzonitrite [20]. The force field for the internal coordinates around the metal atom was initially estimated from the force field of biuret and oxamide complexes [2].

The out-of-plane force constants of the aromatic ring were taken from the 23 parameter force field of fluorobenzene developed by Pearce and Steele [21], and those of the five-membered ring were transferred from the force constant of an oxamide complex [22]. An additional force constant was necessary to adjust the out-of-plane bending of the two rings relative to each other, the so-called butterfly motion of the molecule (π). It was noted that by introducing interaction constants $\infty\gamma$ and $\beta\gamma$ together with the values of the force constants η, ∞, $R\gamma$, $d\varepsilon$ and $s\eta$, the frequency fit could be improved. In Table 5 the final set of force constants used for **Amph** and **Phda** complexes are listed, where the numerical computation and refinement of the force constants were carried out using the PC version of the computer program MOLVIB [23].

Table 5
Set of force constants used in the calculation of **Amph** and **Phda** complexes

Diagonal force constant		Interaction force constants	
r_s^+	6.938	Rr	0.543
r_{as}^-	5.92	RP	−0.046
P	5.17	RR	0.12
R (N)	5.446	RD	0.15
R (O)	5.48	DS	0.23
D (N)	1.39	SR	0.135
D (O)	1.35	$R\infty$	0.75
S_s^+	7.118	$P\infty$	0.0139
S_{as}^-	7.028	$R\gamma$	−0.17
∞	0.654	$R\gamma$	0.0139
γ	0.509	$S\eta$	−0.051
ε (N)	0.48	$\infty\infty$	−0.64
ε (O)	0.437	$\infty\delta$	−0.066
θ	0.310	$\delta\delta$	−0.042
ϕ	0.491		
λ	0.423		
η	0.536		
δ	0.439		
ρ (H)	0.294		
χ (CC)	0.373		
χ (5R)	0.253		
ξ	0.13		

Stretch constants are in units of 10^2 Nm^{-1}; stretch-bend, 10^8 N rad^{-2}; bend and torsion, 10^{18} Nm rad^{-1}.

Figs. 7 and 8 show the i.r. and Raman spectra of the studied compounds; (Tables 6 and 7) list their frequencies. The vibrations of the benzene ring were identified relying on the study of Katritzky and Jones [24]. The calculated P.E.D. indicates that a number of bands are

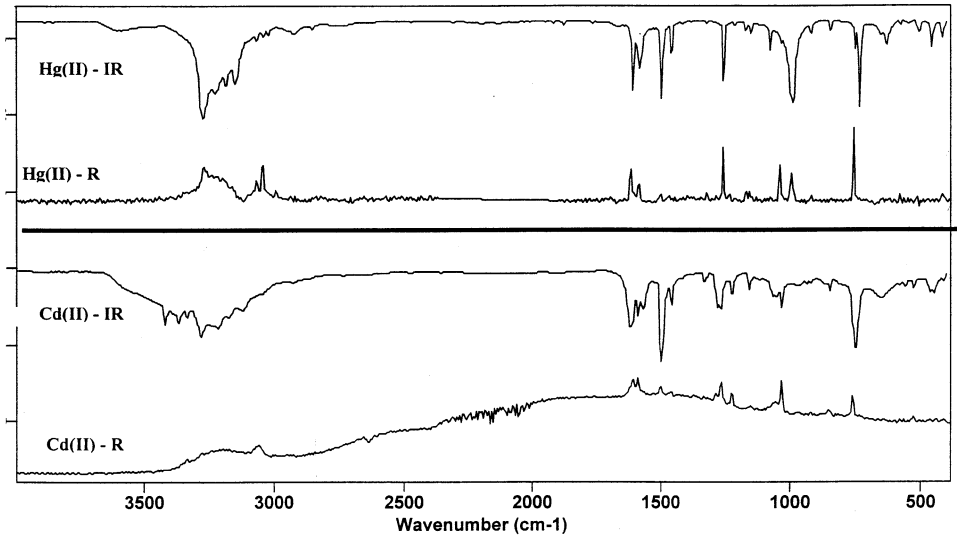


Fig. 7. FTIR and Raman spectra of the **Phda**–Cd(II) and Hg(II) complexes.

Table 6
Comparison of observed and calculated frequencies (cm^{-1}) for 2-phenylenediamine complexes

	$C_6H_4N_2H_4Cd$		$C_6H_4N_2H_4Hg$		Assignment [a](PED)
	ν_{Obs}(IR/R)	ν_{Calc}	ν_{Obs}(IR/R)	ν_{Calc}	
A1					
ν_1	3328/3329	3331	3331/–	3331	ν_sNH(90)
ν_2	3087/3093	3078	3070/3068	3078	ν_{as}CH(97)
ν_3	3042/3062	3042	3044/3040	3042	ν_sCH(97)
ν_4	1625/1626	1630	1627/1620	1630	$\delta_{sc}NH_2(81)+\nu_s$NH(13)+$\nu_s$CN(10)
ν_5	1594/1593	1587	1594/1594	1587	ν_{as}CC(78)+ν_sCN(18)
ν_6	1571/1570	1576	1571/1571	1576	ν_sCC(100)
ν_7	1502/1504	1505	1502/1502	1504	ν_{as}CC(62)+ν_{as}CN(22)+$\delta_{sc}NH_2(12)$
ν_8	1502/1504	1490	1502/1502	1490	ν_{as}CC(46)+ν_sCN(18)+$\delta_{sc}NH_2(15)$
ν_9	1459/1458	1457	1459/1459	1457	ν_sCN(49)+$\delta_{sc}NH_2(22)+\nu_{as}$CC(12)
ν_{10}	1157/1153	1160	1159/1159	1160	δCH(74)+ν_{as}CC(16)
ν_{11}	1122/1120	1120	1119/1119	1121	δCH(48)+ν_sCN(24)+ν_{as}CC(11)
ν_{12}	755/759	750	753/759	750	$\omega NH_2(89)$
ν_{13}	657/647	660	653/651	660	δ5ring(32)+δCC(22)+ν_sCN(18)
ν_{14}	563/566	570	639/634	570	δCC(94)
ν_{15}	447/448	440	457/451	440	ν_sMN(64)+δ5ring(18)+δCC(12)
A2					
ν_{16}	3365/3370	3362	3365/3365	3361	ν_{as}NH(90)
ν_{17}	1267/1267	1274	1268/1260	1274	$\delta_tNH_2(60)+\nu_s$CN(12)
ν_{18}	1224/1226	1220	1225/1236	1220	$\delta_rNH_2(65)+\nu_s$CN(18)
ν_{19}	965/964	964	965/996	964	ωCH(90)
ν_{20}	942/949	931	943/949	930	ωCH(100)
ν_{21}	–/469	461	–/474	461	τCC(79)+ωCH(13)
ν_{22}	–/389	390	–/387	390	τCC(89)+τ5ring(12)
ν_{23}	–/300	310	–/316	310	τ5ring(85)
B1					
ν_{24}	3365/3370	3361	3365/3365	3360	ν_{as}NH(94)
ν_{25}	1267/1267	1255	1268/1260	1255	$\delta_tNH_2(80)+\nu_{as}$NH(13)
ν_{26}	1224/1224	1218	1225/1236	1218	$\delta_rNH_2(73)+\nu_{as}$NH(10)
ν_{27}	926/926	909	926/919	910	ωCH(90)
ν_{28}	855/855	860	853/864	859	ωCH(89)
ν_{29}	–/376	376	–/362	376	τCC(80)+τ5ring(18)
ν_{30}	–/246	246	–/342	246	τ5ring(92)
ν_{31}	–/194	195	–/214	193	π2rings(100)
B2					
ν_{32}	3276/3274	3271	3274/3264	3271	ν_{as}NH(94)
ν_{33}	3060/3056	3056	3060/3065	3056	ν_{as}CH(99)
ν_{34}	3043/3043	3040	3044/3040	3041	ν_{as}CH(100)
ν_{35}	1614/1612	1609	1615/1615	1610	$\delta_{sc}NH_2(78)+\nu_s$CN(18)+$\delta_rNH_2(11)$
ν_{36}	1461/1461	1451	1461/1459	1451	ν_{as}CC(91)+δCH(12)
ν_{37}	1334/1334	1334	1334/1326	1332	ν_sCN(31)+$\delta_rNH_2(27)+\nu_{as}$CC(12)
ν_{38}	1066/1066	1070	1066/1066	1069	δCH(60)+ν_{as}CC(21)+ν_{as}CN(11)
ν_{39}	1054/1054	1046	1052/ -	1046	δCH(53)+ν_{as}CC(31)
ν_{40}	1035/1035	1021	1037/1038	1021	ν_{as}CC(60)+δCH(17)
ν_{41}	736/735	747	743/747	747	$\omega NH_2(95)$
ν_{42}	582/580	598	573/582	597	δCC(90)
ν_{43}	530/530	523	509/514	523	δCC(92)
ν_{44}	468/468	453	466/–	454	δ5ring(90)
ν_{45}	411/409	412	418/418	412	ν_{as}MN(76)+δ5ring(13)

The following abbreviations have been used: ν_s, symmetric stretching; ν_{as}, asymmetric stretching; δ, bending; ω, out-of-plane bending; δ_r, rocking; δ_{sc}, scissoring; τ, torsion; π, torsion of the two rings.

[a] The potential energy distribution defined as $\chi_{ik} = 100$. $F_{ji}L_{ik}^2/\lambda_k$; those less than 10% have been neglected.

due to vibrations localized almost entirely within the benzene ring. Such specified aromatic modes give rise to the bands at 3087, 3060, 3042, 1614, 1594, 1571, 1502, 1334 and 855 cm^{-1} in the i.r. spectra of **Phda**–cadmium complexes and to ones at 3093, 3062, 3056, 1612, 1593, 1570, 1504, 1334 and 855 cm^{-1} in the Raman spectra. These bands assigned to ν_2, ν_3, ν_5, ν_6, ν_7, ν_8, ν_{33}, ν_{34}, ν_{37} and ν_{40} almost at the same wavelengths in **Amph** complex spectra. Absorptions at 580, 565 and 519 cm^{-1} in the i.r. Spectra of **Amph** complexes (ν_{14}, ν_{42}

Table 7
Comparison of observed and calculated frequencies (cm^{-1}) for 2-aminophenol complexes

	$C_6H_4NH_2Ocd$		$C_6H_4NH_2OHg$		Assignment [a](PED)
	ν_{Obs}(IR/R)	ν_{Calc}	ν_{Obs}(IR/R)	ν_{Calc}	
A′					
ν_1	3375/–	3380	3380/3358	3380	ν_{as}NH(90)
ν_2	3302/–	3315	3303/–	3303	ν_sNH(98)
ν_3	3076/3076	3062	3052/–	3061	ν_{as}CH(97)
ν_4	3051/–	3039	3020/–	3042	ν_{as}CH(98)
ν_5	3035/3030	3022	3020/–	3022	ν_{as}CH(99)
ν_6	3022/3009	3018	3020/–	3018	ν_{as}CH(102)
ν_7	1602/1614	1614	1604/1615	1622	$\delta_{sc}NH_2$(100)
ν_8	1590/1606	1593	1583/1588	1591	ν_{as}CC(60)+ν_sCO(18)
ν_9	1562/1563	1552	1565/1579	1552	ν_{as}CC(105)
ν_{10}	1509/1514	1510	1509/1518	1511	ν_sCC(53)+δCH(20)
ν_{11}	1486/1485	1480	1471/1479	1483	ν_{as}CC(46)+δCH(14)+ν_sCO(10)
ν_{12}	1456/1459	1450	1459/1467	1453	ν_sCC(37)+ν_{as}CC(18)+δCH(10)
ν_{13}	1403/–	1401	1382/1389	1400	ν_{as}CC(51)+ν_sCN(13)+ν_sCN(10)
ν_{14}	1272/1268	1275	1268/1268	1276	$\delta_t NH_2$(59)+ν_sNH(18)
ν_{15}	1253/1224	1242	1230/1233	1242	ν_sCO(32)+ν_{as}CC(24)+ν_sCN(14)
ν_{16}	1189/1205	1212	1181/1201	1212	δCH(70)+ν_{as}CC(18)
ν_{17}	1157/1157	1171	1159/1148	1170	$\delta_r NH_2$(74)+ν_sCN(14)
ν_{18}	1108/1108	1109	1085/1079	1109	δCH(80)+ν_{as}CC(24)
ν_{19}	1041/1056	1060	1074/1062	1063	δCH(37)+ν_sCC(33)
ν_{20}	1031/1037	1045	1033/–	1045	δCH(52)+ν_{as}CC(18)+ν_sCO(12)
ν_{21}	855/855	856	847/840	856	ν_{as}CC(54)+δCH(20)
ν_{22}	745/732	745	746/742	745	ωNH_2(100)
ν_{23}	593/599	610	614/602	610	δ5ring(24)+δCC(58)
ν_{24}	580/588	591	582/586	594	δCC(56)+δ5ring(38)
ν_{25}	565/569	560	568/571	560	δCC(44)+δ5ring(54)
ν_{26}	549/–	531	549/551	531	δ5ring(68)+ν_sMN(12)
ν_{27}	519/521	499	512/–	499	δCC(89)
ν_{28}	458/–	461	448/–	459	ν_{as}MO(45)+δ5ring(16)+δCC(12)
ν_{29}	420/–	410	421/–	412	ν_sMN(39)+ν_sMO(12)+δCC(10)
A″					
ν_{30}	977/–	1010	975/–	1010	ωCH(99)
ν_{31}	925/922	930	923/922	930	ωCH(100)
ν_{32}	898/900	891	898/890	891	ωCH(89)+τCC(12)
ν_{33}	761/759	739	766/761	737	ωCH(98)
ν_{34}	487/491	493	496/–	493	τCC(74)+ωCH(11)
ν_{35}	–/472	464	468/–	465	τCC(76)+τ5ring(12)
ν_{36}	–/401	398	398/–	398	τCC(75)+τ5ring(10)
ν_{37}	–/346	340	382/–	340	τ5ring(85)+τCC(18)
ν_{38}	–/264	260	–/251	260	τ5ring(92)
ν_{39}	–	78	–	79	π2rings

The following abbreviations have been used: ν_s, symmetric stretching; ν_{as}, asymmetric stretching; δ, bending; ω, out-of- plane bending; δ_r, rocking; δ_{sc}, scissoring; τ, torsion; π, torsion of the two rings.

[a] The potential energy distribution defined as $\chi_{ik} = 100$. $F_{ji}L_{ik}^2/\lambda_k$; those less than 10% have been neglected.

and ν_{43} in **Phda)** are also related to the benzene ring absorption. The absorption arising from the five-membered ring deformation modes ν_{13} and ν_{44} in **Phda** complexes show very variable intensity, these bands are assigned to ν_{23} and ν_{26} modes at lower wavelengths in the reduced C_s symmetry in **Amph** complexes.

The calculation reveals that the observed vibrational frequencies are generally a complex mixture of different vibrational modes, as shown in different band assignments. However, our calculation for the complexes of **Amph** shows that the (C–O) symmetric stretch, (C–C) and (C–N) are coupled, and would yield a (C–O) stretching mode around 1230 cm^{-1}. Indeed, two bands were observed at 1236 and 1366 cm^{-1} in the i.r. Studies by Fujita and Nakamoto [25] on oxalate complexes have shown the (C–O) symmetric stretch to be about 1230–1400 cm^{-1}, using several force field models in the calculation. The ring-N stretching vibrations are strongly mixed with other motions. The i.r. active vibrations at 1459 and 1334 cm^{-1} and Raman active at 1458 and 1326 cm^{-1} in **Phda**–Hg spectra have the largest contribution from ring-N stretching coordination.

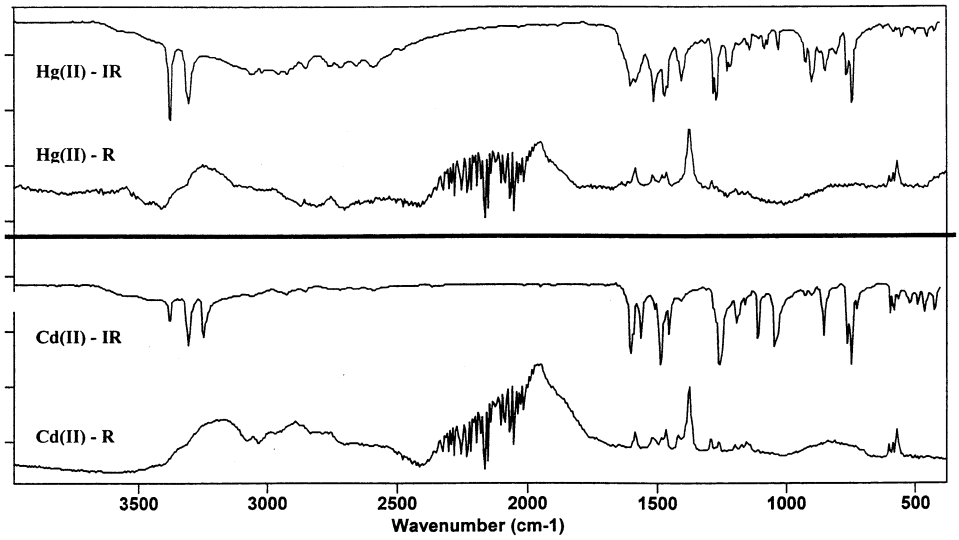


Fig. 8. FTIR and Raman spectra of the **Amph**–Cd(II) and Hg(II) complexes.

The bands observed at 447 and 411 cm^{-1} in the **Phda**–Cd complex and at 457 and 418 cm^{-1} in the spectra of the corresponding mercury complex are all predominantly due to (M–N) stretching. In a recent study of Hg(II) and Cd (II)-aminobenzophenon, a peak at ~ 366 cm^{-1} was tentatively assigned to (Cd–N) and (Hg–N) [26], which is ~ 81 cm^{-1} lower than our calculated value. However, that study did not mention Raman data. In addition Nakamoto [1] have examined the i.r. spectra of bis(glycino) complexes, and have assigned ν(M–N) at 457 cm^{-1} which is very close to our assignment of the same band. ν(M–O), observed at 458 and 448 cm^{-1} in the i.r. spectra of Cd and Hg–**Amph**, are about 124 cm^{-1} higher than the calculated value in the bis(glycino) complex. It should be mentioned that for bis(biuretato) and bis(oxamido) complexes these bands range from 270 to 485 cm^{-1} [2]. Since such a large range for ν(M–N) and ν(M–O) exists for similar complexes, it is not unreasonable to encounter (M–N) and (M–O) frequencies that differ by 81 and 124 cm^{-1} in related compounds.

Acknowledgements

The authors are indebted to Professor G. Keresztury (Chemical Research Center of the Hungarian Academy of Sciences) for infrared and Raman measurements and for helpful discussion about this work.

References

[1] J.R. Kincaid, K. Nakamoto, Spectrochim. Acta 32A (1976) 277.
[2] T.J. Thamann, T.M. Loehr, Spectrochim. Acta 36A (1980) 751.
[3] P. Roezmecnik, M.L. Stephenson, F.F. Scott, Proc. Natl. Acad. Sci. 46 (1960) 811.
[4] T.K. Hzang, J.N. Miller, B.D. Throburn, Anal. Chim. Acta 99 (1978) 305.
[5] J.E. Huheey, Inorganic Chemistry Principles of Structure and Reactivity, Harper and Row, UK, 1975.
[6] F.S. Freeman, B. Carroll, J. Phys. Chem. 62 (1958) 394.
[7] C.D. Doyle, J. Appl. Polym. Sci. (1961) 285.
[8] H.H. Horowitz, G. Metzger, Anal. Chem. 35 (1963) 1464.
[9] E.S. Ibrahim, S.A. Sallam, A.S. Orabi, B.A. El-Shetary, A. Lentz, Monats. Chem. 129 (1998) 159.
[10] Proceedings of the Sixth International Conference in Thermal Analysis, Bayreuth, Germany, 1980.
[11] T.H. Rakha, A.A. El-Asmy, M.M. Mostafa, A. El-Kourshy, Trans. Met. Chem. 12 (2) (1987) 125.
[12] G.O. Piloyan, I.D. Ryabchikov, O.S. Novikova, Nature 212 (1966) 1229.
[13] E.R. Souaya, W.G. Hanna, E.H. Ismail, N.E. Milad, Molecules 5 (2000) 1121.
[14] M. Hernández, S. Dominguez, P. Gili, A. Mederos, C. Ruz-Pérez, Polyhedron II (1992) 1965.
[15] IUPAC commission on Molecular Structure on Spectroscopy, Pure Appl. Chem. 50 (1978) 1707.
[16] G. Fogarsi, X. Zhou, P.W. Taylor, P. Pulay, J. Am. Chem. Soc. 114 (1992) 8191.
[17] E.B. Wilson, J.C. Decius, P.C. Cross, Molecular Vibrations, The Theory of the Infrared and Raman Vibration Spectra, Mc Graw-Hill, London, 1955.
[18] A. Kuwae, K. Machida, Spectrochim. Acta 35A (1979) 27.
[19] R.K. Goel, K.P. Kansal, S.N. Sharma, Indian J. Pure Appl. Phys. 17 (1979) 778.
[20] P.N. Gates, D. Steele, R. Pearce, K. Radclffe, J. Chem. Soc., Perkin Trans. II (1972) 1607.
[21] R. Pearce, D. Steele, K. Radcliffe, J. Mol. Struct. 15 (1973) 409.
[22] P.X. Armendarez, K. Nakamoto, Inorg. Chem. 5 (1966) 796.
[23] T. Sundius, J. Mol. Spectrosc. 82 (1980) 138.
[24] A.R. Katritzky, A.R. Jones, J. Chem. Soc., 3074 (1959).
[25] J. Fujita, A.E. Martell, K. Nakamoto, J. Chem. Phys. 36 (1962) 324.
[26] I.M. Vezzosi, A.F. Zanoli, G. Peyronel, Spectrochim. Acta 36A (1980) 1065.

PERGAMON

Polyhedron 21 (2002) 997–1003

POLYHEDRON

www.elsevier.com/locate/poly

Systematic investigation of the [Ni^{2+}–phen–CrO_4^{2-}] system; dichromate species isolated from alkaline solutions

W. Bronowska [a], Z. Staszak [b], M. Daszkiewicz [c], M. Cieślak-Golonka [c,*], A. Wojciechowska [c]

[a] *Institute of Physics, Wrocław University of Technology, Wybrzeże Wyspiańskiego 27, 50-370 Wrocław, Poland*
[b] *Faculty of Computer Sciences and Management, Wrocław University of Technology, Wrocław, Poland*
[c] *Institute of Inorganic Chemistry and Metallurgy of Rare Elements, Wrocław University of Technology, Wybrzeże Wyspiańskiego 27, 50-370 Wrocław, Poland*

Received 14 November 2001; accepted 25 January 2002

Abstract

Nickel(II) dichromate and chromate complexes with 1,10-phenanthroline were isolated from basic (pH 8–9) solutions. $[Ni(phen)_3]Cr_2O_7\cdot 8H_2O$ (**1**), $NiCrO_4$ (**2**), $[Ni(phen)_3]Cr_2O_7\cdot 3H_2O$ (**3**) and $[Ni(phen)(OCrO_3)(H_2O)_3]\cdot H_2O$ (**4**) were characterized with spectroscopic (UV–Vis, IR, FIR) methods and one (**4**), additionally, with X-ray data. In the complex (**4**) the chromate ion is monodentately coordinated to nickel ion. This complex crystallizes in the triclinic crystal system (space group $P\bar{1}$). The single crystal electronic spectrum of complex (**4**) at 4 K reveals a rare feature when the structured second d–d band (O_h symmetry) is unsplit in spite of lowering symmetry. The filtration process has revealed that this band is vibronically structured in the ν_s Ni–O–Cr quantum. A new broad low intensity band at approximately 14 000 cm^{-1} was assigned to the forbidden transition in the bridge. An attempt to explain precipitation of dichromates from alkaline solutions has been given. © 2002 Published by Elsevier Science Ltd.

Keywords: Nickel(II) chromate and dichromate complexes of phenanthroline; Monodentate coordination of CrO_4^{2-}; Crystal structures; IR and UV–Vis–NIR band analysis

1. Introduction

According to common opinion, the CrO_4^{2-}, $HCrO_4^-$ and $Cr_2O_7^{2-}$ anions are present in basic, slightly acidic and acidic solutions, respectively [1]. However, these oxo species exist in various equilibria depending predominantly on pH and Cr(VI) concentrations [2–7]. Thus, some dichromate anions are present in basic solutions of high Cr(VI) concentrations in amounts corresponding to the magnitude of proper equilibrium constants (for example, calculated abundance of $Cr_2O_7^{2-}$ (10^{-2} M) at pH 8 is 0.1%) [6].

Here we report data showing the effect of 'the environment' of chromium(VI) i.e. accompanying nickel(II) ions and the organic ligand—1,10-phenanthroline (phen) on the chemical composition of precipitated chromium(VI) species. We have isolated from pH 8–9 four complex salts containing the dichromate ($[Ni(phen)_3]Cr_2O_7\cdot 8H_2O$ (**1**), $[Ni(phen)_3]Cr_2O_7\cdot 3H_2O$ (**3**)) and chromate anions ($NiCrO_4$ (**2**), $[Ni(phen)(OCrO_3)(H_2O)_3]\cdot H_2O$ (**4**)).

Generally, the chemistry and geometry of complexes containing Cr(VI) can be interesting as they play an important role in transportation of this cancerogenic metal ion through the cellular membrane and its further metabolization in the cytoplasm [8,9]. Thus, the potential complexation of the Cr(VI) ion may influence its genotoxicity.

2. Experimental

Reagent grade commercially available chemicals were used in all experiments. The system was studied at three different reagent ratios (Ni^{2+}:phen:CrO_4^{2-}): 1:1:1, 1:2:1

* Corresponding author. Tel.: +48-71-32-03666; fax: +48-71-32-84330.
E-mail address: golonka@ichn.ch.pwr.wroc.pl (M. Cieślak-Golonka).

0277-5387/02/$ - see front matter © 2002 Published by Elsevier Science Ltd.
PII: S0277-5387(02)00912-9

and 1:3:1 and with three different nickel(II) salts: $NiSO_4$, $NiCl_2$ and $Ni(NO_3)_2$. The general procedure was the same for all syntheses. The compounds (**1**–**4**) were formed during the reaction of methanolic solutions of phen previously mixed with a water solution of K_2CrO_4 and a water solution of the respective nickel salt. The complexes were precipitated from the reagent mixture in the following order: **1**, **2**, **3** and **4** (see Table 1).

2.1. Syntheses

2.1.1. Reagent ratio 1:1:1

A methanolic solution of 1,10-phenanthroline (5 cm^3, 0.75 M) was mixed by stirring with 15 cm^3 of K_2CrO_4 (0.25 M aqueous solution). The yellow precipitate, which was immediately formed, dissolved upon addition of phen solution. Then 15 cm^3 of 0.25 M $NiSO_4$ ($NiCl_2$, $Ni(NO_3)_2$) aqueous solution, was added. From the resulting orange–red solution, a yellow precipitate (compound **1**) was isolated at pH 8.62. The precipitate was filtered, washed several times with water and finally dried in a desiccator over P_2O_5. After separation of **1** the solution became turbid and a brown powder was obtained (compound **2**) at pH 8.82. The resulting red–orange solution was allowed to stand for 24 h and thin orange crystals were formed (compound **3**) at pH 8.86. The final olive green solution was left to stand overnight. The obtained crystals (compound **4**) were separated at pH 8.90, washed with water and dried in air.

Analytical results:

(**1**) Found: C, 44.70; H, 4.10; Cr, 10.67; Ni, 5.82; N, 8.65. Calc. for $C_{36}H_{40}Cr_2N_6NiO_{15}$: C, 45.07; H, 4.20; Cr, 10.84; Ni, 6.12; N, 8.76%. IR spectrum (cm^{-1}) (KBr): Cr–O: ν_{17}-936s; ν_{21}-367m; Ni–N: ν_{as}-302 and ν_s-250; Cr–O–Cr: ν_{as}-771w, ν_s-559; –C=N–: ν-1517m.

(**2**) Found: H, 4.33; Cr, 18.31; Ni, 20.70. Calc. for $CrNiO_4$: H, 4.28; Cr, 18.39; Ni, 20.76%. IR spectrum (cm^{-1}) (KBr): Cr–O: ν_1-874w; ν_3-912vs; ν_4-392ms; Ni–O: ν_s-425.

(**3**) Found: C, 46.96; H, 3.60; Cr, 12.19; Ni, 6.71; N, 9.11. Calc. for $C_{36}H_{30}Cr_2N_6NiO_{10}$: C, 49.74; H, 3.48; Cr, 11.96; Ni, 6.75; N, 9.67%. IR spectrum (cm^{-1}) (KBr): Cr–O: ν_{17}-936w; ν_{21}-367m; Ni–N: ν_{as}-300, ν_s-250; Cr–O–Cr: ν_{as}-770w, ν_s-558; –C=N–: ν-1516m.

(**4**) Found: C, 33.24; H, 3.92; Cr, 11.43; Ni, 13.17; N, 6.40. Calc. for $C_{12}H_{16}CrN_2NiO_8$: C, 33.76; H, 3.78; Cr, 12.18; Ni, 13.75; N, 6.56%. IR spectrum (cm^{-1}) (KBr): Cr–O: ν_1-855w; ν_2-334m; ν_3-897vs and ν_3-916vs; ν_4-367ms and ν_4-386m; Ni–O: ν_s-447; Ni–N: ν_{as}-294 and ν_s-253; Ni–O–Cr: ν_{as}-818w, ν_s-560; –C=N–: ν-1518m.

Table 1
General characteristics of the compounds isolated from the system [Ni^{2+}–phen–CrO_4^{2-}] in succession

Symbol	Formula	Color	pH
1	$[Ni(phen)_3]Cr_2O_7 \cdot 8H_2O$	yellow powder	8.62
2	$NiCrO_4$	brown powder	8.82
3	$[Ni(phen)_3]Cr_2O_7 \cdot 3H_2O$	orange crystals	8.86
4	$[Ni(phen)(OCrO_3)(H_2O)_3] \cdot H_2O$	olive crystals	8.90

Compounds **1**–**4** were also isolated with various yields in the same order for the 1:2:1 (Ni^{2+}:phen:CrO_4^{2-}) reagent ratio. However, for the 1:3:1 molar ratio, only **1**–**3** were precipitated.

2.2. Physical measurements

Elemental analyses were done using the Kupman (C, H, N) and ICP AES (Ni, Cr) methods.

2.2.1. X-ray data collection, structure solution and refinement for complex (*4*)

The single-crystal measurements were carried out on a four circle X-ray KM4 diffractometer (Kuma Diffraction Company). The data were collected using a CCD detector. Mo Kα graphite-monochromated radiation ($\lambda = 0.71073$ Å) and the omega scan with $\Delta\omega = 0.75^\circ$ for one image were used for data collection at room temperature (r.t.) (300 K). The 960 images for six different runs covered 89.2% of the Ewald sphere. 7755 reflections of $[Ni(phen)(OCrO_3)(H_2O)_3] \cdot H_2O$ were recorded which merged to give a total of 3875 reflections.

The structure of $[Ni(phen)(OCrO_3)(H_2O)_3] \cdot H_2O$ (**4**) was solved by direct methods using the SHELXS-97 program [10]. Refinement was carried out using SHELXL-97 [10]. The initial lattice parameters were calculated from 150 reflections obtained from 30 images for ten runs with different orientations in reciprocal space and the final lattice parameters were refined for all reflections with $I > 2\sigma(I)$. Anisotropic thermal displacement parameters were used for all non-hydrogen atoms. The positions of hydrogen atoms were determined from difference Fourier maps and they were well refined. Empirical absorption correction was applied for observed reflections and no extinction correction was introduced in the refinement. The crystal data and details of the data collection and refinement are shown in Table 2.

2.2.2. Spectroscopic study

FIR (500–50 cm^{-1}) and IR (4000–500 cm^{-1}) spectra were recorded on a FTIR Perkin–Elmer 2000 and Perkin–Elmer 1600 spectrophotometers, respectively. Electronic absorption spectra were obtained on a Cary 500 Scan UV–Vis–NIR Spectrophotometer (Varian).

Table 2
Crystal data and structure refinement for $[Ni(phen)(OCrO_3)(H_2O)_3]\cdot H_2O$ (**4**)

Empirical formula	$C_{12}H_{16}CrN_2NiO_8$
Formula weight	426.98
Temperature (K)	293(2)
Crystal system	triclinic
Space group	$P\bar{1}$
a (Å)	8.163(2)
b (Å)	8.582(2)
c (Å)	11.573(2)
α (°)	91.42(3)
β (°)	91.67(3)
γ (°)	104.12(3)
V (Å^3)	785.5(3)
Z	2
D_{calc} (g cm^{-1})	1.805
λ (Å)	0.71073
μ (cm^{-1})	19.34
R [a]	0.0449
R_w [b]	0.0841

[a] $R = \Sigma(|F_0| - |F_c|)/\Sigma|F_0|$.
[b] $R_w = [\Sigma w(|F_0| - |F_c|)^2/\Sigma w|F_0|^2]^{1/2}$ $w = (\sigma_c{}^2 + (0.02|F_0|)^2)^{-1}$.

The low-temperature (4 K) single crystal spectrum was measured using a Cryostat Optistat CF (Oxford) with an open-cycle helium system with identical conditions as a baseline.

The band analysis of the electronic spectra was performed using the variable digital filter method to obtain the approximate band position values [11–15]. To obtain the exact band positions, intensities and half-widths, the spectra have been deconvoluted into Gaussian components [15–18].

Originally, the variable digital filter method described by Biermann and Ziegler was used for analytical purposes [11] and later adopted for electronic spectra analysis [14]. The filter acts by a single convolution of the spectral data $T(k)$ with a filter function $a(n)$:

$$T(k) = \sum_{n=-N}^{N} a(n) f(k-n)$$

where

$$a(n) = \{[(2\alpha+1)/(2N+1)] - [2\alpha|n|/N(N+1)]\}$$

$T(k)$ is the filtered spectrum with k equally distanced measured points, $a(n)$ is the filter function, f is the unfiltered spectrum, N is the integer number greater than $|n|$, and α is a real number determining the degree of the resolution enhancement. By varying α and N one can achieve different degrees of noise reduction, increase of height and decrease of width of the component bands.

The process of the resolution of the experimental contour into component bands was performed by using a modification of the Non-Linear Least-Squares algorithm [16–18]. The number of bands and their approximate positions were taken from filter analysis described above.

3. Results and discussion

From the mixture of components: Ni(II) salt, K_2CrO_4 and phen at three various molar ratios and three anions of the Ni(II) salts in solutions at pH 8–9, four compounds were isolated in succession (Table 1). The most striking was the isolation of two dichromate salts with a $[Ni(phen)_3]^{2+}$ complex cation: a yellow powder and orange–red crystals, differing only in the various amounts of water (Table 1). The crystal structure of the orange crystals (**3**) was reported recently [19]. Here, we present the respective data for the olive crystals of $[Ni(phen)(OCrO_3)(H_2O)_3]\cdot H_2O$ (**4**), precipitating as the last species.

3.1. Crystal structure analysis

The $[Ni(phen)(OCrO_3)(H_2O)_3]\cdot H_2O$ crystals (**4**) have a triclinic symmetry with space group $P\bar{1}$ and two chemical units forming, at room temperature, the unit cell which is similar to that in $[Ni(phen)(S_2O_3)(H_2O)_3]\cdot H_2O$ [20]. However, the atomic coordinates of $[Ni(phen)(OCrO_3)(H_2O)_3]\cdot H_2O$ were determined independently using the direct method. Selected interatomic distances and angles of $[Ni(phen)(OCrO_3)(H_2O)_3]\cdot H_2O$ are shown in Table 3. Fig. 1 presents the projection of the atom arrangement in the unit cell of this crystal along the a axis. The molecular diagram for $[Ni(phen)(OCrO_3)(H_2O)_3]$ is illustrated in Fig. 2 (displacement ellipsoids are drawn at the 50% probability level). The complex is monomeric. The Ni(II) coordination environment can be considered as a distorted octahedron. The coordination positions are occupied by the two N atoms from 1,10-phenanthroline acting in the usual bidentate mode, three water molecules and one O atom

Table 3
Selected bond lengths (Å) and angles (°) for $[Ni(phen)(OCrO_3)(H_2O)_3]\cdot H_2O$ (**4**)

Bond lengths			
Ni(1)–O(1)	2.1008(11)	Ni(1)–O(11)	2.1089(11)
Ni(1)–O(2)	2.0662(9)	Ni(1)–N(1)	2.0749(10)
Ni(1)–O(4)	2.0553(10)	Ni(1)–N(10)	2.0801(11)
Cr(2)–O(11)	1.6225(10)	Cr(2)–O(13)	1.6499(10)
Cr(2)–O(12)	1.6208(10)	Cr(2)–O(14)	1.6062(11)
Bond angles			
O(1)–Ni(1)–O(2)	86.37(4)	O(2)–Ni(1)–O(4)	94.18(4)
O(1)–Ni(1)–O(4)	88.32(4)	O(2)–Ni(1)–O(11)	88.64(4)
O(1)–Ni(1)–O(11)	174.98(3)	O(2)–Ni(1)–N(1)	174.36(4)
O(1)–Ni(1)–N(1)	92.65(5)	O(2)–Ni(1)–N(10)	93.97(4)
O(1)–Ni(1)–N(10)	87.24(4)	O(11)–Ni(1)–N(1)	92.37(5)
O(4)–Ni(1)–O(11)	91.51(4)	O(11)–Ni(1)–N(10)	93.64(4)
O(4)–Ni(1)–N(1)	91.34(5)	N(1)–Ni(1)–N(10)	80.42(5)
O(4)–Ni(1)–N(10)	170.45(3)	Cr(2)–O(11)–Ni(1)	138.00(5)
O(11)–Cr(2)–O(12)	110.77(6)	O(12)–Cr(2)–O(13)	107.94(5)
O(11)–Cr(2)–O(13)	108.58(5)	O(12)–Cr(2)–O(14)	109.12(5)
O(11)–Cr(2)–O(14)	110.68(5)	O(13)–Cr(2)–O(14)	109.70(5)

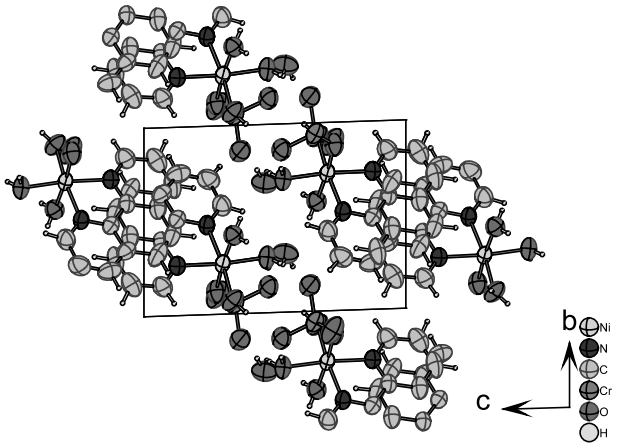


Fig. 1. Projection of the atom arrangement in the unit cell of the $[Ni(phen)(OCrO_3)(H_2O)_3]\cdot H_2O$ crystal along the *a* axis.

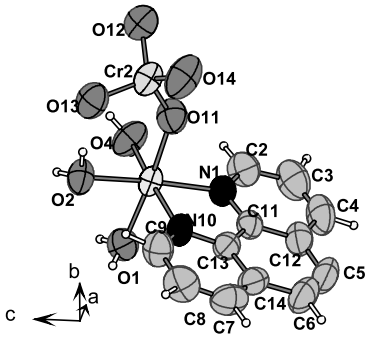


Fig. 2. Molecular diagram for $[Ni(phen)(OCrO_3)(H_2O)_3]$.

from the chromate anion. Two water molecules are situated in equatorial positions whereas one O atom from the water molecule and one O atom from the chromate group occupy the axial positions. The Ni–N bond lengths [2.0749(10) and 2.0801(11) Å] are longer in comparison with other similar complexes [20–22]. The Ni–O distances [2.0662(9) and 2.0553(10) Å] from the equatorial water molecules are shorter than those from the axial water molecule [2.1008(11) Å] and the chromate anion [2.1089(11) Å], and are normal in this type of complex [20,23,24]. Coordination does not seem to affect the geometry of the chromate moiety in this crystal. The mean value of the Cr–O distances agrees well with those reported previously for the uncoordinated unit of CrO_4^{2-} [15,24].

The complex crystallizes with a molecule of water. It takes part in four hydrogen bondings (HBs) with two O atoms from the chromate groups and two water ligands from independent complex molecules. Furthermore, four HBs are formed between two molecules of equatorial water and O atoms from the chromate anion. Amongst these eight HBs, the aqua ligand O(2) forms the shortest [1.820(14) Å] intramolecular HB with O(13) atom from the chromate ion. The strength of the other HB interactions varies from normal to weak. The

Table 4
Hydrogen bonds and angles for $[Ni(phen)(OCrO_3)(H_2O)_3]\cdot H_2O$ (**4**) (Å and °)

D–H···A	d(D–H)	d(H···A)	d(D···A)	<(DHA)
O(1)–H(11)···O(3)	0.779(16)	2.040(15)	2.8083(15)	168.8(16)
O(1)–H(12)···O(3)^{ii}	0.840(16)	1.945(15)	2.7618(15)	163.9(15)
O(2)–H(21)···O(13)	0.854(14)	1.820(14)	2.6716(14)	174.4(16)
O(2)–H(22)···O(12)^{iii}	0.779(18)	1.965(18)	2.7344(15)	169.0(18)
O(3)–H(31)···O(12)^{iv}	0.887(14)	1.874(15)	2.7452(16)	166.8(16)
O(3)–H(32)···O(13)	0.864(17)	1.897(17)	2.7444(16)	166.6(15)
O(4)–H(41)···O(14)^{i}	0.860(16)	1.882(16)	2.7382(14)	173.2(16)
O(4)–H(42)···O(13)^{iii}	0.799(14)	1.958(15)	2.7431(15)	167.3(15)

Symmetry transformations used to generate equivalent atoms: ^{i}, $x+1, y, z$; ^{ii}, $-x, -y+1, -z+1$; ^{iii}, $-x, -y, -z+1$; ^{iv}, $-x-1, -y, -z+1$.

hydrogen-bonding geometry in $[Ni(phen)(OCrO_3)(H_2O)_3]\cdot H_2O$ is shown in Table 4. This three-dimensional network of the HBs involving the molecule of crystallization water, O atoms from the chromate moieties and the aqua ligands appears to be important for the stabilization of the crystal lattice. The small values of the anisotropic temperature factors of all atoms indicate that the structure of the $[Ni(phen)(OCrO_3)(H_2O)_3]\cdot H_2O$ crystals is ordered. The refinement of the crystal structure confirmed that the $[Ni(phen)(OCrO_3)(H_2O)_3]\cdot H_2O$ crystals are isostructural to $[Ni(phen)(S_2O_3)(H_2O)_3]\cdot H_2O$ [20].

3.2. UV–Vis studies

The results of the electronic spectral analysis are shown in Table 5 and in Fig. 3. As the region 20 000–50 000 cm^{-1} is well known both for chromates, dichromates [25–27] and phen [28,29] in this work we have concentrated on the low energy region 5000–20 000 cm^{-1} characteristic of the Ni(II) (d^8) d–d transitions. Moreover, $[Ni(phen)_3]^{2+}$ (**1** and **3**) complexes with the NiN_6 chromophore are also well known in the literature [30] so in this work detailed analysis of the chromate complex (**4**) has been performed.

In spite of the real symmetry (C_{2v}) of the NiN_2O_4 chromophore (**4**), it can be effectively analyzed in the tetragonal D_{4h} symmetry of the metal ion surroundings. During the deconvolution process of the 4 K single crystal $[Ni(phen)(OCrO_3)(H_2O)_3]\cdot H_2O$ spectrum (Fig. 3) it was found that the most reliable crystal field parameters were obtained with the following assumption: the first spin-allowed $^3T_{2g}$ state (O_h) splits into ^3E_g and $^3B_{2g}$, the spin-forbidden ^1E_g state splits into $^1A_{1g}$ and $^1B_{1g}$, whereas the second spin-allowed d–d transition ($^3T_{1g}$) remains unsplit (Fig. 3). Such a rather rare situation where $^3T_{1g}$ is unsplit has been described earlier in the literature [30]. If we assume the splitting of both lowest energy spin-allowed d–d bands, the calculated Racah B parameter gives the wrong result ($B > B^0$!). The

Table 5
The assignment of electronic transitions for the Ni(II) ion in compounds **1**–**4** (energies in [cm^{-1}])

Formula	O_h	$^3T_{2g}$		^1E_g		$^3T_{1g}$	
	D_{4h}	^3E_g	$^3B_{2g}$	$^1A_{1g}$	$^1B_{1g}$	$^3A_{2g}$	^3E_g
1 $[Ni(phen)_3]Cr_2O_7 \cdot 8H_2O$	sn	12 740		11 650			
	sd	12 730		11 570			
2 $NiCrO_4$	sn	–		–			
	sd	8200		–			
3 $[Ni(phen)_3]Cr_2O_7 \cdot 3H_2O$	sn	12 810		11 650			
	sd	11 630		11 570			
4 $[Ni(phen)(OCrO_3)(H_2O)_3] \cdot H_2O$	sn	10 250		13 250		16 500	
	sd	8750	10 690	12 400	13 290	16 310	

third d–d band at $\sim 27\,000$ cm^{-1} is covered under strong CT (O→Cr) bands and was not analyzed. The following crystal field parameters (in cm^{-1}) for the NiN_2O_4 chromophore have been obtained: Dq = 1063; Ds = 145; Dt = −218; B = 825.

The one extra band at approximately 14 000 cm^{-1} (Fig. 3) was assigned to the Ni–O–Cr bridge transition [15,32]. The low intensity of this band suggests that it must be multiple times forbidden, being e.g. an effect of the position of the oxygen between two metal ions and thus its 'frustration' [32].

The filtration process uncovered the vibrational fine structure of the second d–d band (Fig. 3 inset). The differences in the positions of its components (ca. 538 cm^{-1}) indicate that it can be the result of coupling between the electronic transition and the ν_s Ni–O–Cr vibration (ground state at 560 cm^{-1}). This further supports spectroscopically the presence of the bridge found from the crystal data. Both crystallographic and UV–Vis studies exhibit the symmetry of an elongated octahedral environment around the Ni(II) ion. However, the comparison of the Cr–O bond lengths (Table 3, Fig. 2) shows that the longest bond is not Cr(2)–O(14) i.e. with the oxygen atom not coordinated to Ni(II), but that forming the intramolecular hydrogen bond. Such a situation implicates a further decrease of

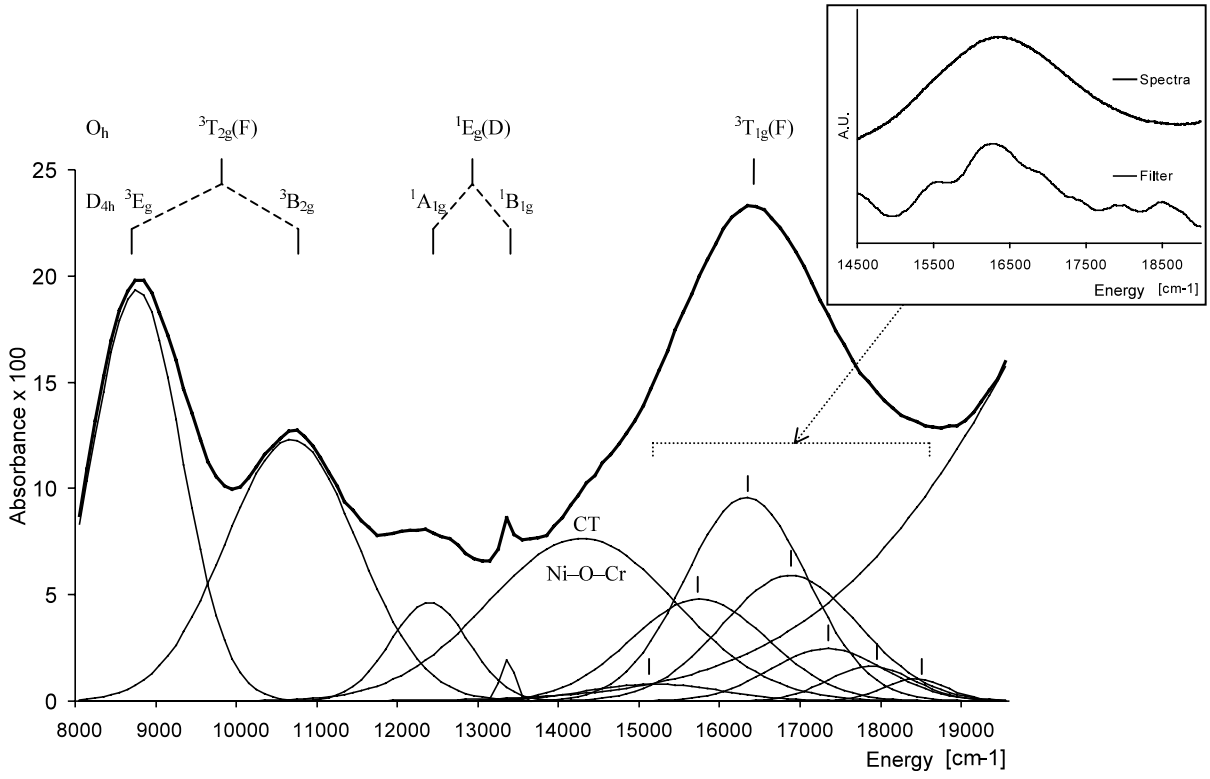


Fig. 3. The GAUSSIAN analysis of the 4 K single crystal electronic spectrum of $Ni(phen)(OCrO_3)(H_2O)_3]H_2O$ in the 8000–20 000 cm^{-1} region. Inset: the part of second d–d band ($^3A_{2g} \rightarrow {}^3T_{1g}$ transition) exhibiting vibrational fine structure as the result of filtration (filter parameters $\alpha = 200$, $N = 30$, step = 10 cm^{-1}).

the CrO_4^{2-} entity symmetry ($C_{3v} \rightarrow C_1$), which is not seen in the IR spectra. The hydrogen bonding interaction, being weaker than a coordination bond, is not able to 'disturb the C_{3v} symmetry' of the chromate to such a degree as to be seen in the IR spectroscopy. A more detailed study (better resolution of the spectra) could exhibit the competition between both types of bonding.

3.3. The precipitation of the dichromate salts from basic solutions

It is well known that Cr(VI) can exist in various oxoforms depending on acidity and chromium(VI) concentration [1–7]. Generally, at pH 8.5–9.5 the predominant species is CrO_4^{2-} and no $Cr_2O_7^{2-}$ entities should be present in a significant amount. In our experiment, among the various species existing in solution that of $[Ni(phen)_3]Cr_2O_7 \cdot 8H_2O$ must have the lowest solubility (**1**) as it is the first to precipitate. The dichromate anion is just withdrawn from the solution due to the lowest solubility of the $[Ni(phen)_3]Cr_2O_7 \cdot 8H_2O$ complex. However, underlying the importance of the solubilities of the species present in solution it would be interesting to analyze the possible influence of other factors e.g. metal ion, phen (and $Hphen^+$) on the chromate–dichromate equilibria. For example, in similar conditions the respective chromates (not dichromates) were isolated from the system [M–bpy–CrO_4] M = Ni, Co, Cu, Zn [15,31–33].

The chromium(VI) equilibria in the presence of complexes of other metal ions are evidently a rich area for further research.

4. Summary

Four Ni(II) compounds; two containing dichromate and two containing chromate species, have been precipitated in succession from basic solutions of the [Ni^{2+}–phen–CrO_4^{2-}] system. As the last of these, olive crystals of the formulae $[Ni(phen)(OCrO_3)(H_2O)_3] \cdot H_2O$ (**4**) with monodentate coordination, untypical (but not unexpected) for the chromates, have been isolated. The structure of these crystals is ordered and isostructural to $[Ni(phen)(S_2O_3)(H_2O)_3] \cdot H_2O$. The three-dimensional network of hydrogen bonds involving the $[Ni(phen)(OCrO_3)(H_2O)_3] \cdot H_2O$ molecule and aqua ligands seems to be essential for the stabilization of the crystal lattice. Monodentate coordination of the chromate group to the Ni(II) ion in these crystals was supported with vibrational and electronic spectroscopic data. The electronic spectral analysis of (**4**) exhibited a tetragonal deformation of the Ni(II) ion in the NiN_2O_4 chromophore.

The precipitation of the dichromate species from alkaline solutions can be an effect of their lowest solubility among the reagents present.

5. Supplementary material

Supplementary data are available from The Director, CCDC, 12 Union Road, Cambridge, CB2 1EZ, UK (fax: +44-1223-336033; e-mail: deposit@ccdc.cam.ac.uk or www: http://www.ccdc.cam.ac.uk) on request, quoting the deposition number 164162.

Acknowledgements

The authors would like to thank Professor A. Pietraszko (Institute of Low Temperature and Structure Research, Polish Academy of Science Wroclaw) for his assistance and stimulating discussions as well as the Wroclaw University of Technology (No. 34256-8) for financial support.

References

[1] G. Wilkinson (Ed.), Comprehensive Coordination Chemistry, vol. 3, 1st ed., Pergamon, Oxford, 1987, p. 699.
[2] J.J. Cruywagen, J.B.B. Heyns, E.A. Rohwer, Polyhedron 17 (1998) 1741.
[3] F. Brito, J. Ascanio, S. Mateo, C. Hernandez, L. Araujo, P. Gili, P. Martin-Zarza, S. Dominguez, A. Mederos, Polyhedron 16 (1997) 3835.
[4] N.E. Brasch, D.A. Buckingham, A. Bram Evans, C.H.R. Clark, J. Am. Chem. Soc. 118 (1996) 7969.
[5] J.B.B. Heyns, J. Cruywagen, J. Raman Spectr. 30 (1999) 335.
[6] R.K. Tandon, P.T. Crisp, J. Ellis, R.S. Baker, Talanta 31 (1984) 227.
[7] T. Ozeki, Y. Kinoshita, H. Adachi, S. Ikeda, Bull. Chem. Soc. Jpn. 67 (1994) 1041.
[8] M. Cieślak-Golonka, Polyhedron 15 (1996) 3667.
[9] R. Codd, C.T. Dillon, A. Levina, P.A. Lay, Coord. Chem. Rev. 216–217 (2001) 537.
[10] G.M. Sheldrick, SHELX-97 Program for the solution and the refinement of crystal structures from diffraction data. University of Göttingen, Germany, 1997.
[11] G. Bierman, H. Ziegler, Anal. Chem. 58 (1986) 536.
[12] J. Myrczek, Spectr. Lett. 23 (1990) 1027.
[13] M. Cieślak-Golonka, M. Raczko, Z. Staszak, Polyhedron 11 (1992) 2549.
[14] J. Myrczek, Spectr. Lett. 20 (1987) 927.
[15] A. Wojciechowska, Z. Staszak, W. Bronowska, A. Pietraszko, M. Cieślak-Golonka, Polyhedron 20 (2001) 2063.
[16] I.A. Slavič, Nucl. Instr. Meth. 134 (1976) 285.
[17] A. Bartecki, Z. Staszak, Comp. Enh. Spectr. 2 (1984) 129.
[18] D. Miernik, A. Arkowska, E. Grażyńska, Z. Staszak, Spectr. Lett. 24 (1991) 371.
[19] J.-K. Tang, E.-Q. Gao, D.-Z. Liao, Z.-H. Jiang, S.-P. Yan, Pol. J. Chem. 74 (2000) 137.
[20] E. Freire, S. Baggio, R. Baggio, L. Suescun, Acta Crystallogr. C55 (1999) 1780.

[21] B.-H. Ye, X.-M. Chen, G.-Q. Xue, L.-N. Ji, J. Chem. Soc., Dalton Trans. (1998) 2827.
[22] F. Walmsley, A.A. Pinkerton, J.A. Walmsley, Polyhedron 8 (1989) 689.
[23] S. Namouchi Cherni, A. Driss, T. Jouini, Acta Crystallogr. C55 (1999) 1248.
[24] D. Poleti, D.R. Stojanković, B.V. Prelesnik, L. Manojlovic-Muir, Acta Crystallogr. C46 (1990) 399.
[25] V. Miskowski, H.B. Gray, C.J. Ballhausen, Mol. Phys. 28 (1974) 729.
[26] Z.G. Szabo, K. Kamaras, S. Szebeni, I. Ruff, Spectrochim. Acta 34A (1978) 607.
[27] M. Cieślak-Golonka, Coord. Chem. Rev. 109 (1991) 223.
[28] S.C. Zhu, J.Q. Xu, J.M. Shi, Z.D. Zhang, S.C. Shang, C.J. Wu, J.J. Lu, Pol. J. Chem. 73 (1999) 2053.
[29] C.C. Phifer, D.R. McMillin, Inorg. Chem. 25 (1986) 1329.
[30] A.B. Lever, Inorganic Electronic Spectroscopy, 2nd ed. (and references therein), Elsevier, New York, 1984.
[31] A. Wojciechowska, W. Bronowska, A Pietraszko, Z. Staszak, M. Cieślak-Golonka, J. Mol. Struct. 608 (2002) 151.
[32] A. Pietraszko, W. Bronowska, A. Wojciechowska, Z. Staszak, M. Cieślak-Golonka, Pol. J. Chem. 76 (2002) 309.
[33] A. Wojciechowska, W. Bronowska, A Pietraszko, Z. Staszak, M. Cieślak-Golonka, J. Inorg. Biochem. 86 (2001) 480.

PERGAMON

Polyhedron 21 (2002) 1005–1015

POLYHEDRON

www.elsevier.com/locate/poly

Thermodynamic studies on supramolecular interactions of metal ions with nucleotides/tripods ligands

Yan-He Guo [a], Qing-Chun Ge [a], Hai Lin [b], Hua-Kuan Lin [a,c,*], Shou-Rong Zhu [a]

[a] Department of Chemistry, Nankai University, Tianjin 300071, People's Republic of China
[b] State Key Laboratory of Functional Polymer Materials for Adsorption and Separation, Nankai University, Tianjin 300071, People's Republic of China
[c] The National Key Laboratory of Coordination Chemistry, Nanjing University, Nanjing 210093, People's Republic of China

Received 20 November 2001; accepted 25 January 2002

Abstract

Four closely related polyamino tripodal ligands 1,3,5-tri(*n*-2′,5′-diaminohexane)-benzene (**L1**), 1,3,5-tri(*n*-2′,5′-diaminoheptane)-benzene (**L2**), 1,3,5-tri(*n*-2′,5′-diaminooctane)-benzene (**L3**) and 1,3,5-tri(*n*-2′,5′-diaminononane)-benzene (**L4**) were synthesized and characterized. Each tripodal ligand forms six protonated species in solution. The binding of these tripodal ligands to the nucleotide anions ATP, ADP and AMP are described in detail, with equilibrium constants given for each species formed. The strength of binding increases with the number of protons, corresponding to an increase in the number of hydrogen bonds and to an increase in the coulombic attractive forces. Moreover, the existence of a benzene spacer takes π-stacking interactions with the nucleobase residue of the nucleotides. At the same time, the coordination properties of the ternary complexes formed from the above tripods and Zn(II) and ATP were studied. The metal complexes of tripods recognize the nucleotides via multiple interactions that are similar to those occurring in the center of enzymes. © 2002 Elsevier Science Ltd. All rights reserved.

Keywords: Supramolecular interactions; Tripodal ammonium; Nucleotides; Ternary complexes; Zn(II)

1. Introduction

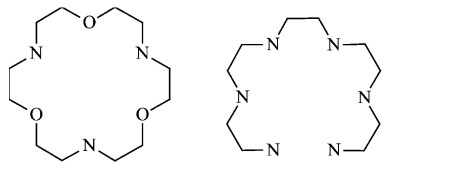
Molecular catalysis represents a major feature of the functional properties of supramolecular systems [1]. In particular, the recent development of anion receptors [2], that is organic ligands which bind organic and inorganic anions, opens the way to the design of molecular catalysts capable of affecting reactions on a bound anionic substrate [3].

The nucleotide adenosine 5′-triphosphate (ATP) and its di- and monophosphate analogs (ADP and AMP, respectively) are of great importance in the life science. It is the principal biological energy store, and about one sixth of all enzyme systems need ATP or a related adenine cofactor [4]. With this fact in mind, it is not surprising that the properties of adenine nucleotides are receiving much attention. ATP is a stable polyvalent anion at neutral pH that is the substrate for a highly efficient group of enzymes termed ATPases. Of particular interest are the factors that contribute to the 10^{10}-fold difference between the uncatalyzed and the ATPase-catalyzed hydrolysis of ATP [5]. Many protonated polyaza ligands, especially polyaza macrocyclic ligands (Scheme 1, compound **1**), have been shown to bind strongly with ATP, ADP and AMP [3,6] and in some instances, are able to catalyze their hydrolysis. On the other hand, the linear pentaethylenehexamine can also produce a rate enhancement [7,8]. However, successful catalysis by polyammonium ligands relies heavily on the recognition and selectivity of the initially bound substrate and the release of the product formed following chemical transformation [7–9].

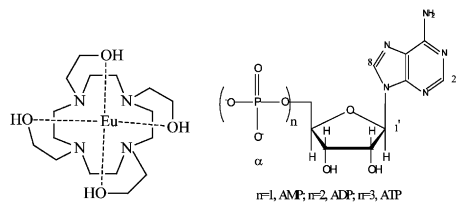
Since metal ions (for example, the Eu^{2+} complex **3** in Scheme 1) take part in the enzymatic hydrolysis of ATP, the metal-ion-promoted non-enzymatic hydrolysis has been extensively investigated [10–14]. In general, the assisted hydrolysis of polyphosphate and ATP by coordinating to a metal ion complex is affected by factors such as electron-withdrawing effects of the metal ion, strain in the chelated ring, proximity of the bound nucleophile [15], and so on. It is believed that a strong

* Corresponding author. Fax: +86-22-235-02458.
E-mail address: hklin@nankai.edu.cn (H.-K. Lin).

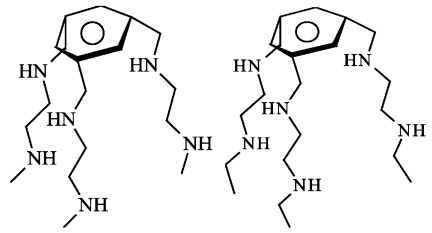
0277-5387/02/$ - see front matter © 2002 Elsevier Science Ltd. All rights reserved.
PII: S0277-5387(02)00916-6



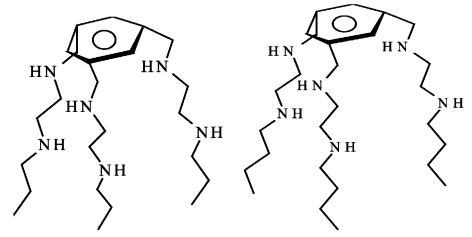
1 2



3 nucleotides



L1 L2



L3 L4

Scheme 1. R = methyl, **L1**; ethyl, **L2**; *n*-propyl, **L3**; *n*-butyl, **L4**.

binding strength of the catalyst with ATP is required but not necessary for ATP-hydrolysis, and the hydrolysis heavily depends on the nature of the additives, which may relate to structural factors as well as protonation at a given pH.

Although numerous studies have been performed to determine the supramolecular interactions between receptors and nucleotides, polyaza tripodal ligands, however, have been rarely investigated in this aspect. Tripodal ligands are capable of forming complexes with metal ions which exhibit unusual coordination features, high thermodynamic stability and kinetic inertness [16–19]. The tripodal ligands can form octahedral complexes by wrapping around the metal ion, leaving an open face with three arms positioned so that it can be capped by suitable reagents. Also, molecules or ionic fragments can enter the cavity and bind the metal ion and at the same time can be involved in hydrogen bonding to the 'semi-cryptand'. In this paper, we report a study of the complexes formed between polyaza tripodal ligands in their various protonated forms as well as their Zn(II) complexes with ATP, ADP and AMP. This investigation constitutes a good basis for ATP-hydrolysis and can lead to a better understanding of certain biological functions as well as to new catalysts of value in chemical synthesis.

2. Experimental

2.1. Materials

Most of the starting materials were obtained commercially and were purified prior to use. The sodium salt of ATP, ADP and AMP were purchased from Aldrich Chemical Co. The aqueous stock solutions of the nucleotides were freshly prepared daily and the exact concentrations were newly measured each time by titration with KOH. All other materials used in the experiments including the potassium hydrogen phthalate, HNO_3, KOH, and the metal ion solution of $Zn(NO_3)_2$ were prepared with redistilled water and stocked in jar bottle. The concentration of KOH used for titration was established with potassium hydrogen phthalate. The exact concentration of the stock $Zn(NO_3)_2$ solution was determined via its EDTA complex.

2.2. Equipments

C H N elemental analyses were made on a Perkin–Elmer 240C Analyzer (American). ^1H and ^{31}P NMR spectra were recorded on a Varian UNITY-plus 400 MHz Spectrometer. IR spectra were recorded by an Euinox 55 FT Spectrometer (Bruker). Titration was carried out with a Beckman pH Meter (model Φ71) equipped with a type 39481 combination glass electrode.

2.3. Potentiometric pH titration

Potentiometric determination was measured in a 50ml jacketed cell thermostatted at 25.0 ± 0.1 °C by a refrigerated circulating water bath. Anaerobic conditions were maintained using pre-purified N_2 as an inert atmosphere, and the ionic strength was maintained through the addition of KNO_3 to each solution to achieve $I = 0.1$ mol dm^{-3}. All the concentrations of tripod, nucleotides and metal ion are 1.0×10^{-3} mol dm^{-3}. The calibration of the glass electrode was the same as described in the literature [20]. The values of $k_\omega = 1.68 \times 10^{-14}$, $\gamma_H^+ = 0.851$ of water were used for calculations.

The protonation constants of the tripodal ligands were determined by adding KOH to the acid forms of the ligand (20.00±0.05 ml). The ligand with a concentration of 1.0×10^{-3} mol dm^{-3} was dissolved in an adequate amount of dilute HNO_3 and then was titrated with approximate 0.1 M KOH. The calculations were carried out through the curve-fitting computer program (TITFIT), which uses a Newton–Gauss–Marquardt non-linear least-squares program [21]. The final results are the averages of at least five independent titrations. For the tripodal ligand L, the pH range used in the calculation was 2.7–11, and for the three nucleotides, ATP, ADP and AMP, all pH ranges were 2.2–11.

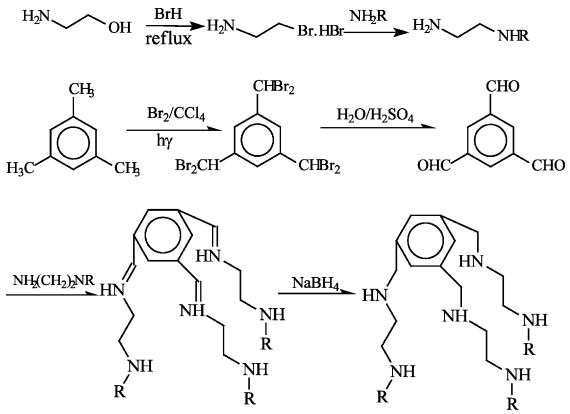
The interactions of protonated polyammonium tripods with nucleotide anions were determined under the same conditions as used for the protonation constants. The ligand L and ATP, ADP or AMP were placed in the jacked cell and titrated using 0.1 mol dm^{-3} KOH. The stoichiometry of L:Nu (that is, ATP^{4-}, ADP^{3-}, AMP^{2-}) was 1:1 and both the concentration of L and Nu were 1.0×10^{-3} mol dm^{-3}. The pH range for calculation was 2.6–10.5. Since it has been reported [3,6] that protonated polyaza ligands can accelerate the rate of ATP hydrolysis in water solution, the titration was carried out at once after the mixing of the reactants and was finished within 15 min. The stability constants of the L–Nu systems were the result of at least six independent pairs of titrations.

The conditions for the determination of the stability constants of Zn(II)–L systems were the same as for the protonation constants, but now $Zn(NO_3)_2$ was added with the stoichiometry of Zn^{2+}:L = 1:1. At the same time, the stability constants of binary systems Zn(II)–Nu as well as the ternary systems Zn(II)–L–ATP were studied. The pH range was 2.7–10 for the two systems. The ratios of the reactants Zn(II):Nu and Zn(II):L:ATP were 1:1 and 1:1:1 (1.0×10^{-3} mol dm^{-3}), respectively. As Zn(II) promotes the dephosphorylation of nucleotides [11], both reactants were only mixed in the last minute before the titration, and this was completed within 15 min. In this way the hydrolysis of ATP was kept to a minimum. The stability constants were computed from five independent pairs of titrations for each system.

3. Results and discussions

3.1. Synthesis

2-Hydroxylethyleneamine was treated with concentrated HBr to give the product 2-bromoethyleneamine, which was reacted with the corresponding R-substituted amine RNH_2 to form N–R–en [22]. The two starting materials 1,3,5-tris-(dibromomethyl)benzene and 1,3,5-tricarboxaldehyde-benzene were synthesized according to reported processes [23]. The synthesis route of tripods is shown in Scheme 2.



Scheme 2. Route of synthesis of the new tripodal ligands.

3.1.1. Synthesis of 1,3,5-tri(n-2′,5′-diazahexane)-benzene (*L1*)

N-methyl-ethylenediamine (3.42 g, 46.2 mmol) was dissolved in ethyl alcohol (200 ml). 1,3,5-tricarboxaldehyde-Benzene (2.5 g, 15.4 mmol) dissolved in ethyl alcohol (40 ml) was added dropwise over 2 h with stirring at room temperature. After the addition was completed, the suspension was stirred for further 12 h at 35 °C and then filtered. $NaBH_4$ was added in small quantities and the mixture reacted for 6 h. The solvent was removed under reduced pressure, leaving a white residue, NH_4HCO_3 (4 g) in 10 ml water was then added to the white residue. The aqueous mixture was extracted with chloroform (4 × 100 ml). The organic fractions were combined, washed with distilled water (3 × 20 ml), and then dried over $MgSO_4$. The solution was filtered and the chloroform was removed on a rotary evaporator to give a yellow oil 2.06 g, yield 41.1%. ^{1}H NMR ($CDCl_3$): δ 7.18 (s, 3H, C_6H_3); δ 3.80 (s, 6H, CH_2-ph); δ 2.50–2.80 (t, 12H, NCH_2–CH_2N); δ 2.18 (s, 9H, CH_3–N). IR (KBr pellet): 1161(ν_{C-N}); 2945(ν_{CH_3}); 865, 456, 1595(Ar); 2845(ν_{CH_2}). Elemental analysis: Calc. for $C_{18}H_{36}N_6$: C, 59.06; H, 7.12; N, 21.35. Found: C, 58.93; H, 7.36; N, 21.35%.

3.1.2. Synthesis of 1,3,5-tri(n-2′,5′-diazaheptane)-benzene (*L2*)

N-ethyl-ethylenediamine (4.10 g, 46.2 mmol) and 1,3,5-tricarboxaldehyde-benzene (2.5 g, 15.4 mmol) were reacted to give **L2** as a oil of 2.21 g, yield 38.0%. The oil was dissolved in alcohol and then hydro bromide was added. The white–yellow precipitate formed was collected and dried on P_2O_5. ^{1}H NMR (D_2O): δ 7.18 (s, 3H, C_6H_3); δ 3.85 (s, 6H, CH_2-ph); δ 2.50–2.80 (t, 12H, NCH_2CH_2N); δ 2.00 (s, 6H, N–CH_2–C); δ 1.15 (t, 9H,

CH_3–C–N). IR (KBr pellet): 1044(ν_{C-N}); 717(δ_{C-C}); 865, 1452, 1595(Ar). Elemental analysis: Calc. for $C_{21}H_{43}N_6 \cdot 6HBr$: C, 55.35; H, 7.38; N, 9.68. Found: C, 55.64; H, 7.05; N: 9.66%.

3.1.3. Synthesis of 1,3,5-tri(n-2′,5′-diazaoctane)-benzene (*L3*)

N-*n*-propyl-ethylenediamine (4.6 g, 45.0 mmol) and 1,3,5-tricarboxaldehyde-benzene (2.5 g, 15.4 mmol) were reacted to give **L3** 3.37 g, yield 51.9%. ^{1}H NMR (D_2O): δ 7.15 (s, 3H, C_6H_3); δ 3.75 (s, 6H, CH_2-ph); δ 2.50–2.80 (t, 12H, NCH_2–CH_2N); δ 1.45 (t, 6H, N–CH_2–C–C); δ 0.95 (m, 15H, CH_3–C–C–). IR (KBr pellet): 1164(ν_{C-N}); 2957(ν_{CH_3}); 863, 1458, 1590(Ar); 2872 (ν_{CH_2}). Elemental analysis: Calc. for $C_{24}H_{49}N_6$: C, 50.56; H, 8.10; N, 10.72. Found: C, 50.84; H, 8.03; N, 10.57%.

3.1.4. Synthesis of 1,3,5-tri(n-2′,5′-diazanonane)-benzene (*L4*)

N-*n*-butyl-ethylenediamine (5.48 g, 47.3 mmol) and 1,3,5-tricarboxaldehyde-benzene (2.5 g, 15.4 mmol) were reacted to give **L4** 3.03 g, yield 42.5%. ^{1}H NMR (D_2O): δ 7.55–7.80 (d, 3H, C_6H_3); δ 4.45 (s, 6H, CH_2-ph); δ 3.38–3.85 (t, 12H, NCH_2CH_2N); δ 3.15 (t, 6H, NCH_2–C–C–C); δ 1.75 (m, 6H, N–C–CH_2–C–C); δ 1.40 (m, 6H, N–C–C–CH_2–C); δ 0.95 (t, 9H, CH_3–). IR (KBr pellet): 1114(ν_{C-N}); 2961(ν_{CH_3}); 862, 1462, 1590(Ar). Elemental analysis: Calc. for $C_{27}H_{55}N_6 \cdot 6HCl$: C, 51.57; H, 8.26; N, 10.59. Found: C, 51.46; H, 8.26; N, 10.44%.

3.2. Protonation of the ligands

The ligands synthesized in the present work consist of a hexaaza tripod with six secondary amino nitrogen atoms, so they are able to bear six protons at the most. The tripods differ from one another in the following respects: (a) the N-substituents and the length of the arms; (b) the size of the 'semi-cavity' formed by the arms of these tripods. The decimal logarithms of stepwise protonation constants of the ligands resulted from potentiometric pH titration are listed in Table 1. The titration curve and the species percentage distribution diagram of **L1** are shown in Fig. 1(a) and (b), respectively. The titration and distribution diagrams of the other three ligands are similar to those of **L1** shown in Fig. 1.

As seen from Fig. 1(a), there are no significant inflection points in the titration curves. In general, the inflection points are only seen when pK_a values are well separated; otherwise the buffering means that only small changes in slope are observed. This indicates that all the six amino nitrogen atoms are considered to be moderately strong bases.

Both basicity and steric effects may play important roles in the protonation process of the ligands. By comparison with the benzylic amino groups, the terminal ones have a smaller space hindrance for proton attraction as well as stronger basicity due to the electron-pushing effect of aliphatic substituents, which is contrary to the electron-withdrawing effect of π-benzene to the former via a methylene group. Thus, the first three protonation constants belong to the terminal amino groups while the others involve the benzylic amino groups. As shown in Table 1, the protonation constants of the first three amino groups of **L1**, **L2** and **L3** are higher than 9.50 while the last three amino groups behave as weaker bases than the former. It is an exception that the first two amino nitrogen atoms of **4** are more basic than the others.

A comparison of the data listed in Table 1 shows the order of **L1** > **L3** > **L2** > **L4** for the first, fourth and fifth protonation constants. Thus, the biggest protonation constant of **L1** indicates that steric effects do play a main role in the first protonation process, in spite of the weakest electrostatic effects of its N-substituent among the four ligands. However, all the smaller values of 5.19–6.01 for the sixth protonation constants respond to cumulative electrostatic repulsion effects.

In conclusion, these protonation features make **L1**–**L4** promising receptors for nucleotides anions. As seen from the species distribution diagram (Fig. 1(b)), the most significant tetraprotic species H_4L^{4+} exists in the wide pH range of 4–10 with its maximum concentration at pH ~ 7.5. Therefore, these polyprotic species at neutral pH containing a polyammonium chain are potential binding sites for the anionic phosphate moiety of nucleotides. Moreover, the benzene unit may give π-stacking interactions with the nucleobase residue.

Table 1
The stepwise protonation constants for the tripodal ligands

Equilibria	L1	L2	L3	L4
$[(LH)^+]/[L][H^+]$	10.98 ± 0.06	10.45 ± 0.02	10.70 ± 0.06	10.34 ± 0.08
$[(LH_2)^{2+}]/[(LH)^+][H^+]$	10.42 ± 0.05	9.81 ± 0.04	9.70 ± 0.03	9.77 ± 0.06
$[(LH_3)^{3+}]/[(LH_2)^{2+}][H^+]$	9.52 ± 0.06	9.54 ± 0.04	9.50 ± 0.04	7.34 ± 0.06
$[(LH_4)^{4+}]/[(LH_3)^{3+}][H^+]$	8.66 ± 0.06	8.12 ± 0.05	8.38 ± 0.05	7.05 ± 0.10
$[(LH_5)^{5+}]/[(LH_4)^{4+}][H^+]$	6.49 ± 0.08	6.34 ± 0.05	6.58 ± 0.06	6.29 ± 0.06
$[(LH_6)^{6+}]/[(LH_5)^{5+}][H^+]$	5.89 ± 0.07	5.30 ± 0.04	5.19 ± 0.05	5.31 ± 0.07

25.0 ± 0.1 °C; $I = 0.1$ mol dm^{-3} KNO_3; $C_L = 1 \times 10^{-3}$ mol dm^{-3}.

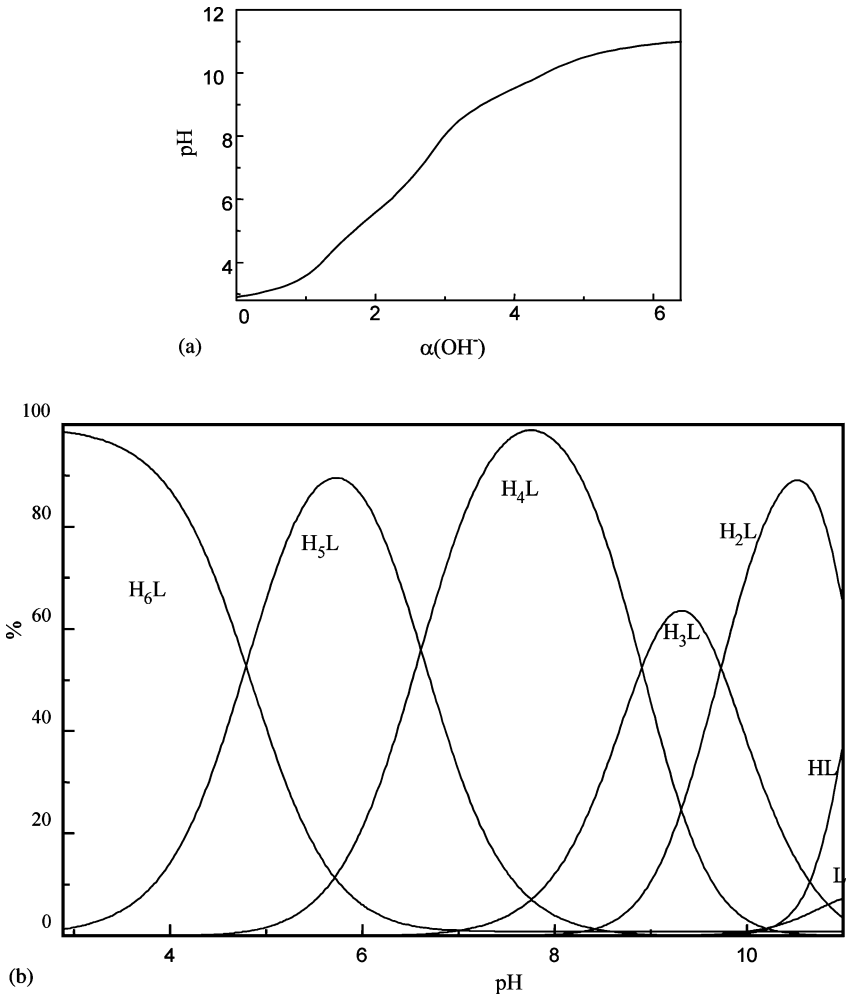


Fig. 1. (a) Titration curve of **L1**–H^+ system, 25.0±0.1 °C, $I = 0.1$ mol dm^{-3} KNO_3, [L] = 1×10^{-3} mol dm^{-3}. (b) Species percentage distribution diagrams of protonated **L1** as a function of pH, 25.0±0.1 °C, $I = 0.1$ mol dm^{-3} KNO_3, [L] = 1×10^{-3} mol dm^{-3}.

3.3. Binding strength between tripods and nucleotides

The protonation constants for nucleotides involved in this study are shown in Table 2. The corresponding values found for ATP, ADP and AMP are consistent with those reported in the literature [24].

Table 2
The stepwise protonation constants for Nu (Nu = AMP, ADP and ATP) and the stepwise stability constants of their Zn^{2+} complexes

Nu	H^+				Zn(II)	
	Literature [a]		Measured		ZnNu [a]	ZnNuH [a]
	HNu	H_2Nu	HNu	H_2Nu		
ATP	6.50	4.02	6.59	4.12	5.16	4.16
ADP	6.36	3.95	6.45	4.01	4.18	
AMP	6.21	3.80	6.27	3.95	2.38	

The protonation constants determined were almost the same as the reported values, and the stability constants were directly used as cited in literature [24].

[a] See reference [24], 25 °C, 0.10 mol dm^{-3} K^+.

Protonation of the receptors gives charged species, for example polyammonium, which can bind a single inorganic phosphate, such as orthophosphate, pyrophosphate and triphosphate as well as nucleotides, such as AMP, ADP and ATP in aqueous solution [3,6,15,25,26]. The interactions of protonated polyammonium ligands with the nucleotides anions have been determined by potentiometric pH titration and the biding strength are listed in Tables 3–5. The percentage distribution diagrams of **L1**–**L4**–ATP are shown in Fig. 2. The binding strengths mean the $-\log K$ value of equilibrium (1), which is obtained from equilibria (2), (3) and (4). The equilibria (2), (3) and (4) stand for the overall stability constants of species $[LATPH_{(m+n)}]^{m+n-4}$, the overall protonation constant of LH_m^{m+} and the overall protonation constant of H_nATP^{4-n}, respectively.

$$LH_m^{m+} + H_nATP^{4-n} = [LATPH_{(m+n)}]^{m+n-4} \quad (1)$$

$$(m+n)H^+ + L + ATP^{4-} = [LATPH_{(m+n)}]^{m+n-4} \quad (2)$$

Table 3
Binding strength of species formed in L–ATP systems determined in 0.1 mol dm^{-3} KNO_3 at 25 °C

Stoichiometry			Equilibrium K	log K			
At	L	H		**L1**	**L2**	**L3**	**L4**
1	1	1	[AtLH]/[HL][At]	2.60 ± 0.03	2.71 ± 0.06	2.84 ± 0.05	2.58 ± 0.07
1	1	2	[AtlH$_2$]/[H$_2$L][At]	3.26 ± 0.04	3.57 ± 0.05	3.89 ± 0.05	2.99 ± 0.07
1	1	3	[AtLH$_3$]/[H$_3$L][At]	4.45 ± 0.04	4.84 ± 0.07	4.93 ± 0.06	3.53 ± 0.08
1	1	4	[AtLH$_4$]/[H$_4$L][At]	6.00 ± 0.05	7.28 ± 0.08	7.59 ± 0.05	5.88 ± 0.06
1	1	5	[AtLH$_5$]/[H$_4$L][HAt]	8.19 ± 0.04	8.75 ± 0.07	9.15 ± 0.02	7.35 ± 0.03
1	1	5	[AtLH$_5$]/[H$_5$L][At]	8.29 ± 0.04	9.00 ± 0.07	9.16 ± 0.02	7.65 ± 0.06
1	1	6	[AtLH$_6$]/[H$_5$L][HAt]	9.38 ± 0.06	9.89 ± 0.06	10.1 ± 0.04	8.40 ± 0.03
1	1	6	[AtLH$_6$]/[H$_6$L][At]	10.08 ± 0.06	11.18 ± 0.06	11.50 ± 0.04	9.68 ± 0.03
1	1	7	[AtLH$_7$]/[H$_5$L][H$_2$At]	8.04 ± 0.05	8.64 ± 0.08	8.92 ± 0.05	6.37 ± 0.07
1	1	7	[AtLH$_7$]/[H$_6$L][HAt]	6.27 ± 0.05	7.46 ± 0.08	7.85 ± 0.05	5.18 ± 0.07

Both the concentration of At (At = ATP) and L are 1×10^{-3} mol dm^{-3}. The charge is omitted. The symbol 116 is representative for species $ATPLH_6^{2+}$.

$$mH^+ + L = LH_m^{m+} \quad (3)$$

$$nH^+ + ATP^{4-} = H_nATP^{n-4} \quad (4)$$

The data in Tables 3–5 show an increase in the binding strength with the number of protons on the hexaaza tripodal ligands increasing to a maximum of six, corresponding to the maximum number of hydrogen bonds between the host and guest. In the systems of L (**L1**–**L4**)–ATP and **L3**–ADP the number of protons reaches a maximum of seven. Thus, when the number of protonated amino nitrogen atoms increases upto six, it can be seen from Tables 3–5 that the stepwise equilibrium constants increase as the number of hydrogen bonds as well as the coulombic attraction between the host and guest increase. However, any further increase in the number of protons of complex H_6LATP (Table 3) or H_6(**L3**)–ADP (Table 4) causes a decrease in the binding constants. This is because under this condition, the additional proton must attach to the guest, decreasing its charge (and thus decreasing the coulombic attraction to the host) and the number of oxygen atoms in the guest that can be hydrogen bound to the host.

It is interesting to discuss the possible structure of the supramolecular binary species as illustrated in Scheme 3. The number of H-bonds of the adducts is shown as equal to or higher than the number of protons present in the complexes, since the H-bonds cannot only form the type NH···O, but also the types NH···N, OH···O and OH···N. As shown in Scheme 3, the non-ligating behavior of α-phosphate of ATP is tested by ^{31}P NMR spectra, which show significant upfield shifts of the chemical resonances of β- and γ-phosphate but only a slight shift of α-phosphate. For example, the ^{31}P signals of α-, β- and γ-phosphate of ATP in the presence of **L2** at pH 7.6 shift upfield by −0.01, 0.78 and 0.17 ppm, respectively. On the other hand, the ^1H NMR spectra reveal that in the **L2**–ATP system H-8, H-2, H-1′ of ATP as well as protons on benzene and the benzylic protons of L shift upfield when compared with free ATP and L at pH 7.6, which indicates that the existence of the benzene ring leads to π-stacking interactions with the nucleobase residue of nucleotides.

Table 4
Binding strength of species formed in L–ADP systems determined in 0.1 mol dm^{-3} KNO_3 at 25 °C

Stoichiometry			Equilibrium K	log K			
Ad	L	H		**L1**	**L2**	**L3**	**L4**
1	1	1	[AdLH]/[HL][Ad]	2.30 ± 0.08	2.42 ± 0.05	2.15 ± 0.05	2.13 ± 0.05
1	1	2	[AdLH$_2$]/[H$_2$L][Ad]	2.93 ± 0.07	3.14 ± 0.08	2.72 ± 0.06	2.69 ± 0.04
1	1	3	[AdLH$_3$]/[H$_3$L][Ad]	4.11 ± 0.10	4.73 ± 0.05	3.35 ± 0.03	3.17 ± 0.04
1	1	4	[AdLH$_4$]/[H$_4$L][Ad]	5.02 ± 0.06	5.26 ± 0.04	4.74 ± 0.05	4.36 ± 0.03
1	1	5	[AdLH$_5$]/[H$_4$L][HAd]	7.07 ± 0.07	7.30 ± 0.06	7.01 ± 0.02	6.33 ± 0.04
1	1	5	[AdLH$_5$]/[H$_5$L][Ad]	7.03 ± 0.07	7.41 ± 0.06	6.88 ± 0.02	6.49 ± 0.04
1	1	6	[AdLH$_6$]/[H$_5$L][HAd]	8.70 ± 0.06	8.40 ± 0.03	7.47 ± 0.04	7.21 ± 0.06
1	1	6	[AdLH$_6$]/[H$_6$L][Ad]	9.26 ± 0.06	9.55 ± 0.03	8.73 ± 0.04	8.35 ± 0.06
1	1	7	[AdLH$_7$]/[H$_5$L][H$_2$Ad]			6.26 ± 0.04	
1	1	7	[AdLH$_7$]/[H$_6$L][HAd]			5.08 ± 0.04	

Both the concentration of Ad (Ad = ADP) and L are 1×10^{-3} mol dm^{-3}. The symbol 116 is representative for $ADPLH_6^{3+}$.

Table 5
Binding strength of species formed in L–AMP systems determined in 0.1 mol dm^{-3} KNO_3 at 25 °C

Stoichiometry			Equilibrium K	log K			
Am	L	H		**L1**	**L2**	**L3**	**L4**
1	1	1	[AmLH]/[HL][Am]	2.14±0.04	2.10±0.05	2.00±0.03	1.89±0.06
1	1	2	$[AmLH_2]/[H_2L][Am]$	2.38±0.07	2.26±0.03	2.17±0.04	2.01±0.07
1	1	3	$[AmLH_3]/[H_3L][Am]$	2.97±0.04	2.63±0.06	2.43±0.06	2.10±0.05
1	1	4	$[AmLH_4]/[H_4L][Am]$	3.56±0.06	3.19±0.07	2.94±0.04	2.77±0.03
1	1	5	$[AmLH_5]/[H_5L][Am]$	5.94±0.08	5.75±0.04	5.32±0.08	4.64±0.04
1	1	6	$[AmLH_6]/[H_5L][HAm]$	6.96±0.05	6.06±0.02	5.83±0.06	5.29±0.05
1	1	6	$[AmLH_6]/[H_6L][Am]$	7.34±0.05	7.03±0.02	6.91±0.06	6.25±0.05

Both the concentration of Am (Am = AMP) and L are 1×10^{-3} mol dm^{-3}. The symbol 116 is representative for $AMPLH_6^{4+}$.

By examining the different values of binding constants, several main features can be readily noted. (1) The present results demonstrate the ability of polyammonium to strongly bind nucleotides, giving a variety of complex species. As seen from Fig. 2, the receptor-substrate adducts mainly form at weakly alkaline to

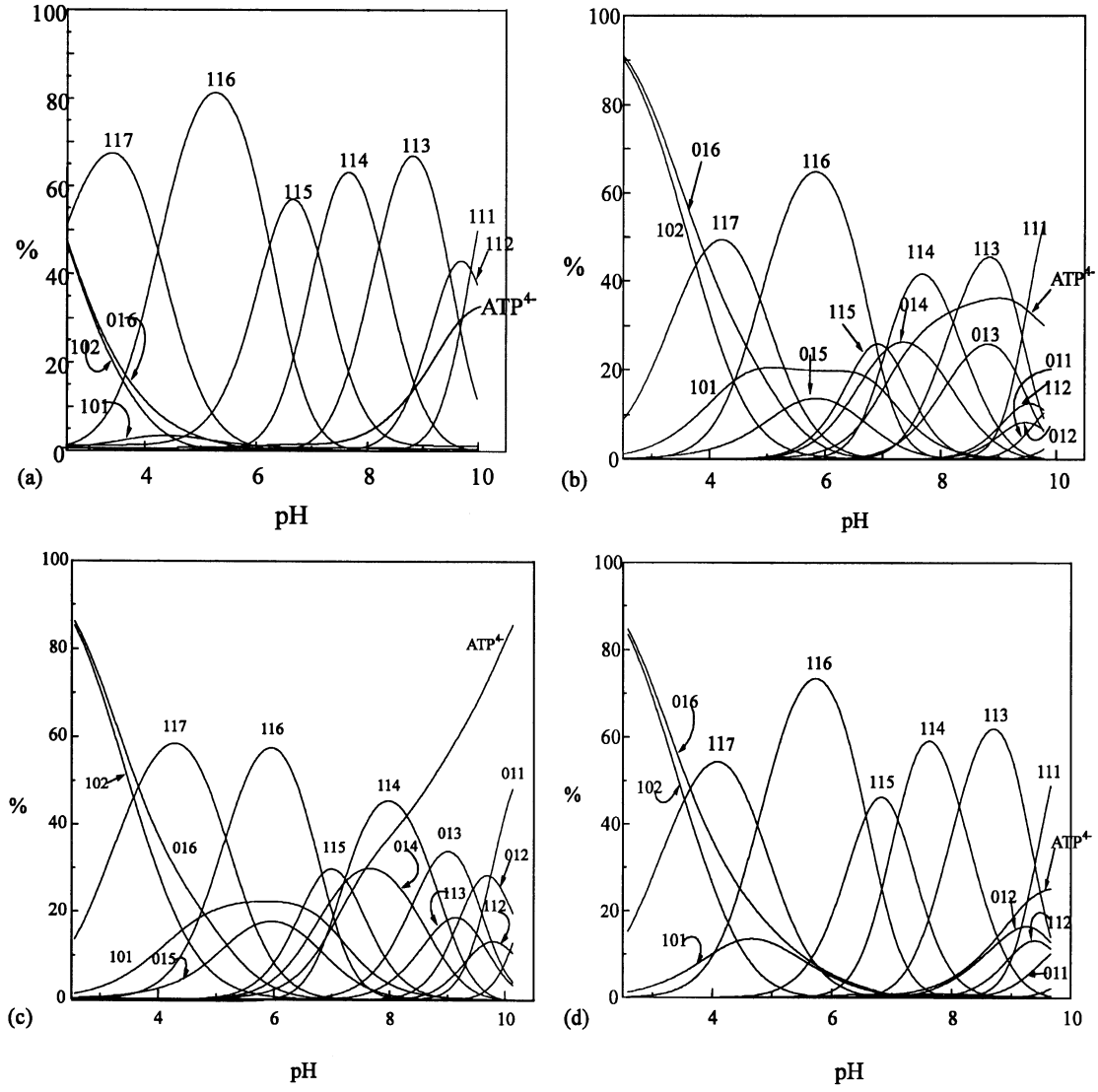
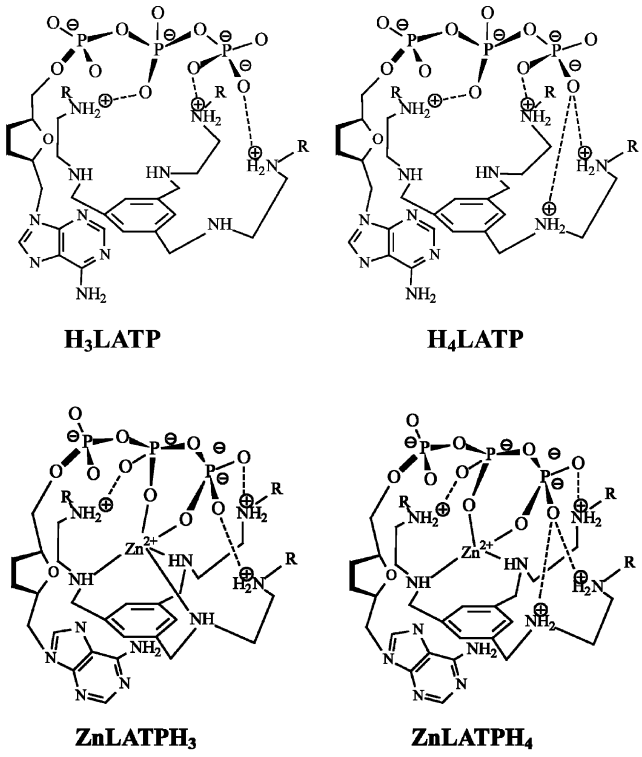


Fig. 2. Distribution diagrams for the species present in solution for the system ATP–L of (a) ATP–**L1** and of (b) ATP–**L2** and of (c) ATP–**L3** and of (d) ATP–**L4**. The secondary species are ATPLH, $ATPLH_2$, $ATPLH_3$, $ATPLH_4$, $ATPLH_5$, $ATPLH_6$ and $ATPLH_7$. The charge of complexes is omitted. The symbols for instance 117 are representative for species $ATPLH_7^{3+}$, (1×10^{-3} mol dm^{-3} L: 1×10^{-3} mol dm^{-3} ATP in water at 25 °C and $I = 0.1$ mol dm^{-3} KNO_3).



Scheme 3. Possible spuramolecular structure species H_3LATP, H_4LATP, $ZnLATPH_3$ and $ZnLATPH_4$.

slightly acidic pH values where the ligands are protonated as shown in Fig. 1(b). It is fairly reasonable to say that there is no interaction when the pH raises above 11. (2) Based on electrostatic predications, more stable complexes are expected to form between the most charged species. (3) For a given ligand, the adducts in the more highly protonated forms are more likely to involve the protonation of the anions, HNu (101 in Fig. 2) and H_2Nu (102 in Fig. 2) which exist at low pH values. With regard to the species H_7LATP^{3+}, at least one proton is located at a phosphate group of the nucleotide since the tripods can bear six protons at the most. On the other hand, the first protonation constant of ATP (6.59) is larger than the sixth protonation constants (5.30–5.89) or even some fifth protonation constants of L, leading to the existence of $HATP^{3-}$ and H_2ATP^{2-} (see Fig. 2, species 101 and 102). However, neutralization of the substrate would decrease the number of H-bonds as well as the electrostatic interactions and then the stability.

The magnitudes of the binding strength between the polyammonium tripodal ligands and the substrates ATP, ADP and AMP increase in the order ATP > ADP > AMP, as one would expect from corresponding decreases in the length of phosphate chain and as a consequence of the hydrogen bonding and coulombic forces. Thus, the recognition of nucleotides by polyammonium ligands via multiple interactions relies on the length of phosphate chain and the charge of substrates. According to the stability constants shown in Tables 3 and 4, the catalytic conversion of ATP → ADP in the presence of protonated polyammonium tripods is reasonable. The product of the reaction, ADP, is less strongly bound than ATP due to its shorter phosphate backbone and the lower negative charge, facilitating the regeneration of the next catalytic cycle.

3.4. Stability constants of metal complexes

The stability constants of Zn^{2+} metal complexes of **L1**–**L4** are given in Table 6. The species distribution diagram of Zn(II)–**L1** (Fig. 3) shows that the mononuclear Zn^{2+} complex ZnL begins to form when pH > 8. The other complexes, $ZnLH^{3+}$, $ZnLH_2^{4+}$, $ZnLH_3^{5+}$ and $ZnLH_4^{6+}$ form stepwisely as pH increase, and reach a maximum at pH around 9, 7.5, 6.5 and 5, respectively. The major species $ZnLH_4^{6+}$ containing four protons exists at pH 4–7 with maximum concentration at pH 5.0, but $ZnLH_4^{6+}$ has low concentration when pH < 5 where the ligand **L1** is mainly in its hexa- or penta-protic forms. Both the species $ZnLH^{3+}$ and $ZnLH_2^{2+}$ are predominant in the pH range 6–8 and their maximum amount are higher than 70%. It is worth noting that $ZnLH_2^{4+}$ gets to its maximum concentration (> 80%) at pH 7.5, the most ideal pH value for bioactivity.

Since the tripodal ligand acts as a three-dimensional receptor, various kinds of its metal complexes would probably coexist in solution. It is also difficult to discern which atoms take part in the coordination as well as the number of the donor atoms in a specific coordination, because the formation of complexes is also controlled by the pH of the solution. We have supposed the configurations for each binary species formed. Tripod L may coordinate with Zn^{2+} through all its six amino groups to form the species ZnL in a distorted octahedral fashion. When protonated, the hydrogen ion is believed to locate at the two amino nitrogen atoms of one arm through an H-bridge. Successively, the H-bridge may be broken down by the attack of the second proton with the formation of the species $ZnLH_2^{4+}$. The protonation pattern for $ZnLH_3^{5+}$ and $ZnLH_4^{6+}$ follow the same pattern. The metal complexes cannot hold five protons since if this occurs the Zn^{2+} will be replaced by H^+ completely. Although all these instances may exist in solution, it is notable that metal ion and tripod prefer to form mononuclear complexes when in a 1:1 ratio, which has been verified by the pH titration measurements.

3.5. Zn(II)–nucleotide interactions

Zn(II) ion has some tendency to bind the polyphosphate of nucleotides. On the other hand, the adenine residue offers metal ions N-1, occasionally N-3, and N-7 as binding sites. Consequently for adenosine this leaves a dichotomy in metal ion binding of N-1 versus N-7 [27].

Table 6
The stability constants of complexes formed by L in the presence of 1:1 Zn^{2-} (25 °C, $I = 0.1$ mol dm^{-3} KNO_3, $C_L = C_{Zn} = 1 \times 10^{-3}$ mol dm^{-3})

Equilibria	L1	L2	L3	L4
$Zn + L + 4H = ZnLH_4$	39.32 ± 0.06	40.03 ± 0.06	40.52 ± 0.02	41.10 ± 0.05
$Zn + L + 3H = ZnLH_3$	34.10 ± 0.07	32.39 ± 0.07	33.18 ± 0.05	35.34 ± 0.04
$Zn + L + 3H = ZnLH_2$	27.42 ± 0.08	25.07 ± 0.04	25.61 ± 0.06	27.23 ± 0.02
$Zn + L + H = ZnLH$	19.18 ± 0.10	17.82 ± 0.05	17.01 ± 0.09	18.40 ± 0.03
$Zn + L = ZnL$	9.85 ± 0.06	8.62 ± 0.03	8.61 ± 0.08	8.43 ± 0.06

The charge of the complexes and hydrogen ions are not given.

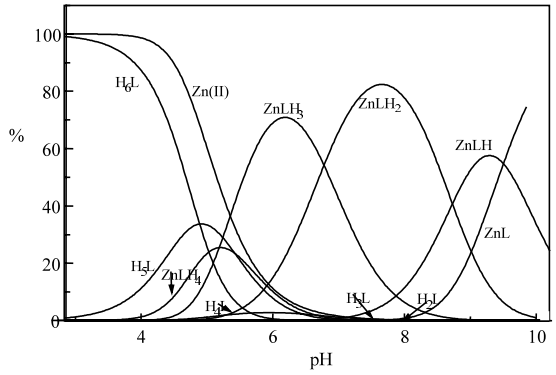


Fig. 3. Distribution diagrams for the species present in solution of Zn(II)–L system. The charge of complexes is omitted for clarification, (1×10^{-3} mol dm^{-3} Zn(II): 1×10^{-3} mol dm^{-3} L in water at 25 °C and $I = 0.1$ mol dm^{-3} KNO_3).

Recently, it has been believed that N-7 of purine chelates the zinc ion when the pH is around 7–9 [28] and N-1–Zn^{2+} binding interaction is reasonable at higher pH values [29]. Mao Xi-an et al. also reported that N1 is the dominant binding site of Zn^{2+} between pH 2 and 5, while takes favors binding with N-7 between pH 5 and 7 [30].

Another feature of metal-nucleotides interactions is the open-macrochelate isomeric equilibrium since N-7 is orientated towards the phosphate group in the dominating anti-conformation of ATP, but N-7 is a weak coordinate point in macrochelate formation. Indeed, the release of N-7 upon mixed ligand complex formation in solution has been demonstrated with different ligands [31]. The stability constants of Zn(II) complexes with nucleotides (AMP, ADP and ATP) are listed in Table 2, which are consistent with literature values [24].

3.6. Interactions of metal complexes and ATP

The binding constants of Zn(II) complexes of L with ATP are listed in Table 7. The ternary species distribution curves of Zn(II)–**L1**–ATP and Zn(II)–**L4**–ATP are shown in Figs. 4 and 5, respectively. The binding strength means the stability constants of equilibrium (5), which is obtained from equilibria (6), (7) and (4),

$$ZnLH_l^{l+2} + H_nATP^{n-4} = [ZnLATPH_{(l+n)}]^{l+n-2} \quad (5)$$

$$Zn^{2+} + (l+n)H^+ + L + ATP^{4-} = [ZnLATPH_{(l+n)}]^{l+n-2} \quad (6)$$

$$Zn^{2+} + lH^+ + L = ZnLH_l^{l+2} \quad (7)$$

Apparently, considerable interactions took place when the nucleotide was introduced to the 1:1 M:L systems. It is interesting to note that the presence of nucleotide stabilizes the ternary system so that species involving up to six protons ($ZnLATPH_6$) can stably form. However, it is reasonable that the additional protons of ZnH_4L to ZnH_5LATP and ZnH_6LATP, bind to the anions. The nucleotides can offer additional coordination sites to the metal ion and thus increase the stability of the ternary complexes.

The tripodal ligand can incorporate a metal ion with two amino groups in the case that the metal ion is also coordinated with the substrate, and thus in turn may form up to four hydrogen bonds between the oxygen atoms of the phosphate chain of ATP and the polyammonium groups of the tripod. Such binding, involving a coordination bond and hydrogen bonds as well as electrostatic interactions, can bind the nucleotide anion quite strongly. For the mononuclear complex $ZnLATPH_2$ (Fig. 4), which is due primarily to coordination bonding of Zn(II) to the tripodal ligand, the stability steadily increases with protonation up to $ZnLATPH_4$ with four hydrogen bonds. Further protonation cause a decrease in stability and the more stable species are found when the polyphosphate groups of the nucleotides are not protonated. The addition of protons beyond this point weakens the hydrogen bonding as well as lowers the charge and hence the coulombic forces.

The distribution diagrams Figs. 4 and 5 show five detected species containing nucleotide bound to coordinated M(II) and/or protonated amino groups. There are four ternary major species in the 1:1:1 systems, namely $ZnLATPH_6$, $ZnLATPH_4$, $ZnLATPH_3$ and $ZnLATPH_2$ (the charge is not given) as well as the species $ZnLATPH_5$ that is in a small amount in Zn(II)–**L1**–ATP and Zn(II)–**L4**–ATP systems. As shown in Fig. 4, the ternary species containing L1 form in a pH range 4–10. When pH < 4, the species H_6L^{6+} and H_2ATP^{2-}

Table 7
Binding strength of Zn(II) complexes of L with nucleotides in 0.1 mol dm^{-3} KNO_3 at 25 °C

Stoichiometry				Equilibrium K	log K			
Zn	L	At	H		**L1**	**L2**	**L3**	**L4**
1	1	1	2	$[ZnH_2LAt]/[ZnH_2L][At]$	4.84 ± 0.02	6.56 ± 0.07	6.36 ± 0.02	3.64 ± 0.04
1	1	1	3	$[ZnH_3LAt]/[ZnH_3L][At]$	6.67 ± 0.05	6.77 ± 0.06	6.15 ± 0.05	3.95 ± 0.05
1	1	1	4	$[ZnH_4LAt]/[ZnH_4L][At]$	8.01 ± 0.08	6.94 ± 0.07	6.75 ± 0.06	5.08 ± 0.05
1	1	1	5	$[ZnH_5LAt]/[ZnH_4L][HAt]$	6.63 ± 0.06	5.25 ± 0.08	5.25 ± 0.08	4.54 ± 0.07
1	1	1	6	$[ZnH_6LAt]/[ZnH_4L][H_2At]$	5.32 ± 0.05	4.28 ± 0.10	4.85 ± 0.03	3.71 ± 0.06

All the concentrations of Zn(II), At (At = ATP) and L are 1×10^{-3} mol dm^{-3}. The symbol 1116 is representative for species $ZnLATPH_6^{4+}$.

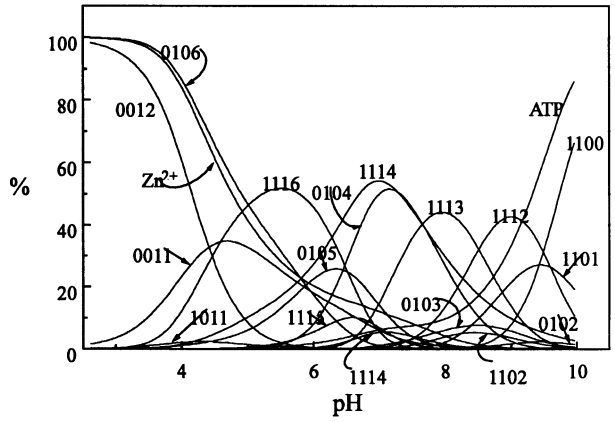


Fig. 4. Percentage distribution diagrams for species present in 1:1:1 Zn(II):**L1**:ATP system. The symbols (for example 1116) are representative for species $ZnLATPH_6^{4+}$, (1×10^{-3} mol dm^{-3} Zn^{2+}, 1×10^{-3} mol dm^{-3} L: 1×10^{-3} mol dm^{-3} ATP in water at 25 °C and $I = 0.1$ mol dm^{-3} KNO_3).

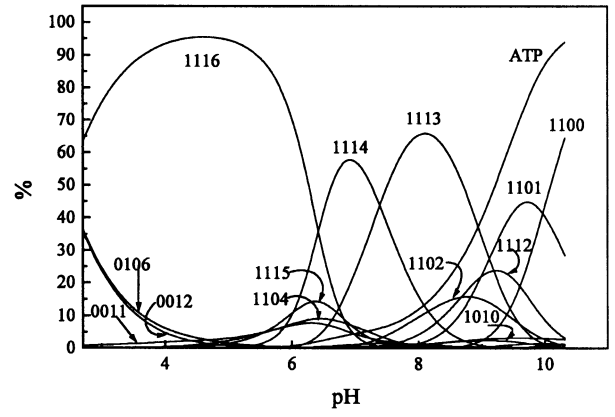


Fig. 5. Percentage distribution diagrams for species present 1:1:1 Zn(II):**L4**:ATP system. The symbols (for example 1116) are representative for species $ZnATPLH_6^{2+}$, (1×10^{-3} mol dm^{-3} Zn^{2+}, 1×10^{-3} mol dm^{-3} L4, 1×10^{-3} mol dm^{-3} ATP in water at 25 °C and $I = 0.1$ mol dm^{-3} KNO_3).

coexist and dominate. In Fig. 5, the species $ZnLATPH_6$ is the major compound from pH 3 to 7 with its maximum at pH about 4–6. In addition, the other ternary species form at a similar pH range in the two systems except for the higher percentage concentration of Zn(II)–**L4**–ATP complexes. Comparing Fig. 4 with Fig. 5, a reasonable conclusion can be drawn that the behavior of the two systems are similar in basic and slightly acidic solution while it is only different at pH below 6.

Due to the different affinity of Zn(II) to oxygen atoms or nitrogen atoms, there exists competitive reaction between the mixed ligands, tripod and nucleotide. The nucleotide acts as a subordinative receptor at higher pH values because of its lower basicity (6.59) compared with that of L. Thus, the polyaza tripodal ligands control the coordination there, which was attested with the results of NMR experiments. For example, at pH 7.6 in the Zn(II)–**L2**–ATP and Zn(II)–ATP systems phosphate signals of α, β and γ-sites of ATP are −0.13, 1.21 and 0.45 ppm for the former, or 0.35, 2.55 and 1.03 ppm for the latter. It is evident that the stronger coordination of L to Zn(II) makes the electron density of the metal ion flux to the amino groups and then decreases the ability for Zn(II) to attract phosphate groups of the substrate. On the other hand, ^1H signals of H-8, H-2 and H-1′ of ATP, as well as protons on benzene and benzylic protons in Zn(II)–L2–ATP are shifted by −0.30, −0.26, −0.32, −0.32 and −0.35 ppm, respectively, while Zn(II) causes the ^1H signals of H-8, H-2 and H-1′ to shift by −0.17, −0.14 and −0.13 ppm, respectively. Comparing ^1H signals of Zn(II)–**L2**–ATP with the corresponding values of **L2**–ATP, −0.45, −0.42, −0.50, −0.40, −0.45 ppm, the downfield shifts of ^1H signals indicate that the bridge of the Zn(II) ion decreases the stacking interactions between benzene and the nucleobase residue. The structures of ternary systems $ZnLATPH_3$ and $ZnLATPH_4$ are drawn in Scheme 3.

From Table 7 we can see that ATP coordinates with Zn(II) complexes of **L1**–**L4** with different binding strength for species with the same stoichiometry. So the nucleotide recognizes the receptors with different size via multiple interactions. For example, at physiological pH values, the coexisted species $ZnLATPH_3$ and $ZnLATPH_4$ have the order of **L1** ~ **L2** > **L3** ≫ **L4** and **L1** > **L2** ~ **L3** > **L4** for binding strength, respectively.

The addition of metal ion to L–Nu systems not only increases the stability of the ternary systems, but also makes competition for L and the substrate to coordinate with Zn(II). Therefore, the action of metal ion can be considered as a 'messenger' between the receptor and the substrate.

3.7. Conclusion

In this paper we primarily investigated the interaction of four polyaza tripodal ligands as well as their Zn(II) complexes with the nucleotides ATP, ADP and AMP. The protonated tripodal ligands can bind anions through hydrogen bonding, and because they are positively charged, through additional coulombic forces. This kind of interaction has been thoroughly explored by Lehn and coworkers [2,3,7,25] for the binding of nucleotides to protonated forms of macrocycle. On the other hand, the existence of aromatic benzene rings makes an additional contribution to the binding strength through π-stacking interactions with the adenosine and/or the ribose of nucleotides. The increased stability of ternary complexes is believed to be caused by substrates, which coordinate to a metal ion complex through such factors as electron-withdrawing effect of the metal ion, strain in the chelated ring and proximity of the bridged receptor/substrate. The results obtained in this study give a quantitative assessment of the different factors governing the receptor-substrate binding interactions. Furthermore, this study extends the coordination chemistry of ions to a class of anionic substrates, which play a fundamental role in the bioenergetics of living organisms.

Acknowledgements

This project 29971018 was supported by the National Science Foundation of People's Republic of China and the National Science Foundation of Tianjin.

References

[1] (a) J.M. Lehn, Pure Appl. Chem. 50 (1978) 871;
(b) J.M. Lehn, Pure Appl. Chem. 51 (1979) 979.
[2] M.W. Hosseini, J.-M. Lehn, J. Am. Chem. Soc 104 (1982) 3525.
[3] M.W. Hosseini, J.-M. Lehn, M.P. Mertes, Helv. Chim. Acta 66 (1983) 8.
[4] N.Z.J. Leonard, Acc. Chem. Res. 15 (1982) 128.
[5] M.W. Hosseini, J.M. Lehn, L. Maggiora, K.B. Mertes, M.P. Mertes, J. Am. Chem. Soc. 109 (1987) 537.
[6] E. Kimura, M. Kodama, T. Yatsunami, J. Am. Chem. Soc. 104 (1982) 3182.
[7] (a) M.W. Hosseini, J.M. Lehn, M.P. Metres, Helv. Chim. Acta 66 (1983) 2454;
(b) M.W. Hosseini, J.M. Lehn, M.P. Metres, Helv. Chim. Acta 68 (1985) 818.
[8] M.W. Hossein, J.M. Lehn, J. Chem. Soc., Chem. Commun. (1985) 1155.
[9] C. Nakai, W. Glinsmann, Biochemistry 16 (1977) 5636.
[10] D.M. Epstein, L.L. Chapel, H. Khalili, R.M. Supkowski, W. DeW Horrocks, Jr., J.R. Maorrow, Inorg. Chem. 39 (2000) 2130.
[11] K.P. McCue, J.R. Morrow, Inorg. Chem. 38 (1999) 6136.
[12] K.P. McCue, D.A. Voss, J.R. Morrow, J. Chem. Soc., Dalton Trans. (1998) 2961.
[13] H. Sigel, F. Hofsterrer, R.B. Martin, R.M. Milburn, V. Scheller-Krattiger, H. Scheller, J. Am. Chem. Soc. 106 (1984) 7935.
[14] B.F. Barker, K. Ramasamy, J. Kiely, J. Bioorg. Med. Chem. Lett. 6 (1996) 1647.
[15] P.W. Hubner, R.M. Milburn, Inorg. Chem. 19 (1980) 1267.
[16] F. Marc, J. Ib, B. Kamal, J. Am. Chem. Soc. 115 (1993) 3752.
[17] V. Amendola, E. Bastianello, L. Fabbrizzi, Angew. Chem., Int. Ed. Engl. 39 (2000) 2917.
[18] M. Kanesato, T. Yokoyama, Chem. Lett. 326 (1999) 137.
[19] M.P. Teulade-Fichou, J.P. Vigeron, J.M. Lehn, J. Chem. Soc., Perkin Trans. 2 (1996) 2169.
[20] S. Ali, A. Sajadi, B. Song, F. Gregán, H. Sigel, Inorg. Chem. 38 (1999) 439.
[21] A.D. Zuberbuhler, T.A. Kaden, Talanta 29 (1982) 201.
[22] R.C. O'Gee, H.M. Woodburn, J. Am. Chem. Soc. 23 (1951) 1370.
[23] M. Li, N. Pan, H.X. ShiJie, 1985, 5, 168; Chemical Abstract, 104 (1986):88214.
[24] R.M. Smith, A.E. Martell, Y. Chen, Pure Appl. Chem. 63 (1991) 1015.
[25] M.W. Hosseini, J.M. Lehn, Helv. Chim. Acta 70 (1987) 1312.
[26] A.E. Martell, R.J. Motekaitis, Q. Lu, D.A. Nation, Inorg. Chem. Acta 18 (1999) 3203.
[27] R.B. Martin, Acc. Chem. Res. 18 (1985) 32.
[28] E.M. Bianchi, A. Ali, A. Sajadi, B. Song, H. Sigel, Inorg. Chim. Acta 300-302 (2000) 487.
[29] J.A. Happe, M. Morales, J. Am. Chem. Soc. 88 (1966) 2077.
[30] F. Du, X. Mao, Spectrochim. Acta, Part A 56 (2000) 2391.
[31] R. Tribolet, R.B. Martin, H. Sigel, Inorg. Chem. 26 (1987) 638.

PERGAMON

Polyhedron 21 (2002) 1017–1022

POLYHEDRON

www.elsevier.com/locate/poly

Mononuclear tungsten(VI) complexes with bis(phenolato) ligands: syntheses, characterisations and activity in ROMP reaction

Ari Lehtonen [a,*], Reijo Sillanpää [b]

[a] Department of Chemistry, University of Turku, FIN-20014 Turku, Finland
[b] Department of Chemistry, University of Jyväskylä, PO Box 35, FIN-40351 Jyväskylä, Finland

Received 26 November 2001; accepted 4 February 2002

Abstract

The reaction of bulky ligand precursor 2,2′-methylenebis(4-methyl-6-*tert*-butylphenol) (H_2mbp) or 2,2′-ethylidenebis(4,6-di-*tert*-butylphenol) (H_2ebp) with trisdiolatotungsten(VI) complex [W(eg)$_3$] **1** (eg = ethanediolate dianion) provides heteroleptic complexes [W(mbp)(eg)$_2$] **2** or [W(ebp)(eg)$_2$] **3**, respectively. Sterically less hindered 2,2′-dihydroxy-1,1′-dinaphtylmethane (H_2dinap) forms heteroleptic disubstituted complex [W(dinap)$_2$(eg)] **4**. The X-ray crystal structure determinations confirmed that the isolated compounds are made of monomeric tris(diolato)tungsten(VI) molecules in which the central tungsten atom is bonded to six oxygen atoms forming a distorted octahedral coordination sphere around the metal ion. Complexes **2** and **3** catalyse the ring opening metathesis reaction of norbornene when activated by Et_2AlCl. © 2002 Elsevier Science Ltd. All rights reserved.

Keywords: X-ray; Mononuclear tungsten(VI) complexes; Ligand; Heteroleptic

1. Introduction

Chelating oxygen donor ligands, e.g. binaphthols and biphenols have confirmed to be useful accessories in organic syntheses with early transition metals [1]. The hard Lewis-base character of the phenoxide group makes these compounds ideal for attaching to the metal ions having high oxidation states (hard Lewis-acids). Sterically hindered auxiliary groups on the bis(phenolato) ligands allow the degree of shielding to be tuned without significantly altering the electronic properties of the ligands. Furthermore, the influence of the number of atoms between the phenoxide oxygen atoms in such ligands to the coordination geometry of metal can be also modified. 1,1′-coupled biphenolates and binaphtholates of W(VI), often with other ligands, have been used successfully as catalyst precursors in olefin metathesis reactions [2]. However, reports on tungsten complexes with bridged bis(phenolate)s are scarce. Heppert's group has reported preparation and spectral characterisation of tungsten(VI) complexes [W(=X)Cl$_2$(mmp)] and [W(=X)Cl$_2$(ebp)] [X=O, NPh-2,6-Me$_2$; H_2mmp = 2,2′-methylenebis(4,6-dimethylphenol); H_2ebp = 2,2′-ethylidenebis(4,6-di-*tert*-butylphenol)] [3]. Nakamura's group has studied complexes of sulfur-bridged bis(phenol), and has characterised several crystal structures, e.g. [W(η^2-EtC≡CEt)(tbp)Cl$_2$] (H_2tbp = 2,2′-thiobis(4,6-dimethylphenol) [4]. In the context of a broader program aimed at developing transition metal catalysts for olefin metathesis reaction, our laboratory has recently become interested in the chemical manipulation of tungsten aryloxide complexes [2b,5]. Our long-term goal is to prepare polymer-based tungsten(VI) phenoxides and use them as recoverable catalyst precursors. To gain a greater degree of understanding this chemistry, we have now prepared three new monomeric tungsten(VI) complexes with bis(phenolato) ligands and used them as catalyst precursors for ring opening metathesis polymerisation of norbornene.

* Corresponding author. Tel.: +358-2-333-6733; fax: +358-2-333-6700.
E-mail address: ari.lehtonen@utu.fi (A. Lehtonen).

0277-5387/02/$ - see front matter © 2002 Elsevier Science Ltd. All rights reserved.
PII: S0277-5387(02)00897-5

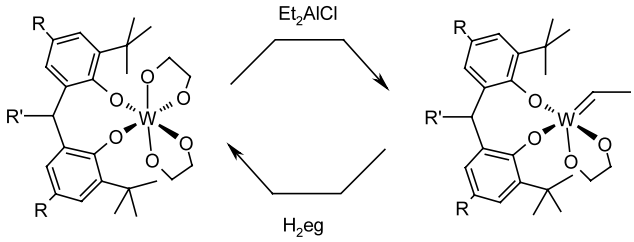
2. Results and discussion

2.1. Synthesis and spectroscopy of the complexes

The addition of 1 equiv. of the ligand precursors 2,2′-methylenebis(4-methyl-6-*tert*-butylphenol) (H_2mbp) or H_2ebp to the refluxing toluene solution of [W(eg)$_3$] **1** (H_2eg = 1,2-ethanediol) leads to the formation of the heteroleptic, monomeric compounds **2** and **3**, respectively (Scheme 1). The red solid products can be purified by crystallisation or by column chromatography to obtain air stable complexes in high yields. They are soluble in chlorinated hydrocarbons, ethers and aromatic solvents but only slightly soluble in hexane. Bulky *tert*-butyl groups in *ortho*-positions of phenoxide moieties seems to prevent further substitution of eg ligands as the use of excess bis(phenol) do not result in complexes of type [W(biphenolate)$_2$(eg)]. However, 2 equiv. of sterically less hindered 2,2′-dihydroxy-1,1′-dinaphtylmethane (H_2dinap) reacts with 1 equiv. of **1** in toluene at reflux temperature to form heteroleptic complex [W(dinap)$_2$(eg)] (**4**) (Scheme 2). This intense red coloured compound is slightly soluble in toluene and chlorinated solvents and it is stable enough to be purified by column chromatography. Unfortunately, **4** was not soluble enough to be used in our catalyst tests (see below).

Earlier studies on transition metal complexes of 2,2′-methylenebisphenoxides have shown that the puckered eight-membered ring formed by chelation to metal centre undergoes slow flipping on the NMR timescale [6–8]. Therefore, the methylene protons in the chelate backbone are typically diastereotopic at ambient temperature.[8] The ^{1}H NMR spectra of complexes **2** and **3** show typical resonances for aromatic protons and alkyl substituents of ligands. In the aliphatic region of the spectra of these complexes are seen two multiplets for ethanediolate groups, which implies that there are two different environments for these methylene protons. The diastereotopic methylene protons in the chelate ring of **2** are separated by 2 ppm showing doublets at 3.3 and 5.4 ppm. Also the methine proton in the chelate ring of **3** shows doublets at 4.4 and 5.8, respectively.

^{1}H NMR spectrum of compound **4** is not very informative. Methylene protons in the bis(naphtolate) rings showed three multiplets at 4.8–5.9 ppm. A sharp singlet at 5.7 ppm was assigned as a signal for ethanediolato protons, as similar signal for that ligand in comparable W(eg)(OAr)$_4$ complex, [W(calix)(eg)] (calix=calix[4]arene), is found at 5.83 [9].



Scheme 2. Activation and regeneration of catalyst precursors.

2.2. Crystal structures

Compounds **2**–**4** form monomeric molecules in which six oxygen donors surround the central tungsten atoms (Figs. 1–3). The distorted octahedral WO_6 units are generally similar, but not identical in all these compounds, as seen from the bonding parameters presented

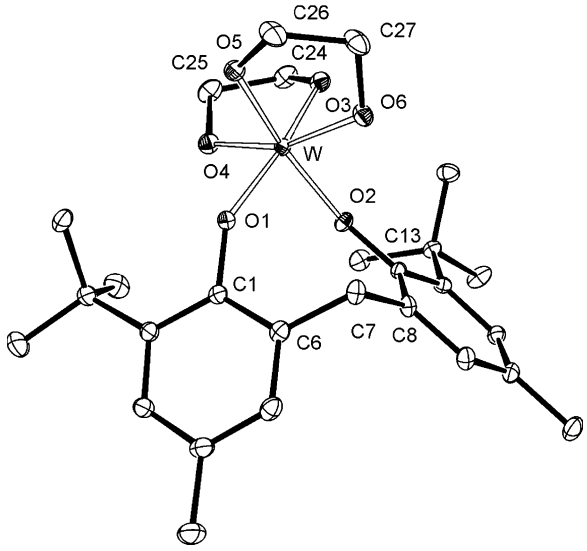
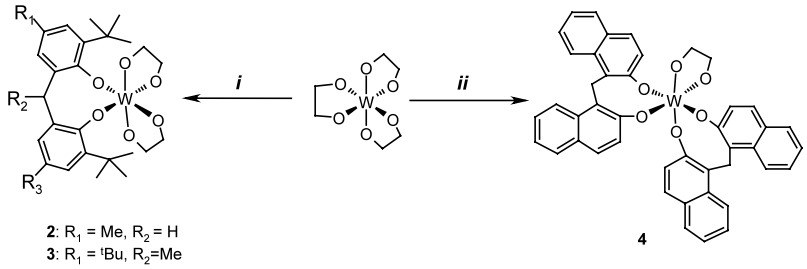


Fig. 1. Molecular structure of [W(mb)(eg)$_2$] (**2**). Hydrogen atoms have been omitted for clarity. Thermal ellipsoids have been drawn at 30% probability level.



Scheme 1. Preparation of complexes. (i) H_2biphe–PhMe, reflux; (ii) 2 H_2dinap–PhMe, reflux.

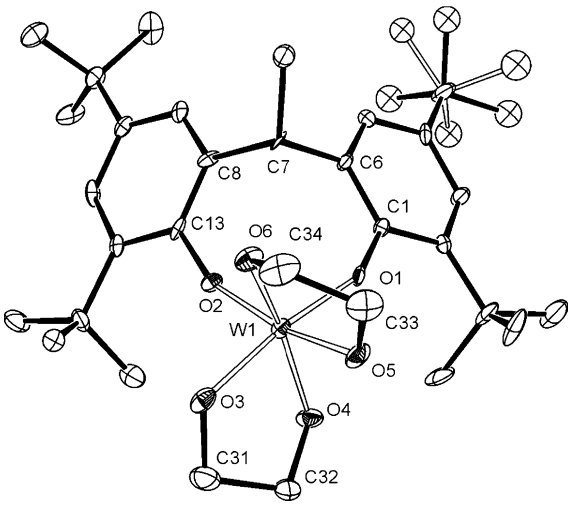


Fig. 2. Molecular structure of [W(ebp)(eg)$_2$] (**3**). Hydrogen atoms have been omitted for clarity. Thermal ellipsoids have been drawn at 30% probability level.

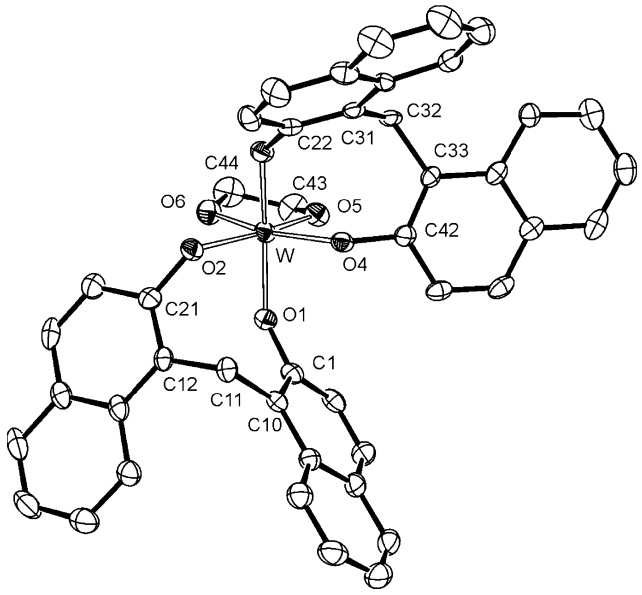


Fig. 3. Molecular structure of [W(dinap)$_2$(eg)] (**4**). Hydrogen atoms have been omitted for clarity. Thermal ellipsoids have been drawn at 30% probability level.

in Table 1. If we have [W(biphenolate)(eg)$_2$] type compound, where biphenolate is a bidentate phenolate dianion (or two monodentate phenolate anions), the shape and rigidity of biphenolate ligand modify the actual octahedral coordination sphere of the W(VI) ion. Comparing the structural parameters of **2** and **3** shows that these have fairly similar overall structure, so the substituents in the main body of the ligand modify the structure of the complexes only slightly. To see the influence of different ligand bodies on the complex structure, we should compare the structures formed by 2,2′-methylenebis(phenolato) ligand and binaphtholato ligand, thus also bonding parameters of [W(bino)(eg)$_2$]

Table 1
Selected bond lengths (Å) and angles (°) for **2**–**4**

	2	**3** [a]	W(bino)(eg)$_2$ [b]	**4**
Bond lengths				
W–O(1)	1.8970(17)	1.891(6)	1.930(8)	1.911(4)
W–O(2)	1.8848(16)	1.899(5)	1.908(8)	1.942(4)
W–O(3)	1.9324(18)	1.923(11)	1.894(7)	1.904(4)
W–O(4)	1.9049(18)	1.899(6)	1.891(8)	1.903(4)
W–O(5)	1.9069(16)	1.925(7)	1.879(8)	1.902(5)
W–O(6)	1.9143(17)	1.888(7)	1.925(8)	1.889(4)
C(1)–O(1)	1.373(3)	1.361(12)	1.397(13)	1.366(7)
C(n)–O(2) [c]	1.368(3)	1.365(10)	1.362(12)	1.362(7)
Bond angles				
O(1)–W–O(2)	87.35(7)	88.7(3)	84.6(3)	84.7(2)
O(1)–W–O(3)	165.66(7)	168.0(3)	164.7(4)	162.9(2)
O(3)–W–O(4)	77.86(8)	78.3(3)	78.0(3)	84.9(2)
O(2)–W–O(5)	162.52(7)	167.5(3)	162.3(4)	164.6(2)
O(5)–W–O(6)	78.72(8)	79.5(3)	78.4(4)	78.4(2)
O(4)–W–O(6)	160.23(8)	159.6(3)	166.4(3)	161.3(2)
C(1)–O(1)–W	148.82(15)	152.9(6)	130.1(7)	141.3(4)
C(n)–O(2)–W	151.18(14)	158.7(6)	127.1(7)	128.6(4)
C(n)–O(3)–W	119.10(17)	119.1(7)	121.0(8)	131.3(4)
C(n)–O(4)–W	120.23(17)	117.2(6)	120.7(8)	138.7(4)
C(n)–O(5)–W	119.79(17)	117.9(7)	121.3(8)	121.0(4)
C(n)–O(6)–W	118.03(17)	118.3(7)	118.1(8)	121.4(4)

[a] Values around W(1).
[b] Binaftolatobis(ethanediolato)tungsten(VI) in ref. [5b].
[c] C(n) is a carbon atom bonded to a host oxygen atom.

have included in Table 1 [5b]. Consequently, we can see large changes in bonding parameters of these bis(phenolato) ligands to W(VI) ion. For ex. W–O(1) bond lengths, as well as O(1)–W–O(2) and C(1)–O(1)–W bond angles are quite different in **2** and [W(bino)(eg)$_2$]. Normally O(phenolato) is bonded more tightly (shorter bond distances) to W(VI) center than O(alcoholato). However, we can see now that a rigid ligand bonds less effectively to W(VI) center. This phenomenon is also seen in the bonding parameters of **4**, where two bis(naphtolato) ligands are attached to W(VI): one of these ligands is quite loosely bonded to W(VI) center. Finally, the bonding parameters of aliphatic diolato groups are quite similar in compounds studied now as in earlier reported tungsten(VI) diolato complexes with simple phenoxides or binaphtholates, e.g. [W(eg)$_2$(OPhR$_2$-2,6)$_2$] [5a] and [W(bino)(eg)$_2$] [5b].

2.3. Polymerisation studies

We have earlier studied ROMP processes employing complexes of type [W(diol)$_2$(OAr)$_2$] and found that the catalytic activities depends on the bulkiness of alkyl substituents at the phenoxide groups [2b]. In this study we used sterically hindered complexes **2** and **3** as precatalysts in ROMP of norbornene and dicyclopentadiene, using a Et$_2$AlCl cocatalyst. Both tungsten precatalysts showed moderate activity for polymerisation of norbornene at 0 °C as the yields of polymers after 15

min reaction were 38% for **2** and 42% for **3**, respectively. Though, they were inactive for the polymerisation of dicyclopentadiene. At 80 °C both precatalysts produced polynorbornene and polydicyclopentadiene in practically quantitative yields. However, the high yields of polydicyclopentadiene were not necessarily due to the increased activity of the catalysts in elevated temperature, but it is possibly simply due to the thermally induced cross-linking reaction [10]. The nature of the active species is unknown, but we can suppose the traditional model for precatalyst activation-dialkylation followed by α-H elimination to produce the reactive Schrock-type alkylidene [11]. Nevertheless, active catalysts can be transformed into compounds **2** or **3**, respectively, by adding excess H_2eg, thus these precatalysts can be recovered from reaction mixtures in nearly quantitative yields (Scheme 2).

3. Conclusion

Bulky methylene-bridged bis(phenol)s react with tris-diolatotungsten(VI) complex [W(eg)$_3$] (eg = ethanediolate dianion) providing heteroleptic complexes [W(biphenolate)(eg)$_2$], where bis(phenol) = 2,2′-CH_2(4-Me-6-^{t}BuPhOH)$_2$ or 2,2′-CHMe(4,6-^{t}Bu$_2$PhOH)$_2$. Sterically less hindered 2,2′-dihydroxy-1,1′-dinaphtylmethane forms disubstituted complex [W(biphenolate)$_2$(eg)]. In solid state these isolated compounds consist of monomeric tris(diolato)tungsten(VI) molecules in which the central tungsten atom is bonded to six oxygen atoms forming a distorted octahedral coordination sphere around the metal ion. Compounds of the type [W(biphenolate)(eg)$_2$] can be activated by Et_2AlCl to catalyse ring opening polymerisation metathesis of norbornene.

4. Experimental

Chemicals were from commercial origins and were used without subsequent purification. Toluene used in polymerisation studies was distilled over sodium under a nitrogen atmosphere. Monomer solutions in toluene were stored over 4 Å molecular sieves. 2,2′-dihydroxy-1,1′-dinaphthylmethane was prepared as described earlier [12]. NMR spectra were recorded on Bruker AM-200 spectrometer. Elemental analyses were obtained using a Perkin–Elmer CHNS-Analyzer 2400. Analytical samples were dried in vacuo at 40 °C for 2 h prior to elemental and spectral analyses.

4.1. Preparation of complexes

[*W*(*eg*)$_2$(*mbp*)] (**2**) 1.09 g of **1** (3.00 mmol) was heated with 1.02 g of H_2mbp (3.00 mmol) in 60 ml of toluene at reflux to form a red solution. The H_2eg that formed was removed by azeotropic distillation with toluene during 4 h. The solvent was evaporated and orange solid residue was column chromatographed (silica–CH_2Cl_2) to give complex **2** as orange–red solid, which was crystallised from 10 ml of acetonitrile to obtain intense red prisms with the formula **2**·CH_3CN in yield of 82% (1.68 g). Samples were dried in vacuo at 40 °C for 6 h before elemental and spectral analyses to remove any solvent of crystallisation. For **2**: δ_H ($CDCl_3$, standard $SiMe_4$): 7.07 (s, 1H, ArH), 6.97 (s, 2H, ArH), 6.92 (s, 1H, ArH), 5.72 (br, s, 2H, –OCH_2–), 5.53 (br, s, 2H, –OCH_2–), 5.38 (d, 1H, –CH_2–), 5.35 (br, s, 2H, –OCH_2–), 5.17 (br, s,2H, –OCH_2–), 3.28 (s, 1H, –CH_2–), 2.34 s, (s, 3H, *p*-CH_3), 2.28 (s, 3H, *p*-CH_3), 1.41 (s, 9H, C(CH_3)$_3$), 1.34 (s, 9H, C(CH_3)$_3$). Found: C, 50.2; H, 5.8. $C_{27}H_{38}O_6W$ requires C, 50.5; H, 6.0%.

[*W*(*ebp*)(*eg*)$_2$] (**3**) 1.09 g of **1** (3.00 mmol) was heated with 1.32 g of H_2ebp (3.00 mmol) in 60 ml of toluene at reflux to form a red solution and the H_2eg that formed was removed by azeotropic distillation with toluene during 4 h. The solvent was evaporated and an orange solid residue was crystallised from 40 ml of hexane to obtain complex **3** as orange-red microcrystals in yield of 90% (2.05 g). Crystals of **3** for X-ray structure analysis were grown from acetonitrile. For **3**: δ_H ($CDCl_3$, standard $SiMe_4$): 7.24 (1H, ArH), 7.17 (m, 3H, ArH), 5.8–5.1 (9 H, several multiplets, –OCH_2– and –CHCH_3), 1.65 (d, 3H, –CHCH_3), 1.32 (q, 36H, C(CH_3)$_3$). Found: C, 55.4; H, 6.9. $C_{34}H_{52}O_6W$ requires C, 55.1; H, 7.1%.

[*W*(*dinap*)$_2$(*eg*)] (**4**) 120 mg of **1** (0.33 mmol) was heated with 200 mg of H_2dinap (0.67 mmol) in 60 ml of toluene at reflux for 4 h to form a red solution. The solution was then concentrated to 15 ml and allowed to stand at r.t. overnight to obtain complex **4** as red powder in 69% yield (190 mg). Crystals of **4**·CH_2Cl_2 for X-ray structure analysis were grown from CH_2Cl_2 by slow evaporation. δ_H ($CDCl_3$, standard $SiMe_4$): 8.80–7.20 (several multiplets, 24H, ArH), 5.90–4,80 (several multiplets, 4H, –CH_2–), 5.73 (s, 4H, –OCH_2–). Found: C, 62.6; H, 4.0. $C_{44}H_{32}O_6W$ requires C, 62.9; H, 3.8%.

4.2. Polymerisation studies

Polymerisations were performed under a nitrogen atmosphere applying the protocol reported by Barnes et al. [2]. Our experiments were carried out employing a 1:4.5:50 tungsten precatalyst: activator:monomer ratio. The precatalyst (2×10^{-5} mol in 10 ml of toluene) was treated with 0.05 ml of Et_2AlCl solution (1.8 M in toluene, 9×10^{-5} mol). The red reaction mixture was stirred for 5 min and 1 ml of 1 M olefinic monomer (1.0 mmol) in toluene was added. After 15 min stirring the solution was treated with 10 ml of methanol to precipitate polymer as a white solid. Polymers were

swelled in toluene, re-precipitated by methanol and dried in vacuo at 40 °C for 8 h.

4.3. Single crystal X-ray diffraction

Crystal data for compounds **2**–**4**, along with other experimental details, are summarised in Table 2. The crystallographic data were collected for **2** and **3** at 173 K on a Nonius Kappa CCD area-detector diffractometer using graphite monochromatised Mo Kα radiation ($\lambda =$ 0.71073 Å). Lattice parameters were determined from ten images recorded with 1° φ scans and subsequently refined on all data. The data collection was performed using φ and ω scans with 1° steps using an exposure time of 5 s per frame for **2** and 2 s per frame for **3.** The crystal-to-detector distances were 30 and 40 mm for **2** and **3**, respectively. The data were processed using DENZO-SMN v0.93.0 [13]. MULABS [14] absorption correction was applied for the data of both compounds, but in final calculations the corrected data were used only for **3**, because corrected data for **2** give higher R-values than the uncorrected one.

Single-crystal data collection for **4** was performed at ambient temperature on a Rigaku AFC5S diffractometer using graphite monochromatised Mo Kα radiation ($\lambda = 0.71069$ Å). Data reduction and subsequent calculations were performed with TEXSAN for Windows [15]. The data were corrected for Lorenz and polarisation effects, for absorption (PSI-scans [16]) and for decay.

Table 2
Crystal data and experimental details of the structure determination of **2**–**4**

	2	**3**	**4**
Formula	$C_{29}H_{41}NO_6W$	$C_{34}H_{52}O_6W$	$C_{45}H_{34}Cl_2O_6W$
M_r	683.48	740.61	925.47
Crystal system	triclinic	orthorhombic	triclinic
Space group (no.)	$P\bar{1}$ (2)	$Pca2_1$ (29)	$P\bar{1}$ (2)
a (Å)	9.1940(1)	15.8055(2)	11.289(3)
b (Å)	10.1566(1)	16.5843(2)	17.342(3)
c (Å)	16.3405(2)	26.5014(3)	10.924(2)
α (°)	77.035(1)	90	95.566(18)
β (°)	82.012(1)	90	117.161(14)
δ (°)	86.927(1)	90	76.898(17)
U (Å^3)	1472.15(3)	6946.63(14)	1853.2(6)
Z	2	8	2
D_{calc} (g cm^{-3})	1.542	1.416	1.658
μ (Mo Kα) (cm^{-1})	39.63	33.65	33.12
Observed reflections	6681	14714	6534
R_{int}	0.0159	0.0600	0.0368
Parameters	332	736	487
R_1	0.022 (0.020) [a]	0.084 (0.048)	0.081 (0.041)
wR_2	0.047 (0.046)	0.104 (0.093)	0.076 (0.068)

$R_1 = \Sigma||F_o|-|F_c||/\Sigma|F_o|$, $wR_2 = \{\Sigma[w(F_o^2-F_c^2)^2]/\Sigma[w(F_o^2)^2]\}^{1/2}$ and $w = 1/[\sigma^2(F_o^2)+(aP)^2+bP)]$, where $P = (2F_c^2+F_o^2)/3$.

[a] Values in parentheses for reflections with $I > 2.0\sigma(I)$.

The structures were solved by direct methods using the SIR-92 program [17] and full-matrix least-squares refinements on F^2 were performed using the SHELXL-97 program [18]. For both all heavy atoms were refined anisotropically. The CH hydrogen atoms were included at the fixed distances with fixed displacement parameters from their host atoms. Compound **3** was refined as a racemic twin (Flack's parameter is 0.65(1). Figures were drawn with ORTEP-3 for *Windows* [19].

5. Supplementary data

Crystallographic data (excluding structure factors) for the structures reported in this paper have been deposited with the Cambridge Crystallographic Data Centre as supplementary publication no. CCDC 174185–174187. Copies of the data can be obtained free of charge on application to CCDC, 12 Union Road, Cambridge CB2 1EZ, UK (fax: +44-1223-336033; e-mail: deposit@ccdc.cam.ac.uk or www: http://www.ccdc.cam.ac.uk).

References

[1] For example, (a) A. Van der Linden, C.J. Schaverien, N. Meijboom, C. Ganter, A.G. Orpen, J. Am. Chem. Soc. 177 (1995) 3008.
(b) M. Chavarot, J. Byrne, P.Y. Chavant, J. Pardillos-Guindet, Y. Vallée, Tetrahedron Asymm. 9 (1998) 3889.
(c) J.B. Alexander, R.R. Schrock, W.M. Davis, K.C. Hultzsch, A.H. Hoveyda, J.H. Houser, Organometallics 19 (2000) 3700.
(d) T. Chen, S.W. Hon, S.S. Weng, Synlett (1999) 816.
[2] (a) D.L. Barnes, N.W. Eilerts, J.A. Heppert, W.H. Huang, M.D. Morton, Polyhedron 13 (1994) 1267;
(b) A. Lehtonen, R. Sillanpää, Inorg. Chem. Commun. 4 (2001) 108.
[3] M.D. Morton, J.A. Heppert, S.D. Dietz, W.H. Huang, D.A. Ellis, T.A. Grant, N.W. Eilerts, D.L. Barnes, F. Takusagawa, D. VanderVelde, J. Am. Chem. Soc. 115 (1993) 7916.
[4] Y. Nakayama, H. Saito, N. Ueyama, A. Nakamura, Organometallics 18 (1999) 3149.
[5] (a) A. Lehtonen, R. Sillanpää, Polyhedron 18 (1999) 175;
(b) A. Lehtonen, R. Sillanpää, Polyhedron 19 (2000) 2579;
(c) A. Lehtonen, R. Sillanpää, Inorg. Chem. 43 (2001) 6047.
[6] J. Okuda, S. Fokken, H.C. Kang, W. Massa, Chem. Ber. 128 (1995) 221.
[7] M.H. Chisholm, J.H. Huang, J.C. Huffman, W.E. Streib, D. Tiedtke, Polyhedron 16 (1997) 2941.
[8] D.R. Mulford, P.E. Fanwick, I.P. Rothwell, Polyhedron 19 (2000) 35.
[9] B. Xu, Y.J. Miao, T.M. Swager, J. Org. Chem. 63 (1998) 8561.
[10] T.A. Davidson, K.B. Wagener, J. Mol. Cat. A: Chem. 133 (1998) 67.
[11] K.J. Ivin, J.C. Mol, Olefin Metathesis and Metathesis Polymerization, Academic Press, London, 1997.
[12] L.E. Mirci, Rom. Pat., 105571, 1992.
[13] Z. Otwinowski, W. Minor, in: C.W. Carter, Jr., R.M. Sweet (Eds.), Methods in Enzymology, Macromolecular Crystallography, Part A, Academic Press, New York, 1997, pp. 307–326.

[14] R.H. Blessing, Acta Crystallogr., Sect. A 51 (1995) 33–38.
[15] TEXSAN for Windows. Structure Analysis Software. Molecular Structure Corporation, Texas 77381, USA, 1997.
[16] A.C. North, D.C. Phillips, F.S. Mathews, Acta Crystallogr., Sect. A 24 (1968) 351.
[17] A. Altomare, G. Cascarano, C. Giacovazzo, A. Gualiardi, M.C. Burla, G. Polidori, M. Camalli, J. Appl. Cryst. 27 (1994) 435.
[18] G.M. Sheldrick, SHELXL-97, In: Program for Crystal Structure Refinement, University of Göttingen, Germany, 1997.
[19] L.J. Farrugia, J. Appl. Cryst. 30 (1997) 565.

PERGAMON

Polyhedron 21 (2002) 1023–1030

POLYHEDRON

www.elsevier.com/locate/poly

Synthesis, characterisation and crystal structure of *cis*-dioxomolybdenum(VI) complexes of some potentially pentadentate but functionally tridentate (ONS) donor ligands

Arindam Rana [a], Rupam Dinda [a], Parbati Sengupta [a], Saktiprosad Ghosh [a,*], Larry R. Falvello [b]

[a] *Department of Inorganic Chemistry, Indian Association for the Cultivation of Science, Jadavpur, Kolkata 700 032, India*
[b] *Departamento de Quimica Inorganica, Universidad de Zaragoza, Zaragoza 50009, Spain*

Received 28 November 2001; accepted 26 February 2002

Abstract

Neutral *cis*-dioxomolybdenum(VI) complexes with potentially pentadentate ONSNO donor Schiff bases of thiocarbodihydrazone of salicylaldehyde (H_3L^1), 5-bromo (H_3L^2), 5-nitro salicylaldehyde (H_3L^3) and 2-hydroxyacetophenone (H_3L^4) acting as tridentate ONS donor ligands have been synthesised. The complexes are found to be of the form $MoO_2LH(R–OH)$ ($R = CH_3$) where, LH = L^1H, L^2H, L^3H and L^4H. The complexes were characterised by elemental analyses, UV, IR, and ^1H NMR spectroscopy, magnetic susceptibility measurement, molar conductivities in solution and by cyclic voltammetry. Two of the complexes $[MoO_2(L^2H)(MeOH)]$ and $[MoO_2(L^4H)(MeOH)]$ were crystallographically characterised. The structures reveal that the molybdenum acceptor centre is present in a distorted octahedral NO_4S donor environment. The presence of a substituent either on the aromatic ring of the salicylaldehyde moiety or on the carbon atom of its carbonyl group is found to exhibit little effect on the corresponding metal ligand bond distances and angles. The sixth coordination site of the complexes harboring the weakly coordinated R–OH moiety is found to act as the binding site for various neutral monodentate Lewis bases. © 2002 Elsevier Science Ltd. All rights reserved.

Keywords: Dioxomolybdenum(VI) complexes; Thiocarbodihydrazone Schiff base; X-ray structures

1. Introduction

Chemistry of the mixed hard–soft nitrogen–sulfur chelating ligands bound to Mo at higher oxidation state is a field of current interest. Such studies did assume greater importance after the revealation that several oxido-reductases like DMSO reductase, xanthine oxidase and other oxo-transferases contain Mo(IV), Mo(V) and Mo(VI) as their prosthetic groups coordinated to nitrogen–sulpur donor points of a macromolecular ligand system [1]. EXAFS study of xanthine oxidase has confirmed the simultaneous presence of nitrogen, sulfur and oxygen donors at its active site [2–4]. The capacity of sulfur donor centres in mixed hard–soft ligand systems to stabilise uncommon oxidation states, to generate unfamiliar coordination number in the resultant transition metal complexes and to take part in diverse type of redox reactions—both chemical and electrochemical, is recognised [5–13]. Our group has been quite active in this field for more than a decade and has reported the synthesis, characterisation, chemical and electrochemical activity of Mo(VI), Mo(V) and Mo(IV) complexes which were found to resemble the oxo-transfer molybdoenzymes [7,14–16]. Schiff bases of thiocarbodihydrazide are known to constitute an interesting ONS chelating ligand system with some other potential donor sites [17]. This work presents a comparative study of the $[Mo(VI)O_2]^{2+}$ complexes of a few multidentate thiocarbodihydrazide-based ONS chelating ligands differing from each other in the nature of the substituent placed at strategic positions with respect to the ONS donor set holding definite possibility of

* Corresponding author. Tel.: +91-33-473-4971/3372; fax: +91-33-473-2805.
E-mail address: icspg@mahendra.iacs.res.in (S. Ghosh).

0277-5387/02/$ - see front matter © 2002 Elsevier Science Ltd. All rights reserved.
PII: S0277-5387(02)00913-0

modifying the over all electron environment around MoO^{2+} centre. Apart from various spectroscopic (UV–Vis, IR, ^{1}H NMR), electrochemical and chemical techniques, crystal and molecular structures of two complexes $[MoO_2(L^2H)(MeOH)]$ and $[MoO_2(L^4H)(MeOH)]$ have been determined by single crystal X-ray diffraction technique.

2. Results and discussion

2.1. Synthesis and characterisation of the ligand

The Schiff base ligands (H_3L^1, H_3L^2, H_3L^3 and H_3L^4) were prepared by condensing thiocarbohydrazide [18] with the appropriate 5-substituted salicylaldehydes in 1:1 molar proportions in refluxing ethanol: glacial acetic acid mixture. The ligands have been satisfactorily characterised by elemental analysis (Table 1), IR (Table 2), and ^{1}H NMR (Table 3) data.

2.2. Synthesis and characterisation of molybdenum(VI) complexes

Dioxomolybdenum(VI) complexes (**1**–**4**) of general formula $MoO_2LH(R–OH)$ were prepared [19] by refluxing $MoO_2(acac)_2$ with the appropriate ligand in 1:1 molar proportion in high yield (80–85%)[Scheme 1] using the appropriate alcohol as the reaction medium. All of them are dark orange–red crystalline solids, which are air and heat stable and diamagnetic as is expected for a species with d^0 Mo(VI) center [20]. They are insoluble in water. They have rather low solubility in common organic solvents but most are quite soluble in polar aprotic co-ordinating solvents like DMF and DMSO. Molar conductivity data in 10^{-3} M DMF solutions indicate that they are non-electrolytes. Cyclic voltammograms and electronic spectra of all the complexes were recorded in DMF (Tables 4 and 5). The solvent (R–OH) molecule at the sixth coordination site is rather weakly coordinated and can be easily replaced by different neutral monodentate Lewis bases like imidazole, substitutet imidazoles, pyridine, methyl pyr-

Table 1
Elemental analyses for the ligands and complexes

Compound	Analysis (%)				
	C	H	N	S	Mo
H_3L^1	57.42(57.32)	4.48(4.45)	17.79(17.83)	9.97(10.19)	
H_3L^2	38.69(38.14)	2.57(2.54)	11.90(11.86)	6.32(6.78)	
H_3L^3	44.45(44.55)	2.95(2.97)	20.72(20.79)	7.86(7.92)	
H_3L^4	59.61(59.65)	5.22(5.26)	16.35(16.37)	9.33(9.36)	
$MoO_2L^1H(MeOH)$ (**1**)	40.55(40.68)	3.50(3.39)	11.70(11.86)	6.45(6.78)	20.10(20.34)
$MoO_2L^2H(MeOH)$ (**2**)	29.74(29.72)	2.19(2.17)	8.64(8.67)	4.83(4.95)	14.75(14.86)
$MoO_2L^3H(MeOH)$ (**3**)	34.10(34.16)	2.52(2.49)	14.93(14.95)	5.50(5.69)	16.89(17.08)
$MoO_2L^4H(MeOH)$ (**4**)	43.17(43.20)	3.89(4.00)	11.16(11.20)	6.12(6.40)	19.00(19.20)

Found (calcuted).

Table 2
Selected IR bands (in cm^{-1}) for the ligands and complexes

Compound	ν(N–H)	ν(O–H)	ν(C=N)	ν(C=S)	ν(MoO_2)
H_3L^1	3190m,br	d	1610,1590 vs	1285vs	f
H_3L^2	3125m,br	3650m,sh	1603vs	1280vs	f
H_3L^3	3180m,br	d	1625,1615vs	1290vs	f
H_3L^4	3220m,br	3550m,sh	1605,1595vs	1290vs	f
$MoO_2L^1H(MeOH)$	3185m,br	3500m,sh	1610,1590vs,sh	f	940,915vs
$MoO_2L^2H(MeOH)$	3180m,br	3610m,sh	1610,1558vs,sh	f	940,908vs
$MoO_2L^3H(MeOH)$	3295m,br	3650m,sh	1610,1558vs,sh	f	940,910vs
$MoO_2L^4H(MeOH)$	3220m,br	3515m,sh	1615,1590vs,sh	f	935,910vs

Abbreviations: vs, very strong; br, broad; m, medium; sh, shoulder; d, not clearly located; f, not existing.

Table 3
^{1}H NMR data for the ligands and complexes in dmso-d_6

Compound	Proton				
	–CH=N–	$-CH_3$	Aromatic proton	–NH–	Aromatic-OH
H_3L^1	8.75 s (1)	f	6.90–8.06 m (8)	11.61 s (1)	12.04 s (1)
	8.49 s (1)			10.02 s (1)	11.88 s (1)
H_3L^2	8.71 s (1)	f	6.87–8.27 m (6)	11.69 s (1)	12.14 s (2)
	8.41 s (1)			10.41 s (1)	
H_3L^3	8.91 s(1)	f	7.11–8.51 m (6)	12.71 s (1)	12.42 s (1)
	8.87 s (1)			11.76 s (1)	12.37 s (1)
H_3L^4	f	2.39s (6)	6.88–7.60 m (8)	11.24 s (2)	12.54 s (2)
$MoO_2L^1H(MeOH)$	8.64 s(1)	f	6.70–7.70 m (8)	10.70 s (1)	11.94 s (1)
	8.31 s(1)				
$MoO_2L^2H(MeOH)$	8.64 s(1)	f	6.86–7.94 m (6)	10.69 s (1)	12.12 s (1)
	8.27 s(1)				
$MoO_2L^3H(MeOH)$	8.88 s(1)	f	7.08–8.51 m (6)	11.81 s (1)	12.36 m (1)
	8.70 s(1)				
$MoO_2L^4H(MeOH)$	f	2.75 s (3)	6.85–7.81 m (8)	10.79 s (1)	12.90 s (1)
	2.39 s (3)				

Abbreviation: s, singlet; m, multiplet; f, not existing.

idines etc. Thus the sixth coordination site around MoO_2^{2+} acceptor centre acts as the site that is utilised to bind substrates like neutral monodentate Lewis bases.

Table 4
Cyclic voltammetric peak potential data (V vs. SCE) in dmf solution

Compound	Cathodic peak potential ($Ec_\perp$ in V)	Cathodic peak potential ($Ec_\parallel$ in V)
H_3L^1	not existing	−1.500
$MoO_2L^1H(MeOH)$	−1.200	−1.713
H_3L^2	not existing	−1.450
$MoO_2L^2H(MeOH)$	−1.025	−1.600
H_3L^3	not existing	−1.338
$MoO_2L^3H(MeOH)$	−0.913	−1.350
H_3L^4	not existing	−1.438
$MoO_2L^4H(MeOH)$	−1.113	−1.488

Solvent: DMF (dry, degassed); supporting electrolyte: 0.1 M TEAP; solution strength: 10^{-3} M; electrode: platinum; reference electrode: SCE; scan rate: 200 mV s^{-1}.

Table 5
Electronic spectra of the [Mo(VI)O_2LH(MeOH)]

Compound	λ_{max} in nm (ε in dm^3 mol^{-1} cm^{-1})
$MoO_2L^1H(MeOH)$	314[19 107], 349[31 089], 362[30 118](sh), 412[8420]
$MoO_2L^2H(MeOH)$	314[19 517], 349[32 630], 366[32 325](sh), 417[10 064]
$MoO_2L^3H(MeOH)$	305[30 152], 338[34 235], 351[34 549](sh), 443[11 621]
$MoO_2L^4H(MeOH)$	303[24 135], 349[30 510], 360[29 144](sh), 506[9107]

Abbreviation: sh, shoulder.

2.3. Structures of complexes

The perspective drawings of the complexes **2** and **4** are given in Figs. 1 and 2, respectively. Experimental details are given in Table 6. Selected bond lengths and angles are listed in Tables 7 and 8, respectively. The tridentate dinegative Schiff base ligand is bonded to the *cis*-$[Mo(VI)O_2]^{2+}$ core on a meridional plane [21,22] through S(1), O(4), and an imine nitrogen atom, which is trans to an oxo group. The sixth coordination site around Mo is occupied by a solvent (MeOH) molecule, thereby providing a distorted octahedral coordination environment around Mo in which the coordinated MeOH lie trans to another oxo group. In both the compounds **2** and **4**, the average O=Mo=O bond angle [106.0(2)°] and Mo–O bond length [1.664(7)–1.700(3) Å] which are very common for *cis*-dioxomolybdenum(VI) complexes [23–26]. The imine nitrogen and methanol oxygen atoms, which are trans to the terminal oxo-groups, are bound to Mo(VI) ions at distance of 2.281(8)–2.290(3) Å for nitrogen and 2.347(3)–2.278(8) Å for oxygen, respectively. The *cis* angles around Mo ranges from 75.5(2)° to 77.53(9)° for N(4)–Mo–S(1) to 105.9(4)°–106.0(2)° for O(1)–Mo–O(2), while the two trans L–Mo–L angles vary from 168.9(2)° to 171.6(3)°

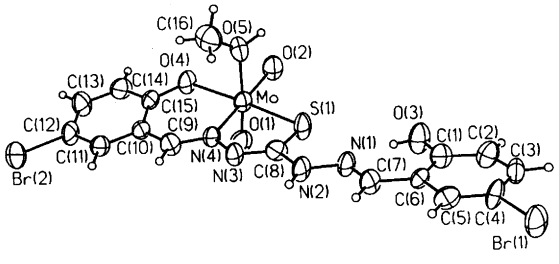
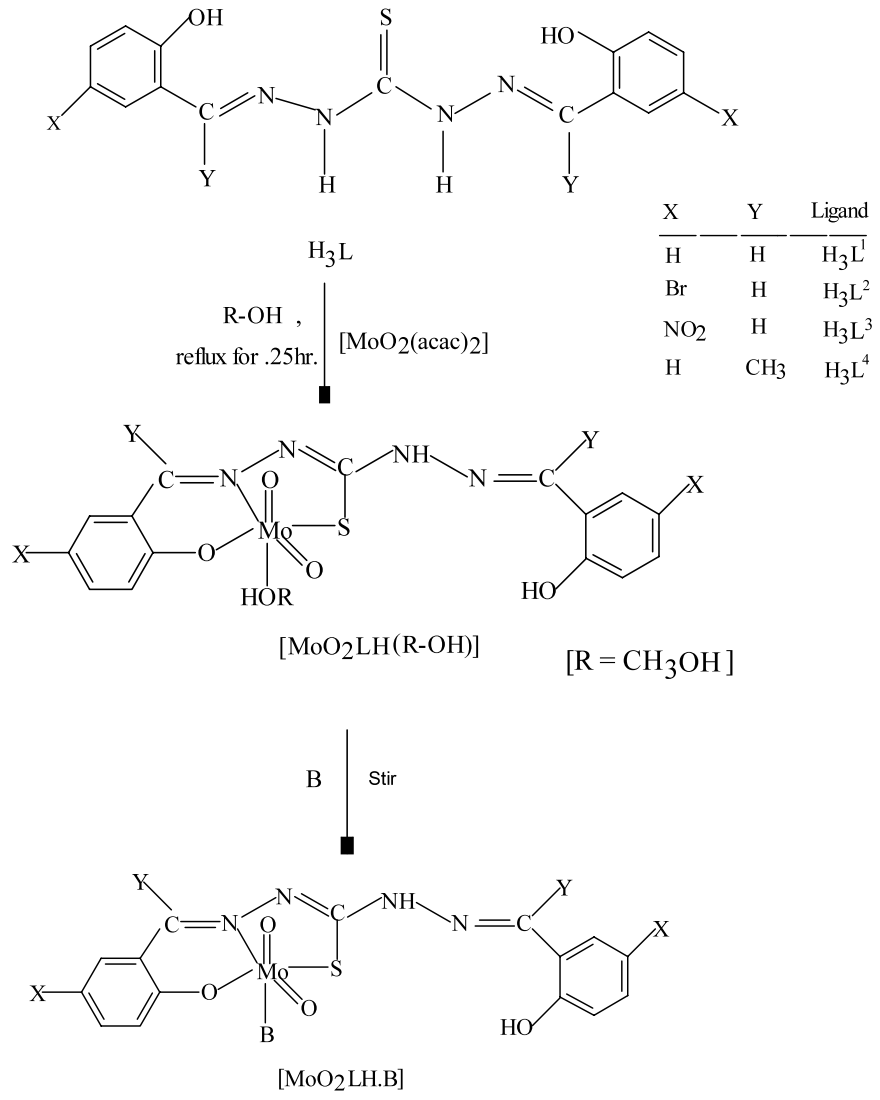


Fig. 1. ORTEP plot of complex **2** [$MoO_2L^2H(MeOH)$].



[B = imidazole, substituted imidazoles, pyridine and methyl pyridines etc.]

Scheme 1. Reaction diagram for the isolation of Mo(VI) complexes.

for O(1)–Mo–O(5) and 150.6(11)°–153.1(2)° for O(4)–Mo–S(1). The C(8)–N(3) bond distance of the two compounds vary from 1.281(5) to 1.297(12) Å is pretty close to the usual C=N length [19,27]. The Mo–S bond distances are found to vary from 2.4299(14) to 2.462(3) Å [22,28,29].

It is observed from the torsional and dihedral angles that, twists occur about three bonds, viz., N(4)–C(9), C(9)–C(10) and N(4)–N(3). Such twists have also been reported previously [21,22,25]. An interesting feature in comparison between two structure is that, in compound **2** the uncoordinated phenolic –OH remains on the same side as the Mo centre with respect to the C(10)–C(9)–N(4)–N(3)–C(8)–N(2)–N(1)–C(7)–C(6) skeleton. However, in compound **4** they are anti to each other, through a primary rotation of ~180° around C(8)–N(2) bond along with a little rotation around N(2)–N(1) and C(7)–N(1) bonds. This is probably to avoid van der waal's interaction between the C(9a) and C(7a) methyl moieties. Careful analysis of the bond lengths and bond angles leads to the following observation. Irrespective of the substitution in the 5-position of the benzene ring or the carbonyl carbon atom of the salicylaldehyde moiety of the ligand, the bonds expected to be affected by such substitution showed no significant differences in length in the MoO_2-complexes reported in this work. Such an observation, though contrary to expectation [30], may be accounted for by invoking the idea of extensive delocalisation of electron density throughout the complex molecule.

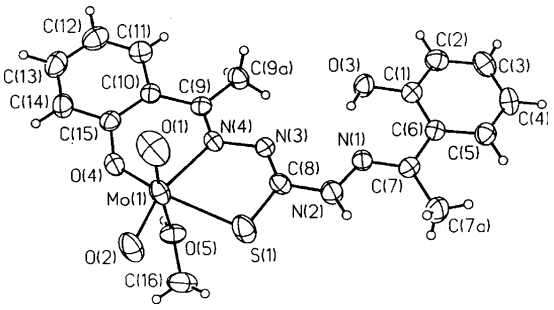


Fig. 2. ORTEP plot of complex **4** [$MoO_2L^4H(MeOH)$].

2.4. IR and ^1H NMR studies

All the four ligands exhibit two to three broad IR bands of medium intensity at 3650–3200 cm^{-1} region, the higher frequency one is due to the ν(O–H) mode while the lower ones are assigned to the ν(N–H) vibrations [31] (Table 2). Presence of these O–H and N–H hydrogens are also revealed in the X-ray crystal structure of the complexes **2** and **4**. Two or more strong ν(C=N) bands are observed in the 1650–1590 cm^{-1} region. Multiplicity of this band may be attributed to the presence of more than one different type of ν(C=N) moieties in the ligands and complexes which is clearly revealed in the crystal structure of the complexes **2** and **4**. Like most of the *cis*-dioxomolybdenum(VI) complexes, two IR bands are observed in the 940–910 cm^{-1} region, the higher frequency band originating from the antisymmetric while the lower one from the symmetric stretching mode of the $[MoO_2]^{2+}$ moiety [25,32,33]. A strong ν(C=S) band was observed around 1295–1280 cm^{-1} for the ligands, which disappeared upon complex formation. Two new bands at $\sim$595 cm^{-1} and in the 510–560 cm^{-1} region are observed in the IR spectra of the complexes. They are assigned to the ν(Mo–N) and ν(Mo–O), respectively, [25,31].

^1H NMR data for the complexes are summarized in Table 3. The non-equivalence of the two N–H moieties in each of the ligand is due to the involvement of the nitrogen atom of one of them in intramolecular hydrogen bonding. NMR spectra of the corresponding complexes (Table 3) exhibit only one N–H proton signal shifted downfield. The spectra of the complexes exhibit only one phenolic O–H proton signal corresponding to the uncoordinated half of the ligand. The broad nature of this O–H proton signal is indicative of intramolecular H-bonding. Coordination from the azomethine nitrogen is reflected in the downfield shift of the CH=N proton in the NMR spectra of the complexes **1**, **2** and **3**. In the complex **4**, the involvement of the azomethine nitrogen is indicated by the shift of the $-CH_3$ proton signal from

Table 6
Crystallographic data for complexes **2** and **4**

	Complex **2**	Complex **4**
Chemical formula	$C_{16}H_{16}Br_2MoN_4O_6S$	$C_{18}H_{20}N_4O_5SMo\cdot 0.5(CH_3OH)$
Formula weight (M)	648.14	516.41
Crystal system	monoclinic	monoclinic
a (Å)	15.251(4)	11.971(1)
b (Å)	9.290(2)	8.318(1)
c (Å)	16.094(6)	21.103(1)
β (°)	10.83(3)	98.51(1)
V (Å^3)	2131(1)	2078.2(2)
Temperature (°C)	22–24±	23–25±
Z	4	4
Space group	$P2_1/c$	$P2_1/n$
μ (Mo Kα) (cm^{-1})	45.0	7.73
Quality of fit	0.908	1.048
Number of data/restraints/parameters	3720/0/286	3642/0/320
$R_1^b(F_o^2 > 2\sigma\ (F_o^2)$	0.0664	0.0427
wR_2^a	0.1599	0.1101
Largest difference peak and hole (e Å^{-3})	0.67, −1.35	0.52, −0.41

Table 7
Selected bond lengths (Å) for complex **2** and **4**

Bond lengths	Complex **2**	Complex **4**
Mo–O(1)	1.664(7)	1.691(4)
Mo–O(2)	1.682(7)	1.700(3)
M0–S(1)	2.462(3)	2.4299(4)
Mo–O(4)	1.945(6)	1.910(3)
Mo–N(4)	2.281(8)	2.290(3)
Mo–O(5)	2.278(8)	2.347(3)
C(8)–S(1)	1.727(11)	1.742(4)
C(8)–N(3)	1.297(12)	1.281(5)
N(3)–N(4)	1.384(10)	1.409(5)
N(4)–C(9)	1.307(12)	1.308(5)
C(9)–C(10)	1.413(13)	1.479(6)
C(10)–C(15)	1.413(13)	1.404(6)
C(15)–O(4)	1.334(11)	1.338(5)
C(8)–N(2)	1.353(11)	1.372(6)
N(2)–N(1)	1.368(11)	1.369(5)

Table 8
Selected bond angles (°) for complex **2** and **4**

Angles	Complex **2**	Complex **4**
O(1)–Mo–O(2)	105.9(4)	106.0(2)
O(1)–Mo–O(4)	98.2(3)	99.7(2)
O(1)–Mo–O(5)	171.6(3)	168.9(2)
O(1)–Mo–N(4)	93.7(3)	90.8(2)
S(1)–Mo–O(1)	97.0(3)	100.8(2)
S(1)–Mo–O(2)	90.5(3)	88.87(12)
S(1)–Mo–O(4)	153.1(2)	150.6(11)
S(1)–Mo–O(5)	82.8(2)	81.17(10)
S(1)–Mo–N(4)	75.5(2)	77.53(9)
O(2)–Mo–O(4)	106.3(3)	105.5(2)
O(2)–Mo–O(5)	82.51(3)	85.0(2)
O(2)–Mo–N(4)	157.3(3)	160.2(2)
O(4)–Mo–O(5)	79.0(3)	74.85(14)
O(4)–Mo–N(4)	81.5(3)	81.31(13)
O(5)–Mo–N(4)	78.1(3)	78.86(12)
N(3)–N(4)–Mo	122.9(6)	120.0(2)

2.39 to 2.75 δ while the other $-CH_3$ proton signal remains unaltered at 2.39 δ corresponding to the uncoordinated part of the ligand.

2.5. Electrochemical properties

Cyclic voltammograms of all the ligands and complexes at a platinum electrode were recorded in dry degassed DMF containing 0.1 M TEAP as the supporting electrolyte over a potential range of 0.0 to −1.9 V. The numerical data are given in Table 4 and representative voltammograms are shown in Fig. 3. All the complexes exhibit two successive reductive responses in the given potential range. The first one is a metal centred $2e^-$ process [19] as was evidenced from a comparison with authentic $1e^-$ systems [6,15,34]. The second reduction wave for the complexes and the corresponding free ligands is found to occur almost at the same potential within the −1.3–−1.8 V region. Such close correspondence of the reduction potential of the ligand–complex pairs points to the ligand based character of this process. Both the reductions observed for all the compounds are irreversible. It is to be noted here that reduction of dioxomolybdenum(VI) complexes in aprotic solvents are generally irreversible [7].

2.6. Electronic spectra

Electronic spectra of the Mo(VI) complexes were recorded in DMF solution and the spectral data is presented in Table 5. The lowest energy absorption maximum is observed in the 510–400 nm range and may be assigned to $S(p\pi) \rightarrow Mo(d\pi)$ LMCT transition caused by the promotion of an electron from the filled HOMO of the ligand of primarily sulfur pπ character to the empty LUMO of molybdenum dπ character. Other LMCT bands are observed in the region 400–300 nm [6,15,19,21]. The bands appearing around 350 and 310 nm may be assigned to the nitrogen to molybdenum and oxygen to molybdenum charge transfer transitions [19]. The bands appearing below 300 nm are due to intra-ligand transitions.

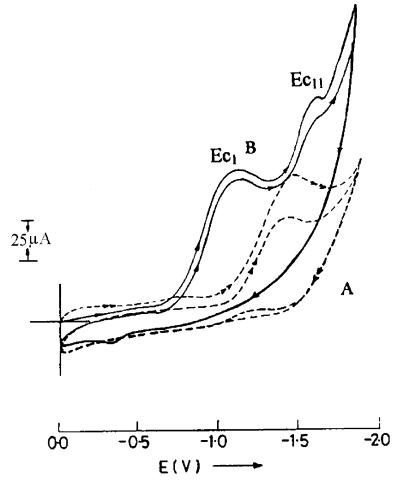


Fig. 3. Cyclic voltammograms for ligand A (H_3L^2) (---) and Mo(VI) complex B [$MoO_2L^2H(MeOH)$] (—) in DMF solution.

2.7. Study of reactivity of $[MoO_2LH(MeOH)]$

Binding of alcohols used as the reaction medium for the preparation of the complexes of the general formula [$MoO_2LH(ROH)$] led us to the idea that this sixth coordination site around Mo(VI) acceptor centre may be utilised for the site of binding of monodentate Lewis base substrates. The weakly coordinated nature of R–OH is apparent from TG-DTA data of the $MoO_2LH(ROH)$ species, which exhibited ready loss of R–OH around 110 °C. This is further substantiated by the facile replacement of R–OH by other neutral monodentate base. Refluxing and even prolonged stirring of a suspension of $MoO_2LH(ROH)$ in dry CH_2Cl_2 or EtOH with the relevant base B such as imidazole, 1-methyl imidazole, 4-methyl imidazole, pyridine, β- and γ-picoline, etc. resulted in formation of $MoO_2LH \cdot B$. So, it is established that the sixth coordination position of the distorted octahedral $MoO_2LH(ROH)$ moiety may be considered as the binding site for various monodentate oxygen (alcohols) and nitrogen (imidazoles and pyridines) donor ligands.

3. Experimental

3.1. Materials

[$MoO_2(acac)_2$] was prepared as described in the literature [35]. Reagent grade solvents were dried and distilled prior to use. All other chemicals were reagent grade, available commercially and used without further purification.

3.2. Physical measurements

Elemental analyses were performed on a Perkin–Elmer 240 C, H, N analyser. The NMR spectra were recorded on a Brüker 300 NMR spectrometer. IR spectra were recorded as KBr pellets on a Perkin–Elmer 783 spectrometer. Electronic spectra were recorded on a Shimadzu UV–Vis recording spectrophotometer Magnetic susceptibility was measured with a PAR model 155 vibrating sample magnetometer with Hg [$Co(SCN)_4$] as calibrant. Electrochemical data were collected with a BAS CV-27 electrochemical analyser and a BAS model X-Y recorder at 298 K, using a three electrode cell, fitted with a purge gas inlet and outlet, consisting of a platinum working electrode, platinum auxiliary electrode and Ag–AgCl reference electrode. Voltammo-

grams were recorded in DMF solutions of the metal complexes containing 0.1 M tetraethylammonium perchlorate as supporting electrolyte.

3.3. Schiff base ligand preparation

All the four ligands were prepared by a method outlined below. $(NH_2NH)_2CS$ (1.83 g, 17.3 mmol) was dissolved in refluxing solution of 21.6 ml glacial acetic acid and 88.4 ml ethanol. Salicyldehyde (4 ml, 34.5 mmol or appropriate mass of the substituted salicylaldehyde) of dissolved in 15 ml ethanol was added to it. The mixture was refluxed on water bath for 4 h. The pale yellow compound that separated on cooling was filtered out, washed with cold dehydrated ethanol and was dried over fused $CaCl_2$. Yield: 80–85%.

3.4. Synthesis of $[MoO_2LH(MeOH)]$ $[LH = L^1H, L^2H, L^3H, L^4H]$

Compounds **1**–**4** were prepared by a method similar to one reported previously [19] using appropriate ligands (Scheme 1). Schiff base ligand (5 mmol) was dissolved in 100 ml dry methanol under reflux. A filtered solution of $[MoO_2(acac)_2]$ in dry methanol was added to this refluxing solution and was stirred for 0.25 h. The dark orange–red crystalline solid so formed was filtered, washed with cold dry methanol and was dried in vacuum over fused $CaCl_2$. Yield 75–80%.

3.5. Crystallographic measurement

Crystal data sets for complexes **2** and **4** were collected on an Nonius CAD-4 four-circle diffractometer [36] (Table 6) employing graphite-monochromated Mo Kα ($\lambda = 0.71073$ Å) radiation, using ω-scans. A decay correction was applied to the data during data reduction [37]. The structures were solved by direct methods [38] and refined to F_0^2 using all data [39,40]. All hydrogen atoms were seen in a difference Fourier map, except for one hydrogen of the methyl group in each structure. The non-methyl hydrogen atoms were refined freely, each with its own isotropic displacement parameter. The non-hydrogen atoms of the molybdenum complexes were all refined with anisotropic displacement parameters.

4. Supplementary data

Crystallographic data have been deposited with the CCDC, 12, Union Road, Cambridge, CB2 1EZ, UK (fax: +44-1223-366033; e-mail: deposit@ccdc.cam.ac.uk or www: http://www.ccdc.cam.ac.uk) and are available on request, quoting the deposition number 162612 and 162613 for the complex **2** and complex **4**, respectively.

Acknowledgements

Financial assistance received by A.R. from the Council of Scientific and Industrial Research, New Delhi, is gratefully acknowledged.

References

[1] (a) A. Müller, B. Krebs, Sulfur, Its Significance for Chemistry, for the Geo-and Cosmosphere and Technology; Studies in Inorganic Chemistry, vol. 5, Elsevier Science Publishers, Amsterdam, 1984; (b) S.D. Conradsson, B.K. Burgess, W.W. Newton, K.O. Hodgson, J.W. McDonald, J.F. Rubinson, S.F. Gheller, L.E. Mortenson, M.W.W. Adams, P.K. Mascharak, W.A. Armstrong, R.H. Holm, J. Am. Chem. Soc. 107 (1985) 7935; (c) P.M. Harisson, Metalloproteins, Part 1, Metalproteins with Redox Roles, Verlag Chemie, Weinheim, FRG, 1985.
[2] (a) R.H. Holm, J.M. Berg, J. Am. Chem. Soc. 107 (1985) 917; (b) J.H. Enemark, C.G. Young, Adv. Inorg. Chem. 40 (1993) 1; (c) L.J. Laughlin, C.G. Young, Inorg. Chem. 35 (1996) 1050; (d) J. Christiansen, R.C. Tittsworth, B.J. Hales, S.P. Cramer, J. Am. Chem. Soc. 117 (1995) 10017.
[3] R.J. Greenwood, G.L. Wilson, J.R. Pilbrow, A.G. Wedd, J. Am. Chem. Soc. 117 (1993) 5385 (and references therein).
[4] (a) E.I. Stiefel, D. Coucouvanis, W.E. Newton (Eds.), Molybdenum Enzymes, Cofactor and Model Systems, ACS Symposium Series, 535, American Chemical Society, Washington, DC, 1993; (b) G.N. George, R.C. Prince, C.A. Kipke, R.A. Sunde, J.H. Enemark, Biochem. J. 256 (1988) 307.
[5] (a) H.J. Kruger, G. Peng, R.H. Holm, Inorg. Chem. 30 (1991) 734; (b) R.H. Holm, Coord. Chem. Rev. 100 (1990) 183.
[6] A.P. Koley, S. Purohit, S. Ghosh, L.S. Prasad, P.T. Manoharan, J. Chem. Soc., Dalton Trans. (1988) 2607.
[7] (a) S. Purohit, A.P. KoLey, L.S. Prasad, P.T. Manoharan, S. Ghosh, Inorg. Chem. 28 (1989) 3735; (b) P. Subramanian, J.T. Spence, R. Ortega, J.H. Enemark, Inorg. Chem. 36 (1997) 2938.
[8] A.P. Koley, S. Purohit, L.S. Prasad, S. Ghosh, P.T. Manoharan, Inorg. Chem. 31 (1992) 305.
[9] A.P. Koley, R. Nirmala, L.S. Prasad, S. Ghosh, P.T. Manoharan, Inorg. Chem. 31 (1992) 1764.
[10] M. Maji, S. Ghosh, S.K. Chattopadhyay, T.C.W. Mak, Inorg. Chem. 36 (1997) 2938.
[11] M. Maji, M. Chatterjee, S. Ghosh, S.K. Chattopadhyay, B.M. Wu, T.C.W. Mak, J. Chem. Soc., Dalton. Trans. (1999) 135.
[12] M. Maji, S. Ghosh, S.K. Chattopadhyay, Trans. Met. Chem. 23 (1998) 81.
[13] M. Hossain, S.K. Chattopadhyay, S. Ghosh, Polyhedron 16 (1997) 143.
[14] S. Ghosh, S. Purohit, Ind. J. Chem. 26A (1987) 131.
[15] S. Purohit, S. Ghosh, J. Chem. Res. (S). (1988) 158.
[16] S. Purohit, A.P. Koley, S. Ghosh, Polyhedron 9 (1990) 881.
[17] T.N. Srivastava, M. Argawal, Indian J. Chem. 17A (1979) 613.
[18] G.R. Burns, Inorg. Chem. 7 (1968) 277.
[19] C. Bustos, O. Burckhardt, R. Schrebler, D. Carrillo, A.M. Arif, A.H. Cowley, C.M. Nunn, Inorg. Chem. 29 (1990) 3996.
[20] E.I. Stiefel, Prog. Inorg. Chem. 22 (1977) 1.
[21] J.A. Craig, E.W. Harlan, B.S. Snyder, M.A. Whitener, R.H. Holm, Inorg. Chem. 28 (1989) 2082.
[22] R. Hahn, U. Kusthardt, W. Scherer, Inorg. Chem. Acta 210 (1993) 177.
[23] J.M. Berg, R.H. Holm, J. Am. Chem. Soc. 106 (1984) 3035.

[24] I. Buchanan, M. Minelli, M.T. Ashby, J.T. King, J.H. Enemark, C.D. Garner, Inorg. Chem. 23 (1984) 495.
[25] S.K. Dutta, D.B. McConville, W.J. Youngs, M. Chaudhury, Inorg. Chem. 36 (1997) 2517.
[26] J. Liimatainen, A. Lehtonen, R. Sillanpaa, Polyhedron 19 (2000) 1133.
[27] R. Mattes, V. Mikloweit, Inorg. Chem. Acta 122 (1986) L19.
[28] B.B. Kaul, J.H. Enemark, S.L. Merbs, J.T. Spence, J. Am. Chem. Soc. 107 (1985) 2885.
[29] E.I. Steifel, in: G. Wilkinson (Ed.), Comprehensive Coordination Chemistry, Pergamon, Oxford, 1987, p. 1375.
[30] J. Topich, J.T. Lyon, Polyhedron 3 (1984) 55.
[31] Y.-L. Zhai, X.-X. Xu, X. Wang, Polyhedron 11 (1992) 415.
[32] R.H. Holm, E.I. Solomon, Chem. Rev. (1996) 2215.
[33] S. Bhattacharyya, S.B. Kumar, S.K. Dutta, E.R.T. Tiekink, M. Chaudhury, Inorg. Chem. 35 (1996) 1967.
[34] P. Ghosh, P. Bandyopadhyay, A. Chakravorty, J. Chem. Soc., Dalton Trans. (1983) 401.
[35] W.C. Fernelius, K. Terada, B.E. Bryant, Inorg. Synth. 6 (1960) 147.
[36] Diffractometer control program: CAD4-PC Version 1.5c, © 1994, Delft Instruments X-ray Diffraction bv, Delft, The Netherlands.
[37] Data were processed on a Local Area VAScluster (VMS V5.5-2), by the program XCAD4B and with the commercial package SHELXTL-PLUS Release 4.21/V: © 1990, Siemens Analytical X-ray Instruments, Inc., Madison, WI.
[38] G.M. Sheldrick, Acta Crystallogr., Sect. A 46 (1990) 467.
[39] G.M. Sheldrick, SHELXL-93: FORTRAN-77 Program for the Refinement of Crystal Structures from Diffraction Data, University of Göttingen, 1993.
[40] Refinement was done on a Hewlett–Packard 9000 Model 715/50 (HP-UX V9.01).

PERGAMON

Polyhedron 21 (2002) 1031–1041

POLYHEDRON

www.elsevier.com/locate/poly

Steric effects on the stereochemistry of copper complexes of 2,6-bis(pyrazol-1-ylmethyl)pyridines

Caroline L. Foster, Colin A. Kilner, Mark Thornton-Pett, Malcolm A. Halcrow *

School of Chemistry, University of Leeds, Woodhouse Lane, Leeds LS2 9JT, UK

Received 4 December 2001; accepted 25 January 2002

Abstract

The stereochemical preferences of copper complexes of 2,6-bis-(3,5-dimethylpyrazol-1-ylmethyl)pyridine (L^1Me_2) and of 2,6-bis-(phenylpyrazol-1-ylmethyl)pyridine (L^1Ph) have been investigated. The single crystal X-ray structures of $[Cu(OH_2)(L^1Me_2)](BF_4)_2$ and $[CuCl(HOMe)(L^1Me_2)]BF_4$ show near-regular tetragonal geometries with one or two axial solvent and/or BF_4^- ligands. In contrast, $[Cu(OH_2)_2(L^1Ph)](BF_4)_2$ adopts an irregular geometry in the crystal mid-way between square-pyramidal and trigonal-bipyramidal. The single crystal X-ray structure of $[Cu(NCMe)(L^1Me_2)]BF_4$ exhibits a distorted tetrahedral geometries, while $[Cu(L^1Ph)]BF_4$ adopts a T-shaped stereochemistry. By a combination of UV–Vis, EPR and conductivity studies, the solution structures of $[CuCl_2(L)]$, $[CuCl(solv)(L)]BF_4$ and $[Cu(solv)_x(L)](BF_4)_2$ ($L = L^1Me_2$, L^1Ph; solv = H_2O, MeCN; $x = 1$, 2) have, in many cases, been shown to be the same as in the crystalline state. The cyclic voltammograms of $[Cu(OH_2)(L^1Me_2)](BF_4)_2$ and $[Cu(OH_2)_2(L^1Ph)](BF_4)_2$ in MeCN/0.1 M $NBu^n_4BF_4$ exhibit chemically reversible Cu(II/I) couples. © 2002 Elsevier Science Ltd. All rights reserved.

Keywords: Copper complexes; Stereochemistry; X-ray structures; Steric properties

1. Introduction

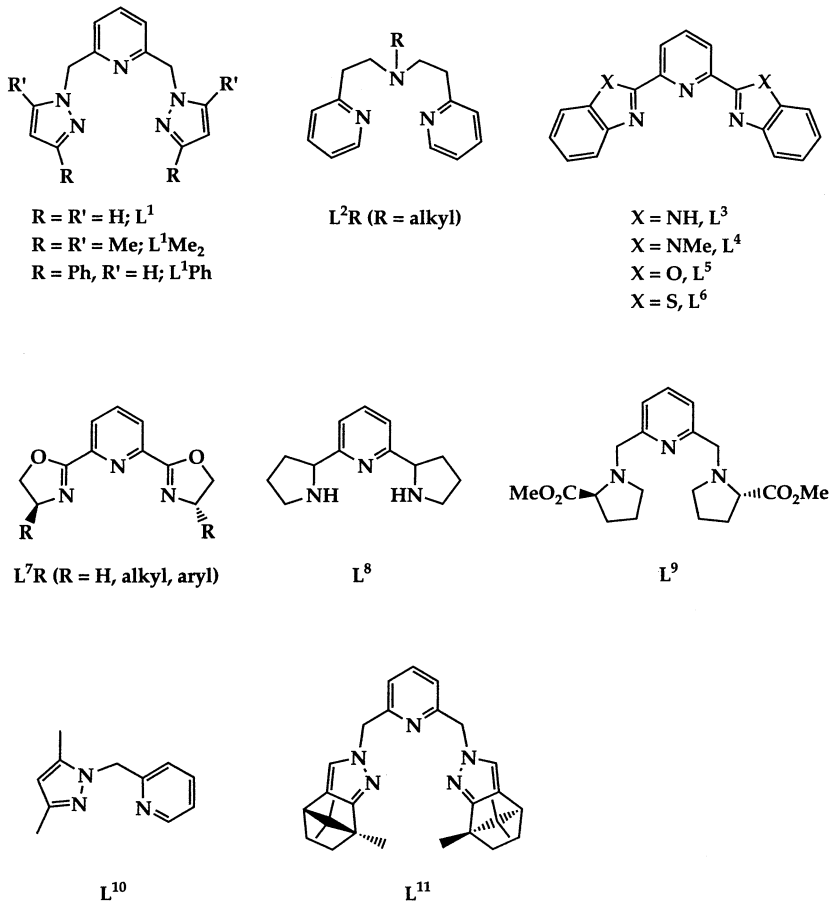
Much of the biomimetic Cu(II) chemistry that has been published over the past 15 years employs facially or meridionally coordinating *tris*-N-donor ligands as protecting groups [1–4]. These are intended to mimic the $[Cu(II)(his)_3L]^{n+}$ ($L = OH^-$, $n = 1$; $L = OH_2$, $n = 2$) centres found in many Type 2 copper [5,6], and all Type 3 and multi-copper [7], proteins. However, despite their utility in this regard, relatively few systematic studies of the stereochemical preferences of Cu(II) centres using this type of ligand have been carried out. This is an important question since, in contrast to many other biometals, the Cu(II) ion readily adopts a wide range of stereochemistries [8]. This can make its chemistry unpredictable and difficult to study, particularly in the absence of strongly coordinating anions.

This paper describes a crystallographic and spectroscopic investigation of the Cu(I) and Cu(II) chemistries of two ligands, L^1Me_2 and L^1Ph (Scheme 1), in the presence and absence of a coordinating anion. Our results complement data from Manoharan and Mukherjee, who reported several compounds of type $[CuX_2(L^1Me_2)]$ (X^- = halide, pseudohalide, NO_2^- or NO_3^-) while our own work was in progress [9–12], and offer a good example of how the Cu(I) and Cu(II) ions adapt their coordination environments in response to steric crowding from the L^1R protecting group. We are aware of only a few similar studies involving other *tris*-N donor ligands. The most relevant example is L^2R, which Karlin and Réglier have shown to cleanly form tetrahedral $[Cu(solv)(L^2R)]^+$ and tetragonal $[Cu(solv)_2(L^2R)]^{2+}$ (solv = MeCN, H_2O) complexes with weakly coordinating anions like triflate and perchlorate [13]. These stereochemistries resemble the structures exhibited by Type 2 and 3 copper biosites, which has contributed to the utility of L^2R ligands in biomimetic Cu chemistry [3,4]. The complexes of L^3–L^9 with Cu(II) salts of weakly coordinating anions have also been studied by Williams [14], Evans [15], and

* Corresponding author. Tel.: +44-113-343-6506; fax: +44-113-343-6565.

E-mail address: m.a.halcrow@chem.leeds.ac.uk (M.A. Halcrow).

0277-5387/02/$ - see front matter © 2002 Elsevier Science Ltd. All rights reserved.
PII: S0277-5387(02)00872-0



Scheme 1. Ligands referred to in this study.

Bernauer [16]. However, L^3–L^5 and L^7R form helical dimeric complexes with Cu(I) that are not biomimetically relevant [17].

2. Results and discussion

The ligand L^1Me_2 was prepared by the literature method [18], while the new ligand L^1Ph was synthesised in good yield from 3{5}-phenylpyrazole [19] and 2,6-bis-(chloromethyl)pyridine [20], following the literature procedure for L^1 [21].

2.1. Copper(I) complexes of L^1R

Complexation of $[Cu(NCMe)_4]BF_4$ by 1 mole equiv. of L^1Me_2 in MeCN under N_2 gave an air-sensitive yellow solution. Layering of this solution with Et_2O afforded air-stable yellow crystals of $[Cu(NCMe)(L^1Me_2)]BF_4$ (**1**) in low yield, together with a larger amount of unreacted $[Cu(NCMe)_4]BF_4$ which was removed manually. Similar reactions in $MeNO_2$ or CH_2Cl_2 afforded a mixture of **1** and a new pale yellow solid, which we were unable to obtain in analytical purity from this mixture. The FAB mass spectrum of this latter species was identical to that of **1**, while its IR spectrum demonstrated the presence of BF_4^- and L^1Me_2 only. Hence, we tentatively formulate this second complex as solvent-free $[Cu(L^1Me_2)]BF_4$. In contrast to the above reactions, treatment of $[Cu(NCMe)_4]BF_4$ with an equimolar amount of L^1Ph in MeCN, followed by precipitation with Et_2O as before, cleanly afforded the pale yellow air-stable compound $[Cu(L^1Ph)]BF_4$ (**2**).

Single crystals of formula $[Cu(NCMe)(L^1Me_2)]BF_4$ (**1**) and $[Cu(L^1Ph)]BF_4$ (**2**) were grown by layering solutions of the complexes in MeCN and $MeNO_2$, respectively, with Et_2O under N_2. The structure of **1** shows an irregular, distorted tetrahedral geometry at Cu(1) (Fig. 1, Table 1), which is, however, similar to those previously described for $[Cu(PPh_3)(L^1Me_2)]ClO_4$ and $[\{Cu(L^1Me_2)\}_2(\mu\text{-dppe})](ClO_4)_2$ [22]. Of particular interest are the unequal angles N(10)–Cu(1)–N(24) and N(18)–Cu(1)–N(24), and the fact that all four Cu–N bond lengths are significantly different. There are no intramolecular steric contacts that would account for these irregularities. However, the packing diagram of **1** shows there is a close contact between C(26) and F(30′) (symmetry operation $x, -1+y, z$) of 3.352(2) Å, which would appear to prevent the MeCN ligand from occupying its idealised position in the coordination

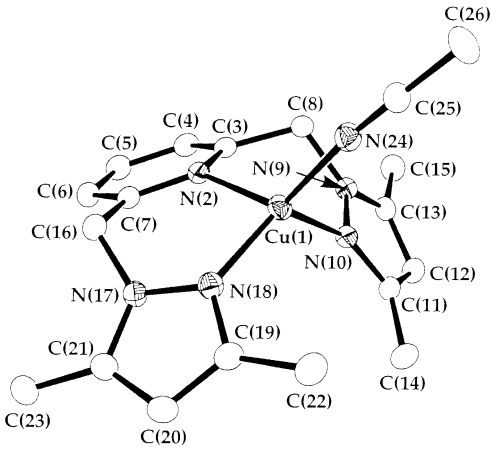


Fig. 1. View of the $[Cu(NCMe)(L^1Me_2)]^+$ complex cation in the structure of **1**, showing the atom numbering scheme employed. Thermal ellipsoids are drawn at the 35% probability level. For clarity, all C-bound H atoms have been omitted.

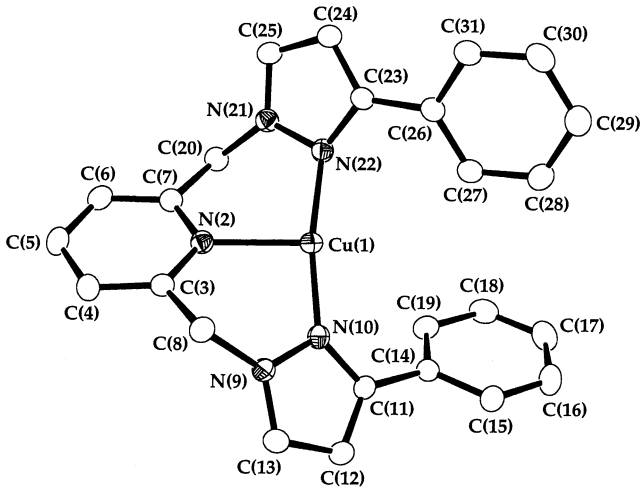


Fig. 2. View of the $[Cu(L^1Ph)]^+$ complex cation in the structure of **2**, showing the atom numbering scheme employed. Details as for Fig. 1.

Table 1
Selected bond lengths (Å) and angles (°) in the single crystal X-ray structures of $[Cu(NCMe)(L^1Me_2)]BF_4$ (**1**) and $[Cu(L^1Ph)]BF_4$ (**2**)

1		**2**	
Bond lengths			
Cu(1)–N(2)	2.1198(12)	Cu(1)–N(2)	2.108(2)
Cu(1)–N(10)	2.1044(13)	Cu(1)–N(10)	1.914(2)
Cu(1)–N(18)	1.9922(13)	Cu(1)–N(22)	1.9175(19)
Cu(1)–N(24)	1.9425(14)		
Bond angles			
N(2)–Cu(1)–N(10)	89.10(5)	N(2)–Cu(1)–N(10)	94.74(8)
N(2)–Cu(1)–N(18)	95.16(5)	N(2)–Cu(1)–N(22)	96.01(8)
N(2)–Cu(1)–N(24)	124.42(6)	N(10)–Cu(1)–N(22)	168.72(8)
N(10)–Cu(1)–N(18)	120.84(5)		
N(10)–Cu(1)–N(24)	103.27(5)		
N(18)–Cu(1)–N(24)	121.04(6)		

sphere. Hence, these molecular distortions can probably be attributed to intermolecular steric contacts.

The complex cation in **2** has a regular T-shaped geometry (Fig. 2, Table 1). The bonds Cu(1)–N(10) and Cu(1)–N(22) are now crystallographically equal, while the angle N(10)–Cu(1)–N(22) has increased to 168.74(8)°, compared with the equivalent angle in **1** of 120.84(5)°. Despite this large variation in *trans*-N–Cu–N angle, the chelate bite angle of the L^1R ligand varies only slightly in the two structures, from an average of 92.14(7)° in **1** to 95.36(11)° in **2**. Rather, these differences reflect differing chelate ring conformations in the structures, which are chair-like in **1** and boat-like in **2**.

2.2. Syntheses and crystal structures of copper(II) complexes of L^1R

Complexation of hydrated $Cu(BF_4)_2$ by an equimolar amount of L^1Me_2 in $MeNO_2$, followed by diffusion of Et_2O into the resultant solution, yielded hygroscopic dark blue microcrystals. Upon prolonged drying in vacuo, these transformed to a blue powder that analysed consistently as $[Cu(OH_2)(L^1Me_2)](BF_4)_2\cdot H_2O$ (**3**·H_2O). Since the crystallographic analysis of this material (see below) showed only 1 mole equiv. of water, it is uncertain whether the second mole of water absorbed by the 'dried' solid is coordinated to the copper ion. A similar reaction employing L^1Ph gave a red–brown crystalline solid $[Cu(OH_2)_2(L^1Ph)](BF_4)_2$ (**4**). Green, sparingly soluble $[CuCl_2(L^1Me_2)]$ (**5**) [9] and $[CuCl_2(L^1Ph)]$ (**6**) were also prepared, by treatment of $CuCl_2$ with the appropriate ligand in MeCN. Reaction of these solids with 1 molar equiv. of $AgBF_4$ in MeCN yielded blue ($L = L^1Me_2$) or green ($L = L^1Ph$) solutions, which were evaporated to dryness. Recrystallisation of the crude materials from MeOH–Et_2O gave $[CuCl(HOMe)(L^1Me_2)]BF_4$ (**7**) and $[CuCl(OH_2)(L^1Ph)]BF_4$ (**8**) as microcrystalline solids.

Single crystals of formula $[Cu(OH_2)(L^1Me_2)](BF_4)_2$ (**3**) and $[CuCl(HOMe)(L^1Me_2)]BF_4$ (**7**) were grown by vapour diffusion from MeOH–Et_2O. Crystals of $[Cu(OH_2)_2(L^1Ph)](BF_4)_2$ (**4**) were similarly obtained from $MeNO_2$–Et_2O. The molecular structures of **3** and **7** are rather similar. Complex **3** contains a near-regular square-planar $[Cu(OH_2)(L^1Me_2)]^{2+}$ centre (Fig. 3, Table 2; structure A in Scheme 2) with a τ index [23] of 0.10, which is very close to the ideal value of 0 for a regular square-pyramid. There are weak axial interactions between Cu(1) and both BF_4^- anions to yield a [4+2] tetragonal Cu(II) ion [Cu(1)···F(26) = 2.531(2), Cu(1)···F(34) = 3.049(3) Å]. Both anions are also involved in hydrogen-bonding to the aqua ligand. One anion interacts with the aqua ligand on the same cation to which it forms an axial interaction. The other (disordered) anion forms hydrogen bonds to a neighbouring cation, yielding a 1-D polymeric lattice composed of alternating Cu···F and F···H–O interactions.

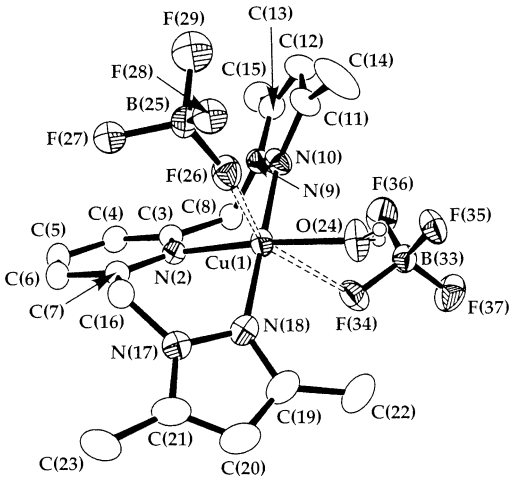


Fig. 3. View of the $[Cu(OH_2)(L^1Me_2)](BF_4)_2$ moiety in the structure of **3**, showing the atom numbering scheme employed. Details as for Fig. 1. For clarity, only one orientation of the disordered BF_4^- anion B(25)–F(29) is shown.

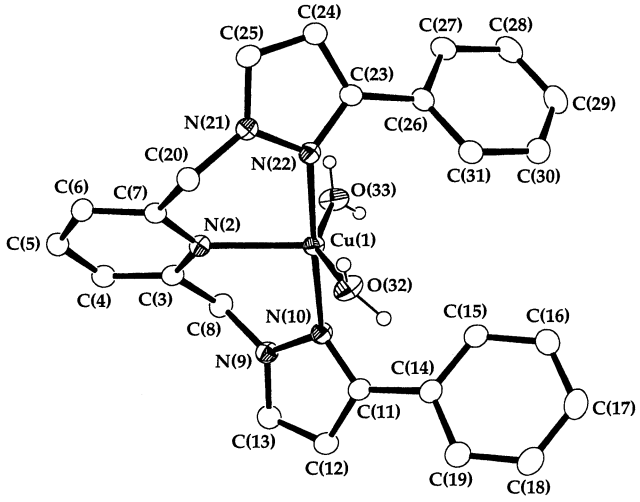


Fig. 4. View of the $[Cu(OH_2)_2(L^1Ph)]^{2+}$ complex dication in the structure of **4**, showing the atom numbering scheme employed. Details as for Fig. 1.

In **7**, the copper ion also adopts structure A (Scheme 2), with an apical MeOH ligand [Cu(1)–O(25) = 2.362(3) Å, $\tau = 0.11$] (Fig. 5, Table 2). The cations in the crystal are arranged into dimers, by hydrogen-bonding between the MeOH hydroxyl proton and a Cl^- ligand of a neighbouring cation related by $1-x, -y, 1-z$.

In contrast to the L^1Me_2 compounds, the copper ion in **4** has an irregular five-coordinate structure, which corresponds to structure B in Scheme 2 (Fig. 4, Table 2). This structure could be considered as trigonal-bipyramidal with the pyrazole N-donors axial [N(10)–Cu(1)–N(22) = 177.84(6)°], or as square-pyramidal with the pyridine N-donor apical [Cu(1)–N(2) = 2.1879(15) Å]. The τ index for this compound is in fact 0.46, almost exactly midway between the limiting values for a regular square-pyramid ($\tau = 0$) or trigonal-bipyramid ($\tau = 1$) [23]. The four protons on the water ligands in **4** are each hydrogen bonded to a different BF_4^- anion, forming a 1-D chain polymer motif in the crystal.

2.3. Conductivity, UV–Vis and EPR measurements

Solution UV–Vis and conductivity data for the Cu(II) compounds in this study, in both MeCN and $MeNO_2$ solutions, are listed in Table 3. Conductivity measurements for all of the Cu(II) complexes in this study were consistent with their solid state molecular structures. Hence, complexes **5** and **6** exhibit molar conductivities consistent with their being non-electrolytes in both these solvents, while **7** and **8** are clearly 1:1 electrolytes and **3** and **4** are 2:1 electrolytes [24]. This demonstrates that Cl^--dissociation does not take place upon dissolution of the chloride-containing complexes in MeCN or $MeNO_2$, which is consistent with an earlier study of **5** in dmf solution [9].

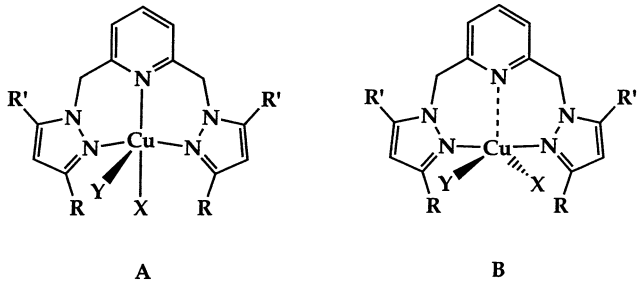
The visible spectra of **3**–**8** each exhibit a single d–d band (Table 3). The d–d spectra of **5**–**7** are essentially identical in MeCN and $MeNO_2$. This shows that they adopt the same molecular structures in these two solvents, and that dissociation of Cl^- or the L^1R ligand does not take place upon dissolution. However, the d–d maximum for **8** lies at a slightly lower wavelength in $MeNO_2$ than in MeCN. This suggests that, although the coordination geometry of **8** probably does not vary between the two solvents, solvent coordination is more important to the solution structure of **8** than **7**. Unsurprisingly, the d–d maxima of **3** and **4** are very solvent dependent. For **3**, **4** and **8**, the d–d maxima lie at longer wavelength in MeCN than in $MeNO_2$, which is consistent with the relative positions in the spectrochemical series of MeCN and H_2O [25] (the probable 'solv' ligand in $MeNO_2$, since $MeNO_2$ itself is an extremely poor ligand [26]).

As solids, the X-band EPR spectra of **4**–**6** and **8** are well-resolved into a clearly rhombic pattern, the g-values for each of these compounds being quite similar (Table 4). We, therefore, propose that **6** and **8** adopt structure B (Scheme 2) in the solid, as do **4** and **5** in the crystal [10]. The solid state EPR spectrum of **7** is distinct from the others and is clearly axial, with the $g_\parallel > g_\perp > g_e$ pattern and an $A_\parallel\{^{63,65}Cu\}$ value typical of a tetragonal $\{d_{x^2-y^2}\}^1$ or $\{d_{xy}\}^1$ Cu(II) species [27]. This is consistent with the crystal structure of this complex. The powder EPR spectrum of **3** is broad and unresolved.

The frozen solution EPR spectra of **6** and **8** in 10:1 MeCN:toluene and 10:1 $MeNO_2$:toluene are isotropic and uninformative. In contrast, **3**–**5** and **7** all exhibit axial or pseudo-axial frozen solution EPR spectra with $g_\parallel > g_\perp > g_e$, that are again consistent with $\{d_{x^2-y^2}\}^1$ or $\{d_{xy}\}^1$ Cu(II) species (Table 4) [27]. Hence, it seems clear that **3** and **7** both retain their crystallographic tetragonal geometry upon dissolution. However, there are some

Table 2
Selected bond lengths (Å) and angles (°) in the single crystal X-ray structures of $[Cu(OH_2)(L^1Me_2)](BF_4)_2$ (**3**), $[Cu(OH_2)_2(L^1Ph)](BF_4)_2$ (**4**) and $[CuCl(HOMe)(L^1Me_2)]BF_4$ (**7**)

3		**4**		**7**	
Bond lengths					
Cu(1)–N(2)	2.011(3)	Cu(1)–N(2)	2.1879(15)	Cu(1)–N(2)	2.063(3)
Cu(1)–N(10)	1.963(3)	Cu(1)–N(10)	1.9935(15)	Cu(1)–N(10)	2.025(3)
Cu(1)–N(18)	1.974(3)	Cu(1)–N(22)	1.9987(16)	Cu(1)–N(18)	2.016(3)
Cu(1)–O(24)	1.958(3)	Cu(1)–O(32)	2.0194(16)	Cu(1)–Cl(24)	2.2573(10)
Cu(1)–F(26)	2.531(2)	Cu(1)–O(33)	2.0276(16)	Cu(1)–O(25)	2.362(3)
Cu(1)–F(34)	3.049(3)				
Bond angles					
N(2)–Cu(1)–N(10)	90.06(12)	N(2)–Cu(1)–N(10)	90.12(6)	N(2)–Cu(1)–N(10)	84.28(12)
N(2)–Cu(1)–N(18)	89.11(12)	N(2)–Cu(1)–N(22)	91.97(6)	N(2)–Cu(1)–N(18)	89.58(12)
N(2)–Cu(1)–O(24)	172.36(14)	N(2)–Cu(1)–O(32)	97.49(7)	N(2)–Cu(1)–Cl(24)	174.32(9)
N(2)–Cu(1)–F(26)	101.11(10)	N(2)–Cu(1)–O(33)	112.24(6)	N(2)–Cu(1)–O(25)	91.52(11)
N(2)–Cu(1)–F(34)	102.25(9)	N(10)–Cu(1)–N(22)	177.84(6)	N(10)–Cu(1)–N(18)	168.02(13)
N(10)–Cu(1)–N(18)	178.64(12)	N(10)–Cu(1)–O(32)	89.44(7)	N(10)–Cu(1)–Cl(24)	93.15(9)
N(10)–Cu(1)–O(24)	90.58(14)	N(10)–Cu(1)–O(33)	87.60(7)	N(10)–Cu(1)–O(25)	103.70(12)
N(10)–Cu(1)–F(26)	91.42(10)	N(22)–Cu(1)–O(32)	89.73(7)	N(18)–Cu(1)–Cl(24)	92.01(10)
N(10)–Cu(1)–F(34)	81.81(10)	N(22)–Cu(1)–O(33)	92.12(7)	N(18)–Cu(1)–O(25)	86.70(12)
N(18)–Cu(1)–O(24)	90.10(14)	O(32)–Cu(1)–O(33)	150.12(7)	Cl(24)–Cu(1)–O(25)	94.02(8)
N(18)–Cu(1)–F(26)	89.80(10)				
N(18)–Cu(1)–F(34)	97.31(10)				
O(24)–Cu(1)–F(26)	86.49(12)				
O(24)–Cu(1)–F(34)	70.32(11)				
F(26)–Cu(1)–F(34)	155.65(7)				



Scheme 2. Coordination geometries exhibited by $[CuXY(L^1R)]^{n+}$ complexes.

differences between the EPR spectra of **4** and **5** in these two phases. Therefore, the detailed stereochemistries of **4**–**6** and **8** in solution are presently uncertain. Importantly, for all complexes where the comparison could be made, these spectra are essentially invariant between solvents, suggesting that changing the identity of solvent ligands to the $[CuCl_x(solv)_{2-x}(L^1R)]^{(2-x)+}$ $(x = 0–2)$ centres barely perturbs the coordination geometry at Cu.

2.4. Electrochemistry

A preliminary voltammetric study was carried out in MeCN/0.1 M $NBu^n_4PF_6$ at 293 K, to elucidate the potentials of the $[Cu(solv)_xL]^{2+}/[Cu(solv)_yL]^{+}$ (L = L^1Me_2, L^1Ph) couples. Cyclic voltammograms (CVs)

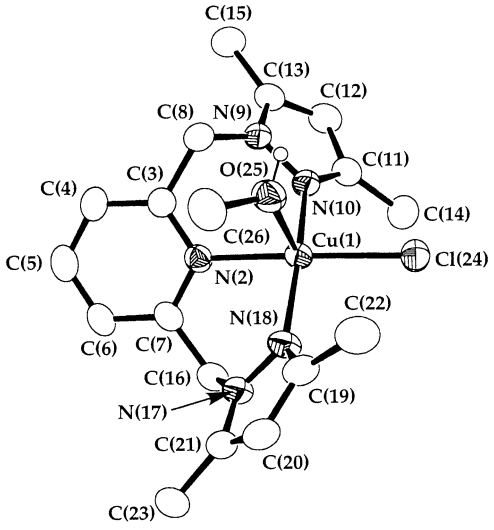


Fig. 5. View of the $[CuCl(HOMe)(L^1Me_2)]^{+}$ complex cation in the structure of **7**, showing the atom numbering scheme employed. Details as for Fig. 1.

of Cu(II) and Cu(I) complexes containing each ligand were run for comparison; in each case, the CVs obtained from the oxidised and reduced congeners of a given couple showed only small differences (Table 5).

For each Cu(II) complex **3** and **4**, a chemically reversible Cu(II/I) couple was obtained. However, plots of Ip versus $v^{1/2}$ (v = scan rate) for these processes did not give a straight line, showing that these couples are

Table 3
Conductivity and UV–Vis spectroscopic data for the Cu(II) compounds in this study (293 K)

	Solvent	Λ_M, Ω^{-1} cm^2 mol^{-1}	λ_{max}, nm (ε_{max}, M^{-1} cm^{-1})
$[Cu(OH_2)(L^1Me_2)](BF_4)_2\cdot H_2O$ (**3**·H_2O)	MeCN	219	260 (6,000), 319 (sh), 645 (69)
	$MeNO_2$	132	612 (70)
$[Cu(OH_2)_2(L^1Ph)](BF_4)_2$ (**4**)	MeCN	207	254 (39,000), 329 (2,200), 458 (280), 802 (70)
	$MeNO_2$	142	689 (70)
$[CuCl_2(L^1Me_2)]$ (**5**)	MeCN	8	267 (6,100), 345 (1,200), 768 (180)
	$MeNO_2$	6	766 (170)
$[CuCl_2(L^1Ph)]$ (**6**)	MeCN	13	254 (87,000), 343 (sh), 453 (150), 807 (139)
	$MeNO_2$	8	808 (135)
$[CuCl(HOMe)(L^1Me_2)]BF_4$ (**7**)	MeCN	128	268 (6,800), 340 (560), 692 (80)
	$MeNO_2$	79	688 (83)
$[CuCl(OH_2)(L^1Ph)]BF_4$ (**8**)	MeCN	112	248 (34,600), 332 (2,800), 413 (sh), 752 (142)
	$MeNO_2$	64	739 (145)

Table 4
X-band EPR data for the Cu(II) complexes in this study

		g_1	g_2	g_3	A_1
$[Cu(OH_2)(L^1Me_2)](BF_4)_2\cdot H_2O$ (**3**·H_2O)	Powder	2.07			
	MeCN	2.28	2.07	2.07	174
	$MeNO_2$	2.26	2.07	2.07	184
$[Cu(OH_2)_2(L^1Ph)](BF_4)_2$ (**4**)	Powder	2.30	2.15	2.04	
	MeCN	2.33	2.12	2.12	144
	$MeNO_2$	2.31	2.13	2.13	143
$[CuCl_2(L^1Me_2)]$ (**5**)	Powder	2.26	2.10	2.03	
	MeCN	2.29	2.10	2.10	161
	$MeNO_2$		2.12		
$[CuCl_2(L^1Ph)]$ (**6**)	Powder	2.28	2.09	2.04	
	MeCN		2.14		
	$MeNO_2$		2.14		
$[CuCl(HOMe)(L^1Me_2)]BF_4$ (**7**)	Powder	2.26	2.06	2.06	170
	MeCN	2.27	2.08	2.08	166
	$MeNO_2$	2.27	2.08	2.08	172
$[CuCl(OH_2)(L^1Ph)]BF_4$ (**8**)	Powder	2.28	2.10	2.04	
	MeCN		2.14		
	$MeNO_2$		2.14		

All spectra were obtained at 120 K. Hyperfine couplings are to ^{63,65}Cu and are in G. All solution spectra were run in solvents containing 10% toluene to aid glassing. Spectra with only one g value quoted are isotropic.

not electrochemically reversible. This probably reflects the kinetics of solvent coordination or decoordination that take place following Cu-based redox at these centres. The **1/3** couple is approximately 0.6 V more positive than the Cu(II/I) reduction previously reported for **5** in dmf [9], consistent with the presence of more strongly donating Cl^- coligands in the latter compound. Interestingly, the **2/4** couple is approximately +0.15 V more positive than the **1/3** couple, showing that the identity of the L^1R 'R' substituents has a substantial effect on the redox chemistry of the coordinated Cu ion.

3. Concluding remarks

Within the $[Cu(solv)_x(L^1R)]^{2+}/[Cu(solv)_y(L^1R)]^+$ system there are substantial structural variations, which appear to depend upon the identity of both 'R' and the exogenous ligands 'solv'. For the Cu(I) complexes, the ability of a $[Cu(L^1R)]^+$ fragment to bind exogenous ligands is dependent on the identity of 'R'. This is

Table 5
Cyclic voltammetric data for the complexes in this study (MeCN/0.1 M $NBu^n_4BF_4$, 298 K, $\nu = 100$ mV s^{-1})

	$E_{1/2}$ {Cu(II/I)} (V) (ΔEp, mV)	Epc{Cu(I/0)} (V)
$[Cu(NCMe)(L^1Me_2)]BF_4$ (**1**)	+0.14 (220)	−1.18
$[Cu(L^1Ph)]BF_4$ (**2**)	+0.29 (88)	−0.91
$[Cu(OH_2)(L^1Me_2)](BF_4)_2\cdot H_2O$ (**3**·H_2O)	+0.18 (244)	−1.20
$[Cu(OH_2)_2(L^1Ph)](BF_4)_2$ (**4**)	+0.33 (146)	−0.89

All potentials quoted vs. an internal ferrocene/ferrocenium standard.

presumably a steric effect, since the greater basicity of 3,5-dimethylpyrazole compared with 3{5}-phenylpyrazole [28] suggests that the $[Cu(L^1Ph)]^+$ moiety should be *less* electron-rich [29], and so more likely to bind exogenous ligands, than $[Cu(L^1Me_2)]^+$. This being the case, it is uncertain whether the lower oxidation potential of **1** compared with **2** is driven by the more donating character of L^1Me_2 compared with L^1Ph [29], or by the higher co-ordination number at Cu in **1**.

Combining our results with earlier work (Table 4), it is clear that $[Cu(II)XY(L^1R)]^{n+}$ (X, Y = halide, pseudohalide or solvent, $n = 0$–2) complexes can adopt one of two limiting geometries; tetragonal, with Y apical (structure A in Scheme 2); or, tetragonal with the L^1R pyridyl group apical (structure B). The available data suggest that these structural types can be distinguished by EPR spectroscopy (Table 6). All structurally authenticated type A complexes exhibit axial $g_\parallel > g_\perp \approx 2.07$ powder EPR spectra, where these can be clearly resolved, while all known type B complexes show strongly rhombic powder EPR spectra, with $g_3 \leq 2.04$. Bulky L^1R 'R' substituents appear to favour structure B, since EPR data show that all of the L^1Ph-containing complexes in this work exhibit structure B in the solid. Most of the L^1Me_2 complexes follow the trend expected on steric grounds, in that $[CuXY(L^1Me_2)]$ (X = Y = Cl, Br) adopt structure B while those complexes containing smaller N- or O-donor X and Y ligands exhibit structure A. However, the anomalous observation that $[Cu(N_3)_2(L^1Me_2)]$ is a structure B complex [9,12] suggests that electronic, as well as steric, factors might play a role in the stereochemistry of Cu(II)–L^1R complexes.

4. Experimental

Unless stated otherwise, all manipulations were performed in air using commercial grade solvents. 2,6-Bis-(chloromethyl)pyridine [20], 3-phenylpyrazole [19], L^1Me_2 [18], $[Cu(NCCH_3)_4]BF_4$ [30] and $[CuCl_2(L^1Me_2)]$ (**5**) [9,10] were prepared by the literature procedures. $Cu(BF_4)_2{\cdot}6H_2O$ (Avocado), KH (Aldrich) and all solvents were used as supplied, except that diglyme was dried over sodium before use. Microanalytical, mass spectrometric, UV–Vis, EPR and conductivity data for the complexes are listed in Tables 3, 4 and 7.

4.1. Synthesis of 2,6-bis-({3-phenylpyrazol-1-yl}methyl)pyridine (L^1Ph)

A mixture of 3-phenylpyrazole (15.9 g, 0.11 mol) and NaH (4.0 g, 0.11 M) in dry THF (50 cm^3) was stirred at 60 °C under N_2 for 30 min. 2,6-Bis-(chloromethyl)pyridine (9.7 g, 0.055 mol) was then added, and the mixture stirred at 60 °C for 24 h. The solvent was removed under reduced pressure and the residue taken up in chloroform (3×50 cm^3). The combined organic fractions were washed with water and saturated aqueous NaCl, then dried over $MgSO_4$. The filtered solution was evaporated to dryness to leave an off-white solid which was recrystallised from thf–Et_2O. Yield 15.0 g, 70% (Found: C, 76.7; H, 5.3; N, 18.1; Calc. for $C_{25}H_{21}N_5$: C, 76.4; H, 5.4; N, 17.8%). M.p. 98–100 °C. EI mass spectrum: m/z 391 $[M]^+$, 248 $[M-pz^{Ph}]^+$, 157 $[CH_2pz^{Ph}]^+$, 144 $[Hpz^{Ph}]^+$, 77 $[C_5H_3N]^+$. NMR spectra ($\{CD_3\}_2SO$, 293 K): ^1H; δ 7.93 (d, 2.3 Hz, 2H, Pz H^5), 7.77 (m, 5H, Ph $H^{2/6}$+Py H^4), 7.38 (m, 6H, Ph $H^{3/5}$+Ph H^4), 6.98 (d, 7.8 Hz, 2H, Py $H^{3/5}$), 6.78 (d, 2.3 Hz,

Table 6
Structural types and powder EPR spectra exhibited by crystallographically characterised Cu(II) 2,6-bis(pyrazolyl-1-ylmethyl)pyridine complexes

	Structure type [a]	τ [b]	g_1	g_2	g_3	Reference
$[Cu(OH_2)(L^1Me_2)](BF_4)_2$ (**3**)	A	0.10		2.07 [c]		This work
$[Cu(ONO_2)_2(L^1Me_2)]$	A	0.10		2.067 [c]		[10]
$[CuCl(HOMe)(L^1Me_2)]BF_4$ (**7**)	A	0.11	2.26	2.06	2.06	This work
$[Cu(ONO)(OClO_3)(L^1Me_2)]$	A	0.13	2.200	2.078	2.078	[12]
$[Cu(L^{10})(L^1Me_2)](ClO_4)_2$ [d]	A	0.14		2.076 [c]		[9]
$[Cu(NCS)_2(L^1Me_2)]$	A	0.26	2.258	2.085	2.085	[10,11]
$[CuBr_2(L^1Me_2)]$	B	0.14	2.236	2.105	2.041	[10]
$[CuCl_2(L^1Me_2)]$	B	0.16	2.252	2.092	2.027	This work, [10]
$[Cu(N_3)_2(L^1Me_2)]$	B	0.37	2.236	2.105	2.041	[9,12]
$[Cu(OH_2)_2(L^1Ph)](BF_4)_2$ (**4**)	B	0.46	2.30	2.15	2.04	This work
$[Cu(NCS)_2(L^{11})]$ [d]	B	0.45		[e]		[20]

[a] Scheme 2.
[b] Ref. [23].
[c] Broad, apparently isotropic spectrum.
[d] Scheme 1.
[e] Not reported.

Table 7
Analytical and selected FAB mass spectrometric data for the complexes in this study

		Found (Calc.)			
	Colour	%C	%H	%N	*m/z*
$[Cu(NCMe)(L^1Me_2)]BF_4$ (**1**)	Yellow	46.8 (46.9)	5.1 (5.0)	17.6 (17.3)	358
$[Cu(L^1Ph)]BF_4$ (**2**)	Pale yellow	55.3 (55.4)	3.9 (3.9)	13.2 (12.9)	454
$[Cu(OH_2)(L^1Me_2)](BF_4)_2\cdot H_2O$ (**3**·H_2O)	Blue	35.7 (35.9)	4.2 (4.4)	12.6 (12.3)	377, 358
$[Cu(OH_2)_2(L^1Ph)](BF_4)_2$ (**4**)	Red-brown	45.0 (45.2)	3.7 (3.8)	10.5 (10.5)	473, 454
$[CuCl_2(L^1Me_2)]$ (**5**)	Green	47.3 (47.5)	4.9 (4.9)	16.5 (16.3)	393, 358
$[CuCl_2(L^1Ph)]$ (**6**)	Green	56.0 (56.9)	3.9 (4.0)	13.5 (13.3)	489, 454
$[CuCl(HOMe)(L^1Me_2)]BF_4$ (**7**)	Blue	42.1 (42.1)	4.8 (4.9)	14.3 (13.6)	393, 358
$[CuCl(OH_2)(L^1Ph)]BF_4$ (**8**)	Brown	50.6 (50.4)	4.1 (3.9)	11.7 (11.8)	489, 454

2H, Pz H^4), 5.50 (s, 4H, CH_2). ^{13}C; δ 157.4 (Py $C^{2/6}$), 151.1 (Pz C^3), 138.0 (Py C^4+Pz C^5), 133.9 (Ph C^1), 129.7 (Ph $C^{2/6}$), 127.2 (Ph $C^{3/5}$), 125.0 (Ph C^4), 120.7 (Py $C^{3/5}$), 103.3 (Pz C^4), 57.6 (CH_2).

4.2. Synthesis of acetonitrile[2,6-bis-({3,5-dimethylpyrazol-1-yl}methyl)pyridine]copper(I) tetrafluoroborate (*1*)

A solution of L^1Me_2 (0.25 g, 8.4×10^{-4} mol) and $[Cu(NCMe)_4]BF_4$ (0.26 g, 8.4×10^{-4} mol) in MeCN (25 cm^3) was stirred under N_2 for 10 min at room temperature (r.t.). The yellow solution was concentrated to approximately 5 cm^3 and layered with Et_2O, affording a mixture of pale yellow needles and colourless blocks that were separated manually for analysis. The colourless crystals were identified as $[Cu(NCMe)_4]BF_4$ by comparison with a genuine sample. Yield of yellow crystals that were sufficiently large to separate by hand 0.064 g, 8%. IR spectrum (Nujol): 2310w, 2275w cm^{-1}.

4.3. Synthesis of [2,6-bis-({3-phenylpyrazol-1-yl}methyl)pyridine]copper(I) tetrafluoroborate (*2*)

A solution of L^1Ph (0.25 g, 6.4×10^{-4} mol) and $[Cu(NCMe)_4]BF_4$ (0.20 g, 6.4×10^{-4} mol) in $MeNO_2$ (25 cm^3) was stirred under N_2 for 10 min at r.t. The yellow solution was concentrated to approximately 5 cm^3 and layered with Et_2O, affording pale yellow needles. Yield 0.16 g, 47%.

4.4. Synthesis of [2,6-bis-({3,5-dimethylpyrazol-1-yl}methyl)pyridine]aquacopper(II) ditetrafluoroborate (*3*)

A solution of L^1Me_2 (0.25 g, 8.4×10^{-4} mol) and $Cu(BF_4)_2\cdot6H_2O$ (0.29 g, 8.4×10^{-4} mol) in $MeNO_2$ (25 cm^3) was stirred for 15 min at r.t. The resultant blue solution was concentrated to approximately 5 cm^3 and filtered. Vapour diffusion of Et_2O into this solution gave a sticky blue solid, which was dried over P_2O_5 and recrystallised from $MeNO_2$–Et_2O to give very hygroscopic blue blocks. Yield 0.29 g, 61%.

4.5. Synthesis of [2,6-bis-({3-phenylpyrazol-1-yl}methyl)pyridine]diaquacopper(II) ditetrafluoroborate (*4*)

A mixture of L^1Ph (0.25 g, 6.4×10^{-4} mol) and $Cu(BF_4)_2\cdot6H_2O$ (0.22 g, 6.4×10^{-4} mol) in $MeNO_2$ (25 cm^3) was stirred for 15 min at r.t., affording a green solution which was concentrated to approximately 5 cm^3 and filtered. Vapour diffusion of Et_2O into this solution yielded red–brown cubes. Yield 0.31 g, 73%.

4.6. Synthesis of dichloro[2,6-bis-({3-phenylpyrazol-1-yl}methyl)pyridine]copper(II) (*6*)

A suspension of L^1Ph (0.66 g, 1.7×10^{-3} mol) and $CuCl_2$ (0.22 g, 1.7×10^{-3} mol) in MeCN (30 cm^3) was stirred for 1 h at r.t., affording a green precipitate. This was filtered, washed with MeCN and Et_2O, and dried in vacuo. This product was analysed without further purification. Yield 0.58 g, 65%.

4.7. Synthesis of chloro[2,6-bis-({3,5-dimethylpyrazol-1-yl}methyl)pyridine](methanol)copper(II) tetrafluoroborate (*7*)

A solution of **5** (0.36 g, 8.4×10^{-4} mol) and $AgBF_4$ (0.16 g, 8.4×10^{-4} mol) in MeCN (25 cm^3) was stirred for 2 h at r.t. The blue solution was filtered, and evaporated to dryness. Recrystallisation of the residue from MeOH–Et_2O yielded dark blue microcrystals. Yield 0.17 g, 40%.

4.8. Synthesis of chloro[2,6-bis-({3-phenylpyrazol-1-yl}methyl)pyridine]aquacopper(II) tetrafluoroborate (*8*)

Method as for **7**, using **6** (0.44 g, 8.4×10^{-4} mol). The product formed green microcrystals from MeOH–Et_2O, which became brown upon drying. Yield 0.16 g, 52%.

4.9. Single crystal X-ray structure determinations

Single crystals of X-ray quality of [Cu(NCMe)-(L^1Me_2)]BF_4 (**1**) were grown by diffusion of ether into a solution of the complex in MeCN. Crystals of [Cu(L^1Ph)]BF_4 (**2**) and [Cu(OH_2)$_2$(L^1Ph)]$(BF_4)_2$ (**4**) were similarly grown from $MeNO_2$–Et_2O, and of [Cu(OH_2)(L^1Me_2)]BF_4 (**3**) and [CuCl(HOMe)(L^1Me_2)]-BF_4 (**7**) from MeOH–Et_2O. Experimental details from the structure determinations are given in Table 8. All structures were solved by direct methods (SHELXS-97 [31]) and refined by full-matrix least-squares on F^2 (SHELXL-97 [32]), with H atoms placed in calculated positions.

4.10. X-ray structure determinations of [Cu(NCMe)(L^1Me_2)]BF_4 (*1*) and [Cu(L^1Ph)]BF_4 (*2*)

No disorder was detected during the refinement of either of these structures, and no restraints were applied. All non-H atoms were refined anisotropically, and all H atoms were placed in calculated positions and refined using a riding model.

4.11. X-ray structure determination of [Cu(OH_2)(L^1Me_2)]$(BF_4)_2$ (*3*)

During refinement, one BF_4^- anion was found to be disordered by rotation about one B–F bond. The disordered F atoms were modelled over two equally occupied orientations. No restraints were applied. All non-H atoms with occupancy >0.5 were refined anisotropically. The H atoms for the aqua ligand were located in the difference map and allowed to refine freely; all other H atoms were placed in calculated positions and refined using a riding model.

4.12. X-ray structure determination of [Cu(OH_2)$_2$(L^1Ph)]$(BF_4)_2$ (*4*)

During refinement, one BF_4^- anion was found to be disordered over three orientations, with occupancy 0.50, 0.30 and 0.20. All B–F distances in the disordered anion were restrained to 1.38(2) Å, and non-bonded F···F distances within a given disorder orientation to 2.25(2) Å. All non-H atoms with occupancy ≥ 0.5 were refined anisotropically. The H atoms for the aqua ligands were located in the difference map and allowed to refine freely; all other H atoms were placed in calculated positions and refined using a riding model.

4.13. X-ray structure determination of [CuCl($HOCH_3$)(L^1Me_2)]BF_4 (*7*)

During refinement, the BF_4^- anion was found to be disordered over three equally occupied orientations. All B–F distances were restrained to 1.36(2) Å, and non-bonded F···F distances within a given disorder orientation to 2.22(2) Å. All wholly occupied non-H atoms were refined anisotropically. The hydroxyl H atom of the methanol ligand was located in the difference map and allowed to refine freely; all other H atoms were placed in calculated positions and refined using a riding model.

4.14. Other measurements

Infra-red spectra were obtained as Nujol mulls pressed between KBr windows, between 400 and 4000 cm^{-1} using a Nicolet Avatar 360 spectrophotometers. UV–Vis spectra were obtained with a Perkin–Elmer Lambda 900 spectrophotometer, operating between 1100 and 200 nm, in 1 cm quartz cells. All NMR spectra were run on a Bruker ARX250 spectrometer, operating at 250.1 MHz (^{1}H) and 62.9 MHz (^{13}C). Electron impact (EI) and positive ion fast atom bombardment (FAB) mass spectra were performed on a VG AutoSpec spectrometer, the FAB spectra employing a 3-NOBA matrix. CHN microanalyses were performed by the University of Leeds School of Chemistry microanalytical service. Melting points are uncorrected. X-band EPR spectra were obtained using a Bruker ER200D spectrometer.

Conductivity measurements were obtained with a Jenway 4310 analyser, at concentrations of approximately 5×10^{-3} mol dm^{-3}. All electrochemical measurements were carried out using an Autolab PGSTAT30 voltammetric analyser, in MeCN containing 0.1 M $NBu^n_4BF_4$ as supporting electrolyte. Cyclic voltammetric experiments involved the use of platinum working and counter electrodes and a silver wire reference electrode; all potentials quoted are referenced to an internal ferrocene/ferrocenium standard and were obtained at a scan rate of 100 mV s^{-1}.

5. Supplementary material

Full crystallographic data for the structure analyses in this study are available on request from the Cambridge Crystallographic Data Centre, 12 Union Road, Cambridge CB2 1EZ, UK (fax: +44-1223-336033; e-mail: deposit@ccdc.cam.ac.uk or www: http://www.ccdc.cam.ac.uk). The CCDC deposition numbers are 165783 (**1**), 165785 (**2**), 165786 (**3**), 165787 (**4**) and 165788 (**7**).

Table 8
Experimental details for the single crystal structure determinations in this study

	[Cu(NCMe)(L^{1}Me$_2$)]BF$_4$ (**1**)	[Cu(L^{1}Ph)]BF$_4$ (**2**)	[Cu(OH$_2$)(L^{1}Me$_2$)](BF$_4$)$_2$ (**3**)
Formula	$C_{19}H_{24}BCuF_4N_6$	$C_{25}H_{21}BCuF_4N_5$	$C_{17}H_{23}B_2CuF_8N_5O$
M_r	486.79	541.82	550.56
Crystal size (mm)	0.66 × 0.45 × 0.12	0.27 × 0.12 × 0.12	0.39 × 0.30 × 0.24
Crystal class	monoclinic	orthorhombic	monoclinic
Space group	$P2_1/c$	$P2_12_12_1$	$P2_1/c$
a (Å)	15.1864(2)	8.0834(2)	13.9278(4)
b (Å)	7.6452(1)	13.6690(3)	10.8144(4)
c (Å)	23.7158(3)	21.1714(5)	19.4236(6)
α (°)			
β (°)	129.4710(5)	–	129.485(2)
γ (°)			
V (Å^3)	2125.53(5)	2339.27(10)	2257.95(14)
Z	4	4	4
μ (Mo Kα) (mm^{-1})	1.081	0.990	1.053
T (K)		150(2)	
Diffractometer		Nonius KappaCCD area-detector	
Radiation, λ (Å)		Graphite-monochromated Mo Kα, 0.71073	
Measured reflections	81608	34397	20524
Independent reflections	4871	5328	4963
R_{int}	0.060	0.066	0.071
Absorption correction		Multi-scan	
Min. transmission	0.54	0.78	0.68
Max. transmission	0.88	0.89	0.79
Observed reflections [$I > 2\sigma(I)$]	4457	4642	4066
Range in 2θ (°)	$3.4 \le 2\theta \le 55.1$	$3.8 \le 2\theta \le 54.9$	$7.7 \le 2\theta \le 55.0$
Range in h	$-19 \le h \le 19$	$-10 \le h \le 10$	$-18 \le h \le 18$
Range in k	$-9 \le k \le 9$	$-17 \le k \le 17$	$-14 \le k \le 13$
Range in l	$-30 \le l \le 30$	$-27 \le l \le 27$	$-25 \le k \le 25$
Parameters/restraints	289/0	326/0	333/0
$R(F)$ [a], $wR(F^2)$ [b]	0.029, 0.080	0.035, 0.078	0.063, 0.166
Goodness-of-fit	1.047	1.031	1.078
Weighting scheme [c]	$w = 1/[\sigma^2(F_o^2)+(0.0397P)^2+1.0105P]$	$w = 1/[\sigma^2(F_o^2)+(0.0381P)^2+0.4381P]$	$w = 1/[\sigma^2(F_o^2)+(0.0352P)^2+0.6207P]$
$\Delta\rho$ (max/min) (e Å^{-3})	0.37/−0.58	0.34/−0.42	0.60/−0.73
Flack parameter	–	−0.009(10)	–

	[Cu(OH$_2$)$_2$(L^{1}Ph)](BF$_4$)$_2$ (**4**)	[CuCl(HOMe)(L^{1}Me$_2$)]BF$_4$ (**7**)
Formula	$C_{25}H_{25}B_2CuF_8N_5O_2$	$C_{18}H_{25}BClCuF_4N_5O$
M_r	664.66	513.23
Crystal size (mm)	0.30 × 0.24 × 0.24	0.51 × 0.30 × 0.18
Crystal class	monoclinic	triclinic
Space group	$P2_1/c$	$P\bar{1}$
a (Å)	18.3780 (3)	10.2687(1)
b (Å)	8.9210(2)	10.9259(1)
c (Å)	16.5700(3)	11.9993(2)
α (°)		89.531(1)
β (°)	94.037(1)	64.997(1)
γ (°)		70.373(1)
V (Å^3)	2709.91(9)	1135.01(2)
Z	4	2
μ (Mo Kα) (mm^{-1})	0.896	1.132
T (K)		150(2)
Diffractometer		Nonius KappaCCD area-detector
Radiation, λ (Å)		Graphite-monochromated Mo Kα, 0.71073
Measured reflections	45581	44356
Independent reflections	6179	5060
R_{int}	0.042	0.151
Absorption correction	Multi-scan	
Min. transmission	0.77	0.60

Table 8 (*Continued*)

	$[Cu(OH_2)_2(L^1Ph)](BF_4)_2$ (**4**)	$[CuCl(HOMe)(L^1Me_2)]BF_4$ (**7**)
Max. transmission	0.81	0.82
Observed reflections $[I > 2\sigma(I)]$	5257	4591
Range in 2θ (°)	$4.4 \le 2\theta \le 55.0$	$3.8 \le 2\theta \le 55.1$
Range in h	$-23 \le h \le 23$	$-13 \le h \le 13$
Range in k	$-11 \le k \le 11$	$-14 \le k \le 14$
Range in l	$-20 \le l \le 21$	$-15 \le l \le 15$
Parameters/restraints	467/30	301/30
$R(F)$ [a], $wR(F^2)$ [b]	0.037, 0.099	0.068, 0.170
Goodness-of-fit	1.024	1.069
Weighting scheme [c]	$w = 1/[\sigma^2(F_o^2)+(0.0517P)^2+1.6824P]$	$w = 1/[\sigma^2(F_o^2)+(0.0746P)^2+1.1726P]$
$\Delta\rho$ (max/min) (e Å^{-3})	0.44/−0.60	0.80/−0.85
Flack parameter		

[a] $R = \Sigma[|F_o|-|F_c|]/\Sigma|F_o|$.
[b] $wR = [\Sigma w(F_o^2-F_c^2)/\Sigma wF_o^4]^{1/2}$.
[c] $P = (F_o^2+2F_c^2)/3$.

Acknowledgements

The authors thank the Royal Society for a research fellowship to M.A.H., the EPSRC for a studentship to C.L.F., and the University of Leeds.

References

[1] N. Kitajima, W.B. Tolman, Prog. Inorg. Chem. 43 (1995) 419.
[2] W.B. Tolman, Acc. Chem. Res. 30 (1997) 227.
[3] K.D. Karlin, A.D. Zuberbühler, in: J. Reedijk, E. Bouwman (Eds.), Bioinorganic Catalysis, second ed., Marcel Dekker, New York, 1999, pp. 469–534.
[4] S. Schindler, Eur. J. Inorg. Chem. (2000) 2311.
[5] J.P. Klinman, Chem. Rev. 96 (1996) 2541.
[6] B.A. Averill, Chem. Rev. 96 (1996) 2951.
[7] E.I. Solomon, U.M. Sundaram, T.E. Machonkin, Chem. Rev. 96 (1996) 2563.
[8] B.J. Hathaway, in: G. Wilkinson, R.D. Gillard, J.A. McCleverty (Eds.), Comprehensive Coordination Chemistry, vol. 5, Pergamon, Oxford, 1987, pp. 596–619.
[9] T.K. Lal, R. Gupta, S. Mahapatra, R. Mukherjee, Polyhedron 18 (1999) 1743.
[10] P. Manikandan, K.R.J. Thomas, P.T. Manoharan, J. Chem. Soc., Dalton Trans. (2000) 2779.
[11] P. Manikandan, K.R.J. Thomas, P.T. Manoharan, Acta Crystallogr., Sect. C 56 (2000) 308.
[12] R. Gupta, R. Mukherjee, Polyhedron 20 (2001) 2545.
[13] (a) K.D. Karlin, M.S. Haka, R.W. Cruse, G.J. Meyer, A. Farooq, Y. Gultneh, J.C. Hayes, J. Zubieta, J. Am. Chem. Soc. 110 (1988) 1196;
(b) I. Blain, M. Giorgi, E. Lojou, D. Lexa, M. Réglier, Eur. J. Inorg. Chem. (1998) 1297;
(c) I. Blain, P. Bruno, M. Giorgi, I. De Riggi, M. Réglier, Eur. J. Inorg. Chem. (2000) 393.
[14] C. Piguet, B. Bocquet, E. Müller, A.F. Williams, Helv. Chim. Acta 72 (1989) 323.
[15] D.A. Evans, M.C. Kozlowski, J.A. Murry, C.S. Burgey, K.R. Campos, B.T. Connell, R.J. Staples, J. Am. Chem. Soc. 121 (1999) 669.
[16] (a) K. Bernauer, F. Gretillat, H. Stoeckli-Evans, R. Warmuth, Helv. Chim. Acta 76 (1993) 545;
(b) K. Bernauer, T. Chuard, H. Stoeckli-Evans, Helv. Chim. Acta 76 (1993) 2263.
[17] (a) C. Piguet, G. Bernardinelli, A.F. Williams, Inorg. Chem. 28 (1989) 2920;
(b) S. Rüttigman, C. Piguet, G. Bernardinelli, B. Bocquet, A.F. Williams, J. Am. Chem. Soc. 114 (1992) 4230;
(c) R.F. Carina, A.F. Williams, C. Piguet, Helv. Chim. Acta 81 (1998) 548.
[18] S. Mahapatra, N. Gupta, R. Mukherjee, J. Chem. Soc., Dalton Trans. (1991) 2911.
[19] S. Trofimenko, J.C. Calabrese, J.S. Thompson, Inorg. Chem. 26 (1987) 1507.
[20] W. Baker, K.M. Buggle, J.W.F. McOmie, D.A.M. Watkins, J. Chem. Soc. (1958) 3594.
[21] A.A. Watson, D.A. House, P.J. Steel, Inorg. Chim. Acta 130 (1987) 167.
[22] (a) P. Manikandan, B. Varghese, P.T. Manoharan, J. Chem. Soc., Dalton Trans. (1996) 371;
(b) P. Manikandan, M. Subramoni, B. Varghese, P.T. Manoharan, J. Chem. Soc., Dalton Trans. (1998) 3219.
[23] A.W. Addison, T.N. Rao, J. Reedijk, J. van Rijn, G.C. Verschoor, J. Chem. Soc., Dalton Trans. (1984) 1349.
[24] W.J. Geary, Coord. Chem. Rev. 7 (1971) 81.
[25] D.F. Shriver, P.W. Atkins, Inorganic Chemistry, third ed., Oxford University Press, Oxford, 1999, p. 228.
[26] See e.g. M. Lanfranchi, M.A. Pellinghelli, G. Predieri, F. Bigi, R. Maggi, G. Sartori, J. Chem. Soc., Dalton Trans. (1993) 1463.
[27] B.A. Goodman, J.B. Raynor, Adv. Inorg. Chem. 13 (1970) 135.
[28] J. Elguero, E. Gonzalez, R. Jacquier, Bull. Soc. Chim. Fr. (1968) 5009.
[29] J.M. Holland, C.A. Kilner, M. Thornton-Pett, M.A. Halcrow, Polyhedron 20 (2001) 2829.
[30] G.J. Kubas, Inorg. Synth. 28 (1990) 68.
[31] G.M. Sheldrick, Acta Crystallogr., Sect. A 46 (1990) 467.
[32] G.M. Sheldrick, SHELXL-97, Program for the refinement of crystal structures, University of Göttingen, 1997.

PERGAMON

Polyhedron 21 (2002) 1043–1050

POLYHEDRON

www.elsevier.com/locate/poly

Synthesis and structural characterization of palladium(II) and platinum(II) complexes containing a chiral *P*,*N*-donor iminophosphine ligand

Hai-Bin Song [a], Zheng-Zhi Zhang [b], Thomas C.W. Mak [a,*]

[a] *Department of Chemistry, The Chinese University of Hong Kong, Shatin, New Territories, Hong Kong SAR, People's Republic of China*
[b] *State Key Laboratory of Elemento-Organic Chemistry, Nankai University, Tianjin 300071, People's Republic of China*

Received 8 January 2002; accepted 8 February 2002

Abstract

A new chiral *P*,*N*-donor iminophosphine ligand was used to synthesize a series of palladium(II) and platinum(II) complexes. Single crystal X-ray analysis showed that in all cases the *P*,*N* ligand forms a six-membered chelate ring, and the square-planar coordination of the metal atom is completed by two halide ions, two methyl groups, or one methyl group and one halide ion. In the latter instance, the methyl group is *cis* to the phosphorus atom. © 2002 Elsevier Science Ltd. All rights reserved.

Keywords: Palladium complexes; Platinum complexes; Chiral iminophosphine ligand

1. Introduction

P,*N*-Donor bidentate ligands are among the most used hemilabile ligands in coordination and organometallic chemistry [1]. Their late transition metal complexes adopt several coordination modes (*P*-monodentate, *N*-monodentate, *P*,*N*-bridging, *P*,*N*-chelate) depending on the ligand bite and the hardness of the metal atoms. In general, the rigid and short-bite *P*,*N*-ligands coordinate to metal atoms in the bridging mode, whereas a non-rigid ligand easily forms a five- or six-member chelate ring. In various catalytic applications, the capability of ligands to adopt different coordination modes is mandatory [2–4].

P,*N*-Donor ligands are expected to exhibit hemilabile behavior when coordinated to a soft metal center such as palladium. The soft P atom coordinates very strongly to palladium whereas the hard N donor is weakly bound. This feature of pyridylphosphine palladium complexes has been employed to catalyze a series of important C–C bond-forming reactions, such as the oligomerization of olefins, the co-polymerization of CO–ethylene, and the telomerization of butadiene [5]. Recently, oligomerization of ethene in polar solvents at higher temperatures is achieved using palladium iminophosphine catalysts, and the oligomer selectivity can be controlled by the nature of the ligand substituents [6]. In the transfer hydrogenation of ketones, bidentate iminophosphine exhibits more efficient catalytic activity than the corresponding amino derivative [7a]. In contrast, the mutidentate *P*,*N*,*N*,*P*-aminophosphine ligand has higher catalytic activity than the corresponding iminophsphine ligand [7b]. A palladium complex bearing *N*-(2-diphenylphosphinobenzylidene)-2-phenylethylamine was found to be more catalytically active than others for the cross-coupling of various types of aryl halides with alkynyl-, alkenyl- and arylstannanes to give the corresponding coupling products in high yields [7c]. A chiral iminophosphine ligand prepared from enantiopure 1-mesitylethylamine and *o*-(diphenylphosphino)benzaldehyde proved to be effective for palladium-catalyzed allylic alkylation. For example, (R)-$MeO_2CCH(CHPhCH{=}CHPh)CO_2Me$ was obtained in 98% yield with 94% ee [7d].

Here we report the preparation of another chiral iminophosphine ligand and its use in synthesizing a

* Corresponding author. Tel.: +852-2609 6279; fax: +852-2603 5057.
E-mail address: tcwmak@cuhk.edu.hk (T.C.W. Mak).

0277-5387/02/$ - see front matter © 2002 Elsevier Science Ltd. All rights reserved.
PII: S0277-5387(02)00914-2

series of palladium(II) and platinum(II) complexes, whose structures were determined by X-ray analysis.

2. Experimental

Na_2PdCl_4, $PtCl_2$(cod) (cod = cyclo-1,5-octadiene), $PtMe_2$(cod) and $HgBr_2$ were obtained from Aldrich and used without further purification. [PdCl(Me)(cod)] [8] and 2-diphenylphosphine-benzaldehyde were synthesized by literature procedures [9].

2.1. Synthesis of the ligand: N-[{2-(diphenylphosphino)phenyl}methylene]-[6,6-dimethyl-{1S-(1α,2β,5α)-bicyclo[3.1.1]heptane}]-2-methaneamine, L

A mixture of 2-diphenylphosphine-benzaldehyde (5.1 g, 13 mmol) and (−)-*cis*-myrtanylamine (2.0 g, 13 mmol) in toluene (25 ml) was refluxed for 18 h on molecular sieves under N_2 atmosphere. After filtration and subsequent evaporation of the solvent under reduced pressure, the crude product was obtained. Recrystallization from CH_2Cl_2–hexane afforded L as a white powder in 85% yield. *Anal.* Found: C 81.72, H 7.61, N 3.28. Calc. for $C_{29}H_{32}NP$: C 81.85, H 7.58, N 3.29%. $^{31}P\{^1H\}$ NMR ($CDCl_3$, 293k, δ): −12.1 ppm.

2.2. Synthesis of palladium and platinum complexes

2.2.1. $PdCl_2(L)$, (**1**)

Ten milliliters MeCN was added to a Schenk tube containing Na_2PdCl_4 (0.1g, 0.34 mmol) and ligand L (0.144 g, 0.34 mmol). The reaction mixture was stirred for 2 h during which brown Na_2PdCl_4 disappeared and a yellow solution with a white NaCl precipitate was obtained. After filtration, the solution was evaporated to give **1** in nearly quantitative yield. After a few days, yellow block-like crystals of **1**·MeCN suitable for X-ray analysis was obtained by slow evaporation of a MeCN solution of **1**. *Anal.* Found: C 57.64, H 5.24, N 2.50. Calc. for $C_{29}H_{32}NCl_2PPd$: C 57.78, H 5.35, N 2.32. $^{31}P\{^1H\}$ NMR ($CDCl_3$, 293k, δ): 32.0 ppm.

2.2.2. PdMeCl(L) (**2**)

PdMeCl(cod) (0.1 g, 0.42 mmol) and L (0.18 g, 0.42 mmol) were mixed in 10 ml MeCN and stirred for 20 min. After filtration, the filtrate was dried in vacuo to give **2** as a yellow solid. *Anal.* Found: C 61.96, H 6.00, N 2.34. Calc. for $C_{30}H_{35}NClPPd$: C 61.86, H 6.06, N 2.40%. $^{31}P\{^1H\}$ NMR ($CDCl_3$, 293k, δ): 38.2. Single crystals of **2**·MeCN were growth from slow evaporation of a solution of **2** in MeCN. Yellow prismatic crystals of **2**·1.5CH_2Cl_2 suitable for X-ray analysis were obtained from diffusion of isopropyl ether into a solution of **2** in CH_2Cl_2.

2.2.3. $PtCl_2(L)$ (**3**)

The procedure was similar to that for **1** using $PtCl_2$(cod) instead of Na_2PdCl_4. *Anal.* Found: C 49.96,H 4.56, N 2.16. Calc. for $C_{29}H_{32}NCl_2PPt$: C 50.37, H 4.66, N 2.03%. $^{31}P\{^1H\}$ NMR ($CDCl_3$, 293k, δ): 3.9 $^1J(^{195}Pt, ^{31}P) = 3735$ Hz.

2.2.4. $PtMe_2(L)$ (**4**)

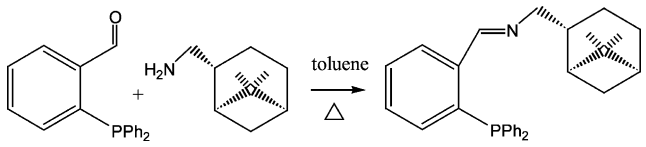
The procedure was similar to that for **1** using $PtMe_2$(cod) instead of Na_2PdCl_4. *Anal.* Found: C 57.04, H 5.68, N 2.26, Calc. for $C_{31}H_{38}NPPt$: C 57.22, H 5.89, N 2.15%. $^{31}P\{^1H\}$ NMR ($CDCl_3$, 293k, δ): 24.5. $^1J(^{195}Pt, ^{31}P) = 1982$ Hz.

2.2.5. PtMeBr(L) (**5**)

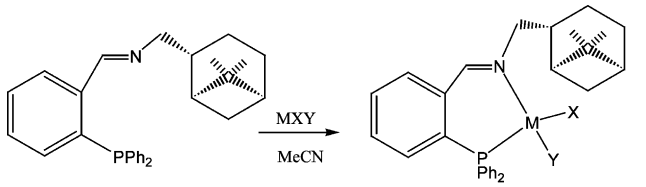
To a solution of **4** (0.1 g, 0.15 mmol) in 5 ml MeCN, $HgBr_2$ (0.09 g, 0.15 mmol) was added. The solution was stirred for 24 h at room temperature (r.t.). The solvent was evaporated in vacuo and the residue was redissolved in 2 ml CH_2Cl_2. Diffusion of isopropyl ether to the solution gave yellow crystals of **5**·0.75CH_2Cl_2. *Anal.* Found: C 50.12, H 5.08, N 1.82. Calc. for $C_{30}H_{35}NBrPPt$: C 50.36, H 4.93, N 1.96%. $^{31}P\{^1H\}$ NMR ($CDCl_3$, 293k, δ): 17.0. $^1J(^{195}Pt, ^{31}P) = 4657$ Hz.

2.3. X-ray crystallography

The intensity data for **1**·MeCN were collected at 293 K in the variable ω-scan mode on a Siemens R3m/V four-circle diffractometer using Mo Kα radiation (λ = 0.71073 Å, 50 kV, 30 mA; $2\theta_{max} = 55^\circ$). An empirical absorption correction was applied using ψ-scan data. For each of complexes **2**·MeCN, **2**·1.5CH_2Cl_2, **3**·MeCN, **4** and **5**·0.75CH_2Cl_2, a selected single crystal was mounted on a Bruker SMART 1000 CCD diffractometer operating at 50 kV and 30 mA using Mo Kα radiation ($\lambda = 0.71073$ Å). Data collection at 293 K and reduction were performed using the SMART and SAINT software [10], with frames of 0.3° oscillation in the θ range $1.5 < \theta < 28^\circ$. An empirical absorption correction was applied using the SADABS program [11]. The structures were solved by direct methods and all non-hydrogen atoms were subjected to anisotropic refinement by full-matrix least-squares on F^2 using the SHELXTL package [12]. Non-hydrogen atoms were subjected to anisotropic refinement. All hydrogen atoms were generated geometrically (C–H bond lengths fixed at 0.96 Å), assigned appropriate isotropic thermal parameters, and included in structure factor calculations in the final stage of F^2 refinement. Flack parameter [13] and the known chiralities of chiral ligands as starting synthetic materials ensured the correct assignment of the absolute configuration of all compounds.



Scheme 1.



M = Pd, X = Y = Cl, **1**

M = Pd, X = Cl Y = Me, **2**

M = Pt, X = Y = Cl, **3**

M = Pt, X = Y = Me, **4**

M = Pt, X = Br Y = Me, **5**

Scheme 2.

3. Results and discussion

The new iminophosphine ligand L was synthesized from the corresponding amine and aldehyde as a white powder in 85% yield (Scheme 1). The ^{31}P NMR $\{^{1}$H$\}$ spectrum of L showed a singlet at −12.1 ppm. The reaction of L with palladium and platinum salts afforded the corresponding chelated product **1**–**5** (Scheme 2).

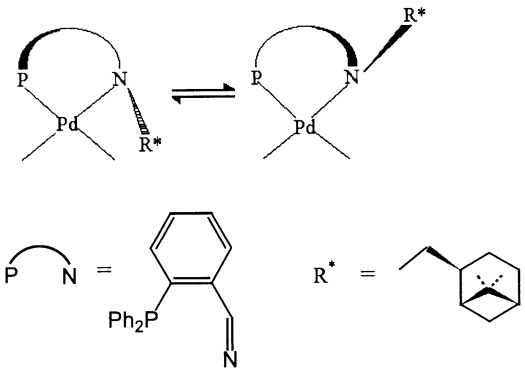


Fig. 1. Two possible configurations of a PdXY(L) complex.

The ^{31}P NMR $\{^{1}$H$\}$ spectrum of $PdCl_2$(L) (**1**) showed a singlet at 32.0 ppm. In **1** the ligand L adopts a κP, κN coordination mode in a square-planar coordination geometry for the palladium center. An ORTEP drawing of **1** is shown in Fig. 1. Selected bond lengths and angles are given in Tables 1 and 2. The least-squares plane through the atoms Pd(1), P(1), N(1), Cl(1) and Cl(2) shows a mean atomic deviation of 0.065 Å. The Pd–P, Pd–N, Pd–Cl(1), and Pd–Cl(2) bond distances are in the normal range [14]. The Pd–Cl bond length *trans* to the P atom (2.380(1) Å) is longer than that *trans* to the N atom (2.281(1) Å) owing to the stronger *trans* influence of a tertiary phosphine with respect to an imine. The bond angles at the Pd(1) atom exhibit only minor deviations from a right angle. The ligand forms a six-membered, puckered chelate ring with the metal so

Table 1

Complex	**1**·MeCN	**2**·MeCN	**2**·1.5CH_2Cl_2	**3**·MeCN	**4**	**5**·0.75CH_2Cl_2
Formula	$C_{31}H_{35}Cl_2N_2PPd$	$C_{32}H_{38}ClN_2PPd$	$C_{315}H_{38}Cl_4NPPd$	$C_{31}H_{35}Cl_2N_2PPt$	$C_{31}H_{38}NPPt$	$C_{30.75}H_{36.5}BrCl_{1.5}NPPt$
M	643.88	623.46	709.80	732.57	650.68	779.25
Crystal system	orthorhombic	monoclinic	orthorhombic	orthorhombic	monoclinic	orthorhombic
Space group	$P2_12_12_1$ (No. 19)	$P2_1$ (No. 4)	$P2_12_12$ (No. 18)	$P2_12_12$ (No. 19)	$P2_1$ (No. 4)	$P2_12_12$ (No. 18)
Crystal size (mm)	0.64 × 0.60 × 0.40	0.42 × 0.38 × 0.32	0.42 × 0.30 × 0.18	0.45 × 0.35 × 0.25	0.60 × 0.45 × 0.20	0.36 × 28 × 0.16
a (Å)	12.039(1)	10.9931(6)	20.764(1)	12.043(2)	10.1793(9)	20.955(4)
b (Å)	15.189(2)	10.1276(5)	12.2591(6)	15.143(3)	9.7873(8)	12.313(3)
c (Å)	16.668(2)	27.186(1)	12.8781(6)	16.780(3)	14.756(1)	13.177(3)
β (°)		94.409(1)			105.420(2)	
U (Å^3)	3047.8(6)	3017.8(3)	3278.1(3)	3060.3(10)	1417.2(2)	3399.7(12)
Z	4	4	4	4	2	4
D_{calc} (g cm^{-3})	1.403	1.372	1.438	1.590	1.525	1.522
F(000)	1320	1288	1452	1448	648	1526
μ (Mo Kα) (mm^{-1})	0.859	0.779	0.962	4.834	5.025	5.485
Total reflections	4888	20718	22453	20586	9319	18602
Unique reflections (R_{int})	4637	11243 (0.0437)	7886 (0.0651)	7353 (0.0337)	6428 (0.0272)	7711 (0.0711)
Observed reflections	3668	8021	5815	6466	5683	5278
Parameters	336	668	351	335	309	324
Flack parameters	−0.03(3)	0.04(3)	−0.05(4)	−0.001(4)	0.0003(2)	−0.029(14)
Goodness-of-fit	1.042	0.936	0.984	0.930	0.957	0.953
R_1, wR_2 [$I > 2\sigma(I)$] [a]	0.0409, 0.0653	0.0427, 0.0867	0.0625, 0.1619	0.0226, 0.0398	0.0301, 0.0623	0.0571, 0.1367
R_1, wR_2 (all data)	0.0634, 0.0719	0.0671, 0.0955	0.0819, 0.1740	0.0292, 0.0411	0.0347, 0.0634	0.0831, 0.1456

[a] $R_1 = \Sigma(|F_o| - |F_c|/\Sigma|F_o|$, $wR_2 = \{w[\Sigma(|F_o| - |F_c|)^2]/\Sigma|F_o|^2\}^{1/2}$.

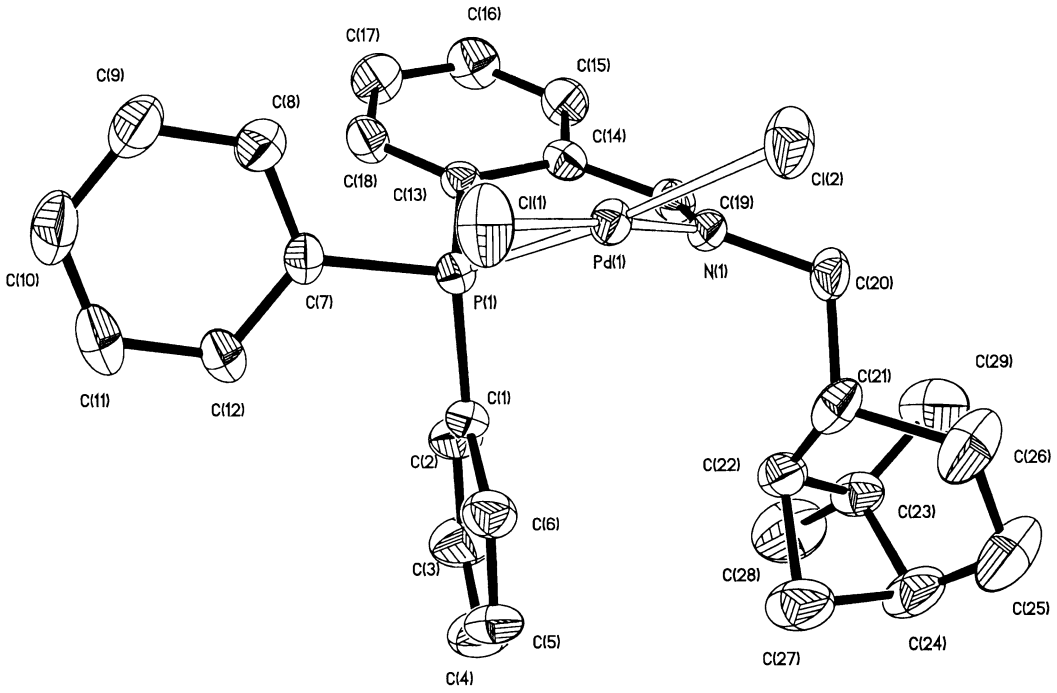


Fig. 2. Perspective drawing (35% thermal ellipsoids) of the molecular structure of $PdCl_2(L)$ (**1**).

that there are two possible isomers of each configuration (Fig. 2). The torsion angle Pd(1)–P(1)–C(13)–C(14) = 42.0(4)° can be conveniently used to indicate the location of the $=CHC_6H_4-$ unit with respect to the $PdCl_2(P,N)$ plane; the plus sign means that the $=CHC_6H_4-$ unit lies above the plane, as seen in a side view from the chloride ligands toward the Pd atom, and the minus sign means the unit lies below the plane.

The reaction of L with PdMeCl(cod) afforded complex **2**, which was crystallized in two solvated forms from different solvents: **2**·MeCN and **2**·1.5CH_2Cl_2. In **2**·MeCN, the asymmetric unit consists of two independent molecules of **2**, in which the $=CHC_6H_4-$ unit lies either below (Fig. 3) or above the PdMeCl(P,N) plane (Fig. 4). The corresponding Pd(1)–P(1)–C(13)–C(14) and Pd(2)–P(2)–C(43)–C(44) torsion angles are

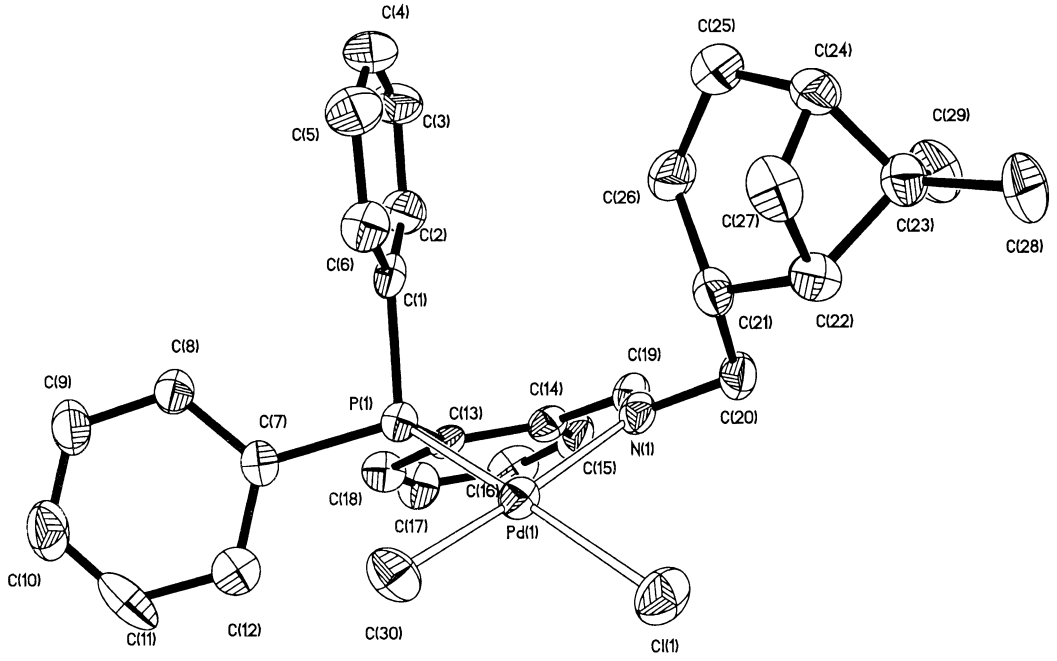


Fig. 3. Perspective drawing (35% thermal ellipsoids) of one of the two independent molecules of PdMeCl(L) (**2**) in **2**·MeCN.

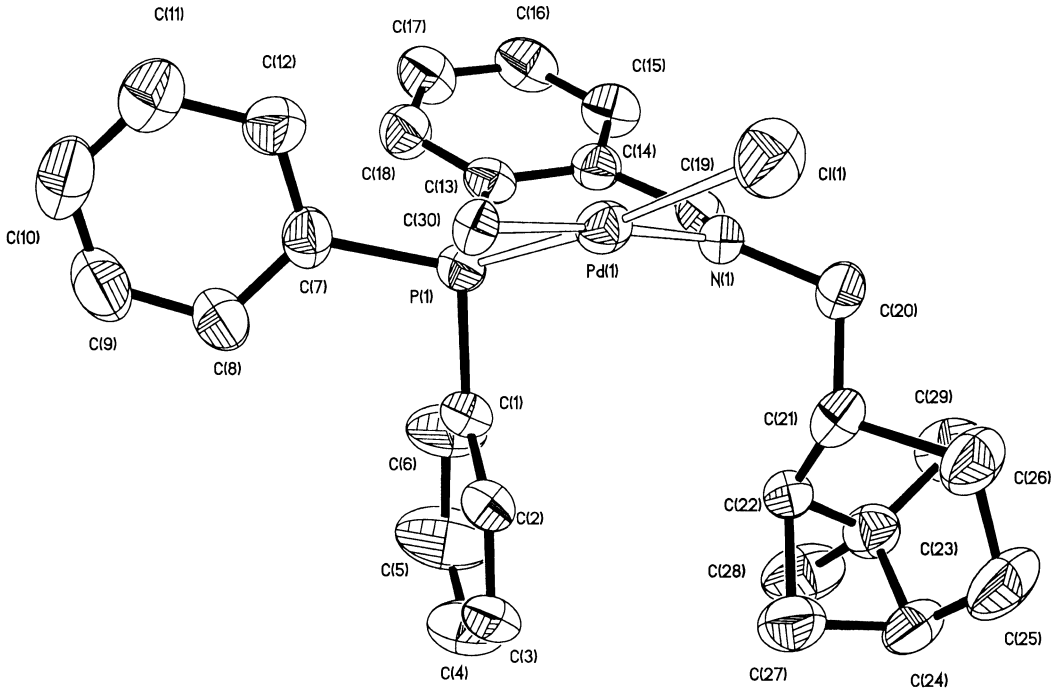


Fig. 4. Perspective drawing (35% thermal ellipsoids) of the second independent molecule of **2** in **2**·MeCN.

−45.4(4)° and 42.4(5)°, respectively. On the other hand, in **2**·1.5CH_2Cl_2 just one configuration exists, in which the =CHC_6H_4– unit lies above the PdMeCl(P,N) plane with torsion angle Pd(1)–P(1)–C(13)–C(14) = 40.4(5)°. The Pd–ligand bond distances and angles are similar in different configurations and different solvate crystals (Table 2). The methyl group is arranged *trans* to the N donor site, as found in other known PdMeCl(P,N) complexes. The least-squares plane through the donor atoms around the palladium atom shows a mean deviation of 0.053 Å for Pd(1), 0.093 Å for Pd(2) in **2**·MeCN and 0.074 Å for Pd(1) in **2**·1.5CH_2Cl_2.

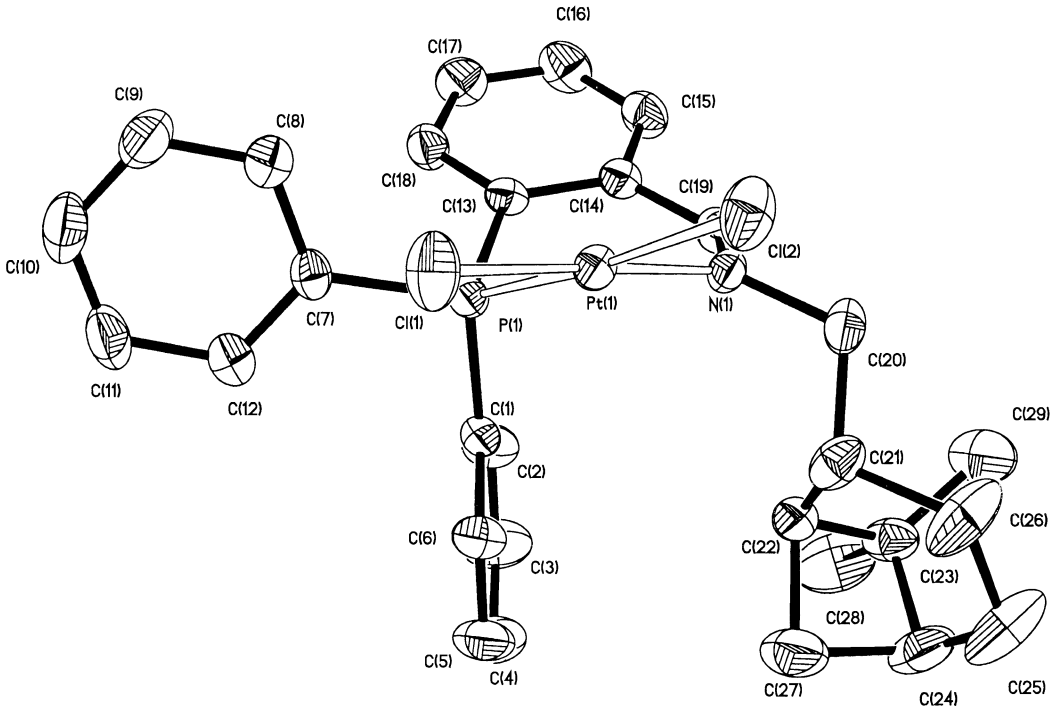


Fig. 5. Perspective drawing (35% thermal ellipsoids) of molecule $PtCl_2$(L) **3** in **3**·MeCN.

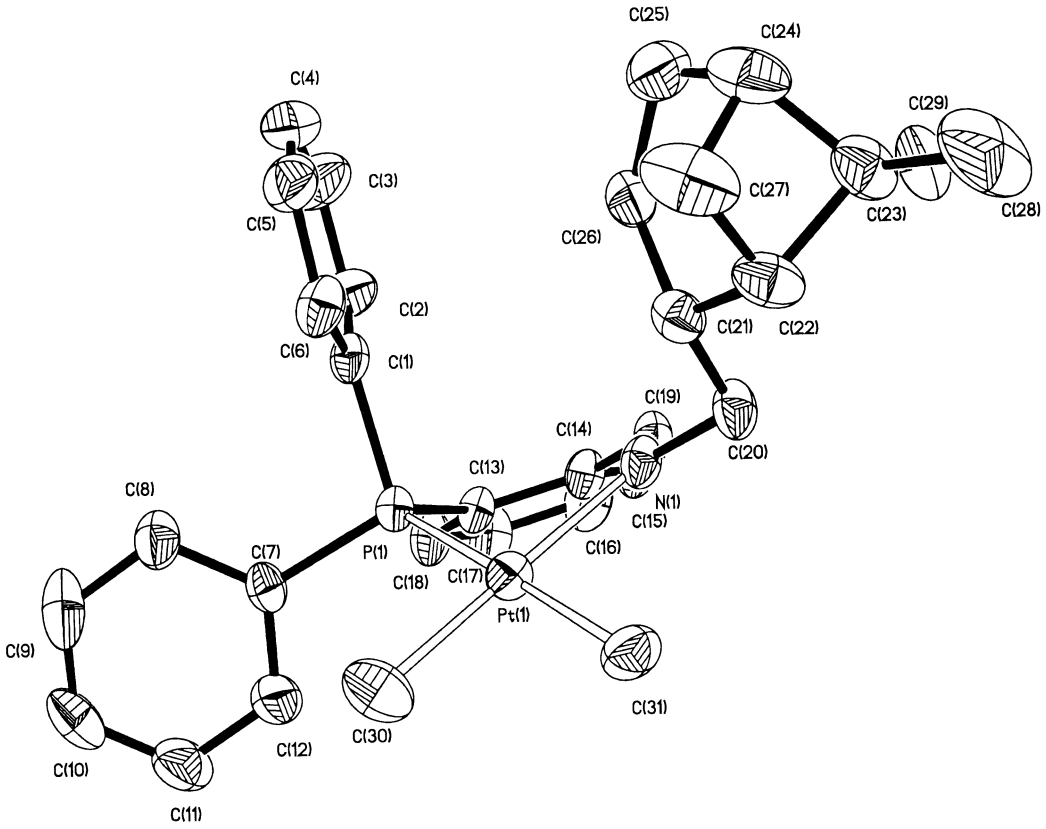


Fig. 6. Perspective drawing (35% thermal ellipsoids) of molecule $PtMe_2(L)$ (**4**).

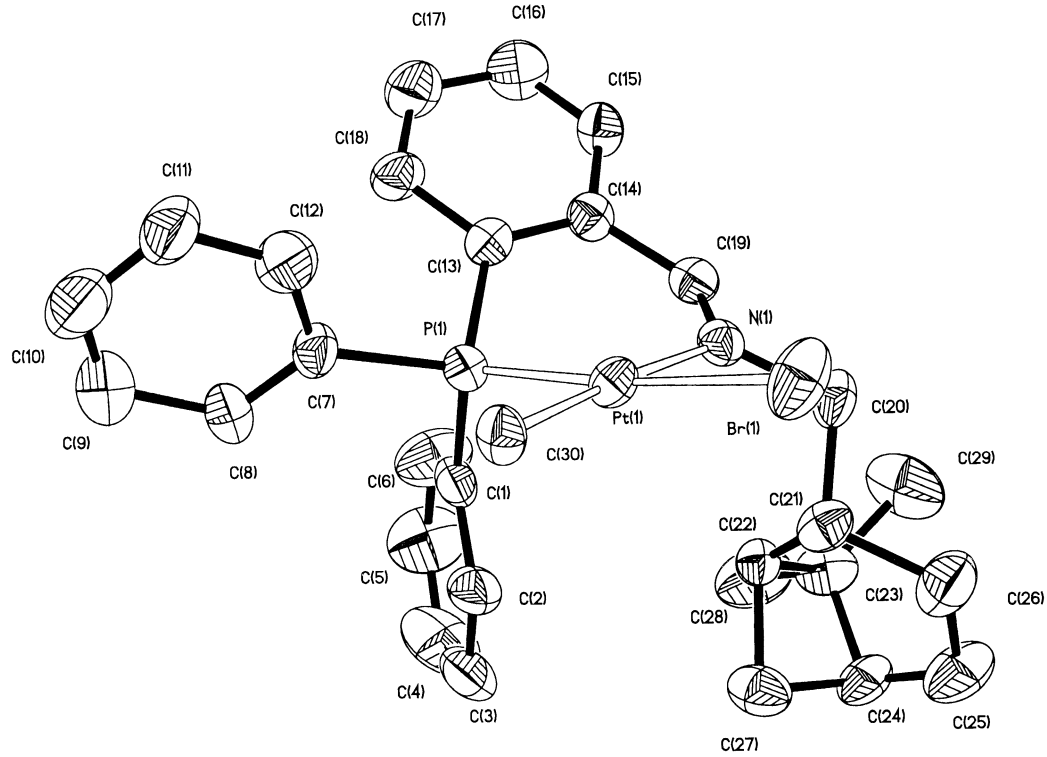


Fig. 7. Perspective drawing (35% thermal ellipsoids) of molecule PtMeBr(L) (**5**) in $\mathbf{5}\cdot 0.75CH_2Cl_2$.

Table 2
Selected bond lengths (Å) and angles (°)

Bond lengths		Bond angles	
***1**·MeCN*			
Pd(1)–N(1)	2.063(4)	N(1)–Pd(1)–P(1)	87.6(1)
Pd(1)–P(1)	2.214(1)	P(1)–Pd(1)–Cl(1)	90.33(5)
Pd(1)–Cl(1)	2.281(1)	N(1)–Pd(1)–Cl(2)	92.84(1)
Pd(1)–Cl(2)	2.380(1)	Cl(1)–Pd(1)–Cl(2)	89.52(5)
P(1)–C(7)	1.794(5)		
***2**·MeCN*			
Pd(1)–C(30)	2.058(6)	C(30)–Pd(1)–P(1)	92.3(2)
Pd(1)–N(1)	2.161(5)	N(1)–Pd(1)–P(1)	86.4(2)
Pd(1)–P(1)	2.199(2)	C(30)–Pd(1)–Cl(1)	88.4(2)
Pd(1)–Cl(1)	2.380(2)	N(1)–Pd(1)–Cl(1)	93.1(2)
Pd(2)–C(60)	2.059(6)	C(60)–Pd(2)–P(2)	91.3(2)
Pd(2)–N(2)	2.164(5)	N(2)–Pd(2)–P(2)	87.8(2)
Pd(2)–P(2)	2.193(2)	C(60)–Pd(2)–Cl(2)	88.4(2)
Pd(2)–Cl(2)	2.388(2)	N(2)–Pd(2)–Cl(2)	93.2(2)
***2**·1.5CH_2Cl_2*			
Pd(1)–C(30)	2.145(4)	C(30)–Pd(1)–P(1)	92.7(1)
Pd(1)–N(1)	2.135(5)	N(1)–Pd(1)–P(1)	88.0(1)
Pd(1)–P(1)	2.203(1)	C(30)–Pd(1)–Cl(1)	86.8(1)
Pd(1)–Cl(1)	2.368(2)	N(1)–Pd(1)–Cl(1)	92.9(1)
***3**·MeCN*			
Pt(1)–N(1)	2.041(3)	N(1)–Pt(1)–P(1)	88.39(8)
Pt(1)–P(1)	2.2031(9)	P(1)–Pt(1)–Cl(1)	91.95(4)
Pt(1)–Cl(1)	2.292(1)	N(1)–Pt(1)–Cl(2)	91.75(8)
Pt(1)–Cl(2)	2.377(1)	P(1)–Pt(1)–Cl(2)	175.57(4)
4			
Pt(1)–C(30)	2.038(7)	C(30)–Pt(1)–C(31)	85.5(3)
Pt(1)–C(31)	2.099(6)	C(31)–Pt(1)–N(1)	93.1(2)
Pt(1)–N(1)	2.131(5)	C(30)–Pt(1)–P(1)	94.7(2)
Pt(1)–P(1)	2.244(1)	N(1)–Pt(1)–P(1)	86.8(1)
***5**·0.75CH_2Cl_2*			
Pt(1)–C(30)	2.12(1)	C(30)–Pt(1)–P(1)	93.3(3)
Pt(1)–N(1)	2.165(9)	N(1)–Pt(1)–P(1)	88.4(2)
Pt(1)–P(1)	2.185(3)	C(30)–Pt(1)–Br(1)	86.7(3)
Pt(1)–Br(1)	2.502(1)	N(1)–Pt(1)–Br(1)	91.8(2)

The reaction of L with $PtCl_2$(cod) afforded $PtCl_2$(L) (**3**), and crystalline **3**·MeCN is isomorphous to the corresponding palladium complex **1**·MeCN. The ^{31}P NMR $\{^1H\}$ spectrum of **3** showed a singlet at 3.9 with $^1J(^{195}Pt, ^{31}P) = 3735$ Hz. An ORTEP drawing of complex **3** is shown in Fig. 5, and selected bond lengths and angles are given in Table 2. A least-squares plane fitted to the metal and surrounding ligand atoms showed a small deviation of 0.055 Å. The torsion angle Pt–P–C(13)–C(14) = 41.5(3)° indicates that the =CHC_6H_4– unit lies above the $PtCl_2$(P,N) plane.

$PtMe_2$(L) (**4**) was obtained from the reaction of L with $PtMe_2$(cod). The ^{31}P NMR $\{^1H\}$ spectrum of **4** showed a singlet at 24.5 with $^1J(^{195}Pt, ^{31}P) = 1982$ Hz. Complex **4** is not isomorphous to **1** and **3**, although single crystals were grown using the same method. An ORTEP drawing of **4** is shown in Fig. 6. The least-squares plane through the atoms Pt(1), P(1), N(1), C(30) and C(31) shows a mean deviation of 0.032 Å. The two methyl groups are arranged in *cis* positions, and the Pt–C bond lengths are similar. The Pt–P and Pt–N distances are similar to those in **3** (Table 2). The torsion angle Pt–P–C(13)–C(14) = −41.7(4)° indicates that the =CHC_6H_4– unit lies below the $PtMe_2$(P,N) plane.

The alkyl platinum(II) complexes of bidentate chelating *N*,*N*-ligands can react with HgX_2 (X = halide or carboxylate) to give adducts containing a Pt→HgX_2 donor–acceptor bond or oxidative addition products containing a PtX(HgX) group [15]. We decided to use $HgBr_2$ to react with **4** to see if there is a similar reaction. However, in the case of the *P*,*N*-bidentate ligand L, the oxidative addition intermediate could not be isolated, and one of the methyl groups of **4** was displaced by the bromide ligand to form complex **5**, whose ^{31}P NMR $\{^1H\}$ spectrum showed a singlet at 17.0 with $^1J(^{195}Pt, ^{31}P) = 4657$ Hz. When we tried to crystallize **5** in MeCN, twinned crystals were obtained. Diffraction-quality single crystals of **5**·0.75CH_2Cl_2 were subsequently grown by diffusing isopropyl ether into a CH_2Cl_2 solution of **5**.

An ORTEP drawing of **5** is shown in Fig. 7, and selected bond lengths and angles are given in Table 2. The methyl group is *trans* to the nitrogen atom of L. The least-squares plane through the atoms Pt(1), P(1), N(1), C(30) and Br(1) shows a mean deviation of 0.069 Å. The P,N-bite angle at Pt(1) is similar to those in **1**–**4**. The torsion angle is 41.6(9)°, indicating that the =CHC_6H_4– unit lies above the PtMeBr(P,N) plane.

4. Supplementary material

Crystallographic data for the structural analysis have been deposited with the Cambridge Crystallographic Data Centre, CCDC reference numbers 176292–176298. Copies of this information may be obtained free of charge from The Director, CCDC, 12 Union Road, Cambridge, CB2 1EZ, UK (fax: +44-1223-336033; e-mail: deposit@ccdc.cam.ac.uk or www: http://www.ccdc.cam.ac.uk).

Acknowledgements

This work is supported by Hong Kong Research Grants Council Earmarked Grant CUHK 4268/00P.

References

[1] (a) For reviews, see: K.N. Gavrilov, A.I. Polosukhin, Russ. Chem. Rev. 69 (2000) 661;
(b) P.J. Guiry, M. McCarthy, P.M. Lacey, C.P. Saunders, S. Kelly, D.J. Connolly, Curr. Org. Chem. 4 (2000) 821;
(c) P. Espinet, J.K. Soulantica, Coord. Chem. Rev. 193 (1999) 499.

[2] H. Cheng, Z. Zhang, Coord. Chem. Rev. 147 (1996) 1.
[3] S.M. Aucott, A.M.Z. Slawin, J.D. Woollins, J. Chem. Soc., Dalton Trans. (2000) 2559 and references therein.
[4] P. Wehman, R.E. Rulke, V.E. Kaasjager, P.C.J. Kamer, H. Kooijmann, A. Spek, C.J. Elsevier, K. Vrieze, P.W.N.M. Van Leeuwen, J. Chem. Soc., Chem. Commun. (1995) 331.
[5] (a) G.M. DiRenzo, P.S. White, M. Brookhar, J. Am. Chem. Soc. 118 (1996) 6225;
(b) L.K. Johnson, S. Mecking, M. Brookhar, J. Am. Chem. Soc. 118 (1996) 267;
(c) R. Patrini, M. Lami, M. Marchionna, F. Benvenuti, A.M. Raspolli Galletti, G. Sbrana, J. Mol. Cat. A. Chem. 129 (1998) 179.
[6] E.K. van den Beuken, W.J.J. Smeets, A.L. Speck, B.L. Feringa, Chem. Commun. (1998) 223.
[7a] P. Crochet, J. Gimeno, S. Garcia-Granda, J. Borge, Organometallics 20 (2001) 4369.
[7b] J.-X. Gao, T. Ikariya, R. Noyori, Organometallics 15 (1996) 1087.
[7c] S. Eiji, H. Hiroto, T. Hidemasa, Tetrahedron Lett. 38 (1997) 3759.
[7d] K. Takehiro, H. Yukihiko, S. Kazuhiko, Synlett 4 (2000) 517.
[8] R.E. Rülke, J.M. Ernsting, A.L. Spek, C.J. Elsevier, P.W.N.M. van Leeuwen, K. Vrieze, Inorg. Chem. 32 (1993) 5769.
[9] T.B. Rauchfuss, D.A. Wrobleski, Inorg. Synth. 21 (1982) 175.
[10] Bruker. SMART 5.0 and SAINT 4.0 for Windows NT: Area Detector Control and Integration Software. Bruker Analytical X-Ray Systems, Inc.: Madison, Wisconsin, USA, 1998.
[11] G.M. Sheldrick, SADABS: Program for Empirical Absorption Correction of Area Detector Data, University of Göttingen, Germany, 1996.
[12] G.M. Sheldrick, SHELXTL 5.10 for Windows NT: Structure Determination Software Programs, Bruker Analytical X-Ray Systems, Inc, Madison, WI, USA, 1997.
[13] (a) H.D. Flack, Acta Crystallogr., Sect. A 39 (1983) 876;
(b) H.D. Flack, D. Schwarzenbach, Acta Crystallogr., Sect. A 44 (1988) 499.
[14] H.A. Ankersmit, B.H. Løken, H. Kooijman, A.L. Spek, K. Vrieze, G. van Koten, Inorg. Chim. Acta 252 (1996) 141.
[15] (a) I. Ara, L.R. Falvello, J. Fornies, V. Sicilia, P. Villarroya, Organometallics 19 (2000) 3091;
(b) A.J. Canty, G. van Koten, Acc. Chem. Res. 28 (1995) 406;
(c) M.C. Janzen, M.C. Jennings, R.J. Puddephatt, Inorg. Chem. 40 (2001) 1728 and references therein.

PERGAMON

Polyhedron 21 (2002) 1051–1055

POLYHEDRON

www.elsevier.com/locate/poly

Synthesis and characterization of tantalum(V) complexes containing bis-sulfamide ligands: X-ray crystal structure of $Ta[N(Me)_2]_3[SO_2(NCMe_3)_2]$

R.C. Mills, P. Doufou, K.A. Abboud, James M. Boncella *

Department of Chemistry and Center of Catalysis, University of Florida, Gainesville, FL 32611, USA

Received 22 May 2001; accepted 28 February 2002

Abstract

The bis-sulfamide compounds, $SO_2[NHCMe_3]_2$ and $SO_2\{NH[CH(Me)Ph]\}$ were successfully employed as chelating diamide ligands in the synthesis of the tantalum complexes $Ta[N(Me)_2]_3[SO_2(NCMe_3)_2]$ (**1**) and $Ta(NMe_2)_3[SO_2(NCH(Me)Ph)_2]$ (**2**). Compound **1** assumes a distorted trigonal pyramidal geometry in the solid state as determined by an X-ray crystallograpic study. Compounds **1** and **2** are fluxional at room temperature. Variable temperature ^1H NMR was used to investigate the nature of these fluxional processes. In addition, preliminary attempts to generate halide and alkyl derivative of **1** and **2** are presented. Specifically, the reaction of **1** with excess AlR_3 (R = Me or Et), in order to generate alkyl derivatives of **1** led to the isolation of AlR_3 adducts.
© 2002 Elsevier Science Ltd. All rights reserved.

Keywords: Bis-sulfamide; Tantalum(V); Diamide; Crystal structures

1. Introduction

The organometallic chemistry of early-transition metal compounds has received increased attention in recent years as applications in α-olefin polymerization have grown. A significant portion of this research has focused on metal complexes supported by cyclopentadienyl based ligand sets [1–3], but there is growing interest in the use of complexes with non-cyclopentadienyl ancillary ligands such as dialkoxide [4–6] or diamide ligands [7–17]. Interest in studying chelating-diamide supported Group 4 complexes as polymerization catalysts is in part due to the ease with which the steric and electronic properties of the catalysts can be altered by varying the nitrogen substituants. Several research groups have shown that d^0 Group 4 metal complexes (Ti, Zr, Hf), supported by diamide ligands are active catalysts for the polymerization of α-olefins [8–27].

In response to the growing interest in alternatives to classical metallocene based catalysts, we have become interested in examining the chemistry of a relatively unexplored class of bis-sulfamide ligands [28–31]. The relative ease with which the steric and electronic properties of bis-sulfamides can be varied is evident in their synthesis (Scheme 1). Typically, the synthesis of these ligands is a high yield, one-step process involving the reaction between SO_2Cl_2 and an amine [32,33]. Therefore, many derivatives are readily available by varying the nature of the amine. In addition, upon coordination the inherent electron withdrawing character of the SO_2 backbone should increase the electronic unsaturation at the metal center. In this paper we describe the reactions of the bis-sulfamide ligands $SO_2[NHCMe_3]_2$ and $SO_2\{NH[CH(Me)Ph]\}$ with $Ta(NMe_2)_5$. The molecular structure and variable temperature ^1H NMR studies of $Ta[N(Me)_2]_3[SO_2(NCMe_3)_2]$ (**1**) are also reported.

2. Experimental

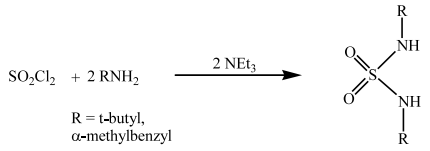
2.1. Materials and methods

All experimental procedures were conducted under an inert atmosphere, either in a N_2 filled dry box or by

* Corresponding author. Tel.: +1-352-392-9512; fax: +1-352-392-3255.

E-mail address: boncella@chem.ufl.edu (J.M. Boncella).

0277-5387/02/$ - see front matter © 2002 Elsevier Science Ltd. All rights reserved.
PII: S0277-5387(02)00933-6



Scheme 1.

using standard Schlenk techniques. Diethyl ether was distilled from sodium benzophenone ketyl; toluene, hexanes, and pentane were distilled from sodium; dichloromethane was distilled from CaH_2. The distilled solvents were stored under an argon atmosphere and over 4 Å molecular sieves. All NMR solvents were degassed and stored over 4 Å molecular sieves in a N_2 filled drybox. $Ta(NMe_2)_5$ was synthesized according to the improved procedure for the preparation of homoleptic metal amide complexes reported by Jordan et al. [34]. The bis-sulfamide compounds $SO_2[NHCMe_3]_2$ and $SO_2\{NH[CH(Me)Ph]\}_2$ were synthesized according to previously published procedures [28–31].

^1H and ^{13}C NMR spectra were measured at 300 MHz on a Varian VXR-300 spectrometer. The chemical shifts are reported in parts per million (ppm) downfield from tetramethylsilane and referenced to residual proton peaks of the NMR solvents. Mass spectrometry was performed by the UF Department of Chemistry Analytical Services.

2.2. $Ta[NMe_2]_3[SO_2(NCMe_3)_2]$ (1)

To a toluene solution of $Ta(NMe_2)_5$ (3.31 g, 8.24 mmol) at room temperature (r.t.) was added a toluene solution of $SO_2(NHCMe_3)_2$ (1.74 g, 8.24 mmol). No immediate color change was observed. The mixture was allowed to stir for 12 h at r.t. (connected to an oil bubbler to release the $HNMe_2$ produced during the reaction). Removal of the reaction solvent under reduced pressure gave a brown oily solid, which was washed with several portions of hexane to yield 3.86 g (74%) of **1** as a light beige solid. Mass Spec. Calc. For $C_{14}H_{37}O_2N_5TaS$ $[M+H]^+$: 520.2143 *m/e*. Found: (FAB) 520.2143 *m/e*. ^1H NMR (25 °C, C_6D_6): δ 1.51 (s, 18H, $SO_2(NC(CH_3)_3)_2$), 3.09 (s, 18H, $N(CH_3)_2$). ^{13}C NMR (25 °C, C_6D_6): δ 32.83, ($SO_2(NC(CH_3)_3)_2$), 45.16 ($N(CH_3)_2$).

2.3. $Ta(NMe_2)_3[SO_2(NCH(Me)Ph)_2]$ (2)

Compound **2** was synthesized from $Ta(NMe_2)_5$ (2.50 g, 6.23 mmol) and $SO_2(NCH(Me)Ph)_2$ (1.90 g, 6.23 mmol) following the same procedure as was used for the synthesis of compound **1**. The reaction yielded 3.41 g (75%) of **2** as a light brown solid. Mass Spec. Calc. For $C_{22}H_{36}O_2N_5TaS$ $[M+H]^+$: 616.5726 *m/e*. Found: (FAB) 616.5725 *m/e*. ^1H NMR (25 °C, C_6D_6): δ 1.76 (d, 6H, $^3J_{H-H} = 6.9$ Hz, $SO_2(NCH\mathit{Me}(C_6H_5))_2$), 2.75 (s,18H, $N(CH_3)_2$), 5.56 (q, 2H, $^3J_{H-H} = 6.9$ Hz, $SO_2(NC\mathit{H}Me(C_6H_5))_2$), 7.01 (t, 2H, $^3J_{H-H} = 6.9$ Hz, *p*-C_6H_5), 7.09 (t, 4H, $^3J_{H-H} = 7.2$ Hz, *m*-C_6H_5), 7.27 (d, 4H, $^3J_{H-H} = 7.2$ Hz, *o*-C_6H_5). ^{13}C NMR (25 °C, C_6D_6): δ 24.43 ($SO_2(NCH\mathit{Me}(C_6H_5))_2$), 43.92 ($SO_2(N\mathit{C}H$-$Me(C_6H_5))_2$), 55.85 ($N(\mathit{C}H_3)_2$), 126.60, 128.13, 146.50 (aromatic).

2.4. X-ray data collection and structure refinement for 1

Single crystals for X-ray crystallography of $Ta[N(CH_3)_2]_3[SO_2(NC(CH_3)_3)_2]$ (**1**) were grown by slow diffusion of pentane in a saturated toluene solution of **1**. Selected bond lengths and angles are given in Table 1. $C_{14}H_{36}N_5O_2STa$; M 519.49; triclinic; space group P_1; $a = 8.9208(1)$, $b = 10.0987(1)$, $c = 13.7290(1)$ Å; $U = 1044.15(2)$ Å^3; $Z = 2$; $D_{calc} = 1.652$ Mg m^{-3}; $\mu = 5.378$ mm^{-1}; $F(000) = 520$; reflections collected 6924; independent reflections 4634 ($R_{int} = 0.0309$).

Data were collected at 173 K on a Siemens SMART PLATFORM equipped with a CCD area detector and a graphite monochromator utilizing Mo Kα radiation ($\lambda = 0.71073$ Å). Cell parameters were refined using up to 6753 reflections. A hemisphere of data (1381 frames) was collected using the ω-scan method (0.3 v frame width). The first 50 frames were remeasured at the end of data collection to monitor instrument and crystal stability (maximum correction on I was $< 1\%$). Ψ scan absorption corrections were applied based on the entire data set.

The structure was solved by Direct Methods SHELXTL-5 [35], and refined using full-matrix least-squares. The non-H atoms were treated anisotropically where the hydrogen atoms were calculated in ideal positions and were riding on their respective carbon atoms. Two hundred and nine parameters were refined

Table 1
Selected bond distances (Å) and angles (°) for **1**

Bond distances	
Ta–N(1)	2.074(3)
Ta–N(2)	2.145(3)
Ta–N(3)	1.961(4)
Ta–N(4)	1.965(3)
Ta–N(5)	1.996(4)
Bond angles	
N(1)–Ta–N(5)	98.78(14)
N(2)–Ta–N(3)	94.94(14)
N(2)–Ta–N(4)	94.65(14)
N(2)–Ta–N(5)	166.32(14)
N(3)–Ta–N(4)	115.70(2)
N(3)–Ta–N(5)	92.40(2)
N(4)–Ta–N(5)	92.50(2)
N(1)–Ta–N(2)	67.54(12)
N(1)–Ta–N(3)	120.90(14)
N(1)–Ta–N(4)	121.45(14)

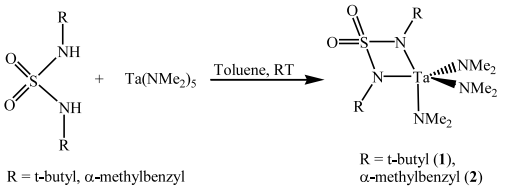
in the final cycle of refinement using 4356 reflections with $I > 2\sigma(I)$ to yield R_1 3.04% and wR_2 7.70%, respectively. Refinement was performed using F^2.

3. Results and discussion

The reaction of 2 equiv. of RNH_2 (R = *t*-butyl or α-methylbenzyl) with 2 equiv. of NEt_3 and O_2SCl_2 yields the bis-sulfamide ligands $SO_2[NHC(CH_3)_3]_2$ and $SO_2\{NH[CH(Me)Ph]\}_2$ [28–31]. Unsuccessful attempts to deprotonate either of these ligands using a wide array of bases and deprotonation techniques led us to examine the amine elimination reaction as a means to incorporate them into a metal coordination sphere [8,27,36–38].

Reaction of the bis-sulfamides $SO_2[NHCMe_3]_2$ and $SO_2\{NH[CH(Me)Ph]\}_2$ with $Ta(NMe_2)_5$ for 12 h at room temperature produced the complexes $Ta[NMe_2]_3[SO_2(NCMe_3)_2]$ (**1**), $Ta[NMe_2]_3[SO_2(NCH(Me)Ph]_2$ (**2**) in high yield (75%) (Scheme 2). The room temperature ^1H NMR spectrum of **1** displays two singlets at 1.46 and 3.12 ppm, corresponding to the CMe_3 and NMe_2 groups, respectively. In the proton NMR spectrum of compound **2**, the sulfamide methyl protons appear as a doublet (1.76 ppm) while the NMe_2 protons appear as a singlet (2.75 ppm) and the methine proton resonates as a quartet (5.56 ppm). Since compounds **1** and **2** are pentacoordinate, they can adopt either a square pyramidal or trigonal bipyramidal idealized geometry [39]. Both of these structures have different chemical environments for their NMe_2 groups. The observed equivalency of the NMe_2 groups at room temperature implies the presence of a fluxional process, which equilibrates the NMe_2 groups on the NMR timescale.

In order to determine the nature of the fluxional process, a variable temperature ^1H NMR study was performed on compound **1** (C_7D_8). The ^1H NMR spectra of **1** at various temperatures are shown in (Fig. 1). At −60 °C, the spectrum of **1** has inequivalent CMe_3 peaks (1.50, 1.56 ppm, 9H each) of equal intensity and three NMe_2 resonances (2.95, 2.98, 3.19 ppm) each integrating to six protons. Two of the NMe_2 resonances, 2.95 and 2.98 ppm, coalesce at −35 °C (2.97 ppm). The CMe_3 resonances coalesce at −30 °C whereas the coalesced NMe_2 resonance at 2.97 ppm coalesces with the resonance at 3.19 ppm at −9 °C.



Scheme 2.

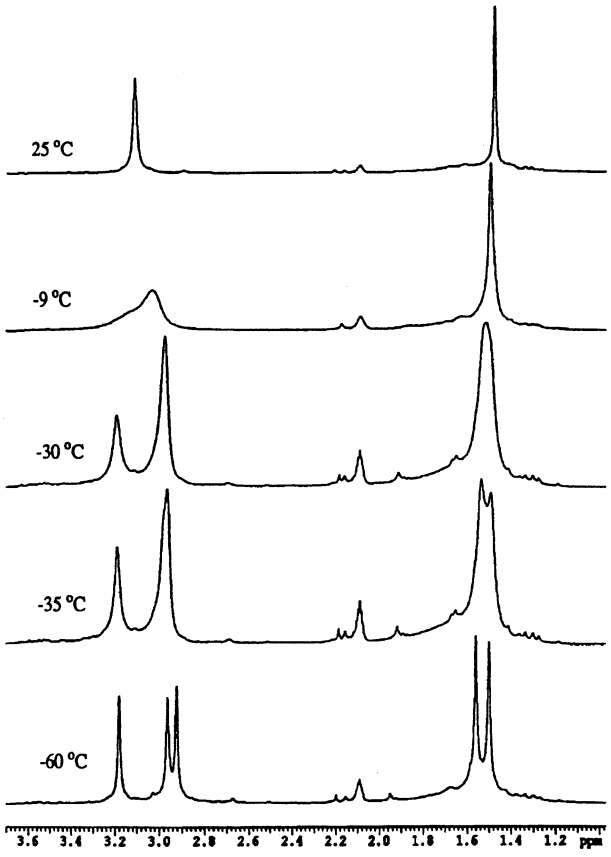


Fig. 1. Variable temperature ^1H NMR spectra of $Ta[N(CH_3)_2]_3[SO_2(NC(CH_3)_3)_2]$ (**1**).

Assuming a trigonal bipyramidal geometry, resolution of the NMe_2 resonance into three peaks instead of two, suggests that at very low temperatures, rotation about the Ta–N bonds of the NMe_2 ligands is slow. Rapid rotation of the equatorial NMe_2 groups at low temperature would produce two peaks in a 2:1 ratio (equatorial:axial). Slow rotation about the Ta–N bonds renders each methyl on the equatorial NMe_2 ligands inequivalent with respect to the other, but equivalent with the adjacent NMe_2 methyl group by a mirror plane that includes the (Fig. 2). The value of $\Delta G^{\ddagger}$ for the coalescence of the NMe_2 (2.95, 2.98 ppm) and the *t*-butyl (1.50, 1.56 ppm) resonances were each estimated to be 12.3 kcal mol^{-1} using the equally populated two-site exchange approximation [40]. Using the unequally populated two-site exchange approximation, the activation energy $\Delta G^{\ddagger}$ for the coalescence of the NMe_2 peaks

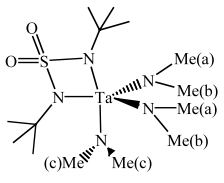


Fig. 2. Proposed structure of **1** to explain the low temperatue ^1H NMR spectrum.

at 2.97 and 3.19 ppm was estimated to be 12.8 kcal mol^{-1}. The similar activation energy values (~12 kcal mol^{-1}) that were calculated for the coalescence of the axial-equatorial NMe_2 groups and the *t*-butyl groups suggest the fluxional process which equilibrates these groups follows a Berry pseudorotation mechanism [39].

A similar variable temperature ^1H NMR study of compound **2** exhibited no significant broadening of the peaks, even at −90 °C. The difference between the dynamic behavior of compounds **1** and **2** may be attributed to the decreased steric bulk of the alkyl substituents of the bis-sulfamide in complex **2**.

The X-ray diffraction study of **1** shows that a trigonal bipyramidal coordination geometry is found in the solid state, which is consistent with the low temperature ^1H NMR spectroscopy of **1**. A molecular drawing of **1** is shown in Fig. 3 and selected bond lengths and angles are presented in Table 1. Compound **1** adopts a distorted trigonal bipyramidal geometry about the Ta metal center with the bidentate sulfamide ligand occupying one axial and one equatorial site. The bite angle of the ligand (67.5°) is smaller than that observed for other bidentate amido complexes reported in the literature due to the four-membered chelate ring. The Ta–N(1) and Ta–N(2) bond lengths of the bis-sulfamide ligand (2.074(3), 2.145(3) Å) are longer than the Ta–N bond lengths of the NMe_2 ligands (1.961(4), 1.965(3), 1.996(4) Å). The angles around N(3) and N(4) and N(5) sum to 360° indicating a trigonal planar geometry at the NMe_2 nitrogen atoms. This suggests that π-donation from the NMe_2 ligands to the metal center is possible and probably plays a role in the observed slow rotation of the NMe_2 groups at low temperature in solution.

In order to explore the reactivity and further derivatization of complexes **1** and **2**, removal of the dimethyl amido ligands was attempted. Attempts to protonate the NMe_2 groups using either Et_3NHCl or $Me_2NH{\cdot}HCl$ or

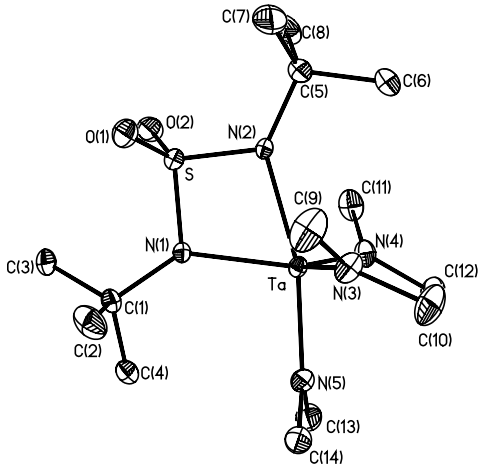


Fig. 3. The structure of $Ta[N(CH_3)_2]_3[SO_2(NC(CH_3)_3)_2]$ (**1**) with the atomic numbering scheme. Ellipsoids are shown at 40% occupancy and the hydrogen atoms have been removed for clarity,

to replace the NMe_2 groups with Cl^- utilizing $SiMe_3Cl$ gave mixtures of uncharacterizable products. Alkyl aluminum reagents have also been useful in converting amido complexes to alkyl derivatives [37,38]. The reaction of compound **1** with either $AlMe_3$ or $AlEt_3$ led to the formation of new complexes, which contain 1 equiv. of AlR_3. It appears that these complexes are coordination complexes between **1** and the aluminum reagent. However, due to inconclusive spectroscopic results and our inability to obtain X-ray quality crystals of these compounds, we do not know whether the AlR_3 groups coordinate to the sulfamide oxygen(s) or the amido N atoms. Further heating of these materials did not lead to characterizable products.

4. Summary

Bis-sulfamide compounds were successfully employed as chelating diamide ligands in the synthesis of the tantalum amido complexes $Ta[NMe_2]_3[SO_2(NCMe_3)_2]$ (**1**) and $Ta(NMe_2)_3[SO_2(NCH(Me)Ph)_2]$ (**2**) via the amine elimination method. Attempts to remove the NMe_2 ligands from either **1** or **2** using Et_3NHCl, $Me_2NH{\cdot}HCl$ or $SiMe_3Cl$ were unsuccessful. The use of AlR_3 reagents to form alkylated derivatives of **1** led to the formation of AlR_3 adduct complexes that have proved difficult to characterize. The synthesis of other metal complexes containing bis-sulfamide ligands is currently being explored.

Acknowledgements

J.M. B. thanks the National Science Foundation (CHE 9523279) for funding of this work and K.A. A. thanks the NSF and the University of Florida for funding X-ray equipment purchases.

References

[1] W.J. Kaminsky, J. Chem. Soc., Dalton Trans. 9 (1998) 1413.
[2] H.H. Brintzinger, D. Fischer, R. Mulhaupt, B. Rieger, R.M. Waymouth, Angew. Chem., Int. Ed. Engl. 34 (1995) 1143.
[3] M.J. Bochmann, J. Chem. Soc., Dalton Trans. (1996) 255.
[4] S. Fokken, T.P. Spaniol, J. Okuda, F.G. Sernetz, R. Mulhaupt, Organometallics 20 (1997) 4240.
[5] F.G. Sernetz, R. Mulhaupt, S. Fokken, J. Okuda, Macromolecules 30 (1997) 1562.
[6] A. Vanderlinden, C.J. Schaverien, N. Meijboom, C. Ganter, A.G. Orpen, J. Am. Chem. Soc. 117 (1995) 3008.
[7] K. Aoyagi, P.K. Gantzel, K. Kalai, T.D. Tilley, Organometallics 15 (1996) 923.
[8] J.D. Scollard, D.H. McConville, J.J. Vittal, Organometallics 14 (1995) 5478.
[9] T.H. Warren, R.R. Schrock, W.M. Davis, Organometallics 15 (1996) 562.

[10] F. Guerin, D.H. McConville, N.C. Payne, Organometallics 15 (1996) 5085.
[11] N.A.H. Male, M. Thornton-Pett, M.J. Bochmann, J. Chem. Soc., Dalton Trans. (1997) 2487.
[12] B. Tsuie, D.C. Swenson, R.F. Jordan, J.L. Petersen, Organometallics 16 (1997) 1392.
[13] S. Pritchett, P. Gantzel, P.J. Walsh, Organometallics 16 (1997) 5130.
[14] R.R. Schrock, F. Schattenmann, M. Aizenberg, W.M. Davis, Chem. Commun. (1998) 199.
[15] F. Guerin, D.H. McConville, J.J. Vittal, G.A.P. Yap, Organometallics 17 (1998) 5172.
[16] L.C. Liang, R.R. Schrock, W.M. Davis, D.H. McConville, J. Am. Chem. Soc. 122 (1999) 5797.
[17] C. Lorber, B. Donnadieu, R. Choukroun, Organometallics 19 (2000) 1963.
[18] S. Tinkler, R.J. Deeth, D.J. Duncalf, A. McCamley, Chem. Commun. (1996) 2623.
[19] J.D. Scollard, D.H. McConville, N.C. Payne, J.J. Vittal, Macromolecules 29 (1996) 5241.
[20] J.D. Scollard, D.H. McConville, J. Am. Chem. Soc. 118 (1996) 10008.
[21] Y.M. Jeon, S.J. Park, J. Heo, K. Kim, Organometallics 17 (1998) 3161.
[22] K. Nomura, N. Naga, K. Takaoki, Macromolecules 31 (1998) 8009.
[23] K. Nomura, N. Naofumi, K. Takaoki, A. Imai, J. Mol. Cat. A-Chem. 130 (1998) L209.
[24] R. Vollmerhaus, P.C. Shao, N.J. Taylor, S. Collins, Organometallics 18 (1999) 2731.
[25] Y.M. Jeon, J. Heo, W.M. Lee, T.H. Chang, K. Kim, Organometallics 18 (1999) 4107.
[26] K. Nomura, K. Oya, Y. Imanishi, Polymer 41 (2000) 2755.
[27] C.H. Lee, Y.H. La, W.J. Park, Organometallics 19 (2000) 344.
[28] R.D.W. Kemmitt, S. Mason, M.R. Moore, J. Fawcett, D.R. Russell, J. Chem. Soc., Chem. Commun. (1990) 1535.
[29] I.P. Parkin, A.M.Z. Slawin, D.J. Williams, J.D. Woollins, J. Chem. Soc., Chem. Commun. (1989) 1060.
[30] I.P. Parkin, J.D. Woollins, J. Chem. Soc., Dalton Trans. (1990) 519.
[31] A.H. Cowley, S.K. Mehrotra, H.W. Roesky, Inorg. Chem. 20 (1981) 712.
[32] M. Bermann, J.R. Wazer, Synthesis (1972) 576.
[33] J.M. Hawkins, K.B. Sharpless, J. Org. Chem. 49 (1984) 3861.
[34] G.M. Diamond, R.F. Jordan, J.L. Petersen, J. Am. Chem. Soc. 118 (1996) 8024.
[35] G.M. Sheldrick, SHELLXT [Nicolet XRD], Madison, WI, 1986.
[36] D.W. Carpenetti, L. Kloppenburg, J.T. Kupec, J.L. Petersen, Organometallics 15 (1996) 2668.
[37] G.M. Diamond, R.F. Jordan, J.L. Petersen, Organometallics 15 (1996) 4030.
[38] G.M. Diamond, R.F. Jordan, J.L. Petersen, Organometallics 15 (1996) 4045.
[39] G.O. Spessard, G.L. Miessler, Organometallic Chemistry, Prentice-Hall, New Jersey, 1997.
[40] J. Sandstrom, Dynamic NMR Spectroscopy, Academic Press, New York, 1982.

PERGAMON

Polyhedron 21 (2002) 1057–1061

POLYHEDRON

www.elsevier.com/locate/poly

Crystal structure, magnetic and spectroscopic properties of copper(II) formato dimethylformamide: a new tetracarboxylato-bridged copper(II) dimer

Rocio Cejudo [a], Gloria Alzuet [a], Joaquín Borrás [a,*], Malva Liu-González [b], Francisco Sanz-Ruiz [b]

[a] *Departamento de Química Inorgánica, Universidad de Valencia, Avda. Vicent Andrés Estellés s/n, 46100 Burjassot, Spain*
[b] *Departamento de Termología, Universidad de Valencia, Dr. Moliner, 50. 46100 Burjassot, Spain*

Received 19 June 2001; accepted 26 February 2002

Abstract

The crystal and molecular structure of a new tetracarboxylato copper(II) dimer [bis(dimethylformamide)tetrakis(μ-formato)dicopper(II)], has been determined by X-ray diffraction methods. The crystal structure consists of a centrosymmetric dimer $[Cu_2(HCOO)_4(dmf)_2]$, where four bidentate formato anions form *syn–syn* bridges between the metal ions which are in a 4+1 environment. Magnetic susceptibility data show that the copper ions are strongly antiferromagnetically coupled with $J = -470$ cm^{-1}. The EPR spectrum shows a characteristic pattern of a triplet state with a D zero field splitting value of 0.27 cm^{-1}. © 2002 Elsevier Science Ltd. All rights reserved.

Keywords: Copper; Formato; Dinuclear complexes; Antiferromagnetic; EPR

1. Introduction

Extensive work on dimeric copper(II) carboxylates has been reported. Among these copper carboxylates, the copper acetates form a large family with many structurally characterised compounds for which magnetic and spectroscopic properties have been measured [1,2]. In contrast, only a very limited amount of detailed structural data is available for dimeric cupric formato adducts [3]. One of the most attractive puzzles in magneto-structural correlations in dimeric copper carboxylates is why do dimeric copper(II) formato complexes show much larger $-2J$ values (approximately 500 cm^{-1}) than the corresponding copper(II) acetate dimers whose $-2J$ values are approximately 300 cm^{-1}.

With the aim of obtaining a better understanding of this phenomenon we have investigated the structural, spectroscopic and magnetic properties of [bis(dimethylformamide)tetra-μ-formatodicopper(II)] reported here.

2. Experimental

All reagents and chemicals were purchased from commercial sources and used without further purification. Elemental analyses (C, H, N) were carried out at the microanalytical laboratory of the ITQ of the Universidad Politécnica of Valencia.

2.1. Physical measurements

The infrared (IR) spectrum ($\nu = 400$–4000 cm^{-1}) was obtained on KBr pellets using a Mattson Satellite FTIR spectrophotometer. Solid electronic spectra were recorded on samples dispersed in Nujol using a Shimadzu 2101 PC spectrophotometer. Electron paramagnetic resonance (EPR) measurements for ground crystals were carried out on a Bruker ELEXSYS at X-band frequencies. The variable temperature magnetic susceptibility measurement on a microcrystalline sample was

* Corresponding author. Tel.: +34-96-3864530; fax: +34-96-3864960.
E-mail address: joaquin.borras@uv.es (J. Borrás).

0277-5387/02/$ - see front matter © 2002 Elsevier Science Ltd. All rights reserved.
PII: S0277-5387(02)00935-X

carried out on a Quantum Design MPMS2 SQUID susceptometer equipped with a 55 kG magnet, operating at 10 kG in the range of 1.8–400 K. The susceptometer was calibrated with $(NH_4)_2Mn(SO_4)_2\cdot 12H_2O$. Corrections for diamagnetism were estimated from Pascal constants.

2.2. Synthesis of the complex

Prismatic green crystals of $[Cu_2(HCOO)_4(dmf)_2]$ were obtained by slow evaporation of a dmf saturated solution of $Cu(HCOO)_2\cdot 4H_2O$ at room temperature. They were isolated by filtration, washed with dmf and air-dried. Yield: 57%. Anal. Calc. for $C_{10}H_{18}Cu_2N_2O_{10}$: C, 26.5; H, 4.0; N, 6.2. Found: C, 26.4; H, 3.9; N, 6.0%. IR (KBr pellet; cm^{-1}): 2935, 2877 $\nu(CH_3)$; 1629 [ν(C=O)dmf, ν_{as}(COO)]; 1460 ν_s(COO); 1377, 1355 $\delta(CH_3)$; 775 δ(COO). Solid electronic spectra (Nujol) (λ_{max}, nm): 720 (d–d).

2.3. Crystal data

$C_{10}H_{18}Cu_2N_2O_{10}$. Mr = 453.34, triclinic space group $P\bar{1}$, $a = 6.488(3)$ Å, $b = 7.3551(12)$ Å, $c = 9.8309(7)$ Å, $\alpha = 100.25(9)^\circ$, $\beta = 99.212(16)^\circ$, $\gamma = 110.53(2)^\circ$, $V = 419.5(2)$ Å^3, $Z = 1$, Dx = 1.794 g cm^{-3}, Mo Kα radiation (graphite crystal monochromator, $\lambda = 0.7173$ Å), $\mu = 2.586$ mm^{-1}, $F(000) = 228$, $T = 293(2)$ K, final conventional $R_1 = 0.0456$ and $wR_2 = 0.1185$ for 1488 observed reflections and 145 variables.

2.4. X-ray crystal structure determination

Green crystal, size $0.40 \times 0.30 \times 0.18$ mm^3. Throughout the experiment Mo Kα was used with a graphite crystal monochromator on an Enraf Nonius CAD-4 [4] single crystal diffractometer ($\lambda = 0.7173$ Å). The unit cell dimensions were determined from the angular settings of 25 reflections with θ between 2.17° and 25.95°. The space group was determined to be $P\bar{1}$ from no systematic absences (ABSEN, [5]). The intensity data of 3250 reflections, in the *hkl* range (−7, −9, −12) to (7, 9, 12) and limits ($1^\circ < \theta < 25^\circ$), were measured, using the ω–2θ scan technique and variable scan rate with a maximum scan time of 60 s per reflection. The intensity of the primary beam was checked throughout the data collection by monitoring three standard reflections every 60 min. On all reflections profile analyses were performed (PROFIT, Profile Fitting Data Reduction, [6]). Lorentz-polarization corrections were applied and then data were reduced to F_o^2 values. The structure was solved using SIR-92 (A program for crystal structure solution, [7]). Isotropic least-squares refinement on F^2 was made using SHELX-93 [8]. During the final stages of the refinement on F^2 the positional parameters and the anisotropic thermal parameters of the non-H atoms were refined. The hydrogen atoms were located by XHYDEX [9]. The final conventional agreement factors were $R_1 = 0.0456$ and $wR_2 = 0.11185$ for 1488 observed reflections and 221 variables. The function minimised was $[\Sigma(w(F_o^2 - F_c^2)^2)/\Sigma[w(F_o^2)]^2]^{1/2}$, $w = 1/[\sigma^2(F_o^2) + (0.0828P)^2]$ with $\sigma(F_o^2)$ from counting statistic and $P = (F_o^2 + 2F_c^2)/3$. The final difference Fourier map showed a peak of 0.851–0.91 Å^3 for the atom Cu1, the other peaks were no deeper—0.977–0.90 Å^3 from Cu(1). The figures were made by ORTEP-3 (for Windows, [10]). Geometrical calculations were made with PARST [11]. Atomic scattering factors were taken from International Tables of Crystallography [12].

3. Results and discussion

3.1. Spectroscopic properties

In the visible region the diffuse reflectance spectrum is characterised by a very broad band at approximately 13 900 cm^{-1} which can be assigned to unresolved d–d transitions. This spectrum is similar to that reported for $[Cu(HCOO)_2(OH_2)_2]2H_2O$ [13].

The IR spectrum of the compound shows a broad and intense band at 1629 cm^{-1} that must correspond to the ν_{as}(COO) vibration of the bridging formato and to the ν(C=O) of the dmf molecules. The ν_s(COO) vibration of the formato appears at 1377 cm^{-1}. Moreover, the spectrum exhibits characteristic vibrations of the methyl groups of the dmf ligands at 2935, 2877 and 1355 cm^{-1}.

3.2. Crystal structure

Fig. 1 shows an ORTEP drawing of the complex with the atomic numbering scheme. Bond distances and angles are reported in Table 1.

The crystal structure consists of a centrosymmetric dimeric unit of copper atoms bridged by four *syn–syn* $HCOO^-$ ions. Each copper ion is coordinated by four formato oxygens as equatorial ligands and by a dmf molecule, occupying the apex of a square pyramid. The coordination of dmf is through the amide oxygen which is sterically favoured over nitrogen. All Cu–O(formato) bond distances are similar and comparable to those of other cupric carboxylates. The Cu(1)–O(formato) bond lengths are in the range from 1.959(3) to 1.973(3) Å. The apical Cu–O(dmf) bond length [2.131(3)] is longer than the equatorial ones. The Cu(II) ions are displaced out of the mean planes formed by formato oxygen atoms [−1.3991 Å Cu]. The tetragonality value [T, defined as (mean in-plane distance R_S)/(mean out-of-plane distance R_L)] [14] for Cu(1) is 0.92.

The equatorial bond angles around Cu(1) are in the range from 88.42(14)° to 90.80(14)°. The value of τ is 0,

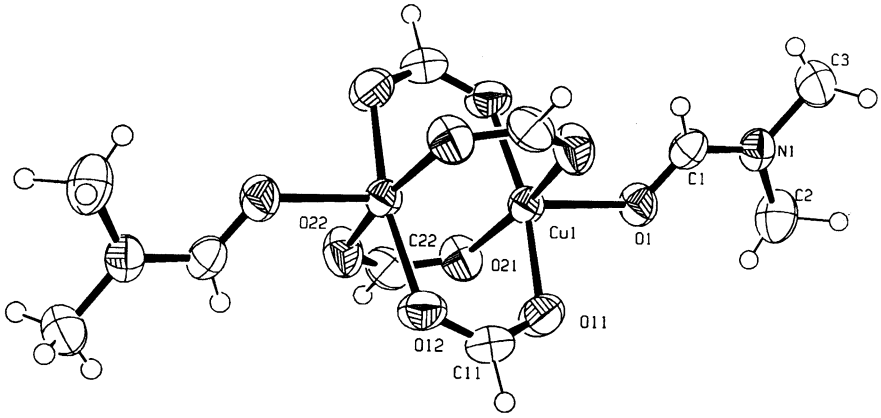


Fig. 1. ORTEP drawing of the $[Cu_2(HCOO)_4(dmf)_2]$ dimer showing 50% probability ellipsoids.

Table 1
Selected bond lengths (Å) and angles (°)

Bond lengths	
Cu(1)–O(21)	1.959(3)
Cu(1)–O(11)	1.967(3)
Cu(1)–O(22) [a]	1.969(3)
Cu(1)–O(12) [a]	1.973(3)
Cu(1)–O(1)	2.131(3)
Cu(1)–Cu(1) [a]	2.6509(19)
Bond angles	
O(21)–Cu(1)–O(11)	88.42(14)
O(21)–Cu(1)–O(22) [a]	167.72(12)
O(11)–Cu(1)–O(22) [a]	89.48(14)
O(21)–Cu(1)–O(12) [a]	88.66(14)
O(11)–Cu(1)–O(12) [a]	167.50(12)
O(22) [a]–Cu(1)–O(12) [a]	90.80(14)
O(21)–Cu(1)–O(1)	97.68(14)
O(11)–Cu(1)–O(1)	96.43(13)

[a] Symmetry transformations used to generate equivalent atoms: $-x+1, -y+1, -z+1$.

indicating that the coordination polyhedron around the Cu(II) ions is square pyramidal [15].

The Cu–Cu separation [2.6509(19) Å] is very similar to the average value of the other four structurally characterised $[Cu_2(HCOO)_4L_2]$ compounds (L = urea, dioxane, dithiocyanate, DMSO) [3,16,17] and is slightly larger (approximately 0.05 Å) than that found for the cupric acetate monohydrate [18].

The lengths of the Cu–O–C–O–Cu bridges (6.42 Å) are identical (6.44 ± 0.02 Å) for all dimeric cupric carboxylates [16].

3.3. EPR

The X-band EPR spectrum exhibits broad features characteristic of a triplet state with non-negligible zero field splitting (Fig. 2).

The spectra can be analysed with the spin Hamiltonian:

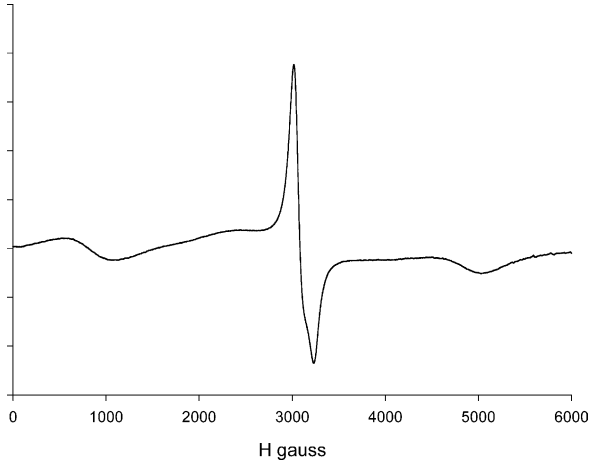


Fig. 2. EPR spectrum of polycrystalline $[Cu_2(HCOO)_4(dmf)_2]$ complex at room temperature.

$$H = \beta HgS + D[S_{z2} - 2/3] + [S_{x2} - S_{y2}]E$$

At the X-band, D is greater than the microwave energy and only two signals are observed, indicating moreover that $E \approx 0$. The two signals corresponds to H_{z1} and H_{z2}. Taking into account the equations proposed by Wasson et al. [19]

$$H_{z1} = (g_e/g_{\|})(H_0 - D')$$

$$H_{z2} = (g_e/g_{\|})(H_0 + D')$$

where $g_e = 2.0023$, $H_0 = h\nu/\beta g_e$ and $D' = D/\beta g_e$. From these expressions, the experimental field positions can be reproduced with $g_{\|} = 2.43$ and $D = 0.27\ cm^{-1}$. The zero field splitting is lower than that reported for $[Cu_2(HCOO)_4(dmso)_2]$ ($D = 0.40\ cm^{-1}$) [3] but similar to that of copper(II) acetate monohydrate ($D = 0.34\ cm^{-1}$) [20] or copper(II) benzoate ($D = 0.33\ cm^{-1}$) [21].

The dipole–dipole contribution, D_{dd}, can be estimated from the following relationship [22]:

$$D_{dd} = \frac{0.650 g_{\|}}{R^3}$$

where the R is the Cu···Cu separation. For this compound, with $R = 2.65$ Å, the dipole–dipole contribution to the experimental D is evaluated to be about 0.205 cm^{-1}. The experimental D is given by $D = D_{dd} + D_{exchange}$, and taking into account that the sign of the experimental D is unknown, a negative sign can be expected for D_{dd} [23], and a positive one for $D_{exchange}$, a $D_{exchange}$ value of 0.478 cm^{-1} is obtained.

3.4. Magnetic properties

The magnetic behaviour of the title compound is illustrated in Fig. 3 by means of a plot of χ_M versus the temperature in the range 100–300 K. The curve shows a strong antiferromagnetic behaviour. The experimental data were fitted to the Bleaney–Bowers equation. The least-squares fitting procedure led to $J = -470$ cm^{-1}, $g = 2.13$, $r_0 = 0.08$[Q1], and $R = 170 \times 10^{-6}$. The absolute value obtained for the singlet–triplet energy gap is similar to that reported for other tetra-μ-formato dicopper adducts and higher than the tetra-μ-acetato dicopper ones [24].

Recently, Rodriguez-Fortea et al. [25] have reported a density functional study of the exchange coupling in carboxylato-bridged dinuclear copper(II) compounds. They compared the J values for several substituents in $[Cu_2(\mu\text{-}RCOO)_4]$ and concluded that the electron-withdrawing groups reduce the strength of the exchange coupling. With respect to the previous studies that suggested a correlation between J and the electronegativity of the atom directly bonded to the carbon atom of the carboxylato group [22,26,27], Rodriguez-Fortea et al. concluded that this correlation is in general valid, but caution is needed when very electronegative atoms are taken into consideration. According to that, it is reasonable that the formato bridge has more exchange coupling than the acetato bridge. Besides, they concluded that the change of the axial ligand induces smaller variations in the coupling constant. They attributed the small changes to indirect effects associated with interactions of the unpaired electrons with lower lying electrons. Another studied factor is the distortion from the square pyramidal to trigonal bipyramidal geometry, which can be determined by the τ parameter. They concluded that for the formato bridge a decrease of the antiferromagnetic coupling occurs when the τ parameter increases. Since the complex is a regular square pyramid ($\tau \approx 0$), the obtained J value must be closed to the maximum expected for this family of compounds.

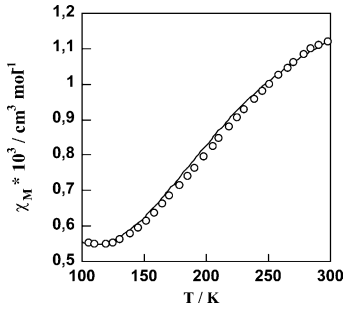


Fig. 3. Experimental χ_M versus T for $[Cu_2(HCOO)_4(dmf)_2]$ compound. The solid line represents the least-squares fit.

4. Supplementary data

Crystallographic data for the structural analysis have been deposited with the Cambridge Crystallographic Data Centre, CCDC No. 165343. Copies of this information may be obtained free of charge from The Director, CCDC, 12 Union Road, Cambridge, CB2 1EZ, UK (fax: +44-1223-336033; e-mail: deposit@ccdc.cam.ac.uk or www: http://www.ccdc.cam.ac.uk).

Acknowledgements

G.A. and J.B. thank CYCIT (project PM97-0105-C02-01) for financial support and Prof. J.A. Real for magnetic measurements.

References

[1] L.P. Battaglia, A. Bonamartini Corradi, L. Menabue, J. Chem. Soc., Dalton Trans. (1986) 1653.
[2] O. Kahn, Molecular Magnetism, VCH, New York, 1993.
[3] F. Sapiña, M. Burgos, E. Escrivá, J.-V. Folgado, D. Beltrán, P. Gómez-Romero, Inorg. Chim. Acta 216 (1994) 185.
[4] CAD-4 Software, Enraf-Nonius, BV Delf, The Netherlands, 1996.
[5] P. McArdle, J. Appl. Crystallogr. 29 (1996) 306.
[6] (a) M.S. Lehman, F.K. Larsen, Acta Crystallogr., Sect. A 30 (1974) 580;
(b) V.A. Strel'tsov, V.E. Zavodnik, Sov. Phys. Crystallogr. 34 (1989) 824;
(c) V.A. Strel'tsov, V.E. Zavodnik, Sov. Phys. Crystallogr. 35 (1990) 281.
[7] A. Altomare, G. Cascarano, C. Giacovazzo, A. Guagliardi, J. Appl. Crystallogr. 26 (1993) 343.
[8] G.M. Sheldrick, SHELXL-93, Program for Crystal Structure Refinement, University of Göttingen, Germany, 1993.
[9] K. Harms, S. Wocadlo, XCAD-4-CAD-4 Data Reduction, University of Marburg, Germany, 1995.
[10] L.J. Farrugia, J. Appl. Crystallogr. 30 (1997) 565.
[11] (a) M. Nardelli, Comput. Chem. 7 (1983) 95;
(b) M. Nardelli, J. Appl. Crystallogr. 28 (1995) 659.
[12] International Tables for X-ray Crystallography, vol. A, Kluwer Academic, Dordrecht, The Netherlands, 1995.
[13] D.E. Billing, B.J. Hathaway, J. Chem. Soc., Part A (1968) 1516.
[14] B.J. Hathaway, in: G. Wilkinson, R.D. Gillard, J.A. McCleverty (Eds.), Comprehensive Coordination Chemistry (Chapter 53), Pergamon, Oxford, 1987, p. 603.
[15] A.W. Addison, T.N. Rao, J. Reedijk, J. van Rijn, G.C. Verchoor, J. Chem. Soc., Dalton Trans. (1984) 1349.
[16] D.B.W. Yawney, R.J. Doerdens, Inorg. Chem. 9 (1970) 1626.

[17] H. Uekusa, S. Ohba, Y. Saito, Acta Crystallogr., Sect. C 45 (1989) 377.
[18] R. Chidambarum, G.M. Brown, Abstracts, American Association Meeting, Gatlinburg, TN, June 1965, No. D3.
[19] J.R. Wasson, C. Chin-I-Shyr, Trap, Inorg. Chem. 7 (1968) 469.
[20] B. Bleaney, K.D. Bowers, Proc. R. Soc. London, Ser. A 214 (1952) 451.
[21] F.G. Herring, R.C. Thompson, C.F. Swerdtfeger, Can. J. Chem. 47 (1969) 55.
[22] N.D. Chasten, R.L. Belford, Inorg. Chem. 9 (1970) 169.
[23] A. Abragam, B. Bleaney, Electron Paramagnetic Resonance of Transition Ions, Clarendon, Oxford, 1970, p. 508.
[24] R.W. Jotham, S.F.A. Kettle, J.A. Marks, J. Chem. Soc., Dalton Trans. (1972) 428.
[25] A. Rodriguez-Fortea, P. Alemany, S. Alvarez, E. Ruiz, Chem. Eur. J. 7 (2001) 627.
[26] R.J. Doedens, Prog. Inorg. Chem. 21 (1976) 209.
[27] M. Melnik, Coord. Chem. Rev. 36 (1981) 1.

PERGAMON

Polyhedron 21 (2002) 1063–1071

POLYHEDRON

www.elsevier.com/locate/poly

Synthesis and catalytic activity of manganese(II) complexes of heterocyclic carboxylic acids: X-ray crystal structures of $[Mn(pyr)_2]_n$, $[Mn(dipic)(bipy)_2]\cdot 4.5H_2O$ and $[Mn(chedam)(bipy)]\cdot H_2O$ (pyr = 2-pyrazinecarboxylic acid; dipic = pyridine-2,6-dicarboxylic acid; chedam = chelidamic acid(4-hydroxypyridine-2,6-dicarboxylic acid); bipy = 2,2-bipyridine)

Michael Devereux [a,*], Malachy McCann [b], Vanessa Leon [a], Vickie McKee [c], Richard J. Ball [c]

[a] *Dublin Institute of Technology, Cathal Brugha Street, Dublin 1, Ireland*
[b] *Chemistry Department, The National University of Ireland Maynooth, Maynooth, Co. Kildare, Ireland*
[c] *Chemistry Department, Loughborough University, Loughborough, Leics., England, LE11 3TU, UK*

Received 9 August 2001; accepted 8 January 2002

Abstract

Reactions of manganese(II) acetate with 2-pyrazine carboxylic acid, 2,6-pyridinedicarboxylic acid and chelidamic acid (4-hydroxypyridine-2,6-dicarboxylic acid) yielded $[Mn(pyr)_2]_n$ (**1**), $[Mn(dipic)]\cdot 1.5H_2O$ (**2**) and $Mn(chedam)]\cdot H_2O$ (**6**), respectively. Reaction of **2** with 2,2′-bipyridine and 1,10-phenanthroline results in the synthesis of $[Mn(dipic)(bipy)]\cdot 2H_2O$ (**3**), $[Mn(dipic)(bipy)_2]\cdot 4.5H_2O$ (**4**) and $[Mn(dipic)(phen)_2]\cdot 2H_2O$ (**5**). Complex **6** reacted with 2,2′-bipyridine and 1,10-phenanthroline to give $[Mn(chedam)(bipy)]\cdot H_2O$ (**7**) and $[Mn(chedam)(phen)_2]\cdot 3H_2O$ (**8**), respectively. Molecular structures for **1**, **4** and **7** were determined by X-ray crystallography. In **1** the structure is essentially polymeric with each pyrazine carboxylate anion coordinated to the manganese ion in a bidentate fashion using one carboxylate oxygen atom and the adjacent nitrogen. The second nitrogen is uncoordinated. For **4** the asymmetric unit consists of one tridentate dipicolinate ligand, two bidentate bipyridine molecules, four full-occupancy water molecules and one half-occupancy water molecule. The structure of **7** contains monomeric [Mn(dicarboxylate)(bipy)H_2O] units in which the Mn(II) ions have very irregular six-coordinate geometry. Spectroscopic, magnetic and physical data for the complexes are presented. All of the manganese complexes catalytically disproportionate hydrogen peroxide in the presence of imidazole. © 2002 Published by Elsevier Science Ltd.

Keywords: Manganese(II) complexes; 2-Pyrazine carboxylic acid; 2,6-Pyridinedicarboxylic acid; Chelidamic acid; Crystal structures; Catalytic disproportionation; Hydrogen peroxide

1. Introduction

The carboxylate group is an important class of ligand in inorganic and bioinorganic chemistry. Metal complexes containing monocarboxylic acids are well known and the publication of many structurally characterised examples of this class of compound has demonstrated the versatility of the carboxylate group as an inner-sphere ligand [1]. The coordination chemistry of dicarboxylic acids is far less developed and indeed structural information for this class of complex is relatively scarce. The main reason for this is due to the fact that dicarboxylic acids generally tend to react with metal salts to yield insoluble polymeric materials which can be difficult to characterise and almost impossible to crystallise. We have shown that reaction of polymeric copper(II), polymeric manganese(II) and polymeric

* Corresponding author. Tel.: +353-45-871-545.
E-mail addresses: michael.devereux@dit.ie (M. Devereux), devereuxm@eircom.net (M. Devereux).

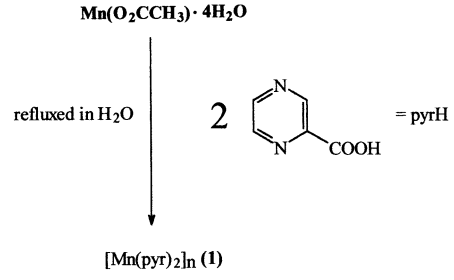
0277-5387/02/$ - see front matter © 2002 Published by Elsevier Science Ltd.
PII: S0277-5387(02)00842-2

cobalt(II) dicarboxylic acid complexes with the *N*,*N*-donor ligands 1,10-phenanthroline and 2,2′-bipyridine can lead to the synthesis of crystalline compounds which are easily structurally characterised by X-ray methods [2–4]. Furthermore, we have found that the reaction of simple transition metal salts with functionalised carboxylic and dicarboxylic acids leads to the isolation of soluble materials which we have structurally elucidated [5–7]. As well as the contribution that such complexes make to the knowledge of the coordination chemistry of the chemically/biologically important carboxylate ligands, further interest is derived from their potential applications. A wide range of the manganese(II) carboxylate complexes that we have generated exhibit excellent catalytic activity towards the disproportionation of hydrogen peroxide [8]. Such compounds are of interest not only because they mimic the activity of the biologically important mangano-catalases but also a number of them have been shown to catalyse the low temperature peroxide bleaching of fabrics [9].

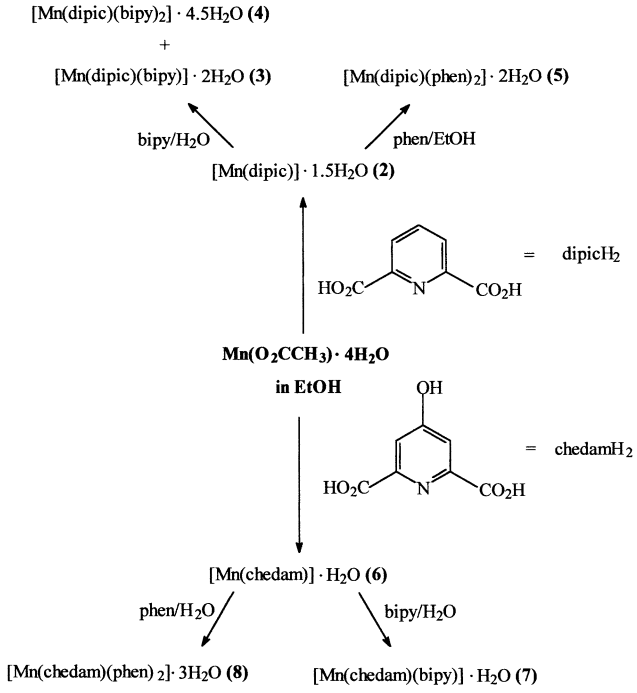
Herein, we report the synthesis, properties and structures for complexes of the heterocyclic carboxylic and dicarboxylic acids; 2-pyrazine carboxylic acid {pyrH}, 2,6-pyridine-dicarboxylic acid {dipicH_2} and chelidamic acid {chedamH_2} (4-hydroxypyridine-2,6-dicarboxylic acid). The disproportionation of hydrogen peroxide by the complexes is also discussed.

2. Results and discussion

Synthetic routes to the complexes **1**–**8** are shown in Schemes 1 and 2. $[Mn(pyr)_2]_n$ (**1**) was prepared in moderate yield by the reaction of 2-pyrazine carboxylic acid with manganese(II) acetate. Reaction of the acetate with 2,6-pyridinecarboxylic acid in ethanol resulted in the high yield formation of $[Mn(dipic)]\cdot 1.5H_2O$ (**2**). Reaction of **2** with excess 2,2′-bipyridine gave a suspension from which $[Mn(dipic)(bipy)]\cdot 2H_2O$ (**3**) was filtered in moderate yield. $[Mn(dipic)(bipy)_2]\cdot 4.5H_2O$ (**4**) was subsequently isolated from the filtrate. When **2** was reacted with 1,10-phenanthroline in ethanol, yellow/green crystals of $[Mn(dipic)(phen)_2]\cdot 2H_2O$ (**5**) were obtained in moderate yield. Chelidamic acid (4-hydroxypyridine-2,6-dicarboxylic acid) reacted with manganese(II) acetate in methanol to give $Mn(chedam)]\cdot H_2O$ (**6**) in high yield. Complex **6** reacted with 2,2′bipyridine and 1,10-phenanthroline to give good yields of $[Mn(chedam)(bipy)]\cdot H_2O$ (**7**) and $[Mn(chedam)(phen)_2]\cdot 3H_2O$ (**8**), respectively.



Scheme 1.



Scheme 2.

The X-ray structure of $[Mn(pyr)_2]_n$ (**1**) is shown in Figs. 1 and 2 and selected bond and angles are listed in Table 1. In the structure each pyrazine carboxylate anion is coordinated to the manganese ion in bidentate fashion using one carboxylate oxygen atom [O(11) and O(21)] and the adjacent nitrogen [N(11) and N(21)]; the second nitrogen atoms [N(12) and N(22)] are not involved in bonding. The manganese ion achieves six-coordination by coordinating to carboxylate groups in adjacent asymmetric units, forming a two-dimensional polymeric sheet in which the two independent pyrazole anions show different coordination behaviour (Fig. 1).

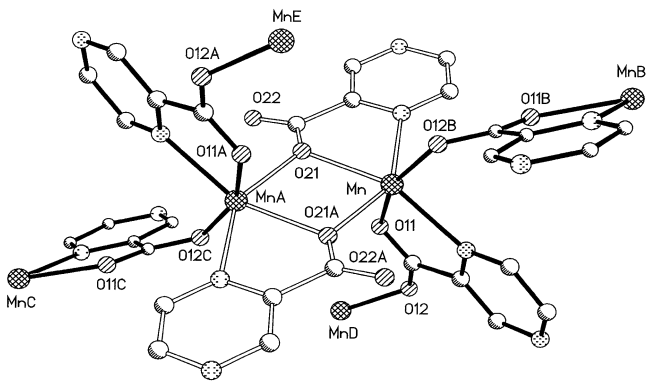


Fig. 1. A view of the pyrazine carboxylate bridging in $[Mn(pyr)_2]_n$ (**1**).

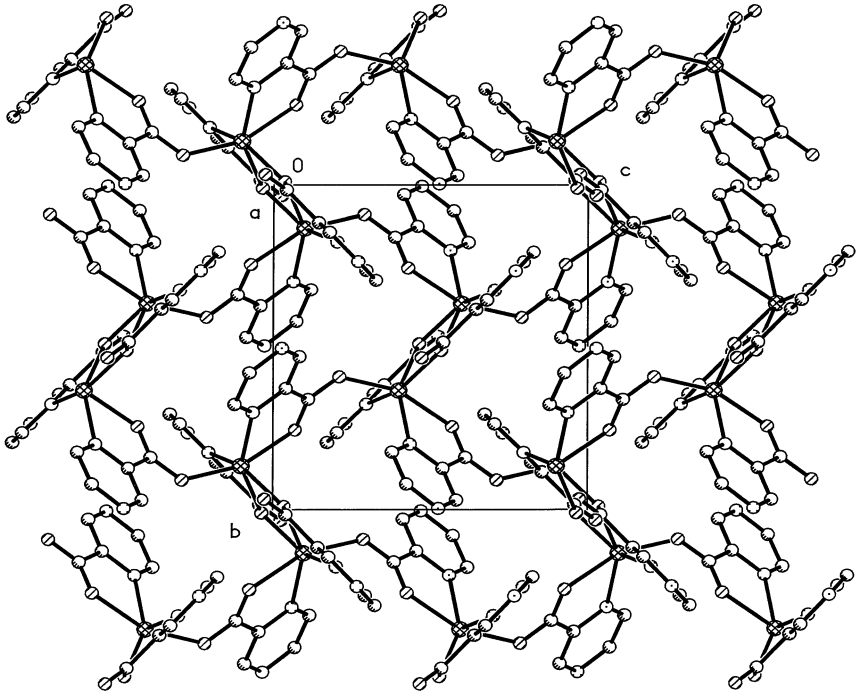


Fig. 2. A view of the π–π stacking in $[Mn(pyr)_2]_n$ (**1**).

Table 1
Selected bond lengths (Å) and angles (°) for $[Mn(pyr)_2]_n$ (**1**)

Bond lengths	
Mn–O(12) [a]	2.1037(12)
Mn–O(21) [b]	2.1394(12)
Mn–O(11)	2.2072(12)
Mn–O(21)	2.2211(12)
Mn–N(21)	2.2826(14)
Mn–N(11)	2.3056(15)
Mn–Mn [b]	3.5046(5)
Bond angles	
O(12) [a]–Mn–O(21) [b]	99.22(5)
O(12) [a]–Mn–O(11)	159.73(5)
O(21) [b]–Mn–O(11)	94.80(5)
O(12) [a]–Mn–O(21)	112.73(5)
O(21) [b]–Mn–O(21)	73.04(5)
O(11)–Mn–O(21)	85.31(5)
O(12) [a]–Mn–N(21)	94.02(5)
O(21) [b]–Mn–N(21)	144.88(5)
O(11)–Mn–N(21)	82.60(5)
O(21)–Mn–N(21)	71.84(5)
O(12) [a]–Mn–N(11)	91.13(5)
O(21) [b]–Mn–N(11)	95.50(5)
O(11)–Mn–N(11)	72.92(5)
O(21)–Mn–N(11)	154.62(5)
N(21)–Mn–N(11)	116.71(5)

Symmetry transformations used to generate equivalent atoms:
[a] $x, 0.5-y, 0.5+z$.
[b] $1-x, -y, -z$.

In the first case, the pyrazine carboxylate anion links two manganese ions via a single-atom bridge [Mn–O(21)–MnA 106.96(5)°, Mn–MnA 3.5046(5) Å] and the carbonyl oxygen remains uncoordinated. The second pyrazine carboxylate bridges two manganese ions via *anti*-1,3-carboxylate bridging [Mn–O(11)–C(15)–O(12)–MnB, Mn–MnB 5.646(1) Å]; this pyrazine carboxylate ion is also involved in a π–π interaction with a symmetrically equivalent neighbour (Fig. 2). The net effect is the formation of two-dimensional sheets perpendicular to the *a* axis with no significant interactions between the layers.

The X-ray crystal structure of $[Mn(dipic)(bipy)_2]\cdot 4.5H_2O$ (**4**) is shown in Figs. 3 and 4 and selected bond lengths and angles are listed in Table 2. The asymmetric unit consists of one tridentate dipicolinate ligand, two bidentate bipyridine molecules, four full-occupancy water molecules and one half-occupancy water molecule. The $[Mn(dipic)(bipy)_2]$ complex lies on

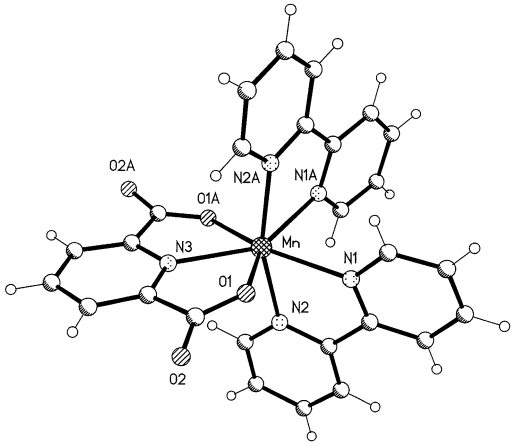


Fig. 3. The asymmetric unit of $[Mn(dipic)(bipy)_2]\cdot 4.5H_2O$ (**4**).

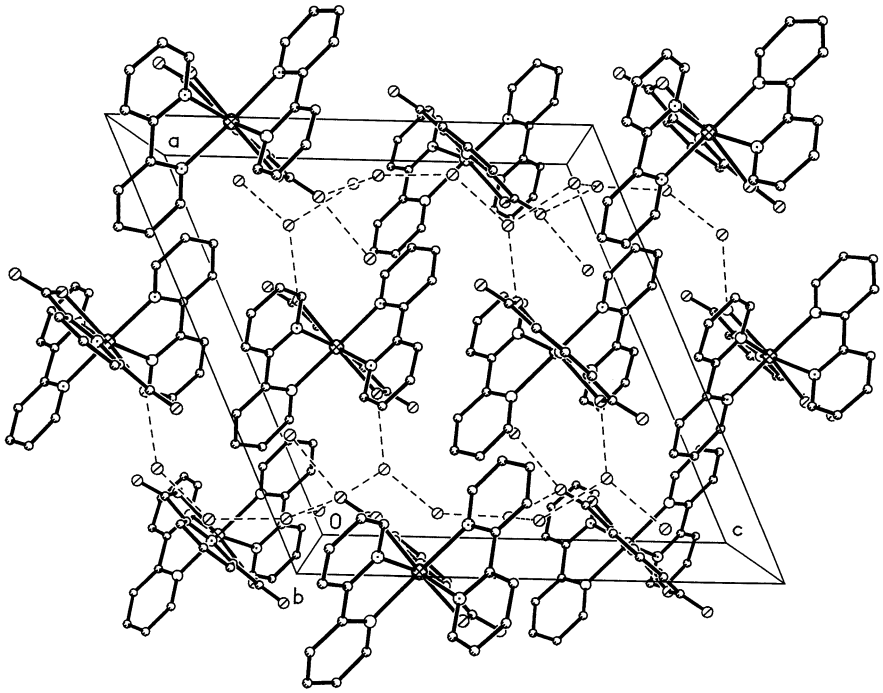


Fig. 4. The packing diagram in $[Mn(dipic)(bipy)_2]\cdot 4.5H_2O$ (**4**).

Table 2
Selected bond lengths (Å) and angles (°) for $[Mn(dipic)(bipy)_2]\cdot 4.5H_2O$ (**4**)

Bond lengths	
Mn–N(2)	2.243(2)
Mn–N(3)	2.272(3)
Mn–N(1)	2.315(2)
Mn–O(1)	2.384(2)
Bond angles	
N(2)–Mn–N(2)#1	162.43(12)
N(2)–Mn–N(3)	98.78(6)
N(2)–Mn–N(1)	71.73(8)
N(2)–Mn–N(1)#1	94.31(8)
N(3)–Mn–N(1)	141.30(6)
N(1)–Mn–N(1)	77.41(11)
N(2)–Mn–O(1)	97.64(7)
N(2)–Mn–O(1)#1	88.76(7)
N(3)–Mn–O(1)#1	68.64(5)
N(1)–Mn–O(1)	75.45(7)
N(1)–Mn–O(1)#1	145.05(7)
O(1)–Mn–O(1)#1	137.29(10)

Symmetry transformations used to generate equivalent atoms: #1: $-x-1, y, -z+1/2$.

Table 3
Hydrogen bonds for $[Mn(dipic)(bipy)_2]\cdot 4.5H_2O$ (**4**) (Å and °)

D–H···A	d(D–H)	d(H···A)	d(D···A)	∠(DHA)
O(1W)–H(1WA)···O(1)	0.92	1.96	2.862(3)	165.4
O(1W)–H(1WB)···O(3W)	0.87	1.88	2.734(3)	166.4
O(2W)–H(2WA)···O(2)	0.87	1.98	2.806(3)	157.3
O(2W)–H(2WB)···O(4W)#2	0.94	1.84	2.776(4)	173.5
O(3W)–H(3WA)···O(2W)#3	0.91	1.90	2.792(3)	168.2
O(3W)–H(3WB)···O(2W)#4	0.89	1.86	2.752(3)	176.1
O(4W)–H(4WA)···O(1W)	0.95	1.81	2.758(3)	174.3
O(4W)–H(4WB)···O(5W)	0.83	1.79	2.598(6)	165.1
O(4W)–H(4WB)···O(5W′)	0.83	2.21	3.012(18)	164.7

Symmetry transformations used to generate equivalent atoms: #2: $-x-1/2, -y-3/2, -z$; #3: $-x-1/2, y+1/2, -z+1/2$; #4: $x+1/2, -y-3/2, z+1/2$.

a twofold axis, passing through Mn, N3 and C14 so that the bipy groups are *cis* to one another and the metal ion has irregular six-coordinate geometry. All the solvate water molecules and all the carboxylate oxygens of the dipic ligand are involved in hydrogen bonding (Fig. 4, Table 3). The bipy ligands are involved in π–π stacking interactions with neighbouring complex molecules.

The X-ray crystal structure of $[Mn(chedam)(bipy)]\cdot H_2O$ (**7**) is shown in Fig. 5 and selected bond lengths and angles are given in Table 4. The structure contains monomeric $[Mn(dicarboxylate)(bipy)H_2O]$ units in which the Mn(II) ions have very irregular six-coordinate geometry. This arrangement is imposed by the small bite angles of the diacid (O11– Mn–O15, 143.44(4)°) and bipy (72.19(5)°) ligands. Individual molecules are linked into chains running parallel to the *c* axis by hydrogen bonding involving the coordinated water molecule, the phenol group and the carboxylate groups (Fig. 6 and Table 5) and the chains are linked by π–π stacking of the bipy ligands parallel to the *b* axis.

The infrared spectrum of **1** contains prominent $\nu_{OCOasym}$ and ν_{OCOsym} stretching bands around 1588 and 1421 cm^{-1}, respectively. The value of Δ_{OCO} ($\nu_{OCOasym}-\nu_{OCOsym}$) calculated for the complex (167

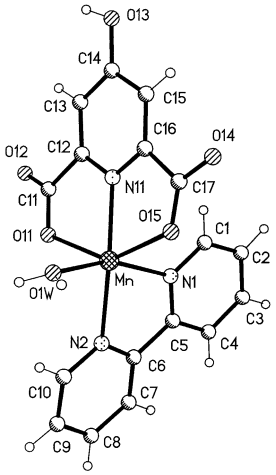


Fig. 5. The asymmetric unit of [Mn(chedam)(bipy)]·H_2O (**7**).

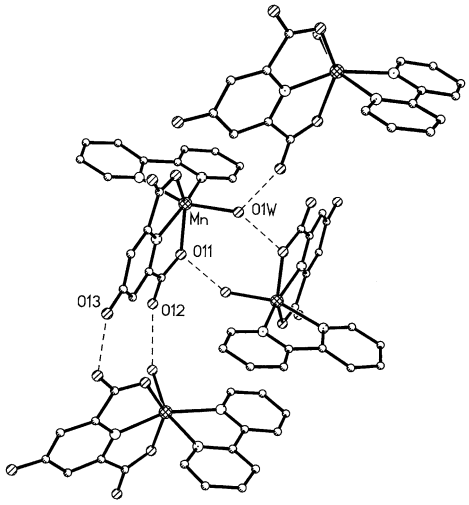


Fig. 6. The hydrogen bonding in [Mn(chedam)(bipy)]·H_2O (**7**).

Table 4
Selected bond lengths (Å) and angles (°) for [Mn(chedam)(bipy)]·H_2O (**7**)

Bond lengths	
Mn–O(1W)	2.1350(12)
Mn–N(11)	2.1697(13)
Mn–N(1)	2.2443(15)
Mn–O(15)	2.2492(12)
Mn–O(11)	2.2755(11)
Mn–N(2)	2.2783(14)
Bond angles	
O(1W)–Mn–N(11)	101.93(5)
O(1W)–Mn–N(1)	159.57(5)
N(11)–Mn–N(1)	97.04(5)
O(1W)–Mn–O(15)	89.12(4)
N(11)–Mn–O(15)	72.10(5)
N(1)–Mn–O(15)	89.55(5)
O(1W)–Mn–O(11)	93.24(4)
N(11)–Mn–O(11)	71.73(4)
N(1)–Mn–O(11)	99.89(5)
O(15)–Mn–O(11)	143.44(4)
O(1W)–Mn–N(2)	91.74(5)
N(11)–Mn–N(2)	159.64(5)
N(1)–Mn–N(2)	72.19(5)
O(15)–Mn–N(2)	123.70(5)
O(11)–Mn–N(2)	92.71(5)

Table 5
Hydrogen bonds for [Mn(chedam)(bipy)]·H_2O (**7**) (Å and °)

D–H···A	d(D–H)	d(H···A)	d(D···A)	∠(DHA)
O(13)–H(13A)···O(14)#1	0.94	1.65	2.5780(17)	171.3
O(1W)–H(1WA)···O(12)#2	0.86	1.86	2.7115(17)	173.9
O(1W)–H(1WB)···O(11)#3	0.87	1.89	2.7677(16)	177.5

Symmetry transformations used to generate equivalent atoms: #1: $x, -y, z-1/2$; #2: $x, -y, z+1/2$; #3: $-x+1, -y, -z$.

cm^{-1}) is close to the value expected for a bridging bidentate coordination mode of the carboxylate moiety [10]. The infrared spectrum of **2** contains prominent $\nu_{OCOasym}$ and ν_{OCOsym} stretching bands around 1588 and 1400 cm^{-1}, respectively. The value of Δ_{OCO} ($\nu_{OCOasym} - \nu_{OCOsym}$) calculated for the complex (188 cm^{-1}) is close to the value expected for a monodentate coordination mode of the carboxylate moiety [10]. Its relative insolubility in most common solvents suggests that it may have a polymeric structure. Complex **2** is sparingly soluble in acetone and its molar conductivity ($\Lambda_M = 0.0$ S cm^2 mol^{-1}) suggests that it is a non-electrolyte in this solvent. The IR spectra of complexes **3**, **4** and **5** contain bands attributable to $\nu_{OCOasym}$ and ν_{OCOsym} that give values of 188, 181 and 195 cm^{-1} for Δ_{OCO}, suggesting that the coordination modes for the dicarboxylate ligands in these complexes may be similar. The molar conductivity values for complexes **3** ($\Lambda_M = 0.0$ S cm^2 mol^{-1}) and **4** ($\Lambda_M = 1.64$ S cm^2 mol^{-1}) showed that these compounds are essentially non-electrolytes in ethanol and methanol, respectively. The IR spectra of complexes **6**,**7** and **8** contain bands attributable to $\nu_{OCOasym}$ and ν_{OCOsym} that give values of 148, 188 and 175 cm^{-1} for Δ_{OCO}, suggesting that the coordination modes for the dicarboxylate ligands in **6** may not be the same as those in **7** and **8**. Whereas complexes **7**and **8** are insoluble in most common solvents, **6** readily dissolved in several solvents, further suggesting possible structural differences between it and the other cheledamic acid complexes. The molar conductivity value for an aqueous solution of complex **6** ($\Lambda_M = 300.76$ S cm^2 mol^{-1}) suggests that it dissociates extensively in that solvent.

The room temperature magnetic moments of powdered samples of complexes **1**, **2**, **3**, **6**, **7** and **8** (5.82, 5.72, 5.95, 5.69, 5.89 and 5.99 BM, respectively) were in the range expected for manganese complexes where there is no significant exchange interactions between metal centres [11]. The room temperature magnetic moments for **4** and **5** (6.44 and 6.11 BM, respectively) fall slightly above this range.

We have recently described the synthesis of a series of manganese carboxylate complexes and demonstrated their ability to catalyse the disproportionation of hydrogen peroxide [12]. Apart from the obvious implications that such mimetic systems have for the biologically important mangano-catalases, further applications in areas such as catalytic low temperature bleaching technologies are attracting significant attention [9,13]. The catalytic activity of complexes **1**–**8** towards the disproportionation of hydrogen peroxide was investigated in the presence of the base imidazole (in the absence of the imidazole the complexes were either inactive or very weak catalysts for this reaction). The results from these reactions are summarised in Tables 6 and 7. Table 6 shows the rate of evolution of oxygen from the respective reactions for the complexes over the first 60 min. Examination of Table 7 shows that over the first minute of the reaction, complex **8** appears to be the most efficient catalyst with 4206 molecules of peroxide disproportionated by one molecule of the complex. Complex **2** appears to be the least efficient catalyst over the first minute, with one molecule of the compound knocking down 742 molecules of the peroxide. Significantly, the activity of complex **1** is relatively low, which is surprising as the Mn–Mn separation in this compound (3.5 Å) is similar to that found in the manganocatalases from *Thermus thermophilus* (3.6 Å) [14]. The catalytic activity of these complexes is relatively moderate when compared to that of the best complexes previously made in this laboratory [2]. It should be noted that imidazole itself causes only a very slight disproportionation of the peroxide (Table 6). Such an enhancement of the catalytic activity in the presence of the imidazole has been previously observed in this laboratory [2,12] and indeed by other workers [15]. This may demonstrate the importance of the heterocyclic bases that are known to exist in the vicinity of the active sites of the manganoenzymes [14].

3. Experimental

Chemicals were purchased from commercial sources and used without further purification. IR spectra were recorded in the region 4000–400 cm^{-1} on a Nicolet-400 Impact spectrometer. Magnetic susceptibility measurements were made using a Johnson Matthey Magnetic Susceptibility balance. $[HgCo(SCN)_4]$ was used as a reference. Conductivity readings were obtained using a Ciba Corning model check-mate 90 conductivity meter. Satisfactory microanalytical data for the complexes were reported by the Microanalytical Laboratory, University College Cork, Ireland.

3.1. $[Mn(pyr)_2]_n$ (**1**)

To a solution of 2-pyrazine carboxylic acid {pyrH} (1.22 g, 9.83 mmol) in water (100 cm^3) was added manganese(II) acetate (1.19 g, 4.85 mmol). The resulting mixture was refluxed for 2 h. The product formed as a yellow powder and yellow crystals (**1**) that were filtered off and then dried in air. Yield: 0.75 g (51.17%). Complex **1** was insoluble in dist. H_2O, EtOH, MeOH, acetone, ether and chloroform. *Anal.* Found: C, 39.52; H, 1.92; N, 18.17. Calc.: C, 39.88; H, 2.01; N, 18.60%. IR: 3482.84, 3415.67, 3093.28, 3066.42, 3026.12, 1662.69, 1622.39, 1588.81, 1521.64, 1474.63, 1420.90, 1387.31, 1353.73, 1165.67, 1038.06, 890.30, 850.00, 789.55, 729.10, 635.07, 554.48, 447.01 cm^{-1}. μ_{eff} = 5.82 B.M.

3.2. $[Mn(dipic)]\cdot 1.5H_2O$ (**2**)

To a solution of 2,6-pyridinedicarboxylic acid {dipicH_2} (1.16 g, 6.94 mmol) in ethanol (100 cm^3) was added manganese(II) acetate (1.52 g, 6.20 mmol), and the reaction mixture was refluxed for 2 h. The product formed as a colourless solid. The mixture was allowed to cool to room temperature and then filtered. The product was washed with two small portions of ethanol and then

Table 6
Time course of O_2 evolution in H_2O_2 disproportionation by the complexes (in the presence of added imidazole) at S.T.P. conditions

Complex	Mass (mg)	Oxygen evolved (ml) and time (min)									
		1	2	5	10	15	20	30	40	50	60
1	10.3	515	633	728	785	813	830	856	877	897	918
2	10.7	36	350	665	814	884	930	986	1021	1048	1069
3	10.1	728	894	1046	1158	1205	1233	1270	1293	1307	1318
4	10.0	605	747	896	981	1015	1046	1075	1092	1103	1110
5	10.1	215	463	676	795	875	931	1042	1089	1125	1157
6	10.7	82	565	849	972	1038	1067				
7	10.3	953	1029	1142	1211	1272	1295	1327	1348	1365	1374
8	10.0	724	815	934	1001	1049	1073	1105	1126		
Imidazole	50	4	12	29	35						

Table 7
Molecules of H_2O_2 disproportionated by the complexes (in the presence of added imidazole) at S.T.P. conditions

Complex	Total number of molecules of H_2O_2 disproportionated by one molecule of complex	Molecules of H_2O_2 disproportionated during first min by one molecule of the complex
1	2397	1345
2	2205	742
3	4525	2499
4	6885	3753
5	6307	1172
6	2263	1739
7	4888	3390
8	6542	4206

dried in air. Yield: 1.48 g (96.62%). Complex **2** was partially soluble in warm acetone and insoluble in dist. H_2O, EtOH, MeOH, ether and chloroform. *Anal*. Found: C, 34.13; H, 1.49; N, 5.60. Calc: C, 34.03; H, 2.44; N, 5.66%. IR: 3402.10, 1642.01, 1588.81, 1568.11, 1441.04, 1400.75, 1373.88, 1279.85, 1192.54, 1158.32, 1085.07, 1017.91, 970.22, 823.13, 769.40, 722.39, 661.19 cm^{-1}. $\mu_{eff} = 5.72$ B.M. Λ_M (acetone) = 0 S cm^2 mol^{-1}.

3.3. [Mn(dipic)(bipy)]·2H_2O (**3**) and [Mn(dipic)(bipy)$_2$]·4.5H_2O (**4**)

To a solution of [Mn(dipic)]·1.5H_2O (**2**) (0.50 g, 2.02 mmol) in water (100 cm^3) 2,2'-bipyridine (0.95 g, 6.09 mmol) was added. The resulting mixture was stirred for 4 h. The product formed as a yellow solid that was then filtered off and allowed to dry in air. Yield: 0.29 g (36.98%). Complex **3** was partially soluble in warm EtOH, MeOH and chloroform, and insoluble in dist. H_2O, acetone and ether. *Anal.* Found: C, 46.31; H, 3.94; N, 10.20. Calc.: C, 46.40; H, 3.89; N, 10.82. IR: 3422.26, 3079.64, 1621.85, 1581.55, 1480.78, 1433.75, 1366.57, 1319.55, 1279.24, 1245.65, 1191.91, 1158.32, 1077.70, 1017.24, 956.78, 923.19, 762.69, 735.82, 701.50, 661.19 cm^{-1}. $\mu_{eff} = 5.95$ B.M. Λ_M (EtOH) = 0 S cm^2 mol^{-1}.

The yellow filtrate was reduced to 50 cm^3 on a hot plate for 1 day. Upon standing at room temperature for 1 week the solution turned clear and complex **4** deposited as yellow crystals. The crystals were filtered off and air-dried. Yield: 0.19g (13.54%). Complex **4** was soluble in MeOH and insoluble in distilled H_2O, EtOH, ether, chloroform and acetone. *Anal.* Found: C, 46.89; H, 3.30; N, 10.02. Calc.: C, 52.86; H, 4.60; N, 11.41%. IR: 3405.17, 3073.13, 2355.17, 1620.69, 1574.14, 1474.63, 1439.66, 1356.90, 1274.14, 1078.36, 1010.34, 762.07, 731.03, 661.94 cm^{-1}. $\mu_{eff} = 6.44$ B.M. Λ_M (MeOH) = 1.64 S cm^2 mol^{-1}.

3.4. [Mn(dipic)(phen)$_2$]·2H_2O (**5**)

To a solution of [Mn(dipic)·1.5H_2O] (**2**) (0.50 g, 2.02 mmol) in ethanol (100 cm^3) 1,10-phenanthroline (0.75 g, 3.78 mmol) was added. The resulting mixture was refluxed for 2 h. The product formed as green crystals that were filtered and then dried in air. Yield: 0.49 g (37.84%). Complex **5** was insoluble in dist. H_2O, EtOH, MeOH, acetone, ether and chloroform. *Anal.* Found: C, 60.49; H, 3.66; N, 11.41. Calc.: C, 60.39; H, 3.76; N, 11.36%. IR: 3422.26, 3220.72, 3052.77, 1648.73, 1622.39, 1588.27, 1514.93, 1500.93, 1427.61, 1373.88, 1359.86, 1273.13, 1225.50, 1138.16, 1104.57, 1071.64, 1024.63, 903.73, 876.17, 843.28, 769.40, 722.39, 701.50, 634.32 cm^{-1}. $\mu_{eff} = 6.11$ B.M.

3.5. Mn(chedam)]·H_2O (**6**)

To a solution of chelidamic acid {chedamH_2} (1.01 g, 5.51 mmol) in methanol (100 cm^3) was added manganese(II) acetate (1.34 g, 5.51 mmol), and the reaction mixture was refluxed for 3 h. The product formed as a colourless solid. The mixture was allowed to cool to room temperature and the product was filtered off and dried in air. Yield: 1.29 g (86.05%). Complex **7** was soluble in dist. H_2O and in soluble in EtOH, MeOH, acetone, ether and chloroform. *Anal*. Found: C, 30.67; H, 2.59; N, 5.15. Calc.: C, 30.90; H, 2.50; N, 5.40%. IR: 3407.85, 1577.57, 1429.53, 1348.79, 1133.46, 1032.52, 817.20, 749.91, 642.24, 588.41 cm^{-1}. $\mu_{eff} = 5.69$ B.M. Λ_M (H_2O) = 300.76 S cm^2 mol^{-1}.

3.6. [Mn(chedam)(bipy)]·H_2O (**7**)

To a solution of [Mn(chedam)]·H_2O (**6**) (0.46 g, 1.88 mmol) in water (100 cm^3) 2,2'-bipyridine (0.59 g, 3.77 mmol) was added. The resulting mixture was refluxed for 12 h. The product formed as a yellow solid and crystals that was filtered off and allowed to dry in air. Yield: 0.52 g (66.95%). Complex **7** was insoluble in dist. H_2O, EtOH, MeOH, acetone, ether and chloroform. *Anal.* Found: C, 50.15; H, 3.08; N, 10.39. Calc.: C, 49.77; H, 3.19; N, 10.24%. IR: 3300.19, 3111.78, 3084.86, 2950.28, 2876.26, 2728.29, 2600.37, 2519.63, 1604.49, 1496.82, 1449.72, 1416.07, 1348.79, 1120.00,

1039.25, 897.94, 823.93, 770.09, 749.91, 642.24 cm^{-1}. $\mu_{eff} = 5.89$ B.M.

3.7. [Mn(chedam)(phen)$_2$]·3H$_2$O (8)

To a solution of [Mn(chedam)]·H_2O (**6**) (0.60 g, 2.36 mmol) in water (100 cm^3) 1,10-phenanthroline (0.96 g, 4.84 mmol) was added. The resulting mixture was refluxed for 5 h. The product formed as a yellow powder that was filtered off and dried in air. Yield: 1.27 g (82.79%). Complex **8** was insoluble in dist. H_2O, EtOH, MeOH, acetone, ether and chloroform. *Anal.* Found: C, 57.76; H, 3.12; N, 10.79. Calc.: C, 57.24; H, 3.87; N, 10.77%. IR: 3434.77, 3057.94, 1611.21, 1517.01, 1436.26, 1335.33, 1261.31, 1106.54, 1025.79, 857.57, 823.93, 736.45, 642.24 cm^{-1}. $\mu_{eff} = 5.99$ B.M.

4. X-ray crystallography

Crystal data for complexes **1**, **4** and **7** are summarised in Table 8. Structures **1** and **7** were solved by direct methods, a Patterson tmap was used to solve the structure of complex **4**. All three data sets were refined by full-matrix least-squares on F^2 and the programs used in the structure solution and refinement are contained in the SHELXTL package [16]. All non-hydrogen atoms were refined with anisotropic atomic displacement parameters except for the partial occupancy water molecule in complex 4 (O5w). Hydrogen atoms bonded to carbon were inserted at calculated positions, those bonded to oxygen were located in difference maps, inserted at these positions and not further refined. Hydrogen atoms on the disordered water molecule on complex 4 (O5w) were not included.

4.1. Hydrogen peroxide disproportionation studies

To a solid sample (ca. 10 mg) of the manganese complex was added aqueous H_2O_2 (35% w/w, 10 cm^3, 114 mmol). The mixture was stirred and thermostated at 25 °C and the evolved O_2 was measured volumetrically (volume ± 0.10 cm^3). In cases where imidazole (50 mg) was added this was introduced into the reaction vessel before the addition of H_2O_2.

5. Supplementary material

Crystallographic data have been deposited with the Cambridge Crystallographic Data Centre, CCDC Nos. 164978, 164979 and 164980, respectively. Copies of this information may be obtained free of charge from The Director, 12 Union Road, Cambridge, CB2 1EZ, UK (fax: +44-1223-336033; e-mail: deposit@ccdc.cam.ac.uk or www: http://www.ccdc.cam.ac.uk).

Acknowledgements

M.D. acknowledges the late Noel O'Reilly (DIT) for technical assistance. V.L. acknowledges the SRD and Seed funding schemes (DIT/EU) for financial support. This work has been carried out (in part) within the

Table 8
Summary of crystal data, data collection, structure solution and refinement details for complexes **1**, **4** and **7**

	Complex **1**	Complex **4**	Complex **7**
Complex	$[Mn(pyr)_2]_n$	$[Mn(dipic)(bipy)_2]\cdot 4.5H_2O$	$[Mn(chedam)(bipy)]\cdot H_2O$
Empirical formula	$C_{10}H_6MnN_4O_4$	$C_{27}H_{37}MnN_5O_{13}$	$C_{17}H_{13}MnN_3O_6$
Description	yellow block	yellow block	yellow block
Diffractometer	Siemens P4	Siemens P4	Bruker SMART
Absorption corr.	none	none	multiscan
λ (Å)	0.71703	0.71703	0.71703
Temperature (K)	153(2)	153(2)	150(2)
a (Å)	10.1903(8)	15.9288(16)	25.513(2)
b (Å)	10.8464(8)	14.5310(15)	9.6237(9)
c (Å)	10.1079(4)	15.4748(13)	14.8053(14)
α, β, γ (°)	90, 108.290(5), 90	90, 113.962(8), 90	90, 102.527(2), 90
U (Å^3)	1060.8(1)	3273.1(5)	3548.6(6)
Crystal system	monoclinic	monoclinic	monoclinic
Space group	$P2(1)/c$	$C2/c$	$C2/c$
Z	4	4	8
θ Range (°)	2.82–24.00	2.09–25.00	1.64–27.50
Reflections collected	2213	3242	15916
Independent reflections	1869	2885	4064
R_{int}	0.0085	0.0227	0.0281
R_1, wR_2 [$I > 2\sigma(I)$]	0.0212, 0.0515	0.0416, 0.1100	0.0304, 0.0727
R_1, wR_2 [all data]	0.0253, 0.0527	0.0564, 0.1174	0.0400, 0.0772

structures of the Facility for Optical Characterisation and Spectroscopy (FOCAS), funded by the Irish Government Programme for Research in Third Level Institutions.

References

[1] R.C. Mehrotra, R. Bohra, Metal Carboxylates, Academic Press, London, 1983.
[2] M.T. Casey, M. McCann, M. Devereux, M. Curran, C. Cardin, M. Convery, V. Quillet, C. Harding, J. Chem. Soc., Chem. Commun. (1994) 2643.
[3] M. McCann, F. Cronin, M. Devereux, G. Ferguson, Polyhedron 14 (1997) 2379.
[4] M. Geraghty, M. McCann, M. Devereux, V. McKee, Inorg. Chim. Acta 293 (1999) 160.
[5] M. McCann, M.T. Casey, M. Devereux, M. Curran, C. Cardin, A. Todd, Polyhedron 15 (1996) 2117.
[6] M. McCann, M.T. Casey, M. Devereux, M. Curran, V. McKee, Polyhedron 15 (1996) 2321.
[7] S. McCann, M. McCann, M.T. Casey, M. Devereux, V. McKee, P. McMichael, J. McCrea, Polyhedron 16 (1997) 4247.
[8] M. Devereux, M. McCann, M.T. Casey, M. Curran, International Patent, 1994, IPA No. S940892.
[9] M. Curan, Ph.D. Thesis, National University of Ireland, 1996.
[10] K. Nakamoto, Infrared and Raman Spectra of Inorganic and Coordination Compounds, 3rd ed., Wiley, New York, 1978.
[11] F.A. Cotton, G.K. Wilkinson, Advanced Inorganic Chemistry, 5th ed., Wiley, New York, 1988, p. 702.
[12] See for example: M. Devereux, M. Jackman, M. McCann, M. Casey, Polyhedron 17 (1998) 153.
[13] R. Hague, J.E. Iburg, J. Kerschner, J.H. Koek, E.L.M. Lempers, R.J. Martens, U.S. Racherla, S.W. Russell, T. Swarthoff, M.R.P. Van Vilet, J.B. Warnaar, L. Van Der Wolf, B. Krijen, Nature 369 (1994) 637.
[14] E. Larson, V. Pecoraro, in: V. Pecoraro (Ed.), Manganese Redox Enzymes (chapter 1 and references therein), VCH, New York, 1992.
[15] Y. Naruta, K. Maruyama, J. Chem. Soc., Chem. Commun. (1994) 2667.
[16] SHELXTL Version 5.1 Bruker Analytical X-ray Systems, Madison, WI, 1997.

PERGAMON

Polyhedron 21 (2002) 1073–1080

POLYHEDRON

www.elsevier.com/locate/poly

Substituted boat-shaped Co_6 carbonyl cluster derivatives containing a semi-interstitial P atom and both bridging dithiolate and heterocyclic phosphido ligands

Shu-Tang Liu *, Xiang Hu, Fei Chang, Ying-Chun Liu, Er-Run Ding, Bin-Fang Wu, Zhi-Rong Zhao

Department of Chemistry, Inner Mongolia University, Huhhot 010021, People's Republic of China

Received 17 August 2001; accepted 8 January 2002

Abstract

The reaction of $Co_2(CO)_8$ with $Cl[PSCH_2CH_2CH_2S]$ gives the Co_6 cluster $Co_6(\mu_6\text{-}P)(\mu\text{-}SCH_2CH_2CH_2S)(\mu\text{-}[PSCH_2CH_2CH_2S])(CO)_{12}$ (**5**). X-ray structural analysis of **5** revealed that six Co atoms form a boat-shaped array consisting of a basal square of four cobalt atoms with two opposite edges bridged by two apical Co atoms, a semi-interstitial P atom, a propanedithiolate ligand doubly bridging a basal side and a heterocyclic phosphido ligand bridging the opposite basal edge. Reaction of **5** with PPh_3 results in the formation of the mono-substituted products $(Co_6(\mu_6\text{-}P)(\mu\text{-}SCH_2CH_2CH_2S)(\mu\text{-}[PSCH_2CH_2CH_2S])(\mu\text{-}CO)(CO)_{10}(PPh_3)$ (**6**) and $(Co_6(\mu_6\text{-}P)(\mu\text{-}SCH_2CH_2CH_2S)(\mu\text{-}[PSCH_2CH_2CH_2S])(\mu\text{-}CO)(CO)_{11}(PPh_3)$ (**7**). Reaction of $(Co_6(\mu_6\text{-}P)(\mu\text{-}SCH_2CH_2S)(\mu\text{-}[PSCH_2CH_2S])(CO)_{12}$ (**4**) with PPh_3 at higher temperature results in the formation of the di-substituted cluster $Co_6(\mu_6\text{-}P)(\mu\text{-}SCH_2CH_2S)(\mu\text{-}[PSCH_2CH_2S])(CO)_{10}\cdot(PPh_3)_2$ (**8**). Reactions of **5** with $P(OEt)_3$ result in the substitution of one or two carbonyl groups to give $(Co_6(\mu_6\text{-}P)(\mu\text{-}SCH_2CH_2CH_2S)(\mu\text{-}[PSCH_2CH_2CH_2S])(CO)_{11}P(OEt)_3)\}$ (**9**) and $\{Co_6(\mu_6\text{-}P)(\mu\text{-}SCH_2CH_2CH_2S)(\mu\text{-}[PSCH_2CH_2CH_2S])(CO)_{11}(P(OEt)_3)\}$ (**9′**) with different spectral data from that of (**9**), and $\{Co_6(\mu_6\text{-}P)(\mu\text{-}SCH_2CH_2CH_2S)(\mu\text{-}[PSCH_2CH_2CH_2S])(\mu\text{-}CO)(CO)_9(P(OEt)_3)_2\}$ (**10**). X-ray structural analysis of 10 identified the sites of phosphite substitution as the two apical Co atoms. A semi-bridging CO group in **10** is located on a basal side. The IR ν(CO) solution spectrum of **10** does indicate the existence of the semi-bridging CO group in the solution as well. © 2002 Published by Elsevier Science Ltd.

Keywords: Crystal structures; Cobalt(I) clusters; Interstitial phosphorus atom; Heterocyclic phosphide; Semi-bridging carbonyl; Substituted site

1. Introduction

The open structures of Co_6 carbonyl clusters which contain an interstitial main group atom have been rarely reported [1,2]. They can be obtained by the insertion of a bulky P atom or a C_2 group into the polyhedral metal arrays, two examples being $(Co_6(\mu_6\text{-}P)(\mu\text{-}CO)_2(CO)_{14})$ (**1**) [3] and $(Co_6(\mu_6\text{-}C_2)(\mu_4\text{-}S)(\mu\text{-}CO)_6(CO)_8$ (**2**) [4]. In **1**, the six metal atoms form a twisted boat arrangement surrounding a semi-interstitial P atom. In **2**, the six metal atoms form a boat-shaped open array which contains a roughly square-planar base with two opposite edges apically bridged by two cobalt atoms. The metal arrangement surrounds a semi-interstitial dicarbide group. We have reported in a previous communication that the reaction of $Co_2(CO)_8$ with $RSPCl_2$ (R = Me, Et) gives the boat-shaped Co_6 carbonyl clusters $(Co_6(\mu_6\text{-}P)(\mu\text{-}SR)_3(CO)_{12})$ (R = Me, (**3**); Et) which contain a semi-interstitial P atom and bridging thiolate ligands [5]. In **3**, the array of the six metal core is similar to that of **2** but with a semi-interstitial P atom in place of the dicarbide group. Another boat shaped (μ_6-P)-containing Co_6 species with a wrongly proposed formula $(Co_6(\mu_6\text{-}P)(\mu_4\text{-}SCH_2CH_2S)(\mu\text{-}[PSCH_2CH_2S])(CO)_{12})$ (**4**) in the previous communication was also reported. We had wrongly imagined that its ligand arrangement pattern might be similar to that in **3**. Since then, more boat-shaped Co_6 carbonyl clusters and their phosphine–

* Corresponding author. Tel.: +86-471-499-2605; fax: +86-471-431-0066.

E-mail address: celtckr@imu.edu.cn (S.-T. Liu).

0277-5387/02/$ - see front matter © 2002 Published by Elsevier Science Ltd.
PII: S0277-5387(02)00855-0

phosphite derivatives which contain a semi-interstitial P atom and both a doubly bridging propanedithiolate and a bridging heterocyclic phosphido ligand $\overline{PSCH_2CH_2CH_2S}$ have been made in our laboratory. Here we report the syntheses and spectral charaterization of the open Co_6 clusters **5**, **6**, **7**, **8**, **9**, **9′** and **10**. The X-ray analysis of clusters **5** and **10** reveal the unusual metal framework geometries and the structural features of P and S-containing ligands.

2. Experimental

2.1. Materials and measurements

All operations were carried out under nitrogen using standard Schlenk techniques. Solvents were purified, distilled from the appropriate drying agents and stored under nitrogen prior to use. Dicobalt octacarbonyl was purchased and the $Cl\overline{PSCH_2CH_2CH_2S}$ was prepared by the literature method [6]. PPh_3 was purchased from Aldrich and $P(OEt)_3$ was made by the literature method [7]. Preparative chromatography was performed on a silica gel column. Infrared spectra were recorded on a Mattson Alpha-Centauri FT-IR spectrophotometer using n-C_6H_{14}–CH_2Cl_2 as solvent. ^1H NMR ($CDCl_3$ as solvent, δ scale relative to $SiMe_4$) and ^{31}P NMR spectra ($CDCl_3$ as solvent, δ scale relative to H_3PO_4) were measured on a Bruker AM-400 instrument and **8** on a BrukerAC-200PFT NMR instrument. FAB MS spectra were recorded on a Finigan MAT 90 instrument using 3-nitrobenzyl alcohol as the matrix. Only the highest mass peaks are given and M^+ = parent ion. Elemental analyses for carbon and hydrogen were conducted on an elemental analyser Perkin–Elmer 2400.

2.1.1. Synthesis of cluster compounds

*2.1.1.1. Synthesis of ($Co_6(\mu_6$-P)(μ-$SCH_2CH_2CH_2S$)-(μ-$\overline{PSCH_2CH_2CH_2S}$)$(CO)_{12}$ (**5**).* $Co_2(CO)_8$ (800 mg, 2.34 mmol) was dissolved in toluene (15 cm^3). A solution of $Cl\overline{PSCH_2CH_2CH_2S}$ (404 mg, 2.34 mmol) in toluene was added dropwise to the $Co_2(CO)_8$ solution and the reaction mixture was stirred at 41 °C for 15 h. After evaporation of the solvent the black residue was dissolved in 3:1 petroleum ether–CH_2Cl_2 v/v, separated by chromatography (eluent: 3:1 petroleum ether–benzene v/v) and recrystallized in 3:1 n-hexane–CH_2Cl_2 v/v (**6**, **7**, **8**, **9**, **9′** and **10** were crystallized using the same solvent mixture) to yield the dark-green cluster compound **5** (200 mg, 26.6%). Spectroscopic data for **5** IR ν(CO): 2077m, 2047vs, 2026vs, 1988m, 1950w cm^{-1}; ^1H NMR: δ 3.31 (d, 6H, $\overline{PSCH_2CH_2CH_2S}$), 2.23–1.26 (m, 6H, $SCH_2CH_2CH_2S$); ^{31}P NMR: δ 811.3 (s, μ_6-P), 322.2 (s, $\overline{PSCH_2CH_2CH_2S}$); FAB MS: M^+ −$PSCH_2CH_2CH_2S$, 826 (Calc. 827). *Anal*. Calc. for $C_{18}H_{12}Co_6O_{12}P_2S_4$ (964.0): C, 22.42; H, 1.24. Found: C, 22.83; H, 1.18%.

*2.1.1.2. Syntheses of ($Co_6(\mu_6$-P)(μ-$SCH_2CH_2CH_2S$)-(μ-$\overline{PSCH_2CH_2CH_2S}$)($\mu$-CO)$(CO)_{10}(PPh_3)$) (**6**) and ($Co_6(\mu_6$-P)($\mu$-$SCH_2CH_2CH_2S$)($\mu$-$\overline{PSCH_2CH_2CH_2S}$)$(CO)_{11}(PPh_3)$) (**7**).* Compound **5** (400 mg, 0.415 mmol) and PPh_3 (280 mg,1.07 mmol) were dissolved in toluene (15 cm^3). The dark–green solution was stirred at 38 °C for 13 h. After evaporation of the solvent the residue was dissolved in 3:1 petroleum ether–CH_2Cl_2 v/v, separated by chromatography and recrystallized to yield the dark-green cluster compound **6** (35 mg, 7%) from the first dark-green band using 3:1 petroleum ether–benzene v/v as eluent and then the cluster compound **7** (30 mg, 6%) from the second green band using 1:1 petroleum ether–benzene v/v as eluent. Spectroscopic data for **6**: IR ν(CO): 2058m, 2022vs, 2017vs, 1990w, 1822w cm^{-1}; ^1H NMR: δ 7.22 (m, 15H, PPh_3), 3.70–3.00 (m, 6H, $\overline{PSCH_2CH_2CH_2S}$), 2.20–1.18 (m, 6H, $\overline{SCH_2CH_2CH_2S}$); FAB MS: M^+ −PPh_3–CO, 909 (Calc. 908); *Anal*. Calc. for $C_{35}H_{27}Co_6O_{11}P_3S_4$ (1198.4): C, 35.06; H, 2.25. Found: C, 35.54; H, 2.60%.

Spectroscopic data for **7**: IR ν(CO): 2058m, 2022vs, 2017vs, 1990w cm^{-1}; ^1H NMR: δ 7.41 (m, 15H, PPh_3), 3.40 (m, 6H, $\overline{PSCH_2CH_2CH_2S}$), 2.63 (m, 6H, $\overline{SCH_2CH_2CH_2S}$); FAB MS: M^+ −3CO, 1115 (Calc. 1114); *Anal*. Calc. for $C_{35}H_{27}Co_6O_{11}P_3S_4$ (1198.4): C, 35.06; H, 2.25. Found: C, 35.51; H, 2.64%.

*2.1.1.3. Synthesis of ($Co_6(\mu_6$-P)(μ-SCH_2CH_2S)(μ-$\overline{PSCH_2CH_2S}$)$(CO)_{10}(PPh_3)_2$ (**8**).* Compound **4** (200 mg, 0.214 mmol) [5], and PPh_3 (280 mg, 1.07 mmol) were dissolved in THF(10 cm^3) and a few drops of Ph_2CONa–THF solution was added to the solution as a catalyst. The mixture was stirred at 47 °C for 10 h. After evaporation of the solvent the black residue was dissolved in benzene and separated by chromatography (eluent: 1:1 petroleum ether–benzene v/v) resulting in a violet eluate which was recrystallized to yield the violet cluster compound **8** (200 mg, 66.6%). Spectroscopic data for **8**: IR ν(CO): 2060m, 2025vs, 2020s, 1990w cm^{-1}; ^1H NMR: 7.40–7.00 (m, 30H, 2 × PPh_3), 3.65 (d, 4H, $\overline{PSCH_2CH_2S}$), 2.63–1.63 (4H, SCH_2CH_2S); ^{31}P NMR: δ 532.5 (s, μ_6-P), 326.8 (s, μ-$\overline{PSCH_2CH_2S}$), 44.5 (s, 2 × PPh_3); *Anal*. Calc. for $C_{50}H_{38}Co_6O_{10}P_4S_4$ (1404.6): C, 34.19; H, 2.71. Found: C, 34.40; H, 2.83%.

*2.1.1.4. Syntheses of {$Co_6(\mu_6$-P)(μ-$\overline{PSCH_2CH_2CH_2S}$)($\mu$-$\overline{SCH_2CH_2CH_2S}$)$(CO)_{11}$-($P(OEt)_3$)} (**9**), {$Co_6(\mu_6$-P)($\mu$-$\overline{PSCH_2CH_2CH_2S}$)($\mu$-$\overline{SCH_2CH_2CH_2S}$)$(CO)_{11}P(OEt)_3$)} (**9′**) and {$Co_6(\mu_6$-P)($\mu$-$\overline{PSCH_2CH_2CH_2S}$)($\mu$-$SCH_2CH_2CH_2S$)($\mu$-CO)-$(CO)_9P(OEt)_3)_2$} (**10**).* Compound **5** (600 mg, 0.622 mmol) was dissolved in toluene (15 cm^3) and then $P(OEt)_3$ (0.54 ml, 3.11 mmol) solution (dissolved in 15

cm^3 toluene) was added dropwise. The mixture was stirred at 40 °C for 18 h. After evaporation of the solvent the black residue was dissolved in 3:1 petroleum ether–CH_2Cl_2 v/v and separated by chromatography. The dark-green cluster compound **9** (41 mg, 6%) was obtained from the first dark-green band using 3:1 petroleum ether–benzene v/v as eluent, the dark-green cluster compound **9′** (25 mg, 3.4%) from the second dark-green band using 2:1 petroleum ether–benzene v/v as eluent and the lighter green cluster compound **10** (20 mg, 2.6%) from the third green band using 1:1 petroleum ether–benzene v/v as eluent.

Spectroscopic data for **9**: IR ν(CO): 2060m, 2025vs, 2012s, 1998w cm^{-1}; ^{1}H NMR: δ 4.02 (m, 6H, $3 \times CH_2$); 2.37 (m, 12H, $SCH_2CH_2CH_2S$ and $\overline{PSCH_2CH_2CH_2S}$), 1.24(t, 9H, $3 \times CH_3$); FAB MS: $M^+ - 3CO$, 1018 (Calc. 1018); *Anal*. Calc. for $C_{23}H_{27}Co_6O_{14}P_3S_4$ (1102.2): C, 25.05; H, 2.45. Found: C, 25.47; H, 2.91%.

Spectroscopic data for **9′**: IR ν(CO): 2065m, 2038vs, 2013vs, 1990w cm^{-1}; ^{1}H NMR: δ 3.76 (m, 6H, $3 \times CH_2$), 2.10 (m, 12H, $SCH_2CH_2CH_2S$ and $\overline{PSCH_2CH_2CH_2S}$), 1.14 (t, 9H, $3 \times CH_3$); ^{31}P NMR: δ 311.3 (s, μ-$\overline{PSCH_2CH_2CH_2S}$), 145.0 (s, $P(OEt)_3$); FAB MS: $M^+ - 5CO$, 962 (Calc. 962); *Anal*. Calc. for $C_{23}H_{27}Co_6O_{14}P_3S_4$ (1102.2): C, 25.05; H, 2.45. Found: C, 25.53; H, 2.94%.

Spectroscopic data for **10**: IR ν(CO): 2055w, 2034w, 2013vs, 1991s, 1823w cm^{-1}; ^{1}H NMR: δ 4.00 (m, 12H, $6 \times CH_2$), 2.63 (m, 12H, $SCH_2CH_2CH_2S$ and $\overline{PSCH_2CH_2CH_2S}$), 1.24(t, 18H, $6 \times CH_3$); ^{31}P NMR: δ 311.2 (s, μ-$\overline{PSCH_2CH_2CH_2S}$), 141.1 (s, $2 \times P(OEt)_3$); FAB MS: $M^+ - 5CO$, 1100 (Calc. 1100); *Anal*. Calc. for $C_{28}H_{42}Co_6O_{16}P_4S_4$ (1240.4): C, 27.10; H, 3.39. Found: C, 27.57; H, 3.81%.

2.1.2. X-ray crystallography and structure determination and refinement of 5 and 10

The X-ray intensities of single crystals **5** ($0.40 \times 0.20 \times 0.15$ mm) and **10** ($0.45 \times 0.30 \times 0.20$ mm) were measured on a Rigaku AFC 6SV diffractometer using graphite–monochromatized Mo Kα radiation ($\lambda =$ 0.71073 Å) in the θ–2θ scan mode. The crystallographic data for clusters **5** and **10** are given in Table 1.

All calculations were performed with the SHELXS-97 program package. Final refinement was conducted through a full-matrix least-squares procedure with non-hydrogen atoms anisotropic and hydrogen atoms isotropic.

Table 1
Crystallographic data for clusters **5** and **10**

Cluster	**5**	**10**
Molecular formula	$C_{18}H_{12}Co_6O_{12}P_2S_4$	$C_{28}H_{42}Co_6O_{16}P_4S_4$
MW	964.04	1240.39
Z	4	4
Crystal dimensions(mm)	$0.40 \times 0.20 \times 0.15$	$0.45 \times 0.30 \times 0.20$
Crystal color/habit	dark-green/plates	light dark-green/plates
Crystal system	triclinic	monoclinic
Space group	$P\bar{1}$	$P2_1/n$
a (Å)	14.623(3)	11.170(2)
b (Å)	17.204(3)	23.554(5)
c (Å)	12.565(3)	17.977(4)
α (°)	100.03(3)	90
β (°)	90.28(3)	99.50(3)
γ (°)	81.87(3)	90
V (Å^3)	3081(1)	4665(2)
D_{calc} (g cm^{-3})	2.078	1.749
μ (Mo Kα) (mm^{-1})	3.585	2.450
Temperature (K)	293(2)	293(2)
F(000)	1800	2496
Absorption correction	ψ scans	ψ scans
T_{max}/T_{min}	1.0000/0.5082	1.0000/0.6013
Number of data collected	11280	8630
Number of unique data	10819	8185
Number of observed data used $I > 2\sigma(I)$	7526	4960
$2\theta_{min}/2\theta_{max}$ (°)	2.01/25.01	2.14/25.00
R_1, wR_2 ($I > 2\sigma(I)$) [a]	0.0401, 0.0936	0.0497, 0.1386
R_1, wR_2 (all data)	0.0801, 0.1068	0.1115, 0.1808
Residual electron density difference features (max/min) (e Å^{-3})	0.873, −0.829	0.755, −0.713

[a] $R_1 = \Sigma||F_o|-|F_c||/\Sigma|F_o|$; $wR_2 = \{\Sigma(W(F_o^2-F_c^2)^2)/\Sigma(W(F_o^2)^2)\}^{1/2}$.

3. Results and discussion

3.1. Syntheses

The reaction of $Co_2(CO)_8$ with $Cl\overline{PSCH_2CH_2CH_2S}$ in toluene at moderate temperature (41 °C) gave the Co_6 cluster **5** in moderate yield (26.6%). The reaction of **5** with PPh_3 in toluene at lower temperature (38 °C) leads to the formation of the phosphine monosubstituted Co_6 clusters **6** and **7** in low yields (7% for **6** and 6% for **7**). The reaction of **4** with PPh_3 in THF at higher temperature (47 °C) results in the formation of the phosphine disubstituted Co_6 cluster **8** in good yield (66%).

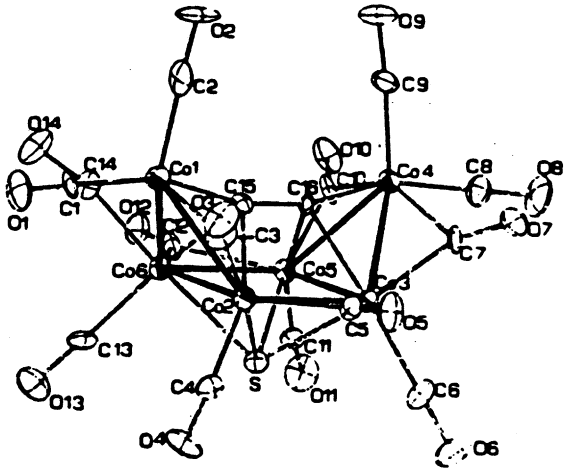
The reaction of **5** with $P(OEt)_3$ in toluene at moderate temperature (40 °C) results in substitution of one or two carbonyl groups to give the monosubstituted Co_6 clusters **9** (yield: 6%) and **9′** (yield: 3.4%) and also the disubstituted Co_6 cluster **10** (yield: 2.6%).

The results demonstrate that the reaction at lower temperature (< 40 °C) mainly leads to the formation of the phosphine–phosphite monosubstituted products and that at higher temperature (> 40 °C) mainly leads to the formation of the phosphine–phosphide disubstituted products.

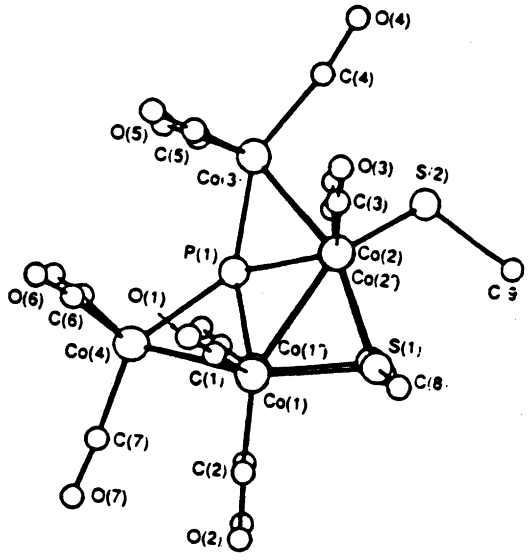
3.2. Description of the structures of clusters 5 and 10

The molecular structures of clusters **5**[1] and **10** are illustrated in Figs. 1 and 2, while selected bond lengths and angles are summarized in Tables 2 and 3, respectively.

The boat-shaped open array of Co_6 atoms in **5** contains a Co_4 basal square with two opposite edges Co(1)–Co(4) and Co(2)–Co(3) bridged by two apical atoms Co(5) and Co(6), respectively, and the metal atoms surround a semi-interstitial P atom. The eight Co–Co bond lengths (2.426(1)–2.677(1) Å) and the eight Co–P bond lengths (2.142(2)–2.299(2) Å) are consistent with the values found in many P-containing cobalt clusters, including **1** and **3** [3,5]. Compound **5** presents an unusual boat-shaped open metal array analogous to that of **2** and **3**. The Co_6 framework of $Co_6(\mu_6\text{-}C_2)$ cluster **2** can be considered to be a finite fragment of metallic cobalt (face-centered cubic and hexagonal close packed) with similar Co–Co distances, Co–Co–Co angles and dihedral angles between triangular and square planes (av. 122° for **2** and 125° for metallic cobalt). The C_2 unit was considered to be inserted into a trigonal–prismatic Co_6 array by breaking an edge and widening the distance between the two apical Co atoms [2]. The dihedral angles between triangular and square planes for 3 (103.5°–106.9°, av. 105.2°) and **5** (104.5°–108.1°, av. 106.3°) are much smaller than that for metallic cobalt and **2**. So, the Co_6 frameworks of **1** and **5** would not be considered to be a finite chunk of metallic cobalt but would be considered as arising from insertion of a P atom into a trigonal prismatic Co_6 array, and the widening degrees between the two apical Co atoms are smaller than that of a C_2 unit. The $Ru_6(\mu_4\text{-}S)$ cluster $\{Ru_6(\mu_4\text{-}S)(\mu_3\text{-}\eta_2\text{-}EtNCSNHEt)(\mu_3\text{-}\eta_2\text{-}EtNCHHEt)(\mu\text{-}CO)_2(CO)_{14}\}$ was reported to present an unusual Ru_6 framework analogous to the boat conformation of cyclohexane (with 109.5° C–C–C angles) but with the dihedral angles 137.3°–143° between Ru triangles and square planes and 54.1°–71.6° triangular Ru interior angles [8]. So neither the Ru_6 framework nor the Co_6 framework of **3** and **5** (with triangular interior angles of 56.4°–61.8°) would be considered to be analogous to the boat conformation of cyclohexane.



2



3

The apical Co atoms bear three terminal carbonyl groups whereas the basal Co(3) and Co(4) bear two and Co(1) and Co(2) only one. The Co(1)–Co(2) side is doubly bridged by a propanedithiolate ligand. We had wrongly proposed that a μ_4-dithiolate ligand with its one S atom bridges the Co(1)–Co(4) edge and the other S atom bridges the opposite Co(2)–Co(3) side in cluster **4** [5], and proposed that a heterocyclic phosphido ligand might be located on the Co(1)–Co(2) side edge such that the ligand arrangements in **4** would look like that in **3**. The real situation is much more complicated. The two donor S atoms of the dithiolate ligand have shown versatile coordination modes in other metal carbonyl polynuclear clusters. For instance, the reaction of

[1] In one crystal structure unit, there are two independent molecules (I and II) having almost the same bond lengths (av. Co–Co distance: 2.5864 Å for I and 2.589 Å for II). The molecule I is chosen to represent cluster 5.

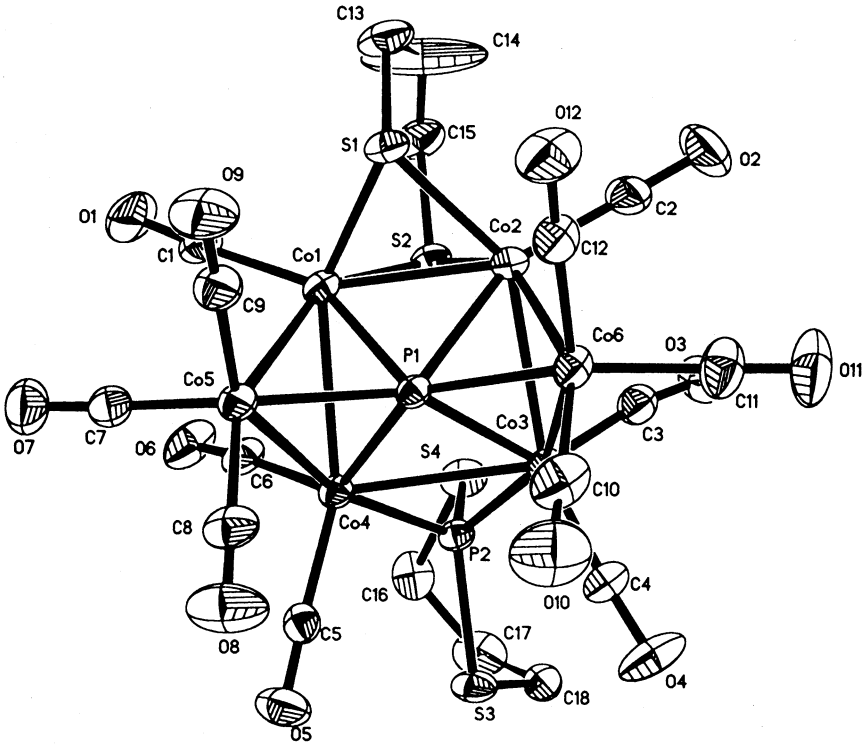


Fig. 1. Molecular structure of $Co_6(\mu_6\text{-}P)(\mu\text{-}SCH_2CH_2CH_2S)(\mu\text{-}\overline{PSCH_2CH_2CH_2S})(CO)_{12}$ (**5**).

$\{Os_6(CO)_{18-n}\{Me(CN)_n\}\}$ $(n = 1,2)$ with thiirane gives $\{Os_6(\mu_3\text{-}S)(\mu\text{-}SCH_2CH_2S)(CO)_{16}\}$, $(Os_6(\mu_3\text{-}SCH_2CH_2S)(CO)_{17}$ and $\{Os_6(\mu_4\text{-}S(CH_2CH_2S)_3)\}$ [9]. In the products, each of the two donor S atoms can be attached to one, two or three Os atoms.

The Co(3)–Co(4) side of cluster **5**, which lies opposite to the Co(1)–Co(2) side, was bridged by a heterocyclic phosphido ligand. During the synthetic reactions, one ligand precursor $Cl\overline{PSCH_2CH_2CH_2S}$ was cleaved at the Cl–P bond and both P–S bonds to yield the P and

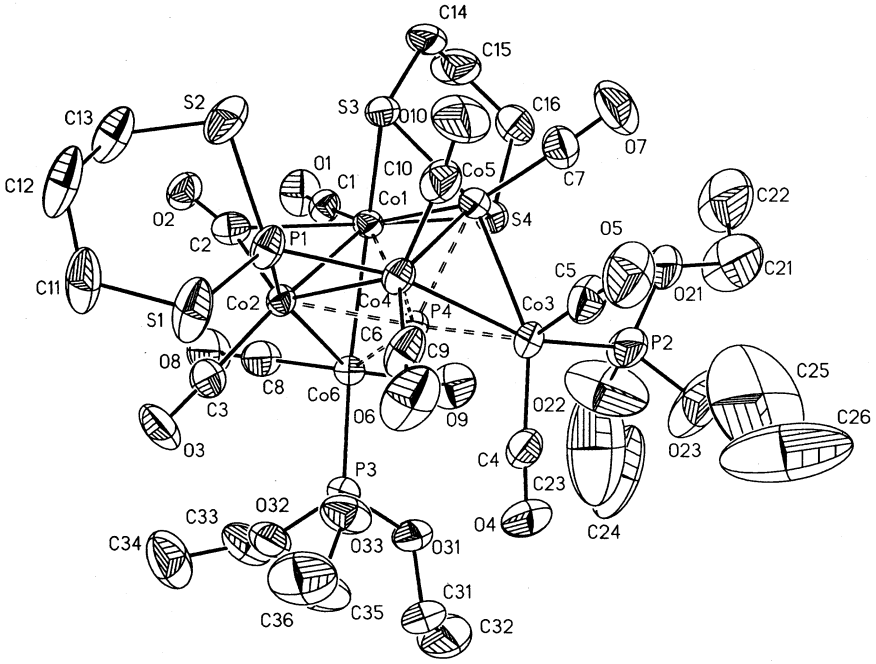


Fig. 2. Molecular structure of $Co_6(\mu_6\text{-}P)(\mu\text{-}SCH_2CH_2CH_2S)(\mu\text{-}\overline{PSCH_2CH_2CH_2S})(\mu\text{-}CO)(CO)_9(P(OEt)_3)_2$ (**10**).

Table 2
Selected bond lengths (Å) and angles (°) for **5**

Bond lengths			
Co(1)–Co(2)	2.426(1)	Co(3)–C(3)	1.757(7)
Co(1)–Co(4)	2.624(2)	Co(3)–C(4)	1.772(7)
Co(1)–Co(5)	2.600(1)	Co(4)–Co(5)	2.588(1)
Co(1)–P(1)	2.287(2)	Co(4)–P(2)	2.142(2)
Co(1)–S(2)	2.199(2)	Co(4)–P(1)	2.237(2)
Co(1)–S(1)	2.226(2)	Co(4)–C(5)	1.794(7)
Co(1)–C(1)	1.767(7)	Co(4)–C(6)	1.775(7)
Co(2)–Co(3)	2.596(1)	Co(5)–P(1)	2.157(2)
Co(2)–Co(6)	2.588(1)	Co(5)–C(7)	1.799(8)
Co(2)–P(1)	2.983(2)	Co(5)–C(9)	1.769(7)
Co(2)–S(2)	2.196(2)	Co(5)–C(8)	1.801(8)
Co(2)–S(1)	2.232(2)	Co(6)–P(1)	2.160(2)
Co(2)–C(2)	1.769(8)	Co(6)–C(12)	1.785(7)
Co(3)–Co(4)	2.677(1)	Co(6)–C(10)	1.808(9)
Co(3)–Co(6)	2.593(1)	Co(7)–C(11)	1.823(8)
Co(3)–P(2)	2.145(2)		
Co(3)–P(1)	2.251(2)		
Bond angles			
Co(2)–Co(1)–Co(4)	93.62(4)	Co(4)–C(5)–O(5)	177.7(6)
Co(2)–Co(1)–Co(5)	107.74(4)	Co(4)–C(6)–O(6)	173.7(6)
Co(4)–Co(1)–Co(5)	59.39(4)	Co(3)–C(3)–O(3)	171.6(6)
Co(1)–Co(2)–Co(3)	91.85(4)	Co(3)–C(4)–O(4)	177.9(7)
Co(1)–Co(2)–Co(6)	108.10(5)		
Co(3)–Co(2)–Co(6)	60.01(4)		
Co(2)–Co(3)–Co(4)	88.63(4)		
Co(2)–Co(3)–Co(6)	59.84(5)		
Co(4)–Co(3)–Co(6)	104.47(5)		
Co(1)–Co(4)–Co(3)	85.82(4)		
Co(1)–Co(4)–Co(5)	59.83(4)		
Co(3)–Co(4)–Co(5)	105.59(4)		
Co(1)–Co(5)–Co(4)	60.78(4)		
Co(2)–Co(6)–Co(3)	60.15(4)		
Co(3)–P(2)–Co(4)	77.28(6)		
Co(1)–S(2)–Co(2)	67.00(6)		
Co(1)–S(1)–Co(2)	65.95(6)		

dithiole fragments as ligands (the negative trivalent 5e donor μ_6-P and the negative bivalent 6e donor μ-$SCH_2CH_2CH_2S$, respectively) and another precursor $Cl\overline{PSCH_2CH_2CH_2S}$ was cleaved only at the Cl–P bond to yield the heterocyclic phosphide fragment as the negative univalent 3e donor μ-$\overline{PSCH_2CH_2CH_2S}$ ligand. They are the essential constituents to build the novel 92e boat-shaped $Co(I)_6$ carbonyl cluster **5** which obeys the EAN rule in having 8 Co–Co bonds (on average each of the six Co atoms is in oxidation state + 1 and has 18e) and contains a semi-interstitial P atom and both bridging P and S-containing ligands.

The phoshite substituted cluster **10** presents the boat-shaped open metal array analogous to that of its parent cluster **5**. The X-ray structural analysis of **10** identified the site of phosphide substitution as the apical Co(3) and Co(6) atoms. The eight Co–Co bond lengths (2.443 (2)–2.710 (2) Å) and the ten Co–P bond lengths (2.124 (2)–2.380 (2) Å) in **10** are consistent with the values found in many P-containing cobalt clusters but delicate differences of bond distance between the bonding types are observed, the Co–P bond with 1.5 bridging phosphide donating valence electrons is the shortest bond (av. 2.127 Å); the Co–P bond with the phosphite lone pair electrons is in the middle (av. 2.157 Å); the Co–P bond with 5/6 μ_6-P donating valence electron is the longest bond (av. 2.260 Å).

The X-ray structural analysis of **10** revealed that a semibridging CO group is linked to the basal Co(1) and Co(2) atoms. The unsymmetrical semibridging C(2)–O(2) group mainly belongs to the Co(2) atom with a Co(2)–C(2) bond length of 1.773(8) Å and Co(2)–C(2)–O(2) bond angle of 162.5(7)°, and it is linked to the Co(1) atom with some minor bonding interaction {Co(1)–C(2) bond length, 2.437(8) Å, Co(1)–C(2)–O(2) bond angle, 123.8(6)°}. An explanation for the semibridging posture of one CO ligand can be given in terms of an inequality of metal atom charges caused by the distribution of the dithiole and the phosphido ligands in the molecule [10]. The valence electron numbers around Co(2) are 18 1/3 and around Co(1) are 17 5/6. The Co(2)–Co(1) bond may be considered to be a dative interaction and written as $Co^+(2) \rightarrow Co^-(1)$, and, therefore, the C(2)–O(2) group originally on Co(2) then moves into a semibridging position to help remove some of this excessive electron density at Co(1). There is a partial transference of electron density from a filled d-orbital of the Co(1) atom into one of the π^* orbitals of the C(2)–O(2) group that is principally bonded to the adjacent Co(2) atom.

The inequality of metal atom charges in these open Co_6 clusters would cause the inequality of metal–metal bonds in the basal square also. In cluster **5** the electron deficient Co(1) and Co(2) (with one CO attached) may demand a shorter Co(1)–Co(2) bond (2.426(1) Å) to increase the electron density around its valence shell to balance the deficiency. In contrast, the electron surfeit Co(3) and Co(4) (with two CO attached) results in a longer Co(3)–Co(4) bond (2.677(1) Å). In cluster **10** the electron deficient Co(1) and Co(5) show a shorter Co(1)–Co(5) bond (2.443(2) Å) and the electron surfiet Co(2) and Co(4) shows a longer Co(2)–Co(4) bond (2.710(2) Å). So, the boat-shaped open array of Co_6 atoms in **5** and **10** contain an approximate square planar base that is better described as a trapezoidal base. The average bond lengths of the eight Co–Co bonds in clusters **3**, **5**, **10** are 2.593, 2.586, 2.571 Å, respectively. The shortest value is for cluster **10** reflecting the fact that both the phosphite and semibridging CO ligands in **10** may have a stabilization interaction for this type of Co_6 open structure.

3.3. Spectral characterizations

The IR ν(CO), ^{1}H NMR, ^{31}P NMR and MS spectral data of clusters **5**, **6**, **7**, **8**, **9**, **9′**, and **10** are given in the Section 2 and the spectrometric characterizations are in

Table 3
Selected bond lengths (Å) and angles (°) for **10**

Bond lengths			
Co(1)–Co(2)	2.577(1)	Co(3)–P(4)	2.178(2)
Co(1)–Co(5)	2.443(2)	Co(3)–C(4)	1.772(9)
Co(1)–Co(6)	2.586(1)	Co(3)–C(5)	1.79(1)
Co(1)–P(4)	2.380(2)	Co(4)–Co(5)	2.574(1)
Co(1)–S(3)	2.226(2)	Co(4)–P(1)	2.124(2)
Co(1)–S(4)	2.226(2)	Co(4)–P(4)	2.276(2)
Co(1)–C(1)	1.760(8)	Co(4)–C(6)	1.786(9)
Co(1)–C(2)	2.437(8)	Co(4)–C(10)	1.75(1)
Co(2)–Co(4)	2.710(2)	Co(5)–P(4)	2.295(2)
Co(2)–Co(6)	2.537(1)	Co(5)–S(3)	2.218(2)
Co(2)–P(1)	2.130(2)	Co(5)–S(4)	2.215(2)
Co(2)–P(4)	2.274(2)	Co(5)–C(7)	1.765(9)
Co(2)–C(2)	1.773(8)	Co(6)–P(3)	2.161(2)
Co(2)–C(3)	1.761(9)	Co(6)–P(4)	2.155(2)
Co(3)–Co(4)	2.561(2)	Co(6)–C(8)	1.800(9)
Co(3)–Co(5)	2.583(1)	Co(6)–C(9)	1.77(1)
Co(3)–P(2)	2.153(3)		
Bond angles			
Co(1)–Co(2)–Co(5)	91.77(5)	Co(1)–C(1)–O(1)	176.5(8)
Co(5)–Co(1)–Co(6)	106.35(5)	Co(2)–C(2)–O(2)	162.5(7)
Co(2)–Co(1)–Co(6)	58.87(4)	Co(1)–C(2)–O(2)	123.8(6)
Co(6)–Co(2)–Co(1)	60.75(4)	Co(1)–C(2)–Co(2)	73.6(3)
Co(6)–Co(2)–Co(4)	105.84(5)	Co(2)–C(3)–O(3)	177.8(9)
Co(1)–Co(2)–Co(4)	88.04(5)	Co(4)–C(6)–O(6)	176(1)
Co(4)–Co(3)–Co(5)	60.06(4)	Co(4)–C(10)–O(10)	168.6(9)
Co(3)–Co(4)–Co(5)	60.39(4)	Co(4)–Co(3)–P(2)	93.3(3)
Co(3)–Co(4)–Co(2)	106.05(5)	C(5)–Co(3)–P(2)	96.3(3)
Co(5)–Co(4)–Co(2)	86.00(5)	C(4)–Co(3)–C(5)	105.84(5)
Co(1)–Co(5)–Co(4)	94.16(5)	C(8)–Co(6)–P(3)	100.7(3)
Co(1)–Co(5)–Co(3)	111.32(5)	C(9)–Co(6)–P(3)	97.2(3)
Co(4)–Co(5)–Co(3)	59.55(4)	C(8)–Co(6)–C(9)	103.3(4)
Co(2)–Co(6)–Co(1)	60.38(4)		
Co(2)–P(1)–Co(4)	79.14(8)		
Co(1)–S(3)–Co(5)	66.67(6)		
Co(1)–S(4)–Co(5)	66.74(7)		

agreement with the confirmed structures determined by X-ray analyses. IR ν(CO) and ^{31}P NMR spectra are selected to explain the characterizations as follows.

3.3.1. Infrared ν(CO) spectra

The five terminal ν(CO) infrared active bands of twelve terminal CO groups in the solution spectrum of **5** are observed at 2077, 2047, 2026, 1988 and 1950 cm^{-1}.

The four terminal ν(CO) infrared active bands of ten terminal CO groups in the spectrum of PPh_3 monosubstituted **6** are observed at 2058, 2022, 2017 and 1990 cm^{-1}. One band of the bridging CO group is observed at 1822 cm^{-1}. The analogous four terminal ν(CO) bands are observed at 2058, 2022, 2017 and 1990 cm^{-1} in the spectrum of **7** but no low frequency ν(CO) band of a bridging CO group is observed in its spectrum. So, **6** is a bridging CO containing isomer and **7** is another isomer containing no bridging CO.

The four terminal ν(CO) bands in the spectrum of PPh_3 disubstituted **8** are observed at 2060, 2025, 2020 and 1990 cm^{-1} and no low frequency ν(CO) band of a bridging CO group is observed.

The four terminal ν(CO) bands in the spectra of $P(OEt)_3$ monosubstituted **9** and **9′** (both with eleven terminal CO groups) are observed at 2060, 2025, 2012 and 1988 cm^{-1} and at 2065, 2038, 2013 and 1990 cm^{-1}, respectively. Clusters **9** and **9′** are isomers and the separations of the three higher frequency ν(CO) bands are different from each other (35 and 13 cm^{-1} for **9**, 27 and 25 cm^{-1} for **9′**).

The four terminal ν(CO) bands of nine terminal CO groups in the spectrum of **10** are observed at 2055, 2034, 2013 and 1991 cm^{-1} and one band of the semibridging CO group is observed at 1823 cm^{-1}.

If CO is replaced by phosphine–phosphite, ν(CO) decreases since the latter is a strong σ donor but a weak π-acceptor [11]. The ν(CO) highest frequency bands in the spectra of mono and disubstituted phosphine clusters **6**, **7**, **8** are shifted 17–19 cm^{-1} toward the lower side from that of the parent cluster **5**. The reason is unclear why the disubstituted **8** and the monosubstituted **6** and **7** are observed to have almost the same vibration frequencies of their four CO bands in the spectra. The ν(CO) highest frequency bands in the spectra of the mono, and disubstituted phosphite clusters **9**, **9′** and **10** are observed to shift 17,12 and 22 cm^{-1} toward the lower side from that of the parent cluster **5**, respectively.

3.3.2. ^{31}P NMR spectra

The ^{31}P NMR spectrum of **5** was found to exhibit the μ_6-P singlet at 811.3 and the μ-$\overline{PSCH_2CH_2CH_2S}$ singlet at 322.2 ppm. The ^{31}P NMR spectrum of PPh_3 disubtituted **8** was found to exhibit the μ_6-P singlet at 532.5, the μ-$\overline{PSCH_2CH_2S}$ singlet at 326.8 and the PPh_3 singlet at 44.5 ppm. The ^{31}P NMR spectrum of $P(OEt)_3$ monosubstituted **9′** and disubstituted **10** were found to exhibit the μ-$\overline{PSCH_2CH_2CH_2S}$ singlets at 311.3, 311.2 and the $P(OEt)_3$ singlets at 145.0, 141.1 ppm, respectively. These are in agreement with the X-ray molecular structural determinations of **5** and **10**. The ^{31}P NMR signal will shift to lower field with a paramagnetic deshielding effect for the compounds which have low-lying exited states associated with M–M and M–P bonding systems [12]. For instance, the phosphorus resonance signal of the ligand precursor Cl$\overline{PSCH_2CH_2S}$ occurs at 171.6 but the signal of μ-$\overline{PSCH_2CH_2S}$ in **8** occurs at 326.8 ppm [13]. As the numbers of metal atoms linked to the P atom are increased in the M–P bonding system, the paramagnetic deshielding effect will be increased with the enhancement of valence electrons being donated to the P atom by more metals so the μ_6-P signals are exhibited in the lowest field.

4. Supplementary data

Supplementary data are available from the CCDC, 12 Union Road, Cambridge, CB2 1EZ, UK (fax: +44-1223-336-033, e-mail: deposit@ccdc.cam.ac.uk), on request quoting the deposition numbers 148272 and 148273.

Acknowledgements

The project was financially supported by the Natural Science Foundation of China.

References

[1] J.N. Nicholls, Polyhedron 3 (1984) 1307.
[2] L. Ma, G.K. Williams, J.R. Shapley, Coord. Chem. Rev. 128 (1993) 261.
[3] G. Ciani, A. Sironi, J. Organomet. Chem. 241 (1983) 385.
[4] G. Gervasio, R.R. Rossetti, P.L. Stanghellini, G. Bor, Inorg. Chem. 23 (1984) 2073.
[5] X. Hu, Q.W. Liu, S.T. Liu, L.P. Zhang, B.F. Wu, J. Chem. Soc., Chem. Commun. (1994) 139
[6] C.M. Kosolapoff, Organophosphorous Compounds, Wiley, New York, 1950, p. 180.
[7] W. Gerrard, M.J.D. Isaacs, G. Machell, K.B. Smith, P.L. Wyvill, J. Chem. Soc. (1953) 1920.
[8] U. Bodensieck, L. Hoferkamp, H. Stoeckli-Evans, G. Süss-Fink, J. Chem. Soc., Dalton Trans (1993) 127.
[9] R.D. Adams, G. Chen, S. Sun, T.A. Wolfe, J. Am. Chem. Soc. 112 (1990) 868.
[10] F.A. Cotton, G. Wilkinson, Advances in Inorganic Chemistry, fourth ed., Wiley, New York, 1980, p. 1059.
[11] K. Nakamoto, Infrared and Raman Spectra of Inorganic and Coordination Compounds, third ed., Wiley, New York, 1978, p. 286.
[12] A.J. Carty, S.A. Maclaughlin, D. Nucciarone, Phosphorus-31 NMR Spectroscopy in Stereochemical Analysis of Organic Compounds and Metal Complexes, VCH, Florida, 1987, p. 561.
[13] E.R. Ding, MSc thesis. Inner Mongolia University, June, 1994, pp. 15.

PERGAMON

Polyhedron 21 (2002) 1081–1087

POLYHEDRON

www.elsevier.com/locate/poly

Preparation and structures of complexes of titanium(IV) and 8-hydroxyquinoline: $TiQ_2(Opr^i)_2$ and $[TiQ_2(\mu\text{-}O)]_4\cdot 6H_2O$

Wen Fong Zeng [a], Yen Shen Chen [a,b], Michael Y. Chiang [c], Shuenn Shing Chern [d], Cheu Pyeng Cheng [b,*]

[a] *Department of Industrial Safety and Hygiene, Tajen Institute of Technology, Ping-Tung, Taiwan, ROC*
[b] *Department of Chemistry, National Tsing Hua University, Hsin-Chu, Taiwan, ROC*
[c] *Department of Chemistry, National Sun Yet-Sen University, Kaoshiong, Taiwan, ROC*
[d] *Institute of Molecular Biology, Academia Sinica, Nankang, Taiwan, ROC*

Received 5 September 2001; accepted 15 January 2002

Abstract

The reaction between $Ti(OPr^i)_4$ and 8-hydroxyquinoline (HQ) resulted in $TiQ_2(OPr^i)_2$, **1** in 90% yield. Further reaction of **1** with water yielded $[TiQ_2(\mu\text{-}O)]_4\cdot n H_2O$, $\mathbf{2}\cdot nH_2O$, $n = 2$ or 6 depending on whether the sample was dried. The structures of **1** and $\mathbf{2}\cdot 6H_2O$ were determined by X-ray diffraction method. In **1** and **2** the bonding situations around the pseudo-octahedrally coordinated Ti(IV) are very similar. The two oxygen atoms from Q^- ligands are *trans* to each other, while the two nitrogen atoms are *cis* to each other and *trans* to the other two oxygen atoms of OPr^i in **1** and μ-O in **2**. The $[Ti(\mu\text{-}O)]_4$ eight-membered ring is puckered. There is extensive hydrogen bonding of four water molecules with $[TiQ_2(\mu\text{-}O)]_4$, two on each side of the eight-membered ring of $[Ti(\mu\text{-}O)]_4$. The two water molecules on the same face of the eight-membered ring are further hydrogen bonded to another water molecule. A novel feature in **2** is that the plane of each Q^- ligand is parallel to that of another Q^- ligand coordinated to a neighboring Ti(IV) in an eclipsed conformation. The average distance between the corresponding atoms in the parallel Q^- ligands is 3.6 Å. It is an indication that there is a strong non-bonding interaction between each pair of parallel Q^- ligands. The hydrogen bonds and the non-bonding interactions lead to the most severely distorted plane of the $[Ti(\mu\text{-}O)]_4$ eight-membered ring. © 2002 Elsevier Science Ltd. All rights reserved.

Keywords: Titanium; Chelate; Coordination chemistry; Structure elucidation; 8-Hydroxyquinolinate

1. Introduction

After losing a proton, *8*-hydroxyquinline (HQ) and its derivatives are capable of forming complexes with a large number of both main group [1] and transition metal ions. The complexes of beryllium [2,3] boron, [4–9] magnesium, aluminum and zinc have attracted particular attentions in recent years because of their applications in organic electroluminescence (OEL) devices [10,11]. For example, AlQ_3 [1] is widely used as an electron transport material because it is chemically stable; can be vacuum deposited to form a stable amorphous film without pin-holes and has high light emitting efficiency in a double layer OEL device. The electroluminescent light frequencies of these 8-hydroxyquinolinate complexes are influenced by the central metal ions. For example, tetrakis(2-methyl-8-hydroxyquinolinato)boron(III)$^-$ emits blue light (470 nm) [4], MgQ_2 emits green light (519 nm)[1]; AlQ_3 emits green light (530 nm) [11] and ZnQ_2 emits yellow light (568 nm) [1]. We were curious to find out the influence of Ti(IV), which does not possess d-electrons like the main group ions, on the light emitting properties of the 8-hydroxyquinolinate–Ti(IV) complex. Although to our disappointment, the Ti(IV)–Q complexes do not fluoresce, these novel Ti(IV) complexes have interesting structural features. The preparations and structures of these complexes are reported herein.

* Corresponding author.

0277-5387/02/$ - see front matter © 2002 Elsevier Science Ltd. All rights reserved.
PII: S0277-5387(02)00873-2

2. Results and discussion

The reaction between 8-hydroxyquinoline (HQ) and $Ti(OPr^i)_4$ in dichloromethane resulted in $TiQ_2(OPr^i)_2$, (**1**), in high yield (90%) as indicated in Eq. (1).

$$Ti(OPr^i)_4 + 2HQ \rightarrow TiQ_2(OPr^i)_2(\mathbf{1}) + 2Pr^iOH \quad (1)$$

The light orange product was characterized by ^1H NMR, mass spectrum, elemental analysis and X-Ray structural analysis. It is interesting to point out that the methyl groups in the two isoproproxide groups split into two doublets. These doublets are due to the vicinal couplings ($J = 5$ Hz) to the protons on the central carbons of the isoproproxide groups. The chemical shift difference of these two doublets(0.915 and 1.097 ppm) is 0.182 ppm (72.8 Hz) which is independent of temperature in the range 20–60 °C in $CDCl_3$. Further examination on the structure of **1** reveals that the two methyl groups on each OPr^i group are diastereotopic. Therefore, the methyl groups are chemically non-equivalent.

When **1** was treated with water in dichloromethane, orange crystalline precipitates were obtained. The quality of the crystals was good enough for a X-ray single crystal analysis. The precipitate, after drying in a vacuum oven, has been characterized by ^1H NMR, UV–Vis spectrum, elemental analysis and thermal gravimetric analysis to be $[TiQ_2(\mu\text{-}O)]_4\cdot 2H_2O$ (**2**·$2H_2O$). However, the X-ray structure indicates that there are six water molecules of hydration. Therefore, the heating in vacuum oven led to a loss of four water molecules of hydration. The hydrolysis reaction and the subsequent heating are summarized in Eqs. (2) and (3).

$$4TiQ_2(OPr^i)_2 + 10H_2O \rightarrow [TiQ_2(\mu - O)]_4 \cdot 6H_2O(\mathbf{2} \cdot 6H_2O) + 8Pr^iOH \quad (2)$$

$$[TiQ_2(\mu - O)]_4 \cdot 6H_2O \xrightarrow{\Delta} [TiQ_2(\mu - O)]_4 \cdot 2H_2O(\mathbf{2} \cdot 2H_2O) + 4H_2O \quad (3)$$

The hydration number of this compound after vacuum heating was confirmed by a thermal gravimetric analysis.

2.1. Structure of $TiQ_2(OPr^i)_2$ (1)

The molecular plot of 30% probability of **1** together with the atomic numbering is shown in Fig. 1. The titanium atom is octahedrally coordinated by two nitrogen atoms and two oxygen atoms from the 8-hydroxyquinolinate ligands, as well as two oxygen atoms from the isopropoxide groups. The two isopropoxide groups are *cis* to each other and they are *trans* to nitrogen atoms. The two oxygen atoms in the Q^- ligands are *trans* to each other.

The selected bond distances and bond angles are summarized in Table 1. The Ti–O(Q) distances (1.961 and 1.963 Å) are ostensibly shorter than the Ti–N bond distances (2.248 and 2.251Å). This large difference can be attributed to the double-bond character between Ti and oxygen atoms. The Ti–O(Pr^i) distances (1.798 and 1.783 Å) are significantly shorter than those of Ti–O(Q) distances. This obvious difference in the two types of Ti–O bond distances is due to the *trans* ligand influence because the isopropoxide groups are *trans* to the

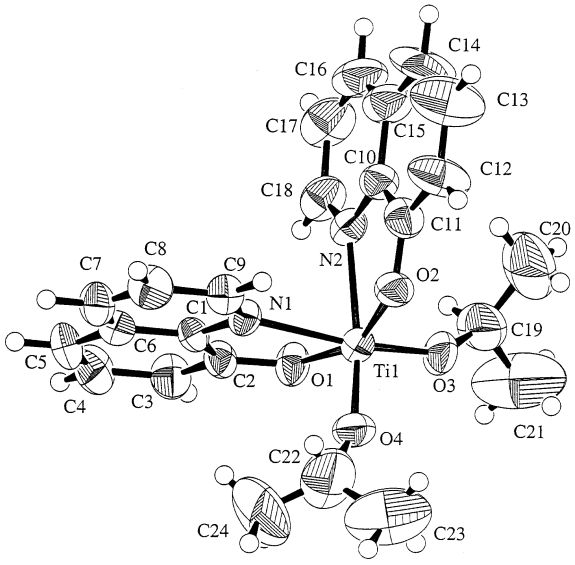


Fig. 1. Molecular plot with atomic numbering of $TiQ_2(OPr^i)_2$ (atoms shown at 30% probability).

Table 1
Relevant bond distances and bond angles for $TiQ_2(OPr^i)_2$ and $[TiQ_2(\mu\text{-}O)]_4\cdot 6H_2O$

$TiQ_2(Opr^i)_2$		$TiQ_2(\mu\text{-}O)_4\cdot 6H_2O$	
Bond distances			
Ti1–O1	1.961(4)	Ti1–O1	1.94(1)
Ti1–O2	1.963(4)	Ti1–O2	1.97(1)
Ti1–O3	1.798(4)	Ti1–O3	1.84(1)
Ti1–O4	1.783(4)	Ti1–O3*	1.79(1)
Ti1–N1	2.248(4)	Ti1–N1	2.26(1)
Ti1–N2	2.251(5)	Ti1–N2	2.29(1)
Bond angles			
O1–Ti1–O2	155.2(2)	O1–Ti1–O2	153.0(5)
O3–Ti1–N1	165.2(2)	O3–Ti1–N1	87.0(5)
O4–Ti1–N2	165.8(2)	O3*–Ti1–N2	164.5(5)
O1–Ti1–N1	75.9(2)	O1–Ti1–N1	75.7(5)
O2–Ti1–N2	75.9(2)	O2–Ti1–N2	74.7(5)
O3–Ti1–O4	103.1(2)	O3–Ti1–O3*	102.9(7)
O2–Ti1–O3	101.2(2)	O2–Ti1–O3*	102.6(5)
O2–Ti1–N1	85.4(2)	O2–Ti1–N1	86.0(5)
O1–Ti1–O3	93.7(2)	O1–Ti1–O3*	92.5(5)
O1–Ti1–O4	101.5(2)	O1–Ti1–O3	105.7(5)
O1–Ti1–N2	84.6(2)	O1–Ti1–N2	83.5(5)
O2–Ti1–O4	94.4(2)	O2–Ti1–O3	92.7(5)
O1–Ti1–N2	84.6(2)	O1–Ti1–N2	83.5(5)
N1–Ti1–O2	85.4(2)	N1–Ti1–O2	86.0(5)
N1–Ti1–N2	79.6(2)	N1–Ti1–N2	83.1(5)

nitrogen atoms. The five-membered rings of Ti(IV) and the coordinating atoms in the 8-hydroxyquinolinate ligands may further lead to the longer Ti–O(Q) distances because of possible ring constraint. The angles between the *trans* atoms and Ti are 155° (∠O1–Ti–O2), 165° (∠N1–Ti–O3) and 166°(∠N2–Ti–O4) which are far from the ideal angle of 180°. The reasons for this octahedral distortion can be attributed to the small bite angles (75.9°) of the coordinated 8-hydroxyquinolinate ligands and the large size of the isopropoxide groups (∠O3–Ti–O4: 103°). Looking at the plane formed by N1, O1, O3, O2 and Ti1, opposite to the small bite angle, there is a large angle ∠O2–Ti–O3 (101.2°) to counter balance it. Likewise, opposite to the small bite angle of the other 8-hydroxyquinolinate ligand, the angle ∠O1–Ti–O4 of 101.5° is observed. The dihedral angle between the two 8-hydroxyquinolinate planes is 88.9°. It indicates that the two Q^- planes are almost perpendicular to each other. The titanium atom is out of the Q^- planes only slightly by 0.03 (Q1) and 0.18 Å (Q2).

There are a total of four structurally characterized titanium(IV) complexes containing the 8-hydroxyquinolinate ligand reported in literature: TiQ_2Cl_2, [12] $TiQ_2Cl(\eta^5\text{-}C_5H_5)$ [13], $TiQ_2(OAr)_2$ [14] and $TiQ'_2(OAr)_2$ (OAr: 2,6-di-isopropylphenoxide; Q'^-: 2-methyl-8-hydroxyquinolinate) [14]. The structure of **1** is remarkably similar to those known structures as far as the arrangement of the two 8-hydroxyquinolinate ligands to the metal are concerned. The bonding parameters such as Ti–O, Ti–N bond distances, ∠O–Ti–O, ∠N–Ti–N bond angles and the bite angles of these complexes are compared in Table 2. These parameters show little variation in each compared category. It is noteworthy that the Ti–O–C(Pr^i) angles are far larger than the values found in simple organic ethers. Similar large angles of Ti–O–C(Ar) are also found in $TiQ_2(OAr)_2$ and $TiQ'_2(OAr)_2$ (OAr: 2,6-di-isopropylphenoxide).[14]

2.2. Structure of $[TiQ_2(\mu\text{-}O)]_4\cdot 6H_2O$

There are six water molecules of hydration in the formula of this crystalline compound. It differs from the number of water molecules of hydration in the bulk sample obtained after drying in a vacuum oven. The single crystal of this compound developed cracks easily when left in the open air for a short period of time. This may be due to the loss of some water molecules of hydration.

The molecular plot of $[TiQ_2(\mu\text{-}O)]_4$ at 30% probability of **2** together with atomic numbering are shown in Fig. 2. The tetramer sits on a crystallographic fourfold inversion axis. In other words, it is composed of two inversion related $[TiQ_2(\mu\text{-}O)]$ pairs. The skeleton of the tetramer is a $[Ti(\mu\text{-}O)]_4$ eight-membered ring. Each Ti atom is coordinated to two 8-hydroxyquinlinate ligands via both the nitrogen atoms and oxygen atoms. In addition two bridging oxo ligands also coordinated to

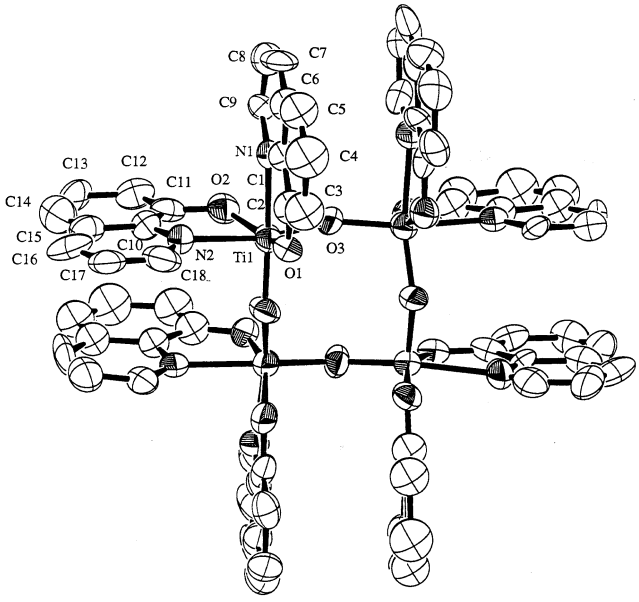


Fig. 2. Molecular plot with atomic numbering of $[TiQ_2(\mu\text{-}O)]_4\cdot 6H_2O$ (atoms shown at 30% probability).

Table 2
The relevant bond distances and bond angles of all structurally characterized Ti(IV) complexes with 8-hydroxyquinolinate ligands

Compound	**1**	**2**	TiQ_2Cl_2	$TiQ_2(\eta^5\text{-}C_5H_5)Cl$	$TiQ_2(Oar)_2$[a]	$TiQ'_2(OAr)_2$[a]
Ti–O(Q) (Å)	1.961, 1.963	1.94, 1.97	1.89	1.987, 1.954	1.953	1.920, 1.921
Ti–N(Q) (Å)	2.248, 2.251	2.26, 2.29	2.20	2.224, 2.270	2.220	2.347, 2.355
Ti–O[b] (Å)	1.798, 1.783	1.79, 1.84			1.818	1.819, 1.813
∠O–Ti–O (°)	155.2	153.0	159.3	150.0	155.5	151.6
∠N–Ti–N (°)	79.6	83.1	82.8	73.8	80.6	84.0
∠N–Ti–O (°(bite angle))	75.9	74.7, 75.7	76.9	75.9, 74.6	75.9	74.5, 74.6
∠Ti–O–C[b] (°)	147.2, 154.9				166.5	151.6

[a] OAr is 2,4,6-trimethylphenoxide, Q'^-: 2-methyl-8-hydroxyquinolinate.
[b] The oxygen atom(s) not in Q^-.

each Ti atom completing the distorted octahedral environment of each Ti atom. Relevant bond distances and bond angles are summarized in Table 1. The Ti–O, and Ti–N distances in **2** are close to the corresponding distances in **1** as well as those of known Ti(IV)–Q complexes (Table 2). The angles around Ti atoms are also remarkably similar to those corresponding angles in **1**. The interplanar angle between the two Q^- ligands is 89.8° which is almost the same as that in **1**.

The skeletal Ti_4O_4 ring is puckered as shown in Fig. 3. The deviations of all atoms from the least-square plane passing through the eight-membered ring are Ti1: −0.26 Å, Ti1a: −0.26 Å, Ti1b: 0.26 Å, Ti1c: 0.26 Å, O3: 0.50 Å, O3a: 0.50 Å, O3b: −0.50 Å, O3c: −0.50 Å. The average deviation from the plane is 0.38 Å. It is clear that the puckering of the ring is extensive and the ring is far from planar. Hydrogen bonding of the water molecules with the oxygen atoms on Q^- ligands as well as the bridging oxygen atoms is shown in Fig. 4. The distances between a representative water oxygen atom O4 with its hydrogen bonded atoms are O4–O2: 2.88(2) Å, O4–O3: 3.05(2) Å and O4–O1*: 3.01(2) Å. These distances indicate that there is a strong hydrogen bonding between O4–O2, and weak hydrogen bonds between O4–O3 and O4–O1*. There are three other symmetry-related water molecules hydrogen bonded in the same fashion. The two oxygen atoms O4, O4* of the two water molecules on the same side of the $[Ti(\mu\text{-}O)]_4$ ring are also hydrogen bonded to another water molecule O5(O5–O4: 2.81(2) Å) which is located on the molecular twofold symmetry axis. The strong hydrogen bonding of O2 and weak hydrogen bonding of O1 to water molecules, resulted in a longer Ti1–O2 distance (1.97(1) Å) than Ti1–O1 (1.94(1) Å).

Careful examination of the orientations of the 8-hydroxyquinolinate ligands reveals that the plane of each Q^- ligand is parallel with the plane of another Q^- ligand coordinated to an adjacent Ti atom. This parallelism can easily be quantified by a small average dihedral angle of 3.5° between these Q^- planes. The parallel Q^- ligands are in an eclipse conformation. Furthermore, the average distance between atoms on the two parallel Q^- planes is 3.6 Å which is close to the sum of van der Waals radii of carbon atoms. Therefore, there

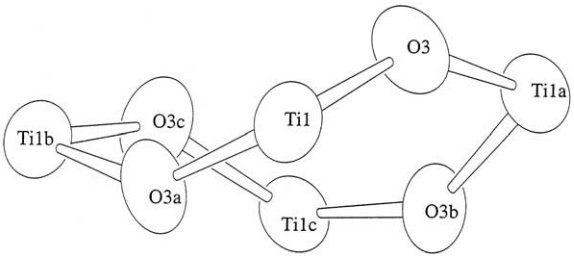


Fig. 3. The puckered conformation of the $[Ti_2(\mu\text{-}O)]_4$ ring in $[TiQ_2(\mu\text{-}O)]_4\cdot 6H_2O$.

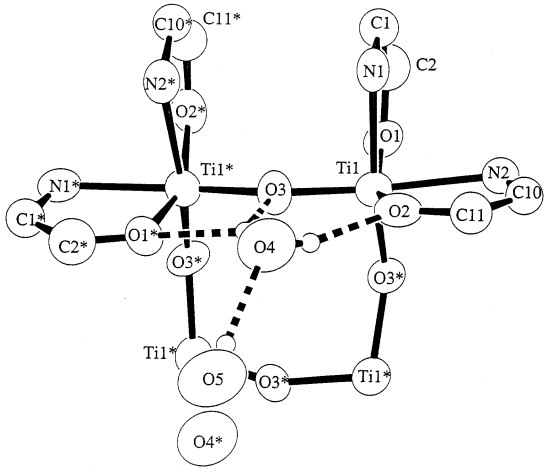


Fig. 4. Hydrogen bonding in $[TiQ_2(\mu\text{-}O)]_4\cdot 6H_2O$. For brevity, only one side of the $[Ti(\mu\text{-}O)]_4$ plane is shown.

are optimal non-bonded interactions in every pair of Q^- ligands. It is likely that these non-bonded interactions, together with hydrogen bonding, are responsible for the special puckered conformation of the $[Ti(\mu\text{-}O)]_4$ ring. The π–π interactions [15] between the pairs of parallel Q^- ligands cannot be important since the eclipsed overlap of the filled π-orbitals on the two Q^- ligands cannot lead to a favorable stabilization energy. The π–π interactions can be significant if the filled π-orbital in one ligand interacts with an empty π*-orbital on the other parallel Q^- ligand. Under this condition, the conformation of the parallel Q^- ligands cannot be eclipsed [15,16] On the other hand, the eclipsed overlap of π-orbitals can lead to significant stabilization when these orbitals are not completely filled [17].

The $[TiQ_2(\mu\text{-}O)]_4\cdot 6H_2O$ molecules pack in a pseudo body-centered cubic arrangement (Fig. 5). One tetramer occupies each corner of the unit cell while another tetramer, rotated about 30° around the *c*-axis, occupies the body center position. Looking down the *a* or *b*-axis the two alternating layer feature (ABABAB–) is obvious. The averaged layer thickness of 8.85 Å (half the length of the *c*-axis) is smaller than the thickness of the hydrated tetramer (10.90 Å), measured from the two tips of the water molecules O5 and O5*. This is because the outer-most water molecule O5 and its symmetry equivalent penetrate into the neighboring layers and point to the central holes that were formed by the groups of four tetramers in the neighboring layer.

There are quite a number of structurally characterized compounds with $[Ti(\mu\text{-}O)]_4$ rings reported. The majority of these complexes contain the cyclopentadienyl ligand or its derivatives coordinated to Ti(IV). In these compounds, each Ti can be viewed as four coordinated if cyclopentadenyl or its derivative is considered to occupy one coordination site. The planarities of the $[Ti(\mu\text{-}O)]_4$ rings of these compounds were analyzed

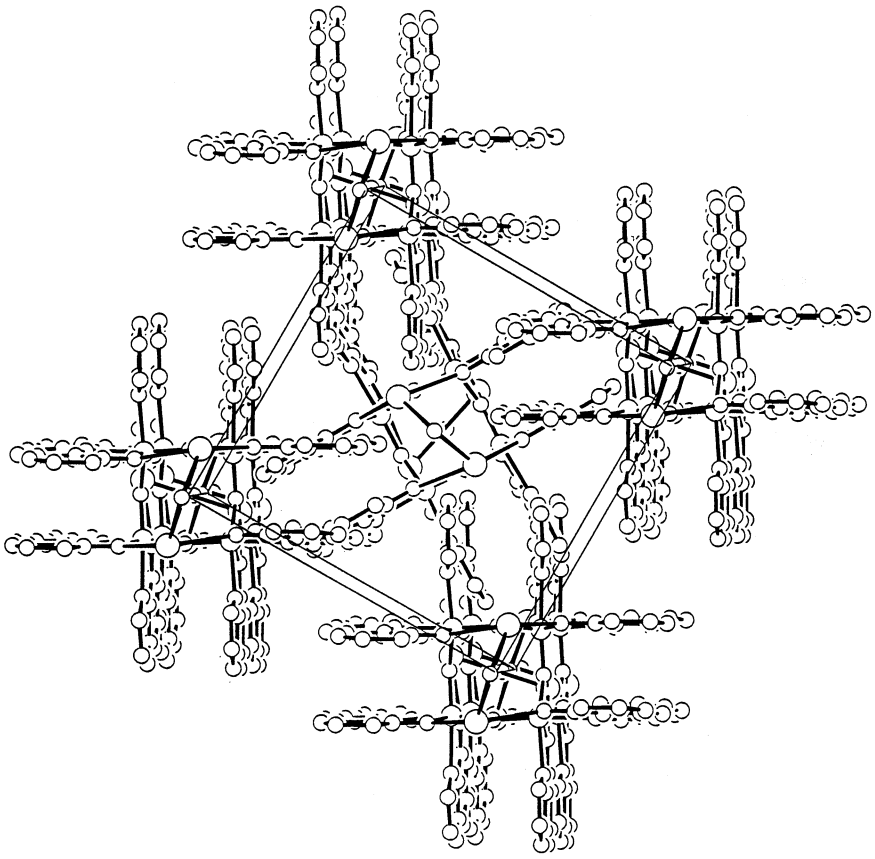


Fig. 5. Pseudo body-centered unit cell packing arrangement of $[TiQ_2(\mu\text{-}O)]_4 \cdot 6H_2O$.

based on the information collected in the Cambridge Structural Database System using Bruker SHELX program. The maximum deviations and the types of atoms above (+) and below(−) the least-square plane of [Ti(μ-O)]$_4$ were used to measure the planarity. The average deviation of all atoms from their least-square plane can also be used to judge whether the [Ti(μ-O)]$_4$ rings is planar. The deviations from planarity for some of the compounds with four coordinated Ti(IV) are given below. [(η^5-C_5Me_5)EtTi(μ-O)]$_4$ [18]: +0.17 Å(Ti), −0.17 Å(Ti), av. 0.09 Å; (η^5-C_5Me_5)$_4F_3$(FAl(CH_2Ph)$_3$)-Ti_4(μ-O)$_4$ [18]: +0.12 Å(Ti), −0.12 Å(Ti), av. 0.07 Å; (η^5-C_5Me_5)$_4$F(FAlMe3)$_3Ti_4$(μ-O)$_4$ [18]: +0.14 Å(Ti), −0.10 Å(O), av. 0.05 Å; [(η^5-C_5Me_5)($FAlMe_3$)Ti(μ-O)]$_4$ [19]: +0.10 Å(Ti), −0.10 Å(Ti), av. 0.05 Å; [(η^5-$C_5H_4SiMe_3$)NCSTi(μ-O)]$_4$ [20]: +0.19 Å(Ti), −0.28 Å(Ti), av. 0.12 Å; [(η^5-C_5Me_5)FTi(μ-O)]$_4$ [21]: +0.03 Å(Ti), −0.03 Å(Ti), av. 0.02 Å; [(η^5-C_5H_5)(O(2,4,6-$C_6H_2Me_3$)Ti(μ-O))$_4$ [22]: +0.46 Å(Ti), −0.44 Å(Ti), av. 0.28 Å. It is clear that the majority of these compounds with four coordinated Ti(IV) have a planar or close to planar [Ti(μ-O)]$_4$ ring. The only exception is [(η^5-C_5H_5)(O(2,4,6-$C_6H_2Me_3$)Ti(μ-O)]$_4$ in which severe distortion from planarity is obvious. It is likely due to the presence of the bulky ligands of 2,4,6-trimethylphenoxide.

In contrast to the four coordinated Ti(IV) compounds with [Ti(μ-O)]$_4$ rings, the structurally characterized six coordinated Ti(IV) compounds with similar rings are rather scarce. Most of them, together with the planarity parameters of the [Ti(μ-O)]$_4$ planes, are given below. [(η^5-N(CH_2COO)$_3$Ti(μ-O))$_4Cs_4$ [23]: +0.12 Å(O), −0.12 Å(O), av. 0.06 Å; [(Me_6acac)$_2$Ti(μ-O)]$_4$ [24]: +0.01 Å(Ti), −0.01 Å(Ti), av. 0.01 Å; [(Cl_2(CH_3CN)$_2$-Ti(μ-O))$_4$ [25]: +0.28 Å(Ti), −0.30 Å(Ti), av. 0.18 Å; [(acac)$_2$Ti(μ-O)Ti(μ-O)(OMe)*c*−(N$MeCH_2CH_2$)$_3$]$_2$ [26]: +0.17 Å(Ti), −0.17 Å(Ti), av. 0.12 Å; [(Oxalato)$_2$Ti(μ-O)]$_4$[NH_4]$_8 \cdot 4H_2O$ [27]: +0.33 Å(Ti), −0.33 Å(Ti), av. 0.24 Å; [(Oxalato)$_2$Ti(μ-O)]$_4Cs_8 \cdot 6H_2O$ [28]: +0.24 Å(O), −0.24 Å(O), av. 0.13 Å. Of these six hexacoordinated Ti(IV) compounds, four of them have planar or nearly planar [Ti(μ-O)]$_4$ rings. The two non-planar compounds have two oxalato ligands coordinated to each Ti(IV) atom. No strong non-bonding interaction among the oxalato ligands can be found. However, both compounds have water molecules of crystallization. Extensive hydrogen bonding exists in these two compounds. The non-planarity can be attributed to the presence of these hydrogen bonds. Therefore, the hydrogen bonding should be one major factor for the non-planarity of **2**. However, the non-bonding interactions must also be important because the distor-

tion from planarity is much more severe in **2**·$6H_2O$ than any known structure with the $[Ti(\mu\text{-}O)]_4$ eight-membered ring.

Fluorescence from both **1** and **2** in chloroform solution or in solid, was not detected. The strong bonding of Q^- ligands to Ti(IV) may be a major factor for the lack of fluorescence. However, a similar strong bonding of Q^- ligands to metal ions also exists in AlQ_3 where the Al–O distances (1.845, 1.847 and 1.857 Å) [29] are also shorter than the Al–N distances (2.073, 2.036 and 2.028 Å) [29], but AlQ_3 has relatively strong fluorescence. We think that the large spin-orbital coupling constant of Ti(IV) relative to that of Al(III) and the involvement of d-orbitals in the bonding of these complexes must be the main reasons why **1** and **2** are non-fluorescent.

3. Experimental

3.1. Physical measurements

^1H NMR spectra were recorded on a Bruker AC-400 spectrometer. Thermal gravimetric analysis was performed on a Seiko SSC 500 Thermal Analyzer under nitrogen stream. UV–Vis spectra were measured on a Perkin–Elmer Lamda-5 spectrophotometer. Elemental analyses were carried out in a Heraeus CHN Rapid Analyzer.

3.1.1. Preparation of $TiQ_2(OPr^i)_2$

$Ti(OPr^i)_4$ (Aldrich) 6 ml (20.4 mmol) was transferred to a 20 ml dichloromethane solution (which was thoroughly dried according to standard procedure) containing 6.0 g (41.3 mmol) HQ (Aldrich). The color of the solution turned orange. The reaction mixture was stirred for 2 h then the solvent was stripped off in a rotary evaporator. Recrystallization of the resulting residue from dichloromethane solution yielded a light orange product. It was dried in a vacuum oven at 70 °C. Yield: 8.45 g (90%). M.p. > 400 °C. δ_H ($CDCl_3$) 0.915(6H, d), 1.097(6H, d), 4.587(2H, t), 6.993(2H, d), 7.092(2H, d), 7.173(2H, t), 7.491(2H, t), 8.053(2H, d) and 8.481(2H, d). (Found: C, 63.31; H: 5.64; N: 6.21. Required for $TiC_{24}H_{26}N_2O_4$: C, 63.44; H: 5.77; N: 6.17%).

3.1.2. Preparation of $[TiQ_2(\mu\text{-}O)]_4\cdot 2H_2O$

To a 40 ml dried dichloromethane solution containing $TiQ_2(OPr^i)_2$ 0.25 g (0.55 mmol), five drops of deionized water were added. After standing for 3 days, orange crystals were obtained by filtration. The crystal were dried in a vacuum oven. Yield 0.153 g (75%). M.p. > 400 °C. λ_{max} nm^{-1} (CH_2Cl_2) 379 (ε dm^{-3} mol^{-1} cm^{-1} 15 700). δ_H (C_6D_6–CD_3OD, 1/1) 6.916 (2H, dd), 7.095 (2H, d), 7.140(2H, d), 7.484(2H, t), 7.870(2H, d), 8.490(2H, d) (Found: C, 58.64; H, 3.99; N, 7.54. $Ti_4C_{72}H_{48}N_8O_{12}\cdot 2H_2O$ requires C, 59.82; H, 3.64; N, 7.75%). Thermal gravimetric analysis indicated that the complex lost 2.7% weight at 53 °C. These data are consistent with a content of two water molecules of hydration in this complex which is expected to be 2.5% theoretically.

3.1.3. X-Ray crystallography

Single crystals of $TiQ_2(OPr^i)_2$ were obtained from a dichloromethane solution by the slow evaporation method. Single crystals of $[TiQ_2(\mu\text{-}O)]_4\cdot 6H_2O$ were obtained directly from its preparative solution. Both crystals of $TiQ_2(OPr^i)_2$ and $[TiQ_2(\mu\text{-}O)]_4\cdot 6H_2O$ were sealed in glass capillaries. Care was taken in the case of $[TiQ_2(\mu\text{-}O)]_4\cdot 6H_2O$ to avoid exposure to air because crystals of $[TiQ_2(\mu\text{-}O)]_4\cdot 6H_2O$ developed cracks easily. Diffraction data measurements were made on a Rigaku AFC6S diffractometer for $TiQ_2(OPr^i)_2$ and an AFC5R diffractometer for $[TiQ_2(\mu\text{-}O)]_4\cdot 6H_2O$ with a graphite monochromater. Empirical absorption corrections were made. The structures were solved by direct methods, [30] and expanded using Fourier techniques. All non-hydrogen atoms in $TiQ_2(OiPr)_2$ were refined anisotropically. However, the weak diffracting nature of the small $[TiQ_2(\mu\text{-}O)]_4$ sample prevents the same treatment. Barely enough data were possible when a rotating anode was used for data collection. Therefore, only non-carbon, non-hydrogen atoms were anisotropically refined. The weak diffracting data (hence less usable data) are also

Table 3
Crystallographic data for $TiQ_2(OPr^i)_2$ and $[TiQ_2(\mu\text{-}O)]_4\cdot 6H_2O$

Compound	$TiQ_2(OPr^I)_2$	$[TiQ_2(\mu\text{-}O)]_4\cdot 6H_2O$
Crystals obtain from	CH_2Cl_2	CH_2Cl_2
Formula	$C_{24}H_{26}N_2O_4Ti$	$C_{72}H_{60}N_8O_{18}Ti_4$
Formula weight	454.38	1516.91
Crystal size (mm)	0.50 × 0.52 × 0.60	0.05 × 0.15 × 0.25
Crystal system	Monoclinic	Tetragonal
Space group	$P2_1/n$	$P2_1c\bar{4}$
a (Å)	11.314(3)	13.862(2)
b (Å)	14.534(2)	
c (Å)	15.332(2)	17.690(7)
β (°)	107.14(1)	
V (Å^3)	2409.1(8)	3399(2)
Z	4	2
D_{calc} (Mg m^{-3})	1.253	1.482
μ (mm^{-1})	0.386(Mo Kα)	4.532(Cu Kα)
$F(000)$	952.00	1560.00
T (K)	296	296
Number of reflections collected	4665	1529
Number of reflections used [$I > 3\sigma(I)$]	1792	947
Goodness-of-fit indicator	2.25	2.28
R [$I > 3\sigma(I)$]	0.050	0.090
R_w [$I > 3\sigma(I)$]	0.026	0.118

responsible for the higher R value obtained. Hydrogen atoms were included but not refined.

The crystal data, important information on the diffraction data collections and refinements of structural data, are presented in Table 3.

4. Supplementary material

Crystallographic data for the structural analysis have been deposited with the Cambridge Crystallographic Data Centre, CCDC No. 155436 for $TiQ_2(OPr^i)_2$ and 155437 for $[TiQ_2(\mu\text{-}O)]_4\cdot 6H_2O$. Copies of this information may be obtained free of charge from The Director, CCDC, 12 Union Road, Cambridge, CB2 1EZ, UK (fax: 44-1223-336033: e-mail: deposit@ccdc.cam.ac.uk or www: http://www.ccdc.cam.ac.uk).

Acknowledgements

We thank the National Science Council of Taiwan (Grant: 89-2113-M-007-027) and Tajen Institute of Technology (Grant: 90060 and 90024) for financial support.

References

[1] (a) Y. Hamada, IEEE Trans. Elect. Dev. 44 (1997) 1208;
(b) Y. Hamada, T. Sano, M. Fjjujita, T. Fujii, Y. Nishio, K. Shibata, Jpn. J. Appl. Phys. 32 (1993) L514.
[2] Y. Yamada, T. Sano, M. Fujita, T. Fujii, Y. Nishio, K. Shibata, Chem Lett. (1994) 905.
[3] Y. Yamada, T. Sano, K. Shibata, K. Kuroki, Jpn. J. Appl. Phys. 34 (1995) L824.
[4] X.T.H. Suzuki, T. Wada, S. Miyata, H. Sasabe, J. Am. Chem. Soc. 121 (1999) 9447.
[5] M. Matsumura, T. Akai, Jpn. J. Appl. Phys. 35 (1996) 5357.
[6] P.E. Burrows, Z. Shen, V. Bulovic, D.M. McCarty, S.R. Forest, J.A. Cronin, M.E. Thompson, J. Appl. Phys. 79 (1992) 7991.
[7] C.H. Chen, J.M. Shi, Coord. Chem. Rev. 171 (1998) 161.
[8] J. Kido, J. Endo, Chem. Lett. (1997) 593.
[9] T.A. Hopkins, K. Meerholz, S. Shaheen, M.L. Anderson, A. Schmidt, B. Kippelen, A.B. Padias, H.K. Hall, N. Peyghamharian, N.R. Armstrong, Chem. Mater. 8 (1996) 344.
[10] S.A. Van Slyke, C.W. Tang, US Pat. 4,539,507, 1995.
[11] C.W. Tang, S.A. Van Slyke, Appl. Phys. Lett. 51 (1987) 913.
[12] B.F. Studd, A.G. Swallow, J. Chem. Soc. (A), 1968, 1961.
[13] J.D. Matthews, N. Singer, A.G. Swallow, J. Chem. Soc. (A) (1970), 2545.
[14] P.H. Bird, A.R. Frazer, C.F. Llau, Inorg. Chem. 12 (1973) 1322.
[15] C.A. Hunter, J.K.M. Sanders, J. Am. Chem. Soc. 112 (1990) 5535.
[16] W.L. Jorgensen, D.L. Severance, J. Am. Chem. Soc. 112 (1990) 4768.
[17] L.L. Miller, K.R. Mann, Acc. Chem. Res. 29 (1996) 417.
[18] P. Yu, T. Poupe, I. Uson, M.A. Said, H.W. Roesky, M.L. Montero, H. -G. Schmidt, A. Demsar, Inorg. Chem. 37 (1998) 5117.
[19] P. Yu, H.W. Roesky, A. Demsar, T. Albers, H.-G. Schmidt, Angew. Chem., Int. Ed. Engl. 36 (1997) 1766.
[20] T. Carofiglio, C. Floriani, A. Sgamelletti, M. Rosi, A. Chiesi-Villa, C. Rizzoli, J. Chem. Soc., Dalton Trans. (1992) 1081.
[21] H.W. Roesky, I. Leichtweis, M. Noltemeyer, Inorg. Chem. 32 (1993) 5102.
[22] U. Thewalt, K. Doppert, J. Organomet. Chem. 320 (1987) 177.
[23] K. Wieghardt, U. Quilitzsch, J. Weiss, B. Buber, Inorg. Chem. 19 (1980) 2541.
[24] S.I. Troyanov, O.Y. Gorbenko, Polyhedron 16 (1997) 777.
[25] G.R. Willey, J. Palin, M.G.B. Drew, J. Chem. Soc., Dalton Trans. (1994) 1799.
[26] P. Jeske, K. Wieghardt, B. Nuber, Z. Naturforsch., Teil B 47 (1992) 1621.
[27] G.M.H. van de Velde, S. Harkema, P.J. Gellings, Inorg. Chim. Acta 11 (1974) 243.
[28] A. Fester, W. Bensch, N. Tromel, Inorg. Chim. Acta 193 (1992) 99.
[29] Mazhar-Ul-Haque, W. Horne, S.J. Lyle, J. Crystallogr. Spectr. Res. (1991) 411.
[30] A. Altomare, M. Casacarano, C. Giacovazzo, J. Appl. Cryst. 26 (1993) 343.

PERGAMON

Polyhedron 21 (2002) 1089–1095

POLYHEDRON

www.elsevier.com/locate/poly

Halogenation of tellurium by SO_2Cl_2. Formation and crystal structures of $(H_3O)[Te_3Cl_{13}]\cdot 1/2SO_2$, $[(C_4H_8O)_2H][TeCl_5]\cdot(C_4H_8O)$, $[(Me_2SO)_2H]_2[TeCl_6]$, and $[Ni(NCCH_3)_6][Te_2Cl_{10}]$

Jarkko Pietikäinen [a], Arto Maaninen [a], Risto S. Laitinen [a,*], Raija Oilunkaniemi [a], Jussi Valkonen [b]

[a] *Department of Chemistry, University of Oulu, P.O. Box 3000, 90014 Oulu, Finland*
[b] *Department of Chemistry, University of Jyväskylä, P.O. Box 35, FIN-40350 Jyväskylä, Finland*

Received 11 October 2001; accepted 12 February 2002

Abstract

The halogenation of elemental tellurium with SO_2Cl_2 in various solvents has been investigated. $(H_3O)[Te_3Cl_{13}]\cdot 1/2SO_2$ (**1**) and $[(C_4H_8O)_2H][TeCl_5]\cdot(C_4H_8O)$ (**2**) were obtained in CS_2 and THF, respectively. When DMSO is added into the THF solution of tellurium and SO_2Cl_2, $[(Me_2SO)_2H]_2[TeCl_6]$ (**3**) is formed. In the acetonitrile solution tellurium and SO_2Cl_2 form $[Ni(NCCH_3)_6][Te_2Cl_{10}]$ (**4**) in the presence of metallic nickel. All compounds **1**–**4** were characterized by ^{125}Te NMR and by X-ray crystallography. The formation of the anions has been discussed. © 2002 Elsevier Science Ltd. All rights reserved.

Keywords: Tellurium dichloride; Chloridotellurate anions; X-ray crystallography; NMR spectroscopy

1. Introduction

Chalcogen dihalides EX_2(E = S, Se, Te; X = Cl, Br, I) are useful reagents for synthetic applications. Of the chalcogen dihalogenides SCl_2 is most stable and can be prepared from the elements or by chlorination of S_2Cl_2 [1,2]. While $SeCl_2$ is stable only in the gas phase [3–5], it survives sufficiently long in coordinating solvents to serve as a synthon [6]. At 25 °C it can be stored for hours, and the appearance of Se_2Cl_2 and $SeCl_4$ due to disproportionation is only observed by ^{77}Se NMR after 24 h. $SeBr_2$ can be obtained by halogen exchange between $SeCl_2$ and Me_3SiBr, but disproportionation to Se_2Br_2 is apparent already after 1 h [6].

Tellurium dichloride has been known for over 100 years [7], but only few synthetic routes for the compound have been reported [8–10]. The reaction between $TeCl_4$ and neat hexamethyldisilane seems to be most promising [10]. In CS_2 solution, however, the formation of polymeric $(MeTeCl_3)_n$ was observed [11]. $TeCl_2$ is only stable in the gas phase and the condensation leads to rapid disproportionation to tellurium and $TeCl_4$ [12].

In this work we report the investigation of the reaction of elemental tellurium and SO_2Cl_2 in various solvents in order to explore the plausibility to produce $TeCl_2$ for synthetic applications. It turned out that in the presence of adventitious water tellurium is easily oxidized to the oxidation state IV with the production of a number of anionic species. The products have been characterized by ^{125}Te NMR and X-ray crystallography.

2. Experimental

2.1. General

All reactions were carried out under an argon atmosphere passed through P_4O_{10}. Tellurium (Aldrich), nickel (Merck), and SO_2Cl_2 (Aldrich) were used without further purification. DMSO (Lab-Scan) was dried by stirring over CaH_2 and acetonitrile (Lab-Scan) by distillation over CaH_2 before use. THF (Lab-Scan)

* Corresponding author. Tel.: +358-8-553-1611; fax: +358-8-553-1608.
E-mail address: risto.laitinen@oulu.fi (R.S. Laitinen).

0277-5387/02/$ - see front matter © 2002 Elsevier Science Ltd. All rights reserved.
PII: S0277-5387(02)00909-9

and CS_2 (Merck) were dried by distillation over Na/benzophenone and P_4O_{10}, respectively.

2.2. Spectroscopy

All ^{125}Te NMR spectra were recorded on a Bruker DPX 400 spectrometer at 300 K operating at 126.241 MHz. The spectral width was 95.24 kHz, yielding the resolution of 2.91 Hz per data point. The pulse width was 6.67 μs corresponding to a nuclear tip angle of 30°. The accumulations contained approximately 30 000 transients. All spectra were recorded unlocked. The ^{125}Te chemical shifts are reported relative to a saturated D_2O solution of H_6TeO_6 [$\delta(Me_2Te) = \delta(H_6TeO_6) + 712$].

TOF MS ES negative ion mass spectra were recorded using a Micromass LCT spectrometer at following voltages: capillary 3200 or 4000 V, sample cone from 15 to 30 V, RF lens 200 V, and extraction cone 3 V. Both the desolvation and source temperatures were 120 °C.

2.3. X-ray crystallography

Diffraction data for **1**–**4** were collected on a Nonius Kappa CCD diffractometer at 150 K using graphite monochromated Mo Kα radiation ($\lambda = 0.71073$ Å) by recording 360 frames via φ-rotation ($\Delta\varphi = 1°$; two times 20–40 s per frame). Crystal data and the details of the structure determinations are given in Table 1. Lorentz and polarization corrections as well as empirical absorption correction were applied to the net intensities.

All structures were solved by direct methods using SHELXS-97 [13] and refined using SHELXL-97 [14]. After the full-matrix least-squares refinement of the non-hydrogen atoms with anisotropic thermal parameters, the methyl and methylene hydrogen atoms were placed in calculated positions (C–H = 0.98 Å). In the subsequent refinements the hydrogen atoms were riding with the carbon atom they were bonded to. The isotropic thermal parameters of these hydrogen atoms were fixed at 1.5 times to that of the corresponding carbon atom. It was possible, however, to locate the oxonium hydrogen atoms in **1**, and the bridging hydrogen atoms in the cations of **2** and **3**. In the final refinement their positional and isotropic thermal parameters were refined normally. The scattering factors for the neutral atoms were those incorporated with the programs.

2.4. Preparation of samples

2.4.1. $(H_3O)[Te_3Cl_{13}]\cdot 1/2SO_2$ (**1**)

Tellurium (0.458 g, 3.59 mmol) was added into 30 ml of dry CS_2. An excess (1.20 g, 8.89 mmol) of SO_2Cl_2 was added into the resulting suspension during which a clear solution was formed. The mixture was stirred for 2 h during which some white solid was precipitated. Fifty ml of CS_2 was added to dissolve the precipitation. The solution was filtered and the filtrate was concentrated under dynamic vacuum. The crystals for the X-ray structure determination were obtained by cooling the filtrate. After 2 days 0.77 g (72% based on tellurium) of almost colorless crystals were obtained. Spectroscopic data: ^{125}Te NMR (CS_2, 25 °C): $\delta = 1803$ ppm.

2.4.2. $[(C_4H_8O)_2H][TeCl_5]\cdot(C_4H_8O)$ (**2**)

$[(C_4H_8O)_2H][TeCl_5]\cdot(C_4H_8O)$ was prepared by adding 1.380 g (10.23 mmol) of SO_2Cl_2 in 30 ml of THF into 0.522 g (4.09 mmol) of elemental tellurium upon stirring. The mixture was further stirred until the reaction was completed and a clear yellow solution was formed. The solution was concentrated under dynamic vacuum. Yellow crystals of **2** were obtained upon crystallization from the concentrated solution at room temperature (r.t.). The yield is approximately 1.9 g (90% based on tellurium). The rapid decomposition of the product in vacuum precluded the elemental analysis. Spectroscopic data: ^{125}Te NMR (THF, 25 °C): $\delta = 1712$ ppm.

2.4.3. $[(Me_2SO)_2H]_2(TeCl_6)$ (**3**)

SO_2Cl_2 (0.16 ml, 2.00 mmol) and 10 ml of THF were added into 0.255 g (2.00 mmol) of elemental tellurium upon stirring. The solution was further stirred for 60 min after which a 0.06 ml (0.75 mmol) portion of SO_2Cl_2 was added. All tellurium reacted and the solution turned yellow upon further stirring of 15 min. At this point 0.28 ml (4.00 mmol) of DMSO in 10 ml of THF was added into the resulting solution. An immediate pale yellow precipitation was observed with a yield of 0.62 g (95% based on DMSO). The precipitate was filtered, dissolved, and the solution was allowed to stand at r.t. overnight during which yellow crystals were formed. *Anal.* Calc. for $C_8H_{26}O_4S_4TeCl_6$: C, 14.67; H, 4.00. Found: C, 15.05; H, 3.62%. Spectroscopic data: ^{125}Te NMR (THF, 25 °C): $\delta = 1548$ ppm.

2.4.4. $[Ni(NCMe)_6][Te_2Cl_{10}]$ (**4**)

Metallic nickel (0.345 g, 5.88 mmol) and 1.508 g (11.82 mmol) of tellurium were mixed in 40 ml of acetonitrile. Upon addition of 3.995 g (29.60 mmol) of SO_2Cl_2 the color of the solution turned first yellow and then dark green. After stirring for 2 h the solvent was evaporated to dryness under dynamic vacuum. The yield is quantitative. The crystals for X-ray structure determination were obtained by recrystallization at r.t. from acetonitrile. *Anal.* Calc. for $C_{12}H_{18}N_6NiTe_2Cl_{10}$: C, 15.76; H, 1.98; N, 9.19. Found: C, 14.94; H, 1.97; N, 8.59%. Spectroscopic data: ^{125}Te NMR (MeCN, 25 °C): $\delta = 1570$ ppm.

Table 1
Details of the structure determination of $(H_3O)[Te_3Cl_{13}]\cdot 1/2SO_2$ (**1**), $[(C_4H_8O)_2H][TeCl_5]\cdot(C_4H_8O)$ (**2**), $[(Me_2SO)_2H]_2[TeCl_6]$ (**3**), and $[Ni(NCMe)_6][Te_2Cl_{10}]$ (**4**)

	1	**2**	**3**	**4**
Empirical formula	$H_3Cl_{13}O_2S_{0.5}Te_3$	$C_6H_{12.5}Cl_{2.5}O_{1.5}Te_{0.5}$	$C_4H_{13}Cl_3O_2S_2Te_{0.5}$	$C_6H_9N_3Cl_5Ni_{0.5}Te$
Relative molecular mass	902.70	522.17	327.41	457.37
Crystal system	trigonal	monoclinic	triclinic	triclinic
Space group	$R\bar{3}m$	$C2/c$	$P\bar{1}$	$P\bar{1}$
a (Å)	11.146(2)	13.753(3)	7.898(2)	8.701(2)
b (Å)		10.648(2)	9.067(2)	9.284(2)
c (Å)	17.552(4)	14.430(3)	10.125(2)	10.172(2)
a (°)			66.95(3)	91.58(3)
β (°)		102.70(3)	71.26(3)	97.64(3)
γ (°)			66.64(3)	104.79(3)
V (Å^3)	1888.2(5)	2061.5(7)	600.5(2)	785.7(2)
T (K)	150	150	150	150
Z	3	8	2	2
$F(000)$	1224	1032	324	434
D_{calc} (g cm^{-3})	2.382	1.682	1.811	1.933
μ (Mo Kα) (mm^{-1})	4.869	2.096	2.264	3.301
Crystal size (mm)	0.30 × 0.15 × 0.10	0.25 × 0.10 × 0.10	0.20 × 0.15 × 0.12	0.15 × 0.12 × 0.10
θ Range (°)	2.41–25.67	3.00–25.61	3.27–25.59	2.94–25.00
Number of reflections collected	3527	5066	2844	4431
Number of unique reflections	810	1836	1911	2484
Number of observed reflections [a]	804	1644	1852	2327
Number of parameters/restraints	49/2	100/0	118/2	146/0
R_{int}	0.0789	0.0390	0.0298	0.0221
R_1 [b]	0.0348	0.0286	0.0215	0.0222
wR_2 [b]	0.0883	0.0619	0.0545	0.0549
R_1 (all data) [b]	0.0353	0.0352	0.0223	0.0250
wR_2 (all data) [b]	0.0887	0.0644	0.0550	0.0560
Goodness-of-fit	1.113	1.067	1.022	1.184
Max. and min. heigthts in final difference Fourier synthesis (e Å^{-3})	0.863, −0.664	0.446, −0.590	0.694, −0.913	0.480, −0.434

[a] $I \geq 2\sigma(I)$.
[b] $R_1 = \Sigma||F_o|-|F_c||/\Sigma|F_o|$, $wR_2 = [\Sigma w(F_o^2-F_c^2)^2/\Sigma wF_o^4]^{1/2}$.

3. Results and discussion

3.1. General

While $SeCl_2$ can conveniently be prepared in coordinating solvents from elemental selenium and SO_2Cl_2 [6], the attempts to treat elemental tellurium with SO_2Cl_2 resulted in the production of chloridotellurate anions in which tellurium is in the oxidation state IV. The reaction route depends on the reaction conditions and is also influenced by the presence of adventitious water. All syntheses are reproducible.

The main products are $(H_3O)[Te_3Cl_{13}]\cdot 1/2SO_2$ (**1**) and $[(C_4H_8O)_2H][TeCl_5]\cdot(C_4H_8O)$ (**2**) in CS_2 and THF, respectively. With the addition of DMSO into the THF solution of the reaction mixture $[(DMSO)_2H]_2[TeCl_6]$ (**3**) is formed. In the presence of elemental nickel in acetonitrile, the reaction produces $[Ni(NCMe)_6][Te_2Cl_{10}]$ (**4**).

The ^{125}Te NMR spectra of all four reaction solutions show only a single resonance each with the chemical shifts of 1803, 1712, 1548, and 1570 ppm for **1**–**4**, respectively. All resonances are expectedly very broad because of the isotopic shifts of the chlorine atoms that are bound to tellurium.

The TOF ES negative ion mass spectra were recorded from every reaction solution. In all cases the most abundant fragment was $TeCl_2^-$ that was assigned on the basis of good agreement between the calculated and observed isotopic distribution. It was also the fragment of highest mass in **1**, **2**, and **3**. In **4** the fragment of highest mass was $TeCl_5^-$.

3.2. Crystal structures

3.2.1. $(H_3O)[Te_3Cl_{13}]\cdot 1/2SO_2$ (1)

The structure of **1** together with the numbering of the atoms is shown in Fig. 1, and the selected bond parameters are presented in Table 2.

The structure of **1** contains discrete $[Te_3Cl_{13}]^-$ and H_3O^+ ions and a disordered SO_2 molecule. The $[Te_3Cl_3]^-$ anion can be thought to be composed of three $TeCl_3^+$ units that are connected together by three bridging μ-Cl^- ligands and by one μ_3-Cl^- ligand that is

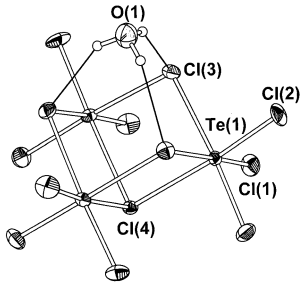


Fig. 1. The molecular structure of $(H_3O)[Te_3Cl_{13}]\cdot 1/2SO_2$ (**1**) indicating the numbering of the atoms. The thermal ellipsoids have been drawn at 50% probability.

coordinated to all three tellurium atoms. The lengths of the terminal Te–Cl bonds Te(1)–Cl(1) and Te(1)–Cl(2) are 2.339(3) and 2.330(4) Å, respectively. The Te(1)–Cl(3) distance of 2.826(2) Å involving a bridging μ-Cl^- ligand is significantly longer than the terminal bonds and the μ_3-Cl^- ligand Cl(4) shows a still longer bond of 2.942(3) Å to tellurium. These values are well in agreement with the corresponding bonds reported for $(Ph_3C)[Te_3Cl_{13}]$ [15,16] and $[(CH_3)_2CHC(NH_2)(OH)][Te_3Cl_{13}]\cdot(CH_3)_2CHCN$ [17]. The terminal Te–Cl bonds span the range of 2.320(5)–2.388(5) Å and 2.313(1)–2.356(1) Å in $(Ph_3C)[Te_3Cl_{13}]$ [15,16] and $[(CH_3)_2CHC(NH_2)(OH)][Te_3Cl_{13}]\cdot(CH_3)_2CHCN$ [17], respectively, those involving the μ-Cl^- ligands show the respective Te–Cl distances of 2.706(5)–2.863(5) Å and 2.798(1)–2.880(1) Å, and the Te–Cl distances involving the μ_3-Cl^- ligand lie in the range of 2.924(5)–2.984(5) Å and 2.913(1)–2.965(1) Å in $(Ph_3C)[Te_3Cl_{13}]$ [15,16] and $[(CH_3)_2CHC(NH_2)(OH)][Te_3Cl_{13}]\cdot(CH_3)_2CHCN$ [17], respectively.

It can be seen from the bond angles in Table 2 that the tellurium atom shows an approximate octahedral coordination and that the anion is a slightly distorted cube with one vertex occupied by the oxonium ion. The O(1)–H(1) bond length is 0.90(1) Å and the H(1)–O(1)–H(1)^a and H(1)–O(1)–H(1)^b bond angles are 106(10)° [see the footnotes in Table 2 for the definition of the symmetry operations *a* and *b*]. The hydrogen atoms of the oxonium ion are involved in weak hydrogen bonds to the bridging chloride Cl(3). The H(1)···Cl(3) contact is 2.6(1) Å. The oxonium oxygen also shows a close contact of 2.39(3) Å to S(1) of the SO_2 molecule.

It is interesting to note that the cation in neither $(Ph_3C)[Te_3Cl_{13}]$ [15,16] nor $[(CH_3)_2CHC(NH_2)(OH)][Te_3Cl_{13}]\cdot(CH_3)_2CHCN$ [17] lies in the open vertex of the cube. In the case of $(Ph_3C)[Te_3Cl_{13}]$ [15,16] there is a close contact between the Ph_3C^+ carbon and the μ_3-Cl^- ligand, and in the case of $[(CH_3)_2CHC(NH_2)(OH)][Te_3Cl_{13}]\cdot(CH_3)_2CHCN$ [17] the $[MeC(H)C(NH_2)O–H\cdots NCCMe_2]^+$ cation interacts through hydrogen bonds of the NH_2 group with one terminal and one μ-Cl^- ligand. These differences in the interionic packing help to understand, why the $[Te_3Cl_{13}]^-$ anion in **1** shows an exact site symmetry of C_{3v}, while the anions in $(Ph_3C)[Te_3Cl_{13}]$ [15,16] and $[(CH_3)_2CHC(NH_2)(OH)][Te_3Cl_{13}]\cdot(CH_3)_2CHCN$ [17] are somewhat distorted from the ideal symmetry.

Table 2
Selected bond lengths (Å) and bond angles (°) in the anions of $(H_3O)[Te_3Cl_{13}]\cdot 1/2SO_2$ (**1**), $[(C_4H_8O)_2H][TeCl_5]\cdot(C_4H_8O)$ (**2**), $[(Me_2SO)_2H]_2[TeCl_6]$ (**3**), and $[Ni(NCMe)_6][Te_2Cl_{10}]$ (**4**)

(*A*) $(H_3O)[Te_3Cl_{13}]\cdot 1/2SO_2$ (**1**)	
Te(1)–Cl(1)	2.339(3)
Te(1)–Cl(2)	2.330(4)
Te(1)–Cl(3)	2.826(2)
Te(1)–Cl(4)	2.942(3)
Cl(1)–Te(1)–Cl(2)	93.8(1)
Cl(1)–Te(1)–Cl(3)	175.38(9)
Cl(1)–Te(1)–Cl(4)	89.50(10)
Cl(1)–Te(1)–Cl(1)^a	92.1(2)
Cl(1)–Te(1)–Cl(3)^b	89.7(1)
Cl(2)–Te(1)–Cl(3)	90.4(1)
Cl(2)–Te(1)–Cl(4)	175.3(1)
Cl(3)–Te(1)–Cl(4)	86.27(6)
Cl(3)–Te(1)–Cl(3)^b	88.2(2)
Te(1)–Cl(3)–Te(1)^c	96.2(1)
Te(1)–Cl(4)–Te(1)^b	91.2(1)
(*B*) $[(C_4H_8O)_2H][TeCl_5](C_4H_8O)$ (**2**)	
Te(1)–Cl(1)	2.515(1)
Te(1)–Cl(2)	2.516(1)
Te(1)–Cl(3)	2.355(1)
Cl(1)–Te(1)–Cl(2)	89.89(4)
Cl(1)–Te(1)–Cl(3)	89.83(2)
Cl(1)–Te(1)–Cl(1)^d	179.66(5)
Cl(2)–Te(1)–Cl(2)^d	179.45(5)
Cl(2)–Te(1)–Cl(3)	89.72(2)
Cl(1)^d–Te(1)–Cl(3)	89.83(2)
Cl(2)^d–Te(1)–Cl(3)	89.72(2)
(*C*) $[(Me_2SO)_2H]_2[TeCl_6]$ (**3**)	
Te(1)–Cl(1)	2.528(1)
Te(1)–Cl(2)	2.547(1)
Te(1)–Cl(3)	2.5354(8)
Cl(1)–Te(1)–Cl(2)	89.30(4)
Cl(1)–Te(1)–Cl(3)	90.41(3)
Cl(2)–Te(1)–Cl(3)	91.05(3)
(*D*) $[Ni(NCMe)_6][Te_2Cl_{10}]$ (**4**)	
Te(1)–Cl(1)	2.783(1)
Te(1)–Cl(2)	2.499(1)
Te(1)–Cl(3)	2.383(1)
Te(1)–Cl(4)	2.352(1)
Te(1)–Cl(5)	2.486(1)
Cl(1)–Te(1)–Cl(2)	94.04(4)
Cl(1)–Te(1)–Cl(3)	176.57(3)
Cl(1)–Te(1)–Cl(4)	87.49(4)
Cl(1)–Te(1)–Cl(5)	88.37(4)
Cl(2)–Te(1)–Cl(3)	89.22(5)
Cl(2)–Te(1)–Cl(4)	89.39(4)
Cl(2)–Te(1)–Cl(5)	177.33(3)
Cl(3)–Te(1)–Cl(4)	91.46(4)
Cl(3)–Te(1)–Cl(5)	88.35(4)
Cl(4)–Te(1)–Cl(5)	89.56(4)

Symmetry operations: [a], $x, x-y, z$. [b], $-x+y+1, -x+1, z$. [c], $-y+1, x-y, z$. [d], $-x, y, -z+1/2$.

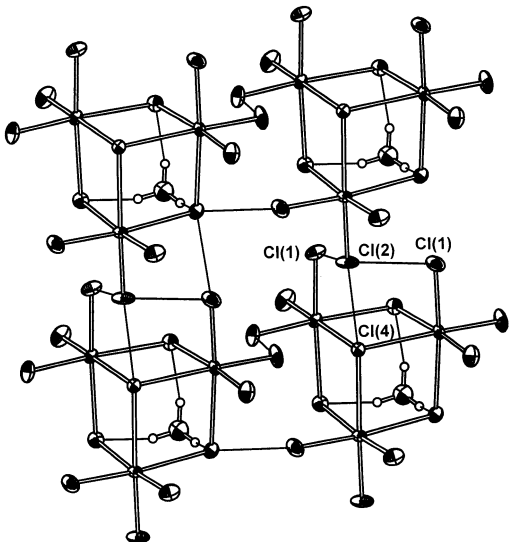


Fig. 2. The packing of the $[Te_3Cl_{13}]^-$ anions in **1**.

It can be seen in Fig. 2 that the anions of **1** are packed into layers involving close Cl···Cl contacts that lie in the range 3.497(6)–3.768(5) Å. It is interesting to note that while the closest Cl···Cl contacts in $(Ph_3C)[Te_3Cl_{13}]$ and $[(CH_3)_2CHC(NH_2)(OH)][Te_3Cl_{13}]\cdot(CH_3)_2CHCN$ are shorter than in **1** {3.328 [15,16] and 3.217(2) Å [17], respectively}, the packing of anions in **1** is more efficient than in either of the two related species. This is reflected by a somewhat higher density of $(H_3O)[Te_3Cl_{13}]\cdot 1/2SO_2$ (2.382 g cm^{-3}) compared with that of $(Ph_3C)[Te_3Cl_{13}]$ {2.127 g cm^{-3} [15,16]} or $[(CH_3)_2CHC(NH_2)(OH)][Te_3Cl_{13}]\cdot(CH_3)_2CHCN$ {2.247 g cm^{-3} [17]} and is a consequence of a significantly smaller cation in **1** that can be incorporated in the cage-structure of the anion.

3.2.2. $[(C_4H_8O)_2H][TeCl_5]\cdot(C_4H_8O)$ (2)

The crystal structure and the numbering of the atoms of **2** is shown in Fig. 3. The selected bond parameters are presented in Table 2. The structure is ionic and is composed of $[(C_4H_8O)_2H]^+$ cations and $[TeCl_5]^-$ anions. In addition there is one discrete THF solvent molecule in the lattice.

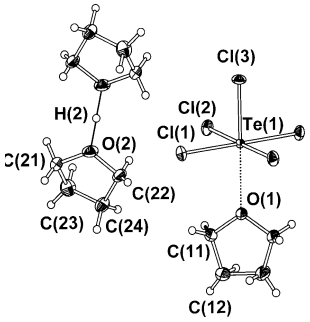


Fig. 3. The molecular structure of $[(C_4H_8O)_2H][TeCl_5]\cdot(C_4H_8O)$ (**2**) indicating the numbering of the atoms. The thermal ellipsoids have been drawn at 50% probability.

The primary coordination sphere of tellurium is a square pyramid. The basal bonds Te(1)–Cl(1) and Te(1)–Cl(2) show the respective lengths of 2.515(1) and 2.516(1) Å. The apical bond Te(1)–Cl(3) is expectedly somewhat shorter [2.355(1) Å]. The basal plane is virtually planar [Σ(Cl–Te–Cl) = 359.1°]. The long Te(1)···O(1) contact of 2.593(4) Å from the solvent molecule completes the octahedral coordination and is consistent with the concept of secondary bonding [18] that has recently been considered for a number of tellurium compounds [19,20]. $(C_8H_8S_2N)[TeCl_5]\cdot 1.5C_4H_8O_2$ [21], $(H_3O)[TeBr_5]\cdot C_4H_8O_2$ [22], and $(AsPh_4)[TeCl_5]\cdot H_2O$ [23] also exhibit a $[TeX_5]^-$ anion with a weak secondary interaction to the dioxane or water oxygen atom. For instance, in $(C_8H_8S_2N)[TeCl_5]\cdot 1.5C_4H_8O_2$ the virtually coplanar basal bonds range 2.494(3)–2.514(3) and the apical Te–Cl bond shows the length of 2.330(4) Å. The secondary Te–O contact is 2.766 Å [21] in agreement with the bond parameters in **2**.

The cation of **2** is a protonated THF dimer $[(C_4H_8O)\cdots H\cdots(OC_4H_8)]^+$. The hydrogen atom H(2) lies at a symmetry element and is thus exactly in the middle of O(2) and its symmetry-related counterpart. The O(2)–H(2) distance is 1.209(3) Å and the O(2)···O(2) separation is 2.418(5) Å. The existence of this kind of protonated dimeric cations with strong hydrogen bonds is well-known and can be exemplified by bis(*N*-nitrosopyrrolidine)hydrogen hexafluorophosphate [24] and $[Me_2NC(H)O\cdots H\cdots O(H)CNMe_2][TeCl_4(OEt)]$ [25]. The $[MeC(H)C(NH_2)O–H\cdots NCCMe_2]^+$ cation that serves as a counterion for one of the $[Te_3Cl_{13}]^-$ structures [17] is also analogous to the dimeric bonding arrangement involving a bridging H^+ ion, as is the dimeric $[Me_2SO–H\cdots OSMe_2]^+$ cation of **3** described below. Reich et al. [23] have suggested that the formation of protonated organic molecules as counterions to halogenidotellurates(IV) is observed, when the electron donating group is more basic than water.

The anions of **2** are chained together involving the solvent THF molecule. In addition to the close Te(1)···O(1) contact to one $[TeCl_5]^-$ anion, there is a Cl(3)···C(12) contact of 3.580(2) Å to another $[TeCl_5]^-$ anion. The closest anion-cation Cl···C distances are 3.672(2) and 3.696(1) Å.

3.2.3. $[(Me_2SO)_2H]_2[TeCl_6]$ (3)

The crystal structure of **3** with the numbering of atoms is shown in Fig. 4, and the selected bond lengths are presented in Table 2. The lattice of **3** consists of discrete $[TeCl_6]^{2-}$ anions and $[(Me_2SO)_2H]^+$ cations. The coordination sphere of tellurium in $[TeCl_6]^{2-}$ is an almost regular octahedron with the Te–Cl bond lengths ranging 2.528(1)–2.547(1) Å. The bond angles are near to 90° ranging 89.30(4)°–91.05(3)°. These values are in

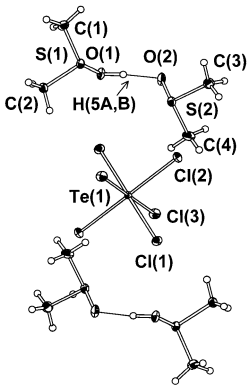


Fig. 4. The molecular structure of $[(Me_2SO)_2H]_2[TeCl_6]$ (**3**) indicating the numbering of the atoms. The thermal ellipsoids have been drawn at 50% probability. Only one hydrogen of the disordered H(5A,B) pair has been displayed.

good agreement with those reported for a large number of species containing the $[TeCl_6]^{2-}$ ion [26].

In an analogous fashion to **2** the cation in **3** is a protonated DMSO dimer. The O(1)···O(2) distance of 2.435(3) Å indicates a relatively strong hydrogen bond. It was possible to detect two electron density maxima along the line connecting O(1) and O(2) and refine the positions of these two hydrogen atoms H(5A) and H(5B) by defining the site occupation factors of 0.5 for both of them (a constant isotropic thermal parameter 0.05 was used in the refinement). Both the O(1)–H(5A) and O(2)–H(5B) bond lengths are 0.9(1) Å with the H(5A)···O(2) and H(5B)···O(1) contacts 1.5(1) Å. The O–H···O bond angles are 175(10)° and 170(5)° for H(5A) and H(5B), respectively.

The crystal structure of $[(Me_2SO)_2H]_2[TeCl_6]$ has also been determined earlier at room temperature [27]. The structure of **3** expectedly shows the same general structural features. In the present low-temperature redetermination, however, it was possible to locate and refine the hydrogen atom positions and establish that the protonation of the two DMSO molecules in the dimeric cation is distributed statistically in the lattice.

3.2.4. *[Ni(NCMe)$_6$][Te$_2$Cl$_{10}$] (4)*

The molecular structure of **4** is shown in Fig. 5 together with the numbering of the atoms. The selected bond lengths and angles of the anion are given in Table 2.

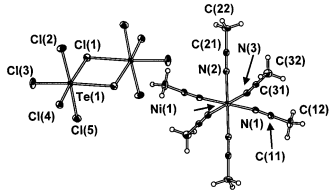


Fig. 5. The molecular structure of $[Ni(NCMe)_6][Te_2Cl_{10}]$ (**4**) indicating the numbering of the atoms. The thermal ellipsoids have been drawn at 50% probability.

The discrete $[Te_2Cl_{10}]^{2-}$ anions consist of two $TeCl_6$ octahedral sharing a common edge. The terminal Te–Cl bond lengths range 2.383(1)–2.352(1) Å. The bridging Cl(1) shows two distances to tellurium, 2.783(1) and 2.909(1) Å. Such an unsymmetrical bridge is a common feature in dinuclear tellurates [28]. The bond angles around tellurium span 87.49(4)°–94.04(4)° indicating a slightly distorted octahedron.

The $[Ni(NCMe)_6]^{2+}$ cation is virtually a regular octahedron. All bond lengths are quite normal for the atoms in question. The anions and the cations form alternating stacks throughout the lattice. The closest cation-anion distances involve the interaction between the chlorido-ligands and the CN group in acetonitrile. The Cl···N contacts range 3.441(3)–3.676(3) Å and the Cl···C contacts 3.336(3)–3.585(4) Å.

3.3. *The structural relationships between the anions and their formation*

All anions formed in this work bear a structural relationship to $TeCl_4$ and to each other. This relationship has initially been proposed by Krebs and Paulat [16] and is presented in Fig. 6. Hasche et al. ([17], and references therein) have also discussed the formation equilibria of the different chloridotellurate anions.

$$3[Te_4Cl_{16}] + 4Cl^- \rightleftharpoons [Te_3Cl_{13}]^-$$

$$4[Te_3Cl_{13}]^- + 4Cl^- \rightleftharpoons 4[Te_2Cl_{10}]^{2-} + [Te_4Cl_{16}]$$

$$[Te_2Cl_{10}]^{2-} + 2Cl^- \rightleftharpoons 2[TeCl_6]^{2-}$$

Hasche et al. [17] suggest that $[TeX_5]^-$ is formed in organic solutions due to disproportionation of TeX_4. This anion is stabilized by the secondary interaction of

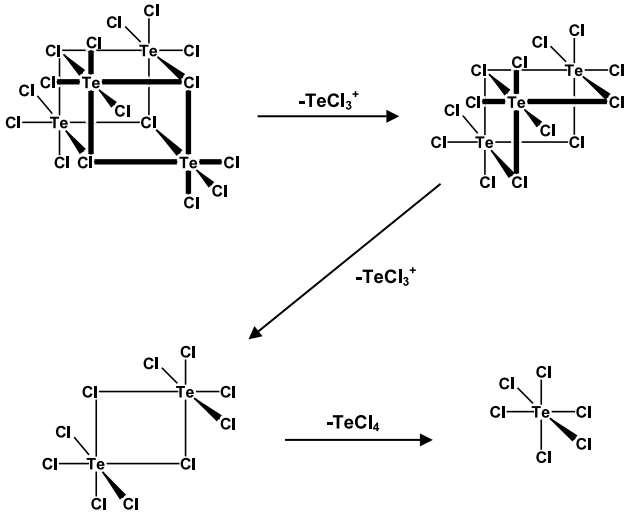


Fig. 6. The structural relationships between the halogenidotellurate anions as suggested by Krebs and Paulat [16].

tellurium to the oxygen atom of the solvent molecules as observed in $(C_8H_8S_2N)[TeCl_5]\cdot 1.5C_4H_8O_2$ [21], $(H_3O)[TeBr_5]\cdot C_4H_8O_2$ [22], $(AsPh_4)[TeCl_5]\cdot H_2O$ [23], and **2**.

These equilibria may well explain the formation of **1**–**4** upon the reaction of elemental tellurium with SO_2Cl_2. It is possible that $TeCl_2$ is an initial product in the reaction, as expected on the basis of the reaction of elemental selenium and sulfuryl chloride in THF that is known to afford $SeCl_2$ in good yields [6]. However, an excess of SO_2Cl_2 needs to be used to facilitate the complete reaction of tellurium. It is possible that in addition to $TeCl_2$ also $TeCl_4$ is formed. Both molecules may play a role in the setting of the above-mentioned equilibria and the isolation of the products **1**–**4**. The solvent and the possible presence of a small amount of residual moisture seem to determine the identity of the main product in each individual case.

4. Supplementary material

Crystallographic information for **1** (excluding tables of structure factors) has been deposited with the Fachinformationzentrum Karlsruhe (FIZ) as supplementary publication number CSD 412153, and that for **2**, **3**, and **4** with the Cambridge Crystallographic Data Center as supplementary publication numbers CCDC 171280-171282, respectively. Copies of the data can be obtained free of charge on application to FIZ, abt. PROKA, 76344 Eggenstein-Leopoldshafen, Germany (tel.: +49-7247-808-205; e-mail: crysdata@fiz-karlsruhe.de), and to CCDC, 12 Union Road, Cambridge CB2 1EZ, UK (fax: +44-1223-336-033; e-mail: deposit@ccdc.cam.ac.uk www:http://www.ccdc.cam.ac.uk).

Acknowledgements

Financial support from the Academy of Finland is gratefully acknowledged.

References

[1] K.J. Palmer, J. Am. Chem. Soc. 60 (1938) 2360.
[2] B. Solouki, P. Rosmus, H. Bock, Chem. Phys. Lett. 26 (1974) 20.
[3] D.M. Yost, C.E. Kircher, J. Am. Chem. Soc. 52 (1930) 4680.
[4] M. Lundqvist, M. Lellep, Acta Chem. Scand. 22 (1968) 291.
[5] G.A. Ozin, A.V. Voet, Chem. Commun. (1970) 896.
[6] A. Maaninen, T. Chivers, M. Parvez, J. Pietikäinen, R.S. Laitinen, Inorg. Chem. 38 (1999) 4093.
[7] A. Michaelis, Ber. 20 (1887) 2488.
[8] K. Lindner, N. Apolant, Z. Anorg. Allg. Chem. 136 (1924) 381.
[9] E.E. Aynsley, J. Chem. Soc. (1953) 3016.
[10] R.C. Paul, A. Arneja, S.P. Narula, Inorg. Nucl. Chem. Lett. 5 (1969) 1013.
[11] J. Pietikäinen, J. Konu, R.S. Laitinen, J. Valkonen, Z. Naturforsch., Teil. B 56b (2001) 1369.
[12] G.C. Christensen, J. Alstad, Radiochem. Radioanal. Lett. 13 (1973) 227.
[13] G.M. Sheldrick, SHELXS-97. Program for Crystal Structure Determination, University of Göttingen, 1997.
[14] G.M. Sheldrick, SHELXL-97. Program for Crystal Structure Determination, University of Göttingen, 1997.
[15] B. Krebs, V. Paulat, Angew. Chem. 85 (1973) 662.
[16] B. Krebs, V. Paulat, Z. Naturforsch. 34b (1979) 900.
[17] S. Hasche, O. Reich, I. Beckmann, B. Krebs, Z. Anorg. Allg. Chem. 623 (1996) 724.
[18] N.W. Alcock, Adv. Inorg. Chem. Radiochem. 15 (1972) 1.
[19] M.J. Collins, J.A. Ripmeester, J.F. Sawyer, J. Am. Chem. Soc. 110 (1988) 8583 (and references therein).
[20] R. Oilunkaniemi, J. Pietikäinen, R.S. Laitinen, M. Ahlgrén, J. Organomet. Chem. 640 (2001) 50 (and references therein).
[21] W. Hinrichs, D. Mandak, G. Klar, Cryst. Struct. Commun. 11 (1982) 1781.
[22] O. Reich, S. Hasche, K. Büscher, I. Beckmann, B. Krebs, Z. Anorg. Allg. Chem. 622 (1996) 1011.
[23] O. Reich, S. Hasche, S. Bonmann, B. Krebs, Z. Anorg. Allg. Chem. 624 (1998) 411 (and references therein).
[24] L.K. Keefer, J.A. Hrabie, L. Ohannesian, J.L. Flippen-Anderson, C. George, J. Am. Chem. Soc. 110 (1988) 3701.
[25] R.A. Zingaro, C. Herrera, E.A. Meyers, Phosphorus Sulfur Silicon Relat. Elem. 48 (1990) 1.
[26] B. Krebs, F.-P. Ahlers, Adv. Inorg. Chem. 35 (1990) 235 (and references therein).
[27] B. Viossat, P. Khodadad, N. Rodier, J. Mol. Struct. 71 (1981) 237.
[28] M.A. James, O. Knop, T.S. Cameron, Can. J. Chem. 70 (1992) 1795.

PERGAMON

Polyhedron 21 (2002) 1097–1103

POLYHEDRON

www.elsevier.com/locate/poly

Lanthanide contraction and anions-controlled dimensional diversity in Ln–Cu–NTA (Ln = lanthanide, H_3NTA = nitrilotriacetic acid) coordination polymers: crystal structure and magnetic properties

Qin-De Liu [a], Song Gao [a,*], Jun-Ran Li [a,*], Bao-Qing Ma [a], Qing-Zhong Zhou [a], Kai-Bei Yu [b]

[a] *State Key Laboratory of Rare Earth Materials Chemistry and Applications and PKU-HKU Joint Laboratory on Rare Earth Materials and Bioinorganic Chemistry, College of Chemistry and Molecular Engineering, Peking University, Beijing 100871, People's Republic of China*
[b] *Chengdu Center for Analysis and Measurement, Academia Sinica, Chengdu 610041, People's Republic of China*

Received 26 October 2001; accepted 16 January 2002

Abstract

A series of lanthanide–copper coordination polymers with nitrilotriacetic acid (H_3NTA) were synthesized as $[LnCuCl(NTA)(H_2O)_6]ClO_4\cdot H_2O$ [Ln=La (**1**), Ce (**2**), Pr (**3**), Gd (**4**, **4′**), Tb (**5**) and Dy (**6**)] and $[LnCuCl(NTA)(H_2O)_6]ClO_4\cdot 3H_2O$ [Ln=Ho (**7**), Er (**8**), Tm(**9**), Lu (**10**) and Y (**11**)] in aqueous solution. The crystal structures of **1**, **4**, **4′**, **8**, **11** were determined and isomorphous relationships of the others identified. They turned out to be diverse, ranging from a two-dimensional (2D) array for **1** to one-dimensional (1D) chains of three different types (**2**–**4**, **4′**–**6**, and **7**–**11**), as controlled by lanthanide contraction and mixed anions Cl^- and ClO_4^-, which were found to play a crucial role in the formation and stabilization of this series of LnCu polymers. Temperature-dependent magnetic susceptibilities for **1**, **3**, **4**, **5** and **8** were studied. **1** shows a weak ferromagnetic-like behavior, whereas the others exhibit an overall antiferromagnetic feature. © 2002 Elsevier Science Ltd. All rights reserved.

Keywords: Lanthanide contraction; Anion controlled assembly; Crystal structures; Magnetic properties

1. Introduction

Lanthanide(Ln)-transition metal coordination polymers are of great interest in view of their interesting magnetic properties [1–4]. From a structural viewpoint, lanthanide contraction may have a crucial effect on the formation of 4f–3d complexes. Recently, it was reported that with the ligand 3,5-pyrazoldicarboxylic acid (H_3pdc), three different types of structures (two-dimensional single layer, two-dimensional double layer and three dimensional structures) could be obtained by using different lanthanides from Lu to La [5]. Kahn and coworkers have also carried out systematic studies on a series of $[Ln_2Cu_3]$ heteronuclear complexes with the 1,3-propylene-bis(oxamato) ligand [6]. They observed the lanthanide contraction controlled dimensional structural diversity ranging from two-dimensional honeycomb patterns (Ln=La–Gd) to one-dimensional ladder-like chains (Ln=Tb–Yb). These results suggest that lighter lanthanides tend to form higher-dimensional structures, while heavier lanthanides tend to generate lower-dimensional structures. However, the contraction from light to heavy lanthanides seems to have little effect on the crystal structure of zero-dimensional high nuclearity clusters, such as $[Cu_{12}Ln_6(OH)_{24}(H_2O)_{18}(pyb)_{12}(ClO_4)]^{17+}$ (Ln = Nd, Gd, Y, Sm, Eu, pyb = pyridine betaine) [7] and the heptanuclear clusters $[LnCu_6(\mu_3\text{-}OH)_3(HL)_2(L)_4]\ (ClO_4)_2\cdot 25H_2O$ (Ln = La, Tb, H_2L = iminodiacetic acid) [8].

Nitrilotriacetic acid (H_3NTA) is an important derivative of glycine. However, only a few rare-earth complexes with NTA have been synthesized [9–11], and we first reported two 4f–3d heteronuclear complexes $[LnCuCl(NTA)(H_2O)_6](ClO_4)\cdot H_2O$ (Ln = La, Gd) **1** and **4′** [12]. As an extension of this work, herein we report the synthesis and structural diversity of a series of Ln–Cu–NTA complexes. We found that with a syn-

* Corresponding authors. Fax: +86-10-6275-1708.
E-mail address: lijunran@pku.edu.cn (J.-R. Li).

0277-5387/02/$ - see front matter © 2002 Elsevier Science Ltd. All rights reserved.
PII: S0277-5387(02)00911-7

thetic method similar to that of **1**, two other kinds of different one-dimensional chains could be obtained as $[GdCuCl(NTA)(H_2O)_6](ClO_4)\cdot H_2O$ (**4**) and $[ErCuCl(NTA)(H_2O)_6]\cdot(ClO_4)\cdot 3H_2O$ (**8**), indicating the dimensional diversity controlled by lanthanide contraction in this series of complexes.

Some earlier reports have mentioned the template effect of inorganic anions in studies on the formation of some cluster compounds, e.g. Cl^- in $[Eu_{15}(Cl)(\mu_3\text{-}Tyr)_{10}(\mu_3\text{-}OH)_{20}(\mu_2\text{-}H_2O)_5(OH)_{12}(H_2O)_8](ClO_4)_2\cdot 56H_2O$ [13], $\mu_{12}\text{-}ClO_4^-$ in $[Ln_6Cu_{12}]$ (Ln = Nd, Sm, Gd and Y) [7], and $\mu_6\text{-}O^{2-}$ in $[Ln_6(\mu_6\text{-}O)(\mu_3\text{-}OH)_8(H_2O)_{24}]\cdot(ClO_4)_8\cdot 6H_2O$ [14,15]. In contrast, as monodentate ligands and counter ions, both Cl^- and ClO_4^- ions play crucial roles in the formation of compounds **1** to **11**.

2. Experimental

2.1. Synthesis of the complexes

All the complexes were synthesized by similar procedures. A mixture of $Cu(OH)_2$ (3 mmol) and H_3NTA (3 mmol) was dissolved in 30 ml H_2O, then aqueous solutions of $Ln(ClO_4)_3$ (0.5 M, 1.5 mmol) and $LnCl_3$ (0.5 M, 1.5 mmol), where Ln stands for La, Ce, Pr, Gd, Tb, Dy, Ho, Er, Tm, Lu and Y, were added. The pH value of the reaction mixture was adjusted carefully to approximately 5.0. The solution was filtered, concentrated to 15 ml and left to stand at r.t. Blue crystalline blocks of $[LnCuCl(NTA)(H_2O)_6]\cdot ClO_4\cdot H_2O$ [Ln=La (**1**), Ce (**2**), Pr (**3**), Gd (**4**), Tb (**5**) and Dy (**6**)] and $[LnCuCl(NTA)(H_2O)_6]ClO_4\cdot 3H_2O$ [Ln=Ho (**7**), Er (**8**), Tm(**9**), Lu (**10**) and Y (**11**)] suitable for X-ray crystallography formed after 2 weeks. C, H, N analyses results of the products are listed in Table 1.

Table 1
Results of C, H and N analyses for complexes **2**–**11** (outside brackets, calculated data; inside brackets, found data)

Complexes	Formula	C (%)	H (%)	N (%)
2	$CeCuC_6H_{20}NCl_2O_{17}$	11.04 (11.35)	3.09 (2.96)	2.15 (1.90)
3	$PrCuC_6H_{20}NCl_2O_{17}$	11.03 (10.98)	3.08 (3.20)	2.14 (2.02)
4	$GdCuC_6H_{20}NCl_2O_{17}$	10.76 (10.69)	3.01 (3.04)	2.09 (1.96)
5	$TbCuC_6H_{20}NCl_2O_{17}$	10.73 (10.33)	3.00 (2.96)	2.09 (2.03)
6	$DyCuC_6H_{20}NCl_2O_{17}$	10.67 (9.93)	2.99 (3.05)	2.07 (1.93)
7	$HoCuC_6H_{24}NCl_2O_{19}$	10.10 (9.99)	3.39 (3.39)	1.96 (1.93)
8	$ErCuC_6H_{24}NCl_2O_{19}$	10.06 (9.64)	3.38 (3.60)	1.96 (1.94)
9	$TmCuC_6H_{24}NCl_2O_{19}$	10.04 (10.09)	3.37 (3.09)	1.95 (1.74)
10	$LuCuC_6H_{24}NCl_2O_{19}$	9.96 (9.66)	3.34 (3.07)	1.94 (1.70)
11	$YcuC_6H_{24}NCl_2O_{19}$	11.30 (11.03)	3.79 (3.41)	2.20 (2.14)

2.2. X-ray data collection and structure determination

Crystals of complexes **1**, **4**, **8** and **11** with suitable dimensions were picked out from paraffin oil and sealed into thin-walled capillaries for structure determination. Intensity data were collected on a Siemens P4 diffractometer with Mo Kα radiation in the ω-scan mode. The unit-cell parameters of the complexes were determined from a least-square refinement. Empirical absorption corrections were applied using the XPRED program [16]. The structures were solved and refined with direct methods and difference Fourier syntheses. The structures were further refined with full-matrix least-square calculations using the Siemens SHELXTL/PC system [16]. All non-hydrogen atoms were refined anisotropically. Details of data collection and refinements are listed in Table 2.

2.3. Magnetic measurements

The dc and ac magnetic susceptibility data for crystalline samples were collected on a MAGLAB2000 system in the temperature range from 2 to 300 K. The data were corrected for the diamagnetism of the samples calculated from Pascal's constants.

3. Results and discussion

3.1. Description of structures

Compound **1** consists of a two-dimensional metal-apex honeycomb-like layer with nine-coordinated lanthanum and five-coordinated copper ions located at the apexes of each hexagon [12(a)].

Compound **4** is not a 2D polymer, but a 1D zigzag chain with nine-coordinated gadolinium and five-coordinated copper ions, which was established by X-ray crystallography. An ORTEP view of **4** is shown in Fig. 1. Selected bond lengths and angles are given in Table 3. Similar to **1**, the Cu in complex **4** is also tetradentately chelated by a NTA ligand through O1, O3, O5 and N. The fifth coordination site is occupied by Cl1. Despite the fact that six water molecules (O7–O12) are coordinated to it, Gd is also bidentately chelated by a carboxyl group of NTA through O1 and O2. The last coordination site of Gd is taken up by a carboxyl oxygen atom (O6A) from another NTA ligand. Therefore, each NTA consists of a chelating carboxyl bridge and a *syn–anti* carboxyl bridge over a copper and two different gadolinium ions. The third carboxyl group of NTA is monodentately coordinated to Cu through O3, and O4 is left non-coordinating. The intra-chain Gd···Cu distances in complex **4** is 4.63 (chelation bridge) and 5.72 Å (*syn–anti* bridge). The *syn–anti* and the chelation bridges interconnect the complex into a 1D zigzag chain

Table 2
Crystallographic data for complexes **4**, **8** and **11**

	4	**8**	**11**
Formula	$GdCuC_6H_{20}NCl_2O_{17}$	$ErCuC_6H_{24}NCl_2O_{19}$	$YCuC_6H_{24}NCl_2O_{19}$
Formula weight	669.92	715.96	637.61
Crystal system	monoclinic	triclinic	triclinic
Space group	$P2_1$	$P\bar{1}$	$P\bar{1}$
T (K)	291	291	291
λ (Å)	0.71073	0.71073	0.71073
ρ_{calcd} (g cm^{-3})	2.327	2.188	1.937
μ (mm^{-1})	4.913	5.146	3.944
a (Å)	8.1475(2)	9.5015(2)	9.5128(2)
b (Å)	12.7277(2)	10.5625(2)	10.5842(4)
c (Å)	9.3964(2)	12.7806(3)	12.7858(5)
α°	90	89.1760(15)	89.1950(16)
β°	101.0789(12)	70.9180(14)	70.959(2)
γ°	90	64.9510(14)	65.196(2)
V (Å^3)	956.24(3)	1086.58(4)	1093.28(6)
Z	2	2	2
Number of independent reflections	2865	6288	5154
R [a]	0.0222	0.0395	0.0449
R_w [b]	0.0552	0.1002	0.1158

[a] $R = \Sigma[|F_o| - |F_c|]/\Sigma|F_o|$.
[b] $R_w = \{\Sigma[w(F_o^2 - F_c^2)]/\Sigma[w(F_o)^2]\}^{1/2}$.

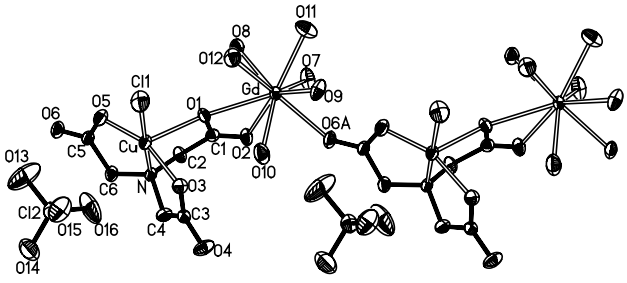


Fig. 1. An ORTEP view of complex **4** showing the connection between Gd^{3+} and Cu^{2+}. Hydrogen atoms and lattice water molecules are omitted for clarity.

(Fig. 2). Under the condition when the concentration of Cl^- was considerably low, we also obtained another Gd–Cu–NTA 1D chain (**4′**) [12(b)], which is a little different from **4**. The structure of **4′** is very similar to that of **4,** except that the carboxyl bridge is *syn–anti* in **4** and *anti–anti* in **4′**. As a result, the crystal system of **4′** is triclinic: space group $P\bar{1}$, $a = 8.483$ Å, $b = 9.642$ Å, $c = 12.838$ Å, $\alpha = 111.17°$, $\beta = 93.52°$, $\gamma = 100.89°$. It is very interesting to find two kinds of Gd–Cu–NTA chains with the same formula and same coordination environments around the metal ions. Since different synthesis methods were employed for **4** and **4′**, it seems that the crystals formed tend to be monoclinic when a higher concentration of Cl^- is used, while a lower concentration of Cl^- is advantageous for the formation of triclinic crystals. The mechanism of crystal formation will be further studied.

As for compounds **8** and **11**, X-ray single crystal diffraction analysis revealed that they are isomorphous.

Table 3
Selected bond lengths (Å) and angles (°) for **4**

Bond lengths			
Gd–O11	2.377(4)	Gd–O7	2.399(4)
Gd–O9	2.423(4)	Gd–O10	2.436(4)
Gd–O6A	2.450(4)	Gd–O8	2.470(3)
Gd–O12	2.476(4)	Gd–O2	2.502(4)
Gd–O1	2.519(3)	Cu–O5	1.939(3)
Cu–O3	1.981(3)	Cu–N1	2.049(4)
Cu–Cl1	2.2234(15)	Cu–O1	2.285(3)
Bond angles			
O11–Gd–O7	72.67(19)	O11–Gd–O9	68.36(16)
O7–Gd–O9	115.76(14)	O11–Gd–O10	138.39(17)
O7–Gd–O10	136.9(2)	O9–Gd–O10	71.35(16)
O11–Gd–O6A	105.51(16)	O7–Gd–O6A	68.74(16)
O9–Gd–O6A	75.08(13)	O10–Gd–O6A	73.10(16)
O11–Gd–O8	73.28(15)	O7–Gd–O8	69.58(14)
O9–Gd–O8	136.41(14)	O10–Gd–O8	136.65(12)
O6A–Gd–O8	136.41(13)	O11–Gd–O12	75.99(17)
O7–Gd–O12	139.62(18)	O9–Gd–O12	73.90(14)
O10–Gd–O12	83.43(18)	O6A–Gd–O12	145.72(15)
O8–Gd–O12	77.50(14)	O11–Gd–O2	141.98(15)
O7–Gd–O2	73.98(14)	O9–Gd–O2	145.06(15)
O10–Gd–O2	79.44(16)	O6A–Gd–O2	78.45(13)
O8–Gd–O2	78.40(13)	O12–Gd–O2	121.92(13)
O11–Gd–O1	133.30(16)	O7–Gd–O1	115.81(13)
O9–Gd–O1	128.21(13)	O10–Gd–O1	68.42(12)
O6–Gd–O1	120.58(13)	O8–Gd–O1	68.57(11)
O12–Gd–O1	70.40(13)	O2–Gd–O1	51.65(11)
O5–Cu–O3	159.02(15)	O5–Cu–N	83.47(15)
O3–Cu–N	84.72(15)	O5–Cu–Cl1	95.53(11)
O3–Cu–Cl1	97.13(11)	N–Cu–Cl1	176.78(12)
O5–Cu–O1	108.88(15)	O3–Cu–O1	86.37(14)
N–Cu–O1	81.46(14)	Cl1–Cu–O1	96.01(10)

Symmetry transformations used to generate equivalent atoms: (A) $x, y, z+1$.

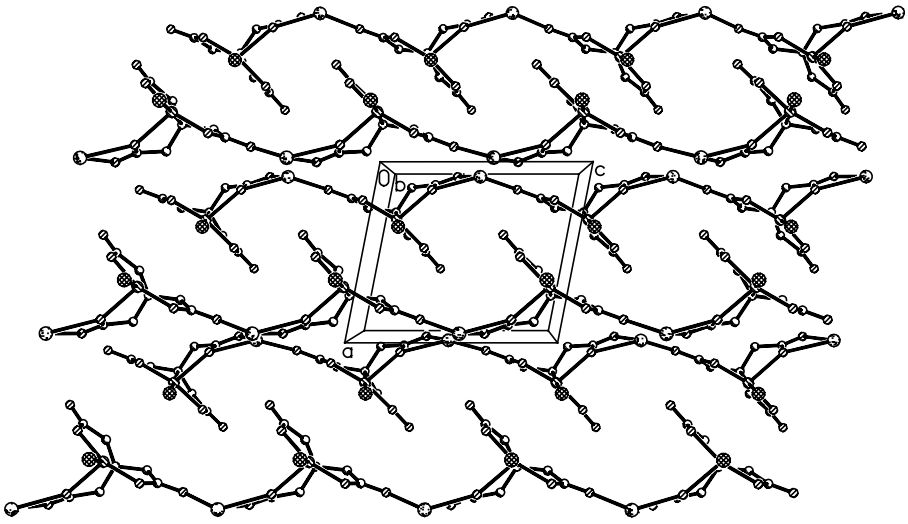


Fig. 2. Viewed along the *c* axis showing the zigzag chains along the *b* axis in **4**. All water molecules and ClO_4^- are omitted for clarity.

Both compounds are 1D chain-like polymers with eight-coordinated lanthanide and five-coordinated copper ions. The ORTEP view of **8** is shown in Fig. 3. Selected bond lengths and angles are given in Table 4. In complex **8**, the coordination environment of Cu is the same as that in **1**, but the environment of Er is different from that of La in **1** and Gd in **4** and **4′**, mainly due to the fact that Er is only eight-coordinated. In addition to six water molecules, Er is only coordinated by two carboxyl oxygen atoms from two different NTA ligands. Thus, each NTA forms a *syn–anti* bridge and an *anti–anti* bridge over one copper and two different erbium ions. The complex is linked into a 1D chain by the *syn–anti* and *anti–anti* bridges of NTA ligands. In general, the length of either the *syn–anti* bridge or the *anti–anti* bridge is much longer than that of the chelating bridge. Both complexes **4** and **4′** contain chelating carboxyl bridges while complex **8** does not. Therefore, the length of chain per unit in **8** (intra-chain Er···Er distance, 10.81 Å) is longer than those in **4** and **4′** (intra-chain Gd···Gd distance: 9.40 Å for **4** and 9.64 Å for **4′**).

Based on the results of elemental analyses and crystal cell parameters (shown in Table 5) for complex **2**, **3**, **5**, **6**, **7**, **9** and **10**, we found that complexes **2** and **3** are isomorphous with **4**, complexes **5** and **6** are isomorphous with **4′**, and complexes **7**, **9** and **10** are isomorphous with **8** and **11**.

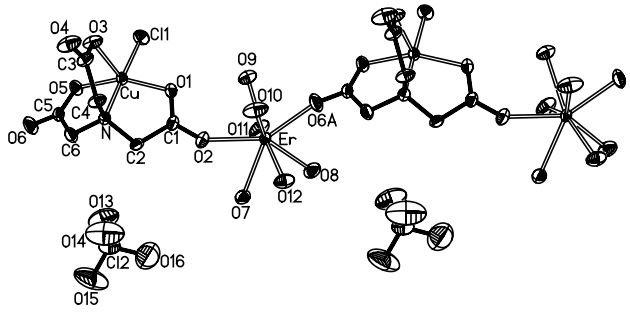


Fig. 3. An ORTEP view of complex **8** showing the connection between Er^{3+} and Cu^{2+}. Hydrogen atoms and lattice water molecules are omitted for clarity.

3.2. Anion controlled assembly

It was found that experiments using either $Ln(ClO_4)_3$ or $LnCl_3$ alone could not give rise to this series of Ln–Cu complexes, suggesting that both Cl^- and ClO_4^- have a synergetic effect on the formation of this series of heteronuclear complexes. On comparing to the Ln_{15} cluster which contains a central Cl^- ion as template and ClO_4^- ions as counter ions [13], the Cl^- ions in the Ln–Cu–NTA complexes are not templates, but are directly coordinate to Cu. Formation of these complexes turned out to be impossible without the presence of Cl^-. The role of ClO_4^- as counter ions may involve it occupying the holes of the honeycomb in complex **1** and the vacuous spaces among the zigzag chains in complex **2**–**11**. The lattices are, therefore, stabilized. Since the size of the Cl^- ion is much smaller than that of ClO_4^-, the lattice may become unstable if the counter ions are changed from ClO_4^- to Cl^-. These facts suggest that the formation of this series of Ln–Cu–NTA complexes is influenced by both Cl^- and ClO_4^-.

3.3. Structural diversity and dimensional change

As all the complexes were synthesized with the same procedure (except for **4′**) except for the use of different starting materials, $Ln(ClO_4)_3$ and $LnCl_3$, the different crystal structures obtained provide a fair assessment of the critical influence of lanthanide contraction. La has the largest ionic radius among all lanthanides. This makes it possible for La^{3+} to be connected to three Cu ions from three different directions through three *anti–*

Table 4
Selected bond lengths (Å) and angles (°) for **8** (Ln=Er) and **11** (Ln=Y)

	8	11
Bond lengths		
Ln–O6A	2.2608(12)	2.2715(12)
Ln–O2	2.2826(10)	2.2868(11)
Ln–O12	2.3212(13)	2.3344(13)
Ln–O10	2.3535(17)	2.3725(16)
Ln–O11	2.3581(14)	2.3684(14)
Ln–O9	2.3674(15)	2.3727(15)
Ln–O8	2.3681(14)	2.3713(14)
Ln–O7	2.3939(14)	2.4072(14)
Cu–O1	1.9777(11)	1.9763(11)
Cu–O5	1.9787(11)	1.9833(12)
Cu–N	2.0323(11)	2.0348(12)
Cu–O3	2.2175(15)	2.2225(15)
Cu–Cl1	2.2412(4)	2.2407(4)
Bond angles		
O6A–Ln–O2	145.40(6)	145.56(6)
O6A–Ln–O12	95.44(5)	94.23(5)
O2–Ln–O12	103.03(4)	103.40(4)
O6A–Ln–O10	79.63(5)	79.93(5)
O2–Ln–O10	78.89(5)	77.86(5)
O12–Ln–O10	71.55(5)	71.94(5)
O6A–Ln–O11	92.93(5)	94.50(5)
O2–Ln–O11	88.44(5)	87.91(5)
O12–Ln–O11	145.04(6)	144.79(6)
O10–Ln–O11	143.41(6)	143.24(5)
O6A–Ln–O9	71.93(5)	71.89(5)
O2–Ln–O9	75.94(4)	76.53(5)
O12–Ln–O9	143.68(6)	143.74(6)
O10–Ln–O9	72.69(5)	72.69(5)
O11–Ln–O9	70.96(6)	71.07(6)
O6A–Ln–O8	73.42(6)	74.05(6)
O2–Ln–O8	139.02(6)	138.46(6)
O12–Ln–O8	76.98(5)	76.89(5)
O10–Ln–O8	135.93(5)	137.35(5)
O11–Ln–O8	73.06(5)	72.92(5)
O9–Ln–O8	127.72(4)	127.33(4)
O6A–Ln–O7	144.68(5)	144.88(5)
O2–Ln–O7	69.65(5)	69.45(5)
O12–Ln–O7	72.36(5)	72.33(5)
O10–Ln–O7	124.25(4)	123.26(4)
O11–Ln–O7	81.32(5)	81.11(5)
O9–Ln–O7	135.98(5)	136.44(5)
O8–Ln–O7	71.57(4)	71.35(5)
O1–Cu–O5	156.19(6)	156.37(6)
O1–Cu–N	82.74(4)	82.80(5)
O5–Cu–N	85.35(5)	85.35(5)
O1–Cu–O3	106.63(5)	106.78(5)
O5–Cu–O3	91.71(5)	91.42(5)
N–Cu–O3	81.09(5)	81.10(5)
O1–Cu–Cl1	95.98(3)	95.66(3)
O5–Cu–Cl1	95.73(3)	96.13(4)
N–Cu–Cl1	178.66(4)	178.46(4)
O3–Cu–Cl1	99.64(3)	99.26(4)

Symmetry transformations used to generate equivalent atoms: (A) $-x+1, -y-1, -z$.

anti carboxyl bridges of NTA ligands, forming a 2D honeycomb layer. The smaller ionic radii of Ce, Pr and Gd ions only allow them to be connected to two Cu ions from two directions through two carboxyl bridges, forming 1D zigzag chains. Owing to the fact that nine-coordinated ions of Ce, Pr and Gd are more stable than the eight-coordinated ones, one of the carboxyl bridges becomes a chelating bridge in order to satisfy the nine-coordination requirement. As Tb^{3+} and Dy^{3+} are smaller than Ce^{3+}, Pr^{3+} and Gd^{3+}, the length of the chelating bridges in complexes **5** and **6** should be shorter than that in **2**, **3** and **4**. In order to make the chain stable, in **5** and **6** longer carboxyl bridges (*anti–anti bridges*) replace the shorter bridges (*syn–anti* bridges) in **2**, **3** and **4,** and the crystal system changes from monoclinic to triclinic. A point should be made that because of the medium ionic radius of Gd, it might yield either monoclinic or triclinic crystals subject to the concentration of Cl^-. The heavy lanthanides, Ho, Er, Tm, Lu and Y, have the smallest ion radii and higher stability with eight-coordinated ions than with nine-coordinated ones. In this case, chelating bridges are no longer necessary and the carboxyl bridges in complexes **7**–**11** are both μ_2 bridges (*anti–anti* and *syn–anti*).

From the above discussion, it is obvious that various coordination modes of carboxyl groups in NTA, caused by lanthanide contraction, give rise to the diverse structures of the Ln–Cu–NTA complexes. In another word, the structural diversity and dimensional change of the Ln–Cu–NTA complexes are controlled by lanthanide contraction. According to this regularity, it may be suitable to divide all lanthanides (including Y) into four groups according to the crystal structures of their resulting Ln–Cu–NTA complexes. La belongs to group 1, the complexes of which have a 2D layered structure, (orthorhombic $Pca2_1$). Ce to Gd, are in group 2, the complexes of which have a 1D chain structure, (monoclinic, $P2_1$). Gd to Dy, form group 3, and the complexes of which have a different type of 1D chain structure, (triclinic, $P\bar{1}$), form group 4. The lanthanides in groups 1–3 are all nine-coordinated. Gd could be assigned to either group 2 or group 3 because its radius is medium sized. Ho to Lu and Y form group 4, the complexes (a 1D chain structure, triclinic, $P\bar{1}$) where the lanthanides are all eight-coordinated.

3.4. Magnetic properties

The temperature dependence of the magnetic susceptibility in the temperature range 2–300 K at an applied field of 10 kOe (**1**, **3**) or 5 kOe (**4**, **5**, **8**) is shown in Fig. 4, where χ_M is the magnetic susceptibility per LnCu unit. The value of $\chi_M T$ is 0.4 $cm^3\ mol^{-1}$ K at 200 K for **1** and increases very slowly to a maximum of 0.47 $cm^3\ mol^{-1}$ K between 13 and 6 K, then decreases upon further cooling. Fitting the data to the Curie–Weiss law gave $C = 0.398$ $cm^3\ mol^{-1}$ K and $\theta = 2.6$ K, indicative of weak ferromagnetic-like behavior. This might be considered as the result of frustration in the 2D triangular array of antiferromagnetic (AF) interacting copper ions

Table 5
Crystal cell parameters for the complexes **1**–**11** and **4′**

Complex	Colour	Crystal system	*a* (Å)	*b* (Å)	*c* (Å)	*α* (°)	*β* (°)	*γ* (°)
[LaCu]	blue	orthorhombic	15.975	9.298	12.726	90	90	90
[CeCu]	blue	monoclinic	8.212	12.846	9.467	90	100.94	90
[PrCu]	green	monoclinic	8.209	12.824	9.455	90	101.07	90
α-[GdCu] [a]	blue	monoclinic	8.148	12.728	9.396	90	101.08	90
β-[GdCu] [a]	blue	triclinic	8.493	9.642	12.838	111.17	93.52	100.89
[TbCu]	blue	triclinic	8.492	9.628	12.838	111.25	93.48	100.93
[DyCu]	blue	triclinic	8.482	9.601	12.838	111.35	93.54	100.87
[HoCu]	green	triclinic	9.504	10.560	12.774	89.15	70.93	65.23
[ErCu]	blue	triclinic	9.501	10.563	12.781	89.18	70.92	64.95
[TmCu]	blue	triclinic	9.500	10.560	12.737	89.02	70.99	65.04
[LuCu]	blue	triclinic	9.500	10.539	12.721	88.81	70.97	64.85
[YCu]	blue	triclinic	9.513	10.584	12.786	89.20	70.96	65.20

[a] α-[GdCu] is the complex **4**, β-[GdCu] is complex **4′**.

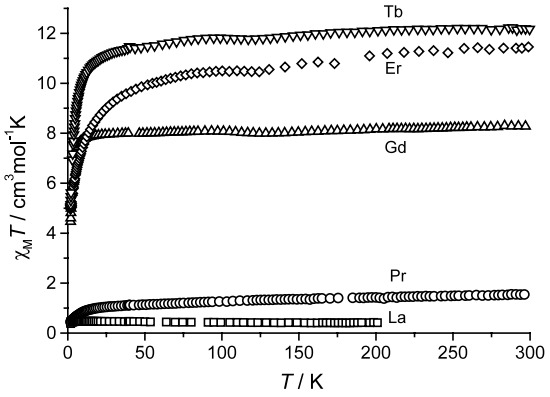


Fig. 4. Temperature dependence of magnetic susceptibility for complexes **1**, **3**, **4**, **8**.

[12(a)]. For other 1D chain compounds **3**, **4**, **5**, **8**, the $\chi_M T$ values are 1.98, 8.28, 12.17, and 11.46 cm^3 mol^{-1} K at 300 K, respectively, which are consistent with the values of 1.87, 8.25, 12.19, 11.87 cm^3 mol^{-1} K, expected for one spin only Cu^{2+} ion and one trivalent rare-earth ion with its *J* quantum number. The $\chi_M T$ of **4** keeps almost a constant above 20 K and decreases remarkably below 10 K, indicating a weak antiferromagnetic coupling between Gd–Cu and/or Gd–Gd at low temperature. The temperature dependence of $\chi_M T$ for **3**, **5**, **8** shows a similar feature: $\chi_M T$ decreases upon cooling, the lower the temperature, the quicker the decrease of $\chi_M T$. The reduction of $\chi_M T$ at low temperature, should mainly arise from the crystal field splitting of Ln^{3+} (here, Pr, Tb, Er) ions, and combine the contribution of the overall antiferromagnetic interactions among the metal ions. However, the nature of the interactions between Ln^{3+} and Cu^{2+} cannot be extracted due to the complication of the system.

As observed in the weak AF interacting 2D LaCu compound **1** [12(a)], field dependent magnetic relaxation was also observed in other 1D LnCu complexes, such as **3** and **4**, shown in Fig. 5. When a dc field (10 kOe for **3**, 5

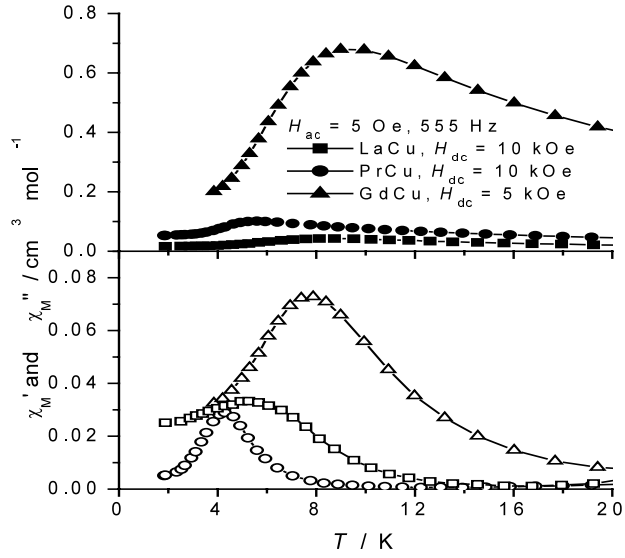


Fig. 5. Temperature dependence of ac magnetic susceptibility for complexes **1**, **3**, **4**, measured at 10 kOe (**1**, **3**) or 5 kOe (**4**) dc field, with 5 Oe, 555 Hz ac field.

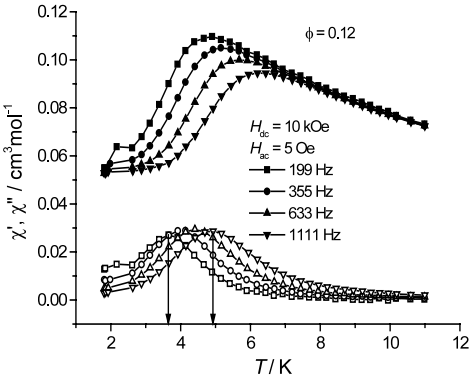


Fig. 6. Temperature dependence of ac magnetic susceptibility for complex **3**, measured at 10 kOe dc field, with 5 Oe ac field at different frequencies (199–1111 Hz).

kOe for **4**) was applied, maxima for ac susceptibility χ' and χ'' are observed, with different peak temperatures (Tp) dependent on the different lanthanide ions. The ac susceptibility is strongly frequency dependent as shown in Fig. 6 for **3**. If we calculate the value of the relative variation of Tp per decade of frequency, $\phi = \Delta T\text{p}/[T\text{p}\Delta(\log f)] = 0.12$, which is distinctly different from the behavior of normal spin glasses ($\phi < 0.1$), and smaller than 1.2 in 2D LaCu (**1**).

The antiferromagnetic (AF) interactions of triangularly arranged metal ions (including inter-chain) should give to rise a spin frustration, which may result in the unusual magnetic relaxation observed in **1**, **3**, and **4**. Similar phenomenon was also observed in other coordination polymers [17].

4. Supplementary material

Supplementary data are available from the CCDC, 12 Union Road, Cambridge CB2 1EZ, UK (fax: +44-1223-336033; e-mail: deposit@ccdc.cam.ac.uk or www: http://www.ccdc.cam.ac.uk) on request, quoting the deposition numbers: $LaCuC_6H_{20}NCl_2O_{17}$ 182/1730, α-$GdCuC_6H_{20}NCl_2O_{17}$ 168442, β-$GdCuC_6H_{20}NCl_2O_{17}$ 168937, $ErCuC_6H_{24}NCl_2O_{19}$ 168441.

Acknowledgements

This work is supported by the National Natural Science Foundation of China (No. 20125104, 29831010), National Key Project for Fundamental Research (G1998061305), and the Excellent Young Teachers Fund of MOE, P.R.C.

References

[1] A. Bencini, C. Benelli, A. Caneschi, R.L. Carlin, A. Dei, D. Gatteschi, J. Am. Chem. Soc. 107 (1985) 8128.
[2] A. Bencini, C. Benelli, A. Caneschi, A. Dei, D. Gatteschi, Inorg. Chem. 25 (1986) 572.
[3] C. Benelli, A. Caneschi, D. Gatteschi, O. Guillou, L. Pardi, Inorg. Chem. 29 (1990) 1750.
[4] M. Andruh, I. Ramade, E. Codjovi, O. Guillou, O. Kahn, C. Trombe, J. Am. Chem. Soc. 115 (1993) 1182.
[5] L. Pan, X.Y. Huang, J. Li, Y.G. Wu, N.W. Zheng, Angew. Chem., Int. Ed. Commun. 39 (3) (2000) 527.
[6] O. Guillou, O. Kahn, R.L. Oushoorn, Inorg. Chim. Acta 200 (1992) 119.
[7] (a) X.M. Chen, S.M.J. Aubin, Y.L. Wu, Y.S. Yang, T.C.W. Mak, D.N. Hendrickson, J. Am. Chem. Soc. 117 (37) (1995) 9600;
(b) X.M. Chen, Y.L. Wu, R.J. Wang, Sci. Chin. Ser. B-Chem. 39 (5) (1996) 536;
(c) X.M. Chen, Y.L. Wu, Y.X. Tong, X.Y. Huang, J. Chem. Soc., Dalton Trans (1996) 2443.
[8] Q.D. Liu, S. Gao, J.R. Li, Q.Z. Zhou, K.B. Yu, B.Q. Ma, S.W. Zhang, X.X. Zhang, T.Z. Jin, Inorg. Chem. 39 (2000) 2488.
[9] L.L. Martin, R.A. Jacobson, Inorg. Chem. 11 (1972) 2785.
[10] L.L. Martin, R.A. Jacobson, Inorg. Chem. 11 (1972) 2789.
[11] Y. Chen, B.Q. Ma, Q.D. Liu, J.R. Li, S. Gao, Inorg. Chem. Commun. 3 (2000) 319.
[12] (a) Q.D. Liu, J.R. Li, S. Gao, B.Q. Ma, Q.Z. Zhou, K.B. Yu H. Liu, J. Chem. Soc., Chem. Commun. (2000) 1685;
(b) Q.D. Liu, J.R. Li, B.Q. Ma, S. Gao, Q.Z. Zhou, K.B. Yu, J. Rare Earths 18 (3) (2000) 161.
[13] R.Y. Wang, Z.P. Zheng, T.Z. Jin, R.J. Staples, Angew. Chem., Int. Ed. 38 (1999) 1813.
[14] R.Y. Wang, M.D. Carducci, Z.P. Zheng, Inorg. Chem. 39 (2000) 1836.
[15] D.S. Zhang, B.Q. Ma, T.Z. Jin, S. Gao, C.H. Yan, T.C.W. Mak, New J. Chem. 24 (2000) 61.
[16] SHELXTL Version 5 Reference Manual; Siemens Industrial Automation, Inc., Madison, WI, 1994.
[17] (a) S. Gao, G. Su, T. Yi, B.Q. Ma, Phys. Rev. B 63 (5) (2001) 054431;
(b) B.Q. Ma, S. Gao, G. Su, G.X. Xu, Angew. Chem. Int. Ed. 40 (2001) 434.

PERGAMON

Polyhedron 21 (2002) 1105–1115

POLYHEDRON

www.elsevier.com/locate/poly

^{1}H, ^{13}C and ^{29}Si NMR study of acetylide and parallel alkyne substituted Ru_3 and Os_3 clusters derived from HC≡CR (R = $SiMe_3$, $SiPh_3$ and CMe_3). X-ray crystallographic study of [(μ-H)$M_3(CO)_9$(CCR)] (M = Ru, R = $SiMe_3$, $SiPh_3$; M = Os, R = $SiPh_3$, CMe_3) and [Ru_3(μ-CO)$(CO)_9$(HCCR)] (R = CMe_3)

Francisco J. Zuno-Cruz, Ana L. Carrasco, María J. Rosales-Hoz *

Departamento de Química, Centro de Investigación y de Estudios Avanzados del I. P. N. Apdo Postal 14-740, 07000 Mexico, D.F. Mexico

Received 1 November 2001; accepted 25 February 2002

Abstract

A series of alkyne parallel μ_3-η_2-(//) substituted trinuclear cluster derivatives has been synthesized, containing the alkynes (HC≡CR, R = $SiMe_3$, $SiPh_3$ and *t*Bu) coordinated to Ru_3 and Os_3 units and then converted into the corresponding chemically related acetylide derivatives. A ^{1}H, ^{13}C and ^{29}Si NMR study was carried out for all the complexes and the results are also analyzed in comparison with results of Extended Hückel Molecular Orbital calculations carried out on the complexes and the free alkynes. In the acetylide derivatives, ^{13}C–^{1}H and ^{187}Os–^{1}H couplings involving the hydride, were measured. The ^{13}C–^{29}Si couplings for all the derivatives which contain silicon shows the changes in hybridization of the C_β. The structures of [(μ-H)$Ru_3(CO)_9$(CCR)] (R = $SiMe_3$ and $SiPh_3$) and [(μ-H)$Os_3(CO)_9$(CCR)] (R = $SiPh_3$ and CMe_3) and [$Ru_3(CO)_{10}$(HCCR)] (R = CMe_3) were determined by single crystal X-ray diffraction methods. © 2002 Elsevier Science Ltd. All rights reserved.

Keywords: Ruthenium; Osmium; Acetylide; Alkyne; Clusters

1. Introduction

The reactions of alkynes with trinuclear metal clusters have been extensively studied [1–10]. The two main coordination modes that have been observed, a parallel μ_3-η^2-(//) and a perpendicular μ_3-η^2-(⊥), have been shown to be dependent on the electron count found in the complex. Thus, the perpendicular mode is found in 46-electron clusters while the parallel one is observed to be present in 48-electron clusters [5–8]. In the case of parallel compounds, [$M_3(CO)_{10}$(μ_3-η^2-(//)-HCCR)] (M = Ru and Os), containing terminal alkynes, these transform into the corresponding acetylide derivatives [$HM_3(CO)_9$(μ_3-η^2-(⊥)-CCR)], (Fig. 1), through the cleavage of the C–H bond, rapidly in the case of ruthenium, more slowly in the osmium compounds [9,11].

The ^{13}C and ^{1}H NMR spectroscopy have been shown to be powerful methods for the assignment of coordination modes for hydrocarbyls [12], but the low natural abundance of the C-13 nuclei combined with the long relaxation times of the coordinated carbon atoms, has limited the studies of coordinated alkynes to cluster units, in particular those reported in the 1970s and early 1980s. Not much information is available on ^{13}C shifts of alkynes or acetylides bonded to trinuclear units [13]. These values could also help to obtain further values of $\delta(C_\alpha)+\delta(C_\beta)$ and $\delta(C_\alpha)-\delta(C_\beta)$, which have been proposed to be related to the total charge alteration in the C≡C triple bond and the polarization of that bond, respectively [14]. More values could also be used to try to evaluate the effect of coordination modes, metal atoms and substituted groups on these values and from there obtain a larger understanding of the reactivity of these systems. The study of shifts and coupling con-

* Corresponding author. Tel.: +52-5-747-3716; fax: +52-5-747-7113.

E-mail address: mrosales@mail.cinvestav.mx (M.J. Rosales-Hoz).

0277-5387/02/$ - see front matter © 2002 Elsevier Science Ltd. All rights reserved.
PII: S0277-5387(02)00932-4

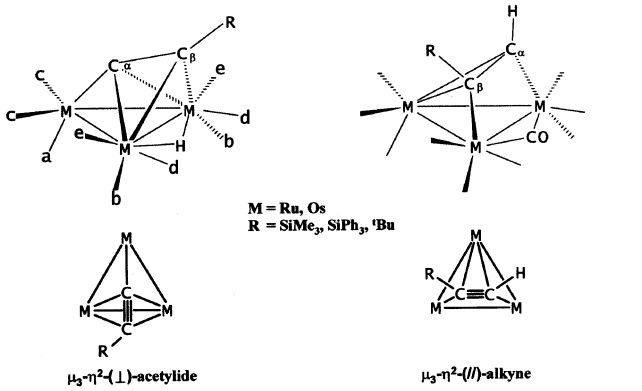


Fig. 1. Structures of the μ_3-η^2-(⊥)-acetylide and μ_3-η^2-(//)-alkyne trinuclear cluster compounds. The carbonyl assignment for compounds **1**–**6** is shown in the acetylide derivative.

stants of the alkyne substituents could also help to determine whether these substituents are affected by the differences in coordination modes.

In an effort to expand the available information on these systems, ^{1}H, ^{13}C and ^{29}Si NMR studies were carried out on both (//)-[$M_3(CO)_{10}(\mu_3$-η^2-HCCR)] and [(μ-H)$M_3(CO)_9(\mu_3$-η^2-CCR)] systems where M = Ru and Os and R = $SiMe_3$, $SiPh_3$ and CMe_3. In the case of acetylide derivatives, ^{13}C–^{1}H of the hydride hydrogen atom and some of the carbonyl groups were also obtained as well as ^{187}Os–^{1}H coupling constants. In the acetylide derivatives, ^{13}C–^{1}H coupling constants for the hydride–acetylide fragment were also measured and ^{1}H–^{13}C couplings between the hydride and some of the carbonyl groups could also be measured. ^{13}C–^{29}Si couplings were obtained in order to attain more information on the changes within the ligand upon coordination to the cluster. EHMO calculations on the 12 compounds were also carried out in order to see whether there is a relationship between calculated charges and experimental NMR chemical shifts. Crystal structures of [$HRu_3(CO)_9$(CCR)] (R = $SiMe_3$ and $SiPh_3$), [$HOs_3(CO)_9$(CCR) (R = $SiPh_3$ and CMe_3) and [$Ru_3(CO)_{10}$(HCCR)] (R = CMe_3) were also obtained and compared with those already described in the literature. Results of these studies are described herein.

2. Results and discussion

2.1. Synthesis

The reactions of terminal alkynes with trinuclear ruthenium and osmium clusters often lead to hydrogen transfer to the metal core and formation of acetylide groups [15]. However, the stabilization of osmium systems containing terminal alkynes coordinated in a (//) mode is possible and seems to be preferred over that of the corresponding ruthenium systems. The (//)-Os_3 systems can then be transformed into the corresponding acetylide derivatives. Very few reports have been published [10,16] of the (//) coordination mode in Ru_3 compounds, in spite of the extensive chemistry carried out on the chemically related acetylide compounds [16]. These few (//)-Ru_3 complexes reported have been usually prepared through the reaction of the activated complex [$Ru_3(CO)_{10}(MeCN)_2$] which permits the preparation of a variety of substituted compounds under mild conditions [17].

Since the synthesis of the acetylide –Ru_3 complexes has been described, reactions of [$Ru_3(CO)_{12}$] with other terminal alkynes HC≡CR (R = $SiMe_3$ and $SiPh_3$), were carried out following the method reported [18] to produce [(μ-H)$Ru_3(CO)_9(\mu_3$-η^2-CCR)] (R = $SiMe_3$, compound **1**, R = $SiPh_3$, compound **2** and R = CMe_3, compound **3**). The corresponding osmium compounds [(μ-H)$Os_3(CO)_9(\mu_3$-η^2-CCR)] (R = $SiMe_3$, compound **4**, R = $SiPh_3$, compound **5** and R = CMe_3, compound **6**), were obtained by heating octane solutions of the parallel derivatives [$Os_3(CO)_{10}$(HCCR)] (compounds **10** [9], **11** and **12**, respectively) prepared by the reaction of [$Os_3(CO)_{10}(MeCN)_2$] with the corresponding alkyne.

As reported [10] for parallel alkyne Ru_3 compounds, the reaction of HC≡CR (R = $SiMe_3$, $SiPh_3$ or ^{t}Bu) with [$Ru_3(CO)_{10}(MeCN)_2$], prepared in situ, yielded [$Ru_3(CO)_{10}$(HCCR)], the (//)-derivatives with R = $SiMe_3$, compound **7**, R = $SiPh_3$, compound **8** and R = ^{t}Bu, compound **9**, which slowly transformed into the acetylide compounds. As an example, the $SiMe_3$ derivative changed from the (//) compound to the acetylide, in 1 h of leaving the solid standing at room temperature in the presence of light. In the dark and at low temperature (−20 °C) the conversion is much slower.

All 12 compounds were characterized by infrared and ^{1}H and ^{13}C NMR spectroscopic methods and ^{29}Si NMR in the case of compounds, which contain silicon groups. Results are given in Tables 1–4. Data on compounds already described (Compounds **3** [18], **4** [9], and **10** [9]) agree with those reported.

As expected, very little difference is observed in the frequency values for the terminal CO stretching bands when moving from one substituent to the other or from one coordination mode to the other. Larger differences are observed in the NMR results, and as observed in other systems [13], ^{13}C chemical shifts for similar compounds appear at higher fields in osmium complexes than in ruthenium ones.

2.2. NMR data for acetylide derivatives (compounds 1–6)

The ^{1}H NMR spectra of compounds **1**–**6** show the presence of a hydride group. Chemical shifts for these hydrides are very similar. Compounds **4**, **5** and **6** show

Table 1
Infrared spectra for **1**–**12**

	Color	IR [a] ν(CO) (cm^{-1})
1	yellow	2096(w), 2070(s), 2054(s), 2022(vs), 1999(vw,sh), 1990(m), 1958(vw)
2	yellow	2098(w), 2072(s), 2054(s), 2022(vs), 1997(vw,sh), 1990(m), 1958(vw)
3	yellow–orange	2096(w), 2068(s), 2052(s), 2024(vs), 2018(sh), 1998(vw,sh), 1990(m), 1958(vw)
4	pale yellow	2100(w), 2074(s), 2052(s), 2020(vs), 2010(s), 1992(vw,sh), 1982(m), 1948(vw)
5	white	2100(w), 2076(s), 2052(s), 2020(vs), 1993(vw,sh), 1980(m), 1948(vw)
6	pale yellow	2100(w), 2072(s), 2052(s), 2020(vs), 2010(s), 1991(vw,sh), 1982(m), 1948(vw)
7	red–orange	2110(vw), 2096(w), 2070(s), 2054(vs), 2022(vs), 2010(s), 1990(m), 1886(w,br)
8	red–orange	2112(vw), 2096(w), 2072(s), 2054(vs), 2028(vs), 2012(s), 1990(m), 1882(w,br)
9	red–orange	2111(vw), 2096(w), 2068(s), 2056(vs), 2052(vs), 2028(vs), 2006(s), 1990(m,sh), 1882(w,br)
10	orange	2098(w), 2074(w,sh), 2058(vs), 2022(s), 2008(m), 1998(m), 1982(w), 1852(w,br)
11	orange	2098(w), 2076(w,sh), 2062(vs), 2054(vs), 2024(s), 2006(m), 2000(m), 1982(w), 1854(w,br)
12	orange	2098(w), 2074(w,sh), 2060(vs), 2052(vs), 2022(s), 2006(m), 1982(w), 1849(w,br)

(vs) Very strong, (s) strong, (m) medium, (w) weak, (vw) very weak, (br) broad, (sh) shoulder.
[a] Hexane.

the presence of satellites due to $^{187}Os-^{1}H$ couplings with J values of 32.5 (compounds **4** and **6**) and 32.6 (compound **5**) Hz. These values are in the same range than those observed in other μ_2-hydride groups [19,20].

^{13}C NMR spectra show that, as reported [13], the chemical shift for C_α is found downfield from that of C_β. This assignment was confirmed in compound **1** by the observation of one bond $^{13}C-^{29}Si$ coupling for C_β while ^{29}Si spectra of **2**, **4** and **5**, showed ^{13}C satellites due to coupling with C_β (a polarization transfer experiment from the methyl group to C_β was carried out in order to augment the C_β signal). Shifts for both C_α and C_β appear in the range reported by Carty and coworkers [13] for this type of acetylide although the value for C_α of compounds **3** and **6** (^{t}Bu derivatives) is observed to be at higher fields than those of the silyl substituted alkynes while the trend for C_β is the opposite one. Furthermore, there are larger differences in chemical shifts of the carbon atoms on going from the free alkyne to the coordinated ones in the ^{t}Bu-acetylene than in the SiR_3 compounds. A much larger separation between C_α and C_β is observed in the silyl substituted compounds than in those containing ^{t}Bu as substituent. In fact the difference in the silyl compounds is larger than that reported for other acetylide compounds [21].

$^{13}C-^{1}H$ couplings with the hydride can be observed for both carbon atoms in some of the compounds. The coupling with C_α is larger than with C_β. In some of the signals due to the carbonyl groups, couplings with the hydride can also be observed. The different types of carbonyl groups in compounds **1**, **2**, **4**, **5** and **6**, were assigned by comparison with those that have been reported for compound **3** [22] as it is shown in Fig. 1. The couplings with the hydride support the assignments since only the carbonyls near the hydride (two bonds),

Table 3
^{29}Si NMR data for **1**–**11**

	^{29}Si δ (ppm)	$^{1}J_{^{13}C-^{29}Si}$ (Hz)	$^{1}\Delta(^{13}C/^{12}C)-^{29}Si$ (ppb)
1	1.2 (s) [a]	64.0 (C_β)	−10.9
2	−13.8 (s) [a]	55.6 (CH_3)	−2.4
4	5.3 (s) [a]	71.7 (C_β)	−25.9
5	−11.4 (s) [a]	63.2 (C_β)	−7.8
7	3.8 (s) [b,c]	55.3 (CH_3)	−1.2
8	−7.7 (s) [b,c]	73.2 (C_β)	−18.4
10	11.7 (s) [b]	65.5 (C_β)	−6.9
11	−0.7 (s) [b]	53.7 (CH_3)	−2.6
		70.5 (C_β)	−18.8
		64.5 (C_β)	−5.5
		53.4 (CH_3)	−1.3
		72.2 (C_β)	−11.4

$CDCl_3$. (s) singlet. Negative values of $^{1}\Delta$ are high field isotope shifts.
[a] Recorded at 53.674 MHz.
[b] Recorded at 79.426 MHz.
[c] Recorded at 243 K.

Table 2
^{1}H NMR data for **1**–**12**

	^{1}H δ (ppm)	$^{1}J_{^{187}Os-^{1}H}$ [$^{2}J_{^{13}C-^{1}H}$] {$^{1}\Delta(^{13}C/^{12}C)-^{1}H$}		^{1}H δ (ppm)
1	0.36 (s) (CH_3); −21.16 (s) (Ru–H–Ru) [a]		**7**	9.18 (s) (CH); 0.04 (s) (CH_3) [a,c]
2	7.74 (m), 7.45 (m) (Ph); −21.08 (s) (Ru–H–Ru) [a]		**8**	8.95 (s) (CH); 7.70 (m), 7.45 (m) (Ph) [a,c]
3	1.40 (s) (CH_3); −21.06 (s) (Ru–H–Ru) [a]		**9**	8.31 (s) (CH); 1.01 (s) (CH_3) [a,c]
4	0.39 (s) (CH_3); −23.70 (s) (Os–H–Os) [b]	32.5 [12.0] (COe) {+1.8}	**10**	10.56 (s) (CH); 0.07 (s) (CH_3) [b]
5	7.74 (m), 7.45 (m) (Ph); −23.44 (s) (Os–H–Os) [b]	32.6 [12.3] (COe) {+1.7}; [3.5] (Cob,d) {−1.7}	**11**	10.32 (s) (CH); 7.68 (m), 7.44 (m) (Ph) [b]
6	1.44 (s) (CH_3); −23.61 (s) (Os–H–Os) [b]	32.5 [12.2] (COe) {+1.5}	**12**	9.63 (s) (CH); 1.02 (s) (CH_3) [b]

$CDCl_3$. J (Hz), Δ (ppb).(s) singlet, (m) multiplet. Negative values of $^{1}\Delta$ are high field isotope shifts.
[a] Recorded at 399.778 MHz.
[b] Recorded at 300.130 MHz.
[c] Recorded at 243 K.

Table 4
^{13}C NMR data for **1**–**12**

	$^{13}C\{^1H\}$ δ (ppm)	$^{13}C-^1H$ [b] $\{^1J_{^{13}C-^1H}\}$ $[^2J_{^{13}C-^1H}]$	$[C_\alpha+C_\beta]$ $\{C_\alpha-C_\beta\}$
1	199.6 (s) (COa) [a]	(d) [3.8]	[254.3]
	197.6 (s) (COb) [a]		
	192.8 (s) (COc) [a]	(d) [3.8]	{107.2}
	189.1 (s) (COd) [a]	(d) [13.8]	
	188.0 (s) (COe) [a]	(d) [2.4]	
	180.6 (s) (C_α) [a]	(d) [1.6]	
	73.7 (s) (C_β) [a]	(q) {119.9}	
	1.4 (s) (CH_3) [a]		
2	199.5 (s) (COa) [a]		
	197.4 (s) (COb) [a]	(d) [3.8]	[253.9]
	192.7 (s) (COc) [a]		
	188.3 (s) (COd) [a]	(d) [3.8]	{114.7}
	187.7 (s) (COe) [a]	(d) [14.1]	
	184.3 (s) (C_α) [a]	(d) [1.9]	
	69.6 (s) (C_β) [a]	(d) [1.7]	
	135.9 (s) (C*o*),		
	133.2 (s) (*Ci*) [a]		
	130.5 (s) (C*p*),		
	128.3 (s) (C*m*) [a]		
3	199.0 (s) (COa) [a]		
	197.3 (s) (COb) [a]	(d) [3.6]	[278.2]
	193.1 (br), (COc) [a]		
	189.5 (s) (COd) [a]	(d) [3.6]	{56.4}
	188.5 (s) (COe) [a]	(d) [13.9]	
	167.3 (s) (C_α) [a]	(d) [2.1]	
	110.9 (s) (C_β) [a]	(d) [1.7]	
	35.5 (s) (C^tBu) [a]	(o) [3.8]	
	34.3 (s) (CH_3) [a]	(q) {127.1}	
4	173.6 (br) (COa,c) [b]		
	172.5 (s) (COb) [b]	(d) [3.4]	[193.1]
	169.5 (s), (COd) [b]	(d) [3.4]	
	162.5 (s) (COe) [b]	(d) [12.0]	{95.5}
	144.3 (s) (C_α) [b]	(d) [1.6]	
	48.8 (s) (C_β) [b]	(br)	
	1.6 (s) (CH_3) [b]	(q) {120.0}	
5	173.8 (br) (COa,c) [b]		
	172.3 (s) (COb) [b]	(d) [3.5]	[194.1]
	169.4 (s) (COd) [b]	(d) [3.5]	
	162.5 (s) (COe) [b]	(d) [12.3]	{102.9}
	148.5 (s) (C_α) [b]	(d) [1.5]	
	45.6 (s) (C_β) [b]	(br)	
	136.6 (s) (C*o*),		
	133.6 (s) (*Ci*) [b]		
	130.9 (s) (C*p*),		
	128.7 (s) (C*m*) [b]		
6	174.2 (br) (COa,c) [b]		
	172.4 (s) (COb) [b]	(d) [3.5]	[224.5]
	170.4 (s) (COd) [b]	(d) [3.5]	
	163.7 (s) (COe) [b]	(d) [12.2]	{47.1}
	135.8 (s) (C_α) [b]	(d) [1.6]	
	88.7 (s) (C_β) [b]	(br)	
	35.6 (s) (C^tBu) [b]	(o) [4.1]	
	34.5 (s) (CH_3)	(q) {127.0}	
7	199.2 (s) (CO) [a,c]		
	193.0 (s) (CO) [a,c]		[324.2]
	189.5 (s) (CO) [a,c]		
	164.6 (s) (C) [a,c]	(d) [4.4]	{−5.0}
	159.6 (s) (CH) [a,c]	(d) {159.9}	
	0.1 (s) (CH_3) [a,c]	(q) {119.1}	
8	201.7 (s) (CO) [a,c]		
	194.4 (s) (CO) [a,c]		[320.6]
	189.7 (s) (CO) [a,c]		
	165.6 (s) (CH) [a,c]	(d) {161.4}	{10.6}
	155.0 (s) (C) [a,c]	(d) [2.3]	
	136.4 (s) (C*o*),		
	135.6 (s) (C*o*) [a,c]		
	133.5 (s) (C*i*),		
	132.6 (s) (C*i*) [a,c]		
	130.4 (s) (C*p*),		
	130.2 (s) (C*p*) [a,c]		
	128.3 (s) (C*m*),		
	128.2 (s) (C*m*) [a,c]		
9	201.5 (s) (CO) [a,c]		
	195.2 (s) (CO) [a,c]		[329.9]
	189.9 (s) (CO) [a,c]		
	193.4 (s) (C) [a,c]	(d) [4.6]	{−56.9}
	136.5 (s) (CH) [a,c]	(d) {158.4}	
	44.1 (s)(C^tBu) [a,c]	(o) [3.1]	
	32.5 (s) (CH_3) [a,c]	(q) {126.1}	
10	176.2 (br)(CO) [b]		
	139.4 (s) (C) [b]	(d) [4.6]	[277.6]
	138.2 (s) (CH) [b]	(d) {156.2}	
	0.2 (s) (CH_3) [b]	(q) {119.2}	{−1.2}
11	176.0 (br) (CO) [b]		
	144.2 (s) (CH) [b]	(d) {159.0}	[275.5]
	131.3 (s) (C) [b]	(d) [2.3]	
	136.7 (s) (C*o*),		{12.9}
	135.4 (s) (C*o*) [b]		
	133.9 (s) (C*i*),		
	133.2 (s) (C*i*) [b]		
	130.6 (s) (C*p*),		
	128.5 (s) (C*m*) [b]		
12	175.7 (br) (CO) [b]		
	180.2 (s) (C) [b]	(d) [4.5]	[292.8]
	112.6 (s) (CH) [b]	(d) {157.5}	
	46.4 (s) (C^tBu) [b]	(o) [3.6]	{−67.6}
	32.5 (s) (CH_3) [b]	(q) {126.0}	

$CDCl_3$. *J* (Hz), Δ (ppb). (s) singlet, (d) doublet, (q) quartet, (o) octet, (br) broad, *o* ortho, *p* para, *m* meta, *i* ipso.
[a] Recorded at 100.5354 MHz.
[b] Recorded at 75.4756 MHz.
[c] Recorded at 243 K.

couple with it. Couplings with COb, and COd show smaller magnitudes than couplings with COe. Therefore, different coupling constant values are explained by different H–M–C angles.

The chemical shift of the quaternary carbon of the ^tBu group show this to be slightly shifted downfield in the complexes with respect to the free alkyne. This trend is also observed in the ^{29}Si spectra.

$^{13}C-^{29}Si$ couplings can be observed in all the compounds. These ^1J values are smaller in the coordinated groups than in the free alkynes and, as expected, the C_β–Si coupling is more affected than the Si–CH_3 coupling. Even though it has been pointed out that a direct relationship between coupling constant values and s character in the bond must be used very cautiously [23]

when one of the atoms involved is large and polarizable, a rehybridization of C_β in compounds **1**–**6** must be expected and a larger sp^2 character seems logical. These is confirmed by the analysis of the values obtained, in free $HC{\equiv}CSiMe_3$ the value of the $^1J_{^{13}C-^{29}Si}$ between the carbon of the methyl group and the silicon atoms is 57 Hz while the coupling alkynic carbon–silicon is 82 Hz. The C_β–Si coupling constant value in compound **1**, 64 Hz, is intermediate between those two values. The same trend is observed in compounds **2**, **4** and **5**.

As can be appreciated in Fig. 2, from the ^{29}Si spectra it was possible to obtain the $^{13}C/^{12}C$ isotope effects on the ^{29}Si chemical shift. Isotope induced shifts, $\Delta\delta^i$, over one bond, have been associated with changes in rotational and vibrational states of the bond under consideration [24,25]. Several studies of isotope effects on different nuclei have been published [26,27], but to our knowledge, nothing has been reported of these type of effects in cluster compounds. This lack of data precludes a more detailed analysis of trends. However, it can be observed that the isotope effect in the compounds reported here, decreases on going from the free ligand to the complexes, and with osmium complexes showing smaller absolute values than ruthenium ones as a consequence of the larger mass of the former.

2.3. NMR data for parallel alkyne derivatives (compounds 7–12)

Proton NMR spectroscopy shows that the chemical shifts for the CH group, move significantly downfield in the coordinated (//) complexes in comparison with the shifts observed in the free ligands. $^{13}C-^1H$ coupling constants of this same group, are much lower on going from the free alkyne to the (//) complex but are very similar in the six complexes. This behavior reflects the rehybridization suffered by the carbon atoms of the alkyne. A similar trend had been previously observed in acetylene-clusters [10,23].

^{13}C NMR of the six compounds show these do not follow a regular trend in the relative position of the carbon atoms of the coordinated alkynes. Depending on the metal and the substituent, their chemical shifts change. Thus, while chemical shift for the carbon of the CH group moves to lower fields in the order ^{t}Bu > $SiMe_3$ > $SiPh_3$; shifts for the CR groups follow the order $SiPh_3$ > $SiMe_3$ > ^{t}Bu, with this last complex being found at much lower fields than the other two. This effect must be a reflection of the higher electronegativity of the ^{t}Bu group.

The quaternary carbon of the ^{t}Bu group also moves downfield on going from the free acetylene to the complexes. The same effect is observed in the ^{29}Si chemical shift of the silyl derivatives. $^1J_{^{13}C-^{29}Si}$ values for compounds **7**, **8**, **10** and **11** range between 64 and 72 Hz. $^{13}C/^{12}C$ isotope effects on the ^{29}Si chemical shift were also observed and follow the same trend observed in acetylide complexes.

The chemical shifts for C_α are found at low fields in both types of compounds, while C_β are shifted to much higher fields when going from the parallel coordination mode to the acetylides. The similarity of the $^{13}C-^{29}Si$

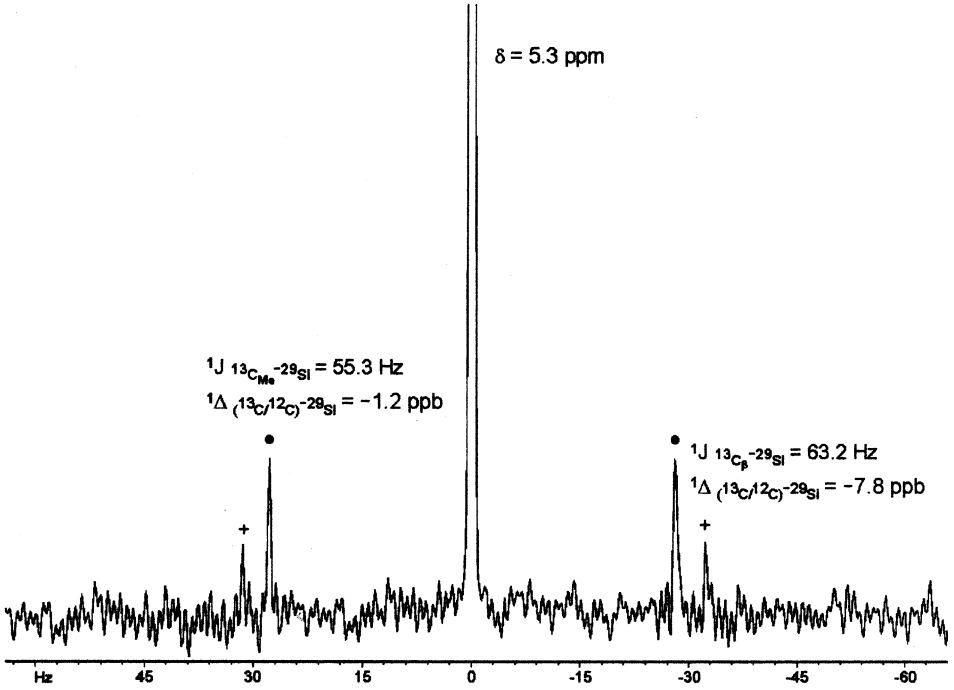


Fig. 2. NMR ^{29}Si spectra for **4**. Negative values are high field isotope shifts.

coupling constants suggests a similar hybridization for C_β.

Given the closely related coordination environment of the two carbon atoms in the alkyne moiety of the (//) systems, the $\Delta\delta$ of these two carbon atoms could be expected to be lower in the (//) systems than in the acetylide ones. Such is the case in the two silyl substituted alkynes both for ruthenium and osmium with $\Delta\delta$ values of around 10 ppm. In the ^{t}Bu derivatives the $\Delta\delta$ (in absolute value) is higher in the (//) derivative than in the acetylide, contrary to what was observed in the silyl compounds. If it is true that $\delta(C\alpha)-\delta(C\beta)$ is related to the polarizability of the CC bond, the $\Delta\delta =$ 67.6 ppm for compound **12**, would suggest that there is a larger polarizability of the CC bond in that complex than in the acetylide derivative, compound **6** ($\Delta\delta = 47.1$ ppm). No values above 100 ppm are observed in other derivatives [21], however, in the silyl acetylides these magnitudes are obtained, therefore, compounds **1** and **3** have the largest polarizability of all.

2.4. Theoretical calculations

In order to observe if the reactivity studies described and the NMR trends could be supported with the results of theoretical studies, EHMO calculations were carried out on the 12 complexes and the free alkynes. In the case of those compounds where crystal structure results were available, these were taken as a basis for the calculation. The (//)-complexes which have not been crystallographically characterized, were modeled taking the structure of $[Os_3(CO)_{10}(EtCCEt)]$ [28,29] as a basis.

CNDO theoretical calculations have been carried out in some (//) and ($\perp$) alkyne clusters [30] but no substituents were included in this calculation. Also, EHMO calculations have been reported previously [31] for several trimetal alkyne clusters including heterometallic derivatives, the results described show a good correlation with structures obtained experimentally. When the substituent of the C_β is a methyl group [32] a large difference in charge is described between Cα and Cβ with Cα showing a positive charge and Cβ a negative charge. In general, our results do not yield such differences in charge, (Fig. 3).

Granozzi and coworkers [32] report to have obtained positive charges on the ruthenium atoms, however, we obtain negative values for these. An opposite behavior is observed, in our results, for the osmium derivatives. It is worth noticing that protonation of compound **3**, has been described [33] to occur initially at the metal centers, therefore, a negative charge on the metal atoms makes this result more logical.

It is also interesting to notice that charge on the acetylenic carbon atoms is much more negative in the osmium compounds than in the ruthenium ones. Both in the free ligand and the osmium complexes, the substituted carbon atom (C_β) of the ^{t}Bu compounds, shows a less negative charge, also indicating a larger electronegativity of the ^{t}Bu group. In order to observe if protonation of the osmium acetylide complexes, showed any differences in reaction with protic acids, we carried out the reaction of these compounds with a large excess of trifluoroacetic acid and no reaction was observed to occur, even after 24 h of reaction. This result is thus consistent with the charge distribution obtained in our calculations.

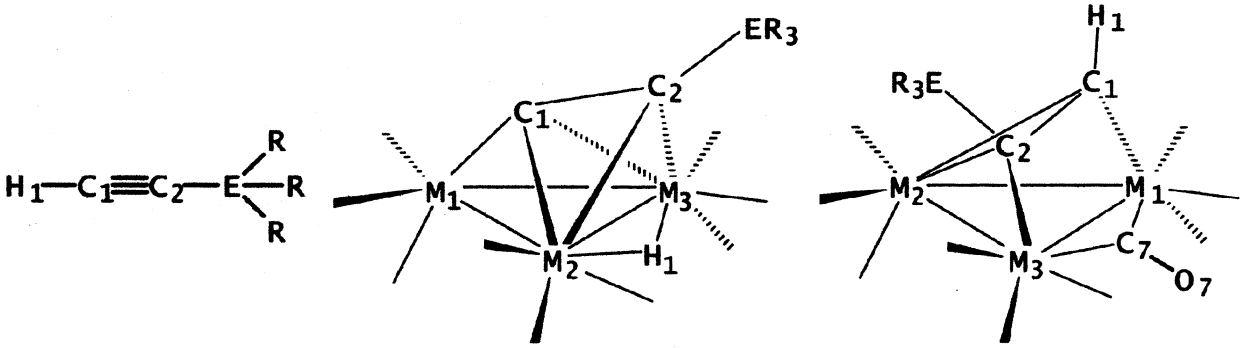
Frontier orbitals from the twelve complexes show that while the LUMO orbitals lie largely on the metal atoms in all cases, there are important differences in the position of the HOMO orbitals. Thus, in the ruthenium complexes, the HOMO orbitals are mainly found on the alkyne ligands. The $SiMe_3$ and ^{t}Bu derivatives have the HOMO situated on the acetylenic carbon atoms, while the $SiPh_3$ derivatives have them on the aromatic rings. In the case of the osmium compounds, the HOMO are also found on the metal atoms with the exception of compound **11** where it is again found on the aromatic rings. EHMO calculations of the free alkynes also show different behavior in the $SiPh_3$ compound where the HOMO orbital is found largely on the aromatic rings while in the other cases, at least part of it, is located on the hydrogen substituted carbon atom of the alkyne.

Osmium (//) complexes show both the HOMO and the LUMO to be lying on the metal atoms while in the (//) ruthenium complexes, the HOMO sit largely on the acetylenic moiety while the LUMO is found on the metal atoms. This might be related to the greater stability of the Os-parallel complexes since the rearrangement towards the acetylide compounds should take place more easily in the case of ruthenium.

In all cases, the HOMO orbitals of the (//) derivatives are observed to be at lower energy values than in the acetylide derivatives, more so in the ruthenium derivatives. The HOMO–LUMO gap is also smaller in the (//) complexes with larger gaps in the osmium complexes than in the ruthenium ones.

2.5. X-ray structures of compounds *1, 2, 5, 6 and 9*

In order to certify there were no important structural differences in the complexes, compounds **1**, **2**, **5**, **6** and **9** were studied by X-ray crystallography. Results are shown in Figs. 4–8 and in Table 5. No significant differences are observed in bond distances and angles in any of the compounds in comparison with the structures already described, compounds **3** [34] and **4** [9]. It is important that although the structure of compound **1** has been reported [35], the data given in this work are the result of the structural results we obtained. Structural details of compound **9** are similar to corresponding values in $[Ru_3(CO)_{10}(HCCH)]$ [11].



	M_1	M_2	M_3	C_1	C_2	E	H_1	C_7	O_7
$SiMe_3$	-	-	-	-0.019	-0.303	1.037	0.108	-	-
$SiPh_3$	-	-	-	-0.046	-0.296	0.954	0.108	-	-
^{t}Bu	-	-	-	-0.341	0.065	0.175	0.115	-	-
1	-1.783	-1.544	-1.537	0.359	0.005	1.141	-0.033	-	-
2	-1.838	-1.500	-1.543	0.336	0.014	0.957	-0.031	-	-
3	-1.847	-1.555	-1.448	0.286	0.282	0.184	-0.030	-	-
4	0.304	0.650	0.639	-0.338	-0.458	1.012	-0.313	-	-
5	0.219	0.691	0.447	-0.333	-0.442	0.919	-0.297	-	-
6	0.346	0.553	0.479	-0.439	-0.154	0.167	-0.315	-	-
7	-1.759	-1.500	-1.687	0.197	-0.064	1.117	0.073	1.039	-0.635
8	-1.781	-1.527	-1.703	0.212	-0.064	0.986	0.076	1.033	-0.639
9	-1754	-1.543	-1.728	0.121	0.244	0.157	0.077	1.034	-0.639
10	0.387	0.641	0.435	-0.320	-0.591	1.057	0.060	0.609	-0.756
11	0.381	0.616	0.412	-0.321	-0.592	0.875	0.062	0.606	-0.757
12	0.383	0.573	0.358	-0.413	-0.232	0.124	0.065	0.602	-0.759

Fig. 3. Calculated atomic charges for ligands and compounds **1**–**12**.

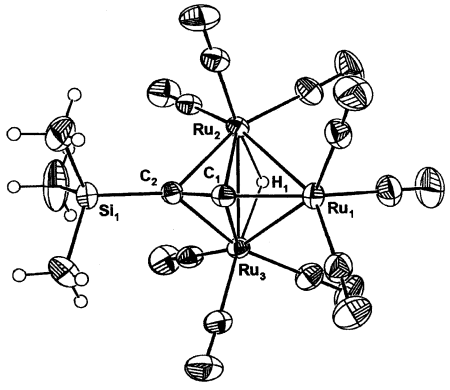


Fig. 4. Molecular structure for compound **1**, including numbering scheme. ORTEPS shown at 40% probability.

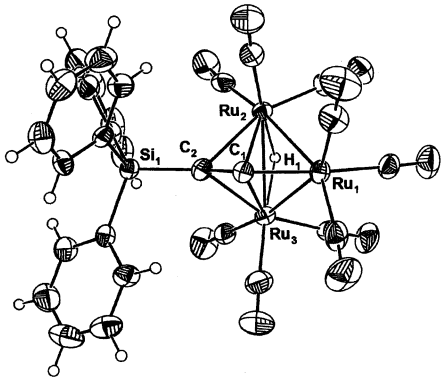


Fig. 5. Molecular structure for compound **2**, including numbering scheme. ORTEPS shown at 40% probability.

The M(1)–C(1)–C(2) angle of the acetylide complexes tends to be in the range of 153°–158° while the C(1)–C(2)–R angle is somewhat smaller, (138°–148° for Ru compounds and about 140° for osmium complexes). The corresponding angles in compound **9** are much smaller (112.6(3)° and 121.8(9)°). Also, in the case of the ruthenium compounds, the larger electronic deformation can be thought to follow the order $SiPh_3 > SiMe_3 > {}^t$Bu while in the osmium derivatives, the trend is the opposite one. The angle formed by the C(1)–C(2) line and the plane formed by the three metal atoms in the acetylides shows different values depending on the metal and the substituent. Thus the two silicon substituted derivatives show larger values than the ^{t}Bu compound in the ruthenium cases while the ^{t}Bu complex shows the largest value for that angle in the osmium compounds.

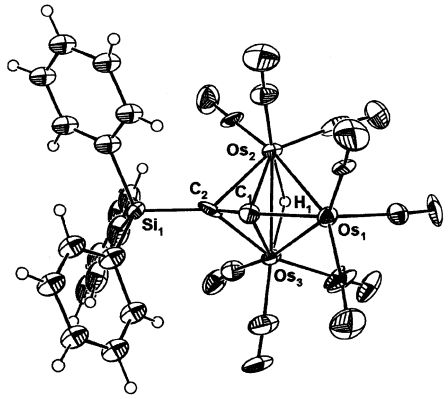


Fig. 6. Molecular structure for compound **5**, including numbering scheme. ORTEPS shown at 40% probability.

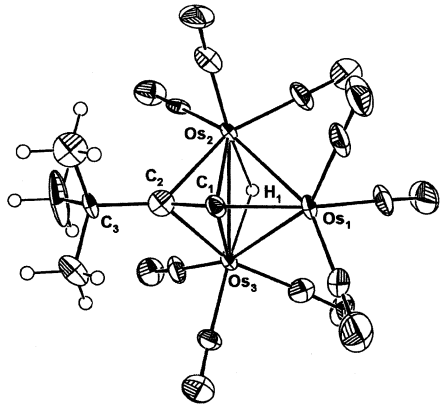


Fig. 7. Molecular structure for compound **6**, including numbering scheme. ORTEPS shown at 40% probability.

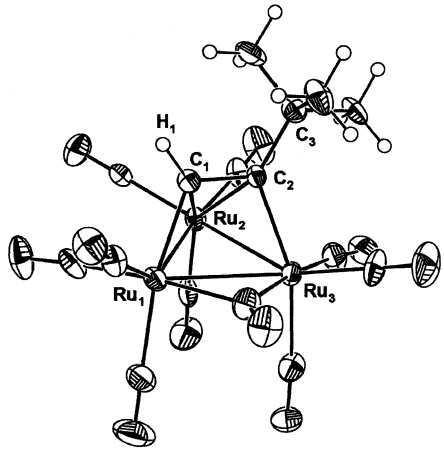


Fig. 8. Molecular structure for compound **9**, including numbering scheme. ORTEPS shown at 40% probability.

A comparison of bond lengths and angles of **5** and **6** with those of $[Os_3(CO)_{10}(EtCCEt)]$ [29] among other (//) complexes [30,36] shows that while the Os–C π interaction, have similar Os–C bond lengths in both (//) and acetylide, the Os–C σ-interaction is slightly shorter in the acetylide complexes. The same trend is observed in the ruthenium compounds **1**, **2** and **9**, in comparison with the structure of $[Ru_3(\mu\text{-}H)_2[\mu_3\text{-}C_2(CO_2Me)_2\}(\mu\text{-}dppm)(CO)_7]$, also a (//) complex [37] although compound **9** shows slightly longer Ru–C σ-bonds. However, it has to be pointed out that angles about the acetylenic carbon atoms show values similar to 120° in the parallel complexes, for example the C–C–R angle is 123.9(18)° in $[Os_3(CO)_{10}(C_2Et_2)]$ and 121.6(4)° for $[Ru_3(\mu\text{-}H)_2[\mu_3\text{-}C_2(CO_2Me)_2\}(\mu\text{-}dppm)(CO)_7]$.

The type of the substituents on Cβ does not affect too much the angle between the C–C bond and the M–M bond. Values go from 87.99(4)° to 89.81(2)°. However, it seems to affect the angle formed by the M_3 plane and the M_2-hydride plane, since values are around 111°–112° in $SiMe_3$ and ^{t}Bu derivatives and around 130° in the two $SiPh_3$ compounds. Hydride positions were calculated by the potential energy method [38].

3. Conclusions

The synthesis of parallel Os_3- and Ru_3-monosubstituted alkyne complexes was accomplished and these compounds were shown to transform into the acetylide complexes. The ^{1}H, ^{13}C and ^{29}Si NMR study of (//)- and acetylide complexes shows important differences in chemical shifts and coupling constants of the acetylenic carbons and the substituents when Ru_3- and Os_3-complexes are found in one coordination mode or the other. The presence of SiR_3 substituents strongly affects the ^{13}C chemical shifts as well as the $\delta(C_\alpha)-\delta(C_\beta)$ values. EHMO calculations also show differences between the two types of coordination modes. Both spectroscopic data and theoretical calculations show that the largest changes in chemical shift and atomic charges are observed in C_β, when changing from one coordination mode to the other. The atomic charges obtained in this work, are consistent with the reactivity of $[(\mu\text{-}H)M_3(CO)_9(CC^tBu)]$ (M = Ru, Os) towards protic acids. Some differences in bond lengths and angles can also be appreciated in the molecular structures of (//) and acetylide derivatives. Angles around C_β change significantly on going from the (//) complexes to the acetylides which could suggest a change in hybridization around this carbon atom. However, $^{13}C-^{29}Si$ coupling constants do not support this change.

4. Experimental

4.1. General procedures

All reactions and other manipulations were carried under a nitrogen atmosphere using standard Schlenk techniques. All solvents were dried and distilled under a

Table 5
Selected bond lengths (Å) and angles (°) for **1**, **2**, **5**, **6** and **9**

	1	**2**	**5**	**6**	**9**
Bond lengths					
M(1)–M(2)	2.8074(7)	2.7915(9)	2.8272(12)	2.8362(8)	2.7375(11)
M(2)–M(3)	2.7955(7)	2.7960(12)	2.8218(13)	2.8297(7)	2.7182(11)
M(3)–M(1)	2.8059(7)	2.7982(10)	2.8190(12)	2.8356(8)	2.8319(11)
C(1)–C(2)	1.300(8)	1.285(10)	1.28(3)	1.328(15)	1.377(14)
C(2)–Si(1)	1.858(5)	1.864(8)	1.89(2)		
C(2)–C(3)				1.503(14)	1.532(15)
C(1)–H(1)					0.990
M(1)–C(1)	1.941(5)	1.953(7)	1.967(19)	1.923(13)	2.110(11)
M(2)–C(1)	2.198(5)	2.188(7)	2.229(19)	2.211(12)	2.229(9)
M(3)–C(1)	2.197(5)	2.199(7)	2.225(17)	2.212(14)	
M(2)–C(2)	2.265(5)	2.306(8)	2.275(17)	2.268(7)	2.295(9)
M(3)–C(2)	2.272(5)	2.312(7)	2.24(2)	2.244(9)	2.118(10)
M(2)–H(1)	1.950	1.943	1.977	1.954	
M(3)–H(1)	1.951	1.952	1.818	1.948	
M(1)–C(7)					2.132(9)
M(3)–C(7)					2.154(10)
Bond angles					
M(1)–M(2)–M(3)	60.11(1)	60.11(2)	59.87(3)	60.06(2)	62.54(3)
M(2)–M(1)–M(3)	59.74(1)	60.03(3)	59.97(3)	59.85(2)	58.40(3)
M(1)–M(3)–M(2)	60.16(1)	59.87(3)	60.16(3)	60.08(2)	59.06(3)
M(1)–C(1)–C(2)	155.6(4)	157.7(6)	152.9(16)	154.9(10)	112.6(3)
C(1)–C(2)–Si(1)	143.6(5)	147.7(6)	140.4(17)		
C(1)–C(2)–C(3)				140.6(12)	121.8(9)
Interline and interplane angles					
C(1)–C(2)/M(2)–M(3)	89.7(3)	89.81(2)	88.9(11)	89.13(1)	
C(1)–C(2)/M(1)–M(3)					−2.1(6)
C(1)–C(2)/M(1)–M(2)–M(3)	19.4(3)	21.67(2)	17.3(10)	18.46(1)	2.3(6)
M(1)–M(2)–M(3)/M(2)–M(3)–H(1)	112.86(2)	131.17(1)	129.28(3)	113.88(1)	
M(1)–M(2)–M(3)/M(1)–M(3)–C(7)					167.5(4)

nitrogen atmosphere prior to use. Infrared spectra were recorded on a Perkin–Elmer 2000 spectrometer, and the solvent is indicated in Table 1. NMR spectra were obtained in a JEOL GSX-270, a JEOL Eclipse 400 or a Bruker Avance™ DPX 300 spectrometers, ^{1}H, ^{13}C and ^{29}Si spectra relative to $SiMe_4$, in $CDCl_3$ solution. $[Ru_3(CO)_{12}]$ and $[Os_3(CO)_{12}]$ and the corresponding alkynes, were purchased from Strem and Aldrich and were used without further purification. $[Ru_3(CO)_{10}(MeCN)_2]$ and $[Os_3(CO)_{10}(MeCN)_2]$ were prepared as reported [17,39]. Elemental analysis were carried out in the University of Oviedo, in Spain.

4.2. Synthesis of (//)-[$Ru_3(CO)_{10}(HCCR)$] (compounds 7, 8 and 9)

$[Ru_3(CO)_{10}(MeCN)_2]$ was synthesized as described in the literature (starting with $[Ru_3(CO)_{12}]$, 100 mg, 0.156 mmol) [17] and the product made to react, in situ, with 6 equiv. of the corresponding alkyne (0.939 mmol). These last reactions were carried out in dichloromethane solution, stirring at room temperature (r.t.) for 15 min. After that time, the solvent was evaporated to dryness under vacuum and the residue immediately dissolved in $CDCl_3$ for NMR studies. Conversion was quantitative in all cases. In the case of compound **7**, the solvent was removed to dryness under vacuum and the red solid was left to stand in the light at r.t.; after an hour, the solid had totally transformed into yellow $[(\mu\text{-H})Ru_3(CO)_9(CCSiMe_3)]$, compound **1**.

4.3. Synthesis of [$(\mu\text{-H})Ru_3(CO)_9(CCR)$] (R = $SiMe_3$, $SiPh_3$ and ^tBu) (compounds 1, 2 and 3)

$[Ru_3(CO)_{12}]$ (1 equiv.) (100 mg, 0.156 mmol) was made to react with 6 equiv. of the alkyne (0.939 mmol) in refluxing hexane for 2 h. The solvent was removed under vacuum and the residues purified by silica column or silica thin layer chromatography using hexane (R = $SiMe_3$ or ^tBu) or hexane–$CHCl_3$ (8:2) for compound **2**. Yields: compound **1**, 79%, compound **2**, 85% and compound **3**, 76%. Elemental analysis, Found (calculated): compound **1**, C, 25.72 (25.72); H, 1.60% (1.54); compound **2**, C, 41.50 (41.48); H, 1.91% (1.92); compound **3**, C, 28.55 (28.27); H, 1.46% (1.56).

4.4. Synthesis of (//)-[$Os_3(CO)_{10}(HCCR)$] (compounds **10**, **11** and **12**) and [(μ-H)$Os_3(CO)_9(CCR)$] (R = $SiMe_3$, $SiPh_3$ and ^tBu) (compounds **4**, **5** and **6**)

$[Os_3(CO)_{10}(NCMe)_2]$ (92.5 mg, 0.099 mmol) and the corresponding alkyne (0.595 mmol), were dissolved in dichloromethane in a 1:6 ratio and stirred at r.t. for 15 min. After that time the solvent was removed under vacuum and the residue separated by silica thin layer chromatography using hexane: $CHCl_3$ (9:1) as eluant. Yields of the (//)-$[Os_3(CO)_{10}(HCCR)]$ derivatives varied depending on the substituent (86% if R = $SiMe_3$, 65% if R = $SiPh_3$ and 80% if R = ^{t}Bu). (//) Compounds could be converted to the corresponding acetylide by heating octane solutions of the compounds for 2 h. Yields for these conversions were 49% if R = $SiMe_3$, 45% if R = $SiPh_3$ and 47% if R = ^{t}Bu). Elemental analysis for compound **4**, Found (calculated): C, 18.25 (18.24); H, 0.965 (1.09); for compound **5**, C, 31.20 (31.44); H, 1.31% (1.45); for compound **6**, C, 20.18 (19.91); H, 0.97% (1.11); for compound **11**, C, 31.47 (31.74); H, 1.34% (1.42); for compound **12**, C, 20.18 (20.61); H, 0.92% (1.08).

4.5. Theoretical calculations

Calculations were carried out using Extended Hückel, as implemented on HyperChem [39]. All calculations included d-orbitals for the silicon atoms.

4.6. Crystallographic studies

Crystals of **1**, **2**, **5** and **6** were grown from hexane–CH_2Cl_2 solutions while those of **9** were grown from a $CDCl_3$ solution. Details of the data collection and structure refinement procedures are summarized in Table 6. Data sets were collected in an Enraf–Nonius CAD4 diffractometer except for those of **9**, these were collected in a Nonius Kappa CCD diffractometer. The samples were mounted in capillary tubes. Both structures were solved by direct methods (SHELXS-93) [40]. All non-hydrogen atoms were found in Fourier maps and refined anisotropically. Hydrogen atoms from phenyl and methyl groups were fixed in idealized positions and their positions refined. Absorption corrections were carried out by empirical methods. All calculations were carried out in PC computers.

Table 6
Data collections parameters and structure refinement procedures for **1**, **2**, **5**, **6** and **9**

	1	**2**	**5**	**6**	**9**
Formula	$C_{14}H_{10}O_9Ru_3Si$	$C_{29}H_{16}O_9Ru_3Si$	$C_{29}H_{16}O_9Os_3Si$	$C_{15}H_{10}O_9Os_3$	$C_{16}H_{10}O_{10}Ru_3$
Molecular weight	652.51	839.72	1107.11	904.83	665.45
Crystal size (mm)	0.51 × 0.41 × 0.40	0.56 × 0.22 × 0.17	0.4 × 0.3 × 0.2	0.15 × 0.19 × 0.21	0.47 × 0.17 × 0.10
Crystal color and habit	yellow rectangular	yellow flake	white rectangular	pale yellow rectangular	red rectangular
System	triclinic	monoclinic	monoclinic	triclinic	orthorhombic
Space group	$P\bar{1}$	$P2_1/c$	$P2_1/c$	$P\bar{1}$	$Pna2_1$
a (Å)	9.1554 (10)	12.757 (3)	12.712 (3)	9.0171 (10)	12.651 (2)
b (Å)	9.2373 (10)	9.310 (2)	0 9.270 (2)	9.0060 (10)	13.255 (2)
c (Å)	13.1229 (10)	25.874 (5)	25.690 (5)	12.8762 (10)	24.605 (4)
α (°)	92.135 (10)	90.00	90.00	92.324 (10)	90.00
β (°)	106.738 (10)	97.68 (3)	97.23 (3)	105.917 (10)	90.00
γ (°)	98.483 (10)	90.00	90.00	100.632 (10)	90.00
V (Å^3)	1045.62 (18)	3045.4 (11)	3003.2 (11)	983.69 (17)	4126.0 (11)
Z	2	4	4	2	8
ρ_{calc} (Mg m^{-3})	2.072	1.831	2.449	3.055	2.143
F(000)	622	1632	2016	800	2544
λ (Mo Kα) (Å)	0.71073	0.71073	0.71073	0.71073	0.71073
μ (Mo Kα) (mm^{-1})	2.236	1.559	12.752	19.370	2.217
2θ range (°)	4.26–51.94	4.82–53.94	4.82–49.92	4.62–51.94	6.98–54.94
Temperature (K)	293 (2)	293 (2)	293 (2)	293 (2)	223 (2)
(h_{min}/h_{max}	−11/10	−16/16	−15/14	−11/10	−16/16
k_{min}/k_{max}	−11/11	0/11	0/11	−11/11	−17/17
l_{min}/l_{max})	0/16	0/33	0/30	0/15	−31/31
Measured reflections collected	4326	6769	5781	4321	9152
Observed reflections, ($F > 4\sigma(F)$)	3469	3684	2964	3081	7552
Unique reflections	4098	6618	5254	3794	8819
(R_{int})	(0.0100)	(0.0453)	(0.0010)	(0.0000)	(0.0010)
R_1 [$F > 4\sigma(F)$]	0.0373	0.0455	0.0510	0.0520	0.0515
wR_2 (on F^2 all data) [a]	0.1108	0.1559	0.1285	0.1659	0.1362
Goodness-of-fit on F^2	1.133	1.060	1.048	1.070	1.048

[a] $w^{-1} = \sigma^2 F_o^2 + (P)^2 + P$, where $P = (F_o^2 + 2F_c^2)/3$.

5. Supplementary material

Crystallographic data for the structural analysis have been deposited with the Cambridge Crystallographic Data Centre, CCDC Nos. 152437–152440 and 169330. Copies of the information may be obtained free of charge from The Director, CCDC, 12 Union Road, Cambridge CB2 1EZ, UK (fax: +44-1223-336063; e-mail: deposit@ccdc.cam.ac.uk or www: http://www.ccdc.cam.ac.uk).

Acknowledgements

We express our gratitude to Dr. Javier Cabeza from the University of Oviedo in Spain and Dr. Bernd Wrackmeyer from the University of Bayreuth, Germany, for their help. We also wish to thank the Consejo Superior de Investigaciones Científicas de España for the award of a license for the use of the Cambridge Crystallographic Data Base. Thanks are also given to Efrén V. García-Baez, Marco A. Leyva and Gloria Sánchez-Cabrera for their help. We wish to thank CONACYT for the award of a grant (To Francisco J. Zuno-Cruz) and for support towards the acquisition of a NMR spectrometer (Project 166-0/PAD).

References

[1] E. Sappa, A. Tiripicchio, P. Braunstein, Chem. Rev. 83 (1983) 203 (and references therein).
[2] P. Raithby, M.J. Rosales, Adv. Inorg. Chem. Radiochem. 29 (1985) 189.
[3] M.I. Bruce, in: Comprehensive Organometallic Chemistry I. vol. 4 Pergamon, Oxford, 1982, and references therein, p. 843.
[4] A.J. Deeming, Adv. Organometal. Chem. 26 (1986) 1.
[5] D. Osella, R. Gobetto, P. Montanegro, P. Zanello, A. Cinquantini, Organometallics 5 (1985) 1247.
[6] R. Schilling, R. Hoffmann, J. Am. Chem. Soc. 101 (1979) 3456.
[7] G. Granozzi, E. Tondello, M. Casarin, S. Aime, D. Osella, Organometallics 2 (1983) 430.
[8] S. Aime, R. Bertoncello, V. Busetti, R. Gobeto, G. Granozzi, D. Osella, Inorg. Chem. 25 (1986) 4004.
[9] J. Lewis, A.D. Massey, M. Monari, B.F.G. Johnson, D. Braga, F. Grepioni, J. Chem. Soc., Dalton Trans. (1992) 249.
[10] S. Aime, R. Gobetto, L. Milone, D. Osella, L. Violano, A.J. Arce, Y. De Sanctis, Organometallics 10 (1991) 2854.
[11] M.I. Bruce, B.W. Skelton, A.H. White, N.N. Zaitseva, J. Chem. Soc., Dalton Trans. (1999) 1445.
[12] S. Doherty, J.F. Carrigan, A.J. Carty, E. Sappa, Adv. Organomet. Chem. 37 (1995) 39.
[13] A.J. Carty, A.A. Cherkas, L.H. Randall, Polyhedron 7 (1988) 1045.
[14] W. Hagens, H.J.T. Bos, J.F. Arens, Recl. Trav. Chim. Pays-Bas 92 (1973) 762.
[15] A.J. Arce, Y. De Sanctis, A.J. Deeming, Polyhedron 7 (1988) 979.
[16] A.K. Smith, Comprehensive Organometallic Chemistry II, vol. 7 (Chapter 13), Pergamon, Oxford, 1995.
[17] C.A. Foulds, B.F.G. Johnson, J. Lewis, J. Organomet. Chem. 296 (1985) 147.
[18] E. Sappa, O. Gambino, L. Milone, G. Cetini, J. Organomet. Chem. 39 (1972) 169.
[19] E.C. Constable, B.F.G. Johnson, J. Lewis, G.N. Paine, M.J. Taylor, J. Chem. Soc., Chem. Commun. (1982) 754.
[20] J.S. Holmgren, J.R. Shapley, P.A. Belmonte, J. Organomet. Chem. 284 (1985) C5.
[21] G. Gervasio, R. Gobetto, P.J. King, D. Marabello, E. Sappa, Polyhedron 17 (1998) 2937.
[22] L.J. Farrugia, S.E. Rae, Organometallics 11 (1992) 196.
[23] S. Aime, D. Osella, E. Giamello, G. Granozzi, J. Organomet. Chem. 262 (1984) C1.
[24] C.J. Jameson, J. Chem. Phys. 66 (1977) 4983.
[25] S. Kerschl, A. Sebald, B. Wrackmeyer, Magn. Reson. Chem. 23 (1985) 514.
[26] W. Gombler, J. Am. Chem. Soc. 104 (1982) 6616.
[27] B. Wrackmeyer, J. Magn. Reson. 42 (1981) 287.
[28] 3D Search and Research using the Cambridge Structural Database. F.H. Allen, O. Kennard., Chemical Dessign Automation News 8 (1993) 31.
[29] E. Rosenberg, J. Bracker-Novak, R.W. Gallert, S. Aime, R. Gobetto, D. Osella, J. Organomet. Chem. 365 (1989) 163.
[30] S. Aime, R. Bertoncello, V. Busetti, R. Gobeto, G. Granozzi, D. Osella, Inorg. Chem. 25 (1986) 4004.
[31] J.F. Halet, J.Y. Saillard, R. Lissillour, M.J. McGlinchey, G. Jaouen, Inorg. Chem. 24 (1985) 218.
[32] G. Granozzi, E. Tandello, R. Bertoncello, S. Aime, D. Osella, Inorg. Chem. 22 (1983) 744.
[33] C. Barner-Thorsen, E. Rosenberg, G. Saatjian, S. Aime, L. Milone, D. Osella, Inorg. Chem. 20 (1981) 1592.
[34] M. Catti, G. Gervasio, S.A. Mason, J. Chem. Soc., Dalton Trans. (1977) 2260.
[35] A.I. Yanovski, Y.T. Struchkov, N.M. Astakhova, A.A. Koridze, Organomet. Chem. USSR 3 (1990) 359.
[36] A.J. Deeming, A.M. Senior, J. Organomet. Chem. 439 (1992) 177.
[37] M.I. Bruce, P.A. Humphrey, H. Miyamaes, B.W. Skelton, A.H. White, J. Organomet. Chem. 429 (1992) 187.
[38] XHYDEX, Potential Energy Calculation for Determining Hydride Positions. A.G. Orpen, J. Chem. Soc., Dalton Trans. (1980) 2509.
[39] HYPER CHEM, Release 5; HyperCube, Inc. (1998).
[40] SHELX-93 Program for Crystal Structure Refinement. G.M. Sheldrick, Institüt für Anorganische Chemie der Universität. Tammanstrastrasse 4, D-3400 Göttingen, Germany, 1993. SHELXS-86 Program for Crystal Structure Refinement. G.M. Sheldrick, Institüt für Anorganische Chemie der Universität. Tammanstrasse 4, D-3400 Göttingen, Germany, 1993.

PERGAMON

Polyhedron 21 (2002) 1117–1123

POLYHEDRON

www.elsevier.com/locate/poly

Synthesis and structural characterization of complexes derived from treatment of gallium trichloride with 3,5-diphenylpyrazole

Zhengkun Yu, Andrey V. Korolev, Mary Jane Heeg, Charles H. Winter *

Department of Chemistry, Wayne State University, Detroit, MI 48202, USA

Received 1 November 2001; accepted 25 February 2002

Abstract

The adduct $GaCl_3(Ph_2pzH)$ (Ph_2pzH, 3,5-diphenylpyrazole) was synthesized in 96% yield upon treatment of equimolar amounts of gallium trichloride with Ph_2pzH in toluene at room temperature. The tetrachlorogallate salt $[Ph_2pzH_2]^+GaCl_4^-$ was obtained in 93% yield by treatment of a 2:1 stoichiometry of gallium trichloride and Ph_2pzH at room temperature, followed by recrystallization from toluene/dichloromethane. The X-ray crystal structures of $GaCl_3(Ph_2pzH)$ and $[Ph_2pzH_2]^+GaCl_4^-$ were determined, and reveal weak hydrogen bond interactions between the nitrogen-bound hydrogen atoms and gallium-bound chlorine atoms. Examination of the formation of $[Ph_2pzH_2]^+GaCl_4^-$ from $GaCl_3(Ph_2pzH)$ and gallium trichloride (1.0 equiv.) revealed that the hydrogen chloride used to form $[Ph_2pzH_2]^+GaCl_4^-$ arises from gallium trichloride-catalyzed chloromethylation of toluene. Under conditions where $[Ph_2pzH_2]^+GaCl_4^-$ was isolated in 82% yield upon treatment of $GaCl_3(Ph_2pzH)$ and gallium trichloride (1.0 equiv.) in toluene/dichloromethane, a mixture of ditolylmethane isomers was isolated in 330% yield based upon gallium trichloride.
© 2002 Elsevier Science Ltd. All rights reserved.

Keywords: Gallium pyrazole complexes; Tetrachlorogallate salt; Gallium trichloride; 3,5-diphenylpyrazole

1. Introduction

The coordination chemistry of complexes containing pyrazolato ligands has been extensively studied [1–3]. However, most of this work has focused on transition metal and organolanthanide complexes. Recently, there has been considerable interest in pyrazolato complexes of the Group 13 elements [4–39]. Most of the recent efforts have related to aluminum complexes [4–19]. Pyrazolato complexes of gallium are well known [20–39], although complexes containing bulky alkyl or aryl substituents in the 3- and 5-positions of the pyrazolato ligand have not been reported. Gallium trichloride is a relatively weak Lewis acid [40], but is known to form adducts with many nitrogen donor ligands [41–44]. The development of new source compounds for use in the chemical vapor deposition of metal nitride films is a long-term interest in our group [45], and complexes of gallium with nitrogen heterocyclic ligands may serve as precursors to GaN films [46]. Of relevance to the present work, GaCl-containing precursors have been recently demonstrated to be extremely selective growth species in epitaxial film growth of gallium-based semiconductor materials [47]. In view of our recent reports of aluminum pyrazolato complexes [17–19], we sought to explore the synthesis of new gallium pyrazolato complexes. Herein, we describe the synthesis and structural characterization of products that are obtained upon treatment of gallium trichloride with diphenylpyrazole. Depending on the reaction conditions, the complexes $GaCl_3(Ph_2pzH)$ and $[Ph_2pzH_2]^+GaCl_4^-$ are obtained. The nitrogen-bound hydrogen atoms in these complexes participate in hydrogen bonding to chlorine atoms. $[Ph_2pzH_2]^+GaCl_4^-$ is obtained upon capture of hydrogen chloride by $GaCl_3(Ph_2pzH)$, and it is demonstrated that the hydrogen chloride originates from gallium trichloride-catalyzed chloromethylation of toluene by dichloromethane. To our knowledge, this is the first example of a Friedel–Crafts reaction with dichloromethane that is promoted by any gallium complex. Dichloromethane is a poor electrophile in Friedel–

* Corresponding author. Tel.: +1-313-577-5224; fax: +1-313-577-1377.

E-mail address: chw@chem.wayne.edu (C.H. Winter).

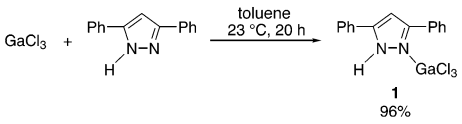
0277-5387/02/$ - see front matter © 2002 Elsevier Science Ltd. All rights reserved.
PII: S0277-5387(02)00931-2

Crafts reactions, and gallium compounds are at best moderate strength Lewis acids that should not be capable of activating dichloromethane [40]. Accordingly, observation of the chloromethylation reaction described herein is surprising.

2. Results and discussion

2.1. Synthesis and characterization

Treatment of gallium trichloride with 3,5-diphenylpyrazole (Ph_2pzH) in a 1:1 molar ratio in toluene at 23 °C led to the formation of the adduct $GaCl_3(Ph_2pzH)$ (**1**), which was isolated as colorless crystals in 96% yield after crystallization from toluene at −20 °C (Eq. (1)). A similar reaction was conducted in an NMR tube in chloroform-*d*. The ^1H NMR spectrum after 24 h indicated that **1** was the only product that formed. The structure of **1** was established by a combination of spectral and analytical data, and by an X-ray crystal structure determination as described below. The ^1H NMR spectrum of **1** in chloroform-*d* showed the nitrogen-bound hydrogen resonance at δ 11.19, consistent with the coordinated Ph_2pzH ligand. The infrared spectrum of **1** revealed a sharp, strong nitrogen–hydrogen absorption at 3350 cm^{-1} and weak nitrogen–hydrogen absorptions between 3274 and 3151 cm^{-1}.

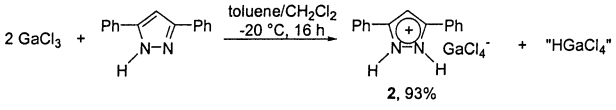


1
96%

(1)

When **1** was prepared using a 1.00:1.00 molar ratio of gallium trichloride and diphenylpyrazole and was recrystallized from toluene, the ^1H and $^{13}C\{^1H\}$ NMR spectra revealed chemically distinct resonances for the two types of phenyl groups present in **1**. Such an observation indicates that cleavage of the gallium–nitrogen bond in **1**, followed by hydrogen atom transfer between the pyrazole nitrogen atoms and recoordination to gallium, is slow on the NMR timescale. In some preparations of **1**, only one type of phenyl group was observed in ^1H and $^{13}C\{^1H\}$ NMR spectra of the product. An NMR tube experiment with recrystallized **1** demonstrated that excess gallium trichloride (up to one full equivalent) had no effect on the ^1H and $^{13}C\{^1H\}$ NMR spectra of **1** in benzene-d_6 at ambient temperature, and two chemically distinct phenyl groups were observed. However, addition of as little as 5% excess diphenylpyrazole to recrystallized **1** led to the observation of a single type of phenyl resonance in the ^1H and $^{13}C\{^1H\}$ NMR spectra at ambient temperature, indicating rapid exchange of the phenyl sites on the NMR timescale. We suggest that the excess diphenylpyrazole promotes the exchange through a low energy associative transition state containing a 5-coordinate gallium center.

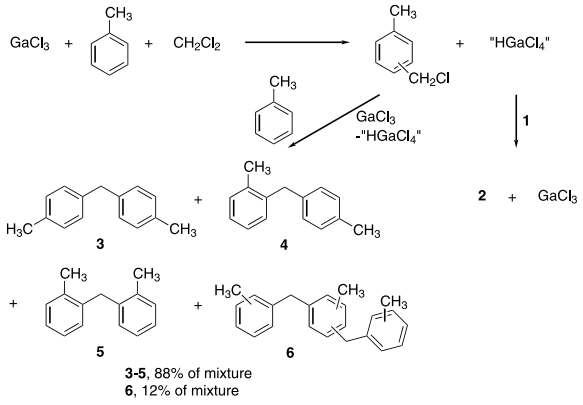
As noted above, **1** could be prepared as a single pure product through careful control of the gallium trichloride:diphenylpyrazole stoichiometry, followed by crystallization from toluene. However, treatment of gallium trichloride with Ph_2pzH in a 2:1 ratio in toluene for 0.5 h, followed by recrystallization from toluene/dichloromethane for 16 h at −20 °C, afforded 3,5-diphenylpyrazolium tetrachlorogallate (**2**, 93%) as a colorless crystalline solid (Eq. (2)). The structure of **2** was established by a combination of spectral and analytical data, and by an X-ray crystal structure determination as described below. The ^1H NMR spectrum of **2** in chloroform-*d* revealed the nitrogen-bound hydrogen resonance at δ 12.76. The infrared spectrum showed medium intensity nitrogen–hydrogen absorptions between 3255 and 3174 cm^{-1}, and the electron impact mass spectrum revealed the cation $[Ph_2pzH_2]^+$ with 100% intensity. The microanalysis was consistent with the formulation of **2**. The formation of **2** from **1** and 1.0 equiv. of gallium trichloride was monitored by ^1H NMR in toluene-d_8 and a toluene-d_8/dichloromethane mixture (1.0 ml/0.2 ml) at ambient temperature. After 20 h in toluene-d_8, the only product present was **1**. However, **1** converted to **2** completely over 16 h at ambient temperature when dissolved in 5:1 toluene-d_8/dichloromethane. During this time, the reaction mixture turned deep red and colorless crystals were observed to deposit on the walls of the NMR tube. These observations are consistent with the preparation of **2** outlined above. In addition, new resonances were observed in the ^1H NMR spectrum, suggesting the formation of new organic products.



2, 93%

(2)

An experiment was performed in which gallium trichloride (1.0 equiv.) was treated with **1** (1.0 equiv.) in 90:10 toluene/dichloromethane at 20 °C for 16 h. Workup as described in the experimental section afforded **2** in 82% yield. In addition, a brown–red oil was isolated that was identified as three ditolylmethane isomers **3**–**5** (88% of mixture) and eight or more isomers of (methylbenzyl)ditolylmethane **6** (12% of mixture) by GLC/MS and by analysis of the ^1H and $^{13}C\{^1H\}$ NMR spectra of the mixture (Scheme 1). The ^1H NMR spectrum indicated an 84:12:4 mixture of *p*,*p*′-ditolylmethane (**3**), *o*,*p*′-ditolylmethane (**4**), and *o*,*o*′-ditolylmethane (**5**). This identification was based upon comparison with methyl and methylene ^1H NMR chemical shifts that have been previously reported for



Scheme 1. Chloromethylation of toluene.

these compounds [48,49]. The GLC/MS of **3**–**5** all showed a parent ion of mass/charge 196, with a base peak of 181 corresponding to loss of a methyl group from the parent ion. In addition to the ditolylmethane isomers, eight or more methylene resonances were observed between δ 3.82 and 3.87 in the ^{1}H NMR spectrum of the red–brown oil. GLC/MS revealed at least eight minor components exhibiting parent ions of mass/charge 300, with base peaks of 195 corresponding to loss of a methylbenzyl group from isomeric (methylbenzyl)ditolylmethanes. The (methylbenzyl)ditolylmethane mixture was not characterized further, due to the small amount and large number of isomers.

Observation of the mixture containing **3**–**6** suggests that the pathway outlined in Scheme 1 is operant in the formation of **2** under the conditions of excess gallium trichloride. Gallium trichloride-promoted chloromethylation of toluene can proceed to afford *ortho*- and *para*-isomers of chloromethyltoluene as well as '$HGaCl_4$'. As noted in the introduction, this is the first example of a Friedel–Crafts alkylation reaction of dichloromethane that is promoted by any gallium compound. Gallium trichloride is considered to be a moderate strength Lewis acid at best [40], and gallium compounds have been frequently used as Friedel–Crafts reaction catalysts with reactive alkyl halides to avoid side products that are observed with more reactive aluminum-based Lewis acids [50–53]. The direct chloromethylation of aromatic compounds with dichloromethane using aluminum halide catalysts has been well documented [40,54–56]. In addition, an aluminum trichloride-promoted chloromethylation of an aluminum-bound phenoxy group by dichloromethane to give non-aromatic product was described [57]. Several reports have described the chloromethylation of toluene using Lewis acid catalysis and various reactive chloromethyl cation equivalents such as methoxyacetyl chloride, bis(chloromethyl) ether, or chloromethyl methyl ether [58]. Once formed, the intermediate chloromethyl-substituted aromatic compounds rapidly react to form diarylmethane derivatives. In the present work, the intermediate chloromethyltoluene isomers react rapidly with toluene to afford the mixtures of **3**–**5**. The yield of **3**–**5** based upon gallium trichloride is about 330%, thus indicating that the formation of **3**–**5** is catalyzed by a gallium species present in the reaction mixture. The first equivalent of hydrogen chloride generated during the chloromethylation reaction is trapped by **1** to form **2**. Thereafter, the fate of the hydrogen chloride is less clear. '$HGaCl_4$' has been previously described as a diethyl ether adduct [59]. However, the strongest bases remaining after complete formation of **2** are toluene and **3**–**6**. It is possible that the deep red coloration of the reaction solution corresponds to the formation of arenium cations, which are known to be deeply colored in solution [60–63].

The central discovery described herein is the Friedel–Crafts chloromethylation of toluene promoted by **1**, **2**, or some other gallium species present in solution. The fact that gallium compounds can promote rapid Friedel–Crafts alkylation reactions using a poor electrophile such as dichloromethane is surprising in view of the extensive literature in this area [40]. The high solubility of **1** in toluene may be the reason why the chloromethylation reaction proceeds at such a rapid rate. In the present work, the Friedel–Crafts alkylation reaction manifested itself initially through the unexpected formation of **2** when **1** was recrystallized from toluene/dichloromethane mixtures. We expect that similar Friedel–Crafts reactions will occur in systems that contain what are presumed to be weak Lewis acids and poorly electrophilic alkyl halides.

2.2. *Molecular structures of **1** and **2***

The solid-state structures of **1** and **2** were determined by X-ray crystallography. Perspective views are shown in Figs. 1 and 2, crystallographic data are provided in Table 1, and selected bond lengths and angles are listed in Tables 2 and 3.

Complex **1** crystallizes as a monomer with distorted tetrahedral geometry about the gallium center. The Ga–N(1) bond distance is 1.971(2) Å. The nitrogen–hydrogen bond length is 0.759(4) Å. The nitrogen-bound hydrogen participates in intramolecular hydrogen bond-

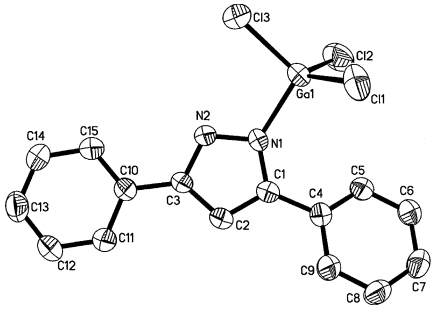


Fig. 1. Perspective view of $GaCl_3(Ph_2pzH)$ (**1**) with thermal ellipsoids at the 50% probability level.

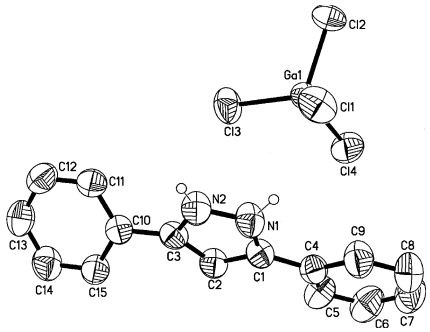


Fig. 2. Perspective view of $[Ph_2pzH_2]^+GaCl_4^-$ (**2**) with thermal ellipsoids at the 50% probability level.

Table 1
Crystallographic data for **1** and **2**

Formula	$C_{15}H_{12}Cl_3GaN_2$ (**1**)	$C_{15}H_{13}Cl_4GaN_2$ (**2**)
Formula weight	396.34	432.79
Space group	$P2_1/n$	$P2_1/n$
a(Å)	10.461(7)	11.8508(7)
b(Å)	12.882(9)	7.3609(4)
C (Å)	11.913(8)	21.0097(12)
β(°)	92.646(18)	96.2560(10)
V (Å^3)	1603.8(19)	1821.8(2)
Z	2	4
T (K)	295 (2)	295(2)
λ (Å)	0.71073	0.71073
$\rho_{calc.}$(g cm^{-3})	1.641	1.578
μ (mm^{-1})	2.208	2.093
$R(F)$ (%)	3.23	2.96
$R_w(F)$ (%)	7.16	7.42

$R(F) = \Sigma||F_o| - |F_c||/\Sigma|F_o|$. $R_w(F)^2 = [\Sigma w(F_o^2 - F_c^2)^2/\Sigma w(F_o^2)^2]^{1/2}$.

Table 2
Selected bond lengths (Å) and angles (°) for **1**

Bond lengths			
Ga–N(1)	1.971(2)	Ga–Cl(1)	2.1448(13)
Ga–Cl(2)	2.1589(15)	Ga–Cl(3)	2.1568(17)
N(1)–N(2)	1.365(5)	N(1)–C(1)	1.348(3)
N(2)–C(3)	1.347(3)	N(2)–H	0.759(3)
(N2)H···Cl(3)	2.625(4)		
Bond angles			
Cl(1)–Ga–Cl(2)	110.85(5)	Cl(1)–Ga–Cl(3)	112.28(6)
Cl(2)–Ga–Cl(3)	110.85(5)	N(1)–Ga–Cl(1)	109.19(8)
N(1)–Ga–Cl(2)	111.79(9)	N(1)–Ga–Cl(3)	101.56(7)
Ga–N(1)–N(2)	116.74(17)	Ga–N(1)–C(1)	135.98(18)
N(2)–H–Cl(3)	127.96(3)		

ing to Cl(3), with a hydrogen-chlorine distance of 2.625(4) Å. The N(2)–H(N2)–Cl(3) angle is 127.96(3)°. There are no significant intermolecular hydrogen bonds. The gallium–chlorine bond distances range from 2.1448(13)–2.1589(15) Å. All three gallium–chlorine bond lengths are identical within the precision of the structure determination, suggesting that the intramolecular hydrogen bond to Cl(3) is weak. The N(1)–Ga–Cl(3) angle (101.56(7)°) is smaller than the related values

Table 3
Selected bond lengths (Å) and angles (°) for **2**

Bond lengths			
Ga–Cl(1)	2.1718(6)	Ga–Cl(2)	2.2032(6)
Ga–Cl(3)	2.1607(7)	Ga–Cl(4)	2.1521(7)
N(1)–N(2)	1.345(3)	N(1)–C(1)	1.339(3)
N(2)–C(3)	1.338(3)	H(N1)–N(1)	0.937(3)
H(N2)–N(2)	0.827(3)	H(N1)–Cl(1)	2.533(3)
H(N2)–Cl(2′)	2.663(3)	H(N2)–Cl(2″)	2.573(3)
Bond angles			
Cl(1)–Ga–Cl(2)	103.90(3)	Cl(1)–Ga–Cl(3)	112.68(3)
Cl(1)–Ga–Cl(4)	111.53(3)	Cl(2)–Ga–Cl(3)	110.15(3)
Cl(2)–Ga–Cl(4)	110.41(3)	Cl(3)–Ga–Cl(4)	108.15(3)
N(1)–N(2)–C(3)	109.5(2)	N(2)–N(1)–C(1)	109.7(2)
N(1)–H(N1)–Cl(1)	132.88(3)	N(2)–H(N2)–Cl(2′)	165.65(3)
N(1)–H(N1)–Cl(2′)	127.68(3)		

for N(1)–Ga–Cl(1) (109.19(8)°) and N(1)–Ga–Cl(2) (111.79(9)°). This distortion may arise from the weak hydrogen bond associated with Cl(3).

Complex **2** crystallizes with a diphenylpyrazolium ion that contains several different hydrogen bonds to the tetrachlorogallate ion. The geometry about the gallium atom is distorted tetrahedral. The gallium–chlorine bond distances range from 2.1521(7) to 2.2032(6) Å, and are slightly longer than the range found in **1** due to the reduced Lewis acidity of the gallium center in the tetrachlorogallate ion. The chlorine–gallium–chlorine angles range between 103.90(3)° and 112.68(3)°. The nitrogen–hydrogen bond lengths are 0.937(5) and 0.827(5) Å. The nitrogen-bound hydrogen atoms are hydrogen-bonded to chlorine atoms of the tetrachlorogallate ion with bond lengths of 2.533(3) ((N1)H···Cl(1)), 2.663(5) ((N1)H···Cl(2′)), and 2.573(4) Å ((N2)H···Cl(2″)). The nitrogen–hydrogen–chlorine angles associated with the hydrogen bonds are 132.88(3)°, 127.68(3)°, and 165.65(3)°, respectively. The nitrogen–hydrogen bond lengths are similar to the value found in **1**. Interestingly, the two chlorine atoms involved in weak hydrogen bonding (Cl(1), Cl(2)) exhibit slightly longer gallium–chlorine bond lengths than the two chlorine atoms that are not involved in hydrogen bonding (Cl(3), Cl(4)). These bond length differences, while small, suggest slightly stronger hydrogen bonding in **2**, compared with **1**. Stronger hydrogen bonding in **2** can be rationalized on the basis of more electrophilic hydrogen atoms and more electron rich chlorine atoms due to the presence of ions in the solid.

The gallium–nitrogen bond length in **1** is very similar to values ranging from 1.97 to 2.00 Å that have been documented in gallium–pyrazolate complexes [20–39]. The X-ray crystal structures of several pyrazolium salts of the formula $[t\text{-}Bu_2pzH]^+X^-$ (X = Cl, Br) have been reported [64,65]. These compounds form distinct dimeric aggregates featuring ten-membered $X_2H_4N_4$ rings in the solid state that are held together by strong, linear N–H···X hydrogen bonding. Ten-membered rings are

present in **2**, but these rings are present as part of an extended hydrogen bonded network, as opposed to the dimeric units in the pyrazolium halide salts. In 3,5-di-*tert*-butylpyrazolium chloride [64,65], the nitrogen–chlorine distance containing the hydrogen bond was 3.057(2) Å, the H···Cl distance was 2.12(3) Å, and the nitrogen–hydrogen–chlorine angle was 175(3)°. By contrast, in **2** the related values were 3.244(2)–3.380(2) Å, 2.533(4)–2.663(4) Å, and 127.68(5)°–165.65(5)°. These values for **2** suggest much weaker hydrogen bonding than is present in 3,5-di-*tert*-butylpyrazolium chloride. The order of hydrogen bonding strength is consistent with the lone pairs of electrons on $GaCl_4^-$ being much less basic than those of chloride ion. Similar weak E–H···X hydrogen bonding (E = O, N; X = halogen) is well established in the solid state structures of other metal halide complexes containing EH fragments within the crystal [66].

3. Experimental

3.1. General considerations

All manipulations were performed under argon using either drybox or Schlenk-line techniques. Gallium trichloride was purchased from Strem Chemical Company. Ph_2pzH was prepared using a reported procedure [67]. ^1H and $^{13}C\{^1H\}$ NMR spectra were obtained at 500 or 300 and 125 or 75 MHz, respectively, in the indicated solvents. Infrared spectra were recorded using KBr discs. Mass spectra were obtained on a Kratos MS-50 spectrometer in the electron impact mode or on a Hewlett–Packard Model 5980 GLC/MS instrument. Elemental analyses were performed by Midwest Microlab, Indianapolis, IN. Melting points are uncorrected.

3.2. Synthesis of $GaCl_3(Ph_2pzH)$ (**1**)

A 100 ml Schlenk flask was charged with a stir bar, gallium trichloride (0.42 g, 2.4 mmol), and diphenylpyrazole (0.52 g, 2.4 mmol). Toluene (30 ml) was added by syringe to form a colorless solution. This mixture was stirred at ambient temperature for 24 h. The volatile components were removed under reduced pressure to afford spectroscopically pure **1** as a white powder (0.91 g, 96%). X-ray and analytical quality crystals were obtained by recrystallization from toluene at −20 °C: m.p. 157–158 °C; IR (KBr, cm^{-1}) 3350 (s), 3274 (w), 3151 (w), 1610 (m), 1569 (s), 1273 (m), 1182 (m), 1108 (m), 1085 (m), 990 (m), 821 (w), 761 (s), 705 (w), 703 (m), 684 (s), 563 (s); ^1H NMR ($CDCl_3$, 23 °C, δ) 11.19 (br. s, 1 H, N***H***), 7.77 (m, 2H, Ph C***H***), 7.65, (m, 2 H, Ph C***H***), 7.57 (m, 3 H, Ph C***H***), 7.51 (m, 3 H, Ph C***H***), 6.91 (d, $J = 3.0$ Hz, 1 H, pyrazole C***H***); $^{13}C\{^1H\}$ NMR ($CDCl_3$, 23 °C, ppm) 156.33 (s, ***C***Ph), 147.39 (s, ***C***Ph), 131.64 (s, *p*-***C***H of Ph), 130.92 (s, *p*-***C***H of Ph), 129.82 (s, *m*-***C***H of Ph), 129.00 (s, *m*-***C***H of Ph), 128.85 (s, *o*-***C***H of Ph), 127.86 (s, *ipso*-***C*** of Ph), 126.34 (s, *o*-***C***H of Ph), 125.39 (s, *ipso*-***C*** of Ph), 105.79 (s, ***C***H of pyrazolato); MS (EI, 70 eV) 220 ($[Ph_2pzH]^+$, 100%).

Anal. Calc. for $C_{15}H_{12}Cl_3GaN_2$: C, 45.46; H, 3.05; N, 7.07. Found: C, 45.68; H, 3.13; N, 6.99%.

3.3. Synthesis of $[Ph_2pzH_2]^+GaCl_4^-$ (**2**)

A 100 ml Schlenk flask, equipped with a stir bar and a rubber septum, was charged with **1** (0.26 g, 0.66 mmol), gallium trichloride (0.12 g, 0.66 mmol), and toluene (10 ml). To this stirred solution was added dichloromethane (0.5 ml). The solution color changed immediately to yellow and deepened to dark red after 0.5 h. The reaction solution was placed in a −20 °C freezer for 16 h. Yellow crystals formed during this time, and a dark red oil separated. The crystals were collected on a medium glass frit and were washed with 1:1 toluene/pentane (18 ml) followed by pentane (18 ml). Vacuum drying afforded white crystals. The washings were combined, producing more white crystals. These crystals were collected on a medium glass frit, washed with pentane (18 ml), and dried under vacuum. The crystals were combined to afford **2** as a colorless solid (0.26 g, 93%): m.p. 135–136 °C; IR (KBr, cm^{-1}) 3255 (m), 3219 (m), 3191 (m), 3174 (m), 1613 (m), 1590 (m), 1262 (w), 1227 (w), 1208 (w), 1188 (w), 1162 (w), 1095 (w), 1070 (w), 1053 (w), 1019 (w), 950 (w), 918 (w), 835 (w),765 (s), 704 (w), 691 (w), 681 (m); ^1H NMR ($CDCl_3$, 23 °C, δ) 12.76 (s, 2H, N***H***), 7.75 (m, 4H, Ph C***H***), 7.62 (m, 6H, Ph C***H***), 7.15 (t, $^4J_{HH} = 3.0$ Hz, 1H, pyrazolato C***H***); $^{13}C\{1H\}$ NMR ($CDCl_3$, 23 °C, ppm) 149.60 (s, pyrazolato ***C***Ph), 132.94 (s, *p*-***C***H of Ph), 130.21 (s, *m*-***C***H of Ph), 126.85 (s, *o*-***C***H of Ph), 123.95 (s, *ipso*-***C*** of Ph), 102.02 (s, ***C***H of pyrazolato); MS (EI, 70 eV) 221 ($[Ph_2pzH_2]^+$, 100%).

Anal. Calc. for $C_{15}H_{13}Cl_4GaN_2$: C, 41.62; H, 3.03; N, 6.47. Found: C, 41.49; H, 3.07; N, 6.55%.

3.4. Isolation of ditolylmethane isomers upon treatment of **1** with excess gallium trichloride

A Schlenk flask was charged with a stir bar, **1** (0.26 g, 0.66 mmol) and gallium trichloride (0.12 g, 0.66 mmol). Toluene (10 ml) was added to the flask to produce a colorless solution. Immediately thereafter, dichloromethane (1 ml) was added. The solution color changed to yellow and deepened to medium red within 0.5 h. The solution was stirred at ambient temperature for 6 h, and the volatiles were removed under reduced pressure to leave a dark red oil. Hexane (20 ml) was added to this oil to afford a pale yellow solution and colorless crystals in the dark red oil. This mixture was kept at ambient temperature for 16 h without stirring. The solution was

decanted from the oily residue, and the oily residue was washed again with hexane (6 ml). The hexane extracts were combined and the volatile components were removed under reduced pressure, leaving a red oil (0.41 g) that was identified as a mixture of **3**–**6** by GLC MS and by correlation of the ^{1}H NMR spectrum with previously reported values for ditolylmethane isomers. For further data, see below and in the text. The hexane-insoluble crystals were collected on a medium glass frit and then washed with 1:1 toluene/hexane (18 ml) and hexane (18 ml). Drying under vacuum for 1 h afforded spectroscopically pure **2** as a pale brown crystalline solid (0.23 g, 82%). The identity of **2** was confirmed by comparison of its ^{1}H and ^{13}C{^{1}H} NMR spectra with those of authentic material described above.

Data for the ditolylmethane mixture:

p,*p*′-ditolylmethane (**3**, 84%): partial ^{1}H NMR ($CDCl_3$, δ) 3.88 (s, C***H***$_2$), 2.29 (s, 2C***H***$_3$) [lit.[28] ^{1}H NMR ($CDCl_3$, δ) 3.89 (s, C***H***$_2$), 2.23 (s, 2C***H***$_3$)]; GLC/MS 196 (M^+, 57%), 181 (M^+–CH_3, 100%).

o,*p*′-ditolylmethane (**4**, 12%): partial ^{1}H NMR ($CDCl_3$, δ) 3.93 (s, C***H***$_2$), 2.28 (s, C***H***$_3$), 2.22 (s, C***H***$_3$) [lit.[27] ^{1}H NMR ($CDCl_3$, δ) 3.93 (s, C***H***$_2$), 2.30 (s, C***H***$_3$), 2.23 (s, C***H***$_3$)]; GLC/MS 196 (M^+, 63%), 181 (M^+–CH_3, 100%).

o,*o*′-ditolylmethane (**5**, 4%): partial ^{1}H NMR ($CDCl_3$, δ) 3.91 (s, C***H***$_2$), 2.28 (s, 2C***H***$_3$) [lit.[28] ^{1}H NMR ($CDCl_3$, δ) 3.91 (s, C***H***$_2$), 2.26 (s, 2C***H***$_3$)]; GLC/MS 196 (M^+, 61%), 181 (M^+–CH_3, 100%).

3.5. X-ray structure determinations of *1* and *2*

Single crystals of **1** and **2** were mounted in thin-walled capillaries under a nitrogen atmosphere. Crystallographic data were collected at room temperature (295 K) on a Siemens–Bruker automated P4/CCD diffractometer with monochromated Mo Kα radiation. Frames (1650) were collected at 10 s and integrated with the manufacturer's SMART and SAINT software. Absorption corrections were applied with Sheldrick SADABS program and the structure was solved and refined using programs of SHELXL-97 [68]. Hydrogen atoms were placed in observed and calculated positions.

4. Supplementary material

Crystallographic data for the structural analyses have been deposited with the Cambridge Crystallographic Data Centre, quoting No. 173005 for **1** and No. 173006 for **2**. Copies of this information may be obtained free of charge from The Director, CCDC, 12 Union Road, Cambridge CB2 1EZ, UK (fax: +44-1233-336033; e-mail: deposit@ccdc.cam.ac.uk or www: http://www.ccdc.cam.ac.uk).

Acknowledgements

We are grateful to the National Science Foundation (Grant No. CHE-9807269) and the Defense Advanced Research Projects Agency for support of this research.

References

[1] A.P. Sadimenko, S.S. Basson, Coord. Chem. Rev. 147 (1996) 247.
[2] G. La Monica, G.A. Ardizzoia, Prog. Inorg. Chem. 46 (1997) 151.
[3] J.E. Cosgriff, G.B. Deacon, Angew. Chem., Int. Ed. Engl. 37 (1998) 286.
[4] G.B. Deacon, E.E. Delbridge, C.M. Forsyth, P.C. Junk, B.W. Skelton, A.H. White, Aust. J. Chem. 52 (1999) 733.
[5] C.C. Chang, T.Y. Her, F.Y. Hsieh, C.Y. Yang, M.Y. Chiang, G.H. Lee, Y. Wang, S.M. Peng, J. Chin. Chem. Soc. (Taipei) 41 (1994) 783.
[6] A. Arduini, A. Storr, J. Chem. Soc., Dalton Trans., (1974) 203.
[7] H.-D. Hausen, K. Locke, J. Weidlein, J. Organomet. Chem. 429 (1992) C27.
[8] J. Lewinski, J. Zhchara, P. Gos, E. Grabska, T. Kopec, I. Madura, W. Marciniak, I. Prowotorow, Chem. Eur. J. 6 (2000) 3215.
[9] A. Looney, G. Parkin, A.L. Rheingold, Inorg. Chem. 30 (1991) 3099.
[10] A. Looney, G. Parkin, Polyhedron 9 (1990) 265.
[11] M.H. Chisholm, N.W. Eilerts, J.C. Huffman, Inorg. Chem. 35 (1996) 445.
[12] D.J. Darensbourg, E.L. Maynard, M.W. Holtcamp, K.K. Klausmeter, J.H. Reibenspies, Inorg. Chem. 35 (1996) 2682.
[13] W. Zheng, N. Mösch-Zanetti, H.W. Roesky, M. Hewitt, F. Cimpoesu, T.R. Schneider, A. Stasch, J. Prust, Angew. Chem., Int. Ed. Engl. 39 (2000) 3099.
[14] W. Zheng, N. Mösch-Zanetti, H.W. Roesky, M. Noltemeyer, M. Hewitt, H.-G. Schmidt, T.R. Schneider, Angew. Chem., Int. Ed. Engl. 39 (2000) 4276.
[15] W. Zheng, H.W. Roesky, M. Noltemeyer, Organometallics 20 (2001) 1033.
[16] W. Zheng, H. Hohmeister, N. Mösch-Zanetti, H.W. Roesky, M. Noltemeyer, H.-G. Schmidt, Inorg. Chem. 40 (2001) 2363.
[17] Z.K. Yu, J.M. Wittbrodt, M.J. Heeg, H.B. Schlegel, C.H. Winter, J. Am. Chem. Soc. 122 (2000) 9338.
[18] Z.K. Yu, M.J. Heeg, C.H. Winter, Chem. Commun., (2001) 353.
[19] Z.K. Yu, J.M. Wittbrodt, A. Xia, M.J. Heeg, H.B. Schlegel, C.H. Winter, Organometallics 20 (2000) 4301.
[20] D.F. Rendle, A. Storr, J. Trotter, J. Chem. Soc., Dalton Trans. (1973) 2252.
[21] D.F. Rendle, A. Storr, J. Trotter, Can. J. Chem. 53 (1975) 2944.
[22] D.F. Rendle, A. Storr, J. Trotter, J. Chem. Soc., Dalton Trans. (1975) 176.
[23] D.J. Patmore, D.F. Rendle, A. Storr, J. Trotter, J. Chem. Soc., Dalton Trans. (1975) 718.
[24] D.F. Rendle, A. Storr, J. Trotter, Can. J. Chem. 53 (1975) 2930.
[25] K.S. Chong, S.J. Rettig, A. Storr, J. Trotter, Can. J. Chem. 56 (1978) 1212.
[26] K.R. Breakell, S.J. Rettig, D.L. Singbeil, A. Storr, J. Trotter, Can. J. Chem. 56 (1978) 2099.
[27] K.S. Chong, S.J. Rettig, A. Storr, J. Trotter, Can. J. Chem. 57 (1978) 1335.

[28] K.R. Breakell, S.J. Rettig, A. Storr, J. Trotter, Can. J. Chem. 57 (1979) 139.
[29] K.S. Chong, S.J. Rettig, A. Storr, J. Trotter, Can. J. Chem. 58 (1980) 1080.
[30] K.S. Chong, S.J. Rettig, A. Storr, J. Trotter, Can. J. Chem. 58 (1978) 1091.
[31] S.J. Rettig, A. Storr, J. Trotter, Can. J. Chem. 59 (1981) 2391.
[32] B.M. Louie, A. Storr, J. Trotter, Can. J. Chem. 62 (1984) 633.
[33] B.M. Louie, A. Storr, J. Trotter, Can. J. Chem. 63 (1985) 3019.
[34] E.C. Onyiriuka, S.J. Rettig, A. Storr, Can. J. Chem. 64 (1986) 321.
[35] G.A. Banta, B.M. Louie, E.C. Onyiriuka, S.J. Rettig, A. Storr, Can. J. Chem. 64 (1986) 373.
[36] D.L. Reger, S.J. Knox, L. Lebioda, Inorg. Chem. 28 (1989) 3092.
[37] D.L. Reger, S.J. Knox, L. Lebioda, Organometallics 9 (1990) 2218.
[38] F. Kratz, B. Nuber, J. Weiss, B.K. Keppler, Polyhedron 11 (1992) 487.
[39] P. Hodge, B. Piggott, Chem. Commun. (1998) 1933.
[40] G.A. Olah (Ed.), Friedel-Crafts and Related Reactions, vol. I–IV, Wiley Interscience, New York, 1963, p. 1965.
[41] D. Pahari, V.K. Jain, Main Group Metal Chem. 20 (1997) 691.
[42] N. Burford, T.S. Cameron, D.J. LeBlanc, P. Losier, S. Sereda, G. Wu, Organometallics 16 (1997) 4712.
[43] S. Schulz, L. Martinez, J.L. Ross, Adv. Mater. Opt. Electron. 6 (1996) 185.
[44] W.R. Nutt, J.S. Blanton, A.M. Boccanfuso, L.A. Silks, A.R. Garber, J.D. Odom, Inorg. Chem. 30 (1991) 4136.
[45] For leading references, see: C.H. Winter, Aldrichimica Acta 33 (2000) 3.
[46] M.A. Munoz-Hernandez, M.S. Hill, D.A. Atwood, Polyhedron 17 (1998) 2237.
[47] T.F. Kuech, Semicond. Sci. Technol. 8 (1993) 967.
[48] D. Guijarro, B. Mancheno, M. Yus, Tetrahedron 49 (1993) 1327.
[49] I.O. Shapiro, M. Nir, R.E. Hoffman, M. Rabinovitz, J. Chem. Soc., Perkin Trans. 2 (1994) 1519.
[50] C.R. Smoot, H.C. Brown, J. Am. Chem. Soc. 78 (1956) 6245.
[51] C.R. Smoot, H.C. Brown, J. Am. Chem. Soc. 78 (1956) 6249.
[52] H. Ulich, A. Keutmann, A. Geierhaas, Z. Elektrochem. 49 (1943) 292.
[53] H. Ulich, Angew. Chem. 55 (1942) 37.
[54] J. Lavaux, M. Lombard, Bull. Soc. Chim. Fr. (1910) 913–915.
[55] H. Wang, L.D. Kispert, H. Sang, J. Chem. Soc., Perkin Trans. II (1989) 1463.
[56] J.H. Clark, K. Martin, A.J. Teasdale, S.J. Barlow, J. Chem. Soc., Chem. Commun. (1995) 2037.
[57] M.D. Healy, J.W. Ziller, A.R. Barron, Organometallics 11 (1992) 3041.
[58] For leading references, see: F.P. DeHaan, M. Djaputra, M.W. Grinstaff, C.R. Kaufman, J.C. Keithly, A. Kumar, M.K. Kuwayama, K.D. Macknet, J. Na, B.R. Patel, M.J. Pinkerton, J.H. Tidwell, R.M. Villahermosa, J. Org. Chem. 62 (1997) 2694.
[59] R.J.H. Clark, B. Crociani, A. Wasserman, J. Chem. Soc. (A) (1970) 2458.
[60] C.A. Reed, N.A.P. Fackler, K.-C. Kim, D. Stasko, D.R. Evans, P.D.W. Boyd, C.E.F. Rickard, J. Am. Chem. Soc. 121 (1999) 6314.
[61] R. Rathore, S.H. Loyd, J.K. Kochi, J. Am. Chem. Soc. 116 (1994) 8414.
[62] G.A. Olah, R.H. Schlosberg, D.P. Kelly, G.D. Mateescu, J. Am. Chem. Soc. 92 (1970) 2546.
[63] H.H. Perkampus, E. Baumgarten, Angew. Chem., Int. Ed. Engl. 3 (1964) 776.
[64] C. Fernandez-Castano, C. Foces-Foces, N. Jagerovic, J. Elguero, J. Mol. Struc. 355 (1995) 265.
[65] C. Foces-Foces, L. Infantes, R.M. Claramunt, C. Lopez, N. Jagerovic, J. Elguero, J. Mol. Struc. 415 (1997) 81.
[66] For leading references, see: G. Aullon, D. Bellamy, L. Brammer, E.A. Bruton, A.G. Orpen, Chem. Commun. (1998) 653.
[67] J. Elguero, E. Gonzalez, R. Jacquier, Bull. Soc. Chim. Fr. (1968) 707.
[68] G. Sheldrick, SHELX-97, Institut für Anorg. Chemie, Tammann-strasse 4, D-37077 Göttingen, Germany.

PERGAMON

Polyhedron 21 (2002) 1125–1131

POLYHEDRON

www.elsevier.com/locate/poly

Hydrogen bonded supramolecular assemblies from uranyl ion complexes of tetrahomodioxacalix[4]arenes with various counterions

Bernardo Masci [a,*], Meri Gabrielli [a], Stefano Levi Mortera [a], Martine Nierlich [b], Pierre Thuéry [b,*]

[a] *Dipartimento di Chimica and Centro CNR di Studio sui Meccanismi di Reazione, Università 'La Sapienza', Box 34, Roma 62, P.le Aldo Moro 5, 00185 Rome, Italy*

[b] *CEA/Saclay, DSM/DRECAM/SCM (CNRS URA 331), Bât. 125, 91191 Gif-sur-Yvette, France*

Received 16 November 2001; accepted 22 January 2002

Abstract

Reaction of the expanded calixarenes *p*-*R*-tetrahomodioxacalix[4]arenes (*R* = methyl, phenyl) with uranyl ions in the presence of amines (butylamine, pyrrolidine, triethylamine) gives complexes in which the metal ion is in a distorted square-planar, tetra-phenoxide, equatorial environment. Changes in *para*-substituents and/or in the amine lead to different supramolecular assemblies, resulting in sheets or columns held by hydrogen bonds and cation–π interactions. The importance of primary or secondary amines, able to give divergent hydrogen bonds, to promote such structures, is evidenced. © 2002 Elsevier Science Ltd. All rights reserved.

Keywords: Uranyl ion; Calixarenes; Homooxacalixarenes; Supramolecular assembly; Crystal structures

1. Introduction

In the course of our investigation of uranyl ion complexes of calixarenes and homooxacalixarenes obtained in a basic medium [1], we have reported previously the first crystal structures of free and complexed *p*-*R*-tetrahomodioxacalix[4]arene (*R* = methyl, *tert*-butyl) [2–4]. In all cases, the conformation of the macrocycle is a distorted *cone* one, held by intramolecular hydrogen bonds involving both phenolic and ether oxygen atoms in the free form, and by internal, tetra-phenoxide uranyl bonding in the complex. We have recently investigated, in the case of the related compound *p*-*R*-hexahomotrioxacalix[3]arene (*R* = methyl, *tert*-butyl), the effect of changes in the base used for deprotonation (and subsequently in the counterion present in the solid state) on uranyl ion complexation [5]. Due to the usual feature of inclusion of the counterion in the macrocycle cavity, these changes result in slight modifications in the homooxacalixarene conformation and in the uranyl ion equatorial coordination geometry, which can be distorted trigonal, tetragonal or pentagonal, depending on the number of coordinating ether oxygen atoms. This study evidenced also the interest of primary or secondary amines as deprotonating agents, due to their ability to be involved in divergent hydrogen bonds and give rise by this way to supramolecular assemblies. We report in the present paper the results of a similar investigation in the case of *p*-*R*-tetrahomodioxacalix[4]arenes with *R* = methyl (L^1H_4) or phenyl (L^2H_4), represented in Scheme 1, and the bases triethylamine (NEt_3), butylamine (NBu) and pyrrolidine (pyr).

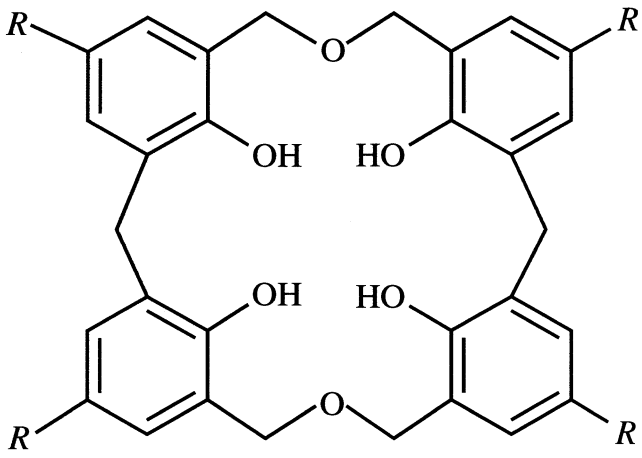
2. Results and discussion

The asymmetric unit in $[Hpyr]_2[UO_2(L^1)]\cdot 3H_2O$ **1** comprises two crystallographically independent but nearly identical complex molecules, denoted A and B in the following. As can be seen in Fig. 1 in the case of molecule A, the uranyl ion is in a slightly distorted square-planar equatorial environment, being bound to the four phenoxide groups, with bond lengths in the

* Corresponding authors. Tel.: +39-06-49-913703; fax: +39-06-49-0631 (B.M.); tel.: +33-01-69-086329; fax: +33-01-69-086640 (P.T.).

E-mail addresses: bernardo.masci@mail.uniroma1.it (B. Masci), thuery@drecam.cea.fr (P. Thuéry).

0277-5387/02/$ - see front matter © 2002 Elsevier Science Ltd. All rights reserved.
PII: S0277-5387(02)00896-3



Scheme 1. The *p*-*R*-tetrahomodioxacalix[4]arenes under study.

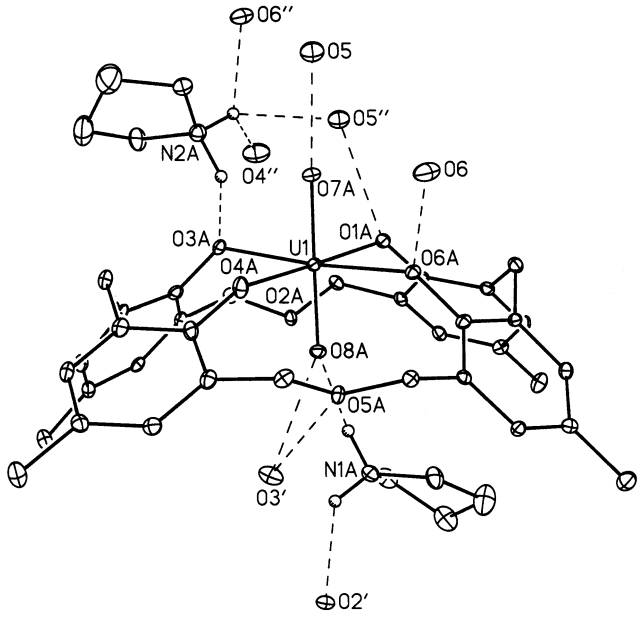


Fig. 1. View of molecule A in $[Hpyr]_2[UO_2(L^1)]\cdot 3H_2O$ **1**. Ellipsoids drawn at the 20% probability level. Hydrogen bonds represented as dashed lines. Ammonium protons drawn as small spheres of arbitrary radii. All other hydrogen atoms omitted for clarity. Symmetry codes: ′, $1-x, 1-y, 2-z$; ″, $1-x, 1-y, 1-z$.

range 2.225(4)–2.306(4) Å [mean value 2.27(3) Å, including both molecules] (Table 1). The uranium atom is consequently in a distorted, axially compressed, octahedral environment. The two ether oxygen atoms are clearly not coordinated, with U···O distances in the range 3.721(4)–3.796(4) Å. The range of $U-O_{phenoxide}$ bond lengths in **1** is comparable to that in the previously reported uranyl complex of *p*-*tert*-butyltetrahomodioxacalix[4]arene **4** (2.252(4)–2.333(4), mean value 2.28(3) Å) [2]. It is also close to the bond lengths in the distorted square–planar uranyl complexes of *p*-*tert*-butyldihomooxacalix[4]arene [2.247(6)–2.275(6), mean value 2.26(1) Å] [6a] and *p*-*tert*-butyltetrahomodioxacalix[6]arene [2.203(5)–2.301(6), mean value 2.26(4) Å] [6b], as well as to those in the more symmetrical uranyl complex of *p*-*tert*-butyltetrathiacalix[4]arene [2.230(2)–2.300(2), mean value 2.27(4) Å] [7a] and even the 'external' uranyl complex of *p*-*tert*-butylcalix[6]arene [2.22(1)–2.31(1), mean value 2.27(4) Å] [7b]. This range thus appears rather independent of the more-or-less regular square–planar geometry, and may be indicative in **1** and **4** of slightly too large donor atoms arrays, preventing the optimal bond length from being reached for all oxygen atoms (narrower ranges are observed for example in the trigonal uranyl complexes of hexahomotrioxacalix[3]arenes [5]). The four donor atoms in **1** define a plane O_4 with a r.m.s. deviation of 0.043 and 0.014 Å in molecules A and B, respectively, and the uranium atoms are located at 0.067(2) and 0.064(2) Å from these mean planes. The distances between the ether oxygen atoms and the O_4 planes are in the range 1.716(6)–2.005(6) Å, which are usual values for non-coordinated ether atoms [5]. The $O_{oxo}-U-O_{phenoxide}$ angles do not deviate much from 90°, but the $O_{phenoxide}-U-O_{phenoxide}$ angles involving adjacent atoms around the macrocycle are significantly different from this value, those between phenolic rings separated by methylenic bridges being smaller than those corresponding to ether bridges (mean values 85.3(4)° and 94.6(3)° in both cases, respectively). The macrocycles in **1** are in the *cone* conformation (a much more regular one than that of uncomplexed L^1H_4 [4]), with dihedral angles between the four aromatic rings and the O_4 plane of 46.4(2)°, 52.5(2)°, 30.3(2)° and 46.5(2)° in molecule A and 46.9(2)°, 49.9(1)°, 43.9(2)° and 30.9(2)° in molecule B. These values span a wider range than in compound **4** [40.0°–48.3°], one of the rings in particular being closer to the mean plane. The ether bridges in both molecules are characterized by *anti* $C-O-C-C_{arom}$ torsion angles [164.6(4)°–170.8(4)°], as in compound **4**. Each complex molecule is accompanied by two protonated pyrrolidine molecules. Both of these counterions possessing two nitrogen-bound protons and, moreover, three water molecules being present for each complex molecule, a most intricated hydrogen bonding pattern is formed (Table 2). In both molecules A and B, one of the pyrrolidinium ions is located near the macrocycle cavity and is hydrogen bonded to the oxo atom directed inwards. These ions are further bonded by their second protons to one or two (bifurcated bond) water molecules. The pyrrolidinium ions located out of the cavities are hydrogen bonded to one phenoxide oxygen atom and possibly, through their second protons, to three water molecules (trifurcated bonds). The water molecules make also hydrogen bonds with oxo, phenoxo and ether oxygen atoms. The resulting tridimensional ar-

Table 1
Environment of the uranium atom in compounds **1**–**3**: selected distances (Å) and angles (°)

1	U1–O(1A)	2.274(4)	O(1A)–U1–O(3A)	94.7(1)	U2–O(1B)	2.294(4)	O(1B)–U2–O(3B)	95.0(1)
	U1–O(3A)	2.306(4)	O(3A)–U1–O(4A)	84.9(1)	U2–O(3B)	2.278(3)	O(3B)–U2–O(4B)	85.6(1)
	U1–O(4A)	2.226(4)	O(4A)–U1–O(6A)	94.4(1)	U2–O(4B)	2.285(4)	O(4B)–U2–O(6B)	94.3(1)
	U1–O(6A)	2.284(4)	O(6A)–U1–O(1A)	85.9(1)	U2–O(6B)	2.225(4)	O(6B)–U2–O(1B)	85.0(1)
	U1–O(7A)	1.813(4)	O(7A)–U1–O(8A)	178.4(2)	U2–O(7B)	1.811(3)	O(7B)–U2–O(8B)	178.0(2)
	U1–O(8A)	1.807(4)			U2–O(8B)	1.811(4)		
2	U–O(1)	2.276(3)	O(1)–U–O(3)	95.1(1)				
	U–O(3)	2.309(3)	O(3)–U–O(1′)	84.6(1)				
	U–O(4)	1.785(4)	O(4)–U–O(5)	180.0				
	U–O(5)	1.803(4)						
3	U–O(1)	2.246(6)	O(1)–U–O(3)	93.7(2)				
	U–O(3)	2.280(5)	O(3)–U–O(4)	85.1(2)				
	U–O(4)	2.299(6)	O(4)–U–O(6)	94.0(2)				
	U–O(6)	2.287(6)	O(6)–U–O(1)	86.5(2)				
	U–O(7)	1.789(5)	O(7)–U–O(8)	179.0(3)				
	U–O(8)	1.783(5)						

Symmetry code: ′, $-x, y, 0.5-z$.

rangement displays hydrogen bonded sheets bisecting the planes *ac* and *bc* (Fig. 2).

$[HNEt_3]_2[UO_2(L^2)]\cdot 2CHCl_3$ **2** involves the same tertiary amine as compound **4**, from which it differs by its *para*-substituent, phenyl in **2**, *tert*-butyl in **4**. The asymmetric unit comprises half a complex molecule, the other half being obtained through the binary axis containing the uranyl ion (Fig. 3). The uranyl ion is bound, as in **1** and **4**, to the four phenoxide groups, with U–O bond lengths of 2.276(3) and 2.309(3) [mean value 2.29(2)] Å, the ether oxygen atoms being at a distance of 3.715(3) Å. The mean O_4 plane presents a r.m.s. deviation of 0.081 Å, the uranium atom being at 0.149(2) Å from it. The main geometrical features around the metal ion are identical to those in compounds **1** and **4** and will not be further described. The macrocycle is in a cone conformation but two aromatic rings are much closer to the O_4 plane than the two other ones [dihedral angles 54.44(9)° and 30.62(8)°, respectively]. The dihedral angles between the phenolic rings and their phenyl substituents are 43.1(1)° and 22.5(2)°. The ether bridges correspond to *anti* C–O–C–C_{arom}

Table 2
Hydrogen bonding geometry in compounds **1**–**3**: selected distances (Å) and angles (°)

	X···Y		X–H		H···Y		X–H···Y	
1	N(1A)···O(8A)	2.942(6)	N(1A)–H(1A)	0.99	H(1A)···O(8A)	2.08	N(1A)–H(1A)···O(8A)	144.7
	N(1A)···O(2′)	2.797(6)	N(1A)–H(2A)	0.96	H(2A)···O(2′)	2.06	N(1A)–H(2A)···O(2′)	132.2
	N(2A)···O(3A)	2.739(6)	N(2A)–H(3A)	1.15	H(3A)···O(3A)	1.66	N(2A)–H(3A)···O(3A)	153.7
	N(2A)···O(4″)	2.908(7)	N(2A)–H(4A)	0.98	H(4A)···O(4″)	2.32	N(2A)–H(4A)···O(4″)	118.2
	N(2A)···O(5″)	2.949(7)	N(2A)–H(4A)	0.98	H(4A)···O(5″)	2.28	N(2A)–H(4A)···O(5″)	124.5
	N(2A)···O(6″)	3.042(7)	N(2A)–H(4A)	0.98	H(4A)···O(6″)	2.31	N(2A)–H(4A)···O(6″)	130.5
	N(1B)···O(8B)	3.025(7)	N(1B)–H(2B)	0.90	H(2B)···O(8B)	2.19	N(1B)–H(2B)···O(8B)	154.7
	N(1B)···O(4)	2.947(9)	N(1B)–H(1B)	0.90	H(1B)···O(4)	2.48	N(1B)–H(1B)···O(4)	112.5
	N(1B)···O(5)	2.794(7)	N(1B)–H(1B)	0.90	H(1B)···O(5)	1.98	N(1B)–H(1B)···O(5)	149.3
	N(2B)···O(1)	3.004(7)	N(2B)–H(3B)	1.08	H(3B)···O(1)	2.23	N(2B)–H(3B)···O(1)	127.1
	N(2B)···O(2)	2.970(7)	N(2B)–H(3B)	1.08	H(3B)···O(2)	2.21	N(2B)–H(3B)···O(2)	125.6
	N(2B)···O(3)	3.024(7)	N(2B)–H(3B)	1.08	H(3B)···O(3)	2.36	N(2B)–H(3B)···O(3)	118.1
	N(2B)···O(1B)	2.770(6)	N(2B)–H(4B)	1.00	H(4B)···O(1B)	1.85	N(2B)–H(4B)···O(1B)	152.0
2	N···O(3)	2.857(5)	N–H(1)	1.03	H(1)···O(3)	1.85	N–H(1)···O(3)	165.7
3	N(1)···O(4)	2.772(8)	N(1)–H(1)	0.81	H(1)···O(4)	1.97	N(1)–H(1)···O(4)	174.1
	N(1)···O(10)	2.799(9)	N(1)–H(2)	0.87	H(2)···O(10)	1.93	N(1)–H(2)···O(10)	178.4
	N(1)···O(11)	2.829(10)	N(1)–H(3)	1.00	H(3)···O(11)	1.89	N(1)–H(3)···O(11)	155.1
	N(2)···O(3″)	2.784(9)	N(2)–H(6)	0.96	H(6)···O(3″)	1.85	N(2)–H(6)···O(3″)	163.7
	N(2)···O(9)	2.741(10)	N(2)–H(4)	0.96	H(4)···O(9)	1.83	N(2)–H(4)···O(9)	157.9
	N(2)···O(10″)	2.849(9)	N(2)–H(5)	1.00	H(5)···O(10″)	1.86	N(2)–H(5)···O(10″)	170.7
	N(3)···O(11)	2.816(10)	N(3)–H(8)	0.93	H(8)···O(11)	1.92	N(3)–H(8)···O(11)	160.2
	N(3)···O(12)	2.764(12)	N(3)–H(7)	1.15	H(7)···O(12)	1.80	N(3)–H(7)···O(12)	137.7
	O(11)···O(2‴)	2.799(8)	O(11)–H(10)	0.89	H(10)···O(2‴)	1.93	O(11)–H(10)···O(2‴)	166.1
	O(11)···O(6)	2.719(8)	O(11)–H(11)	0.87	H(11)···O(6)	1.86	O(11)–H(11)···O(6)	168.1

Symmetry codes: ′, $1-x, 1-y, 2-z$; ″, $1-x, 1-y, 1-z$; ‴, $x, 0.5-y, 0.5+z$.

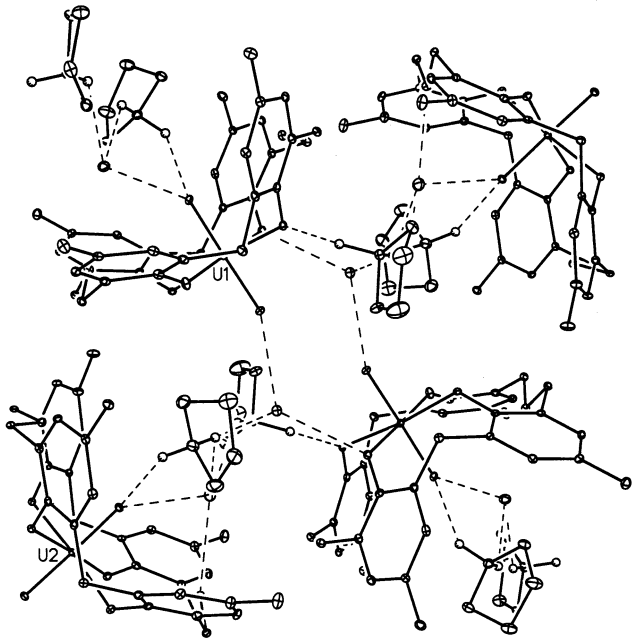


Fig. 2. Partial view of the crystal packing in $[Hpyr]_2[UO_2(L^1)]\cdot 3H_2O$ **1** showing the formation of hydrogen bonded sheets. Ellipsoids drawn at the 10% probability level. Hydrogen bonds represented as dashed lines. Ammonium protons drawn as small spheres of arbitrary radii. All other hydrogen atoms omitted for clarity.

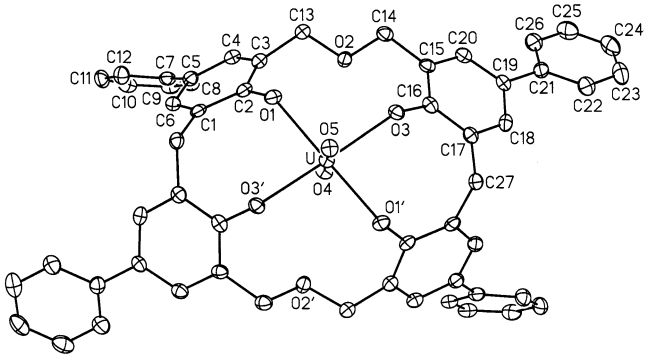


Fig. 3. View of the anionic complex molecule in $[HNEt_3]_2[UO_2(L^2)]\cdot 2CHCl_3$ **2**. Ellipsoids drawn at the 50% probability level. Hydrogen atoms, counterions and solvent molecules omitted for clarity. Symmetry code: ′, $-x, y, 0.5-z$.

torsion angles [−162.3(3)° and 173.4(3)°]. The most original feature is the counterions arrangement and the resulting crystal packing. The triethylammonium ions are not located as they were in compound **4**, i.e. one inside the cavity and hydrogen bonded to an oxo atom and the other outside and linked to a phenoxide group. In compound **2**, the two equivalent ammonium ions are located outside the cavity of the complex molecule to which they are hydrogen bonded through phenoxide oxygen atoms and they are further included in the cavity of the neighboring molecule along the *b*-axis. The location of the counterions, sandwiched between the phenolic rings closer to the mean plane in both neighboring molecules, probably explains the distortion with respect to the *cone* geometry indicated above. The combination of hydrogen bonds and cation–π interactions thus gives rise to a columnar arrangement, as represented in Fig. 4. Several short contacts exist between the carbon atoms of the triethylammonium cation and those of the aromatic rings (either phenolic or phenyl rings) with distances as short as 3.39 Å, comparable to those previously observed in other complexes and discussed in relation with cation–π interactions [5]. Some weaker contacts involve the cations and the phenyl rings of molecules belonging to the neighboring columns, with a shorter distance of 3.80 Å. Few contacts exist between phenolic and phenyl rings from different molecules, the shortest distance being 3.50 Å, and π–π interactions seemingly do not play an important part in this stacking. The disordered chloroform molecules are located in the spaces between the columns.

The complex obtained from the same ligand L^2H_4 and butylamine as a base, $[HNBu]_2[UO_2(L^2)]\cdot(HNBu)\cdot(CH_3COO)\cdot 2H_2O$ **3**, is an example of the ability of primary amines, combined with water molecules, to give rise to extended hydrogen bonded networks, similarly to what is observed with secondary amines in compound **1**.

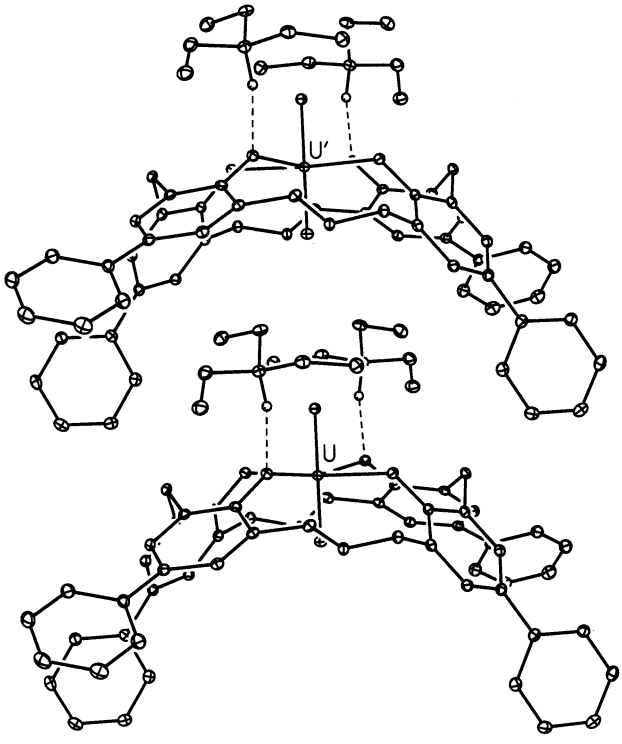


Fig. 4. View of the crystal packing showing the formation of columns along the *b*-axis in $[HNEt_3]_2[UO_2(L^2)]\cdot 2CHCl_3$ **2**. Ellipsoids drawn at the 20% probability level. Hydrogen bonds represented as dashed lines. Ammonium protons drawn as small spheres of arbitrary radii. All other hydrogen atoms and solvent molecules omitted for clarity.

Uranyl complexation in compound **3**, which does not present any crystallographic symmetry, displays the same geometrical features as that in compounds **1**, **2** and **4**, with tetra-phenoxide coordination {range of U–O bond lengths 2.246(6)–2.299(6) [mean value 2.28(2)] Å; ether oxygen atoms at 3.718(5) and 3.678(6) Å from uranium} and a departure of the uranium atom from the O_4 mean plane (r.m.s. deviation 0.023 Å) of 0.118(3) Å. The dihedral angles between the phenolic rings and the O_4 mean plane are 43.0(3)°, 38.9(2)°, 44.7(2)° and 46.8(2)°, evidencing a more regular cone conformation than in compound **2**, and the dihedral angles between phenolic and phenyl rings are 28.4(6)°, 27.1(4)°, 10.8(4)° and 28.4(4)°/29.7(5)° (the last phenyl ring being disordered over two positions). The complex molecule is associated to its two butylammonium counterions and, moreover, an additional butylammonium ion is present, its charge being compensated by that of an acetate ion. Two water molecules complete this assemblage of small molecules and ions. As in compound **1**, all these species and the complex itself are linked by an extended hydrogen bond network, as can be seen in Fig. 5 and Table 2. It can be noted that one of the butylammonium ions [comprising N(3)] is bound to the macrocycle, not directly, but *via* two water molecules [O(11) and O(12)]. As illustrated in Fig. 6, hydrogen bonded undulated sheets parallel to the *bc* plane are formed in **3**, in a way analogous to that in compound **1**, but different from the columnar stacking observed with the same macrocycle in compound **2**. Four species are deeply imbedded in the macrocyclic cavity: two butylammonium ions and the two water molecules. The two butylammonium ions are those corresponding to nitrogen atoms N(1) and N(3), with shortest $C_{ammonium}\cdots C_{phenyl}$ contacts of 3.65 and 3.34 Å, respectively (some shortest contacts between one of the disordered positions of the second cation and one disordered position of a phenyl ring are not physically acceptable and indicate that these two disordered components cannot be occupied simultaneously). These two butylammonium ions occupy the cavity spaces located at the vertical of the methylenic bridges. The spaces at the vertical of the ether bridges are occupied by the two water molecules, each of them being hydrogen bonded to the corresponding ether oxygen atom.

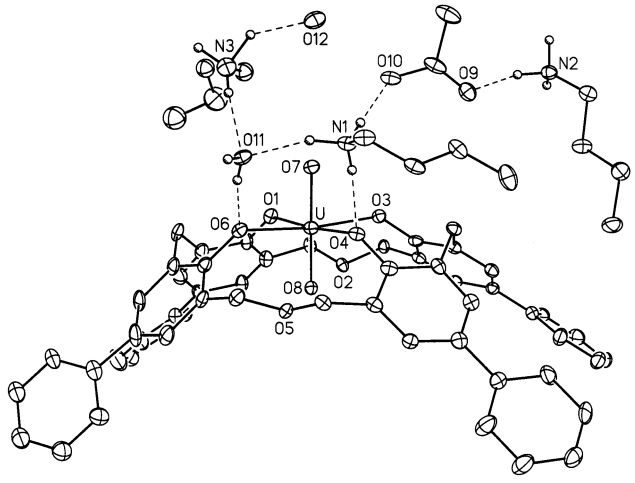


Fig. 5. View of the complex molecule in $[HNBu]_2[UO_2(L^2)]\cdot(HNBu)\cdot(CH_3COO)\cdot 2H_2O$ **3**. Ellipsoids drawn at the 20% probability level. Hydrogen bonds represented as dashed lines. Ammonium and water protons drawn as small spheres of arbitrary radii. All other hydrogen atoms omitted for clarity.

The previous study of *para*-substituent and basic agent replacement in the uranyl complexes of *p*-*R*-hexahomotrioxacalix[3]arene (*R* = methyl, *tert*-butyl) evidenced an effect of these changes on the coordination geometry around the cation, since distorted trigonal, tetragonal and pentagonal equatorial coordinations could be obtained [5]. The propensity of primary and secondary amines (butylamine and dibutylamine) to give rise to hydrogen bonded polymers was also apparent. In the present work, no effect on uranyl coordination is observed, which may be ascribed to the much more stable character of the square planar coordination with respect to the trigonal one. However, the potential of primary and secondary amines for the building of supramolecular assemblies through hydrogen bonding (possibly involving other solvent molecules or ions) and cation–π interactions has been extended and examples have been given of planar or columnar arrangements.

3. Experimental

3.1. Synthesis

The synthesis of L^1H_4 will be described elsewhere [8]. L^2H_4 was prepared as previously reported [9] and purified through column chromatography (silica gel, chloroform–hexane 3:5).

3.1.1. $[Hpyr]_2[UO_2(L^1)]\cdot 3H_2O$ (**1**)

A solution of L^1H_4 (20 mg, 0.037 mmol) and uranyl acetate dihydrate (20 mg, 0.047 mmol) in MeCN (7 ml) was heated to reflux under stirring. Pyrrolidine (150 mg, 1.9 mmol) was then added dropwise. Red–brown crystals suitable for X-ray crystallography separated in a few days.

3.1.2. $[HNEt_3]_2[UO_2(L^2)]\cdot 2CHCl_3$ (**2**)

A solution of L^2H_4 (49 mg, 0.062 mmol) and uranyl acetate dihydrate (30 mg, 0.071 mmol) in MeOH (4 ml) was heated to reflux under stirring. Triethylamine (250 mg, 2.5 mmol) was then added dropwise. The dark-brown solid that separated on slow solvent evaporation at room temperature (r.t.) was recrystallized from $CHCl_3$–MeOH to yield orange crystals suitable for X-ray crystallography.

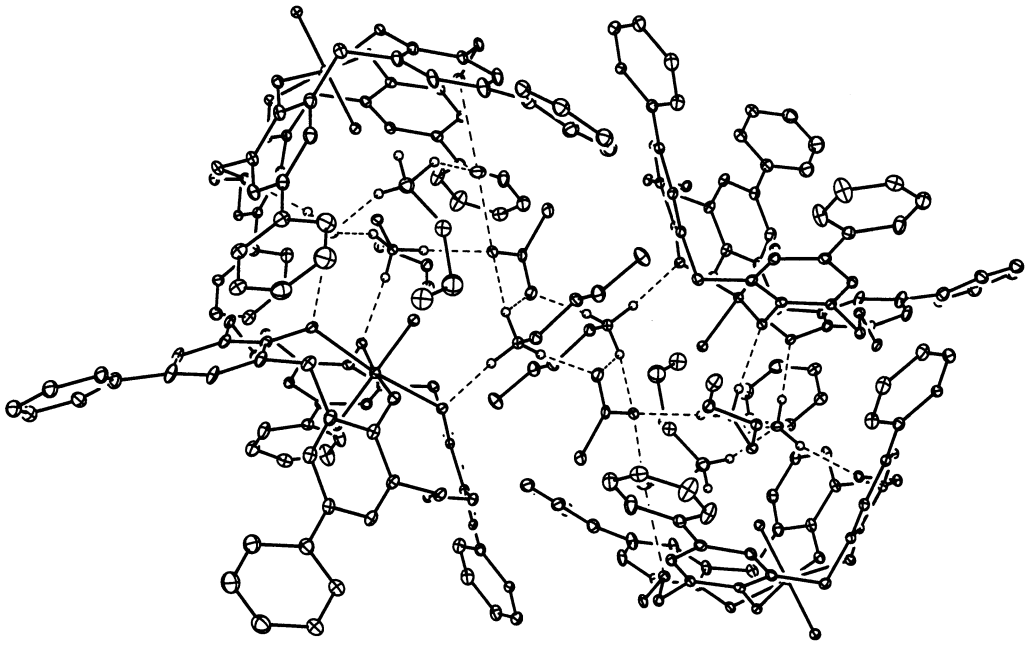


Fig. 6. Partial view of the crystal packing in $[HNBu]_2[UO_2(L^2)]\cdot(HNBu)\cdot(CH_3COO)\cdot 2H_2O$ **3** showing the formation of hydrogen bonded sheets. Ellipsoids drawn at the 10% probability level. Hydrogen bonds represented as dashed lines. Ammonium and water protons drawn as small spheres of arbitrary radii. All other hydrogen atoms omitted for clarity.

3.1.3. $[HNBu]_2[UO_2(L^2)]\cdot(HNBu)\cdot(CH_3COO)\cdot 2H_2O$ (**3**)

A solution of L^2H_4 (15 mg, 0.019 mmol) and butylamine (150 mg, 2.1 mmol) in MeCN (7 ml) was heated to reflux under stirring and uranyl acetate dihydrate (10 mg, 0.024 mmol) was then added gradually. Orange crystals suitable for X-ray crystallography separated in a few days.

3.2. Crystallography

The data were collected at 100(2) K on a Nonius kappa-CCD area detector diffractometer [10] using graphite-monochromated Mo Kα radiation (0.71073 Å). The crystals were introduced in glass capillaries with a protecting 'Paratone' oil (Exxon Chemical Ltd.) coating. The unit cell parameters were determined from the reflections collected on ten frames and were then refined on all data (90 frames, φ-scans, 2° steps). The data were processed with DENZO-SMN [11]. The structures were solved by Patterson map interpretation (compounds **1** and **3**) or by direct methods (compound **2**) with SHELXS-97 [12] and subsequent Fourier-difference synthesis and refined by full-matrix least-squares on F^2 with SHELXL-97 [13]. Absorption effects were corrected empirically with the program DELABS from PLATON [14]. Special features for each structure:

1 The hydrogen atoms bound to nitrogen have been found on the Fourier-difference map, except those bound to N(1B), which have been introduced at calculated positions. The protons of the water molecules have not been found, nor introduced.

2 The chlorine atoms of the chloroform molecule are disordered over two sites which have been refined with some restraints on bond lengths and with occupancy factors constrained to sum to unity. The hydrogen atoms bound to nitrogen and that of the chloroform molecule have been found on the Fourier-difference map.

3 One phenyl substituent and one butylammonium ion were found disordered over two positions, which were refined with occupancy factors constrained to sum to unity. Some restraints on bond lengths have been used and the disordered phenyl rings have been refined as idealized hexagons. The hydrogen atoms bound to nitrogen and oxygen atoms have been found on the Fourier-difference map, except those bound to O(12). The three hydrogen atoms of the disordered butylammonium ion have been kept as found, which clearly does not describe perfectly their disordered nature.

All non-hydrogen atoms were refined with anisotropic displacement parameters, except those of the disordered parts of one butylammonium ion in **3**. All other hydrogen atoms were introduced at calculated positions, except in the disordered parts. The hydrogen atoms were treated as riding atoms with an isotropic displacement parameter equal to 1.2 (OH, NH, CH, CH_2) or 1.5 (CH_3) times that of the parent atom. Crystal data and structure refinement details are given in Table 3. The

Table 3
Crystal data and structure refinement details

	1	2	3
Empirical formula	$C_{42}H_{58}N_2O_{11}U$	$C_{68}H_{74}Cl_6N_2O_8U$	$C_{68}H_{83}N_3O_{12}U$
M (g mol^{-1})	1004.93	1498.02	1372.40
Temperature (K)	100(2)	100(2)	100(2)
Crystal system	triclinic	monoclinic	monoclinic
Space group	$P\bar{1}$	$C2/c$	$P2_1/c$
a (Å)	14.9824(5)	36.490(2)	17.4406(7)
b (Å)	16.8460(5)	8.2821(4)	23.1260(12)
c (Å)	17.7805(7)	22.0199(7)	16.2386(6)
α (°)	86.862(2)		
β (°)	86.610(2)	106.736(2)	92.017(4)
γ (°)	66.507(2)		
V (Å^3)	4106.1(2)	6372.8(5)	6545.5(5)
Z	4	4	4
μ (mm^{-1})	4.015	2.856	2.541
Reflections collected	28 472	21 128	43 906
Independent reflections	14 439	6014	12 293
Observed reflections [$I > 2\sigma(I)$]	11 331	5379	8383
R_{int}	0.044	0.064	0.097
Parameters	1017	417	773
R_1	0.037	0.035	0.069
wR_2	0.077	0.080	0.145
S	1.019	1.072	1.113

molecular plots were drawn with SHELXTL [15]. All calculations were performed on a Silicon Graphics R5000 workstation.

4. Supplementary material

Crystallographic data for the structural analysis have been deposited with the Cambridge Crystallographic Data Center as supplementary publication CCDC no. 174000–174002. Copies of the data can be obtained free of charge from the Director, CCDC, 12 Union Road, Cambridge CB2 1EZ, UK (fax: +44-1223-336033; e-mail: deposit@ccdc.cam.ac.uk or www: http://www.ccdc.cam.ac.uk).

References

[1] For reviews on this topic, see: (a) J. Harrowfield, Gazz. Chim. Ital. 127 (1997) 663;
(b) P. Thuéry, M. Nierlich, J. Harrowfield, M. Ogden, in: Z. Asfari, V. Böhmer, J. Harrowfield, J. Vicens (Eds.), Calixarenes 2001, Kluwer Academic Publishers, Dordrecht, 2001.
[2] P. Thuéry, M. Nierlich, J. Vicens, B. Masci, H. Takemura, Eur. J. Inorg. Chem. (2001) 637.
[3] P. Thuéry, M. Nierlich, J. Vicens, B. Masci, Acta Crystallogr. Sect. C 57 (2001) 70.
[4] P. Thuéry, M. Nierlich, J. Vicens, B. Masci, Acta Crystallogr. Sect. C 57 (2001) 833.
[5] B. Masci, M. Nierlich, P. Thuéry, New J. Chem. 26 (2002) 120.
[6] (a) J.M. Harrowfield, M.I. Ogden, A.H. White, J. Chem. Soc., Dalton Trans. (1991) 979;
(b) P. Thuéry, M. Nierlich, J. Vicens, B. Masci, J. Chem. Soc., Dalton Trans. (2001) 867.
[7] (a) Z. Asfari, A. Bilyk, J.W.C. Dunlop, A.K. Hall, J.M. Harrowfield, M.W. Hosseini, B.W. Skelton, A.H. White, Angew. Chem., Int. Ed. 40 (2001) 721;
(b) P. Thuéry, M. Lance, M. Nierlich, Supramol. Chem. 7 (1996) 183.
[8] B. Masci, to be published.
[9] K. No, Bull. Korean Chem. Soc. 20 (1999) 33.
[10] Kappa-CCD Software, Nonius B.V., Delft, 1998.
[11] Z. Otwinowski, W. Minor, Methods Enzymol. 276 (1997) 307.
[12] G.M. Sheldrick, Acta Crystallogr. Sect. A 46 (1990) 467.
[13] G.M. Sheldrick, SHELXL-97, Program for the Refinement of Crystal Structures, University of Göttingen, 1997.
[14] A.L. Spek, PLATON, University of Utrecht, 2000.
[15] G.M. Sheldrick, SHELXTL, Version 5.1, University of Göttingen, distributed by Bruker AXS Inc., Madison, WI, 1999.

PERGAMON

Polyhedron 21 (2002) 1133–1138

POLYHEDRON

www.elsevier.com/locate/poly

The separation of *cis*- and *trans*-1,3-cyclohexanediol isomers by copper complexation. Crystal structures of *cis*-1,3-cyclohexanediol and copper(II) chloride *cis*-1,3-cyclohexanediol complex

Ari Lehtonen [a], Raikko Kivekäs [b], Reijo Sillanpää [c,*]

[a] *Department of Chemistry, University of Turku, FIN-20014 Turku, Finland*
[b] *Department of Chemistry, University of Helsinki, FIN-00014 Helsinki, Finland*
[c] *Department of Chemistry, University of Jyväskylä, FIN-40351 Jyväskylä, Finland*

Received 8 January 2002; accepted 13 March 2002

Abstract

A 1:1 complex between copper(II) chloride and *cis*-1,3-cyclohexanediol has been synthesized and its crystal structure determined. The structure is composed of two different dinuclear $[CuCl_2(c\text{-}13chd)]_2$ units in which the copper(II) ions are surrounded by the two oxygen atoms of the diol and the two halide ions in a distorted *cis*-square planar arrangement in both cases. A fifth coordination site is occupied by a halide ion in one dinuclear unit for both copper ions and an O atom belonging to the adjacent $CuCl_2(c\text{-}13chd)$ moiety in the other dinuclear unit for both copper ions, thus forming a distorted square pyramidal geometry for the metals in all cases. The ability of $CuCl_2$ to preferentially form a complex with *cis*-1,3-cyclohexanediol renders it amenable to the separation of the *cis*- and *trans*-isomers of 1,3-cyclohexanediol as the *trans*-isomer is not able to form such a complex with $CuCl_2$ and neither are any mixed complexes formed. The crystal structure of *cis*-1,3-cyclohexanediol is also reported for comparative purposes. © 2002 Elsevier Science Ltd. All rights reserved.

Keywords: Crystal structures; Copper(II) complexes; Cyclohexanediols; Separation of isomers

1. Introduction

Neutral diols and polyols form relatively unstable complexes with metal ions [1]. The packing of these complexes in the solid state is mainly controlled by second-sphere coordination [2] with hydrogen bonding playing a dominant role [3]. Due to the moderately low coordination ability of these ligands the syntheses of their metal complexes can usually be accomplished only in weakly coordinating solvents. Aprotic solvents such as tetrahydrofuran, 1,2-dimethoxyethane, or acetonitrile generally suffice for this purpose.

The copper(II) halides that form complexes with 1,2-diols do so with varying degrees of stoichiometry. For example, 1 equiv. of copper(II) chloride can complex with 0.5, 1, 1.5, or 2 equiv. of the diols 1,2-ethanediol, *cis*- or *trans*-1,2-cyclohexanediol, *trans*-1,2-cycloheptanediol, or 2,3-dimethyl-2,3-butanediol. The basic structure of these complexes consists of a $CuCl_2$–(diol) complex unit in which the diol is coordinated to copper as a bidentate ligand, and the complex units are linked as dimers or polymers through halogen bridges. If the stoichiometry is 1.5 or 2, only one diol molecule is directly coordinated to the copper(II) ion, and the $CuCl_2$–(diol) units are linked to the uncoordinated diol molecules through hydrogen bonds [4–7]. If the metal has a weakly coordinating counter anion, e.g. sulfate, then the metal ion can retain its coordination number by bonding to more than two diols as in $[Cu(eg)_3]SO_4$, where eg = 1,2-ethanediol [8a]. However, if strongly coordinating solvents such as water are present, mixed complexes such as $[Cu(eg)_2(H_2O)_2SO_4]$ are formed [8b]. The structure of the latter contains eg ligands which act as a bridge between two copper(II) ions. These observations illustrate that the structure of the 1,2-diol complexes depends on the diol used (the size

* Corresponding author. Tel.: +358-14-260-2603; fax: +358-14-260-2501.
E-mail address: resillan@jyu.fi (R. Sillanpää).

0277-5387/02/$ - see front matter © 2002 Elsevier Science Ltd. All rights reserved.
PII: S0277-5387(02)00934-8

and the shape), the metal-to-diol stoichiometry, the solvent, and the counter anion of the metal ion itself.

For 1,3-diols several transition metal complexes have been prepared, although the 1,3-diols are generally weaker ligands than their comparable 1,2-diols [9]. 1,3,5-Substituted triols, such as *per*-*cis*-1,3,5-cyclohexanetriol [10] and 2-ethyl-2-hydroxymethyl-1,3-propanediol [11], form 1:1 complexes with $CuCl_2$. The former is coordinated to copper(II) in a tridentate manner, whilst the latter is a bidentate ligand to the copper(II) ion. Surprisingly, there appear to be no prior structural reports on the metal complexes of non-mixed 1,3-diols. To address this deficiency we have now extended our work on diol coordination chemistry to the copper(II) complexes of 1,3-cyclohexanediols, and it was found that only *cis*-1,3-cyclohexanediol (*c*-13chd), and not the isomeric *trans*-1,3-cyclohexanediol (*t*-13chd), forms a complex with $CuCl_2$. Furthermore, *c*-13chd does so only in a 1:1 stoichiometry.

Metal complexation as a methodology for the separation of isomeric organic compounds has been successfully accomplished previously. For example, various alcohols and phenols have been resolved using anhydrous $CaCl_2$, $CaBr_2$, and $MnCl_2$ as the complexing substrate [12,13]. In particular, mixtures of the *E* and *Z* isomers of α-hydroxyimino phosphonates have been separated by selective complexation to the Cu(II) ion [14]. Furthermore, the commercially available ligand *N*,*N*′-ethylenebis[2-(*o*-hydroxyphenyl)glycine] has been separated into racemic and *meso* isomers via Fe(III) complexes [15]. The complexation of carbohydrates with calcium(II) ion has also been employed for the separation of sugars and polyols on ion-exchange resins [16]. Given the above divergence in complexation between the *cis*- and *trans*-isomers of 1,3-cyclohexanediol towards $CuCl_2$, this approach was explored as a methodology for the separation of the two isomers. In practice it was found to be a simple and practical method for their separation. The crystal structures of both *cis*-1,3-cyclohexanediol and [$CuCl_2$(*c*-13chd)] complex are also described in this work.

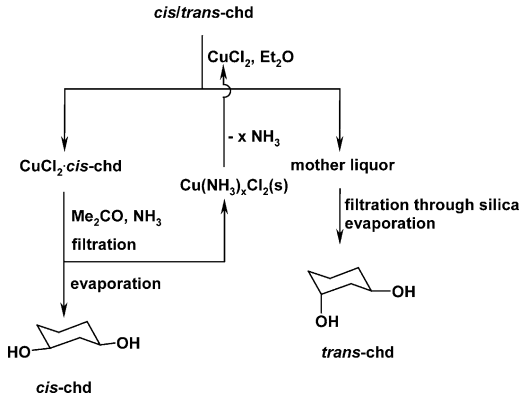
2. Results and discussion

2.1. Syntheses and separation

Copper(II) chloride is only slightly soluble in acetonitrile, resulting in a pale yellow solution. Upon the addition of a mixture of *cis*- and *trans*-1,3-cyclohexanediols to the $CuCl_2$ acetonitrile solution, the color of the solution turned green or greenish–yellow depending on the concentration of the diol. The colors of the various solutions are qualitatively indicative of a low coordination power of the diol for copper. The color, though, is temperature-dependent, and the solution changes to a more intense green upon lowering of the temperature. On standing at room temperature green crystals were found to be formed, which were separated by decanting, and the formula was determined to be [$CuCl_2$(*c*-13chd)]. Variation of the $CuCl_2$ to diol ratio and using only *c*-13chd as a ligand did not result in complexes other than the 1:1 complex. If more than 1.8 equiv. of diol was present in acetonitrile solution, uncoordinated diol was also found to crystallize out together with the complex.

The conventional methodology to separate the isomeric *cis*- and *trans*-1,3-cyclohexanediols is by the sole formation of the cyclic acetal for *c*-13chd which is then separated by distillation from the *trans* isomer. The diol *c*-13chd is regenerated by hydrolysis [18], whilst *t*-13chd is recovered, albeit in a compromised state, from the distillation residues. Although quite satisfactory, the methodology requires extensive repurification of the *t*-13chd isomer, which may not be that well separated from the *c*-13chd isomer, and is somewhat cumbersome for the production of the *c*-13chd isomer. Thus the observations just described suggested a possible avenue for creating a practical and possibly general method for the separation of 1,3-diol isomers via the preferential reaction of $CuCl_2$ with *c*-13chd. Indeed, the separation was accomplished successfully in diethyl ether solution; THF and hexane were also tried as solvents but with only limited success. The underlying reason for the success of diethyl ether is that whilst diols are reasonably soluble in ether, Cu(II)–diol complexes on the other hand are only very slightly soluble. This dramatic difference in solubility means that after the formation of the Cu(II)–diol complex, physical separation is afforded simply by filtration. Regeneration of the *c*-13chd isomer was also found to be similarly accomplished by the hydrolysis of the acetals using mild conditions. The complex was dissolved in acetone, and ammonia gas was bubbled through the solution for a few minutes until $Cu(NH_3)_xCl_2$ precipitated out. (Presumably five ammonias are complexed to the copper, i.e. $x = 5$.) The ammine Cu complex was filtered off and the filtrate solution evaporated to produce pure *cis*-1,3-cyclohexanediol. $CuCl_2$ can be regenerated from the $Cu(NH_3)_xCl_2$ complex simply by heating to release the ligand-bound ammonias for subsequent reuse.

Although the ether filtrate after removal of the Cu(II)–diol complex clearly still contained copper(II) ions as indicated by the light green color of the solution, these impurities were readily and easily removed by filtration through silica gel. From this filtrate, essentially pure *t*-13chd was obtained by removal of the solvent. Unfortunately, X-ray quality crystals were not forthcoming from an ethyl acetate solution. Sublimation provided extremely pure and microcrystalline *t*-13chd, but the material readily softened and became oily upon standing, even within a closed vessel (Scheme 1).



Scheme 1.

2.2. The structure of the complex *1*

The solid-state structure of $CuCl_2$(*c*-13chd) is composed of two distinct dinuclear units. The two different dimeric $[CuCl_2(c\text{-13chd})]_2$ units and their atomic numbering are depicted in Fig. 1 which shows that the diol in order to be able to accommodate coordination to the metal must adopt a cyclohexane ring conformation whereby both OH groups are axially orientated, in this case a chair conformation. Clearly, the adoption of a suitable cyclohexane ring conformation in the *trans* isomer for complexation is unfavorable; hence the distinction in the formation of isolatable complexes. In both dinuclear units (**a** and **b**) the copper(II) ions are surrounded by two oxygen atoms of the diol and two halide ions in a distorted *cis*-square planar arrangement. The fifth coordination site in **a** is occupied by a halide ion. In **b** an O atom that belongs to the adjacent $CuCl_2$(diol) unit fulfils the fifth coordination site. Both structures represent a distorted square pyramidal geometry for a metal ion. Selected bond parameters are presented in Table 2. The halide-bridged $[CuCl_2(c\text{-13chd})]_2$ unit is similar to other dinuclear $[CuCl_2(diol)]_2$ complexes that have been described. The neutral OH-bridged structure seen in the other $[CuCl_2(c\text{-13chd})]_2$ dinuclear unit has not been described previously in diol–metal complexes.

Table 1
Crystal data and experimental details of the structure determination of $CuCl_2 \cdot c$-13chd (**1**) and *c*-13chd (**2**)

	1	**2**
Formula	$C_6H_{12}CuCl_2O_2$	$C_6H_{12}O_2$
M_r	250.61	116.16
Crystal system	monoclinic	monoclinic
Space group (no.)	$P2_1/c$ (14)	$P2_1/n$ (14)
a (Å)	12.1286(13)	5.382(3)
b (Å)	19.002(4)	19.669(2)
c (Å)	8.1452(9)	6.868(2)
β (Å)	90.46 (1)	110.78(3)
U (Å^3)	1877.1(5)	679.8(5)
Z	8	4
μ(Mo Kα) (cm^{-1})	28.46	0.83
Observed reflections	3304	1192
Parameters	212	109
R_1 [a]	0. 092 (0.054) [b]	0.069 (0.046)
wR_2 [c]	0.114 (0.103)	0.121 (0.104)

[a] $R_1 = \Sigma||F_o|-|F_c||/\Sigma|F_o|$.
[b] Values in parentheses for reflections with $I > 2.0\sigma(I)$.
[c] $wR_2 = \{\Sigma[w(F_o^2 - F_c^2)^2]/\Sigma[w(F_o^2)^2]\}^{1/2}$ and $w = 1/[\sigma^2(F_o^2) + (aP)^2 + bP]$, where $P = (2F_c + F_o^2)/3$.

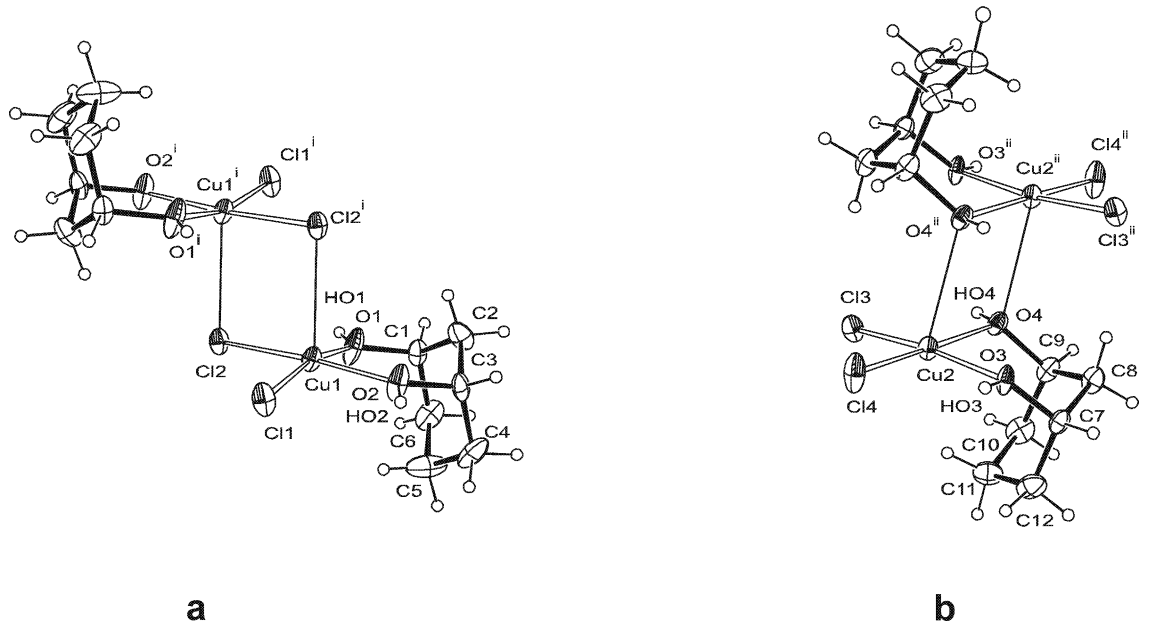


Fig. 1. ORTEP drawing of centrosymmetric $CuCl_2 \cdot c$-13chd dinuclear units with the atomic labeling scheme of heavy atoms: (**a**) the dichloro-bridged unit and (**b**) the oxygen bridged unit. Probability ellipsoids are drawn at 30% level. Symmetry codes: i = $1-x$, $1-y$, $-z$ and ii = $-x$, $1-y$, $-z$.

Table 2
Selected bond lengths [Å] and angles [°] for (**1**)

a		**b**	
Bond lengths			
Cu(1)–O(1)	1.960(5)	Cu(2)–O(3)	1.982(4)
Cu(1)–O(2)	1.961(5)	Cu(2)–O(4)	2.004(5)
Cu(1)–Cl(1)	2.226(2)	Cu(2)–Cl(3)	2.230(2)
Cu(1)–Cl(2)	2.262(2)	Cu(2)–Cl(4)	2.216(2)
Cu(1)–Cl(2^{i})	2.796(2)	Cu(2)–O(4^{ii})	2.835(5)
Bond angles			
O(1)–Cu(1)–O(2)	88.0(2)	O(3)–Cu(2)–O(4)	84.25(18)
O(1)–Cu(1)–Cl(1)	166.8(2)	O(3)–Cu(2)–Cl(3)	169.23(16)
O(1)–Cu(1)–Cl(2)	87.89(15)	O(3)–Cu(2)–Cl(4)	90.23(13)
O(2)–Cu(1)–Cl(1)	88.01(15)	O(4)–Cu(2)–Cl(3)	90.63(14)
O(2)–Cu(1)–Cl(2)	173.22(19)	O(4)–Cu(2)–Cl(4)	172.83(16)
Cl(1)–Cu(1)–Cl(2)	94.86(7)	Cl(3)–Cu(2)–Cl(4)	95.56(7)
Cl(2)–Cu(1)–Cl(2^{i})	90.38(6)	O(4)–Cu(2)–O(4^{ii})	80.0(2)
Cu(1)–Cl(2)–Cu(1^{i})	89.62(6)	Cu(2)–O(4)–Cu(2^{ii})	100.4(2)
C(1)–O(1)–Cu(1)	131.6(4)	C(7)–O(3)–Cu(2)	124.2(4)
C(3)–O(2)–Cu(1)	132.9(4)	C(9)–O(4)–Cu(2)	120.7(4)

Symmetry codes: i = 1−x, 1−y, −z and ii = −x, 1−y, −z.

Structurally, as a result of the different coordinations, there are some distinct differences between the two dinuclear units, as can be seen from Fig. 1. For example, the distances of H-atoms at the top carbons of the chd-ring from the copper atoms are 3.060 Å in **a** and 2.377 Å in **b**, and the O1···O2 and O3···O4 distances are 2.722(6) and 2.674(6) Å, respectively. By comparison, for the Cu(II) complexes of *cis*- and *trans*-1,2-cyclohexanediol the O···O distances in the metal bonded diols are 2.569(4) and 2.571(4) Å, respectively [5]. The longer O···O distances in 1,3-chd complexes are an indication of a different geometric constraint of 1,3-chd compared to that of 1,2-chd in their $CuCl_2$ complexes. Furthermore, the O–Cu–O bond angles, which are 88.0(2)° and 84.25(18)° in **1** and 79.6(1)° in both $CuCl_2$ complexes with the aforementioned 1,2-cyclohexanediols, support the differing geometric constraints of the 1,3- and 1,2-diols under complexation.

The $[CuCl_2(c\text{-13chd})]_2$ units are packed into chains by four OH···Cl hydrogen bonds. The hydrogen bond strength is only moderate, as suggested by a very broad band at 3250 cm^{-1} in the infrared (IR)-spectrum of the compound. The chains are held together by van der Waals' interactions.

2.3. The structure of *cis*-1,3-cyclohexanediol **2**

In the lattice the *c*-13chd molecules (Fig. 2) adopt a chair conformation whereby both OH groups, as expected, are in equatorial positions. The bond parameters are normal and otherwise unexceptional. Both OH hydrogens form intermolecular H-bonds with neighboring molecules (see Fig. 2), and this H-bonding directs the molecules in the layers, which are held together by weak van der Waals interactions.

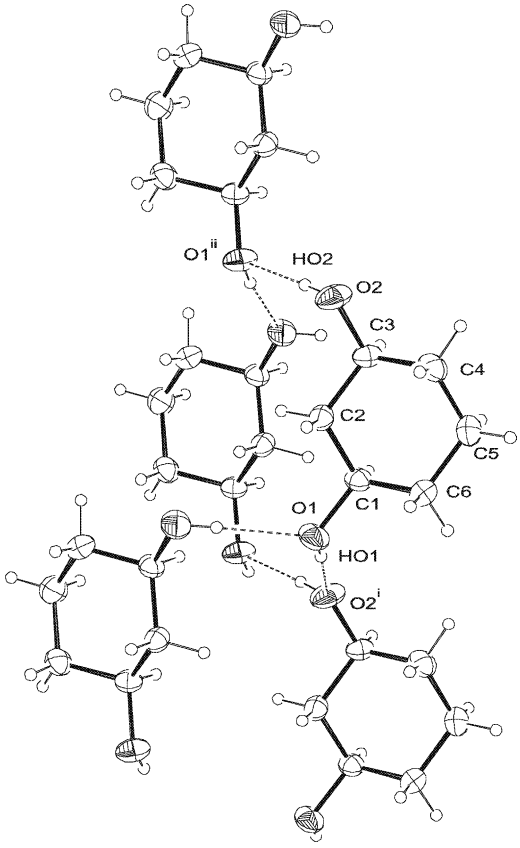


Fig. 2. ORTEP drawing of several *c*-13chd molecules showing the hydrogen bonding system and a part of packing system. The heavy atoms of the asymmetric unit are labeled. Probability ellipsoids are drawn at 30% level. Symmetry codes: i = x, y, z−1 and ii = x−1/2, −y+1/2, z+1/2.

3. Conclusion

$CuCl_2$–(polyol) complexes can be useful intermediaries for the separation of geometric isomeric polyols based on their differing abilities to coordinate the copper(II) cation. The separation potential of such systems is compromised though, when the polyols can form hydrogen bonds to the coordinated OH groups, thus resulting in mixed complexes. In straightforward and limited systems such as the *cis*- and *trans*-1,3-cyclohexanediol isomers, a simple and convenient methodology to separate the two isomers via the copper(II)chloride complex in ether is attainable, as has been amply demonstrated. The method is environmentally acceptable as the solvents, $CuCl_2$, and even the ammonia gas can be recirculated.

4. Experimental

Commercial 1,3-cyclohexanediol is a mixture of *cis* and *trans* isomers of varying proportions. The first 1,3-cyclohexanediol sample from Aldrich (98%) was a 1:1 mixture of isomers according to ^{1}H NMR [17,18] and was used as received for the syntheses. The second sample of 1,3-cyclohexanediol, also from Aldrich (98%), was a mixture of *cis* and *trans* isomers in a 2:1 ratio and was sublimed prior to the separation studies. Solvents were of HPLC grade and used as purchased. $CuCl_2 \cdot 2H_2O$ was held overnight at 120 °C to obtain anhydrous $CuCl_2$.

4.1. Preparation of $CuCl_2 \cdot$ *c*-13chd (method 1)

$CuCl_2$ (793 mg, 5.90 mmol) and commercial 1,3-cyclohexanediol (1.392 g, 11.98 mmol, 1:1 mixture of isomers) were suspended in 20 ml of acetonitrile. The yellow suspension was stored at 4 °C for a week to yield bright green crystals (696 mg, 47% based on copper). The crystals were separated by decanting and washed with ether. IR (Nujol): 3250 (s, v br), 1332 (s), 1281 (vs), 1260 (vs), 1213 (m), 1203 (m), 1101 (vs), 1072 (s), 1007 (m), 943 (vs), 914 (vs), 901 (vs), 873 (m), 839 (s), 777 (m), 720 (s), 708 (s), 617 (w), 536 (w), 444 (m), 421 (m) cm^{-1}. For $C_6H_{12}O_2CuCl_2$: Calc.: Cu, 25.4; Cl, 28.3; Found: Cu, 25.0; Cl, 28.0%.

4.2. Preparation of $CuCl_2 \cdot$ *c*-13chd (method 2)

$CuCl_2$ (50.7 mg, 0.38 mmol) and *cis*-1,3-cyclohexanediol (see preparation below; 61.5 mg, 0.53 mmol) were suspended in 1.0 ml of acetonitrile. The solution, originally yellow, slowly turned green and after overnight at room temperature, the solution yielded bright green, plate-like crystals. After a second night at 7 °C, the crystals were separated by decanting and washed with ether (65 mg, yield 68% based on copper). The IR-spectrum of the sample was identical to the earlier preparation and X-ray diffraction analysis confirmed the structure.

4.3. Separation of *c*-13chd and *t*-13chd

1.80 g of commercial 1,3-cyclohexanediol (15.5 mmol, 1:1 mixture of isomers) and 1.22 g $CuCl_2$ (9.0 mmol) were suspended in 40 ml of diethyl ether, and the suspension was stirred for 2 h to yield a greenish–blue solid and a slightly green solution. The solid, containing $CuCl_2 \cdot$ *c*-13chd and unreacted copper(II) chloride, was filtered off and washed with a small amount of ether (discarded). The solid was then dissolved in 40 ml of acetone and treated with gaseous ammonia precipitating a copper salt, which was removed by filtration and washed with a small amount of acetone. The combined acetone solutions were then evaporated to dryness to obtain 600 mg of *cis*-chd (m.p. 85 °C, lit. 85.5–86 °C [19]). The ether filtrate from above was filtered through a short pad of silica gel and evaporated to yield 1.0 g of *t*-13chd (m.p. 115–117 °C, lit. 117–118 °C [19]). The ^{1}H NMR spectra of both compounds were consistent with previous reports [17,18]. Single crystals of *c*-13chd were grown from ethyl acetate by slow evaporation of the solvent.

4.4. Crystal structure determination

Single-crystal data collections were performed at ambient temperature on a Rigaku AFC5S diffractometer using graphite monochromatized Mo Kα radiation ($\lambda = 0.71069$ Å). The unit cell parameters were determined by least-squares refinement of 25 carefully centered reflections. Data reduction and subsequent calculations were performed with TEXSAN FOR WINDOWS [20]. The data were corrected for Lorenz and polarization effects and for absorption (for **1**) (Ψ-scans [21]). A decay of 3.6% for **1** was also taken into account. The crystal data for compounds **1** and **2**, along with other experimental details, are summarized in Table 1.

The structures were solved by direct methods using the SIR-92 program [22], and full-matrix least-squares refinements on F^2 were performed using the SHELXL-97 program [23]. For **1**, all heavy atoms were refined anisotropically. The CH hydrogen atoms were included at fixed distances with fixed displacement parameters from their host atoms, and the OH hydrogen atoms were refined with fixed displacement parameters. The O–H distances were restrained to 0.82 Å during refinements. For **2**, non-hydrogen atoms were refined with anisotropic displacement parameters, whilst the hydrogen atoms were refined isotropically. Figures were drawn with ORTEP-3 FOR WINDOWS [24].

5. Supplementary material

Crystallographic data (excluding structure factors) for the structural analysis have been deposited with the Cambridge Crystallographic Data Centre, CCDC no. 170018–170019. Copies of this information may be obtained free of charge from The Director, CCDC, 12 Union Road, Cambridge CB2 1EZ, UK (fax: +44-1223-336033; e-mail: deposit@ccdc.cam.ac.uk or www: http://www.ccdc.cam.ac.uk).

References

[1] N.S. Poonia, A.V. Bajaj, Chem. Rev. 79 (1979) 389.
[2] J. Bjerrum, Adv. Chem. Ser. 62 (1967) 178.

[3] H.M. Colquhoun, J.F. Stoddart, D.J. Williams, Angew. Chem., Int. Ed. Engl. 25 (1986) 483.
[4] B.-M. Antti, Acta Chem. Scand., A 30 (1976) 405.
[5] L. Hiltunen, M. Leskelä, L. Niinistö, R. Sillanpää, Acta Chem. Scand., A 38 (1984) 201 (and references therein).
[6] A. Lehtonen, R. Sillanpää, Acta Chem. Scand. 46 (1992) 249.
[7] R. Sillanpää, Inorg. Chim. Acta 82 (1984) 75.
[8a] B.-M. Antti, B.S.K. Lundberg, N. Ingri, Acta Chem. Scand., A 26 (1972) 3984.
[8b] I. Labádi, K. Burger, G. Liptay, M. Czugler, A. Kálmán, J. Therm. Anal. 31 (1986) 1171.
[9] D. Knetsch, Thesis, University of Leiden, Leiden, 1976.
[10] (a) J. Bebendorf, H.-B. Bürgi, E. Gamp, M.A. Hitchman, A. Murphy, D. Reinen, M.J. Riley, H. Stratemeier, Inorg. Chem. 35 (1996) 7419;
(b) C. Boever, J. Gislason, W.P. Jensen, R.A. Jacobson, Inorg. Chim. Acta 284 (1999) 284.
[11] R. Sillanpää, M. Leskelä, L. Hiltunen, Acta Crystallogr., Sect. B 38 (1982) 1591.
[12] K.B. Sharpless, A.O. Chong, J.A. Scott, J. Org. Chem. 40 (1975) 1252.
[13] US. Patent 4,447,658.
[14] D. Gibson, R. Karaman, Inorg. Chem. 28 (1989) 1928.
[15] C.J. Bannochie, A.E. Martell, J. Am. Chem. Soc. 111 (1989) 4735.
[16] S.J. Angyal, G.S. Bethell, R.J. Beveridge, Carbohydr. Res. 73 (1979) 9.
[17] R.J. Abraham, E.J. Chambers, W.A. Thomas, J. Chem. Soc., Perkin Trans. 2 (1993) 1061.
[18] Y. Kikuchi, Y. Kato, Y. Tanaka, H. Toi, Y. Aoyama, J. Am. Chem. Soc. 113 (1991) 1349.
[19] R.A.B. Bannard, A.A. Casselman, E.J. Langstaff, R.Y. Moir, Can. J. Chem. 45 (1967) 2605.
[20] TEXSAN FOR WINDOWS. Structure Analysis Software, Molecular Structure Corporation, Texas 77381, USA, 1997.
[21] A.C. North, D.C. Phillips, F.S. Mathews, Acta Crystallogr., Sect. A 24 (1968) 351.
[22] A. Altomare, G. Cascarano, C. Giacovazzo, A. Gualiardi, M.C. Burla, G. Polidori, M. Camalli, J. Appl. Cryst. 27 (1994) 435.
[23] G.M. Sheldrick, SHELXL-97. Program for Crystal Structure Refinement, University of Göttingen, Germany, 1997.
[24] L.J. Farrugia, J. Appl. Cryst. 30 (1997) 565.

PERGAMON

Polyhedron 21 (2002) 1139–1148

POLYHEDRON

www.elsevier.com/locate/poly

Structures of four types of novel high-valent manganese complexes obtained by the reactions of $KMnO_4$ with tridentate Schiff base ligands

Hideyuki Asada, Minoru Ozeki, Manabu Fujiwara, Takayuki Matsushita *

Department of Materials Chemistry, Faculty of Science and Technology, Ryukoku University, Seta, Otsu 520-2194, Japan

Received 3 August 2001; accepted 26 February 2002

Abstract

X-ray structure analysis revealed that four types of novel manganese complexes, Mn^{IV}(*N*-EtO-sal)$_2$, Mn^{III}(*N*-PhO-sal)(L), [Mn^{IV}(5,6-Benzo-L)$_2$(μ-O)]$_2$ and Mn^{III}(L-4-Me)$_3$ have been found to be obtained by the reactions of $KMnO_4$ with various tridentate Schiff base ligands (*N*-EtOH-salH, *N*-PhOH-salH and its derivatives) in dry MeCN, where *N*-EtOH-salH, *N*-PhOH-salH, LH, 5,6-Benzo-LH and L-4-MeH denote *N*-2-hydroxyethyl-salicylideneamine, *N*-2-hydroxyphenyl-salicylideneamine, 2-(2-hydroxyphenyl)-benzoxazole 2-(2-hydroxynaphthyl)-benzoxazole and 2-(2-hydroxyphenyl)-5-methylbenzoxazole, respectively. The reactions of $KMnO_4$ and *N*-PhOH-salH and its derivatives have especially been found to afford benzoxazole derivatives which may be formed by intramolecular oxidative coupling between the phenolic oxygen atom of aminophenol moiety and the carbon atom of imine moiety. © 2002 Elsevier Science Ltd. All rights reserved.

Keywords: Tridentate Schiff base ligand; Potassium permanganate; Molecular structures; Photosystem II

1. Introduction

Manganese plays an important role in biological redox systems, which is exemplified by the oxygen-evolving complex of photosystem II (PS II, OEC) in green plants [1–10]. In order to understand its function, a number of oxomanganese clusters with various nuclearity, ligation and number and type of oxo-bridges, have been prepared and studied [11–17]. In particular, there have been many reports on the preparation of structurally characterized di-μ-oxo dimanganese complexes, since the close Mn–Mn distance of OEC (2.7 Å) implies a strong interaction between the manganese atoms of the substructure consistent with a di-μ-oxo dimanganese core. So far, most di-μ-oxo dimanganese(IV) complexes [18–33], such as [Mn^{IV}(salpn)(μ-O)]$_2$ (salpnH_2 = *N*,*N*′-disalicylidene-1,3-diaminopropane) [18–20], have been prepared by the reaction of mononuclear manganese(II) or manganese(III) complexes with dioxygen, hydrogen peroxide or other oxidants. We have reported that a series of di-μ-oxo dimanganese(IV) complexes has been prepared by the one step reaction of $KMnO_4$ with bi- and tetradentate Schiff base ligands in MeCN and characterized in order to mimic OEC [30–34].

In this paper, we describe that the reactions of $KMnO_4$ with tridentate Schiff base ligands, *N*-EtOH-salH, *N*-chxOH-salH, *N*-PhOH-salH and its derivatives, gave four types of manganese complexes: Mn^{IV}(*N*-RO-sal)$_2$, Mn^{III}(*N*-PhO-sal)(L), [Mn^{IV}(5,6-Benzo-L)$_2$(μ-O)]$_2$ and Mn^{III}(L-4-Me)$_3$ where *N*-ROH-X-salH, *N*-Y-PhOH-X-salH, LH, 5,6-Benzo-LH and L-4-MeH denote *N*-2-hydroxy-alkyl-X-salicylideneamine, *N*-2-hydroxy-Y-phenyl-X-salicylideneamine, 2-(2-hydroxyphenyl)-benzoxazole, 2-(2-hydroxynaphthyl)-benzoxazole and 2-(2-hydroxyphenyl)-5-methylbenzoxazole, respectively (R = 1,2-C_6H_{10}, C_2H_4, X = H, 5,6-Benzo, 5-Br and Y = H, 4-Me) [35]. In addition, their molecular structures and a reaction scheme forming benzoxazole derivatives are also described.

* Corresponding author. Tel.: +81-77-543-7471; fax: +81-77-543-7483.

E-mail address: matusita@chem.ryukoku.ac.jp (T. Matsushita).

0277-5387/02/$ - see front matter © 2002 Elsevier Science Ltd. All rights reserved.
PII: S0277-5387(02)00936-1

2. Experimental

2.1. Preparation of tridentate Schiff base ligands

All of the tridentate Schiff base ligands were prepared and identified according to the literature methods [36,37].

2.2. Preparation of Mn^{IV}(*N*-EtO-sal)$_2$ (Type I)

The manganese(IV) complex, Mn^{IV}(*N*-EtO-sal)$_2$ (**1**) was prepared by the reaction of *N*-EtOH-salH (1.652 g, 10 mmol) and $KMnO_4$ (790 mg, 5 mmol) in MeCN (150 ml) with stirring at room temperature (r.t.). The solution color changed from purple to brown and was allowed to stand in a dark place at r.t. After 12 h, the resulting precipitates were collected on a glass filter and recrystallized from a mixed solvent of CH_2Cl_2 and MeCN. The other type I manganese complexes which use *N*-ROH-X-salH were obtained in the same manner. Single crystals of Mn^{IV}(*N*-EtO-sal)$_2$ (**1**), Mn^{IV}(*N*-EtO-5,6-Benzo-sal)$_2$ (**2**) and Mn^{IV}(*N*-chxO-sal)$_2$ (**3**) were used for X-ray crystallographic determination and their structures are shown in Figs. 1–3, respectively. Elemental analysis data for all of the complexes are given in Table 1.

2.3. Preparation of Mn^{III}(*N*-PhO-sal)(L) (Type II)

The manganese(III) complex, Mn^{III}(*N*-PhO-sal)(L) (**4**) was prepared by the reaction of *N*-PhOH-salH (2.132 g, 10 mmol) and $KMnO_4$ (790 mg, 5 mmol) in MeCN (200 ml) with stirring at r.t. After 12 h, the resulting precipitates were collected on a glass filter and recrystallized from a mixed solvent of CH_2Cl_2 and MeCN. Single crystals of **4** were used for X-ray crystallographic characterization and the structure is shown in Fig. 4. Elemental analysis data are given in Table 1.

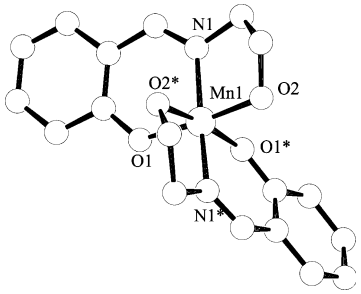


Fig. 1. The molecular structure of Mn^{IV}(*N*-EtO-sal)$_2$ (**1**) with hydrogen atoms omitted for clarity.

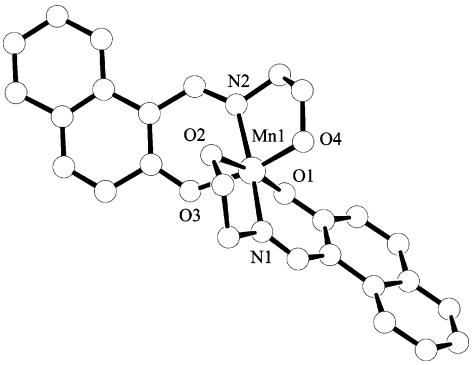


Fig. 2. The molecular structure of Mn^{IV}(*N*-EtO-5,6-Benzo-sal)$_2$ (**2**) with hydrogen atoms omitted for clarity.

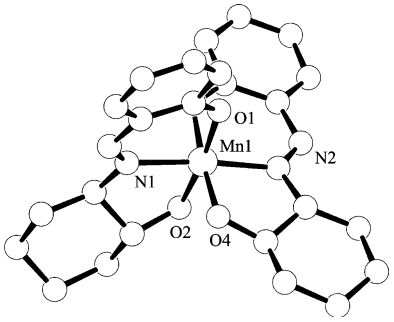


Fig. 3. The molecular structure of Mn^{IV}(*N*-chxO-sal)$_2$ (**3**) with hydrogen atoms omitted for clarity.

2.4. Preparation of [Mn^{IV}(5,6-Benzo-L)$_2$(μ-O)]$_2$ (Type III)

The di-μ-oxo dimanganese(IV) complex, [Mn^{IV}(5,6-Benzo-L)$_2$(μ-O)]$_2$ (**5**) was prepared by the reaction of *N*-PhOH-5,6-Benzo-salH (263 mg, 1.0 mmol) and $KMnO_4$ (80 mg, 0.5 mmol) in MeCN (500 ml) with stirring at r.t. The solution color changed from purple to brown and was allowed to stand in a dark place at r.t. Two weeks later the resulting brownish black crystals were collected on a glass filter. Single crystals of **5** were used for X-ray crystallographic characterization and the structure is shown in Fig. 5. Elemental analysis data are given in Table 1.

2.5. Preparation of Mn^{III}(L-4-Me)$_3$ (Type IV)

The manganese(III) complex, Mn^{III}(L-4-Me)$_3$ (**6**) was prepared by the reaction of *N*-4-Me-PhOH-salH (3.413 g, 15 mmol) and $KMnO_4$ (790 mg, 5 mmol) in MeCN (200 ml) with stirring at r.t. After 12 h, the resulting precipitates were collected on a glass filter and recrystallized from a mixed solvent of CH_2Cl_2 and MeCN. Single crystals of **6** were used for X-ray crystallographic characterization and the structure is shown in Fig. 7. Elemental analysis data are given in Table 1.

Table 1
Elemental analysis of the complexes and ligands

Complex	Formula	Analyses [a]				μ_{eff} (B.M.) [b]
		C (%)	H (%)	N (%)	Mn (%)	
1·1.5MeCN	$C_{22}H_{24}MnN_4O_4$	56.97 (56.96)	5.09 (5.14)	11.26 (11.28)	11.82 (11.86)	3.85
2	$C_{26}H_{22}MnN_2O_4$	62.81 (64.87)	4.84 (4.61)	5.79 (5.82)	10.70 (10.51)	4.02
3·MeCN	$C_{28}H_{33}MnN_3O_4$	62.04 (63.39)	6.53 (6.27)	8.18 (7.92)	10.26 (10.36)	3.88
4·MeCN	$C_{28}H_{20}MnN_3O_4$	66.72 (64.60)	3.79 (3.75)	7.90 (7.98)	10.94 (10.62)	4.80
5·1.25CH_2Cl_2	$C_{69.25}Cl_{2.5}H_{42.5}$ $Mn_2N_4O_{10}$	64.57 (64.52)	3.33 (3.32)	4.58 (4.35)	8.60 (8.52)	2.92
6	$C_{40}H_{30}MnN_3O_6$	69.36 (69.32)	4.07 (4.16)	5.88 (5.78)	7.41 (7.51)	4.87
7	$C_{13}H_9NO_2$	73.51 (73.92)	4.11 (4.30)	6.68 (6.63)		
8	$C_{17}H_{11}NO_2$	77.32 (78.15)	4.52 (4.24)	5.28 (5.36)		
9	$BrC_{13}H_8NO_2$	53.78 (53.82)	2.82 (2.78)	4.82 (4.83)		
10·0.2Me_2CO	$C_{14.6}H_{12.2}NO_{2.2}$	74.13 (74.03)	5.23 (5.19)	5.98 (5.92)		

[a] Required values in parentheses.
[b] Per manganese ion.

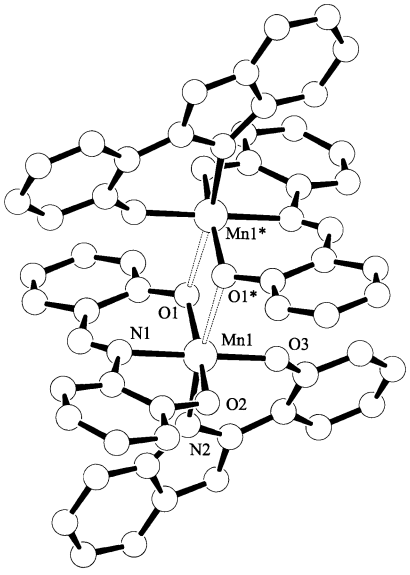


Fig. 4. The molecular structure of Mn^{III}(*N*-PhO-sal)L (**4**) with hydrogen atoms omitted for clarity.

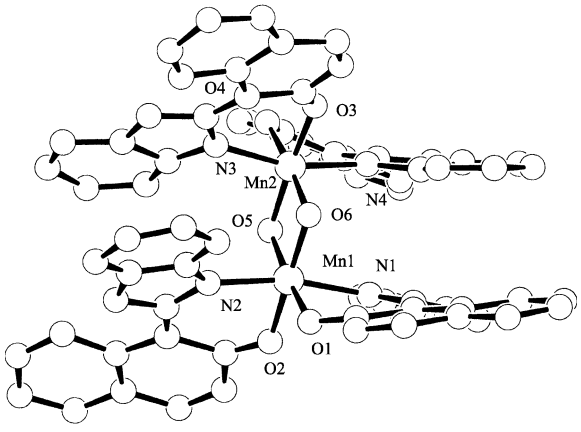


Fig. 5. The molecular structure of $[Mn^{IV}(5,6\text{-Benzo-L})_2(\mu\text{-O})]_2$ (**5**) with hydrogen atoms omitted for clarity.

2.6. Isolation of LH

The bidentate ligand LH (**7**) was isolated from Mn^{III}(*N*-PhO-sal)L (**4**) as follows. To a mixed solvent of *n*-hexane (50 ml) and H_2O (100 ml) containing **4** (500 mg, 1 mmol), glacial acetic acid (1.5 ml) was added and shaken in a separation funnel. The aqueous layer was removed. After the organic layer had been washed with H_2O, it was dried over Na_2SO_4 and evaporated to yield off-white solids. They were recrystallized from *n*-hexane. Other ligands, 5,6-Benzo-LH (**8**), 5-Br-LH (**9**) and L-4-MeH (**10**) were obtained in the same manner from type II-IV complexes where 5,6-Benzo-LH, 5-Br-LH and LH-4-Me denote 2-(2-hydroxynaphthyl)-benzoxazole, 2-(2-hydroxy-5-bromo-phenyl)-benzoxazole and 2-(2-hydroxyphenyl)-5-methylbenzoxazole, respectively. Single crystals of **8** were used for X-ray crystallographic characterization and the structure is shown in Fig. 8. Elemental analysis data for all of the bidentate ligands, X-L-YH, which were isolated from various complexes, are given in Table 1.

2.7. Physical measurements

Elemental analyses were made on a Yanaco Model CHN-CORDER MT-5. UV–Vis and IR spectra were recorded on a Shimadzu Model UV-3100 spectrophotometer and a Shimadzu Model IR-470 infrared spectrophotometer, respectively. Electrochemical studies were performed under argon, using a BAS Model CV-27 voltammograph equipped with a Graphtec Model WX 2400 XY recorder and a standard three-electrode assembly (glassy carbon working, Pt wire auxiliary and Ag–AgCl MeCN 0.1 M *n*-Bu_4NClO_4, TBAP, reference electrode) with 0.1 M TBAP (*n*-Bu_4NClO_4) as the supporting electrolyte. All the redox potentials were corrected to the saturated calomel electrode (SCE).

Magnetic susceptibility measurements were carried out by the Gouy method at r.t.

2.8. X-ray crystallographic measurements

X-ray structure analyses were taken on a Rigaku AFC-7R automatic 4-circle X-ray diffractometer.

Single crystals of all of the manganese complexes and 2-(2-hydroxynaphthyl)-benzoxazole were obtained by recrystallization from a mixed solvent of CH_2Cl_2 and MeCN and *n*-hexane, respectively. The crystals were mounted on a glass capillary. All the data were collected on a Rigaku AFC-7R four circle automated diffractometer with graphite monochromated Cu Kα radiation ($\lambda = 1.54178$ Å) for **1**, **2**, **3**, **4** and **5** and Mo Kα radiation ($\lambda = 0.71069$ Å) for **6** and **8** at 23 °C. Unit-cell parameters were obtained from a least-squares fit of 24 reflections, $25.28^\circ < 2\theta < 51.92^\circ$ for **1**, 25 reflections, $48.40^\circ < 2\theta < 54.36^\circ$ for **2**, $36.89^\circ < 2\theta < 48.54^\circ$ for **3**, $25.38^\circ < 2\theta < 51.40^\circ$ for **4**, 19 reflections, $20.09^\circ < 2\theta < 34.44^\circ$ for **5**, 23 reflections, $22.14^\circ < 2\theta < 24.37^\circ$ for **6** and 14 reflections, $7.17^\circ < 2\theta < 13.67^\circ$ for **8**. Three standard reflections were measured every 150 reflections; they showed no systematic decay throughout the data collection. The data were corrected for Lorentz and polarization effects. All the calculations were carried out using the TEXSAN [38] crystallographic software package. The structures of the complexes and the ligand were solved using direct method for **1**, **2**, **8** (SHELX-86) [39], **3**, **4** (SIR-92) [40], **5** (MULTAN-88) [41], **6** (SIR-88) [42] and expanded using Fourier techniques [43]. These structures were refined by the full-matrix least-squares technique with anisotropic thermal parameters for all non-hydrogen atoms. Hydrogen atoms were introduced in calculated positions but not refined. Crystallographic data for the complexes **1**–**6** and the ligand **8** are summarized in Tables 2 and 3.

2.9. Reagents

The reagents (salicylaldehydes and monoamines) were obtained commercially and used without further purification. $KMnO_4$ was of reagent grade (99.5%). MeCN was purified by distillation over P_4O_{10} twice and then distilled further before use. Other solvents were purified by usual methods.

3. Results and discussion

3.1. Molecular structures

All of the complexes obtained by the reactions of $KMnO_4$ with various tridentate Schiff base ligands are illustrated in Scheme 1, which include the four types of manganese complexes as follows.

Table 2
Crystallographic parameters for **1**, **2** and **3**

Compound	**1**·2MeCN	**2**	**3**·MeCN
Chemical formula	$MnC_{22}H_{24}N_4O_4$	$MnC_{26}H_{22}N_2O_4$	$MnC_{28}H_{33}N_3O_4$
Formula weight	463.39	481.41	530.52
Crystal color, habit	brown, prism	brown, prism	brown, prism
Crystal size	0.17 × 0.15 × 0.15	0.30 × 0.25 × 0.40	0.20 × 0.20 × 0.15
a (Å)	9.385(3)	7.163(2)	11.894(2)
b (Å)	9.818(3)	7.163(2)	10.496(2)
c (Å)	23.953(4)	40.479(3)	20.896(2)
α (°)			
β (°)			90.961(9)
γ (°)			
V (Å^3)	2206(1)	2076(1)	2604.9(6)
Z	4	4	4
Crystal system	orthorhombic	tetragonal	monoclinic
Space group	*Pbcn*	$P4_1$	$P2_1/n$
D_{calc} (g cm^{-3})	1.395	1.540	1.353
Radiation	Cu Kα	Cu Kα	Cu Kα
2*θ* Max	120.1	120.1	120.1
Unique data	1923	1858	4133
Observed data	558	1623	2502
R [a]	0.061	0.052	0.044
R_w [b]	0.079	0.083	0.067
Goodness-of-fit	1.01	1.41	1.33

[a] $R = \Sigma||F_o| - |F_c||/\Sigma|F_o|$.
[b] $R_w = [\Sigma w(|F_o| - |F_c|)^2/\Sigma wF_o^2]^{1/2}$, $w = 4F_o^2/\sigma^2(F_o^2)$.

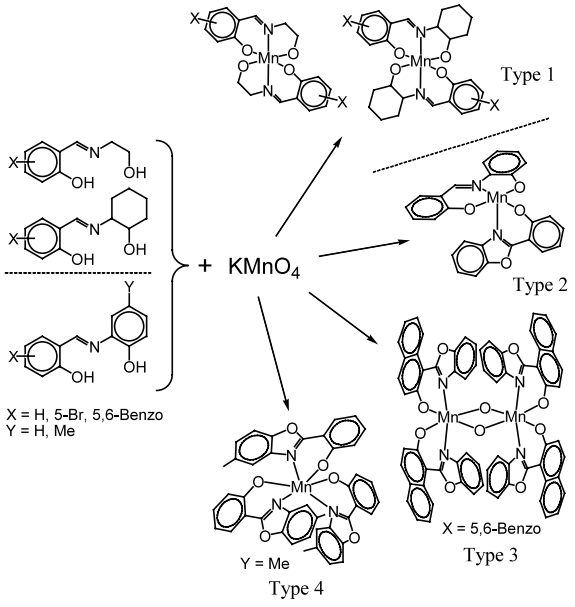
3.1.1. Type I complexes

The molecular structures of Mn^{IV}(*N*-EtO-sal)$_2$ (**1**), Mn^{IV}(*N*-EtO-5,6-Benzo-sal)$_2$ (**2**) and Mn^{IV}(*N*-chxO-sal)$_2$ (**3**) are shown in Figs. 1–3, respectively. Selected bond lengths and angles are listed in Table 4. In the case of the tridentate Schiff base ligands *N*-ROH-X-salH, which were obtained by the condensation of X-salicylaldehyde and ethanolamine and/or 1,2-*trans*-cyclohexanolamine, the mononuclear manganese(IV) complexes were obtained. The X-ray crystallographic determination of these manganese(IV) complexes, Mn^{IV}(*N*-RO-X-sal)$_2$, revealed that their configuration has a meridional octahedron. The manganese ion is surrounded by an octahedral N_2O_4 donor set and is at the center of three axes of N(1)–Mn(1)–N(1)*, O(1)–Mn(1)–O(1)* and O(2)–Mn(1)–O(2)* for **1** and N(1)–Mn(1)–N(2), O(1)–Mn(1)–O(2) and O(3)–Mn(1)–O(4) for **2** and **3**. The molecular structures of the present complexes are very similar to those previously reported for $Mn^{IV}L_2^{NO2}$ such as Mn^{IV}(*N*-PrO-sal)$_2$ and Mn^{IV}(*N*-BzO-sal)$_2$, where *N*-PrOH-salH and *N*-BzOH-salH denote *N*-3-hydroxypropyl-salicylideneamine and *N*-2-hydroxybenzyl-salicylideneamine, respectively. Moreover, the bond lengths and angles are very close to those for these manganese(IV) complexes [44–47].

Table 3
Crystallographic parameters for **4**, **5**, **6** and **8**

Compound	**4**·MeCN	**5**·2CH_2Cl_2	**6**	**8**
Chemical formula	$MnC_{28}H_{20}N_3O_4$	$Mn_2C_{70}H_{44}N_4O_{10}Cl_4$	$MnC_{42}H_{30}N_3O_6$	$C_{17}H_{11}NO_2$
Formula weight	517.42	1352.83	727.65	261.28
Crystal color, habit	brown, prism	dark brown, prism	green, prism	orange, prism
Crystal size	0.20 × 0.10 × 0.05	0.02 × 0.25 × 0.30	0.40 × 0.40 × 0.05	0.20 × 0.20 × 0.05
a (Å)	10.629(3)	13.746(5)	11.995(2)	14.736(5)
b (Å)	12.047(5)	18.247(5)	14.531(5)	17.835(6)
c (Å)	10.456(3)	13.49(1)	10.184(3)	4.856(5)
α (°)	112.72(2)	109.70(4)	97.99(2)	
β (°)	110.24(2)	111.06(4)	107.71(2)	
γ (°)	82.01(3)	89.93(4)	81.04(2)	
V (Å^3)	1158.8(7)	2943(3)	1662.4(8)	1276(1)
Z	2	2	2	4
Crystal system	triclinic	triclinic	triclinic	orthorhombic
Space group	$P\bar{1}$	$P\bar{1}$	$P\bar{1}$	$P2_12_12_1$
D_{calc} (g cm^{-3})	1.483	1.526	1.454	1.360
Radiation	Cu Kα	Cu Kα	Mo Kα	Mo Kα
2θ Max	120.1	120.1	55.0	55.0
Unique data	3434	8771	7631	1638
Observed data	1646	2138	1870	426
R [a]	0.076	0.079	0.055	0.055
R_w [b]	0.104	0.099	0.071	0.063
Goodness-of-fit	1.23	1.20	1.13	1.23

[a] $R = \Sigma||F_o| - |F_c||/\Sigma|F_o|$.
[b] $R_w = [\Sigma w(|F_o| - |F_c|)^2/\Sigma wF_o^2]^{1/2}$, $w = 4F_o^2/\sigma^2(F_o^2)$.



Scheme 1. Four types of complexes obtained by the reactions of $KMnO_4$ with various tridentate Schiff base ligands.

Table 4
Selected bond lengths (Å) and angles (°) for **1**, **2** and **3**

Mn^{IV}(N-EtO-sal)$_2$ (**1**)			
Mn(1)–O(1)	1.904(9)	Mn(1)–O(2)	1.836(8)
Mn(1)–N(1)	1.964(9)		
O(1)–Mn(1)–N(1)	96.9(4)	O(2)–Mn(1)–N(1)	83.5(4)
O(1)–Mn(1)–O(2)	172.4(4)	N(1)–Mn(1)–N(1)*	170.7
Mn^{IV}(N-EtO-5,6-Benzo-sal)$_2$ (**2**)			
Mn(1)–O(1)	1.831(6)	Mn(1)–O(2)	1.942(6)
Mn(1)–O(3)	1.999(6)	Mn(1)–O(4)	1.757(6)
Mn(1)–N(1)	1.920(7)	Mn(1)–N(2)	2.008(7)
O(1)–Mn(1)–N(1)	90.3(3)	O(2)–Mn(1)–N(1)	84.5(3)
O(3)–Mn(1)–N(2)	84.8(3)	O(4)–Mn(1)–N(2)	84.3(3)
O(1)–Mn(1)–O(2)	171.3(3)	O(3)–Mn(1)–O(4)	169.1(3)
N(1)–Mn(1)–N(2)	172.3(3)		
Mn^{IV}(N-chxO-sal)$_2$ (**3**)			
Mn(1)–O(1)	1.913(3)	Mn(1)–O(2)	1.839(3)
Mn(1)–O(3)	1.904(3)	Mn(1)–O(4)	1.850(3)
Mn(1)–N(1)	1.975(4)	Mn(1)–N(2)	1.980(3)
O(1)–Mn(1)–N(1)	91.0(1)	O(2)–Mn(1)–N(1)	84.6(1)
O(3)–Mn(1)–N(2)	90.7(1)	O(4)–Mn(1)–N(2)	84.2(1)
O(1)–Mn(1)–O(2)	175.2(1)	O(3)–Mn(1)–O(4)	173.7(1)
N(1)–Mn(1)–N(2)	174.5(2)		

3.1.2. Type II complex

The molecular structure of Mn^{III}(*N*-PhO-sal)(L) (**4**) is shown in Fig. 4. Selected bond lengths and angles are listed in Table 5. In the case of *N*-PhOH-salH, which was obtained by the reaction of salicylaldehyde and *o*-aminophenol, the six-coordinate manganese(III) complex having mixed ligands **4** was isolated. This ligand L, 2-(2-hydroxy-phenyl)-benzoxazole, may be formed by an intramolecular C–O coupling reaction. In the structure of **4**, one nitrogen and two oxygen atoms of *N*-PhOH-salH and the phenolic oxygen atom of the monoanion of L occupy the equatorial plane and a nitrogen atom of the benzoxazole group is placed at the axial position. The *trans* position to the nitrogen atom

Table 5
Selected bond lengths (Å) and angles (°) for **4**, **5**, **6** and **8**

Mn^{III}(N-PhO-sal)(L) (**4**)			
Mn(1)–O(1)	1.913(9)	Mn(1)–O(2)	1.886(9)
Mn(1)–O(3)	1.868(7)	Mn(1)–N(1)	1.98(1)
Mn(1)–N(2)	2.251(9)		
O(1)–Mn(1)–O(2)	166.4(3)	O(1)–Mn(1)–N(1)	88.5(5)
O(2)–Mn(1)–N(1)	84.3(6)	O(3)–Mn(1)–N(1)	178.2(5)
O(3)–Mn(1)–N(2)	86.9(3)		
[*Mn^{IV}*(5,6-*Benzo*-*L*)$_2$(*μ*-*O*)]$_2$ (**5**)			
Mn(1)–O(1)	1.93(2)	Mn(1)–O(2)	1.85(2)
Mn(1)–N(1)	1.95(2)	Mn(1)–N(2)	2.06(2)
Mn(2)–O(3)	1.85(3)	Mn(2)–O(4)	1.91(2)
Mn(2)–N(3)	2.00(2)	Mn(2)–N(4)	1.96(2)
Mn(1)–O(5)	1.83(2)	Mn(1)–O(6)	1.83(2)
Mn(2)–O(5)	1.80(2)	Mn(2)–O(6)	1.85(2)
Mn(1)–Mn(2)	2.749(7)		
O(1)–Mn(1)–N(1)	83.3(9)	O(3)–Mn(2)–N(3)	85.4(9)
O(2)–Mn(1)–N(2)	85.0(9)	O(4)–Mn(2)–N(4)	86.0(10)
O(1)–Mn(1)–O(6)	174.3(8)	O(3)–Mn(2)–O(6)	174.3(9)
O(2)–Mn(1)–O(5)	172.6(9)	O(4)–Mn(2)–O(5)	174.4(9)
N(1)–Mn(1)–N(2)	164.7(9)	N(3)–Mn(2)–N(4)	167.6(9)
O(5)–Mn(1)–O(6)	82.3(7)	O(5)–Mn(2)–O(6)	82.4(8)
Mn(1)–O(5)–Mn(2)	98.5(9)	Mn(1)–O(6)–Mn(2)	96.8(7)
Mn^{III}(*L*-4-*Me*)$_3$ (**6**)			
Mn(1)–O(1)	1.889(7)	Mn(1)–O(2)	1.873(7)
Mn(1)–O(3)	1.908(3)	Mn(1)–N(1)	2.253(8)
Mn(1)–N(2)	2.109(8)	Mn(1)–N(3)	2.261(9)
O(1)–Mn(1)–N(1)	83.1(3)	O(2)–Mn(1)–N(2)	84.7(3)
O(3)–Mn(1)–N(3)	84.2(3)	O(1)–Mn(1)–O(2)	176.6(4)
O(3)–Mn(1)–N(2)	167.3(3)	N(1)–Mn(1)–N(3)	172.1(3)
5,6-*Benzo*-*LH* (**8**)			
C(1)–O(1)	1.38(1)	C(1)–N(1)	1.28(2)
O(1)–C(1)–N(1)	115(1)		
C(1)–O(1)–C(2)	103(1)	C(1)–N(1)–C(3)	104(1)
O(1)–C(1)–C(4)	117(1)	N(1)–C(1)–C(4)	126(1)

of the benzoxazole group is occupied by a phenolic oxygen atom of the neighboring complex with a Mn(1)···O(3)* separation of 2.47 Å, which is considered to be not so strong an interaction. Thus, it can be seen that along the axis of O(3)–Mn(1)···O(3)* the Jahn–Teller effect may be operating on the manganese(III) ion.

3.1.3. Type III complex

The molecular structure of [Mn^{IV}(5,6-Benzo-L)$_2$(μ-O)]$_2$ (**5**) is shown in Fig. 5. Selected bond lengths and angles are listed in Table 5. The reaction of $KMnO_4$ with *N*-PhOH-5,6-Benzo-salH gave the di-μ-oxo dimanganese(IV) complex, [Mn^{IV}(5,6-Benzo-L)$_2$(μ-O)]$_2$ (**5**). This structure consists of two manganese(IV) centers which are bridged by two oxygen atoms to yield a planar Mn_2O_2 core with a Mn–Mn separation of 2.749 Å and two benzoxazole derivatives are coordinated to each manganese atom. Its Mn–Mn separation is relatively long compared with those of the di-μ-oxo dimanganese(IV) complexes with tetradentate Schiff base ligands (2.688(1)–2.732(3) Å) [18–20,30,33] and shorter than those of the di-μ-oxo dimanganese(IV) complexes with bidentate Schiff base ligands (2.756(3)–2.780(2) Å) [31,34].

In the structure of this complex, benzoxazole derivatives around each manganese atom bond via two phenolic oxygen atoms and two nitrogen atoms to complete the roughly octahedral coordination environment. Adoption of this binding model places two phenolic oxygen atoms *trans* and two benzoxazole nitrogen atoms *cis* toward a bridging oxo group, which is similar to the metal center of the di-μ-oxo dimanganese(IV) complexes with tetradentate Schiff bases [Mn^{IV}(μ-sal-*o*-phen)(μ-O)]$_2$ and [Mn^{IV}(μ-salen)(μ-O)]$_2$ [30,33] and the series of [Mn^{IV}(*N*-R-sal)$_2$(μ-O)]$_2$ (R ≥ Et) [31,34]. Moreover, as can be seen in Fig. 5, one of the most interesting features of **5** is two intramolecular close π–π stackings, between one benzoxazole ring and a second one coordinated to another manganese ion, which are coplanar and separated by only 3.54 Å on average (see Fig. 6A and B).

3.1.4. Type IV complex

The molecular structure of Mn^{III}(L-4-Me)$_3$ (**6**) is shown in Fig. 7. Selected bond lengths and angles are listed in Table 5. In contrast to types I–III complexes mentioned above, with *N*-4-Me-PhOH-salH, having a methyl group at the four-position of aminophenol, a roughly octahedral manganese(III) complex, Mn^{III}(L-4-Me)$_3$ was obtained. This means that all of the tridentate Schiff base ligands are converted to a benzoxazole derivative. The metal center is surrounded octahedrally by a N_3O_3 donor set. The bond distances of Mn(1)–N(1) and Mn(1)–N(3) (2.253(8) and 2.261(9) Å, respectively) are longer than that of Mn(1)–N(2) (2.109(8) Å). On the other hand, the differences among the bond distances of Mn(1)–O(1), Mn(1)–O(2), and Mn(1)–O(3) (1.889(7), 1.873(7), and 1.908(3) Å, respectively) are not so large as the differences in the distances of Mn–N bonds. Thus, the Jahn–Teller effect on the manganese(III) ion may occur along the axis containing *trans* nitrogen atoms (N(1)–Mn(1)–N(3)) of benzoxazole groups. Previously, we have reported the molecular structure of the manganese(III) complex with a bidentate Schiff base ligand, Mn^{III}(*N*-Dod-sal)$_3$, where *N*-Dod-salH denotes *N*-dodecyl-salicylideneamine [32]. In this case, three ligands arrange to form a tetragonally distorted octahedron around the manganese atom; such distortion has been ascribed to the Jahn–Teller effect.

3.2. Electronic spectra

Fig. 9 shows the electronic absorption spectra of the complexes **1**, **4**, **5** and **6** in CH_2Cl_2. In the spectra of **4**, **5** and **6**, characteristic absorption bands with high in-

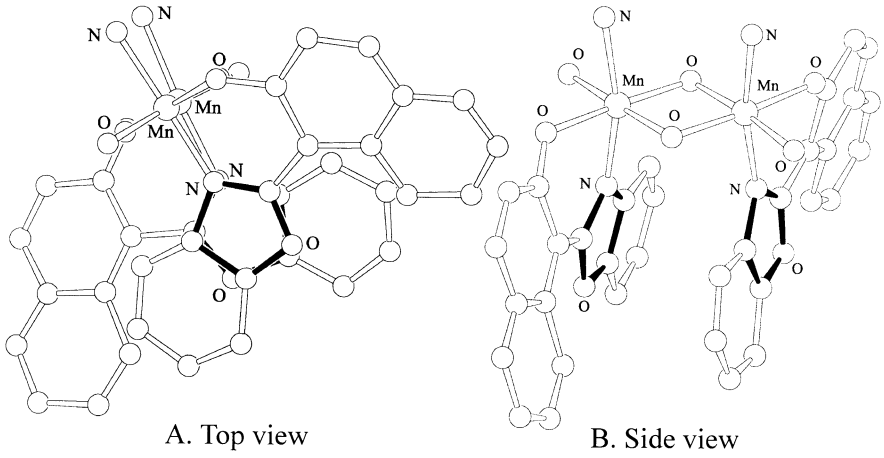


Fig. 6. The intramolecular π–π stacking between benzoxazole rings in **5**.

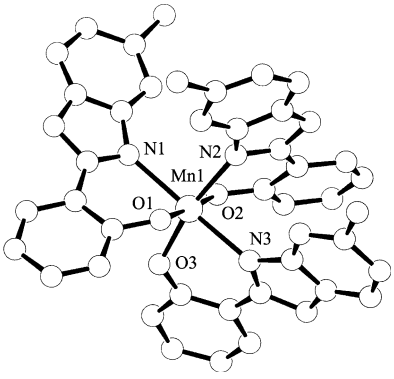


Fig. 7. The molecular structure of $Mn^{III}(L\text{-}4\text{-}Me)_3$ (**6**) with hydrogen atoms omitted for clarity.

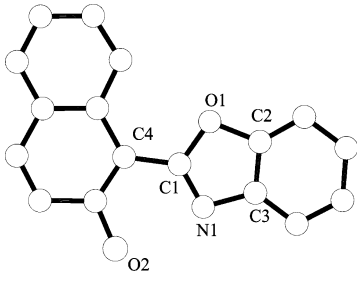


Fig. 8. The molecular structure of the ligand (**8**) with hydrogen atoms omitted for clarity.

tensities around 250–350 nm are observed which are not seen in the spectrum of **1**. These absorption bands can be assigned mainly to ligand transitions due to the benzoxazole groups, which was confirmed by the absorption spectra of the free ligands isolated from these complexes. Moreover, in the spectrum of **5**, high intensity absorption band around 370 nm and moderate ones around 410 and 480 nm are observed. The former absorption bands can be assigned to ligand transitions of the 5,6-Benzo-group, and the latter bands are characteristic for the LMCT from bridging oxygen atoms to the manganese ions [30,31,33,34]. Numerical

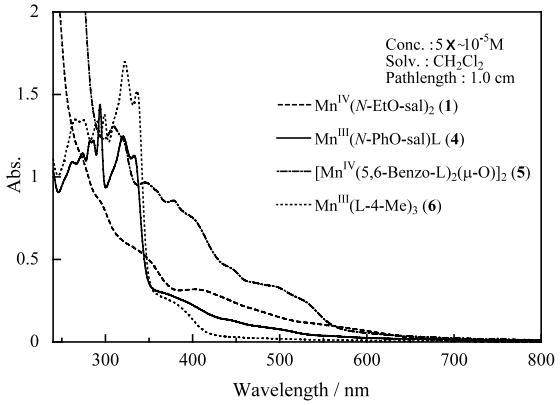


Fig. 9. The electronic absorption spectra of the complexes **1**, **4**, **5** and **6** in CH_2Cl_2.

data for the electronic absorption spectra of all the complexes are listed in Table 6.

3.3. IR spectra

In the IR spectra of the products obtained by the reaction of $KMnO_4$ with *N*-Y-PhOH-X-salH, intense bands around 1250 cm^{-1} were observed, which can be ascribed to the formation of the benzoxazole moiety. Numerical data for the IR spectra of all the complexes are listed in Table 6. It has been reported that IR spectra of di-μ-oxo dimanganese(IV) complexes exhibit sharp absorption bands characteristic for a $Mn_2(\mu\text{-}O)_2$ core in the region around 600–700 cm^{-1}, which can be assigned to the stretching vibrations of $Mn\text{–}O_{oxo}$ bonds [30,31,33,34]. In the IR spectrum of **5**, there are two medium bands at 654 and 633 cm^{-1}. These results suggest that the *N*-PhOH-5,6-Benzo-salH was converted to 5,6-Benzo-LH and formed the di-μ-oxo dimanganese complex.

From the UV–Vis and IR spectra, it can be judged whether the complexes obtained thus include a benzoxazole group as a ligand or not.

Table 6
Absorption spectra and electrochemical data for the complexes and ligands

Complex	λ_{max} (nm) ($\varepsilon \times 10^{-3}$) ($dm^3\ mol^{-1}\ cm^{-1}$)	ν (C–O) [a] (cm^{-1})	$E_{1/2}$ (vs. SCE) (V)
1	273 (22.4), 295 (17.0), 349 (10.1), 405 (6.40), 536 (2.29), 570 (1.91)		−0.44 (IV↔III)
2	260 (36.8), 309 (20.9), 336 (16.6), 436 (5.44), 504 (4.16), 599 (2.75)		−0.52 (IV↔III)
3	292 (20.4), 341 (11.7), 400 (7.06), 475 (3.82), 564 (1.73)		−0.58 (IV↔III)
4	262 (21.8), 274 (22.9), 283 (24.4), 286 (24.4), 294 (28.8), 321 (24.9), 333 (22.6), 389 (5.04), 445 (2.62), 502 (1.52)	1253	−0.36 (III?II) +0.87 (III↔IV)
5	309 (26.2), 321 (24.5), 344 (19.4), 379 (17.1), 401 (14.8), 447 (8.78), 496 (6.70), 531(4.81)	1256	−0.38 (IV↔III)
6	265 (27.0), 275 (26.9), 291 (26.8), 299 (27.6), 312 (27.5), 337 (30.4), 323 (33.9), 378 (4.84)	1252	−0.30 (III↔II) +0.86 (III↔IV)
7	265 (11.8), 274 (13.8), 283 (15.6), 286 (15.7), 294 (20.6), 321 (19.4), 333 (17.4)	1244, 1254	
8	249 (20.8), 256 (25.8), 295 (6.74), 307 (12.5), 321 (16.1), 344 (11.6), 360 (16.8), 376 (13.2)	1259	
9	268 (10.7), 279 (13.6), 289 (16.2), 298 (18.2), 331 (14.6), 343 (14.1)	1251	
10	267 (9.64), 276 (10.8), 291 (10.4), 299 (11.0), 323 (16.5), 337 (14.6)	1256, 1267	

[a] Five membered ring of benzoxazole moiety.

3.4. Magnetic properties

The magnetic moments per manganese ion of the complexes measured at room temperature are 3.85 μ_B for **1**, 4.02 μ_B for **2**, 3.59 μ_B for **3**, 4.80 μ_B for **4**, 2.92 μ_B for **5** and 4.87 μ_B for **6**. Excepting complex **5**, these values are close to the spin only value of 4.90 μ_B and 3.88 μ_B expected for a magnetically diluted high-spin d^4 manganese(III) ion and d^3 manganese(IV) ions, respectively. For complex **4**, as the manganese ion, located on the axis of nitrogen atom of benzoxazole group, interacts with the phenolic oxygen atom of a neighboring complex, it seems to adopt a dimeric structure. However, the value of its magnetic moment indicates that there is little or no intermolecular antiferromagnetic coupling.

On the other hand, for the di-μ-oxo dimanganese(IV) complex **5**, the magnetic moment per manganese ion of the complex measured at room temperature is 2.92 μ_B. This lower value indicates that an intramolecular antiferromagnetic interaction between the two manganese(IV) ions (d^3) exists in complex **5**. Although this value is slightly higher than those for other di-μ-oxo dimanganese complexes [18–33], it may be caused by the effect of π–π stacking between the benzoxazole moieties of each manganese ion.

3.5. Electrochemical properties

Electrochemical data for all the complexes are listed in Table 6. Quasi-reversible redox waves were observed at −0.44 V for **1**, −0.52 V for **2**, −0.58 V for **3**, −0.36 and +0.87 V for **4**, −0.38 V for **5**, and −0.30 and +0.86 V (vs. SCE) for **6**. The redox waves observed for manganese(IV) complexes **1**, **2**, **3** and **5** can be assigned to the redox couple due to Mn(IV)↔Mn(III). The two redox waves around −0.30 and +0.85 V observed for manganese(III) complexes **4** and **6** can be assigned to the redox couples due to Mn(III)↔Mn(II) and Mn(IV)↔Mn(III), respectively.

3.6. Reactions of $KMnO_4$ with tridentate Schiff base ligands

Fig. 10 shows the absorption spectral changes of a MeCN solution of $KMnO_4$ caused by the addition of a MeCN solution of *N*-PhOH-salH in a 1:2 molar ratio, measured at room temperature. As the intensities of characteristic absorption bands around 550 nm due to $KMnO_4$ were decreased, intensities around 300 nm were significantly increased. These absorption bands can be attributed to the five-membered ring formation of the benzoxazole derivative. Moreover, the spectral changes indicate that this ring formation can take place in the

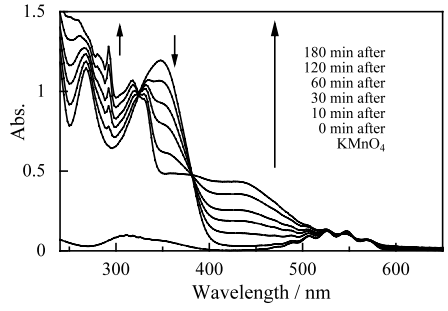


Fig. 10. Spectral changes of a MeCN solution of $KMnO_4$ (5×10^{-4} M) caused by the addition of a MeCN solution of *N*-PhOH-salH. ($KMnO_4$:*N*-PhOH-salH = 1:2, cell length; 1 cm).

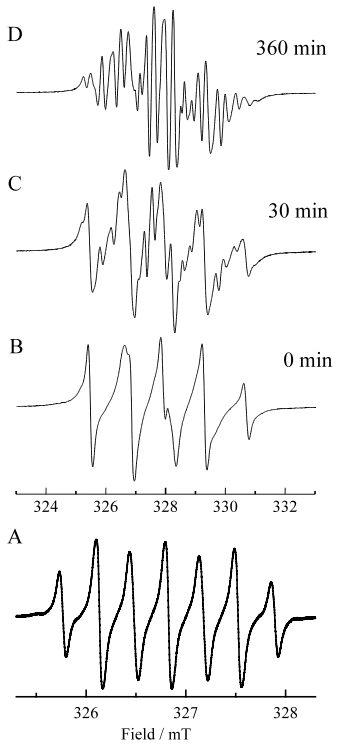


Fig. 11. ESR spectrum of a MeCN solution of $KMnO_4$ in the presence of DMPO (A) and spectral changes during the reaction of $KMnO_4$ and *N*-PhOH-salH (B–D) at 213 K.

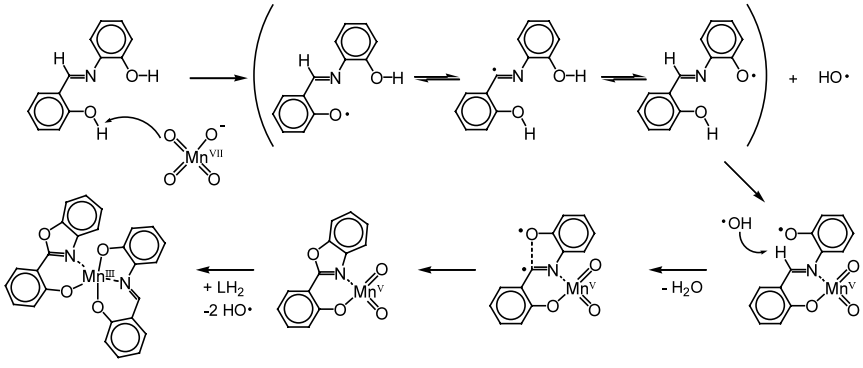
early stages of the reaction of $KMnO_4$ with the tridentate Schiff base ligand.

Oxidation of organic compounds by $KMnO_4$ has been known to proceed via radical formation [48]. Thus, the ESR spectra were measured for the present systems in order to clarify the reaction mechanism. Fig. 11A shows the ESR spectrum of a MeCN solution of $KMnO_4$ plus DMPO (5,5-dimethylpyrroline-N-oxide), which is well-known as a radical trapping agent, measured at 213 K. Seven-line signals centered at $g = 2.0$ were observed. It is conceivable that this signal may be assigned to the DMPO radical which may form by the reaction between DMPO and hydrogen radical, forming by hydrogen abstraction of DMPO by $KMnO_4$. This signal was so stable that further reaction with $KMnO_4$ did not occur.

Next, the ESR spectrum of a MeCN solution of *N*-PhOH-salH plus $KMnO_4$ in the presence of DMPO was measured, as shown in Fig. 11(B). The five-line signals centered at $g = 2.0$ were observed in the early stages of the reaction. Moreover, these signals were split with the passage of time (Fig. 11(C)) and changed to a complicated signal having a hyperfine structure 6 h later (Fig. 11(D)). The ESR spectra for the reaction systems between $KMnO_4$ and other analogous Schiff base ligands, *N*-EtOH-salH and *N*-chxOH-salH and the bidentate one, *N*-Me-salH, which were not oxidized to oxazole derivatives, were measured under almost the same conditions. The ESR spectral changes obtained were similar to that observed for the *N*-PhOH-salH plus $KMnO_4$ system. These results indicate that the signals shown in Fig. 11(B–D) could be attributed to the product formed by the reaction between a phenoxy radical of salicylideneamines and DMPO, which has not yet been identified. Consequently, the reaction of tridentate Schiff base ligands with $KMnO_4$ may be initiated by the hydrogen atom abstraction from the phenol moiety of the ligands to give a phenoxy radical. Scheme 2 shows a tentative reaction pathway for the five-membered ring formation during the reaction of $KMnO_4$ and tridentate Schiff base ligand, *N*-PhOH-salH. In the case of *N*-PhOH-salH, $KMnO_4$ may attack a phenol group of the salicylaldehyde moiety and a phenoxy radical may form. This radical can be stabilized by the aromatic resonance system (π conjugation) and may be delocalized and transferred on the carbon atom of the imino group, which may induce a –N=C–H cleavage to form –N=C, which in turn may couple with a phenoxy radical of an amino phenol moiety to afford a five-membered ring benzoxazole derivative. A further investigation has not been made.

4. Conclusions

Four types of novel manganese complexes can be obtained by the reaction of $KMnO_4$ with various tridentate Schiff base ligands. In the case of *N*-EtOH-



Scheme 2. A tentative reaction pathway for the five-membered ring formation during the reaction of $KMnO_4$ with *N*-PhOH-salH.

salH, the mononuclear manganese(IV) complex, Mn^{IV}(*N*-EtO-sal)$_2$ was obtained. On the other hand, with *N*-PhOH-salH and its derivatives five-coordinate manganese(III) complexes having mixed ligands, Mn^{III}(*N*-PhO-sal)(L), the di-μ-oxo dimanganese(IV) complex, [Mn^{IV}(5,6-Benzo-L)$_2$(μ-O)]$_2$ and the roughly octahedral manganese(III) complex, Mn^{III}(L-4-Me)$_3$ were obtained, depending on the substituents. The reactions between $KMnO_4$ with the tridentate Schiff base ligands have been monitored by UV–Vis and ESR spectroscopies. The results indicate that the five-membered ring formation may proceed via a radical reaction initiated by the oxidation of the ligands with the permanganate ions in the early period of the reaction of $KMnO_4$ with tridentate Schiff base ligands.

5. Supplementary data

Supplementary data are available from The Director, CCDC, 12 Union Road, Cambridge, CB2 1EZ, UK (fax: +44-1223-336033; e-mail: deposit@ccdc.cam.ac.uk or www: http://www.ccdc.cam.ac.uk), deposition numbers 161717 to 161719 for ligand **8** and complexes **3** and **2**, respectively. The complexes **1**, **4**, **5**, **6** are in the CSD with the following refcodes: GAQDUX, GAQFEJ, GAQFUZ and GAQMOA.

References

[1] N.A. Law, M.T. Caudle, V.L. Pecoraro, Adv. Inorg. Chem. 46 (1998) 305.
[2] V.L. Pecoraro, Manganese Redox Enzymes, VCH Publishers, New York, 1992.
[3] V.K. Yachandra, V.J. DeRose, M.J. Latimer, I. Mukerji, K. Sauer, M.P. Klein, Science 260 (1993) 675.
[4] V.L. Pecoraro, M.J. Baldwin, A. Gelasco, Chem. Rev. 94 (1994) 807.
[5] V.K. Yachandra, K. Sauer, M.P. Klein, Chem. Rev. 96 (1996) 2927.
[6] W. Rüttinger, G.C. Dismukes, Chem. Rev. 97 (1997) 1.
[7] C.W. Hoganson, G.T. Babcock, Science 277 (1997) 1953.
[8] C. Tommos, G.T. Babcook, Acc. Chem. Res. 31 (1998) 18.
[9] P.E.M. Siegbahn, R.H. Crabtree, J. Am. Chem. Soc. 121 (1999) 117.
[10] J. Limburg, J.S. Vrettos, L.M. Liable-Sands, A.L. Rheingold, R.H. Crabtree, G.W. Brudving, Science 283 (1999) 1524.
[11] R. Manchanda, G.W. Brudvig, R.H. Crabtree, Coord. Chem. Rev. 1 (1995) 144.
[12] K. Wieghardt, Angew. Chem., Int. Ed. Engl. 28 (1989) 1153.
[13] K. Wieghardt, Angew. Chem., Int. Ed. Engl. 33 (1994) 725.
[14] E. Gallo, E. Solari, S.D. Angelis, C. Floriani, N. Re, A. Chiesi-Villa, C. Rizzoli, J. Am. Chem. Soc. 115 (1993) 9850.
[15] Y. Gultneh, B. Ahvazi, A.R. Khan, R.J. Butcher, J.P. Tuchagues, Inorg. Chem. 34 (1995) 3633.
[16] M. Mikuriya, Y. Yamato, T. Tokii, Bull. Chem. Soc. Jpn. 65 (1992) 2624.
[17] M. Mikuriya, Y. Hashimoto, A. Kawamori, Chem. Lett. (1995) 1095.
[18] E.J. Larson, V.L. Pecoraro, J. Am. Chem. Soc. 113 (1991) 3810.
[19] J.W. Gohodes, W.H. Armstrong, Inorg. Chem. 31 (1992) 368.
[20] E.J. Larson, M.S. Lah, X. Li, J.A. Bonadies, V.L. Pecoraro, Inorg. Chem. 31 (1992) 373.
[21] E. Libby, R.J. Webb, W.E. Streib, K. Folting, J.C. Huffman, D.N. Hendrickson, G. Christou, Inorg. Chem. 28 (1989) 4037.
[22] M. Stebler, A. Ludi, H.B. Bürgi, Inorg. Chem. 25 (1986) 4743.
[23] A.R. Oki, J. Glerup, D.J. Hodgson, Inorg. Chem. 29 (1990) 2435.
[24] P.A. Goodson, J. Glerup, D.J. Hodgson, K. Michelsen, E. Pedersen, Inorg. Chem. 29 (1990) 503.
[25] P.A. Goodson, J. Glerup, D.J. Hodgson, K. Michelsen, H. Weihe, Inorg. Chem. 30 (1991) 4909.
[26] S. Pal, W.H. Armstrong, Inorg. Chem. 31 (1992) 5417.
[27] J.E. Sarneski, M. Didiuk, H.H. Thorp, R.H. Crabtree, G.W. Brudvig, J.W. Faller, G.K. Schulte, Inorg. Chem. 30 (1991) 2833.
[28] S. Pal, M.K. Chan, W.H. Armstrong, J. Am. Chem. Soc. 114 (1992) 6398.
[29] S. Pal, M.M. Olmstead, W.H. Armstrong, Inorg. Chem. 34 (1995) 4708.
[30] H. Torayama, T. Nishide, H. Asada, M. Fujiwara, T. Matsushita, Chem. Lett. (1996) 387.
[31] H. Torayama, H. Asada, M. Fujiwara, T. Matsushita, Chem. Lett. (1996) 1067.
[32] H. Torayama, T. Nishide, H. Asada, M. Fujiwara, T. Matsushita, Polyhedron 17 (1998) 105.
[33] H. Torayama, H. Asada, M. Fujiwara, T. Matsushita, Polyhedron 17 (1998) 3859.
[34] H. Torayama, T. Nishide, H. Asada, M. Fujiwara, T. Matsushita, Polyhedron 16 (1997) 3787.
[35] H. Asada, M. Ozeki, M. Fujiwara, T. Matsushita, Chem. Lett. (1999) 525.
[36] K. Ramesh, R. Mukherjee, J. Chem. Soc., Dalton Trans. 83 (1992).
[37] G. Das, R. Shukla, S. Mandal, R. Singh, P.K. Bharadwaj, Inorg. Chem. 36 (1997) 323.
[38] TEXSAN: Crystal Structure Analysis Package, Molecular Structure Corporation, 1985 and 1992.
[39] SHELXS-86: G.M. Sheldrick, in: G.M. Sheldrick, C. Kruger, R. Goddard (Eds.), Crystallographic Computing 3, Oxford University Press, 1985, pp. 175–189.
[40] SIR-92: A. Altomare, M.C. Burla, M. Camalli, M. Cascarano, C. Giacovazzo, A. Guagliardi, G. Polidori, J. Appl. Cryst. 27 (1994) 435.
[41] MULTAN-88: T. Debaerdemaeker, G. Germain, P. Main, L.S. Refaat, C. Tate, M.M. Woolfson, Computer programs for the automatic solution of crystal structures from X-ray diffraction data, University of York, UK, 1988.
[42] SIR-88: M.C. Burla, M. Camalli, G. Cascarano, C. Giacovazzo, G. Polidori, R. Spagna, D. Viterbo, J. Appl. Cryst. 22 (1989) 389.
[43] DIRDIF-94: P.T. Beurskens, G. Admiraal, G. Beurskens, W.P. Bosman, R. de Gelder, R. Israel, J.M.M. Smits, The DIRDIF-94 program system, Technical Report of the Crystallography Laboratory, University of Nijmegen, The Netherlands, 1994.
[44] D.P. Kessissoglou, W.M. Butler, V.L. Pecoraro, J. Chem. Soc., Chem. Commun. (1986) 1253.
[45] D.P. Kessissoglou, X. Li, W.M. Butler, V.L. Pecoraro, Inorg. Chem. 26 (1987) 2487.
[46] M. Mikuriya, D. Jie, Y. Kakuta, T. Tokii, Bull. Chem. Soc. Jpn. 66 (1993) 1132.
[47] S.K. Chandra, P. Basu, D. Ray, S. Pal, A. Chakravorty, Inorg. Chem. 29 (1990) 2423.
[48] K.A. Gardner, J.M. Mayer, Science 269 (1995) 1849.

PERGAMON

Polyhedron 21 (2002) 1149–1153

POLYHEDRON

www.elsevier.com/locate/poly

Organotin(IV) complexes of 4,6-dimethylpyrimidine-2-thione, Me_2PymtH. Preparation, characterization and crystal structure determination of *cis*-[$Ph_2Sn(Me_2Pymt)_2$] and [$Ph_3Sn(Me_2Pymt)$]

Ramão M. Fernandes [a], Ernesto S. Lang [a], Ezequiel M.V. López [b], Gerimário F. de Sousa [c,*]

[a] *Departamento de Química Inorgânica, Universidade Federal de Santa Maria, 97119-900 Santa Maria, RS, Brazil*
[b] *Departamento de Química Inorgánica, Facultade de Ciencias-Químicas, E-36200 Vigo, Galicia, Spain*
[c] *Instituto de Química, Universidade de Brasília, 70919-970 Brasília, DF, Brazil*

Received 7 September 2001; accepted 19 March 2002

Abstract

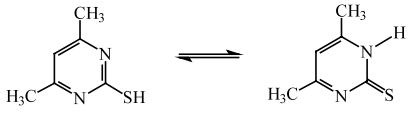
The coordination mode of the ambidentate ligand 4,6-dimethylpyrimidine-2-thione (Me_2PymtH) was investigated with respect to the organotin(IV) compounds, namely Me_2SnCl_2, *n*-Bu_2SnCl_2, Ph_2SnCl_2 and Ph_3SnCl. An X-ray crystal structure determination carried out on *cis*-[$Ph_2Sn(Me_2Pymt)$] (**3**) and [$Ph_3Sn(Me_2Pymt)$] (**4**) revealed that the Me_2Pymt^- ligand is N,S-coordinated in both complexes. The Sn(IV) atom is six-coordinated in **3** and five-coordinated in **4**. The similarities observed in the IR, NMR (^1H, ^{13}C) and mass spectroscopy are indicative of a similar behavior of the ligand in all the complexes, thus suggesting a six-coordination in the dimethyltin (**1**) derivative and five-coordination in the dibutyltin (**2**) one. The complexes were characterized by means of elemental analysis, IR, NMR (^1H, ^{13}C) and mass spectroscopic methods. © 2002 Published by Elsevier Science Ltd.

Keywords: Organotin(IV) complexes; Dimethylpyrimidinethione; Crystal structures

1. Introduction

The variety of coordination modes of 4,6-dimethylpyrimidine-2-thione (Me_2PymtH) has been demonstrated in a number of complexes [1] and their biological applications have been of considerable interest for years [2]. Insofar as many organotin(IV) complexes are also noteworthy for the same reason [3], a combination of the two chemistry is an interesting topic to pursue.

The present work deals with the preparation and characterization of four new organotin(IV) complexes with the Me_2PymtH ligand, whose structure is shown below.



Me_2PymtH

This ligand was chosen since it has the potential to form four-, five-or hexacoordinate metal complexes which the polyhedral of these compounds assuming structures that are considerably distorted from ideal configuration. These distorted structures in many organotin(IV) complexes are thought to be due to a number of factors, such as steric requirements, electronic effects arising from different electronegativities of the ligands, intermolecular interactions and crystal packing requirements [4]. Pyridines and pyrimidines substituted with an SH or an OH group at the two or four positions are fundamentally tautomeric heterocyclic system and many experimental studies have been reported [5,6]. The complexes were studied by microanalyses, IR, NMR (^1H, ^{13}C), mass spectroscopy and crystal X-ray diffraction.

* Corresponding author. Tel.: +55-61-307-2165; fax: +55-61-273-4149.
E-mail address: gfreitas@unb.br (G.F. de Sousa).

0277-5387/02/$ - see front matter © 2002 Published by Elsevier Science Ltd.
PII: S0277-5387(02)00996-8

2. Experimental

Solvents were purified and dried according to standard procedures. Thiourea, pentane-2,4-dione and organotin(IV) chlorides were obtained from Aldrich and used without further purification. IR spectra were recorded on a Bruker IFS-28 spectrophotometer in the 4000–400 cm^{-1} range using KBr pellets. NMR (^{1}H, ^{13}C) spectra were obtained from a Bruker DPX-200 spectrometer using $CDCl_3$ as the solvent with chemical shifts in parts per million downfield from Me_4Si. The mass spectra were recorded on a Micromass 7070-F instrument, using FAB+Xe at 8 eV and alcohol 3-nitrobenzilic as matrix. Microanalyses were performed in a VARIO EL (Elementar Analysensysteme GmbH) instrument.

2.1. Synthesis

The ligand was prepared according to the literature [2] and the complexes by the following procedure: 0.28 g (2 mmol) of Me_2PymtH was dissolved in 30 ml of THF (freshly distilled) in a Schlenk tube kept under N_2 atmosphere. To the solution, 0.84 ml (6 mmol) of triethylamine (Et_3N) was added via a syringe and the resulting solution was stirred for 30 min. To this solution was added, during 10 min, 1 mmol of the appropriate organotin(IV) species dissolved in 3 ml of THF, and the mixture was refluxed for about 4 h. A white flocculent precipitate identified as triethylamine chloride (Et_3NHCl) was produced and filtered. Slowly evaporation of the solvent led to the appearance of white amorphous crystalline solids with yields of the order 70%. Well formed crystals suitable for X-ray studies were only obtained for complexes **3** and **4** by recrystallization from a 1:1 (v/v) mixture of dichloromethane–*n*-hexane. The microanalyses were performed in a Perkin–Elmer 2400C analyzer, giving for C, H and N the following results: [$Me_2Sn(Me_2Pymt)_2$] (**1**): (m.p. 197–199 °C). *Anal*. Found: C, 40.66; H, 4.78; N, 13.55. Calc. for ($C_{14}H_{20}N_4S_2Sn$): C, 39.37; H, 4.72; N, 13.12%. [$Bu_2SnCl(Me_2Pymt)$] (**2**): (m.p. 212–211 °C). *Anal*. Found: C, 43.32; H, 6.46; N, 6.72. Calc. for ($C_{14}H_{25}ClN_2SSn$): C, 41.26; H, 6.18; N, 6.87%. *cis*-[$Ph_2Sn(Me_2Pymt)_2$] (**3**): (m.p. 202–204 °C). *Anal*. Found: C, 52.17; H, 4.58; N, 10.62. Calc. for ($C_{24}H_{24}N_4S_2Sn$): C, 52.29; H, 4.39; N, 10.16%. [$Ph_3Sn(Me_2Pymt)$] (**4**): (m.p. 206–208 °C). *Anal*. Found: C, 58.67; H, 4.57; N, 5.84. Calc. for ($C_{24}H_{22}N_4S_2Sn$): C, 58.92; H, 4.53; N, 5.73%.

2.2. X-ray studies

Colourless single crystals of compounds **3** and **4** which were suitable for X-ray diffractometric studies were selected and data collected on a Bruker Smart CCD for **3** and an Enraf–Nonius MACH3 for **4**. The data were corrected for absorption effects by an empirical correction (SADABS 7b) (**3**) or using ψ-scans 7a (**4**).

Structural solutions were determined by direct methods [8]. Least-squares full-matrix refinement on F2 was performed using the program SHELXL-97 [8]. All non-H atoms were refined anisotropically. H atoms were calculated and refined as ridding atoms (HFIX [8]). Atomic scattering factors and anomalous dispersion corrections for all atoms were taken from International Tables for Crystallography [9]. Graphics were obtained with ZORTEP [10].

3. Results and discussion

3.1. Infrared spectroscopy

Table 1 shows the assignment of the main IR absorptions of the ligand and its complexes. The Me_2PymtH ligand shows a rather complicated spectrum in the 3100–2600 cm^{-1} range where C–H and N–H stretching absorptions occur. Thus, the spectra of complexes retain those absorptions found in free ligand. The ring stretching vibrations, $\nu(C{=}C)+\nu(C{=}N)$, are shifted to lower frequencies, together with the shift in opposite direction of the ligand band at 1235 cm^{-1}, assigned to mixed $\nu(C{-}S)+\nu(C{-}N)$ absorption bands. These results suggest, in accordance with ^{1}H NMR, an N,S-chelation of the aromatic Me_2Pymt^{-} anion around the Sn(IV) ion. Similar results have been reported for tiolate complexes of 2-PySH (2-mercaptopyridine) and 2-PymSH (2-mercaptopyrimidine) and different metal ions such as Ni(II) [11] and Pt(II) [12], as well as with Re(V) complex of Me_2PymtH [13].

In the IR spectrum of [$Me_2Sn(Me_2Pymt)_2$] the asymmetric Sn–C stretching band at 551 cm^{-1} indicates that this complex has the *trans* arrangement of the methyl groups [14].

3.2. NMR spectroscopy

Table 2 lists ^{1}H chemical shifts for the free ligand Me_2PymtH and its complexes. The ^{13}C NMR spectrum to complex **1** showed a $^{1}J(^{119}Sn{-}CH_3)$ coupling constant of 600 Hz and the ^{1}H NMR spectrum showed one doublet and a singlet in the methyl region occurring at 2.37 and 1.03 [$^{2}J(^{119}Sn{-}CH_3)$ 83 Hz] due to two magnetically non-equivalent methyl groups bonded in $N{=}CH{-}CH_3$ and $Sn{-}CH_3$, respectively. These ^{1}J and ^{2}J coupling constants data can be used to estimate the $CH_3{-}Sn{-}CH_3$ angle in complex **1**, and according to the literature [15,16], two empirical equations can be set up for this estimate:

Table 1
Main IR absorptions (cm^{-1}) for Me_2PymtH and its Sn(IV) complexes

Compound	C.N. [a]	ν(N–H)+ν(C–H)	ν(C=C)+ν(C=N)	ν(C–S)+ν(C–N)
Me_2PymtH		2911	1625, 1569, 1432	1235
$[Me_2Sn(Me_2Pymt)_2]$ (**1**)	6	2916	1578, 1543, 1435	1257
$[Bu_2SnCl(Me_2Pymt)]$ (**2**)	5	2921	1578, 1539, 1437	1257
cis-$[Ph_2Sn(Me_2Pymt)_2]$ (**3**)	6	3038	1579, 1525, 1430	1255
$[Ph_3Sn(Me_2Pymt)]$ (**4**)	5	3038	1584, 1524, 1427	1255

[a] C.N. = coordination number.

Table 2
^1H NMR data in $CDCl_3$ solution[a]

Me_2PymtH	6.49 (s, 1H, C–H); 2.39 (t, 6H, C–CH_3)
$[Me_2Sn(Me_2Pymt)_2]$ (**1**)	6.69 (s, 2H, C–H); 2.37 (d, 12H, C–CH_3); 1.03 (s, 6H, Sn–CH_3) $^2J(^{119}Sn–CH_3)$ = 83/75
$[Bu_2SnCl(Me_2Pymt)]$ (**2**)	(s, 2H, C–H); 2.37 (d, 6H, C–CH_3); 1.64-1.55 (m, 4H, Sn–CH_2–C); 1.42–1.26 (m, 4H, C–CH_2–C); 0.79 (t, 6H, Bu–CH_3)
cis-$[Ph_2Sn(Me_2Pymt)_2]$ (**3**)	7.88–7.26 (m, 10H, Sn–C_6H_5); 6.52 (s, 2H, C–H); 2.18 (s, 6H, C–CH_3)
$[Ph_3Sn(Me_2Pymt)]$ (**4**)	7.80–7.23 (m, 10H, Sn–C_6H_5); 6.55 (s, 2H, C–H); 2.13 (s, 6H, C–CH_3)

[a] s = Singlet, d = doublet, m = multiplet, δ in ppm, J in Hz.

$$^1J(^{119}Sn–^{13}CH_3) = 11.4\theta - 875 \quad (1)$$

$$\theta = 0.0161\{^2J(^{119}Sn–CH_3)\}^2 - 1.32\{^2J(^{119}Sn–CH_3)\} + 133.4 \quad (2)$$

Using ^1J into Eq. (1) and ^2J into Eq. (2), one finds values of θ of 135° and 129°, respectively. These angles values might suggests that in solution the dimethyltin derivative is a distorted *trans* octahedral complex and the basic structural features of the solid-state phase remain in $CDCl_3$ solution. For dibutyl derivative, similar structural considerations in solution might hold.

Similar results were reported for octahedral complexes with analogous *trans* arrangement, namely $[Me_2Sn(dtc)_2]$ [17] [$^2J(^{119}Sn–CH_3)$ 84 Hz and $^1J(^{119}Sn–^{13}CH_3)$ 670 Hz], $[Me_2SnCl_2\cdot(DMSO)_2]$ [15] [$^2J(^{119}Sn–CH_3)$ 86 Hz] and $[Me_2Sn(CH_3COO)_2]$ [18] [$^2J(^{119}Sn–CH_3)$ 82 Hz], where Hdtc = ditiocabamic acid and DMSO = dimethylsulfoxide.

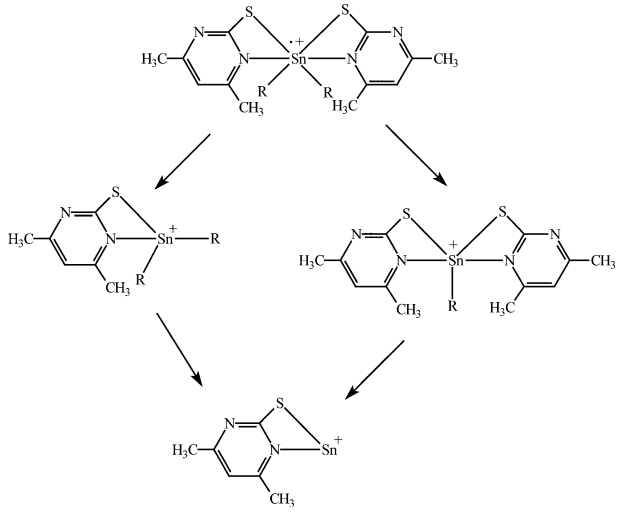


Fig. 1. Fragmentation scheme proposed for complexes **1**–**3**.

3.3. Mass spectroscopy

Table 3 shows the FAB mass spectra of compounds **1**–**4** and Fig. 1 presents a fragmentation scheme proposed for complexes **1**–**3** compatible with literature data [4,19]. The molecular ion for complexes **1**, **3** and **4** were detectable at m/z 429, 553 and 489, respectively.

The spectra of complexes **1** and **3** showed that the base peaks are the ions $R_2Sn(Me_2Pymt)^+$ (R = Me, Ph), in agreement with reported works [4,19]. This contrasts with the spectra of compounds **2** and **4**, in which the base peaks appeared at m/z 882 (not attributed) and m/z 291 (probably due to the ion $Ph_2Sn(H_2O)^+$), respectively.

Table 3
Fragment-ions observed in the FAB mass spectra of compounds **1**–**4**

Fragment-ion	Me_2Sn (**1**) m/z [a] (abundance)	Bu_2Sn (**2**) m/z [a] (abundance)	Ph_2Sn (**3**) m/z [a] (abundance)	Ph_3Sn (**4**) m/z [a] (abundance)
$R_3Sn(Me_2Pymt)^+$				489(8)
$R_2Sn(Me_2Pymt)_2^+$	429(33)		553(15)	
$R_2Sn(Me_2Pymt)^+$	289(100)	373(64)	413(100)	
$RSn(Me_2Pymt)_2^+$	413(16)		258(9)	
$Sn(Me_2Pymt)^+$	259(18)	259(22)	259(24)	259(25)
$(Me_2Pymt)_2^+$	279(9)	279(16)	279(48)	

[a] Nominal values calculated using the most abundant isotope ^{120}Sn.

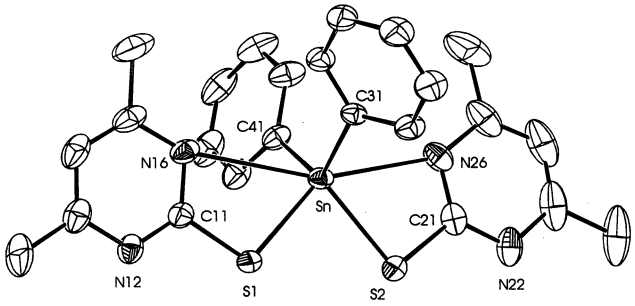


Fig. 2. Perspective view of *cis*-[$Ph_2Sn(Me_2Pymt)_2$] (**3**) showing the atom numbering scheme. Displacement ellipsoids are drawn at the 50% probability level.

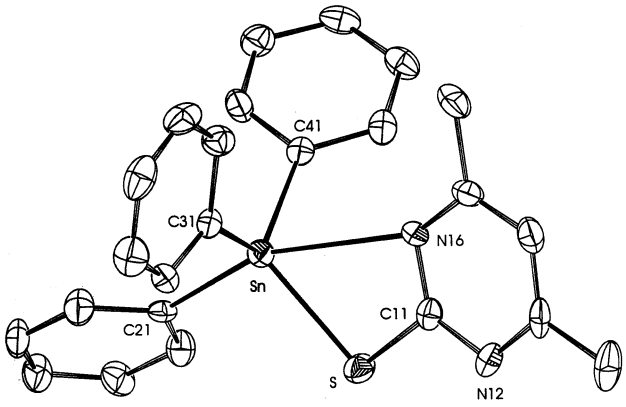


Fig. 3. Perspective view of [$Ph_3Sn(Me_2Pymt)$] (**4**) showing the atom numbering scheme. Displacement ellipsoids are drawn at the 50% probability level.

3.4. X-ray structures of cis-[$Ph_2Sn(Me_2Pymt)_2$] (3) and [$Ph_3Sn(Me_2Pymt)$] (4)

The molecular structures of **3** and **4** are given in Figs. 2 and 3, respectively. Tables 4 and 5 summarize the crystal data and selected bond lengths and bond angles for the two compounds, respectively.

The geometry about Sn(IV) in **3** is best described as a distorted octahedral with the two Me_2Pymt^- anions acting as bidentate ligands with *cis* Ph–Sn–Ph [117.42(13)°] and *cis* S–Sn–S [84.50(3)°] arrangements. The bond distances [2.4476(10); 2.4515(10) Å] in the Sn–S bond lengths found in **3** are shorter than the Sn–S bond distances [2.476(2); 2.485(1) Å], [2.477(3) Å] and [2.487(2) Å] found in [$Ph_2Sn(2\text{-}SPy)_2$] [20], [*n*-$Bu_2Sn(2\text{-}SPy\text{-}5\text{-}NO_2)_2$] [4] and [$Me_2Sn(2\text{-}SPy)_2$] [21], respectively, where 2-SPyH is 2-pyridinethione and 2-SPyH-5-NO_2 is 5-nitropyridinethione.

The Sn–N bond distances [2.754(3) and 3.083(3) Å] found in complex **3** are shorter than the sun of the van der Waals radii (3.75 Å) [20] indicating the bidentate nature of the Me_2Pymt^- ligand. However, these distances are longer than the Sn–N distances [2.636(4); 2.698(3) Å] and [2.702(5) Å] found in [$Ph_2Sn(2\text{-}SPy)_2$] [20] and [$Me_2Sn(2\text{-}SPy)_2$] [21], respectively. Although conclusions are drawn with caution, it would appear most reasonable that the disparate Sn–N bond distances in **3** versus [$Ph_2Sn(2\text{-}SPy)_2$] and [$Me_2Sn(2\text{-}SPy)_2$] [21] is probably due to the electronic effects caused by uncomplexed N(12) and N(22) atoms in complex **3**. The Sn–C bond distances (mean value of 2.12 Å) is typical, and compares favorably with the analogous bond in related compounds, in particular [$Ph_2Sn(2\text{-}SPy)_2$] [20] (2.13 Å) and [$Me_2Sn(2\text{-}SPy)_2$] [21] (2.13 Å), with which it shows striking structural similarities.

Table 4
Crystallographic data for the X-ray diffraction studies for **3** and **4**

	3	**4**
Formula	$C_{24}H_{24}N_4S_2Sn$	$C_{24}H_{22}N_2SSn$
Formula weight	551.28	498.19
Crystal system	monoclinic	orthorhombic
Space group	$P2_1/c$	*Pbca*
Z	4	8
A (Å)	9.6990(3)	8.7994(14)
B (Å)	17.0580(5)	17.513(3)
C (Å)	15.9182(4)	28.826(5)
β (°)	106.0652(8)	90
V (Å^3)	2528.14(13)	4442.2(13)
D_{calc} (g cm^{-3})	1.448	1.463
Crystal size (mm)	0.45 × 0.30 × 0.20	0.48 × 0.16 × 0.08
Index ranges	$-12 \le h \le 12$	$0 \le h \le 10$
	$-18 \le k \le 22$	$0 \le k \le 21$
	$-21 \le l \le 21$	$0 \le l \le 35$
μ (mm^{-1})	1.194	1.255
T (K)	293(2)	293(2)
F(000)	1112	1968
Reflections collected	16755	4477
Independent reflections	6151	4477
Reflections observed	4230	1507
R [$I > 2\sigma(I)$]	0.0397	0.0525
R_w	0.0852	0.0881
Goodness-of-fit	1.016	0.894

The geometry about Sn(IV) in **4** is best described as a strongly distorted trigonal bipyramid (TBP) configuration where two phenyl groups and a S atom are at the equatorial plane while N(16) atom and other phenyl group occupy the axial position.

The Sn–S bond distance [2.433(2) Å] found in **4** is within the range (2.405–2.481 Å) [22,23] recently reported for triphenyltin(IV) thiolates compounds R_3SnL, containing potentially bidentate ligand. Similarly, the Sn–C distances [mean 2.14 Å] agree well with those previously reported [22,23].

The Sn–N bond length [2.835(7) Å] is equal to the length of Sn–N bond [2.836(3) Å] found in [Ph_3Sn(o-quinolinylthiolate)] [22], in which sulfur and nitrogen atoms are bonded to the Sn(IV) atom forming five-membered chelate ring. On the other hand, the Sn–N length in **4** is smaller than that of the Sn–N bond [2.88(5) Å] found in [$Ph_3Sn(2\text{-}Pymt)$] [24], where 2-PymtH is 2-pyrimidinethione, suggesting that the methyl group, C(151), does not cause steric effect. In contrast,

Table 5
Selected bond distances (Å) and angles (°) for **3** and **4**

	3		**4**
Bond distances			
Sn–S(1)	2.4515(10)	Sn–S	2.433(2)
Sn–S(2)	2.4476(10)	Sn–N(16)	2.835(7)
Sn–C(31)	2.124(3)	Sn–C(21)	2.159(8)
Sn–C(41)	2.116(3)	Sn–C(31)	2.117(8)
Sn–N(16)	3.083(3)	Sn–C(41)	2.134(9)
Sn–N(26)	2.754(3)	S–C(11)	1.752(9)
C(11)–N(12)	1.327(5)	C(11)–N(12)	1.334(10)
C(11)–N(16)	1.334(4)	C(11)–N(16)	1.320(10)
C(21)–N(22)	1.341(5)	C(13)–N(12)	1.326(11)
C(21)–N(26)	1.331(5)	C(15)–N(16)	1.344(11)
S(1)–C(11)	1.755(4)	C(13)–C(14)	1.359(13)
S(2)–C(21)	1.740(4)	C(14)–C(15)	1.371(11)
Bond angles			
C(41)–Sn–C(31)	117.42(13)	C(31)–Sn–C(41)	116.8(3)
C(41)–Sn–S(1)	108.81(11)	C(31)–Sn–C(21)	106.9(3)
C(41)–Sn–S(2)	116.30(10)	C(41)–Sn–C(21)	104.3(3)
C(41)–Sn–N(16)	80.65(12)	C(31)–Sn–N(16)	83.3(3)
C(41)–Sn–N(26)	88.44(13)	C(41)–Sn–N(16)	85.7(3)
C(31)–Sn–N(16)	85.23(11)	C(21)–Sn–N(16)	159.7(3)
C(31)–Sn–N(26)	85.04(12)	C(31)–Sn–S	111.0(2)
C(31)–Sn–S(1)	111.93(9)	C(41)–Sn–S	115.2(3)
C(31)–Sn–S(2)	113.03(10)	C(21)–Sn–S	100.7(2)
S(1)–Sn–S(2)	84.50(3)	S–Sn–N(16)	59.03(17)
N(16)–Sn–N(26)	160.02(10)	C(11)–S–Sn	94.6(3)
N(16)–Sn–S(1)	55.75(6)	N(12)–C(11)–N(16)	127.7(9)
N(26)–Sn–S(2)	59.71(8)	N(16)–C(11)–S	116.3(7)
N(16)–Sn–S(2)	140.25(6)	N(12)–C(11)–S	115.9(8)
N(26)–Sn–S(1)	144.21(8)	N(12)–C(13)–C(131)	117.9(11)
N(16)–C(11)–S(1)	117.3(3)	N(16)–C(15)–C(151)	115.5(9)
N(26)–C(21)–S(2)	117.6(4)	C(13)–C(14)–C(15)	118.3(11)

the Sn···N interaction [2.920(3) Å], found in [Ph_3Sn(mimt)] [22], where mimtH is 1-methyl-2(3H)-imidazolinethione, slightly distorts the Sn(IV) coordination geometry from that a perfect tetrahedron.

Around the Sn(IV) atom, the S–Sn–C(31), C(31)–Sn–C(41) and C(41)–Sn–S equatorial angles of 110.0(2)°, 116.8(3)°, 115.2(3)° and the N–Sn–C(21) axial angle of 159.7(3)°, are smaller than the ideal trigonal bipyramid angles.

The bite angle of the chelating ligand is similar for both complexes and quite acute, 59.71(8)° for **3** and 59.03(17)° for **4**. In both cases, the phenyl groups (C31 and C41) bend away the coordinate Sn–S bonds, generating an Ph–Sn–Ph angle of 117.42(13)° in the case **3** and 116.8(3)° in **4**.

4. Supplementary data

Crystallographic data (excluding structure factors) for the structures have been deposited with the Cambridge Crystallographic Data Center as supplementary publication nos. 167994 (**3**) and 167995 (**4**). Copies of the data can be obtained, free of change, on application to CCDC, 12 Union road, Cambridge CB2 1EZ, UK (fax: +44-1223-336033 or e-mail: deposit@ccdc.cam.ac.uk or www: http://www.ccdc.cam.ac.uk).

Acknowledgements

The authors are grateful for financial support from CNPq in Brazil.

References

[1] N.S. Nigan, G.S. Saharia, H.R.J. Sharma, Indian Chem. Soc. 60 (1983) 583.
[2] S.S. Lemos, M.A. Camargo, Z.Z. Cardoso, V.M. Deflon, F.H. Försterling, A. Hagenbach, Polyhedron 20 (2001) 849.
[3] M. Mohan, P. Sharma, M. Kumar, N.K. Jha, Inorg. Chim. Acta 125 (1986) 9.
[4] G. Domazetis, B.D. James, M.F. Mackay, R.J. Magee, J. Inorg. Nucl. Chem. 41 (1979) 1555.
[5] C. Kashima, A. Katoh, M. Shimizu, Y. Omote, Heterocycles 22 (1984) 2591.
[6] S. Stoyanov, I. Petkov, L. Antonov, T. Stoyanova, P. Karagiannidis, P. Aslandis, Can. J. Chem. Soc. 68 (1990) 1482.
[7] (a) A.C.T. North, D.C. Phillips, F.S. Mathews, Acta Crystallogr., Sect. A 24 (1968) 351;
(b) G.M. Sheldrick, SADABS, University of Göttingen, Germany, 1996.
[8] G.M. Sheldrick, SHELX-97, Program for the Solution and Refinement of Crystal Structures, University of Göttingen, Germany, 1997.
[9] International Tables for Crystallography, vol. C, Kluwer Academic, Dordrecht, The Netherlands, 1992.
[10] L. Zsolnai, G. Huttner, ZORTEP, A Program for the Representation of Crystal Structures, University of Heidelberg, 1994.
[11] G.F. de Sousa, C.A.L. Filgueiras, Transition Met. Chem. 15 (1990) 286.
[12] G.F. de Sousa, C.A.L. Filgueiras, Transition Met. Chem. 15 (1990) 290.
[13] G. Battistuzzi, A.B. Corradi, D. Dallari, M. Saladini, R. Battistuzzi, Polyhedron 18 (1998) 57.
[14] M. McGrady, R.S. Tobias, J. Am. Chem. Soc. 87 (1965) 1909.
[15] T.P. Lockhart, W.F. Manders, J. Am. Chem. Soc. 107 (1985) 4546.
[16] T.P. Lockhart, W.F. Manders, J. Organomet. Chem. 25 (1986) 892.
[17] M. Honda, M. Komura, Y. Kawasaki, T. Tanaka, R. Okawara, J. Inorg. Nucl. Chem. 30 (1968) 3231.
[18] Y. Maeda, C.R. Dillard, R. Okawara, Inorg. Nucl. Chem. Lett. 2 (1966) 197.
[19] W.O. George, Spectroscopic Methods in Organometallic Chemistry, Butterworths, London, 1970, pp. 95–131.
[20] R. Schmiedgen, F. Huber, H. Preut, Acta Crystallogr., Sect. C 49 (1993) 1735.
[21] M.V. Castaño, A. Macías, A. Castiñeiras, A.S. González, E.G. Martínez, J.S. Casas, J. Sordo, W. Hiller, E.E. Castellano, J. Chem. Soc., Dalton Trans. (1990) 1001.
[22] J.S. Casas, A. Castiñeiras, E.G. Martínez, A.S. González, A. Sánchez, J. Sordo, Polyhedron 16 (1997) 795.
[23] B.D. James, R.J. Magee, W.C. Patalinghug, B.W. Skelton, A.H. White, J. Organomet. Chem. 467 (1994) 51.
[24] L. Petrilli, F. Caruso, E. Rivarola, Main Group Met. Chem. 17 (1994) 439.

PERGAMON

Polyhedron 21 (2002) 1155–1161

POLYHEDRON

www.elsevier.com/locate/poly

A spirocyclic tetraoxyphosphorane with an apically located chlorine in a trigonal bipyramid and its hydrolysis product

Sudha Kumaraswamy, K.C. Kumara Swamy *

School of Chemistry, University of Hyderabad, Hyderabad 500046, A.P., India

Received 11 October 2001; accepted 7 March 2002

Abstract

The spirocyclic (chloro)tetraoxyphosphorane CH_2(6-*t*-Bu-4-Me-$C_6H_2O)_2$P(Cl)(1,2-$O_2C_6Cl_4$) (**2**) and its hydrolysis product CH_2(6-*t*-Bu-4-Me-$C_6H_2O)_2$P(O)(OC_6Cl_4-2-OH) (**3**) have been synthesized and characterized by X-ray crystallography and solution state NMR. Unlike the previously reported spirocyclic chlorophosphoranes where chlorine occupies an equatorial position of a trigonal bipyramid (TBP), in **2** it is apical. The hydrolysis product **3** is a hydrogen bonded dimer. Compound CH_2(6-*t*-Bu-4-Me-$C_6H_2O)_2$P(Cl)[1,2-O_2–3,5-(*t*-Bu)$_2C_6H_2$] (**4**) was also synthesized in a manner analogous to that of **2**. Attempts to isolate structurally characterizable pentacoordinate compounds by reacting CH_2(6-*t*-Bu-4-Me-$C_6H_2O)_2$PX [X = Cl (**1**), 2,6-$Cl_2C_6H_3O$ (**5**), *cycl*-C_6H_{11}NH (**6**)] with *N*-chlorodiisopropylamine were not successful, although in some cases a pentacoordinate species was detected; the corresponding oxidized products CH_2(6-*t*-Bu-4-Me-$C_6H_2O)_2$P(O)X [X = Cl (**7**), 2,6-$Cl_2C_6H_3O$ (**8**), *cycl*-C_6H_{11}NH (**9**)] were isolated by this route. Variable temperature (^{1}H, ^{31}P) NMR spectra of **2** have been recorded; at low temperatures, two ^{31}P NMR signals of unequal intensity are seen in the pentacoordinate region. A probable intramolecular process involving equatorial–equatorial↔apical–equatorial (for the eight-membered ring) has been invoked to explain the spectral features. © 2002 Elsevier Science Ltd. All rights reserved.

Keywords: Phosphoranes; Pentacoordinated; X-ray structures; Hydrogen bonding

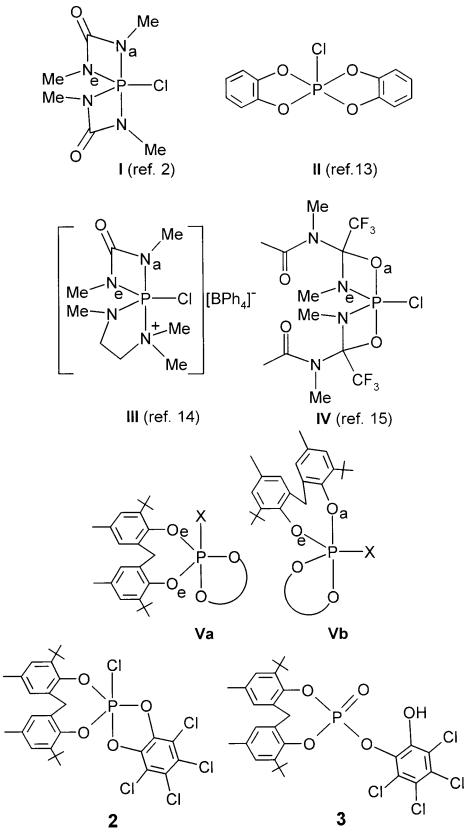
1. Introduction

In spirocyclic phosphoranes with phosphorus as a part of a four to seven membered ring, the rings generally prefer apical–equatorial (a–e) sites irrespective of the substituents when phosphorus has a trigonal bipyramidal geometry [1–10]. Thus, in most spirocyclic phosphoranes, the fifth substituent will have to occupy an equatorial position of the trigonal bipyramid (TBP). If the structure has more square (or rectangular) pyramidal (RP) character, the fifth substituent will take an apical position [11,12]. Compounds **I**–**IV** represent some examples involving chlorine as the fifth substituent [2,13–15]. Thus, in the structures of spirocyclic chlorophosphoranes reported so far, the chlorine has been found to be either in an equatorial position of a TBP or in an apical position of an RP [2,13–20]. The sterically hindered eight-membered ring present in **V** is an interesting system in which the a–e and e–e dispositions are equally feasible for the ring, depending on the fifth substituent [21,22]. In this paper we show the utility of such a ring in placing the chlorine at an apical position of a trigonal bipyramidal phosphorus in the spirocyclic phosphorane CH_2(6-*t*-Bu-4-Me-$C_6H_2O)_2$P(Cl)(1,2-$O_2C_6Cl_4$) (**2**), prepared by starting with CH_2(6-*t*-Bu-4-Me-$C_6H_2O)_2$PCl (**1**), as evidenced by X-ray crystallography. Hydrolysis of **2** leads to the tetracoordinate compound CH_2(6-*t*-Bu-4-Me-$C_6H_2O)_2$P(O)(OC_6Cl_4-2-OH) (**3**) that exists in the solid state as a novel hydrogen-bonded dimer (X-ray). Synthesis of CH_2(6-*t*-Bu-4-Me-$C_6H_2O)_2$P(Cl)(1,2-O_2-3,5-(*t*-Bu)$_2C_6H_2$) (**4**) by a route analogous to that for **2** is also reported herein. In addition, a unique exchange behavior of **2** observed in the variable temperature NMR (^{1}H and ^{31}P) is described. Also described here is our attempt to prepare other chlorophosphoranes by the oxidative addition reaction of CH_2(6-*t*-Bu-4-Me-$C_6H_2O)_2$PX [X = Cl (**1**), 2,6-$Cl_2C_6H_3O$ (**5**), *cycl*-

* Corresponding author. Fax: +91-40-3012-460/3010120.
E-mail address: kckssc@uohyd.ernet.in (K.C. Kumara Swamy).

0277-5387/02/$ - see front matter © 2002 Elsevier Science Ltd. All rights reserved.
PII: S0277-5387(02)01003-3

$C_6H_{11}NH$ (**6**)] with *N*-chlorodiisopropylamine in which only the corresponding oxidized products $CH_2(6\text{-}t\text{-Bu-}4\text{-Me-}C_6H_2O)_2P(O)X$ [X = Cl (**7**), 2,6-$Cl_2C_6H_3O$ (**8**), *cycl*-$C_6H_{11}NH$ (**9**)] were isolated.



2. Experimental

Chemicals were procured from Aldrich/Fluka or from local manufacturers; they were purified when required. Solvents were purified according to standard procedures [23]. All reactions, unless stated otherwise, were performed under dry nitrogen atmosphere. ^1H, and $^{31}P\{H\}$ NMR spectra were recorded on a Bruker 200 MHz spectrometer in $CDCl_3$ or $C_6D_5CD_3$ solutions (unless stated otherwise), with shifts referenced to $SiMe_4$ ($\delta = 0$) or 85% H_3PO_4 ($\delta = 0$). Variable temperature ^1H and ^{31}P NMR spectra were recorded in $C_6D_5CD_3$. Elemental analyses were carried out on a Perkin–Elmer 240C CHN analyzer.

2.1. Synthesis of 2 and 3

A mixture of the P(III) precursor $CH_2\{6\text{-}t\text{-Bu-}4\text{-Me-}C_6H_2O\}_2PCl$ (**1**) [δ(P): 153.7] (0.216 g, 0.53 mmol) and *o*-chloranil (0.131 g, 0.53 mmol) was evacuated for 0.5 h. Then dry heptane (5 ml) was added, the mixture heated at 90 °C for 5 min and brought to room temperature (r.t.). After 0.5 h the clear red solution became colorless. It was concentrated to 1 ml and kept at r.t. Crystals of **2** (0.208 g, 60%) were obtained after 1 day. M.p. 206 °C (dec., darkens slightly at 192 °C). ^1H NMR (C_6D_6): δ 1.36 (br s, 18 H, $C(CH_3)_3$), 2.04, 2.09 (2 s, 6 H, $ArCH_3$), 3.86 (d, $J = 14.0$ Hz, 1 H, CH_AH_X), 4.14 (d, $J = 14.0$ Hz, 1 H, CH_AH_X), 6.96–7.03 (m, 4 H, Ar–*H*). ^{31}P NMR (C_6D_6): δ −35.6. *Anal*. Calc. for $C_{29}H_{30}Cl_5O_4P$: C, 53.52; H, 4.61. Found: C, 53.88; H, 4.75%.

Compound **2** was very susceptible to hydrolysis. Exposure to air for approximately 1 day resulted in the formation of **3**, which could be crystallized from dichloromethane–toluene (1:3) mixture in approximately 70% yield. This compound could also be obtained by stirring a solution of **2** in toluene with 1 mol equiv. of water for 18 h and then allowing to crystallize. M.p. 128–130 °C. IR (KBr): 3350–3600 (br) cm^{-1}. ^1H NMR ($CDCl_3$): δ 1.30 (s, 18 H, $C(CH_3)_3$), 2.31 (s, 6 H, $ArCH_3$), 3.96 (d, $J = 16.0$ Hz, 1 H, CH_AH_X), 4.24 (d, $J = 16.0$ Hz, 1 H, CH_AH_X), 7.00–7.29 (m, 4 H, Ar–*H*). ^{31}P NMR ($CDCl_3$): δ −14.5. *Anal*. Calc. for $C_{29}H_{31}Cl_4O_5P$: C, 55.08; H, 4.94. Found: C, 55.21; H, 4.92%.

Compound **4** was prepared in 54% yield in a manner similar to that for **2**. M.p. 204–210 °C. ^1H NMR: δ 0.35, 1.17, 1.23 (3 br s, 36 H, $C(CH_3)_3$), 2.30 (s, 6 H, $ArCH_3$), 3.62 (br d, 1 H, CH_AH_X), 4.48 (br, 1 H, CH_AH_X), 6.70–7.20 (many lines, 6 H, Ar–*H*). ^{31}P NMR: δ −41.3. Within approximately 10 min a hydrolyzed product [δ(P) −15.6] was also observed. Compound **4** was too moisture sensitive and hence elemental analysis was not attempted.

2.2. Isolation of 7–9 from the reaction of $CH_2\{6\text{-}t\text{-Bu-}4\text{-Me-}C_6H_2O\}_2PX$ [X = Cl (1), 2,6-Cl_2-OC_6H_3 (5), NH-cycl-C_6H_{11} (6)] with N-chlorodiisopropylamine

2.2.1. $CH_2\{6\text{-}t\text{-Bu-}4\text{-Me-}C_6H_2O\}_2P(O)Cl$ (7)

To a solution of **1** (0.390 g, 0.96 mmol) in toluene (10 ml) at −30 °C was added a solution of $ClN(i\text{-Pr})_2$ (0.263 g, 1.94 mmol) in toluene (5 ml) during 5 min. The mixture was slowly brought to r.t., stirred overnight and filtered. Concentration to 0.5 ml and addition of heptane (1 ml) afforded **7** as a crystalline solid (0.28 g, 69%). M.p. 155–156 °C. ^1H NMR: δ 1.52 (s, 18 H, $C(CH_3)_3$), 2.07 (s, 6 H, $ArCH_3$), 3.70–4.10 (AB qrt, 2 H, CH_AH_B), 6.81, 7.06 (2 s, 4 H, Ar–*H*). ^{31}P NMR: δ −3.4 (lit. [24] −3.4) [in C_6D_6: −4.6]. *Anal*. Calc. for $C_{23}H_{30}ClO_3P$: C, 65.63; H, 7.18. Found: C, 66.06; H, 7.49%.

2.2.2. $CH_2\{6\text{-}t\text{-}Bu\text{-}4\text{-}Me\text{-}C_6H_2O\}_2P(O)(2,6\text{-}Cl_2\text{-}OC_6H_3Cl)$ (**8**)

Procedure same as for **7** using **5** [δ(P): 134.8] (0.432 g, 0.81 mmol) and ClN(*i*-Pr)$_2$ (0.222 g, 1.64 mmol). Yield: 0.30 g (67%). M.p. 226 °C. ^{1}H NMR: δ 1.34 (s, 18 H, C(CH_3)$_3$), 2.30 (s, 6 H, ArCH_3), 3.59 (d, $J = 14.2$ Hz, 1 H, CH_AH$_X$), 4.61 (dd, $J = 2.0$, 14.2 Hz, 1 H, CH$_A$$H_X$), 7.04–7.40 (m, 7 H, Ar–H). ^{31}P NMR: δ −21.7. *Anal*. Calc. for $C_{29}H_{33}Cl_2O_3P$: C, 63.62; H, 6.08. Found: C, 64.10; H, 6.15%.

2.2.3. $CH_2\{6\text{-}t\text{-}Bu\text{-}4\text{-}Me\text{-}C_6H_2O\}_2P(O)(NH\text{-}cycl\text{-}C_6H_{11})$ (**9**)

Procedure same as for **7** using **6** [δ(P): 141.5] (0.385 g, 0.82 mmol) and ClN(*i*-Pr)$_2$ (0.225 g, 1.66 mmol). Yield: 0.27 g (68%). M.p. 210 °C. ^{1}H NMR: δ 1.45 (s, 18 H, C(CH_3)$_3$), 1.47–1.49, 1.57–1.68 and 1.70–1.82, 2.15–2.25 (m each, 10 H, cyclohexyl –H), 2.29 (s, 6 H, ArCH_3), 2.95 (dd (?), $J = 9.3$, 13.0 Hz, 1 H, CH_AH$_X$), 3.38–3.58 and 3.50–3.85 (br m, 2 H, CHNH+CHNH), 4.16 (d, $J = 13.0$ Hz, 1 H, CH$_A$$H_X$), 7.21 (s, 4 H, Ar–$H$). ^{31}P NMR: δ −1.8. *Anal*. Calc. for $C_{29}H_{42}NO_3P$: C, 72.02; H, 8.75; N, 2.90. Found: C, 71.88; H, 8.81; N, 2.91%.

Obviously, hydrolysis had occurred in the formation of **7**–**9**. NMR tube experiments were performed in the case of **1** and **6** using C_6D_6 as the solvent at r.t. ^{31}P NMR spectra recorded immediately after the addition of ClN(*i*-Pr)$_2$ showed peaks at δ −15.2 and −38.6, respectively; these peaks may be ascribed to the pentacoordinate species $CH_2\{6\text{-}t\text{-}Bu\text{-}4\text{-}Me\text{-}C_6H_2O\}_2P(N\text{-}(i\text{-}Pr)_2)Cl_2$ and $CH_2\{6\text{-}t\text{-}Bu\text{-}4\text{-}Me\text{-}C_6H_2O\}_2P(N\text{-}(i\text{-}Pr)_2)(NH\text{-}cycl\text{-}C_6H_{11})Cl$, respectively. Over a period of 1–2 days, these peaks disappeared and new peaks at δ −4.6 (in the case of **1**) or −1.8 (in the case of **6**) appeared.

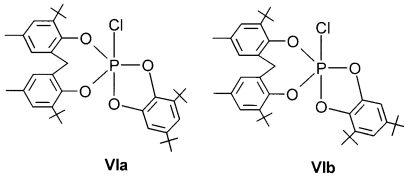
2.2.4. Reaction of **2** with 4-dimethylaminopyridine

Compound **2** (0.410 g, 0.63 mmol) was dissolved in heptane (20 ml) and 4-dimethylaminopyridine (0.154 g, 1.26 mmol) was added to it. The mixture was refluxed for 10 min, solvent removed in vacuo and benzene (carcinogen!) was added to the residue. After warming, the solution was filtered and the filtrate was concentrated to yield a microcrystalline solid (0.130 g). M.p. 206–208 °C. ^{1}H NMR (C_6D_6): δ 1.12 and 1.42 (s each of equal intensity, (18+18) H, C(CH_3)$_3$), 2.05 and 2.12 (s each of equal intensity, (6+6) H, ArCH_3), 3.24 and 3.52 (d each, $J \sim 16.0$ Hz, (1+1) H, CH_AH$_X$), 4.68, 5.21 (dd each, $J \sim 4.0$, 16.0 Hz, (1+1) H, CH$_A$$H_X$), 6.79–7.17 (many lines, (4+4) H, Ar–H). ^{31}P NMR: δ −19.6, −58.1. Due to the moisture sensitive nature, elemental analysis was not taken.

X-ray data were collected on an Enraf-Nonius-MACH3 X-ray diffractometer at 293 K using Mo Kα ($\lambda = 0.71073$ Å) radiation and capillary mounting. The structures were solved by direct methods; [25] all non-hydrogen atoms were refined anisotropically. For the hydrogen atoms bonded to carbon, the riding model was used. The hydrogen atom bonded to the hydroxyl oxygen was located in a difference map. The crystal data are summarized in Table 1.

3. Results and discussion

Compound **2** is synthesized by the oxidative addition of *o*-chloranil to the corresponding phosphite $CH_2\{6\text{-}t\text{-}Bu\text{-}4\text{-}Me\text{-}C_6H_2O\}_2PCl$ (**1**). The ^{31}P NMR chemical shift value confirms that the pentacoordinate structure is preserved in solution (more details discussed below) [8,22]. This compound is quite susceptible towards hydrolysis and exposure to air leads to the hydrolyzed product **3**. Although the reaction of **1** with benzil and 9,10-phenanthrenequinone did not yield any identifiable pentacoordinate compound even upon heating, the reaction with 3,5-di-*t*-butyl-*o*-benzoquinone afforded the moisture sensitive pentacoordinate compound **4**. Two isomers **VIa** and **VIb** differing in the connectivity of oxygens in the five-membered ring are possible, but only one signal is observed in the ^{31}P NMR [δ −41.3].



VIa VIb

The initial product in the reaction of P(III) com-

Table 1
Crystal data for **2** and **3**

Compound	**2**	**3**
Empirical. formula	$C_{29}H_{30}Cl_5O_4P$	$C_{29}H_{31}Cl_4O_5P$
Formula weight	650.75	632.31
Crystal system	triclinic	monoclinic
Space group	$P\bar{1}$	
a (Å)	9.478(2)	14.654(1)
b (Å)	10.014(2)	9.312(3)
c (Å)	17.116(3)	23.316(1)
α (°)	90.22(1)	90.0
β (°)	91.86(2)	106.08(1)
γ (°)	109.04(3)	90.0
V (Å^3)	1534.6(5)	3057.2(10)
Z	2	4
D_{calc} (g cm^{-3})	1.408	1.374
μ (mm^{-1})	0.558	0.476
$F(000)$	672	1312
Data/restraints/parameters	5395/0/361	5366/0/364
S	1.015	1.026
R_1 [$I > 2\sigma(I)$]	0.0593	0.0503
wR_2 (all data)	0.1837	0.1573
Max/min residual electron density (e Å^{-3})	0.33/−0.96	0.36/−0.42

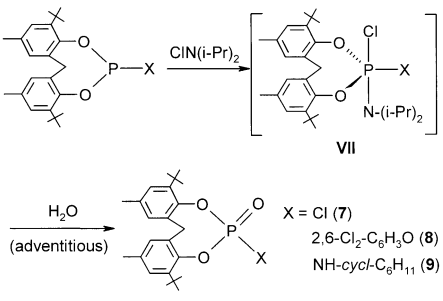
pounds with *N*-chlorodiisopropylamine [ClN(*i*-Pr)$_2$] is expected to be a pentacoordinate phosphorane with a P(*N*-*i*-Pr$_2$)(Cl) unit [26]. We felt that the sterically hindered eight-membered ring in our system would make it possible to isolate stable species of this type and hence reacted the P(III) precursors $CH_2\{6\text{-}t\text{-Bu-4-Me-}C_6H_2O\}_2PX$ [X = Cl (**1**), 2,6-Cl_2-OC_6H_3 (**5**) and NH-*cycl*-C_6H_{11} (**6**)] with ClN(*i*-Pr)$_2$ (Scheme 1). Immediately after addition of ClN(*i*-Pr)$_2$, in the case of **1** or **6**, a peak is observed in the ^{31}P NMR at −15.2 or −36.6 ppm, respectively; this is ascribable to the corresponding pentacoordinate chlorophosphorane of type **VII**. However, this product rapidly hydrolyzed due to adventitious moisture, leading to the tetracoordinate compounds **7**–**9** as isolable products.

We have been interested in utilizing chlorophosphoranes such as **2** for further reactions. One of the reactions we checked was that of **2** with 4-dimethylaminopyridine to obtain a salt of the type $[CH_2(6\text{-}t\text{-Bu-4-Me-}C_6H_2O)_2P(O_2C_6Cl_4)(NC_5H_4\text{-}4\text{-}NMe_2)]^+[Cl]^-$ containing a P–N bond. In this reaction (done in heptane), the hygroscopic solid obtained had two peaks of equal intensity in the ^{31}P NMR [δ −58.1, −19.7] and the peaks corresponding to the 4-dimethylaminopyridine moiety were not seen in the ^{1}H NMR. Although it is difficult to ascertain the exact structure of this product, it appears to be a species with one phosphorus tetracoordinated and the other pentacoordinated [27,28].

3.1. Structural aspects

The molecular structures of **2** and **3** are depicted in Figs. 1 and 2, respectively. Relevant bond parameters for these two and **1** [29] are given in Table 2. The geometry around phosphorus in **2** can be considered to be essentially a TBP based on the O–P–Cl angle; the chlorine occupies an apical position. The eight-membered 1,3,2-dioxaphosphocin ring spans two of the three equatorial positions. The high electronegativity of chlorine coupled with the flexible nature of the phosphocin ring is thus responsible for the chlorine occupying the apical position.

The P–O bond distances of the eight-membered ring in **2** and **3** are similar but longer than what is observed in



Scheme 1.

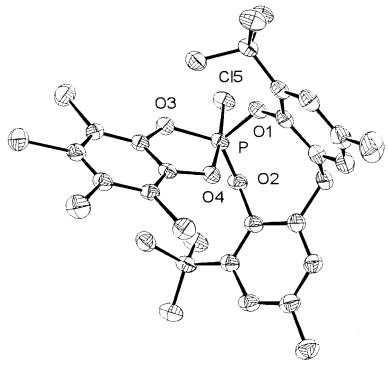
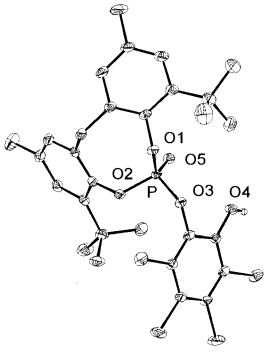


Fig. 1. An ORTEP drawing of **2** showing all non-hydrogen atoms.



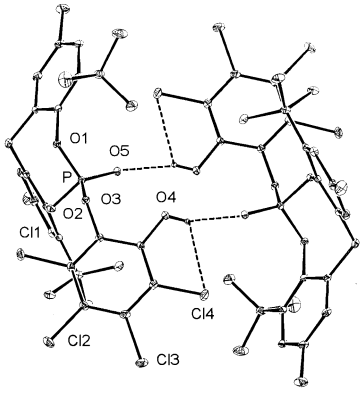


Fig. 2. An ORTEP drawing of **3** showing all non-hydrogen atoms and the OH hydrogen; shown at the bottom is the hydrogen-bonded dimer structure.

the tricoordinate compound **1**. The P–O distances of the five-membered ring are longer than those of the eight-membered ring. The P–Cl distance in **2** is longer than that observed in many other spirocyclic chlorophosphoranes with trigonal bipyramidal geometry, [13,15–18] but this is to be expected since the chlorine in **2** is apically located and such apical bonds are expected to be longer because of the 3c–4e bonds associated with them [30]. The ring angle O(1)–P–O(2) increases in the order: **1** (tricoordinate) < **3** (tetracoordinate) < **2** (pentacoordinate with diequatorial placement). While the

Table 2
Selected bond lengths (Å) and bond angles (°) with su's for **1**–**3**

Compound	**2** [a]	**3** [b]	**1** [c]
Bond lengths			
P–O(1)	1.574(3)	1.571(2)	1.624(3)
P–O(2)	1.573(3)	1.580(2)	1.624(3)
P–O(3)	1.626(3)	1.583(2)	
P–O(4)	1.711(3)		
P–Cl	2.085(1)		2.018(2)
P–O(5)	–	1.447(2)	
Bond angles			
O(1)–P–O(2)	118.0(2)	108.2(2)	103.3(3)
O(1)–P–Cl	88.9(1)		95.7(1)
O(2)–P–Cl	88.4(1)		95.9(1)
O(1)P–O(3)	118.7(2)	95.7(1)	
O(2)P–O(3)	122.8(2)	102.5(1)	
O(4)–P–Cl	175.2(1)		

[a] Other angles at phosphorus: O(2)–P–O(4) 92.9(1); O(1)–P–O(4) 94.6(1); O(3)–P–O(4) 89.5(1); O(3)–P–Cl(5) 86.0(1). Cl(5) is the chlorine atom bonded to phosphorus.

[b] Other angles at phosphorus: O(5)–P–O(1) 115.3(1); O(5)–P–O(3) 119.69(12).

[c] Data for **1** taken from Ref. [29]. We also had performed an X-ray study of this compound; although the *R* values are slightly better in our case the bond parameters are essentially the same as reported.

smaller value in **1** may be attributed to the lone pair on phosphorus trying to occupy more space, the higher value in **2** may be due to the equatorial placement of the eight-membered ring. What is perhaps noteworthy is the flexiblility of this angle (a range of ca. 15° while going from the tricoordinate compound **1** to the pentacoordinate compound **2**).

The eight-membered 1,3,2-dioxaphosphocin ring (Fig. 3) has a boat-chair conformation in **1**–**3**. This feature in **2** is analogous to what was observed by us before when

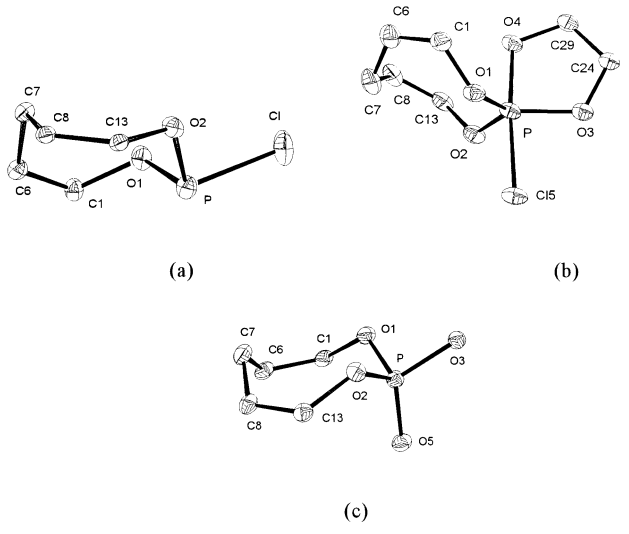


Fig. 3. Selected atoms, highlighting the placement of the substituents on phosphorus and conformation of the eight-membered 1,3,2-dioxaphosphocin ring in (a) **1**, (b) **2** and (c) **3**.

this ring is located diequatorially in a trigonal bipyramidal arrangement [22]. However, for **3**, the boat-chair conformation observed is opposite to that found in the phosphite $CH_2\{6\text{-}t\text{-Bu-4-Me-}C_6H_2O\}_2P(O)H$, [31] phosphate $CH_2\{6\text{-}t\text{-Bu-4-Me-}C_6H_2O\}_2P(O)(OH)$, [32] or the cyclophosphazene $N_4P_4[(4,6\text{-}t\text{-Bu}_2\text{-}C_6H_2O)_2\text{-}CH_2]Cl_6\cdot 1/2C_4H_8Cl_2$ [33]. As can be seen from Fig. 4, it is difficult to define the placement of the other substituents on phosphorus with respect to the eight-membered ring (a–e in the familiar organic terminology). In the tetra-coordinate compound **3** the oxygen atoms O(3) and O(5) are at distances of 1.52 and −1.03 Å from the O(1)–P–O(2) plane; in **1** the chlorine is at 2.028 Å from this plane. In **2**, the atom O(3) is slightly (0.19 Å) away from the O(1)–P–O(2) plane.

Compound **3** exists as a hydrogen-bonded dimer involving O(4)–H and the phosphoryl oxygen O(5) in the solid state [Fig. 2(b)]. However, the O(4)–H(O4)···O(5) angle of 158(4)° is quite far from the expected 180° for a normal hydrogen bond; it is also observed that H(O4) is pretty close to Cl(4) [3.014 Å] of the tetrachlorocatecholate residue although it could have tilted away from this chlorine. This feature, in addition to the lower O(4)–H(O4)···O(5) angle probably suggests that this is a three-center (bifurcated) hydrogen bond [34]. The dimeric structure in **3** contrasts with the intramolecular structure as in **VIII** or intermolecular chain **IX** both of which are phosphates analogous to **3** [35,36].

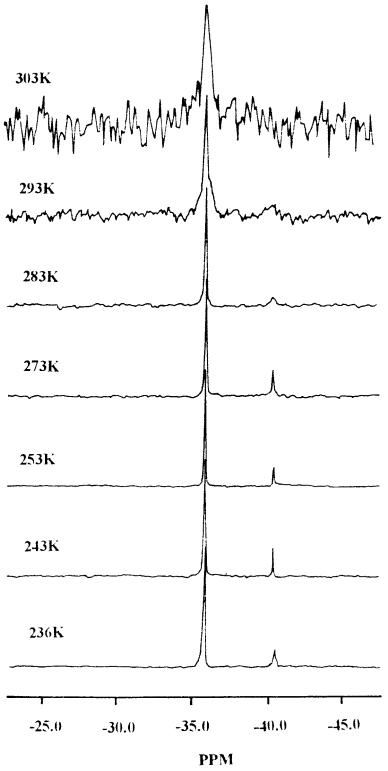
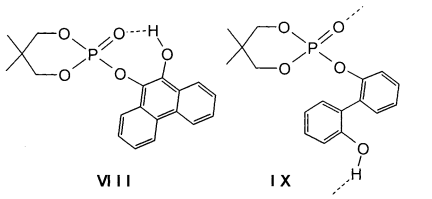


Fig. 4. Variable temperature ^{31}P NMR spectra for **2**.

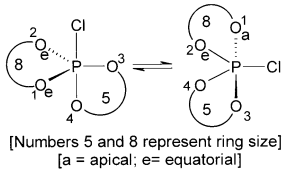


VIII (intramolecular; ref. 35) IX (intermolecular chain; ref. 36)

3.2. Variable temperature NMR behavior

The variable temperature ^{31}P NMR spectra of **2** are shown in Fig. 4. At low temperatures two signals at δ(P) values −35.8 and −40.3 are observed and at >283 K only one peak [δ(P): −35.8] in the pentacoordinate region is observed. We have reported the observation of two ^{31}P NMR signals in compounds of the type CH_2(6-*t*-Bu-4-Me-$C_6H_2O)_2P(X)(O_2C_6Cl_4)$ [X = Ph, Me, NMe_2 (<253 K)] [22]. As regards ^{1}H NMR, at 243 K two signals of unequal intensity for the *t*-Bu-*H* [δ 1.10 (minor), 1.32 (major)] as well as ArCH_3 [δ 2.00(major), 2.10 (minor)] protons are observed. In the ArCH_AH_X region the signals for the minor isomer are mostly buried in those due to the major isomer. At 293 K, only one broad signal each for the *t*-butyl and ArCH_3 protons is observed at δ 1.32 and 2.00, respectively. Unfortunately, at higher temperatures (>293 K) decomposition occurred leading to other signals [this is corroborated by ^{31}P NMR at 323 K which showed a signal at −14.5 ppm in addition to the one due to the pentacoordinate peak at −35.8 ppm].

We assign the downfield signal/s in the ^{31}P NMR spectra of **2** to the Cl(apical) isomer and the upfield signal to the Cl(equatorial) isomer on the basis of observations made in the case of CH_2(6-*t*-Bu-4-Me-$C_6H_2O)_2P(X)(O_2C_6Cl_4)$ [X = Me, NMe_2] [22]. Interconversion between these two isomers is possible through the e–e↔ a–e Berry exchange process for the eight-membered ring with O(2) as the pivotal position (Scheme 2). A similar process involving the five-membered ring would involve much higher energy. In the process shown in Scheme 2, the local environment at phosphorus is likely to change significantly [O(1)–P–O(2) angle could vary from 118.0° in the e–e isomer to approximately 90° in the a–e isomer; there will also be significant changes in the P–Cl bond lengths] and hence the ^{31}P NMR chemical shifts can be expected to show a wide difference for the two isomers. The other point is the unequal population of the two isomers; a rationale for this may come through if the individual isomers can be independently isolated.



[Numbers 5 and 8 represent ring size]
[a = apical; e= equatorial]

Scheme 2.

4. Summary

We have provided here an example of a spirocyclic pentacoordinated phophorane with chlorine at the apical site of a TBP; in previous examples of spirocyclic chlorophosphoranes chlorine had occupied either an equatorial site of a TBP or an apical site of a rectangular pyramid. The low temperature ^{31}P NMR spectra for **2** show two signals of unequal intensity; such an observation has not been made in the previously known chlorophosphoranes. A dimeric formulation for the hydrolysis product of **2** involving O–H···O and possible O–H···Cl interactions is described. Thus, this study has further expanded our understanding of the structural preferences of pentacoordinate phosphorus, which in turn is important in the context of nucleophilic substitution reactions at a tetrahedral phosphorus(V) center.

5. Supplementary data

Supplementary data as cif files are available from the CCDC, 12 Union Road, Cambridge, CB2 1EZ, UK (fax: +44-1223-336033; e-mail: deposit@ccdc.cam.ac.uk or www: http://www.ccdc.cam.ac.uk) on request, quoting the deposition numbers CCDC 171595 and 171596.

Acknowledgements

This work was supported by the Department of Science and Technology (DST), New Delhi. The National Single Crystal Diffractometer Facility at the University of Hyderabad funded by DST (New Delhi) is gratefully acknowledged.

References

[1] R.R. Holmes, Prog. Inorg. Chem. 32 (1984) 119.
[2] D. Schomburg, U. Wermuth, R. Schmutzler, Chem. Ber. 120 (1987) 1713.
[3] K.C. Kumara Swamy, J.M. Holmes, R.O. Day, R.R. Holmes, J. Am. Chem. Soc. 112 (1990) 6092.
[4] J.H. Yu, A.M. Arif, W.G. Bentrude, J. Am. Chem. Soc. 112 (1990) 7451.
[5] T.K. Prakasha, S.D. Burton, R.O. Day, R.R. Holmes, Inorg. Chem. 31 (1992) 5494.
[6] S. Kojima, K. Kajiyama, K.-Y. Akiba, Bull. Chem. Soc. Jpn. 68 (1995) 1785.

[7] M. Gorg, E. Lork, A.A. Kolomcitsev, G.-V. Roschenthaler, Phosphorus, Sulf. Silicon Relat. Elem. 127 (1997) 15.
[8] M.A. Said, M. Pülm, R. Herbst-Irmer, K.C. Kumara Swamy, Inorg. Chem. 36 (1997) 3044.
[9] R. Sonnenburg, I. Neda, H. Thonnessen, P.G. Jones, R. Schmutzler, Z. Anorg. Allg. Chem. 626 (2000) 412.
[10] C. Muthiah, M.A. Said, M. Pülm, R. Herbst-Irmer, K.C. Kumara Swamy, Polyhedron 19 (2000) 63.
[11] A.C. Sau, J.M. Holmes, R.O. Day, R.R. Holmes, Inorg. Chem. 22 (1983) 1771.
[12] I.V. Shevchenko, A. Fischer, P.G. Jones, R. Schmutzler, Chem. Ber. 125 (1992) 1325.
[13] R.K. Brown, R.R. Holmes, Inorg. Chem. 16 (1977) 2294.
[14] T. Kaukorat, L. Ernst, R. Schmutzler, D. Schomburg, Polyhedron 9 (1990) 1463.
[15] A.D. Sinitsa, L.I. Nesterova, D.M. Malenko, V.V. Pirozhenko, E.B. Rusanov, A.N. Chernega, Zh. Obshch. Khim. 65 (1995) 232.
[16] W. Schwarz, E. Fluck, M. Vargas, Phosph. Sulf. 5 (1978) 217.
[17] H.W. Roesky, H. Djarrah, D. Amirzadeh-Asl, W.S. Sheldrick, Chem. Ber. 114 (1981) 1554.
[18] T. Kaukorat, P.G. Jones, R. Schmutzler, Z. Naturforsch., Teil B 47 (1992) 755.
[19] R.O. Day, A. Schmidpeter, R.R. Holmes, Inorg. Chem. 21 (1982) 3916.
[20] Fused ring systems and salts are exceptions and it is possible to place the chlorine apically. See: X.-D. Liu, J.G. Verkade, Inorg. Chem. 37 (1998) 5189.
[21] N.V. Timosheva, A. Chandrasekaran, T.K. Prakasha, R.O. Day, R.R. Holmes, Inorg. Chem. 35 (1996) 6552 (and references therein).
[22] S. Kumaraswamy, C. Muthiah, K.C. Kumara Swamy, J. Am. Chem. Soc. 122 (2000) 964.
[23] D.D. Perrin, W.L.F. Armarego, D.R. Perrin, Purification of Laboratory Chemicals, Pergamon Press, Oxford, UK, 1986.
[24] M. Vijjulatha, K. Praveen Kumar, K.C. Kumara Swamy, J.J. Vittal, Tetrahedron Lett. 39 (1998) 1819.
[25] G.M. Sheldrick, SHELX-97, University of Göttingen, Germany, 1997.
[26] M.A. Said, K.C. Kumara Swamy, K. Chandra Mohan, N. Venkata Lakshmi, Tetrahedron 50 (1994) 6989.
[27] The reaction of **2** with *i*-PrOH and pyridine exhibited a peak at δ −57.0 ppm in the ^{31}P NMR; this peak is ascribable to the pentacoordinate compound CH_2(6-*t*-Bu-4-Me-$C_6H_2O)_2$P(O-*i*-Pr)($O_2C_6Cl_4$). Also see Ref. [25] for some ^{31}P NMR shift correlations.
[28] M.A. Said, M. Pülm, R. Herbst-Irmer, K.C. Kumara Swamy, J. Am. Chem. Soc. 118 (1996) 9841.
[29] D.J. Sherlock, A. Chandrasekaran, R.O. Day, R.R. Holmes, Inorg. Chem. 36 (1997) 5082.
[30] M. Lattman, Hypervalent compounds, in: R.B. King (Ed.), Encyclopedia of Inorganic Chemistry, vol. 3, Wiley, Chichester, UK, 1994, pp. 1496–1511.
[31] S. Kumaraswamy, K. Senthil Kumar, S. Raja, K.C. Kumara Swamy, Tetrahedron 57 (2001) 8181.
[32] K.C. Kumara Swamy, S. Kumaraswamy, P. Kommana, J. Am. Chem. Soc. 123 (2001) 12642.
[33] S. Kumaraswamy, M. Vijjulatha, C. Muthiah, K.C. Kumara Swamy, U. Engelhardt, J. Chem. Soc., Dalton Trans. (1999) 891.
[34] G.A. Jeffrey, W. Saenger, Hydrogen Bonding in Biological Structures, Springer-Verlag, Berlin, 1991, p. 136.
[35] J.C. Gallucci, R.R. Holmes, Inorg. Chem. 19 (1980) 3540.
[36] K.C. Kumara Swamy, M.A. Said, S. Kumaraswamy, R. Herbst-Irmer, M. Pülm, Polyhedron 17 (1998) 3643.

PERGAMON

Polyhedron 21 (2002) 1163–1175

POLYHEDRON

www.elsevier.com/locate/poly

Metal–metal bonding trends in mixed-group, face-shared d^3d^3 bioctahedral dimer systems, $M'M''Cl_9^{n-}$

Simon Petrie, Robert Stranger *

Department of Chemistry, The Australian National University, Canberra, ACT 0200, Australia

Received 14 October 2001; accepted 21 March 2002

Abstract

The results of density functional theory (DFT) calculations on a set of binuclear nonachloride complexes $M'M''Cl_9^{4-}$ ($M' = V$, Nb, Ta; $M'' = Cr$, Mo, W) and $M'M''Cl_9^{2-}$ ($M' = Cr$, Mo, W; $M'' = Mn$, Tc, Re), in which each metal possesses a nominal d^3 valence electronic configuration, are reported. When compared with previous studies on same-group dimers (typified by the $M'M''Cl_9^{3-}$ complexes of the chromium triad), the present results display an increased tendency for electron donation from M′ to M″. Structural trends evident for the $M'M''Cl_9^{4-}$ and $M'M''Cl_9^{2-}$ series of dimers are remarkably consistent: weak ferromagnetic coupling between M′ and M″ is the most favorable intermetallic interaction when M″ is a first-row transition metal, antiferromagnetic coupling dominates when M′ is first-row but M″ is second- or third-row, and metal–metal triple bond formation generally yields the lowest-energy structure when neither metal is first-row. These structural trends, and other characteristics of the dimers described here, can be satisfactorily rationalized in terms of the tendency for electron transfer from M′ to M″, coupled with effects due to spin polarization and ligand field splitting of the valence d orbitals on M′ and M″. © 2002 Elsevier Science Ltd. All rights reserved.

Keywords: DFT calculations; Dinuclear transition metal complexes; Electron transfer; Magnetic coupling; Metal–metal bonding; Spin polarization

1. Introduction

In previous studies [1–7], we have employed DFT to examine metal–metal interactions within face-shared octahedral dimers of the generic formula $M'M''Cl_9^{n-}$. Such dimers exhibit a continuum of metal–metal bonding tendencies ranging from essentially nonbonded to triply bonded structures [8–10]. The broken-symmetry (BS) density functional technique [11] has been found to be especially useful as a method for probing intermetallic interactions in these systems, as is typified by calculations upon the dimers of the Cr(III) triad [1–3]. BS minima corresponding to a weakly coupled structure for $Cr_2Cl_9^{3-}$, possessing a long Cr–Cr separation of 3.22 Å, and a triply-bonded structure for $W_2Cl_9^{3-}$ with a short W–W separation of 2.40 Å, are in excellent agreement with the experimentally determined metal–metal distances in these complexes, and BS calculations on many other complexes also show generally good agreement with experiment.

A feature of the previous studies on same-group d^3d^3 dimers [1–4,6] has been the consistent correlation evident between the energy associated with metal–metal orbital overlap, E_{ovlp}, and the spin polarization (exchange) energy E_{SPE} favoring localization of electrons on the metal centers. Given the very strong correlation between E_{ovlp} and E_{SPE} for same-group dimers of the V, Cr, and Mn triads [2,12], we were motivated to determine whether this correlation was exhibited also by mixed-group d^3d^3 dimers such as $VCrCl_9^{4-}$. While no examples are yet known of experimentally-isolated mixed-group, face-shared complexes, both mixed-valence (e.g. $W(III)W(IV)Cl_9^{2-}$, $[Bu_3P]_3RuCl_3$-$RuCl_2PBu_3$) [13–15] and heterobimetallic (e.g. $CrMoCl_9^{3-}$) [16] face-shared bioctahedra have been structurally characterized, as have a large number of mixed-group bimetallic complexes involving macrocyclic or other bridging ligands. Several studies on such families of compounds have now shown [17–20] that the mode of magnetic coupling in such dimers is strongly

* Corresponding author. Fax: +61-2-62490760.
E-mail address: rob.stranger@anu.edu.au (R. Stranger).

0277-5387/02/$ - see front matter © 2002 Elsevier Science Ltd. All rights reserved.
PII: S0277-5387(02)00999-3

dependent on the identity of the two metal atoms. In a preliminary study of the $MW(III)Cl_9^{n-}$ (M = V(II), Cr(III), Mn(IV)) dimers [21], we noted that the lowest-energy structure undergoes a switch from markedly antiferromagnetic ($VWCl_9^{4-}$) to ferromagnetic ($MnWCl_9^{4-}$) coupling, and that this tendency is consistent with the relative magnitudes of spin polarization and ligand-field splittings of the valence d-orbitals on the nominally more highly oxidized metal atom in each case (i.e. respectively, W(III) and Mn(IV)). By surveying a significantly larger group of mixed-metal complexes, the present study affords an opportunity to further test the influence of electron transfer on the mode of magnetic coupling, and on the broader structural characteristics of mixed-group dimers [22].

2. Computational details

All calculations described in this work were performed on Linux-based Pentium III 600 MHz computers using the Amsterdam Density Functional (ADF) program, version ADF-1999 [23], developed by Baerends et al. [24]. All calculations employed the local density approximation (LDA) to the exchange potential [25,26], and the correlation potential of Vosko, Wilk, and Nusair [27], since previous [3,28] and ongoing [29] studies on other anionic metal dimers have shown that this DFT method performs particularly well for the purposes of characterizing the metal–metal interaction in such species. Basis sets for all atoms were triple-ζ quality Slater type orbitals (Type IV). Electrons in orbitals up to and including 2p {Cl}, 3p {V, Cr, Mn}, 4p {Nb, Mo, Tc}, and 4f (but excluding 5s and 5p) {Ta, W, Re} were treated in accordance with the frozen-core approximation. Test calculations, using smaller frozen cores for the various metals, were also performed but were found to yield very minor differences to the fully optimized geometries (with one exception, discussed within the text). Optimized geometries were obtained using the gradient algorithm of Versluis and Ziegler [30]. Calculations for the BS state, $S = 0$, 2, and 3 associated states, and the 'reference state' were performed in C_{3v} symmetry; all such calculations, except for the reference state, were spin-unrestricted. BS calculations employed an asymmetry in the initial spin densities upon the two metal atoms [11]. Potential energy curves for all pertinent states were obtained by optimization of all other structural parameters for the dimers along a series of fixed metal–metal separations.

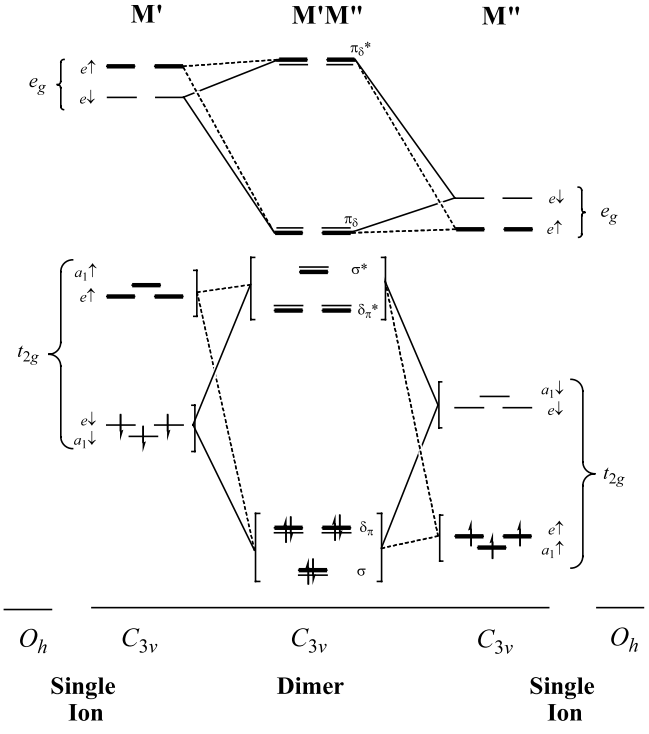


Fig. 1. Representation of localized and delocalized limits for the $S = 0$ BS state of a heteronuclear dimer $M'M''Cl_9^{n-}$. Orbitals are labelled according to the representations of the C_{3v} point group. The energetic ordering of the t_{2g}-derived and e_g-derived orbitals on the two metal atoms permits weak antiferromagnetic coupling, and a d^3d^3 occupation, as the lowest-energy electronic configuration at large intermetallic separations.

3. Results and discussion

3.1. Orbital energies, d-orbital occupancy, and intermetallic interactions: an overview

In a bioctahedral complex $M'M''X_9^{n-}$, the reduction in symmetry (from O_h to C_{3v}) around each metal atom results in a splitting of the t_{2g} orbitals depending on their orientation with respect to the metal–metal axis. Fig. 1 illustrates this principle for a heteronuclear bimetallic complex, depicting both the nonbonded and the triply-bonded limiting cases for the BS state. Due to the disparity between atomic orbital (AO) energies on M′ and M″, the interaction between metal atoms is expected to involve a degree of electron transfer: in the scenario shown here (which is reasonably representative of the species studied in the present work), the imbalance between the orbital energies of M′ and M″ is significant but insufficient to override a d^3d^3 minimum-energy configuration. In the nonbonded case, the t_{2g} orbital splitting produces the symmetry-distinct subsets a_1 and e which have σ and δ_π symmetry ($2/3\delta$, $1/3\pi$), respectively, with reference to the intermetallic axis; stabilization by antiferromagnetic coupling is associated with the splitting of the α- and β-spin orbitals by spin polarization on each metal center. Interaction between the a_1 and e orbitals on neighboring metal centers, for close M–M distances, produces σ, σ*, δ_π and δ_π^* orbitals: here the stabilization results from the energetic

separation between bonding and antibonding orbitals. In the example shown in Fig. 1, stabilization by metal–metal 'polar covalent' bonding exceeds the stabilization offered by antiferromagnetic coupling, and so M–M triple bond formation is favored in this case; but the balance between M–M bond formation and coupling of localized electrons is sensitive to several factors, as we have previously discussed [3].

The tendency to adopt a triply-bonded, singly-bonded, or nonbonded configuration of the two metal centers with increasing M′–M″ separation is most conveniently assessed by comparing three associated pure spin states $S = 0$ (triple bond between M′ and M″, no net excess of α-spin electrons), $S = 2$ (single σ-bond between metals, four α-spin electrons aligned in δ_π and δ_π^* orbitals) and $S = 3$ (no net bonding interaction between metals, six α-spin localized electrons aligned in σ, δ_π, δ_π^*, and σ* orbitals) Orbital occupancies for the $S = 0$, 2, and 3 associated states, and for the hypothetical 'reference state' representing the absence of any stabilization associated with either metal–metal bonding or spin polarization, in which the σ, δ_π, δ_π^*, and σ* orbitals are all half-filled in a spin-restricted calculation [2] are depicted in Fig. 2.

In the discussion which follows, we identify the general bonding trends evident within the set of mixed-group dimers before examining key structural and electronic features of particular dimers. The notation M′ and M″ is used throughout to distinguish between the less highly oxidized (M′) and more highly oxidized (M″) metal atoms within a given mixed-group dimer. We also adopt the convention, pertinent to discussion of electronic configurations and modes of bonding encountered in the $S = 2$ and BS minima, that the unpaired spin density on M″ is always positive (i.e. a net α-spin excess) or zero.

It is perhaps also appropriate to justify the DFT methodology employed in the present study. DFT methods incorporating nonlocal ('gradient') corrections to the exchange and correlation functionals, such as B-LYP, are generally regarded as superior to LDA in their ability to reliably characterize the structural and energetic properties of main-group compounds. There is, however, a sizeable number of studies which have shown that, for certain classes of transition metal compounds (including tetranuclear metal carbonyls [31], mononuclear anionic hexahalide [32] and tetraoxide [33] complexes, and dinuclear halide- [3,29] and oxo-bridged [28] complexes), LDA tends to outperform the gradient-corrected methods on structural, if not energetic, grounds. The transition metal compounds for which LDA performs best are often [32,34,35] but not exclusively [29,31,36–38] anionic species, and in this context the widely-acknowledged 'overbinding' propensity [39] of LDA may be considered to compensate for the absence of stabilizing counterions in these vacuum-phase calculations. While a more rigorous approach would be to pursue calculations including such stabilizing countercharges, either through explicit inclusion of the counterions themselves or via intercalation of point charges at appropriate sites, such calculations are often rather unwieldy (e.g. by not permitting full geometry optimization) or are otherwise subject to a tendency to overemphasize the target species–counterion interaction. In any event, these measures are most likely to influence the metal–*ligand* interaction, whereas it is the metal–*metal* interaction which is the principal focus of the present work; LDA's good performance in characterizing metal–metal interactions has most frequently been explored in the context of polyanionic dimers [3,28], but recent work [29] indicates that such interactions in neutral and cationic metal dimers are also (structurally) better described by LDA than by gradient-corrected methods. Note also that the use of LDA-optimized geometries with gradient-corrected single-point total energies—a combination which has been successfully adopted for several classes of transition metal compounds [31,32,34]—has not been found helpful in the present study, because of the propensity for the

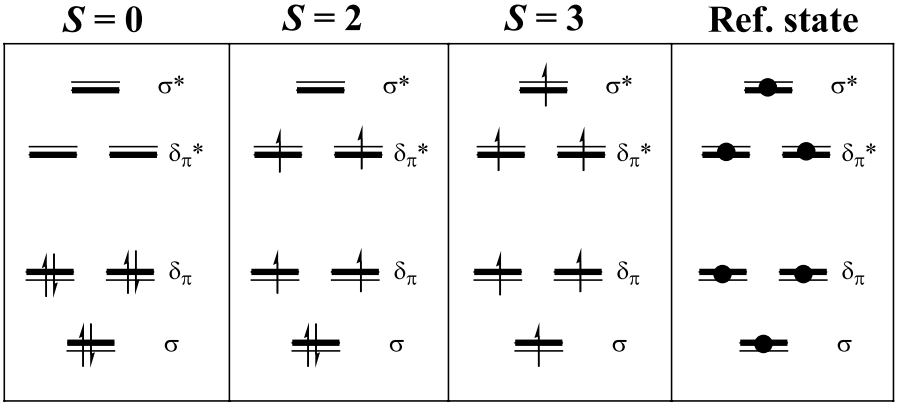


Fig. 2. Representation of t_{2g}-derived orbital occupancy for the $S = 0$, 2, and 3 associated states, and for the reference state, for a generic dimer $M'M''Cl_9^{n-}$.

gradient-corrected methods to favor inappropriately weak metal–metal interactions [3].

3.2. Overall results of calculations upon the mixed-group dimers

Table 1 summarizes the key structural and energetic parameters obtained for the minima of the $S = 0$, 2, and 3 associated states as well as their energies relative to that of the BS minimum for each of the mixed-group dimers.

The spin density calculated for the individual metal atoms is a further diagnostic tool offering useful insights into the electronic structure of the mixed-group dimers. In Table 2, we provide 'covalency-corrected' Mulliken spin densities[40] determined for M′ and M″ for the optimized minima upon the $S = 2$, $S = 3$, and BS potential energy surfaces.

3.3. Trends evident in the $M'M''Cl_9^{n-}$ broken–symmetry potential energy curves

The BS calculations on the mixed-group dimers reveal a trend which is broadly consistent with that already seen for the same-group d^3d^3 $M'M''Cl_9^{n-}$ dimers: that is, dimers in which M′ or M″ is a first-row transition metal (or both M′ and M″ are first-row) exhibit weak antiferromagnetic coupling between M′ and M″ (as evidenced by the unpaired spin densities on the two metal atoms) in complexes characterized by typically large (3.0–3.3 Å) intermetallic separations [41], while dimers in which both M′ and M″ are second- or third-row transition metals yield BS minima characterized by multiple metal–metal bonding (and $\rho_{spin} = 0$ on each metal) and hence small intermetallic distances.

One other result of the calculations deserves comment. For all of the $M'CrCl_9^{4-}$ and $M'MnCl_9^{2-}$ complexes we find that the BS minimum is not the lowest energy structure: ferromagnetic coupling of M′ and M″ is favored over antiferromagnetic coupling, as diagnosed by the negative E_{rel} value (see Table 1) for the $S = 3$ minimum [41]. This result, which extends our previously reported finding of a ferromagnetically coupled global minimum for $WMnCl_9^{2-}$ [21], is exemplified in Fig. 3, which shows the $S = 0$, 2, 3 and BS potential energy curves for the $TaCrCl_9^{4-}$ dimer. We shall return later below to this 'reversal' of the $S = 3$ and BS minimum energies.

When M″ is not first-row, as noted above, the BS minimum is the lowest-energy species found. In such complexes, weak antiferromagnetic coupling is indicated when the less highly oxidized metal, M′, is first-row, with triple M′–M″ bond formation occurring when M′ is second- or third-row. Potential energy curves for $VMoCl_9^{4-}$ and $NbMoCl_9^{4-}$ (Fig. 4) nicely illustrate the influence of M′ upon the location of the BS minimum: for the V/Mo complex, and similarly V/W (not shown), the $S = 0$, 2 and 3 curves possess minima which are

Table 1
Energetic and structural parameters for the $S = 0$, 2, 3, reference state and broken symmetry minima for each dimer system

M′M″ [a]	$E_{rel}(S=0)$ [b]	r_0(M–M) [c]	$E_{rel}(S=2)$ [b]	r_2(M–M) [c]	$E_{rel}(S=3)$ [b]	r_3(M–M) [c]	E_{rel}(ref) [b,d]	E_{tot}(BS) [e]	r_{BS}(M–M) [c]
VCr	1.559	2.217	0.502	3.299	−0.169	3.391	3.369	−1.52800	3.236
VMo	0.310	2.210	0.239	2.924	0.264	3.509	3.040	−1.53289	3.138
VW	0.336	2.341	0.193	2.918	0.297	3.539	2.990	−1.58497	3.028
NbCr	0.288	2.262	−0.029	3.459	−0.357	3.582	2.853	−1.55015	3.250
NbMo	0.0	2.276	0.973	3.000	1.439	3.645	3.697	−1.59435	2.278
NbW	0.0	2.442	0.739	2.983	1.367	3.646	3.505	−1.63972	2.441
TaCr	0.139	2.374	−0.274	3.517	−0.525	3.639	2.729	−1.56659 [f]	3.179
TaMo	0.0	2.443	0.873	3.020	1.420	3.668	3.608	−1.60933	2.443
TaW	0.0	2.463	0.937	2.987	1.738	3.634	3.772	−1.66519	2.463
CrMn	2.085	2.383	0.681	2.954	−0.009	3.172	3.185	−1.90755	3.120
CrTc	1.014	2.361	0.304	2.797	0.095	3.256	2.630	−1.94404	3.135
CrRe	0.885	2.391	0.226	2.816	0.092	3.264	2.555	−1.98420	3.036
MoMn	0.670	2.388	0.152	2.924	−0.126	3.294	2.636	−1.90760	3.059
MoTc	0.0	2.396	0.351	2.866	0.902	3.365	2.773	−1.96294	2.381
MoRe	0.0	2.444	0.305	2.851	0.931	3.373	2.733	−2.00143	2.442
WMn	0.308	2.409	−0.118	3.250	−0.315	3.337	2.528	−1.96689	2.720
WTc	0.0	2.432	0.537	2.875	1.302	3.370	3.068	−2.03174	2.449
WRe	0.0	2.474	0.555	2.861	1.452	3.363	3.136	−2.07180	2.462

[a] Identity of the two metal atoms M′ and M″ in the bioctahedral complex $M'M''Cl_9^{n-}$.
[b] Relative energy of the indicated state, E_{tot}–E_{tot} (BS), in electronvolts.
[c] Optimized intermetallic separation for the $S = 0$, 2, or 3 state, in Angstroms.
[d] Intermetallic separations for the reference state are very similar to those found for the $S = 3$ associated state.
[e] Total bond energy, E_{tot} of the BS optimized geometry, in Hartrees.
[f] For this species, two local minima are obtained on the BS potential energy surface, with the values shown here applying to the global minimum BS (2). Minimum (1) has a geometry characteristic of a $S = 2$ associated state (r(M–M) = 2.767 Å) and an energy $E_{rel} = 0.006$.

Table 2
Mulliken spin densities determined for the $S = 2$, $S = 3$, and BS minima of the mixed-group dimers, adjusted for metal–ligand bond covalency

	$S = 2$ [a]		$S = 3$ [a]		BS [a]		MCl_6^{n-} [b]	
M′M″	$\rho_{spin}(M')$	$\rho_{spin}(M'')$	$\rho_{spin}(M')$	$\rho_{spin}(M'')$	$\rho_{spin}(M')$	$\rho_{spin}(M'')$	$\rho_{spin}(M')$	$\rho_{spin}(M'')$
VCr	0.48	3.48	2.52	3.41	−2.73	2.77	3.15	3.14
VMo	2.13	1.84	2.88	3.10	−2.6	2.66	3.15	2.79
VW	2.15	1.82	2.94	3.01	−2.53	2.58	3.15	2.73
NbCr	0.14	3.77	2.07	3.73	−2.49	2.58	3.06	3.14
NbMo	1.90	2.03	2.59	3.37	0	0	3.06	2.79
NbW	1.93	1.99	2.83	3.11	0	0	3.06	2.73
TaCr	−0.04	3.94	1.86	3.91	−2.35 [c]	2.45 [c]	3.04	3.14
TaMo	1.87	2.08	2.30	3.68	0	0	3.04	2.79
TaW	1.90	2.02	2.66	3.29	0	0	3.04	2.73
CrMn	1.34	2.66	2.68	3.07	−2.70	2.81	3.14	2.90
CrTc	2.23	1.62	2.85	2.93	−2.67	2.80	3.14	2.30
CrRe	2.25	1.58	2.87	2.92	−2.64	2.75	3.14	2.26
MoMn	1.05	2.87	2.03	3.61	−2.29	2.52	2.79	2.90
MoTc	1.83	2.01	2.72	3.07	0	0	2.79	2.30
MoRe	1.85	1.95	2.81	2.97	0	0	2.79	2.26
WMn	−0.09	3.94	1.74	3.89	−1.90	2.22	2.73	2.90
WTc	1.80	2.06	2.54	3.30	0	0	2.73	2.30
WRe	1.85	1.99	2.75	3.05	0	0	2.73	2.26

[a] Covalency-corrected values. The method of covalency correction is described within the text.
[b] Spin densities for the octahedral complexes; these values are not covalency-corrected.
[c] Results for BS(2). For BS(1), values of −1.93 (Ta) and +2.12 (Cr) are obtained.

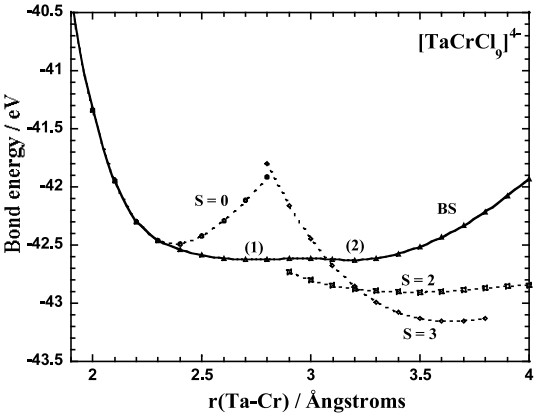


Fig. 3. Potential energy curves for BS and associated states of $TaCrCl_9^{4-}$. Note the presence of two distinct minima (1) and (2) on the BS PES, corresponding to (1) singly-bonded and (2) weakly-coupled metal atoms.

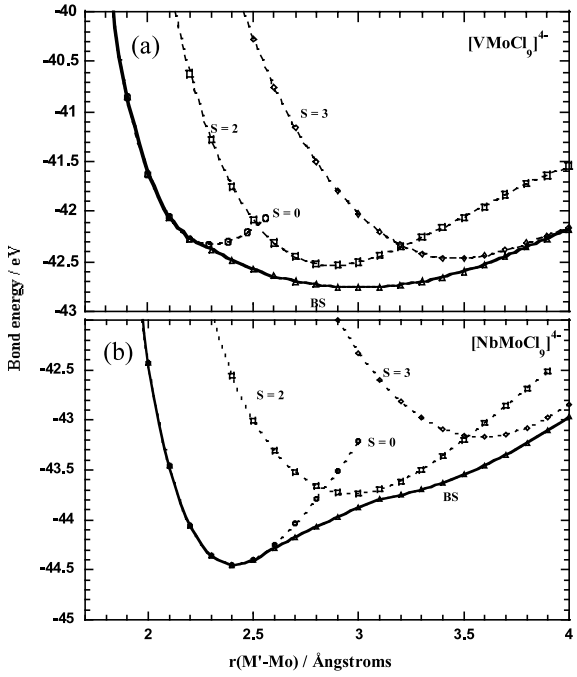


Fig. 4. Potential energy curves for BS and associated states of (a) $VMoCl_9^{4-}$ and (b) $NbMoCl_9^{4-}$. As noted in the text, curves displayed here were obtained with the frozen core on V comprising 1s, 2s, and 2p orbitals, while the frozen cores on Nb and Mo contained all AOs up to 3d.

remarkably close in energy, resulting in a notably shallow BS potential energy curve with a minimum somewhat intermediate between $S = 2$ (σ-bonded) and $S = 3$ (non-bonded), while for the Nb/Mo analogue the $S = 0$ curve is very significantly stabilized (and $S = 2$ to a lesser degree) relative to $S = 3$, due to better overlap between Mo(III) and the larger Nb(II) d orbitals.

A technical point should also be noted with regard to Fig. 4. In this figure we have employed the V '2p' and Nb/Mo '3d' basis sets, where the orbital subshell specifies the highest-lying orbital within the metal atom's frozen core: this approach of 'thawing' the frozen core was found necessary to delivery physically reasonable behavior (i.e. evident repulsion between metal atoms) at intermetallic separations significantly shorter than that of the $S = 0$, 'triply bonded' minimum. This difficulty with the standard (i.e. V '3p' and Nb/Mo

'4p' frozen core) basis sets appears to be important only for M′–M″ separations shorter than those in any of the minima: in only one instance ($VCrCl_9^{4-}$, $S=2$) was there a significant divergence between the 'thawed' (2.97 Å) and 'standard frozen core' (3.3 Å) optimized metal–metal distances. There was no significant difference between 'thawed' and 'standard frozen core' relative energies for the $S=0$, 2, 3, and BS minima for any species.

3.4. Stabilization of ferromagnetic coupling in $M'CrCl_9^{4-}$ and $M'MnCl_9^{2-}$

For each of the $M'CrCl_9^{4-}$ and $M'MnCl_9^{2-}$ dimers, the $S=3$ minimum has a total energy lower than that of the BS minimum; furthermore, for M′M″=NbCr, TaCr, and WMn, the $S=2$ structure is also lower in energy than BS, but above $S=3$. The relative energies of the $S=3$ and BS minima indicate that the $M'CrCl_9^{4-}$ and $M'MnCl_9^{2-}$ dimers are ferromagnetically, rather than antiferromagnetically, coupled. We examine this issue in the molecular orbital (MO) diagrams for $VCrCl_9^{4-}$ and $TaCrCl_9^{4-}$, in Figs. 5–7. These figures also incorporate bar charts indicating the contributions of metallic valence AOs to the key occupied MOs in our DFT calculations.

For the $S=3$ associated state of $VCrCl_9^{4-}$ (Fig. 5), the α-spin $10a_1$, $11a_1$, 13e, and 14e MOs arise from the valence V and Cr AOs, and detailed examination of the composition of these MOs reveals that, for the most part, they remain effectively localized upon either V ($11a_1$) or Cr ($10a_1$ and 13e) with no contamination from the other metal atom. The exception here is the 14e orbital, which is best described as being derived from the V δ_π-symmetry AOs but with significant contamination by the α-spin Cr e_g orbital, which accounts for about 20% of the metal-based character for α-spin 14e. The mixing between the α-spin V δ_π and Cr e_g AOs acts to lower the energy of the 14e MO pair (with a concomitant increase in the energy of the similarly mixed, unoccupied, α-spin 15e MO pair), helping to stabilize the ferromagnetic coupling of the $S=3$ associated state. Furthermore, it is the α-spin 14e level which effectively provides a conduit (by way of the V/Cr AO mixing) for electron transfer from V to Cr in the $S=3$ minimum.

The large metal–metal distance in the BS $VCrCl_9^{4-}$ minimum is consistent with weak antiferromagnetic coupling between V and Cr. Here the valence electrons on V are of opposite spin to those on Cr, and the large spin polarization energies found for each of these first-row TMs (and lower orbital energies for Cr than for V) result in a very large energy separation between the occupied α-spin Cr AOs and the unoccupied vanadium AOs of the same spin. There is thus very little mixing between V and Cr in the α-spin valence MOs, which can be regarded as virtually pure metallic AOs. In contrast, the β-spin AOs on V and Cr are fairly close in energy, and rather more mixing is seen between these: the occupied β-spin $10a_1$ MO is dominated by V, but also significantly contaminated by Cr, $3d_{z^2}$ character, with a

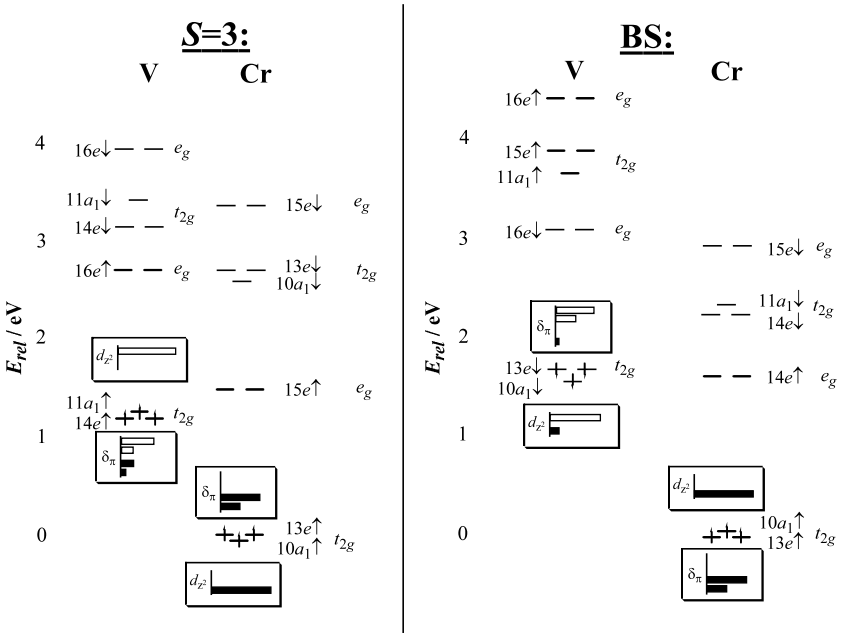


Fig. 5. Electronic configurations of the $S=3$ and broken symmetry minima of $VCrCl_9^{4-}$. In this and subsequent electronic configuration diagrams, the MOs shown, which are labelled according to their hierarchy (excluding 'frozen core' orbitals), are those identified as arising principally from the valence-d AOs of the metal atoms. Metal AO contributions to the occupied MOs are shown as overlaid bar charts, with M′ shown as outlined (white) bars and M″ as filled (black) bars; for a_1- or σ-symmetry MOs, only d_{z^2} content is shown, while for e-symmetry orbitals, the two bars depicted for each metal are: upper bar, $d_{x^2-y^2}$ (or d_{xy}) content; lower bar, d_{xz} (or d_{yz}) content.

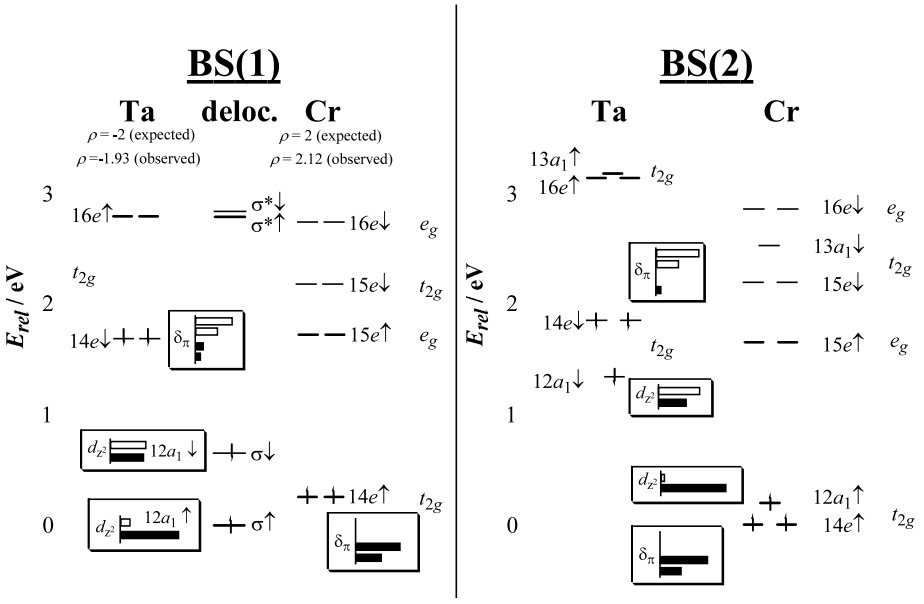


Fig. 6. Electronic configurations of the broken symmetry minima of $TaCrCl_9^{4-}$. The unoccupied α- and β-spin 17e MOs, which correspond to the Ta e_g AOs and which lie more than 1 eV above the highest-energy orbital depicted, are omitted. See Fig. 5 for an explanation of the orbital content bar charts.

converse weighting seen in the unoccupied $11a_1$ MO. Much less contamination is found for the occupied β-spin 13e and unoccupied 14e MOs, despite a similar energy separation, since the AOs concerned lack the direct alignment which exists between the $3d_{z^2}$ orbitals on the two metals. As with $S = 3$, the BS minimum also displays a degree of V → Cr electron transfer, but here it is the β-spin $10a_1$ MO which provides the pathway for this electron migration. We can discern that the β-spin donation manifested in the BS minimum is a less effective method of M′ → M″ electron transfer than is the α-spin donation exhibited by $S = 3$, because the magnitude of the deviation in ρ_{spin} from the expected value of ± 3, on both M′ and M″, is larger for $S = 3$ than for BS (see Table 2). The relative extent of M′ → M″ electron transfer for these two configurations is also consistent with the relative energy separations of the V and Cr AOs involved in the electron transfer: the β-spin $10a_1/11a_1$ gap (implicated in the BS electron transfer) is significantly larger than the α-spin 14e/15e gap (involved in $S = 3$ electron transfer), indicating a greater impediment to electron transfer in the BS electronic configuration.

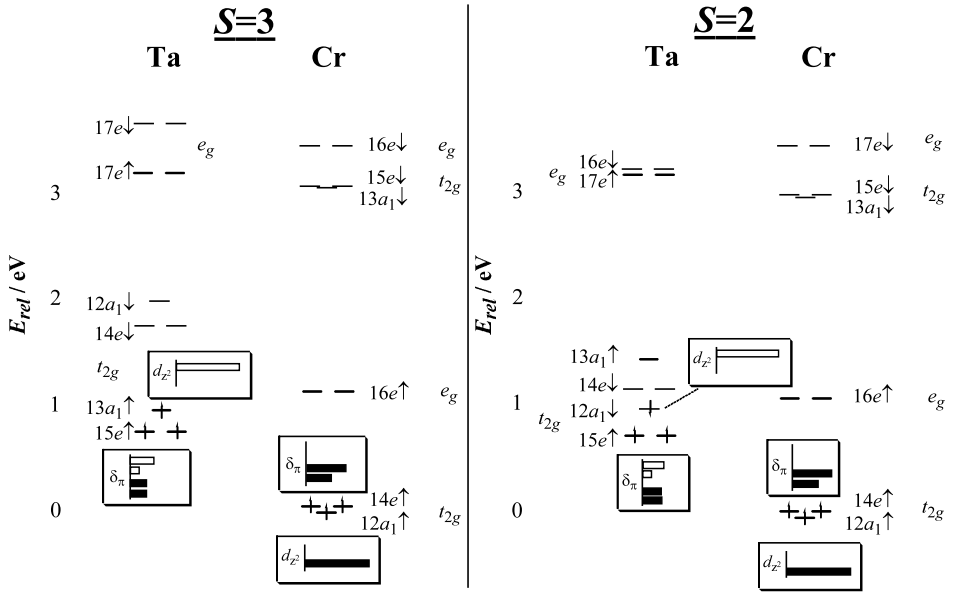


Fig. 7. Electronic configuration of the $S = 3$ and $S = 2$ minima of $TaCrCl_9^{4-}$. See Fig. 5 for an explanation of the orbital content bar charts.

The $TaCrCl_9^{4-}$ BS PES (see Fig. 3) has two local minima at $r(M–M) = 2.77$ Å (BS(1)) and 3.18 A (BS(2)); the two minima and the transition state separating them are all very close in total energy. The bond length for BS(1) is indicative of a Ta–Cr σ bond, while the intermetallic separation in BS(2)—which is marginally the global minimum on the BS surface—is consistent with a weakly coupled antiferromagnetic complex. The BS(2) Ta–Cr distance is also close to that seen in the ferromagnetically-coupled $S = 3$ minimum. Thus, whereas the V/Cr system can be considered a conflict between ferromagnetic and antiferromagnetic coupling, Ta/Cr represents a three-way contest between ferromagnetism, antiferromagnetism, and metal–metal bond formation. Superficial examination of the $TaCrCl_9^{4-}$ $S = 3$ valence MOs in Fig. 6 shows that, as expected, the spin polarization splitting of α- and β-spin orbitals on Cr is much greater than the ligand field splitting of t_{2g}-based and e_g-based orbitals, while for Ta the ligand field splitting is the dominant effect. What influence do these trends have upon the character of the valence MOs in the BS and $S = 3$ states?

For the BS (1) minimum of $TaCrCl_9^{4-}$ (Fig. 6), the M–M distance is suggestive of a metal–metal σ bond. This is reflected in the composition of the MOs, with the a_1-symmetry orbitals identifiable as more-or-less polar σ and σ* delocalized orbitals (the occupied α-spin $12a_1$ is dominated by Cr d_{z^2} character, while the corresponding β-spin $12a_1$ has only a slight excess of Ta d_{z^2} content over Cr) while the *e*-symmetry orbitals are essentially localized on Ta or Cr (although some Cr content is evident in β-spin 14*e*, due to mixing between the Ta and Cr β-spin δ_π-symmetry AOs). While there is clearly a significant degree of overall electron transfer from Ta to Cr, the contributions from α-spin transfer (via $12a_1$) and β-spin transfer (via 14*e*) are of comparable magnitude so that the calculated (covalency-corrected) spin densities on the two metals are very close to the values of −2 and +2, respectively, expected for a straightforward σ-bonded complex.

The longer-bonded BS (2) minimum (Fig. 6) is electronically very similar to BS V/Cr, with the occupied α-spin orbitals ($12a_1$ and 14e) identifiable as the essentially pure t_{2g}-based (σ and δ_π) chromium AOs, while the occupied β-spin $12a_1$ orbital in particular displays very severe mixing between Cr and Ta d_{z^2} AOs.

For the $S = 3$ minimum (Fig. 7), majority-spin $12a_1$, $13a_1$ and 14e occupied MOs display very little mixing between the constituent metal AOs, and these MOs thus correspond, respectively, as the valence Cr $3d_{z^2}$, Ta $5d_{z^2}$, and Cr δ_π-symmetry orbitals. In contrast, severe mixing is found for the α-spin (occupied) 15e and (unoccupied) 16e orbitals, such that these MOs contain virtually equal portions of Ta δ_π-symmetry and Cr e_g character. Since the two electrons occupying the 15e orbital are shared while the other valence electrons are localized, the $S = 3$ state can be considered as involving transfer of a full electron from Ta(II) to Cr(III), resulting in oxidation states of Ta(III) and high-spin Cr(II).

A common feature of the V/Cr and Ta/Cr $S = 3$ and BS minima is the tendency for electron transfer from the vanadium-triad metal to Cr (indeed, all of the various minima for the mixed-group $M'M''Cl_9^{n-}$ dimers show some electron transfer from M′ towards M″). This is the principal factor favoring ferromagnetic coupling when first-row M″ is the recipient of this electron donation: Cr and Mn both have a large spin polarization energy, and this is accentuated when the first-row M″ has an effective share of more than its nominal three valence majority-spin electrons. It is also notable that, while all of the $M'CrCl_9^{4-}$ and $M'MnCl_9^{2-}$ dimers exhibit a preference for ferromagnetic coupling, no dimer with second- or third-row M″ does so. The lower stability of ferromagnetic coupling when, for example, Cr is replaced by Mo or by W, can be reconciled with the comparatively low spin polarization energies, and high ligand field splitting energies, seen for these larger metal ions. This observed trend is consistent with the mechanism by which we have already accounted for the stabilization of ferromagnetic coupling in $WMnCl_9^{2-}$ [21].

The relative energies of vacant α-spin (e_g) and β-spin (t_{2g}) orbitals on the nominally more highly oxidized metal M″ will help to determine the extent of electron transfer in the longbonded BS and $S = 3$ configurations, which we can gauge from the parameter $\Delta(\rho_{spin})$ as listed in Table 3. This parameter measures the deviation (from the value of $\rho_{spin} = 3$ expected in the absence of electron transfer) of the calculated covalency-corrected spin densities on M′ for the series of $M'M''Cl_9^{4-}$ and $M'M''Cl_9^{2-}$ having longbonded BS minima, and can be considered as a measure of the extent of α-spin ($S = 3$) or β-spin (BS) electron transfer from M′ to M″. We can see that, when M″ is first-row, $\Delta(\rho_{spin})$ is consis-

Table 3
Deviation of absolute covalency-corrected Mulliken spin densities on M′, from the expected value of $\rho_{spin} = 3$, for $S = 3$ and longbonded BS minima of $M'M''Cl_9^{n-}$

M′M″	$\Delta(\rho_{spin})$: $S = 3$ [a]	$\Delta(\rho_{spin})$: BS[a]
VCr	0.48	0.27
VMo	0.12	0.40
VW	0.06	0.47
NbCr	0.93	0.51
TaCr	1.14	0.65
CrMn	0.32	0.30
CrTc	0.15	0.33
CrRe	0.13	0.36
MoMn	0.97	0.71
WMn	1.26	1.10

[a] $\Delta(\rho_{spin}) = 3 - |\rho_{spin}|$, where ρ_{spin} is the covalency-corrected value as listed in Table 1.

tently larger for $S=3$ than for BS, while when M″ is second- or third-row, $\Delta(\rho_{spin})$ is larger for BS than for $S=3$. This trend is broadly consistent with our expectations based upon the qualitative arguments presented above, and serves to reiterate the preference for ferromagnetic state stabilization by α-spin electron transfer for the $M'CrCl_9^{4-}$ and $M'MnCl_9^{2-}$ dimers.

3.5. Competition between σ-bonding and electron transfer in the $S=2$ associated state minima

The $S=2$ minima for all of the $M'CrCl_9^{4-}$ and $M'MnCl_9^{2-}$ dimers exhibit very large M–M separations, not greatly shorter than the $S=3$ values, and so an electronic configuration lacking significant σ-bond character appears to be indicated for the $S=2$ minima for these species. In such an $S=2$ minimum featuring purely localized d electrons, we would expect nominal ρ_{spin} values of 3 ($=3\alpha-0\beta$) and 1 ($=2\alpha-1\beta$) for the two metals. This expectation is not precisely met—$\rho_{spin}(M')<1$ and $\rho_{spin}(M'')>3$ for most of the $S=2$ $M'CrCl_9^{4-}$ and $M'MnCl_9^{2-}$ dimers—but examination of the d-orbital composition for these dimers (for example, $S=2$ $TaCrCl_9^{4-}$ in Fig. 7) indicates that the above description is otherwise fairly accurate. As seen in Fig. 7, the occupied α- and β-spin $12a_1$ orbitals are localized on Cr and Ta, respectively. There is negligible contamination of the (Cr δ_π) α-spin 14e, but significant contamination by Cr e_g AOs of the (nominally Ta δ_π) α-spin 15e MO pair. As with the $S=3$ configuration, the mixing between Ta and Cr in the α-spin 15e orbitals is so extreme that this MO pair in fact possesses about as much Cr content as Ta. It is instructive to contrast the $S=2$ structure and electronic configuration against those of the σ-bonded BS(1) minimum (Fig. 6), to which an $S=2$ associated state would normally be expected to conform. If a BS minimum exists for a σ-bonded dimer, why does the $S=2$ surface not also feature such a minimum?

The same factors which favor antiferromagnetic coupling in the $M'M''Cl_9^{n-}$ (M″ = first-row) dimers also favor $S=2$ associated states for these species which effectively lack any metal–metal bonding. Formation of a σ bond in the $S=2$ associated state of $M'M''Cl_9^{n-}$ (M″ = first-row) permits β-spin electron transfer towards M″ (via the polar M′–M″ σ bond) but mitigates against the spin-polarization stabilization of α-spin orbitals on M″. On the other hand, mixing of the α-spin M′ δ_π and M″ e_g AOs at longer M′–M″ separations provides a means for α-spin electron transfer (enhancing the M″ α-orbital stabilization due to spin-polarization splitting of α- and β-spin orbitals) without any requirement for M′–M″ bond formation. For $TaCrCl_9^{4-}$, it is this M′–M″ α-spin δ_π mixing which drives the elongation of the M′–M″ internuclear separation in the $S=2$ associated state compared with that of the BS(1) geometry.

Analysis of the MO composition also allows us to interpret the observation (see Table 2) that dimers having first-row M′ and second-or third-row M″ (e.g. $CrTcCl_9^{2-}$) are the only complexes in which the $S=2$ spin density on M′ exceeds that on M. A comparison between the Mo/Mn and Cr/Tc $S=2$ dimers is instructive. For Mo/Mn, we obtain $\rho_{spin}(M')$ and (M'') values of 1.05 and 2.87, respectively. For Cr/Tc the situation is reversed: $\rho_{spin}(M')=2.23$, while $\rho_{spin}(M'')=1.62$, a result which appears to run contrary to the expected general tendency of electron transfer from M′ to M″.

The spin density distortions described above arise from the different trends in d-orbital splitting for first-row versus second- and third-row transition metal atoms: ligand field splitting of the t_{2g} and e_g orbitals is significantly greater for second and third row transition metals, while splitting of the α and β orbital energies due to spin polarization is generally greatest for first row TMs. Thus, as reflected in the occupied $10a_1$ orbital compositions in Fig. 8, first-row M″ (e.g., in $S=2$ $MoMnCl_9^{2-}$) is a good α-spin electron acceptor but a poor acceptor of β-spin electron density due to its large spin polarization energy. Conversely, second- or third-row M″ (e.g. $S=2$ $CrTcCl_9^{2-}$) is much more able to accept β-spin, than α-spin, electron density by virtue of its ligand field splitting.

3.6. Overall comparison of $M'M''Cl_9^{4-}$ and $M'M''Cl_9^{2-}$ bonding trends

As noted above, the following statements on mixed-group $M'M''Cl_9^{n-}$ dimers are true for both the V(II)/Cr(III) ($M'M''Cl_9^{4-}$) and Cr(III)/Mn(IV) ($M'M''Cl_9^{2-}$) dimer families:

i) when M″ is first-row, the complexes have ferromagnetic lowest-energy configurations
ii) when M′ (but not M″) is first-row, lowest-energy configurations of the complexes exhibit weak antiferromagnetic coupling between M′ and M″
iii) when neither M′ nor M″ is first-row, complexes show a preference for multiple metal–metal bonding
iv) when M″ is first-row, $S=2$ minima have unexpectedly large M′–M″ interatomic distances, and appear deficient in M′–M″ σ bond character.

Notwithstanding these striking qualitative similarities between the V(II)/Cr(III) and Cr(III)/Mn(IV) families, which are generalized schematically in Fig. 9, there are some significant differences in detail. For example, the preference for ferromagnetic complexes is less marked for M″ = Mn than for M″ = Cr (stabilization of the $S=3$ $VCrCl_9^{4-}$ minimum relative to the antiferromagnetic

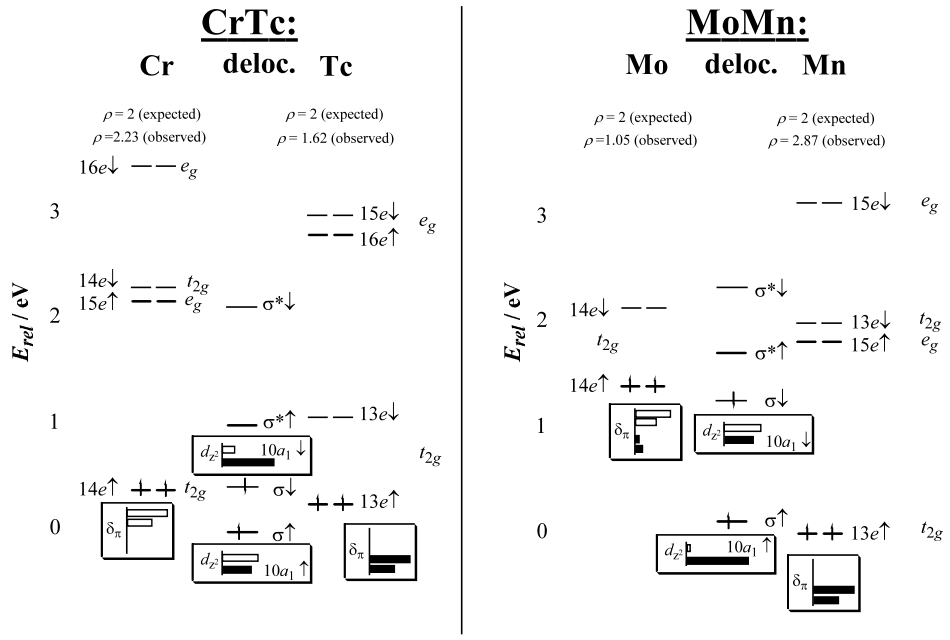


Fig. 8. Electronic configurations of the $S = 2$ minima of $CrTcCl_9^{4-}$ and $MoMnCl_9^{4-}$. See Fig. 5 for an explanation of the orbital content bar charts.

BS minimum is 0.17 eV, whereas the corresponding value for $CrMnCl_9^{2-}$ is only 0.01 eV) [22]. Moreover, we can examine the effect of 'transmuting' the metals such that M′ and M″ both retain their respective row numbers (for example, comparing $VMoCl_9^{4-}$ with $CrTcCl_9^{2-}$, since these are the two complexes having first-row M′ and second-row M″). In such a lateral comparison of the energetic trends across the V(II)/Cr(III) and Cr(III)/Mn(IV) families (see Table 4), it appears that the Cr(III)/Mn(IV) family is more inclined towards weakly-coupled dimers than is the V(II)/Cr(III) family: although the global minima numbers of triply-bonded and weakly-coupled dimers are the same for both families, the total energies of weakly-coupled dimers ($S = 2$, 3, and long M′–M″ bond BS minima) relative to their strongly-bonded counterparts ($S = 0$ minima) are consistently lower for Cr(III)/Mn(IV) mixed triad combinations than for the analogous V(II)/Cr(III) mixed triad combination. As with so many other trends amongst the $M'M''Cl_9^{n-}$ dimers, this observation can be rationalized according to d-orbital size: the larger the d orbitals upon M′ and M″, the greater the strength of any intermetallic bond, and the lower the spin polarization splitting of the valence orbitals of M′ and M″. It is also of interest to note that, while weakly-coupled ($S = 3$, long-bonded BS) and σ-bonded ($S = 2$) minima have generally *shorter* M′–M″ bonds for the Cr(III)/Mn(IV) family than for the V(II)/Cr(III) family, the triply-bonded ($S = 0$) minima exhibit the opposite trend: Cr(III)/Mn(IV) family M′≡M″ bonds are almost invariably *longer* than the corresponding examples from the V(II)/Cr(III) family, again under-

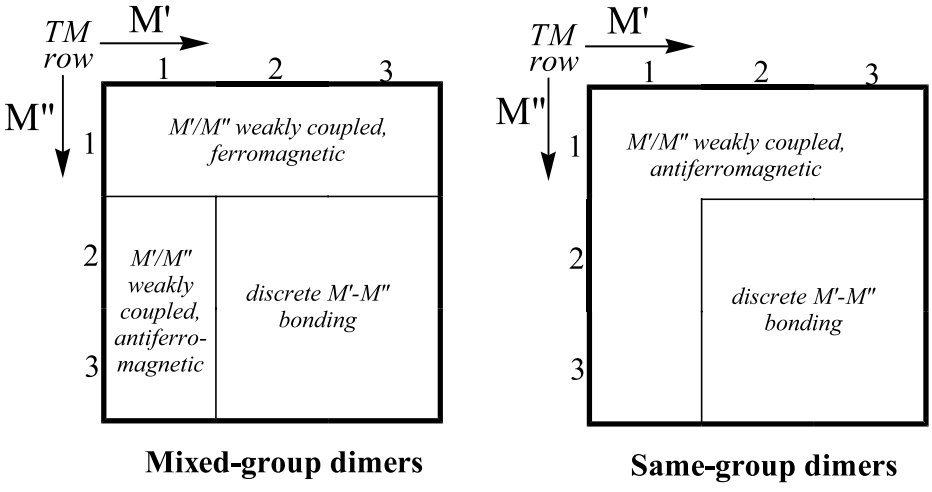


Fig. 9. A summary of metal–metal bonding trends evident for mixed-group and same-group d^3d^3 $M'M''Cl_9^{n-}$ dimers.

Table 4
Lateral comparison of $S = 2$, 3, and weakly-coupled BS minima relative to $S = 0$ structures, for the V(II)/Cr(III) and Cr(III)/Mn(IV) dimer families

Family member		Relative stabilization energies (eV)		
V(II)/Cr(III)	Cr(III)/Mn(IV)	$\Delta(E_{rel,S=0}[S=2])$ [a]	$\Delta(E_{rel,S=0}[S=3])$ [a]	$\Delta(E_{rel,S=0}[BS])$ [a]
VCr	CrMn	0.35	0.37	0.53
NbCr	MoMn	0.64	0.87	0.70
TaCr	WMn	0.53	0.75	0.55
VMo	CrTc	0.20	0.15	0.38
NbMo	MoTc	0.62	0.54	[b]
TaMo	WTc	0.43	0.44	[b]
VW	CrRe	0.01	−0.04	0.17
NbW	MoRe	0.34	0.12	[b]
TaW	WRe	0.38	0.29	[b]

[a] $\Delta(E_{rel,S=0}[S=2]) = (E[S=2]-E[S=0])_{V(II)/Cr(III)}-(E[S=2]-E[S=0])_{Cr(III)/Mn(IV)}$, where the subscripts V(II)/Cr(III) and Cr(III)/Mn(IV) denote the 'equivalent' family members sharing a given row of this table. The parameters $\Delta(E_{rel,S=0}[S=3])$ and $\Delta(E_{rel,S=0}[BS])$ are defined in an entirely analogous fashion.

[b] For these species, the BS minima are coincident with the respective $S = 0$ minima.

scoring the Cr(III)/Mn(IV) family's generally lower propensity for multiple bond formation via d-orbital σ and δ_π overlap.

3.7. The interplay between spin polarization and d-orbital overlap

Investigating the relationship between d-orbital overlap in the triple-bonded metal dimers, and spin polarization in the weakly antiferromagnetically coupled dimers, has been an important aspect of our previous studies on same-group dimers [1–6]. This has been parametrized in the terms E_{ovlp} and E_{SPE}, which are defined as $E_{ovlp} = E_{ref} - E_{S=0}$ and $E_{SPE} = E_{ref} - E_{S=3}$, where E_{ref}, $E_{S=0}$ and $E_{S=3}$ are the energies of the respective minima for the reference state, $S = 0$, and $S = 3$ associated state potential energy surfaces [2]. The significance of E_{ovlp} and E_{SPE} is that they provide a measure of the stabilization due to metal–metal bond formation through d-orbital overlap, and of stabilization due to spin polarization of localized d-orbital electrons. Plots of E_{ovlp} versus E_{SPE} for the same-group dimers of the Cr(III) and Mn(IV) triads have revealed a consistent linear trend [2]: a large E_{ovlp} value is associated with small E_{SPE} for a given dimer, and as E_{ovlp} is reduced, E_{SPE} increases. This is fully consistent with expectations, since d-orbital overlap leading to bond formation is most effective when the d orbitals are large, while spin polarization of the unpaired electrons is most significant when the d orbitals are small.

We have determined E_{ovlp} and E_{SPE} for the mixed-group dimers (see Table 5). When we analyze these parameters (see Fig. 10), we find that the correlation between E_{ovlp} and E_{SPE} is more-or-less maintained, but adherence to a linear relationship is much more poor for the mixed-group dimers than for their same-group counterparts. This is undoubtedly due, in part, to the effect of electron transfer towards the more highly oxidized metal, which will have a much greater distorting effect than any tendency for electron transfer within the same-group dimers. In this respect, it is worth noting that the most significant 'outliers' for the mixed-group families are, (i) the M′Cr and M′Mn species (where M′ is second- or third-row; labels 1 and 3 on Fig. 10), for which the data points are substantially above the best-fit lines for the respective families; and (ii) the VM″ and CrM″ (with M″ second- or third-row; labels 2 and 4 on Fig. 10), for which the data points lie well below the best-fit lines. Case (i) encompasses the most extreme

Table 5
Overlap and spin polarization stabilization energies determined for mixed-group dimers

M′M″	E_{ovlp} [a]	E_{SPE} [a]	$E_{SPE}(M')$ [b]	$E_{SPE}(M'')$ [b]	δ_{SPE} [c]
VCr	1.810	3.538	1.828	1.857	−0.15
VMo	2.730	2.776	1.828	1.128	−0.18
VW	2.654	2.693	1.828	1.004	−0.14
NbCr	2.565	3.210	1.244	1.857	0.11
NbMo	3.697	2.258	1.244	1.128	−0.11
NbW	3.505	2.138	1.244	1.004	0.11
TaCr	2.590	3.254	1.137	1.857	0.26
TaMo	3.608	2.188	1.137	1.128	−0.08
TaW	3.772	2.034	1.137	1.004	−0.11
CrMn	1.100	3.194	1.857	1.636	−0.30
CrTc	1.616	2.535	1.857	0.885	−0.21
CrRe	1.670	2.463	1.857	0.791	−0.19
MoMn	1.966	2.762	1.128	1.636	0.00
MoTc	2.773	1.871	1.128	0.885	−0.14
MoRe	2.733	1.802	1.128	0.791	−0.12
WMn	2.220	2.843	1.004	1.636	0.20
WTc	3.068	1.766	1.004	0.885	−0.12
WRe	3.136	1.864	1.004	0.791	0.07

[a] Parameter, in eV and as defined in text, for the mixed dimer.

[b] Spin polarization stabilization energy (in eV) for the octahedral complex containing the indicated metal ion.

[c] $\delta_{SPE} = E_{SPE}(M'M'') - (E_{SPE}(M') + E_{SPE}(M''))$, expressed in eV.

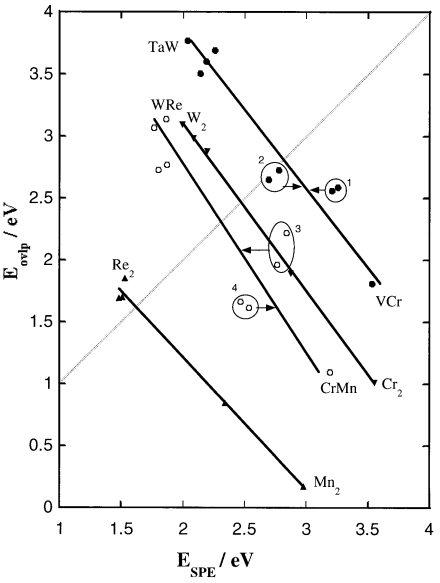


Fig. 10. Graph of E_{ovlp} vs. E_{SPE} (see text for definitions), for the V(II)/Cr(III), Cr(III)/Cr(III), Cr(III)/Mn(IV), and Mn(IV)/Mn(IV) families of $M'M''Cl_9^{n-}$ dimers. Best-fit lines show the general trend within each family, for which the 'terminal' members (i.e. first-row/first-row and third-row/third-row combinations) are labelled; also identified (as numbered ellipses) are groups of significant 'outliers' among the mixed-group dimers [1 = NbCr, TaCr; 2 = VMo, VW; 3 = MoMn, WMn; 4 = CrTc, CrRe]. The dotted line is the boundary between $S = 0$ and 3 absolute stability, which reflects the tendency of dimers to form either multiple metal–metal bonds (upper left section) or weakly coupled complexes (lower right section).

examples of ferromagnetic cf. antiferromagnetic stabilization for each family (in which electron density is transferred from M′ associated with a small spin polarization splitting, to M″ having a large characteristic spin polarization splitting), and we can assume that the effect of electron transfer for these systems is to enhance E_{SPE}; for case (ii), M′ has a larger spin polarization splitting than M″ and so electron transfer will act to diminish E_{SPE} for these species. When these tendencies are accounted for, it appears that the relationship between E_{SPE} and E_{ovlp} for the mixed-group dimers is otherwise broadly similar to that seen for the same-group dimers.

The second noteworthy trend evident in Fig. 10 is due to increasing metal atom oxidation state. We have previously commented [2] that the chromium-triad d^3d^3 dimers display a systematically higher E_{ovlp} term than the corresponding manganese-triad d^3d^3 dimers, in accord with the generally greater spatial extent of d-orbitals for M(III) species than for M(IV), and the mixed-group dimers essentially obey this trend also: the V(II)/Cr(III) data points on Fig. 10 all lie above the best-fit line for the Cr(III)/Cr(III) triad dimers, while (with the exception of WMn, a species heavily influenced by electron-transfer-enhanced ferromagnetic stabilization as noted above) all of the Cr(III)/Mn(IV) family dimers lie between the Cr(III)/Cr(III) and Mn(IV)/Mn(IV) triad dimer best-fit lines, in accord with the trend in d-orbital radii M(II) > M(III) > M(IV) within any given row. The best-fit lines in Fig. 10 also indicate that the change in E_{ovlp} generally exceeds the change in E_{SPE} in moving across a transition row (as can be seen, for example, for the series $VCr \rightarrow Cr_2 \rightarrow CrMn \rightarrow Mn_2$ and $TaW \rightarrow W_2 \rightarrow WRe \rightarrow Re_2$), and this too is consistent with our earlier studies on the same-group dimers [2].

4. Concluding remarks

The various structural and energetic trends reported here for the series of mixed-group, face-shared dimers $M'M''Cl_9^{4-}$ (M′ = V, Nb, Ta; M″ = Cr, Mo, W) and $M'M''Cl_9^{2-}$ (M′ = Cr, Mo, W; M″ = Mn, Tc, Re) can largely be attributed to the interplay between three parameters: the tendency for electron transfer from M′ to M″, the degree of ligand-field splitting Δ for the metal atoms, and the magnitude of the spin-polarization splitting E_{SPE} of the α- and β-spin valence d orbitals on each metal. Our studies on both mixed-group and same-group dimers show that this interplay has consistent results, which may be succinctly summarized: ferromagnetic coupling is adopted in the d^3d^3 $M'M''Cl_9^{n-}$ dimers in which M″ (the more highly oxidized metal) is first-row; weak antiferromagnetic coupling occurs in those dimers in which M′, but not M″, is first-row; and significant metal–metal bonding is always only seen when neither M′ nor M″ is first-row.

Acknowledgements

We gratefully acknowledge the Australian Research Council (ARC) for financial support.

References

[1] T. Lovell, J.E. McGrady, R. Stranger, S.A. Macgregor, Inorg. Chem. 35 (1996) 3079.
[2] J.E. McGrady, T. Lovell, R. Stranger, Inorg. Chem. 36 (1997) 3242.
[3] J.E. McGrady, R. Stranger, T. Lovell, J. Phys. Chem. A 101 (1997) 6265.
[4] J.E. McGrady, R. Stranger, T. Lovell, Inorg. Chem. 37 (1998) 3802.
[5] R. Stranger, J.E. McGrady, T. Lovell, Inorg. Chem. 37 (1998) 6795.
[6] R. Stranger, A. Turner, C.D. Delfs, Inorg. Chem. 40 (2001) 4093.
[7] T. Lovell, R. Stranger, J.E. McGrady, Inorg. Chem. 40 (2001) 39.
[8] F.A. Cotton, R.A. Walton, Multiple Bonds between Metal Atoms, second ed., Clarendon Press, Oxford, 1993.
[9] H.B. Kraatz, P.M. Boorman, Coord. Chem. Rev. 143 (1995) 35.
[10] F.A. Cotton, Inorg. Chem. 37 (1998) 5710.
[11] L. Noodleman, J.G. Norman, Jr., J. Chem. Phys. 70 (1979) 4903.

[12] S. Petrie, R. Stranger, Inorg. Chem. (2002) submitted for publication.
[13] F.A. Cotton, L.R. Falvello, G.N. Mott, R.R. Schrock, L.G. Sturgeoff, Inorg. Chem. 22 (1983) 2621.
[14] F.A. Cotton, R.C. Torralba, Inorg. Chem. 30 (1991) 2196.
[15] F.A. Cotton, E.V. Dikarev, W.Y. Wong, Polyhedron 16 (1997) 3893.
[16] F.A. Cotton, J.L. Eglin, C.A. James, R.L. Luck, Inorg. Chem. 31 (1992) 5308.
[17] F. Birkelbach, M. Winter, U. Flörke, H.J. Haupt, C. Butzlaff, M. Lengen, E. Bill, A.X. Trautwein, K. Wieghardt, P. Chaudhuri, Inorg. Chem. 33 (1994) 3990.
[18] S.K. Dutta, R. Werner, U. Flörke, S. Mohanta, K.K. Nanda, W. Haase, K. Nag, Inorg. Chem. 35 (1996) 2292.
[19] S. Mohanta, K.K. Nanda, L.K. Thompson, U. Flörke, K. Nag, Inorg. Chem. 37 (1998) 1465.
[20] J. Cano, A. Rodriguez-Fortea, P. Alemany, S. Alvarez, E. Ruiz, Chem. Eur. J. 6 (2000) 327.
[21] S. Petrie, R. Stranger, Inorg. Chem. 41 (2002) 2341.
[22] We are currently also studying the mixed dimers $M'M''Cl_9^{3-}$ in which M′ and M″ are, respectively, members of the V and Mn triads. For this set of complexes a d^3d^3 configuration requires formal oxidation states of (M′)(II) and (M″)(IV); however, the magnitude of electron transfer seen in the V(II)/Mn(IV) triad mixed dimers is such that these species are best described by d-electron configurations other than d^3d^3, and for this reason we shall report on the V/Mn triad mixed dimers in detail elsewhere.
[23] E.J. Baerends, A. Bérces, C. Bo, P.M. Boerrigter, L. Cavallo, L. Deng, R.M. Dickson, D.E. Ellis, L. Fan, T.H. Fischer, C. Fonseca Guerra, S.J.A. van Gisbergen, J.A. Groeneveld, O.V. Gritsenko, F.E. Harris, P. van den Hoek, H. Jacobsen, G. van Kessel, F. Kootstra, E. van Lenthe, V.P. Osinga, P.H.T. Philipsen, D. Post, C. Pye, W. Ravenek, P. Ros, P.R.T. Schipper, G. Schreckenbach, J.G. Snijders, M. Sola, D. Swerhone, G. te Velde, P. Vernooijs, L. Versluis, O. Visser, E. van Wezenbeek, G. Wiesenekker, S.K. Wolff, T.K. Woo, T. Ziegler, ADF-1999.
[24] C. Fonseca Guerra, J.G. Snijders, G. te Velde, E.J. Baerends, Theor. Chem. Acc. 99 (1998) 391.
[25] R.G. Parr, W. Yang, Density Functional Theory of Atoms and Molecules, Oxford University Press, New York, 1989.
[26] T. Ziegler, Chem. Rev. (1991) 91.
[27] S.H. Vosko, L. Wilk, M. Nusair, Can. J. Chem. 58 (1980) 1200.
[28] A.J. Bridgeman, G.J. Cavigliasso, Phys. Chem. A 105 (2001) 7111.
[29] S. Petrie, R. Stranger, in preparation.
[30] L. Versluis, T.J. Ziegler, J. Chem. Phys. 88 (1988) 322.
[31] K. Besançon, G. Laurenczy, T. Lumini, R. Roulet, R. Bruyndonckx, Inorg. Chem. 37 (1998) 5634.
[32] R.J. Deeth, H.D.B. Jenkins, J. Phys. Chem. A 101 (1997) 4793.
[33] A.J. Bridgeman, G. Cavigliasso, Polyhedron 20 (2001) 2269.
[34] K. Doclo, D. de Corte, C. Daul, H.U. Güdel, Inorg. Chem. 37 (1998) 3842.
[35] J. Bendix, R.J. Deeth, T. Weyhermuller, E. Bill, K. Wieghardt, Inorg. Chem. 39 (2000) 930.
[36] C. Daul, E.J. Baerends, P. Vernooijs, Inorg. Chem. 33 (1994) 3538.
[37] F. Rogemond, H. Chermette, D.R. Salahub, Chem. Phys. Lett. 219 (1994) 228.
[38] M.R. Bray, R.J. Deeth, V.J. Paget, P.D. Sheen, Int. J. Quantum Chem. 61 (1997) 85.
[39] A.D. Becke, J. Chem. Phys. 96 (1992) 2155.
[40] The raw Mulliken spin densities were corrected by a factor $3/\rho_{M(oct)}$, where $\rho_{M(oct)}$ is the Mulliken spin density obtained for the central metal atom within the isolated high-spin d^3 octahedral complex MCl_6^{n-}. The purpose of this correction factor is to allow for the effect of M–Cl bond covalency within the octahedral complex: covalency reduces the spin density from the value of three expected for a purely ionic complex featuring a d^3 metal atom. We assume for simplicity that the extent of M–Cl bond covalency within the mixed-group dimer is similar to that found for the octahedral complex. This assumption ignores the distorting effect of electron transfer between the two metal atoms within the dimer, but we have previously found that this assumption holds very well within same-group dimers, and within the set of mixed-group dimers described here the sum of the adjusted $\rho(M')$ and $\rho(M'')$ values is always within $\pm 5\%$ of the value of 4.0 expected for the $S=2$ state, while for the $S=3$ state there are only two instances (Mo/Mn and W/Mn) where $\rho(M')+\rho(M'')$ deviates by more than 5% from the expected value of 6.0. We conclude that the 'covalency correction' to the spin densities is essentially appropriate for the mixed-group dimers.
[41] Stabilization of the $S=3$ minimum is systematically more pronounced for the $M'CrCl_9^{4-}$ than the $M'MnCl_9^{2-}$ complexes. The greater preference for $M'CrCl_9^{4-}$ ferromagnetic complexes than for ferromagnetic $M'MnCl_9^{2-}$ species can be rationalized on the basis of the spin polarization energies (SPE) of the metal atoms involved, particularly the relative SPEs for Cr(III) and Mn(IV) [4]. Note that, while the trend in bare metal ions is to d-orbital contraction with increasing oxidation number, the effect of metal-ligand bond covalency is to offset this trend, and the increase in metal-ligand bond covalency in going from Cr(III) to Mn(IV) is sufficient to ensure that the spin polarization splitting for $MnCl_6^{2-}$ is less than that for $CrCl_6^{3-}$.

PERGAMON

Polyhedron 21 (2002) 1177–1187

POLYHEDRON

www.elsevier.com/locate/poly

Coordination chemistry of a new imine-ether ligand, *N*,*N*′-bis(2-pyridylmethylene)-2,2′-(ethylenedioxy)bis(ethylamine): mono-helical and single-helical-strand coordination modes identified by X-ray crystallography

Ana Tesouro Vallina, Helen Stoeckli-Evans *

Institut de Chimie, Université de Neuchâtel, Avenue de Bellevaux 51, Case Postale 2, CH-2007 Neuchâtel, Switzerland

Received 17 October 2001; accepted 11 February 2002

Abstract

A new Schiff base ligand, *N*,*N*′-bis(2-pyridylmethylene)-2,2′-(ethylenedioxy)bis(ethylamine), **L**, and the complexes, [AgL](BF_4) (**1**), $[Zn_2LCl_4]$ (**2**), $[Hg_2LCl_4]$ (**3**), $[Cd_2LI_4]$ (**4**), $[Ni_2L_3](BF_4)_4$ (**5**), and $[M_2L_3](ClO_4)_4$ with M = Co(II) (**6**) Fe(II) (**7**) and Zn(II) (**8**), have been synthesised and characterised crystallographically and spectroscopically. The silver(I) complex **1** consists of a mono-helical structure where one ligand molecule, coordinating in a tetradentate manner, wraps itself around the Ag(I) ion, giving rise to a distorted tetrahedral arrangement. Single-helical-strand binuclear complexes were obtained with zinc(II), mercury(II) and cadmium(II), **2**, **3** and **4**, respectively. Complexes **2** and **3** are isomorphous and both contain one ligand molecule coordinating to two metal atoms via the two pyridylimine N-atoms. The two remaining coordination sites on the metals are occupied by chlorine atoms. In the fivefold coordinate cadmium(II) complex, **4**, the ligand coordinates in a bis-tridentate manner via the two pyridylimine units and the two oxygen atoms. The two remaining coordination sites on the metals are occupied by iodine atoms. It was possible to combine both coordination modes of the ligand, mono-helical and single-helical-strand, in the isomorphous binuclear octahedrally coordinated nickel(II), cobalt(II), iron(II) and zinc(II) complexes, **5**–**8**, respectively. One ligand molecule is wrapped around each metal ion, which in turn are linked by a third ligand molecule, so forming mono-bridged species. © 2002 Elsevier Science Ltd. All rights reserved.

Keywords: Mono-helical; Single-helical-strand; Mono-bridged species; Coordination chemistry; Transition metals; X-ray crystallography

1. Introduction

The design of new nitrogen-donor multidentate ligands, their metallosupramolecular chemistry and the study of their physical properties are of interest not only from the point of view of their potential applications in areas such as catalysis, magnetism, transport processes, sensors or modelling of biological compounds, but also from a strictly structural point of view. The reactivity of transition metals with electron donor organic molecules has been systematically investigated since the last century and continues to be an important area of research [1–7]. One of the main goals today in coordination chemistry is to synthesise molecules with a predefined geometry. To do this, it would be useful to have a library of ligands and a database concerning their characteristics as far as coordination to transition metals is concerned. In this way molecular fragments could be assembled to produce a whole diversity of compounds with predetermined geometry.

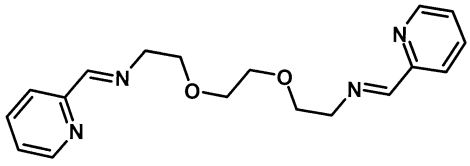
The condensation reaction of an aromatic carbaldehyde with a primary amine has been shown to offer an easy and inexpensive way of forming a variety of bis-bidentate and bis-tridentate Schiff base ligands [8–14]. It has previously been shown that such ligands readily lead to the formation of double and triple binuclear helices [8,9]. Already in 1977 the group of Fenton et al. [15] began a series of studies on what they called 'compartmental ligands'. Later [15b] they prepared a

* Corresponding author. Tel.: +41-32-718-2400; fax: +41-32-718-2511.

E-mail address: helen.stoeckli-evans@unine.ch (H. Stoeckli-Evans).

0277-5387/02/$ - see front matter © 2002 Elsevier Science Ltd. All rights reserved.
PII: S0277-5387(02)01015-X

series of compartmental Schiff bases using pyrrole units and having two dissimilar 'N_2O_2' or 'N_4' donor sites for metal complexation with different bridges. They were used to study the selective preferences of the metal atom and the effect of the bridge extension. Recently, an interesting 'two-compartmental' receptor ligand capable of moving a metal from one site to another by a change of pH was reported [16]. Bridging amino ether units are commonly used for the formation of macro cyclic ligands [17–19] but only a few acyclic related compounds are known [20–22]. The condensation of pyridine-2-carbaldehyde with the bridging amino ether unit, 2,2′-(ethylenedioxy)bis(ethylamine), resulted in the formation of a new N_4O_2 Schiff base. This is the pyridine analogue of ligand H_2L_8 of reference [15b], which was formed by the condensation of pyrrole-2-carbaldehyde and the same bridging amino ether unit. Lam et al. [22] have recently described the formation of mono-helical zinc(II) and europium(II) complexes of a similar ligand formed by the reaction of 3-(pyridine-2-yl)pyrazole with the same bridging amino ether unit.



L

Here we describe some examples of the coordination chemistry of ligand *N*,*N*′-bis(2-pyridylmethylene)-2,2′-(ethylenedioxy)bis(ethylamine) (**L**) and the characterisation of the different complexes formed, by spectroscopic and crystallographic means.

2. Experimental

2.1. Materials and general methods

All chemicals were used as received without further purification. ^{1}H and ^{13}C NMR spectra were recorded on a Bruker AMX-400 (400 MHz) in CD_3OD. Infrared spectra were measured using a Perkin–Elmer FT IR 1720X spectrometer using KBr pellets. The elemental analysis were carried out by the Ecole d'ingénieurs de Fribourg, Switzerland. No elemental analyses were available for compounds containing Hg, Cd or ClO_4^-. Electron impact (EI) mass spectra were obtained using a DELSI-NERMAG R30-10 system. Electrospray (ESI) mass spectra were performed using a BRUKER FTMS 4.7T BioAPEX II system by the MS-Service at the University of Fribourg. UV–Vis spectrophotometric titration measurements were carried out using a Spectramax-250 Plate Reader (equiped with 96-well microtiter plates) at the Department of Chemistry and Biochemistry, University of Bern. The results were analysed using SOFTMAXPRO 2.2.1 and EXCEL 2000.

Caution! Although no problems were encountered in the present study, perchlorate salts are potentially explosive and should be handled in small quantities with the necessary precautions.

2.2. Synthesis of *N*,*N*′-bis(2-pyridylmethylene)-2,2′-(ethylenedioxy)bis(ethylamine) (*L*)

Pyridine-2-carboxaldehyde (20.93 mmol, 2 ml) was added drop-wise to a solution of methanol (50 ml) containing 2,2′-(ethylenedioxy)bis(ethylamine) (10.46 mmol, 1.53 ml). The mixture was heated at reflux with stirring for 4 h. Removal of solvent under vacuum yielded **L** as a yellow–brown oil which was dried under vacuum for several hours (yield: 3.34 g, 98.0%). ^{1}H NMR (CD_3OD, 400 MHz, ppm): see Table 6. ^{13}C NMR (CD_3OD, 400 MHz, ppm): 163.65, 154.11, 149.28, 137.66, 125.65, 121.79, 70.51, 70.24, 60.65. IR (KBr pellet, cm^{-1}): 2863 (vs), 1651 (s), 1588 (vs), 1568 (m), 1469 (s), 1436 (s), 1353 (m), 1294 (w), 1122 (vs), 993 (m), 776 (s), 618 (m). MS (EI, 70 eV), *m*/*z* (%): 349.3 (LNa+), 327.4 (LH+), 238.3, 219.1, 175.1, 134.1, 106.2. *Anal.* for $C_{18}H_{22}N_4O_2$ (326.39 g mol^{-1}) calc. C 66.24, H 6.80, N 17.16. Found: C 66.00, H 7.09, N 17.17%.

2.3. Synthesis of [*AgL*](*BF*$_4$) (*1*)

$AgBF_4$ (0.1704 mmol, 0.0332 g) in MeOH (15 ml) was slowly added to a methanolic (5 ml) solution of **L** (0.1704 mmol, 0.5 ml of a 0.341 M solution), under N_2 and protected from the light. The colour of the reaction mixture changed immediately to yellow. The solution was refluxed for 2 h and then left undisturbed in the dark for at least 2 weeks, whereupon yellow–green crystals were formed. ^{1}H NMR (CD_3OD, 400 MHz, ppm): see Table 6. IR (KBr pellet, cm^{-1}): 1648 (m), 1589 (s), 1479 (w), 1438 (m), 1308 (m), 1225 (w), 1055 (s), 938 (w), 777 (m), 631 (w). *Anal.* for [AgL](BF$_4$)·2(H_2O)(635.01 g mol^{-1}): calc. C 38.81, H 4.70, N 10.06. Found: C 38.85, H 4.10, N 9.75%.

2.4. Synthesis of [*Zn*$_2$*LCl*$_4$] (*2*)

A very dilute solution of **L** (ca. 0.1 mmol in 10 ml CH_2Cl_2) was introduced into a glass tube and layered with approximately 2 ml MeOH as a buffer zone. A dilute solution of $ZnCl_2$ (ca. 0.25 mmol in 10 ml MeOH) was then added very slowly to avoid possible mixing. The glass tube was sealed and left at room temperature (r.t.). After 2 days pale-yellow plate-like crystals were obtained at the interface of the two solutions. IR (KBr pellet, cm^{-1}): 1654 (s), 1599 (vs), 1474 (m), 1445 (s), 1298 (s), 1222 (m), 1121 (s), 1111 (vs), 1099 (vs), 1091 (s),

1017 (s), 942 (m), 781 (s), 642 (m). *Anal.* for $[Zn_2LCl_4](CH_2Cl_2)\cdot 1/2(MeOH)$ (699.93 g mol^{-1}): calc. C 33.10, H 3.84, N 7.94. Found: C 33.53, H 3.67, N 8.24%.

2.5. Synthesis of $[Hg_2LCl_4]$ (3)

A very dilute solution of **L** (ca. 0.1 mmol in 10 ml CH_2Cl_2) was introduced into a glass tube and layered with about 2 ml MeOH as a buffer zone. A dilute solution of $HgCl_2$ (ca. 0.25 mmol in 10 ml MeOH) was then added very slowly to avoid possible mixing. The glass tube was sealed and left at r.t. After 2 days light-yellow plate-like crystals were obtained at the interface of the two solutions. IR (KBr pellet, cm^{-1}): 1658 (s), 1591 (s), 1472 (m), 1438 (s), 1299 (s), 1220 (m), 1118 (vs), 1106 (s), 1081 (s), 1025 (m), 1010 (m), 930 (m), 784 (s), 636 (m).

2.6. Synthesis of $[Cd_2LI_4]$ (4)

A very dilute solution of **L** (ca. 0.1 mmol in 10 ml CH_2Cl_2) was introduced into a glass tube and layered with approximately 2 ml MeOH as a buffer zone. A dilute solution of CdI_2 (ca. 0.25 mmol in 10 ml MeOH) was then added slowly to avoid possible mixing. The glass tube was sealed and left at r.t. After 2 days, light-yellow plate-like crystals were obtained at the interface of the two solutions. IR (KBr pellet, cm^{-1}): 1661 (s), 1594 (vs), 1476 (m), 1442 (s), 1302 (s), 1221 (m), 1106 (s), 1091 (vs), 1077 (s), 1012 (m), 934 (m), 925 (m), 779 (s), 638 (m).

2.7. Synthesis of $[Ni_2L_3](BF_4)_4$ (5)

To a solution of **L** (3 equiv., 0.341 mmol, 1 ml of a solution 0.341 M, 30 ml MeOH) was added 0.054 g of $NiCl_2\cdot 6H_2O$ (2 equiv., 0.227 mmol). The colour of the reaction mixture changed immediately to light orange. The solution was refluxed for 2 h. $[NH_4][BF_4]$ (0.0476 g, 4 equiv., 0.454 mmol) were then added. The clear solution was heated for a further 2 h, cooled and filtered to avoid any impurity, and allowed to slowly evaporate. After 1 week, light orange needle-like crystals of the complex were obtained. The same compound was also obtained by slow diffusion of $Ni(BF_4)_2$ in MeOH over $NaClO_4$ in MeOH and **L** in CH_2Cl_2 in a glass tube. IR (KBr pellet, cm^{-1}): 1647 (m), 1599 (s), 1481 (m), 1448 (m), 1308 (m), 1058 (vs), 777 (m), 643 (w). *Anal.* for $[Ni_2L_3](BF_4)_4\cdot(H_2O)$ (1461.8 g mol^{-1}): calc. C 43.83, H 4.77, N 11.36. Found: C 43.89, H 4.25, N 10.86%.

2.8. Synthesis of $[Co_2L_3](ClO_4)_4$ (6)

A solution of **L** (0.423 mmol, 3 ml of a solution 0.141 M, 30 ml MeOH) was slowly added, under N_2, to a solution of $Co(ClO_4)_2\cdot 6H_2O$ (0.282 mmol, 0.1031 g) in 10 ml MeOH. The colour of the reaction mixture changed immediately to deep orange–red and a precipitate appeared in some minutes. Ten ml MeCN were then added in order to dissolve the precipitate. The orange–red clear solution was heated at reflux during 2 h and an excess of $NaClO_4$ in 10 ml MeOH was added (0.211 mmol, 0.03 g). The solution was refluxed for a further 2 h. After filtration, slow evaporation of the solution yielded orange–red rod crystals. The same compound could also be obtained by slow diffusion of a methanolic solution containing a mixture of $Co(ClO_4)_2\cdot 6H_2O$ and $NaClO_4$ over a solution of **L** in CH_2Cl_2. The addition of $LiClO_4$ or $KClO_4$ did not lead to the formation of any crystals. IR (KBr pellet, cm^{-1}): 1645 (m), 1599 (s), 1480 (m), 1447 (m), 1309 (m), 1084 (vs), 776 (m), 623 (s).

2.9. Synthesis of $[Fe_2L_3](ClO_4)_4$ (7)

A solution of **L** (3 equiv., 0.341 mmol, 1 ml of a solution 0.341 M, 30 ml MeOH) was slowly added, under N_2, to a methanolic (50 ml) solution of $Fe(ClO_4)_2\cdot 6H_2O$ (2 equiv., 0.227 mmol, 0.0082 g). The colour of the reaction mixture changed immediately to deep purple. The solution was refluxed for 2 h, filtered to avoid any impurity, diluted with more MeOH and allowed to evaporate slowly. After approximately 2 weeks, very small purple needle-like crystals were obtained. The same compound was also obtained by slow diffusion of $Fe(ClO_4)_2\cdot 6H_2O$ in MeOH over $NaClO_4$ also in MeOH and **L** in CH_2Cl_2 in a glass tube under N_2. IR (KBr pellet, cm^{-1}): 1615 (m), 1599 (w), 1474 (m), 1448 (m), 1302 (m), 1093 (vs), 771 (w), 623 (m).

2.10. Synthesis of $[Zn_2L_3](ClO_4)_4$ (8)

A very dilute solution of **L** (ca. 0.1 mmol in 10 ml CH_2Cl_2) was introduced into a glass tube and layered with approximately 2 ml MeOH as a buffer zone. A dilute solution of $Zn(ClO_4)_2$ (ca. 0.25 mmol in 10 ml MeOH) was then added very slowly to avoid possible mixing. The glass tube was sealed and left at r.t. After approximately 2 weeks, small light-yellow needle-like crystals were obtained at the interface of the two solutions. IR (KBr pellet, cm^{-1}): 1652 (m), 1599 (s), 1482 (m), 1446 (m), 1310 (m), 1093 (vs), 777 (m), 624 (s).

2.11. X-ray data collection, structure solution and refinement

Crystals of compounds **1**, **2**, **4**, **5**, **6**, **7**, and **8** were mounted on a Stoe Imaging Plate Diffractometer System equipped with a one-circle φ goniometer and a graphite-monochromator. Data collection was per-

formed using Mo Kα radiation ($\lambda = 0.71073$ Å). Two hundred exposures (3 min per exposure) were obtained at an image plate distance of 70 mm (resolution D_{min}–D_{max} 14.23–0.87 Å) with $0° < \varphi < 200°$ and with the crystal oscillating through 1° in φ. For compound **3**, a crystal was mounted on a Stoe STADI4 four-circle diffractometer. Intensity data were measured using graphite-monochromated Mo Kα radiation ($\lambda =$ 0.71073 Å). The ω–2θ scan technique was used for data collection in the range $2.97° < \theta < 25.50°$. The cell parameters were determined by a least-squares treatment of the setting angles of 20 reflections, and their equivalents, with $12.5° < \theta < 14.5°$. The intensity of the two standard reflections measured every 60 min was found to decrease by less than 2%. The structures were solved by either Patterson or direct methods using SHELXS-97 [23] and refined by full-matrix least-squares on F^2 with SHELXL-97 [24]. The hydrogen atoms were included in calculated positions and treated as riding atoms using SHELXL-97 default parameters. All non-hydrogen atoms were refined anisotropically. Complex **1** crystallised in the non-centrosymmetric group *Cc* and was refined as a racemic twin [25] (BASF = 0.37(3)). It crystallised with one highly disordered BF_4^- anion with occupancies of 0.5 for all of the fluorine atoms (F1 to F4 and $F1^a$ to $F4^a$). Part of the ligand was also found to be disordered with occupancies of 0.4 and 0.6 for atoms C9, C10 and $C9^a$, $C10^a$, respectively. The thermal parameters for the fluorine atoms were constrained to be equal in the refinement process. Complex **2** was a twinned crystal with more than 40% overlapped reflections. The reflections relating to the major twin component were used for structure analysis. No disorder was observed in compounds **2**, **3** and **4** and an empirical absorption correction using the DIFABS routine in PLATON [26] was applied. One molecule of dichloromethane per molecule of complex was found for structure **4**. For compound **7**, only a very small crystal was available and it was shown to be isomorphous with compounds **5**, **6** and **8**. The number of observed reflections was too small to permit the complete refinement of this compound, nevertheless, the unit cell parameters were refined and the heavy atom and the main backbone atomic positions were located. The structure is not presented in detail. In compounds **5**, **6** and **8**, one ligand (one pyridine ring and the ether chain) molecule presents conformational disorder. The disordered atomic positions were refined with occupancies of 0.47 for **5**, 0.56 for **6** and 0.44 for **8**, and their thermal parameters were constrained to be equal in the refinement process. The two perchlorate anions were also highly disordered. The thermal parameters for the disordered oxygen atoms were constrained to be equal. The Cl–O bond distances as well as some of the N_{im}–C distances, were constrained to their theoretical values. In compound **5**, the BF_4^- anions were highly disordered and were refined with occupancies of 0.5 for the F atoms. Further crystallographic details are summarised in Tables 1 and 2. Selected bond lengths and bond angles are listed in Tables 3–5.

3. Results and discussion

3.1. Spectral characterisation

The formation of ligand **L** was followed by NMR spectroscopy until the complete disappearance of the aldehyde and the amine proton signals (9.83 and 1.63 ppm, respectively). The ^{1}H NMR spectra of **L** displays five sets of resonances in the aromatic region (Table 6). As the ligand is symmetrical each set of resonances was assigned to a given pair of equivalent H's; one for the imine H's and four for the pyridine H's (ddd (Ha), ddd (Hb), ddt (Hc) and td (Hd)). Two supplementary signals were observed in the CH_2 region, in the form of a multiplet and a singlet, corresponding to the alkane chain protons. The ^{1}H NMR spectrum for the silver complex (**1**) is compared with the corresponding spectrum of the free ligand in Table 6. The ^{1}H NMR spectrum of **1** shows five signals in the aromatic region for the symmetrically coordinated ligand **L** and two more resonance sets in the CH_2 region. The signals were displaced to higher or lower chemical shifts depending on the H-atom. The largest displacement was found, as expected, for the imine hydrogen atom signal due to the coordination of the N_{im}-atom to the metal. Compounds **2**, **3** and **4** were insoluble in all common organic solvents.

The infrared spectra for ligand **L** and compounds **1**–**8** exhibit the characteristic imine, C–N, C–C(pyridine) and C–O–C vibrational frequencies. A small (ca. 10–15 cm^{-1}) shift to higher or lower frequencies was observed in the metal complexes compared with the corresponding frequencies for the free ligand. For compounds **5**–**8**, the vibrational bands of the perchlorate or BF_4^- anions (very strong for all four compounds) overlapped with the C–O–C bands. The perchlorate bands were found in the region of 1084–1093 cm^{-1}, and for the BF_4^- anion at 1058 cm^{-1}, showing typical values for uncoordinated anions.

Complexes **1**, and **5**–**8**, were soluble in several organic solvents, such as methanol and acetonitrile. The positive ESI MS spectrum of **1** in acetonitrile indicated the presence of only one peak at *m*/*z* 435, and was assigned to cation $[AgL]^+$, which corresponds to the solid state cation. The positive ESI MS spectra of **7** and **8** in acetonitrile, and **5** and **6** in methanol–acteonitrile, appear to be more complicated. Each spectrum is composed of several peaks of different intensity. The cation $\{[ML](ClO_4)\}^+$ could clearly be identified in the respective spectra, at *m*/*z* 483 for **5**, 484 for **6**, 481 for **7**,

Table 1
Crystallographic data for complexes **1**, **2**, **3** and **4**

	[AgL](BF$_4$) (**1**)	[Zn$_2$LCl$_4$] (**2**)	[Hg$_2$LCl$_4$] (**3**)	[Cd$_2$LI$_4$] (**4**)
Formula	$C_{18}H_{22}N_4O_2Ag\cdot BF_4$	$C_{18}H_{22}N_4O_2Zn_2Cl_4$	$C_{18}H_{22}N_4O_2Hg_2Cl_4$	$C_{18}H_{22}N_4O_2Cd_2I_4\cdot CH_2Cl_2$
Formula mass	521.08	598.95	869.39	1143.73
Crystal system	monoclinic	triclinic	triclinic	monoclinic
Space group	*Cc*	$P\bar{1}$	$P\bar{1}$	*C*2/*c*
a (Å)	10.151(1)	7.149(1)	7.200(10)	13.325(1)
b (Å)	13.834(1)	7.750(1)	7.856(8)	9.040(1)
c (Å)	15.590(1)	12.434(2)	12.733(2)	26.556(2)
α (°)	90	73.13(2)	72.40(9)	90
β (°)	105.29(1)	79.46(2)	80.53(10)	97.03(1)
γ (°)	90	64.99(2)	64.91(8)	90
V (Å^3)	2111.9(2)	596.0(2)	621.2(4)	3174.9(4)
Z	4	2	2	4
T (K)	223(2)	153(2)	233(2)	153(2)
Crystal size (mm)	0.50 × 0.40 × 0.30	0.35 × 0.15 × 0.10	0.46 × 0.30 × 0.04	0.50 × 0.18 × 0.05
D_{calc} (g cm^{-3})	1.639	1.669	2.324	2.393
μ (mm^{-1})	1.01	2.48	12.80	5.42
T_{min}/T_{max}		0.386/0.788	0.123/0.592	0.446/0.583
Independent reflections	3534	1228	2317	2680
Observed reflections	3146, $I > 2\sigma(I)$	786, $I > 2\sigma(I)$	1893, $I > 2\sigma(I)$	1665, $I > 2\sigma(I)$
R_1 [a]	0.0361	0.0401	0.0533	0.0416
wR_2 [b]	0.0943	0.0991	0.1290	0.0981
Res. dens. (e Å^{-3})	0.441/−0.544	0.379/−0.316	1.542/−1.980	1.142/−1.062

[a] R_1 (observed reflections) $= \Sigma||F_o|-|F_c||/\Sigma|F_o|$.
[b] wR_2 (observed reflections) $= [\Sigma w(|F_o^2|-|F_c^2|)^2/\Sigma wF_o^4]^{1/2}$.

and 489 for **8**. For **5**, the ClO_4^- anion comes from the $NaClO_4$ used during the diffusion reaction. Peaks at *m*/*z* 634 for **5** and 644 for **7** were assigned to species $\{[Ni_2L_3](BF_4)_2\}^{2+}$ and $\{[Fe_2L_3](ClO_4)_2\}^{2+}$, respectively, which correspond to the solid state cations. In **6**, the same aggregate species, *m*/*z* 612, $\{[Co_2L_3](BF_4)(MeO)\}^{2+}$, incorporates a methoxy group instead of a second BF_4 or a perchlorate. In **5** and **7**, peaks at *m*/*z* 797 and 807, respectively, were assigned to $\{[NiL_2](BF_4)\}^+$ and $\{[FeL_2](ClO_4)\}^+$. For **8**, a medium

Table 2
Crystallographic data for complexes **5**, **6**, **7** and **8**

	[Ni$_2$L$_3$](BF$_4$)$_4$ (**5**)	[Co$_2$L$_3$](ClO$_4$)$_4$ (**6**)	[Fe$_2$L$_3$](ClO$_4$)$_4$ (**7**)	[Zn$_2$L$_3$](ClO$_4$)$_4$ (**8**)
Formula	$C_{54}H_{66}N_{12}O_6Ni_2B_4F_{16}$	$C_{54}H_{66}N_{12}O_{22}Co_2Cl_4$	$C_{54}H_{66}N_{12}O_{22}Fe_2Cl_4$	$C_{54}H_{66}N_{12}O_{22}Zn_2Cl_4$
Formula mass	1443.80	1494.84	1488.67	1507.72
System	monoclinic	monoclinic	monoclinic	monoclinic
Space group	*C*2/*c*	*C*2/*c*	*C*2/*c*	*C*2/*c*
a (Å)	18.645(1)	18.635(1)	18.637(3)	18.567(1)
b (Å)	19.801(1)	19.864(1)	19.987(3)	19.956(2)
c (Å)	17.513(1)	17.721(1)	17.340(2)	17.679(1)
α (°)	90	90	90	90
β (°)	99.40(1)	97.28(1)	99.20(2)	100.09(1)
γ (°)	90	90	90	90
V (Å^3)	6379.1(7)	6506.9()	6376.2(2)	6449.1(8)
Z	4	4	4	4
T (K)	223(2)	153(2)	223(2)	293(2)
Crystal size (mm)	0.40 × 0.15 × 0.13	0.60 × 0.13 × 0.10	0.50 × 0.10 × 0.10	0.60 × 0.10 × 0.10
D_{calc} (g cm^{-3})	1.503	1.526	1.551	1.553
μ (mm^{-1})	0.70	0.76	0.71	1.00
Independent reflections	5868	6298	5998	6193
Observed reflections	2480, $I > 2\sigma(I)$	2824, $I > 2\sigma(I)$	537, $I > 2\sigma(I)$	2036, $I > 2\sigma(I)$
R_1 [a]	0.0912	0.0809		0.0723
wR_2 [b]	0.2446	0.2117		0.1773
Res. dens. (e Å^{-3})	1.010/−0.578	1.188/−0.744		1.225/−0.437

[a] R_1 (observed reflections) $= \Sigma||F_o|-|F_c||/\Sigma|F_o|$.
[b] wR_2 (observed reflections) $= [\Sigma w(|F_o^2|-|F_c^2|)^2/\Sigma wF_o^4]^{1/2}$.

Table 3
Selected bond lengths (Å) and bond angles (°) for [AgL](BF$_4$) (**1**)

Bond lengths	
Ag1–N1	2.385(5)
Ag1–N2	2.277(5)
Ag1–N3	2.410(6)
Ag1–N4	2.251(5)
Bond angles	
N1–Ag1–N2	72.49(17)
N1–Ag1–N3	105.74(15)
N1–Ag1–N4	125.99(16)
N2–Ag1–N3	123.12(17)
N2–Ag1–N4	154.37(17)
N3–Ag1–N4	72.57(17)

Table 4
Selected bond lengths (Å) and bond angles (°) for complexes **2**, **3**, **4**

	[Zn$_2$LCl$_4$] (**2**)	[Hg$_2$LCl$_4$] (**3**)	[Cd$_2$LI$_4$] (**4**)
Bond lengths			
M–M [a]	7.409(2)	7.429(9)	6.664(1)
M–N1	2.136(7)	2.436(13)	2.373(7)
M–N2	2.055(6)	2.297(11)	2.293(7)
M–X1 [b]	2.216(2)	2.381(4)	2.713(1)
M–X2 [b]	2.231(2)	2.428(5)	2.714(1)
M···O1	2.705(5)	2.823(10)	2.666(5)
Bond angles			
N2–M–N1	78.6(3)	70.5(4)	70.9(2)
N2–M–X1	122.14(17)	121.5(3)	127.04(17)
N1–M–X1	109.39(17)	114.0(3)	99.88(17)
N2–M–X2	115.32(16)	113.4(3)	119.54(17)
N1–M–X2	101.20(18)	99.3(3)	110.18(15)
X1–M–X2	118.51(10)	122.20(16)	112.62(3)
N1–M–O1	147.90(22)	135.12(32)	138.07(21)
N2–M–O1	70.24(23)	66.39(36)	67.41(22)
X1–M–O1	93.83(13)	98.89(22)	101.11(13)
X2–M–O1	85.85(13)	86.85(23)	94.45(11)

[a] Symmetry operation for **2**: $-x+2$, $-y+1$, $-z+2$; for **3**: $-x+1$, $-y+2$, $-z+1$; for **4**: $-x+1$, y, $-z+3/2$.
[b] X = Cl$^-$ for **2** and **3**, X = I$^-$ for **4**.

intensity peak at m/z 1083 was assigned to a binuclear species $\{[Zn_2L_2](ClO_4)_3\}^+$.

UV–Vis spectrophotometric titrations of ligand **L** in ethanol ([**L**] = 125 μm) were carried out with the metal salts, $AgNO_3$, $Co(BF_4)_2\cdot 6H_2O$, $Fe(ClO_4)_2\cdot 6H_2O$, $Zn(ClO_4)_2$, and $Ni(ClO_4)_2\cdot 6H_2O$. The metal concentration was varied from 0 to 300 μM in eight steps. Upon addition of $AgNO_3$ the ligand π–π* band at 270 nm was progressively displaced to 280 mm. The presence of an isosbestic point at 265 mm was indicative of a clean reaction. In the case of Ni^{2+}, Co^{2+} and Zn^{2+} the ligand band was shifted to 280–285 mm but the isosbestic point at approximately 270 nm was poorly defined. Titration with $Fe(ClO_4)_2\cdot 6H_2O$ was carried out with the metal concentration varying from 0 to 300 μM in 31 steps. The spectra are shown in Fig. 1. An intense band in the UV region due to the ligand π–π* transitions was observed,

Table 5
Selected bond lengths (Å) and bond angles (°) for complexes **5**, **6** and **8**

	[Ni$_2$L$_3$](BF$_4$)$_4$ (**5**)	[Co$_2$L$_3$](ClO$_4$)$_4$ (**6**)	[Zn$_2$L$_3$](ClO$_4$)$_4$ (**8**)
Bond lengths			
M–M^{a} [a]	7.988(2)	7.859(2)	8.055(2)
M–N1	2.108(6)	2.148(5)	2.181(7)
M–N2	2.127(6)	2.148(5)	2.191(6)
M–N3	2.081(7)	2.131(6)	2.177(6)
M–N4	2.067(7)	2.115(5)	2.138(7)
M–N5	2.100(8)	2.116(8)	2.178(8)
M–N6	2.075(7)	2.133(6)	2.161(7)
Bond angles			
N1–M–N2	78.0(2)	77.2(2)	76.2(2)
N1–M–N3	91.2(2)	92.2(2)	92.7(2)
N1–M–N4	91.4(3)	91.9(2)	91.1(3)
N1–M–N5	94.5(3)	97.5(3)	95.1(3)
N1–M–N6	170.8(2)	171.9(2)	169.0(3)
N2–M–N3	97.7(2)	98.7(2)	96.5(2)
N2–M–N4	169.0(3)	168.5(2)	166.0(2)
N2–M–N5	86.5(2)	84.6(2)	87.3(2)
N2–M–N6	94.8(2)	96.3(2)	94.8(3)
N3–M–N4	79.2(3)	78.1(2)	77.9(3)
N3–M–N5	173.5(3)	170.2(3)	171.9(3)
N3–M–N6	95.5(3)	93.4(3)	94.7(3)
N4–M–N5	97.5(3)	100.4(2)	99.9(3)
N4–M–N6	95.9(3)	94.9(2)	98.4(3)
N5–M–N6	79.2(3)	77.1(3)	77.9(3)

[a] Symmetry operation: $-x+1$, y, $-z+3/2$. M and M^a are the respective metal centres.

Table 6
Comparison of ^{1}H NMR data [a] for **L** and complex [AgL](BF$_4$) (**1**)

	Chemical Shifts (δ, ppm)	
	L	[AgL](BF$_4$) (**1**)
Ha	8.62 [ddd, ^{3}J(a,b) = 4.9, ^{4}J(a,c) = 1.7, ^{5}J(a,d) = 1.0, 2H]	8.53 [ddd, ^{3}J(a,b) = 4.8, ^{4}J(a,c) = 1.6, ^{5}J(a,d) = 0.8, 2H]
Hb	7.48 [ddd, ^{3}J(b,c) = 7.5, ^{3}J(b,a) = 4.9, ^{4}J(b,d) = 1.2, 2H]	7.67 [ddd, ^{3}J(b,c) = 7.7, ^{3}J(b,a) = 4.8, ^{4}J(b,d) = 1.2, 2H]
Hc	7.90 [ddt, ^{3}J(c,d) = 7.9, ^{3}J(c,b) = 7.5, ^{4}J(c,a) = 1.7, ^{5}J(c,e) = 0.5, 2H]	8.13 [dt, ^{3}J(c,d) = 7.7, ^{3}J(c,b) = 7.7, ^{4}J(c,a) = 1.6
Hd	8.01 [td, ^{3}J(d,c) = 7.9, ^{4}J(d,b) = 1.2, ^{5}J(d,a) = 1.0, 2H]	7.87 [td, ^{3}J(d,c) = 7.7, ^{4}J(d,b) = 1.2, ^{5}J(d,a) = 0.8, 2H]
He	8.36 (s, broad, 2H)	8.70 (s, broad, 2H)
Hf	3.64 (s, broad, 4H)	3.62 (s, broad, 4H)
Hg,h	3.79 (m, 8H)	3.95 (m, 8H)

[a] Bruker AMX-400 (400 MHz), solvent CD_3OD.

and the metal-to-ligand charge-transfer (MLCT) bands were observed in the Visible region of the spectrum. During the titration, the ligand band was gradually displaced to 280 nm and suffered a hyperchromic effect. A new band appeared at 349 nm and increased in intensity with increasing concentration of Fe^{2+}. Finally a new band emerged at 562 nm and increased in

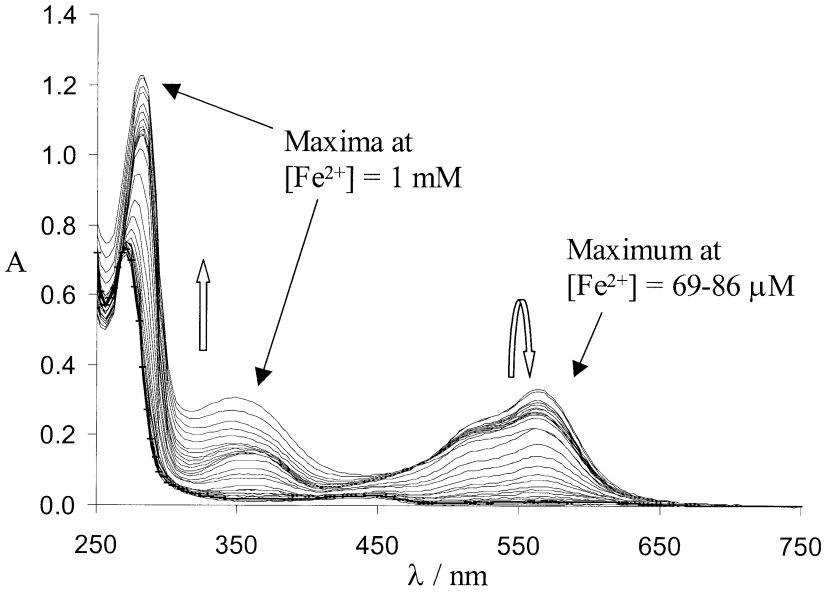


Fig. 1. Spectrophotometric titration of **L** with Fe^{2+} in EtOH.

intensity until the metal concentration reached 69 μM. On continued addition of Fe^{2+} the absorption maximum decreased until the [Fe^{2+}] was 86 μM, after which it decreased only slightly. The diminution in intensity became more pronounced for concentrations greater than 108 μM. This was associated with a net decrease in the intensity of the purple colour of the solution. An isosbestic point appeared at 268 nm, until the metal concentration reached 69 μM. With increasing metal concentration it disappeared, but then a second isosbestic point appeared at 478 nm. This could be indicative of a switch from one species to another. The metal concentration of 69–86 μM corresponds approximately to a M:L ratio of 2:3, which is the same ratio found for the deep purple solid-state species $[Fe_2L_3]^{4+}$. The following solution equilibria can be proposed:

$$2Fe^{2+} + 3L \rightleftharpoons [Fe_2L_3]^{4+} + Fe^{2+} \rightleftharpoons 3[FeL]^{2+}$$

Admitting that the concentration of the $[Fe_2L_3]^{4+}$ species is approximately 3.45×10^{-5} (half of 69 μM) and with $l = 0.5$ cm, a ε value of approximately 19 400 at $\lambda = 562$ nm can be estimated [27]. Compound **7** contains two Fe^{2+} ions; hence the ε value per Fe^{2+} ion is approximately 9700. This can be compared with the value of 11 000 at 510 nm found for the d^6 low-spin mononuclear complex tris–phenanthroline–iron(II) [28]. Hence, it is reasonable to suppose that the Fe^{2+} ion is also in the low-spin state. This is also in agreement with the short Fe–N_{py} bond distances, typical for low-spin iron(II), observed in the solid-state structure (see Table 9). This type of Schiff base ligand does indeed induce high *ligand fields* around the metal and hence it is reasonable to propose that the metal is mainly in the low-spin state. The ^{1}H NMR spectrum of complex **7** (purple crystals in CD_3OD) was poorly resolved. This may be due to the coexistence in solution of both low- and high-spin species.

3.2. X-ray crystallography

3.2.1. Structure of [AgL](BF$_4$) (1)

The reaction of **L** with $AgBF_4$ in a 1:1 ratio lead to the formation of a mononuclear complex. The structure can be considered as a mono-helical complex with the silver atom encapsulated by a single ligand molecule (Fig. 2).

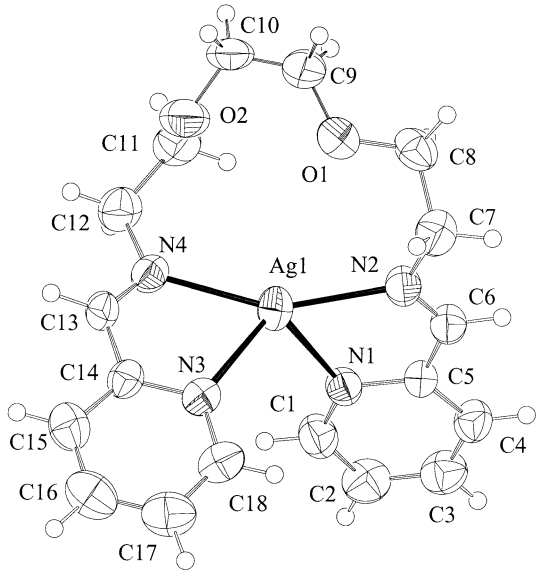


Fig. 2. The molecular structure of cation $[AgL]^+$ (**1**) showing the crystallographic numbering scheme and thermal ellipsoids at 50% probability level.

A number of examples of mono-helical complexes with different ligand molecules have been published [22,29–33]. The silver atom has a distorted tetrahedral geometry and is coordinated to the two pyridylimine units of one ligand molecule. Selected bond distances and bond angles are given in Table 3. The N_{py}–Ag–N_{im} bite angles are very narrow, 72.5(2)°. The average Ag–N_{py} bond length of 2.398(4) Å is significantly longer than the standard value of 2.299 Å [34], while the average Ag–N_{im} bond distance of 2.264(4) Å, is considerably shorter than the standard value for Schiff bases, 2.403 Å [34], see Table 3. The helicity is caused by a twist of **L** about the very flexible C–O–C–C–O–C chain linking the two pyridylimine units. Selected dihedral angles are given in Table 7. The complex crystallises in a non-centrosymmetric space group and in the crystal the molecules stack up the *b*-axis. Molecules with one sense of chirality stack in the one direction (> > > > >) while those with the opposite sense of chirality stack in the opposite direction (< < < < <).

3.2.2. Structure of compounds $[M_2LX_4]$, where M = Zn(II) for 2, Hg(II) for 3 and Cd(II) for 4 and X = Cl^- for 2 and 3 and I^- for 4

The reaction of **L** with $ZnCl_2$, $HgCl_2$ and CdI_2, using diffusion techniques (see Section 2) and in dilute conditions, gave in a few days, crystals of these centrosymmetric binuclear complexes (Figs. 3 and 4). Their overall structures can be considered as single-helical-strand, as clearly illustrated in Fig. 4 for complex **4**. In **2** and **3**, which are isomorphous, the metal atoms (Zn(II) and Hg(II), respectively) are four-coordinate with very distorted tetrahedral geometry and are coordinated to one pyridylimine unit and to two chlorine atoms (Fig. 3). Selected bond distances and bond angles are given in Table 4, and select dihedral angles and inter-planar distances in Table 7. The five-membered chelate pyridylimine ring forces the bond angle, N_{py}–M^{2+}–N_{im}, to be almost 70°, much smaller than the theoretical value of 109° for an ideal tetrahedron. In **2**, the Zn to O1 distance is very long, 2.705(5) Å, compared with the typical Zn–O bonding distance of 2.093 Å [34]. In **3**, it is reasonable to consider that the O-atom participates in the coordination sphere of the metal as the Hg–O distance of 2.823(10) Å is comparable to the literature values of 2.825, 2.909 and 2.935 Å [34]. In **4** the Cd atom is five-coordinate with a distorted square-pyramidal coordination geometry (Fig. 3(a)). Here the Cd-atom adds to its coordination sphere the ether function of the ligand, distance Cd–O is 2.666(5) Å. This is only slightly longer than the standard Cd–O distance of 2.569 Å [34]. The trigonality index τ is 0.42, indicating that the coordination geometry around the Cd^{2+} ion can be described as half-way between an ideal square-pyramidal geometry ($\tau = 0$) and an ideal trigonal-bipyramidal geometry ($\tau = 1$) [35]. The structures of **2** and **3** differ from that of **4** in their overall conformation. In **2** and **3**, the two pyridine rings are strictly parallel while in **4** the bridge is more twisted and the pyridine rings are almost perpendicular to one another (see Table 7). Compound **4** is also more compact than compounds **2** and **3** with the metal centres being separated by 6.645(1) Å in **4** compared with 7.409 (2) Å in **2**, 7.429 (9) Å in **3**. In all three compounds the pyridylimine unit is nearly planar. The pyridine and chelate ring dihedral angles are less than 4°, and the metal atoms are displaced by less than 0.25 Å from the mean plane of the pyridine ring (Table 7).

Table 7
Selected dihedral angles (*t*, °) and inter-planar distances (*d*, Å) for **1**, **2**, **3** and **4**

	[AgL](BF$_4$) (**1**) [a]	[Zn_2LCl_4] (**2**) [b]	[Hg_2LCl_4] (**3**)	[Cd_2LI_4] (**4**)
t (py_1–py_2)	74.6(2)			
t (py_1–che_1)	1.6(3)			
t (py_2–che_2)	9.3(3)			
t (py–py [c])		0.0(4)	0.0(7)	89.4(3)
t (py–che)		3.7(3)	3.0(6)	4.3(5)
d (py–py [c])		2.61(4)	3.18(7)	5.53(4)
d (py–M)		0.18(1)	0.15(2)	0.23(1)
d (py–M [c])		2.44(3)	3.02(5)	3.45(3)

[a] che_1 chelate rings Ag1–N1–C5–C6–N2; che_2 chelate ring Ag1–N3–C14–C13–N4. py1 N1,C1–5; py2 N3,C14–18.
[b] Complexes **2** and **3** are isomorphous.
[c] Symmetry operations: for **2:** $-x+2$, $-y+1$, $-z+2$; for **3:** $-x+1$, $-y+2$, $-z+1$; for **4:** $-x+1$, y, $-z+3/2$. py = pyridine ring, che chelate ring M–N1–C5–C6–N2; M is the respective metal centre.

3.2.3. Structure of compounds $[M_2L_3](X)_4$, where M = Ni(II) for 5, Co(II) for 6, Fe(II) for 7 and Zn(II) for 8 and X = BF_4^- for 5 and ClO_4^- for 6, 7 and 8

The four compounds were obtained either by refluxing a methanolic solution containing 3 equiv. of **L** with 2 equiv. of the correspondent metal salt or by slow diffusion of a methanolic solution of the metal salt into a solution of **L** in dichloromethane. Complexes **5**–**8** have a metal-to-ligand ratio of 2:3 and were obtained even when this ratio was varied. They combine the two coordination modes observed for complexes **1** and **2**–**4**, that is mono-helical and single-helical-strand (see Fig. 5) for complex **8**. One ligand molecule is wrapped around each metal ion, which in turn are linked by a third ligand molecule, giving rise to mono-bridged species. In this way, the metal is coordinated to three pyridine N-atoms and three imine N-atoms. Selected bond distances and bond angles are given in Table 5 and select dihedral angles and inter-plane distances in Table 8. The metals are octahedrally coordinated with distorted octahedral geometry. The distortion is essentially due to the narrow N_{py}–M–N_{im} bite angles (ca. 77°) imposed by the ligand.

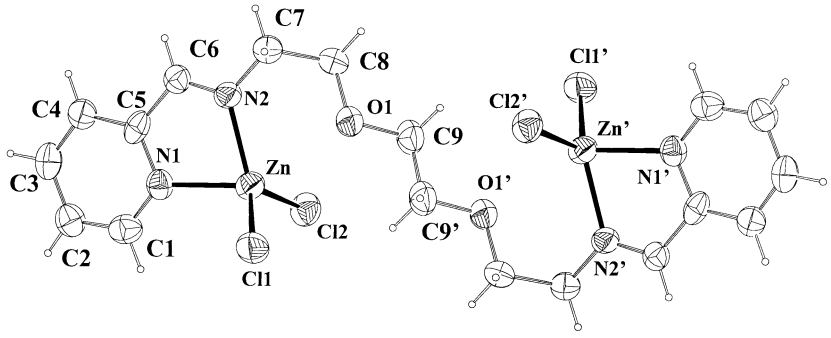


Fig. 3. The molecular structure of complex $[Zn_2LCl_4]$ (**2**), showing the crystallographic numbering scheme and thermal ellipsoids at 50% probability level. (See Table 4 for symmetry operation.)

The metal centres are separated by distances between 7.859(2) and 8.055(2) Å.

It can be seen from Tables 7 and 8 that in complexes **2**–**8**, the metal atoms are only slightly displaced from the best plane through the pyridine rings, and that the pyridine and chelate rings are almost perfectly co-planar, with the dihedral angles varying from 2.6° to 7.1°. The average $C{=}N_{im}$ bond distance of 1.266(4) Å, is close to the standard value of 1.279 Å for a Schiff base system [34]. The average $C_{py}{-}C_{im}$ bond distance, 1.469(4) Å, is close to the standard value of 1.476 Å found for a conjugated system [34]. The $N_{py}{-}M{-}N_{im}$ bite angles vary from 70.5(4)° to 78.6(3)° (see Tables 4 and 5). The standard values [34] for the $Metal{-}N_{py}$ and $Metal{-}N_{im}$ bond distances are compared with the values found in complexes **1**–**8** in Table 9. In the case of complexes **1**–**4** not all the standard values are available. However, it is interesting to note here that the observed $M{-}N_{py}$ bond distances are longer than the standard values and that this trend is reversed for the $M{-}N_{im}$ bond distances. For the first row transition metal complexes, **5**–**8**, the $M{-}N_{py}$ and the $M{-}N_{im}$ bond distances for individual complexes are very similar. However, it can be seen that the $M{-}N_{py}$ bond distances are shorter than the standard values while the $M{-}N_{im}$ bond distances are either similar or longer than the standard values (see Table 9). The difference in the relative M–N bond distances with respect to the standard values, for compounds **1**–**4** compared with compounds **5**–**8**, is probably due to steric overcrowding in the latter.

4. Conclusions

As expected, the ligand **L** was found to be very flexible and reacted readily with transition metals. Two different coordination modes of the ligand were possible; mono-helical and single-helical-strand. Depending on the geometrical preferences of the metal these coordination modes can either be observed separately or combined in the same complex. With silver(I) a mono-helical complex **1** was formed rather than a polymeric structure. With zinc(II), mercury(II) and cadmium(II) single-helical-strand complexes, **2**, **3** and **4**, respectively, were obtained. Finally with the first row transition metals, which favour octahedral coordination, both mono-helical and single-helical-strand coordination modes are present in complexes **5**–**8**. This result was surprising as frequently binuclear complexes

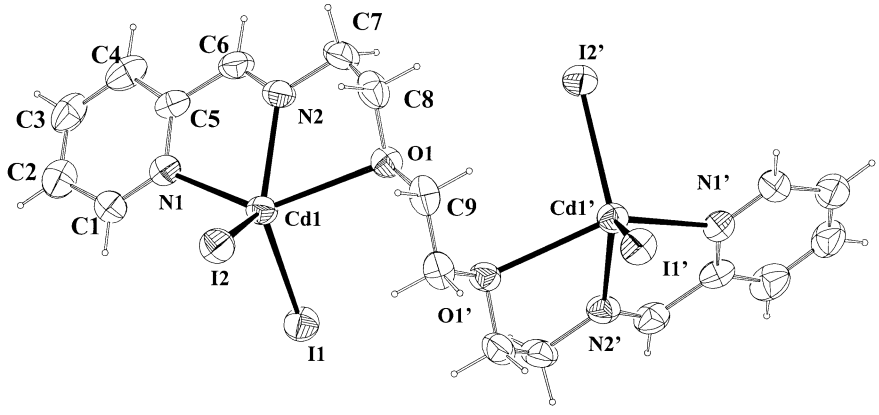


Fig. 4. The molecular structure of the binuclear complex $[Cd_2LI_4]$ (**4**), showing the crystallographic numbering scheme and thermal ellipsoids at 50% probability level. (The solvent molecule was omitted for clarity; see Table 4 for symmetry operation.)

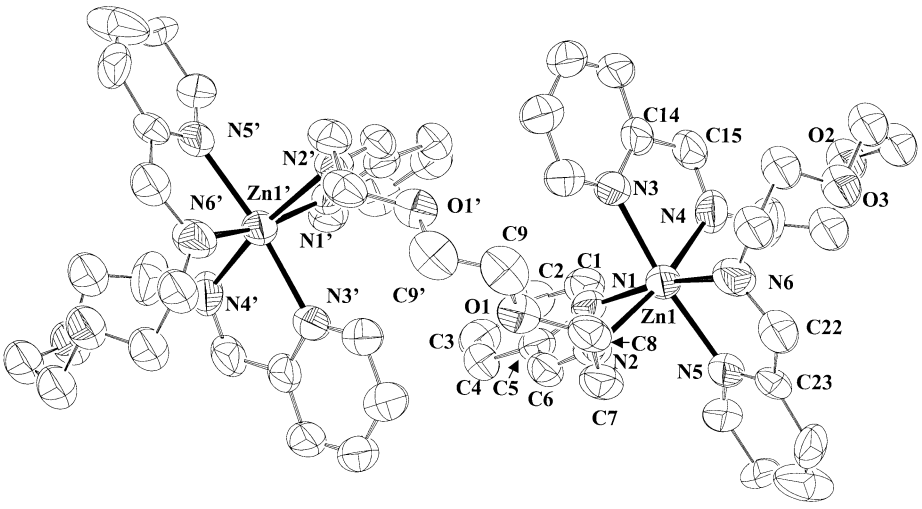


Fig. 5. The molecular structure of cation $[Zn_2L_3]^{4+}$ (**8**), showing the crystallographic numbering scheme and thermal ellipsoids at 50% probability. (The hydrogen atoms have been omitted for clarity; see Table 5 for symmetry operation.)

Table 8
Selected dihedral angles (t, °) and some important distances (d, Å) for **5**, **6** and **8**

	$[Ni_2L_3](BF_4)_4$ (**5**)	$[Co_2L_3](ClO_4)_4$ (**6**)	$[Zn_2L_3](ClO_4)_4$ (**8**)
t (py_1–py_1 [a])	29.6(4)	31.0(3)	30.1(3)
t (py_1–py_2)	86.5(2)	82.4(2)	87.8(2)
t (py_1–py_3)	86.6(4)	82.7(6)	86.4(5)
t (py_2–py_3)	81.3(4)	83.5(6)	79.5(5)
t (py_1–che_1)	4.1(4)	2.6(4)	4.1(4)
t (py_2–che_2)	5.4(5)	7.1(3)	3.5(4)
t (py_3–che_3)	2.2(1.2)	3.1(1.5)	3.2(1.5)
d (py_1–M)	0.15(1)	0.09(1)	0.17(1)
d (py_1–M [a])	4.98(1)	5.20(1)	4.95(1)
d (py_2–M)	0.23(1)	0.32(1)	0.16(1)
d (py_2–M [a])	5.13(1)	5.04(1)	5.18(1)
d (py_3–M)	0.11(2)	0.09(3)	0.14(3)
d (py_3–M [a])	4.92(6)	4.80(8)	5.22(9)

[a] Symmetry operation: $-x+1$, y, $-z+3/2$; py_1 N1,C1–5; py_2 N3,C10–14; py_3 N5,C23–27; che_1 M–N1–C5–C6–N2; che_2 M–N3–C14–C15–N4; che_3 M–N5–C23–C22–N6; when disorder was present, only the mean values are reported.

Table 9
A comparison of $M–N_{py}$ and $M–N_{im}$ bond distances (Å) for compounds **1**–**8**, with standard values [34] given in parentheses

	$M–N_{py}$	$M–N_{im}$
Ag (**1**)	2.385, 2.410(2.299)	2.251, 2.277(2.403)
Zn (**2**)	2.136(2.116)	2.054(2.122)
Hg (**3**)	2.436(2.164)	2.297(–)
Cd (**4**)	2.373(2.381)	2.293(–)
Ni (**5**)	2.081, 2.100, 2.108(2.122)	2.067, 2.075, 2.127(2.051)
Co (**6**)	2.116, 2.131, 2.148(2.185)	2.115, 2.133, 2.148(2.015)
Fe (**7**) [a]	1.945, 1.965, 2.000(1.961) [b]	1.907, 1.911, 2.030(1.958) [c]
Zn (**8**)	2.177, 2.178, 2.181(2.116)	2.138, 2.161, 2.191(2.122)

[a] Approximate values only as the crystal was of very poor quality.
[b] Low-spin 2,2′-bipyridyl (chelating, η^2-bpy).
[c] Low-spin Schiff base (η^1-RN=CR_2).

of this type of ligand, with a M:L ratio of 2:3, and with metals having predilection for octahedral geometry, form triple helical arrangements [8,9]. The flexibility of the central spacer obviously plays an important role and it also appears that the type of complex formed depends upon the counterion used for the reaction. In the case of Zn(II), two different complexes, **2** and **8,** were obtained using chloride or perchlorate, respectively, as counterions. The chloride atoms prefer to coordinate to the metal centre while with $Zn(ClO_4)_2$ the metal prefers to coordinate to the nitrogen atoms only, with an octahedral geometry. Interestingly the mono-helical zinc(II) complex recently obtained by Lam et al. [22] was synthesised using anhydrous $ZnCl_2$ but $NaClO_4$ was later added to the refluxed solution in absolute ethanol. There the zinc atoms are also coordinated to the ether O-atoms with typical Zn–O bond distances of 2.203–2.211 Å. In the case of the pyrrole analogue of **L**, described by Bailey et al. [15b], only a mononuclear copper(II) complex was reported. These studies are being extended to the synthesis of related ligands with different central spacers and chelating units, in order to explore ways in which the ligand flexibility can be controlled.

5. Supplementary material

Crystallographic data (excluding structure factors) for the structures **1**–**8** have been deposited with the Cambridge Crystallographic Data Centre as supplementary

publication nos. CCDC 149607 (**1**), CCDC 149608 (**2**), CCDC 149609 (**3**), CCDC 149610 (**4**), CCDC 149611 (**5**), CCDC 149612 (**6**), CCDC 149613 (**7**—unit cell dimensions only) and CCDC 149614 (**8**). Copies of the data can be obtained free of charge on application to CCDS, 12 Union Road, Cambridge CB2 1EZ, UK (fax: +44-1223-336033; e-mail: deposit@ccdc.cam.ac.uk or www: http://www.ccdc.cam.ac.uk).

Acknowledgements

Financial support from the Swiss National Science Foundation is gratefully acknowledged. We would also like to thank Professor Klaus Bernauer (Neuchâtel) for valuable discussions and the interest he has shown in this work.

References

[1] A.F. Williams, C. Floriani, A.E. Merbach, Perspectives in Coordination Chemistry, VCHA Verlagsgeselleshaft, Weinheim, Germany, 1992.
[2] J.L. Atwood, J.E.D. Davies, D.D. MacNicol, F. Vögtle (Eds.), Comprehensive Supramolecular Chemistry, Vol. 9, J.-P. Sauvage, M. Wais Hosseini (Volume Eds.), Templating Self-assembly and Self-organisation, Pergamon, Oxford, 1996.
[3] J.-M. Lehn, Supramolecular Chemistry—Concepts and Perspectives, VCH Verlagsgeselleshaft, Weinheim, Germany, 1995.
[4] D. Philp, J.F. Stoddart, Angew. Chem., Int. Ed. 35 (1996) 1155.
[5] G.F. Swiegers, T.J. Malefetse, Chem. Rev. 100 (2000) 3483.
[6] C. Piguet, G. Bernadinelli, G. Hopfgartner, Chem. Rev. 97 (1997) 2005.
[7] (a) E.C. Constable, Prog. Inorg. Chem. 42 (1994) 67;
(b) E.C. Constable, in: Comprehensive Supramolecular Chemistry, Vol. 9, J.-P. Sauvage, M. Wais Hosseini (Volume Eds.), Templating Self-assembly and Self-organisation, Pergamon, Oxford, 1996, pp. 213–252;
(c) E.C. Constable, Metals and Ligand Reactivity, VCH Verlagsgeselleshaft, Weinheim, Germany, 1996.
[8] N. Yoshida, K. Ichikawa, Chem. Commun. (1997) 1091.
[9] M.J. Hannon, C.L. Painting, A. Jackson, J. Hamblin, W. Errington, Chem. Commun. (1997) 1807.
[10] M.J. Hannon, S. Bunce, A.J. Clarke, N.W. Alcock, Angew. Chem., Int. Ed. 38 (1998) 1277.
[11] M.R. Bermejo, A. García Deibe, J. Sanmartin, A. Sousa, C.E. Hulme, C.A. McAuliffe, R.G. Pritchard, M. Watkinson, Chem. Commun. (1994) 645.
[12] S. Gourbatsis, S.P. Perlepes, I.S. Butler, N. Hadjuliadis, Polyhedron 18 (1999) 2369.
[13] J.M. Dominguez-Vera, N. Galvez, J.M. Moreno, E. Colacio, Polyhedron 16 (1998) 2713.
[14] F. Franceschi, G. Guillemot, E. Solari, C. Floriani, N. Re, H. Birkedal, P. Pattison, Chem. Eur. J. 7 (2001) 1468.
[15] (a) D.E. Fenton, S.E. Gayda, J. Chem. Soc., Dalton Trans. (1977) 2095;
(b) N.A. Bailey, A. Barrass, D.E. Fenton, M.S. Leal Gonzalez, R. Moody, C.O. Rodriguez de Barbarin, J. Chem. Soc., Dalton Trans. (1984) 2741.
[16] V. Amendola, L. Fabbrizzi, C. Mangano, P. Pallavicini, A. Perotti, A. Taglietti, J. Chem. Soc., Dalton Trans. (2000) 185.
[17] E. Asato, H. Furutachi, T. Kawahashi, M. Mikuriya, J. Chem. Soc., Dalton Trans. (1995) 3897.
[18] I.A. Kahwa, S. Folkes, D.J. Williams, S.V. Ley, C.A. O'Mahoney, G.L. McPherson, J. Chem. Soc., Chem. Commun. (1989) 1531.
[19] M.G.B. Drew, M. McCann, S.M. Nelson, Inorg. Chim. Acta 41 (1980) 213.
[20] M. Mikuriya, Y. Hatano, E. Asato, Bull. Chem. Soc. Jpn. 70 (1997) 2495.
[21] J.R. Hartman, R.W. Vachet, J.H. Callahan, Inorg. Chim. Acta 297 (2000) 79.
[22] M.H.W. Lam, D.Y.K. Lee, S.S.M. Chiu, K.W. Man, W.T. Wong, Eur. J. Inorg. Chem. (2000) 1483.
[23] G.M. Sheldrick, Acta Crystallogr., Sect. A 46 (1990) 467.
[24] G.M. Sheldrick, SHELXL-97, Program for Crystal Structure Refinement, University of Göttingen, Göttingen, Germany, 1997.
[25] H.D. Flack, Acta Crystallogr., Sect. A 39 (1983) 876.
[26] A.L. Spek, Acta Crystallogr., Sect. A 46 (1990) C-34.
[27] Using the Lambert–Beer equation, $A = \varepsilon cl$.
[28] J.O. Edwards, K. Edwards, J. Palma, J. Chem. Ed. 52 (1975) 408.
[29] E. Weber, W. Saenger, F. Vögtle, H. Sieger, Angew. Chem., Int. Ed. Engl. 18 (1979) 226.
[30] N. Beynek, M. McPartlin, B.P. Murphy, I. Scowen, Polyhedron 17 (1998) 2137.
[31] F. Hirayama, V. Zabel, W. Saenger, Acta Crystallogr., Sect. C 41 (1985) 61.
[32] Y.-J. Fu, W.-Y. Sun, W.-N. Dai, M.-H. Shu, F. Xue, D.-F. Wang, T.C.W. Mak, W.-X. Tang, H.-W. Hu, Inorg. Chim. Acta 290 (1999) 127.
[33] Y.-J. Fu, H. Yang, D.-F. Wang, W.-X. Tang, B.-M. Wu, T.C.W. Mak, Polyhedron 16 (1997) 1505.
[34] International Tables for Crystallography C, 2nd ed., Kluwer Academic, Dordrecht, The Netherlands, 1999, pp. 811–875, Table 9.6.3.3.
[35] A.W. Addison, T.N. Rao, J. Reedijk, J. van Rijn, G.C. Verschor, J. Chem. Soc., Dalton Trans. (1984) 1349.

PERGAMON

Polyhedron 21 (2002) 1189–1195

POLYHEDRON

www.elsevier.com/locate/poly

Structure and properties of tetraaquabis(hydrogenmaleato)iron(II)

Rama K. Barman, Rajesh Chakrabarty, Birinchi K. Das *

Department of Chemistry, Gauhati University, Guwahati 781 014, Assam, India

Received 22 October 2001; accepted 6 March 2002

Abstract

The title compound tetraaquabis(hydrogenmaleato)iron(II), $Fe(C_4H_3O_4)_2(H_2O)_4$ (**1**) forms large orange-coloured crystals that are remarkably stable against air-oxidation and weight loss until ~160 °C. Crystal structure analysis of compound **1** has been performed by single crystal X-ray diffraction. The basic octahedral complex consisting of two centrosymmetrically related monodentate hydrogenmaleato ligands and four water molecules coordinated to Fe(II) remains firmly hydrogen-bonded through intra- and inter-molecular interactions to form a robust three-dimensional network structure in the solid state. Comparison between the simulated and experimental powder X-ray diffraction patterns confirms bulk purity of the product. The solid-state UV–Vis–NIR spectrum for this yellow–orange compound shows bands at 227, 383 (broad) and 917 (broad) nm among which the last one is assignable to the expected $^5T_{2g} \rightarrow {}^5E_g$ band for octahedral Fe(II) complexes. The variable temperature magnetic susceptibility measured for compound **1** in the 2–300 K range shows Curie–Weiss behaviour with weak antiferromagnetic interactions occurring at low temperatures as observed from the $\chi_M T$ versus T curve and a Weiss constant of −2.4 K found from the $1/\chi_M$ versus T plot. An aqueous solution prepared by dissolving crystalline samples of **1** is indefinitely stable in air and it is possible to recover **1** from the solution. The yellow–orange solution displays nearly identical redox stability ($E_{1/2} = 0.15$ V vs. Ag/AgCl) with the well-known $Fe(CN)_6^{3-}/Fe(CN)_6^{4-}$ couple. © 2002 Published by Elsevier Science Ltd.

Keywords: Crystal structures; Iron(II) complexes; Hydrogen-bonded network; Hydrogen maleate

1. Introduction

Investigations on the salts of the *cis* and *trans* isomers of 1,4-butenedioic acid are not extensive. Although a few crystal structure analyses on such compounds are available in the literature, the intimate details of the truly intricate structures have remained by and large obscure. These two dicarboxylic acids, maleic and fumaric acid, may bind to a metal ion in either the monoanionic or dianionic form, and given with the possibility of the resulting ligands to act as mono-, bi-, tri-, and tetra-dentate ligands, formation of a variety of compounds displaying a plethora of interesting structures and properties could easily be imagined. In recent times the salts of dicarboxylic acids, including those of fumaric acid, have been found to display porous metal-organic network structures [1].

An example of metal maleate complexes, copper(II) maleate hydrate, is known to display ferromagnetic behaviour resulting from the complicated layered structure of this polymeric compound [2]. In this compound the maleato ligand coordinates in a tetradentate fashion, utilising all four carboxyl oxygen atoms present in the dianion, to produce two-dimensional sheets that finally link through hydrogen bonds to one another to form a three-dimensional structure [3] essential for ferromagnetism [4]. In the case of copper(II) hydrogenmaleate tetrahydrate, the hydrogenmaleate anions remain fully uncoordinated to the metal centre [3a]. Herein we describe the detailed structure and magnetic properties of tetraaquabis(hydrogenmaleato)iron(II), $Fe(C_4H_3O_4)_2(H_2O)_4$ (**1**) where the monoanion of maleic acid acts as a monodentate ligand. Ferrous fumarate is extensively used in commercial medicinal formulations to provide iron supplement to anaemic bodies [5], but the corresponding maleate salt remains largely unknown. On the other hand, several metal hydrogenmaleates, including that of ferrous iron, are known [6,7], but the physico-chemical properties of most of the

* Corresponding author. Tel.: +91-361-570-535; fax: +91-361-570-133.

E-mail address: das_bk@rediffmail.com (B.K. Das).

0277-5387/02/$ - see front matter © 2002 Published by Elsevier Science Ltd.
PII: S0277-5387(02)01002-1

compounds remain unexplored. Although some properties of ferrous hydrogenmaleate tetrahydrate have been previously described [8], the details of its crystal and molecular structure and the correlation of the properties with the structure remain unpublished. In fact, a previous structural report [7] on the compound does not take into account the intermolecular hydrogen-bonding interactions that are likely to play an important role in determining the properties of such metal salt hydrates. To our knowledge, the title compound represents the only structurally characterised example of simple salts or salt hydrates formed by 1,4-butenedioic acid anions with iron in any of its oxidation states. In fact, a search of chemical and structural databases indicates that crystal structure analyses have not so far been published for any complex of iron other than **1** in which either maleato or fumarato ligands remain coordinated to iron through one or more of its oxygen atoms. Compounds of interesting compositions such as calcium tris(maleato)ferrate(III) [9] and $[Fe_3O(OOCCH{=}CHCOOH)_6]OH\cdot 3H_2O$ [10] are known in the literature, but the details of their structure are yet to be published.

2. Experimental

2.1. Materials and methods

All materials were used as obtained from commercial sources. Electrolytic iron powder was purchased from Loba Chemie (India). Infrared (IR) spectrum in the mid-IR region (4000–450 cm^{-1}) was recorded using a Perkin–Elmer 1600 spectrometer. While the solution UV–Vis spectrum was recorded on a Perkin–Elmer Lambda 40 spectrophotometer, the UV–Vis–NIR (200–2600 nm) diffuse-reflectance spectrum for compound **1** in the solid state was obtained using a Shimadzu UV-3101PC scanning Spectrophotometer. $BaSO_4$ powder was used as reference (100% reflectance). Absorption data were calculated from the reflectance data using the Kubelka–Munk function ($a/S = (1-R)^2/2R$ where a is the absorption coefficient, R the reflectance and S the scattering coefficient) [11]. For obtaining the cyclic voltammogram of **1** a computer controlled BAS-100 electrochemical analyser was used. In the three-electrode set-up of the electrochemical cell, the redox potential measured on a platinum microelectrode (in conjunction with a Pt counter electrode) was referenced to an Ag/AgCl electrode. Electrochemical response was measured at 22 °C at the scan rates of 20 and 50 mV s^{-1} for an approximately 10^{-3} M solution of **1** in the presence of $NaClO_4$ (0.1 M) as the supporting electrolyte. Under similar experimental conditions the Fe(III)/Fe(II) couple of potassium hexacyanoferrate(II), was observed at a potential +0.12 V against the Ag/AgCl electrode. Magnetic susceptibility data for **1** were obtained as a function of temperature using an MPMS Quantum Design SQUID magnetometer in the 2–300 °C range. Susceptibility data were corrected for diamagnetism. Details of X-ray crystallographic procedures are given below in a separate section.

2.2. Preparation of $Fe(C_4H_3O_4)_2(H_2O)_4$ (1)

Electrolytic iron powder (0.28 g, 5 mmol) is heated with a solution of maleic acid (1.74 g, 15 mmol) in water (10 ml) under reflux for 2 h to dissolve the iron completely. The resulting solution is filtered and the filtrate is allowed to stand for 24 h at room temperature (r.t.). The orange crystals formed at the bottom of the beaker are filtered off, washed with a small volume of cold water under suction, and dried in air. Yield: 0.76 g (42%). *Anal.* Calc. for $C_8H_{14}O_{12}Fe$: C, 26.61; H, 3.91; Fe, 15.64. Found: C, 26.88; H, 3.74; Fe, 16.49 (titrimetric)%. UV–Vis–NIR spectral data (λ_{max}, nm): (i) aqueous solution: 340 (sh), 947 (br); (ii) solid state: 227, 383(br), 917(br), 1120(sh). IR spectral data (cm^{-1}): 3491(sh), 3412(s), 3054(w), 2932(m), 2852(w), 1680(m), 1618(sh), 1559(s), 1489(s), 1362(s), 1222(m), 1087(br), 897(w), 866(m), 744(s), 669(s), 497(s) [sh, shoulder; s, strong; m, medium; w, weak; br, broad].

2.3. X-ray crystallographic procedures

The thick orange crystals of compound **1** directly obtained from the reaction mixture are suitable for single crystal X-ray diffraction experiments. A relatively large crystal was mounted on a glass fibre for intensity data collection using graphite monochromatized Mo-Kα radiation on a Bruker SMART Platform CCD Diffractometer. Several sets of frames covering a random area of the reciprocal space were collected using 0.3° steps in ω at a detector to sample distance of ~5 cm. Data acquisition, extraction and reduction and empirical absorption correction were performed using the programs SMART, SAINT and SADABS [12], respectively. The structure solution (direct methods) and refinement (full-matrix least-squares) were carried out with the SHELX-97 suite [13] of crystallographic programs. The correct assignment of the triclinic centrosymmetric space group for **1** was made on the basis of successful solution and well-behaved refinement of the structure. All non-hydrogen atoms were refined anisotropically. The hydrogen atoms were located in difference Fourier maps and refined with isotropic displacement parameters. The structural diagrams were drawn using the programs ORTEP-3 and PLUTON available in WINGX [14].

2.3.1. Crystal data

Columnar crystal, $1.03 \times 0.52 \times 0.44$ mm, $[Fe(C_4H_3O_4)_2(H_2O)_4]$, $a = 5.2785(8)$ Å, $b = 7.3987(11)$ Å, $c = 9.3016(14)$ Å, $\alpha = 109.249(2)^\circ$, $\beta = 104.727(2)^\circ$, $\gamma = 93.366(2)^\circ$, $V = 327.62(9)$ Å^3, $\lambda = 0.71073$ Å, triclinic, $P\bar{1}$, $Z = 1$, Bruker SMART CCD platform diffractometer, 3633 reflections of which 1440 unique, $R_{int} = 0.0212$, 96.1% completeness of data to $2\theta = 55^\circ$, $R_1^\dagger = 0.0227$, $wR_2^\dagger = 0.0612$, refinement against all 1440 reflections based on F^2 for 126 parameters, GoF* = 1.046. $^\dagger wR_2 = \{\Sigma[w(F_o^2 - F_c^2)^2]/\Sigma[w(F_o^2)^2]\}^{1/2}$; $R_1 = \Sigma||F_o| - |F_c||/\Sigma|F_o|$, *GoF $= S = \{\Sigma[w(F_o^2 - F_c^2)^2]/(n-p)\}^{1/2}$].

The powder X-ray diffraction pattern was recorded using a Rigaku-Denki/RW400F2 (Rotaflex) rotating-anode powder diffractometer. The calculated powder pattern was generated from the refined atom coordinates using the CERIUS^2 software [15].

3. Results and discussion

3.1. Synthesis and properties

Reaction of iron powder with aqueous maleic acid is rapid at refluxing temperature. The resulting solution is stable against air-oxidation. Yellow–orange crystalline columns and crystals of irregular shape, some of which are over 5 mm in the longest dimension, of compound **1** form slowly when the cooled reaction mixture is allowed to stand at room temperature.

$$Fe + 2C_4H_4O_4 + 4H_2O = Fe(C_4H_3O_4)_2(H_2O)\ \ (\mathbf{1}) + H_2\uparrow$$

For molar ratios higher than 1:3 between the reactants, formation of colourless crystals of maleic acid was observed and due to the similar solubility property of these crystals, purification of **1** was found to be difficult. Vithal and Jagannathan [8] prepared this compound using a 1:4 molar ratio of the reactants under somewhat different conditions. Analogous compounds of manganese [16], cobalt and nickel were previously obtained for crystallographic work by treating MCO_3 with aqueous maleic acid [6].

The crystalline, non-hygroscopic solid of [Fe(hydrogenmaleate)$_2$(H$_2$O)$_4$] (**1**) is indefinitely stable against air-oxidation and water loss. In fact, thermogravimetric data show that there is no loss of water until ~ 160 °C. Slow dissolution of the crystals of **1** in water leads to a slightly acidic (pH 4.2) air-stable solution from which the crystals can be grown again in a slightly different morphology. The solution obtained by dissolving **1** is electrically conducting in nature and the high value of conductivity (equivalent conductance falls in the range of values expected for aqueous 10^{-3} M solutions of 1:2 electrolytes) can be explained by invoking the formation of $[Fe(H_2O)_6]^{2+}$ upon dissolution in water. But this leaves the orange–yellow colour, in contrast to the expected pale green colour of the hexaaqua cation, of the solution unexplained. It seems likely that because the orange colour of the solution could only result from charge-transfer transitions between metal and ligand orbitals, the hydrogenmaleato anions may not dissociate fully in water with the high solution conductivity arising from a partial dissociation of the acidic protons of the coordinated ligands. While the charge-transfer absorption is seen as a shoulder around ~ 340 nm, the expected $^5T_{2g} \rightarrow {}^5E_g$ transition appears as a weak, broad absorption band at 947 nm in the UV–Vis–NIR spectra of compound **1**. The solid state UV–Vis–NIR spectrum (Fig. 1) of compound **1** also shows these absorption features as two broad bands at 383 and 917 nm along with a strong red-shifted UV absorption at 227 nm due to the $\pi \rightarrow \pi^*$ transition of the C=C bond of the hydrogenmaleato ligands. The NIR band with a shoulder at lower energy is strikingly similar to an electronic spectrum of Fe^{2+} [17], and the splitting of this d–d band for high-spin Fe(II) may be attributed [8,17] to a splitting of the excited state in a permanently distorted ligand field. This appears to be acceptable because our structural data to be detailed below show that the Fe^{2+} centre in complex 1 is indeed in a low symmetry environment.

An aqueous solution of **1** was studied by cyclic voltammetry in the presence of $NaClO_4$ as a supporting electrolyte. The observed $E_{1/2}$ value of +0.15 V versus Ag/AgCl is low compared with the values known for aqueous acidic solutions of Fe^{2+}, and is nearly the same with the reduction potential found for the $Fe(CN)_6^{3-}$/$Fe(CN)_6^{4-}$ couple under similar experimental conditions. The quasi-reversible nature ($\Delta E_p = 227$ mV, $i_c/i_a = 0.986$ and $\Delta E_p = 257$ mV, $i_c/i_a = 0.951$ at 20 and 50 mV s^{-1}, respectively) of the electrochemical response is indicative of sluggish electron transfer for the oxidation of Fe^{2+} to Fe^{3+}. Resulting kinetic barrier for the redox process involving the Fe(III)/Fe(II) couple appears to be responsible for the stability of iron(II) in compound **1** against aerial oxidation, a commonly accepted redox property of the ferrocyanide ion in aqueous solution.

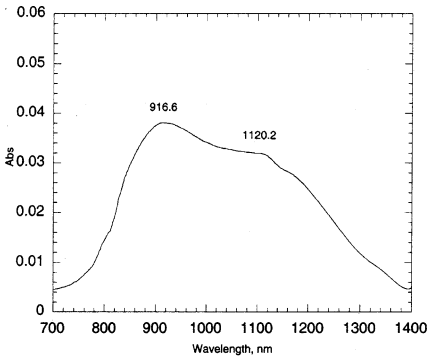


Fig. 1. Electronic spectrum of compound **1** in the near-IR region.

The KBr phase infrared spectrum of $Fe(O_2CCH{=}CHCO_2H)_2(H_2O)_4$ (**1**) displays bands assignable to the presence of the hydrogenmaleato and aqua ligands. Observation of the O–H vibrations at low energies is suggestive of their participation in hydrogen-bonding interactions. The bands at 2932 and 2852 cm^{-1} may also be of similar origin traceable to the likely presence of strong intramolecular hydrogen bonding between the –COOH and $–COO^-$ groups of the hydrogenmaleate anions. The C=O stretching frequency for the acid end of the hydrogenmaleato ligand could be assigned to the medium intensity band at approximately 1680 cm^{-1}. But there are several overlapping bands on the low energy side of this band and accurate assignment of bands to specific stretching vibrations is difficult to make. Assuming the absorption at $\sim$1620 cm^{-1} (the corresponding band for maleic acid is known to occur at 1640 cm^{-1}) to be due to the C=C stretch, the stronger absorptions at 1559 and 1489 cm^{-1} could be traced to the ν_{asym}(carboxyl) and ν_{sym}(carboxyl) vibrations, respectively. More detailed assignment of infrared absorption by a coordinated maleate dianion has been attempted earlier [7,18].

3.2. Crystal structure

Details of the solid-state structure of the compound have been determined by X-ray diffraction. An ORTEP presentation of the molecular structure of **1** is shown in Fig. 2 and a list of selected geometrical parameters are presented in Table 1. The iron atom in $Fe(C_4H_3O_4)_2(H_2O)_4$ (**1**) lies at a crystallographic centre of symmetry (1/2, 0, 1/2). The $HO_2CCH{=}CHCO_2^-$ ligands in the complex are *trans* to one another. However, the effective point symmetry of the central metal atom is only C_i. In spite of this low symmetry the metal complex at hand may, however, be conveniently considered to be approximately octahedral in structure. The Fe–O distances of 2.086(1) and 2.154(1) Å for the aqua ligands

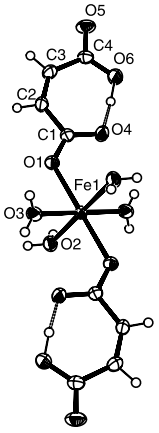


Fig. 2. An ORTEP view of $[Fe(C_4H_3O_4)_2(H_2O)_4]$ (**1**) at 50% probability. Hydrogen atoms are shown by spheres of arbitrary radius.

Table 1
Selected bond lengths (Å) and angles (°) for $Fe(C_4H_3O_4)_2(H_2O)_4$ (**1**)

Bond distances			
Fe(1)–O(3)	2.086(1)	Fe(1)–O(2)	2.154(1)
Fe(1)–O(1)	2.162(1)	O(1)–C(1)	1.259(2)
O(4)–C(1)	1.264(2)	O(5)–C(4)	1.231(2)
O(6)–C(4)	1.296(2)	C(1)–C(2)	1.496(2)
C(2)–C(3)	1.337(2)	C(3)–C(4)	1.494(2)
Bond angles			
O(3)–Fe(1)–O(1)	83.17(4)	O(2)–Fe(1)–O(1)	86.69(4)
O(3)–Fe(1)–O(2)	92.47(5)	O(3)#1–Fe(1)–O(2)	87.53(5)
O(3)–Fe(1)–O(1)#1	96.83(4)	O(2)–Fe(1)–O(1)#1	93.31(4)
C(1)–O(1)–Fe(1)	126.76(9)	O(1)–C(1)–O(4)	122.6(1)
O(1)–C(1)–C(2)	116.5(1)	O(4)–C(1)–C(2)	120.9(1)
C(3)–C(2)–C(1)	129.9(1)	C(2)–C(3)–C(4)	130.6(1)
O(5)–C(4)–O(6)	121.4(1)	O(5)–C(4)–C(3)	118.5(1)
O(6)–C(4)–C(3)	120.0(1)		

Symmetry transformation used to generate equivalent atoms: #1 $-x+1, -y, -z+1$.

and 2.162(1) Å for the carboxyl group show the distorted nature of the FeO_6 octahedron. The expected C=O distance [O5–C4 = 1.231(2) Å] for the acid end (–COOH) is about 0.07 Å shorter compared with the C–O in O=C–O–H. The former distance is also shorter compared with the C–O distances for the coordinated $–COO^-$ group. The O4···O6 intra-molecular hydrogen bond distance of 2.428(2) Å is the shortest of all distinct hydrogen bonds (Table 2). The geometrical constraint of keeping the hydrogen bond as linear as possible [$\angle$ O4···H7–O6, 174(4)°] for the maximisation of bonding ($d_{O6–H7}$: 1.04 Å and $d_{O4\ldots H7}$: 1.39 Å compared with the other O–H distances in the range of 0.74–0.81 Å) leads to the formation of a seven-member ring for each of the hydrogenmaleate anions. Structure of **1** is similar to that of $[M(C_4H_3O_4)_2]\cdot 4H_2O$ (M = Ni, Zn and Mn) [6,16]. Considering the ionic radii of the metal ions involved, the M–O distances in these compounds are comparable to those in **1**. The intramolecular hydrogen bond mentioned above for **1** is also similar in length with those in the other compounds, but the O–H···O bond angle is much closer to the ideal 180° for **1** compared with that in the Mn compound [$\angle$ O···H–O: 165(7)°] [16] and is nearly identical with the corresponding angle in the Zn analogue for which hydrogen atom positions

Table 2
Hydrogen-bonds for $Fe(C_4H_3O_4)_2(H_2O)_4$ (**1**) (Å) and angles (°)

D–H···A	d(D–H)	d(H···A)	d(D···A)	$\angle$ (DHA)
O(3)–H(2)···O(5)#2	0.81(2)	1.99(3)	2.787(2)	169(2)
O(2)–H(3)···O(1)#3	0.81(2)	2.05(2)	2.857(1)	175(2)
O(2)–H(5)···O(5)#4	0.79(3)	2.09(3)	2.864(2)	164(2)
O(3)–H(6)···O(6)#5	0.74(3)	2.23(3)	2.881(1)	149(3)
O(3)–H(6)···O(4)#1	0.74(3)	2.45(3)	2.904(2)	122(2)
O(6)–H(7)···O(4)	1.04(4)	1.39(4)	2.428(2)	174(4)

Symmetry transformations used to generate equivalent atoms: #1 $-x+1, -y, -z+1$; #2 $-x+1, -y, -z+2$; #3 $-x, -y, -z+1$; #4 $-x+1, -y+1, -z+2$; #5 $x-1, y-1, z-1$.

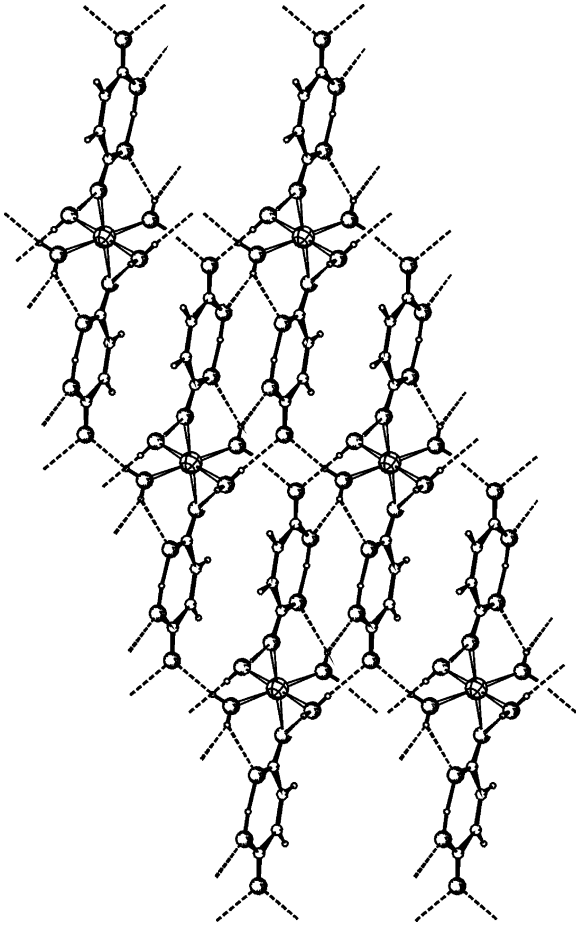


Fig. 3. Crystal packing diagram of $[Fe(C_4H_3O_4)_2(H_2O)_4]$ (**1**) viewed along *a*-axis showing the details of hydrogen-bonding interactions.

have been determined by a more appropriate neutron diffraction analysis [6]. For the example of copper(II) hydrogenmaleate tetrahydrate, the hydrogenmaleate ions present as charge-compensating anions are merely hydrogen bonded to the water molecules that form the tetraaqua copper(II) coordination sphere [3a]. The comparable intra-molecular O···O hydrogen bond distance in this compound is 2.409(3) Å, which is marginally shorter than that in compound **1**. The hydrogen atoms were not located in this structure.

Crystal packing diagram of the discrete $Fe(C_4H_3O_4)_2(H_2O)_4$ molecular units of **1** are given in Fig. 3. All O and O–H groupings participate in hydrogen-bonding and one hydrogen atom (H6) is involved in bifurcated hydrogen-bonding. The resultant supramolecular network thus assumes a rigid three-dimensional structure. The hydrogen-bonded architecture presents approximately hexagonal pores with shortest and the longest void dimensions of 4.8 and 9.4 Å (Fig. 4). A more detailed analysis of the hydrogen-bonding interactions in isostructural compounds, based on neutron diffraction studies on $Zn(C_4H_3O_4)_2(H_2O)_4$, has been made by Sequeira et al. [6].

Purity of the bulk sample of **1** has been confirmed by comparing the simulated powder X-ray diffraction pattern based on the atom coordinates obtained from single crystal X-ray analysis with the experimental pattern. Apart from the fact that the two most intense peaks in the two patterns (Fig. 5) have different d-spacings, both XRD patterns are very similar in appearance to suggest that both patterns tally well with one another.

3.3. Magnetic behaviour

Variable temperature magnetic susceptibility data on compound **1** have been measured in the 2–300 K range.

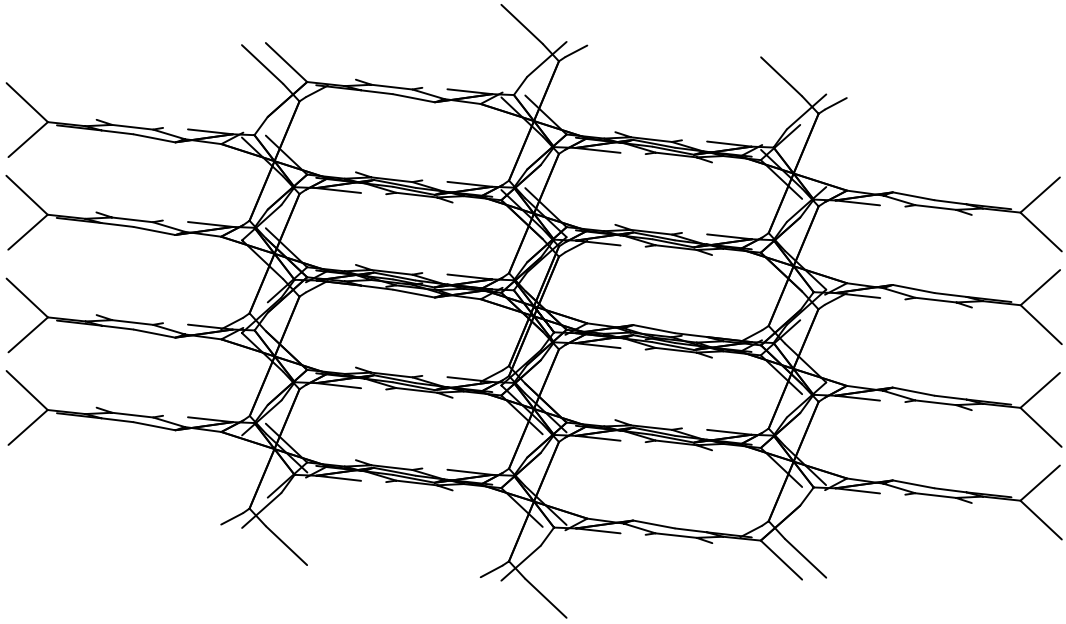


Fig. 4. A view of the supramolecular porous network in **1**.

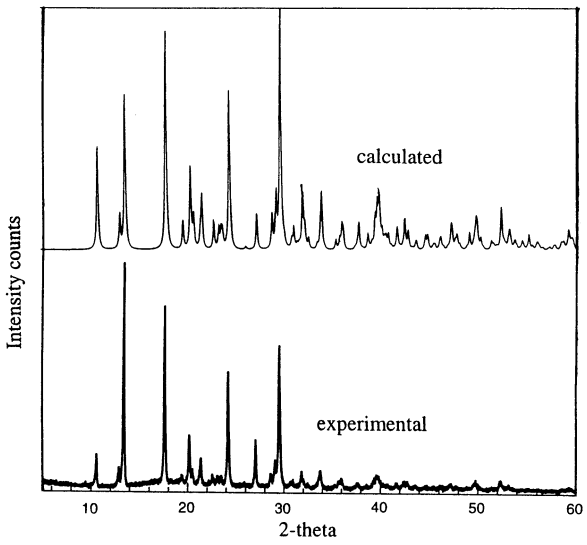


Fig. 5. Observed and calculated powder X-ray diffraction patterns for $[Fe(C_4H_3O_4)_2(H_2O)_4]$ (**1**).

The straight line obtained for the $1/\chi_M$ versus T plot (Fig. 6) makes an intercept with the T axis at -2.4 K. This indicates that the compound remains a Curie–Weiss paramagnet down to very low temperatures. Around 30 K the μ_{eff} ($=5.25$ BM at 300–30 K) value of high-spin iron(II) starts to decrease slowly to reach a minimum value of 3.4 BM at 2 K. Porollo et al. [7] reported two μ_{eff} values of 5.83 and 5.71 BM, respectively, at 290 and 80 K for this compound without indicating whether any antiferromagnetic interaction was involved. The μ_{eff} value for **1** obtained by us appears to be well within the minimum and maximum of such values commonly observed for high-spin iron(II) complexes [19]. The reduction in the μ_{eff} value at low temperatures is suggestive of progressive spin pairing with decreasing temperature. That the high-spin iron(II) complex weakly couples through antiferromagnetic exchange interactions is seen from the negative Weiss constant as well as the downward behaviour of the $\chi_M T$ versus T curve (please see inset in Fig. 6) below ~ 30 K [4]. Although our attempts to obtain a good fit of the data with well-established equations for magnetic susceptibility were unsuccessful, we are of the view that the unpaired electrons couple weakly in an antiferromagnetic manner through the hydrogen-bonded network, because of the lack of covalent bonds to connect the metal centres and also due to the fact that the shortest distance separating the iron(II) centres is over 5 Å in the crystal lattice.

4. Conclusions

The work reported in the paper indicates that detailed knowledge of the crystal structure even for a simple compound such as **1** may prove useful in understanding some bulk properties of the compound in the solid state. Intermolecular association through hydrogen-bonding phenomena may lead to enhanced redox stability of Fe(II) and to weak antiferromagnetism at low temperature.

5. Supplementary material

Cyclic volammogram and crystallographic data for compound **1** in CIF format are available from the authors. CIF is deposited with the Cambridge Crystallographic Data Centre, CCDC (No. 172028). The

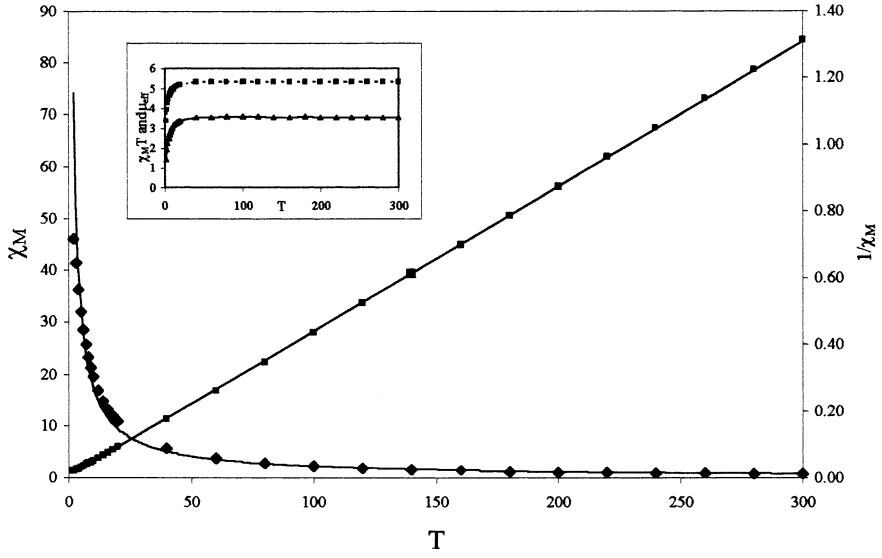


Fig. 6. χ_M vs. T (◆) and $1/\chi_M$ vs. T (■) plots for $[Fe(C_4H_3O_4)_2(H_2O)_4]$ (**1**) with the data fitted to power series and linear expressions, respectively. The inset in the figure shows the variations of $\chi_M T$ (▲)and μ_{eff} (■) with temperature.

crystallographic information file is available free of charge from: The Director, CCDC, 12 Union Road, Cambridge, CB2 1EZ, UK (fax: +44-1223-336033; e-mail: deposit@ccdc.cam.ac.uk; www: http://www.ccdc.cam.ac.uk).

Acknowledgements

We thank the Department of Science & Technology and the University Grants Commission, India for financial support. A part of the work was possible during a visit by B.K.D. to Michigan State University, USA. Financial support under an Academic Affiliate Program from the Centre for Fundamental Materials Research of the University is gratefully acknowledged.

References

[1] (a) K. Seki, S. Takamizawa, W. Mori, Chem. Lett. (2001) 122;
(b) H. Li, M. Eddaoudi, O.M. Yaghi, Nature 402 (1999) 276.
[2] J. Padilla, W.E. Hatfield, J.R. Wasson, W.E. Estes, Transition Met. Chem. 14 (1989) 217.
[3] (a) C.K. Prout, J.R. Carruthers, F.J.C. Rossotti, J. Chem. Soc. (A) (1971) 3342;
(b) B.K. Das, R.S.K. Singh, R.K. Barman, unpublished results, 2000.
[4] O. Kahn, Molecular Magnetism, VCH, Weinheim, 1993.
[5] C.P. Prabhakaran, C.C. Patel, Ind. J. Chem. 7 (1969) 266.
[6] A. Sequeira, H. Rajagopal, M.P. Gupta, F. Vanhouteghem, A.T.H. Lenstra, H.J. Geise, Acta Crystallogr., Sect. C 48 (1992) 1192 (and references therein).
[7] N.P. Porollo, Z.G. Aliev, G.I. Dzhardimalieva, I.N. Ivleva, I.E. Uflyand, A.D. Pomogailo, N.S. Ovanesyan, Russ. Chem. Bull. 46 (1997) 362.
[8] M. Vithal, R. Jagannathan, Transition Met. Chem. 9 (1984) 73.
[9] B.S. Randhawa, K. Sweety, Bull. Mater. Sci. 23 (2000) 305.
[10] A.T. Shuvaev, A.S. Rozenberg, G.I. Dzhardimalieva, I.N. Ivleva, V.G. Vlasenko, T.I. Nedoseikina, T.A. Lyubeznova, I.E. Uflyand, A.D. Pomogailo, Russ. Chem. Bull. 47 (1998) 1460.
[11] (a) H.-H. Perkampus, in: H.-C. Grinter, R. Grinter (translators), Encyclopaedia of Spectroscopy, VCH, Weinheim, 1993;
(b) G. Kortüm, Reflectance Spectroscopy, Springer-Verlag, Berlin, 1969.
[12] Bruker X-ray Analytical Systems, Inc., Madison, WI, 53719, USA.
[13] G.M. Sheldrick, SHELX-97: A Program for the Solution and Refinement of Crystal Structures, University of Göttingen, Göttingen, Germany, 1997.
[14] L. Farrugia, J. Appl. Crystallogr. 32 (1999) 837.
[15] CERIUS^2: Version 3.8, Molecular Simulations Inc., Cambridge, 1999.
[16] T. Lis, Acta Crystallogr., Sect. C 39 (1983) 39.
[17] F.A. Cotton, M.D. Meyers, J. Am. Chem. Soc. 82 (1960) 5023.
[18] J. Černak, J. Chomič, C. Kappenstein, F. Robert, J. Chem. Soc., Dalton Trans. (1997) 2981.
[19] S.F.A. Kettle, Physical Inorganic Chemistry, Oxford University Press, Oxford, 1998, p. 194.

PERGAMON

Polyhedron 21 (2002) 1197–1201

POLYHEDRON

www.elsevier.com/locate/poly

Synthesis and structure of peptide–copper(II)–isocytosine ternary complexes

Angel García-Raso [a,*], Juan J. Fiol [a,*], Bartomeu Adrover [a], Amparo Caubet [b], Enrique Espinosa [c], Ignasi Mata [c], Elies Molins [c]

[a] *Departament de Química, Universitat de les Illes Balears, 07071 Palma de Mallorca, Spain*
[b] *Departament de Química Inorgànica, Universitat de Barcelona, 08028 Barcelona, Spain*
[c] *Institut de Ciència de Materials de Barcelona (CSIC), Campus de la Universitat Autònoma, 08193 Cerdanyola, Spain*

Received 24 October 2001; accepted 15 April 2002

Abstract

Two ternary complexes [Cu(ala–gly)(isocyt)(H_2O)]·H_2O (**1**) and [Cu(L-tyr–gly) (isocyt)]·3H_2O (**2**) have been prepared and characterised by X-ray diffraction, optical, ESR and IR spectral data. Both compounds exist as slightly distorted square-planar complexes, with the four co-ordination sites occupied by the tridentate peptidic dianion [oxygen carboxylic O(7), nitrogen amidic N(13) and nitrogen aminic N(10)] and the N(3) of the pyrimidine base. In complex **1**, obtained as a racemic compound, an additional weak axial interaction exists between the oxygen of a water molecule OW1 and the copper atom [Cu–OW1 distance 2.50 Å]. Spectroscopic data are in accordance with the crystal structures. The isocytosine ligand is approximately orthogonal to the Cu–peptide moiety independently of the nature of the lateral chain. This disposition of the nucleobase contrasts with the coplanarity of the previously described Cu(II)–glygly–creatinine complex. © 2002 Elsevier Science Ltd. All rights reserved.

Keywords: Cu(II) complexes; Ternary complexes; Peptide–Cu(II)–isocytosine complexes; Isocytosine complexes

1. Introduction

The present study is a continuation of our work on ternary metal complexes with peptides and nucleobase related ligands [1–3]. A considerable number of X-ray crystallographic studies on glycylglycinato–copper(II)–cytosine or isocytosine have been reported but X-ray diffraction crystallographic studies on ternary copper(II) complexes containing other peptides are scarce [3–7]. This fact could be related to some experimental difficulties in the preparation of gly-X and X-gly copper(II) ternary compounds and only one copper(II) ternary complex, [Cu(L-tyr–gly)(phen)]·3H_2O has been structurally described [8].

In a previous paper [3] two glycylglycinato isocytosine copper(II) complexes were structurally characterised. Primary co-ordination spheres of copper(II) were very similar to the previously described cytosine [4] and cytidine [5] related compounds. Moreover, additional intramolecular interactions NH_2(glygly)···O=C(pyrimidine) and intermolecular interactions COO(glygly)···NH(pyrimidine) are present. To obtain direct evidence for specific ligand-peptide interactions and the influence of the nature of the lateral chain in the formation and stabilisation of the ternary complex, two new (X-gly)–copper(II)–isocytosine compounds: [Cu(ala–gly)(isocyt)(H_2O)]·H_2O (**1**) and [Cu(L-tyr–gly)(isocyt)]·3H_2O (**2**) have been synthesised and characterised.

2. Experimental

Reagents were used as received from Aldrich.

The synthesis of these type of ternary complexes Cu(peptide)(isocytosine) strongly depends on the nature of the peptide moiety. In our hands we have explored the preparation of the corresponding ternary complexes with gly-D,L-ala, gly–L-ala, gly–L-val, gly–L-phe, gly–

* Corresponding authors. Tel.: +34-971-173-263; fax: +34-971-173-426.
E-mail address: dquagro@clust.uib.es (A. García-Raso).

0277-5387/02/$ - see front matter © 2002 Elsevier Science Ltd. All rights reserved.
PII: S0277-5387(02)01010-0

L-tyr, gly–L-trp and L-val–gly, modifying the reaction conditions (solvent, temperature, stoichiometry of the reagents, pH and reaction time). Unfortunately, all these experiments were unsuccessful yielding the binary copper compounds. Only with L-ala–gly and L-tyr–gly it has been possible to isolate ternary complexes.

2.1. Preparation of [Cu(ala–gly)(isocyt)(H_2O)]·H_2O (**1**)

Isocytosine (0.11 g, 1 mmol) was added, while stirring, to a 3 ml aqueous solution containing $CuSO_4 \cdot 5H_2O$ (0.25 g, 1 mmol) and L-ala–gly (0.15 g, 1 mmol). The mixture was treated with 2 ml of NaOH 1 N and then heated on a steam bath up to boiling and filtered. The resulting solution was allowed to stand at room temperature (r.t.) for a few days until blue crystals of the racemic compound were formed. These crystals were filtered off and air dried (yield: 17%). The complex exhibits a mass decrease between 79 and 133 °C corresponding to the loss of two water molecules per formula unit (mass loss calc., 10.1%; mass loss found, 10.1%). *Anal.* Found: C, 30.47; H, 4.76; N, 19.50. Calc. for $C_9H_{17}CuN_5O_6$: C, 30.47; H, 4.79; N, 19.75%. IR(KBr, cm^{-1}): 282m, 337w, 439w(br), 459s, 577s, 713m, 766w, 790vw, 820s, 877m, 919w, 941w(br), 982m(br), 1020w, 1057m, 1086m, 1099m, 1236m, 1288s, 1399s(br), 1434w, 1465m, 1498m, 1597s(br), 1635s(br), 1683s(br), 3664m(sp). UV–vis (water): λ 639 (ε 94), 284 (5.1×10^3), 261 nm (5.1×10^3 dm^3 mol^{-1} cm^{-1}). Λ_M (Ω^{-1} cm^2 mol^{-1}) of 10^{-3} M in water, 20 °C = 11.6

2.2. Preparation of [Cu(L-tyr–gly)(isocyt)]·3H_2O (**2**)

[Cu(L-tyr-gly)] was freshly prepared by addition of 0.12 g (0.5 mmol) of L-tyr–gly in 1 ml of NaOH 1 N to an aqueous solution (4 ml) containing 0.12 g (0.5 mmol) of $CuSO_4 \cdot 5H_2O$. The resulting suspension was heated for 10 min on a steam bath (85 °C). After cooling the precipitate was filtered off and dried (yield: 89%). To a suspension of 0.10 g (0.33 mmol) of crude [Cu(L-tyr–gly)] in 2 ml of distilled water, heated on a steam bath (70 °C), 0.04 g (0.33 mmol) of isocytosine were added. The temperature of the steam bath was increased to boiling and subsequently the suspension was stirred for 20 min without heating. The blue precipitate was filtered off and air dried (yield: 73%). The product was partially redissolved in hot water and suitable crystals for X-ray diffraction were obtained by slow evaporation for a few days at room temperature. The complex exhibits a mass loss between 27 and 201 °C corresponding to the loss of three water molecules per formula unit (mass loss calc., 11.6%; mass loss found, 10.9%). *Anal.* Found: C, 38.66; H, 5.07; N, 14.96. Calc for: $C_{15}H_{23}CuN_5O_8$: C, 38.75; H, 4.95; N, 15.07%. IR (KBr, cm^{-1}): 288w, 352vw, 373w, 438w, 503w, 544w, 563vw, 577w, 598w, 630vw, 713vw, 731vw, 759vw, 810m, 824m, 854w, 889w, 907vw, 951w, 996vw, 1019m, 1058vw, 1083m, 1117w, 1174vw, 1205vw, 1234w, 1273m, 1300m, 1378m(br), 1401vw, 1431w, 1447w, 1499m(sh), 1513m, 1576s(br), 1613s, 1663m(br), 1689m, 3273vw, 3336w. UV–vis (water): λ 634 (ε 96), 281(sh) (6.9×10^3), 276 nm (7.0×10^3 dm^3 mol^{-1} cm^{-1}). Λ_M ($\Omega^{-1}cm^2$ mol^{-1}) of 10^{-3} M in water, 20 °C = 16.5.

2.3. Physical measurements

Elemental analyses of the complexes were carried out using a Carlo Erba model 1106 microanalyzer. The infrared spectra (KBr pellets) were recorded on a PE 683 with an infrared data station PE 1600 and the electronic spectra were registered on a PE 552 spectrophotometer. Thermogravimetric data in the temperature range from 30 to 700 °C were recorded in a flowing nitrogen atmosphere (heating rate 10 °C min^{-1}) on a PE TGA-2 thermobalance. ESR spectra were recorded at X-band frequencies with a Bruker ESP-300E spectrometer at 298 K. Magnetic measurements were carried out on powdered samples with a pendulum-type magnetometer (Manics DSM8). Diamagnetic corrections were estimated from the Pascal tables.

2.4. Crystallographic studies

X-ray data for single crystals of **1** and **2** were collected on an Enraf Nonius CAD4 diffractometer using monochromatic Mo Kα radiation ($\lambda = 0.71069$ Å). The cell parameters and space group were determined from a least squares refinement of 25 reflections randomly searched. Data collection was realised with scan ω–2θ technique.

The WINGX program [9] was used for applying Lorentz-polarization, decay and ψ-scan empirical absorption corrections. The structures were solved by direct methods and refined by a full-matrix least-squares method using the SHELX97 programs [10]. Non-H atoms were anisotropically refined. H atoms were positioned in calculated positions, except those in water molecules, which were localised in Fourier difference maps. Isotropic thermal vibration of the H-atoms were fixed to 1.2–1.5 times the U_{iso} of the bonded atom. Crystal parameters, data collection details and results of the refinements are summarised in Table 1.

3. Results and discussion

In order to explore specific ligand–peptide interactions and the influence of the lateral chain in the formation and stabilisation of the ternary complex, we have been working on the system Cu–(peptide)–iso-

Table 1
Crystal data and structure refinement for [Cu(ala–gly)(isocyt)(H$_2$O)]·H$_2$O (**1**) and [Cu(L-tyr–gly)(isocyt)]·3H$_2$O (**2**)

	[Cu(ala–gly)(isocyt)(H$_2$O)]·H$_2$O (**1**)	[Cu(L-tyr–gly)(isocyt)]·3H$_2$O (**2**)
Empirical formula	$C_9H_{17}CuN_5O_6$	$C_{15}H_{23}CuN_5O_8$
Formula weight	354.82	464.92
Crystal system	monoclinic	orthorhombic
Space group	*P*c	*P* $2_12_12_1$
Unit cell dimensions		
a (Å)	11.857(1)	8.151(1)
b (Å)	10.368(1)	12.217(4)
c (Å)	12.674(1)	19.881(5)
β (°)	112.18(7)	
V (Å^3)	1442.8(4)	1979.8(9)
Z	4	4
D_{calc} (Mg m^{-3})	1.633	1.560
Absorption coefficient (mm^{-1})	1.549	1.157
F(000)	732	964
Crystal size (mm)	0.42 × 0.16 × 0.09	0.10 × 0.12 × 0.77
θ Range (°)	2.62–28.45	2.64–30.40
Index ranges	$-15 \le h \le 14$, $-13 \le k \le 13$, $0 \le l \le 16$	$0 \le h \le 11$, $-17 \le k \le 0$, $0 \le l \le 28$
Reflections collected	7044	3385
Independent reflections	3776	3385
Data/parameters	3776/383	3385/281
Final *R* indices [$I > 2\sigma(I)$]	$R_1 = 0.0687$, $wR_2 = 0.1511$	$R_1 = 0.0357$, $wR_2 = 0.0841$
R indices (all data)	$R_1 = 0.2298$, $wR_2 = 0.1906$	$R_1 = 0.1025$, $wR_2 = 0.0957$
Goodness-of-fit on F^2	1.036	1.005
Largest difference peak (e Å^{-3})	0.625	0.793
Largest differe. hole (e Å^{-3})	−0.787	−0.761

cytosine. As indicated in the experimental section, the preparation of copper(II) ternary complexes with more complex peptides than glygly presents important difficulties and we have been unsuccessful to obtain the complete family of these compounds. In our hands, we should mention that the nature of the peptide show a great influence in the synthesis of these ternary complexes. Thus, peptides like gly-X (gly-D,L-ala, gly–L-ala, gly–L-val, gly–L-phe, gly–L-tyr and gly–L-trp) have not allowed us to isolate the ternary compound. Contrarily, with X-gly peptides it is possible to obtain the desired complexes and two new compounds were obtained: [Cu(ala–gly)(isocyt)(H$_2$O)]·H$_2$O (**1**) and [Cu(L-tyr–gly)(isocyt)]·3H$_2$O (**2**). It is interesting to note that the reaction conditions for the obtention of the ternary complex with L-ala–gly yield the racemic [Cu(ala–gly) (isocyt)(H$_2$O)]·H$_2$O (**1**) probably due to the high basicity involved in the synthesis. Unfortunately, it has not been possible to isolate the binary Cu(L-ala–gly) to perform the synthesis of the ternary complex in a non-basic conditions.

3.1. Crystal structures

The molecular structures of the compounds are shown in Fig. 1 and Fig. 2. Selected bond distances and angles are given in Table 2.

The crystal structure of **1** presents two molecules per asymmetric unit, having opposite chiralities at C(12).

The complexes [Cu(ala–gly)(isocytosine)(H$_2$O)]·H$_2$O (**1**) and [Cu(L-tyr–gly) (isocyt)]·3H$_2$O (**2**) present a slight distorted square-planar geometry with the four co-ordination sites occupied by the tridentate peptidic dianion [O(7), N(13) and N(10)] [Cu–O(7): 2.020(13) and 2.042(13); Cu–N(13): 1.922(16) and 2.095(15); Cu–N(10): 1.905(17) and 1.883(18) Å for **1** and Cu–O(7): 1.986(2); Cu–N(13): 2.014(3); Cu–N(10): 1.892(3) Å for **2**] and the N(3) [Cu–N(3) 2.003(17) and 2.008(17) Å for **1** and 2.000(3) Å for **2**] of the isocytosine (Figs. 1 and 2). The structures of these two complexes **1** and **2** are similar to the previously described isocytosine complex [Cu(gly–gly)(isocyt)]·2H$_2$O (**3**). Moreover, as observed in compound **3**, additional interactions Cu–water molecules, are present in **1**, although the distance Cu···OW is shorter [2.59 and 2.50 Å for **1** and 2.70 Å for **3**]. On the other hand, in complex **2**, the distances Cu–N(13)

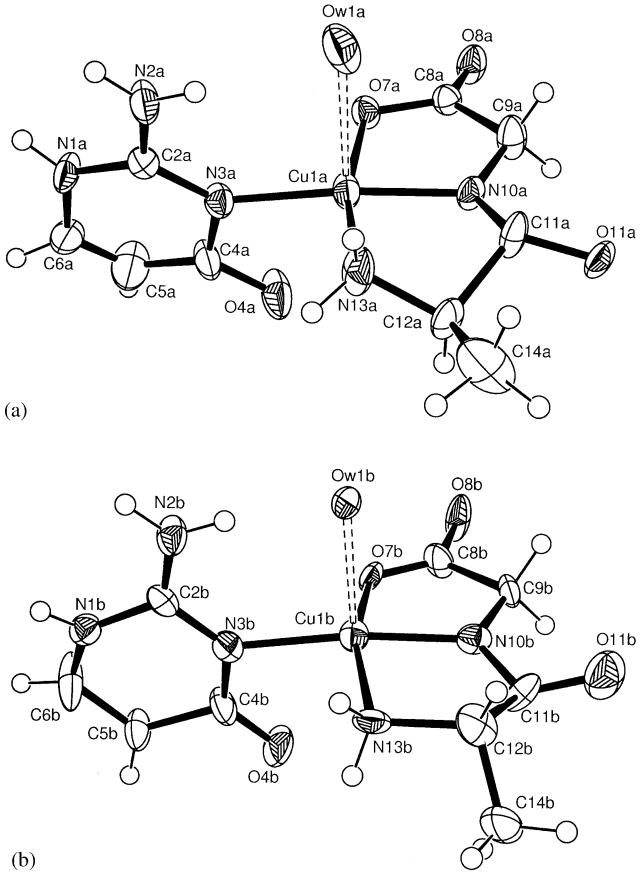


Fig. 1. ORTEP representation of the racemic [Cu(ala–gly)(isocyt)(H$_2$O)]·H$_2$O (**1**). (External water has been supressed for clarity). (a) R form. (b) S form

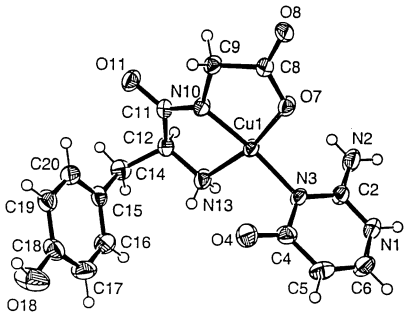


Fig. 2. ORTEP representation of [Cu(L-tyr–gly)(isocyt)]·3H_2O (**2**). (External waters have been supressed for clarity).

Table 2
Selected bond lengths (Å) and angles (°) for [Cu(ala–gly)(isocyt)(H_2O)]·H_2O (**1**) and [Cu(L-tyr–gly)(isocyt)]·3H_2O (**2**)

	[Cu(ala–gly)(isocyt)(H_2O)]·H_2O (**1**)	[Cu(L-tyr–gly)(isocyt)]·3H_2O (**2**)
Bond lengths		
Cu(1)–N(10)	1.905(17) and 1.883(18)	1.892(3)
Cu(1)–O(7)	2.020(16) and 2.042(13)	1.986(2)
Cu(1)–N(13)	1.922(16) and 2.095(15)	2.014(3)
Cu(1)–N(3)	2.003(17) and 2.008(17)	2.000(3)
Cu–O(8)#1		2.566(3)
Cu–O(4)		2.747(3)
Bond angles		
N(10)–Cu(1)–N(3)	168.9(8) and 172.4(8)	168.42(13)
N(10)–Cu(1)–O(7)	81.7(6) and 84.0(6)	83.52(12)
N(3)–Cu(1)–O(7)	94.1(7) and 96.3(7)	94.18(12)
N(10)–Cu(1)–N(13)	84.4(7) and 80.7(7)	82.11(12)
N(3)–Cu(1)–N(13)	100.0(8) and 97.7(7)	99.45(13)
O(7)–Cu(1)–N(13)	165.9(7) and 162.3(6)	165.46(11)
N(10)–Cu–O(8)#1		93.91(10)
O(7)–Cu–O(8)#1		87.45(10)
N(3)–Cu–O(8)#1		97.33(10)
N(13)–Cu–O(8)#1		95.75(12)
N(10)–Cu–O(4)		116.27(10)
O(7)–Cu–O(4)		106.29(11)
N(3)–Cu–O(4)		53.45(10)
N(13)–Cu–O(4)		78.30(12)
O(8)#1–Cu–O(4)		147.66(9)
C(2)–N(3)–Cu(1)	134.2(14) and 130.4(15)	129.3(2)
C(4)–N(3)–Cu(1)	110.4(13) and 102.6(12)	109.1(2)
C(8)–O(7)–Cu(1)	112.4(12) and 113.6(13)	113.9(2)
C(11)–N(10)–C(9)	122.9(18) and 119.2(18)	122.4(3)
C(11)–N(10)–Cu(1)	115.7(13) and 125.4(15)	120.5(2)
C(9)–N(10)–Cu(1)	119.1(13) and 114.0(13)	115.6(2)
C(12)–N(13)–Cu(1)	108.3(10) and 108.2(10)	109.6(2)

[2.023(8) Å for **3**] and Cu–O(7) [2.008(7) Å for **3**] are shorter than in [Cu(gly–gly)(isocyt)]·2H_2O (**3**). In both complexes the distance Cu–N(3) [1.949(7) Å for **3**] is larger than in **3**. The peptide dianion in **1** and **2** show similar angles as observed in other ternary complexes [Cu(glygly)(isocytosine)]·2H_2O (**3**) [3], [Cu(glygly)(6-methylisocytosine)]·H_2O (**4**) [3], [Cu(glygly)(cytosine)] (**5**) [4] and [Cu(glygly)(cytidine)] (**6**) [5]. Complex **2** show a hydrogen bond N(13)(peptide)–H···O(4)=C(pyrimidine ring) at 2.59 Å and an ancillary interaction Cu–O(8)(other complex unit) [Cu–O(8)*, 2.566(3) Å] similar to those observed in other complexes [3–5] but in complex **1**, neither a hydrogen bond N(13)(peptide)–H···O(4)=C(pyrimidine ring) nor ancillary interactions Cu–O(8) (other complex unit) are observed. The crystal structure of **1** is formed by direct interactions between different complex units [N(13)–H···O*(8)=C: 2.29 and 2.19 Å and N(1)–H···O**(8)=C: 1.70 and 2.03 Å] jointly with interactions through a water molecule [N(2)–H···O(W1): 2.206 and 1.842 Å; O(W1)···O*(11): 2.653 and 2.810 Å] similar to that observed in complex **2** where the crystal packing is dominated by a network of H–bonds through one [N(1)–H···O(21)–H···O*(11): 1.91 and 1.90 Å], two [N(1)–H···O(21)···H–O(23)–H···O*(4): 1.91, 1.92 and 1.96 Å] or three [N(1)–H···O(21)···H–O(23)···H–O(22)–H···O*(11): 1.91, 1.92, 1.88 and 1.946 Å] water molecules, besides other direct interactions between two different complex units [N(2)–H···O*(8): 1.96 Å; O(18)–H···O*(7): 1.89 Å].

These results and the previously described [3] show that the ligand is approximately orthogonal to the Cu–peptide moiety independently of the nature of the lateral chain. Moreover, this disposition contrasts with the corresponding Cu(II)–glygly–creatinine complex [1] where, although the distance between the carboxylic oxygen (O=C) and the aminic nitrogen (H_2N–C) of these two ligands is practically the same (4.5±0.1 Å) the torsion angle that implies Cu(II)–peptide and ligand moieties is completely different. Thus, creatinine adopts a nearly planar disposition with two strong intramolecular H-bonds contrarily to isocytosine that present a nearly orthogonal disposition (Fig. 3).

3.2. IR and electronic absorption

As observed in other N(3) metal co-ordinated isocytosine complexes [3], the strong band assigned to ν[C(4)=O] (1679 cm^{-1} for isocytosine) is shifted to higher frequencies (1683 cm^{-1} for **1** and 1689 cm^{-1} for **2**) upon complexation, ruling out direct O(4) binding of isocytosine to the metal ion. In C(2)=O bonded cytosine complexes [11], the ν(C=O) peak is shifted to lower frequencies. The most noticeable changes in frequency are observed on the bands related to the isocytosine ring stretching. The peaks appearing at 1518 and 1476 cm^{-1} assigned to ν(ring), νC–C+νC=N+ν C–N+νN–H in the free ligand [12–16], are shifted to lower frequencies (1498 and 1465 cm^{-1} for **1**, 1513 and 1499 cm^{-1} for **2**) and the intensity of the band at 1476 cm^{-1} decrease noticeably in both complexes. Similar behaviour in these ν(ring) bands have been observed and attributed to co-ordination of isocytosine to the metal ion through the N(3) [3]. In the lower frequency region the new bands at

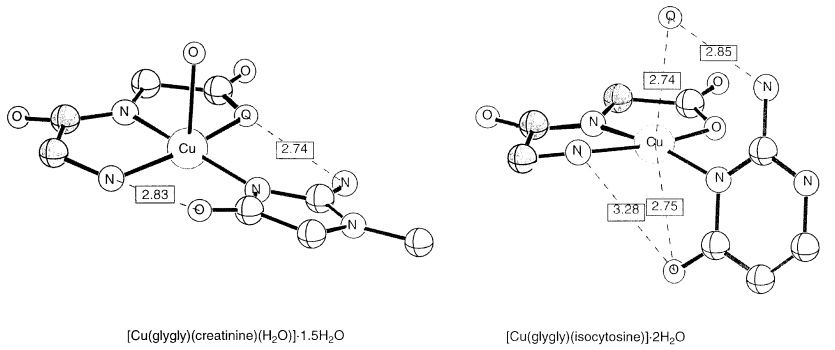


Fig. 3. Isocytosine vs. creatinine: they have similar structure moiety (O=C–N=C–NH_2) but present two different ways of interaction with peptide–Cu(II) binary compounds.

337, 282 cm^{-1} (for **1**) and 288 cm^{-1} (for **2**) are tentatively assigned to ν(Cu–N) [17].

The compounds yield blue solutions in water. The d–d transition spectra of the complexes show broad bands centred at 639 nm ($\varepsilon = 94$), 634 nm ($\varepsilon = 96$) for the isocytosine complexes **1** and **2**, respectively, that are suggestive of approximate square pyramidal geometry about Cu(II) as observed in other Cu(II) peptide complexes [1,18–20]. The π–π* transition bands corresponding to the isocytosine (263sh, $\varepsilon = 3.7 \times 10^3$ and 284, $\varepsilon = 4.5 \times 10^3$) exhibit, in the complex **1**, similar values of intensity and energy (261, $\varepsilon = 5.1 \times 10^3$ and 284, $\varepsilon = 5.1 \times 10^3$) and, in the complex **2**, an increase in intensity and energy (276, $\varepsilon = 7.0 \times 10^3$ and 281, $\varepsilon = 6.9 \times 10^3$). For these complexes, the Λ_M (10^{-3} M) values in water at 20 °C [11.6 (for **1**) and 16.5 (for **2**)] imply the presence of non-electrolyte-type species [21].

3.3. ESR spectra and magnetic properties

The effective magnetic moments $\mu_{eff} = 1.85$ BM (**1**) and 1.72 BM (**2**) at room temperature are normal for magnetically diluted d^9 systems. The X-band ESR spectra of a polycrystalline powder of complexes **1** and **2** recorded at 298 K show a single broad band centred at $g = 2.12$ and 2.11, respectively. Signals of both ESR spectra could be generated by the overlapping of the three components of g according to a rhombically distorted symmetry, particularly in the case of complex **1** in which a small anisotropic feature in $g_\perp$ component is observed.

4. Supplementary material

Crystallographic data for the structural analysis have been deposited with the Cambridge Crystallographic Data Centre, CCDC Nos. 172038 and 172037 for **1** and **2,** respectively. Copies of this information mat be obtained free of charge from The Director, CCDC, 12 Union Road, Cambridge, CB2 1EZ, UK (fax: +44-1223-336033; e-mail: deposit@ccdc.cam.ac.uk or www:http://www.ccdc.cam.ac.uk).

Acknowledgements

We are grateful to Spanish CICYT (PB98-0123) for financial support.

References

[1] A. García-Raso, A. Terrón, J.J. Fiol, E. Molins, C. Miravitlles, Polyhedron 14 (1995) 2537.
[2] A. García-Raso, J.J. Fiol, B. Adrover, E. Molins, C. Miravitlles, Polyhedron 15 (1996) 1829.
[3] A. García-Raso, J.J. Fiol, B. Adrover, V. Moreno, E. Molins, I. Mata, J. Chem. Soc., Dalton Trans. (1998) 1031.
[4] T.J. Kistenmacher, D.J. Szalda, L.G. Marzilli, Acta Crystallogr., Sect. B 31 (1975) 2416.
[5] D.J. Szalda, L.G. Marzilli, T.J. Kistenmacher, Biochem. Biophys. Res. Commun. 63 (1975) 601.
[6] K. Saito, R. Terashima, T. Sakaki, K. Tomita, Biochem. Biophys. Res. Commun. 61 (1974) 83.
[7] D.J. Szalda, T.J. Kistenmacher, Acta Crystallogr., Sect. B 33 (1977) 865.
[8] T. Sugimori, K. Shibakawa, H. Masuda, A. Odani, O. Yamauchi, Inorg. Chem. 32 (1993) 4951.
[9] L.J. Farrugia, J. Appl. Crystallogr. 32 (1999) 837.
[10] G.M. Sheldrick, SHELXL97. Program for Crystal Structure Analysis (Release 97-2). University of Göttingen, Germany, (1997).
[11] G. Cervantes, J.J. Fiol, A. Terrón, V. Moreno, J.R. Alabart, M. Aguiló, M. Gómez, X. Solans, Inorg. Chem. 29 (1990) 5168.
[12] M.M. Stimson, M.J. O'Donnell, J. Am. Chem. Soc. 74 (1952) 1805.
[13] M. Tsuboi, S. Takahasha, I. Harada, in: J. Duchesne (Ed.), Physicochemical Properties of Nucleic Acids, vol. 2, Academic Press, London, 1973, p. 91.
[14] H. Susi, J.S. Ard, J.M. Purcell, Spectrochim. Acta 29A (1973) 725.
[15] E.D. Radchenko, G.G. Sheina, N.A. Smorygo, Y.P. Blagoi, J. Mol. Struct. 116 (1984) 387.
[16] Y. Nishimura, M. Tsuboi, Chem. Phys. 98 (1985) 71.
[17] K. Nakamoto, Infrared an Raman Spectra of Inorganic and Coordination Compounds, Wiley, New York, 1978, p. 243.
[18] C.J. Simmons, M. Lundeen, K. Seff, Inorg. Chem. 17 (1978) 1429.
[19] M.C. Lim, E. Sinn, R.B. Martin, Inorg. Chem. 15 (1976) 807.
[20] A.B.P. Lever, Inorganic Electronic Spectroscopy, second ed., Elsevier, New York, 1986.
[21] W.J. Geary, Coord. Chem. Rev. 7 (1971) 81.

PERGAMON

Polyhedron 21 (2002) 1203–1209

POLYHEDRON

www.elsevier.com/locate/poly

Oxalato complexes of copper(II) with chelating diamines. Crystal structure of $[Cu(dmen)ox(H_2O)]_2[Cu(dmen)_2](ClO_4)_2$

Zdeněk Smékal [a,*], Jiří Kameníček [a], Petra Klasová [a], Grzegorz Wrzeszcz [b], Zdeněk Šindelář [a], Pavel Kopel [a], Zdirad Žák [c]

[a] *Department of Inorganic and Physical Chemistry, Palacký University, Křížkovského 10, 771 47 Olomouc, Czech Republic*
[b] *Faculty of Chemistry, Nicholas Copernicus University, Gagarina 7, 87-100 Toruń, Poland*
[c] *Department of Inorganic Chemistry, Masaryk University, Kotlářská 2, 611 37 Brno, Czech Republic*

Received 26 October 2001; accepted 19 February 2002

Abstract

Four new oxalato complexes of copper(II) of composition $[Cu(dmen)ox(H_2O)]_2$ $[Cu(dmen)_2](ClO_4)_2$ (**1**) (dmen = *N*,*N*-dimethylethylenediamine, H_2ox = oxalic acid), $[(Cu(dmen)H_2O)_2ox](ClO_4)_2 \cdot H_2O$ (**2**), $[Cu(tmen)(H_2O)(ox)Cu(aep)(H_2O)](ClO_4)_2$ (**3**) (tmen = *N*,*N*,*N*′,*N*′-tetramethylethylenediamine, aep = 2-(2-aminoethyl)pyridine) and $[(Cu(dben)NO_3)_2ox]$ (**4**) (dben = *N*,*N*′-dibenzylethylenediamine) have been prepared and characterised by IR and UV–Vis spectroscopies and magnetic measurements. The crystal structure of $[Cu(dmen)ox(H_2O)]_2[Cu(dmen)_2](ClO_4)_2$ (**1**) has been determined by single-crystal X-ray analysis. The structure of **1** contains a neutral $[Cu(dmen)ox(H_2O)]$ complex, a cationic $[Cu(dmen)_2]^{2+}$ complex and perchlorate anions. The copper(II) atom of the neutral $[Cu(dmen)ox(H_2O)]$ unit possesses a distorted square-pyramidal environment with two oxygen atoms of oxalate and two nitrogen atoms of dmen in the basal plane and an oxygen atom of a water molecule in the apical position. The copper(II) atom of the cationic $[Cu(dmen)_2]$ unit shows a square-planar environment with four donor nitrogen atoms of two molecules of dmen. The temperature dependence of magnetic susceptibility for compounds **2**–**4** was measured. Magnetochemical measurements show that copper(II) ions in compounds **2**–**4** are antiferromagnetically coupled through the oxalate bridge, $J = -157$, -175 and -167 cm^{-1} ($H = -2JS_1S_2$, $S_1 = S_2 = 1/2$) for **2**, **3** and **4**, respectively. © 2002 Elsevier Science Ltd. All rights reserved.

Keywords: Copper(II) complexes; Oxalato complexes; Oxalato-bridged complexes; Magnetic properties; Crystal structures

1. Introduction

Binuclear copper(II) complexes with the oxalate dianion (ox) acting as a bis-bidentate bridging ligand are suitable model compounds for magneto-structural correlations. General trends of magnetic behaviour of these compounds are well established, the oxalate bridge being very efficient in transmission of the antiferromagnetic interactions between the two copper(II) atoms. Julve at al. [1,2] described a theory predicting the magnetic interactions in oxalato bridged Cu(II) complexes. Many binuclear copper(II) mixed-ligand complexes with oxalate as bridging ligand have been structurally characterised and it was found copper(II) can be five- or six-coordinated [2–30]. It was demonstrated that μ-oxalato-dicopper(II) complexes possesses *J*-values approximately from 0 to -200 cm^{-1} ($H = -2JS_1S_2$, $S_1 = S_2 = 1/2$). Further, it is known that complexes with tetragonal pyramidal geometry at both copper centres with oxalate coordinated in the basal plane give rise to *J*-values near -200 cm^{-1} [2,6,8,11,13,24,25,28–30]. A weak interaction (the observed *J*-values are in the range from $+1.1$ to -37.4 cm^{-1}) was found in the case of octahedral, trigonal bipyramidal or tetragonal pyramidal (with one oxygen atom of oxalate coordinated in the basal plane and the other in the apical position) arrangements of copper(II) atoms [9,17,23,25]. Recently, we prepared and characterised binuclear μ-oxalato copper(II) complexes $[(Cu(1,3\text{-pn}))_2ox](ClO_4)_2$ (1,3-pn = 1,3-diaminopropane)

* Corresponding author. Tel.: +420-68-563-4352; fax: +420-68-522-5737.
E-mail address: smekal@risc.upol.cz (Z. Smékal).

0277-5387/02/$ - see front matter © 2002 Elsevier Science Ltd. All rights reserved.
PII: S0277-5387(02)01000-8

($J = -127$ cm^{-1}), [(Cu(ept))$_2$ox](ClO$_4$)$_2$ (ept = *N*-(2-aminoethyl)-1,3-diaminopropane) [31], [(Cu(aep)-H$_2$O)$_2$ox](NO$_3$)$_2$ (aep = 2-(2-aminoethyl)pyridine) ($J = -160$ cm^{-1}), [(Cu(ept))$_2$ox](NO$_3$)$_2$·H$_2$O [28], [(Cu(medpt))$_2$ox](ClO$_4$)$_2$ (medpt = 3,3′-diamino-*N*-methyl-dipropylamine) ($J = +1.9$ cm^{-1}), [(Cu-(medpt))$_2$ox](NO$_3$)$_2$·2 2/3H$_2$O [29] ($J = -2.6$ cm^{-1}), [(Cu(trimeen)H$_2$O)$_2$ox](ClO$_4$)$_2$·2H$_2$O (trimeen = *N*,*N*,*N*′-trimethylethylenediamine) ($J = -172$ cm^{-1}), [(Cu(trimeen)H$_2$O)$_2$ox](NO$_3$)$_2$·2H$_2$O ($J = -168$ cm^{-1}) and [(Cu(dieten)H$_2$O)$_2$ox](ClO$_4$)$_2$·H$_2$O (dieten = *N*,*N*′-diethylethylenediamine) ($J = -172$ cm^{-1}) [30].

We have extended the series of amine ligands by dmen (*N*,*N*-dimethylethylenediamine) and dben (*N*,*N*′-dibenzylethylenediamine) with the aim to prepare new binuclear μ-oxalato copper(II) complexes. Therefore, we carried out the reaction of copper(II) perchlorate (or copper(II) nitrate), the appropriate amine and sodium oxalate and prepared binuclear μ-oxalato copper(II) complexes [(Cu(dmen)H$_2$O)$_2$ox](ClO$_4$)$_2$·H$_2$O (**2**) and [(Cu(dben)NO$_3$)$_2$ox] (**4**). Our attempts to prepare the analogous complexes [(Cu(dmen)H$_2$O)$_2$ox](NO$_3$)$_2$ and [(Cu(dben)H$_2$O)$_2$ox](ClO$_4$)$_2$ led only to non-reproducible products. Surprisingly, the reaction of copper(II) perchlorate, *N*,*N*-dimethylethylenediamine, sodium oxalate and potassium cyanate in aqueous solution did not result in a complex with oxalato or cyanato bridging ligands but the mononuclear oxalato complex [Cu(dmen)ox(H$_2$O)]$_2$[Cu(dmen)$_2$](ClO$_4$)$_2$ (**1**).

Julve et al. [2] prepared an interesting binuclear oxalato-bridged complex with non-equal copper(II) centres (each copper atom is coordinated by a different blocking ligand) of composition [Cu(tmen)(H$_2$O)(ox)-Cu(dien)](ClO$_4$)$_2$ (tmen = *N*,*N*,*N*′,*N*′-tetramethylethylenediamine, dien = diethylenetriamine). With the aim to extend the series of these compounds we tried the reaction [Cu(tmen)ox]·4H$_2$O, copper(II) perchlorate and 2-(2-aminoethyl)pyridine (aep) that results in the formation of the complex [Cu(tmen)(H$_2$O)(ox)Cu(aep)-(H$_2$O)](ClO$_4$)$_2$ (**3**).

The prepared compounds were characterised by elemental analysis, IR and UV–Vis spectroscopies and magnetic susceptibility measurements. The crystal structure of the complex [Cu(dmen)ox(H$_2$O)]$_2$[Cu(dmen)$_2$]-(ClO$_4$)$_2$ (**1**) has been determined by a single-crystal X-ray analysis.

2. Experimental

2.1. Chemicals and methods

The starting material Cu(ClO$_4$)$_2$·6H$_2$O was obtained by the reaction of basic copper(II) carbonate and HClO$_4$ (Carlo Erba) in aqueous solution (the reaction mixture was concentrated to crystallisation, the solid was filtered off and dried at 35 °C under an infralamp). *N*,*N*-dimethylethylenediamine, *N*,*N*′-dibenzylethylenediamine and 2-(2-aminoethyl)pyridine (Aldrich), sodium oxalate and Cu(NO$_3$)$_2$·3H$_2$O (Lachema Brno) and KOCN (Fluka) were used without further purification. Compound [Cu(tmen)ox]·4H$_2$O was prepared according to the literature [2].

Elemental analyses (C, H, N) were performed on a Fisons EA1108 CHN instrument. Absorption UV–Vis spectra (33 000–11 000 cm^{-1}) were recorded on a SPECORD M40 instrument in Nujol, IR spectra (4000–400 cm^{-1}) on a SPECORD IR 80 instrument using the Nujol technique. The magnetic susceptibilities were measured in the temperature range liquid nitrogen to room temperature (r.t.) by the Faraday method on the balance constructed in Nicholas Copernicus University (complexes **3** and **4**) and in Palacký University (complex **2**) with Hg[Co(NCS)$_4$] as a calibrant [32]. The molar susceptibilities of all complexes were corrected for diamagnetism using Pascal's constants [33].

Crystals of [Cu(dmen)ox(H$_2$O)]$_2$[Cu(dmen)$_2$](ClO$_4$)$_2$ (**1**) of X-ray quality were obtained from water by slow evaporation of solvent at r.t. The reflections were collected at 150 K on a four-circle κ-axis KUMA KM-4 diffractometer. The structure was solved by the heavy method using atom the program SHELXS-97 [34]. All non-hydrogen atoms were refined anisotropically [35] by a full-matrix least-squares with the weight procedure $w = [\sigma^2(F_o^2) + (w_1P)^2 + w_2P]^{-1}$, where $P = [F_o^2 + 2F_c^2]/3$, $w_1 = 0.0740$, $w_2 = 3.4700$. Parameters of all hydrogen atoms were refined isotropically. The crystal data and structure refinement details for [Cu(dmen)ox(H$_2$O)]$_2$[Cu(dmen)$_2$](ClO$_4$)$_2$ (**1**) are given in Table 1, whereas selected bond lengths and angles are listed in Table 2.

2.2. Syntheses

Caution! Perchlorates and perchlorate salts of metal complexes with organic ligands are potentially explosive. A small amount of material only should be prepared and it should be handled with care.

2.2.1. [Cu(dmen)ox(H$_2$O)]$_2$[Cu(dmen)$_2$](ClO$_4$)$_2$ (1)

A solution of 0.22 g (2.71 mmol) of KOCN and 0.36 g (2.69 mmol) of sodium oxalate in 25 cm^3 of water was added to a solution of 2.00 g (5.40 mmol) of Cu(ClO$_4$)$_2$·6H$_2$O and 0.59 cm^3 (5.37 mmol) of *N*,*N*-dimethylethylenediamine in 10 cm^3 of water. After 1 h of stirring the reaction mixture was concentrated to crystallisation in a water bath. The obtained dark blue crystals were filtered off and dried in air. The yield was 0.6 g (45%).

2.2.2. [(Cu(dmen)H$_2$O)$_2$ox](ClO$_4$)$_2$·H$_2$O (2)

A solution of 0.18 g (1.34 mmol) of sodium oxalate in 15 cm^3 of water was added to a solution of 1.00 g (2.70

Table 1
Crystal data and structure refinement parameters for [Cu(dmen)-ox(H_2O)]$_2$[Cu(dmen)$_2$](ClO_4)$_2$ (**1**)

Formula	$C_{10}H_{26}ClCu_{1.5}N_4O_9$
Formula weight (g mol^{-1})	477.11
Temperature (K)	150(2)
Wavelength (Å)	0.71073
Crystal system	triclinic
Space group	$P\bar{1}$
Unit cell dimensions	
a (Å)	6.4920(10)
b (Å)	8.501(2)
c (Å)	17.079(3)
α (°)	94.38(3)
β (°)	100.68(1)
γ (°)	103.80(3)
V (Å^3)	892.3(3)
Z	2
Calculated density (Mg m^{-3})	1.776
Absorption coefficient (mm^{-1})	2.006
F(000)	493
Crystal size (mm)	0.35 × 0.30 × 0.25
θ Range for data collection (°)	3.67–29.21
Index ranges	$-5 \le h \le 8$, $-11 \le k \le 11$, $-23 \le l \le 23$
Reflection collected/unique	7649/4279 [$R_{int} = 0.0297$]
Refinement method	full-matrix least-squares on F^2
Data/restraints/parameters	4279/0/258
Goodness-of-fit on F^2	1.080
Final R factor [$I > 2\sigma(I)$]	$R_1 = 0.0431$, $wR_2 = 0.1440$
R factor (all data)	$R_1 = 0.0461$, $wR_2 = 0.1454$
Largest difference peak and hole (e Å^{-3})	0.972 and −0.780

Table 2
Selected bond lengths (Å) and angles (°) for[Cu(dmen)ox(H_2O)]$_2$[Cu-(dmen)$_2$](ClO_4)$_2$ (**1**)

Bond lengths	
Cu(1)–O(4)	1.940(3)
Cu(1)–O(3)	1.957(3)
Cu(1)–N(2)	2.015(3)
Cu(1)–N(1)	2.022(3)
Cu(1)–O(9)	2.345(3)
Cu(2)–N(4)	1.994(3)
Cu(2)–N(3)	2.095(3)
Bond angles	
O(4)–Cu(1)–O(3)	84.50(11)
O(4)–Cu(1)–N(2)	95.18(12)
O(3)–Cu(1)–N(2)	164.41(13)
O(4)–Cu(1)–N(1)	175.16(11)
O(3)–Cu(1)–N(1)	92.57(11)
N(2)–Cu(1)–N(1)	86.61(12)
O(4)–Cu(1)–O(9)	87.68(11)
O(3)–Cu(1)–O(9)	105.97(11)
N(2)–Cu(1)–O(9)	89.57(12)
N(1)–Cu(1)–O(9)	96.84(11)
N(4)–Cu(2)–N(3)	85.30(12)
N(4a) [a]–Cu(2)–N(3)	94.70(12)

[a] Symmetry transformations used to generate equivalent atoms: $-x$, $-y+1$, $-z+1$.

mmol) of Cu(ClO_4)$_2$·6H_2O and 0.30 cm^3 (2.73 mmol) of *N*,*N*-dimethylethylenediamine in 25 cm^3 of water. The resulting dark blue solution was concentrated to 15 cm^3 to crystallisation by heating. A small amount of solid formed was discarded. The filtrate was allowed to stand overnight. The light blue microcrystals were filtered off, washed with a small amount of water and dried in air. The yield was 0.35 g (40%).

2.2.3. [Cu(tmen)(H_2O)(ox)Cu(aep)(H_2O)](ClO_4)$_2$ (**3**)

A solution of 0.50 g (1.35 mmol) of Cu(ClO_4)$_2$·6H_2O and 0.16 cm^3 (1.34 mmol) of 2-(2-aminoethyl)pyridine in 20 cm^3 of water was added to a solution of 0.46 g (1.35 mmol) of [Cu(tmen)ox]·4H_2O in 15 cm^3 of water. The resulting dark blue solution was concentrated to 10 cm^3 to crystallisation by heating. A small amount of light blue powder formed was discarded. The filtrate was allowed to stand overnight. The obtained blue polycrystalline product was filtered off and dried in air. The yield was 0.2 g (22%).

2.2.4. [(Cu(dben)NO_3)$_2$ox] (**4**)

A solution of 0.14 g (1.04 mmol) of sodium oxalate in a minimum amount of water was added to a solution of 0.50 g (2.07 mmol) of Cu(NO_3)$_2$·3H_2O and 0.49 cm^3 (2.08 mmol) of *N*,*N*′-dibenzylethylenediamine in ethanol (25 cm^3) and water (10 cm^3). The reaction mixture was filtered and the filtrate was allowed to stand overnight. The blue microcrystalline product was filtered off, washed with water and ethanol and dried in air. The yield was 0.7 g (85%).

3. Results and discussion

3.1. Structure of complex *1*

The structure of [Cu(dmen)ox(H_2O)]$_2$[Cu-(dmen)$_2$](ClO_4)$_2$ (**1**) is made up of neutral [Cu(dmen)-ox(H_2O)] units, cationic [Cu(dmen)$_2$]$^{2+}$ units and un-

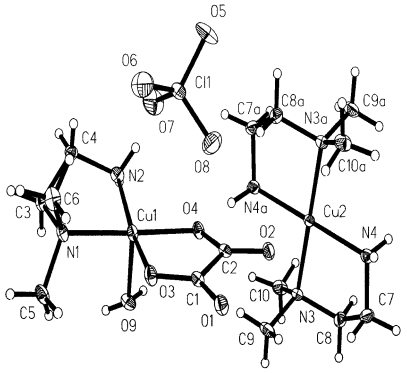


Fig. 1. A view (thermal ellipsoids are drawn at 40% probability level) of [Cu(dmen)ox(H_2O)]$_2$[Cu(dmen)$_2$](ClO_4)$_2$ (**1**).

Table 3
Elemental analysis of the complexes

Complex	Found (Calc.) (%)		
	C	H	N
$[Cu(dmen)ox(H_2O)]_2[Cu(dmen)_2](ClO_4)_2$ (**1**)	24.6 (25.2)	4.7 (5.5)	11.9 (11.8)
$[(Cu(dmen)H_2O)_2ox](ClO_4)_2 \cdot H_2O$ (**2**)	19.1 (18.6)	4.3 (4.7)	7.8 (8.7)
$[Cu(tmen)(H_2O)(ox)Cu(aep)(H_2O)](ClO_4)_2$ (**3**)	26.2 (26.4)	4.4 (4.6)	8.1 (8.2)
$[(Cu(dben)NO_3)_2ox]$ (**4**)	49.8 (49.2)	4.9 (5.2)	10.2 (9.5)

coordinated perchlorate anions (Fig. 1). The $[Cu(dmen)ox(H_2O)]$ complex, $[Cu(dmen)_2]^{2+}$ cation and perchlorate anion, in a 2:1:2 molar ratio, coexist. The copper atom of the neutral $[Cu(dmen)ox(H_2O)]$ unit shows a distorted square-pyramidal environment with the two oxygen atoms of oxalate and two nitrogen atoms of dmen building the basal plane and an oxygen atom of a water molecule in the apical position. The in-plane Cu–N and Cu–O bond lengths ranges from 1.940(3) to 2.022(3) Å and the axial Cu–O bond distance 2.345(3) Å is significantly longer than the in-plane Cu–N and Cu–O bond lengths. The value of the τ parameter (17.9) [36] discloses a square-pyramidal shape of the coordination polyhedron (ideal τ value for square-pyramidal situation is 0 and for trigonal bipyramidal situation is 100). The copper atom of the cationic $[Cu(dmen)_2]^{2+}$ unit is situated on a crystallographic centre of symmetry and shows a square-planar environment with four nitrogen atoms from two molecules of dmen. The one Cu–N bond length (1.994(3) Å) is shorter than the other Cu–N bond length (2.095(3) Å). This difference may be explained by steric hindrance from the methyl groups bonded to donor nitrogen atom.

The neutral complex $[Cu(dmen)ox(H_2O)]$ has square-pyramidal arrangement around the copper(II) atom with the two oxygen atoms of oxalate and two nitrogen atoms of *N*,*N*-dimethylethylenediamine forming the basal plane and an oxygen atom of a water molecule in the apical position as in the analogous complex $[Cu(L)ox(H_2O)]$ (L = *N*,*N*′-dimethylethylenediamine) [37] (its structure has been known since 1973).

3.2. IR and UV–Vis

The characteristic IR spectra group vibrations of the complexes prepared are as follows: $\nu_3(ClO_4)$ 1056–1100 cm^{-1} (s), $\nu_4(ClO_4)$ 624–620 cm^{-1} (s), $\nu_{asym}(OCO)$ 1642–1668 cm^{-1} (s) and $\delta(OCO)$ 752–788 cm^{-1} (m). These values are consistent with coordinated oxalate [7,12,38,39] and uncoordinated perchlorate [28,29,40] anions.

The UV–Vis absorption spectra of Cu(II) complexes are characterised by a strong band in the range 11 000–16 000 cm^{-1} corresponding to a d–d transition [41]. In the present compounds, the maxima for **1** (16 250), **2** (16 450), **3** (14 900) and **4** (15 700 cm^{-1}) with ε_{max} (mol^{-1} dm^3 cm^{-1}; per Cu) equal to 62 (**1**), 115 (**2**), 140 (**3**) and 103 (**4**), respectively, correspond to this band.

3.3. Magnetic properties

The magnetic susceptibility of the mononuclear complex $[Cu(dmen)ox(H_2O)]_2[Cu(dmen)_2](ClO_4)_2$ (**1**) was measured at r.t. only. The observed value of the magnetic moment (1.82μ_B per Cu) is in accordance with the literature data for magnetically diluted compounds of copper(II).

The variable-temperature magnetic moment and magnetic susceptibility in the range 84–295 K (compound **2**) and 78–298 K (compounds **3** and **4**) for solid samples is shown in Figs. 2–4. The magnetic moment are dependent on temperature and decreases from 1.31–1.40 μ_B (per Cu) at 298 (or 295) K to 0.29–0.30 μ_B (per Cu) at 78 (or 84) K (see Tables 3 and 4). This implies rather strong antiferromagnetic coupling mediated by the oxalate bridge.

Magnetic measurements show that complexes **2**–**4** behave like a common copper(II) dimers ($H = -2JS_1S_2$, $S_1 = S_2 = 1/2$) (see Figs. 2–4). The molar magnetic susceptibility was expressed by the modified Bleaney–Bowers equation allowing for the presence of paramagnetic impurity [42]:

Table 4
Magnetic properties of the complexes

Complex	μ_{eff} (per Cu)/T[μ_B] (K)	J (cm^{-1})	g	P (%)
$[Cu(dmen)ox(H_2O)]_2[Cu(dmen)_2](ClO_4)_2$ (**1**)	1.82/294			
$[(Cu(dmen)H_2O)_2ox](ClO_4)_2 \cdot H_2O$ (**2**)	1.40/295–0.30/84	−157	2.150	0
$[Cu(tmen)(H_2O)(ox)Cu(aep)(H_2O)](ClO_4)_2$ (**3**)	1.31/298–0.30/78	−175	2.108	1.63
$[(Cu(dben)NO_3)_2ox]$ (**4**)	1.35/298–0.29/78	−167	2.123	0.86

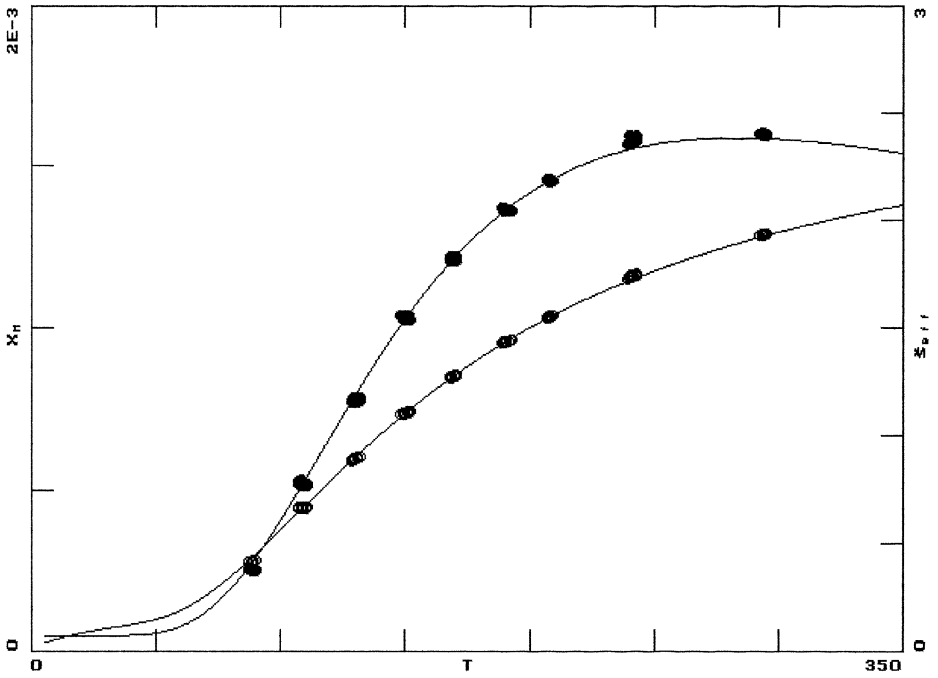


Fig. 2. Variation of corrected molar magnetic susceptibility (●) and effective magnetic moment (○) per mole of $[(Cu(dmen)H_2O)_2ox](ClO_4)_2 \cdot H_2O$ (**2**) complex with temperature. The circles are the experimental points, the solid lines are theoretical lines.

$$\chi_M^{corr} = 2(Ng^2\beta^2/3kT)[1 + 1/3\ \exp(-2J/kT)]^{-1}(1 - P) + (Ngi_i^2\beta^2/4kT)P + N\alpha$$

where χ_M^{corr} is the corrected molar magnetic susceptibility per copper(II) dimer, P is the mole fraction of the monomeric copper(II) impurities, g_i is the average g factor of the impurity which was fixed at 2.15 throughout the present study, $-2J$ is the singlet-triplet separation, $N\alpha$ is the temperature independent paramagnetism equal to 120×10^{-6} cm^3 mol^{-1} (per dimer), and the other symbols have their usual meanings. The best fit parameters J, g and P, were obtained by using a non-linear least-squares program. The exchange integral does not depend on the g_i value within range 2.1–2.2 and $N\alpha$ within the reasonable range, whereas changes on g-value and P are negligible. As a convenient statistical indicator of the quality of the least-squares fits, the discrepancy index σ_{dis} ($\sigma_{dis} = [\Sigma(\chi_{obs} - \chi_{calc})^2/$

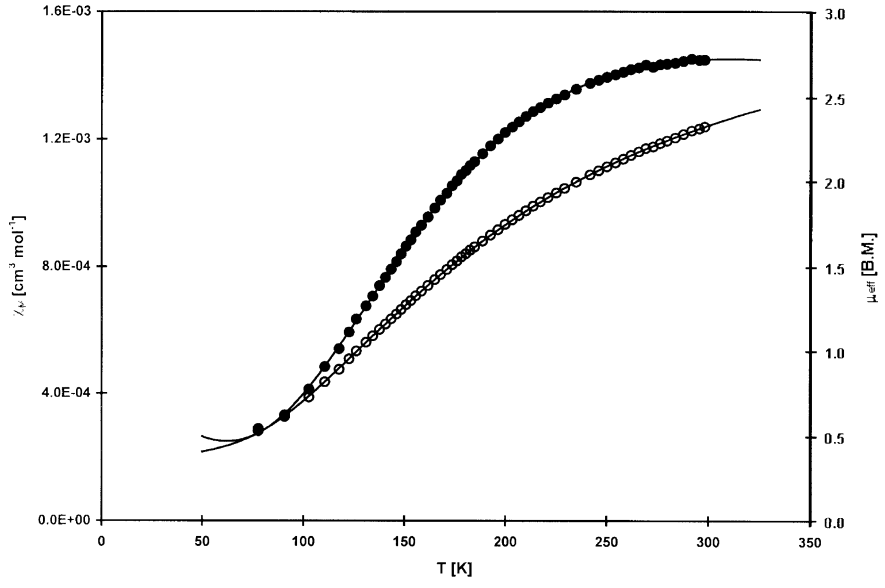


Fig. 3. Variation of corrected molar magnetic susceptibility (●) and effective magnetic moment (○) per mole of $[Cu(tmen)(H_2O)(ox)Cu(aep)(H_2O)](ClO_4)_2$ (**3**) complex with temperature. The circles are the experimental points, the solid lines are theoretical lines.

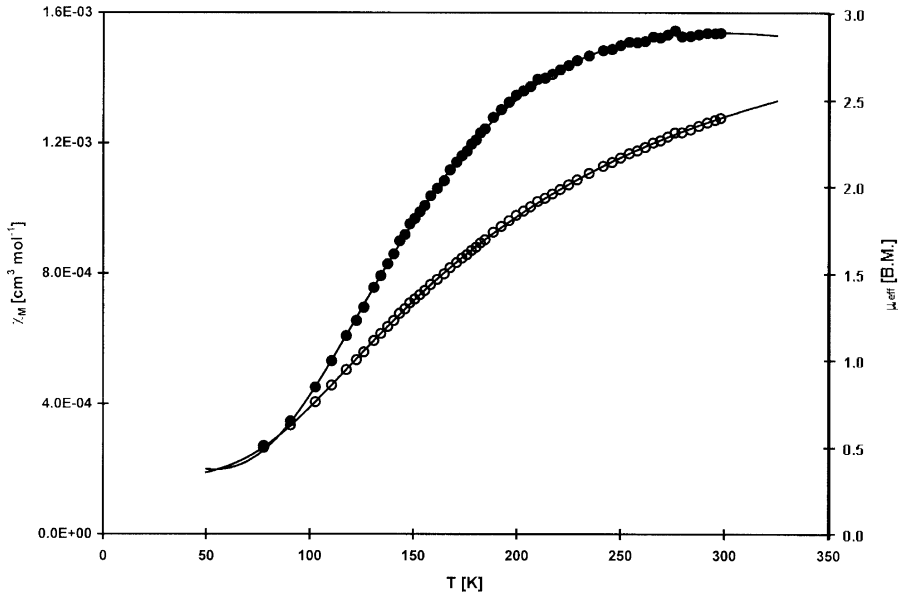


Fig. 4. Variation of corrected molar magnetic susceptibility (●) and effective magnetic moment (○) per mole of [(Cu(dben)NO_3)$_2$ox] (**4**) complex with temperature. The circles are the experimental points, the solid lines are theoretical lines.

$\Sigma(\chi_{obs})^2]^{1/2}$) was employed. The least-square fit (see Table 4) of the data yields $J = -157$ cm^{-1} ($\sigma_{dis} = 3.99 \times 10^{-3}$), $J = -175$ cm^{-1} ($\sigma_{dis} = 3.08 \times 10^{-3}$) and $J = -167$ cm^{-1} ($\sigma_{dis} = 4.74 \times 10^{-3}$) ($H = -2JS_1S_2$, $S_1 = S_2 = 1/2$) for **2**, **3** and **4**, respectively.

Hence, the compounds **2**–**4** exhibit a strong antiferromagnetic exchange interaction that can be explained by the tetragonal pyramidal coordination of copper with oxalate oxygen atoms in basal positions, so that the x^2-y^2 magnetic orbital on Cu is directed ideally for overlap with the oxalate sigma orbitals [1,2]. The observed J-values for **2** (−157), **3** (−175) and **4** (−167 cm^{-1}) are similar to those of [(Cu(L)H_2O)$_2$ox](ClO$_4$)$_2$ (L = *N*,*N*-diethyl-1,2-diaminoethane) ($J = -150$ cm^{-1}) [24], [(Cu(L)H_2O)$_2$ox](ClO$_4$)$_2$·H_2O (L = *N*,*N*′-diethyl-1,2-diaminoethane) ($J = -172$ cm^{-1}) [30], [(Cu(aep)(H_2O))$_2$ox](ClO$_4$)$_2$ ($J = -160$ cm^{-1}) [28] or [(Cu(tmen)H_2O)$_2$ox](ClO$_4$)$_2$·1.25H_2O ($J = -193$ cm^{-1}) [2]. These four complexes [2,24,28,30] contain the square pyramidal arrangement of copper(II) with bridging oxalate and bidentate amine coordinated in the basal plane. The water oxygen atom is coordinated in the apical position. The square pyramidal coordination with oxalate oxygen atoms and blocking diamine nitrogen atoms in basal positions is supposed for complexes **2**, **3** and **4**, too.

4. Supplementary material

Supplementary data are available on request, quoting the deposition number 171583, from the CCDC, 12 Union Road, Cambridge CB2 1EZ, UK (fax: +44-1223-336033; e-mail: deposit@ccdc.cam.ac.uk; or www: http://www.ccdc.cam.ac.uk).

References

[1] M. Julve, M. Verdaguer, O. Kahn, A. Gleizes, M. Philoche-Levisalles, Inorg. Chem. 22 (1983) 368.
[2] M. Julve, M. Verdaguer, M. Philoche-Levisalles, O. Kahn, Inorg. Chem. 23 (1984) 3808.
[3] N.F. Curtis, I.R.N. McCormick, T.N. Waters, J. Chem. Soc., Dalton Trans. (1973) 1537.
[4] I. Castro, J. Faus, M. Julve, M. Mollar, A. Monge, E. Gutierrez-Puebla, Inorg. Chim. Acta 161 (1989) 97.
[5] A. Bencini, A.C. Fabretti, C. Zanchini, P. Zannini, Inorg. Chem. 26 (1987) 1445.
[6] M. Julve, J. Faus, M. Verdaguer, A. Gleizes, J. Am. Chem. Soc. 106 (1984) 8306.
[7] I. Castro, J. Faus, M. Julve, A. Gleizes, J. Chem. Soc., Dalton Trans. (1991) 1937.
[8] L.S. Tuero, J. Garcia-Lozano, E.E. Monto, M.B. Borja, F. Dahan, J.P. Tuchagues, J.P. Legros, J. Chem. Soc., Dalton Trans. (1991) 2619.
[9] J. Glerup, P.A. Goodson, D.J. Hodgson, K. Michelsen, Inorg. Chem. 34 (1995) 6255.
[10] J. Sletten, Acta Chem. Scand. Ser. A 37 (1983) 569.
[11] J. Shi, G.M. Yang, P. Cheng, D.Z. Liao, Z.H. Jiang, G.L. Wang, Polyhedron 16 (1997) 531.
[12] I. Castro, J. Faus, M. Julve, M.C. Muñoz, W. Diaz, X. Solans, Inorg. Chim. Acta 179 (1991) 59.
[13] A. Gleizes, M. Julve, M. Verdaguer, J.A. Real, J. Faus, X. Solans, J. Chem. Soc., Dalton Trans. (1992) 3209.
[14] J. Tang, E. Gao, W. Bu, D. Liao, S. Yan, Z. Jiang, G. Wang, J. Mol. Struct. 525 (2000) 271.
[15] O. Castillo, I. Muga, A. Luque, J.M. Gutierrez-Zorrilla, J. Sertucha, P. Vitoria, P. Roman, Polyhedron 18 (1999) 1235.
[16] J. Li, J. Sun, P. Chen, X. Wu, Cryst. Res. Technol. 30 (1995) 353.
[17] T.R. Felthouse, E.J. Laskowski, D.N. Hendrickson, Inorg. Chem. 16 (1977) 1077.
[18] J.A. Real, J. Borrás, X. Solans, M. Font-Altaba, Transition Met. Chem. (London) 12 (1987) 254.
[19] C. George, A. Purdy, Acta Crystallogr., Sect. C: Crystal Struct. Commun. 48 (1992) 155.
[20] L. Soto, J. Garcia, E. Escriva, J.P. Legros, J.P. Tuchagues, F. Dahan, A. Fuertes, Inorg. Chem. 28 (1989) 3378.

[21] P.E. Kruger, K.S. Murray, E.R.T. Tiekink, Z. Kristallogr. 209 (1994) 624.
[22] Q. Lu, J.J. Reibenspies, A.E. Martell, R.J. Motekaitis, Inorg. Chem. 35 (1996) 2630.
[23] M.L. Calatayud, I. Castro, J. Sletten, F. Lloret, M. Julve, Inorg. Chim. Acta 300 (2000) 846.
[24] R. Vicente, A. Escuer, J. Ferretjans, H. Stoeckly-Evans, X. Solans, M. Font-Bardia, J. Chem. Soc., Dalton Trans. (1997) 167.
[25] Y. Akhriff, J. Server-Carrió, A. Sancho, J. García-Lozano, E. Escrivá, J.V. Folgado, L. Soto, Inorg. Chem. 38 (1999) 1174.
[26] L. Zhang, H.L. Yan, S.P. Yan, Z.H. Jiang, D.Z. Liao, G.L. Wang, Polish J. Chem. 73 (1999) 391.
[27] L. Zhang, W.M. Bu, S.P. Yan, Z.H. Jiang, D.Z. Liao, G.L. Wang, Polyhedron 19 (2000) 1105.
[28] Z. Smékal, Z. Trávníček, M. Nádvorník, Z. Šindelář, R. Klička, J. Marek, Collect. Czech. Chem. Commun. 63 (1998) 783.
[29] Z. Smékal, Z. Trávníček, F. Lloret, J. Marek, Polyhedron 18 (1999) 2787.
[30] Z. Smékal, V. Langer, G. Wrzeszcz, P. Klasová, J. Coord. Chem. 55 (2002) 595.
[31] Z. Smékal, P. Thornton, Z. Šindelář, R. Klička, Polyhedron 17 (1998) 1631.
[32] B.N. Figgis, R.S. Nyholm, J. Chem. Soc. (1958) 4190.
[33] B.N. Figgis, J. Lewis, Modern Coordination Chemistry, Interscience Publishers, NewYork, 1960, p. 430.
[34] G.M. Sheldrick, Acta Crystallogr., Sect. A 46 (1990) 467.
[35] G.M. Sheldrick, SHELXS-97, Program for Crystal Structure Refinement, University of Göttingen, Göttingen, Germany, 1997.
[36] A.W. Addison, T.N. Rao, J. Reedijk, J. van Rijn, G.C. Verschoor, J. Chem. Soc., Dalton Trans. (1984) 1349.
[37] J. Korvenranta, Suom. Kemistil. B 46 (1973) 296.
[38] N.F. Curtis, J. Chem. Soc. (A) (1968) 1584.
[39] D.M. Duggan, E.K. Barefield, D.N. Hendrickson, Inorg. Chem. 12 (1973) 985.
[40] R. Pastorek, Z. Trávníček, E. Kvapilová, Z. Šindelář, F. Březina, J. Marek, Polyhedron 18 (1999) 151.
[41] N.N. Greenwood, A. Earnshaw, Chemistry of the Elements, Informatorium, Praha, 1993.
[42] M. Kato, Y. Muto, Coord. Chem. Rev. 92 (1988) 45.

PERGAMON

Polyhedron 21 (2002) 1211–1215

POLYHEDRON

www.elsevier.com/locate/poly

Syntheses and reactivities of new bis(imido)Mo(VI) complexes of hydrotris(3,5-dimethyl-1-pyrazolyl)borate and X-ray molecular structures of [{HB(3,5-$Me_2C_3N_2H)_3$}Mo(Nmes)$_2$X] (X = Cl or OH; mes = 2,4,6-trimethylphenyl)

Hyun Yong Cho, Soo-Gyun Roh, Jong Hwa Jeong *

Department of Chemistry, Kyungpook National University, Taegu 702-701, South Korea

Received 14 November 2001; accepted 1 March 2002

Abstract

A chloride substitution reaction of a bis(imido) molybdenum(VI) complex, [Mo(Nmes)$_2$Cl$_2$(dme)] (dme = 1,2-dimethoxyethane) with KTp* (Tp* = hydrotris(3,5-dimethyl-1-pyrazole)borate) in THF resulted in [Tp*Mo(Nmes)$_2$Cl] **1** in good yield. The analogous methylated complex [Tp*Mo(Nmes)$_2$(CH_3)] **2** was formed by reaction of **1** with 1 equiv. of CH_3MgCl in THF, while [Tp*Mo(Nmes)$_2$(OH)] **3** was conveniently produced from **2** in the presence of wet methanol under aerobic conditions. The complexes were characterized by ^{1}H NMR and IR spectroscopy. The molecular structures of complexes of **1** and **3** have been determined by X-ray single crystal analyses. The crystal structures of the complexes show that the three nitrogen atoms of Tp* are not equidistant from the respective Mo(VI) centers. Each Mo(VI) centre of **1** and **3** is in a distorted octahedral coordination geometry with a facially co-ordinated Tp* and two Nmes ligands. The complexes of **1** and **3** contain linear imido ligands © 2002 Elsevier Science Ltd. All rights reserved.

Keywords: Pyrazole; Mononuclear bis(imido) Mo(VI) complexes; X-ray crystal structures

1. Introduction

Tris(pyrazolyl)borate is a facially co-ordinating ligand similar to 6e$^-$ donors such as L_{OR} and Cp* ligands (L_{OR} = [η^5-(C_5H_5)Co{P(OR)$_2$(O)}$_3$]; Cp* = pentamethylcyclopentadienyl). The substitution of groups on the pyrazoles can control the steric and electronic effects of the ligand on the metal center [1–5]. Also, the sterically encumbering nature of the Tp* ligand compared with Cp* is widely known and explored in high activity for catalyst systems [6–8].

Imido ligands attached to transition metals form multiple bonds, which may be used to stabilize high oxidation state metals [9,10]. Certain imido complexes can readily be prepared by adding a primary amine to a molybdenum-oxo complex and removing water. Convenient synthetic entries into bis(imido) [11–17] and chelating bis(imido) [18,19] molybdenum(VI) complexes have been reported and [Mo(TADDAMINat)Cl$_2$(dme)] (TADDAMIN = {(4S,5S)-2,2-dimethyl-α,α,α′,α′-tetraphenyl-1,3-dioxolan-4,5-dimethanamine}) [20] containing a chiral diimido ligand is known as a catalyst for C–C and C–N bond formation.

[TpMo(Nmes)$_2$Cl] (Tp = hydrotris(pyrazolyl)borate) and [(L_{OEt})Mo(Nmes)$_2$Cl] (L_{OEt} = [η^5-(C_5H_5)Co{P(O-C_2H_5)$_2$(O)}$_3$]) [21] have been synthesized by the treatment of [Mo(Nmes)$_2$Cl$_2$(dme)] with KTp or NaL_{OEt}, but are not fully characterized. The related bis(imido) molybdenum complex [Tp*Mo(N′Bu)$_2$Cl] [22] was synthesized and its structure was identified by X-ray crystallography. However, studies of the reactivity of bis(imido) molybdenum complexes are limited. The related dioxomolybdenum(VI) complexes [Tp*Mo-(O)$_2$Cl] [22,23] and [Tp*Mo(O)$_2$(R)] [24,25] (R = CH_3 or $CH_2Si(CH_3)_3$) were also reported. Significantly, we have obtained products containing alkyl and hydroxy

* Corresponding author. Tel.: +82-539-506-343; fax: +82-539-506-6330.

E-mail address: jeongjh@knu.ac.kr (J.H. Jeong).

0277-5387/02/$ - see front matter © 2002 Elsevier Science Ltd. All rights reserved.
PII: S0277-5387(02)01008-2

groups from the further reactions with **1** and we report herein the syntheses, molecular structures and reactivities of [Tp*Mo(Nmes)$_2$X] (X = Cl, CH_3 or OH).

2. Experimental

2.1. General

All manipulations were carried out with standard Schlenk techniques under argon. KTp* [26,27] and [Mo(Nmes)$_2$Cl$_2$(dme)] [21] were prepared according to literature procedures. All other chemicals were of reagent grade and the solvents were distilled and degassed under argon prior to use. Elemental analyses were performed by the Chemical Analysis Laboratory of the Korea Basic Science Institute at Kyungpook National University. The ^{1}H NMR spectra were recorded on a Varian 300 NMR spectrometer at ambient temperature. The IR spectra (KBr, pellet) were recorded on Mattsion, Galaxy 7020A spectrophotometers.

2.2. Synthesis of bis(imido)complexes

2.2.1. Synthesis of [Tp*Mo(Nmes)$_2$Cl] (*1*)

To a mixture of KTp* (2.64 g, 7.90 mmol) and [Mo(Nmes)$_2$Cl$_2$(dme)] (4.11 g, 7.90 mmol) was added 150 ml of THF with stirring and the solution was then left to stir at room temperature (r.t.) for 4 days. The resulting green solution was filtered in air and the filtrate was dried in vacuo. The green solid was extracted with Et_2O and dried to afford a dark green solid. Yield 3.80 g (70%). (Found: C, 56.87; H, 6.38; N, 16.13. $C_{33}H_{44}BClN_8Mo$ requires C, 57.03; H, 6.38; N, 16.12%); ν_{max} (cm^{-1}) 2924m, 2523w, 1601w, 1542m, 1447s, 1414s, 1369s, 1274vs, 1209s, 1070m, 1043w, 969w, 855w, 786w, 648w cm^{-1}; δ_H(300 MHz; $CDCl_3$; $SiMe_4$) 6.70 (2H, s, $Me_3C_6H_2$), 6.45 (2H, s, $Me_3C_6H_2$), 5.68 (1H, s, 4-$Me_2C_3N_2H$), 5.65 (2H, s, 4-$Me_2C_3N_2H$), 2.74 (6H, s, 3-$Me_2C_3N_2H$), 2.37 (3H, s, 3-$Me_2C_3N_2H$), 2.29 (12H, s, *o*-$Me_3C_6H_2$), 2.15 (6H, s, *p*-$Me_3C_6H_2$), 1.98 (3H, s, 5-$Me_2C_3N_2H$), 1.12 (6H, s, 5-$Me_2C_3N_2H$).

2.2.2. Synthesis of [Tp*Mo(Nmes)$_2$(CH$_3$)] (*2*)

Complex **1** (1.70 g, 2.45 mmol) was dissolved in 50 ml of THF, cooled in a dry ice–acetone bath. 3 M CH_3MgCl in THF (0.82 ml, 2.45 mmol) was added slowly by syringe. The dark green solution was allowed to warm to r.t. and the solution stirred for 1 day. The resulting solution was filtered off and the solvent was removed in vacuo. The dark green solid was extracted with Et_2O and dried in vacuo. Yield 1.21 g (73%). (Found: C, 60.67; H, 7.18; N, 16.43. $C_{34}H_{47}BN_8Mo$ requires C, 60.54; H, 7.02; N, 16.61%); δ_H(300 MHz; $CDCl_3$; $SiMe_4$) 6.76 (2H, s, $Me_3C_6H_2$), 6.56 (2H, s, $Me_3C_6H_2$), 5.61 (2H, s, 4-$Me_2C_3N_2H$), 5.54 (1H, s, 4-$Me_2C_3N_2H$), 2.87 (6H, s, 3-$Me_2C_3N_2H$), 2.54 (6H, s, *p*-$Me_3C_6H_2$), 2.21 (3H, s, 3-$Me_2C_3N_2H$), 2.12 (6H, s, *o*-$Me_3C_6H_2$), 2.11 (6H, s, *o*-$Me_3C_6H_2$), 2.06 (3H, s, 5-$Me_2C_3N_2H$), 1.81 (3H, s, CH_3), 1.63 (6H, s, 5-$Me_2C_3N_2H$).

Attempts to obtain [Tp*Mo(Nmes)$_2$(CH$_2$(CH$_3$)$_2$Ph)] from the reaction of **1** with $CH_2(CH_3)_2PhMgCl$ failed.

2.2.3. Synthesis of [Tp*Mo(Nmes)$_2$(OH)] (*3*)

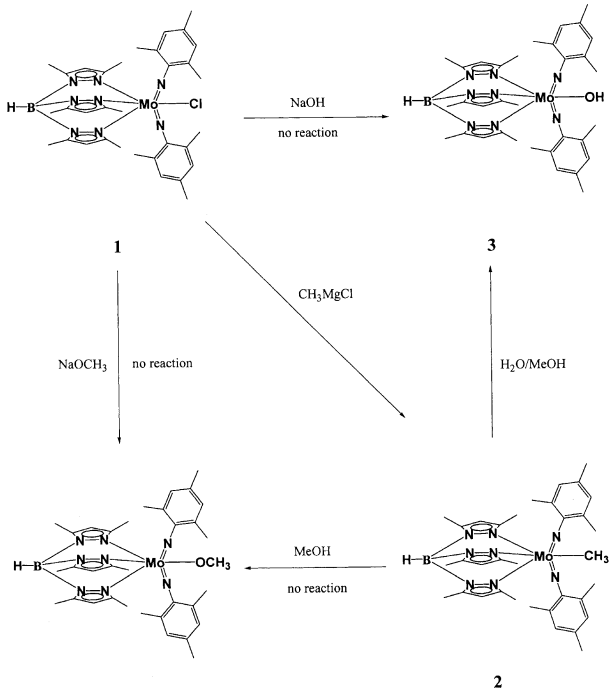
Complex **2** (0.50 g, 0.74 mmol) was dissolved in a mixture of wet methanol (50 ml) and acetone (10 ml), and the solution was stirred at ambient temperature for 1 day. The yellow solution gradually deposited a yellow green solid, which was filtered off and dried in air. Yield 0.37 g (74%). (Found: C, 58.87; H, 6.68; N, 16.53. $C_{33}H_{45}BN_8OMo$ requires C, 58.55; H, 6.67; N, 16.55%); ν_{max} (cm^{-1}) 3404m. br, 2955m, 2923w, 2855w, 1543m, 1447m, 1370w, 1303m, 1278vs, 1211m, 1069m, 1040m, 971m, 854m, 812m 649w cm^{-1}; δ_H(300 MHz; $CDCl_3$; $SiMe_4$) 6.67 (2H, s, $Me_3C_6H_2$), 6.48 (2H, s, $Me_3C_6H_2$), 5.64 (3H, s, 4-$Me_2C_3N_2H$), 2.53 (6H, s, 3-$Me_2C_3N_2H$), 2.34 (3H, s, 3-$Me_2C_3N_2H$), 2.29 (6H, s, *o*-$Me_3C_6H_2$), 2.31 (6H, s, *o*-$Me_3C_6H_2$), 2.23 (6H, s, *p*-$Me_3C_6H_2$), 2.03 (3H, s, 5-$Me_2C_3N_2H$), 1.26 (6H, s, 5-$Me_2C_3N_2H$).

2.3. Crystal structure determination of *1* and *3*

A dark green crystal of **1** and a yellow green crystal of **3** suitable for X-ray diffraction study were obtained from acetonitrile solution and mounted on an Enraf-Nonius CAD-4 diffractometer with graphite-monochromated Mo Kα radiation ($\lambda = 0.71073$ Å). Unit cell dimensions with e.s.d. were determined by least-squares using 25 well-centered reflections in the range of 10°–13°. A total of 6932 unique reflections for **1** were collected in the range of 1.68°–25.47° ($-13 \le h \le 13$, $0 \le k \le 29$, $0 \le l \le 15$) and those (7158) for **3** were collected in the range where ($0 \le h \le 10$, $0 \le k \le 29$, $-21 \le l \le 21$) in the ω–2θ scan mode. The intensities of the reflections were corrected for Lorentz and polarization effects. Crystal data, data collection and refinement for **1** and **3** are listed in Table 2. Data reductions were carried out using a MOLEN program package; a decay correction based on the intensities of two standard reflections and monitoring every hour was performed; empirical absorption corrections were applied based on Ψ scans [28]. The structures in $P2_1/c$ for **1** and **3** were determined by direct methods and refined by full-matrix least-squares using SHELXS-97 and SHELXL-97 program packages [29,30] using reflections with $I > 2\sigma(I)$. All non-hydrogen atoms were refined anisotropically. Hydrogen atoms were constrained by using riding modes. The final cycle of the refinement yielded to $R = 0.055$ and $wR = 0.143$ for **1** and $R = 0.037$ and $wR = 0.103$ for **3**.

3. Results and discussion

A bis(imido) molybdenum complex [Tp*Mo(Nmes)$_2$Cl] was prepared using a similar synthetic procedure to that for [TpMo(Nmes)$_2$Cl]. The dark green crystals of **1** were obtained after recrystallization in acetonitrile and its structure was determined by the X-ray diffraction method. Complex **2** was prepared by the reaction of **1** with 1 equiv. of CH_3MgCl in THF at −78 °C, but [Tp*Mo(Nmes)$_2$($CH_2C(CH_3)_2Ph$)] was not obtained using a similar procedure. Complex **3** was readily obtained from an acetone solution of **2** wet methanol mixture but was not directly produced from NaOH as shown Scheme 1. Attempts to obtain the complex [Tp*Mo(Nmes)$_2$(OCH_3)] from reaction of **1** or **2** with $NaOCH_3$ or MeOH failed. The view of the molecular structure of **1** with the atomic labelling scheme is shown in Fig. 1. Selected bond lengths and angles for **1** are given in Table 1 and the molybdenum atom is in a distorted octahedral geometry surrounded by N(3), N(5) and N(7) nitrogen atoms of Tp*, N(1) and N(2) nitrogen atoms of Nmes and one chlorine atom. While the Mo–N(3), Mo–N(5) and Mo–N(7) bond lengths [2.296(3), 2.325(3) and 2.176(3) A] are slightly shorter than those [2.321(3), 2.472(3) and 2.201(3) Å] in [Tp*Mo(N^{t}Bu)$_2$Cl] [22], the Mo–N(1) and Mo–N(2) bond lengths [1.772(3) and 1.765(3) Å] are somewhat longer than those [1.746(3) and 1.739(3) Å] in [Tp*Mo(N^{t}Bu)$_2$Cl] [22]. The Mo–N bond lengths of Tp* trans to the Nmes ligands are elongated by about 0.135 Å on comparison with that trans to the chloro ligand, which is showing a trans influence. The opening of the bond angle [N(1)–Mo–N(2) 104.7(1)°] is the main distortion of the coordination geometry around the metal center which is similar to that [105.4(2)°] in [Tp*Mo(N^{t}Bu)$_2$Cl] [22]. Both imido ligands are linear having Mo–N(1)–C(1) and Mo–N(2)–C(10) bond angles [177.8(3)° and 174.6(3)°], within the range 160°–180° by comparison with those [170.4(9)° and 164.2(9)°] of [(L_{OEt})Mo(Nmes)$_2$Cl] [21].



Scheme 1.

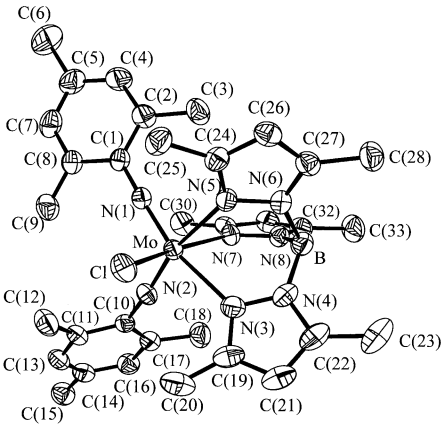


Fig. 1. Molecular structure with the labelling scheme for compound **1**.

Table 1
Selected bond lengths (Å) and angles (°) for **1** and **3**

[Tp*Mo(Nmes)$_2$Cl] **1**		[Tp*Mo(Nmes)$_2$(OH)] **3**	
Bond lengths			
Mo–N(1)	1.772(3)	Mo–N(1)	1.770(3)
Mo–N(2)	1.765(3)	Mo–N(2)	1.770(3)
Mo–N(3)	2.296(3)	Mo–N(3)	2.333(3)
Mo–N(5)	2.325(3)	Mo–N(5)	2.357(3)
Mo–N(7)	2.176(3)	Mo–N(7)	2.228(3)
Mo–Cl	2.3991(9)	Mo–O	2.200(4)
N(1)–C(1)	1.362(5)	N(1)–C(1)	1.375(4)
N(2)–C(10)	1.386(5)	N(2)–C(10)	1.381(4)
Bond angles			
N(1)–Mo–N(2)	104.7(1)	N(1)–Mo–N(2)	105.6(1)
N(1)–Mo–N(3)	166.0(1)	N(1)–Mo–N(3)	166.4(1)
N(1)–Mo–N(5)	89.1(1)	N(1)–Mo–N(5)	90.4(1)
N(1)–Mo–N(7)	90.9(1)	N(1)–Mo–N(7)	92.3(1)
N(2)–Mo–N(3)	87.3(1)	N(2)–Mo–N(3)	87.3(1)
N(2)–Mo–N(5)	166.1(1)	N(2)–Mo–N(5)	164.0(1)
N(2)–Mo–N(7)	96.2(1)	N(2)–Mo–N(7)	100.3(1)
N(3)–Mo–N(5)	78.8(1)	N(3)–Mo–N(5)	76.8(1)
N(3)–Mo–N(7)	80.4(1)	N(3)–Mo–N(7)	81.2(1)
N(5)–Mo–N(7)	81.2(1)	N(5)–Mo–N(7)	79.1(1)
N(1)–Mo–Cl	98.64(9)	N(1)–Mo–O	97.0(1)
N(2)–Mo–Cl	96.2(1)	N(2)–Mo–O	96.3(1)
N(3)–Mo–Cl	87.07(9)	N(3)–Mo–O	85.4(1)
N(5)–Mo–Cl	83.7(8)	N(5)–Mo–O	81.0(1)
N(7)–Mo–Cl	161.89(8)	N(7)–Mo–O	158.1(1)
Mo–N(1)–C(1)	177.8(3)	Mo–N(1)–Cl(1)	175.2(3)
Mo–N(2)–C(10)	174.6(3)	Mo–N(2)–C(10)	177.6(3)

The molecular structure of **3** is shown in Fig. 2. Selected bond lengths and angles are listed in Table 1.

Table 2
Details of the X-ray crystal analyses of **1** and **3**

	[Tp*Mo(Nmes)$_2$Cl] **1**	[Tp*Mo(Nmes)$_2$(OH)] **3**
Empirical formula	$C_{33}H_{44}BClMoN_8$	$C_{33}H_{45}BMoN_8O$
Formula weight (M)	694.96	676.52
T(K)	293(2)	293(2)
Crystal system	monoclinic	monoclinic
Space group	$P2_1/c$	$P2_1/c$
a (Å)	11.561(1)	8.9568(4)
b (Å)	24.259(2)	21.508(1)
c (Å)	12.466(1)	18.1029(8)
β (°)	90.1738(8)	92.665(4)
V(Å^3)	3496.27(6)	3483.6(3)
Z	4	4
μ (mm^{-1})	0.486	0.414
Reflections collected	6932	7158
Independent reflections	6468 [$R_{int} = 0.0219$]	6449 [$R_{int} = 0.0131$]
Data/restraints/parameters	6468/0/398	6449/0/402
Final $R[I > 2\sigma(I)]$	0.055	0.037
wR (all data)	0.143	0.103

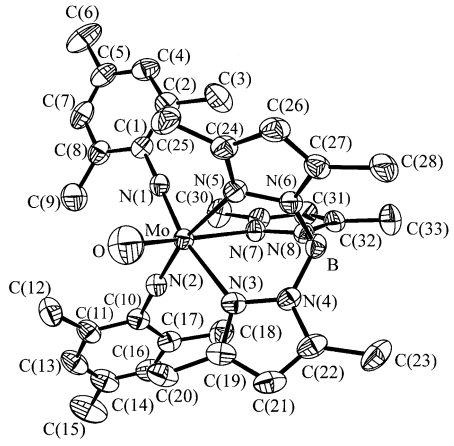


Fig. 2. Molecular structure with the labelling scheme for compound **3**.

The coordination geometry around the Mo atom in **3** is octahedral with three nitrogen atoms of Tp* occupying one face of the octahedron and with two nitrogen atoms of Nmes and one oxygen atom of the hydroxy group occupying the opposite face. The bond lengths of Mo–N(3), Mo–N(5) and Mo–N(7) [2.333(3), 2.357(3) and 2.228(3) Å] are slightly longer than those in **1**, but are similar to those in [Tp*Mo(N^{t}Bu)$_2$Cl] [22]. The Mo–N bond lengths of Tp* trans to the Nmes ligands in **3** are 0.117 Å longer than that trans to the OH ligand. The differences between Mo–N bond lengths for Tp* trans to OH and Nmes ligands in **3** are smaller than that in **1**(0.135Å). The bond angles of N(1)–Mo–N(3), N(2)–Mo–N(5) and N(7)–Mo–O [166.4(1)°, 164.0(1)° and 158.1(1)°] are comparable with those [166.0(1)°, 166.1(1)° and 161.89(8)°] in **1** and those [160.0(1)°, 166.5(1)° and 163.0(1)°] in [Tp*Mo(N^{t}Bu)$_2$Cl] [22]. Both imido ligands can be considered linear having Mo–N(1)–C(1) and Mo–N(2)–C(10) bond angles [175.2(3)° and 177.6(3)°] within the range expected for the related d^0 M(NR) linkages [24,25].

Complexes of **1** and **3** are slightly soluble in hydrocarbon solvents and soluble in THF, $CHCl_3$ and other common polar solvents. Complex **2** is soluble in Et_2O, benzene and toluene. The complexes of **1** and **3** are stable in air for several weeks without noticeable decomposition but **2** decomposed in air within several hours. The ^{1}H NMR spectrum of **1** shows two singlets in a 1:2 ratio at 5.68 and 5.65 ppm for the three 4-H protons of the 3,5-dimethylpyrazolyl groups of Tp*, which are close to those at 5.87 and 5.71 ppm in [Tp*Mo(N^{t}Bu)$_2$Cl] [22]. The ^{1}H NMR spectrum of **2** shows two singlets in a 2:1 ratio for the three 4-H protons of the 3,5-dimethylpyrazolyl groups of Tp* at 5.61 and 5.54 ppm and the ^{1}H NMR of **3** shows a singlet for the three 4-H protons of the 3,5-dimethylpyrazolyl group at 5.64 ppm. The ^{1}H NMR spectra from the 4-H protons of the 3,5-dimethylpyrazolyl of Tp* for **1**, **2** and **3** are shown in Fig. 3. A singlet of one 4-H proton of 3,5-dimethylpyrazole trans to Cl is at low field and a singlet for the 2 equiv. 4-H protons trans to the Nmes ligands is upfield for **1**, while a singlet for two 4-H protons trans to the Nmes ligands is at low field and a singlet for one 4-H proton trans to the methyl group is at up field for **2**, in contrast to **1**. These facts are due to the different trans influences from Cl, methyl and Nmes ligands. However, the ^{1}H NMR of **3** shows a singlet for all three 4-H protons due to the equivalent trans influences of OH and Nmes ligands in comparison with **1** and **2**.

4. Supplementary material

Supplementary data are available from the Cambridge Crystallographic Data Centre, 12 Union Road, Cambridge, CB2 1EZ, UK (fax: +44-1223-336033; e-

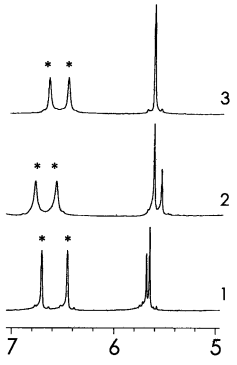


Fig. 3. ^{1}H NMR spectra showing 4-H protons of the 3,5-dimethyl-1-pyrazole for **1**–**3**. Asterisked peaks for aromatic protons of trimethylphenyl.

mail: deposit@ccdc.cam.ac.uk or www: http://www.ccdc.cam.ac.uk) on request, quoting deposit numbers CCDC 174265 and 174266.

Acknowledgements

This work was supported by grant R05-2001-000-00202-0 from the Korea Science and Engineering Foundation.

References

[1] S. Trofimenko, Chem. Rev. 93 (1993) 943.
[2] D.L. Reger, S.S. Mason, A.L. Rheinghold, R.L. Ostrander, Inorg. Chem. 32 (1993) 5216.
[3] A.S. Lipton, S.S. Mason, D.L. Refer, P.D. Ellis, J. Am. Chem. Soc. 116 (1994) 10182.
[4] D.L. Reger, Coord. Chem. Rev. 147 (1996) 571.
[5] W. Klaui, W. Peters, N. Liedtke, S. Trofimenko, A.L. Rheingold, R.D. Sommer, Eur. J. Inorg. Chem. (2001) 693.
[6] N. Kitajima, B.W. Tolman, Prog. Inorg. Chem. 43 (1995) 419.
[7] M.S. Sanford, L.M. Henling, R.H. Grubbs, Organometallics 17 (1998) 5384.
[8] S. Trofimenko, Scorpionates—The Coordination Chemistry of Polypyrazolylborate Ligands, Imperial College Press, London, 1999.
[9] W.A. Nugent, J.M. Mayer, Metal–Ligand Multiple Bonds, Wiley, New York, 1988.
[10] D.E. Wigley, Prog. Inorg. Chem. 42 (1994) 239.
[11] W.D. Philip, V.C. Gibson, W. Clegg, J. Chem. Soc., Dalton Trans. (1995) 3313.
[12] G.L. Casty, T.D. Tilley, G.P.A. Yap, A.L. Rheingold, Organometallics 16 (1997) 4746.
[13] V.C. Gibson, C. Redshaw, G.L.P. Walker, J.A.K. Howard, V.J. Hoy, J.M. Cole, L.G. Kuzmina, D.S. De Silva, J. Chem. Soc., Dalton Trans. 161 (1999) 161.
[14] J.A.M. Brandts, M. van Leur, R.A. Gossage, J. Boersma, A.L. Spek, G. van Koten, Organometallics 18 (1999) 2633.
[15] C.G. Ortiz, K.A. Abboud, J.M. Boncella, Organometallics 18 (1999) 4253.
[16] P.J.A.M. Brandts, J. Boersma, A.L. Spek, G. van Koten, Eur. J. Inorg. Chem. (1999) 1727.
[17] M.C.W. Chan, F.-W. Lee, K.-K. Cheung, C.-M. Che, J. Chem. Soc., Dalton Trans. (1999) 3197.
[18] V.C. Gibson, C. Redshaw, W. Clegg, M.R.J. Elsegood, U. Siemeling, T. Turk, J. Chem. Soc., Dalton Trans. (1996) 4513.
[19] U. Siemeling, T. Turk, W.W. Scheller, C. Redshaw, V.C. Gibson, Inorg. Chem. 37 (1998) 4738.
[20] E.A. Kretzschmar, J. Kipke, J. Sundermeyer, Chem. Commun. (1999) 2381.
[21] A. Galindo, F. Montilla, A. Pastor, E. Carmona, E. Gutierrez-Puebla, A. Monge, C. Ruiz, Inorg. Chem. 36 (1997) 2379.
[22] J. Sundermeyer, J. Putterlik, M. Foth, J.S. Field, N. Ramesar, Chem. Ber. 127 (1994) 1201.
[23] S.A. Roberts, C.G. Young, C.A. Kipke, W.E. Cleland, J.K. Yamanouchi, M.D. Carducci, J.H. Enemark, Inorg. Chem. 29 (1990) 3650.
[24] M. Onishi, K. Ikemoto, K. Hiraki, R. Koga, Bull. Chem. Soc. Jpn. 66 (1993) 1849.
[25] C.Y. Chou, J.C. Huffman, E.A. Maatta, Inorg. Chem. 25 (1986) 822.
[26] S. Trofimanko, J. Am. Chem. Soc. 89 (1967) 6288.
[27] S. Trofimanko, J.C. Calabrese, J.S. Thompson, Inorg. Chem. 26 (1987) 1507.
[28] C.K. Fair, MOLEN, An Interactive Intelligent System for Crystal Structures, Enraf-Nonius, The Netherlands, Deft, 1990.
[29] G.M. Sheldrick, SHELXS-97, Program for The Solution of Crystal Structures, University of Gottingen, 1990.
[30] G.M. Sheldrick, SHELXL-97, Program for Crystal Structure Refinement, University of Gottingen, 1997.

PERGAMON

Polyhedron 21 (2002) 1217–1222

POLYHEDRON

www.elsevier.com/locate/poly

Structural characterization and second-order nonlinear optical properties of zinc halide thiosemicarbazone complexes

Yu-Peng Tian [a,*], Wen-Tao Yu [b], Cun-Yuan Zhao [c], Min-Hua Jiang [b], Zhi-Gang Cai [d], Hoong Kun Fun [e]

[a] *Department of Chemistry, Anhui University, Hefei 230039, People's Republic of China*
[b] *Institute of Crystal Material and State Key Laboratory of Crystal Materials, Shandong University, Jinan 250100, People's Republic of China*
[c] *The State Key Laboratory of Coordination Chemistry, Nanjing University, Nanjing 210093, People's Republic of China*
[d] *Ultrafast Laser Spectroscopic Laboratory Institute of Laser & Spectroscopy, Zhongshan University, Guangzhou 510275, People's Republic of China*
[e] *X-ray Crystallography Unit, School of Physics, University Sains Malaysia, 11800 USM, Penang, Malaysia*

Received 15 November 2001; accepted 20 March 2002

Abstract

Three zinc(II) halide complexes ZnL_2X_2 (X = Cl, Br, I; L = 4-methoxylbenzaldehyde thiosemicarbazone) have been synthesized and characterized by spectroscopic techniques. The complexes exhibit powder SHG efficiency approximately ten times higher than that of urea. The molecular hyperpolarizabilities are calculated to be -2.6×10^{-30} esu for the free ligand L, and -4.6×10^{-30}, -6.2×10^{-30}, -10.1×10^{-30} esu for the three zinc complexes, respectively. The former two complexes crystallize in the noncentrosymmetric space group *Aba*2, whilst ZnL_2I_2 crystallizes in the centrosymmetric space group $P2_1/c$ and does not exhibit any SHG efficiency. The zinc(II) atom in these complexes is tetrahedrally coordinated by two neutral sulfur atoms from the corresponding thiosemicarbazones and two halide anions. The relationships between the molecular structures and nonlinear optical properties were studied based on theoretical calculation and experimental determination methods. © 2002 Elsevier Science Ltd. All rights reserved.

Keywords: Zinc; Halide complexes; Thiosemicarbazones; Ligand

1. Introduction

Nonlinear optical materials exhibiting efficient second-harmonic generation (SHG) at short wavelengths are needed in the fields of high-density optical recording, laser printing, and optical measurement systems and for other applications [1,2]. Compact all-solid-state devices based on the frequency doubling of diode-pumped laser have the potential to meet industrial needs such as efficiency, reliability, and low costing. Recently efficient continuous-wave (cw) green and blue SHG was demonstrated with inorganic crystals such as KTP [3], $KNbO_3$ [4], and β-barium borate (BBO) [5]. The properties of these inorganic devices [5] have made them suitable for practical use. On the other hand, numerous organic SHG materials with nonlinearity superior to that of inorganic materials have been investigated [6,7]. However, only a few organic compounds with large hyperpolarizability (β) have been developed into useful bulk crystalline materials for practical applications [8,9].

Ideally the large nonlinearities of π-conjugated organics and favorable crystal growth characteristics and mechanical properties of ionic salts would be combined into a single NLO crystal [10–17]. Extended π-conjugated networks in organic systems with the largest nonlinearities invariably have significant absorption in the visible portion of the spectrum. Consequently, for SHG into the blue-near-UV regions, more transparent and less extensively delocalized organics must be considered (e.g. urea), albeit at the expense of decreasing the nonlinearity. Semiorganics have the potential for combining the high optical nonlinearity and chemical flexibility of organics with the physical ruggedness of inorganics. Also, for obtaining the materials with large

* Corresponding author. Tel.: +86-551-5107105; fax: +86-551-5107342.
E-mail address: yptian@mars.ahu.edu.cn (Y.-P. Tian).

0277-5387/02/$ - see front matter © 2002 Elsevier Science Ltd. All rights reserved.
PII: S0277-5387(02)01004-5

χ^2, optimization of both the molecular, first hyperpolarizability and their orientation in the bulk should be considered. Towards this end, we have explored a class of crystals in which urea or urea analogs have been stoichiometrically incorporated into an inorganic salt [18–20]. In continuation of these studies, we reported herein the design, synthesis, crystal structure and nonlinear optical properties of zinc halide complexes derived from 4-methoxylbenzaldehyde thiosemicarbazone. The structure of the complexes is shown in Scheme 1.

2. Experimental

All chemicals used were of analytical grade. The solvents were purified by conventional methods.

2.1. Physical measurements

Elemental analysis data were obtained using a Perkin–Elmer 240 analyzer. Infrared spectra were recorded from KBr discs in the range 4000–400 cm^{-1} on a Nicolet FT IR-170SX instrument. Electronic absorption spectra were obtained on a Shimadzu UV-3100 spectrophotometer in DMF solution (1.0×10^{-4} mol dm^{-3}). Solid-state electronic spectra were obtained by the reflection technique on a Shimadzu UV 240 spectrophotometer using MgO as the reference material. DSC and TG of the compounds were carried out using a Perkin–Elmer DSC-2C Differential Scanning Calorimeter and TGS-2 Thermogravimetric Analyzer. The samples were heated at the rate of 20 K min^{-1} in an inert nitrogen atmosphere. The decomposition temperature of the free ligand and its zinc complexes are shown in Table 1.

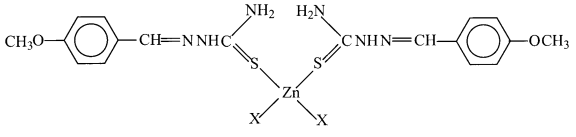
2.2. Synthesis

2.2.1. Preparation of the ligand

4-Methoxylbenzaldehyde thiosemicarbazone (L) was prepared by reacting equimolar amounts of 4-methoxylbenzaldehyde and thiosemicarbazone in hot ethanol.

2.2.2. Preparation of ZnL_2Cl_2

Ethanol solution of (0.42 g, 2 mmol) and zinc chloride (0.69 g, 2 mmol) were mixed. The colorless crystalline solid formed after refluxing for 4 h was isolated and dried in vacuo over P_4O_{10}. Yield: 0.78 g (90%). Crystals



X = Cl, Br, I

Scheme 1.

Table 1
Decomposition temperature of the ligand (L) and its zinc halide complexes (heating rate 20 °C min^{-1} under nitrogen)

Complex	m.p. (°C)	Td (°C)
L	172	201
ZnL_2Cl_2	209	235
ZnL_2Br_2	200	223
ZnL_2I_2	201	221

suitable for X-ray structure analysis were obtained by slowly evaporating an ethanol solution in air. IR data (KBr disc): 3158 (s, N–H), 1607, 1535 (s, C=N), 980 cm^{-1} (s, C=S). UV–Vis: λ_{max} (log ε): 326 nm (3.69). Found: C, 39.3; H, 4.4; N, 15.0; $C_{18}H_{24}N_6O_2S_2ZnCl_2$ Calc.: C, 39.0; H, 4.1; N, 15.2%.

2.2.3. Preparation of ZnL_2Br_2

The complex was synthesized by the same procedure, but from $ZnBr_2$ (yield: 73%). IR data (KBr disc): 3159 (s, N–H), 1604, 1532 (s, C=N), 985 cm^{-1} (s, C=S). UV–Vis: λ_{max} (log ε): 328 nm (3.72). Found: C, 33.5; H, 3.6; N, 13.2; $C_{18}H_{24}N_6O_2S_2ZnBr_2$ Calc.: C, 33.4; H, 3.4; N, 13.0%.

2.2.4. Preparation of ZnL_2I_2

The complex was synthesized by the same procedure, but from ZnI_2 (yield: 69%). IR data (KBr disc): 3289 (s, N–H), 1598, 1548 (s, C=N), 1020 cm^{-1} (s, C=S). UV–Vis: λ_{max} (log ε): 334 nm (3.71). Found: C, 19.4; H, 2.9; N, 7.4; $C_{18}H_{24}N_6O_2S_2ZnI_2$ Calc.: C, 19.1; H, 2.7; N, 7.4%.

2.3. X-ray crystallography and structure solution

The relevant crystal data and structural parameters are summarized in Table 2. Selected bond distances and angles are shown in Tables 3 and 4, respectively. The intensities of ZnL_2Cl_2 was collected at 294 K on a MSC/Rigaku RAXIS-IIC imaging plate diffractometer using Mo Kα radiation ($\lambda = 0.71073$ Å) from a rotating anode operating at 50 kV, 90 mA ($2\theta_{max} = 55.2°$); 60 oscillation frames in the range of 0–180°, expose 8 min per frame for those compounds. Absorption corrections were made using the ABSCOR program based on Fourier-coefficient fitting to the intensities of symmetry-equivalent reflections [21–23].

The structures of ZnL_2Cl_2 was solved by direct methods. All non-hydrogen atoms were refined anistropically by full-matrix least-squares. Hydrogen atoms were placed in calculated positions (C–H = 0.96 Å), assigned fixed isotropic thermal parameters and allowed to ride on their respective parent atoms. The contributions of these hydrogen atoms were included in the structure-factor calculations. All the computations were

Table 2
Crystallographic data for zinc complexes

	$ZnL_{22}Cl_2$	$ZnL_{22}I_2$
Empirical formula	C18H22N6O2S2Cl2Zn	C18H22N6O2S2I2Zn
Mw	554.81	737.71
Crystal color	colorless	colorless
Crystal dimensions (mm)	0.40 × 0.30 × 0.30	0.40 × 0.40 × 0.14
Temperature (K)	293	293
Crystal system	orthorhombic	monoclinic
Space group	*Aba*2	*P*21/*c*
a (Å)	11.971(2)	14.0113(2)
b (Å)	22.153(4)	14.9098(1)
c (Å)	9.090(2)	13.2814(1)
β (°)	90.00 (1)	110.718(1)
V (Å^3)	2374.5(8)	2595.14(5)
Z	4	4
μ (Mo Kα) (mm^{-1})	1.463	3.512
D_{calc} (g cm^{-3})	1.552	1.888
F(000)	1136	1424
Unique reflections	4278	23102
Observed reflections	2305 ($I > 3\sigma(I)$)	9539
R, R_w	0.0400, 0.1129	0.0369, 0.0791
Goodness-of-fit	1.060	1.052
$\Delta\rho_{min}$, $\Delta\rho_{max}$	−0.549, 0.421	−1.541, 1.569

Table 3
Selected bond lengths (Å) and angles (°) for ZnL_2Cl_2 complex

Bond lengths			
Zn(1)–Cl(1)	2.262(1)	Zn(1)–Cl(2)	2.262(1)
Zn(1)–S(1)	2.361(1)	Zn(1)–S(2)	2.361(1)
N(1)–C(1)	1.321(5)	S(1)–C(1)	1.715(3)
N(2)–C(1)	1.343(4)	N(2)–N(3)	1.383(4)
N(3)–C(2)	1.263(5)		
Bond angles			
Cl(1)–Zn(1)–Cl(2)	108.08(12)	Cl(1)–Zn(1)–S(2)	109.11(4)
Cl(2)–Zn(1)–S(1)	112.99(5)	Cl(2)–Zn(1)–S(2)	109.11(4)
S(1)–C(1)–N(1)	120.4(3)	S(1)–Zn(1)–S(2)	104.63(6)
S(1)–C(1)–N(2)	121.2(3)	N(1)–C(1)–N(2)	118.4(3)

Table 4
Selected bond lengths (Å) and angles (°) for ZnL_2I_2 complex

Bond lengths			
I(1)–Zn(1)	2.6056(4)	Zn(1)–S(1)	2.3897(8)
N(2)–N(1)	1.397(3)	N(2)–C(9)	1.334(4)
N(1)–C(8)	1.283(4)	S(1)–C(9)	1.732(3)
N(3)–C(9)	1.313(4)		
Bond angles			
I(2)–Zn(1)–S(2)	108.97(2)	I(1)–Zn(1)–I(2)	114.14(1)
N(3)–C(9)–N(2)	119.2(3)	S(1)–C(9)–N(3)	123.1(2)
S(1)–C(9)–N(2)	117.7(2)	S(1)–Zn(1)–S(2)	105.30(3)
I(2)–Zn(1)–S(1)	111.03(2)	I(1)–Zn(1)–S(1)	107.46(2)

carried out using the SHELXTL-PC program package [24]. Analytical expressions of neutral-atom scattering factors were employed, and anomalous dispersion corrections were incorporated [25].

The data for $[ZnL_2I_2]$ were collected on a Siemens SMART CCD area detector diffractometer equipped with Mo Kα radiation using ω-scan mode. The data collection covered over a hemisphere of reciprocal space by a combination of three sets of exposures; each set had a different ϕ angle (0.88° and 180°) for the crystal and each exposure of 30 s covered 0.3° in ω. The crystal-to-detector distance was 4 cm and the detector swing angle was −35°. Coverage of the unique set is over 99% complete. Crystal decay was monitored by repeating thirty initial frames at the end of data collection and analyzing the duplicate reflections and was found to be negligible.

The unit cell parameters were determined using SMART (Siemens, 1996a) [26]. The three sets of data collected were reduced using the program SAINT (Siemens, 1996b) [27]. The structure was solved with direct methods using the program SHELXTL (Sheldrick, 1997) [28]. All the non-hydrogen atoms were located from the trial structure and then refined anisotropically with SHELXTL using full-matrix least-squares procedure. A weighting scheme of $w = 1/[\sigma^2(F_o^2)+(0.0422P)^2+2.1119P]$, where $P = (F_o^2+2F_c^2)/3$ was applied. The hydrogen atom positions were fixed geometrically at calculated distances.

2.4. Nonlinear optical property measurements

The second order nonlinear optical intensities are estimated by measuring powder samples of 76–154 μm diameter in the form of pellet. The thickness of a pellet is about 0.8 mm. The experimental arrangement for the nonlinear optical properties utilizes a M200 high power Mode-Locked Nd:YAG laser with 200 ps pulse at a repetition rate of 5 Hz. The selected wavelength is 1064 nm. After the selection of the wavelength, the laser beam is split into two parts, one to generate the second harmonic signal in the sample and the other to generate the second harmonic signal in the reference (urea pellet). According to the principle proposed by Kurtz and Perry [29], SHG efficiency can be estimated as 7.6 and 13.2 times higher than that of urea for complexes ZnL_2Cl_2 and ZnL_2Br_2, respectively. However, no SHG response was observed for ZnL_2I_2.

3. Results and discussion

3.1. Spectroscopic characterization

The new Schiff base ligand L was prepared by the reaction of thiosemicarbazide with 4-methoxylbenzaldehyde in a 1:1 molar ratio. The ligand can, in principle, exhibit thione–thiol tautomerism, since it contains a thioamide –HN–C=S functional group [30–32]. The ν(S–H) band at 2570 cm^{-1} is absent from the IR

spectra of the Schiff-base, but ν(N–H) at approximately 3150 cm^{-1} is present, indicating that in the solid state the ligand remains as the thione tautomer. After refluxing the free ligand and zinc halide in ethanol solution, a colorless crystalline solid was formed. It has been shown [33] that the thiosemicarbazide molecule itself exists in the *trans* configuration and while complexing in this configuration, it behaves as a monodentate ligand, bonding only through the sulfur atom. Gerbeleu et al. [34] have shown that bonding may also occur through the hydrazine nitrogen and the amide nitrogen, if the sulfur center is substituted. In most of the complexes studied the thiosemicabazone function coordinates to the metal ion in the *cis* configuration [35], as a bidentate ligand bonding through the thione–thiol sulfur atom and hydrazine nitrogen atom in bidentate manner. The most common stereo chemistries encountered in bidentate thiosemicarbazone complexes are centrosymmetric octahedral and square-planar, so in order to obtained a noncentrosymmetric complex molecule, it is necessary to ensure that the thiosemicarbazone behaves as a monodentate sulfur ligand. HSAB consideration dictates that the softer acid character of Zn(II), Cd(II)and Hg(II) exhibit higher stability constants with this class of sulfur ligands, because of the formation of strong σ-bonds as well as d(π)–d(π) bonds by donation of a pair of electrons to ligands. So it can be expected that the zinc halide complexes might be monodentate S-bonded. The explanation was supported by the IR and UV–Vis spectra of the zinc complexes, which are quite similar to those of the corresponding ligand L, especially with the presence of ν(N–H) at approximately 3150 cm^{-1}.

3.2. Thermal stabilities for the ligand and its zinc complexes

Thermal stabilities for the ligand and its zinc complexes were determined by DSC and TG. The data for them are given in Table 1. From the table, it can be seen that both melting point and decomposition temperature of the complexes are higher than those of their free ligand. So it can be concluded that coordination of the ligand to the metal ion results in greater thermal stability.

3.3. Crystal structure for ZnL_2Cl_2

The ORTEP drawing of ZnL_2Cl_2, with numbering scheme is shown in Fig. 1. The unit cell contents of the complex is shown in Fig. 2. The coordination geometry of the zinc atom is distorted tetrahedral with the two sulfur atoms from the neutral thiosemicarbazone ligand forming bond angles around the Zn(1) in the range of 104.5°–113.2°. The ligand (except the amino atom N(1) is almost planar (mean deviations from the best plane being ca. 0.074 Å). The dihedral angle between the two ligand planes is 75.7°.

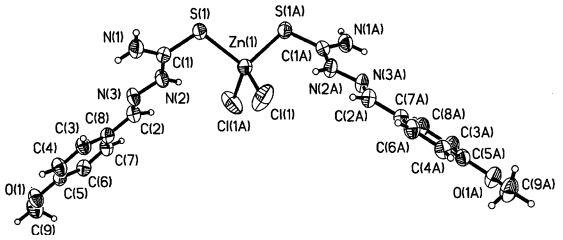


Fig. 1. Molecular structure and atom numbering of ZnL_2Cl_2. The thermal ellipsoids are drawn at the 50% probability level.

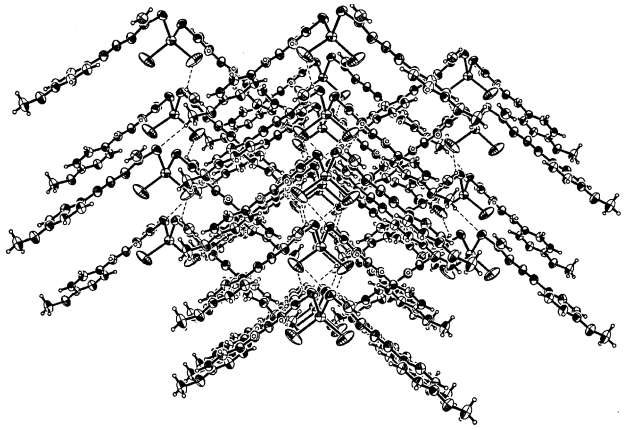


Fig. 2. Packing diagram for ZnL_2Cl_2 viewed approximately along the *c* axis.

The thiosemicarbazone moiety in the complex shows *E* configuration about both C(2)–N(3) and C(1)–N(2). The hydrogen atoms attached to the imine nitrogen atoms N(2) and N(5) are also in cis-configuraion with the sulfur atoms. The six hydrogen atoms attached to amino nitrogen atoms N(1), N(2), N(4) and N(5) have the potential to form donor hydrogen bonds. The two hydrogen atoms attached to the imine nitrogen atoms N(2) and N(5) form intramolecular hydrogen bond with the chloride atoms Cl(1) and Cl(2) (distances of 3.235(7) and 3.215(7) Å for N(2)···Cl(1) and N(5)···Cl(2), respectively and angles around corresponding hydrogen atoms are 152.9(4)° and 152.4(4)°, respectively). Analyses of intermolecular contacts indicated that the hydrogen atoms attached to amino nitrogen atoms N(1) and N(4) formed donor hydrogen bonds of the types N(1)–H(1b)···O(2a) $(-0.5+x, -0.5+y, 1+z)$ and N(4)–H(4b)···O(1b) $(-0.5+x, 0.5+y, z-1)$. The N···O separations are approximately 3.02 and the N–H···O angles are approximately 154°. There are also two intermolecular contacts which can be considered as hydrogen bonds, although the contacts are approximately 3.40 Å. [3.397(8) Å, N(1) and Cl(2c) $(-0.5+x, 0.5-y, 0.5+z)$; 3.405(8) Å, N(4)···Cl(1d) $(-0.5+x, 0+0.5-y, -0.5+z)$], since the bond angles around the corresponding hydrogen atoms are 158.2(5)° and 158.8(5)°, respectively.

The data in Table 3 show that all the bond distances in the side chain of the thiosemicarbazones are intermediate between formal single and double bonds, pointing to extensive electron delocalization over the entire moiety. Examination of the structural data for thiosemicarbazones [36] and their metal complexes [37–40] shows that the N(1)–C(1) and C(1)–S(1) bonds in L^- are longer than those in the neutral form L (1.34 vs. 1.31 and 1.73 vs. 1.71 Å on average, respectively), whereas the N(2)–C(1) bond is shorter than that in L (1.35 vs. 1.33 Å on average).

3.4. Crystal structure for ZnL_2I_2

The crystals contain individual $ZnL_2^2I_2$ neutral molecules. A perspectives drawing with atom-labeling scheme is shown in Fig. 3. Each metal atom is tetracoordinated by two monodentate L ligands bonded through the S atoms, and two terminal iodine atoms (Table 4). The Zn–S and Zn–I distances are almost equal; thus the strong distortion in the tetrahedral environment of the four donor atoms is explained on the basis of strong stereo interactions between the two L ligands in each complex. The Zn–S distance (Table 4) in the complex is in the range of those found for metal–S terminal bonds in other complexes [35]. Zn–I distances are also in the range of those found in other Zn(II) iodine complexes with terminal Zn–I bonds.

3.5. Nonlinear optical properties

Based on MNDO Hamitanian [41] and PM3 parametrization [42] with the MOPAC program package [43], the molecular hyperpolarizability, β_μ, the vector component along the dipole moment direction, of the organic ligand are calculated to be -2.6×10^{-30} esu for the free ligand L, and -4.6×10^{-30}, -6.2×10^{-30}, -10.1×10^{-30} esu for the three zinc complexes, respectively. The molecular hyperpolarizabilities β_μ of organic ligands and their complexes are comparable with that of *p*-nitroaniline (PNA, 6.3×10^{-30}). The absolute values are much greater than that of urea (0.14×10^{-30} esu). This result is easily understood, since the ligand in the free state and in the zinc complexes both present

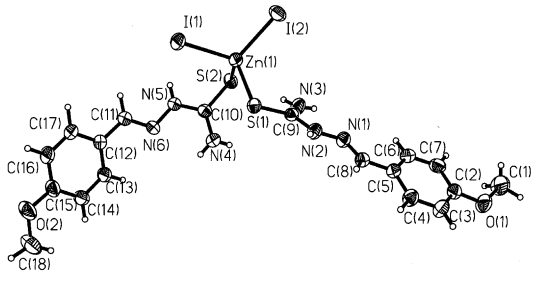


Fig. 3. Molecular structure and atom numbering of ZnL_2I_2. The thermal ellipsoids are drawn at the 50% probability level.

extensive electron delocalization in the whole system with long conjugation length between the donor and acceptor. The negative sign of β_μ can be explained by the smaller dipole moment of the lowest excited state than that of the ground one. The microscopic second-order susceptibility β values of zinc complexes seems to be twice as larger than that of the free ligands. This suggests that the two ligands in complexes may contribute equally to the microscopic second-order nonlinearity of complexes. The β_u value can also be understood by their contribution from lower-energy transition. The linear absorption spectra of the ligand and the zinc complexes in DMF solution exhibit only one intense band near 325 nm. The optical transition associated with this band is mainly the contribution of $\pi^*\leftarrow\pi$ and $\pi^*\leftarrow n$ transitions of nonbonding electron pairs of N and S atoms according to the analysis of molecular orbital components for the ligand and zinc complexes, which are the excitation mainly responsible for the NLO response [19].

Apart from the discussions above, the crystal structures and their alignment is important for the enhancement of nonlinear optical response. The noncentrosymmetric crystals of ZnL_2Cl_2 (molecular dipole moment $\mu=0.39$ D) and ZnL_2Br_2 ($\mu=1.27$ D) serve to hold the molecules in the head-to-tail fashion which give rise to effective dipolar orientation for near-optimum second-order harmonic generation. However, the complex ZnL_2I_2 ($\mu=2.29$ D) showed no SHG response due to its centrosymmetric space group in crystallization, although it has the largest microscopic second-order nonlinear susceptibility. As predicted by PM3 method, the large ground dipolar moment of an isolated molecule in these crystals can lead to strong dipole–dipole interaction and then result in dimers or anti-paralleled molecular alignment in the crystal. Therefore, the centrosymmetric crystals show vanishing SHG efficiency.

Several conclusions can be drawn from the experimental determinations and theoretical calculations above. Combining the conjugated thiosemicarbazide containing donor group with a distorted inorganic tetrahedral center, we may design and synthesize various metal complexes, which possess a large second-order microscopic and macroscopic nonlinear optical (NLO) property. For example, the complexes ZnL_2X_2 (X = Cl, Br, I) have larger molecular hyperpolarizability and greater thermal stability than those of their free ligand. It is interesting to find that the zinc halides are deliquescent whereas the zinc halide thiosemicarbazone complexes are moisture free. The molecules of ZnL_2Cl_2 and ZnL_2Br_2 are arranged noncentrosymmetrically in the crystalline state to have macroscopic second-order nonlinear optical response. Unfortunately, the molecules of $[ZnL_2I_2]$ crystallize centrosymmetrically, leading to vanishing SHG activity. These are associated with

their molecular dipole moment. The results above might give us a general guideline in the synthesis of new nonlinear optical materials. The complexes in this report, are almost colorless, transparent and easy to form crystals. They are also mechanically and thermally stable, thereby making them suitable to be used as potential or practical NLO materials.

4. Supplementary material

Crystallographic data have been deposited with the CCDC (12 Union Road, Cambridge, CB2 1EZ, UK, fax: +44-1223-336033; e-mail: deposit@ccdc.cam.ac.uk; www: http://www.ccdc.cam.ac.uk) and are available on request quoting the deposition number CCDC145742 for ZnL_2Cl_2; CCDC145743 for ZnL_2I_2.

Acknowledgements

This work was supported by a grant for the State Key Program of China, National Natural Science Foundation of China, the Ministry of Education of China, and by research grant R&D No. 190-9609-2801 of the Malaysian Government and Universiti Sains Malaysia.

References

[1] (a) J. Zyss, I. Ledoux, Chem. Rev. 94 (1994) 77;
(b) W.E. Maerner, S.M. Silence, Chem. Rev. 94 (1994) 127.
[2] T. Verbiest, S. Houbrechts, M. Kauranen, A. Persoons, J. Mater. Chem. 7 (1997) 2175.
[3] F. Averseng, C. Lepetit, P.G. Lacroix, J.P. Tuchagues, Chem. Mater. 12 (2000) 2225.
[4] W.J. Kozlovsky, W. Lenth, E.E. Latta, A. Moser, G.L. Bona, Appl. Phys. Lett. 56 (1990) 2291.
[5] H. Yamamoto, S. Funato, T. Sugiyama, J. Opt. Soc. Am. B 13 (1996) 837.
[6] H. Yamamoto, S. Funato, T. Sugiyama, J. Opt. Soc. Am. B 14 (1997) 1099.
[7] Y. Kitaoka, T. Sasaki, S. Nakai, Y. Goto, Appl. Phys. Lett. 59 (1991) 19.
[8] H. Minemoto, Y. Ozaki, N. Sonoda, T. Sasaki, Appl. Phys. Lett. 63 (1993) 3565.
[9] S.R. Marder, J.W. Perry, W.P. Schaefer, Science 245 (1989) 626.
[10] U.B. Ramabadran, A.L. McPherson, D.E. Zelmon, J. Appl. Phys. 76 (1994) 1150.
[11] N.J. Long, Angew. Chem., Int. Ed. Engl. 34 (1995) 21.
[12] C. Dhenaut, I. Ledoux, I.D.W. Saue, J. Zyss, Nature 374 (1995) 339.
[13] V. Venkatarmanan, C.K. Subramanian, H.L. Bhat, J. Appl. Phys. 77 (1995) 6049.
[14] U.B. Ramabadra, R. Vuppuladhadium, D. Small, D.Z.E. Zelmon, G.C. Kennedy, Appl. Optics 35 (1996) 903.
[15] M.J. Gerald, A. Woodward, N.J. Taylor, T.B. Marder, Chem. Mater. 10 (1998) 1355.
[16] (a) R. Andrel, I. Malfant, P.G. Lacroix, H. Gornitzka, Chem. Mater. 11 (1999) 840;
(b) T. Renouard, H.L. Bozec, S. Brasselet, I. Ledoux, J. Zyss, Chem. Commun. (1999) 871;
(c) A. Hilton, T. Renouard, O. Maury, I. Ledoux, J. Zyss, Chem. Commun. (1999) 2521.
[17] W.B. Hou, M.H. Jiang, D.R. Yuan, D. Xu, Mat. Res. Bull. 28 (1993) 645.
[18] D. Xu, M.G. Liu, M.H. Jiang, D.R. Yuan, Mat. Res. Bull. 29 (1994) 73.
[19] Y.P. Tian, C.Y. Duan, Z.L. Lu, X.Z. You, Inorg. Chem. 36 (1997) 1247.
[20] Y.P. Tian, F.X. Xie, Chin. Chem. Lett. 9 (1998) 215.
[21] K.L. Krause, G.N. Phillips, J. Appl. Crystallogr. 25 (1992) 146.
[22] T. Higashi, ABSCOR, Rigaku Corporation, Tokyo, 1995.
[23] G.M. Sheldrick, in: D. Sayre (Ed.), Computational Crystallography, Oxford University Press, New York, 1982, pp. 506–514.
[24] J. Ibers, W.C. Hamilton (Eds.), International Tables for X-ray Crystallography, Kynock Press, Birmingham (now distributed by Kluwer Academic Press, Dordrecht), 1974, pp. 55, 99, 149.
[25] Siemens, SAINT V4 Software Reference Manual, Siemens Analytical X-Ray Systems, Inc., Madison, WI, USA, 1996b.
[26] Siemens, SMART Software Reference Manual, Siemens Analytical X- Ray Systems, Inc., 1996a
[27] G.M. Sheldrick, SHELXTL V5.1 Software Reference Manual, Bruker AXS, Inc, Madison, WI, USA, 1997.
[28] S.K. Kurtz, T.T. Perry, J. Appl. Phys. 39 (1968) 3798.
[29] M.A. Ali, S.E. Livingstone, Coord. Chem. Rev. 13 (1974) 101.
[30] M.J.M. Campbell, Coord. Chem. Rev. 15 (1975) 279.
[31] S.E. Livingstone, Q. Rev. 15 (1965) 386.
[32] P. Dominao, M. Nardelli, P. Sgarabotto, Acta Crystallogr., Sect. B 25 (1969) 343.
[33] N.V. Gerbeleu, M.D. Revenko, V.M. Leovats, Russ. J. Inorg. Chem. 22 (1977) 1009.
[34] S. Padhye, G.B. Kauffman, Coord. Chem. Rev. 63 (1985) 127.
[35] E.W. Ainscough, A.M. Brodie, J.D. Ranford, J.M. Waters, J. Chem. Soc., Dalton Trans. (1991) 1737.
[36] B.M. Wu, C.W. Mak, J. Chem. Soc., Dalton Trans. (1996) 3485.
[37] K.V. Katti, P.R. Singh, C.L. Barnes, J. Chem. Soc., Dalton Trans. (1993) 2135.
[38] G.R. Clark, G. Palennik, J. Crystal Struct. Commun. 9 (1980) 499.
[39] J.S. Case, M.V. Castone, M.C. Rodriguez-Arguelles, A. Sanchez, J. Sordo, J. Chem. Soc., Dalton Trans. (1993) 1253.
[40] M.B. Freeari, G.G. Fava, M. Lanfranchi, C. Pelizzi, P. Tarasconi, J. Chem. Soc., Dalton Trans. (1991) 1951.
[41] M.J.S. Dewar, W.J. Thiel, J. Am. Chem. Soc. 99 (1977) 4907.
[42] J.J.P. Stewart, J. Comp. Chem. 10 (1989) 209.
[43] J.J.P. Stewart, QCPE Program 455, 1983; Version 6.0, 1990.

PERGAMON

Polyhedron 21 (2002) 1223–1227

POLYHEDRON

www.elsevier.com/locate/poly

Direct synthesis of a dimeric mixed-anion lead(II) complex, crystal structure of $[Pb(phen)(_2OCCH_3)(NCS)]_2$

Ali R. Mahjoub *, Ali Morsali

Department of Chemistry, School of Science, Tarbiat Modarres University, PO Box 14155-4838 Tehran, Iran

Received 28 November 2001; accepted 14 March 2002

Abstract

A lead(II) complex with 1,10-phenanthroline (phen) containing two different anions has been synthesized using a direct synthetic method and characterized by IR and CHN elemental analysis. The structure of $[Pb(phen)(_2OCCH_3)(NCS)]_2$ was confirmed by X-ray crystallography. The single crystal X-ray data of this compound shows the complex to be dimeric as a result of acetate ligand bridging. The Pb atom has an unsymmetrical six-coordinate geometry, being coordinated by three nitrogen atoms of 1,10-phenanhroline and the thiocyanate ligand and three oxygen atoms of the acetate ligand. The arrangement of the 1,10-phenanhroline, acetate and thiocyanate ligands exhibits a coordination gap around the Pb(II) ion, occupied possibly by a stereoactive lone pair of electrons on lead(II), with the coordination around lead atoms being hemidirected. There is a $\pi-\pi$ stacking interaction between the parallel aromatic rings that may help to increase the 'gap' in the coordination geometry around the Pb(II) ion. © 2002 Published by Elsevier Science Ltd.

Keywords: Hemidirected; Lead(II) complexes; Thiocyanate ligands; Crystal structures

1. Introduction

The coordination chemistry of lead(II) with N and O-donor ligands has been investigated in the past decade and frequently discussed in regard to the the coordination and stereoactivity of the valence shell lone electron pairs [1–8]. Extensive recent structural studies of lead(II) compounds [9,10] in particular have provided a basis for rather detailed analysis of the evidence for coordination sphere distortions which may be a consequence of the presence of such electron pairs. It appears that in complexes of lead(II) (and probably in those of related species such as Tl(I) [11,12] and Bi(III) [13,14]), the nature and form of the coordination sphere are generally determined by a number of factors, possibly lone pair-bond pair repulsions is important, so that seemingly minor differences in ligands can have quite marked effects upon the coordination stereochemistry. Since the presence of a lone pair is not directly detected but it is inferred on the basis of the spatial distribution of donor atoms surrounding the metal, the identification of these donor atoms is fundamental to the analysis of any particular system. Interestingly, this alone is not a straightforward process. An interesting point is that crystal packing may affect the size and extent of the lone-pair in the coordination sphere. Building new molecular species and modifying their architectures in order to control their physical properties has been a topic for many research groups. Different ligands have been used to bridge in lead(II) complexes, like acetate [2,10,15], thiocyanate [10] or nitrate [16]. The thiocyanate ligand presents an ambidentate ability with an end-on and end-end coordination mode and the acetate ligand presents bridging coordination of both acetate oxygen atoms.

The recent reports of the crystal structures of $Pb(phen)(O_2CCH_3)(O_2ClO_2)$ [2] and $Pb(phen)(O_2CCH_3)(O_2NO)$ [15] described the presence of bridging acetate and its influence upon the coordination stereochemistry of the lead(II) ion and also on their polymeric structures. In the present paper, we report the synthesis and characterization of a dimeric mixed-ligand lead(II) complex of acetate and thiocyanate ligands.

* Corresponding author. Tel.: +21-801-1001; fax: +21-800-6544.
E-mail address: mahjouba@net1cs.modares.ac.ir (A.R. Mahjoub).

0277-5387/02/$ - see front matter © 2002 Published by Elsevier Science Ltd.
PII: S0277-5387(02)00977-4

2. Experimental

2.1. Physical measurements

IR spectra were recorded as Nujol mulls using Perkin–Elmer 597 and Nicolet 510P spectrophotometers. Microanalyses were carried out using a Heraeus CHN-O-RAPID.

2.2. Preparation of [Pb(phen)(O_2CCH_3)(NCS)]

The complex was prepared by dissolving lead(II) acetate (0.36 g, 1 mmol) and potassium thiocyanate (0.097 g, 1 mmol) in distillation water and adding an alcoholic solution of 1,10-phenanhroline ligand, (0.2 g, 1 mmol). The resulting solution was stirred for 5 h at room temperature (r.t.), then it was allowed to stand for 2–3 days in a refrigerator (ca. 6 °C). White crystals of the desired product precipitated, which were filtered off, washed with acetone and ether and air dried (0.356 g yield 70%), m.p. 215 °C. found C, 35.61; H, 2.18; N, 8.43: calculated for $C_{15}H_{11}N_3O_2PbS$; C, 35.65; H, 2.18; N, 8.32%. IR (cm^{-1}) selected bands: 740(s), 1010(s), 1480(s), 1590(s), 1618(s), 2040(vs), 3040(w). Branched tube method: 1, 10-Phenanthroline (0.2 g, 1 mmol) was placed in one arm of the branched tube and a mixture of lead(II) acetate (0.36 g, 1 mmol) and potassium thiocyanate (0.097 g, 1 mmol) in the other. Methanol was carefully added to fill both arms, then the tube was sealed and the ligand-containing arm immersed in a bath at 60 °C while the other was at ambient temperature. After 10 days, white crystals, (m.p. 215 °C) had deposited in the cooler arm.

2.3. Crystallography

2.3.1. Crystal data and refinement details

[Pb(phen)(O_2CCH_3)(NCS)]$_2$. $C_{30}H_{22}N_6O_4Pb_2S_2$, M 1009.04, triclinic, Space group $P\bar{1}$, $a = 8.1581(13)$, $b = 9.0697(15)$, $c = 11.0187(17)$ Å, $\alpha = 68.089(3)$, $\beta = 82.769(3)$, $\gamma = 74.970(3)^\circ$, $V = 730.1(2)$ Å^3, D_c ($Z = 1$ f.u.) 2.295 mg m^{-3}, $F(000)$ 472. Specimen: 0.40 × 0.4 × 0.4 mm; $T_{max,\ min} = 0.9621$, 0.2333, N 12255, N_0 3789, $R = 0.0344$, $R_w = 0.0929$.

2.3.2. Determination of the structure

Crystallographic measurements were made at 140(2) K using a Siemens R3m/V diffractometer. The intensity data were collected within the range $1.99^\circ \le \theta \le 29.58^\circ$ using graphite monochromated Mo Kα radiation ($\lambda = 0.71073$ Å). Accurate unit cell parameters and an orientation matrix for data collection were obtained from least-squares refinement. Intensities of 12 255 unique reflections were measured, from which 3789 with $I > 2\sigma(I)$ were used in the refinement. The structure was solved by direct methods and refined by full-matrix least-squares techniques on F^2.

The positions of hydrogen atoms were idealized and included in the calculations of the structure factors as fixed contributions. Each hydrogen atom was assigned an isotopic thermal parameter. R, R_w, with goodness-of-fit on F^2 $1.088R = 0.0344$, $R_w = 0.0929$. The final difference density map showed a maximum peak and hole of 3.032 and −2.625 e Å^{-3}. Corrections for the Lp effects as well as the empirical correction for absorption using the SADABS programs were applied. All structural calculations were carried out with a PDP-11/23+computer using the SDP-PLUS program package [17,18].

Crystal data and structure refinement are given in Table 1. Selected bond lengths and angles are given in Table 2. Anisotropic thermal parameters, observed and calculated structure factors, full lists of bond distances, bond angles and torsion angles are given as supplementary material. ORTEP diagrams and a perspective view of the packing in the unit cells are shown in Figs. 1 and 2.

Table 1
Crystal data and stucture refinement for Pb(phen)(CH_3COO)(SCN)

Identification code	Pb(phen)(CH_3COO)(SCN)
Empirical formula	$C_{30}H_{22}N_6O_4Pb_2S_2$
Formula weight	1009.4
Temperature (K)	140(2)
Wavelength (Å)	0.71073
Crystal system	triclinic
Space group	$P\bar{1}$
Unit cell dimensions	
a(Å)	8.1581(13)
b(Å)	9.0697(15)
c(Å)	11.0187(17)
α(°)	68.089(3)
β(°)	82.769(3)
γ(°)	74.970(3)
V(Å^3)	730.1(2)
Z	1
D_{calc} (Mg m^{-3})	2.295
Absorption coefficient (mm^{-1})	11.706
$F(000)$	472
Crystal size (mm)	0.4 × 0.4 × 0.4
θ Range for data collection (°)	1.99–29.58
Index ranges	$-11 < h \le 11$, $-12 \le K \le 12$, $-15 < l \le 15$
Reflections collected	12 255
Independent reflections	4063 [$R_{int} = 0.0492$]
Completeness to theta = 29.58° (%)	99.1
Absorption correction	Semi empirical from equivalents
Max./min. transmission	0.9621 and 0.23333
Refinement method	Full matrix least-squares on F^2
Data/restraints/parameters	4063/0/199
Goodness-of-fit on F^2	1.088
Final R indices [for 3789 reflections with $I > 2\sigma(I)$]	$R_1 = 0.0344$, $wR_2 = 0.0946$
R indices (all data)	$R_1 = 0.0368$, $wR_2 = 0.0946$
Largest difference peak and hole (e Å^{-3})	3.032 and −2.625

Table 2
Selected bond lengths and angles for [Pb(phen)(O_2CCH_3)(NCS)]

Bond lengths (Å)	
Pb(1)–N(1S)	2.511(5)
Pb(1)–N(7)	2.564(4)
Pb(1)–N(1)	2.663(4)
Pb(1)–O(1)	2.322(4)
Pb(1)–O(2)	2.674(4)
Pb(1)···O(2) #1	3.190(4)
Bond angles (°)	
O(1)–Pb(1)–N(1S)	85.27(16)
O(1)–Pb(1)–N(7)	82.42(14)
N(1S)–Pb(1)–N(7)	78.86(14)
O(1)–Pb(1)–N(1S)	80.74(13)
N(1S)–Pb(1)–N(1)	141.12(14)
N(7)–Pb(1)–N(1)	63.49(12)
O(1)–Pb(1)–O(2)	51.90(12)
N(1S)–Pb(1)–O(2)	76.43(15)
N(7)–Pb(1)–O(2)	129.06(13)
N(1)–Pb(1)–O(2) #1	119.68(13)
O(1)–Pb(1)–O(2) #1	134.82(12)
N(1S)–Pb(1)–O(2) #1	67.95(14)
N(7)–Pb(1)–O(2) #1	123.99(12)
N(1)–Pb(1)–O(2) #1	141.92(13)
O(1)–Pb(1)–O(2) #1	85.77(13)

#1 $-x+1, -y+1, -z+1$.

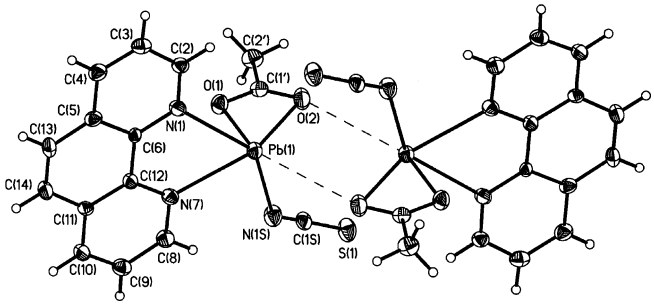


Fig. 1. ORTEP diagram of [Pb(phen)(O_2CCH_3)(NCS)].

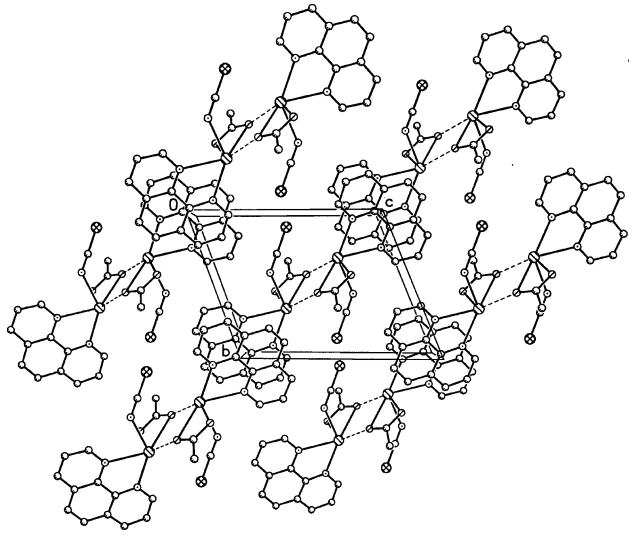


Fig. 2. The unit cell and showing π–π stacking interactions in [Pb(phen)(O_2CCH_3)(NCS)].

3. Discussion

3.1. Synthesis

Reaction between 1,10–phenantroline (phen) and an equimolar mixture of lead(II) acetate and potassium thiocyanate by diffusion along a thermal gradient in methanol solution (the branched tube method), provided crystalline material analyzing as [Pb(phen)(O_2CCH_3)(NCS)]. Attempts to isolate [$(phen)_2$Pb(O_2CCH_3)(NCS)] were not successful and each time, the 1:1 adduct was isolated.

3.2. Crystal structure of [Pb(phen)(O_2CCH_3)(NCS)]$_2$

The crystal structure of this compound consists of dimeric units of [Pb(phen)(O_2CCH_3)(NCS)]$_2$. Each lead atom is chelated by the nitrogens of 1,10-phenanthroline with Pb–N distances of 2.564 and 2.663 Å, and bonded to the thiocyanate with a Pb–N distances of 2.511 Å and also the oxygen atoms of an acetate ligand with Pb–O distances of 2.322 and 2.674 Å. The coordination number in this complex is five (two from the 'phen' ligand, one from thiocyanate and two from the acetate ligand) and the weak interaction of lead(II) with oxygen atoms of an adjacent molecule produce dimer units in the solid state. In fact each Pb atom in this structure with five normal bonds forms two 'weak' Pb···O bonds. Only one of them is symmetry independent and the exact distances is Pb1···O2 = 3.190 Å (Table 2). The presence of a lone pair of electrons on the lead atom is apparently the reason that the bridging interactions are so long.

Determination of the structure of this material by X-ray crystallography (Table 1) showed the complex in the solid state (Fig. 1) to be a dimeric species with various similarities to the polymeric structures of [Pb(phen)(O_2CCH_3)(O_2ClO_2)], [Pb(phen)(NO_3)$_2$(OH_2)] and the dimeric structure of [Pb(phen)(O_2CCH_3)$_2$].

The Pb_2O_2 rings which share edges with PbOCO quadrilaterals to make the dimer core are similar to the central Pb_2O_2 rings of dimeric [Pb(phen)(O_2CCH_3)$_2$] [10], polymeric [Pb(phen)(O_2CCH_3)(O_2ClO_2)] [2] and [(phen)Pb(O_2CCH_3)(O_2NO)] [15], though the long edge of the rings in [Pb(phen)(O_2CCH_3)(NCS)]$_2$ (3.190 Å) is considerably longer than in [Pb(phen)(O_2CCH_3)(O_2NO)]$_n$ (2.804 Å), [Pb(phen)(O_2CCH_3)(O_2ClO_2)]$_n$ (2.736 Å), but shorter than [Pb(phen)(O_2CCH_3)$_2$]$_2$ (3.366 Å). This is consistent with the assumption that the thiocyanate anion should be a stronger ligand than nitrate and perchlorate and weaker ligand than the acetate anion, ($CH_3COO^- > NCS^- > NO_3^- > ClO_4^-$). The arrangement of nitrate and acetate anions suggest a gap or hole in the coordination geometry around the metal ion the [N(1S)–Pb–N(1) angle is 141.12°], occupied possibly by a stereoactive lone pair of electrons on lead(II). The

observed shortening of the Pb–N and Pb–O bonds on the side of the Pb(II) ion opposite to the putative lone pair (2.564 and 2.322 Å) compared with 2.663 and 2.674 Å adjacent to the lone pair) supports the presence of this feature [19]. Hence, the geometry of the nearest coordination environment of every lead atom is likely caused by the geometrical constraints of the coordinated 1,10-phenanhroline ligand, the acetate and thiocyanate anions and by the influence of a stereochemically active lone pair of electrons in an hybrid orbital on the metal atom. Such an environment leaves space for bonding of oxygen atoms of an acetate anion from an adjacent molecule (Fig. 2).

The possible stereochemical activity of the lone pair in divalent lead compounds has recently been discussed by Shimoni-Livny et al. based on a thorough review of crystal data available in the Cambridge Structural Database (CSD) [20]. They classify lead coordination as holodirected which refers to complexes in which the bonds to ligand atoms are directed throughout the surface of an encompassing sphere, while hemidirected refers to those cases in which the bonds to ligand atoms are directed throughout only part of the coordination sphere, leaving a gap in the distribution of bonds to the ligand. The latter, present in all Pb(II) compounds with coordination number 2–5, is quite common in Pb(II) compounds with coordination numbers 6, 7 and 8, and does not exist in lead complexes with higher coordination numbers, here holodirected geometry is the rule. For the structure described here, coordination around the lead atoms is hemidirected with a significant gap trans to the chelating acetate and thiocyanate ligands. The two lone pairs on two lead atoms in a dimeric unit are trans. The striking similarity of $[Pb(phen)(O_2CCH_3)(O_2ClO_2)]_n$ and $[Pb(phen)(O_2CCH_3)(O_2NO)]_n$ with $[Pb(phen)(O_2CCH_3)(NCS)]_2$ is that, there is a π–π stacking interaction [21,22] (charge-transfer arrays) between the parallel aromatic rings belonging to adjacent chains in all three compound, as shown in Fig. 2. A question is, do the π–π stacking interactions between the parallel aromatic rings help to increase the 'gap' in coordination geometry around the metal ion or does the 'gap' arising from the 'stereochemical activity' of valence shell lone electron pairs help to form π–π stacking? The 'gap' in $[Pb(phen)(O_2CCH_3)(O_2ClO_2)]_n$ [2], $[Pb(phen)(O_2CCH_3)(O_2NO)]_n$ [15], and $[Pb(phen)(O_2CCH_3)(NCS)]_2$ is more than in $[(phen)_2Pb(NO_3)_2]$ [10], $[(phen)_2Pb(NO_3)(NCS)]$ [23] and $[(phen)_2Pb(ClO_4)_2]$ [10]. The π–π stacking interactions are rarely observed in complexes with a ratio of ligand to metal of 2:1. In both 1:1 and 2:1 ratios there is a gap and this is greater for 1:1 than in 1:2. It may be that the increased gap to the influence of π–π stacking of aromatic units in these cases.

4. Supplementary material

Complete bond lengths and angles, coordinates and displacement parameters have been deposited at the Cambridge Crystallography Data Centre. Supplementary data are available on request, quoting the deposition number 174596, from the CCDC, 12 Union Road, Cambridge CB2 1EZ, UK (fax: +44-1223-336033; e-mail: deposit@ccdc.cam.ac.uk; www: http://www.ccdc.cam.ac.uk).

Acknowledgements

Support of this investigation by Tarbiat Modarres University is gratefully acknowledeged. We thank the Institute of Organoelement Compounds of the Russian Academy of Science for determining the crystal structure by X-ray crystallography.

References

[1] L.M. Engelhard, D.L. Kepert, J.M. Patrick, A.H. White, Aust. J. Chem. 42 (1998) 329.
[2] A.K. Hall, J.M. Engelhard, A. Morsali, A.A. Soudi, A. Yanovsky, Cryst. Eng. Comm. (2000) 13.
[3] R.D. Hancock, in: A.F. Williams, C. Floriani, A.E. Merbach (Eds.), Pespectives in Coordination Chemistry, VCHA, VCH, Basel, 1992, p. 129.
[4] R.D. Hancock, M.S. Shaikjee, S.M. Dobson, J.C.A. Boeyens, Inorg. Chim. Acta 154 (1988) 229.
[5] P. Pyykkö, Chem. Rev. 88 (1988) 563.
[6] A. Bashall, M. Mcpartlin, B.P. Murphy, D.E. Fenton, S.J. Kitchen, P.A. Tasker, J. Chem. Soc., Dalton Trans. (1990) 505 (and references therein).
[7] P. Schwerdtheger, G.A. Heath, M. Dolg, M.A. Bennett, J. Am. Chem. Soc. 114 (1992) 7518.
[8] K. Byriel, K.R. Dunster, L.R. Gahan, C.H.L. Kennard, J.L. Latten, I.L. Swann, P.A. Duckworth, Polyhedron 11 (1992) 1205.
[9] A. Andres. A. Bencini, A. Garachalios, A. Bianchi, P. Dapporto, E. Garcia-Espna, P. Paoletti, P. Paoli, J. Chem. Soc., Dalton Trans. (1993) 3507.
[10] (a) J.M. Harrowfield, H. Miyamae, B.W. Skelton, A.A. Soudi, A.H. White, Aust. J. Chem. 49 (1996) 1029;
(b) J.M. Harrowfield, H. Miyamae, T.M. Shand, B.W. Skelton, A.A. Soudi, A.H. White, Aust. J. Chem. 49 (1996) 1043;
(c) J.M. Harrowfield, H. miyamae, T.M. Shand, B.W. Skelton, A.A. Soudi, A.H. White, Aust. J. Chem. 49 (1996) 1051;
(d) J.M. Harrowfield, H. Miyamae, B.W. Skelton, A.A. Soudi, A.H. White, Aust. J. Chem. 49 (1996) 1067;
(e) J.M. Harrowfield, H. Miyamae, B.W. Skelton, A.A. Soudi, A.H. White, Aust. J. Chem. 49 (1996) 1081;
(f) G.A. Bowmaker, J.M. Harrowfield, H. Miyamae, B.W. Skelton, A.A. Soudi, A.H. White, Aust. J. Chem. 49 (1996) 1089;
(g) I. Bytheway, L.M. Engelhardt, J.M. Harrowfield, D.L. Kepert, H. Miyamae, J.M. Patrick, B.W. Skelton, A.A. Soudi, A.H. White, Aust. J. Chem. 49 (1996) 1099;
(h) L.M. Engelhardt, J.M. Harrowfield, D.L. Kepert, H. Miyamae, J.M. Patrick, B.W. Skelton, A.A. Soudi, A.H. White, Aust. J. Chem. 49 (1996) 111;
(i) J.M. Harrowfield, H. Miyamae, B.W. Skelton, A.A. Soudi,

A.H. White, Aust. J. Chem. 49 (1996) 1121;
(j) J.M. Harrowfield, H. Miyamae, B.W. Skelton, A.A. Soudi, A.H. White, Aust. J. Chem. 49 (1996) 1127;
(k) L.M. Engelhardt, J.M. Harrowfield, D.L. Kepert, H. Miyamae, J.M. Patrick, B.W. Skelton, A.A. Soudi, A.H. White, Aust. J. Chem. 49 (1996) 1135;
(l) J.M. Harrowfield, D.L. Kepert, H. Miyamae, B.W. Skelton, A.A. Soudi, A.H. White, Aust. J. Chem. 49 (1996) 1147;
(m) J.M. Harrowfield, H. Miyamae, B.W. Skelton, A.A. Soudi, A.H. White, Aust. J. Chem. 49 (1996) 1157;
(n) J.M. Harrowfield, H. Miyamae, B.W. Skelton, A.A. Soudi, A.H. White, Aust. J. Chem. 49 (1996) 1165.

[11] J.M. Harrowfield, R.P. Sharma, B.W. Skelton, A.H. White, Aust. J. Chem. 51 (1998) 735 (and references therein).

[12] A.R Mahjoub, A. Morsali, H. Bagherzadeh, Syntheses and Characterization of Thalium I complexes with Phenoxide Derivation Ligands (Submitted for publication in Polyhedron).

[13] (a) G.A. Bowmaker, F.M.M. Hannaway, P.C. Junk, A.M. Lee, B.W. Shelton, A.H. White, Aust. J. Chem. 51 (1998) 331 (and references therein);
(b) L.J. Barbour, S.J. Belfield, P.C. Junk, M.K. Smith, Aust. J. Chem. 51 (1998) 337.

[14] A. Morsali, A. Tadjarodi, R. Mohammadi, A.R. Mahjoub, Z. Kristallogr. NCS 216 (2001) 379–380.

[15] A. Morsali, M. Payheghader, M.S. Salehi, Zeitschr. Anorg. Allgem. Chem. 628 (2002) 12.

[16] A.R. Mahjoub, A. Morsali, Chem. Lett. 1234 (2001).

[17] G. Ferguson, C. Glidewell, E.S. Lavender, Acta Crystallogr., Sect. B 55 (1999) 591.

[18] G.M. Sheldrick, SHLXTL-97 V5.10, 1997, Bruker AXS Inc., Madison, WI-53719, USA.

[19] R.D. Hancock, M.S. Shaikjee, S.M. Dobson, J.C.A. Boeyens, Inorg. Chim. Acta 154 (1988) 229.

[20] L. Shimonni-Livny, J.P. Glusker, C.W. Bock, Inorg. Chem. 37 (1998) 1853.

[21] A.S. Taylor, in: R. Foster (Ed.), Molecular Complexes, Paul Elek (Scientific Books) Ltd, London, 1973.

[22] N.N. Greenwood, A. Earnshaw, Chemistry of the Elements, Pergamon Press, Oxford, 1984, pp. 235–236.

[23] A.R. Mahjoub, A. Morsali, Z. Kristallogr. NCS 216 (2001) 601–602.

PERGAMON

Polyhedron 21 (2002) 1229–1234

POLYHEDRON

www.elsevier.com/locate/poly

Synthesis and characterization of sulfonamides containing 8-aminoquinoline and their Ni(II) complexes. Crystalline structures of the Ni complexes

Benigno Macías [a,*], Isabel García [a], María V. Villa [a], Joaquín Borrás [b], Alfonso Castiñeiras [c], Francisca Sanz [d]

[a] *Departamento de Química Inorgánica, Facultad de Farmacia, Universidad de Salamanca, Campus Unamuno, Avda. Campo Charro, s.n., E-37007 Salamanca, Spain*

[b] *Departamento de Química Inorgánica, Facultad de Farmacia, Universidad de Valencia, Valencia, Spain*

[c] *Departamento de Química Inorgánica, Facultad de Farmacia, Universidad de Santiago de Compostela, Santiago de Compostela, Spain*

[d] *Servicio de Rayos X, Universidad de Salamanca, Salamanca, Spain*

Received 13 December 2001; accepted 27 March 2002

Abstract

Reaction between 8-aminoquinoline and benzenesulfonyl, toluene-4-sulfonyl and naphthalene-2-sulfonyl chlorides in a basic medium leads to the formation of the corresponding sulfonamides. Reaction of these sulfonamides with Ni(II) salts leads to the formation of the corresponding complexes, with a NiL_2 stoichiometry. Determination of the crystalline structure by X-ray diffraction shows an octahedral environment for the Ni(II) ions, sulfonamides acting as bidentate ligands and two solvent molecules completing the octahedral coordination. The spectroscopic and magnetic properties of these compounds are also discussed. © 2002 Elsevier Science Ltd. All rights reserved.

Keywords: Nickel complexes; Sulfonamide complexes; 8-Aminoquinoline; X-ray crystal structures

1. Introduction

Coordination chemistry of nickel with ligands containing N-donor atoms has been widely studied in the literature and in recent years such studies have been mostly addressed to ligands with a biological interest, such as peptides [1,2]; the Ni(II)-promoted hydrolysis of these peptides has been one of the aims of these sorts of studies [3]. Recent findings showing the role of Ni(II) ions in several processes taking place in living organisms (where it is coordinated by N-donor ligands) have been probably the origin of these studies [4]. However, complexes of this ion with sulfonamides are not well known, and only a few examples have been described in the literature [5], despite the fact that complexes formed by sulfonamides and other transition metal cations, especially copper, have been studied, probably because they may act as chemical nucleases [6–9].

In the present paper, we describe the synthesis of three new sulfonamides derived from 8-aminoquinoline and benzenesulfonyl, toluene-4-sulfonyl and naphthalene-2-sulfonyl chlorides, which have then been used as ligands to coordinate Ni(II) ions.

2. Experimental

2.1. Materials and methods

8-Aminoquinoline and the sulfonyl chlorides were provided by Aldrich and Fluka, respectively, and all reagents were of analytical grade.

Chemical analyses for carbon, hydrogen and nitrogen were performed on a 2400 elemental analyzer from Perkin–Elmer. Nickel was determined on an ICP spectrometer (Perkin–Elmer model 2380 Plasma 2).

* Corresponding author. Tel.: +34-923-294-524; fax: 34-923-294-514.

E-mail address: bmacias@usal.es (B. Macías).

0277-5387/02/$ - see front matter © 2002 Elsevier Science Ltd. All rights reserved.
PII: S0277-5387(02)00997-X

FT-IR spectra were recorded using KBr mulls and a Perkin–Elmer FT-IR 1730 instrument. Electronic spectra were recorded on a Shimadzu 8452A diode spectrophotometer.

Molecular masses were measured by Servicio de Masas (Universidad Autónoma de Madrid, Spain) by the FAB method with samples held on a nitrobenzyl alcohol (NBA) matrix.

Magnetic susceptibility measurements at room temperature (r.t.) were taken with a fully automatized AZTEC DSM8 pendulum-type susceptometer. Mercury tetrakis(thiocyanate)cobaltate(II) was used as a susceptibility standard. Corrections for diamagnetism were estimated from Pascal's constants.

2.2. Synthesis of the ligands

The sulfonamides were prepared by direct synthesis between 8-amino quinoline with the corresponding sulfonyl chloride, using pyridine as solvent. The procedure is as follows: 5 mmol 8-amino quinoline and 5 mmol sulfonyl chloride are dissolved in 10 ml pyridine and the mixture is heated under reflux at 110–120 °C for 30 min. The solution is then left to cool down to 70 °C and is added to a beaker containing 10 ml water. A brown precipitated is formed; this is filtered and washed with distilled water until all pyridine has been removed. Yield is 85–90%.

Analytical data: For N-quinolin-8-yl-benzenesulfonamide, Hqbsa: Found: C, 63.30; H, 4.04; N, 10.25%. Calculated for $C_{15}H_{12}N_2O_2S$: C, 63.37; H, 4.25; N, 9.85%. For N-quinolin-8-yl-*p*-toluenesulfonamide, Hqtsa: Found: C, 64.38; H, 4.69; N, 9.47%. Calculated for $C_{16}H_{14}N_2O_2S$: C, 64.44; H, 4.73; N, 9.43%. For N-quinolin-8-yl-naphthalene-2-sulfonamide, Hqnsa: Found: C, 68.08; H, 4.07; N, 8.32%. Calculated for $C_{19}H_{14}N_2O_2S$: C, 68.24; H, 4.22; N, 8.38%. The most significant IR bands are listed in Table 3. λ_{max} nm (ε, M^{-1} cm^{-1}): 250 (16 000), 320 (7000).

2.3. Synthesis of the nickel complexes

Although direct synthesis between the sulfonamide and the metallic salt is possible with the copper complexes [6], addition of a base is required in the case of the Ni derivatives in order to deprotonate the sulfonamidate nitrogen atom. So 1.5 mmol sulfonamide are dissolved in 75 ml DMF and 2 ml NH_3 2 M are added. Then a solution containing 0.75 mmol Ni(II) chloride dissolved in 25 ml methanol is slowly added dropwise to the former solution. Once the addition has been completed, the original green color of the solution becomes enhanced. Upon very slow evaporation of the solvent, green crystals (suitable for structural determination by X-ray diffraction) were obtained.

Analytical data: $[Ni(qbsa)_2(H_2O)(MeOH)]$: Found: C, 55.31; H, 4.21; N, 8.43; Ni, 8.92%. Calculated for $NiC_{31}H_{28}N_4O_6S_2$: C, 55.13; H, 4.18; N, 8.29; Ni, 8.69%. MS: $m/z = 625$ $[M]^+$

$[Ni(qtsa)_2(H_2O)_2]$: Found: C, 56.01; H, 4.47; N, 8.33; Ni, 8.39%. Calculated for $NiC_{32}H_{30}N_4O_6S_2$: C, 55.75; H, 4.39; N, 8.13; Ni, 8.52%. MS: $m/z = 652.1$ $[M]^+$

$[Ni(qnsa)_2(H_2O)_2]$.2DMF: Found: C, 57.91; H, 4.91; N, 9.06; Ni, 6.55%. Calculated for $NiC_{44}H_{44}N_6O_8S_2$: C, 58.22; H, 4.89; N, 9.26; Ni, 6.47%. MS: $m/z = 725$ $[M]^+$.

The most significant IR bands are listed in Table 3. λ_{max} nm (ε, M^{-1} cm^{-1}): 266 (18 000), 370 (12 000), 585 (20), 785 (30).

2.4. X-ray data collection and processing

A green needle crystal of $[Ni(qtsa)_2(H_2O)_2]$ was mounted on an Enraf Nonius CAD4 automatic drifractometer to be used for the structure determination. X-ray diffraction data for $[Ni(qbsa)_2(H_2O)(MeOH)]$ and $[Ni(qnsa)_2(H_2O)_2]\cdot 2DMF$ were collected on a four circle Seifert XRD 3003 SC diffractometer. Data of these Ni(II) complexes were collected at r.t. using Cu Kα radiation and the $\omega-2\theta$ scan technique. The unit cell parameters were determined by least-squares refinement on the 2θ values of 25 strong well centered reflections in the range $13.5° < \theta < 27°$ for $[Ni(qtsa)_2(H_2O)_2]$ and $8° < \theta < 20°$ for $[Ni(qbsa)_2(H_2O)(MeOH)]$ and $[Ni(qnsa)_2(H_2O)_2]\cdot 2DMF$ compounds. Scattering factors for neutral atoms and anomalous dispersion correction for Ni, C, N, O and S were taken from 'International Tables for X Ray Crystallography' [10]. The structures of $[Ni(qtsa)_2(H_2O)_2]$ and $[Ni(qbsa)_2(H_2O)(MeOH)]$ were resolved by direct methods and refined in the monoclinic space groups $P2_1/c$ and $C2/c$, respectively. The structure of $[Ni(qnsa)_2(H_2O)_2]\cdot 2DMF$ was resolved by Patterson methods and refined in the monoclinic space group $P2(1)/n$. Full-matrix least-squares refinement with anisotropic thermal parameters for non-H atoms was carried out by minimizing $\omega(F_o^2-F_c^2)^2$. Refinement on F^2 for all reflections, weighted R factors ($R\omega$), and all goodness-of-fit S are based on F^2, while conventional R factors (R) are based on F; R factors based on F^2 are statistically about twice as large as those based on F, and R factors based on all data will be even larger.

Most of the calculations for $[Ni(qtsa)_2(H_2O)_2]$ were carried out using CAD4-EXPRESS [11] software for data collection, GENHKL [12] program for data reduction, SHELX-97 [13] to refine the structure and PLATON [14] for molecular graphics. All calculations for $[Ni(qbsa)_2(H_2O)(MeOH)]$ and $[Ni(qnsa)_2(H_2O)_2]\cdot 2DMF$ were performed using CRYSOM [15] software for data collection, X-ray8O [16] for data reduction, SHELXTL™ [17] to resolve and refine the structure and to prepare material for publication.

Table 1
Summary of crystal parameters, data collection and refinement for the three crystal structures

	[Ni(qbsa)$_2$(H$_2$O)(MeOH)]	[Ni(qtsa)$_2$(H$_2$O)$_2$]	[Ni(qnsa)$_2$(H$_2$O)$_2$]2DMF
Empirical formula	$NiC_{31}H_{28}N_4O_6S_2$	$NiC_{32}H_{30}N_4O_6S_2$	$NiC_{44}H_{40}N_6O_8S_2$
Formula weight	675.40	689.43	903.65
Temperature (K)	293(2)	213(2)	293(2)
Wavelength (Å)	1.54180	1.54184	1.54180
Crystal system	monoclinic	monoclinic	monoclinic
Space group	$C2/c$	$P2_1/c$ (No.14)	$P2_1/n$
Unit cell dimensions			
a (Å)	11.868(2)	13.361(12)	10.554(2)
b (Å)	16.161(3)	10.238(4)	30.480(6)
c (Å)	31.417(6)	24.056(16)	14.004(3)
α (°)	90	90	90
β (°)	100.06(3)	101.06(7)	109.58
γ (°)	90	90	90
Volume (Å^3)	5932.8(21)	3229.4(4)	4244.4(15)
Z	8	4	4
D_{calc} (g cm^{-3})	1.441	1.482	1.414
Absorption coefficient (mm^{-1})	0.838	2.491	0.617
$F(000)$	2672	1432	1880
Crystal size (mm)	0.04 × 0.04 × 0.06	0.20 × 0.10 × 0.05	0.30 × 0.04 × 0.06
θ Range for data collection (°)	4.88–67.26	5.48–65.01	1.45–64.34
Index ranges	$-14 < h < 14$	$-15 < h < 1$	$-12 < h < 11$
	$0 < k < 19$	$0 < k < 12$	$0 < k < 36$
	$0 < l < 31$	$-28 < l < 28$	$0 < l < 14$
Reflections collected, unique, R_{int}	5249, 5147, 0.0219	6243, 5476, 0.0509	5096, 4780, 0.0709
Refined method	full-matrix least-squares on F^2	full-matrix least-squares on F^2	full-matrix least-squares on F^2
Data, restraints, parameters	5125, 0, 510	5476, 0, 410	4764, 0, 654
Goodness-of-fit on F^2	1.160	1.039	1.216
Final R indices [$I > 2\sigma(I)$]	$R_1 = 0.0765$, $wR_2 = 0.1556$	$R_1 = 0.0595$, $wR_2 = 0.1184$	$R_1 = 0.0997$, $wR_2 = 0.1730$
R indices (all data)	$R_1 = 0.1130$, $wR_2 = 0.2030$	$R_1 = 0.1551$, $wR_2 = 0.1434$	$R_1 = 0.1724$, $wR_2 = 0.2290$
Largest differential peak and hole (e Å^{-3})	0.481 and −0.875	0.335 and −0.366	0.380 and −0.664

Crystal data and some details of the structural determination are given in Table 1. Table 2 shows some selected geometrical information.

3. Results and discussion

The synthetic route used to prepare the sulfonamides can be depicted as in Scheme 1 for N-quinolin-8-yl-naphthalene-2-sulfonamide, Hqnsa.

Deprotonation of the sulfonamide takes place in an ammonia medium to yield the sulfonamidate anion, qnsa$^-$, which readily reacts with Ni(II) ions to form complexes with a NiL_2 stoichiometry, although solvent molecules also exist completing the coordination around the Ni(II) cations.

3.1. Description of the crystal structures

As it could be readily expected, the local environment around the Ni(II) cations is very similar in all three cases, with a distorted octahedral structure (Figs. 1–3). The coordination polyhedron is formed by four N atoms from both sulfonamide molecules (one nitrogen atom from the sulfonamide group, and another from the quinoline group), which act as bidentate ligands, together with two oxygen atoms from two water molecules. The sulfonamide molecule forms a stable five-member ring with the metal cation. It should be noticed that the hydrogen atoms from the water molecules are not shown in the structural formula of the complex, [Ni(qnsa)$_2$(H$_2$O)$_2$]·2DMF, as they were not located by X-ray diffraction.

Selected bond distances and angles are summarized in Table 2. Only minor differences can be seen in the local environment of the nickel ions among the three complexes prepared, as expected bearing in mind that the organic chains differentiating the three ligands studied are rather far away from the coordinating (donor) sites of these molecules. From the bond angles given, it can be also concluded that the distortion is not too severe, the angle between *trans* atoms being close to 180°, and that between *cis* atoms close to 90°.

The most significant distortions are observed for the complex [Ni(qsba)$_2$(H$_2$O)(MeOH)], where two different molecules (water and methanol) complete the octahedral coordination around the Ni(II) cation, opposite to the findings for the other complexes, where two water molecules exist. Consequently, the O1–Ni–O2 angle decreases to 85.3°, with respect to the values determined

Table 2
Selected bond lengths (Å) and angles (°) for nickel complexes

	$[Ni(qbsa)_2(H_2O)(MeOH)]$	$[Ni(qtsa)_2(H_2O)_2]$	$[Ni(qnsa)_2(H_2O)_2]2DMF$
Bond lengths			
Ni–N(21)	2.077(5)	2.049(4)	2.063(10)
Ni–N(11)	2.048(5)	2.060(5)	2.067(9)
Ni–O(1)	2.122(7)	2.098(4)	2.087(8)
Ni–N(12)	2.139(5)	2.119(4)	2.127(10)
Ni–N(22)	2.101(5)	2.136(4)	2.117(10)
Ni–O(2)	2.068(7)	2.152(4)	2.097(7)
Bond angles			
N(21)–Ni–N(11)	95.0(2)	91.7(19)	91.7(4)
N(21)–Ni–O(1)	176.9(2)	175.8(17)	176.4(4)
N(11)–Ni–O(1)	86.5(3)	92.3(17)	90.5(3)
N(21)–Ni-N(12)	91.1(2)	94.1(17)	94.0(4)
N(11)–Ni–N(12)	79.2(2)	79.4(17)	79.6(4)
O(1)–Ni–N(12)	91.9(3)	88.2 (16)	89.2(3)
N(21)–Ni–N(22)	78.8(2)	79.6(17)	78.4(4)
N(11)–Ni–N(22)	92.3(2)	91.5(18)	94.0(4)
O(1)–Ni–N(22)	98.4(2)	98.7(15)	98.6(3)
N(12)–Ni–N(22)	166.2(2)	168.8(18)	170.0(3)
N(21)–Ni–O(2)	93.2(3)	88.1(17)	90.8(3)
N(11)–Ni–O(2)	171.7(3)	177.4(18)	176.6(4)
O(1)–Ni–O(2)	85.3(3)	88.0(16)	87.0(3)
N(12)–Ni–O(2)	99.9(3)	98.1(17)	97.9(3)
N(22)–Ni–O(2)	90.1(3)	91.0(17)	88.7(3)

for the other two complexes (88.0° and 87.0°); similarly, the N11–Ni–O2 angle also decreases (171.7° vs. 177.43° and 176.6°), while angle N21–Ni–O2 is slightly larger (93.2° instead of 88.1° and 90.8°).

As expected, the angle formed by the Ni(II) cation with the two N atoms belonging to the same ligand molecule (N11–Ni–N12 and N21–Ni–N22) remain constant in all three complexes, although small differences are seen for angles formed between N atoms from both ligands (e. g. N11–Ni–N21), probably as a consequence of the changes in other angles commented above. The Ni–N(sulfonamidate) distances are also slightly larger than the Ni–N(quinoline) ones. In any case, the bond and angle distances measured for these complexes are very similar to those previously reported [5,18] for complexes similar to those prepared here.

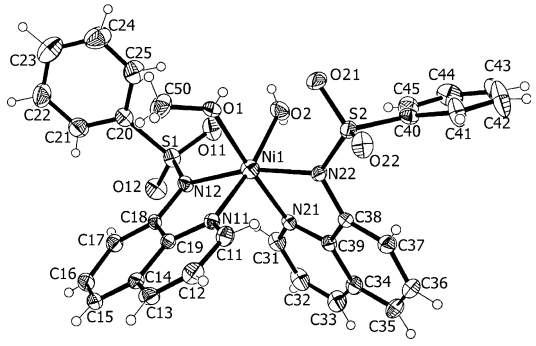
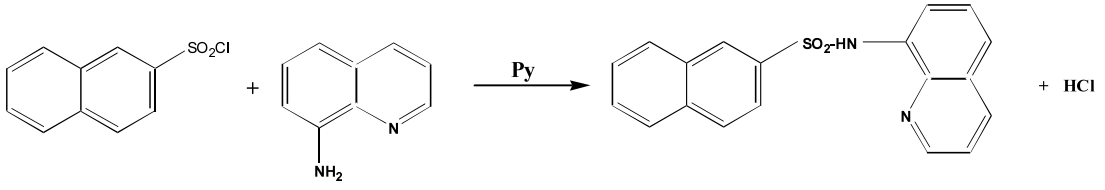


Fig. 1. Molecular structure of $[Ni(qbsa)_2(H_2O)(MeOH)]$ showing the atom numbering scheme.

3.2. FT-IR spectroscopy

Data are summarized in Table 3. It should be noticed that the removal of the band at 3260 cm^{-1}, due to the N–H stretching mode, in the complexes demonstrates the deprotonation of the N(sulfonamide) atom. It should also be mentioned that the splitting of bands due to the symmetric and antisymmetric stretching modes of the SO_2 group, probably because of the different spatial orientation of the S=O bonds upon coordination of the sulfonamide to the metal cation. Both bands shift approximately 30 cm^{-1} downwards when passing from the ligands to the complexes,



Scheme 1. Formation of *N*-quinolin-8-yl-naphthalene-2-sulfonamide.

Table 3
Selected IR bands (cm^{-1})

	Hqbsa	Hqtsa	Hqnsa	$[Ni(qbsa)_2(H_2O)(MeOH)]$	$[Ni(qtsa)_2(H_2O)_2]$	$[Ni(qnsa)_2(H_2O)_2]2DMF$
ν_{N-H}	3218	3260	3245			
SO_2 ν_{as}	1359	1367	1375	1317	1316	1314
				1276	1273	1274
SO_2 ν_{s}	1169	1160	1164	1130	1129	1141
				1114	1115	1122
SO_2 δ_{SO_2}	585	570	558	596	578	567
	559	545	546	584	550	549
ν_{S-N}	926	922	918	952	954	961
ν_{C-S}	686	666	679	692	658	655

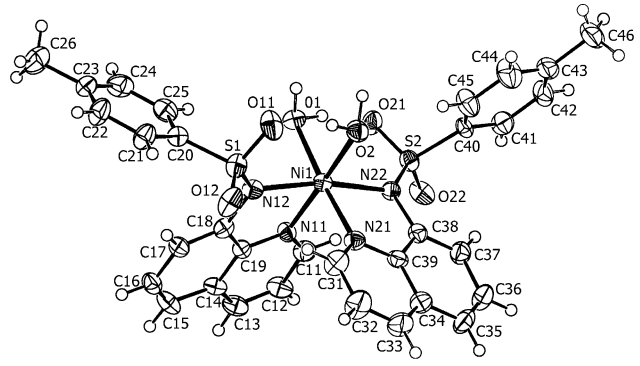


Fig. 2. Molecular structure of $[Ni(qtsa)_2(H_2O)_2]$ showing the atom numbering scheme.

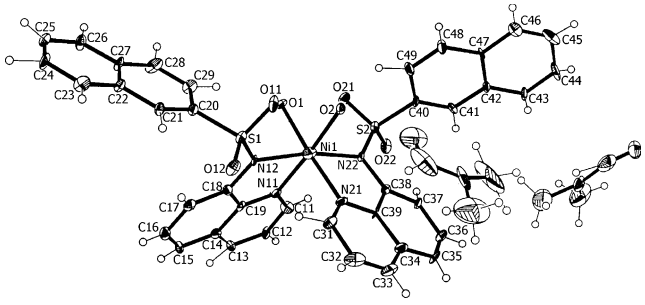


Fig. 3. Molecular structure of $[Ni(qnsa)_2(H_2O)_2]\cdot 2DMF$ showing the atom numbering scheme.

probably due to a charge transfer from the deprotonated, negatively-charge N atom to the oxygen atom of the sulfonyl group [7]; consequently, the double bond character of the S=O group results larger in the free ligands than in the complexes.

The remaining bands are recorded in close positions both for the ligands and for the complexes, except the band due to the S–N stretching mode, which shifts approximately 30 cm^{-1} upwards, thus confirming the donor role of the N atom. Overall, the positions are similar to those previously reported for similar compounds [19].

3.3. Magnetic susceptibility and electronic spectra

The effective magnetic moments at room temperature of the complexes are in the range 2.95–3.13 BM, in agreement with the octahedral environment around the Ni(II) cations. These values are only slightly larger than that corresponding to the spin-only value (2.83 BM), thus suggesting an orbital contribution by mixing of the ground state with low energy excited states, or because the ground state is orbitally degenerated.

The two intense bands recorded in the electronic spectra of the complexes at 266 and 370 nm are probably due to charge transfer processes. The two bands at 785 and 585 nm are recorded in the ranges usually expected for transitions $^3A_{2g} \rightarrow {}^3T_{1g}$ and $^3A_{2g} \rightarrow {}^3T_{1g}(P)$, respectively, of octahedral Ni(II) (d^8) complexes [20].

4. Supplementary material

Complete lists with atomic coordinates, anisotropic displacement parameters, bond lengths and angles have been deposited at the Cambridge Crystallographic Data Center, 912 Union Road, Cambridge CB2 1EZ, UK (fax: +44-1223-336033; e-mail: deposit@ccdc.cam.ac.uk or www: http://www.ccdc.cam.ac.uk) [CCDC 173676, 173677, 173866].

Acknowledgements

The authors thank CICYT (grant PM97-0105-C02-02) for financial support. Critical reading of the manuscript by Professor V. Rives is also acknowledged.

References

[1] H. Sigel, R.B. Martin, Chem. Rev. 82 (1982) 385.
[2] R.B. Martin, in: H. Sigel, A. Sigel (Eds.), Metal Ions in Biological Systems, vol. 23, 1988, p. 123.
[3] G.M. Polzin, J.N. Burstyn, in: H. Sigel, A. Sigel (Eds.), Metal Ions in Biological Systems, vol. 38, 2001, p. 103.
[4] W. Kaim, B. Schwederski, Bioinorganic Chemistry: Inorganic Elements in the Chemistry of Life. An Introduction and guide, Wiley, Chichester, 1994, pp. 172–184.
[5] S. Cabaleiro, J. Castro, E. Vazquez-Lopez, J.A. Garcia-Vazquez, J. Romero, A. Sousa, Polyhedron 18 (1999) 1669.
[6] B. Macias, M.V. Villa, E. Fiz, I. Garcia, A. Castiñeiras, M. Gonzalez-Alvarez, J. Borras, J. Inorg. Biochem. 88 (2002) 101.
[7] C.A. Otter, S.M. Couchman, J.C. Jeffery, K.L.V. Mann, E. Psillakis, M.D. Ward, Inorg. Chim. Acta 278 (1998) 178.
[8] N.P. Farrel (Ed.),Use of Inorganic Chemistry in Medicine, The Royal Society of Chemistry, Cambridge, 1999.
[9] J. Casanova, G. Alzuet, J. Borras, O. Carugo, J. Chem. Soc., Dalton Trans. (1996) 2239.
[10] International Tables for X-ray Crystallography, vol. C, Kluwer Academic Publishers, Dordrecht, The Netherlands, 1995.
[11] B.V. Nonius, CAD4-Express Software, Ver. 5.1/1.2, Enraf Nonius, Delft, The Netherlands, 1994.
[12] M. Kretschmar, GENHKL Program for the reduction of CAD4 Diffractometer data, University of Tübingen, Germany, 1997.
[13] G.M. Sheldrick, SHELXL-97. Program for the Refinement of Crystal Structures, University of Göttingen, Germany, 1997.
[14] A.L. Spek, PLATON. A Multipurpose Crystallographic Tool, Utrecht University, Utrecht, The Netherlands, 2000.
[15] M. Martínez-Ripoll, F.H. Cano, An Interactive Program for Operating Rich. Seifert Single-Crystal Four-Circle Diffractometers, Institute of Physical Chemistry Rocasolano, CSIC, Madrid, Spain, 1996.
[16] J.M. Stewart, F.A. Kundell, J.C. Baldwin, The X-ray80 System, Computer Science Center, University of Maryland, College Park, MD, USA, 1990.
[17] Siemens SHELTXTL™, Version 5.0, Siemens Analytical X-ray Instruments Inc., Madison, WI 53719, 1995.
[18] A.D. Garnovskii, A.S. Burlov, D.A. Garnovskii, I.S. Vasilchenco, A.S. Antsichkina, G.G. Sadikov, A. Sousa, J.A. Garcia-Vázquez, J. Romero, M.L. Duran, A. Sousa-Pedrares, C. Gomez, Polyhedron 18 (1999) 863.
[19] G. Alzuet, S. Ferrer-Llusar, J. Borrás, J. Server-Carrio, R. Martinez-Mañez, J. Inorg. Biochem. 75 (1999) 189.
[20] A.B.P. Lever, Inorganic Electronic Spectroscopy, second ed., Elsevier, New York, 1984.

PERGAMON

Polyhedron 21 (2002) 1235–1244

POLYHEDRON

www.elsevier.com/locate/poly

Synthesis and crystal structures of urea and thiourea derivatives of diruthenium(II,III) tetraacetate

Michael W. Cooke [a], Christopher A. Murphy [a], T. Stanley Cameron [b], Ellen J. Beck [a], George Vamvounis [a], Manuel A.S. Aquino [a,*]

[a] *Department of Chemistry, St. Francis Xavier University, PO Box 5000, Antigonish, Nova Scotia, Canada B2G 2W5*
[b] *Department of Chemistry, Dalhousie University, Halifax, Nova Scotia, Canada B3H 4J3*

Received 16 December 2001; accepted 19 March 2002

Abstract

Diadduct complexes of the mixed-valent form of diruthenium tetraacetate, $[Ru_2(\mu\text{-}O_2CCH_3)_4L_2](PF_6)$, with L = urea (**1**), 1,1,3,3-tetramethylurea (tmu) (**2**) and 1,1,3,3-tetramethyl-2-thiourea (tmtu) (**3**) have been synthesized and characterized by elemental analysis, IR and UV–Vis spectroscopy, magnetic susceptibility, cyclic voltammetry and X-ray crystallography. Compound **1** crystallizes as a co-diadduct system from 1-propanol in which both $[Ru_2(\mu\text{-}O_2CCH_3)_4(urea)_2]^+$ and $[Ru_2(\mu\text{-}O_2CCH_3)_4(1\text{-}propanol)_2]^+$ cations are present in the unit cell. Complex **3** displays a very long Ru–S bond of 2.610(2) Å and is only the second example of a sulfur-donor adduct of a diruthenium tetracarboxylate that has been structurally characterized. Electrochemical measurements on **2** and **3** show them to have reduction potentials of −487 and −541 mV (vs. Fc/Fc^+), respectively, which is in the range of moderate to strong axial donor adducts despite the long Ru–S bond in **3**. Reaction of $[Ru_2(\mu\text{-}O_2CCH_3)_4(H_2O)_2](PF_6)$ with thiourea yields a 1:1 complex, $[Ru_2(\mu\text{-}O_2CCH_3)_4(thiourea)](PF_6)$, which from solubility and infrared evidence appears to be a polymer in which the thiourea bridges through the sulfur and one of the amine nitrogens. © 2002 Elsevier Science Ltd. All rights reserved.

Keywords: Diruthenium carboxylates; Urea and thiourea derivatives; Crystal structures; Infrared spectroscopy

1. Introduction

Paddle-wheel complexes of the type $[Ru_2(\mu\text{-}O_2CR)_4L_2]X$, where L = an axially bound Lewis base, R = an alkyl or aryl group and X = a non-coordinating counterion, have received considerable attention over the last 25 years [1–3]. Until recently the most common Lewis base used was an O-donor such as H_2O, THF or $OPPh_3$. Our group has expanded this somewhat in including a significant number of N-donors [4,5] and the first structurally characterized cases of such adducts containing a P-donor [6] and an S-donor [7]. Reactions of diruthenium tetracarboxylates with various phosphines had already received significant attention but were always hampered by rapid axial to equatorial migration followed by Ru–Ru bond rupture [1–3]. Far less attention has been focussed on S-donor adducts and their properties. We report here on the thiourea and tetramethylthiourea (tmtu) derivatives.

Another area which has had limited study is the axial interaction of ligands of biological relevance with the $[Ru_2(\mu\text{-}O_2CR)_4]^+$ core. Dunbar et al. [8,9] investigated the reaction of 9-ethylguanine with $Ru_2(\mu\text{-}O_2CCH_3)_4Cl$ and found that it displaced two of the bridging acetates. Gangopadhyay and Gangopadhyay [10] synthesized an adenine containing polymer, $[Ru_2(\mu\text{-}O_2CCH_3)_4(adenine)]_x$, in which the adenine bridges adjacent dimers through N^9 and N^3 (or N^1) and a distinct diadduct containing adenosine, $[Ru_2(\mu\text{-}O_2CCH_3)_4(adenosine)_2]Cl$, most likely bound to the ruthenium through N^7. However, no structural characterization of either derivative was reported and doubt about the actual structures remains. Recently the crystal structure of $[Ru_2(\mu\text{-}O_2CC_6H_4\text{-}p\text{-}OMe)_4(2\text{-}mimH)_2](ClO_4)$ where 2-mimH = 2-methylimidazole was reported [11]. It was found that the axial 2-mimH ligands were oriented in a

* Corresponding author. Tel.: +1-902-867-5336; fax: +1-902-867-2414.
E-mail address: maquino@stfx.ca (M.A.S. Aquino).

0277-5387/02/$ - see front matter © 2002 Elsevier Science Ltd. All rights reserved.
PII: S0277-5387(02)00998-1

cis fashion and that there was weak H-bonding between the NH group of the imidazole ring and an oxygen on the perchlorate counterion. In light of the activity shown by $Ru_2(\mu\text{-}O_2CCH_3)_4Cl$ and other derivatives [12,13] against certain cancer cell lines we are beginning an extensive study on the axial and equatorial interaction of various biologically relevant ligands with the diruthenium core. The reactions with urea and tetramethylurea (tmu) are reported here.

2. Experimental

2.1. General procedures

1-Propanol, 2-propanol and diethyl ether were used as received. 1,2-Dichloroethane (dce) was distilled from CaH_2 prior to use. Urea, 1,1,3,3-tetramethylurea (tmu), thiourea and 1,1,3,3-tetramethyl-2-thiourea (tmtu) were used as received. The compounds $Ru_2(\mu\text{-}O_2CCH_3)_4Cl$ and $[Ru_2(\mu\text{-}O_2CCH_3)_4(H_2O)_2](PF_6)$ were prepared using literature procedures [14,15]. Infrared spectra were recorded on a Bruker IFS25 or a Bio-Rad FTS-175 spectrophotometer as KBr discs. UV–Vis spectra were recorded in methanol or 1,2-dichloroethane using a Varian 2300 or Varian 100 spectrophotometer. Effective magnetic moments were determined at room temperature (r.t.) using a Johnson Matthey MSB-1 magnetic susceptibility balance with $HgCo(SCN)_4$ as a calibrant ($\chi_g = 16.17 \times 10^{-6}$ c.g.s.) [16]. Cyclic voltammetry was performed in 1,2-dichloroethane and/or dichloromethane using a BAS CV-50W voltammetric analyzer. The cell system consisted of a platinum button working electrode, platinum wire auxiliary electrode and an Ag/AgCl reference electrode. The ferrocene/ferrocenium couple was used as an internal reference and was consistently measured at 392 mV versus Ag/AgCl. Measurements were normally performed on a 2 mM solution of the complex with 0.100 M $[CH_3(CH_2)_3]_4NPF_6$ as the supporting electrolyte. All solutions were purged with argon for 15 min prior to each scan. Elemental analyses were performed by Canadian Microanalytical Service Ltd., Delta, BC, Canada. X-ray data were collected and the structures solved at the DalX X-ray facility, Dalhousie University, Halifax, NS, Canada.

2.2. Synthesis of $[Ru_2(\mu\text{-}O_2CCH_3)_4(urea)_2](PF_6)$ (**1a**)

$[Ru_2(\mu\text{-}O_2CCH_3)_4(H_2O)_2](PF_6)$ (0.100 g, 0.16 mmol) was dissolved in 4 ml of 2-propanol. An excess of urea (0.038 g, 0.64 mmol) dissolved in 4 ml of 2-proponal was added dropwise with stirring to the first solution. An orange–brown precipitate slowly formed and the solution was allowed to stir for a further 15 min. It was then filtered, washed with 1 ml of cold 2-propanol and dried in vacuo. Additional product could be obtained by adding diethyl ether to the remaining solution. Recrystallization of the product was afforded from hot 2-propanol. Ligand to metal ratios of 0.5:1–6:1 were tried with all giving the same formulation and a 4:1 ratio (described above) giving the optimal yield. Yield = 0.080 g (71%). *Anal*. Calc. for $C_{10}H_{20}F_6N_4O_{10}PRu_2$: C, 17.07; H, 2.86; N, 7.96. Found: C, 17.39; H, 2.78; N, 7.67%. IR (KBr, cm^{-1}): 3474 (s), 3362 (m), 2930 (m), 1648 (s), 1600 (s), 1565 (m), 1452 (s), 1402 (s), 1351 (w), 1156 (m), 1044 (m), 843 (s), 693(s), 563 (m). UV–Vis: λ (nm) (ε, $dm^3\ mol^{-1}\ cm^{-1}$) (methanol): 332 (1800), 420 (950). $\mu_{eff} = 4.1$ B.M.

2.3. Synthesis of $[Ru_2(\mu\text{-}O_2CCH_3)_4(urea)_2](PF_6)$/ $[Ru_2(\mu\text{-}O_2CCH_3)_4(1\text{-propanol})_2](PF_6)$ (**1b**)

Attempts to grow crystals of (**1a**) from 2-propanol that were suitable for X-ray diffraction studies proved unsuccessful, however, we were able to obtain good crystals from 1-propanol. These turned out to be a co-crystallized system of (**1a**) and the solvent (1-propanol) diadduct (see Section 3.2).

2.4. Synthesis of $[Ru_2(\mu\text{-}O_2CCH_3)_4(tmu)_2](PF_6)$ (**2**)

$[Ru_2(\mu\text{-}O_2CCH_3)_4(H_2O)_2](PF_6)$ (0.100 g, 0.16 mmol) was dissolved in 15 ml of 1,1,3,3-tetramethylurea (tmu). The solution was gently heated to completely dissolve the solid. Stirring was continued for 1 h at r.t. Diethyl ether was then added slowly to precipitate the tan colored product. The product was filtered and dried in vacuo. The complex could be recrystallized by diffusion of diethyl ether into a 1,2-dichloroethane (dce) solution of the product. Crystals suitable for X-ray diffraction were also obtained in this fashion. Yield = 0.116 g (89%). *Anal.* Calc. for $C_{18}H_{36}F_6N_4O_{10}PRu_2$: C, 26.51; H, 4.45; N, 6.87. Found: C, 26.44; H, 4.39; N, 6.75%. IR (KBr, cm^{-1}): 2935 (m), 1614 (s), 1551 (s), 1445 (s), 1411 (s), 1357 (m), 1333 (m), 1237 (w), 1163 (m), 1070 (m), 843 (s), 693 (s), 558 (m). UV–Vis: λ (nm) (ε, $dm^3\ mol^{-1}\ cm^{-1}$) (dce): 302 (2320), 436 (880). $\mu_{eff} = 4.0$ B.M.

2.5. Synthesis of $[Ru_2(\mu\text{-}O_2CCH_3)_4(tmtu)_2](PF_6)$ (**3**)

$[Ru_2(\mu\text{-}O_2CCH_3)_4(H_2O)_2](PF_6)$ (0.050 g, 0.08 mmol) was dissolved in a 3 ml of 2-propanol. 1,1,3,3-Tetramethyl-2-thiourea (tmtu) (0.021 g, 0.16 mmol) in 3 ml of 2-propanol was added with stirring and allowed to react for 5 min. The resulting light brown precipitate was filtered and dried in vacuo. Yield = 0.030 g (44%). *Anal.* Calc. for $C_{18}H_{36}F_6S_2N_4O_8PRu_2$: C, 25.44; H, 4.27; N, 6.60; S, 7.53. Found: C, 25.39; H, 4.25; N, 6.35; S, 7.47%. IR (KBr, cm^{-1}): 2936 (m), 2855 (w), 1543 (m), 1437 (s), 1387 (s), 1266 (m), 1163 (m), 1102 (s), 1046 (w),

841 (s), 691 (s). UV–Vis: λ (nm) (ε, dm^3 mol^{-1} cm^{-1}) (dce): 393 (2220), 475 (1130). $\mu_{eff} = 3.8$ B.M.

Recrystallization of **3** from 1,2-dichloroethane (dce) by diethylether diffusion led to the formation of plate-like crystals of the disolvate (**3**)·2dce. Compound **3** can be regenerated by rigorous drying, however, crystal integrity is lost.

2.6. Reaction of $[Ru_2(\mu\text{-}O_2CCH_3)_4(H_2O)_2](PF_6)$ with thiourea (tu) and formation of the polymeric $[Ru_2(\mu\text{-}O_2CCH_3)_4(tu)]_x(PF_6)_x$ (**4**)

Reactions of $[Ru_2(\mu\text{-}O_2CCH_3)_4(H_2O)_2](PF_6)$ with thiourea in various alcohols at stoichiometries of 0.5:1 to 4:1 led, in all cases, to the rapid formation of a dark brown insoluble solid. A typical reaction giving optimum yield of this solid was carried out as follows. $[Ru_2(\mu\text{-}O_2CCH_3)_4(H_2O)_2](PF_6)$ (0.100 g, 0.16 mmol) was dissolved in 4 ml of 2-propanol to which was added 0.013 g (0.16 mmol) thiourea in 3 ml of 2-propanol. A dark brown precipitate formed immediately. The solution was allowed to stir for 5 min, filtered, washed thoroughly with 2-propanol and dried in vacuo. The product was found to be insoluble in most organic solvents. Yield = 0.084 g (80% based on above formulation). *Anal.* Calc. for $C_9H_{16}F_6SN_2O_8PRu_2$: C, 16.39; H, 2.45; N, 4.25; S, 4.86. Found: C, 16.09; H, 2.61; N, 4.33; S, 5.06%. IR (KBr, cm^{-1}): 3396 (m), 3210 (m), 3186 (m), 2924 (m), 1661 (s), 1624 (s), 1536 (s), 1448 (m), 1406 (s), 1102 (w), 1038 (w), 918 (s), 853 (s), 696 (s). $\mu_{eff} = 4.0$ B.M.

2.7. X-ray crystallography

All crystals (**1b**, **2** and **3**·2dce) were mounted in glass capillaries and measurements were made at r.t. on a Rigaku AFC5R diffractometer with graphite monochromated Cu Kα radiation and a rotating anode generator. Procedures for crystal indexing, data collection and data reduction for this instrument were routine and have been described elsewhere [15]. Corrections were made for the effects of absorption anisotropy as well as Lp effects. A correction for secondary extinction was applied in all cases.

All three structures were solved by direct methods and expanded using Fourier techniques [17,18]. All data processing was performed using TEXSAN [19] except for the refinement of complex **1b** which was done using SHELX-97 [20]. Neutral atom scattering factors were taken from Cromer and Waber [21]. The values of the mass attenuation coefficients are those of Creagh and Hubbell [22]. For complex **2** and **3**·2dce anomolous dispersion effects were included in F_{calc} [23] and the values for $\Delta f'$ and $\Delta f''$ were those of Creagh and McAuley [24]. Crystallographic parameters for the three structures discussed are given in Table 1. Bond lengths and angles are presented in Tables 2–4.

3. Results and discussion

3.1. Synthesis

The synthesis of complexes **1**, **3**, and **4** was carried out in a similar fashion in 2-propanol using a simple axial ligand substitution reaction [4] displacing H_2O in the starting $[Ru_2(\mu\text{-}O_2CCH_3)_4(H_2O)_2](PF_6)$ complex with the desired ligand normally in a 2:1–4:1 ligand:metal ratio. The optimum yields of complex **4** were obtained using a 1:1 ratio. Complex **2** was synthesized by using the neat 1,1,2,2-tetramethylurea (tmu) ligand as solvent with precipitation of the product afforded by the addition of diethyl ether. Satisfactory elemental analyses were obtained for all of the thoroughly dried compounds with that of compound **4** being consistent with a 1:1 ligand to complex ratio which is evidence for a possible polymeric structure. Complex **1** was successfully recrystallized from 1-propanol as the co-diadduct system **1b** and **2** and **3**·2dce were obtained from diethyl ether diffusion into a solution of the complex in 1,2-dichloroethane. Complex **4** could not be recrystallized satisfactorily as it was only found to be soluble in DMSO and pyridine in which it decomposed.

3.2. Structure of $[Ru_2(\mu\text{-}O_2CCH_3)_4(urea)_2](PF_6)$/ $[Ru_2(\mu\text{-}O_2CCH_3)_4(1\text{-}propanol)_2](PF_6)$ (**1b**)

Complex **1b** crystallizes in a triclinic system ($P\bar{1}$). Selected bond lengths and angles are listed in Table 2. An ORTEP diagram of each diadduct is shown in Fig. 1. Fig. 2 presents the unit cell diagram which clearly shows the presence of the two distinct diadducts, namely $[Ru_2(\mu\text{-}O_2CCH_3)_4(urea)_2](PF_6)$ and $[Ru_2(\mu\text{-}O_2CCH_3)_4(1\text{-propanol})_2](PF_6)$. Co-crystallization of more than one diadduct is not common but has been seen on four previous occasions. Each of these earlier cases have their own unique characteristics and a brief discussion of each will help to put complex **1b** in context.

McCann et al. [25] synthesized the complex salt, $[Ru_2(\mu\text{-}O_2CC_6H_5)_4(C_2H_5OH)_2][Ru_2(\mu\text{-}O_2CC_6H_5)_4(HSO_4)_2]$, which in the crystal structure was found to contain the $[Ru_2(\mu\text{-}O_2CC_6H_5)_4(C_2H_5OH)_2]^+$ cation and the $[Ru_2(\mu\text{-}O_2CC_6H_5)_4(HSO_4)_2]^-$ anion. These ions linked together in an infinite polymeric chain by a modest hydrogen-bond (2.77 Å) between the ethanol oxygen of one dimer and the hydrogensulfate oxygen of another. Handa et al. [26,27] recently investigated the magnetic properties of two compounds that display co-crystallized adducts. The first, $[Ru_2(\mu\text{-}O_2CCMe_3)_4(tempo)_2][Ru_2(\mu\text{-}O_2CCMe_3)_4(H_2O)_2](BF_4)_2$ where tempo = 2,2,6,6-tetramethylpiperidine-1-oxyl, contains the two

Table 1
Crystal data and structure refinement parameters

Empirical formula	$C_{12}H_{23}O_{10}N_2Ru_2PF_6$ (**1b**)	$C_{18}H_{36}O_{10}N_4Ru_2PF_6$ (**2**)	$C_{22}H_{44}O_8N_4S_2Ru_2PF_6Cl_4$ (**3**)
Molecular weight	702.43	815.61	1045.65
Space group	$P\bar{1}$	$P2_1/c$	$P\bar{1}$
Unit cell dimensions			
a (Å)	11.272(1)	8.002(2)	11.4650(9)
b (Å)	11.655(1)	16.650(2)	11.814(1)
c (Å)	9.838(1)	11.949(2)	8.0367(9)
α (°)	92.802(9)	90.0	108.104(8)
β (°)	107.650(9)	107.94(2)	102.120(7)
γ (°)	70.811(9)	90.0	77.543(7)
V (Å^3)	1161.2(3)	1514.7(5)	998.2(2)
Z	2	2	1
T (K)	296 ± 1	296 ± 1	296 ± 1
D_{calc} (g cm^{-3})	2.009	1.788	1.739
Crystal size (mm)	0.25 × 0.30 × 0.45	0.15 × 0.20 × 0.40	0.09 × 0.30 × 0.40
μ (cm^{-1})	121.32	94.19	106.17
λ (Å)	1.54178	1.54178	1.54178
$2\theta_{max}$ (°)	127.2	127.1	127.1
Number of unique data	3781	2569	3231
R [a]		0.037	0.051
R_w [b]		0.042	0.056
R_1 [c]	0.039		
wR_2 [d]	0.142		
Goodness-of-fit	1.08	2.02	1.93

[a] $R = \Sigma||F_o| - |F_c||/\Sigma|F_o|$.
[b] $R_w = [(\Sigma w(|F_o| - |F_c|)^2/\Sigma wF_o^2)]^{1/2}$.
[c] $R_1 = \Sigma||F_o| - |F_c||/\Sigma|F_o|$.
[d] $wR_2 = [\Sigma w(F_o^2 - F_c^2)^2/\Sigma w(F_o^2)^2]^{1/2}$.

cationic diadducts $[Ru_2(\mu\text{-}O_2CCMe_3)_4(tempo)_2]^+$ and $[Ru_2(\mu\text{-}O_2CCMe_3)_4(H_2O)_2]^+$ and two BF_4^- ions. No evidence of any interactions between the two cations is mentioned. In the second case, $[Ru_2(\mu\text{-}O_2CCMe_3)_4(nitme)_2][Ru_2(\mu\text{-}O_2CCMe_3)_4(H_2O)_2](BF_4)_2$ where nitme = 2,4,4,5,5-pentamethyl-4,5-dihydro-1H-imidazolyl-1-oxyl 3-oxide, the two cations are linked by hydrogen-bonds (2.81 Å) between the N–O groups of the nitme and the water molecules on $[Ru_2(\mu\text{-}O_2CCMe_3)_4(H_2O)_2]^+$ leading to an infinite zig-zag chain. An interesting system investigated by Jimenez-Aparicio et al. [28], $Ru_2(\mu\text{-}O_2CCH_2OEt)_4Cl\cdot H_2O$, showed not only the distinct cationic species $[Ru_2(\mu\text{-}O_2CCH_2OEt)_4(H_2O)_2]^+$ and the anionic $[Ru_2(\mu\text{-}O_2CCH_2OEt)_4Cl_2]^-$ but also the infinite chain $\{Ru_2(\mu\text{-}O_2CCH_2OEt)_4Cl\}_x$ where the Cl^- links adjacent dimers, all in the same crystal lattice.

In the present study the nature of complex **1b** most closely resembles that of Handa's first complex as we have two distinct cations, $[Ru_2(\mu\text{-}O_2CCH_3)_4(urea)_2]^+$ and $[Ru_2(\mu\text{-}O_2CCH_3)_4(1\text{-propanol})_2]^+$ with two PF_6^- anions. While there is no evidence of any significant axial ligand to axial ligand interaction between the cations in **1b** there is a weak hydrogen-bonding interaction (3.18(1) Å) between the urea nitrogen N(2) and an oxygen, O(9), on the equatorial acetate of the 1-propanol containing diadduct and a stronger interaction (2.786(8) Å) between the 1-propanol oxygen, O(10) and an acetate oxygen, O(4), on the urea adduct. The Ru–Ru and Ru–O_{eq} bond lengths in the two cations are typical for these types of compounds [3] as are the two Ru–Ru–O_{axial} bond angles. The Ru–O_{ax}(urea) bond, (Ru(1)–O(5) = 2.245(5) Å) and the Ru–O_{ax}(1-propanol) bond (Ru(1)–O(10) = 2.268(6) Å) are comparable to the tetraacetato complexes $[Ru_2(\mu\text{-}O_2CCH_3)_4(DMSO)_2](PF_6)$ (Ru–O_{ax} = 2.243(5) Å) and $[Ru_2(\mu\text{-}O_2CCH_3)_4(H_2O)_2](PF_6)$ (Ru–O = 2.279(4) Å), respectively [15]. The Ru(1)–O(5)–C(5) bond angle of 134.6(5) Å (urea cation) is somewhat larger than might be expected, possibly due to the hydrogen-bonding mentioned above, whereas the Ru(2)–O(10)–C(10) (1-propanol cation) angle is 123.2(6) Å. In both cases the axial ligands are arranged in an anti geometry with respect to each other.

3.3. Structure of $[Ru_2(\mu\text{-}O_2CCH_3)_4(tmu)_2](PF_6)$ (2)

Complex **2** crystallizes in the monoclinic system ($P2_1/c$) with a center of inversion lying between the two Ru atoms. Selected bond lengths and angles are given in Table 3 and an ORTEP diagram is shown in Fig. 3. The bonding parameters in this complex are similar to those of the urea diadduct in complex **1b** with the Ru–Ru and Ru–O_{eq} bond lengths and the Ru–Ru–O_{ax} bond angle falling into the typical ranges and the axial tmu ligands

Table 2
Selected bond lengths (Å) and angles (°) for $[Ru_2(\mu\text{-}O_2CCH_3)_4(urea)_2](PF_6)$/$[Ru_2(\mu\text{-}O_2CCH_3)_4(1\text{-propanol})_2](PF_6)$ (**1b**)

Bond lengths			
Ru(1)–Ru(1)′	2.264(1)	Ru(2)–Ru(2)′	2.259(1)
Ru(1)–O(1)	2.016(5)	Ru(2)–O(6)	2.024(5)
Ru(1)–O(2)′	2.016(5)	Ru(2)–O(7)′	2.023(5)
Ru(1)–O(3)′	2.018(5)	Ru(2)–O(8)	2.026(6)
Ru(1)–O(4)	2.034(5)	Ru(2)–O(9)′	2.031(6)
Ru(1)–O(5)	2.245(5)	Ru(2)–O(10)	2.268(6)
O(1)–C(1)	1.260(9)	O(6)–C(6)	1.27(1)
O(2)–C(1)	1.278(9)	O(7)–C(6)	1.24(1)
O(3)–C(3)	1.243(9)	O(8)–C(8)	1.28(1)
O(4)–C(3)	1.275(9)	O(9)–C(8)	1.24(1)
O(5)–C(5)	1.25(1)	O(10)–C(10)	1.42(1)
N(1)–C(5)	1.33(1)	C(6)–C(7)	1.50(1)
N(2)–C(5)	1.31(1)	C(8)–C(9)	1.49(1)
C(1)–C(2)	1.47(1)	C(10)–C(11)	1.31(2)
C(3)–C(4)	1.52(1)	C(11)–C(12)	1.50(2)
Bond angles			
Ru(1)′–Ru(1)–O(1)	89.3(1)	Ru(2)′–Ru(2)–O(6)	89.8(2)
Ru(1)–Ru(1)′–O(2)	89.4(1)	Ru(2)–Ru(2)′–O(7)	88.7(2)
Ru(1)–Ru(1)′–O(3)	89.8(1)	Ru(2)′–Ru(2)–O(8)	89.5(2)
Ru(1)′–Ru(1)–O(4)	89.1(1)	Ru(2)′–Ru(2)–O(9)	89.5(2)
Ru(1)′–Ru(1)–O(5)	176.3(2)	Ru(2)′–Ru(2)–O(10)	175.6(1)
O(1)–Ru(1)–O(2)′	178.5(2)	O(6)–Ru(2)–O(7)′	178.5(2)
O(1)–Ru(1)–O(3)′	89.6(2)	O(6)–Ru(2)–O(8)	89.1(2)
O(1)–Ru(1)–O(4)	89.8(2)	O(6)–Ru(2)–O(9)′	89.7(2)
O(1)–Ru(1)–O(5)	93.6(2)	O(6)–Ru(2)–O(10)	93.7(2)
O(2)–Ru(1)′–O(3)	89.7(2)	O(7)′–Ru(2)–O(8)	90.8(2)
O(2)′–Ru(1)–O(4)	90.8(2)	O(7)–Ru(2)′–O(9)	90.4(2)
O(2)′–Ru(1)–O(5)	87.8(2)	O(7)′–Ru(2)–O(10)	87.8(2)
O(3)′–Ru(1)–O(4)	178.7(2)	O(8)–Ru(2)–O(9)′	178.4(2)
O(3)′–Ru(1)–O(5)	92.6(2)	O(8)–Ru(2)–O(10)	87.8(2)
O(4)–Ru(1)–O(5)	88.6(2)	O(9)′–Ru(2)–O(10)	93.2(2)
Ru(1)–O(1)–C(1)	120.1(5)	Ru(2)–O(6)–C(6)	118.2(5)
Ru(1)′–O(2)–C(1)	119.5(5)	Ru(2)′–O(7)–C(6)	120.2(6)
Ru(1)′–O(3)–C(3)	119.0(5)	Ru(2)–O(8)–C(8)	118.4(6)
Ru(1)–O(4)–C(3)	118.1(5)	Ru(2)′–O(9)–C(8)	119.2(6)
Ru(1)–O(5)–C(5)	134.6(5)	Ru(2)–O(10)–C(10)	123.2(6)
O(1)–C(1)–O(2)	121.7(8)	O(6)–C(6)–O(7)	123.2(8)
O(1)–C(1)–C(2)	120.6(8)	O(6)–C(6)–C(7)	118.2(8)
O(2)–C(1)–C(2)	117.7(7)	O(7)–C(6)–C(7)	118.7(8)
O(3)–C(3)–O(4)	124.1(8)	O(8)–C(8)–O(9)	123.3(9)
O(3)–C(3)–C(4)	118.3(7)	O(8)–C(8)–C(9)	117.4(8)
O(4)–C(3)–C(4)	117.6(7)	O(9)–C(8)–C(9)	119.2(9)
O(5)–C(5)–N(1)	118.0(8)	O(10)–C(10)–C(11)	121.0(1)
O(5)–C(5)–N(2)	123.1(8)	C(10)–C(11)–C(12)	122.0(1)
N(1)–C(5)–N(2)	118.9(8)		

arranged in an anti fashion. The Ru–O_{ax}(tmu) bond (Ru(1)–O(5) = 2.249(4) Å) is essentially identical to the ruthenium–urea bond in complex **1b**. Although one might have expected it to be shorter due to the stronger Lewis basicity of tmu versus urea, the steric bulk introduced by the four methyl groups may hinder a closer approach. It is also worthy of note that the Ru(1)–O(5)–C(5) bond angle of 125.3(4)° is smaller than the corresponding bond angle in the urea diadduct in **1b**.

Table 3
Selected bond lengths (Å) and angles (°) for $[Ru_2(\mu\text{-}O_2CCH_3)_4(tmu)_2](PF_6)$ (**2**)

Bond lengths			
Ru(1)–Ru(1A)	2.2750(9)	O(5)–C(5)	1.257(7)
Ru(1)–O(1)	2.024(4)	N(1)–C(5)	1.345(9)
Ru(1)–O(2)	2.029(4)	N(1)–C(6)	1.45(1)
Ru(1)–O(3)	2.024(4)	N(1)–C(7)	1.45(1)
Ru(1)–O(4)	2.017(4)	N(2)–C(5)	1.359(8)
Ru(1)–O(5)	2.249(4)	N(2)–C(8)	1.459(9)
O(1)–C(1)	1.268(7)	N(2)–C(9)	1.444(9)
O(2)–C(1)	1.275(8)	C(1)–C(2)	1.50(1)
O(3)–C(3)	1.268(7)	C(3)–C(4)	1.487(9)
O(4)–C(3)	1.285(7)		
Bond angles			
Ru(1A)–Ru(1)–O(1)	90.1(1)	Ru(1)–O(4)–C(3)	120.1(4)
Ru(1A)–Ru(1)–O(2)	89.0(1)	Ru(1)–O(5)–C(5)	125.3(4)
Ru(1A)–Ru(1)–O(3)	90.0(1)	C(5)–N(1)–C(6)	123.9(7)
Ru(1A)–Ru(1)–O(4)	88.8(1)	C(5)–N(1)–C(7)	119.3(6)
Ru(1A)–Ru(1)–O(5)	174.5(1)	C(6)–N(1)–C(7)	114.4(7)
O(1)–Ru(1)–O(2)	178.5(2)	C(5)–N(2)–C(8)	123.8(6)
O(1)–Ru(1)–O(3)	90.1(2)	C(5)–N(2)–C(9)	119.7(6)
O(1)–Ru(1)–O(4)	89.7(2)	C(8)–N(2)–C(9)	113.8(6)
O(1)–Ru(1)–O(5)	94.6(2)	O(1)–C(1)–O(2)	123.9(6)
O(2)–Ru(1)–O(3)	88.6(2)	O(1)–C(1)–C(2)	119.1(6)
O(2)–Ru(1)–O(4)	91.6(2)	O(2)–C(1)–C(2)	117.0(6)
O(2)–Ru(1)–O(5)	86.4(2)	O(3)–C(3)–O(4)	122.0(6)
O(3)–Ru(1)–O(4)	178.8(2)	O(3)–C(3)–C(4)	118.8(6)
O(3)–Ru(1)–O(5)	92.9(2)	O(4)–C(3)–C(4)	119.2(6)
O(4)–Ru(1)–O(5)	88.3(2)	O(5)–C(5)–N(1)	121.6(6)
Ru(1)–O(1)–C(1)	118.0(4)	O(5)–C(5)–N(2)	119.5(6)
Ru(1)–O(2)–C(1)	118.8(4)	N(1)–C(5)–N(2)	118.8(6)
Ru(1)–O(3)–C(3)	119.0(4)		

3.4. Structure of $[Ru_2(\mu\text{-}O_2CCH_3)_4(tmtu)_2](PF_6)\cdot 2dce$ (**3**)·2dce

Complex **3**·2dce crystallizes in the triclinic system ($P\bar{1}$). Selected bond lengths and angles are presented in Table 4 and an ORTEP diagram is given in Fig. 4. This is the second example of a structurally characterized sulfur-donor adduct of a diruthenium carboxylate. The first, $[Ru_2(\mu\text{-}O_2CCH_3)_4(tht)_2](PF_6)$ where tht = tetrahydrothiophene, was reported earlier by our group [7]. Fig. 4 clearly shows co-ordination of the tmtu ligands through the sulfur atom. The Ru–Ru bond (2.301(2) Å) is slightly longer than is typical for these types of complexes and is second only to the very strong axial donor adduct, $[Ru_2(\mu\text{-}O_2CCH_3)_4(PCy)_2](PF_6)$ (Cy = cyclohexyl), in which Ru–Ru is 2.427(1) Å [6]. The Ru–O_{eq} bonds and the Ru–Ru–S bond angle are normal for these compounds. As with the $[Ru_2(\mu\text{-}O_2CCH_3)_4(tht)_2](PF_6)$ complex in which the Ru–S bond was very long at 2.627 Å, the Ru–S bond in **3** is long at 2.610(2) Å. A similar argument can be used here as for the tht adduct in that there appears to be a strong *trans*-effect across the Ru–Ru bond and very little π-backbonding from the metal centers to the sulfur [7]. Finally the Ru(1)–S(1)–C(5) bond angle is quite small, in compar-

Table 4
Selected bond lengths (Å) and angles (°) for $[Ru_2(\mu\text{-}O_2CCH_3)_4(tmtu)_2](PF_6)\cdot 2dce$ (**3**)·2dce

Bond lengths			
Ru(1)–Ru(1)′	2.301(2)	O(4)–C(3)	1.27(1)
Ru(1)–O(1)	2.033(6)	N(1)–C(5)	1.34(1)
Ru(1)–O(2)′	2.038(6)	N(1)–C(6)	1.46(1)
Ru(1)–O(3)	2.018(7)	N(1)–C(7)	1.46(2)
Ru(1)–O(4)′	2.031(7)	N(2)–C(5)	1.33(1)
Ru(1)–S(1)	2.610(2)	N(2)–C(8)	1.48(1)
S(1)–C(5)	1.72(1)	N(2)–C(9)	1.45(2)
O(1)–C(1)	1.25(1)	C(1)–C(2)	1.49(1)
O(2)–C(1)	1.28(1)	C(3)–C(4)	1.50(1)
O(3)–C(3)	1.28(1)	C(10)–C(11)	1.17(4)
Bond angles			
Ru(1)′–Ru(1)–S(1)	177.2(1)	Ru(1)–O(3)–C(3)	119.3(7)
Ru(1)′–Ru(1)–O(1)	89.0(2)	Ru(1)′–O(4)–C(3)	119.4(6)
Ru(1)–Ru(1)′–O(2)	88.8(2)	C(5)–N(1)–C(6)	123(1)
Ru(1)′–Ru(1)–O(3)	89.3(2)	C(5)–N(1)–C(7)	122(1)
Ru(1)–Ru(1)′–O(4)	88.8(2)	C(6)–N(1)–C(7)	113(1)
S(1)–Ru(1)–O(1)	88.9(2)	C(5)–N(2)–C(8)	122(1)
S(1)–Ru(1)–O(2)	93.3(2)	C(5)–N(2)–C(9)	122(1)
S(1)–Ru(1)–O(3)	92.5(2)	C(8)–N(2)–C(9)	114(1)
S(1)–Ru(1)–O(4)′	89.3(2)	O(1)–C(1)–O(2)	123.4(8)
O(1)–Ru(1)–O(2)	177.8(3)	O(1)–C(1)–C(2)	119.2(9)
O(1)–Ru(1)–O(3)	90.6(3)	O(2)–C(1)–C(2)	117.4(9)
O(1)–Ru(1)–O(4)′	88.7(3)	O(3)–C(3)–O(4)	123.1(9)
O(2)′–Ru(1)–O(3)	89.4(3)	O(3)–C(3)–C(4)	118(1)
O(2)–Ru(1)′–O(4)	91.2(3)	O(4)–C(3)–C(4)	118.4(9)
O(3)–Ru(1)–O(4)′	178.1(3)	S(1)–C(5)–N(1)	119.5(8)
Ru(1)–S(1)–C(5)	104.9(3)	S(1)–C(5)–N(2)	121.2(9)
Ru(1)–O(1)–C(1)	119.7(6)	N(1)–C(5)–N(2)	119(1)
Ru(1)′–O(2)–C(1)	119.1(6)		

ison with the similar angle in the urea type derivatives **1b** and **2**, at 104.9(3)°.

3.5. IR spectroscopy

All four compounds show the characteristic symmetric ν_{sym}(COO) and asymmetric ν_{asym}(COO) carboxylate stretches in the 1380–1450 cm^{-1} region and $\nu(PF_6^-)$ in the range 840–855 cm^{-1} [15]. Of more interest, however, is the nature of the axial ligand binding. A summary of all the bands and assignments mentioned in this section is given in Table 5.

Let us consider the urea, **1**, and tmu, **2**, derivatives first. Bands above 3000 cm^{-1} in **1** can be assigned to N–H stretching frequencies with the band at 2930 cm^{-1} due to the C–H stretch of the acetate methyl groups. In **2** no bands are seen above 3000 cm^{-1} and the C–H stretching frequency is observed at 2935 cm^{-1}. The $\nu_s(C=O)$ values for **1** (1648 cm^{-1}) and **2** (1614 cm^{-1}) represent a decrease in the stretching frequencies from free urea (1683 cm^{-1}) and free tmu (1640 cm^{-1}) [29–31] of 35 and 26 cm^{-1}, respectively. CO stretching frequencies are expected to decrease (by as much as 110 cm^{-1}) when coordination to the metal occurs through the oxygen [29]. Coordination through the nitrogen should

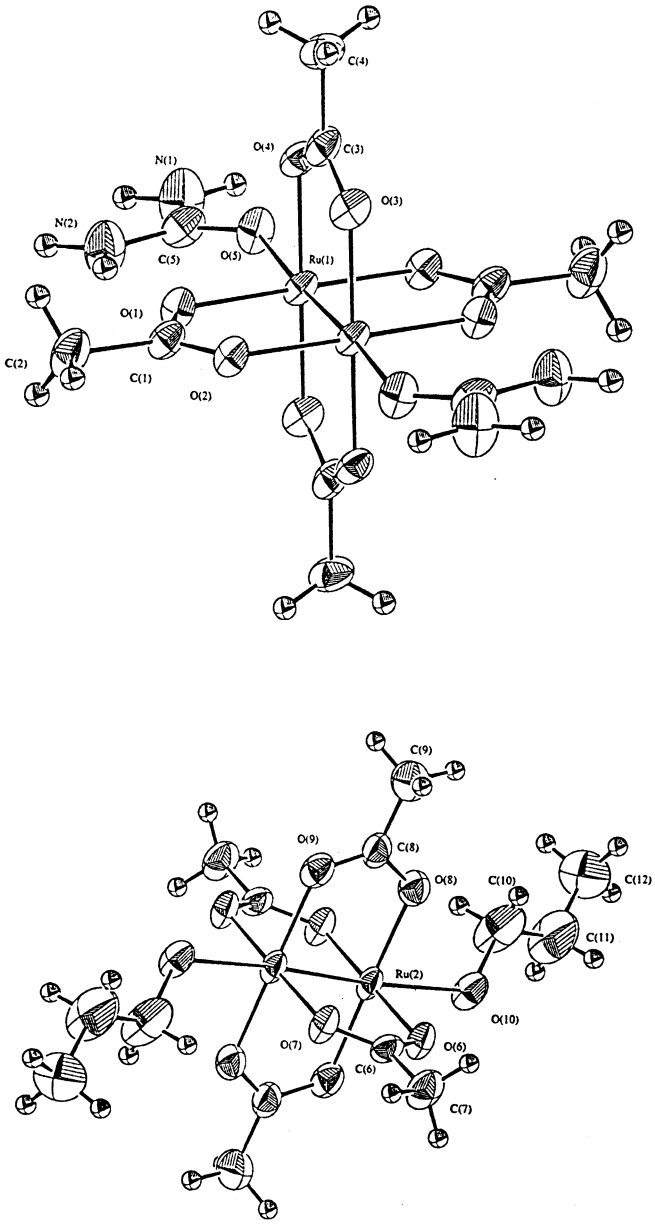


Fig. 1. ORTEP drawing of **1b** showing the $[Ru_2(\mu\text{-}O_2CCH_3)_2(urea)_2]^+$ cation (top) and the $[Ru_2(\mu\text{-}O_2CCH_3)_2(1\text{-propanol})_2]^+$ cation (bottom). The PF_6^- counterion has been omitted for clarity.

lead to an increase in $\nu_s(C=O)$. The band at 1600 cm^{-1} in **1** (absent in **2**) is assigned to an NH_2 bending mode. This is virtually identical to the value for the free urea ligand (1599 cm^{-1}) [32,33]. It has been shown previously that this band remains relatively constant upon urea coordination through oxygen [29,33,34]. The bands at 1565 and 1551 cm^{-1} in complexes **1** and **2**, respectively, are assigned to the antisymmetric N–C–N stretching vibration which has a value of 1506 cm^{-1} in free urea [32,33] and 1499 cm^{-1} in free tmu [30]. An increase of this frequency upon coordination is also consistent with bonding through oxygen.

Let us now consider the tmtu, **3**, and thiourea, **4**, derivatives. As was the case with **2**, complex **3** shows no

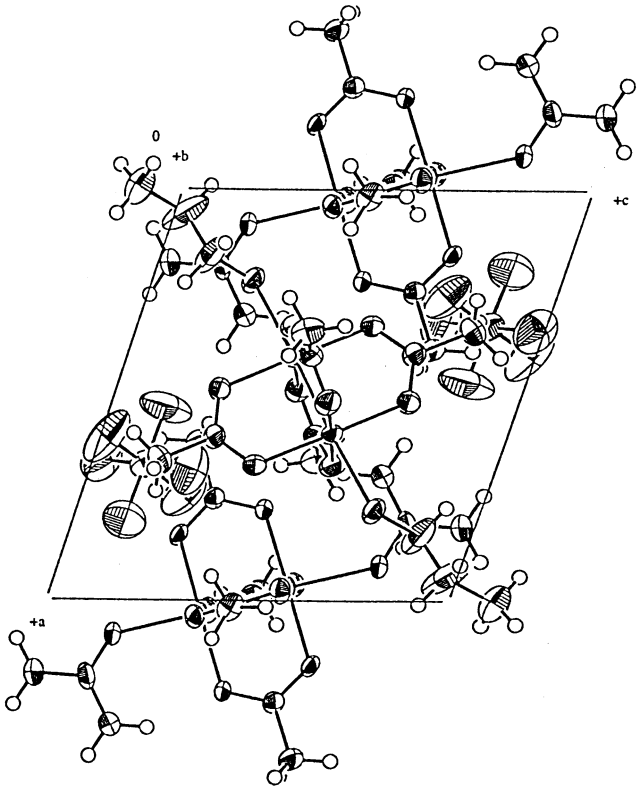


Fig. 2. View of the unit cell looking down the *b*-axis of **1b** showing the two unique diadducts present.

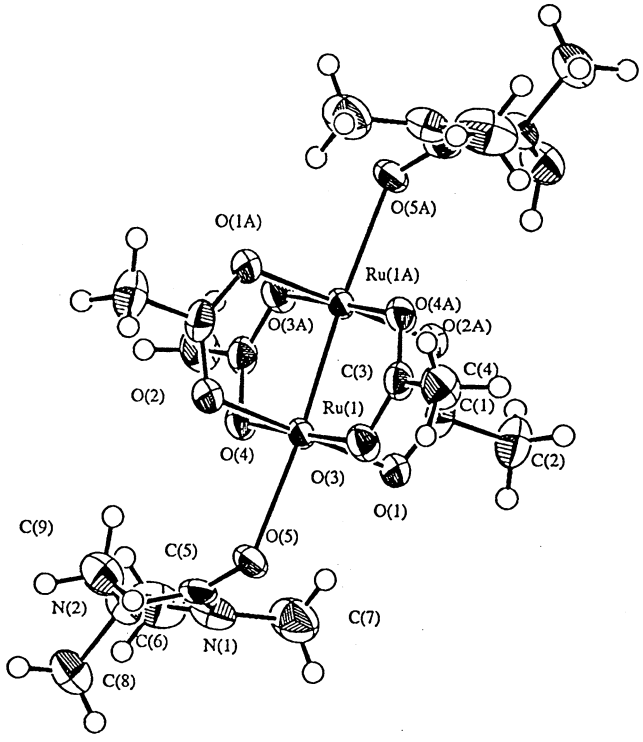


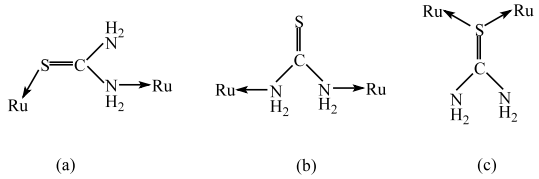
Fig. 3. ORTEP drawing of the $[Ru_2(\mu\text{-}O_2CCH_3)_2(tmu)_2]^+$ cation in **2**. The PF_6^- counterion has been omitted for clarity.

bands above 3000 cm^{-1} (no N–H stretching) and a band at 2936 cm^{-1} due to C–H stretching. Complex **4** shows bands characteristic of both of these modes at 3396, 3210 and 3186 cm^{-1} for N–H and at 2924 cm^{-1} for C–H. It is important to note that there are several N–H stretching modes for **4** and the two lowest lie at lower frequencies than those for **1** and those for free thiourea. According to Nakamoto [29] and Yamaguchi [34] this suggests that there may be coordination through nitrogen rather than (or as well as) sulfur. In the NH_2 bending region **4** shows two strong bands at 1661 and 1624 cm^{-1} which is indicative of two different NH_2 environments, possibly bound and unbound [34]. As with complex **2**, complex **3** shows an antisymmetric N–C–N stretch at 1543 cm^{-1} which is higher than the value for the free tmtu ligand of 1504 cm^{-1} [30]. In complex **4** there is also a positive shift from the free ligand value of 1470–1536 cm^{-1}. In both cases this is indicative of coordination through the sulfur. Finally we consider the two stretching modes due, primarily, to the C=S double bond. In free tmtu these lie at 1126 and 718 cm^{-1} and both are shifted to lower frequencies (1102 and 691 cm^{-1}) upon complexation. This is consistent with a reduction in the double bond character and coordination through the sulfur. In **4** the results are not as clear as there is a shift to higher frequency for ν_1(C=S) from 1083 to 1102 cm^{-1} and to a lower frequency for ν_2(C=S) from 730 to 696 cm^{-1}. The band in **4** at 1102 cm^{-1} is very weak and previous results have been ambiguous in that slight increases are seen despite coordination still taking place at sulfur [34,35]. The decrease in ν_2(C=S) points to bonding through sulfur.

The ligand coordination modes for complexes **1**, **2**, and **3** are clear from the X-ray structures and the infrared data supports this. For compound **4** we can only speculate for now. Assuming that a polymer (or oligomer) is formed, and the elemental analysis and solubility properties appear to support this, there are three likely bridging modes for thiourea. These are shown in Scheme 1. It would appear from the arguments presented above that bridging mode (a) is the most likely as it accommodates both sulfur and nitrogen coordination.

3.6. UV–Vis spectroscopy and magnetic susceptibility

The electronic spectra of complexes **1**–**3** have been recorded in methanol (for **1**) and dce (for **2** and **3**). All of



Scheme 1.

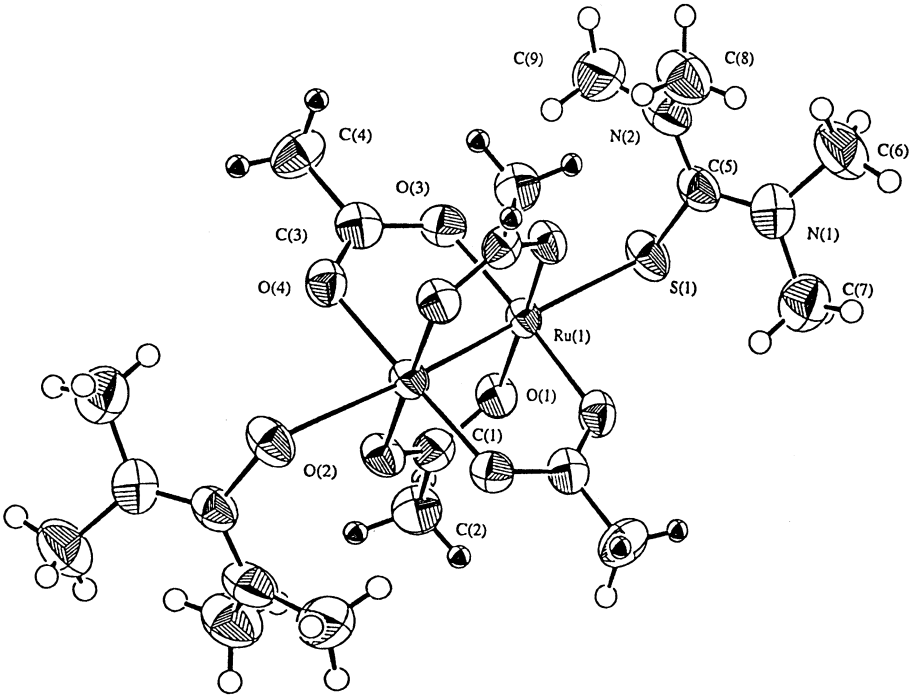


Fig. 4. ORTEP drawing of the $[Ru_2(\mu\text{-}O_2CCH_3)_2(tmtu)_2]^+$ cation in **3**·2dce. The PF_6^- counterion and the dce molecules of solvation have been omitted for clarity.

the complexes display a distinctive electronic transition in the visible in the range 420–475 nm due to a π(RuO, Ru_2) → π*(Ru_2) transition and another in the UV in the range 300–395 nm assigned to a π(axial O or S) → π*(Ru_2) transition [3]. It should be noted that both of the bands for **3** (475 and 393 nm) are red-shifted somewhat from the corresponding bands in **1** (420 and 332 nm) and **2** (436 and 302 nm). A similar shift to lower energies has been seen in the only other S-donor adduct to date, $[Ru_2(\mu\text{-}O_2CCH_3)_4(tht)_2](PF_6)$ [7]. Complex **4** was insoluble in most solvents to obtain a reasonable spectrum. Dissolution in DMSO or pyridine caused decomposition.

The magnetic moment of each complex was measured in the solid state at room temperature and found to be in the range 3.8–4.1 B.M. This is consistent with the ground-state configuration $\sigma^2\pi^4\delta^2(\pi^*\delta^*)^3$ and three unpaired electrons [3].

Table 5
Key infrared bands (cm^{-1}) and their assignments for complexes **1**–**4** and free ligands [a]

Assignment	urea	**1**	tmu	**2**	tmtu	**3**	thiourea	**4**
ν(N–H)	3500	3474					3380	3396
	3350	3362					3260	3210
								3186
ν(C–H)		2930	2942	2935	2941	2936		2924
						2855		
ν(C=O)	1683	1648	1640	1614				
NH_2 bend	1599	1600					1617	1661
								1624
ν_{asym}(NCN)	1506	1565	1499	1551	1504	1543	1470	1536
ν_{asym}(COO)		1452		1445		1437		1448
ν_{sym}(COO)		1402		1411		1387		1406
ν_1(C=S) [b]					1126	1102	1080	1102
ν_2(C = S) [c]					718	691	730	696
ν(PF_6^-)		843		843		841		853

[a] Values for the free ligands are collected from Refs. [29–35].
[b] C=S stretching + symmetric C–N stretching + (NH_2 rocking for thiourea) [34].
[c] C=S stretching + N–C–N stretching [34].

3.7. Electrochemistry

As complex **1** is not sufficiently soluble in an appropriate non-coordinating solvent, measurements carried out in coordinating solvents such as water or methanol suffer from the ambiguity of which is the electroactive species: complex **1**, the solvent-donor adduct or a mixture of the two. For example, cyclic voltammetry measurements on **1** in aqueous media (0.100 M $NaClO_4$) versus Ag/AgCl reference yielded an essentially reversible redox couple at $E_{1/2} = 72$ mV ($\Delta E_p = 68$ mV) at a scan rate of 100 mV s^{-1}. This is the same value as was found for $[Ru_2(\mu\text{-}O_2CCH_3)_4(H_2O)_2](PF_6)$, $[Ru_2(\mu\text{-}O_2CCH_3)_4(DMF)_2](PF_6)$, and $[Ru_2(\mu\text{-}O_2CCH_3)_4(DMSO)_2](PF_6)$ which were measured under identical conditions [15]. This is almost certainly due to substantial hydrolysis of the complexes, with the measured value being essentially that for the $[Ru_2(\mu\text{-}O_2CCH_3)_4(H_2O)_2](PF_6)$ adduct. Subsequent measurements of the DMF and DMSO adducts in the non-coordinating solvents dichloromethane and/or 1,2-dichloroethane showed substantially different values [4].

Complexes **2** and **3** were not hampered by this solubility problem and could readily be measured in 1,2-dichloroethane allowing for direct comparison to several previously measured adducts. Both complexes displayed one quasi-reversible one-electron reduction at a scan rate of 100 mV s^{-1}. For complex **2** this occurred at −487 mV (vs. Fc/Fc^+) with an anodic to cathodic potential separation (ΔE_p) of 123 mV. Complex **3** showed a similar reduction at −541 mV (vs. Fc/Fc^+) with $\Delta E_p = 93$ mV. Table 6 summarizes these results and puts them in the context of selected donor adducts measured under similar conditions. The trend of decreasing $E_{1/2}$ values with increasing Gutmann donor number of the axial ligand has been discussed elsewhere [4]. What we are primarily interested in here is where complex **2** and **3** fit into this trend. With a Gutmann donor number of 31 for tmu [36] complex **2** fits the trend quite nicely, lying between L = DMSO (D.N. = 29.8) and L = pyridine (D.N. = 33.1). The potential for complex **3** lies substantially lower than **2** with a value close to that for L = 4-methylpyridine (D.N. = 35.1). As there is no documented donor number value for tmtu a direct comparison cannot be made and structurally the long Ru–S bond (2.610(2) Å) makes the low $E_{1/2}$ value and hence strong donor character somewhat surprising. However, if one compares the tmtu adduct with the tetrahydrothiophene (tht) adduct ($E_{1/2} = -322$ mV) there is structural consistency. The tht adduct has a longer Ru–S bond (2.627 Å) and shorter Ru–Ru bond (2.285 Å) than complex **3** (Ru–Ru = 2.301 Å). This implies that **3** forms a stronger axial bond and more electron density is transferred into the metal centers leading to an increased population of the antibonding orbitals, a longer Ru–Ru bond and hence a lower $E_{1/2}$ value.

Table 6
Electrochemical data for various $[Ru_2(\mu\text{-}O_2CCH_3)_4L_2]^{+/0}$ couples

L	$E_{1/2}$ (mV) [a]	D.N. [b]	Ref.
PCy_3	−730		6
TMTU (**3**)	−541		This work
4-MePy	−537	35.1	4
Py	−519	33.1	4
TMU (**2**)	−487	31.0	This work
DMSO	−483	29.8	4
THT	−322		7
DMF	−302 [c]	26.6	4
Unligated [d]	−233	1 [e]	38

[a] In 1,2-dichloroethane vs. Fc/Fc^+ (Fc/Fc^+ couple measured at 392 mV vs. Ag/AgCl, $\Delta E = 75-80$ mV).
[b] Refs. [36] and [37].
[c] Cathodic potential only.
[d] For the $[Ru_2(\mu\text{-octanoate})_4]^{0/+}$ couple in dichloromethane [38].
[e] Value for dichloromethane.

4. Conclusion

We have synthesized and fully characterized three (complexes **1**–**3**) new Lewis base adducts of diruthenium(II,III) tetraacetate and partially characterized a fourth (**4**) which appears to be of a polymeric or oligomeric nature. Complex **1** crystallizes from 1-propanol as a rare example of co-solvent diadduct system and complex **3** is only the second known example of a diruthenium tetracarboxylate sulfur-donor adduct. While there is no significant intramolecular hydrogen-bonding in **1** there is evidence for intermolecular H-bonding between the urea nitrogen and an acetate of the 1-propanol diadduct as well as between the 1-propanol oxygen and an acetate oxygen of the diurea adduct. The X-ray structures for **1**–**3** are supported by the infrared and electronic spectroscopy. The cyclic voltammetry of complexes **2** and **3** displays one quasi-reversible reduction, consistent with earlier studied Lewis base adducts [4,6,7]. Despite the long axial Ru–S bond in **3** the electrochemistry implies that tmtu is a moderately strong donor, comparable to 4-methylpyridine.

Evidence for **4**'s polymeric nature comes from its solubility properties and the metal complex to ligand stoichiometry which is shown to be 1:1 from the elemental analysis. IR spectroscopy provides partial evidence that the thiourea ligand in **4** is acting as a bridge between adjacent $[Ru_2(\mu\text{-}O_2CCH_3)_4]^+$ groups and that bridging occurs through both the S and N atoms, but this is not conclusive. Decomposition of **4** in an excess of strong solvents such as DMSO and pyridine is also consistent with the breakdown of a diruthenium tetracarboxylate polymer [39]. Assuming **4** is a polymer, some key questions do remain. What is the exact nature

of the thiourea bridge? Why doesn't the urea analogue form a polymer? Are there significant magnetic and/or electronic interactions through the bridge? We are currently attempting to answer these questions by synthesizing adducts of partially methylated derivatives of thiourea, using slow diffusion processes to grow crystals of **4** and investigating the low temperature magnetic susceptibility of all the compounds.

5. Supplementary material

Crystallographic data (CIF) files for the structural analyses of **1**, **2**, and **3** have been deposited with the Cambridge Crystallographic Data Centre (12 Union Road, Cambridge, CB2 1EZ, UK (fax: +44-1223-336033; e-mail: deposit@ccdc.cam.ac.uk or www: http://www.ccdc.cam.ac.uk)), and are available on request quoting the deposition numbers 175390 for **1**, 175391 for **2**, and 175392 for **3**.

Acknowledgements

M.A.S.A. wishes to thank the Natural Sciences and Engineering Council (NSERC) of Canada and the University Council for Research (UCR) for financial support.

References

[1] F.A. Cotton, R.A. Walton, Multiple Bonds between Metal Atoms, second ed., Oxford University Press, Oxford, 1993.
[2] M.C. Barral, R. Jiménez-Aparicio, J.L. Priego, E.C. Royer, F.A. Urbanos, An. Quim. Int. Ed. 93 (1997) 277.
[3] M.A.S. Aquino, Coord. Chem. Rev. 170 (1998) 141.
[4] G. Vamvounis, J.F. Caplan, T.S. Cameron, K.N. Robertson, M.A.S. Aquino, Inorg. Chim. Acta 304 (1998) 87.
[5] H.J. Gilfoy, K.N. Robertson, T.S. Cameron, M.A.S. Aquino, Acta Crystallogr., Sect. E 57 (2001) m496.
[6] G.G. Briand, M.W. Cooke, T.S. Cameron, H.M. Farrell, T.J. Burchell, M.A.S. Aquino, Inorg. Chem. 40 (2001) 3267.
[7] H.J. Gilfoy, K.N. Robertson, T.S. Cameron, M.A.S. Aquino, Inorg. Chim. Acta 331 (2002) 330.
[8] K.R. Dunbar, J.H. Matonic, V.P. Saharan, C.A. Crawford, G. Christou, J. Am. Chem. Soc. 116 (1994) 2201.
[9] C.A. Crawford, E.F. Day, V.P. Saharan, K. Folting, J.C. Huffman, K.R. Dunbar, G. Christou, J. Chem. Soc., Chem. Commun. (1996) 1113.
[10] S. Gangopadhyay, P.K. Gangopadhyay, J. Inorg. Biochem. 66 (1997) 175.
[11] C. Sudha, A.R. Chakravarty, Ind. J. Chem. 37A (1998) 1.
[12] B.K. Keppler, M. Henn, U.M. Juhl, M.R. Berger, R. Niebl, F.E. Wagner, Prog. Clin. Biochem. Med. 10 (1989) 41.
[13] C.E.J. van Rensburg, E. Kreft, J.C. Swarts, S.R. Dalrymple, D.M. MacDonald, M.W. Cooke, M.A.S. Aquino, Anticancer Res. 22 (2002) 889.
[14] R.W. Mitchell, A. Spencer, G. Wilkinson, J. Chem. Soc., Dalton Trans. (1973) 846.
[15] K.D. Drysdale, E.J. Beck, T.S. Cameron, K.N. Robertson, M.A.S. Aquino, Inorg. Chim. Acta 256 (1997) 243.
[16] B.N. Figgis, R.S. Nyholm, J. Chem. Soc. (1958) 4190.
[17] G.M. Sheldrick, in: G.M. Sheldrick, C. Kruger, R. Goddard (Eds.), SHELXS-86: Crystallographic Computing, third ed., Oxford University Press, Oxford, UK, 1985, pp. 175–189.
[18] DIRDIF-94: P.T. Beurskens, G. Admiraal, G. Beurskens, W.P. Bosman, R. de Gelder, R. Israel, J.M.M. Smits, The DIRDIF-94 program system, Technical Report of the Crystallographic Laboratory, University of Nijmegen, The Netherlands, 1994.
[19] teXsan for Windows: Crystal Structure Analysis Package, Molecular Structure Corporation, 1997.
[20] G.M. Sheldrick, SHELX-97, Program for Refinement of Crystal Structures, University of Göttingen, Germany, 1997.
[21] D.T. Cromer, J.T. Waber, International Tables for X-ray Crystallography, vol. IV (Table 2.2A), Kynoch Press, Birmingham, 1974.
[22] D.C. Creagh, J.H. Hubbell, in: A.J.C. Wilson (Ed.), International Tables for Crystallography, vol. C, Kluwer Academic Publishers, Boston, 1992, pp. 200–206.
[23] J.A. Ibers, W.C. Hamilton, Acta Crystallogr. 17 (1964) 781.
[24] D.C. Creagh, W.J. McAuley, in: A.J.C. Wilson (Ed.), International Tables for Crystallography, vol. C, Kluwer Academic Publishers, Boston, 1992, pp. 219–222.
[25] M. McCann, A. Carvill, C. Cardin, M. Convery, Polyhedron 10 (1993) 1163.
[26] M. Handa, Y. Sayama, M. Mikuriya, R. Nukada, I. Hiromitsu, K. Kasuga, Bull. Chem. Soc. Jpn. 68 (1995) 1647.
[27] Y. Sayama, M. Handa, M. Mikuriya, I Hiromitsu, K. Kasuga, Chem. Lett. (1999) 453.
[28] M.C. Barral, R. Jimenez-Aparicio, J.L. Priego, E.C. Royer, F.A. Urbanos, U. Amador, Inorg. Chem. 37 (1998) 1413.
[29] K. Nakamoto, Infrared and Raman Spectra of Inorganic and Coordination Compounds (Part B), fifth ed., Wiley, New York, 1997.
[30] M. Schafer, C. Curran, Inorg. Chem. 5 (1966) 265.
[31] E. Giesbrecht, M. Kawashita, J. Inorg. Nucl. Chem. 32 (1970) 2461.
[32] C.J. Pouchert, The Aldrich Library of FT-IR Spectra, vol. 1, first ed., Aldrich Chemical Company Inc, Milwaukee, WI, 1985.
[33] A. Yamaguchi, T. Miyazawa, T. Shimanouchi, S. Mizushima, Spectrochim. Acta 10 (1957) 170.
[34] A. Yamaguchi, R.B. Penland, S. Mizushima, T.J. Lane, C. Curran, J.V. Quagliano, J. Am. Chem. Soc. 80 (1958) 527.
[35] R.A. Bailey, T.R. Peterson, Can. J. Chem. 45 (1967) 1135.
[36] V. Gutmann, The Donor–Acceptor Approach to Molecular Interactions, Plenum Press, New York, 1978.
[37] Y. Marcus, J. Solut. Chem. 13 (1984) 599.
[38] M.H. Chisholm, G. Christou, K. Folting, J.C. Huffman, C.A. James, J.A. Samuels, J.L. Wesemann, W.H. Woodruff, Inorg. Chem. 35 (1996) 3643.
[39] M.C. Barral, I. de la Fuente, R. Jiménez-Aparicio, J.L. Priego, M.R. Torres, F.A. Urbanos, Polyhedron 20 (2001) 2537.

PERGAMON

Polyhedron 21 (2002) 1245–1253

POLYHEDRON

www.elsevier.com/locate/poly

Synthesis and properties of $[Cu(L^5)_2][ClO_4]_2 \cdot H_2O$ having square planar and pseudo-octahedral geometries in the same unit cell, and anion-bound complexes $[Cu(L^5)_2X][ClO_4]$ ($X = Cl^-$, NCS^-, N_3^-) [L^5 = 2-(3,5-dimethylpyrazol-1-ylmethyl)pyridine]

Rajeev Gupta, Tapan Kumar Lal, Rabindranath Mukherjee *

Department of Chemistry, Indian Institute of Technology, Kanpur 208 016, India

Received 3 January 2002; accepted 27 March 2002

Abstract

Using a bidentate heterocyclic ligand with mixed hard–soft nitrogen donor set [L^5 = 2-(3,5-dimethylpyrazol-1-ylmethyl)pyridine] two types of copper(II) complexes have been synthesized and characterized: (i) $[Cu(L^5)_2][ClO_4]_2 \cdot H_2O$ (**1**) and (ii) $[Cu(L^5)_2X][ClO_4]$ ($X = Cl^-$ (**2**), NCS^- (**3**) and N_3^- (**4**)). Structural analysis of **1** reveals that its unit cell consists of a 1:1 mixture of square planar $[Cu(L^5)_2]^{2+}$ (coordination by two pyrazoles and two pyridines) and tetragonal $[Cu(L^5)_2(H_2O)_2]^{2+}$, having additional weak interaction with the water molecules in the axial positions. Preliminary X-ray structural analysis of **3** with a poor data set, which is not reported here, revealed that the thiocyanate group is S-coordinated. For each complex the stereochemistry of the copper(II) centre has been investigated in the solid state as well as in MeCN solution, by absorption and EPR spectroscopy. In the polycrystalline state as well as in MeCN solution complex **1** displays axial EPR spectra having a $d_{x^2-y^2}$ ground state. However, solid samples of **2**–**4** exhibit rhombic EPR spectral features, characteristic of a compressed d_{z^2} ground state. In the solution phase (80 K) **2** exhibits an isotropic signal; **3** and **4** exhibit axial spectra, characteristic of a $d_{x^2-y^2}$ ground state. The observed $E_{1/2}$ values for the Cu^{II}–Cu^{I} redox couple [cyclic voltammetry: MeCN solution; V vs. saturated calomel electrode (SCE)] are fairly positive: 0.41 (**1**), 0.29 (**2**), 0.30 (**3**) and 0.19 (**4**). © 2002 Elsevier Science Ltd. All rights reserved.

Keywords: 2-(3,5-Dimethylpyrazol-1-ylmethyl)pyridine; Bis-ligand and anion-bound copper(II) complexes; X-ray structure; Absorption and EPR spectra; Cyclic voltammetry

1. Introduction

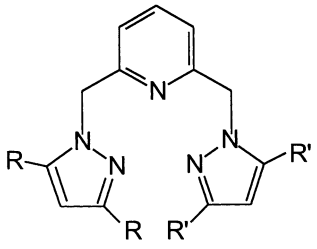
Investigations of the coordination chemistry of copper(II) with chelating ligands continue to be stimulated by interest in developing models for copper proteins and in understanding the factors which give rise to the relationship between the coordination geometry and the nature of the donor atoms and redox potentials [1–6]. As a result of 'plasticity effect' due to Jahn–Teller active ground state, copper(II) forms compounds of coordination number 4–6 with many kinds of irregular coordination geometries. The geometry of the coordination polyhedron around copper(II) is also influenced by subtle ligand characteristics: ligand constraints/flexibility, steric hindrance and the strength of the donor atoms. Systematic variation of Cu^{II} stereochemistry provides an opportunity to identify the effect of ligands' electronic and/or imposed steric factors responsible for subtle stereochemical preferences for a particular molecular structure, associated electronic structure and reactivity behaviour.

In the past few years we have investigated [7–13] the coordination chemistry using nonplanar bi- and tridentate heterocyclic ligands (L^1–L^5) to control the stereochemistry at metal centres, including copper(II) [10,11,13]. These ligands contain both pyridine (soft) and pyrazole (hard) donors in a given ligand system. However, their electronic communication is prevented due to placement of methylene spacer(s) between the rings. The effects of such an electronic feature and the

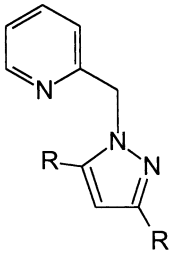
* Corresponding author. Tel./fax: +91-512-597-437.
E-mail address: rnm@iitk.ac.in (R. Mukherjee).

0277-5387/02/$ - see front matter © 2002 Elsevier Science Ltd. All rights reserved.
PII: S0277-5387(02)01014-8

presence of methyl substituents near the donor site (L^2, L^3 and L^5) were revealed in the structural and electronic properties of transition-metal centres. We [10,11,13] and others [14,15] have demonstrated that using ligands L^1, L^3 or L^5 the coordination polyhedra around mononuclear Cu^{II} centres could be systematically tuned. X-ray crystallographic investigations on $[Cu(L^3)X_2]$ ($X = Cl^-$, Br^- or SCN^-) [14,15], $[Cu(L^3)(N_3)_2]$ [13], $[Cu(L^3)(ONO)(OClO_3)]$ [13], $[Cu(L^3)(L^5)][ClO_4]_2$ [11] and $[Cu(L^5)_2(ONO)][ClO_4]$ [10] complexes have given credence to our expectation. These observations prompted our interest in the synthesis of bis-ligand $Cu^{II}N_4$ complexes of L^5 to probe the coordination geometry around copper(II). To reveal stereochemical changes around the Cu^{II} centre by coordination of the bidentate ligand L^5 with additional binding of simple inorganic anions, we have synthesized complexes like dark violet $[Cu(L^5)_2][ClO_4]_2\cdot H_2O$ (**1**) and green $[Cu(L^5)_2X][ClO_4]$ ($X = Cl^-$ (**2**), NCS^- (**3**) and N_3^- (**4**)) and determined the crystal structure of **1**. Interestingly, the crystal structure of **1** reveals that it contains a 1:1 mixture of square planar $[Cu(L^5)_2]^{2+}$ and tetragonal $[Cu(L^5)_2(H_2O)_2]^{2+}$, having weak interaction with the water molecules in the axial positions. This paper is also concerned with the spectral and redox properties of these complexes. Given the scarcity [7,10,11,13–15] of structural investigation of copper(II) complexes with this class of ligands, the structural information on the bis-ligand complex **1** would be of interest to rationalize the chemical significance of the results observed.



R = R' = H; L^1
R = H, R' = Me; L^2
R = R' = Me; L^3



R = H; L^4
R = Me; L^5

2. Experimental

2.1. Materials

All chemicals were obtained from commercial sources and used as received. Solvents were purified/dried following standard procedures [10,11,13]. The ligand L^5 and tetra-*n*-butylammonium perchlorate were synthesized as before [9,10].

2.2. Synthesis of copper(II) complexes

2.2.1. $[Cu(L^5)_2][ClO_4]_2\cdot H_2O$ (1)

To a magnetically stirred solution of $Cu(ClO_4)_2\cdot 6H_2O$ (0.1 g, 0.27 mmol) in EtOH (3 cm^3) a solution of the ligand L^5 (0.1 g, 0.54 mmol) in EtOH (3 cm^3) was added dropwise. The resulting clear blue solution was stirred for 15 min and kept in air for slow evaporation. After 12 h, a dark violet microcrystalline solid that formed was collected by filtration, washed thoroughly with EtOH and dried in vacuo. Recrystallization was achieved from MeCN/EtOH to afford a dark violet product (yield: approximately 60%). *Anal.* Found: C, 40.2; H, 4.2; N, 12.7. Calc. for $C_{22}H_{28}N_6O_9Cl_2Cu$: C, 40.3; H, 4.3; N, 12.8%. IR (KBr, cm^{-1}, selected peaks): 3400 ν(OH), 1085, 620 $\nu(ClO_4^-)$. Conductivity (MeCN, $\approx 10^{-3}$ mol dm^{-3} solution at 298 K): $\Lambda_M = 286\ \Omega^{-1}\ cm^2\ mol^{-1}$ (expected range [16] for 1:2 electrolyte: 220–300 $\Omega^{-1}\ cm^2\ mol^{-1}$). UV–Vis: λ_{max} (nm) (ε, $dm^3\ mol^{-1}\ cm^{-1}$): 950 (sh), 602 (80), 350 (sh), 262 (sh) (MeCN); 980 (sh), 505, 364, 273 (Nujol mull). μ_{eff} (MeCN, 298 K) 1.87 μ_B. Variable-temperature magnetic moment data (T/K, μ_{eff}/μ_B): 300, 1.88; 280, 1.86; 260, 1.87; 240, 1.86; 220, 1.87; 200, 1.86; 180, 1.85; 160, 1.85; 140, 1.83; 120, 1.82; 100, 1.77; 81, 1.81. Cyclic voltammetry (V vs. SCE; MeCN): $E_{1/2} = 0.41$ V, $\Delta E_p = 120$ mV and $E_{pc} = -0.56$ V.

2.2.2. $[Cu(L^5)_2Cl][ClO_4]$ (2)

2.2.2.1. Method A. To a magnetically stirred solution of **1** (0.1 g, 0.153 mmol) in MeCN (8 cm^3) was added dropwise a solution of $Et_4NCl\cdot xH_2O$ (0.025 g, 0.153 mmol) in H_2O. The green reaction mixture thus obtained was allowed to stand for 3 days in air. Green crystals thus obtained were washed thoroughly with water and dried in vacuo (yield: approximately 98%). *Anal.* Found: C, 46.2; H, 4.5; N, 14.6. Calc. for $C_{22}H_{26}N_6O_4Cl_2Cu$: C, 46.1; H, 4.5; N, 14.7%. IR (KBr, cm^{-1}, selected peaks): 1100, 620 $\nu(ClO_4^-)$. Conductivity (MeCN, $\approx 10^{-3}$ mol dm^{-3} solution at 298 K): $\Lambda_M = 132\ \Omega^{-1}\ cm^2\ mol^{-1}$ (expected range [16] for 1:1 electrolyte: 120–160 $\Omega^{-1}\ cm^2\ mol^{-1}$). UV–Vis: λ_{max} (nm) (ε, $dm^3\ mol^{-1}\ cm^{-1}$): 980 (sh), 710 (160), 355 (800), 280 (sh), 260 (8270) (MeCN); 980 (br), 720 (br), 620 (sh), 370 (sh), 271 (Nujol mull). μ_{eff} (MeCN, 298 K) 1.90 μ_B. Variable-temperature magnetic moment data (T/K, μ_{eff}/μ_B): 300, 1.90; 280, 1.87; 260, 1.87; 240, 1.87; 220, 1.88; 200, 1.86; 180, 1.84; 160, 1.85; 140, 1.82; 120, 1.79; 100, 1.77; 81, 1.75. Cyclic voltammetry (V vs. SCE; MeCN): $E_{1/2} = 0.29$ V, $\Delta E_p = 180$ mV and $E_{pc} = -0.66$ V.

2.2.2.2. Method B. To a magnetically stirred solution of $Cu(ClO_4)_2\cdot 6H_2O$ (0.050 g, 0.135 mmol) in MeCN (1 cm^3) was added dropwise a solution of L^5 (0.050 g, 0.27 mmol) in MeCN (2 cm^3). After 2 min of stirring the

resulting blue solution, a solution of $Et_4NCl \cdot xH_2O$ (0.029 g, 0.18 mmol) in H_2O (1 cm^3) was added dropwise and the resulting faint greenish-blue solution was stirred for an additional 1 h at 298 K. It was then left for slow evaporation in air. After 2 days fine needle-like light blue crystals precipitated, which were collected by filtration, washed with water and dried in vacuo (yield: approximately 65%).

2.2.3. $[Cu(L^5)_2(SCN)][ClO_4]$ (3)

2.2.3.1. Method A. A similar procedure as that for **2** was followed with KSCN (0.015 g, 0.153 mmol). (yield: approximately 95%). *Anal.* Found: C, 46.5; H, 4.4; N, 16.5. Calc. for $C_{23}H_{26}N_7ClSO_4Cu$: C, 46.4; H, 4.4; N, 16.5%. IR (KBr, cm^{-1}, selected peaks): 2105, 2060 ν(CN) of NCS^-; 1100, 620 $\nu(ClO_4^-)$. Conductivity (MeCN, $\approx 10^{-3}$ mol dm^{-3} solution at 298 K): $\Lambda_M = 154\ \Omega^{-1}\ cm^2\ mol^{-1}$. UV–Vis: λ_{max} (nm) (ε, $dm^3\ mol^{-1}\ cm^{-1}$): 950 (sh), 690 (140), 412 (1100), 254 (11 470), 224 (21 300) (MeCN); 712, 390, 268 (Nujol mull). μ_{eff} (MeCN, 298 K) 1.82 μ_B. Cyclic voltammetry (V vs. SCE; MeCN): $E_{1/2} = 0.30$ V, $\Delta E_p = 140$ mV and $E_{pc} = -0.64$ V.

2.2.3.2. Method B. To a magnetically stirred solution of $Cu(ClO_4)_2 \cdot 6H_2O$ (0.050 g, 0.135 mmol) in MeCN (2 cm^3) was added dropwise a solution of L^5 (0.050 g, 0.27 mmol) in MeCN (3 cm^3). After stirring for 2 min, a solution of KSCN (0.013 g, 0.135 mmol) in EtOH (2 cm^3) was added dropwise to generate a dark green solution. After 1 h it was left for slow evaporation in air. After 2 days, green crystals that precipitated were collected by filtration, washed with water and dried in vacuo (yield: approximately 75%).

2.2.3.3. Method C. To a magnetically stirred solution of **2** (0.02 g, 0.035 mmol) in MeCN (3 cm^3) was added dropwise an aqueous solution (1 cm^3) of KSCN (0.004 g, 0.041 mmol) and the resulting solution was allowed to stand for 2 days. Green crystals that precipitated were collected by filtration, washed with water and dried in vacuo (yield: approximately 96%).

2.2.4. $[Cu(L^5)_2(N_3)][ClO_4]$ (4)

2.2.4.1. Method A. A similar procedure as that for **2/3** was followed with NaN_3 (0.015 g, 0.153 mmol) (yield: approximately 95%). *Anal.* Found: C, 45.6; H, 4.4; N, 21.7. $C_{22}H_{26}N_9ClO_4Cu$: C, 45.6; H, 4.5; N, 21.8%. IR (KBr, cm^{-1}, selected peaks): 2042, 2005 $\nu(N_3^-)$ of N_3^-; 1080, 620 $\nu(ClO_4^-)$. Conductivity (MeCN, $\approx 10^{-3}$ mol dm^{-3} solution at 298 K): $\Lambda_M = 144\ \Omega^{-1}\ cm^2\ mol^{-1}$. UV–Vis: λ_{max} (nm) (ε, $dm^3\ mol^{-1}\ cm^{-1}$): 717 (370), 425 (1950), 417 (2350), 254 (9500) (MeCN); 800, 440, 270 (Nujol mull). μ_{eff} (MeCN, 298 K) 1.85 μ_B. Cyclic voltammetry (V vs. SCE; MeCN): $E_{1/2} = 0.19$ V, $\Delta E_p = 260$ mV and $E_{pc} = -0.65$ V.

2.2.4.2. Method B. To a magnetically stirred solution of $Cu(ClO_4)_2 \cdot 6H_2O$ (0.050 g, 0.135 mmol) in MeCN (2 cm^3) was added dropwise a solution of L^5 (0.050 g, 0.27 mmol) in MeCN (3 cm^3). After stirring the resulting blue solution for 2 min, a solution of NaN_3 (0.009 g, 0.135 mmol) in H_2O (3 cm^3) was added dropwise to generate a dark green solution. After 1 h it was filtered and left for slow evaporation in air. After 3 days, green crystals that precipitated were collected by filtration, washed with water and dried in vacuo (yield: approximately 70%).

2.2.4.3. Method C. A similar procedure as that for **3** was followed with NaN_3 (0.015 g, 0.035 mmol) (yield: approximately 95%).

Caution! Perchlorate salts of compounds containing organic ligands are potentially explosive.

2.3. Measurements

Elemental analyses (C, H, N) were obtained at the Microanalysis Service Centre of the Department of Inorganic Chemistry, Indian Association for the Cultivation of Science, Kolkata. Infrared spectra were recorded on a Perkin Elmer M-1320 spectrophotometer using KBr discs or Nujol mulls. Electronic spectra were recorded using a Perkin Elmer Lambda 2 spectrophotometer. Solution electrical conductivity measurements (298 K) were carried out at a concentration of $\sim 1 \times 10^{-3}$ $dm^3\ mol^{-1}\ cm^{-1}$ with an Elico (Hyderabad, India) Type CM-82 T conductivity bridge. Variable temperature (81–300 K) magnetic susceptibility measurements in the solid state were performed using a locally-built Faraday balance [17] comprising an electromagnet with constant gradient pole caps (Polytronic Corporation, Mumbai, India), an ultravacuum Sartorius M25-D/S Balance (Germany), a closed-cycle refrigerator and a Lake Shore temperature controller (Cryo Industries, USA). All measurements were made at a fixed main field strength of ~ 10 kG. Solution state magnetic susceptibility was obtained by the NMR technique of Evans [18] in MeCN with a PMX-60 JEOL (60 MHz) NMR spectrometer. Susceptibilities were corrected for the diamagnetic contribution [19]. Cyclic voltammograms were recorded at 298 K on a PAR model 370 electrochemistry system consisting of a model 174A polarographic analyzer with a model 175 universal programmer. A planar Beckman platinum electrode (model 39273) was used as the working electrode. All potentials were measured referenced to SCE; no corrections were made for junction potentials.

2.4. Structure determination and refinement

A violet crystal of **1** was used for data collection (θ–2θ scan technique) on an Enraf Nonius CAD-4-Mach four-circle diffractometer using graphite-monochromated Mo Kα radiation ($\lambda = 0.71073$ Å). Lattice parameters were obtained from least-squares analyses of 25 machine-centred reflections. A total of 5306 reflections were measured of which 4986 were unique and 3104 reflections with $I > 3\sigma(I)$ were used in the structure refinement.

2.4.1. Crystal data

$C_{22}H_{28}Cl_2CuN_6O_9$, $M = 654.54$, triclinic, space group $P\bar{1}$, $a = 9.824(5)$, $b = 10.208(7)$, $c = 14.750(1)$ Å, $\alpha = 90.39(6)$, $\beta = 104.51(4)$, $\gamma = 95.72(5)^\circ$, $V = 1424(2)$ Å^3, $Z = 2$, $D_c = 1.485$ g cm^{-3}, $\mu = 10.1$ cm^{-1}.

Data were corrected for Lorentz-polarization effects; anomalous dispersion was applied for all non-hydrogen atoms and analytical absorption corrections were also applied. The structure was solved initially with SIR-92 and refined isotropically with the SHELX-97 package incorporated in WINGX 1.61 crystallographic collective package [20]. Using the XTAL 3.2 crystallographic software package [21], anisotropic refinements were performed by full-matrix least-squares procedure on F, where the function minimized was $\Sigma w(F_o - F_c)^2$ with $w = 1$. The positions of the hydrogen atoms were calculated assuming ideal geometries, but not refined. Except for O atoms, which were refined isotropically, all other atoms were refined with anisotropic thermal parameters. The ClO_4^- anions were disordered; eight peaks were located as possible oxygen positions, each of them was given a site occupation factor of 0.5. We could not locate the hydrogen atoms of the water molecule. The final cycle of refinement included 371 variable parameters and converged with $R = 0.074$, $R_w = 0.079$, $S = 2.071$, final difference Fourier synthesis: $-0.68 \leq \Delta\rho \leq 0.78$ e Å^{-3}.

3. Results and discussion

3.1. Synthesis and properties

Dark violet bis-ligand copper(II) complex $[Cu(L^5)_2][ClO_4]_2 \cdot H_2O$ (**1**) was readily prepared by the stoichiometric reaction of $[Cu(H_2O)_6][ClO_4]_2$ with L^5 in EtOH. Green anion-bound complexes $[Cu(L^5)_2X][ClO_4]$ (X = Cl^- (**2**), NCS^- (**3**) and N_3^- (**4**)) were prepared in MeCN–H_2O/EtOH mixture by (i) reaction between **1** and $Et_4NCl \cdot xH_2O$, KSCN or NaN_3 in a 1:1 molar ratio and (ii) direct reaction of $[Cu(H_2O)_6][ClO_4]_2$, L^5 and $Et_4NCl \cdot xH_2O$, KSCN or NaN_3 in the molar ratio 1:2:1. Complexes **3** and **4** were also prepared from the reaction between **2** and KSCN or NaN_3 in the molar ratio 1:1. Microanalytical, IR [11,22] and conductivity data (in MeCN, **1** behaves as a 1:2 electrolyte and **2**–**4** behave as 1:1 electrolytes) are in conformity with the suggested formulations for **1**–**4**. For **1** an interesting observation is that it reacts with Br^- ion giving rise to green colouration, which was revealed during KBr pellet formation for IR studies. This inspired us to explore the possibility of synthesizing anion-bound complexes and successful synthesis of **2**–**4** from **1**, is the outcome of such an effort. Complex **1** is highly soluble in MeCN, MeOH, DMF and moderately soluble in $MeNO_2$ and Me_2CO, however, generating blue solutions. Complexes **2**–**4** are highly soluble in MeCN and DMF.

In order to determine unambiguously the structure of the bis-ligand complex **1**, a single-crystal structure determination was undertaken (vide infra). Although we succeeded in growing single crystals of **3**, the X-ray data collected at 295 K using such a crystal [monoclinic, space group $P2_1$ (no. 4); $a = 9.465(3)$, $b = 18.364(7)$, $c = 15.496(9)$ Å, $\beta = 102.7(4)^\circ$, $V = 2628(2)$ Å^3, $Z = 4$] has not allowed us to solve the structure satisfactorily, due to a poor data set. However, the presence of $[Cu(L^5)_2(SCN)][ClO_4]$ is clearly observable in the difference Fourier map. The asymmetric unit contains two such units, and in each molecule the copper(II) centre is distorted towards trigonal bipyramidal and the thiocyanate group is S-coordinated in the equatorial plane [23].

3.2. Description of the structure of $[Cu(L^5)_2][ClO_4]_2 \cdot H_2O$

The asymmetric unit of the crystal of the complex $[Cu(L^5)_2][ClO_4]_2 \cdot H_2O$ contains a 1:1 mixture of square planar $[Cu(L^5)_2][ClO_4]_2$ and tetragonal $[Cu(L^5)_2(H_2O)_2][ClO_4]_2$. The molecular structures of both the cations together with the atom numbering scheme used are shown in Fig. 1. Relevant bond distances and angles are given in Table 1. In each $[Cu(L^5)_2]^{2+}$ cation the copper(II) ion sits on a crystallographically imposed centre of inversion, with the two pyridyl [N1 and its symmetry related N1′ for Cu(1); N1a and N1a′ for Cu(2)] and two pyrazole [N3 and its symmetry related N3′ for Cu(1); N3a and N3a′ for Cu(2)] nitrogens in mutually *trans* positions. The coordination angles very slightly deviate from the ideal angle of 90° (Table 1). The water molecules are not in contact distances with the Cu(1) centre [Cu(1)–O(1w) distance 10.82(1) Å]. For the Cu(2) centre two extremely long interactions with the O atoms of water molecules in the axial positions is clearly observable (Fig. 1(b)). The observed Cu(2)–O(1w) bond distance [2.729(8) Å] can at most be regarded as semi-coordination [24,25], then the structure would correspond to CuN_4O_2 coordination. Each cation is thus effectively a four-coordinate bis-ligand complex and the geometry of the copper(II) centre is square planar. The Cu–N(pyridyl) and Cu–N(pyrazole) bond distances are

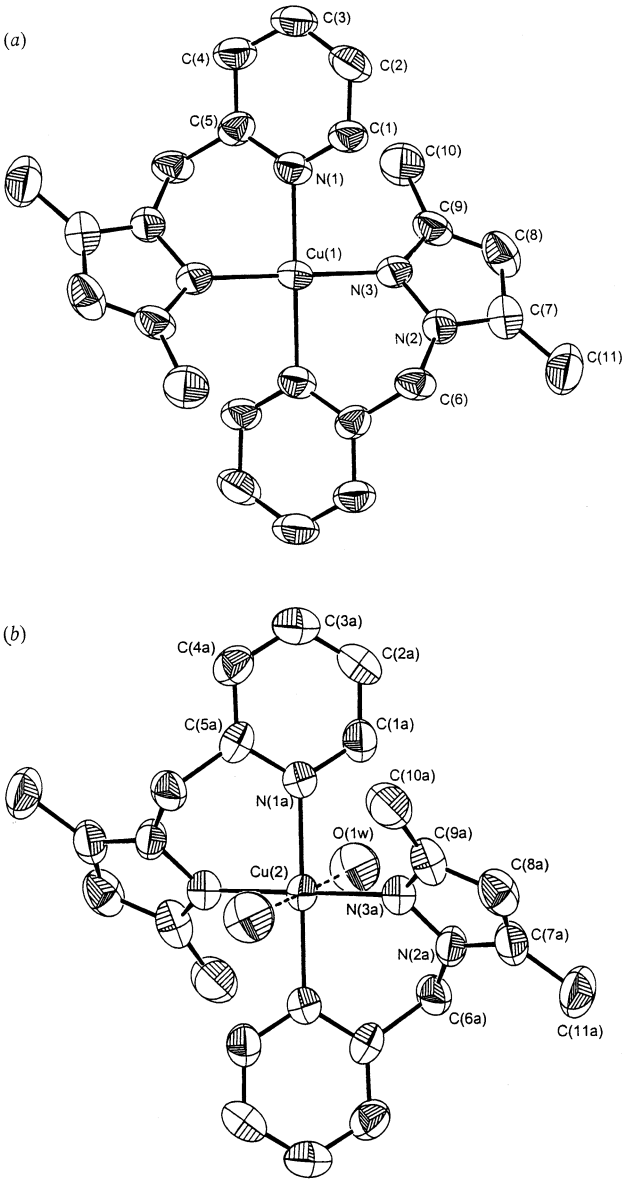


Fig. 1. Molecular structure of (a) $[Cu(L^5)_2]^{2+}$ and (b) $[Cu(L^5)_2(H_2O)_2]^{2+}$ in the unit cell of $[Cu(L^5)][ClO_4]_2 \cdot H_2O$ (**1**). The thermal ellipsoids are at the 50% probability level. Hydrogen atoms are omitted.

Table 1
Selected bond distances (Å) and bond angles (°) for $[Cu(L^5)_2][ClO_4]_2 \cdot H_2O$ (**1**)

Bond lengths			
Cu(1)–N(1)	2.026(7)	Cu(2)–N(1a)	2.029(8)
Cu(1)–N(3)	1.981(8)	Cu(2)–N(3a)	1.990(7)
Bond angles			
N(1)–Cu(1)–N(3)	92.3(3)	N(1a)–Cu(2)–N(3a)	92.0(3)
N(1)–Cu(1)–N(3′)	87.7(3)	N(1a)–Cu(2)–N(3a′)	88.0(3)

2.026(7) and 1.981(8) Å for Cu(1) and 2.029(8) and 1.990(7) Å for Cu(2), respectively. The Cu–N(pyridyl) distances are longer than Cu–N(pyrazole) distances (Table 1). The observed behaviour is in line with this trend and the distances are also in good agreement with values observed in $[Cu(L^3)(ONO)(OClO_3)]$ [13] and $[Cu(L^3)(NCS)_2]$ [14]. The pyridyl and pyrazole rings are each planar. However, a pyridyl ring of a given ligand is twisted to a pyrazole ring by an angle of $\sim 57^\circ$ or $\sim 65^\circ$. Thus, the six-membered chelate rings exist in boat conformations [7,10].

Within the present class of non-planar pyrazolylmethylpyridine ligands, the structure of **1** has two distinct noteworthy features. This is for the first time the metric parameters of a mononuclear copper(II) complex with coordination solely by two chelating ligands L^5 have become available. To the best of our knowledge, this is the second report of two different cationic copper(II) coordination geometries in the same unit cell, one four-coordinate and the other six-coordinate. The other report [25] demonstrated the existence in the same unit cell one hexa-coordinate and the other penta-coordinate cations.

3.3. Absorption spectral properties

The electronic spectra of complexes **1**–**4** were measured both in the solid state (dispersed in mineral oil mull) and in MeCN solution (Section 2). The diffuse reflectance spectrum of **1** displays a visible band at 505 nm, suggestive of a predominantly square planar stereochemistry [26], in conformity with the X-ray structural result. In MeCN solution it displays a band due to a d-d transition at 602 nm. This indicates a square pyramidal geometry [26] around Cu^{II}, implying that in going from solid to the solution phase, a stereochemical change around Cu(II) from square planar to square pyramidal has occurred. For **2**, the solid state reflectance spectrum displays two overlapping bands in the region 600–1000 nm. Similar behaviour was observed for $[Cu(L^1/L^3)Cl_2]$ [11], exhibiting Cu_2Cl_2 core formation (vide infra). For **3** and **4** broad absorptions are observed at 710 and 800 nm, respectively. This is indicative of a distorted trigonal bipyramidal geometry around Cu^{II} [26]. However, in MeCN solution the positions of the d–d transition are 710 nm (**2**), 690 nm (**3**) and 717 nm (**3**). The observed blue shift implies that a change in copper(II) stereochemistry has occurred in going from solid to solution (vide infra) and the effect is more pronounced in the case of **4**.

3.4. EPR spectral properties

To extract more information about the stereochemistry at the copper(II) centre, the X-band EPR spectra of all the complexes have been recorded as microcrystalline solids (at 298 and at 80 K) and in frozen MeCN solution or as glass at 80 K. The data are summarized in Table 2.

Table 2
EPR spectral data for the complexes [a]

Compound	Medium	$g_{\|}$	$A_{\|}$	$g_{\perp}$	g_1	g_2	g_3
1 $[Cu(L^5)_2][ClO_4]_2\cdot H_2O$	polycrystalline powder at 298 K	2.214	207	2.048			
	polycrystalline powder at 80 K	2.209	214	2.043			
	MeCN solution at 80 K	2.232	198	2.063			
2 $[Cu(L^5)_2Cl][ClO_4]$ [b]	polycrystalline powder at 298 K				2.222	2.149	2.014
	polycrystalline powder at 80 K				2.192	2.150	2.007
3 $[Cu(L^5)_2(SCN)][ClO_4]$	polycrystalline powder at 298 K				2.192	2.143	2.011
	polycrystalline powder at 80 K				2.190	2.146	2.010
	CH_2Cl_2–C_6H_7 solution (2:1 v/v) at 80 K	2.269	169	2.061			
4 $[Cu(L^5)_2(N_3)][ClO_4]$	polycrystalline powder at 298 K				2.173	2.131	2.017
	polycrystalline powder at 80 K				2.175	2.134	2.013
	CH_2Cl_2–C_6H_7 solution (2:1 v/v) at 80 K	2.250	163	2.050			

[a] $A_{\|}$ values are in $\times 10^{-4}$ cm^{-1}. For the complex $[Cu(L^5)_2(ONO)][ClO_4]$ in CH_2Cl_2–C_6H_7 solution (2:1 v/v) at 80 K the EPR parameters: $g_{\|} = 2.266$, $A_{\|} = 169 \times 10^{-4}$ cm^{-1}, $g_{\perp} = 2.060$.
[b] $g_{iso} = 2.121$ in MeCN/MeCN–C_6H_7 solution (1:1 v/v) at 80 K.

Complex **1** exhibits in the solid state as well as in MeCN solution, axial spectra typical for monomeric tetragonal copper(II) species with $d_{x^2-y^2}$ ground-state ($g_{\|} > g_{\perp} > 2.0$) [26]. The behaviour of **1** in the polycrystalline state at 298 K is displayed in Fig. 2. For **1**, the change from solid state to MeCN solution affects the EPR spectral parameters only slightly. A convenient EPR spectral empirical index is the $g_{\|}/A_{\|}$ ratio [27], which provides information about distortion in the geometry around copper(II). For **1**, an increase in $g_{\|}$ and a decrease in $A_{\|}$ rendering the ratio to increase from 103 cm (solid state at 80 K) to 113 cm (MeCN solution at 80 K), however, is clearly observable. This indicates that the copper environment in **1** has been modified in solution due to increased in-plane ligand-field strength or increased axial interaction. It is well known [28] that as the axial interaction in copper(II) complexes increases, ν_{max} of the ligand-field spectral band decreases (vide supra), $g_{\|}$ increases and $A_{\|}$ decreases (Table 2). For **1**, the axial interaction, manifested by giving blue solutions in common organic solvents, is clearly weak.

The polycrystalline EPR spectra of **2**–**4**, in contrast to that of **1**, displayed rhombic pattern from which three distinct g values ($g_1 > g_2 > g_3$) could be derived. The behaviour of **2** at 298 K is displayed in Fig. 2. The fact that the lowest g-value is < 2.03 indicates that these complexes have a compressed rhombic site with a d_{z^2} ground state [26]. For **2**–**4** the values of R [$= (g_2-g_3)/(g_1-g_2)$] [26] at 298 K are 1.85, 2.69 and 2.71, respectively. The observed R values, which are > 1, also justify the fact that these complexes have a predominant d_{z^2} ground state [26]. Interestingly, for **2** the frozen MeCN solution spectrum is isotropic. This could be due to a relaxed (more toward octahedral) coordination sphere, due to the existence of a 'pseudo dimeric structure' with additional coordination of a Cl^- ion

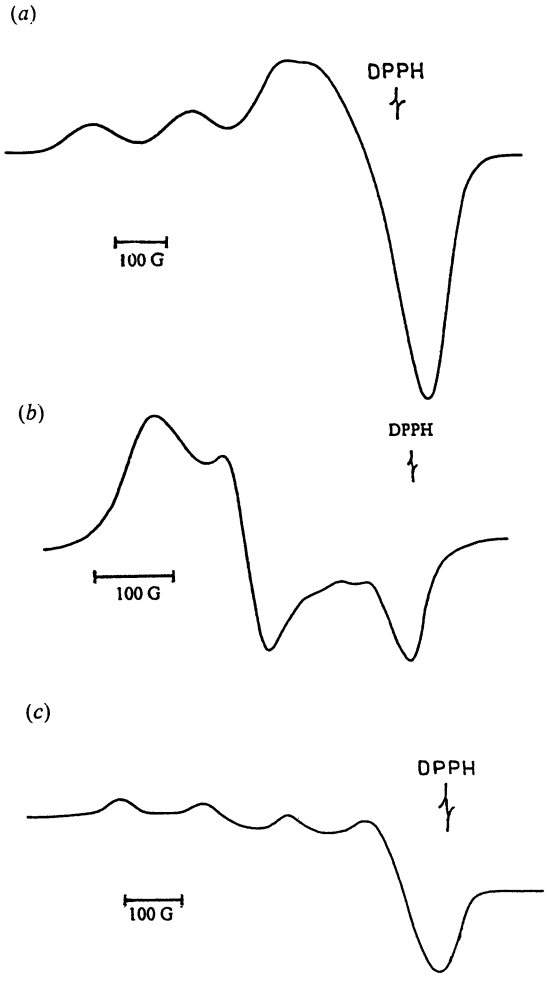


Fig. 2. X-band EPR spectra of (*a*) $[Cu(L^5)_2][ClO_4]_2\cdot H_2O$ (**1**) in the polycrystalline state at 298 K, (b) $[Cu(L^5)_2Cl][ClO_4]$ (**2**) in the polycrystalline state at 298 K and (c) $[Cu(L^5)_2(SCN)][ClO_4]$ (**3**) in CH_2Cl_2–C_6H_7 glass (2:1 v/v) at 80 K.

from a Cu(II) centre to a nearby Cu(II) centre. The existence of such a Cu_2Cl_2 core is well documented in Cu^{II} coordination chemistry, including our own report [29]. However, for **2**, such an interaction must be very weak (cf. magnetism data). Given the results at hand for **2**, we are not in a position to comment more specifically on this behaviour. It should be mentioned here that the complex $[Cu(L^3)(ONO)(OClO_3)]$ [13] behaved similarly. On the other hand, complexes **3** and **4** in 2:1 (v/v) CH_2Cl_2–C_7H_8 glass (80 K) show well resolved four-line tetragonal spectra, characteristic of a $d_{x^2-y^2}$ ground state (Fig. 2 and Table 2). In fact, the spectra are closely similar to that of the structurally characterized square pyramidal complex $[Cu(L^5)_2(ONO][ClO_4]$ ($g_{\|}/A_{\|} = 134$ cm, under identical experimental conditions) [10]. We can therefore infer that the Cu^{II} centre in $[Cu(L^5)_2(SCN)][ClO_4]$ assumes a tetragonal geometry in MeCN solution (cf. absorption spectral result), implying a structural change in going from solid to solution. Given the X-ray structures of $[Cu(L^3)(L^5)][ClO_4]_2$ [11] and $[Cu(L^5)_2(ONO)][ClO_4]$ [10] we believe that in the square pyramidal geometry one of the pyrazole groups acts as the axial ligand. The EPR spectra for the present complexes indicate that it adopts a similar geometry in frozen solution (barring the behaviour of **2** in solution) despite the fact that in the solid state the Cu^{II} geometry of **3** and **4**, is considerably distorted from square pyramidal towards trigonal bipyramidal. Presumably the energy difference between square pyramidal and trigonal bipyramidal geometries is small, and at lower temperature there is a shift toward square pyramidal geometry. Similar changes in stereochemistry have been observed for other Cu^{II} complexes [1].

3.5. Magnetic properties

To confirm whether or not compound **2** is a monomer, we decided to investigate its variable-temperature (81–300 K) magnetic susceptibility behaviour in the solid state using the Faraday method. We have also done temperature-dependent measurement for bis-ligand complex **1**, for which the X-ray structure is available. The complexes followed the Curie–Weiss law. The $1/\chi_M$ versus T plots are linear. The effective magnetic moments of the complexes in the solid state at 300 K are 1.88 and 1.90 μ_B for **1** and **2**, respectively. The solution-state values for all the complexes lie in the range 1.8–2.0 μ_B, expected for copper(II) complexes in a magnetically dilute environment [26] Thus, in the absence of X-ray structural proof, the temperature-dependent magnetic studies clearly demonstrate the mononuclear nature of **2**.

3.6. Redox properties

Cyclic voltammetric measurements of the copper(II) complexes **1**–**4** were carried out in MeCN at a platinum working electrode. Each complex displayed chemically reversible ($i_{pc}/i_{pa} \approx 1$) and electrochemically quasireversible (ΔE_p, in the range 120–260 mV) redox waves corresponding to the reduction of copper(II) to copper(I). The observation of larger ΔE_p values for these complexes is expected given the differing stereochemical requirements of the Cu^{II} and Cu^{I} states [30]. For each complex a second redox process was also observed. This reduction, which was irreversible, led to a copper stripping peak in the subsequent oxidation cycle, indicative of decomposition of a zerovalent complex to elemental copper at the platinum electrode. Such an effect has been described for closely similar complexes [10,11,13].

Interestingly, compared to similar types of complex the $E_{1/2}$ values (V vs. SCE) for the present complexes are fairly positive [10,11,13,15]. The factors [2,10,31–35] which contribute to tune the Cu^{II}–Cu^{I} reduction potentials are: (i) the flexibility of or constraints imposed by the chelating ligands, which might favour a geometry preferred by one metal ion oxidation state, but not the other, (ii) the types of the coordinated donor atoms (i.e. O vs. N vs. S, etc.), (iii) the coordination geometries of the copper sites and (iv) hydrophobicity in the copper complex environment. The complexes **1**–**4**, including previously reported complex $[Cu(L^5)_2(ONO)][ClO_4]$ [10], have given us an unique opportunity to pinpoint each subtle effect. (i) On the cyclic voltammetric time scale, the formation of the comparatively stable copper(I) complex upon reduction will mostly require concomitant distortion of the square planar arrangement of the complex toward a tetrahedral geometry. The flexible ligand L^5 must be contributing to the geometrical requirement. (ii) For a given ligand L^5, the $E_{1/2}$ values for the present solvent-/anion-bound complexes are significantly more positive in the order: MeCN (0.41) > NCS^- (0.30) > Cl^- (0.29) > N_3^- (0.19). In this series **1** has the highest $E_{1/2}$ value. This is possibly because reduction of the Cu^{II} centre to Cu^{I} is expected to trigger a decrease in coordination number from five to four. It is understandable that a weaker axial bond would facilitate bond dissociation and hence electron addition and makes the reduction potential more positive.

The complex $[Cu(L^5)_2(ONO)][ClO_4]$ [10] exhibits a Cu^{II}–Cu^{I} wave at −0.32 V, albeit irreversible, under identical conditions. As the nitrito group in $[Cu(L^5)_2(ONO)][ClO_4]$ [10] or the NCS^- group in **3** [23] is coordinated in the equatorial position it is reasonable to assume that in **2** and **4** the X^- anions are present in the equatorial position, as well. For the mononuclear copper(II) complexes with the composition $[Cu(L^5)_2$-

(X)][ClO_4], a stronger equatorial ligation by X^- is expected to bring about an increase in repulsion between the $d_{x^2-y^2}$ orbital and X^-, which in turn would lead to an increase in the energy of the $d_{x^2-y^2}$ orbital. This would make the addition of an electron into this orbital difficult, i.e. the $E_{1/2}$ values would be more cathodic. It is worth noting here that the Cu–ONO bond distance in [$Cu(L^5)_2$(ONO)][ClO_4] is quite short [2.091(5) Å] [10]. As the Cu^{II}–SCN bond is quite long ($\approx$2.37 Å) [23] the observed trend $ONO^- < NCS^-$ is thus justifiable. Moreover, the S-bound NCS^- group in **3** raises the $Cu^{II}-Cu^{I}$ redox potential by destabilizing the copper(II) state. It is worth noting here that thioether coordination behaves similarly [5]. If we assume a similar Cu–Cl bond distance ($\approx$2.34 Å) as that observed in [$Cu(L^3)Cl_2$] [15], then the observed trend in $E_{1/2}$ values between **2** and **3** is understandable. (iv) Complex **2** exhibits a more negative $E_{1/2}$ value than **1**, undoubtedly caused by the presence of the anionic chloride ligand, which favours ligation to Cu^{II} compared to MeCN [34].

Interestingly, it is well documented that pyrazole-containing complexes have more positive $E_{1/2}$ values than the corresponding pyridine complexes [35]. This is illustrated by comparing (in MeCN) complex **1** (0.41) with [CuL_2][ClO_4]$_2$ [L = di(2-pyridyl)methane] (0.25) [36]. This result suggests that the pyrazole-containing ligands are weaker ligands than the pyridine ones and that the coordination environment of the complexes is softer for the pyrazole complexes. The presence of methyl substituents near the donor site provides 'environmental effects' [11,32]. We believe that the comparatively higher Cu^{II}–Cu^{I} redox potential observed for **1**–**4** is primarily due to reduced ligand field strength exerted around the copper(II) centre by the ligand L^5. Generally speaking, these ligands (L^1–L^5) do not possess good σ-donor ability to stabilize the copper(II) centre [7].

4. Conclusions

Although numerous four, five and six-coordinate mononuclear copper(II) complexes are known in the literature, examples of such structural varieties with non-planar heterocyclic ligands having both soft and hard donor sets are quite uncommon. In this investigation we have provided examples of such complexes with a pyridyl and pyrazole containing bidentate ligand L^5. Interestingly, the crystal structure reveals that [$Cu(L^5)_2$][ClO_4]$_2$·H_2O contains a 1:1 mixture of square planar $[Cu(L^5)_2]^{2+}$ and tetragonal $[Cu(L^5)_2(H_2O)_2]^{2+}$, having additional weak interaction with the water molecules in the axial positions. The properties in the solid state have been systematically compared with those in MeCN solution, revealing that the structure of these complexes in solution is predominantly square pyramidal. Taken together the results presented here and that recently reported [10,11,13–15], indicate that a change in the nature of the anion can substantially influence the geometry (square pyramidal or trigonal bipyramidal) and Cu^{II}–Cu^{I} redox potentials of the copper(II) complexes. This tuning of ligand makeup and resulting metal complex will continue to be useful in the design of desired reactivity [6,30,33,34]. The effects of various factors, which contribute to tune the Cu^{II}–Cu^{I} reduction potentials, have been carefully analyzed. These ligands considerably stabilize the copper(I) state over Cu(II), due to reduced donation by the pyrazole groups. In essence, the bidentate ligand L^5 having non-communicable hard–soft N-donor sets offers a wealth of interesting copper chelate chemistry.

5. Supplementary material

Full tables of bond lengths and angles, tables of non-hydrogen and hydrogen atomic coordinates, anisotropic thermal parameters for non-H atoms as well as hydrogen atom parameters have been deposited with the Cambridge Crystallographic Data Centre, CCDC No. 171047. Copies of this information may be obtained free of charge from The Director, CCDC, 12 Union Road, Cambridge, CB2 1EZ, UK (fax: +44-1223-336033; e-mail: deposit@ccdc.cam.ac.uk or www: http://www.ccdc.cam.ac.uk).

Acknowledgements

This work was supported by the Department of Science and Technology (DST) and the Council of Scientific and Industrial Research, Government of India. The financial assistance of the National X-ray diffractometer facility by DST at this Department is gratefully acknowledged. We sincerely thank Mr. V. Balamurugan for his help in X-ray structural work.

References

[1] G.A. McLachlan, G.D. Fallon, R.L. Martin, L. Spiccia, Inorg. Chem. 34 (1995) 254.
[2] C.F. Martens, A.P.H.J. Schenning, M.C. Feiters, H.W. Berens, J.G.M. van der Linden, G. Admirral, P.T. Beurskens, H. Kooijman, A.L. Spek, R.J.M. Nolte, Inorg. Chem. 34 (1995) 4735 (and references therein).
[3] R.T. Jonas, T.D.P. Stack, Inorg. Chem. 37 (1998) 6615.
[4] E.A. Ambundo, M.-V. Deydier, A.J. Grall, N. Aguera-Vega, L.T. Dressel, T.H. Cooper, M.J. Heeg, L.A. Ochrymowycz, D.R. Rorabacher, Inorg. Chem. 38 (1999) 4233 (and references therein).
[5] R. Balamurugan, M. Palaniandavar, R.S. Gopalan, Inorg. Chem. 40 (2001) 2246.

[6] M. Schatz, M. Becker, F. Thaler, F. Hampel, S. Schindler, R.R. Jacobson, Z. Tyeklár, N.N. Murthy, P. Ghosh, Q. Chen, J. Jubieta, K.D. Karlin, Inorg. Chem. 40 (2001) 2313 (and references therin).
[7] R. Mukherjee, Coord. Chem. Rev. 203 (2000) 151.
[8] S. Mahapatra, R.J. Butcher, R. Mukherjee, J. Chem. Soc., Dalton Trans. (1993) 3723.
[9] Z. Shirin, R. Mukherjee, J.F. Richardson, R.M. Buchanan, J. Chem. Soc., Dalton Trans. (1994) 465 (and references therein).
[10] T.K. Lal, J.F. Richardson, M.S. Mashuta, R.M. Buchanan, R. Mukherjee, Polyhedron 16 (1997) 4331.
[11] T.K. Lal, R. Gupta, S. Mahapatra, R. Mukherjee, Polyhedron 18 (1999) 1743.
[12] S. Mahapatra, R.J. Butcher, R. Mukherjee, Indian J. Chem. 40A (2001) 973 (and references therein).
[13] R. Gupta, R. Mukherjee, Polyhedron 20 (2001) 2545.
[14] P. Manikandan, K.R. Justin Thomas, P.T. Manoharan, Acta Crystallogr., Sect. C 56 (2000) 308.
[15] P. Manikandan, K.R. Justin Thomas, P.T. Manoharan, J. Chem. Soc., Dalton Trans. (2000) 2779.
[16] W.J. Geary, Coord. Chem. Rev. 7 (1971) 81.
[17] R. Gupta, S. Mukherjee, R. Mukherjee, J. Chem. Soc., Dalton Trans. (1999) 4025.
[18] D.F. Evans, J. Chem. Soc. (1959) 2003.
[19] C.J. O'Connor, Prog. Inorg. Chem. 29 (1982) 203.
[20] L.J. Farrugia, WINGX ver 1.61, An Integrated System of Windows Programs for the Solution, Refinement and Analysis of Single-Crystal X-ray Diffraction Data, Department of Chemistry, University of Glasgow.
[21] S.R. Hall, H.D. Flack, J.M. Stewart, The XTAL 3.2 Reference Manual, Universities of Western Australia, Geneva and Maryland, 1992.
[22] J.G. Haasnoot, W.L. Driessen, J. Reedijk, Inorg. Chem. 23 (1984) 2803.
[23] R. Gupta, T.K. Lal, R. Mukherjee, Unpublished results.
[24] R.H. Bode, J.E. Bol, W.L. Driessen, F.B. Hulsbergen, J. Reedijk, A.L. Spek, Inorg. Chem. 38 (1999) 1239.
[25] M. Palaniandavar, R.J. Butcher, A.W. Addison, Inorg. Chem. 35 (1996) 467.
[26] B.J. Hathaway, in: G. Wilkinson, R.D. Gillard, J.A. McCleverty (Eds.), Comprehensive Coordination Chemistry, vol. 5 (and references therein), Pergamon, Oxford, 1987, pp. 533–594.
[27] U. Sakaguchi, A.W. Addison, J. Chem. Soc., Dalton Trans. (1979) 600.
[28] K. Miyoshi, H. Tanaka, E. Kimura, S. Tsuboyama, S. Murata, H. Shimizu, K. Ishizu, Inorg. Chim. Acta 78 (1983) 23.
[29] R. Gupta, R. Mukherjee, Polyhedron 19 (2000) 719.
[30] D. Ghosh, R. Mukherjee, Inorg. Chem. 37 (1998) 6597.
[31] G.S. Patterson, R.H. Holm, Bioinorg. Chem. 4 (1974) 257.
[32] T.N. Sorrell, D.L. Jameson, Inorg. Chem. 21 (1982) 1014.
[33] N. Wei, N.N. Murthy, K.D. Karlin, Inorg. Chem. 33 (1994) 6093.
[34] D.-H. Lee, N.N. Murthy, K.D. Karlin, Inorg. Chem. 36 (1997) 5785.
[35] M.R. Malachowski, H.B. Huynh, L.J. Tomlinson, R.S. Kelly, J.W. Furbee, Jr., J. Chem. Soc., Dalton Trans. (1995) 31.
[36] E. Spodine, J. Manzur, M.T. Garland, J.F. Fackler, Jr, R.J. Staples, B. Trzcinska-Bancroft, Inorg. Chim. Acta 203 (1993) 73.

PERGAMON

Polyhedron 21 (2002) 1255–1260

POLYHEDRON

www.elsevier.com/locate/poly

The thermodynamic studies of the molecular interactions of methyltin(IV) tribromide with free base *meso*-tetraarylporphyrins

Mozaffar Asadi [a,*], Abedien Zabardasti [a], ValiAllah Karimivand [a], Jahanbakhsh Ghasemi [b]

[a] *Chemistry Department, College of Sciences, Shiraz University, I.R. Shiraz, Iran*
[b] *Chemistry Department, College of Sciences, Razi University, I.R. Kermanshah, Iran*

Received 3 January 2002; accepted 28 March 2002

Abstract

The thermodynamic parameters for the interactions of $MeSnBr_3$ with *para*- and *meta*-substituted *meso*-tetraphenylporphyrins ($H_2T(4\text{-}X)PP$; $X = OCH_3$, CH_3, H, Cl, NO_2 and $H_2T(3\text{-}X)PP$; $X = CH_3$, Cl) have been studied. The formation constants have been elucidated by using spectrophotometric titration and computer SQUAD program data refinement. The adducts of composition 2:1 and 1:1 of $MeSnBr_3$ to $H_2T(4\text{-}X)PP$ with stability constants K_1 and K_2 coexist in solution, but *meta*-substituted porphyrins form adducts of the composition 1:1 of $MeSnBr_3$ to $H_2T(3\text{-}X)PP$ with stability constant K_1. Formation constants decrease with decreasing electron donation of *para*-substituted porphyrins as follow: $H_2T(4\text{-}CH_3O)PP > H_2T(4\text{-}CH_3)PP > H_2TPP > H_2T(4\text{-}Cl)PP > H_2T(4\text{-}NO_2)PP$. Despite the electron donation of the methyl group, $H_2T(3\text{-}Cl)PP$ forms more stable adducts than $H_2T(3\text{-}CH_3)PP$ with $MeSnBr_3$. © 2002 Published by Elsevier Science Ltd.

Keywords: Porphyrins; Sitting–Atop complexes; Methyltin(IV) tribromide; Organotin(IV) halide adducts; Tin compounds; Spectral method

1. Introduction

Thermodynamics of organotin(IV) halides adducts with various uni- and bidentate ligands [1–4], specially with biological systems, have been the subject of lots of studies [5–9]. In addition, a particularly attractive idea in the kinetics and mechanism of metallation of free base porphyrins is that of the Sitting–Atop (SAT) complexes [10,11]. In 1960, Fleischer and Wang [10] first proposed the so-called Sitting–Atop complexes as intermediates of metallation of the protoporphyrin dimethyl ester in chloroform. According to the SAT idea the metallation of free base porphyrin begins with a pre-equilibrium step involving partial bonding of the metal ion to two of the pyrrolenine nitrogens to form an intermediate, the so-called Sitting–Atop complex, in which two protons on the pyrrole nitrogens still remain. Some controversy exists as to whether this kinetically detected complex is of the Sitting–Atop type or is best represented as an outer-sphere ion pair [12]. Recently Funahashi et al. [13–15] have succeeded in the direct detection of SAT complexes of *meso*-tetraphenylporphyrin (H_2TPP), *meso*-tetrakis(4-chlorophenyl)porphyrin ($H_2T(4\text{-}Cl)PP$), *meso*-tetramesitylporphyrin (H_2TMP), and octaethylporphyrin (H_2OEP), with the Cu(II) ion in acetonitrile as solvent. Continuing these encouraging studies for the direct characterization of SAT complexes, led us to investigate the organotin(IV) halide adducts with a number of free base *para*-substituted *meso*-tetraphenylporphyrins, $H_2T(4\text{-}X)PPs$, in non-basic solvents. With a suitable selection of acceptor species and solvent, we successfully prepared some adducts of diorganotin(IV) dichlorides as the acceptor with free base *para*-substituted *meso*-tetraphenylporphyrin as the donor [16], these adducts have structures close to SAT complexes. Here we believe that tetraarylporphyrin as a bidentate bridging ligand makes a bridge between two molecules of organotin(IV) halide and produces a stable Sitting–Atop adduct.

In the earlier works we investigated the interactions of R_2SnCl_2, (R = Me [17], Et and Bu [18]) with tetraar-

* Corresponding author. Tel.: +98-71-1228-2380; fax: +98-71-1228-0926.
E-mail address: asadi@chem.susc.ac.ir (M. Asadi).

0277-5387/02/$ - see front matter © 2002 Published by Elsevier Science Ltd.
PII: S0277-5387(02)01013-6

ylporphyrins. The present work is on the investigation of thermodynamic parameters for the interaction of methyltin(IV) tribromide with H_2TPP (*meso*-tetraphenylporphyrin), H_2T(4-Cl)PP (*meso*-*tetrakis*-(*4*-chlorophenyl)porphyrin), H_2T(3-Cl)PP (*meso*-*tetrakis*-(*3*-chlorophenyl)porphyrin), H_2T(4-NO_2)PP (*meso*-*tetrakis*-(*4*-nitrophenyl)porphyrin), H_2T(4-CH_3)PP (*meso*-*tetrakis*-(*4*-methylphenyl)porphyrin), H_2T(3-CH_3)PP (*meso*-*tetrakis*-(*3*-methylphenyl)porphyrin) and H_2T(4-CH_3O)PP (*meso*-*tetrakis*-(*4*-methoxyphenyl)porphyrin) in chloroform as solvent.

2. Experimental

2.1. Reagents

Benzaldehyde and *para*- and *meta*-substituted benzaldehydes (Merck and Fluka) were used as received. Pyrrole (Fluka) was distilled before use. Propionic acid and chloroform (Merck) employed for the synthesis and the purification of porphyrins were used as received. Me_4Sn (Fluka) was used without further purification. Chloroform solvent for UV–Vis measurements was distilled over K_2CO_3 before use.

2.2. Instrumental

UV–Vis measurements were carried out on a JASCO V-530 UV–Vis spectrometer equipped with a LAUDA Ecoline RE 104 thermostat.

2.3. Preparations

Methyltin(IV) tribromide was prepared by the reaction between Me_4Sn and anhydrous $SnBr_4$, and purified by sublimation [19]. H_2T(4-X)PP; X = OCH_3, CH_3, H, Cl, NO_2 and H_2T(3-X)PP; X = CH_3, Cl were prepared and purified by usual methods [20–22].

2.4. General method

UV–Vis measurements were carried out by the titration method at 5.0, 10.0, 15.0, 20.0 and 25.0 ± 0.1 °C. In a typical measurement, 2.5 ml solution of H_2TPP (5×10^{-6} M) in chloroform was titrated by $MeSnBr_3$ (6.25×10^{-4} M). UV–Vis spectra were recorded in the range of 396–710 nm approximately 10 min after each addition. In this range of spectra, about 20–30 wavelengths that have suitable variations of absorbance were selected, and the formation constants and other thermodynamic parameters of adduct formation were calculated. Formation constants were calculated by squad program [23,24].

3. Results

On addition of $MeSnBr_3$ to a solution of porphyrin in chloroform its purple color changes to green. This change is due to adduct formation between $MeSnBr_3$ and the porphyrins. These adduct formations are reversible and show a different order of stability with respect to temperature. For example rising of the temperature to 60 °C caused the [$(MeSnBr_3)_2H_2$T(4-Cl)PP], Fig. 2, and [$(MeSnBr_3)_2H_2$T(4-NO_2)PP] adducts to return to $MeSnBr_3$ and free bases H_2T(4-Cl)PP and H_2T(4-NO_2)PP, respectively. Dissociation of [$(MeSnBr_3)_2H_2$TPP] and [$(MeSnBr_3)_2H_2$T(4-CH_3)PP] at this temperature occurred to a lesser extent, while the [$(MeSnBr_3)_2H_2$T(4-CH_3O)PP] adduct showed a high degree of stability with respect to temperature. Interactions of $MeSnBr_3$ with porphyrins were studied by means of UV–Vis spectrophotometry.

By interaction of tetraarylporphyrins with $MeSnBr_3$ Lewis acid the original peaks of the tetraarylporphyrins (Soret band and Q bands) undergo considerable changes with a range of isosbestic points. For example by addition of $MeSnBr_3$ to H_2T(4-CH_3O)PP, Fig. 1, the original peaks of the free base (421, 518, 556, 589 and 646 nm) were diminished and two new peaks appeared at (456 and 696 nm) with isosbestic points around 428, 480, 574, 598 nm. Table 1 gives the original peaks of free base porphyrins and new peaks produced by addition of $MeSnBr_3$ to a solution of porphyrins in chloroform. It seems that the positions of the adduct peaks mainly relate to a step of the adduct formation which leads to a deformation of the porphyrin plane and other steps only exert a minor effect on the λ_{max} of the adducts. On the other hand, since the distortion of porphyrin plane occurred during the 1:1 adduct formation, the attachment of the second Lewis acid is not accompanied by a significant displacement in the position of these bands (about 2–4 nm shift to longer wavelength for the Soret band). This statement can be better understood by comparison of electronic absorption spectra of a planar free base porphyrin such as 5,10,15,20-tetrabutylporphyrin; UV–Vis (CH_2Cl_2): Soret band (417 nm) and Q bands (520, 555, 600, 659 nm) with a severely ruffled (distorted) one like free base 5,10,15,20-tetrakis(*tert*-butyl)porphyrin: Soret band (446 nm) and Q bands (552, 596, 628, 691 nm) [25]. This example clearly shows that the observed bathochromic shift resulted mainly from distortion of the porphyrin structure.

However λ_{max} (corresponding to the Soret band) of electronic absorption spectra of adducts and also the positions of the isosbestic points change by a limited range of wavelengths (about 2–6 nm) during adduct formation. It is noticeable while there are a few (2–4 nm) displacements for the Soret band of adducts from the beginning up to completion of adduct formation, this displacement reached 20–45 nm upon completion of

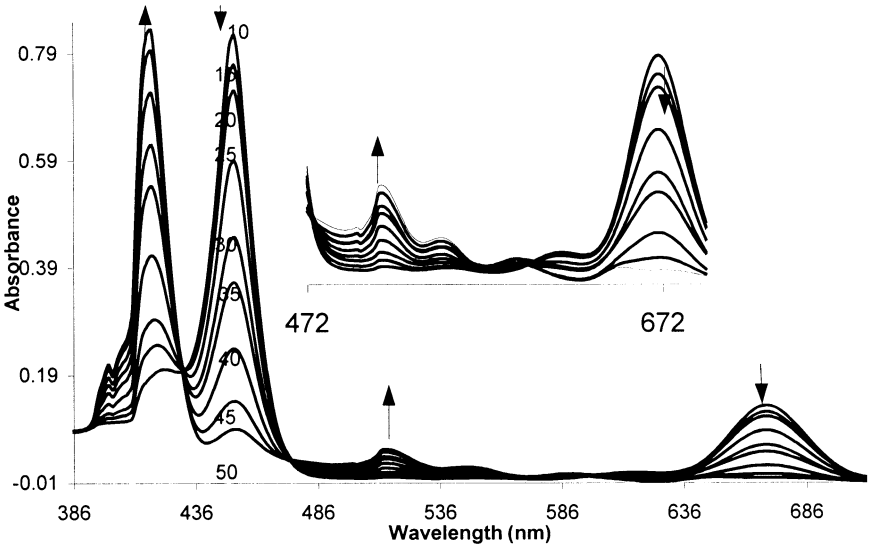


Fig. 2. Temperature dependence spectra of: $(MeSnBr_3)_2H_2T(4\text{-}Cl)PP$ adduct. By addition of $MeSnBr_3$ (6.25×10^{-4} M) to 2.5 ml of the solution of $H_2T(4\text{-}Cl)PP$ (2.5×10^{-6} M) in chloroform in a UV–Vis cell at 5 °C, the $(MeSnBr_3)_2H_2T(4\text{-}Cl)PP$ adduct was formed. Then the composition of the cell remained constant and the temperature was raised to 60 °C stepwisely, isosbestic point around 430, 476, 570, 596 nm. This spectrum has a similarity to the previous work on acidic dissociation of ClHg–TPP–HgCl complex [30], in which ClHg–TPP–HgCl returned to H_2TPP and $HgCl_2$.

the reaction for the band that appeared beyond 660 nm for different adducts.

The thermodynamic parameters were studied for these interactions and formation constants were determined at several temperatures by analyzing the concentration and the temperature dependence of UV–Vis electronic absorptions spectra by the SQUAD program. These absorption spectra were analyzed by using the following mole ratios of acid to base as models of interaction between $MeSnBr_3$ and a typical porphyrin: (1) formation of the 1:1 adduct; (2) formation of the 2:1 adduct; (3) simultaneous formation of the 1:1 and 2:1 adducts. The fit of the model to the experimental data, 15 points, is measured by the sum of the squares of the deviations of the experimental points from the point calculated by the model. For *para*-substituted porphyrins the proposed model is the coexistence of 2:1 and 1:1 adducts of acceptor to donor and in the case of *meta*-substituted porphyrins only 1:1 adducts have the best fitting and the produced error sum of squares was between 10^{-2} and 10^{-3}. The mole ratio plot of these adducts has good agreement with the stoichiometry

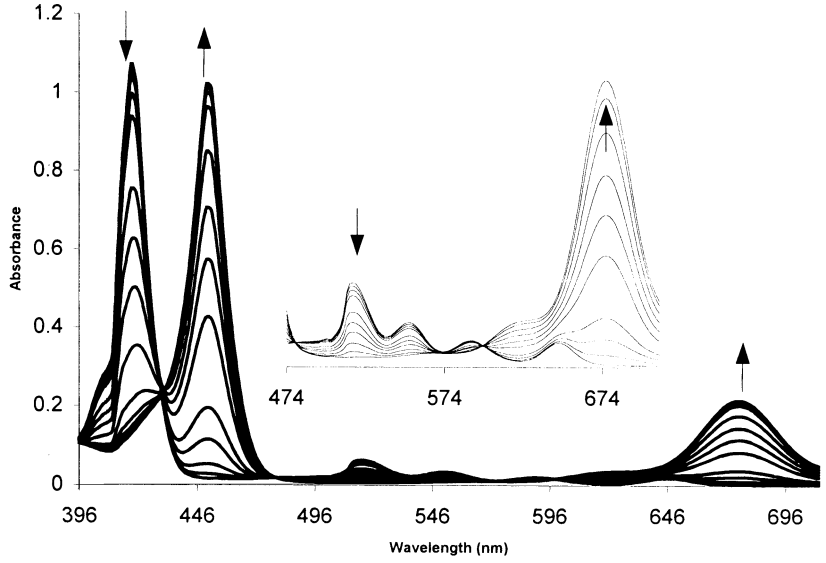


Fig. 1. Titrametric absorption spectra of $H_2T(4\text{-}CH_3O)PP$ with $MeSnBr_3$ in chloroform; 396–710 nm bands appeared at 450 and 476 nm are related to the adduct. Inset expanded of 474–710 nm region. Isosbestic points around 428, 480, 574, 598 nm.

Table 1
UV–Vis peaks λ ($CHCl_3$/nm) of the free bases $H_2T(X)PP$ and their adducts with $MeSnBr_3$

Compound	Wavelength (nm)				
H_2TPP	417	514	549	589	646
$(MeSnBr_3)_2H_2TPP$	448				666
$H_2T(4\text{-Cl})PP$	418	514	550	590	646
$(MeSnBr_3)_2H_2T(4\text{-Cl})PP$	452				670
$H_2T(3\text{-Cl})PP$	418	514	550	590	646
$(MeSnBr_3)H_2T(3\text{-Cl})PP$	450				674
$H_2T(4\text{-}NO_2)PP$	424	516	550	590	646
$(MeSnBr_3)_2H_2T(4\text{-}NO_2)PP$	458				664
$H_2T(4\text{-}CH_3)PP$	419	516	553	591	649
$(MeSnBr_3)_2H_2T(4\text{-}CH_3)PP$	450				676
$H_2T(3\text{-}CH_3)PP$	419	514	548	591	646
$(MeSnBr_3)H_2T(3\text{-}CH_3)PP$	448				666
$H_2T(4\text{-}CH_3O)PP$	421	518	555	594	649
$(MeSnBr_3)_2H_2T(4\text{-}CH_3O)PP$	456				696

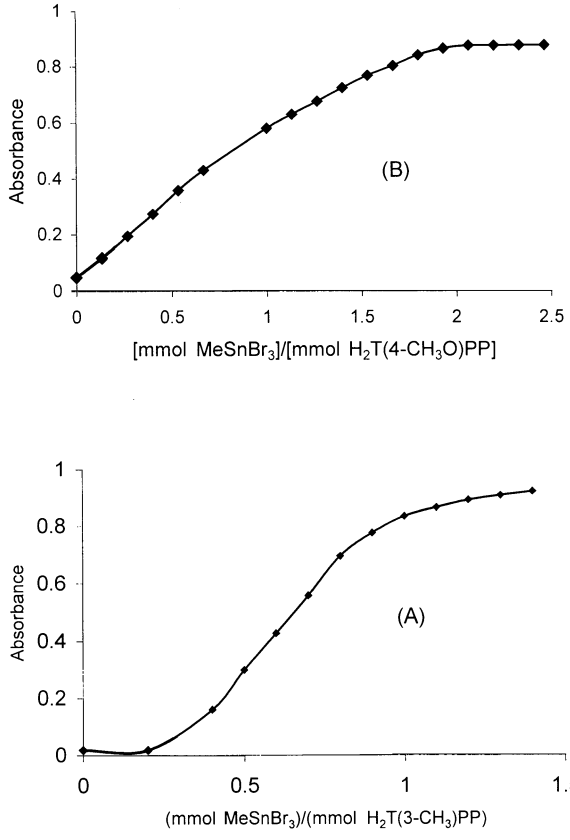


Fig. 3. Mole ratio plots for titration of: (A) $H_2T(3\text{-}CH_3)PP$ with $MeSnBr_3$ at 448 nm, 1:1 adduct; and (B) $H_2T(4\text{-}CH_3O)PP$ with $MeSnBr_3$ at 456 nm, simultaneous presence of 1:1 and 2:1 adducts.

indicated by the SQUAD program, Fig. 3. Van 't Hoff plots of these formation constants, K_1 and K_2, and the overall formation constant β_2 lead to the other thermodynamic parameters ΔH° and ΔS°, Tables 4–6.

4. Discussion

4.1. $(MeSnBr_3)_2H_2T(4\text{-}X)PP$ adducts

The data of Table 2 show that the equilibrium constants of the adducts undergo a regular increase from $H_2T(4\text{-}NO_2)PP$, $H_2T(4\text{-Cl})PP$, H_2TPP, $H_2T(4\text{-}CH_3)PP$ to $H_2T(4\text{-}CH_3O)PP$. For example at 5 °C we have the following order of formation constants:

$(MeSnBr_3)_2H_2T(4\text{-}NO_2)PP < (MeSnBr_3)_2H_2T(4\text{-Cl})PP < (MeSnBr_3)_2H_2TPP < (MeSnBr_3)_2H_2T(4\text{-}CH_3)PP < (MeSnBr_3)_2H_2T(4\text{-}CH_3O)PP$

$\log K_1 \quad 3.13 < 5.31 < 5.68 < 6.30 < 6.58$

$\log K_2 \quad 3.55 < 6.10 < 6.65 < 7.31 < 7.70$

Tables 4 and 5 show the thermodynamic parameters obtained for the interactions of $MeSnBr_3$ with $H_2T(4\text{-X})PP$ in chloroform.

The successive adducts $(MeSnBr_3)(H_2T(4\text{-X})PP)$ and $(MeSnBr_3)_2(H_2T(4\text{-X})PP)$ have negative values of ΔH° and ΔS°.

4.2. $(MeSnBr_3)H_2T(3\text{-}X)PP$ adducts

The data of Table 3 show that interactions in the $(MeSnBr_3)H_2T(3\text{-Cl})PP$ system are stronger than $(MeSnBr_3)H_2T(3\text{-}CH_3)PP$. For example at 5 °C we have the following order of formation constants:

$(MeSnBr_3)H_2T(3\text{-}CH_3)PP < (MeSnBr_3)H_2T(3\text{-Cl})PP$

$\log K_1 \quad 6.30 < 8.42$

Table 6 shows the thermodynamic parameters obtained for the interactions of $MeSnBr_3$ with $H_2T(3\text{-X})PP$ in chloroform. The negative values of ΔH° are indicating favorable adduct formations, but a negative entropy contribution is unfavorable for adduct formation.

Our results are in agreement with a pre-equilibrium step as demonstrated by previous studies on the kinetics of incorporation of some divalent metal ions into the free base porphyrins. Tanaka et al. [26] have studied the incorporation of Cu(II), Zn(II) and Cd(II) in the free base H_2TPP in DMF. They suggested a pre-equilibrium between metal ions and H_2TPP prior to metal insertion and proton release. Their values of K were 1.6×10^4 M^{-1} for Cu(II), 7.2×10^2 M^{-1} for Zn(II), and no kinetic evidence for complex formation was found for Cd(II). Pasternack's group [27] kinetically found a $K = 5$ M^{-1} for Cu(II)–H_2TPP reaction in DMSO. Hambright and Rabinson [28] obtained the following values of K (M^{-1}) for Zn(II) SAT complexes with tetraphenylporphyrin (12.3×10^3), tetrakis(2,6-difluorophenyl)porphyrin (2.8×10^3), tetra(4-aminophenyl)porphyrin (7.7×10^3), tetrakis(4-*N*,*N*-dimethylaminophenyl)porphyrin (6.0×10^3) and tetra(4-hydroxyphenyl)porphyrin

Table 2
The formation constants K (M^{-1}) for $MeSnBr_3$ adducts with $H_2T(4\text{-}X)PP$ in $CHCl_3$ solvent

Adduct		Temperature (°C)				
		5	10	15	20	25
$(MeSnBr_3)_2H_2TPP$	log K_1	5.68±0.06	5.33±0.03	4.80±0.03	4.48±0.03	3.97±0.02
	log K_2	6.65±0.06	5.97±0.03	5.66±0.03	5.10±0.03	4.48±0.02
$(MeSnBr_3)_2H_2T(4\text{-}Cl)PP$	log K_1	5.31±0.05	4.86±0.04	4.60±0.02	4.35±0.02	3.76±0.02
	log K_2	6.10±0.03	5.70±0.04	5.15±0.02	4.80±0.02	4.19±0.02
$(MeSnBr_3)_2H_2T(4\text{-}NO_2)PP$	log K_1	3.13±0.01	2.91±0.03	2.60±0.05	2.28±0.08	2.03±0.04
	log K_2	3.55±0.01	3.20±0.03	2.98±0.05	2.62±0.07	2.38±0.04
$(MeSnBr_3)_2H_2T(4\text{-}CH_3)PP$	log K_1	6.30±0.06	5.66±0.06	5.30±0.04	4.65±0.04	4.25±0.05
	log K_2	7.31±0.06	6.83±0.06	6.23±0.04	5.80±0.04	5.06±0.05
$(MeSnBr_3)_2H_2T(4\text{-}CH_3O)PP$	log K_1	6.58±0.03	6.00±0.03	5.34±0.02	5.02±0.02	4.34±0.09
	log K_2	7.70±0.03	7.12±0.02	6.62±0.02	5.86±0.02	5.42±0.09

(9.5×10^3) in DMF as solvent [29]. They suggested that metal ions and porphyrins formed an intermediate with composition [M–H_2P; M = Zn(II), Cd(II), Cu(II)] [26–29] in which coordination of H_2P with metal ion causes a deformation of the porphyrin plane in such a manner that a second metal ion is more readily able to incorporate into this bent porphyrin structure on the opposite side. Then formation of M–H_2P–Zn follows by dropping the Zn(II) ion into the porphyrin cavity [26–29]. These studies show that SAT stability has a strict dependence on the basicity of the solvent. But here attending to the non basic properties of our solvent and more importantly because of our bulky Lewis acids ($MeSnBr_3$), which could not drop into the porphyrin cavity under these conditions we deal with more stable SAT complexes. Comparing the results in Tables 2–6 with results given in our last works [17,18], the present adducts are more stable than the corresponding adducts with dialkyltin(IV) dichlorides. This greater stability of adducts returns to the higher acceptor property of $MeSnBr_3$ compared to R_2SnCl_2 Lewis acids. The results in Tables 2–6 show that the kind and the the position of substituent (X) on phenyl rings of $H_2T(X)PP$ significantly influences the interactions of the corresponding porphyrin with $MeSnBr_3$. We think that primarily 1:1 adduct formation, [$(MeSnBr_3)H_2T(4\text{-}X)PP$], for *para*-substituted porphyrins induces a distortion in the porphyrin plane; this deformation enhances the coordinating ability of the nitrogen lone pairs by directing them away from the central porphyrin cavity. Therefore, the distorted porphyrin readily accepts the second $MeSnBr_3$ molecule on the opposite side and eventually favors the formation of the 2:1 adduct [$(MeSnBr_3)_2H_2T(4\text{-}X)PP$], so we are dealing with a $K_2 > K_1$ for these adducts. Both the free energy and the enthalpies of adduct formation become more negative through the series $H_2T(4\text{-}NO_2)PP$, $H_2T(4\text{-}Cl)PP$, H_2TPP, $H_2T(4\text{-}CH_3)PP$ to $H_2T(4\text{-}CH_3O)PP$, which indicates stronger interactions and favoring adduct formations with increasing electron donation of free base porophyrins along this series.

In the case of $H_2T(3\text{-}X)PP$ porphyrins a behavior different to $H_2T(4\text{-}X)PP$ was observed. Our studies give acceptable results only for formation of 1:1 adducts between *meta*-substituted porphyrins and $MeSnBr_3$, perhaps steric hindrance arising from *meta*-substituents prevents the attachment of a second $MeSnBr_3$ molecule to $H_2T(3\text{-}X)PP$ on the opposite side. Also the greater magnitude of the binding constants, K_1, for the corresponding *meta*- relative to K_1 of *para*-substituted porphyrins is probably due to a more distorted structure of *meta*- free base than the corresponding *para*- isomer that increases the N-lone pairs coordinative property toward the first $MeSnBr_3$ molecule. It seems that this distortion depends on the weight and the bulkiness of the substituent, so that the weightier groups lead to better deformation in porphyrin structure and a greater tendency for 1:1 adduct formation.

Adducts have negative values of ΔH°, ΔS° and ΔG°. Generally, the negative values of ΔS° refer to an associative reaction between donor and acceptor and has an unfavorable contribution on adduct formation. These results show the following order for interactions of *para*- and *meta*-substituted porphyrin with methylti-

Table 3
The formation constants K (M^{-1}) for $MeSnBr_3$ adducts with $H_2T(3\text{-}X)PP$ in $CHCl_3$ solvent

Adduct		Temperature (°C)				
		5	10	15	20	25
$(MeSnBr_3)_2H_2T(3\text{-}Cl)PP$	log K_1	8.42±0.14	7.80±0.04	7.40±0.06	6.60±0.05	6.10±0.04
$(MeSnBr_3)_2H_2T(3\text{-}CH_3)PP$	log K_1	6.30±0.17	5.66±0.15	5.30±0.08	4.65±0.06	4.25±0.05

Table 4
The thermodynamic parameters for interaction of $MeSnBr_3$ with $H_2T(4\text{-}X)PP$ in chloroform [a]

Adduct	ΔH_1°	ΔH_2°	ΔS_1°	ΔS_2°	ΔG_1° [b]	ΔG_2° [b]
$(MeSnBr_3)_2H_2TPP$	-135 ± 6	-165 ± 10	-377 ± 22	-467 ± 36	-28 ± 6	-33 ± 10
$(MeSnBr_3)_2H_2T(4\text{-}Cl)PP$	-114 ± 11	-150 ± 9	-310 ± 39	-420 ± 27	-26 ± 11	-31 ± 9
$(MeSnBr_3)_2H_2T(4\text{-}NO_2)PP$	-90 ± 4	-93 ± 4	-262 ± 13	-266 ± 13	-15 ± 4	-17 ± 4
$(MeSnBr_3)_2H_2T(4\text{-}CH_3)PP$	-162 ± 8	-175 ± 10	-464 ± 27	-489 ± 34	-31 ± 8	-36 ± 10
$(MeSnBr_3)_2H_2T(4\text{-}CH_3O)PP$	-173 ± 9	-185 ± 8	-498 ± 32	-516 ± 27	-32 ± 9	-39 ± 8

[a] ΔH° (kJ mol^{-1}) and ΔS° (J K^{-1} mol^{-1}).
[b] ΔG° at 10 °C (kJ mol^{-1}).

Table 5
The overall thermodynamic parameters [a] for $(MeSnBr_3)_2H_2T(4\text{-}X)PP$ adducts [b]

Adduct	ΔH°	ΔS°	ΔG° [c]
$(MeSnBr_3)_2H_2TPP$	-301 ± 11	-845 ± 37	-61 ± 11
$(MeSnBr_3)_2H_2T(4\text{-}Cl)PP$	-264 ± 17	-730 ± 60	-57 ± 17
$(MeSnBr_3)_2H_2T(4\text{-}NO_2)PP$	-182 ± 5	-528 ± 17	-32 ± 5
$(MeSnBr_3)_2H_2T(4\text{-}CH_3)PP$	-337 ± 8	-953 ± 28	-67 ± 8
$(MeSnBr_3)_2H_2T(4\text{-}CH_3O)PP$	-358 ± 2	-1014 ± 8	-71 ± 2

[a] Are calculated from $\beta_2 = K_1K_2$.
[b] ΔH° (kJ mol^{-1}) and ΔS° (J K^{-1} mol^{-1}).
[c] ΔG° at 10 °C (kJ mol^{-1}).

Table 6
The thermodynamic parameters ΔH°, ΔS° and ΔG° for $(MeSnBr_3)H_2T(3\text{-}X)PP$ adducts [a]

Adduct	ΔH°	ΔS°	ΔG° [b]
$(MeSnBr_3)H_2T(3\text{-}Cl_3)PP$	-185 ± 36	-504 ± 10	-42 ± 36
$(MeSnBr_3)H_2T(3\text{-}CH_3)PP$	-162 ± 8	-463 ± 27	-31 ± 8

[a] ΔH° (kJ mol^{-1}) and ΔS° (J K^{-1} mol^{-1}).
[b] ΔG° at 10 °C (kJ mol^{-1}).

n(IV) tribromide:

$$H_2T(4\text{-}CH_3O)PP > H_2T(4\text{-}CH_3)PP > H_2TPP > H_2T(4\text{-}Cl)PP > H_2T(4\text{-}NO_2)PP$$

and

$$H_2T(3\text{-}CH_3)PP < H_2T(3\text{-}Cl)PP$$

Acknowledgements

We are grateful to Shiraz University Research Council for their financial support.

References

[1] B. Albert, A.S. Gonzalez, E. Garcia, J.S. Casas, J. Sordo, E.E. Castellano, J. Organomet. Chem. 338 (1988) 187.
[2] C.H. Yoder, D. Mokrynka, J.N. Spencer, S.M. Coley, J.C. Otter, R.E. Haines, A. Grushow, L.J. An Sel, J.W. Horick, J. Mikus, M.A. Shermak, Organometallics 6 (1987) 1679.
[3] H. Fujiwara, F. Sakai, Y. Mikawa, Y. Sakai, Bull. Chem. Soc. Jpn. 58 (1985) 1741.
[4] Y. Farhagi, D.P. Garddon, J. Organomet. Chem. 87 (1975) 67.
[5] A. Jancso, B. Henry, P. Rubini, G. Vanko, T. Gajda, J. Chem. Soc., Dalton Trans. (2000) 1941.
[6] A.J. Crowe, Drugs Future 2 (1987) 255.
[7] M.M. Shoukry, Talanta 43 (1996) 177.
[8] J. McManus, D. Cunningham, M.J. Hynes, J. Organomet. Chem. 468 (1994) 87.
[9] R. Barbieri, A. Silvestri, A.M. Giuliani, V. Piro, F. Di Simone, G. Madonia, J. Chem. Soc., Dalton Trans. (1992) 585.
[10] E.B. Fleischer, J.H. Wang, J. Am. Chem. Soc. 82 (1960) 3498.
[11] F.R. Longo, E.M. Brown, W.G. Rau, A.D. Alder, in: D. Dolphin (Ed.), The Porphyrins, vol. V, Academic Press, New York, 1979, p. 459.
[12] M.J. Bain-Ackerman, D.K. Lavalee, Inorg. Chem. 18 (1979) 3358.
[13] S. Funahashi, M. Inamo, N. Kamiya, Y. Inada, M. Nomura, Inorg. Chem. 40 (2001) 5636.
[14] S. Funahashi, M. Inamo, M. Nomura, Y. Nakano, Y. Inada, Inorg. Chem. 39 (2000) 4793.
[15] S. Funahashi, Y. Inada, Y. Sugimoto, Y. Nakano, Y. Itoh, Inorg. Reac. Mech. 37 (1998) 5519.
[16] M. Asadi and A. Zabardasti, in preparation.
[17] M. Asadi, A. Zabardasti, J. Ghasemi, Polyhedron 21 (2002) 653.
[18] M. Asadi, A. Zabardasti, J. Ghasemi, Bull. Chem. Soc. Jpn., in press.
[19] A.C. Smith, Jr, E.G. Rochow, J. Am. Chem. Soc. 75 (1953) 4103.
[20] A. Bettelheim, B.A. White, S.A. Raybuck, R.W. Murray, Inorg. Chem. 26 (1987) 1009.
[21] A.M. d'A.R. Gonsalves, J.M.T.B. Vare Jao, M.M. Pereira, J. Heterocyclic Chem. 28 (1991) 635.
[22] R.A.W. Johnstone, M.L.P.G. Nunes, M.M. Pereira, A.M.R. Gonsalves, A.C. Serra, Heterocycles 43 (1996) 1423.
[23] D.J. Leggett, Computational Methods for the Determination of Formation Constant, Plenum Press, New York, 1985.
[24] D.J. Leggett, S.L. Kelly, L.R. Shiue, Y.T. Wu, Talanta 30 (1983) 579.
[25] M.O. Senge, I. Bischoff, N.Y. Nelson, K.M. Smith, J. Porphyrins Phthalocyanines 3 (1999) 99.
[26] S. Funahashi, Y. Yamaguchi, M. Tanaka, Bull. Chem. Soc. Jpn. 57 (1984) 204.
[27] R.F. Pasternack, G.C. Vogel, C.A. Skowronek, R.K. Harris, J.G. Miller, Inorg. Chem. 20 (1981) 3763.
[28] L.R. Robinson, P. Hambright, Inorg. Chim. Acta 185 (1991) 17.
[29] B. Shah, B. Shears, P. Hambright, Inorg. Chem. 10 (1971) 1828.
[30] M.F. Hudson, K.M. Smith, Tetrahedron 32 (1976) 597.

PERGAMON

Polyhedron 21 (2002) 1261–1265

POLYHEDRON

www.elsevier.com/locate/poly

Phosphine nickel(0) π-complexes with vinylcyclosilazane —synthesis and structure

Hieronim Maciejewski *, Maciej Kubicki, Bogdan Marciniec, Agnieszka Sydor

Faculty of Chemistry, Adam Mickiewicz University, Grunwaldzka 6, 60-780 Poznań, Poland

Received 8 January 2002; accepted 13 March 2002

Abstract

Synthesis, spectroscopic (^{1}H, ^{13}C, ^{31}P, ^{29}Si NMR) characterisation and X-ray structure of the first nickel(0) π-complex with vinylcyclosilazane [{Ni(PPh$_3$)}$_2${μ-(η-CH$_2$=CH(Me)Si(μ-NH))$_4$}] (**1a**) have been presented. This is the first report on the structure of a TM complex with a vinylsilazane ligand. Complex **1a** is synthesised by the reaction of [Ni(cod)$_2$] with cyclotetra (vinylmethylsilazane). The complex occupies a special position of the space group $P2_1/c$ on the centre of symmetry that lies in the middle of the cyclotetrasilazane ring. The coordination of nickel is close to triangular one. © 2002 Elsevier Science Ltd. All rights reserved.

Keywords: Nickel(0); Vinylcyclosilazane complexes; Crystal structure

1. Introduction

The recent interest in the chemistry of transition metal olefin complexes containing vinyl derivatives of organosilicon compounds as π-ligands is fully justified not only by the particular nature of the bond between vinylsilicon derivatives and transition metals, but mainly by the possible application of this kind of complex as catalysts in hydrosilylation of olefins [1]. Hydrosilylation is also used to a much greater extent in industry to produce crosslinked products [2]. Such processes generally require the use of highly active platinum—containing catalysts. One class of platinum compounds used as hydrosilylation catalysts includes Pt(0) complexes containing vinyl-siloxane ligands. An example is the Karstedt's catalyst, which contains both bridging and chelating divinyl ligands [{Pt(η-CH$_2$=CHSiMe$_2$)$_2$O}$_2${μ-(η-CH$_2$=CHSiMe$_2$)$_2$O}] [3,4]. Besides showing a high catalytic activity, this complex is also a good starting compound for synthesis of other platinum(0) π-complexes. The treatment of the Karstedt's catalyst with maleic anhydride, styrene or divinyltetramethyldisiloxane gave [{Pt(η-CH$_2$=CHSiMe$_2$)$_2$O}{η^2-CHC(O)OC(O)CH}] [4], [{Pt(η-CH$_2$=CHSiMe$_2$)$_2$O}-(η^2-CH$_2$=CHPh)] [4] and [{Pt(η-CH$_2$=CHSiMe$_2$)$_2$O}-{η^2-(CH$_2$=CHSiMe$_2$)$_2$O}] [5].

Due to the fact that tertiary phosphine ligands play a crucial role in many industrially important metals—catalysed organic reactions, phosphine metal—vinylsilicon complexes were also synthesised [6,7]. The reaction between Karstedt's catalyst [{Pt(LL)}$_2$(μ-LL)] (where LL = {CH$_2$=CHSiMe$_2$}$_2$O) and mono-, bis- or tris(tertiary phosphine) led to complexes of the type [Pt(LL)(PR$_3$)] [6], [{Pt(LL)}$_2$(DIPHOS)] or [{Pt(LL)}$_3$(TRIPHOS)] [7], respectively. Moreover there is arousing interest in complexes with cyclic π-vinylsilicon ligands. Cyclotetrakis[vinyl(methyl)siloxane] has been used to generate the platinum complex [{Pt(PPh$_3$)}$_2${μ-(η-CH$_2$=CH(Me)Si(μ-O))$_4$}] acting as a hydrosilylation catalyst equivalent to Karstedt's catalyst [2,5,9].

The cost of platinum compounds has stimulated much research to check other transition metal compounds as potential hydrosilylation catalysts. By analogy to Karstedt's catalyst, the nickel complex [{Ni(η-CH$_2$=CHSiMe$_2$)$_2$O}$_2${μ-(η-CH$_2$=CHSiMe$_2$)$_2$O}] was obtained and showed high catalytic activity in the hydrosilylation and related reactions (dehydrogenative coupling especially of vinyl derivatives) [10]. In analogy to platinum

* Corresponding author. Tel.: +48-61-82-91366; fax: +48-61-82-91508.

E-mail address: maciejm@main.amu.edu.pl (H. Maciejewski).

0277-5387/02/$ - see front matter © 2002 Elsevier Science Ltd. All rights reserved.
PII: S0277-5387(02)01001-X

complexes, those of the type [Ni(LL)(PR_3)] were also prepared [6,7]. Very recently, nickel complexes with cyclotetrasiloxane [{Ni(PR_3)}$_2${μ-(η-CH_2=CH(Me)Si-(μ-O))$_4$}] were synthesised and the X-ray structure of one of them was determined [11]. There are also well known platinum or nickel complexes with vinylsilanes (i.e. vinyltrimethylsilane [12,13] or divinyldimethylsilane [7]) used as ligands, however, the application of vinyl derivatives of silazane as ligands in organometallic chemistry has been rather rare. Hitherto only two examples of the synthesis of nickel complexes with linear divinyltetramethyldisiloxane, i.e. [{Ni(η-CH_2=CHSiMe_2)$_2$NH}$_2$ {μ-(η-CH_2=CHSiMe_2)$_2$NH}] and [Ni(PR_3)(η-CH_2=CHSiMe_2)$_2$NH}], have been reported in Ph.D. Theses [8,14], however, they have not been fully characterised and their crystallographic structures have not been resolved.

In this paper, we present a synthetic procedure, spectroscopic characterisation and X-ray structure of phosphine–nickel complexes with vinylcyclosilazane ligands. To the best of our knowledge this is the first example of a fully characterised TM complex with a vinylsilazane ligand.

2. Experimental

2.1. General procedures

All reagents were dried and purified before use by the usual procedures. [Ni(cod)$_2$] was prepared as described in literature [15]. Other chemicals were purchased from Fluka. The NMR spectra (^{1}H, ^{13}C, ^{31}P, ^{29}Si) were recorded on a Varian XL 300 spectrometer. In all cases C_6D_6 was used as a solvent.

2.2. Synthesis of complexes

2.2.1. [{Ni(PPh_3)}$_2${μ-(η-CH_2=CH(Me)Si(μ-NH))$_4$}] (**1a**)

Cyclotetrakis [vinyl(methyl)silazane] (2 ml) was added slowly to a stirred red suspension of [Ni(cod)$_2$] (0.5 g, 1.8 mmol) and PPh_3 (0.47 g, 1.8 mmol) in diethyl ether (10 ml) at ambient temperature, yielding a yellow solution. The reaction mixture was allowed to stir overnight. The volatiles were removed in vacuo to give a yellow oil, which was extracted into pentane (2 × 2 ml). The extract was filtered through Celite. The filtrate was concentrated, then set aside at −30 °C to yield a yellow solid compound (0.66 g, 0.72 mmol, 79%). Yellow crystals of **1a** suitable for X-ray diffraction, were grown from benzene at ambient temperature over a period of 24 h.

^{1}H NMR (C_6D_6, 298 K, 300 MHz,) δ 0.09 (s, 12H), 2.68 (td, 4H), 3.04 (dd, 8H), 7.08–7.76 (m, 30H); $^3J(^1H_1-^1H_2) = 12.0$ Hz, $^3J(^1H_1-^1H_3) = 16.0$ Hz, $^3J(^1H_1-^{31}P) = 4.6$ Hz, $^3J(^1H_2-^{31}P) = 7.7$ Hz, $^3J(^1H_3-^{31}P) = 6.0$ Hz.

^{13}C NMR (C_6D_6, 298 K, 125.8 MHz); δ 2.66 (s, CH_3), 60.66 (d, =CH–), 62.93 (s, =CH_2), 129.00–134.00 (m, Ph), $^2J(^{13}C_1-^{31}P) = 6.7$ Hz.

^{29}Si NMR (C_6D_6, 298 K, 99.4 MHz); δ −12.07(d), $^3J(^{29}Si-^{31}P) = 3.8$ Hz.

^{31}P NMR (C_6D_6, 298 K, 101.2 MHz); δ 38.59.

2.2.2. [{NiP(C_6H_4Me-4)$_3$}$_2${μ-(η-CH_2=CH(Me)Si(μ-NH))$_4$}] (**1b**)

Compound **1b** (0.76 g, 0.74 mmol, 82%) was prepared in a similar manner to **1a**, except that P(C_6H_4Me-4)$_3$ was used in the place of PPh_3. Yellow crystals of **1b** were obtained by recrystalisation from benzene, at ambient temperature.

^{1}H NMR (C_6D_6, 298 K, 300 MHz); δ 0.15 (s, 12H), 2.10 (s, 9H), 2.72 (td, 4H), 3.12 (dd, 8H), 6.90–7.34 (m, 24H).

^{13}C NMR (C_6D_6, 298 K, 125.8 MHz); δ 2.39 (s, CH_3), 21.58 (s, CH_3), 58.28 (s, =CH–), 61.86 (s, =CH_2), 127.90–139.22 (m, tol).

^{29}Si NMR (C_6D_6, 298 K, 99.4 MHz); δ −12.57 (d).

^{31}P NMR (C_6D_6, 298 K, 101.2 MHz); δ 39.24.

2.2.3. [{NiP(C_6H_{11}-c)$_3$}$_2${μ-(η-CH_2=CH(Me)Si(μ-NH))$_4$}] (**1c**)

Compound **1c** (0.65 g, 0.66 mmol, 72%) was prepared in a similar manner to **1a**, except that P(C_6H_{11}-c)$_3$ was used in the place of PPh_3. Yellow crystals of **1c** were obtained by recrystalisation from benzene at ambient temperature.

^{1}H NMR (C_6D_6, 298 K, 300 MHz); δ 0.17 (s, 12H), 1.21–1.82 (m, 33H), 2.63 (td, 4H), 3.08 (dd, 8H).

^{13}C NMR (C_6D_6, 298 K, 125.8 MHz); δ 2.54 (s, CH_3), 26.23–35.54 (m, C_6H_{11}-c), 59.76 (s, =CH–), 61.34 (s, =CH_2).

^{29}Si NMR (C_6D_6, 298 K, 99.4 MHz); δ −12.94(d).

^{31}P NMR (C_6D_6, 298 K, 101.2 MHz); δ 38.27.

2.3. Crystal structure determination of **1a**

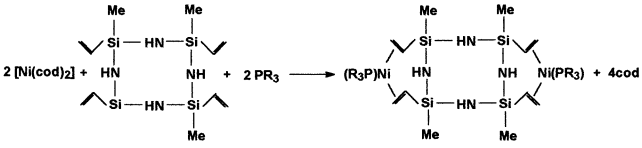
Diffraction data from a yellow, prism-shaped crystal with dimensions 0.2 × 0.2 × 0.15 mm, sealed in a glass capillary, were collected on a KUMA KM4CCD diffractometer [16] at room temperature (r.t.), using graphite-monochromated Mo Kα radiation (λ = 0.71073 Å). The data collection was performed in six separate runs in order to cover the symmetry-independent part of the reciprocal space. The ω-scan was used with a step of 0.75°, two reference frames were measured after every 50 frames, they did not show any systematical changes either in the peaks positions or in their intensities. A total of 782 frames was collected, giving 22 024 reflections up to $2\theta = 60°$. The unit-cell parameters were determined by the least-squares treatment

of the setting angles of 2400 highest-intensity reflections, chosen from the whole experiment. The Lorentz and polarisation corrections were applied [17], and then the reflexes were merged and corrected for absorption ($A_{min} = 0.747$, $A_{max} = 0.767$) with Sortav [18]. The merging procedure produced 6003 unique data with R_{int} of 0.13. The structure was solved by direct methods with SHELXS-97 program [19], and refined with full-matrix least-squares by SHELXL-97 [20]. Non-hydrogen atoms were refined anisotropically, hydrogen atoms were generated geometrically and were refined as a 'riding model' with their U_{iso} parameters set at 1.2 times U_{eq} of the appropriate carrier atom. Selected geometric parameters are listed in Table 1.

Crystallographic data for $[Ni_2(PPh_3)_2(Si_4N_4C_{12}H_{28})]$: empirical formula $Ni_2P_2Si_2N_4C_{48}H_{58}$, monoclinic, space group $P2_1/c$, $a = 13.5628(17)$ Å, $b = 9.7290(12)$ Å, $c = 18.605(2)$ Å, $\beta = 90.349(10)^\circ$, $V = 2454.9(5)$ Å^3, $Z = 2$, $d_x = 1.332$ g cm^{-3}, μ(Mo Kα) = 0.97 mm^{-1}, $F(000) = 1032$, $R(F)$ $[F_o > 4(F_o)] = 0.057$, $wR(F^2) = 0.127$, where $w^{-1} = [\sigma^2(F_o)^2 + (0.01P)^2 + 5P]^{-1}$, $P = (\mathrm{Max}(F_o{}^2, 0) + 2F_c{}^2/3)$, $S = 1.29$, $(\Delta/\sigma)_{max} = 0.001$ in the last cycle of refinement, $\Delta\rho_{max} = 0.42$ e Å^{-3}, $\Delta\rho_{min} = -0.35$ e Å^{-3}.

3. Results and discussion

The reaction of $[Ni(cod)_2]$ with cyclotetra(vinylmethylsilazane) in the presence of tertiary phosphine was effective for the preparation of the corresponding phosphine nickel–vinylcyclosilazane complexes according to the following equation.



1a R = C_6H_5, **1c** C_6H_{11}-c

1b C_6H_4Me-4,

The above reaction seems to be a very simple and convenient route to synthesise various phosphine complexes with vinylsilicon ligands. As mentioned earlier, the nickel phosphine complexes with cyclotetra(vinylmethylsiloxane) $[\{Ni(PR_3)\}_2\{\mu\text{-}(\eta\text{-}CH_2{=}CH(Me)Si(\mu\text{-}O))_4\}]$ (**2**) (where $R = C_6H_5$ (**a**), C_6H_4–Me (**b**) and c-C_6H_{11} (**c**)) were synthesised previously [11].

Table 1
Selected bond lengths (Å), bond angles (°) and torsion angles (°) with e.s.d.'s in parentheses

Bond lengths			
Ni(1)–X(1)	1.890(10)	Ni(1)–X(2)	1.920(10)
Ni(1)–P(1)	2.175(3)	P(1)–C(21)	1.836(10)
P(1)–C(31)	1.850(12)	P(1)–C(11)	1.859(12)
Si(1)–N(2)	1.710(9)	Si(1)–N(1) [a]	1.722(8)
Si(1)–C(1A)	1.840(10)	Si(1)–C(1)	1.873(10)
C(1A)–C(1B)	1.364(14)	C(2A)–C(2B)	1.417(15)
C(2A)–Si(2)	1.841(11)	N(2)–Si(2)	1.724(9)
Si(2)–N(1)	1.722(7)	Si(2)–C(2)	1.872(11)
Bond angles			
X(1)–Ni(1)–X(2)	127.5(4)	X(1)–Ni(1)–P(1)	113.6(3)
X(2)–Ni(1)–P(1)	117.1(4)	C(21)–P(1)–Ni(1)	123.1(4)
C(31)–P(1)–Ni(1)	116.8(4)	C(11)–P(1)–Ni(1)	108.1(4)
N(2)–Si(1)–N(1) [a]	111.0(4)	N(2)–Si(1)–C(1A)	108.9(5)
N(1)^i–Si(1)–C(1A)	111.3(5)	N(2)–Si(1)–C(1)	112.1(5)
N(1)^i–Si(1)–C(1)	105.4(5)	C(1A)–Si(1)–C(1)	108.1(4)
C(1B)–C(1A)–Si(1)	121.6(8)	C(2B)–C(2A)–Si(2)	121.2(8)
Si(1)–N(2)–Si(2)	129.7(5)	N(1)–Si(2)–N(2)	111.3(4)
N(1)–Si(2)–C(2A)	111.1(5)	N(2)–Si(2)–C(2A)	109.1(4)
N(1)–Si(2)–C(2)	105.8(4)	N(2)–Si(2)–C(2)	110.7(5)
C(2A)–Si(2)–C(2)	108.9(5)	Si(1) [a]–N(1)–Si(2)	132.7(5)
Torsion angles			
N(2)–Si(1)–C(1A)–C(1B)	−134.2(8)	N(1) [a]–Si(1)–C(1A)–C(1B)	−11.5(10)
C(1)–Si(1)–C(1A)–C(1B)	103.8(9)	N(1) [a]–Si(1)–N(2)–Si(2)	−99.9(7)
C(1A)–Si(1)–N(2)–Si(2)	23.1(8)	C(1)–Si(1)–N(2)–Si(2)	142.6(6)
Si(1)–N(2)–Si(2)–N(1)	101.8(7)	Si(1)–N(2)–Si(2)–C(2A)	−21.1(8)
Si(1)–N(2)–Si(2)–C(2)	−140.8(6)	C(2B)–C(2A)–Si(2)–N(1)	7.4(10)
C(2B)–C(2A)–Si(2)–N(2)	130.4(9)	C(2B)–C(2A)–Si(2)–C(2)	−108.8(9)
N(2)–Si(2)–N(1)–Si(1) [a]	−29.2(9)	C(2A)–Si(2)–N(1)-Si(1) [a]	92.6(8)
C(2)–Si(2)–N(1)–Si(1) [a]	−149.4(8)		

X1 and X2 denote the middlepoints of the C1A–C1B and C2A–C2B bonds, respectively.
[a] Symmetry transformations used to generate equivalent atoms: $-x+1$, $-y$, $-z+1$.

All kinds of analyses of the crystalline yellow complexes **1a**–**c** have brought satisfactory results. The NMR spectra taken for complexes **1a**–**c**, were very similar to those for complexes **2a**–**c**. The NH signal was not observed in the spectra which is consistent with the ^{1}H spectrum obtained for hexamethyldisilazane [21].

The ^{1}H NMR spectra of **1a**–**c** reveals one signal from the methyl group and two signals from the vinyl group in the region appropriate for vinylsilicon complexes of this type. The ^{13}C NMR spectra also confirm the structure of complexes **1a**–**c**. These spectra showed one signal assigned to the methyl carbons and the signals corresponding to the vinyl carbons at frequencies lower than those observed for the free ligand. The ^{31}P NMR spectra of each of the complexes obtained revealed a single signal. The signals in these spectra showed some differences in positions, depending on the type of phosphine used, however, they always appeared in the region typical of a coordinated phosphine. The values of spectroscopic chemical shifts in ^{1}H, ^{13}C and ^{31}P NMR spectra for complexes **1a**–**c** are quite similar to those for complexes **2a**–**c**, but some differences are observed in the ^{29}Si NMR spectra. For the complexes with vinylsiloxane ligands, the ^{29}Si NMR spectrum showed signals at -24 ppm but in the spectra of complexes with vinylsilazane these signals were observed at -12 ppm. The difference depends on the nature of the vinylsilicon compounds used.

The crystal structure of **2b** is very similar to that one established for **1a.**

The complex **1a** lies in a special position of the space group $P2_1/c$, on the centre of symmetry that lies in the middle of the cyclotetrasilazane ring. The coordination of nickel is close to a triangular (regarding the middlepoints of the double bonds as coordination centres), however, some degree of pyramidalization can be noticed. The sum of the angles around nickel is 358.2(3)° and the Ni1 atom is displaced by 0.156(5) Å from the plane defined by P1, X1 and X2 (X1 and X2 denote the middlepoints of C1A–C1B and C2A–C2B

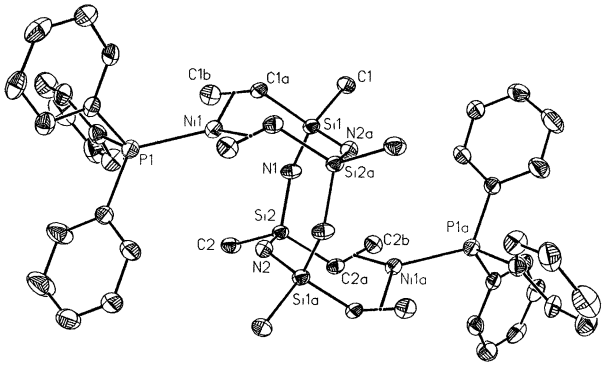


Fig. 1. The thermal ellipsoid view of the complex **1a** (at 50% probability level) with the numbering scheme [23]. The hydrogen atoms are omitted for clarity.

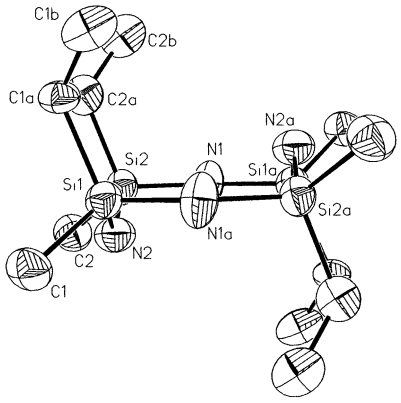


Fig. 2. The conformation of the tetrasilazane ring. The thermal ellipsoids are drawn at 50% probability level, only symmetry-independent atoms are labelled.

double bonds, respectively). The Ni–P bond length of 2.175(3) Å is within the range for short Ni–P bonds (the Ni–P lengths distribution is bimodal [22]).

The eight-membered silazane ring adopts the chair conformation; six atoms N1, Si2, Si1, N1′, Si2′ and Si1′ are almost perfectly coplanar (the prime denotes the atoms created by the centre of symmetry), with the largest deviation from the least-square plane of 0.012(5) Å, while the N2 and N2′ atoms are tilted out of this plane by + and −0.729(9) Å, respectively, (Figs. 1 and 2). This different character of N1 and N2 nitrogen atoms is reflected in differences of the Si–N–Si angles: 132.7(5)° for N1 and 129.7(5)° for N2, while the Si–N bond lengths are almost equal with the mean value of 1.720(2) Å. The methyl substituents are in quasi-equatorial positions, and the vinyl ones in quasi-axial ones (cf. Table 1).

The phenyl rings are planar within experimental error, the mean value of the C_{ar}–C_{ar} bond length is 1.380(7) Å, and agrees well with the typical value. The mutual disposition of these rings can be described by the dihedral angles between their least-squares planes A/B 85.1(4)°, B/C 72.6(4)°, A/C 82.8(3)°, where A, B, and C denote the rings with C11, C21, and C31 atoms, respectively. The crystal packing is determined mainly by van der Waals interactions.

4. Conclusions

1) Nickel complexes of the type $[\{Ni(PR_3)\}_2\{\mu\text{-}(\eta\text{-}CH_2{=}CH(Me)Si(\mu\text{-}NH))_4\}]$ are the first examples of TM complexes with vinylsilazane whose crystal structure has been determined.
2) The NMR and crystal structure data obtained have proved that the compounds **1a**–**c** and **2a**–**c** are similar. They both are binuclear nickel(0) complexes with a inversion centre at the mid-point of the chair-shaped $(SiO)_4$ or $(SiNH)_4$ ring.

3) Phosphine nickel(0) π-complexes with vinylcyclosilazane ligands seem to be promising potential catalysts for hydrosilylation and related reactions; the catalytic aspects will be considered in a separate paper.

5. Supplementary data

Supplementary data are available from the CCDC, 12 Union Road, Cambridge, CB2 1EZ (fax: +44-1223-336033; e-mail: deposit@ccdc.cam.ac.uk; or www: http://www.ccdc.cam.ac.uk) on request, quoting the deposition number CCDC 168038.

Acknowledgements

This work was supported by funds from the State Committee for Scientific Research, Poland, Project No. 2 T09A 122 17.

References

[1] B. Marciniec (Ed.),Comprehensive Handbook on Hydrosilylation, Pergamon, Oxford, 1992.
[2] L.N. Lewis, J. Stein, Y. Gao, R.E. Colborrn, G. Hutchins, Platinum Metals Rev. 4 (12) (1997) 66.
[3] B.D. Karstedt, US Patent 3775452, 1973.
[4] P.B. Hitchcock, M.F. Lappert, N.J.W. Warhurst, Angew. Chem., Int. Ed. Engl. 30 (1991) 438.
[5] M.F. Lappert, F.A. Scott, J. Organometal. Chem. 492 (1995) C11.
[6] P.B. Hitchcock, M.F. Lappert, C. MacBeath, F.P.E. Scott, N.J.W. Warhurst, J. Organomet. Chem. 528 (1997) 185.
[7] P.B. Hitchcock, M.F. Lappert, C. MacBeath, F.P.E. Scott, N.J.W. Warhurst, J. Organomet. Chem. 534 (1997) 139.
[8] C. MacBeath, Ph.D. Thesis, University of Sussex, 1996.
[9] J. Stein, L.N. Lewis, J. Am.Chem. Soc. 121 (1999) 3693.
[10] H. Maciejewski, B. Marciniec, I. Kownacki, J. Organomet. Chem. 597 (2000) 175.
[11] P.B. Hitchcock, M.F. Lappert, H. Maciejewski, J. Organomet. Chem. 605 (2000) 221.
[12] L.S. Isaeva, T.A. Peganova, P.V. Petrovskii, F.F. Kayumov, F.G. Yusupova, V.P. Yur'ev, J. Organomet. Chem. 248 (1983) 375.
[13] J.W. Fitch, K.C. Chan, J.A. Froelich, J. Organomet. Chem. 160 (1978) 477.
[14] B. Proft, PH.D. Thesis, University of Dusseldorf, 1993.
[15] D.J. Krysan, P.B. Mackenzie, J. Organomet. Chem. 55 (1990) 4229.
[16] CRYSALIS v.162, KUMA Diffraction, Wroclaw, Poland, 2000.
[17] CRYSALISRED v. 162, KUMA Diffraction, Wroclaw, Poland, 2000.
[18] R.H. Blessing, J. Appl. Crystallogr. 22 (1989) 396.
[19] G.M. Sheldrick, Acta Crystallogr. A46 (1990) 467.
[20] G.M. Sheldrick, SHELXL-93. Program for the Refinement of Crystal Structures, University of Göttingen, Germany, 1993.
[21] The Aldrich Library of NMR Spectra, second ed., vol. 2, 99C.
[22] International Tables for Crystallography, vol. C: Mathematical, Physical and Chemical Tables, Kluwer, Dordrecht, 1995.
[23] Siemens, Stereochemical Workstation, Siemens Analytical X-ray Instruments Inc, Madison, WI, USA, 1989.

PERGAMON

Polyhedron 21 (2002) 1267–1271

POLYHEDRON

www.elsevier.com/locate/poly

Synthesis of silver(I) complexes of thiones and their characterization by ^{13}C, ^{15}N and ^{107}Ag NMR spectroscopy

Anvarhusein A. Isab *, Saeed Ahmad, Mohammed Arab

Department of Chemistry, King Fahd University of Petroleum and Minerals (KFUPM), Dhahran 31261, Saudi Arabia

Received 8 January 2002; accepted 28 March 2002

Abstract

Silver(I) complexes of thiones (L), $[LAgNO_3]$ and $[AgL_2]NO_3$ have been prepared and characterized by elemental analysis, IR and NMR (^1H, ^{13}C, ^{15}N and ^{107}Ag) spectroscopy. An upfield shift in the C=S resonance of thiones in ^{13}C NMR and downfield shifts in N–H resonances in ^1H and ^{15}N NMR are consistent with the sulfur coordination to silver(I). In ^{107}Ag NMR, the $AgNO_3$ signal is deshielded by 300–500 ppm on its coordination to thiones. Greater upfield shifts in ^{13}C NMR are observed for $[LAgNO_3]$ compared with $[AgL_2]NO_3$ complexes, whereas the opposite trend is observed for ^1H, ^{15}N and ^{107}Ag chemical shifts. © 2002 Elsevier Science Ltd. All rights reserved.

Keywords: Silver(I) complexes; Thiones; NMR studies

1. Introduction

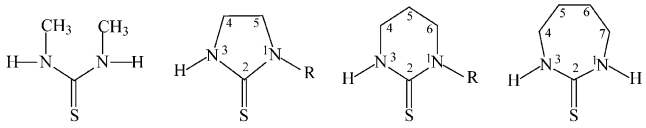
Complexes of heterocyclic thiones such as imidazolidine-2-thione (Imt), diazinane-2-thione (Diaz) and their derivatives with transition metals are of interest in bioinorganic chemistry because of the search for simple model compounds for metal proteins [1,2]. In view of this, Cu(I) [3], Ag(I) [4,5], Au(I) [6–8], Hg(II) [9] and Cd(II) [10] complexes with thiones have been widely studied in recent years. In our previous work on silver-thione complexes, we reported the synthesis and spectroscopic characterization of various $[LAgNO_3]$ (where L = Imt, Diaz and their derivatives) [4] and $Ag(Tu)_xNO_3$ (Tu = thiourea and $x = 1$–4) complexes [11]. The present report describes the synthesis of silver(I) complexes of the stoichiometry, $[AgL_2]NO_3$ for a series of thiones and their characterization by ^{13}C, ^{15}N and ^{107}Ag NMR spectroscopy. The results of ^{15}N and ^{107}Ag NMR for $[LAgNO_3]$ complexes are also presented. Among $[LAgNO_3]$ complexes, $[DmTuAgNO_3]$ and $[DiapAgNO_3]$ were not reported earlier. The main goal of the study is to provide a data base of ^{13}C and ^{107}Ag NMR spectra for silver(I) complexes of thiones.

The structures of the thiones used in this study are described in Scheme 1.

2. Experimental

2.1. Chemicals

N,*N*′-dimethylthiourea, methanol, acetone, acetonitrile and DMSO-d_6 were obtained from Fluka Chemical Co. The thione ligands were synthesized according to



(a) (b-f) (g-h) (i)

Scheme 1. (a) *N*,*N*′-dimethylthiourea (DmTu); (b) R = H; imidazolidine-2-thione (Imt); (c) $R = CH_3$; *N*-methylimidazolidine-2-thione (MeImt); (d) $R = C_2H_5$; *N*-ethylimidazolidine-2-thione (EtImt); (e) $R = C_3H_7$; *N*-propylimidazolidine-2-thione (PrImt); (f) R = *i*-C_3H_7; *N*-(*i*-propyl)imidazolidine-2-thione (*i*-PrImt); (g) R = H; 1,3-diazinane-2-thione (Diaz); (h) $R = C_2H_5$; *N*-ethyl-1,3-diazinane-2-thione (EtDiaz); (i) 1,3-diazipane-2-thione (Diap).

* Corresponding author. Tel.: +966-3-860-2645; fax: +966-3-860-4277.

E-mail address: aisab@kfupm.edu.sa (A.A. Isab).

0277-5387/02/$ - see front matter © 2002 Elsevier Science Ltd. All rights reserved.
PII: S0277-5387(02)00981-6

the procedure described in the literature (by the addition of CS_2 to diamines in ether and then heating the resulting adduct at 100–110 °C for 2–3 h, followed by its crystallization in methanol) [12,13]. The ligands Imt and Diaz contain 2–3% ^{15}N labelled nitrogen (by using a mixture of ^{15}N labelled and unlabeled diamine in preparation of thiones).

2.2. Preparation of complexes

All the complexes were prepared by adding thiones in methanol (20–25 ml) to $AgNO_3$ in 15 ml acetonitrile in the required molar ratios and stirring for 15 min. For the complexes of DmTu, Imt and Diaz ligands, white or yellow precipitates were formed on mixing the two solutions (dark brown for [ImtAgNO$_3$]), which were filtered and washed with methanol. The $[Ag(Diaz)_2]NO_3$ complex was crystallized from a water-methanol mixture. For the complexes of MeImt, EtImt, PrImt, *i*-PrImt and EtDiaz mixing resulted in a colorless or yellow solution. White or yellow solids were obtained on evaporation of the solvent. In the case of EtImt and *i*-PrImt the products were washed with water and acetone. $[Ag(EtDiaz)_2]NO_3$ was isolated from acetone. The experimental yield of the products was around 60–70% (40% for $[Ag(EtDiaz)_2]NO_3$]). The elemental analyses, melting points (m.p.) and molar conductance of the complexes are given in Table 1.

2.3. NMR measurements

The ^1H NMR spectra were obtained on a JEOL JNM-LA 500 NMR spectrometer operating at a frequency of 500.00 MHz. The ^{13}C NMR spectra were obtained at the frequency of 125.65 MHz with ^1H broadband decoupling at 297 K. The spectral conditions were: 32 K data points, 0.967 s acquisition time, 1.00 s pulse delay and 45° pulse angle.

The ^{15}N NMR spectra were recorded at 50.55 MHz using 2.1 M $NH_4^{15}NO_3$ in D_2O as an external reference, which lies at 375.11 ppm relative to pure CH_3NO_2, 380.2 ppm [14]. The spectral conditions for ^{15}N were: 32 K data points, 0.721 s acquisition time 2.50 s delay time, 60° pulse angle and 15 000 scans.

The ^{107}Ag NMR spectra were obtained at the frequency of 20.13 MHz using 10 mm low frequency probe with 9.1 M aqueous $AgNO_3$ as an external reference. The spectral conditions were: 32 K data points, 1.02 s acquisition time, 6.0 s delay time, 45° pulse angle and approximately 4000 scans.

3. Results and discussion

Selected IR spectroscopic vibrational bands for the free ligands and their silver(I) complexes are given in Table 2. A low frequency shift in the ν(C=S) band and a high frequency shift in ν(N–H) band in the complexes compared with free ligands indicate the existence of

Table 2
Selected IR absorption (cm^{-1}) for free ligands and their silver(I) complexes

Species	ν(C=S)	$\nu(NH_2)$	$\delta(NO_3^-)$
DmTu	722	3204	
[DmTu $AgNO_3$]	718	3282	826
$[Ag(DmTu)_2]NO_3$	718	3288	833, 822
Imt	510	3200	
$[Ag(Imt)_2]NO_3$	496	3214	834, 820
MeImt	520	3200	
$[Ag(MeImt)_2]NO_3$	506	3232	822
EtImt	515	3200	
$[Ag(EtImt)_2]NO_3$	504	3210	824
i-PrImt	525	3210	
$[Ag(i\text{-}PrImt)_2]NO_3$	522	3208	826
Diaz	510	3200	
$[Ag(Diaz)_2]NO_3$	522	3230	820
EtDiaz	505	3210	
$[Ag(EtDiaz)_2]NO_3$	487	3220	825
Diap	527	3224	
[$DiapAgNO_3$]	524	3224	812

Table 1
Elemental analysis of silver(I)-thione complexes ([L_2AgNO_3])

Complex	Found (Calc.)%				M.p. (°C)	Molar [a] conductance
	C	H	N	S		
[$DmTuAgNO_3$]	14.97 (13.14)	3.71 (2.94)	15.56 (15.34)	13.47 (11.70)	157–159	22.3
$[Ag(DmTu)_2]NO_3$	18.70 (19.05)	3.91 (4.26)	17.06 (18.52)	15.42 (16.95)	169–170	29.8
$[Ag(Imt)_2]NO_3$	17.98 (19.26)	3.12 (3.23)	17.61 (18.72)	15.23 (17.14)	217–219	37.5
$[Ag(MeImt)_2]NO_3$	23.77 (23.89)	3.90 (4.01)	17.04 (17.41)	17.53 (15.94)	154–155	32.2
$[Ag(EtImt)_2]NO_3$	27.82 (27.91)	5.10 (4.68)	16.07 (16.28)	16.56 (14.90)	118–120	33.5
$[Ag(i\text{-}PrImt)_2]NO_3$	31.10 (31.44)	5.76 (5.28)	15.72 (15.28)	15.04 (13.99)	126–128	30.6
$[Ag(Diaz)_2]NO_3$	21.84 (23.89)	3.79 (4.01)	16.62 (17.41)	14.46 (15.94)	204–206	32.5
$[Ag(EtDiaz)_2]NO_3$	31.10 (31.44)	5.76 (5.28)	15.72 (15.28)	15.04 (13.99)	118–120	26.5
[$DiapAgNO_3$]	19.82 (20.01)	3.39 (3.36)	13.50 (14.01)	11.27 (10.68)	156–158	32.5

[a] λ, in mho cm^2 mol^{-1} (for free silver nitrate in DMSO, $\lambda = 38.0$ mho cm^2 mol^{-1}).

thione forms in the solid state. A sharp band around 825 cm^{-1} for NO_3^- bending was observed for all the complexes indicating that NO_3^- ion is not coordinated [5,15].

The molar conductivity measurements in DMSO show that for $[LAgNO_3]$ complexes, the NO_3^- ion is weakly coordinated except in the complexes of Diaz, EtDiaz and Diap. For $[AgL_2]NO_3$ complexes, the conductance values lie in the range acceptable for a 1:1 electrolyte except in EtDiaz and DmTu complexes, which indicates that these two complexes are polymeric (Table 1). The polymeric structure of $[Ag(DmTu)_2]ClO_4$ is already known [16].

The ^1H and ^{13}C NMR chemical shifts of 0.10 M solutions of the complexes in DMSO-d_6 are summarized in Table 3. In ^1H NMR spectra of the complexes, the N–H signal of thiones became less intense upon coordination and shifted downfield by 0.7–1.0 ppm from their positions in free ligands. The deshielding of the N–H proton is related to an increase of the π electron density in the C–N bond upon complexation [17]. The appearance of a N–H signal shows that the ligands are coordinating to silver(I) via the thione group.

In all complexes, the C-2 resonance appears upfield by 4–7 ppm compared wth free ligands in accordance with the data observed for other complexes of Cu(I), Ag(I) and Au(I) with heterocyclic thiones [3–7]. The upfield shift is attributed to a lowering of the >C=S bond order upon coordination and a shift of N→C electron density producing partial double bond character in the C–N bond [17,18]. The upfield shift decreases as the number of ligands attached to silver(I) increases from one in $[LAgNO_3]$ to two in $[AgL_2]NO_3$. This is because of the increase in number of electronegative groups attached to silver(I). A small shift of 1–2 ppm is observed in other carbon atoms, which shows that the nitrogen atoms are not involved in coordination. In the complexes of Imt and its derivatives a deshielding effect is observed at C-4/5 while in Diaz and EtDiaz complexes, a deshielding effect is observed at C-4 and C-6, but C-5 bears a shielding effect. The deshielding at C-4/6 is due to an increase in π character of the C–N bond.

The difference in shielding at C-2 is related to the strength of the metal-sulfur bond, which arises from the back donation of silver(I) to sulfur [17]. In mono complexes, the smallest C-2 shift, amounting to 5.18 ppm was detected in [*i*-PrImtAgNO$_3$], while the greatest one was found in [DiapAgNO$_3$]. Among the bis complexes, the DmTu complex with the most significant shift in C-2 was found to be the most stable. From Table

Table 3
^1H and ^{13}C chemical shifts of thiones and their silver(I)-thione complexes in DMSO-d_6

Species	N–H	C-2	C-4	C-5	C-6	N–C1	N–C2
DmTu	7.38	182.64				30.66	
[DmTuAgNO$_3$]	8.32, 8.53	174.69				29.74 [a]	32.29 [a]
[Ag(DmTu)$_2$]NO$_3$	8.27, 8.53	175.18				29.65 [a]	32.16 [a]
Imt	7.98	183.44	43.97	43.97			
[ImtAgNO$_3$] [c]	9.04	176.96	45.14	45.14			
[Ag(Imt)$_2$]NO$_3$	8.95	177.81	44.85	44.85			
MeImt	8.02	182.90	40.60	50.18		33.39	
[MeImtAgNO$_3$] [c]	8.81	177.13	51.30	41.32		33.79	
[Ag(MeImt)$_2$]NO$_3$	8.76	178.27	51.25	33.82		33.82	
EtImt	7.99	182.05	40.68	47.03		40.41	11.80
[EtImtAgNO$_3$] [c]	8.74	176.83	48.33	41.42		41.33	12.02
[Ag(EtImt)$_2$]NO$_3$	8.78	177.26	41.28	48.22		41.42	12.04
PrImt	7.99	182.55	40.79	47.70		47.38	19.86, 11.00 [b]
[PrImtAgNO$_3$] [c]	8.7	173.68	41.93	49.12		48.28	19.84, 10.88 [b]
i-PrImt	7.96	181.44	40.85	42.02		45.64	18.92
[*i*-PrImtAgNO$_3$] [c]	8.65	176.26	43.40	47.30		41.47	19.25
[Ag(*i*-PrImt)$_2$]NO$_3$	8.73	176.47	41.38	47.09		43.19	19.15
Diaz	7.81	175.62	39.76	19.19	39.76		
[DiazAgNO$_3$] [c]	8.96	167.83	40.08	18.08	40.08		
[Ag(Diaz)$_2$]NO$_3$	8.82	168.91	40.04	18.24	40.04		
EtDiaz	7.89	176.05	45.03	20.84	40.48	47.54	12.05
[EtDiazAgNO$_3$] [c]	8.71	168.07	46.29	19.66	40.48	48.91	12.36
[Ag(EtDiaz)$_2$]NO$_3$	8.40	171.18	45.79	20.01	40.12	48.41	12.18
Diap	7.76	187.91	44.76	27.12	27.12		
[DiapAgNO$_3$]	8.87	174.92	44.58	25.85	25.85	44.58	

[a] Resonances due to nonequivalent CH_3 groups.
[b] N–C3.
[c] ^{13}C Resonances for these complexes in a 50:50 (v/v) mixture of DMSO and acetone are reported in Ref. [4]; the values given here are in DMSO and are mentioned to show a comparison with other complexes.

3, it can be seen that as the size of the ring is increasing the shift difference at C-2 also increases. Thus, Diap forms more stable complexes with $AgNO_3$ compared with Imt and Diaz. Also, for the complexes of *N*-ethyl derivatives (EtImt and EtDiaz), the shift is greater for EtDiaz complexes than for the EtImt one. Changing the group at the *N*-1 position has a little effect on the C-2 shift.

The ^{15}N NMR chemical shifts of Imt, Diaz and their complexes are given in Table 4. The ^{15}N NMR of the complexes shows an opposite trend compared with that observed in ^{13}C NMR. The ^{15}N NMR signal shifts towards downfield position on coordination consistent with an increase in double bond character of the C–N bond [17]. A similar observation was found in other silver(I) and gold(I) complexes of thiones [5,11,19]. As found in ^{13}C NMR, a greater shift in ^{15}N NMR is observed for Diaz complexes compared with those of Imt (Tables 3 and 4). The ^{15}N signal undergoes a slight shift suggesting that the nitrogen of thiones is not involved in bonding with silver(I) [11,19]. The metal binding through nitrogen involves an upfield shift of at least 50 ppm as is observed in some Pt(II) complexes [20,21].

In ^{107}Ag NMR the signal for $AgNO_3$ is deshielded by 166 ppm when recorded in DMSO compared with that in aqueous solution showing that the ^{107}Ag chemical shift is not only sensitive to the nature of ligands but is also affected by changing the solvent. The complexation with thiones shifts the signal further downfield by approx. 300–500 ppm. This very large reduction in shielding indicates the silver(I) binding to sulfur of the thiones [22]. In the case of bonding through nitrogen a smaller shift of around 100 ppm would have been observed in ^{107}Ag NMR [22]. This provides a clear evidence that thiones bind to silver(I) through sulfur only. The ^{107}Ag chemical shifts of all the complexes are listed in Table 5. For $[LAgNO_3]$ type complexes, two categories of ^{107}Ag chemical shifts are found, one around 500 ppm and the other around 600 ppm or greater. The larger downfield shifts suggest that the compounds should be polymeric, since the electronegative ligands are coordinating from both sides of the metal ion. The smaller shifts for MeImt, EtImt, PrImt and *i*-PrImt indicate that they are forming monomeric complexes. For Imt and its derivatives, ^{107}Ag chemical shifts are greater in bis complexes than for mono complexes, while for DmTu and Diaz, the trend is opposite. The opposite trend suggests that they exist in the form of polymers or involve some change in the geometry of the complex. The same trend was observed for $[Ag(Tu)_xNO_3]$ complexes ($x = 1$–4), which are also polymeric [11,23,24]. The crystal structure of $[Ag(DmTu)_2]ClO_4$ also shows that the compound is polymeric, having a tetrahedral geometry around silver(I) [16]. The more downfield shifts for bis complexes than for mono complexes are because of the increase in the number of electronegative groups attached to silver(I). The ^{107}Ag NMR chemical shifts for the complexes are comparable to the reported complexes of other thiones with the same stoichiometries [5,11].

Table 4
^{15}N NMR chemical shifts of Imt, diaz and their silver(I) complexes in DMSO-d_6

Species	δ (^{15}N)
Imt	112.24
$[ImtAgNO_3]$	119.09
$[Ag(Imt)_2]NO_3$	117.88
Diaz	108.47
$[DiazAgNO_3]$	115.66
$[Ag(Diaz)_2]NO_3$	114.62

Table 5
^{107}Ag NMR chemical shifts of various silver(I)-thione complexes in DMSO-d_6

Thione (L)	δ (^{107}Ag) for $[LAgNO_3]$	δ (^{107}Ag) for $[AgL_2]NO_3$
DmTu	657.86	656.12
Imt	571.03	608.29
MeImt	493.73	645.39
EtImt	480.15	645.15
PrImt	506.97	
i-PrImt	489.58	650.27
Diaz	708.73	678.00
EtDiaz	612.01	731.01
Diap	664.04	

In this study we have shown that thiones react with silver nitrate to form complexes of the type, $[LAgNO_3]$ and $[AgL_2NO_3]$ in which the ligands exist in thione form both in solution as well as in the solid state. The study provides useful information about the nature of bonding in silver(I) complexes. The chemical shifts for different complexes presented here are useful, especially if the ^{107}Ag NMR is used to study silver(I) complexes with sulfur containing biological ligands.

Acknowledgements

This research was supported by the KFUPM Research Committee under project no. CY/NMR-STUDIES/214.

References

[1] E.S. Raper, Coord. Chem. Rev. 153 (1996) 199.
[2] P.D. Akrivos, Coord. Chem. Rev. 213 (2001) 181.
[3] A.A. Isab, M.S. Hussain, Transition Met. Chem. 11 (1986) 298.
[4] A.A. Isab, Transition Met. Chem. 17 (1992) 374.

[5] J.S. Casas, E.G. Martinez, A. Sanchez, A.S. Gonzalez, J. Sordo, U. Casellato, R. Graziani, Inorg. Chim. Acta 241 (1996) 117.
[6] A.A. Isab, C.F. Shaw, III, J. Inorg. Biochem. 38 (1990) 95.
[7] A.A. Isab, M.S. Hussain, Polyhedron 4 (1985) 1683.
[8] A.A. Isab, M.S. Hussain, J. Coord. Chem. 15 (1986) 125.
[9] A.A. Isab, H.P. Perzanowski, Polyhedron 15 (1996) 2397.
[10] U. Rajalingam, P.W.A. Dean, H.A. Jenkis, Can. J. Chem. 78 (2000) 590.
[11] S. Ahmad, A.A. Isab, H.P. Perzanowski, Transition Met. Chem. (2002) in press.
[12] G.D. Thorn, Can. J. Chem. 33 (1955) 1278.
[13] L. Maier, Helv. Chim. Acta 53 (1970) 1417.
[14] M.N. Akhtar, A.A. Isab, A.R. Al-Arfaj, M.S. Hussain, Polyhedron 16 (1997) 125.
[15] M.M. El-Etri, W.M. Scovell, Inorg. Chim. Acta 187 (1991) 201.
[16] C. Pakawatchai, K. Sivakumar, H.K. Fun, Acta Crystallogr., Sect. C 52 (1996) 1954.
[17] Z. Popovic, G. Pavlovic, D. Matkovic-Calogovic, Z. Soldin, M. Rajic, D. Vikic-Topic, D. Kovacek, Inorg. Chim. Acta 306 (2000) 142.
[18] U. Bierbach, T.W. Hambly, N. Farrell, Inorg. Chem. 37 (1998) 708.
[19] S. Ahmad, A.A. Isab, J. Inorg. Biochem. 88 (2002) 43.
[20] T.G. Appletone, J.R. Hall, S.T. Ralph, Inorg. Chem. 24 (1985) 637.
[21] F.M. Macdonald, P.J. Sadler, Magn. Res. Chem. 29 (1991) S52.
[22] P.M. Henrichs, S. Sheard, J.J.H. Jackerman, G.E. Maciel, J. Am. Chem. Soc. 101 (1979) 3222.
[23] P.M. Henrichs, J.J.H. Jackerman, G.E. Maciel, Inorg. Chem. 16 (1977) 2544.
[24] E.A. Vizzini, I.F. Taylor, E.L. Amma, Inorg. Chem. 7 (1968) 1351.

PERGAMON

Polyhedron 21 (2002) 1273–1278

POLYHEDRON

www.elsevier.com/locate/poly

Copper(II) complexes of 1,3-dithian-2-ylidenemalonate: doubly layered 2D sheet induced by alkali metal ions

Jung Su Park, Kyoung-Tae Youm, Moo-Jin Jun *

Department of Chemistry, Yonsei University, Seoul 120-749, South Korea

Received 8 January 2002; accepted 6 March 2002

Abstract

Novel doubly layered 2D sheets of $M_2[Cu(DTAYM)_2(H_2O)_m]\cdot nH_2O$ (M = K, $m = 0$, $n = 2$ for compound **1**; M = Na, $m = 1$, $n = 4$ for compound **2**; M = Rb, $m = 1$, $n = 2$ for compound **3**) have been synthesized and characterized by single crystal X-ray structure studies. In compounds **1**, **2** and **3** the alkali metal ions hold each layer by binding oxygen donor atoms from hydrated water and DTAYM. Basic frameworks are an oxo-bridged dimer for **1** and monomers for **2** and **3** of which the apical site is occupied by hydrate water. © 2002 Published by Elsevier Science Ltd.

Keywords: Alkali metal ions; Doubly layered 2D sheet; Copper(II) complexes

1. Introduction

There has been great interest in the coordination chemistry of alkali metal ions since the fact was discovered that macrocyclic polyethers have been found to act as efficient ligands for alkali metals. Many works have focused on understanding the vital role played by alkali metal ions in biological systems, followed by exploiting macrocyclic multidentate ligands such as crownethers, cryptands and the relates [1]. Recently alkali metal aggregates of metal complexes ligating donor atom rich ligands have been studied [2]. In view of structural studies many examples of multidimensional polymers induced by alkali metals have been reported [3,4]. In some instances they show remarkable magnetic properties [5], which are caused by the high coordination number of alkali metals [6]. One of the strategies in making heterometallic coordination polymers containing alkali metals is that complexes with residual donor atoms such as oxygen, nitrogen or sulfur are designed. In this respect the ligand 1,3-dithian-2-ylidenemalonate (DTAYM) should be a particularly promising one in that it has many binding sites (four oxygen and two sulfur atoms). The complex, $[MnCu(MTM)_2(H_2O)_2\text{-}(CH_3OH)_2]_n$, a transition–transition metal aggregate containing bis(methylthio)methylidene)malonate (MTM) which is similar to DTAYM, affords a ferrimagnetic layered compound where four carboxylates of two MTM ligands bridge Mn and Cu atoms in a *syn-anti* bonding mode [7]. Here we report $M_2[Cu(DTAYM)_2(H_2O)_m]\cdot nH_2O$ (M = K, $m = 0$, $n = 2$ for compound **1**; M = Na, $m = 1$, $n = 4$ for compound **2**; M = Rb, $m = 1$, $n = 2$ for compound **3**), all of which show doubly layered 2D sheet frameworks in the solid state.

2. Experimental

2.1. Materials

DTAYM was prepared by the hydrolysis of the diethylester of DTAYM with an equivalent of $Ba(OH)_2$ in MeOH at boiling temperature [8]. Elemental analyses (C, H, O, S) were performed with Elementa Analysensysteme GmbH Vario EL instrument by Korea Basic Science Institute Seoul branch Lab.

* Corresponding author. Tel.: +82-2-2123-2639; fax: +82-2-364-7050.

E-mail address: mjjun@yonsei.ac.kr (M.-J. Jun).

0277-5387/02/$ - see front matter © 2002 Published by Elsevier Science Ltd.
PII: S0277-5387(02)01009-4

Table 1
Crystal data and structure refinement for $K_2[Cu(DTAYM)_2]\cdot 2H_2O$ (**1**), $Na_2[Cu(DTAYM)_2(H_2O)]\cdot 4H_2O$ (**2**), and $Rb_2[Cu(DTAYM)_2(H_2O)]\cdot 2H_2O$ (**3**)

	1	**2**	**3**
Empirical formula	$C_{14}H_{16}CuK_2O_{10}S_4$	$C_{14}H_{22}CuNa_2O_{13}S_4$	$C_{14}H_{18}CuO_{11}Rb_2S_4$
Formula weight	614.28	636.11	725.04
Temperature (K)	293(2)	293(2)	293(2)
Wavelength (Å)	0.71073	0.71073	0.71073
Crystal system	monoclinic	triclinic	triclinic
Space group	$P2_1/C$	$P\bar{1}$	$P\bar{1}$
a (Å)	9.005(5)	9.651(2)	10.0096(16)
b (Å)	22.088(5)	11.430(2)	11.513(3)
c (Å)	12.2598(18)	11.6962(15)	11.592(2)
α (°)		84.475(12)	82.159(17)
β (°)	104.50(3)	65.921(15)	66.585(14)
γ (°)		72.261(16)	67.576(16)
Volume (Å^3)	2360.9(15)	1121.4(4)	1133.0(4)
Z	4	2	2
Calculated density (g cm^{-3})	1.728	1.884	2.125
Absorption coefficient (mm^{-1})	1.678	1.444	5.655
$F(000)$	1244	650	714
Crystal size (mm)	$0.35 \times 0.25 \times 0.10$	$0.4 \times 0.3 \times 0.1$	$0.22 \times 0.16 \times 0.14$
θ range for data collection	1.84–22.98	1.87–24.98	1.91–24.97
Reflections collected/unique	2940/2741 [$R_{int} = 0.0220$]	3833/3605 [$R_{int} = 0.0145$]	3474/3274 [$R_{int} = 0.0184$]
Data/restraints/parameters	2741/0/280	3605/0/304	3274/0/289
Goodness-of-fit on F^2	1.160	1.181	1.150
Final R indices [$I > 2\sigma(I)$]	$R_1 = 0.0677$, $wR_2 = 0.1963$	$R_1 = 0.0686$, $wR_2 = 0.1942$	$R_1 = 0.0526$, $wR_2 = 0.1383$
R indices (all data)	$R_1 = 0.0682$, $wR_2 = 0.1971$	$R_1 = 0.0688$, $wR_2 = 0.1944$	$R_1 = 0.0533$, $wR_2 = 0.1390$

2.2. Synthesis

2.2.1. $K_2[Cu(DTAYM)_2]\cdot 2H_2O$ (**1**)

$CuSO_4\cdot 5H_2O$ (0.25 g, 1 mmol) and K_2SO_4 (0.175 g, 1 mmol) were added to a solution of Ba(DTAYM) (0.711 g, 2 mmol) in H_2O (30 ml). After vigorous stirring for 2 h, the white precipitate ($BaSO_4$) was removed by filtration. The filtrate was evaporated to dryness and then the resultant solid was dissolved in MeOH (30 ml), the resulting solution was filtered, concentrated to a half of its original volume and left undisturbed for a week. Single crystals were separated. Yield: 91% (based on Ba(DTAYM)). *Anal*. Calc. for $C_{14}H_{16}CuK_2O_{10}S_4$: C, 27.37; H, 2.63; O, 26.05; S, 20.88. Found: C, 27.43; H, 2.89; O, 26.32; S; 20.52%.

2.2.2. $Na_2[Cu(DTAYM)_2(H_2O)]\cdot 4H_2O$ (**2**)

Compound **2** was prepared via a similar method as that for compound **1**, using Na_2SO_4 (0.284 g, 2 mmol) in place of K_2SO_4. After removing $BaSO_4$ the filtrate was concentrated to approximately half of its original volume under reduced pressure and layered with MeOH slowly. After a day single crystals were separated and washed with MeOH, acetone and air-dried. Yield: 85% (based on Ba(DTAYM)). *Anal*. Calc. for $C_{14}H_{22}CuNa_2O_{13}S_4$: C, 26.43; H, 3.49; O, 32.70; S, 20.16. Found: C, 26.80; H, 3.37; O, 33.05; S, 20.49%.

2.2.3. $Rb_2[Cu(DTAYM)_2(H_2O)]\cdot 2H_2O$ (**3**)

Compound **3** was prepared via a similar method as that for compound **2**, using Rb_2SO_4 (1.534 g, 2 mmol) instead of Na_2SO_4. Yield: 89% (based on Ba(DTAYM)). *Anal*. Calc. for $C_{14}H_{18}CuO_{11}Rb_2S_4$: C, 23.19; H, 2.50; O, 24.27; S, 17.69. Found: C, 22.87; H, 2.75; O, 24.51; S; 17.58%.

2.2.4. X-ray diffraction measurement

All the X-ray data were collected on Enraf–Nonius CAD-4 automated diffractometer with Mo Kα radiation ($\lambda = 0.71073$ Å) at ambient temperature. The orientation matrix and unit cell dimensions were determined from 25 machine-centered reflections in the 2θ range from 15 to 25°. The variation of intensities were monitored with repeated check of intensities of three reflections every 1 h during the data collection period. An absorption correction was applied by an empirical ψ-scan on two or three reflection planes with a κ-value near 90°. A direct method (SHELX-86) [9] was employed to locate heavy atoms and subsequent cycles of Fourier map and least-square refinements located the other atoms (SHELX-97) [10]. Hydrogen atoms were included in the structure factor calculation using a riding model. All the calculations were carried out using a VAX and a PC. Detailed crystal parameters and procedural information corresponding to data collection and structure refinement are given in Table 1.

Table 2
Selected bond lengths (Å) and angles (°) for **1**

Bond lengths	
Cu–O(1)	1.927(5)
Cu–O(3)	1.920(5)
Cu–O(5)	1.907(5)
Cu–O(7)	1.921(5)
Cu–O(1)#1	2.418(4)
Cu···Cu#1	3.3409(17)
K(1)–O(1)	2.740(5)
K(1)–O(2)	3.054(6)
K(1)–O(3)#1	3.109(5)
K(1)–O(4)#5	2.848(6)
K(1)–O(7)	2.801(5)
K(1)–OW1	2.890(7)
K(1)–OW1#4	2.685(6)
K(2)–O(2)	2.717(6)
K(2)–O(5)#1	2.968(5)
K(2)–O(6)#6	2.661(7)
K(2)–O(6)#1	2.704(6)
K(2)–OW2	2.646(10)
K(1)···K(1)#4	3.612(4)
Bond angles	
O(1)–Cu–O(3)	88.93(19)
O(1)–Cu–O(5)	173.1(2)
O(1)–Cu–O(7)	89.3(2)
O(3)–Cu–O(5)	92.0(2)
O(3)–Cu–O(7)	164.0(2)
O(5)–Cu–O(7)	91.7(2)
O(1)–Cu–O(1)#1	80.11(18)
O(3)–Cu–O(1)#1	90.31(19)
O(5)–Cu–O(1)#1	93.06(18)
O(7)–Cu–O(1)#1	104.99(19)
K(2)#1–O(6)–K(2)#3	106.2(2)
O(1)–K(1)–OW1#4	102.64(17)
O(7)–K(1)–OW1#4	135.24(18)
OW1–K(1)–OW1#4	99.33(19)
O(6)#1–K(2)–O(6)#6	73.8(2)
O(1)–K(1)–O(2)#4	3.80(14)

Symmetry operation: #1: $-x+2$, $-y+1$, $-z+2$; #2: $x+1$, y, z; #3: x, y, $z-1$; #4: $-x+1$, $-y+1$, $-z+2$; #5: $x-1$, y, z; #6: x, y, $z+1$.

3. Result and discussion

DTAYM is a very feasible ligand in that it has four oxygen atoms (two carboxylates) and two sulfur atoms, which are potential donors to act as a metal acceptor. A similar ligand, MTM, coordinates to a Pt(II) ion via one of the three distinct modes of O, O′-, O, S′- and S, S′-chelation [8]. Recently, it has been reported that selective affinity of oxygen and sulfur of similar derivative, bis(ethylthio)methylenepropanedithiolate (BETMP) to particular metal ions gives the trinuclear complex $[[(dach)Pt(BETMP)]_2[Cu(BF_4)_2]]$ which is dimerized in MeOH to give an inorganic tennis ball via a non-covalent interaction [11]. As mentioned above, DTAYM is a donor-rich ligand which can give unpredictable polymorphs.

The reaction of Ba(DTAYM) with Cu(II) ion and M_2SO_4 (M = Na, K, Rb) affords compounds **1**, **2** and **3**.

Table 3
Selected bond lengths (Å) and angles (°) for **2**

Bond lengths	
Cu–O(1)	1.935(4)
Cu–O(3)	1.922(4)
Cu–O(5)	1.920(4)
Cu–O(7)	1.917(4)
Cu–O(9)	2.396(5)
Na(1)–O(1)	2.412(4)
Na(1)–O(4)#1	2.519(5)
Na(1)–O(7)	2.500(5)
Na(1)–OW1	2.349(5)
Na(1)–OW2	2.395(6)
Na(1)–OW3	2.319(2)
Na(2)–O(4)#4	2.456(4)
Na(2)–O(5)	2.544(4)
Na(2)–O(8)#3	2.283(5)
Na(2)–O(9)	2.589(6)
Na(2)–OW1#5	2.517(6)
Na(2)–OW4	2.538(14)
Na(2)–OW4#4	2.820(16)
Bond angles	
O(1)–Cu–O(3)	90.47(17)
O(1)–Cu–O(5)	173.25(17)
O(1)–Cu–O(7)	87.30(17)
O(1)–Cu–O(9)	101.52(17)
O(3)–Cu–O(5)	91.27(17)
O(3)–Cu–O(7)	176.26(17)
O(3)–Cu–O(9)	88.20(17)
O(5)–Cu–O(7)	90.61(17)
O(5)–Cu–O(9)	85.05(17)
O(7)–Cu–O(9)	95.19(17)
O(1)–Na(1)–O(7)	65.51(14)
Na(1)–Na(1)–OW1–Na(2)#2	97.60(19)
Na(1)–OW3–Na(1)#6	180.0
Na(1)#1–O(4)–Na(2)#4	94.81(15)

Symmetry operation: #1: $-x$, $-y+1$, $-z+2$; #2: $x-1$, y, z; #3: $-x+1$, $-y$, $-z+2$; #4: $-x+1$, $-y+1$, $-z+2$; #5: $x+1$, y, z; #6: $-x$, $-y$, $-z+2$.

All of the complexes show U-shaped frameworks like horseshoes, which face each other. This inward connection is caused by the alkali metal ions, hydrated water and oxygen from DTAYM, resulting in a doubly layered 2D sheet. Selected bond lengths and angles are listed in Table 2 for **1**, Table 3 for **2** and Table 4 for **3**. In compound **1** the elucidative framework is horseshoes in which the copper ion is surrounded by five oxygens (four from DTAYM (O1, O3, O5, O7) and the rest from neighboring DTAYM ligands (O1#1)). As a result the basic framework of **1** is a bis-μ-oxo-bridged dimer. The length of Cu–O1#1 and bond angle of O1–Cu–O1#1 are 2.418(4) Å and 80.11(18)°, respectively. These dimers are aggregated via an interaction of potassium ions and oxygen atoms. As shown in Fig. 1, the environment of each potassium ion is different, where K1 has the coordination number of seven. K1 ions are bridged by two hydrated water and two carboxylate groups. More interestingly two carboxylate groups bridge two K1 ions in a *syn–syn* bonding mode and hydrated waters (OW1)

Table 4
Selected bond lengths (Å) and angles (°) for **3**

Bond lengths	
Cu–O(1)	1.916(4)
Cu–O(3)	1.921(5)
Cu–O(5)	1.921(4)
Cu–O(7)	1.922(5)
Cu–O(9)	2.363(5)
Rb(1)–O(2)#1	2.878(6)
Rb(1)–O(3)	2.972(5)
Rb(1)–O(5)	2.985(4)
Rb(1)–O(6)#3	3.113(5)
Rb(1)–O(9)	3.136(6)
Rb(1)–OW1#1	2.982(5)
Rb(1)–OW1#2	3.101(6)
Rb(2)–O(1)	2.926(4)
Rb(2)–O(2)#5	2.861(5)
Rb(2)–O(6)#4	2.904(5)
Rb(2)–O(9)	3.103(6)
Rb(2)–OW2	3.021(6)
Rb(2)–OW2#5	2.962(6)
Rb(2)–Rb(2)#5	3.8458(17)
Bond angles	
O(1)–Cu–O(5)	178.7(2)
O(1)–Cu–O(3)	91.83(19)
O(1)–Cu–O(7)	89.09(19)
O(1)–Cu–O(9)	90.15(19)
O(3)–Cu–O(5)	88.6(2)
O(3)–Cu–O(7)	173.0(2)
O(3)–Cu–O(9)	90.5(2)
O(5)–Cu–O(7)	90.39(19)
O(5)–Cu–O(9)	91.1(2)
O(7)–Cu–O(9)	96.4(2)
OW1#1–Rb(1)–OW1#2	85.01(16)
OW2–Rb(2)–OW2#5	100.01(15)
Rb(1)#1–O(2)–Rb(2)#5	103.15(15)

Symmetry operation: #1: $-x+2$, $-y+1$, $-z+1$; #2: x, $y-1$, z; #3: $-x+2$, $-y$, $-z+1$; #4: $-x+3$, $-y$, $-z+1$; #5: $-x+3$, $-y+1$, $-z+1$.

bridge two K1 ions in a μ-mode. The distance between K1 (K1–K1#4) is 3.612(4) Å and the rest of the coordination environment is completed with η^2-chelating of another carboxylate and η^1-bonding of the other carboxylate group. The coordination number of K2 is five, where the oxygen atoms from the carboxylate group chelate the potassium ion in a η^2-mode, one of which bridges the other potassium ion to form a bis-μ-oxo K_2O_2 plane. As a result these interactions induce the doubly layered 2D sheets (Fig. 2).

In the case of compounds **2** and **3**, the interacting patterns are somewhat different from that of the compound **1**. The basic unit of the double layer is composed of the asymmetric units of **2** and **3** as a monomer, where an hydrated water occupies an apical site of the copper ion and four oxygen atoms from DTAYM complete the five coordination environment of the Cu atom.

In compound **2**, the Na1 ion lies coplanar against the least-squared plane made up of O1, O3, O5 and O7 and Na2 is located above that plane to interact with apically occupied water and the oxygen atoms belonging to a neighboring monomer and hydrated waters (Ow1, Ow4), resulting in doubly layered 2D sheet frameworks. The coordination number of sodium ions (Na1 and Na2) is six (Figs. 3 and 4). Ow3 bridges Na1 and Na1#6 with an angle of 180°, which is related by an inversion symmetry operation. Sodium ions (Na1 and Na2#2) are bridged through Ow1 and O4#4 via a bis-μ-oxo-bridging mode to afford a bent plane composed of Na1, Na2#2, Ow1 and O4#4. The resultant dihedral angle between the Na1, Ow1, O4#4 plane and the Na2#2, Ow1, O4#4 plane is 126.19°.

It is very interesting to see the position of the

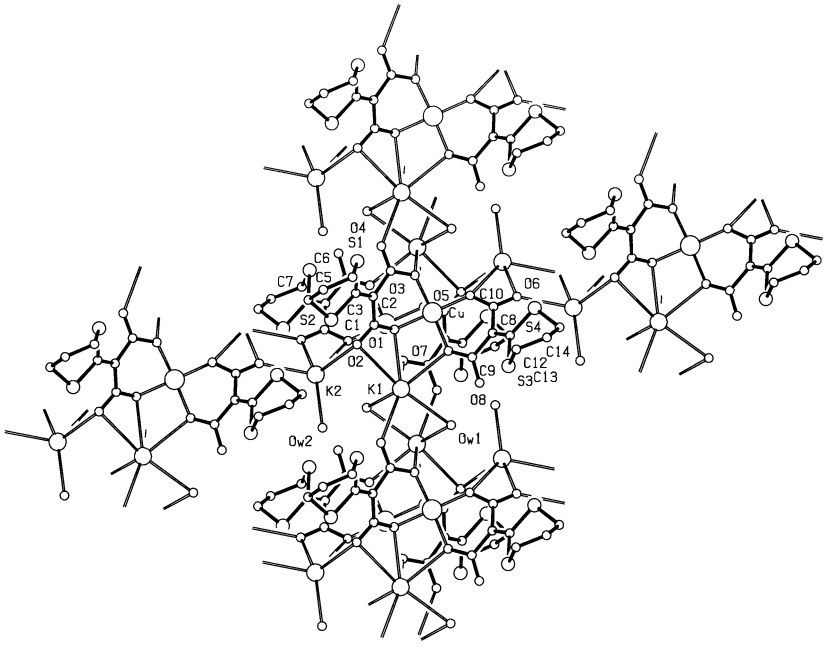


Fig. 1. Extended structure of **1** showing binding mode of K ions [12]. All hydrogen atoms are omitted for clarity.

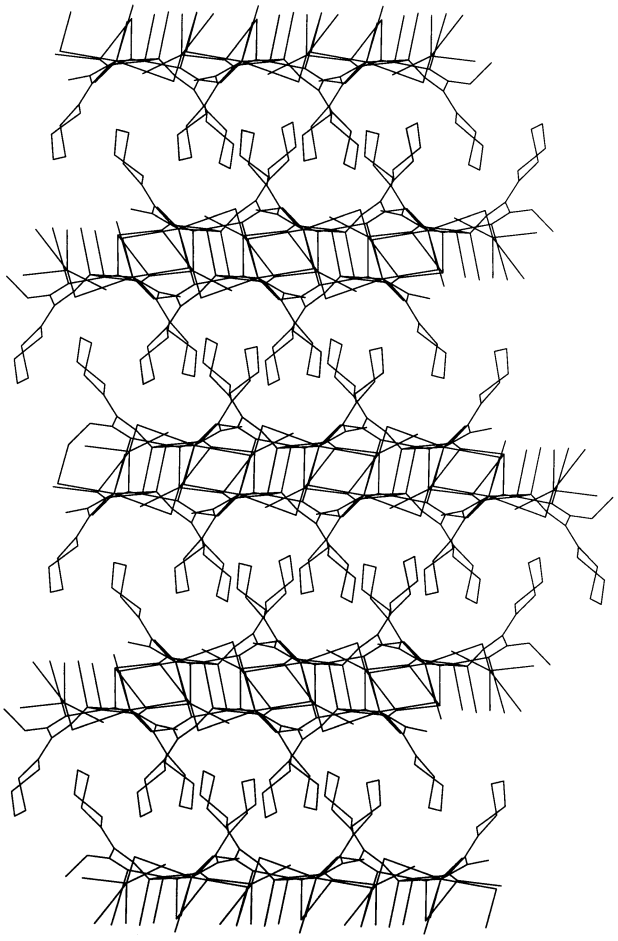


Fig. 2. Doubly layered 2D sheet as viewed from the [100] side plane of coordination polymer.

rubidium ions in compound **3**. Here the apically occupied water (O9) pushes down the face of copper ions and hold the rubidium ions a μ-3 mode. The angle of ∠Rb1–O9–Rb2 is 167.53(17)°, and the Rb1 lies in the bisect plane against the O3–Cu–O5 plane. The Rb2 ion interacts with only O1 atom in the asymmetric unit of compound **3**. The coordination numbers of Rb1 and Rb2 are seven and six, respectively (Fig. 3). Rb1 ions are bridged through hydrate waters (Ow1) and two carboxylate groups via a *syn–syn* bonding mode, as is the case for the Rb2 ions. But the distances between the rubidium ions are quite different. Whereas Rb1 ions are separated by approximately 4.48 Å, the length between two Rb2 ions (Rb(2)–Rb(2)#5) is 3.8458(17) Å. As a result these interactions in compounds **2** and **3** induce doubly layered 2D sheets similar to compound **1**.

In summary, the affinity of the alkali metal ions to oxygen atoms plays a pivotal role for all compounds to afford doubly layered 2D sheets where all oxygen atoms and alkali metal ions protrude inward in the double layer.

4. Supplementary material

Lists of full data collection and processing parameters, atomic coordinates, anisotropic displacement coefficient, hydrogen coordinates, full bond distances, angles and torsional angles can be obtained on request from the Cambridge Crystallographic Data Center, 12 Union Road, Cambridge CB21 1EZ, UK (fax: +44-1223-336033; e-mail: deposit@ccdc.cam.ac.uk or www: http://www.ccdc.cam.ac.uk) (CCDC Nos. 176300, 176301, and 176302 for **1**, **2**, and **3**).

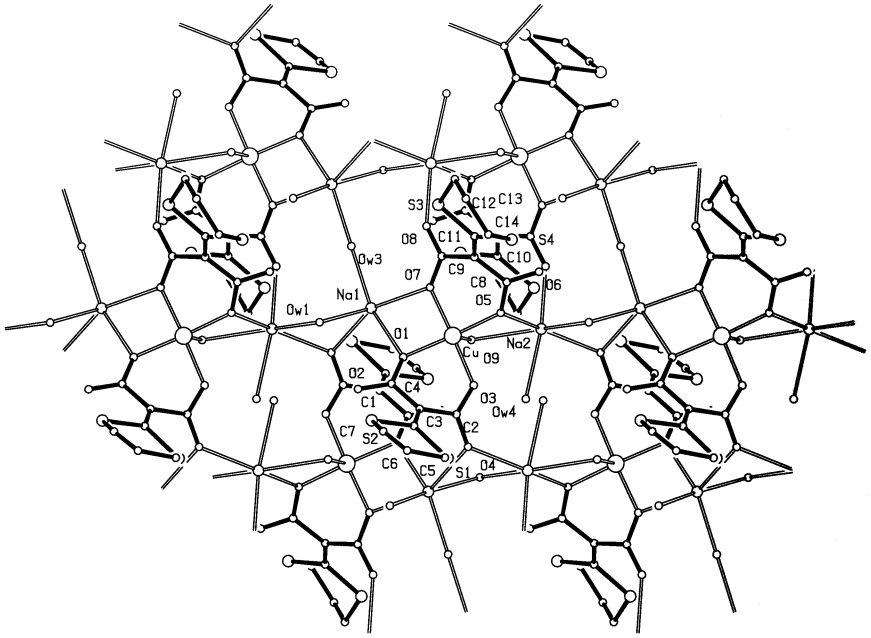


Fig. 3. Extended structure of **2** showing binding mode of Na ions [12]. All hydrogen atoms are omitted for clarity.

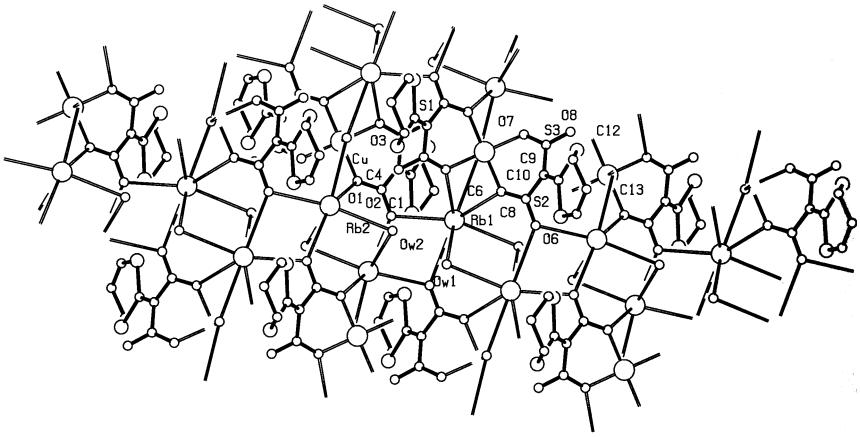


Fig. 4. Extended structure of **3** showing binding mode of Rb ions [12]. All hydrogen atoms are omitted for clarity.

Acknowledgements

The authors wish to acknowledge the financial support of Yonsei University for the year 2000 (2000-1-0072).

References

[1] (a) D.E. Fenton, in: S.G. Wilkinson (Ed.), Comprehensive Coordination Chemistry, vol. 3, first ed., Pergamon, Oxford, 1987, p. 1;
(b) H. Tsukube, Y. Mizutani, S. Shinoda, T. Okazaki, M. Tadokoro, K. Hori, Inorg. Chem. 38 (1999) 3506;
(c) T. Nabeshima, Coord. Chem. Rev. 148 (1996) 151.

[2] (a) S. Gambarotta, F. Urso, C. Floriani, A. Chiesi-Villa, C. Guastini, Inorg. Chem. 22 (1983) 3966;
(b) S.D. Augelis, E. Solari, E. Gallo, C. Floriani, A. Chiesi-Villa, C. Rozzoli, Inorg. Chem. 35 (1996) 6086;
(c) U. Riarulli, A.J. Rogers, C. Floriani, G. Gervasio, D. Viterbo, Inorg. Chem. 36 (1997) 6127;
(d) D. Cunningham, P. McAdle, M. Mitchell, N.N. Chonchubhair, M. O'Gara, F. Franceschi, C. Floriani, Inorg. Chem. 39 (2000) 1639.

[3] (a) F.D. Rochon, R. Melanson, M. Andruh, Inorg. Chem. 35 (1996) 6086;
(b) J. Heo, S.-K. Kim, D. Whang, K. Kim, Angew. Chem., Int. Engl. Ed. 38 (1999) 641;
(c) J. Heo, J. Kim, D. Whang, K. Kim, Inorg. Chim. Acta 39 (2000) 1639.

[4] (a) W.S. Sheldrick, I.M. Müller, Coord. Chem. Rev. 182 (1999) 125;
(b) T. Rottgers, W.S. Sheldrick, J. Solid State Chem. 152 (2000) 271.

[5] (a) N. Re, E. Gallo, E. Gallo, C. Floriani, H. Miyasaka, N. Matsumoto, Inorg. Chem. 35 (1996) 5964;
(b) H. Miyasaka, N. Matsumoto, H. Okawa, N. Re, E. Gallo, C. Floriani, J. Am. Chem. Soc. 118 (1996) 981.

[6] (a) G. Liu, Y.-G. Wei, J. Liu, Q. Liu, S.-W. Zhang, Y.-Q. Tang, J. Chem. Soc., Dalton. Trans. (2000) 1013;
(b) J.C. Bryan, K. Kavallieratos, R.A. Sachleben, Inorg. Chem. 39 (2000) 1568.

[7] J. Kim, J.M. Lim, Y. -K. Choi, Y. Do, Angew. Chem., Int. Engl. Ed. 35 (1996) 998.

[8] Y.S. Sohn, K.M. Kim, S.J. Kang, O.-S. Jung, Inorg. Chem. 35 (1996) 4274.

[9] G.M. Sheldrick, SHELXS-86: Program for Solution of Crystal Structure, University of Göttingen, Germany, 1986.

[10] G.M. Sheldrick, SHELXL-97: Program for Refinement of Crystal Structure, University of Göttingen, Germany, 1997.

[11] K.M. Kim, J.S. Park, Y. -S. Kim, Y.J. Jun, T.Y. Kang, Y.S. Sohn, M.-J. Jun, Angew. Chem., Int. Engl. Ed. 40 (2001) 2458.

[12] A.L. Spek, PLATON for Window graphic program, University of Utrecht, The Netherlands, 1998.

PERGAMON

Polyhedron 21 (2002) 1279–1288

POLYHEDRON

www.elsevier.com/locate/poly

The coordination chemistry of mono and bis(di-2-pyridylamine)copper(II) complexes: preparation, characterization and crystal structures of $[Cu(L)(NO_2)_2]$, $[Cu(L)(H_2O)_2(SO_4)]$, $[Cu(L)_2(NCS)](SCN)\cdot 0.5DMSO$ and $[Cu(L)_2(SCN)_2]$

Sujittra Youngme [a,*], Narongsak Chaichit [b], Chaveng Pakawatchai [c], Saksit Booncoon [a]

[a] *Department of Chemistry, Faculty of Science, Khon Kaen University, Khon Kaen 40002, Thailand*
[b] *Department of Physics, Faculty of Science and Technology, Thammasart University Rangsit, Pathumthani 12121, Thailand*
[c] *Department of Chemistry, Faculty of Science, Prince of Songkla University, Hatyai 90112, Thailand*

Received 8 January 2002; accepted 13 March 2002

Abstract

The crystal structures of two mono(dpyam)copper(II) complexes, $[Cu(dpyam)(NO_2)_2]$ (**1**) and $[Cu(dpyam)(H_2O)_2(SO_4)]$ (**2**) and two dithiocyanate compounds containing bis(dpyam)copper(II) units, $[Cu(dpyam)_2(NCS)](SCN)\cdot 0.5DMSO$ (**3**) and $[Cu(dpyam)_2(SCN)_2]$ (**4**) have been determined by X-ray crystallography. The second orthorhombic form of the monomeric Cu(II) complex **1** was obtained by the reaction of di-2-pyridylamine (dpyam) with CuCl and $NaNO_2$ in water–methanol solution. Each copper(II) ion in **1** exhibits a tetrahedrally-distorted square base of the CuN_2O_2 chromophore, with off-the-z-axis coordinated nitrito groups weakly bound in approximately axial positions. Complex **2** is an example of a polymeric copper(II) derivative containing the bidentate bridging sulfate ligand in the long-bonded axial positions. Each copper(II) ion in **2** shows an elongated tetragonal octahedral stereochemistry. The CuN_4N' chromophore of **3** involves a square-based pyramidal structure, slightly distorted towards a trigonal bipyramidal stereochemistry, $\tau = 0.13$. One of the SCN^- anions is bonded to the copper(II) ion via the N atom in the axial position of the square pyramid. Complex **4** is centrosymmetric and octahedrally elongated, with the SCN^- anions coordinating in axial positions via the S atom. The structures of complexes **1**–**4** and their ESR and electronic reflectance spectra are compared with those of related complexes. © 2002 Elsevier Science Ltd. All rights reserved.

Keywords: Crystal structures; Copper(II) complexes; Nitrite complexes; Sulfate complexes; di-2-Pyridylamine complexes; Thiocyanato complexes

1. Introduction

Reported complexes of copper(II) and bidentate mono(chelate) ligands with mono- and divalent oxyanions may be grouped in many classes for each type of oxyanions depending on the coordinating nature. Complexes with monovalent oxyanions formulated as $Cu(chelate)(OXO)_2\cdot nH_2O$ or $Cu(chelate)(OXO)(OYO)\cdot nH_2O$, where OXO and OYO = NO_2^-, NO_3^-, ClO_4^-, $CH_3CH_2COO^-$, CH_3COO^- or $HCOO^-$, exhibit three classes of local molecular structures: (A) monomeric tetrahedrally-distorted elongated octahedron with an extremely asymmetric bidentate coordination of both oxyanions [1–10]; (B) polymeric elongated tetragonal (or rhombic) octahedron with the nearly symmetric bidentate coordination of a basal oxyanion and the bridging bidentate coordination in the axial positions of the second one [10–13] and (C) dimeric tetrahedrally-distorted square pyramid with monodentate and bidentate bridging oxyanions [8,14]. While complexes with divalent oxyanions formulated as $Cu(chelate)(OZO)\cdot nH_2O$, where OZO = CO_3^{2-} and SO_4^{2-}, involve five classes of local molecular structures: (I) monomeric distorted square-based pyramid with bidentate oxyanions [15]; (II) polymeric distorted square-based pyramid with the tridentate bridging oxyanions [16]; (III) monomeric square-based pyramid with unidentate oxyanions [17]; (IV) polymeric elongated octahedron with

* Corresponding author. Tel.: +66-43-241-3319x2370-74; fax: +66-43-243-338.
E-mail address: sujittra@kku.ac.th (S. Youngme).

0277-5387/02/$ - see front matter © 2002 Elsevier Science Ltd. All rights reserved.
PII: S0277-5387(02)01011-2

bidentate bridging oxyanions [18,19]; (V) dimeric distorted square-based pyramid with double bridges of tridentate oxyanions [20]. In order to continue exploring the coordinating and bridging natures of mono- and divalent oxyanions on these types of complexes, [Cu(dpyam)$(NO_2)_2$] (**1**) and [Cu(dpyam)$(H_2O)_2(SO_4)$] (**2**) complexes were prepared and the structures investigated and compared with other relevant complexes.

More interesting of **1** is that it was reported by us in 1999 to crystallize in orthorhombic form of the $P2_12_12_1$ space group but the title complex **1** of the same composition shows differences both in color and electronic spectra. We have characterized this second form crystallographically and found that it crystallized in space group $Pca2_1$ of the orthorhombic system. Both forms were each unique in their unit cell content and their local molecular environments. Herein we have reported differences in their molecular geometries and their spectroscopic properties.

The bis(chelate)copper(II) complexes formulated as Cu(chelate)$_2$XY, with chelate being 2,2′-bipyridyl (bpy) and 1,10-phenanthroline (phen) and X, Y various counter anions, coordinated or not, are known to display a large variation of non-regular stereochemistry [1,21] with a large number of investigated structural data [22–26]. Structural data are more limited for the corresponding complexes in which the chelate is the more flexible di-2-pyridylamine (dpyam) [24,27a,27b,28–35]. In order to examine the chelate function of bpy or phen and the more flexible dpyam ligand upon the range of stereochemistries observed in this family of complexes, this paper also reports the crystal structures and electronic properties of two bis(dpyam) complexes [Cu(dpyam)$_2$(NCS)](SCN)·0.5DMSO (**3**) and [Cu(dpyam)$_2$(SCN)$_2$] (**4**) and these are compared with other analogous complexes.

2. Experimental

All reagents were commercial grade materials and were used with out further purification. Elemental analyses (C, H, N) were performed by the Microanalytical Service of Science and Technological Research Equipment Centre, Chulalongkorn University on a Perkin–Elmer PE2400 CHNS/O Analyzer. The infrared spectra were recorded on a Biorad FTS-7/PC FTIR spectrophotometer as KBr pellets in the 4000–450 cm^{-1} region. Solid-state (diffuse reflectance) electronic spectra were recorded as polycrystalline samples on a Perkin–Elmer Lambda2S spectrophotometer over the range 8000–18 000 cm^{-1}. The X-band ESR spectra were recorded on polycrystalline samples at room temperature (r.t.) with a JEOL ESR JES-RE2X spectrometer (operating at the X-band) by the service of Scientific and Technological Research Equipment Centre, Chulalongkorn University.

2.1. Preparation

2.1.1. Preparation of [Cu(dpyam)$(NO_2)_2$] (1)

A solution of CuCl (99 mg, 1.0 mmol) in 25 ml water was mixed with a solution of dpyam (85.5 mg, 0.5 mmol) in 25 ml methanol and 69 mg (1.0 mmol) of solid $NaNO_2$ were added to the mixed solution. Bright green needle crystals were deposited when allow to stand for slow evaporation in air. They were filtered off, washed with mother liquor and were dried in air. Yield approximately 60%. *Anal.* Calc. for $C_{10}H_9CuN_5O_4$: C, 36.76; H, 2.78; N, 21.43. Found: C, 36.68; H, 2.70; N, 21.39%.

The first form of **1** (compound **5**) was also reprepared following the method previously described [7] for spectral comparison to that of **1**, starting differently with the $Cu(O_2CCH_3)_2·H_2O$: dpyam: $NaNO_2$ ratio of 1:2:4 in methanolic aqueous solution (20:30 ml). Dark green crystals were obtained as [Cu(dpyam)$(NO_2)_2$]. Yield approximately 83%. *Anal.* Calc. for $C_{10}H_9CuN_5O_4$: C, 36.76; H, 2.78; N, 21.43. Found: C, 36.82; H, 2.83; N, 21.50%.

2.1.2. Preparation of [Cu(dpyam)$(H_2O)_2(SO_4)$] (2)

2.1.2.1. Method a. To a stirring aqueous solution (75 ml) containing $CuCl_2·2H_2O$ (169 mg, 1.0 mmol) and $Na_2S_4O_6$ (307 mg, 1.0 mmol), a solution of dpyam (171 mg, 1.0 mmol) in MeOH (20 ml)–DMSO (35 ml) mixed solvent was added. The solution was heated to approximately 40 °C with continuous stirring for 3 h. A light green precipitate was filtered off resulting in a light green filtrate. From the light green solution, light green needle crystals were deposited on slow evaporation at r.t. Yield approximately 48%. *Anal.* Calc. for $C_{10}H_{13}CuN_3O_6S$: C, 32.74; H, 3.57; N, 11.46. Found: C, 32.80; H, 3.65; N, 11.51%.

2.1.2.2. Method b. To a stirring aqueous solution (15 ml) containing $CuSO_4·5H_2O$ (250 mg, 1.0 mmol) and $Na_2S_2O_3·5H_2O$ (268 mg, 1.0 mmol), a solution of dpyam (171 mg, 1.0 mmol) in MeOH (10 ml) was added. The solution was heated with continuous stirring for 15 min. Light green precipitates were developed and filtered off. The solids were dissolved in DMSO (50 ml) with heating and stirring for 14 h resulting in a bluish-green solution. On slow evaporation at r.t., light green needle crystals of **2** were obtained. Yield approximately 40%.

2.1.3. Preparation of [Cu(dpyam)$_2$(NCS)](SCN)·0.5DMSO (3)

The complex [Cu(dpyam)$_2$(NCS)](SCN)·0.5DMSO (**3**) was prepared by adding a hot solution of dpyam (0.34 g, 2.0 mmol) in 20 ml methanol to a hot DMSO solution (20 ml) of Cu(SCN) (0.12 g, 1.0 mmol). Dark green and rod-like crystals of [Cu(dpyam)$_2$(SCN)$_2$] (**4**) deposited together with the green, rectangular-shaped crystals of **3**, which were separated by hand. Yield approximately 50%. *Anal.* Calc. for $C_{24}H_{24}N_8CuOS_3$: C, 49.23; H, 3.77; N, 19.97. Found: C, 49.17; H, 3.69; N, 19.92%.

2.1.4. Preparation of [Cu(dpyam)$_2$(SCN)$_2$] (4)

The complex [Cu(dpyam)$_2$(SCN)$_2$] (**4**) was prepared by adding a hot solution of dpyam (0.34 g, 2 mmol) in 30 ml ethanol to a hot aqueous solution (30 ml) containing $Cu(CH_3CO_2)_2·H_2O$ (0.18 g, 1 mmol) and KSCN (0.19 g, 2 mmol). Dark-green and rod-like crystals of **4** were formed after a few days. Yield approximately 92%. *Anal.* Calc. for $C_{22}H_{18}N_8CuS_3$: C, 50.61; H, 3.48; N, 21.46. Found: C, 50.55; H, 3.53; N, 21.41%.

The complex [Cu(dpyam)$_2$Br$_2$]·2H$_2$O (**6**) was reprepared in order to compare its electronic spectrum to that of the present compound **4**. This compound was structurally reported [29] but there was no electronic reflectance spectrum reported. Complex **6** was prepared by adding a hot solution of dpyam (0.34 g, 2.0 mmol) in 20 ml methanol to a hot aqueous solution (30 ml) of $CuBr_2$ (0.22 g, 1 mmol). Dark green needle-like crystals of **6** were formed after slow evaporation at r.t. for several days. Yield approximately 86%. *Anal.* Calc. for $C_{20}H_{22}N_6CuBrO_2$: C, 39.92; H, 3.69; N, 13.97. Found: C, 39.86; H, 3.74; N, 14.01%.

2.2. Crystallography

Reflection data for complexes **1**–**4** were collected at 293 K on a 1K Bruker SMART CCD area-detector diffractometer using graphite monochromated Mo Kα radiation ($\lambda = 0.71073$ Å) at a detector distance of 4.5 cm and swing angle of $-35°$. A hemisphere of the reciprocal space was covered by a combination of three sets of exposures; each set had a different ϕ angle (0, 88, 180°) and each exposure of 30 s for all complexes except that of **1** (35 s), covered 0.3° in ω. Data reduction and cell refinements were performed using the program SAINT [36]. An empirical absorption correction by using the SADABS [37] program was applied, which resulted in transmission coefficients ranging from 0.705 to 1.000 for **1**, 0.723 to 1.000 for **2**, 0.806 to 1.000 for **3** and 0.908 to 1.000 for **4**. The structures were solved by direct methods and refined by full-matrix least-squares method on F^2_{obs} with anisotropic thermal parameters for all non-hydrogen atoms using the SHELXTL-PC V 5.03 [38] software package. All hydrogen atoms in **1** and **2** were located by difference synthesis and refined isotropically, except hydrogen atoms of a water molecule in **2** and nine dpyam hydrogens in **1** which are geometrically fixed and allowed to ride on attached atoms. The methyl hydrogens of DMSO were not located but the bond parameters of DMSO are reasonable with average S–O and S–C distances of 1.563 and 1.663 Å, respectively. The molecular graphics were created by using SHELXTL-PC. The crystal and refinement details for complexes **1**–**4** are listed in Table 1. Selected bond lengths and angles are given in Tables 2–5. Figs. 1–4 illustrate the structures of complexes **1**–**4**, respectively, and the atom numbering scheme used.

3. Results and discussion

3.1. Structure of [Cu(dpyam)(NO$_2$)$_2$] (1)

The structure of **1** (Fig. 1) consists of a neutral [Cu(dpyam)(NO$_2$)$_2$] unit. The local molecular structure of the copper(II) ion involves a tetrahedrally-distorted elongated octahedral $CuN_2O_2O'_2$ chromophore. The dpyam ligand bonds symmetrically in-the-plane with Cu–N distances of 1.970(2) and 1.984(2) Å, and a N(1)–Cu–N(2) dpyam bite angle of 93.5(1)°. Two oxygen atoms from each nitrite group also bond in-the-plane with Cu–O distances of 1.984(2) and 2.012(2) Å, forming a markedly tetrahedral distorted square base with the dihedral angle of 38.6(1)° at which the N–Cu–N and O–Cu–O planes cross. The four N(1), N(2), O(2), O(3) basal donor atoms are out from their least-squares plane as 0.474(1), −0.472(1), −0.476(1), 0.475(1) Å, respectively. The second oxygen atom from each nitrite group are bent towards the Cu atom to complete the fifth and sixth coordination sites in the approximately axial positions at longer distances of 2.471(2) and 2.535(2) Å and with an O(1)–Cu–O(4) angle of 128.6(3)° which is markedly less than 180°, giving the extremely distorted octahedron.

There are no unusual bond lengths or bond angles in the dpyam ligand [39]. The separate pyridine rings are planar, (r.m.s.d. 0.003 and 0.005 Å) and the dihedral angle is 6.0(1)°. The nitrite ions show the expected geometry, with the longer N–O bonds involved in coordination with respect to the weakly coordinated N–O bonds (1.276(2) and 1.222(2) Å, and 1.267(2) and 1.230(2) Å, respectively, for both nitrite groups). However, the variations are less than that found in a purely monodentate nitrite (1.290 and 1.207 Å) [40]. In addition, the angles at the in-plane oxygen atoms [106.9(2)° and 109.4(2)°] are intermediate between the value of 119.5° in the monodentate nitrito-complex [40] and of 93°–100° in the bidentate nitrito-complex [41]. The angles at the nitrogen atoms of the nitrite groups

Table 1
Crystal and refinement data for complexes **1**, **2**, **3** and **4**

Complex	**1**	**2**	**3**	**4**
Molecular formulae	$[Cu(dpyam)(NO_2)_2]$	$[Cu(dpyam)(H_2O)_2(SO_4)]$	$[Cu(dpyam)_2(NCS)](SCN)\cdot 0.5DMSO$	$[Cu(dpyam)_2(SCN)_2]$
Molecular weight	326.73	366.78	561.15	522.09
T (K)	293(2)	293(2)	293(2)	293(2)
Crystal system	orthorhombic	monoclinic	triclinic	monoclinic
Space group	$Pca2_1$	Cc	$P\bar{1}$	$P2_1/c$
a (Å)	12.4083(3)	16.1695(8)	9.6326(2)	7.6835(2)
b (Å)	6.7322(2)	11.8116(6)	12.0156(2)	17.6246(4)
c (Å)	14.8457(2)	7.0266(4)	13.4225(2)	8.4275(2)
α (°)	90	90	68.29(2)	90
β (°)	90	99.53(2)	75.48(2)	102.58(2)
γ (°)	90	90	89.67(2)	90
V (Å^3)	1240.14(4)	1323.47(12)	1390.6(3)	1113.85(3)
Z	4	2	2	2
D_{calc} (g cm^{-3})	1.750	1.836	1.433	1.557
μ (mm^{-1})	1.783	1.840	1.044	1.197
$F(000)$	660	744	618	534
Crystal size (mm)	0.43 × 0.38 × 0.30	0.05 × 0.33 × 0.08	0.33 × 0.18 × 0.18	0.38 × 0.35 × 0.28
θ range (°)	2.74–30.47	2.15–30.45	1.69–30.51	2.73–30.36
Index ranges	$-14 \le h \le 17$, $-9 \le k \le 7$, $-20 \le l \le 21$	$-21 \le h \le 22$, $-16 \le k \le 11$, $-9 \le l \le 9$	$-8 \le h \le 13$, $-16 \le k \le 16$, $-18 \le l \le 19$	$-10 \le h \le 9$, $-24 \le k \le 23$, $-8 \le l \le 11$
Number of reflection collected	8559	4861	10279	8061
Number of unique reflections	3529	3327	7502	3191
Number of observed reflection	2843	2837	5879	2849
Absorption correction	Semi-empirical	Semi-empirical	Semi-empirical	Semi-empirical
T_{max} and T_{min}	1.0000, 0.7053	1.0000, 0.7234	1.0000–0.8057	1.0000–0.9085
Data/restraints/parameter	3529/1/217	3327/2/230	7502/0/380	3191/0/187
Goodness-of-fit	1.040	1.094	1.058	1.055
Final R indices [$I > 2\sigma(I)$]	$R_1 = 0.0320$, $wR_2 = 0.0632$	$R_1 = 0.0295$, $wR_2 = 0.0710$	$R_1 = 0.0595$, $wR_2 = 0.1857$	$R_1 = 0.0261$, $wR_2 = 0.0720$
R indices (all data)	$R_1 = 0.0484$, $wR_2 = 0.0703$	$R_1 = 0.0395$, $wR_2 = 0.0805$	$R_1 = 0.0764$, $wR_2 = 0.2045$	$R_1 = 0.0306$, $wR_2 = 0.0741$
Largest difference peak and hole (e Å^3)	0.226, −0.369	0.300, −0.408	1.353, −0.427	0.339, −0.400

Table 2
Selected bond lengths (Å) and angles (°) with e.s.d.s. in parentheses of $[Cu(dpyam)(NO_2)_2]$ (**1**)

Bond lengths			
Cu–N(1)	1.970(2)	Cu–N(2)	1.980(2)
Cu–O(3)	1.984(2)	Cu–O(2)	2.012(2)
Cu–O(1)	2.471(2)	Cu–O(4)	2.535(2)
O(1)–N(4)	1.222(2)	O(2)–N(4)	1.276(2)
O(3)–N(5)	1.267(2)	O(4)–N(5)	1.230(2)
Bond angles			
N(1)–Cu–N(2)	93.5(1)	N(1)–Cu–O(3)	152.3(1)
N(1)–Cu–O(2)	93.6(1)	N(1)–Cu–O(1)	111.9(2)
N(1)–Cu–O(4)	99.8(3)	N(2)–Cu–O(1)	98.5(3)
N(2)–Cu–O(3)	94.4(1)	N(2)–Cu–O(4)	119.4(2)
N(2)–Cu–O(2)	152.4(1)	O(2)–Cu–O(1)	54.2(2)
O(2)–Cu–O(3)	91.6(1)	O(2)–Cu–O(4)	85.5(2)
O(3)–Cu–O(1)	93.1(3)	O(3)–Cu–O(4)	53.5(2)
O(1)–Cu–O(4)	128.6(3)	O(1)–N(4)–O(2)	113.0(2)
O(3)–N(5)–O(4)	113.7(2)		

Table 3
Selected bond lengths (Å) and angles (°) with e.s.d.s. in parentheses of $[Cu(dpyam)(H_2O)_2(SO_4)]$ (**2**)

Bond lengths			
Cu–N(1)	2.011(8)	Cu–O(2)	2.012(7)
Cu–O(1)	1.999(6)	Cu–N(2)	2.015(7)
Cu–O(3)	2.482(9)	Cu–O(6′)	2.447(9)
S(1)–O(3)	1.448(9)	S(1)–O(4)	1.461(7)
S(1)–O(5)	1.512(7)	S(1)–O(6)	1.477(9)
Bond angles			
N(1)–Cu–O(2)	90.9(3)	N(1)–Cu–O(1)	168.2(3)
N(1)–Cu–N(2)	92.8(1)	N(1)–Cu–O(3)	101.0(3)
N(1)–Cu–O(6′)	85.5(2)	N(2)–Cu–O(2)	168.6(3)
N(2)–Cu–O(6′)	97.5(2)	N(2)–Cu–O(1)	91.9(3)
N(2)–Cu–O(3)	85.8(3)	O(1)–Cu–O(2)	86.5(1)
O(1)–Cu–O(3)	89.3(3)	O(1)–Cu–O(6′)	84.0(2)
O(2)–Cu–O(6′)	94.8(2)	O(2)–Cu–O(3)	81.6(3)
O(3)–Cu–O(6′)	172.5(4)	O(4)–S–O(5)	108.6(1)
O(4)–S–O(3)	107.9(6)	O(5)–S–O(3)	107.5(5)
O(5)–S–O(6)	112.8(6)	O(3)–S–O(6)	110.3(2)
O(4)–S–O(6)	109.7(5)		

Table 4
Selected bond lengths (Å) and angles (°) with e.s.d.s. in parentheses of $[Cu(dpyam)_2(NCS)](SCN)\cdot 0.5DMSO$ (**3**)

Bond lengths			
Cu–N(1)	2.017(3)	Cu–N(2)	1.997(3)
Cu–N(4)	2.017(3)	Cu–N(5)	2.164(3)
Cu–N(7)	1.976(4)		
Bond angles			
N(1)–Cu–N(2)	87.4(2)	N(1)–Cu–N(4)	90.5(2)
N(1)–Cu–N(5)	97.4(2)	N(1)–Cu–N(7)	158.6(2)
N(2)–Cu–N(4)	166.2(2)	N(2)–Cu–N(5)	104.9(2)
N(2)–Cu–N(7)	88.9(2)	N(4)–Cu–N(5)	88.9(2)
N(4)–Cu–N(7)	88.1(2)	N(5)–Cu–N(7)	103.9(2)

Table 5
Selected bond lengths (Å) and angles (°) with e.s.d.s. in parentheses of $[Cu(dpyam)_2(SCN)_2]$ (**4**)

Bond lengths			
Cu–N(1)	2.036(2)	Cu–N(2)	2.020(2)
Cu–S(1)	2.944(3)		
Bond angles			
N(1)–Cu–N(2)	93.8(2)	N(1A)–Cu–N(2)	86.2(2)
S(1)–Cu–N(1)	96.0(2)	S(1)–Cu–N(2)	87.8(2)
S(1)–Cu–N(1A)	84.0(2)	S(1)–Cu–N(2A)	92.2(2)
S(1)–Cu–S(1A)	180.0(3)	S(1A)–Cu–N(1)	84.0(2)
S(1A)–Cu–N(2)	92.2(2)	S(1A)–Cu–N(1A)	96.0(2)
S(1A)–Cu–N(2A)	87.8(2)		

Symmetry code: #1; $-x, -y+1, -z+1$.

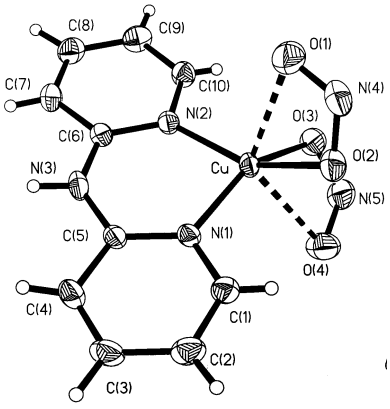


Fig. 1. The molecular structure of $[Cu(dpyam)(NO_2)_2]$ (**1**).

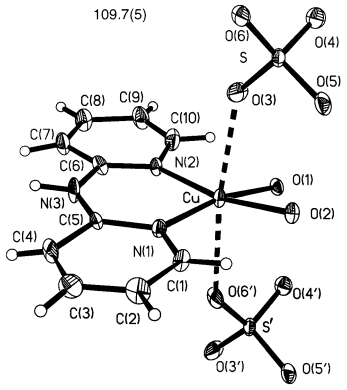


Fig. 2. The complex unit of $[Cu(dpyam)(H_2O)_2(SO_4)]$ (**2**).

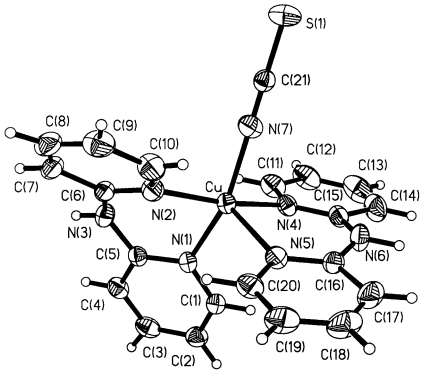


Fig. 3. The molecular structure of $[Cu(dpyam)_2(NCS)](SCN)\cdot 0.5DMSO$ (**3**).

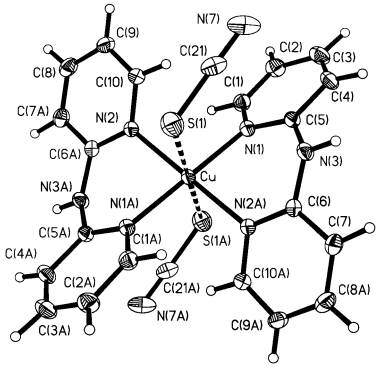


Fig. 4. The molecular structure of $[Cu(dpyam)_2(SCN)_2]$ (**4**).

[113.0(2)° and 113.7(2)°] are between that found in the purely monodentate nitrito-coordination (115.0°) [40] and the bidentate nitrito-coordination (111°–112°) [41,42]. Consequently, the coordination mode of the weakly coordinated oxygen atoms to the copper in **1** is intermediate between the purely monodentate nitrito-coordination [40] and the bidentate nitrito-coordination [41].

The coordination geometry of the nitrite groups in **1** is similar to that of the first previous reported isomer **4** [7]. The planes of the dinitrite groups in each complex are almost perpendicular to each other [87.0(3)° for **1** and 82.0(2)° for **4**]. In spite of the same composition of the orthorhombic system for both complexes, their local molecular geometries around the copper(II) ions are not comparable, with a slightly more elongated and asymmetric coordination in the axial positions for **1** [2.471 and 2.535 Å, $\Delta O = 0.068$ Å for **1**, and 2.431 and 2.469 Å, $\Delta O = 0.038$ Å for **4**]. Both complexes have significant differences in the tetrahedral twist of the basal plane [38.6(1)° in **1** and 31.2(2)° in **4**], the O(1)–Cu–O(4) angle [128.6(3)° in **1** and 133.7(2)° in **4**] and the dihedral angle

between pyridine rings [6.0(1)° in **1** and 25.6(2)° in **4**]. These cause differences in the electronic spectra of both complexes and these differences in the local molecular arrangements of **1** and **4** arise due to a difference of the packing forces in the lattices of both complexes. Another closely related complex is observed in the dimeric tetranitrito copper(II) complex, $[Cu(dpyam)(NO_2)_2]_2 \cdot 2CH_3CN$ [8] containing double bridges of asymmetrically-O-bridging nitrito groups and the asymmetrically-bidentate chelating nitrito ligands. The coordination around each copper atom in this compound is best described as tetrahedrally-distorted elongated octahedral with off-the-*z*-axis coordination in the axial positions rather than the distorted square pyramidal geometry described by the authors. The local molecular structure is comparable to those of **1** and **4** but with a larger O–Cu–O axial angle of 144.6(1)° and a reasonably lower tetrahedral twist [deviations of basal atoms from the mean plane: 0.209(3), 0.223(3), 0.557(5), 0.217(3)] [8]. The dihedral angle of 23.1(1)° between pyridine rings also corresponds to the lesser tetrahedral twist with respect to that of **1** (6.0°) and is not too different from that of **4** (25.6°).

The N–H groups [N(3)–H] of both complexes **1** and **4** are involved in intermolecular hydrogen bonds. In **1**, the N–H group is involved in a N–H···O hydrogen bonds with an oxygen atom of the nitrite (O(4)) group which is translated one unit cell along the '*c*' direction. Where as in **4**, it is involved in N–H···N hydrogen bond with the nitrite [N(4)] group of the molecule which is translated one unit cell along the '*a*' direction.

3.2. Structure of $[Cu(dpyam)(H_2O)_2(SO_4)]$ (2)

The asymmetric unit of **2** consists of the neutral $[Cu(dpyam)(H_2O)_2(SO_4)]$ complex unit. The local molecular structure of the copper(II) ions involves the six coordinate $CuN_2O_2O_2'$ chromophore, with elongated tetragonal octahedral stereochemistry (Fig. 2). The basal planes with four nearly equal short bonds involve two pyridyl nitrogen atoms from dpyam ligand [Cu–N, 2.011(8) and 2.015(7) Å] and two oxygen atoms from each water molecule [Cu–O, 2.012(7) and 1.999(6) Å]. These basal planes are linked into an infinite chain by the bidentate bridging sulfate group. The two donor atoms from the almost-symmetrically-bridging sulfate groups occupy axial positions above and below the CuN_2O_2 planes, with Cu–O distances of 2.447(9) and 2.482(9) Å, giving the tetragonality (T) of 0.815. The four in-plane ligand atoms are reasonably planar (r.m.s.d. = 0.195 Å), with a slight tetrahedral twist [dihedral angles between CuN_2 and CuO_2 planes = 15.8(1)°]. The axial O–Cu–O angle is 172.5(4)°. The separate pyridine rings are planar and the dpyam ligands as a whole are nearly planar [dihedral angle between pyridine rings is 3.5(2)°].

The S–O distances of the coordinated O atoms are shorter [1.448(9) and 1.477(9) Å] than those of the uncoordinated oxygen atoms [1.461(7) and 1.517(7) Å], except that of the coordinated S(1)–O(6) [1.477(9) Å]. However, the internal geometry of the sulfate anion is quite regular in spite of their coordinations. Both the bond distances and angles are not too different and are within the range for ionic sulfate [43]. The six O–S–O angles vary from 107.5° to 112.8°. These deviations may be due to the hydrogen-bonding network involving all water molecules, non-coordinated sulfate oxygen atoms and the dpyam amino groups.

The structure of **2** is comparable to those of $[Cu(en)(H_2O)_2(SO_4)]$ [18] and $[Cu(bpy)(H_2O)_2(SO_4)]$ [19], all of which involve polymeric chain structures with bidentate bridging sulfate groups. However, they differ from the square pyramidal monomeric complex, $[Cu(tmen)(H_2O)_2(SO_4)] \cdot H_2O$ [17] in which the coordination geometry (4+1) around copper consists of a water molecule at the apex and four base sites occupied by two nitrogen atoms from the chelated diamine and two oxygen atoms from a monodentate sulfate and a second water molecule. In comparison to the copper(II) complexes with the divalent carbonate anion, they exhibit the marked difference both in the nature of coordinating and bridging modes between the carbonate and sulfate anions, and the local molecular geometries [15,16,20]. However, the structure of **2** with the divalent bidentate bridging sulfate group is similar to those of complexes with monovalent oxyanions, $[Cu(dpyam)(NO_3)_2]$ [10], $[Cu(dpyam)(O_2CCH_3)(ClO_4)]$ [11], $[Cu(dpyam)(O_2CCH_3)(NO_3)]$ [12] and $[Cu(dpyam)(O_2CCH_2CH_3)(NO_3)]$ [13], all of which involve polymeric chain structures with bidentate bridging nitrate or perchlorate groups.

3.3. Structure of $[Cu(dpyam)_2(NCS)](SCN) \cdot 0.5DMSO$ (3)

The asymmetric unit of **3** consists of a $[Cu(dpyam)_2(NCS)]^+$ cation, a thiocyanate ion and a half molecule of disordered, non-coordinated dimethylsulfoxide. The cation involves a five coordinate CuN_4N' chromophore, with an approximately trigonal bipyramidal stereochemistry, Fig. 3 [21]. The out-of-plane bond lengths, Cu–N(2) and Cu–N(4), are not significant different, with values of 1.997(3) and 2.017(3) Å. The in-plane bond lengths, Cu–N(1), Cu–N(7) and Cu–N(5), are significantly different, with values of 2.017(3), 1.976(4) and 2.164(3) Å, respectively. The N(1,2) dpyam ligand is thus nearly symmetrically coordinated, but the N(4,5) dpyam ligand is very asymmetrically coordinated. The CuN_4N' chromophore stereochemistry is distorted from regular trigonal pyramidal. The N(2)–Cu–N(4) (α_8) angle of 166.2(1)° is significantly different from 180° and is distorted away from the Cu–N(7) direction [44].

The in-plane angles, N(1)–Cu–N(7) (α_1), N(5)–Cu–N(7) (α_2) and N(1)–Cu–N(5) (α_3), are all significantly different from 120°, namely 158.6(2)°, 103.9(1)° and 97.4(1)°, respectively.

The largest in-plane angle of 158.6(2)° lies opposite the longest in-plane bond length, namely, the Cu–N(5) bond. This could be taken as the basal angle of a square-based pyramidal stereochemistry with elongation in the Cu–N(5) direction. The τ-value defined to describe the degree of trigonal distortion is 0.13 $\{\tau = (\alpha_8 - \alpha_1)/60\}$ [25]. As the regular trigonal bipyramid and square-based pyramid have τ values of 1.00 and 0.00, respectively, the stereochemistry of the CuN_4N' chromophore of **3** is best described as square-based pyramidal, with a slight trigonal distortion, rather than square pyramidal distorted trigonal bipyramidal [44]. The Cu(II) ion is displaced 0.31 Å from the N(1), N(2), N(4), N(7) basal plane. There are unusual bond lengths and bond angles in the coordination of the dpyam ligands [39]. The dihedral angles between the pyridine rings within the same dpyam ligand, are 31.1(1)° and 11.5(3)° and the N–Cu–N bite angles of the N(1,2) and N(4,5) dpyam ligands are 87.4(1)° and 88.9(2)°, respectively. The full mean planes of the dpyam ligands are inclined to each other at 62.3(1)°.

The non-coordinated thiocyanate group is well-ordered with C–N and C–S distances of 1.168(9) and 1.620(7) Å, compared with the coordinated isothiocyanato moiety C–N and C–S distances of 1.157(5) and 1.622(4) Å, respectively. Those of the isothiocyanato group are comparable to those reported for $[Cu(phen)_2(NCS)](ClO_4)$ (1.138 and 1.629 Å, respectively) [26a]. The crystal structure is stabilized by cooperative hydrogen bonds N–H···O (DMSO) and N–H···N (NCS counterion).

The τ-value of 0.13 for the trigonal bipyramidal distorted square-based pyramidal (TBDSBP) CuN_4N' chromophore of **3** is the lowest value found in the five-coordinated bis(dpyam)copper(II) complexes known to date. Most close geometries are the chromophores of $[Cu(dpyam)_2(NCS)]^+$ cation ($\tau = 0.18$) [33], $[Cu(dpyam)_2Cl]Cl\cdot 4H_2O$ ($\tau = 0.25$) [30], $[Cu(dpyam)_2(NCO)]_2(SO_4)(dpyam)_2\cdot H_2O$ ($\tau = 0.30$) [28] and $[Cu(dpyam)_2Cl]_2I_2\cdot 2CH_3CN$ ($\tau = 0.32$) [29]. The geometry of the last compound should be TBDSBP rather than distorted trigonal bipyramidal as previously reported [29]. In the corresponding compounds $[Cu(dpyam)_2Cl]Cl$ ($\tau = 0.57$) [32] and $[Cu(dpyam)_2I]_2I(ClO_4)$ ($\tau = 0.63$ and 0.65) [31] the trigonal bipyramidal geometry is considerably more pronounced, giving the square-based pyramidal distorted trigonal bipyramidal (SBPDTB) stereochemistry. There is a substantial number of monomeric five-coordinated $[Cu(bpy \text{ or } phen)_2X]^+$ complexes with coordination geometries ranging from TBDSBP ($\tau = 0.19$–0.22) to SBPDTB ($\tau = 0.56$–0.80) and to near regular trigonal bipyramidal (RTB) ($\tau > 0.80$–1.00) [25]. These series of cation distortion isomers have been used to suggest a structural pathway from a RTB ($\tau = 1.0$) to distorted square-based pyramidal ($\tau = 0.0$) stereochemistry [25] and suggest that **3** forms a point in a most extensive ($\tau = 0.13$) structural pathway for the CuN_4N' chromophore.

Most of the complexes of the bpy or phen ligand mentioned above have geometries ranging from SBPDTB to near RTB ($\tau \approx 0.6$–1.0). Only two complexes have very close to TBDSBP geometry, namely, $[Cu(phen)_2Cl](BPh_4)$ ($\tau = 0.19$) [25b] and $[Cu(phen)_2Br](BPh_4)$ ($\tau = 0.22$) [25d]. The more closely related CuN_4N' chromophores from these complexes also involve the above geometric range, e.g. $[Cu(bpy)_2(NCS)](NO_3)$ ($\tau = 0.89$) [45], $[Cu(bpy)_2(NCS)](NCS)$ ($\tau = 0.65$) [46], $[Cu(bpy)_2(NCS)](BF_4)$ ($\tau = 0.61$) [47], $[Cu(bpy)_2(NH_3)](BF_4)_2$ ($\tau = 0.77$) [48] and $[Cu(phen)_2(NCS)](ClO_4)$ ($\tau = 0.81$) [26a]. It thus appears that the near RSBP and TBDSBP geometries may be better attained with di-2-pyridylamine as ligands.

3.4. Structure of $[Cu(dpyam)_2(SCN)_2]$ (4)

The complex **4** involves an elongated centrosymmetric octahedral geometry of the six-coordinate CuN_4S_2 chromophore of a neutral $[Cu(dpyam)_2(SCN)_2]$ unit. The copper ion is equatorially bonded to two bidentate dpyam ligands [Cu–N = 2.020(1) and 2.036(1) Å] and axially, weakly bonded to the thiocyanato group (S-bonded) [Cu–S = 2.944(1) Å] giving an elongated tetragonal octahedral stereochemistry with the tetragonality (T = mean in-plane Cu–N distance/mean out-of-plane Cu–S distance) of 0.69. The basal CuN_4 plane is exactly planar, attributed to the large dihedral angle of 41.8(1)° between the pyridine rings of the dpyam ligand. The N–Cu–N bite angle of the dpyam ligands is 86.2(1)°.

The coordination chemistry of the thiocyanato group (S-bonded) in the six-coordinate complex **4** differs from those of the five-coordinate complexes $[Cu(bpy)_2(NCS)]Y$, $Y = SCN^-$ [46], NO_3^- [45] and BF_4^- [47], $[Cu(phen)_2(NCS)](ClO_4)$ [26a], $[Cu(dpyam)_2(NCO)](SO_4)_{0.5}\cdot dpyam\cdot(H_2O)_{0.5}$ [28] and the present complex **3**, involving the isothiocyanato or isocyanato coordination (N-bonded). The five-coordinate and six-coordinate complex units, $[Cu(dpyam)_2(NCS)]^+$ and $[Cu(dpyam)_2(NCS)_2]$, respectively, of the compound $[Cu(dpyam)_2(NCS)_{1.5}(ClO_4)_{0.5}][Cu(dpyam)_2(NCS)]_2(ClO_4)_2$ [33] also involve the N-bonded isothiocyanato group. Hence, complex **4** is rare example involving the S-bonded SCN^- group as in general, Class A metals (first transition series) form M–N bonds, whereas Class B metals form M–S bonds [23,24,25a,25b]. This could be understood as the S-bonded coordination mode in **4** give rises to the N–H···N (NCS) hydrogen bonds in order to stabilize the crystal structure.

The elongated centrosymmetric octahedral geometry found in **4** ($T = 0.69$) has also been observed in the $[Cu(dpa)_2]X_2$ (X = *O*-tricyanoethyleneoate) [49], $[Cu(dpyam)_2(NCS)_2]$ ($T = 0.83$) [33] and $[Cu(dpyam)_2(OH_2)_2](PF_6)_2$ ($T = 0.82$) [27a] complex units and complexes $[Cu(dpyam)_2(NO_3)_2]$ ($T = 0.81$) [33], $[Cu(dpyam)_2(Br)_2]\cdot 2H_2O$ ($T = 0.65$) [29] and $[Cu(dpyam)_2(OH_2)_2](SO_4)\cdot 7H_2O$ ($T = 0.81, 0.82$) [50]. The complexes $[Cu(dpyam)_2(CF_3SO_3)_2]$ ($T = 0.81$) [27a] and $[Cu(dpyam)_2(OH_2)_2](S_4O_6)$ ($T = 0.82$) [27a], which are although not centrosymmetric, also have structures similar to the above complexes. The equatorial Cu–N distances in these complexes range from 1.983 to 2.047 Å. The planar equatorial CuN_4 plane is only possible because of the flexibility of the dpyam ligands. This results in a great range of values of the dihedral angles between the pyridine rings, which are comparable for all complexes (35.6°–46.5°). The N–Cu–N bite angles within these complexes are also comparable (85.3°–86.4°). An analogous coordination geometry has not been found in complexes with the less flexible bpy and phen ligands. Complexes $[Cu(bpy)_2(O_2ClO_2)](ClO_4)$ [50] and $[Cu(bpy)_2(F_2BF_2)](BF_4)$ [50] although involving the six-coordinated elongated octahedral chain structure are not centrosymmetric and involve a strong tetrahedral distortion (dihedral angles = 37.9° and 44.6°, respectively). The coordination geometries in $[Cu(bpy)_2(NO_3)](NO_3)\cdot H_2O$ [51] and $[Cu(phen)_2Br]Br\cdot 2H_2O$ [52] are totally different from those of the closely related dpyam complexes $[Cu(dpyam)_2(NO_3)_2]$ [33] and $[Cu(dpyam)_2Br_2]\cdot 2H_2O$ [29], respectively. The former involves a distorted bicapped square pyramidal geometry of the CuN_4OO' chromophore with a marked asymmetric bidentate coordination of the nitrato group while the latter involves the five-coordinate CuN_4Br complex of the near RTB geometry with a slight distortion towards the square-based pyramidal geometry ($\tau = 0.87$). Hence, the analogous coordination geometry has not been found in complexes with the less flexible bpy or phen ligand. These observations demonstrate a noticeable difference between the chelate functions of bpy or phen and the more flexible dpyam ligand.

3.5. ESR spectra

The polycrystalline ESR spectrum of **3** is axial with $g_{//} \gg g_{\perp} > 2.0 = 2.310 \gg 2.054 > 2.0$, consistent with a $d_{x^2-y^2}$ ground state for the distorted square-based pyramidal geometry of the CuN_4N' chromophore [21]. This type of ESR spectrum is similar to those of **1**, **2** and **4** which also are of the axial type, consistent with a $d_{x^2-y^2}$ ground state for the tetrahedrally-distorted elongated tetragonal octahedral geometry with off-the-*z*-axis coordination in the axial positions of **1** and the elongated tetragonal octahedral stereochemistry of **2** and **4**.

3.6. Electronic and IR spectra

The significant crystallographic differences between **1** and **5** are reflected in their color (bright green for **1** and dark green for **5**) and their electronic spectra. The electronic reflectance spectra of **1** and **5** involve a broad peak ranging from 11 500 to 13 500 cm^{-1} (centered at ca. 12 500 cm^{-1}) for **1** and 13 300 to 14 400 cm^{-1} (centered at ca. 13 890 cm^{-1}) for **5**. The lower frequencies in electronic spectrum of **1** are consistent with the higher tetrahedral twist of the equatorial plane in **1** compared with **5** [7]. The most relevant feature of the IR spectra in complexes **1** and **2** is the evidence for the coordination of the nitrite and sulfate anions, respectively. As some interest regions are obscured by absorption peaks deriving from dpyam, the precise assignment, which we have usually made, is by comparison with the prepared $[Cu(dpyam)_2Cl]Cl$ complex. The IR spectrum of **1** shows two strong bands at 1370 and 1140 cm^{-1} and a medium peak at 860 cm^{-1} corresponding to the $\nu_{as}(NO_2)$, $\nu_s(NO_2)$ and $\delta(NO_2)$ absorption bands, respectively [1,7,53]. The latter appears to be superimposed on a weak intensity dpyam peak. The IR spectrum of the present batch of **5** has peaks at 1365, 1180 and 860 cm^{-1} for $\nu_{as}(NO_2)$, $\nu_s(NO_2)$ and $\delta(NO_2)$, respectively [7] in which the latter two peaks are superimposed on the lower intensity dpyam peaks.

The light green complex **2** exhibits a single broad band at 13 700 cm^{-1} with a poorly resolved shoulder at 10 260 cm^{-1}. The local molecular geometry around the copper(II) ion in **2** is very comparable to that of the relevant polymeric chain complex, $[Cu(dpyam)(NO_3)_2]$ involving the monovalent nitrate oxyanions [10], but with a higher tetrahedral twist (15.8° in **2**) than the dinitrate complex (7.0° and 3.8° for both units). Consequently, complex **2** exhibits lower energies in the electronic spectrum than the dinitrate complex. The higher tetrahedral twist of the basal planes results in the smaller dihedral angle between the pyridine rings [3.5° in **2**, and 10.0° and 6.1° in the dinitrate complex]. The IR spectrum of **2** shows a strong band (ν_3) splitting into 1160, 1140 and 1115 cm^{-1} and a medium band (ν_4) at 619 cm^{-1} attributed to the coordinated sulfate group [1,19].

The polycrystalline electronic reflectance spectrum of **3** shows a high-energy peak at 15 740 cm^{-1}, with a low-energy peak at lower intensity at 10 660 cm^{-1}, consistent with the near RSBP with a slight trigonal distortion of **3** ($\tau = 0.13$) [25], and similar to that of the closely related CuN_4N' chromophore in $[Cu(dpyam)_2(NCO)]_2(SO_4)\cdot(dpyam)_2\cdot H_2O$ (14 230 and 10 630 cm^{-1}) ($\tau = 0.30$) [28]. The IR spectrum of **3** shows a strong band ($\nu_{as}(CN)$) splitting into three bands at 2100, 2080 and 2055 cm^{-1}, several weak bands ($\nu_s(CS)$) at 820, 795, 745 cm^{-1} and several weak bands ($\delta(NCS)$) at 485, 475 and 470 cm^{-1}. The splitting into several peaks of the

frequencies in **3** could imply two distinct crystallographic sites of a coordinated isothiocyanate group and a free thiocyanate anion. The bands at 2055(ν_{as}(CN)), 745(ν_s(CS)) and 485(δ(NCS)) cm^{-1} may be attributed to the free ligand [43a]. However, the ν_s(CS) and δ(NCS) bands are rather weak and some are partially obscured by the presence of the dpyam ligand in the same region. Hence the ν_{as}(CN) frequencies are used as a criteria to determine the bonding type of the SCN^- group, which are generally lower in N-bonded complexes than S-bonded complexes [43a].

The electronic spectrum of **4** involves an asymmetric broad peak occurring at 16 700 cm^{-1} with some evidence for a possible low-energy shoulder at approximately 14 080 cm^{-1}, consistent with its stereochemistry, and similar to those of the comparable structures in $[Cu(dpyam)_2X_2]$, $X = Br^- \cdot 2H_2O$ (17 200 cm^{-1}) [27b], $CF_3SO_3^-$ (18 120, 15 430(sh) cm^{-1}) [27a], NO_3^- (17 870, 14 700(sh) cm^{-1}) [24,27b]. That of the most similar complex $[Cu(dpyam)_2Br_2]\cdot 2H_2O$ (**6**) prepared in the present work also shows an asymmetric broad peak at 16 790 cm^{-1} with some evidence for a low-energy shoulder at approximately 14 170 cm^{-1}. The suggested one-electron ground state configuration is $d_{x^2-y^2} > d_{z^2} > d_{xy} > d_{xz} \approx d_{yz}$ for the complexes. For complexes **2**–**4**, the transitions may be assigned as the $d_{z^2} \rightarrow d_{x^2-y^2}$ transition for the low-energy peak and the d_{xz}, $d_{yz} \rightarrow d_{x^2-y^2}$ transition for the high-energy peak, with the position of the $d_{xy} \rightarrow d_{x^2-y^2}$ transition being uncertain. The single broad peak in **1** may be assigned as the d_{z^2}, d_{xy}, d_{xz}, $d_{yz} \rightarrow d_{x^2-y^2}$ transition. The IR spectrum of **4** appears as a strong band (ν_{as}(CN)) splitting into two peaks at 2140 and 2110 cm^{-1} and two weak bands at approximately 810–790 (ν_s(CS)) and 470 (δ(NCS)) cm^{-1}, corresponding to the S-bonded thiocyanato groups in **4**.

While this paper was accepted, we noted that the structure of $[Cu(dpyam)_2(SCN)_2]$ (**4**) has been published as a short communication in *Acta Chem. Scand.* (1999) 53, 634. This is to indicate the duplication of the structure **4**.

4. Supplementary material

Crystallographic data for the structures in this paper have been deposited with the Cambridge Crystallographic Data Centre as supplementary publication no. CCDC No. 168990, 168991, 169167 and 169168 for structures **1**–**4**, respectively. Copies of the data can be obtained free of charge from The Director, CCDC, 12 Union Road, Cambridge CB2 1EZ, UK (fax: +44-1223-336033; e-mail: deposit@ccdc.cam.ac.uk www: http://www.ccdc.cam.ac.uk).

Acknowledgements

The authors would like to thank the National Research Council of Thailand and Khon Kaen University for a research grant. Support of the Postgraduate Education and Research Program in Chemistry is also gratefully acknowledged.

References

[1] I.M. Procter, B.J. Hathaway, P.G. Hodgson, Inorg. Nucl. Chem. 34 (1972) 3689.
[2] S.F. Pavkovic, D. Miller, Acta Crystallogr., Sect. B 33 (1977) 2894.
[3] D.L. Lewis, D.J. Hodgson, Inorg. Chem. 12 (1973) 2935.
[4] F.S. Stephens, J. Chem. Soc., Sect. A (1969) 2081.
[5] M.C. Munoz, J.M. Lazaro, J. Faus, M. Julve, Acta Crystallogr., Sect. C 49 (1993) 1756.
[6] S. Youngme, C. Pakawatchai, H.K. Fun, K. Chinnakali, Acta Crystallogr., Sect. C 54 (1998) 1586.
[7] S. Youngme, S. Tonpho, K. Chinnakali, S. Chantrapromma, H.K. Fun, Polyhedron 18 (1999) 851.
[8] A. Camus, N. Marsich, A.M.M. Lanfredi, F. Ugozzoli, C. Massera, Inorg. Chim. Acta 309 (2000) 1.
[9] A. Tadsanaprasittipol, H.B. Kraatz, G.D. Enright, Inorg. Chim. Acta 278 (1998) 143.
[10] S. Youngme, N. Chaichit, K. Damnatara, Polyhedron 21 (2002) 943.
[11] N. Ray, S. Tyagi, B.J. Hathaway, Acta Crystallogr., Sect. B 38 (1982) 1574.
[12] S. Aduldecha, B.J. Hathaway, Acta Crystallogr., Sect. C 47 (1991) 84.
[13] S. Youngme, C. Pakawatchai, H.K. Fun, Acta Crystallogr., Sect. C 54 (1998) 451.
[14] S. Youngme, W. Somjitsripunya, K. Chinnakali, S. Chantrapromma, H.K. Fun, Polyhedron 18 (1999) 857.
[15] P. Akhter, P. Fitzsimons, B. Hathaway, Acta Crystallogr., Sect. C 47 (1991) 308.
[16] J. Sletten, Acta Chem. Scand., Sect. A 38 (1984) 491.
[17] J. Balvich, K.P. Fivizzani, S.F. Pavkovic, J.N. Brown, Inorg. Chem. 15 (1976) 71.
[18] M. Dunai-Jurio, M.A. Porai-Koshits, Chem. Zvesti 20 (1966) 783.
[19] J.C. Tedenac, N.D. Phung, C. Avinens, M. Maurin, Inorg. Nucl. Chem. 38 (1976) 85.
[20] S. Youngme, N. Chaichit, P. Kongsaeree, G.A. van Albada, J. Reedijk, Inorg. Chim. Acta 20 (2001) 232.
[21] B.J. Hathaway, Comprehensive coordination chemistry, in: G. Wilkinson, R.D. Gillard, J.A. McCleverty (Eds.), The Synthesis, Reactions, Properties and Applications of Coordination Compounds, vol. 5 (Section 53), Pergamon Press, Oxford, 1987, pp. 533–774.
[22] C.J. Simmons, B.J. Hathaway, K. Amornjarusiri, B.D. Santarsiero, A. Clearfield, J. Am. Chem. Soc. 109 (1987) 1947 (And references therein).
[23] W. Fitzgerald, B.J. Hathaway, C.J. Simmons, J. Chem. Soc., Dalton Trans. (1985) 141.
[24] S. Youngme, K. Poopasit, K. Chinnakali, S. Chantrapromma, H.K. Fun, Inorg. Chim. Acta 292 (1999) 57 (and references therein).
[25] (a) G. Murphy, C. Murphy, B. Murphy, B.J. Hathaway, J. Chem. Soc., Dalton Trans. (1997) 2653;
(b) G. Murphy, P. Nagle, B. Murphy, B.J. Hathaway, J. Chem. Soc., Dalton Trans. (1997) 2645;
(c) P. Nagle, E. O'Sullivan, B.J. Hathaway, J. Chem. Soc., Dalton

Trans. (1990) 3399;
(d) G. Murphy, C. O'Sullivan, B. Murphy, B.J. Hathaway, Inorg. Chem. 37 (1998) 240.
[26] O.J. Parker, J.L. Manson, G.L. Breneman, Acta Crystallogr., Sect. C 50 (1994) 1201.
[27a] S. Youngme, N. Chaichit, Polyhedron 21 (2001) 247.
[27b] J.C. Lancaster, W.R. McWhinnie, P.L. Welham, J. Chem. Soc., Sect. A (1971) 1742.
[28] P. Akhter, B.J. Hathaway, Acta Crystallogr., Sect. C 47 (1991) 86.
[29] A. Camus, A. Facchinetti, N. Marsich, A.M.M. Lanfredi, F. Ugozzoli, Inorg. Chim. Acta 290 (1999) 180.
[30] W.P. Jensen, R.A. Jacobson, Inorg. Chim. Acta 49 (1981) 199.
[31] J.E. Johnson, R.A. Jacobson, J. Chem. Soc., Dalton Trans. (1973) 580.
[32] R.A. Jacobson, W.P. Jensen, Inorg. Chim. Acta 114 (1986) L9.
[33] (a) J. Sletten, K. Svardal, A. Sϕrensen, Acta Chem. Scand. 47 (1993) 1091;
(b) J.E. Johnson, R.A. Jacobson, Am. Cryst. Assn. Abstr. (1971).
[34] S. Aduldecha, M.E. Keniry, P. Akhter, S. Tyagi, B.J. Hathaway, Acta Crystallogr., Sect. C 47 (1991) 1378.
[35] S. Youngme, C. Pakawatchai, W. Somjitsripunya, S. Chantrapromma, K. Chinnakali, H.K. Fun, Inorg. Chim. Acta 303 (2000) 181.
[36] Siemens SAINT, Version4, Software Reference Manual, Siemens Analytical X-Ray Systems, Inc., Madison, WI, USA, 1996.
[37] G.M. Sheldrick, SADABS, Program for Empirical Absorption correction of Area Dectector Data, University of Göttingen, Germany, 1996.
[38] Siemens SHELXTL, Version 5, Reference Manual, Siemens Analytical X-Ray Systems, Inc., Madison, WI, USA, 1996.
[39] N. Ray, B.J. Hathaway, Acta Crystallogr., Sect. B 34 (1978) 3324.
[40] M.G.B. Drew, D.M.L. Goodgame, M.A. Hitchman, D. Rogers, Proc. Chem. Soc. (1964) 363.
[41] I.M. Procter, F.S. Stephans, J. Chem. Soc., Sect. A (1969) 1248.
[42] M.G.B. Drew, D. Rogers, Chem. Commun. (1965) 476.
[43] (a) K. Nakamoto, Infrared and Raman Spectra of Inorganic and Coordination Compounds, fourth ed., Wiley, New York, 1986;
(b) Y. Iitaka, K. Shimizu, T. Kwan, Acta Crystallogr. 20 (1966) 803.
[44] W.D. Harrison, D.M. Kennedy, M. Power, R. Sheahan, B.J. Hathaway, J. Chem. Soc., Dalton Trans. (1981) 1556.
[45] V. Manriquez, I. Brito, C. Andrade, O. von Wittke, H.G. Schnering, K. Peters, Acta Crystallogr., Sect. C 44 (1988) 1191.
[46] A. Sedov, J. Kozisek, M. Dunaj Jurco Kabesová, J. Gazo, J. Garaj, Inorg. Chim. Acta 75 (1983) 73.
[47] S. Tyagi, B.J. Hathaway, J. Chem. Soc., Dalton Trans. (1981) 2029.
[48] F.S. Stephens, J. Chem. Soc., Dalton Trans. (1972) 1350.
[49] C.C. Fuller, R.A. Jacobson, Inorg. Chim. Acta 48 (1981) 191.
[50] J. Foley, D. Kennefick, D. Phelan, S. Tyagi, B.J. Hathaway, J. Chem. Soc., Dalton Trans. (1983) 2333.
[51] R.J. Fereday, P. Hodgson, S. Tyagi, B.J. Hathaway, J. Chem. Soc., Dalton Trans. (1981) 2070.
[52] G. Murphy, C. O'Sullivan, B. Murphy, B.J. Hathaway, Inorg. Chem. 37 (1998) 240.
[53] (a) R.T. Stibrany, J.A. Potenza, H.J. Schugar, Inorg. Chim. Acta 243 (1996) 33;
(b) M.A. Hitchman, G.L. Rowbottom, Coord. Chem. Rev. 42 (1982) 55.

PERGAMON

Polyhedron 21 (2002) 1289–1297

POLYHEDRON

www.elsevier.com/locate/poly

Synthesis and physical and structural characterization of Ag(I) complexes supported by non-fluorinated β-diketonate and related ancillary ligands

Silvana C. Ngo, Kulbinder K. Banger, Paul J. Toscano *, John T. Welch *

Department of Chemistry and NYS Center for Advanced Thin Film Technology, The University at Albany, State University of New York, 1400 Washington Ave., Albany, NY 12222, USA

Received 9 January 2002; accepted 21 March 2002

Abstract

A series of Ag(I) complexes, [Ag(X)L], where X is the anion of 2,2,6,6-tetramethyl-3,5-heptanedione (tmhdH), 2,2,7-trimethyl-3,5-octanedione (tmodH), 2-sila-2,2,6,6-tetramethyl-3,5- heptanedione (tmshdH), 5-mercapto-2,2,6,6-tetramethyl-4-hepten-3-one (*S*-tmhdH), 5-mercapto-2,2,7-trimethyl-4-octen-3-one (*S*-tmodH), or 5-amino-2,2,6,6-tetramethyl-4-hepten-3-one (*N*-tmhdH) and L = triphenylphosphine (PPh_3) or tri-*n*-butylphosphine (PBu_3), were prepared by treatment of silver nitrate with either the diketone derivative in the presence of a base or with the preformed sodium salt of the diketone derivative. The thermal properties of the new complexes were investigated for potential application in chemical vapor deposition (CVD) processes. Results of thermogravimetric analysis showed that the vast majority of the silver complexes have little promise for CVD, since the ligands dissociate at elevated temperatures without volatilization. The first ever reported single crystal X-ray diffraction studies of silver complexes, with simple, ancillary, non-fluorinated β-diketonate supporting ligands, revealed [Ag(tmhd)(PPh_3)] (**1a**) to be monomeric and [Ag(*S*-tmhd)(PPh_3)]$_2$ (**4a**) to be dimeric in the solid state, respectively. © 2002 Elsevier Science Ltd. All rights reserved.

Keywords: Silver(I) complexes; Non-fluorinated β-diketonate ligands; Monothio-β-ketonate; β-Ketoiminate; Chemical vapor deposition; Crystal structures

1. Introduction

Currently, there is ongoing interest in the search for electroluminescent materials. Applications range from lighting appliances, such as fluorescent tubes, to display apparatus such as cathode ray tubes or projection television [1]. One of the most rapidly advancing and growing areas is the development of thin film electroluminescent displays. Inorganic phosphor materials currently are widely used in these applications, while research on organic phosphors is ongoing [2]. The most commonly employed phosphor, the ZnS–Mn with SrS–Ce combination, generates red and green output by filtering the yellow emission from the ZnS–Mn couple while the SrS–Ce couple provides a bluish green light [3]. Unfortunately, the SrS–Ce couple is only a weak blue emitter and as such, a need remains for the development of brighter blue sources. Recent work suggests SrS–Cu is a suitable alternative, with a good blue emission with CIE color coordinates of $x = 0.15$ and $y = 0.23$ [3,4]. Codoping of the SrS–Cu couple with Ag gave an even truer blue color with $CIE_x = 0.17$, $CIE_y = 0.13$ [3,5]. However, the strategy for silver doping is currently limited by a lack of suitable volatile silver-containing precursors.

One of the techniques for preparation of thin films of these phosphors is metallo-organic chemical vapor deposition (MOCVD). As such, precursor volatility and stability are important issues for doping strategy. Research on the preparation of stable, yet volatile, complexes is central to the development of new, more efficient MOCVD precursors.

β-Diketonates and allied derivatives are among the most common ancillary ligand types for the preparation

* Corresponding authors. Tel.: +1-518-442-3127; fax: +1-518-442-3462.

E-mail addresses: ptoscano@csc.albany.edu (P.J. Toscano), jwelch@uamail.albany.edu (J.T. Welch).

0277-5387/02/$ - see front matter © 2002 Elsevier Science Ltd. All rights reserved.
PII: S0277-5387(02)00980-4

of MOCVD precursors. Structural variations of the supporting β-diketonate ligand can impart desired chemical and physical properties to the precursor complex as well as modulate the volatility. Introduction of a second, supporting ligand in a ternary complex can have complementary effects, while improving the stability of the complex. Combination of both strategies clearly can lead to highly desirable enhancements in performance for MOCVD.

Previously, the preparation of silver β-diketonate complexes for use in MOCVD have focused on fluorinated β-diketonate ligands, such as hfac (anion of 1,1,1,5,5,5-hexafluoro-2,4-pentanedione) and fod (anion of 2,2-dimethyl-6,6,7,7,8,8,8-heptafluoro-3,5-octanedione) [6]. While these ligands impart volatility to the Ag complexes, a crucial property for applications in MOCVD, fluoride ion contamination in the resultant films is frequently observed. The initial aim of the present study was to investigate alternatives to the use of fluorinated silver β-diketonates for MOCVD applications. Although there were some previous studies that indicated that silver complexes containing non-fluorinated β-diketonate ligands had limited volatility [7], we decided to explore a much wider range of structural alterations to the β-diketonate backbone, including unsymmetrically substituted ligands, as well as those in which silylated substituents were incorporated or in which an oxygen donor atom was replaced by sulfur [8] or imino nitrogen [9]. The replacement of one of the oxygen donor atoms of the β-diketonate was investigated, since such ancillary ligands might facilitate reduction of oxygen contamination, which accompanies the MOCVD processing of silver β-diketonates. We report here the synthesis and physical characterization of a series of binary and ternary silver complexes, [Ag(X)] and [Ag(X)L], where X is the anion of 2,2,6,6-tetramethyl-3,5-heptanedione (tmhdH), 2,2,7-trimethyl-3,5-octanedione (tmodH), 2,2,6,6-tetramethyl-2-sila-3,5-heptanedione (tmshdH), 5-mercapto-2,2,6,6-tetramethyl-4-hepten-3-one (*S*-tmhdH), 5-mercapto-2,2,7-trimethyl-4-octen-3-one (*S*-tmodH), or 5-amino-2,2,6,6-tetramethyl-4-hepten-3-one (*N*-tmhdH) and L is triphenylphosphine (PPh_3) or tri-*n*-butylphosphine (PBu_3). We also present structural results on the first two non-fluorinated β-diketonate silver complexes characterized by single crystal X-ray diffraction.

2. Experimental

2.1. Materials and physical measurements

Unless otherwise noted, all experiments were performed under an inert atmosphere of nitrogen utilizing standard Schlenk techniques or in a Vacuum Atmospheres drybox filled with nitrogen. Reagents and solvents obtained commercially were of reagent grade and used as received unless otherwise noted. Tetrahydrofuran (thf), toluene, and anhydrous diethyl ether (Et_2O) were distilled from sodium–benzophenone ketyl under nitrogen. Pentane and hexane were distilled from sodium–benzophenone–diglyme under nitrogen. The β-diketone tmshdH was prepared according to our procedure [10], while tmodH was made analogously by condensing 3-methylbutyryl chloride with pinacolone in the presence of lithium diisopropylamide. The heteroatom substituted β-diketone derivatives, *S*-tmhd [8], *S*-tmod [8], and *N*-tmhd [9] were prepared by literature procedures. The sodium salts of the β-diketonate compounds were prepared by modification of the literature procedure for Na(hfac) [11].

^1H, ^{13}C, and ^{19}F NMR spectra were recorded on a Gemini-300 MHz NMR spectrometer at 300, 75.46, and 282.3 MHz, respectively. TGA data were obtained on a TA Instrument TGA 2050 Thermogravimetric Analyzer. Sample sizes were 1–3 mg. The ramp rate was 5.0° min^{-1} and the nitrogen purge rate was 100 cm^3 min^{-1}. Elemental analyses were performed by MHW Laboratories.

2.2. [Ag(tmhd)] (**1**)

This complex was prepared following a slight modification of the literature procedure [12]. Under an inert atmosphere, a stirring slurry of $AgNO_3$ (0.42 g, 2.5 mmol) in acetonitrile (0.14 ml) and methanol (5 ml) was cooled to 0 °C. To this slurry was added a solution of tmhdH (0.55 ml, 2.6 mmol) and triethylamine (0.35 ml, 2.5 mmol) in methanol (5 ml). The mixture was stirred at 0 °C for 1 h and then filtered quickly. The white-colored silver complex was washed with methanol and dried in vacuo. Yield: 0.40 g (55%). *Anal.* Calc. for $C_{11}H_{19}AgO_2$: C, 45.38; H, 6.58. Found: C, 45.52; H, 6.39%. ^1H NMR (C_6D_6): δ 5.71 (s, 1H, C(O)C*H*C(O)), 1.06 (s, 18H, ^tBu–CH_3). ^{13}C NMR (C_6D_6): δ 201.6 (*C*=O), 90.7 (C(O)*C*HC(O)), 39.4 (*C*(CH_3)$_3$), 27.4 (C(*C*H_3)$_3$).

2.3. [Ag(tmhd)(PPh_3)] (**1a**) (method A)

A stirred slurry of **1** (0.21 g, 0.72 mmol) and triphenylphosphine (0.19 g, 0.71 mmol) in toluene (10 ml) was cooled to 0 °C. The mixture was stirred at 0 °C for 1 h giving a clear solution. Removal of the solvent in vacuo afforded the silver complex as an off-white solid. Yield: 0.33 g (83%). *Anal.* Calc. for $C_{29}H_{34}AgO_2P$: C, 62.94; H, 6.19. Found: C, 62.78; H, 6.09%. ^1H NMR (C_6D_6): δ 7.28–6.88 (m, 15H, C_6H_5), 6.06 (s, 1H, C(O)C*H*C(O)), 1.49 (s, 18H, ^tBu–CH_3). ^{13}C NMR (C_6D_6): δ 200.4 (*C*=O), 134.3 (d, $^2J_{CP} = 17.0$ Hz, *o*-*C* Ph), 132.1 (d, $^1J_{CP} = 35.8$ Hz, *ipso*-*C* Ph), 130.4 (*p*-*C*

Ph), 129.0 ($^3J_{CP} = 10.4$ Hz, *m-C* Ph), 88.5 (C(O)*C*HC(O)), 42.4 (*C*(CH_3)$_3$), 29.4 (C(*C*H_3)$_3$).

2.4. [Ag(tmhd)(PPh$_3$)] (**1a**) (method B)

Na(tmhd) (0.45 g, 2.2 mmol) was dissolved in Et_2O (15 ml) and added to a stirred slurry of $AgNO_3$ (0.37 g, 2.2 mmol) and triphenylphosphine (0.57 g, 2.2 mmol) in Et_2O (15 ml). The mixture was allowed to react for 24 h forming a gray slurry. The volatile components were removed in vacuo affording the crude product. Extraction with toluene (2 × 20 ml), followed by filtration and evaporation in vacuo, gave the silver complex as a white solid. Yield: 1.2 g (56%). The ^{1}H NMR spectrum of the product was identical to that formed via Method A.

2.5. [Ag(tmhd)(PBu$_3$)] (**1b**)

Tri-*n*-butylphosphine (1.0 ml, 4.0 mmol) was added to a stirred slurry of **1** (1.2 g, 4.0 mmol) in toluene (45 ml) at 0 °C. The mixture was stirred at 0 °C for 1 h giving a red–brown solution. Removal of the toluene in vacuo afforded the silver complex as a reddish brown oily liquid. Yield: 1.8 g (93%). *Anal.* Calc. for $C_{23}H_{46}AgO_2P$: C, 55.98; H, 9.40. Found: C, 55.82; H, 9.29%. ^{1}H NMR (C_6D_6): δ 5.82 (s, 1H, C(O)C*H*C(O)), 1.42 (s, 18H, ^{t}Bu–CH_3), 1.32–1.22 (m, 18H, PCH_2CH_2-CH_2CH$_3$), 0.88 (t, 9H, $^3J_{HH} = 6.9$ Hz, PCH$_2$CH$_2$CH$_2$-CH_3). ^{13}C NMR (C_6D_6): δ 198.9 (*C*=O), 87.2 (C(O)*C*HC(O)), 42.1 (*C*(CH_3)$_3$), 29.5 (C(*C*H_3)$_3$), 27.9 (d, $^3J_{CP} = 6.0$ Hz, PCH$_2$CH$_2$*C*H$_2$CH$_3$), 25.9 (d, $^1J_{CP} =$ 14.8 Hz, P*C*H$_2$CH$_2$CH$_2$CH$_3$), 24.7 (d, $^2J_{CP} = 13.8$ Hz, PCH$_2$*C*H$_2$CH$_2$CH$_3$), 14.0 (PCH$_2$CH$_2$CH$_2$*C*H$_3$).

2.6. [Ag(tmod)] (**2**)

This complex was prepared using a similar procedure as that for **1**, starting with $AgNO_3$ (0.51 g, 3.0 mmol) and tmodH (0.59 g, 3.2 mmol). Yield of white solid: 0.57 g (66%). *Anal.* Calc. for $C_{11}H_{19}AgO_2$: C, 45.38; H, 6.58. Found: C, 45.58; H, 6.54%. ^{1}H NMR (C_6D_6): δ 5.43 (s, 1H, C(O)C*H*C(O)), 2.12–1.96 (m, 1H, ^{i}Bu–C*H*), 1.93 (s, 1H, ^{i}Bu–CH_2), 1.91 (br s, 1H, ^{i}Bu–CH_2), 1.05 (s, 9H, ^{t}Bu–CH_3), 0.80 (d, 6H, $^3J_{HH} = 6.6$ Hz, ^{i}Bu–CH_3). ^{13}C (C_6D_6): δ 201.1 (*C*=O), 194.1 (*C*=O), 95.9 (C(O)*C*HC(O)), 47.7 (^{i}Bu–*C*H$_2$), 39.3 (*C*(CH_3)$_3$), 27.3 (C(*C*H_3)$_3$), 26.2 (^{i}Bu–*C*H), 22.5 (^{i}Bu–*C*H$_3$).

2.7. [Ag(tmod)(PPh$_3$)] (**2a**)

This complex was prepared by a similar method to that for the preparation of **1a** (Method A). Triphenylphosphine (0.12 g, 0.46 mmol) was added to a stirred slurry of **2** (0.13 g, 0.46 mmol) in toluene (15 ml) at 0 °C. The mixture was stirred at 0 °C for 1 h, after which the toluene was removed in vacuo. Trituration of the oily residue with pentane gave the silver complex as a gray solid. Yield: 0.20 g (79%). *Anal.* Calc. for $C_{29}H_{34}AgO_2P$: C, 62.94; H, 6.19. Found: C, 62.77; H, 6.24%. ^{1}H NMR (C_6D_6): δ 7.28–6.86 (m, 15H, C_6H_5), 5.82 (s, 1H, C(O)C*H*C(O)), 2.60–2.45 (m, 1H, ^{i}Bu–C*H*), 2.41 (br s, 2H, ^{i}Bu–CH_2), 1.47 (s, 9H, ^{t}Bu–CH_3), 1.12 (d, 6H, $^3J_{HH} = 6.0$ Hz, ^{i}Bu–CH_3). ^{13}C NMR (C_6D_6): δ 199.9 (*C*=O), 194.1 (*C*=O), 134.3 (d, $^2J_{CP} = 16.9$ Hz, *o-C* Ph), 131.9 (d, $^1J_{CP} = 36.8$ Hz, *ipso-C* Ph), 130.5 (d, $^4J_{CP} = 1.9$ Hz, *p-C* Ph), 129.0 (d, $^3J_{CP} = 10.7$ Hz, *m-C* Ph), 94.3 (C(O)*C*HC(O)), 53.2 (^{i}Bu–*C*H$_2$), 41.9 (*C*(CH_3)$_3$), 29.3 (C(*C*H_3)$_3$), 27.2 (^{i}Bu–*C*H), 23.3 (^{i}Bu–*C*H$_3$).

2.8. [Ag(tmod)(PBu$_3$)] (**2b**)

This complex was prepared by a similar method to that for **1b**, instead utilizing tri-*n*-butylphosphine (0.11 ml, 0.42 mmol) and **2** (0.13 g, 0.46 mmol). Yield of reddish–black oily liquid: 0.20 g (97%). *Anal.* Calc. for $C_{23}H_{46}AgO_2P$: C, 55.98; H, 9.40. Found: C, 56.12; H, 9.30%. ^{1}H NMR (C_6D_6): δ 5.66 (s, 1H, C(O)C*H*C(O)), 2.51–2.36 (m, 1H, ^{i}Bu–C*H*,), 2.29 (br s, 2H, ^{i}Bu–CH_2), 1.38 (s, 9H, ^{t}Bu–CH_3), 1.21–1.01 (complex, 24H, PCH_2CH_2CH_2CH$_3$ and ^{i}Bu–CH_3), 0.80 (t, 9H, $^3J_{HH} = 6.9$ Hz, PCH$_2$CH$_2$CH$_2$CH_3). ^{13}C NMR (C_6D_6): 199.3 (*C*=O), 193.5 (*C*=O), 93.9 (C(O)*C*HC(O)), 53.1 (^{i}Bu–*C*H$_2$), 41.6 (*C*(CH_3)$_3$), 29.2 (C(*C*H_3)$_3$), 27.9 (d, $^3J_{CP} = 5.6$ Hz, PCH$_2$CH$_2$*C*H$_2$CH$_3$), 27.1 (^{i}Bu–*C*H), 25.7 (d, $^1J_{CP} = 18.4$ Hz, P*C*H$_2$CH$_2$CH$_2$CH$_3$), 24.4 (d, $^2J_{CP} = 14.2$ Hz, PCH$_2$*C*H$_2$CH$_2$CH$_3$), 23.3 (^{i}Bu–*C*H$_3$), 13.8 (PCH$_2$CH$_2$CH$_2$*C*H$_3$).

2.9. [Ag(tmshd)] (**3**)

A mixture of $AgNO_3$ (0.92 g, 5.4 mmol) in CH_3CN (0.5 ml) and CH_3OH (11 ml) at 0 °C was transferred by cannula to a cooled flask containing a stirring mixture of tmshdH (1.15 g, 5.7 mmol), triethylamine (0.8 ml, 5.7 mmol), and CH_3OH (11 ml) at 0 °C. Immediate formation of white precipitate was observed. The mixture was stirred at 0 °C for an hour, filtered and the precipitates washed with minute amounts of cold CH_3OH. The pale colored precipitates darkened over time even at −25 °C and were used immediately for the preparation of the ternary complex **3a**. Yield: 0.33 g (20%).

2.10. [Ag(tmshd)(PPh$_3$)] (**3a**)

A mixture of **3** (0.14 g, 0.46 mmol) and triphenylphosphine (0.12 g, 0.46 mmol) in Et_2O (30 ml) was stirred at 0 °C for 3 h. Removal of the solvent at 0 °C gave a light brown powder. Yield: 0.25 g (95%). *Anal.* Calc. for $C_{28}H_{34}AgO_2PSi$: C, 59.05; H, 6.02. Found: C, 59.27; H, 5.99%. ^{1}H NMR ($CDCl_3$): δ 7.50–7.34 (m, 15H, C_6H_5),

5.80 (s, 1H, C(O)C*H*C(O)), 1.16 (s, 9H, ^{t}Bu–CH_3), 0.17 (s, 9H, Si–CH_3).

2.11. [Ag(S-tmhd)] (4)

A yellow slurry of $AgNO_3$ (0.26 g, 1.5 mmol) and Na(*S*-tmhd) (0.34 g, 1.5 mmol) in thf (20 ml) was stirred for 24 h giving a dark gray mixture. The solvent was removed in vacuo and the residue extracted with toluene (20 ml). Filtration and removal of all volatiles in vacuo gave the silver complex as a yellow brown solid. Yield: 0.38 g (81%). *Anal.* Calc. for $C_{11}H_{19}AgOS$: C, 43.01; H, 6.23. Found: C, 42.91; H, 6.02%. ^{1}H NMR ($CDCl_3$): δ 6.74 (s, 1H, C(O)C*H*C(S)), 1.31 (s, 9H, ^{t}Bu–CH_3), 1.10 (s, 9H, ^{t}Bu–CH_3). ^{13}C NMR ($CDCl_3$): δ 206.9 (*C*=O), 173.5 (*C*=S), 118.2 (C(O)*C*HC(S)), 44.7 (*C*$(CH_3)_3$), 42. (*C*$(CH_3)_3$), 31.0 (C(*C*$H_3)_3$), 27.2 (C(*C*$H_3)_3$).

2.12. [Ag(S-tmhd)(PPh$_3$)] (4a)

A slurry of $AgNO_3$ (0.26 g, 1.5 mmol), Na(*S*-tmhd) (0.33 g, 1.5 mmol) and triphenylphosphine (0.39 g, 1.5 mmol) in thf (20 ml) was stirred for 44 h giving a lemon yellow slurry. The solvent was removed in vacuo and the residue extracted with toluene (25 ml). Filtration and removal of all volatiles in vacuo gave the silver complex as a lemon yellow solid. Yield: 0.61 g (72%). *Anal.* Calc. for $C_{29}H_{34}AgOPS$: C, 61.16; H, 6.02. Found: C, 61.32; H, 6.15%. ^{1}H NMR ($CDCl_3$): δ 7.60–7.30 (m, 15H, C_6H_5), 6.85 (s, 1H, C(O)C*H*C(S)), 1.36 (s, 9H, ^{t}Bu–CH_3), 1.14 (s, 9H, ^{t}Bu–CH_3). ^{13}C NMR ($CDCl_3$): δ 205.5 (*C*=O), 134.1 (d, $^2J_{CP} = 16.6$ Hz, *o*-*C* Ph), 131.4 (d, $^1J_{CP} = 34.6$ Hz, *ipso*-*C* Ph), 130.6 (d, $^4J_{CP} = 1.9$ Hz, *p*-*C* Ph), 128.9 (d, $^3J_{CP} = 10.4$ Hz, *m*-*C* Ph), 113.6 (C(O)*C*HC(S)), 44.5 (*C*$(CH_3)_3$), 44.4 (*C*$(CH_3)_3$), 31.5 (C(*C*$H_3)_3$), 27.7 (C(*C*$H_3)_3$).

2.13. [Ag(S-tmhd)(PBu$_3$)] (4b)

A mixture of $AgNO_3$ (0.20 g, 1.2 mmol), Na(*S*-tmhd) (0.26 g, 1.2 mmol) and tri-*n*-butylphosphine (0.30 g, 1.1 mmol) in thf (20 ml) was stirred for 24 h giving a yellow mixture. The solvent was removed in vacuo and the residue extracted with toluene (20 ml). Filtration and removal of all volatiles in vacuo gave the silver complex as a yellow brown oil. Yield: 0.56 g (96%). *Anal.* Calc. for $C_{23}H_{46}AgOPS$: C, 54.22; H, 9.10. Found: C, 54.42; H, 8.86%. ^{1}H NMR ($CDCl_3$): δ 6.74 (s, 1H, C(O)C*H*C(S)), 1.61–1.32 (complex, 18H, PCH_2CH_2-CH_2CH$_3$), 1.29 (s, 9H, ^{t}Bu–CH_3), 1.07 (s, 9H, ^{t}Bu–CH_3), 0.85 (t, 9H, $^3J_{HH} = 7.2$ Hz, PCH$_2$CH$_2$CH$_2$CH_3). ^{13}C NMR ($CDCl_3$): δ 204.8 (*C*=O), 185.0 (*C*=S), 113.4 (C(O)*C*HC(S)), 43.7 (*C*$(CH_3)_3$), 43.5 (*C*$(CH_3)_3$), 30.8 (C(*C*$H_3)_3$), 27.2 (d, $^3J_{CP} = 5.6$ Hz, PCH$_2$CH$_2$*C*H$_2$CH$_3$), 27.1 (C(*C*$H_3)_3$), 24.8 (d, $^1J_{CP} = 18.8$ Hz, P*C*H$_2$CH$_2$-CH$_2$CH$_3$), 23.7 (d, $^2J_{CP} = 14.3$ Hz, PCH$_2$*C*H$_2$CH$_2$CH$_3$), 13.1 (PCH$_2$CH$_2$CH$_2$*C*H$_3$).

2.14. [Ag(S-tmod)] (5)

This complex was prepared by the same method as for **4**, instead using $AgNO_3$ (0.26 g, 1.5 mmol) and Na(*S*-tmod) (0.34 g, 1.53 mmol). Yield of dark yellow brown product: 0.36 g (76%). *Anal.* Calc. for $C_{11}H_{19}AgOS$: C, 43.01; H, 6.23. Found: C, 43.18; H, 6.03%. ^{1}H NMR ($CDCl_3$): δ 6.48 (s, 1H, C(O)C*H*C(S)), 2.34 (s, 1H, ^{i}Bu–CH_2), 2.32 (s, 1H, ^{i}Bu–CH_2), 2.24–2.05 (m, 1H, ^{i}Bu–C*H*), 1.09 (s, 9H, ^{t}Bu–CH_3), 0.85 (d, 6H, $^3J_{HH} = 6.3$ Hz, ^{i}Bu–CH_3). ^{13}C NMR ($CDCl_3$): δ 204.8 (*C*=O), 120.7 (C(O)*C*HC(S)), 59.3 (^{i}Bu–*C*H$_2$), 43.6 (*C*$(CH_3)_3$), 27.8 (^{i}Bu–*C*H), 27.0 (C(*C*$H_3)_3$), 22.4 (^{i}Bu–*C*H$_3$).

2.15. [Ag(S-tmod)(PPh$_3$)] (5a)

This complex was prepared analogously to **4a** using $AgNO_3$ (0.26 g, 1.5 mmol), Na(*S*-tmod) (0.33 g, 1.5 mmol) and triphenylphosphine (0.39g, 1.5 mmol). Yield of yellow–brown product: 0.71 g (83%). *Anal.* Calc. for $C_{29}H_{34}AgOPS$: C, 61.16; H, 6.02. Found: C, 61.34; H, 5.87%. ^{1}H NMR ($CDCl_3$): δ 7.46–7.26 (m, 15H, C_6H_5), 6.45 (s, 1H, C(O)C*H*C(S)), 2.33 (bs, 2H, ^{i}Bu–CH_2), 2.27–2.04 (m, 1H, ^{i}Bu–C*H*), 1.01 (s, 9H, ^{t}Bu–CH_3), 0.82 (d, 6H, $^3J_{HH} = 6.3$ Hz, ^{i}Bu–CH_3). ^{13}C NMR ($CDCl_3$): δ 204.6 (*C*=O), 133.9 ($^2J_{CP} = 16.6$ Hz, *o*-*C* Ph), 131.8 (d, $^1J_{CP} = 30.2$ Hz, *ipso*-*C* Ph), 130.3 (*p*-*C* Ph), 128.8 (d, $^3J_{CP} = 10.0$ Hz, *m*-*C* Ph), 117.6 (C(O)*C*HC(S)), 59.7 (^{i}Bu–*C*H$_2$), 43.5 (*C*$(CH_3)_3$), 28.4 (^{i}Bu–*C*H), 27.3 (C(*C*$H_3)_3$), 22.3 (^{i}Bu–*C*H$_3$).

2.16. [Ag(S-tmod)(PBu$_3$)] (5b)

Na(*S*-tmod) (0.26 g, 1.2 mmol) was added to a stirring slurry of $AgNO_3$ (0.20 g, 1.2 mmol) and tri-*n*-butylphosphine (0.30 ml, 1.1 mmol) in thf (20 ml). The reaction mixture was allowed to react for 24 h, resulting in a gray slurry. The volatile components were removed in vacuo affording the crude product. Extraction with toluene (20 ml) followed by filtration and evaporation in vacuo gave the silver complex as an orange brown oily liquid. Yield: 0.42 g (72%). *Anal.* Calc. for $C_{23}H_{46}AgOPS$: C, 54.22; H, 9.10. Found: C, 54.12; H, 9.27%. ^{1}H NMR ($CDCl_3$): δ 6.47 (s, 1H, C(O)C*H*C(S)), 2.33 (s, 1H, ^{i}Bu–CH_2), 2.31 (s, 1H, ^{i}Bu–CH_2), 2.25–2.05 (m 1H, ^{i}Bu–C*H*), 1.60–1.31 (complex, 18H, PCH_2CH_2-CH_2CH$_3$), 1.07 (s, 9H, ^{t}Bu–CH_3), 0.80 (d, 6H, $^3J_{HH} = 6.3$ Hz, ^{i}Bu–CH_2), 0.79 (t, 9H, $^3J_{HH} = 7.2$ Hz, PCH$_2$CH$_2$CH$_2$CH_3). ^{13}C NMR ($CDCl_3$): δ 203.7 (*C*=O), 179.2 (*C*=S), 119.7 (C(O)*C*HC(S)), 59.8 (^{i}Bu–*C*H$_2$), 43.3 (*C*$(CH_3)_3$), 28.7 (^{i}Bu–*C*H), 27.6 (d, $^3J_{CP} = 5.6$ Hz, PCH$_2$CH$_2$*C*H$_2$CH$_3$), 27.4 (C(*C*$H_3)_3$), 25.5 (d, $^1J_{CP} = 13.6$ Hz, P*C*H$_2$CH$_2$CH$_2$CH$_3$), 24.4 (d, $^2J_{CP} = 13.3$ Hz,

$PCH_2CH_2CH_2CH_3$), 22.5 ($^{i}Bu-CH_3$), 13.6 ($PCH_2CH_2CH_2CH_3$).

2.17. [Ag(N-tmhd)(PPh$_3$)] (6a)

A stirring slurry of $AgNO_3$ (0.13 g, 0.77 mmol) and Na(*N*-tmhd) (0.16 g, 0.78 mmol) was dissolved in Et_2O (20 ml). A solution of triphenylphosphine (0.20 g, 0.76 mmol) in Et_2O (40 ml) was added. The reaction mixture was allowed to react for 24 h resulting in a gray slurry. The volatile components were removed in vacuo affording the crude product as a black solid. Extraction with toluene (2×20 ml) followed by filtration and evaporation in vacuo gave the silver complex as a salmon pink colored solid. Yield: 0.24 g (56%). *Anal.* Calc. for $C_{29}H_{35}AgNOP$: C, 63.05; H, 6.39. Found: C, 63.22; H, 6.50%. ^{1}H NMR ($CDCl_3$): δ 7.44–7.16 (m, 15H, C_6H_5), 5.32 (s, 1H, C(O)C*H*C(NH)), 1.14 (s, 9H, $^{t}Bu-CH_3$), 1.12 (s, 9H, $^{t}Bu-CH_3$). ^{13}C NMR ($CDCl_3$): δ 205.3 (*C*=O), 173.5 (*C*=NH), 133.8 (d, $^2J_{CP} = 16.4$ Hz, *o*-*C* Ph), 131.8 (d, $^1J_{CP} = 29.2$ Hz, *ipso*-*C* Ph), 130.1 (*p*-*C* Ph), 128.6 (d, $^3J_{CP} = 9.8$ Hz, *m*-*C* Ph), 86.4 (C(O)*C*HC(NH)), 41.9 ($C(CH_3)_3$), 35.9 ($C(CH_3)_3$), 28.7 ($C(CH_3)_3$), 27.8 ($C(CH_3)_3$).

2.18. [Ag(N-tmhd)(PBu$_3$)] (6b)

A stirred mixture of $AgNO_3$ (0.20 g, 1.18 mmol) and (*N*-tmhd) (0.24 g, 1.18 mmol) was dissolved in thf (10 ml). Tri-*n*-butylphosphine (0.31 ml, 1.18 mmol) was added and the mixture stirred for 18 h. All volatiles were removed from the resulting greenish black mixture. Extraction of the residue with toluene (2×20 ml) followed by filtration and evaporation in vacuo gave the silver complex as a reddish brown oil. Yield: 0.51 g (88%). *Anal.* Calc. for $C_{23}H_{47}AgNOP$: C, 56.10; H, 9.62. Found: C, 55.95; H, 9.49%. ^{1}H NMR ($CDCl_3$): δ 10.2 (br s, 1H, N*H*), 5.18 (s, 1H, C(O)C*H*C(NH)), 1.53–1.21 (complex, 18H, $PCH_2CH_2CH_2CH_3$), 1.04 (s, 9H, $^{t}Bu-CH_3$), 0.98 (s, 9H, $^{t}Bu-CH_3$), 0.75 (t, 9H, $^3J_{HH} = 6.9$ Hz, $PCH_2CH_2CH_2CH_3$). ^{13}C NMR ($CDCl_3$): δ 204.9 (*C*=O), 173.4 (*C*=NH), 86.2 (C(O)*C*HC(NH)), 41.7 ($C(CH_3)_3$), 35.8 ($C(CH_3)_3$), 28.6 ($C(CH_3)_3$), 27.7 ($C(CH_3)_3$), 27.4 (d, $^3J_{CP} = 2.9$ Hz, $PCH_2CH_2CH_2CH_3$), 24.8 (d, $^1J_{CP} = 16.6$ Hz, $PCH_2CH_2CH_2CH_3$), 24.0 (d, $^2J_{CP} = 13.5$ Hz, $PCH_2CH_2CH_2CH_3$), 13.3 ($PCH_2CH_2CH_2CH_3$).

2.19. X-ray crystallography

Crystals of **1a** and **4a** suitable for X-ray diffraction studies were obtained by dissolving the corresponding complex in thf and layering pentane over the solution. The mixture was cooled to -35 °C, while allowing the pentane to diffuse slowly through the mixture. Crystals formed over a period of five to nine days (yield of **1a**: 30%; yield of **4a**: 75%). X-ray data were collected at ambient temperature using a Bruker R3m diffractometer in the $\omega-2\theta$ mode with variable scan speed (3–20 ° min^{-1}) and graphite monochromated Mo Kα radiation ($\lambda = 0.71073$ Å). Check reflections were measured every 200 reflections during data collection and gave no indication of crystal decay. Data were corrected for background, attenuators, Lorentz and polarization effects in the usual fashion [13]. A semi-empirical absorption correction was applied to **4a** using the Ψ-scan method.

Both structures were solved by direct methods and refined by full matrix least-squares procedures on $|F^2|$ with the SHELXTL Plus package of programs. All non-hydrogen atoms were refined anisotropically; hydrogen atom positions were calculated geometrically and fixed at a C–H distance of 0.96 Å and were not refined. Crystal data and further data collection parameters are summarized in Table 1.

Table 1
Crystallographic data and parameters for **1a** and **4a**

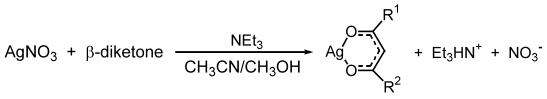
	1a	**4a**
Formula	$C_{29}H_{34}AgO_2P$	$C_{58}H_{68}Ag_2O_2P_2S_2$
Formula weight	553.4	1138.9
Crystal color, Habit	Pale yellow, plate	Pale yellow, rectangular prism
Crystal dimensions (mm)	$0.15 \times 0.30 \times 0.45$	$0.15 \times 0.20 \times 0.45$
Crystal system	monoclinic	triclinic
Space group	$P2_1/c$	$P\bar{1}$
a (Å)	13.253(6)	11.194(3)
b (Å)	11.756(3)	13.639(3)
c, (Å)	17.722(5)	20.431(5)
α (°)	90	75.32(2)
β (°)	102.40(3)	78.61(2)
γ (°)	90	72.37(2)
V Å^3	2696.7(16)	2851.0(12)
Z	4	2
D_{calc} (g cm^{-3})	1.363	1.327
μ (Mo Kα) (cm^{-1})	8.29	8.54
F(000)	1144	1176
2θ max (°)	45.0	45.0
Reflections collected	3698	7678
Independent reflections	3521 ($R_{int} = 1.44\%$)	7427 ($R_{int} = 2.68\%$)
Observed reflections	2081 ($F > 6.0\sigma(F)$)	4351 ($F > 4.0\sigma(F)$)
T_{min}/T_{max}	N/A	0.868/0.953
Number of parameters	298	595
R [a]	0.0422	0.0817
R_w [a]	0.0437	0.0826
Goodness-of-fit [b]	1.19	1.51

[a] $R = \Sigma||F_o| - |F_c||/\Sigma|F_o|$; $R_w = [\Sigma\, w(|F_o| - |F_c|)^2/\Sigma\, w|F_o|^2]^{1/2}$; $w = 1/\sigma^2(F_o) + g(F_o)^2$; $g = 0.001$ and 0.002 for **1a** and **4a**, respectively.
[b] GOF $= [\Sigma\, w(|F_o| - |F_c|)^2/(NO - NV)]^{1/2}$, where NO is the number of observations and NV is the number of variables.

3. Results and discussion

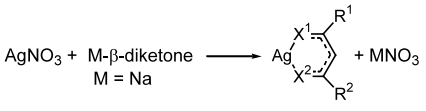
3.1. Synthesis

Two routes were employed for the syntheses of the binary silver complexes, [Ag(X)]. For complexes **1** (X = tmhd), **2** (X = tmod), and **3** (X = tmshd), a modification of the method of Wakeshima [13] was employed. In this approach, $AgNO_3$ was reacted with the β-diketone in the presence of a base (Eq. (1)). Alternatively for **4** (X = *S*-tmhd) and **5** (X = *S*-tmod), the complexes were readily formed by displacement of nitrate using the sodium salt of the β-diketonate derivative (Eq. (2)) [14]. The method described in Eq. (1) was somewhat preferable, in that it afforded spectroscopically pure products, suitable for further reaction with neutral coordinating ligands to form ternary complexes (vide infra). On the other hand, separation of the silver product obtained in Eq. (2) from unreacted sodium β-diketonate was difficult due to the similar solubilities of these substances in most solvents. Attempts to prepare the complexes via reaction of Ag_2O with the β-diketone, as described for hfac [7], failed to provide the desired compounds. This result may be attributed to the decreased acidity of the nonfluorinated β-diketones relative to the fluorinated analogs.



(1)

1: $R^1 = R^2 = t$-Bu
2: $R^1 = t$-Bu, $R^2 = i$-Bu
3: $R^1 = t$-Bu, $R^2 = SiMe_3$



4: X^1 = O, X^2 = S, $R^1 = R^2 = t$-Bu
5: X^1 = O, X^2 = S, $R^1 = t$-Bu, $R^2 = i$-Bu
6: X^1 = O, X^2 = NH, $R^1 = R^2 = t$-Bu

(2)

Ternary complexes, [Ag(X)L], were prepared in two ways. In the first method, reaction of Ag(tmhd) **1**, Ag(tmod) **2**, and Ag(tmshd) **3** with 1 equiv. of PPh_3 or PBu_3 gave the corresponding desired complexes **1a**–**3a** (L = PPh_3) and **1b**–**2b** (L = PBu_3) in >80% yield. The complexes are air-stable; the PPh_3 derivatives were white to grayish-white in color, while the PBu_3 compounds were orange or reddish-brown viscous liquids, perhaps due to slight amounts of oxidation products. In all cases, good elemental analyses [15] and NMR spectroscopic data were obtained, so contamination must have been quite small. Slight downfield shifts of the CH resonance of the β-diketonate ligands were observed in the ^{1}H NMR spectra, while slight upfield shifts were found for the carbonyl and CH carbon atoms in the ^{13}C NMR spectra, upon coordination of the phosphine ligands. Although slight darkening occurred over long periods of time, no changes were observed in the NMR spectra of the compounds.

Complex **1a** could also be obtained by direct reaction of $AgNO_3$ with Na(tmhd) in the presence of PPh_3. This method was employed successfully for the preparation of [Ag(X)L], X = *S*-tmhd, L = PPh_3 **4a** or PBu_3 **4b**; X = *S*-tmod, L = PPh_3 **5a** or PBu_3 **5b**. The complexes were air-stable, yellow to yellow–brown compounds, probably due to the coloration of the ligands. The ^{1}H NMR resonance for the CH resonance of the monothio-β-diketonate ligands in the silver complexes experienced a downfield shift compared to the corresponding silver β-diketonate complexes, a result previously noted by Musso and coworkers for an analogous silver complex [16]. We also observed a downfield shift of the CH resonance in the ^{13}C NMR spectra of the coordinated ligands upon sulfur substitution.

Attempts to isolate pure Ag(*N*-tmhd) proved unsuccessful, perhaps due to ease of hydrolysis [17]. However, [Ag(*N*-tmhd)L], L = PPh_3 **5a** or PBu_3 **5b** could be prepared in acceptable yield by direct reaction of $AgNO_3$ with Na(*N*-tmhd) in the presence of the appropriate phosphine ligand. The CH resonance of the β-diketoiminate ligands in **5a** and **5b** was slightly upfield of the chemical shifts observed for the β-diketonate analogs, **1a** and **1b**, in both the ^{1}H and ^{13}C NMR spectra.

3.2. Thermal studies

Thermogravimetric analysis was employed to determine the suitability of the silver complexes for MOCVD processing. Experiments were conducted at atmospheric pressure under a nitrogen purge. Typical temperatures of maximum weight loss were in the range of 160–240 °C. For most of the complexes, weight loss was accompanied by residues in the TGA pan, the amount of which was comparable to the theoretical percentage of silver present in the complex. In fact in some cases, the residue appeared to be a silver mirror. Evidently, these complexes lose the ancillary ligands upon heating, without significant volatilization of the intact complex. One exception was **1b**, which had maximum rate of weight loss at 204 °C and a residue of only 11% (theoretical %Ag, 22%). Thus, at atmospheric pressure, the majority of the studied complexes showed little utility for MOCVD applications.

3.3. X-ray diffraction studies

While numerous solid-state structures have been reported for silver complexes supported by fluorinated β-diketonate ligands [6a,6b,6c,6f,6h,6f,6h,7,17–23], we

have determined the first structures of ternary silver complexes containing either a non-fluorinated β-diketonate or a monothio-β-diketonate ligand.

The asymmetric unit for [Ag(tmhd)(PPh_3)] **1a** contains one molecule of the mononuclear complex. The geometry is best described as highly distorted trigonal planar (Fig. 1); selected bond lengths and angles are summarized in Table 2. Ag(1), P(1), O(1), and O(2) are planar to within ±0.066 Å; the silver atom is 0.18 Å out of the plane defined by the three donor atoms of the ligands.

Structural features for **1a** are reminiscent to those reported for similar, three-coordinate analogs, [Ag(hfac)L], L = PMe_3 [6a,6b,6c], MeNC [6f], and PPh_3 [17]. Comparisons to the latter complex are probably most fruitful. The silver atom in **1a** is unsymmetrically bonded to the tmhd ligand with the Ag(1)–O(1) bond almost 0.08 Å longer than Ag(1)–O(2). Not surprisingly, the longer Ag–O bond occurs on the side of the complex with the smaller P–Ag–O angle (Table 2 and Fig. 1). Similar results are observed for [Ag(hfac)(PPh_3)] [17]. The reasons for these distortions are not clear, though sterics may play a part; the hfac ligand is more symmetrically coordinated in [Ag(hfac)L], L = PMe_3 [6a,6b,6c] and MeNC [6f]. The Ag–O bonds in **1a** are slightly shorter than those observed for [Ag(hfac)(PPh_3)] (2.218 (5) and 2.341(5) Å) [17], which can be attributed to the absence of the electron-withdrawing trifluoromethyl substituents. However, no appreciable lengthening of the C–O bonds of the tmhd ligand was observed for **1a**. The Ag–P bond length in **1a** is comparable to those in previously reported monomeric, three-coordinate silver β-diketonate complexes [6a,6b,6c,6f,17]. The packing diagram shows a head-to-tail stacking of β-diketone ligands for adjacent molecules. Stacking of phenyl rings is also observed for alternating molecules.

The asymmetric unit for [Ag(*S*-tmhd)(PPh_3)] **4a** contains two crystallographically independent halves of centrosymmetric dimers; thus, the triclinic unit cell contains two dimers. Selected bond lengths and angles are collected in Table 3. To our knowledge, **4a** is the first complex for which a monothio-β-diketonate serves as a bridging ligand [24,25], though a weak, long-range bridging interaction is observed in a Hg(II) monothio-β-diketonate complex [9].

The two dimers of **4a** have similar overall structures (see Fig. 2 for dimer molecule 1). The *S*-tmhd ligands in both **4a** dimers can be considered to be bridging in a μ_4:η^2,η^2 mode, that is analogous to that seen for the hfac ligands in [Ag(hfac)L]$_2$, where L is 1,5-dimethyl-1,5-cyclooctadiene [18] or diglyme [19a]. The dihedral angle between the planes defined by the bridging *S*-tmhd ligands in each dimer is a crystallographically-enforced 0.00°. The Ag···Ag distances in the dimers are

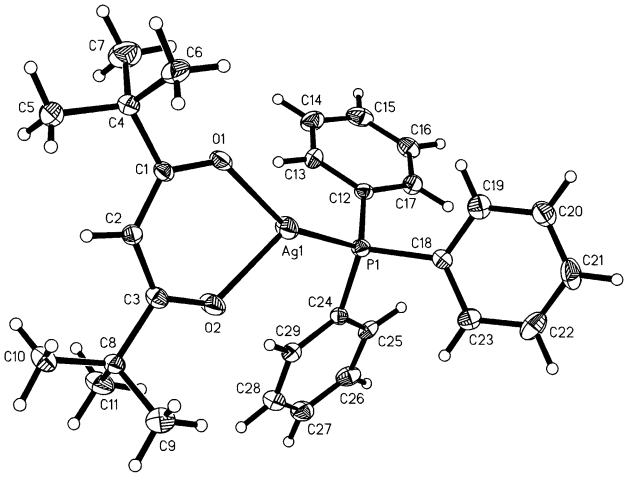


Fig. 1. Molecular structure and atom numbering scheme for **1a**.

Table 2
Selected bond lengths (Å) and angles (°) for **1a**

Bond lengths	
Ag(1)–P(1)	2.320(2)
Ag(1)–O(1)	2.176(5)
Ag(1)–O(2)	2.254(6)
O(1)–C(1)	1.260(8)
O(2)–C(3)	1.257(8)
C(1)–C(2)	1.385(11)
C(2)–C(3)	1.417(10)
Bond angles	
P(1)–Ag(1)–O(1)	152.3(2)
P(1)–Ag(1)–O(2)	122.7(2)
O(1)–Ag(1)–O(2)	82.5(2)
Ag(1)–O(1)–C(1)	130.0(5)
Ag(1)–O(2)–C(3)	128.8(5)
C(1)–C(2)–C(3)	127.7(6)

Table 3
Selected bond lengths (Å) and angles (°) for **4a**

Molecule 1			
Ag(1)–P(1)	2.382(3)	P(1)–Ag(1)–S(1)	132.6(1)
Ag(1)–S(1)	2.540(4)	P(1)–Ag(1)–O(1)	118.2(2)
Ag(1)–O(1)	2.604(9)	S(1)–Ag(1)–O(1)	75.9(2)
Ag(1)–S(1a)	2.608(4)	P(1)–Ag(1)–S(1a)	116.7(1)
Ag(1)–O(1a)	2.830(9)	P(1)–Ag(1)–O(1a)	126.0(2)
S(1)–C(1)	1.720(13)	S(1)–Ag(1)–S(1a)	110.7(1)
O(1)–C(3)	1.335(16)	O(1)–Ag(1)–O(1a)	114.9(2)
C(1)–C(2)	1.364(21)	Ag(1)–S(1)–C(1)	115.2(4)
C(2)–C(3)	1.435(18)	Ag(1)–O(1)–C(3)	119.6(7)
Molecule 2			
Ag(1′)–P(1′)	2.372(3)	P(1′)–Ag(1′)–S(1′)	130.7(1)
Ag(1′)–S(1′)	2.540(4)	P(1′)–Ag(1′)–O(1′)	117.0(2)
Ag(1′)–O(1′)	2.575(9)	S(1′)–Ag(1′)–O(1′)	77.4(2)
Ag(1′)–S(1′a)	2.634(5)	P(1′)–Ag(1′)–S(1′a)	117.4(1)
Ag(1′)–O(1′a)	2.750(9)	P(1′)–Ag(1′)–O(1′a)	128.2(2)
S(1′)–C(1′)	1.624(16)	S(1′)–Ag(1′)–S(1′a)	111.8(1)
O(1′)–C(3′)	1.499(18)	O(1′)–Ag(1′)–O(1′a)	114.1(2)
C(1′)–C(2′)	1.376(19)	Ag(1′)–S(1′)–C(1′)	117.5(4)
C(2′)–C(3′)	1.446(17)	Ag(1′)–O(1′)–C(3′)	115.7(7)

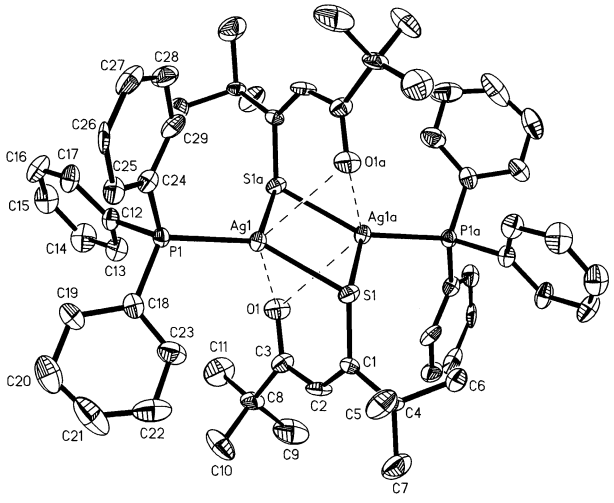


Fig. 2. Molecular structure for and atom numbering scheme for dimer molecule 1 for **4a**. Hydrogen atoms are omitted for clarity.

2.929(2) and 2.900(2) Å, for dimer molecules 1 and 2, respectively.

The Ag–S bond lengths for the dimers of **4a** are clearly within bonding range, but are somewhat longer on average than those observed in silver clusters containing bridging thiolate ligands [26] or for metal-to-sulfur bond distances in comparable, monomeric monothio-β-diketonate complexes involving metals from the second and third transition series [9,24]. The Ag–O distances are longer than the Ag–S bonds and include one long and one very long interaction per silver center from different bridging *S*-tmhd ligands. These interactions are weak at best; if the longer interaction is ignored, then the geometry about each silver ion is distorted tetrahedral. On the other hand, each silver ion can be considered to be distorted trigonal planar, if all Ag–O bonds are omitted. Interestingly, the shorter Ag–O bond distance is similar to that found in monomeric [Hg(*S*-tmhd)$_2$], a linear complex with two weak Hg–O interactions [9]. The Ag–P bond distances in the **4a** dimers are somewhat longer than those found for **1a** and [Ag(hfac)(PPh$_3$)] [17], presumably due to increased steric congestion in the dimers.

4. Conclusions

We have presented a series of silver complexes containing non-fluorinated β-diketonate derivatives. These complexes are air-stable, though slightly light and temperature sensitive. We have also reported on the first solid-state structures for this class of complexes, including [Ag(tmhd)(PPh$_3$)] **1a** and [Ag(*S*-tmhd)(PPh$_3$)] **4a**. The former is a monomeric, three-coordinate complex, while the latter is a dimer with two bridging *S*-tmhd ligands.

In general at atmospheric pressure, the complexes under study decompose without volatilization to give silver via loss of the supporting ligands. One exception was **1b**, [Ag(tmhd)(PBu$_3$)], which exhibited some ability to volatilize before total decomposition. We note that while our work was in progress, Edwards, et al. reported on the utility of [Ag(X)(PPh$_3$)] complexes for CVD processes, where X is various β-diketonate or β-ketoiminate ligands [17]. This group found a significant variation in volatility and quality of deposited silver films as a function of X. While many silver β-diketonate derivatives, [Ag(X)L], including those in the present study, are either too ionic [22] or too unstable to be employed for CVD applications, it appears that judicious choice of X and L ancillary ligands will possibly allow for useful complexes to be obtained [6f,17,20,21].

5. Supplementary material

Full lists of crystallographic data for **1a** (CCDC 169487) and **4a** (CCDC 169488), including atomic coordinates, bond lengths and angles, and anisotropic thermal parameters have been deposited with the Cambridge Crystallographic Data Center. Copies of this information may be obtained from The Director, CCDC, 12 Union Road, Cambridge, CB2 1EZ, UK (fax: +44-1233-336033; e-mail: deposit@ccdc.cam.ac.uk or www: http://www.ccdc.cam.ac.uk).

Acknowledgements

We gratefully acknowledge the generous support for this study by Planar Systems, Inc. and thank Dr. Richard Tuenge for helpful advice.

References

[1] (a) G. Blasse, B.C. Grabmeier, Luminescent Materials, Springer-Verlag, Berlin, 1994;
(b) K.A. Franz, W.G. Kehr, A. Siggel, J. Wieczoreck, W. Adam, Ullmanns Encyclopedia of Industrial Chemistry, vol. A15, VCH, Weinheim, 1990, p. 519;
(c) T. Welker, J. Lumin. 48–49 (1991) 49;
(d) G. Blasse, J. Alloys Compd. 192 (1993) 17;
(e) C.R. Ronda, J. Alloys Compd. 225 (1995) 534;
(f) C.R. Ronda, J. Lumin. 72-74 (1997) 49.
[2] J. Kido, M. Kimura, K. Nagai, Chem. Lett. (1996) 47 and references therein.
[3] S.S. Sun, E. Dickey, J. Kane, P.N. Yocom, Proceedings of the International Display Research Conference and International Workshops on LCD and Emissive Technology, Toronto, Canada, 15–17 September, 1997.
[4] (a) N. Yamashita, Jpn. J. Appl. Phys. Part 1 30 (1991) 3335;
(b) T.C. Jones, W. Park, E. Mohammed, B.K. Wagner, C.J. Summers, S.S. Sun, Mater. Res. Soc., Symp. Proc. 508 (1998) 281;
(c) W. Lehmann, J. Electrochem. Soc. 117 (1970) 1389.

[5] S.-S Sun, Fouth International Conference on the Science and Technology of Display Phosphors, Extended Abstracts Bend, OR, USA, 1998, p. 183.
[6] (a) W. Lin, T.H. Warren, R.G. Nuzzo, G.S. Girolami, J. Am. Chem. Soc. 115 (1993) 11644;
(b) N.H. Dryden, J.J. Vittal, R.J. Puddephatt, Chem. Mater. 5 (1993) 765;
(c) Z. Yuan, N.H. Dryden, J.J. Vittal, R.J. Puddephatt, Chem. Mater. 7 (1995) 1696;
(d) S. Serghini-Monim, Z. Yuan, K. Griffiths, P.R. Norton, R.J. Puddephatt, J. Am. Chem. Soc 117 (1995) 4030;
(e) C. Xu, M.J. Hampden-Smith, T.T. Kodas, Chem. Mater. 7 (1995) 1539;
(f) Z. Yuan, N.H. Dryden, X. Li, J.J. Vittal, R.J. Puddephatt, J. Mater. Chem. 5 (1995) 303;
(g) R. West, R. Riley, J. Inorg. Nucl. Chem. 5 (1958) 295;
(h) C. Xu, M.J. Hampden-Smith, T.T. Kodas, E.N. Duesler, A.L. Rheingold, G. Yap, Inorg. Chem. 34 (1995) 4767;
(i) D.B. Beach, J.M. Jasinski, US Patent 4 948 (1990) 623;
(j) E.T. Eisenbraun, A. Klaver, Z. Patel, G. Nuesca, A.E. Kaloyeros, J. Vac. Sci. Technol. B 19 (2001) 585.
[7] A. Bailey, T.S. Corbitt, M.J. Hampden-Smith, E.N. Duesler, T.T. Kodas, Polyhedron 12 (1993) 1785.
[8] (a) M. Das, Inorg. Chim. Acta 48 (1981) 33;
(b) S.H.H. Chaston, S.E. Livingstone, T.N. Lockyer, V.A. Pickles, J.S. Shannon, Aust. J. Chem. 18 (1965) 673;
(c) R.K.Y. Ho, S.E. Livingstone, T.N. Lockyer, Aust. J. Chem. 19 (1966) 1179;
(d) S.H.H. Chaston, S.E. Livingstone, Aust. J. Chem. 20 (1967) 1065;
(e) S.H.H. Chaston, S.E. Livingstone, Aust. J. Chem. 20 (1967) 1079;
(f) E. Uhlemann, U. Eckelmann, Z. Anorg. Allg. Chem. 383 (1971) 321;
(g) E. Uhlemann, P. Thomas, Z. Anorg. Allg. Chem. 356 (1967) 71.
[9] K. Dietrich, K. König, G. Mattern, H. Musso, Chem. Ber. 121 (1988) 1277.
[10] K.K. Banger, A. Kornilov, R.U. Claessen, E.T. Eisenbraun, A.E. Kaloyeros, P.J. Toscano, J.T. Welch, Inorg. Chem. Commun. 4 (2001) 496.
[11] H.-K. Shin, K.M. Chi, J. Farkas, M.J. Hampden-Smith, T.T. Kodas, E.N. Duesler, Inorg. Chem. 31 (1992) 424.
[12] I. Wakeshima, H. Ohgi, I. Kijima, Synth. React. Inorg. Met.-Org. Chem. 23 (1993) 1507.
[13] A. Bruce, J.L. Corbin, P.L. Dahlstrom, J.R. Hyde, M. Minelli, E.I. Stiefel, J.T. Spence, J. Zubieta, Inorg. Chem. 21 (1982) 917.
[14] W. Partenheimer, E.H. Johnson, Inorg. Chem. 11 (1972) 2840.
[15] A reviewer pointed out that the elemental analyses and NMR spectra can not exclude the presence of a mixture of Ag(β-diketonate)$(L)_n$, $n = 0$, 1, and 2. Low temperature NMR in a noncoordinating solvent could resolve the issue, but the complexes were not sufficiently soluble to answer this question.
[16] K. Dietrich, H. Musso, R. Allmann, J. Organomet. Chem. 93 (1975) 15.
[17] D.A. Edwards, R.M. Harker, M.F. Mahon, K.C. Molloy, J. Mater. Chem. 9 (1999) 1771.
[18] P. Doppelt, T.H. Baum, L. Ricard, Inorg. Chem. 35 (1996) 1286.
[19] (a) J.A. Darr, M. Poliakoff, A.J. Blake, W.-S. Li, Inorg. Chem. 37 (1998) 5491;
(b) J.A. Darr, M. Poliakoff, W.-S. Li, A.J. Blake, J. Chem. Soc., Dalton Trans. (1997) 2869.
[20] (a) K.-M. Chi, K.-H. Chen, S.-M. Peng, G.-H. Lee, Organometallics 15 (1996) 2575;
(b) K.-M. Chi, C.-T. Lin, S.-M. Peng, G.-H. Lee, Organometallics 15 (1996) 2660;
(c) K.-M. Chi, K.-H. Chen, H.-C. Lin, K.-J. Lin, Polyhedron 16 (1997) 2147;
(d) K.-M. Chi, Y.-H. Lu, Chem. Vap. Deposit. 7 (2001) 117.
[21] C. Xu, T.S. Corbitt, M.J. Hampden-Smith, T.T. Kodas, E.N. Duesler, J. Chem. Soc., Dalton Trans. (1994) 2841.
[22] Z. Yuan, N.H. Dryden, J.J. Vittal, R.J. Puddephatt, Can. J. Chem. 72 (1994) 1605.
[23] A.J. Blake, N.R. Champness, S.M. Howdle, P.B. Webb, Inorg. Chem. 39 (2000) 1035.
[24] (a) L.M. Shkol'nikova, Y.M. Yutal', E.A. Shugam, A.N. Knyazeva, J. Struct. Chem. (Engl. Transl.) 14 (1973) 80;
(b) L.E. Pope, J.C.A. Boeyens, Acta Crystallogr., Sect. B 32 (1976) 1599;
(c) G. Bandoli, U. Mazzi, H. Spies, R. Münze, E. Ludwig, E. Ulhemann, D. Scheller, Inorg. Chim. Acta 132 (1987) 177;
(d) L.W. Tari, G.A. Stern, J.B. Westmore, A.S. Secco, Acta Crystallogr., Sect. C 46 (1990) 197.
[25] (a) J. Coetzer, J.C.A. Boeyens, J. Cryst. Mol. Struct. 1 (1971) 277;
(b) J. Sieler, P. Thomas, E. Uhlemann, E. Höhne, Z. Anorg. Allg. Chem. 380 (1971) 160;
(c) O. Siiman, D.D. Titus, C.D. Cowman, J. Fresco, H.B. Gray, J. Am. Chem. Soc. 96 (1974) 2353;
(d) D.C. Craig, M. Das, S.E. Livingstone, N.C. Livingstone, Cryst. Struct. Commun. 3 (1974) 283;
(e) B.F. Hoskins, C.D. Pannan, Inorg. Nucl. Chem. Lett. 11 (1975) 409;
(f) J. Ollis, M. Das, V.J. James, S.E. Livingstone, K. Nimgirawath, Cryst. Struct. Commun. 5 (1976) 679;
(g) C. Sreelatha, V.D. Gupta, C.K. Narula, H. Nöth, J. Chem. Soc., Dalton Trans. (1985) 2623.
[26] (a) K. Tang, M. Aslam, E. Block, T. Nicholson, J. Zubieta, Inorg. Chem. 26 (1987) 1488;
(b) E. Block, M. Gernon, H. Kang, G. Ofori-Okai, J. Zubieta, Inorg. Chem. 28 (1989) 1263;
(c) K. Tang, J. Yang, Q. Yang, Y. Tang, J. Chem. Soc., Dalton Trans. (1989) 2297;
(d) E. Block, D. Macherone, S.N. Shaikh, J. Zubieta, Polyhedron 9 (1990) 1429;
(e) X. Jin, K. Tang, W. Liu, H. Zeng, H. Zhao, Y. Ouyang, Y. Tang, Polyhedron 15 (1996) 1207.

PERGAMON

Polyhedron 21 (2002) 1299–1304

POLYHEDRON

www.elsevier.com/locate/poly

Crystal structure and heat capacity of the mixed-valence trinuclear iron monoiodoacetate complex, $[Fe(III)_2Fe(II)O(O_2CCH_2I)_6(H_2O)_3][Fe(III)_3O(O_2CCH_2I)_6(H_2O)_3]I$☆

Tadahiro Nakamoto [a,*], Qi Wang [b], Yuji Miyazaki [a], Michio Sorai [a,*]

[a] *Research Center for Molecular Thermodynamics, Graduate School of Science, Osaka University, 1-1 Machikaneyama, Toyonaka, Osaka 560-0043, Japan*

[b] *Department of Chemistry, Zhejiang University, Hangzhou 310027, People's Republic of China*

Received 14 January 2002; accepted 18 March 2002

Abstract

The crystal structure of a trinuclear iron monoiodoacetate complex was determined. Although it has been incorrectly characterized as $[Fe_3O(O_2CCH_2I)_6(H_2O)_3]$, the correct chemical formula turned out to be $[Fe(III)_2Fe(II)O(O_2CCH_2I)_6(H_2O)_3]$-$[Fe(III)_3O(O_2CCH_2I)_6(H_2O)_3]I$ (**1**). The two kinds of Fe_3O molecules ($Fe(III)_2Fe(II)O$ and $Fe(III)_3O$) are crystallographically indistinguishable. All the Fe atoms are crystallographically equivalent because of a crystallographic threefold symmetry. Heat capacities of **1** seem to exhibit no thermal anomaly in the temperature range 5.5–309 K, although the valence detrapping phenomenon has been observed in this temperature range. This fact indicates that the valence-detrapping phenomenon in **1** occurs without any phase transition, leading **1** to a glassy state, probably because the crystal of **1** is just like a solid solution of distorted mixed-valence $Fe(III)_2Fe(II)O$ molecules and permanently undistorted $Fe(III)_3O$ molecules which may act as an inhibitor for a cooperative valence-trapping. © 2002 Elsevier Science Ltd. All rights reserved.

Keywords: Mixed-valence compound; Electron transfer; Iron; Trinuclear; Iodoacetate; Heat capacity

1. Introduction

^{57}Fe Mössbauer spectra of mixed-valence trinuclear iron carboxylate complexes $[Fe(III)_2Fe(II)O(O_2CR)_6L_3]$ (R: substituent group, L: monodentate neutral molecule) have been known to exhibit a temperature-dependent valence transformation between a valence-detrapped state at high temperatures and a valence-trapped state at low temperatures in the solid state [1]. Recent studies on this type of complex have shown that the valence trapping-detrapping process is accompanied by phase transitions [2] and that the mixed-valence state observed by ^{57}Fe Mössbauer spectroscopy is sensitively affected by the solid state environment [3]. It has been observed that the solvent molecule in crystals of solvated acetate complexes, $[Fe_3O(O_2CCH_3)_6L_3]S$ (S: solvate molecule), can modulate the lattice dynamics and can determine the rate of intramolecular electron transfer [3].

The valence detrapping phase transition has also been found in non-solvated mixed-valence trinuclear iron carboxylate complexes, $[Fe_3O(O_2CR)_6L_3]$ [4]. The cyanoacetate complex $[Fe_3O(O_2CCH_2CN)_6(H_2O)_3]$ [5] is an appropriate substance for the study of valence-detrapping phase transitions because of the lack of solvate molecules. From the crystal structure determinations above and below T_c, a clear change in the molecular-core structure formed by three iron atoms from an equilateral triangle to an isosceles triangle was observed for the first time. The most essential factor controlling the valence-trapping phenomenon (not valence-trapping phase transition) has been suggested to be the electric

☆ Contribution number 64 from the Research Center for Molecular Thermodynamics.

* Corresponding authors. Tel.: +81-6-6850-5523; fax: +81-6-6850-5526.

E-mail addresses: tadahiro@chem.sci.osaka-u.ac.jp (T. Nakamoto), sorai@chem.sci.osaka-u.ac.jp (M. Sorai).

0277-5387/02/$ - see front matter © 2002 Elsevier Science Ltd. All rights reserved.
PII: S0277-5387(02)00976-2

dipole moment ascribed to the distorted Fe_3O molecule itself in this complex [5].

In the course of our investigations, we found that the monoiodoacetate-aqua complex previously reported as $[Fe_3O(O_2CCH_2I)_6(H_2O)_3]$ [6] is an unusual compound. Its correct formula turned out to be $[Fe(III)_2Fe(II)O(O_2CCH_2I)_6(H_2O)_3][Fe(III)_3O(O_2CCH_2I)_6(H_2O)_3]I$ (**1**). Two types of (mixed-valence and homo-valence) Fe_3O clusters coexist in the same crystal, just like a solid solution. In the case of the mixed-valence solid solutions, $[Fe(III)_2Fe(II)_{1-x}Co(II)_xO(O_2CCH_3)_3(py)_3]\cdot py$ [7], it has been found that the Fe_2CoO molecule acts as unusual quenched disorder for the valence trapping phase transition, hindering the ordering of trapped-valence Fe_3O molecules in the solid solution even before the percolation threshold is reached [8]. Adachi et al. [8] examined the effect of doping of permanently distorted Fe_2CoO molecules in the mixed-valence Fe_3O complex, which exhibits a cooperative valence trapping phase transition. The present system can be regarded as a solid solution of a Fe_3O complex doped with permanently undistorted Fe_3O monocations, although the undoped crystal of each complex has not been isolated. Thermal properties of such a system are of great interest and will give some insight into the valence trap-detrapping phenomenon. In the present paper, we report the single crystal structure determination and heat capacity measurement of **1**.

2. Experimental

2.1. Compound preparation

2.1.1. $[Fe(III)_2Fe(II)O(O_2CCH_2I)_6(H_2O)_3][Fe(III)_3O(O_2CCH_2I)_6(H_2O)_3]I$ (**1**)

A solution of CH_2ICO_2H (50.2 g, 0.27 mol) and NaOH (3.4 g, 0.066 mol) in 50 ml of water was added to a solution of $FeCl_2\cdot 4H_2O$ (13.2 g, 0.066 mol) in 50 ml of water. The resulting mixture was allowed to stand for several weeks in air. Black needle-like crystals were filtered off, washed with water and acetone, and dried under a nitrogen atmosphere. *Anal.* Found: C, 10.46; H, 1.25; I, 58.22. Calc. for $C_{24}H_{36}O_{32}Fe_6I_{13}$: C, 10.22; H, 1.29; I, 58.47%.

2.2. Crystal structure determination

All measurements were made by using graphite monochromated Mo Kα (0.71069 Å) radiation and a rotating anode generator (40 kV, 150 mA) on a Rigaku AFC-5R diffractometer at 296 K. A crystal with dimensions of $0.20 \times 0.20 \times 0.50$ mm^3 cut from a long needle-like crystal was mounted on the end of a glass fiber by epoxy cement. Data collection was made by using the ω–2θ scan to a maximum 2θ value of 55.0°.

Table 1
Crystallographic data of $[Fe_3O(O_2CCH_2I)_6(H_2O)_3]I_{0.5}$ at 296 K

Temperature (K)	296
Empirical formula	$C_{12}H_{18}I_{6.5}Fe_3O_{16}$
Formula weight	1410.74
Crystal system	trigonal
Space group	$R\bar{3}$ (# 148)
a (Å)	13.846(2)
c (Å)	28.625(2)
V (Å^3)	4752(1)
Z	6
D_{calc} (g cm^{-3})	2.96
μ (cm^{-1})	77.5
Radiation (Å)	Mo Kα, 0.71069
2θ Range (°)	5–55
Goodness-of-fit	1.61
R_1 [a]	0.046
R_w [b]	0.114

[a] $R_1 = (\Sigma||F_o|-|F_c||)/(\Sigma|F_o|)$.
[b] $R_w = [\Sigma w(|F_o|-|F_c|^2)/(\Sigma w|F_o|^2)]^{1/2}$.

The structure was solved by direct method SHELXS-86 [9] and expanded by using Fourier techniques. An intense peak found in the difference Fourier map was regarded as the I^- ion. None of the refinements locating the other possible atoms such as O, Na and Cl could converge with any reasonable thermal parameters. All the non-hydrogen atoms were refined anisotropically. Hydrogen atoms of iodoacetate ligands were located in idealized positions of the tetrahedral methylen group with a fixed distance of 0.95 Å by calculation but not refined. Hydrogen atoms of water could not be located. Crystallographic data are presented in Table 1. Selected bond lengths and angles are summarized in Tables 2 and 3, respectively. The final positional parameters are provided as Supporting Information in CIF format.

2.3. Heat capacity measurement

Heat capacity measurements between 6 and 309 K were made with a home-built adiabatic microcalorimeter [10,11]. The mass of the sample **1** used for the calorimetry was 2.50608 g, but we determined molar heat capacities by assuming as if it were 1.77650 mmol of $[Fe_3O(O_2CCH_2I)_6(H_2O)_3]I_{0.5}$. A small amount of helium gas was sealed in the calorimeter cell to aid the heat transfer.

3. Results and discussion

The mixed-valence Fe_3O type complex with monoiodoacetate anion was first reported by Yakubov et al. [12,13], and a valence detrapping phenomenon was observed by ^{57}Fe Mössbauer spectroscopy. Sato et al. [6] also studied the crystalline sample of this complex and observed a valence detrapping phenomenon by ^{57}Fe

Table 2
Selected bond lengths (Å) for $[Fe_3O(O_2CCH_2I)_6(H_2O)_3]I_{0.5}$ at 296 K

Fe1–O1	1.896(1)
Fe1–O2	2.122(5)
Fe1–O3	2.039(5)
Fe1–O4 [a]	2.096(5)
Fe1–O5	1.997(5)
Fe1–O6	2.014(5)
O3–C1	1.259(9)
O4–C1	1.250(9)
C1–C2	1.50(1)
C2–I1	2.12(1)
O5–C3	1.260(8)
O6–C3 [b]	1.267(8)
C3–C4	1.477(9)
C4–I2	2.158(8)

[a] Symmetry codes; $-x+y-1$, $-x+2$, z.
[b] Symmetry codes; $-y+2$, $x-y+3$, z.

Table 3
Selected bond angles (°) for $[Fe_3O(O_2CCH_2I)_6(H_2O)_3]I_{0.5}$ at 296 K

O1–Fe1–O2	176.7(3)
O1–Fe1–O3	96.1(2)
O1–Fe1–CH	93.0(2)
O1–Fe1–O5	98.7(2)
O1–Fel–O6	96.0(2)
Fe1–O3–C1	132.4(5)
Fe1–O4–C1 [a]	131.0(5)
Fe1–O5–C3	132.9(5)
Fe1–O6–C3 [b]	131.1(5)
O3–C1–O4	125.4(7)
O3–C1–C2	117.2(7)
O4–C1–C2	117.4(7)
C1–C2–I1	108.5(6)
O5–C3–O6 [a]	124.5(6)
O5–C3–C4	117.8(2)
O6–C3–C4 [a]	117.6(2)
C3–C4–I2	105.4(5)
Fe1–O1–Fe1 [a]	119.90(3)

[a] Symmetry codes; $-x+y-1$, $-x+2$, z.
[b] Symmetry codes; $-y+2$, $x-y+3$, z.

Mössbauer spectroscopy. At 8.5 K two quadrupole split doublets were observed and ascribed to a high-spin Fe(II) and a high-spin Fe(III). With increasing temperature, two doublets became indistinguishable and seemed to coalesce into one broad peak at room temperature, but there was a peculiar feature in the Mössbauer spectra, i.e. the area ratio of Fe(II) and Fe(III) seemed to be much smaller than 1/2 even at liquid helium temperature. Unfortunately, however, there has been no structure report on this complex, so as to solve the mysterious situation, before the present structure determination.

An ORTEP plot of **1** is shown in Fig. 1. There is only one independent molecular site in the crystal. The ratio of Fe_3O complex site and I^- ion site is 2:1 owing to the crystallographic necessity. As the occupancy factor of each site is 1.0, the chemical formula of **1** should be

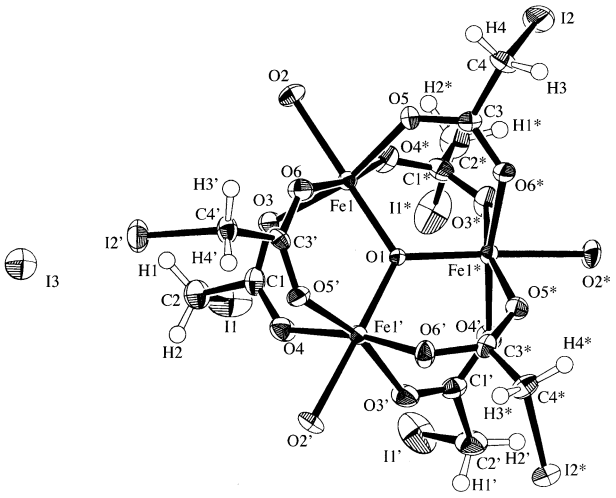


Fig. 1. ORTEP drawing of **1**. The thermal ellipsoids are drawn at the 50% probability level. This molecular structure is a time average and space average of two kinds of molecules.

$[Fe_3O(O_2CCH_2I)_6(H_2O)_3]_2I$. To maintain the whole charge balance, the crystal of **1** should consist of two kinds of Fe_3O complexes, $[Fe(III)_2Fe(II)O(O_2CCH_2I)_6(H_2O)_3]$ and $[Fe(III)_3O(O_2CCH_2I)_6(H_2O)_3]I$ in the ratio of 1:1. Probably these two kinds of Fe_3O complexes are arranged in the crystal with some regularity, but they are crystallographically indistinguishable. It is very likely that the source of I^- ion is monoiodoacetic acid. The elimination of I^- ion from $CH_2ICO_2^-$ may occur in the reaction mixture. It was difficult to distinguish the present complex from $[Fe_3O(O_2CCH_2I)_6(H_2O)_3]$ by elemental analysis, because there is no significant difference in the contents of C and H between **1** and $[Fe_3O(O_2CCH_2I)_6(H_2O)_3]$. For example, the calculated values for $[Fe_3O(O_2CCH_2I)_6(H_2O)_3]$ ($C_{12}H_{18}O_{16}Fe_3I_6$) are C, 10.70; H, 1.35; I, 56.52%. The difference on the contents of I is insignificant beyond the experimental error of approximately 0.3%. Since the correct formula was found to be different from that of the normal mixed-valence Fe_3O type complex, the ^{57}Fe Mössbauer spectrum of **1** should be re-analyzed by assuming the existence of two Fe_3O complexes: one quadrupole split doublet ascribed to high spin Fe(III) at any temperatures, and an $Fe(III)_2Fe(II)O$ complex showing temperature-dependent spectra from valence trapped at low temperature to valence detrapped at room temperature.

The selected bond lengths are listed in Table 2. It has been established that the Fe–(μ_3-O) distance determined by single crystal X-ray structure determination well corresponds to the 'effective' valence state of the Fe atom [1]. For example, the distances Fe(II)–O = ~2.0 Å and Fe(III)–O = ~1.85 Å are observed in a fully trapped Fe_3O complex at room temperature. Recently, the longest and the shortest distances for a mixed-valence Fe_3O complex were reported for $[Fe_3O(O_2CC-$

Table 4
Molar heat capacities of the spin crossover complex $[Fe_3O(O_2CCH_2I)_6(H_2O)_3]I_{0.5}$ (relative molar mass 1410.69)

Temperature (K)	C_p (J K^{-1} mol^{-1})	Temperature (K)	C_p (J K^{-1} mol^{-1})	Temperature (K)	C_p (J K^{-1} mol^{-1})
5.525	10.85	58.013	270.17	139.053	496.87
5.598	11.08	59.018	275.15	141.077	500.99
5.825	12.02	59.955	278.56	143.100	505.79
6.134	14.03	60.959	281.79	145.126	510.46
6.557	16.44	61.904	284.66	147.150	514.96
7.038	18.85	62.903	288.73	149.176	519.36
7.592	22.17	63.856	289.88	151.707	524.90
7.960	24.29	64.851	294.94	154.736	532.86
8.172	25.77	65.809	297.19	157.741	539.16
8.807	29.08	66.801	301.80	160.721	545.01
9.404	32.21	67.764	304.88	163.699	551.30
10.103	36.66	68.757	308.03	166.680	557.43
10.816	41.33	69.724	311.86	169.663	563.31
11.540	46.15	70.712	315.19	172.646	569.51
12.278	51.34	71.690	317.92	175.630	576.04
13.027	56.37	72.671	321.14	178.616	582.03
13.786	61.46	73.660	324.72	181.601	587.94
14.561	66.50	74.630	327.89	184.584	594.04
15.346	72.19	75.632	332.31	187.570	600.18
16.155	77.22	76.595	334.41	190.556	606.11
16.984	82.51	77.607	337.53	193.540	612.03
17.775	87.32	78.564	340.57	196.524	617.86
18.606	92.37	79.582	343.73	199.508	623.83
18.922	94.21	80.535	346.20	202.494	629.60
19.441	97.90	81.562	349.73	205.482	635.48
19.990	101.12	82.506	352.38	208.468	640.75
20.319	102.92	83.541	355.79	211.454	646.44
21.291	108.33	84.586	358.82	214.439	651.65
22.275	114.10	85.524	361.91	217.424	656.76
22.744	116.97	86.571	364.09	220.408	662.70
23.332	120.61	87.507	368.10	223.393	667.92
24.127	124.91	88.559	369.88	226.378	673.78
24.440	126.66	89.490	374.52	229.364	679.74
25.560	132.31	90.547	376.29	232.350	685.63
26.859	138.92	91.476	379.32	235.337	690.82
28.211	146.15	92.537	381.72	238.324	696.45
29.693	154.19	93.462	384.77	241.312	702.00
31.046	159.66	94.529	386.83	244.298	707.46
32.461	166.27	95.450	389.59	247.282	712.86
33.874	172.44	96.522	392.48	250.268	718.65
35.293	178.99	98.515	398.36	253.255	723.92
36.839	186.38	100.510	403.78	256.241	729.10
38.276	192.81	102.730	409.43	259.226	734.57
39.717	198.13	104.741	415.13	262.211	739.89
41.164	204.71	106.755	419.97	265.194	745.01
42.604	210.86	108.771	425.41	268.179	750.82
44.046	216.21	110.789	430.13	271.163	756.42
45.489	222.13	112.805	435.41	274.146	761.79
46.934	228.08	114.821	440.14	277.130	767.10
48.383	234.16	116.838	444.61	280.114	773.18
49.636	238.71	118.855	449.36	283.098	779.17
50.291	240.39	120.873	454.51	286.080	784.45
51.325	244.41	122.891	459.13	289.061	790.46
52.217	248.48	124.908	463.72	292.042	796.76
53.242	251.90	126.926	468.78	295.021	802.77
49.636	238.71	128.944	473.27	296.791	805.88
54.142	256.07	130.964	478.43	299.805	811.87
55.157	260.96	132.985	483.04	302.817	819.25
56.075	263.30	135.008	487.52	305.835	824.79
57.083	268.58	137.030	492.36	308.851	830.57

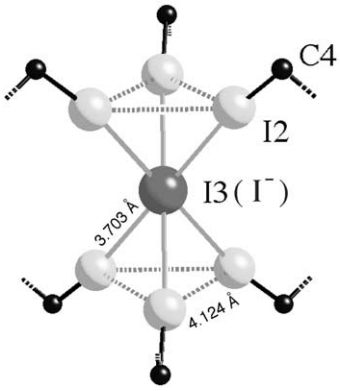


Fig. 2. Bicapped trigonal antiprism structure constructed by the I^- ion and surrounding six I atoms of $CH_2ICO_2^-$.

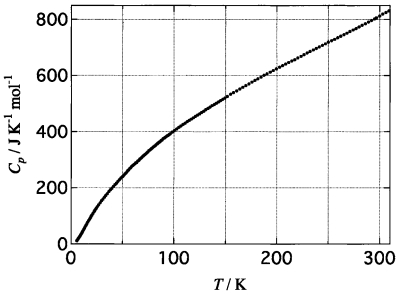


Fig. 3. Plot of the molar heat capacity of $[Fe_3O(O_2CCH_2I)_6(H_2O)_3]I_{0.5}$ vs. temperature.

$Me_3)_6(py)_3]$: 2.046 Å attributable to Fe(II)–O (28 K) and 1.824 Å attributable to Fe(III)–O (10 K) [14]. In the case of a valence fluctuation system, the Fe–O distance shows an intermediate value depending on the mixing ratio of Fe(II) and Fe(III) at each Fe site, because the single crystal structure determination provides a space and/or time averaged structure. In a valence detrapped system, the Fe–(μ_3-O) distance of a molecule with crystallographic threefold symmetry is usually $\sim$1.9 Å, corresponding to a weighted-average of the three distances in a trapped molecule, while those of a Fe_3O molecule located on a crystallographically lower symmetric site are usually in a range between 1.85 and 2.0 Å and exhibit a temperature dependence [3,15]. The three distances sometimes exhibit a curious temperature dependence [15], but finally they become close to one at 2.05 Å and two at 1.85 Å at low temperature [3,5,15]. On the other hand, the Fe(III)–O length in $Fe(III)_3O$ complex is $\sim$1.9 Å, slightly longer than that in a mixed-valence molecule. These lengths are known to be slightly varied by some anisotropy effect or packing force [1]. In the case of **1**, all the Fe–(μ_3-O) lengths are 1.896 Å at room temperature. This value is close to both the Fe(III)–O length in a $Fe(III)_3O$ complex and the averaged length in a $Fe(III)_2Fe(II)O$ complex.

It is worth stating here about another interesting feature of the structure. Fig. 2 illustrates a bicapped trigonal antiprism structure constructed by the I^- ion and surrounding six I atoms of monoiodoacetate ligands. The interatomic distance of $I^-\cdots I$ is 3.703 Å and the shortest $I\cdots I$ distance in the bicapped trigonal antiprism is 4.124 Å. These distances are much longer than 2.715 Å, the intramolecular I–I distance of I_2 in the solid sate, implying no chemical bond between the I atoms and I^- ion. However, they are close to the shortest interatomic approaches between the I_2 molecules, 3.50 Å within the layer and 4.27 Å between layers, in solid I_2 [16], indicating a contact of van der Waals radius.

The molar heat capacities under constant pressure, C_p, of **1** at temperatures between 5.5 and 309 K are plotted in Fig. 3 and listed in Table 4. It has so far been known that the valence trapping phase transition takes place below room temperature in any mixed-valence Fe_3O complexes which have crystallographic threefold symmetry at room temperature as a result of valence fluctuation [2,3,5]. If some ordering of Fe_3O molecules takes place in **1**, the entropy change of $(R \ln 3)/2 = 4.567$ J K^{-1} mol^{-1} per mole of $[Fe_3O(O_2CCH_2I)_6(H_2O)_3]I_{0.5}$ should be observed as some type of thermal anomaly. However, neither phase transition nor thermal anomaly was observed in the measured temperature region, although the valence detrapping phenomenon has been observed in the same temperature region based on ^{57}Fe Mössbauer spectroscopy [6]. This is copmprehensible if the crystal of **1** becomes glassy state at low temperatures. In that case, the permanently undistorted $Fe(III)_3O$ cations will act as an inhibitor for the cooperative lattice distortion due to the electron trapping. As there is no phase transition in **1** below room temperature, the crystallographic threefold symmetry will remain at low temperatures even if the mobile electron ceases to itinerate. At low temperatures, the orientational motion of the distorted Fe_3O molecules due to the intramolecular electron transfer will be randomly frozen in three directions, implying a glassy state. Only this situation can explain how **1** interconvertes between the valence-trapped and valence-detrapped states without any phase transition or any thermal anomaly.

4. Supplementary material

Supplementary data are available from the CCDC, 12 Union Road, Cambridge CB2 1EZ, UK (fax: +44-1223-336033; e-mail: deposit@ccdc.cam.ac.uk or www: http://www.ccdc.cam.ac.uk) on request, quoting the deposition number 177652.

References

[1] R.D. Cannon, R.P. White, Prog. Inorg. Chem. 36 (1988) 195.
[2] M. Sorai, D.N. Hendrickson, Pure Appl. Chem. 63 (1991) 1503.
[3] C.-C. Wu, S.A. Hunt, P.K. Gantzel, P. Gütlich, D.N. Hendrickson, Inorg. Chem. 36 (1997) 4717 (and references therein).
[4] T. Nakamoto, M. Katada, H. Sano, Inorg. Chim. Acta 291 (1999) 127 (and references therein).
[5] T. Nakamoto, M. Hanaya, M. Katada, K. Endo, S. Kitagawa, H. Sano, Inorg. Chem. 36 (1997) 4347.
[6] T. Sato, M. Katada, K. Endo, M. Nakada, H. Sano, J. Radioanal. Nucl. Chem. 173 (1993) 107.
[7] H.G. Jang, K. Kaji, M. Sorai, R.J. Wittebort, S.J. Geib, A.L. Rheingold, D.N. Hendrickson, Inorg. Chem. 29 (1990) 3547.
[8] S.H. Adachi, A.E. Panson, R.M. Stratt, J. Chem. Phys. 88 (1988) 1134.
[9] G.M. Sheldrick, SHELXS-86, Program for the solution of crystal structure.
[10] Y. Ogata, K. Kobayashi, T. Matsuo, H. Suga, J. Phys. E; Sci. Instrum. 17 (1984) 1054.
[11] Y. Kume, Y. Miyazaki, T. Matsuo, H. Suga, J. Phys. Chem. Solids 53 (1992) 1297.
[12] (a) K.M. Yakubov, V.V. Zelentsov, T.A. Zhemchuzhnikova, S.K. Abdullaev, V.R. Fisher, Dokl. Akad. Nauk. SSSR. 250 (1980) 402;
(b) K.M. Yakubov, V.V. Zelentsov, T.A. Zhemchuzhnikova, S.K. Abdullaev, V.R. Fisher, Dokl. Phys. Chem. 49 (1980).
[13] (a) S.K. Abdullaev, T.A. Nasonova, K.M. Yakubov, K.I. Turte, V.V. Zelentsov, R.A. Stukan, Zh. Neorg. Khim. 33 (1988) 1765;
(b) S.K. Abdullaev, T.A. Nasonova, K.M. Yakubov, K.I. Turte, V.V. Zelentsov, R.A. Stukan, Russ. J. Inorg. Chem. 33 (1988) 1004.
[14] C. Wilson, B.B. Iversen, J. Overgaard, F.K. Larsesn, G. Wu, S.P. Palii, G.A. Timco, N.V. Gerbeleu, J. Am. Chem. Soc. 122 (2000) 11370.
[15] G. Wu, Y. Zhang, L. Ribaud, P. Coppens, C. Wilson, B.B. Iversen, F.K. Larsesn, Inorg. Chem. 37 (1998) 6078.
[16] N.N. Greenwood, A. Earnshaw, Chemistry of the Elements, 1st ed., Pergamon Press, Oxford, 1984, p. 937.

PERGAMON

Polyhedron 21 (2002) 1305–1310

POLYHEDRON

www.elsevier.com/locate/poly

Diphosphazane supported platinum(II) triflate, amine, and amido complexes: synthesis and X-ray crystal structures

Aibing Xia, Paul R. Sharp *

125 Chemistry, University of Missouri, Columbia, MO 65211, USA

Received 24 January 2002; accepted 19 March 2002

Abstract

Treatment of L_2PtCl_2 ($L_2 = MeN[P(OPh_2)]_2$) with $AgSO_3CF_3$ gives the triflate complex $L_2Pt(SO_3CF_3)_2$ (**1**). Addition of 2,6-dimethylaniline to **1** in CH_2Cl_2 gives the monomeric diamine complex $[L_2Pt(NH_2Ar)_2](SO_3CF_3)_2$ (**2**, $Ar = 2,6\text{-}Me_2C_6H_3$), while reaction of **1** with lithium 2,6-dimethylanilide gives the dimeric bridging amido complex $[L_2Pt(\mu\text{-}NHAr)]_2(SO_3CF_3)_2$ (**3** $Ar = 2,6\text{-}Me_2C_6H_3$). Cyclometalation is observed when **1** is treated with lithium 2,4,6-triphenylanilide yielding the neutral complex $L_2Pt\{NH[2\text{-}(3,5\text{-}Ph_2C_6H_2)C_6H_4]\}$ (**4**). The structures of all four complexes were determined by X-ray diffraction methods. All display the expected four-coordinate square planar Pt geometry. The amine (**2**) and amido (**3**) complexes show N–H hydrogen bonding to the triflate anions. © 2002 Elsevier Science Ltd. All rights reserved.

Keywords: Amido; Amine; Triflate; Platinum; Diphosphazane; Cyclometalation

1. Introduction

Late transition metal amido complexes [1] have attracted considerable interest for their potential in organic synthesis [2] and for their usefulness as synthetic precursors [1,3,4]. Platinum(II) and palladium(II) amido complexes have been widely studied and their structural features and reactivities found to be influenced by differences in the supporting ligands [2,5,6]. A common feature of amido complexes is a relatively high amido ligand electron density. Since one of our major interests is deprotonation of amido ligands to imido ligands we are interested in factors that reduce amido ligand electron density and enhance acidity. Diphosphazanes ($RN(PX_2)_2$) are versatile supporting ligands that can be easily modified on both nitrogen and phosphorus centers to tune steric and electronic properties [7]. Here we report the synthesis and structures of several platinum(II) complexes, including amido complexes, employing the supporting diphosphazane ligand $MeN[P(OPh)_2]_2$.

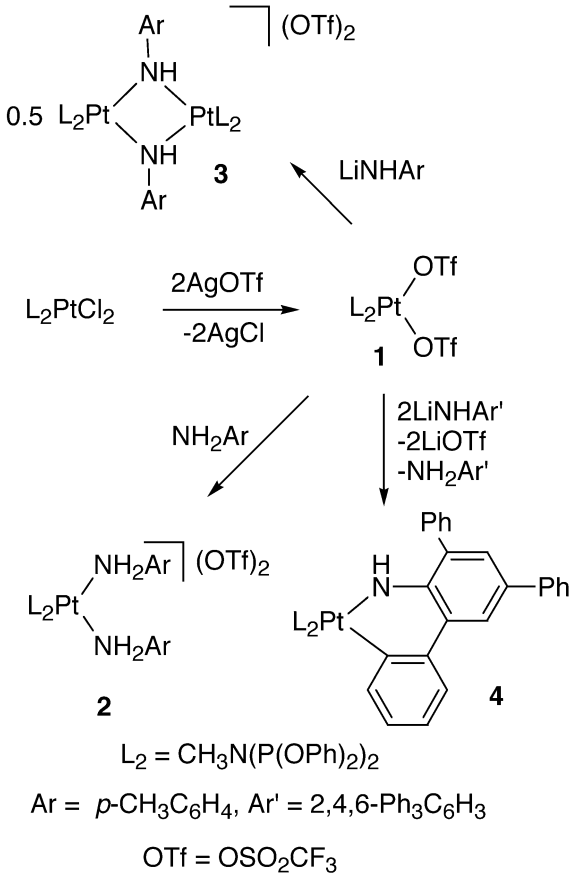
2. Results and discussion

The high lability of the triflate ligand makes metal triflate complexes excellent synthetic precursors [8]. The triflate complex $L_2Pt(SO_3CF_3)_2$ (**1**) is readily obtained from the reaction of L_2PtCl_2 ($L_2 = MeN[P(OPh)_2]_2$) [9] with $AgSO_3CF_3$ in CH_2Cl_2 at ambient temperatures (Scheme 1). The ^{31}P NMR signal of the diphosphazane ligand shifts upfield by about 36 ppm (from 43.5 ppm for the dichloride to 7.5 ppm for the triflate). Along with this upfield shift, the Pt–P coupling constant increases almost 1000 Hz (from 5036 to 6008 Hz). These data imply a stronger P–Pt interaction consistent with the expected weaker *trans*-influence of the triflate ligand [10]. An X-ray crystal structure analysis of **1** (Fig. 1, Table 1) shows the expected square planar Pt center with a *cis*-disposition of the triflate ligands. Selected distances and angles are given in Table 2. There are two known structures of Pt(II) triflate complexes with a phosphorus ligand *trans* to the triflate ligand. The most closely related to **1** is the diphosphine complex $\{1,2\text{-}(PMePh)_2C_6H_4\}Pt(OTf)_2$ [11]. The Pt–O bond lengths in this complex are 2.142(9) and 2.091(8) Å, similar to those in **1** (2.080(3) and 2.096(3) Å). The Pt–O–S angles of 136.1(5)° and 131.1(6)° are slightly greater than those in **1** (130.19(17)° and 128.06(16)°). The more open Pt–

* Corresponding author. Tel.: +1-573-882-7715; fax: +1-573-882-2754.

E-mail address: sharpp@missouri.edu (P.R. Sharp).

0277-5387/02/$ - see front matter © 2002 Elsevier Science Ltd. All rights reserved.
PII: S0277-5387(02)00979-8



Scheme 1.

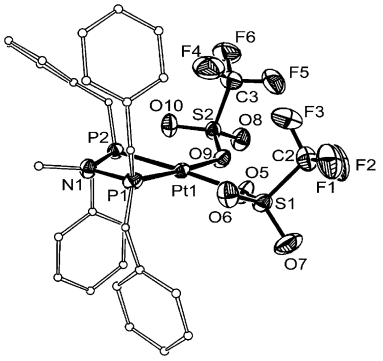


Fig. 1. ORTEP drawing of $L_2Pt(SO_3CF_3)_2$ (**1**). Hydrogen atoms are omitted for clarity. Atoms, except phenoxide atoms and the N–Me carbon (arbitrary spheres), are represented by 50% probability thermal ellipsoids.

O–S angle of $\{1,2\text{-}(PMePh)_2C_6H_4\}Pt(OTf)_2$ may result from steric crowding. Such factors are absent in **1** with its smaller bite angle diphosphazane and less sterically demanding OPh phosphorus substituents. The second complex for comparison is the diphosphine complex $\{(C_2F_5)_2PCH_2CH_2P(C_2F_5)_2\}Pt(Me)(OTf)$ [12]. The Pt–O distance (2.090(6) Å) and the Pt–O–S angle (130.2(3)°) in this complex are almost identical to those of **1** suggesting minimal steric congestion, as in **1**.

As expected, the triflate ligands of **1** are labile and **1** reacts readily with 2,6-dimethylaniline at ambient temperature to afford the diamine complex $[L_2Pt(NH_2Ar)_2](SO_3CF_3)_2$ (**2**, Ar = 2,6-$Me_2C_6H_3$). Complex **2** gives a ^{31}P NMR signal at 16.5 ppm with a Pt–P coupling constant of 4900 Hz. This decrease in the Pt–P coupling constant from that of **1** and L_2PtCl_2 is indicative of the stronger *trans*-influence of the amine ligand relative to the triflate and chloride ligands [10]. The NH peak is observed in the ^1H NMR spectrum of **2** at 7.04 ppm (CD_2Cl_2), shifted downfield by about 2 ppm from that of the free ligand in the same solvent. An X-ray crystal structure analysis of **2** (Fig. 2, Table 1) shows the expected square planar Pt center with a *cis*-disposition of the amine ligands. The amine ligands interact with the two triflate anions through bifurcated hydrogen bonds. Metrical parameters are given in Table 3. Comparison structures with mononuclear *cis*-P_2PtN_2 cores are mostly limited to complexes incorporating the amine nitrogen in a chelate ring. An exception is the simple ammonia complex *cis*-$[(Ph_3P)_2Pt(NH_3)_2](NO_3)_2$ [13]. This complex shows a similar hydrogen bonding pattern of the coordinated amine to the counter anion, and an average Pt–N distance of 2.098(9) Å. Structures incorporating the amine into a chelate ring have average Pt–N distances ranging from 2.07(11) to 2.110(8) Å [14]. The Pt–N distances of **2** are in this range (2.118(4) and 2.129(4) Å).

Attempts to deprotonate **2** with $LiN(SiMe_3)_2$ to obtain an amido complex were not successful. ^1H NMR spectra of the reaction mixtures showed the loss of the diphosphazane N–Me triplet signal indicating disruption of the diphosphazane ligand, probably through nucleophilic attack on the phosphorus center.

As an alternative to the formation of an amido complex by deprotonation of **2**, **1** was treated with lithium 2,6-dimethylanilide in THF at −30 °C. The amido-bridged dimer $[L_2Pt(\mu\text{-}NHAr)]_2(SO_3CF_3)_2$ (**3**, Ar = 2,6-$Me_2C_6H_3$) was obtained as the only isolated product with anilide to Pt ratios of 1:1–2:1 (Scheme 1). Complex **3** gives a ^{31}P signal at 29.9 ppm with a Pt–P coupling constant of 4628 Hz. The ^1H NMR spectrum shows an N–H peak at 4.93 ppm, an upfield shift compared with the monomeric diamine complex **2** and suggestive of greater electron density on the nitrogen centers in the anilido dimer **3**. However, this shift is lower than that observed for analogous diphosphine complexes (4.6–2.6 ppm) [6] suggesting that the reduced donor properties of the diphosphazane ligand result in less electron density at the amido ligand. An X-ray crystal structure analysis of **3** (Figs. 3 and 4, Table 1) shows the expected edge-shared dimer with a *syn*-orientation of the amido aryl groups. One triflate anion is hydrogen-bonded to the amido groups. The Pt_2N_2 core is slightly bent at the N–N hinge. Factors involved in the bending of di-bridged d^8-square-planar dimers of

Table 1
Crystallographic and data collection parameters at 173 K [a]

Formula	$C_{27}H_{23}F_6N\ O_{10}P_2PtS_2$ (**1**)	$C_{43}H_{45}F_6N_3O_{10}P_2PtS_2$ (**2**)	$C_{68}H_{66}F_6N_4O_{14}P_4Pt_2S_2$ (**3**)·DME [d]	$C_{49}H_{40}N_2O_4P_2Pt$ (**4**)·1.5DME [d]
Color/habit	colorless/block	colorless/needle	yellow/prism	yellow/plate
Size (mm)	0.5 × 0.2 × 0.2	0.5 × 0.05 × 0.05	0.2 × 0.15 × 0.15	0.2 × 0.2 × 0.05
Crystal system	triclinic	monoclinic	monoclinic	triclinic
Space group (Z)	$P\bar{1}$ (2)	Cc (4)	$P2_1/n$ (4)	$P\bar{1}$ (2)
a (Å)	10.7182(6)	13.185(2)	19.809(3)	13.3686(6)
b (Å)	11.2575(6)	17.330(2)	20.117(3)	13.3859(6)
c (Å)	15.7721(9)	21.515(3)	21.242(3)	15.9724(7)
α (°)	82.078(1)	90	90	91.497(1)
β (°)	83.812(1)	101.394(7)	112.780(2)	108.834(1)
γ (°)	64.575(1)	90	90	112.315(1)
Total reflections	13 552	14 825	48 486	19 793
Unique/R_{int}	7337/0.026	8833/0.028	17 226/0.056	10 675/0.029
Observed ($>2\sigma(I)$)	6501	8157	11 169	9391
θ_{max}/%measured	27.13/97.3	27.13/98.9	27.19/99.2	27.15/97.7
R_1 [b]	0.0249	0.0292	0.0381	0.0300
wR_2 [c]/No. var.	0.0582/443	0.0709/604	0.0780/963	0.0691/608

[a] Siemens CCD system (omega scans), SADABS absorption correction, λ (Mo Kα) = 0.71073 Å, refined on F_o^2, H atoms riding/refined.
[b] $R_1 = (\Sigma||F_o|-|F_c||)/\Sigma|F_o|$.
[c] $wR_2 = [(\Sigma(F_o^2-F_c^2)^2)/\Sigma\ w(F_c^2)^2]^{1/2}$ with weight $= 1/[\sigma^2(F_o^2)+(xP)^2+yP]$; $x = 0.0333$, $y = 0$ for **1**; $x = 0.0420$, $y = 4.7556$ for **2**; $x = 0.0299$, $y = 0$ for **3**; $x = 0.0379$, $y = 0$ for **4**; $P = (F_o^2+2F_c^2)/3$.
[d] Solvent of crystallization, DME = $MeOCH_2CH_2OMe$ ($C_4H_{10}O_2$).

Table 2
Selected distances (Å) and angles (°) for $L_2Pt(OTf)_2$ (**1**)

Bond distances			
Pt1–O5	2.080(3)	S2–O10	1.430(3)
Pt1–O9	2.096(3)	S2–O9	1.487(3)
Pt1–P2	2.182(1)	S2–C3	1.819(5)
Pt1–P1	2.190(1)	F5–C3	1.327(5)
S1–O7	1.416(3)	F1–C2	1.325(5)
O5–S1	1.485(3)	F6–C3	1.333(6)
S1–C2	1.814(5)	F3–C2	1.326(6)
S1–O6	1.422(3)	F4–C3	1.325(6)
S2–O8	1.419(3)	F2–C2	1.311(5)
Bond angles			
O5–Pt1–P2	176.53(8)	P2–Pt1–P1	71.21(3)
O5–Pt1–O9	78.21(11)	O9–Pt1–P1	176.03(7)
O5–Pt1–P1	105.65(8)	S1–O5–Pt1	130.19(17)
O9–Pt1–P2	104.96(8)	S2–O9–Pt1	128.06(16)

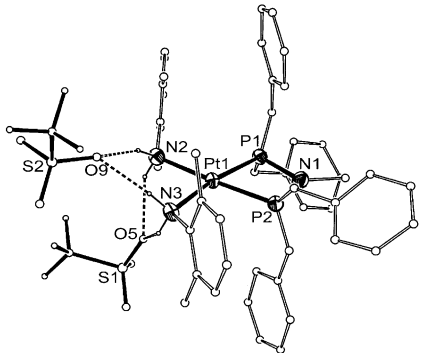


Fig. 2. ORTEP drawing of $[L_2Pt(NH_2Ar)_2](SO_3CF_3)_2$ (**2**, Ar = 2,6-$Me_2C_6H_3$). Hydrogen atoms, except the amine hydrogen atoms, are omitted for clarity. Arbitrary spheres represent the atoms except for the Pt, P, and N atoms, which are represented by 50% probability thermal ellipsoids.

Table 3
Selected distances (Å) and angles (°) for $[L_2Pt(NH_2Ar)_2](SO_3CF_3)_2$ (**2**, Ar = 2,6-$Me_2C_6H_3$)

Bond lengths			
Pt1–P1	2.211(4)	Pt1–P2	2.209(1)
Pt1–N2	2.118(4)	Pt1–N3	2.129(4)
P1–N1	1.664(4)	P2–N1	1.684(4)
N3–C1n	1.472(6)	N2–C1n2	1.475(6)
Bond angles			
P1–Pt1–P2	70.85(5)	N2–Pt1–N3	86.24(16)
Pt1–P1–N1	94.49(17)	Pt1–P2–N1	94.97(16)
P1–N1–P2	99.69(25)		

this type have been studied [15]. Selected bond distances and angles are given in Table 4 and are similar to those of related structurally characterized amido complexes with $P_2Pt(\mu\text{-}N)_2PtP_2$ cores [6,16].

Previous work has shown that $[L_2Pt(\mu\text{-}NHAr)]_2^{2+}$ complexes can be converted to imido complexes by deprotonation if L_2 is the small bite-angle ligand $(Ph_2P)_2NMe$ [3]. We, therefore, anticipated that **3**, with its more weakly donating $[(PhO)_2P]_2NMe$ ligand, would deprotonate even more readily to produce an imido complex. However, treatment of **3** with $LiN(SiMe_3)_2$ does not give an imido complex but rather appears to lead to disruption of the diphosphazane ligand. As in the attempted deprotonation of **2** (see above), this is indicated by the loss of the N–Me triplet signal in the ^1H NMR spectrum of the reaction mixture.

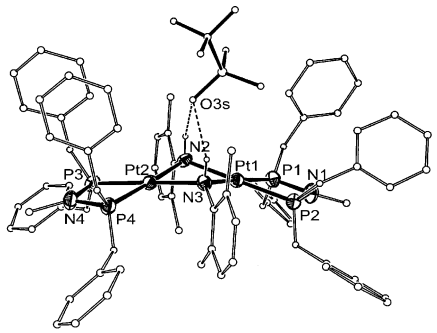


Fig. 3. ORTEP drawing of the cationic portion of $[L_2Pt(\mu\text{-}NHAr)]_2(SO_3CF_3)_2$ (**3**, Ar = 2,6-$Me_2C_6H_3$). Hydrogen atoms, except the N–H hydrogen atoms, are omitted for clarity. All atoms, except phenoxide atoms and the N–Me carbon (arbitrary spheres), are represented by 50% probability thermal ellipsoids.

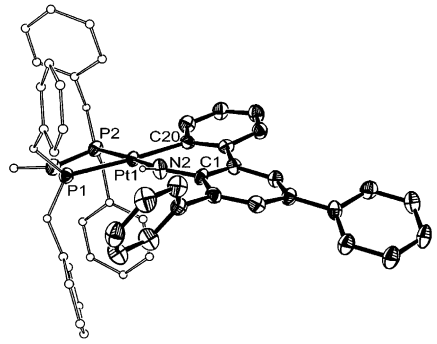


Fig. 4. ORTEP drawing of the cationic portion of $L_2Pt\{NH[2\text{-}(3,5\text{-}Ph_2C_6H_2)C_6H_4]\}$ (**4**). Hydrogen atoms, except the amine hydrogen atoms, are omitted for clarity. Atoms, except phenoxide atoms and the N–Me carbon (arbitrary spheres), are represented by 50% probability thermal ellipsoids.

Table 4
Selected distances (Å) and angles (°) for $[L_2Pt(\mu\text{-}NHAr)]_2(SO_3CF_3)_2$ (**3**, Ar = 2,6-$Me_2C_6H_3$)

Bond lengths			
Pt1–Pt2	3.1732(5)	Pt1–N2	2.115(4)
Pt1–N3	2.104(4)	Pt1–P1	2.210(2)
Pt1–P2	2.206(1)	Pt2–N2	2.113(4)
Pt2–N3	2.104(4)	Pt2–P3	2.220(2)
Pt2–P4	2.208(2)		
Bond angles			
P1–Pt1–P2	70.54(5)	P3–Pt2–P4	70.77(5)
P1–Pt1–N2	106.3(1)	P3–Pt2–N2	105.7(1)
P1–Pt1–N3	175.2(1)	P3–Pt2–N3	175.7(1)
P2–Pt1–N2	176.8(1)	P4–Pt2–N2	176.4(1)
P2–Pt1–N3	104.7(1)	P4–Pt2–N3	105.7(1)
N2–Pt1–N3	78.53(15)	N2–Pt2–N3	78.58(15)
P1–N1–P2	99.53(25)	P3–N4–P4	100.6(3)
Pt1–N2–Pt2	97.26(15)	Pt1–N3–Pt2	97.90(16)

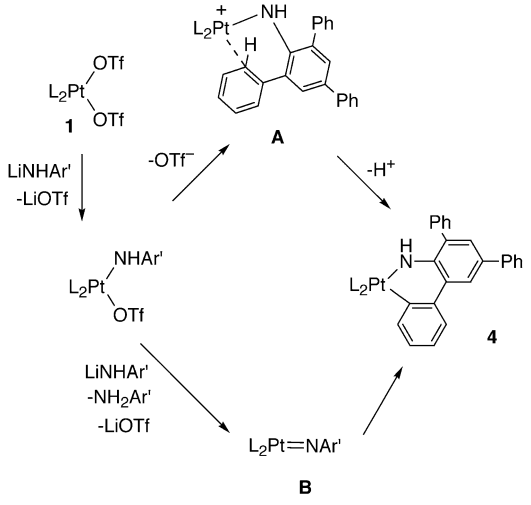
In an effort to block dimer formation as observed in **3**, **1** was treated with 2 equiv. of the bulky anilide LiNH(2,4,6-$Ph_3C_6H_2$). Instead of the expected mononuclear diamido complex, cyclometalation product

Table 5
Selected distances (Å) and angles (°) for $L_2Pt\{NH[2\text{-}(3,5\text{-}Ph_2C_6H_2)C_6H_4]\}$ (**4**)

Bond lengths			
Pt1–P1	2.284(2)	Pt1–P2	2.209(2)
Pt1–N2	1.995(5)	Pt1–C20	2.049(6)
P1–N1	1.673(6)	P2–N1	1.678(6)
Bond angles			
P1–Pt1–P2	69.48(6)	N2–Pt1–C20	89.9(2)
Pt1–P1–N1	96.4(2)	Pt1–P2–N1	93.6(2)
P1–N1–P2	99.7(3)		

$L_2Pt\{NH[2\text{-}(3,5\text{-}Ph_2C_6H_2)C_6H_4]\}$ (**4**) was obtained (Scheme 1). The ^{31}P NMR spectrum of **4** shows two doublets ($J_{P-P} = 49.1$ Hz) at 70.8 ppm ($J_{P-Pt} = 3920$ Hz) and 95.9 ppm ($J_{P-Pt} = 1959$ Hz). The high-shift doublet with the small Pt–P coupling constant is assigned to the phosphorus atom *trans* to the carbon atom consistent with the strong *trans*-influence of a carbon anion [10]. An X-ray crystal structure analysis of **4** (Fig. 4, Table 1) confirms the cyclometalation of the amido ligand. Selected distances and angles are given in Table 5. Remarkably, despite the commercial availability of the aniline, this is apparently only the second report of a transition metal complex formed from this aniline [17]. This is in sharp contrast to other terphenyl ligands, [18] the related phenol, 2,6-$Ph_2C_6H_3OH$, [19] and other substituted anilines, [20] which have been used for the preparation of a number of metal complexes. Cyclometalations, like that observed here, have been reported with the phenoxo ligand 2,6-$Ph_2C_6H_3O$ for a number of early transition metals [19] and for Sn [21] and Ge [22].

Two possible pathways to cyclometalation product **4** are considered in Scheme 2. Both begin by formation of the amido triflate complex $L_2Pt(NHAr')(OTf)$. This species may loose a triflate anion to generate the three-coordinate species $[L_2Pt(NHAr')]^+$ (**A**). (A



Scheme 2.

Ni(II) analog of **A** has been isolated [23]). Three-coordinate species are thought to be required for significant cyclometalation rates in Pt(II) systems [24]. The second pathway requires formation of the terminal imido complex $L_2Pt{=}NAr'$ (**B**) either by deprotonation of $L_2Pt(NHAr')(OTf)$ (or **A**) or formation of $L_2Pt(NHAr')_2$ followed by elimination of H_2NAr'. Addition of the C–H bond across the Pt–N double bond, a process known for terminal early transition metal imido complexes, [25] would then yield **4**. Although never observed, terminal Pt(II) oxo complexes analogous to **B** have been postulated [26] and a Ni(II) analog of **B** has been recently reported [23]. Given the lack of evidence for imido complex **B**, we favor the well-established [24] electrophilic cyclometalation through three-coordinate **A**. However, future work will be directed at establishing the possible existence of **A** with aryl groups that are less susceptible to cyclometalation and supporting ligands (L_2) that discourage approach of the aryl group to the Pt center.

3. Experimental

3.1. General procedures

Experiments were performed under a nitrogen atmosphere in a Vacuum Atmospheres Corp. drybox. Solvents were dried by standard techniques and stored under nitrogen over 4 Å molecular sieves. The compounds 2,6-dimethylaniline, 2,4,6-triphenylaniline, and $AgSO_3CF_3$ were purchased from Aldrich or Acros Chemicals and were used as received. The lithium anilides were prepared from the anilines and $LiBu^n$ (2.5 M) in hexane. $L_2 = MeN[P(OPh)_2]_2$ and L_2PtCl_2 were prepared by literature procedures [9]. NMR spectra were recorded on a Bruker AMX-250 spectrometer. ^1H NMR (250 MHz) and ^{13}C NMR (62.9 MHz) spectra are referenced to TMS or to solvent impurities referenced back to TMS. ^{31}P NMR (101 MHz) spectra are referenced to external 85% H_3PO_4. All NMR shifts are in ppm with negative shift upfield from the reference. Spectra were recorded at ambient temperatures (22 °C) unless otherwise indicated. Melting points are uncorrected.

3.2. Preparation of $L_2Pt(OTf)_2$ (**1**)

Silver trifluoromethane sulfonate (0.257 g, 1.00 mmol) was added to a suspension of L_2PtCl_2 (0.365 g, 0.500 mmol) in 2.0 ml of CH_2Cl_2. The mixture was stirred at ambient temperature overnight and then filtered. Addition of Et_2O (10 ml) to the filtrate afforded a white precipitate of the product. This was collected by filtration, washed twice with Et_2O (3 ml), and dried in vacuo to give 0.400 g (83.5%) of white solid. Colorless single crystals suitable for X-ray diffraction were obtained from CH_2Cl_2–Et_2O. *Anal*. Calc. (Found): C 33.90 (34.12), H 2.42 (2.41), N 1.46 (1.49)%. M.p.: 180–182 °C. ^1H NMR (CD_2Cl_2): 2.91 (t, $^3J_{H-P} = 13.3$ Hz, 3H, Me), 7.20–7.41 (m, 20H, phenyl). ^{13}C NMR (CD_2Cl_2): 31.71 (s, Me), 120.92 (t, $J_{C-P} = 2.4$ Hz, C_{ortho} of Ph), 127.85 (s, C_{para} of Ph), 131.15 (s, C_{meta} of Ph), 149.39 (t, $J_{C-P} = 4.0$ Hz, C_{ipso} of Ph). ^{31}P (CD_2Cl_2): 7.49 ($J_{P-Pt} = 6008$ Hz).

3.3. $[L_2Pt(NH_2Ar)_2](SO_3CF_3)_2$ (**2**, $Ar = 2,6\text{-}Me_2C_6H_3$)

2,6-dimethylaniline (0.032 g, 0.260 mmol) was added to a solution of $(L_2Pt)(OTf)_2$ (0.126 g, 0.132 mmol) in CH_2Cl_2 (2 ml). The solution was stirred for 2 h at ambient temperature. Addition of Et_2O (10 ml) afforded a white precipitate of the product. This was collected by filtration, washed twice with Et_2O (3 ml), and dired in vacuo (0.135 g, 85.4%). Colorless single crystals suitable for X-ray diffraction were obtained from CH_2Cl_2–Et_2O. *Anal*. Calc. (Found): C 43.08 (42.87), H 3.78 (3.87), N 3.50 (3.50)%. M.p.: 196–200 °C. ^1H NMR (CD_2Cl_2): 1.75 (t, $^3J_{H-P} = 12.0$ Hz, 3H, Me), 2.67 (s, 12H, Me), 7.04 (s, overlapped with Ph, NH), 6.87–7.49 (m, 30H, Ph). ^{13}C NMR (CD_2Cl_2): 15.00, 18.11, 110.09, 119.63, 124.53, 126.95, 127.62. ^{31}P (CD_2Cl_2): 16.47 ($J = 4909$ Hz).

3.4. $[L_2Pt(\mu\text{-}NHAr)]_2(OTf)_2$ (**3**, $Ar = 2,6\text{-}Me_2C_6H_3$)

A solution of lithium 2,6-dimethylanilide (0.010 g, 0.079 mmol) in THF (1 ml) was added to a solution of $(L_2Pt)(OTf)_2$ (0.039 g, 0.040 mmol) in THF (1 ml) at −30 °C. The mixture was kept at −30 °C overnight then warmed to ambient temperatures and the volume reduced in vacuo. Et_2O (10 ml) was added and the resulting precipitate was filtered and washed with Et_2O (3 ml) to afford the pale yellow solid product (0.020 g, 50%). Yellow crystals for the X-ray analysis were obtained from DME–$^iPr_2O$. M.p.: 205–208 °C. ^1H NMR (CD_2Cl_2): 2.13 (t, $^3J_{H-P} = 12.0$ Hz, 6H, Me), 2.42 (s, 6H, Me), 3.52 (s, Me), 4.93 (bs, 2H, NH), 6.73–7.45 (m, 26H, Ph). ^{13}C NMR (CD_2Cl_2): 19.18, 22.97, 120.14, 120.21, 127.34, 129.10, 130.80, 130.99, 131.44, 149.49. ^{31}P (CD_2Cl_2): 29.93 ($J_{P-Pt} = 4628$ Hz).

3.5. $L_2Pt\{NH[2\text{-}(3,5\text{-}Ph_2C_6H_2)C_6H_4]\}$ (**4**)

A solution of lithium 2,4,6-triphenylanilide (0.013 g, 0.040 mmol) in THF (1 ml) was added to a solution of $(L_2Pt)(OTf)_2$ (0.020 g, 0.020 mmol) in THF (1 ml) at −30 °C. The mixture was kept at −30 °C overnight and the volume was reduced under reduced pressure. Et_2O (10 ml) was added and the precipitate was filtered and washed with Et_2O (3 ml) to afford a pale yellow solid

(0.010 g, 50%). Yellow crystals for the X-ray analysis were obtained from DME–$^{i}Pr_2O$. M.p.: 196–200 °C. ^{1}H NMR (CD_2Cl_2): 3.00 (t, $^{3}J_{H-P} = 8.0$ Hz, 3H, Me of L_2), 6.60 (1H, NH), 6.64–7.74 (38H, Phenyl). ^{13}C NMR (CD_2Cl_2): 14.27, 126.62, 126.72, 127.28, 127.77, 128.33, 128.62, 128.66, 129.10, 129.38, 131.10, 140.18, 140.95, 141.25. ^{31}P (CD_2Cl_2): 70.80 ($^{2}J_{P-P} = 49.1$ Hz, $J_{P-Pt} =$ 3920 Hz, *trans* to N), 95.86 ($^{2}J_{PP} = 49.1$ Hz, $J_{P-Pt} =$ 1959 Hz, *trans* to C).

4. Supplementary data

Full crystal structure information has been deposited with the Cambridge Crystallographic Data Center (deposition numbers CCDC 178035-CCDC 178038). Copies of this information are available upon request from The Director, CCDC, 12 Union Road, Cambridge CB2 1EZ, UK (fax: +44-1223-336033; e-mail: deposit@ccdc.cam.ac.uk or www: http://www.ccdc.cam.ac.uk).

Acknowledgements

We thank the Division of Chemical Sciences, Office of Basic Energy Sciences, Office of Energy Research, US Department of Energy (Grant DF-FG02-88ER13880) for support of this work. A grant from the National Science Foundation provided a portion of the funds for the purchase of the NMR (CHE 9221835) equipment.

References

[1] Reviews: (a) H.E. Bryndza, W. Tam, Chem. Rev. 88 (1988) 1163; (b) M.D. Fryzuk, C.D. Montgomery, Coord. Chem. Rev. 95 (1989) 1.
[2] For examples see: (a) B.H. Yang, S.L. Buchwald, J. Organomet. Chem. 576 (1999) 125; (b) J.F. Hartwig, Angew. Chem., Int. Ed. Engl. 37 (1998) 2047 (c) L.A. Villanueva, K.A. Abboud, J.M. Boncella, Organometallics 11 (1992) 2963 (d) C.M. Jensen, W.C. Trogler, J. Am. Chem. Soc. 108 (1986) 723.
[3] (a) P.R. Sharp, J. Chem. Soc., Dalton Trans. (2000) 2647; (b) P.R. Sharp, Comments Inorg. Chem. 21 (1999) 85.
[4] K. Koo, G.L. Hillhouse, Organometallics 17 (1998) 2924.
[5] (a) S. Kannan, A.J. James, P.R. Sharp, Polyhedron 19 (2000) 155; (b) H. Shan, A.J. James, P.R. Sharp, Inorg. Chem. 37 (1998) 5727.
[6] J.J. Li, W. Li, A.J. James, T. Holbert, T.P. Sharp, P.R. Sharp, Inorg. Chem. 38 (1999) 1563.
[7] (a) M.S. Balakrishna, V.S. Reddy, S.S. Krishnamurthy, J.F. Nixon, J.C.T.R. Burckett, Coord. Chem. Rev. 129 (1994) 1; (b) M. Witt, H.W. Roesky, Chem. Rev. 94 (1994) 1163.
[8] G.A. Lawrance, Chem. Rev. 86 (1986) 17–33.
[9] (a) M.S. Balakrishna, S.S. Krishnamurthy, R. Murugavel, M. Nethaji, I.I. Mathews, J. Chem. Soc., Dalton Trans. (1993) 477; (b) M.S. Balakrishna, T.K. Prakasha, S.S. Krishnamurthy, U. Siriwardane, N.S. Hosmane, J. Organomet. Chem. 390 (1990) 203.
[10] (a) T.G. Appleton, H.C. Clark, L.E. Manzer, Coord. Chem. Rev. 10 (1973) 335; (b) F.R. Hartley, The Chemistry of Platinum and Palladium, Appl. Sci. Publishers, 1973; (c) E.M. Shustorovich, M.A. Porai-Koshits, Y.A. Buslaer, Coor. Chem. Rev. 17 (1975) 1.
[11] A. Appelt, V. Ariaratnam, A.C. Willis, S.B. Wild, Tetrahedron: Asymmetry 1 (1990) 9.
[12] B.L. Bennett, J. Birnbaum, D.M. Roddick, Polyhedron 14 (1995) 187.
[13] A.D. Burrows, D.M.P. Mingos, S.E. Lawrence, A.J.P. White, D.J. Williams, J. Chem. Soc., Dalton Trans. (1997) 1295.
[14] (a) A.M.Z. Slawin, M.B. Smith, New J. Chem. 23 (1999) 777; (b) Y. Matsuura, K. Okude, H. Ichida, T.K. Miyamoto, Y. Sasaki, Acta Crystallogr. Sect. C: Cryst. Struct. Commun. 48 (1992) 357; (c) E.K. van den Beuken, A. Meetsma, H. Kooijman, A.L. Spek, B.L. Feringa, Inorg. Chim. Acta 264 (1997) 171; (d) T. Suzuki, A. Morikawa, K. Kashiwabara, Bull. Chem. Soc. Jpn. 69 (1996) 2539.
[15] (a) R.H. Summerville, R. Hoffmann, J. Am. Chem. Soc. 98 (1976) 7240; (b) G. Aúllon, G. Ujaque, A. Lledós, S. Alvarez, P. Alemany, Inorg. Chem. 37 (1998) 804; (c) G. Aúllon, G. Ujaque, A. Lledós, S. Alvarez, Chem. Eur. J. 5 (1999) 1391.
[16] (a) C.A. O'Mahoney, I.P. Parkin, D.J. Williams, D.J. Woollins, Polyhedron 8 (1989) 1979; (b) N.W. Alcock, P. Bergamini, T.J. Kemp, P.G. Pringle, S. Sostero, O. Traverso, Inorg. Chem. 30 (1991) 1594.
[17] G.R. Clark, A.J. Nielson, C.E.F. Rickard, J. Chem. Soc., Dalton Trans. (1996) 4265.
[18] B. Twamley, S.T. Haubrich, P.P. Power, Adv. Organomet. Chem. 44 (1999) 1.
[19] Leading references: (a) D.R. Mulford, J.R. Clark, S.W. Schweiger, P.E. Fanwick, I.P. Rothwell, Organometallics 18 (1999) 4448; (b) M.G. Thorn, P.E. Fanwick, I.P. Rothwell, Organometallics 18 (1999) 4442.
[20] (a) P.P. Power, Comments Inorg. Chem. 8 (1989) 177; (b) D.E. Wigley, Prog. Inorg. Chem. 42 (1994) 239–482.
[21] (a) G.D. Smith, P.E. Fanwick, I.P. Rothwell, J. Am. Chem. Soc. 111 (1989) 750; (b) G.D. Smith, V.M. Visciglio, P.E. Fanwick, I.P. Rothwell, Organometallics 11 (1992) 1064.
[22] W. Maringgele, A. Meller, Phosphorus Sulfur Silicon Relat. Elem. 90 (1994) 235–241.
[23] D.J. Mindiola, G.L. Hillhouse, J. Am. Chem. Soc. 123 (2001) 4623.
[24] A.D. Ryabov, Chem. Rev. 90 (1990) 403.
[25] (a) P.J. Walsh, F.J. Hollander, R.G. Bergman, J. Am. Chem. Soc. 110 (1988) 8729; (b) S.Y. Lee, R.G. Bergman, J. Am. Chem. Soc. 117 (1995) 5877; (c) J.L. Bennett, P.T. Wolczanski, J. Am. Chem. Soc. 116 (1994) 2179; (d) C.P. Schaller, C.C. Cummins, P.T. Wolczanski, J. Am. Chem. Soc. 118 (1996) 591; (e) C.P. Schaller, P.T. Wolczanski, Inorg. Chem. 32 (1993) 131.
[26] M.A. Andrews, G.L. Gould, E.J. Vos, Inorg. Chem. 35 (1996) 5740.

PERGAMON

Polyhedron 21 (2002) 1311

POLYHEDRON

www.elsevier.com/locate/poly

Preface

Thermodynamics of Metal Complexes ISMEC XII, Parma, Italy, June 6–9, 2001

This special Issue of POLYHEDRON contains the contributions presented at the Meeting ISMEC 2001 (XII Italian–Spanish Congress on Thermodynamics of Metal Complexes and XXVIII Congress of the Italian 'Gruppo di Termodinamica dei Complessi', GTC). The Meeting has taken place at the University of Parma, Italy from the 6th to 9th of June 2001. The articles are dedicated to the members of the group that have recently retired or are going to retire: Professors Giorgio Ostacoli (University of Turin), Carla Riolo Bertoglio (University of Pavia), Fernando Pulidori (University of Ferrara), Vincenzo Carunchio (University of Rome, La Sapienza), Piero Paoletti (University of Florence), and Antonio Braibanti (University of Parma). Vincenzo Carunchio has described the history of the development of the thermodynamics of Metal Complexes, and of GTC in particular, in his article published in this Issue. The personal scientific contributions by these researchers who, for about three decades, have taken part to the activities of the Group since its foundation, are documented by the titles of their papers contained in the list of publications of the GTC (the updated list can be requested from Professor Diego Ferri, University of Naples, Italy, e-mail: ferri@chemistry.unina.it). Their researches have permitted to obtain significant achievements in the field of thermodynamics of metal complexes from the integrated points of view of inorganic, analytical and physical chemistry.

The human participation to the activities of the Group lives in the memory of all those who have had the opportunity to meet them or to work with them. It is continuously renovated by the contacts they maintain after retirement.

The warm applause by the whole assembly of participants and Academic Authorities that has accompanied the assignment to them of dedicated medals has been the best reward offered to the senior researchers by their Italian and Spanish friends and pupils.

A. Braibanti, E. Fisiccaro
Physical Chemistry Section,
Pharmaceutical Department,
University of Parma,
Parco Area delle Scienze 27/A,
I-43100 Parma, Italy
E-mail addresses: braiban@unipr.it (A. Braibanti)
fisicaro@unipr.it (E. Fisicaro)
Guest Editors

0277-5387/02/$ - see front matter © 2002 Published by Elsevier Science Ltd.
PII: S0277-5387(02)01017-3

PERGAMON

Polyhedron 21 (2002) 1313–1318

POLYHEDRON

www.elsevier.com/locate/poly

Metal complexes: from pioneers to the GTC

Vincenzo Carunchio *

Department of Chemistry, University 'La Sapienza' Piazzale Aldo Moro 5, 00185 Rome, Italy

Received 1 October 2001; accepted 29 October 2001

Abstract

The lecture takes into consideration the main and significant stages of the history of metal complexes. The story begins with the first empirical observations at the end of the XVIII Century, to the attempts for explaining some supposed anomalous behaviours, to the different interpretations by Jorgensen and Werner, to the Ziegler and Natta's achievements. Particular attention is devoted to the development of the study of complex formation equilibria in solution, and kinetic of complexation reactions. Together with these historical passages, consideration is also given to the different scientific fields in which the study of metal complexes gave a noteworthy contribution to increase in knowledge by suggesting some original solutions and supporting other fields of research, especially in biochemistry. With the aim of keeping alive the interest on the fundamental researches in these fields, the Group of Thermodynamics of Complexes (GTC) was constituted in Italy in 1973. The GTC has organised yearly congress and some summer schools, and has produced a wealth of scientific papers. © 2002 Published by Elsevier Science Ltd.

Keywords: Complex history; Complex pioneers; Thermodynamics group; Coordination chemistry

We were taught that 'History is Master of Life', and presuming this saying is correct, its scope can be extended also to the life of that small portion of knowledge represented by the 'Group of Thermodynamics of Complexes' (GTC), that was founded mainly with the aim of preserving the heritage of experiences on this subject, both those already collected, and those yet to be realised. An outline of the articulated history of the complexes, which in its initial phases alterned between critical and fascinating, may be a valid support for the 'complex researchers'.

The term, 'complex', as well as the general concept of 'complex' appear for the first time in the literature in an article by Werner in 1893 [1]. He introduced such innovation being pressed by the obvious desire of every researcher to provide an explanation for everything that he has under study, all the more so when the observed phenomenon appears strange or, at least, anomalous and unpredictable. In that case the attention was focused on solutions containing particular salts, which reacting with one another did not maintain their original chemical properties, but presented new and different ones.

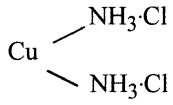
In the previous literature there had been references describing casual events of this type but they were presented with no explanations at all or by interpretations that the later chemists could not accept. The first report of an event that can be related with a metal complex dates back at the beginning of the XVIII century, and refers to the case of a manufacturer from Berlin. He, combining potassium cyanide with iron cyanide, casually obtained a dark blue stain, (also called soluble Prussian Blue) and a blue precipitate (Prussian blue). In later times, they were attributed the formulae $KFe(III)[Fe(II)(CN)_6]$ (soluble) and $Fe(III)_4[Fe(II)(CN)_6]_3$ (precipitate), respectively. The moiety enclosed in squared parentheses is just the 'complex' with secondary valence recognised by Werner. Nevertheless the first article that in the literature [2] refers to a real preparation of a complex mentions $CoCl_3 \cdot 6NH_3$, obtained by Tassaert in 1798. The properties of such compound were pretty peculiar because they were different from those of each single component, but at the time such phenomenon could not find an explanation consistent with current knowledge. The possibilities of combination of these two stable compounds, alleg-

* Tel.: +39-06-495-8251; fax: +39-06-490-631.
E-mail address: carunchio@arma.uniromal.it (V. Carunchio).

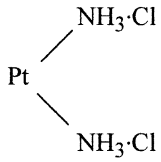
0277-5387/02/$ - see front matter © 2002 Published by Elsevier Science Ltd.
PII: S0277-5387(02)00961-0

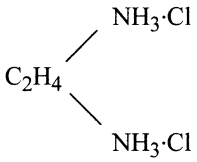
edly having saturated (primary) valences, such as $CoCl_3$ and NH_3, represented an incentive to conduct further researches aimed at the comprehension of the behaviour of some apparently anomalous other salt.

We find also further references to the formation of compounds included in the typology of the complexes, however, they were accompanied with elementary and not convincing explanations which often seemed to depend on the prevailing culture of the organic chemistry. To recall some examples, we can mention the case of the copper(II) complex prepared by Graham (1837), who postulated, the following formula:



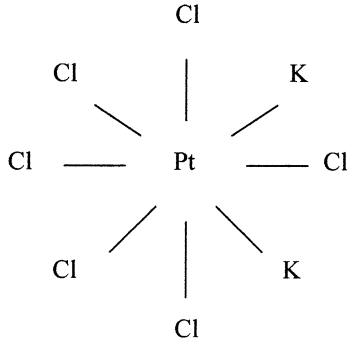
This structure, nevertheless, allowed for no explanation for a metal/amine ratio higher than 1:2.





Another example to be mentioned is a platinum(II) compound obtained by Odling (1870), proposing a sort of analogy between a metal and an ethylene group.

Another interesting attempt to explain the structure of a compound on the basis of the ratio of the elements was proposed by Horstman (1885) for $2KCl–PtCl_4$ in which the metal is attached in the same manner to six atoms of chlorine and two of potassium.



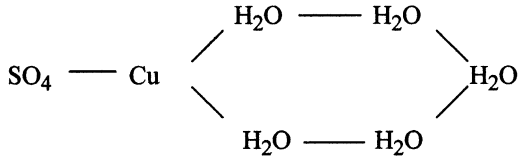
In the meantime, Reset [3] in 1844 and Peyrone [4] in 1845 described almost contemporaneously two compounds responding to the same stoichiometrical ratio ($Pt(NH_3)_2Cl_2$), but presenting different properties. The news of these compounds gave rise to contrasting exchanges of opinion, since the concept of isomerism for the complexes had not yet been achieved.

Summarizing what said before, in the literature we may find several references to such findings of compounds of this kind 'on a chance basis', although, as mentioned above, it was only in 1893 that Werner started to refer to them as 'complexes'. The metal atom (particularly transition metal) was considered as the centre of a whole system, so that we might very easily set the molecules connected or coordinated to it at the corners of an octahedron. Specifically, Werner introduced the concept that metal atoms have two types of valence, primary and secondary. Every metal tends to satisfy both types of valence. The secondary valence is directed toward fixed positions, which form a coordination polyhedron. It is worth noting that Werner introduced also the term 'coordination number', used until today, as well as the entire nomenclature to indicate the complexes. Werner was awarded Nobel Prize in 1913 for such achievements. In this manner he revolutionised-as was later stated by Pauling- the original global concept of valence, giving rise to new 'dissociated' (or 'articulated') concepts, to which we still make reference to today, although obviously in terms of the modern electronic structure of the atoms.

A concrete attempt to interpret analogous compounds was tried also in 1886 by S.M. Jorgensen [5], another pioneer of the chemistry of complexes. Jorgensen, prompted by organic chemistry, supported 'the theory of the chain', the same one that in 1869 inspired Blomstrand [6] to propose for hexamminocobalt(II) a linear formula similar to that of a hydrocarbon,

$Cl–NH_3–NH_3–NH_3–Co–NH_3–NH_3–NH_3–Cl$

It is no wonder that, according to this view, for some compounds, as for example the cupric(II) sulphate pentahydrate, the following ring-structure was proposed:



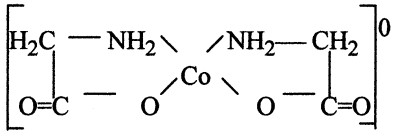
The diversity of opinions between Werner and Jorgensen gave rise to an increase in the development of knowledge relevant to the complexes that, independently from the result of the dispute, the two chemists' names are often recalled together as the pioneers of this branch of the science. In this regard, it is interesting to mention Basolo and Pearson [7] who, in the introduction of their well-known text 'Mechanisms of inorganic reactions' propose an imaginaring meeting between the two famous competitors, a meeting that during their lifetime they did not have the opportunity to arrange.

During the first stage of the historical development of Werner's theory, a notable confirmation derived from the experimental demonstration of the variation of the electric conductivity. In tetramminoplatinum(II), $Pt(NH_3)^{+2}$, the gradual substitution of the chloride ions for ammonia molecules produces a modification of the charge, while maintaining the unity of the 'complex-

ion'. The occasion for this demonstration occurred to Werner as a result of the enunciation of the theory of the electrolytic dissociation, which Arrhenius was formulating in that period. The coordinated complex ion exists as a unit in the solution and the stepwise substitution occurs as a consequence of equilibria between the central metal (in general a transition metal) and one or more ligand. The binding of neutral ligands to the metal ion was explained by introducing the idea of 'coordinative' or 'dative' bond. These coordinated compounds gave rise to the widely used definition of Coordination Chemistry for the study of metal complexes.

During the first 20 years of the XX century, the methods of synthesis of the complexes witnessed considerable development, and the discussions on the relative structures were thoroughly analysed. Among them, particularly those referring to the isomers, determined a definite progress in highlighting the diversities (both logic and real) presented by compounds sharing the same stoichometry but holding different properties, as those previously mentioned [3,4]. And on this occasion too, the culture of organic chemistry inspired concrete analogies for debates and definitions.

Significant progress was also made through the process involving the 'chelation' and related applications [8], although it was a long time before the actual interpretation was arrived at. In fact, the current term, as well as its relevant meaning, was proposed as late as 1920 by Morgan and Drew [9]. The methods of preparation, however, were already known for many of the compounds, even if not yet classified as 'chelates', and Ley [10] had referred some of these electrically neutral complexes as 'metal complex salts' as long ago as 1904:



Subsequently Lewis, [11] in order to interprete the complexation reactions proposed considering them as 'acid–base reactions' in which the metal ions are the acids and the ligands are the bases.

The studies focused particularly on the synthesis and on the structural properties of the complexes were continually growing. Nevertheless, interest in those compounds could not be confined to those targets, albeit of utmost importance.

This very long initial period, which we can actually define as a 'period of pioneers', was the prelude to new phases. After the Second World War, coordination chemistry was undergoing tremendous development mainly under the leadership of inorganic chemists. The main factor, however, was undoubtedly that coordination chemistry is a branch tending to integrate the whole of chemistry. The physical chemists studied the spectroscopic, theoretical, electrochemical, thermochemical, structural and crystallographic properties. The inorganic chemists studied the preparative, spectrochemical, magnetic and structural properties. The organic chemists contributed with preparation of ever new and complicated ligands, and with the study of kinetic, mechanistic, and catalytic properties. The analytical chemists provided the search for new complexing agents for precipitation and spectroscopic identification, and devoted their attention to speciation in solution searching for modern and sophisticated instrumental and computational methods. Subsequently the basic research was intensified both to reach a better comprehension of the experimental data and to obtain some benefits in the applications by means of the implementation of some various scientific and technological branches in a more rational and clear way.

An ever-increasing role was being played by the study of the mechanisms of metal–ligand interactions. Consequently, the studies on the thermodynamics and kinetics of the complexes increased. They represent a large portion of the chemical research, being the basis for fruitful use of application in different areas and for providing large interpretative contributions to other branches of the basic research. Precious contributions to the thermodynamics were developed by the prestigious schools of Bjerrum, Biedermann, Sillen, and Schwarzenbach. The school of Guttmann analysed the effects of the solvent on the equilibria. Other scientists (Ingold, Basolo) addressed themselves successfully to the study of the kinetics of the coordination compounds in solution, the main goal being to identify the mechanism of substitution reactions. This period of intense research on coordination compounds produced a considerable development, and led to technological improvements in organic chemistry, in electrochemistry through the development of processes of controlled and guided electrodeposition, as well as in analytical chemistry.

We have to recall here the studies on thermal analysis of the solid state complexes developed in particular by the School of Duval, already well known scientist for its thermoanalytical researches in geology and in the area of the materials. Other groups, first of all that of Wenndlandt' further developed these types of research.

Greater perspectives were opened for the use of the complexes in industry, first of all for the catalytic activity presented by some of them. Ziegler and Natta, in particular, were awarded the Nobel Prize for Chemistry in 1963 for their success in the stereospecific polymerisation of ethylene at low pressure in the presence of a complex of aluminium and titanium as catalyst.

Biochemistry, pharmacology and industrial production as well as environmental problems, in addition to

the application in analytical chemistry can be considered the main branches where the complexes have given rise to a considerable impact.

A very important subject of the research studies is the role that the metal ions exert upon the biological activity of the organism, by means of complexing, and in particular on the enzymatic activity. The best known coordination compounds in biological systems consist of ions of a transition metal and, as ligands, of atoms of nitrogen of a tetrapyrrole system. For example, it is absolutely necessary for the relevant complexing and activation of molecular oxygen, that a metal centre in the protein is responsible for the storage and transport of the oxygen itself as in hemocyanins, hemoglobin, hemerythrin and others. The same holds for some enzymes as oxigenase and oxidase.

In a number of biological systems the coordination compounds exert a function of great relevance since they constitute, in many systems, the active site for some essential process for the life of the cells. The catalytic functioning of about one third of all known enzymes requires the presence of a metal ion. The metal, more or less closely connected with the protein moiety of the enzyme, participates in the process either by binding to the substrate, thus activating it for the reaction, or through redox reactions by means of reversible variations of the oxidation state of the metal.

In this comprehensive view of innovative aspects, a newer frontier for research has been opened up under the stimulation of the large universe represented by the biothecnologies, which—as is well known—have given rise to a very considerable increase in every field connected to them. This trend has resulted as being particularly useful for the enzymatic systems, to which a considerable attention has been devoted in order to study the effects caused by the occurrence of certain cations on the coordination sites present in the enzyme molecules.

At cell level the sequence of the redox reactions is controlled by systems present in the cytochrome C, consisting of iron complexed in a porphyrin ring that shifts from the reduced to oxidised state and back, during the transport of the electrons. Beyond that, studies on the biomodel have been undertaken in order to interpret the effect produced by the presence of different kinds of ligands on the cobalt oxidation as well as on the formation and stability of oxygenated intermediate species [12–15]. It is also worthwhile to recall the mechanism activated by the main plants' photoreceptors and, above all, in vegetal biology. The well-known photosynthetic action of the chlorophyll is due to its structure in which one atom of magnesium is coordinated to the nitrogens of four pyrrolic rings, analogous to that of haemoglobin.

In the bio-medical field the main results from the study of the complexes have been attained through the examination of the interactions of the metal ions with several biologically active substances. Often the amount of data collected leads to a major awareness of the action mechanism that represents the base for the application to practical problems, mainly in the pharmacological field. In fact, the possibility of using inorganic compounds as pharmaceutical agents has been known for centuries. Nevertheless, the interest in 'bio-inorganic medical chemistry' is mainly related to the recent therapeutic innovating features achieved using, for example, radioactive and not radioactive metal complexes employed in imagery diagnosis, lithium compounds in neurology, complexes of gold in reumathology and, above all, some coordination compounds for anti-tumour action. This is the case of bleomycin [16–22], an antibiotic of the family of the glycopeptide derivates used in the Hogkin's lynphoma as well as in skin, head, and neck carcinomas. Its action seems to be connected to the formation of complexes as the copper(II), which is able to penetrate the tumour cells where, through a process of de-complexing, it causes the scission of the DNA strain. The major contribution to the use of coordination compounds in therapy is represented by the discovery [23] of the activity of the *cis*-diamminedichloroplatinum(II) (*cis*-DDP or *cis*-Platinum), on the tumours of the head, neck or genital-urinary apparatus. From this discovery, research studies were performed, with the purpose of identifying anti-tumor properties of 'new' coordination compounds as well as organo-metal compounds with ions other than Platinum [24].

The knowledge of the thermodynamic properties of the complexes species allows for metal ions to be used for regulating the concentration of biologically active substances in the living organism, but also as vehicles of medicaments through the cell membranes. In fact, it may be necessary to examine the properties of the complexes in more depth by identifying the chemical species effectively present in the solutions, that is their 'speciation'. These further studies have made possible to explain the effects of particular elements in fluids that represent the basis of the investigations, particularly in environmental refluents and in biological fluids. Their contribution to the interpretation of relevant and specific effects, in environmental chemistry is of vital importance. They represent the best interpretation of the causes of the deviations from normal state and consequently of the study of protective and curative applications. By means of speciation, it is possible to know the behaviour of a metal in solution, because of the different chemical–physical forms in which it 'actually' exists. Through the thermodynamic study of the equilibria in solution we obtain the knowledge of the real species and, from the values obtained, we can find out the number, the nature and the concentration of the different species that exist in the solution investigated

[25]. The knowledge of such data is of the utmost importance on account of its potential benefits in dealing with contaminating agents and constitutes a tool for solving problems related to the mobility of metals, in addition to explaining, rationalising and highlighting the potential toxic features of the species. These latter are also particularly relevant in the case of heavy metals.

The study of toxicity for living organisms is also connected to 'speciation', since the permeability of the cell membrane is different according to the species coming in contact with it. In particular, the toxicity of the metal in water solution was investigated, mainly in connection with unicellular organism as algae and phytoplankton. The toxicity of the free-metal ion emphasised as has that of the neutral stable complexes of a lipophilic type [26], able to penetrate directly the layer of cell membranes in which they are soluble.

The knowledge of 'speciation' of an environmental system is particularly important both for theoretical and implementation [27] purposes. In fact, it is possible to interpret or to predict the performance of a natural system and potentially to plan interventions upon it in terms of both resolution or prevention, merely by knowing the relationships and mutual influences of the chemical components, as well as the physical parameters that characterise such a system.

In the field of analytical chemistry, new, important applications have been carried out following the studies on complexation, which have proved to be of particular advantage regarding two subjects: (1) as titration indicators of metal ions, as murexide, or 'eriochrome black T'; (2) as reagents in colorimetry for the qualitative and quantitative analysis, such as dithizone, dimethylglyoxime, hydroxyquinoline, cupferron, *o*-phenanthroline. In most cases, the resulting coordination compounds are chelates, as for example in the quantitative volumetric analysis. As far as these complexometric titrations are concerned, many reactions lead to the formation of soluble complexes but only a few of them can be used for analytical purposes since they must meet the fundamental requirements for the volumetric analysis, quickness, univocality and fulfilment. It is also worthmentioning that, apart from those related to the formation of halogenic (as with Hg(II)) or cyanidric (as with Ag (I)) complexes, the reactions mainly used for complexometric titrationd analysis are those involving chelation [28]. In accordance with that, the term 'chelometry' identifies the related part of volumetry.

In the titrations of metal ions of different types, the multidentate ligands are used more frequently, since it is possible to find in their structures different donor atoms, as oxygen and nitrogen. Among those, the best known is ethylene-diamminetraacetic acid (EDTA) that, being able to form stable chelates with almost all the polivalent metal cations, is used for the direct determination, of ions, as for Ca^{2+}, Mg^{2+}, Zn^{2+}, Bi^{3+}, Fe^{3+}, Co^{2+}. Other multidentate chelating agents are diethylenetriaminepentaacetic acid (DTPA), which provides a better result than the EDTA in the titrations of cations with a high coordination number, cyclohexanediamine tetraacetic acid (CyDTA), whose complexes are, in contrast, characterised by a partial liability, and some other synthesised products, including, for example, tris-(2pyridylmethyl) amine (TPA). We may take into account that in different analytical methods applied to matrixes containing many species the reagents play a determining role since, through them, it is possible to 'sequestrate', in a selective manner, the ions provoking interferences.

We have already mentioned the outstanding success attained by the Nobel Prizewinners Ziegler and Natta in the synthesis of the isotactic polypropylene, a compound of great relevance both for scientific and industrial applications. Their great success was not achieved by chance but was the result of thorough research involving the chemistry of the complexes since almost all processes in the chemical industry are based on the implementation, selection and application of catalysts. Thus, in the literature we find reports of several reactions indicating complexes, or, rather, the metal ions that form coordination compounds with the substrata, acting as catalysts. We also need to say here that, when the catalysed reaction of the metal ion is completed, the catalyst can be recovered also, although in most cases in an oxidation state different from the initial one and coordinated to groups that are different from the initial ones.

The reaction catalysed by hydrogen ions can be activated also by metal ions able to produce the formation of chelates with the substrata. There are several examples of this, ranging from the reaction of the bromuration of acetacetic ester catalysed by copper ion [29] to decarboxylation of some keto-acids, such as 'oxalacetic acid', or the hydrolysis of esters and amides of α-aminoacids.

The complexes also play a fundamental role as catalysts in the processes of hydrogenation and of the acid-catalysed reactions. Such reactions find their main application in food industry and in particular in the production of edible fats starting from oils of animal or vegetal origin, varying in mono and poly-unsaturated fatty acids.

The coordination compounds are also involved in the mechanism of condensation leading to the production of molecules that are important from an industrial point of view. We have, for example, acrylonitrile, starting from acetylene and from hydrocyanic acid in the presence of copper chloride as a catalyst [30], or derived from acrylic acid obtained from the reaction of carbon monoxide and water, alcohol, or amines, with carbonyl nickel as a catalyst.

Another subject of great interest is the use of transition metal complexes as catalysts in the oxidation reactions. The catalytic oxidation of hydrocarbons in the presence of oxygen, in fact, finds a considerable number of applications. In industry, mention can be made of those conducted on the *p*-xylene [31] for producing acids, used in the production of polymers for synthetic fibres, as well as those for the production of hydroperoxides, used as sources of free radicals for their function of starter in the polymerisation reactions [32,33].

In the light of what has been said above, it is clearly important to know the chemistry of the complexes in solution for: (1) the interpretations of some interactions that can explain the mechanism of the reactions, in which the complexes are involved, and (2) some applications in specific fields, for which the data collected through such study provide basic information for the planned targets. It is reasonable to assess that further research on coordination compounds will lead to further knowledge of the interpretations and applications involving chemistry as a whole. This support provided by the thermodynamic and kinetic studies of the complexes in solution will also lead to their application in the many and varied fields in which chemistry is directly or indirectly interested.

I was with the purpose of contributing to further studies in this field, requiring deep commitment and engagement, that the Group of Thermodynamics of the Complexes, 'GTC' was founded in 1973, in Italy, just in Parma, by researchers from a sizeable number of Italian universities. The GTC was constituted to create a common background to increase specific knowledge, and to compare with the experiences of the individual members by means of debates. Distinguished by the qualified experience of its members, the Group has attained important international recognition, without being bound by the bureaucracy of statutes or rigorous regulations. GTC has had the resolve and the tenacity to remain operational for the last 28 years. GCT each year is seeking confrontation in a Congress, having found interests and met challenges that go well beyond any barriers that may exist between various academic fields. This is confirmed, on the one hand, by its extremely friendly and fruitful relationship with the corresponding groups in the Spanish universities, and, on the other, by the high number of publications of its members. The GTC's main policy is to foster and intensify basic research by the setting up of 'Summer Schools', which are held with the purpose of providing constant updating through didactics.

I would like to end with a much appreciated quotation by Professor Luigi Sacconi, one of the most eminent scientists involved in the chemistry of complexes: 'The aim of fundamental research is, mainly, to understand'.

References

[1] A. Werner, Z. Anorg. Chem. 3 (1893) 267.
[2] B.M. Tassaert, Ann. Chim. Phys. 28 (1798) 92.
[3] J. Reset, Compt. Rend. 18 (1844) 1103.
[4] M. Peyrone, Annals 51 (1845) 15.
[5] S.M. Jorgensen, J. Prakt. Chem. 33 (1886) 489.
[6] C.W. Blomstrand, Chemie der Jetztzeit vom Standpunkte der electrochemischen Auffassung aus Berzelius Lehre entwickelt, Heidelberg, 1869.
[7] F. Basolo, R.G. Pearson, Mechanisms of Inorganic Reactions, Wiley, New York, 1958.
[8] D.P. Mellor, in: R. Dwyer, D.P. Mellor (Eds.), Chelating Agents and Metal Chelates, Academic Press, New York, 1964.
[9] G.T. Motgan, H.D.K. Drew, J. Chem. Soc. 117 (1920) 1456.
[10] H. Ley, Z. Elektrochem. 52 (1904) 954.
[11] G.N. Lewis, Valence and the Structure of Atoms and Molecules, The Chemical Catalog Company, New York, 1923.
[12] S. Canepari, V. Carunchio, A. Messina, Transition Met. Chem. 16 (1991) 296.
[13] R. Antiochia, S. Canepari, V. Carunchio, Transition Met. Chem. 19 (1994) 359.
[14] S. Cabani, N. Ceccanti, M.R. Tinè', J. Chem. Soc., Dalton Trans. (1988) 373.
[15] S. Cabani, N. Ceccanti, M.R. Tinè', A. Bencini, A. Bianchi, P. PaolettiI, J. Chem. Soc., Dalton Trans. (1993) 695.
[16] M. Zimmer, Chem. Rev. 95 (1995) 2629.
[17] J.C. Dabrowiac, in: H. Siegel (Ed.), Metal Ions in Biological Systems, vol. 11, Marcel Dekker, New York, 1980, p. 305.
[18] J.C. Dabrowiac, F.T. Greemaway, F.S. Santillo, in: S.M. Hecht (Ed.), Bleomycin, Chemical, Biochemical and Biological Aspects, Springer-Verlag, New York, 1979, p. 137.
[19] J.C. Dabrowiac, J. Inorg. Biochem. 13 (1980) 317.
[20] E.A. Rao, L.A. Saryan, W.E. Antholine, D.H. Petering, J. Med. Chem. 23 (1980) 1310.
[21] D. Solaiman, E.A. Rao, W.E. Antholine, D.H. Petering, J. Inorg. Biochem. 12 (1980) 201.
[22] S. Lyman, B. Ujjiani, K. Renner, W.E. Antholine, D.H. Petering, J.W. Whetstone, J.M. Knight, Cancer Res. 46 (1986) 4470.
[23] B. Rosenberg, L. Van Camp, J.E. Trosko, V.H. Mansour, Nature (London) 222 (1969) 385.
[24] S. Spinelli, M. Valsecchi, Complessi Metallici Come Antitumorali, in Metalli in Medicina, Società Chimica Italiana, 1993, p. 21.
[25] J. Buffle, Complexation Reactions in Aquatic Systems, Ellis Horwood, Chichester, 1988.
[26] G.M.P. Morrison, G.E. Batley, T.M. Florence, Chem. Britain (1989) 791.
[27] A. De Robertis, C. De Stefano, S. Sammartano, Chem. Speciation Bioavailability 6 (1994) 65.
[28] A.E. Martell, M. Calvin, Chemistry of the Metal Chelate Compounds, Prentice Hall, New York, 1952.
[29] I.K. Pedersen, Acta Chem. Scand. 2 (1948) 252.
[30] C.W. Bradley, H.S. Davis, Chem. Abstr. 40 (1946) 1867.
[31] P.W. Sherwood, Chim. Ind. 71 (1954) 300.
[32] R.J. Orr, H.L. Williams, J. Am. Chem. Soc. 78 (1956) 3273.
[33] E. Collison, F.S. Dainton, Nature 177 (1956) 1224.

PERGAMON

Polyhedron 21 (2002) 1319–1327

POLYHEDRON

www.elsevier.com/locate/poly

Equilibrium study on Cd(II) and Zn(II) chelates of mercapto carboxylic acids

Guido Crisponi [a,*], Angelo Diaz [a], Valeria Marina Nurchi [a], Tiziana Pivetta [a], María José Tapia Estévez [b]

[a] *Dipartimento di Chimica Inorganica e Analitica, Complesso Universitario di Monserrato, 09042 Monserrato-Cagliari, Italy*
[b] *Área de Química Física, Departamento de Química, Universidad de Burgos, Plaza Misael Bañuelos, 09001 Burgos, Spain*

Received 11 December 2001; accepted 25 January 2002

Abstract

Cadmium(II) and zinc(II) complexes with the chelating agents *meso*-2,3-dimercapto succinic acid, *meso*-monomethyl dimercapto succinate, *meso*-dimethyl dimercapto succinate and the related methylmercapto acetate and mercapto succinic acid were studied potentiometrically in 0.1 M KCl at 25 °C. Models and hypotheses of coordination for the solution complexes are proposed. IR characterisation and stoichiometry of the solid state compounds evaluated by elemental analysis are presented. The obtained formation constants, together with the previously measured ionisation constants of the ligands, were used to compute pCd and pZn values and then to evaluate the effectiveness of the studied chelating agents in binding Cd(II) and Zn(II) in intoxication treatments.
© 2002 Published by Elsevier Science Ltd.

Keywords: Mercapto-carboxylic acid; Potentiometry; IR; Formation constants; Ionisation constants

1. Introduction

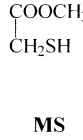
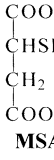
The use of chelating agents in heavy metal intoxication treatment is a very complex field that requires the collaboration of several branches of Science. The main contribution of Chemistry to this field is the determination of both coordination models and formation constants of complexes between metal ions and chelating agents to compare the strength and characteristic of the formed complexes. In the coordination processes using chelating agents in vivo, it should be taken into account that there is always competition for the coordinating positions between toxic and essential metal ions such as calcium(II), magnesium(II), zinc(II), manganese(II), iron(III) or copper(II) [1,2]. For this reason, it is of great interest from a chemical point of view to study the chelating agent coordination with both toxic and essential metal ions. In recent years our group has focused on the thermodynamic study of the complexation of DMSA (*meso*-2,3-dimercapto succinic acid) and some derivatives with platinum group metals [3,4]. DMSA is a widely used oral chelating agent with two kinds of binding positions involved in metal coordination: the carboxylic and mercapto groups [5–7]. However, DMSA hydrophilicity prevents it from permeating cell membranes and entering into cells. For this reason, it would be useful to study the mono and dimethyl DMSA ester derivatives which, apart from being good chelating agents, are also more lipophylic compounds.

In this paper, the equilibrium studies of complexation between Zn(II) and Cd(II) with DMSA, mono and dimethyl dimercapto succinates, and the other structurally related molecules shown in Table 1 are presented. Zinc is the second more abundant trace metal in the human body [1] and can be considered as non-toxic to humans [8]. It is essential for the structure, regulation, and/or catalytic action of over 300 enzymes, as for example those responsible for DNA and RNA synthesis [9]. It has also a physiological action in collagen synthesis, bone metabolism, immune system integrity, anti-inflammatory action and protection against free radicals [10]. As a consequence, zinc should not be removed by chelating agents used *in vivo*. Cadmium, on the contrary, is a very toxic metal widely used in many

* Corresponding author. Fax: +39-070-675-4478.
E-mail address: crisponi@unica.it (G. Crisponi).

0277-5387/02/$ - see front matter © 2002 Published by Elsevier Science Ltd.
PII: S0277-5387(02)00973-7

Table 1
Names, formulae and acronyms of the used compounds

methylmercapto acetate	mercapto succinic acid	*meso*-2,3-dimercapto succinic acid	*meso*-monomethyl dimercapto succinate	*meso*-dimethyl dimercapto succinate
				
MS	**MSA**	**DMSA**	**MMS**	**DMS**

industrial processes to produce batteries, plastic, pigments and semiconductors [1]. It is estimated that humans absorb 5% of ingested cadmium, while absorption of cadmium by the lungs (cigarette smoke) is approximately 10–40% [1]. Immediately after systemic entrance, cadmium localises intracellularly and kidney, liver, lung and pancreas [11] are the main organs for its accumulation. In the kidneys it has a 30-year biological half-life causing renal dysfunction [1]. Other syndromes produced by cadmium toxicity are: hepatic injury, lung damage, bone defects dependent on altered calcium metabolism [12], mutagenic and carcinogenic effects [13,14]. Orally administered DMSA has been shown to reduce intestinal cadmium uptake but, to mobilise aged cadmium depots from the liver or kidney, monoalkylesters or monoalkylamides derivatives of *meso*-2,3-dimercapto succinic acid have been proved to be more effective chelators [15,16]. The main aim of this work is to compare quantitatively the strength of the Cd(II) and Zn(II) complexes formed with DMSA, alkyl ester derivatives and related molecules to evaluate the efficiency of these compounds in cadmium removal and in the possible side-effects on the zinc level. This study follows previous works on the complexation of DMSA [17–23] or other related molecules[24–26] with Cd(II) and Zn(II) and can provide insights into the proposed complexation models.

2. Experimental

2.1. Reagents

HCl standard solution, KOH, $CdCl_2$, $ZnCl_2$, KCl, methylmercapto acetate, mercapto succinic acid, *meso*-2,3-dimercapto succinic acid were Aldrich products; *meso*-monomethyl dimercapto succinate and *meso*-dimethyl dimercapto succinate were synthesised according to Gerecke [27]. The purity of the synthesised compounds was checked by elemental analysis with a CHN-S Fisons instrument and by ^{13}C NMR and IR spectra. The commercial compounds were used without further purification. Due to their redox properties, the solutions of mercapto-compounds were prepared daily by dissolving weighed amounts with freshly double-distilled water saturated with Argon. Potassium hydroxide carbonate free solutions were prepared according to Albert [28].

2.2. Potentiometric measurements

Titrations were performed on a Dosimat 665 Metrohm automatic titrator connected to a Metrohm 654 pH meter. A thermostated glass-cell was used equipped with a magnetic stirring system, a Metrohm combined LL Unitrode glass electrode, a thermometric probe, a microburet delivery tube, and an inlet-outlet tube for Argon. The solutions (20 ml at ionic strength 0.1 M KCl) were titrated at 25 °C with carbonate-free KOH, whose titre was checked daily. The electrode was calibrated for hydrogen ion concentration by titration of HCl with KOH; the resulting data were analysed with Gran [29] procedure using our granplot program. We titrated, for each ligand, 20 ml ligand–metal mixtures with KOH 0.1 M using ligand 10^{-3} M and metal variable in order to have 4:1, 2:1, 4:3 and 1:1 ligand–metal molar ratios. Ionisation and formation constants were calculated by the psequad [30] program operating on the experimental data (ml, $-\log[H^+]$). Since the analysis of results led us to assume polymeric complexes, we repeated the measurements at four different ligand concentrations (1×10^{-4}, 4×10^{-4}, 7×10^{-4} and 1×10^{-3} M) using the same scheme as above i.e. 4:1, 2:1, 4:3 and 1:1 ligand–metal molar ratios.

2.3. Synthesis of metal complexes

2.3.1. Zinc complexes

A mixture of 50 mmoles (or 100 mmoles in the case of 2:1 molar ratio) of ligand and 50 mmoles of zinc chloride in ethanol was left for 1 h in reflux under nitrogen. The resulting solution was evaporated to dryness under vacuum to give a white solid product, which was washed with a 1:1 isopropanol–ethyl ether mixture, and filtered off to dryness under vacuum. In both 1:1 and 2:1 molar ratio preparations the same

Table 2
Ionisation constants for the five molecules in Table 1

	pK_{C1} [a]	pK_{C2}	pK_{S1}	pK_{S2}
Methylmercapto acetate			7.99(2)	
Mercapto succinic acid	3.12(1)	4.52(1)	10.24(3)	
meso-2,3-Dimercapto succinic acid	2.71(1)	3.43(2)	9.65(3)	12.05(3)
meso-Monomethyl dimercapto succinate	2.80(1)		7.15(2)	9.98(2)
meso-Dimethyl dimercapto succinate			5.23(1)	7.32(3)

[a] pK_{C1} and pK_{C2} refer to the first and second ionisations of COOH; pK_{S1} and pK_{S2} to the first and second ionisations of SH; values in parentheses are standard deviations in units of the last significant figure.

products were obtained. In the case of MS ligand colourless oil was obtained.

2.3.2. Cadmium complexes

A mixture of 50 mmoles (or 100 mmoles in the case of 2:1 molar ratio) of ligand and 50 mmoles of cadmium chloride in water was stirred under nitrogen for 1 h. Freezing this solution, a solid residue was obtained and filtered off under vacuum, washed with cool water, and then dried under vacuum. In both 1:1 and 2:1 molar ratio preparations the same products were isolated.

2.4. IR measurements

IR spectra were recorded with a Perkin–Elmer 983 instrument in the range $4000 \div 180$ cm^{-1} using KBr pellets for solid compounds, and CsI disks for liquid compounds.

3. Results and discussion

The ionisation constants of the five ligands, previously determined [31], are reported in Table 2. Since the studied equilibria involve formation of polynuclear complexes we took the measurements at four different metal concentrations ranging from 10^{-4} to 10^{-3} M and for each metal concentration at four different metal–ligand ratios. For each system the data relative to all the performed titrations (4×4) were processed at the same time using psequad program.

The estimated models and related formation constants for zinc and cadmium are reported in Tables 3 and 4, respectively. The solid complexes obtained as reported in Section 2.3 were characterised by IR spectroscopy to give evidence of SH and COOH group involvement in complex formation, and the frequencies of the significant bands are reported in Table 5.

Table 3
Models, ligand proticity, logarithm of formation constants, and pK of complex deprotonations for the zinc(II)–ligand systems

	Models	Ligand proticity	log(β)	pK
MS	methylmercaptoacetate	HL		
$[Zn_2L_2]^{2+}$			12.54(4) [a]	7.50
$[Zn_2L_2H_{-1}]^{+}$			5.04(4)	8.16
$[Zn_2L_2H_{-3}]^{-}$			−11.27(3)	9.62
$[Zn_2L_2H_{-4}]^{2-}$			−20.89(5)	
ZnL_2			8.87(3)	
$[ZnL_3]^{-}$			13.51(3)	
MSA	mercaptosuccinic acid	H_3L		
$[Zn_2L_2]^{2-}$			18.74(3)	8.48
$[Zn_2L_2H_{-1}]^{3-}$			10.26(4)	9.44
$[Zn_2L_2H_{-2}]^{4-}$			0.82(4)	
$[ZnL_2H]^{3-}$			20.3(2)	6.1
$[ZnL_2]^{4-}$			14.16(3)	
DMSA	*meso*-dimercaptosuccinic acid	H_4L		
$[Zn_2L_2H_2]^{2-}$			44.10(8)	4.4
$[Zn_2L_2H]^{3-}$			39.73(3)	6.44
$[Zn_2L_2]^{4-}$			33.29(4)	
MMS	*meso*-monomethyl dimercaptosuccinate	H_3L		
$[Zn_4L_4H]^{3-}$			62.7(1)	5.3
$[Zn_4L_4]^{4-}$			57.4(1)	9.2
$[Zn_4L_4H_{-1}]^{5-}$			48.2(1)	
$[Zn_2L_4H_2]^{6-}$			53.6(3)	7.6
$[Zn_2L_4H]^{7-}$			46.0(1)	10.6
$[Zn_2L_4]^{8-}$			35.4(3)	
DMS	*meso*-dimethyl dimercaptosuccinate	H_2L		
$[ZnL_2]^{2-}$			14.84(3)	

[a] Values in parentheses are S.D. in units of the last significant figure.

Table 4
Models, ligand proticity, logarithm of formation constants, and pK of complex deprotonations for cadmium(II)–ligand systems

	Models	Ligand proticity	log(β)	Pk
MS	methylmercaptoacetate	HL		
CdL_2			12.5(1) [a]	
MSA	mercaptosuccinic acid	H_3L		
$[Cd_4L_4H]^{3-}$			52.4(1)	5.5
$[Cd_4L_4]^{4-}$			46.9(1)	9.6
$[Cd_4L_4\cdot H_{-1}]^{5-}$			37.3(1)	
$[Cd_3L_4]^{6-}$			41.12(7)	
$[CdL_2H_2]^{2-}$			27.4(1)	5.1
$[CdL_2H]^{3-}$			22.3(1)	7.5
$[CdL_2]^{4-}$			14.83(4)	
DMSA	*meso*-dimercaptosuccinic acid	H_4L		
$[Cd_4L_4H_5]^{3-}$			105.4(2)	4.5
$[Cd_4L_4H_4]^{4-}$			100.9(2)	6.1
$[Cd_4L_4H_3]^{5-}$			94.8(2)	7.4
$[Cd_4L_4H_2]^{6-}$			87.4(2)	8.0
$[Cd_4L_4H]^{7-}$			79.4(2)	10.0
$[Cd_4L_4]^{8-}$			69.4(2)	
MMS	*meso*-monomethyl dimercaptosuccinate	H_3L		
$[Cd_4L_4H_3]^{-}$			80.29(3)	4.93
$[Cd_4L_4H_2]^{2-}$			75.36(3)	6.40
$[Cd_4L_4H]^{3-}$			68.96(3)	10.51
$[Cd_4L_4]^{4-}$			58.45(3)	
$[Cd_2L_4H_4]^{4-}$			70.88(2)	5.74
$[Cd_2L_4H_3]^{5-}$			65.14(2)	6.70
$[Cd_2L_4H_2]^{6-}$			58.44(2)	7.99
$[Cd_2L_4H]^{7-}$			50.45(2)	
DMS	*meso*-dimethyl dimercaptosuccinate	H_2L		
CdL			14.3(1)	
CdL_2H_2			34.1(1)	4.8
$[CdL_2H]^{-}$			29.3(1)	5.9
$[CdL_2]^{2-}$			23.4(1)	

[a] Values in parentheses are S.D. in units of the last significant figure.

3.1. Zinc complexes

Examined ligands form 1:1 and 2:1 complexes with Zn(II) except MS that also forms a $[ZnL_3]^{-}$ complex. Polymeric structures must be assumed in the majority of cases. The distribution curves for zinc(II) complexes at 1:1 molar ratio are reported in Fig. 1.

The lower stability (complex formation starting at pH > 5) of complexes with ligands characterised by a single SH group (MS and MSA) is observed, compared with those with ligands having two SH groups, already formed at pH 4. The 2:2 complexes with monothiolic ligands can be hypothesised as in Scheme 1(A) and Scheme 2(A), in which two zinc atoms in a tetrahedral configuration are joined by two bridging sulfur atoms. Four water molecules complete metal coordination in the first case, while only two water molecules are required for MSA where a COO^{-} group per ligand binds zinc forming a five membered ring.

Their different configurations as well as the total charges (2+ for MS and 2-for MSA) determine their pH behaviour: $[Zn_2L_2]^{2+}$ with MS loses protons from the

Table 5
Frequencies of significant IR bands of zinc and cadmium complexes

Ligand	Pure ligand (cm^{-1})	Zn complex (cm^{-1})	Stoichoimetry	Cd complex (cm^{-1})	Stoichoimetry
MS	2570–2550 (SH)	broad bands	oil product	no SH band	CdLCl
MSA	2570–2550 (SH) 1700 (COOH)	1700 (COOH) 1600 (COO–Zn)	$ZnLH\cdot 2H_2O$	1700 (COOH) 1570 (COO–Cd)	CdLH
DMSA	2550–2525(SH) 1700 (COOH)	1700 (COOH) 1600 (COO–Zn)	$Zn_2LHCl\cdot 3H_2O$	2550 (SH) 1700 (COOH) 1537–1340 (COO–Cd)	$CdLH_2$
MMS	2550–2515(SH) 1730 ($COOCH_3$) 1700 (COOH)	1730 ($COOCH_3$) 1600 (COO–Zn)	Zn_2LCl	1730 ($COOCH_3$) 1575 (COO–Cd)	Cd_2LCl
DMS	2520 (SH) 1730 ($COOCH_3$)	2525 (SH) very weak 1630–1730 ($COOCH_3$)	ZnLHCl	1730–1675 ($COOCH_3$)	CdL

four coordinated water molecules at pH 7.50, 8.16 (two protons) and 9.62, while $[Zn_2L_2]^{2-}$ with MSA ionises at pH 8.48 and 9.44. At higher pH, the monodentate MS forms both ZnL_2 and $[ZnL_3]^-$ complexes (Scheme 1(B)), being this last the prevailing species at 4:1 molar ratio. The bidentate MSA besides $[Zn_2L_2]^{2-}$ forms only $[ZnL_2]^{4-}$, whose structure is proposed in Scheme 2(B).

We were not able to obtain a solid compound with MS. The structure of the white solid obtained with MSA, characterised by elemental analysis as $ZnLH\cdot 2H_2O$, is analogous to that presented in Scheme 2(A), protonated on the two uncoordinated carboxylates. This agrees with IR findings: the SH bands at 2570–2550 cm^{-1} of pure ligand totally disappear while the COOH band at 1700 cm^{-1} decreases with the simultaneous appearance of a band at 1600 cm^{-1} assigned to a coordinated COO^-.

The greater stability of $[Zn_2L_2H_2]^{2-}$ with DMSA compared with that of $[Zn_2L_2]^{2-}$ with MSA implies a coordination through both S^- groups as reported in Scheme 3. This structure suits the pK values 4.4 and 6.4, which can be attributed to COOH ionisation from a

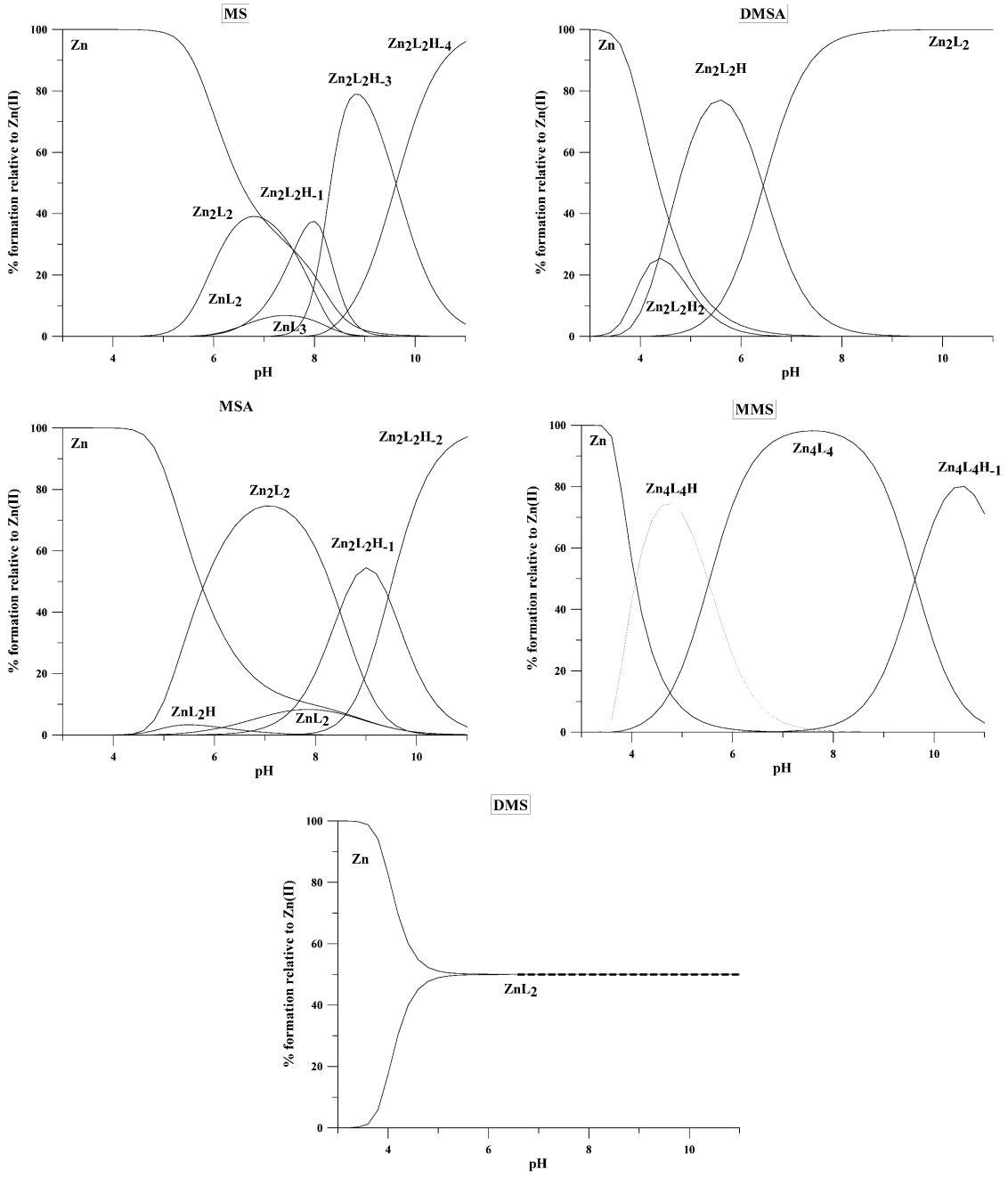
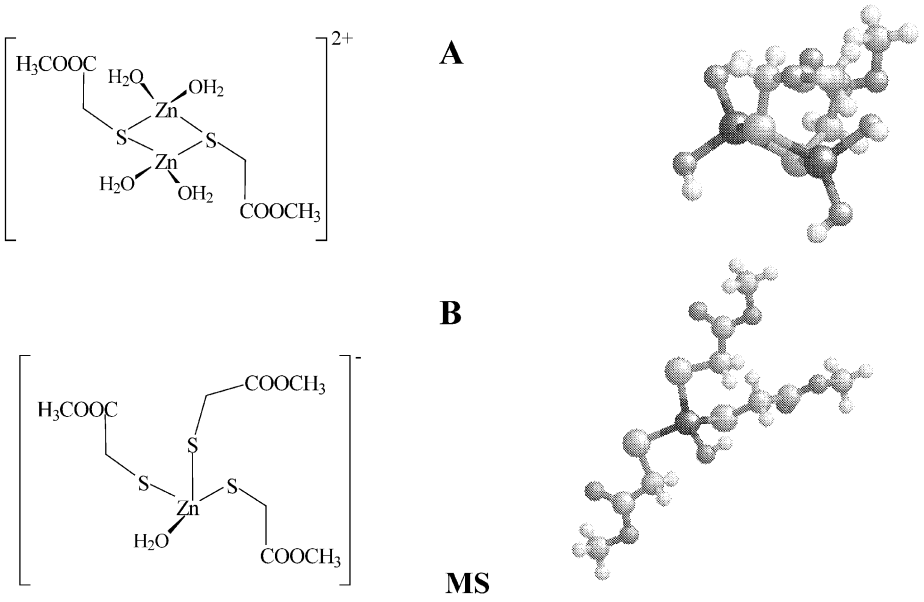
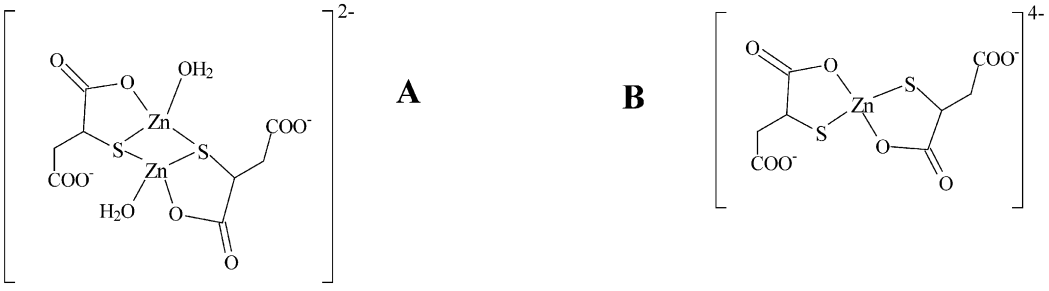


Fig. 1. Distribution curves for Zn(II) complexes versus pH, calculated with concentration of Zn(II) and ligands 1 mM.



Scheme 1.

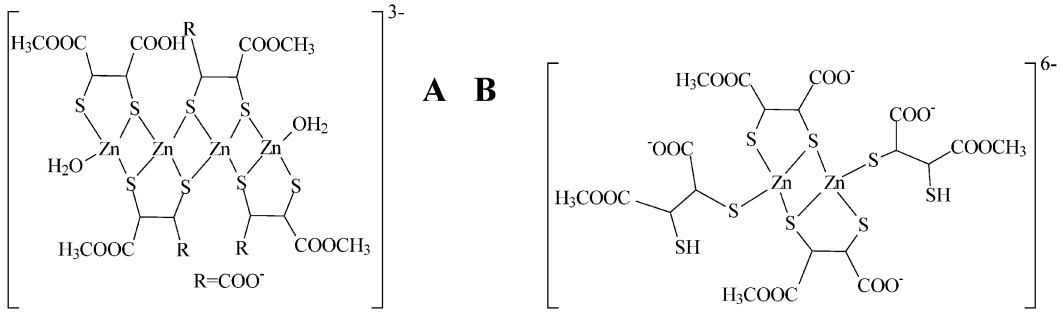


Scheme 2.



Scheme 3.

MMS



Scheme 4.

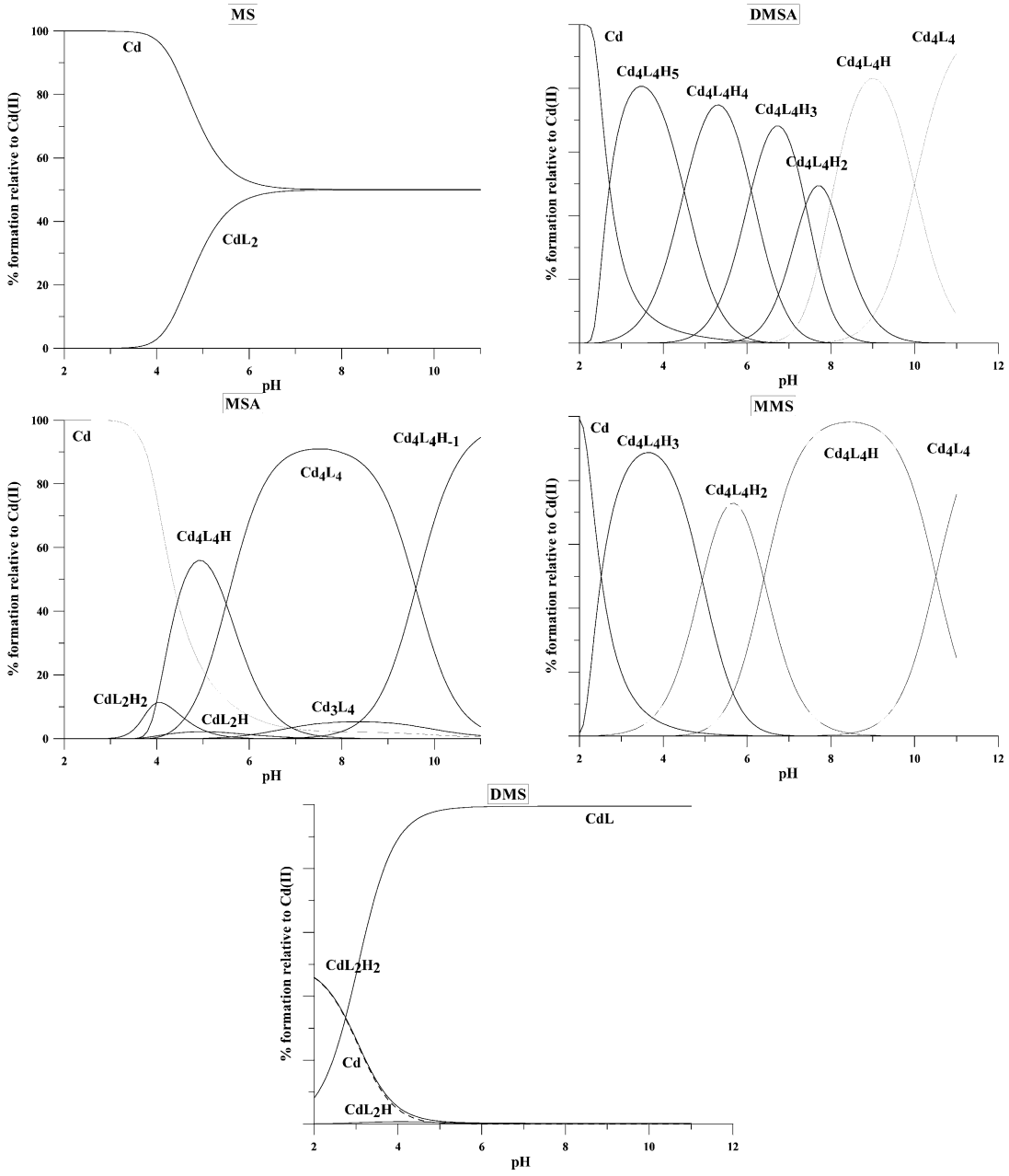


Fig. 2. Distribution curves for Cd(II) complexes versus pH, calculated with concentrations of Cd(II) and ligands 1 mM.

negatively charged molecule. The obtained solid compound with DMSA, characterised as $Zn_2LHCl\cdot 3H_2O$, does not correspond to the solution model.

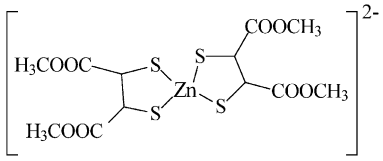
A polymeric structure, Scheme 4(A), has to be invoked for $[Zn_4L_4H]^{3-}$ with MMS; the first pK 5.3 agrees with the carboxylic group ionisation, while the value 9.2 can be ascribed to one coordinated water molecule. In the $[Zn_2L_4H_2]^{6-}$ structure, Scheme 4(B), two MMS molecules coordinate via both thiolato groups and two via a S^- alone. The isolated compound, as in DMSA case, involves zinc coordination by a single thiolato group and it does not correspond to the solution model.

At any metal ratio, a $[ZnL_2]^{2-}$ complex is formed by DMS in which zinc is coordinated by both S^- groups as suggested in Scheme 5. At molar ratios lower than 2:1 excess zinc precipitates as hydroxide at pH > 6.5. In a different way from DMSA and MMS, only a zinc per ligand is coordinated in the solid compound, via a S^- group.

3.2. Cadmium complexes

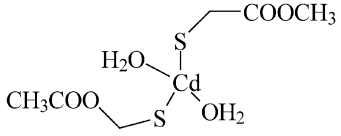
The distribution curves of cadmium(II) complexes are reported in Fig. 2. Also in this case, the greatest stability

DMS



Scheme 5.

MS



Scheme 6.

of complexes of ligands with two thiolic groups is evident.

At any molar ratio MS forms only the CdL_2 complex, Scheme 6. The much higher stability of CdL_2 than ZnL_2 prevents formation of 2:1 and 3:1 complexes. A CdLCl compound was isolated in the solid state.

As with zinc, cadmium forms with MSA 1:1 and 1:2 polymeric complexes. In the proposed structure for $[Cd_4L_4]^{4-}$, Scheme 7(A), the inner cadmium(II) ions are linked by two S-bridges while the coordination sphere of the external ions is completed by two water molecules. All four ligands coordinate both by thiolato and carboxylate groups. Moreover a $[Cd_3L_4]^{6-}$ complex is formed, Scheme 7(B), where all the ligands coordinate again by thiolato and carboxylate groups. A solid compound of formula CdLH, analogous to ZnLH, was obtained.

The cadmium(II) tendency to form polymeric structures of multiplicity four was confirmed by DMSA

Table 6
pZn and pCd, for the studied ligands, defined according Raymond [32]

	pZn	pCd
MS	6.0	7.0
MSA	6.0	6.1
DMSA	7.9	7.9
MMS	8.2	9.5
DMS	10.1	18.7

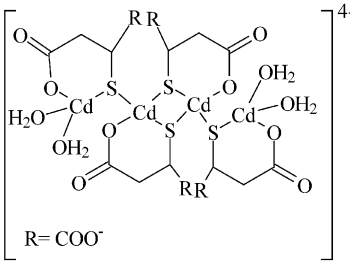
complexes, for which a structure similar to that in Scheme 4(A) for $[Zn_4L_4H]^{3-}$ can be proposed. IR spectrum of the solid $CdLH_2$ suggests a coordination via one S^- and one COO^- group.

A structure as in Scheme 4(A) could be proposed again for 4:4 MMS complexes. The $[Cd_4L_4H_3]^-$, existing at pH < 4, loses the first two protons at pH 4.93 and 6.40, starting from 1-and 2-charged molecules. This behaviour is similar to that of DMSA in which the reactions $[Cd_4L_4H_5]^{3-} \rightarrow [Cd_4L_4H_4]^{4-} \rightarrow [Cd_4L_4H_3]^{5-}$ take place at pH 4.5 and 6.1 but starting from 3-and 4-charged molecules. A structure similar to that for Zn(II) in Scheme 4(B), can be proposed for $[Cd_2L_4H_4]^{4-}$. In this case the two protons on carboxylic groups are removed at pH 5.74 and 6.70, due to the high negative charge on the complex, and the third from the SH group at pH 7.99. A solid Cd_2LCl compound was isolated, analogous to the Zn_2LCl.

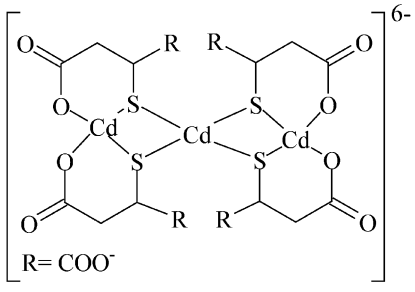
In excess of the dimethylated DMS cadmium forms CdL_2H_2 coordinated by only one thiolato group per ligand, Scheme 8, while at higher pH is coordinated by both thiolato groups as in Scheme 5. At 1:1 molar ratio the prevailing compound is CdL, coordinated by both thiolato groups, with the same stoichiometry of the solid compound.

MSA

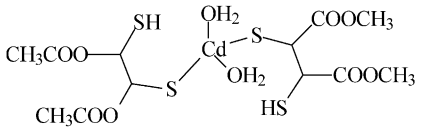
A



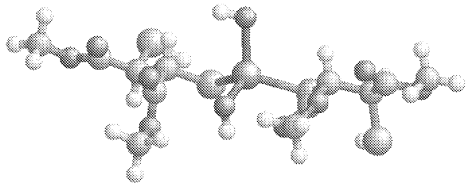
B



Scheme 7.



DMS



Scheme 8.

In literature solution equilibria between zinc(II) and DMSA has been studied by different authors; leaving out the oldest [17,18] the models and the numerical values of recent works [19,21,23] are in good agreement with our results. A good agreement has been also found with MSA results [24,25]. No other ligand is reported, except DMS whose equilibria with zinc(II) were examined [26] in a water-ethanol 50% mixture. No comparison with literature was possible for cadmium(II) since its complexes have been scarcely studied (DMSA [19] and MSA [25] at 37 °C). We only remark that with these two ligands we had to assume polymeric structures.

4. Conclusions

The evaluation of the clinical success of a ligand involves the knowledge of the amount of chelated metal ions. This amount depends on binding properties of the ligand at physiological pH, taking into account the competition of the proton towards the same binding sites. To compare the effectiveness of ligands we made use of pM introduced by Raymond [32]. It is defined as the concentration, expressed as negative logarithm, of free metal ion in a solution at pH 7.4 that is 10 μM in ligand and 1 μM in metal. A high pM value signifies that the ligand is a successful chelating agent. In Table 6 we report the pCd and pZn values for the studied ligands. On the basis of these values we can state that monothiolic, different from dithiolic ligands, are not good chelators. The dithiolic ligands can be classified in the order DMSA < MMS ≪ DMS, according to their efficiency, that increases with methylation of carboxylic groups. Methylation has two cooperative effects, one inductive and one electrostatic. These two effects act synergistically, the first increasing the strength of S–Cd bond and the second decreasing proton competition. Furthermore, methylated compounds have different behaviour in vivo for their different lipophilicity, which should allow them to pass through cellular membranes.

Acknowledgements

Financial support by MURST (COFIN2000) is gratefully acknowledged.

References

[1] J.K. Dunnick, B.A. Fowler, in: H.G. Seiler, H. Sigel, A. Sigel (Eds.), Handbook on Toxicity of Inorganic Compounds (Ch. 14), Marcel Dekker, New York, 1988, p. 155.
[2] A. Catsch, A.E. Harmuth-Hoene, Pharm. Ther. A 1 (1976) 1.
[3] G. Crisponi, F. Cristiani, V.M. Nurchi, R. Pinna, M.J. Tapia Estevez, Polyhedron 18 (1999) 3257.
[4] G. Crisponi, F. Cristiani, V.M. Nurchi, R. Pinna, R. Pivetta, M.J. Tapia Estevez, Polyhedron 19 (2000) 2435.
[5] J. Aaseth, Hum. Toxicol. 2 (1983) 257.
[6] H.V. Aposhian, C. Hsu, T.D. Hoover, Toxicol. Appl. Pharmacol. 69 (1983) 206.
[7] H.V. Aposhian, Ann. Rev. Pharmacol. Toxicol. 23 (1983) 193.
[8] National Research Council, Subcommittee on Zinc, Zinc, University Park Press, Baltimore, MD, 1979.
[9] L. Thunus, R. Lejeune, in: H.G. Seiler, H. Sigel, A. Sigel (Eds.), Handbook on Metals in Clinical and Analytical Chemistry (Ch. 58), Marcel Dekker, New York, 1994.
[10] R.L. Willson, in: C.F. Mills (Ed.), Zinc in Human Biology, Springer, London, 1989.
[11] W.H. Cherry, in: J.O. Nriagu (Ed.), Cadmium in the Environment, Wiley, New York, 1981, pp. 69–536.
[12] R.E. Gosselin, R.P. Smith, H.C. Hodge, Clinical Toxicology of Commercial Produts, V ed., Williams and Wilkin, Baltimore, MD, 1984.
[13] Environmental Protection Agency, Updated Mutagenicity and Carcinogenicity Assessment of Cadmium PB 82-115-163. Office of Health and Environmental Assessment, Washington, DC, 1984.
[14] International Agency for Research on Cancer, Cadmium and Cadmium Compounds, vol. 2, Lyon, France 1976, pp. 39–74.
[15] M.M. Jones, P.K. Singh, G.R. Gale, A.B. Smith, L.M. Atkins, Pharmacol. Toxicol. 70 (1992) 336.
[16] P.K. Singh, M.M. Jones, K. Rostial, M. Blanusa, M. Piasek, N. Restek-Samarzija, Chem. Res. Toxicol. 9 (1996) 965.
[17] A. Agren, G. Schwarzenbach, Helv. Chim. Acta, 1921 (1955).
[18] G. Cheney, Q. Fernando, H. Freiser, J. Am. Chem. Soc. 63 (1959) 2055.
[19] W.R. Harris, Y. Chen, J. Stenback, B. Shah, J. Coord. Chem. 23 (1991) 173.
[20] M. Rivera, W. Zheng, H. Vasken Aposhian, Q. Fernando, Tox. Appl. Pharm. 100 (1989) 96.
[21] D. Ceri Jones, G.L. Smith, P.M. May, D.R. Williams, Inorg. Chim. Acta 93 (1984) 93.
[22] L.G. Egorova, V.L. Nirenburg, Z. Obshchei Khim. 50 (1980) 426.
[23] X. Fang, Q. Fernando, Chem. Res. Toxicol. 7 (1994) 770.
[24] R.S. Saxena, K.C. Gupta, M.L. Mittal, Can. J. Chem. 46 (1968) 311.
[25] M. Filella, A. Izquierdo, E. Casassas, J. Inorg. Biochem. 28 (1986) 1.
[26] M. Rivera, Q. Fernando, Chem. Res. Toxicol. 5 (1992) 142.
[27] M. Gerecke, E.A.H. Friedheim, A. Brossi, Helv. Chim. Acta 44 (1961) 955.
[28] A. Albert, E.P. Serjant, The Determination of Ionization Constants (Ch. 2), Chapman & Hall, London, 1984.
[29] G. Gran, Analyst 77 (1952) 661.
[30] L. Zekany, I. Nagypal, in: D.J. Leggett (Ed.), Computational Methods for the Determination of Formation Constants (Ch. 8), Plenum, New York, 1985.
[31] M.C. Aragoni, M. Arca, G. Crisponi, F. Cristiani, F. Isaia, V.M. Nurchi, Talanta 43 (1996) 1357.
[32] W.R. Harris, K.N. Raymond, F.L. Weitl, J. Am. Chem. Soc. 103 (1981) 2667.

PERGAMON

Polyhedron 21 (2002) 1329–1335

POLYHEDRON

www.elsevier.com/locate/poly

Cd(II) complexation in aqueous solution with dipyridine- and phenanthroline-containing polyamine macrocycles

Andrea Bencini *, Antonio Bianchi *, Patrizia Fornasari, Claudia Giorgi, Piero Paoletti *, Barbara Valtancoli

Department of Chemistry, University of Florence, Via della Lastruccia 3, 50019-Sesto Fiorentino, Firenze, Italy

Received 10 September 2001; accepted 1 October 2001

Abstract

The coordination features toward Cd(II) of four phenanthroline-containing and three dipyridine-containing macrocyclic polyamines have been studied by means of potentiometric and spectrophotometric UV–Vis measurements in aqueous solutions. All ligands form stable 1:1 metal complexes. The stability constants of the Cd(II) are generally lower than those reported for Cd(II) complexes with aliphatic macrocyclic polyamines containing the same number of nitrogen donors. This effect is mainly related to the stiffening of the ligands, due to the insertion of a large and rigid heteroaromatic moiety within the aliphatic polyamine framework. This structural feature does not allow the nitrogen donor to achieve an optimal arrangement around the metal ion. The decreased stability is often accompanied by facile protonation of the complexes, suggesting that some amine groups are not involved in metal binding. © 2002 Elsevier Science Ltd. All rights reserved.

Keywords: Macrocycles; Cadmium; Polyamines; Dipyridine; Phenanthroline

1. Introduction

Macrocyclic ligands may contain central hydrophilic cavities, ringed with electronegative binding atoms, and exterior frameworks exhibiting hydrophobic behavior [1–15]. The hydrophobic exteriors may allow them to solubilize metal ions in nonaqueous solvents or in membrane media, resulting in their employment as models for carrier molecules in the study of active ion transport phenomena as well as in their potential use as sequestering agents for metals of environmental importance, such as Pb(II) or Cd(II). The coordination features of several saturated polyamine macrocycles have been investigated in order to design selective binding agents for these metals [16–26].

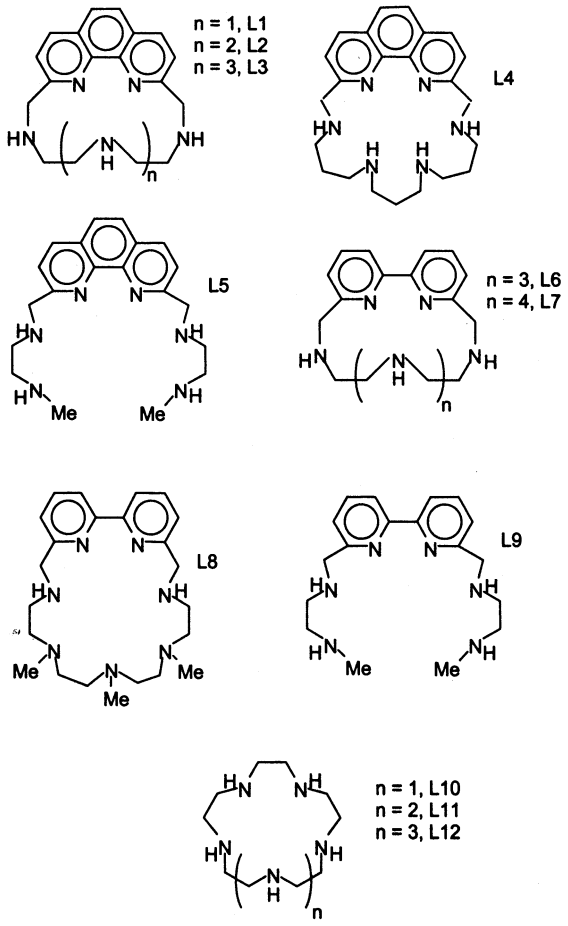
Earlier, we reported the synthesis of a series of macrocyclic polyamine ligands containing a dipyridine or a phenanthroline unit, namely **L1**–**L4** [24,27–29] and **L6**–**L8** [30]. These heteroaromatic moieties can provide a further binding site for metal cations. Furthermore, these units are rather rigid, and may provide two aromatic nitrogens whose unshared electron pairs may act cooperatively in binding cations.

Previous studies on Cu(II) [28,31], Zn(II) [27,32,33], Ni(II) [34] and Pb(II) [24] coordination have shown that the heteroaromatic nitrogens are generally involved in metal coordination. Only in the case of Pb(II) complexation, however, this structural feature leads to an enhancement of the stability of the complexes with respect to the saturated polyamine ligands with the same number of nitrogen donors, such as **L10**–**L12**, containing an ethylendiamine unit which replaces the heteroaromatic moiety ([3*k*]aneN$_k$ series) [35]. This was attributed to the higher affinity of the heteroaromatic nitrogens toward the soft Pb(II) ion than aliphatic amine groups [24]. On the contrary, in the case of Cu(II) [28], Zn(II) [27,32,33] and Ni(II) [34], the replacement of an ethylendiamine chain of **L10**–**L12** with a dipyridine or a phenanthroline unit gives rise to a destabilization of the complexes. The rigidity of these heteroaromatic units, in fact, does not allow all the nitrogen donors to bind simultaneously to the smaller Cu(II), Zn(II) or Ni(II) ions.

* Corresponding authors. Tel.: +39-055-354-841; fax: +39-055-354-845.

E-mail address: andrea.bencini@unifi.it (A. Bencini).

0277-5387/02/$ - see front matter © 2002 Elsevier Science Ltd. All rights reserved.
PII: S0277-5387(02)00967-1



We have now extended this analysis to Cd(II), in order to further elucidate the relationship between the structural features of these ligands and their coordination properties. In this paper we report a potentiometric and UV spectrophotometric study on the interaction with this metal in aqueous solutions. The coordination features of the two open-chain polyamines **L5** and **L9** [26,36], which contain a phenanthroline or a dipyridine unit, are also analyzed. The results are compared with those previously obtained with saturated polyazacycloalkanes not containing heteroaromatic units, such as **L10**–**L12** [35].

2. Experimental

2.1. General procedures

Ligands **L1** and **L2** [24], **L3** [28], **L4** [29], **L5** and **L9** [36], **L6**–**L8** [30] were obtained as previously reported.

2.2. EMF measurements

Equilibrium constants for the complexation reactions were determined by pH-metric measurements ($pH = -\log [H^+]$) in 0.1 mol dm^{-3} NMe_4Cl at 298.1 ± 0.1 K, by using the potentiometric equipment that has been already described [37]. The combined glass electrode was calibrated as a hydrogen concentration probe by titrating known amounts of HCl with CO_2-free NaOH solutions and determining the equivalent point by the Gran's method [38], by which you may determine the standard potential E°, and the ionic product of water ($pK_w = 13.83(1)$ at 298.1 K in 0.1 mol dm^{-3} NMe_4Cl, $K_w = [H^+][OH^-]$). Also 1×10^{-3}–2×10^{-3} mol dm^{-3} ligands and metal ion concentrations were employed in the potentiometric measurements performing three titration experiments (about 100 data points each one) in the pH ranges 2.5–10.5. Protonation constants of ligands are from references [33] (**L1** and **L2**), [28] (**L3**), [29] (**L4**), [27] (**L6**), [25] (**L7** and **L8**) and [26] (**L5** and **L9**). The computer program HYPERQUAD [39] was used to calculate equilibrium constants from e.m.f. data. All titrations were treated either as single sets or as separated entities, for each system, without significant variation in the values of the determined constants.

2.3. Spectrophotometric measurements

Absorption spectra were recorded on a Perkin–Elmer Lambda 9 spectrophotometer. HCl and NaOH were used to adjust the pH values that were measured on a Metrohm 713 pH meter.

3. Results and discussion

Cd(II) coordination by ligands **L1**–**L4** and **L6**–**L8** was studied by means of potentiometric measurements and the formation constants of the complexes formed in aqueous solutions are listed in Tables 1 and 2 for the phenanthroline and dipyridine complexes, respectively. The stability constants of the complexes with **L5** and **L9** are reported for comparison [26].

Considering the data in Tables 1 and 2, some general features can be outlined.Firstly, all ligands form mononuclear $[CdL]^{2+}$ complexes (**L** = **L1**–**L9**) in aqueous solutions. The data analysis with the program HYPERQUAD [39] under our experimental conditions revealed 1:1 stoichiometries for all the species detected. The stability constants of the **L1**–**L9** complexes are generally lower than those of the corresponding complexes with polyamine ligands with the same number of nitrogen donors but not containing heteroaromatic units [35]. Secondly, with the exception of **L1**, Cd(II) forms stable complexes with protonated species of the ligands. **L3**, **L4**, **L5**, **L6** and **L9** can bind up to three protons in aqueous solution, while **L7** can also form a tetraprotonated species $[CdL7H_4]^{6+}$. Consequently, protonated species of the complexes are often present in solution at neutral or slightly acidic pH values. Some exemplifying distribution diagrams are reported in Figs. 1 and 2.

Table 1
Formation constants of the Cd(II) complexes with the phenanthroline-containing ligands **L1**–**L5** (0.1 M NMe_4Cl, 298.1 K)

Reaction	L1	L2	L3	L4	L5 [a]
$Cd^{2+} + L = [CdL]^{2+}$	17.30(1) [b]	16.91(1)	15.89(2)	10.82(1)	16.03(2)
$[CdL]^{2+} + H^+ = [CdLH]^{3+}$		4.00(7)	5.60(8)	8.65(1)	5.19(2)
$[CdLH]^{3+} + H^+ = [CdLH_2]^{4+}$			5.16(2)	7.20(3)	4.67(5)
$[CdLH_2]^{4+} + H^+ = [CdLH_3]^{5+}$			2.91(2)	6.07(9)	3.43(5)
$[CdL]^{2+} + OH^- = [CdL(OH)]^+$	2.72(6)				

[a] Values from Ref. [26].
[b] Values in parenthesis are standard deviations on the last significant figure.

Table 2
Formation constants of the Cd(II) complexes with the dipyridine-containing ligands **L6**–**L9** (0.1 M NMe_4Cl, 298.1 K)

Reaction	L6	L7	L8	L9 [a]
$Cd^{2+} + L = [CdL]^{2+}$	15.70(1) [b]	14.27(1)	13.23(2)	16.31(2)
$[CdL]^{2+} + H^+ = [CdLH]^{3+}$	5.22(2)	5.45(2)	6.05(2)	4.92(4)
$[CdLH]^{3+} + H^+ = [CdLH_2]^{4+}$	4.90(1)	5.42(1)	5.41(4)	4.88(2)
$[CdLH_2]^{4+} + H^+ = [CdLH_3]^{5+}$	3.74(3)	4.72(3)		3.73(7)
$[CdLH_3]^{5+} + H^+ = [CdLH_4]^{6+}$		2.64(5)		

[a] Values from Ref. [26].
[b] Values in parenthesis are standard deviations on the last significant figure.

3.1. Cd(II) complexation by phenanthroline-containing polyamines

The phenanthroline-containing ligands **L1**–**L3** present aliphatic chains, linking the 2, 9 positions of phenanthroline, with an increasing number of amine groups separated by ethylenic spacers. In Fig. 3 the logarithms of the stability constants corresponding to the general reaction $Cd^{2+} + \mathbf{L} = [Cd\mathbf{L}]^{2+}$ are plotted for the phenanthroline-containing polyamines **L1**–**L3** and for the macrocycles of the $[3k]aneN_k$ series containing the same number of nitrogen donors (**L10**–**L12**) [35]. Although ligands **L1**–**L3** show a good ability to coordinate Cd(II), the stability constants of their complexes are remarkably lower than those of the complexes with macrocycles of the $[3k]aneN_k$ series with the same number of donors. This would be ascribed, in principle, to the different binding ability of phenanthroline and/or to steric effects exerted by this heteroaromatic unit, which replaces, in **L1**–**L3**, one ethylenic chain of **L10**–**L12**. In order to get further information on the role played by the phenanthroline unit in Cd(II) coordination, the reaction of complex formation was followed by means of UV spectra recorded on aqueous solutions containing ligands and Cd(II) in various molar ratios. Metal binding by 1,10 phenanthroline usually does not change the position of the typical UV band of this heterocycle at 270 nm, but leads to a marked change in the molar absorbance [24,26,28]. For instance, in the case of **L1** the aromatic moiety gives a rather sharp band

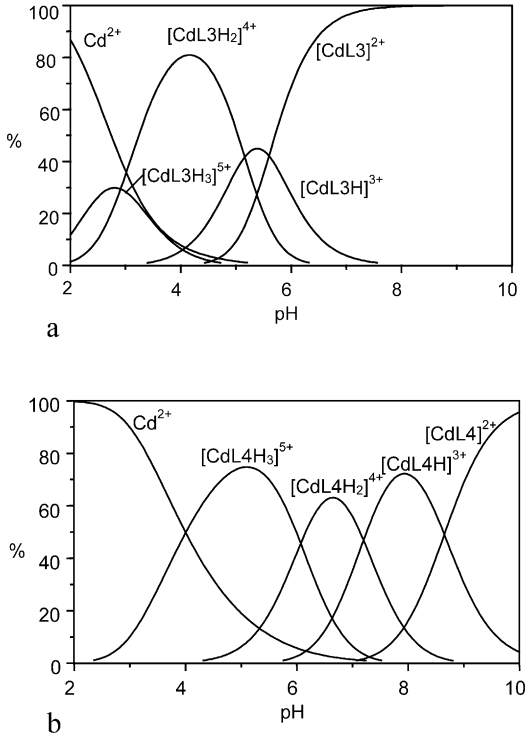


Fig. 1. Distribution diagrams of the species for the systems **L3**/Cd(II) (a) and **L4**/Cd (b) (NMe_4Cl 0.1 mol dm^{-3}, 298.1 K, $[\mathbf{L3}] = [\mathbf{L4}] = [Cd^{2+}] = 1 \times 10^{-3}$ M).

at 273 nm ($\varepsilon = 21\,200$ dm^3 mol^{-1} cm^{-1}). Solutions containing **L1** and increasing amounts of Cd(II) at neutral pH values, up to 1:1 molar ratio, show a marked decrease of the absorbance. A linear correlation between the ε values and the Cd(II):**L1** ratio is found up to 1:1 molar ratio (in this condition $\lambda_{max} = 273$, $\varepsilon = 17\,400$ dm^3 mol^{-1} cm^{-1}). Similar decreases of the ε values in presence of Cd(II) are also found for the other phenanthroline-containing ligands, as summarized in Table 3. These data account for the involvement of the phenanthroline moiety in metal coordination in the $[Cd\mathbf{L}]^{2+}$ complexes in aqueous solution. On the other hand, 1,10-phenanthroline and the aliphatic amine *N*,*N*′-dimethyl-ethylendiamine show almost equal binding ability toward Cd(II) (log $K = 4.9$ and 5.2 for the equilibrium $Cd^{2+} + \mathbf{L} = [Cd\mathbf{L}]^{2+}$ with **L** = 1,10 phenan-

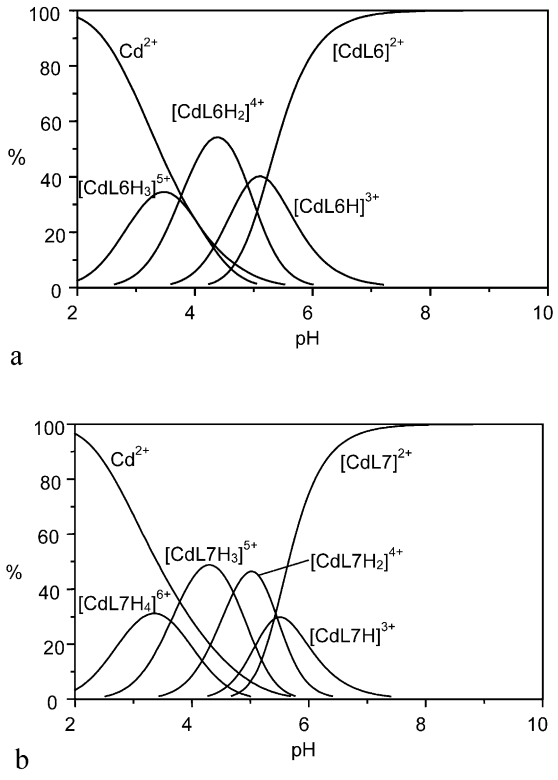


Fig. 2. Distribution diagrams of the species for the systems **L6**/Cd(II) (a) **L7**/Cd (b) and **L9**/Cd(II) (c) (NMe_4Cl 0.1 mol dm^{-3}, 298.1 K, [**L6**] = [**L7**] = [**L9**] = $[Cd^{2+}] = 1 \times 10^{-3}$ M).

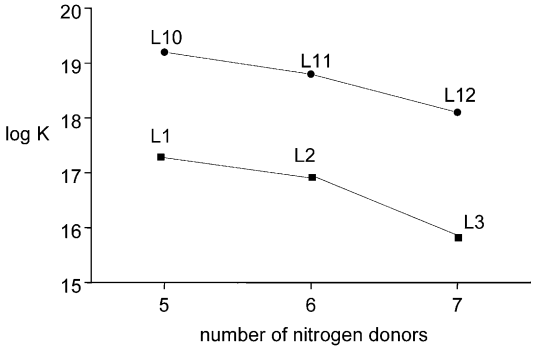


Fig. 3. Plot of the stability constants of Cd(II) complexes with phenanthroline-containing ligands **L1**–**L3** (■) and with [3*k*]aneN$_k$ macrocycles **L10**–**L12** (●) as a function of the number of nitrogen donors.

throline and *N*,*N*′-dimethyl-ethylendiamine, respectively) [40]. This consideration suggests that the lower stability of the **L1**–**L3** complexes cannot be simply ascribed to the different binding ability of phenanthroline with respect to an ethylediamine chain, but it is mainly ascribed to the stiffening of the macrocyclic structure, due to the insertion of a large and rigid heteroaromatic unit, which does not allow all the nitrogen donors to achieve an optimal arrangement around the metal ion.

Comparing the formation constants of the Cd(II) complexes with the **L1**–**L3** ligands, the stability slightly decreases on passing from the pentadentate **L1** to the hexadentate **L2**, while a larger decrease is observed for **L3** (Table 1 and Fig. 3). The small decrease in stability experienced by **L2** with respect to **L1** may be explained considering that a nitrogen donor in the **L2** complex is weakly bound, or not bound, to the metal. The formation of a monoprotonated $[Cd\mathbf{L2}H]^{3+}$ complex, not observed in the case of the **L1** complex, confirms this hypothesis. For **L3**, assuming that the metal is coordinated, once again, by only five out of the seven nitrogens, two amine groups would remain uncoordinated. These nitrogens should be located either far from each other or in adjacent positions, yielding respectively the formation of two eight-membered chelate rings or of one eleven-membered chelate ring. Both possibilities may account for the lower stability of the $[Cd\mathbf{L3}]^{2+}$ complex with respect to that of $[Cd\mathbf{L2}]^{2+}$, but the second one is in contrast to the fact that the two first stepwise protonation constants of $[Cd\mathbf{L3}]^{2+}$ have similar values. Interestingly, the electronic spectra recorded at pH 5 and 4, where the $[Cd\mathbf{L3}H]^{3+}$ and $[Cd\mathbf{L3}H_2]^{4+}$ predominate in solution (Fig. 1(a)), are almost equal ($\lambda_{max} = 273$, $\varepsilon = 17\,530$ dm^3 mol^{-1} cm^{-1} at pH 5 and $\lambda_{max} = 273$, $\varepsilon = 17\,700$ dm^3 mol^{-1} cm^{-1} at pH 4) to that of the $[Cd\mathbf{L3}]^{2+}$ complex ($\lambda_{max} = 273$, $\varepsilon = 17\,400$ dm^3 mol^{-1} cm^{-1}), indicating that these two protonation steps take place on nitrogen donors of the aliphatic pentaamine chain. This fact is not surprising, considering the by far higher basicity of secondary amine groups with respect to the phenanthroline nitrogens [41].

Ligand **L4** contains four aliphatic amine groups separated by propylenic chain. The spectral features of this complex (Table 3) account for the involvement of the phenanthroline nitrogen in metal binding. Ligand **L4**, however, forms a Cd(II) complex which is remarkably less stable than **L2**, where the four amine groups are spaced by ethylenic chains. Actually, open-chain or macrocyclic tetraamines containing propylenic chains linking the nitrogen donors usually form less stable Cd(II) complexes than the corresponding ligands with ethylenic chains (for instance log $K = 14.32$ for the formation of the Cd(II) complex with 1,4,7,10-tetraazacyclododecane, while log $K = 12.65$ in the case of the Cd(II) complex with 1,5,9,13-tetraazacyclohexadecane) [40]. This fact is usually ascribed to the formation of larger chelate ring, due to the larger bite of the propylenic chain with respect to the ethylenic ones. The resulting molecular strain may also lead to a weak interaction of some nitrogen donors with the metal, as testified by the tendency of the $[Cd\mathbf{L4}]^{2+}$ to form protonated species (Table 1 and Fig. 1(b)). The constants for successive additions of H^+ to the $[Cd\mathbf{L4}]^{2+}$ complex are far higher than those of $[Cd\mathbf{L2}]^{2+}$ and $[Cd\mathbf{L3}]^{2+}$, due to the larger +I inductive effect exerted

Table 3
UV–Vis data of phenanthroline-containing ligands **L1**–**L5** and their Cd(II) complexes

	L1	**L2**	**L3**	**L4**	**L5**
λ (nm) [ε ($dm^3\ mol^{-1}\ cm^{-1}$)]	273 [21 200]	267 [24 200]	273 [21 200]	264 [27 900]	271 [27 000]
	$[Cd\mathbf{L1}]^{2+}$	$[Cd\mathbf{L2}]^{2+}$	$[Cd\mathbf{L3}]^{2+}$	$[Cd\mathbf{L4}]^{2+}$	$[Cd\mathbf{L5}]^{2+}$
λ (nm) [ε ($dm^3\ mol^{-1}\ cm^{-1}$)]	273 [17 400]	270 [18 500]	270 [18 600]	269 [22 700]	266 [20 200]

by the propylenic chains with respect to ethylenic chains. Furthermore, propylenic linkages can also better minimize the electrostatic repulsion between charged ammonium groups, leading to a stabilization of the protonated forms of the complex.

As previously found in the case of **L3**, the electronic spectra recorded in the pH range 8–5, where the formation of protonated species $[Cd\mathbf{L4}H_n]^{(n+2)+}$ occurs (Fig. 1(b)), are almost equal to that of $[Cd\mathbf{L4}]^{2+}$, indicating that protonation takes place on aliphatic amine groups.

The open-chain ligand **L5** contains two ethylendiamine side arms linked to the 2,9 positions of phenanthroline. The stability of its Cd(II) complex is somewhat lower than the corresponding complex with **L2**, which can be considered the cyclic ligand analogous to **L5**. The higher stability observed for the complexes with cyclic ligands with respect to the corresponding acyclic ligands is generally ascribed to the 'macrocyclic effect' [2,6]. It should be noted, however, that in the present case the extent of the macrocyclic effect is rather small, the stability constant of the **L2** complex being less than one log. unit higher than that of the **L5** complex. For instance, the formation constant of the Cd(II) complex with the aliphatic macrocyclic hexamine **L10** is approximately 3 log units higher than that of the complex with the corresponding acyclic hexamine 1,14-bis(methylamino)-3,6,9,12-tetraazatetradecane [42]. Among the factors that determine the macrocyclic effect, cyclic ligands usually offer preorganized binding sites, with a preformed optimal disposition of the donors for metal binding to the metal, while the open-chain ligands would rearrange themselves to coordinate the metal cation, with a consequent energy cost. On the other hand, a previous study on the metal binding features of **L5** [26] showed that the particular molecular architecture of this ligand gives rise to a preformed coordinating 'cleft', delimited by the phenanthroline unit and the two ethylendiamine side-arms, where the metal ions can be lodged with a low energetic cost for the process of ligand rearrangement upon metal complexation. On the contrary, as discussed above, the rigid macrocyclic ligand **L2** does not seem to offer to the metal an optimal arrangement of the donors, and severe conformational stress could accompany the formation of its Cd(II) complex. Although other factors, such ligand and metal desolvation in the process of complex formation, may contribute to the macrocyclic effect, i.e. to the stabilization of the complex with macrocycle **L2**, the effect of 'ligand preorganization' would not favor the formation of the complex with the cyclic ligand **L2**, giving a reasonable explanation to the observed low difference in stability between the **L2** and **L5** complexes.

3.2. Cd(II) complexation by dipyridine-containing polyamines

A similar binding ability is shown by 2,2′-dipyridine toward Cd(II) with respect to 1,10-phenanthroline ($\log K = 4.9$ and 4.6 for the equilibrium $Cd^{2+} + \mathbf{L} = [Cd\mathbf{L}]^{2+}$ with **L** = 1,10-phenanthroline and 2,2′-dipyridine, respectively) [40]. Although in 2,2′-dipyridine the two aromatic rings can rotate along the C–C axis which connects the two pyridine units, X-ray crystallographic studies on Cu(II) [36], Zn(II) [27] and Pb(II) [25] coordination by ligands **L6**–**L9** showed that in their complexes the two heteroaromatic nitrogens are bound to the metal with an almost coplanar disposition of the two pyridine moieties. On the basis of these considerations it is expected that the present dipyridine-containing polyamines show similar binding features with respect to the corresponding phenanthroline-containing ligands. Actually, the stability constants of the complexes with **L6** and **L9** (Table 2) are almost equal to those previously found for **L3** and **L5**, where the dipyridine unit of **L6** and **L9** is simply replaced by a phenanthroline one.

The protonation behavior of $[Cd\mathbf{L6}]^{2+}$ and $[Cd\mathbf{L9}]^{2+}$ is also similar to that found for the $[Cd\mathbf{L3}]^{2+}$ and $[Cd\mathbf{L5}]^{2+}$ complexes, with rather high equilibrium constants for the successive addition of the first and the second H^+ to the complexes. As suggested for $[Cd\mathbf{L3}]^{2+}$, it can be proposed that, at least in the case of the $[Cd\mathbf{L6}]^{2+}$ complex, two nitrogen donors are not involved, or at least weakly involved, in metal coordination, and facile protonation may occur on these amine groups.

As previously observed in the case of Zn(II) binding [27], Cd(II) coordination by the dipyridine unit leads to marked changes in the absorption spectra of the ligands, with the appearance of a new red-shifted absorption band at approximately 305 nm. This new band can be used as a diagnostic tool to prove the effective involvement of dipyridine in metal binding. Fig. 4 reports the electronic spectra of **L6** and its Cd(II) complexes at different pH values. The remarkable red shift of the UV band observed with the formation of $[Cd\mathbf{L6}]^{2+}$ indicate that dipyridine is indeed coordinated to the metal. Similar features are also found in the spectra recorded at acidic pH values (c and d spectra in Fig. 4), where the mono- and diprotonated $[Cd\mathbf{L6}H]^{3+}$ and $[Cd\mathbf{L6}H_2]^{4+}$ species predominates in solution (Fig. 2(a)), suggesting that the heteroaromatic nitrogens are still involved in Cd(II) coordination. The first two protonation steps of the complex, therefore, occur on the nitrogens of the aliphatic chain. Similar results are also found for the other dipyridine-containing ligands; Table 4 summarizes the spectral features of **L6**–**L9** and their Cd(II) complexes.

Ligand **L7** displays a molecular architecture similar to **L6**, containing a longer hexamine chain linking the 6, 6′ positions of 2,2′-dipyridine. The addition of a nitrogen donor and the increased length of the aliphatic chain determine a marked decrease of the stability of the $[Cd\mathbf{L7}]^{2+}$ complex with respect to the $[Cd\mathbf{L6}]^{2+}$ complex. This result can be explained assuming that, as in $[Cd\mathbf{L6}]^{2+}$, only five out of the eight nitrogen donors of **L7** are coordinated to the metal, leading to the formation of one or more large chelate rings, containing uncoordinated nitrogen atoms. This hypothesis is confirmed by the rather high values of the first three protonation constants of $[Cd\mathbf{L7}]^{2+}$. As previously found for $[Cd\mathbf{L6}]^{2+}$, protonation of the complex does not significantly change the shape and position of the band at 304 nm in the UV spectrum, indicating that protonation takes place on aliphatic amine groups.

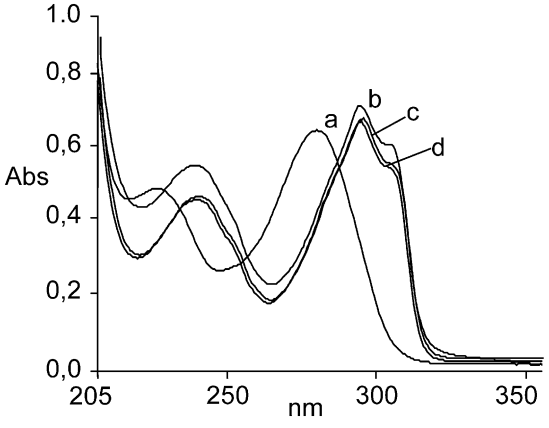


Fig. 4. UV spectra of **L6** and its Cd(II) complex at different pH values. **L6** at pH 11 (a); $[Cd\mathbf{L6}]^{2+}$ at pH 10 (b), at pH 5.2 (c) and at pH 4.5 (d).

Table 4
UV–Vis data of dipyridine-containing ligands **L6**–**L9** and their Cd(II) complexes

	L6	**L7**	**L8**	**L9**
λ (nm)	288	290	288	290
[ε ($dm^3\ mol^{-1}\ cm^{-1}$)]	[11 700]	[12 300]	[12 200]	[12 400]
	$[Cd\mathbf{L6}]^{2+}$	$[Cd\mathbf{L7}]^{2+}$	$[Cd\mathbf{L8}]^{2+}$	$[Cd\mathbf{L9}]^{2+}$
λ (nm)	304	304	304	305
[ε ($dm^3\ mol^{-1}\ cm^{-1}$)]	[14 030]	[12 550]	[13 770]	[13 200]

The macrocyclic ligand **L8** contains a pentaamine aliphatic moiety. The only structural difference with respect to **L6** is the presence of methyl groups on the three central nitrogens of the pentaamine chain. This apparently small structural modification strongly affects the stability of the Cd(II) complex, leading to a remarkable decrease of the formation constant with respect to the complex with **L6**. This fact can be related to the electronic and steric effects of N-methylation. N-methylation, in fact, reduces the σ-donating properties of the amine groups, due to the absence of M–N–H···O hydrogen bonds to the solvent, that make them weaker σ-donors [43]. Furthermore, steric hindrance due to the insertion of methyl groups within the ligand framework can cause elongation of the M–N bond as well as distortions of the coordination sphere of the metal in its complexes and thus reduces the overall metal–ligand interaction [43].

4. Concluding remarks

Phenanthroline- and dipyridine-containing macrocycles and open-chain ligands generally form stable water-soluble 1:1 Cd(II) complexes. In all the complexes under investigation the two heteroaromatic nitrogens are involved in metal coordination. Although the binding ability of 1,10-phenanthroline and 2,2′-dipyridine toward Cd(II) is similar to that of an ethylendiamine chain, the insertion of these large and rigid heteroaromatic units within a macrocyclic framework lead to a decrease of the thermodynamic stability of the complexes, i. e., the stability constants are lower than those reported for Cd(II) complexes with cyclic aliphatic polyamines containing the same number of nitrogen donors. This effect is mainly due to the stiffening of the macrocyclic structure, which does not allow the nitrogen donor to achieve an optimal arrangement around the metal ion. Among ligands **L1**–**L3**, the stability of the complexes decreases from **L1** to **L3**. The potentiometric results indicate that in the $[Cd\mathbf{L1}]^{2+}$ complex all nitrogens are involved in metal coordination, while in $[Cd\mathbf{L2}]^{2+}$ and $[Cd\mathbf{L3}]^{2+}$ some of the amine groups are

weakly bound or not bound to the metal. Other structural modifications, such as replacement of the ethylenic chain connecting the amine groups with propylenic linkages or methylation of some nitrogen donors further decrease the complex stability.

The decreased stability is generally accompanied by facile protonation of the complexes, suggesting that some nitrogen donors are not involved in metal binding. In the protonated complexes the acidic protons are located on the aliphatic amine groups, due to their higher basicity with respect to the heteroaromatic nitrogens.

Acknowledgements

Financial support by the Italian Ministero dell'Università e della Ricerca Scientifica e Tecnologica (COFIN 2000) is gratefully acknowledged.

References

[1] M.N. Hughes, The Inorganic Chemistry of the Biological Processes, Wiley, New York, 1981.
[2] J.S. Bradshaw, Aza-crown Macrocycles, Wiley, New York, 1993.
[3] R.M. Izatt, J.S. Bradshaw, S.A. Nielsen, J.D. Lamb, J.J. Christensen, D. Sen, Chem. Rev. 85 (1985) 271.
[4] R.M. Izatt, K. Pawlak, J.S. Bradshaw, Chem. Rev. 91 (1991) 1721.
[5] M. Dobler, Ionophores and their Structure, Wiley Interscience, New York, 1981.
[6] L.F. Lindoy, The Chemistry of Macrocyclic Ligand Complexes, Cambridge University Press, Cambridge, 1989.
[7] A.J. Blake, N.R. Champness, P. Hubberstey, W.S. Li, M. Schröder, M.A. Withersby, M.A. Coord, Chem. Rev. 183 (1999) 117.
[8] E. Garcia-España, J. Latorre, S.V. Luis, J.F. Miravet, P. Pozuelo, J.A. Ramirez, C. Soriano, Inorg. Chem. 35 (1996) 4591.
[9] T.A. Kaden, D. Tschudin, M. Studer, U. Brunner, Pure Appl. Chem. 61 (1989) 879.
[10] J. Nelson, V. McKee, G. Morgan, in: K.D. Karlin (Ed.), Progr. Inorganic Chemistry, vol. 47, Wiley, New York, 1998, p. 167.
[11] D.A. Nation, A.E. Martell, R.I. Carroll, A. Clearfield, Inorg. Chem. 35 (1996) 7246.
[12] G.W. Gokel, in: J.F. Stoddart (Ed.), Crown Ethers and Cryptands, The Royal Society of Chemistry, Cambridge, UK, 1991.
[13] J.M. Lehn, Supramolecular Chemistry, VCH, New York, 1995.
[14] N.W. Alcock, E.W. Curzon, P. Moore, J. Chem. Soc., Dalton Trans. (1984) 605.
[15] P. Guerriero, S. Tamburini, P.A. Vigato, P.A. Coord, Chem. Rev. 139 (1995) 17.
[16] K. Wieghardt, M. Kleine-Boymann, B. Nuber, J. Weiss, L. Zsolnai, G. Huttner, Inorg. Chem. 25 (1986) 1647.
[17] M.G.B. Drew, A. Rodgers, M. McCann, S.M. Nelson, J. Chem. Soc., Chem. Commun. (1978) 415.
[18] R.D. Hancock, M.S. Shaikjee, S.M. Dobson, C.A. Boeyens, Inorg. Chim. Acta 154 (1988) 229.
[19] V.J. Thöm, M.S. Shaikjee, R.D. Hancock, Inorg. Chem. 25 (1986) 2992.
[20] V.J. Thöm, G.D. Hosken, R.D. Hancock, Inorg. Chem. 24 (1985) 3378.
[21] V.J. Thöm, R.D. Hancock, J. Chem. Soc., Dalton Trans. (1985) 1877.
[22] A. Andres, A. Bencini, A. Charachalios, A. Bianchi, P. Dapporto, E. Garcia-España, P. Paoletti, P. Paoli, J. Chem. Soc., Dalton Trans. (1993) 3507.
[23] A. Bencini, A. Bianchi, M. Castello, M Di Vaira, J. Faus, E. Garcia-España, M. Micheloni, P. Paoletti, Inorg. Chem. 28 (1989) 347.
[24] C. Bazzicalupi, A. Bencini, V. Fusi, C. Giorgi, P. Paoletti, B. Valtancoli, J. Chem. Soc., Dalton Trans. (1999) 393.
[25] P. Arranz, C. Bazzicalupi, A. Bencini, A. Bianchi, C. Giorgi, P. Fornasari, S. Ciattini, V. Valtancoli, submitted for publication.
[26] C. Bazzicalupi, A. Bencini, E. Berni, A. Bianchi, C. Giorgi, P. Fornasari, A. Masotti, B. Valtancoli, J. Phys. Org. Chem. 14 (2001) 432.
[27] C. Lodeiro, A.J. Parola, F. Pina, C. Bazzicalupi, A. Bencini, A. Bianchi, C. Giorgi, A. Masotti, B. Valtancoli, Inorg. Chem. 40 (2001) 2968.
[28] C. Bazzicalupi, A. Bencini, V. Fusi, C. Giorgi, P. Paoletti, B. Valtancoli, Inorg. Chem. 37 (1998) 941.
[29] C. Bazzicalupi, A. Beconcini, A. Bencini, V. Fusi, C. Giorgi, A. Masotti, B. Valtancoli, J. Chem. Soc., Perkin Trans. 2 (1999) 1675.
[30] A. Bencini, A. Bianchi, V. Fusi, C. Giorgi, A. Masotti, P. Paoletti, J. Org. Chem. 65 (2000) 7686.
[31] D.K. Chand, H.-J. Schneider, A. Bencini, A. Bianchi, C. Giorgi, S. Ciattini, B. Valtancoli, Chem. Eur. J. 6 (2000) 4001.
[32] C. Bazzicalupi, A. Bencini, A. Bianchi, V. Fusi, C. Giorgi, B. Valtancoli, F. Pina, M.A. Bernardo, Inorg. Chem. 37 (1999) 3806.
[33] C. Bazzicalupi, A. Bencini, A. Bianchi, V. Fusi, C. Giorgi, B. Valtancoli, F. Pina, M.A. Bernardo, Eur. J. Inorg. Chem. (1999) 1911.
[34] C. Bazzicalupi, A. Bencini, A. Bianchi, C . Giorgi, P. Paoletti, F. Secco, M.R. Tinè, B. Valtancoli, M. Venturini, Phys. Chem. Chem. Phys. 2 (2000) 4864.
[35] A. Bianchi, M. Micheloni, P. Paoletti, Coord. Chem. Rev. 110 (1991) 17.
[36] C. Bazzicalupi, A. Bencini, S. Ciattini, C. Giorgi, A. Masotti, P. Paoletti, B. Valtancoli, N. Navon, D. Meyerstein, J. Chem. Soc., Dalton Trans. (2000) 2383.
[37] A. Bianchi, L. Bologni, P. Dapporto, M. Micheloni, P. Paoletti, Inorg. Chem. 23 (1984) 1201.
[38] G. Gran, Analyst (London) 77 (1952) 661.
[39] P. Gans, A. Sabatini, A. Vacca, Talanta 43 (1996) 807.
[40] R.M. Smith, A.E. Martell, NIST Critical Stability Constants Database, version 2, 1995.
[41] A. Bencini, A. Bianchi, E. Garcia-España, M. Micheloni, J.A. Ramirez, Coord. Chem. Rev. 118 (1999) 97.
[42] J. Aragò, A. Bencini, A. Bianchi, E. Garcia-España, M. Micheloni, P. Paoletti, J.A. Ramirez, A. Rodriguez, J. Chem. Soc., Dalton Trans. (1993) 3507.
[43] G. Golub, H. Cohen, P. Paoletti, A. Bencini, L. Messori, I. Bertini, D. Meyerstein, J. Am. Chem. Soc. 117 (1995) 8353.

PERGAMON

Polyhedron 21 (2002) 1337–1342

POLYHEDRON

www.elsevier.com/locate/poly

The influence of *N*-alkylation and chain length in the coordination ability of diamines towards silver(I) in dimethylsulfoxide

Clara Comuzzi *, Veronica Novelli, Roberto Portanova, Marilena Tolazzi *

Dipartimento di Scienze e Tecnologie Chimiche, Università di Udine, Via del Cotonificio 108, I-33100 Udine, Italy

Received 27 September 2001; accepted 16 October 2001

Abstract

The thermodynamic functions for the complexation of Ag(I) by the following diamines: *N*,*N*-dimethyldiethylenediamine (*N*,*N*-dmen), *N*,*N*-dimethyl-1,3-propanediamine (*N*,*N*-dmtn) and *N*,*N*,*N*′,*N*′-tetramethyl-1,3-propanediamine (tmtn) have been determined in dimethylsulfoxide (dmso) by potentiometric and calorimetric techniques at 298 K and 0.1 mol dm^{-3} ionic strength (NEt_4ClO_4). Only mononuclear complexes are formed (AgL_j^+, $j = 1, 2$) where the ligands act as monodentate or chelate agents. All the complexes are enthalpy stabilized whereas the entropy changes counteract the complexation. The different basicities and steric requirements of both the ligands and complexes formed together with the size of the chelate rings are taken into account to discuss the results presented here. © 2002 Elsevier Science Ltd. All rights reserved.

Keywords: Silver(I); *N*-methylated polyamines; Complexes; Dimethylsulfoxide; Thermodynamics

1. Introduction

In the last few years there has been a great deal of interest in the field of complex formation of metal ions with neutral N-donors in water [1–8] as well as in nonaqueous or mixed solvents [9–17]. The aim of these works has been to improve the knowledge of the coordination chemistry of soft and hard metal ions with these ligands, to investigate the strong influence of different basicities and steric properties of the ligands on the stability and nature of the complexes and to design ligands for selective complexation of metal ions.

These studies have now also attracted renewed interest as the coordination properties of open chain polyamines towards different cations have been taken as models allowing direct comparison with corresponding macrocyclic systems [18].

In particular many papers have reported data concerning Group 11 metal complexation with these ligands [1,3,7,12,16,17]. These data have shown that the coordination properties of amines towards these ions may be modulated through the number and the basicity of nitrogen atoms present in the ligand, the different chelate ring sizes the ligands can form, the different N-functionalization and the nature of the solvent.

In this context and as an extension of previous works, we report here the results of a thermodynamic study on the complex formation of Ag(I) with the following diamines in the aprotic solvent dimethylsulfoxide (dmso): *N*,*N*-dimethyldiethylenediamine (*N*,*N*-dmen), *N*,*N*-dimethyl-1,3-propanediamine (*N*,*N*-dmtn) and *N*,*N*,*N*′,*N*′-tetramethyl-1,3-propanediamine (tmtn).

The ligands have been chosen in order to provide further information on how the different alkylation and/or the different size of the potential chelate rings formed may affect their coordination ability toward metal ions. For this purpose also a comparison with data previously reported on Ag(I) complex formation with similar diamines possessing the same skeleton, but differently methylated, i.e. ethylenediamine (en) [12c], *N*,*N*′-dimethylethylenediamine (dmen) [12e], *N*,*N*,*N*′*N*′-tetramethylethylenediamine (tmen) [12e] and 1,3-propanediamine (tn) [12c], will be carefully taken into account.

Potentiometric and calorimetric measurements have been used to obtain the free energy and enthalpies of the

* Corresponding authors. Tel.: +39-0432-558852/558882; fax: +39-0432-558803.

E-mail addresses: comuzzi1@dstc.uniud.it (C. Comuzzi), tolazzi@dstc.uniud.it (M. Tolazzi).

0277-5387/02/$ - see front matter © 2002 Elsevier Science Ltd. All rights reserved.
PII: S0277-5387(02)00970-1

reactions, respectively. All measurements have been performed at 298 K in an ionic medium adjusted to 0.1 mol dm^{-3} with NEt_4ClO_4 as neutral salt. ^1H NMR spectroscopy has been used to provide insight into the coordination modes of the ligands.

2. Experimental

Anhydrous silver perchlorate was obtained from $AgClO_4 \cdot H_2O$ (Fluka puriss) as described previously [12a]. Dimethylsulfoxide (Fluka >99%) was purified by distillation according to the described procedures [12a] and stored over activated 4 Å molecular sieves. The background salt NEt_4ClO_4 was recrystallized twice from MeOH and dried at 110 °C. The ligands *N*,*N*-dmen (Aldrich 95%), *N*,*N*-dmtn (Aldrich 99%) and tmtn (Aldrich 98%) were purified by fractional distillation [19].

The Ag(I) solutions were prepared from anhydrous $AgClO_4$ and freshly distilled dmso. (*Warning*! Although we encountered no problems when handling $AgClO_4$, metal perchlorates solvated by dmso are powerful explosives under certain conditions [20] and should be handled with caution!)

The metal concentration in these solutions was checked by potentiometric titrations with chloride. Solutions of the ligands were prepared by dissolving weighted amounts in the anhydrous solvent. NEt_4ClO_4 was used to obtain the required ionic strength.

All the solutions were prepared afresh before each experiment in a MB Braun 150 glove box under atmosphere of dry nitrogen. The water content in the solutions, typically 10–20 ppm, was determined by a Metrohm 684 KF Coulometer.

2.1. Potentiometric measurements

All measurements were carried out in the MB Braun 150 glove box in a thermostated cell maintained at 298.0 ± 0.1 K. The experimental data required for the determination of the stability constants of the complexes were the equilibrium concentrations of the Ag(I) ion, which were obtained from the emf of a galvanic cell previously described [12a]. The emf were measured by means of an Amel 338 pH meter equipped with a Metrohm 6.0328.000 Ag electrode as a working electrode and a Metrohm 6.0718.000 Ag electrode as a reference. An experimental run consisted in collecting many equilibrium data points when solutions of silver perchlorate ($2.00 < C^\circ_M < 20.0$ mmol dm^{-3}) were titrated with solutions of the ligands ($50 < C^\circ_L < 200$ mmol dm^{-3}). Titrations were performed with at least three different initial Ag(I) concentrations and some titrations were carried out in duplicate to verify the reproducibility of the system. The electrode couple was periodically checked in dmso solutions containing no coordinating ligands. In the concentration range $10^{-6} < [Ag^+] < 10^{-2}$ mol dm^{-3}, the emf values varied with the metal ion concentration according to Nernst's law.

The computer program HYPERQUAD [21] was used for the calculation of the stability constants.

2.2. Calorimetric measurements

A Tronac model 87-558 precision calorimeter was employed to measure the heat of reaction. The calorimeter was checked by titration of tris(hydroxymethyl)aminomethane (tham) with a standard solution of HCl in water. The experimental value of the heat of neutralization of tham was found to be $\Delta H^\circ = -47.61$ kJ mol^{-1}, in good agreement with the accepted value of -47.53 ± 0.13 kJ mol^{-1} [1].

The calorimetric titrations were performed at 298.00 ± 0.02 K by adding known volumes of ligand solutions ($50 < C^\circ_L < 200$ mmol dm^{-3}) to 20 ml of Ag(I) solution ($2.00 < [Ag^+] < 20.0$ mmol dm^{-3}). The heats of dilution of the reactants, determined in separate runs, were found negligible. The least-squares computer program LETAGROP KALLE [22] was used for the calculation of the enthalpy changes.

2.3. NMR measurements

^1H NMR spectra were recorded at 298 K on a Brucker AC 200F QNP spectrometer. ^1H chemical shifts refer to $SiMe_4$. Measurements were performed on dmso-d_6 solutions containing the dissolved salt $AgClO_4 \cdot 4$dmso (approximately 20 mmol dm^{-3} in Ag^+) and the ligand *N*,*N*-dmtn in the molar ratio $R_c = C_L/C_M = 0.5$. Analogous measurements were carried out on a solution containing only the ligand concerned.

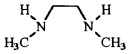
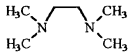
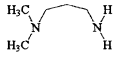
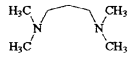
3. Results

The computer treatment of the potentiometric data shows that the best fit is obtained when the mononuclear species reported in Table 1 are taken into account. In the table, the overall stability constants and free energies of formation, with the limits of error indicated, are listed for the reactions: $Ag^+ + jL \rightleftharpoons AgL_j^+$ ($j = 1, 2$; L is the ligand concerned). In Fig. 1, the distribution of Ag(I) between the different complexes as a function of the ligand-to-metal ratio, $R_c = C_L/C_M$, is plotted for all the systems studied.

The experimental data obtained from the calorimetric measurements are reported in Fig. 2 as Δh_v, the total heats of reaction per mole of metal ion versus R_c.

From an examination of the shape of these curves some conclusions can be drawn about the prevalent

Table 1
Overall stability constants and thermodynamic functions for the reaction $Ag^{+} + jL \rightleftharpoons AgL_j^{+}$ in dmso at 298 K and $I = 0.1$ mol dm^{-3}

Ligand	Complex	Logβ_j	-$\Delta G°_{\beta j}$/kJmol^{-1}	-$\Delta H°_{\beta j}$/kJmol^{-1}	-$\Delta S°_{\beta j}$/Jmol^{-1}K^{-1}
en[a]	AgL	5.34	30.5	63	109
	AgL_2	9.50	54.2	85	103
dmen[b]	AgL	4.31	24.6	43.7	64
	AgL_2	8.31	47.4	79.3	107
N,N-dmen	AgL	4.75(0.09)	27.1(0.5)	42.1(0.7)	50
	AgL_2	8.86(0.08)	50.6(0.4)	86.5(0.3)	120
tmen[b]	AgL	3.25	18.6	30.8	41
	AgL_2	6.24	35.6	69.3	113
tn[a]	AgL	5.9	34	80.8	157
	Ag_2L	8.06	46.0	71.6	86
	Ag_2L_2	14.4	82	146.8	217
N,N-dmtn	AgL	3.95(0.04)	22.5(0.2)	40.9(0.4)	62
	AgL_2	7.49(0.03)	42.7(0.2)	73.4(0.5)	103
tmtn	AgL	1.67(0.07)	9.5(0.4)	21.7(0.5)	41
	AgL_2	2.83(0.06)	16.1(0.4)	39.6(0.6)	79

The errors quoted correspond to three standard deviations. [a]Ref. [12c]. [b]Ref. [12e].

coordinated species formed, which are consistent with the information obtained from the analysis of the potentiometric data.

For Ag(I)–tmtn system, the splitting of the curves is only indicative of formation of weak complex(es), whereas for Ag(I)–*N*,*N*-dmen and *N*,*N*-dmtn systems the enthalpy data which coincide up to $R_c = 1$, slightly diverge at the inflection point ($R_c = 2$) and superimpose at higher R_c values can be easily explained by the formation of only two successive, almost equally stable, mononuclear complexes.

The enthalpy values and the overall stability constants in Table 1 were used to calculate the full lines in Fig. 2. The match of the experimental data is quite good indicating that all the systems are satisfactorily described. Also in Table 1, the stability constants and the thermodynamic functions for the complexation reactions of Ag(I) by the ligands en [12c], dmen, tmen [12e] and tn [12c] previously determined in dmso are reported, for comparison.

Fig. 3 shows the ^{1}H NMR spectra of *N*,*N*-dmtn and of its [Ag(*N*,*N*-dmtn)]$^+$ complex in dmso-d_6.

4. Discussion

As a consequence of the formation of strong covalent Ag(I)–N bonds and the relatively weak solvation of the species [9] favourable enthalpy values are obtained whereas the entropy terms oppose the complex formation.

In a previous work [12e] the drop in the stability constant values between en, dmen and tmen, all behaving as chelating agents, was explained as due to: (i) the

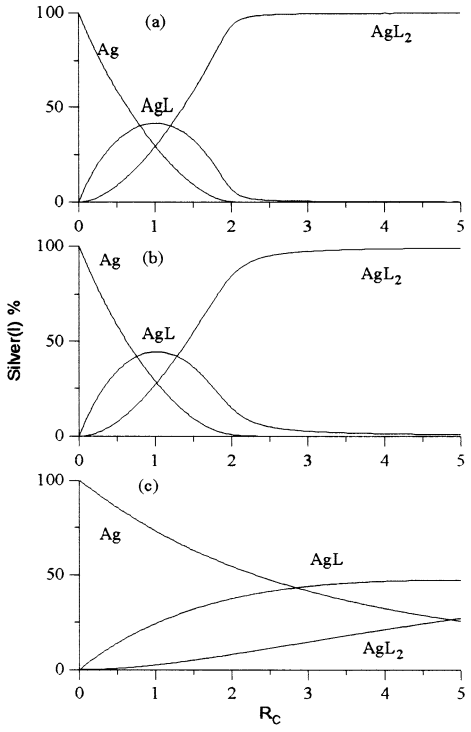


Fig. 1. The percent distribution of the metal ion in the Ag(I)–diamine systems in dmso at $C^{\circ}_{Ag} = 10$ mmol dm^{-3}. (a) *N*,*N*-dmen; (b) *N*,*N*-dmtn; (c) tmtn.

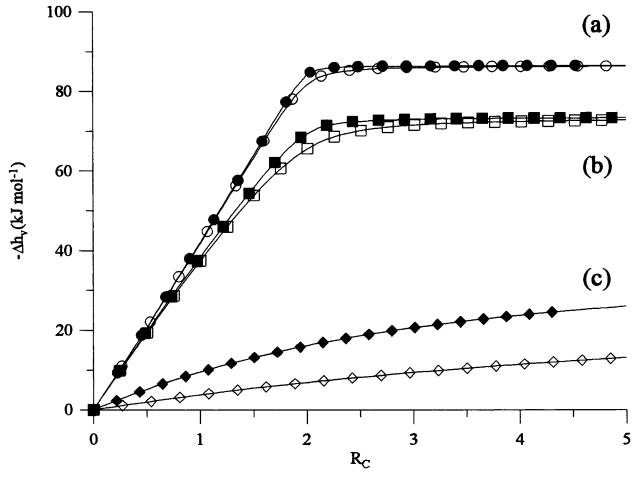


Fig. 2. The total molar enthalpy changes, Δh_v, as a function of $R_c = C_L/C_M$ for Ag(I)–diamine systems in dmso. (a) *N*,*N*-dmen: (○) 5.10, (●) 19.85 mmol dm^{-3} in Ag^+; (b) *N*,*N*-dmtn: (□) 4.85, (■) 19.98 mmol dm^{-3} in Ag^+; (c) tmtn: (◇) 4.91, (◆) 19.55 mmol dm^{-3} in Ag^+. Only some of the experimental points, chosen at random, have been plotted. The solid lines have been calculated from the values of β_j and $\Delta H^{\circ}_{\beta_j}$ in Table 1.

different basicity of amino group, which decreases in the order $-NH_2 > -NHR > -NR_2$ in dmso [23]; (ii) the elongation of M–N bonds, as a consequence of the steric hindrance of the ligands [7]; and (iii) the decreased solvation of the complexes as a consequence both of their increased radii and of the minor extent of hydrogen bonding brought about by the *N*-alkylated amines [7].

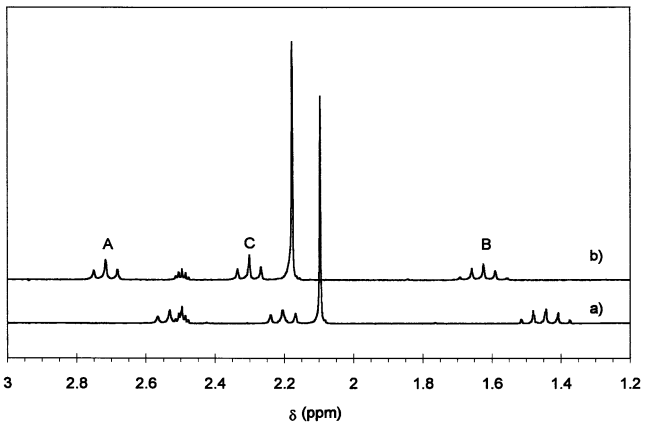


Fig. 3. ^{1}H NMR spectra at 298 K of: (a) *N*,*N*-dmtn = 10.1 mmol dm^{-3}; (b) $C^{\circ}_{Ag} = 20.0$, *N*,*N*-dmtn = 10.1 mmol dm^{-3} in dmso-d_6.

The log β_1 value here reported for the Ag(I)–*N*,*N*-dmen system is about of the same order of magnitude as that of dmen: this indicates that the ligand behaves as bidentate as confirmed by the enthalpy and entropy values.

It is of interest to note that the major difference in the thermodynamic values between dmen and *N*,*N*-dmen lies in the entropy term which is less unfavourable for the latter system. This points out that no great differences in the medium M–N bond strength are found when changing two secondary nitrogens with one primary and one tertiary ones whereas the asymmetric *N*-methylation in *N*,*N*-dmen influences the first step of complexation from an entropic point of view.

Evidently, both the ligand and the complex formed should be seen as less hydrogen bonded by the dmso molecules with respect to dmen system where the solvent may well interact with alongside –NHR groups, due to the formation of less crowded solvates.

The thermodynamic data associated with the second complexation step indicate that in the AgL_2 complex the ligand behaves also as bidentate. The higher exothermic enthalpy value of the second complexation step, ΔH°_{K2}, as compared with ΔH°_{K1} is probably due to a particular desolvation occurring in the first step of complexation: the enthalpy needed for desolvating causes the ΔH°_{K1} to be less exothermic than ΔH°_{K2} in spite of the larger exothermicity associated to the Ag(I) interaction in the first complexation step. This hypothesis is confirmed by the unfavourable high stepwise entropy term which is also in line with the above mentioned relatively scanty outer sphere solvation of the $[Ag(N,N\text{-dmen})]^+$ complex.

As far as *N*,*N*-dmtn is concerned, the thermodynamic data are somewhat ambigous in indicating the ligand coordination mode, i.e. if it acts as mono- or bi-dentate.

A comparison of the data previously reported for monoamines [12a,12b] and tn [12c] in dmso shows that: (i) the values of log β_1 and ΔH°_1 for *N*,*N*-dmtn are

slightly more favourable and the ΔS°_1 value much more unfavourable than those found previously for the monodentate *n*-butylamine (*n*-but) ($\log \beta_1 = 3.58$; $-\Delta H^{\circ}_1 = 31.4$ kJ mol^{-1}; $-\Delta S^{\circ}_1 = 37.3$ J mol^{-1} K^{-1} [12b]; (ii) $\log \beta_1$ for *N*,*N*-dmtn is about two orders of magnitude lower than that found for tn and ΔH°_1 about half the enthalpy value for tn, which has been found to be linearly chelated to Ag(I) [12c], whereas the same differences between the two chelated en and dmen are much less important (see Table 1).

Point (i) seems to indicate that *N*,*N*-dmtn is able to act as a chelating agent, whereas point (ii) seems to imply a different conclusion. Nevertheless the trend in thermodynamic functions discussed in (ii) should also be due to different geometric requirements in Ag(I)–*N*,*N*-dmtn and Ag(I)–tn systems. In fact, as mentioned above, tn was found to behave as linear bidentate in dmso according with the observed fact that large metal ions such as Ag(I) and Hg(II) will tend to have low coordination numbers and therefore large N–M–N angles [24]: this is an exception to the general behaviour of metal ions whose coordination numbers tend to become higher as metal ions become larger, behaviour which generally favours five-membered chelate ring formation more than six-membered ones [24].

As a consequence of this exception, the decreased complex stability expected for large metal ions when chelate ring size is changed from five- to six-membered, is not observed when Ag(I) is considered (see also data reported in Table 1 for en and tn systems) but, on the contrary, an increase in complex stability occurs.

In conclusion, the trend in the thermodynamic data here reported seems to indicate that, if the ligand acts as bidentate, the tetrahedral configuration of the Ag(I) solvate [9] is retained: likewise, when *N*-methyl groups are present in *N*,*N*-dmtn other steric requirements are added to the six-membered chelate ring formed which prevents Ag(I) from being coordinated linearly.

The ^{1}H NMR spectra of *N*,*N*-dmtn and of its Ag(I) complex may be of some help in investigating the coordination mode of the ligand concerned. In Fig. 3, a $\Delta\delta$ ($\Delta\delta = \delta_{complex} - \delta_{ligand}$) of about 0.1 is observed for both *N*-methyl groups (from 2.18 to 2.08) and the CH_2 (C) (see Scheme 1) (from 2.32 to 2.22) whereas the $\Delta\delta$ of CH_2 (A) is about 0.2 ppm (from 2.72 to 2.52).

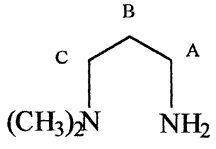
For comparison also the ^{1}H NMR spectra of the monodentate *n*-but and of its Ag(I) complex were collected and it was observed that the multiplet signal of CH_2 (at 1.30) in γ position with respect to $-NH_2$ is unaffected by complexation. The small downfield shift of CH_2 (C) (and of methyl protons) observed in Ag(I)–*N*,*N*-dmtn system should be therefore taken as reflecting an interaction between the $-NR_2$ moiety and the metal ion.

Nevertheless, this M–NR_2 interaction is weak, given that the formation of a six-membered chelate ring, normally more strained than that of a five-membered ring in a tetrahedral arrangement [24], is assisted by a tertiary, low basic, amino group [23]. The weakness of this interaction is supported not only by the values of the thermodynamic functions associated to [Ag(*N*,*N*-dmtn)]$^+$ formation, but also by the absence of polynuclear species which have usually been found to be formed in dmso when chelating ligands having primary nitrogen atoms separated by more than two methylene groups were considered [12c,12d].

The thermodynamic parameters associated to the second complexation step are very close to those corresponding to the formation of [Ag(*n*-but)$_2$]$^+$ complex ($\log \beta_2 = 7.34$; $-\Delta H^{\circ}_2 = 71.5$ and $-\Delta S^{\circ}_2 = 99.6$) [12b], thus indicating that *N*,*N*-dmtn behaves as monodentate in this complexation step.

For tmtn system, the data clearly indicate that the ligand behaves as monodentate in both the complexation steps: the $\log \beta_1$ value is even lower than that found for Ag(I)–tributylamine (tribut) system ($\log \beta_{1\ tribut} = 2.2$) [17]. The enthalpy value for 1:1 Ag(I)–tribut complex has not been reported: therefore the most reliable comparison with literature data is with the enthalpy values relative to the secondary monodentate dibutylamine (dibut) which are, respectively $\Delta H^{\circ}_1 = -31.80$ and $\Delta H^{\circ}_2 = -61.60$ kJ mol^{-1} for the 1:1 and 1:2 Ag(I)–dibut complexes [12b]. These values are certainly much more favourable than those found for tmtn system further confirming monodentation.

In conclusion, it is of interest to note that symmetric dimethylation of an amino group in a potential six-membered *N*,*N*-dmtn chelate ligand reverses the peculiar feature of silver ion to form more stable six-membered chelate rings with respect to five-membered chelate ones, strongly influencing the efficiency of the ligands concerned toward Ag(I). In the case of the tetramethylated 1,3-propanediamine the low basicity of the tertiary amino groups and the important steric requirement of the ligand even prevent chelation.



Scheme 1.

5. Supplementary material

The material is available from the authors on request.

Acknowledgements

This work has been supported by the Ministero dell'Università e della Ricerca Scientifica e Tecnologica (MURST, Rome) within the program COFIN 2000. We thank Pierluigi Polese for technical assistance.

References

[1] (a) R.M. Smith, A.E. Martell, Critical Stability Constants, vol. 6 (2nd Supplement), Plenum Press, New York, 1989;
(b) A.E. Martell, R.M. Smith, R.J. Motekaitis, Critically Selected Stability Constants of Metal Complexes Database, version 5.0, 1998.
[2] R.M. Clay, S. Corr, M. Micheloni, P. Paoletti, Inorg. Chem. 24 (1985) 3330.
[3] R. Hancock, A.E. Martell, Chem. Rev. 89 (1989) 1875.
[4] A. Bencini, A. Bianchi, P. Paoletti, Coord. Chem. Rev. 120 (1992) 51.
[5] F.C.J.M. van Veggel, W. Verboom, D.N. Reinboudt, Chem. Rev. 94 (2) (1994) 279.
[6] C. Bazzicalupi, A. Bencini, A. Bianchi, V. Fusi, E. Garcia-Espana, P. Paoletti, P. Paoli, B. Voltancoli, Inorg. Chem. 32 (1995) 4900.
[7] D. Meyerstein, Coord. Chem. Rev. 185–186 (1999) 141 (and references therein).
[8] G. Golub, H. Cohen, P. Paoletti, A. Bencini, D. Meyerstein, J. Chem. Soc., Dalton Trans. (1996) 2055.
[9] S. Ahrland, in: J.J. Lagowsky (Ed.), The Chemistry of Non-aqueous Solvents, vol. 5a (and references therein), Academic Press, New York, 1978.
[10] B.G. Cox, J. Garcia-Rosas, H. Schneider, J. Am. Chem. Soc. 103 (1981) 1384.
[11] H.K. Chantooni, I.M. Kolthoff, J. Solution Chem. 14 (1985) 1.
[12] (a) A. Cassol, P. Di Bernardo, P.L. Zanonato, R. Portanova, M. Tolazzi, J. Chem. Soc., Dalton Trans. (1987) 657;
(b) A. Cassol, P. Di Bernardo, P.L. Zanonato, R. Portanova, M. Tolazzi, G. Tomat, J. Chem. Soc., Dalton Trans. (1988) 1781;
(c) A. Cassol, P. Di Bernardo, P.L. Zanonato, R. Portanova, M. Tolazzi, G. Tomat, V. Cucinotta, D. Sciotto, J. Chem. Soc., Faraday Trans. I 85 (8) (1989) 2445;
(d) A. Cassol, P. Di Bernardo, P.L. Zanonato, R. Portanova, M. Tolazzi, G. Tomat, J. Chem. Soc., Faraday Trans. 86 (16) (1990) 2841;
(e) C. Comuzzi, V. Novelli, R. Portanova, M. Tolazzi, Supramol. Chem. 13 (3) (2001) 455.
[13] A.F. De Namor, J. Chem. Soc., Faraday Trans. 1 84 (7) (1988) 2441.
[14] A. Lewandowski, A. Szukalska, M. Galinski, J. Chem. Soc., Faraday Trans. 91 (7) (1995) 1097 (and references therein).
[15] F. Arnaud-Neu, Chem. Soc. Rev. (1994) 235.
[16] N. Heidari, A. Thaler, H. Schneider, B.G. Cox, Inorg. Chim. Acta 279 (1998) 186.
[17] A. Thaler, N. Heidari, B.G. Cox, H. Schneider, Inorg. Chim. Acta 286 (1999) 160.
[18] I. Bertini, L. Messori, G. Galub, H. Cohen, D. Meyerstein, Inorg. Chim. Acta 235 (1995) 5.
[19] D.D. Perrin, W.L.F. Armarego, D.R. Perrin, Purification of Laboratory Chemicals, 2nd ed., Pergamon, Oxford, 1980.
[20] (a) S. Ahrland, I. Persson, Acta Chem. Scand., Sect. A 34 (1980) 645;
(b) D. Martin, H.G. Hauthal, Dimethyl Sulfoxide, van Nostrand Reinhold, Wokingham, Berkshire, 1975, pp. 448–449.
[21] P. Gans, A. Sabatini, A. Vacca, Talanta 43 (1996) 1739.
[22] R. Arnek, Ark. Kemi 32 (1970) 81.
[23] (a) A. Mucci, R. Domain, R.L. Benoit, Can. J. Chem. 58 (1980) 953;
(b) R.L. Benoit, M.J. Mackinnon, L. Bergeron, Can. J. Chem. 59 (1981) 1501.
[24] A.E. Martell, R.D. Hancock, in: J.P. Fackler, Jr. (Ed.), Metal Complexes in Aqueous Solutions, Plenum, New York, 1996.

PERGAMON

Polyhedron 21 (2002) 1343–1350

POLYHEDRON

www.elsevier.com/locate/poly

Investigation of the complexation properties of a natural water towards copper(II), manganese(II) and aluminium(III), based on sorption of metal ions on a complexing resin

Maria Pesavento *, Raffaela Biesuz, Flavia Dalla Riva, Giancarla Alberti

Dipartimento di Chimica Generale, Università di Pavia, Viale Taramelli 12, 27100 Pavia, Italy

Received 24 September 2001; accepted 25 November 2001

Abstract

A competion method is proposed to characterize natural metal complexes present in a high salinity spring water. The competitor is a strong complexing resin containing the iminodiacetic group, Chelex 100. Its sorbing properties towards the metal ions here considered, Cu(II), Mn(II) and Al(III), are well known and could be quantified through K^*, the ratio of the concentration of the metal in the resin phase to that of the free metal in solution. It can be calculated for the considered metal ion for the particular experimental conditions. From the fraction of metal experimentally sorbed on the resin it is possible to obtain information about the distribution of the metal in the original water solution. Two different methods are proposed. In the resin titration (RT), different volumes of sample are treated with the same amount of resin. RT allows to determine the total metal concentration and the reaction coefficient of that metal in solution. In the ligand titration (LT), the free metal is added stepwise into the original sample, and the ligand concentration and the complexation constant are determined. This was done by the Ruzic linearization method, modified to take unto account the variation of the pH of the solution. Also the data from RT were elaborated by the modified Ruzic linearization. The study of metal ions distribution among different chemical species by the combined methods is discussed in detail. The three metal ions in the considered high salinity water were found to be mainly combined in complexes with high complexation constant. The concentration of the strong ligands involved was near to that of the metals. © 2002 Elsevier Science Ltd. All rights reserved.

Keywords: Natural metal complexes; Natural ligands; Resin titration; Ligand titration; Chelex 100

1. Introduction

The metal ions in natural waters can be complexed by ligands of different nature and concentration, for instance inorganic anions, included OH^-, and organic molecules or ions, at low and high molecular weight. The metal ions can be also adsorbed or combined in micellar particles [1,2]. This distribution among different species determines the geochemical mobility, bioavailability and toxicity of heavy metals in natural waters. The stability of the species is very important, since the most toxic form is often the free metal ion, and the weak species which are easily dissociated.

The stability of the metal complexes in aqueous solution can be determined by a number of well established experimental methods [3], but most of them can not be applied for the direct investigation of natural waters, due to the very low concentration of the metal ions and of the ligands and to the complexity of these samples. This is the reason why these investigations are usually carried out in model solutions, under exactly controlled conditions, and usually at relatively high concentration of metals and ligands. The results are transferred to the real systems, as for instance natural waters, using dedicated calculation programs. Obviously this can be done only if the system is exactly characterized, i.e. if the nature and the total concentration of all the metals and the ligands are exactly known. This is only seldom true in the case of natural waters. The experimental methods which can be used for the direct determination of the stability of the metal complexes in

* Corresponding author. Tel.: +39-0382-507580; fax: +39-0382-528544.

E-mail address: pesaven@unipv.it (M. Pesavento).

0277-5387/02/$ - see front matter © 2002 Elsevier Science Ltd. All rights reserved.
PII: S0277-5387(02)00969-5

solution must be specific and with a low detection limits. For this reason they are often based on some kind of preconcentration procedures. For instance in the widely used voltammetric methods ASV and CSV [4,5] the metal is concentrated at the working electrode in the first step of the determination. Other preconcentration methods are based on the sorption of a species on a solid phase, for example the metal ions on an ion exchange resin [6,7]. In this way, the labile fraction of a metal ion in a sample is obtained. This is an operationally defined quantity, which has been found to be correlated to the toxicity of a metal [6].

In this work, a method is proposed based on the sorption of a metal ion on a complexing resin. The metal ions complexed by the active groups present in the resin are strongly sorbed, and can be specifically separated also from complex matrices, for instance natural waters [8–10]. By this method it is possible to evaluate the concentration of free metal ion in solution, in the presence of the resin, based on the experimental determination of the concentration of metal ion sorbed on the resin, c, according to Eq. (4) described later on. To illustrate the application of the method, a natural water was considered, with a very complex composition. It is a high salinity spring water, whose main components are reported in Table 1. The sodium and chloride concentration is higher than in seawater, the alkaline earth metals are also present at high concentration. Sulfide is present at high concentration immediately after drawing the sample from the spring. Then its concentration decreases due to the bacterial activity, which transforms it into sulfur and sulfate.

An investigation method similar to that here proposed has been previously applied in the case of some synthetic solutions [11] and freshwaters [8,9], for different metal ions. In this investigation, it is used for the determination of the complexation of copper(II), manganese(II) and aluminium(III) in the particular sample describe above.

Table 1
Major components of the sample considered (high salinity water), dry residue at 180° = 52 g l^{-1}, pH 7.29, $\chi = 6.4\ 10^4$ μS cm^{-1}

Na^+	1.20 mol l^{-1}
K^+	2.60 mmol l^{-1}
Ca^{2+}	47.7 mmol l^{-1}
Mg^{2+}	32.1 mmol l^{-1}
NH_4^+	3.2 mmol l^{-1}
Cl^-	0.98 mol l^{-1}
HCO_3^-	8.19 mmol l^{-1}
H_2S(tot)	5.11 mmol l^{-1}
SO_4^{2-}	0.14 mmol l^{-1}
Br^-	1.87 mmol l^{-1}

1.1. Description of the method

The complexation of a metal in a given solution can be considered characterized, from a thermodynamic point of view, when the concentration of the ligands and the complexation constant are known. This can be done for instance by the simple method proposed by Ruzic and van der Berg [12,13]. This method is widely used in environmental determinations. Here the ligand concentration is usually not known, and it must determined together with the conditional complexation constant.

Suppose that the following complexation equilibrium is set up in solution, where I is the natural ligand, M is the metal and charges are omitted, here and in the following:

$$\mathrm{M} + \mathrm{I} \rightleftarrows \mathrm{MI} \quad K_{\mathrm{M(I)}} = \frac{[\mathrm{MI}]}{[\mathrm{M}]c_{\mathrm{I}}'} \tag{1}$$

where $K_{\mathrm{M(I)}}$ is the conditional equilibrium coefficient and c_{I}' is the total concentration of the not complexed ligand.

The reaction coefficient $\alpha_{\mathrm{M(I)}}$ pertinent to this complexation, as defined by Ringbom [14], is:

$$\alpha_{\mathrm{M(I)}} = \frac{c_{\mathrm{M}}}{[\mathrm{M}]} = 1 + K_{\mathrm{M(I)}}c_{\mathrm{I}}' \tag{2}$$

Considering the mass balance of I, $c_{\mathrm{I}} = c_{\mathrm{I}}' + [\mathrm{MI}]$, and the mass balance of M, $c_{\mathrm{M}} = [\mathrm{M}] + [\mathrm{MI}]$, the following relationship is obtained, from which both c_{I} and $K_{\mathrm{M(I)}}$ can be evaluated:

$$\frac{[\mathrm{M}]}{[\mathrm{MI}]} = \frac{1}{K_{\mathrm{M(I)}}c_{\mathrm{I}}} + \frac{[\mathrm{M}]}{c_{\mathrm{I}}} \tag{3}$$

In the method originally proposed by Ruzic and van den Berg, [M], the concentration of free, uncomplexed metal ion was determined by voltammetric techniques, as ASV and CSV, which have the required low detection limits. Here the concentration of free metal ion in solution in equilibrium with a complexing resin can be evaluated by the following relationship [15]:

$$[\mathrm{M}] = \frac{cV}{wK^*} \tag{4}$$

where c is the concentration of the metal ion sorbed on the resin.

The mass balance of M is in this case $c_{\mathrm{M}} = c + [\mathrm{M}] + [\mathrm{MI}]$, since the metal ion is partially sorbed on the resin. The evaluation can be done only if the metal is partially sorbed on the resin, so that a properly selected resin must be used. It has been previously shown [8,11] that this is so when $\alpha_{\mathrm{M(I)}}/K^*$ ranges between 0.1 and 10 w/V (V is the volume of the solution phase, and w that of the solvent in the resin phase). K^* is the ratio of the

concentration of metal ion sorbed in the resin phase to the concentration of the free metal ion in the solution phase. The accurate knowledge of K^* is required for the evaluation of [M] by Eq. (4). It can be obtained either experimentally or by calculation, if the sorption equilibria are known, as described in a number of previous works [8,11].

The reaction coefficient $\alpha_{M(I)}$ can be evaluated from the concentration of sorbed metal c from the relationship:

$$c = \frac{c_M}{1 + \frac{\alpha_{M(I)} V}{K^* w}} \quad (5)$$

It should be considered that $K_{M(I)}$ is a conditional equilibrium coefficient, since the ligand I not complexed with the metal ion M can be present in different forms, and in particular at different protonation degree. In this case its value depends on the acidity of the solution. The complexation constant, independent of the pH, is $K_{M(I)t}$ which is correlated to the conditional equilibrium coefficient by the following relation:

$$K_{M(I)t} = \frac{[MI]}{[M][I]} = \frac{K_{M(I)}\, c_I'}{[I]} = K_{M(I)}\,(1 + \sum \beta_{ap}[H]^p) \quad (6)$$

where β_{ap} is the p-protonation constant of the ligand I, to form the p-protonated species, H_pI, and $c_I'/[I]$ is the reaction coefficient of the I form of the ligand, α_I.

If $K_{M(I)}$ depends on the acidity, the reaction coefficient, $\alpha_{M(I)}$, too changes with the pH. The following simplified relationship can be obtained:

$$\log \alpha_{M(I)} = \log \frac{c_I' K_{M(I)t}}{\beta_{an}} + n\mathrm{pH} \quad (7)$$

holding for $\alpha_{M(I)}$ and $\alpha_I \gg 1$. n is the average number of protons linked to I in the considered pH range. It can also have fractional values. If $K_{M(I)}$ depends on the acidity, Eq. (3) (Ruzic linearization) strictly holds only when the acidity is constant. In the present investigation, a modification of the original equation is proposed, to take into account the pH variations. It is obtained by substituting Eqs. (4) and (6) into Eq. (3) and assuming for simplicity that $[M] \ll c_M - c$:

$$\frac{cV}{(c_M - c)K^*[H]^n w} = \frac{1}{\frac{K_{M(I)t}}{\beta_{an}}\, c_I} + \frac{cV}{c_I\, K^*[H]^n w} \quad (8)$$

From the parameters of the straight line obtained by considering the two variables $cV/(c_M - c)K^*[H]^n w$ and $cV/K^*[H]^n w$ (n has the value experimentally found by Eq. (7)) the concentration of the ligand I in solution (c_I) and the complexation constant are evaluated.

1.2. Procedures

In this investigation two procedures were used to obtain the information:

1.2.1. Resin titration (RT)

[M] and [MI] are varied by changing the ratio V/w, while c_M is kept constant. Different fractions of the metal ion are sorbed on the resin at different V/w, so that the metal ion is actually titrated by the resin. This is the reason for the name of the method. This procedure was used in the case of different natural waters [10,16], to determine the value of the reaction coefficient $\alpha_{M(I)}$. The total concentration of metal ion in solution, which is labile for the considered resin, c_M, can also be evaluated. The concentration of the metal sorbed on the resin is given by Eq. (5), where the two unknown quantities are c_M and $\alpha_{M(I)}$. The reaction coefficient is an interesting quantity for the characterization of the stability of the complex.

1.2.2. Ligand titration (LT)

[M] is varied by adding increasing concentrations of metal ion M to the sample. Here the ligands are titrated by the added metal ion. The ligand titration (LT) is widely used in the investigation of the complexing capacity of natural waters, often in connection with amperometric techniques for the determination of the labile metal [4,5,13]. The LT of copper(II) and aluminium(III) in freshwater [10] and synthetical solutions [15] using complexing resins was described. Eq. (8) is applied to obtain the required information about c_I and $K_{M(I)}$.

2. Experimental

2.1. Chemicals

All the reagents were of analytical reagent grade.

The spring water was analyzed without any modification of the sample, after filtration on 0.22 μm polycarbonate Nucleopore filter.

Chelex 100 (Na-form, 50–100 mesh) was obtained from Bio-Rad Laboratories, Richmond, CA. Its capacity (mmoles of active groups per g of dry resin), and the amount of water sorbed under different conditions were previously determined [11,17].

Chelex-100 in Na^+ form was transformed in H^+ form as previously reported [16].

2.2. Instrumentation

The determination of the metal concentrations was made by AAS. A Shimadzu AA-6601 G/GFA 6500 electrothermal atomic spectrometer with Shimadzu

autosampler ASC 6100 was used for Al(III), Cu(II) and Mn (II) determinations. L'vov platform pyrolytic graphite tube was used and analysis was performed according to operating instruction of the producer [9].

When the concentration was sufficiently high a Perkin–Elmer 1100 B flame AAS was used, following the standard condition of the operating instruction of the producer.

The concentration of H^+ in the solution phase was measured potentiometrically by a combined glass electrode (Orion 9102 SC, saturated KCl filling solution) standardized in H^+ concentration by the standard addition method in NaCl 1.1 M solution. The standard potential $E^{\circ\prime}$ was determined by the Gran linearization as described elsewhere [11,16].

2.3. Experimental procedure

All the titrations were made dividing the sample in a number of subsamples (5–8), whose volume ranged from 25 to 100 ml. Each subsample was contacted with a measured amount of resin, from 0.2 to 0.5 g of dry resin. In the case of RT the subsamples had different volumes, while all other variables were the same. In the case of LT only the total concentration of the metal was varied. In both cases, the subsamples were equilibrated at the considered acidity, and after 12 h the liquid phase was separated by filtration, the resin rapidly washed with water and eluted with 10 ml of HNO_3 0.1 M. The concentration of the metal ion in the eluting solution was determined by AAS. By this technique the required low detection limits were obtained.

2.4. Evaluation of K*

This quantity, which is of foundamental importance for the investigation of the speciation by the method proposed, was calculated as previously described from the sorption equilibria of the metals on Chelex 100, which have been investigated elsewhere [8,9,17]. As a matter of fact the knowledge of the exchange coefficient of the considered metal on Chelex 100 is required for the evaluation of K^*. The exchange coefficients are calculated from the intrinsic complexation constants of the metal, on the basis of the Gibbs–Donnan model for the resin [18,19].

The intrinsic complexation constants of copper(II), manganese(II) and aluminium(III), used in this investigation, have been previously reported [8,9].

Table 2
Concentration of some metals in the solid phase collected in a 0.22 μm filter after the filtration of 1 l of the high salinity water sample

	μmol l^{-1}
Iron	52.5
Calcium	21.7
Magnesium	14.0
Copper	1.82
Manganese	2.67
Aluminium	9.11

Concentrations of metal ions are referred to the volume of the filtered sample.

3. Results and discussion

3.1. Resin titration of the high salinity spring water

The complexation of copper(II), manganese(II) and aluminium(III) in a high salinity spring water was investigated by the resin titration (RT) procedure, as described under 'Methods'. The major constituents of this water sample are reported in Table 1. The speciation investigation was performed in solution, after filtration through a 0.22 μm filter. In Table 2 the concentration of copper, manganese and aluminium retained in the filter is reported. It was determined by AAS, after dissolution with concentrated HNO_3 (3 ml) of the filtrate obtained from 1 l of sample. A large amount of copper(II) and aluminium(III) is in the solid fraction, while manganese is almost totally in the solution phase, as seen by comparing these results with the concentration of the metals in the solution phase (see Table 4).

The strongly sorbing resin Chelex 100 was used for RT, since in the considered sample a high concentration of competing metals, like alkaline hearth metals, is present.

The results of the RT of the solution phase are reported in Fig. 1, which shows the concentration of metal ion sorbed in the resin phase c against the volume of the solution phase, at constant amount of resin. The data for the three metals were obtained by the same resin equilibration, determining the concentration of the sorbed metals in the same eluate, as described in the experimental section. This is very convenient since informations about different metals can be obtained at the same time. The average acidity was pH 5.6, but it ranged from 5.08 to 6.06 in the different subsamples, as reported in Table 3. The pH of the subsamples, obtained spontaneously after equilibration with the resin, was much lower, since Chelex 100 was used in the H^+ form, and this H^+ is almost completely exchanged for other ions, in particular the alkaline earth metals, which are present at high concentration in the sample here considered. The acidity is partially neutralized by addition of NaOH, up to the final pH reported in Table 3. This neutralization is poorly reproducible, and very time consuming, so that it is practically impossible to obtain subsamples at the same final acidity. For this reason a data treatment is used which takes into account the pH variations among the different subsamples (see

Table 4
Results of RT of the high salinity water sample

	c_{tot} (mol l^{-1})	$\alpha_{M(I)}$ at pH 5.6 [a]	n [b]	log $c_I' K_{M(I)t}/\beta_{an}$ [c]	$K_{M(I)}c_I$ [d]
Cu(II)	4.90×10^{-8}	4.0×10^{9}	2.04(0.14)	−1.77(0.88)	4.5×10^{9}
Mn(II)	2.06×10^{-5}	1.1×10^{0}	1.43(0.11)	−8.06(0.62)	9.0×10^{-1}
Al(III)	5.00×10^{-7}	9.8×10^{5}	2.71(0.23)	−9.04(1.34)	1.3×10^{6}

[a] Evaluated from the RT curve.
[b] Slope of Eq. (7).
[c] Ordinate at the origin of Eq. (7).
[d] Calculated from the ordinate at the origin of Eq. (7), at pH 5.6, assuming that $c_I = c_I'$.

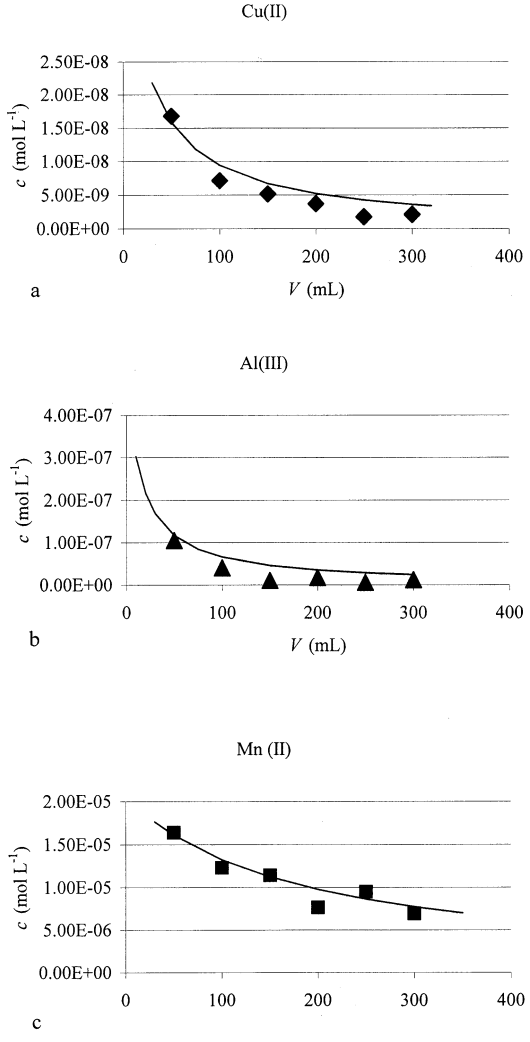


Fig. 1. RT curves obtained treating different volumes of high salinity spring water with 0.3 g of dry Chelex 100. Graph (a) copper Graph (b) aluminium Graph (c) manganese.

Eq. (8)). The values of K^* which have been used for the three metals are those reported in Table 3.

The fact that K^* varies with the conditions is usually observed, also for Chelex 100. It is important for the accuracy of the method to know the value of K^* exactly at the operating conditions.

Table 3
Final pH of the subsamples of the high salinity water, after equilibration with 0.3 g of Chelex 100 in H^+ form and after control of the acidity

V (ml)	Ph	K^*(Cu)	K^*(Mn)	K^*(Al)
50	5.69	3.9×10^{11}	$5.7\ 10^{2}$	4.3×10^{7}
100	5.58	2.3×10^{11}	$3.7\ 10^{2}$	2.4×10^{7}
150	6.06	2.0×10^{12}	$2.7\ 10^{3}$	3.4×10^{8}
200	5.08	2.4×10^{10}	$8.9\ 10^{1}$	1.9×10^{6}
250	6.32	6.2×10^{12}	$8.3\ 10^{3}$	1.7×10^{9}
300	5.22	4.5×10^{10}	$1.2\ 10^{2}$	3.9×10^{6}

Calculated K^* values at the operating conditions are reported for the three metal ions.

The RT curves of each metal are fitted by Eq. (5), whose parameters c_M and $\alpha_{M(I)}$ are evaluated assuming that $\alpha_{M(I)}/K^*$ is constant. The results are reported in Table 4 as c_{tot} and $\alpha_{M(I)}$ at an intermediate pH. The reaction coefficient $\alpha_{M(I)}$ at different pH was evaluated, and the function log $\alpha_{M(I)}$ versus pH is reported in Fig. 2 for the three metals. It is a straight line, as expected from Eq. (7), whose slope indicates the number of protons removed from the ligand I when the metal ion combines. The ordinate at the origin is related to the stability of the complexes formed in solution.

The parameters of the straight lines corresponding to Eq. (7) are reported in Table 4 for each metal ion. Different values of n are obtained for the three metals, in the same pH range, indicating that probably different ligands are involved in the respective complexation. In the case of manganese a value of $\alpha_{M(I)}$ near to 1 indicates that it is not correct to use the simplified Eq. (7) for this metal. The parameters obtained are reported in Table 4 as well, together with those of the other metals.

The reaction coefficients $\alpha_{M(I)}$ of the three metals have widely different values. It is very high in the case of copper(II), as previously found in some seawater samples [16]. Also aluminium has a high reaction coefficient, somewhat higher than that ascribable to the hydrolysis (log $\alpha_{hydr} = 4.0$ at pH 5.6 [9]), while the reaction coefficient of manganese corresponds to the free metal ion, or to a very weak complexation.

An attempt was made to determine stability constant and the concentration of ligands responsible for the

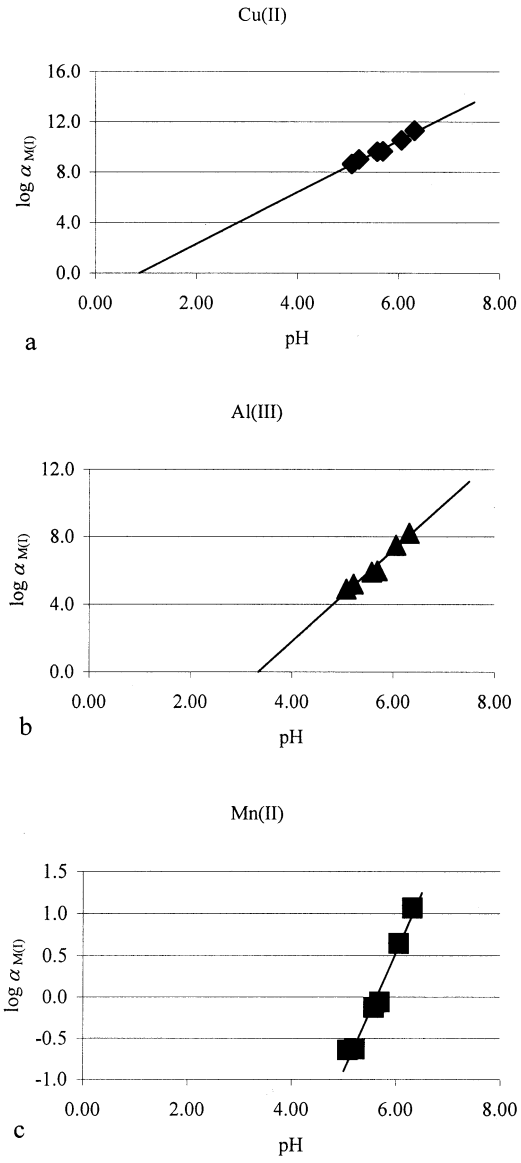


Fig. 2. Log $\alpha_{M(I)}$ at different pH of the subsamples, obtained from the RT (Eq. (7)). Graph (a) copper Graph (b) aluminium Graph (c) manganese.

complexation, by treating the data of RT by a method similar to that proposed by Ruzic in the early 1980s [12]. A modification of the equation originally proposed was used, as shown in Eq. (8), to take into account the pH variations in the different subsamples.

The results obtained in the present investigation are reported in Table 5. The ordinate at the origin was negative in the case of copper(II) and aluminium(III).

The negative intercept indicates that the complexation constant in solution $K_{M(I)}$ is too high to be evaluated by the proposed procedure. It should be observed that the fraction of sorbed metal was low for both the metals, lower than 0.1 in the majority of the points obtained by RT. The high imprecision of the metal ion determination when a low concentration is sorbed on the resin is responsible for the irreproducibility of the ordinate a the origin. In both these cases, the slope is significantly different from 0, and thus the concentration of the ligands could be evaluated. It was, respectively, 3.9×10^{-8} M for copper(II) and 3.8×10^{-7} M for Al(III). These ligands are at concentration close to that of the metal ions, forming complexes of very high stability, whose conditional complexation constants at pH 5.6 can be evaluated to be approximately 1.0×10^{17} (copper) and 2.5×10^{12} (aluminium).

The slope of the straight line in the case of manganese is not significantly different from zero. This indicates that the ligand of manganese (if any ligand is present, detectable by the proposed method) is at concentration much higher than that of the metal ion ($c_I \gg [MI]$). Obviously in this situation the concentration of the ligands can not be evaluated. The ordinate at the origin is significantly different from 0. In this case the fraction of sorbed metal ranged from 0.79 to 0.33, so it is always significant. From the ordinate at the origin $c_I K_{M(I)t}$ was evaluated to be 0.58, a value near to that obtained by the log $\alpha_{M(I)}$ versus pH straight line.

3.2. Ligand titration of the high salinity spring water

To investigate the presence of other ligands, a LT of the high salinity spring water sample was carried out with manganese(II) and copper(II). This could not be done with aluminium since a precipitate was formed when aluminium(III) was added to the solution as titrant. The same was observed in the case of copper(II) at concentration higher than 2×10^{-5} M. The LT was carried out independently for each metal ion. The data of the titration are reported in Table 6. The pH of each subsample is also shown, together with other informations of interest for the considered LT. In this procedure too it was experimentally difficult to maintain the same acidity in all the subsamples. On the other hand, the pH variation may allow us to obtain other information about the complexation, i.e. the dependence of the reaction coefficient on the acidity, as in the case of RT. Here again, as described above, log $\alpha_{M(I)}$ for each pH can be obtained, and the parameters n and log $c_I' K_{M(I)t}/\beta_{an}$ of Eq. (7) can be evaluated. They are reported in Table 7, together with the other results of the LT, obtained by Eq. (8).

In the case of copper(II) only a concentration of titrant up to 1.6×10^{-5} M could be considered, since at higher concentration a precipitate was formed. The fraction of metal sorbed never exceeded 10%, so it is evident that strong complexes are formed in solution and the ligands are far from being saturated by the added copper(II). For these reasons the quantitative evaluation of the ligand concentration and stability constant was affected by a high inaccuracy, as discussed elsewhere [15].

Table 5
Results obtained from the Ruzic linearization of the RT data of the high salinity water (according to Eq. (8))

	Slope	intercept	c_I (mol l^{-1})	$K_{M(I)t}c_I/\beta_{an}$	$K_{M(I)}$
Cu(II)	$2.54(0.26)\times10^{7}$	$-5.00(3.68)\times10^{0}$	$3.92(0.14)\times10^{-8}$	–	1.0×10^{17} [a]
Mn(II)	$-1.91(4.00)\times10^{4}$	$1.76(0.58)\times10^{12}$	$c_I \gg c_M$	$5.66(1.88)\times10^{-9}$	–
Al(III)	$2.64(0.18)\times10^{6}$	$-2.87(0.77)\times10^{8}$	$3.78(0.26)\times10^{-7}$	2.5×10^{12} [a]	–

[a] Approximate conditional constant at pH 5.6 (average pH of the RT), obtained from the average $\alpha_{M(I)}$ reported in Table 4, and c_I here obtained.

Table 6
LT with copper and manganese ($V=25$ ml) of the high salinity thermal water, in the presence of Chelex 100 (0.25 g of dry resin)

c_{tot} (M)	pH [a]	K^*	f [b]	Log $\alpha_{M(I)}$
Copper				
6.79×10^{-7}	3.50	6.86×10^{6}	0.131	5.66
1.31×10^{-6}	2.88	2.48×10^{5}	0.064	4.56
3.20×10^{-6}	3.63	1.30×10^{7}	0.096	6.09
6.34×10^{-6}	4.41	5.17×10^{8}	0.056	7.94
1.58×10^{-5}	3.67	1.58×10^{7}	0.071	6.32
Manganese				
2.17×10^{-5}	5.49	1.93×10^{2}	0.194	0.91
2.72×10^{-5}	5.70	4.39×10^{2}	0.288	1.04
3.63×10^{-5}	5.68	4.05×10^{2}	0.386	0.81
3.99×10^{-5}	5.34	1.12×10^{2}	0.468	0.11
7.63×10^{-5}	5.63	3.32×10^{2}	0.549	0.44
1.13×10^{-4}	5.49	1.93×10^{2}	0.589	0.13
1.68×10^{-4}	5.29	0.96×10^{2}	0.587	−0.17
2.04×10^{-4}	5.97	12.8×10^{2}	0.679	0.78

[a] Acidity of the different subsamples.
[b] f is the fraction of metal ion sorbed on the resin (c/c_M).

However, the quantity $\log c_I K_{M(I)t}/\beta_{an}$ can be evaluated from the ordinate at the origin of Eq. (7), and is reported in Table 7. The value has a high uncertainty, due to the fact that the fraction of sorbed metal is lower than 10%. If it has any meaning, the value of $\log c_I' K_{M(I)t}/\beta_{an}$ is very near to that determined by RT, (see Table 4). On the contrary the concentration of the ligands can not be determined, even if it can be said that they are at concentration higher than that of the maximum amount of copper added for the titration. In any case these ligands are not the strong ligands detected by RT, which are at a concentration very near to that of the metal.

In the LT with manganese(II) both c_I and $K_{M(I)t}/\beta_{an}$ (see Eq. (8)) could be determined, even if with a large uncertainty. A considerably high fraction of metal was always sorbed on Chelex 100, and the last metal additions were sorbed as expected if the ligand were completely saturated. It has been previously shown [15] that in this situation accurate values can be obtained for $K_{M(I)}$ and c_I. The results are reported in Table 7. The concentration of the ligands is higher than that of the metal ion, as expected from RT. Considering the results obtained from the modified Ruzic linearization, the quantity $\log c_I' K_{M(I)t}/\beta_{an} = -6.7$ is probably not significantly different from that obtained by RT, considering the high uncertainty. This confirms that the same complexes are detected by the two methods. The reaction coefficient, evaluated at pH 5.56, is 11.4 with a standard deviation (S.D.) of 5.9, obtained by the error propagation. Thus the hypothesis on which Eq. (7) is based should hold. The reaction coefficient of the species of manganese in the high salinity water here examined is slightly higher than that ascribable to the complexation produced by the major inorganic components, since the conditional complexation constant can be evaluated to be 2.9×10^{5}.

4. Conclusions

Some interesting results have been obtained in the investigation of some metal ions complexation in a high salinity spring water.

The reaction coefficient of aluminium obtained by RT was found to be somewhat higher than that due to the hydrolytic species, which are usually believed to be the most important aluminium species in natural waters. As an example, the strongly complexing synthetic ligand EDTA has a conditional complexation constant with aluminium of 4.7×10^{11} at pH 6 [20], which is only slightly lower than that here determined. This is the

Table 7
Results of the LT of the high salinity water sample with copper and manganese

	Results from Eq. (8) (Ruzic equation at different acidity)		Results from Eq. (7)	
	c_I (mol l^{-1})	$K_{M(I)t}/\beta_{an}$	n	$\log c_I' K_{M(I)t}/\beta_{an}$
Cu(II) pH 3.88	$>1.6\times10^{-5}$ [a]	–	2.2(0.1)	−1.9(0.5)
Mn(II) pH 5.56	$3.9(0.8)\times10^{-5}$	$4.8(2.3)\times10^{-3}$	1.4(0.6)	−7.6(3.2)

[a] Slope not significantly different from 0.

opposite of what observed in the case of manganese, whose conditional complexation constant with EDTA at these conditions is $10^{9.24}$ [20], much higher than that found here. Very strong are also the complexes of copper(II), and detected by RT. The conditional complexation constant was around 10^{17}, while that of EDTA is 1.5×10^{14} [20]. Other ligands of copper(II) were detected by the LT procedure, which are at concentration higher than 1.6×10^{-5} M, and must have a conditional stability constant lower than 2.4×10^{11}. This is true also considering that the LT was carried out at a pH lower than that of the RT. The complexing properties of the ligands of copper(II) detected by LT could be near to that of EDTA, since the conditional complexation constant Cu-EDTA at pH 4 is 2.4×10^{10}. The comparison with EDTA for the three metals is only reported as an example. It is likely that different ligands are involved for copper(II), manganese(II) and aluminium(III) complexation in the considered sample.

The methods based on the sorption of a metal ion on a complexing resin are useful for the characterization of the metal ion complexation in natural waters, at the very low concentration, and to detect metal ligands.

The characterization consists in the determination of the reaction coefficient, of the concentration of the ligands, and of the complexation constant. Informations about the dependence of the complexation equilibria on the acidity of the solution can be obtained, if the experiments are performed at different acidities. Of course the accuracy of the results depends on the accuracy of the knowledge of the sorption equilibria, since the evaluations are based on the existing relationship between the concentration of free metal in solution and that sorbed on the resin phase in equilibrium conditions, shown by Eq. (4).

The reproducibility of the experimental method is also important, and it should be improved to obtain more reliable results. Best and more complete information is obtained when the experiment is properly set up, by using a suitable resin and proper conditions, as for instance acidity and V/w. Only those complexes with $\alpha_{M(I)}$ ranging from 0.1 to 10 K^*w/V can be detected and investigated. The metal ion combined in complexes with $\alpha_{M(I)}$ lower than 0.1 K^*w/V are completely sorbed on the resin, while those with $\alpha_{M(I)}$ higher than 10 K^*w/V are not sorbed at all [15].

For instance in the sample here considered a better characterization of the strong complexes of copper and aluminium should be obtained by changing the conditions of the experiment, in particular by decreasing V/w. In this paper, the results obtained by a standard procedure are reported, which in any case give us interesting information about the considered sample. On the basis of this preliminary knowledge, most suitable conditions can be selected for a most accurate characterization.

In this paper, the results obtained using Chelex 100 are reported. This resin strongly sorbs the heavy metal ions, and makes it possible the detection of very strong complexes, which are hardly observed by other methods. This is interesting, since for instance the presence of strong ligands in solution increases the mobility of the metals, and has an influence on the toxicity. Usually strong complexes are less toxic than the weak complexes and the free metal ions.

References

[1] J. Buffle, Complexation Reactions in Aquatic Systems: An Analytical Approach, Ellis Horwood, Chichester, 1988.
[2] W. Stumm, J.J. Morgan, Acquatic Chemistry, Wiley, New York, 1996.
[3] A. Braibanti, V. Carunchio, I Complessi Metallici in Soluzione, Aracne Editrice, Rome, 1999.
[4] J.R. Donat, K.A. Lao, K.W. Bruland, Anal. Chim. Acta 248 (1994) 547.
[5] C.M.G. van den Berg, Anal. Chim. Acta 250 (1991) 265.
[6] T.M. Florence, Analyst 117 (1992) 551.
[7] J.B. Christensen, J.J. Botma, T.H. Christensen, Wat. Res. 33 (1999) 3231.
[8] M. Pesavento, R. Biesuz, Anal. Chim. Acta 346 (1997) 381.
[9] M. Pesavento, R. Biesuz, C. Palet, Analyst 123 (1998) 1295.
[10] M. Pesavento, G. Alberti, Wat. Res. 34 (2000) 4482.
[11] M. Pesavento, R. Biesuz, Anal. Chem. 67 (1995) 3558.
[12] I. Ruzic, Anal. Chim. Acta 140 (1982) 99.
[13] C.M.G. van den Brg, J.R. Donat, Anal. Chim. Acta 257 (1992) 281.
[14] A.J. Ringbom, Complexation in Analytical Chemistry, Interscience, New York, 1963.
[15] M. Pesavento, G. Alberti, A. Profumo, Anal. Chim. Acta 405 (2000) 309.
[16] M. Pesavento, R. Biesuz, F. Baffi, C. Gnecco, Anal. Chim. Acta 401 (1999) 265.
[17] M. Pesavento, R. Biesuz, M. Gallorini, A. Profumo, Anal. Chem. 65 (1993) 2522.
[18] F. Helfferich, Ion Exchange, McGraw Hill, New York, NY, 1962, p. 125.
[19] J.A. Marinsky, T. Miyajima, M. Muhammed, React. Pol. 11 (1989) 279.
[20] A.E. Martell, R.M. Smith, Critical Stability Constants, Plenum, New York, 1974.

PERGAMON

Polyhedron 21 (2002) 1351–1356

POLYHEDRON

www.elsevier.com/locate/poly

Two triaza-polyamine units linked together by different aromatic spacers, coordination properties towards metal cations of a new compartmental ligand

Mauro Formica, Luca Giorgi, Vieri Fusi *, Mauro Micheloni *, Roberto Pontellini

Institute of Chemical Sciences, University of Urbino, Piazza Rinascimento 6, I-61029 Urbino, Italy

Received 24 July 2001; accepted 18 October 2001

Abstract

The synthesis of the flexible ligand 2,6-bis-{[bis-(2-aminoethyl)amino]methyl}-benzene (**L1**) is reported. The basicity behavior of the ligand in aqueous solution was studied by potentiometry (25 °C, $I = 0.15$ mol dm^{-3}, Me_4NCl). **L1** behaves as pentaprotic base ($\log K_1 = 10.39(2)$, $\log K_2 = 9.72(1)$, $\log K_3 = 9.11(1)$, $\log K_4 = 8.72(1)$, $\log K_5 = 2.03(2)$). The stability constants for Mn(II), Co(II), Ni(II), Cu(II), Zn(II), Cd(II) and Pb(II) complexes were determined by potentiometry under the same experimental conditions and they were compared with those of ligands **L2** having the same two tri-amine subunits linked by a phenol, rather than a benzene, spacer. **L1** forms mono nuclear species with $\log K_{ML} = 9.65(1)$ for Co(II), 13.92(1) for Ni(II), 17.59(1) for Cu(II), 10.45(1) for Zn(II) and 9.24(1) for Cd(II) and binuclear species with $\log K_{M2L} = 15.28(1)$ for Co(II), 19.24(3) for Ni(II), 28.32(2) for Cu(II), 16.94(1) for Zn(II) and 14.88(1) for Cd(II). The role of the benzene and phenol as spacers of two amine functions in metal ion coordination is discussed. © 2002 Elsevier Science Ltd. All rights reserved.

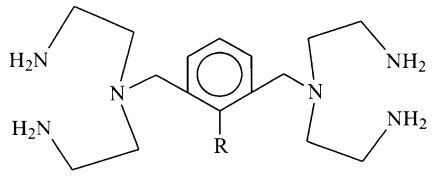
Keywords: Synthesis; Equilibria; Binuclear complexes; Polyamines

1. Introduction

Due to the key roles they play in a variety of fields, binuclear transition metal complexes and ligands capable to form them have been attracting interest from the standpoints of synthetic and biological chemistry [1–4]. Various hydrolytic metal-enzymes contain two divalent transition metal ions in close proximity, forming their active site [5–12]. For this reason, the distance between the two metals is the crucial feature allowing the cooperation of both metal ions in the active center. Recently, we reported the synthesis and the coordination properties toward M(II) metal cations of the non-cyclic ligand **L2** (Chart 1) containing a phenol moiety separating two *triaza*-polyamine fragments, highlighting its capability to assemble two transition metal ions in close proximity [13]. In this way, the two metals cooperate to bind a new species (OH^-, Cl^-, $R–O^-$, N_3^-, O_2, and other), which are coordinated in a bridge disposition between the two metals [13–15]. **L3** includes the same two tri-amine moieties but in this case, they are separated by the anisolic group (Chart 1). The presence of this spacer permits the formation of binuclear complexes with various M(II) metal ions in which, the two metals are far from each other; in this way, they can bind secondary ligands independently to saturate their coordination sphere [16]. To learn more about the structural parameters needed to obtain a bimetallic center using simple triamine subunits, we designed the new ligand **L1**, which has a different rigid spacer linking two amine moieties. The acid–base behavior and the coordination properties toward M(II) transition cations of this ligand were determined and are reported and compared with the coordination properties of **L2** toward the same M(II) cations.

* Corresponding authors. Tel./fax: +39-722-350-032.
E-mail address: vieri@chim.uniurb.it (V. Fusi).

0277-5387/02/$ - see front matter © 2002 Elsevier Science Ltd. All rights reserved.
PII: S0277-5387(02)00960-9



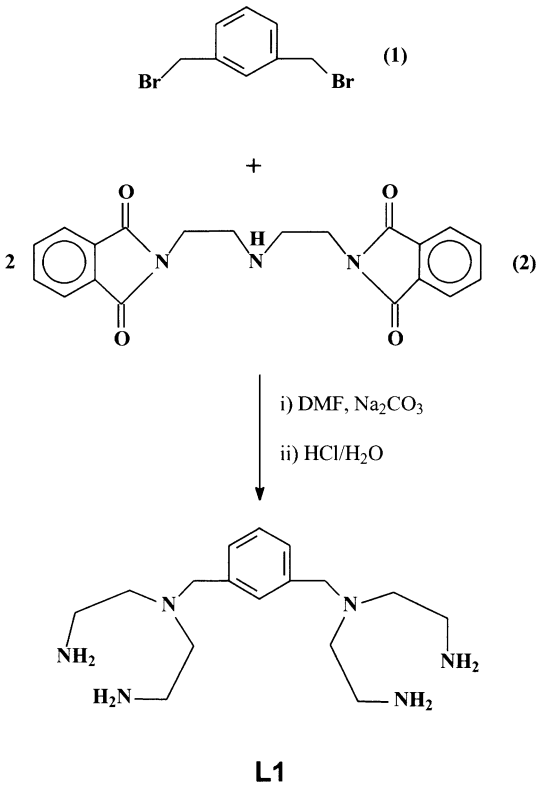
L1, R = H
L2, R = OH
L3, R = OCH_3

Ligands

2. Experimental

2.1. Synthesis

The synthesis of ligands **L1** was obtained following the procedure reported in Scheme 1. 2,6-bis(Bromomethyl)-benzene (**1**) [19] and *N*,*N*′-imminodiethylene-bis-phthalimide (**2**) [20] were prepared as previously described. Solvents and starting materials were used as purchased.



Scheme 1. Synthetic pathway followed to obtain compound **L1**.

2.1.1. 2,6-bis{[bis(2-Phthalimidoethyl)amino]methyl}benzene

Over a period of 3 h, a solution of **1** (2.6 g, 0.01 mol) in 200 cm^3 of dimethylformamide was added to a refluxing suspension of **2** (7.3 g, 0.02 mol) and of Na_2CO_3 (5.3 g, 0.05 mol) in 250 cm^3 of dimethylformamide. The reaction mixture was maintained under reflux for a further 3 h. Subsequently, the mixture was cooled to room temperature (r.t.) and the resulting suspension was filtered. The solution was concentrated to 100 cm^3 under reduced pressure and poured into cold water (500 cm^3), obtaining the product as a white solid. Yield: 7.4 g (89%). *Anal*. Calc. for $C_{48}H_{40}N_6O_8$: C, 69.55; H, 4.86; N, 10.14. Found: C, 69.4; H, 4.8; N, 10.1%. ^{1}H NMR ($CDCl_3$, 25 °C): 2.74 (t, 8H), 3.39 (s, 4H), 3.72 (t, 8H), 6.51 (t, 1H), 6.79 (d, 2H), 6.89 (s, 1H), 7.71 (m, 16H) ppm.

2.1.2. 2,6-bis{[bis-(2-Aminoethyl)amino]methyl}benzene (*L1*)

2,6-bis{[bis-(2-Phthalimidoethyl)-amino]methyl}-benzene (4.1 g, 5.0 mmol) was suspended in HCl 6 M (50 cm^3). The reaction mixture was maintained under reflux for 1 day. Subsequently, the mixture was cooled to r.t. and the resulting suspension was filtered to eliminate the phthalic acid. The solution was evaporated under reduced pressure to give a white solid, which was recrystallized with hot ethanol, achieving **L1** as *hexa*-hydrochloride salt. Yield: 2.2 g (83%). *Anal*. Calc. for $C_{16}H_{38}N_6Cl_6$: C, 36.45; H, 7.26; N, 15.94. Found: C, 36.6; H, 7.4; N, 15.8%. ^{1}H NMR D_2O, (pH 3, 25 °C): 3.42 (m, 16H), 4.46 (s, 4H), 7.60 (m, 3H), 7.68 (s, 1H) ppm. ^{13}C NMR 35.3, 50.7, 59.2, 131.7, 132,0 134.0, 134.7 ppm.

2.2. General

2.2.1. NMR spectroscopy

^{1}H and ^{13}C NMR spectra were recorded on a Bruker AC-200 instrument, operating at 200.13 and 50.33 MHz, respectively. Peak positions are reported in relation to TMS ($CHCl_3$) or HOD at 4.75 ppm (D_2O). Dioxane was used as reference standard in ^{13}C NMR spectra (δ = 67.4 ppm).

2.2.2. UV–Vis spectroscopy

UV absorption spectra were recorded at 298 K on a Varian Cary-100 spectrophotometer equipped with a temperature control unit.

2.2.3. Potentiometric measurements

Equilibrium constants for complexation reactions were determined by pH-metric measurements (pH = $-\log[H^+]$) in 0.15 mol dm^{-3} Me_4NCl at 298.1 ± 0.1 K, using the fully automatic equipment that has already been described; the EMF data were acquired with the

PASAT computer program [21]. The combined glass electrode was calibrated as a hydrogen concentration probe by titrating known amounts of HCl with CO_2-free Me_4NOH solutions and determining the equivalent point by Gran's method [22], which gives the standard potential E° and the ionic product of water ($pK_w = 13.73(1)$ at 298.1 K in 0.15 mol dm^{-3} Me_4NCl, $K_w = [H^+][OH^-]$). Ligand and metal ion concentrations of 1×10^{-3}–2×10^{-3} were employed in the potentiometric measurements, performing at least three measurements in the pH range 2–11. The HYPERQUAD [23] computer program was used to process the potentiometric data. All titrations were treated either as single sets or as separate entities, for each system, without significant variation in the values of the determined constants.

3. Results and discussion

3.1. Synthesis

The synthetic pathway used to obtain ligand **L1** is depicted in Scheme 1. The reaction of 2,6-bis(bromomethyl)-benzene (**1**) with 2 equiv. of *N*,*N*′-iminodiethylenebisphthalimide (**2**), in the presence of a base gives the intermediate molecule 2,6-bis[[bis-(2-phthalimidoethyl)-amino]methyl]-benzene in high yield. The cleavage reaction of the phthalic groups was carried out with HCl 6 M, obtaining **L1**, after the work up, as hydrochloride salt.

3.2. Solution studies

3.2.1. Basicity

Table 1 summarizes the basicity constants of **L1** with those of **L2** [15], potentiometrically determined in 0.15 mol dm^{-3} Me_4NCl aqueous solution at 298.1 K. **L1** can bind up to five protons under the experimental conditions used. The first four protonation steps lead to a slight decrease in the log *K* values: from $\log K_1 = 10.39 - \log K_4 = 8.72$, while a greater decrease in the log *K* value was observed for the fifth protonation step (see Table 1).

Table 1
Equilibrium constants (298.15 K, $I = 0.15$ mol dm^{-3}, Me_4NCl) for the protonation equilibria of **L1** and **L2** in aqueous solution

Reaction	Log *K*	
	L1	**L2**
$L + H^+ = HL^+$	10.39(2) [a]	10.49 [b]
$HL^+ + H^+ = H_2L^{2+}$	9.72(1)	9.68
$H_2L^{2+} + H^+ = H_3L^{3+}$	9.11(1)	9.21
$H_3L^{3+} + H^+ = H_4L^{4+}$	8.72(1)	7.59
$H_4L^{4+} + H^+ = H_5L^{5+}$	2.03(2)	2.31

[a] Values in parentheses are the S.D. on the last significant figure.
[b] Values from [15].

Considering the number of the protonation sites and their localization, this trend in the constant values can be easy explained in terms of minimization of the electrostatic repulsion between positive charges in the protonated species. In other words, the first four protons, binding the four primary amine functions, occupy positions far from each other and thus experience little charge repulsion. On the contrary, the fifth proton must be bound to a nitrogen atom (a tertiary amine) having the two other nitrogens of the same subunit protonated; this situation implies significant charge repulsion and is the cause of the drop in the log *K* value for the fifth protonation step. The differences between the stepwise basicity constants $\log K_1 - \log K_2 = 0.67$, $\log K_2 - \log K_3 = 0.61$ and $\log K_3 - \log K_4 = 0.39$ are similar to the critical and statistical value of $\Delta pK_a = pK_2 - pK_1 = 0.6$ of the successive dissociation of H_2L species having 2 equiv. but not-interacting dissociable protons. These data suggest that the four primary amines do not interact and they behave independently to the protonation processes. Furthermore, the first four protonation constants of **L1** are very similar to the first two basicity constants of diethylenetriamine, indicating again the independency of the two amine subunits [17]. In contrast, the differences of stepwise protonation constants of **L2**, show different values (0.81, 0.47, 1.59 logarithmic units, respectively) due to the interaction between the protonable sites during the protonation processes, produced by the insertion of the phenolic moiety.

3.2.2. Coordination of metal ions

The coordination behavior of **L1** towards the bipositive metal cations Mn(II), Co(II), Ni(II), Cu(II), Zn(II), Cd(II) and Pb(II) was potentiometrically studied in 0.15 mol dm^{-3} NMe_4Cl aqueous solution at 298.1 K and the data are reported in Table 2. For comparison, the binding properties of ligand **L2** towards the same metal cations are reported in Table 3. The data for **L2** were taken from the literature or determined under the same experimental conditions used for **L1**. **L1** forms stable mono and binuclear complexes with Co(II), Ni(II), Cu(II), Zn(II), and Cd(II); in addition, Mn(II) and Pb(II) are bound by **L2**, forming both mono and binuclear species.

The trends of the log *K* values for the addition of one M(II) ion to the neutral species are reported in Fig. 1; they are in agreement with the Irving–Williams sequence, although for the same metals **L2** always shows higher addition values than **L1**.

This behavior can be explained taking into account the fact that **L2** contains the phenolic function, which provides one more active coordination site in the ligand, thus permitting a better stabilization of the metal ion.

Table 2
Equilibrium constants (298.15 K, $I = 0.15$ mol dm^{-3}, Me_4NCl) for the metal complex equilibria of **L1** in aqueous solution

Reaction	log K				
	Co	Ni	Cu	Zn	Cd
$M+L=ML$ [a]	9.65(1) [b]	13.92(1)	17.59(1)	10.45(1)	9.24(1)
$M+L+H=MLH$	18.32(2)		26.68(1)	19.41(1)	17.91(3)
$M+L+2H=MLH_2$	26.93(1)	29.43(3)	33.60(1)	27.81(1)	26.57(5)
$M+L+3H=MLH_3$			36.15(4)		
$M+L+H_2O=MLOH+H$	−1.09(2)	2.04(4)	6.63(2)	0.32(2)	−1.97(5)
$2M+L=M_2L$	15.28(1)	19.24(3)	28.32(2)	16.94(1)	14.88(1)
$2M+L+H_2O=M_2LOH+H$	4.45(5)		18.96(3)	7.02(2)	4.13(2)
$2M+L+2H_2O=M_2L(OH)_2+2H$	−6.33(6)		9.18(4)	−2.97(3)	−7.41(8)
$ML+H=MLH$	8.7		9.1	9.0	8.7
$MLH+H=MLH_2$	8.6		6.9	8.4	8.7
$ML+OH=MLOH$	3.0	1.85	2.8	3.6	2.5
$M_2L+OH=M_2LOH$	2.9		4.4	3.8	3
$M_2LOH+OH=M_2L(OH)_2$	2.9		3.9	3.7	2.2

[a] Charges omitted for clarity.
[b] Values in parentheses are the S.D. on the last significant figure.

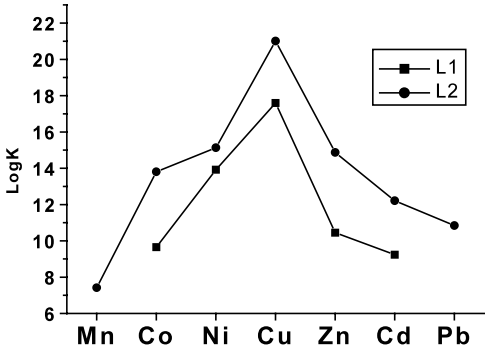


Fig. 1. Trend of the formation constants (log K) for the mononuclear species $[ML]^{2+}$ of **L1** (■) and **L2** (●).

As already demonstrated, the phenol of **L2** is involved in the coordination with its deprotonated form even at low pH values; in the mononuclear $[MH_{-1}L2]^{+}$ species the metal is probably bound by it and by three nitrogen atoms of one tri-amine subunit. Moreover, Tables 2 and 3 report the formation of complexed protonated species for all $[ML]^{2+}$ species; they easily give the $[MLH_2]^{4+}$ species indicating that the two protons are located on donor atoms not involved in the coordination of the metal ion. The molecular topology of the ligands, which have two symmetrical tri-amine subunits kept apart by a rigid spacer, can justify this behavior since it prevents the two tri-amine moieties from simultaneously binding

Table 3
Equilibrium constants (298.15 K, $I = 0.15$ mol dm^{-3}, Me_4NCl) for the metal complex equilibria of **L2** in aqueous solution

Reaction	log K						
	Mn	Co	Ni	Cu	Zn	Cd	Pb
$M+L=ML$ [a]	7.42(4) [b]	13.81 [c]	15.13 [d]	21.01 [d]	14.87 [e]	12.21(3)	10.84(3)
$M+L+H=MLH$	16.57(1)	22.46	23.96	28.27	23.51	20.73(4)	20.05(3)
$M+L+2H=MLH_2$	24.08(4)	27.52	28.64	33.02	28.67	26.82(7)	26.76(2)
$M+L+3H=MLH_3$				36.61			
$M+L=MH_{-1}L+H$	−2.17(2)	4.24	5.49	11.60	5.63	−2.25(4)	1.05(2)
$M+L+H_2O=MH_{-1}OH+2H$			−5.94				
$2M+L=M_2L$				30.27			
$2M+L=M_2H_{-1}L+H$	2.32 (5)	14.25	15.94	25.95	17.64	11.85(2)	10.19(2)
$2M+L+H_2O=M_2H_{-1}LOH+2H$	−5.89(4)	5.68	7.04	19.87	9.08	0.89(5)	−1.28(5)
$2M+L+3H_2O=M_2H_{-1}L(OH)_2+3H$	−16.55(4)	−5.27					
$ML+H=MLH$	9.2	8.6	8.1	7.3	8.6	8.5	9.2
$MLH+H=MLH_2$	7.5	5.1	6.5	4.8	5.2	6.1	6.7
$M_2H_{-1}L+OH=M_2H_{-1}LOH$	5.5	5.2	5.2	7.6	5.2	2.8	2.3

[a] Charges omitted for clarity.
[b] Values in parentheses are the S.D. on the last significant figure.
[c] [15].
[d] [13].
[e] [14].

the same metal ion, leaving one of the units involved in the protonation process unbound.

The molecular topology also facilitates the formation of binuclear species; however, because the subunits are close to each other and not independent, the addition of the second metal ion is affected by the presence of the first one and is less favorable, as reported in Tables 2 and 3. It is of note that the addition of the second metal ion takes place on the $[MH_{-1}\mathbf{L2}]^{+}$ species for **L2**, again highlighting the involvement of the phenolate in stabilizing the mononuclear species. The log K values for the addition of the second metal ions (Fig. 2) reveal that **L2** again shows higher addition constant values than **L1**. This is again due to the fact that **L2** provides a further binding site, since it is well know that the phenolate is able to simultaneously bind two metal ions in a bridge disposition [13–15,18].

All the mononuclear species $[M\mathbf{L1}]^{2+}$ have a great tendency to form *mono*-hydroxo species, indicating that the coordination requirement of the metal ion is not satisfied by the donor atoms present in the molecule. Comparison of the data for the addition of one OH^{-} to the *mono*-nuclear species shows that, while **L1** forms $[M\mathbf{L1}OH]^{+}$ species with all the metal ions, in the case of **L2** the monohydroxo species are present only for the Ni(II) species (see Table 3). This once again indicates the better saturation of the coordination sites of the metal by **L2** than **L1**.

The binuclear species of both ligands show the addition of at least one hydroxide to the $[M_2\mathbf{L1}]^{4+}$ or $[M_2H_{-1}\mathbf{L2}]^{3+}$ species, respectively, (the precipitation of hydroxo species of Ni(II) prevents detection of the addition of OH^{-} to the binuclear complex of **L1**). The addition constants of the first OH^{-} are always greater for **L2** than for **L1** by about two logarithmic units for the binuclear species of the metal ions of the first transition row. On the contrary, the addition process of the OH^{-} to the Cd(II) and Pb(II) binuclear species of **L2** shows log K values that are similar between them and also similar to the value found for the addition of the anion to the Cd(II) binuclear species of **L1**. Moreover, while the addition of a second hydroxide was observed only for the Mn(II) and Co(II) binuclear species of **L2**, this speciation was found for all the metal ions except for Ni(II), for the above reason, in the case of **L1.** This different behavior for the hydroxylated binuclear species can be ascribed to the different disposition of the two metals in the complexes of **L1** or **L2**. In the case of **L1** the two metals are independent and quite far from each other; in this way, the addition of one hydroxide to form the *mono*-hydroxylated species takes place only in one of the two metal ions, while the other one remains unaffected and tends to bind a second hydroxide anion. This is confirmed by the similar values for the addition of the second hydroxide to such species (see Table 2). In the case of **L2**, the two metals are most likely brought close to each other by forming the phenolate bridge; therefore, the first hydroxide anion can be bound in a bridge disposition by both metal ions, giving rise to higher addition constant values and moreover, at the same time saturating their coordination requirement. This assumption is contradicted in the cases of Cd(II) and Pb(II) binuclear complexes of **L2**, where the larger dimension of the ions probably prevents the formation of the hydroxo-bridge. In other words, the presence of the phenolate oxygen bridging two metal ions of the first transition row permits the assembling of two metals close to each other, allowing them to cooperate to bind molecules having two close lone pairs such hydroxide anion; on the contrary, this cooperation is unfavorable for the bigger Cd(II) and Pb(II) metal ions; in the case of **L1**, where the spacer does not have binding properties, the two amine subunits show independent coordination behavior. In this case, each metal ion must fulfil its coordination requirement on each side of the molecule by using external donor atoms; indeed, all of the metal ions investigated form binuclear *di*-hydroxo species (see Table 2).

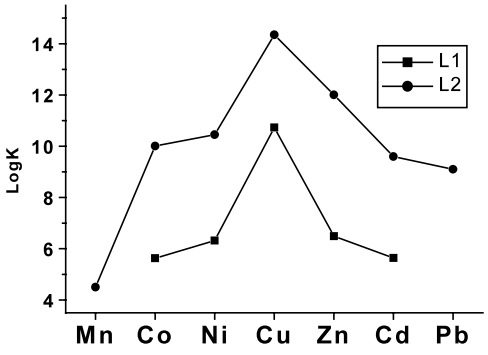


Fig. 2. Trend of the addition constants (log K) for the second M(II) ions to the mononuclear species of [**ML1**] (■) and $[MH_{-1}\mathbf{L2}]$ (●).

3.3. Conclusions

The insertion of benzene (**L1**) instead of phenol (**L2**) as spacer to separate two triamine units produces changes in the coordination properties of the two resulting ligands towards metal cations, exalting the compartmental behavior of **L1** as compared with **L2**. The basicity constants of both ligands are approximately the same in aqueous solution, while the formation constants of the *mono*- and *bi*-nuclear species with the M(II) metal ions studied are always higher for the phenolic ligand **L2** than **L1**. This is ascribed to the presence of one more coordination site in **L2** due to the oxygen of the phenol, which moreover has the possibility to bridge two metal ions in the binuclear species, furnishing a further coordination site. However, **L1** forms stable binuclear complexes with many of the ions

investigated. The metal is coordinated by a single triamine sub-unit of the ligand in both *mono*- and binuclear complexes; in the *mono*-nuclear species, the other amine subunit remains unbound. In all cases, however, the metal ions show an unsaturated coordination environment; for this reason, these species are able to bind at least another ligand, giving rise to cascade complexes. The presence of the phenolic function in **L2** gives binuclear complexes in which the two metal ions are located close to each other due to the formation of one metal–oxygen–metal phenol bridge; on the contrary, this situation is unfavorable for the binuclear species of **L1** in which the benzene spacer exalts the compartmental behavior of the ligand, due to the long distance between the two metal ions. In this way, the two metal centers of **L2** can cooperate to bind a substrate, while the same centers in **L1** are able to bind substrates independently in order to saturate their coordination requirement.

Acknowledgements

Financial support from the Italian Ministero dell'Università e della Ricerca Scientifica e Tecnologica (COFIN2000) is gratefully acknowledged.

References

[1] (a) C.J. Pedersen, J. Am. Chem. Soc. 89 (1967) 7017;
(b) J.M. Lehn, Pure Appl. Chem. 49 (1977) 857;
(c) D.J. Cram, J.M. Cram, Science 183 (1984) 4127;
(d) J.M. Lehn, Angew. Chem., Int. Ed. Engl. 27 (1988) 89.

[2] (a) P. Guerriero, S. Tamburini, P.A. Vigato, Coord. Chem. Rev. 110 (1995) 17;
(b) C. Bazzicalupi, A. Bencini, V. Fusi, C. Giorgi, P. Paoletti, B. Valtancoli, Inorg. Chem. 37 (1998) 941 (and references therein).

[3] (a) Q. Lu, J.J. Reibespiens, A.E. Martell, R.I. Carroll, A. Clearfield, Inorg. Chem. 35 (1996) 7246;
(b) T. Koike, M. Inoue, E. Kimura, M. Shiro, J. Am. Chem. Soc. 118 (1996) 3091.

[4] C. Bazzicalupi, A. Bencini, A. Bianchi, V. Fusi, E. Garcia-España, C. Giorgi, J.M. Llinares, J.A. Ramirez, B. Valtancoli, Inorg. Chem. 38 (1999) 620 (and references therein).

[5] (a) S.J. Lippard, J.M. Berg, Principles of Bioinorganic Chemistry, University Science Books, Sausalino, CA, 1994;
(b) J. Reedijk (Ed.), Bioinorganic Catalysis, M. Dekker, New York, 1993.

[6] (a) K.D. Karlin, Science 261 (1993) 701;
(b) D.E. Wilcox, Chem. Rev. 96 (1996) 2435.

[7] M.N. Hughes, The Inorganic Chemistry of the Biological Processes, Wiley, New York, 1981.

[8] Y.L. Agnus, Copper Coordination Chemistry: Biochemical and Inorganic Perspective, Adenine Press, New York, 1983.

[9] N.E. Dixon, C. Gazzola, R.L. Blakeley, B. Zerner, J. Am. Chem. Soc. 97 (1975) 4131.

[10] A. Abb, in: I. Bertini, C. Luchinat, W. Marek, M. Zeppezauer (Eds.), Zinc Enzymes, Birkhauser, Boston, MA, 1986.

[11] (a) C.J. Cooksey, P.J. Garratt, E.J. Land, S. Pavel, C.A. Ramsden, P.A. Riley, N.P.M. Smit, J. Biol. Chem. 272 (1997) 26226;
(b) L.M. Sayre, D.V. Nadkarni, J. Am. Chem. Soc. 116 (1994) 3157;
(c) A. Sánchez-Ferrer, J.N. Rodríguez-López, F. García-Cánovas, F. García-Carmona, Biochim. Biophys. Acta 1 (1995) 1247.

[12] B. Linzen, N.M. Soeter, A.F. Riggs, H.-J. Schneider, W. Schartau, M.D. Moore, E. Yokota, P.Q. Beherens, H. Nakashima, T. Takagi, T. Remoto, J.M. Vewreijken, H.J. Bak, J.J. Beintema, A. Volbeda, W.P.J. Gaykema, W.G.J. Hol, Science 229 (1985) 519.

[13] P. Dapporto, M. Formica, V. Fusi, M. Micheloni, P. Paoli, R. Pontellini, P. Rossi, Inorg. Chem. 39 (2000) 4663.

[14] P. Dapporto, M. Formica, V. Fusi, M. Micheloni, P. Paoli, R. Pontellini, P. Rossi, Inorg. Chem. 40 (2001) 6186.

[15] N. Ceccanti, M. Formica, V. Fusi, M. Micheloni, R. Pardini, R. Pontellini, M.R. Tinè, Inorg. Chim. Acta 321 (2001) 153.

[16] P. Dapporto, M. Formica, V. Fusi, M. Micheloni, P. Paoli, R. Pontellini, P. Rossi, Supramol. Chem. 13 (2001) 369.

[17] R.M. Smith, A.E. Martell, Critical Stability Constant (and supplements), Plenum, New York, 1975.

[18] (a) F.H. Allen, O. Kennard, Cambridge Structural Database Chem. Des. Autom. News 8 (1993) 31;
(b) J.S. Seo, T.H. Hynes, D. Williams, J. Chin, J. Am. Chem. Soc. 120 (1998) 9943;
(c) N.M. Murthy, M. Mahroof-Tahir, K.D. Karlin, Inorg. Chem. 40 (2001) 628;
(d) S. Torelli, I. Gautier-Luneau, J.L. Pierre, Inorg. Chem. 39 (2000) 3526;
(e) P. Dapporto, M. Formica, V. Fusi, M. Micheloni, P. Paoli, R. Pontellini, P. Romani, P. Rossi, Inorg. Chem. 39 (2000) 2156.

[19] W. Zazulak, E. Chapoteau, B.-P. Czech, A. Kumar, J. Org. Chem. 25 (1992) 6720.

[20] G.H. Searle, S.F. Lincoln, S.G. Teague, D.G. Rowe, Aust. J. Chem. 32 (1979) 519.

[21] M. Fontanelli, International Spanish–Italian Conference, Thermodynamics of Metal Complexes, Peñiscola, June 3–6, University of Valencia, Spain, 1990, pp. 41.

[22] (a) G. Gran, Analyst 77 (1952) 661;
(b) F.J. Rossotti, H. Rossetti, J. Chem. Educ. 43 (1996) 1739.

[23] P. Gans, A. Sabatini, A. Vacca, Talanta 43 (1996) 1739.

PERGAMON

Polyhedron 21 (2002) 1357–1361

POLYHEDRON

www.elsevier.com/locate/poly

Calculation of organic solvent–water partition coefficients of iron–sulfur protein models

Francisco Torrens *

Institut Universitari de Ciència Molecular, Universitat de València, Dr Moliner 50, E-46100-Burjassot, València, Spain

Received 6 June 2001; accepted 29 October 2001

Abstract

A method is presented that permits semiquantitative estimation of the partitioning of many solutes between many pairs of media. As an example, the organic solvent–water partition coefficients P are calculated. The only needed parameters are the dielectric constant and molecular volume of the organic solvent. $Fe_4S_4Cys_n$ models of high-potential FeS proteins are studied. The Gibbs free energies of solvation and partition coefficients for $Fe_4S_4Cys_n$ are calculated. The organic solvent–water partition coefficients for 1-octanol P_o, cyclohexane P_{ch} and chloroform P_{cf} decrease 4.41, 6.22 and 4.60 log units per cysteine (Cys) ligand, respectively. P_o results are compared with CDHI calculations and P_{ch} and P_{cf} results are compared with calculations carried out with a method by Leo et al. With these reference methods, P_o, P_{ch} and P_{cf} decrease 4.12, 4.70 and 5.63 log units per Cys ligand, respectively. log P_o, log P_{ch} and log P_{cf} mean relative errors (MRE) are 17, 26 and −16%, respectively. These represent a MRE of 9% but a mean unsigned relative error (URE) of 19%. For Fe_4S_4, P_o, P_{ch} and P_{cf} are close to 0 log unit. On varying the number of Cys units, the structures show hydrophobic moments indicative of particularly amphipathic structures as Fe_4S_4Cys. © 2002 Elsevier Science Ltd. All rights reserved.

Keywords: Solvation parameter model; Partition coefficient; Hydrophobic moment; Iron–sulfur protein; Mixed-valence non-integer oxidation number; Cysteine ligand

1. Introduction

High-potential iron–sulfur proteins (HiPIPs) are a class of small electron-transfer metalloproteins that have been predominantly found in purple sulfur bacteria [1–8]. The cubane [4Fe–4S] cluster of HiPIPs is widespread in nature, functioning in electron transfer, catalytic or other roles in various proteins including ferredoxins, hydrogenase, aconitase and gene regulatory proteins. In addition, the [4Fe–4S] cluster is an element of more complex centers such as the P-cluster of nitrogenase. HiPIPs are amenable to study by a variety of biophysical techniques and are thus important paradigms in elucidating the structural determinants of the physicochemical properties of both [4Fe–4S] clusters and, more generally, biological metallocenters.

As their name implies, HiPIPs have relatively high midpoint reduction potentials, varying between 50 and 450 mV. The cluster of the reduced HiPIP has an overall charge of +2 and a net spin of 0. Mössbauer spectra indicate that the iron atoms are in equivalent, $Fe^{2.5+}$, oxidation states. The oxidized HiPIP cluster, with an overall charge of +3 and a net spin of 1/2, is made up of two antiferromagnetically coupled spin pairs. One spin pair consists of two Fe^{3+}, whereas the other consists of two $Fe^{2.5+}$. The chemical shift of the βCH_2 protons of the cluster cysteine (Cys) ligands and their temperature dependence are consistent with this interpretation. Extensive nuclear magnetic resonance (NMR) work demonstrates that the position of the spin pairs within the protein framework varies from one HiPIP to another and may be determined by the relative reduction potentials of the individual iron atoms. A third oxidation state of the [4Fe–4S] cluster possesses a charge of +1. This corresponds to the reduced ferredoxin cluster and has only been observed in HiPIPs when the protein is partially denatured.

The valence distribution within the 4-Fe cluster of oxidized HiPIPs is not well understood and may be

* Tel.: +34-96-398-3182; fax: +34-96-398-3156.
E-mail address: francisco.torrens@uv.es (F. Torrens).

0277-5387/02/$ - see front matter © 2002 Elsevier Science Ltd. All rights reserved.
PII: S0277-5387(02)00956-7

relevant to elucidating the factors determining the redox potential. The cluster contains two Fe^{3+} ions and a mixed-valence $Fe^{2.5+}$ pair [9,10]. The cluster of HiPIP II from *Ectothiorhodospira halophila* is the best understood system: its electron spin resonance spectrum at 4 K is consistent with an $S = 1/2$ ground state [11], and magnetic Mössbauer data indicate that this $S = 1/2$ state is the result of antiferromagnetic coupling between the mixed-valence pair and the Fe^{3+} pair, the former having a larger subspin than the latter [12,13]. This arises because the hyperfine coupling with ^{57}Fe of $Fe^{2.5+}$ has a regular sign while that of Fe^{3+} has a reversed sign, indicative of negative and positive $\langle S_z \rangle$ for the $Fe^{2.5+}$ pair and for the Fe^{3+} pair, respectively. This interpretation of the electronic structure of the oxidized cluster of HiPIP II from *E. halophila*, which is also valid for model compounds, is consistent with NMR data [14,15]. The NMR spectrum of this protein possesses two clearly divided sets of four signals arising from Cys βCH_2 proton signals, one set being upfield and the other, downfield [16]. This spectrum was interpreted by assigning a negative $\langle S_z \rangle$ to the $Fe^{2.5+}$ pair, thus accounting for the dawnfield hyperfine shifts of the βCH_2 protons of the Cys ligated to the $Fe^{2.5+}$ pair, and a positive $\langle S_z \rangle$ to the Fe^{3+} pair, accounting for the upfield hyperfine shifts of the βCH_2 protons of the Cys ligated to the Fe^{3+} pair [17,18]. With increasing temperature, the upfield shifted signals move rapidly toward the diamagnetic region of the spectrum, and at infinite temperature, their shifts extrapolate to far downfield. This behavior, which was termed pseudo-Curie, is observed because the excited states of the Fe^{3+} ions, which increase in population, have negative $\langle S_z \rangle$ [19].

In all other characterized HiPIPs, only one of the two Cys bound to the Fe^{3+} ions has upfield-shifted βCH_2 protons, while the βCH_2 protons of the other Cys are downfield shifted, albeit to a lesser extent than those of the Cys bound to the $Fe^{2.5+}$ ions [20–22]. The temperature dependence of the latter pair of signals is of anti-Curie type. The signals of both pairs extrapolate far downfield at infinite temperature. These data were interpreted by assuming the existence of an equilibrium between two electronic distributions in the cluster; both distributions have $Fe^{2.5+}$ and Fe^{3+} pairs, but one $Fe^{2.5+}$ ion in one distribution becomes Fe^{3+} in the other and vice versa [23]. This equilibrium is fast on the NMR time scale. According to this interpretation, the Fe^{3+} ion, which exists transiently in the $Fe^{2.5+}$ state, induces a small downfield shift on the Cys proton signals. Conversely, the $Fe^{2.5+}$ ion, which exists transiently in the Fe^{3+} state, induces a downfield shift, which, while still sizable, is smaller than that induced by the 100% $Fe^{2.5+}$ ion.

Bertini et al. performed the sequence-specific assignment of ligand Cys protons of oxidized, recombinant HiPIP I from *E. halophila* [24]. They investigated the unfolding properties of HiPIP from *Chromatium vinosum* [25] and compared them with those of other proteins representative of various classes of FeS proteins [26].

The present model is an extension of the solvent-dependent conformational analysis program (SCAP) 1-octanol–water model to organic solvents. It uses extended versions of the functional forms developed in that work [27]. The method was previously applied to the calculation of the organic solvent–water partition coefficients of porphyrins, phtahlocyanines, benzobisthiazoles, fullerenes, acetanilides, local anaesthetics [28], lysozyme [29], barbiturates, polystyrene [30] and hydrocarbons [31]. In this work, $Fe_4S_4Cys_n$ $(0 \leq n \leq 4)$ models of HiPIP have been studied. Section 2 presents the improvements in the solvation model. Section 3 is devoted to the results. The last section summarizes the conclusions.

2. Solubilities and partition coefficients for general organic solvents

SCAP is based on the model of Hopfinger parameterized for the 1-octanol–water solvent pair with solute molecules composed of H, C, N, O, F, S, Cl and Br, and containing a wide variety of functional groups [32,33]. SCAP was initially used to calculate the Gibbs free energy of solvation of molecules. From these data and with the equation

$$RT \ln P = \Delta G^{\circ}_{solv}\ (\text{water}) - \Delta G^{\circ}_{solv}\ (\text{1-octanol}) \qquad (1)$$

one can calculate the logarithm log P at a given T which is taken as 298 K. R is the gas constant, and ΔG°_{solv} (1-octanol) and ΔG°_{solv} (water) (in kJ mol^{-1}) are the standard-state free energies of solvation of a given solute considered in 1-octanol and water, respectively.

SCAP manages up to four fitting parameters for a given solvent: (1) n, maximum number of solvent molecules allowed for filling the solvation sphere; (2) Δg°, variation of Gibbs free energy associated with the extraction of one solvent molecule out of the solvation sphere; (3) R_v, radius of the solvation sphere and (4) V_f, free volume available for a solvent molecule in the solvation sphere. In order to generalize SCAP for a different organic solvent, it was decided not to fit new parameters, because of the lack of available experimental data for many solvents. Instead, the four parameters of 1-octanol have been used, but modified taking into account the effect of only the new dielectric constant and molecular volume on the original parameters of 1-octanol.

For a general organic solvent (e.g. cyclohexane), the maximum number of solvent molecules allowed to fill the solvation sphere is related to the molecular volume of the solvent molecule as

$$n_s = n_o \left(\frac{V_s}{V_o}\right)^{\log\frac{n_o}{n_w}/\log\frac{V_o}{V_w}} \quad (2)$$

where V_o, V_w and V_s are the molecular volumes of 1-octanol, water and a general organic solvent, respectively; n_o, n_w and n_s are the maximum numbers of molecules of 1-octanol, water and a general organic solvent, respectively, allowed to fill the solvation sphere.

The variation in the standard Gibbs free energy associated with the extraction of one solvent molecule out of the solvation sphere Δg_s° is calculated using the generalized Born equation,

$$\Delta g_s^\circ = \Delta g_o^\circ \frac{1-\frac{1}{\varepsilon_s}}{1-\frac{1}{\varepsilon_o}} = \Delta g_o^\circ \frac{\varepsilon_o(\varepsilon_s-1)}{\varepsilon_s(\varepsilon_o-1)} \quad (3)$$

where ε_o and ε_s are the relative dielectric constants [34]. Previous results for benzene suggested a variation of only 80% of that (Eq. (3)). However, the calculation of more molecules showed that it is a better rule to expand this variation up to 100%.

The radius of the solvation sphere is related to the molecular volume of the solvent molecule as

$$R_{v,s} = R_{v,o}\left(\frac{V_s}{V_o}\right)^{1/3} \quad (4)$$

Finally, the free volume available for a solvent molecule in the solvation sphere is related to the molecular volume of the solvent molecule as

$$V_{f,s} = V_{f,o}\frac{V_s}{V_o} \quad (5)$$

The only parameters needed are the relative dielectric constant ε and molecular volume V_s of the organic solvent. V_s values have been calculated with a new version of our program TOPO version 2001 [35], which includes an actualized database of van der Waals radii [36]. In the present work, the following values have been used: $\varepsilon = 10.34$ (1-octanol), 2.023 (cyclohexane) and 4.806 (chloroform); $V_s = 155.0$ (1-octanol), 93.4 (cyclohexane) and 72.1 Å^3 (chloroform) [37]. The 1-octanol is a linear molecule, very mobile, and thus it has very different volumic properties than the cyclohexane and the chloroform.

The algorithm of Kyte and Doolittle has been used to calculate the hydropathy profile of the structures [38]. The hydrophobicity of each molecule is calculated from its atomic contributions as:

$$H = \sum_{i=1}^{M} h_i$$

where h_i is the hydrophobicity of atom i and the sum extends to the number of atoms in the molecule, M.

The hydrophobic moment calculation is based on the Eisenberg et al. formula:

$$\mu = \left[\left(\sum_{i=1}^{M} h_i \cos\delta_i\right)^2 + \left(\sum_{i=1}^{M} h_i \sin\delta_i\right)^2\right]^{1/2}$$

where the gyration angle δ_i is the successive angle between an atom and the next, around the z axis [39–41]. For instance, δ increases 97° in the successive C^α atoms of an α-helical structure (Fig. 1). This hydrophobic moment is a widely used method for determining amphipathic helices in a protein [42,43].

3. Calculation results and discussion

The free energies of solvation, partition coefficients and hydrophobic moment for $Fe_4S_4Cys_n$ $(0 \le n \le 4)$ models of HiPIP are reported (Table 1). The organic solvent–water partition coefficients P_o, P_{ch} and P_{cf} decrease monotonically 4.41, 6.22 and 4.60 log units per Cys ligand, respectively. Notice that for values of $\log P < 3$, more than 99.9% of the solute is in the aqueous phase. Therefore, some results predict a negligible quantity of solute in the organic phase. The value $1-\log P_{ch}$ is greater than the Avogadro number exponent 23 ($P_{ch} < 10^{-23}$). This means that no solute molecule would be present in the organic solvent to allow experiments for validation. However, all the log P figures are only kept for the purpose of comparison along the series. P_o results are on the same order of magnitude as CDHI computations [44]. P_{ch} and P_{cf} results are on the same order of magnitude as calculations carried out with a method by Leo et al. [45]. With these reference methods, P_o, P_{ch} and P_{cf} decrease monotonically 4.12, 4.70 and 5.63 log units per Cys ligand, respectively. log P_o, log P_{ch} and log P_{cf} mean relative errors (MRE) are 17, 26 and −16%, respectively. These represent globally a MRE of 9%. However,

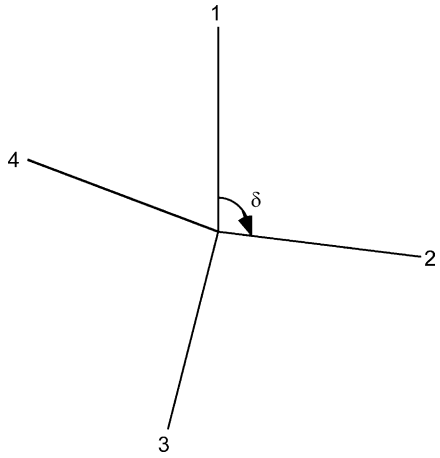


Fig. 1. Top view of an α-helix showing the gyration angle ($\delta = 97°$) in the successive C^α atoms of the first four amino acids.

Table 1
Free energy of solvation, partition coefficient and hydrophobic moment results for iron–sulfur protein models

Cluster	$\Delta G^{\circ}_{solv.w}$ [a]	$\Delta G^{\circ}_{solv.o}$ [b]	$\Delta G^{\circ}_{solv.ch}$ [c]	$\Delta G^{\circ}_{solv.cf}$ [d]	log P_o (SCAP) [e]	log P_o (CDHI) [f]	log P_{ch} (SCAP) [g]	log P_{ch} [h]	log P_{ch} (SCAP) [i]	log P_{cf} [h]	μ [j]
Fe_4S_4	−2.56	−2.76	−1.39	−2.01	0.04	0.28	−0.21	−0.70	−0.10	0.22	0.25
Fe_4S_4Cys	−61.74	−36.64	−24.86	−34.73	−4.41	−3.66	−6.48	−5.42	−4.74	−5.46	4.42
$Fe_4S_4Cys_2$	−216.4	−166.8	−144.6	−163.6	−8.72	−7.21	−12.6	−10.0	−9.28	−11.0	3.49
$Fe_4S_4Cys_3$	−454.9	−380.5	−348.0	−376.1	−13.1	−11.2	−18.8	−14.6	−13.8	−16.5	0.77
$Fe_4S_4Cys_4$	−648.4	−548.1	−505.5	−542.9	−17.6	−16.2	−25.1	−19.5	−18.5	−22.3	2.62

[a] Gibbs free energy of solvation in water (kJ mol^{-1}).
[b] Gibbs free energy of solvation in 1-octanol (kJ mol^{-1}).
[c] Gibbs free energy of solvation in cyclohexane (kJ mol^{-1}).
[d] Gibbs free energy of solvation in chloroform (kJ mol^{-1}).
[e] P_o is the 1-octanol–water partition coefficient.
[f] CDHI, calculations carried out with a method developed by Kantola et al.
[g] P_{ch} is the cyclohexane–water partition coefficient.
[h] Calculations carried out with a method developed by Leo et al.
[i] P_{cf} is the chloroform–water partition coefficient.
[j] μ is the hydrophobic moment.

this result should be taken with care because the mean unsigned relative error (URE) is 19%. The error for chloroform is rather smaller than for cyclohexane. This is due to the greater similarity in relative dielectric constant between the former solvent and 1-octanol. In particular, for Fe_4S_4 the three P are close to 0 log unit.

On the other hand, the hydrophobic moment μ differentiates well the $Fe_4S_4Cys_n$ structures. On varying the number of Cys units, the structures show μ values indicative of particularly amphipathic structures as Fe_4S_4Cys.

4. Conclusions

From the previous results the following conclusions can be drawn.

1) The three organic solvent–water P for $Fe_4S_4Cys_n$ ($0 \leq n \leq 4$) models of HiPIP decrease approximately 5.1 log units per Cys ligand. With reference methods the three P decrease 4.8 log units per Cys ligand. log P_o, log P_{ch} and log P_{cf} MRE are 17, 26 and −16%, respectively. These represent a MRE of 9% but a URE of 19%.
2) The organic solvents similar to 1-octanol in relative dielectric constant are those that are best modeled by SCAP.
3) The hydrophobic moment μ differentiates well $Fe_4S_4Cys_n$ structures. On varying the number of Cys units, the structures show μ indicative of particularly amphipathic structures as Fe_4S_4Cys. An extension of the present study to other proteins would give an insight into a possible generality of this conclusion. Further work is in progress on the characterization of lysozyme.

Acknowledgements

The author acknowledges the financial support of the Dirección General de Enseñanza Superior of the Spanish MEC (Project PB97-1383).

References

[1] E.T. Adman, L.C. Sieker, L.H. Jensen, J. Biol. Chem. 251 (1976) 3801.
[2] M.M. Benning, T.E. Meyer, I. Rayment, H.M. Holden, Biochemistry 33 (1994) 2476.
[3] R. Langen, G.M. Jensen, U. Jacob, P.J. Stephen, A. Warshel, J. Biol. Chem. 267 (1992) 25625.
[4] C.W.J. Carter, J. Kraut, S.T. Freer, N.-H. Xuong, R.A. Alden, R.G. Bartsch, J. Biol. Chem. 249 (1974) 4212.
[5] D.R. Breiter, T.E. Meyer, I. Rayment, H.M. Holden, J. Biol. Chem. 266 (1991) 18660.
[6] C.T. Przysiecki, T.E. Meyer, M.A. Cusanovich, Biochemistry 24 (1985) 2542.
[7] G. Backes, Y. Mino, T.M. Loehr, T.E. Meyer, M.A. Cusanovich, W.V. Sweeney, E.T. Adman, J. Sanders-Loehr, J. Am. Chem. Soc. 113 (1991) 2055.
[8] J. Huang, R.L. Ostrander, A.L. Rheingold, Y. Leung, M.A. Walters, J. Am. Chem. Soc. 116 (1994) 6769.
[9] P. Middleton, D.P.E. Dickson, C.E. Johnson, J.D. Rush, Eur. J. Biochem. 104 (1980) 289.
[10] I. Bertini, A.P. Campos, C. Luchinat, M. Teixeira, J. Inorg. Biochem. 52 (1993) 227.
[11] H. Beinert, A.J. Thomson, Arch. Biochem. Biophys. 222 (1983) 333.
[12] T.H. Moss, A.J. Bearden, R.G. Bartsch, M.A. Cusanovich, Biochemistry 7 (1968) 1591.
[13] D.P.E. Dickson, C.E. Johnson, R. Cammack, M.C.W. Evans, D.O. Hall, K.K. Rao, Biochem. J. 139 (1974) 105.
[14] J.M. Mouesca, G.J. Rius, B. Lamotte, J. Am. Chem. Soc. 115 (1993) 4714.
[15] J. Gloux, P. Gloux, B. Lamotte, J.M. Mouesca, G.J. Rius, J. Am. Chem. Soc. 116 (1994) 1953.
[16] R. Krishnamoorthi, J.L. Markley, M.A. Cusanovich, C.T. Przysiecki, T.E. Meyer, Biochemistry 25 (1986) 60.

[17] L. Banci, I. Bertini, F. Briganti, C. Luchinat, A. Scozzafava, M. Vicens Oliver, Inorg. Chim. Acta 180 (1991) 171.
[18] L. Banci, I. Bertini, F. Capozzi, P. Carloni, S. Ciurli, C. Luchinat, M. Piccioli, J. Am. Chem. Soc. 115 (1993) 3431.
[19] I. Bertini, F. Briganti, C. Luchinat, A. Scozzafava, M. Solá, J. Am. Chem. Soc. 113 (1991) 1237.
[20] L. Banci, I. Bertini, F. Briganti, C. Luchinat, A. Scozzafava, M. Vicens Oliver, Inorg. Chem. 30 (1991) 4517.
[21] I. Bertini, F. Capozzi, C. Luchinat, M. Piccioli, Eur. J. Biochem. 212 (1993) 69.
[22] I. Bertini, A. Gaudemer, C. Luchinat, M. Piccioli, Biochemistry 32 (1993) 12887.
[23] L. Banci, I. Bertini, S. Ciurli, S. Ferretti, C. Luchinat, M. Piccioli, Biochemistry 32 (1993) 9387.
[24] I. Bertini, F. Capozzi, L.D. Eltis, I.C. Felli, C. Luchinat, M. Piccioli, Inorg. Chem. 34 (1995) 2516.
[25] I. Bertini, J.A. Cowan, C. Luchinat, K. Natarajan, M. Piccioli, Biochemistry 36 (1997) 9332.
[26] I. Bertini, C. Luchinat, M. Piccioli, A. Soriano, Inorg. Chim. Acta 283 (1998) 12.
[27] F. Torrens, J. Sánchez-Marín, I. Nebot-Gil, J. Chromatogr. A 827 (1998) 345.
[28] F. Torrens, J. Chem. Inf. Comput. Sci. 40 (2000) 236.
[29] F. Torrens, J. Chromatogr. A 908 (2001) 215.
[30] F. Torrens, V. Soria, Sep. Sci. Technol. 37 (2002) 1.
[31] F. Torrens, Chromatographia 53 (2001) S199.
[32] A.J. Hopfinger, Macromolecules 4 (1971) 731.
[33] A.J. Hopfinger, R.D. Battershell, J. Med. Chem. 19 (1976) 569.
[34] M. Born, Z. Phys. 1 (1920) 45.
[35] F. Torrens, E. Ortí, J. Sánchez-Marín, J. Chim. Phys. Phys.-Chim. Biol. 88 (1991) 2435.
[36] D.R. Flower, J. Mol. Graphics Mod. 15 (1997) 238.
[37] A.A. Maryott, E.R. Smith, Table of Dielectric Constants of Pure Liquids, National Bureau of Standards Circular No. 514, United States Department of Commerce-National Bureau of Standards, Washington, 1951.
[38] J. Kyte, R.F. Doolittle, J. Mol. Biol. 157 (1982) 105.
[39] D. Eisenberg, E. Schwarz, M. Komaromy, R. Wall, J. Mol. Biol. 179 (1984) 125.
[40] D. Eisenberg, Annu. Rev. Biochem. 53 (1984) 595.
[41] D. Eisenberg, R.M. Weiss, T.C. Terwilliger, Proc. Natl. Acad. Sci. U.S.A. 81 (1984) 140.
[42] J.L. Pellequer, E. Westhof, J. Mol. Graphics 11 (1993) 204.
[43] X. Gallet, F. Festy, P. Ducarme, R. Brasseur, A. Thomas-Soumarmon, J. Mol. Graphics Mod. 16 (1998) 72.
[44] A. Kantola, H.O. Villar, G.H. Loew, J. Comput. Chem. 12 (1991) 681.
[45] A. Leo, C. Hansch, J. Org. Chem. 36 (1971) 1539.

PERGAMON

Polyhedron 21 (2002) 1363–1367

POLYHEDRON

www.elsevier.com/locate/poly

Copper(II) and nickel(II) uptake from aqueous solutions by cork wastes: a NMR and potentiometric study

Isabel Villaescusa [a,*], Núria Fiol [a], Franco Cristiani [b], Costantino Floris [c], Simona Lai [c], Valeria Marina Nurchi [b]

[a] *Departament d'Enginyeria Química, Agrària i Tecnologia Agroalimentària, Universitat de Girona, Avda.Lluis Santaló, s/n, 17002 Girona, Spain*
[b] *Dipartimento di Chimica Inorganica ed Analitica, Università di Cagliari, Complesso di Monserrato, 09042 Cagliari, Italy*
[c] *Dipartimento di Scienze Chimiche, Università di Cagliari, Complesso di Monserrato, 09042 Cagliari, Italy*

Received 10 July 2001; accepted 18 February 2002

Abstract

Due to the increasing interest in the use of biomasses from agriculture as removing agents for heavy metals in waste effluents, we present here a joint potentiometric and ^{13}C MAS and cross polarization-magic angle spinning NMR (CP-MAS NMR) study on cork interaction with Cu(II) and Ni(II). Through potentiometry we were able to distinguish two kind of interactions, a stronger one which involves protonated sites on cork and a second that allows hydroxide precipitation of the bound metal ion into the cork structure. NMR signal analysis suggests a specific metal complexation on the carbohydrate moieties of polymeric cork matrix. The ^{13}C MAS NMR suggests that the dynamics in the MHz range and the overall arrangement of polymeric matrix is not affected by metal binding; and the spin relaxation times $T_{1\rho}(^{1}H)$ and $T_{1\rho}(^{13}C)$ show that no significant difference of relaxation processes in the KHz range is introduced by metal coordination. © 2002 Published by Elsevier Science Ltd.

Keywords: Cork; Solid state ^{13}C MAS and CP-MAS NMR; Copper; Nickel; Potentiometric titration; Metal uptake

1. Introduction

Considering the harmful effects of heavy metals, it is necessary to almost totally remove them from waste effluents. When contaminants are in low concentrations chemical precipitation, reverse osmosis and other methods can become inefficient. In these conditions, adsorption is one of the best options. Heavy metal adsorption from wastewater is generally achieved with polymer resins, activated carbon, activated alumina, which are expensive and non-regenerable. In the last decade many studies have been carried out to evaluate the metal removal potential of different kinds of biomass. Increasing attention has been devoted to the use of biomass generated from the waste by-products of agriculture or industry, such as sun-flowers stalks [1], apple wastes [2], pine, yohimbe and cork barks [3,4]. In one of our recent studies, cork wastes generated from wine cork manufacture were found to be efficient in the removal of Ni(II) and Cu(II) from aqueous solutions [4]. In this study, the influence of pH, NaCl and metal concentration on metal uptake was investigated, and maximum adsorption for both metals was found at around pH 6–7; an increase of NaCl concentration caused a decrease of metal removal. Absorption isotherms were expressed by the non-competitive Langmuir model. The metal binding mechanism responsible for metal uptake is, however, unknown: mechanisms like complexation, coordination, chelation, ion exchange, physical adsorption, inorganic microprecipitation or a combination of any of them might be involved [5].

The cork bark of *Quercus suber* L. is widely used for stoppers; floor and wall insulation from noise and temperature; decoration, etc. The main polymeric components of cork are suberin (40%), lignin (22%) and polysaccharides (cellulose and hemicellulose 20%). The remainder comprises waxes, tannins and other extractable compounds [6]. Cork has been extensively studied by solid state ^{13}C NMR spectroscopy, and information

* Corresponding author. Tel.: +34-972-418-416; fax: +34-972-418-399.
E-mail address: isabel.villaescusa@udg.es (I. Villaescusa).

0277-5387/02/$ - see front matter © 2002 Published by Elsevier Science Ltd.
PII: S0277-5387(02)00957-9

was obtained on the polymeric structure and dynamics of the main components of untreated cork [7–10], but to our knowledge no studies have yet been performed on metal cork interactions. The aim of this work is the investigation of the role of chemical groups in the different cork components in Ni(II) and Cu(II) uptake. This study has been carried out characterizing the cork bark before and after metal uptake. The Ni(II) and Cu(II) affinities toward cork polymeric matrix were investigated by potentiometric titrations, while the structure and local dynamics of the cork samples in the absence and in the presence of these paramagnetic metal ions were studied by means of solid state ^{13}C MAS and cross polarization-magic angle spinning NMR (CP-MAS NMR).

2. Experimental

2.1. Reagents

Cork wastes were kindly supplied by the company Oller Germans, Cassà de la Selva (Catalunya). Cork was ground and sifted to the desired particle size (20–40 and >20 mesh) and used without further treatment. $NiCl_2 \cdot 6H_2O$, $CuCl_2$, KCl, NaOH and HCl volumetric standard 0.1 N solutions and ICP standards for Cu and Ni 1000 mg l^{-1} were Aldrich products. Metal ion solutions were prepared by dissolving proper amounts of chlorides in bidistilled water.

2.2. Cork metal uptake

In order to study by potentiometry and NMR the behavior of cork containing metal we prepared the samples at different metal concentrations in the following way: 0.5 g of cork was put into 50 ml of variable metal concentration solutions and shaken with a magnetic stirrer for 24 h. Metal concentrations lay in the range 0.03–1.0 M for potentiometry and 0.24 and 1.0 M for NMR measurements. Then, the samples were vacuum filtered through a Gooch number 1, and abundantly rinsed with bi-distilled water to remove the not bound metal ions. These experiments were performed with cork of two different particle sizes, 20–40 and >20 mesh. The second size was chosen for the following experiments since it gave more reliable results.

2.3. Potentiometric titrations

Untreated and metal treated 0.125 g cork samples were suspended in 20 ml of a solution 0.1 M KCl and titrated both with 0.1 M NaOH and with 0.1 M HCl, added stepwise each 30 s (100 points). This time delay allows reproducible titration curves (without any differences from those, for example, with 120 s of time delay). Titrations were performed on a DOSIMAT 655 Metrohm automatic titrator connected to a Metrohm 654 pH-meter, in a glass cell thermostated at 25 °C, equipped with a magnetic stirring system, a Metrohm glass electrode for highly alkaline solutions, and a microburet delivery tube. The electrode was calibrated daily for hydrogen ion concentration by titrating standard HCl with carbonate free 0.1 M NaOH; the resulting potentiometric data were analyzed with Gran procedure [11] using our GRANPLOT program. The results of potentiometric titrations were processed with the PSEQUAD program[12] operating on the experimental data (titrant volume, $\log[H^+]$). These data were processed simplifying the system as a single phase one.

2.4. ICP-AES measurements

The ICP measurements were made on a Liberty 200 ICP Varian spectrometer set up with Argon plasma flow at 15 l min^{-1}; with auxiliary gas flow 1.5 l min^{-1}; at a power 1.0 kW. The sample was aspired at a flow of 1.0 ml min^{-1} through a nebulizer of the V-grove type. Atomic emissions were determined at 324.7 for Cu and 231.6 for Ni. No spectral interferences were observed. Fresh working calibration solutions were prepared by properly diluting the commercial standards with double distilled water. Calibrations, within the expected ranges for each element, were obtained with nine equally spaced concentrations.

2.5. NMR studies

Solid-State ^{13}C NMR spectra were obtained on a Varian 400 Unity Inova spectrometer operating at 100.57 MHz, equipped with 7 mm CPMAS probeheads by a cross-polarization tecnique (CP) with magic-angle spinning (MAS). A matched Hartmann–Hann condition was established by using radio-frequency field of 38 KHz for ^1H and 152 KHz for ^{13}C. The rotor was spun at spinning rate (frequency) of 4 KHz and, working at room temperature (r.t.), a contact time of 1000 μs was applied to obtain polarization transfer. An acquisition time of 0.010 s and the 90° pulse of 6.6 ms were used. Chemical shifts of CP-MAS spectra were originally obtained with respect to the methylene carbon resonance of solid adamantine, 38.3 ppm with respect to Me_4Si, measured before each measurement. Proton spin-lattice relaxation times in the rotating frame, $T_{1\rho}H$, were determined in a CP-MAS experiment from the decay of the carbon signal as a function of d3, the time before cross polarization. The $T_{1\rho}H$ values were calculated from exponential fits (proton signal height) versus time d3. Carbon rotating-frame relaxation time, $T_{1\rho}C$, were measured by recording the ^{13}C signal as a function of carbon spin-lock time following cross polarization. Value of $T_{1\rho}C$ were determined from

exponential fits (carbon signal height) versus spin-lock time. For these studies cork samples previously contacted with 0.24 and 1.0 M metal (nickel and copper) solutions were used.

3. Results and discussion

In a previous work [4], the Langmuir isotherm model provided a maximum uptake of 2.64 $mg \cdot g^{-1}$ for Cu(II) and 4.09 $mg \cdot g^{-1}$ for Ni(II) at pH 6. Further metal desorption from biomaterials was observed using HCl as eluent, up to 90% for Cu(II) and 10% for Ni(II). To better quantify these last results, in the present work we have examined more thoroughly the behavior of pure cork before and after metal absorption when subjected to acid and basic treatments. Therefore, different cork samples, according to Section 2.2, suspended in 20 ml of 0.1 M KCl, were titrated both with 0.1 M HCl and 0.1 M NaOH. The titration plots for nickel and copper treated samples are presented in Figs. 1 and 2 for acid and basic titrations, respectively. These titrations allow interesting conclusions to be made, although some differences are found among similar samples in repeated experiments, to be ascribed both to non-homogeneous cork and to different contacts between solution and stirred sample.

As can be seen from the acid titration curves in Fig. 1, the pure cork curve lies above that of KCl. This implies that suspended cork binds H^+ on some basic groups, according to the reaction Cork $+ H^+ \rightleftharpoons H^+$ Cork. The dashed curve can be reproduced by assuming a concentration of basic groups equal to 0.1 mmoles l^{-1}, which corresponds to $\sim 1.6 \cdot 10^{-5}$ moles of basic groups per gram of cork. The curves of metal treated cork start at acidic pH 4.5–5 and then overlap the reference KCl solution curve.

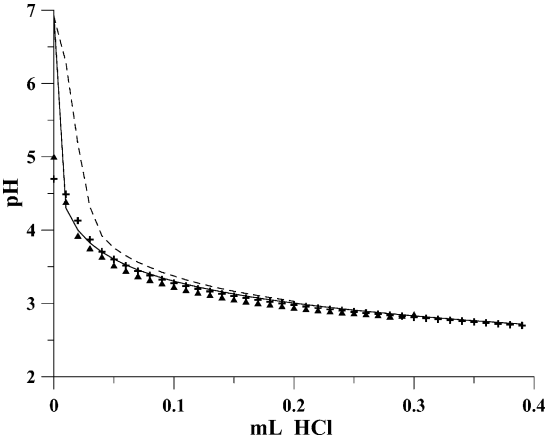


Fig. 1. Titration curves with 0.1 M HCl of 20 ml of 0.1 M KCl in which 0.125 g of cork samples were suspended: untreated (dashed line), treated with (■) Cu(II) and (▲) Ni(II) and titration curve of 0.1 M KCl alone (full line).

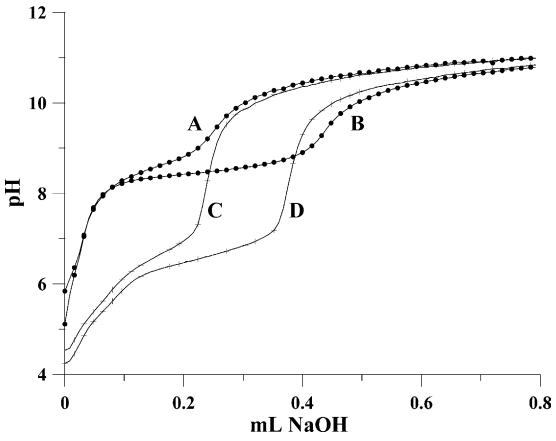


Fig. 2. Titration curves with NaOH 0.1 M of 20 ml of 0.1 M KCl in which were suspended 0.125 g of cork, (A) treated with Ni(II) 0.24 M; (B) with Ni(II) 1.0 M; (C) with Cu(II) 0.24 M; and (D) with Cu (II) 1.0 M.

The starting acidity and the curve shapes imply that cork binds the metal ions via some acidic groups, therefore, releasing H^+ ions which are bonded by free basic sites on cork. The titration protons, which compete for the same binding sites, release the metal ions coordinated by cork, as quantified by ICP-AES analysis. These measurements showed that all coordinated metal ions are totally released, contrary to that observed for nickel in our previous study[4]. This can be attributed to the used ionic strength KCl 0.1 M, i.e. to K^+ competition with copper and nickel for the same binding sites. The data shown in Fig. 2 for the basic titration show that (a) curves A and B for nickel are characterized by a first part (0.09 ml of added base) whose width does not depend on the previous cork treatment, and by a second part, attributed to the formation of nickel hydroxide at pH $\sim$ 8.5, whose width instead depends on nickel concentration; (b) a similar trend is observed for curves C and D relative to copper(II), taking into account copper(II) hydroxide formation at pH $\sim$ 6.6; (c) it must be pointed out that the titration curve of untreated cork did not show easily titrable acidic groups (less than pK 9).

These plots were fitted, using the PSEQUAD program [11] for the calculation of solution equilibria, by assuming the models and the concentration reported in Table 1.

These models can be interpreted assuming that during the preliminary treatment the metal ions are coordinated by cork via some acidic groups which, due to metal coordination, lose their protons that transfer to less basic sites. Therefore, the first part of the curve can be considered proportional to the maximum concentration of tightly bound metal. In the second part we observe, on the other hand, the precipitation of metal hydroxides, at the same pH values as solutions of the same ionic strength. The hydroxide formation involves less

Table 1
Models and concentrations assumed for fitting the curves in Fig. 2 with PSEQUAD program

	Curve	Cork acidic sites	Metal hydroxide	Model	Log β
Ni	A	2.5×10^{-4}	4.8×10^{-4}	HCork(site3)	6.9
	B	2.7×10^{-4}	9.2×10^{-4}	$Ni(OH)_2$	−17.1
Cu	C	$(3.0+3.0) \times 10^{-4}$	2.8×10^{-4}	Hcork(site1), Hcork(site2)	4.8, 5.8
	D	$(3.0+3.0) \times 10^{-4}$	6.4×10^{-4}	$Cu(OH)_2$	−13.3

In the third and fourth columns cork titrable protons (different sites with proper pK values) and metal titrable as hydroxydes are reported, respectively.

tightly bound metal ions, whose amount depends on Cu(II) or Ni(II) concentrations in the preparative procedure. It should be noted that hydroxide formation takes place inside the cork framework, since no turbidity appears in the titration vessel. This second kind of interaction is also favored for Ni(II) with respect to Cu(II).

As far as NMR measures are concerned, Fig. 3(a) shows the ^{13}C CP-MAS NMR spectrum of a cork sample. The attribution of the observed peaks, collected in Table 2, corresponds to that found in previous works [8,13,14]. The intense signals at 30 and 33 ppm originate from suberin chain methylens; the peak $a(3.0+3.0)t$ 56 ppm corresponds to O–CH_3 groups from suberin, lignin or hemicellulose. The signals in the range 62–105 ppm are due to the carbohydrate and to the aliphatic carbons of suberin and/or lignin, while the unsaturated and aromatic ring carbon signals appear in the 105–148 ppm range. Finally, the peak at 173 ppm is attributed to the ester groups of suberin and hemicellulose or to carboxyls in aromatic structures of suberin and/or lignin and in uronic acids.

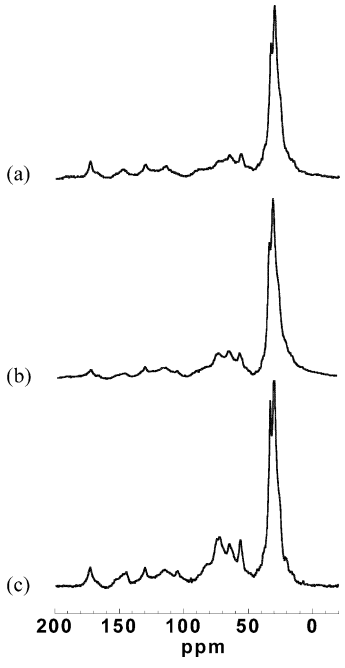


Fig. 3. ^{13}C CP-MAS NMR spectra of untreated (a), and treated cork with aqueous solutions of Ni(II) 0.24 M (b) and 1.0 M (c).

Adding aqueous Ni(II) or Cu(II) to cork particles resulted in beyond detection broadenings of a part of the signals at 72 and 105 ppm suggesting that a specific complexation occurs between each of these paramagnetic metal ions and, especially the carbon-hydrated moieties of the polymeric matrix, which originates an electron dipole-nuclear dipole relaxation. In Fig. 3(b and c), such broadening is shown as an example for the Nickel-cork sample. It can be clearly seen that when contacting cork with increasing concentrations of Ni(II) the peaks at 72 ppm and 105 ppm progressively disappear, while the remaining resonances do not show any appreciable effect.

To investigate possible changes in the structure and/or dynamics of those polymeric domains not involved in the binding with the paramagnetic metal ions, ^{13}C MAS NMR spectra of a cork sample in the absence and in the presence of nickel were performed as a function of the recycle delay between spectral acquisitions. As shown in Fig. 4(a) (I–IV), shortening the recycle delay from 50 to 0.1 s causes a progressively large decrease of signal intensities of carbon atoms with the longest relaxation times in the MHz range, especially the signals at 173 and 80 ppm.

A comparison between the ^{13}C MAS NMR spectra of Fig. 4(a) (I–IV) and Fig. 2(b) (I–IV) indicates that very similar behaviour occurs in the Ni(II) treated cork sample, suggesting that the dynamics in the MHz range and possibly the overall arrangement of the polymeric matrix is not affected by the metal binding.

Additional information on the dynamics of the polymeric domains in these samples was obtained from the spin relaxation times $T_{1\rho}(^1H)$ and $T_{1\rho}(^{13}C)$, which are sensitive to the motions in the KHz range. More specifically, the former is affected by ^1H spin diffusion and, therefore, depends on the neighbouring spin reservoirs, while the latter gives information on the site- and arrangement-specific motions. The average $T_{1\rho}$'s are collected in Table 2. Comparing the data for the untreated and treated cork it can be seen that, within experimental error, no important differences exist in the efficiency of the relaxation processes in the KHz range for the polymeric domains of the two samples.

Table 2
$T_{1\rho}(^{13}C)$ and $T_{1\rho}(^{1}H)$ of cork untreated and treated with an aqueous solution of 1 M Ni(II)

Carbon type	Chemical shift (ppm)	$T_{1\rho}(^{13}C)$ (ms)		$T_{1\rho}(^{1}H)$ (ms)	
		Cork	Cork-Ni(II)	Cork	Cork-Ni(II)
COO	172	18.5	19.9	3.3	3.3
Aromatics	130	6.3	6.4	1.5	2.0
Alkenes	114	5.2	5.9	2.8	2.3
Aromatic polysaccarid. Carbon 1	105	7.8	/	3.3	/
Polysaccarid hydrated. Carbons 2,3,5	72.0	4.0	2.2	2.8	2.3
Aliphatic	64.6	3.9	4.0	2.8	2.2
OCH_3	56.2	9.7	6.1	1.2	/
$(CH_2)_n$	33.0	3.2	2.9	3.5	3.5
$(CH_2)_n$	30.0	4.3	2.7	1.7	2.1

These values have an estimated uncertainty of less than 15%.

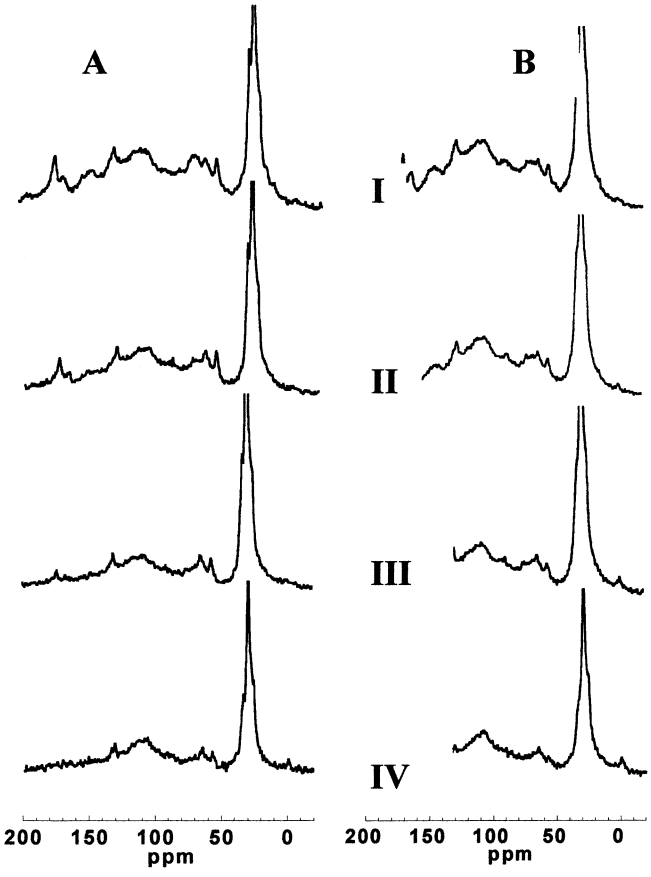


Fig. 4. ^{13}C MAS NMR spectra of untreated (A), and treated cork with Ni(II) 1 M (B) with the recycle times 0.1 s (I), 1.0 s (II), 5.0 s (III), 50 s (IV).

Despite the complexity and heterogeneity of the polymeric matrix of cork, precious information has been obtained on the affinity and binding sites of Ni(II) and Cu(II) on cork. These encouraging results have been obtained thanks to the joint use of potentiometric and ^{13}C NMR solid state methods.

Acknowledgements

Thanks are due to Miss Marta Bruguera and Dr. Roberta Silvagni for their help in the experimental work. I.V. thanks the Generalitat de Cataluna for the grant 2000BEAI400093. F.C. and V.M.N acknowledge the financial support by MURST (COFIN 2000).

References

[1] G. Sun, W. Shi, Ind. Eng. Chem. Res. 37 (1998) 1324.
[2] L. Sung-ho, Y. Ji-Won, Sep. Sci. Technol. 32 (1997) 1371.
[3] S. Al-Asheh, Z. Duvnjak, Sep. Sci. Technol. 33 (1998) 1303.
[4] I. Villaescusa, M. Martinez, N. Miralles, J. Chem. Tech. Biotech. 75 (2000) 812.
[5] K.H. Chong, B. Volesky, Biotech. Bioeng. 47 (1995) 451.
[6] H. Pereira, Wood Sci. Technol. 22 (1988) 211.
[7] C.P. Neto, N. Cordeiro, A. Seca, F. Domingues, A. Gandini, D. Robert, Holzforschung 50 (1996) 563.
[8] C.P. Neto, J. Rocha, A. Gil, N. Cordeiro, A.P. Esculcas, S. Rocha, I. Delgadillo, J.D. Pedrosa de Jesus, A.J.F. Correia, Solid State NMR 4 (1995) 143.
[9] N. Cordeiro, M.N. Belgacem, A.J.D. Silvestre, D. Pascoal Neto, A. Gandini, Int. J. Biol. Macromol. 22 (1998) 71.
[10] M. Lopes, C. Pascoal Neto, D. Evtuguin, A.J.D. Silvestre, A. Gil, N. Cordeiro, A. Gandini, Hozforschung 52 (1998) 146.
[11] G. Gran, Analyst 77 (1952) 661.
[12] L. Zekany, I. Nagjpal, in: D.J. Leggett (Ed.), Computational Methods for the Determination of Formation Constants (Ch. 8), Plenum, New York, 1985.
[13] G.R. Hatfield, G.E. Maciel, H.A. Schroeder, Anal. Chem. 59 (1987) 172.
[14] A. Gil, M. Lopes, J. Rocha, C.P. Neto, Int. J. Biol. Macromol. 20 (1997) 293.

PERGAMON

Polyhedron 21 (2002) 1369–1373

POLYHEDRON

www.elsevier.com/locate/poly

The determination of mineral acidity excess in solutions containing Ga(III), Al(III), Bi(III)

Diana Amorello, Vincenzo Gambino, Vincenzo Romano *, Roberto Zingales

Department of Inorganic Chemistry, University of Palermo, Viale Delle Scienze, Parco D'Orleans II, 90128 Palermo, Italy

Received 24 July 2001; accepted 24 September 2001

Abstract

A new procedure is proposed to carry out volumetric determinations of the strong acid content of a solution in the presence of inorganic cations such as Ga^{3+}, Al^{3+}, Bi^{3+} which, showing in aqueous solution an acidic behaviour, introduce non negligible interferences in these determinations. Before the acid–base titration, an equivalent amount of a ligand, such as dihydrogen ethylendiamino tetraacetate is added, in order to strongly complex the cation masking it toward the successive addition of a strong base. Interferences are thus removed, and the volumetric determination of the strong acid excess plus the hydrogen ions set free from the ligand, as a consequence of the complex forming reaction, can be accurately carried out, in the presence of a colorimetric indicator. © 2002 Elsevier Science Ltd. All rights reserved.

Keywords: Solutions; Equilibria; Cations; Hydrolysis; Titration; Masking

1. Introduction

It is well known that the sharpness index at the equivalence point in the titration of a strong acid with a strong base is lowered by the presence of a weak acid. This lowering will be the greater, the greater the strength of the weak acid, and the greater the ratio of its concentration to that of the strong acid [1].

The same problem arises, of course, when dealing with a mixture of a strong acid and a salt whose cation shows acidic properties such as, for instance, Fe^{3+}, Al^{3+}, Ga^{3+}.

Aqueous solutions of these cations must often be prepared by adding an excess of a strong acid to avoid the formation of slightly soluble hydrolysis products [2]. Moreover, their salts are commonly hygroscopic and the small quantities of retained water can give rise to the formation of hydrolysis products long before their dissolution.

When investigating complex or hydrolysis equilibria involving these cations, the analytical composition of both the metal and the hydrogen ions content of the stock solutions must be accurately known, both for the metal and the hydrogen ions content. This could be accomplished by mixing known amounts of the solution components in a high degree of purity. Concerning the commercially available salts of the hydrolizable cations, these often contain small quantities of the mineral acid excess used in the process of their preparation and crystallisation. So, the composition derived from the amount of the mixed chemicals to give the stock solution may result erratic, and accurate analytical procedure become obliged.

Usually, the analysis of the cation does not give great difficulties, but its behaviour as a weak acid can make the determination of the strong acid excess troublesome, just for the reasons above discussed.

This problem must not be under-evaluated, because for example in the study of the hydrolysis equilibria, even a slight error in the strong acid analytical excess content of the stock solution can generate a wrong assumption for the hydrolysis model. For instance, this systematic error, which is different at the different metal ion concentrations, can suggest a polynuclear hydrolysis model even if only mononuclear species are present.

We met this problem in the study of gallium(III) hydrolysis, when analysing the stock solution of $Ga(ClO_4)_3$ containing some $HClO_4$ excess. To avoid

* Corresponding author. Fax: +39-91-427584.
E-mail address: viromano@unipa.it (V. Romano).

0277-5387/02/$ - see front matter © 2002 Elsevier Science Ltd. All rights reserved.
PII: S0277-5387(02)00959-2

the occurrence of these troubles, we thought to change the free Ga^{3+} ion in a stable complex ion, so that the titration of the perchloric acid excess could be carried out as the titration of the strong acid alone. The ligand chosen was the EDTA ion (Y^{4-}) which was introduced into the solution in the usual form of $Na_2H_2Y\cdot H_2O$.

2. The method

In order to test the method we had to prepare an aqueous solution of defined Ga(III) content, moreover containing a known amount of H^+.

As already discussed, this can be done by mixing chemicals of high purity: under this respect, gallium(III) chloride appears to be the best choice, as it can be prepared by direct reaction of metallic gallium with gaseous hydrochloric acid [3]; gaseous acid is preferred to its aqueous solutions, as its excess can be easily completely removed from the reaction mixture, leaving an anhydrous product, free from any contaminant.

An accurately weighed amount of metallic gallium was put into a multi-necked vessel kept at 190 °C in which gaseous dry HCl was driven to quantitatively convert the metal into its chloride. To avoid losses of the quite volatile solid $GaCl_3$, the vessel was kept under water reflux. Once the reaction was completed, the residual gaseous HCl was removed from the reaction vessel by passing a stream of dry, purified nitrogen. Then, after cooling, a defined amount of a standard HCl solution was introduced into the vessel through the reflux by means of a weight burette. The chloride was completely dissolved and the so obtained solution quantitatively transferred to a volumetric flask and diluted to the mark.

The Gallium content (C_M) of this solution was checked by titration with standard EDTA according to [4] (see Section 4). The agreement was quite good, differences being less than 0.1%. The hydrochloric acid excess content (C_H) of this solution was determined by means of the potentiometric and volumetric acid–base titrations, which form our proposed method.

To a measured amount of the solution, standard EDTA of concentration C_L was added, in order to have a ratio $C_L/C_M = 1$. In this way, gallium(III) ions were stoichiometrically converted into the stable Gallium–EDTA complex [5], setting free two hydrogen ions for each gallium ion, according to reaction (1):

$$Ga^{3+} + H_2Y^{2-} = GaY^- + 2H^+ \quad (1)$$

So the hydrolysable species was masked, and only a strong acid, whose total concentration was equal to $C_H + 2C_M$, was left in solution. The stepwise addition of a strong base solution should now give rise to a strong acid–strong base titration curve.

The vessel containing the solution was equipped with a glass (GE) and a saturated calomel electrode (SCE), and the potentiometric titration carried out by stepwise additions of a standard NaOH solution C_b molar. The e.m.f. of cell (G)

G.E.|Solution|S.C.E (G)

was read after each addition, waiting long enough (5 min) to have steady e.m.f. values.

An example of the so obtained titration curves is reported in Fig. 1. It can be seen that the curve exhibits two sharp jumps, one for $C_b = 2C_M + C_H$ and another one, larger, for $C_b = 3C_M + C_H$.

If the potentiometric titration is carried out including thymol blue or phenolphthalein indicators, a sharp change of colour can be observed at the second jump. No indicator seems to be useful for detecting the first jump observed in the potentiometric titration curve.

3. Results and discussion

According to our hypothesis on the occurrence of reaction (1), the first jump in the mentioned curve can be explained as corresponding to the titration of the hydrogen ions due to the mineral acid excess (C_H), plus those made free in reaction (1) which are equal to $2C_M$. The second pH jump in the titration curve can be ascribed to the completion of a second acid–base titration. As the moles of added base, going from the first to the second inflection point, are exactly equal to the moles of Gallium ion, we can ascribe it to a reaction involving the gallium–EDTA complex, such, for instance:

$$[GaY]^- + OH^- = [GaYOH]^{2-} \quad (2)$$

We do not have elements to decide if reaction (2) is an OH^- addition to $[GaY]^-$ or a proton extraction from a water molecule bound to $[GaY]^-$ [6].

We want to emphasise that the differences of the NaOH volumes used between the second and the first jump gives $C_b = C_M$ and is a further check of the Gallium content analysis.

In Table 1 some results of different titrations with colorimetric or potentiometric detection of the end point are summarised. It can easily be seen that the match between the expected and the measured value is quite good (differences not higher than 0.1–0.2%) for Ga(III) solutions.

Once we succeeded in checking the validity of the proposed analytical method, we turned to the original problem of preparing a stock solution of $Ga(ClO_4)_3$ containing an excess of perchloric acid. As the previously reported methods suffer the inconvenience of giving solid $Ga(ClO_4)_3$ contaminated by small amounts of chloride ions and perchloric acid [7], we tried a

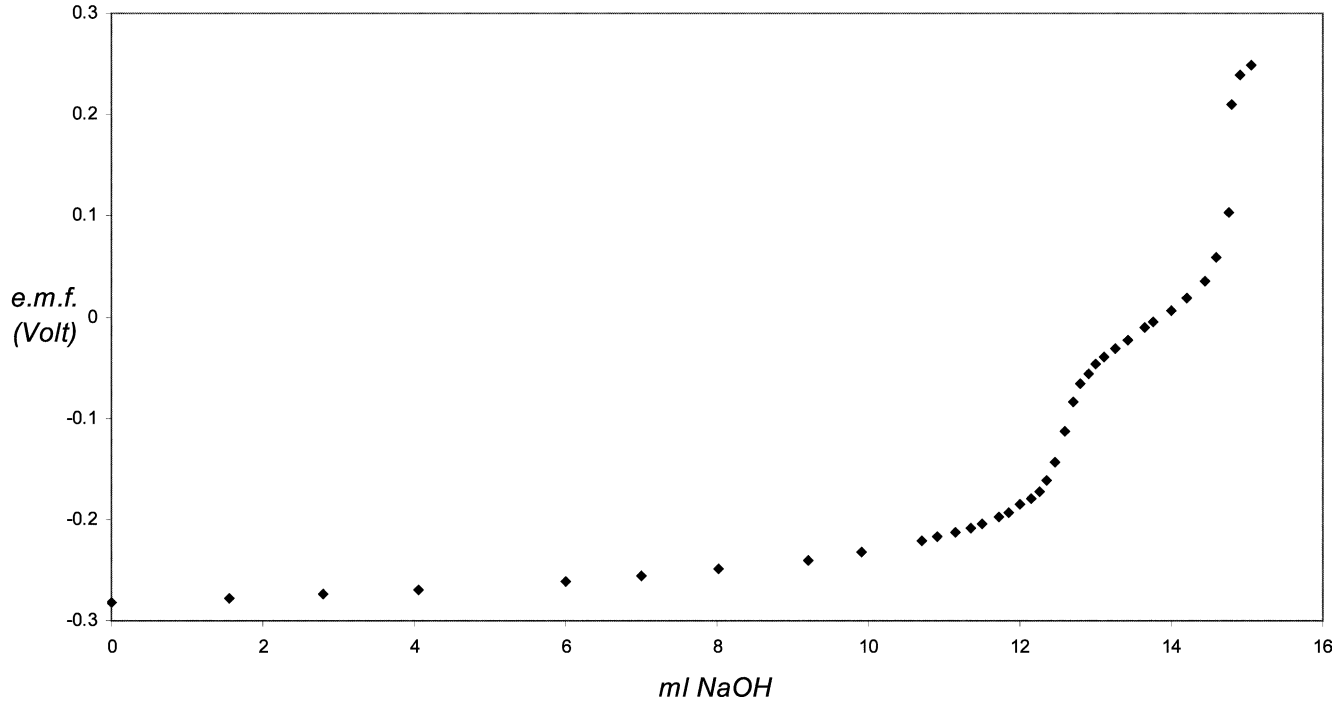


Fig. 1. Potentiometric curve for the titration of hydrochloric acid with standard sodium hydroxide, in the presence of a known amount of gallium(III) ions masked by means of EDTA.

different approach. A weighed amount of metallic Gallium was dissolved in a slight excess of a hot redistilled HBr solution. A platinum wire was dipped into the liquid gallium pool to speed up its dissolution. When this was completed, the obtained gallium(III) bromide complex, probably $[GaBr_4]^-$, was then converted into gallium(III) perchlorate, by treating it with a measured slight excess of a $HClO_4$ solution. Bubbling gaseous ozone into the solution, kept at about 90 °C, bromide ions were oxidised to bromine. The bromine excess was then driven off by a nitrogen stream. This long procedure led to unavoidable slight losses of the solution components and finally gave a stock $Ga(ClO_4)_3$ solution containing a slight excess of $HClO_4$. In it, C_M and C_H could be determined, using the above described method.

Finally, we decided to check if the method could be applied to other cations, especially the trivalent ones, which show similar acidic properties. To an acidic solution of Al(III) ions, the equivalent amount of a Na_2H_2Y solution was added, warming it near to boiling for about 2 min, and then cooling to room temperature. The solution was then titrated in the presence of phenolphtalein, giving good agreement between expected and measured values (see Table 1).

A slight different behaviour is shown by the Bi(III) solutions, for which the titration curve shows only one jump giving evidence that the reaction with NaOH and

Table 1
C_H values in metal salt solutions obtained by volumetric titrations with colorimetric detection of the end point

Cation	Weight of analysed solution (g)	C_H found (in mol kg^{-1} of solution)	Expected value
Ga^{3+}	0.6299	0.493	
	0.5622	0.495	
	0.5917	0.492	
Average		0.493 ± 0.001	0.493 ± 0.001
Al^{3+}	2.0147	0.615	
	2.1412	0.617	
	1.6822	0.615	
Average		0.616 ± 0.001	0.612 ± 0.001
Bi^{3+}	1.4368	0.757	
	1.5401	0.760	
	1.9922	0.759	
Average		0.759 ± 0.002	0.758 ± 0.001

H_2Y^{2-} proceeds only to the formation of BiY^- so that the acid excess is given by $C_H = C_b - 2C_M$. No evidence could be detected of any further reaction with OH^- ions.

The data reported quite clearly indicate that the proposed masking method can give accurate values in the determination of the acid excess content of gallium, aluminium and bismuth salt solutions either by potentiometric or volumetric titrations in the presence of colour indicators. Due to its simplicity, we are confident that the method will give accurate results also in the presence of any strong mineral acids such as sulphuric, nitric, hydrobromic.

This fact is important and probably extendible to other ions whose perchlorates are usually obtained in the presence of an unknown slight acid excess, added to suppress the hydrolysis of the metal ions. In fact it exists a great variety of chelating ligands which can mask completely most ions already before the equivalence point, so making it possible the acid excess determination.

An accurate knowledge of the title of this acid excess is important to get accurate data when studying for example, complex formation or ion hydrolysis equilibria. As we will show in a coming paper, the usual method of carrying out the titration of a metal ion and hydrogen ion mixture with a strong base, detecting the end point with a Gran plot [8] gives systematically higher titles, which can result in a wrong hydrolysis model, wrong equilibrium constants and chemical artefacts.

4. Experimental

All the solutions were prepared using water twice distilled from an alkaline solution of potassium permanganate.

Their composition, if not specified, has been determined using standard methods of analysis [4,9].

4.1. Gallium(III) chloride solution

This solution has been prepared as above detailed; although these procedures allowed us to know the correct composition of the solution from the steps of its preparations, anyway a check was carried out.

Gallium (III) content was determined by EDTA titration, following two different procedures: the first consisted in the addition of a measured excess of a standard EDTA solution, buffering the mixture at pH 9 and then back titrating with a standard zinc sulphate solution, in the presence of Black Eriochrome T as indicator, following the details reported in [10]. In the second procedure, the gallium solution was buffered at pH 3.5, boiled and then titrated with standard EDTA in the presence of PAN as indicator [11]. Both methods gave results agreeing with the expected value, into the experimental uncertainties.

The chloride content was determined argentimetrically, according to [12]. In this case too the found chloride concentration agreed with the expected one. Moreover, as a further check, the H^+ ion excess could be estimated according to

$$C_H = C_{Cl} - 3C_M \quad (3)$$

which gave C_H values in excellent agreement with those obtained with the here proposed method and with the expected ones, reported in Table 1.

4.2. Aluminium(III) solution in perchloric acid

A weighed amount of potassium aluminium sulphate, $KAl(SO_4)_2$, was dissolved in a weighed amount of water containing a known amount of perchloric acid. Its aluminium content was determined by adding a measured excess of a standard EDTA solution, boiling for a couple of minutes, cooling to room temperature and back titrating the excess with a standard zinc sulphate solution, in the presence of Black Eriochrome T as indicator, following the details reported in [13].

4.3. Bismuth(III) solution in perchloric acid

A weighed amount of $Bi(NO_3)_3 \cdot 5H_2O$ was dissolved in a weighed amount of water containing a known amount of perchloric acid. Its bismuth content has been determined adding a measured excess of a standard EDTA solution which was then back titrated with standard zinc sulphate, as above.

4.4. Sodium hydroxide solutions

Their title was determined by titration with a standard perchloric acid solution, standardised, at its time, against potassium hydrogen carbonate. A weighed amount of this solid was dissolved in water and treated with the solution to be standardised; the mixture was boiled just before the equivalence point to drive off the formed carbon dioxide. A mixed indicator was used, consisting of three volumes of methyl red and one volume of bromocresol green; it turned from green to red at pH near 7.

4.5. EDTA solutions

In the proper volume of water, it was dissolved a weighed amount of the disodium salt, which had been stored overnight in an oven at 80 °C. Its content was checked by titration with standard zinc sulphate [13].

4.6. Potentiometric titrations

Cell (G) was used, containing one Ingold GE and one Ingold reference SCE, connected to a Keithley model 624 high impedance electrometer, giving e.m.f. values on a digital display.

References

[1] J.N. Butler, Ionic Equilibria, Addison Wesley Publishing Company, Reading, MA, 1964.
[2] (a) L.G. Sillèn, E.A. Martell, Stability Constants, The Chemical Society, London, Special Publication 17 (1964);
(b) L.G. Sillèn, E.A. Martell, Stability Constants, The Chemical Society, London, Special Publication 25 (1971);
(c) E. Högfeldt, Stability Constants of Metal-Ion Complex, IUPAC Chemical Data Series 21 (1982).
[3] W.C. Johnson, C.A. Jaskew, Inorganic Syntheses, vol. 1, McGraw-Hill, New York, 1939, pp. 26–27.
[4] I.M. Kolthoff, E.B. Sandell, E.J. Meehan, S. Bruckenstein, Quantitative Chemical Analysis, McMillan, London, 1969.
[5] G. Schwarzwenbach, H. Flaschka, Complexometric Titrations, Methuen and Co, London, 1964, p. 10.
[6] K. Saito, H. Terrey, J. Chem. Soc. (1956) 4701.
[7] L.S. Foster, Inorganic Syntheses, vol. 2, McGraw-Hill, New York, 1946, pp. 26–29.
[8] G. Gran, Analyst (London) 77 (1961) 661.
[9] A.I. Vogel, Quantitative Inorganic Analysis, third ed., Longmans, London, 1961.
[10] G. Schwarzwenbach, H. Flaschka, Complexometric Titrations, Methuen and Co, London, 1964, p. 273.
[11] I.M. Kolthoff, P.J. Elving, Treatise on Analytical Chemistry, Part II, vol. II, Interscience, New York, 1962, p. 86.
[12] A.I. Vogel, Quantitative Inorganic Analysis, third ed., Longmans, London, 1961, p. 266.
[13] A.I. Vogel, Quantitative Inorganic Analysis, third ed., Longmans, London, 1961, p. 436.

PERGAMON

Polyhedron 21 (2002) 1375–1384

POLYHEDRON

www.elsevier.com/locate/poly

Evaluation of chemical equilibria with the use of artificial neural networks

Josef Havel *, Přemek Lubal, Marta Farková

Department of Analytical Chemistry, Faculty of Science, Masaryk University, Kotlářská 2, 611 37 Brno, Czech Republic

Received 6 June 2001; accepted 22 October 2001

Abstract

Multivariate calibration with experimental design (ED) and artificial neural networks (ANN) modeling can be used to estimate equilibria constants from any kind of protonation or metal–ligand equilibrium data like potentiometry, polarography, spectrophotometry, extraction, etc. The method was tested on evenly or randomly distributed experimental error-free data and data with random noise and the results show that even rather higher experimental errors do not influence significantly the prediction power and correctness of ANN prediction. ANN with appropriate ED can provide accurate prediction of stability constants with the relative errors in the range of $\pm 4\%$ or smaller while the approach is very robust. Comparison with a hard model evaluation based on non-linear regression techniques shows excellent agreement. Proposed ANN method is of a general nature and, in principal, can be adopted to any analytical technique used in equilibria studies. © 2002 Elsevier Science Ltd. All rights reserved.

Keywords: Artificial neural networks; Experimental design; Stability constants; Metal complexes; Ion selective electrodes; Metal–ligand equilibria

1. Introduction

Protonation and/or metal–ligand equilibria play substantial role in analytical, organic and/or other chemistries, especially bio-organic or bio-inorganic and theirs knowledge is substantial to understand chemical processes.

During the second half of the last century great effort was devoted to the development of computational methods for the determination of protonation or complexation equilibria. From single graphical methods used from the beginning, almost solely computer-aided methods are used now. A good overview of solution equilibria computation can be found elsewhere ([1,2] and references therein).

In spite of the fact that many computer programs has been developed, still the problem of chemical model determination (stability constants, stoichiometry of complexes, etc.) is alive. Mostly potentiometry, spectrophotometry, extraction, NMR, etc. experimental techniques are used, while computation is based on so called 'hard' modeling, solving mass balance equations while stability constants are searched for by a computer-aided 'curve fitting' applying general least-squares method and suitable optimizing technique.

The aim of this work was to study other alternatives for evaluation of equilibrium data. We have turned our attention towards the artificial intelligence methods among which artificial neural networks (ANN) are increasingly applied in chemistry. As for basic review we refer here to a paper by Gasteiger and Zupan [3]. ANN represent so called 'soft' modeling without the need to know or establish a mathematical model. Recently, ANN has successfully been applied in capillary zone electrophoresis [4–6], for modeling in ion chromatography [7] or in electrokinetic micellar chromatography [8] without necessity to know or determine physicochemical parameters.

In chemical equilibria Havel et al. showed recently that another 'soft' modeling method, partial least-squares (PLS) multivariate calibration method, can be used to evaluate equilibrium data in potentiometry [9]. ANN has been successfully applied in differential pulse polarography to evaluate equilibria for fully inert [10] or labile [11] metal complexes. The purpose of this work

* Corresponding author. Tel.: +420-5-41-129568; fax: +420-5-41-211214.

E-mail address: havel@chemi.muni.cz (J. Havel).

0277-5387/02/$ - see front matter © 2002 Elsevier Science Ltd. All rights reserved.
PII: S0277-5387(02)00955-5

was to study the possibility of applying ANN for the chemical equilibria computation from a general point of view for any kind of data.

In order to calculate the unknown parameters from a data set, the programs such as LETAGROP, SQUAD, POLET [2,12,13], OPIUM [14] were prepared. In 1950s Sillén created the theory of normalized projection maps [15–19]. A survey is given of graphical methods for the determination of unknown parameters from a data set by fitting normalized curves. By the application of the 'hard' programs is in every iterative cycle solved mass balance (equations system). By normalized projection maps using, once we are getting normalized graphs no more mass balance is necessary to solve. If we have calculated projection maps, it is possible to predict the required parameters immediately. If we train a neural network, we get corresponding weights and biases. We use this trained network for consecutive determinations the parameters. Every determination is ready at once, immediately. We do not solve mass balance equations (only once, when we train the neural network).

2. Theoretical

2.1. Experimental design

Experimental designs (ED) are methods, based on statistics, for making plan of experiments. The use of ED strongly reduces the number of needed experiments. The most important aspect of statistical ED is that they provide a strict mathematical framework for changing all pertinent factors simultaneously, and achieve this in a small number of experimental runs. There are various types of ED [20]. The selection of a specific type of design depends primarily on both the nature and the extent of the information we want to obtain.

2.2. Artificial neural networks

One of the most common is the feedforward neural network of multilayer perceptrons. The training data for this network contain examples (patterns) of inputs together with the corresponding outputs, and the network learns to infer a relationship between the two.

The network consists of artificial neurons sorted in input layer, hidden layer(s) (one or more) and output layer. Input neurons accept the input data characterizing each observation, output neurons provide the predicted value or pattern, and hidden neurons neither receive inputs directly nor provide output values directly. Neurons are connected by weights, which are modified in the course of network operation. Each neuron has an activity level that is determined by an input signal received from the other units in the network.

The use of ANN consists of two steps: 'learning' and 'prediction'. In the 'learning' phase the optimum structure, weight coefficients and biases are searched for. These parameters are found from a training data set. After the 'learning' phase the network can be used to predict (calculate) the outputs from an arbitrary set of inputs. Although the 'learning' phase can be quite lengthy, once trained, the network produces prediction almost instantaneously.

The input neurons activities introduce the inputs to the neural networks. The hidden and output neurons activities are defined by the relations:

$$x_i = t(\xi_i) \tag{1}$$

$$\xi_i = \sum_j w_{ij} x_j + \upsilon_i \tag{2}$$

where υ_i is the bias, w_{ij} is the weight and ξ_i is the sum of the weighted inputs (see Fig. 1).

Function $t(\xi)$ is so called transfer function with these properties:

1) t: $R \rightarrow (0, 1)$ is a continuous and monotonously increasing function;
2) $t(\xi) \rightarrow 0$ for $\xi \rightarrow -\infty$ and $t(\xi) \rightarrow 1$ for $\xi \rightarrow \infty$.

Commonly, the sigmoid function for $t(\xi)$ is used:

$$t(\xi) = \frac{1}{1 + e^{-\xi}} \tag{3}$$

The aim of the neural network training is by the changes of weights and biases to minimize the error E:

$$E = \sum_{i=1}^{r} E^{(i)} = \frac{1}{2} \sum_{i=1}^{r} (\underline{x}_0^{(i)} - \underline{\hat{x}}_0^{(i)})^2 \tag{4}$$

where r is the number of input–output vector pairs in the training set, $\underline{\hat{x}}_0^{(i)}$ is required output vector and $\underline{x}_0^{(i)}$ is the neural network response to the adequate input vector.

The error E can be minimized for example using gradient methods. Most often the steepest descent method is used. The weights and the biases are changed by the relations:

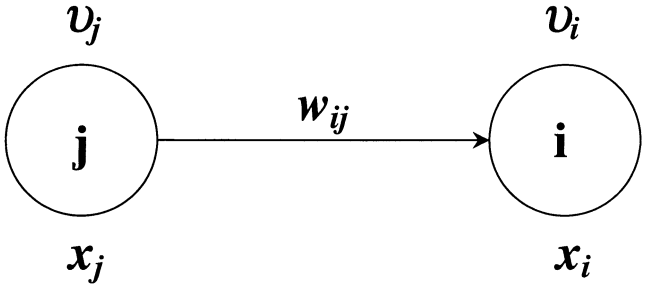


Fig. 1. Two neurons from the neighboring layers of the feedforward multilayer neural network, their activities, biases and the weight between them.

$$w_{ij}^{(k+1)} = w_{ij}^{(k)} - \mu\frac{\partial E}{\partial w_{ij}} + \mu\Delta w_{ij}^{(k)} \quad (5)$$

$$\vartheta_j^{(k+1)} = \vartheta_j^{(k)} - \lambda\frac{\partial E}{\partial \vartheta_j} + \mu\Delta\vartheta_j^{(k)} \quad (6)$$

$$\Delta v_j^{(k)} = v_j^{(k)} - v_j^{(k-1)} \quad (7)$$

$$\Delta w_{ij}^{(k)} = w_{ij}^{(k)} - w_{ij}^{(k-1)} \quad (8)$$

where k is the iteration number, λ the learning rate, $\mu\Delta w_{ij}^{(k)}$ and $\mu\Delta v_j^{(k)}$ are the momentum members. The minimization process is done until no improvement of root mean square (RMS) is observed.

RMS error is used to follow minimizing process. To obtain this value the individual errors are squared, added together, divided by the number of individual errors, and then square rooted. RMS gives a single number which summarizes the overall error (equals to squared sum of residuals divided by $N \times M$ and squared root of):

$$\mathrm{RMS} = \sqrt{\frac{\sum_{i=1}^{N}\sum_{j=1}^{M}(t_{ij} - y_{ij})^2}{N \times M}} \quad (9)$$

where t_{ij} are elements of the matrix for the training or the test set, y_{ij} are elements of the output matrix of the neural network, N is the number of patterns and M is the number of outputs for the training or the test set.

A standard technique is to train the network using one data set (training set). For a check that the network is able to perform well on previously-unseen data is necessary to have also a verification set not used in training. As training progresses, the RMS value for the training set drops, and providing training is minimizing the true error function, the RMS value for the verification set drops too. If the RMS value for the verification set stops to decrease, or starts to rise, this indicates that the network is starting to overfit the data. It is necessary to stop training in this case.

2.3. Computer data treatment

The data were processed on a Pentium PC computer using ANN TRAJAN 3.0 software package [21]. POLET [2,12,13], LETAGROP, SQUAD and OPIUM [14] programs were used for the simulation of experimental data needed for training ANN or for the treatment of experimental data.

3. Results and discussion

3.1. Case (1) potentiometry–dissociation of a weak acid in two steps with two near pK values

In this case, we have studied the possibility to use ANN modeling for normalized potentiometric data.

Let us consider an acid which splits off consecutively two protons:

$$H_2L \rightleftarrows H^+ + L^-H^- \quad K_{a1}$$

$$H_2L \rightleftarrows 2H^+ + L^{2-} \quad K_{a1} \times K_{a2}$$

We can define Z as a function of pH:

$$Z = \frac{c_H - 10^{-pH} + 10^{pH-pK_w}}{c_L}$$

where c_H is analytical concentration of protons, c_L the analytical concentration of acid present in solution and pK_w is the negative decadic logarithm of ionic product of water.

A pattern is a curve consisting of a number of data, each one being a Z value calculated at pH value for adequate pK_1 and pK_2 values. Number of pH values selected in pH range 1–6 was 21.

The pK_1 and pK_2 values are selected according to the ED used. In this way the error-free training set containing 13 patterns was generated. The training set is shown in the Fig. 2. Then four patterns as a test set were randomly generated.

The Z values were used as input for the ANN, the pK_1 and pK_2 values were used as output. The ANN architecture was searched for automatically by the TRAJAN program computation and then used further for the training process and the prediction, as well. This architecture (21:6:2) is shown in Fig. 3. We have also tried 'manual' search of the best architecture with the same result as using Trajan Automatic Network Designer. As training algorithm we have usually used Back Propagation (BP). Other training algorithms were tried too (Conjugate Gradients, Levenberg-Marquardt, and Quick Propagation) but the same results were obtained. Therefore, BP was used throughout the paper. In this

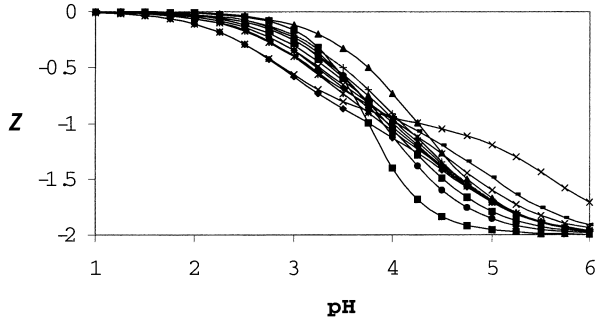


Fig. 2. Normalized Z-pH data concerning Case (1) of two overlapping protonation equilibria.

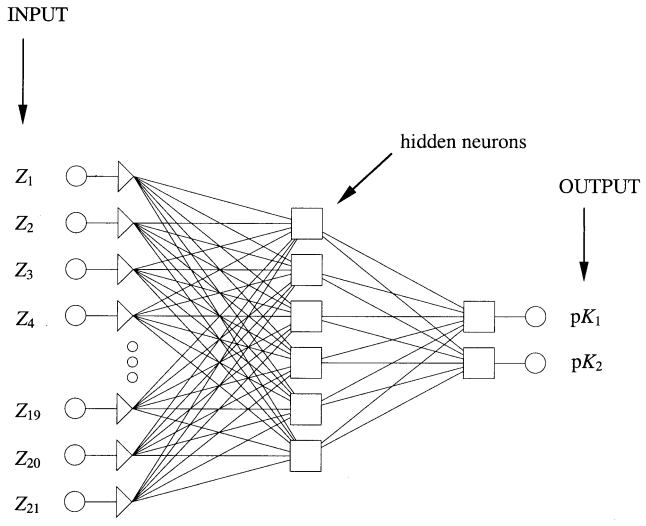


Fig. 3. Optimal ANN architecture (21:6:2) applicable for modeling Z-pH data and estimation of near pK_a values in Case (1).

case, number of epochs needed was 1200. For this value no overtraining was observed (Fig. 4). Table 1 shows the corresponding weight matrix. The RMS value obtained for the training set was 0.0352, the value for the test set was 0.0359. The predicted and correct pK_1 and pK_2 values for the test set are given in Table 2.

In the next stage, the simulated patterns with random noise were generated. Using a random number generator, error values were obtained (normal distribution with S.D. 0.001 and 0.01, respectively) and then were added to the error-free data in the patterns of the test set. The ANN structure with weights obtained on the error-free data was used to evaluate the ANN resistance to the noise. The results obtained for the test sets are seen in Table 2. The RMS values (0.03184 and 0.0306, respectively) are near to the value for error-free test set and the results obtained can be regarded as highly satisfactory. In addition, as it can be seen, the agreement was also achieved with the results obtained by OPIUM program [14] (Table 2).

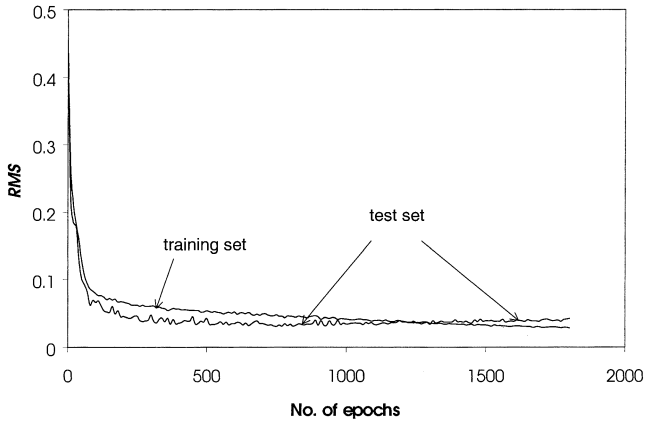


Fig. 4. Demonstration of the convergency of BP algorithm for optimal ANN architecture.

3.2. Case (2) determination of equivalence point and simultaneous glass-electrode calibration in potentiometry

3.2.1. Stage (A)

As the example, titration of acetic acid (p$K_a = 4.56$, p$K_w = 13.78$, $I = 0.1$ M) of initial concentration c_{HA} ($V_0 = 5$ ml, $T = 298.15$ K) with 0.1 M sodium hydroxide using a glass electrode was chosen. The task was to determine c_{HA}, electrode potential E_0 and electrode slope g from real titration curve in one step.

The input vector contains the electrode potential values measured for equidistant additions of sodium hydroxide solution in the range from 0 to 1.3 ml (totally 66 values).

The three-level factorial design for three parameters in combination with a star design for three parameters were used and for each combination of c_{HA}, E_0 and g values 32 titration curves were calculated by OPIUM software package [14] for a simulated titration generating always 66 values of emf for 66 additions of sodium hydroxide solution. Error-free training set containing 32 patterns was then generated by simulation using program, ten patterns randomly generated were used as a verification set and four patterns randomly generated were used as a test set. Example of selected titration curves is given in Fig. 5.

Values of the emf were used as inputs for the ANN, while c_{HA}, E_0 and g parameters of the electrode were used as outputs. Suitable ANN architecture for modeling was selected automatically by the TRAJAN program and used further for the training process. The optimal architecture found was (66:27:3). The RMS value for the training set was 0.00022, for the verification set 0.00065 and for the test set 0.00075. The predicted and given c_{HA}, E_0 and g values for the test set are given in Table 3.

In the next stage, the simulated patterns with random noise were generated. Using a pseudo-random numbers generator, error values with normal distribution were obtained and then were loaded to the error-free data in the patterns of the test set. The ANN structure with weights obtained on the error-free data was used to evaluate the ANN resistance to the noise. The results obtained for the test sets are seen in Table 3. In order to compare results obtained from hard modeling, the noise loaded data were treated by OPIUM program. The results are comparable (Table 3) and show that ANN are able to predict acid concentration, electrode potential and the slope of the electrode while the prediction errors are acceptable and within common experimental errors.

3.2.2. Stage (B)

A weak acid with dissociation constant pK_a in aqueous solution showing dissociation constant of water pK_w were titrated with sodium hydroxide ($c = 0.1$ M) using a glass electrode. The acids of initial concentration

Table 1
The values of weights and biases concerning results of ANN modeling for the Case (1)

	h1	h2	h3	h4	h5	h6	o1	o2
Biases	0.0953	0.0295	−2.231	−0.7919	−4.106	1.032	0.0753	1.42
i1	0.2784	−0.4336	0.8547	−0.4558	−0.3331	1.073		
i2	−0.7188	−0.6154	−0.3257	0.2479	−0.2031	1.284		
i3	−0.8336	1.135	−0.3489	−0.6902	0.3065	−0.4563		
i4	−0.5826	0.5747	1.081	−0.3873	0.557	0.8587		
i5	0.8921	−0.3179	−0.4476	−0.8369	−0.4105	0.7929		
i6	−0.0221	1.11	0.3635	0.3876	−0.407	1.154		
i7	−0.553	0.8014	−0.363	−0.0224	0.5217	0.5866		
i8	0.7112	1.3	−1.192	0.6296	−0.286	0.2272		
i9	−0.3975	1.314	−1.414	0.4535	0.2699	−0.2366		
i10	0.6753	0.4446	−1.304	−0.8485	−0.3692	−0.4898		
i11	0.6246	0.1104	−0.7822	−0.2736	−1.099	1.149		
i12	−1.219	−0.2435	−0.9842	1.673	−1.892	0.8004		
i13	−0.1727	0.2907	0.1533	1.489	−0.5968	0.5686		
i14	−0.8753	0.5152	0.7257	1.527	0.0953	0.2722		
i15	−0.0802	0.3945	1.048	0.1365	0.6927	−0.5789		
i16	−0.3861	−0.105	0.5588	0.8887	−0.5595	−0.927		
i17	−1.084	−0.5132	0.1363	1.375	−0.7429	−0.0729		
i18	0.3158	0.0092	0.0282	−0.2087	−0.8077	−0.3777		
i19	−0.8538	−0.7321	0.857	0.1054	−1.422	−0.6868		
i20	0.3977	−0.0762	0.8419	1.187	−0.914	0.7175		
i21	0.2581	−0.6958	0.5325	−0.6886	−1.289	−0.6206		
h1							−0.479	1.259
h2							−3.119	0.0267
h3							3.139	−0.2787
h4							1.51	−2.23
h5							2.139	6.63
h6							−2.761	−1.831

Remark: i1–i21 are order numbers of input neurons, h1–h6 are order numbers of the hidden neurons and o1–o2 are order numbers of output neurons.

c_{HA} ($V_0 = 5$ ml, $T = 298.15$ K) were titrated, while electrode potential E_0 and electrode slope g were studied.

The input vector contains the electrode potential values calculated for volumes of volumetric solution added from 0 to 1.3 (in sum 66 values).

The pK_a, pK_w, c_{HA}, E_0 and g values are selected according to the ED used. Training set containing 480 error free titration curves (patterns) was generated by simulation using program. Then 50 patterns were randomly generated as a verification set and two patterns were randomly generated as a test set.

Table 2
Comparison of calculated and given pK_1 and pK_2 values for the test set (Case 1)

Curve numbers	Theoretical values		Estimated values				Noise $s(Z)$
	pK_1	pK_1+pK_2	pK_1		pK_1+pK_2		
			OPIUM	ANN	OPIUM	ANN	
1	3.40	8.30	3.400	3.438	8.300	8.332	0
2	3.70	8.10	3.700	3.707	8.100	8.135	0
3	3.80	7.80	3.800	3.779	7.800	7.763	0
4	3.20	8.40	3.200	3.267	8.400	8.420	0
1	3.40	8.30	3.399(3)	3.429	8.300(3)	8.321	0.001
2	3.70	8.10	3.703(3)	3.707	8.102(4)	8.143	0.001
3	3.80	7.80	3.809(4)	3.773	7.797(5)	7.770	0.001
4	3.20	8.40	3.200(1)	3.249	8.400(2)	8.411	0.001
1	3.40	8.30	$3.43_1(1_2)$	3.409	$8.31_1(1_6)$	8.279	0.01
2	3.70	8.10	$3.78_8(4_0)$	3.697	$8.02_3(4_8)$	8.080	0.01
3	3.80	7.80	$3.75_2(4_8)$	3.795	$7.80_8(5_5)$	7.715	0.01
4	3.20	8.40	3.190(7)	3.225	8.389(9)	8.410	0.01

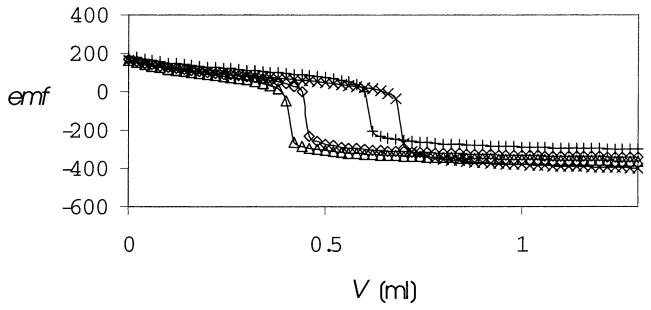


Fig. 5. Selected titration curves concerning Case (2A).

Values of the emf were used as inputs for the ANN, while pK_a, pK_w, c_{HA}, E_0 and g parameters of the electrode were used as outputs. Suitable ANN architecture for modeling was selected automatically by the TRAJAN program and used further for the training process. This architecture was (66:12:5). The RMS value for the training set was 0.005227, for the verification set 0.006166 and for the test set 0.00648. The average prediction errors for these three sets are given in Table 4. The predicted and given pK_a, pK_w, c_{HA}, E_0 and g values for the test set are compared in Table 5.

Table 4
Comparison of average prediction errors for the determination of five parameters (pK_a, pK_w, c_{HA}, E_0 and g) concerning potentiometric titration

Type of set	Estimated parameters				
	pK_a	pK_w	c_{HA}	E_0	g
Training	−0.41%	0.11%	1.01%	0.39%	−1.18%
Verification	1.32%	1.27%	0.90%	0.18%	−2.08%
Test	−3.10%	0.27%	2.03%	−0.26%	0.13%

Results given for training, verification and test sets (Case 2B).

Then the simulated patterns with random noise were generated. Using a random number generator, error values were obtained (normal distribution with S.D. 0.1, 0.3, 0.6, 1.2 and 3 mV corresponding with pH uncertainity 0.002, 0.006, 0.01, 0.02 and 0.05, respectively) and then were added to the error-free data in the patterns of the test set. The ANN structure with weights obtained on the error-free data was used to evaluate the ANN resistance to the noise. The results obtained for the test sets are seen in Table 5. In addition, the results are similar to those obtained by OPIUM program.

Table 3
Evaluation of potentiometric titration data of a weak monoprotic acid

Curve numbers	Theoretical values			Estimated values						Noise $s(E)$ (mV)
	C_{HA} (mM)	E_0 (mV)	g	c_{HA} (mM)		E_0 (mV)		g		
				ANN	OPIUM	ANN	OPIUM	ANN	OPIUM	
1	9.000	366.8	59.5	9.000	9.003	366.8	366.2	59.5	59.53	0
1	9.000	366.8	59.5	9.000(1)	8.993	366.78(3)	366.1	59.498(3)	59.52	0.1
1	9.000	366.8	59.5	8.998(2)	9.012	366.9(1)	366.2	59.51(1)	59.55	0.3
1	9.000	366.8	59.5	8.998(4)	8.957	366.9(2)	366.2	59.51(2)	59.61	0.6
1	9.000	366.8	59.5	8.989(6)	8.967	366.4(4)	365.7	59.45(4)	59.43	1.2
1	9.000	366.8	59.5	$8.99_0(1_6)$	9.056	$366._3(1_1)$	365.8	59.6(1)	59.54	3.0
2	8.045	369.3	61.3	8.045	8.178	369.3	369.3	61.3	61.48	0
2	8.045	369.3	61.3	8.045(0)	8.177	369.25(4)	369.2	61.297(4)	61.47	0.1
2	8.045	369.3	61.3	8.045(0)	8.184	369.2(1)	369.1	61.29(1)	61.44	0.3
2	8.045	369.3	61.3	8.044(1)	8.192	369.2(3)	369.1	61.29(3)	61.44	0.6
2	8.045	369.3	61.3	8.043(2)	8.112	369.6(5)	369.9	61.35(5)	61.7	1.2
2	8.045	369.3	61.3	8.045(6)	8.171	$369._5(1_4)$	370.4	61.3(1)	61.79	3.0
3	13.89	375.1	65.8	13.89	13.27	375.1	374.2	65.8	65.05	0
3	13.89	375.1	65.8	$13.89_0(_0)$	13.27	375.11(3)	374.3	65.802(3)	65.05	0.1
3	13.89	375.1	65.8	$13.89_0(_1)$	13.27	375.1(1)	374.3	65.80(1)	65.05	0.3
3	13.89	375.1	65.8	$13.89_0(_2)$	13.27	375.3(2)	374.5	65.80(2)	65.05	0.6
3	13.89	375.1	65.8	$13.90_0(_4)$	13.27	375.6(4)	375	65.86(4)	65.14	1.2
3	13.89	375.1	65.8	13.88(1)	13.27	373.1(9)	372.8	65.6(1)	65.13	3.0
4	12.12	370.8	56.8	12.12	12.12	370.8	369.8	56.8	57.04	0
4	12.12	370.8	56.8	$12.12_0(_0)$	12.12	370.82(3)	369.9	56.800(3)	57.04	0.1
4	12.12	370.8	56.8	$12.12_2(_1)$	12.13	370.8(1)	369.4	56.79(1)	56.99	0.3
4	12.12	370.8	56.8	$12.11_9(_2)$	12.12	371.3(2)	370.2	56.85(2)	57.09	0.6
4	12.12	370.8	56.8	$12.12_1(_6)$	12.11	371.3(5)	369.6	56.84(5)	56.86	1.2
4	12.12	370.8	56.8	12.12(1)	12.15	371.5(8)	371.6	56.85(9)	57.13	3.0

Comparison of calculated and given c_{HA}, E_0 and g values for the titration curves of the test set (Case 2A).

Table 5
Comparison of calculated and given pK_a, pK_w, c_{HA}, E_0 and g values for the test set (Case 2B)

Curve numbers	Theoretical values					Estimated values					Noise $s(E)$ (mV)
	c_{HA} (mM)	E_0 (mV)	g	pK_a	pK_w	OPIUM; ANN					
						c_{HA}	E_0	g	pK_a	pK_w	
1	11.80	366	60.0	3.80	13.90	11.80; 11.99	366.0; 370.5	60.00; 58.95	3.800; 3.543	13.90; 14.21	0
1	11.80	366	60.0	3.80	13.90	11.801(1); 11.99	366.0(1); 370.5	60.00(3); 58.96	3.801(3); 3.544	13.901(6); 14.21	0.1
1	11.80	366	60.0	3.80	13.90	11.800(1); 11.99	365.4(4); 370.5	59.83(9); 58.96	3.802(9); 3.540	$13.92_3(1_8)$; 14.21	0.3
1	11.80	366	60.0	3.80	13.90	11.805(4); 12.00	363.8(8); 370.5	59.9(2); 58.92	$3.77_2(1_8)$; 3.530	$13.89_4(3_8)$; 14.21	0.6
1	11.80	366	60.0	3.80	13.90	11.803(6); 12.00	$366._5(1_3)$; 370.4	60.2(3); 58.88	$3.79_6(3_1)$; 3.523	$13.87_4(6_2)$; 14.22	1.2
1	11.80	366	60.0	3.80	13.90	11.78(1); 11.97	$362._4(3_2)$; 370.3	59.4(8); 58.70	$3.77_3(7_8)$; 3.501	$13.9_5(1_6)$; 14.23	3.0
2	10.00	368	57.8	5.40	13.70	10.00; 10.04	368.0; 372.9	57.80; 56.91	5.400; 5.503	13.70; 13.96	0
2	10.00	368	57.8	5.40	13.70	$10.000_0(1_1)$; 10.04	368.1(2); 372.9	57.79(3); 56.90	5.403(4); 5.504	13.704(6); 13.96	0.1
2	10.00	368	57.8	5.40	13.70	$10.000_0(1_1)$; 10.04	368.6(5); 373.0	57.76(8); 56.92	$5.41_5(1_1)$; 5.507	$13.71_9(1_6)$; 13.96	0.3
2	10.00	368	57.8	5.40	13.70	$10.000_0(4)$; 10.03	$368._8(1_2)$; 372.9	57.6(2); 56.87	$5.43_6(2_5)$; 5.501	$13.76_3(3_7)$; 13.97	0.6
2	10.00	368	57.8	5.40	13.70	$9.999_9(7)$; 10.10	$362._5(2_4)$; 373.1	57.2(3); 56.99	$5.35_1(5_0)$; 5.469	$13.72_3(7_4)$; 13.94	1.2
2	10.00	368	57.8	5.40	13.70	9.997(1); 10.11	$364._8(5_8)$; 373.1	58.4(8); 57.05	$5.2_8(1_2)$; 5.504	$13.5_3(1_8)$; 13.94	3.0

The results show that ANN are able to predict pK_a, pK_w, c_{HA}, E_0 and g values with sufficient accuracy.

3.3. Case (3) NMR

Nuclear magnetic resonance (NMR) spectroscopy is a powerful tool for the determination of structural information of complexes in solution. It can also be used for the determination of equilibrium constant of species present in solution. As example, we took example of dissociation constant determination of hydrogen cyanide followed by means of ^{13}C NMR spectroscopy [22].

The input vector contains the chemical shift as observed values were calculated for 56 pH values from 2 to 13.

The δ_{HA}, δ_A (both measured in ppm) and pK_a values were selected according to the three-level factorial design. This design is demonstrated in the Fig. 6. In this way, the error-free learning set containing 27 patterns was created. Then six patterns as a test set were randomly generated.

Observed values of chemical shift were used as inputs for the ANN, the δ_{HA}, δ_A and pK_a values were used as outputs. The optimal ANN architecture (56:16:3) was found by computing using the TRAJAN program and was then used further for the training process and data evaluation. The RMS value for the training set was 0.05897, for the test set 0.0601. The predicted and given δ_{HA}, δ_A and pK_a values for the test set are in Table 6.

In the next stage the simulated patterns with random noise were generated. Using a random generator, appropriate values of noise with normal distribution were calculated and were then loaded to the error-free data in test set patterns. Optimal ANN structure with weights obtained on the error-free data was then applied to evaluate with ANN approach to study the resistance of the method with respect to the noise level. The results obtained for the test sets by means of ANN and OPIUM program are given in Table 6.

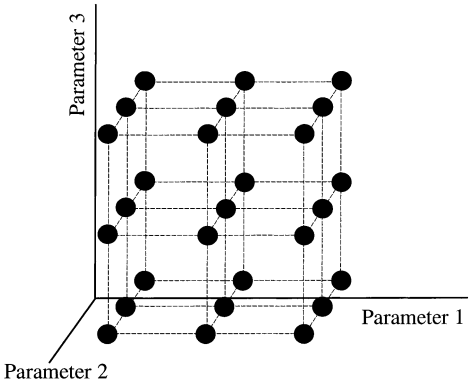


Fig. 6. Scheme of a three-level factorial design for three parameters used in Case (3).

The RMS values obtained were 0.06038 and 0.08332, respectively. The increase in the RMS values when increasing the level of noise is not very large. The results obtained with ANN are acceptable and then indicate that ANN approach is usable for NMR data evaluation.

Further the evaluation of experimental data was accomplished. Results obtained can be seen from Table 6 and can be regarded as highly satisfactory. The difference between the expected and ANN predicted value is within the experimental errors.

3.4. Case (4) potentiometry-determination of uranyl hydrolytic constants

The hydrolytic reaction of uranyl can be written

$$pUO_2^{2+} + qH_2O \overset{K_{h,pq}}{\rightleftarrows} (UO_2)_p(OH)_q^{2p-q} + qH^+$$

where the equilibrium hydrolytic constant is defined as

$$K_{h,pq} = [(UO_2)_p(OH)_q^{2p-q}][H^+]^q[UO_2^{2+}]^{-p}$$

We will continue in abbreviating hydrolytic species using their indices in brackets (p, q).

As training data, 192 curves for ANN were simulated by means of OPIUM package for the following parameters: uranyl concentration 2, ..., 100 mM, $-\log[H^+]$ 3, ..., 5, $\log K_{2-2} = -5.8$, ..., -6.5, $\log K_{3-4} = -12.6$, ..., -13.2, $\log K_{3-5} = -16.5$, ..., -17.2. The following Z function

$$Z = \frac{c_{OH} - K_w/[H^+] + [H^+]}{c_U}$$

where c_{OH} is analytical concentration of hydroxide ions, c_U is analytical concentration of uranyl present in solution, K_w is the ionic product of water under given experimental conditions and $[H^+]$ is concentration of free protons which can be determined e.g. by glass electrode. Z-function is dependent on parameters mentioned above. The change of parameters was proposed according to central composite design. The simulated data are presented in Fig. 7. As data for ANN verification, 50 curves were generated under the same conditions as for training data but for different values. Experimental data [23] were then evaluated using simulated curves of the training set by ANN approach.

For ANN computation, a trial set $(c_M, -\log[H^+], Z)_n$ was used as input data while the output data were $-\log K_{2-2}$, $-\log K_{3-4}$, and $-\log K_{3-5}$. The architecture of ANN was optimized and it was found to be (33:3:3). The results of experimental data evaluation by means of ANN were compared with the results obtained by POLET program. The results of experimental data analysis by soft and hard model technique are given in Table 7 and it is evident that ANN approach is giving good agreement with 'hard' computing.

Table 6
Comparison of results for NMR data

Curve numbers	Theoretical values			Estimated values						Noise $s(\delta)$
	pK_a	δ_{HA}	δ_A	pK_a		δ_{HA}		δ_A		
				OPIUM	ANN	OPIUM	ANN	OPIUM	ANN	
1	9.00	112	167	9.000	9.017	112.00	111.4	167.00	166.7	0
2	9.05	117	172	9.050	9.034	117.00	117.2	172.00	173.3	0
3	9.05	117	175	9.050	9.122	117.00	117.6	175.00	173.7	0
4	9.05	120	175	9.050	9.045	120.00	118.8	175.00	174.4	0
5	9.15	120	175	9.150	9.127	120.00	118.9	175.00	174.5	0
6	9.15	110	175	9.150	9.143	110.00	110.5	175.00	174.0	0
1	9.00	112	167	9.004(1)	9.018	112.02(2)	111.4	166.98(2)	166.7	0.1
2	9.05	117	172	9.052(2)	9.035	117.00(2)	117.2	172.03(3)	173.4	0.1
3	9.05	117	175	9.152(1)	9.122	116.98(2)	117.5	172.02(3)	173.8	0.1
4	9.05	120	175	9.052(2)	9.047	120.00(2)	118.8	175.00(3)	174.4	0.1
5	9.15	120	175	9.147(2)	9.123	120.00(2)	118.9	174.98(3)	174.5	0.1
6	9.15	110	175	9.148(1)	9.143	110.03(2)	110.5	175.02(3)	174.0	0.1
1	9.00	112	167	$8.98_2(1_4)$	9.018	$111.9_7(1_7)$	110.9	$166.8_7(2_4)$	166.5	1.0
2	9.05	117	172	$9.05_4(1_4)$	9.023	$116.5_5(1_7)$	117.6	$172.2_3(2_4)$	173.9	1.0
3	9.05	117	175	$9.14_5(1_8)$	9.133	$117.0_8(2_1)$	117.9	$172.0_2(3_0)$	173.6	1.0
4	9.05	120	175	$9.04_3(1_5$	9.050	$120.0_7(1_8)$	119.4	$175.0_8(2_5)$	174.3	1.0
5	9.15	120	175	$9.12_3(1_4)$	9.108	$119.8_7(1_7)$	118.9	$174.4_8(2_5)$	174.3	1.0
6	9.15	110	175	$9.15_1(1_{4)}$	9.148	$109.9_5(2_0)$	110.5	$174.9_4(2_9)$	174.0	1.0
Experimental data				9.028(3)	9.056	114.76(4)	114.8	$168.0_3(1_1)$	167.0	

Calculated and given δ_{HA}, δ_A and pK_a values for the test set (Case 3).

Table 7
The results of experimental data concerning hydrolysis of uranium(VI) analysis by soft (ANN) and hard model (POLET) techniques

Hydrolytic constant	Uranyl concentration (mM)				
	ANN				POLET [a]
	8.28	16.56	33.13	Average	
$\log K_{2-2}$	−6.200	−6.196	−6.195	−6.197	−6.22(2)
$\log K_{3-4}$	−12.890	−12.892	−12.893	−12.892	−12.9(1)
$\log K_{3-5}$	−16.800	−16.805	−16.806	−16.804	−16.78(4)

[a] Calculated for all concentrations together.

4. Conclusions

The use of ANN multivariate calibration approach to estimate stability constants tested on error-free data and on data with random noise shows high rigidity of ANN method to random errors, while equilibrium constants can be obtained with sufficient accuracy and the results do not differ significantly from the correct values or those obtained by a general regression optimization programs.

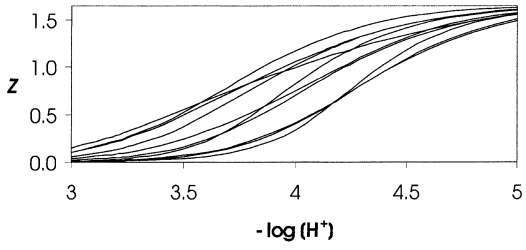


Fig. 7. Simulated ($-\log[H^+]$, Z) curves concerning hydrolysis of uranium with experimental points concerning Case (4). For the sake of clarity, only each 20th curve of the total number of curves are given (total number of the curves was 192).

The method proposed is quite general and, in principal, can be applied for evaluation of any kind of experimental data in equilibria studies.

On the base of ED-ANN, 'normalized equilibrium data base' can be created. Once evaluated (trained) it can yield the equilibrium constants very fast without solving mass balance equations, for any data with the same chemical model. This can be a completely general and NEW approach towards equilibrium data evaluation.

Acknowledgements

We would like to thank Professor J. Glaser (KTH Stockholm, Sweden) for providing ^{13}C NMR spectra of HCN. This work was supported by the project FRVŠ 541/2001 of the Ministry of Education and Youth, Czech Republic.

References

[1] M. Meloun, J. Havel, E. Högfeldt, Computation of Solution Equilibria, Ellis Horwood, Chichester, 1985.
[2] D.J. Leggett (Ed.),Computational Methods for the Determination of Formation Constants, Plenum, New York, 1985.
[3] J. Gasteiger, J. Zupan, Angew. Chem. 32 (1993) 503.
[4] J. Havel, E.M. Peña-Méndez, A. Rojas-Hernández, J.-P. Doucet, A. Panaye, J. Chromatogr. A 793 (1998) 317.
[5] M. Farková, E.M. Peña-Méndez, J. Havel, J. Chromatogr. A 848 (1999) 365.
[6] V. Dohnal, M. Farková, J. Havel, Chirality 11 (1999) 616.
[7] J. Havel, J.E. Madden, P.R. Haddad, Chromatographia 49 (1999) 481.
[8] J. Havel, M. Breadmore, M. Macka, P.R. Haddad, J. Chromatogr. A 850 (1999) 345.
[9] J. Perutka, J. Havel, L. Galindo, F.G. Montelongo, J.J. Arias León, Chem. Papers 50 (4) (1996) 162.
[10] I. Cukrowski, J. Havel, Electroanalysis 12 (2000) 1481.
[11] I. Cukrowski, M. Farková, J. Havel, Electroanalysis 13 (2001) 295.
[12] J. Havel, M. Meloun, Talanta 32 (1985) 171.
[13] E. Mikanová, M. Bartušek, J. Havel, Scr. Fac. Sci. Nat. Univ. Purk. Brunensis 10 (1980) 3.
[14] (a) M. Kývala, P. Lubal, I. Lukeš, in: IX Spanish–Italian Congress on Thermodynamics of Metal Complexes, Girona, 1998, Abstract book, p. 94;
(b) M. Kývala, Ph.D. thesis, Charles University, Prague, 2000.;
(c) http://prfdec.natur.cuni.cz/ ~ kyvala/opium.html.
[15] L.G. Sillén, Acta Chem. Scand. A 10 (1956) 186.
[16] G. Biedermann, L.G. Sillén, Acta Chem. Scand. A 10 (1956) 203.
[17] D. Dyrssen, N. Ingri, L.G. Sillén, Acta Chem. Scand. A 15 (1961) 604.
[18] G. Biedermann, T.G. Spiro, Chem. Scr. 1 (1971) 193.
[19] D. Ferri, O. Wahlberg, E. Högfeldt, Acta Chem. Scand. A 27 (1973) 3591.
[20] D.L. Massart, B.G.M. Vandeginste, S.M. Deming, Y. Michotte, L. Kaufman, Chemometrics: A Textbook, Elsevier, Amsterdam, 1988.
[21] Trajan Neural Network Simulator, Release 3.0 D. Copyright Trajan Software Ltd., 1996–1998.
[22] I. Bányai, J. Blixt, J. Glaser, I. Tóth, Acta Chim. Scand. 46 (1992) 138–142.
[23] P. Lubal, J. Havel, Chem. Papers 51 (1997) 213.

PERGAMON

Polyhedron 21 (2002) 1385–1391

POLYHEDRON

www.elsevier.com/locate/poly

Affinity of lanthanide(III) ions for oxygen- and mixed oxygen–nitrogen-donor ligands in dimethylsulfoxide: a thermodynamic and spectroscopic investigation

Clara Comuzzi [a,*], Plinio Di Bernardo [b], Roberto Portanova [a], Marilena Tolazzi [a,*], Pierluigi Zanonato [b]

[a] *Dipartimento di Scienze e Tecnologie Chimiche, Università di Udine, Via del Cotonificio 108, 33100 Udine, Italy*
[b] *Dipartimento di Chimica Inorganica, Metallorganica e Analitica, Università di Padova, Via Loredan 4, 35131 Padova, Italy*

Received 30 July 2001; accepted 3 October 2001

Abstract

The interactions of lanthanide(III) ions with the following oxygen- and mixed oxygen–nitrogen-donor ligands: 2-methoxyethylamine (**L1**), 2-aminoethanol (**L2**), 2-methoxyethylether (**L3**), di(ethyleneglycol) (**L4**), 2,2′-oxydiethylamine (**L5**) and 1,5-diaminopentane (**L6**) have been investigated in dimethylsulfoxide (DMSO) at 298 K and $I = 0.1$ mol dm^{-3} (Et_4NClO_4). Calorimetric and ^{1}H NMR results show that **L1**–**L4** and **L6** are not able to complex Ln(III) ions. **L5** is shown to be able to bind heavier Ln(III) ions (Ln=Ho–Lu). Potentiometric and calorimetric measurements have been carried out to obtain the Ln(III)–**L5** thermodynamic parameters of complexation. All the complexes are formed in exothermic reactions being the entropy terms generally negative or slightly positive. Comparison between the complexing abilities of **L1** and **L5** shows that at least two $-CH_2CH_2NH_2$ side-arms added to an ether function are needed to promote effective interaction between an ether O atom and Ln(III) ions in the high coordinating solvent DMSO. The results are discussed in terms of different donor properties and solvation of –NR– and –O– groups towards metal ions. A comparison with data previously obtained in DMSO for the complex formation of Ln(III) with the purely N donor diethylenetriamine (dien) is made. © 2002 Elsevier Science Ltd. All rights reserved.

Keywords: Lanthanides(III); Oxygen donors; 2,2′-Oxydiethylamine; Dimethylsulfoxide; Complexes; Thermodynamics

1. Introduction

The past decade has witnessed a growth in research into the coordination chemistry of lanthanide(III) ions, due to the importance of their compounds in homogeneous and heterogeneous catalysis [1], in biochemistry as luminescent probes [2], in analytical chemistry as ion-selective reagents [3], in NMR as shift reagents [4] and, as shown by recent studies, in magnetic resonance imaging (MRI) [5], where they are used as contrast reagents. Their development also concerns the fields of glass, ceramics, magnets, optics and electronics [6] and also extends to studies as catalytic active metals in synthetic hydrolases [7].

This enlargement in the scientific and technological interest of lanthanides consequently means that additional information concerning particular aspects of their coordination chemistry is of interest and usefulness.

So far, much attention has been paid to the aqueous solution chemistry of lanthanides, which is dominated by their oxophilicity, most ligands containing carboxylato or phosphinato oxygen donors [1,8–10]. In this context, only slightly basic N-donors have been studied in water, as strongly basic amines do not survive hydrolysis [9,11]: these studies have shown that amines are poor donors for lanthanides in water whereas, when incorporated into aminocarboxylates or aminophosphonate, they form quite stable Ln(III) complexes, much more stable than the analogous oxoacids [10].

* Corresponding authors. Tel.: +39-0432-558-852/882; fax: +39-0432-558-803.
E-mail addresses: comuzzi1@dstc.uniud.it (C. Comuzzi), tolazzi@dstc.uniud.it (M. Tolazzi).

0277-5387/02/$ - see front matter © 2002 Elsevier Science Ltd. All rights reserved.
PII: S0277-5387(02)00965-8

Recently, some attention has been also paid to non-aqueous media, where strongly basic ligands can be more easily investigated [12–14]. In particular, our resaerch group has recently studied [15] the thermodynamic and luminescent properties of lanthanide(III) complexes with linear amines and polyamines in the following solvents of differing coordinating properties [16,17]: dimethylsulfoxide (DMSO), (donor number, DN = 29.8), acetonitrile, an, (DN = 14.1), and *N*,*N*′-dimethylformamide (DMF) (DN = 26.6). These studies have shown that: (i) the formation constants of LnL_j complexes in DMSO (L = en, $J = 1–3$; L = dien and trien, $j = 1, 2$) increase almost linearly with the increasing atomic number of the metal ion, indicating ion–dipole interactions; (ii) complex formation in all aprotic solvents is accompanied by high negative enthalpy and entropy values, as a consequence of strong Ln–N coordination and relatively weak desolvation of the species; (iii) strong chelate effects are at play, as complex stability increases with the N atoms present in the ligand concerned; (iv) solvation effects greatly influence complex formation in such a way that complexes unstable in DMSO are stabilized in DMF and, to a greater extent, in an.

Up to date, few studies concerning the affinity of Ln(III) ions for the ether or alcohol O-function inserted in neutral ligands have been reported in water or other strong donor solvents such as DMF [13,14,18] or DMSO [19,20]: in the latter solvent, the formation of stable lanthanide (III) complexes with cryptands 4,7,13,16,21,24-hexaoxa-1,10-diazabicyclo[8.8.8]hexacosane and 4,7,13,16,21-pentaoxa-l,10-diazabicyclo[8.8.5]tricosane, claimed by some authors [19], has been ruled out by independent experimental evidence [20]. However, data on Ln(III) interactions with neutral macrocycles containing O and other heteroatoms, N or S, in less coordinating solvents such as propylenecarbonate (4-methyl-l,3-dioxolan-2-one, pc) or acetonitrile (an) show that lanthanides have considerable affinity not only for –NH– but also for –O– functions, though maintain a greater preference for –NH– coordination [13,14,21].

With the aim of improving our understanding of Ln(III) behavior towards the coordination of the neutral oxygen atom in strong donor solvents, we present here an investigation on the interactions of some oxygen- and mixed oxygen–nitrogen-donor ligands with some lanthanide(III) ions in DMSO. The ligands studied are 2-methoxyethylamine (**L1**), 2-aminoethanol (**L2**), 2-methoxyethylether (**L3**) di(ethyleneglycol) (**L4**) and 2,2′-oxydiethylamine (**L5**) (Scheme 1). They were chosen as being able to form five-membered chelate rings, which should maximize their complexing ability [22]. In order to clarify if the ether function in **L5** contributes to stabilizing Ln(III)–2,2′-oxydiethylamine complexes or if it simply acts as a spacer between the amino groups, some experimental measurements were carried out in DMSO to verify the complexing ability towards lanthanides(III) of 1,5-diaminopentane (**L6** in Scheme 1), were the O atom of **L5** is substituted by a $–CH_2–$ moiety.

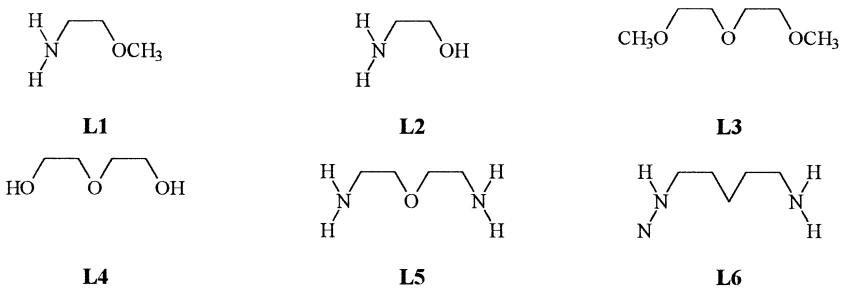
A number of preliminary experiments, run using solutions of moderately high concentrations of the above-mentioned ligands proved that (see Section 3) only **L5** shows some affinity for lanthanide ions: the present thermodynamic investigation was therefore focused on the study of **L5** complexation with the heavier Ln(III) ions ($Ln=Ho^{3+}–Lu^{3+}$), as their high charge density should maximize ion–dipole interactions.

The stability constants of the complexes formed by metal ions with **L5** were obtained by means of potentiometric measurements using the method of competitive reactions [23]: silver(I) was the auxiliary metal ion. The method requires the preliminary determination of the stability constants of the silver(I) complexes with **L5** [23]. Enthalpy changes were determined by direct calorimetric titration.

The present study was performed at 298 K by adjusting the ionic medium to 0.1 mol dm^{-3} with tetraethylammonium perchlorate as supporting electrolyte. To provide insight into the nature of Ln(III)–**L5** coordination, spectroscopic NMR studies were also performed.

2. Experimental

Warning! Although we did not have any problems, organic solvates of perchlorate salts are powerful



Scheme 1.

explosives and should be handled with great caution! [24]

$Ln(III)(ClO_4)_3 \cdot n$DMSO (n decreasing almost regularly from 7.9 for La to 7.1 for Lu) were prepared, crystallized and characterized as described earlier [15a]. Stock anhydrous solutions of the salts were prepared by dissolving weighed amounts of the adducts in anhydrous DMSO. The metal ion concentration in the stock solution was determined by complexometry with EDTA [25].

Silver (I) perchlorate (Fluka puriss × H_2O) and NEt_4ClO_4 (Fluka purum >99%) were dehydrated and purified as previously described [26].

DMSO (Fluka >99%) was distilled under reduced pressure [27] and stored with 4 Å molecular sieves in dark bottles.

Pure 1,5-diaminopentane was obtained by distillation under reduced pressure of the commercial product (Aldrich 95%) [27]. 2-Methoxyethylamine (Aldrich 99%), 2-aminoethanol (Aldrich 99+%), 2-methoxyethylether (Aldrich 99%) and di(ethylene glycol) (Aldrich 99%) were dehydrated with 4 Å molecular sieves and used without further purification.

The free base 2,2′-oxydiethylamine (**L5**) was obtained by percolation of an aqueous solution of the dihydrochloride salt (Aldrich 97%) through an Amberlite-IRA-400(OH) ion exchange resin. Water was then removed from the eluate by distillation and the anhydrous product (purity >99% by gas chromatography) was finally obtained by distillation under reduced pressure.

Stock solutions of the ligands were prepared by dissolving weighed amounts of the pure substances in anhydrous DMSO. All solutions were prepared and stored in a glove box under controlled atmosphere of N_2 (H_2O <2 ppm). The water content in the stock solutions (10–30 ppm) was determined on a Metrohm 684 KF coulometer.

2.1. Potentiometric measurements

Data for calculating the stability constants of the Ln(III)–2,2′-oxydiethylamine complexes were obtained by monitoring the equilibrium concentration of silver(I) in solutions containing different initial concentration of silver(I)–lanthanide(III) and known concentrations of the ligands. All measurements were carried out in a thermostatted cell maintained at 298.0±0.1 K. The e.m.f. values were collected by means of a data acquisition system using an Amel model 338 pH-meter equipped with a Metrohm 6.0328.000 silver electrode as working electrode and a Metrohm 6.0718.000 silver electrode as reference. Typically, a titration run was carried out by adding known volumes of the ligand solution ($100 < C^\circ_L < 300$ mmol dm^{-3}) to 20 ml of a lanthanide(III)–silver(I) solution ($5 < C^\circ_{Ln} < 33$ mmol dm^{-3}; K $C^\circ_{Ag} < 10$ mmol dm^{-3}).

The e.m.f. values of cells containing Ln^{3+} and Ag^+ ions proved that the silver(I) electrode behaved in DMSO according to Nernst's law in the range $10^{-5} < [Ag] < 10^{-2}$ mol dm^{-3}. To exclude moisture, all titrations were performed in a dry MB Braun 150 glove box. The computer program HYPERQUAD [28] was used for the calculation of the stability constants.

2.2. Calorimetric measurements

A Tronac model 87-558 precision calorimeter was employed to measure reaction heats. The calorimeter accuracy was checked by titration of tris(hydroxymethyl)aminomethane (THAM) with a standard solution of HCl in water. The experimental value of the neutralization heat of tham was found to be $\Delta H^\circ = -47.58$ kJ mol^{-1}, in good agreement with the accepted value of -47.53 ± 0.13 kJ mol^{-1} [9].

Calorimetric titrations were performed at 298.00±0.02 K by adding known volumes of ligand solutions ($30 < C^\circ_L < 120$ mmol dm^{-3}) to 20 ml of lanthanide(III) ($5 < C^\circ_{Ln} < 33$ mmol dm^{-3}) solutions. The dilution heats of the reactants, determined in separate runs, were found to be negligible. The LETAGROP KALLE least-squares computer program [29] was used to calculate enthalpy changes.

2.3. NMR measurements

^{1}H NMR spectra were recorded at 298 K on a Brucker AC 200F QNP spectrometer.^{1}H chemical shifts refer to $SiMe_4$. Measurements were performed on DMSO-d_6 solutions containing the metal ions (~33 mmol dm^{-3}) and the ligands in the molar ratio $R_c = C_L/C_M = 0.3$. Analogous measurements were carried out on solutions containing only the ligand concerned.

3. Results

The overall stability constants obtained after the minimization procedure of the potentiometric data, with the limits of error indicated, are listed in Table 1 for reactions $M + jL \rightleftarrows ML_j$ ($M = Ln^{3+}$, **L** = **L5**). Computer treatment of experimental data showed that the best fit was achieved when one (Ho) or two (Er–Lu) successive mononuclear complexes formed.

Fig. 1 shows plots of $\bar{n}$, the average number of ligands per metal ion, versus $-\log[\mathbf{L}]$ for the formation of **L5** complexes of Ho^{3+} and Lu^{3+}, where [**L**] is the free ligand concentration. The relationship $\bar{n} = (C_L - \bar{n}' C_{Ag} - [\mathbf{L}])/C_M$ was used to calculate $\bar{n}$, where $\bar{n}'$ is the average number of ligands bound to silver(I) ion and C_L is the analytical ligand concentration. The values of

Table 1
Overall stability constants and thermodynamic functions for the lanthanide(III)–**L5** complexes in DMSO at 25 °C and $I = 0.1$ mol dm^{-3}

Ln(III)	r (Å) [a]	ML$_j$	Log β_j	$-\Delta G^\circ_{\beta j}$	$-\Delta H^\circ_{\beta j}$	$-T\Delta S^\circ_{\beta j}$
Ho	0.894	$J = 1$	2.3(1)	13.1(6)	12(1)	−1.1
Er	0.881	$J = 1$	2.6(2)	15(1)	12(3)	−3
		$J = 2$	4.4(2)	25(1)	26(3)	1
Tm	0.869	$J = 1$	2.68(3)	15.3(2)	12(2)	−3.3
		$J = 2$	4.64(1)	26.7(1)	30(3)	3.3
Yb	0.858	$J = 1$	2.70(8)	15.4(5)	14(1)	−1.4
		$J = 2$	4.7(1)	26.8(6)	35(3)	8.2
Lu	0.848	$J = 1$	2.82(7)	16.1(4)	17(1)	0.9
		$J = 2$	4.79(8)	27.3(5)	37(3)	9.7

$\Delta G^\circ_{\beta j}$, $\Delta H^\circ_{\beta j}$ and $T\Delta S^\circ_{\beta j}$ in kJ mol^{-1}. Estimated three S.D. in parentheses.
[a] Ref. [31]

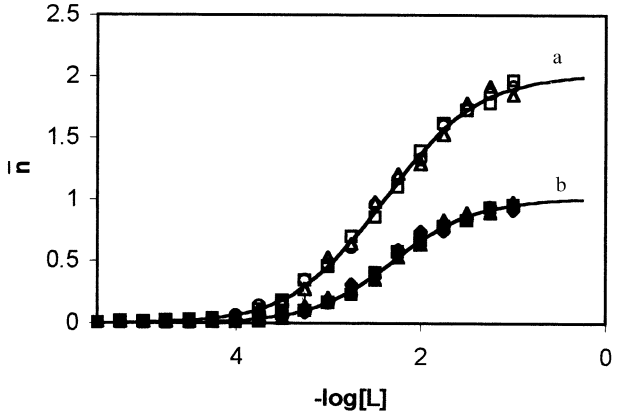


Fig. 1. Complex formation functions for (a) Lu(III) and (b) Ho(III)–**L5** systems. Concentrations in mmol dm^{-3}. (a) (○) C°_{Lu} 9.05, C°_{Ag} 1.77; (△) C°_{Lu} 17.8 C°_{Ag} 4.78; (□) C°_{Lu} 26.6, C°_{Ag} 1.77; (b) (▲) C°_{Ho} 10.0, C°_{Ag} 4.23; (◆) C°_{Ho} 18.6, C°_{Ag} 4.23, (■) C°_{Ho} 32.7, C°_{Ag} 7.91. Only some experimental points chosen at random are plotted. Full curves are calculated from the stability constants in Table 1.

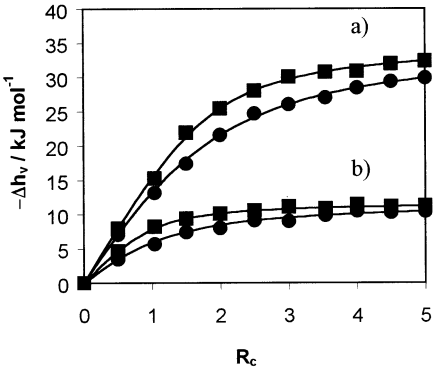


Fig. 2. Total molar enthalpy changes, Δh_v, as a function of $R_c = C_L/C_M$ for (a) Lu(III)- and (b) Ho(III)–**L5** systems. Total Ln(III) concentrations in mmol dm^{-3}: (a) (●) 9.96, (■) 30.10; (b) (●)11.6, (■) 32.7. Only some experimental points chosen at random are plotted. Full curves calculated from stability constants and enthalpy changes in Table 1.

$\bar{n}'$ and [**L**] were obtained from the measured free silver(I) concentration calculated from e.m.f. data and the stability constants of the silver(I) complexes with **L5** previously obtained [30].

The complex–formation curves in Fig. 1, almost superimposing, show that neither polynuclear nor mixed complexes form in appreciable amounts in the adopted conditions [23].

The total reaction heats per mole of metal ion, Δh_v, are reported as a function of $R_c = C_L/C_M$ in Fig. 2 for Ho and Lu, respectively. The experimental reaction heats and overall stability constants of Table 1 were used to calculate the full lines in Fig. 2. The fit of the experimental data is quite good, indicating that the systems are satisfactorily described. As the results for the other lanthanides are quite similar, they are not reported here. Calorimetric measurements carried out on the lanthanide(III)–**L1**–**L4** and **L6** systems gave negligible reaction heats, indicating that no appreciable interactions exist between Ln(III) ions and these ligands in DMSO. This evidence is further supported by the ^{1}H NMR measurements on DMSO solutions of ligands alone and on solutions also containing Lu(III): the shapes and chemical shifts of the signals observed in the latter solutions did coincide with those observed in the solutions containing the ligands alone.

Fig. 3 shows that a difference exists between the ^{1}H NMR spectrum of **L5** and that of its [Lu**L5**]$^{3+}$ complex in DMSO-d_6. From the values of the stability constants and from the used Lu(III) concentration, one can calculate that at $R_c = 0.3$ the percentual of 1:1 Lu(III)–**L5** complex formed was about 90%.

4. Discussion

The experimental data (see above) clearly show **L1**–**L4** and **L6** cannot interact with Ln(III) ions in DMSO.

The following considerations are applied to explain, ligand by ligand, their inability to interact with Ln(III) ions: (i) it has previously been shown that the chelate ring size of non-macrocyclic ligands plays an important role in controlling the affinity and selectivity for metal

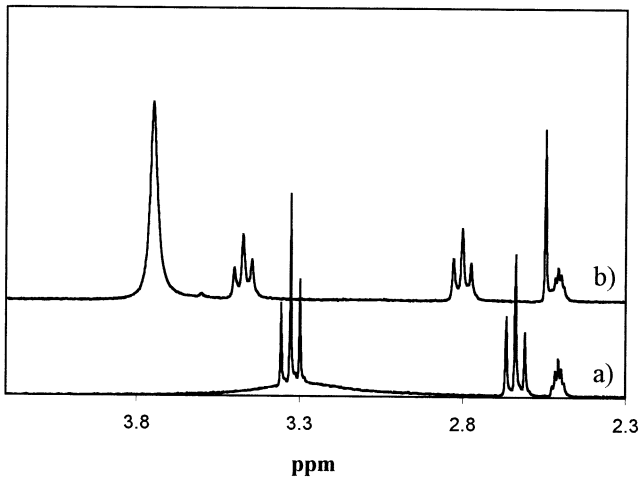


Fig. 3. NMR spectra at 298 K of: (a) **L5** = 11.0 mmol dm^{-3}; (b) $C^{\circ}_{Lu} = 33.2$, **L5** = 11.0 mmol dm^{-3} in DMSO-d_6.

ions [22], and in particular that increasing the number of the $-CH_2-$ groups separating the N atoms decreases the stability of block f lanthanide(III) complexes with polyaminocarboxylates in water [31] and of uranyl(VI) complexes with polyamines in DMSO [32], the stability of these complexes being maximized when five-membered chelate rings are formed. Evidently the eight-membered chelate ring that **L6** should have formed in the hypothesis of chelate complex formation is greatly hindered and so no Ln(III)–complex(es) is(are) form. The lack of interaction not only of L6 but also of **L1**–**L4** with Ln(III) ions is also in line with the observed inability of monoamines to coordinate block f ions in DMSO [15f, 32]; (ii) the absence of interactions between metal ions and **L3** or **L4**, oxygen donors having the same molecular framework as dien or **L5**, shows that purely O-donors do not exhibit any affinity for Ln(III) in DMSO. Many factors must be considered when attempting to explain ligand affinity for metal ions, i.e. donor strength of donor atoms, strain effects in the formation of chelate rings, steric and inductive effects of substituents, and the role of donor group orientation [22,33]. Strain energy effects in five-membered chelate rings, whether they contain oxygen or nitrogen donors, are similar [33a] and the role of donor group orientation may not be important in interactions with f-block lanthanide ions. The important difference between O- and N-donor ligands is that neutral oxygen donors are not better bases than DMSO, as the relative basicity of saturated neutral oxygen donors, measured in the gas phase, decreases in the order DMSO > ROH > ROR [34a,34b], this trend being retained, for example, in aqueous solution [34c]. For most metal ions, nitrogen donors are generally better donors than DMSO [16,17,34,35]. Since the ligand donor atoms must compete with DMSO for coordination sites on metal ions, the poorer basicity of alcohols and ethers with respect to the solvent is probably responsible for the results obtained here, despite the potential chelate effect which the ligand should cause; (iii) the fact that potential chelate ligands such as **L1** and **L2**, containing both nitrogen and oxygen atoms, cannot interact with Ln(III) ions shows that the cooperativity of one N and one O atom is not efficient enough to create a chelate in DMSO [16,17,34]. Otherwise, when **L5** is concerned, the coordination of Ln(III) ions is possible and one or two complexes are formed. Certainly, on the basis of the above discussed inability of **L6** to complex lanthanide(III), in this case the –O– group must be active part in the complex formation.

The ^{1}H NMR spectra of **L5** (A_2X_2 system) and of its lutetium complex (AA′XX′ system) reported in Fig. 3 show a $\Delta\delta$ ($\Delta\delta = \delta_{complex} - \delta_{ligand}$) of about 0.2 ppm for both $-CH_2-$ protons near the O atom (from 3.32 in the free ligand to 3.48 in the complex) and $-CH_2-$ protons near the amino function (from 2.63 to 2.80): despite the downfield shift is low, this shift should be considered as a possible diagnostic tool of the interaction of –NH– and –O– donor groups with the central metal ion.

One interesting piece of evidence which emerges from this study is that complex formation depends on a synergic effect between donor groups in the ligand: at least two $-CH_2CH_2NH_2$ side-arms added to an ether function are needed to make the ligand capable of forming two five-membered chelate rings, giving rise to effective interaction between O atom and Ln(III) ions.

The complex formation of Ln(III) ions with **L5** is always accompanied by negative enthalpy changes, which are typical of aprotic solvent reactions involving complexation by neutral ligands [13,15,18,21,26,36]. This behavior has already been observed in other Ln(III)–amine systems in DMSO [15] and has been interpreted as the formation of complexes in which interactions of metal ions with donor atoms are quite strong and fully capable of compensating the energy required to set off from the co-ordination sphere of the metal ion one or more solvent molecules. As lanthanides are strongly solvated in DMSO [15a], this implies that inner-sphere complexes are formed.

The entropy terms are generally negative or, when positive, only slightly favorable. This is in accord with the formation of complexes generally involving large conformational entropy losses not, or only slightly, compensated by gains due to desolvation of reacting species. That is, when neutral ligands are considered, complex formation does not cause substantial modifications in the metal-charge ordering effect of the bulk solvent, and thus no large positive entropy changes take place [36].

The data in Table 1 and Fig. 4 show that the stability constants of 1:1 Ln(III)–**L5** complexes increase almost regularly with the increasing charge density of the metal ions, indicating that the ion–dipole character of the

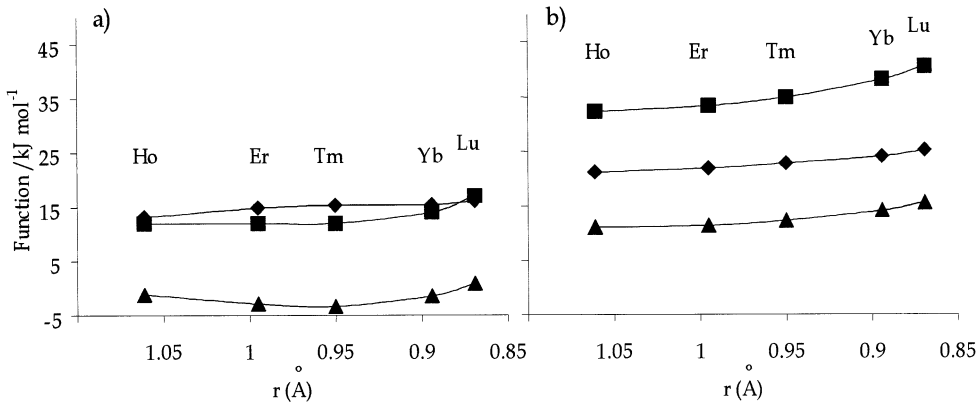


Fig. 4. Thermodynamic functions for 1:1 complex formation of (a) Ln(III)–**L5** and (b) Ln(III)–dien [15c] systems at 298 K and $I = 0.1$ mol dm^{-3}. (◆) $-\Delta G^{\circ}_{\beta 1}$; (■) $-\Delta H^{\circ}_{\beta 1}$; (▲) $-T\Delta S^{\circ}_{\beta 1}$.

interaction is an important feature of these complexes. Similar behavior was observed (Fig. 4) for the formation of Ln(III)–dien complexes in DMSO 15b. The stabilities of the complexes of **L5** are lower than those of dien. This is reasonably due to two main factors: the intrinsic higher basicity of the central –NH– group in dien with respect to that of –O– group in **L5** [16,17,34]; the lower solvation energies of the complexes formed by **L5** [33,37], due to the presence of an ether function which cannot give rise to hydrogen bonds with the solvent, like the –NH– group in dien. The magnitude of enthalpy gains for the formation of the lanthanide(III)–**L5** complexes are much lower than those found for homologous dien complexes. Certainly, the decreased strength of the Ln(III)–O interaction with respect to that of Ln(III)–NH is reflected in this result, but other effects should also be considered to explain this enthalpy trend and, even more, to provide deeper insight into the entropy values. As mentioned above, the entropy term for 1:1 complex formation contributes in a slightly favorable way to complex formation (apart from the Lu(III)–**L5** system), whereas the contribution of entropy always opposes it in Ln(III) dien systems (Fig. 4).

Solvation of **L5** is certainly less considerable than that of dien, because of the lesser hydrogen bonding with the solvent: this effect alone would increase the net enthalpy gain and decrease the entropy term for Ln(III)–**L5** systems with respect to dien ones and therefore it does not explain the trend in the data reported here. As both **L5** and dien are probably responsible for the removal of the same number of solvent molecules from the first solvation sphere of the metal ion, these results may be explained by taking into account the effect that –NH– substitution with the –O– group has on the outer-sphere solvation energy of the resulting complexes.

In particular, it is to be considered that the minor extent of hydrogen bonding of **L5** should also cause less outer-sphere solvation energy of the metal complex [37], reflected in a lower enthalpy gain and a less unfavorable entropy term.

From the thermodynamic data and for the reasons discussed above (point (i) at the beginning of discussion), it may be presumed that **L5** acts as a tridentate also in ML_2 complexes. The higher exothermic enthalpy value of the second complexation step, ΔH°K2, compared with ΔH°K1 is probably due to a particular kind of desolvation occurring in the first complexation step: the enthalpy required for desolvating causes ΔH°K1 to be less exothermic than ΔH°K2, in spite of the greater exothermicity associated with the Ln(III) interaction in the first step.

Acknowledgements

This work was supported by the Ministero dell'Università e della Ricerca Scientifica e Tecnologica (MURST, Rome) within the COFIN 2000 program. We thank Mr. Pierluigi Polese for technical assistance.

References

[1] (a) G.R. Choppin, J. Less-Common Met. 112 (1985) 193;
(b) G.R. Choppin, Lanthanide Probes in Life, Chemical and Earth Sciences (Chapter 1), Elsevier, Amsterdam, 1989;
(c) J.C.G. Bunzli, in: G.R. Choppin, J.C.G. Bunzli (Eds.), Lanthanide Probes in Life, Chemical and Earth Sciences (Chapter 7), Elsevier, Amsterdam, 1989;
(d) G.X. Xu, Pure Appl. Chem. (1988) 8;
(e) E.N. Rizkalla, G.R. Choppin, in: K.A. Gschneider, L. Eyring (Eds.), Handbook on the Physics and Chemistry of Rare Earths, vol. 15, North-Holland, Amsterdam, 1991, pp. 393–441;
(f) S.I. Ishiguro, K. Kato, R. Takahashi, S. Nakasone, Rare Earths 27 (1995) 61 (and references therein);
(g) J.C.G. Bünzli, A. Milicic-Tang, Handbook of the Physics and Chemistry of Rare Earths, vol. 21, Elsevier, Amsterdam, 1995;
(h) C. Piguet, J.C. Bunzli, Chem. Soc. Rev. 28 (1999) 347 (and references therein).
[2] (a) N. Sabbatini, M. Guardigli, J.-M. Lehn, Coord. Chem. Rev. 123 (1993) 201;
(b) G. Choppin, D.R. Peterman, Coord. Chem. Rev. 174 (1998) 283;

(c) G.F. de Sa, O.L. Malta, C. de Mello Donega, A.M. Simas, R.L. Longo, P.A. Santa-Cruz, E.F. da Silva, Jr., Coord. Chem. Rev. 196 (2000) 165;
(d) B. Mastsuhico, M. Campos-Vallette, J. Canales, M. Villagraz, J. Vargas, M.J. Aguirre, Coord. Chem. Rev. 196 (2000) 125.
[3] K. Kumar, A. Alien Chang, M.F. Tweedle, Inorg. Chem. 32 (1993) 587.
[4] (a) J.A. Peters, J. Huskens, D.J. Raber, Prog. NMR Spectrosc. 28 (1996) 283;
(b) U. Casellato, S. Tamburini, P. Tomasin, P.A. Vigato, S. Aime, M. Botta, Inorg. Chem. 38 (1999) 2906.
[5] (a) S. Aime, M. Botta, M. Fasano, E. Terreno, Chem. Soc. Rev. 27 (1998) 19 (and references therein);
(b) S.M. Cohen, J. Xu, E. Radka, K.N. Raymond, M. Botta, A. Barge, S. Aime, Inorg. Chem. 39 (2000) 5747.
[6] K. Mashima, A. Nakamura, J. Chem. Soc., Dalton. Trans. (1999) 3899.
[7] (a) D.M. Epstein, L.L. Chappel, H. Khaiili, R.M. Supkowski, W. DeW. Horrocks, J.L. Morrow, Inorg. Chem. 39 (10) (2000) 2130;
(b) R. Kramer, Coord. Chem. Rev. 182 (1999) 243;
(c) V. wing-Wah Yam, K. Kam-Wmg Lo, Coord. Chem. Rev. 184 (1999) 157;
(d) J.R. Morrow, Inorg. Chem. 16 (1998) 3989;
(e) E.R. Hegg, J.N. Burstyn, Coord. Chem. Rev. 173 (1998) 133.
[8] R.M. Smith, A.E. Martell, Sci. Total Environ. 64 (1987) 125.
[9] A.E. Martell, R.M. Smith, R.J. Motekaitis, Critically Selected Stability Constants of Metal Complexes Database, version 6.0, 2001.
[10] P. Caravan, T. Hedlund, S. Liu, S. Sjoberg, C. Orvig, J. Am. Chem. Soc. 117 (1995) 11230 (and references therein).
[11] R.D. Hancock, G. Jackson, A. Evers, J. Chem. Soc., Dalton. Trans. (1979) 1384.
[12] J.H. Forsberg, Coord. Chem. Rev. 10 (1973) 195.
[13] F. Arnaud-Neu, Chem. Soc. Rev. (1994) 235.
[14] M.A.M. Kervey, M.J. Schwing-Weill, F. Arnaud-Neu, in: G.W. Gokel (Ed.), Comprehensive Supramolecular Chemistry, vol. 1 (and references therein), Elsevier, Oxford, 1996, p. 537.
[15] (a) A. Cassol, P. Di Bernardo, R. Portanova, M. Tolazzi, G. Tomat, P. Zanonato, J. Chem. Soc., Dalton Trans. (1992) 469;
(b) Z. Wang, G.R. Choppin, P. Di Bernardo, P.L. Zanonato, R. Portanova, M. Tolazzi, J. Chem. Soc., Dalton Trans. (1993) 2791;
(c) A. Cassol, G.R. Choppin, P. Di Bernardo, R. Portanova, M. Tolazzi, G. Tomat, P. Zanonato, J. Chem. Soc., Dalton Trans. (1993) 1695 (and references therein);
(d) P. Di Bernardo, G.R. Choppin, R. Portanova, P.L. Zanonato, Inorg. Chim. Acta 207 (1993) 85;
(e) A. Cassol, P. Di Bernardo, R. Portanova, M. Tolazzi, P.L. Zanonato, Inorg. Chim. Acta 262 (1997) 1–32;
(f) C. Comuzzi, P. Di Bernardo, P. Polese, R. Portanova, M. Tolazzi, P.L. Zanonato, Polyhedron 19 (2000) 2427.
[16] V. Guttmann, Coordination Chemistry in Non-Aqueous Solution, Springer, Vienna, 1968.
[17] V. Guttmann, The Donor Acceptor Approach to Molecular Interactions, Plenum Press, New York, 1978.
[18] I. Marolleau, J.-P. Gisselbrecht, M. Gross, F. Arnaud-Neu, M.J. Schwing-Weil, J. Chem. Soc., Dalton Trans. (1989) 367.
[19] R. Pizer, R. Selzer, Inorg. Chem. 22 (1983) 1359.
[20] A. Cassol, P. Di Bernardo, G. Pilloni, M. Tolazzi, P.L. Zanonato, J. Chem. Soc., Dalton Trans. (1995) 2689.
[21] Y. Liu, T.B. Lu, M.Y. Tan, T. Hakushi, Y. Inoue, J. Phys. Chem. 97 (1993) 4548.
[22] A.E. Martell, R.D. Hancock, in: J.P. Fackler, Jr. (Ed.), Metal Complexes in Aqueous Solutions, Plenum Press, New York, 1996.
[23] F.J.C. Rossotti, H. Rossotti, The Determination of Stability Constants, McGraw-Hill, New York, 1961.
[24] (a) W.L. Reynolds, Prog. Inorg. Chem. 12 (1970) 1;
(b) D. Martin, H.G. Hauthal, Dimethyl Sulfoxide, van Nostrand Reinhold, Wokingham, Berkshire, 1975, pp. 448–449.
[25] A.I. Vogel, Textbook of Quantitative Chemical Analysis, 5th ed., Longman, London, 1989.
[26] (a) A. Cassol, P. Di Bernardo, P. Zanonato, R. Portanova, M. Tolazzi, J. Chem. Soc., Dalton Trans. (1987) 657;
(b) A. Cassol, P. Di Bernardo, P. Zanonato, R. Portanova, M. Tolazzi, G. Tomat, V. Cucinotta, D. Sciotto, J. Chem. Soc., Faraday Trans 1 85 (1989) 2445;
(c) A. Cassol, P. Di Bernardo, P. Zanonato, R. Portanova, M. Tolazzi, G. Tomat, J. Chem. Soc., Faraday Trans. 86 (1990) 2841.
[27] D.D. Perrin, W.L.F. Amarego, D.R. Perrin, Purification of Laboratory Chemicals, 2nd ed., Pergamon Press, Oxford, 1980.
[28] P. Cans, A. Sabatini, A. Vacca, Talanta 43 (1996) 1739.
[29] R. Arnek, Ark. Kemi 32 (1970) 81.
[30] Log β values for $AgL = 6.25(0.03)$; $AgL_2 = 7.76(0.09)$; $Ag_2L = 7.70(0.10)$. The errors in parentheses are three times the standard deviation.
[31] F.A. Cotton, G. Wilkinson, Advanced Inorganic Chemistry, 4th ed., Wiley, New York, 1980, p. 1011.
[32] E.N. Rizkalla, C. Niu, G.R. Choppin, Inorg. Chim. Acta 146 (1988) 135.
[33] (a) R.D. Hancock, A.E. Martell, Chem. Rev. 89 (1989) 1875;
(b) B.P. Hay, R.D. Hancock, Coord. Chem. Rev. 212 (2001) 61.
[34] (a) A.E. Marteil, M. Calvin, Chemistry of the Metal Chelate Compounds, Prentice-Hall, New York, 1952;
(b) A. Bagno, G. Lovato, G. Scorrano, J. Chem. Soc., Perkin Trans. 2 (1993) 1091;
(c) A. Bagno, G. Scorrano, J. Chem. Am. Soc. 110 (1988) 4577.
[35] A. Cassol, P. Di Bernardo, R. Portanova, M. Tolazzi, P.L. Zanonato, J. Chem. Soc., Dalton Trans. (1995) 733.
[36] S. Ahrland, in: J.J. Lagowski (Ed.), The Chemistry of Nonaqueous Solvents, vol. 5a (Chapter 1), Academic Press, New York, 1978.
[37] D. Meyerstain, Coord. Chem. Rev. 185–186 (1999) 141 (and references therein).

PERGAMON

Polyhedron 21 (2002) 1393–1396

POLYHEDRON

www.elsevier.com/locate/poly

Complexation of lanthanide(III) with a tripodal polyaza polycatecholate ligand

Arturo Bismondo [a], Plinio Di Bernardo [b,*], Roberto Portanova [c], Marilena Tolazzi [c], Pier Luigi Zanonato [b]

[a] *Istituto di Chimica e Tecnologie dei Materiali Avanzati del CNR, Corso Stati Uniti 4, 35127 Padova, Italy*
[b] *Dipartimento di Chimica Inorganica Metallorganica e Analitica, Via Loredan 4, 35131 Padova, Italy*
[c] *Dipartimento di Scienze e Tecnologie Chimiche, Via del Cotonificio 108, 33110 Udine, Italy*

Received 1 October 2001; accepted 22 November 2001

Abstract

The interaction of La(III), Gd(III), and Yb(III) with Tris((2,3-dihydroxybenzylamino)ethyl)amine) (TRENCAT) was investigated by means of potentiometric measurements in 0.1 mol dm^{-3} aqueous solution of sodium perchlorate at 25 °C. The formation of complexes between the partially protonated ligand and lanthanides has been observed and the values of their formation constants are reported. © 2002 Elsevier Science Ltd. All rights reserved.

Keywords: Lanthanide; Polyaza ligands; Catecholate ligands; Stability constants; Potentiometry

1. Introduction

In the last few years, many multidentate ligands of several kinds have been prepared in the quest for lanthanide(III) complexes useful in the medical field. The greatest interest focuses on the use of these complexes, gadolinium compounds in particular, as contrast agents in magnetic resonance imaging (MRI) [1].

For this purpose, the most stringent requirement for these complexes is good thermodynamic stability. Enhanced stability has generally been achieved by introducing two or more carboxyl groups in various positions into the frame of the ligand, together with other neutral donor groups.

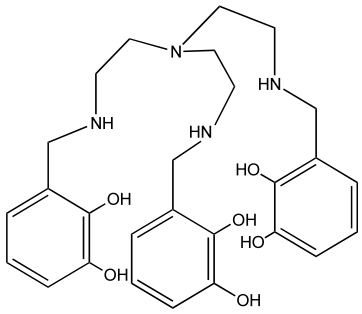
While a large number of publications regarding this kind of polycarboxyl ligands reveal growing interest, only a few studies on the interaction of lanthanides(III) with ligands bearing a phenol group as possible anion donor have been published. The main reason why this kind of ligand is less appealing than polycarboxyl ones is the low acidity of the hydroxyl group. In most cases, lanthanide ions, which are themselves weak Lewis acids in water, are not as competitive as hydrogen ions towards the phenol group, so that Ln(III) ions, unable to create stable complexes with phenol ligands, show a marked tendency to form hydroxo complexes in solution. Nevertheless, it has recently been demonstrated that the introduction of phenol groups into a well preorganised structure allows the ligand to form strong lanthanide(III) complexes [2].

In line with these findings, in our most recent publication [3] we demonstrated the very high complexing power of Tris((2,3-dihydroxybenzylamino)ethyl)amine (TRENCAT; a new ligand containing three catechol groups linked via ethylene moieties to the backbone of Tris(2-aminoethyl)amine) towards 'hard' cations like thorium(IV) and H^+ (Scheme 1).

The present study extends investigations to some trivalent lanthanide ions. To verify the effect of lanthanoid contraction, three metal ions were chosen. Two (La^{3+} and Yb^{3+}) occupy the extremes of the lanthanide series and the third (Gd^{3+}) lies in the middle. The study, carried out with the potentiometric technique in water at 25 °C with 0.1 M $NaClO_4$ as ionic medium, yielded the

* Corresponding author. Present address: Dipartimento di Chimica Inorganica Metallorganica e Analitica, Via Loredan 4, 35131 Padova, Italy. Tel.: +39-049-275213; fax: +39-049-8275161.
E-mail address: plinio.dibernardo@unipd.it (P. Di Bernardo).

0277-5387/02/$ - see front matter © 2002 Elsevier Science Ltd. All rights reserved.
PII: S0277-5387(02)00962-2



Scheme 1. Schematic drawing of TRENCAT

formation constants of all the metal species involved in the detected equilibria.

As already reported [3], TRENCAT is a potentially hexa-protic acid. However, in the experimental conditions adopted here, deprotonation of only one of the two weak acid functions of each catechol group could be studied. Accordingly, in the following discussion, neutral TRENCAT is called H_3L and the fully protonated form H_6L^{3+}. In the latter form, protons are presumed to be bound only to the secondary nitrogens of the molecule, as the tertiary one could not be protonated in our experimental conditions ($p[H+] > 2$) [2].

2. Experimental

2.1. Reagents

Stock solutions of lanthanoid perchlorates were prepared by dissolving the appropriate oxide (Aldrich $>99.9\%$ pure) in a small excess of perchloric acid. Working solutions were prepared from stock solutions by dilution. Metal ion concentration was determined by titration with EDTA using Xylenol Orange as indicator and acetate buffer [4]. The concentration of free perchloric acid in the lanthanide(III) solutions was determined by Gran's potentiometric method [5].

The stock solution of perchloric acid was prepared by dilution of concentrated perchloric acid (Aldrich 70% ACS reagent) with doubly-distilled deionised water and standardised by titration with Tris(hydroxymethyl)aminomethane (Aldrich, ultrapure grade).

Diluted sodium hydroxide solutions were prepared from a saturated NaOH solution (50% NaOH, 50% H_2O) left standing in a polyethylene bottle for several days. Standardisation of these solutions was carried out with potassium hydrogenphthalate (Aldrich, ACS acidimetric standard).

A stock solution of sodium perchlorate was prepared with recrystallised reagent grade product (Fluka, puriss. p.a. ACS). The solution titre was obtained by ion-exchange analysis on a cationic resin in the hydrogen form.

The trihydrochloride monohydrate salt of the ligand was prepared and purified as already reported [3].

2.2. Apparatus

Potentiometric measurements were carried out at 25 °C in solutions in which the total concentration of sodium ion was maintained at 0.1 mol dm^{-3} by adding a standard $NaClO_4$ solution. A 50-ml glass cell with a thermostated water jacket maintained the temperature at 25 ± 0.1 °C.

Potentiometric measurements were performed on a Metrohm (model 654) pH-meter equipped with a Metrohm 6.0204.100 combined glass electrode. The original electrode filling solution (3 mol dm^{-3} KCl) was replaced with a 100 mmol dm^{-3} NaCl solution to avoid clogging of the electrode frit glass septum by $KClO_4$. The electrode was calibrated (25 ml of $NaClO_4$ 0.1 mol dm^{-3} titrated with standard 0.1 mol dm^{-3} $HClO_4$) before each titration, in order to measure hydrogen ion concentration H^+ and liquid-junction potential E_j.

The computer-controlled potentiometric apparatus collected e.m.f. data (ΔE) at intervals determined by the data collection criterion, i.e. $\Delta E = 0.0$ mV for 2 min, a value usually reached within 3–7 min.

2.3. Procedures

The experimental method consisted of potentiometric titrations of the ligand acid in the presence of metal ion, by adding standard NaOH solution. Ligand solutions were prepared immediately prior to experiments with deoxygenated water, as ligands may slowly oxidise in aerated solutions. Six titrations with the following initial concentrations of lanthanide(III) ($C_M°$) and ligand ($C_L°$) were carried out: ($M = La^{3+}$) $C_M°/C_L° = 0.55/0.55$, 0.29/0.58; ($M = Gd^{3+}$) $C_M°/C_L° = 0.50/0.49$; 0.50/1.00; ($M = Yb^{3+}$) $C_M°/C_L° = 0.56/0.56$; 0.29/0.56 mmol dm^{-3}/mmol dm^{-3}. The low concentrations adopted in these experiments were imposed by the poor solubility of the unprotonated neutral ligand.

Stability constants for lanthanide(III)–TRENCAT complexes were obtained with the help of the SUPERQUAD computer program [6]. Only data points for which the absence of a solid phase was clearly assessed were considered in data processing. The six protonation constants of the ligand (log β_n ($1 \le n \le 6$) 11.23, 21.84, 31.59, 40.10, 47.68, 54.00), previously reported [3], were used as input data to evaluate the formation constants of the metal complexes.

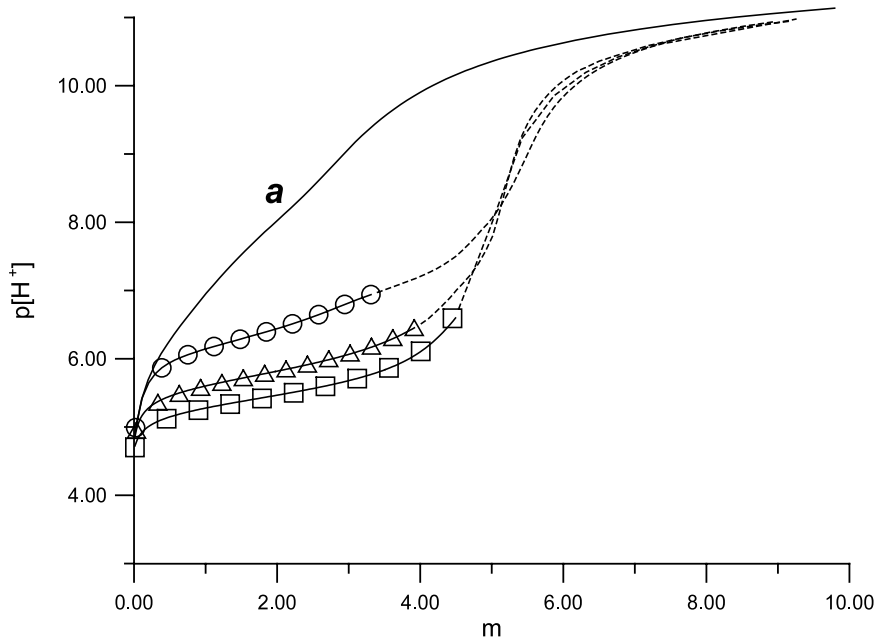


Fig. 1. Titration curves of H_6L^{3+} in absence (***a***) and presence of metal ions La^{3+} (○), Gd^{3+} (△) and Yb^{3+} (□). For all curves, Ln^{3+}–H_6L^{3+} ratio was 1/1.

3. Results and discussion

Fig. 1 compares p[H^+] versus m (m = moles of NaOH per mole of metal ion) for each Ln^{3+}–TRENCAT system studied. Open symbols (○, △, □) represent equilibrium points collected when no solid phase was present in solution. Dashed lines represent points collected when solid phase was or might be present in solution. Line ***a***, which represents p[H^+] as a function of m (m = moles of base per mole of ligand) for a solution in which only the ligand was present, was calculated with the protonation constants reported above.

Qualitatively, Fig. 1 gives the following indications: (i) TRENCAT has considerable affinity for lanthanide ions (as clearly illustrated by the difference in the shapes of the titration curves of the ligand alone and those in which Ln^{3+} is present); (ii) the stability of the complexes depends to a significant extent on the charge density of the metal ion (Yb^{3+} complexes form at the lowest pH values and La^{3+} at the highest); (iii) due to complexation reactions, more than three protons are set free per mole of ligand before a solid phase forms in solution. On the basis of these preliminary observations, many sets of possible lanthanide(III)–TRENCAT complexes were tested by the minimisation program. Table 1 lists the stability constants which best represent the experimental data. MH_2L^{2+} and MH_3L^{3+} are the main species for low p[H^+] regions (see Fig. 2). At higher p[H^+] these complexes lose protons, as depicted in Eqs. (1a) and (1b):

$$MH_3L \leftrightarrows MH_2L + H \quad \log K_M = -7.28_{La},\ -5.91_{Gd},\ -6.51_{Yb} \tag{1a}$$

$$MH_2L \leftrightarrows MHL + H \quad \log K_M = -6.97_{La},\ -6.66_{Gd},\ -5.20_{Yb} \tag{1b}$$

giving, before precipitation, a complex (MHL) in which the neutral ligand has lost two protons. It may be a matter of debate exactly which of these protons are removed, as they may be either the more acid ones, for which pK_a values may be evaluated, or catechol ones, for three of which the deprotonation values are unknown. Naturally, the two hypotheses lead to clearly distinct structures for the resulting complexes (MH_2L and MHL). In the first case, the metal ion is 'encapsulated' in the upper cavity of the ligand. In the second case, Ln^{3+} remains outside the nitrogen–oxygen cage. Starting from the initial 'capped' configuration, it forms five-membered chelate rings in sequence, being at-

Table 1
Logarithms of overall formation constants (log $\beta_{M,H,L} \pm 3\sigma$) at 25 °C and $I = 0.1$ mol dm^{-3} (Na)ClO_4

Reaction (charges omitted for clarity)	M = La^{3+}	M = Gd^{3+}	M = Yb^{3+}
M + H + L ⇆ MHL	24.28 ± 0.12	27.51 ± 0.09	29.08 ± 0.12
M + 2H + L ⇆ MH_2L	31.25 ± 0.21	34.17 ± 0.06	35.59 ± 0.12
M + 3H + L ⇆ MH_3L	38.53 ± 0.06	40.08 ± 0.06	40.79 ± 0.09
M + 6H + 2L ⇆ MH_6L_2	76.41 ± 0.12	79.10 ± 0.12	80.64 ± 0.18
M + H_3L ⇆ M(H_3L)	6.94	8.49	9.20
M(H_3L) + H_3L ⇆ M(H_3L)$_2$	6.29	7.43	8.26
M + TRNS ⇆ M(TRNS)	5.65	6.67	8.53
M(TRNS) + TRNS ⇆ M(TRNS)$_2$	6.34	7.69	9.73

Data for TRNS ($\mu = 0.16$, 25 °C) taken from Ref. [2].

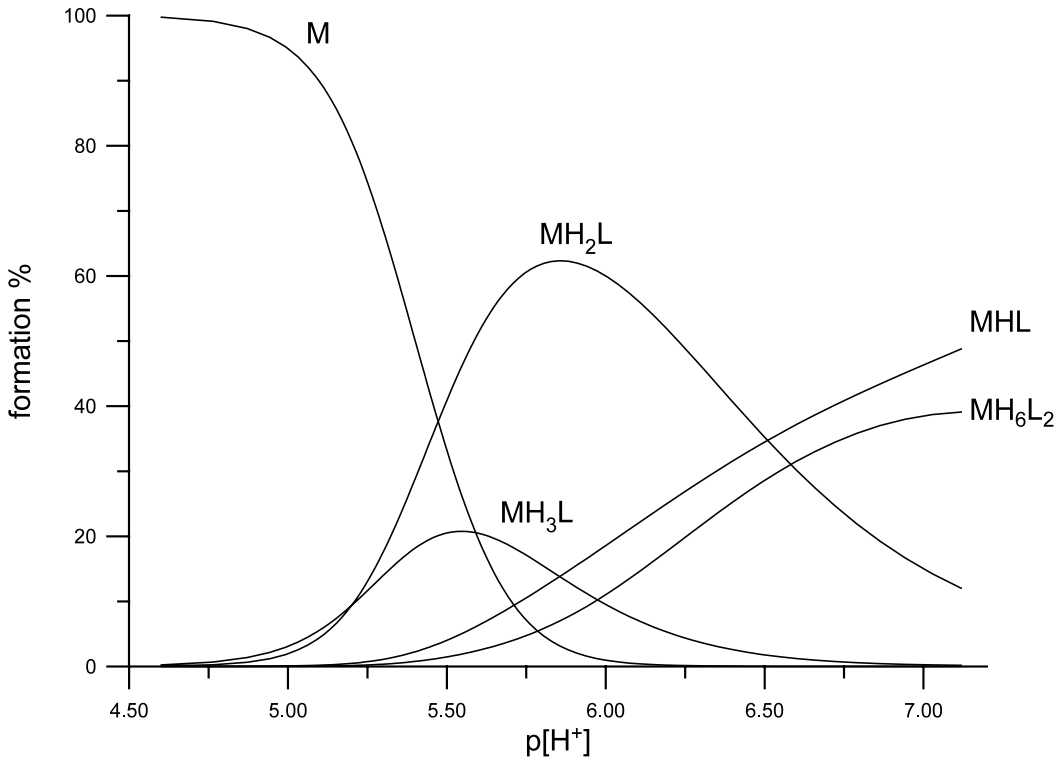


Fig. 2. Speciation diagram calculated for a 1/2 = Yb^{3+}–TRENCAT system. [Yb^{3+}] = 0.5 mmol dm^{-3}.

tracted, step by step as the p[H^+] increases, into the lower cavity formed by the three catechol units.

From the electrostatic point of view, the 'encapsulated' configuration does not appear to be probable. This is because the stability of 'hard' cation complexes depends mainly upon the difference in electrical charge density of the interacting species (either ions or neutral atoms): i.e. the larger the difference, the stronger the interaction. Thus, in the 'encapsulated' configuration, Ln^{3+} would interact with neutral nitrogen and, in the more reliable 'capped' version, with negatively charged oxygens.

Table 1 compares the stability constants of the lanthanide(III) complexes formed by triprotonated TRENCAT and TRNS [tris((2-hydroxy-5-sulfobenzylamino)ethyl) amine [2], a parent compound of TRENCAT containing sulfophenol instead of catechol units.

The stability of the 'capped' complexes formed by TRENCAT, higher ($\Delta \log \beta = 0.67$ for Yb^{3+}) or much higher ($\Delta \log \beta = 1.29$ and 1.82 for La^{3+} and Gd^{3+}, respectively) than that of TRNS complexes, reflects the stabilising effect of the phenol in *ortho* which probably forms chelate complexes, favouring co-ordination of lanthanides to TRENCAT. In addition, formation of stronger 1:1 complexes: (i) removes the anomalous behaviour in the formation constants observed for TRNS complexation ($K_2 > K_1$): in this case, K_1 is always higher than K_2; (ii) allows much easier deprotonation of two of the three highly basic catechol hydrogens of the molecule. Reactions 1a and 1b show that complete deprotonation of catechol takes place at nearly physiological pH levels. This is an important result when we consider these ligands as potential candidates for the formation of very stable lanthanide complexes, for use as contrast agents in magnetic resonance imaging.

Acknowledgements

This work was supported by the Italian Ministero dell'Università e della Ricerca Scientifica e Tecnologica (MURST, Rome) within the COFIN 2000 program and by the Consiglio Nazionale delle Ricerche (CNR, Rome).

References

[1] G.R. Choppin, K.M. Schaab, Inorg. Chim. Acta 252 (1996) 299.
[2] P. Caravan, T. Hedlund, S. Liu, S. Sjoberg, C. Orvig, J. Am. Chem. Soc. 117 (1995) 11230.
[3] (a) A. Bismondo, A. Cassol, P. Di Bernardo, P.L. Zanonato, in: S. Daolio, E. Tondello, P.A. Vigato (Eds.), Syntheses and Methodologies in Inorganic Chemistry, vol. 7, 1997, p. 396;
(b) A. Bismondo, C. Comuzzi, P. Di Bernardo, P.L. Zanonato, Inorg. Chim. Acta 286 (1999) 103.
[4] S.L. Lyle, M.M. Rahman, Talanta 10 (1963) 1177.
[5] G. Gran, Analyst 77 (1952) 661.
[6] P. Gans, A. Sabatini, A. Vacca, J. Chem. Soc., Dalton Trans. (1985) 1995.

PERGAMON

Polyhedron 21 (2002) 1397–1404

POLYHEDRON

www.elsevier.com/locate/poly

Open-chain polyazaalkanes functionalised with pyrene groups as sensing fluorogenic receptors for metal ions

Felix Sancenón, Ana Bélen Descalzo, José Manuel Lloris, Ramón Martínez-Máñez *, Teresa Pardo, María Jesús Seguí, Juan Soto

Departamento de Química, Universidad Politécnica de Valencia, Camino de Vera s/n, 46071 Valencia, Spain

Received 8 October 2001; accepted 12 November 2001

Abstract

The new open-chain polyazaalkanes ligands L^1, L^2, L^3 and L^4 functionalised with one or two pyrene groups were synthesised and characterised and their potential use as selective cation and anion sensing chemosensors studied. Solution studies by potentiometric methods were carried out in the presence of the metal cations Cu^{2+} and Zn^{2+} in acetonitrile–water (70:30 v/v, 0.1 mol dm^{-3} tetrabutylammonium perchlorate, 25 °C) The results are compared with those reported for the analogous non-functionalised ligand triethylentetraamine (*tta*). The fluorescence behaviour of the ligands L^1–L^4 has been studied as a function of the pH in the presence of the metal cations Ni^{2+}, Cu^{2+}, Zn^{2+}, Cd^{2+}, Hg^{2+} and Pb^{2+} in acetonitrile–water 70:30 v/v mixtures. The Zn^{2+} and Cd^{2+} cations enhance the fluorescence emission of the L^1–L^4 chemosensors at basic pH, whereas Cu^{2+} induce quenching of the fluorescence emission at acid pH. The fluorescence behaviour of L^1–L^4 receptors was also studied as a function of the pH in acetonitrile–water 70:30 v/v in the presence of anions. © 2002 Elsevier Science Ltd. All rights reserved.

Keywords: Polyazaalkanes ligand; Fluorogenic receptors; Chemosensors

1. Introduction

The development of chemosensors is an area of current interest [1–3]. This usually involves the design and synthesis of molecules containing binding sites and signalling subunits able to display selective changes in observable features such as colour [4–6], fluorescence emission intensity [7–10], electrochemical shifts [11–13], etc upon guest binding. Chemosensors showing fluorescence emission changes are of interest due to the usually low detection limits that can be reached using fluorimetric techniques. Among different coordinating environments polyamines have been used as binding sites for both cations and anionic species. Polyamines are known to form stable complexes with metal cations and are good receptors for anions. The functionalisation of polyamines with fluorescent groups such as anthracene has resulted in systems that act as chemosensors for transition metal ions and anions [14–16]. In fact, anthracene is one of the fluorescent groups most widely used in the development of fluorescent chemosensors. In contrast, other aromatic hydrocarbons have been less studied as fluorescent signalling subunits. We report here the synthesis and characterisation of new open-chain polyazaalkanes functionalised with pyrene groups, and have studied the fluorescence behaviour of these receptors in the presence of metal cations and anions in acetonitrile–water 70:30 v/v (0.1 mol dm^{-3} tetrabutylammonium perchlorate, 25 °C) in order to find pH ranges of selective response.

2. Experimental

2.1. Physical measurements

The fluorescence behaviour was studied with a FS900CDT Steady State T-Geometry Fluorimeter, Edinburgh Analytical Instruments. All solution for photophysical studies were previously degassed. The concentration of ligands and metal ion were approxi-

* Corresponding author. Tel.: +34-96-387-7340; fax: +34-96-387-9349.

E-mail address: rmaez@qim.upv.es (R. Martínez-Máñez).

0277-5387/02/$ - see front matter © 2002 Elsevier Science Ltd. All rights reserved.
PII: S0277-5387(02)00963-4

mately 1.0×10^{-4} mol dm^{-3} in acetonitrile–water (the metal ions were perchlorate or nitrate salts of Ni^{2+}, Cu^{2+}, Zn^{2+}, Cd^{2+}, Hg^{2+} and Pb^{2+}). In all photophysical studies the data were collected at fixed values of $\lambda_{ex} = 340$ nm and $\lambda_{em} = 395$ nm. The ^{1}H NMR spectra were recorded with Varian Gemini spectrometer. Chemical shifts were reported in parts per million downfield from TMS. Spectra taken in $CDCl_3$ were referenced to residual $CHCl_3$.

Potentiometric titrations were carried out in acetonitrile–water (70:30 v/v, 0.1 mol dm^{-3} tetrabutylammonium perchlorate, 25 °C) for L^1, L^2, L^3 and L^4 using a reaction vessel water-thermostatted at 25.0 ± 0.1 °C under nitrogen. The titrant was added by a Crison microburete 2031. The potentiometric measurements were made using a Crison 2002 pH-meter and a combined glass electrode. A PC computer automatically controlled the titration system. The electrode was calibrated as a hydrogen concentration prove by titration of well-known amounts of HCl with CO_2-free KOH solution and determining the equivalent point by the Gran's method [17] which gives the standard potential E'° and the ionic product of water ($K'_w = [H^+][OH^-]$). The computer program SUPERQUAD [18] was used to calculate the protonation and stability constants. The titration curves for each system (ca. 250 experimental points corresponding to at least three titration curves, pH −log[H] range investigated 2.5–10.5, concentration of the ligand and cations was ca. 1.1×10^{-3} mol dm^{-3}) were treated either as a single set or as separated entities without significant variations in the values of the stability constants.

2.1.1. Synthesis of receptors L^1–L^4

1-Pyrenecarboxaldehyde, the correspondent open-chain polyamine and 20 g of molecular sieve (3 Å) were heated to reflux in dry dichlorometane (100 ml) for 2 h. The solution was filtered off, evaporated to dryness, dissolved in dry ethanol (100 ml) and the imine obtained as an orange oil reduced with $NaBH_4$ at reflux under argon for 2 h and then 16 h at room temperature (r.t.). The resulting solution was evaporated to dryness, dissolved in dichloromethane and washed with NaOH 1 M (3 × 25 ml). HCl 35% was added dropwise to the dichloromethane phase until total precipitation of the final product in its chlorohydrate form. The yellow–orange solid was filtered off, washed with dichloromethane and dried in vacuum.

2.1.2. Synthesis of 1-(1-methylpyrenyl)-1,4,7,10-tetraazadecane (L^1)

1-Pyrenecarboxaldehyde (500 mg, 2.17 mmol), triethylentetraamine (*tta*; 2020 mg, 10.85 mmol) and reduction of the imine with $NaBH_4$ (125 mg, 3.26 mmol) give, after HCl treatment, 1-(1-methylpyrenyl)-1,4,7,10-tetraazadecane in its tetraprotonated form (935 mg, 85%). NMR ($CDCl_3$): ^{1}H δ 2.50–2.85 (m, 12H), 4.44 (s, 2H), 7.93 (m, 3H), 8.12 (m, 4H), 8.34 (d, 2H). ^{13}C δ 46.83 (CH_2), 48.70 (CH_2), 49,15 (CH_2), 49.17 (CH_2), 49.25 (CH_2), 49.52 (CH_2), 51.70 (CH_2), 123.16 ($C_{16}H_9$), 124.60 ($C_{16}H_9$), 124.91 ($C_{16}H_9$), 124.97 ($C_{16}H_9$), 125.01 ($C_{16}H_9$), 125.81 ($C_{16}H_9$), 126.89 ($C_{16}H_9$), 127.39 ($C_{16}H_9$), 127.51 ($C_{16}H_9$), 128.96 ($C_{16}H_9$), 130.57 ($C_{16}H_9$), 130.76 ($C_{16}H_9$), 131.24 ($C_{16}H_9$), 133.88 ($C_{16}H_9$). HRMS. Calc. for $C_{23}H_{32}N_4Cl_4$ 506.6422, obs. 506.4434.

2.1.3. Synthesis of 1,10-bis(1-methylpyrenyl)-1,4,7,10-tetraazadecane (L^2)

1-Pyrenecarboxaldehyde (1000 mg, 4.34 mmol), *tta* (405 mg, 2.17 mmol) and reduction of the imine with $NaBH_4$ (410 mg, 10.85 mmol) give, after HCl treatment, 1,10-bis(1-methylpyrenyl)-1,4,7,10-tetraazadecane in its tetraprotonated form (1250 mg, 80%). NMR ($CDCl_3$): ^{1}H δ 2.57 (s, 4H), 2.68 (t, 4H), 2.80 (t, 4H), 4.37 (s, 4H), 7.93 (m, 6H), 8.10 (m, 8H), 8.28 (d, 4H). ^{13}C δ 49,11 (CH_2), 49.18 (CH_2), 51.65 (CH_2), 123.16 ($C_{16}H_9$), 124.60 ($C_{16}H_9$), 124.92 ($C_{16}H_9$), 125.01 ($C_{16}H_9$), 125.81 ($C_{16}H_9$), 126.91 ($C_{16}H_9$),126.97 ($C_{16}H_9$), 127.39 ($C_{16}H_9$), 127.40 ($C_{16}H_9$), 127.49 ($C_{16}H_9$), 128.93 ($C_{16}H_9$), 130.55 ($C_{16}H_9$), 130.64 ($C_{16}H_9$), 130.71 ($C_{16}H_9$), 130.75 ($C_{16}H_9$), 131.21 ($C_{16}H_9$), 131.24 ($C_{16}H_9$), 132.85 ($C_{16}H_9$), 133.85 ($C_{16}H_9$). HRMS. Calc. for $C_{40}H_{42}N_4Cl_4$ 720.6135, obs. 720.5537.

2.1.4. Synthesis of 1-(1-methylpyrenyl)-1,4,7,10,13-pentaazatridecane (L^3)

1-Pyrenecarboxaldehyde (220 mg, 0.95 mmol), tetraethylenpentaamine (890 mg, 4.70 mmol) and reduction of the imine with $NaBH_4$ (60 mg, 1.43 mmol) give, after HCl treatment, 1-(1-methylpyrenyl)-1,4,7,10,13-pentaazatridecane in its pentaprotonated form (483 mg, 87%). NMR ($CDCl_3$): ^{1}H δ 2.50–2.90 (m, 16H), 4.45 (s, 2H), 7.97 (m, 3H), 8.12 (m, 4H), 8.35 (d, 2H). ^{13}C δ 46.79 (CH_2), 49.10 (CH_2), 49.16 (CH_2), 49.24 (CH_2), 49.25 (CH_2), 49.30 (CH_2), 49.49 (CH_2), 51.72 (CH_2), 123.19 ($C_{16}H_9$), 124.63 ($C_{16}H_9$), 124.90 ($C_{16}H_9$), 124.94 ($C_{16}H_9$), 125.03 ($C_{16}H_9$), 125.79 ($C_{16}H_9$), 126.92 ($C_{16}H_9$), 127.41 ($C_{16}H_9$), 127.53 ($C_{16}H_9$), 129.00 ($C_{16}H_9$), 130.58 ($C_{16}H_9$), 130.73 ($C_{16}H_9$), 131.26 ($C_{16}H_9$), 133.86 ($C_{16}H_9$), 137.95 ($C_{16}H_9$). HRMS. Calc. for $C_{25}H_{38}N_5Cl_5$ 585.8764, obs. 585.8033.

2.1.5. Synthesis of 1,13-bis(1-methylpyrenyl)-1,4,7,10,13-pentaazatridecane (L^4)

1-Pyrenecarboxaldehyde (1640 mg, 7.10 mmol), tetraethylenpentaamine (670 mg, 3.55 mmol) and reduction of the imine with $NaBH_4$ (400 mg, 10.65 mmol) to give, after HCl treatment, 1,13-bis(1-methylpyrenyl)-1,4,7,10,13-pentaazatridecane in its pentaprotonated form (2350 mg, 83%). NMR ($CDCl_3$): ^{1}H δ 2.60–2.69 (m, 12H), 2.79 (t, 4H), 4.39 (s, 4H), 7.90–8.15 (m, 14H),

8.28 (d, 4H). ^{13}C δ 49,05 (CH_2), 49.13 (CH_2), 51.60 (CH_2), 123.16 ($C_{16}H_9$), 124.58 ($C_{16}H_9$), 124.91 ($C_{16}H_9$), 125.00 ($C_{16}H_9$), 125.80 ($C_{16}H_9$), 126.92 ($C_{16}H_9$), 126.97 ($C_{16}H_9$), 127.39 ($C_{16}H_9$), 127.40 ($C_{16}H_9$), 127.48 ($C_{16}H_9$), 127.54 ($C_{16}H_9$) 128.96 ($C_{16}H_9$), 130.56 ($C_{16}H_9$), 130.76 ($C_{16}H_9$), 131.24 ($C_{16}H_9$), 133.88 ($C_{16}H_9$). HRMS. Calc. for $C_{42}H_{48}N_5Cl_5$ 800.1431, obs. 800.1846.

3. Results and discussion

Reaction of the corresponding amine and 1-pyrenecarboxaldehyde gave Schiff-base derivatives that were reacted without further purification with $NaBH_4$ to obtain the receptors L^1, L^2, L^3 and L^4 (see Scheme 1) [19]. The receptors were isolated in their chlorohydrate form. ^1H NMR spectra of the receptors show pyrenyl protons in the 7.5–8.5 range and CH_2 groups as multiplets between 2.5 and 3.0. ^{13}C NMR, elemental analysis and mass spectra of L^1–L^4 were also in agreement with the proposed formulation.

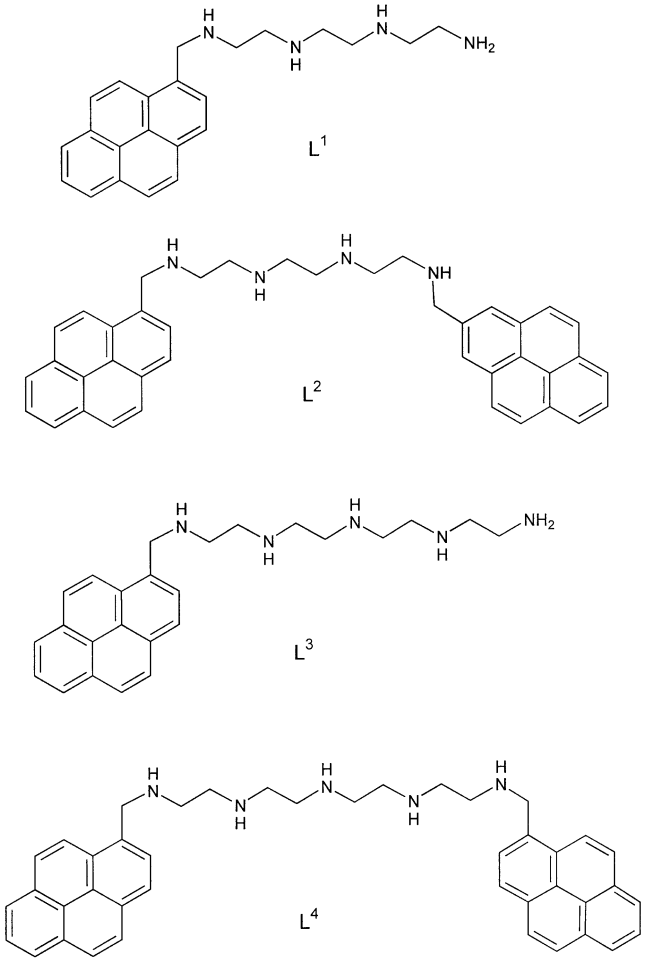
Table 1
Protonation constants (log K) of L^1 and L^2 determined in acetonitrile–water 70:30 v/v at 298.1 K in 0.1 mol dm^{-3} tetrabutylammonium perchlorate

Reaction	L^1	L^2
$L+H \leftrightarrow HL$ [a]	10.32(1) [b]	9.47(1)
$L+2H \leftrightarrow H_2L$	19.49(1)	18.10(1)
$L+3H \leftrightarrow H_3L$	26.02(1)	25.22(1)
$L+4H \leftrightarrow H_4L$	29.06(2)	30.21(2)
$L+H \leftrightarrow HL$ [a]	10.32	9.47
$HL+H \leftrightarrow H_2L$	9.17	8.63
$H_2L+H \leftrightarrow H_3L$	6.53	7.12
$H_3L+H \leftrightarrow H_4L$	3.04	4.99

[a] Charges have been omitted for clarity.
[b] Values in parentheses are standard deviations (S.D.) on the last significant figure.

4. Protonation and coordination behaviour

The protonation and coordination behaviour of the L^1 and L^2 ligands was studied by potentiometric titrations with KOH of previously acidified solutions of the corresponding system in acetonitrile–water (70:30



Scheme 1.

Table 2
Logarithms of the stability constants for the interaction of L^1 and L^2 with Cu^{2+} and Zn^{2+} in acetonitrile–water 70:30 v/v (0.1 mol dm^{-3} tetrabutylammonium perchlorate, 298.1 K)

Reaction	L^1	L^2	
	Cu^{2+}	Cu^{2+}	Zn^{2+}
$L+M^{2+}+2H^+ \leftrightarrow [M(H_2L)]^{4+}$	26.22(2) [a]	27.32(3)	23.58(3)
$L+M^{2+}+H^+ \leftrightarrow [M(HL)]^{3+}$	20.62(3)	20.98(3)	16.16(3)
$L+M^{2+} \leftrightarrow [M(L)]^{2+}$	13.50(3)	13.70(2)	6.11(2)
$L+M^{2+}+OH^- \leftrightarrow [M(L)(OH)]^+$	4.38(2)	4.17(1)	−6.40(3)
$L+M^{2+}+2OH^- \leftrightarrow [M(L)(OH)_2]$	−7.57(3)	−4.75(3)	−20.69(3)

[a] Values in parentheses are the S.D. in the last significant digit.

v/v, 0.1 mol dm^{-3} tetrabutylammonium perchlorate, 25 °C). Table 1 shows the protonation constants. Both L^1 and L^2 behave as tetra-protic bases and their basicity constants are similar to those obtained for other open-chain tetraazaalkanes [20]. Table 2 shows the complex stability constants found for L^1 with Cu^{2+} and for L^2 with Cu^{2+} and Zn^{2+}. For Cu^{2+} similar stability constants have been obtained for both L^1 and L^2 ligands. The logarithms of the stability constant for the formation of the complexes $[Cu(L^1)]^{2+}$ and $[Cu(L^2)]^{2+}$ are 13.50 and 13.70, respectively. These values are similar to those obtained for the formation of copper complexes with the analogous tetraamine 1,12-diferrocenyl-2,5,8,11-tetraazadodecane (L^5) (analo-

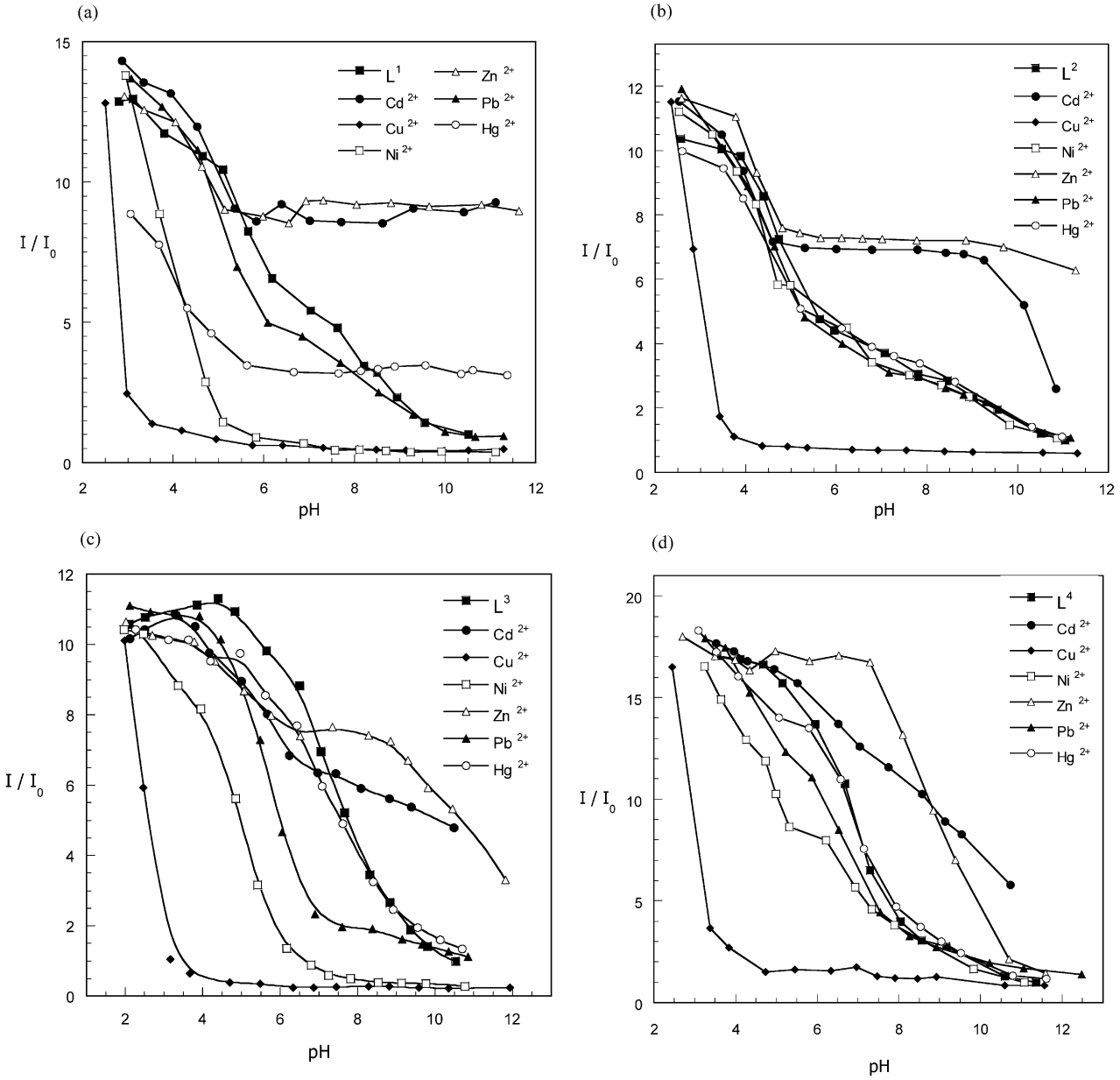


Fig. 1. Fluorescence emission intensity vs. pH for the systems (a) L^1–H^+–M^{2+}, (b) L^2–H^+–M^{2+}; (c) L^3–H^+–M^{2+} and (d) L^4–H^+–M^{2+}. M^{2+}=Ni^{2+}, Cu^{2+}, Zn^{2+}, Cd^{2+}, Hg^{2+} and Pb^{2+} (λ_{ex} = 340 nm, λ_{em} = 395 nm).

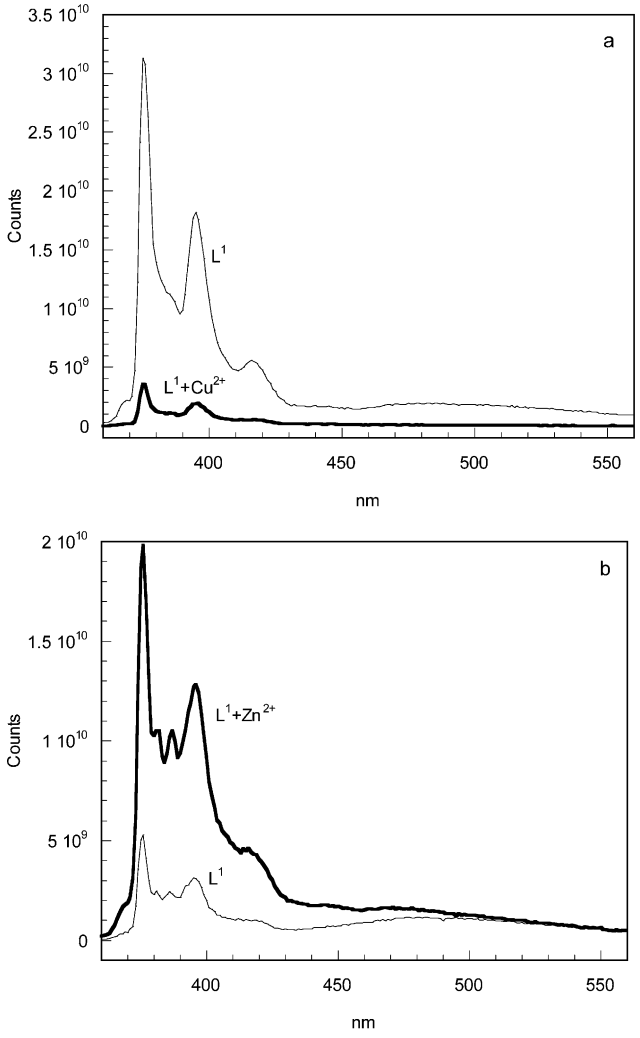


Fig. 2. Fluorescence emission spectra for (a) L^1 and L^1 in the presence of Cu^{2+} cation at pH 3.0, (b) L^1 and L^1 in the presence of Zn^{2+} cation at pH 9.0 ($\lambda_{ex} = 340$ nm, concentration of ligand and metal ions were equal and approximately 1.0×10^{-4} mol dm^{-3}).

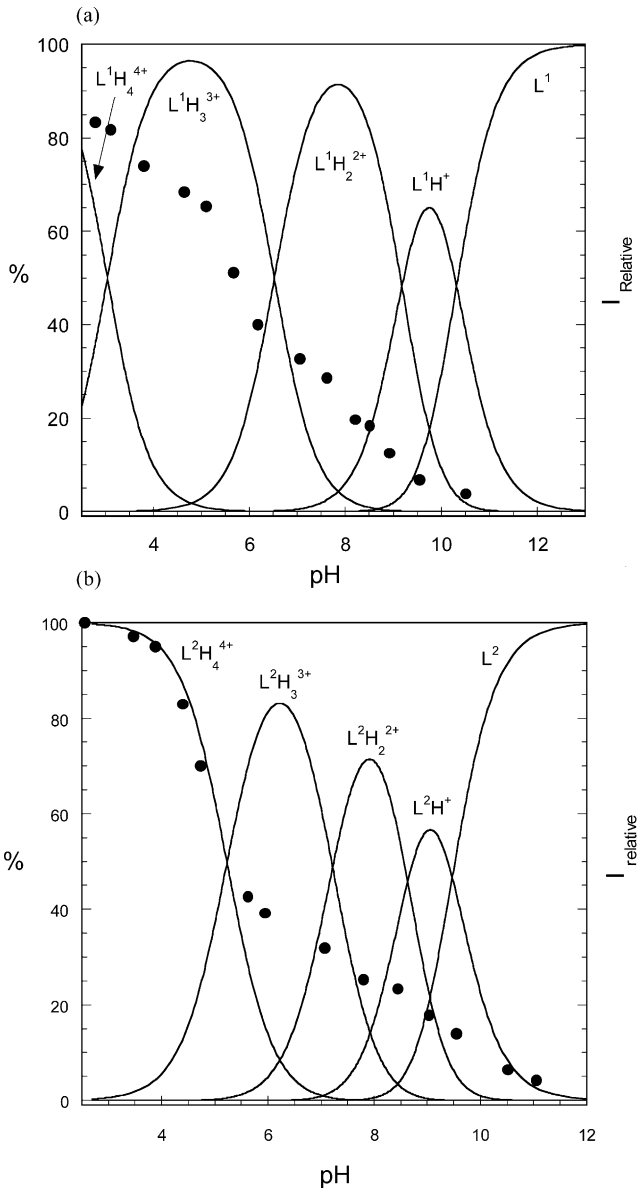


Fig. 3. Distribution diagrams of the species for (a) L^1–H^+ and (b) L^2–H^+ (full line) and the fluorescence emission titration curves (●) for those systems (concentration of L^1 and L^2 were equal and approximately 1.0×10^{-4} mol dm^{-3}, acetonitrile–water 70:30 v/v, 0.1 mol dm^{-3} tetrabutylammonium perchlorate, 298.1 K).

gous to L^2 but functionalised with ferroceneylmethyl groups) [20]. In this case, the logarithm of the constant for the formation of the $[Cu(L^5)]^{2+}$ complex was 14.34 in water. These values obtained for L^1 and L^2 with copper are remarkably lower that than found for the analogous non-functionalised ligand *tta* [20]. In water, the logarithm of the stability constant found for the formation of the $[Cu(tta)]^{2+}$ complex was 20.4. Despite the use of a different solvent, this large difference between the stability constants of L^1, L^2 and that of the *tta* with Cu^{2+} could be attributed to the different number of nitrogens coordinating the metal cation. Thus, the logarithm of the first protonation step of the species $[Cu(L)]^{2+}$ $\{[Cu(L)]^{2+} + H^+ = [Cu(HL)]^{3+}$, $\log K = 7.12$ for L^1 and $\log K = 7.28$ for $L^2\}$ are larger than the logarithm of the third protonation step of the corresponding ligand $\{(H_2L)^{2+} + H^+ = (H_3L)^{3+}$, $\log K = 6.53$ for L^1 and 7.12 for $L^2\}$. In contrast, the $[Cu(tta)]^{2+}$ complex shows a logarithm for the first protonation constant lower than the third protonation of the free *tta* amine (3.5 and 6.67, respectively), indicating that the protonation of the $[Cu(tta)]^{2+}$ complex involves the cleavage of M–N bonds and suggesting that the number of nitrogens coordinating the Cu^{2+} cation in the $[Cu(tta)]^{2+}$ complex is four. This is not the case for $[Cu(L)]^{2+}$ ($L = L^1$ or L^2) for which the stability constants suggested that the number of coordinated nitrogens are less than four. The large difference in stability constants between *tta* and L^1 or L^2 (due to the different number of coordinated nitrogens atoms to the metal cation) has to the attributed to the

presence of bulky pyrene groups in the functionalised L^1 and L^2 receptors. The logarithm of the stability constant for the formation of the $[Zn(L^2)]^{2+}$ complex is much lower than that found for Cu^{2+}. A detailed study of the stability constants for the L^2–Zn^{2+}–H^+ system also suggests that the number of nitrogen atoms coordinating the Zn^{2+} metal cation in the $[Zn(L^2)]^{2+}$ complex is less than four.

5. Cation sensing

The cation sensing behaviour of receptors L^1, L^2, L^3 and L^4 in the presence of the metal ions Ni^{2+}, Cu^{2+}, Zn^{2+}, Cd^{2+}, Hg^{2+} and Pb^{2+} was studied in acetonitrile–water 70:30 v/v as a function of the pH. The relative fluorescence intensity versus pH for L^1, L^2, L^3 and L^4 are shown in Fig. 1(a–d), respectively. The fluorescence emission of the receptors L^1–L^4 is pH-dependent. Maximum fluorescence emission was found for all receptors at acidic pH (when protonated). At basic pH there is a partial quenching. This is a similar behaviour to that found for analogous open-chain polyazaalkanes functionalised with anthrylmethyl groups [21]. At basic pH there is a photo-induced electron transfer form the lone pair of the nitrogen atom from the amines to the photo-excited pyrene group. When the pH is acid, the amines are protonated and the photo-induced electron-transfer process from the nitrogen to the pyrene is inhibited [22].

In the presence of metal ions three different behaviours are observed; namely, fluorescence enhancement, fluorescence quenching and no effect. Fluorescence enhancement is observed at basic pH for the diamagnetic cations Zn^{2+} and Cd^{2+} [23]. For all four receptors there is an enhancement of the fluorescence in the 7–10 pH range in the presence of these two cations. The maximum enhancement is observed for L^1 at pH 10–11 (enhancement factor of ca. 10). In contrast to this enhancement behaviour some other metal ions induce in all receptors a fluorescence quenching. This is the case for the paramagnetic cations Cu^{2+} and Ni^{2+} [24]. The quenching is more remarkable for Cu^{2+}. There is also a fluorescence quenching in the presence of Ni^{2+} for the receptors L^1, L^3, and in a lesser extension for L^4. At acid pH there is a remarkable selective sensing of Cu^{2+} using

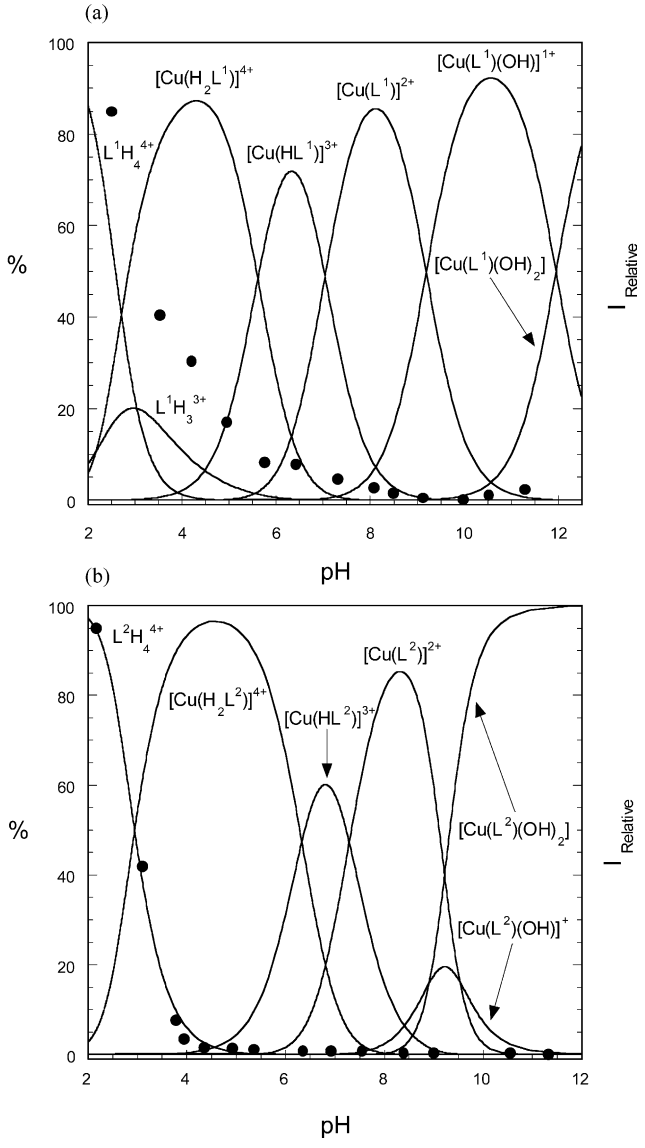


Fig. 4. Distribution diagrams of the species for (a) L^1–Cu^{2+}–H^+ and (b) L^2–Cu^{2+}–H^+ (full line) and the fluorescence emission titration curves (●) for those systems (concentration of L^1, L^2 and Cu^{2+} were equal and approximately 1.0×10^{-4} mol dm^{-3}, acetonitrile–water 70:30 v/v, 0.1 mol dm^{-3} tetrabutylammonium perchlorate, 298.1 K).

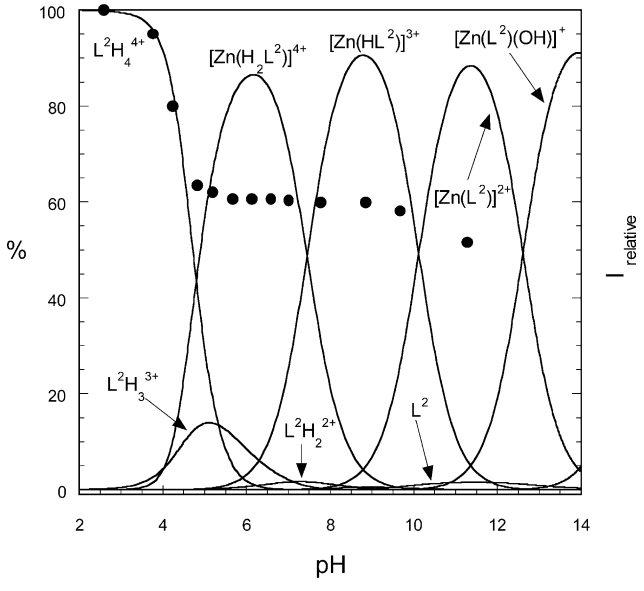


Fig. 5. Distribution diagrams of the species for the L^2–Zn^{2+}–H^+ system (full line) and the fluorescence emission titration curves (●) for those systems (concentration of L^2 and Zn^{2+} were equal and approximately 1.0×10^{-4} mol dm^{-3}, acetonitrile–water 70:30 v/v, 0.1 mol dm^{-3} tetrabutylammonium perchlorate, 298.1 K).

receptor L^2. A quenching factor of approximately 8 is found for Cu^{2+}, whereas other metal cations (Ni^{2+}, Zn^{2+}, Cd^{2+}, Hg^{2+} and Pb^{2+}) do not change the fluorescence behaviour of the L^2 receptor. Neither Hg^{2+} nor Pb^{2+} have any remarkable effect on the fluorescence emission of L^2 and L^4. Addition of Hg^{2+} to a solution of L^1 results in a partial fluorescence quenching in the 3–8 pH range, whereas Pb^{2+} has little effect. In contrast, receptor L^3 is able to sense Pb^{2+} in the pH range 5–9 whereas Hg^{2+} does not induce any effect. Emission spectra of L^1 in the absence and in the presence of Cu^{2+} and Zn^{2+} cations at different pH values (pH 3.0 for the system L^1+Cu^{2+} and pH 9.0 for the system L^1+Zn^{2+}) are shown in Fig. 2.

Fig. 3 shows the distribution diagrams of the L^1–H^+ and L^2–H^+ systems and the fluorescence emission (in arbitrary units) of L^1 and L^2 as a function of the pH. From this figure it can be seen that the fluorescence emission intensity increases remarkably when the species $(H_2L^1)^{2+}$, $(H_3L^1)^{3+}$ and $(H_4L^1)^{4+}$ exists. The maximum fluorescence emission is observed for the tetraprotonated species $(H_4L^1)^{4+}$. For L^2 a similar behaviour is observed. Fig. 4 shows the distribution diagram for the L^1–Cu^{2+}–H^+ and L^2–Cu^{2+}–H^+ systems and the relative fluorescence emission as a function of the pH. The maximum fluorescence emission is found when the metal cation is not coordinating the ligand at acid pH. When the pH is basified an abrupt decrease of the fluorescence emission is observed. This corresponds to coordination of the copper cation. Thus the species $[Cu(L)(OH)_2]$, $[Cu(L)(OH)]^+$, $[Cu(L)]^{2+}$, $[Cu(HL)]^{3+}$ and $[Cu(H_2L)]^{4+}$ quench the fluorescence emission significantly. Fig. 5 shows the distribution diagram for the L^2–Zn^{2+}–H^+ system and the fluorescence emission. The fluorescence behaviour of the Zn^{2+} species is very different to that of the Cu^{2+} cation and the $[Zn(L)(OH)_2]$, $[Zn(L)(OH)]^+$, $[Zn(L)]^{2+}$, $[Zn(HL)]^{3+}$ and $[Zn(H_2L)]^{4+}$ species do not quench the fluorescence significantly as do the analogous copper complexes. This is a similar behaviour to that reported for polyazaalkanes functionalised with anthracene [21–24].

6. Anion sensing

The fluorescence behaviour of receptors L^1, L^2, L^3 and L^4 was studied as a function of the pH in the presence of the anions chloride, bromide, iodide, sulfate, phosphate and ATP. Despite the well-known ability of the polyamines to act as anion receptors, the curve of the fluorescence emission intensity versus pH of L^1–L^4 is not modified in the presence of those anions. This contrasts with the selective ATP sensing found for related systems containing anthryl signalling subunits [25].

7. Conclusions

We have synthesised and characterised the new ligands L^1, L^2, L^3 and L^4 containing pyrene groups as signalling subunits and amino groups as binding sites. The protonation, coordination and fluorescence behaviour of those ligands has been studied in acetonitrile–water 70:30 v/v mixtures. The new ligands have proved to be suitable chemosensors for the fluorimetric sensing of certain metal cations. All four receptors show a remarkable fluorescence enhancement at basic pH in the presence of the Zn^{2+} and Cd^{2+} metal cations. Addition of Cu^{2+} to acidic solutions of the L^1–L^4 receptors results in a remarkable quenching of the fluorescence emission.

Acknowledgements

We should like to thank the DGICYT (proyecto PB98-1430-C02-02, 1FD97-0508-C03-01 and AMB99-0504-C02-01) for support. F.S. also thanks the Ministerio de Ciencia y Tecnología for a Doctoral Fellowship.

References

[1] B. Valeur, I. Leray, Coor. Chem. Rev. 205 (2000) 3.
[2] P.D. Beer, P.A. Gale, Angew. Chem., Int. Ed. 40 (2001) 486.
[3] A.P. de Silva, H.Q.N. Gunaratne, T. Gunnlaugsson, A.J.M. Huxley, C.P. McCoy, J.T. Rademacher, T.E. Rice, Chem. Rev. 97 (1997) 1515.
[4] O. Brümmer, J.J. La Clair, K.D. Janda, Bioorg. Med. Chem. 9 (2001) 1067.
[5] M. Micheloni, M. Formica, V. Fusi, P. Romani, R. Pontellini, P. Dapporto, P. Paoli, P. Rossi, B. Valtancoli, Eur. J. Inorg. Chem. (2001) 51.
[6] F. Sancenón, R. Martínez-Máñez, J. Soto, Tetrahedron Lett. 42 (2001) 4321.
[7] S.A. McFarland, N.S. Finney, J. Am. Chem. Soc. 123 (2001) 1260.
[8] C. Erk, Ind. Eng. Chem. Res. 39 (2000) 3582.
[9] T. Hirano, K. Kikuchi, Y. Urano, T. Higuchi, T. Nagano, Angew. Chem., Int. Ed. 39 (2000) 1052.
[10] K. Rurack, U. Resch-Genger, J.L. Bricks, M. Spieles, Chem. Commun. (2000) 2103.
[11] J.M. Lloris, R. Martínez-Máñez, J. Soto, T. Pardo, M.E. Padilla-Tosta, A. Benito, M.D. Marcos, Polyhedron 18 (1999) 3689.
[12] J.M. Lloris, R. Martínez-Máñez, M.E. Padilla-Tosta, T. Pardo, J. Soto, P.D. Beer, J. Cadman, D.K. Smith, J. Chem. Soc., Dalton Trans. (1999) 2359.
[13] R. Martínez-Máñez, J. Soto, J.M. Lloris, T. Pardo, Trends Inorg. Chem. 5 (1998) 183.
[14] J.A. Sclafani, M.T. Maranto, T.M. Sisk, S.A. Van Arman, Tetrahedron Lett. 37 (1996) 2193.
[15] J. Yoon, N.E. Ohler, D.H. Vance, W.D. Aumiller, A.W. Czarnik, Tetrahedron Lett. 38 (1997) 3845.
[16] A. Bencini, M.A. Bernardo, A. Bianchi, V. Fusi, C. Giorgi, F. Pina, B. Valtancoli, Eur. J. Inorg. Chem. (1999) 1911.

[17] G. Gran, Analyst (London) 77 (1952) 661.
[18] F.J. Rossotti, J. Chem. Edu. 42 (1965) 375.
[19] J.A. Sclafani, M.T. Maranto, T.M. Sisk, S.A. Van Arman, J. Org. Chem. 61 (1996) 3221.
[20] J.M. Lloris, R. Martínez-Máñez, M.E. Padilla-Tosta, T. Pardo, J. Soto, M.J.L. Tendero, J. Chem. Soc., Dalton Trans. (1998) 3657.
[21] M.A. Bernardo, F. Pina, B. Escuder, E. García-España, M.L. Godino-Salido, J. Latorre, S.V. Luis, J.A. Ramírez, C. Soriano, J. Chem. Soc., Dalton Trans. (1999) 915.
[22] L. Fabbrizzi, M. Licchelli, P. Pallavicini, D. Sacchi, A. Taglietti, Analyst 121 (1996) 1763.
[23] F. Pina, M.A. Bernardo, E. García-España, Eur. J. Inorg. Chem. (2000) 2143.
[24] S. Alves, F. Pina, M.T. Albelda, E. García-España, C. Soriano, S.V. Luis, Eur. J. Inorg. Chem. (2001) 405.
[25] M.T. Albelda, M.A. Bernardo, E. García-España, M.L. Godino-Salido, S.V. Luis, M.J. Melo, F. Pina, C. Soriano, J. Chem. Soc. Perkin Transactions 2 (1999) 2545.

PERGAMON

Polyhedron 21 (2002) 1405–1410

POLYHEDRON

www.elsevier.com/locate/poly

Detection of heterologous bovine pancreatic trypsin inhibitor by capillary zone electrophoresis

Alvaro Galli [a], Lisa Ghezzi [b], Giorgio Raspi [c], Fernando Secco [b,*], Maria Spinetti [b]

[a] *Laboratorio di bioterapia molecolare (I.M.D.), C.N.R., Area della ricerca di Pisa, Via Moruzzi 1, 56124 Pisa, Italy*
[b] *Dipartimento di Chimica e Chimica Industriale, University of Pisa, Via Risorgimento 35, 56126 Pisa, Italy*
[c] *Istituto di Chimica Analitica Strumentale, C.N.R., Area della ricerca di Pisa, Via Moruzzi 1, 56124 Pisa, Italy*

Received 10 October 2001; accepted 30 November 2001

Abstract

A method based on the use of capillary zone electrophoresis (CZE) is proposed for the determination of the heterologous protein bovine pancreatic trypsin inhibitor (BPTI) expressed in yeast. *Saccharomyces cerevisiae* cells were transformed with plasmid pCB235U and the amount of inhibitor expressed in yeast was measured both in the culture medium (supernatant) and the cell extract. Supernatant samples were investigated by the CZE method preceded by affinity chromatography (the BPTI yield was between 2 and 5 μg ml^{-1}); direct determination of BPTI in cell extract was performed taking advantage of the complex formation of BPTI and trypsin (BPTI yield was 5 μg ml^{-1}). © 2002 Elsevier Science Ltd. All rights reserved.

Keywords: Capillary electrophoresis; Hydrophobic interaction chromatography; Heterologous protein; BPTI; *Saccharomyces cerevisiae*

1. Introduction

Bovine pancreatic trypsin inhibitor (BPTI), commonly known as aprotinin, is widely used in clinical and biochemical research; it is a strongly basic protein (isoelectric point close to 10.5, $M_r = 6512$ Da) with a remarkable stability to heat, acid or basic treatment, organic solvents and proteolytic degradation; it strongly inhibits trypsin as well as various trypsin-like enzymes [1].

Various immunological or enzyme assays for the determination of the polypeptide concentration were proposed [2–6]. Immunological assays [2–4] are specific and highly sensitive, but they require relatively complex and time-consuming sample preparations. Furthermore, immunological methods show a non-linear calibration function, which does not go through the origin: calibration based on non-linear standard curves is tedious, and reproducibility varies over the measuring range. The enzymic methods [1,5,6] are based on the BPTI inhibition of bovine trypsin-catalysed hydrolysis of an appropriate chromogenic substrate, under defined conditions, followed by spectrophotometric detection. BPTI undergoes a reversible reaction with bovine trypsin at about pH 8.0 to form a very stable complex with 1:1 stoichiometry [1]. These procedures can only be used with relatively pure inhibitor samples; they also posses rather low sensitivity, involve an indirect determination procedure and are limited by competition between the substrate and the inhibitor for the active center of the enzyme.

Therefore, the development of economical, time-saving, routine, direct assay systems which allow a reliable estimation of BPTI in various biological matrices is of interest. In previous papers [7–11] we have considered the direct determination of BPTI in pre-purified solutions, by using various HPLC columns with different hydrophobicities. In a recent work [12], carried out by capillary zone electrophoresis (CZE), we describe the effects of inhibitor interaction with trypsin on the electrophoretic pattern.

It is known that the yeast *Saccharomyces cerevisiae* is recognized as an ideal eukaryotic microorganism used for biological and genetic studies: BPTI is representative of the class of proteins well suited to yeast expression

* Corresponding author. Tel.: +39-050-918-259; fax: +39-050-918-260.
E-mail address: ferdi@dcci.unipi.it (F. Secco).

0277-5387/02/$ - see front matter © 2002 Elsevier Science Ltd. All rights reserved.
PII: S0277-5387(02)00964-6

and it has been studied as a model system for the folding of globular polypeptide domains and for secretion [13,14]. Owing to higher efficiency and resolution, shorter analysis time and the lower operating cost of CZE technique in comparision with HPLC, in particular when highly complex matrices are examined, and availing ourselves of previous experience, we developed a CZE approach to the direct determination of BPTI expressed in different laboratory strains of *S. cerevisiae*.

In this paper, we propose a direct electrophoretic assay which allows a reliable routine estimation of effective inhibitor concentrations in such biological matrices. The method permits a specific and direct determination of BPTI; the analysis of the inhibitor is accomplished without the use of any substrate and is effective in very diluted solution.

2. Experimental

2.1. Reagents and materials

Buffer 1: 0.1 M sodium phosphate buffer [NaH_2PO_4–Na_2HPO_4], pH 7.2. Buffer 2: 0.1 M sodium phosphate buffer [H_3PO_4–$Na_2H_2PO_4$], pH 2.5. Buffer 3: 1: 2 dilution (0.05 M) of buffer 2. Buffer 4: 0.1 M sodium hydrogencarbonate in 0.5 M sodium chloride, pH 8.3.

HPLC grade ammonium sulphate and buffer 2 were purchased from Bio-Rad (Richmond, VA, USA); bovine Trypsin was from Sigma (St. Louis, MO, USA) and native BPTI, as physiologic solution, was from Istituto Behring (Scoppito, L'Aquila, Italy). All other chemicals were of analytical grade.

A stock solution of bovin trypsin was prepared by dissolving the appropriate amount of commercial enzyme in buffer 2 to yield a 1 mg ml^{-1} solution. A stock solution of native BPTI was prepared by diluting 100 μl of physiologic solution with 900 μl of buffer 1. Working standard solutions were prepared by diluting stock solutions with the appropriate buffer. Stock and standard solutions were stored at 4 °C when not in use. Information concerning the stabilities of stock and standard solutions has been previously reported [7–12].

Bovine trypsin was bound to cyanogen bromide (CNbr)-activated Sepharose 4B according to the method of the manufacturer (Pharmacia, Uppsala, Sweden); prolonged washing cycles of the affinity chromatography column (Econo columns, 10 × 1.0 cm I.D. (Bio-Rad)) with solutions of alternately high and low pH were necessary to obtain an accettable HPLC background.

S. cerevisiae strains, RSY12 and RS112, constructed by Robert H. Schiestl (UCLA, Los Angeles, CA, USA) were available in our laboratory. The BJ5464 strain was provided by K. Dane Wittrup (MIT, Cambridge, MA, USA). Yeast strains were transformed with the plasmid pCB235U which was obtained from K. Dane Wittrup (MIT); yeast transformation was performed as described by Gietz and Schiestl [15]. Liquid and solid media were prepared according to a standard procedure [16].

All the strains of *S. cerevisiae* were maintained in complete medium. They were grown for 24 h in a culture medium containing glucose and then were resuspended in a medium containing galactose to induce expression of BPTI. Yeast cells (10^8 cells ml^{-1}) were inoculated in 20–50 ml liquid medium lacking uracile plus galactose for 24 h at 30 °C. The cells (5×10^9) were collected by centrifugation at 4390 g for 5 min and washed with ultrapure water; the cell extract was prepared as described by Kimmerly et al. [17]. Subsequently, the cells were incubated for 96 h at 30 °C in galactose medium, the culture was centrifuged and the supernatant collected for analysis.

Cell extracts were either stored at −70 or at −20 °C; whereas the supernatants were stored at 4 °C. All chemicals were stored as recommended by the manufacturer. Water used in every operation was deionized through a Milli-Q water purification system (Millipore, Bedford, MA, USA).

Before injecting cell extract in CZE each sample was clarified to avoid formation of colloidal suspensions; for this purpose samples were ultracentrifuged through a 0.2 μm Anopore Plus filter (Whatman). All solutions were filtered through a Millipore 0.45 μm filter.

2.2. Apparatus and operating conditions

2.2.1. Chromatography

Hydrophobic interaction chromatography (HIC) measurements were carried out using a LKB Pharmacia DfB HPLC System One which includes a LC 2249 gradient pump, variable-wavelength 2141 monitor connected to a 2221 integrator (LKB-Pharmacia). The UV detector was operated at 220 nm. A Model 7125 sample injector (Rheodyne, Cotati, CA, USA) equipped with 100-μl loop was used. The separations were performed by a TSKgel Phenyl-5PW (TosoHaas), at room temperature (r.t.) and a flow-rate of 1.0 ml min^{-1} with a 30 min linear salt-gradient from 100% high salt buffer (buffer 1, 1.8 M ammonium sulphate) to 100% low-salt buffer (buffer 1). The mobile phase as well as all the solutions were filtered through a 0.45 μm cellulose acetate filter (Millipore). When necessary, the eluted fractions were recovered by means of a Pharmacia Frac-100 Collector.

2.2.2. Electrophoresis

The CZE experiments were performed with a Biofocus 2000 Capillary Electrophoresis System (Bio-Rad) equipped with a non-coated silica capillary (total length = 50 cm, length to detector 45.5 cm and internal diameter = 50 μm).

The following optimised operating conditions were selected. The capillary was conditioned prior to its first use by flushing with 0.1 M NaOH (15 min), ultrapure water (10 min), buffer 2 (10 min), ultrapure water (5 min) and finally running buffer (15 min). The running buffer was buffer 3 with a voltage of 20 kV. Samples were injected by hydrodynamic injection at 5 psi × s. Electropherograms were recorded at 200 nm. The capillary was flushed with buffer 3 before starting daily experiments (15 min) and between two separations (3 min); it was filled with ultrapure water when not in use. Triplicate injections of the solution were performed and average corrected peak areas (area/migration time) were used for the quantitation. All experiments were carried out at 20 °C.

3. Procedures

3.1. Analysis of yeast supernatant

A known volume of sample (20–50 ml) was adjusted to pH 8.0 and applied to the trypsin-Sepharose 4B column (bed volume ca. 1.0 ml), previously equilibrated with buffer 4. The column was washed with at least ten bed volumes of starting buffer to remove unbound substances prior to elution. BPTI, tightly bound to the immobilized trypsin, was fully recovered in a 5.0 ml calibrated flask by elution, in order, with the following volumes and concentrations of phosphoric acid: 0.8 ml (0.01 M), approximately 1.0 ml (1.0 M) and 2.0 ml (0.01M). After adjustment of the pH to the value of 2.5, the resulting solution was brought to the mark with ultrapure water and appropriate aliquots were injected into the CZE capillary or in HIC column. The concentration of BPTI was determined from a calibration curve of peak areas versus amounts (μg) of inhibitor, constructed from directly injected BPTI standard solutions.

3.2. Analysis of cell extract

To a known volume of sample (3 ml) 1.0 M phosphoric acid was added to bring the pH value to approximately 2.5 and the mixture was gently stirred for 10 min. The precipitate was removed by centrifugation (4390 *g*) for 40 min and the supernatant was further centrifuged through a 0.2 μm Anopore Plus membrane filter to drive away the persistent cloudiness. The pH value of the resulting clear solution was adjusted to approximately 7.0 and a moderate excess (10–20 μmol) trypsin was added to allow the rapid formation of the BPTI–trypsin complex. The mixture was collected in a 5 ml calibrated flask and brought to the mark with buffer 3. An aliquot of the resulting solution was assayed by CZE; the concentration of the inhibitor was determined by calibrated additions of BPTI to standard solutions containing trypsin.

4. Results and discussion

In order to produce BPTI, *S. cerevisiae* cells were transformed with the expression vector pCB235U. Selection of transformed yeast cells was carried out in solid medium lacking uracile; BPTI expression was induced by growth in galactose conditions. By contrast, no BPTI presence was detected in cells grown under glucose conditions. BPTI expression led to secretion into the culture medium and to intracellular accumulation.

4.1. Analysis of yeast supernatant

The proposed procedure includes a specific isolation of BPTI on immobilized trypsin; this step is followed by analysis by CZE technique.

Preliminary experiments were carried out under the same conditions used for the analysis of BPTI by HIC [9–11]. The possibility of determining the inhibitor by direct injection of an aliquot of the yeast supernatant solution was discarded, because the chromatogram obtained from injected fresh galactose medium, where the inhibitor has not been induced, already showed a wide absorption in the time range where the BPTI peak appears. Instead, the chromatographic peak for BPTI was obtained by injecting an aliquot of the solution resulting after the passage of the yeast supernatant through the column of immobilized trypsin (Fig. 1,

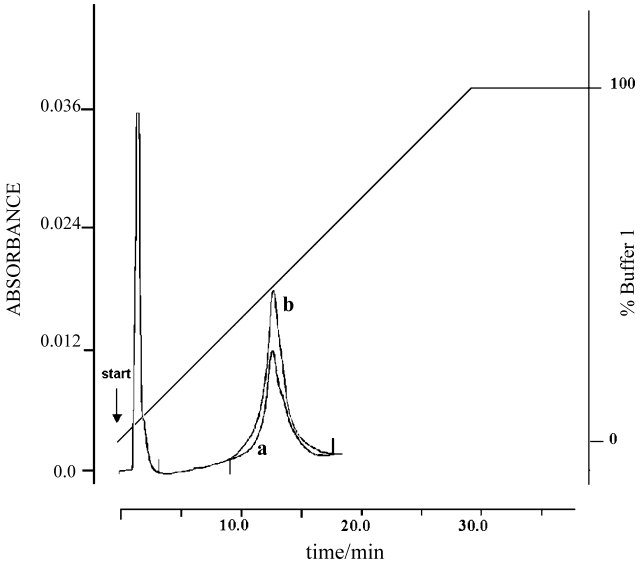


Fig. 1. Chromatogram of heterologous BPTI (29.5 μg ml^{-1}) before (curve a) and after addition of native BPTI (100 μl, 4×10^{-6} M) (curve b). Conditions: TSKgel Phenyl-5PW column; flow rate, 1.0 ml min^{-1} with 30 min linear gradient ammonium sulphate 1.8–0 M in 0.1 M sodium phosphate buffer (pH 7.2); volume injected 100 μl; $\lambda = 280$ nm.

curve a). The peak ascribed to the inhibitor appeared at the expected retention time; an identically shaped peak, without distortions, was obtained (Fig. 1, curve b) from the injection of another aliquot of the same solution, spiked with the standard solution of the inhibitor.

Owing to the enrichment effect resulting from the affinity chromatography step, the possibility of revealing the BPTI signal by CZE technique was considered. Fig. 2(a) shows the electrophoretic peak: its migration time coincides with the previously reported time [12].

To ascertain that no other components interfered with BPTI, 50 ml of a freshly prepared galactose medium (blank) was subjected to the procedure described in this work: the results demonstrated that even high sample volumes do not produce interfering peaks.

A calibration equation for the external addition method was previously established [12] by the regression of the peak area on standard concentration with a correlation coefficient higher than 0.9998. The limit of determination, defined here as the lowest injected amount of BPTI that gave a 5:1 signal-to-noise ratio, was 2 μg ml^{-1}.

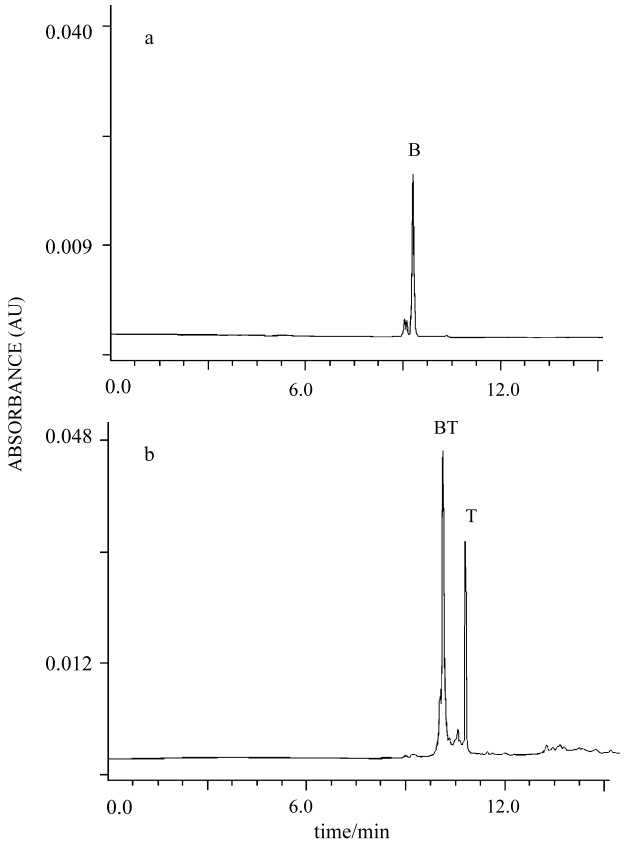


Fig. 2. (a) Electropherogram of heterologous BPTI (B) (1.0×10^{-5} M); (b) electropherogram of the same sample in the presence of bovine trypsin (T) in excess (2.5×10^{-5}); BT represents the inhibitor–trypsin complex. Conditions: 50 μm × 50 cm non-coated silica capillary containing 0.05 M sodium phosphate buffer (pH 2.5). Hydrodynamic injection at 5 psi × s; $V = 20$ KV; $T = 20$ °C; $\lambda = 200$ nm.

Recoveries of BPTI from spiked fresh galactose medium samples were determined in duplicate at BPTI concentrations 5.0 and 10.0 μg ml^{-1}. An identical series of BPTI amounts in buffer standard solution provided the 100% values. Three injections for each sample, test and reference, were performed. The mean (±S.D.) recovery from the six determinations over the calibration range indicated was 99.2 ± 1.24%.

From the results of the described experiment it was concluded that sensitivity due to the preconcentration of the inhibitor; accuracy, precision and freedom from interference make the described procedure a suitable routine tool for monitoring the levels of BPTI in yeast supernatant. Table 1 shows the results obtained by applying the method to the supernatant collected from *S. cerevisiae* strains (RSY12, RS112, BJ5464); the expression levels ranged between 2 and 5 μg ml^{-1}.

4.2. Analysis of cell extract

A fast determination of BPTI in cell extracts obtained from BJ5464 strain was considered representative of all *S. cerevisiae* strains analyzed. In fact, the three strains (RSY12, RS112, BJ5464) showed almost the same profile when analyzed either by CZE or HIC, thus indicating that cell extract and supernatant have nearly the same composition.

A typical electropherogram obtained from cell extract treated as described under 'Procedures', but with no added trypsin, is reported in Fig. 3(a). The electrophoretic profile shows numerous peaks; however, the high efficiency and resolution achieved by CZE technique enabled us to single out peak B as that due to the inhibitor we looked for. This assumption was supported through spiking experiments with a BPTI standard solution and by comparison of the electrophoretic pattern with that displayed by the yeast extract from cells grown on a glucose medium (i.e. under no induction conditions). Decisive confirmation was achieved through the analysis of the BPTI-trypsin complex. As it has recently been demonstrated [12], the electrophoretic signal of the complex BPTI–trypsin appears at a migration time somewhere between those of pure BPTI and trypsin. When increasing amounts of

Table 1
Yield of inhibitor (BPTI) produced by different strains of *S. cerevisiae* both in supernatant and cell extract

Strain	Amount of BPTI (μg ml^{-1})	
	Supernatant	Cell extract
RSY12	4.8	n.d
RS112	2.2	n.d
BJ5464	4.2	5.0

n.d: Not determined.

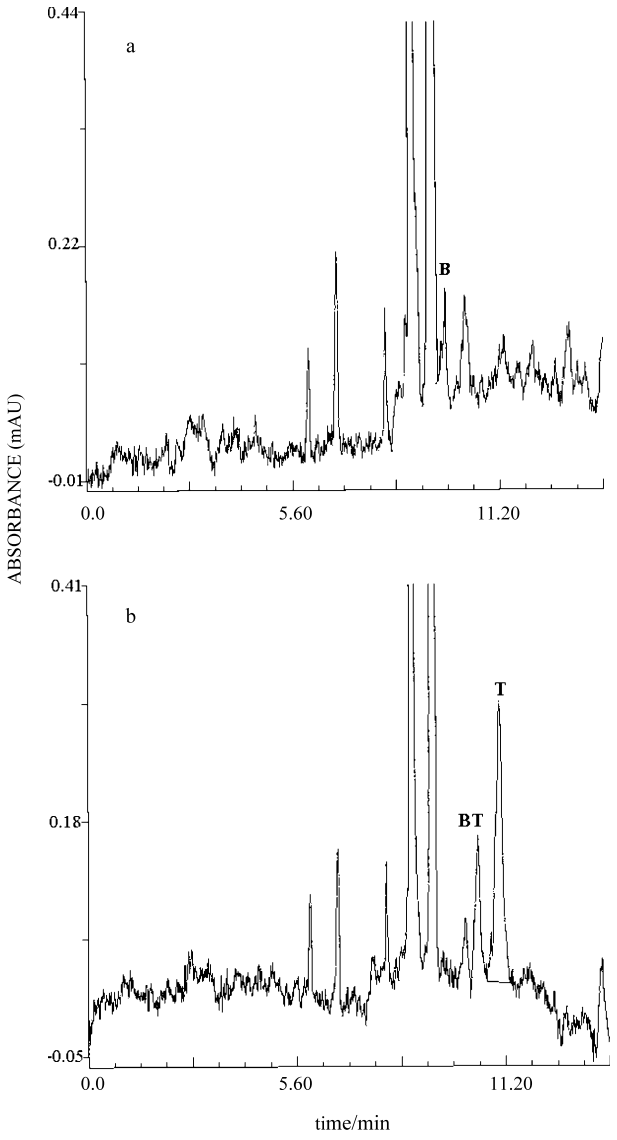


Fig. 3. (a) Electropherogram of cell extract, amount of BPTI (B) 1.6 μg ml^{-1}; (b) Electropherogram of the same sample in the presence of bovine (T) trypsin in excess; BT represents the inhibitor–trypsin complex. Electropherogram obtained from cell extract treated as described under 'Procedures'. Conditions: 50 μm × 50 cm non-coated silica capillary containing 0.05 M sodium phosphate buffer (pH 2.5). Hydrodynamic injection at 5 psi × s; $V = 20$ KV; $T = 20$ °C; $\lambda = 200$ nm.

trypsin are added to a solution containing BPTI, the corresponding electrophoretic patterns show the progressive decrease of the BPTI peak and the increase of the complex peak: in the presence of excess trypsin the disappearance of the BPTI peak is paralleled by the increase of the trypsin peak. The same result was obtained with heterologous BPTI (Fig. 2(b)).

By adding excess trypsin to the solution of cell extract, the corresponding electropherogram shows (Fig. 3(b)) a change with respect to that reported in Fig. 3(a) which agrees upon the appearance and disappearance of the described peaks. The wider area of the complex peak allows an enhancement of the sensivity of the determination.

A calibration curve was constructed for the BPTI–trypsin complex from a series of standard working solutions (2–20 μg ml^{-1}) of BPTI to which an excess (five times molar concentration of inhibitor) of trypsin was added. The analytical recovery was found to be almost complete, the correlation coefficient (six points) being 0.9994. Limits of determination (0.5 μg ml^{-1}), limits of quantitation (1 μg ml^{-1})and coefficient of variation $< 4.0\%$ were ascertained by a series of experiments. In order to evaluate the possible matrix effect, the method of standard addition was used for the determination of BPTI in the cell extract. The calibration curves obtained by standard addition to the sample and by using external standard solutions were significantly parallel; owing to the limited number of determinations, the standard addition method was preferred. Each peak area was measured three times: the mean BPTI level in the cell extract was found to be 5.0 μg ml^{-1}.

The results obtained from the series of experiments performed to determine the amount of BPTI expressed into both the supernatants and the cell extract area are summarized in Table 1.

5. Conclusions

The results of the chromatographic and electrophoretic experiments in the biological matrices described above show that heterologous BPTI produced by the *S. cerevisiae* expression/secretion system is indistinguishable from the natural material. We have been able to detect and quantify low levels of BPTI with a direct method which is simpler and more rapid than the commonly used immunological assays. Given the increasing interest in genetically modified microorganisms and plants, which involve heterologous proteins, other experiments are in progress to apply the CZE method to detect specific heterologous proteins directly in yeast extracts.

Acknowledgements

This work was financially supported by MURST (Cofin 2000) and by the Consiglio Nazionale delle Ricerche (C.N.R.), Italy. The authors are indebted to Mrs M. Ciampini for her invaluable technical support.

References

[1] H. Fritz, G. Wunderer, Arzneim-Forsh./Drug Res. 33 (1983) 479.
[2] T. Shikimi, J. Pharm. Dyn. 5 (1982) 708.

[3] I. Trautshold, Life Sci. 16 (1975) 830.
[4] W. Muller-Esterl, A. Oettl, E. Truscheit, H. Fritz, Fresenius' Z. Anal. Chem. 317 (1984) 718.
[5] W. Gebhard, H. Tschesche, H. Fritz, in: J.T. Dingle, J.L. Gordon (Eds.), Proteinase Inhibitors, Elsevier, Amsterdam, 1986, p. 375.
[6] M. Jochum, V. Jonakova, H. Dittmer, H. Fritz, Fresenius' Z. Anal. Chem. 317 (1984) 719.
[7] G. Raspi, A. Lo Moro, M. Spinetti, M. Molinari, Analyst 114 (1989) 1017.
[8] G. Raspi, A. Lo Moro, M. Spinetti, J. Chromatogr. 525 (1990) 426.
[9] G. Raspi, A. Lo Moro, M. Spinetti, Chromatographia 35 (1993) 93.
[10] G. Raspi, A. Lo Moro, M. Spinetti, Chromatographia 35 (1993) 381.
[11] G. Raspi, A. Lo Moro, M. Spinetti, Chromatographia 37 (1993) 471.
[12] F. Braca, F. Secco, M. Spinetti, G. Raspi, Chromatographia (2002), in print.
[13] C.B. Marks, M. Vasser, P. Ng, W. Henzel, S. Anderson, J. Biol. Chem. 16 (1986) 7115.
[14] N. Parekh, K.D. Wittrup, Biotechnol. Prog. 13 (1997) 117.
[15] R.D. Gietz, R.H. Schiestl, Methods Mol. Cell. Biol. 5 (1995) 255.
[16] C. Kaiser, S. Michaelis, A. Mitchell, Methods in Yeast Genetics, Cold Spring Harbor Laboratory, Cold Spring Harbor, NY, 1994.
[17] W. Kimmerly, A. Buchman, R. Kornberg, J. Rine, EMBO J. 7 (1988) 2241.

PERGAMON

Polyhedron 21 (2002) 1411–1420

POLYHEDRON

www.elsevier.com/locate/poly

Spectrophotometric study of uranyl–oxalate complexation in solution

Josef Havel *, Julio Soto-Guerrero, Přemysl Lubal

Department of Analytical Chemistry, Faculty of Science, Masaryk University, Kotlářská 2, 611 37 Brno, Czech Republic

Received 15 October 2001; accepted 30 November 2001

Abstract

Uranyl–oxalate complex equilibrium in aqueous solution was studied by UV–Vis spectrophotometry. Due to high spectra correlation, derivative spectrophotometry was also applied during the search for the best chemical model. The absorption spectra of all the complexes were calculated and found in a good agreement with theoretical considerations. Overall protonation constants of oxalate, necessary for accurate calculation of uranyl–oxalate formation constants, were also determined under the same conditions and the following values were obtained $\log K_1 = 3.83 \pm 0.01$; $\log K_2 = 4.92 \pm 0.01$. Stability constants determined for the $[(UO_2)_p(C_2O_4)_q]^{2p-2q}$ species were: $\log \beta_{11} = 6.31 \pm 0.02$, $\log \beta_{12} = 11.21 \pm 0.07$, $\log \beta_{13} = 13.8 \pm 0.04$, $\log \beta_{23} = 18.5 \pm 0.2$, $\log \beta_{25} = 28.5 \pm 0.1$ ($I = 3.0$ M $NaClO_4$; 25 °C). The equilibrium constants were extrapolated to infinite dilution by applying specific ion interaction theory (SIT) and are the following: $\log \beta_{11}{}^0 = 7.41 \pm 0.01$, $\log \beta_{12}{}^0 = 11.80 \pm 0.02$, $\log \beta_{13}{}^0 = 13.96 \pm 0.07$. Formation of polynuclear $[(UO_2)_2(C_2O_4)_3]^{2-}$ and $[(UO_2)_2(C_2O_4)_5]^{6-}$ species was proved and confirmed independently by conductometry and vapor pressure osmometry. © 2002 Published by Elsevier Science Ltd.

Keywords: Uranyl oxalates; Oxalic acid; UV–Vis spectrophotometry; Speciation; Stability constants; Aqueous solutions

1. Introduction

Modeling of chemical processes governing the migration of actinides and fission products requires reliable thermodynamic data concerning metal ion complexation. Knowledge of uranyl–oxalate complexation equilibrium is important as oxalate can be formed in nuclear waste depositories by decomposition of organic compounds. It is known that in aqueous solution, uranyl reacts with oxalate forming $[UO_2(C_2O_4)_n]^{2-2n}$ ($n = 1$–3) complexes and a great effort has been made to determine the reliable values of the stability constants under different conditions. Also protonated complexes were mentioned in the literature [1,2] to explain different grades of complexation as a function of pH. Potentiometry [3], solvent extraction [1,4], Raman spectroscopy [5], etc. methods have been used and the system is apparently well known. However, the stability constant of the complex $[UO_2(C_2O_4)_3]^{4-}$, $\log \beta_{13}$, is still not well established and there is great discrepancy in literature values. In 1969, using UV-spectrophotometry, Havel [6] determined a value for $\log \beta_3 = 11.0$ confirming the decrease of stepwise constants ($\log K_{11} = 5.99$, $\log K_{12} = 4.65$, $\log K_{13} = 0.36$ in 1 M $NaClO_4$). Also, structural–theoretical considerations with regard to the actual value of $\log K_{13}$ conclude that this should be relatively small, since a third oxalate is expected to bind differently to the uranyl than the first two oxalate molecules do [7]. Furthermore, studies of single-crystal X-ray diffraction of the mono-, bis- and trisoxalato dioxouranium(VI) compounds in solid state have been made [8–11] and they show that the third oxalate is actually bound differently.

Recently, Ferri et al. [12,13] developed a second kind electrode, based on the $Hg_2(C_2O_4)(s)$–Hg couple, which was used to determine the stability constants of $[UO_2(C_2O_4)_n]^{2-2n}$ ($n = 1$–3) complexes in 1, 2 and 3 M $NaClO_4$, ascribing the variation of $\log \beta_3$ (14.0 in 1 M and 15.2 in 3 M $NaClO_4$) to the different ionic strength employed. In that study, the third stepwise formation constant is $\log K_{13} = 3.45$ in 1 M $NaClO_4$ [12].

In spite of the fact that uranyl polynuclear complexes such as $M_2[(UO_2)_2(C_2O_4)_3]\cdot nH_2O$ with M = NH_4, K, Cs, Tl, and $M_6[(UO_2)_2(C_2O_4)_5(H_2O)_2]\cdot nH_2O$ with M = N_2H_5, NH_4, Na, K, Cs have also been known for a long

* Corresponding author. Fax: +420-5-41-211214.
E-mail address: havel@chemi.muni.cz (J. Havel).

0277-5387/02/$ - see front matter © 2002 Published by Elsevier Science Ltd.
PII: S0277-5387(02)00947-6

time [8,14–16], their possible formation in aqueous solution has always been neglected. The only information published so far concerns the reaction (A)

$$[(UO_2)_2(C_2O_4)_5]^{6-} = 2\,[UO_2(C_2O_4)_2]^{2-} + C_2O_4^{2-} \quad (A)$$

with an equilibrium constant $K = 5 \times 10^{-7}$ [17].

Spectrophotometric study of the uranyl–oxalate system is complicated by photolysis and numerous investigators have studied it [2,18–22]. An UV–Vis spectrophotometric study of uranyl species also has to deal with high correlation of absorption spectra as this has been observed not only for hydrolyzed uranium(VI) species [23,24], but also for uranium(VI)–selenate complexes [25].

The aim of this paper is to perform a detailed multiwavelength spectrophotometric study (in UV–Vis range) in order to verify uranyl–oxalate stability constants, applying computational methods and investigating systematically the possible formation of polynuclear and protonated complexes in aqueous solution.

2. List of symbols

All the concentrations are expressed as molarities (mol dm^{-3}). c_L, total concentration of $C_2O_4^{2-}$; c_M, total concentration of UO_2^{2+} and $[H^+]$ the free hydrogen ion concentration. The equilibria of interest are:

$$rH^+ + C_2O_4^{2-} = H_rC_2O_4^{r-2} \quad (B)$$

$$pUO_2^{2+} + qC_2O_4^{2-} + rH = [(UO_2)_p(C_2O_4)_qH_r]^{2p-2q+r} \quad (C)$$

for which the equilibrium constants, expressed in terms of the concentrations, are defined by Eqs. (1)–(2):

$$K_r = [H_rC_2O_4^{r-2}][C_2O_4^{2-}]^{-1}[H^+]^{-r} \quad (1)$$

$$\beta_{pqr} = [(UO_2)_p(C_2O_4)_qH_r^{2p-2q+r}][UO_2^{2+}]^{-p}[C_2O_4^{2-}]^{-q} \times [H^+]^{-r} \quad (2)$$

For simplicity, β_{pq} means $r = 0$ and β_q means $p = 1$, $r = 0$.

3. Experimental

3.1. Chemicals

Stock solution of uranium(VI) perchlorate (1.66 M) was prepared as described elsewhere [23]. Sodium oxalate, potassium oxalate and oxalic acid, purity pro analysis, were purchased from Lachema (Brno, Czech Republic) and used as such without any further purification. Sodium perchlorate (from the same company) was recrystallized twice and traces of metals removed according to the procedure [26] and air-dried. Stock solution of 8.77 M $NaClO_4$ was analyzed, by drying defined volumes of the solution in a drying box at 120 °C to constant weight. Traces of perchloric acid in sodium perchlorate solution were determined by potentiometry. Concentrated perchloric acid (70%) was from Merck (Darmstadt, Germany).

3.2. Synthesis of $K_6[(UO_2)_2(C_2O_4)_5(H_2O)_2]\cdot 8H_2O$

The compound was prepared from a concentrated aqueous solution of $UO_2(C_2O_4)\cdot 3H_2O$ and $K_2C_2O_4\cdot H_2O$ mixed in stoichiometric ratio 2:3. The mixture was heated and then partly evaporated at 60 °C and formed crystals were isolated [8].

3.3. Apparatus

All emf and absorbance measurements were performed at 25.0 ± 0.2 °C, using $NaClO_4$ at constant perchlorate concentration, $[ClO_4^-] = 3.00$ M. A combined glass electrode 01-29 B of Monokrystaly (Turnov, Czech Republic) was used, in which the inner saturated potassium chloride solution of reference electrode was replaced with 3 M sodium perchlorate saturated with silver chloride. The emf of the cell was measured to ± 0.2 mV with a Radelkis OP-208 Precision Digital pH-meter (Budapest, Hungary). The electrode parameters were determined titrating a known amount of diluted perchloric acid by a standard sodium hydroxide solution also in 3 M $NaClO_4$. The free hydrogen-ion concentrations, $[H^+]$, were determined by calculating the $-\log[H^+]$ values from the measured emf by means of Eqn. (3),

$$E = E^\circ - g\log[H^+] + E_j \quad (3)$$

where, E° is the potential of the cell at $\log[H^+] = 0$, g the Nernstian slope given by the term $2.30259(RT/F)$ and E_j the liquid junction potential.

Spectrophotometric measurements were done on a single-beam, diode-array, HP 8452A spectrophotometer of Hewlett–Packard (Palo Alto, USA). A quartz cell with 1 cm of path-length was used.

3.4. Preparation of the solutions for experiments

Two different methods were used to mix oxalate and uranium(VI). In one method, the total uranyl plus oxalate concentration ($c_L + c_M$) was kept constant, while the total oxalate concentration (c_L) was varied (continuous variation or Job's method). In the other method, the total uranyl concentration (c_M) was kept constant, while the oxalate concentration was varied (molar-ratio method). In each experiment, the pH was fixed either with $HClO_4$ or NaOH and the emf was measured after every mixing. At least one of the quantities $-\log[H^+]$,

$c_M + c_L$ or c_M was varied in the different experiments. This represented more than 90 000-absorbance values for about 640 different spectra (solutions).

The vapor-pressure osmometry (VPO) measurements were done with a thermostated osmometer of Knauer (Berlin, Germany) and conductivity was measured with a conductometer type OK-104 and an electrode for conductivity type OK-0902P, Radelkis (Budapest, Hungary).

3.5. Computation

The number of light-absorbing species was estimated by SIBYLA [27] factor analysis program. The equilibria constants were calculated and refined with SQUAD [28], LETAGROP-SPEFO [29] or with OPIUM [30] least-squares programs. All experimental points were given unit weight in the least-square refinement. Hence, we had to use approximately the same number of experimental points in the regions where the different complexes were predominant.

The derivative spectra were calculated either with the standard software provided in HP-spectrophotometer or with a spreadsheet based on the Savitzky–Golay algorithm [31] and its corrections [32]. No differences in calculated derivative spectra were observed. First and third derivative spectra were calculated using a sixth order polynomial, while for second and fourth derivative, a fourth order polynomial was used. In all the cases, a 13-point convolution operation was employed.

4. Results and discussion

Equilibria in H^+–$C_2O_4^{2-}$–UO_2^{2+} system can be described by a general reaction (C). In order to make realistic and correct evaluation of uranium–oxalate equilibria, reliable values of oxalate protonation constants are needed and they have therefore been carefully checked.

4.1. H^+–oxalate system

The values of oxalate protonation constants in 3 M $NaClO_4$ were checked by spectrophotometry. As traces of carbonate in sodium hydroxide were absorbing strongly in the same region as oxalate, the protonation constants of oxalate were determined via titration of diluted sodium oxalate with perchloric acid.

An initial volume equal to 40 ml of 0.001 M of sodium oxalate was titrated with 0.1 or 0.8 M perchloric acid. The UV-spectra for 59 different hydrogen-ion concentrations and wavelengths in the range 200–250 nm (step 1 nm) were measured. The value of $-\log[H^+]$ was varied from 6.7 to 0.7 and the total concentration of oxalate was varied from 1.0 to 0.61 mM. An example of selected data is given in Fig. 1.

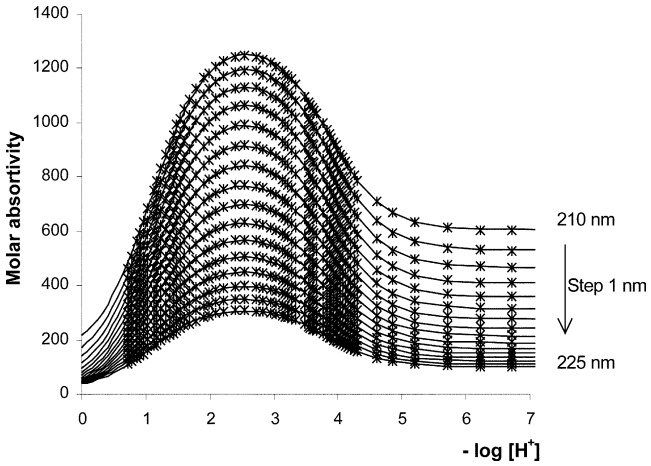


Fig. 1. The apparent absortivity of oxalate (A/c_L, where $c_L = 0.6$–1.0 mM) vs. $-\log[H^+]$. The stars are experimental points and the solid lines were calculated using the protonation constants ($\log K_1 = 3.83 \pm 0.01$and $\log K_2 = 4.92 \pm 0.01$) and molar absortivities obtained in this work.

Protonation constants were calculated with a SQUAD computer program and the complete data matrix (1770 absorbances) was evaluated with OPIUM. The resulting logarithmic constants agree up to the second decimal. Satisfactory agreement of protonation constants obtained in this work (Table 1) with those of literature was reached. For further calculations, the values $\log K_1 = 3.83$ and $\log K_2 = 4.92$ ($pK_{a1} = 1.09$, $pK_{a2} = 3.83$) were used.

4.2. Uranium(VI)–oxalate system

An example of absorption spectra in visible range concerning uranyl complexation with oxalate in acid solutions is given in Fig. 2. We have chosen to work at pH 4, as hydrolysis of uranyl ion or the formation of mixed uranyl–hydroxo–oxalate species [8,13] can thus be neglected. Increasing oxalate:uranyl ratio, the absorption bands of uranyl are more intense and a slight

Table 1
Survey of the oxalate protonation constants in 3 M $NaClO_4$ at 25 °C

Equilibrium	log K	Method	References
$H^+ + C_2O_4^{2-} = HC_2O_4^-$	3.85 ± 0.1	gl	[1]
	3.81 ± 0.01	sp and gl	[33]
	3.81 ± 0.02	ise-ox	[13]
	3.83 ± 0.01	sp	this work
$2H^+ + C_2O_4^{2-} = H_2C_2O_4$	$4.8_5 \pm 0.3_2$	gl	[1]
	5.09 ± 0.02	sp and gl	[33]
	4.95 ± 0.02	ise-ox	[13]
	4.92 ± 0.01	sp	this work

gl, Glass electrode; sp, spectrophotometry; ise-ox, ion selective electrode for oxalate.

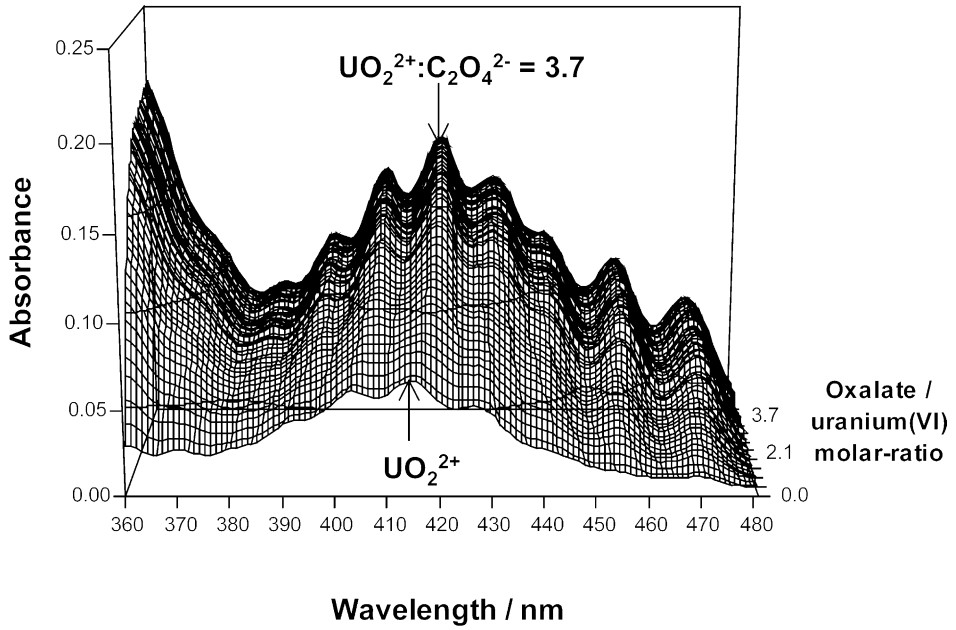


Fig. 2. Absorption spectra of uranyl ($c_M = 8.3$ mM) at various oxalate concentrations (0.0–30.0 mM) and $-\log[H^+] = 2.7$.

shift toward higher wavelengths is observed. Results of factor analysis (FA) are summarized in Table 2. A factor is considered significant if the variance is larger than 0.01% [27]. Hence, the variance test suggests three factors. The fourth column holds the residual standard deviation of absorbance, $s_k(\mathbf{A})$. This value accepts a factor if the corresponding $s_k(\mathbf{A})$ is larger than the standard deviation of the measured absorbance. For two factors ($k = 2$), $s_k(\mathbf{A})$ is 0.00334 AU (absorbance units) which is larger than estimated experimental noise (± 0.001–0.002). Therefore, three factors (species) are needed to explain the data sufficiently as the spectra are very similar (and perhaps correlated).

Derivative spectra from the first up to the fourth derivative with the aim to prove the number of species formed in solution were also used. In this case, the value of the rank of derivative spectra matrices was also found to be equal to three. FA was applied systematically throughout the work also for other data.

Concluding, FA of normal and derivative spectra confirms the formation of three absorbing species in acid solution, which might be UO_2^{2+} and 1:1, 1:2 $[UO_2(C_2O_4)_n]^{2-2n}$ complexes.

4.3. Continuous variation method (CVM)

In spite of the fact that stoichiometry of uranium(VI)–oxalate species is well known, continuous variation method was applied here as a way to study the formation of 1:1 complex in acid solutions and the possible occurrence of protonated species. Job's plots for $c_L + c_M = 16.6$ mM and different pH are presented in Fig. 3. It is observed that as pH increases, the maximum shifts towards higher values of oxalate molar fraction. It means that in addition to 1:1 complex, complexes with a higher number of oxalates are starting to be formed. Selected data of CVM were treated by SQUAD program to determine the formation constants and testing

Table 2
An example of factor analysis of selected data

K	Eigen value $\times 10^3$	Variance (%)	Cumulative variance (%)	$s_k(\mathbf{A}) \times 10^3$
1	504.5003	99.3311	99.3311	9.5822
2	2.9949	0.5897	99.9208	3.3432
3	0.3529	0.0695	99.9902	1.1891
4	0.0421	0.0083	99.9985	0.4653
5	0.0035	0.0007	99.9992	0.3402
6	0.0021	0.0004	99.9994	0.2335
7	0.0007	0.0001	99.9998	0.1815
8	0.0002	0.0000	99.9998	0.1603
Number of factors		3	3	3

Experimental data: 38 spectra × 41 wavelengths (350–470 nm, step 3 nm); uranyl concentration: 4.1, 8.3 and 16.6 mM; oxalate concentration, 0–36 mM; $1.2 < -\log[H^+] < 3.7$.

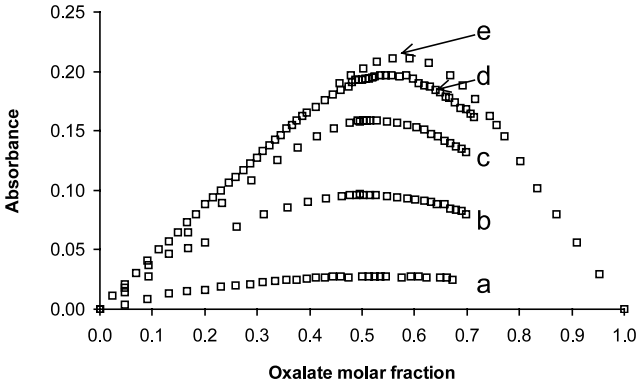


Fig. 3. Continuous variation curves (350 nm) for uranyl–oxalate system at $c_L + c_M = 16.6$ mM and different $-\log[H^+]$ values: (a) 0.0; (b) 0.5; (c) 1.0; (d) 1.5; (e) 2.4.

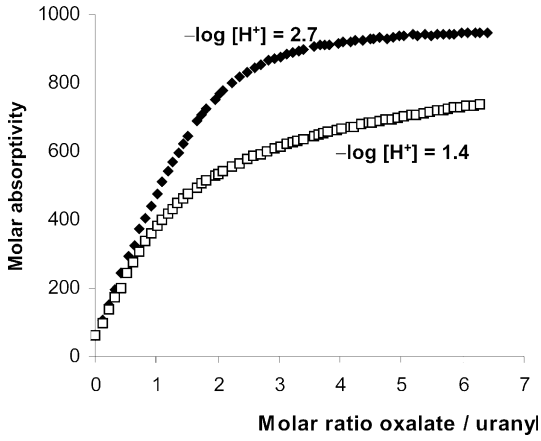


Fig. 4. Apparent molar absorbtivity of uranium(VI) (A/c_M, where, $c_M = 1.7$ mM) at 300 nm vs. ligand to metal molar-ratio.

different protonated species. No protonated species was accepted. The results of computation are presented in Table 3. For the experiments carried out at $-\log[H^+] = 1.5$, it was possible to calculate also $\log \beta_{12}$ in addition to $\log \beta_{11}$. Negligible difference in $\log \beta_{11}$ at $-\log[H^+] = 0.5$, 1.0 and 1.5 proves no formation of protonated complexes, which was also verified by factor analysis. The higher absorbances for higher pH and other changes in the range $0.5 < -\log[H^+] < 3.0$ are satisfactorily explained on the bases of acid–base equilibria involving oxalate and binary uranyl–oxalate complexes.

4.4. Molar-ratio method

In molar-ratio method, the total uranyl concentration is kept constant, pH was fixed (but measured through the whole experiment), and the concentration of oxalate was varied. Two examples of molar-ratio curves for 1.7 mM uranyl and different pH are shown in Fig. 4. Data matrix was divided to several parts according to uranyl concentration and also subdivided according to either the pH or the ligand to metal ion molar-ratio (θ). In each division and subdivision the data were evaluated, i.e. different species were tested and constants calculated with SQUAD program. Addition of 1:2 complex (uranium(VI):oxalate) greatly improved the fit. The initial calculations allowed rationalizing the data selection and implementing a good strategy for the final test of models and constants refinement. In the second evaluation stage, a typical calculation started with two sets of data for one metal concentration. The first set was a matrix (usually with $\theta \leq 3$ for pH 1.5 and $\theta \leq 1.5$ for pH 2.0) for the refinement of β_{11} and β_{12}. In the next step (generally with the remaining data) β_{12} and β_{13} were refined with β_{11} fixed together with the molar absortivities of 1:1 complex (obtained from previous experiments). Then returning to the first data to refine β_{11} while β_{13} and the molar absortivities of 1:3 complex were fixed. In this calculation step, the parameters of complex 1:2 were either fixed or refined. The whole procedure was repeated three to four times until the whole set of stability constants remained unchanged.

The results for different experiments and data subsets presented in Table 4 were calculated assuming only mononuclear species. In this table, the presence of 1:3 complex, $[UO_2(C_2O_4)_3]^{4-}$ was examined. Experiment 1 in Table 4 contains spectra in the UV-range (300–349 nm), where no new band is observed. Evaluation of experiments 2 and 3 takes data in the visible range, where different bands are observed (cf. Fig. 2). Different data were evaluated in this way with similar results, while $\log \beta_{13}$ obtained was lower than 14. Generally, these results show acceptable consistency among $\log \beta$ values, although some slight discrepancy for $\log \beta_{12}$ values was observed. Finally, the recommended values of the present work are presented in Table 5. These values were chosen among the several results obtained and considered reliable on the basis of not only statistical parameters but also following the species spectra and the relationship between experimental conditions and constants refined.

Table 3
Equilibrium constants, $\log \beta_{pq}$, for the reactions $p\,UO_2^{2+} + q\,C_2O_4^{2-} = [(UO_2)_p(C_2O_4)_q]^{2p-2q}$ $(p = 1)$ determined from data of continuous variation method ($c_L + c_M = 16.6$ mM) in a 3.00 M $NaClO_4$ ionic medium at 25 °C

$-\log[H^+]$	Formation constants
1.5	$\log \beta_{11} = 6.26 \pm 0.05$
	$\log \beta_{12} = 11.4_2 \pm 0.1_3$
1.0	$\log \beta_{11} = 6.25 \pm 0.01$
0.5	$\log \beta_{11} = 6.2_6 \pm 0.1_8$

The uncertainties of $\log \beta_{pq}$ values are given as a S.D. obtained in the least-square refinement of data. Each input file contained 24 spectra with 41 wavelengths (350, 353, …, 470 nm) and SQUAD program was used.

Table 4
Equilibrium constants, $\log \beta_{pq}$, for the reactions $p UO_2^{2+} + q C_2O_4^{2-} = [(UO_2)p(C_2O_4)q]^{2p-2q}$ ($p = 1$) determined from data of molar ratio method in a 3.00 M $NaClO_4$ ionic medium at 25 °C

Model	Experiment 1	Experiment 2	Experiment 3
$\log \beta_{11}$	6.19 ± 0.01	6.38 ± 0.02	6.25 ± 0.02
$\log \beta_{12}$	11.05 ± 0.01	10.93 ± 0.01	11.08 ± 0.01
$s(A)$	3.59×10^{-3}	5.36×10^{-4}	2.63×10^{-3}
U	1.48×10^{-2}	2.71×10^{-4}	6.52×10^{-3}
$\log \beta_{11}$	6.20 ± 0.01	6.43 ± 0.01	6.42 ± 0.02
$\log \beta_{12}$	11.07 ± 0.01	11.02 ± 0.01	11.52 ± 0.01
$\log \beta_{13}$	13.81 ± 0.04	13.81 fixed	13.73 ± 0.05
$s(A)$	2.29×10^{-3}	3.40×10^{-4}	8.69×10^{-4}
U	5.77×10^{-3}	1.04×10^{-4}	6.80×10^{-4}

The uncertainties of $\log \beta_{pq}$ values are given as a S.D. obtained in the least-square refinement of data. Experiment 1. Data matrix: 24 spectra (solutions) × 50 wavelengths (300, 301, ..., 349 nm). $c_M = 1.7$ mM; $5.0 < c_L < 10.2$ mM for $-\log[H^+] = 1.4$ and $3.4 < c_L < 15.1$ mM for $-\log[H^+] = 2.7$. Experiment 2. Data matrix: 24 spectra (solutions) × 25 wavelengths (398, 401, ..., 470 nm). $c_M = 4.1$ mM; $4.3 < c_L < 18.9$ mM for $-\log[H^+] = 1.3$ and $4.0 < c_L < 18.9$ mM for $-\log[H^+] = 2.3$. Experiment 3. Data matrix: 24 spectra (solutions) × 41 wavelengths (350, 353, ..., 470 nm). $c_M = 8.3$ mM; $16.7 < c_L < 33.3$ mM for $-\log[H^+] = 1.3$ and $17.4 < c_L < 36.1$ mM for $-\log[H^+] = 2.7$.

5. Search of the presence of polynuclear complexes

Similar strategy as described above was used to investigate whether the formation of polynuclear species takes place in solution or not. The starting file involved absorbance data for lower uranyl and oxalate concentrations and in the next stage higher concentrations were included (where complexes different from 1:1 and 1:2 might be formed). The candidates being examined to improve the fit were: $[UO_2(C_2O_4)_3]^{4-}$, $[(UO_2)_2(C_2O_4)_3]^{2-}$ and $[(UO_2)_2(C_2O_4)_5]^{6-}$ species. Stoichiometry of soluble polynuclear complexes was suggested by the composition of such complexes, obtained in solid state via synthesis [8]. Other dimers, such as $[(UO_2)_2(OH)_2(C_2O_4)_2]^{2-}$, suggested by Ferri et al. [13] but in much more basic conditions than those we used here, are of low probability and therefore were not tested.

In addition to normal spectra, up to fourth derivative spectra were used here to test the different models. As an example, the results corresponding to first derivative, similar to the other derivative orders, are presented in Table 6. It can be seen that the addition of the polynuclear species improves the fit. Although the improvement is not too high, it is statistically significant. The stability constant of equilibrium (A) given by Grinberg et al. [17] can be used to estimate $\log \beta_{25} = 28.7$, which agrees very well with the calculated value of the present work (Table 5).

The spectra for the individual species presented in Fig. 5 concord with theoretical considerations. The absorption spectrum of a solution of synthesized $K_6[(UO_2)_2(C_2O_4)_5(H_2O)_2]\cdot 8H_2O$ compound was measured and the spectrum matched well with that calculated in this work for 2:5 complex, as well as with the spectrum of $(N_2H_5)_6[(UO_2)_2(C_2O_4)_5]\cdot 2H_2O$ as published by Govindarajan et al. [16].

Table 5
Review of some selected formation constants of $[(UO_2)_p(C_2O_4)_q]^{(2p-2q)}$ species ($p = 1, 2$; $q = 1, 2, 3, 5$)

$[NaClO_4]$ (M)	t (°C)	$\log \beta_{11}$	$\log \beta_{12}$	$\log \beta_{13}$	Method	References
0.1	not given		11.08 ± 0.03		dis	[4]
0.1	20	4.63 ± 0.03	8.69 ± 0.03	12.0 ± 0.05	UV sp	[34]
0.1	20	6.36 ± 0.07	10.59 ± 0.07		UV sp	[6]
0.11	25	$6.1_0 \pm 0.1_1$			ix	[35]
1.0	20	5.99 ± 0.03	10.64 ± 0.06	11.0 ± 0.2	UV sp	[6]
1.0	25.00	6.03 ± 0.03	10.87 ± 0.07	14.0 ± 0.3	ise-ox	[12]
2.0	25.00	6.20 ± 0.02	11.21 ± 0.02	14.9 ± 0.1	ise-ox	[13]
3.0	25.00	6.39 ± 0.01	11.52 ± 0.02	15.2 ± 0.1	ise-ox	[13]
3.0	25.0	6.31 ± 0.02	11.21 ± 0.07	13.8 ± 0.04	UV–Vis sp	this work [a]
3.0	25	6.00 ± 0.05 [b]	$11.2_1 \pm 0.1_8$ [b]		dis	[1]
		6.126 ± 0.007 [c]	11.09 ± 0.09 [c]			
5.0	25	$6.5_5 \pm 0.2_8$ [b]	11.28 ± 0.1$_1$ [b]		dis	[1]
		6.917 ± 0.008 [c]	12.92 ± 0.01 [c]			
7.0	25	$6.55 \pm 0.3_3$ [b]	$12.94 \pm 0.4_0$ [b]		dis	[1]
		7.40 ± 0.03 [c]	13.74 ± 0.14 [c]			
9.0	25	7.37 ± 0.05 [b]	14.08 ± 0.1$_1$ [b]		dis	[1]
		7.71 ± 0.02 [c]	14.12 ± 0.07 [c]			

dis, Distribution between two phases; sp, spectrophotometry; ix, ion exchange; ise-ox, ion selective electrode for oxalate.
[a] Chemical model with formation of polynuclear species, $\log \beta_{23} = 18.5 \pm 0.2$; $\log \beta_{25} = 28.5 \pm 0.1$.
[b] The protonated species MHL and $M(HL)_2$ were taken into account.
[c] The protonated species MHL and $M(HL)_2$ were not taken into account.

Table 6
Test of the different possible models evaluating first derivative spectra (A')

Model	Species				$s(A') \times 10^4$	$U \times 10^5$
	ML_2	ML_3	M_2L_3	M_2L_5		
1	11.17(0.01)				2.644	6.583
2	11.06(0.02)	15.26(0.05)			2.089	3.927
3	11.22(0.01)	18.3(0.2)			1.932	3.363
4	11.06(0.02)			28.68(0.05)	2.019	3.667
5	11.14(0.02)	14.9(0.1)	18.0(1.0)		1.811	2.818
6	10.95(0.03)	15.2(0.1)		28.4(0.2)	1.935	3.214
7	11.09(0.02)	18.3(0.4)		28.4(0.1)	1.809	2.812
8	11.05(0.03)	14.0(1.0)	18.5(0.2)	28.5(0.1)	1.804	2.660

Equilibrium constants, log β_{pq}, for the reactions $pM+qL=M_pL_q$ (where, M is UO_2^{2+} and L is $C_2O_4^{2-}$) determined in a 3.00 M $NaClO_4$ medium at 25 °C. In all models log $\beta_{11}=6.29\pm0.03$ was kept constant. *, Compare to log $\beta_{25}=28.7$, recalculated from [17]. The uncertainty (in parentheses) is equal to once the e.s.d. in the least-squares refinement of the experimental data. Data matrix: 24 first derivative spectra (solutions) × 41 wavelengths (396, 398, …, 476 nm). $c_M=8.3$ mM: $9.9<c_L$ mM^{-1} <36.5 for $-\log[H^+]=1.3$ and $8.9<c_L$ mM^{-1} <35.2 for $-\log[H^+]=3.4$; $c_M=16.6$ mM: $16.6<c_L$ mM^{-1} <33.2 for $-\log[H^+]=1.2$ and $16.9<c_L$ mM mM^{-1} <23.2 for $-\log[H^+]=2.2$. The protonation constants, log K_r, for the reactions $rH^+ + C_2O_4^{2-} = H_rC_2O_4^{r-2}$ from this work are equal to log $K_1=3.83\pm0.01$ and log $K_2=4.92\pm0.01$.

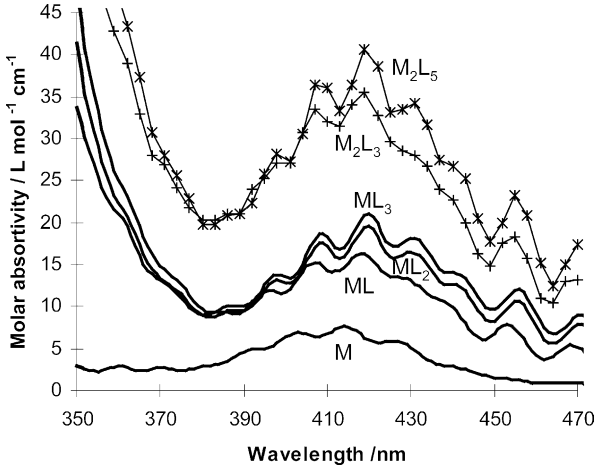


Fig. 5. Calculated spectra of individual species (M is UO_2^{2+} and L is $C_2O_4^{2-}$).

5.1. Vapor-pressure osmometry (VPO) and conductivity experiments

In order to independently check the formation of polynuclear complexes, these two techniques was applied in order to study the behavior of more concentrated solutions of uranyl and oxalate (in absence of $NaClO_4$, i.e. without constant ionic strength).

Solutions of $K_2C_2O_4$ and $UO_2(NO_3)_2$ in ratio 2:3 were prepared at concentrations suited to be studied by VPO, in the limit of their solubility. As shown in Fig. 6(a), a deviation from linearity in VPO experiments for mixtures 2:3 uranium(VI)–oxalate is observed for approximately 0.060 M uranium(VI) (0.180 M oxalate) and higher concentrations.

A saturated solution (ca. 47 g l^{-1}) of $K_6[(UO_2)_2(C_2O_4)_5(H_2O)_2]\cdot 8H_2O$ was used to prepare different dilutions, for which VPO and conductivity measurements were made. Conductivity results are shown in Fig. 6(b) and deviation from linearity is observed both in VPO and conductivity experiments at about 0.030 M uranium(VI) (0.150 M oxalate) and higher concentrations.

The deviation of the linearity in these experiments can be explained by the formation of polynuclear species. Concluding, the presence of polynuclear compounds in aqueous solution might be observed at 0.060 M uranium(VI) or higher concentrations. Rather low improvement of the fit to the spectrophotometric equilibrium data after introducing polynuclear species might be due to the low concentration of these species at the conditions investigated and spectra correlation. The stability constants determined for 2:3 and 2:5 complexes should be regarded as an upper limit of their real values. Studies at the suggested concentrations (0.060 M uranium(VI) or higher) cannot be made at 1 or 3 M $NaClO_4$ since both sodium oxalate and $UO_2(C_2O_4)$ compound are barely soluble at high ionic strength.

Distribution diagram of uranium as a function of oxalate concentration is presented in Fig. 7. Complex 2:3 is a minor species and it explains why most of the previous authors overlook its formation. Polynuclear 2:5 complex is present simultaneously with 1:2 and 1:3 complexes, which explains the discrepancies found in the literature, particularly for the β_{13} value. The relative stability of the 1:3, 2:3 and 2:5 complexes may be explained on the basis of their structures as investigated in solid state. In 2:5 complex, uranyl groups are five-coordinated by oxygen atoms of three oxalate ions, resulting in an approximately pentagonal bipyramidal coordination for uranium. Two oxalate groups are chelating as bidentate (1,4-coordination), while the third one acts as a bridging bidentate (1,4-coordination) [16]. The peculiarity of 1:3 complex is that uranyl group is

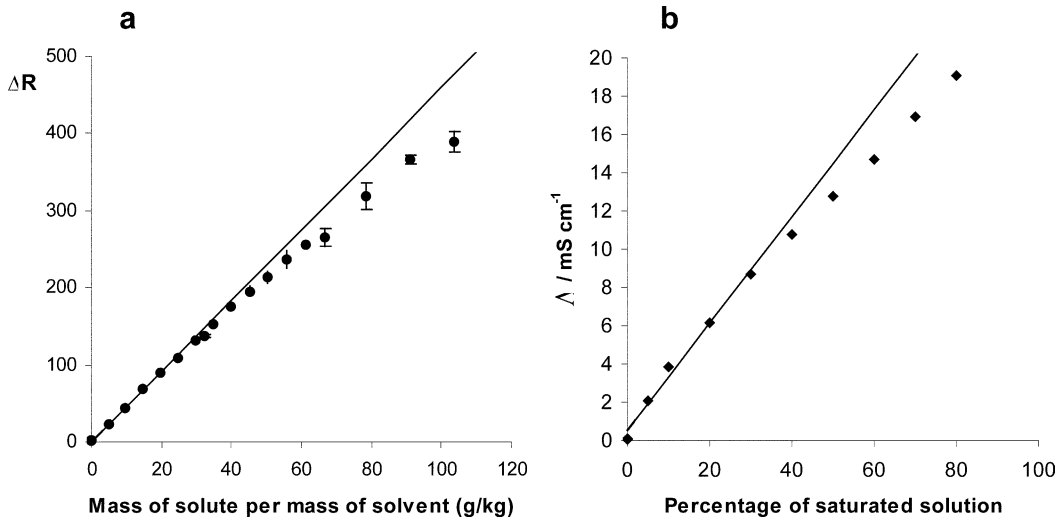


Fig. 6. (a) Vapor pressure osmometry. The solute is a mixture of uranyl nitrate and potassium oxalate in ratio 2–3. The straight line represents the linear regression of the first five points. Three S.D. are shown. (b) Conductivity measurements. The solute is $K_6[(UO_2)_2(C_2O_4)_5(H_2O)_2]\cdot 8H_2O$ and an aqueous saturated solution contains approximately 47 g l^{-1}. The straight line represents the linear regression of the first five points.

not five, but six-coordinated by oxygen atoms of three oxalate ions, one of which is chelating bidentate with 1,3-coordination to give an unique four-membered ring among this family of complexes [11]. The main distinctive characteristic of 2:3 complex (at least as observed in the cell of its crystal form) is that the bridging oxalate is quadridentate, 1,4-coordinated to two uranium atoms [14,15]. All these structural properties fit nicely with the relative stability of 1:3, 2:3 and 2:5 complexes.

5.2. SIT analysis

The extrapolation of experimental stability constants to zero ionic strength was done using specific ion interaction theory (SIT) [7,36,37]. The basic SIT equation for uranyl–oxalate system is

$$\log {}^{*}\beta_{pq} - \Delta z^2 \times D - n \log a(H_2O) = \log {}^{*}\beta^{0}_{pq} - \Delta\varepsilon \times I_m \quad (4)$$

where, ${}^{*}\beta_{pq}$ is a conditional stability constant, Δz^2 the

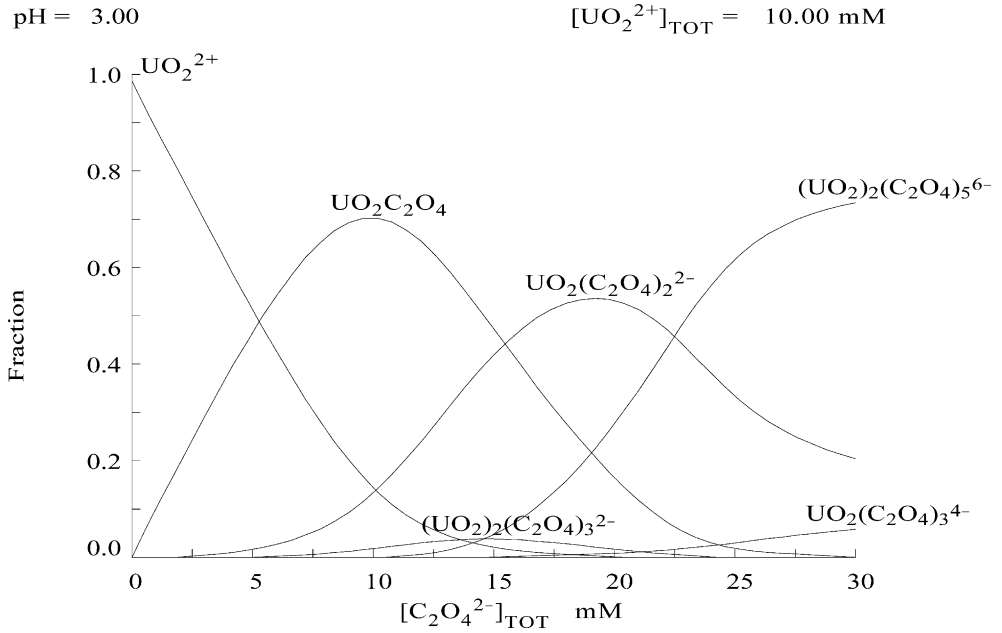


Fig. 7. Distribution diagram for solutions of $[UO_2^{2+}]_{total} = 10$ mM, pH 3 and $[C_2O_4^{2-}]_{total}$ varying from 0 to 30 mM at 25 °C.

charge change in course of reaction, D the Debye–Hückel term, ${}^{*}\beta_{pq}{}^{0}$ the thermodynamic constant at zero ionic strength, $\Delta\varepsilon$ the change of ion interaction coefficients of species involved in the reaction, and I_m is ionic strength in molality scale.

Applying Eq. (4) to uranyl–oxalate system, the following equations are obtained

$$\log \beta_1 + 8D = \log \beta_1{}^{0} - \Delta\varepsilon' \times I_m \quad (5)$$

$$\log \beta_2 + 8D = \log \beta_2{}^{0} - \Delta\varepsilon'' \times I_m \quad (6)$$

$$\log \beta_3 + 0D = \log \beta_3{}^{0} - \Delta\varepsilon''' \times I_m \quad (7)$$

where

$$\Delta\varepsilon' = \varepsilon(UO_2(C_2O_4),\ Na^+ + ClO_4{}^-) - \varepsilon(UO_2{}^{2+},\ ClO^{4-}) - \varepsilon(C_2O_4{}^{2-},\ Na^+) \quad (8)$$

$$\Delta\varepsilon'' = \varepsilon(UO_2(C_2O_4)_2{}^{2-},\ Na^+) - \varepsilon(UO_2{}^{2+},\ ClO^{4-}) - 2\varepsilon(C_2O_4{}^{2-},\ Na^+) \quad (9)$$

$$\Delta\varepsilon''' = \varepsilon(UO_2(C_2O_4)_3{}^{4-},\ Na^+) - \varepsilon(UO_2{}^{2+},\ ClO^{4-}) - 3\varepsilon(C_2O_4{}^{2-},\ Na^+) \quad (10)$$

In order to apply SIT analysis, we need reliable data for different ionic strengths. The system uranium(VI)–oxalate has been studied by means of different experimental techniques in perchlorate as inert supporting electrolyte (Table 5). However, the stability constants in some of those papers [1,34] are lower in comparison with other values. These discrepancies can be ascribed either to some side reactions (e.g. photochemical decomposition of uranium(VI) oxalate), incorrect evaluation of experimental data or wrong chemical model. The formation of protonated species MHL and $M(HL)_2$ was deduced from pH dependence of stability constants obtained [1] but it was not detected by another experimental technique allowing determination of chemical structure in solution (e.g. NMR, EXAFS, etc.). Furthermore, the species are not formed under the experimental conditions given in that paper and, as it was proved here, the stability constants are not dependent on the solution acidity. Hence the stability constants were recalculated as a weighted average of values taken from paper [1] and the new values are given in Table 5. As it can be seen in some cases, there is a large difference between old and new estimates of stability constants.

The experimental stability constants found in literature for various ionic strengths up to 9 M $NaClO_4$ were evaluated (Table 5) and then the chosen values were treated using SIT [7] and following parameters were obtained: $\log \beta_1{}^{0} = 7.41_4 \pm 0.01_4$, $\Delta\varepsilon' = -0.230 \pm 0.004$ kg mol^{-1}, $\log \beta_2{}^{0} = 11.79_6 \pm 0.02_4$, $\Delta\varepsilon'' = -0.462 \pm 0.006$ kg mol^{-1}. Using the ion interaction coefficient $\varepsilon(UO_2{}^{2+},\ ClO_4{}^-) = 0.46 \pm 0.03$ kg mol^{-1} [36] and $\varepsilon(C_2O_4{}^{2-},\ Na^+) = -0.07_9 \pm 0.01_2$ kg mol^{-1} [38], the ion interaction coefficients $\varepsilon(UO_2(C_2O_4),\ Na^+ + ClO_4{}^-) = 0.15_1 \pm 0.03_3$ kg mol^{-1} and $\varepsilon(UO_2(C_2O_4)_2{}^{2-},\ Na^+) = 0.07_2 \pm 0.06_1$ kg mol^{-1} are obtained. The stability constant $\log \beta_3{}^{0} = 13.96_4 \pm 0.06_7$ was obtained by extrapolation to zero ionic strength using $\Delta\varepsilon''' = -0.23 \pm 0.05$ kg mol^{-1} for the formation of uranium(VI) tricarbonate complex [36] and then calculated as weighted average of four values ([12,13] and this work). The extrapolated stability constants at zero ionic strength are in a good agreement with those obtained by Ferri et al. ($\log \beta_1{}^{0} = 7.38 \pm 0.07$, $\log \beta_2{}^{0} = 11.7_2 \pm 0.1$, $\log \beta_3{}^{0} = 13.6 \pm 0.2$) [13]. In addition, the value of ion interaction coefficient $\varepsilon(UO_2(C_2O_4),\ Na^+ + ClO_4{}^-)$ is not zero as it has to be assumed according to SIT but it is comparable with other values obtained for other chemical species [7] ($\varepsilon(CdCl_2{}^0,\ Na^+ + ClO_4{}^-) = 0.15 \pm 0.02$ kg mol^{-1}, $\varepsilon(CdCl_2{}^0,\ Na^+ + ClO_4{}^-) = 0.15 \pm 0.02$ kg mol^{-1}, $\varepsilon(CdCl_2{}^0,\ Li^+ + ClO_4{}^-) = 0.23 \pm 0.05$ kg mol^{-1}, $\varepsilon(CdI_2{}^0,\ Na^+ + ClO_4{}^-) = 0.25 \pm 0.05$ kg mol^{-1}, $\varepsilon(Hg(OH)_2{}^0,\ Na^+ + ClO_4{}^-) = 0.06 \pm 0.05$ kg mol^{-1}, $\varepsilon(HgCl_2{}^0,\ Na^+ + ClO_4{}^-) = 0.06 \pm 0.03$ kg mol^{-1}, $\varepsilon(PbCl_2{}^0,\ Na^+ + ClO_4{}^-) = 0.13 \pm 0.02$ kg mol^{-1}).

The stability constants for uranium(VI)–oxalate at zero ionic strength are much lower than analogous complexes of uranyl-carbonate ($\log \beta_1{}^{0} = 9.67 \pm 0.05$, $\log \beta_2{}^{0} = 16.9_4 \pm 0.1_2$, $\log \beta_3{}^{0} = 21.60 \pm 0.05$ [36,37]) due to its five membered chelate ring in comparison with the four membered one in the case of carbonate.

6. Conclusions

In uranium–oxalate system, the formation of $[(UO_2)_p(C_2O_4)_q]^{2p-2q}$ complexes with composition (p, q) = 1:1, 1:2, 1:3, 2:3 and 2:5 was found and their equilibrium constants determined. Stability constants of mononuclear complexes ($p = 1$, $q = 1$–2), agree with those of Ferri et al. [13]. The difference concerning $\log \beta$ of 1:3 complex at 3 M $NaClO_4$ can be explained by the competing formation of polynuclear 2:3 and 2:5 complexes. The occurrence of polynuclear species in aqueous solution (reported before only in solid state) was also confirmed by conductometry and vapor-pressure osmometry. Absorption spectra of all uranyl–oxalate complexes were calculated and were found to be in good agreement with theoretical considerations.

Acknowledgements

This work was supported by project CEZ:J07/98:143100011 of Ministry of Education and Youth, Czech Republic. J.S.G. would like to thank to the Mexican National Council of Science and Technology (CONACYT) for the fellowship given for his doctorate study at Masaryk University.

References

[1] H.N. Erten, A.K. Mohammed, G.R. Choppin, Radiochim. Acta 66/67 (1994) 123.
[2] A.G. Brits, R. van Eldik, J.A. van den Berg, Z. Phys. Chem. Neue Folge 99 (1976) 107.
[3] V. Kumari, G.K. Chaturvedi, J. Indian Chem. Soc. 56 (1979) 854.
[4] J. Starý, Coll. Czech. Chem. Commun. 25 (1960) 2630.
[5] C. Nguyen-Trung, G.M. Begun, D.A. Palmer, Inorg. Chem. 31 (1992) 5280.
[6] J. Havel, Coll. Czech. Chem. Commun. 34 (1969) 2348.
[7] I. Grenthe, I. Puigdomenech (Eds.),Modelling in Aquatic Chemistry, NEA-TDB, OECD, North-Holland, Amsterdam, 1997, p. 102.
[8] I.I. Chernayev (Ed.),Kompleksnyje sojedinenija urana (Complex Compounds of Uranium), Nauka, Moscow, 1964.
[9] N.C. Jayadevan, D.M. Chackraburty, Acta Crystallogr., Sect. B 28 (1972) 3178.
[10] N.W. Alcock, J. Chem. Soc., Dalton. (1973) 1614.
[11] N.W. Alcock, J. Chem. Soc., Dalton. (1973) 1610.
[12] E. Vasca, T. Caruso, M. Iuliano, C. Manfredi, C. Fontanella, M. Trifuoggi, Ann. Chim. (Rome) 90 (2000) 181.
[13] D. Ferri, M. Iuliano, C. Manfredi, E. Vasca, T. Caruso, M. Clemente, C. Fontanella, J. Chem. Soc., Dalton Trans. (2000) 3460.
[14] N.W. Alcock, Chem. Commun. (1968) 1327.
[15] N.W. Alcock, J. Chem. Soc., Dalton (1973) 1616.
[16] S. Govindarajan, K.C. Patil, M.D. Poojary, H. Manohar, Inorg. Chim. Acta 120 (1986) 103.
[17] A.A. Grinberg, B.V. Ptitsyn, E.N. Tekster, Trudy Radievovo inst. AN SSSR 7, Khimia I geokhimia 74, 1956.
[18] H.D. Burrows, T.J. Kemp, Chem. Soc. Rev. 3 (1974) 139.
[19] E. Rabinowitch, R.L. Belford, Spectroscopy and Photochemistry of Uranyl Compounds, Pergamon, Oxford, 1964.
[20] A.G. Brits, R. van Eldik, J.A. van den Berg, Z. Phys. Chem. Neue Folge 102 (1976) 203.
[21] A.G. Brits, R. van Eldik, J.A. van den Berg, Z. Phys. Chem. Neue Folge 102 (1976) 213.
[22] A.G. Brits, R. van Eldik, J.A. van den Berg, J. Inorg. Nucl. Chem. 39 (1977) 1195.
[23] P. Lubal, J. Havel, Chem. Papers 51 (1997) 213.
[24] G. Meinrath, S. Lis, Z. Stryla, C. Noubactep, J. Alloys Comp. 300–301 (2000) 107.
[25] P. Lubal, J. Havel, Talanta 44 (1997) 457.
[26] Some Laboratory Methods, Stockholm, KTH, 1981.
[27] J. Havel, L. Jancár, Scr. Fac. Sci. Nat. Uni. Purk. Brun. 28 (1990) 295.
[28] D.J. Legett, W.A.E. McBryde, Anal. Chem. 47 (1975) 1065.
[29] L.G. Sillén, B. Warnqvist, Ark. Kemi 31 (1968) 377.
[30] (a) M. Kývala, I. Lukeš, International Conference of Chemometrics 1995, Pardubice, Czech Republic, 1995, p. 63.;
(b) M. Kývala, P. Lubal, I. Lukeš, IX Spanish–Italian Congress on Thermodynamics of Metal Complexes, Girona, 1998, Abstract book, p. 94.;
(c) http://www.natur.cuni.cz/ ~ kyvala/opium.html.
[31] A. Savitzky-Golay, Anal. Chem. 36 (1964) 1627.
[32] J. Steinier, Y. Termonia, J. Deltour. Anal Chem. 44 (1972) 1909.
[33] J.J. Cruywagen, J.B.B. Heyns, Talanta 30 (1983) 197.
[34] C. Miyake, H.W. Nürnberg, J. Inorg. Nucl. Chem. 29 (1967) 2411.
[35] L.R. van Loon, Z. Kopajtic, Radiochim. Acta 54 (1991) 193.
[36] I. Grenthe, J. Fuger, R.J.M. Konings, R.J. Lemire, A.B. Muller, C. Nguyen-Trung, H. Wanner, Chemical Thermodynamics of Uranium, Elsevier, Amsterdam, 1992.
[37] R.J. Silva, G. Bidoglio, M.H. Rand, P.B. Robouch, H. Wanner, I. Puigdomenech, Chemical Thermodynamics of Americium, Elsevier, Amsterdam, 1995.
[38] I. Puigdomenech, W. Hummel, Abstract No. PC1-04, Eighth International Conference on Chemistry and Migration Behaviour of Actinides and Fission Products in the Geosphere MIGRATION'01, Bregenz, 2001.

PERGAMON

Polyhedron 21 (2002) 1421–1427

POLYHEDRON

www.elsevier.com/locate/poly

Acidity in bile acid systems

Adamo Fini [a,*], Giorgio Feroci [a], Aldo Roda [b]

[a] *Istituto di Scienze Chimiche, Università di Bologna, Via S. Donato 15, 40133 Bologna, Italy*
[b] *Dipartimento di Scienze Farmaceutiche, Università di Bologna, Bologna, Italy*

Received 24 September 2001; accepted 15 November 2001

Abstract

The acidity parameter in bile acid systems was re-examined in an attempt to unify the many contrasting results reported in the literature. Discrepancies originate not only through differences in experimental approaches but mainly through the peculiar behaviour of bile acids and their salts, which can be present in aqueous solution as monomers, or simple and/or mixed aggregates. The acidity (and the pK_a values) of bile acid could also be affected by parameters which do not usually play a major role (e.g. hydroxy groups, far from the reaction centre). The microenvironment, where the bile acid is partitioned (e.g. inside a mixed micelle), also makes the carboxyl group less acidic than it would commonly be, considering only structural factors. When the system is made simpler, avoiding problems of solubility and self-aggregation (e.g. in mixed solvents), unconjugated and glycine-conjugated bile acids display acidity behaviour which matches their molecular structure. © 2002 Published by Elsevier Science Ltd.

Keywords: Acidity parameter; Aqueous solution; Hydroxy groups; Glycine-conjugated bile acids

1. Introduction

Bile acids are a group of acidic compounds, which are present in biological fluid mostly in their ionised form; they are produced by cholesterol (and, therefore, possess its steroid skeleton) and are responsible for its transport in the intestine via formation of mixed micelles or vescicles, composed also of phospolipids. In a physiological medium bile salts interact not only with cholesterol but also with fairly soluble lipid materials such as fatty acids and hydrophobic drugs, since, above a narrow range of concentration value (CMC), they self-associate to form micelles, which are able to solubilise or emulsify endogenous and exogenous materials and, therefore, to improve their transport and absorption or, in any case, to prevent their precipitation [1–4].

Bile acids are synthesised in the liver as unconjugated C-24 carboxylic acids and, after amidation, are secreted into the bile. They are exclusively amidated with glycine and taurine and accumulated in these forms. The most relevant bile acids in humans are the two primary bile acids i.e. cholic acid, 3α7α12α tri-hydroxy-5β-cholan-24-oic acid and chenodeoxycholic acid, 3α7α di-hydroxy-5β-cholan-24-oic acid; by the action of intestinal bacterial 7-dehydrogenase enzyme they are converted, respectively, to deoxycholic acid, 3α,12α di-hydroxy-5β-cholan-24-oic acid and lithocholic acid, 3α monohydroxy 5β-cholan-24-oic acid [4]. Most of the physical chemistry studies dealing with their behaviour in aqueous solution in terms of micelle formation and the little accurate data on solubility, acidity and other properties has only recently been defined [5–11].

On the other hand little data is available regarding their action towards hydrogen or metal ions [12–24].

Moreover, the importance of having experimental data as close as possible to a physiological medium greatly limited the possibility of obtaining results with thermodynamic meaning. In addition the behaviour in solution of these acids (poorly soluble in water) and anions (self-aggregated in micelles) imposed non-canonic experimental conditions or suggested the use of indirect approaches to the determination of acidity constants, that, therefore, appear as a set of scattered values. These could have been interpreted as not very precise if the values were not read in the light of the different conditions used for measurements or if the micro-environment surrounding the molecules during

* Corresponding author. Tel.: +39-051-24-4540; fax: +39-051-24-9770.
E-mail address: fini@biocfarm.unibo.it (A. Fini).

0277-5387/02/$ - see front matter © 2002 Published by Elsevier Science Ltd.
PII: S0277-5387(02)00968-3

the determinations was not taken into account. In the classic review regarding bile acid chemistry and physiology [4] very different pK_a values are still wrongly reported among a class of unconjugated bile acids and these data lead to misinterpretation of their physiopathological role [5].

In a previous paper [25] we preliminarily reported and discussed the difference in behaviour between monomers and aggregates, the latter playing an important role in the optimisation of bile acid functions in biological systems, in such a way as to represent a preorganised and privileged substrate for reaction with hydrophilic species, such as, for instance, hydrogen or metal ions, not only for hydrophobic substances.

In this paper, by reviewing the suggestions and considerations that have emerged during more than 30 years of experimental work on these topics, we wish to discuss the influence of the surrounding medium on the acidity constant of bile acids and that of the experimental conditions, in an attempt to find a relationship between the values obtained in different conditions by different authors and establish the 'true' pK_a value for bile acid systems.

2. The bile acid molecule

Bile acids consist of a steroid nucleus, containing 1, 2 or 3 hydroxy groups, that differentiate the single compounds by number, position and orientation; they also bear a short side chain terminating with a carboxy group, that can be free (unconjugated bile acid, UCBA), conjugated with the glycine (GCBA) or taurine (TCBA). Irrespective of their structure the terms bile salt or bile acid anion both refer to the ionised forms, which is the form present in solution in most of the physiological medium [1].

Thus the steroid structure of a bile acid is identified by the hydroxy groups: e.g. a pattern such as 3α, 7α, 12α indicates the moiety typical of the cholic acid (CA, for the unconjugated form), that remains unchanged when the side chain carboxylic group binds, through a peptide moiety –CONH–, to glycine (glycocholic acid, GCA) or taurine (taurocholic acid, TCA). Different bile acids of the same class do not, therefore, differ due to the nature of the acidic group; researchers took advantage of this fact, using the most soluble compounds for each class for measurements and extending the results to all others [1].

3. Behaviour in aqueous solution

UCBA and GCBA are rather poorly soluble in water in their unionised form; while TCBA, bearing the strongly hydrophilic sulphonic group, does not display problems for solubility in water in both forms [5,6]. The water solubility of the bile acids is also influenced by the nature of their solid state; see, for example, the difference between two di-hydroxy bile acids, such as 3α7α and 3α7β di-hydroxy epimers [26,27].

Solubility increases with the pH according to the anionic species formation; a CMpH can be defined, whose value represents the lowest pH, which ensures a sufficiently high concentration of the ionised form to originate micelles:

$$\mathrm{CMpH} = \mathrm{p}K_a + \log(\mathrm{CMC}/S_w)$$

where S_w is the water solubility of the unionised form. This parameter is related to the dissolution of a bile acid when orally administered as a solid and in dissociated form (see for instance the UCDA administration for gallstone dissolution) [11].

Bile salts behave in aqueous solutions as association colloids. They are atypical surface active agents: in this class of compounds the molecular polarity originates from a dissimilarity between the two faces of the steroid rings: the one containing the hydroxy groups is defined as α-face; while the one formed by the hydrocarbon skeleton is the β-face [28]. The aggregation occurs via a 'back-to-back' contact between the β-faces of two monomers to minimise the contact with water of these hydrophobic surfaces (primary micelles) [28].

In most of the physiological bile acids all the hydroxy groups are oriented in the same direction, even if other bile acids present not in human but in other animal species present a structure in which the continuity of the hydrophobic β-face is partially interrupted by the presence of hydroxyls, which are no longer oriented in the α-face. Typical examples are represented by ursodeoxycholic acid (UDCA), 3α7β di-hydroxy-5β-cholan-24-oic acid and ursocholic acid (UCA), 3α7β12α trihydroxy-5β-cholan-24-oic acid.

Aggregation starts above a so-called critical micelle concentration (CMC). The CMC values are affected by the number, position and orientation of hydroxyls, and bile acids, like those reported above, exhibit high CMC values with respect to conventional bile acids (compare UDCA vs. CDCA and CA vs. UCA) [5,29].

The aggregation number is generally low and micelles can increase their size and number as the bile salt concentration increases; as a consequence, the aggregation is not really co-operative and critical.

In other words in bile salt micelles the hydrophobic effect is weak, since the molecular size and the mode of association prevent the building of large and compacted structures. The term CMC, however, is widely used, even though it also refers to a (narrow) concentration range rather than to a single concentration, as is usually reported. Dimers represent the starting and more frequent form of association, especially for hydrophilic bile salt (such as cholate). Electrostatic repulsion of

charged groups does not occur in dimerisation since the charged chains are positioned as far as possible from each other, that is diagonally opposite in a dimer structure [29].

Association could also be present at low concentrations, and may even not be detectable when using in a appropriate techniques; the study of the isolated monomers can, therefore, be carried out only at very low concentrations, below the CMC. In most cases the concentration ranges useful for acidity constant determination are too low and too narrow to allow accuracy. Moreover, the low solubility in water of the unionised forms for UCBA and GCBA limit direct determinations in water.

This introduction is necessary to understand the results obtained with bile salts towards hydrogen ions as well as heavy metal ions and the differences between monomers and aggregates, since many parameters undergo a fairly sharp change around the CMC.

4. Hydrolysis

At low concentrations the bile salts behave like a 1:1 electrolyte. Since UCBA are weak acids, the pH of the sodium deoxycholate (which is a 3α12α UCBA) aqueous solutions steadily increases with concentration, as expected. When aggregates start to form, pH shows a dramatic increase, as a consequence of a higher hydrolysis reaction, as if the strength of the acid undergoes a sudden drop after the aggregation [30]. In fact, when anions in large aggregates are forced into a closer spatial contiguity than that of monomers in solution, an increased electrostatic repulsion occurs. To attenuate this repulsion, some surface charges are protonated by water and consequently produce OH^- ions. At the same time, an electrode sensitive to sodium ions reveals a parallel increase of activity of Na^+ ions, that, as a consequence of the protonation, are freed from the micellar surroundings. It must be pointed out that deoxycholate forms the largest micelles of all bile salts examined and its behaviour is opposite to that of cholate.

These results suggest that a bile salt micelle can be considered a polyanion, like that formed by the ionisation of a poly(carboxylic acid), where single components are kept together by hydrophobic effects, rather than by covalent bonds, such as in the polymer, and where a polyelectrolyte effect operates to increase the affinity of the anion groups towards protons. In this particular polyanion, charged and uncharged groups coexist, solvated by the ions present in the original salt form. When a charged group is protonated, precipitation of the poorly soluble unionised form does not occur immediately, despite its low solubility: this is maintained in solution, precisely because of its participation in this assembled structure. This can, at the same time, explain the resistance to precipitation of the protonated bile acid after an abrupt decrease of pH [31].

This fact has some practical implications, since simple measurements of pH, as a function of concentration, could be sufficient to determine the CMC of bile salts without invasive techniques or the addition of extraneous substances to the system. This fact also explains the possibility of obtaining different acidity constants when the concentration is above or below the CMC, which, therefore, represents a critical concentration border around which a bile salt exists in different forms (monomer/micelle) affecting the experimental results. Qualitatively this suggests that the acidity of a bile acid (when in micelles) is a function of the aggregation degree and, therefore, of all the parameters affecting the aggregation, such as, for instance, concentration and nature of electrolytes controlling the ionic strength.

5. Acidity constant of aggregates

$C_{tot} = CMC$ represents the highest concentration of the monomer, which remains rather constant also at $C_{tot} > CMC$, where excess bile salts self aggregate and the solution contains monomer and aggregates. At $C_{tot} = 0.1$ M, a proton added by titration more frequently encounters a micellar rather than a monomer bile salt anion. Previous data concerning pK_a values [32] did not take into account possible differences between monomers and aggregates; therefore, acid–base titrations provided different results depending on the total concentration used (in parentheses): deoxycholate: 5.3 (2 mM); 6.3 (23 mM); chenodeoxycholate: 5.88 (2 mM); 6.18 (23 mM); glycocholate: 3.95 (2 mM); 3.8 (20 mM); glycodeoxycholate: 4.69 (2 mM); 4.77 (20 mM); glycochenodeoxycholate: 4.23 (1.5 mM); 4.20 (76 mM).

Let us consider the difference between cholate and chenodeoxycholate, two UCBA having 3α7α12α and 3α7α hydroxy groups, respectively. The first one contains three hydroxy groups and is known to form only dimers in a large concentration range. In this case the poly-electrolyte effect can be considered practically negligible, since, according to the 'back-to-back' aggregation, the charged chains are completely separated from each other and behave independently as far as their affinity to protons is concerned. By titrating this system it was observed that the acidity constant is unaffected by the total concentration of cholate (at least in the concentration range examined, where the system remains homogeneous) and its value ($pK_a = 5.02$) concords with the value expected for the structure of such an acid: that is an aliphatic carboxylic acid, where the steroid moiety has very limited influence on the acidic behaviour, like a simple alkyl group [33,34].

On the contrary, chenodeoxycholate (that is a 3α7α UCBA, more hydrophobic than cholate) forms aggregates of a larger size and in this case the polyelectrolyte effect plays a major role: the observed pK_a value (6.38) is much higher than that expected from the structure of the monomer. The carboxylate groups, kept together in the structure of a micelle, display a synergetic affinity to protons. The assembly of monomers by hydrophobic effect is very efficient, since during titration the precipitation of unionised species is slowed down; protonated monomers are kept solubilised as long as the system globally maintains a favourable hydrophilic/hydrophobic balance: also metastable, the system allows the collection of precise experimental data [33,34].

These results confirm that intra and intermolecular interactions affect acidity: acidity constants determined in these conditions are thus also a function of the hydroxy groups, despite their distance from the reaction centre and a completely aliphatic bonding system. In fact they are involved in the formation of secondary micelles, mainly by intermicellar hydrogen bonds, and are responsible for the aggregation number of micelles [35–38].

6. Acidity constant of monomers

At the same time, however, it is well known that an aliphatic structure, such as that of the steroid ring and its substituents, especially when far from the reaction centre, should not have any influence; the acidity constant should be the same for each bile acid in each bile acid class.

To minimise the polyelectrolyte effect, which alters the behaviour of the anions, and to study the behaviour of monomers different approaches were used.

First, acidity constants were measured [39] in a mixed solvent (methanol/water 50% w/w), where the hydrophobic effect does not operate and aggregation does not occur, since both bile acids and bile salts are freely soluble.

As expected, within the UCBA class, where the side chain bears a carboxyl group, all the components display the same acidity constant; steroid hydroxy does not influence the acidity. They are too far from the reaction centre and their inductive or mesomer effects cannot be transmitted through the aliphatic structures of the steroid ring. This test was carried out only with UCBA, available in a very large variety of structures [40].

A second approach [41] considered potentiometric measurements in mixed solvents of different composition and extrapolation of experimental data to a zero content of the organic solvent, that is to pure water. Using two different solvent systems (DMSO and methanol) and two bile acid classes (UCBA and GCBA), values in agreement with each other, both for cholic and glycocholic acid, were obtained. The pK_a value (5.05) for the UCBA is a little higher that that of the GCBA (3.91), because of the -I effect of the peptide group near the acidic centre. This pair of values was confirmed also for deoxycholic and glycodeoxycholic acid [41].

Finally we carried out direct potentiometric measurements on UCA, a 3α7β12α tri-hydroxy semi-synthetic bile acid. This compound has both a high CMC and solubility in water, thus allowing reliable direct data, without the possible interference of aggregates, formation of precipitate or presence of organic solvent. Titration of the sodium salt afforded a value of 4.76 (25 °C and 0.1 M NaCl), which concords very well with previous values obtained by extrapolation and without controlling the ionic strength; moreover the measured $\Delta H = +0.1$ Kcal mol^{-1} can be easily associated with the ionisation of a mono-carboxyl aliphatic acid. The same results were obtained with cholic acid [19].

More recently an interesting result was obtained [42] again using a semisynthetic sodium bile salt, namely UDCA , whose two hydroxy groups were sulphated, giving rise to an anion with three negative charges, freely soluble in water. By titrating the carboxylate group in carefully controlled conditions (0.25 M KCl or Et_4NI, at 25 °C) the following was found: absence of monomeric species in the solution, either protonated or complexed; initial presence of a completely deprotonated dimer (L_2^{6-}) that converts into partially (HL_2^{5-} and $H_2L_2^{4-}$) protonated forms in the course of titration. The values obtained for the acidity constants (5.25 and 4.80) refer to the protonation of the two carboxylate groups [42].

These results suggest a few comments.

It is not clear whether the formation of a dimer found for this compound, at the concentrations used, is a general feature for each bile salt or peculiar to this particular compound: nevertheless, this fact suggests [42] that experimental conditions for the study of isolated monomers of bile salts must be carefully controlled since the association cannot simply be ignored, even in a dilute solution of bile salts and especially at high ionic strength.

The effect of the ionic strength on the CMC is dependent on the nature of the electrolyte, since it was reported that the disulphated ursodeoxycholate forms a complex with K^+ ions. In addition this fact suggests the need to specify the nature of the electrolyte used in every experiment with bile salts and to control the occurrence of unforeseen interactions between the cations of the electrolyte and the bile salt anions (monomer or micelle).

7. Influence of the medium

Previous data suggested that the different acidity of monomers and aggregates originates from the micro environment surrounding the centre of the reaction [43,44].

As a consequence, the differences observed in the case of cholic acid when inserted into mixed micelles with phosphatidylcholine or bound to serum albumin are not surprising: these results were obtained measuring the ^{13}C chemical shift of the C24 of the carboxyl group, as a function of pH [43,44].

Different pK_a values can be found for the same compound according to the nature of the medium: the ionisation ability of a bile acid tends to decrease as far as the hydrophobicity of the medium surrounding the acidic group increases, as a consequence of increasing difficulty for the anion to be solvated.

Cholic acid shows an apparent pK_a 4.98 in 2 mM solution in water (below CMC), 5.2 in 3 mM solution cholic acid solubilised in 90 mM sodium taurocholate, 5.5 in 100 mM solution (above CMC) [46] and two values in phospholipid vesicles as 3 wt.% were 6.8 for the first and 7.3 for the second. This last value is attributed to the molecules inside the layer of the vesicle, the carboxyl group being more shielded than that on the outside [45]. Finally cholic acid bound to albumin has an apparent p$K_a \approx 4.2$. These values overlap those found for the oleic acid in similar experimental conditions, suggesting that the state of ionisation of carboxyl carbon of fatty acids strongly depends on the surrounding medium: a hydrophobic environment destabilised a charged moiety, increasing its affinity for hydrogen and metal ions [45].

8. Affinity for Me^{2+} ions

The affinity of bile salts also increases towards the metal cations when in the form of aggregates [46–53]. Metal ions form complexes with small aggregates that can saturate the solution or remain in solution as colloidal species. Measurements were carried out by polarographic techniques. This first behaviour is typical of hydrophobic bile salts; the precipitation, as a consequence of the formation of very simple (dimers?) and poorly soluble species, is accompanied by a marked decrease of the metal ion concentration (in most cases the precipitation of a salt was observed); in the second case, the depletion of the metal ion in the solution is less pronounced, because hydrophilic complexes are formed and solubilisation and a clarification of the system is observed, as the bile salt concentration increases due to the formation of more soluble complexes with larger bile salt aggregates [53–55].

Solubilisation occurs when larger aggregates are formed and the basicity of the system increases: when this ability is scarce, the bile salt is not able to maintain metal ions in the solution, forming soluble complexes [54]. This can be the case of ursodeoxycholate that only forms aggregates of a small size. During ursotherapy to dissolve cholesterol gallstones, bile is enriched with this exogenous bile acid, increases its ability to interact with cholesterol, but decreases the solubilising ability for metal ions, which can precipitate in an insoluble form. In fact long-term ursotherapy leads to the formation of a thin film of calcium carbonate on gallstones and prevents continuing solubilisation. But when the pool of bile acids has the physiological composition [55], precipitation of complexes or salts with heavy metal ions is very rare, this system displaying a notable buffering action towards the activity of hydrogen and heavy metal ions in bile [53–58].

9. Conclusions

Each bile acid of the UCBA and GCBA classes behaves like common aliphatic carboxylic acids, when the experimental conditions cancel its peculiarities (poor solubility for the acids and self aggregation for the anions). Due to their acidic strength, TCBA were not

Table 1
Chemical and physical properties of some bile acids and salts at 25 °C [56–58]

Bile acids	Symbol	Hydroxy group	log P	CMC (mM)	Solubility (μM)	CMpH (mM)
Cholic	CA	3α7α12α	2.02	11	273	6.71
Taurocholic	TCA	3α7α12α	–	6	–	–
Glycocholic	GCA	3α7α12α	1.65	10	32	5.72
Ursocholic	UCA	3α7β12α	0.92	39	1670	6.73
Hyocholic	HCA	3α6α7α	2.80	8	45	7.53
Chenodeoxycholic	CDGA	3α7α	3.28	4	27	7.59
Ursodeoxycholic	UDCA	3α7β	3.00	7	9	8.44
Hyodeoxycholic	HDCA	3α6α	3.08	6	15	8.16
Deoxycholic	DCA	3α12α	3.50	3	28	7.30
Lithocholic	LA	3α	–	–	–	–

Table 2
pK_a values for the cholic acid under different experimental conditions

pK_a	Experimental conditions	References
5.02	Above CMC	[10,11]
5.21	At 22 mM	[4]
5.5	At 80 mM	[4]
4.98	Below CMC (2 mM)	[18]
6.30	Aqueous methanol 50% v/v	[12,13]
5.05	Extrapolated from potentiometric measurements in aqueous methanol and DMSO	[14]
I = 6.8; II = 7.3	Phospholipid vesicles	[19]
5.2	In 3 mM sodium taurocholate	[18]

examined here. Precise pK_a for any taurine conjugates are not yet known; they will probably be between −1.5 and +1.5 [28].

Some pK_a values for the cholic acid are summarised in Tables 1 and 2 for comparison.

When in aggregated form, anionic micelles can refer to single anions as a polycarboxylic polymer relates to its monomers: in both cases the polyelectrolyte effect increases the affinity of the anion to protons (or metal ions) and higher pK_a are found.

A hydrophobic environment destabilises charged moieties, increasing their affinity for protons to acquire an uncharged form: again higher pK_a values are produced. Different values obtained for the same compounds, in different situations, must be related to the experimental conditions, and each value has an intrinsic meaning.

Acknowledgements

This investigation was supported by the Bologna University Funds (Funds for selected research topics) and by MURST Funds (ex-40%).

References

[1] A. Fini, The physical chemical properties of bile acids and their role in drug delivery, in: D.D. Breimer, D.J.A. Crommelin, K.K. Midha (Eds.), Topics in Pharmaceutical Sciences (Ch. 32), F.I.P, The Hague, The Netherlands, 1989, pp. 459–471.
[2] P. Zuman, A. Fini, Solubilization of organic compounds in the presence of bile salts and related phenomena, in: W.L. Hinze Series (Ed.), Organized Assemblies in Chemical Analysis. Bile Acids/Salts Surfactant Systems, vol. 2, JAI Press Inc, Stamford, CT, 2000, pp. 117–145.
[3] A. Fini, A.L. Fini, M. Gonzalez Cordero, G. Feroci, Acidi biliari e solubilizzazione di farmaci, in: A. Roda, E. Roda, A.F. Hofman (Eds.), Acidi Biliari 2000: aggiornamento per il futuro, Masson, Milan, 2000, pp. 227–246.
[4] P.P. Nair, D. Kritchevsky, The Bile Acids: Chemistry, Physiology and Metabolism, vol. 1, Plenum, New York, 1971.
[5] A. Roda, A.F. Hofmann, K.J. Mysels, J. Biol. Chem. 258 (1983) 6362.
[6] A.F. Hofmann, A. Roda, J. Lipid Res. 25 (1984) 1477.
[7] F. Scagnolari, A. Roda, A. Fini, B. Grigolo, Biochim. Biophys. Acta 791 (1984) 274.
[8] A. Roda, A. Fini, B. Grigolo, P. Simoni, E. Roda, Composizione e stato chimico-fisico della bile, in: A. Roda, E. Roda, G. D'Ascenzo, L. Barbara (Eds.), La bile: aspetti chimici, farmacologici e fisiopatologici, Bologna, 1985, pp. 49–60.
[9] A. Fini, A. Roda, Hepatology 4 (1984) 72S.
[10] A. Roda, G. Cappelleri, R. Aldini, E. Roda, L. Barbara, J. Lipid Res. 23 (1982) 490.
[11] A. Roda, B. Grigolo, A. Minutello, A. Fini, R. Pellicciari, B. Natalini, Relazione struttura-funzione degli acidi biliari, I: Proprietà chimico-fisiche, in: A. Roda, R. Pellicciari (Eds.), Acidi Biliari: Ricerca e Applicazioni Terapeutiche, Momento Medico, Bologna, 1991, pp. 51–72.
[12] E.W. Moore, L. Celic, J.D. Ostrow, Gastroenterology 84 (1982) 1079.
[13] C.A. Jones, A.F. Hofmann, K.J. Mysels, A. Roda, J. Colloid Interface Sci. 114 (1986) 452.
[14] N. Rajagopalan, S. Lindenbaum, Biochim. Biophys. Acta 711 (1982) 66.
[15] A.J. Sanyal, J.I. Hirsch, E.W. Moore, Gastroenterology 10 (1989) 116A.
[16] A. Fini, A. Roda, Ioni inorganici e bile, in: A. Roda, E. Roda, G. D'Ascenzo, L. Barbara (Eds.), La bile: aspetti chimici, farmacologici e fisiopatologici, Atti del Seminario Interdisciplinare di Studio, Bologna, 1985, pp. 65–70.
[17] A. Fini, A. Roda, Interazione tra anioni biliari e cationi metallici, in: A. Roda, R. Pellicciari (Eds.), Acidi Biliari: Ricerca e Applicazioni Terapeutiche, Momento Medico, Bologna, 1991, pp. 89–106.
[18] G. Feroci, A. Fini, G. Fazio, P. Zuman, J. Colloid Interface Sci. 166 (1994) 180.
[19] A. Fini, G. Feroci, G. Fazio, A. Roda, P. Zuman, Curr. Top. Solution Chem. 1 (1994) 69.
[20] G. Feroci, G. Fazio, A. Fini, P. Zuman, J. Pharm. Sci. 84 (1995) 119.
[21] G. Feroci, A. Fini, G. Fazio, P. Zuman, Anal. Chem. 67 (1995) 4077.
[22] G. Feroci, A. Fini, G. Fazio, P. Zuman, J. Colloid Interface Sci. 178 (1996) 339.
[23] G. Feroci, A. Fini, G. Fazio, A. Roda, P. Zuman, Microchem. J. 55 (1997) 382.
[24] A. Fini, G. Feroci, G. Fazio, P. Zuman, J. Inorg. Biochem. 68 (1997) 251.
[25] A. Fini, G. Feroci, G. Fazio, P. Zuman, A. Roda, in: A. Fini (Ed.), Bile salt aggregates as pre-organized substrates for binding H^+ and Me^{2+} ions. Incontro su recettori pre-organizzati per metalli e substrati, Bologna, 1993, pp. 71–82.
[26] A. Fini, A. Roda, R. Fugazza, B. Grigolo, J. Solution Chem. 14 (1985) 595.
[27] Y. Moroi, M. Kitagawa, H. Itoh, J. Lipid Jpn. 33 (1992) 49.
[28] M.C. Carey, Measurement of physical-chemical properties of bile salt solutions, in: L. Barbara, R.H. Dowling, A.F. Hofmann, E. Roda (Eds.), Bile Acids in Gastroenterology, Cortina, Italy, 1985, pp. 19–56.
[29] A. Roda, C. Cerrè, A. Fini, A.M. Sipahi, M. Baraldini, J. Pharm. Sci. 84 (1995) 593.
[30] G. Sugihara, M. Tanaka, Bull. Chem. Soc. Jpn. 49 (1976) 3457.
[31] G. Sugihara, K. Yamakawa, Y. Murata, M. Tanaka, J. Phys. Chem. 86 (1982) 2784.
[32] D.M. Small, The physical chemistry of cholanic acids, in: P.P. Nair, D. Kritchevsky (Eds.), The bile acids, Chemistry, Physiology and Metabolism, vol. 1, Plenum, New York, 1971, pp. 1249–1355.

[33] P. Ekwall, E.V. Lindstrom, K. Setala, Acta Chem. Scand. 5 (1951) 990.
[34] H. Igimi, M.C. Carey, J. Lipid Res. 21 (1980) 72.
[35] L.J. Kunze, S. Lindenbaum, J. Pharm. Biomed. Anal. 7 (1989) 947.
[36] M. Vadnere, S. Lindenbaum, J. Pharm. Sci. 71 (1982) 881.
[37] M. Vadnere, S. Lindenbaum, J. Pharm. Sci. 71 (1982) 875.
[38] N. Rajagopalan, S. Lindenbaum, Biochim. Biophys. Acta 711 (1982) 66.
[39] P. DeMaria, A. Fini, A. Roda, Gazz. Chim. It. 111 (1981) 95.
[40] A. Fini, A. Roda, P. DeMaria, Eur. J. Med. Chem.-Chim. Ther. 17 (1982) 467.
[41] A. Fini, A. Roda, J. Lipid Res. 28 (1987) 755.
[42] A. De Robertis, C. De Stefano, Modelli di protonazione di acidi biliari in diverse condizioni di concentrazione e di mezzo ionico: un approccio metodologico, in: A. Roda, R. Pellicciari (Eds.), Acidi biliari: ricerca e applicazioni terapeutiche, Momento Medico, Bologna, 1990, pp. 33–49.
[43] D.J. Cabral, J.A. Hamilton, D.M. Small, J. Lipid Res. 27 (1986) 334.
[44] D.M. Small, D.J. Cabral, D.P. Cistola, J.S. Parks, J.A. Hamilton, Hepatology 4 (1984) 77S (and references therein).
[45] D.M. Small, S.A. Penkett, D. Chapman, Biochim. Biophys. Acta 176 (1969) 178.
[46] E.W. Moore, J.D. Ostrow, Gastroenterology 109 (1995) 662.
[47] A.J. Sanyal, J.I. Hirsch, E.W. Moore, Gastroenterology 106 (1994) 866.
[48] A.J. Sanyal, J.I. Hirsch, E.W. Moore, Am. J. Physiol. 266 (1994) G318.
[49] A.J. Sanyal, J.I. Hirsch, E.W. Moore, Gastroenterology 102 (1992) 1997.
[50] A.J. Sanyal, M.L. Shiffmann, J.I. Hirsch, E.W. Moore, Gastroenterology 101 (1991) 382.
[51] E.W. Moore, Hepatology 12 (1990) 206S.
[52] A.J. Sanyal, J.I. Hirsch, E.W. Moore, J. Lab. Clin. Med. 116 (1990) 76.
[53] G. Feroci, A. Fini, P. Zuman, Bioelectrochem. Bioenerg. 29 (1992) 91.
[54] A. Fini, G. Feroci, Heavy metal ions and physiological bile salt pool. X Italian-Spanish congress on thermodynamics of complexes. S.Martino al Cimino (Viterbo, Italy, 6-10 June, 1999).
[55] A. Fini, G. Feroci, G. Fazio, P. Zuman, Quimica Analitica 15 (1996) 558.
[56] A. Roda, A.M. Gioacchini, A.C. Manetta, C. Cerrè, M. Montagnani, A. Fini, Ital. J. Gastroenterol. 27 (1995) 327.
[57] A. Roda, A. Minutello, M.A. Angellotti, A. Fini, J. Lipid Res. 31 (1990) 1433.
[58] A. Roda, A. Fini, B. Grigolo, P. Simoni, G. Rusticali, B. Natalini, Ann. Chim. 78 (1988) 15.

PERGAMON

Polyhedron 21 (2002) 1429–1437

POLYHEDRON

www.elsevier.com/locate/poly

Liquid–liquid extraction of palladium(II) and gold(III) with *N*-benzoyl-*N*′,*N*′-diethylthiourea and the synthesis of a palladium benzoylthiourea complex

Mercè Domínguez [a], Enriqueta Anticó [a], Lothar Beyer [b], Angel Aguirre [c], Santiago García-Granda [c], Victoria Salvadó [a,*]

[a] *Dept. de Química, Universitat de Girona, Campus Montilivi, 17071 Girona, Spain*
[b] *Institut für Anorganishe Chemie, Universität Leipzig, Johannisallee 29, D-04103 Leipzig, Germany*
[c] *Depto. de Química Física y Analítica, ClJulián Clavería 8, 33006 Oviedo, Spain*

Received 23 October 2001; accepted 3 December 2001

Abstract

N-Benzoylthioureas have been reported to form complexes with gold (III) and palladium (II) and other transition metals. In this study, an *N*-benzoyl-*N*′,*N*′-diethylthiourea (**3f**) ligand was used in the solvent extraction of palladium(II) and gold(III) from aqueous chloride media (0.1 mol l^{-1} NaCl). The distribution coefficient was determined as a function of both metal concentration in the aqueous phase and extractant concentration in the organic phase. The experimental distribution data were numerically analysed by LETAGROP-DISTR software in order to obtain the thermodynamic model corresponding to the metal extraction. It is found that pH does not affect the metal extraction process in the 1–2 pH range. Synthesis of the palladium benzoyl thiourea complexes was carried out by mixing quantities of metal and ligand solutions in methanol in a 1:2 ratio stoichiometric. Yields of 74 and 80.9% were obtained for the Pd-3c and Pd-3f complexes. In order to confirm the formation of the palladium complexes, NMR, FTIR and MS analyses were performed. From MS analyses a complex stoichiometry 1:2 (metal:ligand) was confirmed. The formation of crystals of palladium *N*-benzoyl-*N*′,*N*′-diethylthiourea complex (Pd-3f) in the methanolic solution allows the characterisation of the complex structure by XRD. The resulting structure is described and discussed. Bis(1,1,-diheptadecyl-3-benzoyl-thioureate)palladium(II) (Pd-3c) and bis(1,1,-diheptadecyl-3-benzoyl-thioureate)palladium(II) (Pd-3f) were used as ionophores in polymeric membrane electrodes. Their potentiometric responses to different anionic metal chlorocomplexes are evaluated and discussed taking into consideration the results obtained in the liquid–liquid distribution studies. A nernstian response was only obtained for $AuCl_4^-$ (PDL = 8.8×10^{-8}) and $PdCl_4^{2-}$ (PDL = 1.5×10^{-4} M) with a selectivity coefficient of $K^{pot}_{AuCl_4^-,\ PdCl_4^{2-}} = -3.4$, calculated taking $AuCl_4^-$ as being the primary anion. © 2002 Elsevier Science Ltd. All rights reserved.

Keywords: *N*-Benzoylthiourea derivatives; Gold; Palladium; Solvent extraction; Ion selective electrode; Crystal and molecular structure

1. Introduction

The development of selective extractants for the separation and concentration of precious metals at trace levels reflects an increasing need for these metals to be recovered and analysed. Chelating extractants have been found to be more selective than solvating reagents and anion exchangers, and, in accordance with Pearson's theory [1], better performance is obtained with sulfur-containing compounds in the cases of Au(III) and Pd(II). Of the extractants containing soft atoms, a novel group of benzoylthioureas has been reported to form complexes with Cu, Fe(III), Pb, Ni, Zn, Cd, Co, Ag, Pd, Hg and Au [2]. In particular, *N*-benzoyl-*N*′,*N*′-diheptadecylthiourea (**3c**) and *N*-benzoyl-*N*′,*N*′-diethylthiourea (**3f**) (see Fig. 1) have been successfully used in the extraction of copper(II) [3] and gold(III) [4] from acidic media. These reagents have also been implemented in a solid supported liquid membrane system for the selective

* Corresponding author. Tel.: +34-972-418-271; fax: +34-972-418-150.
E-mail address: victoria.salvado@udg.es (V. Salvadó).

0277-5387/02/$ - see front matter © 2002 Elsevier Science Ltd. All rights reserved.
PII: S0277-5387(02)00948-8

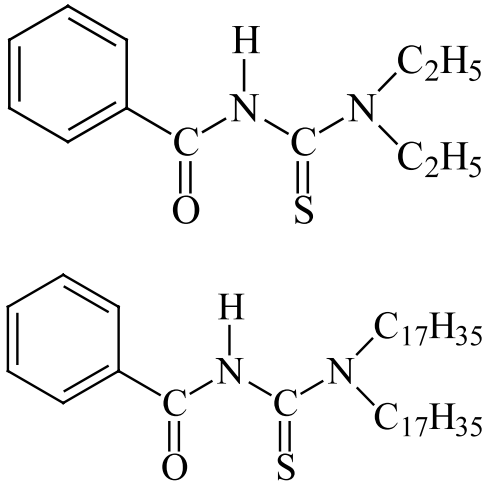


Fig. 1. Chemical structure of the ligands *N*-benzoyl-*N*′,*N*′-diheptadecylthiourea (**3c**) and *N*-benzoyl-*N*′,*N*′-diethylthiourea (**3f**).

transport of palladium(II) [5] and gold(III) [6]. Recently, the field of organic extractant applications has broadened since metal complexes of reagents used in solvent extraction have also been studied in the development of polymeric membrane electrodes taking advantage of the specific interactions between the carrier, i.e. the metal complex and the target ion. This is the case of several metallomacrocyclic and organometallic compounds, for example metalloporphyrin [7] and vitamin B_{12} [8] derivatives, as well as silver(I)–thiourea complexes [9] and several M–triisobutylphosphine sulfide complexes (M = Au, Ag or Hg) [10–12].

In this study, the thermodynamic characterisation of the solvent extraction of palladium(II) and gold(III) from aqueous chloride media by *N*-benzoyl-*N*′,*N*′-diethylthiourea in $CHCl_3$ is undertaken in order to determine the stoichiometry of the complexes formed in the organic solution and their corresponding extraction constants.

Taking advantage of the palladium complexation properties of these ligands, the solid complexes bis-(1,1,-diheptadecyl-3-benzoyl-thioureate)palladium(II) (Pd-3c) and bis(1,1,-diheptadecyl-3-benzoyl-thioureate)palladium(II) (Pd-3f) were obtained and isolated from a mixture of ethanol–methanol solutions. The metallic compounds were characterised and the structure of the crystal Pd-3f was redetermined by means of XRD and compared with previous published results [13]. Pd-3c and Pd-3f were used as ionophores in an ISE system and the potentiometric response of the ion selective membrane to the aqueous chlorocomplexes of precious metals was studied. The selectivity of the potentiometric response is related to the distribution of the metal between the solution and the membrane phases [14].

2. Experimental

2.1. Reagents and solutions

N-benzoyl-*N*′,*N*′-diheptadecylthiourea (**3c**) and *N*-benzoyl-*N*′,*N*′-diethylthiourea (**3f**) were synthesised by Professor Beyer et al. [15]. Organic solutions of these ligands were prepared in $CHCl_3$ (HPLC grade, Panreac, Spain).

Stock solutions of the metals were prepared from the solid compounds, Na_2PdCl_4 (Aldrich, UK) and $HAuCl_4$ (Fluka, Switzerland). Working solutions were prepared by dilution and appropriate volumes of NaCl and HCl standardised solutions were added to adjust the ionic strength (0.1 M) and the H^+ concentration to the desired value.

Pro analysis-grade Na_2PdCl_4 (Aldrich), methanol (Fluka) and ethanol (Fluka) were used for the synthesis of solid palladium complexes Pd-3c and Pd-3f.

High molecular weight poly(vinylchloride) (PVC) and *o*-nitrophenyl octyl ether (*o*-NPOE), used to prepare the polymeric membranes, were purchased from Fluka.

All other reagents were of analytical grade (Panreac, Spain) and all standard solutions and buffers were prepared with deionised (Milli-Q, Millipore, Bedford, USA) distilled water.

2.2. Apparatus

A Labinco rotary mixer was employed to agitate aqueous and organic solutions.

A Spectra A-300 atomic absorption spectrometer (Varian, Australia) was employed to analyse the metal remaining in the aqueous phase.

All pH measurements were carried out using a pH-meter GLP 22 (Crison, Spain) equipped with a combined electrode model 50-02 (Crison).

IR spectra, which were obtained through the use of with KBr pellets, were recorded on a Satellite FTIR equipped with a WINFIRST LITE software package form Mattson Instruments.

The ^1H NMR and ^{13}C NMR spectroscopy was performed on a Brucker DPX200. Samples were run in CD_3CN (for Pd-3f) or $CDCl_3$ for (Pd-3c).

Elemental analyses were performed using a CHNS-O elemental analyser EA-1108 from Fisons.

ESI MS spectra were obtained with a Finnigan AQA™ (ThermoQuest, Manchester, UK). The temperature of the probe was 170 °C and the voltage of the source was 30 eV. The mobile phase was a mixture of acetonitrile:water 70:30 and the flow rate 150 μl min^{-1}.

X-Ray data were collected on a Nonius CAD4 single-crystal diffractometer Potentiometric responses were measured with a digital pH/mV meter (micropH-2002, Crison) and registered on a Yokogawa (LR 4120, Japan) strip-chart recorder. In order to test different

units simultaneously, we used a custom built three-way commuter.

2.3. Procedure for the liquid–liquid distribution studies

Experiments were carried out by shaking equal volumes (10 ml) of the aqueous and organic phases at known concentrations in stoppered glass tubes. After equilibrium was reached, the liquid phases were separated and an aliquot was taken from the aqueous phase for analysis by atomic absorption spectrometry (AAS). Equilibrium time was determined in preliminary experiments by measuring the metal content in the aqueous phase as a function of time until the metal concentrations in the aqueous solutions did not vary. The equilibrium times needed for the extraction of gold and palladium were 16 h and 5 h, respectively. The equilibrium metal concentration in the organic phase was calculated as the difference between the initial and remaining concentrations in the aqueous phase. In some experiments, metal concentration in the organic phase was determined after stripping in order to verify the mass balance.

The initial metal concentration in the aqueous phase was varied from 1×10^{-4} to 1×10^{-3} mol l^{-1} and the total ligand (**3f**) concentration in the organic phase was varied within the range 1×10^{-5}–1×10^{-3} mol. l^{-1}. In order to study the pH dependence of the extraction process, experiments were performed with the aqueous solution at both pH 1 and 2. All experiments were performed at least in duplicate at a controlled room temperature (r.t.) of 22 ± 1 °C.

2.4. Preparation of compounds Pd-3f and Pd-3c

Stoichiometric quantities of metal and ligand in a 1:2 ratio were mixed in order to prepare the Pd-3c and Pd-3f complexes [16]. *N*-benzoyl-*N*′,*N*′ -diheptadecylthiourea palladium complex was obtained by dropwise addition of a methanolic solution of 0.333 mmol of Na_2PdCl_4 to an ethanolic solution of the ligand (0.665 mmol). The mixture was then shaken during 10 min and left to precipitate at −22 °C. The resulting dark yellow solid was vacuum filtered and washed with methanol. *N*-benzoyl-*N*′,*N*′-diethylthiourea (**3f**) palladium complex was prepared following the same steps as for Pd-3c. In this case, 0.250 mmol of Na_2PdCl_4 was added to a 0.500 mmol **3f** ligand resulting in the formation of orange crystals.

$C_{84}H_{150}N_4S_2O_2Pd$ (Pd-3c) (1418.68) *Anal*. Calc. for: C, 71.12; H, 10.66; N, 3.95; S, 4.52. Found: C, 70.82; H, 10.29; N, 3.87; S, 4.24%. Yield: 74%. M.p.: 41–42 °C.

^{1}H NMR δ (ppm) 8.29–8.25 (m, 4H, Ph); 7.52–7.30 (m, 6H, Ph); 3.86–3.74 (m, 8H, CH_2); 1.3 (s, 120H, CH_2); 0.95–0.88 (t, 12H, CH_3). ^{13}C NMR δ (ppm) 14.1 (CH_3); 27.0–31.9, 53.1, 51.9 (CH_2); 127.9, 129.7, 131.3, 137.1 (Ph); 170.5, 171.5 (CS–, CO–). IR (cm^{-1}) 2923, 2852 (C–H st), 1492, 1427.

$C_{24}H_{30}N_4S_2O_2Pd$ (Pd-3f) (577.07) *Anal*. Calc. for: C, 49.95; H, 5.24; N, 9.71; S, 11.11%. Found: C, 50.01; H, 5.13; N, 9.63; S, 10.93%. Yield: 80.9%. M.p.: 128–130 °C.

^{1}H NMR δ (ppm) 8.30 (m, 4H, Ph), 7.63–7.50 (m, 6H, Ph); 3.80–3.40 (m, 8H, CH_2); 1.3 (m, 12H, CH_3). ^{13}C NMR δ (ppm) 11.7, 12.3 (CH_3); 46.2, 47.3 (CH_2); 128.3, 129.4, 131.8, 136.8 (Ph); 170.3, 170.5 (CS–, CO–). IR (cm^{-1}) 2981, 2931 (C–H st), 1517, 1456, 1411, 1372. ES$^+$ MS *m*/*z* (Fragment Ion) 577.4 (M–[H]$^+$).

2.5. Procedure for crystal structure determination

Unit cell dimensions were determined from the angular settings of 25 reflections in the $10 \leq \theta \leq 15°$ range. The space group was inferred by systematic absences to be $P2_1/n$. Intensities were measured using the ω–2θ scan technique with a scan angle of 1.5° and a variable scan rate of 60 s per reflection. The intensity of the primary beam was checked throughout the collection by monitoring three standard reflections every 60 min. Profile analysis was performed on all reflections [17]. Symmetry-equivalent reflections were averaged and Lorentz and polarisation corrections were applied. The structure was solved by direct methods using SHELXS-97 [18]. Isotropic least-square refinement on F^2 was obtained using SHELXS-97 [19]. During the final stages, all positional parameters and the anisotropic temperature factors of all the non-H atoms were refined. The H-atoms were located by Fourier difference synthesis and refined free or riding with common isotropic thermal parameters. The function minimised was $[(\Sigma w F_o^2 - F_c^2)/\Sigma w(F_o^2)]^{1/2}$ where $w = 1/[\sigma(F_o^2) + (0.0661P)^2 + 1.3168P]$ and with $\sigma(F_o^2)$ from counting statistics and $P = (\text{Max}(F_o^2, o) + 2*F_c^2)/3$. Atomic scattering factors were taken from International tables for X-ray Crystallography [20]. Plots were made with the EUCLID package [21]. Geometrical calculations were made with PARST [22]. Relevant crystal and refinement data are collected in Table 1. All calculations were made at the Scientific Computer Centre of the University of Oviedo and on the X-ray group computers.

2.6. Procedure for the potentiometric measurements

Solvent polymeric membranes were prepared by mixing the ionophore (2 wt.%), the plasticiser (66 wt.%) and the polymer, PVC (32 wt.%). The mixture was dissolved in 1 ml THF and cast in a 16 mm i.d. glass ring [23]. The solvent was allowed to evaporate overnight and a membrane was obtained from which 16 mm diameter disks were cut and mounted on a Phillips IS-561 electrode body (Glassblaserei, W. Moller, Switzer-

Table 1
Crystal data and structure refinement for Pd-3f

Empirical formula	$C_{24}H_{30}N_4S_2O_2Pd$
Crystal system	monoclinic
Space group	$P2_1/n$
a (Å)	10.443 (3)
b (Å)	18.55 (2)
c (Å)	13.503 (2)
β (°)	104.70 (2)
V (Å^3)	2530 (3)
Z	4
Formula weight	577.04
T (K)	293 (2)
λ (Å)	0.71073
d_{calc} (mg cm^{-3})	1.515
$F(000)$	1184
Crystal size (mm)	0.33 × 0.23 × 0.20
θ Range for data collection (°)	1.91–25.97
Index ranges	$0 \le h \le 12$, $0 \le k \le 22$, $-16 \le l \le 16$
Reflections collected/unique	5236/4959 [$R_{int} = 0.0239$]
Completeness to $2\theta = 25.97$	96.8%
Max/min transmission	0.8363 and 0.7496
Refinement method	Full-matrix least-square on F^2
Data/restraints/parameters	4959/0/298
Goodness-of-fit on F^2	1.045
Final R indices [$I > 2\sigma(I)$]	$R_1 = 0.0352$, $wR_2 = 0.1000$
R indices (all data)	$R_1 = 0.0606$, $wR_2 = 0.1121$
Extinction coefficient	0.0094(6)
Largest difference peak and hole (e Å^{-3})	0.651 and −0.446

land). In this study, between calibrations we stored electrodes which were either dry or soaked in diluted 10^{-4} M Pd(II) chloride solution after having tested different conditioning solutions (10^{-3} or 10^{-4} M Pd(II) chloride) for periods of between 2 h and 24 h without observing any significant improvement in their slope and stability.

The membranes were conditioned for between 2 h and 24 h in 10^{-3} or 10^{-4} M $PdCl_4^{2-}$ solutions or were kept dry.

An Orion double-junction Ag–AgCl electrode (90-02-00) was used as the reference electrode. The outer compartment was filled with the same solution as in the test solution.

Different volumes of standard analyte solutions were added to a 10.0 ml aliquot of 0.100 M KCl–HCl pH 3.0 to determine the response of the ISE to precious metal chlorocomplexes. Differences in potential were measured with the pH/mV meter and registered on the strip-chart recorder. All experiments were carried out in a thermostatic cell at 25.0 ± 0.1 °C. Calibration plots were obtained by representing the potential of the electrode versus the logarithm of the concentration of the analyte in the sample solution. Response time was calculated as the time elapsed to be within 1 mV of the steady-state potential. Analytical parameters, i.e. slope of the linear portion, practical detection limit (PDL), linear range, operational lifetime and selectivity coefficients were determined in accordance with IUPAC recommendations [24–26].

3. Results and discussion

3.1. Liquid–liquid extraction

The metal distribution coefficient (D) between the organic and aqueous phase was calculated as the ratio of total metal concentration in both phases:

$$D = \frac{[\text{Metal}]_{org}}{[\text{Metal}]_{aq}} \quad (1)$$

The experimental data are presented in Figs. 2 and 3 in the form of log D versus log[*3f*] for several concentrations of the metals and at different initial pH of the aqueous solutions. The great extractability of both metals, especially gold(III), with **3f** has restricted the metal and ligand concentration ranges which can be used as when the metal content is low, errors in the analysis lead to inaccurate D values. The dependence of the metal extraction processes on pH range 1–2 was studied varying the proton concentration in the aqueous phase while keeping the total concentration of chloride at 0.1 mol l^{-1}. As seen in Fig. 3 there is no dependence of the gold(III) and palladium(II) extraction by **3f** on the pH.

In order to determine the composition and formation constants of the extracted species, the distribution data was analysed using LETAGROP-DISTR software [27]. The best set of equilibrium constants for a given model is found by a numerical analysis based on the minimisation of the square sum, U, defined as:

$$U = \sum_N (\log D_{calc} - \log D_{exp})^2 \quad (2)$$

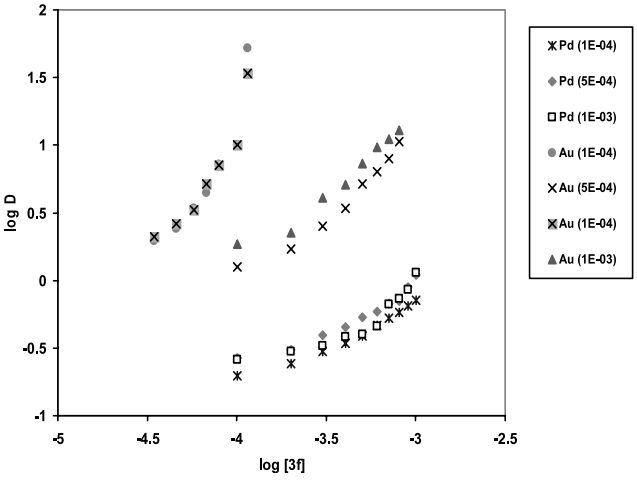


Fig. 2. Experimental distribution data of gold(III) and palladium(II) at pH 1. The total ligand concentration in the organic phase was varied from 3.16×10^{-5} to 1×10^{-3} M.

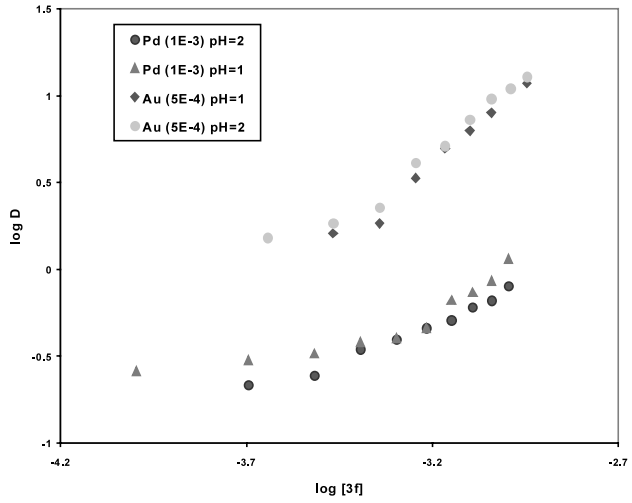


Fig. 3. Experimental distribution data of gold(III) and palladium(II) as a function of pH. The total ligand concentration in the organic phase was varied from 1.0×10^{-4} to 1.0×10^{-3} M.

where D_{exp} represents the experimental values of the distribution coefficient and D_{calc} is the corresponding value calculated by the program solving the mass balance equation for the ligand, the metal and H^+, assuming a proposed set of chemical species and formation constants. N_p is the number of experimental points.

In the experimental conditions used in this work (0.1 M NaCl and low pH), palladium and gold are present in the aqueous solution as the chlorocomplexes $PdCl_4^{2-}$ and $AuCl_4^-$ and the experiments were performed at such low metal concentration that only mononuclear species are present. Then, the metal extraction reaction can by described by using the following equation:

$$MeCl_4^{n-} + qH^+ + rL_{(org)} \Leftrightarrow MeCl_sH_qL_{r(org)} + (4\text{-}s)Cl^- \quad (3)$$

By considering ideal behaviour in the organic phase and assuming the activity coefficients of the aqueous solution to be constant, the equilibrium constant of the reaction can be written as:

$$K_{qr} = \frac{[MeCl_sH_qL_r]_{org}[Cl^-]^{(4-s)}}{[MeCl_4^{n-}][H^+]^q[L]^r_{org}} \quad (4)$$

The distribution coefficient, D, for metal extraction can be expressed by:

$$D = \sum_1^q \sum_1^r K_{qr}[H^+]^q[L]^r_{org}[Cl^-]^{(4-s)} \quad (5)$$

Hence, a plot of log D versus log L would give a preliminary estimation of the stoichiometric coefficients by slope analysis [28]. The values obtained from this graphical treatment were considered as the starting point of the numerical calculations and were introduced into the input of the program along with the constants related to the equilibria involved in the system i.e. hydrolysis of the metal, formation of the metal chlorocomplexes. The results of the numerical analysis are given in Table 2. The goodness-of-fit for any model may be evaluated from the values of U and σ (log D) defined as σ (log D) $= (U/N-N_K)^{1/2}$ where N_K is the number of constants to be adjusted.

The best fit to the experimental data is given by models consisting of one species with a 1:1 stoichiometry i.e. $AuCl_3L$ and $PdCl_2L$. As can be seen in Table 2, the model formed by the species with stoichiometries 1:1 and 1:2 (metal:ligand) gave the same values of U and σ as the models formed by the 1:1 species. This result means that the addition of the 1:2 species to the latter model did not improve the fit of the data and, hence, the most realistic model is that composed by 1:1 species.

Previous studies on gold(III) solvent extraction from aqueous chloride media by *N*-benzoylthiourea derivatives [4] found that the species responsible for gold extraction by **3f** in cumene was $AuCl_3L_2$ and its extraction constant log $K_2 = 5.9 \pm 0.4$. In our case, the use of chloroform, which is more polar than cumene, favours the formation of 1:1 species. Mühl et al. [2] studied the extraction of palladium and gold (10^{-4} M) with *N*-benzoyl-*N*′,*N*′-dibuthylthiourea (**3e**) in benzene, whose concentration was varied from 2.5×10^{-4} to 10^{-2} M. From the representation of log D versus log[*3e*], they obtained slopes of two for palladium and approximately one for gold which indicated the formation of a palladium species of 1:2 (metal:ligand) stoichiometry and a 1:1 gold: ligand complex. The differences in the results of Mühl et al. with respect to the stoichiometry of the palladium species is attributable to the higher ligand concentrations at which they have conducted their experiments.

The extraction of gold by *N*-benzoylthiourea derivatives can take place after the reduction of gold(III) to gold(I) by the ligand as was found in the characterisa-

Table 2
Results of the numerical treatment of experimental data on gold(III) and palladium(II) extraction by *N*-benzoyl-*N*′,*N*′-diethylthiourea in chloroform

Model	Species	log K	U	σ (log D)
Model 1 (Au extraction)	$AuCl_3L$	4.07 ± 0.10	0.7165 ($N_p = 58$)	0.1151
	$AuCl_3L_2$	7.78 max. 7.40		
Model 2 (Au extraction)	$AuCl_3L$	4.07 ± 0.06	0.7165 ($N_p = 58$)	0.1151
Model 3 (Pd extraction)	$PdCl_2$ L	3.72 ± 0.18	0.413 ($N_p = 51$)	0.09
	$PdCl_2L_2$	7.69 max. 8.29		
Model 4 (Pd extraction)	$PdCl_2L$	3.73 ± 0.20	0.413 ($N_p = 51$)	0.09

Table 3
Selected interatomic and intermolecular bond distances (Å) and angles (°) for complex Pd-3f

Bond distances	
Pd–O′	2.015 (3)
Pd–O	2.016 (3)
Pd–S′	2.224 (2)
Pd–S	2.231 (1)
Bond angles	
O′–Pd–O	86.3 (1)
O′–Pd–S′	93.41 (8)
O–Pd–S′	178.9 (1)
O′–Pd–S	176.7 (1)
O–Pd–S	93.43 (8)
S′–Pd–S	86.79 (4)

tion by XRD of the crystal obtained by mixing a $AuCl_4^-$ solution with a solution of **3f** in $CHCl_3$ [29]. The 1:1 (gold:ligand) complex formed has a Au(I) centre, one ligand molecule in which the sulfur atoms are oxidised and one chloride atom.

3.2. Spectral properties

The IR spectra of the complexes Pd-3c and Pd-3f described in this work are assigned in the Section 2. Comparison of these spectra with those of ligands **3c** and **3f** (not shown here) reveals the absence of the bands corresponding to the N–H and C=O bonds which were present in the ligands. The resonance signals in the ^1H NMR and in the ^{13}C NMR spectra can be assigned easily (see Section 2). The disappearance of the N–H signal in the ^1H NMR spectra and the shift in the ^{13}C NMR spectra of the signals assigned to the C–O and C–S bonds, which in the complex appear close together, shows once more the co-ordination of the palladium through the O and S atoms of the ligand.

The ES^+ MS spectrum of the Pd-3f complex shows a peak at $m/z = 577.4$ which corresponds to a 1:2 (metal:ligand) stoichiometry. In Fig. 4, the experimental and calculated isotopic patterns of compound Pd-3f (which agree with the presence of the Pd atom in the complex) are depicted showing the complete correlation between them. The high degree of fragmentation of Pd-3c makes it difficult to interpret the mass spectrum (not shown).

3.2.1. X-ray structure determination

In order to achieve more accurate solid state structural data for the complex compound, the crystal structure of Pd-3f was determined. The structure found agrees with previously published results [13]. In Tables 1 and 3, the crystallographic data and selected bond length and angles are presented. That the new determination is a significant improvement is shown by the *R* factor, the hydrogen atom locations and the refinement of the H bonding description, and the overall decrease in e.s.d. Fig. 5 shows the molecular structure of the complex with the atomic labelling.

3.2.2. Potentiometric results

Potentiometric responses to $PdCl_4^{2-}$ have been accurately determined in 0.10 M KCl–HCl pH 3.0, which was chosen to ensure that more than 95% of the added analyte was in the $PdCl_4^{2-}$ form. The influence of the membrane composition and working conditions on the electrode response to this palladium chlorocomplex was evaluated by systematically changing certain variables. Both palladium ionophores (Pd-3c and Pd-3f) were tested and a significantly greater signal stability was achieved when Pd-3c was used as the ionophore. The drift in potential obtained with Pd-3f membranes is explained by the leaching of the ionophore into the test solution due to the lower lipophilicity of ligand **3f** in comparison to **3c**, which has longer alkylic side chains (see Fig. 1). Subsequent experiments were mainly focussed on Pd-3c based membrane ISEs. Preliminary experiments were undertaken in order to evaluate the optimum composition of the liquid membranes and their conditioning. No significant improvement in the slope and stability of the electrodes was made by varying the time and the composition of the conditioning solution. The best reproducibility of the Nerstian response was obtained with 2 wt.% Pd-3c as the ionophore and *o*-nitrophenyl octyl ether (*o*-NPOE) as the solvent mediator.

After testing all precious metal chlorocomplexes (Fig. 6), a Nernstian response was only obtained for $AuCl_4^{2-}$ and $PdCl_4^{4-}$ in 0.100 M KCl pH 3.0 medium. $RhCl_5(H_2O)^{2-}$, $PtCl_6^{2-}$ and $PtCl_4^{2-}$ did not give any response and, therefore, would not have interfered in the measurement of $PtCl_4^{2-}$ in a mixed PGM solution. The calibration parameters for $AuCl_4^-$ potentiometric responses were determined by using the optimum working conditions described above for $PtCl_4^{2-}$. The electrodes, with membranes containing 2% of Pd-3c ionophore, presented Nernstian slopes of 59.6 ± 1.9 mV per decade for $AuCl_4^-$. However, the sensitivity and linear dynamic range are very different for the two chlorocomplexes. The measured PDL value for $AuCl_4^-$ was 8.8×10^{-8} M while for $PdCl_4^{2-}$ it was only 2×10^{-4} M. A selectivity coefficient of $K^{pot}_{AuCl_4^-,\ PdCl_4^{2-}} = -3.4$ was calculated taking $AuCl_4^-$ as being the primary anion. These selectivity coefficients were calculated by the matched potential method [30,31]. The greater response of the ISE system for gold is a result of the higher extraction constant obtained for gold in the liquid–liquid system.

4. Conclusions

Solutions of *N*-benzoyl-*N*′,*N*′-diethylthiourea (**3f**) in $CHCl_3$ were used in the solvent extraction of gold (III)

and palladium (II) from aqueous chloride media (0.1 M NaCl) giving high extraction rates especially for gold. By treating equilibrium data with the LETAGROP-DISTR software we have concluded that gold and palladium extraction can be explained by the formation of 1:1 (metal:ligand) species with extraction constants of log K ($AuCl_3L$) = 4.07 and log K ($PdCl_2L$) = 3.73. The pH of the aqueous solution does not affect the metal extraction process in the 1–2 pH range

The solid complexes bis(1,1,-diheptadecyl-3-benzoyl-thioureate)palladium(II) (Pd-3c) and bis(1,1,-diheptadecyl-3-benzoyl-thioureate)palladium(II)Pd-3f were prepared and isolated from a mixture of ethanol–methanol solution obtaining yields of 74 and 80.9%,

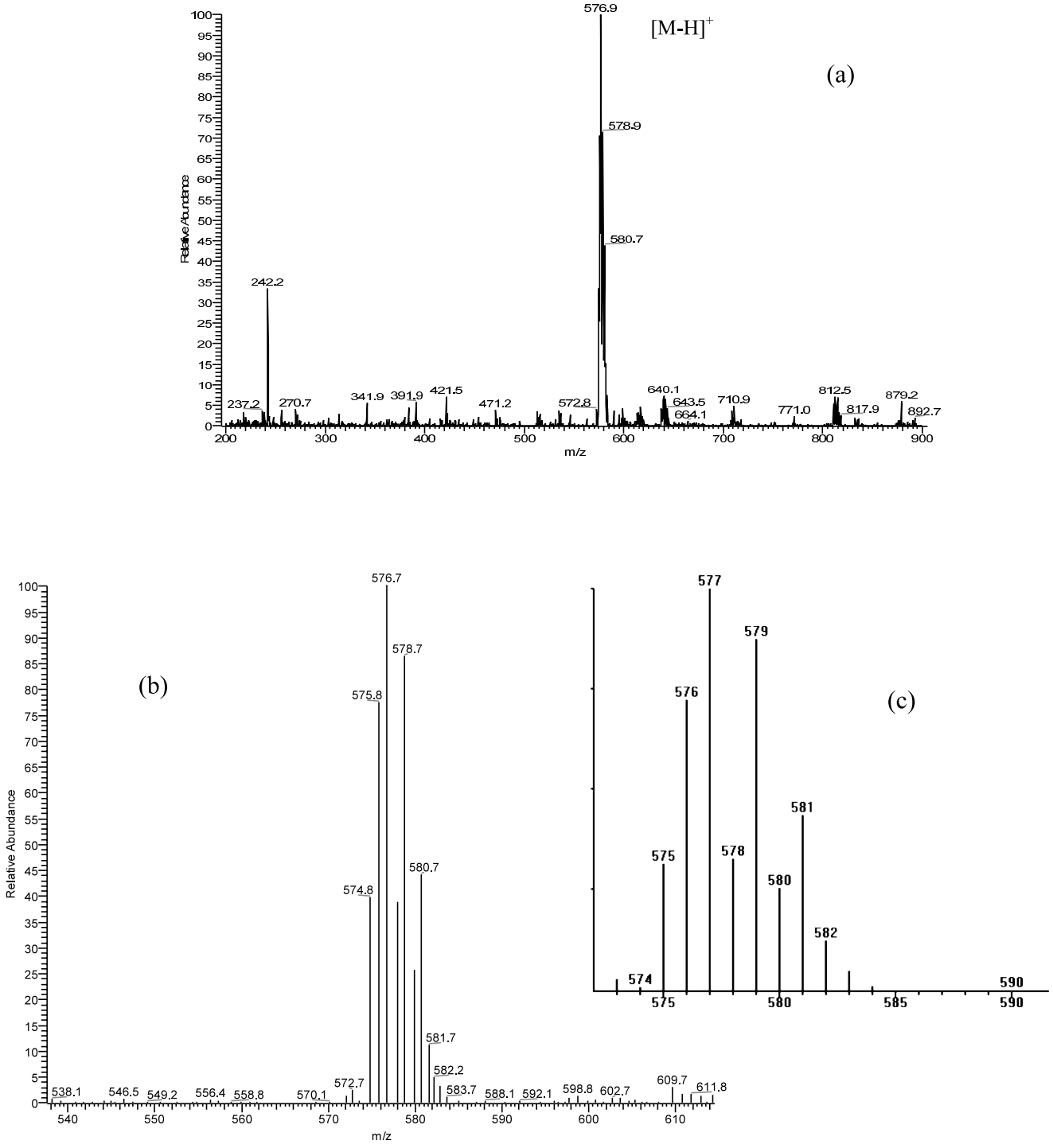


Fig. 4. ES^+ MS mass spectra of Pd-3f. Comparison of the (b) found and (c) calculated isotopic pattern of compound Pd-3f.

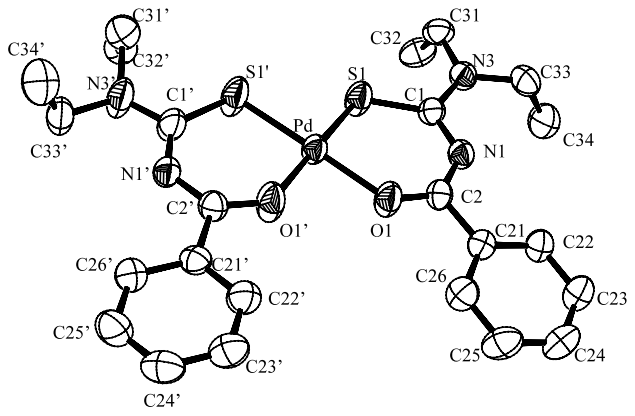


Fig. 5. Molecular structure of bis(1,1,-diheptadecyl-3-benzoylthiourea)palladium(II) with the atom numbering scheme.

respectively. The characterisation of these complexes was performed by NMR, FTIR and MS analyses and their stoichiometry was confirmed to be 1:2 (metal:ligand) by MS.

The structure of the Pd-3f crystal was redetermined by means of XRD. The *R* factor, hydrogen atom locations and the refinement of the H bonding description, and the decrease in e.s.d. are significant improvements.

The Pd-3c and Pd-3f complexes were used as ionophores in the development of polymeric membrane electrodes. The membranes prepared with 2% of Pd-3c gave Nernstian responses to $PdCl_4^{2-}$ and $AuCl_4^-$, with an average of -30.9 ± 0.8 mV per decade and a PDL of 1.5×10^{-4} M for palladium, and a slope of -59.6 mV per decade and a PDL of 8.8×10^{-8} M for gold.

5. Supplementary data

Further details of the complex Pd-3f structure determination are available as a cif (crystallographic information file) magnetic file from The Director, CCDC, 12 Union Road, Cambridge CB2 1EZ, UK (fax: +44-1223-336033; e-mail: deposit@ccdc.cam.ac.uk or www: http://www.ccdc.cam.ac.uk) on request quoting deposition number 172658.

Acknowledgements

This study has been part-financed by CYCIT projects (QUI99-0749-C03-03 and BQU2000-0219). We would like to thank J. Delós for carrying out the liquid–liquid distribution experiments and Dr. A. Roglans for her help in the interpretation of MS spectra.

References

[1] R.G. Pearson, J. Am. Chem. Soc. 85 (1963) 3533.
[2] P. Mühl, K. Gloe, F. Dietze, L. Beyer, Z. Chem. 26 (1986) 81.
[3] F.Z. El Aamrani, A. Kumar, J.L. Cortina, A.M. Sastre, Anal. Chim. Acta 382 (1999) 205.
[4] F.Z. El Aamrani, A. Kumar, L. Beyer, J.L. Cortina, A.M. Sastre, Solv. Extr. Ion Exch. 16 (6) (1998) 1389.
[5] E. Anticó, A. Masana, M. Hidalgo, V. Salvadó, M. Valiente, Hydrometallurgy 35 (1994) 343.
[6] F.Z. El Aamrani, A. Kumar, L. Beyer, J.L. Cortina, A.M. Sastre, Hydrometallurgy 50 (1998) 315.
[7] D. Gao, J.-Z. Li, R.-Q. Yu, G.-D. Zheng, Anal. Chem. 66 (1994) 2245.
[8] C. Palet, M. Muñoz, S. Daunert, L.G. Bachas, M. Valiente, Anal. Chem. 65 (1993) 1533.

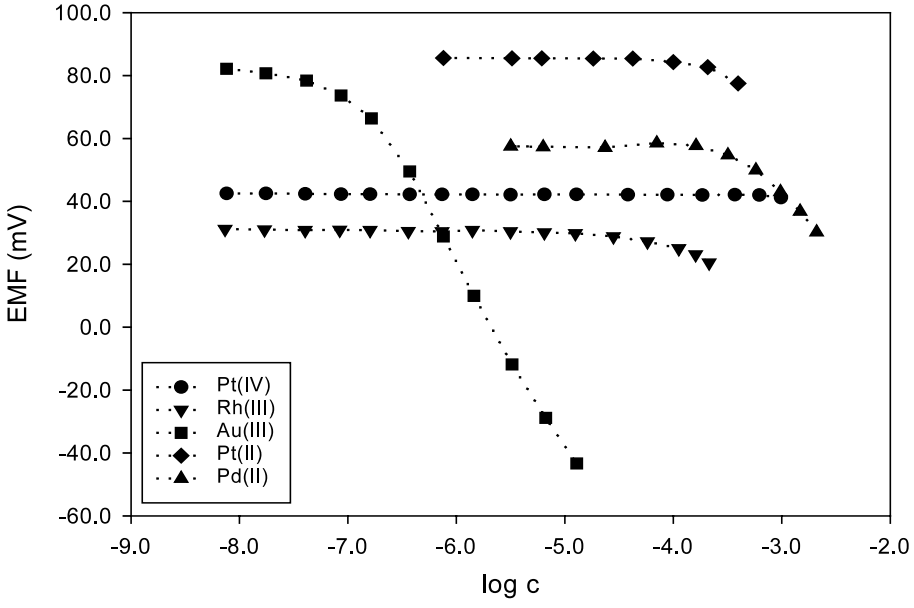


Fig. 6. Potentiometric response. Selectivity pattern of noble metal chlorocomplexes.

[9] F.Z. El Aamrani, A. Sastre, M. Aguilar, L. Beyer, A. Florido, Anal. Chim. Acta 329 (1996) 247.
[10] A. Florido, L.G. Bachas, M. Valiente, M. Villaescusa, Analyst 119 (1994) 2421.
[11] J. Bricker, S. Daunert, L.G. Bachas, M. Valiente, Anal. Chem. 63 (1991) 1586.
[12] S. Daunert, A. Florido, J. Bricker, W. Dunaway, L.G. Bachas, M. Valiente, Electroanalysis 5 (1993) 839.
[13] G. Fitze, L. Beyer, J. Sieler, R. Richter, J. Kaiser, E. Hoyer, Z. Anorg. Allg. Chem. 433 (1977) 237.
[14] E. Bakker, P. Bühlmann, E. Pretsch, Chem. Rev. 97 (1997) 3083.
[15] H. Hartmann, I. Reuther, J. Prakt. Chem. 315 (1973) 144.
[16] J. Hartung, G. Weber, L. Beyer, R. Szargan, Z. Anorg. Allg. Chem. 523 (1985) 153.
[17] (a) M.S. Lehman, F.K. Larsen, Acta Crystallogr. Sect. A 30 (1974) 580;
(b) D.F. Grant, E.J. Gabe, J. Appl. Crystallogr. 11 (1978) 114.
[18] G.M. Sheldrick, SHELXS-97. Program for the Solution of Crystal Structures, University Göttingen, 1997.
[19] G.M. Sheldrick, SHELXS-97. Program for the Refinement of Crystal Structures, University Göttingen, 1997.
[20] International Tables for X-Ray Crystallography, 1974, vol. IV. Kynoch Press, Birmingham: (Present distributor: Kluwer Academic, Dordrecht).
[21] A.L. Spek, in: D. Sayre (Ed.), Computational Crystallography, Clarendon, Oxford, 1982, p. 528.
[22] M. Nardelli, Comput. Chem. 7 (1983) 95.
[23] G.J. Moody, R.B. Oke, J.D.R. Thomas, Analyst 95 (1970) 910.
[24] G.G. Guibault, R.A. Durst, M.S. Frant, H. Freiser, E.H. Hansen, T.S. Light, E. Pungor, G. Rechnitz, N.M. Rice, T.J. Rohm, W. Simon, J.D.R. Thomas, Pure Appl. Chem. 48 (1976) 129.
[25] Y. Umezawa, K. Umezawa, H. Sato, Pure Appl. Chem. 67 (1995) 508.
[26] R.P. Buck, V.V. Cosofret, Pure Appl. Chem. 65 (1993) 1849.
[27] D.H. Liem, Acta Chem. Scand. 25 (1971) 1521.
[28] M. Aguilar, in: S. Alegret (Ed.), Developments in Solvent Extraction, Ellis Horwood, Chichester, 1988.
[29] W. Bensch, M. Schuster, Z. Anorg. Allg. Chem. 611 (1992) 99.
[30] V.P.Y. Gadzepko, G.D. Christian, Anal. Chim. Acta 164 (1984) 279.
[31] A.S. Attiyat, A.M. Kagry, M.A. Badawy, H.R. Hanna, Y.A. Ibrahim, G.D. Christian, Electroanalysis 2 (1990) 119.

PERGAMON

Polyhedron 21 (2002) 1439–1449

POLYHEDRON

www.elsevier.com/locate/poly

Molecular energy parameters by solution thermodynamics

Antonio Braibanti *

Physical Chemistry Section, Pharmaceutical Department, University of Parma, Parco Area delle Scienze 27/A, I-43100 Parma, Italy

Received 10 July 2001; accepted 17 September 2001

Abstract

The relationships between statistical thermodynamics and equilibrium constants, either cumulative, stepwise or specific site constants are investigated. In order to show the link between equilibrium constants and statistical thermodynamic microscopic properties, a distinction has been introduced between non-reacting and reacting systems. The non-reacting systems are those for which continuous statistical distributions of enthalpies can be assumed. The distribution function can be obtained as an integral of the interparticle potential extended to the whole ensemble. Molecular partition functions ζ_A, are used to describe the properties of the ensembles. The reacting ensemble is represented by distinct distributions of enthalpies, each distribution being grouped around a mean value. Each level is representative of one species. Around each mean level the distribution is continuous as in non-reacting ensembles. The reacting ensemble of particles is described by a grand canonical molar partition function $Z_M = (1+k\gamma(i)[A])^t$ where k is the specific site constant, $\gamma(i)$ is the cooperativity function, [A] is the concentration of free ligand, and the power t indicates the maximum number of i sites in one class. The specific site constant k is proportional to the affinity of binding and is related to the depth of the minimum of the potential function. The factor γ_i is the cooperativity factor given by the value of the cooperativity function $\gamma(i)$ at the ith level and indicates how the depth of the potential function is affected by previous binding of a ligand. The values of the stability constant and cooperativity factor can be optimized by a computer program. The derivatives of the partition function Z_M with respect to ln[A] correspond to the formation function $\langle n \rangle$ (first derivative) and to the buffer capacity B_C (second derivative). The derivatives of the partition function Z_M with respect to temperature are reaction enthalpy ΔH (first derivative with $-(1/T)$) and apparent heat capacity $\Delta C_{p,app}$ (second derivative with ln T). The denaturation heat obtained by integration of $\Delta C_{p,app}\, dT$ for many proteins explains why the denaturation enthalpy depends linearly upon T. © 2002 Elsevier Science Ltd. All rights reserved.

Keywords: Partition function; Equilibria in solution; Cooperativity; Site affinity; Buffer capacity; Heat capacity

1. Introduction

Statistical thermodynamics provides a bridge linking the thermodynamic properties of a macroscopic system to molecular parameters of its microscopic constituents; thus giving a molecular basis to the thermodynamic laws.

Materials in bulk will contain some multiple of Avogadro's number (e.g. 10^{10} or higher) of particles (atoms, molecules, or their constituent nuclei and electrons). We will refer to such collections of particles as macroscopic (experimental) systems where we use the term 'system' to refer to any collection of material particles enclosed by a boundary. Anything not included in a defined system is considered as the surroundings. Any macroscopic system, therefore, has a microscopic model description, i.e. a description in terms of properties of its individual particles. A macroscopic system such as one drop of water, or 1 carat of diamond corresponds to a model containing many microscopic particles or elements.

2. Non-reacting and reacting systems

Appropriate relationships between macroscopic experimental properties and motions of collection of molecules can be found not only for gases but also for liquids, solids, and solutions. We have now investigated the relationships between equilibrium constants, either

* Corresponding author. Tel.: +39-52-190-5024; fax: +39-52-190-5006.

E-mail address: braiban@unipr.it (A. Braibanti).

0277-5387/02/$ - see front matter © 2002 Elsevier Science Ltd. All rights reserved.
PII: S0277-5387(02)00958-0

cumulative, stepwise, or specific site constants, in solution and the properties of statistical thermodynamic ensembles. In order to establish the correspondence between real macroscopic systems and molecular models it has been necessary to distinguish between non-reacting and reacting systems [1–4].

The non-reacting systems are represented by ensembles of cells for which continuous distributions of enthalpies can be assumed. The distribution function of energy or enthalpy can be obtained as an integral of the interparticle potential extended to the whole ensemble. Molecular partition functions ζ_A appropriate to microcanonical, canonical and grand canonical ensembles, respectively, are used to describe the properties of the ensembles.

The reacting system is represented by an ensemble of cells presenting distinct distributions of energies or enthalpies; each distribution being grouped around a mean energy or enthalpy value. Each mean level is representative of one species. Around each mean level the distribution is continuous as in non-reacting ensembles.

The fundamental assumption of the statistical approach to thermodynamics is that the behaviour of materials in bulk can be described by appropriate averages obtained from sums or powers of activities of the constituent parts. By reference to a solution, we can imagine a subdivision of the whole volume of the solution in a very large number of microscopic cells. Each cell has its own energy and the mean energy can be obtained as the mathematical average of the sum of single energies. Each cell has its own concentration c_i; then the concentration of the typical cell from an ensemble of n cells is obtained by taking the nth root (i.e. geometrical average) of the product of n concentrations.

The possible configurations of a system where the total energy E is given by the sum of all the energies of the particles

$$E = \sum_i n_i \varepsilon_i \tag{1}$$

are given by the Boltzmann distribution, whereby the probability p_i of state i is

$$p_i = \exp(-\varepsilon_i/k_B T)/\sum_i \exp(-\varepsilon_i/k_B T) \tag{2}$$

and is equal to the ratio n_i/N between the population n_i of the ith state and the total number N of states ($k_B = 1.381 \times 10^{-23}$ J K^{-1} is the Boltzmann constant).

The denominator of Eq. (2) is the partition function

$$\zeta = \sum_i \exp(-\varepsilon_i/k_B T) \tag{3}$$

of the system and indicates how the particles are distributed over the different states.

The total internal energy of a macroscopic system is the sum of the kinetic and potential energy associated with the various active modes of motion of the individual microscopic particles together with the sum of the microscopic potential energies resulting from interactions between the particles. We assume that there is a distribution of kinetic energies among the individual particles and among their several modes of motion and that the kinetic energy of a single particle is constantly changing as a result of energy exchange occurring during collisions or in the coupling of internal motions. This distribution of energies can be related to the model of an ideal gas. The ideal gas is assumed to be formed by a large set of particles with mass m and velocity u. There is no net interaction (either attractive or repulsive) between molecules. The volume of the molecules is very small with respect to the volume V of the container. Any molecule has equal statistical probability to be found in any part of the volume. On the other hand not all the molecules have the same and constant velocity and the directions of the motion of these molecules are completely random.

The distribution of energy can be also calculated by assuming that it is quantized. The energy levels for a single molecule can be calculated by quantum mechanics methods. In principle, the energy level of any molecule can be calculated, although the actual computation can be very difficult and in many cases is not yet possible.

For an ideal gas the energy levels of a molecule can be assigned, with good approximation, to translational, rotational, and electronic motion. The spacing between energy levels is smallest for translational energy levels and largest for electronic levels. The values of the energy levels can be calculated from quantum mechanics and the partition function can be obtained (for volume $V = abc$)

$$\zeta = (2\pi m k_B T/h^2)^{3/2} V \tag{4}$$

that can be written

$$\zeta = V/\Lambda^3 \tag{5}$$

where

$$\Lambda = (2\pi m k_B T/h^2)^{-1/2} \tag{6}$$

has the dimension of length and is called the thermal wavelength. Correspondingly, Λ^3 is a length to the third power and hence a volume. This continuous distribution of energies is a distinctive example of a non-reacting system. The identification of volume in Eq. (6) as 'dilution' volume qualifies it as an entropy probability factor $\zeta = \exp(S/R)$ (see Section 3). The expression (4) shows how the exponential probability factor is a function of the kinetic energy $(m/2)u^2$.

3. Potential functions and non-reacting systems

The fundamental problem in statistical mechanics is to find a relationship between the interparticle interactions and the energy differences contained in the partition function. The possibility to predict thermodynamic properties of liquids resides in finding accurate potential functions to describe the interparticle interactions [5].

Intermolecular potential theory is based upon two assumptions: (i) that intermolecular potentials are a function of internuclear separations (Born–Oppenheimer approximation), (ii) that the total potential energy of a system of N atoms whose nuclei are at positions $\boldsymbol{r}_1, \ldots \boldsymbol{r}_i, \ldots \boldsymbol{r}_N$ may be written (in the absence of external fields) as a sum of two-body; three-body, four-body,... potential functions

$$\Phi(\boldsymbol{r}_1, \ \ldots \ \boldsymbol{r}_i, \ \ldots \boldsymbol{r}_N) = \sum_{i<j} \phi^{(2)}(\boldsymbol{r}_{ij}) + \sum_{i<j<k} \phi^{(2)}(\boldsymbol{r}_{ij}, \ \boldsymbol{r}_{jk}, \boldsymbol{r}_{ik}) + \ldots \tag{7}$$

In general we can truncate the series to the two-body potential [$\Sigma\phi^{(2)}$] and calculate the canonical partition function

$$Z_N = \{((\Lambda^3)^N/(N!)\ldots \mathrm{d}\mathbf{r}_1 \ldots \mathbf{r}_N) \exp[-\Phi(\mathbf{r}_1 \ldots \mathbf{r}_N)]/k_\mathrm{B}T\} \tag{8}$$

It is assumed that the particles are obeying the laws of classical mechanics. The partition function is divided by $N!$ because it refers to a collection of indistinguishable particles. The most realistic two-body potential function is the Lennard–Jones (12, 6) potential

$$\phi(\boldsymbol{r}) = 4\eta[(\sigma/r)^{12} - (\sigma/r)^6] \tag{9}$$

In this potential, σ is a measure of the diameter of the particle and η gives the potential at its minimum. The microscopic enthalpy η is related to the microscopic energy ε by $\eta = \varepsilon + p\phi$, where ϕ is the microscopic volume accessible to one molecule. The shape of the potential curve is that reported in Fig. 1. The total energy produced by two-body interactions between the particles is transformed into kinetic energy which is measured by an entropy increase. It is worth noting that the partition function for non-reacting systems can be an extremely large number [6].

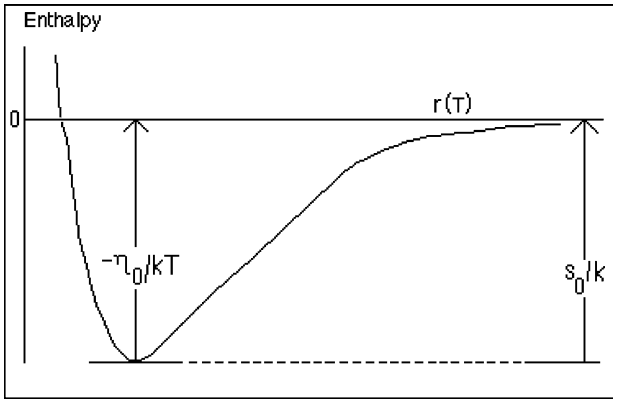


Fig. 1. Potential function in non-reacting ensemble.

The non-reacting system can be represented by the partition function which can be derived with respect to temperature to give an average enthalpy

$$-\partial \ln \zeta/\partial(1/T) = \sum\nolimits_i (\eta_i/k_\mathrm{B})\{\exp(-\eta_i/k_\mathrm{B}T)/\sum\nolimits_i \exp(-\eta_i/k_\mathrm{B}T)\} = \langle \eta_i/k_\mathrm{B} \rangle = \langle H/R \rangle \tag{10}$$

where

$$\zeta = \sum\nolimits_i \exp(-\eta_i/k_\mathrm{B}T) \tag{11}$$

is the partition function of the system. The ensemble can be represented by the mean enthalpy value with average partition function $\zeta_\mathrm{av} = \exp(-\langle \eta \rangle/k_\mathrm{B}T)$. Note that the derivation of $\ln \zeta_\mathrm{av}$ with respect to $(1/T)$ leads to the same result as the derivation of $\ln \zeta$ (cfr. Eq. (10)). The multiplicity of the state ω, i.e. the number of accessible states (cfr. dilution factor below), is an entropy factor

$$\omega = \sum\nolimits_i \exp(s_i/k_\mathrm{B}) \tag{12}$$

In non-reacting systems, $\zeta = \omega$, which means that the partition function is a measure of the probability of the state and corresponds to the number of accessible states. Therefore, the following equality holds

$$\exp(-\langle \eta \rangle/k_\mathrm{B}T) = \exp(\langle s/k_\mathrm{B} \rangle) \tag{13}$$

The distribution of enthalpies, as well as that of entropies, of a non-reacting ensemble is continuous, centred around the most probable state. According to Eq. (13) in the diagram of Fig. 1, the total energy $(-\eta/k_\mathrm{B}T)$ of each elementary process is transformed into kinetic energy (s/k_B). The intermolecular interactions do not give origin to definite compounds.

The partition function of a non-reacting ensemble is suited to represent the thermal properties of the system. For example, the isobaric heat capacity C_p is by definition the quantity of heat supplied to one mole of substance (or solute) necessary to increase by 1 °C the temperature of the substance. More immediately, the specific heat capacity applies to 1 g of substance. This experimental quantity corresponds, for the model, to the derivative of Eq. (10) and, therefore, to the double derivative of the partition function

$$\partial \langle H/R \rangle/\partial T = -\partial^2 \ln \zeta/\partial(1/T)\partial T = C_\mathrm{p}/R \tag{14}$$

On the other hand, it can be shown that the variance of enthalpy is

$$\mathrm{var}(H) = C_\mathrm{p}RT^2 \tag{15}$$

By calculating the dispersion of enthalpy as the square

root of variance, the mean enthalpy can be written

$$\langle H\rangle = 5/2RT \pm (C_p R)^{1/2} T \quad (16)$$

The non-reacting ensemble can be open to exchange of matter. Therefore, the partition function (Eqs. (11)–(13)) is expressed as the function of the multiplicity factor ω, which represents the dependence upon the dilution. In order to show the relation between the multiplicity and an experimental quantity such as the concentration or its reciprocal, the dilution, we can refer to Fig. 2. In (a) the dilution of solute A in (conventional) standard state d_1 indicates a ratio of one molecule A in every 5 cells, whereas in (b) the dilution is d_2 and it has been increased to one molecule A in every 14 cells ($d_2 = 2.8d_1$). The state d_2 (corresponding to a larger number of accessible states) is more probable than the state d_1. The dilution is an entropy factor because it is a probability factor which measures the trend of the molecules to occupy the maximum accessible volume [7]. In fact, any non-reacting solute moves towards less occupied cells, so that it becomes as sparse as possible. The more diluted solution is, therefore, the more probable state. The change of probability is measured on a molar scale by an entropy change corresponding to a dilution change

$$\mathrm{d}S = R\ \mathrm{d}\ \ln\ 1/[\mathrm{A}] = R\ \mathrm{d}\ \ln\ d_\mathrm{A} \quad (17)$$

On the molecular scale, the change of entropy is

$$\mathrm{d}s = k_\mathrm{B}\ \mathrm{d}\ \ln\ \omega \quad (18)$$

where ω is the number of accessible states or multiplicity.

Not only a change of dilution but also a change of temperature in non-reacting systems produces a change of entropy, which is proportional to the isobaric heat capacity $C_{p,A}$ of the solute A. In fact

$$\mathrm{d}S = C_{p,A}\ \mathrm{d}\ \ln\ T \quad (19)$$

By equating Eqs. (17) and (19) we obtain a virtual change of dilution produced by a change of temperature

$$-R\partial\ \ln[\mathrm{A}]/\partial\ \ln\ T = C_{p,A}/R \quad (20)$$

which can be called thermal equivalent dilution [8]. This principle raises a question: Can we assume that the thermal equivalent dilution is an experimental demonstration of the so-called ergodic hypothesis whereby the 'mean toss over time' (temperature) is equal to the 'mean toss over space' (dilution)? On the other hand, it has been asserted that Maxwell–Boltzman statistics with corrections for the quantum character of energy changes and the indistinguishable nature of molecules, works perfectly well when we consider systems of non-interacting molecules [9].

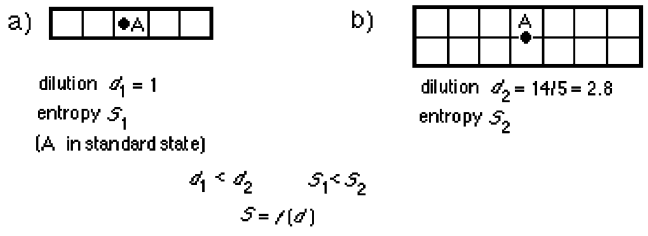


Fig. 2. Dilution and entropy: $d = \exp(S/R)$. (a) The dilution of solute A is d_1 (one molecule A every 5 cells. (b) Dilution of solute A is d_2 (one molecule A every 14 cells) ($d_2 = 2.8d_1$).

4. Reacting systems

The reacting system is composed of two or more non-reacting ensembles of energy (or enthalpy) levels. Each non-reacting sub-system represents a continuous distribution of energies, at constant volume, or of enthalpies, at constant pressure. Examples of the latter subsystems are those represented by the integral of Eq. (8) and by the partition function of Eq. (12). Each group of energies or enthalpies is centred about its mean value $\langle \varepsilon/k_\mathrm{B}T\rangle$ or $\langle \eta/k_\mathrm{B}T\rangle$ and the same holds for mean entropy $\langle s/k_\mathrm{B}\rangle$ and mean free energy $\langle \gamma/k_\mathrm{B}T\rangle$, respectively.

Therefore the whole partition function, by taking 1 the probability of occupation of the ground level is

$$Z_\mathrm{M} = 1 + \exp(-\Delta\gamma/k_\mathrm{B}T) \quad (21)$$

The distribution of molecules is of the order of moles and on this scale the exponential term can be written by multiplying numerator and denominator of the exponent by N_L (Avogadro number)

$$Z_\mathrm{M} = 1 + \exp(-\Delta G/RT) \quad (22)$$

The potential function of the reacting system can be represented in Fig. 3 where the total energy corresponds to the enthalpy change ($\Delta H/RT$), the kinetic energy to the entropy change ($\Delta S/R$) and the potential energy to the free energy change ($\Delta G/RT$). Note that the entropy change is not equal to the enthalpy change, which is different from the non-reacting systems.

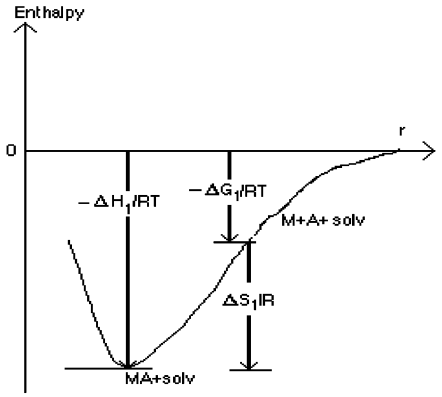


Fig. 3. Potential energy function in a reacting system.

Following the line of Poland [10], I want to find the relation between this kind of partition function employed as molecular descriptor and experimental quantities, such as analytical total amounts, equilibrium constants and site constants. The total analytical amount of molecules in a system with a receptor M and a ligand A forming mononuclear complexes MA, MA_2, MA_3... is represented by the sum of all the species containing M

$$[T_M] = [M] + [MA] + [MA_2] + \ldots + [MA_i] \ldots + [MA_t] \quad (23)$$

where $t = i(\max)$ is the number of binding sites of the receptor M. By dividing by [M] we obtain

$$Z_M = 1 + [MA]/[M] + [MA_2]/[M] + \ldots + [MA_i]/[M] + \ldots + [MA_t]/[M] \quad (24)$$

which has the same structure of the partition function of Eq. (22), provided that each exponential free energy term corresponds to a concentration ratio and, hence, to a relative probability of occupation [11,12]. In fact, the binding of M with iA is ruled by a cumulative binding constant

$$\beta_i = [MA_i][M]^{-1}[A]^{-i} \quad (25)$$

and, therefore, each term

$$\beta_i[A]^i = [MA_i][M]^{-1} \quad (26)$$

can be substituted for each term of Eq. (24), thus obtaining ($\beta_0 = 1$)

$$Z_M = 1 + \beta_1[A] + \beta_2[A]^2 + \ldots \beta_i[A]^i \ldots + \ldots \beta_t[A]^t \quad (27)$$

Each term of Eq. (27) corresponds to an exponential factor $\exp(-\Delta G_i/RT)$ where $-\Delta G_i$ is the free energy change for the binding of M with iA. At [A] = 1, we obtain the cumulative standard free energy change for each step i

$$\exp(-\Delta G_i^\circ/RT) = \beta_i \quad (28)$$

The cumulative binding constant depends on the site affinity constant. The affinity of A to M is measured by the site binding constant k which, in the absence of cooperativity, should be the same for every site of the same class. The whole probability of binding as a function of site constant k can be obtained as the tth power of the probability of binding to one site

$$Z_M = (1 + k\gamma(i)[A])^t \quad (29)$$

where $\gamma(i)$ is a cooperativity function which depends on the cooperativity between sites. The cooperativity is the average weakening (the most general cases) of affinity when other sites are previously occupied by the ligand. The product of Eq. (29) can be transformed to a polynomial and written

$$Z_M = \sum_i m_i\{k\gamma_i[A]\}^i \quad (30)$$

where m_i is the statistical factor and γ_i the cooperativity factor i.e. the value of the cooperativity function of the ith term. Each term of Eq. (30) corresponds to each term of Eq. (27) and hence

$$\beta_i = m_i\{k\gamma_i\}^i \quad (31)$$

The cumulative constant is therefore a function of the statistical factor m_i, of the site constant k, and of the cooperativity factor γ_i. The statistical factor m_i is a dilution indicator depending on the multiplicity of the site in one class and, as such, is an entropy factor. The specific site constant k is proportional to the affinity of binding and is related to the depth of the minimum of the potential function and on the change in kinetic energy. The factor γ_i is the cooperativity factor given by the value of the cooperativity function $\gamma(i)$ at the ith level

$$\gamma(i) = \exp(-b(i-1)) \quad (32)$$

and indicates how the depth and distance of the minimum of the potential function are affected by previous binding of a ligand.

When self-association takes place, the partition function is no longer exactly proportional to the total stoichiometric amount $[T_M]$. In fact, the partition function is composed of as many terms as independent species in solution and, in case of self-association, $Z_M < [T_M]/[A]$ (see Eq. (47b)). When there are more classes of sites, then the partition function becomes a product of probability functions

$$Z_M = (1 + k_1\gamma(i_1)[A])^{t(1)}(1 + k_2\gamma(i_2)[A])^{t(2)} \quad (33)$$

If there is self-association, the molecules, for instance with three M, are considered as a combination between M (receptor) and 2M (ligands).

5. Derivatives of partition function and observables

The partition function as a whole is equal to an exponential probability factor

$$\exp(-\Delta G_i/RT) = Z_M \quad (34)$$

The derivative of $\ln Z_M$ with respect to the variable ln[A] is therefore a change of free energy and corresponds, for mononuclear complexes, to the formation function of Bjerrum

$$\partial \ln Z_M/\partial \ln[A] = \langle n \rangle \quad (35)$$

where $\langle n \rangle$ measures the number of ligand bound per molecule of receptor against ln[A]. The plot is practically a titration curve and the elementary area

$$\langle n \rangle \, \mathrm{d} \ln[A] = \mathrm{d}(-\Delta G_i/RT) \quad (36)$$

is the differential of free energy [13]. By integration between [A] = 0 and [A] = 1, provided that the satura-

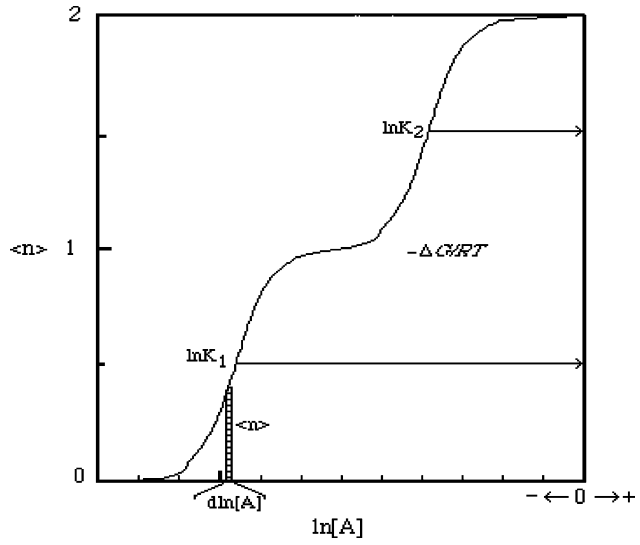


Fig. 4. The integral area below the formation curve is proportional to $-\Delta G_t/RT$.

tion of receptor has been reached, we obtain (Fig. 4)

$$\int_{[A]=0}^{[A]=1} \langle n\rangle \, \mathrm{d}\ln[A] = -\Delta G_t/RT \tag{37}$$

where

$$-\Delta G_t/RT = \ln \beta_t \tag{38}$$

is the free energy change for the whole reaction

$$M + tA = MA_t \tag{39}$$

The formation fraction of each species is

$$\beta_i[A]^i/Z_M = \alpha_i \tag{40}$$

and the formation function can be rewritten as a sum of formation fractions

$$\langle n\rangle = \sum_{i=1}^{i=t} i\alpha_i \tag{41}$$

that can be rearranged to a double summation

$$\langle n\rangle = \sum_{i=1}^{i=t} \sum_{i=i}^{i=t} \alpha_i \tag{42}$$

In the case, for example, with $t=2$, $\langle n\rangle = (\alpha_1+\alpha_2)+(\alpha_2)$ which, when multiplied by d ln[A] and integrated, yields the whole area corresponding to free energy $-\Delta G_t/RT$ as the sum of two areas (Fig. 5), each of which corresponds to one $\ln K_i$. This $\ln K_i$ is the stepwise constant for the ith step. In fact, by recalling Eq. (38)

$$\sum_{i=1}^{i=t} \ln K_i = \ln \beta_t \tag{43}$$

The differences between the areas are proportional to

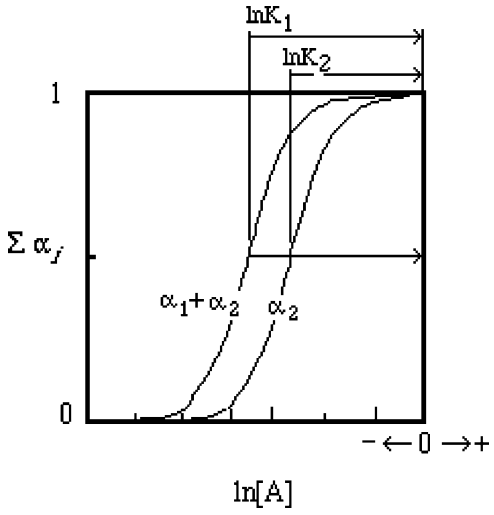


Fig. 5. The cumulative fraction curves delimit areas proportional to $-\Delta G_i/RT$ for each step.

the logarithm of the statistical factor and to the logarithm of the cooperativity factor.

The stepwise constants, however, are not indicative of the real ligation process. In fact, successive binding of ligands to the sites of the receptor (Fig. 6) takes place by rearrangement of the previous bonds [13]. For instance, when the second ligand binds, the bond (if the cooperativity is negative) of the first ligand is weakened and becomes equal to that of the second one. In terms of potential function, this means that the mean minimum of the well is less deep and further from the origin for both ligands The cooperativity might be also positive and the bond lengths would become uniformly shorter.

6. Cooperativity function

In order to verify the model of specific site affinity constant and class cooperativity function, we can recall Eqs. (42) and (43) and calculate

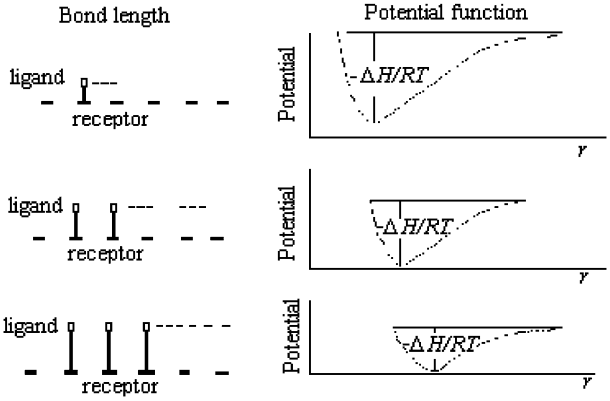


Fig. 6. Successive binding of ligands produces weakening of all the bonds. The reduction of the potential function well is represented on the right.

$$\ln K_{\gamma} = (1/i)(\ln \beta_t \ln m) = \ln k - \ln \gamma(i)$$
$$= \ln k - (i-1)b \quad (44)$$

whereby we calculate the mean cooperativity per site at each binding step and, by extrapolation to $i=1$, the specific site affinity constant. Then by plotting this function [13] against $(i-1)$, a straight line should be obtained with slope b. This behaviour has been observed for several sets of experimental data such as the cumulative constants for complexes Ni(II)–ammonia, Cu(II)–bovine serum albumin (BSA), Co(II)–ammonia, Ni(II)–hydrazine, and Cd(II)–ammonia. The determination of the cooperativity function with cooperativity factor b for BSA is reported in Fig. 7. The Scatchard function

$$\partial \ln Z_{\mathrm{M}}/\partial[\mathrm{A}] = \langle n \rangle/[\mathrm{A}] \quad (45)$$

plotted against $\langle n \rangle$ is a straight line with slope proportional to the site constant k whenever there is no cooperativity, i.e. when the sites are independent. The Scatchard function, however, is curved downward with respect to the straight line of non-cooperativity when the cooperativity is negative and upward when the cooperativity is positive. By applying to the original data of the cumulative constants the cooperativity factor calculated according to Eq. (45), the curve is transformed into a straight line (Fig. 8).

7. Site affinity constants and cooperativity coefficients

In a sufficiently general case, we can assume that there are three independent components M, A, and H forming complexes $\mathrm{M}_P\mathrm{A}_Q\mathrm{H}_R$ defined by the cumulative constants

$$\beta_{PQR} = [\mathrm{M}_P\mathrm{A}_Q\mathrm{H}_R][\mathrm{M}]^{-P}[\mathrm{A}]^{-Q}[\mathrm{H}]^{-R} \quad (46)$$

We can describe the thermodynamic state of the system by means of three partition functions, Z_{M}, Z_{A}, and Z_{H}, respectively

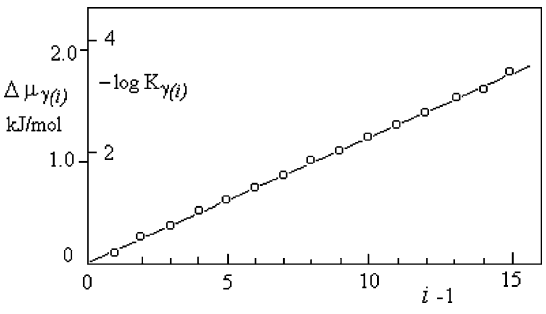


Fig. 7. The cooperativity function reported against $(i-1)$ shows a slope corresponding to b of Eq. (44).

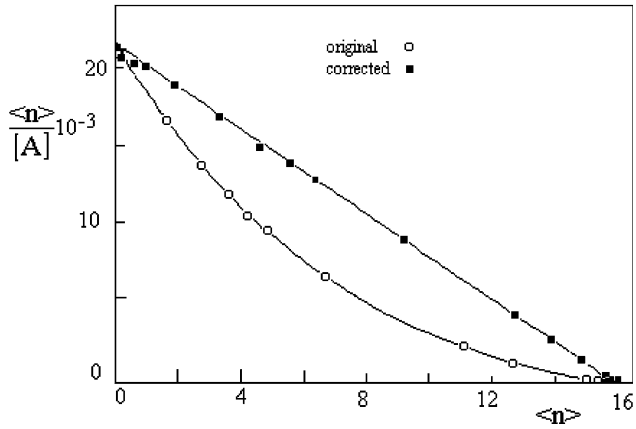


Fig. 8. Scatchard function calculated with original and corrected data of cumulative constants for BSA (Bovine Serum Albumin).

$$Z_{\mathrm{M}} = \sum_{P=1}^{P_t}\sum_{Q=0}^{Q_t}\sum_{R=0}^{R_t}\beta_{PQR}[\mathrm{M}]^{(P-1)}[\mathrm{A}]^{Q}[\mathrm{H}]^{R} \quad (47a)$$

$$Z_{\mathrm{A}} = \sum_{P=0}^{P_t}\sum_{Q=1}^{Q_t}\sum_{R=0}^{R_t}\beta_{PQR}[\mathrm{M}]^{P}[\mathrm{A}]^{(Q-1)}[\mathrm{H}]^{R} \quad (48a)$$

$$Z_{\mathrm{H}} = \sum_{P=0}^{P_t}\sum_{Q=0}^{Q_t}\sum_{R=1}^{R_t}\beta_{PQR}[\mathrm{M}]^{(P-1)}[\mathrm{A}]^{Q}[\mathrm{H}]^{(R-1)} \quad (49a)$$

where P_t, Q_t, and R_t are the maximum values of the indexes P, Q, and R, respectively. The total balance equations become

$$[T_{\mathrm{M}}] = [\mathrm{M}]\{Z_{\mathrm{M}}\} + [\mathrm{M}]\{\partial Z_{\mathrm{M}}/\partial[\mathrm{M}]\} \quad (47b)$$
$$[T_{\mathrm{A}}] = [\mathrm{A}]\{Z_{\mathrm{A}}\} + [\mathrm{A}]\{\partial Z_{\mathrm{A}}/\partial[\mathrm{A}]\} \quad (48b)$$
$$[T_{\mathrm{H}}] = [\mathrm{H}]\{Z_{\mathrm{H}}\} + [\mathrm{H}]\{\partial Z_{\mathrm{H}}/\partial[\mathrm{H}]\} \quad (49b)$$

Each cumulative constant in Eqs. (47a), (48a) and (49a) can be expressed as sums of terms as in Eq. (31) which are functions of statistical factor, site constant of the class j, and cooperativity coefficient $\gamma_{i,j} = \exp(b_j(i-1))$ of the i element of class j. Therefore, it is possible to express the mass balance equations Eqs. (47b), (48b) and (49b) via Eqs. (47a), (48a) and (49a) as functions of the variables k_j and $\gamma_{i,j}$. The derivatives of the mass balance equations with respect to the variables k_j and $\gamma_{i,j}$ can be calculated analytically. Then these derivatives can be employed to construct the normal equations necessary to refine the values of the site constants and of the cooperativity coefficients by means of a non-linear least-squares optimization procedure. A computer program called SITECON has been prepared [14]. This program has been employed to calculate the affinity site constant and the cooperativity constant in a set of titrations of polyamines [15]. The values of the cumulative equilibrium constants calculated by introducing the values of the site constant and of the cooperativity coefficient obtained in the refinement have been compared with (see Table 1) values of the cumulative constants obtained by direct refinement by the computer method

SUPERQUAD [16]. In the series of aliphatic diamines, the value of the cooperativity factors b obtained in the refinement shows a negative cooperativity effect decreasing with the increase of the molecular length (Table 2). This conforms to the hypothesis that the reciprocal influence of the two binding sites is smaller the greater is the distance between them. The question can be raised whether the cooperativity effect, which is a free energy difference, is purely enthalpic or partially enthalpic and partially entropic. The results obtained so far are not conclusive in this respect.

8. Partition function derivatives: buffer capacity and heat capacity

The formation function, which is the first derivative of partition function with respect to ln[A] can be derived again, thus obtaining, as the second derivative, the buffer capacity B_C. The buffer capacity is an element of the matrix formed by the second derivatives of the partition function. The B_C values of the different parts are important features of the titration curve. It is important, however, to emphasize that the buffer capacity is the second derivative of ln Z_M

$$B_C = \partial^2 \ln Z_M / \partial(\ln[A])^2 \quad (50)$$

and as such it indicates the spreading (variance) of the free energy around values of ln β_t. The buffer capacities are independent for each cumulative constant and are a good indicator of the multimodal distribution of the reacting ensemble (Fig. 9).

In the cases where there is only one site, the formation function is identical with the molar fraction α_1 of the complex and its derivative with ln[A] can be rewritten as

$$B_C = \partial\alpha_1/\partial \ln[A] = \alpha_1(1-\alpha_1) \quad (51)$$

whereby B_C becomes the convolution of α_1 with its complement to unity. Because of this property, every cumulative curve can be convoluted with its own complement to unity to produce a set of buffer capacity curves, one curve for each ln β_t.

Every constant either cumulative or stepwise can be derived with respect to the reciprocal temperature thus yielding the reaction enthalpy for the corresponding reaction

$$(\partial \ln K_i/\partial(-1/T))_p = (\Delta H_{i,i-1}/R) \quad (52)$$

or

$$(\partial \ln \beta_i/\partial(-1/T))_p = (\Delta H_i/R) \quad (53)$$

where $\Delta H_{i,i-1}$ is the enthalpy of the reaction $MA_{i-1} + A = MA_i$ and ΔH_i is the enthalpy of the reaction $MA_{i-1} + iA = MA_i$. By further derivation with respect to T, we obtain the heat capacity

$$\partial^2 \ln \beta_i/\partial(-1/T)\partial T = \partial^2 \ln\beta_i/\partial(\ln T)^2 = (\Delta C_{p,i}/R) \quad (54)$$

If the equilibrium constant matches exactly the species involved, then $(\Delta H_i/R)$ is constant $(\Delta C_{p,i} = 0)$. By plotting ln β_i against $(1/T)$ we obtain a straight line whose slope yields the reaction enthalpy. If, however, other reactants are involved in the reaction but are not explicitly included in the equilibrium constant, particularly the solvent, then the enthalpy is altered by the contribution of these reactants and we do not obtain a constant slope any more $(\Delta C_{p,i} \neq 0)$, but rather a curve at a variable slope.

The partition function can be also derived with respect to ln T thus obtaining another element of the

Table 1
Comparison between cumulative constants obtained with SITECON [14] and SUPERQUAD [15]

	SITECON				SUPERQUAD			
	lg β_1	lg β_2	lg β_3	lg β_4	lg β_1	lg β_2	lg β_3	lg β_4
DAP	10.864	20.754			10.757	20.546		
DAB	9.718	17.265			10.302	17.922		
DAHP	9.595	17.564			9.580	17.560		
DETA					9.840	18.860	23.090	
EDDC	9.936	17.047			9.937	17.059		
PDDC	10.506	19.255			10.876	19.877		
BDDC	10.717	20.717			10.743	20.227		
BTATC	6.432	10.278			6.365	10.639		
DETA	9.815	18.651	26.509		9.692	18.793	23.201	
TETA	10.004	18.505	25.577	31.146	9.822	18.913	25.490	28.855
HEDTA	9.846	15.130	17.571		9.901	15.192	17.519	
EDTA	10.182	16.344	19.060	21.118	10.176	16.327	19.033	21.114

DAP, 1,5-diaminopentane dihydrochloride; DAB, 1,4-diamine-butanone; DAHP, 1,3-diamine-hydroxy-propane; DETA, diethylentriamine; EDDC, ethylendiamine dihydrochloride; PDDC, 1,3-diamepropane dihydrochloride; BDDC, 1,4-diamine-butane dihydrochloride; BTATC, 1,2,3,4-benz.tetramine tetrachloride; TETA, triethylintetram tetrachloride; HEDTA, N(hyd.ethyl)ethylendiaminetriac acid; EDTA, ethylendiaminetetrac acid.

Table 2
Cooperativity calculated by SITECON [a]

Amine	No. class	No. sites	log k	σ	b	σ	$\Delta\mu^\circ$ (kJ mol^{-1})
DAP	1	2	10.404	0.005	0.279	0.014	1.592
DAB	1	2	9.417	0.034	1.807	0.067	10.309
DAHP	1	2	9.294	0.015	1.179	0.036	6.726
DETA	1	2	9.598	0.082	0.408	0.178	2.328
EDDC	1	2	9.634	0.001	2.557	0.003	14.6
PDDC	1	2	10.205	0.003	1.239	0.008	7.6
BDDC	1	2	10.416	0.025	0.767	0.069	4.4
BTATC	1	2	6.131	0.082	1.823	0.141	10.4
DETA	1	3	9.337	0.055	0.577	0.095	3.3
TETA	1	4	9.402	0.048	1.240	0.074	7.1
HEDTA	2	2	9.545	0.036	4.560	0.090	26.0
		1(COOH)	2.441				
EDTA	2	2	9.881	0.013	3.935	0.009	22.4
		2(COOH)	2.415				

DAP, 1,5-diaminopentane dihydrochloride; DAB, 1,4-diamine-butanone; DAHP, 1,3-diamine-hydroxy-propane; DETA, diethylentriamine; EDDC, ethylendiamine dihydrochloride; PDDC, 1,3-diaminepropane dihydrochloride; BDDC, 1,4-diamine-butane dihydrochloride; BTATC, 1,2,3,4-benz.tetramine tetrachloride; TETA, triethylenetetram tetrachloride; HEDTA, N(hyd.ethyl)ethylendiaminetriac acid; EDTA, ethylendiaminetetrac acid.

[a] Data from Ref. [16].

derivative matrix. The first derivation with respect to ln T yields the molar fraction obtained from the change of temperature α_T

$$(\partial \ln(1+k[\mathrm{A}])/\partial(\ln T))_\mathrm{p} = (1/R)\{(\Delta H_i/T) - n_\mathrm{A} C_{\mathrm{p,A}}\}\alpha = (1/R)\alpha_T \quad (55)$$

and the second derivation yields

$$(\partial^2 \ln(1+k[\mathrm{A}])/\partial(\ln T)^2)_\mathrm{p} = (1/R)\alpha_T(1-\alpha_T)\{(\Delta H_i/T) - n_\mathrm{A} C_{\mathrm{p,A}}\} \quad (56)$$

which by comparison with Eq. (51) can be recognized as an apparent (buffer) heat capacity.

$$(\partial^2 \ln(1+k[\mathrm{A}])/\partial(\ln T)^2)_\mathrm{p} = (1/R)\Delta C_{\mathrm{p,app}} \quad (57)$$

Therefore, we obtain an explicit expression for the apparent heat capacity $\Delta C_{\mathrm{p,app}}$

$$\Delta C_{\mathrm{p,app}} = \alpha_T(1-\alpha_T)\{(\Delta H_{\mathrm{reac}}/T) - n_\mathrm{A} C_{\mathrm{p,A}}\} \quad (58)$$

This heat capacity is called *apparent* because it is dependent not only upon the heat supplied to the system to increase the temperature by one degree but also upon the endogenous heat produced or absorbed by the advancement of the reaction produced by the change of temperature. (We recall that the definition of molar heat capacity is the amount of heat supplied to the system necessary to increase the temperature of one mole of substance by one degree).

By multiplication of Eq. (58) by dT and integration (Fig. 10) between the limits T_1 (beginning of the reaction) and T_2 (end), we obtain the denaturation heat Q_{den}

$$Q_{\mathrm{den}} = \Delta H_{\mathrm{reac}} - n_\mathrm{A} C_{\mathrm{p,A}} T_{\mathrm{av}} \quad (59)$$

where T_{av} has been substituted for the mean temperature between T_1 and T_2. If the reaction is denaturation with water as ligand the result is

$$\Delta H_{\mathrm{den}} = (\Delta H^\circ + n_\mathrm{w} T_{\mathrm{den}} C_{\mathrm{p,w}}) \quad (60)$$

where T_{den} has been substituted for the mean temperature. This means that, according to this model, the denaturation enthalpy is changing linearly with the temperature following the expression

$$\Delta H_{\mathrm{den}} = \Delta H^\circ + \Delta C_\mathrm{p} T_{\mathrm{den}}, \quad (61)$$

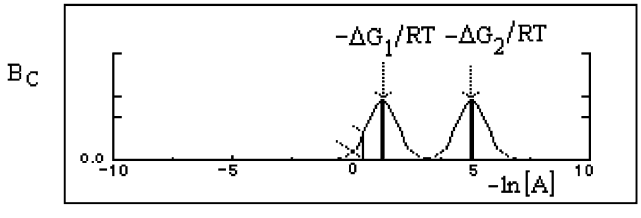


Fig. 9. Buffer capacity B_C as indicative of a multimodal distribution in a reacting system.

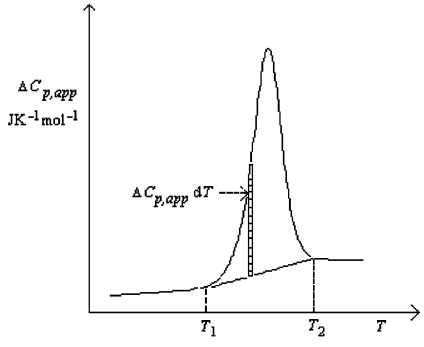


Fig. 10. Denaturation calorimetric profile for one-step process.

with ($\Delta C_p \neq 0$)

$$\Delta C_p = n_w C_{p,w} \tag{62}$$

It is then possible from the slope of the line ΔH_{den} against T to obtain the number n_w of water molecules involved in the denaturation process, by assuming $C_{p,w} = 75.38$ J K^{-1} mol^{-1}. The real changes in $C_{p,w}$ between 0 and 100 °C are very small and no appreciable error ($< 0.2\%$) is introduced by assuming a constant value and hence a non-reacting system. These calculations have been applied [17] to several sets of data of different origin and in any case the number of water molecules has been calculated. An example is represented in Fig. 11. The values n_w of water molecules calculated for different proteins range from 66.8 for β-lactoglobulin to 283 for ribonuclease. It depends on the size of the molecule, on the pH, and the hydrophobic character of the substituents.

Similarly for micelles [17], by plotting the micellization enthalpy against T, a straight line is obtained with negative slope, thus indicating that $n_w < 0$. This is in accordance with a possible mechanism of micellization opposite to that occurring in denaturation, whereby the separated chains are initially surrounded in the solution by a cavity which has been produced by some water molecules relaxed during the solubilization process. When the two hydrophobic moieties come close to one another, they need a volume which is smaller than the sum of the original cavities. As a consequence, a certain number n_w of released water molecules need to be restructured to occupy the available space.

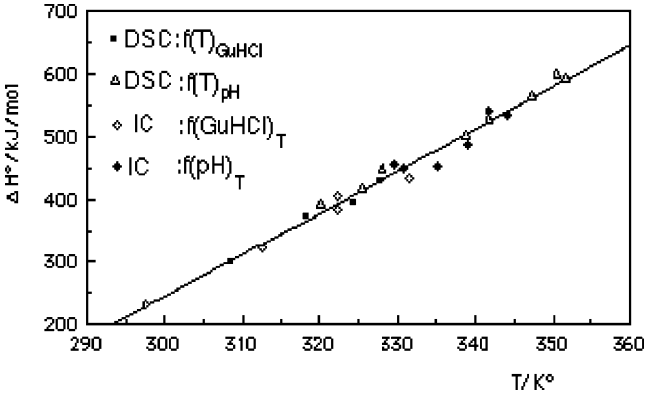


Fig. 11. Denaturation enthalpy of HEW lysozyme versus T. (Data from Ref. [18].) DSC, differential scanning calorimetry (denaturation by varying the temperature T at various constant concentrations of GuHCl or at various constant pH). IC, isothermal calorimetry (denaturation by adding GuHCl or by changing pH at various constant temperatures T).

9. Probability space, thermodynamic space, and energy space

The partition function belongs to the probability space and through Eq. (34) can be transformed into a function of the thermodynamic space [4]

$$\ln Z_M = -\Delta G/RT \tag{63}$$

The thermodynamic space is the domain of the relative changes of probability. In the thermodynamic space, the function can be expanded in a Taylor series following the maximum entropy method [19–21]. The logarithmic function can be written

$$\ln Z_M = (\ln Z_M)_0 + \sum\nolimits_n M^{(n)} x^n \tag{64}$$

where $(\ln Z_M)_0$ is the value of the function at the centre of expansion, x is a thermodynamic variable that can be either ln[A], ln T, or $1/T$, and $M^{(n)}$ is the nth derivative of the function with respect to the variable chosen

$$M^{(n)} = \partial^n \ln Z_M / \partial x^n \tag{65}$$

For instance, if $x = (\ln[A] - \ln[A]_0)$, then the first moment is given by $\langle n \rangle$ of Eq. (35) and the second moment by the buffer capacity B_C of Eq. (50). Higher moments can be calculated as derivatives of the partition function with respect to ln[A]. Poland has shown how this expansion can be used to calculate the partition function starting from the knowledge of the higher moments [19].

If the variable is $x = (\ln T - \ln T_0)$, then the first moment is given by Eq. (55) and the second moment by Eq. (57). If the variable is $x = (1/T - 1/T_0)$, then the first moment is the reaction enthalpy of Eq. (52) and the second moment is a function of the heat capacity $C_p^* = T^2 C_p$ [22]. An application of the variable $x = (1/T - 1/T_0)$ has been given in the study of the dependence upon the temperature of the protonation constant of carboxylic acids [23]. On the other hand, by multiplication of both members of Eq. (63) by RT, we perform a transformation to the energy–affinity space

$$-RT \ln Z_M = \Delta G \tag{66}$$

for which the derivative with respect to the variable $x = T$ is

$$M^{(1)} = \partial(\Delta G)/\partial x = \partial(\Delta H - T\Delta S)/\partial x = -\Delta S \tag{67}$$

It is possible, however, to expand the function ΔH, which is to conform to the energy space, in a Taylor series, for which the first moment is the heat capacity ΔC_p and higher moments can be calculated by expanding the heat capacity as a function of $x = (T - T_0)$. Poland [20,21] has shown how the expression for heat capacity as the function of the variable x can be used to calculate the enthalpy by integration, starting from the knowledge of the moments of heat capacity.

Acknowledgements

This work is part of the Project "Molecular Systems and Metallo-receptors for the Activation and Transport of Dioxygen, Nitric Oxide, and Biosubstrates" supported by MURST, COFIN 2000.

References

[1] A. Braibanti, E. Fisicaro, C. Compari, Thermochim. Acta 320 (1998) 253.
[2] A. Braibanti, E. Fisicaro, C. Compari, Thermochim. Acta 320 (1998) 265.
[3] A. Braibanti, E. Fisicaro, C. Compari, Thermochim. Acta 320 (1998) 101.
[4] A. Braibanti, E. Fisicaro, C. Compari, Thermochim. Acta 320 (1998) 277.
[5] R.O. Watts, Integral Equation Approximations in the Theory of Fluids, Statistical Mechanics, vol. 1, The Chemical Society, London, 1973.
[6] J.W. Whalen, Molecular Thermodynamics: a Statistical Approach, Wiley, New York, 1991.
[7] A. Braibanti, E. Fisicaro, F. Dallavalle, J.D. Lamb, J.L. Oscarson, J. Phys. Chem. 97 (1993) 8054.
[8] A. Braibanti, E. Fisicaro, C. Compari, J. Phys. Chem. B 102 (1998) 8357.
[9] E. Fisicaro, A. Braibanti, J.D. Lamb, J.L. Oscarson, Biophys. Chem. 36 (1990) 1.
[10] D. Poland, Cooperative Equilibria in Physical Biochemistry, Clarendon, Oxford, 1978.
[11] E. Fisicaro, A. Braibanti, J.D. Lamb, J.L. Oscarson, Biophys. Chem. 36 (1990) 15.
[12] A. Braibanti, F. Dallavalle, E. Fisicaro, Ann. Chim. 78 (1988) 679.
[13] A. Braibanti, E. Fisicaro, M.C. Monguidi, F. Dallavalle, Inorg. Chim. Acta 138 (1993) 17.
[14] E. Fisicaro, A. Braibanti, R. Sambasiva Rao, C. Compari, A. Ghiozzi, G. Nageswara Rao, Talanta 45 (1998) 1267.
[15] C. Compari, E. Fisicaro, A. Braibanti, Polyhedron 21 (2002), 1503 (this issue).
[16] P. Gans, A. Sabatini, A. Vacca, J. Chem. Soc., Dalton Trans. (1985) 1195.
[17] A. Braibanti, E. Fisicaro, C. Compari, J. Therm. Anal. Calc. 61 (2000) 461.
[18] P.L. Privalov, Pure Appl. Chem. 47 (1976) 293.
[19] D. Poland, J. Chem. Phys. 113 (2000) 4774.
[20] D. Poland, J. Chem. Phys. 112 (2000) 6554.
[21] D. Poland, Biopolymers 58 (2001) 89.
[22] A. Braibanti, E. Fisicaro, F. Dallavalle, J.D. Lamb, J.L. Oscarson, J. Phys. Chem. 97 (1993) 8062.
[23] A. Braibanti, E. Fisicaro, F. Dallavalle, J.D. Lamb, J.L. Oscarson, F.X. Ughi, J. Phys. Chem. 97 (1993) 8071.

atom by the N(9) donor (as mono-dentate) [1,3,4,7,9,10] or in a μ-N(3),N(9) bridging mode (oligomers) [2,5,6,8]. Such coordination modes in non-substituted adenine species are understood on the basis that the N(9) donor atom is the most basic among its five nitrogen atoms, followed by N(1) [1]. Interestingly a single metal–N(3)–adenine coordination has been proved in the structure of [Ni(AdeH)(tren)Cl]Cl [11] and [Pd(thiacyclophane)(AdeH)]BF_4 [12]. A variety of structures concerning adeninium(1+) and adeniniun(2+) ions (for this latter, four inorganic salts [13–15]) are also known. Compounds which have $AdeH_2^+$ cation are a broad variety of salts with inorganic or organic counter-anions as well as adeninium(1+)–metal complexes of nickel(II) [16], copper(II) [8–10], zinc(II) [17–19] cadmium(II) [20] and silver(I) [21]. In the Cd(II) derivative the $AdeH_2^+$ ligand acts as a bridge, with an unexpected μ-N3,N7 coordination mode [20]. In Ag(I) complexes, $AdeH_2^+$ ion links the metal by N(9) atom [21], whereas in Ni(II) [16] and Zn(II) [17–19] derivatives the donor is unusually the N(7) atom. Keeping this in mind, as a part of the laboratory work for our students in Inorganic Aspects of Biological Processes [22], the following proposal was made: to carry out the reaction of AdeH and aqua(dihydrogen-ethylenediaminetetraacetato)copper(II), [Cu(H_2EDTA)(H_2O)], an acid-complex derivative of ethylenediaminetetraacetic acid (H_4EDTA) whose structure was reported by Stephens a long time ago [23]. In this octahedral complex the pentadentate H_2EDTA^{2-} ligand has one coordinated and one free acetic arms. We could expect that this acidic complex should react with neutral AdeH to give the $AdeH_2^+$ ion. This adeninium(1+) ion could or could not bind the copper(II) atom. In this latter case it probably replaces the aqua ligand, which in the parent complex is among the four closest donors. The best way to find definitive answers to these hypotheses is to perform the X-ray structure determination of the corresponding reaction product. In this connection, we have carried out the synthesis, structure and properties of the title compound.

2. Experimental

All chemicals were commercially available products of reagent grade and used without further purification.

2.1. Synthesis of title compound *1*

Adeninium [aqua(ethylenediamine-*N*,*N*,*N*′-triacetato-*N*′-acetic acid)copper(II) dihydrate} (**1**) ($AdeH_2$)[Cu(HEDTA)(H_2O)]·$2H_2O$, was obtained by reaction of $Cu_2CO_3(OH)_2$ (221 mg, 1 mmol, Probus or Aldrich) and H_4EDTA (588.5 mg, 2 mmol, Sigma) in water (100 ml) in a Kitasato flask, by heating (15 min, $t < 50$ °C) and stirring under reduced pressure (to remove the CO_2, by-product). The resulting blue solution was stirred and heated at 60 °C during 30 min. After leaving it to cool to room temperature (r.t.), it was slowly filtered (without vacuum, to remove a very small amount of CuO) on an Erlenmeyer flask. Adenine (270 mg, 2 mmol) was added to this clear blue solution and stirred. No appreciable change of colour occurs in the solution, which was filtered without vacuum on crystallisation device. By slow evaporation of the clear solution at r.t. (1–2 weeks), crystals of compound **1** were observed. First poly-crystals were removed by filtration. The evaporation of the remaining solution (partially covered with a plastic film) gives many well-shaped crystals of the desired product suitable for X-ray diffraction studies. Several fractions of the product were collected by filtration, washed with cold water and air-dried. The blue compound is stable at r.t. without apparent water loss. It can be re-crystallised at r.t. from water. Yield: 980 mg (90%). $C_{15}H_{25}CuN_7O_{11}$: Calc.: H 4.64, C 33.18, N 18.06. Found: H 5.13, C 32.99, N, 18.19%. Calc. Cu 11.7. Found: Cu 17.6% (EDTA complexometry [24]). If the solution of compound **1** became microbiologically contaminated, ethanol should be added, the solution covered with a plastic film, filtered without vacuum 2 or more days after, and left to evaporate as before. Using a molar ratio Cu(II)/H_4EDTA/AdeH 1:1:2, a pale blue powder of the type Cu(EDTA)·$(AdeH_2)_2$·nH_2O is also obtained. However, no suitable crystals for X-ray diffraction studies of such compound have yet been obtained. The analytical data of this product is close to a 1:2 metal/ligand molar ratio, but at the present time it seems not consistent enough to a well-defined stoichiometry.

2.2. Crystal structure determination

A blue prismatic crystal of (AdeH)[Cu(HEDTA)(H_2O)]·$2H_2O$ was mounted on a glass fibre and used for data collection. Crystal data were collected at 291(2) K, using a Bruker SMART CCD 1000 diffractometer. Graphite monochromated Mo Kα radiation ($\lambda =$ 0.71073 Å) was used throughout. The data were processed with SAINT [25] and corrected for absorption using SADABS (transmission factors: 0.9189–0.6729) [26]. The structure was solved by direct methods using the program SHELXS-97 [27] and refined by full-matrix least-squares techniques against F^2 using SHELXL-97 [28]. Positional and anisotropic atomic displacement parameters were refined for all non-hydrogen atoms. Hydrogen atoms were located unambiguously from difference Fourier maps and refined isotropically. Atomic scattering factors from 'International Tables for X-ray Crystallography' [29]. Molecular graphics were obtained with the program PLATON [30]. A summary of the crystal data, experimental details and refinement results are listed in Table 1.

Table 1
Crystal data and structure refinement for compound **1**

Empirical formula	$C_{15}H_{25}CuN_7O_{11}$
Formula weight	542.96
Temperature (K)	293(2)
Wavelength (Å)	0.71073
Crystal system	monoclinic
Space group	$P2_1/c$
Unit cell dimensions	
a (Å)	7.053(1)
b (Å)	42.540(5)
c (Å)	7.4978(1)
β (°)	104.24(1)
Volume (Å^3)	2180.5(2)
Z	4
Calculated density (Mg m^{-3})	1.654
Absorption coefficient (mm^{-1})	1.075
$F(000)$	1124
Crystal size (mm)	0.40 × 0.14 × 0.08
θ range for data collection (°)	1.91–28.01
Index ranges	$-9 < h < 9$, $-56 < k < 55$, $-8 < l < 9$
Reflections collected/unique	13576/5113 [$R_{int} = 0.0509$]
Completeness to $\theta = 28.02°$	95.9%
Absorption correction	SADABS
Max and min transmission	0.9189 and 0.6729
Refinement method	Full-matrix least-squares on F^2
Data/restraints/parameters	5113/0/407
Goodness-of-fit on F^2	0.910
Final R indices [$I > 2\sigma(I)$]	$R_1 = 0.042$, $wR_2 = 0.064$
R indices (all data)	$R_1 = 0.087$, $wR_2 = 0.072$
Largest difference peak and hole (e Å^{-3})	0.394 and −0.394

2.3. Physical measurements

Elemental analysis was performed on a Fisons–Carlo Erba EA 1108 microanalyser (C, H, N) or by standard EDTA complexometry (Cu). The infrared spectrum was obtained by the KBr disc technique on a JASCO FT-IR 410 instrument. TG analysis (pyrolysis) of the studied compound (295–875 K) in air flown (100 ml min^{-1}) and corresponding IR spectra of evolved gasses were recorded using a Shimazu Thermobalance TGA-DTG-50H coupled with an FT-IR Nicolet Magna 550. Electronic (reflectance) spectrum (175–3300 nm) was obtained in a Varian Cary-5E spectrophotometer. RSE spectrum of a polycrystalline sample was recorded without magnetic dilution in a spectrophotometer Bruker ESP 300E (X band) at r.t. Magnetic susceptibility was measured at the temperature range 80–300 K using a Manics DM magnetometer. The susceptometer was calibrated with mercury tetrakis(thiocyanato)cobaltato(II). Corrections for the diamagnetism (-271.47×10^{-6} cm^3 mol^{-1}) were estimated from Pascal's constants [31]. Experimental susceptibilities were also corrected for the temperature-independent paramagnetism (60×10^{-6} cm^3 mol^{-1}).

3. Results and discussion

3.1. Cu(II) coordination, conformation of ligands and crystal packing in compound 1

Bond lengths and angles of the copper(II) coordination in the complex $[Cu(HEDTA)(H_2O)]^-$ of compound **1** are listed in Table 2. Structural data of the adeninium(1+) ion are given in Table 3. Hydrogen bonding data of the studied crystal are showed in Table 4. The studied compound consists of a salt of the complex anion $[Cu(HEDTA)(H_2O)]^-$ and the adeninium(1+) cation with two non-bonded to the metal water molecules (Fig. 1). The copper(II) atom exhibits a distorted octahedral coordination supplied by a penta-dentate $HEDTA^{3-}$ anion and one aqua ligand. This coordination polyhedron is of the general type 4+1 and closely related to those reported for the parent complex $[Cu(H_2EDTA)(H_2O)]$ [23] (hereafter compound **2**) and the bimetallic derivative $Ag[Cu(HEDTA)(H_2O)]\cdot H_2O$ [32] (hereafter compound **3**). The metal falls at 0.083(1) Å from the mean plane P-1 [O1,O11,O15,N12] of the four closest donor atoms (0.075(1) and 0.13(1) Å in compounds **2** and **3**, respectively). In the three compounds which we are considering now, the partially protonated EDTA ligand acts as pentadentate giving a Cu(II)–ethylendiamine-like ring (E ring) and three Cu(II)–glycinato-like rings (one of them is a Cu(II)–glycine-like ring in compound **2**). Two of these three rings are so-called R rings (nearly perpendicular to the plane P-2 [Cu1,N11,N12]), and the

Table 2
Bond lengths (Å) and angles (°) for copper(II) coordination in compound **1**

Bond lengths	
Cu(1)–O(15)	1.941(1)
Cu(1)–O(11)	1.953(1)
Cu(1)–O(1)	1.954(1)
Cu(1)–N(12)	2.066(1)
Cu(1)–N(11)	2.373(1)
Cu(1)–O(17)	2.405(1)
Bond angles	
O(15)–Cu(1)–O(11)	176.64(1)
O(15)–Cu(1)–O(1)	89.06(1)
O(11)–Cu(1)–O(1)	92.51(1)
O(15)–Cu(1)–N(12)	85.69(1)
O(11)–Cu(1)–N(12)	93.48(1)
O(1)–Cu(1)–N(12)	166.28(1)
O(15)–Cu(1)–N(11)	97.48(1)
O(11)–Cu(1)–N(11)	79.19(1)
O(1)–Cu(1)–N(11)	110.65(1)
N(12)–Cu(1)–N(11)	82.64(1)
O(15)–Cu(1)–O(17)	91.35(1)
O(11)–Cu(1)–O(17)	91.49(1)
O(1)–Cu(1)–O(17)	94.29(1)
N(12)–Cu(1)–O(17)	73.20(1)
N(11)–Cu(1)–O(17)	153.57(1)

Table 3
Bond lengths (Å) and angles (°) for adeninium(1+) ion in compound **1**

Bond lengths	
N(21)–C(21)	1.313(1)
N(22)–C(22)	1.341(1)
N(22)–C(21)	1.375(1)
N(23)–C(22)	1.308(1)
N(23)–C(23)	1.350(1)
N(24)–C(25)	1.313(1)
N(24)–C(24)	1.377(1)
N(25)–C(25)	1.353(1)
N(25)–C(23)	1.355(1)
C(21)–C(24)	1.384(1)
C(23)–C(24)	1.390(1)
Bond angles	
C(22)–N(22)–C(21)	123.40(1)
C(22)–N(23)–C(23)	111.43(1)
C(25)–N(24)–C(24)	102.54(1)
C(25)–N(25)–C(23)	106.25(1)
N(21)–C(21)–N(22)	119.44(1)
N(21)–C(21)–C(24)	126.74(1)
N(22)–C(21)–C(24)	113.83(1)
N(23)–C(22)–N(22)	125.88(1)
N(23)–C(23)–N(25)	127.34(1)
N(23)–C(23)–C(24)	127.46(1)
N(25)–C(23)–C(24)	105.18(1)
N(24)–C(24)–C(21)	130.65(1)
N(24)–C(24)–C(23)	111.31(1)
C(21)–C(24)–C(23)	118.00(1)
N(24)–C(25)–N(25)	114.73(1)

Table 4
Bond distances (Å) and angles (°) for the hydrogen bonds in the crystal of compound **1**

D–H···A	*d*(D–H)	*d*(H···A)	*d*(D···A)	<(DHA)
O(3)–H(30B)···O(11)	0.791(3)	2.058(3)	2.847(1)	175.0(3)
O(3)–H(30A)···O(16)^{i}	0.784(2)	1.992(2)	2.767(1)	169.8(2)
O(2)–H(20B)···O(3)^{ii}	0.621(1)	2.114(2)	2.726(1)	169.2(2)
O(2)–H(20A)···N(24)^{iii}	0.837(3)	2.020(3)	2.849(1)	170.4(3)
N(25)–H(25A)···O(2)^{iv}	0.783(2)	1.889(2)	2.673(1)	178.4(2)
N(22)–H(22A)···O(17)	0.847(2)	1.795(2)	2.638(1)	172.9(1)
N(21)–H(21B)···N(23)^{v}	0.824(1)	2.417(2)	3.118(1)	143.4(1)
N(21)–H(21A)···O(18)	0.986(3)	1.821(3)	2.804(1)	174.6(2)
O(13)–H(13)···O(12)^{vi}	0.816(3)	1.822(3)	2.638(1)	177.8(3)
O(1)–H(10B)···O(16)^{vii}	0.759(2)	1.918(3)	2.663(1)	166.8(2)
O(1)–H(10A)···O(18)^{viii}	0.837(1)	1.848(2)	2.657(1)	162.4(1)

Symmetry codes: i = $x+1, y, z+1$; ii = $x, y, z-1$; iii = $-x+1, -y, -z+1$; iv = $-x, -y, -z+1$; v = $x+1, y, z$; vi = $x-1, -y+1/2, z-1/2$; vii = $x, y, z+1$; viii = $x-1, y, z$.

other, is a G ring (nearly coplanar to P-2) [32,33]. The G ring is more strained than the R ones [34], as the corresponding bond angles on the metal atom reveal (73.2° for the G ring, and 79.2 and 85.6° for R1 and R2 rings involving the O(18), O(15) and O(11) donor atoms, respectively). The free carboxymethyl arm in the three compounds could be considered as an 'opened G ring'.

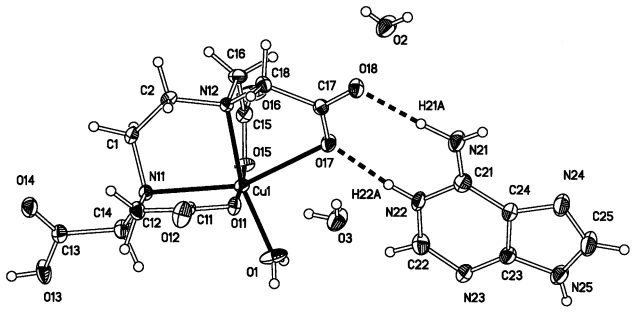


Fig. 1. Asymmetric unit in the crystal of $(AdeH_2)[Cu(HEDTA)(H_2O)]\cdot 2H_2O$ (compound **1**) with the numbering scheme. The two rather linear hydrogen bonds involved in the cation–anion recognition are depicted as dashed links.

Among the three methylene groups linked to the same N atom, those of the E and G rings fall to the same side of the plane P-2, and that of the R ring, to the opposite side [33]. The partially protonated EDTA ligand exhibits in **1** a E,G/R conformation, as in all mononuclear octahedral metal–EDTA chelates [33]. The E ring is puckered. The G and R1 rings have unsymmetrical envelope conformations whereas the R2 ring adopts a less common puckered form [35].

On the other hand, assuming that the N–H bond in neutral AdeH corresponds to the most basic N9 atom (formula 1) and was reported for the crystal structure of the free base [36]), the protonation of the adenine is made in the called N1 atom (formula 2). Indeed, such N1 protonation has been reported for the crystal structure of the adenine hydrochloride *hemi*-hydrate [37] and all known structures involving the adeninium(1+) cation. The N1 protonation is consistent with the C(21)–N(22)–C(22) bond angle (123.4(3)°) which is larger than that of the free base by 4.7°. A similar difference (5°) corresponds to the Ni(II)-bounded adeninium in $[Ni(NTA)(AdeH_2)(H_2O)]\cdot 2.5H_2O$ [16]. The adeninium(1+) cation is planar within ±0.025(1) Å.

In contrast to all other known Cu(II)–adeninium derivatives [8–10], which have coordinated adenium(1+) ligand, compound **1** consists, as referred above, of a salt. This means that the complex **2** reacts with AdeH to give the anion $[Cu(HEDTA)(H_2O)]^-$ which seems unable to recognise the cation $AdeH_2^+$ by means of a complexation process (for example, by a substitution reaction of aqua by the adeninium(1+) ligand). In contrast, Aoki et al. [16] have proved that the octahedral anion diaqua(nitrilotriacetate)nickel(II) recognises selectively the adeninium(1+) ion forming the neutral complex adeninium-aqua(nitrilotriacetato)nickel(II) (described as $[Ni(NTA)(H_2O)(AdeH_2)]_2\cdot 5H_2O$ in the crystalline state [16]) where the unusual Ni–N7($AdeH_2^+$) bond is reinforced by an intra-molecular

bond between an exocyclic N–H bond and one or two O-carboxylate atoms of the NTA ligand. Remarking that complexes $[Ni(NTA)(H_2O)_2]^-$ and $[Cu(HEDTA)(H_2O)]^-$ are both octahedral anions, we suggest that the difficulty of the latter in accepting the adeninium(1+) ion as a 'secondary' ligand arises from steric constraints favouring the recognition by the formation of an ion pair stabilised by inter-ionic hydrogen bonds. Consistently, the data of Table 4 reveal that, among others, there are two rather linear hydrogen bonds [the 'onium' $N(22)^+$–H(22A)···O(17) and exocyclic N(21)–H(21A)···O(18) interactions] where the adeninium(1+) ion acts twice as H-donor for the two O atoms of the same carboxylate group of the $HEDTA^-$ (Figs. 1 and 2). A detailed analysis [38] of the short aromatic ring–ring interactions (with centroid–centroid distances < 6.0 Å and its angles with the normal to the stacked ring planes, β and $\gamma < 60°$) reveals that such ion pairs recognise themselves to form aggregates $\{(AdeH_2)[Cu(HEDTA)(H_2O)]\}_2$ by a π,π-ring stacking interaction (Fig. 2). In the present case, for symmetry reasons, such interaction is displayed by the parallel six-membered rings of two adjacent $AdeH_2^+$ ions (symmetry code $\#5 = -x, -y, 1-z$). With a centroid–centroid vector of 3.39 Å and slipping angles (between the centroid–centroid vector and the normal to each stacked plane) $\beta = \gamma = 10.1°$, the inter-planar distance is 3.34 Å. Such stacking is rather close to, but not strictly, a 'face-to-face' interaction. In addition of the two referred inter-ionic hydrogen bonds, the remaining polar bonds (O–H from the $HEDTA^{3-}$ carboxyl group or water molecules and heterocyclic and exocyclic N–H of $AdeH_2^+$ ion) interact with carboxylate or water O atoms or adeninium N3 and N7 atoms (see Table 4). These hydrogen bonds involve nine different asymmetric units building the crystal as an extensive 3D network. The shortest hydrogen-bridges (2.638–2.672(4) Å) are those involving the aqua ligand, the free carboxylic group of $HEDTA^{3-}$ and both heterocyclic N–H bonds of $AdeH_2^+$ ion.

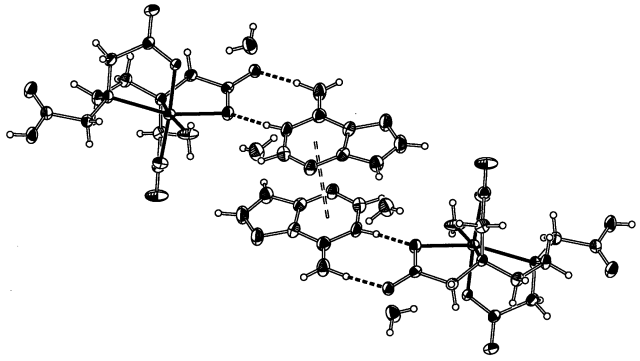


Fig. 2. Formation of aggregates $\{(AdeH_2)[Cu(HEDTA)(H_2O)]\}_2$ by anti-parallel π,π-stacking interaction between adeninium(1+) cations in the crystal of $(AdeH_2)[Cu(HEDTA)(H_2O)]\cdot 2H_2O$.

The structural results reported here offer a definitive answer to the main question of the aim of the present work. In this context, we can also consider that hypoxanthine (6-hydroxopurine) is unable to bind directly to the Ni–NTA chelate, because it has not the possibility to form an appropriate inter-ligand hydrogen bond, whereas the hypoxanthinato(1−) ion acts as a bridging ligand in $[\{Cu(tren)\}_2(\mu\text{-hypoxanthinato})](ClO_4)_3$ (tren = tris(2-aminoethyl)amine) [1] because each tren ligand forms an inter-ligand hydrogen bond with the bridging base. In addition, the Ni–NTA chelate is unable to coordinate the cytosinium(1+) ion because of the protonation of the 'N3' donor, but three inter-ligand hydrogen bonds are used in the inter-ionic recognition process in the salt (cytosinium)$[Ni(NTA)(H_2O)_2]\cdot 2H_2O$ [16]. This latter compound resembles the compound **1** in the out-spherical attachment of the protonated base to the metal chelate. However, it should be noted that the cytosynium(1+) ion has not an available N-heterocyclic donor, whereas the N-heterocyclic coordination of the adeninium(1+) ion to the copper(II) [8–10] and other metal ions [11,12] is well known.

3.2. Properties of compound *1*

The TG/DTG analysis of compound **1** (5.834 mg, 20 °C min^{-1}, in air flown) reveals its thermal decomposition in four steps. Selected FT-IR spectra of the evolved gasses are shown in Fig. 3. The first one (115–180 °C, maximum rate of weight loss at 151 °C, experimental weight loss 6.980% > calculated for $2H_2O$ 6.636%) is due to the loss on non-coordinated water, and lead to a starting actual 'TG-formula' $(AdeH_2)[Cu(HEDTA)(H_2O)]\cdot 2.1H_2O$ (FW 544.747; calculated weight loss 6.945% for $2H_2O$, in good agreement with the experimental value 6.980%). The second step (180–310 °C, weight loss of 36.582%) corresponds reasonably to the estimated loss (35.453%) of the aqua ligand and the pyrolysis of the free carboxymethyl arm ($-CH_2COOH$) and two acetate arms ($-CH_2COO^-$) from $HEDTA^{3-}$ ligand. Consistently, only water loss is observed during the first step, whereas FT-IR spectra during the second step show bands of H_2O, CO_2 and CO. The third step (310–440 °C) produces H_2O, CO_2, N_2O, and lower amounts of NH_3 and CO, whereas the last step (440–480 °C) gives H_2O, CO_2, N_2O, NO and a little CH_4 and NH_3. These steps correspond to the overlapped pyrolysis of the $HEDTA^{3-}$ residue and $AdeH_2^+$ ligand, giving a residue of CuO (experimental 14.651% and calculated 14.602% for the TG-formula). It seems rather improbable that the adeninium(1+) ion pyrolyses at so higher temperatures (> 300 °C) and perhaps adeninate(1−) is formed before this process occurs.

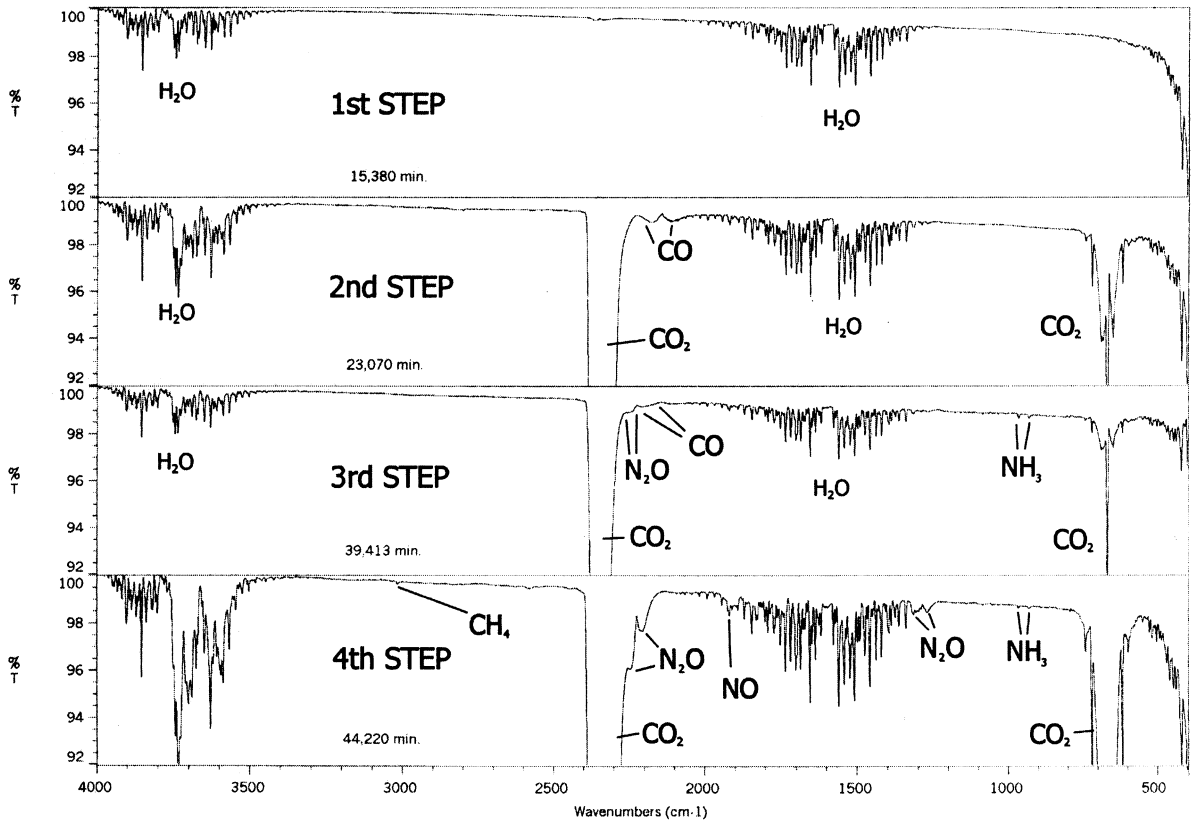


Fig. 3. Selected FT-IR spectra for identification of evolved gasses in the four steps of decomposition and pyrolysis of $(AdeH_2)[Cu(HEDTA)(H_2O)]\cdot 2H_2O$.

The IR spectrum has many peaks and bands expected for contributions of water and/or aqua, $HEDTA^{3-}$ and $AdeH_2^+$ ligands. Tentative assignments (in cm^{-1}) are as follows: $\nu_{as}(H_2O)$, 3440; $\nu_s(H_2O)+\nu_{as}(NH_2)$, 3356; $\nu_s(NH_2)$, 3242; the N^+–H chromophore gives a typical series of peaks in the range 2800–2250 [39] (six peaks in this case), including one at 2760 of $\nu(N^+–H)$; $\nu(C{=}O)$ of hydrogen bonded –COOH, 1720 and 1693; $\delta(H_2O)+\nu_{as}(COO)$, 1595; $\delta(NH_2)$ and $\delta(N^+–H)$, 1537 (shoulder) and 1495 (peak), respectively; $\nu(C–O)+\delta(O–H)$ of –COOH, 1404; and $\nu_s(COO)$, 1381. A large difference $\Delta=\nu_{as}(COO)-\nu_s(COO)=214\ cm^{-1}$ suggests the main ionic character of the Cu(II)–O(carboxyl) bonds [40]. The electronic spectrum shows an unsymmetrical d–d band at $\nu_{max}=13\,260\ cm^{-1}$ (with a shoulder $\sim 8360\ cm^{-1}$) in agreement with the elongated octahedral chromophore $CuNO_3+N+O$. The powder ESR spectrum at r.t. is *quasi*-isotropic type with $\sim g_{//}=2.17>g_{av}=2.14>\sim g_{\perp}=2.13>2.03$, which yields no useful g value information but is in accordance with a d_{x2-y2} Cu(II) ground state, long metal–metal separations (Cu(1)–Cu(1^i) = 7.053(1) Å) and local molecular axes clearly misaligned in the crystal [41]. A plot of χ data versus T (K) ($T=79$–290 K) is linear ($1/\chi=(1/C)T-(\theta/C)$ with a statistical r^2 factor of 0.9965) according to a Curie–Weiss behaviour, $\chi=C/(T-\theta)$ [31]. The Curie constant is $C=0.43$ K emu mol^{-1} with Weiss constant of $\theta=7.46$. The estimated value of μ_{eff} for Cu(II) atom is 1.86 BM, according to the structure reported here.

4. Concluding remarks

We can consider that the chelated anions $[Cu(HEDTA)(H_2O)]^-$ and $[Ni(NTA)(H_2O)_2]^-$ [16] display different mechanisms to recognise the adeninium(1+) ion. The former by means of an ion pair stabilised by two inter-ionic hydrogen bonds, and the latter, as a secondary ligand also reinforced by an inter-ligand NTA–$AdeH_2^+$ hydrogen bond. In addition, ion-pairs of compound **1** recognise themselves forming a slightly slipped π,π-stacking interaction between the six-membered rings of anti-parallel symmetry related adjacent $AdeH_2^+$ cations. In contrast, such aromatic π,π-ring stacking seems not to take part in the crystal packing of the related compound $[Ni(NTA)(AdeH_2)(H_2O)]\cdot 2.5H_2O$ [16].

5. Supplementary material

Crystallographic data for the structural analysis have been deposited with the Cambridge Crystallographic Data Centre CCDC No. 172659 for compound $(AdeH_2)[Cu(HEDTA)(H_2O)]\cdot 2H_2O$. Copies of this information may be obtained free of charge form The Director, CCDC, 12 Union Road, Cambridge, CB2 1EZ, UK (fax: +44-1223-336033; e-mail: deposit@ccdc.cam.ac.uk or www: http://www.ccdc.cam.ac.uk).

Acknowledgements

The authors are gratefully indebted to the DGESIC (MECD, Spain) for financial support (Research Projects PB98-0605-C03-02 and -03). E.S.P. thanks the Department of Inorganic Chemistry of the University of Granada the opportunity to participate in this work during the course Inorganic Aspects of Biological Processes. D.Ch.L. thanks the AECI (MAE, Spain) the financial support of a Doctoral research grant. A research grant to E.B.A. from MECD is also gratefully acknowledged.

References

[1] M. Abdus Salam, K. Aoki, Inorg. Chim. Acta 314 (2001) 71 (and references therein).
[2] A. Marzotto, A. Ciccarese, D.A. Clemente, G. Valle, J. Chem. Soc., Dalton Trans. (1995) 1461.
[3] H. Sakaguchi, H. Anzai, K. Furuhata, H. Ogura, Y. Iitaka, T. Fujita, T. Sakaguchi, Chem. Pharm. Bull. 26 (1978) 2465.
[4] E. Sletten, Acta Crystallogr., Sect. B 25 (1969) 1480.
[5] A. Terzis, A.L. Beauchamp, R. Rivest, Inorg. Chem. 12 (1973) 1166.
[6] P. de Meester, A.C. Skapski, J. Chem. Soc. A (1971) 2167.
[7] K. Tomita, T. Izuno, T. Fujiwara, Biochem. Biophys. Res. Commun. 54 (1973) 96.
[8] P. de Meester, A.C. Skapski, J. Chem. Soc., Dalton Trans. (1972) 2400.
[9] P. de Meester, A.C. Skapski, J. Chem. Soc., Dalton Trans. (1973) 424.
[10] D.B. Brown, J.W. Hall, H.M. Helis, E.G. Walton, D.J. Hodgson, W.E. Hatfield, Inorg. Chem. 16 (1977) 2675.
[11] A. Marzotto, D.A. Clemente, A. Ciccarese, G. Valle, J. Crystallogr. Spectroscop. Res. (1993) 23.
[12] W.M. Beck, J.C. Calabrese, N.D. Kotmair, Inorg. Chem. 18 (1979) 176.
[13] G.L. Hardgrove Junior, J.R. Einstein, B.E. Hingerty, C.H. Wei, Acta Crystallogr., Sect. C 39 (1983) 88.
[14] V. Langer, K. Huml, Acta Crystallogr., Sect. A 40 (1984) C86.
[15] V. Langer, K. Huml, Acta Crystallogr., Sect. B 34 (1978) 1157.
[16] M. Abdus Salam, K. Aoki, Inorg. Chim. Acta 311 (2000) 15 (and references therein).
[17] M.R. Taylor, Acta Crystallogr., Sect. B 29 (1973) 884.
[18] P.T. Muthiah, S.K. Mazumdar, S. Chaudhuri, J. Inorg. Biochem. 19 (1983) 237.
[19] M.R. Taylor, J.A. Westphalen, Acta Crystallogr., Sect. A 37 (1981) C63.
[20] C.H. Wei, K.B. Jacobson, Inorg. Chem. 20 (1981) 356.
[21] C. Gagnon, J.H. Huber, R. Rivest, A.L. Beauchamp, Inorg. Chem. 16 (1977) 2469.
[22] Inorganic Aspects of Biological Processes in an optional subject proposed by one of us (J.N.-G.) to the University of Granada authorities, at the Faculty of Pharmacy. It covers essential theoretical (30 h) and experimental (30 h) aspects of inorganic chemistry regarding their bioinorganic implications. Bioinorganic Chemistry is also offered at this Faculty as an optional subject, covering theoretical (40 h) and practical (20 h) seances.
[23] F.S. Stephens, J. Chem. Soc. A (1969) 1723.
[24] W.B. Guenther, Quantitative Chemistry: Measurements and Equilibrium, Addison-Wesley, Reading, MA, USA, 1968.
[25] SMART and SAINT, Area detector control and integration software, Bruker Analytical X-ray Instruments Inc., Madison, WI, USA, 1997.
[26] G.M. Sheldrick, SADABS. Program for Empirical Absorption Correction of Area Detector Data, University of Göttingen, Göttingen, Germany, 1997.
[27] G.M. Sheldrick, Acta Crystallogr., Sect. A 46 (1990) 467.
[28] G.M. Sheldrick, SHELXL-97, Program for the Refinement of Crystal Structures, University of Göttingen, Göttingen, Germany, 1997.
[29] International Tables X-ray Crystallography, Vol. C, Kluwer Academic, Dordrecht, The Netherlands, 1995.
[30] A.L. Spek, PLATON, A Multipurpose Crystallographic Tool, Utrecht University, Utrecht, The Netherlands, 2000.
[31] F.E. Mabbs, D.J. Machin, Magnetism and Transition Metal Complexes, Chapman & Hall, London, 1973.
[32] C. Brouca-Cabarrecq, B. Marrot, A. Mosset, Acta Crystallogr., Sect. C 52 (1996) 1903.
[33] M.A. Porai-Koshits, A.I. Pozhidaev, T.N. Polynova, Russ. J. Inorg. Chem. 15 (1974) 991.
[34] B.E. Douglas, D.J. Radanovic, Coord Chem. Rev. 128 (1993) 139.
[35] C.J. Hawkins, Absolute Configuration of Metal Complexes (Ch. 3), Wiley-Interscience, New York, USA, 1971.
[36] D. Voet, A. Rich, Prog. Nucleic Acid Res. 10 (1970) 183.
[37] L.M. Cunane, M.R. Taylor, Acta Crystallogr., Sect. B 49 (1993) 524.
[38] C. Janiak, J. Chem. Soc., Dalton Trans. (2000) 3885.
[39] L.J. Bellamy, The Infrared Spectra of Complex Molecules, Vol. 1, Chapman & Hall, London, UK, 1975.
[40] K. Nakanishi, Practical Infrared Absortion Spectroscopy, Nakondo Co Ltd, Tokyo, Japan, 1962.
[41] (a) B.J. Hathaway, In: G. Wilkinson, R.D. Gillard, J.A. McCleverty (Eds.), Comprehensive Coordination Chemistry, Pergamon, Vol. 5, Oxford, UK, 1987 (Ch. 53).;
(b) R.R. Conry, K.D. Karlin, in: R.B. King (Ed.), Encyclopedia of Inorganic Chemistry, Vol. 2 (Copper: Inorganic & Coordination Compounds and references therein), Wiley, New York, 1994, pp. 712–733.

PERGAMON

Polyhedron 21 (2002) 1459–1467

POLYHEDRON

www.elsevier.com/locate/poly

Basicity and coordination ability of linear hexa-amines in relation to N-$(CH_2)_n$-N chain-link lengths. A solution study

Andrea Bencini [a], Emanuela Berni [b], Françoise Chuburu [b], Claudia Giorgi [a], Henri Handel [b,*], Michel Le Baccon [b], Piero Paoletti [a,*], Barbara Valtancoli [a]

[a] *Department of Chemistry, University of Florence, Via della Lastruccia 3, 50019 Sesto Fiorentino, Firenze, Italy*
[b] *Lab. de Chimie, Electrochimie Moléculaires et Chimie Analytique, Université de Bretagne Occidentale, 6, Av. Victor Le Gorgeu (UMR CNRS No 6521), BP 809, F-29285 Brest Cedex, France*

Received 24 October 2001; accepted 20 November 2001

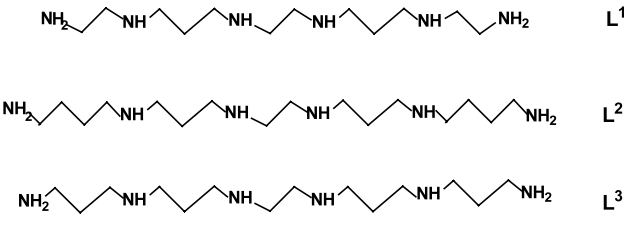
Abstract

The synthesis of the two new linear hexa-amines, 3,7,10,14-tetraazahexadecane-l,16-diamine (L^1) and 5,9,12,16-tetraazaicosane-l,20-diamine (L^2) has been reported. Ligand protonation and Cu(II) and Zn(II) coordination have been studied in aqueous solution by means of potentiometric, microcalorimetric (298.1 K, $I = 0.1$ mol dm^{-3}) and spectrophotometric (UV–Vis, ^{1}H and ^{13}C NMR) measurements. The species present in solution and their stability constants have been determined. L^1 forms mono- and binuclear complexes in aqueous solution with Cu(II). In the $[ML^1]^{2+}$ complexes, the metal ion is coordinated by five nitrogen atoms, while in the $[ML^2]^{2+}$ complexes the metal ion is four-coordinate. This different behavior is explained in terms of the different numbers of methylene groups between adjacent nitrogen atoms. © 2002 Elsevier Science Ltd. All rights reserved.

Keywords: Linear polyamines; Metal complexes; Polyamine complexes

1. Introduction

In recent years [1] much effort has been devoted to the synthesis and characterization of large macrocyclic polyamines such as those in the series [3k]aneN$_k$ (k = 5–12) [2] and their complexes. These ligands are able to hold more than one metal ion inside the ring structure. The ligands are sufficiently flexible so that they can wrap themselves around various metal ions in a way that achieves an optimal match between the stereochemical requirements of both metal and ligand atoms [3–5]. Also, the protonated forms of these ligands are able to encapsulate anions [6]. Recently, some of us [7–9] reported that linear polyamines containing a similar number and type of nitrogen donor atoms have very similar metal coordination chemistry, both in terms of the equilibrium speciation and of the stabilities of the different complexes formed, though there are much more data for macrocyclic polyamines than for linear ones. It has been shown that cyclic polyamines which produce a sequence of alternating five- and six-membered rings form stronger complexes than ligands which produce all five-membered or all six-membered chelate rings [10,11]. In order to get further insight into the chemistry of long open-chain polyamines we have synthesized the two ligands L^1 and L^2, which differ in the size of the chelate rings that may be formed and have examined the formation of complexes of these ligands with Cu(II) and Zn(II).



* Corresponding author. Fax: +39-055-4573364.
E-mail addresses: claudia.giorgi@unifi.it (C. Giorgi), henri.handel@univ-brest.fr (H. Handel).

0277-5387/02/$ - see front matter © 2002 Elsevier Science Ltd. All rights reserved.
PII: S0277-5387(02)00950-6

2. Experimental

2.1. Synthesis of 3,7,10,14-tetraazahexadecane-l,16-diamine (L^1) and 5,9,12,16-tetraazaicosane-1,20-diamine (L^2)

The synthesis of compounds L^1 and L^2 was carried out by the general synthetic route depicted in Scheme 1.

Perhydro-4,5,8a,10a-tetraazaphenanthrene (**1**) was prepared as previously described [12].

2.2. Synthesis of 4,5-bis(phthalimidoalkyl)-perhydro-4,5,8a,10a-tetraazaphenanthrene

To a solution of **1** (3.9 g, 20 mmol) in 60 cm^3 of dry CH_3CN, K_2CO_3 (200 mmol) and a solution of ω-bromoalkylphthalimide (40 mmol) in 50 cm^3 of CH_3CN were added. The reaction mixture was refluxed for 3 days. After reaction, the base was filtered, washed with CH_2C1_2 (3×10 cm^3) and solvents evaporated in vacuo. The resulting solid was recrystallized in CH_3CN affording L^1 and L^2 as white crystals. For L^1 alkyl = ethyl: yield 50% (the mono phthalimidoethyl adduct was also formed and separated by recrystallization from CH_3CN). NMR ^{13}C ($CDCl_3$): 168.3 (CO), 133.6, 132.3, 122.8 (C_{ar}), 79.7 (C_{aminal}), 56.6, 53.1, 50.8, 44.8 (NCH_2), 36.8 (CH_2N_{phth}), 19.9 ($NCH_2CH_2CH_2N$).

For L^2 alkyl = butyl: yield 92%. NMR ^{13}C ($CDCl_3$): 168.3 (CO), 133.6, 132.1, 122.9 (C_{ar}), 80.3 (C_{aminal}), 56.7, 53.4, 49.9, 45.2 (NCH_2), 37.8 (CH_2N_{phth}), 26.3, 26.1 ($CH_2CH_2CH_2CH_2$), 19.4 ($NCH_2CH_2CH_2N$).

2.3. General procedure for deprotection of $L^{1\prime}$ and $L^{2\prime}$: synthesis of ligands L^1 and L^2

4,5-Bis(phthalimidoalkyl)-perhydro-4,5,8a,10a-tetraazaphenanthrene (10 mmol), hydrazine monohydrate (30 cm^3) and ethanol (90 cm^3) were refluxed overnight. After cooling, the white precipitate was filtered and the solvent rotary evaporated. The resulting oil was stirred in chloroform and the white precipitate formed was filtered. After evaporation of the solvent, hexaamine was isolated as colorless oil. These compounds were converted into the corresponding hydrochloride salts using the classical procedure (EtOH–HCl) and then recrystallized from EtOH–H_2O.

3,7,10,14-Tetraazahexadecane-1,16-diamine hexahydrochloride [$L^1 \cdot 6HCl$]: white crystals (yield 82%). NMR ^{13}C (D_2O): 47.8, 47.7, 47.2, 46.0, 38.3 (CH_2N), 25.5 ($NCH_2CH_2CH_2N$). $C_{12}H_{32}N_6 \cdot 6HC1 \cdot (479.19)$: Calc.: C, 30.08; H, 7.99; N, 17.54; Cl, 44.39; Found: C, 30.03; H, 7.77; N, 17.37; Cl, 44.68%.

5,9,12,16-Tetraazaicosane-1,20-diamine hexahydrochloride [$L^2 \cdot 6HCl$]: white crystals (yield 95%). NMR ^{13}C (D_2O): 50.0, 48.0, 47.2, 46.0, 41.7 (CH_2N), 26.8, 25.6, 25.5 ($NCH_2CH_2CH_2CH_2N$ and $NCH_2CH_2CH_2N$). $C_{16}H_{40}N_6 \cdot 6HCl \cdot (535.29)$: Calc.: C, 35.90; H, 8.66; N, 15.74; Cl, 39.74; Found: C, 35.73; H, 8.55; N, 15.56; Cl, 39.68%.

Caution: Perchlorate salts of metal complexes with organic ligands are potentially explosive; these compounds must be handled with great caution.

2.4. Preparation of $[CuL^1](ClO_4)_2$

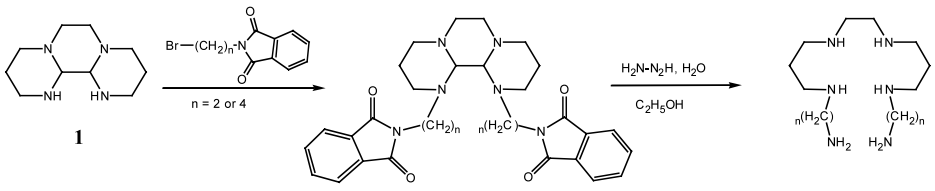
A solution of $Cu(ClO_4)_2 \cdot 6H_2O$ (37 mg, 0.1 mmol) in water (5 cm^3) was slowly added to a solution of $L^1 \cdot 6HCl$ (48 mg, 0.1 mmol) in water (10 cm^3). The pH was adjusted at 10.0 with NaOH and $NaClO_4$ (100 mg) was added to the resulting solution. The complex was obtained as a blue powder by slow evaporation of this solution at room temperature. Yield: 40 mg (76.5%) (Found: C, 27.6; H, 6.2; N, 16.1%. Calc. for $C_{12}H_{32}Cl_2CuN_6O_8$: C, 27.57; H, 6.17; N, 16.07%.)

2.5. Preparation of $[CuL^2](ClO_4)_2$

This compound was synthesized from L^2 (53.5 mg, 0.1 mmol) and $Cu(ClO_4)_2 \cdot 6H_2O$ (37 mg, 0.1 mmol) following the procedure given above for $CuL^1(ClO_4)_2$. Yield: 46 mg (79.5%) (Found: C, 33.2; H, 7.0; N, 14.5%. Calc. for $C_{16}H_{40}Cl_2CuN_6O_8$: C, 33.19; H, 6.96; N, 14.51%.).

2.6. Potentiometric measurements

A combined Ingold 405 S7/120 electrode was calibrated in terms of pH ($pH = -\log[H^+]$) by titrating a known amount of HCl with CO_2-free NMe_4OH solution; Gran's method [13] was applied to determine the



1

L1': n=2
L2': n=4

L1: n=2
L2: n=4

Scheme 1.

standard electrode potential E°, and the ionic product of water: $pK_w = 13.83(1)$. Stability constant titrations were carried out in a 0.1 mol dm^{-3} NMe_4Cl medium at 298.1 K using equipment and procedures which have been already described [14]. Ligand and metal ion concentrations were in the range 1×10^{-3}–2×10^{-3} mol dm^{-3}, and the $[M^{2+}]$ was varied in the range $0.8[L] < [M^{2+}] < 1.5[L]$. At least four titrations, each with about 150 data points, were performed for each system. The pH range covered was 2.5–10.5. The stability constants were derived with the aid of the computer program HYPERQUAD [15]; the values obtained are shown in Tables 1, 3 and 4.

2.7. Microcalorimetric measurements

The enthalpies of both ligand protonation and metal ion complexation reactions were determined in 0.1 mol dm^{-3} Me_4NCl solution by means of an automated system composed of a Thermometric AB thermal activity monitor (model 2277) equipped with a perfusion–titration device and a Hamilton Pump (model Microlab M) coupled with a 0.250 cm^3 gas-tight Hamilton syringe (model 1750 LT). The microcalorimeter was calibrated by determining the enthalpy of reaction of strong base (Me_4NOH) with strong acid (HCl). The value obtained, $-13.55(5)$ kcal mol^{-1} was in good agreement with the literature value [16]. As a further check the enthalpies of protonation of ethylenediamine (en) were determined by addition of a Me_4NOH solution (0.15 mol dm^{-3}, addition volumes 15 μl) to acidified solutions of en (5×10^{-3} mol dm^{-3}, 1.5 cm^3). For heats of complexation, acidified solutions containing a ligand (5×10^{-3} mol dm^{-3}, 1.5 cm^3) and a metal ion were titrated with Me_4NOH solution. Corrections for the heats of dilution were applied. The corresponding enthalpies of reaction were determined from the calorimetric data by least-squares fitting using the AAAL computer program [17]. At least three titrations (each with about 120 data points) were performed for each system.

Table 1
Logarithms of the protonation constants of ligand L^1 [a], L^2 [a] and L^3 [b]

	L^1	L^2	L^3	
$L + H^+ = LH^+$	9.86(2)	10.57(1)	10.83(4)	Log K_1
$LH^+ + H^+ = LH_2^{2+}$	9.63(1)	10.35(2)	10.15(5)	Log K_2
$LH_2^{2+} + H^+ = LH_3^{3+}$	8.65(1)	9.57(1)	9.30(4)	Log K_3
$LH_3^{3+} + H^+ = LH_4^{4+}$	6.81(1)	8.99(2)	8.45(5)	Log K_4
$LH_4^{4+} + H^+ = LH_5^{5+}$	5.90(1)	7.79(3)	7.30(5)	Log K_5
$LH_5^{5+} + H^+ = LH_6^{6+}$	4.92(1)	5.23(3)	4.98(6)	Log K_6

[a] This work. Values determined at 298.1 ± 0.1 K, in 0.1 mol dm^{-3} NMe_4Cl.
[b] Values taken from [19], at 298.1 ± 0.1 K, in 0.1mol dm^{-3} $NaClO_4$.
Values in parentheses are S.D. in the last significant figure.

2.8. NMR measurements

^1H and ^{13}C spectra in D_2O solution were recorded at 298 K and different pD values using a Varian Unity 300 MHz spectrometer. In the ^1H NMR spectra, peak positions are taken relative to HOD at 4.75 ppm. ^1H–^1H and ^1H–^{13}C 2-dimensional correlation experiments were performed to assign the signals. pD was adjusted by adding small amounts of 0.01 mol dm^{-3} NaOD or DCl solution. The pH was calculated from the measured pD value using the following relationship [18]:

$$pH = pD - 0.40$$

3. Results and discussion

The ligand L^1 has the sequence 2,3,2,3,2 of methylene groups between nitrogen atoms and is capable, in principle, of forming a sequence of alternating 5- and 6-membered rings in a metal-ion complex. L^2 has the sequence 4,3,2,3,4 and, therefore, may also form 7-membered rings. The thermodynamic data for protonation and complexation are shown in Tables 1–4, together with data for the related hexa-amine L^3 which has the methylene group sequence 3,3,2,3,3 [19].

3.1. Protonation

Each hexa-amine can accept up to six protons in a regular sequence over the pH range 2.5–11, as shown in Fig. 1. For each protonation step, except the first one, the protonation constant values increase in the order $L^2 > L^3 > L^1$. This sequence can be rationalized in terms of inductive and charge minimization effects, as has been discussed previously [19–23]. The higher basicities of L^2 compared with those of L^1 is also reflected by the higher $-\Delta H^\circ$ values in each protonation step, except the last step, illustrated in Table 2.

The enthalpy terms are favorable for all protonation steps. The entropy terms are favorable for the first three

Table 2
Thermodynamic parameters for ligands, L^1 and L^2, protonation reactions, determined in 0.1 mol dm^{-3} NMe_4Cl, 298.1 ± 0.1 K [a]

	$-\Delta H^\circ$(kJ mol^{-1})		$T\Delta S^\circ$ (kJ mol^{-1})	
	L^1	L^2	L^1	L^2
$L + H^+ = LH^+$	41.63(7)	53.5(1)	14.6(1)	6.7(1)
$LH^+ + H^+ = LH_2^{2+}$	48.78(9)	48.99(7)	6.3(1)	10.0(1)
$LH_2^{2+} + H^+ = LH_3^{3+}$	43.51(9)	51.62(9)	5.8(1)	2.9(1)
$LH_3^{3+} + H^+ = LH_4^{4+}$	41.17(7)	47.94(9)	−2.5(1)	3.3(1)
$LH_4^{4+} + H^+ = LH_5^{5+}$	35.49(7)	43.0(1)	−1.7(1)	1.2(1)
$LH_5^{5+} + H^+ = LH_6^{6+}$	38.75(8)	35.9(1)	−10.9(1)	−6.3(1)

[a] Values in parentheses are S.D. in the last significant figure.

Table 3
Formation constants and corresponding thermodynamic parameters for the copper(II) with ligands L^1 and L^2 determined in 0.1 mol dm^{-3} NMe_4Cl, 298.1 ± 0.1 K [a]

	Log K		$-\Delta H^\circ$ (kJ mol^{-1})		$T\Delta S^\circ$ (kJ mol^{-1})	
	L^1	L^2	L^1	L^2	L^1	L^2
$L + Cu^{2+} = CuL^{2+}$	21.3(1)	16.63(6)	116.6(1)	79.4(1)	4.6(1)	15.5(1)
$CuL^{2+} + H^+ = Cu(HL)^{3+}$	9.47(8)	10.17(6)	43.9(1)	54.3(1)	10.0(1)	3.8(1)
$Cu(HL)^{3+} + H^+ = Cu(H_2L)^{4+}$	6.37(1)	8.99(4)	29.3(1)	53.9(1)	53.9(1)	−2.5(1)
$Cu(H_2L)^{4+} + H^+ = Cu(H_3L)^{5+}$		6.20(2)		27.6(1)		7.5(1)
$CuL^{2+} + OH^- = CuL(OH)^+$	2.99(1)	2.97(9)	3.8(1)	−0.4(1)	13.4(1)	17.1(1)
$CuL^{2+} + Cu^{2+} = Cu_2L^{4+}$	8.73(3)		31.3(1)		18.4(1)	
$Cu_2L^{4+} + OH^- = Cu_2LOH^{3+}$	6.32(7)		35.5(1)		0.4(1)	

[a] Values in parentheses are S.D. in the last significant figure.

protonation steps, much less favorable for the fourth and fifth ones and unfavorable for the last one.

The location of attachment of each proton during the protonation sequence has been determined by relating ^1H and ^{13}C chemical shifts to calculated solution compositions. Firstly, individual resonances were assigned on the basis of ^1H–^1H homonuclear and ^1H–^{13}C heteronuclear correlation experiments, as shown in ligand drawing 1.

Then, changes in chemical shift were correlated with changes in concentration on the speciation diagrams, Fig. 1.

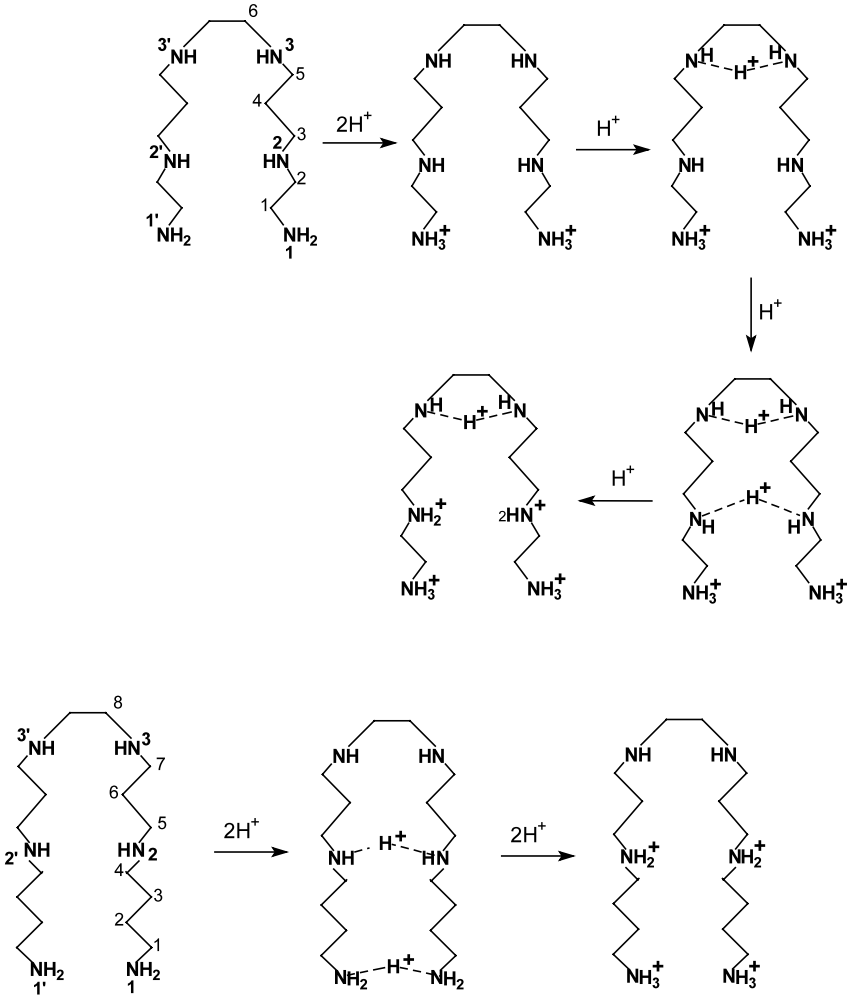


Table 4
Formation constants and corresponding thermodynamic parameters for the zinc(II) with ligands L^1 and L^2 determined in 0.1 mol dm^{-3} NMe_4Cl, 298.1 ± 0.1 K [a]

	log K		$-\Delta H^\circ$ (kJ mol^{-1})		$T\Delta S^\circ$ (kJ mol^{-1})	
	L^1	L^2	L^1	L^2	L^1	L^2
$L + Zn^{2+} = ZnL^{2+}$	13.84(2)	8.66(5)	64.4(1)	24.2(1)	14.2(1)	25.1(1)
$ZnL^{2+} + H^+ = Zn(HL)^{3+}$	6.58(3)	9.71(4)	26.3(1)	51.0(1)	11.3(1)	4.2(1)
$Zn(HL)^{3+} + H^+ = Zn(H_2L)^{4+}$	6.40(2)	8.55(4)	37.2(1)	47.6(1)	−0.8(1)	1.2(1)
$Zn(H_2L)^{4+} + H^+ = Zn(H_3L)^{5+}$		8.11(6)		41.4(1)		5.0(1)
$ZnL^{2+} + OH^- = ZnL(OH)^+$	2.66(7)	3.77(4)	−0.4(1)	5.4(1)	15.5(1)	15.9(1)

[a] Values in parentheses are S.D. in the last significant figure.

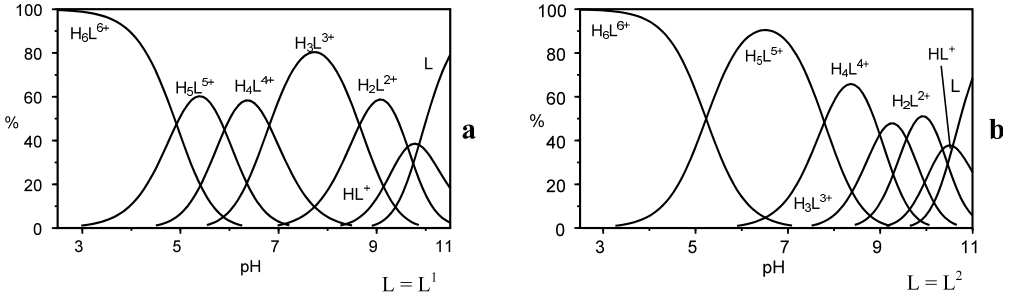


Fig. 1. Distribution diagrams of the protonated species formed by L^1 and L^2 as a function of pH (NMe_4Cl 0.1 mol dm^{-3}, 298.1 K).

At pH 11 the unprotonated amine, L^1, predominates in solution and the ^{13}C spectrum exhibits six peaks, at 28.97 (C4), 40.32 (Cl), 46.90 (C3), 47.10 (C5), 48.07 (C6), and 51.16 (C2). The ^1H spectrum of L^1 at this pH shows a quintuplet at 1.61 ppm (integrating to four protons and attributed to the protons, H4, of the central methylene group in a $-(CH_2)_3-$ group), a multiplet at 2.55 (8 protons), for the protons H3 and H5, a singlet at 2.65 (four protons, H6) and a multiplet at 2.70 ppm (H1 and H2). These spectral features indicate a time-averaged C_{2V} symmetry. This symmetry is preserved throughout the pH range investigated.

Fig. 2(a) and (b) show the ^1H and ^{13}C NMR chemical shifts of L^1 as a function of pH. In the pH range 11–8.5, where the first two protons bind to the ligand, the signal of H1, which is α to N1, shows the largest downfield shift. In ^{13}C NMR spectra of polyamines, it is known that the signal of a carbon atoms β to a nitrogen atom shifts upfield when that nitrogen atom is protonated [24]. The signal of the carbon atom C2, which is β to N1, displays the most pronounced upfield shift. These spectral features suggest that the first two protonation steps involve the primary nitrogens N1 and N1′, as would be expected considering that primary amines are more basic than secondary amines in aqueous solutions.

The third protonation step occurs in the pH range 8.5–7. In the ^1H NMR spectra H5 and H6 show the largest downfield shift whilst C4 and C6 show the largest upfield shift in the ^{13}C spectra. This protonation step therefore occurs at N3 and N3′. In the structure of $[H_3L^1]^{3+}$ each protonated nitrogen atom is separated from the next one by the unprotonated N2 and N2′, an arrangement which minimizes the electrostatic repulsion between charged $-NH_2^+-$ groups.

The atoms N2 and N2′ are protonated when $[H_4L^1]^{4+}$ and $[H_5L^1]^{5+}$ are formed, in the pH range 7.5–5. The protonation process is accompanied by significant shift of the H2, H3, C1 and C4 resonances. Below pH 5 protonation occurs on N3 and N3′ with an upfield shift of the C6 and C4 signals.

The ^1H and ^{13}C NMR spectra of L^2 indicate that this polyamine also has time-averaged C_{2V} symmetry over the whole of the observed pH range. The variation of chemical shift with pH is illustrated in Fig. 3.

With L^2, the first four protons go onto N1, N1′, N2 and N2′, as indicated by the way the resonances associated with H1, H4, H5, C2, C3, and C6 move with pH. This protonation sequence is different from that of L1. The main reason for this difference is the presence of two more methylene groups between N1 and N2. This has the effect increasing the distance between N1 and N2 and so decreasing the electrostatic repulsion when both atoms are protonated. Also N2 is slightly more basic due to inductive effects. Obviously the last two protons must go onto N3 and N3′ and this is confirmed by the movements of H7, H8, C6 and C8 signals in the region pH < 7.

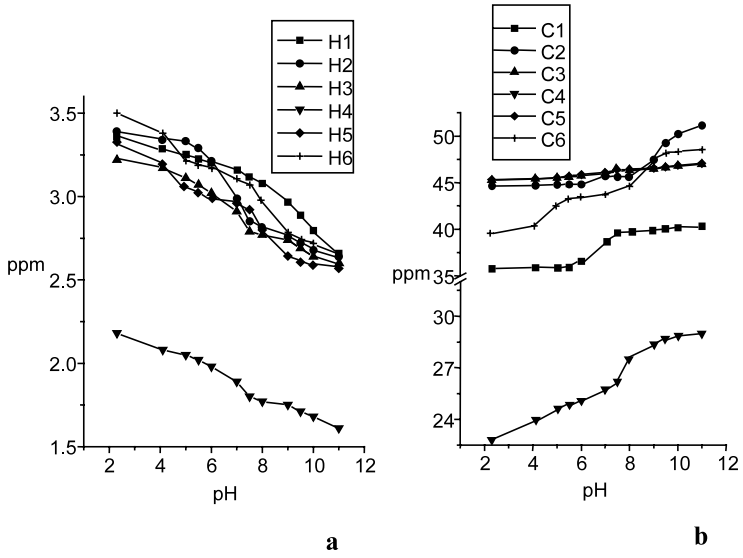


Fig. 2. (a) ^{1}H and ^{13}C (b) NMR chemical shifts of the L^1 signals as a function of pH.

3.2. Complexes of L^1 and L^2 with Cu(II)

Both ligands form the expected 1:1 complex CuL. The complexes can accept two protons to form $[CuLH]^{3+}$ and $[CuLH_2]^{4+}$ or an hydroxyl ion to form $[CuL(OH)]^{+}$. In addition binuclear complexes are formed with L^1 but not L^2 whereas a tris-protonated complex is formed with L^2 but not L^1. Stability constants and enthalpies are in Table 3 and speciation diagrams are in Figs. 4 and 5.

All the indications are that $[CuL^1]^{2+}$ is a 5N-coordinate species whereas L forms only 4N-coordinated complexes.

(i) K_{CuL} for L^2 is much lower than K_{CuL} for L^1. The difference is much larger than might be expected on the basis of ring-size differences and this suggests that $[CuL^2]^{2+}$ has a lower coordination number than $[CuL^1]^{2+}$.

(ii) The constant for the first protonation of the $[CuL]^{2+}$ ($L = L^1$ or L^2) complex is higher than those corresponding to the third protonation of the free amine. These data point out that the first protonation step of the complex occurs on a nitrogen atom not involved in metal coordination. The constant for the second protonation of the complex $[CuHL^1]^{3+}$ is smaller than those of the fourth protonation step of the free amine therefore in the $[CuL^1]^{2+}$ complex the copper ion is probably pentacoordinated. On the other hand the log K value for the protonation of $[CuHL^2]^{3+}$ is equal to

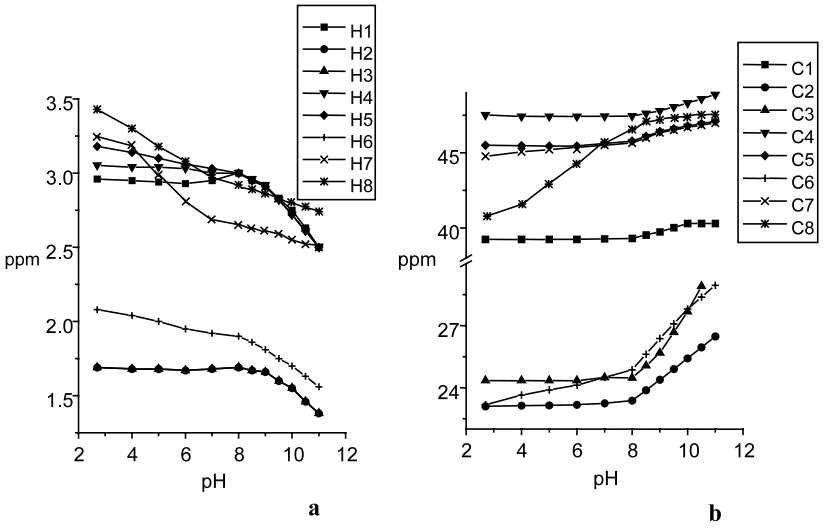


Fig. 3. (a) ^{1}H and ^{13}C (b) NMR chemical shifts of the L^2 signals as a function of pH.

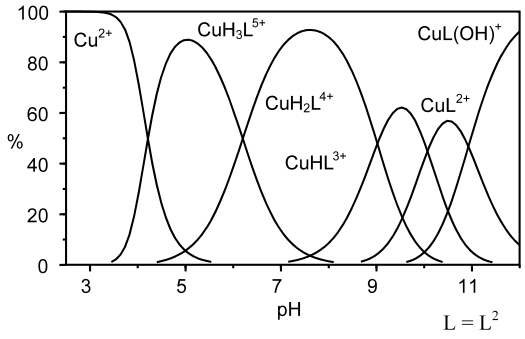


Fig. 4. Distribution diagrams of the species for the systems L^2–Cu(II) ($[L^2] = [Cu^{2+}] = 1 \times 10^{-3}$ mol dm^{-3}) as a function of pH (NMe_4Cl 0.1 mol dm^{-3}, 298.1 K).

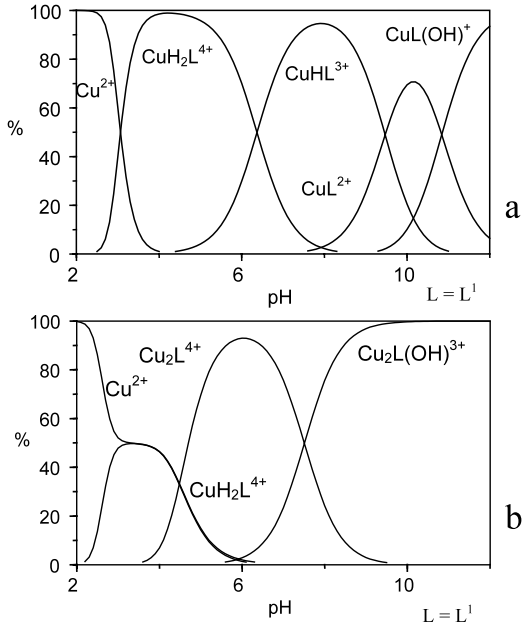


Fig. 5. Distribution diagrams of the species for the systems L^1–Cu(II) ($[L^1] = [Cu^{2+}] = 1 \times 10^{-3}$ mol dm^{-3} (a), $[L^1] = 1 \times 10^{-3}$ mol dm^{-3} and $[Cu^{2+}] = 2 \times 10^{-3}$ mol dm^{-3} (b) as a function of pH (NMe_4Cl 0.1 mol dm^{-3}, 298.1 K).

that for fourth protonation of the free ligand. These data suggest that in the $[CuL^2]^{2+}$ complex two of the nitrogens of L^2 remain uncoordinated.

(iii) The UV–Vis spectra of solutions in conditions where the species $[CuH_2L^2]^{4+}$, $[CuHL^2]^{3+}$ and $[CuL^2]^{2+}$, respectively, predominate all show a broad band at the same position and with the same intensity (λ_{max} 560 nm, ε 180 dm^3 mol^{-1}), suggesting that the copper ion environment is the same in all three complexes. However, the complex $[CuH_3L^2]^{5+}$ has a different spectrum (λ_{max} 610 nm, ε 110 dm^3 mol^{-1}), consistent with a decrease in ligand field strength due to the detachment of a nitrogen donor atom.

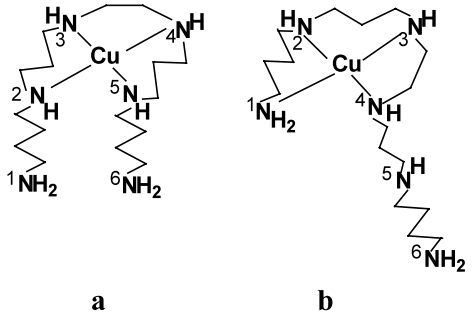
(iv) The UV–Vis spectrum of the species $[CuL^1]^{2+}$ (λ_{max} 538 nm, ε 110 dm^3 mol^{-1}) is consistent with the Cu(II) ion having a 5N- environment with a stronger ligand field splitting than in the 4-N complex formed with L^2.

v) The enthalpy of formation of $[CuL^1]^{2+}$ (116.6 kJ mol^{-1}) is comparable to the enthalpy of formation of the complex of Cu(II) with the linear polyamine 1,4,7,10,15-pentaazatridecane (105 kJ mol^{-1}) which is known to act as a pentadentate ligand towards Cu(II) [19].

It is interesting to note that even though the ligand L^1 could form a hexadentate complex with alternating 5- and 6-membered chelate rings, it does not do so, but instead forms a pentadentate complex. By comparison, the Cu(II) complex with the ligand 1,16-dimethyl-1,4,7,10,13,16-hexaazahexadecane [19,25,26], which forms a pentadentate complex with all 5-membered rings has a stability constant of log $K = 21.6$, which is almost the same as for the ligand L^1. The greater stability of complexes with alternating chelate ring sizes is well established with macrocyclic ligands, which effectively form square–planar complexes. L^2, which could form a 7-membered ring in fact only donates four nitrogen atoms.

In the structure of $[CuL^1]^{2+}$ one nitrogen atom, presumably at the end of the chain is not attached to the metal. In the structure of $[CuL^2]^{2+}$ two nitrogen atoms are unattached. Two proposed structures for this complex are reported in Fig. 6. The metal ion can be coordinated by four secondary nitrogen atoms (N2, N3, N4 and N5, see Fig. 6(a)) or by the terminal nitrogen atom Nl and the three adjacent secondary donors (N2, N3 and N4, see Fig. 6(b)). The spectral and potentiometric data do not allow us to discern between these two hypothesis.

The formation of binuclear complexes with L^1 has a clear analogy with the inclusion of two metal ions in large macrocyclic polyamines. A reasonable structure would have both copper atoms coordinated by three nitrogen atoms. The binuclear complex $[Cu_2L^1]^{4+}$ has a very high stability constant for the formation of the hydroxo complex $[Cu_2L^1(OH)]^{3+}$ (log $K = 6.32$ compared with the value of 2.99 for the formation of the



a b

Fig. 6. Proposed solution structures for the $[CuL^2]^{2+}$ complex.

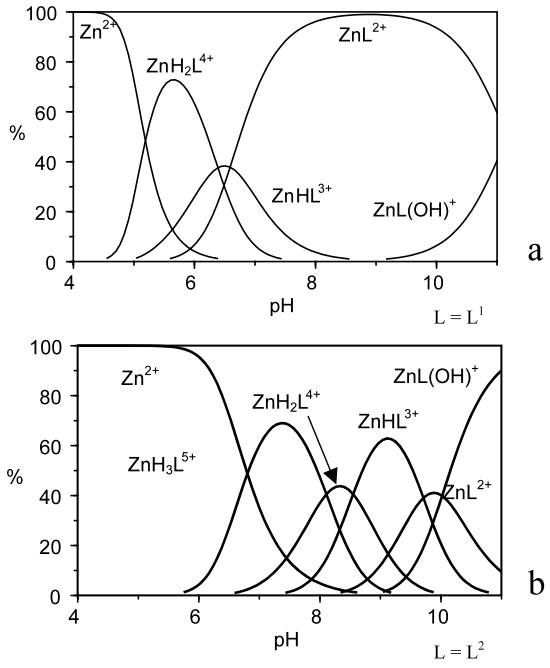


Fig. 7. Distribution diagrams of the species for the systems L^1–Zn(II) (a) and L^2–Zn(II) (b) ($[L^1] = [L^2] = [Zn^{2+}] = 1 \times 10^{-3}$ mol dm^{-3}) as a function of pH (NMe_4Cl 0.1 mol dm^{-3}, 298.1 K).

mononuclear hydroxo complex.). This suggests that the hydroxo group is bridging between two Cu(II) ions, so that both have a N_3O 4-coordinate environment.

3.3. Complexes of L^1 and L^2 with Zn(II)

Thermodynamic data for the complexes formed by Zn(II) with L^1 and L^2 are given in Table 4 and speciation diagrams are illustrated in Fig. 7. The main difference between Zn(II) and Cu(II) coordination is that the Zn(II) complexes are weaker and all mononuclear. Otherwise the coordination chemistry appear to be similar, with L^1 forming a 5-N complex and L^2 forming a 4-N complex. The complexes $[ZnL^1]^{2+}$ and $[ZnL^2]^{2+}$ can both accept two protons or an hydroxyl group whereas the latter can also accept a third proton. The complex $[ZnL^2]^{2+}$ is much less stable than $[ZnL^1]^{2+}$; this is clearly due to the fact that the formation of the complex with L^2 is much less exothermic. As with the Cu(II) complexes this difference in stability is a reflection of the fact that the 5th nitrogen atom necessarily forms an unfavorable 7-membered ring if it coordinates.

Acknowledgements

Financial support by the Italian Ministero dell'Universita e della Ricerca Scientifica e Tecnologica, within the program COFIN 2000, and by Italian Research Council (CNR) is gratefully acknowledged. C.G. wishes to express her thanks to Peter Gans for his ongoing interest and support.

References

[1] R.M. Izatt, K. Pawlak, J.S. Bradshaw, R.L. Bruening, Chem. Rev. 91 (1991) 1721.
[2] A. Bianchi, M. Micheloni, P. Paoletti, Coord. Chem. Rev. 110 (1991) 17.
[3] A. Bencini, A. Bianchi, M. Castellò, P. Dapporto, J. Faus, E. Garcia-España, M. Micheloni, P. Paoletti, P. Paoli, Inorg. Chem. 28 (1989) 3175.
[4] A. Bencini, A. Bianchi, M. Castello, P. Dapporto, E. Garcia-España, M. Micheloni, P. Paoletti, P. Paoli, J. Chem. Soc., Chem. Commun. (1990) 1382.
[5] A. Bencini, A. Bianchi, M. Castellò, P. Dapporto, E. Garcia-España, M. Micheloni, P. Paoletti, P. Paoli, Inorg. Chem. 29 (1990) 1716.
[6] A. Bianchi, C. Bowman-James, E. Garcia-España, (Eds.), Supramolecular Chemistry of Anions, Wiley, New York, 1997.
[7] J. Aragò, A. Bencini, A. Bianchi, E. Garcia-España, M. Micheloni, P. Paoletti, J.A. Ramirez, P. Paoli, Inorg. Chem. 30 (1991) 1843.
[8] J. Aragò, A. Bencini, A. Bianchi, E. Garcia-España, M. Micheloni, P. Paoletti, J.A. Ramirez, A. Rodriguez, J. Chem. Soc., Dalton Trans. (1991) 3077.
[9] A. Bencini, A. Bianchi, V. Fusi, P. Paoletti, B. Valtancoli, A. Adrés, J. Aragò, E. Garcia-España, Inorg. Chim. Acta 204 (1993) 221.
[10] (a) L. Fabbrizzi, R. Barbucci, P. Paoletti, J. Chem. Soc., Dalton Trans. (1972) 1529;
(b) P. Paoletti, L. Fabbrizzi, R. Barbucci, Inorg. Chem. 12 (1973) 1861.
[11] R. Barbucci, L. Fabbrizzi, P. Paoletti, Inorg. Chim. Acta 157 (1973).
[12] G. Hervé, N. Le Bris, H. Bernard, J.J. Yaouanc, H. des Abbayes, H. Handel, J. Organomet. Chem. 585 (1999) 259.
[13] G. Gran, Analyst (London) 77 (1952) 661.
[14] A. Bianchi, L. Bologni, P. Dapporto, M. Micheloni, P. Paoletti, Inorg. Chem. 23 (1984) 1201.
[15] P. Gans, A. Sabatini, A. Vacca, Talanta 43 (1996) 1739.
[16] J.P. Hall, R.M. Izatt, J.J. Christensen, J. Phys. Chem. 67 (1963) 2605.
[17] AAAL is the 1st version of the KK77 program written by A. Vacca, University of Florence, 1997. See A. Bianchi, B. Escuder, E. Garcia-España, S.V. Luis, V. Marcelino, J.F. Miravet, J.A. Ramirez, J. Chem. Soc., Perkin Trans. 2 (1994) 1253 for a program description.
[18] A.K. Covington, M. Paabo, R.A. Robinson, R.G. Bates, Anal. Chem. 40 (1968) 700.
[19] J.A. Aguilar, A. Bianchi, E. Garcia-España, S.V. Luis, J.M. Llinares, J.A. Ramirez, C. Soriano, J. Chem. Soc., Dalton Trans. (1994) 637.
[20] J. Aragò, A. Bencini, A. Bianchi, E. Garcia-España, M. Micheloni, P. Paoletti, J.A. Ramirez, P. Paoli, Inorg. Chem. 30 (1991) 1843.
[21] B. Dietrich, M.W. Hosseini, J.-M. Lehn, R.B. Sessions, Helv. Chim. Acta 66 (1983) 1262.
[22] M. Micheloni, P. Paoletti, A. Bianchi, E. Garcia-España, Inorg. Chim. Acta 117 (1986) 165.
[23] A. Bencini, A. Bianchi, E. Garcia-España, M. Micheloni, J.A. Ramirez, Coord. Chem. Rev. 188 (1999) 97.

[24] (a) J.C. Batchelor, J.H. Prestegard, R.J. Cushley, S.R. Lipsy, J. Am. Chem. Soc. 95 (1973) 6558;
(b) A.R. Quirt, J.R. Lyerla, I.R. Peat, J.S. Cohen, W.R. Reynold, M.F. Freedman, J. Am. Chem. Soc. 96 (1974) 570;
(c) J.C. Batchelor, J. Am. Chem. Soc. 97 (1975) 3410;
(d) J.E. Sarnessky, H.L. Surprenant, F.K. Molen, C.N. Reilley, Anal. Chem. 47 (1975) 2116.

[25] J. Aragò, A. Bencini, A. Bianchi, E. Garcia-España, M. Micheloni, P. Paoletti, J.A. Ramirez, A. Rodriguez, J. Chem. Soc., Dalton Trans. (1991) 3077.

[26] A. Bencini, A. Bianchi, V. Fusi, P. Paoletti, B. Valtancoli, A. Andrés, J. Aragò, E. Garcia-España, Inorg. Chim. Acta 204 (1993) 221.

PERGAMON

Polyhedron 21 (2002) 1469–1474

POLYHEDRON

www.elsevier.com/locate/poly

Copper and nickel complex-formation equilibria with Lys–Gly–His–Lys, a fragment of the matricellular protein SPARC

Chiara Conato [a], Henryk Kozłowski [b], Piotr Młynarz [b], Fernando Pulidori [a], Maurizio Remelli [a,*]

[a] *Department of Chemistry, University of Ferrara, via L. Borsari 46, I-44100 Ferrara, Italy*
[b] *Faculty of Chemistry, University of Wroclaw, F. Joliot-Curie 14, 50-383 Wrocław, Poland*

Received 25 October 2001; accepted 20 December 2001

Abstract

Complex-formation equilibria of the tetrapeptide Lys–Gly–His–Lys with the Cu(II) and the Ni(II) ions have been studied in aqueous solution, at $I = 0.1$ mol dm^{-3} (KNO_3) and $T = 25$ °C. Protonation and complex-formation constants have been potentiometrically determined. The structure of the main complex species is discussed on the basis of thermodynamic data obtained by direct calorimetry as well as the CD, ESR and electronic spectra. The participation of two amide nitrogens in complex-formation is suggested for both the metal ions, while no evidence supports the participation of the ε-NH_2 side groups of Lys residues in coordination. © 2002 Elsevier Science Ltd. All rights reserved.

Keywords: Copper complexes; Nickel complexes; Complex-formation equilibria; Lysyl–glycyl–histidyl–lysine

1. Introduction

Secreted Protein, Acidic and Rich in Cysteine (SPARC) is a matricellular calcium-binding glycoprotein, which mediates the cell–matrix interactions without covering any primarily structural role [1,2]. It is the product of a single-copy gene and its sequence has been highly conserved during vertebrate evolution and among species, with the mammalian, amphibian and avian proteins showing more than 70% amino acid identity [3]. SPARC is highly expressed during embryonic development while its expression in the adult is generally associated with tissues undergoing remodelling or renewal, also as a response to injury. It has also been reported as product of some tumours and this result has been associated to the SPARC activity in angiogenesis [4]. The human protein consists of 286 residues divided into three distinct domains [5]. The N-terminal domain is an acidic region which binds several calcium ions with low affinity. The second domain is a Cys-rich, follistatin-like (FS) domain (residues 53–137), in which all the Cys residues are disulfide-bonded and with an N-linked complex carbohydrate at Asn99. This domain is characterised by the presence of two copper binding sites, the strongest of which contains the sequence Lys–Gly–His–Lys (KGHK) (residues 120–123). Both KGHK and longer peptides containing this sequence and deriving from the proteolysis of SPARC have been recognised to regulate angiogenesis in vitro and in vivo [6]. Domain III (residues 138–286) is largely α-helical and contains high-affinity calcium binding sites.

The side-chain amino group of Lys residues is a potential donor group for oligopeptide and protein coordination to metal ions [7]. Literature data on this topic are growing, but real ability of this group to participate in metal-complex formation is still a vexed question. No evidence of ε-NH_2–metal ion binding has been observed for Cu(II)/Lys [8] and Ni(II)/dipeptide [9] complexes. On the other hand, recent investigations on the complex-formation equilibria of Lys-containing oligopeptides with the Cu(II) ion [10–12], supported the hypothesis that the ε-NH_2 of Lys residue interacts with copper, but only at alkaline pH; no deprotonation of ε-NH_2 (and subsequent interaction with copper) was found at neutral pH, thus supporting the hypothesis that, under physiological conditions protonated Lys residue of

* Corresponding author.
E-mail address: rmm@unife.it (M. Remelli).

0277-5387/02/$ - see front matter © 2002 Elsevier Science Ltd. All rights reserved.
PII: S0277-5387(02)00952-X

metallo-peptides can act as an 'anchor' for biological receptors [13].

In the present paper, the complex-formation equilibria of the tetrapeptide Lys–Gly–His–Lys (Fig. 1) with both, Cu(II) and the Ni(II) ions have been investigated, at $I = 0.1$ mol dm^{-3} (KNO_3) and $T = 25$ °C. Protonation and complex-formation constants have been potentiometrically determined; formation enthalpies have been measured by direct solution calorimetry; complex-formation model and species stoichiometry have been carefully checked by means of UV–Vis absorption, CD and ESR spectroscopies. On the basis of the obtained data, the structures of the complex species have been discussed.

2. Experimental

KGHK was a high purity product (Sigma) and was used without further purification. Cu(II) nitrate and Ni(II) chloride were extra pure Merck products.

Aliquots (2.5 cm^3) of sample solution, containing suitable amounts of the metal ion, the ligand, HNO_3 (when the initial pH value needed to be adjusted) and KNO_3 (to adjust the ionic strength to 0.1 mol dm^{-3}) were potentiometrically titrated with standard NaOH, in the pH range 3.0–11.0 (or till a precipitate or opalescence was observed in solution), in a thermostatted potentiometric vessel ($T = 25.0$ °C). Metal ion concentration ranged from 1×10^{-3} to 3×10^{-3} mol dm^{-3}, and metal to ligand ratios were 1:1.1 with Cu(II), while it was 1:3.5 with Ni(II). A minimum of three pairs of potentiometric titrations for each system were performed.

CD, ESR and UV–Vis spectra were recorded on solutions of the same composition as above, varying the pH by addition of suitable amounts of standard NaOH or HNO_3, under potentiometric control. Spectra every 0.5 pH units were recorded.

Calorimetric titrations were performed by means of an Isoperibolic Calorimeter (Tronac), at 25.0 °C, by addition of standard HNO_3 to solutions of ionic strength equal to 0.1 mol dm^{-3} (KNO_3). The sample solution volume was 2.5–2.8 ml. The ligand concentration ranged from 2×10^{-3} to 4×10^{-3} mol dm^{-3}; the metal-to-ligand ratios were 1:1.1 and 1:2 for the Cu(II) and Ni(II) ions, respectively. For protonation and Cu(II) complex-formation studies at least three pairs of calorimetric titrations containing not less than 250 experimental points were utilised to calculate the thermodynamic quantities. The slow complex-formation kinetics, encountered in the Ni(II)/KGHK system, did not allow the normal calorimetric titrations. In fact, the isoperibolic method requires a maximum run time of about 30 min, calibrations included. Only one titrant addition was then performed during each run and the total heat was recorded after a suitable waiting time. The same experiment was repeated eight to ten times, in order to cover the desired pH range (5.0–6.0). Three series of measurements were performed on different sample solutions.

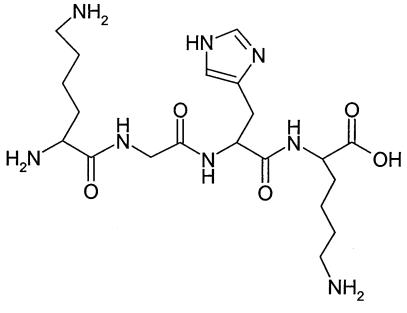


Fig. 1. Structure of Lys–Gly–His–Lys.

Further experimental details, equipment and software used are reported elsewhere [11].

Throughout, the complex species are indicated by means of the corresponding stoichiometric indexes pqr, referred to the equilibrium $pM + qL + rH = M_pL_qH_r$.

3. Results and discussion

3.1. Protonations

Thermodynamic data for KGHK protonation are reported in Table 1.

The most basic groups are the two Lys-residue ε-amino groups: the corresponding protonation constants are slightly higher and slightly lower than those of free Lys [8], respectively. The same is true for the corresponding enthalpies, which are always favourable. Entropy changes, however, are ambiguous in their sign: negative for the first protonation process and positive for the second. This difference should not be due to the position of the two Lys-residues (which are potentiometrically and calorimetrically indistinguishable). In fact, literature data concerning protonation of Lys residues in oligopeptides do not significantly depend on the nature of the other neighbouring amino acids of the chain [14]. Some role is certainly played by the different ligand charge during the first and the second protonation step. Moreover, the formation of an intramolecular hydrogen-bond, between the two side ε-amino groups, as a consequence of the first protonation, could explain the corresponding thermodynamic parameters. However, further investigation is required to confirm such hypothesis.

The terminal amino group is less basic than the ε-amino group of Lys residue due to the former's proximity to the electron-withdrawing carbonyl group of the first peptidic bond. The corresponding pK value is 1.8 U lower than that of free Lys [8]. As a consequence

Table 1
Thermodynamic parameters for KGHK protonation steps, at 25 °C and $I = 0.1$ mol dm^{-3} (KNO_3)

Residue	Donor group	log K	$-\Delta G^\circ$ (kJ mol^{-1})	$-\Delta H^\circ$ (kJ mol^{-1})	ΔS° (J mol^{-1} K^{-1})
Lys	$NH_2(\varepsilon)$	10.97 (6)	62.6 (3)	69 (3)	−23 (15)
Lys	$NH_2(\varepsilon)$	10.16 (8)	57.9 (5)	41 (3)	59 (11)
Lys_1	NH_2 (α)	7.34 (6)	41.9 (3)	39 (3)	8 (12)
His	N(Im)	6.16 (4)	35.2 (2)	23 (4)	42 (15)
Lys_4	COO^-	3.0 (1)	17.1 (7)		

of the formation of peptide linkage, the imidazolic-nitrogen pK value is about 0.3 U higher than the corresponding values of His (6.03) [15]. This difference is mainly of entropic nature. Finally, the terminal carboxylic-group protonation-constant is in agreement with literature data on oligopeptides.

3.2. Cu(II)/Lys–Gly–His–Lys complexes

As the distribution diagram shows (Fig. 2), coordination starts under pH 4, with the 110 complex formation. The concentration of this species reaches its maximum at pH 5, binding all the Cu(II) ion and remaining the only species in solution up to pH 7. At higher pH values, the 110 complex undergoes three deprotonation steps leading to the species 11-1, 11-2 and 11-3. The log $K^{110}_{11\text{-}1}$ value is compatible with the deprotonation of a bound water molecule, while the following log $K^{11\text{-}1}_{11\text{-}2}$ and log $K^{11\text{-}2}_{11\text{-}3}$ values are very close to the protonation pK values of the two side Lys residues (see Table 1), suggesting that no interaction occurs between the ε-NH_2 groups and the copper ion. The corresponding ΔH°_{step} and ΔS°_{step} values, which can be computed from Table 2, can be considered in agreement with this suggestion, taking into account the high standard deviations. If the above hypothesis is true, neither the complex geometry nor the donor-atom set should vary when pH is raised from 5 to 11. This conclusion is fully supported by spectroscopic results, reported in Figs. 3 and 4 and summarised in Table 3.

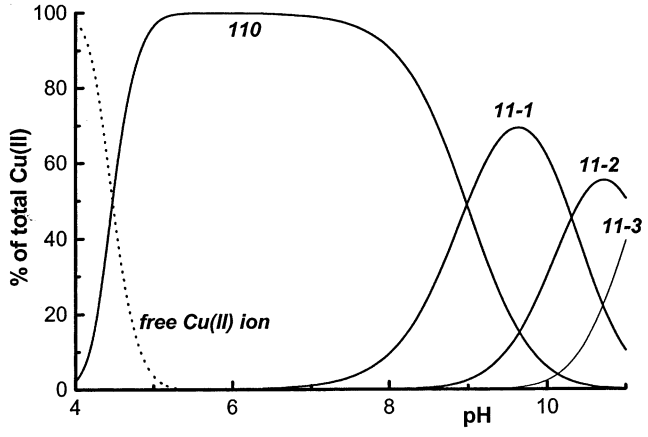


Fig. 2. Distribution diagram of Cu(II)/KGHK complexes, $T = 25$ °C, $I = 0.1$ mol dm^{-3} (KNO_3); [Cu(II)] = 3.0×10^{-3} mol dm^{-3}; [KGHK] = 3.3×10^{-3} mol dm^{-3}.

Absorption spectra (Fig. 3) are characterised by the onset of one single band, due to complex-formation, the intensity of which increases from pH 4 to 5, remaining then constant up to pH 11 (see also Table 3). The wavelength of maximum absorption is 524 nm, very close to the value of 530 nm, which can be computed by means of the empirical formula developed by Sigel and Martin [16] for the coordination of four nitrogen atoms to Cu(II) (α-NH_2, $2N^-$ and N_{Im}). CD spectra (Fig. 4) exhibit an oppositely signed curve for the d–d transition (as His-containing peptides usually do), with the negative extremum centred at 580 nm and the positive one at 495 nm. This result is consistent with the hypothesis of four nitrogen atoms involved in coordination. A CT band at 306 nm is also present in the CD spectra: it can be ascribed to the coordination of deprotonated amido nitrogens to copper. An additional negative band is present, at 272 nm, attributable to an α-$NH_2 \rightarrow$ Cu(II) CT transition. It is remarkable that neither the band shape nor the position depends on pH, but only the signal intensity, as already found for the UV–Vis absorption. Finally, a similar behaviour is also shown by ESR spectra, giving constant $A_{||}$ and $g_{||}$ values, in the pH range 4–11 (see Table 3); such values are once again compatible with the hypothesis of a 4N complex.

The most likely structure hypothesis for the 1:1 Cu(II)/KGHK complex is shown in Fig. 5. In this complex the ligand binds the copper ion in a tetradentate way, i.e. by means of its terminal amino group, the first two [deprotonated] amido nitrogens and the side imidazolic group. This way of coordination is typical of oligopeptides containing His in third position, like Gly–Gly–His (GGH) [17], for which it has also been observed that the 11-2 complex (corresponding to the 110 complex in the present Cu/KGHK system, where the ligand contains two additional-protonated-side chains) is the only species in solution, even in the presence of a ligand excess. The above structural hypothesis is also supported by the results of an X-ray study on the crystal structure of Cu(II)/Gly–Gly–His–N-methylamide 1:1 complex [18]. In order to compare the stability of the corresponding Cu(II) complexes in the two systems, it is useful to compute the respective

Table 2
Thermodynamic parameters of Cu(II) and Ni(II)/KGHK binary-complex formation, at 25 °C and $I = 0.1$ mol dm^{-3} (KNO_3)

Metal ion	Complex stoichiometry	log β	log K_{step}	$-\Delta G^\circ$ (kJ mol^{-1})	$-\Delta H^\circ$ (kJ mol^{-1})	ΔS° (J mol^{-1} K^{-1})
Cu(II)	110	19.51 (2)		111.3 (1)	132 (7)	−70 (25)
	11-1	10.52 (8)	9.0	60.0 (5)	121 (8)	−207 (30)
	11-2	0.21 (7)	10.3	1.2 (4)	55 (11)	−180 (41)
	11-3	−10.9 (1)	10.7	−62.1 (6)	13 (18)	−253 (62)
Ni(II)	110	15.30 (6)		87.3 (3)	134 (9)	−160 (30)

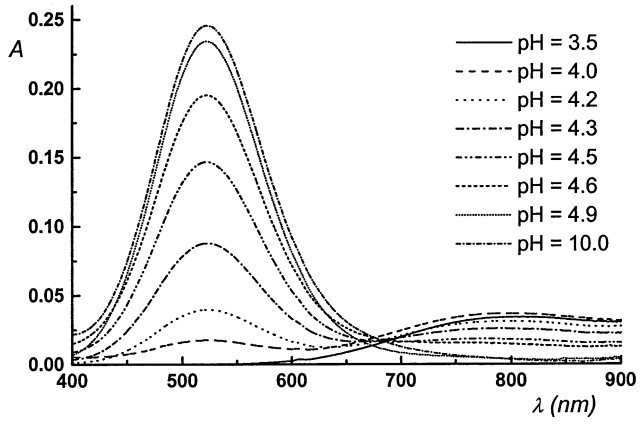


Fig. 3. Absorption spectra of Cu(II)/KGHK solutions. [Cu(II)] = 3.0×10^{-3} mol dm^{-3}, [KGHK] = 3.3×10^{-3} mol dm^{-3}, $T = 25$ °C, $I = 0.1$ mol dm^{-3} (KNO_3).

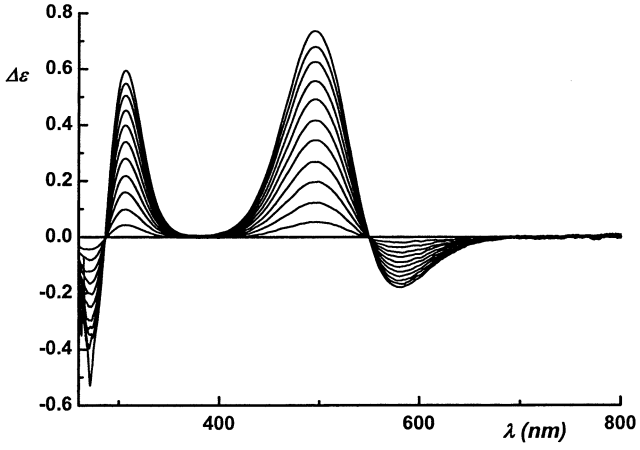


Fig. 4. Circular Dichroism spectra of Cu(II)/KGHK solutions. [Cu(II)] = 3.0×10^{-3} mol dm^{-3}, [KGHK] = 3.3×10^{-3} mol dm^{-3}, $T = 25$ °C, $I = 0.1$ mol dm^{-3} (KNO_3).

log K^* values (log $K^* = \log \beta_{pqr} - pK_{\alpha\text{-}NH2} - [\Sigma pK_{\varepsilon\text{-}NH2}] - pK_{N\text{-}imidazole}$, where pqr is 110 in the case of KGHK and 11-2 for GGH), which measure the binding strength of the ligand, 'normalised' for the basicity of the donor sites and for the presence of additional protonated groups [7]. The computed values are the following: $\log K^*_{Cu(II)/GGH} = -16.43$ [17] and $\log K^*_{Cu(II)/KGHK} = -15.13$ (Table 2). These data show that KGHK is a Cu(II) ligand stronger than GGH: the former's K^* value is higher than the latter's of more than one magnitude order. However, KHGK is weaker than other albumin-like chelators containing the hydroxymethylserine (HmS) residue, like HmS–HmS–His ($\log K^*_{Cu(II)/HmS-HmS-His} = -13.12$ [19]). The extra-stability of the Cu(II)/HmS–HmS–His complex has been ascribed to electronic effects which render the terminal amino group of the ligand more acidic than the imidazole nitrogen and the amido nitrogens much more effective donors [19]. Additional intramolecular interactions among the side chains of the ligand and the metal ion have been excluded in the case of HmS–HmS–His [19]; the same is reasonable here, where no evidence was found for the participation of the ε-amino groups in complex formation (see above). The substitution of Gly with Lys as first residue and the presence of an additional amino acid in the polypeptidic chain most likely influences the basicity of the donor atoms and the complexing strength of KGHK with respect to GGH. Unfortunately, complex-formation enthalpies for GGH or HmS–HmS–His are not available. A systematic study on other peptidic ligands, containing His in the third position, could shed more light on these phenomena, but is beyond the aim of the present work.

3.3. Ni(II)/Lys–Gly–His–Lys complexes

Ni(II)/KGHK coordination starts from pH 5, where the solution colour starts to change from pale blue–green to yellow and the 110 complex is formed. This species, less stable than the corresponding Cu(II) complex, reaches its formation maximum at pH 6, binding the 100% of the Ni(II) ion present in solution; it remains the only species in the whole investigated pH range. Similar results were previously been reported for the Ni(II)/GGH [17] and Ni(II)/HmS–HmS–His systems [19], except for the formation of low amounts of some minor protonated species, not found with KGHK (see Table 2). To compare the Ni(II)/KGHK, Ni(II)/GGH and Ni(II)/HmS–HmS–His complex stabilities, the corresponding log K^* values can, once again, be computed: $\log K^*_{Ni(II)/GGH} = -21.31$ [17], $\log K^*_{Ni(II)/KGHK} = -19.42$, $\log K^*_{Ni(II)/HmS-HmS-His} = -17.92$ [19]). As in the case of copper complexes,

Table 3
Spectroscopic parameters of Cu(II)/KGHK binary-complex formation, at 25 °C and $I = 0.1$ mol dm^{-3} (KNO_3)

pH	Main species	Vis		CD		ESR	
		λ (nm)	ε	λ (nm)	$\Delta\varepsilon$	$A_{\|\|}$	$g_{\|\|}$
3.0–3.5	Cu_{aq}	812	12			120	2.415
4.0	*110*	524	15	272	−0.08	203	2.184
				306	0.10		
				495	0.12		
				580	−0.04		
4.5	*110*	524	54	306	0.45	202	2.184
				495	0.56		
				580	−0.14		
5.0–9.0	*110*	524	92	306	0.60	202	2.184
				495	0.74		
				580	−0.18		
10.0–11.0	*11-1*, *11-2*	524	91	306	0.60	202	2.182
				495	0.74		
				580	−0.18		

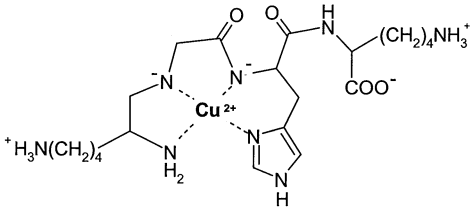


Fig. 5. Structural hypothesis for the complex [Cu(II)/KGHK]$^+$, in aqueous solution.

HmS–HmS–His is the strongest ligand, while KGHK binds the nickel ion with more efficacy than GGH, in the whole investigated pH range. Electronic spectra of Ni(II)/KGHK solutions (Fig. 6) show a single absorption band the intensity of which steadily increases from pH 4 to 6, then remaining constant up to pH 10. The wavelength of maximum absorption is 420 nm, in agreement with the values found for GGH (423 nm [17]) and HmS–HmS–His (420 nm [19]), as well as for other peptides giving a 4N square-planar coordination [16]. Matching results were obtained by CD spectroscopy (see Fig. 7). As in the case of copper complexes discussed above, KGHK should bind the nickel ion in a tetradentate way, i.e. by means of its terminal amino group, the imidazole and two deprotonated amide nitrogens, which provide a strong ligand field leading to singlet ground state Ni(II). No evidence has been found for the involvement of the ε-NH_2 side groups of the two Lys residues in Ni(II) coordination. These hypotheses are in good agreement with the corresponding ΔH°_{110} value, shown in Table 2 (last row). In fact, subtracting the contribution of the two side-amino-group protonations (−110 kJ mol^{-1}, Table 1), a cleansed value of −24 kJ mol^{-1} is obtained; it is very close to the double of the $\Delta H^\circ_{11\text{-}1}$ value for the Ni(II)/

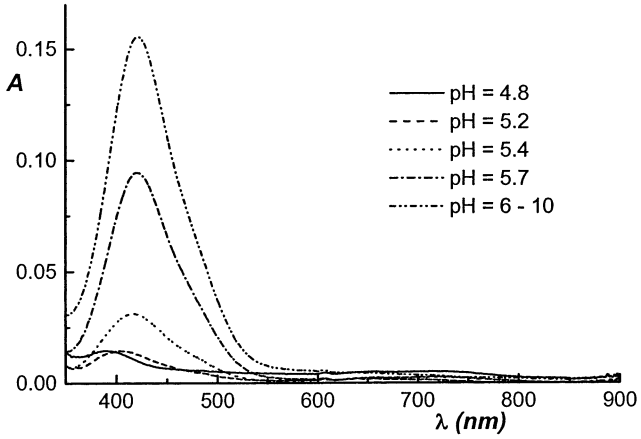


Fig. 6. Absorption spectra of Ni(II)/KGHK solutions. [Ni(II)] = 1.0×10^{-3} mol dm^{-3}, [KGHK] = 3.5×10^{-3} mol dm^{-3}, T = 25 °C, $I = 0.1$ mol dm^{-3} (KNO_3).

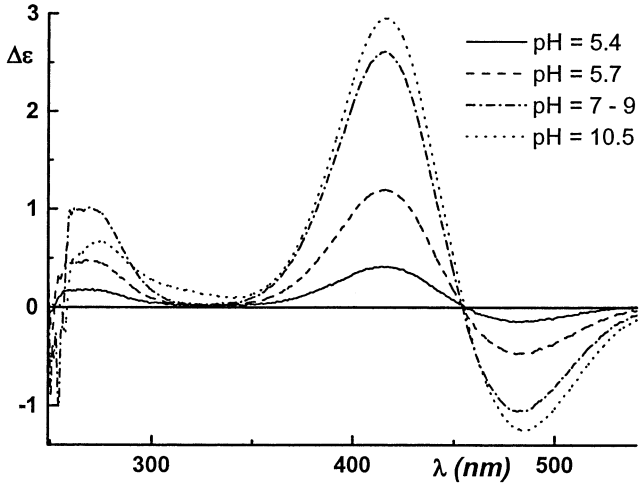


Fig. 7. Circular Dichroism spectra of Ni(II)/KGHK solutions. [Ni(II)] = 1.0×10^{-3} mol dm^{-3}, [KGHK] = 3.5×10^{-3} mol dm^{-3}, T = 25 °C, $I = 0.1$ mol dm^{-3} (KNO_3).

Gly–Ala system [9], which accounts for the formation of one Ni(II)–NH_2 and one Ni(II)–N^- bonds. Moreover, such a ΔH°_{110} value is very close to the corresponding value for the Cu(II)/KGHK system, also reported in Table 2. These results suggest that the lower stability of the Ni(II) complex could be ascribed to a more unfavourable entropic contribution, possibly due to the higher rigidity of the Ni(II) geometry.

4. Conclusions

The tetrapeptide KGHK binds both the Cu(II) and the Ni(II) ions in a tetradentate fashion, forming mono-complexes in the whole investigated pH range; the formation of neither bis-complexes nor polynuclear species has been observed. KGHK binds both the Cu(II) and Ni(II) ions more strongly than GGH, although the complex geometry and the donor-atom set are the same in both the cases. This extra-stability can be ascribed to electronic effects caused by the different side chains on the peptide backbone, which influence the amido-nitrogen donor capability. In fact, the two ε-NH_2 groups of Lys residues proved not to be involved in coordination.

Acknowledgements

The financial support by Italian MURST (CO-FIN'98) is gratefully acknowledged.

References

[1] R.A. Brekken, E.H. Sage, Matrix Biol. 19 (2000) 569.
[2] A.D. Bradshaw, E.H. Sage, J. Clin. Invest. 107 (2001) 1049.
[3] Q. Yan, E.H. Sage, J. Histochem. Cytochem. 47 (1999) 1495.
[4] E.H. Sage, Nature Med. 3 (1997) 144.
[5] E. Hohenester, P. Maurer, R. Timpl, EMBO J. 16 (1997) 3778.
[6] T.F. Lane, M.L. Iruela-Arispe, R.S. Johnson, E.H. Sage, J. Cell Biol. 125 (1994) 929.
[7] L.D. Pettit, J.E. Gregor, H. Kozlowski, in: R.W. Hay, J.R. Dilworth, K.B. Nolan (Eds.), Perspectives on Bioinorganic Chemistry, vol. 1, JAI Press, London, 1991, p. 1.
[8] C. Conato, A. Contino, G. Maccarrone, A. Magrì, M. Remelli, G. Tabbì, Therm. Acta 362 (2000) 13 (and references therein).
[9] C. Conato, S. Ferrari, H. Kozlowski, F. Pulidori, M. Remelli, Polyhedron 20 (2001) 615.
[10] B. Radomska, I. Sovago, T. Kiss, J. Chem. Soc., Dalton Trans. (1990) 289.
[11] M. Remelli, C. Conato, A. Agarossi, F. Pulidori, P. Mlynarz, H. Kozlowski, Polyhedron 19 (2000) 2409.
[12] C. Conato, R. Gavioli, R. Guerrini, H. Kozlowski, P. Mlynarz, C. Pasti, M. Remelli, Biochim. Biophys. Acta 1526 (2001) 199.
[13] L. Pickart, J. Freedman, W.J. Loker, J. Peisach, C.M. Perkins, R.E. Stenkamp, B. Weinstein, Nature 288 (1980) 715.
[14] L.D. Pettit, H.K.J. Powell, The IUPAC Stability Constants Database, Academic Software and IUPAC, Royal Society of Chemistry, London, 1992–1997.
[15] G. Borghesani, F. Pulidori, M. Remelli, R. Purrello, E. Rizzarelli, J. Chem. Soc., Dalton Trans. (1990) 2095.
[16] H. Sigel, R.B. Martin, Chem. Rev. 82 (1982) 385.
[17] R.H. Hay, M.H. Hassan, C. You-Quan, J. Inorg. Biochem. 52 (1993) 17.
[18] N. Camerman, A. Camerman, B. Sarkar, Can. J. Chem. 54 (1976) 1309.
[19] P. Mlynarz, N. Gaggelli, J. Panek, M. Stasiak, G. Valensin, T. Kowalik-Jankowska, M.T. Leplawy, Z. Latajka, H. Kozlowski, J. Chem. Soc., Dalton Trans. (2000) 1033.

purification of the inhibitors carried out by a variety of techniques like ultrafiltration, gel chromatography, ion-exchange. Unfortunately many of them are time consuming or associated with appreciable loss of analyte, thus requiring the treatment of a huge quantity of urine samples to obtain the desired amount of product. Moreover, the inhibitor of interest is always analyzed by enzymic-spectrophotometric assay, which is indirect and non-specific.

Another example of enrichment is the one proposed [18] for UTIs concentration by foam fractionation. This is a type of adsorptive bubble separation technique (adsubble technique [19]) in which surface-active substances, such as proteins and enzymes [20] because of their strong amphipathic nature, are removed from the solution by selective adsorption at the surface of bubbles rising through the solution forming a foam at the top of the solution.

Within adsubble techniques, bubble extraction process used to preconcentrate inorganic species [21–23] appears as a promising technique that could be applied to large samples to concentrate analytes from very diluted solutions obtaining quantitative recoveries.

In this paper we describe a three-step procedure including preconcentration of UTIs by bubble extraction, binding to immobilized trypsin, recovery and separation of the inhibitors at controlled pH by affinity chromatography. This procedure displays a unique capability for retaining full bioactivity of the isolated components. For the direct monitoring of the inhibitors at the intermediate and final steps we adopted a RP-HPLC method developed by our research group [24,25].

2. Experimental

2.1. Reagents and materials

All chemicals were of the highest purity available and were stored, when necessary, as recommended. Aprotinin, bovine pancreas trypsin, Nα-Benzoyl-L-arginine *p*-nitroanilide (L-BAPNA, a cromogenic substrate for trypsin and other proteolytic enzymes) and antifoam A were obtained from Sigma Chemicals (St. Louis, MO, USA). Water was distilled once and then further purified by a Milli-Q purification system (Millipore Systems, Bedford, MA, USA).

2.2. Human urine samples

Urine obtained from healthy volunteers was collected in flasks containing sodium azide (0.02%, w/v) and stored at −20 °C before it was processed.

2.3. Buffer solutions

Buffer solution A (pH 2.2): 10.0 mM H_3PO_4 in 0.2 M $NaClO_4$. Buffer solution B (pH 8.3): 0.1 M Tris–HCl in 0.5 M NaCl. Buffer solution C (pH 3.5): 0.1 M CH_3COONa–CH_3COOH in 1.0 M NaCl.

2.4. Inhibition assays

Inhibition assays were performed by an enzymic-spectrophotometric method based on the inhibition by UTIs of the trypsin-catalysed hydrolysis of L-BAPNA, followed at 405 nm, which takes advantage of the stable complex that UTIs form at approximately pH 8.0 with the enzyme. The UTI concentration in the sample was determined from the decrease in the trypsin activity caused by the sample using aprotinin as standard [26]. For absorbance measurements a Perkin–Elmer H.200 spectrophotometer was used.

2.5. Bubble extraction

The apparatus for bubble extraction utilizing a hydrodynamic trap principle has already been described [22]. In this series of experiments, a column having loading capacity of 5 l was employed.

2.6. Chromatography

Trypsin-affinity chromatography was performed as previously reported [27] taking care of washing the affinity gel phase to obtain an acceptable chromatographic background; econo-columns (1.0 × 10 cm from Bio-Rad) were used.

To perform chromatographic analyses, a Twincle Model JASCO Liquid Chromatograph was used. The instrument equipment included: VL-614 injector loop capacity 100 μl; JASCO Model Uvidec 100-III variable wavelength UV-detector connected to a Chromatopac C-R3A data elaborator; JASCO Model GP-A30 Gradient Programmer.

The chromatographic column was kept in a Violet Thermostat Clar 0.55. Buffer solutions were filtered through a 0.45 Millipore filter, and mobile phases were deareated by helium bubbling. When necessary, the eluted fractions were recovered using a Pharmacia Frac-100 collector.

2.6.1. Chromatographic conditions

Column: LiChrosorb RP18, 250 × 4.6 mm I.D (Merck); temperature: 30 ± 0.1 °C; flow rate: 1.0 ml min^{-1}; injection volume: 100 μl; elution: isocratic step over 15 min with mobile phase 1 (buffer solution A–acetonitrile, 70:30) and then linear gradient with phase mobile 2 (buffer solution A–Acetonitrile, 40:60); detection UV: 200 nm.

3. Procedure

The proposed procedure was experimented with urine collected from healthy volunteers and involved the following steps.

3.1. Step A—preconcentration

For UTIs enrichment and collection a bubble extraction apparatus was used equipped with a column having a loading capacity of 5 l (Fig. 1). The column was filled at the lower end with a detachable section furnished with a gas sparger of fine porosity (G 4), ending in its upper part with a coning tapering at its outlet which fitted for about 1.5 cm above the collected liquid level. A 0.5 l separating funnel was employed as the collecting vessel.

The column was filled with urine and an aqueous dispersion (100 μl in 10 ml) of Fluka Antifoam A was added and ran along the wall of the collecting vessel before its assembly. The gas (N_2) flow was then regulated to obtain the proper run of foam: a flow rate of about 20–30 ml min^{-1}, measured by a soap-bubble flowmeter, was found effective. The suitable operation time of enrichment was about 90–120 min.

3.2. Step B—binding of the inhibitors

The urine collected (ca. 200 ml) was transferred to a vessel, adjusted to pH 8.3 with 2.0 N NaOH, and centrifuged for 10 min at $4390 \times g$.

The supernatant and washings were percolated through a trypsin-Sepharose 4B column (bed volume ca. 1.0 ml; loading capacity approximately 200 nmol of active trypsin) previously equilibrated with buffer solution B. The eluate was then passed through two other econo-columns identical to the first and used in series. The three columns were then washed with at least ten bed volumes of the same buffer solution to remove unbound substances prior to UTIs elution.

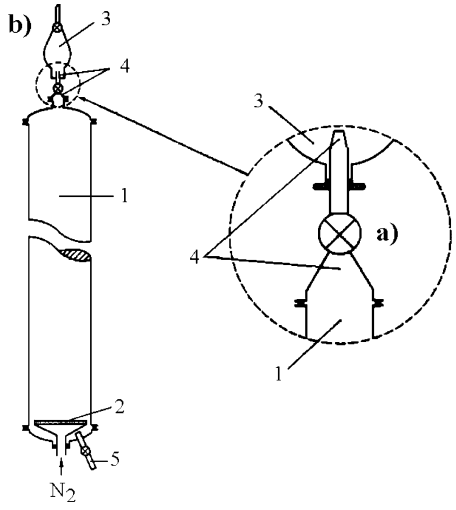


Fig. 1. Bubble extraction apparatus. Experimental set up: 1 column; 2 sparger; 3 collecting funnel; 4 trapping device, 5 column solution outlet.

3.3. Step C—elution at controlled pH values

The first trypsin-Sepharose column was subjected to elution (flow rate: 1 ml min^{-1}) with buffer solution C. The eluate containing UTI_{72} and UTI_{18} was collected in a 250 ml calibrated flask (flask 1). The same column was then subjected to elution with 0.8 ml of 1.0 M H_3PO_4 and buffer solution A; the eluate containing UTI_6 was collected in a 5 ml calibrated flask (Flask 2). From the other two econo-columns the remaining UTI_{72} and UTI_{18} were recovered in flask 1 by eluting any column with 0.8 ml of 1.0 M H_3PO_4 and buffer solution A.

4. Results and discussion

In urine samples of healthy individuals, the Kunitz-type inhibitor (UTI_{72}) occurs at low concentration, approximately 0.3 μmol l^{-1}, which is, however, far higher than that of the Kazal-type (UTI_6), approximately 3 nmol l^{-1}. Bubble extraction combined with affinity chromatography appears promising for the enrichment and separation of considered inhibitors from biological fluids.

As already reported, the extraction bubble apparatus operates substantially by dividing the liquid solution into two portions: the lower part constituting the fractionation column and the upper one the enriched solution. Surface-active substances as proteins, owing to gas bubbling, are progressively transferred from the column into the collecting vessel together with an easy collection of the enriched solution. When biological fluids, as urine, are manipulated according to this technique an antifoam should be added to prevent production of foam excess that can come out from the collecting vessel.

In affinity chromatography the optimal elution conditions are determined by protein stability and strength of binding of UTI types to the adsorbent. Desorption is generally effected by pH decrease because the pH variation alters the ionization degree of the charged groups at the binding site. In our previous studies [24,25], UTIs were desorbed from immobilized trypsin with buffer solution pH 2.2 (Fig. 2). As the inhibitors showed different affinities to immobilized trypsin, in this study UTI_{72}, UTI_{18} and UTI_6 were sequentially eluted at pH 3.5 and 2.2, respectively, in order to obtain a selective separation. When the trypsin inhibitor-binding capacity of the column is exceeded, the UTI_6 is found to bind preferentially to the column at the expense of the UTI_{72} and UTI_{18}. Consequently, under our experimen-

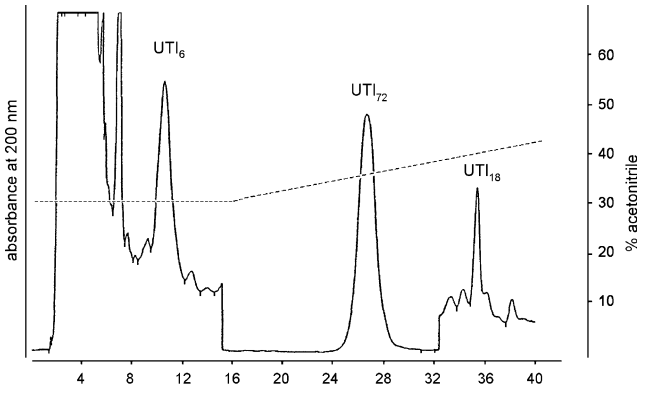


Fig. 2. Separation of UTIs resulting by pH 2.2 elution of a trypsin-Sepharose 4B column after passage of urine sample. See Section 2 for chromatographic conditions.

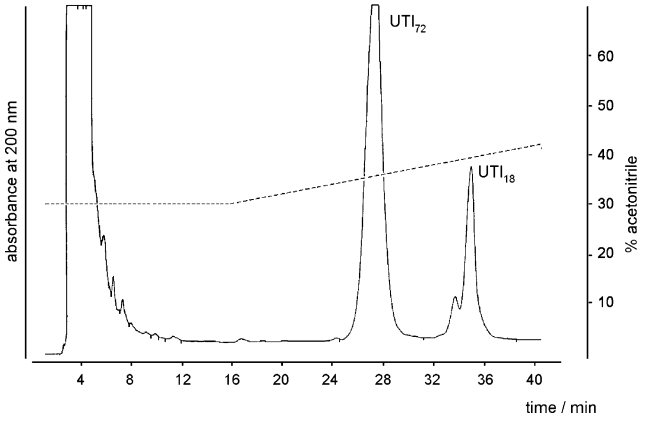


Fig. 3. Chromatogram of solution from flask 1, containing UTI_{72} (and its degradation product UTI_{18}) only. Chromatographic conditions as in Fig. 2.

tal conditions, UTI_6 was found only in the first immobilized trypsin column. UTI_{72} and UTI_{18} were removed from the column by eluting with buffer solution pH 3.5. After passage of about 150 ml of buffer solution C, the decrease until disappearance of the two inhibitors in the eluate was monitored. For this purpose, a 100 μl aliquot of the eluate was tested by RP-HPLC injection. A total elution volume of about 200 ml was found to be effective in any case. The complete

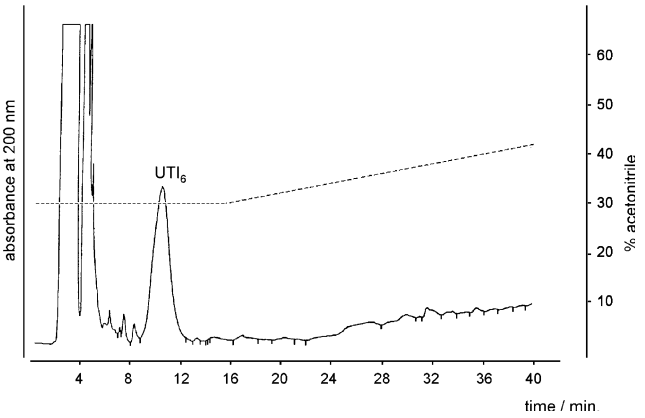


Fig. 4. Chromatogram of solution from flask 2, containing UTI_6 only. Chromatographic conditions as in Fig. 2.

recovery of UTI_6 was achieved by eluting the first column with 0.8 ml of 1.0 M H_3PO_4 and buffer solution A. Finally, flasks 1 and 2 contained only UTI_{72}, UTI_{18} and UTI_6, respectively, as confirmed by the analyses performed by our RP-HPLC method (Figs. 3 and 4).

The analytical recovery of the two inhibitors from urine was determined by inhibition assays and by chromatographic measurements. Each test was performed by comparison of the response obtained by analysis of 200 ml of urine processed without any preconcentration step, which provided the 100% value, with that obtained from 5000 ml of the same urine processed as described, after suitable correction for precocentration factors. The results are shown in Table 1: for both inhibitors, the recoveries were higher than 70%, and the retaining of bioactivity was tested.

The preconcentration step is particular suitable for Kazal-type recovery, owing to the low concentration of this inhibitor in urine of healthy individuals. Some authors processed samples of urine obtained from subjects affected by particular diseases with very high amounts of the inhibitor (ca. 1 mg $^{-1}$): in this instance our procedure could be simplified, avoiding the preconcentration step.

Concluding, the proposed procedure is advantageous for its speed, specificity and, chiefly, for the reliability of monitoring.

Table 1
Recovery of Kazal-type and Kunitz-type inhibitors from human urine (%)

Experiment number	Kazal-type (UTI_6)		Kunitz-type (UTI_{72})	
	By chromatographic measurement	By inhibition assay	By chromatographic measurement	By inhibition assay
1	80	77	91	88
2	78	80	85	87
3	71	73	86	84
4	75	72	92	90

Acknowledgements

This work was financially supported by the Ministero dell'Università per la Ricerca Scientifica e Tecnologica (MURST, Rome) within the program COFIN 2000 and by Consiglio Nazionale delle Ricerche (CNR) of Italy. The authors are grateful to Mrs. M. Campini for her skilful technical assistance.

References

[1] W.L. McKeehan, Y. Sagakami, H. Hoshi, K.A. McKeehan, J. Biol. Chem. 261 (1986) 5378.
[2] U. Turpeinen, E. Koivunen, U.H. Stenman, J. Biochem. 254 (1988) 911.
[3] R.J. Read, M.N.G. James, in: A.J. Barrett, G. Salvesen (Eds.), Proteinase Inhibitors, Elsevier, Amsterdam, 1986, p. 301.
[4] T. Dietl, W. Dobrinski, K. Hochstrasser, Hoppe-Seylers' Z. Physiol. Chem. 360 (1979) 1313.
[5] W. Gebhard, K. Hochstrasser, in: A.J. Barrett, G. Salvesen (Eds.), Proteinase Inhibitors, Elsevier, Amsterdam, 1986, p. 389.
[6] H. Iwama, S. Ohmori, T. Tsutsumi, J. Neurosurg. Anesthesiol. 12 (2000) 29.
[7] A. Karmowski, K.A. Sobiech, I. Maruk-Kertyńska, L. Terpiłowski, B. Malik, B. Palczyński, Ginekol. Pol. 71 (2000) 395.
[8] G. Sparro, S. Bonaiuto, G. Galdenzi, A.M. Eleuteri, M. Angeletti, G. Lupidi, R. Tacconi, E. Giannandrea, A. Vesprini, E. Fioretti, Dis. Markers 13 (1996) 31.
[9] A.M. Piette, J. Saba, N. Bernard, M. Pougheon, O. Abat, J. Fermanian, J.C. Piette, A. Chapman, Eur. J. Med. 1 (1992) 273.
[10] H. Kobayashi, M. Fujie, H. Shinohara, H. Ohi, M. Sugimura, T. Terao, Int. J. Cancer 57 (1994) 378.
[11] J.K. Perry, G.K. Scott, C.A. Tse, Biochim. Biophys. Acta 1221 (1994) 145.
[12] H. Kobayashi, J. Gotoh, M. Fujie, T. Terao, J. Biol. Chem. 269 (1994) 20642.
[13] H. Kobayashi, H. Shinohara, J. Gotoh, M. Fujie, S. Fujishiro, T. Terao, Br. J. Cancer 72 (1995) 1131.
[14] M.L. Huhtala, K. Pesonen, N. Kalkkinen, H.U. Stenman, J. Biol. Chem. 257 (1982) 13713.
[15] K. Matsuda, M. Ogawa, T. Kitahara, M. Ishida, T. Mori, Enzyme 34 (1985) 129.
[16] Y. Tanaka, S. Maehara, H. Sumi, N. Toki, S. Moriyama, Biochim. Biophys. Acta 705 (1982) 192.
[17] M. Balduyck, A. Hayem, J.P. Herckaert, C. Mizon, J. Mizon, Biochem. Biophys. Res. Commun. 109 (1982) 1247.
[18] Y. Yuki, K. Nakanishi, H. Hiratani, US Patent, 4,780,209, 25 October, 1988.
[19] R. Lemlich, Adsorptive Bubble Separation Techniques, Academic Press, New York, 1972.
[20] F. Uraizee, G. Narsimhan, Enzyme Microb. Technol. 12 (1990) 232.
[21] G. Vallebona, G. Raspi, Sep. Sci. Technol. 32 (1997) 2011.
[22] G. Vallebona, G. Banchini, A. Borraccini, G. Raspi, Fresenius Z. Anal. Chem. 331 (1988) 584.
[23] G. Vallebona, G. Raspi, Z. Fresenius, J. Anal. Chem. 341 (1991) 542.
[24] G. Raspi, A. Lo Moro, M. Spinetti, Fresenius Z. Anal. Chem. 332 (1988) 48.
[25] G. Raspi, A. Lo Moro, M. Spinetti, Analyst 115 (1990) 641.
[26] H. Fritz, G. Wunderer, Arzneim-Forsch/Drug. Res. 33 (1983) 479.
[27] G. Raspi, A. Lo Moro, M. Spinetti, Fresenius Z. Anal. Chem. 329 (1988) 786.

containing species, such as HPO_4^{2-}, ATP and ADP, in forming metal-ion complexes.

Few thermodynamic data have been reported for the formation of PCr complexes and those that have are so contradictory that it is stated that the published data do not meet the criteria required for a critical selection in the NIST database [3]. Formation constants have been published for MgPCr [4] and $KPCr^-$ [5], but nothing has been reported for $NaPCr^-$. This is strange as the sodium and potassium complexes of ATP and ADP are usually quite similar [3,6]. Another disquieting aspect of the published data is the small difference between the formation constants of MgPCr and $KPCr^-$, since with analogous ligands magnesium complexes are much more stable than the corresponding potassium complexes [3,6].

Information regarding the stability of PCr complexes is essential for the determination of the concentrations of the species present in the cytosolic medium. We have, therefore, undertaken a systematic study, using ^{31}P NMR spectroscopy, of complexation of the phosphate ligands PCr, ATP, ADP and AMP with the three cations Na^+, K^+ e Mg^{2+}, under physiological conditions ($T = 37$ °C and $I = 0.25$ M). We now report the results for phosphocreatine.

2. Experimental

2.1. Chemicals

$Na_2PCr \cdot 4.5H_2O$ (Sigma) was used without further purification (Calc. for $C_4H_{17}N_3O_{9.5}PNa_2$, C, 14.29; H, 5.10; N, 12.50. Found: C, 14.20; H, 5.21; N, 12.50%). The ^{31}P NMR spectra of this substance show that hydrolysis is negligible in aqueous solution as the intensity of the phosphate ion signal was always less than 1% of the total integrated intensity. Analytical grade reagents (Merck) were used to prepare stock solutions of Me_4NCl, NaCl, KCl and $MgCl_2$ using weighed amounts of solute and solvent. D_2O (99.8%, Merck) and reagent grade Bu_4NCl (Fluka) and Bu_4PCl (50% aqueous solution, Merck) were used as supplied.

2.2. NMR measurements

$^{31}P\{^1H\}$ NMR spectra were recorded at 81.02 MHz using a Bruker AC 200 spectrometer. The probe temperature was 37.0 ± 0.2 °C. Field frequency stabilisation was established by using as solvent H_2O–D_2O (80:20 by volume). All chemical shifts are reported in ppm toward higher frequency relative to external 85% aqueous H_3PO_4. No corrections were made for differences in bulk susceptibly in the various samples. Digital resolution was 0.216 Hz per point. In all cases $\pi/3$ pulses were used. The feed was accumulated in 32 k data points with zero filling to 64 k data points before Fourier transformation. The acquisition time was 4.62 s.

2.3. Spectra and compositions of the solutions used

At least ten solutions were prepared for each system. Solutions were stored at approximately 4 °C to prevent hydrolysis. The concentration of Na_2PCr was approximately 0.02 mol dm^{-3} in all solutions. The concentrations of the metal halides (NaCl, KCl and $MgCl_2$) ranged between zero and the concentration corresponding to an ionic strength of 0.25 mol dm^{-3}. Where necessary, the solutions were made upto constant ionic strength of 0.25 mol dm^{-3} by addition of Me_4NCl for the NaCl–PCr and KCl–PCr systems or NaCl for the $MgCl_2$–PCr system. A further series of 11 replicate solutions in the NaCl–PCr system was prepared, but with Bu_4PCl added as an internal reference and replacing Me_4NCl by Bu_4NCl.

2.4. Computational procedures

In the course of this work the new computer program HYPNMR-2000 has been written and developed. This is a generalised program for the determination of stability constants from NMR chemical shift data in systems where exchange is rapid on the NMR time-scale. It has a novel structure. The main program is written in VISUAL BASIC and runs as a typical WINDOWS application. The main program contains extensive facilities for data input and preliminary calculations including the possibility of interactive data fitting with graphical displays of observed and calculated data. The stability constant refinement is a compiled FORTRAN module, called from the main program, which is based on the earlier HYPNMR program [7]. The refinement module reads data from an input file and records the results of the computation in an output file. On termination of the refinement the output file is automatically opened in the main program and is displayed in a customised viewer.

HYPNMR-2000 can handle any number of individual resonances, including resonances from more than one nucleus, such as ^{13}C and ^1H, at the same time. There are no limitations on the number of reagents or stability constants that can be specified. Further details are available at http://www.chem.leeds.ac.uk/people/peter_gans/hypnmr.htm.

3. Results and discussion

All spectra showed a single narrow resonance, as illustrated in Fig. 1. This indicates that all the species related to phosphocreatine are in rapid equilibrium on the NMR time-scale. Confirmation of this state of affairs is provided by the smooth variation of the

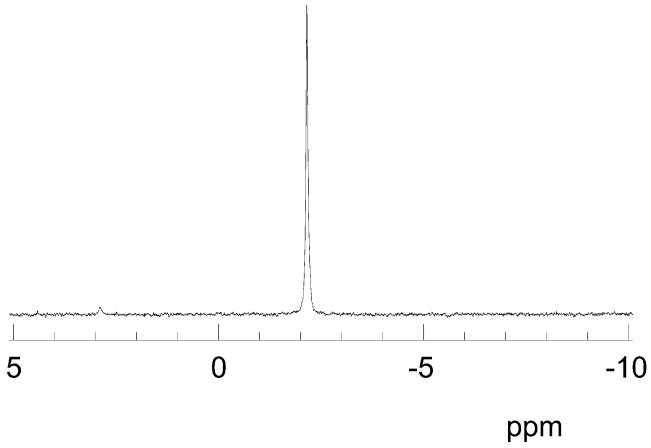


Fig. 1. ^{31}P NMR spectrum of a solution containing Na_2PCr 0.020 mol dm^{-3}; $T = 37$ °C and $I = 0.25$ mol dm^{-3}, made up with Me_4NCl.

chemical shift with changes in concentration of the metallic cations: with Na^+ and K^+ there is a slight drift to low field with increasing metal ion concentration and

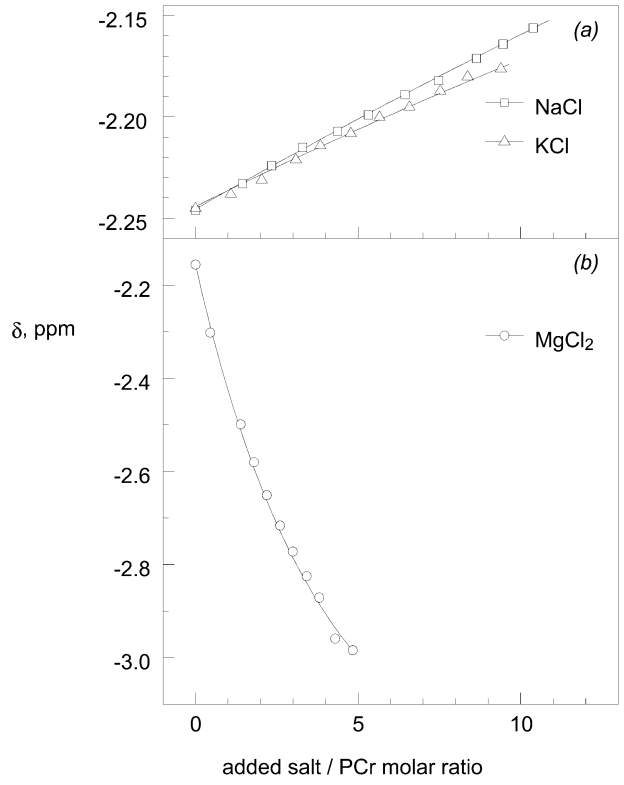


Fig. 2. ^{31}P chemical shifts of phosphocreatine at 37 °C as a function of added salt–phosphocreatine molar ratio. Hollow symbols represent the experimental points, solid lines refer to calculated titration curves. Chemical shifts were calculated on the basis of a constant analytical concentration of PCr equal to the average in each system: 0.01944 mol dm^{-3} for NaCl, and 0.2075 for KCl and $MgCl_2$. (a) Experimental values and titration curves for the systems NaCl–PCr and KCl–PCr, ionic strength adjusted with Me_4NCl; (b) experimental values and titration curve for the system $MgCl_2$–PCr, ionic strength adjusted with NaCl.

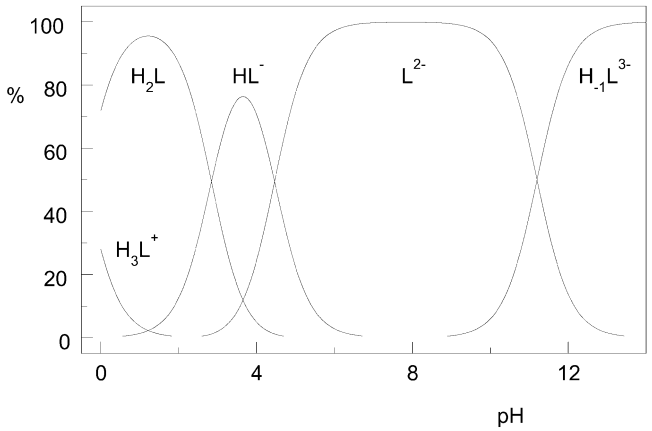


Fig. 3. Hyss distribution diagram of phosphocreatine as a function of pH. The pK_a values were taken from Ref. [8].

with Mg^{2+} there is a marked displacement to high field. These trends are illustrated in Fig. 2.

Four protonation constants have been determined for phosphocreatine [8]. The three pK_a values, −0.41, 2.84 and 4.46, were assigned to dissociation of one proton from the $-PO_3H_2$ group, dissociation of the carboxyl group proton and dissociation of a second proton from the phosphate group, respectively. The fourth pK_a value, 11.2, relates to further deprotonation of PCr^{2-}. A diagram showing the distribution of the species as a function of pH is shown in Fig. 3. This diagram, produced by the program HYSS-2000 [9], shows that PCr^{2-} is the only species present between pH 7 and pH 9. With the same program the pH of an aqueous solution of 0.02 mol dm^{-3} Na_2PCr is calculated to be 7.80 with PCr^{2-} being present at a relative concentration of more than 99.9%. These results mean that any protonated or deprotonated form of PCr^{2-} is present in negligible concentration and can, therefore, be ignored.

The stability constants for $NaPCr^-$, $KPCr^-$ and MgPCr were determined with the aid of the program HYPNMR-2000 by fitting all the data points (with unit weights) with the further inclusion of a stability constant for MgCl (log $K = 0.43$) [5] as a constant entity. The refined stability constants are shown in Table 1. The

Table 1
Logarithms of the formation constants of phosphocreatine complexes with sodium, potassium and magnesium ions at 37 °C, $I = 0.25$ mol dm^{-3} set by addition of Me_4NCl

Reaction	log K	
	This work	Literature
$Na^+ + PCr^{2-} \rightarrow NaPCr^-$	-0.5 ± 0.2	
$K^+ + PCr^{2-} \rightarrow KPCr^-$	-0.3 ± 0.2	1.30 [a]
$Mg^{2+} + PCr^{2-} \rightarrow MgPCr$	1.43 ± 0.03	1.6 ± 0.2 [b]

[a] From [5]; $T = 25$ °C, $I = 0.15$ mol dm^{-3}.
[b] From reference [4]; $T = 30$ °C, in 0.1 mol dm^{-3} *N*-ethylmorpholine buffer at pH 8.0.

value obtained for the complex MgPCr is in satisfactory agreement with a previous determination [4], but with the complex $KPCr^-$ our value is much smaller that the published value [5]. For $NaPCr^-$ there is no previously reported value for comparison and the value is quite similar to that of the potassium complex, as expected.

The chemical shifts of PCr^{2-}, $NaPCr^-$, $KPCr^-$ and MgPCr were refined along with the stability constants. The values found are -2.264 ± 0.001, -0.9 ± 0.6, -1.4 ± 0.3 and -3.44 ± 0.03 ppm, respectively.

Agreement between observed and calculated resonances is excellent, as indicated by a value of 0.00085 ppm for the S.D. on all the residuals. The calculated resonances are also shown on Fig. 2. The good agreement also provides confirmation that the only complexes formed have 1:1 metal:PCr stoichiometry.

Although the fit of the experimental data is very good the standard deviations calculated for both stability constants and chemical shifts of the sodium and potassium complexes are rather large. The main reason for this is that these complexes are rather weak so that even in the most concentrated solutions the degree of formation is small, 7.7% for NaCl–PCr and 8.7% for KCl–PCr. The magnesium complex is stronger and the degree of formation is much larger (reaching a maximum of 61%) so the standard deviations of both stability constant and chemical shift are an order of magnitude smaller.

Two assumptions underlie the results given in this work. Firstly, that the magnetic susceptibility of the medium was not affected by the progressive replacement of Me_4NCl by NaCl or KCl or of NaCl by $MgCl_2$. Secondly, that the Me_4N^+ cation does not associate with PCr^{2-}. The validity of these assumptions was tested by replicating the NMR measurements in the series NaCl–PCr with two significant differences: Bu_4PCl was added as an internal standard for the measurement of chemical shifts and Bu_4NCl was used instead of Me_4NCl for the background electrolyte. It is generally accepted that the tetrabutylammonium ion does not associate with phosphate-containing ligands [10,11]. The ^{31}P chemical shift of the tetrabutylphosphonium ion was found to be constant, 34.2456 ± 0.0009 relative to external 85% H_3PO_4. This shows that variation of solution composition over the experimental range has no significant effect on bulk magnetic susceptibility. The second assumption was tested by comparing the calculated stability constants. With the tetrabutylammonium salt log K was found to be -0.4 ± 0.3. This value is practically the same as the value obtained with the tetramethylammonium salt which demonstrates that neither cation interacts significantly with PCr.

Acknowledgements

The authors thank MURST, Italy, for financial support of this work. Further support was received by the CNR target project Biotechnology, grant 97.01029.PF, and the 'Fondazione Cassa di Risparmio di Bologna'.

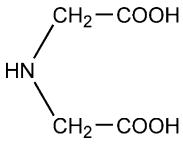
References

[1] I. Wadsö, H. Gutfreund, P. Privlov, J.T. Edsall, W.P. Jenks, G.T. Strong, R.L. Biltonen, J. Biol. Chem. 251 (1976) 6879.
[2] I. Wadsö, R.L. Biltonen, Eur. J. Biochem. 153 (1985) 429.
[3] R.M. Smith, A.E. Martell, NIST Critically Selected Stability Constants of Metal Complexes Database, US Department of Commerce, National Institute of Standards and Technology, Gaithersburg, MD, USA, 1997.
[4] W.J. O'Sullivan, D.D. Perrin, Biochemistry 3 (1964) 18.
[5] H.R. Halvorson, A.M.Q. Vande Linde, J.A. Helpern, K.M.A. Welch, NMR Biomed. 5 (1992) 53.
[6] L.D. Pettit, H.K.J. Powell, IUPAC Stability Constants Database, Academic Software, Sourby Old Farm, Otley, LS21 2PW, UK, 1999.
[7] C. Frassineti, S. Ghelli, P. Gans, A. Sabatini, M.S. Moruzzi, A. Vacca, Anal. Biochem. 231 (1995) 374.
[8] G.W. Allen, P. Haake, J. Am. Chem. Soc. 98 (1976) 4990.
[9] L. Alderighi, P. Gans, A. Ienco, D. Peters, A. Sabatini, A. Vacca, Coord. Chem. Rev. 184 (1999) 311.
[10] R.M. Smith, R.A. Alberty, J. Phys. Chem. 60 (1956) 180.
[11] R.M. Smith, R.A. Alberty, J. Am. Chem. Soc. 78 (1956) 2376.

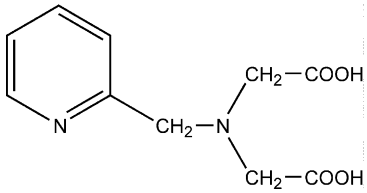
pounds have afforded various structural co-relations. For example, IDA (or IDA-like) conformation changes from *fac*- to *mer*-conformation when aqua is replaced in $[Cu(IDA)(H_2O)_2]$ (or a related chelate) by a monodentate N-heterocyclic imidazole (Him) or Him-derivative. Subsequently, a *mer*- to *fac*-IDA (or IDA-like) conformation is systematically observed going from these 1/1/1 Cu–IDA–N-heterocyclic donor compounds [1c,2–11] to others having a 1/1/2 Cu–IDA–N-heterocyclic donor ratio [12,13] or closely related complexes [14–17]. Some of these later compounds [14,15,17] reveal in addition that in the secondary ligand there is a preference of the N-heterocyclic donor for the *trans*-position to the Cu–N(IDA or IDA-like) bond. In this broad context, we became increasingly interested on new mixed-ligand copper(II) complexes having a *N*-R-IDA derivative with a R non-chelatable [16,17] or chelatable [18]18a aromatic side chain as primary ligand, and various N-heterocyclic secondary ligand of remarkable aromaticity. These kinds of mixed-ligand complexes could be 'structural model systems' with possibilities of displaying 'aromatic π,π-stacking interaction's. Such weak interactions are extensively studied because they seem to play essential roles in molecular recognition processes and in supra-molecular assemblies of relevant biological (and non-biological) systems [19,20].

It is well known that 2-(aminomethyl)pyridine or α-picolyamine (pca) acts as *N,N*-bidentate diamine ligand for copper(II) in $[Cu(pca)_3]Cl_2\cdot Cl_2CH_2$ [21a] and in several 'mixed-ligand' complexes (such as, $[Cu(pca)_2(H_2O)_2]Cl_2$ [21b] or $[Cu(pca)_2(L)_2]$ (L = various anions) both in solution and/or in solid state [21c,21d,21e,21f,21g,21h,21i]. Pyridyl π,π-stacking interactions have recently been reported for a polymeric non-chelated pca–silver(I) complex [22]. In this sense, a suggestive H_2IDA-derivative (as primary ligand) is the anion of *N*,*N*-bis(carboxymethyl)-2-(aminomethyl)pyridine or *N*-(2-pyridylmethyl)iminodiacetic acid (H_2pmda), namely *N*-(2-pyridylmethyl)iminodiacetate(2-) (hereafter pmda) (Schemes 1 and 2).

The stability constants of pmda-complexes in solution have been reported for a large variety of mono-(Li, Na, Ag, Tl), di-(alkaline-earths, Mn, Fe, Co, Ni, Cu, Zn, Cd, Hg, Pb), tri-(lanthanide series, Am, Cm) and tetravalent (vanadyl) metal ions [23]. As expected, the tripodal pmda ligand forms a very stable Cu(II) chelate (log $K = 14.2$ at 20 °C) [23d,23h,23i]. Crystal structure reports on pmda-derivatives are surprisingly limited to one dinuclear complex of iron(III) [24], two vanadium



Scheme 1. H_2IDA.



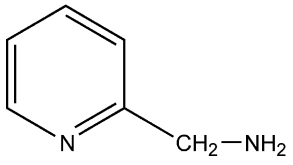
Scheme 2. H_2pmda.

compounds [25] and a tricarbonyl–technetium derivative [26]. In these cases pmda acts as tetradentate, but no mention is made of 'aromatic ring stacking' interactions. In contrast, we have recently found that in the polymeric structure of $\{[Cu(pmda)]\cdot 2H_2O\}_n$ there is a multi-π,π-stacking interaction between pyridyl rings of the complex chains [18b]. This paper deals with the synthesis and molecular and crystal structure of the free acid (H_2pmda·0.5H_2O) and of two pmda–copper(II) chelates having pca or 2-(2′-pyridyl)benzimidazole (Hpb) as secondary ligand. The aim of the present work is to study the coordination preferences of N donor atoms of these unsymmetrical diamines to the *trans*-position versus the Cu–N(tertiary amino pmda) bond. The inter-ligand aromatic ring π,π-stacking interactions in the studied compounds are also discussed (Schemes 3 and 4).

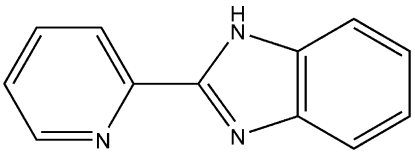
2. Experimental

2.1. Synthesis of the acid H_2pmda·0.5H_2O

The pmda ligand has been obtained as free acid by reaction of potassium chloroacetate and pca in aqueous alkaline solution at room temperature (r.t.). In a standard essay the solution of chloroacetic acid (79.36 g, 0.84 mol) in 200 ml of water was stirred and cooled in a salt–ice bath. A solution of KOH (94.08 g, 1.68 mol) in 200 ml of water was drop-wise added. To the resulting alkaline solution pca (41.24 ml, 0.40 mmol) was slowly added and the mixture was left to react in a 500 ml cooled flask in the dark for 2 weeks. HCl 6N (33 ml) was added to neutralize the solution, which was concentrated under reduced pressure and cooled (salt–ice bath) to remove KCl (by-product, 40 g). HCl 6N was newly added to fit the pH near 2.5. The desired acid precipitates and is removed by filtration. An additional amount of HCl 6N was added to the mother liquor (pH ~4) to bring down the pH to 2.5. A new amount of



Scheme 3. Pca.



Scheme 4. Hpb.

H_2pmda was removed by filtration. The product was re-crystallized in a hot fifty–fifty ethanol–water mixture, filtered and air-dried. Many well-shaped prismatic crystals of H_2pmda·0.5H_2O suitable for crystallographic work were obtained in this way. This product can also be re-crystallized from water or water:methanol (1:4). Yield: 50.38 g, 54%. *Anal.* Calc. for $C_{10}H_{12}N_2O_4$·0.5H_2O: C, 51.50; H, 5.62; N, 12.01. Found: C, 51.41; H, 5.68; N, 11.96%. Alternative syntheses of this acid were reported in the literature [23i,27]. ^{1}H NMR (300 MHz, *d*6-DMSO; δ, ppm): 3.47 (s, 4H), 3.97 (s, 2H), 7.27 (m, 1H), 7.53 (d, 1H), 7.77 (m, 1H), 8.46 (d, 1H) and 11.99 (exchangeable H). ^{13}C NMR (d_6-DMSO; δ, ppm): 54.44 (N–CH_2–COO^-), 59.01 (C_{arom}–CH_2–N), 122.29, 122.71, 136.64, 148.44 and 158.98 (C_{arom}), and 172.47 (–COO^-). FTIR spectrum (cm^{-1}): 3449, ν(OH); 3110, $\nu(CH_{arom})$; 3065 and 3002 $\nu_{as}(CH_2)$; 2964, $\nu_s(CH_2)$; 1690 and shoulders, ν(C=O), pyridyl ring breathing I and $\delta(H_2O)$; 1595, ν_{as}(COO) and pyridyl ring breathing II; 1480, pyridyl ring breathing III; 1437, pyridyl ring breathing IV, and 1389, ν_s(COO). TG+FTIR of pyrolysis gasses: In a dry-air flow it becomes nearly anhydrous (water: 0.58% exp., calc. 3.86%) and the anhydrous sample gives three pyrolytic steps (190–575 °C) with production of H_2O, CO_2, CO, NH_3 and N_2O. The decomposition starts by de-carboxylation of a free carboxylic group (190–200 °C).

2.2. Synthesis of [Cu(pmda)(pca)]·3H_2O

The stoichiometric reaction of bluish copper(II) hydroxycarbonate ($Cu_2(CO_3)(OH)_2$) and (H_2pmda·0.5H_2O) in water yields a blue solution of the complex [Cu(pmda)(H_2O)$_2$] (from which a polymeric solid {[Cu(pmda)]·2H_2O}$_n$ could be obtained [18b]). In a typical essay a mixture of 466.4 mg (2.0 mmol) of H_2pmda·0.5H_2O and 221.1 mg (1.0 mmol, Probus) of $Cu_2CO_3(OH)_2$ in 150 ml of water was heated and stirred under controlled vacuum (to remove the CO_2, by-product). The solution was stirred and heated at 60 °C for 30 min, left to cool at r.t. and then slowly filtered to remove any insoluble by-product (mainly a small amount of CuO). The clear blue solution was stirred and 0.21 ml (2 mmol, Aldrich) of pca was dropwise added. By slow evaporation of the solution at r.t. the volume was reduced to a few millilitres, and then isopropanol and acetone was added just to initiate the precipitation. The crystallization device was covered with a watch glass and slowly evaporated. A very variable and limited amount of needle-shaped crystals of the desired product (compound **1**) were formed, many of them being poly-crystals. Some single crystals were picked up for the X-ray diffraction study. The remaining product was filtered-off and air-dried for elemental analysis and FTIR spectral characterization. Frequently the reaction mixture is degraded, probably by pca oxidation, which is observed from a change from blue to greenish color. These changes are promoted by heating. Yield: < 5%. *Anal*. Calc. for $C_{32}H_{48}Cu_2N_8O_{14}$: C, 42.90; H, 5.40; N, 12.51. Found: C, 42.96; H, 5.44; N, 12.56%. The FTIR spectrum (cm^{-1}): ~3400 and 1629, ν and $\delta(H_2O)$; 3263, 3130 and 1571, ν_{as}, ν_s and $\delta(NH_2)$; 3083 and 3058, $\nu(CH_{arom})$; 2978, $\nu_{as}(CH_2)$; 2863, $\nu_s(CH_2)$; 1680, pyridyl ring breathing I; 1608, ν_{as}(COO) and pyridyl ring breathing II; 1482, pyridyl ring breathing III; 1446 or 1438, pyridyl ring breathing IV; and 1394, ν_s(COO). Δ(COO) = 214 cm^{-1}.

2.3. Synthesis of [Cu(pmda)(Hpb)]·5H_2O

To a clear blue solution of pmda–Cu(II) complex prepared in 200 ml of water, as referred before, 390.5 mg of Hbp (1 mmol, Aldrich) was added. The mixture was stirred 48 h at r.t. and filtered, and the blue solution was left to evaporate in a crystallization device. After 2 weeks, blue crystals of the desired product (compound **2**) were formed, some of them suitable for X-ray crystallography. The product was collected by filtration, washed with water and ethanol, and air-dried. Successive amounts of **2** can be collected. The product can be re-crystallized several times from water. Yield: 75%. *Anal*. Calc. for $C_{22}H_{29}CuN_5O_9$ C, 46.27; H, 5.12; N, 12.26; Cu, 11.13. Found: C, 46.46; H, 5.46; N, 12.48; Cu, 10.93% (EDTA complexometry [1,15]). FTIR spectrum data (cm^{-1}): ~3420 $\nu_{as}(H_2O)$; 3263(broad), $\nu_s(H_2O)$ and ν(NH) of Hpb; 3098 and 3060, $\nu(CH_{arom})$; 2977 and 2926, $\nu_{as}(CH_2)$; 2861 and 2813, $\nu_s(CH_2)$; 1639, pyridyl ring breathing I and $\delta(H_2O)$; 1613, ν_{as}(COO) and pyridyl ring breathing II; 1598, ν_{as}(COO); 1541, δ(NH) of Hpb; 1482, pyridyl ring breathing III; 1443 or 1425, pyridyl ring breathing IV; 1394 and 1382, ν_s(COO). Δ(COO) = 219–216 cm^{-1}.

2.4. X-ray data collection, solution of the structures and refinement

2.4.1. Acid H_2pmda·0.5H_2O

A colorless prismatic crystal of H_2pmda·0.5H_2O was mounted on a glass fibre and used for data collection. Cell constants and an orientation matrix for data collection were obtained by least-squares refinement of the diffraction data from 25 reflections in the range of $12.152° < \theta < 42.972°$ in an Enraf–Nonius CAD4 diffractometer [28]. Data were collected at 293 K using Cu

Kα radiation ($\lambda = 1\,54\,184$ Å) and the ω-scan technique and corrected for Lorentz and polarization effects [29]. A semi-empirical absorption correction (Psi-scans) was made [30]. The structure was solved by direct methods [31], which revealed the position of all non-hydrogen atoms, and refined on F^2 by a full-matrix least-square procedure using anisotropic displacement parameters [32]. All hydrogen atoms were located from difference maps and refined isotropically. Atomic scattering factors were taken from the International Tables for X-ray Crystallography [33]. Molecular graphics plotted from PLATON-98 [34]. A summary of the crystal data, experimental details and refinement results is given in Table 1.

2.4.2. *[Cu(pmda)(pca)]·3H$_2$O and [Cu(pmda)(Hpb)]·5H$_2$O (compounds **1** and **2**)*

Crystallographic data for these two blue compounds were collected on a Bruker Smart CCD diffractometer at 293 K using graphite monochromated Mo Kα radiation ($\lambda = 0.71073$ Å), and were corrected for Lorentz and polarization effects. The frames were integrated with the Bruker SAINT [35a]; software package and the data were corrected for absorption using the program SADABS [35b]. The structures were solved by direct methods using the SHELXS-97 program [36]. All non-hydrogen atoms were refined with anisotropic thermal parameters by full-matrix least-squares calculations on F^2 using the program SHELXL-97 [37]. The position of most H atoms was calculated geometrically and included in structure factor calculations, but in compound **2** the H atom bonded to N23 was located in difference maps and its position was refined isotropically. Crystal data and structure refinement parameters are listed in Table 1. Molecular graphics were obtained using SHELXTL [38].

2.5. Physical measurements

NMR spectra were recorded in a Bruker AM300 spectrophotometer. Infrared spectra were obtained by the KBr disc technique on a JASCO FTIR 410 instrument. In addition the TG (pyrolysis) of studied compounds and analysis of evolved gasses were recorded (295–775 K) in air flow (100 ml min^{-1}) using a Shimazu Thermobalance TGA-DTG-50H coupled with an IRFT Nicolet Magma 550 (and mass spectrometer Fisons Thermolab). Electronic (reflectance) spectra (175–3300 nm) were obtained in a Cary 5E spectrophotometer.

Table 1
Crystal data and structure refinement for compounds H$_2$pmda·H$_2$O, [Cu(pmda)(pca)(H$_2$O)]·3H$_2$O (**1**) and [Cu(pmda)(Hbp)]·5H$_2$O (**2**)

	H$_2$pmda·0.5H$_2$O	Compound **1**	Compound **2**
Empirical formula	$C_{10}H_{13}N_2O_{4.5}$	$C_{16}H_{24}CuN_4O_7$	$C_{22}H_{19}CuN_5O_9$
Formula weight	233.22	895.86	571.04
Temperature (K)	293(2)	293(2)	293(2)
Wave length (Å)	1.54184	0.71073	0.71073
Crystal system	monoclinic	monoclinic	monoclinic
Space group	$C2/c$	$P2_1/n$	$P2_1/n$
Unit cell dimensions			
a (Å)	28.655(4)	15.612(1)	11.632(1)
b (Å)	5.7937(3)	7.833(1)	9.285(1)
c (Å)	12.4235(3)	32.678(2)	23.344(2)
β (°)	114.42(1)	98.95(1)	92.19(1)
Volume (Å^3)	2151.8(5)	3947.6(4)	2519.4(3)
Z	8	8	4
D_{calc} (Mg m^{-3})	1.440	1.507	1.505
Absorption coefficient (mm^{-1})	0.975	1.152	0.927
$F(000)$	984	1864	1188
Crystal size (mm)	0.35 × 0.15 × 0.10	0.42 × 0.29 × 0.16	0.36 × 0.15 × 0.15
θ Range for data collection (°)	3.39–74.24	1.55–28.02	1.75–28.03
Index ranges	$0 < h < 35$, $0 < k < 7$, $-17 < l < 16$	$-9 < h < 20$, $-9 < k < 10$, $-42 < l < 42$	$-15 < h < 15$, $-11 < k < < 12$, $-30 < l < 24$
Reflections collected/unique	2238/2193, [R(int) = 0.0127]	22679/9028, [R(int) = 0.0404]	14863/5848, [R(int) = 0.0480]
Completeness (to 2θ)	45.2% (74.24)	94.4% (28.02)	95.8% (28.03)
Absorption correction	Psi-scan	empirical (SADABS)	empirical (SADABS)
Max/min transmission	0.965, 0.916	1.0000, 0.7485	1.0000, 0.7908
Refinement method	full-matrix least-square F^2	full-matrix least-square F^2	full-matrix least-square F^2
Data/restraints/param.	2193/0/200	9028/0/505	5848/0/338
Goodness-of-fit on F^2	1.038	0.913	0.960
Final R indices[$I > 2\sigma(I)$]	$R_1 = 0.042$, $wR_2 = 0.112$	$R_1 = 0.042$, $wR_2 = 0.099$	$R_1 = 0.053$, $wR_2 = 0.137$
R indices (all data)	$R_1 = 0.055$, $wR_2 = 0.121$	$R_1 = 0.084$, $wR_2 = 0.108$	$R_1 = 0.102$, $wR_2 = 0.152$
Extinction coefficient	0.0046(3)	none	none
Largest difference on peak and hole (e Å^{-3})	0.703/−0.304	0.534/−0.436	0.616/−0.243

RSE spectra of a polycrystalline sample were recorded without magnetic dilution in a spectrophotometer Bruker ESP 300E (X band) at r.t. The magnetic susceptibility of **I** was measured at the temperature range 80–300 K using a Manics DM magnetometer. The susceptometer was calibrated with mercury tetrakis(thiocyanato)–cobaltato(II). Corrections for the diamagnetism ($122 \cdot 10^{-6}$ cm^3 mol^{-1}) were estimated from Pascal constants [39]. Experimental susceptibilities were also corrected for the temperature-independent paramagnetism (60×10^{-6} cm^3 mol^{-1} per Cu(II) atom) [40].

3. Results and discussion

3.1. Description of the structures

Bond lengths and angles between non-hydrogen atoms and hydrogen bond distances and angles of H_2pmda·0.5H_2O are given in Table 2. Fig. 1 shows a drawing of two adjacent symmetrically related units, with the numbering scheme. According to the relative magnitude of its pK_a values (for example, p$K_0 = 2.65$, p$K_1 = 2.74$ and p$K_2 = 8.16$ for a proton dissociation from H_3pmda$^+$, H_2pmda and Hpmda$^-$, respectively, at $I = 0.1$(KNO_3) and 25 °C [23d]) the molecule of this diamino-diacid will exist as a zwitterion in solution of polar solvents. Such dipolar ions H_2pmda$^{\pm}$ are also found in the crystal, as it has usually been observed for a variety of free amino-polycarboxylic acids [41].

Two structural features of the studied amino-polycarboxylic acid are of major interest. First, is the conformation intra-stabilised by a trifurcated hydrogen bond formed by the 'onium' proton with two carboxylate atoms, O(12) and O(22), and the pyridyl atom N(2) as 'acceptors'. In accordance, its planar pyridyl ring forms similar dihedral angles with the planes of both carboxylic (86.2°) and carboxylate (89.3°) groups. Similar kind of zwitterions have been largely referred for the structure of a variety of amino-polycarboxylic acids such as iminodiacetic acid [41]. The presence of similar trifurcated hydrogen bonds governing a zwitterion conformation is also known, for example, in the crystal structures of β-(hydroxyethyl)iminodiacetic acid (H_2heida) [42] and nitrilopropionicdiacetic acid (H_3npda) [43], both with appropriate O-acceptor atoms in the 'third arm'. In H_2heida the 'onium' hydrogen atom interacts with two O-carboxyl and one O-alcoholic atoms, whereas in H_3npda three O-carboxyl atoms interact with the onium N–H$^+$ group. Second, pyridyl rings from pairs of adjacent dipolar ions H_2pmda$^{\pm}$ (related by the symmetry code #2 = ii = $1/2-x$, $-1/2-y$, $2-z$) lie parallel and stacked (dihedral angle between planes $\alpha = 0.2°$) at a distance of 3.57(1) Å (Fig. 1). This

Table 2
Bond lengths (Å) and angles (°) and data concerning hydrogen bonds in H_2pmda·0.5H_2O with e.s.d. in parentheses

Bond lengths				
O(11)–C(12)	1.299(2)	N(2)–C(6)	1.341(2)	
O(12)–C(12)	1.207(2)	C(1)–C(2)	1.506(2)	
O(21)–C(22)	1.234(2)	C(2)–C(3)	1.387(3)	
O(22)–C(22)	1.268(2)	C(3)–C(4)	1.381(3)	
N(1)–C(11)	1.492(2)	C(4)–C(5)	1.378(3)	
N(1)–C(1)	1.495(2)	C(5)–C(6)	1.379(3)	
N(1)–C(21)	1.497(2)	C(11)–C(12)	1.512(2)	
N(2)–C(2)	1.337(2)	C(21)–C(22)	1.520(2)	
Bond angles				
/c>				
C(11)–N(1)–C(1)	112.4(2)	C(4)–C(5)–C(6)	118.4(2)	
C(11)–N(1)–C(21)	111.5(2)	N(2)–C(6)–C(5)	123.6(2)	
C(1)–N(1)–C(21)	111.1(2)	N(1)–C(11)–C(12)	109.2(2)	
C(2)–N(2)–C(6)	117.2(2)	O(12)–C(12)–O(11)	126.7(2)	
N(1)–C(1)–C(2)	111.6(2)	O(12)–C(12)–C(11)	121.9(2)	
N(2)–C(2)–C(3)	123.1(2)	O(11)–C(12)–C(11)	111.5(2)	
N(2)–C(2)–C(1)	117.3(2)	N(1)–C(21)–C(22)	111.8(2)	
C(3)–C(2)–C(1)	119.6(2)	O(21)–C(22)–O(22)	127.2(2)	
C(4)–C(3)–C(2)	118.5(2)	O(21)–C(22)–C(21)	117.2(2)	
C(5)–C(4)–C(3)	119.2(2)	O(22)–C(22)–C(21)	115.6(2)	
Hydrogen bonds				
D–H···A	d(D–H)	d(H···A)	d(D···A)	<(DHA)
N(1)–H(1)···N(2)	0.94(2)	2.32(2)	2.687(2)	102.3(2)
N(1)–H(1)···O(12)	0.94(2)	2.23(2)	2.669(2)	107.4(2)
N(1)–H(1)···O(22)	0.94(2)	2.28(2)	2.680(2)	105.0(2)
O(11)–H(11)···O(22)#1 [a]	1.12(4)	1.38(4)	2.479(2)	165.0(3)
O(1)–H(1O)···O(21)#1 [a]	1.12(2)	1.77(2)	2.830(2)	157.4(1)

[a] Symmetry code: #1 = x, $-y+1$, $z-1/2$.

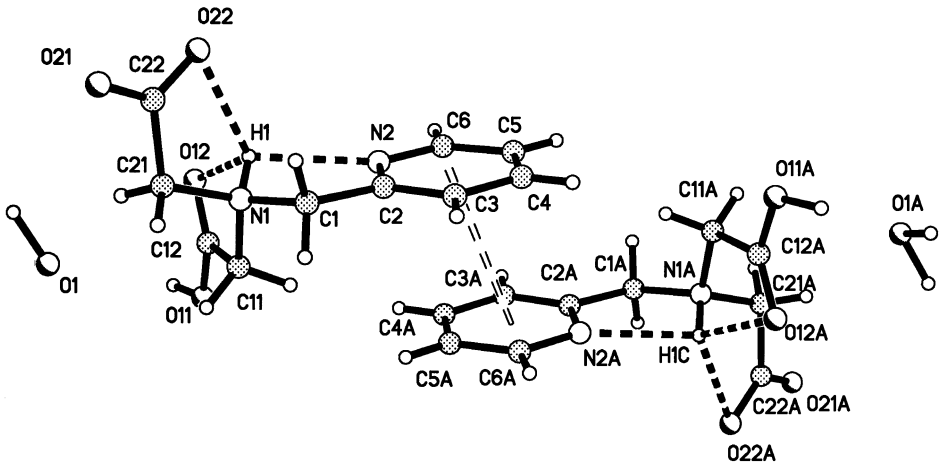
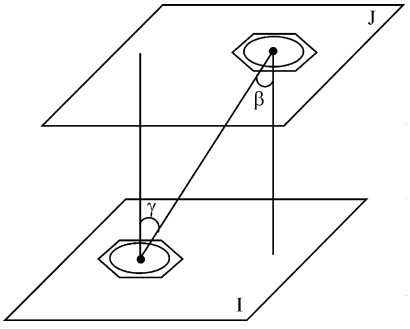


Fig. 1. Structure of the acid *N*-(2-pyridylmethyl)iminodiacetic acid hemi-hydrate showing the stacking between pyridyl rings of two adjacent zwitterions, which are intra-stabilised by a tri-furcated hydrogen bond.



Scheme 5. β and α angles in a ring–ring π,π-stacking interaction.

π,π-interaction will have a significant σ,π-contribution because of the long centroid–centroid distance (3.94 Å) and the remarkable displacement between the stacked rings (angles of the centroid–centroid vector with the perpendicular to each stacked ring plane are $\beta = \gamma =$ 25.0°; see scheme 5 below). In addition, each zwitterion acts as H-donor to an adjacent one (related by the symmetry code #1 = $i = x, -y+1, z-1/2$; see Table 2). These latter –COOH···$^{-}$OOC–hydrogen bonds and the ring–ring stacking interactions generate a 2D framework with the carboxyl groups toward the external surfaces and stacked pyridyl rings toward the inside (Fig. 2). In the crystal, each water molecule forms two symmetry related and equivalent hydrogen bonds of the type O(1)–H(10)···O(21)#1 (Table 2) toward opposite sides connecting the closest external faces of two adjacent bi-layers (Fig. 2) (Scheme 5).

Since the internal geometry of the ligands could be considered normal (see appropriate refs. for pmda [24–26], pca [21,22] and Hpb [44]), only coordination bond lengths and selected *trans*-angles of (α-picolylamine)(*N*-(2-pyridylmethyl)iminodiacetato)copper(II) thi-hydrate

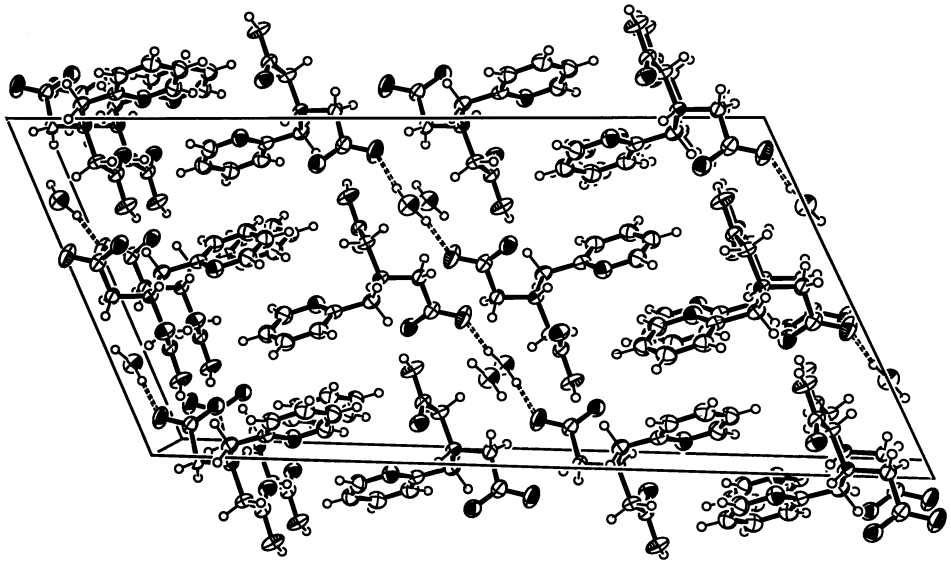


Fig. 2. 2D frameworks of $H_2pmda^{\pm}$ zwitterions and inter-layered connected by the hydrogen bonded water molecules in the unit cell of the acid $H_2pmda \cdot 0.5H_2O$.

Table 3
Copper(II) coordination bond lengths (Å) and *trans*-bond angles (°) in [Cu(pmda)(pca)]·3H_2O (compound **1**) with e.s.d. in parentheses

Bond lengths			
Cu(1)–O(2)	1.970(2)	Cu(2)–O(24)	1.961(2)
Cu(1)–N(11)	1.993(2)	Cu(2)–N(31)	1.987(2)
Cu(1)–N(16)	2.010(2)	Cu(2)–N(36)	2.019(2)
Cu(1)–N(1)	2.073(2)	Cu(2)–N(2)	2.054(2)
Cu(1)–N(6)	2.418(3)	Cu(2)–N(26)	2.640(3)
Cu(1)–O(4)	2.439(2)	Cu(2)–O(22)	2.359(2)
Bond angles			
N(11)–Cu(1)–N(1)	176.39(1)	N(31)–Cu(2)–N(2)	177.42(1)
O(2)–Cu(1)–N(16)	173.29(1)	O(24)–Cu(2)–N(36)	166.67(1)
N(6)–Cu(1)–O(4)	151.56(8)	O(22)–Cu(2)–N(26)	150.92(8)

Table 4
Copper(II) coordination bond lengths (Å) and *trans*-bond angles (°) in [Cu(pmda)(Hpb)]·5H_2O (compound **2**) with e.s.d. in parentheses

Bond lengths	
Cu–N(22)	1.970(3)
Cu–O(11)	2.018(2)
Cu–N(11)	2.029(3)
Cu–N(12)	2.032(3)
Cu–O(13)	2.260(3)
Cu–N(21)	2.535(3)
Bond angles	
N(22)–Cu–N(11)	175.75(12)
O(13)–Cu–N(21)	167.44(11)
O(11)–Cu–N(12)	162.56(12)

([Cu(pmda)(pca)]·3H_2O, compound **1**) and (2-(2′-pyridyl)benzimidazole)(*N*-(2-pyridylmethyl)iminodiacetato)copper(II) pentahydrate ([Cu(pmda)(Hpb)]·5H_2O, compound **2**) are listed in Tables 3 and 4, respectively.

The asymmetric unit of compound **1** (Fig. 3) consists of a pair of crystallographically independent molecules [Cu(pmda)(pca)], very similar from a chemical point of view, and six non-coordinated water molecules. Coordination bond lengths (averaged, in Å): Cu–N(aliphatic) 2.064(2), Cu–O(equat.) 1.966(2), Cu–O(apex) 2.399(2) and Cu–N(py ring) 2.529(3) to pmda; Cu–N(py ring) 1.990(2) and Cu–N(primary amino) 2.015(2) to pca ligand. The closest four donors around the copper(II) atom are both N atoms of pca, and the N aliphatic and one O carboxyl atoms of pmda. It is remarkable that the N(pyridyl) and one O carboxyl atom from pmda occupy the apexes of the asymmetrically elongated coordination of copper(II). Two main structural features arise from this structure: (1) the conformational flexibility of the tripodal tetradentate pmda ligand, which occupy two equatorial and two apical coordination sites (instead of three equatorial and an apical ones), and (2) the coordination preference of the *N*(pyridyl)-heterocyclic atom from the secondary pca ligand to occupy the *trans*-position to the Cu–N(aliphatic) bond of pmda.

Compound **2** has one complex molecule and five water molecules in the asymmetric unit (Fig. 4). In this complex, the pmda exhibits a tripodal tetradentate role occupying three equatorial sites and one apical donor site, whereas the *N*,*N*-bidentate Hpb ligand supplies one equatorial atom and one apical donor atom. The structure of the compound **2** shows the preference of the *N*(imidazolyl) donor versus the *N*(pyridyl) donor of

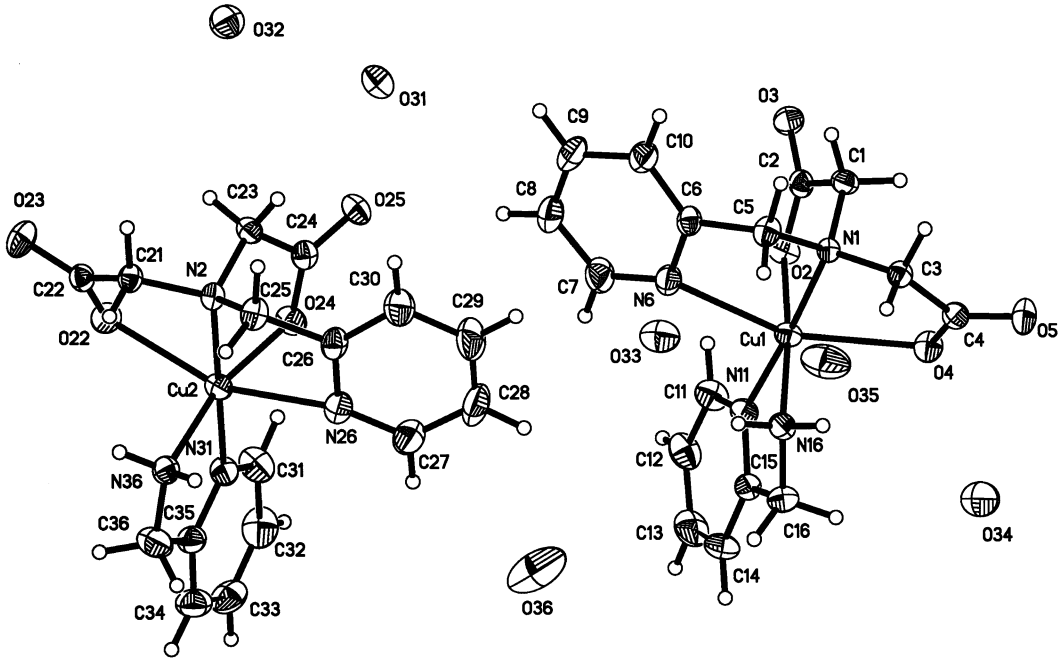


Fig. 3. Asymmetric unit in the crystal of compound **1**, [Cu(pmda)(pca)]·3H_2O, showing the two crystallographically independent complex units and the six independent water molecules.

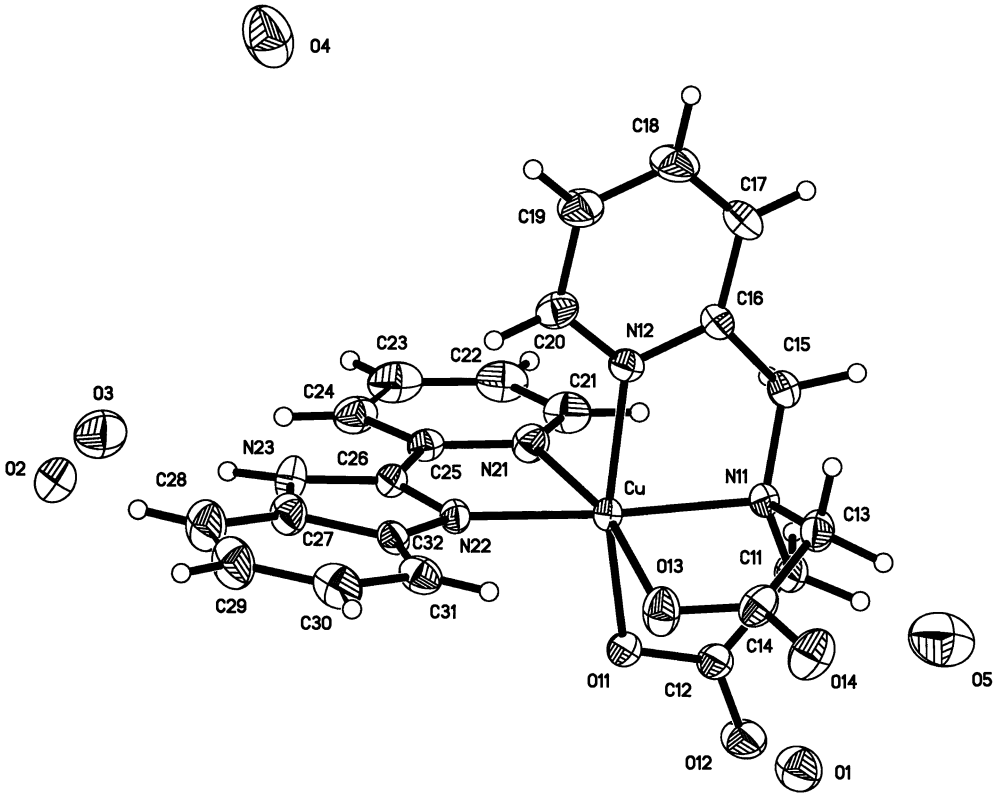


Fig. 4. Asymmetric unit in the crystal of [Cu(pmda)(Hpb)]·5H_2O (compound **2**).

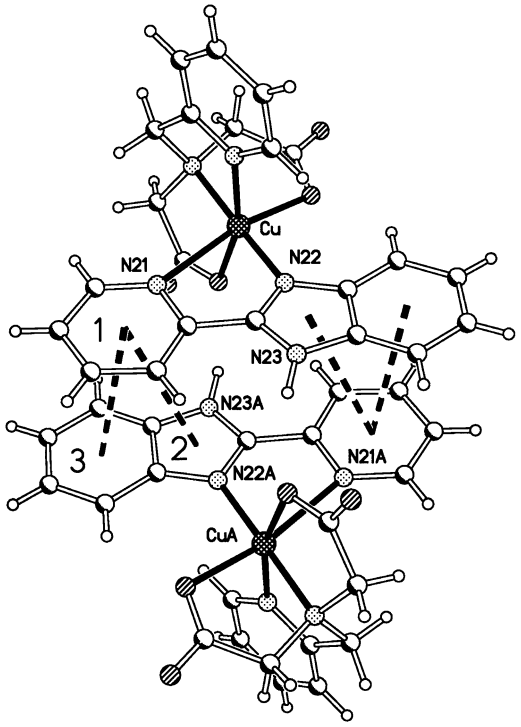


Fig. 5. Aromatic ring–ring π,π-stacking interaction between Hpb ligands of a pair of adjacent molecules in the crystal of [Cu(pmda)(Hpb)]·5H_2O (compound **2**).

Hpb to occupy one among the four closest donor atoms in the distorted octahedral coordination of copper(II) atom; that is just in *trans* to the Cu–N(1) bond of the tertiary amino atom of pmda ligand. In this crystal, pairs of adjacent complex molecules (symmetry related by the code $i = 2-x,\ 1-y,\ z$) have the corresponding Hpb ligands anti-parallel stacked at 3.41 Å (Fig. 5). This π,π-stacking interaction relates approximately the pyridyl ring (ring 1) of each Hpb ligand with the five and six-member rings of the benzimidazolyl moiety from the stacked Hpb ligand (rings 2 and 3, respectively). The analysis of this stacking interaction gives the following structural parameters. Centroid–centroid distances dc_1–$dc_2 = 3.67$ Å and dc_1–$dc_3 = 3.56$ Å. The dihedral angle between stacked rings (α) and angles β and γ of the c–c vector to the normal to the first and second planes (see Scheme 5) are $\alpha = 5.3$, $\beta = 25.6$ and $\gamma = 21.9^\circ$ for planes of rings 1 and 2, and $\alpha = 5.6$, $\beta = 17.2$ and $\gamma = 16.6^\circ$ for planes of rings 1 and 3. The perpendicular distances from the centroid of the ring 1 to the planes 2 and 3 are 3.40 and 3.41 Å, respectively. The perpendicular distances from the centroid of the ring 2 or 3 to the plane of ring 1 are 3.31 and 3.40 Å, respectively. These structural parameters for the stacking between Hpb ligands are consistent with a π,π-interaction with some σ,π-contribution [20]. The crystal is supposedly built linking

pairs of complex molecules and water molecules in a hydrogen-bonding array.

In both complexes the copper(II) atom falls in a distorted and asymmetrically elongated octahedral coordination (type 4+1+1), with the four shortest R_S bonds and the two out-of-plane or *trans*-apical longest R_L bonds. In compound **1** there is a remarkable difference in the asymmetry of two molecules, as reflected by the *trans*-apical R_L bond lengths and the tetragonality (T = mean in-plane distance/mean out-of-plane distance) [45] of 0.828 and 0.802 for Cu(1) and Cu(2), respectively. In this complex the individual and the averaged tetragonality (mean $T = 0.815$) falls below that of compound **2** ($T = 0.839$), which has also rather different *trans*-apical R_L bond distances, Cu–O(13) and Cu–N(21). Consequently, the overall elongation of the copper(II) coordination polyhedron is higher in **1** (with lower T) than in **2**.

In the new mixed-ligand Cu(II) complexes, the pmda ligand acts as a tripodal tetradentate as referred in all known structures of complexes with this chelating agent and other metal ions [24–26]. However, the conformation of pmda ligand around the copper(II) in reported chelates is different, because it supplies two equatorial and two apical donors (in **1**) or three equatorial and one axial donors (see above). We found surprising that in compound **1** the rather flexible pca diamine occupies two among the four closest coordination sites around the copper(II) atom, whereas in compound **2** the very rigid Hpb heterocyclic diamine supplies one equatorial and one axial N donors. This apparent controversy can be rationalised considering that both pmda conformations enable the formation of two types of metal-glycinate rings in the complexes studied here. These are the G ring (nearly coplanar to the plane [Cu, N, N] and more strengthened) and the R ring (nearly perpendicular to the plane [Cu, N, N] and less constrained). In the compounds considered here, the G ring falls approximately coplanar with a mean plane P defined by metal and three N donors (two from the pmda ligand and the other from the auxiliary diamine ligand). In contrast, the R ring is roughly perpendicular to the G ring and to the mean plane P of the Cu and three N atoms.

3.2. Properties of compound 2

3.2.1. Thermal stability

The TG-DTA diagram of compound **2** showed that the studied compound loses all non-bonded to the metal water molecules in air-dry flow before starting the pyrolytic decomposition (190 °C) of the anhydrous complex (5.469 mg, 10 °C min^{-1}) in two overlapped processes. The infrared spectra of evolved gasses in the first step (190–235 °C) showed a significant production of CO_2, H_2O and N_2O. The lost weight corresponds approximately to the pyrolysis of the pmda–IDA moiety (calc. 27.045%, exp. 28.572%). The second step (235–405 °C) shows the decomposition of remaining organic fragments (with production of CO_2, CO, H_2O and N_2O) to yield CuO (exp. 17.584%, calc. residue 16.539%).

3.2.2. Electronic and ESR spectra

The electronic spectrum of **2** shows a d–d band with $\nu_{max} = 13\,320$ cm^{-1} with shoulder at 9000 cm^{-1} and intensity baricenter near 12 500 cm^{-1}. These values are in accordance with a distorted octahedral chromophore CuN_2O_2+N+O (type 4+1+1) [45]. A polycrystalline sample of this compound gives an axial ESR spectrum that is 'reverse' in type ($g_{//} = 2.06 < g_{\perp} = 2.19$) with the lowest g value significantly above 2.00. This behaviour is referred as an antiferrodistortive ordering [45] with total misalignment of the CuN_2O_2+O+N cromophores in the crystal lattice, and is consistent unambiguously with a d_{x2-y2} ground state for the copper(II) atom.

3.2.3. Magnetic susceptibility

A plot of χ data versus T(K) ($T = 79$–290 K) is linear ($1/\chi = (1/C)T - (\theta/C)$ with a statistical r^2 factor of 0.9987) according to a Curie–Weiss behaviour, $\chi = C/(T-\theta)$ [39,45]. The Curie constant is $C = 0.437$ K emu mol^{-1} with Weiss constant of $\theta = 5.45$. The estimated value of μ_{eff} for Cu(II) atom is 1.87 BM. The ESR spectrum and the magnetic susceptibility data are in accordance with the structure reported here and a $Cu\cdots Cu^{ii}$ separation of 7.165(1) Å (symmetry code: ii = $-x$, $1-y$, $-z$).

4. Concluding remarks

From the molecular recognition point of view, it is interesting to note the way in which an inter-molecular hydrogen bond and the pyridyl–pyridyl π,π-stacking interaction co-operate to build the 2D molecular framework of zwitterions in the crystal of H_2pmda·0.5H_2O. The pyridyl–pyridyl inter-planar stacking distance in the free acid (3.57(1) Å) is larger than in compounds $\{[Cu(pmda)]\cdot 2H_2O\}_n$ (3.19(1) Å) [18b] and [2-(aminomethyl)-pyridine]silver(I) nitrate (3.21(1) Å [22]). It is noteworthy that compounds **1** and **2** do not involve the pmda pyridyl ring in aromatic π,π-stacking forces, whereas compound **2** displays such inter-ligand interactions between adjacent Hpb heterocycles to recognize itself forming pairs of complex units. The most important structural consequence of the insertion of a *N*-(α-pycolyl) arm in the IDA skeleton is an efficient increase of denticity from three (IDA) to four (pmda). In addition, the studied Cu(II) complexes reveal a remarkable conformational flexibility of the tripodal tetradentate pmda ligand. As for the coordination

preference for the *trans*-position to the Cu–N(aliphatic) bond, these structures enable to propose the following donor order N(imidazolyl) > N(pyridyl) > N(aliphatic).

5. Supplementary material

Crystallographic data for the structural analysis have been deposited with the Cambridge Crystallographic Data Centre, CCDC No. 129246 for H_2pmda·0.5H_2O, CCDC No. 172576 for [Cu(pmda)(pca)]·3H_2O (compound **1**) and CCDC No. 172577 for [Cu(pmda)(Hpb)]·5H_2O (compound **2**). Copies of this information may be obtained free of charge from The Director, CCDC, 12 Union Road, Cambridge, CB2 1EZ, UK (fax: +44-1223-336-033; e-mail: deposit@ccdc.cam.ac.uk or www:http://www.ccdc.cam.ac.uk).

Acknowledgements

We are grateful to the DGESIC (MEC, Spain) for financial support (Research Projects PB-98-0605-C03-02 and -03). A research grant to B.C. from the Consellería de Educación e Ordenación Universitaria (Xunta de Galicia, Spain) is gratefully acknowledged. D.Ch.L. thanks the AECI (MAE, Spain) for the financial support of a Doctoral research grant.

References

[1] (a) A. Podder, J.K. Dattagupta, N.N. Saha, N. Saenger, Acta Crystallogr., Sect. B 35 (1979) 53;
(b) F.G. Kramanenco, T.N. Polynova, M.A. Porai-Koshits, V.P. Chalvi, G.N. Kumivanova, L.I. Martynenko, Zh. Strukt. Khim. 14 (1973) 744;
(c) M.J. Román-Alpiste, J.D. Martín-Ramos, A. Castiñeiras-Campos, E. Bugella-Altamirano, A.G. Sicilia-Zafra, J.M. González-Pérez, J. Niclós-Gutiérrez, Polyhedron 15 (1999) 439 (and references therein).
[2] X. Duanjun, C. Chaorong, X. Yuanzhi, Z. Kangjing, Jiegou Xuaxue 6 (1987) 39.
[3] X. Duanjun, C. Chaorong, X. Yuanzhi, Z. Kangjing, Jiegou Xuaxue 6 (1987) 106.
[4] J.M. González Pérez, J. Nguyen-Huy Dung, Niclós-Gutiérrez, B. Viossat, A. Busnot, M.L. Vicente-Gelabert, Inorg. Chim. Acta 166 (1989) 115.
[5] B. Nguyen-Huy Dung, Viossat, A. Busnot, J.M. Pérez, J. Niclós Gutiérrez, F. Gardette, Inorg. Chim. Acta 174 (1990) 145.
[6] J. Niclós Gutiérrez, E. Abarca García, B. Viossat, A. Nguyen-Huy Dung, A. Busnot, J.F. Hemidy, Acta Crystallogr., Sect. C 49 (1993) 19.
[7] A. Castiñeiras Campos, A. Busnot, M.E. Abarca, A.G. Sicilia Zafra, J.M. González Pérez, J. Niclós Gutiérrez, Inorg. Chim. Acta 215 (1994) 73.
[8] A. Castiñeiras Campos, J.M. Tercero, A. Matilla, J.M. González, A.G. Sicilia, J. Niclós, J. Coord. Chem. 35 (1995) 61.
[9] A. Castiñeiras Campos, A.G. Sicilia Zafra, J.M. González-Pérez, J. Niclós Gutiérrez, E. Chinea, A. Mederos, Inorg. Chim. Acta 241 (1996) 39.
[10] (a) A.G. Sicilia Zafra, E. Bugella Altamirano, J.M. González-Pérez, J.D. Martín Ramos, J. Niclós Gutiérrez, VIII Italian-Spanish Congress on Thermodynamics of Metal Complexes, Cagliari, Italy, 1997, p. 56;
(b) E. Bugella, A.G. Sicilia, J.M. González, A. Castiñeiras, J. Niclós, IX Spanish–Italian Congress on Thermodynamics of Metal Complexes, Girona, Spain, 1998, report P-2;
(c) A. Castiñeiras, A.G. Sicilia, J.M. González, E. Bugella, J. Niclós, IX Spanish–Italian Congress on Thermodynamics of Metal Complexes, Girona, Spain, 1998, report P-5.
[11] M. Tribet, B. Covelo, A. Castiñeiras, J.M. González-Pérez, J. Niclós-Guiérrez, Reunión de Bioinorgánica 2001, Universidad de Granada, Granada, Spain, 2001, report P-68.
[12] Nguyen-Huy Dung, B. Viossat, A. Busnot, A.G. Sicilia Zafra, J.M. González-Pérez, J. Niclós Gutiérrez, Inorg. Chim. Acta 169 (1990) 9.
[13] (a) G. Nardin, L. Randaccio, R.P. Bonomo, E. Rizzareli, J. Chem. Soc., Dalton Trans. (1980) 369;
(b) A. Castiñeiras, M.E. Abarca, I. de la Cueva, J.M. González, J. Niclós, J. Coord. Chem. 30 (1993) 273.
[14] I.S. de la Cueva, A.G. Sicilia, J.M. González, E. Bugella, A. Castiñeiras, J. Niclós-Gutiérrez, React. Funct. Polym. 36 (1998) 211.
[15] E. Bugella-Altamirano, J.M. González-Pérez, D. Choquesillo-Lazarte, J. Niclós-Gutiérrez, A. Castiñeiras-Campos, Z. Anorg. Allg. Chem. 626 (2000) 930 (and references therein).
[16] A. Castiñeiras Campos, J.D. Martín Ramos, E. Bugella Altamirano, J.M. González-Pérez, D. Choquesillo-Lazarte, J. Niclós Gutiérrez, X Italian–Spanish Congress on Thermodynamics of Metal Complexes, S. Maruno al Cimino, Italy, 1999, report C-18.
[17] E. Bugella-Altamirano, J.M. González-Pérez, A.G. Sicilia-Zafra, A. Castiñeiras-Campos, J. Niclós-Gutiérrez, XI Spanish–Italian Congress on Thermodynamics of Metal Complexes, Valencia, Spain, 2000, report P-18.
[18] (a) E. Bugella Altamirano, A. Castiñeiras Campos, J.M. González-Pérez, A.G. Sicilia Zafra, J. Niclós Gutiérrez, X Italian–Spanish Congress on Thermodynamics of Metal Complexes, S. Maruno al Cimino, Italy, 1999, report C-17;
(b) D. Choquesillo-Lazarte, A. Castiñeiras Campos, E. Bugella Altamirano, J.M. González-Pérez, J. Niclós Gutiérrez, X Italian–Spanish Congress on Thermodynamics of Metal Complexes, S. Maruno al Cimino, Italy, 1999, report C-16.
[19] A.M. Davis, S.J. Teague, Angew. Chem., Int. Ed. 38 (1999) 736.
[20] C. Janiak, J. Chem. Soc., Dalton Trans. (2000) 3885.
[21] (a) A.W. Maverick, M.L. Ivie, F.R. Fronczek, J. Coord. Chem. 21 (1990) 315;
(b) A.G. Hatzidimitriou, M. Uddin, Polyhedron 16 (1997) 1651;
(c) C.J. O'Connor, E.E. Eduok, F.R. Fronczek, O. Kahn, Inorg. Chim. Acta 105 (1985) 107;
(d) H.M. Helis, W.H. Goodman, R.B. Wilson, J.A. Morgan, D.J. Hodgson, Inorg. Chem. 16 (1977) 2412;
(e) H. Kooijman, A.L. Spek, D. Rehorst, W.L. Driessen, J. Reedijk, Acta Crystallogr., Sect. C 53 (1997) 1596;
(f) C.J. O'Connor, E.E. Eduok, J.W. Owens, E.D. Stevens, C.L. Klein, Inorg. Chim. Acta 117 (1986) 175;
(g) H.-M. Hu, D.-L. Long, H.-Y. Zeng, W.-D. Cheng, J.-S. Huang, Acta Crystallogr., Sect. C 55 (1999) 9900049;
(h) M.E. Quiroz-Castro, G.A. van Albada, I. Mutikainen, U. Turpeinen, J. Reedijk, Inorg. Chim. Acta 297 (2000) 129;
(i) C.A. Crawford, E.F. Day, W.E. Streib, J.C. Huffman, G. Christou, Polyhedron 13 (1994) 2933.
[22] G. Swarnabala, M.V. Rajasekharan, Polyhedron 16 (1997) 921.
[23] (a) M. Nishizawa, Y. Sasaki, K. Saito, Inorg. Chem. 24 (1985) 767;

(b) J. Felcman, J. da Silva, Talanta 30 (1983) 565;
(c) G. Anderegg, J. Coord. Chem. 11 (1981) 171;
(d) M. Israeli, L. Pettit, J. Chem. Soc. Dalton Trans. (1975) 414;
(e) S. Eberle, I. Bayat, Inorg. Nucl. Chem. Lett. 5 (1969) 229;
(f) T. Kadenand, S. Fallab, Chimia 20 (1966) 51;
(g) P. Souchey, N. Israily, P. Gouzerh, Bull. Soc. Chim. Fr. 12 (1966) 3917;
(h) L. Thompson, Inorg. Chem. 3 (1964) 1015;
(i) H. Irving, J. Frausto da Silva, J. Chem. Soc. (1963) 945;
(j) Y. Nishida, A. Goto, T. Akamatsu, H. Ohba, T. Fujita, S. Okada, Chem. Lett. (1994) 641.

[24] Y. Nishida, A. Goto, T. Akamatsu, S. Fujita, S. Okada, Chem. Lett. (1994) 641.

[25] (a) S. Ooi, M. Nishizawa, K. Matsumoto, H. Kuroya, K. Saito, Bull. Chem. Soc. Jpn. 52 (1979) 452;
(b) J.P. Launay, Y. Jeannin, M. Daoudi, Inorg. Chem. 24 (1985) 1052.

[26] R. Alberto, R. Schibli, A. Egli, A.P. Schubiger, J. Am. Chem. Soc. 120 (1998) 2026.

[27] D.D. Cox, S.J. Benkovic, L.M. Bloom, F.C. Bradley, M.J. Nelson, L. Que, D.E. Wallik, J. Am. Chem. Soc. 110 (1988) 2026.

[28] B.V. Nonius, CAD4-Express software. Version 5.1/5.2, Enraf Nonius, Delft, The Netherlands, 1994.

[29] M. Kretschmar, GENHKL Program for the Reduction of CAD4 Diffractometer Data, University of Tuebingen, Germany, 1997.

[30] A.C.T. North, D.C. Phillips, F.S. Mathews, Acta Crystallogr., Sect. A 24 (1968) 351.

[31] G.M. Sheldrick, Acta Crystallogr., Sect. A 46 (1990) 467.

[32] G.M. Sheldrick, SHELXL97. Program for the solution and refinement of crystal structures, University of Göttingen, Germany, 1997, http://shelx.uni-ac.gwdg.de/.

[33] International Tables for X-ray Crystallography, vol. C, Kluwer Academic, Dordrecht, The Netherlands, 1995.

[34] A.L. Spek, PLATON: A Multipurpose Crystallographic Tool, Utrecht University, The Netherlands, 1998.

[35] (a) SMART (control) and SAINT (integration) software, Bruker Analytical X-ray Systems, Madison, WI, USA, 1994;
(b) G.M. Sheldrick, SADABS: Program for Absorption Corrections, University of Göttingen, Göttingen, Germany, 1996.

[36] G.M. Sheldrick, SHELXS97. A Program for the Solution of Crystal Structures from X-Ray Data, University of Göttingen, Germany, 1997.

[37] G.M. Sheldrick, SHELXL-97. Program for crystal structure refinement, University of Göttingen, Germany, 1997; http://shelx.uni-ac.gwdg.de/shelx/index.html.

[38] SHELXTL: Integrated system for the determination of crystal structures, Bruker AXS Inc., Madison, WI, USA, 2000.

[39] (a) F.E. Mabbs, D.J. Machin, Magnetism and Transition-Metal Complexes, Chapman & Hall, London, 1973;
(b) W.E. Hatfield, in: R.B. King (Ed.), Encyclopedia of Inorganic Chemistry, vol. 4, Wiley, New York, 1994, pp. 2066–2075: Magnetism of Transition Metal Ions, and references therein.

[40] O. Khan, Molecular Magnetism, VCH Publishers, New York, USA, 1993.

[41] L.M. Shkol'nikova, M.A. Porai-koshits, N.M. Dyatlova, Zh. Strukt. Khim. 27 (1986) 138.

[42] L.M. Shkol'nikova, A.E. Obodovskaya, Zh. Strukt. Khim. 27 (1986) 125.

[43] A.E. Obodovskaya, L.M. Shkol'nikova, A.L. Poznyak, Kristallografiya 37 (1992) 382.

[44] (a) L.P. Battaglia, M.B. Ferrari, A.B. Corradi, G.G. Fava, C. Pelizzi, M.E.V. Tani, J. Chem. Soc., Dalton Trans. (1976) 2197.;
(b) G. Bernardinelli, G. Hopfgartner, A.F. Williams, Acta Crystallogr., Sect. C 46 (1990) 1642;
(c) S.-M. Peng, H.-F. Chen, Bull. Inst. Chem. Acad. Sin. 37 (1990) 49;
(d) T.A. Kabanos, A.D. Keramidas, D. Mentzafos, U. Russo, A. Terzis, J.M. Tsangaris, J. Chem. Soc., Dalton Trans. (1992) 2729;
(e) B.C. Dave, R.S. Czernuszewicz, Inorg. Chim. Acta 227 (1994) 33;
(f) M. Maekawa, M. Munakata, T. Kuroda-Sowa, K. Hachiya, Inorg. Chim. Acta 227 (1994) 137;
(g) V. Tangoulis, D.A. Malamatari, K. Soulti, V. Stergiou, C.P. Raptopoulou, A. Terzis, A. Kabanos, D.P. Kessissoglou, Inorg. Chem. 35 (1996) 4974;
(h) M. Munakata, S.-G. Yan, M. Maekawa, M. Akiyama, S. Kitagawa, J. Chem. Soc., Dalton Trans. (1997) 4257;
(i) J.S. Casas, A. Castiñeiras, Y. Parajó, M.L. Pérez-Parallé, A. Sánchez, A. Sánchez-González, S. Sordo, Reunión de Bioinorgánica 2001, Universidad de Granada, Granada, Spain, 2001, report P-10.

[45] B.J. Hathaway, in: G. Wilkinson, R.D. Gillard, J.A. McCleverthy (Eds.), Comprehensive Coordination Chemistry, vol. 5 (Ch. 53), Pergamon, Oxford, 1987.

to better explain thermodynamic data in terms of microscopic interactions and to understand the role of intra- and/or intermolecular hydrogen bonding on the structure, we have synthesized and studied the aqueous solutions of some potassium salts of 3-((alkylcarbonyl)amino)-4-hydroxybenzoic acid ($KAHB_n$) and 4-((alkylcarbonyl)amino)- benzoic acid ($KPAB_n$) [4]. The present work is devoted to the study of potassium salts of *p*-*n*-hexylbenzoic acid (HBA), *p*-*n*-heptylbenzoic acid (HEBA), *p*-*n*-octylbenzoic acid (OBA) and it is aimed to understand the role played by the amido group bridging the benzoic moiety and the alkyl chain.

2. Experimental

2.1. Materials

p-*n*-Hexylbenzoic acid (HBA), *p*-*n*-heptylbenzoic acid (HEBA), *p*-*n*-octylbenzoic acid (OBA), were prepared at Department of Chemistry of Kyushu University, as already described [2]. The purity of the reagents was checked by elemental analysis and gas chromatography. Inorganic chemicals of analytical reagent grade were used without further purification. Freshly boiled doubly distilled water, stored under nitrogen, was used throughout. Potassium hydroxide solutions (ca. 2 and 0.2 mol l^{-1}) were prepared by diluting the content of Merck Titrisol ampoules with the proper quantity of water and standardized with potassium hydrogen phthalate (C. Erba; dried at 120 °C).

The surfactant solutions were prepared under nitrogen adding to the acid the quantity of KOH needed both to neutralize the carboxylate group and to reach the required excess of hydroxide ion in the final solution (KOH 0.1 m excess). Solution concentrations are expressed as molality, m (mol kg^{-1}).

2.2. Measurements

The enthalpies of dilution were measured by means of the Thermometric TAM (flow mixing cell) microcalorimeter, equipped with 221 Nano Amplifier, at 298 K. The freshly prepared surfactant solutions, kept before injection at the experimental temperature by means of a Heto cryothermostatic bath, were diluted into the 'mixing' measuring cell of the microcalorimeter in ratio 1:1 by using CO_2-free water. The injection of the solutions and of water into the calorimeter was done by means of a Gilson peristaltic pump, Minipuls 2, and their flows were determined by weight.

Densities of the solutions were measured by a vibrating tube densimeter (PAAR DMA602) controlled by an IBM personal computer, calibrated with water and air. The temperature was kept constant at ± 0.002 °C by a Heto proportional temperature controller.

3. Results

The experimental data have been expressed in terms of apparent and partial molar quantities of the solute, as is usual in solution thermodynamics, assuming the infinite dilution as reference state.

With reference to this state, we recall [1,5–10] that, the molar enthalpy of dilution, ΔH_d, is given by:

$$\Delta H_d = \Phi_{L,f} - \Phi_{L,i} \quad (1)$$

where Φ_L is the apparent molar relative enthalpy and the indexes f and i stand for the final and initial concentrations, respectively.

For ionic surfactant in the premicellar region:

$$\Phi_L = A_L m^{1/2} + B_L m + C_L m^{3/2} \quad (2)$$

where A_L is the limiting Debye–Huckel slope for relative enthalpies, accounting for the long range electrostatic solute–solute interactions. Parameters B_L and C_L are averaged on the experimental points in the premicellar region.

In the micellar region, the apparent molar enthalpies are evaluated by means of equation 1 and by graphical interpolation.

The partial molar enthalpies L_2 are determined by drawing the best curve for the apparent molar enthalpies versus m and then by calculating the partial molar quantities as $\Delta(m\Phi_L)/\Delta m$ from points interpolated at regular intervals.

The heats of dilution and apparent and partial molar enthalpies at 298 K, obtained by means of Eq. (1)–(2), for the compounds under study are listed in Tables 1–3. In Figs. 1 and 2, the plots of the apparent and partial molar enthalpies, respectively, as a function of molality for the different chain length are shown.

The apparent molar volumes, V_Φ of surfactants were calculated by means of the following equation:

$$V_\Phi = \frac{M}{d} - \frac{10^3(d - d_o)}{m d d_o} \quad (3)$$

where d is the density of the solution of molality m, M is the molecular weight of the surfactants and d_o is the density of the KOH 0.1 m solution.

4. Discussion

In the literature, dissolution and micellization of HBA and OBA in aqueous solution were examined by the phase rule in relation to the solution pH [2]. The experimental data were interpreted under the light of

Table 1
Enthalpies of dilution, apparent and partial molar enthalpies of KHB, in water at 298 K

m_i (mol Kg^{-1})	m_f (mol Kg^{-1})	ΔH_d (J mol^{-}1)	$\Phi_{L,i}$ (J mol^{-1})	$\Phi_{L,f}$ (J mol^{-1})	$L_{2,i}$ (J mol^{-1})	$L_{2,f}$ (J mol^{-1})
0.0050	0.0024	−54	170	108	184	172
0.0080	0.0039	−96	237	144	414	236
0.0100	0.0042	−131	282	151	504	249
0.0150	0.0071	−195	394	216	794	373
0.0201	0.0098	−235	512	276	996	492
0.0240	0.0117	−269	611	318	1214	578
0.0301	0.0146	−393	766	385	1565	719
0.0401	0.0190	−487	982	488	1560	942
0.0502	0.0244	−457	1100	620	1455	1236
0.0602	0.0251	−427	1150	636	1375	1271
0.0702	0.0333	−309	1180	855	1310	1570
0.0803	0.0391	−204	1180	970	1250	1565
0.1005	0.0488	−121	1190	1090	1175	1470
0.1511	0.0724	−5	1180	1180	1010	1300
0.2021	0.1050	60	1130	1190	880	1152
0.2525	0.1193	123	1080	1192	775	1100
0.3034	0.1439	164	1015	1189	690	1025
0.3548	0.1676	214	950	1162	605	960
0.4060	0.1922	232	900	1150	500	905
0.5093	0.2387	280	810	1088	300	800
0.6132	0.2823	347	695	1040	178	730

the mass action model to obtain the micellization constant K_n, the micelle aggregation number n, and the number of counterion bound per micelle, m. In presence of undissolved acid as a separate phase, the pH plays a role similar to that of temperature, because the concentration of the dissociated anion showing surface active properties increases linearly with $1/a_{H^+}$ till to a range of values (micellar pH range) at which micellization starts. This pH range, as the cmc, is typical of the insoluble acid under study. This paper deals with the potassium salts of the above mentioned acids and of HEBA, in KOH 0.1 m excess, i.e. when the concentration of the undissociated acid is negligible and hydrolysis is avoided. In the same conditions we studied, as mentioned before, the enthalpic properties of the potassium salts of PAS_n, PAB_n, and AIB_n solutions [1,4]. The comparison of the behavior of the above mentioned compounds in the same conditions could give

Table 2
Enthalpies of dilution, apparent and partial molar enthalpies of KHEB, in water at 298 K

m_i (mol kg^{-1})	m_f (mol kg^{-1})	ΔH_d (J mol^{-1})	$\Phi_{L,i}$ (J mol^{-1})	$\Phi_{L,f}$ (J mol^{-1})	$L_{2,i}$ (J mol^{-1})	$L_{2,f}$ (J mol^{-1})
0.0020	0.0010	−14	64	47	95	66
0.0040	0.0020	−36	96	63	162	94
0.0060	0.0029	−52	132	78	247	124
0.0081	0.0040	−132	227	95	350	160
0.0100	0.0048	−126	235	110	300	195
0.0131	0.0064	−27	166	138	−160	265
0.0150	0.0074	111	60	159	−240	316
0.0181	0.0088	159	10	230	−280	360
0.0201	0.0097	219	−16	235	−310	345
0.0301	0.0147	224	−144	80	−410	−230
0.0502	0.0249	191	−278	−88	−550	−360
0.0804	0.0394	189	−399	−210	−668	−475
0.1008	0.0487	188	−453	−265	−715	−538
0.1511	0.0732	188	−558	−370	−858	−650
0.2016	0.0985	195	−645	−450	−975	−712
0.3037	0.1449	227	−777	−550	−1150	−842
0.4064	0.1925	276	−906	−630	−1312	−958
0.4579	0.2156	294	−954	−660	−1390	−998
0.5382	0.2569	324	−1040	−715	−1500	−1070
0.6130	0.2813	372	−1122	−750	−1590	−1113
0.7159	0.3387	408	−1228	−820	−1640	−1215

Table 3
Enthalpies of dilution, apparent and partial molar enthalpies of KOB, in water at 298 K

m_i (mol Kg^{-1})	m_f (mol Kg^{-1})	ΔH_d (J mol^{-1})	$\Phi_{L,i}$ (J mol^{-1})	$\Phi_{L,f}$ (J mol^{-1})	$L_{2,i}$ (J mol^{-1})	$L_{2,f}$ (J mol^{-1})
0.0030	0.0015	189	429	618	−503	746
0.0040	0.0020	605	18	622	−1400	485
0.0050	0.0024	911	−340	571	−1600	149
0.0060	0.0030	887	−460	433	−1660	−486
0.0080	0.0040	779	−760	18	−1710	−1400
0.0101	0.0050	681	−1000	−340	−1750	−1600
0.0200	0.0098	415	−1415	−990	−1860	−1750
0.0401	0.0196	266	−1678	−1390	−1985	−1855
0.0601	0.0302	212	−1785	−1570	−2070	−1935
0.0804	0.0398	191	−1868	−1678	−2140	−1982
0.1359	0.0657	180	−2010	−1810	−2270	−2090
0.1816	0.0870	191	−2090	−1890	−2370	−2160
0.2020	0.0989	194	−2120	−1920	−2430	−2192
0.2543	0.1249	174	−2190	−1975	−2545	−2248
0.3578	0.1720	257	−2320	−2060	−2750	−2340
0.5088	0.2306	355	−2522	−2160	−2950	−2495
0.6134	0.2789	375	−2591	−2220	−3000	−2595

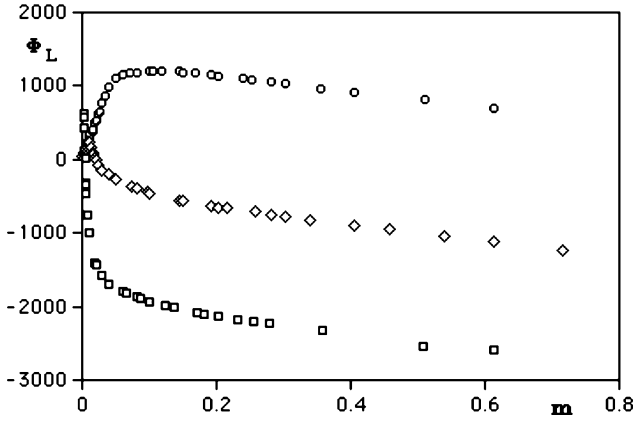


Fig. 1. Apparent molar relative enthalpies (Φ_L, J mol^{-1}) of potassium salts of *p*-*n*-hexylbenzoic acid (KHB, empty circles), *p*-*n*-heptylbenzoic acid (KHEB, empty rhombs), *p*-*n*-octylbenzoic acid (KOB, empty squares) in KOH 0.1 m as a function of surfactant molality, *m*.

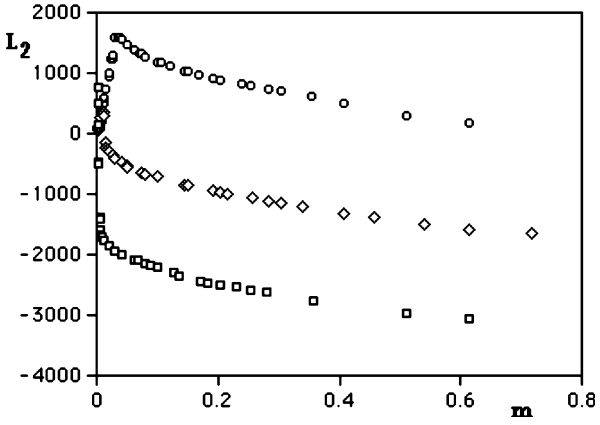


Fig. 2. Partial molar relative enthalpies (L_2, J mol^{-1}) of potassium salts of *p*-*n*-hexylbenzoic acid (KHB, empty squares), *p*-*n*-heptylbenzoic acid (KHEB, empty rhombs), *p*-*n*-octylbenzoic acid (KOB, empty circles) in KOH 0.1 m as a function of surfactant molality, *m*.

us information about the role played by the different fragments of the molecule in the micellization process. In Fig. 1 and in Tables 1–3, the curves of the apparent molar enthalpies versus *m* at 298 K are reported for different chain lengths. The general trends concord with the expectations for ionic surfactants: the curves, after increasing in the premicellar region, tend to level off at concentrations above the cmc, where they are almost parallel. The lowering of the curves in the micellar region is proportional to the number of carbon atoms in the alkyl chain. It is possible to extract the group contribution of the $-CH_2-$ group in the postmicellar region: it results -1.6 kJ mol^{-1} per $-CH_2-$. This value is comparable with that obtained in the case of cationic surfactants [6]. This group contribution proves to apply specifically to the methylene group and to be independent of the charge in the polar head, too.

It is very interesting to evaluate the effect of the amido group, bound in para position in respect to the carboxylic moiety, by the comparison of the trends of the compounds under study with those of potassium 4-((alkylcarbonyl)amino)- benzoate ($KPAB_n$) [4]. In Fig. 3, as an example, the comparison between the apparent molar enthalpies versus *m* of the terms having seven carbon atoms in the alkyl chain is reported. The effect of the substitution of a methylene group by an amido group results in a strong increase in hydrophilicity for the $KPAB_n$: the effect is comparable with that brought about by a removal of a methylene group in the alkyl chain. The group contribution results $+1.7$ kJ mol^{-1}. The electron withdrawing amido group behaves as a part of the polar head. Some of us have shown for a series of dodecyl cationic surfactants with the same counterion that, from the trends of the apparent and

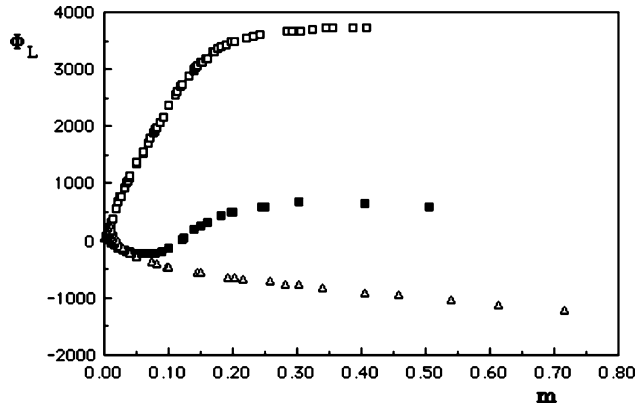


Fig. 3. Comparison between apparent molar enthapies (Φ_L, J mol^{-1}) as a function of molality, m of potassium salts of *p*-*n*-heptylbenzoic acid (KHEB, empty triangles), 4-((hexylcarbonyl)amino-benzoic acid ($KPAB_7$, full squares) [4] and 4-((hexylcarbonyl)amino-2-hydroxybenzoic acid ($KPAS\text{-}C_7$, empty squares) in KOH 0.1 m [1].

partial molar enthalpies, a sort of 'charge delocalization scale' for the polar head could be obtained. The more delocalized is the charge, the more similar is the behavior to that of non-ionic surfactants [10]. The same observation seems to hold also for the anionic surfactants, as shown in Fig. 3.

In the case of cationic surfactants, we have studied the effect of an amido group in meta position by comparing *N*-alkylpyridinium (C_nPC) and *N*-alkylnicotinamide chlorides (C_nNAC). It has been shown that when the amido group is bound in three position to the pyridinic ring, it acts in the opposite way, strongly enhancing the hydrophobicity of the C_nNAC surfactants [10].

4.1. Changes in thermodynamic properties upon micelle formation

In order to obtain the changes in thermodynamic properties upon micellization, we have applied a pseudo-phase transition model, in which the aggregation process is considered like a phase transition, taking place at equilibrium. In this model, it is assumed that, at the cmc, the partial molar properties present a discontinuity due to the formation of a pseudo-phase. The micellization parameters are obtained by extrapolating at the cmc the trends of partial molar properties before and after cmc [1,5–10]. Rather sharp changes occur around the cmc, but they are never discontinuous, especially for surfactants with short hydrophobic chains. In order to evaluate the micellization enthalpy change, ΔH_m of the compounds under investigation, we have to know the values of the cmc. Previous studies on solubility and micelle formation of *p*-*n*-alkylbenzoic acids have shown that the cmc values at the critical micelle pH were 4.80×10^{-2} at 298 K for NaHBA and 1.30×10^{-2} for NaOBA at 308 K [2]. The experimental conditions of this work are very different both as pH value at which only the basic dissociated form is present and as counterion (K^+ instead of Na^+). So it is reasonable to expect that also the cmc values are different. We have evaluated the cmc by a thermodynamic method, assuming as cmc the abscissa of the first inflection point of the curves of Φ_L versus m. The values so obtained for the cmc and the micellization enthalpies of the compounds under investigation are reported in Table 4.

The logarithms of the cmc are nicely linearly correlated (see Fig. 4) with the number of carbon atoms, the slope of the straight line so obtained being proportional to the free energy of transfer of each $-CH_2-$ from the aqueous phase to the micellized state. It results $-1.27kT$ per$-CH_2-$. This value appears to be a slightly greater quantity (in terms of absolute value) than that reported in ref [11]. The difference could be explained in terms of higher ionic strength, reducing the electrostatic repulsion between the polar head groups. The reported micellization enthalpies for the studied compounds are linearly correlated with the number of carbon atoms in the alkyl chain. It is, therefore, possible to extract a group contribution for the methylene group: thus we have -1.5 kJ mol^{-1} per group, which is comparable with that obtained in the case of potassium 3-((alkyl-

Table 4
Critical micelle concentration (cmc), enthalpy changes for the micellization process (ΔH_m) and partial molar volume in micellar phase (V_s) for the surfactants studied

	KOB	KHEB	KHB
Cmc (mol kg^{-1})	0.0016	0.0069	0.020
L_{2m} (kJ mol^{-1})	+0.714	+0.390	+0.980
L_{2s} (kJ mol^{-1})	−1.429	−0.181	+1.847
ΔH_m (kJ mol−1)	−2.143	−0.571	+0.857
V_s (cm^3 mol^{-1})	201	184	167

Indices m and s stand for the value of the quantity for the monomer and for the micelle, respectively.

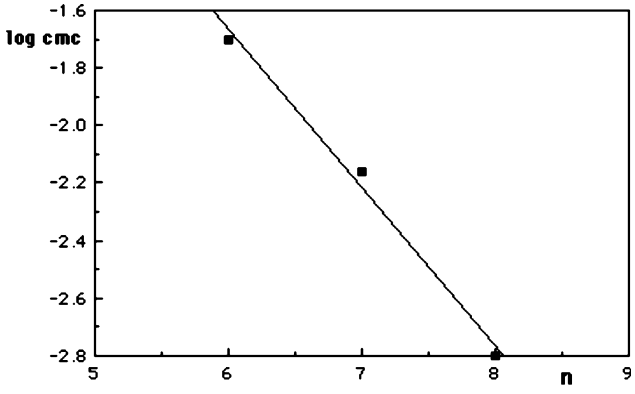


Fig. 4. Log cmc, obtained as the abscissa of the first inflection point of the curves of Φ_L vs. m, as a function of the number of carbon atoms, n in the alkyl chain for the compounds under investigation in the experimental conditions.

carbonyl)amino)-4-hydroxybenzoates (–1.4 kJ mol^{-1} per group) and 4-((alkylcarbonyl)amino)-benzoates (–1.33 kJ mol^{-1} per group) [4], but greater than the average group contribution obtained in the case of cationic surfactants (−1.1 kJ mol^{-1} per group) [6].

In Table 4 partial molar volumes of the surfactants under study in micellar phase are also reported. It is easy to see that the values differs by 17 cm^3 mol^{-1} per $-CH_2-$. The $-CH_2-$ group contribution obtained in micellar region is the same as that obtained for pyridine and nicotinamide type cationic surfactants [6].

5. Conclusions

The study of thermodynamic properties of the aqueous solutions of potassium salts of KHB, KHEB, KOB in KOH 0.1 m has shown that also in the case of anionic surfactants derived from benzoic acid, the group contribution of the $-CH_2-$ is additive both in the plateau (−1.6 kJ mol^{-1} per $-CH_2-$) and in the micellization enthalpy changes (−1.5 kJ mol^{-1} per group). The values are comparable with those obtained in the case of cationic surfactants and for similar anionic compounds in the same experimental conditions. The behavior of the compounds under study was compared with that of the potassium salts of 4-((alkylcarbonyl)amino)-benzoic acids, in order to understand the role played by the amido group bridging the benzoic moiety and the alkyl chain. Thus, we see that the amido group behaves as a part of the polar head, strongly increasing the hydrophilicity of the molecule.

Acknowledgements

The authors are grateful to the Italian Ministry for the University and the Scientific and Technological Research (MURST), COFIN 2000–project 'Molecular Systems and Metallo-receptors for the Activation and Transport of Dioxygen, Nitric Oxide, and Biosubstrate' for financial support.

References

[1] E. Fisicaro, E. Pelizzetti, M. Barbieri, P. Savarino, G. Viscardi, Thermochim. Acta 162 (1990) 277.
[2] Y. Moroi, Y. Sakamoto, J. Phys. Chem. 92 (1988) 5189.
[3] E. Pelizzetti, E. Pramauro, E. Barni, P. Savarino, M. Corti, V. Degiorgio, Ber. Busenges. Phys. Chem. 86 (1982) 529.
[4] E. Fisicaro, C. Compari, G. Viscardi, P.L. Quagliotto, in preparation.
[5] E. Fisicaro, M. Barbieri, E. Pelizzetti, P. Savarino, J. Chem. Soc., Faraday Trans. 87 (1991) 2983.
[6] (a) E. Fisicaro, A. Ghiozzi, E. Pelizzetti, G. Viscardi, P.L. Quagliotto, J. Coll. Interf. Sci. 182 (1996) 549;
(b) E. Fisicaro, A. Ghiozzi, E. Pelizzetti, G. Viscardi, P.L. Quagliotto, J. Coll. Interf. Sci. 184 (1996) 147.
[7] J.E. Desnoyers, G. Perron, in: R. Zana (Ed.), Surfactant Solutions-New Methods of Investigation (and references therein), Marcel Dekker, New York, 1987, p. 1.
[8] E. Fisicaro, Cell. Mol. Biology Lett. 2 (1) (1997) 45.
[9] E. Fisicaro, C. Compari, B. Rozycka-Roszak, G. Viscardi, P.L. Quagliotto, Curr. Top. Coll. Interf. Sci. 2 (1997) 53.
[10] E. Fisicaro, E. Pelizzetti, M. Barbieri, P. Savarino, G. Viscardi, Thermochim. Acta 168 (1990) 143.
[11] K. Shinoda, T. Nakagawa, B. Tamamushi, T. Isemura, Colloidal Surfactants, Academic Press, New York, NY, 1963, pp. 37–42.

or base, etc.) and substrate (proton or metal or ligand) as the functions of affinity constants, k_j and cooperativity coefficients, b_j, respectively, specific for each class of sites.

The probability of state of a solution referred to one mole of reacting receptor is given by:

$$Z_A = \exp(-\Delta G/RT) \quad (1)$$

The joined probability of the state of a solution of a receptor A with t binding sites for ligand H in one class is represented by the product of t factors, each representing the probability of single binding:

$$Z_A = \exp(-\Delta G/RT) = (1 + k\gamma(i)[H])^t \quad (2)$$

where k is the site constant and $\gamma(i)$ is the cooperativity function:

$$\gamma(i) = \exp\{b(i-1)\} \quad (3)$$

When we refer to one class, we can drop the index j. The Newton binomial of the RHS of Eq. (2) produces a polynomial with $t+1$ terms:

$$Z_A = \sum_{i=0}^{t} m_i(k\gamma_i[H])^i \quad (4)$$

where $m_i = t!/\{(t-i)!i!\}$is the multiplicity factor (an entropic factor) that indicates the number of possible microspecies and γ_i is the cooperativity factor that is the value of the cooperativity function at the protonation step i. The microspecies are isomeric complexes AH_i with ligand H occupying equivalent binding sites [19,20].

When two classes, p and q are present with $t(p)$ and $t(q)$ binding sites for the same ligand, respectively, the joined probability of the state of the solution is a product of polynomials:

$$Z_A = (1 + k_p\gamma_p[H])^{t(p)}(1 + k_q\gamma_q[H])^{t(q)} \quad (5)$$

The self-association of receptor units A_1, A_2, $A_{i+1}\ldots A_t$ can be considered a complexation between the first A as the receptor with $(t-1)$ sites and the successive A as the ligands.

For one class of sites without self-association, the probability of the state is given by the polynomial of Eq. (4) that can be rewritten in the form of a summation of cumulative constant terms multiplied by powers of concentrations:

$$Z_A = \sum_{i=0}^{t} \beta_i[H]^i \quad (6)$$

By comparison with Eq. (4), we obtain the cumulative constant β_i as:

$$\beta_i = m_i(k\gamma_i)^i \quad (7)$$

The determination, therefore, of the site affinity constant k for a class is connected to the determination of the cumulative binding constants β_i. For example, the cumulative formation constant of the complex HA in a class with three sites is $\beta_1 = 3\gamma_1 k$, where three is the multiplicity factor, m_1 and $\gamma_1 = 1$ is the cooperativity factor. The formation constant of the complex AH_2 in the same class with three sites is $\beta_2 = 3\gamma_2 k^2$, where three is the multiplicity factor m_2 and $\gamma_2 = \exp b$ is the cooperativity factor. The formation constant of the complex AH_3 in the same class with three sites is $\beta_3 = \gamma_3 k^3$, where one is the multiplicity factor m_3 and $\gamma_3 = \exp 2b$ is the cooperativity factor.

There is one partition function for each component of the system. If the complexes are of type $H_P A_R$ there are two partition functions, namely Z_H and Z_A.

The relationships between partition functions and total analytical concentrations $[T_H]$ and $[T_A]$, respectively, are given by:

$$[T_A] = [A]\{Z_A\} + [A]\{\partial Z_A/\partial[A]\} \quad (8)$$

$$[T_H] = [H]\{Z_H\} + [H]\{\partial Z_H/\partial[H]\} \quad (9)$$

These equations show how one can calculate the analytical quantities T_H and T_A from the partition functions and hence from the cumulative constants. On the other hand, being the cumulative constant function of the site constant k and of cooperativity coefficient b through Eq. (6), then the analytical quantities T_H and T_A can be calculated as functions of these variables (k and b) too.

If the binding of a ligand to the receptor is not affected by the presence of other ligands already bound, the cooperativity factors are all equal to unity ($b = 0$), the cumulative constants are functions of the site affinity k and of the statistical factor m_i only. The latter is a calculated quantity (cf. Eq. (4)) and not a variable. When the cooperativity takes place, the affinity of the ligand for the receptor site can be enhanced (positive cooperativity) or depressed (negative cooperativity) by previous occupation of sites. The cooperativity effect can be accounted for by introducing a cooperativity function $\gamma_j(i)$ for each class j.

By taking the logarithms of Eq. (7), one can calculate [21] a mean affinity constant devoid of statistical factor:

$$\ln K_{\gamma(i)} = (1/i)(\ln \beta_i - \ln m_i) = \ln k - \ln \gamma_i = \ln k - (i-1)b \quad (10)$$

By plotting $\ln K_{\gamma(i)}$ against $(i-1)$, a straight line is obtained with slope b. The validity of the cooperativity function thus obtained can be checked by means of the Scatchard function:

$$\langle n\rangle/[A] = \{\sum_i im_i\{k_{\gamma_i}\}^i[H]^{i-1}\}/\{\sum_i m_i\{k_{\gamma i}[H]\}^i\} = \{\sum_i i\beta_i[H]^{i-1}\}/\{\sum_i \beta_i[H]^i\} \quad (11)$$

The Scatchard diagram with cooperativity is characterised by a concavity upward if the cooperativity is

negative ($\gamma < 1$), or downward if the cooperativity is positive ($\gamma > 1$). The diagram, is a straight line when there is no cooperativity effect ($\gamma = 1$). The Scatchard function can be corrected for cooperativity, obtaining the corrected Scatchard function $\langle n_{corr}\rangle/[A]$

$$\langle n_{corr}\rangle/[A] = \{\sum_i im_i\{k\}^i[H]^{i-1}\}/\{\sum_i m_i\{k[H]\}^i\} = \{\sum_i i\beta_{i,corr}[H]^{i-1}\}/\{\sum_i \beta_{i,corr}[H]^i\} \quad (12)$$

This function is calculated by introducing the constants $\beta_{i,corr}$:

$$\beta_{i,corr} = \beta_i/(\gamma_i)^i \quad (13)$$

corrected for cooperativity effect, by dividing each β_i by the corresponding i-th power of cooperativity factor. If the correction is valid, then the curved plot should be transformed into a straight line.

The existence of the cooperativity function makes the cumulative constants β_i dependent from one another through the affinity constant k_j and cooperativity coefficient b_j. The use, therefore, of the cumulative constants β_i as independent variables in a refinement process by least-squares procedures should be avoided because it is biased. A new algorithm has been proposed [22,23] whereby the independent variables to be refined are class site constants k_j and class cooperativity coefficients b_j. The algorithm has been obtained by introducing the appropriate types of expressions of Eqs. (5) and (3) for Z_H and Z_A into the Eqs. (8) and (9), respectively. It is thus possible to calculate explicitly the derivatives $\partial[T_H]/\partial k_j$, $\partial[T_H]/\partial(\exp b_j)$, $\partial[T_A]/\partial k_j$, $\partial[T_H]/\partial(\exp b_j)$ of the functions T_H and T_A, with respect to the variables to be refined. A set of normal equations for least-squares calculations can be set up where the unknown are the increments to the variables that minimise the difference between observed and calculated values of both T_H and T_A. The program SITECON calculates these increments and has been tested for several systems [23,24]. In this work, this program has been applied to the potentiometric data for the protonation of polyamines. The compounds to be studied have been chosen on the basis of the increasing number of classes and sites in each class.

3. Experimental

The experimental data have been obtained by potentiometric titrations of aqueous solutions of aliphatic polyamines at $T = 298$ K and ionic medium $I = 0.1$ KCl.

3.1. Materials

Ethylenediamine dihydrochloride (Aldrich 98%), 1,3-diaminepropane dihydrochloride (Aldrich 98%, melting point (m.p.) 246°–250°), 1,4-diaminebutane dihydrochloride (Aldrich 97%, m.p. 280°), 1,5-diaminopentane dihydrochloride (Aldrich 99%, m.p. 260°–262°), 1,4-diaminebutanone dihydrochloride (Aldrich 99% m.p. 221°), 1,3-diamine-2-hydroxypropane (Aldrich 95%), diethylenetriamine (Acros 98%, m.p. 90°), triethylenetetramine tetrachloride (Aldrich 97%, m.p. 269°–270°), *N*-(2-hydroxyethyl)ethylenediaminetriacetic acid (Acros 99%), Ethylenediaminetetracetic acid (Aldrich 98.5%). All the compounds have been recrystallized from water. Bidistilled water was used as solvent, deairated by N_2 stream.

3.2. Measurements

Sensor Electrode: Glass electrode (CRISON 52–50). Reference Electrode: Calomel electrode (RADIOMETER REF 401) with 0.1 KCl bridge, ionic medium: KCl 0.1 M. The titrations have been performed by an automatic potentiometric apparatus. The concentration of titrant KOH has been determined by titration of a weighed amount of potassium hydrogen phthalate. The standard potential of the electrometric chain E_0 and pK_w have been determined every day by titration with KOH solution of a fixed volume of hydrochloric acid of known concentration. The neutralisation point was determined by a computer program based on Gran's method [25]. The concentration of polyamine solutions to be titrated has been obtained by weight. The temperature has been maintained constant at 298 K by thermostatting the circulating water by a ISCO CRIOTERM 190 (precision ± 0.1). The volume of the liquid in the cell has been measured at 25 °C (usually 50 ml).

3.3. Calculations

The titration data (emf and volume), the total analytical concentrations $[T_A]$ and $[T_H]$ the guessed value of site constants k_j and cooperativity factors b_j are the input data of the program SITECON. The program refines the values of k_j and $\exp b_j$, by successive iterations. SITECON can be operated on a personal computer in DOS.

4. Results and discussion

The program SITECON was employed to calculate the affinity site constants and the cooperativity parameters in the set of titrations of polyamines (Table 1). In order to identify the classes of sites, the sets of cumulative protonation constants β_i were obtained by means of

Table 1
Site constants, k and cooperativity coefficients, b (cooperativity potential $\Delta\mu_\gamma$) refinement by SITECON (σ = S.D.) at 298 K

Amine	Number of class	Number of sites	log k	σ (log k)	$-b$	σ (b)	$\Delta\mu_\gamma$ (kJ mol^{-1})
EN	1	2	9.634	0.001	2.557	0.003	14.595
PD	1	2	10.205	0.003	1.329	0.008	7.586
BD	1	2	10.416	0.025	0.767	0.069	4.378
DAP	1	2	10.404	0.005	0.279	0.014	1.592
DAB	2	1	9.716	0.034			
		1	7.550	0.048			
DAHP	1	2	9.294	0.015	1.179	0.036	6.729
DIEN	2	2	9.391	0.050	0.000		
		1	4.407	0.123			
TRIEN	2	2	9.460	0.008	0.000		
		2	6.294	0.047	2.923	0.067	16.684
HEDTA	2	2	9.545	0.036	4.556	0.090	26.005
		3	1.866	0.193	0.280	0.918	1.598
EDTA	2	2	9.881	0.006	3.934	0.009	22.454
		4	2.119	0.012	0.321	0.051	1.832

EN, ethylenediamine; PD, 1,3-diaminepropane; BD, 1,4-diaminebutane; DAP, 1,5-diaminopentane; DAB, 1,4-diaminebutanone; DAHP, 1,3-diamine-2-hydroxypropane; DIEN, diethylenetriamine; TRIEN, triethylenetetramine tetrachloride; HEDTA, *N*-(2-hydroxyethyl)ethylenedinitrilo-*N*,*N*′,*N*′-triacetic acid; EDTA, ethylenedinitrilotetracetic acid.

SUPERQUAD algorithm [26]. By using the β_i so obtained, it has been possible to calculate and plot the Scatchard function $\langle n\rangle$/[H] as the function of $\langle n\rangle$. An example is given in Fig. 1 for the compound DIEN. The diagram shows that there are two classes of sites, without cooperativity as shown by the two straight lines. The Scatchard plot of the compound TRIEN shows how this compound presents two classes of sites with two sites each. In the first class, the most basic sites, there is no cooperativity, whereas in the second class there is high cooperativity. After having refined the site constants, the values of the cumulative equilibrium constants were calculated with the values of the constants, k_j and of the cooperativity coefficients, b_j. These cumulative constants were compared with the values of the cumulative constants obtained by direct refinement by the program SUPERQUAD (Table 2).

The values of the site constants, k_j and of the cooperativity coefficients, b_j obtained in the refinement are reported in Table 3 and compared with the values of the site constants and cooperativity coefficients obtained graphically by applying Eq. (10). The values of b_j were then used to calculate the corrected cumulative constants $\beta_{i,\mathrm{corr}}$, according to Eq. (13) and then the corrected Scatchard plot (Table 4). The curve is transformed into a straight line. An example is given for the compound EN in Fig. 2.

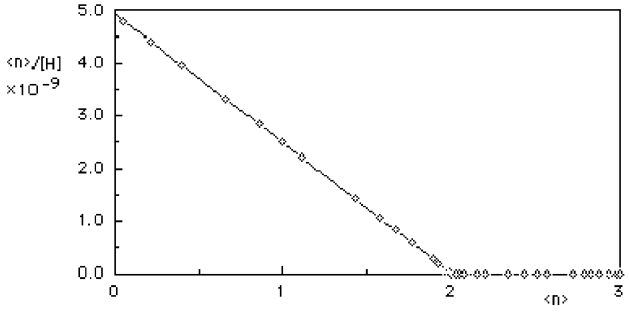


Fig. 1. Scatchard plot for DIEN: two classes and no cooperativity.

The values of b are on the same scale of the natural logarithm of equilibrium constant. Therefore b can be transformed into cooperativity potential, $\Delta\mu_\gamma$ in kJ mol^{-1} scale according to

$$\Delta\mu_\gamma = -bRT \tag{14}$$

We can examine the changes of $\Delta\mu_\gamma$ at $T = 298$ K for the protonation of the amine group $-NH_2$ in the amines of Table 1. By considering the series, $_2HN-(CH_2)_n-NH_2$ with $n = 2$, 3, 4, 5, we observe that these compounds show a mild exponential decrease of the cooperativity effect with the increase of the molecular length (Fig. 3). ($\ln(\Delta\mu_\gamma) = -0.7194n_C + 4.1799$, with $r^2 = 0.9819$). This conforms to the idea that the reciprocal influence of the two sites is smaller the greater is the distance between them. On the contrary, the site affinity constant is scarsely affected by the chain length.

The cooperativity effect can be compared in other analogous or partially analogous molecules. The difference between the site constants in DAB (1,4-diaminebutanone) can be compared with cooperativity in EN (ethylenediamine): the two compounds show a remarkable difference of cooperativity but this could be due to intrinsically different site affinities of the two nitrogens in DAB which are not structurally equivalent. The comparison of PD (1,3-diaminepropane) and DAHP (1,3-diaminehydroxypropane) shows a similar behaviour for the two compounds. On the other hand, we can consider the polyamines DIEN (diethylenetriamine) and TRIEN (triethylenetetramine); the external $-NH_2$ groups do not show any cooperativity. The two

Table 2
Cumulative protonation constants by different refinement programmes

	SITECON [23]				SUPERQUAD [26]			
Amine	log β_1	log β_2	log β_3	log β_4	Log β_1	log β_2	log β_3	log β_4
EN	9.936	17.047			9.937	17.059		
PD	10.506	19.255			10.876	19.877		
BD	10.717	20.165			10.743	20.227		
DAP	10.705	20.566			10.757	20.546		
DAB	9.719	17.266			10.302	17.922		
DAHP	9.595	17.564			9.580	17.560		
DIEN	9.692	18.829	23.236		9.692	18.793	23.201	
TRIEN	9.762	18.922	25.515	28.969	9.822	18.913	25.490	28.855
HEDTA [a]	9.846	15.132	17.474		9.901	15.192	17.519	
EDTA [b]	10.182	16.344	19.065	21.081	10.176	16.327	19.033	21.114

$I = 0.1$ KCl, $T = 298$ K.
[a] (SITECON) log $\beta_4 = 19.096$, log $\beta_5 = 19.998$..
[b] (SITECON) log $\beta_4 = 22.465$, log $\beta_5 = 23.145$.

Table 3
Site constant and cooperativity coefficient refinement by SITECON and by graphical interpolation by Eq. (10)

Amine	Number of class	Number of sites	$-b$ SITECON	$-b_{graph}$ Eq. (10)	log k SITECON	log k_{graph} Eq. (10)
EN	1	2	2.558	2.464	9.634	9.636
PD	1	2	1.329	1.467	10.205	10.575
BD	1	2	0.767	0.758	10.416	10.442
DAP	1	2	0.279	0.419	10.404	10.456
DAB	2	1			9.716	
		1			7.550	
DAHP	1	2	1.179	1.149	9.294	9.279
DIEN	2	2	0.000	−0.005	9.391	9.391
		1			4.407	
TRIEN	2	2	0.000	0.006	9.460	9.521
		2	2.923	3.005	6.294	6.276
HEDTA	1	2	4.556	4.614	9.545	9.600
EDTA	1	2	3.934	3.940	9.881	9.875

Table 4
Cumulative protonation constants corrected for cooperativity effect (Eq. (13))

Amine	Number of class	Number of sites	β_2 SUPERQUAD	$-b$ SITECON	$\beta_{2,corr}$ (corrected by γ_i^2)
EN	1	2	1.145×10^{17}	2.558	1.909×10^{19}
PD	1	2	7.534×10^{19}	1.329	1.075×10^{21}
BD	1	2	1.687×10^{20}	0.767	7.818×10^{20}
DAP	1	2	3.516×10^{20}	0.279	6.516×10^{20}
DAB	1	1			
	1	1	8.356×10^{17}		
DAHP	1	2	3.631×10^{17}	1.179	3.830×10^{18}
DIEN	1	2	6.745×10^{18}	−0.000	6.745×10^{18}
	1	1			
TRIEN	1	2	8.750×10^{9}	2.923	3.008×10^{12}
	1	2	1.114×10^{10}	0.000	1.114×10^{10}
HEDTA	1	2	1.556×10^{15}	4.556	1.411×10^{19}
	1	3 [a]			
EDTA	1	2	2.123×10^{16}	3.394	5.546×10^{19}
	1	4 [a]			

[a] Carboxylic groups.

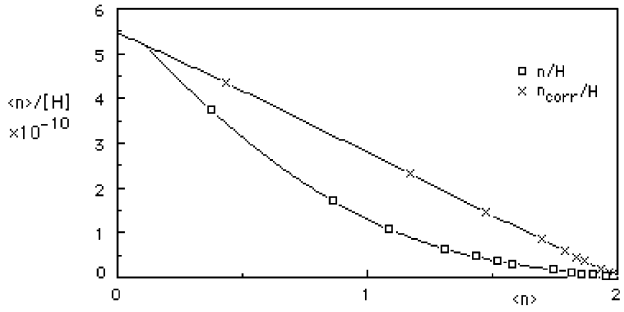


Fig. 2. Scatchard plots for EN: the corrections for cooperativity effect transform the curve into a straight line.

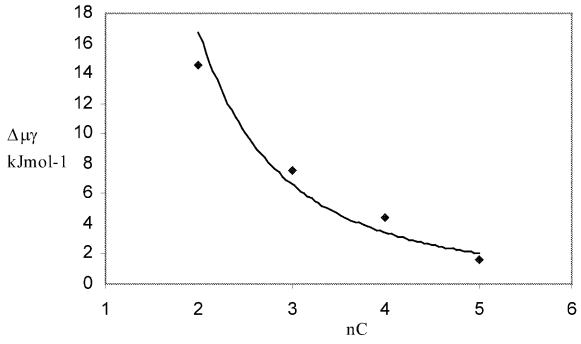


Fig. 3. Cooperativity potential, $\Delta\mu_\gamma$ ($T = 298$ K) in diamines as the function of the chain length.

compounds are structurally similar in the sense that, in both, aliphatic chains containing alternating $-CH_2-CH_2-$ and weakly basic $-NH-$ groups, separate the external $-NH_2$ sites. The two compounds do not show any cooperativity between the external $-NH_2$ groups. It seems that a screen interrupts the electrostatic interaction between the sites. The interaction between the adjacent $-NH-$ groups in TRIEN is highly negatively cooperative. Finally the comparison of HEDTA (*N*(hydroxyethyl)ethylenediaminetriacetic acid) and EDTA (ethylenediaminetetracetic acid) provides evidence for a substantially homogeneous behaviour of the cooperativity between the basic sites, although much higher than that of ethylenediamine. This cooperativity enhancement is due to the influence of the carboxylic substituents.

The values of the site affinity constants are specific for nitrogen sites and can be compared with those of corresponding monoamines [27] as shown in Table 5. The comparison between amine of correspondent chain length shows how the substitution of $-NH_2$ for $-CH_3$ produces a weakening effect, which is lower, the longer the distance from the basic site ($\Delta\log k$ $-RNH_2$). The weakening effect of the charged groups $R-NH_3^+$ can be calculated directly from the cooperativity coefficients divided by 2.303 ($\Delta\log k$ $-RNH_3^+$). The division brings the cooperativity coefficients to the scale of σ_x Hammett constants [28].

The weakening effect of one protonated site over the neighbouring sites can be evaluated by means of the cooperativity coefficient b or from the site constants of the different classes. For instance, in EN with primary amine group, the site constant is $\log k = 9.634$ and the cooperativity coefficient $b = -2.557$. The affinity constant after cooperativity becomes $\log k = 8.702$. It is then possible to evaluate the Taft [29] constant of the protonated or unprotonated substituent by assuming an equation set up by Barlin and Perrin [30]

$$\log k = 11.59 - 1.89 \sum \sigma_R^* \tag{15}$$

The values thus obtained are reported in Table 6, together with substituent constants for secondary and tertiary amines. For secondary and tertiary amines, the Eq. (15) becomes:

$$\log k = 11.59 - 1.89 \sum \sigma_R^* \tag{16}$$

where the additivity rules have been assumed to hold. The calculation of the protonation constant at secondary nitrogen in the symmetric compound DIEN gives a Taft constant $\Sigma\,\sigma^* = 2\sigma_R^*$ from which a value σ_R^* for the single substitutent $(R'H^+) = (H_3N^+-(CH_2-)_2)$ can be obtained. Then this value can be used to calculate, by subtraction from $\Sigma\,\sigma^*$, the contribution of the longer moiety in the asymmetric compound TRIEN.

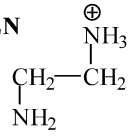
Where tertiary amine groups appear as in EDTA, an average $\sigma^*_{\langle R\rangle} = (1/3)\Sigma\,\sigma_R^*$ can be obtained.

5. Conclusions

The computer program SITECON was applied to the protonation equilibria of polyamines; it is based on a function of affinity constant, k_i and cooperativity coefficient, b_i specific for each class of sites. Thus, the evaluation of the cooperativity potential $\Delta\mu_\gamma = -RTb_i$ can be made. The cooperativity potential between two basic sites depends on the length of the molecule i.e. on the distance between sites and can be attributed to electrostatic interactions. Binding of a proton to one site yields a weaker electrostatic attraction by the second site for the next proton. Introduction of basic $-NH_2-$ groups in the chains between the sites exerts a screening effect removing the cooperative effect. The addition to the basic sites of EDTA and HEDTA of carboxylic groups enhances the cooperativity effect. The cooperativity coefficient divided by 2.303 brings the cooperativity effect to the scale of the base weakening effects as expressed by the Hammett equation and Taft equation. It is then possible to calculate Taft substituent constants σ^* for substitution in primary, secondary and tertiary amines.

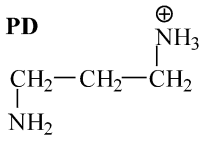
Table 5
Specific site constants and base weakening effects in polyamines

EN



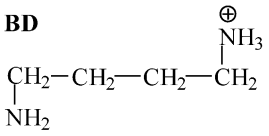
$\log k = 9.634$
propylamine [27] $\log k = 10.566$
$\Delta\log k(\text{R-NH}_2) = -0.932$
$\Delta\log k\ (\text{R-NH}_3^+) = -1.110$

PD



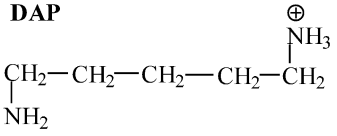
$\log k = 10.205$
butylamine [27] $\log k = 10.75$
$\Delta\log k(\text{R-NH}_2) = -0.545$
$\Delta\log k\ (\text{R-NH}_3^+) = -0.577$

BD



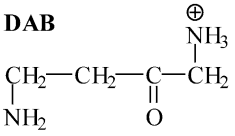
$\log k = 10.416$
pentylamine [27] $\log k = 10.60$
$\Delta\log k(\text{R-NH}_2) = -0.184$
$\Delta\log k\ (\text{R-NH}_3^+) = -0.333$

DAP



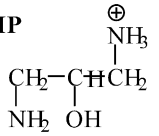
$\log k = 10.404$
hexylamine[27] $\log k = 10.63$
$\Delta\log k(\text{R-NH}_2) = -0.226$
$\Delta\log k\ (\text{R-NH}_3^+) = -0.121$

DAB



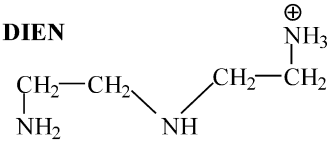
$\log k = 9.716$
$\log k = 7.550$
$\Delta\log k\ (\text{R-NH}_2) = -2.166$

DAHP



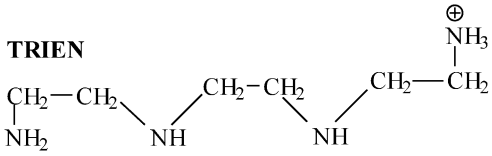
$\log k = 9.294$
1,3-diamino-2-propanolo[27] $\log k = 9.58$
$\Delta\log k(\text{R-NH}_2) = -0.286$
$\Delta\log k\ (\text{R-NH}_3^+) = -0.512$

DIEN



$\log k = 9.391$
$\log k = 4.407$
$\Delta\log k\ (2\text{R-NH}_3^+) = -4.984$

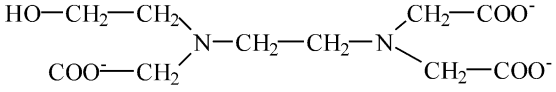
TRIEN



$\log k = 9.460$
triethylamine [27] $\log k = 10.75$
$\Delta\log k\ (\text{R-NH}_2) = -1.290$

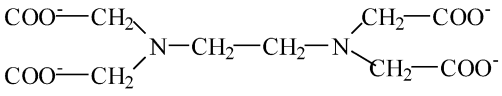
$\Delta\log k\ (\text{R-NH}_2^+\text{-R}') = -1.2692$
$\Delta\log k\ (2\text{R-NH}_3^+) = -1.366$

HEDTA



$\log k = 9.545$
$\Delta\log k\ (\text{R-NH}_3^+) = -1.290$

EDTA



$\log k = 9.881$
$\Delta\log k\ (\text{R-NH}_3^+) = -1.708$

Table 6
Taft constants σ^*_R for substituent R at primary, secondary or tertiary amines

Name	Formula	log k	Substituent R	Amine group R–NH_2 or R′–NH–R″ or R′–N(R‴) R″	σ^*_R
EN	$H_2N-(CH_2-)_2-NH_2$	9.634	$H_2N-(CH_2-)_2$	R–NH_2	1.03
Id.	$H_3N^+-(CH_2-)_2-NH_2$	8.702	$H_3N^+-(CH_2-)_2$	$(H^+R)-NH_2$	1.53
EthAm	$CH_3-CH_2-NH_2$	10.636	CH_3-CH_2-	R–NH_2	0.504
PD	$H_2N-(CH_2-)_3-NH_2$	10.205	$H_2N-(CH_2-)_3$	R–NH_2	0.73
	$H_3N^+-(CH_2-)_3-NH_2$	9.628	$H_3N^+-(CH_2-)_3$	$(H^+R)-NH_2$	1.04
PropAm	$CH_3-(CH_2-)_2NH_2$	10.566	$CH_3-(CH_2-)_2$	R–NH_2	0.54
BD	$H_2N-(CH_2-)_4NH_2$	10.416	$H_2N-(CH_2-)_4$	R–NH_2	0.62
	$H_3N^+-(CH_2-)_4NH_2$	10.083	$H_3N^+-(CH_2-)_4$	$(H^+R)-NH_2$	0.80
ButlAm	$CH_3-(CH_2-)_3NH_2$	10.750	$CH_3-(CH_2-)_3$	R–NH_2	0.44
DAP	$H_2N-(CH_2-)_5NH_2$	10.404	$H_2N-(CH_2-)_5$	R–NH_2	0.63
	$H_3N^+-(CH_2-)_5NH_2$	10.283	$H_3N^+-(CH_2-)_5$	$(H^+R)-NH_2$ [a]	0.69
DAB	$H_2N-(CH_2-)_2-CO-CH_2-NH_2$	9.716	$H_2N-(CH_2-)_2-CO-CH_2-$	R–NH_2	0.99
	$H_3N^+-(CH_2-)_2-CO-CH_2-NH_2$	7.550	$H_3N^+-(CH_2-)_2-CO-CH_2-$	$(H^+R)-NH_2$ [a]	2.14
DAHP	$H_2N-CH_2-CH(OH)-CH_2-NH_2$	9.294	$H_2N-CH_2-CH(OH)-CH_2-$	R–NH_2	1.21
	$H_3N^+-CH_2-CH(OH)-CH_2-NH_2$	8.782	$H_3N^+-CH_2-CH(OH)-CH_2-$	$(H^+R)-NH_2$ [a]	1.49
DIEN	$H_2N-(CH_2-)_2NH-(CH_2-)_2NH_2$	9.391	$H_2N-(CH_2-)_2NH-(CH_2-)_2$	R′–R‴–NH_2 [b]	1.16
	$H_3N^+-(CH_2-)_2NH-(CH_2-)_2NH_2$	4.407	$(H_3N^+-(CH_2-)_2)$	$(R'H^+)_2NH$ [a]	1.17
TRIEN	$H_2N-(CH_2-)_2-(NH-(CH_2-)_2)_2NH_2$	9.460	$H_2N-(CH_2-)_2-(NH-(CH_2-)_2)_2$	R′–(R‴–)$_2NH_2$ [c]	1.12
	$H_3N^+-(CH_2-)_2-(NH-(CH_2-)_2)_2NH_2$	8.191	$H_3N^+-(CH_2-)_2-(NH)-(CH_2-)_2$	$(R'H^+)NH(R''H^+)$ [a,c]	0.63
	$H_3N^+-(CH_2-)_2-(NH_2^+-(CH_2-)_2)_2NH_2$	6.825	$H_3N^+-(CH_2-)_2-(N^+H_2-(CH_2-)_2)$ [d]	$(R'H^+)NH(R'H^+-R''H^+)$ [a,c]	1.36
HEDTA	$(^-O_2C)(HO(CH)_2)N-(CH_2-)_2-N(CO_2^-)_2$	9.545	$\langle R-(CH_2-)_2N(CO_2^-)_2\rangle$ [e]	$\langle R\rangle$ [e]	0.36
	$(^-O_2C)(HO(CH)_2)NH^+-(CH_2-)_2-N(CO_2^-)_2$	8.255	$\langle H^+R-(CH_2-)_2\ N(CO_2^-)_2\rangle$ [f]	HR^+ [f]	1.04
EDTA	$(^-O_2C)_2N-(CH_2-)_2-N(CO_2^-)_2$	9.881	$\langle R-(CH_2-)_2\ N(CO_2^-)_2\rangle$ [g]	$\langle R\rangle$ [g]	0.30
	$(^-O_2C)_2NH^+-(CH_2-)_2-N(CO_2^-)_2$	8.173	$\langle H^+R-(CH_2-)_2\ N(CO_2^-)_2\rangle$ [h]	HR^+ [h]	1.207

$\log k = 11.59-1.89\ (\Sigma\ \sigma^*_R)$.
[a] $(R'H^+) = (H_3N^+-(CH_2-)_2)$.
[b] $R'-R''' = H_2N-(CH_2-)_2-(NH-(CH_2-)_2$.
[c] $(R''H^+) = H_3N^+-(CH_2-)_2-(NH)-(CH_2-)_2$.
[d] $(R'H^+-R''H^+)- = H_3N^+-(CH_2-)_2-(N^+H_2-(CH_2-)_2)$.
[e] $\langle R\rangle = \langle R-(CH_2-)_2N(CO_2^-)_2\rangle$ with $R = (^-O_2C)(HO(CH)_2)N$.
[f] $HR^+ = \langle H^+R-(CH_2-)_2N(CO_2^-)_2\rangle$ with $H^+R = (^-O_2C)(HO(CH)_2)NH^+$.
[g] $\langle R\rangle = \langle R-(CH_2-)_2N(CO_2^-)_2\rangle$ with $R = (^-O_2C)_2N$.
[h] $HR^+ = \langle H^+R-(CH_2-)_2N(CO_2^-)_2\rangle$ with $H^+R = (^-O_2C)_2NH^+$.

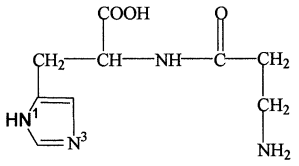
Acknowledgements

The authors are grateful to the Italian Ministry for the University and the Scientific Technological Research (MURST), COFIN 2000—project 'Molecular System and Metallo-Receptor for the Activation and Transport of Dioxygen, Nitric Oxide, and Biosubstrate' for financial support.

References

[1] A. Braibanti, E. Fisicaro, F. Dallavalle, J.D. Lamb, J.L. Oscarson, J. Phys. Chem. 97 (1993) 8054.
[2] A. Braibanti, E. Fisicaro, F. Dallavalle, J.D. Lamb, J.L. Oscarson, J. Phys. Chem. 97 (1993) 8062.
[3] A. Braibanti, E. Fisicaro, F. Dallavalle, J.D. Lamb, J.L. Oscarson, R. Sambasiva Rao, J. Phys. Chem. 98 (1994) 626.
[4] A. Braibanti, E. Fisicaro, C. Compari, Thermochim. Acta 320 (1998) 253.
[5] A. Braibanti, E. Fisicaro, C. Compari, Thermochim. Acta 320 (1998) 265.
[6] A. Braibanti, E. Fisicaro, C. Compari, Thermochim. Acta 320 (1998) 101.
[7] A. Braibanti, E. Fisicaro, C. Compari, Thermochim. Acta 320 (1998) 277.
[8] A. Braibanti, E. Fisicaro, C. Compari, A. Ghiozzi, Reactive Functional Polym. 36 (1998) 235.
[9] A. Braibanti, E. Fisicaro, C. Compari, Ann. Chim. 89 (1999) 63.
[10] A. Braibanti, E. Fisicaro, C. Compari, A. Ghiozzi, M. Panelli, J. Solution Chem. 24 (1995) 703.
[11] A. Braibanti, E. Fisicaro, C. Compari, Polyhedron 19 (2000) 2457.
[12] A. Braibanti, E. Fisicaro, C. Compari, J. Thermal Anal. Calorimetry 61 (2000) 461.
[13] J. Wyman, Adv. Prot. Chem. 19 (1964) 223.
[14] E. Di Cera, S.J. Gill, A. Wyman, Proc. Natl. Acad. Sci. 85 (1988) 449.
[15] A. Wyman, S.J. Gill, Binding and Linkage, University Science Books, Mill Valley, CA, 1990.
[16] F. Rusling, T.F. Kumosinski, Non-linear Computer Modelling of Chemical and Biochemical Data, Academic Press, San Fransisco, CA, 1996.
[17] M. Brunori, M. Coletta, E. Di Cera, Biophys. Chem. 23 (1986) 215.
[18] C. Rivetti, A. Mozzarelli, G.L. Rossi, E.R. Henry, Biochemistry 32 (1993) 2888.

[19] E. Fisicaro, A. Braibanti, J.D. Lamb, J.L. Oscarson, Biophys. Chem. 36 (1990) 1.
[20] E. Fisicaro, A. Braibanti, J.D. Lamb, J.L. Oscarson, Biophys. Chem. 36 (1990) 15.
[21] A. Braibanti, E. Fisicaro, C. Monguidi, F. Dallavalle, Inorg. Chim. Acta 138 (1987) 17.
[22] A. Braibanti, R. Sambasiva Rao, A. Ravindrababu, G. Nageswara Rao, Ann. Chim. 85 (1995) 17.
[23] A. Braibanti, E. Fisicaro, C. Compari, R. Sambasiva Rao, Talanta 45 (1998) 1267.
[24] A. Braibanti, E. Fisicaro, C. Compari, A. Ghiozzi, Reactive Functional Polym. 36 (1998) 249.
[25] F.J.C. Rossotti, H. Rossotti, J. Phys. Chem. 68 (1964) 3773.
[26] P. Gans, A. Vacca, A. Sabatini, J. Chem. Soc. Dalton Trans. (1985) 1195.
[27] R.M. Smith, A. Martell, Critical Stability Constants, vol. 2, Plenum Press, New York, 1975.
[28] L.P. Hammett, Physical Organic Chemistry, McGraw-Hill, New York, 1940.
[29] (a) R.W. Taft, J. Am. Chem. Soc. 74 (1952) 3120;
(b) R.W. Taft, J. Am. Chem. Soc. 75 (1953) 4231.
[30] G.B. Barlin, D.D. Perrin, Dissociation constants in the elucidation of structure, in: K.W. Bentley, G.W. Kirby (Eds.), Elucidation of Organic Structures by Physical and Chemical Methods. Part I, Wiley, New York, 1972.



Scheme 1.

complexes formed strongly depends on metal cation, ligand–metal ratios, and pH of the solution [13].

Carnosine forms complexes with metals of the first transition metal series [13]. Thus, with Zn^{II}, complexes in the ratio metal–ligand 1:1 such as $[ZnLH]^{2+}$ and $[ZnL]^{+}$ which show [14,15] interesting pharmacological activity, are formed [16]. With Cu^{II}, complexes of the type $[CuLH]^{2+}$, $[CuL]^{+}$, $[CuLH_{-1}]^{0}$, $[Cu_2L_2H_{-2}]^{0}$ [13,17,18] and $[CuL_2]$ [19] are found. It has also been shown that the Cu^{II}-carnosine complex possesses a SOD-like activity [20]. For Co^{II}, complexes $[CoLH]^{2+}$, $[CoL]^{+}$ and $[CoLH_{-1}]^{0}$ are found [14,21]. The structure of the Co^{III} mixed ligand complex $[Co(Hcar)(en)(H_2O)]Cl_2 \cdot H_2O$, (Hcar = carnosine, en = etilenediamine) shows that carnosine is coordinated through the deprotonated peptide nitrogen, one carboxylic oxygen and the N^1 atom of the imidazole ring [22]. Studies with other metals such as Ni^{II} [14], Mn^{II}, Mg^{II}, Ca^{II} and Sr^{II} [23] and Cd^{II} [24] have also been carried out.

The interaction of carnosine with the biologically relevant oxovanadium (IV) [25–29] has been investigated by means of ENDOR techniques in frozen solutions [30] and electron absorption spectroscopy at high ligand–metal ratios, in the pH range 6.0–8.5 [31], suggesting the formation of the complex $[VO(car)_4(H_2O)]^{2+}$ with the coordination of the imidazole group of four different ligand molecules. Spectra, however, obtained in the pH range 2.0–4.0, point out a coordination through oxygen atoms of the carboxylate group [31]. The study of complex species formation in aqueous solution in order to determine the stability constants of the complexes formed has not been carried out so far.

In a recent work [32] we have investigated the oxovanadium(IV)–glutathione system in aqueous solution both potentiometrically and spectrophotometrically. The experimental data were analysed by means of least-square computer program LETAGROP: version NERNST [33,34] (potentiometric data) and version SPEFO [35] (spectrophotometric data). Similarly, in this work we have performed an investigation of the oxovanadium(IV)–carnosine system in aqueous solution in the pH range 2.0–9.0 by means of emf and UV–Vis measurements.

2. Experimental

2.1. Materials

Vanadyl(IV) sulfate trihydrate (99.99+%, Aldrich) and L-Carnosine (99%, Sigma) were used as supplied. The solutions of HCl and KCl were prepared by dissolving the respective acid and salts (Merck, analytical grade) in doubly glass-distilled water that has been boiled in order to remove dissolved CO_2. A carbonate-free hydroxide solution (NaOH) were prepared from an ampoule of Titrisol Merck and standardized against potassium hydrogen phthalate. The emf and spectrophotometric UV–Vis measurements were carried out in aqueous solution at ionic strength 0.15 mol dm^{-3} in KCl. Argon free of O_2 and CO_2 was used.

2.2. Emf measurements

We have used ionic strength 0.15 ($I = 0.15$ mol dm^{-3} KCl ionic medium) that is typical for biological systems. However, due to the low stability of the carnosine complexes with first row transition metals [13,14], the study of complex formation at pH 5–7 is not possible since precipitation of hydrolytic species of oxovanadium(IV) occurs. Therefore, ligand–metal ratios up to 60:1 were employed to repress the hydrolysis and to study the pH range 5–7. This high ligand–metal ratio implies that C_L increases to 0.344 mol dm^{-3} and consequently the ionic strength is not mantained practically constant. Due to this, we have carried out experiments at ionic strength $I = 1.5$ mol dm^{-3} in KCl for the ratio ligand–metal 60:1, to confirm the suitability of the model of complex species present in solution and the order of magnitude of the values of stability constants.

We have proceeded as follows.

At low ligand–metal ratios, $6 \leq R \leq 25$, C_B 0.0084–0.0124 mol dm^{-3} and C_L 0.071–0.214 mol dm^{-3} for vanadium(IV) and carnosine, respectively, the potentiometric study was carried out in the pH range 2.5–5 (acid zone) and 7–9 (basic zone), since precipitation occurs between pH 5 and 7 in the experimental conditions stated above.

For ligand–metal (R) ratios ≥ 60, the precipitation was not observed in the pH range 5–7. Thus, for $R \geq 60$ the study was carried out in the pH range 2.5–9 using concentrations of the vanadium(IV) and carnosine in the range 0.0047–0.0058 and 0.330–0.344 mol dm^{-3}, respectively.

Finally at ionic strength $I = 1.5$ mol dm^{-3} in KCl we have confirmed the model (ligand–metal ratio 60:1) of the species present in solution and the order of magnitude of the values of the stability constants.

The symbols used in the present paper are the same as those adopted in previous works [36–41].

The emf and UV–Vis measurements were done using the following instruments: pH meter Radiometer PHM85, Crisson Microbur 2031 piston buret, titration vessel Crisson, thermostat bath Heto, Shimadzu UV-2101 PC spectrophotometer. The sealed 100 ml thermostated double-walled glass titration vessel was fitted with a Red Rod combined pH electrode Radiometer PHG201-7 and titrant inlet, magnetic stirrer, inert argon atmosphere inlet and outlet tubes. The titrant was delivered through an immersed capillary tip from the piston buret. The temperature was maintained at 25.00(1) °C by regular circulation of water from the thermostat bath.

The measurements have been carried out by means of the cell REF//S/EV, where REF = Hg–Hg_2Cl_2(calomel)–saturated KCl solution; S = equilibrium solution and EV = glass electrode. At 25 °C the emf (mV) of this cell follows Nernst's equation $E = E^\circ + Jh + 59.16 \log h$, where h represents the free hydrogen ion concentration, E° the standard potential and J a constant which takes into account the liquid junction potential [39].

The experiments were carried out as follows [40]: a fixed volume of 0.100 mol dm^{-3} HCl was titrated with succesive additions of 0.100 mol dm^{-3} NaOH until near neutrality, in order to get the parameters E° and J. Then, determined weights of carnosine and $VOSO_4$ were added, in this order. Finally, the titration was continued from pH 2–2.5 to 8.5–9 with NaOH 1.000 mol dm^{-3}.

The ionization constants of carnosine have been determined by means of the LETAGROP program at $I = 0.15$ mol dm^{-3} and $I = 1.5$ mol dm^{-3} in KCl. The pK_i values obtained are listed in Table 1 and compared with other literature data at different ionic strength and temperature [44–48]. Fig. 1 shows the formation function Z (pH) [36–41], where Z represents the average number of H^+ associated per mole of carnosine (HL), according to the reaction $L^- + pH^+ \rightleftarrows H_pL^{(p-1)+}$, β_{pr}. The curve shows the formation of the species HL ($Z = 1$), H_2L^+ ($Z = 2$) and H_3L^{2+} ($Z = 3$).

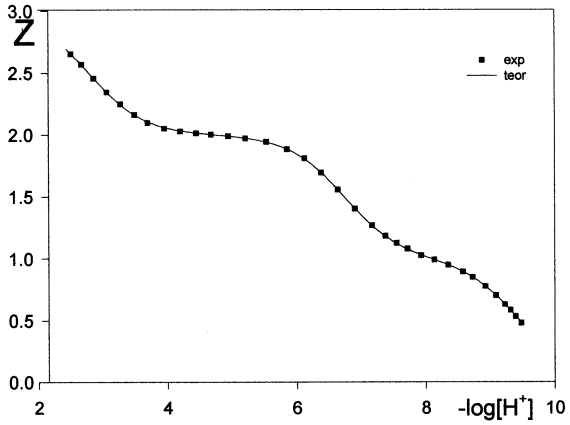


Fig. 1. Z, average number of H^+ associated per mol of the deprotonated carnosine, according the reaction $L^- + pH^+ \rightleftarrows H_pL^{(p-1)+}$, in 0.15 mol dm^{-3} KCl ionic medium at 25 °C. The continuous–draw curve made using the stability constants of Table 1.

We have also carried out theoretical calculations of the pK_i of the carnosine using PALLAS 3.0 program [42]. The method of calculation is based on the consideration that the substituents in the parent compound produce free energy changes that are linearly additive. This assumption led to the Hammet and Taft equations [43], which are the starting points of pK_i predictions (Table 1).

Subsequently, the system VO^{2+}-carnosine was studied according to the reaction

$$pH^+ + qVO^{2+} + r\,L^- \rightleftarrows [H_p(VO)_q(L)_r]^{(2q-r+p)+}, \quad \beta_{pqr}$$

Table 1
Values of β_{pr} and pK_i for the H^+–carnosine system (25 °C, $I = 0.15$ and 1.5 mol dm^{-3} KCl ionic medium)

$I = 0.15$ mol dm^{-3} KCl pr	log β_{pr} emf							
11	9.46(3)							
21	16.21(3)							
31	18.99(4)							
σ(Z)	0.03_6							
Experimental number	3							
Point number	482							
pH range	2.4–9.5							
L($\times 10^3$ mol dm^{-3})	1–7							
Equilibrium	pK_I							
	This work $I = 0.15$ emf	$I = 1.5$ emf	PALLAS program	Ref. [44]	Ref. [45]	Ref. [46]	Ref. [47]	Ref. [48]
H_3L^{2+}–H_2L^+	2.79(4)	2.87(5)	3.61	2.64	2.619	2.77	2.64	2.594
H_2L^+–HL	6.75(3)	6.92(4)	6.42	6.59	6.656	6.90	6.58	6.774
HL–L^-	9.46(3)	9.34(2)	9.26	9.04	9.237	9.70	9.04	9.372

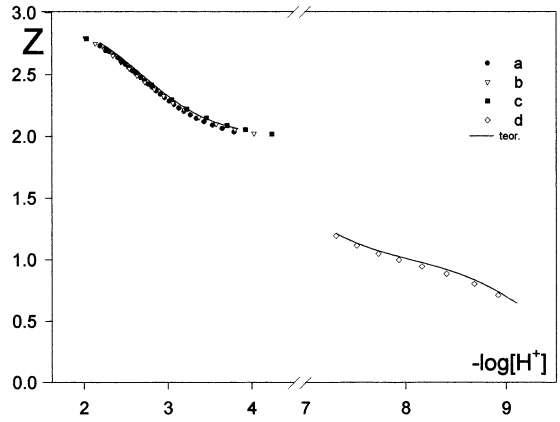


Fig. 2. Z, average number of H^+ associated per mol of deprotonated carnosine L^- vs. pH, according to the reaction $p\,H^+ + q\,VO^{2+} + r\,L^- \rightleftarrows [H_p(VO)_q(L)_r]^{(2q-r+p)+}$, in 0.15 mol dm^{-3} KCl ionic medium at 25 °C and the following B and R ranges: 0.0084 mol dm$^{-3} \leq B \leq$ 0.0124 mol dm^{-3} and $6 \leq R \leq 25$. The continuous-draw curve was made using the stability constants (Table 2, minimising Z_f). (a, b) $R =$ 15/1, $B = 0.01$ mol dm^{-3}, (c, d) $R = 15/1$, $B = 0.0084$ mol dm^{-3}.

As a consequence of the high L–M ratio used, the experimental data are practically situated on the same theoretical curve of the ligand (Fig. 2), similarly to the study of the glutathione–oxovanadium(IV) system [32]. This fact constitutes the main difficulty in the interpretation of this system. The buffer capacity of the ligand prevents detecting the stoichiometry (p, q, r) of the VO^{2+}-carnosine complexes, overlapping it.

The experimental data were analysed by means of both LETAGROP program [33,35] and LETAGROP/FONDO treatment [49,50]. LETAGROP minimizes the function $Z_C = (H-h)/C$ whereas LETAGROP/FONDO minimizes the function $Z_f = ((H-h)-\Sigma p c_{p01})/(L-\Sigma c_{p01})$, (reference L^-) where c_{p01} represents the equilibrium concentrations of the ligand species, in order to eliminate the excess of ligand.

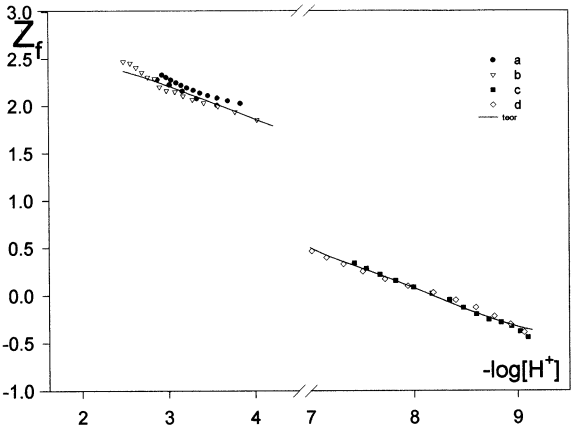


Fig. 3. Z_f $(= (BZ-\Sigma p c_{p01})/(L-\Sigma c_{p01}))$ average number of H^+ associated per mol of deprotonated carnosine L^- as VO^{2+}–carnosine complexes vs. pH, according the reaction $p\,H^+ + q\,VO^{2+} + r\,L^- \rightleftarrows [H_p(VO)_q(L)_r]^{(2q-r+p)+}$, in 0.15 mol dm^{-3} KCl ionic medium at 25 °C. The continuous–draw curve was made using the stability constants (Table 2, minimizing Z_f). (a) $R = 6/1$, $B = 0.0123$ mol dm^{-3}, (b, c) $R = 10/1$, $B = 0.0113$ mol dm^{-3}, (d) $R = 6/1$, $B = 0.012$ mol dm^{-3}.

In both treatments, the model best fitting the experimental data, for ligand–metal ratio $6 \leq R \leq 25$, was that formed by species 512, 412 and 312 for the acid zone (Table 2, $2.5 \leq$ pH ≤ 5), and for species 112, 012 and-112 for the basic zone (Table 2, $7 \leq$ pH ≤ 9). In Fig. 3, we can observe: the formation in acid zone of species 512, ($Z \approx 2.5$, pH ≈ 2.5); 412 with H_2L^+ ligand, ($Z_f \approx 2$, pH ≈ 3.5); and species 312, ($Z_f \approx 1.5$, pH ≈ 4.5). The species 112, ($Z_f \approx 0.5$, pH ≈ 7.3) with HL and L^- as ligands, species 012 with L^- ligand, ($Z_f \approx 0$, pH ≈ 8.3); and -112, with L^- and L^{2-} ligands, ($Z_f \approx -0.5$, pH $\approx$ 9), in basic zone. Complexes with $Z_f \approx 1$ were not observed due to the precipitation of the oxovanadium(IV) hydroxide.

The precipitation of oxovanadium(IV) hydroxide in the pH range 5–7 makes impossible the determination of the stability constant for the species 212. At the ligand–metal ratios $R \geq 60$ the precipitation of the hydroxide was not observed. Therefore, we carried out the titrations in the ratio L–M 60:1. The analyses of the experimental data by LETAGROP allowed us to determine the value of the formation constant corresponding to the complex 212 (Table 2). Although with such an excess of ligand, the values obtained are not so precise, they are in the same order of magnitude as the values obtained for log β_{pqr} at smaller L–M ratios (≤ 25).

In the calculations the hydrolytic species of VO^{2+} $[VO(OH)]^+$ and $[V_2O_2(OH)_2]^{2+}$ were considered [51,52]. In agreement with Baes and Mesmer [51], by means of the equations 10.5 and 10.6, we calculated the following values:

	$I = 0$	$I = 0.15$ mol dm^{-3}	$I = 1.5$ mol dm^{-3}
$[VO(OH)]^+$	−5.67	−5.98	−6.44
$[V_2O_2(OH)_2]^{2+}$	−6.67	−6.98	−7.44

which were used in the calculations.

Fig. 4 shows the species distribution diagram of the system VO^{2+}–carnosine as a function of pH, at $B =$ 0.011 mol dm^{-3} and R 60:1.

2.3. Spectrophotometric measurements

The spectrophotometric measurements were performed using the same experimental conditions (concentration ranges and ligand–metal ratios) as those used in the potentiometric study.

The VO^{2+}–carnosine system in the acidic range gives blue solutions which are slightly more intense in colour than that corresponding to an aqueous solution of the VO^{2+} [53,54], and its spectrum shows a band at 625 nm and another band more intense at 764 nm (Fig. 5). The spectrum of $[VO(H_2O)_5]^{2+}$ (C_{4v} geometry) presents

Table 2
Equilibrium constants for the carnosine–VO^{2+} system (25 °C, 0.15 mol dm^{-3} KCl ionic medium)

L/B: 6/1, 10/1. 2.5 ≤ pH ≤ 5 (acid zone) log $\beta_{pqr}(\pm 3\sigma)$				L/B: 6/1, 10/1. 7 ≤ pH ≤ 9 (basic zone) log $\beta_{pqr}(\pm 3\sigma)$				Simultaneous treatment both acid and basic zone log $\beta_{pqr}(\pm 3\sigma)$			
(p, q, r)		emf		(p, q, r)		emf		(p, q, r)		emf	
512	39.03(5)	39.01(6)	39.06(5)	112	18.93(5)	18.6(< 18.8)	18.87(5)	512	39.3(2)	39.1(2)	
412	36.09(7)	36.07(7)	36.14(5)	012	11.11(4)	10.9(3)	11.18(5)	412	36.4(2)	36.2(2)	
312	32.01(1)	31.9(1)	31.95(5)	−112	2.28(4)	2.4(2)	2.49(5)	312	32.3(1)	32.1(2)	
$\sigma(Z_C)$	0.008_2			σ(Z_C)	0.007_6			212			
$\sigma(Z_{Cf})$		0.04_0		σ(Z_{Cf})		0.1_6		112	18.9(2)	18.6(2)	
$\sigma(E)$ mV			1.5 mV	σ(E) mV			7.2 mV	012	11.1(2)	10.9(2)	
								−112	2.3(2)	2.4(2)	
								$\sigma(Z_C)$	0.032		
								$\sigma(Z$Cf)		0.12_5	

L/B: 15/1, 25/1. 2.5 ≤ pH ≤ 5 (acid zone) log $\beta_{pqr}(\pm 3\sigma)$			L/B: 15/1, 25/1. 7 ≤ pH ≤ 9 (basic zone) log $\beta_{pqr}(\pm 3\sigma)$						
(p, q, r)	emf		(p, q, r)	emf			(p, q, r)	emf	
512	38.85(9)	39.0(1)	112	18.7(1)	19.03(6)		512	38.89(8)	39.03(9)
412	36.1(1)	36.3(1)	012	11.04(3)	11.20(6)		412	36.09(8)	36.24(9)
312	32.0(2)	31.9(2)	−112	2.42(6)	2.32(6)		312	32.2(1)	32.1(2)
σ(Z_C)	0.01_2		σ(Z_C)	0.0030			212		
σ(E)		2.4 mV	σ(Z_{Cf})		0.01_0		112	18.8(2)	19.3(2)
							012	11.2(2)	11.2(2)
							−112	2.6(2)	2.1(2)
							σ(Z_C)	0.009_6	
							σ(Z_{Cf})	0.085	

L/B: 6/1, 10/1, 15/1. 2.0 ≤ pH ≤ 4.3 (acid zone) log $\beta_{pqr}(\pm 3\sigma)$		L/B: 60/1. 2.19 ≤ pH ≤ 9.14 $I = 0.15$ mol dm^{-3} in KCl log $\beta_{pqr}(\pm 3\sigma)$								L/B: 60/1 2.5 ≤ pH ≤ 10.10. I = 1.5 mol dm^{-3} in KCl log $\beta_{pqr}(\pm 3\sigma)$	
(p, q, r)	UV–Vis	(p, q, r)	emf			UV–Vis				(p, q, r) emf	
						440–485 nm	585–630 nm	758–780 nm	830–875 nm		
512	37.4(< 38.6)	412	36.3(< 36.9)	36.5(< 36.9)	36.4(1)	37.6(2)	35.4(< 35.7)	35.4(< 35.7)	35.8(2)	412	35.8(< 36.5)
412	36.1(1)	312	31.8(< 32.6)	32.0(< 32.7)	31.5(< 31.9)	32.95(8)	31.52(8)	31.75(6)	31.78(7)	312	31.9(< 32.7)
312	26.5(< 32.1)	212	27.4(< 27.8)	27.6(< 27.9)	27.4(1)		27.02(7)	27.37(5)	27.43(6)	212	27.5(< 27.8)
σ(D)	0.009	112	18.5(< 18.9)	18.1(< 19.0)	17.7(< 17.8)	19.1(3)	18.4(2)	18.4(< 18.7)	19.0(< 19.2)	112	
nm no.	19	012	8.6(< 10.0)	9.4(< 10.0)	9.4(< 10.0)	9.72(1)	11.0(2)	8.9(2)	9.4(2)	012	7.7(< 8.3)
solution no	37	$\sigma(Z_C)$	0.011							$\sigma(Z_C)$	0.017
bx10^3mol dm^{-3}	8–12	$\sigma(Z_{Cf})$		0.315							
		σ(E)			1.5 mV						
		σ(D)				0.025	0.016	0.019	0.025		
		nm no				10	10	10	10		
		solution no				26	26	26	26		
		B × 10^3mol dm^{-3}				5.73	5.73	5.73	5.73		

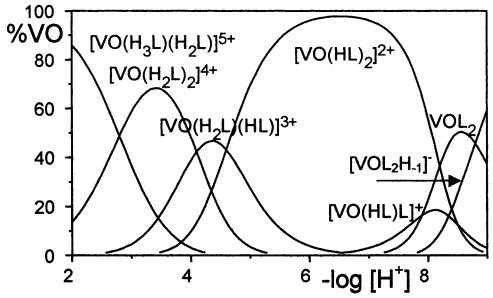


Fig. 4. Species distribution diagram as a function of pH for $B = 0.011$ mol dm^{-3} and ligand–metal $R = 60/1$, in 0.15 mol dm^{-3} KCl ionic medium at 25 °C. Calculated from β_{pqr} values of 512, 412, 312, 112, 012 and −112, Table 2, $R = 6/1,10/1$ and 212 value, Table 2, $R = 60/1$.

three bands corresponding to $b_2 \rightarrow e$, $b_2 \rightarrow b_1$ and $b_2 \rightarrow a_1$ transitions (the latter generally obscured by overlapping with a charge transfer band) [55]. When carboxylate coordinates to oxovanadium(IV) the $b_2 \rightarrow e$ and $b_2 \rightarrow b_1$ bands shifts to the red and to the blue, respectively, due to the stronger ligand crystal field [56]. When the pH is higher than 4 (ratios $\geq 60:1$), the band $b_2 \rightarrow b_1$ is shifted at 480–500 nm and therefore the solution turns dark blue (Fig. 5(a)). The band $b_2 \rightarrow e$ is also shifted to the red. Finally at pH > 7 both bands disminish their intensity to an amber colour (Fig. 5(b)).

Using the program LETAGROP/SPEFO [35,57] for the treatment of the UV–Vis data (pH, B, C, $(D)_{N\lambda})_{NSOL}$, where D is the absorptivity of each solution, Nλ is the number of wave lengths and NOSL is the number of solutions, we select one group of NOSL = 37 solutions and NL = 10 wave lengths at the following ranges: $2.0 \leq pH \leq 4.3$, $0.006 \leq B \leq 0.012$ mol dm^{-3} and $6 \leq R \leq 15$. This analysis gives β_{pqr} values of the same order of magnitude than the *emf* data (Table 2), being its value for the 412 species the stability constant determined with greater precision. But, in the basic zone the values of equilibrium constants could not be determined with enough precision. Fig. 5(b) shows the spectra for $B = 8.4\ 10^{-3}$ mol dm^{-3} and $R = 15/1$. As in this ratio precipitation occurs at pH ≈ 4.5, we could not obtain absorptivity data in the range $4.5 \leq pH \leq 7$.

However, for $R = 60/1$ the hydrolysis is repressed and precipitation is not observed. In this conditions we can see the spectra in this zone ($4.5 \leq pH \leq 7$) in Fig. 5(a).

The spectrophotometric data in the ligand–metal ratio 60/1 and pH range $2.19 \leq pH \leq 9.14$ were analysed by LETAGROP/SPEFO [35,37], using four different zones four λ: 440–485, 585–630, 758–780 and 830–875 nm, respectively (Table 2). The values obtained for log β_{pqr} corresponding to the complexes 412, 312, 212, 112 and 012, are, in general more precise than those obtained from potentiometric data. In particular, the value obtained log β_{212} is good (Table 2).

3. Results and discussion

3.1. Ionization constants of the carnosine

The pK_i constants of the carnosine, HL, (25 °C, $I =$ 0.15 and 1.5 mol dm^{-3} in KCl) are presented in Table 1. The pK_1 corresponds to the deprotonation of the carboxylate group in the species H_3L^{2+}; pK_2 corresponds to the deprotonation of the protonated N^3 imidazole group in the species H_2L^{+}; and pK_3 corresponds to the deprotonation of the NH_3^+ group, in the species HL. The deprotonation of the amide group –CONH– becomes important mainly in the presence of the cation metals [13].

3.2. Stability constants of the complexes formed

From β_{pqr} (Table 2) and β_{pr} constants of the carnosine (Table 1), the formation constants of the complex species formed can readily be calculated according to the following equilibria (Table 3).

The log K value for the species $[VOL_2]$ of the present work (see Table 3) is in agreement with the value reported in the literature for $[CuL_2]$ complex (log $K =$ 14.4) in the carnosine–copper(II) system [19].

The values calculated for pK_i corresponding to the ionization of the protonated complexes are displayed in Table 4.

Taking into account pK_i values of carnosine (Table 1), we can deduce that pK_{a_1} (Table 4) corresponds to the deprotonation of the carboxylic group (Scheme 2). The species distribution diagram (Fig. 4) indicates that the specie $[VO(H_2L)_2]^{4+}$ is the most important in the pH range 3–4. The electronic spectra (Fig. 5(a and b)) up to pH 4 is in accordance with the coordination through oxygen donors [13,31]. The carboxylate group and the oxygen of the peptide group of the carnosine molecules only occupy a part of the coordination site, whereas the remaining ones are occupied by water molecules [31]. The application of SPEFO-LETAGROP program to the spectrophotometric data (Fig. 5(b)) allows to obtain a good value for the stability constants of 412 complex, $[VO(H_2L)_2]^{4+}$ (Table 2). In the specie $[VO(H_3L)(H_2L)]^{5+}$, the ligand H_3L^{2+} (Scheme 2) only can coordinate through oxygen of the peptide group. The values of log K for species $[VO(H_3L)(H_2L)]^{5+}$ and $[VO(H_2L)_2]^{4+}$ (Table 3) indicate that carnosine is a weak complexing agent toward VO^{2+}. The electronic spectra in the ligand–metal ratio 60/1, pH range 5–7 (Fig. 5(a)) change widely, with an increase of the spectral intensity. In pH range 4–7, the band $b_2 \rightarrow b_1$ is shifted [55] to 480–500 nm (solution dark blue) and the band $b_2 \rightarrow e$ is shifted [55] to the red. These changes in the spectra can be explained by the coordination of the N^3 imidazol nitrogen (Scheme 2). The application of SPEFO-LETAGROP program to the spectrophotometric

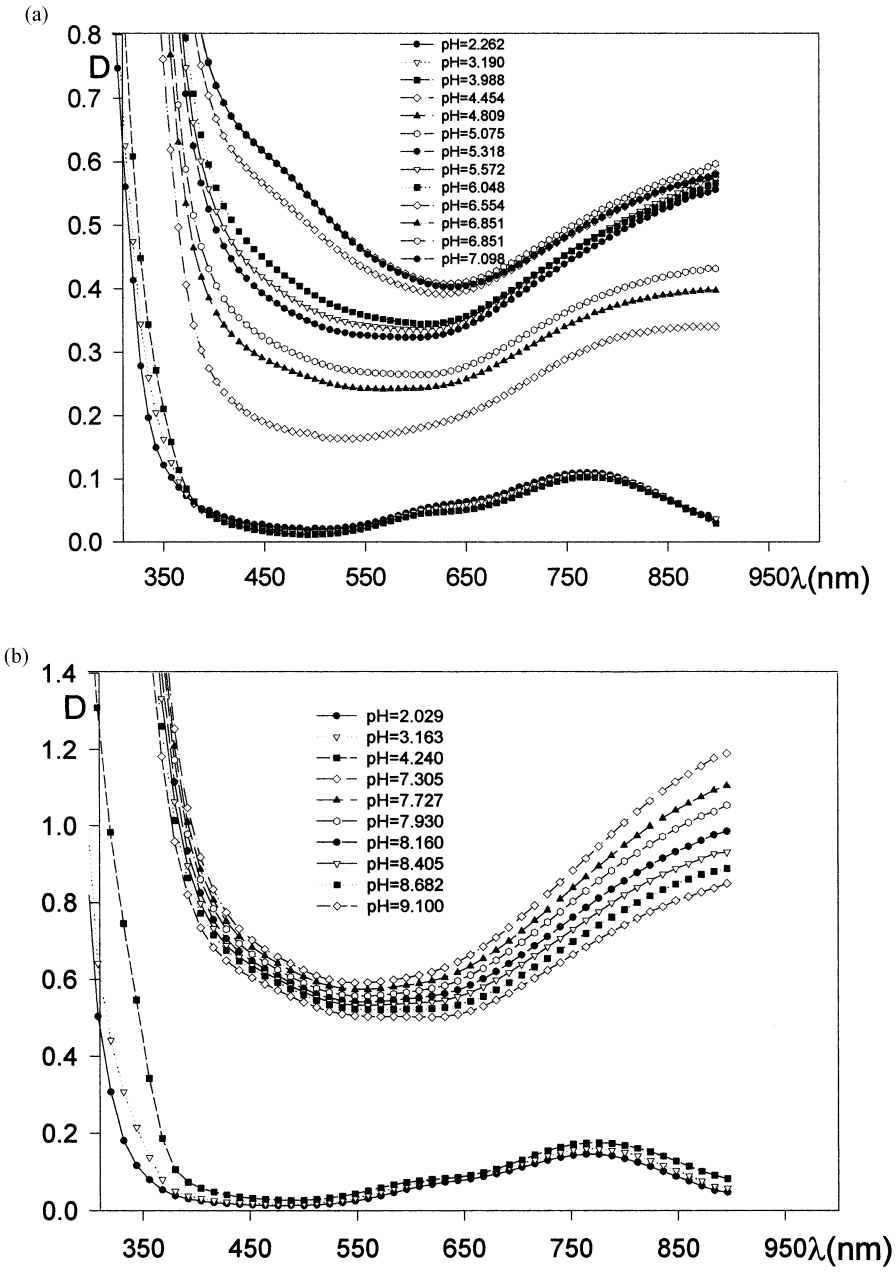


Table 3

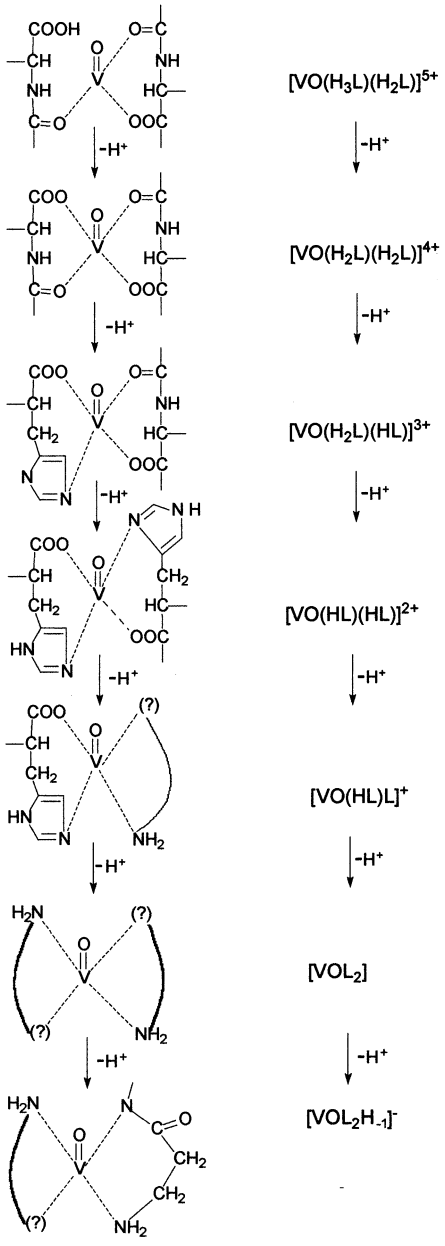
Pqr	Equilibrium	log K
512	$VO^{2+} + H_3L^{2+} + H_2L^{+} \rightleftarrows [VO(H_3L)(H_2L)]^{5+}$	~4
412	$VO^{2+} + 2\ H_2L^{+} \rightleftarrows [VO(H_2L)_2]^{4+}$	~4
312	$VO^{2+} + H_2L^{+} + HL \rightleftarrows [VO(H_2L)(HL)]^{3+}$	6.5
212	$VO^{2+} + 2\ HL \rightleftarrows [VO(HL)_2]^{2+}$	8.6
112	$VO^{2+} + HL + L^{-} \rightleftarrows [VO(HL)L]^{+}$	9.5
012	$VO^{2+} + 2\ L^{-} \rightleftarrows [VOL_2]$	11.2

data in the ligand–metal ratio 60/1 (Table 2) permits to obtain good values for the stability constants of the complexes 312, $[VO(H_2L)(HL)]^{3+}$, and 212, $[VO(HL)_2]^{2+}$. The formation of the complexes $[VO(H_2L)(HL)]^{3+}$ and $[VO(HL)_2]^{2+}$ in the pH range 4–7 can be observed in the species distribution diagram (Fig. 4). Comparing pK_{a_2} and pK_{a_3} (Table 4) with pK_2 (Table 1) we can deduce that the N^3 imidazole atom of the carnosine is involved in coordination to VO^{2+} (Scheme 2), as stated in other work [31]. The HL, species which represents carnosine with a protonated amino group (NH_3^+), also coordinates through the N^3 imidazole nitrogen to Cu^{II} [13]. The species $[VO(HL)_2]^{2+}$ is the most important of the complexes formed in carnosine-oxovanadium(IV) system in accordance with the species distribution diagram, (pH 5–7

Table 4

	pK_{a_i}
$[VO(H_5L_2)]^{5+} \rightleftarrows [VO(H_2L)_2]^{4+} + H^+$	pK_{a_1} ~ 3
$[VO(H_4L_2)]^{4+} \rightleftarrows [VO(H_3L_2)]^{3+} + H^+$	pK_{a_2} ~ 4
$[VO(H_3L_2)]^{3+} \rightleftarrows [VO(HL)_2]^{2+} + H^+$	pK_{a_3} 4.5
$[VO(H_2L_2)]^{4+} \rightleftarrows [VO(HL_2)]^{+} + H^+$	pK_{a_4} 8.5
$[VO(HL_2)]^{+} \rightleftarrows [VOL_2] + H^+$	pK_{a_5} 8
$[VOL_2] \rightleftarrows [VOL_2H_{-1}]^{-} + H^+$	pK_{a_6} 8.7

(Fig. 4)). However, the value of the formation constant (Table 3) indicates that the complex is not very stable since it is necessary a high ratio ligand–metal to avoid the precipitation of the hydroxide.



Scheme 2.

At pH > 7, the electronic spectra (Fig. 5(b), ratio ligand–metal 15:1, similar spectra in ratio 60:1) show that the intensity of the bands diminish, indicating a change of the coordination of the ligand. The curve Z_f(pH) (Fig. 3) and species distribution diagram (Fig. 4) show the formation of the complexes $[VO(HL)L]^+$, $[VOL_2]$ and $[VOL_2H_{-1}]$ in the range pH 7–9. The values of the pK_{a_4} and pK_{a_5} (Table 4) (comparing them with pK_3 of the carnosine (Table 1)) indicate a weak interaction of the nitrogen atom of the amino group with VO^{2+} in the complexes $[VO(HL)L]^+$ and $[VOL_2]$ (Scheme 2). The formation of the complex with a $Z_f = -0.5$ (Fig. 3) can be due either to hydrolysis of the hydroxocomplex $[VOL_2(H_2O)]$ [31] or to the coordination of the deprotonated N-atom of the peptide group –CONH–. The value of the pK_{a_6} (Table 4) is in better agreement with the deprotonation of the peptide nitrogen atom (Scheme 2). In a potentiometric and ^{51}V NMR study in aqueous solution of the H^+-vanadate(V)-L-α-alanyl–L-histidine system [58], the coordination through the amino nitrogen (NH_2), peptide nitrogen and carboxylate oxygen in the complexes (1, 1, 1) and (0, 1, 1) has been proposed. The coordination of the nitrogen atom of the peptide group is also proposed in other work [59]. For the carnosine–copper(II) system, in species $[CuHL]^{2+}$, the ligand behaves as monodentate, coordinating only through N^3 imidazole atom; in the species $[CuL]^+$ the coordination involves the participation of the terminal amino group and deprotonated peptide N-atom; in the species $[CuLH_{-1}]^0$ moreover coordination through N^3 imidazole nitrogen is observed. In the dimeric $[Cu_2L_2H_{-2}]^0$ complex, the carboxylate is also coordinated: each Cu^{II} is coordinated to N-amino, N-peptide, N^3 imidazole nitrogens and to a carboxylate oxygen [13,17].

Acknowledgements

We wish to thank the Ministerio de Ciencias y Tecnología, España (Grant no. PM98-0148) and the Consejería de Educación, Cultura y Deportes, Gobierno de Canarias (Grant COFI 2000/11). Thanks are also due to the Consejo Nacional de Investigaciones Científicas y Tecnológicas (CONICIT, Venezuela) (Project S1-9500494) and the Consejo de Desarrollo Científico y Humanístico (CDCH) of the Universidad Central de Venezuela (UCV, Caracas) (Projects C03-12.3492.95 and PI-03.12.4377.99) as well as CONICET and ANPCyT (PICT 00119), Argentina. M.T.A. is grateful to Caja Canarias-Universidad de La Laguna for a fellowship. S.V.-J. thanks the Agencia Española de Cooperación Internacional (AECI) (Programa de Cooperación Interuniversitaria América Latina-España, AI-E.2000) for a visit grant to the Department of Inorganic

Chemistry, University of La Laguna, Tenerife, Spain, during 2000.

References

[1] W.S. Gulewitsch, S. Amiradzibi, Ber. Deutsch. Chem. Ges. 33 (1900) 1902.
[2] A. Bakardjiev, K. Bauer, Biochemistry (Moscow) 65 (2000) 779.
[3] F.L. Margolis, Science 184 (1974) 709.
[4] P.V. Skulachev, Biochemistry (Moscow) 65 (2000) 749.
[5] A.A. Boldyrev, Biochemistry (Moscow) 65 (2000) 751.
[6] E.A. Decker, S.A. Livisay, S. Zhou, Biochemistry (Moscow) 65 (2000) 766.
[7] P.Q. Trombley, M.S. Horning, L.J. Blakemore, Biochemistry (Moscow) 65 (2000) 807.
[8] S. De Marchins, C. Modena, P. Peretto, A. Migueli, F.L. Margolis, A. Fasolo, Biochemistry (Moscow) 65 (2000) 824.
[9] H. Abe, Biochemistry (Moscow) 65 (2000) 757.
[10] S.L. Stvolinsky, D. Dobrota, Biochemistry (Moscow) 65 (2000) 849.
[11] S. Gallant, M. Semyonova, M. Yuneva, Biochemistry (Moscow) 65 (2000) 866.
[12] H. Itoh, T. Yamane, T. Ashida, M. Kakudo, Acta Crystallogr., Sect. B 33 (1977) 1959.
[13] E.J. Baran, Biochemistry (Moscow) 65 (2000) 789.
[14] E. Farkas, I. Sovago, A. Gergely, J. Chem. Soc. Dalton Trans. (1983) 1545.
[15] T. Gajda, B. Henry, J.J. Delpuech, J. Chem. Soc. Perkin Trans. 2 (1994) 157.
[16] T. Matsukura, H. Tanaka, Biochemistry (Moscow) 65 (2000) 81.
[17] P.G. Daniele, E. Prenesti, V. Zelano, G. Ostacoli, Spectrochim. Acta A 49 (1993) 1299.
[18] I. Sovago, E. Farkas, A. Gergely, J. Chem. Soc. Dalton Trans. (1982) 2159.
[19] R.P. Agarwal, D.D. Perrin, J. Chem. Soc. Dalton (1975) 268.
[20] R. Kohen, R. Misgav, I. Ginsburg, Free Radic. Res. Commun. 12/13 (1991) 179.
[21] R.P. Agarwal, D.D. Perrin, J. Chem. Soc. Dalton (1975) 1045.
[22] K. Okamoto, T. Yasui, H. Kawaguchi, T. Ama, J. Hidaka, Chem. Lett. (1988) 335.
[23] G.R. Lenz, A.E. Martell, Biochemistry 3 (1964) 750.
[24] P.C. Daniele, P. Amino, G. Ostacoli, Inorg. Chim. Acta 66 (1982) 65.
[25] D. Rehder, Biometals 5 (1992) 3.
[26] C. Slebodnick, B.J. Hamstra, V.L. Pecoraro, Struct. Bonding 89 (1997) 51.
[27] D.N. Chasteen (Ed.), Vanadium in Biological Systems, Kluwer Academic, Dordrecht, 1990.
[28] E.J. Baran, Bol. Soc. Chil Quím. 42 (1997) 247.
[29] E.J. Baran, J. Inorg. Biochem. 80 (2000) 1.
[30] C.F. Mulks, B. Kirste, H. Van Willigen, J. Am. Chem. Soc. 104 (1982) 5906.
[31] E.G. Ferrer, P.A.M. Williams, E.J. Baran, Biol. Trace Elem. Res. 55 (1996) 79.
[32] M.T. Armas, A. Mederos, P. Gili, S. Domínguez, R. Hernández-Molina, P. Lorenzo, E.J. Baran, M.L. Araujo, F. Brito, Polyhedron 20 (2001) 799.
[33] (a) F. Brito, J. Gocalves: Project S1-1228, CONICIT, Caracas, 1981;
(b) F. Brito, Project 14/02.06.87, Education Council, Canary Islands Government, Tenerife, Spain, 1987.
[34] (a) N. Ingri, L.G. Sillén, Ark. Kemi 23 (1964) 97;
(b) P. Brauner, L.G. Sillén, R. Whiteker, Ark. Kemi 31 (1969) 365.
[35] J. Sanchiz, S. Domínguez, A. Mederos, F. Brito, J.M. Arrieta, Inorg. Chem. 36 (1997) 4108.
[36] N. Ingri, F. Brito, Acta Chem. Scand. 13 (1959) 1971.
[37] S. Mateo, F. Brito, An. Quim. 68 (1972) 37.
[38] F. Brito, J. Ascanio, S. Mateo, C. Hernández, L. Araujo, P. Gili, P. Martin-Zarza, S. Dominguez, A. Mederos, Polyhedron 16 (1997) 3835.
[39] G. Biedermann, L.G. Sillén, Ark. Kemi 5 (1952) 425.
[40] V. Lubes, Complejos de V(III) y los Acidos Aminopolicarboxílicos NDAP, NPAD y NTP (25 °C, KCl 3.0 M), Tesis de Licenciatura, Facultad de Ciencias, UCV, 1997.
[41] C.A. González, M. Hernández-Padilla, S. Domínguez, A. Mederos, F. Brito, J.M. Arrieta, Polyhedron 16 (1997) 2925.
[42] Pallas 3.0 for Windows. PKALC 3.2, PROLOGP 5.1, PROLOG 2.0, ELUEX 4.0, METABOLEXPERT 11.0, HAZARDEXPERT 3.1, CompuDrug International, Inc., South San Francisco, CA, 94080, USA.
[43] D.D. Perrin, B. Dempsey, E.P. Serjeant, pK_a Prediction for Organic Acids and Bases, Chapman & Hall, London, 1981.
[44] P.C. Daniele, P. Amico, G. Ostacoli, Inorg. Chim. Acta 66 (1982) 65.
[45] P.G. Pietta, A. Chersi, Gazz. Chim. Ital. 98 (1968) 1503.
[46] H. Dobbie, W.O. Kermack, Biochem. J. 59 (1955) 246.
[47] R.P. Agarwal, D.D. Perrin, J. Chem. Soc. Dalton Transact., (1975) 268.
[48] P.G. Daniele, E. Prenesti, V. Zelano, G. Ostacoli, Spectrochim. Acta A49 (1993) 1299.
[49] A. Mederos, S. Domínguez, M.J. Morales, F. Brito, E. Chinea, Polyhedron 6 (1987) 303.
[50] F. Brito, L. Araujo, Estudios sobre Características de Elementos de Transición en Solución. 1. Química de los Vanadatos(IV, V), Proyecto no. S1-95000494, CONICIT, Caracas, 1996.
[51] C.F. Baes, Jr., R.E. Mesmer, The Hydrolysis of Cations, Wiley, New York, 1976, p. 200.
[52] D.T. Richens, The Chemistry of Aqua Ions, Wiley, New York, 1997, p. 237.
[53] D.T. Richens, The Chemistry of Aqua Ions, Wiley, New York, 1997, p. 236.
[54] A.B.P. Lever, Inorganic Electronic Spectroscopy, second ed., Elsevier, Amsterdam, 1984, p. 390.
[55] C.J. Ballhausen, H.B. Gray, Inorg. Chem. 1 (1972) 111.
[56] Y. Alegretti, E.G. Ferrer, A.C. González-Barró, P.A.M. Williams, Polyhedron 19 (2000) 2613.
[57] L.G. Sillén, B. Warnqvist, Ark. Kemi 31 (1969) 377.
[58] K. Elvingson, M. Fritzche, D. Rehder, L. Pettersson, Acta Chem. Scand. 48 (1994) 878.
[59] M. Fritzsche, V. Vergopoulos, D. Rehder, Inorg. Chim. Acta 211 (1993) 11.

polyamine chain to a bithiophene unit through thenylic carbons. In many ways, these novel products might be considered as an initial approach for designing more soluble oligothiophene compounds with interesting properties. In this respect and focusing on future potential applications in the fields of pharmacology and that of sensory materials, some co-ordination studies in aqueous solution with metal ions have been carried out.

2. Experimental

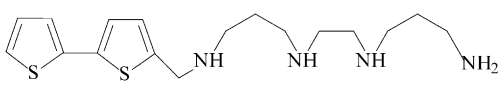
2.1. Materials

The starting materials for the synthesis of **L1** and **L2** were purchased from commercial sources and used without further purification. The solvents were dried using standard techniques.

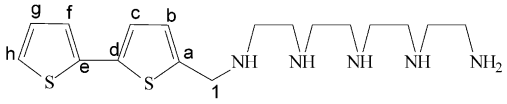
All solutions used in the pH-metric and electrochemical studies have been prepared using milipore H_2O.

The CO_2-free NaOH and HCl, solutions used in the potentiometric measurements were prepared following the procedure reported in ref. [9].

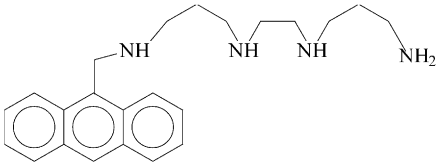
L1



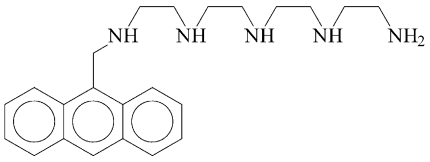
L2



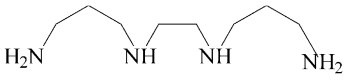
L3



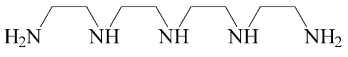
L4



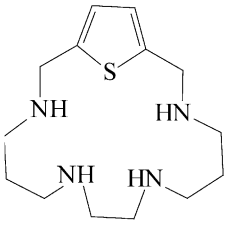
L5



L6



L7



2.2. Synthesis

2.2.1. 2,2′-Bithiophene-5-carboxaldehyde (*1*)

This compound was obtained by a modification of the procedure described in ref. [10] for the preparation of bis(5-formyl-2-thienyl)methane using 2,2′-bithiophene (0.5 g, 3.2 mmol), $POCl_3$ (9.4 mmol) and DMF (9.4 mmol) as starting materials. Yield: 43%, δ_H (300 MHz, $CDCl_3$, J in Hz) 7.09 (t, $J = 4$, 1H), 7.25 (d, $J = 5$, 1H), 7.38 (d, $J = 5$, 2H), 7.68 (d, $J = 4$, 1H), 9.88 (s, 1H); δ_C

(300 MHz, $CDCl_3$) 124.5, 126.4, 127.3, 128.6, 136.3, 137.5, 141.9, 147.4, 182.8.

Synthesis of compounds **L1** and **L2** has been accomplished as described in Ref. [11] for the preparation of some related compounds containing anthracene units.

2.2.2. *N-(3-aminopropyl)-N′-3-(2,2′-bithien-5-ylmethyl)aminopropylethane-1,2-diamine (**L1**)*

*2.2.2.1. **L1**·4HCl.* 1,5,8,12-Tetraazadodecane (1.25 g, 7.2 mmol) and 2,2′-bithiophene-5-carboxaldehyde (0.70 g, 3.6 mmol) were dissolved in ethanol (25 ml) and allowed to react for 24 h at room temperature (r.t.). Then, $NaBH_4$ (0.14 g, 3.6 mmol) was added portionwise and the resulting solution kept for 24 h at r.t. The solvent was distilled off under reduced pressure and the residue treated with water and extracted with dichloromethane (3 × 100 ml). Then, it was dried over Na_2SO_4 and the solvent removed by rotatory evaporation. The final residue was dissolved in ethanol and treated with an excess of aqueous HCl. The yellowish precipitate formed was filtered off and dried under vacuum. Yield: 11%, m.p. 265–270 °C (Found: C, 40.7; H, 6.2; N, 10.9. Calc. for $C_{17}H_{31}S_2N_4Cl_4$: C, 40.9; H, 6.5; N, 11.2%); δ_H (400 MHz, D_2O, J in Hz) 1.99–2.04 (m, 4H), 2.9 (t, $J=8$, 2H), 2.9–3.15 (m, 6H), 3.36 (s, 2H), 4.36 (s, 2H), 6.98 (dd, $J=5$, $J=1$, 1H), 7.07 (d, $J=4$, 1H), 7.12 (d, $J=4$, 1H), 7.20 (dd, $J=5$, $J=1$, 1H), 7.29 (dd, $J=5$, $J=1$, 1H); δ_C (400 MHz, D_2O) 22.8, 23.9, 36.6, 43.2, 43.5, 43, 45.2, 45.3, 45.4, 45, 124.3, 125.0, 126.2, 128.5, 130.0, 132.3, 136, 140.1; FAB mass spectrum: m/z 353 ($[M+H]^+$).

2.2.3. *N-(2-aminoethyl)-N″-2-(2,2′-bithien-5-ylmethyl)aminoethyl diethylen-1,4,7-triamine (**L2**)*

*2.2.3.1. **L2**·5HCl.* To prepare this compound the same procedure was used as for **L1**. Yield: 17%, m.p. 270–272 °C (Found: C, 37.7; H, 6.1; N, 12.9. Calc. for $C_{17}H_{33}S_2N_5C_{15}$: C, 37.2; H, 6.1; N, 12.8%); δH (400 MHz, D_2O) 3.23–3.41 (m, 16H), 4.44 (s, 4H), 7.02 (dd, $J=5$ Hz, $J=1$ Hz, 1H), 7.14 (d, $J=4$ Hz, 1H), 7.17 (d, $J=4$ Hz, 1H), 7.25 (dd, $J=5$ Hz, $J=1$ Hz, 1H), 7.35 (dd, $J=5$ Hz, $J=1$ Hz, 1H); δ_c (300 MHz, D_2O) 36.2, 43.4, 43.7, 44.5, 44.7, 45.1, 45.2, 45.4, 45.6, 124.3, 125.0, 126.2, 128.5, 129.0, 132.5, 140.0, 140.0; FAB mass spectrum: m/z 368 ($[M+H]^+$).

2.3. Spectroscopy

The ^1H and ^{13}C NMR spectra were recorded on Varian UNITY 300 and UNITY 400 spectrometers, operating at 299.95 and 399.95 MHz for ^1H and at 75.43 and 100.58 MHz for ^{13}C, respectively. The spectra were obtained at r.t. in $CDCl_3$ or D_2O solutions. For the ^{13}C NMR spectra the $CDCl_3$ signal or the dioxane (67.4 ppm) were used as a reference standard and for the ^1H spectra, the solvent signal. Adjustments to the desired pH values were made using drops of DCl or NaOD solutions. The pH was calculated from the measured pD values using the correlation, pH = pD − 0.4 [12]

2.4. Electromotive force measurements

The potentiometric titrations were carried out at 298.1 ± 0.1 K using NaCl 0.15 mol dm^{-3} as supporting electrolyte. The experimental procedure and the potentiometric equipment (burette, potentiometer, cell, stirrer, microcomputer, etc.) have been fully described elsewhere [13]. The acquisition of the emf data was performed with the computer program PASAT [14]. The reference electrode was an Ag–AgCl electrode in saturated KCl solution. The glass electrode was calibrated as a hydrogen-ion concentration probe by titration of previously standardised amounts of HCl with CO_2 free NaOH solutions. The equivalent point was determined by the Gran's method [15], which gives the standard potential, $E^{\circ\prime}$, and the ionic product of water [$pK_w = 13.73(1)$]. The concentration of the different metal ions solutions employed was determined gravimetrically by standard methods. The computer program HYPERQUAD [16] was used to calculate the protonation and stability constants. The pH range investigated was 2.5–10.5 and the concentration of the different metal ions and of **L1** and **L2** ranged from 1×10^{-3} to 5×10^{-3} mol dm^{-3}. The different titration curves for each system (ca. 150 experimental points corresponding to at least three measurements) were treated either as single or as separate sets without significant variations in the values of the stability constants. Finally, the sets of data were merged together and treated simultaneously to give the final stability constants.

2.5. Electrochemistry

Cyclic voltammograms (CV) were obtained using a BAS CV50 W equipment. Linear scan (LSV) and differential pulse voltammograms (DPV) were performed with a Metrohm E506 polarecord. Glassy carbon (0.120 cm^2 surface) was used as a stationary working electrode, a platinum wire was used as the counter electrode, and an aqueous saturated calomel reference electrode (SCE), separated from the bulk solution by a salt bridge containing the solvent and supporting electrolyte, only was used as a reference electrode. Prior to series of experiments, the working electrode was cleaned and activated. Pre-treatment was performed in blank solutions by applying +1.50 V versus SCE for 10 min followed by −1.0 V for 1 min. Before each run, the electrodes were polished with an

aqueous suspension of alumina on a soft surface, dried and cleaned.

Single-sweep conditions were used for cyclic voltammetry, the potential scan rate ranging from 0.1 to 50 mV s^{-1}. For DPV, a potential scan rate of 4 mV s^{-1} was used; pulse amplitude was 10 mV.

Electrochemical experiments were performed under an argon atmosphere in solutions of $Cu(NO_3)_2 \cdot 6H_2O$ or $CuCl_2 \cdot 2H_2O$ prepared with doubly distilled water. As supporting electrolytes were used solutions of 0.15 M NaCl and 0.15 M $NaClO_4$, being their pH adjusted to the required value by adding the appropriate amounts of $HClO_4$ and/or NaOH.

3. Results and discussion

3.1. Acid–base behaviour

The protonation trends of **L1** and **L2** (see Ligand Drawing) have been studied in 0.15 mol dm^{-3} NaCl at 298.1 ± 0.1 K. In Table 1 are presented the logarithms of the stepwise basicity constants of the new compounds conjointly with those of the analogue compounds containing an anthracene unit (**L3** and **L4**) [10]. By means of comparison, the constants for the corresponding open-chain non-terminally substituted polyamines **L5** and **L6** have also been included [17].

In order to discuss the data, it is helpful to separate the polyamines in two groups according to the nature of the polyamine chain. When propylenic units are present, slight differences in the individual basicity constants have been found, being the overall basicity of the polyamine **L5** the highest of this group. **L1**, **L3** and their counterpart **L5**, all of them with four basic centres, present relatively large constants for the first three protonation steps and a much lower one for the last protonation. This trend of the stepwise protonation constants can be largely interpreted in terms of minimisation of coulombic repulsions among same sign charges [18]. Thus, the possibility of arranging the first three protons binding **L1**, **L3** and **L5** in non-neighbouring nitrogen atoms together with the presence of the two propylenic chains makes the electrostatic repulsions not very large at this stage. However, the fourth protonation step yields an important basicity decrease because it has to occur necessarily adjacent to two already protonated nitrogen atoms. Another point to be considered is the great resemblance between the data of the compounds with an anthracene unit and the one with the bithiophene fragment, particularly in the values of the three last constants. This would imply that the type of aromatic unit does not seem to be an important factor in defining the acid–base behaviour of these two ligands (**L1** and **L3**).

On the other hand, while the basicity trend of **L4** and **L6** can be explained also in terms of coulombic repulsion, the behaviour of **L2** is rather different. Indeed, according to the literature [19], **L4** and **L6** containing an odd number of nitrogen atoms present two groups of constants, so that their protonation constants decrease sharply upon passing from the third to fourth step; the difference between $\log K_{H_3L}$ and $\log K_{H_4L}$ being approximately 3 logarithmic units. However, for **L2** such a jump is not observed and the decrease in the values on the successive constants are more steady. The largest drop in basicity is observed with the fifth protonation of the ligand. After going through the individual constants, the large basicity of **L2** can be especially attributed to the two last protonations, which are much higher than expected. Therefore, in the ligands with only ethylenic chains the bithiophene unit plays a significant role on its basicity. This observation could be related with the electron-rich characteristic of the thiophene ring [20], and with its much more robust π-conjugation than in related systems.

In order to clarify this point we have carried out a variable pH NMR study of **L2**. The protonation pattern inferred from the displacements of the chemical shifts with the pD values reproduces the one observed in analogous systems [17]. At this respect, a noticeable information stems from changes on the ^{1}H or ^{13}C

Table 1
Logarithms of the stepwise protonation constants and global basicity for **L1**–**L6** at 298.1 ± 0.1 K

Reaction [a]	**L1** [b]	**L2** [b]	**L3** [d]	**L4** [d]	**L5** [e]	**L6** [e]
$L \rightleftarrows H\Delta HL$	10.56(2) [c]	10.81(2)	10.28	10.27	10.53	9.70
$HL + H \rightleftarrows H_2L$	9.29(2)	9.37(3)	9.21	9.17	9.77	9.14
$H_2L + H \rightleftarrows H_3L$	7.65(3)	8.19(4)	7.65	7.84	8.30	8.05
$H_3L + H \rightleftarrows H_4L$	5.51(4)	6.66(5)	5.59	4.71	5.59	4.70
$H_4L + H \rightleftarrows H_5L$	–	4.23(6)	–	2.95	–	2.97
$\log(\Sigma K_{HjL})$	33.01	39.26	32.70	34.95	34.19	34.56

[a] Charges are omitted for clarity.
[b] This work, $I = 0.15$ mol dm^{-3} NaCl.
[c] Values in parentheses are S.D. on the last significant figure.
[d] Taken from ref. 9c, $I = 0.15$ mol dm^{-3} NaCl.
[e] Taken from ref. [16], $I = 0.1$ mol dm^{-3}.

Table 2
Logarithms of the formation constants of the Cu^{2+} and Zn^{2+} complexes with the ligands **L1**–**L6** determined at 298.1 ± 0.1 K

	Cu^{2+}					
	L1 [b]	**L2** [b]	**L3** [d]	**L4** [d]	**L5** [e]	**L6** [e]
Reaction [a]						
M + L ⇄ ML	18.54(5) [c]	24.21(9)	19.45	18.15	21.69	22.8
ML + H ⇄ MHL	5.52(2)	5.51(4)	4.31	7.57	3.53	5.2
MHL + H ⇄ MH_2L		4.33(3)		4.61		3.8
ML + OH ⇄ ML(OH)				3.66		
	Zn^{2+}					
	L1	**L2**	**L3**	**L4**	**L5**	**L6**
Reaction						
M + L ⇄ ML	9.41(1)	14.10(5)	8.62	11.73	11.25	15.1
ML + H ⇄ MHL	7.10(3)	8.71(1)	7.35	8.28		
MHL + H ⇄ MH_2L				5.40		
ML + OH ⇄ ML(OH)			3.82	5.38		

[a] Charges are omitted for clarity.
[b] This work, $I = 0.15$ mol dm^{-3} NaCl.
[c] Values in parentheses are S.D. on the last significant figure.
[d] Taken from ref. 9c, $I = 0.15$ mol dm^{-3} NaCl.
[e] Taken from ref. [16], $I = 0.1$ mol dm^{-3}.

resonances corresponding to the nucleus in position 1 (for the labelling, see ligand drawing), which is the one that acts as a link between the chain and the aromatic system (thenylic carbon or protons). In this way, the ^1H resonance for the protons linked to this carbon does not change very much on going from the pH region where the free ligand predominates (pH > 11) to the one where the existence of the monoprotonated form prevails; this indicates that the first equivalent of added acid protonates mainly the primary nitrogen of the chain. However, the second equivalent (pH 9.5–10.0) induces a large upfield shift on this signal, suggesting this proton is located on the nitrogen closest to the aromatic fragment (thenylic nitrogen). Finally, the remaining positive charges should enter successively at the middle of the chain. In spite of the fact that the aliphatic signals are the most affected by protonation, the aromatic signals result also affected. In these bithiophenic systems slight upfield movements when the pH becomes more basic are observed on the doublets attributed to H_b and H_c (see ligand drawing), so they seem to be affected by the protonation of nitrogen linked to thenylic carbon [21–23].

4. Metal co-ordination

4.1. Emf measurements

Table 2 reports the stability constants for the formation of Cu^{2+} and Zn^{2+} complexes of ligands **L1** and **L2**. Following the same criteria used in the discussion of the protonation data we have also included in this Table the values for the related ligands **L3**–**L6**.

At first glance, the collected data reveal that **L1** forms $[ML]^{2+}$ and $[MHL]^{3+}$ species with both metal ions, while for **L2** an additional $[CuH_2L]^{4+}$ species is detected. In the ligand containing propylenic units the stability tendency of the copper complexes is **L5** > **L3** > **L1**. In this way, the lower stability of $[Cu(\mathbf{L1})]^{2+}$ and $[Cu(\mathbf{L3})]^{2+}$ with respect to that of $[Cu(\mathbf{L5})]^{2+}$ is a well documented fact based on the different kind of nitrogen donors present in these molecules [9,16]. Effectively, **L5** is a molecule which has two primary amino groups at both ends, in **L1** and **L3** one of such nitrogens has been linked to a bulky hydrophobic substituent through a methylene group. This affects the solvation of the molecules and consequently the stability of their complexes. The close stability displayed by $[Cu(\mathbf{L1})]^{2+}$ (log $K = 18.54(5)$ and $[Cu(\mathbf{L3})]^{2+}$, in which full involvement of all the nitrogen atoms in the co-ordination of the metal ion was ascertained by its X-ray crystal structure [10], suggests a similar co-ordination environment in both complexes. The previous copper data analysis can be extrapolated for the Zn^{2+} complex with the exception of the reverted **L1**–**L3** stability; $[Zn(\mathbf{L1})]^{2+}$ is slightly more stable than $[Zn(\mathbf{L3})]^{2+}$.

The behaviour of the Cu^{2+}–**L2** complexes is particularly different. The complex $[Cu(\mathbf{L2})]^{2+}$ is remarkably more stable than the analogous one $[Cu(\mathbf{L4})]^{2+}$ with the anthracene derivative (Table 2). Although the differences in stability are not as large as in the case of Cu^{2+}, the $[Zn(\mathbf{L2})]^{2+}$ complex is also more stable than $[Zn(\mathbf{L4})]^{2+}$. The stability of the $[Cu(\mathbf{L2})]^{2+}$ species is closer to that displayed by the open-chain polyamine

L6, although slightly higher. The higher stability of $[Cu(\mathbf{L2})]^{2+}$ with respect to $[Cu(\mathbf{L4})]^{2+}$ might be ascribed to the full involvement of all the nitrogen atoms in the co-ordination to the metal ion in the first case. The reduced protonation constant of $[Cu(\mathbf{L2})]^{2+}$ with respect to $[Cu(\mathbf{L4})]^{2+}$ lends support to this point. The slightly higher apparent stability of $[Cu(\mathbf{L4})]^{2+}$ with respect to $[Cu(\mathbf{L6})]^{2+}$ can be related to its higher basicity. The Zn^{2+} complexes of this ligand follow the tendency previously advanced for **L1** which denotes higher stability of the complex with the bithiophene unit with respect to that with the anthracenyl fragment. Although it is difficult to explain such behaviour, factors like participation of the sulfur atoms of the bithiophene ring in the stabilisation of the complexes cannot be discarded.

4.2. Electrochemistry of the Cu^{2+}–*L1* system

The electrochemical activity of **L1** in aqueous solution is confined to oxidation processes which develop close to +1.0 V versus SCE. As described in the literature [5], this electrochemical behaviour would be attributable to two successive one-electron transfer steps coupled with a nucleophilic attack of water. On the contrary, at negative potentials coupled reduction and protonation processes occur at −1.2 V, according to the general scheme proposed for aromatic systems [24–26].

The electrochemical response of the Cu^{2+}–**L1** system has been studied by linear scan, cyclic, and differential pulse voltammetry in the 3–11 pH range. At low scan rates, the CVs exhibit two well defined cathodic peaks at −0.32 (C_1) and −0.58 (C_2) V versus SCE followed by anodic peaks at −0.51 (A_2) and −0.20 (A_1) V, as depicted in Fig. 1.

The cyclic voltammetric pattern remains essentially unchanged upon repetitive cyclic voltammetry and the voltammetric response of freshly prepared solutions remains unchanged with time, denoting the absence of kinetic complications. Peak potentials and peak currents are essentially pH-independent in the pH range where the species $[Cu(\mathbf{L1})]^{2+}$ predominates (pH 7−11). Moreover, no changes in the C_1–A_1 couple are detected if the potential sweep is reversed in the first scan before the appearance of the peak C_2. On increasing the potential scan rate, v, the peak C_1 decreases whereas the peak C_2 increases. Although it is not easy to find an explanation for this behaviour, it could be suggested that the C_1 and C_2 peaks must correspond to the reduction of different Cu(II) species for which a relatively slow inter-conversion equilibrium occurs (Eq. (1)). Neither colour decoloration nor changes in the electrochemical response have been detected after the storage of well deareated solutions of an excess of ligand in the presence of a wire of metallic copper, we can conclude that no stable intermediate Cu(I) species are formed. Then, a dual CE mechanism involving Cu(II) complexes with different co-ordination environment can be proposed:

$$Cu^{II}L \overset{k}{\rightarrow} (Cu^{II}L)' \quad (1)$$

$$Cu^{II}L + 2e^- \rightleftarrows Cu^0 + L \quad (2)$$

$$(Cu^{II}L)' + 2e^- \rightleftarrows Cu^0 + L \quad (3)$$

These data are confirmed by differential pulse voltammetry, a technique that allows an increased peak

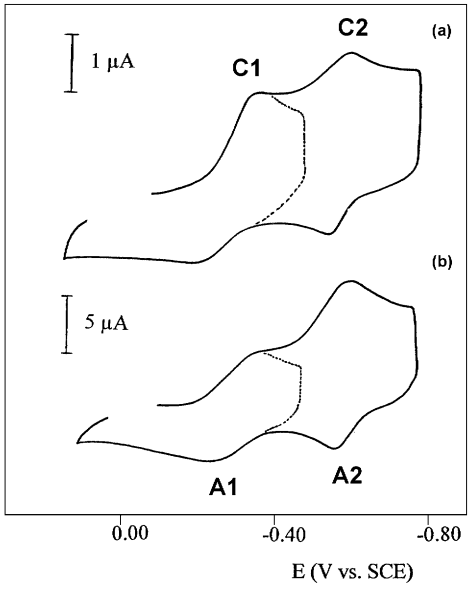


Fig. 1. GCE cyclic voltammograms for a 0.15 M NaCl solution containing $Cu(NO_3)_2 \cdot 6H_2O$ (0.40 mM) plus **L1** (0.85 mM) at pH 8.95. (a): $v = 5$ mV s^{-1}; (b): $v = 50$ mV s^{-1}. Dotted lines represent the CVs when the potential scan is reversed at −0.45 V vs. SCE.

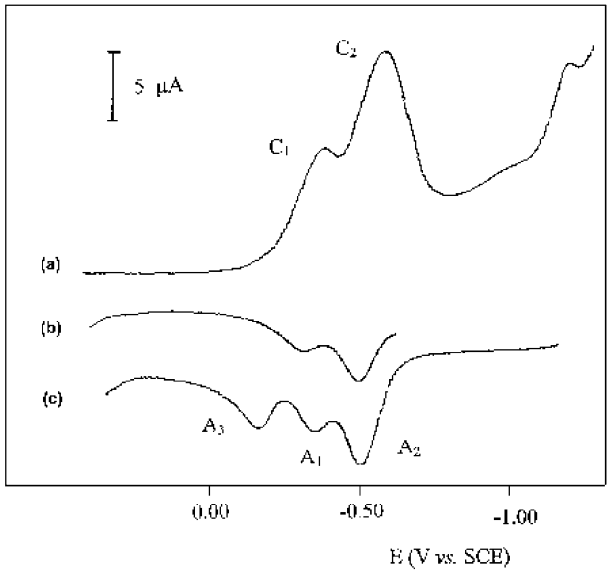


Fig. 2. DPVs for a 0.15 M NaCl solution containing $Cu(NO_3)_2 \cdot H_2O$ (0.30 mM) plus **L1** (0.35 mM) at pH 9.50. (a) Cathodic scan starting at +0.50 V; (b) anodic scan starting from −0.60 V; (c) anodic scan starting from −1.20 V. GCE; $v = 20$ mV s^{-1}; $\Delta U = 80$.

resolution. As can be seen in Fig. 2(a) for the Cu^{2+}–**L1** system, cathodic DPVs exhibit peaks at −0.38 (C_1) and −0.58 (C_2) V clearly separated and followed by a ligand-centred reduction at potentials close to −1.2 V. Interestingly, anodic DPVs depend on the starting potential. As shown in Fig. 2(b), for anodic scans starting from −0.6 V, anodic peaks A_1 and A_2 appear at −0.38 and −0.52 V.

In contrast, on starting the potential scan at −1.2 V, a third peak, A_3, appears at −0.18 V (Fig. 2(c)). Since the ligand is partly reduced at the potentials applied at the beginning of the scan, it appears that Cu^{2+} atoms can also co-ordinate with the reduced ligand, **L***. Thus, the anodic peaks A_1 and A_2 must correspond to the inverse/reverse of processes described by Eqs. (2) and (3), while peak A_3 is attributable to the oxidation reaction described by Eq. (4):

$$Cu^0 + \mathbf{L}^* \rightleftarrows Cu^{II}\mathbf{L}^* + 2e^- \quad (4)$$

This electrochemical behaviour differs from that previously described for macrocyclic thiophenophane ligands for which relatively stable Cu(I) intermediates were detected [23]. Although additional electronic, steric and solvation factors can be adduced to discuss the relative stability of Cu(II) and Cu(I) complexes [27–31], the difference between the cyclic thiophenophane **L7** [23] (see Ligand Drawing) and **L1** could be explained by balancing the number of donor atoms which co-ordinates the metal ion and the flexibility of the polyamine chain. Effectively, the presence of the aromatic spacer supplies rigidity enough to prevent the simultaneous co-ordination of both thenylic nitrogen and so, in the macrocyclic system, the maximum number of nitrogens able to co-ordinate the Cu^{2+} ions would be three. This situation would provide the adequate geometry required for the stabilisation of Cu(I) complexes. On the contrary, in the most flexible linear polyamine chain **L1** the co-ordination of copper probably would take place through four nitrogen atoms and consequently, there are major difficulties to satisfy the structure demanded for the stabilisation of Cu(I) species. The notable destabilisation of Cu(I) complexes observed for macrocyclic polyamines containing biphenyl spacers [32] and for macrocyclic benzene-containing ligands upon incorporation of an axial ligand [33] are consistent with the foregoing considerations.

5. Conclusions

The bithiophene open-chain polyaminic ligands here described show several interesting properties. Firstly, the synthesis, although it does not provide a very high yield is straight forward and allows obtaining the products on a large scale. The basicity and the metal ion studies denote the amphipilic characteristics of the compounds although the chelating characteristics of the parent polyamines are preserved a large extent. All these factors make these compounds promising candidates for potential applications with different purposes.

Acknowledgements

We are indebted to DGICYT Project no. PBQU2000-1424 (Spain) for financial support; P.D. wants to thank Ministerio de Investigación y Ciencia for her Ph.D. grant.

References

[1] (a) D. Fichou, G. Horowitz, F. Garnier, Synth. Met. 39 (1990) 125;
(b) J.V. Caspar, V. Ramamurthy, D.R. Corbin, J. Am. Chem. Soc. 113 (1991) 600;
(c) M.G. Hill, K.R. Mann, L.L. Miller, J.F. Penneau, J. Am. Chem. Soc. 114 (1992) 2728.
[2] (a) F. Garnier, G. Horowitz, D. Fichou, Synth. Met. 28 (1989) C705;
(b) Z.G. Xu, D. Fichou, G. Horowitz, F. Garnier, Adv. Mater. 3 (1991) 150;
(c) K. Yoshino, Synth. Met. 28 (1989) C669;
(d) G. Horowitz, D. Fichou, X.Z. Peng, Z.G. Xu, F. Garnier, Solid State Commun. 72 (1989) 38;
(e) G. Horowitz, X.Z. Peng, D. Fichou, F. Garnier, J. Appl. Phys. 67 (1990) 528.
[3] (a) D. Grebner, M. Helbig, S. Rentsch, J. Phys. Chem. 99 (1995) 16991;
(b) R.S. Becker, J. Seixas de Melo, A.L. Maçanita, F. Elisei, J. Phys. Chem. 100 (1996) 18683;
(c) F. Garnier, G. Horowitz, X.Z. Peng, D. Fichou, Synth. Met. 45 (1991) 163;
(d) S. Hotta, K.J. Waragai, J. Mater. Chem. 1 (1991) 835.
[4] J. Kagan, S.K. Arora, J. Org. Chem. 48 (1983) 4317.
[5] J. Roncali, Chem. Rev. 92 (1992) 711.
[6] (a) M.P. Keane, S. Svenson, A. Naves de Brito, N. Correia, S. Lunell, B. Sjogen, O. Inganas, R. Salaneck, J. Chem. Phys. 93 (1993) 6357;
(b) C. Poux, M. Leclerc, Macromolecules 251 (1992) 2141;
(c) L. Robitaille, M. Leclerc, Macromolecules 27 (1994) 1847;
(d) K. Faïd, M. Fréchette, M. Ranger, M. Mazerolle, I. Lévesque, M. Leclerc, J. Chem. Mater. 7 (1995) 1390.
[7] (a) D.J. Sandman, TRIPS 7 (1994) 1390;
(b) O. Inganas, TRIPS 2 (1994) 189.
[8] (a) C. Roux, J.-Y. Bergeron, M. Leclerc, Makromol. Chem. 194 (1993) 869;
(b) C. Roux, K. Faïd, M. Leclerc, Chem. Mater. 6 (1994) 620;
(c) C. Roux, K. Faïd, M. Leclerc, Polym. News 19 (1994) 6.
[9] M. Micheloni, A. Sabatini, A. Vacca, Inorg. Chim. Acta 25 (1977) 41.
[10] T. Sone, Y. Ohb, R. Watanabe, Bull. Chem. Soc. Jpn. 62 (1989) 1346.
[11] (a) A.A. Van Arman, A.W. Czarnik, J. Am. Chem. Soc. 112 (1990) 5736;
(b) M.A. Bernardo, F. Pina, B. Escuder, E. García-España, M.L. Godino-Salido, J. Latorre, S.V. Luis, J.A. Ramírez, C. Soriano, J. Chem. Soc., Dalton Trans. (1999) 915.;
(c) M.T. Albelda, S. Alves, E. García-España, S.V. Luis, F. Pina, C. Soriano, Eur. J. Inorg. Chem. (2001) 405.

[12] A.K. Convigton, M. Paabo, R.A. Robinson, R.G. Bates, Anal. Chem. 40 (1968) 700.
[13] E. García-España, M.-J. Ballester, F. Lloret, J.-M. Moratal, J. Faus, A. Bianchi, J. Chem. Soc., Dalton Trans (1988) 101.
[14] M. Fontanelli, M. Micheloni, in: Proceedings of the I Spanish–Italian Congress on Thermodynamics of Metal Complexes, Diputación de Castellón, Spain, 1990.
[15] (a) G. Gran, Analyst (London) 77 (1952) 881;
(b) F.J. Rossotti, H. Rossotti, J. Chem. Educ. 42 (1965) 375.
[16] A. Sabatini, A. Vacca, A. Gans, Coord. Chem. Rev. 120 (1992) 389.
[17] R.M. Smith, A.E. Martell, Critical Stability Constants, Plenum Press, New York, 1975, p. 2.
[18] A. Bencini, A. Bianchi, E. García-España, M. Micheloni, J.A. Ramírez, Coord. Chem. Rev. 188 (1999) 97.
[19] J. Aragó, A. Bencini, E. García-España, M. Micheloni, P. Paoletti, J.A. Ramírez, P. Paoli, Inorg. Chem. 30 (1991) 1843.
[20] T.A. Skotheim (Ed.),Handbook of Conducting Polymers, Marcel Dekker, New York, 1986.
[21] A. Bianchi, B. Escuder, E. García-España, S.V. Luis, V. Marcelino, J.F. Miravet, J.A. Ramírez, J. Chem. Soc. Perkin Trans. 2 (1994) 1253.
[22] M.I. Burguete, B. Escuder, E. García-España, J. Latorre, S.V. Luis, J.A. Ramírez, Inorg. Chim. Acta (2000) 970.
[23] J.A. Aguilar, P. Díaz, A. Doménech, E. García-España, J.M. Llinares, S.V. Luis, J.A. Ramírez, C. Soriano, J. Chem. Soc. Perkin Trans. 2 (1999) 1159.
[24] P. Zuman, C.L. Perrin, Organic Polarography, Interscience, New York, 1969.
[25] J. Simonet, M.-A. Michel, H. Lund, Acta Chem. Scand. B 29 (1975) 489.
[26] D. Lexa, J.-M. Savéant, K.-B. Su, D.-L. Wang, J. Am. Chem. Soc. 110 (1988) 7671.
[27] A.B.P. Lever, Inorg. Chem. 29 (1990) 1271.
[28] M.M. Bernardo, M.J. Heeg, R.R. Schroeder, L.A. Ochrymowiycz, D.B. Rorabacher, Inorg. Chem. 31 (1992) 191.
[29] G. Golub, H. Cohen, P. Paoletti, A. Bencini, L. Messori, I. Bertini, D. Meyerstein, J. Am. Chem. Soc. 117 (1995) 8353.
[30] M. Saphier, A. Burg, S. Sheps, H. Cohen, D. Meyerstein, J. Chem. Soc., Dalton Trans (1999) 1845.
[31] G. Golub, H. Cohen, D. Meyerstein, J. Chem. Soc., Chem. Commun. (1992) 398.
[32] Unpublished results.
[33] A. Doménech, E. García-España, S.V. Luis, V. Marcelino, J.F. Miravet, Inorg. Chim. Acta 299 (2000) 238.

PERGAMON

Polyhedron 21 (2002) 1531–1536

POLYHEDRON

www.elsevier.com/locate/poly

Synthesis and coordination properties of functionalized β-cyclodextrins. Thermodynamic of proton and copper(II) complexes of 3A-deoxy-3A-(2-methylaminopyridine)-2A(*S*),3A(*R*)-β-cyclodextrin in aqueous solution

Giuseppe Maccarrone [a], Enrico Rizzarelli [a,b,*], Graziella Vecchio [a]

[a] *Dipartimento di Scienze Chimiche, Università di Catania, viale A. Doria 8, 95125 Catania, Italy*
[b] *Istituto per lo Studio delle Sostanze Naturali di Interesse Alimentare e Chimico-Farmaceutico del CNR, V.le A.Doria 8, 95125 Catania, Italy*

Received 10 January 2002; accepted 8 February 2002

Dedicated to Professor Dr. Antonio Braibanti

Abstract

The 3A-deoxy-3A-(2-methylaminopyridine)-2A(*S*),3A(*R*)-β-cyclodextrin (CDampy3) was synthesized and characterized by NMR spectroscopy. The proton and copper(II) complex formation and stability of this new β-cyclodextrin derivative were determined by potentiometric and calorimetric investigations, carried out in aqueous solution at 25 °C and $I = 0.1$ mol dm^{-3} (KNO_3). The ΔH° and ΔS° values allowed to bring to light the role of the hydrogen bond between the amine and the hydroxyl groups in the basicity decrease of NH group of this 3-functionalized β-cyclodextrin. The comparison between the log K values of copper(II) complexes with CDampy3 and those of 6-deoxy-6-(2-methylaminopyridine)-β-cyclodextrin (CDampy6) allowed to determine the donor atoms involved in the coordination to metal ion. The high stability constant of $[Cu(CDampy3)]^{2+}$ in comparison with $[Cu(CDampy6)]^{2+}$ was attributed to the involvement of the OH groups in the binding to copper(II) ion. © 2002 Elsevier Science Ltd. All rights reserved.

Keywords: Cyclodextrins; Copper(II) complexes; 2-Methylaminopyridine

1. Introduction

Cyclodextrins (CDs) are cyclic oligosaccharides consisting of six or more α-D-glucopyranose units, which have attracted interest in a variety of contexts [1–6]. The direct coordination of native cyclodextrins to the metal ion has been found only for some metal ions because of the poor coordinating ability of their hydroxy groups [7–10]. The secondary OHs act as coordinating groups in the characterized complexes. The only metal complexes with high stability constants described are derivatives in which, the cyclodextrin torus serves as a framework for attaching complexing functional groups [11–33]. In this context mainly six-functionalized cyclodextrins metal complexes have been synthesized and fully characterized [12,15–18,21–28]. This in spite of the fact that the first metallo-enzyme model by cyclodextrins, 'Breslow enzyme' [30], has been the nickel(II) complex with a functional group attached to a secondary alcohol group on the secondary face of CD. Furthermore a CD 3-derivative cobalt(III) complex in comparison to the analogous six-derivative shows larger activity as hydrolase model [15,16]. The reason for the less extensive investigation on the secondary side derivatives is related to the fact that, primary hydroxyl groups are more nucleophilic than secondary OHs and they are easily modified into other functional groups. The secondary side is more crowded than the primary side due to the presence of twice the number of hydroxyl groups [1,2]. Hydrogen bonds between the 2-OH and 3-OH make these OHs less flexible and less reactive. The C-3 functionalization gives chemical modification of

* Corresponding author.
E-mail address: erizzarelli@dpchi.unict.it (E. Rizzarelli).

0277-5387/02/$ - see front matter © 2002 Elsevier Science Ltd. All rights reserved.
PII: S0277-5387(02)00975-0

functionalized unit in altrose and furthermore the tosylation of cyclodextrin, useful starting reaction, is a low yield reaction. New synthetic routes have been reported to give with high yield the CD tosylate [35]. In order to investigate on the complexing features of three-derivatives, recently the thermodynamic characterization of three-functionalized cyclodextrin with ethylendiamine and of its copper(II) complexes have been reported by our group [33]. The ability of this class of derivatives to complex the metal ion with 2-OH of the functionalized ring in addition to the donor atoms present of the functionalizing moiety has been brought to light. The stability constant of copper(II) complex constant complex formation of the CDen3 is larger than that of the analogous six-derivative. To further investigate on the three-derivative properties, we report the potentiometric and calorimetric investigations on a new three-functionalized derivative, the 3A-deoxy-3A-(2-methylaminopyridine)-2A(*S*),3A(*R*)-β-cyclodextrin (CDampy3) (Fig. 1). The formation and stability of copper(II) complexes of CDampy3 were characterized by means of potentiometric measurements.

2. Experimental

2.1. Material

Commercially available reagents were used directly unless otherwise noted. TLC was carried out on silica gel plates 60F-254 (Merck). Cyclodextrin derivatives were detected with UV light and the anisaldehyde reagent. Merck lichroprep RP-8 (40–60 mm) was used for reversed phase column chromatography. NMR spectra were performed at 25 °C in D_2O on a Bruker AC-200 spectrometer. DSS was used as an external standard.

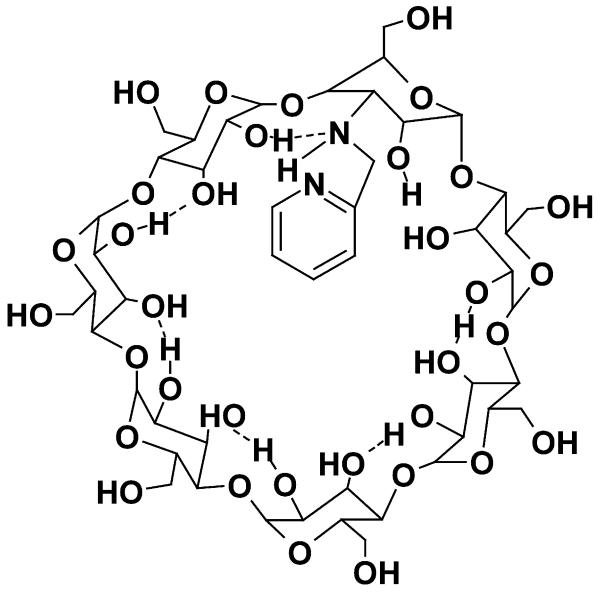


Fig. 1. 3A-deoxy-3A-(2-methylaminopyridine)-2A(*S*),3A(*R*)-β-cyclodextrin.

2.2. Synthesis of 3A-deoxy-3A-(2-methylaminopyridine)-2A(S),3A(R)-β-cyclodextrin

A solution of 500 mg of 2-CDOts [34,35] and 970 mg of $NaHCO_3$ in 7 ml of water was stirred at 60 °C for 3.5 h. The formed epoxide was not isolated. The 2-methylaminopyridine (ampy) in excess was directly added to the solution. The reaction mixture was stirred under nitrogen at 60 °C for 5 h. The solution was evaporated to dryness in vacuo, precipitated in acetone, and purified by elution from a column (35 × 900 mm) of CM-Sephadex C-25 column (NH_4^+ form) with water 1 l, then with a 0–0.25 M NH_4HCO_3 linear gradient (total volume 2 l). The appropriate fractions were concentrated to give CDampy3, $Rf = 0.46$ (5/3/1 PrOH–H_2O–NH_3), yield: 45%.

^{1}H NMR (D_2O, 200 MHz): 2.97 (dd,1H, H-3A), 3.34–4.05 (m, 40H, H-2,H-4, H-5, H-6, H-3), 4.28 (m, 1H, H-5A), 4.76 (d, 1H, H-1A) 4.95–5.10 (m, 6H, H-1), 8.46 (d, 1H, H-1 of pyridine ring), 7.84 (t, 1H, H-3 of pyridine ring), 7.46 (d, 1H, H-4 of pyridine ring), 7.36 (m, 1H, H-2 of pyridine ring).

^{13}C NMR: 160.57 (C-2 py), 151.1 (C-6 of py), 140.9 (C-4 of py), 126.0,125.7 (C-3,5 of py), 106.1 (C-1A), 104.5-104 (C-1 CD), 83.7 (C-4 CD), 78.6 (C-3A CD), 75.9–74.6 (C-2,3,5 CD), 62.9–62.8 (C-6 CD), 54 (CH_2).

2.3. Potentiometric and calorimetric measurements

Copper(II) nitrate was prepared from copper(II) basic carbonate by adding a slight excess of HNO_3. Stock solution concentration was determined by EDTA titrations with a murexide indicator. The concentrations of HNO_3 and KOH stock solutions were determined by titration with the primary standard *tris*(hydroxymethyl)aminomethane (THAM) and potassium hydrogen phthalate, respectively. Potassium nitrate (Suprapur Merck) was used without further purification. All solutions were prepared with doubly distilled water.

Stability constants for proton and copper(II) complexes were calculated from potentiometric titrations carried out at 25 °C (total volumes: 2.5 cm^3). Duplicate or triplicate titrations were carried out at 1:1 and 1:2 Cu–L ratios, with KOH. The KOH solution was added using Hamilton burettes equipped with 0.25 or 0.50 cm^3 syringes. pH changes were measured using a combined Metrohm 125 microelectrode, standardised on the pH $-\log[H^+]$ scale by titrating HNO_3 solutions with CO_2 free KOH. The ionic strength of all solutions was 0.1 mol dm^{-3} (KNO_3).

ΔH° values were determined by calorimetric titrations using a LKB TAM 2277 instrument in isothermal condition at $T = 25.000 \pm 002$.

Other details were as previously described [13,18].

2.4. Calculations

Calculations for the electrode system E° values, ligand purity, and HNO_3 excess in the metal stock solution were performed using the Gran method [36] or the least-squares ACBA computer program [37]. All other potentiometric data were handled using the program SUPERQUAD [38], thus minimizing the error-square sum of the differences between measured and calculated electrode potentials. In this paper, errors in stability constant values are expressed as three times standard deviations. The ΔH° values of complex formation were calculated by the DOEC program [39]. Distribution diagram for the copper(II)–CDampy3 system (1:1 ratio, $c = 5 \times 10^{-3}$ mol dm^{-3}) was calculated by the DISDI program.

3. Results and discussion

The new ligand CDampy3 was synthesized in good yield from the 2-deoxy-2-[(*p*-tosyl)oxy]-β-cyclodextrin treated with an aqueous solution of $NaHCO_3$ to give 2,3-manno-epoxide. Ampy was added in excess to the mixture containing the epoxide. The CDampy3 was isolated by chromatography. As described in the literature [40,41], the ring opening of the manno-epoxide generally gives rise to derivative in position three having modified altrose residue. The ^{1}H NMR were assigned by COSY. The introduction of one altroside into the cyclodextrin caused unequivalency of the glucose units in the NMR spectrum. After the three-functionalization in addition to the two groups of peaks observed in the 4.1–3.5 ppm region due to the CD protons, peaks are present at 2.97 and 4.28 ppm due to the H-3A and H-5A (A is the functionalized ring). All the other protons of the modified ring are easily assigned on the COSY spectra.

3.1. Proton and copper(II) binary complexes: formation, stability and bonding details

The generalized formation reaction of the ligand with protons and copper(II) ions is given in Eq. (1), where L is CDampy3. For the sake of clarity, charges on the copper(II) complexes have been omitted.

$$m\mathrm{Cu}^{2+} + l\mathrm{L} + h\mathrm{H} \rightleftarrows \mathrm{Cu}_m\mathrm{L}_l\mathrm{H}_h \quad (1)$$

The stability constant β_{mlh} is defined in Eq. (2).

$$\beta_{mlh} = \frac{[\mathrm{Cu}_m\mathrm{L}_l\mathrm{H}_h]}{[\mathrm{Cu}^{2+}]^m[\mathrm{L}]^l[\mathrm{H}]^h} \quad (2)$$

Analysis of the titration data for CDampy3 in the absence of copper(II) provides the formation constants for amino and pyridine nitrogen protonation (Eqs. (3) and (4)).

$$\mathrm{L} + \mathrm{H}^+ \rightleftarrows \mathrm{LH}^+ \quad (3)$$

$$\mathrm{L} + 2\mathrm{H}^+ \rightleftarrows \mathrm{LH}_2^{2+} \quad (4)$$

The proton and copper(II) complex formation constants determined in this study are given in Table 1 together with those found for 6-deoxy-6-(2-methylaminopyridine)-β-cyclodextrin (CDampy6) [18], 2-aminomethylpyridine (ampy) [42], *N*-methyl-2-aminomethylpyridine (CH_3ampy) [42]. The equilibria necessary to fit the experimental titration curves for the solutions of copper(II) complex formation with the CDampy3 under study are given in Eqs. (5)–(8).

$$\mathrm{Cu}^{2+} + \mathrm{L} \rightleftarrows \mathrm{CuL} \quad (5)$$

$$\mathrm{Cu}^{2+} + \mathrm{L} \rightleftarrows \mathrm{CuLH}_{-1} + \mathrm{H}^+ \quad (6)$$

$$\mathrm{Cu}^{2+} + \mathrm{L} \rightleftarrows \mathrm{CuLH}_{-2} + 2\mathrm{H}^+ \quad (7)$$

$$2\mathrm{Cu}^{2+} + 2\mathrm{L} \rightleftarrows \mathrm{Cu}_2\mathrm{L}_2\mathrm{H}_{-2} + 2\mathrm{H}^+ \quad (8)$$

The complex formations are listed in Table 2, together with those of CDampy6 [18], ampy [42] and CH_3ampy [42].

The log K for the amino group protonation of CDampy3 (6.35) is about 2.5 log units lower than that for ampy (8.74) and CH_3ampy (9.01) and slightly lower than that of CDampy6 (6.86). The decrease in the amino nitrogen basicity of this latter CD isomer derivative was attributed to the proximity of the NH group to the cavity, in agreement with what previously reported for this type of functionalized cyclodextrins [13,18,21,43]. The main difference between the two CDampy isomers consists in the involvement of the NH group of CDampy3 in the hydrogen bonding network between the 2-OH and the 3-OH groups that stabilizes the toroidal structure of the β-CD (Fig. 1). Thus the low basicity of the NH group can be attributed to the existence of this hydrogen bond that is destroyed in the formation of the monoprotonated species. At the same time this cleavage of the hydrogen bond should imply a significant decrease of rigidity of the cavity, with a sort of collapse of the toroidal structure.

The comparison between the enthalpy and entropy changes (Table 1) associated to the proton complex formation of the two CDampy isomers support what suggested on the basis of the differences in log K values. In fact the ΔH° value of $[(\mathrm{CDampy3})\mathrm{H}]^+$ species (−1.7 kcal mol^{-1}) is less exothermic than that of $[(\mathrm{CDampy6})\mathrm{H}]^+$ species (−9.3 kcal mol^{-1}) due to the fact that the lone pair of the NH group of CDampy3 is less available to interact with the proton than the amino

Table 1
Thermodynamic parameters of protonation of CDampy3, CDampy6 [18], ampy [a] [43] and CH_3ampy[a] [43] at 25 °C and $I = 0.1$ mol dm^{-3} (KNO_3)

Equilibrium	log K	$-\Delta G^\circ$ kcal mol^{-1}	$-\Delta H^\circ$ kcal mol^{-1}	ΔS° cal mol^{-1} °
Cdampy3 + H^+ = [(CDampy3)H]$^+$	6.35(1)	8.65(1)	1.7(2)	23.0(7)
[(Cdampy3)H^+] + H^+ = [(Cdampy3)H_2]$^{2+}$	1.42(1)	1.94(1)	2.7(3)	−2.3(1)
Cdampy6 + H^+ = [(CDampy6)H]$^+$	6.855	9.36	9.3	0.2
[(Cdampy6)H]$^+$ + H^+ = [(Cdampy6)H_2]$^{2+}$	2.05	2.80	2.7	0.4
ampy + H^+ = [(ampy)H]$^+$	8.74	11.93	10.98	3.2
[(ampy)H]$^+$ + H^+ = [(ampy)H_2]$^{2+}$	2.25 [a]	3.07	2.95	0.4
CH_3ampy + H^+ = [(CH_3ampy)H]$^+$	9.01	12.29	9.88	8.1
[(CH_3ampy)H]$^+$ + H^+ = [(CH_3ampy)H_2]$^{2+}$	1.91 [a]	2.61	2.34	0.9

3σ In parentheses.
[a] $I = 0.5$ mol dm^{-3}.

Table 2
Logarithmic stability constant values for copper(II) complexes of CDampy3, CDampy6 [18], ampy [a] [43] and CH_3ampy[a] [43] at 25 °C and $I = 0.1$ mol dm^{-3} (KNO_3)

Equilibrium	log β
Cu^{2+} + Cdampy3 = [Cu(Cdampy3)]$^{2+}$	7.97(2)
Cu^{2+} + Cdampy3 = [Cu(Cdampy3)H_{-1}]$^+$ + H^+	2.79(3)
Cu^{2+} + Cdampy3 = [Cu(Cdampy3)H_{-2}] + 2H^+	−4.95(4)
2Cu^{2+} + 2Cdamp3 = [Cu_2(Cdampy3)$_2H_{-2}$]$^{2+}$ + 2H^+	7.52(4)
Cu^{2+} + Cdampy6 = [Cu(Cdampy6)]$^{2+}$	6.876
Cu^{2+} + ampy = [Cu(ampy)]$^{2+}$	9.55
Cu^{2+} + CH_3ampy = [Cu(CH_3ampy)]$^{2+}$	9.09

3σ In parentheses.
[a] $I = 0.5$ mol dm^{-3}.

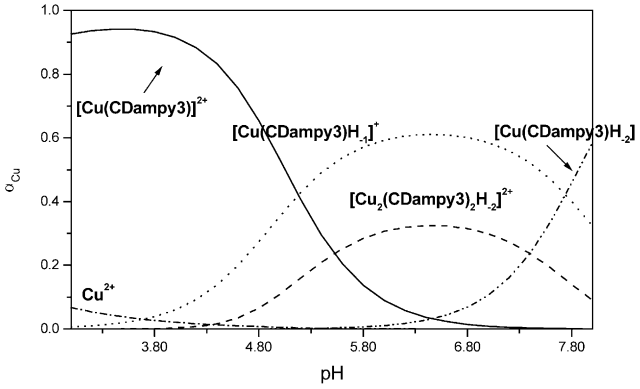


Fig. 2. Distribution diagram for the copper(II)–CDampy3 system (1:1 ratio, $c = 5 \times 10^{-3}$ mol dm^{-3}).

residue of CDampy6. The much less favourable enthalpy changes of [(CDampy3)H]$^+$ accompanying the break-up of the hydrogen bond is counterbalanced by the unusually large entropy change. The ΔS° value reflects the conformational change associated with the monoprotonated species. The larger rim of the β-CD partially loses the rigid ordered structure due to hydrogen bonding network to assume a more flexible partly disordered conformation. The altrose unit could interconvert easily in the $^4C_1$ or $^0S_2$ conformation, in a similar way to altrocyclodextrin [44]. The thermodynamic data bring to light this change, namely by the positive ΔS° value of [(CDampy3)H]$^+$ (23 cal mol^{-1} °) higher not only than that of [(CDampy6)H]$^+$ (0.2 cal mol^{-1} °), but also of ampy and CH_3ampy (Table 1). The decrease of basicity is much less marked in the second protonation step of CDampy3 with respect to CDampy6 as well as the ampy and CH_3ampy. For the second protonation step, ΔH° values are more or less equal and the slight differences in ΔS° values can be attributed to small effects of the cavity environment.

[Cu(CDampy3)]$^{2+}$ is the major species from pH 3 to 5, then CDampy3 forms monomeric and dimeric deprotonated species (Fig. 2). Comparing the stability constant values of the copper(II) mono complexes of the two CDampy isomers with those of the analogous species of ampy and CH_3ampy, the higher stability of these latter follows the differences in the basicity of the amine groups (Table 2). Despite similar basicity CDampy3 displays a stability constant value higher than that of CDampy6 in the CuL species. It is necessary to invoke the involvement of the OH groups of the larger rim of the β-CD to explain this behavior (Fig. 3(a)). Increasing the pH, this tendency of the OH groups to bind to copper(II), verified for other three-functionalized derivatives of CD [7–10] and for some diaminoalcohols [45], is evident in the mono- and bis-deprotonated species as well as in the dimeric species. Structures of copper(II) complexes with native β-CD have been reported, showing the involvement of OH groups [10]. On this basis, the complexation of the deprotonated 2-OH of the A ring can be hypothesized to explain the high stability constant for the [Cu(CDampy3)H_{-1}]$^+$ species. Analogously it is reasonable to suggest that the deprotonated 2-OH group of the A and G rings could coordinate the copper(II) ion (Fig. 3(c)). A possible structure of dimeric species [Cu_2(CDampy3)$_2H_{-2}$]$^{2+}$ is sketched in Fig. 4, as reported for some amino alcohol complexes [45]. The inclusion of the pyridine ring into the CD cavity could stabilize this species.

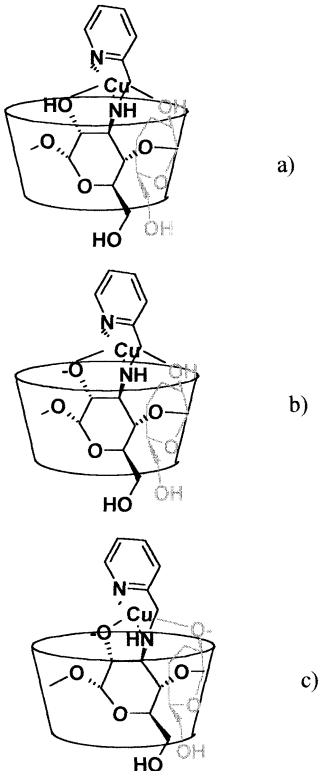


Fig. 3. Schematic representation of $[Cu(CDampy3)]^{2+}$ (a), $[Cu(CDampy3)H_{-1}]^{+}$ (b), $[Cu(CDampy3)H_{-2}]$ (c) species.

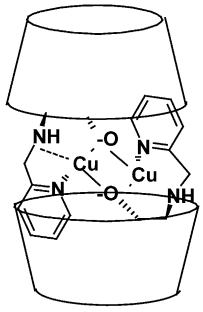


Fig. 4. Schematic representation of $[Cu_2(CDampy3)_2H_{-2}]^{2+}$ species.

4. Concluding remarks

A number of thermodynamic investigations have been carried out on proton and metal complex formation of six functionalized derivatives [13,16–18,21–26,32]. Thus the features of six amino derivatives in terms both of basicity and of complexing ability have been widely explored. The thermodynamic data here reported deals with the protonation and complexation reaction of three functionalized β-cyclodextrin. The involvement of functionalizing group on the C-3 carbon in the H-bond formation has been verified by calorimetry. The OH groups adjacent to the altrose unit, that is the 2-OH of A and 2-OH of G ring, seem bind to the metal ion in the deprotonated form and in the native form, thus determining high complexation stability constants if compared with the analogous six derivatives. These results could be used in the rationalization of the features of three and of six derivatives in the enzyme mimicking [12].

Acknowledgements

We thank MURST (E.R., PRIN 2000–2002) and CNR for partial support of this work.

References

[1] M.L. Bender, M. Komiyama, Cyclodextrin Chemistry, Springer, Berlin, 1978.
[2] W. Saenger, Angew. Chem., Int. Ed. Engl. 19 (1980) 344.
[3] Various author, Chem. Rev. J. (1998).
[4] L. Atwood, J.E.D. Davies, D.D. MacNicol, F. Vogtle (Eds.),-Comprehensive Supramolecular Chemistry, vol. 3, Pergamon, Oxford, 1996.
[5] G. Wenz, Angew. Chem., Int. Ed. Engl. 33 (1994) 803.
[6] C.J. Easton, S.F. Lincoln, Chem. Soc. Rev. (1996) 163.
[7] R. Fuchs, N. Habermann, P. Klufers, Angew. Chem., Int. Ed. Engl. 32 (1993) 852.
[8] P. Klufers, J. Schuhmacher, Angew. Chem., Int. Ed. Engl. 33 (1994) 1863.
[9] K. Yamanari, M. Nakamichi, Y. Shimura, Inorg. Chem. 28 (1989) 248.
[10] Y. Matsui, T. Kurida, M. Yagi, T. Okayama, Bull. Chem. Soc. Jpn. 48 (1975) 2187.
[11] I. Tabushi, Tetrahedron 40 (1984) 269.
[12] E. Rizzarelli, G. Vecchio, Coord. Chem. Rev. 188 (1999) 343 (and references therein).
[13] R.P. Bonomo, V. Cucinotta, F. D'Alessandro, G. Impellizzeri, G. Maccarrone, G. Vecchio, E. Rizzarelli, Inorg. Chem. 30 (1991) 2708.
[14] E.U. Akkaya, A.W. Czarnik, J. Am. Chem. Soc. 110 (1988) 8553.
[15] U.E. Akkaya, A.W. Czarnik, J. Phys. Org. Chem. 5 (1992) 540.
[16] G. Impellizzeri, G. Maccarrone, E. Rizzarelli, G. Vecchio, R. Corradini, M. Marchelli, Angew. Chem., Int. Ed. Engl. 30 (1991) 1348.
[17] R. Corradini, A. Dossena, G. Impellizzeri, G. Maccarrone, R. Marchelli, E. Rizzarelli, G. Sartor, G. Vecchio, J. Am. Chem. Soc. 116 (1994) 10267.
[18] R.P. Bonomo, V. Cucinotta, F. D'Alessandro, G. Impellizzeri, G. Maccarrone, E. Rizzarelli, G. Vecchio, L. Carima, R. Corradini, G. Sartor, R. Marchelli, Chirality 9 (1997) 341.
[19] I. Tabushi, Coord. Chem. Rev. 86 (1988) 1–42 (and reference therein).
[20] V. Cucinotta, F. D'Alessandro, G. Impellizzeri, G. Vecchio. J. Chem. Soc., Chem. Commun. (1992) 1743.
[21] R. Bonomo, V. Cucinotta, F. D'Alessandro, G. Impellizzeri, G. Maccarrone, E. Rizzarelli, G. Vecchio, J. Inclus. Phen. Mol. Rec. 15 (1993) 167.
[22] R. Bonomo, B. Di Blasio, G. Maccarrone, V. Pavone, C. Pedone, E. Rizzarelli, M. Saviano, G. Vecchio, Inorg. Chem. 35 (1996) 4497.
[23] S.E. Brown, J.H. Coates, C.J. Easton, S.J. van Eyk, S.F. Lincoln, B.L. May, M.A. Stile, C.B. Whalland, M.L. Williams, J. Chem. Soc., Chem. Commun. (1994) 47.
[24] E. Brown, J.H. Coates, C.J. Easton, S.F. Licoln, J. Chem. Soc., Faraday Trans. 90 (1994) 739.

[25] S.E. Brown, C.A. Haskard, C.J. Easton, S.F. Lincoln, J. Chem. Soc., Faraday Trans. 91 (1995) 1013.
[26] C.A. Haskard, C.J. Easton, B.L. May, S.F. Lincoln, Inorg. Chem. 35 (1996) 1059.
[27] T. Campagna, G. Grasso, E. Rizzarelli, G. Vecchio, Inorg. Chim. Acta 275/276 (1998) 395.
[28] R. Bonomo, S. Pedotti, G. Vecchio, E. Rizzarelli, Inorg. Chem. 35 (1996) 6873.
[29] I. Tabushi, Y. Kuroda, J. Am. Chem. Soc. 106 (1984) 4580.
[30] R. Breslow, L.E. Overman, J. Am. Chem. Soc. 92 (1970) 1076.
[31] V. Cucinotta, G. Grasso, S. Pedotti, E. Rizzarelli, G. Vecchio, B. Di Blasio, C. Isernia, M. Saviano, C. Pedone, Inorg. Chem. 35 (1996) 7535.
[32] R.P. Bonomo, V. Cucinotta, G. Maccarrone, E. Rizzarelli, G. Vecchio, J. Chem. Soc., Dalton Trans. (2001) 1366.
[33] R.P. Bonomo, G. Maccarrone, E. Rizzarelli, G. Vecchio, submitted for publication.
[34] R. Breslow, A.W. Czarnik, M. Lauer, R. Leppkes, J. Winkler, S. Zimmerman, J. Am. Chem. Soc. 108 (1986) 1969.
[35] K. Teranishi, K. Watanabe, T. Hisamatu, Yamada, J. Carbohydr. Chem. 17 (1998) 489.
[36] G. Gran, Analyst 77 (1952) 661.
[37] G. Arena, E. Rizzarelli, S. Sammartano, C. Rigano, Talanta 26 (1979) 1.
[38] P.P. Gans, A. Sabatini, A. Vacca, J. Chem. Soc., Dalton Trans. (1985) 1195.
[39] C. Rigano, E. Rizzarelli, S. Sammartano, Thermochim. Acta 33 (1979) 211.
[40] J. Yan, R. Watanabe, M. Yamaguchi, Tetrahedron Lett. 40 (1999) 1513.
[41] D.-Q. Yuan, K. Ohta, K. Fujita, Chem. Commun. (1996) 821.
[42] R.M. Smith, A.E. Martell, Critical Stability Constants, vol. 2, Plenum, New York, 1975.
[43] B.L. May, S.D. Kean, C.J. Easten, S.F. Lincoln, J. Chem. Soc., Perkin Trans 1 (1997) 3157.
[44] Y. Nogami, K. Nasu, T. Koga, K. Ohta, K. Fujita, S. Immel, H.J. Linder, G.E. Schmitt, F.W. Lichtenthaler, Angew. Chem., Int. Engl. 36 (1997) 1899.
[45] M. Jezowska-Bojczuk, S. Lamotte, H. Kozlowski, A. Temeriusz, I. Zajaczkowski, J. Stepinski, P. Decock., J. Chem. Soc., Dalton Trans. (1995) 3849.

ELSEVIER

Polyhedron 21 (2002) 1537–1538

POLYHEDRON

www.elsevier.com/locate/poly

Author Index of ISMEC XII, Thermodynamics of Metal Complexes

Aguirre, A., see Domínguez, M., 1429
Alberti, G., see Pesavento, M., 1343
Amorello, D., Gambino, V., Romano, V. and Zingales, R., The determination of mineral acidity excess in solutions containing Ga(III), Al(III), Bi(III), 1369
Anticó, E., see Domínguez, M., 1429
Araujo, M.L., see Armas, M.T., 1513
Armas, M.T., Mederos, A., Gili, P., Domínguez, S., Hernández-Molina, R., Lorenzo, P., Vaz-Júnior, S., Baran, E.J., Araujo, M.L., Lubes, V. and Brito, F., Speciation in oxovanadium(IV)–carnosine system, 1513

Baran, E.J., see Armas, M.T., 1513
Bencini, A., Berni, E., Chuburu, F., Giorgi, C., Handel, H., Le Baccon, M., Paoletti, P. and Valtancoli, B., Basicity and coordination ability of linear hexa-amines in relation to N-$(CH_2)_n$-N chain-link lengths. A solution study, 1459
Bencini, A., Bianchi, A., Fornasari, P., Giorgi, C., Paoletti, P. and Valtancoli, B., Cd(II) complexation in aqueous solution with dipyridine- and phenanthroline-containing polyamine macrocycles, 1329
Berni, E., see Bencini, A., 1459
Beyer, L., see Domínguez, M., 1429
Bianchi, A., see Bencini, A., 1329
Biesuz, R., see Pesavento, M., 1343
Bismondo, A., Di Bernardo, P., Portanova, R., Tolazzi, M. and Zanonato, P.L., Complexation of lanthanide(III) with a tripodal polyaza polycatecholate ligand, 1393
Braibanti, A., Molecular energy parameters by solution thermodynamics, 1439
Braibanti, A. and Fisicaro, E., Preface, 1311
Braibanti, A., see Compari, C., 1503
Brito, F., see Armas, M.T., 1513
Bugella-Altamirano, E., see Serrano-Padial, E., 1451

Carballo, R., see Serrano-Padial, E., 1451
Carunchio, V., Metal complexes: from pioneers to the GTC, 1313
Castiñeiras, A., see Choquesillo-Lazarte, D., 1485
Castiñeiras, A., see Serrano-Padial, E., 1451
Cecconi, F., Frassineti, C., Gans, P., Iotti, S., Midollini, S., Sabatini, A. and Vacca, A., Complex formation equilibria of phosphocreatine with sodium, potassium and magnesium ions, 1481
Choquesillo-Lazarte, D., Covelo, B., González-Pérez, J.M., Castiñeiras, A. and Niclós-Gutiérrez, J., Metal chelates of *N*-(2-pyridylmethyl)iminodiacetate(2-) ion (pmda). Part I. Two mixed-ligand copper(II) complexes of pmda with *N*,*N*-chelating bases. Synthesis, crystal structure and properties of $H_2pmda \cdot 0.5H_2O$, $[Cu(pmda)(pca)] \cdot 3H_2O$ (pca = α-picolylamine) and $[Cu(pmda)(Hpb)] \cdot 5H_2O$ (Hpb = 2-(2′-pyridyl)benzimidazole), 1485
Choquesillo-Lazarte, D., see Serrano-Padial, E., 1451
Chuburu, F., see Bencini, A., 1459
Compari, C., Fisicaro, E. and Braibanti, A., Cooperativity effects in the protonation of aliphatic polyamines, 1503
Compari, C., see Fisicaro, E., 1497
Comuzzi, C., Novelli, V., Portanova, R. and Tolazzi, M., The influence of *N*-alkylation and chain length in the coordination ability of diamines towards silver(I) in dimethylsulfoxide, 1337
Comuzzi, C., Di Bernardo, P., Portanova, R., Tolazzi, M. and Zanonato, P., Affinity of lanthanide(III) ions for oxygen- and mixed oxygen–nitrogen-donor ligands in dimethylsulfoxide: a thermodynamic and spectroscopic investigation, 1385
Conato, C., Kozłowski, H., Młynarz, P., Pulidori, F. and Remelli, M., Copper and nickel complex-formation equilibria with Lys–Gly–His–Lys, a fragment of the matricellular protein SPARC, 1469
Covelo, B., see Choquesillo-Lazarte, D., 1485
Crisponi, G., Diaz, A., Nurchi, V.M., Pivetta, T. and Tapia Estévez, M.J., Equilibrium study on Cd(II) and Zn(II) chelates of mercapto carboxylic acids, 1319
Cristiani, F., see Villaescusa, I., 1363

Díaz, P., Doménech, A., García-España, E. and Soriano, C., Synthesis, acid–base behaviour, co-ordination and electrochemistry studies on new open-chain bithiophene receptors, 1523
Descalzo, A.B., see Sancenón, F., 1397
Diaz, A., see Crisponi, G., 1319
Di Bernardo, P., see Bismondo, A., 1393
Di Bernardo, P., see Comuzzi, C., 1385
Doménech, A., see Díaz, P., 1523
Domínguez, S., see Armas, M.T., 1513
Domínguez, M., Anticó, E., Beyer, L., Aguirre, A., García-Granda, S. and Salvadó, V., Liquid–liquid extraction of palladium(II) and gold(III) with *N*-benzoyl-*N*′,*N*′-diethylthiourea and the synthesis of a palladium benzoylthiourea complex, 1429

Farková, M., see Havel, J., 1375
Feroci, G., see Fini, A., 1421
Fini, A., Feroci, G. and Roda, A., Acidity in bile acid systems, 1421
Fiol, N., see Villaescusa, I., 1363
Fisicaro, E., Compari, C. and Moroi, Y., Apparent and partial molar enthalpies of some potassium *p*-*n*-alkyl-benzoate aqueous solutions, 1497
Fisicaro, E., see Braibanti, A., 1311
Fisicaro, E., see Compari, C., 1503
Floris, C., see Villaescusa, I., 1363
Formica, M., Giorgi, L., Fusi, V., Micheloni, M. and Pontellini, R., Two triaza-polyamine units linked together by different aromatic spacers, coordination properties towards metal cations of a new compartmental ligand, 1351
Fornasari, P., see Bencini, A., 1329
Frassineti, C., see Cecconi, F., 1481
Fusi, V., see Formica, M., 1351

Galli, A., Ghezzi, L., Raspi, G., Secco, F. and Spinetti, M., Detection of heterologous bovine pancreatic trypsin inhibitor by capillary zone

PII: S0277-5387(02)01073-2

electrophoresis, 1405
Gambino, V., see Amorello, D., 1369
Gans, P., see Cecconi, F., 1481
García-España, E., see Díaz, P., 1523
García-Granda, S., see Domínguez, M., 1429
Ghezzi, L., see Galli, A., 1405
Gili, P., see Armas, M.T., 1513
Giorgi, C., see Bencini, A., 1329
Giorgi, C., see Bencini, A., 1459
Giorgi, L., see Formica, M., 1351
González-Pérez, J.M., see Choquesillo-Lazarte, D., 1485

Handel, H., see Bencini, A., 1459
Havel, J., Lubal, P. and Farková, M., Evaluation of chemical equilibria with the use of artificial neural networks, 1375
Havel, J., Soto-Guerrero, J. and Lubal, P., Spectrophotometric study of uranyl–oxalate complexation in solution, 1411
Hernández-Molina, R., see Armas, M.T., 1513

Iotti, S., see Cecconi, F., 1481

Kozłowski, H., see Conato, C., 1469

Lai, S., see Villaescusa, I., 1363
Le Baccon, M., see Bencini, A., 1459
Lloris, J.M., see Sancenón, F., 1397
Lorenzo, P., see Armas, M.T., 1513
Lubal, P., see Havel, J., 1375
Lubal, P., see Havel, J., 1411
Lubes, V., see Armas, M.T., 1513

Maccarrone, G., Rizzarelli, E. and Vecchio, G., Synthesis and coordination properties of functionalized β-cyclodextrins. Thermodynamic of proton and copper(II) complexes of 3A-deoxy-3A-(2-methylaminopyridine)-2A(*S*),3A(*R*)-β-cyclodextrin in aqueous solution, 1531
Martínez-Máñez, R., see Sancenón, F., 1397
Mederos, A., see Armas, M.T., 1513
Micheloni, M., see Formica, M., 1351
Midollini, S., see Cecconi, F., 1481
Młynarz, P., see Conato, C., 1469
Moroi, Y., see Fisicaro, E., 1497

Niclós-Gutiérrez, J., see Choquesillo-Lazarte, D., 1485
Niclós-Gutiérrez, J., see Serrano-Padial, E., 1451
Novelli, V., see Comuzzi, C., 1337
Nurchi, V.M., see Crisponi, G., 1319
Nurchi, V.M., see Villaescusa, I., 1363

Paoletti, P., see Bencini, A., 1329
Paoletti, P., see Bencini, A., 1459
Pardo, T., see Sancenón, F., 1397
Pesavento, M., Biesuz, R., Riva, F.D. and Alberti, G., Investigation of the complexation properties of a natural water towards copper(II), manganese(II) and aluminium(III), based on sorption of metal ions on a complexing resin, 1343
Pivetta, T., see Crisponi, G., 1319
Pontellini, R., see Formica, M., 1351
Portanova, R., see Bismondo, A., 1393
Portanova, R., see Comuzzi, C., 1337
Portanova, R., see Comuzzi, C., 1385
Pulidori, F., see Conato, C., 1469

Raspi, G., see Sbrana, E., 1475
Raspi, G., see Galli, A., 1405
Remelli, M., see Conato, C., 1469
Riva, F.D., see Pesavento, M., 1343
Rizzarelli, E., see Maccarrone, G., 1531
Roda, A., see Fini, A., 1421
Romano, V., see Amorello, D., 1369

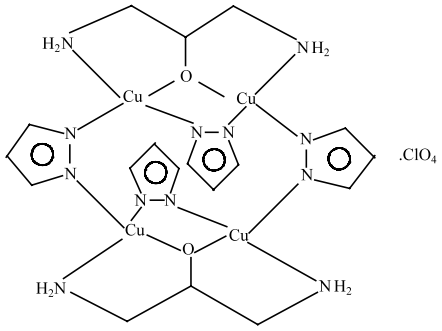
Sabatini, A., see Cecconi, F., 1481
Salvadó, V., see Domínguez, M., 1429
Sancenón, F., Descalzo, A.B., Lloris, J.M., Martínez-Máñez, R., Pardo, T., Seguí, M.J. and Soto, J., Open-chain polyazaalkanes functionalised with pyrene groups as sensing fluorogenic receptors for metal ions, 1397
Sbrana, E., Spinetti, M., Secco, F. and Raspi, G., Bubble extraction and affinity chromatography techniques for human trypsin inhibitors enrichment and purification, 1475
Secco, F., see Galli, A., 1405
Secco, F., see Sbrana, E., 1475
Seguí, M.J., see Sancenón, F., 1397
Serrano-Padial, E., Choquesillo-Lazarte, D., Bugella-Altamirano, E., Castiñeiras, A., Carballo, R. and Niclós-Gutiérrez, J., New copper(II) compound having protonated forms of ethylenediaminetetraacetate(4−) ion (EDTA) and adenine (AdeH): synthesis, crystal structure, molecular recognition and physical properties of $(AdeH_2)[Cu(HEDTA)(H_2O)]\cdot 2H_2O$, 1451
Soriano, C., see Díaz, P., 1523
Soto, J., see Sancenón, F., 1397
Soto-Guerrero, J., see Havel, J., 1411
Spinetti, M., see Galli, A., 1405
Spinetti, M., see Sbrana, E., 1475

Tapia Estévez, M.J., see Crisponi, G., 1319
Tolazzi, M., see Bismondo, A., 1393
Tolazzi, M., see Comuzzi, C., 1337
Tolazzi, M., see Comuzzi, C., 1385
Torrens, F., Calculation of organic solvent–water partition coefficients of iron–sulfur protein models, 1357

Vacca, A., see Cecconi, F., 1481
Valtancoli, B., see Bencini, A., 1329
Valtancoli, B., see Bencini, A., 1459
Vaz-Júnior, S., see Armas, M.T., 1513
Vecchio, G., see Maccarrone, G., 1531
Villaescusa, I., Fiol, N., Cristiani, F., Floris, C., Lai, S. and Nurchi, V.M., Copper(II) and nickel(II) uptake from aqueous solutions by cork wastes: a NMR and potentiometric study, 1363

Zanonato, P.L., see Bismondo, A., 1393
Zanonato, P., see Comuzzi, C., 1385
Zingales, R., see Amorello, D., 1369

takes place through the oxygen and pyrazolate bridge. In Ten Hoedt's study the distortion of the geometry around the Cu atom from square planar toward tetrahedral was considered as the main reason for the small J value, and in Manzur's study the exchange mechanism was explained by the countercomplementary effect without molecular orbital analysis [13]. In this study, we have synthesized a similar tetranuclear copper(II) complex $[Cu_4(pz)_4L_2]\cdot(ClO_4)$ (LH = 1,3-diamino-2-propanol, Hpz = pyrazole) and investigated its crystal structure and magnetic properties. Molecular orbital analysis of the compound have been done by the ab initio restricted Hartree–Fock molecular orbital method [14] to determine the influence of bridging ligands between the metal ions on the magnetic superexchange interaction and to explain the main reason of the weak antiferromagnetic coupling.



2. Experimental

2.1. Synthesis of $[Cu_4(pz)_4L_2]\cdot(ClO_4)$

The copper(II) complex was synthesized by mixing $Cu(ClO_4)_2\cdot 6H_2O$ (0.741 g, 2 mmol) with pyrazole (0.136 g, 2 mmol) in methanol at room temperature (r.t.), followed by the addition of 1,3-diamino-2-propanol (0.090 g, 1 mmol) and triethylamine (0.304 g, 3 mmol) in a methanol-water mixture (5:1, 50 ml). The product is well formed dark blue crystals (yield 0.11 g ca. 49%). *Anal*. Found: C, 23.9; H, 3.5; N, 18.7. Calc. for $C_{18}H_{30}ClCu_4N_{12}O_6$: C, 24.0; H, 3.4; N, 18.8%. Absorption spectra [λ_{max} (nm) (ε, $dm^3\ mol^{-1}\ cm^{-1}$)]: (DMF solution) 275 (14 500), 345 (6270), 604 (600).

CAUTION! Perchlorate salts of metal complexes are potentially explosive and should be handled in small quantities with care.

2.2. Crystal structure determination and refinement

X-ray data collection was carried out on an Enraf-Nonius CAD4 diffractometer [15] using a single crystal with dimensions $0.20 \times 0.15 \times 0.10$ mm with graphite monochromatized Mo Kα radiation ($\lambda = 0.71073$ Å). Precise unit cell dimensions were determined by least-squares refinement on the setting angles of 25 reflections ($2.52^\circ \leq \theta \leq 13.83^\circ$) carefully centered on the diffractometer. Data were collected at 298 K using the ω–2θ scan technique. A total of 4520 reflections were recorded, with Miller indices $h_{min} = -11$, $h_{max} = 5$, $k_{min} = -11$, $k_{max} = 0$, $l_{min} = -20$, $l_{max} = 20$.

2.2.1. Crystal data

$C_{18}H_{30}ClCu_4N_{12}O_6$, $M = 449.8$, monoclinic, space group $P2_1/c$, $a = 9.490(1)$, $b = 9.221(2)$, $c = 16.980(3)$ Å, $\beta = 95.83(1)^\circ$, $V = 1478.2(4)$ $Å^3$, $Z = 2$, $D_{calc} = 2.021$ g cm^{-3}, $\mu = 29.82$ cm^{-1}, $F(000) = 904$.

The structure was solved by direct methods using SHELXS-97 [16] and refined by full-matrix least-squares and Fourier techniques using SHELXL-97 [17]. The positions of the H atoms bonded to C atoms were calculated (C–H distance 0.96 Å), and refined using a riding model, and H atom displacement parameters were restricted to be $1.2U_{eq}$ of the parent atom. Final $R(F^2)$ and $wR(F^2)$ factor as were 0.0340 and 0.0753 and goodness-of-fit = 1.002 for 244 parameters using the I values of 1929 ($I > 2\sigma(I)$) reflections. The highest and the lowest peaks in the final difference map were 1.066 and -0.614 e $Å^{-3}$.

2.3. Susceptibility measurements

Magnetic susceptibility measurements of the powdered sample were performed on a Faraday-type magnetometer consisting of a CAHN D-200 microbalance, a Leybold Heraeus VNK 300 helium flux cryostat and a Bruker BE 25 magnet connected with a Bruker B-Mn 200/60 power supply in the temperature range 4.5–306.8 K. Details of the apparatus have already been described [18]. Diamagnetic corrections of the molar magnetic susceptibility of the compound were applied using Pascal's constants [1]. The applied field was ≈ 1.2 T. Magnetic moments were obtained from the relation $\mu_{eff} = 2.828(\chi T)^{1/2}$.

2.4. Measurements

Chemical analyses were performed by the Scientific and Technical Research Council of Turkey. The UV–Vis spectra of the title compound were recorded on a Perkin–Elmer Lambda-2 spectrophotometer using 1 cm quartz cells and solution concentrations of 10^{-4} mol l^{-1}.

3. Results and discussion

3.1. X-ray crystal structure

A perspective drawing of the title compound is shown in Fig. 1 [19] and consists of a tetranuclear copper(II) complex and perchlorate anion which is bound to the tetrameric unit by hydrogen bonds. Selected bond lengths and angles are summarized in Table 1. In the solid state, the title compound resides on an inversion center so that only half of the molecule is crystallographically unique. The structure contains a pair of dimeric units. The two copper(II) centers are bridged by the alkoxide oxygen atom of the ligand and a pyrazolate ligand and these two dimeric units are linked by two pyrazolate ligands, Cu(1) is bound to Cu(2) and Cu(1a) is bound to Cu(2a) to give the investigated tetrameric copper(II) complex.

In the title compound two different types copper coordination geometry is observed. The coordination around the Cu(1) center (or Cu(1a)) can be described as almost planar formed by N(2), N(4), N(5) and O(1). The maximum deviation of the atoms from the least-squares plane does not exceed 0.04 Å. The deviations of the atoms from the least-squares plane are as follows: N(2) = 0.039(2), N(4) = −0.021(2), N(5) = 0.039(2), O(1) = −0.030(2) Å, while Cu(1) deviates by −0.027(2) Å. However, a small in-plane distortion is reflected by the bond angles N(4)–Cu(1)–O(1) = 179.6(1)° and N(5)–Cu(1)–N(2) = 167.3(2)°. The coordination geometry around the Cu(2) center (or Cu(2a)) is tetrahedrally distorted square planar. The Cu(2) atom is coordinated by N(3), N(6), N(1a) and O(1a). The tetrahedral distortion is evidenced with the distances of the five atoms from the least-squares plane through the atoms: N(3) = −0.331(3), N(6) = 0.361(2), N(1a) = −0.347(2), O(1a) = 0.441(2), Cu(2) = −0.124(2) Å. Besides that the tetrahedrally distorted square planar geometry is reflected by trans-atom bond angles smaller than 180°: N(3)–Cu(2)–O(1a) = 174.4(2)° and N(6)–Cu(2)–N(1a) = 166.7(2)°.

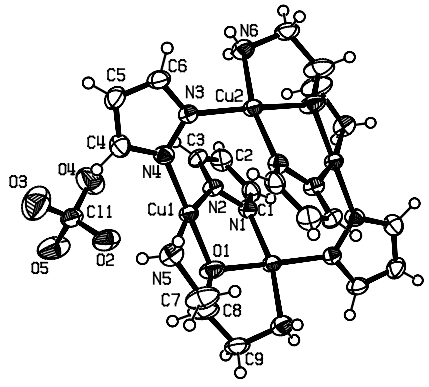


Fig. 1. View of the molecule. Displacement ellipsoids are plotted at the 50% probability level and H atoms are presented as spheres of arbitrary radii.

Table 1
Selected bond lengths (Å) and angles (°) characterizing the inner coordination sphere of the copper ions (see Fig. 1 for labelling scheme adopted)

Bond lengths	
N(1)–Cu(2)	1.959(4)
N(2)–Cu(1)	1.963(4)
N(3)–Cu(2)	1.958(4)
N(4)–Cu(1)	1.948(3)
N(5)–Cu(1)	2.024(4)
N(6)–Cu(2)	2.021(4)
O(1)–Cu(1)	1.921(3)
O(1)–Cu(2)	1.935(3)
Bond angles	
Cu(1)–O(1)–Cu(2)	113.4(2)
O(1)–Cu(1)–N(4)	179.6(2)
O(1)–Cu(1)–N(2)	84.6(2)
N(4)–Cu(1)–N(2)	95.8(2)
O(1)–Cu(1)–N(5)	83.3(2)
N(4)–Cu(1)–N(5)	96.4(2)
N(2)–Cu(1)–N(5)	167.3(3)
O(1a)–Cu(2)–N(3)	174.4(2)
O(1a)–Cu(2)–N(1)	84.5(2)
N(3)–Cu(2)–N(1a)	96.8(2)
O(1a)–Cu(2)–N(6)	82.7(2)
N(3)–Cu(2)–N(6)	96.3(2)
N(1a)–Cu(2)–N(6)	166.7(2)

In the structure, the four copper atoms are situated at the corners of a nearby rectangle with side lengths of 3.223(2)Å (Cu(2)–Cu(1a)) and 3.575(2)Å (Cu(1)–Cu(2)). Cu(1)–Cu(2)–Cu(1a) and Cu(2)–Cu(1)–Cu(2a) angles are 88.8(2)° and 91.2(2)°, respectively. The Cu–O–Cu bridging angle is 113.4(2)° in the super-exchange pathway and in good agreement with data of similar compounds [12,13].

3.2. UV–Vis spectroscopic properties

We have investigated the UV–Vis spectroscopic properties of the title compound to gain insight into the coordination geometry of the title compound. The spectra of the complex were recorded in DMF in the range 250–700 nm. UV–Vis spectroscopic studies revealed that the title compound has ligand-metal charge transfer band at $\lambda = 345$ nm. The bands near 275 nm are attributed to $\pi \rightarrow \pi^*$ transitions within the ligands. A broad d–d transition is observed at near 605 nm is indicative of a square-based geometry around copper(II).

3.3. Magnetic properties

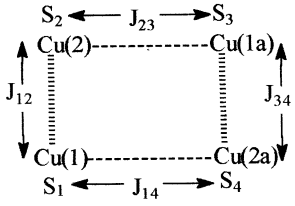
Magnetic susceptibility measurements for a powdered sample of the complex were performed by the Faraday method in the temperature range 4.5–306.8 K. The

observed and calculated magnetic moment ($\mu_{eff} = 2.828 (\chi T)^{1/2}$) decreases with decreasing temperature. The μ_{eff} value per copper center at room temperature is 2.49 μ_B for the title compound. This value is higher than the spin-only value of 1.73 μ_B for a copper(II) ion; this means that the title compound is weakly antiferromagnetically coupled. The magnetic susceptibilities and the effective magnetic moments versus temperature are shown in Fig. 2. The title compound shows a maximum in magnetic susceptibility at approximately 208 K which is typical of antiferromagnetic behavior. The rapid increase in magnetic susceptibility at low temperatures is due to the presence of a small amount of monomeric impurity (1%) which are commonly encountered in such systems [20].

The molar magnetic susceptibility is calculated by using the isotropic (Heisenberg) exchange Hamiltonian which was first used by Kambe for this purpose [21] (Eq. (1)).

$$H = -2\sum_{ij} JS_i \cdot S_j \quad (1)$$

In keeping with the structure of the title compound, the magnetic data were analyzed with the spin Hamiltonian for a rectangular system of four S = 1/2 spins.



$J_{12} = J_{34} = J_1$ and $J_{14} = J_{23} = J_2$

J_1 and J_2 values cannot be determined separately by a fitting procedure. This may show that as a result of antiferromagnetic coupling only the first two lowest energy levels (S = 1 first excited state and S = 0 ground state) are thermally populated at temperatures up to ≈ 300 K. Consequently, the tetrameric complex can be described magnetically as a two-energy level model. Therefore, the experimental data were fitted to the Bleaney–Bowers equation [22] which is used for copper dimers. A fixed value of 60×10^{-6} cm^3 mol^{-1} per Cu atom was employed for the temperature-independent paramagnetism (N_a) contribution. This fit leads to $J = -98.5$ cm^{-1}, $g = 1.96$, $x_p = 1\%$. x_p is the molar fraction of a monomeric impurity.

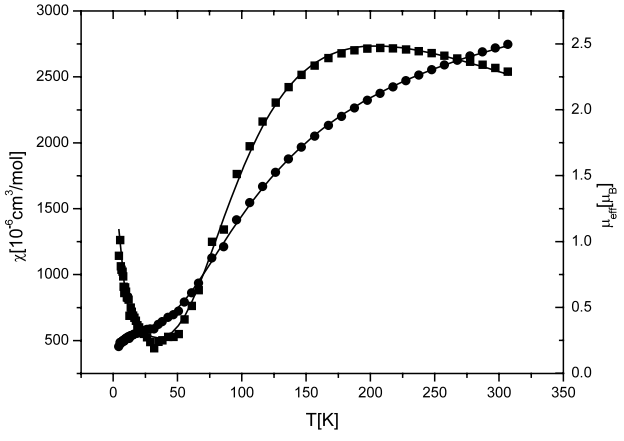


Fig. 2. Molar susceptibility (■) and effective magnetic moment (●) per copper(II) vs. temperature curve.

The good quality of fit to the dimer equation supports that only the first singlet–triplet gap is accessible in magnetic susceptibility measurements. This treatment also shows that two J values (J_1 and J_2) are strongly different from each other. Consequently, the title compound can be considered as being composed of two weakly associated pairs of dimers. At this point, we should decide which of the possible magnetic exchange pathway is more important, Cu(1)–Cu(2a) via the oxygen and pyrazolate bridge or Cu(1)–Cu(2) via the secondary pyrazolate bridge.

3.4. Magnetostructural correlations

Magnetostructural correlations have been established for dinuclear copper(II) complexes in the last two decades [4,5,23–25]. All these correlations show that a linear relationship exists between exchange integral and the Cu–O–Cu bridging angle [4]. This factor also influences the sign of the exchange interaction. In all cases the bridging angle at the point where the sign of the exchange interaction changes is nearly the same, namely 97.5° ±1°. In the title compound the Cu–O–Cu angle is larger than 100° (Cu(1)–O(1)–Cu(2a) = 113.4(2)°). Therefore, if magnetostructural correlations of dinuclear copper(II) complexes are considered for the title compound, antiferromagnetic interactions would be expected. In addition, recent studies have shown that antiferromagnetic interactions via pyrazolate bridges are weaker than substituted oxide bridges [26–29]. As a result of the above conclusions and owing to the shorter bond distance of Cu(1)–Cu(2a) than the bond distance of Cu(1)–Cu(2), the alkoxide oxygen can be considered as a main pathway of magnetic exchange interaction. So, the magnetic super exchange interaction via the oxygen and pyrazolate bridge for Cu(1)–Cu(2a) are a more important pathway than via the secondary pyrazolate bridges between Cu(1) and Cu(2) or Cu(1a) and Cu(2a). However, when we consider the linear dependency between 2J and the Cu–O–Cu bridging angle, as reported by Hatfield et al. [4] the 2J value of the title compound is relatively small. In the case of similar tetranuclear copper(II) complexes, weak antiferromagnetic coupling have been also observed [12,13].

In this study, we considered overlap interactions between the metal d-orbitals and ligand orbitals by molecular orbital calculations to explain the weak antiferromagnetic coupling of the title compound.

The sign and the magnitude of the coupling constant is influenced by bridging ligands between the metal ions because of the various types of overlap interactions between the metal d-orbitals and the ligand orbitals. The difference in the magnitude of the coupling constant may be explained by metal–ligand overlap interactions. Single μ-alkoxo-bridged dinuclear copper complexes are antiferromagnetically coupled [30,31]. When the Cu–O–Cu angle is larger than 90°, in such systems the d_a overlap with oxygen p_x is larger than d_s with p_y, so d_a and d_s split as illustrated in (Fig. 3(a)). Thus, $d_a{}^{I}$ and $d_s{}^{I}$ molecular orbitals are formed. The larger energy seperation of $d_a{}^{I}$ and $d_s{}^{I}$ gives a stronger antiferromagnetic interaction. In the presence of a second bridging ligand according to the orbital symmetries, $d_a{}^{I}$ and $d_s{}^{I}$ interact with antisymmetric (ψ_a) and symmetric (ψ_s) combinations of ligand orbitals, respectively. This interaction forms new molecular orbitals $d_a{}^{II}$ and $d_s{}^{II}$ (Fig. 3(b)). The energy difference between the two new molecular orbitals ($d_a{}^{II}$ and $d_s{}^{II}$) determines the magnitude of the $-2J$ value [32].

According to Hoffmann, the second bridging ligand can act in a complementary or countercomplementary fashion with the alkoxide oxygen atom to enhance or attenuate the strength of the antiferromagnetic coupling [32]. We investigated the overlap interaction between the HOMO's of the pyrazolate nitrogens and the magnetic d-orbitals to understand the influence of the pyrazolate ligand (see Fig. 4). Molecular orbitals of the pyrazolate ion have been calculated by the ab initio restricted Hartree–Fock method using the GAUSSIAN-98 computer program [14]. STO-3G [33] minimal bases sets were adopted for the carbon and nitrogen atoms. The HOMO's are expressed in terms of LCAO's in the appendix for the title compound.

Nishida et al. [34] showed that the energies of $d_a{}^{II}$ and $d_s{}^{II}$ depend on two factors (i) energies of the interacting

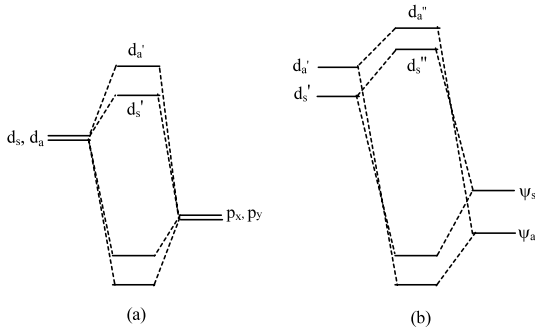


Fig. 3. The orbital energy level diagrams showing the interaction between the magnetic orbitals and bridging group orbitals (a) for single-alkoxide-bridged system; (b) for additional bridging ligand.

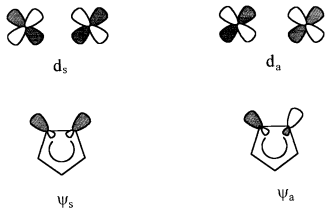


Fig. 4. Orbital symmetry combinations of metal d-orbitals and pyrazolate HOMOs.

orbitals and (ii) the overlap integrals between the interacting orbitals. When ψ_s is higher in energy than ψ_a, the energy gap between $d_a{}^{II}$ and $d_s{}^{II}$ is decreased. In our complex, since the orbital energy of ψ_s is higher than that of ψ_a by 0.260 eV, the energies of the interacting orbitals cause the pyrazolate bridge to work in a countercomplementary fashion with the alkoxide bridge. In additon, overlap integrals of the interacting orbitals is an important factor to increase or decrease the energy separation of $d_a{}^{II}$ and $d_s{}^{II}$. If ψ_s overlaps more effectively with d_s than ψ_a with d_a, the overlap integrals of the interacting orbitals may affect the pyrazolate bridge to act in a countercomplementary fashion with the alkoxide bridge again.

We determined approximate values for the overlap integrals $S(d_a,\psi_a)$ and $S(d_s,\psi_s)$ and calculated the difference between $S(d_a,\psi_a)$ and $S(d_s,\psi_s)$ for the title compound. The rigorous definition and the process of the calculation are given in the Appendix A. The difference between $S(d_a,\psi_a)$ and $S(d_s,\psi_s)$ is denoted as $S(a-s)$.

In the case of the title compound $\alpha = 5.8°$,

$$\begin{aligned} S(a-s) &= S(d_a,\ \psi_a) - S(d_s,\ \psi_s) \\ &= 0.1556(\cos(11.6)) \cdot S(3d,\ 2s) \\ &\quad - 0.0425(\sin(11.6)) \cdot S(3d_p,\ 2p_p) \\ &\quad - 0.3916(\cos(11.6)) \cdot S(3d_s,\ 2p_s) \end{aligned} \tag{5}$$

The rough overlap integrals are evaluated by using data from Jaffe and Kuroda [35,36]: $S(3d,\ 2s) \approx 0.04$, $S(3d_p,\ 2p_p) \approx 0.02$, $S(3d_s,2p_s) \approx 0.06$. For the title compound $S(a-s)$ is negative,

$$S(d_s,\ \psi_s) > S(d_a,\ \psi_a)$$

According to factor (ii) the pyrazolate bridge acts in a countercomplementary fashion to reduce the energy seperation between $d_a{}^{II}$ and $d_s{}^{II}$.

In the title compound, the energy spacing of the pyrazolate HOMO's indicates that the pyrazolate ligand and alkoxide oxygen act in a countercomplementary fashion. Since the symmetric molecular orbitals overlap is more effective (note that $S(a-s)$ is negative) this overlap factor supports the energy factor. Thus, the weak antiferromagnetic coupling of the complex is interpreted in terms of the countercomplementary effect

of the different bridging ligands which participate in the super-exchange interactions.

4. Concluding remarks

The title compound can be considered as being composed of two weakly associated pairs of dimers. The magnetic exchange interaction occurs more possibly via the alkoxide oxygen and pyrazolate bridge. The observed relatively weak antiferromagnetic exchange within the tetranuclear compound is explained by the countercomplementary behavior of the bridging pyrazolate ion which participates in the super-exchange interaction with alkoxide oxygen by means of ab initio restricted Hartree–Fock molecular orbital calculations.

5. Supplementary material

Further details of the structure determination, including atomic coordinates, bond lengths and angles, thermal parameters of all non-hydrogen atoms for the structure are available on request as supplementary material from The Director, Cambridge Crystallographic Data Center, 12 Union Road, Cambridge CB2 1EZ, UK (fax: +44-1223-336033; e-mail: deposit@ccdc.cam.ac.uk or www: http//www.ccdc.cam.ac.uk) (CCDC deposition number, 162126).

Acknowledgements

We thank Professor Dr. W. Haase for giving us the opportunity to do of magnetic susceptibility measurement. This work was supported by the Research Fund of the University of Ankara under grant number 98-25-00-03.

Appendix A: Determination of the orientation of magnetic d-orbitals

The orientation of the magnetic d-orbitals was determined according to Nishida [34]. In order to fulfill the requirement of maximum overlapping, the following function was minimized:

$$F(\alpha) = \alpha^2 + \beta^2 + \gamma^2 + \delta^2 \quad (1')$$

where, α, β, γ and δ are the angles formed by the coordination bonds and the axes of the d-orbitals (Fig. 5).

For the title compound, when the value of

$$\beta = \alpha + 90 - 95.76$$

$$\gamma = \alpha + 180 - 95.76 - 96.36$$

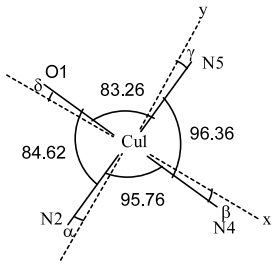


Fig. 5. Projection of Cu1 and donor atoms onto the best plane formed by these atoms (the broken lines are the axes of the magnetic d-orbital) for the title compound.

$$\delta = \alpha + 270 - 95.76 - 96.36 - 83.26$$

are used in Eq. (1), Eq. (1) becomes

$$F(\alpha) = \alpha^2 - 11.63\alpha + 52.25 \quad (2)$$

$$\frac{dF(\alpha)}{d\alpha} = 2\alpha - 11.63 \quad \alpha = 5.8^\circ$$

Determination of overlap integrals between d_s and ψ_s and between d_a and ψ_a:

The HOMOs are expressed in terms of LCAOs in Eqs. (3) and (4) for the title compound

$$\psi_s = 0.1272[s(N1) + s(N2)] + 0.2865[p_x(N1) - p_x(N2)] + 0.3167[p_y(N1) + p_x(N2)] \quad (3)$$

$$\psi_a = 0.2372[s(N1) - s(N2)] + 0.1221[p_x(N1) + p_x(N2)] + 0.0920[p_y(N1) - p_y(N2)] \quad (4)$$

According to Nishida, when the x and y axes in Fig. 5 are rotated by α, the d_1-orbital is expressed in terms of the new coordinate system as

$$d_1 = (\cos(2\alpha))d_{x^2-y^2} + (\sin(2\alpha))d_{xy} \quad (5')$$

The ψ_s and ψ_a orbitals of the pyrazolate ion can be expressed as the sum of the orbitals on N1 and N2 and the neigbouring carbon atoms

$$\psi_s = \phi_{s1} + \phi_{s2} + \phi_{sc} \quad (6)$$

$$\psi_a = \phi_{a1} + \phi_{a2} + \phi_{ac} \quad (7)$$

These orbitals can be expressed in terms of the new coordinate system in which the y axis is on the Cu1–N2 bond.

$$\phi_{s1} = 0.1272[s(N1) + s(N2)] + 0.2865[(\cos 30)p_x + (\sin 30)p_y] + 0.3167[-(\cos 60)p_x + (\sin 60)p_y]$$

$$\phi_{s1} = 0.1272s + 0.0897p_x + 0.4176p_y \quad (8)$$

From Eqs. (5) and (8)

$$S(d_1, \phi_{s1}) = 0.1272(\cos(2\alpha)) \cdot S(3d, 2s) + 0.0897(\sin(2\alpha)) \cdot S(3d_p, 2p_p) + 0.4176((\cos(2\alpha)) \cdot S(3d_s, 2p_s)$$

Since $d_s = (d_1 - d_2)/2^{1/2}$ and $S(d_2, \phi_{s2}) = -S(d_1, \phi_{s1})$

$$S(d_s, \psi_s) = 2S(d_1, \phi_{s1})/2^{1/2}$$

The overlap integral can be expressed as

$$\begin{aligned} S(d_s, \psi_s) = {} & 0.1796(\cos(2\alpha)) \cdot S(3d, 2s) \\ & + 0.1269(\sin(2\alpha)) \cdot S(3d_p, 2p_p) \\ & + 0.5906((\cos(2\alpha)) \cdot S(3d_s, 2p_s) \end{aligned} \quad (9)$$

In a similar way, $S(d_a,\psi_a)$ was obtained as follows

$$\begin{aligned} S(d_a, \psi_a) = {} & 0.3352(\cos(2\alpha)) \cdot S(3d, 2s) \\ & + 0.0844(\sin(2\alpha)) \cdot S(3d_p, 2p_p) \\ & + 0.1990((\cos(2\alpha)) \cdot S(3d_s, 2p_s) \end{aligned} \quad (10)$$

where α is the angle between the Cu–N bond vector and the nearest lobe of the local magnetic d-orbital.

References

[1] O. Kahn, Molecular Magnetism, VCH Publishers, New York, 1993.
[2] K.D. Karlin, Z. Tyeklor (Eds.), Bioorganic Chemistry of Copper, Chapman & Hall, New York, 1993.
[3] L.Q. Jun, A.E. True, Prog. Inorg. Chem. 38 (1990) 97.
[4] V.H. Crawford, H.W. Richardson, J.R. Wasson, D.J. Hodgson, W.E. Hatfield, Inorg. Chem. 15 (1976) 2107.
[5] L. Merz, W. Haase, J. Chem. Soc. Dalton Trans. (1980) 875.
[6] M.A. Halcrow, J.-S. Sun, J.C. Huffman, G. Christou, Inorg. Chem. 34 (1995) 4167.
[7] P.E. Kruger, G.D. Fallon, B. Moubaraki, K.J. Berry, K.S. Murray, Inorg. Chem. 34 (1995) 4808.
[8] P.E. Kruger, B. Moubaraki, K.S. Murray, Polyhedron 15 (1997) 2659.
[9] C.J. Matthews, K. Avery, Z. Xu, L.K. Thompson, L. Zhao, D.O. Miller, K. Biradha, K. Poirer, M.J. Zaworotko, C. Wilson, A.E. Goeta, J.A.K. Howard, Inorg. Chem. 38 (1999) 5266.
[10] A.M. Atria, A. Vega, M. Contresas, J. Valenzula, E. Spodine, Inorg. Chem. 38 (1999) 5681.
[11] R. Ruiz, F. Lloret, M. Julve, J. Faus, M.C. Munoz, X. Solans, Inorg. Chim. Acta 268 (1998) 263.
[12] R.W.M. Ten Hoedt, F.B. Hulsbergen, G.C. Verschoor, J. Reedijk, Inorg. Chem 21 (1982) 2369.
[13] J. Manzur, A.M. Garcia, M.T. Garland, V. Acuna, Polyhedron 15 (1996) 821.
[14] GAUSSIAN 98, Revision A. 3, M.J. Frisch, G.W. Trucks, H.B. Schlegel, G.E. Scuseria, M.A. Robb, J.R. Cheeseman, V.G. Zakrzewski, J.A. Montgomery, R.E. Stratmann, J.C. Burant, S. Dapprich, J.M. Millam, A.D. Daniels, K.N. Kudin, M.C. Strain, O. Farkas, J. Tomasi, V. Barone, M. Cossi, R. Cammi, B. Mennucci, C. Pomelli, C. Adamo, S. Clifford, J.Ochterski, G.A. Petersson, P.Y. Ayala, Q. Cui, K. Morokuma, D.K. Malick, A.D. Rabuck, K. Raghavachari, J.B. Foresman, J. Cioslowski, J.V. Ortiz, B.B. Stefanov, G. Liu, A. Liahenko, P. Piskorz, I. Komaromi, R. Gomberts, R.L. Martin, D.J. Fox, T. Keith, M.A. Al-Laham, C.Y. Peng, A. Nanayakkara, C. Gonzalez, M. Challacombe, P.M.W. Gill, B. Johnson, W. Chen, M.W. Wong, J.L. Andres, M. Head-Gordon, E.S. Replogle, J.A. Pople, Gaussian, Inc., Pittsburgh PA, 1998.
[15] Enraf-Nonius diffractometer control software, Release 5.1., Enraf-Nonius, Delft, Netherlands, 1993.
[16] G.M. Sheldrick, SHELXS-97, Program for the Solution of Crystal Structures, University of Göttingen, Germany, 1997.
[17] G.M. Sheldrick, SHELXL-97, Program for the Refinement of Crystal Structures, University of Göttingen, Germany, 1997.
[18] S. Gehring, P. Fleischhauer, H. Paulus, W. Haase, Inorg. Chem. 32 (1993) 54.
[19] L.J. Farrugia, ORTEPIII. J. Appl. Cryst. 30 (1997) 565.
[20] W. Mazurek, B.J. Kennedy, K.S. Murray, M.J. O'Connor, J.R. Rodgers, M.R. Snow, A.G. Wedd, P.R. Zwack, Inorg. Chem. 24 (1985) 3258.
[21] K. Kambe, J. Phys. Soc. Jpn. 5 (1950) 48.
[22] B. Bleaney, K.D. Bowers, Proc. R. Soc. London, Ser. A 214 (1952) 451.
[23] M. Handa, N. Koga, S. Kida, Bull. Chem. Soc. Jpn. 61 (1988) 3853.
[24] L.K. Thompson, S.K. Mandal, S.S. Tandon, J.N. Bridson, M.K. Park, Inorg. Chem. 35 (1996) 3117.
[25] R. Fletcher, J.J. Hansen, J. Livermore, R.D. Willet, Inorg. Chem. 22 (1983) 330.
[26] L. Banci, A. Bencini, P. Dapporto, A. Dei, D. Gatteshi, Inorg. Chem. 19 (1980) 3395.
[27] E.D. Estes, D.J. Hodgson, Inorg. Chem. 15 (1976) 348.
[28] H.E. Lemay, Jr., D.J. Hodgson, P. Pruettiangkura, L.J. Theriot, J. Chem. Soc., Dalton. Trans. (1979) 781.
[29] J.M. Dominguez-Vera, E. Colacio, Acta Chem. Scand. 46 (1992) 1055.
[30] P.K. Coughlin, S.J. Lippard, J. Am. Chem. Soc., 103 (1981) 3228.
[31] P.L. Burk, J.A. Osborn, M.T. Youinou, J. Am. Chem. Soc., 103 (1981) 1273.
[32] P.J. Hay, J.C. Thibeault, R. Hoffmann, J. Am. Chem. Soc. 97 (1975) 4884.
[33] W.J. Hehre, R.F. Stewart, J.A. Pople, J. Chem. Phys. 51 (1969) 2657.
[34] Y. Nishida, S. Kida, Inorg. Chem. 27 (1988) 447.
[35] (a) H.H. Jaffe, G.O. Doal, J. Chem. Phys. 21 (1953) 196; (b) H.H. Jaffe, J. Chem. Phys. 21 (1953) 258.
[36] Y. Kuroda, K. Ito, Nippon Kagaku Zasshi 76 (1955) 545.

the published methods [19]. The infrared spectra (4000–400 cm^{-1}) were recorded from KBr disks with a SHIMADZU IR-470 spectrometer. UV–Vis spectra of the ligands and complexes were recorded on a JASCO model 7850 spectrophotometer. ^1H NMR spectra were obtained using a Bruker DRX 500 AVANCE spectrometer.

2.2. Preparation of $WOS_3Cu_3Pz_3Cl$ (**1**)

$[NH_4]_2[WOS_3]$ (0.2 g, 0.6 mmol) was partially dissolved in analar acetone (50 ml). Solid CuCl (0.12 g, 1.2 mmol) was added to the solution and the mixture was stirred at room temperature for 45 min. in an erlenmeyer flask. This produced a yellow–orange solution. Pyrazole (0.16 g, 2.3 mmol) was added to this solution and the mixture was stirred for another 2 h. The precipitate was filtered off and the filtrate was vacuum evaporated to dryness, leaving a yellow-orange solid. This product was washed with diethyl ether (2×2 ml) and vacuum dried for 6 h. Yield 55%. *Anal.* Calc. for $C_9H_{12}ClCu_3N_6OS_3W$: C 14.87, H 1.65, N 11.56. Found: C 14.6, H 2.0, N 12.0%.

2.3. Preparation of $[PPh_4]_4[\{WOS_3(CuCNSe)_3\}_2]$ (**2**)

$[PPh_4]_2[WOS_3]$ (0.2 g, 0.2 mmol) was partially dissolved in analar acetone (70 ml). Solid CuCl (0.06 g, 0.61 mmol) and KSeCN (0.09 g, 0.6 mmol) were added to the solution and the mixture was stirred for 12 h. A small amount of yellow precipitate was removed by filtration. Yellow crystals suitable for X-ray crystallography were obtained by slow evaporation of the solvent; they were washed with diethyl ether and air dried. Yield 60%. *Anal.* Calc. for $C_{102}H_{80}Cu_6N_6O_2P_4S_6Se_6W_2$: C 41.38, H 2.72, N 2.84. Found: C 41.0, H 2.8, N 2.8%.

2.4. Attempted preparation of $[PPh_4]_2[Co(WO_2S_2)_2(CuNCS)_2]$

The method was similar to that for **2**. $[PPh_4]_2[Co(WO_2S_2)_2]$ (0.245 g, 0.189 mmol) [20] was dissolved in acetonitrile (50 ml). Solid CuCl (0.752 g, 0.75 mmol) and KSCN (0.732 g, 0.75 mmol) were added to the solution. The resulting mixture was stirred for 5 h. and then filtered. The filtrate was vacuum evaporated to dryness. A solution of this complex in dichloromethane is unstable and storing the solution at room temperature (r.t.) in air deposited a few crystals identified crystallographically as $[PPh_4]_2[Cu(NCS)_4]$. Yield and analysis were not measured.

2.5. X-ray crystallography

Crystal data together with other relevant information on the structure determinations are listed in Table 1. All measurements were made on a Bruker SMART CCD diffractometer with narrow frames (0.3° in ω). Mo Kα radiation ($\lambda = 0.71073$ Å) was employed for data collection at 160 K. Absorption corrections were based on the high redundancy of symmetry-equivalent and repeated reflections. The structures were solved by direct methods and refined by full-matrix least-squares on all F^2 values. Non-hydrogen atoms were refined with anisotropic displacement parameters. Hydrogen atoms were included in calculated positions and refined with isotropic displacement parameters, riding on their parent atoms. The dimeric bridged anion of compound **2** lies on an inversion center, while the monomeric anion of compound **3** has crystallographic twofold rotation symmetry. In compound **1**, twofold disorder with relative occupancies 0.533:0.467(16) was resolved for one Cu atom and its attached Pz ligand; refinement involved restraints on the geometry and displacement parameters of the disordered ligand, and the disorder reduces the overall precision of the structure. Programs were standard Bruker AXS control and integration software, SADABS [21] and SHELXTL [22].

3. Results and discussion

3.1. Infrared spectra

The infrared spectrum of complex **1** shows bands at 3100–3400, 1516, 1462, 1132, 1060 and 759 cm^{-1} characteristic of the pyrazole ligands. The W–S stretching frequency of $[WOS_3]^{2-}$ in the complex (433 cm^{-1}) is shifted to a lower frequency relative to that for free $[WOS_3]^{2-}$ (470 cm^{-1}, ammoniun salt) [19]. This indicates a decrease in the stretching force constant, showing that the $[WOS_3]^{2-}$ ligand is coordinated through the sulfur atoms. Furthermore, the W–O stretching frequency (as expected when W–O is terminal) shifts to higher frequency (905–916 cm^{-1}) compared with the average ν(W–O) frequency of free $[WOS_3]^{2-}$ (860 cm^{-1}).

In the infrared spectrum of complex **2**, two bands are found for the ν(CN) stretching mode at 2084 cm^{-1} (for bridging SeCN ligands) and 2048 cm^{-1} (for terminal N-bonded SeCN ligands). This assignment was confirmed by the crystal structure of the complex. The terminal ν(W–O) stretching freqency has been identified as a strong absorption band at 922 cm^{-1} in accordance with literature values [23]. The band at 429 cm^{-1} is assigned to the stretch of the W–S bridges.

The infrared spectrum of complex **3** exhibits a ν(CN) band at 2075 cm^{-1}, which indicates monodentate N-coordination of the SCN^- anion to the Cu^{2+} ion [24].

Table 1
Crystallographic data for compounds **1**, **2** and **3**

Compound	**1**	**2**	**3**
Chemical formula	$C_9H_{12}ClCu_3N_6OS_3W$	$C_{102}H_{80}Cu_6N_6O_2P_4S_6Se_6W_2$	$C_{52}H_{40}CuN_4P_2S_4$
Formula weight	726.35	2960.66	974.60
Crystal system	monoclinic	triclinic	monoclinic
Space group	*I*2/*a*	$P\bar{1}$	*C*2/*c*
a (Å)	18.592(3)	12.3630(10)	22.3297(15)
b (Å)	12.799(2)	12.9462(10)	14.9842(10)
c (Å)	16.932(3)	18.7189(15)	14.7801(10)
α (°)		84.753(2)	
β (°)	112.015(2)	74.142(2)	108.392(2)
γ (°)		65.513(2)	
V (Å^3)	3735.3(11)	2622.0(4)	4692.7(5)
Z	8	1	4
D_{calc} (g cm^{-3})	2.583	1.875	1.379
μ (mm^{-1})	10.00	5.69	0.75
Crystal size (mm)	0.5 × 0.3 × 0.2	0.50 × 0.35 × 0.15	0.47 × 0.23 × 0.12
θ_{max} (°)	28.6	28.6	28.8
Reflections collected	11059	30233	20091
Unique reflections, R_{int}	4374, 0.0520	12292, 0.0347	5639, 0.0437
Transmission factors	0.059–0.153	0.158–0.296	0.719–0.915
Number of parameters	272	605	285
R (F, $F^2 > 2\sigma$)	0.0872	0.0351	0.0539
R_w (F^2, all data)	0.1557	0.0746	0.1436
Goodness-of-fit on F^2	1.430	1.054	1.021
El. density extremes (e Å^{-3})	2.05, −2.69	1.46, −1.23	0.53, −1.19

3.2. Solution spectroscopic studies

3.2.1. Electronic spectra

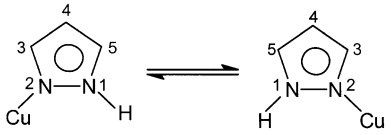
The UV–Vis spectrum of complex **1** shows the existence of $[WOS_3]^{2-}$ in the cluster by the internal transitions of this anion. The major peak in the electronic spectrum of $WOS_3Cu_3Pz_3Cl$ (345 nm) is red-shifted from the position of this transition in the free $[WOS_3]^{2-}$ ion (334 nm). The spectrum of the complex also shows a shoulder in the region 212–203 nm, which corresponds to the $d\pi \rightarrow \pi^*$ and $\pi \rightarrow \pi^*$ transitions [25]. The UV–Vis spectrum of complex **2** is essentially the same as that of complex **1**.

3.2.2. ^1H NMR spectrum

Though the polymeric structure of the title compound **1** was established in the solid state by X-ray crystallography, it was of interest to investigate both the integrity and rigidity of this structure in solution.

The proton magnetic resonance spectrum of the complex in d^6-acetone indicates magnetic equivalence of the H3 and H5 protons of the pyrazole ring at r.t. The spectrum exhibits resonances at 7.9 ppm (br, H-3, 5; Pz) and 6.6 ppm (H4, Pz). This result indicates that rapid exchange is occurring between coordinated copper and the H1 proton of the pyrazole ring (Scheme 1).

^{1}H NMR spectra were recorded down to −65°C in d_6-acetone. The integrals of these resonances are in the ratio of 2:1 (H3, H5: H4). The r.t. ^{1}H NMR spectrum also exhibits three broad peaks at 7.38, 7.50 and 7.61 ppm, which are due to the N–H proton of the pyrazole rings. As the temperature decreases from r.t. to −65 °C, the spectrum shows 1:1 resonances at 7.45 ppm (H3) and 7.8 ppm (H5) due to the non-equivalent H5 and H3 protons of the pyrazole ring, which would indicate proximity to the slow exchange limit between coordinated copper and the N–H proton of the pyrazole ring. The ^{1}H NMR spectrum at −65 °C also exhibits a resonance at 6.2 ppm due to H4, and three other resonances at 7.4, 7.5 and 7.6 ppm due to the N–H proton of pyrazole rings.



Scheme 1.

3.2.3. ^{13}C NMR spectrum

The ^{13}C NMR spectrum of the complex in DMSO at r.t. exhibits two main resonances at 105.23 and 134.65 ppm. The resonance at 105.23 ppm is assigned to C4 and the resonance at 134. 65 ppm is assigned to C3 and C5 of the pyrazole ring. This result agrees with the ^{1}H NMR spectrum, which also indicates that rapid exchange of the coordinated copper and N–H proton of the pyrazole ring is occurring at r.t.

3.3. Description of crystal structures

3.3.1. Crystal structure of $WOS_3Cu_3Pz_3Cl$

Views of a single monomer and the polymeric arrangement of this complex are presented in Figs. 1 and 2, respectively. Table 2 lists selected bond distances (Å) and angles (°), excluding any involving the minor disorder component.

In the complex, there are two distinctly different coordination geometries about copper atoms. The Cu(1) and Cu(3) atoms have a distorted trigonal planar geometry with bond angles ranging from 109.8(2)° to 126.8(2)° and they are coordinated by two sulfur atoms from thiometallate ligands with average Cu–S distances of 2.244 Å, and one nitrogen atom from a pyrazole ring with a Cu–N distance of 1.93(2) or 1.961(12) Å, while Cu(2) has a distorted tetrahedral arrangement with bond angles ranging from 96.9(3)° to 122.4(4)° and coordination by two sulfur atoms from thiotungstate with an average Cu–S distance of 2.228 Å and one nitrogen atom from pyrazole ring with a Cu–N distance of 1.974(11) Å. The fourth ligand atom is Cl^- with a Cu–Cl distance of 2.472(4) Å. The Cu–Cl distance is in the range previously reported for tetrahedral copper(I) geometry [26]. Cl(1) has a weak interaction with a neighboring copper atom at 2.781 Å, linking the anions together into infinite chains (Fig. 2). Bonds involving Cu with primary four coordination are somewhat longer than those for three-coordinate Cu.

The coordination of pyrazole to copper appears to have only minor effects on the structure of the pyrazole molecule. The N=N bond distance of 1.35(1) Å [6] in the uncoordinated pyrazole molecule shows little change [1.344(16), 1.355(13) and 1.359(17) Å] on forming a terminal Cu–N bond in the title compound.

In this complex all metal atoms and sulfur atoms form an incomplete cubane-type framework (the WS_3Cu_3 fragment); the eighth vertex opposite W is vacant. Completion of the pseudo-cubane would either involve rare fivefold coordination for Cu(I), or would displace the chloro ligand from its asymmetric bridging role linking the molecules into a polymeric chain. Around

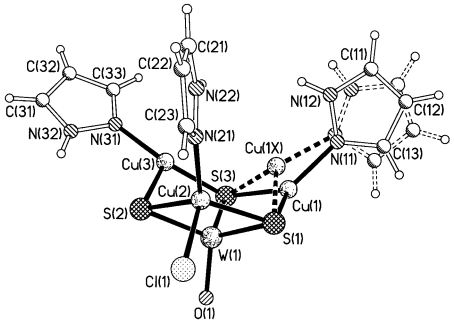


Fig. 1. Structure of the asymmetric unit of $WOS_3Cu_3Pz_3Cl$, with atom labeling, showing the disorder of one copper atom and one Pz ligand.

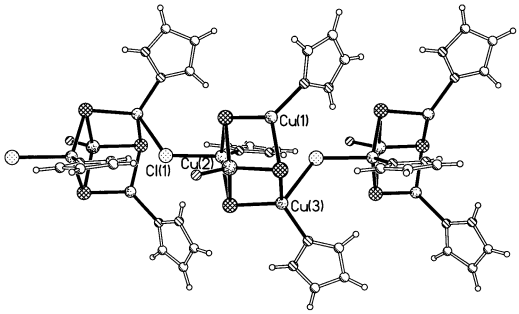


Fig. 2. The polymeric chain structure of $WOS_3Cu_3Pz_3Cl$ formed by chloro bridges, with the Cu and Cl atoms of the basic monomer unit labeled.

Table 2
Selected bond lengths (Å) and angles (°) for compound **1**

Bond lengths			
W(1)–O(1)	1.731(11)	W(1)–S(1)	2.262(4)
W(1)–S(2)	2.264(3)	W(1)–S(3)	2.262(3)
S(1)–Cu(1)	2.221(5)	S(1)–Cu(2)	2.276(4)
S(2)–Cu(2)	2.291(4)	S(2)–Cu(3)	2.295(4)
S(3)–Cu(3)	2.251(4)	S(3)–Cu(1)	2.260(5)
Cu(1)–N(11)	1.93(2)	Cu(2)–N(21)	1.974(11)
Cu(2)–Cl(1)	2.472(4)	Cu(3)–N(31)	1.961(12)
N(11)–N(12)	1.359(17)	N(21)–N(22)	1.355(13)
N(31)–N(32)	1.344(16)		
Bond angles			
O(1)–W(1)–S(3)	110.2(4)	O(1)–W(1)–S(1)	111.8(5)
S(3)–W(1)–S(1)	108.25(14)	O(1)–W(1)–S(2)	110.6(5)
S(3)–W(1)–S(2)	108.06(13)	S(1)–W(1)–S(2)	107.82(13)
Cu(1)–S(1)–W(1)	70.97(15)	Cu(1)–S(1)–Cu(2)	117.9(3)
W(1)–S(1)–Cu(2)	72.79(12)	W(1)–S(2)–Cu(2)	72.49(11)
W(1)–S(2)–Cu(3)	71.39(11)	Cu(2)–S(2)–Cu(3)	106.23(16)
Cu(3)–S(3)–Cu(1)	106.3(2)	Cu(3)–S(3)–W(1)	72.22(11)
Cu(1)–S(3)–W(1)	70.28(14)	N(11)–Cu(1)–S(1)	119(2)
N(11)–Cu(1)–S(3)	126.8(18)	S(1)–Cu(1)–S(3)	109.8(2)
N(21)–Cu(2)–S(1)	122.4(4)	N(21)–Cu(2)–S(2)	116.6(3)
S(1)–Cu(2)–S(2)	106.43(14)	N(21)–Cu(2)–Cl(1)	96.9(3)
S(1)–Cu(2)–Cl(1)	105.40(14)	S(2)–Cu(2)–Cl(1)	107.03(15)
N(31)–Cu(3)–S(3)	133.5(4)	N(31)–Cu(3)–S(2)	112.5(4)
S(3)–Cu(3)–S(2)	107.37(15)		

two dozen such structures are known (containing either W or Mo), all with halide or pseudo-halide as the eighth vertex. In compound **1**, the W atom has a distorted tetrahedral coordination geometry with one terminal O and three μ_3-S atoms. Thus the $[WOS_3]^{2-}$ ion acts as a bidentate ligand toward each copper atom, as has been predicted from the vibrational spectrum. All atoms of the WS_3Cu_3 core are distributed in three planar four-membered rings, having the central W atom as common point.

The W–O distance of 1.731(11) Å is typical for a W=O double bond. The average W–S bond length, 2.262 Å, falls in the range of a typical W–S single bond.

The O–W–S angles range from 110.2(4)° to 111.8(5)°, whereas the three S–W–S angles range from 107.82(2)° to 108.25(4)°. Clearly, the W atom has basically retained

the pseudo-tetrahedral geometry of the free $[WOS_3]^{2-}$ anion. The inter-metal Cu···W distances range from 2.603(4) to 2.713(5) Å, and are sufficiently short to permit a direct Cu–W interaction.

Of about 50 structures in the Cambridge Structural Database [27] containing a MOS_3Cu_3 core (M = Mo or W), including those with the eighth vertex of the cube occupied, the majority are monomeric with terminal ligands attached to Cu. Dimers are formed through halide or thiocyanate bridges, and cyanide ligands give polymers. Although there are several known structures with pyridine as a ligand for Cu, compound **1** is the first reported cluster of this kind to contain pyrazole.

3.3.2. Crystal structure of $[PPh_4]_4[\{WOS_3(CuNCSe)_3\}_2]$

This complex is isostructural with $[PPh_4]_4[\{MoOS_3(CuNCS)_3\}_2]$ [28]. The cluster ion consists of two nest-shaped $[WOS_3(CuNCSe)_3]^{2-}$ fragments connected by a pair of CuNCSeCu bridges to form centrosymmetric dimers (Fig. 3). The $[WOS_3(CuNCSe)_3]^{2-}$ anion has a WS_3Cu_3 chromophore with atoms at seven vertices of a trigonally distorted cube; the eighth vertex, opposite W, is vacant. W is tetrahedrally coordinated by one terminal O^{2-} ligand and by three bridging S^{2-} ligands, each of which also bonds to two Cu atoms. In this anion two distinctly different coordination geometries of copper exist. The Cu(1) and Cu(2) atoms adopt trigonal planar geometry (coordinated by two S^{2-} and one $NCSe^-$ ligand bonded via its N atom), while Cu(3) adopts distorted tetrahedral geometry (coordinated by two S^{2-} and one $NCSe^-$ ligand bonded via N, the fourth ligand atom being Se of a $NCSe^-$ ligand of a neighboring anion, acting as a bridge).

The W–O distance of 1.736(3) Å is typical for a W=O double bond. The three W–S bonds, 2.2569(10)–2.2815(10) Å, fall in the range of a typical W–S single bond. The O–W–S angles range from 110.29(10)° to 111.74(10)°, whereas the three S–W–S angles range from 107.53(4)° to 108.46(4)°. Thus, the W atom has retained the pseudo-tetrahedral geometry of the free $[WOS_3]^{2-}$ anion. Cu–S bond lengths range from 2.2540(11) to 2.3111(11) Å, Cu–N from 1.881(4) to 1.909(4) Å, Cu···W distances from 2.6513(5) to 2.6998(6) Å; Cu–Se is 2.6467(7) Å. Bonds involving four-coordinate Cu are somewhat longer than those for three-coordinate Cu. The CuNCSe linkages are essentially linear at C, and only slightly bent at N. The selenocyanate bridges are markedly bent at Se. Table 3 gives selected bond lengths and bond angles for the anion.

Table 3
Selected bond lengths (Å) and angles (°) for compound **2**

Bond lengths			
W(1)–O(1)	1.736(3)	W(1)–S(2)	2.2569(10)
W(1)–S(3)	2.2710(10)	W(1)–S(1)	2.2815(10)
Cu(1)–N(1)	1.883(4)	Cu(1)–S(1)	2.2540(11)
Cu(1)–S(3)	2.2698(11)	Cu(2)–N(2)	1.881(4)
Cu(2)–S(1)	2.2592(11)	Cu(2)–S(2)	2.2622(11)
Cu(3)–N(3)	1.909(4)	Cu(3)–S(2)	2.2912(12)
Cu(3)–S(3)	2.3111(11)	Cu(3)–Se(2′)	2.6467(7)
Bond angles			
O(1)–W(1)–S(2)	110.71(10)	O(1)–W(1)–S(3)	110.29(10)
S(2)–W(1)–S(3)	108.46(4)	O(1)–W(1)–S(1)	111.74(10)
S(2)–W(1)–S(1)	107.53(4)	S(3)–W(1)–S(1)	107.98(4)
N(1)–Cu(1)–S(1)	122.53(12)	N(1)–Cu(1)–S(3)	126.78(12)
S(1)–Cu(1)–S(3)	108.99(4)	N(2)–Cu(2)–S(1)	131.42(12)
N(2)–Cu(2)–S(2)	119.30(12)	S(1)–Cu(2)–S(2)	108.12(4)
N(3)–Cu(3)–S(2)	115.30(11)	N(3)–Cu(3)–S(3)	122.43(11)
S(2)–Cu(3)–S(3)	105.92(4)	N(3)–Cu(3)–Se(2′)	108.01(11)
S(2)–Cu(3)–Se(2′)	108.29(3)	S(3)–Cu(3)–Se(2’)	94.31(3)
Cu(1)–S(1)–Cu(2)	103.25(5)	Cu(1)–S(1)–W(1)	71.54(3)
Cu(2)–S(1)–W(1)	71.58(3)	W(1)–S(2)–Cu(2)	71.97(3)
W(1)–S(2)–Cu(3)	72.82(3)	Cu(2)–S(2)–Cu(3)	96.96(4)
Cu(1)–S(3)–W(1)	71.45(3)	Cu(1)–S(3)–Cu(3)	103.66(4)
W(1)–S(3)–Cu(3)	72.20(3)	C(1)–N(1)–Cu(1)	156.4(3)
N(1)–C(1)–Se(1)	177.7(4)	C(2)–N(2)–Cu(2)	171.9(4)
N(2)–C(2)–Se(2)	178.1(4)	C(2)–Se(2)–Cu(3′)	116.87(13)
C(3)–N(3)–Cu(3)	167.3(4)	N(3)–C(3)–Se(3)	178.6(4)

Symmetry operation for primed atoms (inversion center): $-x+1$, $-y+1$, $-z+1$.

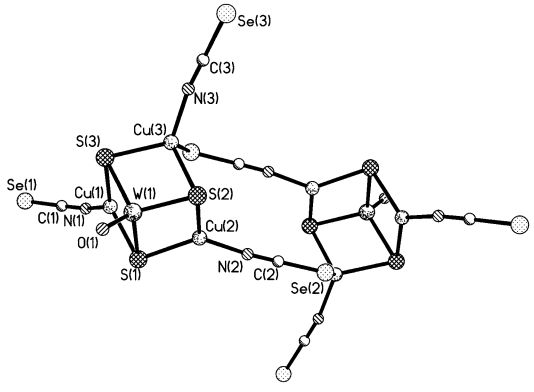


Fig. 3. Structure of the dimeric $[\{WOS_3(CuNCSe)_3\}_2]^{2-}$ anion in **2**, with atom labeling.

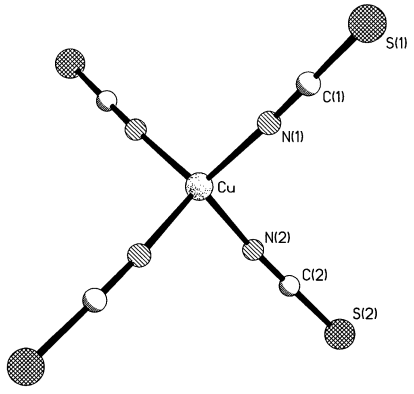


Fig. 4. The essentially tetrahedral $[Cu(NCS)_4]^{2-}$ anion in **3**, with atom labeling.

Table 4
Selected bond lengths (Å) and angles (°) for compound **3**

Bond lengths			
Cu–N(1)	1.945(3)	Cu–N(2)	1.959(3)
N(1)–C(1)	1.158(4)	C(1)–S(1)	1.617(3)
N(2)–C(2)	1.154(4)	C(2)–S(2)	1.625(3)
Bond angles			
N(1)–Cu–N(1')	112.01(17)	N(1)–Cu–N(2)	110.46(13)
N(1)–Cu–N(2')	109.39(12)	N(2)–Cu–N(2′)	104.90(18)
C(1)–N(1)–Cu	171.0(3)	N(1)–C(1)–S(1)	179.2(3)
C(2)–N(2)–Cu	170.8(3)	N(2)–C(2)–S(2)	177.7(3)

Symmetry operation for primed atoms (twofold rotation axis): $-x+1, y, -z+1/2$.

3.3.3. Crystal structure of $[PPh_4]_2[Cu(NCS)_4]$

The crystal structure consists of $[PPh_4]^+$ cations and discrete $[Cu(NCS)_4]^{2-}$ anions (Fig. 4). The bond lengths and bond angles (Table 4) in the $[Cu(NCS)_4]^{2-}$ anion indicate that the copper atom has an only slightly distorted tetrahedral coordination geometry, which is rare for Cu(II) compounds and much more common for Cu(I), and the NCS^- ligands are bonded via their N atoms. N–Cu–N bond angles range from 104.90(18)° to 112.01(17)°. Cu–N distances range from 1.945(3) to 1.959(3) Å. The CuNCS linkages are essentially linear at C and only slightly bent at N. In a previously reported salt of the same anion, this has a geometry intermediate between tetrahedral and square planar, with two opposite N–Cu–N angles of 135.0° and 139.5° [29]; it thus appears to be quite flexible, depending on the counter-ion and crystal packing interactions.

4. Supplementary material

Crystallographic data for the structural analyses have been deposited with the Cambridge Crystallographic Data Center, CCDC No. 164129 for compound **1**, 164128 for compound **2**, and 164127 for compound **3**. Copies of this information may be obtained free of charge from The Director, CCDC, 12 Union Road, Cambridge CB2 1IZ, UK (fax: +44-1223-336033; e-mail: deposit@ccdc.cam.ac.uk or www: http://www.ccdc.cam.ac.uk).

Acknowledgements

We thank EPSRC (UK) and the National Research Council (Iran; grant number 2016) for financial support.

References

[1] R.H. Holm, Chem. Soc. Rev. 10 (1981) 455.
[2] E.D. Simhon, N.C. Baenziger, M. Kanatzidis, M. Draganjic, D. Coucouvanis, J. Am. Chem. Soc. 103 (1981) 1218.
[3] A. Bose, C.R. Saha, J. Mol. Catal. 49 (1989) 271.
[4] F. Sécheresse, M. Salis, C. Potvin, J.M. Manoli, Inorg. Chim. Acta 114 (1986) L19.
[5] J.M. Manoli, C. Potvin, F. Sécheresse, J. Chem. Soc., Chem. Commun. (1982) 1159.
[6] F. Sécheresse, S. Bemes, F. Robert, Y. Jeannin, J. Chem. Soc., Dalton. Trans. (1991) 2875.
[7] F. Sécheresse. J.M. Manoli, C. Potvin, S. Marzak, J. Chem. Soc., Dalton. Trans. (1988) 3055.
[8] Y. Jeannin, F. Sécheresse, S. Bemes, F. Robert, Inorg. Chim. Acta 198 (1992) 493.
[9] F. Sécheresse, F. Robert, S. Marzak, J.M. Manoli, C. Potvin, Inorg. Chim. Acta 182 (1991) 221.
[10] S. Bemés, F. Sécheresse, Y. Jeannin, Inorg. Chim. Acta 191 (1992) 11.
[11] A. Müller, U. Schimanski, J. Schimanski, Inorg. Chim. Acta 76 (1983) L245.
[12] J.R. Nicholson, A.C. Flood, C.D. Garner, W. Clegg, J. Chem. Soc., Chem. Commun. (1983) 1179.
[13] M. Minelli, J.H. Nicholson, C.D. Garner, Inorg. Chem. 23 (1984) 4384.
[14] A. Müller, M. Dartmann, C. Römer, W. Clegg, G.M. Sheldrick, Angew. Chem., Int. Ed. Engl. 20 (1981) 1060.
[15] S.F. Gheller, P.A. Gazzana, A.F. Masters, R.T.C. Brownlee, M.J.O. Connor, A.G. Wedd, J.R. Rodgers, M.R. Snow, Inorg. Chim. Acta 54 (1981) L131.
[16] S.F. Gheller, T.A. Hambley, J.R. Rodgers, R.T.C. Brownlee, M.J.O. Connor, M.R. Snow, A.G. Wedd, Inorg. Chem. 23 (1984) 2519.
[17] J.M. Manoli, C. Potvin, F. Sécheresse, S. Marzak, J. Chem. Soc., Chem. Commun. (1986) 1557.
[18] J.M. Manoli, C. Potvin, F. Sécheresse, S. Marzak, Inorg. Chim. Acta 150 (1988) 257.
[19] J.W. McDonald, G.D. Friesen, L.D. Rosenhein, W.E. Newton, Inorg. Chim. Acta 72 (1983) 205.
[20] A. Müller, H.H. Heinsen, G. Vandrish, Inorg. Chem. 13 (1974) 1001.
[21] G.M. Sheldrick, SADABS, Program for Correction of CCD Data, University of Göttingen, Germany, 1997.
[22] G.M. Sheldrick, SHELXTL User Manual, Bruker AXS Inc, Madison, WI, USA, 1997.
[23] A.B.M. Shamsur Rahman, H. Boller, K.O. Klepp, Inorg. Chim. Acta 305 (2000) 91.
[24] R.A. Bailey, S.L. Kozak, T.W. Michelsen, W.N. Mills, Coord. Chem. Rev. 6 (1971) 407.
[25] T.N. Sorrell, A.S. Borovik, J. Am. Chem. Soc., 108 (1986) 5636.
[26] S. Ogo, T. Suzuki, K. Isobe, Inorg. Chem. 34 (1995) 1304.
[27] F.H. Allen, O. Kennard, Chem. Des. Autom. News 8 (1993) 31.
[28] W. Clegg, A. Beheshti, C.D. Garner, Acta Crystallogr., Sect. C 44 (1988) 170.
[29] D. Reinen, R. Allmann, G. Baum, B. Kakob, U. Kaschuba, W. Massa, G.J. Miller, Z. Anorg. Allg. Chem. 548 (1987) 7.

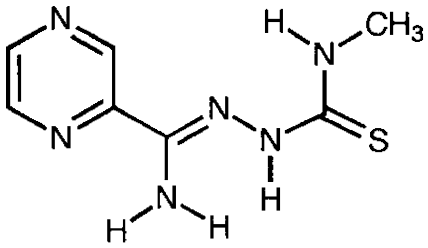


Fig. 1. Representation of pyrazineformamide N(4)-methylthiosemicarbazone, HPzAm4M.

addition of another 25 ml of MeOH, the mixture was refluxed for a minimum of 4 h. Slow evaporation of the MeOH produced the orange pyrazineformamide N4-methylthiosemicarbazone, HPzAm4M, NMR (DMSO-d_6): N(2)H at $\delta = 10.18$, N(4)H at $\delta = 9.72$, N–CH_3 at $\delta = 3.02$ (d), NH_2 at $\delta = 6.95$; m.p., 234–235 °C.

$[Zn(AmPz4M)]_2$ was prepared by electrochemical oxidation of zinc in a solution of HPzAm4M (0.186 mmol, 39.0 mg) in CH_3CN (40 ml) containing 10 mg of tetraethylammonium perchlorate for 1 h at 5 mA. A loss of 6.1 mg of the anode resulted. $[Cd(AmPz4M)]_2$ was prepared by electrochemical oxidation of cadmium in a solution of HAmPz4M (0.25 mmol, 52.5 mg) in CH_3CN (50 ml) containing 10 mg of tetraethylammonium perchlorate for 1 h at 5 mA. A loss of 13.4 mg of the anode resulted.

2.2. X-ray data collection and reduction

Orange crystals of HPzAm4M obtained by slow evaporation of ethanol, dark orange prismatic crystals of $[Zn(PzAm4M)_2]$ grown from MeCN and red prismatic hygroscopic crystals of $[Cd(PzAm4M)_2]$ obtained from MeCN were mounted on glass fibers and used for data collection. Data were collected on a Nonius MACH 3 diffractometer (HPzAm4M) or Bruker Smart CCD area-detector diffractometer at ambient conditions using Cu Kα radiation ($\lambda = 1.54184$ Å) for HPzAm4M and Mo Kα radiation ($\lambda = 0.71073$ Å) for $[Zn(PzAm4M)_2]$ and $[Cd(PzAm4M)_2]$. The structures were solved by direct methods [11] which revealed the position of all non-hydrogen atoms, and refined on F^2 by full-matrix least-square procedure using anisotropic displacement parameters [12]. The hydrogen atoms attached to carbons in the three compounds were located in their calculated positions and were refined using a riding model; the hydrogens attached to nitrogens were found and refined isotropically. Atomic scattering factors were taken from the International Table for X-ray Crystallography [13] and molecular graphics are from PLATON (HPzAm4M) [14] or ORTEP [15].

3. Results and discussion

The molecular structures of HPzAm4M, $[Zn(PzAm4M)_2]$ and $[Cd(PzAm4M)_2]$ are shown in Figs. 2–4, respectively. Table 1 has summaries of crystal data and intensity collection for the three compounds. A selection of bond distances and angles in the thiosemicarbazone fragment and coordination sphere of these complexes are listed in Tables 2 and 3. Hydrogen-bonding interactions for the three compounds are listed in Table 4 and their mean plane deviations, atoms showing the greatest deviation for each plane and the angles between planes are shown in Table 5.

3.1. Crystal structure of HPzAm4M

HPzAm4M crystallizes in the monoclinic space group $P2_1/c$ like 2-pyridineformamide N4-methylthiosemicarbazone, HAm4M [7], while 2-formylpyridine N4-methylthiosemicarbazone, HFo4M, crystallizes in the orthorhombic space group $P2_12_12_1$ with $Z = 4$ [16]. However, HAm4M [7] crystallizes with four unique molecules in the unit cell and $Z = 16$ compared with $Z = 4$ for HPzAm4M. HPzAmM, HAm4M and HFo4M are all E with respect to the imine C=N bond, the conformation that is most often found for heterocyclic N4-alkylthiosemicarbazones [16]. Like other heterocyclic N4-alkylthiosemicarbazones [7,16], the arrangement with respect to the N–C(S) bond, which has considerable double bond character, is also E. This allows for a weak interaction by N14H (Fig. 2) with the imine nitrogen, N12 and another weak interaction occurs between one of the N15 hydrogens and the pyrazine nitrogen, N11, that is unique to these recently studied heterocyclic amide thiosemicarbazones [7]. The bond distances for the thiosemicarbazone moiety of HPzAm4M, HAm4M [7] and HFo4M [16] are not very different except that the two amide thiosemicarbazones, HPzAm4M and HAm4M, have a C17–S1 bond that is approximately 0.05 Å longer and the C17–N13 and

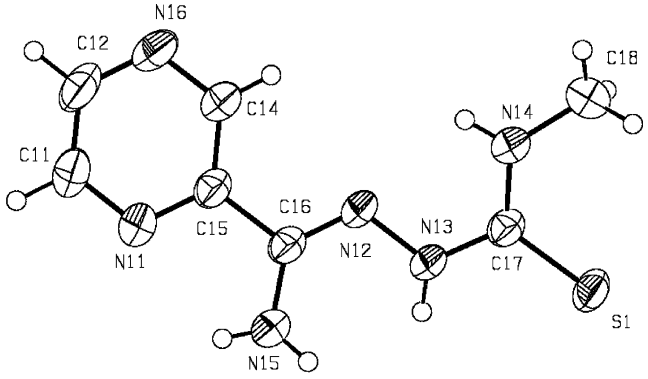


Fig. 2. ORTEP drawing of HPzAm4M with atom numbering scheme and displacement ellipsoids at 50% probability level.

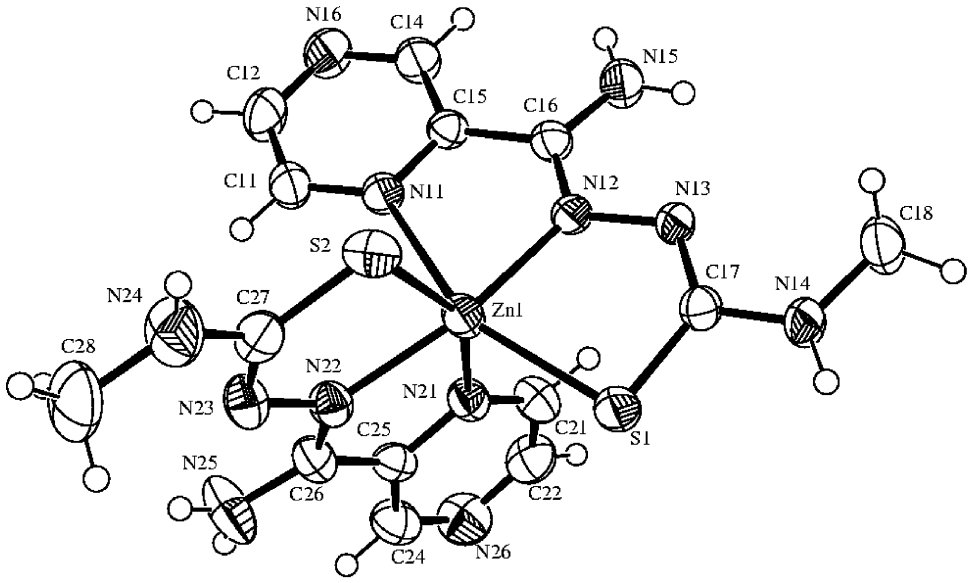


Fig. 3. ORTEP drawing of $[Zn(PzAm4M)_2]$ with atom numbering scheme and displacement ellipsoids at 50% probability level.

C17–N14 bonds are marginally shorter suggesting greater delocalization of electron density. While HPzAm4M and HAm4M have C15–C17–N12 bond angles of approximately 116°, this angle is more than 120° for HFo4M [16], which is consistent with a recent report comparing the structures of 4-formylpyridine and 4-acetylpyridine N(4)-methyl- and N(4)-ethylthiosemicarbazones [17]. The remainder of the thiosemicarbazone bond angles in HPzAm4M, HAm4M [7] and HFo4M [16] are more similar.

As indicated previously, two weak intramolecular hydrogen bonds, N14–H14···N12 and N15–H15B···N11, are present in HPzAm4M. Although the arrangement of HFo4M [16] is the same, the N14–H14···N12 interaction was not found because of the inductive effect of a the aldehyde hydrogen compared with the electron donating amino function. In the four unique molecules of HAm4M, the N14–H14···N12 interaction has an average non-bonding distance of 2.575(5) Å and average angle of 113(4)° which are similar to the values for HPzAm4M (Table 4). The distances and angles for the N15H15B···N11 interaction are essentially the same for HPzAm4M and HAm4M. Unique to HPzAm4M is that H14 is also involved in an interaction with the second nitrogen of the pyrazine ring, N16, which is weaker, based on the H14···N distances, than its intramolecular interaction with N12. The second N15 hydrogen, H15A, interacts weakly with the thione sulfur of a second neighboring molecule.

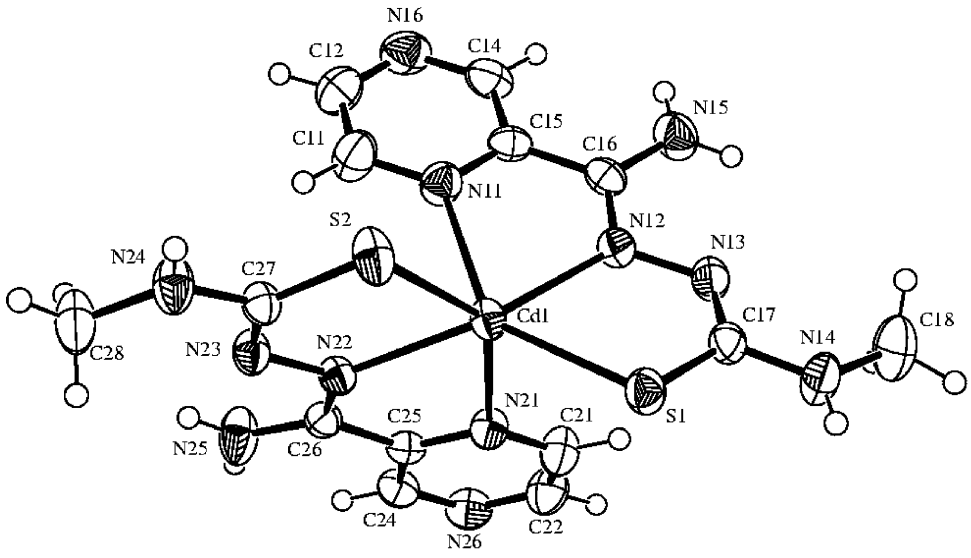


Fig. 4. ORTEP drawing of $[Cd(PzAm4M)_2]$ with atom numbering scheme and displacement ellipsoids at 50% probability level.

Table 1
Crystal data and structure refinement for HPzAm4M, $[Zn(PzAm4M)_2]\cdot 2CH_3CN$, and $[Cd(PzAm4M)_2]\cdot 0.5CH_3CN$

Empirical formula	$C_7H_{10}N_6S$	$C_{18}H_{24}N_{14}S_2Zn$	$C_{15}H_{19.5}CdN_{12.5}S_2$
Color; Habit	orange, prism	dark orange, prism	red, prism
Formula weight	210.27	566.0	551.45
Temperature (K)	293(2)	293(2)	293(2)
Crystal size (mm)	$0.32 \times 0.24 \times 0.12$	$0.20 \times 0.20 \times 0.12$	$0.26 \times 0.17 \times 0.12$
Crystal system	monoclinic	triclinic	triclinic
Space group	$P2_1/c$ (#14)	$P\bar{1}$ (#2)	$P\bar{1}$ (#2)
Unit cell dimensions			
a (Å)	11.1334(8)	7.9278(12)	9.6613(16)
b (Å)	5.0612(3)	11.036(1)	11.1091(18)
c (Å)	17.9215(11)	16.000(2)	11.831(2)
α (°)	90(0)	78.117(16)	89.329(5)
β (°)	99.569(5)	88.668(14)	73.568(5)
γ (°)	90(0)	68.428(14)	64.279(4)
Volume (Å^3)	995.80(11)	1271.8(4)	1088.1(3)
Z	4	2	2
Density (Mg m^{-3})	1.403	1.478	1.683
Absorption coefficient (mm^{-1})	2.669	1.167	1.227
θ Range for data collect. (°)	4.03–74.92	2.61–30.43	1.81–30.58
Index ranges	$-13 \le h \le 13$, $0 \le k \le 6$, $0 \le l \le 22$	$-11 \le h \le 11$, $-15 \le k \le 15$, $-22 \le l \le 0$	$-12 \le h \le 13$, $-15 \le k \le 15$, $-16 \le l \le 16$
Absorption correction	ψ-scan	ψ-scan	SADABS
Reflections collected	2103	7944	19424
Independent reflections (R_{int})	2031 (0.0406)	7688 (0.0861)	6577 (0.0434)
Max., min. transmissions	0.967, 0.916	0.8727, 0.8001	0.8668, 0.7410
Data/restraints/parameters	2031/0/167	7688/0/326	6576/0/289
Final R Indices [$I > 2\sigma(I)$]	$R_1 = 0.0360$, $wR_2 = 0.0999$	$R_1 = 0.0466$, $wR_2 = 0.0795$	$R_1 = 0.0321$, $wR_2 = 0.0604$
R Indices (all data)	$R_1 = 0.0484$, $wR_2 = 0.1061$	$R_1 = 0.2042$, $wR_2 = 0.1063$	$R_1 = 0.0584$, $wR_2 = 0.0666$
Goodness-of-fit	1.060	0.959	0.925
Largest difference peak/hole (e Å^{-3})	0.189/−0.215	0.463/−0.724	0.706/−0.451

The thiosemicarbazone moiety of HPzAm4M, C16–N12–N13–C17–S1–N14, has a larger mean plane deviation (Table 5) than HAm4M, 0.0339 Å. The mean plane of the pyridine ring forms an angle of 9.912(12)° with the thiosemicarbazone moiety mean plane, which is smaller than found for HAm4M, 14.1(4)°.

Table 2
Selected bond distances (Å) for HPzAm4M (**1**); $[Zn(PzAm4M)_2]\cdot 2CH_3CN$ (**2**); and $[Cd(PzAm4M)_2]\cdot 0.5CH_3CN$ (**3**)

Bond	**1**	Bond	**2**	Bond	**3**
S1–C17	1.6939(15)	S1–C17	1.743(3)	S1–C17	1.756(3)
C16–N12	1.290(2)	C16–N12	1.298(3)	C16–N12	1.295(3)
N12–N13	1.3879(18)	N12–N13	1.389(3)	N12–N13	1.389(3)
N13–C17	1.351(2)	N13–C17	1.316(3)	N13–C17	1.307(3)
C17–N14	1.324(2)	C17–N14	1.346(4)	C17–N14	1.349(3)
C16–N15	1.350(2)	C16–N15	1.349(4)	C16–N15	1.361(3)
		S2–C27	1.750(3)	S2–C27	1.744(2)
		C26–N22	1.298(4)	C26–N22	1.292(3)
		N22–N23	1.401(3)	N22–N23	1.391(2)
		N23–C27	1.297(4)	N23–C27	1.317(3)
		C27–N24	1.366(4)	C27–N24	1.343(3)
		C26–N25	1.347(4)	C26–N25	1.348(3)
		Zn–S1	2.4056(10)	Cd–S1	2.5805(7)
		Zn–S2	2.4405(10)	Cd–S2	2.5693(8)
		Zn–N12	2.072(2)	Cd–N12	2.327(2)
		Zn–N22	2.071(2)	Cd–N22	2.2987(19)
		Zn–N11	2.415(2)	Cd–N11	2.481(2)
		Zn–N21	2.333(2)	Cd–N21	2.5260(19)

Table 3
Selected bond angles (°) for HPzAm4M (**1**); $[Zn(PzAm4M)_2]\cdot 2CH_3CN$ (**2**); and $[Cd(PzAm4M)_2]\cdot 0.5CH_3CN$ (**3**)

Angle	**1**	Angle	**2**	Angle	**3**
N15–C16–N12	127.74(15)	N15–C16–N12	123.1(3)	N15–C16–N12	124.1(2)
C15–C16–N12	115.97(14)	C15–C16–N12	116.5(3)	C15–C16–N12	116.8(2)
C16–N12–N13	115.87(14)	C16–N12–N13	113.3(2)	C16–N12–N13	114.09(19)
N12–N13–C17	118.27(14)	N12–N13–C17	113.6(2)	N12–N13–C17	114.57(19)
N13–C17–N14	116.99(14)	N13–C17–N14	115.6(3)	N13–C17–N14	116.2(2)
N13–C17–S1	119.40(12)	N13–C17–S1	127.8(2)	N13–C17–S1	128.70(18)
N14–C17–S1	123.59(13)	N14–C17–S1	116.6(2)	N14–C17–S1	115.1(2)
		N25–C26–N22	123.7(3)	N25–C26–N22	123.6(2)
		C25–C26–N22	116.1(3)	C25–C26–N22	117.1(2)
		C26–N22–N23	113.6(2)	C26–N22–N23	113.38(19)
		N22–N23–C27	113.5(3)	N22–N23–C27	115.00(19)
		N23–C27–N24	116.0(3)	N23–C27–N24	115.2(2)
		N23–C27–S2	128.3(2)	N23–C27–S2	128.93(17)
		N24–C27–S2	115.7(3)	N24–C27–S2	115.91(18)
		S1–Zn1–N22	115.08(7)	S1–Cd1–N22	136.06(5)
		S1–Zn1–N12	81.81(7)	S1–Cd1–N12	74.74(5)
		S1–Zn1–N11	151.79(6)	S1–Cd1–N11	139.83(5)
		S1–Zn1–N21	90.54(7)	S1–Cd1–N21	96.93(5)
		S1–Zn1–S2	105.31(4)	S1–Cd1–S2	104.41(2)
		S2–Zn1–N22	80.97(7)	S2–Cd1–N22	75.99(5)
		S2–Zn1–N12	112.29(7)	S2–Cd1–N12	130.97(5)
		S2–Zn1–N11	93.33(6)	S2–Cd1–N11	91.39(5)
		S2–Zn1–N21	153.25(6)	S2–Cd1–N21	142.08(5)
		N11–Zn1–N22	88.28(9)	N11–Cd1–N22	83.26(7)
		N11–Zn1–N12	71.47(8)	N11–Cd1–N12	67.231(7)
		N11–Zn1–N21	81.21(8)	N11–Cd1–N21	92.06(7)
		N21–Zn1–N22	72.75(9)	N21–Cd1–N22	66.97(6)
		N21–Zn1–N12	90.90(9)	N21–Cd1–N12	84.59(7)
		N12–Zn1–N22	155.91(9)	N12–Cd1–N22	138.23(7)
		Zn1–S1–C17	94.06(10)	Cd1–S1–C17	97.06(8)
		Zn1–N12–C16	124.7(2)	Cd1–N12–C16	123.04(16)
		Zn1–N12–N13	122.01(17)	Cd1–N12–N13	122.85(14)
		Zn1–S2–C27	94.02(11)	Cd1–S2–C27	97.05(8)
		Zn1–N22–C26	123.0(2)	Cd1–N22–C26	123.58(15)
		Zn1–N22–N23	123.18(19)	Cd1–N22–N23	122.58(13)

Table 4
Hydrogen-bonding interactions for HPzAm4M (**1**); $[Zn(PzAm4M)_2]\cdot 2CH_3CN$ (**2**); and $[Cd(PzAm4M)_2]\cdot 0.5CH_3CN$ (**3**)

Compound	D–H···A	d(D–H)	d(H···A)	d(D···A)	∠ (DHA)
1[a]	N14–H14···N12	0.84(2)	2.20(2	2.614(2)	110.3(17)
	N14–H14···N16#1	0.84(2)	2.45(2)	3.124(2)	138.0(18)
	N15–H15A···S1#2	0.84(3)	2.84(3)	3.2886(18)	116(2)
	N15–H15B···N11	0.80(3)	2.26(3)	2.681(2)	113(2)
2[b]	N14–H14···N16#1	0.77(3)	2.29(3)	3.027(4)	163(3)
	N15–H15A···N13	0.80(3)	2.25(3)	2.588(4)	106(2)
	N15–H15B···S2#2	0.92(4)	2.53(4)	3.445(3)	172(3)
	N25–N25B···N23	0.83(4)	2.21(4)	2.612(5)	109(3)
	N25–H25B···N1(MeCN)#3	0.87(4)	2.26(4)	3.117(5)	166(3)
3[c]	N14–H14···N26#1	0.79(3)	2.65(3)	3.358(3)	150(3)
	N24–H24···N26#2	0.79(3)	2.36(3)	3.112(3)	161(3)
	N15–H15A···S2#3	0.93(3)	3.00(3)	3.518(3)	116.5(19)
	N15–H15A···N13	0.93(2)	2.25(3)	2.626(4)	103(2)
	N25–H25A···S1#4	0.81(3)	2.76(3)	3.526(3)	159(3)
	N25–H25BN23	0.81(3)	2.19(3)	2.596(3)	111(2)

Symmetry transformations used to generate equivalent atoms: [a]#1: $-x+3$, $y+1/2$, $-z+3/2$; #2: $-x+2$, $-y$, $-z+1$.[b]#1: $x+1$, $y-1$, z; #2: $-x+1$, $-y+2$, $-z+1$; #3: x, y, $z+1$. [c]#1: $x+1$, y, z; #2: x, $y+1$, z; #3: $-x+2$, $-y+1$, $-z$; #4: $-x+1$, $-y+1$, $-z+1$.

Table 5
Rms planes for HPzAm4M (**1**); $[Zn(PzAm4M)_2]\cdot 2CH_3CN$ (**2**); and $[Cd(PzAm4M)_2]\cdot 0.5CH_3CN$ (**3**)

Compound	Plane	rms dev.	Largest dev.	∠ with previous plane
1	N11–C11–C12–N16–C14–C15	0.0083	C15, 0.0116(0.0014)	
	C16–N12–N13–C17–S1–N14	0.0449	N12, 0.0906(0.0013)	9.912(0.12)
2	N11–C11–C12–N16–C14–C15	0.0012	C12, 0.0017(0.0024)	
	C16–N12–N13–C17–S1–N14	0.0451	C16, 0.0683(0.0016)	7.05(0.14)
	C26–N22–N23–C27–S2–N24	0.0195	N22, 0.0375(0.0021)	89.86(0.06)
	N21–C21–C22–N26–C24–C25	0.0083	C25, 0.0117(0.0021)	5.62(0.19)
3	N11–C11–C12–N16–C14–C15	0.0024	N11, 0.0040(0.0018)	
	C16–N12–N13–C17–S1–N14	0.0637	N12, 0.1112(0.0017)	8.88(0.13)
	C26–N22–N23–C27–S2–N24	0.0248	N23, 0.0445(0.0018)	75.83(0.04)
	N21–C21–C22–N26–C24–C25	0.0013	C24, 0.0019(0.0017)	6.50(0.07)

3.2. Crystal structure of [Zn(PzAm4M)$_2$] and of [Cd(PzAm4M)$_2$]

In both complexes, the metal center has a coordination number of six binding the imine and the pyridine nitrogen atoms, as well as the thiolato sulfur, of two anionic tridentate thiosemicarbazone ligands. The coordinated polyhedron about the metal in both complexes is distorted octahedral with the two ligands in a meridional arrangement. This distortion from octahedral symmetry is illustrated by the three angles defined by pairs of *trans* donor atoms and the metal atom, in the range of 151.77(6)°–155.91(9)° for $[Zn(PzAm4M)_2]$ and 138.23(7)°–142.10(5)° for $[Cd(PzAm4M)_2]$, significantly different from 180°. The small bite angle of chelate rings is the main source of distortion as found previously with Group 12 metal complexes, as well as iron(III), cobalt(III) and nickel(II) complexes with bis(heterocylic thiosemicarbazone) metal centers [7a]. The bond angles (Table 3) of the two ligands, which involve the metal ions, are similar in the two complexes, and, in particular, those angles involving donor atoms within the same ligand. The greatest difference occurs in comparing analogous angles between the two ligands; for example, S1–Zn1–N22 is 115.08(7)°, but S2–Zn1–N12 is 112.29(7)°. The difference is even larger in $[Cd(PzAm4M)_2]$, S1–Cd1-N22 is 136.07(5)° and S2–Cd1–N12 is 130.97(5)°. As would be expected due to the larger size of cadmium(II) compared with zinc(II), the bond angles involving the metals ions in the two complexes are significantly different.

In both complexes the M–N(imine) bonds (i.e. M–N12, M–N22) are the shortest metal–ligand distances and in $[Cd(PzAm4M)_2]$ the Cd–S distances are longer than the Cd–N(pyridine) distances. However, in $[Zn(PzAm4M)_2]$ the Zn–S and Zn–N(pyridine) bond distances are similar. $[Fe(Am4M)_2]ClO_4$ and $[Co(Am4M)_2]ClO_4$ have the same order of ligand bond distances [7a] as $[Cd(PzAm4M)_2]$. To date the only zinc and cadmium complexes of HAm4M for which we have obtained crystals are four-coordinate, $[Zn(Am4M)OAc]_2$ and five-coordinate $[Cd(HAm4M)Cl_2]\cdot DMSO$ [18]. Compared with the bond distances of the thiosemicarbazone moiety of HPzAm4M, the following bond distances have been altered in $[Zn(PzAm4M)_2]$ and $[Cd(PzAm4M)_2]$: C17–S1 (and C27–S2) is longer consistent with it formally changing from a double bond to a single bond, N13–C17 (and N23–C27) is shorter consistent with it formally changing from a single bond to a double bond and C17–N14 (and C27–N24) is marginally longer. The remaining bond distances of the thiosemicarbazone moiety, as well as C16–N15 (and C26–N25) are unchanged in the two complexes from their distances in HPzAm4M. The bond angles of the thiosemicarbazone moieties (Table 3) also are different in the two complexes than in HPzAm4M; N13–C17–S1 (and N23–C27–S2) and N14–C17–S1 (and N24–C27–S2) show the largest differences.

These complexes of 2-pyridineformamide thiosemicarbazones feature hydrogen-bonding involving the amide hydrogens, $N15H_2$ [7,18]. One of the hydrogens from both ligands in $[Zn(PzAm4M)_2]\cdot 2CH_3CN$ is involved in hydrogen-bonding, one to sulfur of the other ligand in a neighboring molecule, and the other to the nitrogen of an acetonitrile solvent molecule. In $[Cd(PzAm4M)_2]\cdot 0.5CH_3CN$ only N25–H25...S1 is present, and it is substantially weaker than the analogous interaction in $[Zn(PzAm4M)_2]\cdot 2MeCN$. Unique to these pyrazine thiosemicarbazones is hydrogen-bonding to the second ring nitrogen, N16. Both complexes, as well as HPzAm4M, involve the atom in an intermolecular interaction and it is either of comparable strength or a stronger interaction in the complexes.

Formation of the anion on coordination retains the planarity of the thiosemicarbazone moiety in the two complexes. The average of the mean planes of the two ligands in $[Zn(PzAm4M)_2]$ is less than that of HPzAm4M, but the mean plane average of the two ligands in $[Cd(PzAm4M)_2]$ is comparable to HPzAm4M. Both ligands in each complex have angles between the mean planes of the pyrazine ring and the thiosemicarbazone moiety that are marginally less than

found for HPzAm4M. This is expected because of the greater conjugation present in the anionic ligand compared with the neutral molecule.

4. Supplementary material

Crystallographic data (excluding structure factors) for the structures reported in this paper have been deposited with the Cambridge Crystallographic Data Center as supplementary publication no. CCDC-172573 for HPzAm4M, and, CCDC-172574 for $[Zn(PzAm4M)_2]\cdot 2CH_3CN$, and CCDC-172575 for $[Cd(PzAm4M)_2]\cdot 0.5CH_3CN$. Copies of available material can be obtained, free of charge, on application to the Director, CCDC, 12 Union Road, Cambridge CB21EZ, UK (fax: +44-1223-336033 or e-mail: deposit@ccdc.cam.ac.uk or www: http://www.ccdc.cam.ac.uk).

References

[1] M.C. Miller, III, K.F. Bastow, C.N. Stineman, J.R. Vance, S.C. Song, D.X. West, I.H. Hall, Archiv der Pharmazie 331 (1998) 121.
[2] J.K. Swearingen, D.X. West, Transition Met. Chem. 26 (2001) 252.
[3] E. Bermejo, R. Carballo, A.Castiñeiras, R. Domínguez, A.E. Liberta, C. Maichle-Mössmer, M.M. Salberg, D.X. West, Eur. J. Inorg. Chem. (1999) 965.
[4] D.X. West, J.K. Swearingen, T.J. Romack, I.S. Billeh, J.P. Jasinski, Y. Li, R.J. Staples, J. Mol. Struct., in press.
[5] D. Kovala-Demertzi, M. Demertzis, P. Nath Yadav, A. Castiñeiras, D.X. West, Transition Met. Chem. 24 (1999) 642.
[6] J.K. Swearingen, D.X. West, Transition Met. Chem. 26 (2001) 252.
[7] (a) D.X. West, J.K. Swearingen, J. Valdés-Martínez, S. Hernández-Ortega, A.K. El-Sawaf, F. van Meurs, A. Castiñeiras, I. Garcia, E. Bermejo, Polyhedron 18 (1999) 2919;
(b) D.X. West, J.K. Swearingen, A.K. El-Sawaf, Transition Met. Chem. 25 (2000) 80.
[8] C. Maichle-Mössmer, A. Castiñeiras, R. Carballo, H. Gebremedhin, M.A. Lockwood, C.E. Ooms, T.J. Romack, D.X. West, Transition Met. Chem. 20 (1995) 228.
[9] D.X. West, M.A. Lockwood, M.D. Owens, A.E. Liberta, Transition Met. Chem. 22 (1997) 366.
[10] J. van Koningsbruggen, J.G. Haasnoot, R.A.G. De Graaff, J. Reedijk, Inorg. Chim. Acta 234 (1995) 87.
[11] G.M. Sheldrick, Acta Crystallogr., Sect. A 46 (1990) 467.
[12] G.M. Sheldrick, SHELXL-97. Program for the Refinement of Crystal Structures, University of Göttingen, Germany, 1997.
[13] International Tables for X-ray Crystallography, vol. C, Kluwer Academic Publishers, Dordrecht, The Netherlands, 1995.
[14] A.L. Spek, PLATON. A Multipurpose Crystallographic Tool, Utrecht University, Utrecht, The Netherlands, 2000.
[15] L.J. Farrugia, J. Appl. Crystallogr. 30 (1997) 565.
[16] D.X. West, G.A. Bain, R.J. Butcher, J.P. Jasinski, Y. Li, R.Y. Pozdniakiv, J. Valdés-Martínez, R.A. Toscano, S. Hernández-Ortega, Polyhedron 15 (1996) 665.
[17] H. Beraldo, R. Lima, L.R. Teixeira, A.A. Moura, D.X. West, J. Mol. Struct. 559 (2001) 99.
[18] I. Garcia, E. Bermejo, A.K. El-Sawaf, A. Castiñeiras, D.X. West, submitted.

containing one [4] or two pyNO groups [5] were investigated. Finally, since 1989 more complex ligands with the pyNO fragment have appeared in the literature. Besides linear tridentate, tetradentate and potentially pentadentate chelating ligands [6], the syntheses of penta-, hexa- and heptadentate tripodal ligands were described [7]. Recently, some macrocyclic systems were synthesised, which contain two pyNO groups and which are able to form binuclear complexes [8].

We have studied Cu(II) complexes of 2,2′-bipyridine N,N′-dioxide (bipyO) [9] and of 1,10-phenanthroline N-oxide [10]. For bipyO, the first structurally characterised couple of binuclear Cu(II) isomers with and without a pyridine N-oxide bridge was reported. The magnetic properties of these isomers stimulated our general interest in pyridine N-oxide ligands and in the magnetism of the corresponding transition metal complexes. We, therefore, began to undertake a systematic study on such systems [11].

The present contribution deals with the spectral and structural properties of Cu(II) complexes formed with the tridentate Schiff base ligand 2-(*o*-hydroxyphenyliminomethyl)pyridine N-oxide (Hpoxap) prepared according to Scheme 1. Some preliminary data on these complexes have been already reported [12].

2. Experimental

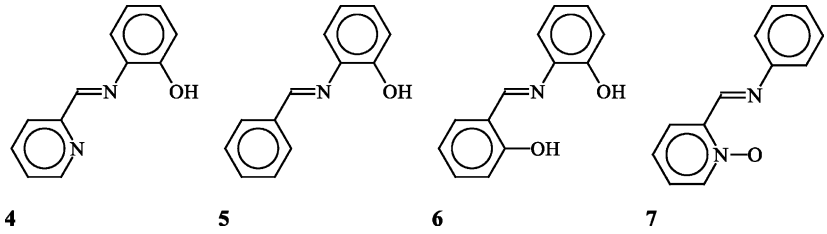
2.1. Preparation of the ligands

2.1.1. Hpoxap

A solution of 15.5 g (11.0 mmol) of 2-pyridinecarboxaldehyde N-oxide, monohydrate (prepared by the method of Jerchel [13]) in 150 cm^3 of EtOH was added to a solution of 12.0 g (11.0 mmol) of freshly recrystallised *o*-aminophenol in 50 cm^3 of EtOH at room temperature (r.t.) under stirring. The resulting solution was heated to 60–70 °C until a yellow Schiff base began to precipitate. The mixture was cooled to r.t. under stirring. After 2 h the solid was filtered, washed with EtOH and air-dried. Yield 17.2 g (73%). *Anal*. Found: C, 67.43; H, 4.62; N, 13.23. Calc. for $C_{12}H_{10}N_2O_2$: C, 67.28; H, 4.70; N, 13.08%. Melting point (m.p.), 204–205 °C.

2.1.2. Other ligands

The remaining ligands, namely 2-(*o*-hydroxyphenyliminomethyl)pyridine (**4**), *N*-phenyl-methylidene(*o*-aminophenol) (**5**), 2-(*o*-hydroxyphenyliminomethyl)phenol (**6**), and 2-(phenyliminomethyl)pyridine *N*-oxide (**7**) were prepared according to literature recipes [14,15] (Eq. (2)).



4 **5** **6** **7** (2)

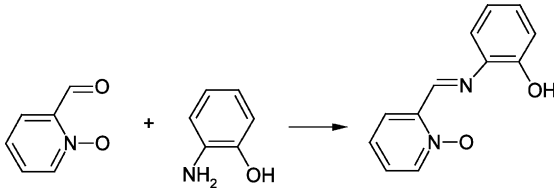
2.2. Preparation of the complexes

2.2.1. Cu(poxap)(OAc) (*8*)

A solution of 2.00 g (10 mmol) of $Cu(OAc)_2.H_2O$ in 150 cm^3 of EtOH was slowly added to the mixture of 2.14 g (10 mmol) of Hpoxap in 90 cm^3 of EtOH under rigorous stirring at r.t. The dark red suspension was stirred and slowly heated for 10 min. After that stirring at r.t. was continued for 60 min. The dark solid product was filtered, washed twice with EtOH and air-dried. Yield 2.96 g (88%). *Anal*. Found: C, 50.01; H, 3.67; N, 8.27; Cu, 19.02. Calc. for $C_{14}H_{12}N_2O_4Cu$: C, 50.07; H, 3.60; N, 8.34; Cu, 18.92%. Cube-shaped crystals, suitable for X-ray structure determination, were received from the mother liquid after 6 weeks.

2.2.2. Cu(poxap)(H_2O)(NO_3) (*9*)

A solution of 1.62 g (7 mmol) of $Cu(NO_3)_2 \cdot 3H_2O$ in 25 cm^3 of ethanol was added to the mixture of 1.50 g (7 mmol) of Hpoxap in 100 cm^3 of boiling EtOH under rigorous stirring. The solution became dark red and



Scheme 1. Preparation route of Hpoxap.

crystals were formed in few seconds. The mixture was cooled to r.t. under stirring within 2 h. The solid product was filtered, washed with EtOH and air-dried. Yield 2.28 g (91%). *Anal*. Found: C, 40.30; H, 3.03; N, 11.67; Cu, 17.82. Calc. for $C_{12}H_{11}N_3O_6Cu$: C, 40.40; H, 3.11; N, 11.78; Cu, 17.81%. Brownish-red needles, suitable for X-ray structure determination, were received by the slow diffusion of diethylether vapour into the solution of the complex **9** in EtOH during 4 months.

2.2.3. Remaining complexes Cu(poxap)(BF_4) (**10**), Cu(poxap)(H_2O)(SiF_6)$_{0.5}$ (**11**), Cu(poxap)(ClO_4) (**12**)

These complexes were prepared according to the procedure described for **9**. Yield for **10**, 85%. *Anal*. Found: C, 39.82; H, 2.51; N, 7.69; Cu, 17.33. Calc. for $C_{12}H_9N_2BCuF_4O_2$: C, 39.64; H, 2.50; N, 7.07; Cu, 17.48%. Yield for **11**, 90%. *Anal*. Found: C, 38.57; H, 2.88; N, 7.47; Cu, 16.73. Calc. for $C_{12}H_{11}N_2CuF_3O_3Si_{0.5}$: C, 39.40; H, 3.03; N, 7.66; Cu, 17.48%. Yield for **12**, 89%. *Anal*. Found: C, 38.53; H, 2.39; N, 7.47. Calc. for $C_{12}H_9N_2ClCuO_6$: C, 38.31; H, 2.41; N, 7.45%.

2.3. Instrumentation

IR spectra were recorded in the 200–4000 cm^{-1} range in Nujol suspension between CsI windows (Philips, PU 9800 FT-IR spectrometer). DRIFT spectra were recorded in the 3000–15 000 cm^{-1} range (Nicolet, Magna 750 FTIR spectrometer).

Electronic solution spectra were recorded in the range 11 000–31 000 cm^{-1} (Zeiss, Specord M 40, and Hewlett-Packard, model 8451).

Conductivity measurements—Radelkis, OK-104.
Powder diffraction patterns were scanned using the STOE, STADI-P apparatus.
Electron spin resonance spectra were recorded at X-band frequency (Bruker, SRC 200D).

The mass magnetisation was measured using the SQUID magnetometer at the field $B = 0.1$ T as well as at the AC susceptometer (LakeShore, model 7221). This was converted to the molar magnetic susceptibility and corrected: (i) for the underlying diamagnetism evaluated on the basis of Pascal constants (χ_{dia}(**8**) $= -1.83 \times 10^9$ m^3 mol^{-1} and χ_{dia}(**9**) $= -1.87 \times 10^9$ m^3 mol^{-1}); (ii) for the temperature-independent paramagnetism per copper atom ($\chi_{TIP} = +0.75 \times 10^9$ m^3 mol^{-1}). The effective magnetic moment is calculated as usual: $\mu_{eff}/\mu_B = 798(\chi'_{mol}T)^{1/2}$ where the SI units are employed.

2.4. X-ray structure determination

Single-crystal data collection was performed with an Enraf–Nonius CAD-4 diffractometer [16]. The unit cells were determined by least-squares refinements from θ values of 25 accurately measured reflections. Intensities were recorded with an ω–2θ scan technique, and graphite-monochromated Mo Kα radiation was used. Corrections for Lorentz polarisation and ψ empirical absorption were applied. The crystallographic data are given in Table 1.

Table 1
Crystal data and structure refinement for **8** and **9**

	8	**9**
Empirical formula	$C_{14}H_{12}CuN_2O_4$	$C_{12}H_{11}CuN_3O_6$
Formula weight	335.82	356.80
Temperature (K)	299(2)	299(2)
Wavelength (Å)	0.71069	0.71069
Crystal system	monoclinic	Triclinic
Space group	$P2_1/n$	$P\bar{1}$
Unit cell dimensions		
a (Å)	7.709(2)	7.410 (1)
b (Å)	14.955(3)	9.222 (1)
c (Å)	11.746(1)	10.359 (1)
α (°)	90	72.68 (1)
β (°)	102.95(1)	74.87 (1)
γ (°)	90	75.47 (1)
Volume (Å^3)	1319.7(4)	640.74(13)
Z	4	2
$D_{calc.}$ (Mg m^{-3})	1.690	1.849
Absorption correction (mm^{-1})	1.674	1.661
F(000)	684	362
Crystal size (mm)	0.08 × 0.08 × 0.08	0.15 × 0.03 × 0.03
θ range for data collection (°)	2.24–22.98	2.10–22.97
Index ranges, h; k; l	−8 to +2; 0 to +16, −12 to +12	−8 to +2, −10 to +10, −11 to +11
Reflections collected	2572	2510
Independent reflections	1836 [$R_{int} = 0.0442$]	1777 [$R_{int} = 0.0304$]
Absorption coefficient	Empirical ψ scan	Empirical ψ scan
Max and min transmission	0.999 and 0.874	0.999 and 0.928
Refinement method	Full-matrix least-squares on F^2	Full-matrix least-squares on F^2
Data/restraints/parameters	1836/0/202	1777/0/211
Goodness-of-fit on F^2	0.997	1.065
Final R indices [$I > 2\sigma(I)$]	$R_1 = 0.0343$, $wR_2 = 0.0722$	$R_1 = 0.0355$, $wR_2 = 0.0741$
R indices (all data)	$R_1 = 0.1037$, $wR_2 = 0.0884$	$R_1 = 0.0861$, $wR_2 = 0.0852$
Largest difference peak and hole (e Å^{-3})	0.322 and −0.290	0.432 and −0.334

The structures were solved by direct methods [17] and all the positions of the non-hydrogen atoms were obtained from the Fourier map. The positions of the hydrogen atoms of the coordinated water molecule in **9** were also obtained from the Fourier map. Refinements were carried out by common least-squares methods [18]. The positions of hydrogen atoms other than water hydrogen atoms were refined with fixed distances from the parent carbon atoms. The function minimised

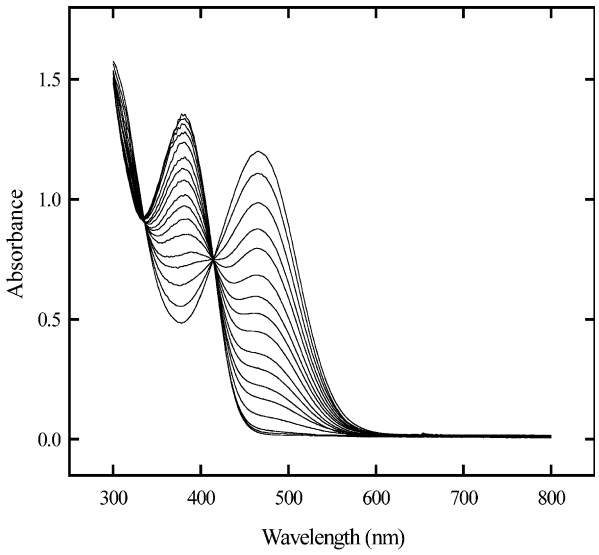


Fig. 1. Titration of Hpoxap with Bu_4NOH in 50% *i*-PrOH/MeOH.

during the least-squares refinements was $\Sigma w(|F_o|-|F_c|)^2$, where $w = 1/[\sigma^2(F_o^2)+(0.0427P)^2+0.0166P]$ for **8**, and $w = 1/[\sigma^2(F_o^2)+(0.0376P)^2+0.1151P]$ for **9**, with $P = (F_o^2+2F_c^2)/3$.

3. Results and discussion

3.1. Electronic spectra of Hpoxap and of the complexes in solution

A yellow solution of Hpoxap in MeOH ($\lambda_{max} = 382$ nm) turns orange–red after deprotonation and a new band appears at 464 nm (Fig. 1). For comparison, the absorption spectra of compounds **4**, **5** and **6** were recorded in MeOH and analogous spectral changes were observed upon addition of base (the absorption maxima were shifted to lower energies). The addition of copper(II) or zinc(II) acetate caused the same sort of red shift (Table 2). Similar shifts of the absorption bands were already described for oxovanadium, chromium and aluminium complexes with **4** and/or **6** [19]. No spectral changes were observed for compound **7** upon addition of NaOH. It is important to note that this is in line with the appearance of new bands in the orange–red range due to phenolate formation and charge transfer from the phenolate oxygen [14,20].

As shown in Table 3, Hpoxap and the poxap anion are subject to solvatochromism.

The UV–Vis spectra of the various complexes Cu(poxap)X ($X^- = NO_3^-$, OAc^-, ClO_4^-, $1/2SiF_6^{2-}$) provide the following information: (i) the strong CT absorption covers the d ← d bands of copper; (ii) there is no anion effect on the spectra (Table 3); (iii) the complex Cu(poxap)(OAc) is subject to solvatochromism. These findings mean that the counteranions X are obviously not coordinated to the copper(II) in solution and the coordination sphere is formed by the anionic ligand poxap and possibly completed by solvent molecules.

The data obtained for the molar conductance of the complexes Cu(poxap)X ($X^- = NO_3^-$, OAc^-, ClO_4^-, $1/2SiF_6^{2-}$, BF_4^-) are in the range typical for 1:1 electrolytes [21] (Table 3). The somewhat lower value of Λ for the acetate complex could indicate that this complex dissociates only partially at the given concentration.

Table 2
Maxima (nm) of the electronic absorption spectra in solution [a]

Reagents		NaOH	$Cu(OAc)_2$	$Zn(OAc)_2$
Hpoxap	379	459	502	484
4	≈370sh	≈480sh	464	
5	345	≈410sh	410	415 375
6	350 442	≈390sh 444 464	418 ≈440sh	412
7	≈350sh	[b]	[b]	[b]

[a] Solvent MeOH.
[b] No spectral change.

3.2. Crystal structures of Cu(poxap)(OAc) (**8**) and Cu(poxap)(H_2O)(NO_3) (**9**)

Figs. 2 and 3 present views and the atom numbering of Cu(poxap)(OAc) and Cu(poxap)(H_2O)(NO_3), respectively. The coordinates of all atoms are contained in Section 4.

In both structures, copper atoms have approximately square-planar coordination formed by two oxygen atoms and one nitrogen atom from the chelating anionic ligand poxap and one oxygen atom (labelled O(3)) from the acetate anion for **8** or water molecule for **9**. In both complexes the ligand poxap is almost planar. Bond angles around the copper atom for both complexes are similar and are probably determined by the ligand geometry.

In **8**, Cu(1) and O(3) lie in the calculated mean plane of the ligand without significant deviations (Table 4). The plane formed by the non-hydrogen atoms of the acetate anion is almost perpendicular to the $Cu(poxap)^+$ fragment (dihedral angle of 88.1°) with a rather long distance (2.745(1) Å) between O(4) and Cu(1). The O(4) oxygen deviates from the theoretically calculated apical position towards copper by 33.4°. This means that the acetate anion can be considered as a monodentate ligand.

In **9**, the copper atom is five-coordinate with the O(5) atom of the nitrate anion in the apical position, thus completing the square-pyramidal surrounding of the copper. The fragment $Cu(poxap)^+$ possesses some deviation from planarity. For the best fit calculations the Plane 3 was chosen, which is formed by the ligand poxap without the O(2) atom. The deviations of Cu(1)

Table 3
Electronic spectral data and molar conductance of Cu(poxap)X complexes

Compound	Solvent	λ_{max} (ε) nm (M^{-1} cm^{-1})	Molar conductance Λ (Ω^{-1} cm^2 mol^{-1})
Hpoxap	Methanol	379 (7300)	
	50% (v/v) *i*-propanol-methanol	382	
Poxap [a]	Methanol	462	
	50% (v/v) *i*-propanol-methanol	464	
	Ethanol	470	
	Acetonitril	470	
	Chloroform	486	
	Pyridine	500	
Cu(poxap)(OAc)	Methanol	502 (9800) [b]	54.0 [c]
	50% (v/v) i-propanol-methanol	506 (9400)	
	Ethanol	510 (6200)	
	Acetonitril	520 (3000)	
	Chloroform	554 (3000)	
Cu(poxap)(ClO_4)	Methanol	502 (9800) [b]	101.5 [c]
Cu(poxap)(H_2O)(NO_3)	Methanol	502 (9800) [b]	81.0 [c]
Cu(poxap)(H_2O)(SiF_6)$_{0.5}$	Methanol	500 (9800) [b]	84.0 [d]
Cu(poxap)(BF_4)			81.8 [c]

[a] Hpoxap was deprotonated by addition of Bu_4NOH.
[b] At 2×10^{-4} M.
[c] At 1×10^{-3} M.
[d] At 3.6×10^{-4} M.

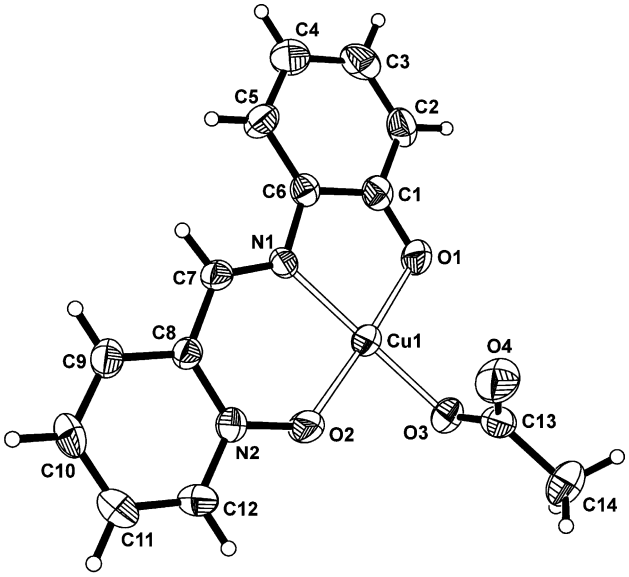


Fig. 2. View of the [Cu(poxap)(OAc)] (**8**) molecule.

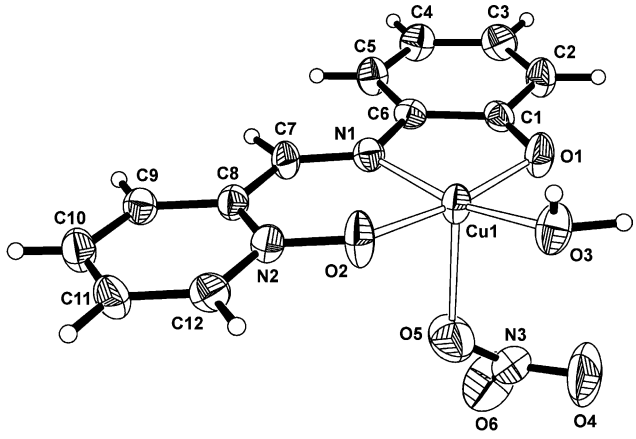


Fig. 3. View of the [Cu(poxap)(H_2O)(NO_3)] (**9**) molecule.

(−0.030 Å), O(2) (0.25 Å) and O(3) (0.40 Å) from this plane were calculated (Table 4). The Cu(1) atom lies nicely in the plane. The deviations of O(2) and O(3) lead to a dihedral angle of 7.6° between Plane 3 and 4 (defined by the four basal donor atoms). The position of Cu(1) is 0.18 Å below Plane 4. It means it is slightly shifted towards the apical O(5) donor. The O(5) atom deviates only by 3.6° from the regular axial position with respect to copper.

It seems to be a common feature of pyridine N-oxides **1** and phenolates **2** that the oxygen atom can deviate from the mean plane of the aromatic ring [22]. However, in **8** and **9**, this deviation is small. The dihedral angle between the N–O group and the normal to the pyridine ring is 92.9° for **8** and 93.9° for **9**, instead of 90°. The values for the N(2)–O(2)–Cu(1) bond angles are 128.4(3)° for **8**, and 127.4(3)° for **9** (Table 5). The relative small deviation of oxygen from the pyridine plane together with the observed values of the N(2)–O(2)–Cu(1) angles and the location of the central Cu(II) atom in the plane of the chelating ligand indicates the sp^2 character of the N-oxide oxygen donor atom.

While the crystal packing of **8** is determined only by van der Waals forces (the nearest interatomic distances between neighbouring molecules Cu(poxap)(OAc),

Table 4
Deviations (Å) from least-squares planes and interplanar angles (°) for **8** and **9** [a]

	Equation	Atom/deviation
Planes for **8**		
1	$0.847x+0.498y-0.187z-3.158=0$	C(1)/−0.012, C(2)/−0.028, C(3)/−0.032, C(4)/−0.026, C(5)/−0.008, C(6)/−0.006, C(7)/0.055, C(8)/−0.053, C(9)/−0.057, C(10)/0.000, C(11)/−0.104, C(12)/−0.087, O(1)/0.014, N(1)/0.036, N(2)/0.011, O(2)/0.076, Cu(1) [e]/0.093, O(3) [e]/0.211, O(4) [e]/2.385
2 [b]	$-0.461x+0.883y+0.082z-6.681=0$	C(13)/0.001, C(14)/0.000, O(3)/−0.001, O(4)/−0.001, Cu(1)/−0.078
Planes for **9**		
3	$0.785x+0.522y+0.335z-6.246=0$	C(1)/−0.040, C(2)/0.004, C(3)/0.043, C(4)/0.032, C(5)/0.006, C(6)/−0.023, C(7)/−0.008, C(8)/0.015, C(9)/−0.033, C(10)/−0.045, C(11)/−0.020, C(12)/0.052, O(1)/−0.054, N(1)/−0.022, N(2)/0.092, O(2) [e]/0.248, Cu(1) [e]/−0.030, O(3) [e]/0.404
4 [c]	$0.697x+0.615y+0.368z-6.683=0$	O(1)/−0.046, O(2)/−0.045, O(3)/0.045, N(1)/0.045, Cu(1)[e]/−0.177
5 [d]	$0.049x+0.995y+0.084z-3.224=0$	O(4)/−0.005, O(5)/−0.004, O(6)/−0.004, N(3)/0.013

[a] Direction cosines of the planes refer to the orthogonal axis system.
[b] The dihedral angle between Plane 1 and 2 is 88.1°.
[c] The dihedral angle between Plane 3 and 4 is 88.1°.
[d] The dihedral angle between Plane 3 and 5 is 54.1° and between Plane 4 and 5 is 47.4°.
[e] Atoms not involved into the plane calculation.

Table 5
Interatomic distances (Å) and bond angles (°) involving the chromophore for **8** and **9**

	8	**9**
Bond lengths		
Cu(1)–N(1)	1.946(3)	1.951(4)
Cu(1)–O(1)	1.911(3)	1.913(3)
Cu(1)–O(2)	1.924(3)	1.930(3)
Cu(1)–O(3)	1.917(3)	1.955(4)
Cu(1)–O(5)		2.258(2)
Bond angles		
O(1)–Cu(1)–O(2)	176.1(2)	171.8(2)
O(3)–Cu(1)–N(1)	178.0(2)	166.9(2)
O(1)–Cu(1)–O(3)	95.4(2)	93.3(2)
O(1)–Cu(1)–N(1)	85.4(2)	85.2(2)
O(2)–Cu(1)–O(3)	87.4(2)	88.3(2)
O(2)–Cu(1)–N(1)	91.9(2)	91.5(2)
O(5)–Cu(1)–N(1)		93.9(4)
O(5)–Cu(1)–O(1)		96.9(4)
O(5)–Cu(1)–O(2)		91.7(4)
O(5)–Cu(1)–O(3)		99.2(4)
C(7)–N(1)–Cu(1)	126.0(3)	125.9(3)
C(6)–N(1)–Cu(1)	110.5(3)	110.8(3)
C(1)–O(1)–Cu(1)	111.8(3)	111.9(3)
N(2)–O(2)–Cu(1)	128.4(3)	127.4(3)
C(13)–O(3)–Cu(1)/N(3)–O(5)–Cu(1)	110.5(3)	123.4(4)

O(4)···H(7) 2.384(3), O(4)···H(9) 2.506(4), O(2)···H(10) 2.531(5), O(1)···H(12) 2.428(3) and O(3)···H(14) 2.533(3) Å, are too long to be considered as interactions), the molecular packing of **9** is affected by two different types of hydrogen bonds.

One hydrogen bond between coordinated water and the phenolic oxygen atom of the neighboring molecule (O(3)···O(1)′ distance is 2.685(1) Å and O(1)′···H(31)–O(3) angle is 158.3(1)°) forms a dimer. Molecules Cu(poxap)(H_2O)(NO_3) are related centrosymmetrically

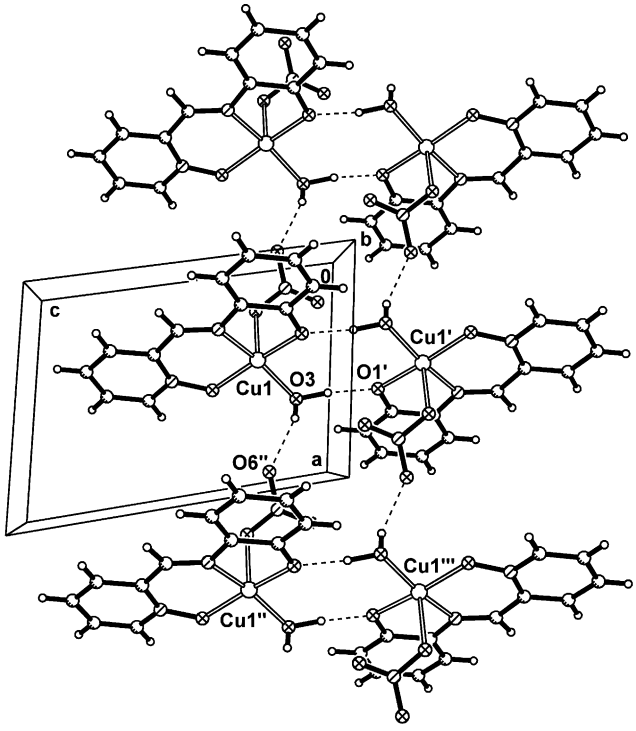


Fig. 4. Crystal packing of **9**. Projection along the *b* axis showing a formation of a 'ladder' structure via a net of hydrogen bonds.

to each other in the dimer. The least-square planes of the neighbouring Cu(poxap)(H_2O)$^+$ fragments in the dimeric unit are parallel as a result of the centre of inversion and separated by 0.12(4) Å.

The dimers are joined into a polymeric chain of dimers (Fig. 4) through another type of hydrogen bond between the other hydrogen atom of coordinated water and the oxygen atom of the apically coordinated nitrato group (O(3)···O(6)″ distance is 2.691(1) Å and O(6)″···H(32)–O(3)) angle is 159.8(1)°).

3.3. ESR spectra

The r.t. X-band ESR spectra of polycrystalline **8** and **9** exhibit signals typical for axial spectra ($g_{||} = 2.19$ and $g_{\perp} = 2.05$ for **8** and $g_{||} = 2.25$ and $g_{\perp} = 2.06$ for **9**) of copper(II) ions with a $d_{x^2-y^2}$ ground state. In frozen ethanol solution (80 K) the hyperfine structure of the $g_{||}$ component is clearly resolved ($g_{||} = 2.26$, $A_{||} = 181$ G and $g_{\perp} = 2.05$ for **8** and $g_{||} = 2.27$, $A_{||} = 173$ G and $g_{\perp} = 2.05$ for **9**). The frozen solution spectrum of **9** exhibits a well resolved feature of medium intensity at $g = 1.90$, which might be attributed to a component of a pair of zero-field split transitions, indicating the presence of a binuclear species in solution. This band disappeared after the addition of pyridine, but the axial character of the spectrum was not affected ($g_{||} = 2.25$, $A_{||} = 177$ G and $g_{\perp} = 2.05$). This indicates that pyridine can substitute the water molecule in the equatorial position and break the hydrogen bonds forming binuclear units. It must be pointed out that no half-field signal was found for solid compound **9**.

3.4. Powder diffraction patterns

As it will be evidenced later, compound **9** exhibits unusual magnetic behaviour. However, the powder sample has been under investigation and thus an important question arises: is the structure of the powder material identical with that determined for the single crystal? For that reason the powder diffraction patterns have been scanned twice: for the original sample of **9a** and a freshly prepared sample of **9b** by the same recipe. According to Fig. 5, the experimental diffraction patters match the theoretical prediction based upon the atomic positions known from the single-crystal data.

3.5. Magnetic data

The temperature variation of the molar magnetic susceptibility and the effective magnetic moment for **8** and **9** is shown in Fig. 6.

The monomeric complex **8** shows features typical for isolated copper(II) ions possessing $s = 1/2$: (i) the almost constant effective magnetic moment at higher temperature being close to the spin-only value of 1.73 μ_B; (ii) some drop at low temperature due to intermolecular interactions of the antiferromagnetic nature. The fitting procedure for the Curie–Weiss law of the form $\chi_{mol} = (N_A\mu_0\mu_B^2/k)g_{eff}^2 s(s+1)/[3(T-\Theta)]$ gave $g_{eff} = 2.092$ and $\Theta = -0.74$ K (discrepancy factor $R = 0.01$).

Complex **9** exhibits features typical for copper(II) dimers: (i) at high temperature the effective magnetic moment reaches the spin-only limit (per copper ion); (ii) on cooling the magnetic susceptibility passes through a maximum and then turns down to zero indicating the singlet ground state of the dimer, $S = 0$; (iii) at very low temperature the vanishing susceptibility of the dimer is superimposed by the Curie-like signal of the paramagnetic impurity. In calculating the molar magnetic susceptibility a doubled value of the formula weight resulting from the single-crystal X-ray analysis has been applied. The fitting procedure for the Bleaney–Bowers equation $\chi_{mol} = (N_A\mu_0\mu_B^2/kT)g_{eff}^2[(1-x_{PI})2/(3+\exp(-J/kT))+2x_{PI}s(s+1)/3]$ gave $g_{eff} = 1.96$, $J/hc = -26.6$

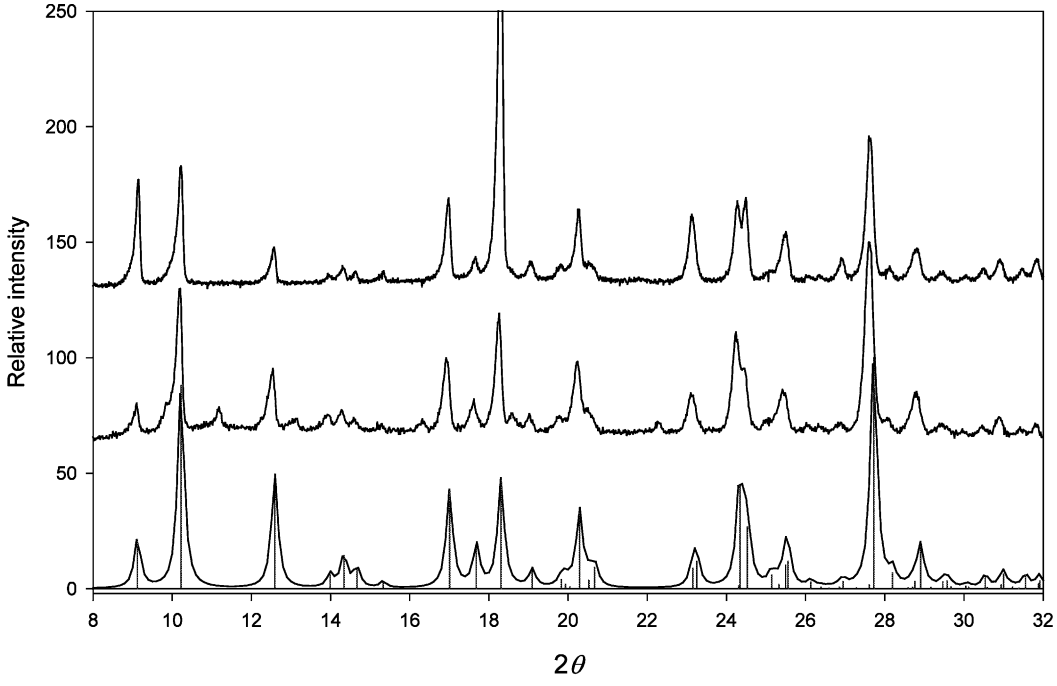


Fig. 5. Experimental powder diffraction patterns for **9b** (top) and **9a** (centre); theoretical patterns—bottom.

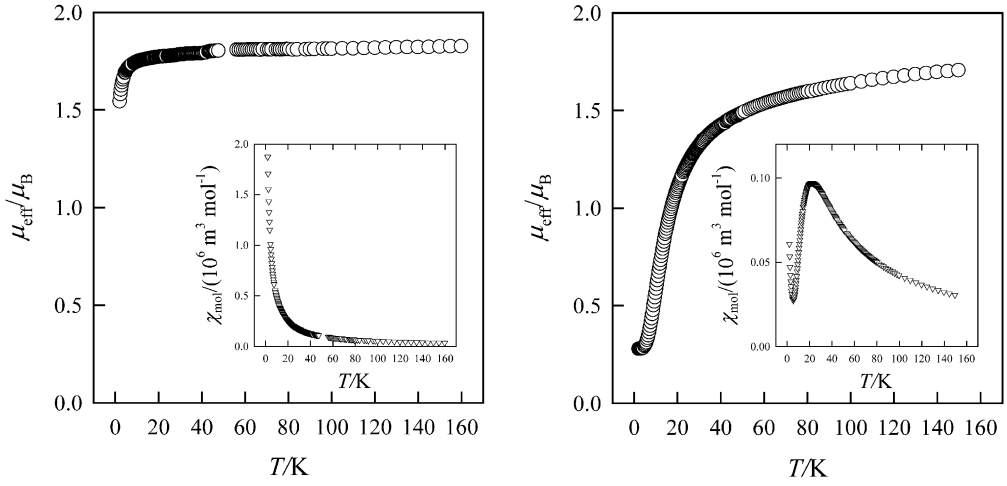


Fig. 6. Temperature dependence of the effective magnetic moment for **8** (left) and **9** (right, per monomer). Inset—the molar magnetic susceptibility.

cm^{-1} and the mole fraction of the paramagnetic impurity $x_{PI} = 0.030$ ($R = 0.028$). The used model [23,24] is partially successful since it does not account for the ladder-type arrangement of the copper(II) centres. The abstraction from the inter-dimer exchange interaction may be the origin of the sub-normal value of the g-factor. The negative value of the coupling constant matches the available experimental data [25–27].

The AC susceptibility data taken for the freshly prepared sample **9b** match perfectly the SQUID data for the sample **9a**. No new information or altered conclusions can be drawn from them except the important statement that the synthesis and the properties of the complex **9** are reproducible.

3.6. IR spectra

The IR spectra of the complexes were studied to obtain more information on the O-coordination of the pyridine N-oxide from the shift of the N–O stretching frequency, relative to the free ligand. Shifts of the (NO) bending vibration could also support the oxygen–metal

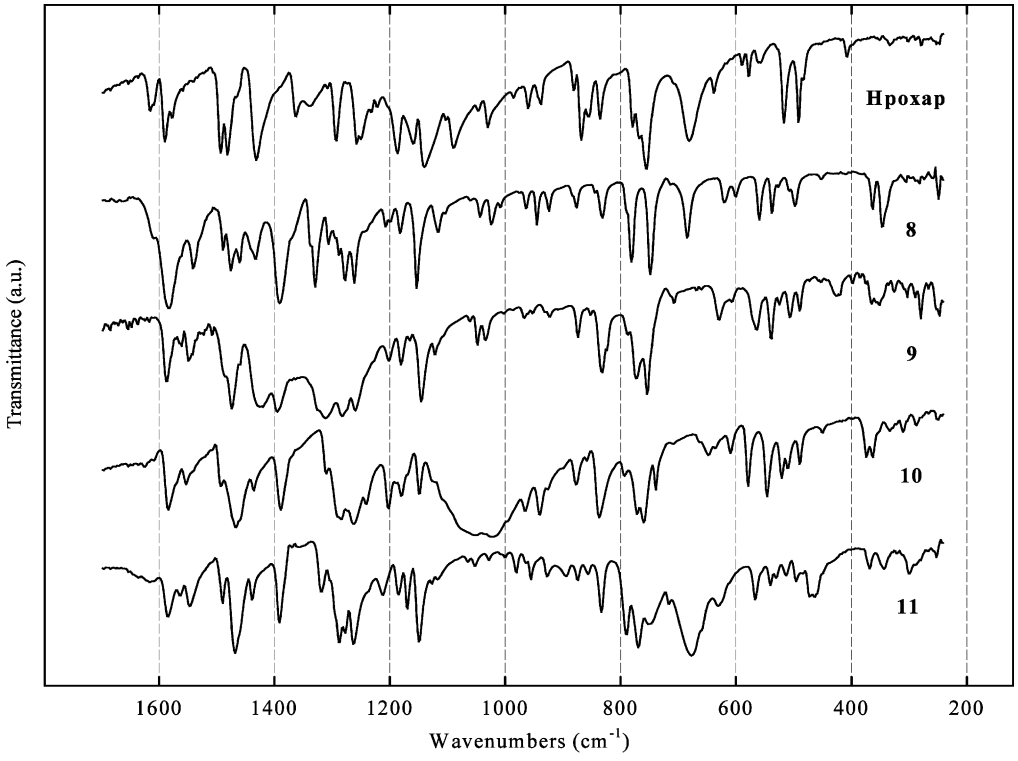


Fig. 7. IR spectra of Hpoxap and its Cu(II) complexes measured in Nujol suspension between CsI windows (absorptions from Nujol were subtracted).

coordination. Unfortunately, even for simple substituted pyridine N-oxides, there are different assignments for the N–O group in literature [28].

The present ligand Hpoxap has a rather complicated IR spectrum (Fig. 7). To assign the observed absorptions, the IR spectrum of Hpoxap was compared with those of **4**, **5** and **7**. Spectra of all four compounds were also simulated (gas phase) using the standard semi-empirical AM1 method of quantum chemistry [29] for better understanding of possible vibrations.

The simulations showed that, the ν(NO) frequency of Hpoxap is shifted to energies, higher than it is usually assumed for substituted pyridine N-oxides [3–6]. The calculated ν(NO) frequency is indeed close to the C=N stretching mode. This supports the assignments recommended by Thornton and Watkins [28]. In addition, ν(NO) is strongly combined with CN pyridine ring stretching. Even more complicated is the identification of the NO bending mode, which is dominated by CN pyridine ring stretching. The combined vibration (with the minor contribution due to the NO bending) should occur in the region of combined ν(ring)/γ(CH) vibrations.

The observed vibrations of the ligands and complexes studied together with the suggested assignments are listed in Table 6. These assignments are:

i) The ν(C=N) vibration is observed in the region 1590–1624 cm^{-1} for the free ligands and is shifted approximately 2–8 cm^{-1} to lower energies for complexes **8**, **9**, **10** and **11**.
ii) There is single vibration at 1615 cm^{-1} in the ν(ring) region (1600–1400 cm^{-1}) of Hpoxap, which disappears upon coordination and new vibrations at about 1550 cm^{-1} appear in the IR spectra of the complexes. These absorptions are assigned as ν(NO). A similar behaviour is observed for a strong band at 1516 cm^{-1} in the spectrum of **7**.
iii) A strong absorption at approximately 1430 cm^{-1}, assigned as ν(CN) aromatic ring vibration, is found in the spectra of all ligands (except of **5**, which does not contain any pyridine ring).
iv) The complexes exhibit a very strong ν(C–O) vibration at approximately 1390 cm^{-1}. No absorption at 1390 cm^{-1} is found neither for Hpoxap nor for the other ligands. In contrast, there are two medium intensity vibrations at 1362 (ν(C–O)), and 1339 cm^{-1} (δ(O–H)) found for Hpoxap as well as for **4** and **5**, but not for **7** (**7** does not contain the phenolic group). Due to the deprotonation of Hpoxap the broad peak at 1339 cm^{-1} disappears upon complexation. The shift of ν(C–O) to higher energies can be explained by an increase of electron density between C and O atoms after the deprotonation of Hpoxap.
v) The bending NO vibration is usually misaligned in the literature. Simulations of IR spectra yielded three combined absorptions. The one with the highest energy is a combination of NO bending mode with the aromatic ring stretching and should be observed in the range of aromatic ring stretching (1300–950 cm^{-1}). In this range a very strong band at 1140 cm^{-1} is found for Hpoxap (and a medium band at 1142 cm^{-1} for **7**, but no for **4**, nor for **5**). In the complexes Cu(poxap)X, this band shifts to

Table 6
Selected IR frequences (cm^{-1}) of Hpoxap, related ligands and Cu(II) complexes of Hpoxap

Hpoxap	**4**	**7**	**5**	**8**	**9**	**10**	**11**	Assignment
≈ 3340w			≈ 3320w		≈ 3220wb		≈ 3250wb	ν(OH)
1590s	1593vs	1603vs	1624vs	1582vs	1588s	1584s	1584s	ν(C=N–)
1615m		1516m		1541m	1549m	1553m	1547m	ν(N–O)
1578m	1570m	1584m	1593m	≈ 1563sh	1561m	≈ 1569sh	1562m	
1493s	1559w	1561w	1584m	1489m	≈ 1489sh	1493m	1489m	
1482s	1539w	≈ 1530sh	1574s	1476m	1474vs	1466vs	1468vs	
1466vs	1507s	1497s	1559m	1460m	1458m	≈ 1459sh	1458sh	
≈ 1460sh	1497s	1489s	1541w					ν(ring$_{CC}$)
	1491s		1507w					
	1476m		1482s					
			≈ 1473sh					
			1451m					
1431vs	1435vs	1429vs	1418w	1433m	[a]	1435m	1439m	ν(ring$_{CN}$)
1362m	≈ 1360sh		1379m	1391vs	1395vs	1389s	1391s	ν(C–O)
1339mbr	1339mbr		1356mbr					δ(O–H)
1140vs		1142m		1154s	1146s	1150m	1150vs	δ(N–O)
				1582 [b]	1426vsbr	980–1100	677vsbr	
				≈ 1440sh	1312vsbr		473m	ν(anions)
	1426vsbr				≈ 824sh		463m	

[a] The band possibly overlapped with anion absorption.
[b] An overlap with ν(C=N–).

slightly higher energy (Table 6). Two another absorptions with a contribution of NO bending mode were not localised, but should be found at lower energies in the range of the ring breathing modes.

vi) The contribution of the anions X to the IR spectra of complexes Cu(poxap)X is clearly observable. The assignment of the ν(COO) vibrations in **8** is possible after a detailed band shape analysis. Compared with the spectra of the other complexes, the absorption at 1582 cm^{-1} is broader possibly due to the overlap of ν_a(COO) with ν(C=N). A shoulder at approximately 1440 cm^{-1} could be assigned to the ν_s(COO) vibration. In **9**, the splitting of $\nu_3(NO_3)$ was observed (1426 and 1312 cm^{-1}) as a product of the symmetry lowering of the nitrato group. The value of 114 cm^{-1} for the splitting is consistent with the monodentate character of the coordinated nitrato anion [30]. Complex **10** exhibits a very broad and strong band in the range 980–1100 cm^{-1}, which corresponds to non-coordinated BF_4^- anion. Analogously, the anion SiF_6^{2-} is most probably not coordinated in **11**, due to the appearance of strong bands (677, 463 and 473 cm^{-1}), which are almost identical with those found for Na_2SiF_6.

4. Supplementary material

Crystallographic data (X-ray data in *.cif files) for the structures reported in this paper have been deposited with the Cambridge Crystallographic Data Centre, CCDC No. 165961 for compound **8** and CCDC No. 165962 for compound **9**. Copies of this information may be obtained from the Director, CCDC, 12 Union Road, Cambridge, CB2 1EZ, UK (fax: +44-1223-336033; e-mail: deposit@ccdc.cam.ac.uk or http://www.ccdc.cam.ac.uk).

Acknowledgements

The work was supported by the Slovak Grant Agency and by the DAAD within the framework of the cooperation between the Technische Hochschule Darmstadt and the Slovak Technical University Bratislava, and the Fonds der Chemischen Industrie. The authors are thankful to Dr. Christina Arnold (Darmstadt) for taking the electron spectra, Dr. Gernot Wltschek (Darmstadt) for taking the magnetic data, Dr. L′ubica Gelieňová and Dr. Milan Gembický (Bratislava) in assistance with chemical synthesis.

References

[1] (a) A. Bencini, D. Gatteschi, C. Zanchini, Inorg. Chem. 25 (1986) 2211;
(b) W.H. Watson, Inorg. Chem. 8 (1969) 1879;
(c) M. Kato, Y. Muto, H.B. Jonassen, Bull. Chem. Soc. Jpn. 40 (1967) 1738;
(d) M. Kato, H.B. Jonassen, J.C. Fanning, Chem. Rev. 64 (1964) 99.

[2] C. Klofutar, S. Paljk, D. Kremser, Spectrochim. Acta 29A (1973) 139.

[3] (a) R.L. Carlin, J. Am. Chem. Soc. 83 (1961) 3773;
(b) J.V. Quagliano, J. Fujita, G. Franz, D.J. Phillips, J.A. Walmsley, S.Y. Tyree, J. Am. Chem. Soc. 83 (1961) 3770;
(c) V.K. Issleib, A. Kreibich, Z. Anorg. Allg. Chem. 313 (1961) 338;
(d) C.M. Harris, E. Kokot, S.L. Lenzer, T.N. Lockyer, Chem. Ind. (1962) 651;
(e) W.E. Hatfield, Y. Muto, H.B. Jonassen, J.S. Paschal, Inorg. Chem. 4 (1965) 97;
(f) H.L. Schäfer, J.C. Morrow, H.M. Smith, J. Chem. Phys. 42 (1965) 504;
(g) W.E. Hatfield, J.C. Morrison, Inorg. Chem. 5 (1966) 1390;
(h) S.J. Gruber, C.M. Harris, E. Kokot, S.L. Lenzer, T.N. Lockyer, E. Sinn, Aust. J. Chem. 20 (1967) 2403;
(i) R. Whyman, W.E. Hatfield, Inorg. Chem. 6 (1967) 1859;
(j) M.R. Kidd, R.S. Sager, W.H. Watson, Inorg. Chem. 6 (1967) 946;
(k) S. Ščavnicar, B. Matkovic, Chem. Commun. (1967) 297;
(l) R. Whyman, D.B. Copley, W.E. Hatfield, J. Am. Chem. Soc. 89 (1967) 3135;
(m) R.S. Sager, W.H. Watson, Inorg. Chem. 7 (1968) 2035;
(n) D.S. Brown, J.D. Lee, B.G.A. Melsom, Chem. Commun. (1968) 852;
(o) R.S. Sager, R.J. Williams, W.H. Watson, Inorg. Chem. 8 (1969) 694;
(p) R.S. Sager, W.H. Watson, Inorg. Chem. 8 (1969) 308;
(q) D.R. Johnson, W.H. Watson, Inorg. Chem. 10 (1971) 1068;
(r) D.R. Johnson, W.H. Watson, Inorg. Chem. 10 (1971) 1281;
(s) A.D. Michell, C.W. Reimann, A. Santoro, Acta Crystallogr., Sect. B 28 (1972) 126;
(t) R.W. Jotham, S.F.A. Kettle, J.A. Marks, J. Chem. Soc., Dalton Trans. (1972) 1133;
(u) J.C. Morrow, J. Cryst. Mol. Struct. 4 (1974) 243;
(v) R.J. Williams, W.H. Watson, A.C. Larson, Acta Crystallogr., Sect. B 31 (1975) 2362;
(w) E.D. Estes, D.J. Hodgson, Inorg. Chem. 15 (1976) 348;
(x) D.A. Krost, G.L. McPherson, J. Am. Chem. Soc. 100 (1978) 987;
(y) J.A. Paulson, D.A. Krost, G.L. McPherson, R.D. Rodgers, J.L. Atwood, Inorg. Chem. 19 (1980) 2519;
(z) M. Gawron, R.C. Palenik, G.J. Palenik, Acta Crystallogr., Sect. C 44 (1988) 170.

[4] (a) A.N. Speca, N.M. Karayannis, L.L. Pytlewski, L.J. Winters, D. Kandasamy, Inorg. Chem. 12 (1973) 1221;
(b) A.N. Speca, N.M. Karayannis, L.L. Pytlewski, Inorg. Chim. Acta 17 (1976) 29;
(c) R.K. Agarwal, Croat. Chem. Acta 60 (1987) 749;
(d) D.X. West, J. Inorg. Nucl. Chem. 43 (1981) 3169;
(e) A.E. Landers, D.J. Phillips, Inorg. Chim. Acta 25 (1977) L39;
(f) A.E. Landers, D.J. Phillips, Inorg. Chim. Acta 51 (1981) 109;
(g) A.E. Landers, D.J. Phillips, Inorg. Chim. Acta 59 (1982) 125;
(h) A.E. Landers, D.J. Phillips, Inorg. Chim. Acta 74 (1983) 43;
(i) A.E. Landers, D.J. Phillips, Inorg. Chim. Acta 86 (1984) 77;
(j) A.E. Landers, D.J. Phillips, Inorg. Chim. Acta 59 (1982) 41;
(k) S.F. Pavkovic, J.N. Brown, Acta Crystallogr., Sect. B 38

(1982) 274;
(l) F. Jiang, M. Hong, X.X. Xie, R. Cao, B. Kang, D. Wu, H. Liu, Inorg. Chim. Acta 231 (1995) 153.
[5] (a) P.G. Simpson, A. Vinciguerra, J.V. Quagliano, Inorg. Chem. 2 (1963) 282;
(b) A. Vinciguerra, P.G. Simpson, Y. Kakiuti, J.V. Quagliano, Inorg. Chem. 2 (1963) 286;
(c) S.K. Madan, W.E. Bull, J. Inorg. Nucl. Chem. 26 (1964) 2211.
[6] (a) M. Antolovich, D.J. Phillips, A.D. Rae, J. Chem. Soc., Chem. Commun. (1984) 582;
(b) M. Antolovich, D.J. Phillips, A.D. Rae, Inorg. Chim. Acta 156 (1989) 189;
(c) D.C. Craig, D.J. Phillips, F.M.Z. Kaifi, Inorg. Chim. Acta 161 (1989) 247;
(d) S. Gou, X. You, Z. Xu, K. Yu, Z. Zhou, Polyhedron 9 (1990) 2981;
(e) Y. Zang, Z. Yin, G. Wang, C. Zeng, A. Dai, Z. Zhou, Inorg. Chem. 29 (1990) 560;
(f) Z. Zhou, K. Yu, S. Gou, X. You, Z. Xu, Polyhedron 10 (1991) 37;
(g) S. Gou, X. You, Z. Xu, Z. Zhou, K. Yu, Polyhedron 10 (1991) 1363;
(h) Z. Xu, E.C. Alyea, G. Ferguson, M.C. Jennings, Polyhedron 10 (1991) 1625;
(i) S. Gou, X. You, Z. Xu, Z. Zhon, K. Yu, Polyhedron 10 (1991) 2659;
(j) A.A. Russell, R.L. Meline, E.N. Duesler, R.T. Paine, Inorg. Chim. Acta 231 (1995) 1;
(k) M. Antolovich, D.J. Phillips, A.D. Rae, Inorg. Chim. Acta 230 (1995) 139.
[7] (a) S. Gou, X. You, Z. Xu, S. Liu, C. Lin, Acta Crystallogr., Sect. C 47 (1991) 708;
(b) S. Gou, Z. Xu, X.Z. You, K.B. Yu, Chin. Chem. Lett. 2 (1991) 801;
(c) S. Gou, X. You, K. Yu, J. Lu, Inorg. Chem. 32 (1993) 1883.
[8] A.B. Blake, E. Sinn, A. Yavari, B. Moubaraki, K.S. Murray, Inorg. Chim. Acta 229 (1995) 281.
[9] (a) P. Baran, M. Koman, D. Valigura, J. Mrozinski, J. Chem. Soc., Dalton Trans. (1991) 1385;
(b) M. Koman, P. Baran, D. Valigura, Acta Crystallogr., Sect. C 47 (1991) 2529;
(c) H. Paulus, H. Fuess, P. Baran, D. Valigura, Z. Kristallogr. 202 (1992) 134;
(d) H. Paulus, H. Fuess, P. Baran, D. Valigura, Z. Kristallogr. 202 (1992) 140;
(e) P. Baran, D. Valigura, I. Svoboda, H. Fuess, Z. Kristallogr. 203 (1993) 279.
[10] (a) J. Kožišek, P. Baran, D. Valigura, Acta Crystallogr., Sect. C 48 (1992) 31;
(b) J. Kožišek, P. Baran, D. Valigura, R. Boča, Contributions to Development of Coordination Chemistry, Proceedings XIV. Conference on Coordination Chemistry, Smolenice, Bratislava, 1993, p. 239.
[11] P. Baran, H. Elias, Ľ. Gelieňová, M. Valko, Contributions to Development of Coordination Chemistry, Proceedings XIV. Conference on Coordination Chemistry, Smolenice, Bratislava, 1993, p. 85.
[12] P. Baran, H. Elias, I. Svoboda, G. Wltschek, Current Trends in Coordination Chemistry, Proceedings XV. Conference on Coordination Chemistry, Smolenice, Bratislava, 1995, p. 309.
[13] D. Jerchel, J. Heider, H. Wagner, Annalen 613 (1958) 153.
[14] M. Otomo, K. Kodama, Bull. Chem. Soc. Jpn. 46 (1973) 2421.
[15] R.K. Parashar, R.C. Sharma, A. Kumar, G. Mohan, Inorg. Chim. Acta 151 (1988) 201.
[16] ENRAF-NONIUS Diffractometer Control Software, release 5.1, Enraf-Nonius, Delft, 1993.
[17] G.M. Sheldrick, SHELXS-86. Program for the Solution of Crystal Structures, University of Göttingen, Göttingen, Germany, 1986.
[18] G.M. Sheldrick, SHELXS-93. Program for Crystal Structure Determination, University of Göttingen, Göttingen, Germany, 1993.
[19] (a) A. Syamal, L.J. Theriot, J. Coord. Chem. 2 (1973) 193;
(b) N.S. Biradar, V.H. Kulkarni, Rev. Roum. Chim. 16 (1971) 1203;
(c) K. Dey, K.C. Ray, Inorg. Chim. Acta 10 (1974) 139;
(d) R.J. Argauer, C.E. White, Anal. Chem. 36 (1964) 2141.
[20] E.W. Ainscough, A.M. Brodie, J.E. Plowman, K.L. Brown, A.W. Addison, A.R. Gainsford, Inorg. Chem. 19 (1980) 3655.
[21] W.J. Geary, Coord. Chem. Rev. 7 (1971) 81.
[22] (a) H. Elias, E. Hilms, H. Paulus, Z. Naturforsch. B37 (1982) 1266;
(b) J.R. Röper, H. Paulus, H. Elias, Inorg. Chem. 28 (1989) 2323;
(c) B. Chiari, W.E. Hatfield, O. Piovesana, T. Tarantelli, L.W. ter Haar, P.F. Zanazzi, Inorg. Chem. 22 (1983) 1468;
(d) Y.M. Chumakov, V.N. Biyushkin, T.I. Malinovskii, S. Kulemu, V.I. Tsapkov, N.M. Samus, Koord. Khim. 15 (1989) 1074;
(e) A. Emali, O. Atakol, I. Svoboda, H. Fuess, Z. Kristallogr. 205 (1993) 146;
(f) C.E. Xanthopoulos, M.P. Sigalas, G.A. Katsoulos, C.A. Tsipis, A. Terzis, A. Hountas, Inorg. Chim. Acta 214 (1993) 153;
(g) C.E. Xanthopoulos, M.P. Sigalas, G.A. Katsoulos, C.A. Tsipis, A. Terzis, M. Mentzafos, A. Hountas, Inorg. Chem. 32 (1993) 5433;
(h) T. Ueki, T. Ashida, Y. Sasada, M. Kakudo, Acta Crystallogr., Sect. B 25 (1969) 328;
(i) T. Ueki, T. Ashida, Y. Sasada, M. Kakudo, Acta Crystallogr. 22 (1967) 870;
(j) D.J. Szalda, L.G. Marzilli, T.J. Kistenmacher, Inorg. Chem. 14 (1975) 2076;
(k) T.J. Kistenmacher, D.J. Szalda, C.C. Chiang, M. Rossi, L.G. Marzilli, Inorg. Chem. 17 (1978) 2582;
(l) J. Sivy, F. Pavelcik, J. Kratschmar-Smogrovic, M. Zemlicka, V. Seresova, Collect. Czech. Chem. Commun. 55 (1990) 2924;
(m) C.E. Xanthopoulos, M.P. Sigalas, G.A. Katsoulos, C.A. Tsipis, C.C. Hadjikostas, A. Terzis, M. Mentzafos, Inorg. Chem. 32 (1993) 3743;
(n) E. Labisbal, J.A. Garcia-Vazquez, J. Romero, S. Picos, A. Sousa, A. Castineiras, C. Maichle-Mossmer, Polyhedron 14 (1995) 663.
[23] O. Kahn, Molecular Magnetism, VCH, New York, 1993.
[24] B. Bleaney, K. Bowers, Proc. R. Soc. London, Ser. A 214 (1952) 451.
[25] E.J. Laskowski, D.M. Duggan, D.N. Hendrickson, Inorg. Chem. 14 (1975) 2449.
[26] (a) G. Niewpoort, G.C. Verschoor, J. Reedijk, J. Chem. Soc., Dalton Trans. (1983) 531;
(b) H. Muhonen, Inorg. Chem. 25 (1986) 4692;
(c) J.A. Bertrand, E. Fujita, D.G. VanDerveer, Inorg. Chem. 19 (1980) 2022;
(d) J.A. Bertrand, T.D. Black, P.G. Eller, F.T. Helm, R. Mahmood, Inorg. Chem. 15 (1976) 2965.
[27] E. Colacio, J.P. Costes, R. Kivekäs, J.P. Laurent, J. Ruiz, M. Sundberg, Inorg. Chem. 30 (1991) 1475.
[28] D.A. Thornton, G.M. Watkins, Spectrsc. Lett. 25 (1992) 1023.
[29] (a) M.J.S. Dewar, W. Thiel, AUSTIN METHOD 1 Package, University of Texas, Austin, TX, 1986;
(b) M.J.S. Dewar, E.G. Zoebisch, E.F. Healy, J.J.P. Stewart, J. Am. Chem. Soc. 107 (1985) 3902.
[30] K. Nakamoto, Infrared Spectra of Inorganic and Coordination Compounds, Wiley, New York, 1978.

novel family of rod-shaped supramolecular materials. If the geometrical arrangement holds for the coordination polymers formed from PyPN and silver alkylsulfonates, the polymers would be expected to take a hairy-rod structure, which is composed of a rigid-rod polymer backbone and alkylsulfonate anions as the side chains.

In this paper we report the formation and organization behavior of novel coordination polymers with hairy-rod structure by self-assembling of PyPN and silver alkylsulfonates (AgC_{12}, AgC_{14}, AgC_{16} and AgC_{18}).

2. Experimental

2.1. Materials

Hexakis(4-pyridylmethoxy)cyclotriphosphazene (PyPN) was synthesized from the reaction of hexachlorocyclotriphosphazene with sodium 4-pyridylmethoxide prepared from 4-pyridinemethanol (Koei Chemical) and NaH in THF, according to the method reported previously [21]. Silver alkylsulfonates (silver dodecylsulfonate (AgC_{12}), silver tetradecylsulfonate (AgC_{14}), silver hexadecylsulfonate (AgC_{16}) and silver octadecylsulfonate (AgC_{18})) were prepared from the corresponding sodium alkylsulfonates and $AgNO_3$ [24]. Other reagents and solvents were commercially available and used without further purification.

2.2. Preparation of coordination polymers

A DMSO solution (5 ml) of PyPN (51 mg, 6.5×10^{-5} mol) was added dropwise to a stirred DMSO solution (15 ml) of AgC_{12} (70 mg, 1.9×10^{-4} mol) at room temperature (r.t.). The resulting precipitate was redissolved in acetonitrile solution at 80 °C and slowly cooled to r.t. giving white solids (PyPN–AgC_{12}). Similarly, other coordination polymers (PyPN–AgC_{14}, PyPN–AgC_{16} and PyPN–AgC_{18}) were obtained. PyPN–AgC_{12} was obtained in 52% yield. *Anal.* Found (Calc. for $C_{72}H_{111}N_9Ag_3O_{15}P_3S_3$): C, 46.37 (46.61); H, 5.90 (6.03); N, 6.82 (6.79)%. FT-IR (KBr, cm^{-1}): 2923, 2852, 1618, 1241, 1192, 1055–1035. PyPN–AgC_{14} was obtained in 35% yield. *Anal.* Found (Calc. for $C_{78}H_{123}N_9Ag_3O_{15}P_3S_3$): C, 47.79 (48.30); H, 6.50 (6.39); N, 6.56 (6.50)%. FT-IR (KBr, cm^{-1}): 2920, 2850, 1618, 1241, 1193, 1055–1035. PyPN–AgC_{16} was obtained in 53% yield. *Anal.* Found (Calc. for $C_{84}H_{135}N_9Ag_3O_{15}P_3S_3$): C, 49.60 (49.85); H, 6.58 (6.72); N, 6.19 (6.23)%. FT-IR (KBR, cm^{-1}): 2919, 2848, 1618, 1240, 1192, 1055–1035. PyPN–AgC_{18} was obtained in 42% yield. *Anal.* Found (Calc. for $C_{90}H_{147}N_9Ag_3O_{15}P_3S_3$): C, 51.10 (51.28); H, 6.95 (7.03); N, 6.05 (5.98)%. FT-IR (KBr, cm^{-1}): 2919, 2848, 1618, 1241, 1192, 1055–1035.

2.3. Measurements

Elemental analyses were carried out with a Perkin–Elmer 240C elemental analyzer (Advanced Instrumentation Center for Chemical Analysis, Ehime University). FT-IR spectra were recorded on a JASCO FT-IR 230 spectrophotometer applying the KBr pelleting techniques. Wide-angle X-ray diffraction patterns were obtained on a Rigaku RINT 2000 diffractometer using graphite-monochromated Cu Kα radiation (40 kV, 20 mA). Differential scanning calorimetry (DSC) was done using a Shimadzu DSC-50 calorimeter in sealed aluminum pans at a heating rate of 10 °C min^{-1}.

3. Results and discussion

The supramolecular materials obtained by self-assembling of hexakis(4-pyridylmethoxy)cyclotriphosphazene (PyPN) and silver alkylsulfonates were stable indefinitely in air, and are insoluble in water and common organic solvents such as acetone, methanol, chloroform and tetrahydrofuran. Combination of PyPN and sodium alkylsulfonates did not give rise to supramolecular assemblies, suggesting that the present supramolecular materials are not formed through the formation of the salt of alkylsulfonate anions with PyPN. This is supported by the fact that the band at 994 cm^{-1} of PyPN remains as a shoulder in the FT-IR spectrum of PyPN–AgC_{16} (Fig. 2), because the band at 993 cm^{-1} of the pure poly(4-vinylpyridine) disappears completely on fully protonation of the pyridyl groups [25]. We have already shown that the pyridyl groups of PyPN coordinate to the Ag^+ ion for the coordination polymer obtained from PyPN and $AgNO_3$ from extended X-ray absorption fine structure (EXAFS) measurements [23]. In the FT-IR spectrum of PyPN–AgC_{16}, the peak at 1605 cm^{-1}, assignable to free PyPN disappeared and shifted to 1618 cm^{-1} (Fig. 2), indicating that all of the pyridyl units in PyPN, participate in the coordination bonding with Ag^+. A similar result was obtained for the other polymers. From elemental analysis and ^1H NMR spectra, the stoichiometry was shown to be PyPN/silver alkylsulfonates = 1:3 for all supramolecular assemblies. These suggest that the coordination bonding with an alternating sequence of one PyPN and three silver alkylsulfonates gives supramolecular (coordination) polymers composed of $[PyPN{\cdot}3Ag^+]_x{\cdot}3x(SO_3C_nH_{2n+1})$, as shown in Fig. 1.

FT-IR spectra also provide information about the conformation of the alkyl chains in the coordination polymers (Fig. 3). The C–H asymmetric and symmetric bands of the alkyl chains for PyPN–AgC_{16} and PyPN–AgC_{18} are observed at 2919 and 2848 cm^{-1}, respectively, indicating that the alkyl chains are in all-*trans* conformation [26,27]. These bands for PyPN–AgC_{14},

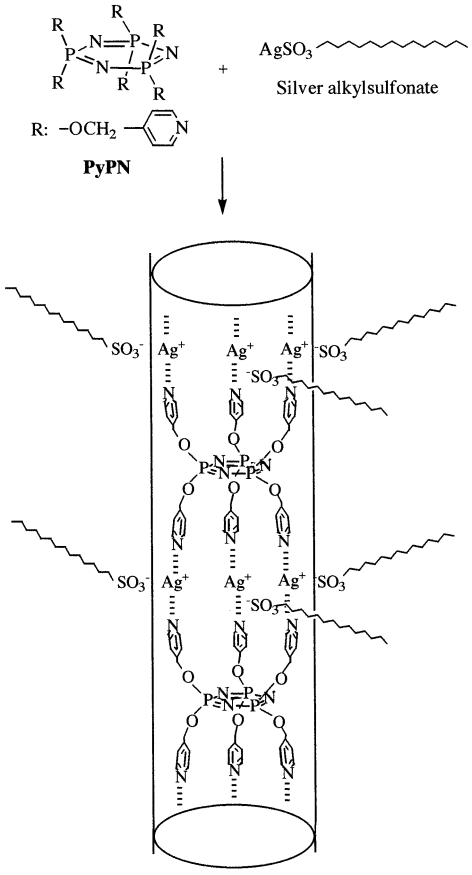


Fig. 1. Formation of coordination polymers by supramolecular assembly of PyPN and silver alkylsulfonates.

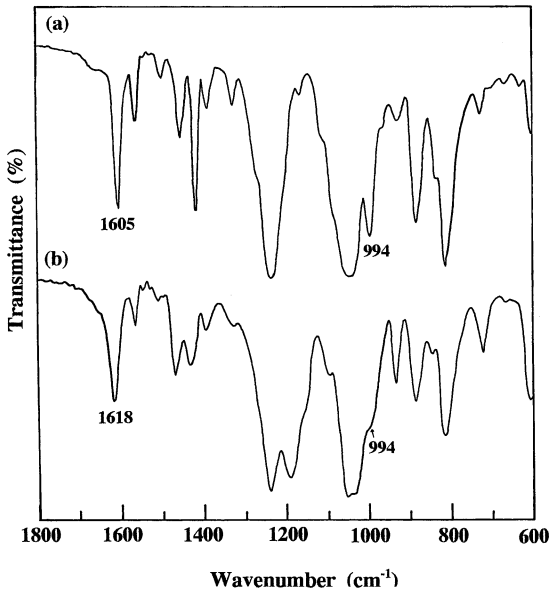


Fig. 2. FT-IR spectra of PyPN (a) and PyPN–AgC_{16} (b).

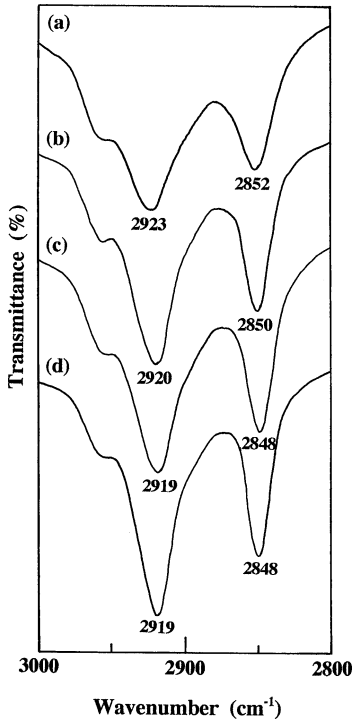


Fig. 3. FT-IR spectra of the coordination polymers in the 2800–3000 cm^{-1} region: (a) PyPN–AgC_{12}, (b) PyPN–AgC_{14}, (c) PyPN–AgC_{16} and (d) PyPN–AgC_{18}.

which were observed at 2920 and 2850 cm^{-1}, suggest that the alkyl chains are almost in extended form. In contrast, PyPN–AgC_{12} gave the C–H stretching bands at higher frequencies of 2923 and 2852 cm^{-1}, indicative of disordered packing of the alkyl chains involving a considerable amount of gauche conformers [26,27].

X-ray diffraction (XRD) patterns for the coordination polymers, PyPN–AgC_n ($n = 12$, 14, 16, 18) are shown in Fig. 4 and the diffraction data are listed in Table 1. The low-angle diffraction comes from the characteristic lattice repeat, i.e. the long range ordering of the polymers, whereas the wide-angle region is indicative of the surfactant alkyl side-chain packing, i.e. the short range ordering [28,29].

PyPN–AgC_{14}, PyPN–AgC_{16} and PyPN–AgC_{18} exhibited peaks centered at Bragg spacings of 4.4, 4.4 and 4.0 Å, and 4.4, 4.0 and 3.8 Å, respectively. These peaks indicate that the alkyl chains in the coordination polymers are organized in the crystal lattice. The spacings of 4.4 and 4.0 Å were in agreement with the values reported for poly(γ-alkyl-L-glutamates) with ten or more carbon atoms in the side chains, which are believed to indicate triclinic packing of the alkyl chains [15].

For the PyPN–AgC_{18} system, three sets of Bragg spacing were observed, one set with the primary reflection at 26.0 Å together with a second order at 13.0 Å, another set having the first-order reflection located at 23.9 Å and second-order at 12.1 Å, and the last set having the first-order reflection located at 21.0

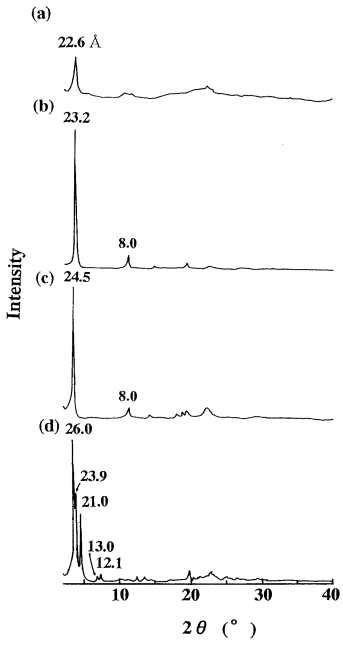


Fig. 4. X-ray diffraction patterns of the coordination polymers: (a) PyPN–AgC_{12}, (b) PyPN–AgC_{14}, (c) PyPN–AgC_{16} and (d) PyPN–AgC_{18}.

Table 1
X-ray diffraction data of the coordination polymers

Sample	Representative X-ray diffraction			
	Before heating		After heating (150 °C)	
	Long spacing	Short spacing	Long spacing	Short spacing
PyPN–AgC_{12}	22.6			
PyPN–AgC_{14}	23.2	4.4	22.6	
PyPN–AgC_{16}	24.5	4.4, 4.0	23.9	4.4, 4.0
PyPN–AgC_{18}	26.0, 23.9, 21.0	4.4, 4.0, 3.8	25.2	4.4, 3.9

Å. Muller has shown in XRD studies of $C_{18}H_{38}$ and $C_{20}H_{42}$, the coexistence of crystalline modification such as α-hexagonal phase and β-triclinic phase [30]. PyPN–AgC_{18} exhibited endothermic transitions, which correspond to the melting of the side-chain crystallites, at 67, 73, 83 °C in its DSC heating curve (Fig. 5). This result is consistent with the observation of the peaks due to the short range packing in the XRD pattern. Taking into consideration the three sets of Bragg spacing and the three melting points of the side-chain crystallites for PyPN–AgC_{18}, it seems reasonable to assume that the alkyl side-chains in PyPN–AgC_{18} organize themselves in multiple crystalline modifications.

PyPN–AgC_{12}, PyPN–AgC_{14} and PyPN–AgC_{16} showed a peak with a Bragg spacing of 22.6, 23.2 and 24.5 Å in the small angle region of their XRD patterns, respectively, although the peak of PyPN–AgC_{12} was

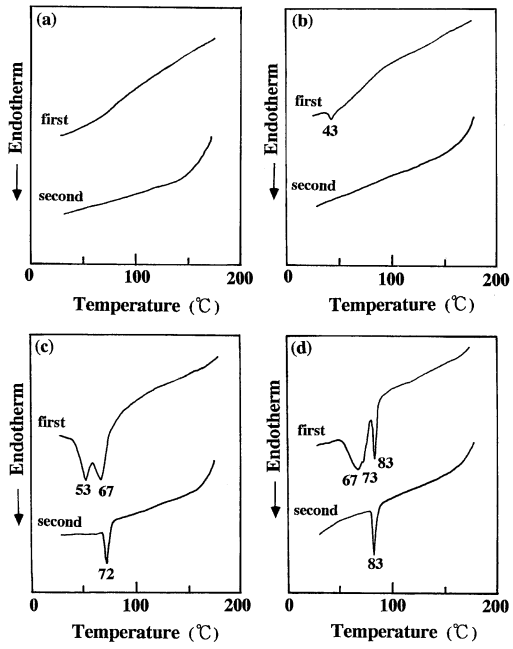


Fig. 5. DSC heating curves of the coordination polymers: (a) PyPN–AgC_{12}, (b) PyPN–AgC_{14}, (c) PyPN–AgC_{16} and (d) PyPN–AgC_{18}.

very broad compared to that of the other polymers. When the coordination polymers were heated up to 150 °C, the Bragg spacing of PyPN–AgC_{14}, PyPN–AgC_{16} and PyPN–AgC_{18} decreased from 23.2 to 22.6, 24.5 to 23.9 and 26.0 to 25.2 Å, respectively (Fig. 6). The DSC second heating curves of these coordination polymers were also different from the DSC first heating curves. These behaviors could be attributed to the disordering and reorganization of the alkyl side chains bound to the polymer backbones by the heating and the subsequent cooling process.

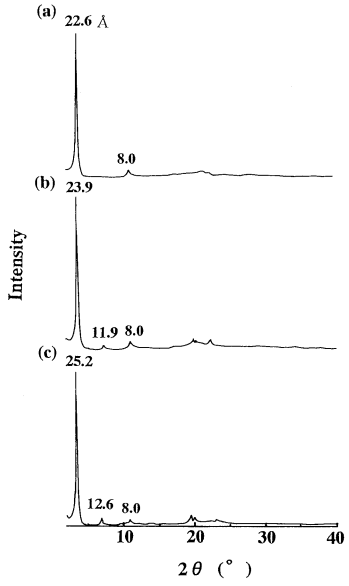
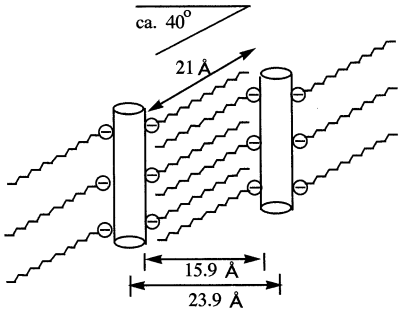


Fig. 6. X-ray diffraction patterns of the coordination polymers after heating up to 150 °C: (a) PyPN–AgC_{14}, (b) PyPN–AgC_{16} and (c) PyPN–AgC_{18}.

The XRD profile of heated PyPN–AgC_{18} was identified by a single reflection with a Bragg spacing of 25.2 Å together with a second-order peak of 12.6 Å. This result suggests that PyPN–AgC_{18}, with a hairy-rod structure [31] i.e. the skeleton is a cylindrical rod consisting of alternating PyPN and three Ag^+ ions bearing alkylsulfonate anions as the side chain, self-organizes into a lamellar structure. The hairy-rod structure is formed by the preference of metal anion (Ag^+)–pyridyl group interaction over the salt formation of the sulfonate anion with the pyridyl group [32], as mentioned above. In the case of PyPN–AgC_{16}, a peak with a spacing of 11.9 Å that corresponds to the second-order spacing of 23.9 Å appeared clearly, showing that the heating treatment brings about a more ordered packing of the hairy-rod coordination polymers and, consequently, the lamellar interface is more sharply defined [33]. PyPN–AgC_{14} did not exhibit a second-order peak of the spacing of 22.6 Å, but the difference (1.30 Å) of the spacing between PyPN–AgC_{14} and PyPN–AgC_{16} is equal to that between PyPN–AgC_{16} and PyPN–AgC_{18}. The above results imply that the PyPN–AgC_{16} and PyPN–AgC_{14} also take a lamellar packing in analogy with PyPN–AgC_{18}. In the XRD patterns of both PyPN–AgC_{16} and PyPN–AgC_{14}, a peak with the spacing of 8.0 Å was observed (Figs. 4 and 6), but, at present, the origin remains unclear.

On the other hand, from the results of FT-IR and XRD measurements, PyPN–AgC_{12} seems distinctly not to form a lamellar structure. In the DSC curve of PyPN–AgC_{12}, an endothermic peak was not observed in both first and second scans, indicative of the absence of a crystalline state of side-chains. It appears that the dodecyl side chains are too short to crystallize.

The orientation of the alkyl side-chains with respect to the polymer backbone in the lamellar structure can be guessed from the dependence of the long period spacing on the number of methylene groups in the side chain. In the case of comb-like polymers [34], the increment of lamellar thickness with side chain length is reported to be about 1.25 Å per methylene group if the alkyl chains are fully extended and perpendicular to the polymer backbone. The increment is less than 1.25 Å if the side chains are tilted. In the coordination polymers composed of PyPN and silver alkylsulfonates, the increment of lamellar thickness with side chain length is estimated to be about 0.65 Å per methylene group, indicating that the alkyl chains are tilted with respect to the polymer backbone. For the PyPN–AgC_{16} assembly, the diameter of rod with the alternating sequence of PyPN and three Ag^+ ions is about 8 Å [23], and the length of fully extended hexadecylsulfonate ion is about 21 Å. Thus, the experimental value (23.9 Å) of the long period of the lamellar of PyPN–AgC_{16} suggests that the alkyl chains of neighboring polymers should be interdigitated and tilted with respect to the polymer backbone by about 40° (Scheme 1).



Scheme 1. Packing model of the lamellar structure of PyPN–AgC_{16}.

Finally, we describe the thermal stability of the coordination polymers composed of PyPN and silver alkylsulfonates. In the second scans for all coordination polymers, an exothermic process occurs from about 170 °C (Fig. 5), indicating the decomposition of the coordination polymers. The temperature of decomposition was higher than that of PyPN (100 °C). The pure PyPN shows an endothermic melting peak at 75 °C, but melting of PyPN is not visible in the DSC curves of the coordination polymers. These indicate that PyPN becomes thermally stable in the coordination polymers with hairy-rod structure. In the DSC curves, an endothermic peak due to the coordination bond scission was not observed. Thus, the coordination polymers decompose due to the pyrolysis of PyPN in the polymers rather than the scission of the coordination bond.

4. Conclusions

The self-assembly of hexakis(4-pyridylmethoxy)cyclotriphosphazene (PyPN) and silver alkylsulfonates through the combination of coordination bonding and ionic interaction has generated novel supramolecular hairy-rod polymers. These coordination polymers with hairy-rod structure were self-organized into ordered structures that depend on the variation of the length of alkyl side chains. The tetradecyl, hexadecyl and octadecyl side chains bound to the rod-shaped coordination polymer composed of PyPN and Ag^+ ions can crystallize intermolecularly, leading to the organization into a lamellar structure. On the basis of the present results, we would now like to go on to exploit new supramolecular rigid-rod polymers controlled nanoscale structures.

Acknowledgements

We are grateful to the Center for Cooperative Research and Development of Ehime University for

supplying the X-ray diffraction equipment. This research was partly supported financially by the grant-in-aid for scientific research from the Ministry of Education, Science and Culture, Japan.

References

[1] J.M. Lehn, Angew. Chem., Int. Ed. Engl. 29 (1990) 1304.
[2] S. Ujiie, K. Iimura, Macromolecules 25 (1992) 3174.
[3] O. Ikkala, M. Knaapila, J. Ruokolainen, M. Torkkeli, R. Serimae, K. Jokela, L. Horsburgh, A. Monkman, G. Brike, Adv. Mater. 11 (1999) 1206.
[4] L.M. Wilson, Macromolecules 27 (1994) 6683.
[5] M.R. Ghadiri, J.R. Granja, L. Buehler, Nature 369 (1994) 301.
[6] T. Kato, Y. Kubota, T. Uryu, S. Ujiie, Angew. Chem., Int. Ed. Engl. 36 (1997) 1617.
[7] I. Nakazawa, M. Masuda, Y. Okada, T. Hanada, K. Yasa, M. Asai, T. Shimizu, Langmuir 15 (1999) 4757.
[8] R. Maki-Ontto, K. Moel, W. Odarico, J. Ruokolajnen, M. Starnm, G. Brike, O. Ikkala, Adv. Mater. 13 (2001) 117.
[9] M. Fujita, Y.J. Kwon, M. Miyazawa, K. Ogura, J. Chem. Soc., Chem. Commun. (1994) 1977.
[10] V.A. Russell, C.C. Evans, W. Li, M.D. Ward, Science 276 (1997) 575.
[11] M. Kondo, M. Shimamura, S. Noro, S. Minakoshi, A. Asami, K. Seki, S. Kitagawa, Chem. Mater. 12 (2000) 1288.
[12] J. Ruokolainen, H. Eerikainen, M. Torkkelo, R. Serimaa, M. Jussila, O. Ikkala, Macromolecules 33 (2000) 9272.
[13] J. Watanabe, Y. Takashima, Macromolecules 24 (1991) 3423.
[14] T.R. Vierheller, M.D. Foster, A. Schmidt, K. Mathauer, W. Knoll, G. Wegner, S. Satija, K. Majkrzak, Macromolecules 27 (1994) 6893.
[15] J. Watanabe, H. Ono, I. Uematsu, A. Abe, Macromolecules 18 (1985) 2141.
[16] H.R. Allcock, Acc. Chem. Res. 11 (1978) 81.
[17] T. Itaya, Y. Sasaki, T. Tanigaki, A. Matsumoto, K. Inoue, Chem. Lett. (1996) 305.
[18] A.P. Primrose, M. Parvez, H.R. Allcock, Macromolecules 30 (1997) 670.
[19] W. Marsh, J. Trotter, J. Chem. Soc. (A), (1971) 169.
[20] G. Bandoli, U. Casellato, M. Grassi, E. Montoneri, G.C. Pappalardo, J. Chem. Soc., Dalton Trans. (1989) 757.
[21] K. Inoue, T. Itaya, N. Azuma, Supramol. Sci. 5 (1998) 163.
[22] T. Itaya, N. Azuma, K. Inoue, Supramol. Chem. 9 (1998) 121.
[23] T. Itaya, K. Inoue, Bull. Chem. Soc. Jpn. 73 (2000) 2615.
[24] T. Itaya, K. Inoue, Kobunshi Ronbunshu 57 (2000) 665.
[25] O. Ikkala, J. Ruokolainen, G. ten Brinke, M. Torkkeli, R. Serimaa, Macromolecules 28 (1995) 7088.
[26] R.G. Snyder, H.L. Strauss, J. Phys. Chem. 86 (1982) 5154.
[27] M.D. Porter, T.B. Bright, D.L. Allara, C.E. Chidsey, J. Am. Chem. Soc. 109 (1987) 3559.
[28] M. Goto, J. Jpn. Oil Chem. Soc. 19 (1970) 583.
[29] T. Shimizu, M. Masuda, J. Am. Chem. Soc. 119 (1997) 2812.
[30] A. Muller, Proc. R. Soc. Lond., Ser. A 127 (1930) 417.
[31] E.A. Ponomarenko, A.J. Waddon, D.A. Tirrell, W.J. MacKnight, Langmuir 12 (1996) 2169.
[32] L. Carlucci, G. Ciani, D.M. Proserpio, A. Sirani, Inorg. Chem. 37 (1998) 5941.
[33] A.M. Donald, A.H. Windle, Liquid Crystalline Polymers, Cambridge University Press, Cambridge, 1992, p. 156.
[34] N.A. Plate, V.P. Shibaev, J. Polym. Sci. Macromol. Rev. 8 (1974) 117.

4, although NMR studies show that often the solutions contain a mixture of species. The isolated complexes were identified by a combination of analysis, IR, ^{1}H, $^{31}P\{^{1}H\}$ and ^{45}Sc NMR spectroscopy, which also revealed that many retain lattice solvent even after prolonged drying in vacuum. The very poorly soluble $ScF_3 \cdot 1/2H_2O$ did not react with Ph_3PO or Me_3PO in boiling ethanol or acetone even with extended reaction times.

2.2. $[ScX_2(Ph_3PO)_4]X$

The reaction of $ScX_3 \cdot nH_2O$ with Ph_3PO in ethanol in molar ratios 1:3–6 resulted in white $[ScCl_2(Ph_3PO)_4]Cl$, $[ScBr_2(Ph_3PO)_4]Br$ and yellow $[ScI_2(Ph_3PO)_4]I$ (Table 1). Attempts to isolate $[ScX_3(Ph_3PO)_3]$ using low ScX_3:Ph_3PO ratios or other solvents were unsuccessful. The presence of six-coordinate cations with O_4X_2 donor sets was confirmed by an X-ray crystal structure of $[ScBr_2(Ph_3PO)_4]Br \cdot 1/2Et_2O$, which (Fig. 1, Table 2)

Table 1
^{45}Sc and $^{31}P\{^{1}H\}$ NMR data [a]

	$^{45}Sc(w_{1/2}$ (Hz))	$^{31}P\{^{1}H\}$	Solvent
$[ScCl_2(Ph_3PO)_4]Cl$	75(850)	34.5	CH_2Cl_2–$CDCl_3$
$[ScCl_3(Ph_3PO)_3]$ [b]	121(1400)	34.0, 33.0	CH_2Cl_2–$CDCl_3$
$[ScBr_2(Ph_3PO)_4]Br$	108(4500)	35.8	CH_2Cl_2–$CDCl_3$
$[ScCl(Me_3PO)_5]Cl_2$	47.0(250)	56.0, 54.5	$MeNO_2$–$CDCl_3$
$[ScCl_2(Me_3PO)_4]Cl$ [b]	85.0(360)	54.0(?)	$MeNO_2$–$CDCl_3$
$[Sc(Me_3PO)_6]Br_3$ [c]	4.4(sept)	57.0(eight lines)	$MeNO_2$–$CDCl_3$
$[ScBr(Me_3PO)_5]Br_2$ [b]	51.5(850)	56.5, 55.0	$MeNO_2$–$CDCl_3$
$[Sc(Me_3PO)_6]I_3$ [c]	4.2(sept)	57.0 (eight lines)	$MeNO_2$–$CDCl_3$
$[Sc(Ph_3AsO)_4Cl_2]Cl$	96(4000)		CH_2Cl_2–$CDCl_3$
$[Sc(Ph_3AsO)_4Br_2]Br$	140(20 000)		CH_2Cl_2–$CDCl_3$
$[Sc(Me_3AsO)_6]Cl_3$	56(80)		$MeNO_2$–$CDCl_3$
$[Sc(Me_3AsO)_6]Br_3$	56(70)		$MeNO_2$–$CDCl_3$
$[Sc(Me_3AsO)_6]I_3$	56(70)		$MeNO_2$–$CDCl_3$
$[ScCl_3(Ph_2MePO)_3]$	123(1100)	40.5, 42.5	CH_2Cl_2–$CDCl_3$
$[ScCl_2(Ph_2MePO)_4]Cl$ [b]	80(2000)	42.4	CH_2Cl_2–$CDCl_3$
$[ScBr_2(Ph_2MePO)_4]Br$	100(8000)	41.0	CH_2Cl_2–$CDCl_3$

[a] All spectra obtained at 295 K in solvent specified.
[b] Species obtained only in solution.
[c] $^{2}J(^{45}Sc-^{31}P) = 19$ Hz.

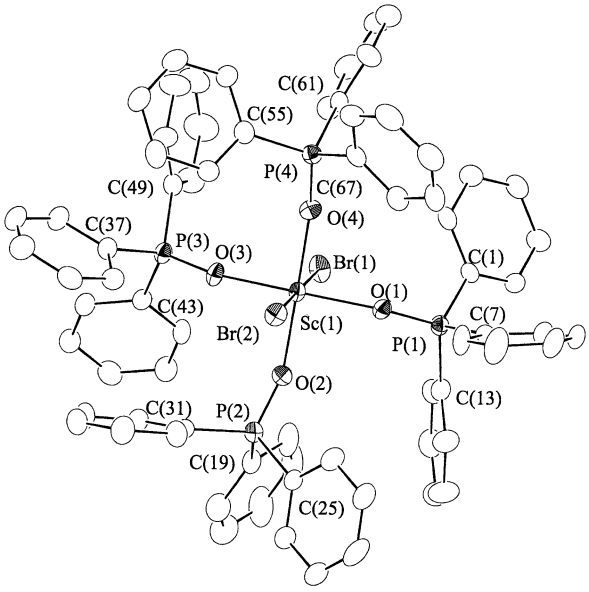


Fig. 1. View of the cation in $[ScBr_2(Ph_3PO)_4]Br \cdot 1/2Et_2O$ showing the atom numbering scheme. Ellipsoids are drawn at the 40% probability level and H atoms omitted for clarity.

reveals a *trans* octahedral cation with Br–Sc–Br very close to linear 179.04(5)° and Br–Sc–O 88.6(3)°–91.3(3)°. The angles Sc–O–P are variable approximately 154–166°. The Sc–O(P) distances, approximately 2.07 Å, are very similar to the values [7] in $[Sc(Ph_3PO)_2(NO_3)_3]$ or $[Sc(Ph_2MePO)_4(NO_3)_2]^{+}$, whilst the Sc–Br distances 2.652(1), 2.661(1) Å appear to be the first reported. The IR spectrum of each complex contains one very strong broad feature in the range 1150–1130 cm^{-1} assignable as ν(PO), which may be compared with 1195 cm^{-1} in the 'free' ligand [7]. In CH_2Cl_2 solution $[ScCl_2(Ph_3PO)_4]Cl$ approximates to a 1:1 electrolyte[1] and in the $^{31}P\{^{1}H\}$ NMR spectrum there is a main feature at δ 34.5 attributed to the tetrakis(Ph_3PO) complex, and weaker features at 26.0 (Ph_3PO), 34.0, 33.0. The corresponding ^{45}Sc NMR spectrum has a broad resonance at δ 75 and a weaker broader resonance at δ 121. Addition of excess Ph_3PO to these solutions results in the loss of the weaker

Table 2
Selected bond lengths (Å) and angles (°) for $[ScBr_2(Ph_3PO)_4]Br \cdot 1/2Et_2O$

Bond lengths			
Sc(1)–Br(1)	2.652(1)	Sc(1)–Br(2)	2.661(1)
Sc(1)–O(1)	2.090(4)	Sc(1)–O(3)	2.059(4)
Sc(1)–O(2)	2.057(4)	Sc(1)–O(4)	2.074(4)
P–O	1.504(4)–1.512(4)		
Bond angles			
Br(1)–Sc(1)–Br(2)	179.04(5)	Br–Sc(1)–O	88.6(3)–91.3(3)
Sc(1)–O(1)–P(1)	153.6(2)	Sc(1)–O(3)–P(3)	163.0(2)
Sc(1)–O(2)–P(2)	159.1(3)	Sc(1)–O(4)–P(4)	166.5(2)

$^{31}P\{^{1}H\}$ NMR features at 34.0 and 33.0 and the ^{45}Sc NMR resonance at 121 which are attributed to *mer*-$[ScCl_3(Ph_3PO)_3]$. In the presence of excess Ph_3PO, $[ScCl_2(Ph_3PO)_4]Cl$ is the only complex present in significant amounts, but in its absence some decomposition into *mer*-$[ScCl_3(Ph_3PO)_3]$ occurs. Even a large excess of Ph_3PO fails to produce substitution of further chloride ligands, in contrast to the corresponding yttrium systems [10]. The $^{31}P\{^{1}H\}$ NMR spectra of $[ScX_2(Ph_3PO)_4]X$ (X = Br or I) in CH_2Cl_2 solution show only a single resonance in each and the conductances do not change significantly on addition of Ph_3PO, consistent with $[ScX_2(Ph_3PO)_4]X$ as the only species present. The ^{45}Sc NMR spectrum of the bromide confirms this with a broad feature at δ 108, but the ^{45}Sc resonance of the iodo-complex is extremely broad (δ ca. 200, $w_{1/2}$ ca. 20 000 Hz) and whilst the δ value is reasonable for a O_4I_2 set, the line-width could clearly obscure any other species present.

2.3. $[ScCl(Me_3PO)_5]Cl_2$ and $[Sc(Me_3PO)_6]X_3$ (X_3 = Br or I)

The reaction of $ScX_3 \cdot nH_2O$ with Me_3PO in a 1:6 molar ratio in ethanol gave $[Sc(Me_3PO)_6]X_3$ (X = Br or I), but only $[ScCl(Me_3PO)_5]Cl_2$ for the lightest halide. The complexes are insoluble or poorly soluble in chlorocarbons, alcohols or acetone, but dissolve in nitromethane. In nitromethane solution, the ^{1}H, $^{31}P\{^{1}H\}$ and ^{45}Sc NMR spectra of $[ScCl(Me_3PO)_5]Cl_2$ show a mixture of species present, which can be identified as $[ScCl(Me_3PO)_5]Cl_2$, $[ScCl_2(Me_3PO)_4]Cl$ (in ca. equal amounts), Me_3PO and some unassigned minor species. In the presence of excess Me_3PO, only $[ScCl(Me_3PO)_5]Cl_2$ (δ $^{45}Sc = 47$) is present in large amounts, but two weak resonances at δ ^{45}Sc 11 and 4 are also seen, the latter due to a small amount of $[Sc(Me_3PO)_6]^{3+}$ (see below). The molar conductivity of a 10^{-3} mol dm^{-3} solution in $MeNO_2$ is 117 Ω^{-1} cm^2 mol^{-1}, intermediate between 1:1 and 1:2 electrolytes and this increases with addition of Me_3PO to 180 Ω^{-1} cm^2 mol^{-1}, showing that excess phosphine oxide shifts the equilibrium in favour of the pentakis complex. An attempt to extract the chloride ligand from $[ScCl(Me_3PO)_5]Cl_2$ with $SbCl_5$ in the presence of Me_3PO was unsuccessful. Dissolution of $[Sc(Me_3PO)_6]Br_3$ in $MeNO_2$ also produces a mixture of complexes which can be identified by the NMR spectra as $[Sc(Me_3PO)_6]^{3+}$ (δ ^{45}Sc 4.5, δ $^{31}P\{^{1}H\}$ 56.5), $[ScBr(Me_3PO)_5]^{2+}$ (δ ^{45}Sc 51.5, δ $^{31}P\{^{1}H\}$ 56.0, 55.0), Me_3PO, and a minor species at δ 11 in the ^{45}Sc NMR spectrum. Addition of excess Me_3PO shifts the equilibria in favour of $[Sc(Me_3PO)_6]^{3+}$, although very small amounts of the other complexes remain evident. In contrast to the initial solution where the resonances of $[Sc(Me_3PO)_6]^{3+}$ in both ^{45}Sc and $^{31}P\{^{1}H\}$ NMR spectra are broad with ill-defined coupling, in the presence of excess Me_3PO well resolved couplings are seen (Fig. 2) confirming the presence of the quadrupolar scandium in a cubic symmetry environment where relaxation is slow. The trends are continued in $[Sc(Me_3PO)_6]I_3$ in that the $[Sc(Me_3PO)_6]^{3+}$ cation is the only major species in solution even in the absence of added Me_3PO (there is also a feature at δ 11 in the ^{45}Sc spectrum). The weak feature in the ^{45}Sc NMR spectra of all three complexes at δ approximately 11 is attributed to a solvento-complex $[Sc(Me_3PO)_{6-n}(MeNO_2)_n]^{3+}$ since the resonance is suppressed by addition of Me_3PO, and moreover is absent if the spectra are recorded in Me_2CO solution (although solubility in acetone is very poor).

2.4. $[ScX_2(Ph_3AsO)_4]X$

The reaction of $ScX_3 \cdot nH_2O$ with Ph_3AsO in 1:4 molar ratio in ethanol gave the *trans*-$[ScX_2(Ph_3AsO)_4]X$ (X = Cl or Br) complexes. The iodide complex failed to give reproducible analytical data, it would appear to be obtained with a mixture of polyiodide–iodide counter-anions, although spectroscopically the cation seems analogous to those with the lighter halides (cf. $[YI_2(Ph_3AsO)_4]I_5$) [9]. The identity as *trans* octahedral

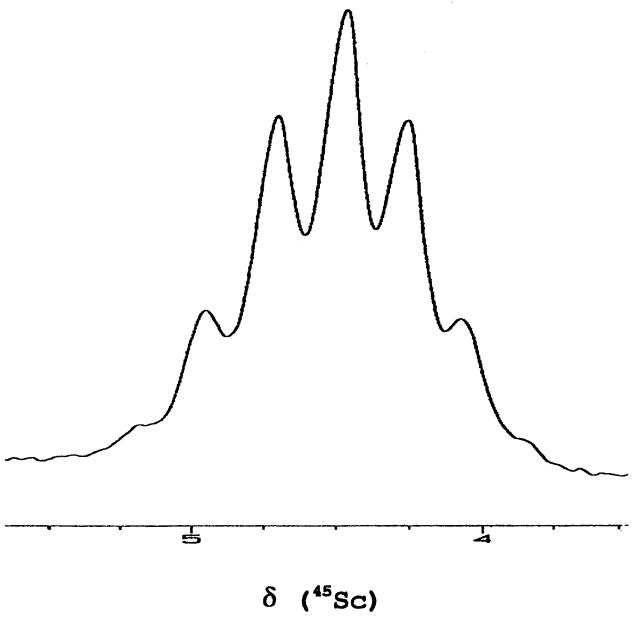


Fig. 2. ^{45}Sc NMR spectrum of $[Sc(Me_3PO)_6]^{3+}$ in $MeNO_2$ at 295 K in the presence of excess Me_3PO.

[1] CH_2Cl_2 has rarely been used as a solvent for conductivity measurements and in the standard review (W.J. Geary, Coord. Chem. Rev., 7 (1971) 81), some doubts were raised about its value for this purpose. We have used it here and in previous papers (refs [7–9]) to correlate with the NMR data obtained in CH_2Cl_2 solution, and with the typical conductances for the electrolyte types established using appropriate tetra-alkylammonium salts.

Table 3
Selected bond lengths (Å) and angles (°) for $[ScCl_2(Ph_3AsO)_4]Cl$

Bond lengths			
Sc(1)–Cl(1)	2.562(4)	Sc(1)–Cl(2)	2.545(4)
Sc(1)–O(1)	2.079(7)	Sc(1)–O(3)	2.059(7)
Sc(1)–O(2)	2.089(7)	Sc(1)–O(4)	2.063(7)
As–O	1.651(7)–1.668(7)		
Bond angles			
Cl(1)–Sc(1)–Cl(2)	179.8(1)	Cl–Sc(1)–O	88.6(3)–91.3(3)
Sc(1)–O(1)–As(1)	146.6(4)	Sc(1)–O(3)–As(3)	147.3(5)
Sc(1)–O(2)–As(2)	145.4(5)	Sc(1)–O(4)–As(4)	147.5(5)

cations was established by the X-ray structure of $[ScCl_2(Ph_3AsO)_4]Cl$ (Table 3, Fig. 3). Like the Ph_3PO complex (above) the scandium cation is *trans* octahedral with bond angles at scandium very close to those of a regular octahedron. The Sc–Cl distances 2.562(4), 2.545(4) Å are approximately 0.15 Å longer than observed in $[ScCl_3(thf)_3]$ [10] or scandium chloride complexes of crown ethers [11]. The Sc–O(As) distances are very similar to those [8] in the eight-coordinate $[Sc(Ph_3AsO)_4(NO_3)_2]^+$, but the Sc–O–As angles (Table 3) are rather more acute than the Sc–O–P angles in $[ScBr_2(Ph_3PO)_4]^+$. In CH_2Cl_2 solution the complexes are 1:1 electrolytes and the conductances increase little in the presence of added ligand. For $[ScCl_2(Ph_3AsO)_4]Cl$ the ^{45}Sc NMR spectrum is a broad ($w_{1/2}$ 4000 Hz) resonance at δ 96 and there was no evidence for any dissociation into a tris(Ph_3AsO) complex (compare $[ScCl_2(Ph_3PO)_4]Cl$ above). The ^{45}Sc NMR spectrum of $[ScBr_2(Ph_3AsO)_4]Br$ has a very broad resonance ($w_{1/2}$ 18 000 Hz) centred at approximately δ 140 ($\pm$20), whilst we have been unable to observe a ^{45}Sc resonance from the iodocomplex.

2.5. $[Sc(Me_3AsO)_6]X_3$

The reaction of $ScX_3 \cdot nH_2O$ with Me_3AsO in boiling ethanol readily affords the hexakis(Me_3AsO) complexes; the contrast with $[ScCl(Me_3PO)_5]Cl_2$ is notable. The complexes are characterised by a sharp singlet in the ^1H NMR spectra at approximately δ 2.1, and a sharp ^{45}Sc NMR signal at δ 56. The IR spectra show three strong bands in the region 925–840 cm^{-1} attributable to ν(As–O) and methyl rocking modes. These data compare well with those reported [7] for $[Sc(Me_3AsO)_6](NO_3)_3$, and the presence of $[Sc(Me_3AsO)_6]^{3+}$ cations was confirmed by an X-ray crystal structure of $[Sc(Me_3AsO)_6]Br_3$ (Fig. 4, Table 4). As expected the dimensions of the cation are very similar to those reported previously for the corresponding nitrate salt

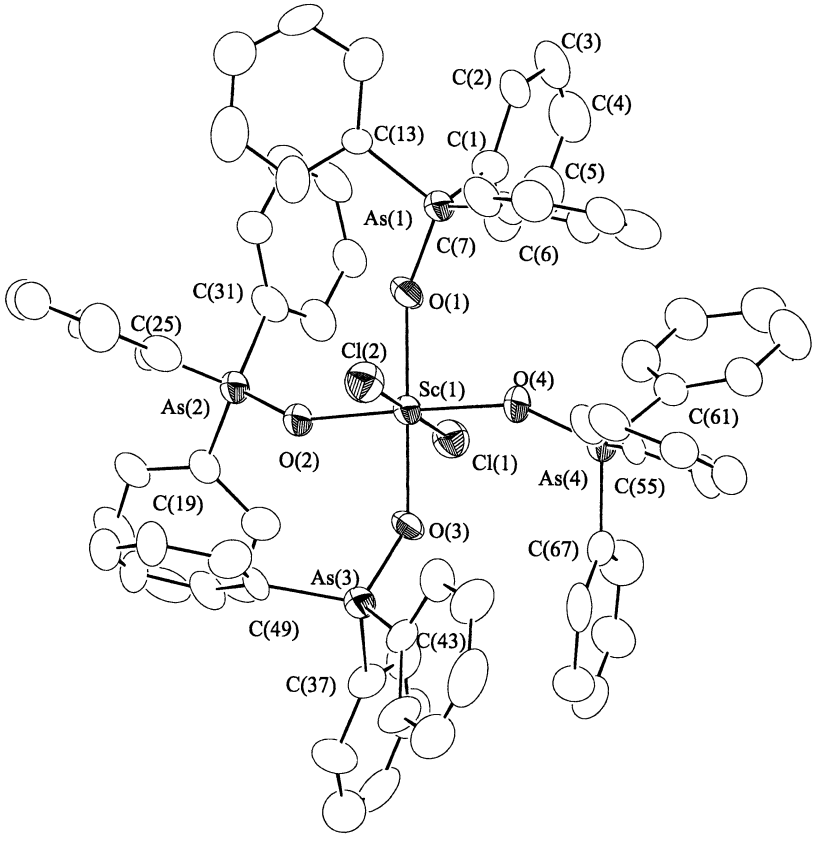


Fig. 3. View of the cation in $[ScCl_2(Ph_3AsO)_4]Cl$ showing the atom numbering scheme. Ellipsoids are drawn at the 40% probability level and H atoms omitted for clarity.

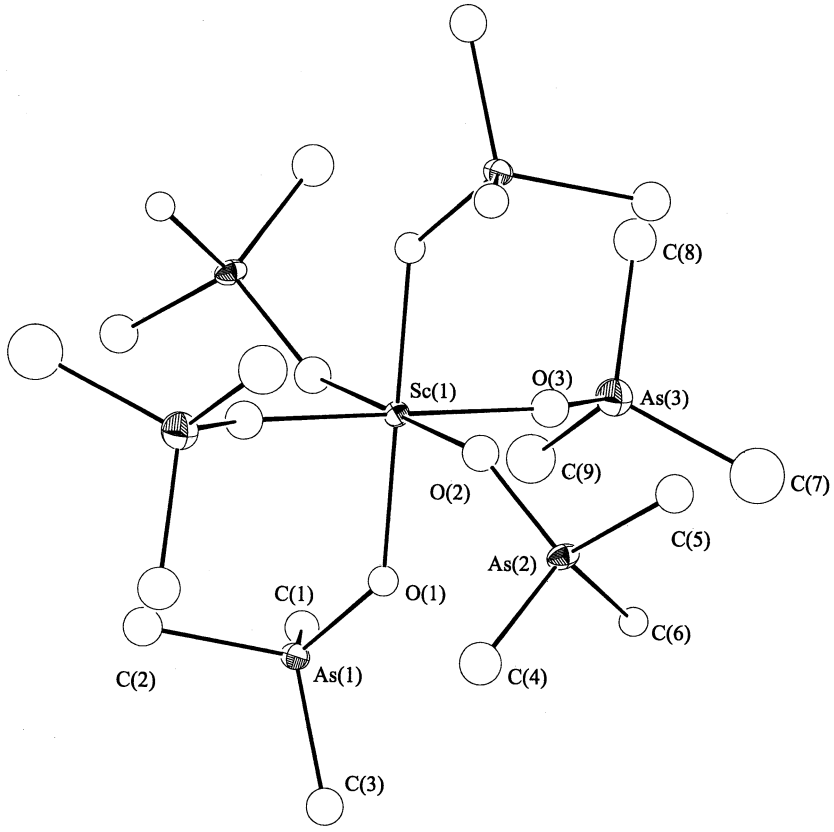


Fig. 4. View of the cation in $[Sc(Me_3AsO)_6]Br_3$ showing the atom numbering scheme. Ellipsoids are drawn at the 40% probability level. The Sc(1) is located on a centre of symmetry.

Table 4
Selected bond lengths (Å) and angles (°) for $[Sc(Me_3AsO)_6]Br_3$

Bond lengths			
Sc(1)–O(1)	2.08(2)	Sc(1)–O(3)	2.11(2)
Sc(1)–O(2)	2.11(2)		
As–O	1.65(2)–1.69(2)		
Bond angles			
O(1)–Sc(1)–O(2)	89.5(6)	Sc(1)–O(1)–As(1)	133.8(9)
O(1)–Sc(1)–O(3)	90.5(7)	Sc(1)–O(2)–As(2)	132.6(10)
O(2)–Sc(1)–O(3)	88.3(6)	Sc(1)–O(3)–As(3)	146.3(10)

[8], but the structure serves to confirm the ScO_6 environment with uncoordinated bromide ions. All three complexes are 3:1 electrolytes in 10^{-3} mol dm^{-3} $MeNO_2$ solution, although the conductivities increase a little on addition of Me_3AsO, possibly indicating some small amounts of coordination of halide, which is suppressed by excess ligand. However, only for $[Sc(Me_3AsO)_6]Cl_3$ is there any NMR evidence for a second complex in $MeNO_2$ solution, with a very weak singlet at δ 2.05 in the ^1H, and a broad weak feature at δ 84 in the ^{45}Sc spectrum, which we propose are due to small amounts of $[ScCl(Me_3AsO)_5]^{2+}$, although this is $\sim$5% of the concentration of the hexakis-complex.

2.6. $[ScCl_3(Ph_2MePO)_3]$ and $[ScBr_2(Ph_2MePO)_4]Br$

Isolation of pure complexes containing Ph_2MePO proved difficult and attempts to obtain reproducible products from the $ScI_3 \cdot 8H_2O$–Ph_2MePO system in either ethanol or acetone were unsuccessful. The white solid isolated from the reaction of hydrated $ScCl_3$ with Ph_2MePO in ethanol or acetone was identified as the $[ScCl_3(Ph_2MePO)_3]$ complex by analysis. In CH_2Cl_2 solution this complex partially rearranges into $[ScCl_2(Ph_2MePO)_4]^+$ readily identified by a combination of ^{45}Sc and $^{31}P\{^1H\}$ NMR spectroscopy. A small amount of Ph_2MePO is also present and there are weak features in the ^{45}Sc NMR spectrum which have no corresponding resonances in the $^{31}P\{^1H\}$ NMR spectrum. From the NMR spectra the two scandium species are tentatively assigned as *mer*-$[ScCl_3(Ph_2MePO)_3]$ and *trans*-$[ScCl_2(Ph_2MePO)_4]^+$ isomers. Addition of excess Ph_2MePO to the solution converts the scandium to the $[ScCl_2(Ph_2MePO)_4]^+$ and this is accompanied by the expected increase in conductance. In contrast the bromide complex isolated was $[ScBr_2(Ph_2MePO)_4]Br$, and in solution in CH_2Cl_2 this appears to be the only significant species present and the conductance is that of a 1:1 electrolyte, showing that $[ScBr_3(Ph_2MePO)_3]$ does not form.

2.7. ^{45}Sc NMR data

The use of ^{45}Sc and ^{31}P NMR spectroscopy to identify solution species has been discussed in previous sections. There are advantages and disadvantages to both nuclei in these systems. The $I = 1/2$ ^{31}P nucleus is very sensitive, but the chemical shifts vary little between complexes in each ScX_3–R_3PO system, and coincidence or only partial resolution of resonances is a concern when identifying minor species or isomers present. The ^{45}Sc nucleus is also inherently very sensitive, but the line widths (Table 1) vary greatly and in some systems this also causes problems. The ^{45}Sc NMR spectra often show a number of weak and usually sharp resonances in addition to those of the major species, which we tentatively assign to hydrolysis/solvolysis impurities in solution, although there remains the possibility that some are due to other isomers of the phosphine oxide complexes. In situ ^{45}Sc NMR studies by Kirakosyan et al. [12,13], on $ScCl_3$–$(RO)_3PO$ (L) systems (R = Me, Et or Bu) identified a range of complexes including $[ScClL_5]^{2+}$, *cis*- and *trans*-$[ScCl_2L_4]^{2+}$, *fac*- and *mer*-$[ScCl_3L_3]$, *cis*- and *trans*-$[ScCl_4L_2]^{-}$. In these phosphate systems the line-widths are much smaller than in the present phosphine oxides and often partial resolution of ^{45}Sc–^{31}P couplings were seen. The line widths in the present complexes increase Cl < Br ≪ I and in several cases we were unable to observe resonances from the iodo-complexes. There is also a significant increase in line-width $R_3PO < R_3AsO$ in the halide systems. The broad lines indicate that the electric field gradient is substantial, promoting fast quadrupolar relaxation of the ^{45}Sc nucleus. The increasing line width Cl → Br → I is predictable as the disparity in electron density increases between the hard O (of Ph_3AsO) and the increasingly soft halide, but clearly the effect is much greater than in the Ph_3PO analogues. We have shown elsewhere [8] that the donor power towards oxophilic metals is $R_3AsO > R_3PO$ and this is manifested here in increased electric field asymmetry. The ^{45}Sc NMR chemical shifts show systematic trends with donor set (Table 1, Scheme 1) the $\delta(^{45}Sc)$ shifting to high frequency with halide Cl → Br → I and $R_3PO \rightarrow R_3AsO$. This pattern is also seen in the ^{89}Y NMR shifts of the yttrium analogues [9]. As discussed above, only for $[Sc(Me_3PO)_6]^{3+}$ were ^{31}P–^{45}Sc couplings resolved (Fig. 2). We also note that intermolecular exchange with added R_3PO or R_3AsO is slow on the NMR time-scales in these systems.

3. Conclusions

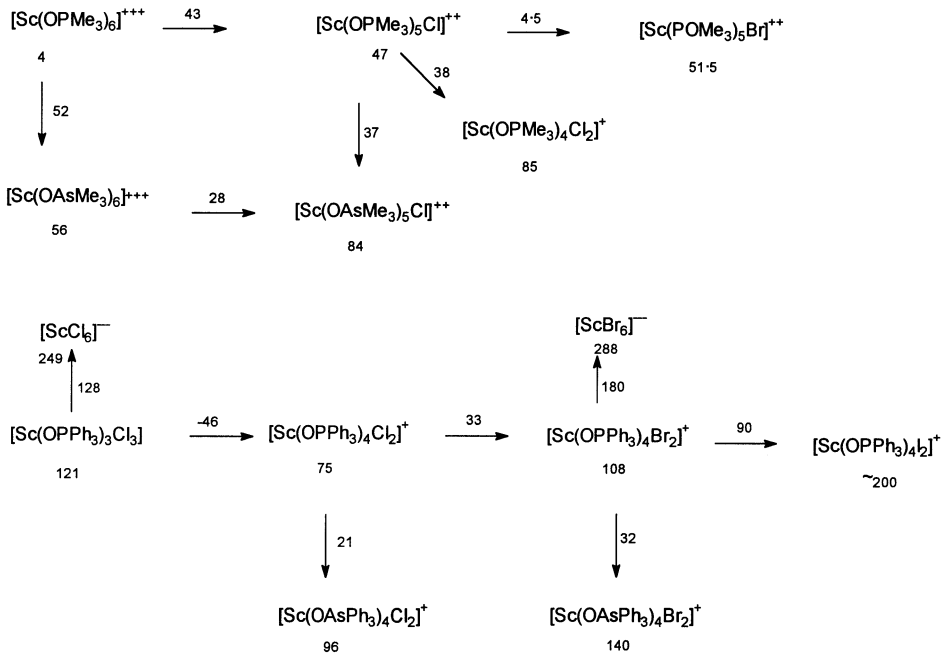
All the scandium halide complexes isolated are based upon six-coordinate metal centres. The results also suggest that the affinity of scandium for chloride is much greater than for the heavier halides; compare $[ScCl(Me_3PO)_5]Cl_2$ and $[Sc(Me_3PO)_6]X_3$ (X = Br or I), and that $[ScX_3(R_3PO)_3]$ form only with X = Cl. Comparison with the yttrium halide systems [9] shows that whilst both metals form $[MX_2(Ph_3EO)_4]X$ (E = As or P), in the presence of excess Ph_3PO, the yttrium systems also form $[YX(Ph_3EO)_5]^{2+}$, whereas we have no evidence for pentakis complexes in the scandium systems. This is probably due to the smaller radius of scandium ($r = 83$ vs. 106 pm for Y) which may be unable to accommodate more than four bulky Ph_3EO ligands. For both metals the affinity for R_3AsO is greater than for R_3PO.

4. Experimental

Multinuclear NMR spectra were obtained on a Bruker DPX400 at 161.9 MHz ($^{31}P\{^1H\}$) and referenced to external 85% H_3PO_4, 97.2 MHz (^{45}Sc) and referenced to 1 mol dm^{-3} $Sc(NO_3)_3$ in water at pH 1. Other physical measurements were made as before [7]. Ph_3PO, Ph_2MePO, Ph_3AsO (Aldrich) and Me_3PO (ALFA) were used as received. Me_3AsO was made by H_2O_2 oxidation of Me_3As in diethyl ether and purified by sublimation in vacuo [8]. $ScF_3 \cdot 1/2H_2O$ was made by precipitation from aqueous solutions of $Sc_2(SO_4)_3$ and NaF, washed with water and dried in vacuo. $ScBr_3 \cdot 6H_2O$ was prepared by evaporating Sc_2O_3 with 48% HBr, and recrystallising the product from H_2O. Yield 79% (Found: Br, 60.8. Calc. for $ScBr_3 \cdot 6H_2O$: Br, 61.0%). $ScCl_3 \cdot 6H_2O$ and $ScI_3 \cdot 8H_2O$ were made by metathesis of aqueous solutions of scandium sulfate and the appropriate barium halide, removal of the precipitated $BaSO_4$, and evaporation to dryness in vacuo. $ScCl_3 \cdot 6H_2O$ yield 90% (Found: Cl, 40.8. Calc. for $ScCl_3 \cdot 6H_2O$: Cl, 41.0%). $ScI_3 \cdot 8H_2O$ yield 86% (Found: I, 66.7. Calc. for $ScI_3 \cdot 8H_2O$: I, 66.8%).

4.1. $[ScCl(Me_3PO)_5]Cl_2$

Ice-cold ethanol solutions (10 cm^3) of $ScCl_3 \cdot 6H_2O$ (0.13 g, 0.5 mmol) and Me_3PO (0.28 g, 3.0 mmol) were mixed, stirred for 1 h and then concentrated to approximately 5 cm^3 and refrigerated overnight. The white solid was filtered off and dried in vacuo. Yield 0.24 g, 63%. (Found: C, 29.7; H, 8.1. Calc. for $C_{15}H_{45}Cl_3O_5P_5Sc$: C, 29.4; H, 7.4%). IR (cm^{-1}) (CsI disc): 2964w, 2896w, 1421w, 1360w, 1299m, 1182w, 1109br,vs (PO), 959s, 872s, 845m, 762s, 682m, 559w, 427s. ^1H NMR (300 K, CD_3NO_2): 1.5(d) $^2J(^{31}P-^1H) = 14$ Hz (Me_3PO); 1.90(d) $^2J(^{31}P-^1H) = 14$ Hz ($[ScCl_2(Me_3PO)_4]^+$); 1.8(d) [4H] 1.70(d) [H] $^2J(^{31}P-^1H) = 14$ Hz ($[ScCl(Me_3PO)_5]^{2+}$). $^{31}P\{^1H\}$ NMR ($MeNO_2$) 36.5 (Me_3PO), 54.0 ($[ScCl_2(Me_3PO)_4]^+$), 54.5 [P], 56.0 [4P] $[ScCl(Me_3PO)_5]^{2+}$). ^{45}Sc NMR ($MeNO_2$) 47.0 ($[ScCl(Me_3PO)_5]^{2+}$), 84.5



Scheme 1. Systematic trends in the ^{45}Sc NMR chemical shifts. The values under formulae are the chemical shift, values over arrows the chemical shift differences. Data for the hexahaloscandate ions are taken from Ref. [6].

($[ScCl_2(Me_3PO)_4]^+$). Λ_M (10^{-3} mol dm^{-3} $MeNO_2$) = 117 Ω^{-1} cm^2 mol^{-1}, +XS Me_3PO 180.

4.2. $[Sc(Me_3PO)_6]Br_3$

A solution of $ScBr_3\cdot 6H_2O$ (0.20 g, 0.50 mmol) in ice-cold ethanol (10 cm^3) was treated with Me_3PO (0.28 g, 3.0 mmol) in ethanol (5 cm^3), resulting in an immediate white precipitate. After stirring for 1 h, the solid was filtered off and dried in vacuo. Yield 0.29 g, 54%. (Found: C, 25.2; H, 6.6. Calc. for $C_{18}H_{54}Br_3O_6P_6Sc$: C, 25.8; H, 6.5%). IR (cm^{-1}) (CsI disc): 2964w, 2897w, 1422m, 1361w, 1312m, 1299m, 1183w, 1110vbr s (PO), 960s, 872s, 762m, 682m, 428s, 418s. ^1H NMR (300 K, CD_3NO_2): 1.5(d) $^2J(^{31}P-^1H) = 14$ Hz (Me_3PO); 1.85(d) $^2J(^{31}P-^1H) = 14$ Hz ($[Sc(Me_3PO)_6]^{3+}$); 1.70(d) [H], 1.85(d) [4H] $^2J(^{31}P-^1H) = 14$ Hz ($[ScBr(Me_3PO)_5]^{2+}$). $^{31}P\{^1H\}$ NMR ($MeNO_2$) 36.5 (Me_3PO), 56.5(m) ($[Sc(Me_3PO)_6]^{3+}$), 56.0 [4P], 55.0 [P] ($[ScBr(Me_3PO)_5]^{2+}$). ^{45}Sc NMR ($MeNO_2$) 51.5 ($[ScBr(Me_3PO)_5]^{2+}$), 4.5 ($[Sc(Me_3PO)_6]^{3+}$). Λ_M (10^{-3} mol dm^{-3} $MeNO_2$) = 179 Ω^{-1} cm^2 mol^{-1}, +XS Me_3PO 221.

4.3. $[Sc(Me_3PO)_6]I_3\cdot EtOH$

Me_3PO (0.14 g, 1.5 mmol) and $ScI_3\cdot 8H_2O$ (0.11 g, 0.25 mmol) were dissolved separately in boiling ethanol (2×5 cm^3) and the solutions mixed to yield a pale yellow precipitate. After stirring for 1 h this was filtered off and dried in vacuo. Yield 0.14 g, 67%. (Found: C, 24.2; H, 6.1. Calc. for $C_{20}H_{60}I_3O_7P_6Sc$: C, 23.6; H, 5.9%). IR (cm^{-1}) (CsI disc): 3480br, 2964w, 2898w, 1421m, 1360w, 1312m, 1299m, 1184w, 1108vbr s (PO), 957s, 871s, 761m, 681m, 427s. ^1H NMR (300 K, CD_3NO_2): 1.1(t) [3H], 3.4(q) [2H] (EtOH), 1.88(d) [54H] $^2J(^{31}P-^1H) = 13$ Hz ($[Sc(Me_3PO)_6]^{3+}$); 1.82–1.78(br). $^{31}P\{^1H\}$ NMR ($MeNO_2$) approximately 57.5(s) ($[Sc(Me_3PO)_6]^{3+}$). ^{45}Sc NMR ($MeNO_2$) 4.0 ($[Sc(Me_3PO)_6]^{3+}$), 9.0. Λ_M (10^{-3} mol dm^{-3} $MeNO_2$) = 189 Ω^{-1} cm^2 mol^{-1}, +XS Me_3PO 242.

4.4. $[ScCl_2(Ph_3PO)_4]Cl$

Warm (60 °C) ethanol solutions (10 cm^3) of $ScCl_3\cdot 6H_2O$ (0.13 g, 0.5 mmol) and Ph_3PO (0.55 g, 2.0 mmol) were mixed, concentrated to approximately 10 cm^3 and then refrigerated for 1 h. The white solid was filtered off and dried in vacuo. Yield 0.35 g, 50%. (Found: C, 68.4; H, 4.7. Calc. for $C_{72}H_{60}Cl_3O_4P_4Sc$: C, 68.4; H, 4.8%). IR (cm^{-1}) (CsI disc): 3055w, 1624w, 1591w, 1439m, 1358w, 1191w, 1152s (PO), 1122s, 1091s, 1046w, 1029w, 999m, 751m, 726s, 697s, 544s, 473m, 460m, 445m, 430m. ^1H NMR ($CDCl_3$) 7.0–7.9(m). $^{31}P\{^1H\}$ NMR (CH_2Cl_2) 34.5 ($[ScCl_2(Ph_3PO)_4]^+$), 34.0 [2P], 33.0 [P] ($[ScCl_3(Ph_3PO)_3]$), 26.0 (Ph_3PO). ^{45}Sc NMR (CH_2Cl_2) 76 ($[ScCl_2(Ph_3PO)_4]^+$), 121 ($[ScCl_3(Ph_3PO)_3]$). Λ_M (10^{-3} mol dm^{-3} CH_2Cl_2) = 17 Ω^{-1} cm^2 mol^{-1}, +XS Ph_3PO 22.

4.5. $[ScBr_2(Ph_3PO)_4]Br\cdot CH_2Cl_2$

A solution of $ScBr_3\cdot 6H_2O$ (0.39 g, 1.0 mmol) in ice-cold ethanol (10 cm^3) was added to Ph_3PO (1.11 g, 4.0 mmol) in ethanol (5 cm^3) and stirred for 1 h. The

solution was refrigerated and the white solid filtered off and dried in vacuo. It was recrystallised by dissolving in CH_2Cl_2 and diffusion of diethyl ether. Yield 0.84 g, 60%. (Found: C, 59.0; H, 4.5. Calc. for $C_{73}H_{62}Br_3Cl_2O_4P_4Sc$: C, 59.1; H, 4.2%). IR (cm^{-1}) (CsI disc): 3056w, 1620w, 1591w, 1438m, 1358w, 1188w, 1137s(PO), 1120s, 1084s, 1028m, 1000m, 750m, 725s, 692s, 547s, 465m, 454m, 426w, 317m, 306m, 269m, 255m. ^1H NMR ($CDCl_3$) 7.0–7.6(m) [30H], 5.2 [H] (CH_2Cl_2). $^{31}P\{^1H\}$ NMR (CH_2Cl_2) 35.8. ^{45}Sc NMR (CH_2Cl_2) 108. Λ_M (10^{-3} mol dm^{-3} CH_2Cl_2) = 21 Ω^{-1} cm^2 mol^{-1}, +XS Ph_3PO 23.

4.6. $[ScI_2(Ph_3PO)_4]I{\cdot}2H_2O$

This was made similarly to the chloride analogue, as a pale yellow solid. Yield 44%. (Found: C, 54.7; H, 3.7. Calc. for $C_{72}H_{64}I_3O_6P_4Sc$: C, 54.9; H, 4.1%). IR (cm^{-1}) (CsI disc): 3466br, 3054w, 1624w, 1590w, 1438m, 1359w, 1187w, 1132s(PO), 1122s, 1073s, 1027m, 999m, 750m, 725s, 693s, 543s, 464m, 452m, 425w. ^1H NMR ($CDCl_3$) 7.0–7.7(m) [60H], 1.7 [4H] (H_2O). $^{31}P\{^1H\}$ NMR (CH_2Cl_2) 38.0. ^{45}Sc NMR (CH_2Cl_2) approximately 200 vbr. Λ_M (10^{-3} mol dm^{-3} CH_2Cl_2) = 22 Ω^{-1} cm^2 mol^{-1}.

4.7. $[ScCl_2(Ph_3AsO)_4]Cl{\cdot}2EtOH$

An ethanol solution (5 cm^3) of Ph_3AsO (0.32 g, 1.0 mmol) was added to a solution of $ScCl_3{\cdot}6H_2O$ (0.06 g, 0.25 mmol) in boiling ethanol (10 cm^3). The mixture was concentrated to 5 cm^3 and refrigerated overnight. The white solid was separated and dried in vacuo. Yield 0.24 g, 64%. (Found: C, 58.9; H, 4.5. Calc. for $C_{76}H_{72}As_4Cl_3O_6Sc$: C, 59.5; H, 4.7%). IR (cm^{-1}) (CsI disc): 3407br, 3055w, 1583w, 1485m, 1440m, 1358w, 1187w, 1162w, 1089s, 1070w, 1027m, 999m, 908vs (AsO), 883m, 745s, 692s, 480s, 458m. ^1H NMR ($CDCl_3$) 7.0–7.7(m) [60H], 1.2(t) [6H], 3.4(q) [4H] (EtOH). ^{45}Sc NMR (CH_2Cl_2) 96. Λ_M (10^{-3} mol dm^{-3} CH_2Cl_2) = 20 Ω^{-1} cm^2 mol^{-1}, +XS Ph_3AsO 24.

4.8. $[ScBr_2(Ph_3AsO)_4]Br{\cdot}5H_2O$

$[ScBr_2(Ph_3AsO)_4]Br{\cdot}5H_2O$ was made similarly (54%) (Found: C, 51.4; H, 3.6. Calc. for $C_{72}H_{70}As_4Br_3O_9Sc$: C, 51.9; H, 4.3%). IR (cm^{-1}) (CsI disc): 3400br, 3051w, 1654m, 1582w, 1485m, 1440s, 1354w, 1185m, 1162w, 1088s, 1027w, 999m, 883s (AsO), 762s, 744s, 691s, 482s, 473s, 457m, 413m. ^1H NMR ($CDCl_3$) 7.1–6.6(m) [60H], 1.8(br) [11H] (H_2O). ^{45}Sc NMR (CH_2Cl_2) approximately 140. Λ_M (10^{-3} mol dm^{-3} CH_2Cl_2) = 19 Ω^{-1} cm^2 mol^{-1}, +XS Ph_3AsO 23.

4.9. $[ScI_2(Ph_3AsO)_4]I$

$[ScI_2(Ph_3AsO)_4]I$ was made similarly as a mustard coloured solid (46%). Not obtained analytically pure see text. IR (cm^{-1}) (CsI disc): 3300m, 1636w, 1439m, 1359w, 1185w, 1161w, 1088s, 1027w, 998m, 883s,br (AsO), 739s, 690s, 477m, 457m, 419m. ^1H NMR ($CDCl_3$) 7.15–7.7(m). ^{45}Sc NMR (CH_2Cl_2) not observed. Λ_M (10^{-3} mol dm^{-3} CH_2Cl_2) = 20 Ω^{-1} cm^2 mol^{-1}, +XS Ph_3AsO 23.

4.10. $[Sc(Me_3AsO)_6]Cl_3$

Scandium chloride hydrate (0.05 g, 0.19 mmol) was dissolved in boiling ethanol (10 cm^3) and added to a solution of Me_3AsO (0.21 g, 1.5 mmol) in ethanol (10 cm^3), resulting in a white suspension. The solution was concentrated to approximately 10 cm^3 and the white solid filtered off and dried in vacuo. Yield 0.13 g, 71%. (Found: C, 22.1; H, 5.6. Calc. For $C_{18}H_{54}As_6Cl_3O_6Sc$: C, 22.3; H, 5.6%). IR (cm^{-1}) (CsI disc): 2981w, 2904w, 1418m, 1359w, 1295w, 1269m, 1114w, 924s, 874s, 844s, 647s, 420m. ^1H NMR (300 K, CD_3NO_2): 2.1(s), 2.05(w). ^{45}Sc NMR ($MeNO_2$) 56.0 ($[Sc(Me_3AsO)_6]^{3+}$), 84(vw) ($[ScCl(Me_3AsO)_5]Cl_2$). Λ_M (10^{-3} mol dm^{-3} $MeNO_2$) = 214 Ω^{-1} cm^2 mol^{-1}, +XS Me_3AsO 251.

4.11. $[Sc(Me_3AsO)_6]Br_3$

$[Sc(Me_3AsO)_6]Br_3$ was made similarly. Yield 62%. (Found: C, 19.0; H, 5.0. Calc. for $C_{18}H_{54}As_6Br_3O_6Sc$: C, 19.6; H, 5.0%). IR (cm^{-1}) (CsI disc): 2982w, 2920w, 1653w, 1418m, 1359m, 1268m, 1088m, 926s, 874s, 846s, 648s, 420m. ^1H NMR (300 K, CD_3NO_2): 2.05(s). ^{45}Sc NMR ($MeNO_2$) 56.0 ($[Sc(Me_3AsO)_6]^{3+}$). Λ_M (10^{-3} mol dm^{-3} $MeNO_2$) = 239 Ω^{-1} cm^2 mol^{-1}, +XS Me_3AsO 281.

4.12. $[Sc(Me_3AsO)_6]I_3{\cdot}3H_2O$

A solution of $ScI_3{\cdot}8H_2O$ (0.10 g, 0.17 mmol) in warm (60 °C) ethanol (10 cm^3) was added to a solution of Me_3AsO (0.14 g, 1.0 mmol) resulting in immediate precipitation of a yellowish solid. After stirring for 1 h this was filtered off and dried in vacuo. Yield 0.11 g, 53%. (Found: C, 15.8; H, 3.9. Calc. for $C_{18}H_{60}As_6I_3O_9Sc$: C, 16.7; H, 4.6%). IR (cm^{-1}) (CsI disc): 3440br, 2978w, 2902w, 1647w, 1417m, 1359w, 1265m, 1088w, 921s, 872s, 844s, 646s, 420m. ^1H NMR (300 K, CD_3NO_2): 2.1(s) [10H], 2.05(vw) 1.7 [H] (H_2O). ^{45}Sc NMR ($MeNO_2$) 56.0 ($[Sc(Me_3AsO)_6]^{3+}$). Λ_M (10^{-3} mol dm^{-3} $MeNO_2$) = 253 Ω^{-1} cm^2 mol^{-1}, +XS Me_3AsO 280.

4.13. $[ScCl_3(Ph_2MePO)_3]\cdot H_2O$

Solutions of $ScCl_3\cdot 6H_2O$ (0.06 g, 0.25 mmol) and Ph_2MePO (0.16 g, 0.75 mmol) in boiling acetone (2×10 cm^3) were mixed resulting in a white suspension. Hexane (10 cm^3) was added and the white sticky solid separated and stirred with diethyl ether for 24 h. The white powder was dried in vacuo. Yield 0.17 g, 59%. (Found: C, 56.8; H, 5.1. Calc. for $C_{39}H_{41}Cl_3O_4P_3Sc$: C, 57.2; H, 5.0%). IR (cm^{-1}) (CsI disc): 3420br, 3056w, 2913w, 1643m, 1439s, 1359w, 1143s(PO), 1127sh, 1099m, 1028w, 998w, 901s, 783m, 746s, 720m, 696s, 517s, 507sh, 429w. ^1H NMR ($CDCl_3$): 1.7br (H_2O), 1.9(d) $^2J_{PH}=13$ Hz, 2.03(d) $^2J_{PH}=13$ Hz, 2.5(d) $^2J_{PH}=13$ Hz, 7.3–7.9(m). ^{45}Sc NMR (CH_2Cl_2) 123 ($[ScCl_3(Ph_2MePO)_3]$), 80(w) ($[ScCl_2(Ph_2MePO)_4]^+$). $^{31}P\{^1H\}$ NMR (CH_2Cl_2) 29.0 (Ph_2MePO), 40.5 [P], 42.5 [2P] $[ScCl_3(Ph_2MePO)_3]$], 42.4 $[ScCl_2(Ph_2MePO)_4)]^+$. Λ_M (10^{-3} mol dm^{-3} CH_2Cl_2) = 8 Ω^{-1} cm^2 mol^{-1}, +XS Ph_2MePO 23.

4.14. $[ScBr_2(Ph_2MePO)_4]Br$

To a solution of Ph_2MePO (0.22 g, 1.0 mmol) in ice-cold acetone (10 cm^3) was added a solution of $ScBr_3\cdot 6H_2O$ (0.09 g, 0.25 mmol) in acetone (5 cm^3). After stirring for 1 h, the solution was concentrated to approximately 5 cm^3 and refrigerated overnight. The white precipitate was filtered off and dried in vacuo. Yield 0.14 g, 49%. (Found: C, 55.3; H, 4.8. Calc. for $C_{52}H_{52}Br_3O_4P_4Sc$: C, 54.3; H, 4.6%). IR (cm^{-1}) (CsI disc): 3420br, 3050w, 2908w, 1638m, 1486m, 1438s, 1363w, 1138s (PO), 1094m, 1073w, 1028m, 998w, 894s, 787m, 746s, 719m, 695s, 515s. ^1H NMR ($CDCl_3$): 1.92(d) $^2J_{PH}=13$ Hz, 7.3–7.9(m). ^{45}Sc NMR (CH_2Cl_2) 100, $w_{1/2}=5000$ Hz. $^{31}P\{^1H\}$ NMR (CH_2Cl_2) 41.0, 40.3(w). Λ_M (10^{-3} mol dm^{-3} CH_2Cl_2) = 22 Ω^{-1} cm^2 mol^{-1}.

4.15. X-ray crystallographic studies

Crystallographic details together with data collection and refinement parameters are given in Table 5. Crystals were obtained by vapour diffusion from $MeNO_2$–Et_2O systems (with excess Me_3AsO added for that complex), or from CH_2Cl_2–Et_2O. Data were recorded from small, modest quality crystals at low temperature using a Nonius Kappa CCD diffractometer. The structure solutions and refinements (on F or F^2 (Cl compound)) were carried out using standard methods [14–17] except for $[ScCl_2(Ph_3AsO)_4]Cl$ which was initially solved and refined in the triclinic space group $P\bar{1}$ (no. 2) (with $Z=4$). The value of Z caused concern [18]; subsequent re-examination of the data showed systematic absences consistent with a monoclinic space group and the structure was re-solved and refined in this higher symmetry space group. Anisotropic refinement of

Table 5
Crystallographic data [a]

	$[ScBr_2(Ph_3PO)_4]Br\cdot 1/2Et_2O$	$[ScCl_2(Ph_3AsO)_4]Cl$	$[Sc(Me_3AsO)_6]Br_3$
Formula	$C_{72}H_{60}Br_3O_4P_4Sc+1/2(C_4H_{10}O)$	$C_{72}H_{60}As_4Cl_3O_4Sc$	$C_{18}H_{54}As_6Br_3O_6Sc$
M	1434.89	1440.19	1100.82
Crystal system	triclinic	Monoclinic	monoclinic
Space group	$P\bar{1}$ (no. 2)	$P2_1/n$ (no. 14)	$C2/c$ (no. 15)
a (Å)	14.2119(4)	18.436(2)	17.7475(5)
b (Å)	14.7923(4)	18.946(3)	16.9358(5)
c (Å)	17.6032(5)	18.393(3)	12.5771(4)
α (°)	66.695(2)	90.0	90.0
β (°)	80.919(1)	90.04(1)	96.643(1)
γ (°)	89.302(1)	90.0	90.0
U (Å^3)	3351.0(2)	6424.5(18)	3754.9(2)
T (K)	150	120	120
Z	2	4	4
$F(000)$ (e)	1462	2912	2136
Total number of observations	46 706	31 012	14 955
Number of unique observations (R_{int})	15012 (0.054)	9826 (0.16)	4371 (0.093)
Max/min transmission	0.668/0.581	0.269/0.240	0.314/0.288
Number of data in refinement	8868 ($I>3\sigma(I)$)	9826	1581 ($I>3\sigma(I)$)
Number of parameters/restraints	777/0	758/0	96/0
μ (cm^{-1})	20.5	23.33	86.7
S	2.13	0.92	1.80
R ($I>n\sigma(I)$)	0.059 ($n=3$)	0.081 ($n=2$, 4002 reflections)	0.065 ($n=3$)
R (all data)		0.217	
wR_2 (all data)		0.265	
wR ($I>n\sigma(I)$)	0.073 ($n=3$)		0.114 ($n=3$)

$R=\Sigma||F_o|-|F_c||/\Sigma|F_o|$; $wR_2=[\Sigma\ w(F_o^2-F_c^2)^2/\Sigma\ wF_o^4]^{1/2}$; $wR=[\Sigma\ w(F_o-F_c)^2/\Sigma\ wF_o^2]^{1/2}$.

[a] Common data: Mo Kα ($\lambda=0.71073$ Å).

$[Sc(Me_3AsO)_6]Br_3$ gave some npd thermal parameters for O and C and all were subsequently refined with an isotropic model.

5. Supplementary data

Crystallographic data for the structures have been deposited with the Cambridge Crystallographic Data Centre (CCDC) and given numbers 173058 $[ScBr_2(Ph_3PO)_4]Br\cdot 1/2Et_2O$, 173059 $[Sc(Me_3AsO)_6]Br_3$, 173060 $[ScCl_2(Ph_3AsO)_4]Cl$. Copies of the data can be obtained on request from The Director, CCDC, 12 Union Road, Cambridge, CB2 1EZ, UK (fax: +44-1223-336033; e-mail: deposit@ccdc.ac.uk or www: http://www.ccdc.cam.ac.uk) quoting the deposition numbers.

Acknowledgements

We thank the EPSRC for support and Professor M.B. Hursthouse for access to the Nonius Kappa CCD diffractometer.

References

[1] P.J. Shapiro, W.D. Cotter, W.P. Schaefer, J.A. Labinger, J.E. Bercaw, J. Am. Chem. Soc. 116 (1994) 4623.
[2] S. Hajela, W.P. Schaefer, J.E. Bercaw, J. Organomet. Chem. 532 (1997) 45.
[3] S. Kobayashi, Eur. J. Org. Chem. (1999) 15.
[4] M. Nakajima, Y. Yamaguchi, S. Hashimoto, Chem. Commun. (2001) 1596.
[5] D. Grosso, P.A. Sermon, J. Mater. Chem. 10 (2000) 359.
[6] D. Rehder, in: P.S. Pregosin (Ed.), Transition Metal NMR, Elsevier, New York, 1991.
[7] L. Deakin, W. Levason, M.C. Popham, G. Reid, M. Webster, J. Chem. Soc., Dalton Trans. (2000) 2439.
[8] W. Levason, B. Patel, M.C. Popham, G. Reid, M. Webster, Polyhedron 20 (2001) 2711.
[9] N.J. Hill, W. Levason, M.C. Popham, G. Reid, M. Webster, Polyhedron 21 (2002) 445.
[10] J.L. Atwood, K.D. Smith, J. Chem. Soc., Dalton Trans. (1974) 921.
[11] (a) G.R. Willey, M.T. Lakin, N.W. Alcock, J. Chem. Soc., Dalton Trans. (1993) 3407.;
(b) G.R. Willey, P.R. Meehan, M.D. Rudd, M.G.B. Drew, J. Chem. Soc., Dalton Trans. (1995) 811.
[12] G.A. Kirakosyan, V.P. Tarasov, Y.A. Buslaev, Mag. Res. Chem. 27 (1989) 103.
[13] Y.A. Buslaev, G.A. Kirakosyan, V.P. Tarasov, Dokl. Akad. Nauk. SSSR 264 (1982) 1405.
[14] PATTY, The DIRDIF Program System. P.T. Beurskens, G. Admiraal, G. Beurskens, W.P. Bosman, S. Garcia-Granda, R.O. Gould, J.M.M. Smits, C. Smykalla, Technical Report of the Crystallography Laboratory, University of Nijmegen, The Netherlands, 1992.
[15] G.M. Sheldrick, SHELXS 97, Program for crystal structure solution, University of Göttingen, 1997.
[16] TEXSAN: Crystal Structure Analysis Package, Molecular Structure Corporation, The Woodlands, TX, 1997.
[17] G.M. Sheldrick, SHELXL 97, Program for crystal structure refinement, University of Göttingen, 1997.
[18] R.E. Marsh, Acta Crystallogr., Sect. B 55 (1999) 931.

described [10] some years ago, showing a new mode of bidentate coordination for this ligand, involving an N–C–O bridging unit.

We report here the preparation of new dinuclear orthometallated palladium(II) derivatives with bridging succinimide, maleimide or phthalimide ligands acting in the coordination mode mentioned above. We also present a novel synthesis route of mononuclear N-bonded succinimidato derivatives, by reaction of the corresponding dinuclear precursor with neutral ligands. Spectroscopic characterization of the new compounds and the structure elucidation by X-ray diffraction analyses of both mononuclear and binuclear derivatives is also given.

2. Experimental

2.1. Materials and physical measurements

C, H and N analysis were carried out with a Perkin–Elmer 240C microanalyser. IR spectra were recorded on a Perkin–Elmer spectrophotometer 16F PC FT-IR, using nujol mulls between polyethylene sheets. NMR data (^{1}H, ^{13}C, ^{31}P) were recorded on a Bruker AC 200E or a Varian Unity 300 spectrometer. Mass spectrometric analyses were performed on a Fisons VG Autospec double-focusing spectrometer, operated in the positive mode. Ions were produced by fast atom bombardment (FAB) with a beam of 25-KeV Cs atoms. The mass spectrometer was operated with an accelerating voltage of 8 kV and a resolution of at least 1000.

The cyclometallated precursors [{Pd(μ-OOCMe)-(C^N)}$_2$] [C^N = azobenzene or 2-phenylpyridine] were prepared as described in the literature [12]. The commercially available chemicals were purchased from Aldrich Chemical Co. and were used without further purification, and all the solvents were dried by standard methods before use.

2.2. Preparation of the complexes [{Pd(μ-NCO)-(C^N)}$_2$] [C^N = azobenzene (azb); –NCO– = succinimide (suc) (**1a**), phthalimide (**2a**) (phtal) or maleimide (mal) (**3a**); C^N = 2-phenylpyridine (phpy); –NCO– = succinimide (**1b**), phthalimide (**2b**) or maleimide (**3b**)]

The azobenzene or 2-phenylpyridine complexes were obtained by treating the appropriated precursor ([{Pd(μ-OOCMe)(azb)}$_2$] or [{Pd(μ-OOCMe)(phpy)}$_2$], respectively) with the corresponding imide (molar ratio 1:2) in acetone, according to the following general method. To an acetone (20 ml) solution of [{Pd(μ-OOCMe)(C^N)}$_2$] (0.07 g, 0.101 mmol if C^N = azb; 0.07 g, 0.109 mmol if C^N = phpy) the stoichiometric amount of ligand was added. The solution was refluxed for 2 h and then concentrated to one-fifth of the initial volume. Slow addition of diethyl ether caused the precipitation of the title complexes, which were filtered off, air-dried and recrystallized from acetone–ether.

2.2.1. [{Pd(μ-suc)(azb)}$_2$] (**1a**)

Yield: 57% (*Anal.* Calc. for $C_{32}H_{26}N_6O_4Pd_2$: C, 49.8; H, 3.4; N, 10.9. Found: C, 49.7; H, 3.5; N, 10.7%). IR (cm^{-1}): 1722s, 1566s (C=O str.). FAB MS (positive mode) *m/z*: 772 [{Pd(μ-suc)(azb)}$_2$]$^+$, 673 [{Pd$_2$(suc)(azb)$_2$}]$^+$, 575 [{Pd(azb)}$_2$]$^+$, 287 [Pd(azb)]$^+$. . $^{13}C\{^1H\}$ NMR ((CD$_3$)$_2$CO, δ ppm): 194.2 (coordinated C=O, suc), 187.9 (non-coordinated C=O, suc), 163.5 (azb), 152.6 (azb), 150.5 (azb), 134.5 (azb), 132.0 (azb), 130.7 (azb), 130.0 (azb), 127.8 (azb), 125.4 (azb), 123.6 (azb), 32.0 (–CH$_2$–, suc). ^1H NMR ((CD$_3$)$_2$CO, δ ppm, *J* Hz): 7.31 (m, 10H, H^{2,3,4,5,6}), 7.15 (m, 2H, H$^{5'}$), 7.12 (d, 2H, H$^{6'}$, $J_{HH} = 7.5$), 6.74 (m, 2H, H$^{4'}$), 6.19 (d, 2H, H$^{3'}$, $J_{HH} = 7.8$), 2.69 (m, 8H, –CH$_2$– suc).

2.2.2. [{Pd(μ-phtal)(azb)}$_2$] (**2a**)

Yield: 65% (*Anal.* Calc. for $C_{40}H_{26}N_6O_4Pd_2$: C, 55.4; H, 3.0; N, 9.7. Found: C, 55.6; H, 3.0; N, 9.7%). IR (cm^{-1}): 1731s, 1569s (C=O str.). FAB MS (positive mode) *m/z*: 868 [{Pd(μ-phtal)(azb)}$_2$]$^+$, 722 [{Pd$_2$(phtal)(azb)$_2$}]$^+$, 287 [Pd(azb)]$^+$, $^{13}C\{^1H\}$ NMR ((CD$_3$)$_2$CO, δ ppm): 183.6 (coordinated C=O, phtal), 178.0 (non-coordinated C=O, phtal), 163.2 (azb), 152.6 (azb), 150.6 (azb), 136.8 (phtal), 135.5 (phtal), 134.5 (azb), 132.4 (phtal), 132.3 (phtal), 132.0 (azb), 130.6 (azb), 129.8 (azb), 127.7 (azb), 125.3 (azb), 123.5 (azb), 123.2 (phtal), 122.1 (phtal). ^1H NMR ((CD$_3$)$_2$CO, δ ppm, *J* Hz): 7.69 (m, 6H, H$^{6'}$, 4H phtal), 7.56 (m, 4H, phtal), 7.40 (m, 4H, H^{2,6}), 7.12 (m, 8H, H^{3,4,5}, H$^{5'}$), 6.59 (m, 2H, H$^{4'}$), 6.22 (d, 2H, H$^{3'}$, $J_{HH} = 7.4$).

2.2.3. [{Pd(μ-mal)(azb)}$_2$] (**3a**)

Yield: 69% (*Anal.* Calc. for $C_{32}H_{22}N_6O_4Pd_2$: C, 50.1; H, 2.9; N, 10.9. Found: C, 50.3; H, 3.1; N, 10.9%). IR (cm^{-1}): 1727s, 1571s (C=O str.). FAB MS (positive mode) *m/z*: 768 [{(Pd(μ-mal)$_2$(azb)}]$^+$, 672 [{Pd$_2$(mal)-(azb)$_2$}]$^+$, 575 [{Pd(azb)}$_2$]$^+$, 287 [Pd(azb)]$^+$, $^{13}C\{^1H\}$ NMR ((CD$_3$)$_2$CO, δ ppm): 186.9 (coordinated C=O, mal), 180.9 (non-coordinated C=O, mal), 163.2 (azb), 152.5 (azb), 150.6 (azb), 136.1 (mal), 134.7 (mal), 132.4 (azb), 132.0 (azb), 131.8 (azb), 131.4 (azb), 127.8 (azb), 125.1 (azb), 123.1 (azb). ^1H NMR ((CD$_3$)$_2$CO, δ ppm, *J* Hz): 7.72 (m, 2H, H$^{6'}$), 7.26 (m, 12H, H^{2,3,4,5,6}, H$^{5'}$), 6.46 (m, 6H, H$^{4'}$, 4H mal), 6.19 (m, 2H, H$^{3'}$).

2.2.4. [{Pd(μ-suc)(phpy)}$_2$] (**1b**)

Yield: 63% (*Anal.* Calc. for $C_{30}H_{24}N_4O_4Pd_2$: C, 50.2; H, 3.4; N, 7.8. Found: C, 50.5; H, 3.4; N, 7.8%). IR (cm^{-1}): 1720s, 1587s (C=O str.). FAB MS (positive mode) *m/z*: 718 [{Pd(μ-suc)(phpy)}$_2$]$^+$, 620 [{Pd$_2$(suc)-(phpy)$_2$}]$^+$, 415 [{Pd(phpy)}$_2$]$^+$, 260 [Pd(phpy)]$^+$.

$^{13}C\{^1H\}$ NMR ($(CD_3)_2CO$, δ ppm): 195.1 (coordinated C=O, suc), 187.9 (non-coordinated C=O, suc), 163.7 (phpy), 150.8 (phpy), 148.8 (phpy), 144.9 (phpy), 137.8 (phpy), 133.7 (phpy), 128.8 (phpy), 123.8 (phpy), 122.7 (phpy), 121.2 (phpy), 117.2 (phpy), 32.2 ($-CH_2-$, suc), 32.0 ($-CH_2-$, suc). ^1H NMR ($(CD_3)_2CO$, δ ppm, J Hz): 7.63 (m, 2H, H^6), 7.28 (m, 2H, H^3), 7.01 (m, 2H, H^4), 6.72 (m, 6H, H^5, $H^{5',6'}$), 6.51 (m, 4H, $H^{3',4'}$), 2.76 (m, 8H, $-CH_2-$ suc).

2.2.5. [{Pd(μ-phtal)(phpy)}$_2$] (**2b**)

Yield: 76% (*Anal.* Calc. for $C_{38}H_{24}N_4O_4Pd_2$: C, 56.1; H, 3.0; N, 6.9. Found: C, 56.4; H, 2.7; N, 6.9%). IR (cm^{-1}): 1728s, 1597s (C=O str.). FAB MS (positive mode) m/z: 812 $[\{Pd(\mu\text{-phtal})(phpy)\}_2]^+$, 668 $[\{Pd_2(phtal)(phpy)_2\}]^+$, 415 $[\{Pd(phpy)\}_2]^+$, 260 $[Pd(phpy)]^+$. $^{13}C\{^1H\}$ NMR ($(CD_3)_2CO$, δ ppm): 184.6 (coordinated C=O, phtal), 178.6 (non-coordinated C=O, phtal), 163.7 (phpy), 151.0 (phpy), 148.9 (phpy), 144.7 (phpy), 137.3 (phpy), 137.0 (phtal), 135.9 (phtal), 134.1 (phpy), 132.2 (phtal), 132.0 (phtal), 128.7 (phpy), 123.7 (phpy), 122.6 (phpy), 122.0 (phpy), 121.7 (phpy), 121.2 (phpy), 117.1 (phpy). ^1H NMR ($(CD_3)_2CO$, δ ppm, J Hz): 7.70 (m, 2H, H^6), 7.50 (m, 8H, phtal), 7.33 (m, 2H, H^3), 7.05 (m, 2H, H^4), 6.68 (m, 2H, $H^{6'}$), 6.62 (m, 8H, H^5, $H^{3',4',5'}$).

2.2.6. [{Pd(μ-mal)(phpy)}$_2$] (**3b**)

Yield: 71% (*Anal.* Calc. for $C_{30}H_{20}N_4O_4Pd_2$: C, 50.5; H, 2.8; N, 7.8. Found: C, 50.8; H, 3.0; N, 7.9%). IR (cm^{-1}): 1724s, 1620s (C=O str.). FAB MS (positive mode) m/z: 714 $[\{Pd(\mu\text{-mal})(phpy)\}_2]^+$, 618 $[\{Pd_2(mal)(phpy)_2\}]^+$, 415 $[\{Pd(phpy)\}_2]^+$, 260 $[Pd(phpy)]^+$. $^{13}C\{^1H\}$ NMR ($(CD_3)_2CO$, δ ppm): 195.0 (coordinated C=O, mal), 188.5 (non-coordinated C=O, mal), 163.7 (phpy), 148.9 (phpy), 144.9 (phpy), 137.9 (mal), 137.6 (mal), 134.1 (phpy), 131.8 (phpy), 129.6 (phpy), 128.9 (phpy), 123.9 (phpy), 122.7 (phpy), 121.0 (phpy), 117.4 (phpy). ^1H NMR ($(CD_3)_2CO$, δ ppm, J Hz): 7.78 (m, 2H, H^6), 7.26 (m, 2H, H^3), 7.06 (m, 2H, H^4), 6.65 (m, 10H, H^5, $H^{5',6'}$, 4H mal), 6.45 (m, 4H, $H^{3',4'}$).

2.3. Preparation of complexes [Pd(C^N)(suc)(L)] [C^N = azb; L = PPh_3 (**4a**), PPh_2Me (**5a**), $PPhMe_2$ (**6a**), P(4-F–C_6H_4)$_3$ (**7a**), P(4-MeO–C_6H_4)$_3$ (**8a**); C^N = phpy; L = PPh_3 (**4b**), PPh_2Me (**5b**), $PPhMe_2$ (**6b**), P(4-F–C_6H_4)$_3$ (**7b**), P(4-MeO–C_6H_4)$_3$ (**8b**)]

The complexes were obtained by treating the precursors [{Pd(μ-suc)(azb)}$_2$] (**1a**) or [{Pd(μ-suc)(phpy)}$_2$] (**1b**) with the corresponding neutral ligand (molar ratio 1:2) in dichloromethane, according to the following general method. To a dichloromethane (20 ml) solution of **1a** (0.07 g, 0.091 mmol) or **1b** (0.07 g, 0.112 mmol) the stoichiometric amount of ligand (**a** compounds: 0.183 mmol; **b** compounds: 0.225 mmol) was added. The solution was refluxed for 2 h, then concentrated until approximately one-fifth of the initial volume. Slow addition of hexane caused the precipitation of the title complexes, which were filtered off, washed with hexane, air-dried and recrystallized from acetone–hexane.

2.3.1. [Pd(azb)(suc)(PPh_3)] (**4a**)

Yield: 62% (*Anal.* Calc. for $C_{34}H_{28}N_3O_2PPd$: C, 63.0; H, 4.4; N, 6.5. Found: C, 63.0; H, 4.4; N, 6.5%). IR (cm^{-1}): 1580s (C=O str.); 534m, 514m, 493m (PPh_3). ^1H NMR ($(CD_3)_2CO$, δ ppm, J Hz): 7.81 (d, 1H, $H^{6'}$, $J_{HH} = 6.2$), 7.72, (m, 6H, Ph), 7.52 (m, 3H, Ph), 7.38 (m, 11H, $H^{2,3,4,5,6}$, 6H Ph), 7.09 (m, 2H, $H^{5'}$), 6.69 (m, 2H, $H^{4'}$), 6.50 (m, 2H, $H^{3'}$), 1.80 (dd, 2H, $-CH_2-$ suc, $J_{HH\ syn} = 5$, $J_{HH\ anti} = 16$), 1.55 (dd, 2H, $-CH_2-$ suc, $J_{HH\ syn} = 5$, $J_{HH\ anti} = 16$). $^{31}P\{^1H\}$ NMR ($(CD_3)_2CO$, δ ppm): 42.3 (s, PPh_3).

2.3.2. [Pd(azb)(suc)(PPh_2Me)] (**5a**)

Yield: 68% (*Anal.* Calc. for $C_{29}H_{26}N_3O_2PPd$: C, 59.5; H, 4.5; N, 7.2. Found: C, 59.4; H, 4.7; N, 7.5%). IR (cm^{-1}): 1572s (C=O str.); 512m, 482m, 446m (PPh_2Me). ^1H NMR ($(CD_3)_2CO$, δ ppm, J Hz): 7.76 (d, 1H, $H^{6'}$, $J_{HH} = 7.4$), 7.28, (m, 15H, $H^{2,3,4,5,6}$, 10H Ph), 7.19 (m, 1H, $H^{5'}$), 7.12 (m, 1H, $H^{4'}$), 6.68 (m, 1H, $H^{3'}$), 2.19 (m, 3H, Me–), 1.88 (m, 2H, suc), 1.57 (m, 2H, suc). $^{31}P\{^1H\}$ NMR ($(CD_3)_2CO$, δ ppm): 23.4 (s, PPh_2Me).

2.3.3. [Pd(azb)(suc)($PPhMe_2$)] (**6a**)

Yield: 72% (*Anal.* Calc. for $C_{24}H_{24}N_3O_2PPd$: C, 55.0; H, 4.6; N, 8.0. Found: C, 55.2; H, 4.8; N, 7.9%). IR (cm^{-1}): 1580s (C=O str.); 540m, 510m, 488m ($PPhMe_2$). ^1H NMR ($(CD_3)_2CO$, δ ppm, J Hz): 7.91 (m, 3H, $H^{6'}$, 2H Ph), 7.41, (m, 8H, $H^{2,3,4,5,6}$, 3H Ph), 7.19 (m, 1H, $H^{5'}$), 6.96 (m, 1H, $H^{4'}$), 6.66 (m, 1H, $H^{3'}$), 2.24 (m, 4H, suc), 1.71 (m, 6H, Me). $^{31}P\{^1H\}$ NMR ($(CD_3)_2CO$, δ ppm): 11.2 (s, $PPhMe_2$).

2.3.4. [Pd(azb)(suc)(P(4-F–C_6H_4)$_3$)] (**7a**)

Yield: 63% (*Anal.* Calc. for $C_{34}H_{25}F_3N_3O_2PPd$: C, 58.2; H, 3.6; N, 6.0. Found: C, 58.3; H, 3.7; N, 6.2%). IR (cm^{-1}): 1586s (C=O str.); 536m, 518m, 452m (P(4–F–C_6H_4)$_3$). ^1H NMR ($(CD_3)_2CO$, δ ppm, J Hz): 8.02 (d, 1H, $H^{6'}$, $J_{HH} = 7.0$), 7.75, (m, 6H, Ph *ortho*), 7.53 (m, 6H, Ph *meta*), 7.38 (m, 6H, $H^{2,3,4,5,6}$, $H^{5'}$), 6.72 (m, 1H, $H^{4'}$), 6.40 (m, 1H, $H^{3'}$), 1.91 (m, 2H, suc), 1.62 (m, 2H, suc). $^{31}P\{^1H\}$ NMR ($(CD_3)_2CO$, δ ppm): 40.0 (s, P(4-F–C_6H_4)$_3$).

2.3.5. [Pd(azb)(suc)(P(4-MeO–C_6H_4)$_3$)] (**8a**)

Yield: 70% (*Anal.* Calc. for $C_{37}H_{34}N_3O_5PPd$: C, 60.2; H, 4.6; N, 5.7. Found: C, 60.2; H, 4.7; N, 5.7%). IR (cm^{-1}): 1566s (C=O str.); 538m, 518m, 498m (P(4-Me–C_6H_4)$_3$). ^1H NMR ($(CD_3)_2CO$, δ ppm, J Hz): 7.99 (d, 1H, $H^{6'}$, $J_{HH} = 6.2$), 7.58, (m, 8H, $H^{2,6}$, 6H Ph *ortho*), 7.33 (m, 3H, $H^{3,4,5}$), 7.10 (m, 1H, $H^{5'}$), 6.85 (m, 6H Ph

meta), 6.73 (m, 1H, $H^{4'}$), 6.54 (m, 1H, $H^{3'}$), 3.79 (s, 9H, MeO–), 1.86 (dd, 2H, –CH_2– suc, $J_{HH\ syn} = 5.2$, $J_{HH\ anti} = 16.4$), 1.58 (dd, 2H, –CH_2– suc, $J_{HH\ syn} = 5.2$, $J_{HH\ anti} = 16.4$). $^{31}P\{^1H\}$ NMR ($(CD_3)_2CO$, δ ppm): 38.9 (s, P(4-MeO–C_6H_4)$_3$).

2.3.6. [Pd(phpy)(suc)(PPh_3)] (**4b**)

Yield: 71% (*Anal.* Calc. for $C_{33}H_{27}N_2O_2PPd$: C, 63.8; H, 4.4; N, 4.5. Found: C, 63.9; H, 4.2; N, 4.7%). IR (cm^{-1}): 1614s (C=O str.); 534m, 514m, 492m (PPh_3). ^1H NMR ($(CD_3)_2CO$, δ ppm, J Hz): 8.19 (m, 1H, H^6), 7.82, (m, 7H, $H^{3,4}$, 5H Ph), 7.46 (d, 1H, $H^{6'}$, $J_{HH} = 7.8$), 7.40 (m, 10H, Ph), 7.11 (m, 1H, H^5), 6.91 (m, 1H, $H^{5'}$), 6.52 (m, 2H, $H^{3',4'}$), 2.22 (dd, 2H, –CH_2– suc, $J_{HH\ syn} = 3$, $J_{HH\ anti} = 11.6$), 1.25 (m, 2H, –CH_2– suc). $^{31}P\{^1H\}$ NMR ($(CD_3)_2CO$, δ ppm): 42.1 (s, PPh_3).

2.3.7. [Pd(phpy)(suc)(PPh_2Me)] (**5b**)

Yield: 66% (*Anal.* Calc. for $C_{28}H_{25}N_2O_2PPd$: C, 60.2; H, 4.5; N, 5.0. Found: C, 60.2; H, 4.6; N, 5.1%). IR (cm^{-1}): 1634s (C=O str.); 516m, 488m, 448m (PPh_2Me). ^1H NMR ($(CD_3)_2CO$, δ ppm, J Hz): 8.10 (m, 1H, H^6), 7.68, (m, 5H, $H^{3,4}$, 3H Ph), 7.45 (d, 1H, $H^{6'}$, $J_{HH} = 7.8$), 7.31 (m, 7H Ph), 6.89 (m, 2H, $H^{3',4'}$), 2.18 (m, 5H, ME, 2H suc), 1.63 (m, 2H, suc). $^{31}P\{^1H\}$ NMR ($(CD_3)_2CO$, δ ppm): 23.5 (s, PPh_2Me).

2.3.8. [Pd(phpy)(suc)($PPhMe_2$)] (**6b**)

Yield: 76% (*Anal.* Calc. for $C_{23}H_{23}N_2O_2PPd$: C, 55.6; H, 4.7; N, 5.6. Found: C, 55.5; H, 4.6; N, 5.5%). IR (cm^{-1}): 1622s (C=O str.); 488m, 470m, 442m ($PPhMe_2$). ^1H NMR ($(CD_3)_2CO$, δ ppm, J Hz): 8.10 (s, 1H, H^6), 7.71, (m, 2H, Ph), 7.66 (m, 2H, $H^{3,4}$), 7.36 (m, 5H, $H^{6'}$, 4 Ph), 7.06 (m, 1H, H^5), 6.90 (m, 1H, $H^{5'}$), 6.57 (m, 2H, $H^{3',4'}$), 2.60 (m, 4H, suc), 1.69 (m, 6H, Me). $^{31}P\{^1H\}$ NMR ($(CD_3)_2CO$, δ ppm): 10.8 (s, $PPhMe_2$).

2.3.9. [Pd(phpy)(suc)(P(4-F–C_6H_4)$_3$)] (**7b**)

Yield: 81% (*Anal.* Calc. for $C_{33}H_{24}F_3N_2O_2PPd$: C, 58.7; H, 3.6; N, 4.1. Found: C, 58.8; H, 3.8; N, 4.3%). IR (cm^{-1}): 1622s (C=O str.); 540m, 454m, 441m (P(4-F–C_6H_4)$_3$). ^1H NMR ($(CD_3)_2CO$, δ ppm, J Hz): 8.16 (m, 1H, H^6), 7.49, (m, 8H, $H^{3,4}$, 6H Ph *ortho*), 7.10 (d, 1H, $H^{6'}$, $J_{HH} = 7.2$), 6.92 (m, 8H, H^5, $H^{5'}$, 6H Ph), 6.47 (m, 2H, $H^{3'}$, $H^{4'}$), 2.33 (m, 2H, suc), 0.86 (m, 2H, suc). $^{31}P\{^1H\}$ NMR ($(CD_3)_2CO$, δ ppm): 40.8 (s, P(4-F–C_6H_4)$_3$).

2.3.10. [Pd(phpy)(suc)(P(4-MeO–C_6H_4)$_3$)] (**8b**)

Yield: 67% (*Anal.* Calc. for $C_{36}H_{33}N_2O_5PPd$: C, 60.8; H, 4.7; N, 3.9. Found: C, 60.9; H, 4.7; N, 3.9%). IR (cm^{-1}): 1624s (C=O str.); 544m, 506m, 494m (P(4-MeO–C_6H_4)$_3$). ^1H NMR ($(CD_3)_2CO$, δ ppm, J Hz): 8.18 (m, 1H, H^6), 7.74 (m, 1H, $H^{6'}$), 7.72, (m, 8H, $H^{3,4}$, 6H Ph *ortho*), 6.94 (m, 1H, H^5), 6.92 (m, 7H, $H^{5'}$, 6H Ph *meta*), 6.56 (m, 2H, $H^{3',4'}$), 3.78 (s, 9H, MeO–), 2.25 (m, 2H, suc), 1.71 (m, 2H, suc). $^{31}P\{^1H\}$ NMR ($(CD_3)_2CO$, δ ppm): 39.4 (s, P(4-MeO–C_6H_4)$_3$).

2.4. Crystal structure determination of [{Pd(phpy)(μ-suc)}$_2$] (**1b**) and [Pd(azb)(suc)(PPh_3)] (**4a**)

Data for **1b** were collected using a single crystal of approximate dimensions $0.5 \times 0.5 \times 0.3$ mm. Accurate cell parameters were determined by least-squares fitting of 25 high-angle reflections. The scan method was ω with the range of *hkl* ($-22 \le h \le 22$, $-14 \le k \le 0$, $0 \le l \le 23$) corresponding to $2\Theta_{max} = 60.84°$. The structure was solved by direct methods and refined anisotropically on F^2 [33]. Hydrogen atoms were introduced in calculated positions. The final R factor was 0.0481 [$R_w = 0.1139$, where $w = 1/\sigma^2(F_o^2) + (0.0678P)^2$ and $P = (F_o^2 + 2F_c^2)/3$] over 5115 observed reflections [$I > 2\sigma(I)$].

Data for **4a** were collected using a single crystal of approximate dimensions $0.2 \times 0.4 \times 0.3$ mm on a Siemens SMART diffractometer under a stream of N_2 at 173 K. Crystallographic data are summarized in Table 1. An empirical absorption (SADABS) was applied [34]. The structure was solved by direct methods and refined on all F^2 data using the SHELX suite of programs on a Silicon Graphics computer [35]. All non-hydrogen atoms were anisotropic refined, hydrogen atoms were introduced in calculated positions. The final R factor was 0.0264 [$R_w = 0.0712$, where $w = 1/[\sigma^2(F_o^2) + (0.0652P)^2 + 6.4628P]$ and $P = (F_o^2 + 2F_c^2)/3$] over 5439 observed reflections [$I > 2\sigma(I)$].

Table 1
Crystal data and summary of data collection and refinement for [{Pd(phpy)(μ-suc)}$_2$] (**1b**) and [Pd(azb)(suc)(PPh_3)] (**4a**)

	1b	**4a**
Empirical formula	$C_{30}H_{24}N_4O_4Pd_2$	$C_{34}H_{28}N_3O_2PPd$
Formula weight	717.33	647.96
Crystal system	monoclinic	monoclinic
Space group	$P2_1/n$	$P2_1/n$
Unit cell dimensions		
a (Å)	16.090(4)	10.8781(19)
b (Å)	10.323(3)	16.079(3)
c (Å)	16.571(2)	16.014(3)
β (°)	105.97(2)	91.560(3)
V (Å^3)	2646.0(11)	2799.9(9)
Z	4	4
D_{calc} (Mg m^{-3})	1.801	1.537
F (mm^{-1})	1.404	0.758
λ (Å)	0.71073	0.71073
Observed reflections	5115	5439
R_1, wR_2	0.0481, 0.1139	0.0264, 0.0712
Goodness-of-fit	1.043	0.663

3. Results and discussion

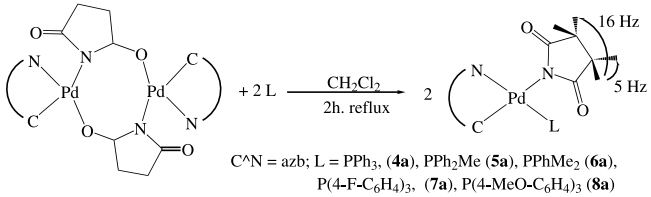
In acetone, the acetato-bridged cyclometallated dimers $[\{Pd(\mu\text{-}OOCMe)(C\hat{}N)\}_2]$ (C^N = azb or phpy) react under the conditions described in the experimental section with succinimide, phthalimide or maleimide to give dinuclear complexes (**1a**–**3a**, **1b**–**3b**) in which the imidato ligands replace the bridging acetate group as presented in Scheme 1.

The new azobenzene derivatives are air-stable brown solids, while the 2-phenylpyridine complexes present a yellow colour. Infrared spectra of all compounds show the characteristic absorptions of the corresponding cyclometallated ligand, partially overlapped with those attributed to imidato–carbonyl stretching. Thus, two medium intensity bands at 1595 and 1552 cm^{-1} were occasionally observed in the IR spectra of the azobenzene compounds, whilst relevant bands for 2-phenylpyridine derivatives appeared at 1604 and 1576 cm^{-1}. Two strong bands in the range 1731–1720 and 1600–1566 cm^{-1} suggested coordination of one carbonyl group to the metal as a part of an –NCO– bridging unit, according to previously reported data [10]. It has been claimed that this bridging structure would remove the twofold symmetry of the free or N-bonded imidato ligand increasing the intensity of the symmetric absorption. This higher frequency mode $\nu_{sym}(CO)$ is normally weak in cyclic imides, as shown later for compounds (**4a**–**8a**, **4b**–**8b**) in whose spectra the band has negligible intensity compared with the antisymmetric $\nu(CO)$ absorption.

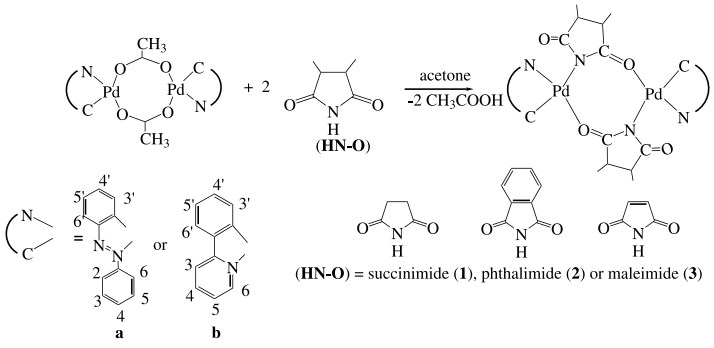
Further evidence for the dinuclearity of complexes (**1a**–**3a**, **1b**–**3b**) comes from the FAB mass spectrometry, as can be implied by the *m*/*z* values for the observed fragments (see Section 2). Spectra of the new bridged compounds show a similar fragmentation pattern which includes the peaks corresponding to $[\{Pd(NCO)(C\hat{}N)\}_2]^+$ and $[\{Pd_2(NCO)(C\hat{}N)_2\}]^+$. The abundances of the signals around the pattern ion are consistent with the natural isotopic abundances.

The ^1H and ^{13}C NMR data are collected in the experimental section and Scheme 1 shows the labelled cyclometallated ligands. The ^1H spectra exhibit the expected resonances for these ligands, together with the corresponding signals of the bridging imidato units that are partly overlapped with the former in the case of phthalimide and maleimide derivatives. Moreover, the succinimidato protons in the 2-phenylpyridine derivative (**1b**) appear as a broad singlet at 2.76 ppm, whereas the spectrum of the azobenzene analogue (**1a**) shows a complex multiplet centered at 2.69 ppm. By analogy with previously reported results in related systems [10], this behaviour may be explained in view of the fact that the azophenyl and methylene groups were close in complex **1a**. On the other hand, the distinction of two different carbonyl signals, shifted downfield from the one observed for the corresponding free ligand, is the only remarkable feature in the ^{13}C NMR spectra of the new compounds. On the basis of previously reported data [27,28], the singlet that appears at lowest field has been assigned to the carbonyl atom coordinated to palladium.

We have also investigated the reaction of the succinimidato-bridged compounds (**1a**,**1b**) with tertiary phosphines, in an attempt to obtain a parallel behaviour to that shown by the well known halide-bridged dimers: bridge splitting to yield the mononuclear derivatives [Pd(C^N)(X)(L)]. The halogen-like character of the succinimido ligand suggested by McCleverty and coworkers [10] should play an important role in the formation of the mononuclear N-bonded imidato derivatives presented in Scheme 2.



Scheme 2.



Scheme 1.

Table 2
Selected bond lengths (Å) and bond angles (°) for **1b** and **4a**

1b		**4a**	
Bond lengths			
Pd(1)–C(1)	1.970(4)	Pd(1)–C(1)	2.008(2)
Pd(1)–N(1)	2.028(3)	Pd(1)–N(3)	2.0970(18)
Pd(1)–N(2)	2.048(3)	Pd(1)–N(1)	2.0998(18)
Pd(1)–O(3)	2.162(3)	Pd(1)–P(1)	2.2580(6)
Pd(1)–Pd(2)	2.9544(7)	C(13)–O(1)	1.222(3)
Pd(2)–C(26)	1.963(4)	C(16)–O(2)	1.220(3)
Pd(2)–N(4)	2.023(3)	C(13)–N(3)	1.361(3)
Pd(2)–N(3)	2.046(3)	C(16)–N(3)	1.362(3)
Pd(2)–O(2)	2.179(3)		
C(12)–O(1)	1.219(5)		
C(19)–O(4)	1.202(5)		
C(15)–O(2)	1.238(5)		
C(16)–O(3)	1.239(5)		
C(12)–N(2)	1.371(5)		
C(15)–N(2)	1.328(5)		
C(16)–N(3)	1.339(5)		
C(19)–N(3)	1.403(5)		
Bond angles			
C(1)–Pd(1)–N(1)	81.47(15)	C(1)–Pd(1)–N(3)	174.71(8)
C(1)–Pd(1)–N(2)	95.96(15)	C(1)–Pd(1)–N(1)	78.45(8)
N(1)–Pd(1)–N(2)	173.60(13)	N(3)–Pd(1)–N(1)	97.10(7)
C(1)–Pd(1)–O(3)	172.76(14)	C(1)–Pd(1)–P(1)	93.28(6)
N(1)–Pd(1)–O(3)	93.57(13)	N(3)–Pd(1)–P(1)	91.15(5)
N(2)–Pd(1)–O(3)	89.51(12)	N(1)–Pd(1)–P(1)	171.74(5)
C(26)–Pd(2)–N(4)	81.55(16)	O(1)–C(13)–N(3)	124.9(2)
C(26)–Pd(2)–N(3)	95.32(15)	O(2)–C(16)–N(3)	125.1(2)
N(4)–Pd(2)–N(3)	173.51(14)		
C(26)–Pd(2)–O(2)	173.88(14)		
N(4)–Pd(2)–O(2)	94.03(13)		
N(3)–Pd(2)–O(2)	89.49(12)		
N(2)–C(12)–O(1)	123.4(4)		
N(3)–C(19)–O(4)	124.4(4)		
N(2)–C(15)–O(2)	126.2(4)		
N(3)–C(16)–O(3)	126.2(4)		

Reactions take place in dichloromethane under continued reflux, yielding brown (**a** compounds) or yellow (**b** compounds) air stable solids with negligible molar conductivity values. Acetone was avoided as a solvent since we found that it tends to stay occluded (lost at 118 °C) in the new complexes. The subsequent strong IR band around 1720 cm^{-1} interfered the monitoring of the reactions by this technique, as it appears in the typical range of absorption for imidato bridging units discussed before. Thus, the spectra show the expected bands for the corresponding cyclometallated backbone, together with those attributed to the incoming neutral ligand and one strong carbonyl band in the range 1566–1586 or 1600–1634 cm^{-1} for azobenzene and 2-phenylpyridine derivatives, respectively.

The ^{1}H and ^{31}P NMR data of the mononuclear complexes are collected in Section 2, the latter consisting of singlets with chemical shifts in the usual range for Pd(II) complexes. With regard to the ^{1}H NMR spectra, they show the expected resonances of the cyclometallated and succinimidato ligands, together with those attributed to the corresponding coordinated phosphine. The assignment of the cyclometallated protons was made by comparison with our previously published data [11]. An interesting aspect, also found before in cyclometallated complexes with iminophosphines [11], is the appreciable coupling to the phosphorus atom exhibited by the $H^{3'}$ in azobenzene derivatives, and $H^{3'}$, H^{6} in compounds with 2-phenylpyridine. On the other hand, basically two different behaviours were observed for aliphatic protons of succinimidato, depending on the steric hindrance introduced by the phosphine ligand in the *cis*-position. Thus, rotation about the Pd–N axis might be hindered when bulky phosphines (**4**, **5**, **7**, **8a**,**b**) coordinate the metal, and two resonances that integrate two protons each (*syn*-/*anti*-, see Scheme 2) are observed, while just one multiplet signal appears in the spectra of compounds **6a** and **6b** with less voluminous substituents. VT ^{1}H NMR experiments were carried out in an attempt to get coalescence of signals and to calculate the energy barrier associated with the Pd–N rotation, but it could not be achieved in the range of temperatures allowed by usual deuterated solvents. Nevertheless, similarly hindered rotations about M–N bonds have been attributed previously to steric factors [27,36,37].

3.1. X-ray structures of [{Pd(μ-suc)(phpy)}$_2$] (**1b**) and [Pd(azb)(suc)(PPh_3)] (**4a**)

Selected bond distances and angles are presented in Table 2. The coordination around the Pd atoms is

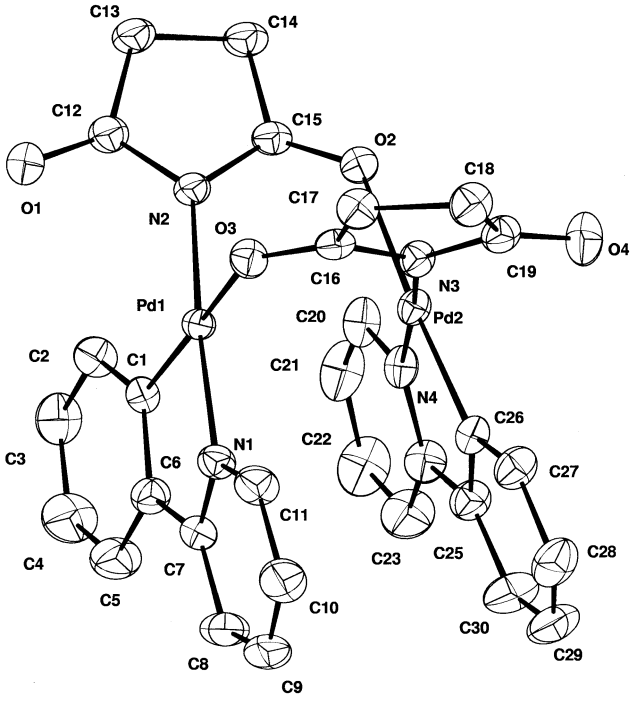


Fig. 1. Molecular structure of complex **1b**.

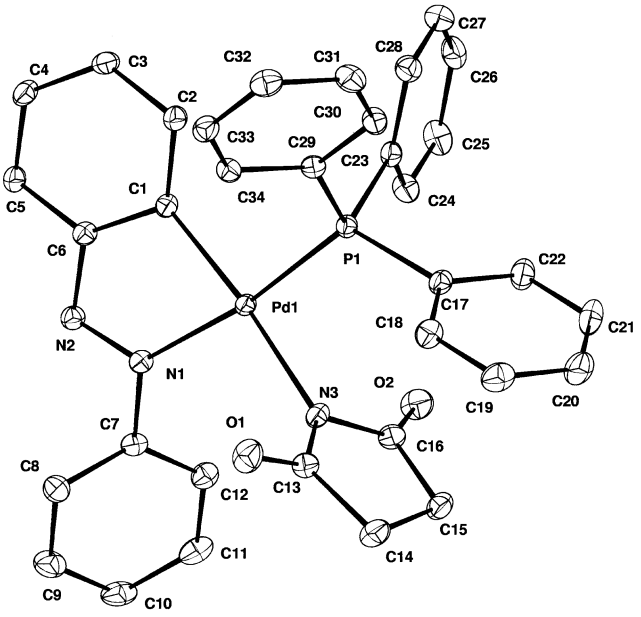


Fig. 2. Molecular structure of complex **4a**.

approximately planar. The narrow NPdC angle, (80.8° and 78.4° in the dinuclear and mononuclear complexes, respectively), in the *ortho*-metallated moiety is similar to that found in complexes containing the same ligand [11]. The structural analysis of complex **4a** confirms the relative *cis*-position of the phosphine ligand and the metallated carbon atom suggested by the NMR data. This is the typical arrangement of the phosphine group in cyclopalladated complexes of the type [Pd(C^N)(phosphine)(X)] (X = anionic monodentate ligand) due to the so-called *transphobia* effect [38,39].

In the succinimide ligand the C=O distance, 1.239(5) Å, is elongated in the bridged group with respect to the non-coordinated C=O, 1.211(5) Å, and to the mononuclear one, 1.221(3) Å. The Pd–N distance is larger in the mononuclear complex and the Pd(1)–Pd(2) distance in dinuclear compound **1b** is rather short (2.9544(7) Å). The angle between the best plane through the succinimide and the coordination plane is 72.40° in dinuclear **1b** (Fig. 1) and 79.22° in mononuclear **4a** (Fig. 2). In the bridged complex the 2-phenylpyridine ligands are nearly parallel, (dihedral angle = 12.89°), while the planes through the succinimide ligands form an angle of 85.96°.

4. Supplementary material

Crystallographic data for the structural analysis have been deposited with the Cambridge Crystallographic Data Centre, CCDC Nos. 173327 for compound **1b** and 173328 for compound **4a**. Copies of this information may be obtained free of charge from The Director, CCDC, 12 Union Road, Cambridge, CB2 1EZ, UK (fax: +44-1223-336033; e-mail: deposit@ccdc.cam.ac.uk or www: http://www.ccdc.cam.ac.uk).

Acknowledgements

Financial support of this work by the Dirección General de Investigación (project BQU2001-0979) Spain is acknowledged. José Pérez thanks the PFMP-UPCT-2001 program for a grant to visit the University of Bristol.

References

[1] I.I. Omae, Coord. Chem. Rev. 83 (1988) 137.
[2] A.C. Cope, R.W. Siekman, J. Am. Chem. Soc. 87 (1965) 3273.
[3] A. Kasahara, Bull. Chem. Soc. Jpn. 41 (1968) 1272.
[4] E.C. Constable, A.M.W. Cargill Thompson, T.A. Leese, D.G.F. Reese, D.A. Tocher, Inorg. Chim. Acta 182 (1991) 93.
[5] D.L. Weaver, Inorg. Chem. 9 (1970) 2250.
[6] M.A. Gutiérrez, G.R. Newkome, J. Selbin, J. Organomet. Chem. 202 (1980) 341.
[7] J.M. Vila, M. Gayoso, M. Pereira, A. Romar, J.J. Fernández, M. Thornton-Pett, J. Organomet. Chem. 401 (1991) 385.
[8] M.M. Mdleleni, J.S. Bridgewater, R.J. Watts, P.C. Ford, Inorg. Chem. 34 (1995) 2334.
[9] C.A. Craig, R.J. Watts, Inorg. Chem. 28 (1989) 309.
[10] H. Adams, N.A. Bailey, T.N. Briggs, J.A. McCleverty, H.M. Colquhoun, D.J. Williams, J. Chem. Soc., Dalton Trans. (1986) 813.
[11] G. Sánchez, J.L. Serrano, M.A. Moral, J. Pérez, E. Molins, G. López, Polyhedron 18 (1999) 3057.
[12] I. Aiello, A. Crispini, M. Ghedini, M. La Deda, F. Barigelletti, Inorg. Chim. Acta 308 (2000) 121.
[13] M.M. Mdleleni, J.S. Bridgewater, R.J. Watts, P.C. Ford, Inorg. Chem. 34 (1995) 2334.
[14] C.A. Craig y, R.J. Watts, Inorg. Chem. 28 (1989) 309.
[15] Y. Ohsawa, S. Sprouse, A. King, M.K. De Armond, K.W. Hanck, R.J. Watts, J. Phys. Chem. 91 (1987) 1047.
[16] K.A. King, P.J. Spellane, R.J. Watts, J. Am. Chem. Soc. 107 (1985) 1431.
[17] L. Chassot, A. Von Zelewsky, Inorg. Chem. 26 (1987) 2814.
[18] L. Chassot, E. Muller, A. Von Zelewsky, Inorg. Chem. 23 (1984) 4249.
[19] A.D. Ryabov, L.G. Kuz'mina, N.V. Dvortsova, D.J. Stufkens, R. van Eldik, Inorg. Chem. 32 (1993) 3166.
[20] J. Matsunami, H. Urata, K. Matsumoto, Inorg. Chem. 34 (1995) 202.
[21] Y. Dohta, M. Kodaka, T. Okada, K. Okamoto, H. Okuno, Inorg. Chim. Acta 5 (1996) 252.
[22] U. Beyer, M. Krüger, P. Schumacher, C. Unger, F. Kratz, Chem. Monthly 128 (1997) 91.
[23] M.T. Schütte, P. Schumacher, C. Unger, R. Mülhaupt, F. Kratz, Inorg. Chim. Acta 267 (1998) 133.
[24] D.M. Roundhill, Inorg. Chem. 9 (1970) 254.
[25] B. Nestler, E. Uhligh, Z. Anorg. Allg. Chem. 530 (1985) 196.
[26] J.L. Serrano, Y. Zheng, J.R. Dilworth, G. Sánchez, Inorg. Chem. Commun. 2 (1999) 407.
[27] I. Dubuc, M. Dubois, F. Belanger-Gariepy, D. Zargarian, Organometallics 18 (1999) 30.

[28] T. Ikariya, S. Takizawa, M. Shirado, S. Yoshikawa, J. Organomet. Chem. 171 (1979) C47.
[29] G. Carturan, V. Belluco, M. Graziani, J. Organomet. Chem. 112 (1976) 243.
[30] E.J. Schier, W. Sacher, W. Beck, Z. Naturforsch., Teil. B Chem. Sci. 42 (1987) 1424.
[31] M.S. Islam, M.M. Uddin, J. Bangladesh Chem. Soc. 7 (1994) 39.
[32] M.S. Islam, R.K. Roy, M.A.J. Miah, Synth. React. Inorg. Met.-Org. Chem. 21 (1991) 869.
[33] G.M Sheldrick, SHELX-97 Programs for Crystal Structure Analysis (Release 97-2), University of Göttingen, Germany, 1998.
[34] G.M. Sheldrick, SADABS: A Program for Absorption Correction with the Siemens SMART system, University of Göttingen, Göttingen, Germany, 1996.
[35] SHELXTL Program System, version 5.03, Siemens Analytical X-ray Instrument, Madison, WI, 1995.
[36] P.L. Holland, R.A. Andersen, R.G. Bergman, J. Huang, S. Nolan, J. Am. Chem. Soc. 119 (1997) 12800.
[37] G.L. Hilhouse, A.R. Bulls, B.D. Santarsiero, J.E. Bercaw, Organometallics 7 (1988) 1309.
[38] J. Vicente, A. Arcas, D. Bautista, P.G. Jones, Organometallics 16 (1997) 2127.
[39] J. Vicente, J.A. Abad, A.D. Frankland, M.C. Ramírez de Arellano, Chem. Eur. J. 5 (1999) 3066.

UV–Vis spectra (CH_2Cl_2 solution), IR spectra (KBr disk), and ^1H NMR spectra ($CDCl_3$) were recorded on a Shimadzu UVPC 1601 spectrophotometer, a Perkin–Elmer 783 spectrometer, and a Bruker FT 300 MHz spectrometer, respectively. The numbering scheme used for ^1H NMR assignment is the same as in crystallography. Spin-spin structures are abbreviated as follows: s, singlet; d, doublet; t, triplet; m, multiplet. Cyclic voltammetry (in MeCN, 0.1M TEAP) was done at a platinum working electrode under nitrogen atmosphere on a PAR model 370-4 electrochemistry system [23]. Microanalyses (C, H, N) were performed using a Perkin–Elmer 2400 Series II elemental analyzer.

2.2. Synthesis of chlorbis(2-amidothiophenolato)triphenylphosphinerhenium(V), [Re(atp)$_2$(Cl)(PPh$_3$)] (**2a**)

To a suspension of $ReOCl_3(PPh_3)_2$ (100 mg, 0.120 mmol) in 10 ml of toluene was added 30 mg (0.240 mmol) of 2-aminothiophenol, (H_2atp). The resulting mixture was heated to reflux for 15 min affording a reddish brown solution. The solvent was then removed under reduced pressure, and the solid thus obtained was dissolved in 5 ml of dichloromethane, and the solution was subjected to chromatography on a silica gel column (20 × 1 cm; 60–120 mesh, BDH). A deep reddish brown band was eluted out with a benzene-acetonitrile (25:1) mixture. Removal of solvent under reduced pressure afforded the pure complex which was dried in vacuo over fused calcium-chloride Yield: (57 mg, 65%). *Anal* Calc. for $C_{30}H_{25}ClN_2S_2PRe$: C, 49.34; H, 3.45; N, 3.84. Found: C, 49.28; H, 3.49; N, 3.87%. UV–Vis (λ_{max}, nm (ε, $M^{-1}cm^{-1}$)): 447(11450); 326(5730). IR(cm^{-1}, KBr pellet): 3250(NH), 320(Re–Cl). ^1H NMR ($CDCl_3$) δ: H5, H11 7.80 (d, *J* 8.1 Hz); H2, H8 7.56 (d, *J* 8.4 Hz); H4, H10 7.08 (t, *J* 7.2 Hz); H3, H9 6.92 (t, *J* 7.3 Hz). N–H, 12.46(s); aromatic multiplets, 7.28–7.48.

2.3. Synthesis of bromobis(2-amidothiophenolato)triphenylphosphinerhenium(V), [Re(atp)$_2$(Br)(PPh$_3$)] (**2b**)

To suspension of $[ReO(OEt)Br_2(PPh_3)_2]$ (100 mg, 0.102 mmol) in 10 ml of toluene was added 25.6 mg (0.204 mmol) of 2-aminothiophenol, H_2atp. The same procedure as in the previous preparation was then followed affording the reddish brown complex. Yield: (53.9 mg, 68%). *Anal.* Calc. for $C_{30}H_{25}BrN_2S_2PRe$: C, 46.51; H, 3.25; N, 3.62. Found: C, 46.46; H, 3.29: N, 3.65%. UV–Vis (λ_{max}, nm (ε, $M^{-1}cm^{-1}$): 453(6740); 335(4284). IR (cm^{-1}, KBr pellet): 3252(NH). ^1H NMR ($CDCl_3$) δ: H5, H11 7.89 (d, *J* 8.0 Hz); H2, H8 7.65 (d, *J* 8.3 Hz); H4, H10 7.15 (t, *J* 7.5 Hz). H3, H9 7.03 (t, *J* 7.4 Hz); N–H 12.77(s); aromatic multiplets, 7.28–7.35.

2.4. Synthesis of iodobis(2-amidothiophenolato)triphenylphosphinerhenium(V), [Re(atp)$_2$(I)(PPh$_3$)] (**2c**)

This was synthesized in the same manner as (**2b**) using $[ReO(OEt)I_2(PPh_3)_2]$ (100 mg, 0.098 mmol) and H_2atp (24.4 mg, 0.196 mmol) Yield: (52 mg, 65%). *Anal* Calc. for $C_{30}H_{25}IN_2S_2PRe$: C, 43.84; H, 3.06; N, 3.41. Found: C, 43.78; H, 3.11; N, 3.45%. UV–Vis (λ_{max}, nm (ε, $M^{-1}cm^{-1}$)): 463(8090); 347(8760). IR (cm^{-1}, KBr pellet): 3250 (NH). ^1H NMR ($CDCl_3$) δ: H5, H11 7.93 (d, *J* 7.7 Hz); H2, H8 7.67 (d, *J* 8.4 Hz). H4, H10 7.12(m); H3, H9 7.12(m); N–H 13.08(s); aromatic multiplets, 7.33–7.52.

2.5. Conversion of [Re(atp)$_2$(Cl)(PPh$_3$)] to [Re(atp)$_3$]

To a solution of [Re(atp)$_2$(Cl)(PPh$_3$)] (100 mg, 0.137 mmol) in 10 ml of toluene was added 17.12 mg (0.137 mmol) of H_2atp. The resulting mixture was heated to reflux for 60 min affording a deep green solution. The solvent was then removed under reduced pressure and the solid thus obtained was dissolved in 10 ml of acetone and kept for slow evaporation for a few days to get the pure complex which was dried in vacuo over fused calcium chloride, Yield: (62.3 mg, 83%). The [Re(atp)$_2$(Br)(PPh$_3$)] and [Re(atp)$_2$(I)(PPh$_3$)] complexes could be similarly converted to [Re(atp)$_3$].

2.6. X-ray crystallography

Single crystal of $[Re(atp)_2(Cl)(PPh_3)].2CH_2Cl_2$ were grown by slow diffusion of hexane into dichloromethane solution the crystals rapidly lost the solvent of crystallization and crystallinity in air. A crystal was sealed over the mother liquor for crystallography. Cell parameters were determined by a least-squares fit of 30 machine-centered reflections ($14^\circ \le 2\theta \le 28^\circ$). Data were collected by the ω scan technique in the range $3^\circ \le 2\theta \le 50^\circ$ for [Re(atp)$_2$(Cl)(PPh$_3$)] on a Siemens R3 *m*/*V* four-circle diffractometer with graphite monochromated Mo Kα ($\lambda = 0.71073$ Å) radiation at 25 °C. Two check reflections after each 198 reflections showed no significant intensity reduction. All data were corrected for Lp effects and absorption [24].

The metal atom was located from Patterson maps, and the rest of the nonhydrogen atoms emerged from successive Fourier synthesis. The structure were refined by full-matrix least-squares procedures on F^2. All nonhydrogen atoms were refined anisotropically. Hydrogen atoms were included at calculated positions. Calculations were performed using the SHELXTL V5.03 [25] program package. The two dichloromethane molecules in the lattice are disordered. Significant crystal data are listed in Table 1.

Table 1
Crystallographic data for $[Re^{V}(atp)_2(Cl)(PPh_3)]\cdot 2\ CH_2Cl_2$ (**2a**)

Empirical formula	$C_{32}H_{28}Cl_5N_2PReS_2$
Formula weight	899.10
Crystal system	triclinic
Space group	$P\bar{1}$
a (Å)	9.693 (3)
b (Å)	13.529 (5)
c (Å)	14.944 (4)
α (°)	115.61 (2)
β (°)	97.78 (2)
γ (°)	92.27 (3)
V (Å^3)	1740.2 (10)
Z	2
$D_{calc.}$ (Mg m^{-3})	1.716
μ (mm^{-1})	4.067
θ Range (°)	1.70–25.00
R [a], wR_2 [b] $[I > 2\sigma(I)]$	0.0744, 0.1796
Goodness-of-fit on F^2	1.046

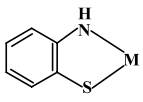
[a] $R = ||F_o| - |F_c||/\Sigma|F_o|$.
[b] $wR_2 = [\Sigma w(F_o^2 - F_c^2)^2/\Sigma w(F_o^2)^2]^{1/2}$.

The twist angle (ϕ) is defined and calculated according to a published procedure [26]. In the case of $[Re(atp)_2(Cl)(PPh_3)]$, let cen a and cen b be the centroids of the faces N1, N2, Cl1 and S1, S2, P1, respectively. The dihedral angles between planes of cen a, cen b, N1 and cen a, cen b S1; cen a, cen b, N2 and cen a, cen b, S2 and cen a, cenb, Cl1 and cen a, cen b P1 are respectively 5.5°, 8.8° and 9.7°. The average value, 8.0°, is taken as ϕ. The angular parameters for $[Re(atp)_3]$ were either taken directly from the published work or were computed using the available atomic coordinates [15]. Here the twist angle is 7.9° is the average of the three dihedral angles 7.4°, 7.8° and 8.5° between planes defined in the same manner as in the case of $[Re(atp)_2(Cl)(PPh_3)]$.

3. Results and discussion

3.1. Synthesis and characterization

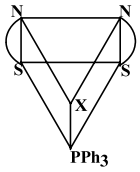
The bidentate ligand used in the present work is 2-aminothiophenol (H_2atp) which is prone to chelate metal ions in diionised form as in (**1**). The basis of this choice is the



1

proven ability of this ligand to stabilize the trigonal prismatic geometry upon tris chelation as in $[Re^{VI}(atp)_3]$ [15,16], $[Tc^{VI}(atp)_3]$ [27] and $[Mo^{VI}(atp)_3]$ [28].

The reaction of $[Re^{V}OCl_3(PPh_3)_2]$ with H_2atp in boiling toluene afforded a reddish brown solution from which $[Re^{V}(atp)_2(Cl)(PPh_3)]$ of coordination type (**2a**) could indeed be isolated in satisfactory yield. For the success of the synthesis it is crucial to control both the reaction time (15 min) and metal: ligand (1:2) mole ratio. Use of $[Re^{V}O(OEt)Br_2(PPh_3)_2]$ and $[Re^{V}O(OEt)I_2(PPh_3)_2]$ in place of $[Re^{V}OCl_3(PPh_3)_2]$ in the above synthesis afforded the bromo (**2b**) and iodo (**2c**) complexes, respectively.



(**2a**), X = Cl

(**2b**), X = Br

(**2c**), X = I

Our interest in oxorhenium chemistry [29–31] prompted us to examine the above $Re^{V}O$ reagents incorporating X(Cl, Br, I) and PPh_3 coligands as starting materials for the reaction with H_2atp. It was hoped that ionised H_2atp would displace the oxo atom forming chelate rings of type (**1**) but with retention of some X/PPh_3 coordination. This happened in practice.

Selected characterization data for (**2a**–**2c**) are given in the Section 2. The complexes are uniformly diamagnetic corresponding to the spin paired d^2 configuration (idealized $a_1'^2$) [1]. In solution the complexes display two characteristic allowed bands in the UV–Vis region. Their energy decreases slightly as in the order (**2a**) (447, 326 nm) > (**2b**)(453, 335 nm) > (**2c**) (463 nm, 347 nm). In IR the N–H stretch is seen as a sharp feature near 3250 cm^{-1}.

The two coordinated atp^{2-} ligands are equivalent in solution giving rise to two ^{1}H NMR doublets and two triplets in the aromatic region, 6.5–8.0 ppm (J, 7.0–8.5 Hz). The N–H proton resonance occurs as a characteristic singlet at 12.46°, 12.77° and 13.08 ppm for (**2a**), (**2b**) and (**2c**), respectively. The signal 'disappears' upon addition of D_2O to the solution.

3.2. Crystal and molecular structure

Only complex (**2a**) afforded single crystals in the form of loosely held solvate $(\mathbf{2a})\cdot 2CH_2Cl_2$ which was stable only in presence of the mother liquor. A molecular view of the complex is shown in Fig. 1 and selected bond parameters are listed in Table 2. The CH_2Cl_2 molecules are highly disordered and occupy cavities in the lattice.

The ReS_2N_2ClP coordination sphere has distorted trigonal prismatic geometry as in (**2a**). The synthetic procedure used always afforded the same complex and no evidence of the existence of the possible geometrical isomers could be found. The areas of the triangular faces defined by S1, S2, P1 and N1, N2, Cl1 are 4.38 and 3.97 Å^2, respectively. The prism is thus tapered.

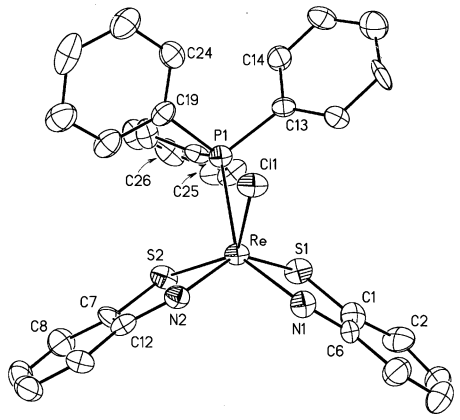


Fig. 1. Molecular view and atom-labeling scheme for $[Re(atp)_2(Cl)(PPh_3)]$. All nonhydrogen atoms are represented by 30% thermal probability ellipsoids.

Certain angular parameters diagnostic of the geometry are: twist angle (ϕ), dihedral angle (ω_1) between one coordination plane and another, dihedral angle (ω_2) between a coordination plane and a triangular face and angle (θ) at the metal site between two donors in *trans* positions. In the present complex the ϕ value is 8.0°. The other angles (Table 2) span the ranges: ω_1, 113.7°–124.7°; ω_2, 80.2°–98.7° and θ, 123.3°–142.7°. It is instructive to compare these parameters with those of the structurally characterized tris chelate $[Re(atp)_3]$ [15] as well as with those of idealised D_{3h} and O_h geometries (Table 3).

Whereas the span of the angular parameters of $[Re(atp)_2(Cl)(PPh_3)]$ is generally higher, the averages invariably lie close to those in $[Re(atp)_3]$.

Even though the metal oxidation state in $[Re(atp)_2(Cl)(PPh_3)]$ is lower than that in $[Re(atp)_3]$ the average Re–N (1.97 Å) and Re–S (2.30 Å) lengths in the former are slightly shorter than those (2.00 and 2.35 Å, respectively) in $[Re(atp)_3]$ [15]. In absence of the third chelate ring the two atp^{2-} ligands are pulled closer to the metal in $[Re(atp)_2(Cl)(PPh_3)]$. We are unable to compare the Re–Cl(2.438(3)) and Re–P (2.450(4)) lengths with those in other trigonal prismatic systems, since no such system exist. In pseudooctahedral species Re^{V}–Cl [29–31] and Re^{V}–P [20,32,33] lengths usually lie in the ranges 2.31–2.39 and 2.46–2.52 Å, respectively.

Table 3
Angular parameters [a] of $[Re(atp)_2(Cl)(PPh_3)]\cdot 2CH_2Cl_2$ and $[Re(atp)_3]$

Parameters [b]	$[Re(atp)_2(Cl)(PPh_3)]$	$[Re(atp)_3]$	D_{3h}	O_h
ϕ (°)	8.0	7.9	0	60
ω_1 (°)	113.7–124.7(119.3)	119.0–119.8(119.3)	120	90
ω_2 (°)	80.2–98.7(90.5)	84.4–95.1(91.4)	90	54.7
θ (°)	123.3–142.7(134.4)	128.2–140.3(134.3)	135.6	180

[a] Average values are given in parenthesis.
[b] For definition see text.

The similarity of the properties of (**2b**) and (**2c**) with those of (**2a**) strongly suggest that the former species also have gross trigonal prismatic geometry, although the extent of distortion could be different in the three species. We thus have here the first examples of the trigonal prismatic complexes of type $M(bidentate)_2(monodentate)_2$. Further unusual feature of (**2**) include the presence of the bulky PPh_3 as a ligand and the presence of the d^2 metal ion (Re^{V}). Structurally characterized trigonal prismatic metal complexes of good standing (using $\phi < 10°$ as a criterion) generally contain only d^0 or d^1 metal ions [9–11,14,15,18,27,28]. We are excluding

Table 2
Selected bond distances (Å) angles (°) and dihedral angles (°) for $[Re(atp)_2(Cl)(PPh_3)]\cdot 2CH_2Cl_2$ (**2a**)

Bond distances			
Re–N(1)	1.956(11)	Re–N(2)	1.988(12)
Re–S(1)	2.306(4)	Re–S(2)	2.289(4)
Re–Cl(1)	2.438(3)	Re–P(1)	2.450(4)
Bond angles			
N(1)–Re–S(1)	79.0(3)	N(1)–Re–S(2)	142.7(3)
N(2)–Re–S(1)	134.0(4)	N(2)–Re–S(2)	79.1(4)
N(1)–Re–N(2)	86.7(5)	S(1)–Re–S(2)	86.5(2)
N(1)–Re–Cl(1)	82.2(3)	N(1)–Re–P(1)	123.3(3)
N(2)–Re–Cl(1)	81.4(4)	N(2)–Re–P(1)	140.2(4)
S(1)–Re–Cl(1)	137.9(2)	S(1)–Re–P(1)	81.4(13)
S(2)–Re–Cl(1)	128.5(2)	S(2)–Re–P(1)	87.5(14)
Cl(1)–Re–P(1)	78.1(12)		
Dihedral angles			
Re, N(1), S(1)–Re, N(2), S(2) 124.7		Re, N(1), S(1)–Re, P(1), Cl(1) 113.7	
Re, N(2), S(2)–Re, P(1), Cl(1) 119.4			
Re, N(1), S(1)–Cl(1), N(1), N(2) 80.2		Re, N(1), S(1)–P(1), S(1), S(2) 86.5	
Re, N(2), S(2)–Cl(1), N(1), N(2) 93.5		Re, N(2), S(2)–P(1), S(1), S(2) 86.5	
Re, Cl(1), P(1)–Cl(1), N(1), N(2) 98.7		Re, Cl(1), P(1)–P(1), S(1), S(2) 97	

the cases where the geometry is forced by ligand structure (clathro-chelates) [34].

3.3. Metal redox and reaction with H_2atp

In acetonitrile solution the $[Re(atp)_2(Cl)(PPh_3)]$ species display a quasireversible cyclic voltrametric response near 0.7 V versus SCE (Table 4). The response is assigned to the Re^{VI}–Re^{V} couple, the reduction potential of which decreases slightly in the order **(2a)** > **(2b)** > **(2c)**.

Upon treating the type **(2)** species with one mole of H_2atp in boiling toluene in air for 1 h, the PPh_3 and X^- ligands are replaced by atp^{2-} affording the tris chelate $[Re(atp)_3]$ in excellent yield. In this reaction the metal undergoes spontaneous aerial oxidation ($Re^{V} \rightarrow Re^{VI}$). This happens because of the large decrease in the Re^{VI}–Re^{V} reduction potential ($E_{1/2}$ of $[Re(atp)_3]$, −0.12 V [16]) upon tris chelation. The stabilization of the d^2 configuration (Re^{V}) in the present complex is promoted by the PPh_3, X pair of ligands.

4. Conclusion

The synthesis and characterization of the first family of trigonal prismatic complexes, $[Re^{V}(atp)_2(X)(PPh_3)]$, belonging to type M(bidentate)$_2$ (monodentate)$_2$ has been achieved by reacting $Re^{V}O$ reagents with H_2atp. The species are further unusual in having a bulky ligand (PPh_3) and d^2 configuration.

Pentavalent rhenium is redox stabilized in the family by the PPh_3, X ligand pair. The complexes react with H_2atp in air affording the tris chelate $[Re^{VI}(atp)_3]$ where the hexavalent metal is stabilized. Further work on the design and isolation of different molecular trigonal prismatic chelate type are in progress.

5. Supplementary material

Crystallographic data for the structural analysis have been deposited with the Cambridge Crystallographic Data Centre, CCDC No. 174267 for compound **(2a)**. Copies of this information may be obtained free of charge from: The Director, CCDC, 12 Union Road, Cambridge, CB2 1EZ, UK (fax: +44-1223-336033; e-mail: deposit@ccdc.cam.ac.uk or www: http://www.ccdc.cam.ac.uk).

Table 4
Cyclic voltametric data in acetonitrile solution (0.1 M TEAP) [a]

Compound	$\frac{E_{1/2}/V(\Delta E_p/mV)}{Re^{VI}/Re^{V}}$
(2a)	0.72(80)
(2b)	0.70(120)
(2c)	0.68(120)

[a] Conditions: working electrode, platinum; reference electrode, SCE; scan rate 50 mV s^{-1}. $E_{1/2} = 1/2\ (E_{pa} + E_{pc})$, where E_{pa} and E_{pc} are anodic and cathodic peak potentials, respectively, $\Delta E_p = E_{pa} - E_{pc}$.

Acknowledgements

We thank the Department of Science and Technology, and the Council of Scientific and Industrial Research, New Delhi, for financial support.

References

[1] R. Hoffmann, J.M. Howell, A.R. Rossi, J. Am. Chem. Soc. 98 (1976) 2484.
[2] S.K. Kang, T.A. Albright, O. Eisenstein, Inorg. Chem. 28 (1989) 1611.
[3] C.R. Landis, T. Cleveland, T.K. Firman, J. Am. Chem. Soc. 120 (1998) 2641.
[4] A. Haaland, A. Hammel, K. Rypdal, H.V. Volden, J. Am. Chem. Soc. 112 (1990) 4547.
[5] M. Kaupp, J. Am. Chem. Soc. 118 (1996) 3018.
[6] P.M. Morse, G.S. Girolami, J. Am. Chem. Soc. 111 (1989) 4114.
[7] J. Friese, A. Krol, C. Puke, K. Kirschbaum, D. Giolando, Inorg. Chem. 39 (2000) 1496.
[8] T.P. Vaid, A.S. Veige, E.B. Lobkovsky, W.V. Glassey, P.T. Wolczanski, L.M. Liable-Sands, A.L. Rheingold, T.R. Cundari, J. Am. Chem. Soc. 120 (1998) 10067.
[9] R. Eisenberg, J.A. Ibers, J. Am. Chem. Soc. 87 (1965) 3776.
[10] A.E. Smith, G.N. Schrauzer, V.P. Mayweg, W. Heinrich, J. Am. Chem. Soc. 87 (1965) 5798.
[11] D.L. Kepert, Prog. Inorg. Chem. 1 (1977) 23 (and references therein).
[12] D. Argyropoulos, E. Lyris, C.A. Mitsopoulou, D. Katakis, J. Chem. Soc., Dalton Trans. (1997) 615.
[13] D. Argyropoulos, C.A. Mitsopoulou, D. Katakis, Inorg. Chem. 35 (1996) 5549.
[14] P. Rosa, L. Ricard, P.L. Floch, F. Mathey, G. Sini, O. Eisenstein, Inorg. Chem. 37 (1998) 3154.
[15] A.A. Danopoulos, A.C.C. Wong, G. Wilkinson, M.B. Hursthouse, B. Hussain, J. Chem. Soc., Dalton Trans. (1990) 315.
[16] J.K. Gardner, N. Pariyadath, J.L. Corbin, E.I. Stiefel, Inorg. Chem. 17 (1978) 897.
[17] A. Mohlenkamp, R. Mattes, Z. Naturforsch. Teil. B 47 (1992) 969.
[18] K. Yamanouchi, J.H. Enemark, Inorg. Chem. 17 (1978) 1981.
[19] J. Chatt, G.A. Rowe, J. Chem. Soc. (1962) 4019.
[20] G. Francociani, G. D'Alfonso, P. Romiti, A. Sironi, M. Freni, Inorg. Chim. Acta 72 (1983) 29.
[21] G.K. Lahiri, S. Bhattacharya, B.K. Ghosh, A. Chakravorty, Inorg. Chem. 26 (1987) 4324.
[22] D.T. Sawyer, J.L. Roberts, Jr., Experimental Electrochemistry for Chemists, Wiley, New York, 1974, p. 167.
[23] A. Pramanik, N. Bag, D. Ray, G.K. Lahiri, A. Chakravorty, Inorg. Chem. 30 (1991) 410.
[24] A.C.T. North, D.C. Philips, F.S. Mathews, Acta Crystallogr., Sect. A 24 (1968) 351.
[25] G.M. Sheldrick, SHELXTL V5.03; Bruker Analytical X-ray Systems: Part Number 269-015900, Madison, WI, 1994.
[26] K.R. Dymock, G.J. Palenik, Inorg. Chem. 14 (1975) 1220.
[27] J. Baldas, J. Boas, J. Bonnyman, M.F. Mackay, G.A. Williams, Aust. J. Chem. 35 (1982) 2413.

[28] K. Yamanouchi, J.H. Enemark, Inorg. Chem. 17 (1978) 2911.
[29] B.K. Dirghangi, M. Menon, A. Pramanik, A. Chakravorty, Inorg. Chem. 36 (1997) 1095.
[30] S. Banerjee, S. Bhattacharyya, B.K. Dirghangi, M. Menon, A. Chakravorty, Inorg. Chem. 39 (2000) 6.
[31] I. Chakraborty, S. Bhattacharyya, S. Banerjee, B.K. Dirghangi, A. Chakravorty, J. Chem. Soc., Dalton Trans. (1999) 3747.
[32] J.E. Fergusson, Coord. Chem. Rev. 1 (1966) 459.
[33] D. Bright, J.A. Ibers, Inorg. Chem. 7 (1968) 1099.
[34] R.A.D. Wentworth, Coord. Chem. Rev. 9 (1972) 171.

The coordination chemistry of copper is important for a variety of reasons such as modelling its sites present in biological systems, display of stereochemical diversity on interaction with organic substrates, formation of oligomers and polymers, interesting magnetic properties etc. [1–23]. In view of our interest in the study of metal–sulfur bonds, structural and spectroscopic properties of interaction of heterocyclic thiones, thiosemicarbazones and phosphine sulfuides/selenides with several transition and non-transition metals have been reported [9–42].

In the literature, neutral heterocyclic thiones form sulfur-bridged dinuclear copper(I) complexes, namely $[Cu_2(C_5H_5NS)_4I_2]$ (**5**) [24], $[Cu_2(imdtH_2)_4Cl_2]$ (**6**) {imdtH$_2$ = 1,3-imidazolidine-2-thione, II} [25], $[Cu_2(meimtH)_4Cl_2]$ (**7**) [26], $[Cu_2(meimtH)_4(SCN)_2]$ (**8**) [27], $[Cu_2(C_5H_5NS)_6]X_2$ {X = Cl, **9**, Br, **10**} [28,29], $[Cu_2(meimtH)_6](BF_4)_2$ (**11**) {meimtH = 1-methylimidazoline-2-thione, III} [30], $[Cu_2(imdtH_2)_6](ClO_4)_2$ (**12**) [31], $[Cu_2(pymtH)_2Cl_2(p\text{-}Tol_3P)_2]$ (**13**) {pymtH = pyrimidine-2-thione, IV} [32],$[Cu_2(C_5H_5NS)_2Br_2(m\text{-}Tol_3P)_2]$ (**14**) [33], $[Cu_2(C_5H_5NS)_2Br_2(PPh_3)_2]$ (**15**) [34], $[Cu_2(C_5H_5NS)_2I_2(p\text{-}Tol_3P)_2]$ (**16**) [6], $[Cu_2(tzdtH)_2Cl_2(p\text{-}Tol_3P)_2]$ (**17**) (tzdtH = 1,3-thiazolidine-2-thione, V} [35] and $[Cu_2(meimtH)_5](SO_4)\cdot 3H_2O$ (**18**) [36].

In this paper, copper(I) complexes with C_5H_5NS containing tertiary phosphines as co-ligands are reported with the objectives of: (i) understanding the effect of substituents on Ph groups attached to P atoms and anion on the Lewis acidity of the Cu(I) centre; (ii) studying the Cu(I)···Cu(I) interaction; and (iii) analysing factors controlling the formation of sulfur-bridged dinuclear copper(I) complexes with various heterocyclic thioamides. It may be mentioned that preparations and other details of the complexes have appeared elsewhere [12,32,34].

2. Experimental

2.1. Preparation of complexes

2.1.1. $[CuBr(\eta^2\text{-}S\text{–}\mu\text{-}C_5H_5NS)(p\text{-}Tol_3P)]_2$ (*1*)

NMR spectroscopy and also preparation details of compound **1** are described earlier [6]. To $CuBr_2(C_5H_5NS)_2$ {0.100 g, 0.22 mmol} suspended in $CHCl_3$ (15 cm^3) was added a solution of excess p-Tol$_3$P (0.136 g, 0.44 mmol) in $CHCl_3$ (15 cm^3) and the mixture was refluxed for 2 h. The clear solution formed was filtered and concentrated. A yellow solid started forming on cooling to room temperature (r.t.), which was filtered, washed with EtOH and dried in vacuo. Yield: 70%, m.p. 208–210 °C. *Anal*. Found: C, 55.3; H, 4.22; N, 2.50. Calc. for $C_{52}H_{52}Br_2Cu_2N_2P_2S_2$: C, 55.9; H, 4.65; N, 2.50%. UV data (λ_{max}, nm): 367mb (CS), 288s (py), 251s (Ph). IR data (cm^{-1}): 3162w (νN–H), 1127s (νC=S), 1098s (νP–C), 809s (ρC–CH$_3$), 219sb (νCu–Br) [7,8]. The crystals were grown from CH_2Cl_2–$CHCl_3$–MeOH mixture.

2.1.2. $[CuCl(C_5H_5NS)(Ph_3P)]_2$ (*2*)

To $CuCl(C_5H_5NS)$ {0.100 g, 0.48 mmol} suspended in $CHCl_3$ (15 cm^3) was added a solution of Ph_3P (0.125 g, 0.48 mmol) in $CHCl_3$ (15 cm^3) and the mixture was refluxed for 2 h. The clear solution formed was filtered and concentrated. A yellow solid started forming on cooling to r.t., which was filtered, washed with EtOH and dried in vacuo. Yield: 65%, m.p. 190–192 °C. *Anal*. Found: C, 57.6; H, 4.40; N, 2.94. Calc. for $C_{46}H_{40}Cl_2Cu_2N_2P_2S_2$: C, 58.5; H, 4.23; N, 2.97%. UV data (λ_{max}, nm): 367mb (CS), 285s (py), 250s (Ph). IR data (cm^{-1}): 1126s (νC=S), 1097s (νP–C), 327sb (νCu–Cl).

2.1.3. $[CuI(C_5H_5NS)(Ph_3P)]_2$ (*3*)

To CuI {0.100 g, 0.52 mmol} suspended in $CHCl_3$ (20 cm^3) was added solid C_5H_5NS (0.058 g, 0.52 mmol) and a solution of Ph_3P (0.138 g, 0.52 mmol) in $CHCl_3$ (15 cm^3) and the mixture was refluxed for 2 h. The clear solution formed was filtered, concentrated to 1/3 of its initial volume and addition of 10 cm^3 of petroleum–ether (60–80 °C) formed a bright yellow solid which was filtered, washed with Et_2O and dried in vacuo. Yield: 70%, m.p. 218–220 °C. *Anal*. Found: C, 49.2; H, 3.69; N, 2.56. Calc. for $C_{46}H_{40}Cu_2I_2N_2P_2S_2$: C, 49.0; H, 3.55; N, 2.49%. UV data (λ_{max}, nm): 355wb (CS), 285s (py), 247 (Ph). IR data (cm^{-1}): 3105w (νN–H), 1124s (νC=S), 1096s (νP–C), 136sb (νCu–I).

2.1.4. $[CuCl(\eta^1\text{-}S\text{–}\mu\text{-}C_5H_5NS)(Ph_3P)_2]$ (*4*)

The crystallisation of **2** from CH_2Cl_2–EtOH mixture resulted in the formation of the monomer **4** as revealed by its X-ray crystal determination.

2.2. Elemental analyses and spectroscopic techniques.

The C, H and N elemental analyses were obtained with a Carlo-Erba 1108 microanalyser. The m.p. was determined with a Gallenkamp electrically heated apparatus. The electronic absorption spectra were recorded on a Shimadzu Graphicord 240 UV–Vis spectrophotometer. The IR spectra were recorded in KBr pellets (4000–400 cm^{-1}) or Nujol mull in polythene sheets (500–100 cm^{-1}) on a Bruker IFS 66V spectrometer. The NMR spectra were recorded in $CDCl_3$ using a Bruker AMX 300 spectrometer at 300.14, and 75.48 MHz probe frequencies (^{1}H and ^{13}C, respectively) with TMS as the internal reference.

2.3. Crystal structure determinations

A yellow crystal of **1** (or yellow plate crystals of **4**) was mounted on a glass fibre and used for data collection. Cell constants and orientation matrix for data collection were obtained by least-squares refinement of the diffraction data from 25 reflections in the range of $14.077^\circ < \theta < 42.253^\circ$ for **1** and $16.036^\circ < \theta < 19.597^\circ$ for **4** on an Enraf–Nonius CAD 4 automatic diffractometer [43]. Data were collected at 293 K using Cu Kα radiation ($\lambda = 1.54184$ Å) and the ω-scan technique and corrected for Lp effects [44]. A semi-empirical absorption correction (ψ-scan) was made [45].

The structure was solved by direct method [46] and subsequent difference Fourier maps, and refined on F^2 by a full-matrix least-squares procedure using anisotropic displacement parameters [47]. For **1** all hydrogen atoms were located from difference Fourier maps while for **4** all hydrogens were located in their calculated positions (C–H 0.93 Å) except the one bonded to N1, which was located from the Fourier map. The located hydrogens were refined isotropically whereas calculated ones were refined using a riding model. Atomic scattering factors were taken from International Tables for X-ray crystallography [48] and molecular graphics from ZORTEP [49]. A summary of the crystal data, experimental details and refinement results are listed in Table 1. Tables 2 and 3 contain bond lengths and angles while NMR data are given in Tables 4 and 5.

Table 1
Summary of crystal data for compounds **1** and **4**

	1	**4**
Empirical formula	$C_{52}H_{52}Br_2Cu_2N_2P_2S_2$	$C_{41}H_{35}ClCuNP_2S$
Formula weight (MW)	1117.92	734.69
T (K)	293(2)	293(2)
λ (Å)	1.54184	1.54184
Crystal system	triclinic	monoclinic
Space group	$P\bar{1}$	$P2_1/c$
Unit cell dimensions		
a (Å)	9.790(5)	14.4776(13)
b (Å)	10.391(7)	10.1609(14)
c (Å)	14.600(5)	24.5402(9)
α (°)	83.64(4)	
β (°)	73.82(3)	93.367(14)
γ (°)	62.16(4)	
V (Å^3)	1261.0(11)	3603.8(6)
Z	1	4
D_{calc} (g cm^{-3})	1.472	1.354
μ(Cu Kα) (mm^{-1})	4.543	3.144
$F(000)$	568	1520
Scan type	$\omega-2\theta$	$\omega-2\theta$
Crystal size (mm)	0.30 × 0.10 × 0.05	0.20 × 0.20 × 0.10
2θ Range (°)	3.15–74.33	3.06–64.92
Index ranges	$-12 \le h \le 0$, $-12 \le k \le 11$, $18 \le l \le 17$	$-17 \le h \le 0$, $0 \le k \le 11$, $-28 \le l \le 28$
Reflections collected	5438	6380
Unique reflections, R_{int}	5122, 0.0227	6117, 0.0672
Max./min. transmission	0.978 and 0.907	0.910 and 0.803
Reflections with $[I > 2\sigma(I)]$, parameters	5122, 384	6117, 429
Final R indices	$R_1 = 0.0414$, $wR_2 = 0.1011$	$R_1 = 0.0705$, $wR_2 = 0.1433$
R indices (all data)	$R_1 = 0.0867$, $wR_2 = 0.1195$	$R_1 = 0.2669$, $wR_2 = 0.2092$
S on F^2	1.010	1.067
Peak and hole (e Å^{-3})	0.324 and −0.711	0.466 and −0.410

3. Results and discussion

3.1. Synthesis, IR and NMR spectral studies

Reaction of $CuBr_2(C_5H_5NS)_2$ with p-Tol_3P in $CHCl_3$ in a 1:2 mole ratio formed dinuclear compound **1** which yielded crystals in the CH_2Cl_2–$CHCl_3$–CH_3OH solvent mixture. Similarly $CuCl(C_5H_5NS)$ reacted with Ph_3P in $CHCl_3$ (1:1 mole ratio) to form **2**; while compound **3** was formed by reacting CuI with C_5H_5NS and Ph_3P in a 1:1:1 mole ratio. The melting points of complexes **2** and **3** are different, though close, to the reported values {lit. value [34], **2**, 196–199 °C; **3**, 210–212 °C} and the difference may be attributed to the different packing densities. The crystallisation of **2** from a CH_2Cl_2–C_2H_5OH mixture resulted in the formation of **4** as revealed by X-ray crystallography. It is significant to note that reaction of $CuCl(C_5H_5NS)$ with Ph_3P in a 1:2 mole ratio formed the monomer **4** [12]. Compound **3** did not yield good quality crystals.

The IR spectra of the complexes showed characteristic peaks due to C_5H_5NS and tertiary phosphines at altered positions and some important ones are listed in Section 2. The presence of a ν(N–H) peak in the region 3105–3164 cm^{-1} as a weak peak in the complexes shows that C_5H_5NS is not deprotonated in the complexes and a strong ν(C=S) peak at 1139 cm^{-1} in the free ligand shifts to the low energy region, 1124–1127 cm^{-1}, again as a strong peak in the complexes. This shows that C_5H_5NS coordinates to the Cu(I) centre via its thione sulfur and the magnitude of the coordination shift is similar to that reported in the literature [6]. Tentative assignments to ν(Cu–X) X = halogen bands are also made (cf. Section 2) [6–8].

The presence of a broad signal due to NH protons in the range δ 13.93–14.92 ppm at a lowfield shows that pyridine-2-thione is coordinating to the Cu(I) centre as a neutral ligand (free ligand, $\delta_{NH} = 13.40$ ppm) (Table 4). There is a lowfield shift in H(6), H(5) and H(4) protons of C_5H_5NS, while H(3) protons remain nearly unaffected. The ^3J coupling constants show variable trends for different ring protons; for example, the J_5 value for H(6) proton decreases, for H(4) proton J_3 and J_5 become equal, for H(3) J_4 and for H(5) J_4 and J_6

Table 2
Bond lengths (Å) and angles (°) for compounds **1** and **4**

Parameters	**1**	Parameters	**4**
Bond lengths			
Cu–P	2.2376(13)	Cu–P1	2.300(2)
		Cu–P2	2.288(2)
Cu–S	2.3895(19)	Cu–S1	2.381(2)
Cu–S*	2.415(2)	Cu–Cl	2.367(2)
Cu–Br	2.4455(11)	S(1)–C(2)	1.688(9)
Cu–Cu*	3.250(2)	N(1)–H(1)	1.14(12)
S–S*	3.539(3)	H(1)···Cl	1.94(12)
S(1)–C(2)	1.717(4)		
N(1)–H(1)	0.93(5)		
H(1)···Br	2.41(5)		
Bond angles			
S–Cu–S*	94.86(6)	P(2)–Cu–P(1)	122.31(9)
Cu–S–Cu*	85.14(6)	P(2)–Cu–Cl	111.84(9)
Cu–S–C(2)	108.41(14)	P(1)–Cu–Cl	99.46(8)
Cu*–S–C(2)	113.12(16)	P(2)–Cu–S(1)	102.83(9)
		P(1)–Cu–S(1)	111.10(9)
		Cl–Cu–S(1)	109.08(9)
		Cu–S(1)–C(2)	113.3(4)

Symmetry transformations used to generate equivalent atoms: $-x+2$, $-y+1$, $-z+1$.

decrease marginally. As regards phosphines, *o*-, *m*- and *p*-protons show lowfield shifts but are unresolved for Ph_3P (Table 4).

The C(2) signal of coordinated C_5H_5NS shows a significant upfield shift relative to the free ligand; C(6) and C(3) signals show small lowfield shifts; C(4) signals are nearly unaffected and finally C(5) signals also show upfield shift (Table 5). The upfield shift of C(2) signals shows that coordination of Cu(I) to the S atom of C_5H_5NS increases the aromatic character of the pyridyl ring. The anionic $C_5H_4NS^-$ shows upfield shifts if it binds to a metal centre via S only and it is attributed to increased aromatic character of the pyridyl ring [6]. As regards ^{13}C NMR signals for the phosphines, the behaviour is summarised as follows: (i) *ipso*-carbons for both ligands show upfield shifts; (ii) *ortho*-carbons for Ph_3P also show the same behaviour, but for *p*-Tol_3P they are nearly unaffected; (iii) the *para*-carbon for Ph_3P also shows an upfield shift and for *p*-Tol_3P it is reversed; and finally (iv) for *meta*-carbons the trend is irregular and nearly unaffected.

3.1.1. Crystal and molecular structures

The atomic numbering schemes of $[CuBr(\eta^2\text{-}S\text{–}\mu\text{-}C_5H_5NS)(p\text{-}Tol_3P)]_2$ (**1**) and $[CuCl(\eta^1\text{-}S\text{–}\mu\text{-}C_5H_5NS)(Ph_3P)_2]$ (**4**) are shown in Figs. 1 and 2, respectively. The selected bond lengths and angles are given in Table 2. The basic structural unit of **1** is a centrosymmetric dimer with no interaction between the dimers and the S atoms of C_5H_5NS molecules bridge two Cu atoms forming a strictly planar Cu_2S_2 core. Each Cu atom is further bonded to a P atom of *p*-Tol_3P and one bromine atom and thus Cu acquires a distorted tetrahedral geometry. Two tetrahedra share a S–S edge and the *trans*-bromine atoms stabilise the dimer with strong intramolecular hydrogen bonds [N–H···Br, 3.319(5); H···Br, 2.41(5) Å and N–H–Br bond angle = 163(5)°] similar to those observed in literature [6,25]. The pyridyl ring of the thione ligand is planar and makes an angle of 63.66° with the plane of the Cu_2S_2 core.

The Cu–Br bond distance, 2.446 Å, is shorter than that (2.493 Å) in $[Cu_2(C_5H_5NS)_2Br_2(m\text{-}Tol_3P)_2]$ (**14**) [33] (the sum of ionic radii, 2.73 Å) [50]. The two short and two longer Cu–S bonds, 2.389 and 2.415 Å form a parallelogram of the Cu_2S_2 core, similar to other dimeric Cu(I) complexes listed in Table 3 and bond lengths are similar in value. The Cu–P bond distance of 2.238 Å is

Table 3
Bond lengths (Å) and angles (°) for Cu_2S_2 core of dinuclear copper(I)-heterocyclic thione complexes

Compound	Cu···Cu	S···S	Cu–Sb_{br}	Cu–S–Cu	S–Cu–S	Reference
1	3.250	3.539	2.389, 2.415	85.14	94.9	this work
5	3.139		2.328, 2.577	79.4	96.1	[24]
6	4.506		2.204, 2.631	137.3		[25]
7	2.914		2.301, 2.572	73.2	106.8	[26]
8	2.861		2.377, 2.457	72.6	107.4	[27]
9	2.950		2.308, 2.498	74.3	105.7	[28,29]
10	2.907		2.297, 2.534	73.8	106.2	[28,29]
11	3.007	3.766	2.358, 2.459	77.2	110.1	[30]
12	2.686		2.362, 2.490	67.2	112.8	[31]
13	3.316	3.508	2.356, 2.470	86.7	93.2	[32]
14	2.691	4.005	2.335, 2.488	67.7	112.3	[33]
15	3.420	3.332	2.383, 2.392	91.5	88.5	[34]
16	3.263	3.545	2.393, 2.425	85.2	94.7	[6]
17	3.508		2.386, 2.470	87.5	92.5	[35]
18	3.308		2.243, 2.151	94.8		[36]

Table 4
^{1}H NMR data (δ ppm, J, Hz) for the compounds [a]

	CH_3	*o*-H	*m*-H	*p*-H
p-Tol_3P [b]	2.36s	7.23t (6H) (7.8,$^3J_{H-H}$,$^3J_{H-P}$)	7.15d (6H) (7.3,$^3J_{H-H}$)	
Ph_3P		7.23m [c]		
1 [b]	2.27s	7.30dd (6H) (8.1,$^3J_{H-H}$, 10.3,$^3J_{H-P}$	7.07d (6H) (7.4, $^3J_{H-H}$)	
2		7.39–7.45m [c]	7.23–7.31m [c]	7.39–7.45m [c]
3		7.44–7.51m [c]	7.29–7.36m [c]	7.44–7.51m [c]
	H(6)	H(4)	H(3)	H(5)
1 [b]	7.71d (4.1, J_5)	7.43td (8.9, J_3, J_5, 1.6, J_6)	7.46d (7.3, J_4)	6.84td (6.2, J_4, J_6, 2.0, J_3)
2	7.70	[c]	[c]	6.81td (6.4, J_4, J_6, 1.6, J_3)
3	7.70d (6.2, J_5)	[c]	[c]	6.91td (5.9, J_4, J_6, 2.7, J_3)
C_5H_5NS [b,d]	7.56ddd (6.3, J_5, 1.6, J_4, 0.8, J_3)	7.34ddd (8.7, J_3, 7.0, J_5, 1.8, J_6)	7.49dt (8.7, J_4, 0.8, J_5, J_6)	6.73td (6.7, J_4, J_6,1.2, J_3)

[a] d, doublet; t, triplet; dd, doublet of doublets; td, triplet of doublets; dt, doublet of triplets.
[b] From Ref. [6].
[c] Unresolved signals.
[d] Unresolved signals δ_{NH} for **1**–**3** and ligand are 14.43, 14.92, 13.93, 13.40 ppm, respectively.

comparable to that (2.243 Å) in analogous $[Cu_2(C_5H_5NS)_2I_2(p\text{-}Tol_3P)_2]$ (**16**) [6], but shorter than in monomeric tetrahedral complexes [12,33]. The C–S bond distance of 1.717 Å is longer than (1.690 Å) in analogous **16**, but close to those in **13** [32], **14** [33] and **15** [34]. The Cu–S–C angles (108.41°, 113.12°) are similar to those (107.0(4)°, 116.5(5)°) in analogous **16**.

The bond angles around Cu in compound **4** reveal a distorted tetrahedral geometry with different Cu–P and Cu–S bond distances unlike those observed in the dimer **1** (Table 2). The structural parameters are similar to the ones reported earlier in literature [12]. In **1**, the non-bonded H(1)···Br bond distance of 2.41(5) Å is longer than that (2.348(2) Å) in $[Cu_2(C_5H_5NS)_2Br_2(m\text{-}Tol_3P)_2]$ (**14**) [33], but shorter than that (2.49 Å) in $[Cu_2(C_5H_5NS)_2Br_2(PPh_3)_2]$ (**15**) [34]; all these are longer than that (2.39 Å) in the monomer $[Cu(C_5H_5NS)Br(PPh_3)_2]$ (**22**) [34]. The H···Br separation is about 0.6 Å shorter than the sum of the van der Walls radii (3.00–3.45 Å) [50] and therefore fulfils Hamilton's criterion for hydrogen bond formation [51]. The H···Cl bond separation of 1.94(12) Å in **4** is much shorter than that (2.23 Å) in analogous monomer $[Cu(bztzdtH)Cl(PPh_3)_2]$ (**23**) {bztzdtH = benz-1, 3-thiazolidine-2-thione} [52] as well as that (2.30 Å) in the related dimer $[Cu_2(pymtH)_2Cl_2(p\text{-}Tol_3P)_2]$ (**13**) {pymtH = pyrimidine-2-thione} [32].

From the reactions of copper(I) halides with tertiary phosphines reported to date, it is noted that there is no monomeric tetrahedral complex with a substituted tertiary phosphine; however monomeric trigonal planar copper(I) complexes, viz. $[CuBr(o\text{-}tol_3P)$(thiazolidine-2-thione)] [37], $[CuCl(o\text{-}tol_3P)$(pyrimidine-2-thione)] and $[CuI(o\text{-}tol_3P)$(pyridine-2-thione)] [38] have been reported. The large cone angles of substituted tertiary phosphines appear responsible for the different behaviour [39]. Our efforts to get tetrahedral or trigonal planar complexes using pyridine-2-thione and *m*- or *p*-tol_3P resulted in the formation of dinuclear copper(I) complexes [6]. However, copper(I) bromide with unsubstituted tertiary phosphines, e.g. triphenyl phosphine, formed both monomeric $[Cu(C_5H_5NS)Br(PPh_3)_2]$ (**22**)

Table 5
^{13}C NMR data (δ ppm, J, Hz) for the compounds

Compound	CH_3	*i*-C ($^1J_{C-P}$)	*o*-C ($^2J_{C-P}$)	*m*-C ($^3J_{C-P}$)	*p*-C ($^4J_{C-P}$)
p-Tol_3P [a]	20.30	133.0 (8.8)	132.6 (19.5)	128.3 (7.2)	137.6
PPh_3		132.5 (10.0)	134.2 (19.5)	128.9 (10.8)	129.1 (9.3)
1 [a]	20.38	131.0	132.8 (15.1)	128.4 (9.9)	138.9
2		131.7	132.9 (14.9)	129.5 (9.4)	128.8
3		131.9	133.0 (14.5)	127.6 (9.4)	128.9
	C(2)	C(6)	C(4)	C(5)	C(3)
1 [a]	171.5	137.8	136.0	128.7	114.6
2	173.3	137.6	136.2	131.0	114.4
3	170.6	137.8		131.3	114.6
C_5H_5NS [a]	175.6	137.0	135.9	132.8	113.4

[a] From Ref. [6].

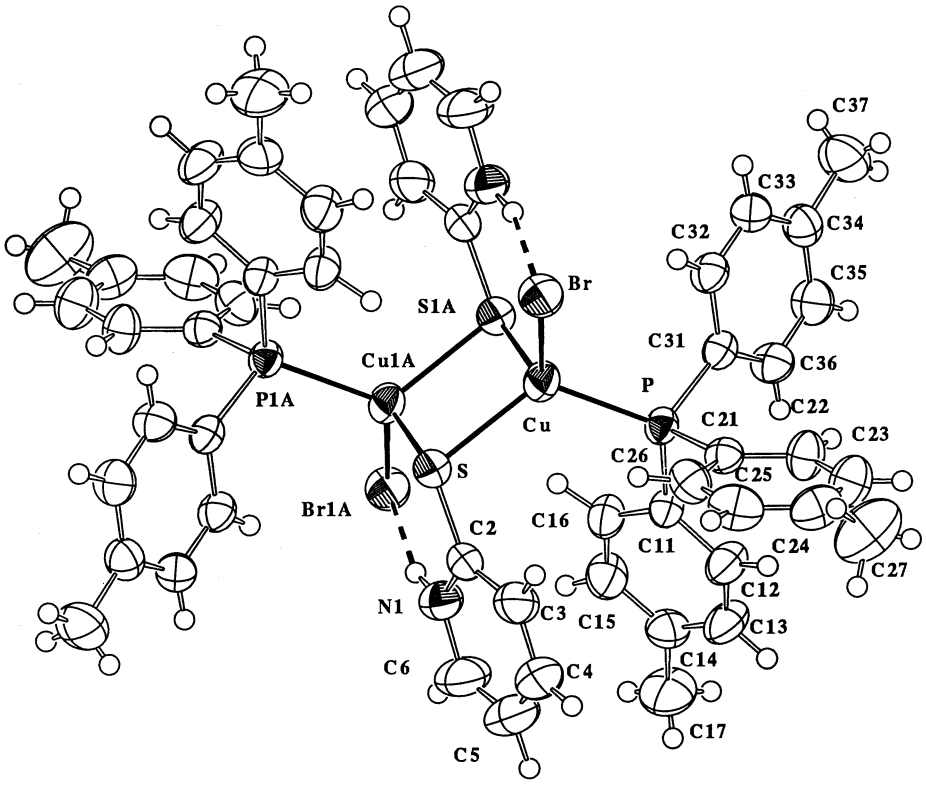


Fig. 1. A perspective view of the structure of compound **1** with atomic numbering scheme.

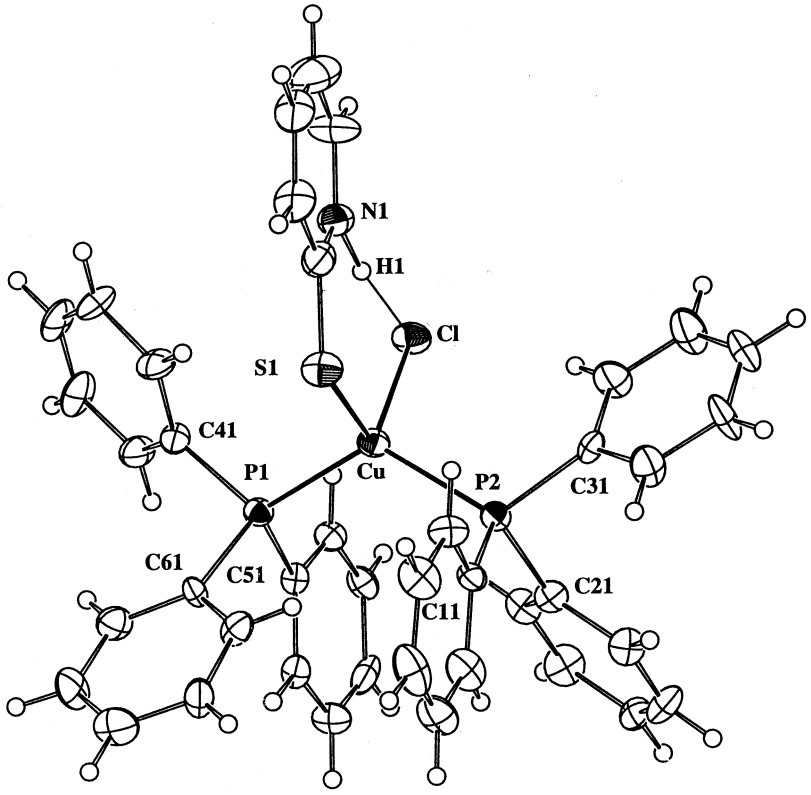


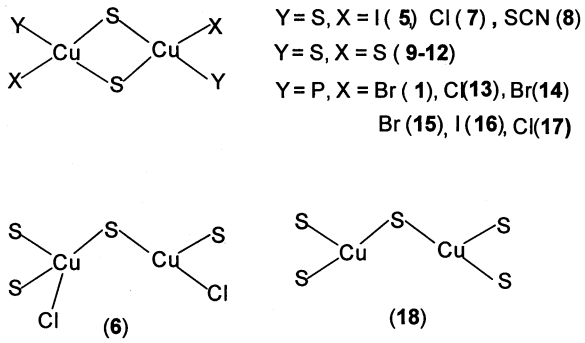
Fig. 2. A perspective view of the structure of compound **4** with atomic numbering scheme.

and dimeric $[Cu_2(C_5H_5NS)_2Br_2(PPh_3)_2]$ (**15**) [34] complexes. Similarly, with copper(I) iodide there are monomeric $[CuI(PPh_3)_2$(pyrimidine-2-thione)] (**24**) with a NH···I separation of 2.65 Å [40] and probably dinuclear $[Cu_2(C_5H_5NS)_2I_2(PPh_3)_2]$ (structurally uncharacterised) [34]. Whereas pyridine-2-thione with copper(I) chloride formed only the monomeric $[Cu(C_5H_5NS)Cl(PPh_3)_2]$ complex [12], benzothiazole-2-thione however stabilised the dinuclear complex [CuCl(benzothiazole-2-thione)$(PPh_3)]_2$ (**25**) [41]. Relatively strong NH···Cl hydrogen bonding in **4** favours the monomeric complex while dinuclear **25** has a NH···Cl separation of 2.169 Å indicating a weak interaction [41].The analytical data of the stoichiometric reaction of copper(I) chloride with Ph_3P presumably showed the formation of a dinuclear complex (cf complex **2**, Section 2); however, the crystallisation of **2** led to the formation of the monomer **4** and it creates doubt about the existence of the dinuclear copper(I) chloride complex **2** [34]. It may be concluded from the above discussion that the intramolecular NH···X(halogen) bonding and nature of the heterocyclic thioamide both determine the formation of monomeric or dimeric copper(I) complexes.

3.2. Cu···Cu bond distances in homologous dinuclear copper(I) complexes

Table 3 contains a list of dinuclear copper(I) complexes with a series of heterocyclic-2-thiones namely pyridine-2-thione (C_5H_5NS), 1,3-imidazolidine-2-thione ($imdtH_2$), 1-methylimidazoline-2-thione (meimtH), pyrimidine-2-thione (pymtH) and 1,3-thiazolidine-2-thione (tzdtH) with tertiary phosphines as co-ligands in some cases. These compounds can be categorised into four types: (i) $[Cu_2(\mu\text{-S–NH})_2X_2]$ (**5**, **7**, **8**); (ii) $[Cu_2(\mu\text{-S–NH})_6]X_2$ (**9**, **10**, **11**, **12**); (iii) $[Cu_2(\mu\text{-S–NH})_2X_2L_2]$ (**1**, **13**, **14**, **15**, **16**, **17**); and (iv) $[Cu_2(\mu\text{-S–NH})(S\text{–NH})_3Cl_2]$ (**6**), $[Cu_2(\mu\text{-S–NH})(S\text{–NH})_4](SO_4)\cdot 3H_2O$ (**18**) {μ-S–NH indicates bridging S-bonding and S–NH indicates terminal S-bonding; X = halogen, and L = a tertiary phosphine}. Except in *type* (*iv*), all other complexes contain a Cu_2S_2 core with two heterocyclic-2-thione ligands bridging the Cu centres via S-donor atoms and in these compounds it can be noted that Cu···Cu and S···S distances (based on reported values) vary in a complementary manner. Generally a decrease in Cu···Cu bond distance is accompanied by an increase in S···S distance.

In the parallelogram Cu_2S_2, the Cu···Cu bond distances vary with the change in ligand and the anion and in *type* (*i*) compounds (**5**, **7**, **8**), the shortest distance is observed in **8** with each copper bonded to four S atoms unlike three S and one halogen atom to each Cu in **5** and **7** (distances 2.861–3.139 Å). Thus the more polarisable SCN^- group has a strong influence in bringing two Cu atoms closer for interaction. In *type* (*ii*) compounds, with each Cu bonded to four S atoms, the Cu···Cu distances (2.686–3.007 Å) vary in the sequence: **12** < **10** < **9** < **11** and it is certainly the



effect of the ligands and the non-bonded anions. It may be noted that the shortest Cu···Cu distance is observed in **12** among all the dinuclear compounds listed in Table 3. Similarly, in *type* (*iii*) compounds with each Cu bonded to two S, one P atom and one halogen atom, Cu···Cu distances fall in the range 3.250–3.508 Å except compound **14** which has a distance of 2.691 Å close to that in **12**. Finally in *type* (*iv*) compounds with one S atom bridging the two Cu atoms, the Cu···Cu distances (3.308–4.506 Å) are among the longest.

Some general trends in Cu···Cu bond distances are revealed as follows: (i) when each copper is bonded to four sulfur atoms, the Cu···Cu bond distances decrease (2.686–3.007 Å; compounds **8**, **9**–**12**) because the electron rich Cu atoms enhance metal–metal interaction; (ii) when each copper is bonded to two S, one P and one halogen atom, the Cu···Cu distances increase (3.250–3.508 Å; compounds **1**, **13**–**17**, except **14**) and this behaviour can be explained in terms of reduction in electron density at the Cu centres in view of pi-bonding from the metal to d-orbitals on phosphorus and this increases the Cu···Cu distance. Whereas complex **14**, having a *m*-tol_3P ligand, showed the short Cu···Cu distance of 2.691 Å, the same was not true for $[Cu_2Br_2$(thiazolidine-2-thione$)_2$(*m*-$tol_3P)_2]$ (**26**) [42] in which the Cu···Cu distance increased to 3.347 Å. It shows that Cu···Cu distance varies with the nature of the thione ligand and is independent of the substituent on the Ph group.

For compounds having three S atoms (2.914–3.139 Å; compounds **5**, **7**) and one halogen bonded to each Cu atom, though many examples are not available, the distances in between the two extremes are observed. Finally in *type* (*iv*) compounds (**6**, **18**), the Cu···Cu distance is longest (4.506 Å) in **6** because one Cu is bonded to three S and one halogen atom and the second Cu is bonded to two S and one halogen atom and this decreases electron density at the Cu centres thus weakening the Cu···Cu interaction. Interestingly in **18**, with each Cu bonded to three S atoms, the distance (3.308 Å) is quite short and comparable to that observed

in the compounds **1**, **13**–**17**. In short, an electron withdrawing halogen or a metal to ligand pi-bonding group decreases Cu···Cu interaction and an increase in number of sulfur groups bonded to Cu enhances Cu···Cu interaction.

The Cu–S–Cu and S–Cu–S bond angles in compounds with a Cu_2S_2 core vary with Cu···Cu distance. A shorter distance is accompanied by smaller Cu–S–Cu and larger S–Cu–S bond angles and vice versa and for *type* (*iv*) compounds the Cu–S–Cu bond angles are the largest. It is interesting to note that the angular flexibility at S is very large (67.2°–137.3°) and is of great consequence for controlling metal–metal interactions.

4. Supplementary material

Supplementary data are available from the Cambridge Crystallographic Data Centre, CCDC Nos. 164391–164390 for compounds **1** and **4**. Copies of this information may be obtained free of charge from The Director, CCDC, 12 Union Road, Cambridge, CB2 1EZ, UK (fax: +44-1223-336033; e-mail: deposit@ccdc.cam.ac.uk or www: http://www.ccdc.cam.ac.uk).

Acknowledgements

One of us (T.S.L.) is thankful to Professor J.S. Casas of University of Santiago, Spain, for instrumental facilities. Financial help from CSIR for a computer grant is also gratefully acknowledged. Authors thank the referees for useful comments on the manuscript.

References

[1] E.S. Raper, Coord. Chem. Rev. 61 (1985) 115.
[2] E.S. Raper, Coord. Chem. Rev. 153 (1996) 199.
[3] E.S. Raper, Coord. Chem. Rev. 129 (1994) 91.
[4] E.S. Raper, Coord. Chem. Rev. 165 (1997) 475.
[5] T.S. Lobana, Renu Verma, Geeta Hundal, A. Castineiras, Polyhedron 19 (2000) 899 (and references cited therein).
[6] T.S. Lobana, Seema Paul, A. Castineiras, Polyhedron 16 (1997) 4023.
[7] P. Aslanidis, S.K. Hadjikakou, P. Karagiannidis, B. Kojic-Prodic, M. Luic, Polyhedron 13 (1994) 3119.
[8] R. Bettistutzzi, G. Peyronel, Transition Met. Chem. 3 (1978) 345.
[9] T.S. Lobana, M.K. Sandhu, E.R.T. Tiekink, J. Chem. Soc., Dalton Trans. (1988) 1401.
[10] T.S. Lobana, M.K. Sandhu, M.J. Liddell, E.R.T. Tiekink, J. Chem. Soc., Dalton Trans. (1990) 691.
[11] T.S. Lobana, Randhir Singh, M.K. Sandhu, E.R.T. Tiekink, J. Coord. Chem. 24 (1991) 29.
[12] (a) T.S. Lobana, P.K. Bhatia, E.R.T. Tiekink, J. Chem. Soc., Dalton Trans. (1989) 749;
(b) S. Skoulika, Inorg. Chim. Acta 156 (1991) 207.
[13] T.S. Lobana, P.K. Bhatia, D.C. Povey, G.W. Smith, J. Crystallogr. Spectrosc. Res. 21 (1991) 9.
[14] E.R.T. Tiekink, T.S. Lobana, Randhir Singh, J. Crystallogr. Spectrosc. Res. 21 (1991) 205.
[15] T.S. Lobana, P.K. Bhatia, J. Chem. Soc., Dalton Trans. (1992) 1407.
[16] E. Horn, T.S. Lobana, Randhir Singh, E.R.T. Tiekink, Z. Kristallogr. 205 (1993) 291.
[17] T.S. Lobana, A. Sanchez, J.S. Casas, A. Castineiras, J. Sordo, M.S. Garica-Tasende, E.M. Vazquez-Lopez, J. Chem. Soc., Dalton Trans. (1997) 4289.
[18] T.S. Lobana, Renu Verma, Randhir Singh, A. Castineiras, Transition Met. Chem. 23 (1998) 25.
[19] T.S. Lobana, Renu Verma, A. Castineiras, Polyhedron 17 (1998) 3753.
[20] T.S. Lobana, Seema Paul, Geeta Hundal, Sangeeta Obrai, Transition Met. Chem. 24 (1999) 202.
[21] T.S. Lobana, A. Sanchez, J.S. Casas, A. Castineiras, J. Sordo, M.S. Garica-Tasende, Polyhedron 17 (1998) 3701.
[22] T.S. Lobana, Seema Paul, A. Castineiras, J. Chem. Soc., Dalton Trans. (1999) 1819.
[23] T.S. Lobana, R. Verma, R. Mahajan, E.R.T. Tiekink, Z. Kristallogr. NCS 214 (1999) 513.
[24] D. Mentzafos, A. Terzis, P. Karagiannidis, P. Aslanidis, Acta Crystallogr., Sect. C 45 (1989) 54.
[25] L.P. Battaglia, A.B. Corradi, M. Nadelli, M.E.V. Tani, J. Chem. Soc., Dalton Trans. (1976) 143.
[26] J.R. Creighton, D.J. Gardiner, A.C. Gorvin, C. Gutteridge, A.R.W. Jackson, E.S. Raper, P.M.A. Sherwood, Inorg. Chim. Acta 103 (1985) 195.
[27] E.S. Raper, W. Clegg, Inorg. Chim. Acta 180 (1991) 239.
[28] G.A. Stergioudis, S.C. Kokkou, P.J. Rentzeperis, P. Karagiannidis, Acta Crstallogr., Sect. C 43 (1987) 1685.
[29] E.C. Constable, P.R. Raithby, J. Chem. Soc., Dalton Trans. (1987) 2281.
[30] E.S. Raper, J.R. Creighton, D. Robson, J.D. Wilson, W. Clegg, A. Milne, Inorg. Chim. Acta 143 (1988) 95.
[31] E.S. Raper, J.D. Wilson, W. Clegg, Inorg. Chim. Acta 194 (1992) 51.
[32] P. Karagiannidis, S.K. Hadjikakou, P. Aslanidis, A. Hountas, Inorg. Chim. Acta 178 (1988) 27.
[33] P. Aslanidis, S.K. Hadjikakou, P. Karagiannidis, B. Kojic-Prodic, M. Luic, Polyhedron 13 (1994) 3119.
[34] P. Karagiannidis, P. Aslanidis, D.P. Kessissoglou, B. Krebs, M. Dartmann, Inorg. Chim. Acta 156 (1989) 47.
[35] S.K. Hadjikakou, P. Aslanidis, P. Karagiannidis, D. Mentzafos, A. Terzis, Polyhedron 10 (1991) 935.
[36] E.R. Atkinson, E.S. Raper, D.J. Gardiner, H.M. Dawes, N.P.C. Walker, A.R.W. Jackson, Inorg. Chim. Acta 100 (1985) 285.
[37] S.K. Hadjikakou, P. Aslanidis, P. Karagiannidis, D. Mentzafos, A. Terzis, Inorg. Chim. Acta 186 (1991) 199.
[38] S. Skoulika, Inorg. Chim. Acta 193 (1992) 192.
[39] C.A. Tolman, J. Am. Chem. Soc. 92 (1970) 2956.
[40] P. Aslanidis, Polyhedron 12 (1993) 2221.
[41] T. Shibahara, S. Kobayashi, D. Long, X. Xin, Acta Crystallogr., Sect. C, Cryst. Struct. Commun., Sect. C 53 (1997) 58.
[42] S.K. Hadjikakou, P. Aslanidis, P.D. Akrivos, P. Karagiannidis, M. Luic, Inorg. Chim. Acta 197 (1992) 31.
[43] CAD 4-Express Software, Ver. 5.1/1.2, Enraf–Nonius, Delft, The Netherlands, 1995.
[44] (a) A.L. Spek, HELENA. A Program for data reduction of CAD4 data, University of Utrecht, The Netherlands, 1997 (for **1**);
(b) M. Kretschmar, GENHKL Program for the reduction of CAD4 Diffractometer data, University of Tübingen, Germany, 1997 (for **4**).
[45] (a) A.L. Spek. PLATON. A Multipurpose Crystallographic Tool, Utrecht University, Utrecht, The Netherlands, 1997 (for **1**);

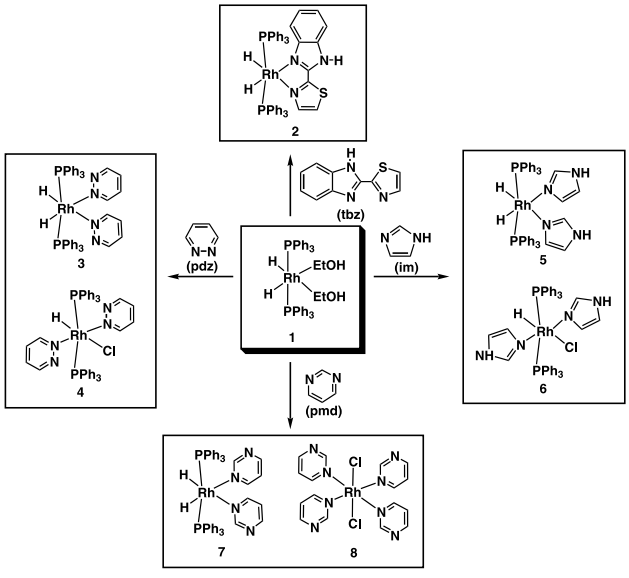
(b) A.C.T. North, D.C. Phillips, F.S. Mathews, Acta Crystallogr., Sect. A 24 (1968) 351(for **4**).
[46] G.M. Sheldrick, Acta Crystallogr., Sect. A 46 (1990) 467.
[47] G.M. Sheldrick, SHELXL-97. Program for the Refinement of Crystal Structures, University of Göttingen, Germany, 1997.
[48] International Tables for X-ray Crystallography vol. C, Kluwer Academic Publishers, Dordrecht, The Netherlands, 1995.
[49] L. Zsolnai, ZORTEP. A Program for the Presentation of Thermal Ellipsoids, The University of Heidelberg, Germany, 1997.
[50] J.E. Huheey, E.A. Keiter, R.L. Keiter (Eds.),Inorganic Chemistry: Principles of Structure and Reactivity, 4th ed., Harper Collins College Publishers, New York, 1993.
[51] W.C. Hamilton, in: A. Rich, N. Davidson (Eds.), Structural Chemistry and Molecular Biology, W.H. Freeman, San Francisco, CA, 1968, p. 466.
[52] G.P. Voutsas, S.C. Kokkou, C.J. Cheer, P. Aslanidis, P. Karagiannidis, Polyhedron 14 (1995) 2287.

reductive elimination of hydrogen. The reaction of complex **1** with pyrazine (pyz) in CH_2Cl_2 afforded the triangular Rh_3 complex $[Rh_3(PPh_3)_6(pyz)_3](ClO_4)_3\cdot CH_2Cl_2$, in contrast to the formation of the dinuclear Rh hydrido complex $[Rh_2(H)_4(PPh_3)_4(Me_2CO)_2(pyz)](ClO_4)_2\cdot EtOH$ in Me_2CO. The reaction of complex **1** with 4,4'-trimethylenedipyridine (tmdp), having a long spacer, in CH_2Cl_2 provided the dinuclear Rh non-hydrido complex $[Rh_2(PPh_3)_4(tmdp)_2](ClO_4)_2$. In this study, as further investigations, the reactions of complex **1** with nitrogen ligands such as 2-(4-thiazolyl)benzimidazole (tbz), pyridazine (pdz), imidazole (im) and pyrimidine (pmd) in CH_2Cl_2 were examined according to Scheme 1. Several mononuclear Rh complexes were isolated and their structures were crystallographically characterized.

2. Experimental

2.1. General procedures

All operations were carried out using standard Schlenk techniques under N_2 atmosphere. All the organic solvents were distilled by general methods before use. $RhCl_3\cdot 3H_2O$, 2-(4-thiazolyl)benzimidazole, pyridazine, imidazole and pyrimidine were commercially purchased from Steam and Aldrich and used without further purifications. $[Rh(H)_2(PPh_3)_2(EtOH)_2]ClO_4$ (**1**) was synthesized according to the literature [8]. IR spectra were recorded on a Perkin–Elmer System 2000 FT IR spectrometer as a KBr pellet. UV–Vis spectra were recorded on a HITACHI U-3500/U-4000 spectrometer. ^1H NMR spectra were measured at room temperature (r.t.) on a JEOL JNM-A 500 FT NMR spectrometer. Trimethylsilane was used as an internal reference.



Scheme 1.

2.2. Preparation of Rh complexes with nitrogen ligands

2.2.1. $[Rh(H)_2(PPh_3)_2(tbz)]ClO_4$ (**2**)

A 5 ml CH_2Cl_2 solution of $[Rh(H)_2(PPh_3)_2(EtOH)_2]ClO_4$ (**1**) (41.1 mg, 0.05 mmol) was added to the tbz ligand (10.1 mg, 0.05 mmol) in CH_2Cl_2 (5 ml). After stirring for 30 min, the reaction solution was filtered. The yellow filtrates were introduced into 5 mm diameter glass tubes and were layered with hexane as the diffusion solvent. The glass tubes were sealed and allowed to stand at r.t. for 2 days. Light yellow crystals of complex **2** were collected. Yield: 43.7 mg (94%). IR (KBr pellet, cm^{-1}): 2081 (Rh–H), 1435, 1095, 696 and 519. ^1H NMR (CD_2Cl_2, 23 °C, ppm): δ 11.98 (N–H of benzimidazole), 8.19 (2-H of thiazolyl), 8.08 (4-H of benzimidazole), 7.00–7.59 (Ph of PPh_3), 6.03 (5-H of benzimidazole), −15.60 (Rh–H) and −16.30 (Rh–H). *Anal.* Calc. for $C_{46}H_{39}P_2N_3SRhO_4Cl$: C, 59.40; H, 4.23; N, 4.52. Found: C, 59.26; H, 3.97; N, 4.33%.

2.2.2. $[Rh(H)_2(PPh_3)_2(pdz)_2]ClO_4\cdot 2CH_2Cl_2$ (**3**) and $[Rh(H)Cl(PPh_3)_2(pdz)_2]ClO_4\cdot CH_2Cl_2$ (**4**)

Complex **3** was prepared in the same manner as for complex **2**, using the pdz ligand (8.0 mg, 0.10 mmol). Light yellow crystals of complex **3** were obtained 2 days later at the middle part of the glass tubes. Yield: 43.4 mg (82%). IR (KBr pellet, cm^{-1}): 2046 (Rh–H), 1435, 1093, 697 and 521. ^1H NMR (CD_2Cl_2, 23 °C, ppm): δ 9.16 (3,6-H of prd), 8.57 (5-H of prd), 8.21 (4-H of prd), 7.20–7.48 (Ph of PPh_3), and −16.89 (Rh–H). *Anal.* Calc. for $C_{46}H_{44}P_2N_4RhO_4Cl_5$: C, 52.17; H, 4.19; N, 5.29. Found: C, 51.68; H, 4.11; N, 5.33%.

The reaction solution was allowed to stand for a further 2 weeks and colorless crystals of complex **4** were collected at the upper part of the glass tubes. Yield: 4.0 mg (8%). IR (KBr pellet, cm^{-1}): 2174 (Rh–H), 1435, 1093, 696 and 523. *Anal.* Calc. for $C_{45}H_{41}P_2N_4RhO_4Cl_4$: C, 53.59; H, 4.10; N, 5.56. Found: C, 53.32; H, 4.03; N, 5.86%.

2.2.3. $[Rh(H)_2(PPh_3)_2(im)_2]ClO_4\cdot 2CH_2Cl_2$ (**5**) and $[Rh(H)Cl(PPh_3)_2(im)_2]ClO_4\cdot CH_2Cl_2$ (**6**)

Complex **5** was prepared in the same manner as for complex **3**, using the im ligand (6.7 mg, 0.10 mmol). The reaction solution was allowed to stand at r.t. for 2 days and light yellow crystals of complex **5** were obtained at the middle part of the glass tubes. Yield: 38.1 mg (74%). IR (KBr pellet, cm^{-1}): 2051 (Rh–H), 1435, 1095, 695 and 520. ^1H NMR (CD_2Cl_2, 23 °C, ppm): δ 10.09 (N–H of im), 7.21–7.61 (Ph of PPh_3), 6.71 (2-H of im), 6.57 (4-H of im), 6.31 (5-H of im) and −16.85 (Rh–H). *Anal.* Calc. for $C_{44}H_{44}P_2N_4RhO_4Cl_5$: C, 51.06; H, 4.28; N, 5.41. Found: C, 51.44; H, 4.42; N, 5.57%.

The reaction solution was allowed to stand at r.t. for another 2 weeks and colorless crystals of complex **6** were collected at the upper part of the glass tubes. Yield: 1.0 mg (2%). IR (KBr pellet, cm^{-1}): 2133 (Rh–H), 1434, 1094, 696 and 523. *Anal.* Calc. for $C_{43}H_{41}P_2N_4RhO_4Cl_4$: C, 52.46; H, 4.20; N, 5.69. Found: C, 52.51; H, 4.11; N, 5.53%.

2.2.4. $[Rh(H)_2(PPh_3)_2(pmd)_4]ClO_4\cdot CH_2Cl_2$ (7) and $[RhCl_2(pmd)_4]ClO_4$ (8)

Complex **7** was prepared in the same manner as for complex **3**, using the pmd ligand (8.0 mg, 0.10 mmol). Complex **7** was obtained as white precipitates. Yield: 36.0 mg (74%). IR (KBr pellet, cm^{-1}): 2060 (Rh–H), 1584, 1435, 1094, 696 and 520. ^1H NMR (CD_2Cl_2, 23 °C, ppm): δ 9.17 (2-H of pmd), 8.73 (6-H of pmd), 8.28 (4-H of pmd), 7.26–7.38 (Ph of PPh_3), 7.01 (5-H of pmd) and −17.30 (Rh–H). *Anal.* Calc. for $C_{45}H_{42}P_2N_4RhO_4Cl_3$: C, 55.49; H, 4.35; N, 5.75. Found: C, 55.92; H, 4.20; N, 5.58%.

Yellow crystals of complex **8** were collected 4 days later at the lower part of the glass tubes. Yield: 3.5 mg (12%). IR (KBr pellet, cm^{-1}): 1595, 1411, 1122, 706 and 625. *Anal.* Calc. for $C_{16}H_{16}N_8RhO_4Cl_3$: C, 32.37; H, 2.72; N, 18.88. Found: C, 32.68; H, 2.61; N, 18.69%.

2.3. X-ray crystallography

For each complex, a suitable crystal was sealed into the glass capillary (0.7 mm, GLAS) and mounted on the crystal goniometer. The intensity data of all the single crystals were collected on the Rigaku/Mercury CCD system using graphite monochromated Mo Kα radiation ($\lambda = 0.710691$ Å). The structures of complexes **2**, **5** and **6** were solved by the direct method (SIR-92 for **2** and **5**; SIR-97 for **6**) [9], and expanded using Fourier techniques [10]. The structure of complex **3** was solved by the heavy-atom Patterson method [11] and expanded using Fourier techniques [10]. The hydride hydrogen atoms were located and refined isotropically. All other hydrogen atoms were included but not refined. The non-hydrogen atoms were refined anisotropically. The final cycle of full-matrix least-squares refinement was based on 5251, 4348, 4418 and 6594 observed reflections ($I > 3\sigma(I)$) for complexes **2**, **3**, **5** and **6**, respectively. The unweighted and weighted agreement factors of $R = \Sigma||F_o|-|F_c||/\Sigma|F_o|$ and $R_w = [\Sigma\, w(F_o^2-F_c^2)^2/\Sigma\, w(F_o^2)^2]^{1/2}$ were used. The atomic scattering factors and anomalous dispersion terms were taken from ref. [12]. All calculations were performed using the TEXSAN crystallographic software package [13]. The detailed crystal data of all complexes are summarized in Table 1.

3. Results and discussion

3.1. Crystal structures

3.1.1. $[Rh(H)_2(PPh_3)_2(tbz)]ClO_4$ (2)

In the reaction of complex **1** with the nitrogen ligand, the tbz ligand acted as a bidentate chelate ligand and led to the typical mononuclear Rh hydrido complex **2**. Since no crystallographic structures of Rh complexes containing the tbz ligand have been reported, complex **2** is the first example of a Rh hydrido complex with the tbz ligand. Fig. 1 shows the cation moiety of complex **2** together with the atomic labelling scheme. The Rh atom is coordinated by two P atoms, two N atoms and two hydride atoms in a distorted octahedral environment. The two PPh_3 ligands are nearly in *trans*-positions with a P(1)–Rh–P(2) angle of 167.06(8)°. The Rh coordination plane defined by two N atoms of the tbz ligand and two hydride atoms are coplanar with the mean deviation of 0.0365 Å. Two heterocyclic rings of the tbz ligand are nearly coplanar with a mean deviation of 0.0707 Å. The average Rh–P, Rh–N and Rh–H distances of 2.299, 2.197 and 1.58 Å are similar to those of other analogous hydrido complexes [14]. The H···H distance of 2.08 Å is characteristic of hydrido complexes [15]. The N(1)–Rh–N(2) angle of 76.1(2)° is within the range of values of other Rh complexes with bidentate nitrogen ligands [16]. Selected bond distances and bond angles are listed in Table 2.

3.1.2. $[Rh(H)_2(PPh_3)_2(pdz)_2]ClO_4\cdot 2CH_2Cl_2$ (3)

The structure of the cation moiety of complex **3** is presented in Fig. 2. The Rh atom is coordinated by two PPh_3 ligands, two pdz ligands and two hydride atoms to afford a mononuclear Rh complex in a slightly distorted octahedral geometry. In each pdz ligands, one of the two N atoms is bonded to the Rh atom. The two pdz ligands, in *cis*-positions, are inclined against the N_2RhH_2 coordination plane at an angle of 31.2(2)°. On the other hand, two PPh_3 ligands in *trans*-positions are bent toward the two hydrides with a P(1)–Rh–P(1′) angle of 163.89(5)°. The Rh–P, Rh–N and Rh–H distances of 2.3033(9), 2.181(3) and 1.44(4) Å are similar to those of other Rh hydrido complexes [14]. The H···H distance of 2.03 Å is within the range of values found in other hydrido complexes [15]. Selected bond distances and angles are listed in Table 3.

Metal complexes with the pdz ligand as a heterocyclic ligand have been relatively limited, in comparison with those with the pyrazine ligand [17]. Although recently there have been several crystallographic reports on complexes with pdz ligands [18], Rh complexes with the pyz ligand are few. The crystal structure of complex **3** is remarkable as a Rh hydrido complex with the pdz ligand.

Table 1
Crystal data and measurement conditions for **2**, **3**, **5** and **6**

Complexes	**2**	**3**	**5**	**6**
Formula	$RhP_2N_3ClO_4C_{46}H_{39}S$	$RhP_2N_4Cl_5O_4C_{46}H_{44}$	$RhP_2N_4Cl_5O_4C_{44}H_{44}$	$RhP_2N_4Cl_4O_4C_{43}H_{41}$
M	930.20	1059.00	1034.97	984.49
Crystal system	monoclinic	orthorhombic	orthorhombic	Monoclinic
Space group	$P2_1/c$	$P2_12_12_1$	$P2_12_12_1$	$P2_1/n$
a (Å)	13.2040(9)	15.362(6)	15.020(2)	22.608(1)
b (Å)	13.7074(9)	15.404(1)	15.3277(3)	14.2621(5)
c (Å)	23.268(1)	10.048(2)	10.1368(2)	13.7827(5)
β (°)	99.3724(8)			104.3593(7)
V (Å^3)	4155.0(5)	2377(1)	2333.8(4)	4305.3(3)
D_{calc} (g cm^{-3})	1.487	1.479	1.473	1.519
$F(000)$	1904	1080	1056	2008
Z	4	2	2	4
μ (Mo Kα) (cm^{-1})	6.50	7.53	7.65	7.65
Number of reflections	24430 (total)	14955 (total)	14544 (total)	27180 (total)
	9159 (unique)	2854 (unique)	2783 (unique)	9470 (unique)
Number of observations	5251 [$I > 3.00\sigma(I)$]	4348 [$I > 3.00\sigma(I)$]	4418 [$I > 3.00\sigma(I)$]	6594 [$I > 3.00\sigma(I)$]
R	0.078	0.042	0.044	0.054
R_w	0.081	0.055	0.062	0.068

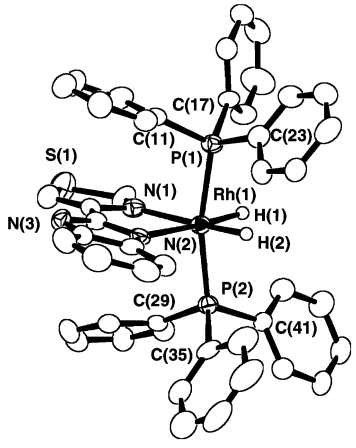


Fig. 1. The crystal structure of the cation moiety of complex **2**. Only Rh(1), N(1), N(2), N(3), S(1), P(1), P(2), C(11), C(17), C(23), C(29), C(35), C(41), H(1) and H(2) in the coordination sphere are labelled.

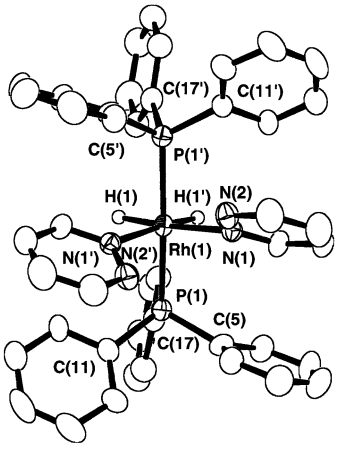


Fig. 2. The crystal structure of the cation moiety of complex **3**. Only Rh(1), N(1), N(1′), N(2), N(2′), P(1), P(1′), C(5), C(11), C(17), C(5′), C(11′), C(17′), H(1) and H(1′) in the coordination sphere are labelled.

Table 2
Selected bond lengths (Å) and bond angles (°) of **2**

Bond lengths			
Rh(1)–P(1)	2.317(2)	Rh(1)–P(2)	2.282(2)
Rh(1)–N(1)	2.192(7)	Rh(1)–N(2)	2.203(6)
Rh(1)–H(1)	1.59(6)	Rh(1)–H(2)	1.57(8)
Bond angles			
P(1)–Rh(1)–P(2)	167.06(8)	P(1)–Rh(1)–N(1)	93.5(2)
P(1)–Rh(1)–N(2)	92.9(2)	P(2)–Rh(1)–N(1)	96.8(2)
P(2)–Rh(1)–N(2)	97.1(2)	N(1)–Rh(1)–N(2)	76.1(2)
Rh(1)–P(1)–C(11)	112.2(3)	Rh(1)–P(1)–C(17)	117.4(3)
Rh(1)–P(1)–C(23)	113.6(3)	Rh(1)–P(2)–C(29)	111.9(2)
Rh(1)–P(2)–C(35)	114.3(3)	Rh(1)–P(2)–C(41)	118.0(3)
H(1)–Rh(1)–H(2)	82.0(3)		

Table 3
Selected bond lengths (Å) and bond angles (°) of **3**

Bond lengths			
Rh(1)–P(1)	2.3033(9)	Rh(1)–N(1)	2.181(3)
Rh(1)–H(1)	1.44(4)		
Bond angles			
P(1)–Rh(1)–P(1′) [a]	163.89(5)	P(1)–Rh(1)–N(1)	98.8(1)
P(1)–Rh(1)–N(1′) [a]	92.3(1)	P(1) [a]–Rh(1)–N(1)	92.3(1)
P(1)[1]–Rh(1)–N(1′) [a]	98.8(1)	N(1)–Rh(1)–N(1′) [a]	92.7(2)
Rh(1)–P(1)–C(5)	112.0(2)	Rh(1)–P(1)–C(11)	115.7(2)
Rh(1)–P(1)–C(17)	117.0(1)	H(1)–Rh(1)–H(1′) [a]	89.0(3)

[a] Symmetry codes $-X-1, -Y-1, Z$.

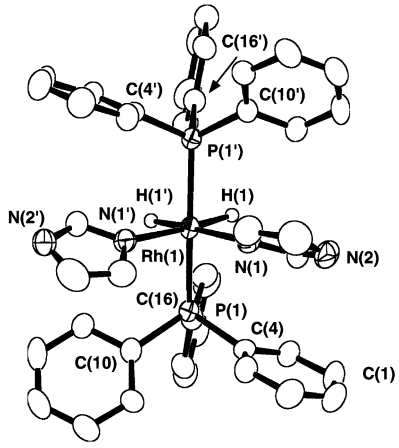


Fig. 3. The crystal structure of the cation moiety of complex **5**. Only Rh(1), N(1), N(1′), N(2), N(2′), P(1), P(1′), C(4), C(10), C(16), C(4′), C(10′), C(16′), H(1) and H(1′) in the coordination sphere are labelled.

3.1.3. $[Rh(H)_2(PPh_3)_2(im)_2]ClO_4{\cdot}2CH_2Cl_2$ (5)

The structure of the cation moiety of complex **5** is shown in Fig. 3. The structure of complex **5** essentially resembles that of complex **3**. The Rh atom is coordinated by two PPh_3 ligands, two im ligands and two hydride atoms in a distorted octahedral geometry. The two im ligands in *cis*-positions are slightly inclined against the N_2RhH_2 coordination plane at an angle of 27.7(2)°, which is smaller than that (31.2(2)°) of complex **3**. The two PPh_3 ligands are in *trans*-positions and the P(1)–Rh–P(1′) angle of 163.13(5)° is similar to that (163.89(5)°) of complex **3**. The Rh–P, Rh–N and Rh–H distances of 2.2955(9), 2.189(3) and 1.50(4) Å are close to those of other Rh hydrido complexes [14]. The H···H distance of 2.07 Å is in the range of those found in other hydrido complexes [15]. Selected bond distances and angles are listed in Table 4.

Our survey of Rh complexes with the im ligand and its derivatives described the tetranuclear complex [Rh(2-Meim)$(CO)_2]_4$ (2-Meim = 2-methylimidazole) [19a], the dinuclear complex $[NBu_4][Rh_2(cod)_2(dcbi)]{\cdot}2^i$PrOH (dcbi = 4,5-dicarboxyimida-zole) [19b], the mononuclear complexes $[RhCl_2(N\text{-Meim})_4]Cl{\cdot}2H_2O$ (Meim = *N*-methyl-imidazole) [19c] and [imH][*trans*-$RhCl_4(im)_2$] [19d]. However, there are no reports of X-ray structures of Rh hydrido complexes with the im ligand. To the best of our knowledge, this is the first crystal structure of a Rh hydrido complex with the im ligand.

Table 4
Selected bond lengths (Å) and bond angles (°) of **5**

Bond lengths			
Rh(1)–P(1)	2.2955(9)	Rh(1)–N(1)	2.189(3)
Rh(1)–H(1)	1.50(4)		
Bond angles			
P(1)–Rh(1)–P(1′) [a]	163.13(5)	P(1)–Rh(1)–N(1)	96.6(1)
P(1)–Rh(1)–N(1′) [a]	94.9(1)	P(1) [a] –Rh(1)–N(1)	94.9(1)
P(1)[1]–Rh(1)–N(1′) [a]	96.6(1)	N(1)–Rh(1)–N(1′) [a]	93.3(2)
Rh(1)–P(1)–C(4)	112.6(1)	Rh(1)–P(1)–C(10)	116.5(1)
Rh(1)–P(1)–C(16)	117.1(1)	H(1)–Rh(1)–H(1′) [a]	87.0(3)

[a] Symmetry codes: $-X+2, -Y, Z$.

3.1.4. $[Rh(H)Cl(PPh_3)_2(im)_2]ClO_4{\cdot}CH_2Cl_2$ (6)

After light-yellow single crystals of complex **5** were obtained according to Scheme 1, colorless single crystals of complex **6** were collected from the same reaction solution 2 weeks later. The structure of the cation moiety of complex **6** is revealed in Fig. 4. The coordination sphere around the Rh atom consists of two PPh_3 ligands, two im ligands, one Cl atom and one hydride atom, providing a distorted octahedral geometry. It is interesting that the two im ligands are located in the *trans*-positions and are separated by the Cl atom and the hydride atom. This structural feature is greatly different from that in complex **5**. The P(1)–Rh–P(2) angle of 177.26(4)° is much larger than those of 163.89(5)° and 163.13(5)° in complexes **3** and **5**, respectively. Therefore the PPh_3 ligands in the *trans*-positions are almost linearly located. The average Rh–P distance of 2.362 Å is longer than those of normal Rh and Ir hydrido complexes [4,7]. The average Rh–N distances of 2.056 Å are shorter than those of 2.181(3) and 2.189(3) Å in complexes **3** and **5**, respectively. The Rh–Cl distance of 2.498(1) Å is longer than those found in other hydrido complexes [4] owing to the *trans* influence of the nitrogen ligands. Selected bond distances and angles are listed in Table 5.

3.2. Reactions of $[Rh(H)_2(PPh_3)_2(EtOH)_2]ClO_4$ with nitrogen ligands in CH_2Cl_2

According to Scheme 1, the reactions of the Rh hydrido complex **1** with nitrogen ligands were attempted and their reaction processes were monitored by ^{1}H NMR and UV–Vis spectra. The addition of the tbz

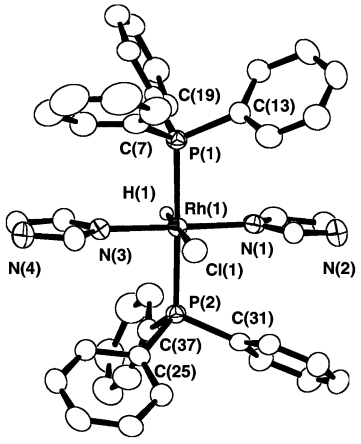


Fig. 4. The crystal structure of the cation moiety of complex **6**. Only Rh(1), Cl(1), N(1), N(2), N(3), N(4), P(1), P(2), C(7), C(13), C(19), C(31), C(25), C(37) and H(1) in the coordination sphere are labelled.

Table 5
Selected bond lengths (Å) and bond angles (°) of **6**

Bond lengths			
Rh(1)–Cl(1)	2.498(1)	Rh(1)–P(1)	2.360(1)
Rh(1)–P(2)	2.364(1)	Rh(1)–N(1)	2.061(4)
Rh(1)–N(3)	2.051(4)	Rh(1)–H(1)	1.47(6)
Bond angles			
Cl(1)–Rh(1)–P(1)	90.94(4)	Cl(1)–Rh(1)–P(2)	91.46(4)
Cl(1)–Rh(1)–N(1)	93.5(1)	Cl(1)–Rh(1)–N(3)	92.2(1)
P(1)–Rh(1)–P(2)	177.26(4)	P(1)–Rh(1)–N(1)	91.6(1)
P(1)–Rh(1)–N(3)	88.8(1)	P(2)–Rh(1)–N(1)	89.6(1)
P(2)–Rh(1)–N(3)	89.8(1)	Rh(1)–P(1)–C(7)	114.5(2)
Rh(1)–P(1)–C(13)	114.5(2)	Rh(1)–P(1)–C(19)	116.4(2)
Rh(1)–P(2)–C(25)	115.2(2)	Rh(1)–P(2)–C(31)	112.4(1)
Rh(1)–P(2)–C(37)	117.9(2)	N(1)–Rh(1)–H(1)	87.0(2)
N(3)–Rh(1)–H(1)	86.0(2)		

ligand to complex **1** in CD_2Cl_2 initially showed two new quintet ^{1}H NMR signals of hydride species at −15.60 and −16.30 ppm at r.t., together with the quintet ^{1}H NMR signal of an hydride species at −22.16 ppm, which should be attributed to hydrides of complex **1**. After about 1 h, the ^{1}H NMR signal of complex **1** completely disappeared and the two new ^{1}H NMR signals only remained. These facts indicate that Rh hydrido complex **2** with the tbz ligand was formed in CH_2Cl_2 solution. Similarly, on the reaction of complex **1** with pdz, im and pmd ligands, the ^{1}H NMR signals of the hydride species could be observed at −16.89, −16.85 and −17.30 ppm for complexes **3**, **5** and **7**, respectively. On the other hand, as shown in the time-course UV–Vis spectra (Fig. 5), complex **1** dissolved in CH_2Cl_2 at 23 °C displayed the color change from yellow to the dark brown solution of $[Rh_2(PPh_3)_2\{(\eta^6\text{-}C_6H_5)Ph_2P\}]_2]^{2+}$ ($\lambda_{max} = 410$ nm ($\varepsilon = 3056\ cm^{-1}\ M^{-1}$)) [7]. The further addition of tbz ligand to the CH_2Cl_2 solution exhibited the color change from dark-brown to a yellow solution ($\lambda_{max} = 420$ nm ($\varepsilon = 2235\ cm^{-1}\ M^{-1}$)) and the formation of complex **2** was completed after about 50 min. On the basis of these structural studies in solution and the above-mentioned crystallographic

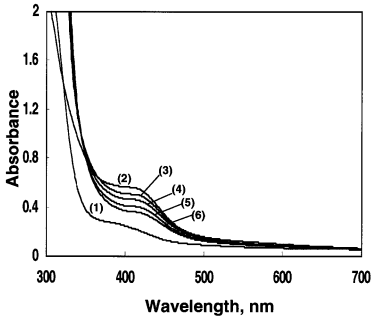


Fig. 5. The time-course UV–Vis spectra in CH_2Cl_2 at 23 °C. After the dissolving of complex **1**: 10 (1) and ≥ 50 (2) min. After the addition of the tbz ligand to complex **1**: 20 (3), 30 (4), 40 (5) and ≥ 50 (6) min. $[c] = 1.7 \times 10^{-4}$ M.

studies, it was concluded that the reaction of complex **1** with nitrogen ligands such as tbz, pdz, im and pmd ligands provided mononuclear Rh hydrido complexes without the reductive elimination of hydrogen. We previously demonstrated that the reactions of complex **1** with nitrogen bridging ligands such as pyrazine and 4,4′-bipyridine derivatives in CH_2Cl_2 could afford di- and trinuclear Rh non-hydrido complexes[7] with the reductive elimination of hydrogen. The results in this study are greatly different from those previously found. Although the detailed reason is not obvious at the present, it is probably considered that nitrogen ligands such as tbz, pdz and im ligands are structurally difficult to bridge Rh centers owing to the steric repulsion against the phenyl group of the PPh_3 ligand and should lead to mononuclear Rh hydrido complexes with nitrogen ligands, without the reductive elimination of hydrogen.

As mentioned in the Section 2, when the reaction solution of the Rh hydrido complex **1** with pdz, im and pmd ligands was allowed to stand for more than 2 weeks, Rh complexes **4**, **6** and **8** [20] with a coordinated Cl atom were collected in the same glass tubes, respectively. The reaction solution of complex **1** with the tbz ligand did not provide the corresponding Rh complex with a coordinated Cl atom since the tbz ligand played a role as a bidentate chelate ligand. In this study, the monitoring of their formation process by ^{1}H NMR and UV–Vis spectra over 2 weeks has not been carried out and the structure of **6** could only be crystallographically characterized. At the present, although their formation mechanisms are not obvious in detail, it is considered that the Cl atom is probably derived from the CH_2Cl_2 solvent since it has been known that $[RhCl(PPh_3)_2]_2$ was produced by the reaction of $[Rh_2(H)_2(PPh_3)_4(Me_4Si_2O)_2]$ with CH_2Cl_2 as the solvent [21].

3.3. Consideration on crystallographic study

The four crystallographic studies revealed the significant structural differences among their bond distances and bond angles of complexes **2**, **3**, **5** and **6**. In complex **6** with the Cl atom, the average Rh–N distance of 2.056 Å is shorter than those (**2** (2.197(7) Å), **3** (2.181(3) Å) and **5** (2.189(3) Å)) of the other Rh complexes without the Cl atom. In contrast, the average Rh–P distance of complex **6** (2.362 Å) is slightly longer than those of **2** (2.299 Å), **3** (2.3033 Å) and **5** (2.2955 Å). The P–Rh–P angle of **6** (177.26(4)°) is rather larger than those of **2** (167.06(8)°), **3** (163.89(5)°), **5** (163.13(5)°) and other Rh hydrido complexes [4,7]. These changes should probably be caused by the repulsion between the bulky Cl atom and the *trans*-nitrogen ligands. The Rh–Cl distance of 2.499(1) Å in complex **6** is also longer than those of

other Rh hydrido complexes [4] owing to the *trans* influence of the nitrogen ligands.

It is suggested that complex **2** possesses a meaningful inter-planar interaction between the nitrogen ligand and the corresponding phenyl group of PPh_3. The mean inter-planar distance between the benzimidazole portion of the tbz ligand and the phenyl group including the C(11) atom is 3.409 Å with a dihedral angle of 10.2°, and that between the thiazolyl group of the tbz ligand and the phenyl group including C(29) atom is 3.422 Å with an angle of 27.1°. A similar intra-molecular interaction has been known in previous reports [22]. This consideration is also supported by other structural parameters in complex **2**: the Rh(1)–P(1)–C(11) bond angle of 112.2(3)° is smaller than Rh(1)–P(1)–C(17) of 117.4(3)° and Rh(1)–P(1)–C(23) of 113.6(3)°. The Rh(1)–P(2)–C(29) bond angle of 111.9(2)° is smaller than Rh(1)–P(2)–C(41) of 118.0(3)° and Rh(1)–P(2)–C(35) of 114.3(3)°.

In complex **6**, it should be noted that the intra-molecular C–H···Cl hydrogen bonds exist between the Cl atom and hydrogen atom at the 2-position in im ligands. The C(1)···Cl(1) and C(4)···Cl(1) distances are 3.339(5) and 3.306(6) Å, respectively. Thus interactions are probably caused by the steric repulsion within the bulky PPh_3 ligands. The possibility of Rh···H agostic interaction and attractive Cl···H–C hydrogen bonds in Rh complexes with the PPh_3 ligand has recently been reported [23]. This suggestion is consistent with the results of the density functional analysis [23]: the intra-molecular steric repulsion can force one of the phenyl rings of the PPh_3 ligands toward the metal center.

4. Supplementary materials

Crystallographic data for the X-ray crystal structural analyses have been deposited with the Cambridge Crystallographic Data Centre, CCDC, Nos. 169897 (**2**), 169896 (**3**), 169895 (**5**) and 169898 (**6**). Copies of this information may be obtained free of charge from The Director, CCDC, 12 Union Road, Cambridge, CB2 1EZ, UK (fax: +44-1233-336033; e-mail: deposit@ccdc.cam.ac.uk or www: http://www.ccdc.cam.ac.uk).

Acknowledgements

This work was partially supported by Grants-in-Aids from the Ministry of Education, Science, Culture, Sports and Technology in Japan and research funds from Kinki University. Miss. X.-Y. Yu is also grateful to the Ministry of Education, Science, Culture, Sports and Technology in Japan for financial support.

References

[1] (a) C. Bianchini, D. Fabbri, S. Gladiali, A. Meli, W. Phol, F. Vizza, Organometallics 15 (1996) 4604;
(b) C. Bianchini, H.M. Lee, A. Meli, F. Vizza, Organometallics 19 (2000) 849;
(c) A. van Rooy, E.N. Orij, P.C.J. Kamer, P.W.N.M. van Leeuwen, Organometallics 14 (1995) 34.

[2] (a) J.F. Young, J.A. Osborn, F.H. Jardine, G. Wilkinson, Chem. Commun. (1965) 131;
(b) J.A. Osborn, F.H. Jardine, J.F. Young, G. Wilkinson, J. Chem. Soc. (1966) 1711;
(c) S.B. Duckett, C.L. Newell, R. Eisenberg, J. Am. Chem. Soc. 116 (1994) 10548.

[3] P.A. Chaloner, M.A. Esteruelas, F. Joó, L.A. Oro, Homogeneous Hydrogenation, Kluwer, Dordrecht, 1994.

[4] (a) J.K. Huang, E.D. Stevens, S.P. Nolan, Organometallics 19 (2000) 1194;
(b) F.T. Ladipo, J.S. Merola, Inorg. Chem. 29 (1990) 4172;
(c) M.E. van der Boom, S.-Y. Liou, Y. Ben-David, M. Gozin, D. Milstein, J. Am. Chem. Soc. 120 (1998) 13415;
(d) K. Osakada, T. Koizumi, T. Yamamoto, Angew. Chem., Int. Ed. 37 (1998) 349;
(e) M. Mediati, G.N. Tachibana, C.M. Jensen, Inorg. Chem. 31 (1992) 1827.

[5] (a) A.P. Sadimenko, S.S. Basson, Coord. Chem. Rev. 147 (1996) 247;
(b) S. Trofimenko, Chem. Rev. 93 (1993) 943;
(c) S. Trofimenko, Prog. Inorg. Chem. 34 (1986) 115;
(d) C. Tejel, J.M. Villoro, M.A. Ciriano, J.A. López, E. Eguizábal, F.J. Lahoz, V.I. Bakhmutov, L.A. Oro, Organometallics 15 (1996) 2967 (and references therein).

[6] (a) R. Halesha, G.K.N. Reddy, S.P.S. Rao, H. Manohar, J. Organomet. Chem. 252 (1983) 231;
(b) M. Maekawa, K. Sugimoto, T. Kuroda-Sowa, Y. Suenaga, M. Munakata, J. Chem. Soc., Dalton Trans. (2000) 4160.

[7] (a) X.-Y. Yu, M. Maekawa, M. Kondo, S. Kitagawa, G.-X. Jin, Chem. Lett. (2001) 168;
(b) X.-Y. Yu, M. Maekawa, T. Morita, H.-C. Chang, S. Kitagawa, G.-X. Jin, Bull. Chem. Soc. Jpn., 75 (2002) 267.

[8] R.R. Schrock, J.A. Osborn, J. Am. Chem. Soc. 98 (1976) 2134.

[9] (a) SIR-92, A. Altomare, M.C. Burla, M. Camalli, M. Cascarano, C. Giacovazzo, A. Guagliardi, G. Polidori, J. Appl. Crystallogr. 27 (1994) 435;
(b) SIR-97, A. Altomare, M.C. Burla, M. Camalli, M. Cascarano, C. Giacovazzo, A. Guagliardi, G. Polidori, R. Spagna, J. Appl. Crystallogr. 32 (1999) 115.

[10] DIRDIF-94, P.T. Beurskens, G. Admiraal, G. Beurskens, W.P. Bosman, R. de Gelder, R. Israel, J.M.M. Smits, The DIRDIF-94 program system, Technical report of the crystallography laboratory, University of Nijmegen, 1994.

[11] DIRDIF-94 PATTY, P.T. Beurskens, G. Admiraal, G. Beurskens, W.P. Bosman, R. de Gelder, R. Israel, J.M.M. Smits, The DIRDIF-94 program system, Technical report of the crystallography laboratory, University of Nijmegen, 1994.

[12] D.T. Cromer, J.T. Waber, International Tables for X-Ray Crystallography, vol. IV, Kyonoch Press, Birmingham, 1974.

[13] TEXSAN: Crystal Structure Analysis Package, Molecular Structure Corporation 1985 and 1999.

[14] (a) M. Iglesias, C. del Pino, S. Martínez-Carrera, J. Organomet. Chem. 317 (1986) 363;
(b) M. Iglesias, C. del Pino, J.L. Nieto, S. Martínez-Carrera, Inorg. Chim. Acta 145 (1988) 91;
(c) J. Ott, L.M. Venanzi, C.A. Ghilardi, S. Midollini, A. Orlandini, J. Organomet. Chem. 291 (1985) 89.

[15] P.G. Jessop, R.H. Morris, Coord. Chem. Rev. 121 (1992) 155.

[16] (a) L. Dadci, H. Elias, U. Frey, A. Hörnig, U. Koelle, A.E. Merbach, H. Paulus, J.S. Schneider, Inorg. Chem. 34 (1995) 306;
(b) A. Zucca, S. Stoccoro, M.A. Cinellu, G. Minghetti, M. Manassero, J. Chem. Soc., Dalton Trans. (1999) 3431.;
(c) B.A. Jackson, L.M. Henling, J.K. Barton, Inorg. Chem. 38 (1999) 6218.
[17] P.J. Steel, Coord. Chem. Rev. 106 (1990) 221.
[18] (a) J. Cano, G. De Munno, F. Lloret, M. Julve, Inorg. Chem. 39 (2000) 1611;
(b) T. Otieno, S.J. Rettig, R.C. Thompson, J. Trotter, Inorg. Chem. 34 (1995) 1718;
(c) T. Felzer, A. Lentz, T. Debaerdemacker, O.Z. Abou-El-Wafa, Z. Naturforsch., Teil. B 45 (1990) 199 (and references therein).
[19] (a) A. Tiripicchio, M. Tiripicchio Camellini, R. Uson, L.A. Oro, M.A. Ciriano, M.T. Pinillos, J. Organomet. Chem. 224 (1982) 207;
(b) J.C. Bayón, G. Net, P.G. Rasmussen, J.B. Kolowich, J. Chem. Soc., Dalton Trans. (1987) 3003;
(c) Z.D. Matovic, S.R. Trifunovic, G. Ponticelli, L.P. Battaglia, G. Pelizzi, I.A. Efimenko, D.J. Radanovic, Inorg. Chim. Acta 278 (1998) 209;
(d) G. Mestroni, E. Alessio, A. Sessanta o Santi, S. Geremia, A. Bergamo, G. Sava, A. Boccarelli, A. Schettino, M. Coluccia, Inorg. Chim. Acta 273 (1998) 62.
[20] The crystal data could be only collected in complex **8**: complex **8**, formula $C_{16}H_{16}N_8RhO_4Cl_3$, M 593.62, crystal system tetragonal, space group $P4/n$, $a = 10.592(2)$, $b = 10.592(2)$ and $c = 9.5780(6)$ Å, $V = 1074.6(3)$ Å^3, $D_{calc} = 1.834$ g cm^{-3}, $Z = 2$, μ(Mo Kα) 12.08 cm^{-1} and number of total reflections 6412.
[21] M.D. Curtis, W.M. Butler, J. Greene, Inorg. Chem. 17 (1978) 2928.
[22] (a) S. Onaka, Y. Katsukawa, M. Yamashita, Chem. Lett. (1998) 525.;
(b) N.G. Spitsina, V.V. Gritsenko, O.A. S'yachenko, B.B. Safoklov, Y.M. Shul'ga, E.B. Yagubskii, Russ. Chem. Bull. 49 (2000) 367;
(c) H.-C. Chang, T. Ishii, M. Kondo, S. Kitagawa, J. Chem. Soc., Dalton Trans. (1999) 2467.
[23] (a) R. Cini, A. Cavaglioni, Inorg. Chem. 38 (1999) 3751;
(b) J. Fawcett, J.H. Holloway, G.C. Saunders, Inorg. Chim. Acta 202 (1992) 111.

dimensional complexes such as discrete complex ions, complex molecules and catena polymeric chains. Mixed ligand complexes with 2D networks are very rare. Additionally, most work was restricted to the low members of the saturated α,ω-dicarboxylate anions and only a few studies have been carried out using sebacate anions ($OOC–(CH_2)_8–COO$) as ligands [39]. Recently, McCann et al. have found that Cu(II) and Mn(II) α,ω-dicarboxylato complexes possess antimicrobial and anti-Candida activity [40,41]. In this paper, we report two sebacato-bridged Cu(II) complexes $^2_\infty[Cu_2(phen)_2L_{4/2}](H_2O)_6$ (**1**) and $[(phen)_2Cu(\mu\text{-}L)Cu(phen)_2](HL)_2(H_2L)(H_2O)_4$ (**2**). Within complex **1**, the $[Cu_2(phen)_2]$ subunits are interlinked by sebacato ligands into 2D grid-like open networks. The principal building blocks in complex **2** are the dinuclear $[(phen)_2Cu(\mu\text{-}L)Cu(phen)_2]^{2+}$ complex cations resulting from two $[Cu(phen)_2]$ moieties bischelated by sebacato ligands. In both complexes, significant π–π stacking interactions play important roles in supramolecular assembly.

2. Results and discussion

2.1. Syntheses

Our earlier investigation indicated that reactions of equimolar $CuCl_2$, 1,10-phenanthroline, sebacic acid ($H_2L = HOOC–(CH_2)_8–COOH$) with Na_2CO_3 in CH_3OH/H_2O produced $[Cu(phen)L]\cdot 3H_2O$ [42] and $[Cu_2(phen)_2(H_2O)_2(OH)_2](HCO_3)_2\cdot 6H_2O$ [43] at pH = 6.4 and 10.2, respectively. However, reactions of phenanthroline, sebacic acid and $Cu(OH)_2$, which was freshly precipitated by addition of NaOH to an aqueous solution of $CuCl_2\cdot 2H_2O$, yielded $^2_\infty[Cu_2(phen)_2L_{4/2}](H_2O)_6$ (**1**) and $[(phen)_2Cu(\mu\text{-}L)Cu(phen)_2](HL)_2(H_2L)(H_2O)_4$ (**2**) at pH = 6.4 in EtOH/H_2O (1:1 v/v) and CH_3OH/H_2O (1:1 v/v), respectively. This finding implies that a neutral solution is obviously favorable for the sebacate anions to coordinate to Cu atoms. Additionally, self-assembly of Cu(II) ions with phen and sebacic acid is solvent dependent and the products rely on the Cu(II) sources used even though the same solvent mixture was employed.

2.2. Structure of $^2_\infty[Cu_2(phen)_2L_{4/2}](H_2O)_6$ (1)

The basic building subunits in **1** are the centrosymmetric $[Cu_2N_4O_4]$ dimers resulting from edge-sharing of two $[CuN_2O_3]$ square pyramids via two μ_2 carboxylato O atoms at the canted edges (Fig. 1). As usual, the basal Cu–O bond distances of 1.944 and 1.963 Å are slightly shorter than the Cu–N bond distances of 2.020 and 2.035 Å, and the axial Cu–O bond distance is 2.407 Å (Table 2). The Cu atom is displaced by 0.049(1) Å from the best plane defined by O(1), N(1), N(2) and O(3)^a towards the apical O(3)^b atom. The Cu···Cu distance within the dimer is 3.419(1) Å. The $[Cu_2N_4O_4]$ dimers are interlinked by the bridging sebacato ligands into 2D $^2_\infty[Cu_2(phen)_2L_{4/2}]$ open layers with rhombus-like 52-membered rings and the chelating phen ligands disposed on both sides (Fig. 1). Such grid-like networks extend infinitely parallel to (101) and are arranged so that adjacent phen planes from different layers face antiparallel to each other with the interplanar phen-to-phen distance of 3.51 Å, suggesting substantial π–π stacking interactions [44–49]. The chelating phen ligands of the 2D layers exhibit nearly perfect coplanarity.

Each carboxylate group of the bridging sebacato ligand offers one O atom, respectively, to coordinate one Cu atom and to bridge two Cu atoms. As expected, the C–O bond length to the bidentate carboxylate O atom is 1.282 Å, slightly longer than that (1.273 Å) to the monodentate carboxylate O atom, and the C–O bond lengths to the non-coordinating carboxylate O atoms are averaged at 1.239 Å.

Out of the three crystallographically distinct H_2O molecules intercalated between 2D $^2_\infty[Cu_2(phen)_2L_{4/2}]$ layers, one donates two hydrogen atoms to two non-coordinating carboxyl O atoms of different sebacato ligands belonging to the same layer, while the remaining two participate in hydrogen bonds both to the non-coordinating carboxyl O atom and to the third water O atom ($d(O\cdots O) = 2.785–2.852$ Å, $\angle(O–H\cdots O) = 144^\circ–177^\circ$).

2.3. Structure of $[(phen)_2Cu(\mu\text{-}L)Cu(phen)_2](HL)_2(H_2L)(H_2O)_4$ (2)

The crystal structure is composed of the centrosymmetric dinuclear $[(phen)_2Cu(\mu\text{-}L)Cu(phen)_2]^{2+}$ complex cations, twisted hydrogensebacate anions, linear sebacic acid molecules and lattice H_2O molecules.

The dinuclear complex cations are generated from two $[Cu(phen)_2]$ moieties bischelated by one 'Z' shaped sebacato ligand (Fig. 2). The Cu atoms are each octahedrally surrounded by four N atoms from two phen ligands and two O atoms from one carboxyl group of the bridging sebacato ligand to complete '4+1+1' coordination geometry with one pyridyl N atom and one carboxyl O atom at the apical positions. The basal Cu–O(3) bond length is 1.976 Å and the basal Cu–N bond distances fall in the range 2.014–2.044 Å. The axial Cu–N(4) and Cu–O(4) bond lengths are 2.241 and 2.692 Å, respectively. Two phen planes and the carboxyl plane around the Cu atom stand nearly perpendicularly to one another.

Within the crystal structure, the divalent complex cations are arranged so that the symmetry related phen ligands of the adjacent complex cations face antiparallel

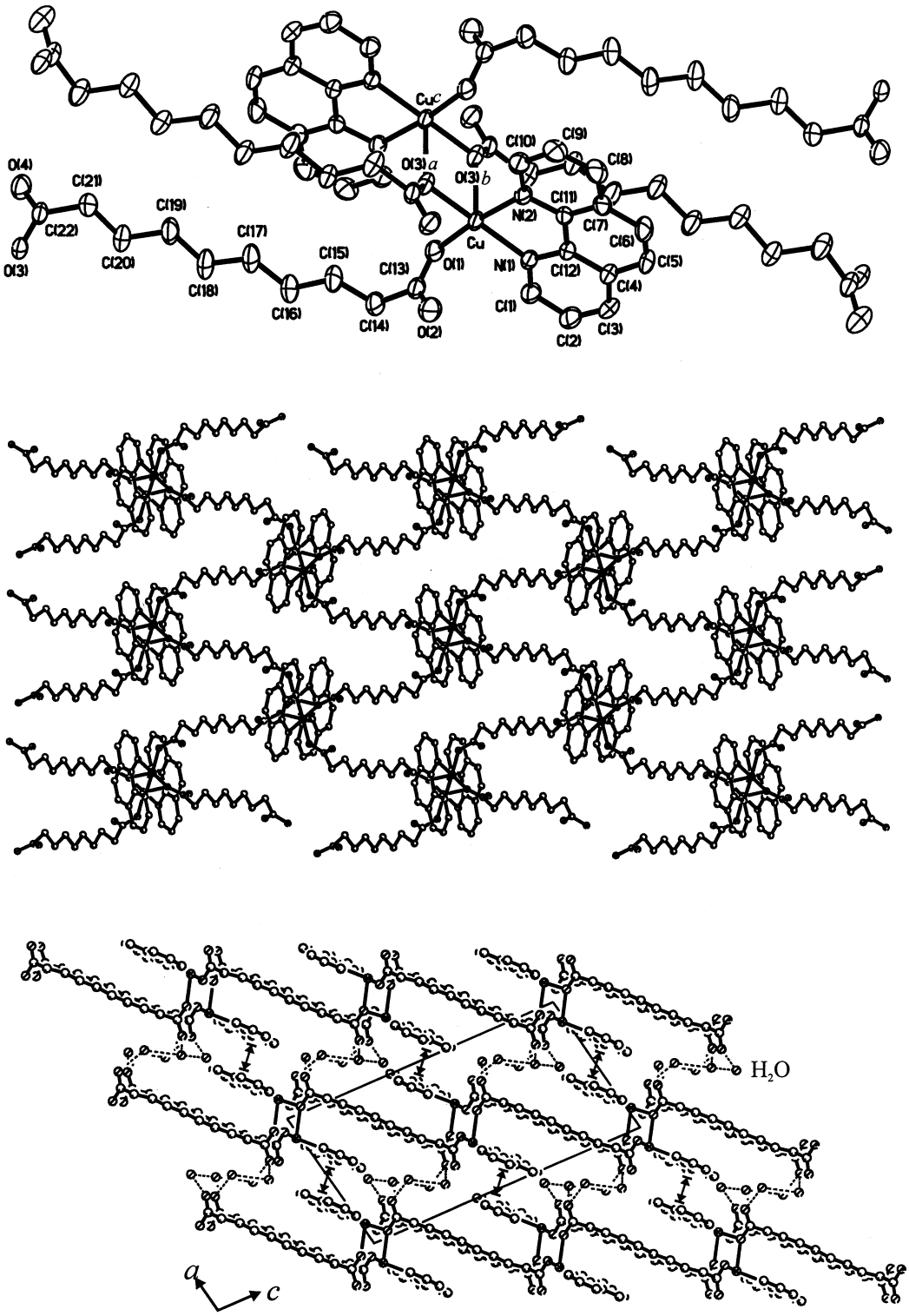


Fig. 1. (Top) ORTEP view of a selected subunit of the 2D $^{2}_{\infty}[Cu_2(phen)_2L_{4/2}]$ layer with displacement ellipsoids (45% probability) and atomic labeling, (middle) a section of the 2D $^{2}_{\infty}[Cu_2(phen)_2L_{4/2}]$ layer, and (bottom) supramolecular assembly of 2D $^{2}_{\infty}[Cu_2(phen)_2L_{4/2}]$ layers with H_2O molecules in tunnels parallel to [010] in **1**; the π–π stacking interactions and hydrogen bondings are indicated by double arrows and dashed lines, respectively.

to each other and the mean phen-to-phen distance of 3.43 Å indicates strong intercationic π–π stacking interactions [44–49]. Through such interactions, the complex cations are assembled into positively charged open networks extending infinitely parallel to (100) (Fig. 3).

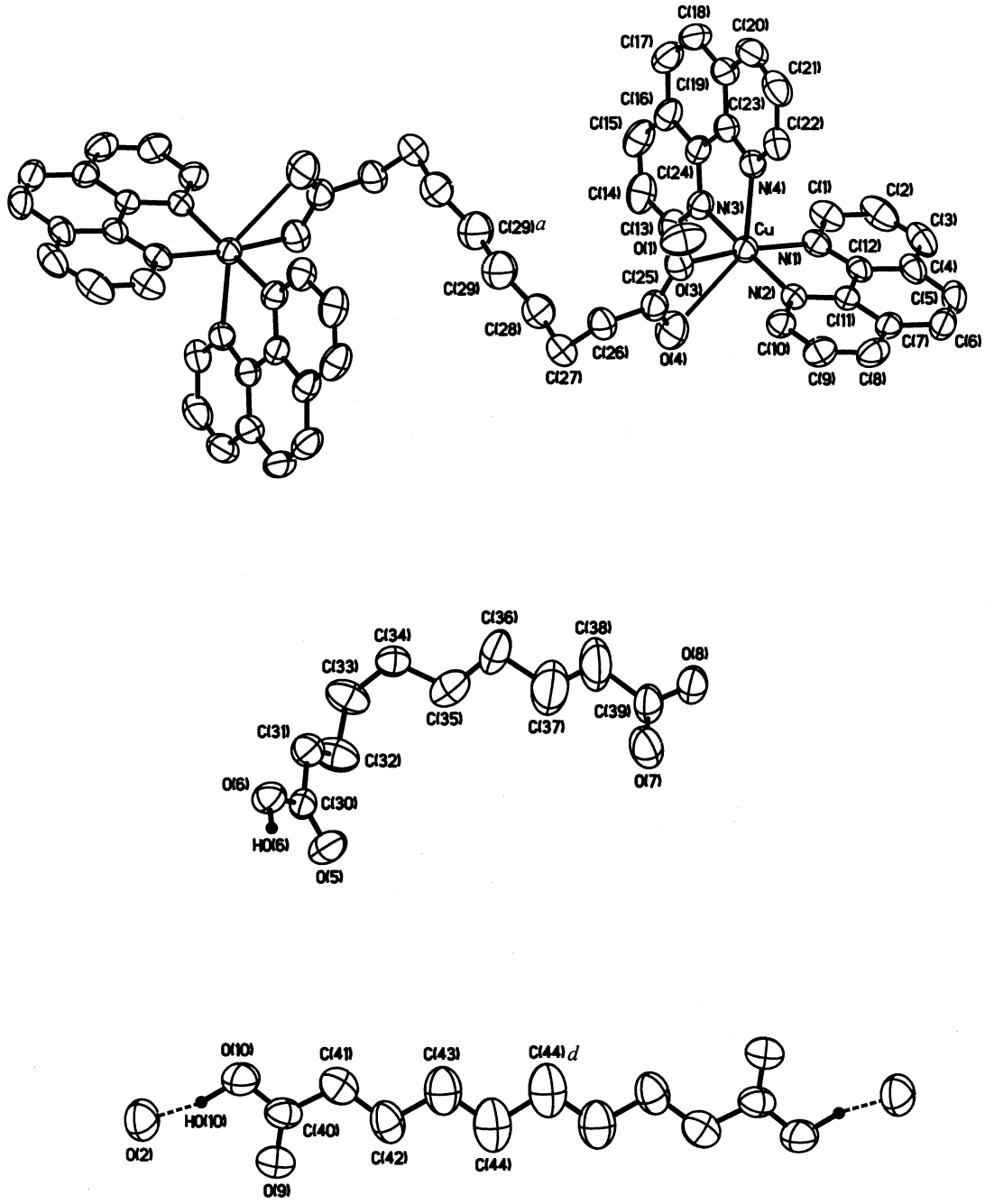


Fig. 2. ORTEP view of (top) divalent $[(phen)_2Cu(\mu\text{-}L)Cu(phen)_2]^{2+}$ complex cation, (middle) hydrogensebacate anion and (bottom) sebacic acid molecule in **2** with displacement ellipsoids (45% probability) and atomic labeling.

Along the [100] direction, the twisted hydrogensebacate anions are linked into 1D zigzag chains via strong head-to-tail hydrogen bonds ($d(O(6)\cdots O(8)^b) = 2.562$ Å, $\angle(O(6)\text{–}H\cdots O(8)^b) = 166^\circ$, b: $x+1$, y, z). Additionally, the carboxylate group of the hydrogensebacate anion, via two carboxylate O atoms, is hydrogen bonded to two crystallographically distinct H_2O molecules (Table 2), of which one accepts hydroxyl hydrogen atom from the linear sebacic molecule to form a strong hydrogen bond with $d(O(10)\cdots O(2)) = 2.531$ Å and $\angle(O(10)\text{–}H\cdots O(2)) = 167^\circ$. Moreover, the H_2O molecules are hydrogen bonded to each other. Such extensive hydrogen bonds assemble the twisted hydrogensebacate anions, linear sebacic molecules and water molecules to form negatively charged open bilayers parallel to (001). The resulting bilayers are held together by the interweaving of the positively-charged open networks (Fig. 4). Furthermore, the carboxylate O(3) strongly coordinated to Cu atom forms hydrogen bond to one water molecule, which is found important for the interdigita-

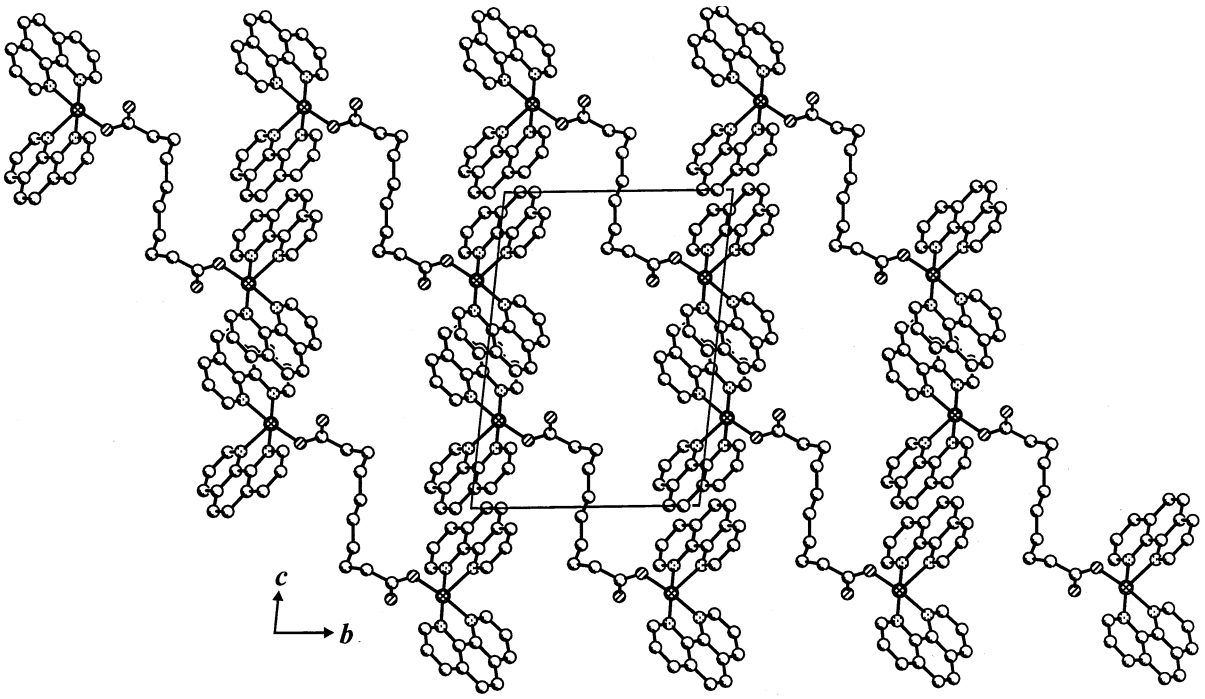


Fig. 3. Supramolecular assembly of the divalent $[(phen)_2Cu(\mu\text{-}L)Cu(phen)_2]^{2+}$ complex cations via π–π stacking interactions into 2D positively charged network in **2**.

tion of the negatively charged bilayers and the positively charged networks.

For the present 'Z' shaped twisted sebacato ligands, the C–O bond length to the coordinating O(3) atom is 1.272 Å, significantly longer than that to the O(4) atom (1.224 Å), and the bite O(3)–C(25)–O(4) bond angle is 122.7(4)°. As far as the hydrogensebacate anions and sebacic acid molecules are concerned, all the C–C and C–O bond lengths are of normal values.

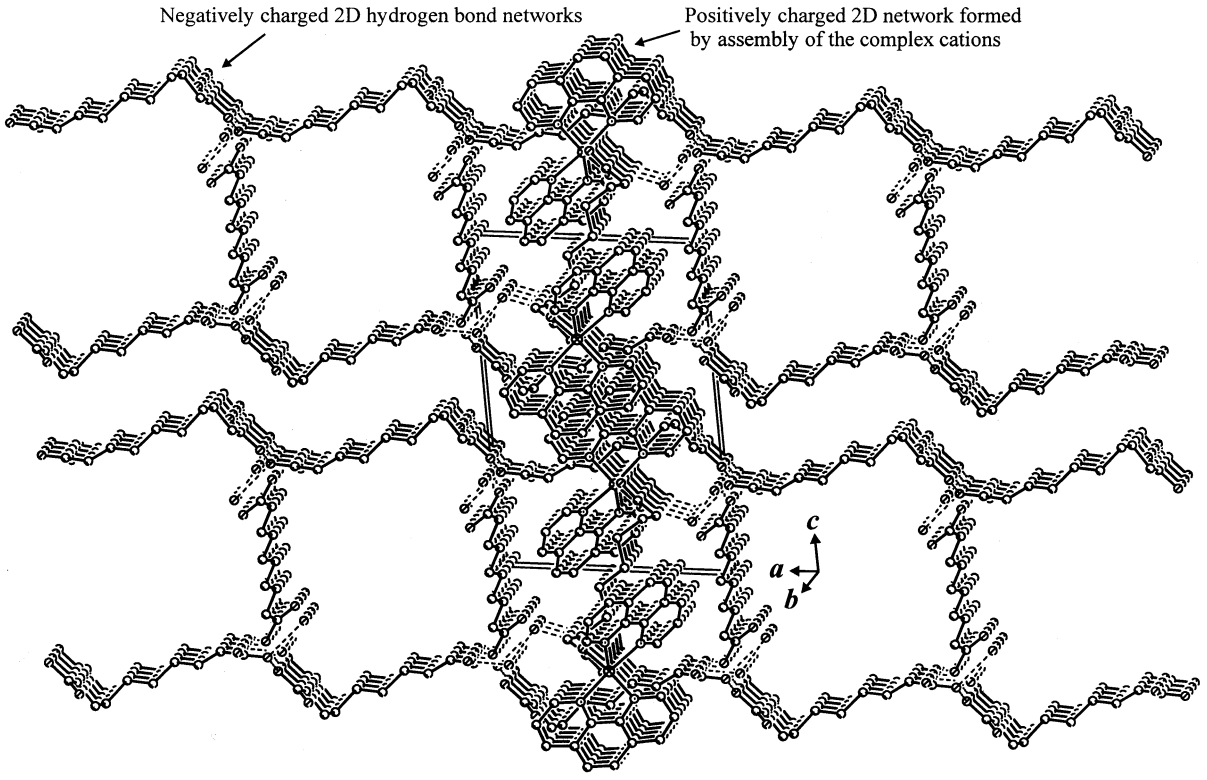


Fig. 4. Negatively charged 2D hydrogen bonded networks with the complex cations in **2**.

Comparison of the title complexes **1** and **2** with the previously-reported [Cu(phen)L]·3H_2O indicates that the sebacate anion is an interesting flexible ligand bridging Cu atoms in three modes, that is, (i) the 'L' shaped twisted sebacato ligands in [Cu(phen)L]·3H_2O bis-monodentately link Cu atoms into 1D chains which are assembled via π–π stacking interactions into supramolecular bi-chains [42], (ii) the nearly linear sebacato ligands in **1** tridentately interlink Cu atoms into 2D open networks and (iii) the 'Z' shaped twisted sebacato ligand bis-chelate two Cu atoms to form dinuclear complex cations in **2**.

3. Experimental

All chemicals of p.a. grade were commercially available and used without further purification. The C, H and N microanalyses were performed with a Heraeus Rapid—CHNO elemental analyzer. The FT-IR spectra were recorded from KBr pellets in the range 4000–400 cm^{-1} on a Protege 460 spectrometer.

3.1. Preparation of $^{2}_{\infty}[Cu_2(phen)_2L_{4/2}](H_2O)_6$ (1)

Addition of 6.0 ml (1 M) NaOH to a stirred aqueous solution of $CuCl_2·2H_2O$ (0.43 g, 2.50 mmol) in 5.0 ml H_2O yielded a blue precipitate, which was separated, washed with distilled water several times until free from detectable Cl^- ions and finally added to a stirred solution of sebacic acid (0.51 g, 2.50 mmol) in 50 ml EtOH/H_2O (1:1 v/v). To the resulting suspension was added phenanthroline monohydrate (0.50 g, 2.50 mmol). The mixture was further stirred for approximately 30 min and the insoluble solid was filtered off. The filtrate (pH = 6.4) was allowed to stand at room temperature. Slow evaporation for several days afforded a small amount of dark blue crystals. *Anal.* Calc. for $C_{44}H_{60}Cu_2N_4O_{14}$: C, 53.06; H, 6.07; N, 5.62. Found: C, 53.39; H, 5.98; N, 5.36%.

3.2. Preparation of $[(phen)_2Cu(\mu\text{-}L)Cu(phen)_2](HL)_2(H_2L)(H_2O)_4$ (2)

An analogous procedure was employed except that 50 ml CH_3OH/H_2O (1:1 v/v) was used instead of EtOH/H_2O. Blue crystals were formed in a blue filtrate (pH 6.4) by slow evaporation for several days. Yield: approximately 65%. *Anal.* Calc. for $C_{44}H_{60}Cu_2N_4O_{14}$: C, 61.26; H, 6.31; N, 6.50. Found: C, 60.83; H, 6.12; N, 6.89%. IR (cm^{-1}): 3410vs (br), 2929s, 2853s, 1570vs, 1515vs, 1426vs, 1302m, 1226m, 1146m, 1105m, 953vs, 724vs, 647m.

3.3. Crystal structure determination

The reflection intensities for complexes **1** and **2** were collected at 293 K on a Bruker P4 diffractometer with graphite-monochromated Mo Kα radiation (λ = 0.71073 Å) using the ϑ–2ϑ scan technique. SHELXS-97 [50] and SHELXL-97 [51] programs were used for structure determination and refinements. The structures were solved by direct methods and refined with full-matrix least-squares techniques. Non-hydrogen atoms were refined anisotropically. Hydrogen atoms associated with carbon atoms were generated geometrically, while the aqua and hydroxyl hydrogen atoms were located from the difference Fourier syntheses. Details of crystal data, collection and refinement of the two

Table 1
Summary of crystal data, data collection, structure solution and refinement details for complexes **1** and **2**

	1	**2**
Empirical formula	$C_{44}H_{60}Cu_2N_4O_{14}$	$C_{88}H_{108}Cu_2N_8O_{20}$
Formula weight	498.02	1724.90
Description	blue block	blue block
Crystal size (mm)	0.47 × 0.22 × 0.18	0.36 × 0.22 × 0.22
Temperature (K)	293(2)	293(2)
Crystal system	monoclinic	triclinic
Space group	$P2_1/n$	$P\bar{1}$
Unit cell dimensions		
a (Å)	11.095(2)	11.746(1)
b (Å)	10.199(1)	12.259(1)
c (Å)	21.221(4)	16.338(2)
α (°)		80.03(1)
β (°)	101.26(1)	79.18(1)
γ (°)		69.16(1)
Volume ($Å^3$)	2355.1(7)	2145.0(4)
Z	2	1
D_{calc} (g cm^{-3})	1.405	1.335
$F(000)$	1044	910
Absorption coefficient (mm^{-1})	0.971	0.571
Absorption correction	empirical	empirical
Maximum and minimum transmission	0.499, 0.478	0.806, 0.755
θ Range (°)	0.95–27.50	1.00–27.50
Refinement method	full-matrix least-squares on F^2	full-matrix least-squares on F^2
Reflections collected	6926	11290
Independent reflections (R_{int})	5419 (0.0415)	9842 (0.0372)
Data/restraints/parameters	3755/0/316	5645/0/537
Goodness of fit on F^2	1.085	1.029
R_1, wR_2 [$I \geq 2\sigma(I)$] [a]	0.0506, 0.1229	0.0697, 0.1595
R_1, wR_2 (all data) [a]	0.0833, 0.1443	0.1340, 0.1950
A, B values in weighting scheme [b]	0.0778, 0.0000	0.0960, 0.4437
Extinction coefficient	0.010(1)	0.008(1)
Largest difference peak and hole (e $Å^{-3}$)	0.868, −0.706	0.693, −0.408

[a] $wR_2 = [\Sigma\, w(F_o^2 - F_c^2)^2/\Sigma\, w(F_o^2)^2]^{1/2}$.
[b] $w = [\sigma^2(F_o^2) + (AP)^2 + BP]^{-1}$ with $P = (F_o^2 + 2F_c^2)/3$.

Table 2
Selected bond lengths (Å) and angles (°) for **1** and **2**

$^{2}_{\infty}[Cu_2(phen)_2L_{4/2}](H_2O)_6$ (**1**) [a]					
Bond lengths					
Cu–O(1)	1.944(2)	Cu–N(1)	2.020(2)	Cu–O(3)^b	2.407(2)
Cu–O(3)^a	1.963(2)	Cu–N(2)	2.035(2)		
Bond angles					
O(1)–Cu–O(3)^a	90.5(1)	O(3)^a–Cu–N(1)	174.7(1)	N(1)–Cu–O(3)^b	106.3(1)
O(1)–Cu–N(1)	93.3(1)	O(3)^a–Cu–N(2)	94.8(1)	N(2)–Cu–O(3)^b	95.1(1)
O(1)–Cu–N(2)	174.3(1)	O(3)^a–Cu–O(3)^b	77.5(1)	Cu–O(3a)–Cu^c	102.5(1)
O(1)–Cu–O(3)^b	88.2(1)	N(1)–Cu–N(2)	81.3(1)		
$[(phen)_2Cu(\mu\text{-}L)Cu(phen)_2](HL)_2(H_2L)(H_2O)_4$ (**2**) [b]					
Bond lengths					
Cu–O(3)	1.976(3)	Cu–N(2)	2.014(3)	Cu–N(4)	2.241(3)
Cu–N(1)	2.044(3)	Cu–N(3)	2.035(3)	Cu–O(4)	2.692(4)
Bond angles					
O(3)–Cu–N(1)	173.2(1)	N(1)–Cu–N(2)	81.4(1)	N(2)–Cu–N(3)	174.0(1)
O(3)–Cu–N(2)	93.3(1)	N(1)–Cu–N(3)	94.0(1)	N(2)–Cu–N(4)	105.2(1)
O(3)–Cu–N(3)	91.0(1)	N(1)–Cu–N(4)	93.7(1)	N(2)–Cu–O(4)	93.3(1)
O(3)–Cu–N(4)	91.8(1)	N(1)–Cu–O(4)	122.4(1)	N(3)–Cu–N(4)	78.9(1)
O(3)–Cu–O(4)	53.3(1)	N(1)–Cu–O(4)	141.8(1)	N(3)–Cu–O(4)	85.8(1)
Hydrogen bonding contacts					
D–H···A	D–H	H···A	D···A	D–H···A	
O(1)–H(AO1)···O(8)^b	0.661	2.222	2.879	173	
O(1)–H(BO1)···O(3)	0.965	1.886	2.822	163	
O(2)–H(AO2)···O(1)^c	0.866	2.040	2.851	155	
O(2)–H(BO2)···O(7)	0.767	1.933	2.664	159	
O(6)–H(O6)···O(8)^b	0.875	1.703	2.562	166	
O(10)–H(O10)···O(2)	1.083	1.465	2.531	167	

[a] Symmetry codes: (*a*) $-x-1/2, y+1/2, -z+1/2$; (*b*) $x+1/2, -y+3/2, z-1/2$; (*c*) $-x, 2-y, -z$.
[b] Symmetry codes: (*a*) $-x+1, -y+1, -z+2$; (*b*) $x+1, y, z$; (*c*) $x-1, y, z$; (*d*) $-x, -y+3, -z+2$.

complexes are summarized in Table 1, while selected interatomic distances and bond angles are listed in Table 2.

4. Supplementary data

Supplementary data for the two structures are available upon request quoting the deposition numbers CCDC 169477 and CCDC 169478 for **1** and **2**, respectively, from the Director, CCDC, 12 Union Road, Cambridge, CB2 1EZ, UK (fax: +44-1223-336033; e-mail: deposit@ccdc.cam.ac.uk or www: http://www.ccdc.cam.ac.uk).

Acknowledgements

The project was supported by the Zhejiang Provincial Natural Science Foundation (RC99034), the Ningbo Municipal Natural Science Foundation (01J201301-1) and the K.C. Wong Magna Fund in Ningbo University. The authors are grateful to Mr. Jian-Li Lin for the collection of the X-ray diffraction data.

References

[1] K. Inoue, T. Hayamizu, H. Iwamura, D. Hashizume, Y. Ohashi, J. Am. Chem. Soc. 118 (1996) 1803.
[2] T. Kitazawa, S. Nishikiori, R. Kuroda, T. Iwamoto, J. Chem. Soc., Dalton Trans. (1994) 1029.
[3] M. Fujita, Y.J. Kwon, S. Washizu, K. Ogura, J. Am. Chem. Soc. 116 (1994) 1151.
[4] (a) O. Ermer, Adv. Mater. 3 (1991) 608;
(b) C. Janiak, Angew. Chem., Int. Ed. Engl. 36 (1997) 1431.
[5] J.L. Manson, C. Campana, J.S. Miller, Chem. Commun. (1998) 251.
[6] O.R. Evans, R.-G. Xiong, Z. Wang, G.K. Wong, W. Lin, Angew. Chem., Int. Ed. Engl. 38 (1999) 536.
[7] W. Lin, O.R. Evans, R.-G. Xiong, Z. Wang, J. Am. Chem. Soc. 120 (1998) 13272.
[8] Y.-Q. Zheng, K. Peters, H.G. von Schnering, Chem. Res. Chin. Univ. 17 (2001) 19.
[9] J.M. Lehn, Supramolecular Chemistry: Concepts and Perspectives, VCH, Weinheim, Germany, 1995.
[10] R. Robson, B.F. Abrahames, S.R. Batten, R.W. Gable, B.F. Hoskins, J. Liu, Supramolecular Architecture (Chapter 19), American Chemical Society, Washington, DC, 1992.
[11] G.F. Swiegers, T.J. Malefeste, Chem. Rev. 100 (2000) 3483.
[12] C. Kaes, A. Katz, M.W. Hosseini, Chem. Rev. 100 (2000) 3553.
[13] T. Rajendran, B. Manimaran, F.-Y. Lee, G.-H. Lee, S.-M. Peng, C.M. Wang, K.-L. Lu, Inorg. Chem. 39 (2000) 2016.
[14] O. Teichert, W.S. Sheldrick, Z. Anorg. Allg. Chem. 626 (2000) 1509.

[15] P.M. Graham, R.D. Pike, M. Sabat, R.D. Bailey, W.T. Pennington, Inorg. Chem. 39 (2000) 5121.
[16] O.R. Evans, W. Lin, Inorg. Chem. 39 (2000) 2189.
[17] S.S.-Y. Chui, S.M.-F. Lo, J.P.H. Charmant, A.G. Orpen, I.D. Williams, Science 283 (1999) 1148.
[18] Z. Wang, R.G. Xiong, B.M. Foxman, S.R. Wilson, W. Lin, Inorg. Chem. 38 (1999) 1523.
[19] Y.Q. Zheng, K. Peters, H.G. von Schnering, 12th International Conference on Solid Compounds of Transition Elements, Saint-Malo, France, (1997) Abstract O-04.
[20] E. Suresh, M.M. Bhadbhade, K. Venkatasubramanian, Polyhedron 18 (1999) 657.
[21] Y.-Q. Zheng, J.-L. Lin, J. Sun, H.-L. Zhang, Z. Kristallogr., NCS 215 (2000) 163.
[22] Y.-Q. Zheng, J.-L. Lin, A.-Y. Pan, Z. Anorg. Allg. Chem. 626 (2000) 1718.
[23] M. Fleck, E. Tillmanns, L. Bohaty, Z. Kristallogr., NCS 215 (2000) 429.
[24] Y.-Q. Zheng, J. Sun, J.-L. Lin, 9th International Conference on Inorganic Ring Systems, Saarbrücken, Germany (2000) Abstract O-61.
[25] C. Ruiz-Pérez, M. Hernandez-Molina, P. Lorenzo-Luis, F. Lioret, J. Cano, M. Julve, Inorg. Chem. 39 (2000) 3845.
[26] J. Li, H. Zeng, J. Chen, Q. Wang, X. Wu, Chem. Commun. (1997) 1213.
[27] J.M. Li, Y.G. Zhang, J.H. Chen, L. Rui, Q.M. Wang, X.T. Wu, Polyhedron 19 (2000) 1117.
[28] E. Suresh, M.M.B. Bhadbhade, Acta Crystallogr., Sect. C 53 (1997) 422.
[29] S. Leslaw, B.-S. Maria, Acta Crystallogr., Sect. C 56 (2000) 19.
[30] E. Suresh, M.M.B. Bhadbhade, Acta Crystallogr., Sect. C 53 (1997) 193.
[31] M.T. Casey, M. McCann, M. Devereux, M. Curran, C. Cardin, M. Convery, V. Quillet, C. Hardivy, J. Chem. Soc., Chem. Commun. 22 (1994) 2643.
[32] M. McCann, J.F. Cronin, M. Devereux, G. Feruson, Polyhedron 14 (1995) 2379.
[33] M. Devereux, M. McCann, J.F. Cronin, Polyhedron 15 (1996) 785.
[34] M. Devereux, M. Curran, M. McCann, M.T. Casey, V. McKee, Polyhedron 14 (1995) 2247.
[35] M. McCann, M.T. Casey, M. Devereux, M. Curran, V. McKee, Polyhedron 16 (1997) 2741.
[36] M. McCann, M. Casey, M. Devereux, M. Curran, G. Ferguson, Polyhedron 16 (1997) 2547.
[37] M. Geraghty, M. McCann, M. Casey, M. Curran, M. Devereux, V. McKee, J. Mcrea, Inorg. Chim. Acta 277 (1998) 257.
[38] M. Devereux, M. McCann, J.F. Cronin, G. Ferguson, V. McKee, Polyhedron 18 (1999) 2141.
[39] S. Leslaw, B.-S. Maria, Acta Crystallogr., Sect. C 55 (1999) 1230.
[40] M. Geraghty, J.F. Cronin, M. Devereux, M. McCann, BioMetals 13 (2000) 1.
[41] M. McCann, M. Geraghty, M. Devereux, D.M.J. O'shea, L. O'Sullivan, Met. Based Drugs 7 (2000) 185.
[42] Y.-Q. Zheng, J. Sun, J.-L. Lin, Z. Anorg. Allg. Chem. 626 (2000) 1274.
[43] Y.-Q. Zheng, J. Sun, J.-L. Lin, Z. Anorg. Allg. Chem. 626 (2000) 613.
[44] M. Munakata, L.P. Wu, M. Yamamoto, T. Kuroda-Sowa, M. Maekawa, J. Am. Chem. Soc. 118 (1996) 3117.
[45] T. Sugimori, H. Masuda, N. Ohata, K. Koiwai, A. Odani, O. Yamauchi, Inorg. Chem. 36 (1997) 576.
[46] J. Dai, M. Yamamoto, T. Kuroda-Sowa, M. Maekawa, Y. Suenaga, M. Munakata, Inorg. Chem. 36 (1997) 2688.
[47] Y.-Q. Zheng, J. Sun, J.-L. Lin, Z. Anorg. Allg. Chem. 627 (2001) 90.
[48] Y.-Q. Zheng, J. Sun, J.-L. Lin, Z. Anorg. Allg. Chem. 627 (2001) 1059.
[49] J.-L. Lin, Y.-Q. Zheng, Z.-P. Kong, H.-L. Zhang, Z. Anorg. Allg. Chem. 627 (2001) 1066.
[50] G.M. Sheldrick, SHELXS-97, Programm zur Lösung von Kristallstrukturen, Göttingen, 1997.
[51] G.M. Sheldrick, SHELXL-97, Programm zur Verfeinerung von Kristallstrukturen, Göttingen, 1997.

The only magnesium-containing oxo-derivative known so far was $[Mg(^nBuOH)TaO(OBu^n)_5]_4$, in the center of the molecule of which was found a cube with Mg atoms and μ_4-oxogroups in its vertices [6]. The present work reports the results of investigation on the interaction of magnesium and niobium methoxides and also the structure of crystalline magnesium oxomethoxoniobate.

2. Experimental

All operations were carried out in dry nitrogen atmosphere using a dry box. MeOH was dehydrated by refluxing over magnesium methoxide with subsequent distillation. The starting alkoxides were prepared by conventional techniques—$Mg(OMe)_2 \cdot 3.5MeOH$ was crystallized from solutions obtained by dissolution of magnesium metal in methanol [7], and $Nb(OMe)_5$ was obtained by anodic oxidation of the metal in alcohol, using LiCl as the electrolyte [8]. IR spectra of **2** and the Nujol mulls of **1** were registered using a Perkin–Elmer FTIR 1600 spectrometer, mass-spectra—with a MI 1201 spectrometer (direct probe insertion, 70 eV, 220 °C). X-ray powder patterns were registered with a STOE STADY-P diffractometer (Cu Kα radiation). ^{1}H NMR spectra were obtained for $CDCl_3$ solutions of **2** and **1** using a Bruker 400 MHz spectrometer.

2.1. Synthesis and isolation of *1* and *2*

On partial evacuation of a solution containing 3.17 g (0.0368 mol) of $Mg(OMe)_2$ and 18.29 g (0.0736 mol) $Nb(OMe)_5$ in 100 ml MeOH up to the total concentration of alkoxides of approximately 40% and subsequent cooling to ~0 °C was achieved the crystallization of complex **1**. The yield after washing with a minimal amount of alcohol was 5.36 g (25%). *Anal.* Found: C 24.1; H 6.23; **M** Mg+Nb 33.6. Calc. for $C_7H_{23}O_8MgNb$: C 23.8; H 6.5; M Mg+Nb 33.2%. IR, cm^{-1}: 3420 s (*ν*-OH), 1456 m, 1376 w, 1148 sh. w, 1108 s, 1072 vs, 1056 sh. vs, 1034 s, 878 vs (*ν*-Nb=O), 528 sh. m, 482 vs, 440 sh.w.

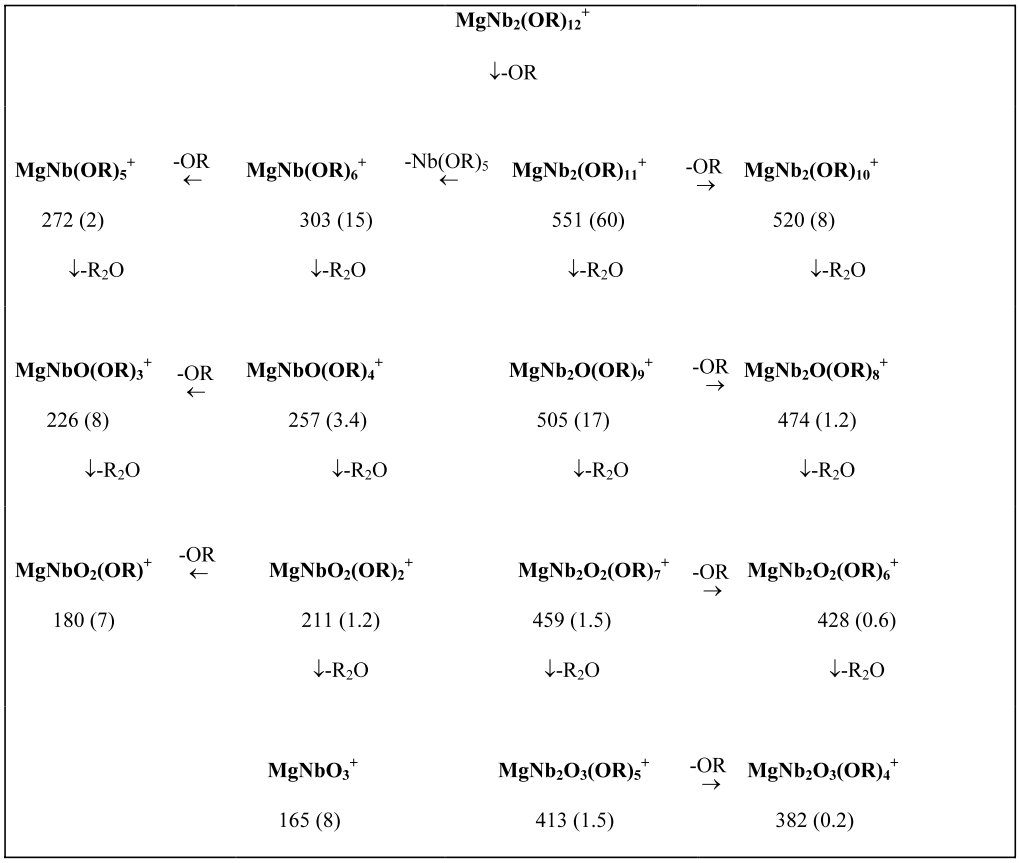
Compound **1** is insoluble in hydrocarbons and poorly soluble in the parent alcohol at room temperature (r.t.). It is not transferred into the gas phase under the conditions of mass-spectrometric experiment. Its X-ray powder pattern can be indexed using the parameters obtained in the single crystal X-ray experiment. *I* (%); *d* (Å); (*hkl*): 33, 8.82 (011); 100, 7.85 (−101); 12, 7.41 (110); 22, 7.07 (−111); 12, 5.78 (120); 9, 5.44 (111); 12, 4.99 (012); 6, 4.37 (−122); 7, 4.20 (200); 8, 3.72 (032); 7, 3.57 (−113); 7, 3.46 (211); 5, 3.21 (023); 5, 3.16 (042); 5, 2.98 (−223); 5, 2.96 (231); 8, 2.95 (301); 7, 2.92 (202); 7, 2.83 (21-2).

The ^{1}H NMR spectrum of the solution obtained by extraction of crystals of **1** with boiling deuterochloroform contains in addition to a comparably rather strong methanol signal (3.48 ppm, singlet) originating apparently from elimination of the solvating methanol molecules from **1**, three well-defined singlets at 4.27, 4.16 and 3.20 ppm with approximately 2:2:1 integration ratio (their positions being temperature-independent in the 0–50 °C temperature interval). The latter can be assigned to the protons of the methyl groups of the terminal, doubly bridging and triply bridging methoxide groups, respectively, in the molecule of **1**.

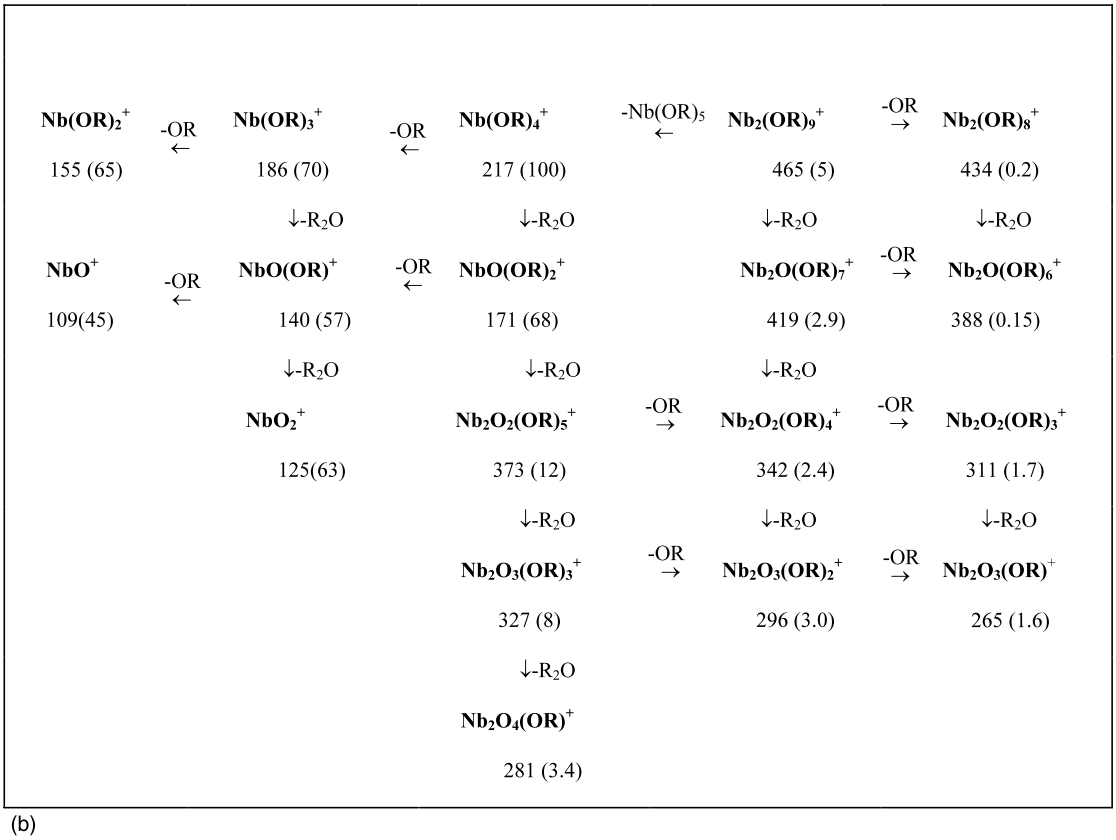
Further concentration of the mother liquor, separated from the crystals of **1**, led to formation of a viscous liquid containing $MgNb_2(OMe)_{12} \cdot 2MeOH$ (**2**) and excess of $Nb(OMe)_5$ (formed on crystallization of **1**), that turned into a glass-like solid at −20 °C. The IR spectrum of the latter was very close to that of **1** except for the absence of the Nb=O band. The mass-spectrum of **2** is shown in Fig. 1. The ^{1}H NMR spectrum of **2** is rather simple in analogy with the spectra of other alkaline earth alkoxoniobates [9]: there is only one signal present for protons of the alkoxide groups (4.00 ppm, singlet) and one signal for the solvating alcohol molecules (3.46 ppm, singlet). It should be noted that the spectra of **2** do usually contain rather weak but distinguishable signals corresponding to **1** (their intensity varies with respect to that of the signal at 4.00 ppm). This fact confirms the supposition that **1** is formed on spontaneous decomposition of **2**.

2.2. Crystallography

X-ray quality crystals of **1** were grown from MeOH at −5 to 8 °C. The crystals were placed in glass capillaries, and sealed under nitrogen atmosphere. Complex **1**, $C_{14}H_{46}O_{16}Mg_2Nb_2$, $M = 704.95$, Monoclinic, Space group $P2(1)/n$, $a = 8.863(2)$ Å, $b = 15.902(4)$ Å, $c = 11.111(4)$ Å, $\beta = 107.63(3)^\circ$, $V = 1492.3(7)$ Å^3, $D_{calc} = 1.569$ g cm^{-3} for $Z = 2$, λ(Mo Kα) = 0.71073 Å, 2615 [$R_{int} = 0.0400$] independent reflections which were collected at 22 °C up to $2\theta_{max} = 50.00^\circ$ with a Bruker SMART CCD 1k diffractometer. The empirical absorption correction was made using Bruker SADABS program ($\mu = 0.871$ mm^{-1}). The structure was solved by standard direct methods; the coordinates of all non-hydrogen atoms were obtained from the initial solution and refined together with the temperature factors first in isotropic and then in anisotropic approximation. The hydrogen atom coordinates, except for those of the active hydrogen atoms H(1) and H(2) located in the difference Fourier syntheses, were calculated geometrically and included into the final solution in isotropic approximation. Final discrepancy factors are $R_1 = 0.0341$, $wR_2 = 0.0753$. The largest difference peak and hole 0.329 and −0.428 e Å^{-3} were located in the direct proximity of niobium atoms. All calculations were



(a)



(b)

Fig. 1. Fragmentation schemes for $MgNb_2(OMe)_{12}2MeOH$ (**2**) (100% corresponds to the intensity of the $Nb(OMe)_4^+$ ion) and $Nb(OMe)_5$.

Table 1
Selected bond distances (Å) and angles (°) in the structure of $Mg_2Nb_2O_2(OMe)_{10}(MeOH)_4$ (**1**)

Bond lengths			
Nb(1)=O(8)	1.741(2)	Mg(2)–O(4)	2.087(3)
Nb(1)–O(5)	2.008(3)	Mg(2)–O(7)	2.088(3)
Nb(1)–O(6)	1.914(3)	Mg(2)–O(1)	2.056(3)
Nb(1)–O(1)	2.071(3)	Mg(2)–O(3)#1	2.055(3)
Nb(1)–O(3)	2.065(2)	Mg(2)–O(2)	2.141(3)
Nb(1)–O(2)	2.246(2)	Mg(2)–O(2)#1	2.077(3)
Bond angles			
O(8)–Nb(1)–O(6)	98.77(13)	O(3)#1–Mg(2)–O(1)	170.09(11)
O(8)–Nb(1)–O(5)	104.26(13)	O(3)#1–Mg(2)–O(2)#1	76.94(10)
O(6)–Nb(1)–O(5)	90.52(12)	O(1)–Mg(2)–O(2)#1	93.30(10)
O(8)–Nb(1)–O(3)	97.06(12)	O(3)#1–Mg(2)–O(4)	92.63(12)
O(6)–Nb(1)–O(3)	93.62(11)	O(1)–Mg(2)–O(4)	91.31(12)
O(5)–Nb(1)–O(3)	157.39(11)	O(2)#1–Mg(2)–O(4)	103.59(12)
O(8)–Nb(1)–O(1)	94.50(12)	O(3)#1–Mg(2)–O(7)	99.32(12)
O(6)–Nb(1)–O(1)	166.40(10)	O(1)–Mg(2)–O(7)	89.82(12)
O(5)–Nb(1)–O(1)	83.36(11)	O(2)#1–Mg(2)–O(7)	166.74(13)
O(3)–Nb(1)–O(1)	87.61(10)	O(4)–Mg(2)–O(7)	89.21(14)
O(3)–Nb(1)–O(2)	73.09(9)	O(3)#1–Mg(2)–O(2)	99.33(11)
O(1)–Nb(1)–O(2)	74.88(9)	O(1)–Mg(2)–O(2)	77.51(10)

Symmetry transformations used to generate equivalent atoms: #1 $-x, -y, -z+1$.

performed on an IBM PC using the SHELXTL-NT program package [10].

3. Results and discussion

Interaction of magnesium and niobium methoxides in MeOH was found to lead to a liquid complex with $MgNb_2(OMe)_{12}\cdot 2MeOH$ (**2**) composition. The formation of **2** was in our experiments accompanied by precipitation of minor amounts of the crystalline poorly soluble oxocomplex, $[MgNbO(OMe)_5(MeOH)_2]$ (**1**). The yields of the latter increased on subsequent storage of solutions even rigorously protected from moisture, indicating that a slow non-hydrolytic decomposition process leading to the formation of the oxospecies took place in this case. This result provides one more confirmation to the observation that bimetallic oxocomplexes are often formed in the systems containing liquid $M^{II}M^{V}_2(OR)_{12}\cdot 2ROH$ (M^V = Nb, Ta) complexes due to decomposition of the latter. Examples can be taken from $[SrTaO(OMe)_5(MeOH)_{2.5}]_4$, $[MgTaO(OBu^n)_5(^n\text{-}BuOH)_4]_4$ and $[BaM^VO(OEt)_5(EtOH)_{1.5}]_4$ [2,6], $[Pb_6Nb_4O_4(OEt)_{24}]$ etc. [11].

The $MgNb_2(OMe)_{12}\cdot 2MeOH$ (**2**) compound is in all its properties, such as composition, physical state and behavior in the gas phase, analogous to its tantalum analog [3], but possesses a lower stability. Its mass spectrum (Fig. 1) contains along with the ions corresponding to the fragmentation pattern of **2**, all the major peaks of $Nb(OMe)_5$, having much higher intensity, which is caused by the thermal dissociation of **2**, and possibly also the presence of niobium methoxide admixture in the samples. The fragmentation of **2** is very close to that described for $MgTa_2(OMe)_{12}\cdot 2MeOH$ [3], which also undergoes even partial thermal dissociation. Fig. 1 contains also the mass spectrum of free $Nb(OMe)_5$ (displaying better completeness compared with that reported earlier in [12]). Its fragmentation pattern differs substantially from that of $Ta(OMe)_5$, where the major transformations are connected with elimination of OH and HCHO groups [13].

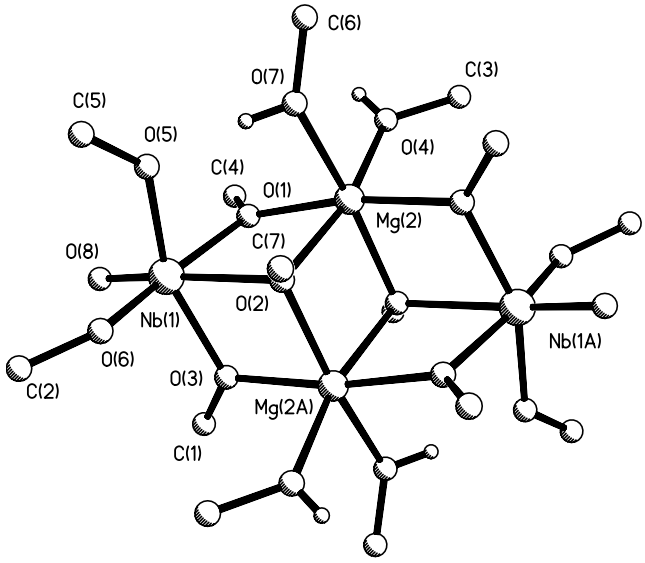


Fig. 2. The molecular structure of $Mg_2Nb_2O_2(OMe)_{10}(MeOH)_4$ (**1**).

$Mg_2Nb_2O_2(OMe)_{10}(MeOH)_4$ (**1**), is, as many other oxoalkoxides, rather scarcely soluble in alcohol at room temperature but dissolves on heating with partial destruction of the molecules.

The dimeric molecule of **1** (Table 1, Fig. 2) belongs to the well-known $Ti_4(OMe)_{16}$ type [14] characterized by a planar arrangement of four metal atoms. Such molecules contain two different kinds of metal positions, one (M^1) with two terminal groups and two bonds with tridentate ligands and the other (M^2) with three terminal groups and one bond to a tridentate ligand. In the molecule of **1** the M^1 positions are occupied by magnesium atoms (2MeOH molecules being the terminal ligands) and the M^2 ones by niobium atoms (two OMe- and one oxogroup as the terminal ligands). This arrangement with a less electronegative metal atom in the M^1 position and more electronegative transition metal atom in the M^2 one is characteristic of the majority of the structures of this type such as $Li_2Ti_2(OR)_{10}$, $R = Pr^i$, $C_5H_{11}^{neo}$ [15,16], $[Li_2Nb_2(OCH_2SiMe_3)_{12}]$ [17], $[Mg_2(MoO_2)_2(OMe)_{10}(MeOH)_4]$ [18] and $[Na(EtOH)_2]_2(WO)_2(OEt)_{10}$ [19]. A less common alternative arrangement is exemplified in particular by the structure of $[LiNbO(OEt)_4(EtOH)]_2$, where the octahedrally coordinated Nb atom occupies the M^1

position and the tetrahedrally coordinated Li, the M^2 position [2].

In the octahedral coordination sphere of niobium atoms in the molecule of **1** the Nb–O bond lengths increase regularly with the increase in number of bonds formed by the oxygen atom from the shortest Nb(1) = O(8) 1.741(2) Å, the doubly bonded 'ylous' oxygen via terminal OMe, 1.914(3) and 2.008(3) Å; the bidentate bridging, 2.065(2) and 2.071(3) Å, to the tridentate methoxide ones, 2.246(2) Å. At the same time all the bond lengths in the octahedron around the magnesium atom lie in the interval of 2.055(3)–2.141(3) Å independent of the function of the ligands, indicating thus a predominantly ionic character of bonding. This permits us to consider the complex **1** as an ion pair, $[Mg(ROH)_2]_2^{2+}$ $[NbO(OR)_5]_2^{2-}$ (in analogy with $[Na(EtOH)_2]_2^{+}$ $[WO(OEt)_5]_2^{-}$ [19]), all the Nb–O bond lengths in the molecule of **1** are 0.1–0.15 Å longer in comparison with its structural analog $[LiNbO(OEt)_4(EtOH)]_2$ [2], the Mg–O bond lengths being quite close to those observed in the known structures such as $Mg(OMe)_2 \cdot 3.5$ MeOH [7] or $[Mg(^nBuOH)TaO(OBu^n)_5]_4$ [6]).

However, the C–O bond lengths in the coordination arrangement of both metals correlate with the bonding character of the ligands (average distances being 1.397 Å for terminal, 1.411 Å for bidentate and 1.424 Å for the tridentate ones). The same can be noticed for the M–O–C angles, which are 130.1°–139.6° for the terminal groups, 123.2°–129.1° for the bidentate and 116.9°–119.6° for the tridentate bridges. The same regularities in the changes of molecular parameters have been observed in the molecules of $[LiNbO(OEt)_4(EtOH)]_2$ or $Ti_4(OMe)_{16}$ [2,14].

The alcohol molecule containing the O(7) atom forms an intramolecular hydrogen bond with a length of 2.606(6) Å with the O(5) atom of an alkoxide group, while that containing the O(4) atom form an intermolecular hydrogen bond with a length of 2.676(6) Å, with the O(8) atom of the neighboring molecule.

Compound **1** provides one more example of rather scarce niobium alkoxides containing terminal 'ylic' oxygen atoms. To this group belong $NbO(OR)_3$ [20], $[NbO(OC_6H_3Ph_2\text{-}2,6)_3]$ [21], and also the bimetallic complexes such as $[LiNbO(OEt)_4(EtOH)]_2$ [2] and $[Li_2(NbO)_2O(OCMe_2CH_2OMe)_6]$ [22]. More stable supposedly and definitely more represented are the structures containing oxo-bridges, such as $[NbO(OC_6H_3Pr^i_2\text{-}2,6)_3]_2$ [23], $[Nb_3O_2[O(CMe_2)_2O]_4[O(CMe_2)_2OH]$, $[Nb_4O_4[O(CMe_2)_2O]_2[OPr^i)_8]$ [24], $Pb_6Nb_4O_4(OEt)_{24}$ [11], $(ReO_4)_2Nb_4O_{12}(OMe)_{14}$, [25], and also $Nb_8O_{10}(OEt)_{20}$ originating from the decomposition of $NbO(OR)_3$ [20].

The decrease in the M=O bond multiplicity in the series V, Nb, Ta (due to the increase in the energy of d_π-orbitals of the metal atom) causes inability to form the terminal 'ylic' bonds for tantalum. This results, in particular, in the absence for tantalum of the monomeric $MO(OR)_3$ oxoalkoxides (known for niobium [20]), with stable dinuclear $Ta_2O(OR)_8$ molecules with 2 μ-O- and one μ-OR bridges being formed instead [13]. It turns then natural that the oxoalkoxides of niobium and tantalum turn to be isomorphous only when the 'ylic' groups are absent at Nb atoms such as, for example, in $M^V_8O_{10}(OEt)_{20}$ [26], and $[BaM^VO(OEt)_5(EtOH)_{1.5}]_4$ [2,6]. It is interesting in this sense to compare the decomposition products of $LiM^V(OEt)_6$, where M^V = Nb, Ta. In the first case it leads to $[LiNbO(OEt)_4(EtOH)]_2$, containing a terminal doubly bonded oxygen atom, while in the case of tantalum the polyoxotantalates—$[LiTa_9O_{13}(OEt)_{20}(EtOH)]$ and $[Li_8Ta_8O_{14}(OEt)_{20}(EtOH)_8]$—containing numerous oxobridges have been isolated [26][1]. Taking into consideration these circumstances it is possible to suppose that magnesium alkoxotantalates should on decomposition give only molecules containing oxobridges like $[Mg(^nBuOH)TaO(OBu^n)_5]_4$ [6].

4. Supplementary material

Crystallographic data for the structural analysis have been deposited with the Cambridge Crystallographic Data Center, CCDC no. 177452 for compound **1**. Copies of this information may be obtained free of charge from the CCDC, 12 Union Road, Cambridge, CB2 1EZ, UK (fax: +44-1223-336033; e-mail: deposit@ccdc.cam.ac.uk or www: http://www.ccdc.cam.ac.uk).

Acknowledgements

The authors would like to express their gratitude to Mr. E.V. Alexeev for the assistance in carrying out the synthetic experiments, to Rolf Andersson for the aid with the NMR studies and the Swedish Council for Scientific Research for financial support of this work.

References

[1] R.C. Mehrotra, A.K. Ray, P.N. Kapoor, R. Bohra, Inorg. Chim. Acta 16 (1976) 237.
[2] E.P. Turevskaya, N.Y. Turova, A.V. Korolev, A.I. Yanovsky, Y.T. Struchkov, Polyhedron 14 (1995) 1531.
[3] D.E. Tchebukov, N.Y. Turova, A.V. Korolev, A.I. Belokon', Russ. J. Inorg. Chem. 42 (1997) 1498.

[1] The earlier published data on existence of $[LiTaO(OEt)_4]_2$ [3] should be considered erroneous.

[4] D.E. Chebukov (Tchebukov), N.Y. Turova, A.I. Belokon', Russ. J. Inorg. Chem. 44 (1999) 807.
[5] M.Y. Antipin, Z.A. Starikova, A.I. Yanovskii, F.M. Dolgushin, K.A. Lysenko, V.N. Khrustalev, I.I. Vorontsov, A.A. Korlyukov, G.B. Andreev, I.S. Neretin, Russ. J. Coord. Chem. 27 (2001) 221.
[6] Z.A. Starikova, A.I. Yanovsky, D.E. Chebukov, E.P. Turevskaya, N.Y. Turova, Russ. J. Inorg. Chem. 43 (1998) 1203.
[7] Z.A. Starikova, A.I. Yanovsky, D.E. Chebukov, E.P. Turevskaya, N.Y. Turova, Polyhedron 16 (1997) 967.
[8] V.A. Shreider, E.P. Turevskaya, N.I. Kozlova, N.Y. Turova, Inorg. Chim. Acta 13 (1981) L73.
[9] S. Boulmaaz, R. Papiernik, L.G. Hubert-Pfalzgraf, J.C. Daran, Eur. J. Solid State Inorg. Chem. 30 (1993) 583.
[10] SHELXTL-NT Reference Manual, Brucer AXS, Madison, WI, 1998.
[11] R. Papiernik, L.G. Hubert-Pfalzgraf, J.C. Daran, Y. Jeannih, J. Chem. Soc., Chem. Commun. (1990) 695.
[12] L.G. Hubert-Pfalzgarf, J.G. Riess, Inorg. Chem. 14 (1975) 2854.
[13] N.Y. Turova, A.V. Korolev, D.E. Tchebukov, A.I. Belokon', Polyhedron 15 (1996) 3869.
[14] N.Y.a. Turova, E.P. Turevskaya, V.G. Kessler, M.I. Yanovskaya, Metal Alkoxides Chemistry Handbook, Kluwer Academic Publishers, Dordrecht, 2001.
[15] T.J. Boyle, D.C. Bradley, M.J. Hampden-Smith, A. Patel, Inorg. Chem. 34 (1995) 5893.
[16] M.J. Hampden-Smith, D.S. Williams, A.L. Rheingold, Inorg. Chem. 29 (1990) 4076.
[17] S.C. Goel, J.A. Hollingsworth, A.M. Beatty, K.D. Robinson, W.E. Buhro, Polyhedron 17 (1998) 781.
[18] M. Antipin, Y. Struchkov, A. Shilov, A. Shilova, Gazz. Chim. Ital. 123 (1993) 265.
[19] N.Y. Turova, V.G. Kessler, S.I. Kucheiko, Polyhedron 10 (1991) 2617.
[20] V.G. Kessler, N.Y. Turova, A.I. Yanovsky, A.I. Belokon', Y.T. Struchkov, Russ. J. Inorg. Chem. 36 (1991) 938.
[21] J.S. Yu, P.E. Fanwick, I.P. Rothwell, Acta Crystallogr., Sect. C 48 (1992) 1759.
[22] W.A. Herrmann, N.W. Huber, O. Runte, Angew. Chem., Int. Ed. 34 (1995) 21877.
[23] V.M. Visciglio, P.E. Fanwick, I.P. Rothwell, Acta Crystallogr., Sect. C. 50 (1994) 90.
[24] L.G. Hubert-Pfalzgarf, V. Abada, J. Vaissermann, J. Roziere, Polyhedron 18 (1999) 845.
[25] G.A. Seisenbaeva, A.V. Shevel'kov, J. Tegenfeldt, L. Kloo, D.V. Drobot, V.G. Kessler, J. Chem. Soc., Dalton Trans. (2001) 2762.
[26] E.P. Turevskaya, N.Y. Turova, A.I. Belokon', D.E. Chebukov, Russ. J. Inorg. Chem. 43 (1998) 975.

complexes than can prepared in the presence of water should be potentially more useful catalysts, and the synthetic routes based on aqueous solutions of alkali molybdates in hydrobromic acid attain special relevance.

The existence of the species $MoO_2Br_2(H_2O)_2$ in solutions of alkali molybdates in concentrated hydrobromic acid, and in the ether extracts, is well established [18]. Recently we reported that $MoO_2Br_2(H_2O)_2$ can be readily extracted from aqueous solutions with diethyl ether in an almost quantitative manner, and the resulting ether solution stored for weeks at room temperature [16]. Here we report on the utility of the ether solution in the synthesis of anhydrous addition compounds of MoO_2Br_2 with representative amides, sulfoxides and phosphine oxides, some of them previously prepared by other procedures.

2. Experimental

2.1. General procedures and measurements

Unless otherwise specified all operations were carried out in air. Diethyl ether was distilled over Na-benzophenone ketyl prior to use. DMSO was dried over calcium hydride and distilled in vacuo. DMF, DMA, NMP and HMPA were distilled under reduced pressure. Phosphine oxides were prepared by oxidation of the parent phosphines with hydrogen peroxide and characterized by elemental analysis (C, H) and NMR spectroscopy. $(CH_3)_3CSH$ was purified by distillation under nitrogen prior to use. All other reagents were commercial products and were used without further purification. Conductivity measurements were made with a Crison 522 conductivimeter. Elemental analyses (C, H, N) were performed on a LECO CHNS-932 analyzer (Module VTF-900 for O). Bromine was eventually determined by gravimetry as AgBr and molybdenum by titration with lead(II) nitrate [19]. IR spectra were recorded on a Nicolet Impact 410 (Software OMNIC for Windows) spectrometer. NMR spectra were recorded on a Varian Unity Inova-400 spectrometer (400 MHz for ^1H and 161.92 MHz for ^{31}P). Chemical shifts are relative to TMS (^1H), or external 85% H_3PO_4 (^{31}P), with downfield values reported as positive. Coupling constants J are given in Hz.

2.2. Preparation of the complexes

2.2.1. Preparation of the diethyl ether solution of $MoO_2Br_2(H_2O)_2$

One gram (4.14 mmol) of powdered $Na_2MoO_4\cdot 2H_2O$ was added with stirring on 8 g (ca. 46.5 mmol) of concentrated hydrobromic acid at room temperature (r.t.) to obtain a clear yellow solution. Then 10 ml of dry diethyl ether was added slowly with stirring. The reaction is exothermic and a significant part of diethyl ether dissolves in the HBr solution. The upper ether phase was collected and the extraction process repeated twice more. The combined extract was stirred for 5 min with 1 g of anhydrous magnesium sulfate. The solution was collected by filtration and the magnesium sulfate washed with three 3-ml portions of diethyl ether. About 30 ml of a light yellow solution containing more than 95% of the original molybdenum, was obtained. This solution was used for the synthesis of addition compounds, for which the yield is given with respect to $Na_2MoO_4\cdot 2H_2O$.

2.2.2. Preparation of $MoO_2Br_2L_2$ ($L = DMF$, HMPA, Ph_2SO)

A solution prepared as above was treated with 8.3 mmol of L in 10 ml of diethyl ether. The light yellow precipitate was filtered, washed with three 3-ml portions of diethyl ether and dried under vacuum.

$MoO_2Br_2(DMF)_2$: Yield 1.73 g (96%). IR(cm^{-1}): ν(Mo=O) 904, 941; ν(C=O) 1646. ^1H NMR ($CDCl_3$): 8.37 ppm (s, 1H, H–CO), 3.15 ppm (s, 3H, N–CH_3), 3.08 ppm (s, 3H, N–CH_3). *Anal*. Found: C, 16,82; H, 3.32; Mo, 21.80; N, 6.38. Calc. for $C_6H_4Br_2MoN_2O_4$: C, 16.61; H, 3.25; Mo, 22.11; N, 6.46%.

$MoO_2Br_2(HMPA)_2$: Yield 2.51 g (94%). IR(cm^{-1}): ν(Mo=O) 902, 939; ν(P=O) 1193, 989. ^1H NMR ($CDCl_3$): 2.72 ppm (d, $^3J_{H-P} = 9.7$ Hz, 18H, N–CH_3). ^{31}P NMR ($CDCl_3$): 29.0 ppm. *Anal*. Found: C, 22.1; H, 5,48; Mo, 14.51; N, 12.80. Calc. for $C_{12}H_{36}Br_2MoN_6O_4P_2$: C, 22.31; H, 5.62; Mo, 14.85; N, 13.01%.

$MoO_2Br_2(Ph_2SO)_2$: Yield 2.72 g (95%). IR(cm^{-1}): ν(Mo=O) 902, 929; ν(S=O) 987, 1001. ^1H NMR ($CDCl_3$): 7.3–7.8 ppm (m, 10H, Ph). *Anal*. Found: C, 41.40; H, 2.99; Mo, 13.66. Calc. for $C_{24}H_{20}Br_2MoO_4S_2$: C, 41.64; H, 2.91; Mo, 13.86%.

2.2.3. Preparation of $MoO_2Br_2L_2$ ($L = DMSO$, MePhSO)

The $MoO_2Br_2(H_2O)_2$ solution was treated with 8.0 mmol of L in 5 ml of acetone. The light yellow solid was filtered, washed with three 3-ml portions of diethyl ether and dried under vacuum.

$MoO_2Br_2(DMSO)_2$: Yield 1.71 g (93%). IR(cm^{-1}): ν(Mo=O) 889, 924; ν(S=O) 989, 1034. ^1H NMR ($CDCl_3$): 2.64 ppm (s, 6H, CH_3). *Anal*. Found: C, 10.80; H, 2.68; Mo, 21.50. Calc. for $C_4H_{12}Br_2MoO_4S_2$: C, 10.82; H, 2.72; Mo, 21.61%.

$MoO_2Br_2(MePhSO)_2$: Yield 2.05 g (87%). IR(cm^{-1}): ν(Mo=O) 900, 929; ν(S=O) 987, 1001. ^1H NMR ($CDCl_3$): 7.4-7.7 ppm (m, 5H, Ph), 2.95 ppm (s, 3H, CH_3). *Anal*. Found: C, 29.82; H, 2.93; Mo, 16.63. Calc. for $C_{14}H_{16}Br_2MoO_4S_2$: C, 29.60; H, 2.84; Mo, 16.89%.

2.2.4. Preparation of $MoO_2Br_2(OPPh_3)_2$

The $MoO_2Br_2(H_2O)_2$ solution was treated with 8.0 mmol of $OPPh_3$ in 30 ml of acetone. The mixture is stirred for 10 min and the light yellow microcrystalline precipitate was filtered, washed with three 3-ml portions of diethyl ether and dried under vacuum. Yield 3.36 g (96%). IR(cm^{-1}): ν(Mo=O) 904, 946; ν(P=O) 1174. ^1H NMR ($CDCl_3$): 7.2–7.9 ppm (m, 30H, Ph). ^{31}P NMR ($CDCl_3$): 41.9 ppm. *Anal*. Found: C, 50.66; H, 3.41; Mo, 11.49. Calc. for $C_{36}H_{30}Br_2MoO_4P_2$: C, 51.21; H, 3.58; Mo, 11.36%.

2.2.5. Preparation of $MoO_2Br_2(dppmO_2)$

The $MoO_2Br_2(H_2O)_2$ solution was treated with 4.0 mmol of $dppmO_2$ in 10 ml of dichloromethane. The light yellow microcrystalline precipitate was filtered, washed with three 3-ml portions of diethyl ether and dried under vacuum. Yield 2.71 g (93%). IR(cm^{-1}): ν(Mo=O) 900, 941; ν(P=O) 1153. ^1H NMR ($CDCl_3$): 7.3–7.6 ppm (m, 12H, Ph), 7.7–7.9 ppm (m, 8H, Ph), 3.87 ppm (t, $^2J_{H-P} = 12.3$ Hz, 2H, CH_3). ^{31}P NMR ($CDCl_3$): 39.6 ppm. *Anal*. Found: C, 42.55; H, 3.08; Mo, 13.84. Calc. for $C_{25}H_{22}Br_2MoO_4P_2$: C, 42.64; H, 3.15; Mo, 13.62%.

2.2.6. Preparation of $MoO_2Br_2(OPMePh_2)_2$

The $MoO_2Br_2(H_2O)_2$ solution was treated with 8.0 mmol of $OPMePh_2$ powder. The mixture was stirred for 30 min and then the solvent was removed in vacuo. The resulting solid was dissolved in acetone (5 ml) and diethyl ether (25 ml) was added with stirring. The white precipitate was filtered, washed with three 3-ml portions of diethyl ether and dried under vacuum. Yield 2.59 g (87%). IR(cm^{-1}): ν(Mo=O) 901, 941; ν(P=O) 1163. ^1H NMR ($CDCl_3$): 7.3–7.9 ppm (m, 10H, Ph), 2.25 ppm (d, $^2J_{H-P} = 13.2$ Hz, 3H, CH_3). ^{31}P NMR ($CDCl_3$): 46.2 ppm. *Anal*. Found: C, 43.10; H, 3.48; Mo, 13.51. Calc. for $C_{26}H_{26}Br_2MoO_4P_2$: C, 43.36; H, 3.64; Mo, 13.32%.

2.2.7. Preparation of $MoO_2Br_2L_2$ ($L = OPBu_3$, $OPOct_3$)

An ether solution of $MoO_2Br_2(H_2O)_2$ prepared as above, and containing 4.0 mmol of molybdenum, was treated with 8.0 mmol of L in 5 ml of diethyl ether. The solution was evaporated in vacuo at r.t. and the resulting light yellow waxy material pumped at 10^{-3} mbar for 10 h.

$MoO_2Br_2(OPBu_3)_2$: Yield 2.94 g (98%). IR(cm^{-1}): ν(Mo=O) 900, 939; ν(P=O) 1186. ^1H NMR ($CDCl_3$): 1.98 ppm (c, $^3J_{H-H} = 8.2$ Hz, $^2J_{H-P} = 18.2$ Hz, 2H, $-C_\alpha H_2-$), 1.63 ppm (m, $^3J_{H-H} = 8.2$ and 7.5 Hz, 2H, $-C_\beta H_2-$), 1.44 ppm (m, $^3J_{H-H} = 7.3$ and 7.5 Hz, 2H, $-C_\gamma H_2-$), 0.93 ppm (t, $^3J_{H-H} = 7.3$ Hz, 3H, CH_3). ^{31}P NMR ($CDCl_3$): 67.9 ppm. *Anal*. Found: Br, 21.72; Mo, 13.51. Calc. for $C_{24}H_{54}Br_2MoO_4P_2$: Br, 22.06; Mo, 13.24%.

$MoO_2Br_2(OPOct_3)_2$: Yield 4.35 g (99%). IR(cm^{-1}): ν(Mo=O) 900, 939; ν(P=O) 1199. ^1H NMR ($CDCl_3$): 1.96 ppm (c, $^3J_{H-H} = 7.5$ Hz, $^2J_{H-P} = 18.2$ Hz, 2H, $-C_\alpha H_2-$), 1.60 ppm (c, 2H, $-C_\beta H_2-$), 1.30 ppm (m, 2H, $-C_\gamma H_2-$), 1.26 ppm (m, 8H, $-CH_2-$), 0.87 ppm (t, $^3J_{H-H} = 7.3$ Hz, 3H, CH_3). ^{31}P NMR ($CDCl_3$): 67.2 ppm. *Anal*. Found: Br, 14.77; Mo, 9.23. Calc. for $C_{48}H_{102}Br_2MoO_4P_2$: Br, 15.06; Mo, 9.04%.

2.2.8. Preparation of $MoO_2Br_2(NMP)_2$

The $MoO_2Br_2(H_2O)_2$ solution was treated with 8.3 mmol of NMP in diethyl ether (5 ml). A green oil immediately was formed. The oil was dissolved in acetone (5 ml) and filtered. To the resulting clear solution diethyl ether (25 ml) was added with stirring. The light yellow precipitate was filtered, washed with three 3-ml portions of diethyl ether and dried under vacuum. Yield 1.67 g (83%). IR(cm^{-1}): ν(Mo=O) 906, 947; ν(C=O) 1634. ^1H NMR ($CDCl_3$): 3.55 ppm (t, $^3J_{H-H} = 7.5$ Hz, 2H, $N-CH_2-$), 3.03 ppm (s, 3H, $N-CH_3$), 2.99 ppm (t, $^3J_{H-H} = 7.5$ Hz, 2H, CH_2-CO), 2.15 ppm (s, $^3J_{H-H} = 7.5$ Hz, 2H, $-CH_2-$). *Anal*. Found: C, 24.30; H, 3.61; Mo, 19.59; N, 5.59. Calc. for $C_{10}H_{18}Br_2MoN_2O_4$: C, 24.71; H, 3.73; Mo, 19.74; N, 5.76%.

2.3. Oxidant ability of the complexes

The oxidant ability of the complexes to transform $(CH_3)_3CSH$ into $(CH_3)_3CS-SC(CH_3)_3$ has been determined by measuring the ratio thiol/disulphide by ^1H NMR spectroscopy. In a NMR tube, 0.01 mol of the bromocomplex finely powdered was placed. Then 0.3 ml of $(CD_3)_2CO$ was added and finally 0.3 ml of 0.04 mol dm^{-3} solution of $(CH_3)_3CSH$ in the same solvent. The tube was flame sealed in a nitrogen atmosphere, shaken and immersed in a water bath at 55 °C. For adducts with $OPBu_3$ and $OPOct_3$, 0.3 ml of 0.01 mol dm^{-3} solution of each compound and 0.3 ml of 0.04 mol dm^{-3} solution of $(CH_3)_3CSH$ were used. The conversion of thiol to disulphide was followed by measuring the intensity of the methyl signals ($\delta = 1.39$ ppm for $(CH_3)_3CSH$, and 1.29 ppm for $(CH_3)_3CS-SC(CH_3)_3$) at 3, 6, 9, 21 and 24 h. Solutions of $(CH_3)_3CSH$ (0.02 mol dm^{-3}) and L (0.01 mol dm^{-3}) in $(CD_3)_2CO$ were used as blanks. Table 1 shows the percent oxidation of the thiol to disulphide for each bromocomplex at 3 and 24 h.

2.4. Crystal-structure determinations

Suitable single crystals were grown at r.t. by diffusion of diethyl ether on acetone solutions of the complexes in a dry atmosphere. Crystal data for $MoO_2Br_2(HMPA)_2$: tetragonal, *I4(1)cd*, yellow, $a = 14.61730(10)$, $b = 14.61730(10)$, $c = 24.4423(3)$ Å, $\alpha = \beta = \gamma = 90°$, $V =$

Table 1
Percent oxidation of $(CH_3)_3CSH$ to $(CH_3)_3CS-SC(CH_3)_3$ by $MoO_2Br_2L_2$ in $(CD_3)_2CO$ at 55 °C, after 3 and 24 h

$MoO_2Br_2L_2$	3 h	24 h
$MoO_2Br_2(OPPh_3)_2$	6	19
$MoO_2Br_2(OPBu_3)_2$	8	22
$MoO_2Br_2(OPOct_3)_2$	17	30
$MoO_2Br_2(OPMePh_2)_2$	8	20
$MoO_2Br_2(dppmO_2)$	6	27
$MoO_2Br_2(DMF)_2$	17	24
$MoO_2Br_2(NMP)_2$	19	28
$MoO_2Br_2(HMPA)_2$	7	20
$MoO_2Br_2(DMSO)_2$	100	
$MoO_2Br_2(MePhSO)_2$	81	98
$MoO_2Br_2(Ph_2SO)_2$	31	84

5222.48(8) Å^3, $Z = 8$, $R = 0.0277$, $R_w = 0.0574$. Crystal data for $MoO_2Br_2(dppmO_2)$: tetragonal, *I4(1)*, yellow, $a = 19.2795(4)$, $b = 19.2795(4)$, $c = 28.7288(8)$ Å, $\alpha = \beta = \gamma = 90°$, $V = 10678.5(4)$ Å^3, $Z = 16$, $R = 0.0390$, $R_w = 0.0549$.

Crystals of $MoO_2Br_2(HMPA)_2$ (block, yellow, dimensions $0.25 \times 0.15 \times 0.05$ mm) and $MoO_2Br_2(dppmO_2)$ (block, yellow, dimensions $0.25 \times 0.25 \times 0.20$ mm) were used for the structure determination. X-ray data were collected using a Brucker SMART CCD area detector single-crystal diffractometer with graphite monochromatized Mo Kα radiation ($\lambda = 0.71073$ Å) by the phi-omega scan method. A total of 1271 frames of intensity data were collected for each compound. The first 50 frames were recollected at the end of data collection to monitor for decay. The integration processes yield a total 16760 for $MoO_2Br_2(HMPA)_2$ and 32541 for $MoO_2Br_2(dppmO_2)$, of which 2992 and 10537, respectively, were independent. Absorption corrections were applied using SADABS program (maximum and minimum transmission coefficients 0.836 and 0.457 for $MoO_2Br_2(HMPA)_2$; and 1.000 and 0.831 for $MoO_2Br_2(dppmO_2)$). The structures were solved using the Brucker SHELXTL-PC software by direct methods and refined by full-matrix least-squares methods on F^2. Hydrogen atoms were included in calculated positions and refined in the riding mode. For $MoO_2Br_2(HMPA)_2$ convergence was reached at a final $R_1 = 0.0277$ [for $I > 2\sigma(I)$], $wR_2 = 0.0635$ (for all data), 129 parameters, with allowance for the thermal anisotropy for all non-hydrogen atoms. Residual electron densities extremes were 0.19 and -0.62 eÅ^{-3} and the goodness-of-fit on F^2 was 0.996 for all observed reflections. For $MoO_2Br_2(dppmO_2)$ convergence was reached at a final $R_1 = 0.0390$ [for $I > 2\sigma(I)$], $wR_2 = 0.0812$ (for all data), 613 parameters, with allowance for the thermal anisotropy for all non-hydrogen atoms. Residual electron densities extremes were 0.45 and -0.48 eÅ^{-3} and the goodness-of-fit on F^2 was 0.884 for all observed reflections. Crystal data and details on the data collection and refinement are given as supplementary material.

3. Results and discussion

3.1. Synthesis and characterization of the complexes

Representative classes of simple ligands that are able to displace water from the coordination sphere of hard metallic centers without significant hydrolysis are amides, sulfoxides and phosphine oxides. Only a very reduced number of addition compounds of MoO_2Br_2 with these ligands has been obtained from aqueous solutions of molybdates in hydrobromic acid [9,12,15]. In our experience it is difficult to obtain pure products by addition of the ligands to aqueous solutions. A large excess of ligand is required to compete successfully with the water present in the system. According to this the use of non aqueous solutions of $MoO_2Br_2(H_2O)_2$ is expected to be superior to the aqueous ones for preparative purposes.

We have found that a number of addition compounds of MoO_2Br_2 with amides, sulfoxides and phosphine oxides can be readily obtained by addition of the stoichiometric, or slightly higher, amount of the ligand to a diethyl ether solution of $MoO_2Br_2(H_2O)_2$. The use of solutions of $MoO_2Br_2(H_2O)_2$ in methyl isobuthyl ketone, a more efficient extractant than diethyl ether for this species, led to less pure products. Other O-donor ligands such as amine oxides and arsine oxides, represented by pyridine oxide and triphenyl arsine oxide, seem to be too basic for the proton to prevent the formation of the corresponding adducts. We also failed in preparing compounds with trimethyl, tributhyl and triphenyl phosphates.

The choice of the solvents and conditions to prepare each compound was essentially based on the solubility of the reactants and the insolubility of the products. We found it is important to dry the starting ether solution with a desiccant inert toward the hydrated dioxomolybdenum(VI) bromide such as magnesium sulfate, as well as to use anhydrous freshly distilled solvents for dissolving the ligands and for the washings, to obtain dry products in high yield. This is surely due to the need of removing the water displaced from the coordination sphere of molybdenum. Indeed, the crude ether extract is water-saturated and usually contains finely dispersed droplets of the aqueous solution so that the precipitates retain the excess water initially present or released in the reaction. The capability of pure diethyl ether to dissolve water helps to obtain dry products.

We failed to find a solvent in which the addition compounds of $OPBu_3$ and $OPOct_3$ were insoluble or could be crystallized. Attempts to purify these bromo-complexes by chromatography on silica or alumina led

to partial decomposition as evidenced by the appearance of blue by-products. So special care is required in the preparation of these compounds by using stoichiometric amounts of reactants. The existence of these waxy compounds should be regarded with caution because of the difficulty for full characterization. However, we propose the usual stoichiometry specially based on ^{31}P NMR evidence.

It is also worth noting that the NMP complex has tendency to form green oils, even when a very pure amide is used. Related to this is the fact that all our attempts to obtain the derivative with *N*,*N*-dimethyl acetamide (DMA) failed, whereas we could prepare $MoO_2Cl_2(DMA)_2$ by a parallel procedure. It is probable that the size of the halogen, plays a decisive role in the low stability of $MoO_2Br_2(NMP)_2$ and in precluding the formation of a stable adduct of MoO_2Br_2 with DMA.

As expected, all compounds have a low thermal stability. However, with the exception of the NMP derivative, they can be stored for weeks at room temperature, and heated to 60 °C in an inert atmosphere for hours, without significant decomposition.

The compounds -excluding those of $OPBu_3$ and $OPOct_3$- are slightly soluble in dichloromethane and chloroform and noticeably more soluble in acetone, solvent in which they are non electrolytes. $MoO_2Br_2(DMSO)_2$ is very soluble in DMSO and behaves as a 1:2 electrolyte. However, the complex can not be readily recovered from the solution. Waxy materials are obtained in all attempts to recover the original product by precipitation with organic solvents, presumably because the displacement of coordinated DMSO in the cationic species $[MoO_2(DMSO)_n]^{2+}$ ($n > 2$) by the bromide ion is difficult.

The IR spectra of the compounds are characterized by two strong bands in the region 880–950 cm^{-1} which indicates that, as usual for dioxomolybdenum(VI) species, all of them contain the *cis*-MoO_2 moiety [3]. A relationship between the position of these bands and the nature of the neutral ligands is expected since the electronic pi-donation from the oxo ligands to molybdenum should be influenced by the electronic density on the metal, in turn affected by the remaining ligands. In this regard it is worth noting that the mean value for ν(Mo=O), $\bar{\nu}(\bar{\nu} = (\nu_s + \nu_{as})/2)$, is lower for sulfoxide than for phosphine oxide complexes. A closer look to these values shows that for each series of compounds $\bar{\nu}$ decreases as the number of aliphatic chains in the ligand increases. According to this, sulfoxides should be stronger donor than phosphine oxides, and alkyl stronger donor than arylderivatives. In the same context, the high $\bar{\nu}$ values displayed by amide complexes suggest that amides are less basic than sulfoxides and phosphine oxides. Consistent with this we have observed that the readily available $MoO_2Br_2(DMF)_2$ is an excellent starting material for the synthesis of sulfoxide and phosphine oxide complexes.

The stretching bands for O–C, O–S and O–P in the coordinated ligands are shifted to lower wavenumbers with respect to those of the free ligands. This is indicative of coordination to molybdenum via the oxygen atom [20].

No special features are observed in the ^1H and ^{31}P NMR spectra of the complexes. The signals characteristic for the free ligands are shifted, as usual, to lower fields upon coordination. However, we have found evidence that the exchange between coordinated and free phosphine oxides does not proceed rapidly at room temperature. Indeed, upon addition of phosphine oxide to samples of the corresponding phosphine oxide complex in $CDCl_3$, two well separated signals are apparent in the ^{31}P NMR spectra. For example, the system $MoO_2Br_2(OPBu_3)_2$–$OPBu_3$ shows two signals at 50.0 ppm for free, and at 68.1 ppm for coordinated ligand. This behavior can be exploited to test the purity of the tributhyl and triocthyl phosphine oxide complexes, difficult to prepare and characterize, and eventually to transform a non stoichiometric product into the stoichiometric one.

3.2. Molecular structures

Based on the stoichiometry and structure for similar adducts it is probable that all compounds be closely related. The molecular structure for $MoO_2Br_2(HMPA)_2$ and $MoO_2Br_2(dppmO_2)$ was determined from single-crystal X-ray diffraction analysis. A view of $MoO_2Br_2(HMPA)_2$ is shown in Fig. 1. Fig. 2 shows the two distortional isomers, (a) and (b), of $MoO_2Br_2(dppmO_2)$ present in the unit cell. Selected bond lengths and angles are listed in Table 2.

As expected, the molybdenum is coordinated in a pseudo-octahedral fashion by two *cis* oxo, two *trans* bromide, and two *cis* O-donor ligands. Distortions from

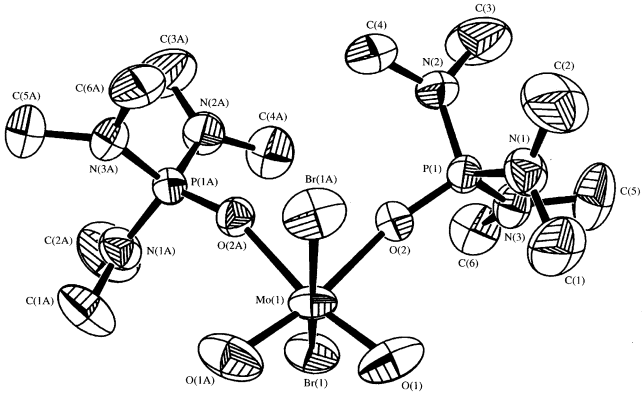


Fig. 1. Molecular structure and atom-labeling scheme for $MoO_2Br_2(HMPA)_2$, (50% probability ellipsoids); hydrogen atoms are omitted.

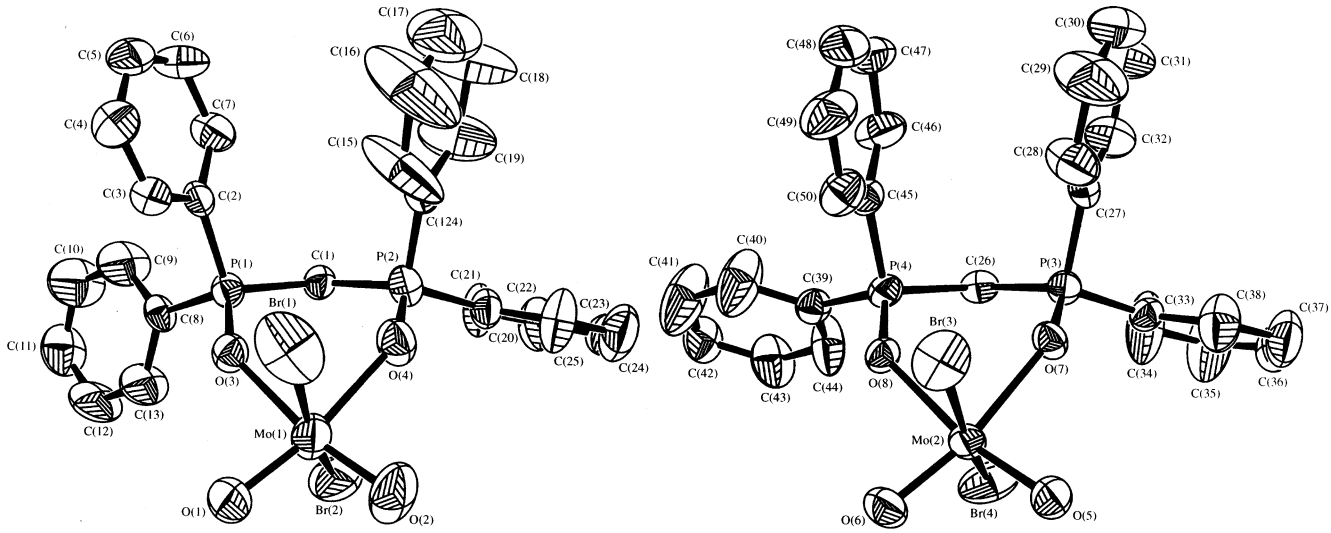


Fig. 2. Molecular structure and atom-labeling scheme for $MoO_2Br_2(dppmO_2)$, (50% probability ellipsoids); hydrogen atoms are omitted.

the theoretical octahedral geometry (see Table 2) are explained in terms of interligand repulsions.

The Mo–O(oxo) bond lengths, and the *cis*-$MoO(oxo)_2$ angles, are within the narrow range usually found in dioxomolybdenum(VI) compounds (1.65–1.75 Å and 95–110°, respectively). The Mo–Br distances, and the Br–Mo–Br angles, are comparable to those reported for other $MoO_2Br_2L_2$ complexes [5,11–16].

$MoO_2Br_2(HMPA)_2$ shows three couples of identical Mo-ligand distances. However, in $MoO_2Br_2(dppmO_2)$ the Mo-ligand distances in each pair of bonds with the same ligand are slightly different, which is probably due

Table 2
Selected bond lengths (Å) and angles (°) for $MoO_2Br_2(HMPA)_2$ and $MoO_2Br_2(dppmO_2)$

$MoO_2Br_2(HMPA)_2$		$MoO_2Br_2(dppmO_2)$			
		Unit A		Unit B	
Bond lengths					
Mo(1)–O(1)	1.690(3)	Mo(1)–O(1)	1.677(4)	Mo(2)–O(6)	1.678(4)
Mo(1)–O(1A)	1.690(3)	Mo(1)–O(2)	1.680(4)	Mo(2)–O(5)	1.690(4)
Mo(1)–O(2)	2.164(2)	Mo(1)–O(3)	2.163(4)	Mo(2)–O(8)	2.192(3)
Mo(1)–O(2A)	2.164(2)	Mo(1)–O(4)	2.197(4)	Mo(2)–O(7)	2.212(3)
Mo(1)–Br(1)	2.5617(3)	Mo(1)–Br(1)	2.5166(11)	Mo(2)–Br(3)	2.5295(8)
Mo(1)–Br(1A)	2.5617(3)	Mo(1)–Br(2)	2.5825(10)	Mo(2)–Br(4)	2.5566(8)
P(1)–O(2)	1.480(2)	P(1)–O(3)	1.518(4)	P(4)–O(8)	1.502(4)
P(1A)–O(2A)	1.480(2)	P(2)–O(4)	1.507(4)	P(3)–O(7)	1.488(4)
Bond angles					
O(1)–Mo(1)–O(1A)	101.9(3)	O(1)–Mo(1)–O(2)	102.3(2)	O(6)–Mo(2)–O(5)	101.92(17)
O(2)–Mo(1)–O(2A)	77.85(12)	O(3)–Mo(1)–O(4)	78.28(14)	O(8)–Mo(2)–O(7)	77.49(13)
O(1)–Mo(1)–O(2A)	167.96(15)	O(1)–Mo(1)–O(3)	88.75(17)	O(6)–Mo(2)–O(8)	90.36(16)
		O(2)–Mo(1)–O(4)	90.47(19)	O(5)–Mo(2)–O(7)	90.20(15)
O(1)–Mo(1)–O(2)	90.15(13)	O(1)–Mo(1)–O(4)	166.29(18)	O(6)–Mo(2)–O(7)	167.85(16)
		O(2)–Mo(1)–O(3)	168.50(18)	O(5)–Mo(2)–O(8)	167.42(16)
Br(1)–Mo(1)–Br(1A)	167.05(3)	Br(1)–Mo(1)–Br(2)	163.59(4)	Br(3)–Mo(2)–Br(4)	166.43(3)
Br(1)–Mo(1)–O(1)	93.55(9)	O(1)–Mo(1)–Br(1)	98.21(16)	O(6)–Mo(2)–Br(3)	94.59(15)
Br(1)–Mo(1)–O(1A)	94.60(9)	O(1)–Mo(1)–Br(2)	93.04(17)	O(6)–Mo(2)–Br(4)	93.59(15)
Br(1)–Mo(1)–O(2)	85.40(5)	O(4)–Mo(1)–Br(1)	85.11(11)	O(7)–Mo(2)–Br(3)	84.74(9)
Br(1)–Mo(1)–O(2A)	84.54(5)	O(4)–Mo(1)–Br(2)	81.25(11)	O(7)–Mo(2)–Br(4)	84.99(9)
P(1)–O(2)–Mo(1)	158.59(15)	P(1)–O(3)–Mo(1)	144.0(2)	P(4)–O(8)–Mo(2)	140.6(2)
P(1A)–O(2A)–Mo(1)	158.59(15)	P(2)–O(4)–Mo(1)	141.6(2)	P(3)–O(7)–Mo(2)	140.8(2)

to different interligand repulsions derived from the non planar conformation of the chelate ring. The Mo–O(neutral ligand) in the HMPA complex is significantly shorter than those in that of $dppmO_2$, as expected according to the superior basicity of HMPA with respect to phosphine oxides.

In $MoO_2Br_2(dppmO_2)$ the diphosphine dioxide behaves in the usual manner, bidentate chelate [21], although the ligand is also known to function in other complexes as bridging [22] and monodentate [23]. It should be noted that in the unit cell there are two distinct molecules, that can be regarded as distortion isomers. This fairly peculiar behavior is presumably due to packing forces.

3.3. Oxidant ability of the complexes

In a previous paper we reported that $MoO_2Br_2(DMSO)_2$ catalyzes the oxotranfer from DMSO to PPh_3 [17]. Here, we have found that these compounds react with excess of common organophosphines and phosphites at room temperature leading to brown or green solutions. This is indicative of oxotransfer processes from the dioxomolybdenum center to the P-oxoaceptor. The evolution of the foul-smelling dimethyl sulphide was detected with the DMSO complex, suggesting the potential of the sulfoxide complexes to work as oxotransfer catalysts from sulfoxides to phosphorus(III) compounds.

As these compounds are relatively resistant to hydrolysis, it is worth testing their oxidant capability in reactions in which water is produced. That some dioxomolybdenum complexes are able to oxidize thiols to disulphides was proved years ago [24]. To compare the oxidizing potential of the bromocomplexes for this transformation we have measured the rate of oxidation of *tert*-buthylmercaptan, a thiol somewhat resistant to oxidation, to the corresponding disulphide. For this study, we used a molar ratio thiol/bromocomplex = 4, on the assumption that Mo(VI) could be reduced to Mo(IV) in the oxidation process and that replacement of bromide by thiolate in the coordination sphere of molybdenum might eventually occur.

Table 1 shows the percent conversion of thiol to disulphide at 3 and at 24 h, when the reaction is virtually stopped in all cases except that of the Ph_2SO complex which requires about 3 days for completion. The results from these observations can be summarized as follows.

No evidence of replacement of bromide by thiolate was found during the process, according to the persistence in the position of the signals corresponding to the thiol.

For amide and phosphine oxide complexes the reaction stops in the vicinity of 25% thiol oxidation. As the reaction progresses a green or brown color develops in the solution and a blue solid forms. This suggests that, in case oxomolybdenum(IV) species were initially formed, they comproportionate with the parent dioxomolybdenum(VI) complex to afford oxomolybdenum(V) products resistant to reduction. Examination by IR spectroscopy of the solids formed at the end of the process showed the absence of dioxomolybdenum(VI) species, but the information was insufficient to demonstrate that only a dinuclear oxomolybdenum(V) product was formed. It is probable that deviations from 25% conversion (the ideal value for reduction of Mo(VI) to Mo(V)) are due to decomposition processes.

The sulfoxide bromocomplexes oxidize complete and selectively the thiol to disulphide. The rate of oxidation decreases from DMSO to MePhSO to Ph_2SO. Under these conditions the free sulfoxides do not react with the thiol. Since the thiol is unable to reduce dioxomolybdenum(VI) beyond oxomolybdenum(IV) we conclude that these complexes behave as oxotransfer catalysts for the oxidation of *tert*-buthylmercaptan to *tert*-buthyldisulphide.

4. Supplementary material

Crystallographic data for the structural analysis have been deposited with the Cambridge Crystallographic Data Centre, CCDC Nos. 156946 and 175434 for $[MoO_2Br_2(OP[N(CH_3)_2]_3)_2]$ and $[MoO_2Br_2(CH_2[P(O)(C_6H_5)_2]_2)]$, respectively. Copies of this information may be obtained free of charge from The Director, CCDC, 12 Union Road, Cambridge, CB2 1EZ, UK (fax: +44-1223-336033; e-mail: deposit@ccdc.cam.ac.uk or www: http://www.ccdc.cam.ac.uk).

Acknowledgements

This work was supported by the Junta de Castilla y Leon (Grant BU14/98).

References

[1] R.H. Holm, Chem. Rev. 87 (1987) 1401 (and references therein).
[2] R.H. Holm, Coord. Chem. Rev. 100 (1990) 183 (and references therein).
[3] J.H. Enemark, C.G. Young, Adv. Inorg. Chem. 40 (1994) 2.
[4] R.H. Holm, P. Kennepohl, E.I. Solomon, Chem. Rev. 96 (1996) 2239 (and references therein).
[5] F.E. Kuhn, E. Herdtweck, J.J. Haider, W.A. Herrmann, I.S. Goncalves, A.D. Lopes, C.C. Romao, J. Organomet. Chem. 583 (1999) 3.
[6] E.I. Stiefel, in: G. Wilkinson, R.D. Gillard, J.A. McCleverty (Eds.), Comprehensive Coordination Chemistry, vol. 3 (Chapter 36.5), Pergamon, Oxford, 1987, p. 1375.
[7] R. Colton, I.B. Tomkins, Aust. J. Chem. 18 (1965) 447.
[8] A. Levason, R. Narayanaswamy, J.S. Ogden, A.J. Rest, and J.W. Turff, J. Chem. Soc., Dalton Trans. (1982) 2009.

[9] R.J. Butcher, H.P. Ganz, R.G.A.R Maclagan, H. Kipton, J. Powell, C.J. Wilkins, Y.S. Hian, J. Chem. Soc., Dalton Trans. (1975) 1223.
[10] Y. Hayashi, S. Shioi, M. Togani, T. Sakan, Chem. Lett. (1973) 651.
[11] R.H. Fenn, J. Chem. Soc. (A) (1969) 1764.
[12] R.J. Butcher, B.R. Penfold, E. Sinn, J. Chem. Soc., Dalton Trans. (1979) 668.
[13] H. Arzoumanian, G. Agrifoglio, H. Krentzien, M. Capparelli, Chem. Commun. 6 (1995) 655.
[14] J.R. Backhouse, H.M. Lowe, E. Sinn, S. Suzuki, S. Woodward, J. Chem. Soc., Dalton Trans. (1995) 1489.
[15] M.J. Taylor, C.E.F. Rickard, L.A. Kloo, J. Chem. Soc., Dalton Trans. (1998) 3195.
[16] F.J. Arnáiz, R. Aguado, M.R. Pedrosa, J. Mahia, M.A. Maestro, Polyhedron 20 (2001) 2781.
[17] F.J. Arnáiz, R. Aguado, J.M. Martínez-Ilarduya, Polyhedron 13 (1994) 3257.
[18] J.M. Coddington, M.J. Taylor, J. Chem. Soc., Dalton Trans. (1990) 41.
[19] R. Pürschel, E. Lassner, R. Scharf, Zeitschr. Anal. Chem. 163 (1958) 104.
[20] see, e.g.: K. Nakamoto, Infrared and Raman Spectra of Inorganic and Coordination Compounds, 5th ed., Wiley, New York, 1997.
[21] see, e.g.: E. Bermejo, A. Castineiras, R. Dominguez, C. Schule, J. Coord. Chem. 33 (1994) 353.
[22] E.J. Fernandez, P.G. Jones, A. Laguna, A. Mendia, Inorg. Chim. Acta 215 (1994) 229.
[23] S. Bhattacharyya, I. Chakravorty, B.K. Dirghangi, A. Chakravorty, Chem. Commun. (2000) 1813.
[24] J.P. Caradonna, E.W. Harlan, R.H. Holm, J. Am. Chem. Soc. 108 (1986) 7856.

water molecule to the copper(II) ion in the complexes with *N*,*N*-dimethyl isoleucine, or *N*,*N*-dimethyl-valine.

The interactions of amino acid side-chains in the metal ion complexes were studied by potentiometric pH-titrations [4,5]. Sigel and coworkers pointed out that in organic solvents interactions between aliphatic amino acid side-chains can be formed only if 2N–2O atoms in the ligand field of the copper(II) ion in the complex were arranged in the *trans*-fashion. In such an arrangement, the amino acid side-chains are located on the same side of the metal-ion coordination sphere allowing aliphatic van der Waals contacts. Upon addition of organic solvents the shift in equilibrium between *cis*- and *trans*-isomers was detected in a number of copper(II) complexes by EPR spectroscopy [6].

The crystal structures of the two modifications of bis[*N*,*N*-dimethyl-isoleucinato]copper(II), with [7] and without [8] apical water, showed different conformations of the amino acid side-chains. In the complex with bound water amino acid side-chains were located in the equatorial plane, while in the absence of apical water, in the axial position. The crystal structure of bis[*N*,*N*-dimethyl-alaninato]copper(II), resolved recently, showed the copper(II) coordination polyhedron strongly distorted [9].

In this work, the role of the water molecule coordinated to the copper(II) on the motional properties of bis[*N*,*N*-dimethyl-isoleucinato]copper(II) complex dissolved in deuterated methanol is investigated. Our hypothesis is that in the methanol solution exchange of the apical water molecule between the copper(II) ion and the solvent in bis[*N*,*N*-dimethyl-L-α-isoleucinato]copper(II) may be related to the conformation change of the amino acid side-chains.

2. Experimental

2.1. Methods

The EPR spectra of the two complexes were studied as a function of temperature (from 276 to 334 K) at two microwave frequencies (S-band, $\nu = 3.860$ GHz, and X-band, $\nu = 9.346$ GHz). The X-band EPR spectra were taken on a Varian E-109 spectrometer, equipped with a Bruker variable temperature control unit. The aqueous solution cell was previously dried with nitrogen stream.

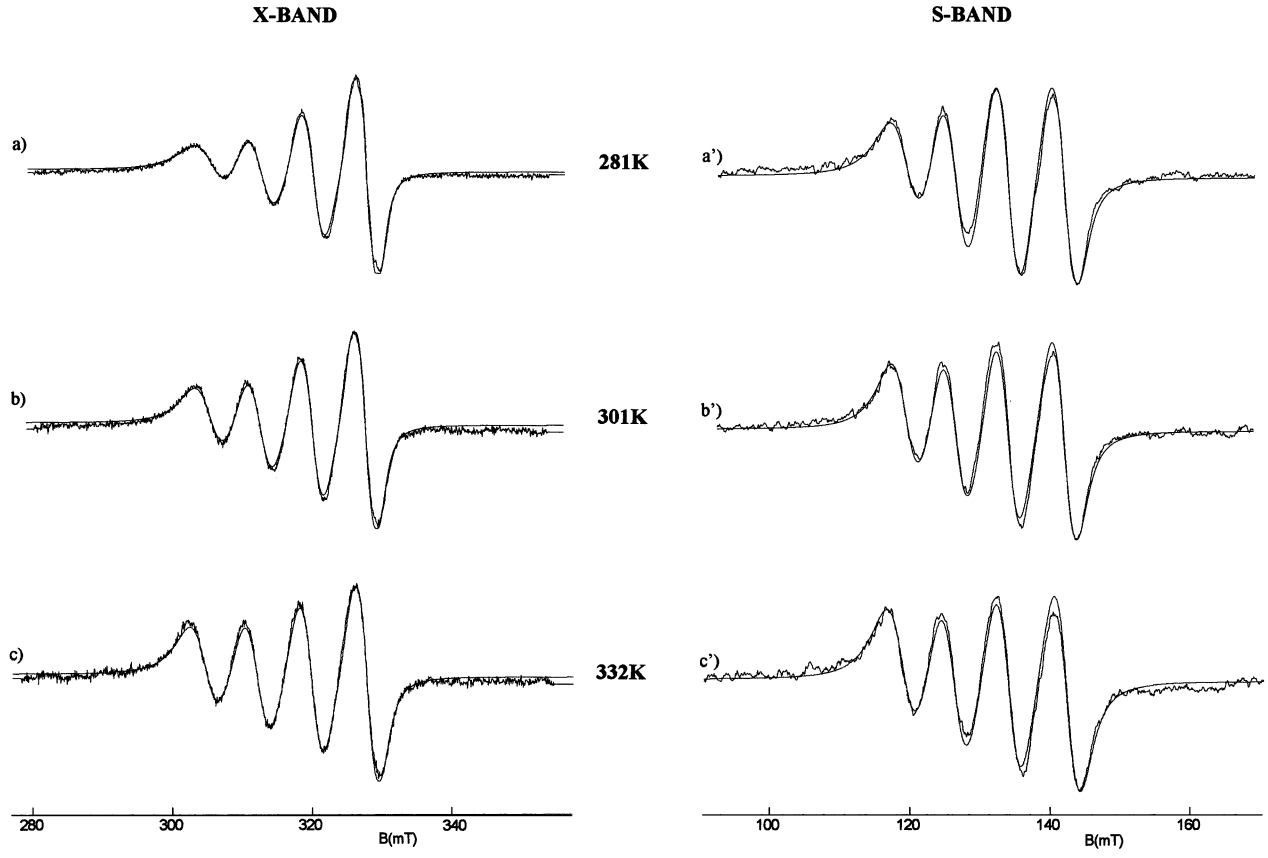


Fig. 1. EPR spectra of bis[*N*,*N*-dimethyl-L-α-alaninato]copper(II) dissolved in dried deuterated methanol and taken at X-band ($\nu = 9.346$ GHz) at; a, 281 K; b, 301 K; c, 332 K and at S-band ($\nu = 3.870$ GHz) at a′, 281 K; b′, 301 K; c′, 332 K. The spectra are fitted with the COSMOS program and the EPR spectral parameters characteristic for the blue complex with bound water are reported in Table 1.

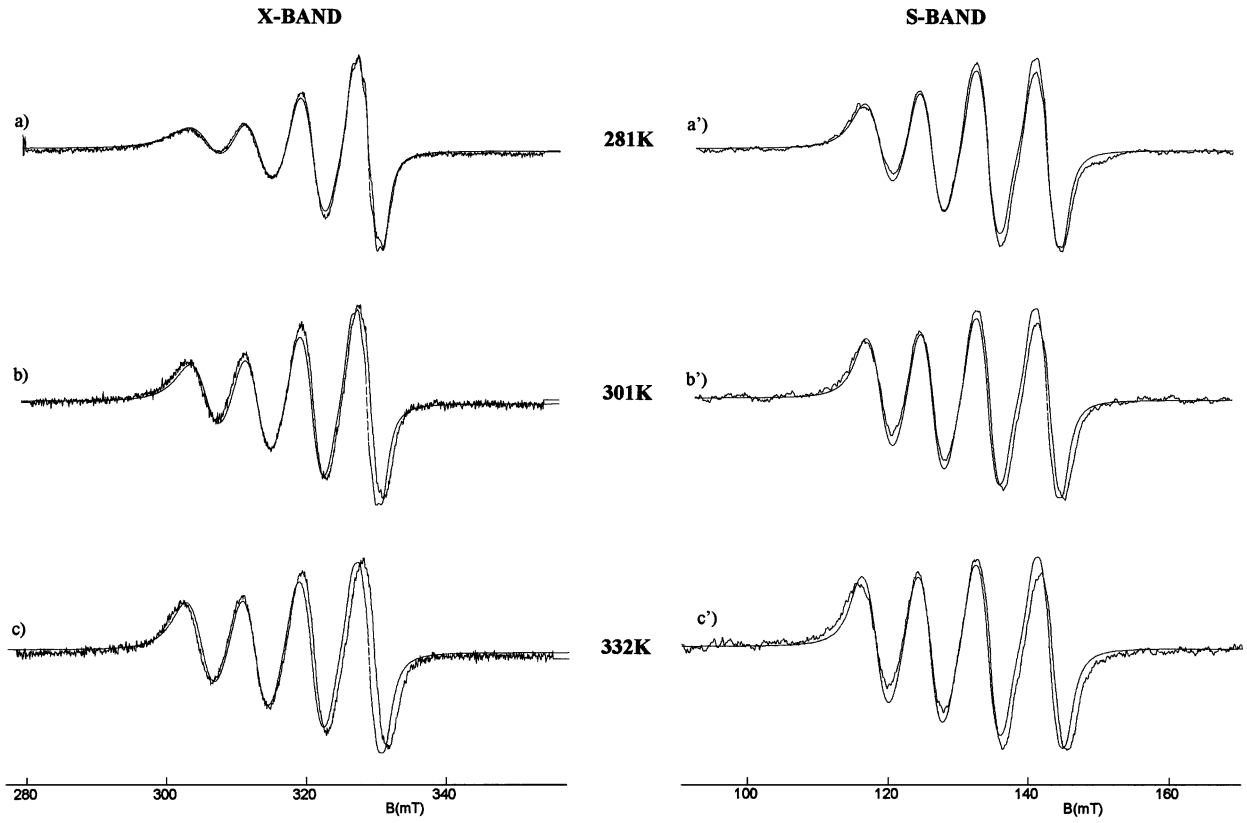


Fig. 2. EPR spectra of bis[*N*,*N*-dimethyl-L-α-isoleucinato]copper(II) dissolved in dried deuterated methanol and taken as a function of the temperature at X-band ($\nu = 9.346$ GHz) at: a, 281 K; b, 301 K; c, 332 K; and at S-band ($\nu = 3.870$ GHz) at a′, 281 K; b′, 301 K; c′, 332 K. The spectra are fitted with the COSMOS program and the EPR spectral parameters characteristic for the blue water complex are reported in Table 1(a).

The S-band EPR spectra were recorded with a microwave bridge, equipped with the loop-gap resonator, from Jagmar (Krakow, Poland) and with a Bruker variable temperature control unit. Microwave frequencies were measured with an XL Microwave Model 3120 counter (Jagmar).

The *g*-factor was measured relative to diphenyl-picryl-hydrazil (DPPH), as an external marker ($g_{DPPH} = 2.0036 \pm 0.0003$). The extra dry (dried over molecular sieves) deuterated methanol was purchased from Cambridge isotope Laboratory USA. The EPR flat cell was closed with the stopper and protected from air humidity with parafilm. Concentrations of about 0.1 mmol dm^{-3} of the complexes were used. Temperature dependence of the methanol viscosity was measured in the viscosimeter with a falling ball.

2.2. Complexes preparation

Amino acids (Merck) were methylated by the method of Bowman and Stroud [10]. Ligands were characterized by elemental analysis, NMR and mass spectroscopy.

2.2.1. Elemental analysis

N,*N*-dimethyl-L-α-alanine (M.W. = 117.0), white crystals (melting point, m.p. = 182–183 °C), elemental analysis: C (Calc. 51.26%) 51.2%; N (Calc. 11.96%) 11.99%; H (Calc. 9.46%) 9.34%. *N*,*N*-dimethyl-L-α-isoleucine (M.W. = 159 150), white hygroscopic crystals (m.p. = 162–163 °C), elemental analysis: C (Calc. 60.34%) 60.21%; N (Calc. 8.79%) 9.02%; H (Calc. 10.76%) 10.66%. The copper(II) complexes were prepared by the method by Nash and Shaefer [11].

3. Theory

EPR spectra of bis[aminoacidato]copper(II) complexes are determined by four resonance transitions arising from the hyperfine coupling between the electron spin of the copper(II) (configuration $3d^9$) and the nuclear spin ($I_{Cu} = 3/2$). The position of the lines are determined by the hyperfine tensor A_{Cu} and a *g*-tensor related to the spin-orbit coupling. The average of the diagonal values of *g* and A_{Cu} tensors is observed in solutions, and the rotational correlation time of the complex (τ_2), the time modulating the energies related to *g* and *A* anisotropy, describes the dynamics of the system in solutions [12–17].

The EPR spectra were calculated by COSMOS program developed by G. della Lunga, R. Pogni and R. Basosi [18,19]. The EPR simulation program COSMOS can cover

Table 1
EPR magnetic parameters of the copper(II) complexes

	g_{xx}	g_{yy}	g_{zz}	A_{xx} (mT)	A_{yy} (mT)	A_{zz} (mT)	a_N (mT)
$Cu(DMA)_2$ [a] (276–332) K	2.041±0.001	2.044±0.001	2.251±0.001	2.56±0.1	2.56±0.1	17.8±0.1	1.02±0.05
$Cu(DMil)_2$ [a](276–300) K (a)	2.036±0.001	2.036±0.001	2.247±0.001	2.58±0.01	2.59±0.01	18.5±0.01	1.08±0.05
(308–332) K (b)	2.032±0.002	2.036±0.001	2.247±0.001	2.79±0.1	2.87±0.1	18.9±0.1	1.10±0.05

[a] Cu(DMA)2-bis[*N*,*N*-dimethyl-L-α-alaninato]copper(II); $Cu(DMil)_2$-bis[*N*,*N*-dimethyl-L-α-isoleucinato]copper(II).

virtually all of the dynamic conditions of copper(II) complexes, from 'fast tumbling' to 'incipient slow motion' in the computer program. The program allows the simultaneous occurrence of the two copper(II) isotopes to be considered. A procedure for the best fit of the experimental spectrum, based on the minimization program [19] is to allow variations of the input magnetic parameters, as well as the rotational correlation time τ_2. The program calculates line-positions, lineshapes and linewidths. In the program, the spin-rotational contribution [13] was included. In the fast motion region the approximation for the rotational correlation time holds:

$$\tau_2 = \frac{1}{6\sqrt{D_{xy}D_{zz}}}$$

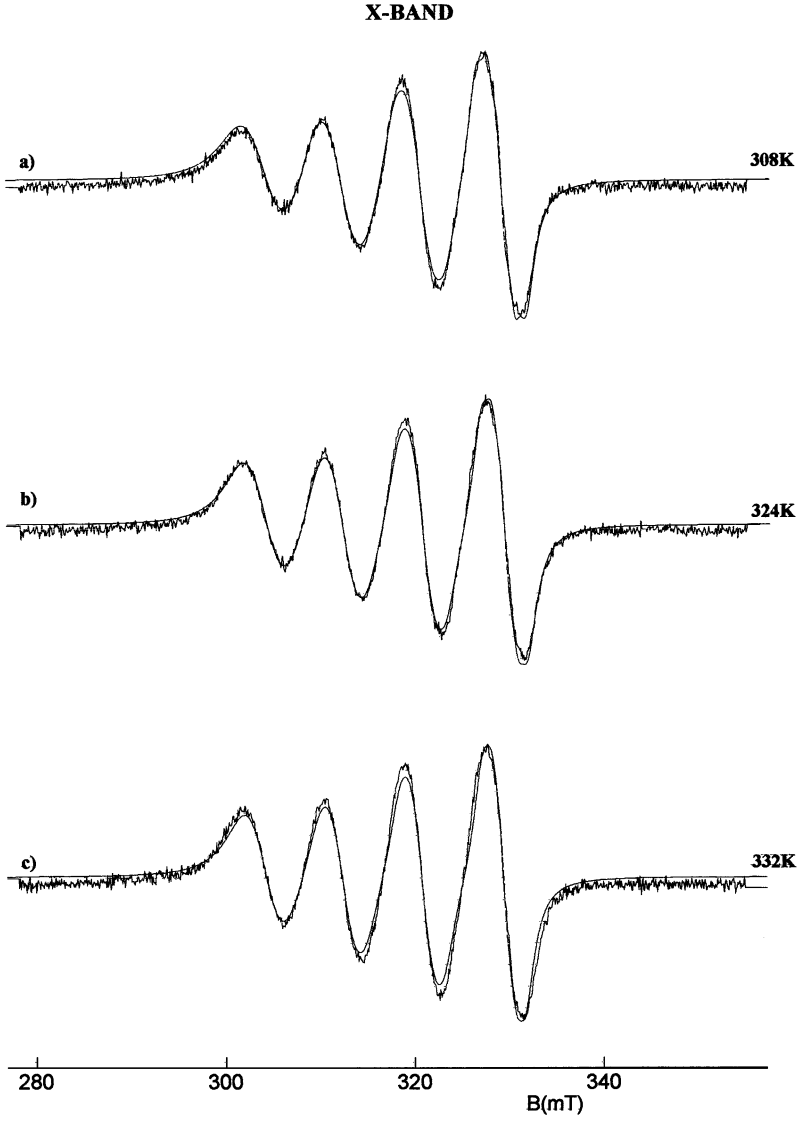


Fig. 3. X-band ($\nu = 9.346$ GHz) EPR spectra of bis[*N*,*N*-dimethyl-L-α-isoleucinato]copper(II) dissolved in dried deuterated methanol and taken at, a, 308 K; b, 324 K; c, 332 K. The spectra are fitted with the COSMOS program with EPR parameters characteristic for the complex without apical water, Table 1(b).

where D_{xy} and D_{zz} are the diffusion tensor components. For the isotropic motion the diffusion tensor components can be considered equal. The best fit of the experimental spectra was found using the Simplex and Levenberg–Marquardt optimization procedures.

4. Results and discussion

Multifrequency EPR analysis [15,16] combined with computer simulations of the EPR spectra in solutions, is a useful tool for determination of the chemical structures and dynamic properties of copper(II) complexes in systems of biological interest. The requirements for a good fit of the copper(II) spectra recorded at different microwave frequencies put constraints on the chosen EPR parameters. Then, computer simulations of the EPR spectra minimize problems arising from the lack of details of the room temperature (r.t.) experimental spectra, and permit determination of dynamic properties of the copper(II) complexes (i.e. the rotational correlation time, τ_2).

The reorientation correlation time τ_2, describes Brownian motion of the Cu(II) complex in solution and is expressed as: $\tau_2 = (1/k)V_{\text{eff.}}(\eta/T)\kappa$, where $V_{\text{eff.}}$ is the effective volume of the complex, η is the viscosity of the solvent, k is the Boltzman constant, T is the temperature (in K) and κ is the anisotropic interaction parameter, the second rank tensor related to EPR spectral parameters [20]. If the copper(II) complex retains one conformation in the examined temperature interval, τ_2 will be a linear function of η/T, with the coefficient of linearity proportional to the effective volume of the solvatized complex.

In Fig. 1, the EPR spectra of bis[*N*,*N*-dimethyl-L-α-alaninato]copper(II) in dried deuterated methanol solution taken at 281 K (a) 301 K (b) 332 K (c) at X-band, and (a′), (b′), (c′), at S-band, are reported. In Fig. 2, the EPR spectra of bis[*N*,*N*-dimethyl-L-α-isoleucinato]copper(II) dissolved in dried deuterated methanol taken at, 281 K (a), 308 K (b), 332 K (c) at X-band, and (a′), (b′), (c′) at S-band are displayed. For each temperature, the line shapes of the spectra were fitted with COSMOS program. The starting magnetic parameters for the fast motion simulations were obtained from the corresponding low temperature EPR spectra ($T = 77$ K).

The simulated spectra of the bis[*N*,*N*-dimethyl-L-α-alaninato]copper(II) complex (Fig. 1), show a good fit with the experimental ones. The simulations have been obtained using the same g and a parameters (Table 1) for all the temperatures at both frequencies. Only the diffusion tensor components were free to vary in order to fit properly the line shapes of the EPR spectra with the temperature variation. On the other hand, in the case of bis[*N*,*N*-dimethyl-L-α-isoleucinato]copper(II) (Fig. 2) the fit (Table 1(a)) is not so good for all the examined temperatures. Above 300 K, a shift of g_o to lower values, concomitant with an increase of a_o is observed for all the recorded spectra.

In Fig. 3, the X-band EPR spectra of the bis[*N*,*N*-dimethyl-isoleucinato]copper(II) taken at 308 K (spectrum a), 324 K (spectrum b) and 332 K (spectrum c), are

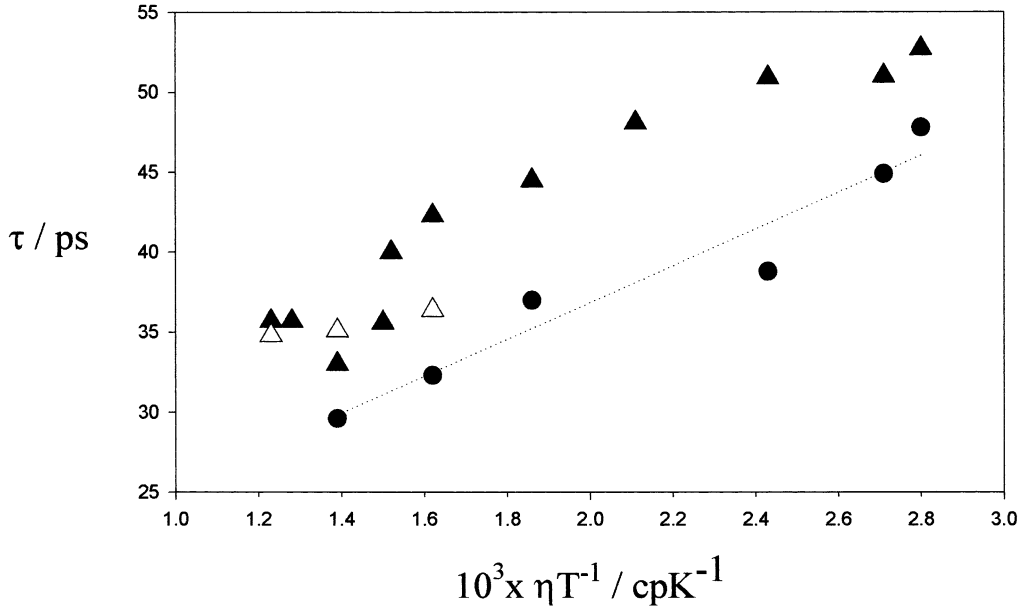


Fig. 4. Reorientation correlation times, τ_2 (ps), of the two complexes dissolved in CD_3OD, as a function of the viscosity of the solvent, η (poise $\times 10^{-3}$), over the temperature, T (K) are reported. Each point on the curve is obtained by fitting the experimental EPR spectra with the COSMOS program: circles, bis[*N*,*N*-dimethyl-L-α-alaninato]copper(II); black triangles, bis[*N*,*N*-dimethyl-L-α-isoleucinato]copper(II); white triangles, τ_2 (ps) values for the bis[*N*,*N*-dimethyl-L-α-isoleucinato]copper(II) complex without apical water.

displayed. The spectra are paired with the simulations that gave the best fit with the parameters reported in Table 1(a). As the simulated spectra reported in Fig. 2 do not fit well the experimental ones, a new fit with different g and a values for the EPR spectra above 300 K is attempted (see Fig. 3 and Table 1(b)). The difference in the parameters (Table 1(a and b)) in the two cases, may be ascribed to the release of the apical water from the copper coordination sphere above 300 K with the concomitant formation of the complex without apical water [3].

The values of the rotational correlation time, τ_2, determined from the calculated EPR spectra are plotted as a function of η/T and are compared in Fig. 4 for the two copper(II) complexes studied. A linear dependence of the rotational correlation time, τ_2, on η/T for bis[*N*,*N*-dimethyl-L-α-alaninato]copper(II) (circles) is observed. The slope of the straight line determined for the alaninato complex is related to the effective volume of the complex and suggests one conformation of the complex in the whole temperature range measured. A reversible temperature dependence was obtained.

More complex and irreversible dependence of τ_2 on η/T is obtained for bis[*N*,*N*-dimethyl-isoleucinato]copper(II) (Fig. 4, triangles). Smaller values of the rotational correlation time τ_2 than predicted for the linear dependence of τ_2 on η/T are obtained at the temperatures above 300 K, suggesting a smaller effective volume of the solvated complex. The change may be related to the release of the apical water molecule from the complex, because EPR spectra taken above 300 K were fitted better (Fig. 3) with the parameters (Table 1(b)) similar to the complex dissolved in the dried CH_2Cl_2. The complex dissolved in CH_2Cl_2 was fitted well with parameters: $g_o = 2.109$; $g_{||} = 2.248$; $g_{\perp} = 2.040$; $a_o = 9.1$ mT; $a_{||} = 18.5$ mT; $a_{\perp} = 4.4$ mT (Simfonia, Bruker). The straight line of τ_2 on η/T in the whole temperature interval 245–300 K was obtained [21].

The τ_2 values displayed in Fig. 4 are obtained using the equation reported in the experimental part, under the reasonable assumption of the isotropic motion of the

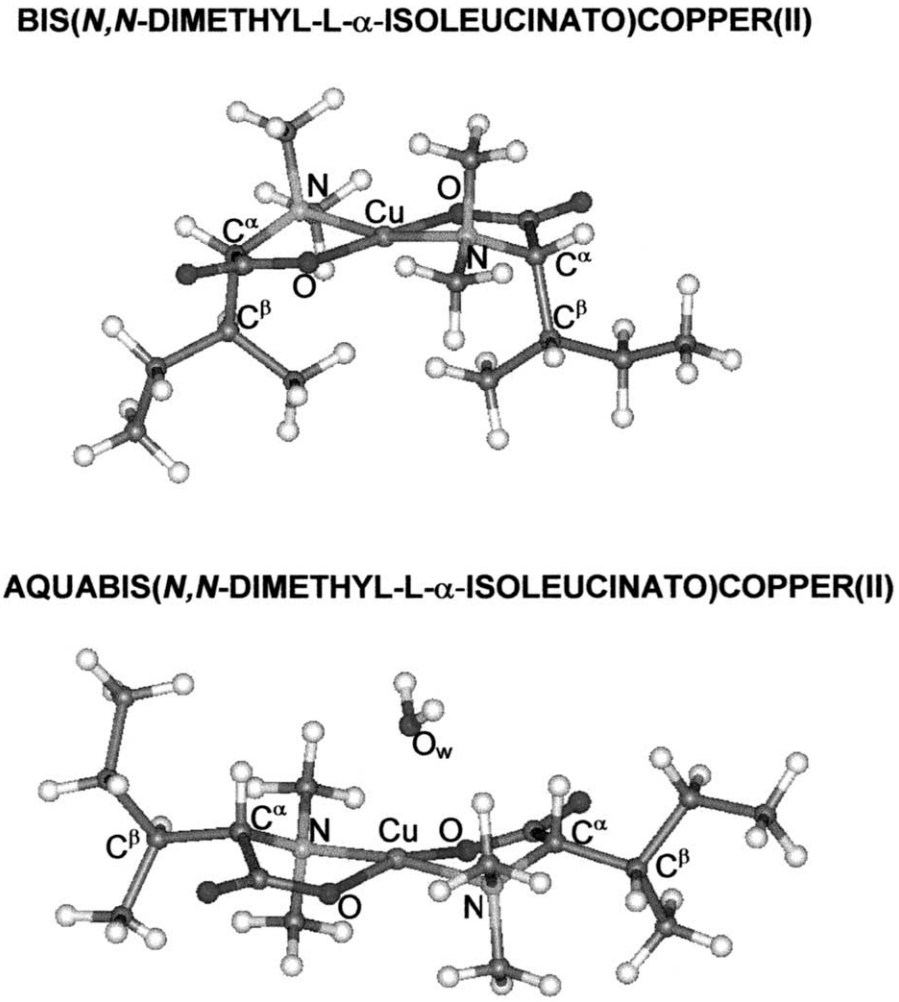


Fig. 5. Proposed conformation change for binding of water molecule to bis[*N*,*N*-dimethyl-L-α-isoleucinato]copper(II).

two complexes. Nevertheless, a more careful analysis of the diffusion tensor components for the two complexes had to be attempted. In the case of the bis[*N*,*N*-dimethyl-L-α-alaninato]copper(II) complex, the best fit of the spectra was obtained if D_{zz} was kept unchanged in the whole range of temperatures. For the bis[*N*,*N*-dimethyl-isoleucinato]copper(II) complex a more anisotropic motion might be inferred, because the best fit could only be obtained with decreasing values of D_{zz} with increase of temperature. This is evident in the whole range of temperature examined, probably due to the longer aliphatic side-chains (2-methyl-buthyl-) compared with that of the bis[*N*,*N*-dimethyl-L-α-alaninato]copper(II) complex (–methyl). Above 300 K, the anisotropic motion of the isoleucinato complex is always present, but the differences in the diffusion tensor components are accompanied by changes in the magnetic parameters suggesting formation of another complex, probably one without the apical water.

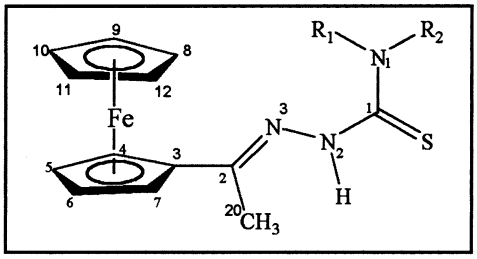
5. Conclusions

Temperature dependence of the Brownian motion of the examined copper(II) complexes in dried deuterated methanol solutions is studied by EPR spectroscopy. Linear temperature dependence of the rotational correlation time, τ_2 on η/T is obtained for bis[*N*,*N*-dimethyl-L-α-alaninato]copper(II), of short amino acid side-chains (–methyl). In the whole temperature range examined (276–332 K), EPR spectra of this complex are fitted well with the parameters that we ascribe to the complex with bound water, suggesting one type of the complex solute–solvent interaction.

More complex temperature dependence of τ_2 on η/T is obtained for the bis[*N*,*N*-dimethyl-L-α-isoleucinato]copper(II), of the longer aminoacid side-chains (2-methyl–butyl–). The EPR parameters characteristic for the complex with bound water could not fit the EPR spectra above 300 K. The parameters that fit well the EPR spectra of this complex above 300 K, are very close to those of the copper(II) complex without the apical water [21]. Smaller values of τ_2 than predicted above 300 K, indicate conformation change of the complex above that temperature, concomitant with the release of the apical water from the copper(II) coordination sphere (Fig. 5).

References

[1] V.A. Davankov, A.A. Kurganov, Chromatographia 17 (1993) 86.
[2] V. Noethig-Laslo, N. Paulić, Polyhedron 18 (1999) 1609.
[3] V. Noethig-Laslo, N. Paulić, Z. Anorg. Allg. Chem. 621 (1995) 84.
[4] B.E. Fischer, H. Sigel, J. Am. Chem. Soc. 102 (1980) 2998.
[5] G. Liand, R. Tribolet, H. Sigel, Inorg. Chim. Acta 155 (1989) 273.
[6] V. Noethig-Laslo, N. Paulić, J. Chem. Soc., Dalton Trans. (1992) 2045.
[7] B. Kamenar, M. Penavić, A. Škorić, N. Paulić, N. Raos, V.I. Simeon, J. Coord. Chem. 17 (1988) 85.
[8] B. Kaitner, N. Paulić, N. Raos, J. Coord. Chem. 22 (1991) 269.
[9] B. Kaitner, G. Pavlović, N. Paulić, N. Raos, J. Coord. Chem. 43 (1998) 309.
[10] R.E. Bowman, H.H. Stroud, J. Chem. Soc. 20 (1951) 1342.
[11] C.P. Nash, W.P. Schaefer, J. Am. Chem. Soc. 91 (1969) 1319.
[12] H.M. Mc Connell, J. Phys. Chem. 25 (1964) 709.
[13] P.W. Atkins, D. Kivelson, J. Chem. Phys. 44 (1966) 169.
[14] A.M. Dezor, Acta Phys. Pol. A 56 (1979) 385.
[15] J.S. Hyde, W. Froncisz, Ann. Rev. Biophys. Bioeng. 11 (1982) 391.
[16] B.N. Misra, R. Kripal, Acta Phys. Pol. A76 (1989) 869.
[17] R. Basosi, W. Antholine, J.S. Hyde, Biol. Magn. Res. 13 (1993) 103.
[18] G.della Lunga, R. Pogni, R. Basosi, J. Phys. Chem. 98 (1994) 3937.
[19] G.della Lunga, R. Pogni, R. Basosi, Mol. Phys. 95 (1998) 1275.
[20] J. Hwang, D. Kivelson, W. Plachy, J. Chem. Phys. 58 (1973) 1753.
[21] K. Mirosavljević, Thesis B.Sc. degree (2002) p. 25.



HL[1] $R_1=R_2=H$
HL[2] $R_1=H$, $R_2=Me$
HL[3] $R_1=H$, $R_2=Ph$
HL[4] $R_1=H$, $R_2=Et$
HL[5] $R_1=R_2=Me$

Scheme 1.

HL^1–HL^5 (see Scheme 1), and of their complexes with the cation $TlMe_2^+$. X-ray studies showed marked variability in coordination mode, including the relatively uncommon formation of four-membered chelate rings. The preparation and structure of HL^1 have previously been reported by Fang et al. [16].

2. Results and discussion

2.1. Structures of the ligands

Table 1 lists selected bond lengths and angles of HL^{3-5}, and Fig. 1 shows the structures and numbering schemes of HL^3, HL^4 and one of the two crystallographically independent molecules of HL^5. Like HL^1 [16] and most thiosemicarbazones [4b,15], both HL^3 and HL^4 adopt E configuration with respect to the C(1)–N(2) bond. The main cause of this is probably that it allows N(1) and N(3) to form an intramolecular hydrogen bond [17]; both of the HL^5 molecules, in which this bond is impossible because of the disubstitution of N(1), adopt Z configuration. In all three compounds the bond lengths in the thiosemicarbazone chain C(2)N(3)N(2)C(1)S(1)N(1) are within the usual ranges [4b,15,18].

In crystals of HL^5 there are two similar but crystallographically independent molecules, **a** and **b**. Their bond lengths and angles are generally similar, but in some cases are clearly not identical in view of the corresponding standard deviations (Table 1).

2.2. Structures of the complexes

The structures and numbering schemes of the $TlMe_2^+$ complexes of HL^2–HL^4 are shown in Figs. 2 and 3, and selected bond lengths and angles are listed in Table 2.

In $[TlMe_2(L^2)]$ and $[TlMe_2(L^4)]$ the ligands chelate the metal through their N(2) and S atoms, forming four-membered chelate rings (Fig. 2(a/b)). This coordination

Table 1
Selected bond lengths (Å) and angles (°) for HL^3, HL^4 and HL^5

	HL^3	HL^4	HL^5	
			(a)	**(b)**
Bond lengths				
S1–C1	1.672(3)	1.694(2)	1.695(6)	1.716(6)
N1–C1	1.339(4)	1.319(3)	1.359(7)	1.345(7)
N2–C1	1.349(4)	1.352(2)	1.330(7)	1.324(7)
N2–N3	1.389(3)	1.396(3)	1.362(6)	1.357(6)
N3–C2	1.281(4)	1.285(3)	1.306(7)	1.296(7)
C2–C3	1.455(4)	1.467(3)	1.429(8)	1.440(8)
C2–C20	1.496(4)	1.494(3)	1.503(7)	1.501(7)
Bond angles				
N1–C1–S1	124.8(3)	124.21(17)	121.2(5)	120.7(5)
N1–C1–N2	114.8(3)	116.84(19)	114.3(6)	116.1(6)
N2–C1–S1	120.4(3)	118.94(17)	124.5(5)	123.2(5)
C1–N2–N3	120.4(3)	118.36(17)	112.3(5)	113.0(5)
C2–N3–N2	117.5(3)	116.04(18)	123.9(5)	123.5(5)
N3–C2–C3	117.1(3)	115.24(19)	117.4(5)	117.9(6)
N3–C2–C20	124.0(3)	125.9(2)	120.2(5)	120.9(6)
C3–C2–C20	118.8(3)	118.86(19)	122.3(6)	121.0(6)
N(1)–H···N(3)	2.613(4)/120(3)	2.629(2)/107.6		
N(2)–H···S(1)#1		3.460(2)/134.2		

Symmetry operation: #1: $-x$, $-y+1$, $-z$.

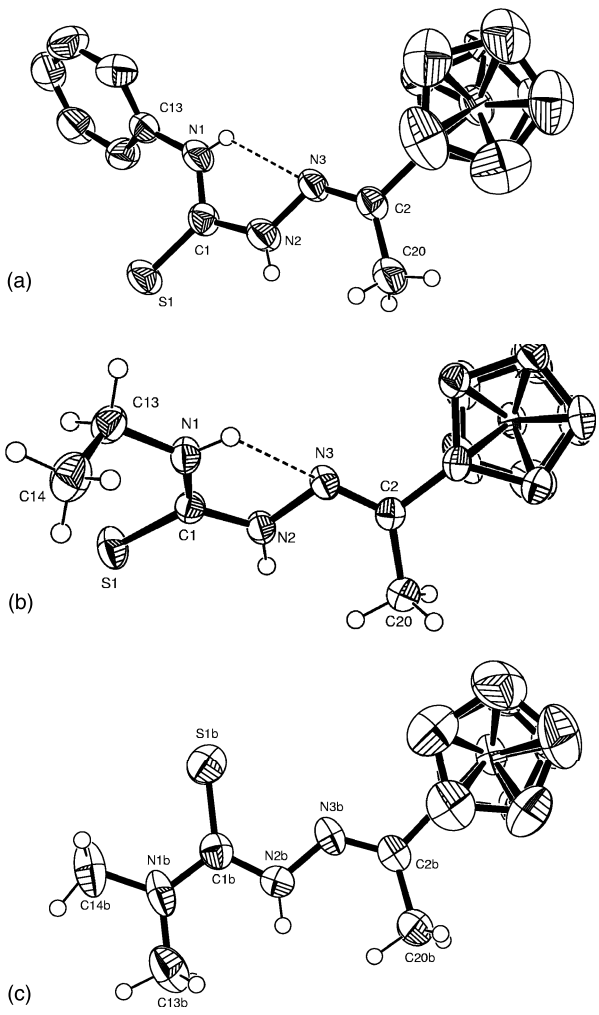


Fig. 1. ORTEP drawings of (a) HL^3, (b) HL^4 and (c) HL^5, showing their molecular structures and the labeling schemes used.

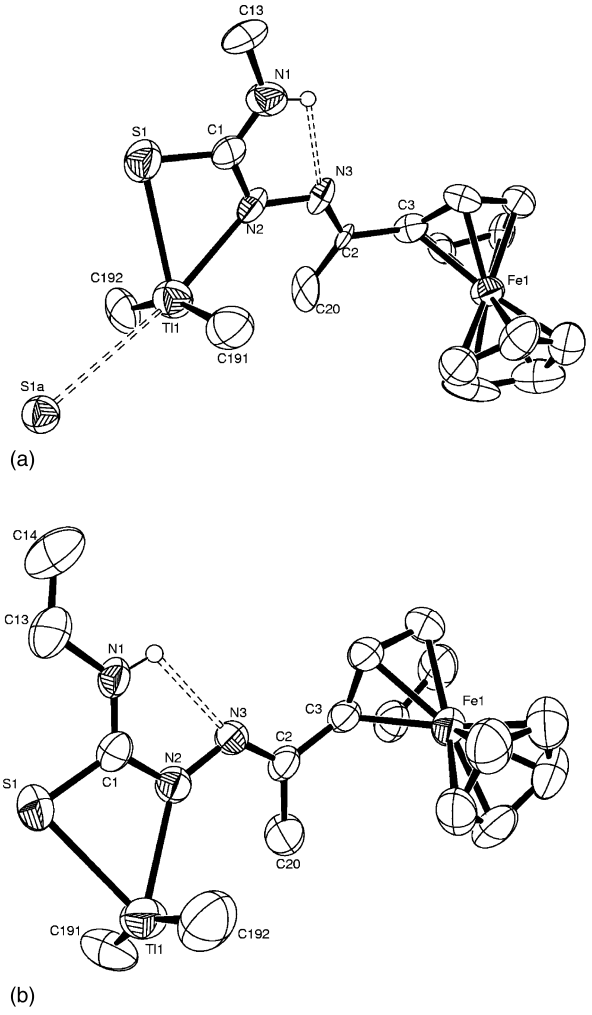


Fig. 2. ORTEP drawings of (a) $[TlMe_2(L^2)]$ and (b) $[TlMe_2(L^4)]$, showing their molecular structures and the labeling schemes used.

mode, which is unusual among thiosemicarbazones, was first observed in this class of compounds in another dimethylthallium(III) complex [19], and later in complexes with organometallic derivatives of Group 13 elements (Al, Ga and In) [20–22] and with Pd [23]. It allows the deprotonated ligand to retain its stabilizing N(1)–H···N(3) hydrogen bond, which in $[TlMe_2(L^4)]$ is actually stronger than in the free ligand, with an N(1)···N(3) distance of 2.580(6) Å as against 2.629(2) Å. In the $(L^4)^-$ complex, thione-to-thiol evolution is reflected by the lengthening of C(1)–S and the shortening of C(1)–N(2) with respect to their lengths in free HL^4.

The Tl–C distances and C–Tl–C angles in the $(L^2)^-$ and $(L^4)^-$ complexes are similar to those found in other complexes of dimethylthallium(III) with thiosemicarbazone ligands [4b,15], but the Tl–N distances (both about 2.50 Å) are somewhat shorter than those previously observed (2.55–2.59 Å), although this difference does not seem to be sufficient to give rise to qualitative differences in coordination geometry. The Tl–S distances (2.78 and 2.75 Å) are also shorter than those found in most other $TlMe_2^+$ complexes of thiosemicarbazones (2.80–2.99 Å) [4b], the only exception being the complex with cyclopentanonethiosemicarbazone, in which Tl–S has a length of 2.627(5) Å [4b].

In $[TlMe_2(L^2)]$ the Tl–S and Tl–N(2) bonds are supplemented by a weak Tl···S interaction with a neighboring molecule that serves to link the molecules in chains. If this interaction is taken into account, the coordination polyhedron is a square pyramid according to Addison's [24] criterion ($\tau = 0.12$). As in the free ligand [25], the C(2)N(3)N(2)C(1)S(1)N(1)C(13) chain is practically flat (the rms deviation from the least squares plane is 0.041), and it makes angles of 32.1° with the cyclopentadiene ring and 71.5° with the least-squares plane through S(1), Tl, C(191) and C(192) (from which the rms deviation is 0.029).

In $[TlMe_2(L^4)]$, there are no intermolecular interactions and the coordination polyhedron is a highly distorted tetrahedron [C(191–Tl(1)–C(192) = 159.2(3)° and N(2)–Tl(1)–S(1) = 59.62(11)°]. A coordination

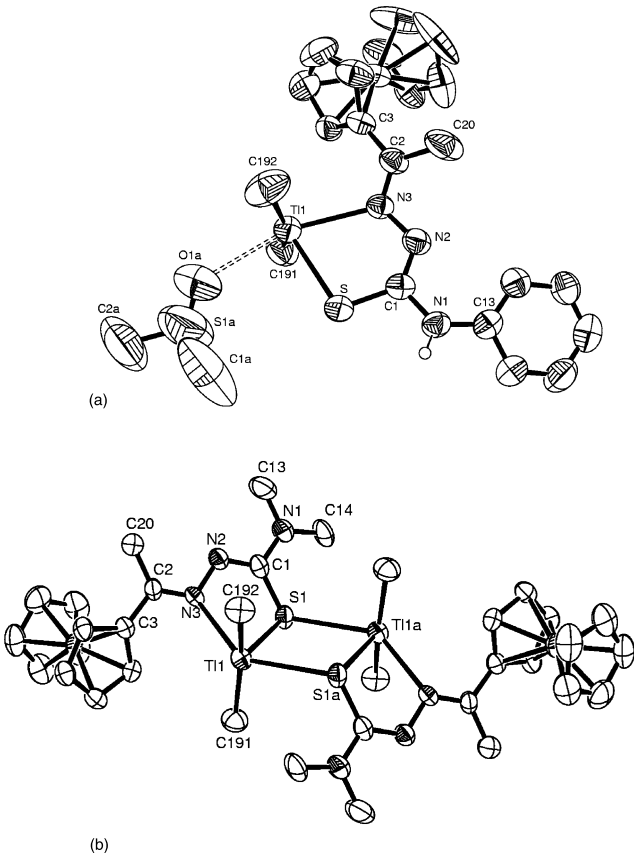


Fig. 3. ORTEP drawing of (a) $[TlMe_2(L^3)(dmso)]\cdot dmso$ and (b) $[TlMe_2(L^5)]$, showing their molecular structures and the labeling schemes used.

number of four is unusually low for $TlMe_2^+$ compounds, and this is the first time it has been found in a thiosemicarbazone complex of this cation; hitherto, all such complexes have had coordination numbers of five, six or seven. In $[TlMe_2(L^4)]$, the thiosemicarbazide/acetyl chain (rms = 0.083) makes angles of 25.3° with the cyclopentadiene ring and 70.2° with the S(1)TlC(191)C(192) plane (rms = 0.027).

The most significant difference between $[TlMe_2(L^2)]$ and $[TlMe_2(L^4)]$ is thus the presence in the former of an intermolecular Tl···S interaction that determines a different coordination environment for the metal and creates a supramolecular structure consisting of chains running parallel to the *y*-axis. It may also be noted that this intermolecular interaction appears to weaken the intramolecular Tl–S bond, which has a length of 2.779(7) Å in $[TlMe_2(L^2)]$ as against 2.7545(18) Å in $[TlMe_2(L^4)]$.

In $[TlMe_2(L^3)(dmso)]\cdot dmso$ the deprotonated ligand chelates the organometallic cation via its N(3) and S atoms, as is usual in this kind of thiosemicarbazone complex [4b,15], so forming a five-membered chelate ring. The coordination number of the thallium atom is made up to five by a bond with a dmso oxygen atom, the resulting coordination polyhedron being a square pyramid with the sulfur atom apical (τ [24] = 0.0017). The lengths of the Tl–S, Tl–N and Tl–C bonds are within the ranges observed in similar compounds [4b], but the Tl–O bond is rather long [2.803(8) Å], though considerably shorter than the sum of the van der Waals radii (3.50 Å [26]). This coordination mode appears to shorten Tl–S and lengthen Tl–N with respect to the N(2),S-coordination of the L^2 and L^4 complexes.

The phenyl ring in $[TlMe_2(L^3)(dmso)]\cdot dmso$ is practically coplanar with the rest of the thiosemicarbazide moiety [rms deviation for C(2)N(3)N(2)C(1)S(1)N(1)-C(13)C(14)C(15)C(16)C(17)C(18), 0.1193]. This structure makes angles of 63.7° with the planes of the ferrocene rings, and 89.9° with the S(1)TlC(191)C(192) plane. The second dmso molecule is occluded in the lattice.

In $[TlMe_2(L^5)]$ a thiolic thiosemicarbazonato anion chelates the metal via its N(3) and S atoms. In addition, the S atoms of pairs of neighboring molecules bridge between the metal atoms, forming weakly bound centrosymmetric dimers (the Tl–$S^{\#2}$ distance, 3.07(16) Å, is longer than usual, though shorter than the sum of the van der Waals radii, 3.76 Å [26]). The coordination polyhedron is a highly distorted square pyramid (τ [24] = 0.31) in which the tightly bound sulfur is apical. The Tl–S, Tl–N(3) and Tl–C distances are similar to those found in other complexes of dimethylthallium(III) with monoanionic organic ligands [14], although the replacement of the weak Tl···O bond of the $(L^3)^-$ complex by a Tl···S bond lengthens both Tl–S and Tl–N. The C(3)C(2)C(20)N(3)N(2)C(1)S(1)N(1)C(13)C(14) chain is almost flat (rms = 0.0981) and makes angles of 25.6° with the cyclopentadienyl ring and 55.4° with the S(1)Tl(1)C(191)C(192) plane (rms = 0.0293).

In the solid state, all the complexes retain the E configuration of the ligands about the C(2)–N(3) bond (see [16,25] for HL^1 and HL^2 and Fig. 1 for HL^3–HL^5).

2.3. IR spectra

The chief IR bands of the ligands were identified on the basis of data for similar compounds [7].

In the 3400–3100 cm^{-1} region, where the ν(N–H) bands lie, deprotonation makes the spectra of the complexes simpler than those of the free ligands, leaving only the ν(N(1)–H) bands. The shifts of these bands in $[TlMe_2(L^1)]$–$[TlMe_2(L^4)]$ with respect to their positions in the spectra of the free ligands must be attributed to changes in hydrogen bonding, since in $[TlMe_2(L^1)]$–$[TlMe_2(L^4)]$ N(1) is not coordinated to the metal.

The coordination via the sulfur atom shifts ν(C=S) to lower wavenumbers than in the free ligands, where it appears near 800 cm^{-1}. The C=N stretching vibration also shifts to lower wavenumbers; this occurs regardless of whether the ligand coordinates via N(2) (as in $(L^2)^-$ and $(L^4)^-$) or N(3) (as in $(L^3)^-$ and $(L^5)^-$), and the

Table 2
Selected bond lengths (Å) and angles (°) for $[TlMe_2(L^2)]$, $[TlMe_2(L^3)(dmso)]\cdot dmso$, $[TlMe_2(L^4)]$ and $[TlMe_2(L^5)]$

	$[TlMe_2(L^2)]$	$[TlMe_2(L^3)(dmso)]\cdot dmso$	$[TlMe_2(L^4)]$	$[TlMe_2(L^5)]$
Bond lengths				
Tl(1)–C(191)	2.11(3)	2.150(7)	2.114(7)	2.148(6)
Tl(1)–C(192)	2.12(2)	2.140(7)	2.123(8)	2.152(6)
Tl(1)–S(1)	2.779(7)	2.6632(16)	2.7545(18)	2.7203(15)
Tl(1)–N(2)	2.50(2)		2.504(5)	
Tl(1)–N(3)		2.577(4)		2.657(4)
Tl(1)–S(1)#1	3.508(7)			
Tl(1)–S(1)#2				3.0709(15)
Tl(1)–O(1A)		2.803(8)		
S(1)–C(1)	1.73(3)	1.734(6)	1.729(6)	1.757(6)
N(1)–C(1)	1.30(3)	1.386(6)	1.330(7)	1.374(6)
N(2)–C(1)	1.33(3)	1.303(7)	1.335(6)	1.318(6)
N(2)–N(3)	1.42(2)	1.391(6)	1.384(6)	1.396(5)
N(3)–C(2)	1.28(2)	1.285(6)	1.286(6)	1.292(6)
C(2)–C(3)	1.43(3)	1.459(7)	1.460(7)	1.459(7)
C(2)–C(20)	1.52(3)	1.515(8)	1.494(8)	1.493(7)
Bond angles				
C(191)–Tl(1)–C(192)	159.2(10)	156.7(3)	159.2(3)	158.9(2)
N(2)–Tl(1)–S(1)	58.0(4)		59.62(11)	
N(3)–Tl(1)–S(1)		70.39(10)		66.16(9)
N(2)–Tl(1)–S(1)#1	166.2(4)			
S(1)–Tl(1)–S(1)#1	109.76(15)			
N(3)–Tl(1)–S(1)#2				140.32(9)
S(1)–Tl(1)–S(1)#2				83.78(4)
N(3)–Tl(1)–O(1A)		156.5(2)		
S(1)–Tl(1)–O(1A)		88.07(17)		
S(1)–C(1)–N(2)	113.9(19)	130.2(4)	117.2(5)	126.2(4)
C(1)–N(2)–N(3)	110.0(18)	115.3(4)	112.7(5)	114.4(4)
N(2)–N(3)–C(2)	115.7(18)	114.2(4)	116.6(5)	113.9(4)
N(3)–C(2)–C(3)	114.7(19)	118.7(5)	115.9(5)	117.3(5)
N(1)–H···N(3)	2.55(3)/105.6		2.580(6)/105.8	

Symmetry operations: #1: $-x+0.5$, $y-0.5$, $-z+0.5$; #2: $-x+1$, $-y$, $-z+1$.

magnitude of the shift is likewise uncorrelated with the coordination mode, probably because it is also influenced by the involvement of N(3) in hydrogen bonds when it does not coordinate to the metal.

The 1650–1450 cm^{-1} region of the IR spectrum of $[TlMe_2(L^1)]$, from the X-ray data for which it was not possible to calculate a structure, shows two strong bands similar to those found in the spectra of N(2)-coordinated N(1)-unsubstituted thiosemicarbazones [19,27]. It is, therefore, reasonable to infer that the ligand is also N(2)-coordinated in $[TlMe_2(L^1)]$.

Coordination does not significantly affect the ferrocene bands [28].

2.4. NMR spectra

The NMR spectra of the ligands and complexes in dmso-d_6 (see Section 4) are in some cases complicated by the presence of several different species (*vide infra*) and were interpreted with the aid of ^1H–^{13}C HMQC and HMBC experiments.

The ^1H NMR spectra of all the ligands except HL^5 show a single series of strong signals, suggesting that in these cases there is a single predominant species present. That of HL^1 shows the two protons on N(1) to be non-equivalent, which is attributable to one of them being involved in an N(1)–H···N(3) hydrogen bond.

The ^1H NMR spectrum of HL^5 shows two series of signals, which differ most as regards the N(2)H signal and which we attribute to distinct species HL^5**a** and HL^5**b** with different conformations with respect to the C(1)–N(2) bond, one being Z and the other E.

Coordination induces a number of changes in the ^1H NMR spectra of the ligands. In all cases, the signal located near 10 ppm disappears as the result of deprotonation. In the spectrum of the $(L^1)^-$ complex the two N(1) protons are now equivalent, probably due to there now being no N(1)–H···N(3) hydrogen bond and to a coordination-induced change in the multiplicity of C(1)–N(1) (this bond is longer in the complexes than in the free ligands). The spectra of the $(L^2)^-$, $(L^4)^-$ and $(L^5)^-$ complexes indicate the presence of more than one species (two for $(L^4)^-$ and $(L^5)^-$, three for $(L^2)^-$), determination of the relative abundances of which was unfortunately prevented by the complexity of the spectra. The presence of three species of $[TlMe_2(L^2)]$

(**a**, **b** and **c**) suggests that these species may differ with respect to C(2)–N(3) as well as C(1)–N(2), i.e. as regards the relative positions of the ferrocene group and the thiosemicarbazide chain.

The ^{1}H NMR signals of the ferrocene group lie between 4.1 and 4.9 ppm in the spectra of the free ligands. Of the slight shifts observed upon coordination, the most important are, as expected, those affecting the signals of C(4) and C(7) (see the scheme in the Section 1), which though less than 0.2 ppm in the cases of $(L^1)^-$, $(L^2)^-$ and $(L^4)^-$ reach 0.3 ppm for $(L^5)^-$ and 0.4 ppm for $(L^3)^-$. These shifts doubtless reflect extension of the delocalized π-system of the thiosemicarbazide chain into the cyclopentadiene ring.

The $TlMe_2^+$ moiety shows up as a single signal in the ^{1}H NMR spectra of all the complexes, including those that are present in more than one form. This means that either the organometallic cation is rapidly exchanged between ligands with different configurations, or that the breadth of these signals is too great to allow observation of the difference between the signals of N(2),S- and N(3),S-coordinated species, which is probably small. The existence of coordination in solution, which is expected in view of the generally poor ionogenicity of dimethylthallium(III) complexes of thiosemicarbazones in dmso [20], is supported by the values of $^{2}J(^{1}H–^{205}Tl)$, 394–408 Hz, being considerably smaller than the 438 ± 2.1 Hz found for dimethylthallium(III) perchlorate [29].

The ^{13}C NMR spectra of all the compounds are in keeping with their ^{1}H NMR spectra. C(1) can be seen to be much more shielded in the complexes than in the free ligands, which indicates a shift from the thione form N(2)–C(1)=S towards the thiol form N(2)=C(1)–S consequent upon coordination of the sulfur atom to the metal. The $^{1}J(^{205}Tl–^{13}C)$ values of the $(L^1)^-$, $(L^2)^-$ and $(L^5)^-$ complexes, 2935–2967 Hz, are larger than that of dimethylthallium(III) perchlorate (2918.2 Hz), but that of $[TlMe_2(L^4)]$ is smaller, 2911 Hz; in the case of $[TlMe_2(L^3)]$, poor solubility prevented identification of $TlMe_2^+$ signals.

3. Conclusions

In conclusion, we have prepared five previously unsynthesized acetylferrocene thiosemicarbazonates of dimethylthallium(III), in yields of about 50% or better, by reacting a solution of the corresponding thiosemicarbazone in methanol or ethanol with a freshly prepared aqueous solution of dimethylthallium hydroxide. The structures of three of the thiosemicarbazones and four dimethylthallium(III) complexes were determined by X-ray crystallography. The complexes differ as regards the coordination number of the metal (four or five), the size of the chelate rings (four- or five-member) and the presence or absence of intermolecular Tl···S interactions, showing that this type of ligand has considerable coordinational versatility. One of the complexes also acquired a dmso ligand molecule upon recrystallization from this solvent. The ^{1}H and ^{13}C NMR spectra of the complexes in dmso-d_6 solution suggest that the thiosemicarbazone ligand remains coordinated in this solvent, and also indicate the presence of more than one species, which probably differ as regards the relative positions of the ferrocene group and the thiosemicarbazone chain.

4. Experimental

4.1. Materials and methods

Thiosemicarbazide (from Fluka), acetylferrocene and 4-methyl-3-thio-, 4-phenyl-3-thio-, 4-ethyl-3-thio- and 4,4-dimethylthiosemicarbazides (all from Aldrich) were used as received. Me_2TlI was prepared as per Gilman and Jones [30], and dimethylthallium hydroxide by stirring Me_2TlI with excess freshly precipitated silver oxide in deionized water and removing AgI by filtration.

Elemental analyses were performed on a Fisons Instruments EA1108CHNS-O microanalyser. Melting points (m.p.) were determined with a Büchi apparatus. Mass spectra were recorded on a Kratos MS50TC spectrometer and the mass for the metallated peaks (*vide infra*) is refereed to the isotopes ^{205}Tl and ^{56}Fe. IR spectra were recorded using KBr discs on a Bruker IFS66V FT-IR spectrometer and are reported in cm^{-1}. The ^{1}H and ^{13}C NMR spectra of dmso solutions were recorded on Bruker WM-250, AMX-300 or AMX-500 apparatuses; chemical shifts are expressed on the δ scale (downfield shifts positive) relative to tetramethylsilane. All physical measurements (including the X-ray diffraction studies) were carried out in the RIAIDT services of the University of Santiago de Compostela.

4.2. Preparation of the ligands HL^n

A solution (HL^1, HL^4, HL^5) or suspension (HL^2, HL^3) of the appropriate thiosemicarbazide (6.60 mmol) in water (45 ml) was added dropwise to a stirred hot solution of acetylferrocene (6.60 mmol) in ethanol (40 ml). Acetic acid (1 ml) was added, and the mixture was refluxed for 15 min and then stirred for a further 12 h. The resulting orange (HL^1–HL^4) or red (HL^5) solid was filtered out and dried under vacuum (yield 75–85%). Single crystals suitable for X-ray study were obtained from the mother liquor (HL^5) or by recrystallization from dichloromethane–hexane (HL^3) or chloroform–cyclohexane (HL^4).

4.2.1. HL^1

M.p. 169 °C. Found: C, 52.3; H, 5.6; N, 13.4. $C_{13}H_{15}N_3SFe$ requires: C, 51.8; H, 5.0; N, 13.9%. MS (FAB, nitrobenzyl alcohol), *m/z*(%): 301 (100) [M], 226 (9) [M–NHC(S)NH_2], 185 (14) [M–C(Me)NNHC(S)NH_2]. IR: 3419s, 3224m, 3136m, ν(N–H); 1585s, ν(C=N); 823m, ν(C=S). ^{1}H NMR: δ[N(2)*H*] 9.93s(1); δ[N(1)H_2] 8.08s(1), 7.65s(1); δ[C(20)*H*] 2.18s(3). ^{13}C NMR: δ[C(1)] 177.8; δ[C(2)] 150.5; δ[C(3)] 83.0; δ[C(20)] 15.0.

4.2.2. HL^2

M.p. 141 °C. Found: C, 53.3; H, 5.7; N, 13.3. $C_{14}H_{17}N_3SFe$ requires: C, 53.4; H, 5.4; N, 13.3%. MS (FAB, nitrobenzyl alcohol), *m/z*(%): 315 (63) [M], 226 (6) [M–NHC(S)NH(Me)], 185 (9) [M–C(Me)NNHC(S)NH(Me)]. IR: 3310m, 3210m, ν(N–H); 1554vs, ν(C=N); 809m, ν(C=S). ^{1}H NMR: δ[N(2)*H*] 9.93s(1); δ[N(1)*H*] 8.20s(1); δ[N(1)CH_3] 2.99d(3); δ[C(20)*H*] 2.18s(3). ^{13}C NMR: δ[C(1)] 177.9; δ[C(2)] 150.0; δ[C(3)] 83.1; δ[C(20)] 15.0; δ[N(1)*C*H_3] 30.9.

4.2.3. HL^3

M.p. 125 °C(dec.). Found: C, 60.4; H, 5.0; N, 10.7. $C_{19}H_{19}N_3SFe$ requires: C, 60.5; H, 5.1; N, 11.1%. MS (FAB, nitrobenzyl alcohol), *m/z*(%): 377 (94) [M], 226 (16) [M–NHC(S)NH(Ph)], 185 (26) [M–C(Me)NNHC(S)NH(Ph)]. IR: 3327m, 326 m,br, ν(N–H); 1590m, ν(C=N); 819m, ν(C=S). ^{1}H NMR: δ[N(2)*H*] 10.34s(1); δ[N(1)*H*] 9.79s(1); δ[N(1)C_6H_5] (7.59d(2) H_o, 7.34t(2) H_m, 7.17t(1) H_p); δ[C(20)*H*] 2.27s(3). ^{13}C NMR: δ[C(1)] 175.3; δ[C(2)] 151.6; δ[C(3)] 82.3; δ[C(20)] 15.0; δ[N(1)C_6H_5] (138.6 C_{13}, 127.5 C_o, 124.7 C_m, 124.5 C_p).

4.2.4. HL^4

M.p. 160 °C. Found: C, 54.7; H, 6.1; N, 12.5. $C_{15}H_{19}N_3SFe$ requires: C, 54.7; H, 5.8; N, 12.8%. MS (FAB, nitrobenzyl alcohol), *m/z*(%): 329 (100) [M], 226 (9) [M–NHC(S)NH(Et)], 185 (16) [M–C(Me)NNHC(S)NH(Et)]. IR: 3280m, 3155m, ν(N–H); 1599m, ν(C=N); 815m ν(C=S). ^{1}H NMR: δ[N(2)*H*] 9.86s(1); δ[N(1)*H*] 8.22s(1); δ[N(1)CH_2] 3.57m(2); δ[N(1)CH_3] 1.13t(3); δ[C(20)*H*] 2.18s(3). ^{13}C NMR: δ[C(1)] 176.85; δ[C(2)] 150.24; δ[C(3)] 83.20; δ[C(20)] 14.63; δ[N(1)*C*H_2] 38.24; δ[N(1)*C*H_3] 15.12.

4.2.5. HL^5

M.p. 123 °C. Found: C, 54.5; H, 5.7; N, 12.8. $C_{15}H_{19}N_3SFe$ requires: C, 54.7; H, 5.8; N, 12.8%. MS (FAB, nitrobenzyl alcohol), *m/z*(%): 329 (100) [M], 226 (15) [M–NHC(S)NMe_2], 185 (21) [M–C(Me)NNHC(S)NMe_2]. IR: 3114m, ν(N–H); 1620m, ν(C=N); 833m ν(C=S). ^{1}H NMR: δ[N(2)*H*] (**a**: 9.34s, **b**: 13.34s)(1); δ[N(1)CH_3] (**a**: 3.21s, **b**: 3.17s)(6); δ[C(20)*H*] **a**,**b**: 2.16s(3). ^{13}C NMR: δ[C(1)] **a**,**b**: 181.9; δ[C(2)] **a**: 150.2, **b**: 154.2; δ[C(3)] **a**: 76.4, **b**: 83.0; δ[C(20)] **a**: 15.1, **b**: 16.5; δ[N(1)*C*H_3] **a**,**b**: 42.4.

4.3. Synthesis of the complexes

4.3.1. $[TlMe_2(L^1)]$

A freshly prepared aqueous solution of $Me_2Tl(OH)$ (0.60 mmol) was added dropwise, with stirring, to a solution of HL^1 (0.2 g, 0.60 mmol) in methanol (10 ml) cooled in an ice-bath. The orange solid so obtained was filtered out and dried under vacuum. Yield 50%. M.p. 119 °C. Found: C, 34.5; H, 3.8; N, 7.9. $C_{15}H_{20}N_3SFeTl$ requires: C, 33.7; H, 3.7; N, 7.9%. MS (FAB, nitrobenzyl alcohol), *m/z*(%): 535 (58) [M], 301 (28) [HL^1], 235 (100) [Me_2Tl], 205 (63) [Tl], 185 (16) [HL^1–C(Me)NNHC(S)NH_2]. IR: 3447s, 3326s,br, ν(N–H); 1568vs,br, ν(C=N); 807m, ν(C=S); 528m, ν_{asim}(C–Tl–C). ^{1}H NMR: δ[N(1)H_2] 6.63s(2); δ[C(20)*H*] 2.02s(3); δ[Tl(CH_3)$_2$] 0.87d(6); [J(^{1}H–^{205}Tl)] 396.3 Hz. ^{13}C NMR: δ[C(1)] 171.7; δ[C(2)] 150.2; δ[C(3)] 85.1; δ[C(20)] 15.6; δ[Tl(*C*H_3)$_2$] 21.1; [J(^{13}C–^{205}Tl)] 2935.0 Hz.

4.3.2. $[TlMe_2(L^2)]$

A freshly prepared aqueous solution of $Me_2Tl(OH)$ (0.64 mmol) was added dropwise, with stirring and mild heating, to a solution of HL^2 (0.2 g, 0.64 mmol) in ethanol (40 ml). Upon concentration under vacuum the mixture afforded an orange solid that was filtered out and dried under vacuum. Yield 53%. Single crystals suitable for X-ray study were obtained by recrystallization from ethanol–water. M.p. 179 °C dec. Found: C, 35.5; H, 4.0; N, 7.7. $C_{16}H_{22}N_3SFeTl$ requires: C, 35.0; H, 4.0; N, 7.7%. MS (FAB, nitrobenzyl alcohol), *m/z*(%): 549.0 (18) [M], 315.0 (33) [HL^2], 235.0 (49) [Me_2Tl], 205.0 (37) [Tl], 185.0 (10) [HL^2–C(Me)NNHC(S)NH(Me)]. IR: 3356s, ν(N–H); 1528vs, ν(C=N); 786m, ν(C=S); 530m, ν_{asim}(C–Tl–C). ^{1}H NMR: δ[N(1)*H*] (**a**: 7.05s, **b**: 6.17s, **c**: 6.31s)(1); δ[N(1)CH_3] (**a**: 2.85m, **b**: 2.72m, **c**: 2.79m)(3); δ[C(20)*H*] (**a**: 2.00s, **b**: 2.31s, **c**: 2.26s)(3); δ[Tl(CH_3)$_2$] 0.77d(6); [J(^{1}H–^{205}Tl)] 401.2 Hz. ^{13}C NMR: δ[C(1)] **a**: 176.3, **b**: 170.1; δ[C(2)] **a**: 148.9, **b**: 156.9, **c**: 152.6; δ[C(3)] **a**: 85.4, **b**: 87.4; δ[C(20)] **a**: 15.3, **b**: 19.2, **c**: 23.2; δ[N(1)*C*H_3] **a**,**c**: 30.3, **b**:30.4; δ[Tl(*C*H_3)$_2$] 20.3; [J(^{13}C–^{205}Tl)] 2954.3 Hz.

4.3.3. $[TlMe_2(L^3)(dmso)]\cdot dmso$

A freshly prepared aqueous solution of $Me_2Tl(OH)$ (0.66 mmol) was added dropwise, with stirring and mild heating, to a solution of HL^3 (0.25 g, 0.66 mmol) in ethanol (45 ml). One-third of the solvent was removed under vacuum, and the remaining solution was stored in a refrigerator for 12 h. The orange solid so obtained was filtered out and dried under vacuum. Yield 81%. Single crystals suitable for X-ray study were obtained by

Table 3
Crystallographic data for the ligands HL^3, HL^4 and HL^5

	HL^3	HL^4	HL^5
Empirical formula	$C_{19}H_{19}FeN_3S$	$C_{15}H_{19}FeN_3S$	$C_{15}H_{19}FeN_3S$
Formula weight	377.28	329.24	329.24
Color, habit	Brown, prism	brown, prism	brown, needle
Crystal size (mm)	$0.32 \times 0.20 \times 0.16$	$0.40 \times 0.25 \times 0.12$	$0.48 \times 0.12 \times 0.04$
Crystal system	monoclinic	monoclinic	Monoclinic
Space group	$P2(1)/n$	$P2(1)/c$	$P2(1)/c$
Unit cell dimensions			
a (Å)	11.761(3)	15.8166(9)	9.410(2)
b (Å)	7.857(3)	7.6969(6)	169.374(4)
c (Å)	18.764(14)	13.2504(9)	20.238(5)
β (°)	91.59(4)	108.630(4)	103.118(4)
Volume (A^3)	1733.1(15)	1528.56(18)	3036.9(13)
Z	4	4	8
Calculated density (Mg m^{-3})	1.446	1.431	1.440
Absorption coefficient (mm^{-1})	0.995	1.116	1.124
T (K)	293	293	293
$F(000)$	784	688	1376
Reflections collected/unique	3749/3574 [$R_{int} = 0.0340$]	19636/4612 [$R_{int} = 0.0602$]	32552/6268 [$R_{int} = 0.1431$]
Final R indices [$I > 2\sigma(I)$]	$R_1 = 0.0402$ $wR_2 = 0.0805$	$R_1 = 0.0347$ $wR_2 = 0.0702$	$R_1 = 0.0529$ $wR_2 = 0.1178$

recrystallization from dmso. M.p. 105 °C dec. Found: C, 38.6; H, 5.3; N, 5.5. $C_{21}H_{24}N_3SFeTl \cdot 2dmso$: C, 39.2; H, 4.7; N, 5.5%. MS (FAB, nitrobenzyl alcohol), m/z(%): 611.0 (59) [M–2dmso], 377.0 (28) [HL^3], 235.0 (60) [Me_2Tl], 205.0 (45) [Tl], 185.0 (26) [HL^3-C(Me)NNHC(S)NH(Ph)]. IR: 3291m,br, ν(N–H); 1570m, ν(C=N); 810m, ν(C=S); 540sh, ν_{asim}(C–Tl–C). ^{1}H NMR: δ[N(1)H] 8.54s(1); δ[N(1)C_6H_5] (7.76m(2) H_o, 7.19m(2) H_m, 6.82m(1) H_p); δ[C(20)H] 2.37s(3); δ[Tl(CH_3)$_2$] 0.69d(6); [J(^{1}H–^{205}Tl)] 408.1 Hz. ^{13}C NMR: δ[C(1)] 167.3; δ[C(2)] 160.0; δ[C(3)] 86.8; δ[C(20)] 20.2; δ[N(1)C_6H_5] (86.8 C_{13}, 128.2 C_o, 119.0 C_m, 120.3 C_p).

4.3.4. [$TlMe_2(L^4)$]

A freshly prepared aqueous solution of $Me_2Tl(OH)$ (0.61 mmol) was added dropwise, with stirring, to a gently heated solution of HL^4 (0.2 g, 0.61 mmol) in ethanol (50 ml). One-half of the solvent was removed under vacuum, and the remaining solution was stored in a refrigerator for 12 h. The crystalline orange solid so obtained was filtered out and dried under vacuum. Yield 48%. Single crystals suitable for X-ray study were obtained from the mother liquor. M.p. 164 °C. Found: C, 36.8; H, 5.0; N, 7.6. $C_{17}H_{24}N_3SFeTl$ requires: C, 36.3; H, 4.3; N, 7.5%. MS (FAB, nitrobenzyl alcohol), m/z (%): 563.0 (38) [M], 329.0 (31) [HL^4], 235.0 (63) [Me_2Tl],

Table 4
Crystallographic data for the complexes [$TlMe_2(L^2)$], [$TlMe_2(L^3)$(dmso)]·dmso, [$TlMe_2(L^4)$] and [$TlMe_2(L^5)$]

	[$TlMe_2(L^2)$]	[$TlMe_2(L^3)$(dmso)]·dmso	[$TlMe_2(L^4)$]	[$TlMe_2(L^5)$]
Empirical formula	$C_{16}H_{22}FeN_3STl$	$C_{25}H_{36}FeN_3O_2S_3Tl$	$C_{17}H_{24}FeN_3STl$	$C_{17}H_{24}FeN_3STl$
Formula weight	548.65	766.97	562.67	562.67
Color, habit	brown, prism	red, prism	red, needle	red, prism
Crystal size (mm)	$0.16 \times 0.08 \times 0.02$	$0.46 \times 0.35 \times 0.32$	$0.44 \times 0.21 \times 0.20$	$0.49 \times 0.17 \times 0.16$
Crystal system	monoclinic	monoclinic	monoclinic	Orthorhombic
Space group	$P2(1)/n$	$P2(1)/c$	$P2(1)/n$	$Pbca$
Unit cell dimensions				
a (Å)	12.671(3)	14.367(2)	12.400(3)	11.508(2)
b (Å)	7.7998(15)	9.4409(16)	8.2554(19)	14.846(3)
c (Å)	18.788(4)	22.447(4)	19.627(5)	22.834(4)
β (°)	108.674(4)	93.049(4)	106.473(5).	
Volume (A^3)	1759.0(6)	3040.4(9)	1926.7(8)	3901.2(12)
Z	4	4	4	8
Calculated density (Mg m^{-3})	2.072	1.676	1.940	1.916
Absorption coefficient (mm^{-1})	10.092	6.002	9.216	9.103
T (K)	293	293	293	293
$F(000)$	1048	1512	1080	2160
Reflections collected/unique	5472/2491 [$R_{int} = 0.1315$]	37808/8527 [$R_{int} = 0.0530$]	9875/3943 [$R_{int} = 0.0390$]	21179/3992 $R_{int} = 0.0563$]
Final R indices [$I > 2\sigma(I)$]	$R_1 = 0.0557$ $wR_2 = 0.1141$	$R_1 = 0.0383$ $wR_2 = 0.0968$	$R_1 = 0.0339$ $wR_2 = 0.0613$	$R_1 = 0.0273$ $wR_2 = 0.0554$

205.0 (49) [Tl], 185.0 (27) [HL^4–C(Me)NNHC(S)NH(Et)]. IR: 3339m, 3279w, ν(N–H); 1520vs, ν(C=N); 804m, ν(C=S); 530m, ν_{asim}(C–Tl–C). ^{1}H NMR: δ[N(1)*H*] (**a**: 6.15s, **b**: 6.24s) (1); δ[N(1)CH_2] **a**,**b**: 3.22m(2); δ[N(1)CH_3] **a**,**b**: 1.11m(3); δ[C(20)*H*] (**a**: 2.03s, **b**: 2.29s)(3); δ[Tl(CH_3)$_2$] 0.77d(6); [J(^{1}H–^{205}Tl)] 394.0 Hz. ^{13}C NMR: δ[C(1)] **a**: 175.4, **b**: 169.4; δ[C(2)] **a**: 149.2, **b**: 156.7; δ[C(3)] **a**: 77.1, **b**: 87.4; δ[C(20)] **a**,**b**: 19.2; δ[N(1)*C*H$_2$] **a**,**b**: 37.9; δ[N(1)*C*H$_3$] **a**: 14.6, **b**: 15.4; δ[Tl(*C*H$_3$)$_2$] 22.4; [J(^{13}C–^{205}Tl)] 2911.3 Hz.

4.3.5. [$TlMe_2(L^5)$]

A freshly prepared aqueous solution of $Me_2Tl(OH)$ (0.61 mmol) was added dropwise, with stirring, to a solution of HL^5 (0.2 g, 0.61 mmol) in ethanol (15 ml). The orange solid so obtained was filtered out and dried under vacuum. Yield 62%. Single crystals suitable for X-ray study were obtained by recrystallization from dmso. M.p. 119 °C. Found: C, 36.6; H, 4.3; N, 8.0. $C_{17}H_{24}N_3SFeTl$ requires: C, 36.3; H, 4.3; N, 7.5%. MS (FAB, nitrobenzyl alcohol), m/z(%): 563.0 (26) [M], 329.0 (52) [HL^5], 235.0 (69) [Me_2Tl], 205.0 (45) [Tl], 185.0 (39) [HL^5–C(Me)NNHC(S)NMe_2]. IR: 1569m, ν(C=N); 824m, ν(C=S); 545m, ν_{asim}(C–Tl–C). ^{1}H NMR: δ[N(1)CH_3] (**a**: 3.13s, **b**: 3.19s)(6); δ[C(20)*H*] (**a**: 2.30s, **b**: 2.28s)(3); δ[Tl(CH_3)$_2$] 0.57d(6); [J(^{1}H–^{205}Tl)] 396.6 Hz. ^{13}C NMR: δ[C(1)] **a**: 172.9, **b**: 174.3; δ[C(2)] **a**: 156.6, **b**: 152.1; δ[C(3)] **a**: 87.5, **b**: 77.3; δ[C(20)] **a**: 19.4, **b**: 23.3; δ[N(1)*C*H$_3$] **a**,**b**: 39.7; δ[Tl(*C*H$_3$)$_2$] 19.4; [J(^{13}C–^{205}Tl)] 2967.6 Hz.

4.4. X-ray crystallography

Crystal data were collected at room temperature (r.t.) on either a Bruker SMART CCD 1000 diffractometer [31] or an Enraf–Nonius MACH3 automatic diffractometer [32] using graphite-monochromated Mo Kα radiation (wavelength 0.71073 Å). The structures were solved using direct methods followed by normal difference Fourier techniques. The hydrogen atoms were included in the model at ideal geometrical positions. In [$TlMe_2(L^3)$(dmso)]·dmso the hydrogens of C(1B) and C(2B) are disordered and were not included in the model. Full-matrix least-squares refinement was performed treating the non-H atoms anisotropically. The atomic scattering factors used were those provided with SHELX-97 [33]. Other programs used were ORTEP-3 [34] and PLATON-98 [35]. Crystal and refinement data for the ligands and compounds are listed in Tables 3 and 4, respectively.

5. Supplementary material

Crystallographic data (excluding structure factors) for the structures reported in this paper have been deposited with the Cambridge Crystallographic Data Center as supplementary publication number CCDC 168313 (HL^3), 168314 (HL^4), 168315 (HL^5), 168316 [$TlMe_2(L^2)$], 168317 [$TlMe_2(L^3)$(dmso)]·dmso, 168318 [$TlMe_2(L^4)$], 168319 [$TlMe_2(L^5)$]. Copies of the data can be obtained free of charge on application to CCDC, 12 Union Road, Cambridge CB2 1EZ, UK (fax: +44-1223-336033; e-mail: deposit@ccdc.cam.ac.uk.or www: http://www.ccdc.cam.ac.uk).

Acknowledgements

We thank the Xunta de Galicia (Spain) for financial support under projects XUGA 20308B97 and PGIDT00PX120301PR.

References

[1] R.W. Brockman, J.R. Thomson, M.J. Bell, H.E. Skipper, Cancer Res. 16 (1956) 167.
[2] S. Padhy, G.B. Kaufman, Coord. Chem. Rev. 63 (1985) 127.
[3] D.L. Klayman, J.P. Scovill, J.F. Bartosevich, J. Bruce, J. Med. Chem. 26 (1983) 35.
[4] (a) D.X. West, S.B. Padhye, P.B. Sonawane, Struct. Bond. 76 (1991) 1;
(b) J.S. Casas, M.S. García-Tasende, J. Sordo, Coord. Chem. Rev. 209 (2000) 197.
[5] F. Chen-jie, D. Chun-ying, H. Cheng, M. Qing-jin, Chem. Commun. (2000) 1187.
[6] B.S. Garg, L. Kapur, Inorg. Chim. Acta 173 (1990) 223.
[7] D.M. Wiles, T. Suprunchuk, Can. J. Chem. 46 (1968) 1865.
[8] (a) S.K. Segupta, O.P. Pandey, B.K. Srivastava, Transition Met. Chem. 23 (1998) 349;
(b) S.K. Segupta, O.P. Pandey, A.K. Srivastava, S.K. Srivastava, Indian J. Chem. 38A (1999) 1066.
[9] Y. Omote, R. Kobayashi, N. Sugiyama, Bull. Chem. Soc. Jpn. 46 (1973) 2896.
[10] F. Chen-jie, D. Chun-ying, H. Cheng, H. Gang, M. Qing-jin, New J. Chem. 24 (2000) 697.
[11] J. Eugenio, J.C. Graúdo, N.L. Speziali, A. Abras, M. Horner, C.A.L. Filgueiras, Polyhedron 18 (1999) 2483.
[12] A.O. Baghlaf, K. Banaser, H.Y. Hashem, A. Albishry, M. Ishaq, Transition Met. Chem. 21 (1996) 16.
[13] O.F. Schedlbauer, K.G. Heumann, Appl. Organomet. Chem. 14 (2000) 330.
[14] J.S. Casas, M.S. García-Tasende, J. Sordo, Coord. Chem. Rev. 193-195 (1999) 283.
[15] J.S. Casas, E.E. Castellano, M.S. García-Tasende, A. Sánchez, J. Sordo, Inorg. Chim. Acta 304 (2000) 283.
[16] C.J. Fang, G. Han, Y.J. Liu, C.Y. Duan, Q.J. Meng, Acta Crystallogr., Sect. C 55 (1999) 2058.
[17] (a) D. Chattopadhyay, S.K. Mazumdar, T. Banerjee, W.S. Sheldrick, Acta Crystallogr., Sect. C 45 (1989) 314;
(b) J.N. Brown, K.C. Agrawal, Acta Crystallogr., Sect. B. 34 (1978) 2038.
[18] G.J. Palenik, D.F. Rendle, W.S. Carter, Acta Crystallogr., Sect. B. 30 (1974) 2390.
[19] J.S. Casas, E.E. Castellano, A. Macías, M.C. Rodríguez-Argüelles, A. Sánchez, J. Sordo, J. Chem. Soc., Dalton Trans. (1993) 1253.

[20] (a) C. Paek, S.O. Kang, J. Ko, P.J. Carroll, Organometallics 16 (1997) 2110;
(b) C. Paek, S.O. Kang, J. Ko, P.J. Carroll, ibid 16 (1997) 1503.
[21] Y. Kang, N. Kang, S. O: Kang, J. Ko, C.-H. Lee, Y.-H. Lee, Organometallics 16 (1997) 5522.
[22] C. Paek, S. O: Kang, J. Ko, P.J. Carroll, Organometallics 16 (1997) 4755.
[23] A. Castiñeiras, E. Bermejo, D.X. West, A.K. El-Sawaf, J.K. Swearingen, Polyhedron 17 (1998) 2751.
[24] A.W. Addison, T.N. Rao, J. Reedijk, F. van Rijn, C.C. Verschoor, J. Chem. Soc., Dalton Trans. (1984) 1349.
[25] J.S. Casas, E.-E. Castellano, J. Ellena, M.-S. García-Tasende, A. Sánchez, J. Sordo, F. Velo, 5th FGIPS meeting in inorganic chemistry, Toulouse (1999).
[26] A. Bondi, J. Phys. Chem. 68 (1964) 441.
[27] (a) J.S. Casas, A. Castiñeiras, M.C. Rodríguez-Argüelles, A. Sánchez, J. Sordo, A. Vázquez-López, E.M. Vázquez-López, J. Chem. Soc., Dalton Trans. (2000) 2267;
(b) J.S. Casas, A. Castiñeiras, M.C. Rodríguez-Argüelles, A. Sánchez, J. Sordo, A. Vázquez-López, E.M. Vázquez-López, J. Chem. Soc., Dalton Trans. (2000) 4056.
[28] H.E. Rubalcava, B. Thomson, Spectrochim. Acta 18 (1962) 449.
[29] J.F. Hinton, K.R. Metz, R.W. Briggs, Prog. NMR Spectrosc. 20 (1988) 423.
[30] H. Gilman, R.G. Jones, J. Am. Chem. Soc. 68 (1946) 517.
[31] Bruker, SMART and SAINT. Area Detector Control and Integration Software, Bruker Analytical X-ray Instruments Inc, Madison, WI, USA, 1997.
[32] B.V. Nonius, CAD4-EXPRESS Software, Ver. 5.1/1.2, Enraf Nonius, Delft, The Netherlands, 1994.
[33] G.M. Sheldrick, SHELX-97 Programs for solution and refinement of crystal structures, University of Göttingen, Germany, 1997.
[34] L. Farrugia, J. Appl. Cryst. 30 (1997) 565.
[35] A.L. Spek, in: PLATON. A Multipurpose Crystallographic Tool, Utrecht University, Utrecht, The Netherlands, 1998.

extracts [14,15]. This suggests that, under physiological conditions, the reductive release of iron from its hydroxamate siderophore complex is a viable process, particularly in the presence of an iron(II) trap such as porphyrin.

The electrochemical behavior of iron(III) complexes with aminohydroxamic acids has not been investigated to date. In the present paper, the cyclic voltammetric behavior of iron(III) complexes with alanine- (**1**), serine- (**2**), lysine- (**3**), histidine- (**4**) and glutamo-γ-hydroxamic acid (**5**) (Scheme 1) has been studied at hanging mercury drop electrodes. The objective was to determine the mechanism involved in the electron transfer processes and to gain some insight into the influence of ligand substituent effects on the redox potentials. The rate constants for the irreversible dissociation of iron(II) complexes were calculated. Comparison of the redox potentials with the redox potentials of some natural hydroxamates identified as siderophores is discussed.

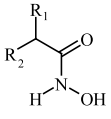
2. Experimental

2.1. Materials

All aminohydroxamic acids were used as purchased from Sigma. Iron(III) perchlorate stock solution was prepared from recrystallized solid iron(III) perchlorate hydrate (Aldrich) and standardized for Fe^{3+} ion spectrophotometrically in strong acid [16]. All other chemicals were of analytical grade and were obtained from Merck, except for sodium dihydrogen phosphate, which was purchased from Kemika (Zagreb, Croatia).

2.2. Methods

Cyclic voltammetry experiments were performed with an EG&G Princeton Applied Research Model 273A potentiostat controlled by the Model 270/250 Research Electrochemistry Software v. 4.30. Cyclic voltammetric studies were carried out using a hanging mercury drop working electrode (EG&G Princeton Applied Research Model 303A), a platinum wire auxiliary electrode and an Ag/AgCl reference electrode. The potentials were scanned from −0.1 to −1 V, employing scan rates between 10 mV s^{-1} and 20 V s^{-1}. All measurements were performed with positive feedback iR compensation.



	R_1	R_2
1	NH_3^+	CH_3
2	NH_3^+	CH_2OH
3	NH_3^+	$CH_2CH_2CH_2CH_2\ NH_3^+$
4	NH_3^+	
5	H	$CH_2CH(COO^-)\ NH_3^+$

Scheme 1. Structures of the aminohydroxamate ligands.

The studied complexes were generated in situ by addition of an appropriate amount of acidic iron(III) perchlorate stock solution to a solution of ligand in 0.05 M phosphate buffer at constant ionic strength ($I = 1.0$ M $NaClO_4$) thermostatted at 25 °C. The pH measurements were made with a Radiometer PHM 85 pH-Meter using a combined glass electrode (Radiometer PHC 2406L). All solutions were purged for 15 min with water-saturated argon, whereafter a continuous stream of argon was passed over the solutions throughout the measurement.

3. Results and discussion

3.1. Solution behavior of iron(III) aminohydroxamates

Equilibria occurring in aqueous solutions of iron(III) with **1**, **2**, **3**, **4** and **5** have been studied by a spectrophotometric method [17–21]. The species distribution diagrams based on the determined stability constants for iron(III) aminohydroxamates were calculated using the same experimental conditions under which their cyclic voltammetric measurements were performed. These data illustrate that the electrochemical behavior of all complexes was investigated under the conditions where the hexacoordinated iron(III) complex (FeL_3 or FeL_2 for **4**) is the main complex species (98.3–100%) present in solution at pH 7 and an iron(III)/ligand ratio of 1:40. In the pH range studied all the aminohydroxamate complexes investigated have the amino group in its protonated form.

3.2. Electrochemical behavior of iron(III) aminohydroxamates

Electrochemical studies of a solution of iron(III) with $c_M = 1 \times 10^{-3}$ M and excess of ligand ($c_L/c_M = 20$–80) at pH 6–8 were carried out by cyclic voltammetry using a hanging mercury drop electrode. Although the cathodic peaks with their anodic counterparts were observed (Fig. 1), these systems do not display simple redox behavior and a detailed analysis is therefore required. In cyclic voltammograms, one well-defined reversible or quasi-reversible cathodic peak was observed for all of the aminohydroxamate complexes investigated. Free

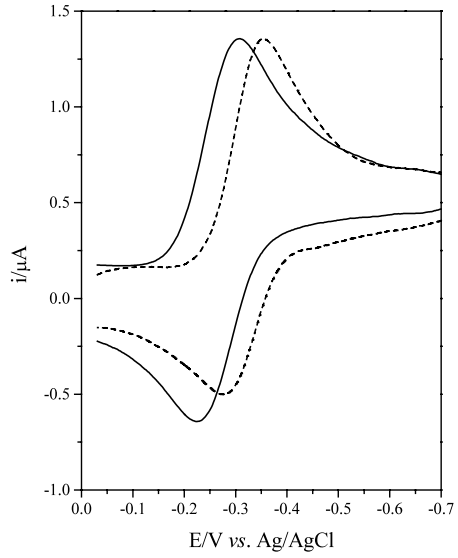


Fig. 1. Cyclic voltammograms of the iron(III) complex with alanine- (solid line) and glutamo-γ-hydroxamic acid (dashed line). Conditions: $c_{Fe} = 1 \times 10^{-3}$ M, $c_L/c_{Fe} = 40{:}1$, 0.05 M NaH_2PO_4, 0.05 M $Na_2B_4O_7$ at pH 7 and 1 M $NaClO_4$, $T = 25.0$ °C; hanging mercury drop electrode at 100 mV s^{-1} scan rate.

ligands are electrochemically inactive in the potential range investigated. The current peak height (i_p^c) is linear with the scan rate, v, and with $v^{1/2}$ for $v < 5$ V s^{-1}, suggesting a diffusion control, although at higher scan rates a weak adsorption of the complexes at the mercury surface was observed. Peak separations $\Delta E_p = E_p^c - E_p^a$ of about 60 mV were noticed in all cases, except for **4**, as expected for a reversible one-electron reduction process (Table 1).

A reduction wave with a typical quasi-reversible pattern was observed for the complex with histidinehydroxamic acid. The values of ΔE_p of about 90 mV were found at low scan rates, but increased up to 120 mV when the scan rate changed from 0.5 to 20 V s^{-1}. The quasi-reversible character of this system was also confirmed by the observation of a cathodic shift of E_p^c of about 30 mV for a tenfold increase in the scan rate. The current function ($i_p^c/v^{1/2}$) is independent of the scan rate and the ratio of anodic to cathodic peak current, i_p^a/i_p^c, is equal to unity, indicating that the iron(II) complex formed in the electro-reduction is stable within the time scale of the experiment.

The reversibility of the systems investigated was checked at a scan rate of 10 mV s^{-1} (Fig. 2). The irreversibility of cathodic current peaks obtained clearly

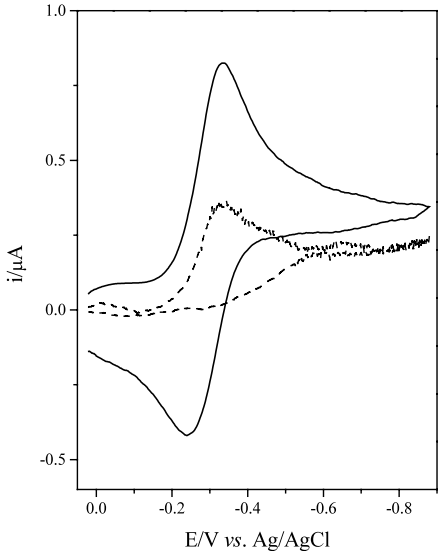


Fig. 2. Cyclic voltammograms of the iron(III) complex with lizinehydroxamic acid at the hanging mercury drop electrode at scan rates of 10 (dashed line) and 50 mV s^{-1} (solid line). Conditions: $c_{Fe} = 1 \times 10^{-3}$ M, $c_L/c_{Fe} = 40{:}1$, 0.05 M NaH_2PO_4, 0.05 M $Na_2B_4O_7$ at pH 7 and 1 M $NaClO_4$, $T = 25.0$ °C.

Table 1
Voltametric data for the iron(III) complex with (a) serine- and (b) histidinehydroxamic acid

	v (V s^{-1})	E_p^c (mV)	$i_p^c \times 10^6$ (A)	i_p^a/i_p^c	ΔE_p (mV)
(a)	0.01	−310	0.42	Irrever.	Irrever.
	0.05	−320	1.03	0.57	64
	0.1	−322	1.32	0.61	66
	0.2	−330	1.77	0.69	64
	0.5	−338	2.74	0.79	68
	1	−348	3.99	0.84	74
	5	−356	9.56	0.88	82
(b)	0.01	−290	0.64	0.97	84
	0.05	−296	1.13	1.13	90
	0.1	−310	1.63	1.03	104
	0.2	−316	2.11	1.00	112
	0.5	−324	3.59	0.99	120
	1	−338	5.39	0.97	128
	5	−346	14.61	0.96	132

Conditions: $c_{Fe} = 1 \times 10^{-3}$ M, $c_L/c_{Fe} = 40{:}1$, 0.05 M NaH_2PO_4, 0.05 M $Na_2B_4O_7$ at pH 7 and 1 M $NaClO_4$, $T = 25.0$ °C; hanging mercury drop electrode.

shows that charge transfer is followed by a homogeneous chemical reaction, except in the case of **4**. Analysis of the effect of scan rates on the voltammograms shows that the values of $i_p^c/v^{1/2}$ are approximately constant with scan rate. On the other hand, a dependence of the reduction potentials on the scan rates was noticed (Table 1), namely E_p^c for all the complexes investigated changes cathodically by about 20–30 mV when the scan rate changes from 0.1 to 1 V s^{-1}. The ratios of i_p^a/i_p^c were changed from 0.52 to 0.98 for scan rates between 0.1 and 1 V s^{-1}. The increase of i_p^a with scan rates is due to the fact that at higher scan rates there is less time for an irreversible chemical reaction. For the iron(III) complexes with **5**, the highest value of i_p^a/i_p^c is about 0.79 when $v = 5$ V s^{-1}, which means that the chemical reaction is fast enough for its influence on anodic peak current to be observed at very high scan rates. All of these electrochemical results suggest a typical EC mechanism, which includes a reversible electrochemical process (E) followed by an irreversible chemical reaction (C) [22].

The reduction potentials in these systems were observed to become more cathodic with increasing pH. The pH dependence on the redox potential can be used to determine the proton stoichiometry of the electrode reaction. For pH values between 6 and 8, a cathodic shift of E_p^c was observed, at an approximate rate of 70 mV per pH unit (Fig. 3). This observation is consistent with protonation of the reduced species, the iron(II) complexes, indicating involvement of one proton and one electron in the redox processes according to Eqs. (1) and (2):

$$Fe(III)L_3 + e^- \Leftrightarrow Fe(II)L_3 \quad (1)$$

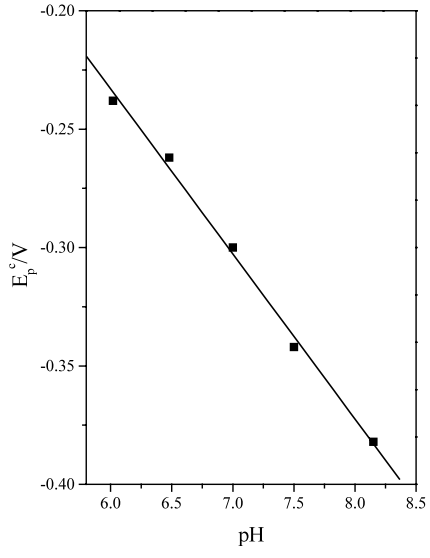


Fig. 3. Cathodic shift of the reduction peak (E_p^c) observed in the cyclic voltammograms of the iron(III) alaninehydoxamate as a function of pH at scan rate $v = 100$ mV s^{-1}. Conditions are as given in Fig. 2.

$$Fe(II)L_3 + H^+ \Rightarrow Fe(II)L_2 + HL \quad (2)$$

Thus, the global mechanisms include an electrochemical step (E), followed by an irreversible chemical dissociation of the reduced complexes.

It is possible to calculate the stability constant of the iron(II) complex from the difference between the peak potentials for the reduction of the $Fe(H_2O)_6^{3+}$ ion and of its complex in a situation where the iron(III) and iron(II) complexes are fully coordinated and no ligand exchange occurs in the reduced form of the complex during the time frame of the experiment [23]. The necessary conditions are an excess of the ligand and a sufficiently high pH. Since it was impossible to find any conditions with complete reversibility for the electrochemical reaction without disturbance by a coupled chemical reaction, no evaluation of the stability constant for the reduced complexes of aminohydoxamate was carried out. However, literature data [12] for the stability constants of the acetohydroxamate iron(II) complexes suggest that the $Fe(II)L_2$ species is highly favored (94.8%) under the same experimental conditions used for the cyclic voltammetric measurements. This may explain why the chemical reaction (eq. 2) is favored despite a high free ligand concentration present in solution.

The rate constants for the irreversible dissociation decomposition of the iron(II) complexes, following the reversible reduction of the iron(III) complexes (eqs 1 and 2) have been determined using the Nicolson and Shain theoretical approach [22]. The pseudo-first order kinetics is assumed because the solutions were buffered, which means that the H^+ concentration was essentially unchanged during the voltammetric measurement. The working curve of i_p^a/i_p^c, as a function of $\log k_d\tau$, was used, where τ is the time in s required to scan from $E_{1/2}$ to the switching potential $E_\chi = -900$ mV. Redox potentials $E_{1/2}$ were determined from cyclic voltammograms by taking an average of the cathodic and anodic peak potentials $[(E_p^c + E_p^a)/2]$. The calculated values k_d were obtained as an average of several single point

Table 2
Scan rate effect on the i_p^a/i_p^c ratio and calculated kinetics parameters for the iron(III) lizinehydroxamate at pH 7, $c_{Fe} = 1 \times 10^{-3}$ M, $c_L/c_{Fe} = 40{:}1$, $T = 25.0$ °C, $I = 1.0$ ($NaClO_4$)

v (V s^{-1})	i_p^a/i_p^c	$k_d\tau$	$E_{1/2}$ (mV)	k_d (s^{-1})
0.1	0.79	0.24	−300	0.040
0.2	0.86	0.14	−304	0.047
0.3	0.90	0.10	−308	0.051
0.4	0.91	0.09	−302	0.060
0.5	0.94	0.06	−320	0.052
0.6	0.95	0.05	−316	0.052
0.7	0.96	0.04	−320	0.048
0.8	0.97	0.03	−320	0.041
0.9	0.97	0.03	−326	0.047

calculations (Table 2), corresponding to the different scan rates in the range 100–900 mV s^{-1}, where adsorption effects were neglected.

3.3. Ligand substituent effects

Electrochemical studies of the iron siderophore and model siderophore complexes reveal a strong influence of the type and the number of metal binding groups on the redox potential, with relatively little influence of the ligand structure, although the latter statement is based on limited data. On the other hand, investigations of the ligand substituent effects on the redox potentials in the substituted benzohydroxamic acid complexes of iron indicate that the more electron donating groups shift the potential to more negative values [24]. In order to determine the effect of the electronic and steric properties of the R substituent in the ligand side chain on the redox potential, different aminohydroxamate ligands were chosen. The presence of other functional groups in the hydroxamic acid molecules, such as amino, hydroxyl or carboxyl ones, offers the possibility of formation of the complex in which they participate as electron pair donors. In spite of these possibilities, the spectrophotometric results show that complexation occurs by coordinating both the carbonyl and OH oxygen atoms of the hydroxamate group to the iron(III) center for all the complexes investigated, except for **4**. Involvement of the amino group and the imidazole ring nitrogen atom in the coordination of histidinehydroxamic acid to iron was detected [25]. The shift in the coordination mode from bi- to tridentate, from O to N atom and from five- to six-membered ring was reflected in a change of the mechanism involved in the electron transfer process. On the other hand, it is reasonable to expect that the participation of nitrogen atoms in the complexation should be reflected more in the difference of the redox potential. A comparison of the reduction peak potentials obtained for the various iron(III) aminohydroxamates is given in Table 3. The reduction potential of **5** is more negative than the potentials of other complexes. This behavior could be explained taking into account that the amino group in the γ-position relative to the carbonyl group has a less pronounced electron withdrawing effect compared with the effect of the NH_3^+ group in an α-position. Complex **1** ($R = CH_3$) has a more positive potential than **2** ($R = CH_2OH$), consistent with the electron donating effect of the hydroxyl group, although their stability constants for the tris complexes are very similar. If the observed difference in the redox potential between the investigated complexes could be explained on the basis of the electronic effect of the substituent on the carbonyl group, the most positive redox potential would be expected for **3**, due to a longer alkyl chain with a positively charged amine terminal group. The obtained results show that this complex has a more negative potential than **1**. However, this observation may be reasonably rationalized by a comparison of the stability constants of these complexes, which indicates that the redox potential was shifted to more negative values as the stability of the complex increased (Table 3). It is obvious that the differences in aminohydroxamate ligands influence the rate constants for irreversible dissociation of the iron(II) complexes, as the ligand increases the stability of the iron(III) complex relative to the corresponding Fe(II) complex. Why complex **3** has a lower k_d value than the complexes with more positive potentials is unclear.

Table 3
Reduction peak potentials, logarithmic equilibrium constants of the iron(III) aminohydroxamate complexes and the rate constants for the irreversible dissociation of the iron(II) complexes

Complex	$E_{1/2}$ (mV)	log K [a]	k_d (s^{-1}) [b]
1	−272	−3.638	0.15(1)
2	−290	−3.628	0.19(2)
3	−300	−2.886	0.05(1)
4	−258		
5	−324	0.653	0.51(3)

Standard deviations are shown in parentheses.
[a] $K = [Fe(III)L_3][H^+]^3/[Fe(III)][HL]^3$.
[b] Conditions: $c_{Fe} = 1 \times 10^{-3}$ M, $c_L/c_{Fe} = 40{:}1$, 0.05 M NaH_2PO_4, 0.05 M $Na_2B_4O_7$ at pH 7 and 1 M $NaClO_4$, $T = 25.0$ °C; hanging mercury drop electrode.

4. Conclusion

Analysis of the reduction potentials shows that the values obtained are much lower than those found for the naturally occurring siderophores, including ferrioxamine B ($E_{1/2} = -0.69$ V vs. the standard Ag/AgCl electrode), which has a positively charged amine side chain as well [10]. The potentials are in the range of potentials for physiological reductants such as NADH [26]. Such electrochemical behavior, namely the easy reduction accompanied by dissociation of the reduced species, gives some support for considering these compounds as potential siderophore models. Furthermore, in all the investigated complexes, except for **4**, the NH_3^+ groups may remain free for eventual hydrogen binding interaction with proteins in the required molecular recognition functions, as proposed by the outer-membrane receptor protein involved in ferrioxamine transport [27].

References

[1] A.L. Crumbliss, in: G. Winkelmann (Ed.), Handbook of Microbial Iron Chelates, CRC Press, New York,, 1991.

[2] K.N. Raymond, Pure Appl. Chem. 66 (1994) 773.
[3] A.-M. Albrecht-Gary, A.L. Crumbliss, in: A. Sigel, H. Sigel (Eds.), Metal Ions in Biological Systems, vol. 35, Marcel Dekker, New York,, 1998, p. 239.
[4] A.E. Martell, W.F. Anderson, D.G. Badman (Eds.), Development of Iron Chelators for Clinical Use, Elsevier, New York, 1981.
[5] G. Winkelman, D. Van der Helm, J.B. Neilands (Eds.), Iron Transport in Microbes, Plants and Animals, VCH, Weinheim, Germany, 1987.
[6] V. Braun, K. Hantke, in: G. Winkelmann, C.J. Carrano (Eds.), Transition Metals in Microbial Metabolism, Harwood Academic Publishers, London,, 1997, p. 81.
[7] S.R. Cooper, J.V. McArdle, K.N. Raymond, Proc. Natl. Acad. Sci. USA 75 (1978) 3551.
[8] C.J. Carrano, S.R. Cooper, K.N. Raymond, J. Am. Chem. Soc. 101 (1979) 599.
[9] E.F. Wawrousek, J.V. McArdle, J. Inorg. Biochem. 17 (1982) 169.
[10] R. Helman, G.D. Lawrence, Biochem. Bioenerg. 22 (1987) 187.
[11] I. Spasojević, S.K. Armstrong, T.J. Brickman, A.L. Crumbliss, Inorg. Chem. 38 (1999) 449.
[12] K. Abu-Dari, S.R. Cooper, K.N. Raymond, Inorg. Chem. 17 (1978) 3394.
[13] M.A. Santos, M.A. Esteves, M.C.T. Vaz, M.L. Goncalves, J. Chem. Soc., Dalton Trans. (1993) 927.
[14] J.F. Ernst, G.F. Winkwlmann, Biochim. Biophys. Acta 500 (1977) 27.
[15] J.B. Straka, T. Emery, Biochim. Biophys. Acta 569 (1979) 277.
[16] R. Bastian, R. Weberling, F. Palilla, Anal. Chem. 28 (1956) 459.
[17] N. Kujundžić, V. Bačić, M. Pribanić, Acta Pharm. Jugosl. 35 (1985) 221.
[18] N. Kujundžić, A. Tešija, V. Todorić-Kovačević, Acta Pharm. Jugosl. 41 (1991) 17.
[19] N. Kujundžić, V. Boban, V. Todorić-Kovačević, Pharmazie 47 (1992) 433.
[20] N. Kujundžić, S. Inić, V. Todorić-Kovačević, Acta Pharm. 44 (1994) 61.
[21] N. Kujundžić, S. Inić, V. Todorić-Kovačević, Acta Pharm. 45 (1995) 83.
[22] R.S. Nicholson, I. Shain, Anal. Chem. 36 (1964) 706.
[23] D. DeFord, D.H. Hume, J. Am. Chem. Soc. 73 (1951) 532.
[24] P. Ghosh, A. Chakravorty, Inorg. Chim. Acta 56 (1981) L77.
[25] D.A. Brown, B.S. Sekhon, Inorg. Chim. Acta 91 (1984) 103.
[26] K.N. Raymond, C.J. Carrano, Acc. Chem. Res. 12 (1979) 183.
[27] I. Berner, P. Yakirevitch, J. Libman, A. Shanzer, G. Winkelman, Biol. Metals 4 (1991) 186.

bonds prevented sensible conclusions being obtained, in particular regarding the Sn–X bonds. In addition to the X-ray data, solution ^{1}H, ^{13}C and ^{119}Sn NMR and far-IR spectral data are presented.

2. Experimental

NMR spectra were run on Bruker 300 and Varian 400 MHz instruments, IR spectra on Nicolet Magna 760 FTIR and Nicolet Fourier-transform spectrometers. Melting points were measured on a Melt-TempII instrument and are uncorrected.

2.1. Synthesis

Compound **1** (X = Neo) [9] was obtained by a published procedure and **1** (X = OSn(Neo)$_3$) was a gift from Dow Chemical Co.

Compound **1** (X = Neo). IR (CsI, cm^{-1}): *v*: 462, 391, 259, 158. [**1**: X = OSn(Neo)$_3$]. IR (CsI, cm^{-1}): *v*: 454, 419, 396, 374, 256, 157.

2.1.1. 1 (X = Cl)

To a solution of **1** (X = OSn(Neo)$_3$) (0.5 mmol) in Et_2O was added aqueous HCl (2 ml of 1.0 M solution). After sonification for 5 min, the organic phase was collected and evaporated. Crystals of **1** (X = Cl) were obtained by slow evaporation from an Et_2O solution; m.p. 117–119 °C; lit. [3] value 117.5–118.5 °C.

IR (CsI, cm^{-1}): *v*: 461, 394, 311(Sn–Cl), 266, 160.

2.1.2. 1 (X = Br)

To a solution of **1** (X = Neo) (2.0 mmol) in $CHCl_3$ was added, dropwise with stirring, a solution of Br_2 (2.0 ml) in $CHCl_3$ at −10 °C. After addition was complete, the temperature was allowed to rise to ambient. Complete reaction occurred after 2 h as shown by the decoloration of the reaction mixture. The solvent was removed under vacuum to leave a solid, which was washed with cold MeOH. Crystals of **1** (X = Br) were obtained by slow evaporation from an Et_2O solution; m.p. 112–113 °C; lit. [3] value 109.5–110 °C.

IR (CsI, cm^{-1}): *v*: 457, 398, 266, 212(Sn–Br), 164.

2.1.3. 1 (X = I)

To a solution of **1** (X = Br) (0.55 mmol) in Me_2CO was added a solution of KI (1.75 mmol) in warm Me_2CO. The reaction mixture was stirred at room temperature (r.t.) for 1 h, filtered and the filtrate evaporated. The residue was extracted with CH_2Cl_2 and the extractions were partially evaporated. Colorless crystals of **1** (X = I) were obtained by further slow evaporation; m.p. 117–118 °C; lit. [3] value 116.5–117.5 °C.

IR (CsI, cm^{-1}): *v*: 454, 396, 268, 172(Sn–I).

2.1.4. 1 (X = F)

Solutions of **1** (X = Br) (0.60 mmol) in Et_2O and NaF (3.66 mmol) in water were mixed. A little decyltrimethylammonium bromide was added and the mixture was sonicated for 10 min. Sodium sulfate was added and the organic phase collected. Slow evaporation of the organic solution gave crystals of **1** (X = F); m.p. 99–100 °C; lit. [3] value 98–100 °C.

IR (CsI, cm^{-1}): *v*: 497(Sn–F), 444, 263, 178.

2.1.5. 1 (X = N_3)

To a solution of **1** (X = Br) (0.25 mmol) in EtOH was added a solution of NaN_3 (2.5 mmol) in warm EtOH. The reaction mixture was stirred at r.t. for 30 min, filtered and the filtrate evaporated. The residue was extracted with Et_2O and the extracts gave colorless crystals of **1** (X = N_3) on slow evaporation; m.p. 98–99.5 °C; lit. [3] value 96–96.5 °C.

IR (CsI, cm^{-1}): *v*: 2069 (N_3), lit. [3] value 2072, 456, 386, 266, 153.

2.1.6. 1 (X = NCS)

To a solution of **1** (X = Br) (0.3 mmol) in Me_2CO was added a solution of KNCS (2.2 mmol) in warm acetone. The reaction mixture was stirred at r.t. for 1 h, filtered and the filtrate evaporated. The residue was extracted with CH_2Cl_2 and the extracts gave colorless crystals of **1** (X = NCS) on slow evaporation; m.p. 98–99.5 °C.

IR (CsI, cm^{-1}): *v*: 2021(NC), 459, 399, 303(Sn–N), 268, 167.

2.1.7. 1 (X = OAc)

Compound **1** (X = OSn(Neo)$_3$] (0.15 mmol) was dissolved in acetic acid (3 ml, 5.2 mmol). The solution was evaporated under vacuum and gently heated to leave a residue of **1** (X = OAc). This was recrystallized from acetic acid; m.p. 85–88 °C; lit. [3] value 86.5–87 °C.

IR (CsI, cm^{-1}): *v*: 1667 (CO) (lit. [3] value 1660), 456, 402, 292, 266, 160.

Selected ^{1}H, ^{13}C and ^{119}Sn NMR spectral data for **1** are displayed in Table 1.

2.2. Crystallography

2.2.1. Data collection

Intensity data for **1** (X = Br, I, N_3 and OAc) were obtained, at 150 K in all cases, by means of the Enraf Nonius KappaCCD area detector diffractometer of the EPSRC's crystallography service at Southampton. The entire process of data collection, cell refinement and data reduction was accomplished by means of the programs DENZO [16] and COLLECT [17]. Correction for absorption by a semi-empirical method based upon the variation in intensity of equivalent reflections was achieved with the program SORTAV [18]. Data for **1**

Table 1
Selected NMR spectral data for **1** in $CDCl_3$

X	δ^{119}Sn	δ^{1}H(CH_2) [J(^{119,117}Sn–H)]	δ^{1}H(Me) [J(^{119,1117}Sn–H)]	δ^{13}C(CH_2) [J(^{119,117}Sn–^{13}C)]	δ^{13}C(Me) [J(^{119,117}Sn–^{13}C)]	$\delta^{13}C$(CMe_2) [J(^{119,117}Sn–^{13}C)]	δ(others)
F	138.8	1.01	1.18	39.8	38.6	33.8	^{1}J(Sn–F) = 2301
	[146] [a]	[48.9]	[ca. 5]	[350]	[20.5]	[44.1]	^{3}J(F–CH_2) = 3.1
							^{2}J(F–CH_2) = 7.6
		0.95 [c]	1.22				
		[52.4] [c]	[–]				
Cl	118.4	1.11	1.18	40.4	38.9	33.9	
		[47.2]	[5.8]	[334,319]	[21.3]	[46.4]	
	[118] [a]						
	[117.7] [b]	1.05 [c]	1.19 [c]				
		[47.8] [c]	[5.8] [c]				
Br	92.3	1.23	1.19	39.1	38.1	32.9	
		[46.5]	[5.8]	[323,309]	[22.0]	[46.4]	
		1.07 [c]	1.20 [c]				
		[48.4] [c]	[5.9] [c]				
I	14.7	1.38	1.19	39.3	39.6	34.0	
		[45.1]	[6.2]	[309,295]	[22.0]	[46.3]	
		1.34 [c]	1.19 [c]				
		[44.5] [c]	[6.2] [c]				
NCS	47.9	1.05	1.22	37.5	37.6	32.8	^{1}J(Sn–N) = 125
		[49.0]	[6.2]	[354,339]	[22.8]	[46.0]	
N_3		1.03	1.19	37.5	37.6	32.8	
		[48]	[6.2]	[–]	[–]	[–]	
OAc	83.4	1.07	1.12	37.3	37.8	32.87	δ^{13}C(CO) = 176.2
		[50.6]	[5.1]	[356]	[20.1]	[44.1]	δ^{13}C(CH_3) = 22.6
	[79] [a]						δ^{1}H(CH_2) = 1.89
		1.04 [c]	1.25 [c]				δ^{1}H(CH_2) = 1.82 [c]
		[51.7] [c]	[5.2] [c]				
OH	77.1	0.99	1.20	37.8	37.3	33.1	
	[75.9] [b]	[50.4]	[4.6]	[–]	[–]	[41.9]	
Neo	−52.5	0.80	1.16	31.2	38.5	33.6	
		[47.9]	[–]	[–]	[18.6]	[34.5]	

[a] [10].
[b] [12].
[c] [3].

(X = NCS) were obtained at 297 K with a Bruker SMART 1000 CCD area detector diffractometer. SMART software [19] was used for data collection and the program SAINT [19] for cell refinement and data reduction. A semi-empirical correction for absorption similar to that noted above was applied by means of the program SADABS [19].

2.2.2. Structure solution and refinement

The same procedure was used for all **1**. Structure solutions providing positions for the majority of the non-H atoms were obtained by application of the direct methods procedure of SHELXS-97 [20]. Thereafter difference map calculations to find any missing non-H atoms and completion of the refinement process were carried out with SHELXL-97 [21]. In the final stages of refinement H atoms were placed in calculated positions and refined with a riding model. Further details of the processes of data collection and structure refinement are available in Table 2. The program, ORTEP-3 [22], was used to obtain the Figures.

3. Results and discussion

3.1. General

The syntheses of the various compounds **1** were achieved by bromo-dealkylation of **1** (X = Neo) or by anion exchange using as reagents either **1** (X = Br), with Y^- (Y = F, I, NCS or N_3), or **1** (X = OSn(Neo)$_3$), with HCl or HOAc. Complete anion exchanges were indicated from the physical properties, including NMR and far IR spectra.

3.2. Crystallography

The solid state structures were not merely studied to determine the coordination at tin, but to investigate the conformations and molecular arrangements in **1**, compounds in which there are three relative bulky hydrophobic groups (the neophyl ligands) and a relatively small polar region (the Sn–X fragment).

Table 2
Crystal data and structure refinement [a] for (**1**: X = Br, I, N_3, NCS and OAc)

X	Br	I	N_3	NCS	OAc
Empirical formula	$C_{30.25}H_{39.25}BrCl_{0.75}Sn$	$C_{30.25}H_{39.25}Cl_{0.75}ISn$	$C_{30}H_{39}N_3Sn$	$C_{31}H_{39}NSSn$	$C_{32}H_{42}O_2Sn$
M	628.05	675.04	560.33	576.38	577.35
T (K)	150(2)	150(2)	150(2)	297(2)	150(2)
Wavelength (Å)	0.71073	0.71073	0.71073	0.71073	0.71073
Space group	$P2_1$	$P2_1$	$P2_1/n$	$P2_1/c$	$P1$
Cell dimension					
a (Å)	17.9633(4)	18.0069(3)	18.7224(2)	17.7105(7)	12.2476(2)
b (Å)	17.9225(4)	17.9500(3)	17.2884(2)	18.7575(8)	15.3004(2)
c (Å)	18.3954(6)	18.4313(4)	19.4326(4)	18.3223(8)	16.9444(2)
α (°)	90	90	90	90	104.3450(8)
β (°)	103.9165(9)	103.4000(7)	117.2747(5)	100.7760(10)	103.4030(7)
γ (°)	90	90	90	90	100.7490(6)
V (Å^3)	5748.5(3)	5795.25(19)	5590.63(14)	5979.4(4)	2890.50(7)
Z	8	8	8	8	4
Calculated density (Mg m^{-3})	1.451	1.547	1.331	1.281	1.327
Absorption coefficient (mm^{-1})	2.365	2.032	0.936	0.942	0.909
F(000)	2548	2692	2320	2384	1200
Crystal color	colorless	colorless	colorless	colorless	colorless
Crystal size (mm)	0.10 × 0.10 × 0.10	0.35 × 0.10 × 0.04	0.20 × 0.20 × 0.10	0.30 × 0.20 × 0.20	0.20 × 0.20 × 0.12
θ Range for data collection (°)	2.91–27.44	3.00–30.83	3.13–27.51	2.08–32.51	2.94–30.77
Index range	$-23 \le h \le 22$, $-19 \le k \le 21$, $-19 \le l \le 23$	$-24 \le h \le 24$, $-22 \le k \le 22$, $-21 \le l \le 26$	$-24 \le h \le 21$, $-20 \le k \le 21$, $-25 \le l \le 25$	$-26 \le h \le 17$, $-28 \le k \le 25$, $-25 \le l \le 27$	$-16 \le h \le 17$, $-19 \le k \le 21$, $-23 \le l \le 20$
Reflections collected/ unique	36 214/22 983	45 544/26 606	42 274/12 668	61 105/21 502	30 901/22 786
[R_{int}]	0.0754	0.0451	0.0523	0.0533	0.0341
Completeness to 2θ limit (%)	27.44, 95.6%	30.83, 82.1%	27.51, 98.4%	32.51, 99.2%	30.77, 74.4%
Max. and min. transmission	0.838 and 0.733	0.995 and 0.908	0.904 and 0.828	0.912 and 0.808	0.910 and 0.846
Data/restraints/ parameters	22 983/1/1213	26 606/1/1213	12 668/0/625	21 502/0/625	22 786/3/1261
Goodness-of-fit on F^2	1.002	1.010	1.030	0.807	1.103
Final R indices [$I > 2\sigma(I)$]	$R_1 = 0.0604$, $wR_2 = 0.1275$	$R_1 = 0.0470$, $wR_2 = 0.0947$	$R_1 = 0.0410$, $wR_2 = 0.0915$	$R_1 = 0.0356$, $wR_2 = 0.0633$	$R_1 = 0.0374$, $wR_2 = 0.1049$
R indices (all data)	$R_1 = 0.1199$, $wR_2 = 0.1687$	$R_1 = 0.0763$, $wR_2 = 0.1081$	$R_1 = 0.0678$, $wR_2 = 0.1022$	$R_1 = 0.1258$, $wR_2 = 0.0816$	$R_1 = 0.0450$, $wR_2 = 0.1209$
Absolute structure parameter	0.001(11)	−0.042(15)			−0.047(14)
Largest diff. peak and hole (e Å^{-3})	0.862 and −1.050	0.967 and −1.593	0.904 and −1.074	0.623 and −0.369	0.877 and −1.362

[a] In all cases, absorption correction was semi-empirical from equivalents and refinement by full-matrix least-squares on F^2.

The crystals used in the crystallography were grown by evaporation of $CHCl_3$ solutions. Unsolvated compounds were obtained for **1** (X = N_3, NCS and OAc), while solvates, [**1**·1/4$CHCl_3$] were isolated for **1** (X = Br and I).

As well as the structures of **1** (X = Br, I, N_3, NCS and OAc), the structure of the previously reported compound **1** (X = Cl) [6] at 150 K is also discussed here. All these molecules are themselves not inconsiderable in size requiring the placement, in the absence of coincident crystallographic and molecular symmetry, of at least 32 non-H atoms per molecule. The situation is further complicated by the fact that the asymmetric unit of **1** (X = N_3) and **1** (X = NCS) contains two complete molecules and that of **1** (X = Br), **1** (X = I) and **1** (X = OAc) no less than four. This has prompted the following labeling convention. The atoms of every neophyl group have been labeled numerically in the same manner (Fig. 1), e.g. in every case C1 is bonded to Sn1 and the methyl and phenyl groups are C3 and C4 and C5 to C10, respectively. There is not, however, complete consistency in the numbering of the atoms of the methyl and phenyl groups in relation to their orientation with respect to the molecule as a whole.

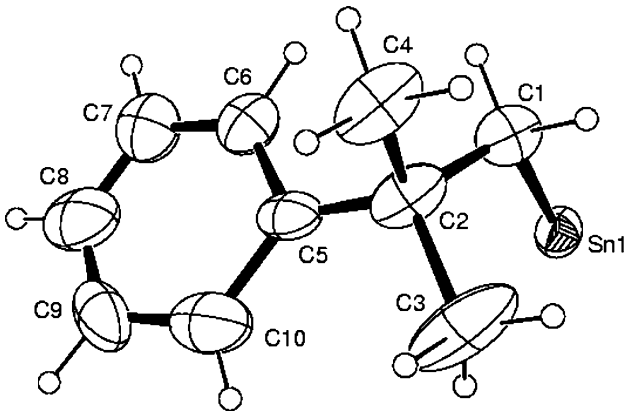


Fig. 1. The general atom numbering scheme used for the carbon atoms of the neophyl groups in **1**, see text. The example shown is the asymmetric unit of **1** (X = Cl) omitting the Cl atom. Non-H atoms are shown as 30% ellipsoids and H atoms as small circles.

For **1** (X = N_3) and **1** (X = NCS), the two independent molecules are termed I and II: in molecule I, the tin atom is Sn1a, the three neophyl ligands/their constituent atoms are identified by the suffices A/a, B/b and C/c, while in molecule II, the tin atom is Sn1b and the suffixes used for the three neophyl groups/atoms are D/d, E/e and F/f. In each of **1** (X = Br), **1** (X = I) and **1** (X = OAc), which have four independent molecules in the asymmetric unit, a similar system is utilized. The four independent molecules are termed I, II, III and IV, having tin atoms Sn1a, Sn1b, Sn1c and Sn1d, respectively. The neophyl group suffices are here A, B and C (in molecule I), D, E and F (in molecule II), G, H and I (in molecule III) and J, K and L (in molecule IV): the atoms within each neophyl ligand take the appropriate lower case suffix. A similar strategy as used for Sn has been applied to the labeling of the halide, X, in molecules of **1** (X = Br) and **1** (X = I). The general numbering of the other X group atoms are (Sn1)–N1–N2–N3 in **1** (X = N_3), and (Sn1)–N1–C11–S1 in **1** (X = NCS) and (Sn1)–O1–C11(O2)–C12 in **1** (X = OAc).

3.2.1. Geometry at tin

Selected bond lengths and angles for **1** (X = Cl, Br, I, N_3 and NCS) are listed in Tables 3 and 4, while selected geometric data for **1** (X = OAc) are provided in Table 5. Molecules of **1** (X = Cl, Br, I, N_3 and NCS) clearly contain four-coordinate tin centers, with distorted tetrahedral geometries. Each independent molecule of each compound **1** (X = Cl, Br, I, N_3 and NCS) has a very similar geometry, with relatively small differences in the C–Sn–X and C–Sn–C bond angles for each X. In each molecule, the three smallest angles subtended at tin are the C–Sn–X angles. The bulk of the neophyl groups results in the opening up of the C–Sn–C angles. The average C–Sn–X angles are 99.67°, 101.6°, 102.5°, 100.6° and 99.7° in **1** (X = Cl, Br, I, N_3 and NCS) and are influenced by both the size of the ligand X and the length of the Sn–X bond. The Sn–X bond lengths, averages for all but **1** (X = Cl), are 2.382(3), 2.545(2), 2.714(8) Å for X = Cl, Br and I, respectively, and are close to the appropriate sums of the covalent radii of 2.39, 2.54 and 2.73 Å [23].

The average Sn–N bond lengths in **1** (X = NCS) and **1** (X = N_3) are 2.119(2) and 2.247(12) Å, respectively, compared with the sum of the covalent radii for Sn and N of 2.15 Å [24]. There are no intermolecular Sn···N contacts in **1** (X = N_3) or Sn···S contacts in **1** (X = NCS) less than 4.0 Å. The closest intermolecular contacts in a particular molecule of **1** (X = NCS) are S···S at 3.6429(16) Å—that is close to the sum of the van der Waals radii. Smaller triorganotin *N*-thiocyanates, such as Me_3SnNCS {Sn–N and Sn–S = 2.15(6) and 3.13(2) Å} [24], Ph_3SnNCS {Sn–N and Sn–S = 2.199(11)–2.248(10), and 2.897(4)–2.952(4) Å} [25,26] and (p-$MeC_6H_4)_3SnNCS$ {Sn–N and Sn–S = 2.195(5) and 3.0255(2) Å} [26], exist in the solid state as zig-zag polymers due to NCS bridging with five-coordinate tin atoms. The more hindered compounds, $Me_2[(PhMe_2Si)_3C]SnNCS$ {Sn–N = 2.12(3) Å} [27] and (o-$MeC_6H_4)_3SnNCS$ {Sn–N = 2.067(6) and 2.066(6) Å} [26], on the other hand, are monomeric in the solid state with four-coordinate tin centers. Compound (o-$MeOC_6H_4)_3SnNCS$ {Sn–N = 2.090(5) Å} [26], is also molecular, but here there is a suggestion of a weak intramolecular Sn–O interaction [Sn–O 2.961(4) Å, ∠ N–Sn–O = 152.19(17)°] and hence an increase in the coordination number at Sn to 5, but this clearly has little effect on the Sn–N bond length.

The Sn–N bond length in monomeric t-Bu_3SnN_3 [28] is a little shorter, at 2.101(4) Å, than those found in **1** (X = N_3). Smaller triorganotin azides, e.g. Me_3SnN_3 [29], are N-bridged in the solid state. The Sn–N bond lengths in [(**1**: X = triazole)·0.5H_2O] [5] are 2.123(6) and 2.105(7) Å.

Compound **1** (X = OAc) was the only trineophyltin compound studied here that was other than four-coordinate, as a result of the acetate group tending to be a bidentate chelating ligand and the tin centers becoming five-coordinate (Fig. 2). As shown by the Sn–O distances, there is a strong asymmetry in the acetate chelate bonding, with one strong and one weak bond: the primary Sn–O1 bond lengths fall in the range 2.070(5)–2.117(4) Å with the Sn–O2 separations between 2.963 and 3.069 Å. These values can be compared with sums of covalent radii and van der Waals radii of 2.15 and 3.70 Å [23]. Noticeably too, the primary C–Sn–O1 angles fall into three distinct groupings, with ranges of 93.84° ± 0.82°, 103.13° ± 1.33° and 107.75° ± 0.55°, see Table 5. The C–Sn–C angles in **1** (X = OAc) also show a slightly greater variation than those in **1** (X = Cl, Br, I, N_3 and NCS). The geometry at tin is best described as being on the pathway from tetrahedral to

Table 3
Selected bond lengths (Å) for **1** (X = Cl, Br, I, N_3 and NCS) [a]

X	Mol	Sn1–X1	Sn1–C1(n)		
			[n]	[n]	[n]
Cl		2.382(3)	2.149(5)	2.149(5)	2.149(5)
Br	I	2.5473(14)	2.150(12) [a]	2.157(10) [c]	2.172(9) [b]
	II	2.5427(13)	2.147(12) [e]	2.147(10) [f]	2.171(9) [d]
	III	2.5440(15)	2.151(11) [g]	2.170(11) [h]	2.172(10) [i]
	IV	2.5438(14)	2.170(10) [j]	2.173(10) [l]	2.184(11) [k]
I	I	2.7496(6)	2.154(6) [b]	2.162(7) [a]	2.164(6) [c]
	II	2.7333(6)	2.159(6) [f]	2.160(7) [d]	2.163(7) [e]
	III	2.7441(6)	2.143(7) [g]	2.156(7) [h]	2.163(6) [i]
	IV	2.7424(6)	2.161(6) [l]	2.166(6) [j]	2.166(6) [k]
N3	I	2.259(5)	2.147(3) [b]	2.150(3) [a]	2.156(3) [c]
	II	2.235(3)	2.143(3) [e]	2.150(3) [f]	2.150(3) [d]
NCS	I	2.117(3)	2.138(3) [b]	2.142(2) [a]	2.147(2) [c]
	II	2.121(3)	2.141(2) [e]	2.141(2) [f]	2.149(2) [d]

[a] The three Sn—C1(n) bond lengths in each molecule have been placed in order of increasing bond length. The particular C1(n) atom involved in each bond has been indicated by the lower case letter, a, b, c etc., which, as indicated in the text, are associated with neophyl ligands, A, B, C etc.

trigonal bipyramidal, with the carbonyl oxygens, O2, in quasi axial positions and O1 in the quasi equatorial sites. A similar situation of a *cis*-R_3SnO_2 arrangement pertains in **1** (X = O_2CCH_2OPh) [7] and in other hindered triorganotin carboxylates [30]. The most frequently found structural type, however, for unhindered triorganotin carboxylates is a carboxylate bridged polymeric chain with *trans*-R_3SnO_2 cores [31], for example, as found in Me_3SnOAc [32].

3.2.2. The existence of rotamers

In all of the structures discussed here the molecules are propeller shaped (Fig. 3) and as a consequence can, and do, exist in two rotameric forms. In one form (type R), when viewed along the Sn–X bond from X to Sn, the phenyl groups of the neophyl substituents are displaced in a clockwise direction. In the other (type L) the displacement is anticlockwise. In **1** (X = Cl), the example shown in Fig. 3, both forms are present due to the operation of the crystallographic bar4 (fourfold rotary inversion axis) and equivalently the *d*-glide of the cubic space group *I*-43*d* and the structure is racemic. It is, however, polar because the space group lacks a center of symmetry and the bar4 creates a molecular arrangement with the overall symmetry of a regular tetrahedron whose orientation relative to the unitcell edges can differ from one crystal to another. The structures of **1** (X = N_3) and **1** (X = NCS), being centrosymmetric, are of course racemic and non-polar. By accident of choice in both cases both molecules of the bimolecular asym-

Table 4
Selected bond angles (°) [a] in **1** (X = Cl, Br, I, N_3 and NCS)

X	Mol	C1(n)–Sn1–X1			C1(n)–Sn1–C1(n′)		
		[n]	[n]	[n]	[n,n′]	[n,n′]	[n,n′]
Cl		99.67(15)	99.67(15)	99.67(15)	117.24(8)	117.24(8)	117.24(8)
Br	I	99.6(3) [c]	102.2(4) [a]	103.2(3) [b]	115.0(4) [c,b]	115.7(4) [a,c]	B117.3(4) [a,b]
	II	100.9(3) [e]	101.4(3) [f]	102.5(3) [d]	115.3(4) [e,f]	116.2(4) [e,d]	116.7(4) [f,d]
	III	100.2(4) [h]	101.8(3) [g]	102.9(3) [i]	114.7(4) [g,h]	116.5(4) [g,i]	116.9(4) [h,i]
	IV	100.3(4) [l]	101.4(3) [j]	102.8(3) [k]	115.4(4) [j,l]	115.5(4) [l,k]	117.4(4) [j,k]
I	I	100.7(2) [c]	102.8(2) [a]	104.41(18) [b]	114.8(3) [a,c]	115.3(2) [b,c]	116.0(2) [b,a]
	II	101.14(19) [e]	101.90(19) [f]	103.13(18) [d]	115.6(3) [f,d]	115.7(2) [f,e]	116.0(2) [d,e]
	III	102.24(17) [g]	C103.2(2) [h]	I04.2(2) [i]	114.9(3) [g,h]	114.9(3) [h,i]	115.0(3) [g,i]
	IV	100.8(2) [l]	102.71(18) [j]	102.78(19) [k]	115.3(2) [l,j]	115.9(2) [j,k]	116.0(2) [l,k]
N3	I	98.72(15) [c]	102.18(15) [a]	102.49(16) [b]	115.69(12) [b,c]	115.92(11) [b,a]	117.50(12) [a,c]
	II	100.39(12) [f]	100.58(12) [d]	101.04(12) [e]	115.68(12) [e,d]	117.10(12) [e,f]	117.18(12) [f,d]
NCS	I	99.65(11) [b]	99.92(11) [c]	100.72(12) [a]	116.38(10) [b,a]	116.56(10) [a,c]	118.05(10) [b,c]
	II	98.09(12) [e]	99.28(11) [d]	100.70(12) [f]	116.67(10) [f,d]	117.48(10) [e,f]	118.09(10) [e,d]

[a] The three C1(n)—Sn1—X1, and three C1(n)—Sn—C1(n′) bond angles in each molecule have been placed in order of increasing size. The particular C1(n) and C1(n′) atoms involved have been indicated by the lower case letter, a, b, c etc., which, as indicated in the text, are associated with neophyl ligands, A, B, C etc.

Table 5
Selected geometric parameters for **1** (X = OAc) [a]

Molecule	I	II	III	IV
C1	C1c	C1d	C1I	C1l
C2	C2b	C2f	C2h	C2j
C3	C3a	C3e	C3g	C3k
Bond lengths				
Sn1–O1	2.070(5)	2.117(4)	2.086(4)	2.074(4)
Sn1–O2	3.069(7)	3.052(5)	3.004(5)	2.963(4)
Sn1–C1	2.137(6)	2.142(6)	2.151(5)	2.147(5)
Sn1–C2	2.143(6)	2.145(5)	2.152(5)	2.150(5)
Sn1–C3	2.163(5)	2.155(5)	2.170(5)	2.164(5)
C11–O1	1.266(8)	1.266(8)	1.279(8)	1.295(7)
C11–O2	1.221(10)	1.202(8)	1.214(9)	1.221(7)
C11–C12	1.498(10)	1.489(10)	1.5222(9)	1.489(8)
Bond angles				
Equatoriallequatorial				
O1–Sn1–C1	108.3(2)	107.2(2)	107.79(19)	104.46(18)
O1–Sn1–C2	102.6(2)	102.0(2)	101.8(2)	107.68(17)
C1–Sn1–C2	115.0(2)	118.7(2)	118.5(2)	119.63(19)
Axiallequatorial (*C3*)				
C3–Sn1–O1	93.3(2)	93.11(19)	94.65(19)	93.02(19)
C3–Sn1–C1	116.3(2)	115.1(2)	114.2(2)	114.1(2)
C3–Sn1–C2	117.2(2)	115.7(2)	115.6(2)	113.6(2)
Axiallequatorial (*O2*)				
O2–Sn1–O1	45.2(2)	45.45(15)	47.30(16)	47.94(13)
O2–Sn1–C1	77.2(3)	79.10(19)	78.08(18)	84.36(16)
O2–Sn1–C2	87.4(2)	85.4(2)	84.9(2)	81.26(16)
Trans axial				
O2–Sn1–C3	137.1(2)	137.93(19)	141.11(19)	140.78(17)

[a] Distance and angle table for bidentate acetate anion comprising carboxyl O1, O2 and C11 and methyl group C12 which creates a trigonal bipyramidal coordination around Sn1 with equatorial O1, C1 and C2 (Sn1—C1 ⇐ Sn1—C2) and axial O2 and C3.

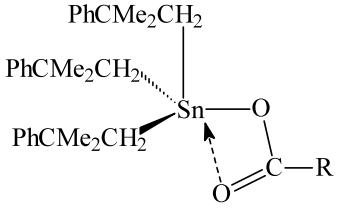


Fig. 2. Trineophyltin carboxylates (**1**: X = OAc or O_2CCH_2COPh).

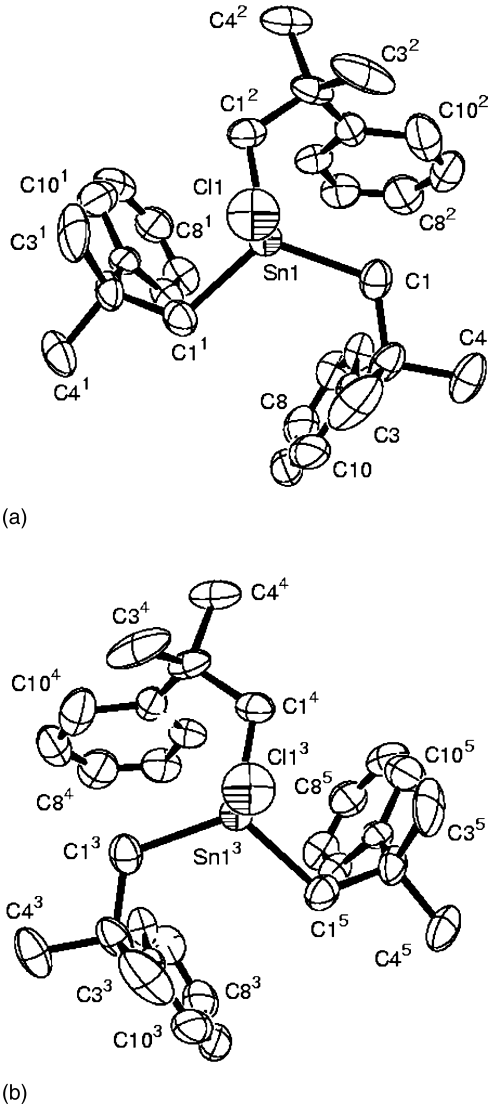


Fig. 3. Two molecules of **1** (X = Cl) displaying (a) the 'clockwise' type R rotamer and (b) the 'anticlockwise' type L rotamer. Non-H are shown as 30% ellipsoids and H have been omitted for clarity. Selected atoms are labeled with symmetry codes for (a) 1: z, x, y; 2: y, z, x and (b) 3: $1/4+x, 1/4+z, 1/4+y$; 4: $1/4+y, 1/4+x, 1/4+z$ and 5: $1/4+z, 1/4+y, 1/4+x$.

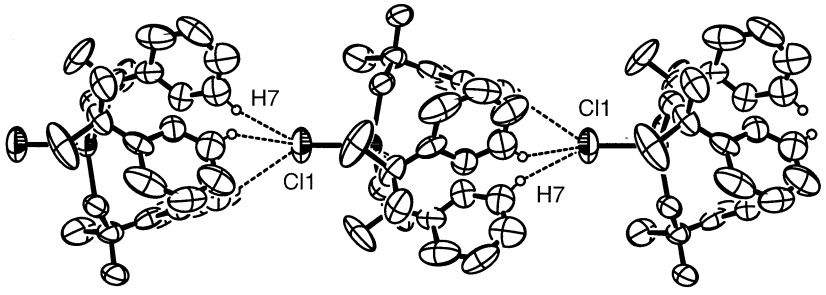


Fig. 4. A portion of a linear chain of head to tail molecules, as indicated by PLATON [39] of **1** (X = Cl) propagated in the direction of a diagonal of the cubic unitcell [111]. Non-H are shown as 30% ellipsoids and H7, involved in C—H···Cl intermolecular contacts (dashed lines), is the only H shown. The molecules in the portion of the chain shown alternate in terms of rotameric type as R at the extremes and L in the center. The parameters associated with the C7—H7···Cl contacts are C—H, H···Cl and C···Cl 0.95, 2.79 and 3.622(8) Å, respectively, and C—H···Cl 146.47°.

metric unit are of the same hand but of type L for **1** (X = N_3) and type R for **1** (X = NCS). In each of **1** (X = Br), **1** (X = I) and **1** (X = OAc) all of the molecules in the asymmetric unit are of the same hand, type R for **1** (X = Br) and isostructural **1** (X = I) and type L for **1** (X = OAc). Since all of these last three structures lack a center of symmetry or any other form of crystallographic symmetry element to bring about inversion of molecular symmetry, all of the molecules in a particular crystal must then be of the same hand. However, since there is no element of handedness in the synthesis of the compounds, and no evidence of disorder, a bulk sample of any one of them must contain crystals of one hand in admixture with crystals of the other in equal parts by volume which allows for variation in crystal size.

3.2.3. Molecular packing

With one slight exception, all of the compounds have entirely molecular structures with only van der Waals forces controlling the packing of the molecules and three situations arise. The first is the exception namely **1** (X = Cl). Here the molecules, with crystallographic threefold axial symmetry, are packed head to tail in rigorously linear rows (Fig. 4). This arrangement permits weak H-bond like intermolecular contacts of the form C7–H7···Cl′ with, for the 150 K structure [6] (CSD ref. code FOZRER) [33], symmetry code $5/4-y$, $3/4-x$, $z-1/4$ and C–H, H···Cl and C···Cl 0.95, 2.79 and 3.622(8) Å, respectively, and C–H···Cl 146.47°. The second case is that of **1** (X = OAc) in which the molecules can be perceived as forming layers parallel to (001) with molecules II and III forming one layer centered approximately on $z = 0.15$ and molecules I and IV forming the other centered on $z = 0.65$ (Fig. 5). The third and last case applies to all of the other structures. The molecules are now found in columns in which all of the molecules are the same (all molecule I or all molecule II etc. but never mixed) and all of the same rotameric type (R or L, see above) because each molecule is related to the next by the operation of a crystallographic twofold screw axis propagating the columns in the direction of *b* (Fig. 6).

In all of **1** (X = Br, I, N_3 and NCS), four such columns pass through the unit cell and in **1** (X = Br) and **1** (X = I) all of the molecules in all of the columns are of the same type and, as it happens, of type R. In centrosymmetric and therefore racemic **1** (X = N_3) and **1** (X = NCS), however, it is the all-molecule I or all-molecule II columns which are related in pairs by the crystallographic centers of symmetry and hence there is still no mixture of R and L type molecules within a single column. The chloroform solvate molecules of **1** (X = Br) and **1** (X = I), simply occupy cavities between the columns.

3.3. Spectroscopy

NMR spectral data obtained for **1** in this study were in agreement with those reported in the literature. In the humid atmosphere of Rio de Janeiro, **1** [X = OSn(Neo)$_3$] in solution was rapidly hydrolyzed to **1** (X = OH), as shown by the δ^{119}Sn value 77.1 ppm, obtained after several minutes in solution. Lockhart [12] reported values of 54.8 and 75.9 ppm for **1** (X = OSn(Neo)$_3$) and **1** (X = OH), respectively, in $CDCl_3$ solution. The

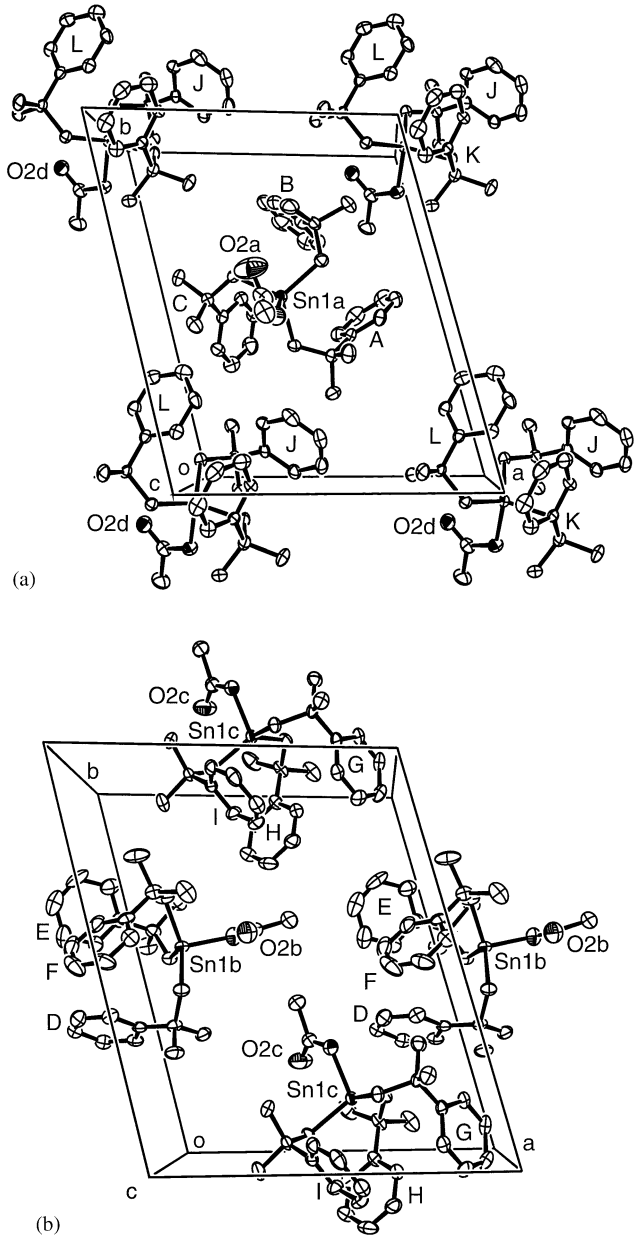


Fig. 5. Molecules of **1** (X = OAc) in layers parallel to (001) comprising (a) molecules I and IV in a layer centered on $z = 0.65$ and (b) molecules II and III in a layer centered on $z = 0.15$. Non-H are shown as 50% ellipsoids and H have been omitted for clarity. Labels on selected Sn and O and group suffices (see text) identify the molecules and neophyl groups.

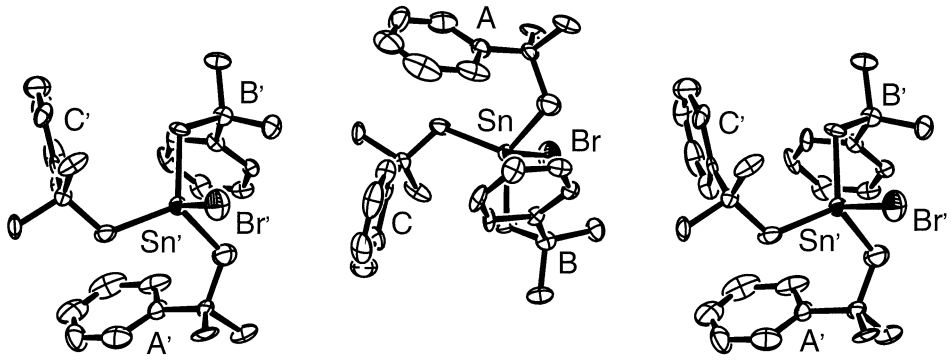


Fig. 6. A portion of a chain of molecules I in **1** (X = Br) propagated in the direction of b. Non-H atoms are shown as 50% ellipsoids and H have been omitted for clarity. In addition to labeled Sn and Br atoms, neophyl groups are identified by group suffices, A, B and C. Symmetry codes for primed atoms: $-x, y+1/2, 1-z$ (left) and $-x, y-1/2, 1-z$ (right).

product isolated from solutions, however, was always **1** [X = OSn(Neo)$_3$]. Lockhart also indicated similar effects [12].

Triorganotin chlorides, bromides and iodides, R_3SnX (R = unfunctionalised organyl group; X = Cl, Br or I), are generally monomeric four-coordinate species in non-coordinating solvents and in the solid state [34]. Hence there are much data available on spectral parameters for such species in solution. On the other hand, R_3SnF, except the most hindered compounds, such as (2.4,6-$Me_3C_6H_2)_3SnF$ [35], $Ph_2[(Me_3Si)_3C]SnF$ [36], $Me_2[(PhMe_2Si)_3C]SnF$ [36] and **1** (X = F), are aggregated species in the solid state and are poorly soluble in organic solvents. Reported NMR data for triorganotin fluorides in solution are thus limited. The $^1J(^{119}Sn-^{19}F)$ value for **1** (X = F) = 2301 ppm in $CDCl_3$ solution is similar to the reported values for other monomeric R_3SnF compounds, $Ph_2[(Me_3Si)_3C]SnF$, $Me_2[(PhMe_2Si)_3C]SnF$ and $Me_2[(Me_3Si)_3C]SnF$ [24] [$^1J(^{119}Sn-^{19}F) = 2376$, 2374 and 2463 ppm, respectively]. The $\delta^{119}Sn$ values for the monomeric trialkyltin fluorides are also similar: $\delta^{119}Sn$ values for **1** (X = F), $Me_2[(PhMe_2Si)_3C]SnF$ and $Me_2[(Me_3Si)_3C]SnF$ are 138.8, 124.5 and 146.9 ppm, respectively. The $^1J(^{119}Sn-^{14}N)$ values in **1** (X = NCS) and $Me_2[(PhMe_2Si)_3C]SnNCS$ [27] are very close, 125 and 123 Hz, respectively, and are appreciably greater than those [90 ± 4 Hz] quoted for (o-$MeC_6H_4)_3SnNCS$ and (o-$MeOC_6H_4)_3SnNCS$ [26]. The $\nu(NC) = 2021$ cm^{-1} value in **1** (X = NCS) is lower than quoted values for four-coordinate triorganotin *N*-thiocyanates, e.g. $Me_2[(PhMe_2Si)_3C]SnNCS$ {2066 cm^{-1}} [27] and (o-$MeC_6H_4)_3SnNCS$ {2045 cm^{-1}} [26].

Values of ν(Sn–X) in simple R_3SnX (e.g. R = Me, Et, Bu, Ph) are generally in the regions: 170–210 (X = I), 220–265 (X = Br), and 325–385 cm^{-1} (X = Cl), irrespective of phase [37], whereas values for R_3SnF depend on the phase, due to differences in aggregation. Gas phase values for R_3SnF (e.g. R = Me, Et, Bu, Ph) (i.e. for monomeric species) have been reported to be in the range 555–590 cm^{-1}, while values for the aggregated species as solids are quoted as 340–380 cm^{-1} [37]. The ν(Sn–X) values for **1** (X = Cl, Br or I) in CsI, viz. 311, 212 and 172 cm^{-1} respectively, fall in the expected regions. The ν(Sn–F) value [497 cm^{-1}] in molecular **1** (X = F) can be compared with the values, 535 and 537 cm^{-1}, found in (2.4,6-$Me_3C_6H_2)_3SnF$ [35] and (o-$MeOC_6H_4)_3SnF$ [38], respectively, both shown by X-ray crystallography to be monomeric. The latter compound, just like (o-$MeOC_6H_4)_3SnNCS$ [26], has indications of S–O intramolecular interaction and hence a higher coordination.

4. Supplementary material

Crystallographic data for the structural analyses have been deposited with the Cambridge Crystallographic Data Center, CCDC numbers 178628–178632 for compounds (**1**: X = Br, I, N_3, NCS and OAc), respectively. Copies of this information may be obtained free of charge from the Director, CCDC, 12 Union Road, Cambridge CB2 1EZ, UK (fax: +44-1223-336033; e-mail: deposit@ccdc.cam.ac.uk).

Acknowledgements

The authors thank the ESPSRC X-ray service at the University of Southampton for data collection, and CPNq and FAPERJ, Brazil for financial support. We acknowledge the use of the Chemical Database of EPSRC at Daresbury.

References

[1] C.J. Evans, in: P.J. Smith (Ed.), Chemistry of Tin, 2nd ed., Chapman and Hall, London, 1998.
[2] (a) H. Zimmer, O.A. Homberg, M. Jayawant, J. Org. Chem. 31 (1966) 3857;

(b) H. Zimmer, I. Hachenbleiker, O.A. Homberg, M. Danzik, J. Org. Chem. 29 (1964) 2632.
[3] W.T. Reichle, Inorg. Chem. 5 (1966) 87.
[4] (a) R.H. Herber, H.A. Stoecker, Trans. New York Acad. Sci. 26 (1964) 929;
(b) V. Kotkhekar, V.S. Shpinel, Zh. Strukt. Khim. 10 (1969) 37;
(c) R. Gupta, B. Majee, J. Organomet. Chem. 49 (1973) 203.
[5] D. Schomberg, M. Link, H. Linoh, R. Tacke, J. Organomet. Chem. 339 (1988) 69.
[6] J.N. Low, J.L. Wardell, J.A.S. Bomfim, S.M.S.V. Wardell, Acta Crystrallogr., Sect. C 56 (2000) 554.
[7] M. Bao, Q. He, B. Liu, Y. Xing, Y. Liu, Wuji Huaxue Xuebao 14 (1998) 114.
[8] H. Reuter, R. Pawlak, Z. New Cryst. Struct. 213 (1998) 147.
[9] J.N. Low, J.L. Wardell, Acta Crystrallogr., Sect. C 56 (2000) e3.
[10] W.D. McFarlane, R.I. Wood, J. Organomet. Chem. 40 (1972) c17.
[11] (a) M. Devaud, D. Gula, Electrochim. Acta 23 (1978) 563;
(b) H.U. Buschhaus, M. Lehnig, W.P. Neumann, J. Chem. Soc., Chem. Commun. (1977) 129;
(c) A.B. Chope, A.E. Zuniga, J.C. Podesta, J. Chem. Res., S (1989) 234.
[12] T.P. Lockhart, J. Organomet. Chem. 287 (1985) 179.
[13] (a) K.A. Barnes, R.J. Fussell, J.R. Startin, H.J. Mobbs, R. James, S.L. Reynolds, Rapid. Commun. Mass Spectrom. 11 (1997) 159;
(b) K. Sasaki, T. Tatsuno, M. Nakamura, M. Kaneko, N. Goto, Y. Kondo, K. Takahata, Y. Miura, M. Toyoda, J. Food Hyg. Soc. Jpn. 42 (2001) 210.
[14] A. Gray, A.J. Dutton, C.V. Ebsforth, Pestic. Sci. 43 (1995) 295.
[15] (a) G.J. Devine, M. Barber, I. Denholm, Pest Manage. Sci. 57 (2001) 443;
(b) R. Nauen, N. Stumpf, A. Elbert, C.P.W. Zebitz, W. Kraus, Pest Manage. Sci. 57 (2001) 253.
[16] Z. Otwinowski, W. Minor, in: C.W. Cater, R.M. Sweet (Eds.), Methods in Enzymology: Macromolecular Crystallography, Part A, vol. 276, Academic Press, New York, 1997, pp. 307–326.
[17] R. Hooft, COLLECT, Nonius BV, Delft, The Netherlands, 1998.
[18] (a) R.H. Blessing, Acta Crystallogr., Sect. A 51 (1995) 33;
(b) R.H. Blessing, J. Appl. Crystallogr. 30 (1997) 421.
[19] Bruker, 1999. SADABS, SMART and SAINT. Bruker AXS Inc., Madison, WI, USA.
[20] G.M. Sheldrick, SHELXS-97, Program for the Solution of Crystal Structures, University of Göttingen, Germany, 1997.
[21] G.M. Sheldrick, SHELXL-97; Program for the Refinement of Crystal Structures, University of Göttingen, Germany, 1997.
[22] L.J. Farrugia, J. Appl. Crystallogr. 30 (1997) 565.
[23] J.E. Huheey, E.A Keiter, R.L. Keiter, Inorganic Chemistry, Principles of Structure and Reactivity, 4th ed., Harper Collins, New York, 1993.
[24] R.A. Forder, G.M. Sheldrick, J. Organomet. Chem. 21 (1970) 115.
[25] (a) L.E. Khoo, X.-M. Chen, T.C.W. Mak, Acta Crystallogr., Sect. C 47 (1991) 2647;
(b) A.M. Domingos, G.M. Sheldrick, J. Organomet. Chem. 67 (1974) 257.
[26] I. Wharf, M.G. Simard, Inorg. Chim. Acta 282 (1998) 30.
[27] S.S. Al-Juaid, M. Al-Rawi, C. Eaborn, P.B. Hitchcock, J.D. Smith, J. Organomet. Chem. 446 (1993) 161.
[28] D. Hänssgen, M. Jensen, C. Leben, T. Oster, J. Organomet. Chem. 49 (1995) 223.
[29] R. Allmann, R. Hohefeld, A. Waskowska, J. Lorbeth, J. Organomet. Chem. 192 (1980) 353.
[30] (a) S.W. Ng, V.G. Kumar Das, F. van Meurs, J.D. Schagen, L.H. Staver, Acta Crystallogr., Sect. C 45 (1989) 569;
(b) E.R.T. Tiekink, Appl. Organomet. Chem. 5 (1991) 1;
(c) R.R. Holmes, R.O. Day, V. Chadrasekhar, J.F. Vollano, J.M. Holes, Inorg. Chem. 25 (1986) 2490.
[31] R. Willem, A. Bouhdid, M. Biesemans, J.C. Martins, D. de Vos, E.R.T. Tiekink, M. Gielen, J. Organomet. Chem. 514 (1996) 203.
[32] D.R. Smyth, E.R.T. Tiekink, Z. Krist. 213 (1998) 605.
[33] (a) F.H. Allen, O. Kennard, Chem. Des. Autom. News 8 (1993) 1 and 31–37;
(b) D.A. Fletcher, R.F. McMeeking, D. Parkin, J. Chem. Inf. Comput. Sci. 36 (1996) 746.
[34] P.J. Smith (Ed.),Chemistry of Tin, 2nd ed., Chapman and Hall, London, 1998.
[35] H. Reuter, H. Puff, J. Organomet. Chem. 379 (1989) 223.
[36] S.S. Al-Juaid, S.M. Dhaher, C. Eaborn, P.B. Hitchcock, J.D. Smith, J. Organomet. Chem. 325 (1987) 117.
[37] K. Light, H. Geissler, P. Koehler, K. Hottmann, H. Schorr, H. Kriegsman, Z. Anorg. Allg. Chem. 385 (1971) 271.
[38] I. Wharf, A.-M. Lebus, G.A. Roper, J. Organomet. Chem. 294 (1999) 224.
[39] A.L. Spek, Acta Crystallogr., Sect. A 46 (1995) 34.

enthalpy of sublimation of 1 mol of adduct is equal to the enthalpy of sublimation of one mol of the ligand [1]. So it was assumed that the intermolecular forces in the adduct and ligand should be very similar since the crystalline structure of the ligand complex remains virtually unchanged in the gaseous phase. Such hypothesis was confirmed by experimental results, since the obtained enthalpy values exhibited a variation [4] within ± 10 kJ mol^{-1}.

The purpose of this paper is to report the non-isothermal kinetic thermogravimetric study for the adducts $ZnX_2 \cdot 2hmpa(c)$ (X = Cl, Br, I and hmpa = hexamethylphosphoramide), as well as showing that some thermochemical parameters normally measured or calculated by using reaction-solution calorimetry data, can also be estimated from thermogravimetric or spectroscopic (IR) data. So, a series of empirical correlations involving calorimetric, t.g. and IR data are established.

2. Experimental

The adducts of the general formula $ZnX_2 \cdot 2hmpa$ (X = Br and I; hmpa = hexamethylphosphoramide) were prepared as previously described [5]. A slight excess of the ligand in relation to the desired stoichiometry was added to the metal halide solution in light petroleum ether. The resulting solution was stirred and warmed to 60 °C to allow the complete dissolution of the salt. Upon cooling, the adduct started to settle and the solid was filtered off, washed with ether and dried in vacuum.

The adduct $ZnCl_2 \cdot 2hmpa$ was obtained by the direct dissolution of a stoichiometric amount of the metal halide in pure ligand. The product was washed with double distilled water and dried under vacuum at 30 °C for 10 h.

The elemental analysis was performed on a Perkin–Elmer CHN analyzer. The IR spectra were obtained on a Bomem spectrophotometer in KBr discs. The thermogravimetric curves were obtained on a DuPont apparatus, model 1090B, under argon atmosphere, with a heating rate of 5 °C min^{-1}. The scanning differential calorimetric (DSC) curves were obtained under the same conditions, by using DuPont 2000 equipment.

The kinetic parameters for the thermal degradation of the three adducts were calculated through the Coats–Redfern method [6], employing the data collected in the non-isothermal thermogravimetric curves.

3. Results and discussion

3.1. Solution calorimetry, t.g. and d.s.c data

The obtained IR results are in agreement with a coordination involving the P=O group of the hmpa molecule [5]. The thermogravimetric curves for the three synthesized adducts are shown in Fig. 1. All calculated kinetic parameters obtained through the Coats–Redfern method [6] are listed in Table 1.

The profile of the thermogravimetric curves of these adducts clearly showed that the thermal stability of the

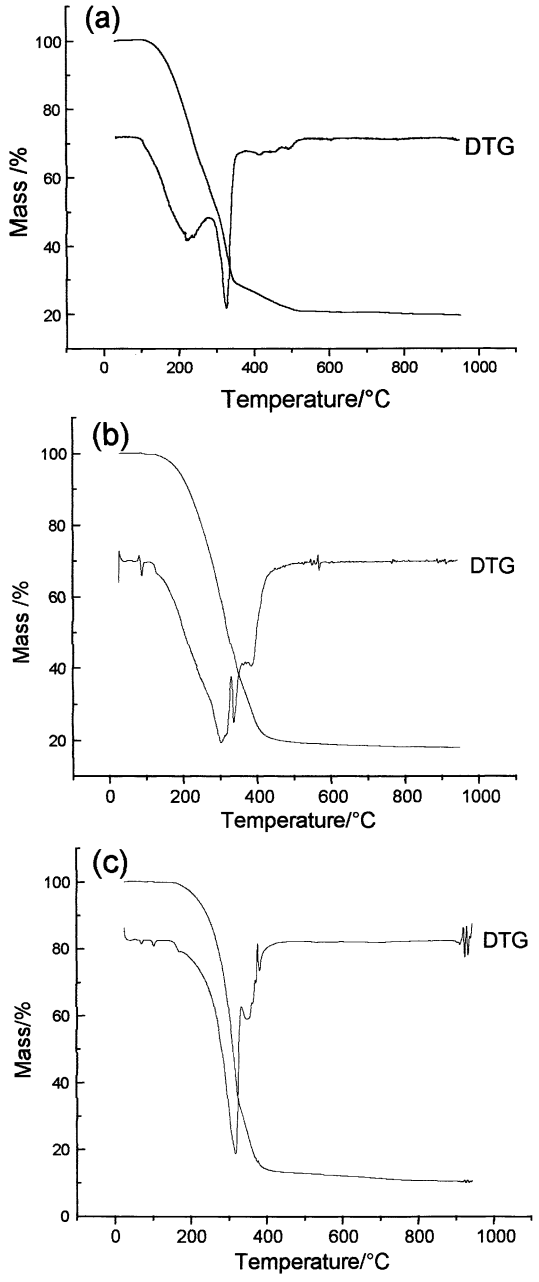


Fig. 1. Thermogravimetric curves for the adducts $ZnX_2 \cdot 2hmpa$: X = chloride (a), bromide (b) and iodide (c).

Table 1
Kinetic parameters calculated through Coats–Redfern method for the non-isothermal degradation of the adducts $ZnX_2 \cdot 2hmpa$

$ZnX_2 \cdot 2hmpa$	E_a (kJ mol^{-1})	A	n
Cl	44	3.1×10^3	1
Br	94	6.6×10^6	1
I	215	4.4×10^{23}	1

E_a is the activation energy, A is the frequency or pre-exponential factor and n is the order of reaction.

compounds decreased in the order: Cl < Br < I. This is the same sequence found for the activation energy (E_a) values for the corresponding thermal degradation processes: $ZnX_2 \cdot 2hmpa(c) \rightarrow ZnX_2(c) + 2hmpa(g)$.

Based on the collected data, the ratio between t_i, the Kelvin temperature of the beginning of the thermal degradation, and the corresponding E_a values listed in Table 1, gives: 387/44 = 2.63 395/94 = 4.20 and 440/215 = 8.80. These data can be summarized by the empirical equation: t_i (K)/E_a (kJ mol^{-1}) $\cong 2^b$, which exponential value ranges from 1 to 3. A plot of E_a values as function of t_i is shown in Fig. 2. As can be observed, a straight line is obtained with a coefficient of correlation of 0.99, providing the empirical equation:

$$E_a = 3.043 \times t_i - 1122.130 \quad (1)$$

The standard molar enthalpy of formation of the considered adducts in the condensed phase presented the following values: −1596, −1532 and −1408 kJ mol^{-1} for chloride, bromide and iodide [5], respectively. By plotting this sequence of values as function of the E_a values, again a straight line was obtained as shown in Fig. 3. Then, a new empirical equation was established as:

$$\Delta_f H^\circ_m = 1.086 \times E_a - 1639.738 \quad (2)$$

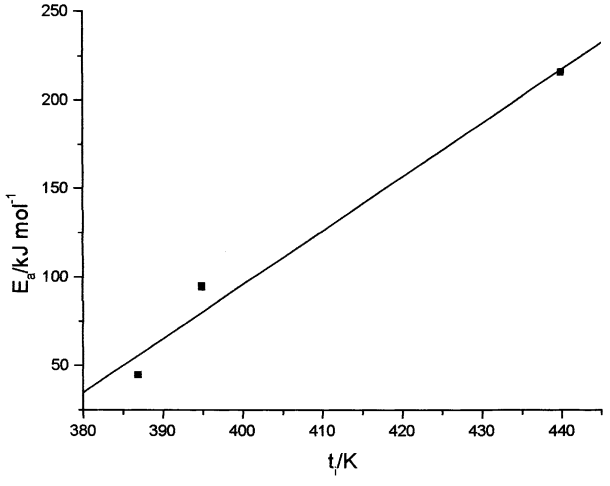


Fig. 2. Activation energy values (E_a kJ mol^{-1}) as a function of the Kelvin temperature for the beginning of the thermal degradation (t_i K), for the $ZnX_2 \cdot 2hmpa$ adducts.

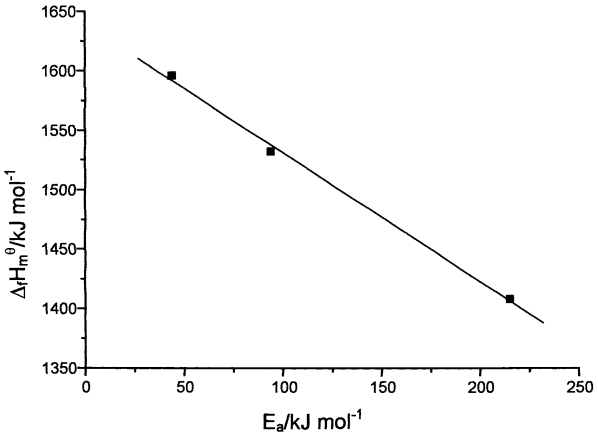


Fig. 3. Standard molar enthalpy of formation ($\Delta_f H^\circ_m$ kJ mol^{-1}) as function of the activation energy for the thermal degradation process (E_a kJ mol^{-1}), for $ZnX_2 \cdot 2hmpa$ adducts.

This obtained equation opens the possibility of estimates for an enthalpic value, which is normally obtained from calorimetric measurements, by using a simple kinetic parameter derived from thermogravimetric data.

The order of reaction 'n' obtained for the thermal degradation processes gives a unity value for these three adducts, as listed in Table 1. Such a fact suggests a similar behavior for the adducts on heating, which implies a certain degree of isomorphism [7]. The temperatures of fusion, t_{fus}, determinated by DSC analysis gave the values 108, 125 and 166 °C for the chloride, bromide and iodide adducts, respectively. The increase in melting temperature values suggests an enhancement of the intermolecular interactions of the adducts from chloride to iodide. This sequence is in agreement with t_i as well as E_a values. The relationship t_i/t_{fus} is almost constant and near to unity for the three adducts: 1.02, 0.99 and 1.00 for Cl, Br and I adducts, respectively.

The lattice enthalpy ($\Delta_M H^\circ_m$) for the adducts, associated with the process: $ZnX_2 \cdot 2hmpa(c) \rightarrow ZnX_2(g) + 2hmpa(g)$, was calculated to give [5] 375; 380 and 365 kJ mol^{-1}, for Cl, Br and I, respectively. These values enabled the acquisition of an interesting empirical equation related to melting temperature, t_{fus}. As observed for dimethylethyleneurea adducts [8], the lattice enthalpy values are adjusted to the empirical equation [9]:

$$\Delta_M H^\circ_m = 0.11 \times M \times \Delta^1_{cr} H^\circ_m (t_{fus}) \quad (3)$$

where M is the molar mass of the ligand and $\Delta^1_{cr} H^\circ_m (t_{fus})$ is the enthalpy of melting of these adducts, at the melting temperature, as determined by DSC data, whose values are 18.90, 19.52 and 16.46 kJ mol^{-1}, for chloride, bromide and iodide adducts, respectively.

3.2. Themochemistry and IR spectroscopy

From the point of view of coordination chemistry, the nature of the donor atom on the ligand molecule as well as the number of ligands involved in bond formation are associated to important features related with the mean metal–ligand bond enthalpy, ⟨D⟩(M–L) [4,10,11].

To establish an equation relating thermochemical and IR data, only adducts of zinc halides with two ligands, which are generally tetrahedral, were chosen. The selected adducts of zinc halides are those with urea (u) [12], methylurea (mu) [13], dimethylurea (dmu) [14], dimethylformamide (dmf) [15] tetramethylurea (tmu) [16], dimethylacetamide (dma) [17], dimethylethyleneurea (dmeu) [8], ε-caprolactam (cl) [18], γ-butyrolactam (bul) [19] and hexamethylphosphoramide (hmpa) [5]. In these adducts, all ligands coordinate through oxygen, and so C=O or P=O stretching frequencies of such ligands decrease upon coordination [1–5,7–19]. For this series of adducts, it is observed that the mean zinc–oxygen bond enthalpy ⟨D⟩(Zn–O) is correlated to the variation (decrease) in the stretching frequency $\Delta\nu$, of the C=O or P=O groups (free ligand-coordinated ligand). Based on this fact, the following empirical equation is proposed:

$$\langle D\rangle(Zn\text{–}O) = \alpha + \beta + \Delta\nu \quad (4)$$

where α and β represent the acidic and basic contributions associated with metal halide and ligand, respectively.

The decrease in α values from chloride to iodide, as shown in Table 2, is followed by the tendency in increasing the anionic radii, which also imply an enhancement of their polarizability. On the other hand, β values comprise the donor ability as well as the steric effect of the molecule of the ligand. For example, by considering a sequence of similar ligands, an increase in β values occurred from urea to methyurea, giving 73 and 92, respectively. However, these values decrease progressively from methyl- to tetramethylurea, which has a value of 27. This behavior can be explained taking into account the positive inductive effect of the methyl groups (increased basicity of the donor atom) as well as their effect from the point of view of steric hindrance (larger metal–ligand bond lengths). So, the β values reflects the basicity as well as volume of the ligand molecule.

The α and β values shown in Table 2 were established as follows: the $\Delta\nu$ experimental values for adducts with zinc halides and dmf [15] were chosen and a value of 25 was attributed for α, associated with $ZnCl_2$. From this value, α values for $ZnBr_2$ and ZnI_2 were also calculated as well as β for the same ligand. Afterwards, using the experimental data from adducts of $ZnCl_2$ and the other ligands, a complete series of β values were established.

The second step is dedicated to the application of the proposed equation by using the parameters shown in Table 2 for the adducts $ZnX_2{\cdot}2L$ (X = Br, I and L = u, mu, dmu, tmu, dma, dmeu, cl, bul, hmpa). The collected results obtained are listed in Table 3, where the thermochemical (calorimetric) and IR ⟨D⟩(Zn–O) values are compared.

The results derived from IR data shows a relatively good agreement with the thermochemical data. To evaluate how good the IR results are, one needs to bear in mind that: (a) thermochemical data for ⟨D⟩(M–O) are obtained from $\Delta_g H^\circ_m$ values. In that case, the adduct must be found in the gaseous phase, whereas $\Delta\nu$ values are calculated from infrared spectra obtained for solid adducts; (b) α and β values for metal halides and ligands were obtained from ⟨D⟩(M–O) thermochemical data, which were calculated considering that the enthalpy of sublimation for adducts is equal to the enthalpy of sublimation for the respective ligands. Such a hypothesis is based on a series of sublimable adducts, and could not be true for all adducts; (c) $\Delta\nu$

Table 2
Values of α for zinc halides, ZnX_2, and β for a series of oxygen donor atom ligands

ZnX_2	α	Ligand	β
Cl	25	dmf	82
Br	19	u	73
L	15	mu	92
		dmu	88
		tmu	27
		dma	60
		dmeu	84
		cl	96
		bul	77
		hmpa	90

Table 3
The mean zinc–ligand bond enthalpy ⟨D⟩(Zn–O) (kJ mol^{-1}) values, based on thermochemical (ther.) and infrared (IR) data for $ZnX_2{\cdot}2L$ adducts

Adduct	Thermochemical	Infrared	Δ% [a]
$ZnBr_2{\cdot}2u$	139	130	−6.5
$ZnI_2{\cdot}2u$	145	138	4.8
$ZnBr_2{\cdot}2mu$	123	141	14.6
$ZnBr_2{\cdot}2dmu$	136	145	6.6
$ZnBr_2{\cdot}2tmu$	135	141	4.4
$ZnI_2{\cdot}2tmu$	149	140	−6.0
$ZnBr_2{\cdot}2dma$	136	129	−5.1
$ZnI_2{\cdot}2dma$	131	116	−11.5
$ZnBr_2{\cdot}2cl$	128	145	13.3
$ZnI_2{\cdot}2cl$	121	144	19.0
$ZnBr_2{\cdot}2bul$	122	119	−2.5
$ZnI_2{\cdot}2bul$	118	130	10.2
$ZnBr_2{\cdot}2hmpa$	162	155	−4.3
$ZnI_2{\cdot}2hmpa$	154	151	−1.0
$ZnBr_2{\cdot}2dmeu$	137	137	0.0

[a] Δ% = (infrared − thermochemical) × 100.

were assumed to contain only C=O or P=O stretching vibrational modes. In reality, there are other components included in such vibrational modes [20,21] that could not be completely considered and are, of course, different for each ligand molecule. Nevertheless, taking into account all these facts, the results obtained may be considered quite good.

For adducts of zinc halides with dmf [15] the metal–ligand stretching frequency values, ν(M–L) are available in the range from 412 to 420 cm^{-1}. From these values an empirical correlation was also established. Then, the relationship between ν(M–L) and $\langle D\rangle$(Zn–O) values was obtained and the results are presented in Table 4.

The ratio involving ν(M–L)/$\langle D\rangle$(M–L) increases from chloride to iodide, reflecting the increase of the anion radii. Another observation related to these values comes from the fact that the considered ratio is nearly equal to $n+1$, where n is the number of ligands.

These series of data open the possibility of estimating $\langle D\rangle$(M–O) values by using IR results, establishing an exciting connection between spectroscopy and calorimetry.

4. Conclusion

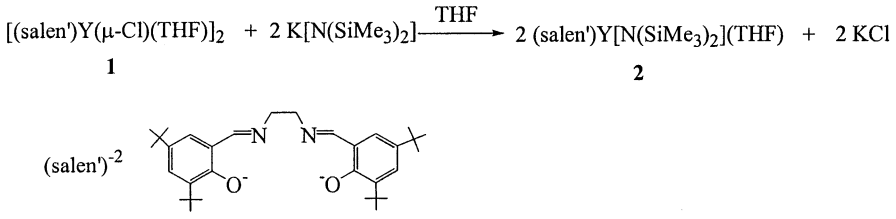
The obtained experimental results lead to the establishment of a series of empirical equations relating calorimetric, thermogravimetric and IR data. The very simple observed empirical relations could be explored to achieve a most profound knowledge of the physical and chemical behavior of adducts. These kinds of correlations were not restricted to zinc adducts, since they were also observed for copper and cobalt adducts with cyclic amides [22,23] or amino acids [24].

Table 4
ν(Zn–L)/$\langle D\rangle$(Zn–L) values for $ZnX_2\cdot$ndmf adducts

Adduct	ν(Zn–L)/$\langle D\rangle$(Zn–L)
$ZnCl_2\cdot$2dmf	3.0
$ZnBr_2\cdot$2dmf	3.1
ZnI_2.2dmf	3.3
$ZnCl_2\cdot$dmf	2.1
$ZnBr_2\cdot$dmf	2.2
$ZnI_2\cdot$dmf	2.3

References

[1] C. Airoldi, A.P. Chagas, Coord. Chem. Rev. 119 (1992) 29.
[2] R.F. de Farias, O.A. de Oliveira, J.V. de Medeiros, C. Airoldi, Thermochim. Acta 328 (1999) 241.
[3] S.J. Ashcroft, J. Chem. Soc. A (1970) 1020.
[4] P.M. Burkinshaw, C.T. Mortimer, J. Chem. Soc., Dalton Trans. (1984) 75.
[5] J.C. de Queiroz, C. Airoldi, A.P. Chagas, J. Chem. Soc., Dalton Trans. (1985) 1103.
[6] A.W. Coats, J.P. Redfern, Nature 201 (1964) 68.
[7] R.F. de Farias, O.A. de Oliveira, H. Scatena, Jr., F.M. de M. Borges, A.O. da Silva, Quím. Nova 21 (1998) 164.
[8] R.F. de Farias, O.A. de Oliveira, Quím. Nova 19 (1996) 100.
[9] R.F. de Farias, Quím. Nova 22 (1999) 205.
[10] E.F. Lot, C. Airoldi, A.P. Chagas, Polyhedron 13 (1994) 27.
[11] M.J. Gallagher, D.P. Graddon, A.R. Sheiker, Thermochim. Acta 27 (1979) 269.
[12] M.R.M.C. Santos, C. Airoldi, Thermochim. Acta 125 (1988) 295.
[13] C. Airoldi, A.P. Chagas, F.P. Assunção, Can. J. Chem. 60 (1982) 2132.
[14] C. Airoldi, A.P. Chagas, F.P. Assunção, J. Chem. Soc., Dalton Trans. (1980) 1823.
[15] O.A. de Oliveira, C. Airoldi, A.P. Chagas, Inorg. Chem. 22 (1983) 136.
[16] J. de, A. Simoni, C. Airoldi, A.P. Chagas, J. Chem. Soc., Dalton Trans. (1980) 156.
[17] Z.R. da Silva, J.C. de Queiroz, E.F.S. Vieira, F.S. Dias, Thermochim. Acta 285 (1996) 289.
[18] E.F.S. Vieira, J.C. de Queiroz, F.S. Dias, Thermochim. Acta 256 (1995) 249.
[19] L.C.R. Santos, A.G. de Souza, C. Airoldi, Thermochim. Acta 317 (1998) 99.
[20] S. Milicev, D. Hadzi, Inorg. Chim. Acta 21 (1977) 201.
[21] R.J. Berni, R.R. Benerito, W.M. Ayres, H.B. Jonassen, J. Inorg. Nucl. Chem. 25 (1963) 807.
[22] R.F. de Farias, G.C. Petrucelli, C. Airoldi, Thermochim. Acta 376 (2001) 1.
[23] R.F. de Farias, L.M. Nunes, Transition Met. Chem. 26 (2001) 477.
[24] R.F. de Farias, Transition Met. Chem., in press.



Scheme 1.

salen′. Complexometric analysis was consistent with the formula (salen′)Y[N(SiMe$_3$)$_2$](THF), **2**.

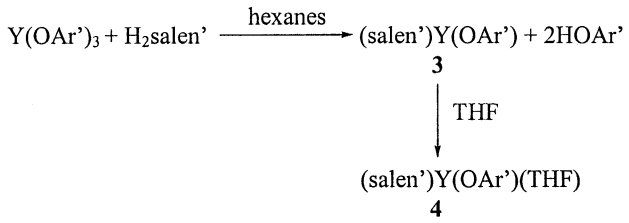
2.2. Synthesis of [(salen′)Y(OC$_6$H$_3^t$Bu$_2$-2,6)], 3, and [(salen′)Y(OC$_6$H$_3^t$Bu$_2$-2,6)] (THF), 4

The synthesis of an aryloxide complex from **1** was subsequently attempted since it had been reported previously that (salen′)Y(OC$_6$H$_3^t$Bu$_2$-2,6)](THF) could be made [7]. Ionic metathesis of **1** with LiOAr′ (OAr′ = OC$_6$H$_3^t$Bu$_2$-2,6) did not produce a pure aryloxide by ^{1}H NMR spectroscopy. Instead, the ^{1}H NMR spectrum of the product was complicated and suggested that multiple products had formed.

However, reaction of Y(OAr′)$_3$ [15] and H$_2$salen′ in hexanes precipitated a yellow solid that had a simple NMR spectrum consistent with (salen′)Y(OAr′), **3**. Complex **3** displayed high solubility in coordinating solvents, such as THF, and was moderately soluble in benzene and toluene, but had only limited solubility in alkanes. Attempts to crystallize **3** in a non-coordinating medium were unsuccessful. However, when **3** is concentrated in a 50/50 mixture of toluene–THF and cooled to −35 °C, yellow crystals are obtained which were analyzed by X-ray crystallography and determined to be the THF adduct (salen′)Y(OAr′)(THF), **4** (Scheme 2, Fig. 1). As expected [7], **2** could be transformed quantitatively to **4** by reaction with HOAr′ in THF, Scheme 3.

2.3. Synthesis of (salen′)Y(hfac)(THF)$_2$, 5

Although **3** was not easily synthesized by ionic metathesis, this synthetic approach did succeed with the chelating oxygen donor ligand hexafluoroacetylacetonate (hfac). **1** reacts with Na(hfac) to form a yellow solution and a white precipitate according to Scheme 4.



Scheme 2.

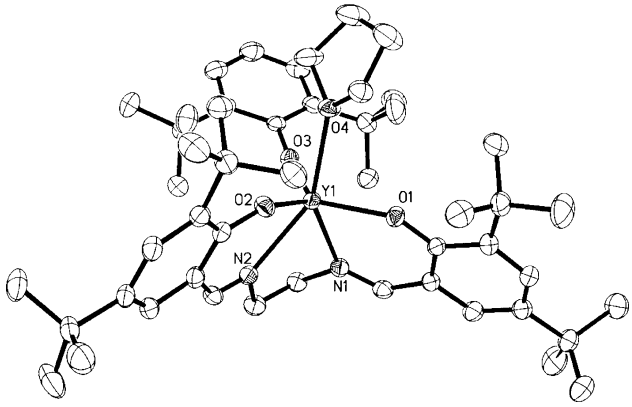


Fig. 1. Thermal ellipsoid plot of [(salen′)Y(OC$_6$H$_3$Bu$_2^t$-2,6)(THF)], **4**, drawn at the 50% probability level with hydrogen atoms omitted for clarity.

The yellow product had a ^{1}H NMR spectrum consistent with the formula (salen′)Y(hfac)(THF)$_2$, **5**, and the IR spectrum contained two strong absorbances at 1660 and 1613 cm^{-1} attributable to [C=O]$_{hfac}$ and [C=N]$'_{salen}$. X-ray diffraction confirmed the identity of this product as (salen′)Y(hfac)(THF)$_2$, **5**, Fig. 2.

2.4. Synthesis of organoyttrium salen′ complexes

In attempt to isolate an organometallic complex of the salen′ yitrium system, the reaction of **1** and KC$_5$Me$_5$ was examined. (salen′)Y(C$_5$Me$_5$), **6** could be isolated in good yields (Scheme 5) and was fully characterized by NMR, IR and X-ray diffraction (Fig. 3). In contrast, when **1** reacts with simple lithium alkyls, LiR (R = Me, CH$_2$SiMe$_3$, CH(SiMe$_3$)$_2$), in toluene at −78 °C, a mixture is indicated by the complicated ^{1}H NMR spectrum. These mixtures could result from attack of the alkyl on the imine portion of the salen′ ligand as has been reported to occur in Group IV systems [16,17]. The susceptibility of the imine bonds to nucleophilic attack could be further enhanced by coordination to the highly electropositive metal.

2.5. Structural comparison of yttrium–salen′ complexes

The Y–O(salen′) distances in **4**, **5**, and **6** range from 2.141(2) to 2.240(2) Å while the Y–N(salen′) interactions range from 2.392(3) to 2.559(3) Å (Table 1). These

$$\underset{\mathbf{2}}{\text{(salen')Y[N(SiMe}_3)_2\text{](THF)}} + \text{HOAr'} \xrightarrow{\text{THF}} \underset{\mathbf{4}}{\text{(salen')Y(OAr')(THF)}} + \text{HN(SiMe}_3)_2$$

Scheme 3.

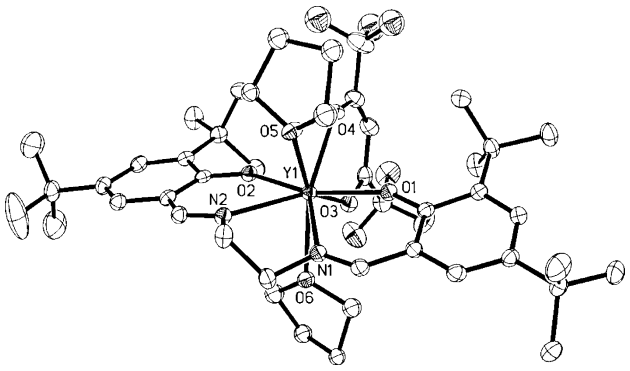


Fig. 2. Thermal ellipsoid plot of (salen′)Y(hfac)(THF)$_2$, **5**, drawn at the 50% probability level with hydrogen atoms omitted for clarity.

distances are consistent with Ln–O and Ln–N salen′ distances in other reported Schiff base complexes when metal sizes are taken in consideration [20] (Ln–O and Ln–N): [(salen′)Y(μ-Cl)(THF)]$_2$ [14], 2.143(2) and 2.492(3) Å; (salen′)Y[N(SiMe$_2$H)$_2$](THF) [7], 2.16 and 2.27 Å; [(*N*-(2,4,6-trimethylphenyl)salicylideneimine)$_2$La(μ-Cl)(THF)] [10], 2.295(11) and 2.659(16) Å; [(*trans*-(±)-*N*,*N*′-bis(salicylidene)-1,2-cyclohexanediamine)Sm(C$_5$H$_5$)]$_2$(μ-THF)(THF)$_2$ [9], 2.30(6) and 2.56(5) Å.

The salen′ moieties in complexes **4**–**6** adopt bent geometries about the yitrium metal center as measured by the dihedral angle between the two phenyl rings. The aryloxide, **4**, which has the largest deviation from planarity, 60.2°, is followed by the pentamethylcyclopentadienyl, complex **6**, with a 44° angle, and the hfac complex, **5**, with a 17° angle. These angles show that the salen′ ethylene backbone is flexible and is able to adopt a preferred orientation with respect to the steric bulk of the second ligand in the complex, i.e. the alkoxide, hfac, or cyclopentadienyl group.

The 2.128(2) Å Y–O(OAr′) distance in **4**, the 2.383(2) and 2.404(2) Å Y–O(hfac) distances in **5**, and the 2.372 Å Y-(C$_5$Me$_5$ ring centroid) length in **6** are similar to analogous bond lengths in other yttrium complexes containing these groups: e.g. 2.096(4) Å, Y–O(OAr′) in (C$_5$Me$_5$)Y(OC$_6$H$_3^t$Bu$_2$-2,6)$_2$ [18]; 2.283(7) and 2.322(6) Å, Y–O(hfac) in [(triglyme)Y(hfac)$_2$]$^+$ [19]; and 2.381 Å, Y-(C$_5$Me$_5$ ring centroid) in (C$_5$Me$_5$)$_2$YCl(THF) [20]. These comparisons suggest that salen′ can provide coordination equivalent to that of (C$_5$Me$_5$)(OC$_6$H$_3^t$Bu$_2$-2,6), (hfac)(triglyme), or (C$_5$Me$_5$)Cl(THF).

3. Conclusion

These studies have shown that the readily obtainable chloride, [(salen′)Y(μ-Cl)(THF)]$_2$ and ionic metathesis reactions are synthetically useful in making yttrium complexes ligated by salen′. Reactions of **1** with KN(SiMe$_3$)$_2$, Na(hfac), and KC$_5$Me$_5$ all form the corresponding products in high yields. Although the chemistry of salen′ as an ancillary ligand is promising, it contains a reactive imine functional group that is prone to nucleophilic attack. This can interfere with the isolation of complexes of reactive alkyl and hydride groups.

4. Experimental

The chemistry described below was performed under nitrogen with rigorous exclusion of air and water by Schlenk, vacuum line, and glovebox techniques. Solvents were purified by distillation over sodium or potassium benzophenone ketyl. KN(SiMe$_3$)$_2$ was purchased from Aldrich and used as received. [(salen′)Y(μ-Cl)(THF)]$_2$ [14] and Y[(OC$_6$H$_3$Bu$_2^t$-2,6)$_2$]$_3$ [15] were prepared by literature methods. NMR spectra were recorded using a Bruker DRX400 or a General Electric GE500 spectrometer. Infrared spectra were recorded on a ReactIR1000 system (Applied System Inc.) as thin films in toluene. X-ray crystallographic data were obtained on a Bruker CCD platform diffractometer. Complexometeric analyses were obtained as previously described [21].

4.1. (Salen′)Y[N(SiMe$_3$)$_2$](THF), 2

In a glovebox KN(SiMe$_3$)$_2$ (52 mg, 0.26 mmol) was added to a slurry of **1** (180 mg, 0.26 mmol) in 5 ml of toluene. After stirring for 12 h, the dark orange–red slurry was centrifuged to remove KCl. The solvent was removed by rotary evaporation and the dark orange–

$$\underset{\mathbf{1}}{\text{[(salen')Y(μ-Cl)(THF)]}_2} + 2\ \text{Na(hfac)} \xrightarrow{\text{THF}} 2\ \underset{\mathbf{5}}{\text{(salen')Y(hfac)(THF)}_2} + 2\ \text{NaCl}$$

Scheme 4.

$$\underset{\mathbf{1}}{[(\text{salen'})\text{Y}(\mu\text{-Cl})(\text{THF})]_2} + 2\ \text{K}(\text{C}_5\text{Me}_5) \xrightarrow{\text{THF}} \underset{\mathbf{6}}{2\ (\text{salen'})\text{Y}(\text{C}_5\text{Me}_5)} + 2\ \text{KCl}$$

Scheme 5.

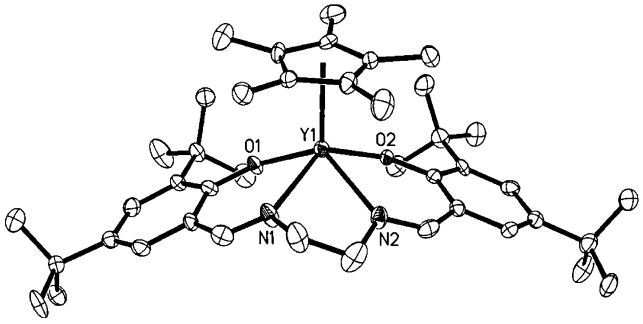


Fig. 3. Thermal ellipsoid plot of (salen′)Y(C_5Me_5), **6**, drawn at the 50% probability level with hydrogen atoms omitted for clarity.

Table 1
Selected bond lengths for [(salen′)Y(μ-Cl)(THF)]$_2$, **1**; (salen′)-Y(OAr′)(THF), **4**; (salen′)Y(hfac)(THF)$_2$, **5**; (salen′)Y(C_5Me_5), **6**

Complex	Y–O(salen′)	Y–N(salen′)	Y–O(THF)
1	2.143(2)	2.492(3)	2.463(3)
	2.143(2)	2.418(3)	
4	2.165(2)	2.430(3)	2.457(2)
	2.179(2)	2.483(3)	
5	2.205(2)	2.511(3)	2.379(2)
	2.240(2)	2.559(3)	2.425(2)
6	2.141(2)	2.392(3)	
	2.148(2)	2.418(3)	

red oil was stirred for 15 min in hexanes. Removal of solvent by rotary evaporation gave a dark orange powder (155 mg, 72%). *Anal*. Calc. for $C_{42}H_{72}N_3O_3Si_2Y$: Y, 10.9. Found: Y, 11.2%. ^{1}H NMR (C_6D_6): δ 7.73 (s, 2H), 7.69 (d, 2H, $J = 2.5$ Hz), 7.03 (d, 2H, $J = 2.5$ Hz), 4.39 (q, 2H, $J = 6.0$ Hz), 4.10 (b, 4H, $\Delta\nu_{1/2} = 125$ Hz), 2.82 (q, 2H, $J = 6.0$ Hz), 1.63 (s, 18H), 1.50 (b, 4H, $\Delta\nu_{1/2} = 120$ Hz), 1.36 (s, 18H), 0.26 (s, 18H). ^{13}C{^{1}H} NMR: δ (C_6D_6) 170.6, 164.4, 139.2, 136.8, 130.0, 129.7, 122.6, 70.2, 59.0, 35.7, 34.1, 31.7, 30.3, 25.4, 5.3. IR 2957vs, 2907s, 2868s, 1617vs, 1536s, 1463s, 1440s, 1413s, 1390s, 1274w, 1235w, 1200w, 1166s, 1054w, 1027w, 980w, 837m cm^{-1}.

4.2. (Salen′)Y($OC_6H_3Bu^t_2$-2,6)(THF)$_{0,1}$, **3**, **4**

Addition of H_2salen′ (111 mg, 0.22 mmol) to a white slurry of Y(OAr′)$_3$ (159 mg, 0.22 mmol) in 5 ml of hexanes immediately generated a yellow solution. Within a few minutes, a yellow precipitate appeared. The reaction was stirred overnight and the slurry was centrifuged to separate a yellow solid and light yellow solution. The yellow solid was isolated and dried by rotary evaporation (151 mg, 85%). X-ray quality crystals were grown from a 50/50 mixture of toluene–THF at −35 °C. *Anal*. Calc. for $C_{50}H_{75}N_2O_4Y$: Y, 10.4. Found: Y, 9.9%. ^{1}H NMR (C_6D_6): δ 7.73 (d, 2H, $J = 2.4$ Hz), 7.65 (s, 2H), 7.31 (d, 2H, $J = 7.7$ Hz), 7.06 (d, 2H, $J = 2.4$ Hz), 6.82 (t, 1H, $J = 7.7$ Hz), 3.73 (q, 2H, $J = 6.5$ Hz), 2.76 (q, 2H, $J = 6.5$ Hz), 1.69 (s, 18H), 1.46 (s, 18H), 1.36 (s, 18H). ^{13}C{^{1}H} NMR (C_6D_6): δ 170.9, 164.1, 139.8, 138.0, 137.8, 130.6, 129.6, 129.3, 124.9, 122.7, 116.7, 58.2, 35.7, 34.7, 34.1, 31.7, 30.6, 30.1. IR 2958vs, 2912s, 2873s, 1614vs, 1537s, 1437m, 1321m, 1259a, 1205w, 1166m, 1097w, 1027w, 841w, 803w cm^{-1}.

4.3. (Salen′)Y(hfac)(THF)$_2$, **5**

Na(hfac) (51 mg, 0.22 mmol) was added to a yellow slurry of **1** (152 mg, 0.22 mmol) in 5 ml of THF. After stirring for 12 h, the yellow slurry was centrifuged and the solvent was removed from the yellow solution under vacuum (169 mg, 82%). X-ray quality crystals were grown from a toluene solution at room temperature (r.t.). *Anal*. Calc. for $C_{45}H_{63}N_2O_6F_6Y$: Y, 9.6. Found: Y, 9.4%. ^{1}H NMR (C_6D_6): δ 7.91 (s, 2H), 7.70 (d, 2H, $J = 2.6$ Hz), 7.11 (d, 2H, $J = 2.6$ Hz), 6.48 (s, 1H), 3.40 (b, 8H, $\Delta\nu_{1/2} = 116$ Hz), 3.28 (s, 4H), 1.64 (s, 18H), 1.37 (s, 18H), 1.14 (b, 8H, $\Delta\nu_{1/2} = 124$ Hz). ^{13}C{^{1}H} NMR (C_6D_6): δ 168.6, 165.0, 140.5, 135.7, 129.7, 129.1, 120.8, 91.9, 69.4, 63.3, 35.5, 34.0, 31.8, 29.9, 25.2. IR 2957vs, 2914s, 2868s, 1660vs, 1613s, 1552w, 1498m, 1463w, 1440m, 1413m, 1393w, 1363w, 1339m, 1332s, 1254s, 1200s, 1146s, 1100s, 1023s, 911w, 872w cm^{-1}.

4.4. (Salen′)Y(C_5Me_5), **6**

KC_5Me_5 (33 mg, 0.19 mmol) was added to **1** (133 mg, 0.19 mmol) in 5 ml of THF. The reaction was stirred for 12 h, the yellow slurry was centrifuged, and the solvent was removed from the yellow solution by rotary evaporation to give a yellow oil. Hexanes were added, the mixture was stirred, and solvent was removed from the oil by rotary evaporation to give a yellow solid (103 mg, 75%). X-ray quality crystals were grown from a 50/50 toluene–hexanes mixture at r.t. *Anal*. Calc. for $C_{46}H_{80}N_3O_4Si_2Y$: Y, 12.4. Found: Y, 11.6%. ^{1}H NMR (C_6D_6): δ 7.71 (d, 2H, $J = 2.3$ Hz), 7.70 (s, 2H), 7.07 (d, 2H, $J = 2.3$ Hz), 3.60 (q, 2H, $J = 6.5$ Hz), 2.68 (q, 2H, $J = 6.5$ Hz), 2.00 (s, 15H), 1.75 (s, 18H), 1.36 (s, 18H).

$^{13}C\{^{1}H\}$ NMR (C_6D_6): δ 169.9, 164.9, 140.2, 136.8, 130.0, 129.5, 122.4, 116.7, 58.3, 35.8, 34.1, 31.7, 30.3, 11.1. IR 2957vs, 2907s, 2868s, 1610vs, 1532s, 1463w, 1440m, 1413m, 1390m, 1359w, 1316s, 1274s, 1254s, 1200m, 1166s, 1096w, 1058w, 1027w, 984w, 930w, 911w, 876w, 849m cm^{-1}.

4.5. X-ray data collection, structure determination, and refinement for [(salen′)Y($OC_6H_3Bu^t_2$-2,6)(THF)], 4

A colorless crystal of approximate dimensions 0.16 × 0.19 × 0.25 mm was mounted on a glass fiber and transferred to a Bruker CCD platform diffractometer. The SMART [22] program package was used to determine the unit-cell parameters and for data collection (30 s per frame scan time for a sphere of diffraction data). The raw frame data was processed using SAINT [23] and SADABS [24] to yield the reflection data file. Subsequent calculations were carried out using the SHELXTL [25] program. The diffraction symmetry was 2/*m* and the systematic absences were consistent with the centrosymmetric monoclinic space group $P2_1/n$ which was later determined to be correct. Details are in Table 2.

The structure was solved by direct methods and refined on F^2 by full-matrix least-squares techniques. The analytical scattering factors [26] for neutral atoms were used throughout the analysis. There were 2.5 molecules of toluene solvent present per formula unit. The half molecule of solvent was modeled as a disorder over an inversion center. Hydrogen atoms were included using a riding model. At convergence, $wR_2 = 0.1788$ and GOF = 0.0631 for 586 variables refined against 15 186 unique data. As a comparison for refinement on *F*, $R_1 = 0.0631$ for those 9780 data with $I > 2.0\sigma(I)$. Subsequent complexes were handled as described for **4**.

4.6. (Salen′)Y(hfac)(THF)$_2$, 5

A yellow crystal of approximate dimensions 0.17 × 0.20 × 0.33 mm was mounted on a glass fiber and transferred to a Bruker CCD platform diffractometer (30 s per frame scan time for a hemisphere of diffraction data). The diffraction symmetry was 2/*m* and the systematic absences were consistent with the centrosymmetric monoclinic space group $P2_1/c$ which was later determined to be correct.

Disorder was present in the CF_3 group and both THF molecules. Atoms F(4)–F(5), C(38)–C(40), C(43) and C(44) were disordered and included using multiple components with partial site-occupancy factors. Hydrogen atoms were included using a riding model. At convergence, $wR_2 = 0.1533$ and GOF = 1.032 for 518 variables refined against 10 952 data. As a comparison for refinement on *F*, $R_1 = 0.0576$ for those 8653 data with $I > 2.0\sigma(I)$.

4.7. (Salen′)Y(C_5Me_5), 6

A yellow crystal of approximate dimensions 0.10 × 0.15 × 0.25 mm was mounted on a glass fiber and transferred to a Bruker CCD platform diffractometer (30 s per frame scan time for a hemisphere of diffraction data). The diffraction symmetry was *mmm* and the systematic absences were consistent with the orthorhombic space group $P2_12_12_1$ which was later determined to be correct.

Hydrogen atoms were included using a riding model. At convergence, $wR_2 = 0.0592$ and GOF = 0.934 for 424 variables refined against 9633 data. As a comparison for refinement on *F*, $R_1 = 0.0452$ for those 6021 data with $I > 2.0\sigma(I)$. The absolute structure was assigned by refinement of the Flack parameter [26].

Table 2
X-ray crystallographic data on Y(salen′)($OC_6H_3Bu^t_2$-2,6)(THF), **4**, Y(salen′)hfac$(THF)_2$, **5**, (salen′)Y(C_5Me_5), **6**

Compound	4	5	6
FW	$C_{50}H_{73}N_2O_4Y \cdot 2.5(C_7H_8)$	$C_{45}H_{63}F_6N_2O_6Y$	$C_{42}H_{61}N_2O_2Y$
Temperature (K)	178 (2)	158 (2)	158 (2)
Crystal system	monoclinic	monoclinic	orthorhombic
Space group	$P2_1/n$	$P2_1/c$	$P2_12_12_1$
a (Å)	16.5331(7)	13.7169(6)	10.4859(9)
b (Å)	16.0380(6)	21.1351(10)	15.7481(13)
c (Å)	23.5698(9)	16.7430(7)	24.370(2)
α (°)	90	90	90
β (°)	92.4660(10)	109.0750(10)	90
γ (°)	90	90	90
V (Å^3)	6243.9(4)	4587.4(4)	4024.2(6)
Z	4	4	4
ρ_{calc} (Mg m^{-3})	1.157	1.348	1.180
μ (mm^{-1})	0.980	1.343	1.484
Final $R_1[I > 2\sigma(I)]$	0.0631	0.0576	0.0452
Final wR_2 (all data)	0.1788	0.1533	0.0592

5. Supplementary material

Crystallographic data for the structural analysis have been deposited with the Cambridge Crystallographic Data Centre, CCDC Numbers CCDC 172137–172139 for compounds **4**–**6**, respectively. Copies of this information may be obtained free of charge from The Director, CCDC, 12 Union Road, Cambridge, CB2 1EZ, UK (fax: +44-1223-336033; e-mail: deposit@ccdc.cam.ac.uk or www: http//www.ccdc.cam.ac.uk).

Acknowledgements

For support of this research, we thank the Division of Chemical Sciences of the Office of Basic Energy Sciences of the Department of Energy.

References

[1] R. Duchateau, C.T. van Wee, A. Meetsma, J.H. Teuben, J. Am. Chem. Soc. 115 (1993) 4931.
[2] L. Lee, D.J. Berg, G.W. Bushnell, Organometallics 14 (1995) 8.
[3] C.J. Schaverien, A.G. Orpen, Inorg. Chem. 10 (1991) 4968.
[4] T. Dube, S. Gambarotta, G.P.A. Yap, Organometallics 19 (2000) 817.
[5] Y. Cai, H. Ma, B. Kang, C. Su, W. Zhang, J. Sun, Y. Xiong, J. Organomet. Chem. 628 (2001) 99.
[6] Q. Liu, M. Ding, Y. Lin, Y. Xing, Polyhedron 17 (1998) 555.
[7] R. Anwander, T. Priermeier, O. Runte, Chem. Commun. (1996) 1385.
[8] Q. Liu, M. Ding, Y. Lin, Y. Xing, J. Organomet. Chem. 548 (1997) 139.
[9] Q. Liu, M. Ding, Y. Lin, Y. Xing, Polyhedron 17 (1998) 2327.
[10] P. Blech, C. Floriani, A. Chiesi-Villa, C. Guastini, J. Chem. Soc., Dalton Trans. (1990) 3557.
[11] T. Dube, S. Gambarotta, G. Yap, Organometallics 17 (1998) 3967.
[12] G.W. Coates, T.M. Ovitt, J. Am. Chem. Soc. 121 (1999) 4072.
[13] J.P. Morken, C.M. Mascarenhas, S.P. Miller, P.S. White, Angew. Chem., Int. Ed. 30 (2001) 601.
[14] W.J. Evans, C.H. Fujimoto, J.W. Ziller, Chem. Commun. (1999) 311.
[15] P.B. Hitchcock, M.F. Lappert, R.G. Smith, Inorg. Chim. Acta 139 (1987) 183.
[16] F. Cobrazza, E. Solari, C. Floriani, A. Chiesi-Villa, C. Guastini, J. Chem. Soc., Dalton Trans. (1990) 1334.
[17] E.B. Tjaden, D.C. Swenson, R.F. Jordan, Organometallics 14 (1995) 371.
[18] C.J. Schaverien, J.H.G. Frijns, H.J. Heeres, J.R. van den Hende, J.H. Teuben, J. Chem. Soc., Chem. Commun. (1991) 642.
[19] K.D. Pollard, J.J. Vittal, G.P.A. Yap, R.J. Puddephatt, J. Chem. Soc., Dalton Trans. (1998) 1265.
[20] W.J. Evans, J.W. Grate, K.R. Levan, I. Bloom, T.T. Peterson, R.J. Doedens, H. Zhang, J.L. Atwood, Inorg. Chem. 25 (1986) 3614.
[21] M.D. Taylor, C.D. Carter, J. Inorg. Nucl. Chem. 24 (1962) 387.
[22] SMART Software Users Guide, Version 5.1, Bruker Analytical X-Ray Systems, Madison, WI, 1999.
[23] SAINT Software Users Guide, Version 6.0, Bruker Analytical X-Ray Systems, Madison, WI, 1999.
[24] G.M. Sheldrick, SADABS, Bruker Analytical X-Ray Systems, Madison, WI, 1999.
[25] G.M. Sheldrick, SHELXTL Version 5.10, Bruker Analytical X-Ray Systems, Madison, WI, 1999.
[26] International Tables for X-Ray Crystallography, vol. C, Kluwer Academic Publishers, Dordrecht, 1992.

Table 1
Crystal data for **1**, **2** and **3**

	1	**2**	**3**
Empirical formula	$C_{18}H_{16}OSi.C_{11}H_9N$	$C_{18}H_{16}OSi.C_{10}H_8N_2$	$C_{18}H_{16}OSi.C_{13}H_9N$
Colour, habit	colourless blocks	colourless blocks	colourless irregular shape
Crystal size (mm)	$0.45 \times 0.35 \times 0.28$	$0.40 \times 0.33 \times 0.15$	$0.22 \times 0.20 \times 0.15$
Crystal system	triclinic	triclinic	triclinic
a (Å)	9.1913(10)	9.2547(9)	10.984(3)
b (Å)	9.3733(11)	9.3329(13)	11.077(3)
c (Å)	15.6990(17)	15.3755(19)	11.276(3)
α (°)	81.291(9)	83.675(15)	100.147(3)
β (°)	89.381(10)	89.194(12)	111.809(3)
γ (°)	65.344(9)	63.861(7)	101.899(3)
Volume (Å^3)	1213.0(2)	1184.1(2)	1197.2(6)
Space group	$P\bar{1}$	$P\bar{1}$	$P\bar{1}$
Z	2	2	2
Temperature (K)	293(2)	293(2)	120(2)
Reflections measured	4617	4508	14617
Unique reflections, R_{int}	4441, 0.013	4334, 0.017	6511, 0.019
Completeness to $\theta = 25°$	100%	100%	100%
Reflections with $I > 2\sigma(I)$	2559	2092	5531
Number of L.S. parameters	291	291	407
Weighting scheme parameters a and b	0.0423, 0.04213	0.0285, 0.6316	0.0568, 0.3770
R, wR_2	0.0467, 0.0957	0.0555, 0.0947	0.0389, 0.1024

erally contain tertiary amino groups and are often labelled as sila-drugs, e.g. siladifendol, (3-piperidinopropyl)diphenylsilanol which contains intra-molecular O–H···N hydrogen bonds [6] or silapridinol, (2-piperidinoethyl)diphenylsilanol which contains inter-molecular O–H···N hydrogen bonds [7]. A related secondary amine derivative, 3-(*cyclo*hexylamino)propyldimethylsilanol, has been reported to form inter-molecular O–H···N hydrogen bonds [8].

2. Experimental

The adducts **1**–**3** were obtained as crystals from dichloromethane solutions of Ph_3SiOH and the amine at room temperature (r.t.). The 1:1 adducts were obtained from solutions of the reagents in 1:x ratio of silanol:amine for $x = 1$ or 2 for 4-phenylpyridine or acridine, $x = 1$, 2 or 4 for 4,4′-bipyridine. Infrared spectra were recorded on a Perkin–Elmer Paragon 1000 Fourier Transform Spectrometer. Samples were prepared as KBr discs. All ^{1}H NMR spectra were recorded on a Bruker Avance 300 MHz spectrometer. Tetramethylsilane was used as the standard and deuterated chloroform as the solvent. All NMR spectra were recorded at ambient temperature. Melting points (m.p.) were recorded on an Electrothermal IA 9000 Series digital m.p. apparatus. Elemental (C/H) analyses were carried out on an Exeter Analytical Inc., CE 440 Elemental Analyser at the Microanalytical Laboratory, University College, Cork.

Bulk samples of the 4-phenylpyridine adduct **1**, m.p. 53–55 °C, the 4,4′-bipyridine adduct **2**, m.p. 103–106 °C, and the acridine adduct **3**, m.p. 96–97 °C afforded satisfactory chemical (C, H and N) analysis.

Adduct **1**, Ph_3SiOH:4-phenylpyridine. Found: C, 80.7; H, 5.9; N, 3.2. $C_{29}H_{25}NOSi$ requires: C, 80.7; H, 5.8; N, 3.2%. IR (KBr disc) ν_{max} (cm^{-1}): (only very strong or strong vibrations are reported) 1428, 1118, 1115, 899, 739, 709, 698, 511. NMR (ppm): ^{1}H 3.69 (s, 1H), 7.31 to 7.43 (m, 15H), 7.55 to 7.58 (m, 7H), 8.51 (d, 2H).

Adduct **2**, Ph_3SiOH:4,4′-bipyridine. Found: C, 77.8; H, 5.8; N, 6.6. $C_{28}H_{24}N_2OSi$ requires: C, 77.7; H, 5.6; N, 6.5%. IR (KBr disc) ν_{max} (cm^{-1}): (only very strong or strong vibrations are reported) 1589, 1428, 1118, 1112, 895, 804, 708, 612, 510. NMR (ppm): ^{1}H 4.15 (s, 1H), 7.18 to 7.36 (m, 9H), 7.43 to 7.45 (m, 4H), 7.56 to 7.58 (m, 6H), 8.59 (d, 4H).

Adduct **3**, Ph_3SiOH:acridine. Found: C, 81.9; H, 5.6; N, 3.1. $C_{31}H_{25}NOSi$ requires: C, 81.75; H, 5.5; N, 3.1%. IR (KBr disc) ν_{max} (cm^{-1}): (only very strong or strong vibrations are reported) 1516, 1428, 1116, 1112, 888, 741, 708, 699, 510, 506. NMR (ppm): ^{1}H 3.28 (s, 1H), 7.25 to 7.39 (m, 9H), 7.46 to 7.50 (m, 2H); 7.55 to 7.58 (m, 6H), 7.69 to 7.73 (m, 2H), 7.92 (d, 2H), 8.13 (d, 2H), 8.60 (s, 1H).

2.1. Crystal structure analysis for compounds *1*, *2* and *3*

Crystal data are given in Table 1. Data for **1** and **2** were collected on a Nonius MACH 3 diffractometer using graphite monochromatised Mo Kα radiation, $\lambda =$

0.71073 Å. Data for **3** were collected on a Bruker SMART-1K CCD area detector diffractometer using graphite monochromatised Mo Kα radiation and an Oxford Cryosystems open-flow N_2 gas cryostat [9]. Unit cell parameters were determined using the SMART [10] program from the centroids of 828 reflections with 2θ values between 27.4° and 59.7°. Reflection intensities were integrated using the SAINT program [11]. For all three compounds no absorption correction was performed. The structures were solved by direct methods [12], refined by full-matrix least-squares on F^2 [13] and analysed for non-covalent interactions [14]. The weighting scheme employed was $w = 1/[\sigma^2(F_o^2)+(aP)^2+bP]$ where $P = (F_o^2+F_c^2)/3$.

For **1** and **2**, the hydroxyl hydrogen was located from a difference Fourier electron density map and all other hydrogen atoms were geometrically placed in calculated positions. All hydrogen atoms were allowed to ride on their parent atom with $U_{iso}(H) = 1.2\ U_{eq}(C)$ and $1.5\ U_{eq}(O)$. Idealised C–H distances were fixed at 0.93 Å. For **3**, all hydrogen atoms were found from difference Fourier maps and their coordinates and isotropic atomic displacement parameters were refined.

3. Results and discussion

All adducts reported here were formed with the triphenylsilanol: amine ratio 1:1. This occurred even when a 2:1 ratio of Ph_3SiOH: 4,4′-bipyridine was reacted together. Views of the structures of **1**, **2** and **3** are shown in Figs. 1–3. Important distance and angle data are given in the legends to the Figures. Compounds **1**, **2** and **3** are monomeric with single O–H···N hydrogen bonds. In all adducts the silicon is tetrahedrally coordinated and all the angles at silicon are close to 109.5°. The

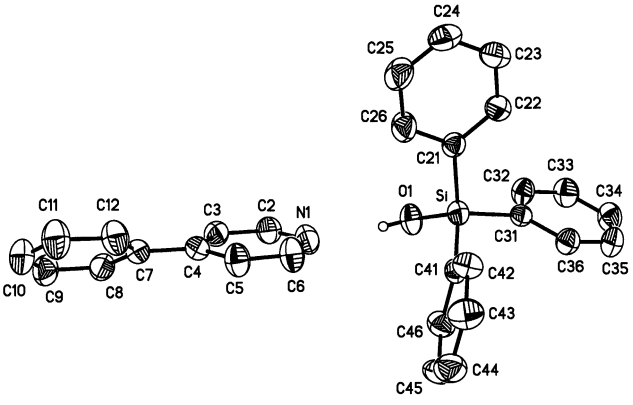


Fig. 1. A view of **1** showing the numbering scheme. Selected distances (Å) and angles (°): N1–C6 1.327(4), N1–C2 1.325(4), C2–C3 1.378(4), C3–C4 1.392(4), C4–C5 1.381(4), C4–C7 1.480(4), C5–C6 1.378(4), C7–C12 1.383(4), C7–C8 1.381(4), C8–C9 1.398(4), C9–C10 1.366(5), C10–C11 1.355(5), C11–C12 1.377(5), Si–O1 1.625(2), Si–C41 1.867(3), Si–C31 1.869(3), Si–C21 1.872(3), C6–N1–C2 115.6(3), N1–C2–C3 124.4(3), C2–C3–C4 119.9(3), C5–C4–C3 115.5(3), C5–C4–C7 121.9(3), C3–C4–C7 122.6(3), C4–C5–C6 120.4(3), N1–C6–C5 124.2(3), C12–C7–C8 117.9(3), C12–C7–C4 120.8(3), C8–C7–C4 121.3(3), C7–C8–C9 120.2(3), C10–C9–C8 120.0(3), C11–C10–C9 120.3(3), C10–C11–C12 119.9(4), C7–C12–C11 121.6(3), O1–Si–C41 110.40(12), O1–Si–C31 106.14(12), C41–Si–C31 110.63(12), O1–Si–C21 111.56(13), C41–Si–C21 109.09(13), C31–Si–C21 108.98(12).

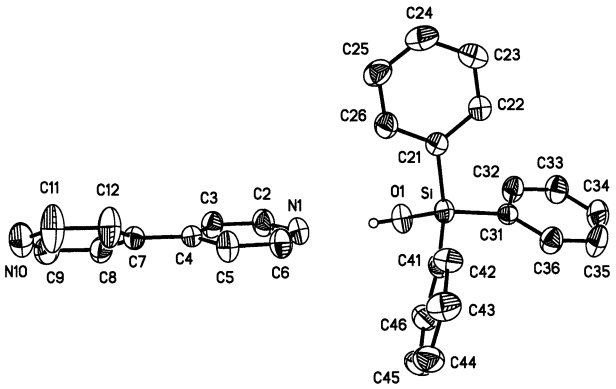


Fig. 2. A view of **2** showing the numbering scheme. Selected distances (Å) and angles (°): N1–C6 1.317(5), N1–C2 1.322(5), C2–C3 1.380(5), C3–C4 1.382(5), C4–C5 1.371(5), C4–C7 1.478(5), C5–C6 1.379(5), C7–C8 1.371(5), C7–C12 1.372(5), C8–C9 1.401(6), C9–N10 1.311(6), N10–C11 1.307(6), C11–C12 1.376(6), Si–O1 1.630(3), Si–C41 1.863(4), Si–C31 1.863(4), Si–C21 1.877(4); C6–N1–C2 115.0(4), N1–C2–C3 124.6(4), C2–C3–C4 119.7(4), C5–C4–C3 115.9(4), C5–C4–C7 122.2(4), C3–C4–C7 121.9(4), C4–C5–C6 120.0(4), N1–C6–C5 124.8(4), C8–C7–C12 115.8(4), C8–C7–C4 122.5(4), C12–C7–C4 121.7(4), C7–C8–C9 119.6(4), N10–C9–C8 123.9(5), C11–N10–C9 115.7(5), N10–C11–C12 124.8(5), C7–C12–C11 120.1(5), O1–Si–C41 110.68(16), O1–Si–C31 105.78(15), C41–Si–C31 110.74(16), O1–Si–C21 110.77(17), C41–Si–C21 109.70(16), C31–Si–C21 109.12(16).

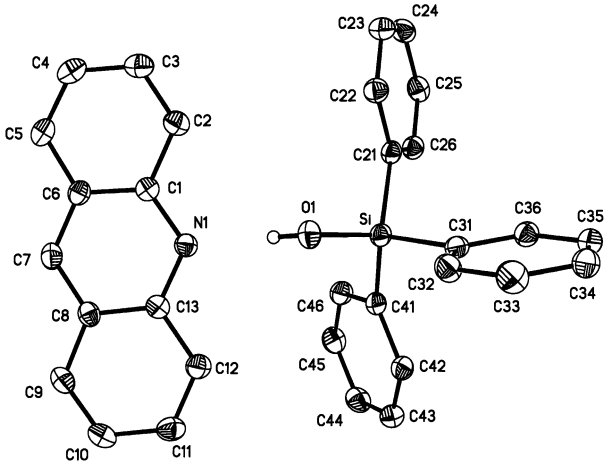


Fig. 3. A view of **3** showing the numbering scheme. Selected distances (Å) and angles (°): Si1–O1 1.6355(10), Si1–C31 1.8705(12), Si1–C41 1.8714(13), Si1–C21 1.8755(13), N1–C1 1.3512(15), N1–C13 1.3524(15), C1–C6 1.4334(16), C6–C7 1.3961(17), C7–C8 1.3943(18), C8–C13 1.4351(16), O1–Si1–C31 104.69(5), O1–Si1–C41 110.45(5), C31–Si1–C41 112.53(5), O1–Si1–C21 110.78(5), C31–Si1–C21 108.56(5), C41–Si1–C21 109.74(5), C1–N1–C13 118.65(10), N1–C1–C6 122.79(11), C7–C6–C1 117.69(11), C8–C7–C6 120.45(11), C7–C8–C9 123.12(11), C7–C8–C13 117.97(11), N1–C13–C8 122.40(11).

average Si–C distances in **1**, **2** and **3** are 1.869(3), 1.867(4) and 1.8725(13) Å. There are no unusual distances or angles within the aromatic rings in any of the sections of the adducts. The structures of **1**, **2** and **3** are remarkably simple compared with the reported structures of some amine adducts of disiloxanediols or trisiloxanediols which may be either discrete molecules or contain infinite chains formed through either O–H···N or O–H···O hydrogen bonds, [3,4,15] (see Table 2).

The O···N bond distances and O–H···N angles are 2.768(3), 2.789(4) and 2.7631(14) Å and 163°, 164° and 176(2)° in **1**, **2** and **3**, respectively, Table 2. The distances in **1** and **2** are the same within 3σ and likewise for **1** and **3**. However, the distances in **2** and **3** are not the same within 3σ vide infra. The O(H)···N distances are indicative of moderately strong inter-molecular hydrogen bonds [13] and are at the lower end of the reported range of such distances in silanol–amine adducts which extends from 2.681(6) Å in $\{Ph_2SiOSi(OH)_2O\}_2$(pyridine)$_2$ [16] to 3.054(4) Å in $\{(HO)SiPh_2OSiPh_2OSiPh_2(OH)\}_2$(pyridine)$_3$ [4]. The related dimensions in the $[\{(Me_3Si)_3C\}Ph_2SiOH]_2$·TMEDA adduct are 2.75 Å and 158° [5], and in the secondary amine derivative, 3-(*cyclo*hexylamino)propyldimethyl silanol, the mean values for the two independent molecules in the unit cell are 2.75 Å and 171° [8]. In general, inter-molecular O(H)···N hydrogen bond distances are greater than intra-molecular distances as in, for example the siladrugs (3-piperidinopropyl)diphenylsilanol which contains intra-molecular O–(H)···N hydrogen bonds of 2.685 Å [6] and (2-piperidinoethyl)diphenylsilanol which contains inter-molecular O–H···N hydrogen bonds of 2.758 Å [7]. In the latter two compounds the O(H)···N angles are essentially the same at 173.2° and 172.5(2)°, respectively.

Table 2
Hydrogen-bonding in adducts of silanols with aromatic amines

	Type of complex	Types of hydrogen bonding present	Manner of chain propagation
Ph_3SiOH adducts			
4-Phenylpyridine (1:1) [a]	Discrete molecule	O–H···N	None
4,4′-Bipyridine (1:1) [b]	Discrete molecule	O–H···N	None
Acridine (1:1) [c]	Discrete molecule	O–H···N	None
$(HO)SiPh_2OSiPh_2(OH)$ adducts			
Pyridine (1:1) [d]	Infinite chain	O–H···N and O–H···O	O–H···O
Pyrimidine (1:1) [e]	Infinite chain	O–H···N and O–H···O	O–H···O
Pyrazine (2:1) [f]	Infinite chain	O–H···N and O–H···O	O–H···N
2,2′-Bipyridine (1:1) [g]	Infinite chains	O–H···N	O–H···N
Pyridazine (3:2) [h]	Discrete molecule	O–H···N and O–H···O	None
$(HO)SiPh_2OSiPh_2OsiPh_2(OH)$ adducts			
Pyridine (2:3) [i]	Discrete molecule	O–H···N and O–H···O	None
Pyrazine (4:1) [j]	Discrete molecule	O–H···N and O–H···O	None
(D) $[\{Ph_2SiOSi(OH)_2O\}_2]$ adduct			
Pyridine (1:2)[k]	Infinite chain	O–H···N and O–H···O	O–H···O

[a] O···N 2.768(3) Å, O–H···N 163°, Si–O 1.625(2) Å (this work).
[b] O···N 2.789(4) Å, O–H···N 164°, Si–O 1.630(3) Å (this work).
[c] O···N 2.7631(14) Å, O–H···N 176(2)°, Si–O 1.6355(10) Å (this work).
[d] O···N 3.001(3) Å, Si–O 1.6201(14) Å [4].
[e] O···N 2.963(5) Å, O–H···N 163°, Si–O 1.624(2) Å [4].
[f] O···N 2.718(3) Å, O–H···N 168°, Si–O 1.6267(17) Å [4].
[g] O···N 2.869(2) and 2.846(2) Å, O–H···N 159 and 167°, Si–O 1.622(2) and 1.6201(12) Å [4].
[h] O···N 2.75(1) and 2.75(2) Å [3], Si–O 1.62 and 1.63 Å [17].
[i] O···N 2.722(3) and 3.054(4) Å, O–H···N 150 and 174°, Si–O 1.6096(14) and 1.6250(15) Å [4].
[j] O···N 2.706(2) Å, O–H···N 168°, Si–O 1.6282(14) Å [4].
[k] O···N 2.699(6) and 2.681(6) Å, O–H···N 175(3) and 177(3)° [16], Si–O 1.609 and 1.610 Å [17].

The Si–O distances, 1.625(2), 1.630(3) and 1.6355(10) Å for **1**, **2** and **3**, respectively, are almost indistinguishable at the 3σ. All the Si–O distances are typical of measured Si–O distances in amine adducts of silanols and siloxanediols [4,17]. The average Si–O distance in crystalline Ph_3SiOH, which exists as two independent tetrameric O–H···O hydrogen bonded species, is 1.645(7) Å [18].

Comparing compounds **1**–**3**, it is notable that **3** has the shortest O···N distance, the longest Si–O distance and a Si–O–N angle closest to linearity. These features suggest that **3** contains the strongest O–H···N hydrogen bond in these three adducts.

In both **1** and **2** there is an interplanar twist of the amine's aromatic rings. The twist angles for planes containing the C(3)–C(4)–C(7) and C(4)–C(7)–C(8) atoms, see Figs. 1 and 2 are 33.6(4)° and 27.6(6)° for **1** and **2**, respectively. In comparison, the interplanar twist angles in 4,4′-bipyridine [19], which possess two crystallographically independent molecules, are 18.50(12)° and 34.85(10)°. Theoretical studies indicate that a value of 48.6° can be expected and this may be compared with 37.2° determined from gas phase measurements [20]. There is no significantly enhanced inter-ring π overlap in the amine portions of the adducts.

For **1** and **2**, there is a layer structure present parallel to the *yz* plane. The layers containing the triphenylsilanol molecules are shown in Fig. 4. The silanol molecules are arranged in layers which contain an hydrophobic core formed by numerous interactions of both π–π stacking and C–H···π type between phenyl groups. The π–π stacking interactions are characteristic

of multi-phenyl systems [21] with, for example, the shortest centroid–centroid distance in **1** at 4.4 Å for the ring containing atoms C(41)–C(46) and its centrosymmetrically related neighbour with the rings aligned in a parallel fashion. In general, C–H···π interactions may be characterised by the angle at the hydrogen atom (the angle α in Fig. 5) and the perpendicular distance of the H atom from the plane of the ring. Typical values may be between 120° to 180° with distances of up to 3.2 Å [21]. The values found in **1** and **2** are normal for such systems; for example, in **1** the distance from H(24) to the ring containing atoms C(31)–C(36) is 2.9 Å and the angle α is 148°. The silanol groups are orientated away from the hydrophobic core and form a hydrophilic exterior which interacts with the layers of amines via hydrogen bonding. The amine layers are held together by π–π stacking between the phenyl and/or pyridyl rings, for example in **1** the centroid–centroid distance is 4.5 Å and the dihedral angle between the planes is 34°. There are C–H···π interactions present as well, for example in **1** the distance is 3.0 Å at 118°. The structure of **3** also contains π–π stacking which is notably stronger than in **1** and **2**, with the centroid–centroid distance in **3** being 3.6 Å and the dihedral angle between the planes is 2.3°. There are also seven C–H···π interactions present in **3** and these involve both the amine and the silanol.

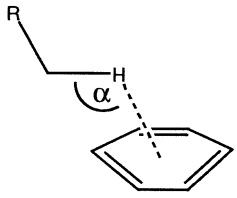


Fig. 5. Schematic diagram of the pertinent features for describing C–H···π interactions.

It is not clear why Ph_3SiOH does not form a 2:1 adduct with 4,4′-bipyridine when the reaction is carried out with a molar ratio $\geq$2:1 since both nitrogen donor sites in 4,4′-bipyridine appear to be identical. Indeed, the N–C bond distances and C–N–C angles in both the 4,4′-bipyridine and 4-phenylpyridine parts of the adducts **1** and **2** are the same at the 2σ level. It is possible that no 2:1 adduct is observed because there would be no contribution to the overall stability of the crystal from π–π stacking between the 4,4′-bipyridine molecules.

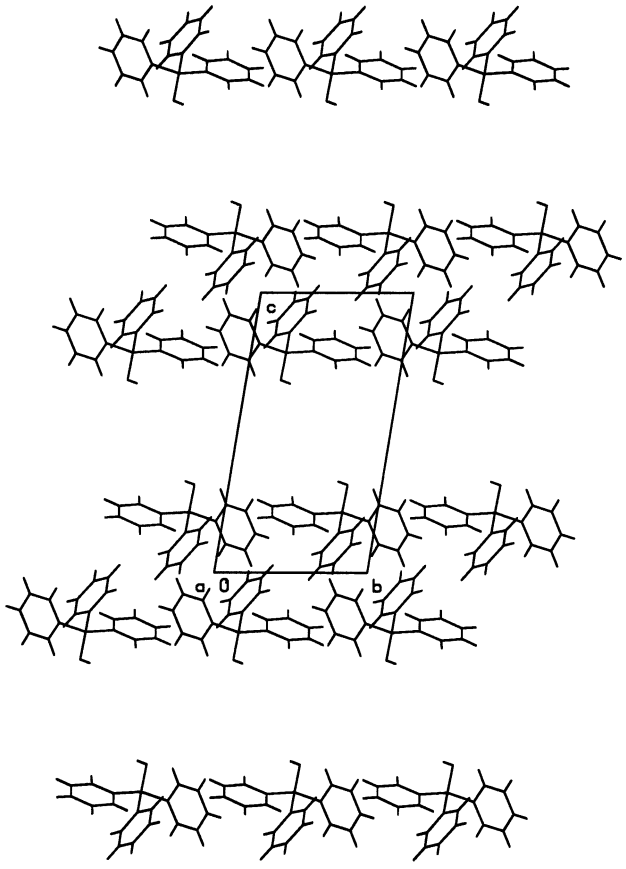


Fig. 4. Packing diagram for **1** showing the hydrophilic exterior and the hydrophobic core of the silanol double layer sheets. The amine molecules have been omitted for clarity.

4. Supplementary material

Supplementary crystallographic data are available from the CCDC, 12 Union Road, Cambridge CB2 1EZ, UK (fax: +44-1223-336033; e-mail: deposit@ccdc.cam.ac.uk or www: http://www.ccdc.cam.ac.uk) on request, quoting the deposition numbers 169134 (for **1**), 169133 (for **2**), and 169135 (for **3**).

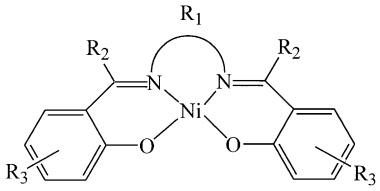
Acknowledgements

We thank Cork University Foundation for help with the purchase of an X-ray diffractometer.

References

[1] (a) R. Corriu, P. Jutzi, Tailor-made Silicon-Oxygen Compounds, F. Vieweg & Sohn, Braunschweig/Wiesbaden, 1996;
(b) Z. Zhang, H. Wakabayashi, Y. Tanigami, R. Terai, Thin Solid Films 349 (1999) 24.
[2] D.F. Shantz, R.F. Lobo, Micropor. Mesopor. Mater. 43 (2001) 127.
[3] (a) K.A. Ruud, J.S. Sepeda, F.A. Tibbals, D.C. Hrncir, J. Chem. Soc., Chem. Commun. (1991) 629;
(b) L. Clausen, I. Fabricius, L. Madsen, J. Environ. Qual. 30 (2001) 846.
[4] B.J. O'Leary, T.R. Spalding, C. Glidewell, G. Ferguson, Acta Crystallogr. Sect. B 56 (2000) 273.
[5] I. Baxter, L.D. Cother, C. Dupuy, P.D. Lickiss, A.J.P. White, D.J. Williams, obtained on the Internet at http://www.ch.ic.ac.uk/ectoc/ectoc-3/pub/010/index.htm, 1997.

[6] R. Tacke, M. Strecker, W.S. Sheldrick, E. Heeg, B. Berndt, K.M. Knapstein, Z. Naturforsch. Teil B., Anorg. Chem. Org. Chem. 34B (1979) 1279.
[7] R. Tacke, M. Strecker, W.S. Sheldrick, E. Heeg, B. Berndt, K.M. Knapstein, R. Niedner, Chem. Ber. 113 (1980) 1962.
[8] W. Ziche, B. Herrschaft, F. Hahn, P. John, J. Weis, N. Auner, J. Organometal. Chem. 536/537 (1997) 375.
[9] J. Cosier, A.M. Glazer, J. Appl. Cryst. 19 (1986) 105.
[10] SMART-NT. Data Collection Software. Version 5.0, Bruker Analytical X-ray Instruments Inc, Madison, WI, USA, 1998.
[11] SAINT-NT. Data Reduction Software. Version 5.0, Bruker Analytical X-ray Instruments Inc, Madison, WI, USA, 1998.
[12] G.M. Sheldrick, Acta Crystallogr. Sect. A. 46 (1990) 467.
[13] G.M. Sheldrick, SHELXL-97, University of Göttingen, Göttingen, Germany, 1997.
[14] A.L. Spek, PLATON, University of Utrecht, Utrecht, Holland, 2000.
[15] B.J. O'Leary, Ph.D. Thesis, University College, Cork, Ireland (1998).
[16] V.E. Shklover, I.L. Dubchak, Y.T. Struchkov, E.S. Khynku, A.A. Zhdanov, J. Struct. Chem. (Engl. Translation) 22 (1981) 229.
[17] F.H. Allen, O. Kennard, Chem. Design. Automation News 8 (1993) 525.
[18] H. Puff, K. Braun, H. Reuter, J. Organomet. Chem. 409 (1991) 119.
[19] N.M. Boag, K.M. Coward, A.C. Jones, M.E. Pemble, J.R. Thompson, Acta Crystallogr. Sect. C 55 (1999) 672.
[20] L. Ould-Moussa, O. Poizat, M. Casellà-Ventura, G. Buntinx, E. Kassab, J. Phys. Chem. 100 (1996) 2072.
[21] J.A.R.P. Sarma, G.R. Desiraju, Acc. Chem. Res. 19 (1986) 222.



(1)	[Ni(salen)]	R_1=CH_2CH_2	R_2=H	R_3=H
(2)	[Ni(saltMe)]	R_1=$C(CH_3)_2C(CH_3)_2$	R_2=H	R_3=H
(3)	[Ni(3,5-Cl_4saltMe)]	R_1= $C(CH_3)_2C(CH_3)_2$	R_2=H	R_3=3-Cl; 5-Cl
(4)	[Ni(salhd)]	R_1=cyclo-C_6H_{10}	R_2=H	R_3=H
(5)	[Ni(α,α'-Me_2salen)]	R_1=CH_2CH_2	R_2=CH_3	R_3=H
(6)	[Ni(salpd)]	R_1=$CH_2CH_2CH_2$	R_2=H	R_3=H
(7)	[Ni(salbd)]	R_1=$CH_2CH_2CH_2CH_2$	R_2=H	R_3=H
(8)	[Ni(saloph)]	R_1=cyclo-C_6H_4	R_2=H	R_3=H
(9)	[Ni(saloph-Cl_2)]	R_1=cyclo-3,4-Cl_2-C_6H_2	R_2=H	R_3=H

Scheme 1. Structure of nickel(II) complexes.

characterised in some of the solvents used, [1a,1c,1d,5] but they are included to provide a coherent framework for the overall study reported.

2. Results and discussion

2.1. Cyclic voltammetry of nickel(II) complexes

The complexes studied can be divided in two groups, based on their electrochemical response (Table 1). Complexes with non-aromatic imine bridges (**1**–**7**; group **A**) show, in the potential range used, one reduction process in all solvents used. With increasing scan rates (v), a linear dependence between i_p and $v^{1/2}$ is observed (similar slopes for the i_{pc} vs. $v^{1/2}$ and i_{pa} vs. $v^{1/2}$ plots), and the cathodic–anodic peak potential separations are similar to those observed for the couple Fc^+–Fc, and the ratios i_{pa}/i_{pc} are solvent independent, constant and equal to 1 for all the scan rates used. Electrochemical data for complexes of group **A** are thus consistent with one electron, diffusion-controlled, reversible reduction process [6].

Complexes with aromatic imine bridges (**8** and **9**; group **B**) present, in all solvents and for scan rates in the range 0.02–0.5 V s^{-1}, cyclic voltammograms with one cathodic wave at 1.210 V $< -E_{pc} <$ 1.378 V and one anodic wave at 0.282 V $< -E_{pa} <$ 0.630 V (Fig. 1(a)). Despite their large separation ($\approx$0.75 V), the two waves are related, as no anodic wave could be detected when the potential is cycled from 0 to −1.0 V.

With increasing scan rate a linear dependence between i_p and $v^{1/2}$ is also observed, but with quite different slopes for the i_{pc} versus $v^{1/2}$ and i_{pa} versus $v^{1/2}$ plots, which implies different diffusion coefficients for the reduced and oxidised species, and suggests significant structural changes upon reduction.

Peak potential dependence with complex concentration at a constant scan rate in dmf was also studied. For **8** and **9**, the values of E_{pa} are independent of complex concentration, whereas those of E_{pc} are shifted to more negative potentials when the complex concentration is reduced. For a scan rate of 200 mV s^{-1}, E_{pc} is shifted by 21 mV for [Ni(saloph)] (**8**) and 20 mV for [Ni(saloph-Cl_2)] (**9**), when the complex concentration is tenfold reduced.

Similar results have been described in literature for dmf solutions of complex **8** [5,7] and have been interpreted as a one-electron reversible reduction process followed by a fast chemical reaction leading to the formation of a stable new product, which is oxidised to the original complex.

Floriani et al. [8,9] have isolated the product of sodium reduction in the solution of [Ni(saloph)]. X-ray and magnetic data show that the product, formulated as $[Ni(saloph)]_2Na_2$, is a diamagnetic Ni(II) dimeric compound which is composed of two monomeric units linked by one of the carbon imine atoms that has been reduced to an amide carbon. Vianello et al. [5], based on the similarity between the cyclic voltamograms of $[Ni(saloph)]_2Na_2$ and [Ni(saloph)] in dmf, suggested that the electro-reduction of [Ni(saloph)] in this solvent produces in a first step a nickel(II) anion radical due to reduction of the imine bond to an amide bond, followed by a fast dimerisation reaction to yield the Ni(II) dimeric species, $[Ni(saloph)]_2^{2-}$. These species are then reversibly oxidised to the parent complex by cleavage of the bonding between the two monomer units. We presuppose the same mechanism for reduction of complexes **8** and **9** in all solvents used, and experimental evidence for the formation of the radical intermediate species have been obtained by EPR (see below).

Cyclic voltammograms recorded in dmf using very high scan rates, typically in the 1–60 V s^{-1} range exhibit in the reverse scan a new anodic wave at potentials similar to those of the cathodic wave, whereas the anodic wave at more positive potentials looses intensity as the scan rate is increased (Fig. 1(b)). When the scan rate reaches 60 V s^{-1}, the cyclic voltammograms, in all solvents, resemble those of a reversible type system with $E_{1/2} = 1/2(E_{pa} + E_{pc}) = -1.380$ for **8** and $E_{1/2} = -1.298$ V for **9**, and the ratio i_{pa}/i_{pc} reaches 1. The new anodic wave is attributed to the oxidation of the reduced monomeric species, in the absence of dimerisation; by using very fast scan rates the monomeric reduced species are oxidised before the dimerisation reaction takes place.

An estimate of the dimerisation rate constant, k_{dim}, can be obtained from the difference between E_{pc} (obtained for a scan rate of 50 mV s^{-1}, where the system is kinetically controlled by the dimerisation

Table 1
Electrochemical data for nickel(II) complexes [a]

Complex	Solvent	E_{pc} (V)	E_{pa} (V)	$-\Delta E$ (V)	$E_{1/2}$ (V) [b]	$-i_{pc}$(μA)	i_{pa} (μA)	$-i_{pc}/i_{pa}$	q (∞)/C [c]	n [c]
[Ni(salen)] (**1**)	CH_3CN	−1.715	−1.650	0.065	−1.682	8.50	7.75	1.10	5.44	1.07
	dmf	−1.633	1.565	0.068	−1.599	5.00	4.90	1.02		
	$(CH_3)_2SO$	−1.627	−1.563	0.064	−1.595	2.48	2.22	1.12		
[Ni(saltMe)] (**2**)	CH_3CN	−1.781	−1.710	0.071	−1.735	5.60	5.60	1.00	5.46	1.07
	dmf	−1.707	−1.636	0.071	−1.672	4.18	3.84	1.09		
	$(CH_3)_2SO$	−1.704	−1.639	0.065	−1.672	1.53	1.32	1.16		
[Ni(Cl_2-saltMe)] (**3**)	CH_3CN	−1.488	−1.413	0.075	−1.450	3.18	3.12	1.02	5.15	1.01
	dmf	−1.408	−1.330	0.078	−1.369	4.04	4.00	1.01		
	$(CH_3)_2SO$	−1.406	−1.328	0.078	−1.367	4.70	4.70	1.00		
[Ni(salhd)] (**4**)	CH_3CN	−1.760	−1.685	0.075	−1.722	3.18	3.12	1.02	5.20	1.12
	dmf	−1.662	−1.594	0.068	−1.628	4.04	4.00	1.01		
	$(CH_3)_2SO$	−1.676	−1.584	0.092	−1.630	3.55	3.20	1.11		
[Ni(α,α′-Me_2salen)] (**5**)	CH_3CN	[d]								
	dmf	−1.740	−1.675	0.065	−1.707	3.28	3.10	1.06	3.75	1.08
	$(CH_3)_2SO$	−1.727	−1.669	0.058	−1.698	2.38	2.21	1.08		
[Ni(salpd)] (**6**)	CH_3CN	[d]								
	dmf	−1.386	−1.330	0.056	−1.358	3.36	3.40	0.99	3.09	1.23
	$(CH_3)_2SO$	−1.400	−1.322	0.078	−1.361	3.70	3.70	1.00		
[Ni(salbd)] (**7**)	CH_3CN	[d]								
	dmf	−1.402	−1.335	0.067	−1.369	3.10	2.92	1.06	3.12	1.20
	$(CH_3)_2SO$	−1.435	−1.352	0.083	−1.393	2.50	2.35	1.06		
[Ni(saloph)] (**8**)	CH_3CN	−1.378	−0.631	0.747		7.61	1.89	4.02	2.94	1.02
	dmf	−1.300	−0.555	0.745	−1.380 [e]	5.24	1.40	3.74		
	$(CH_3)_2SO$	−1.298	−0.555	0.743		5.56	2.11	2.63		
[Ni(saloph-Cl_2)] (**9**)	CH_3CN	−1.292	−0.364	0.928		10.5	3.94	2.66	3.00	1.01
	dmf	−1.210	−0.282	0.928	−1.298 [e]	7.00	2.80	2.50		
	$(CH_3)_2SO$	−1.210	−0.284	0.926		6.47	2.71	2.39		

[a] The values were obtained at 0.05 V s^{-1}.
[b] The $E_{1/2}$ values are calculated as $1/2(E_{pc}+E_{pa})$.
[c] Refers to electrolysis.
[d] Complexes have low solubility in this solvent.
[e] Obtained at 60 V s^{-1}, see text for details.

reaction) and $E_{1/2}$ for a scan rate of 60 V s^{-1}, where the system is approximately reversible and diffusion controlled. Under the experimental conditions in which the system is kinetically controlled by the dimerisation reaction, E_{pc} is expressed by the equation [5,7]:

$$E_{pc} = E_{1/2} - 0.058 + 0.0197 \log k_{dim} + 0.0197 \log(c/v)$$

For complex solutions with $c = 2.00 \times 10^{-3}$ mol dm^{-3} in dmf and using the $E_{1/2}$ calculated at 60 V s^{-1}, k_{dim} was found to be: $4.08 \pm 0.67 \times 10^5$ mol^{-1} dm^3 s^{-1} ($E_{pc} = -1.355$ V) for [Ni(saloph)] (**8**) and $3.23 \pm 0.53 \times 10^5$ mol^{-1} dm^3 s^{-1} ($E_{pc} = -1.275$ V) for [Ni(saloph-Cl_2)] (**9**). The presence of electron withdrawing Cl groups in the imine bridge reduces the electronic density in the imine bond which would hinder the dimerisation process.

2.2. Coulometry of nickel(II) complexes

Electrochemical reduction of complexes of group **A** produces a colour change from reddish to dark blue (**1**–**5**) or dark green (**6** and **7**), whereas reduction of **8** and **9** (group **B**) led to brown–green solutions, implying the formation of new species that depend on the precursor. Plots of the cathodic current, i_c, against the time of electrolysis exhibit exponential decay typical of first-order processes for all complexes. On the other hand, plots of i_c versus q (charge transferred during the electrolysis) are quasi-linear, which suggests the transference of a constant number of electrons during electrolysis [6]. The i_c–q plots were used to obtain the values of q (∞) by extrapolation to $i_c = 0$, which has enabled the estimation of the number of electrons, n, involved in the reduction process (Table 1) [6]. The observation that the resulting n values are ≈1 for complexes **1**–**7** (Table 1), provides additional confirmation that only one electron is involved in the reduction process of these complexes. For complexes **8** and **9**, the values of n are also ≈1, which indicates that only one imine bond is involved in the reduction and dimerisation reactions. The values of n were not corrected for blank solutions, but reduction of these solutions under the experimental conditions used produces only a small contribution for the cathodic current. Thus, the small deviations from unity can be attributed to residual charge from oxidation of traces of molecular oxygen or support electrolyte reductions.

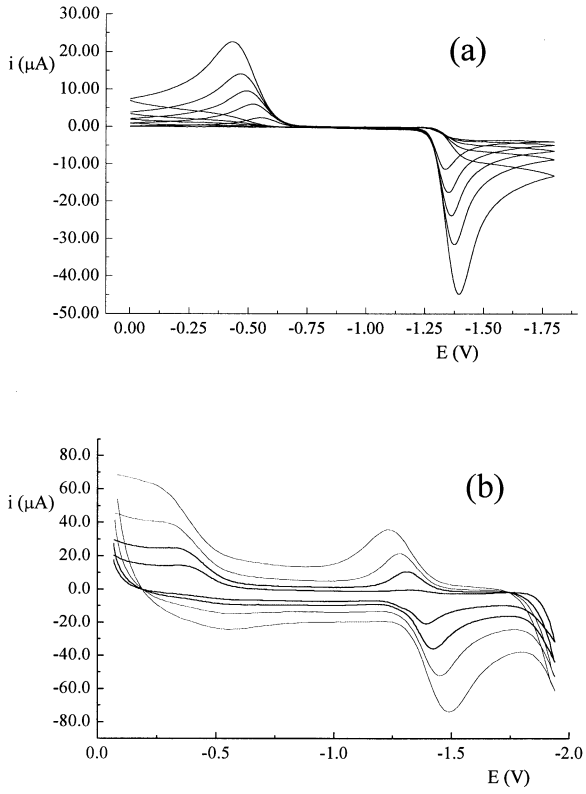


Fig. 1. Cyclic voltammograms of the complex [Ni(saloph)] (**8**) (group B) in dmf at scan rates in the range: (a) 0.02, 0.05, 0.10, 0.20 and 0.5 V s^{-1} and (b) 5, 10, 20, and 40 V s^{-1}.

2.3. EPR and electronic spectroscopy of reduced species

Analysis of electrochemical data has shown that all complexes of group **A** and **B** are reduced by an electron charge transfer process, but that different species are produced by complexes with aromatic and non-aromatic imine bridges, a consequence of different reduction processes. Coupling EPR and electronic spectroscopy provides further characterisation of the reduced species.

It must be pointed out that all complexes were also reduced with Na(Hg) and in the same solvents used for coulometric reductions. As the resulting solutions have the same colours and identical frozen solution EPR spectra it is possible to conclude that the same reduced species are formed by chemical and electrochemical reduction. The following description is thus applicable to chemically and electrochemically reduced nickel(II) complexes.

Frozen solution EPR spectra of reduced species from group **A** in any of the solvents are very similar, and show large g tensor anisotropy with $g_{av} \approx 2.12$–2.15, typical of metal centred reduced species, in this case nickel(I) complexes. The spectra of reduced solutions of **1**–**5** are rhombic and exhibit hyperfine splittings in the two high magnetic field regions ($a \approx 0.6$–1.0 mT) due to the interaction of the unpaired electron with two nitrogen atoms of the polydentate ligand (Fig. 2(a)). For reduced **6** and **7**, the EPR spectra are apparently axial, with no detectable hyperfine splittings in any g region (Fig. 2(b)).

In the absence of single crystal EPR measurements for these complexes, the observed similarity between the g features from both type of spectra with those of other Ni(I) complexes with similar ligands and with tetraaza macrocyclic ligands, [10–13] and of analogous isoelectronic d^9 Cu(II) complexes, [14–16] can be taken as support for the following orientation scheme for tensor axes in complexes **1**–**7**: $g_1 = g_z$, $g_2 = g_x$ and $g_3 = g_y$, where g_1 and g_3 refer to the lowest and highest magnetic field values, respectively (obviously, $a_1 = a_z$; $a_2 = a_x$ and $a_3 = a_y$). The observation that $g_z > g_x$; g_y implies a $B_{1g}(d_{xy})^1$ ground state for all the Ni(I) complexes [17–21]. All EPR spectra were manipulated and simulated as described in the Section 4; EPR parameters are summarised in Table 2. Spectra of each complex are practically independent of the solvent used, thus providing an indication that the reduced nickel complexes keep their four-coordinate geometry.

Analysis of the g and a(N) values show that complexes **1**–**5**, which possess an ethylenediimine based bridge, exhibit very similar values, but that their g values are smaller and their a(N) are larger than those of complexes with three and four atoms in the imine bridge (**6** and **7**). By taking into account data for Cu(II) complexes, [22] this observation provides an indication that the Ni(I) complexes with a long diimine bridge exhibit larger tetrahedral distortions than those with ethylenediimine based bridges (**1**–**5**). Additional indirect evidence for the larger tetrahedral distortion of Ni(I) complexes **6** and **7**, can be gathered from the existence of larger distortions in the corresponding Ni(II) complexes, as observed in the crystallographic structures of the latter complexes [23,24].

Frozen EPR spectra of electro-reduced complexes of group **B** (**8**–**9**) are quite different: they exhibit a low intensity pseudo isotropic signal at $g \approx 2.007$–2.010 (Fig. 2(c)), assigned to a radical, which provides an indication that reduction of these complexes involves ligand based processes. The low intensity isotropic signal must thus be due to monomeric Ni(II) radical species present in solution, probably a consequence of the existence in solution of an equilibrium between monomeric and dimeric species.

Electronic spectra of the Ni(I) species obtained by reduction of the corresponding Ni(II) complexes can also be divided into two sets. Spectra of reduced complexes **8**–**9** are similar to those of the parent Ni(II) complexes, thus suggesting a similar electronic structure in dimeric complex.

On the other hand, electronic spectra in dmf of all Ni(I) species obtained by reduction of **1**–**7**, are practically identical for all complexes and comparable to those

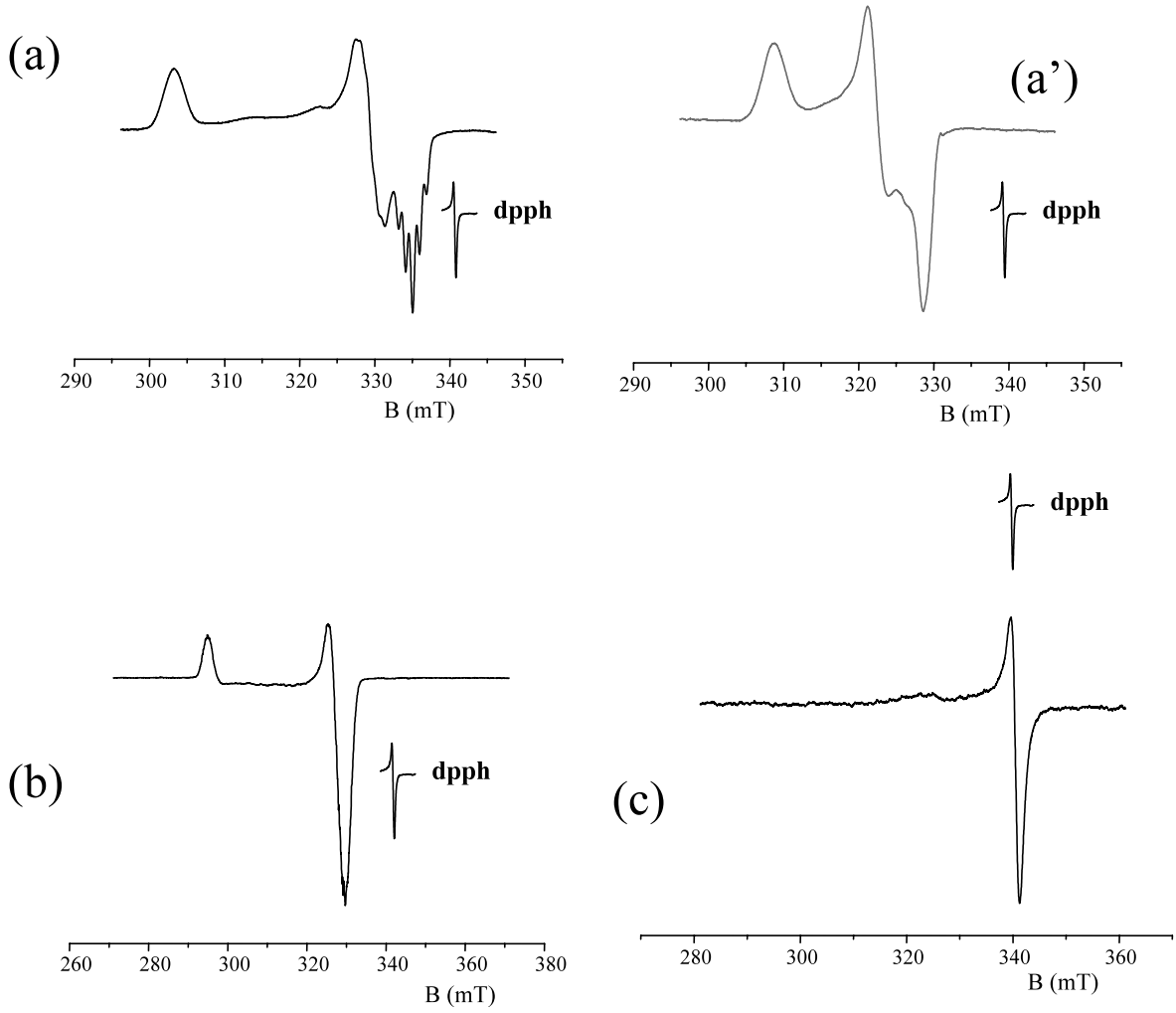


Fig. 2. Frozen solution EPR spectra of the reduced species in dmf (−120 °C): (a) $[Ni(\alpha,\alpha'\text{-}Me_2salen)]^-$; (b) $[Ni(salbd)]^-$ and (c) $[Ni(saloph)]_2^{2-}$ in N_2 atmosphere and (a′) $[Ni(\alpha,\alpha'\text{-}Me_2salen)]^-$ in CO atmosphere.

of similar Ni(I) compounds described in literature [13,25–29]; they show a medium intensity band at $\lambda = 800–830$ nm ($\varepsilon = 1100–1800$ dm^{-3} mol^{-1} cm^{-1}) with a shoulder at higher energies $\lambda = 637–760$ nm ($\varepsilon = 3200–5100$ dm^{-3} mol^{-1} cm^{-1}), and high-intensity bands in the UV region $\lambda < 400$ ($\varepsilon > 10\,000$ dm^{-3} mol^{-1} cm^{-1}) (Fig. 3(a) and Table 2). On the basis of their extinction coefficients the low energy band can be tentatively assigned to a d–d transition, albeit with a large contribution from ligand orbitals, and the shoulder at higher energy to charge transfer bands. The wavelength of the d–d band in spectra of reduced species is bathochromic shifted by about 30% relative to the d–d transitions of the precursor Ni(II) complexes, which occur in the range $\lambda = 550–500$ nm (Table 2) [13,25–29]. This indicates a weakening in the ligand field caused by the decrease in effective nuclear charge of the metal centre concomitant with its reduction. The extinction coefficients for Ni(I) complexes are usually much larger than those observed for similar Ni(II) complexes which is attributed to a large degree of covalency in the metal–ligand bonds (see below) [13,25–29].

Using the splitting scheme proposed by Nishida et al. [30,31] for the d-orbitals in isoelectronic square–planar copper(II) complexes with di-negatively charged tetradentate ligands, $d_{x^2-y^2} < d_{z^2} < d_{xz} \leq d_{yz} < d_{xy}$, and assuming the same d-splitting for the isoelectronic Ni(I) complexes used in this work, the low energy band in each spectrum can be assigned to the transition $d_{xz} \approx d_{yz} \leftarrow d_{x^2}$.

Confirmation for this assignment is provided by EPR data. Ni(I) complexes are at best of D_{2h} symmetry and using the g equations deduced for d^9 systems with B_{1g} ground state, the values of σ and π-out-of plane covalency parameters, α^2 and δ'^2, respectively, can be estimated from the g_x and g_y values [18–21]. This calculation was made using the methodology outlined in [13], with the further assumption that the low-energy electronic band corresponds to the transition $d_{xz} \approx d_{yz} \leftarrow d_{z^2}$. The values of these parameters, summarised

Table 2
EPR parameters and electronic data for nickel reduced species

Complex	Solvent	g_z	g_x	g_y	g_{av} [a]	A_z(N) [b]	A_x(N) [b]	A_y(N) [b]	λ_{max} (ε/M^{-1} cm^{-1}) [c]	λ_{max} nm (ε/M^{-1} cm^{-1}) [d]	α^2	δ'^2
[Ni(salen)]$^-$	CH_3CN	2.264	2.084	2.043	2.131							
	dmf	2.250	2.081	2.040	2.124	0.82	0.94	0.98	806 (1700); 637 (5100)	540 (230)	0.81	0.48
	$(CH_3)_2SO$	2.261	2.086	2.044	2.130							
[Ni(saltMe)]$^-$	CH_3CN	2.264	2.084	2.046	2.132							
	dmf	2.253	2.081	2.041	2.125	0.82	0.94	0.96	820 (1800); 668 (5000)	545 (160)	0.80	0.49
	$(CH_3)_2SO$	2.250	2.081	2.040	2.124							
[Ni(Cl_2-saltMe)]$^-$	CH_3CN	2.273	2.088	2.047	2.136							
	dmf	2.252	2.080	2.040	2.124	0.82	0.93	0.96	819 (1750); 668 (4700)	545 (180)	0.79	0.49
	$(CH_3)_2SO$	2.273	2.088	2.047	2.136							
[Ni(salhd)]−	CH_3CN	2.266	2.083	2.044	2.131							
	dmf	2.254	2.081	2.041	2.125	0.81	0.92	0.96	803 (1880); 663 (4900)	540 (200)	0.81	0.49
	$(CH_3)_2SO$	2.267	2.085	2.045	2.132							
[Ni(α,α′-Me_2salen)]−	CH_3CN	2.263	2.077	2.042	2.127							
	dmf	2.255	2.076	2.041	2.124	0.78	0.88	0.96	828 (1500); 674 (4600)	545 (190)	0.74	0.53
	$(CH_3)_2SO$	2.263	2.077	4.042	2.127							
[Ni(salpd)]−	CH_3CN	[e]										
	dmf	2.300	2.083	2.055	2.146	0.71	0.73	0.76	807 (1200); 672 (3500)	500 (140)	0.83	0.65
	$(CH_3)_2SO$	2.304	2.084	2.058	2.149							
[Ni(salbd)]−	CH_3CN	[e]										
	dmf	2.314	2.088	2.070	2.157	0.60	0.63	0.69	805 (1100); 763 (3200)	505 (140)	0.88	0.79
	$(CH_3)_2SO$	2.322	2.094	2.076	2.164							
$[Ni(saloph)]_2^{2-}$	CH_3CN				2.010 [f]						[g]	
	dmf				2.007 [f]				622 (60); 462 (1200)	575 (240); 475 (8400)	[g]	
	$(CH_3)_2SO$				2.010 [f]						[g]	
[Ni(saloph-Cl_2)] $^2_2$	CH_3CN				2.009 [f]						[g]	
	dmf				2.006 [f]				620 (75); 465 (1500)	565 (260); 485 (9200)	[g]	
	$(CH_3)_2SO$				2.010 [f]						[g]	

[a] g_{av} is calculated as $1/2(g_x+g_y+g_z)$.
[b] A_N(N) are expressed in mT and have been obtained as described in Section 4.2; only in dmf the spectra have the appropriate resolution.
[c] The electronic bands have been deconvoluted with the program ORIGIN.
[d] Refers to parent Ni(II) complexes.
[e] The complexes are not soluble in this solvent.
[f] The signal is pseudo isotropic and the value corresponds to g_{av}.
[g] No metal reduction occurs.

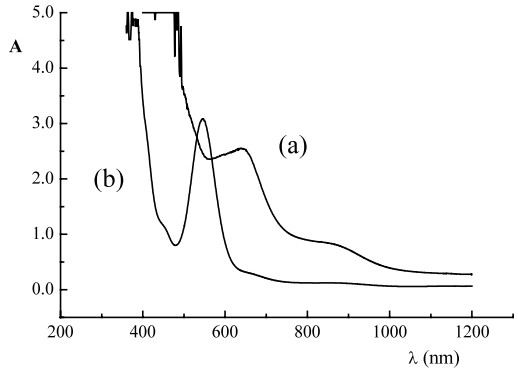


Fig. 3. UV–Vis spectra in dmf of $[Ni(salen)]^-$ (1 mmol dm^{-3}) in: (a) N_2 and (b) CO atmospheres.

in Table 2, compare with those observed for other Ni(I) complexes with similar ligands [11–13,32,33] which provides indirect support for the assignment. The values indicate that covalency is greater for the π-out-of plane bonding, suggesting large π delocalisation between the ligand and the metal centre. The lower planarity of the Ni(I) complexes with a long aliphatic diimine bridge (**6**, **7**) is also evidenced by the larger values calculated for δ'^2.

2.4. Reactivity of reduced species towards Lewis bases

No changes in the frozen EPR spectra or electronic spectra were observed upon addition of pyridine, imidazole or triphenylphosphine (in stoichiometric or excess molar ratio) to nickel reduced solutions, either freshly electrolysed or chemically reduced, an indication that neither these Ni(I) species interact with the strong Lewis bases, nor do the nickel(II) dimeric species. Probably the monodentate N and P donors ligands act as weaker π acceptors than the tetradentate ligand in stabilising the Ni(I) species.

2.5. Reactivity of reduced species towards carbon monoxide

The binding of CO, a stronger π acceptor ligand, with complexes **1**–**9** was assessed by studying the reduction process by cyclic voltammetry and coulometry under a CO atmosphere, and the reduced species were characterised by EPR and electronic spectroscopy.

2.6. Cyclic voltammetry and electrolysis

No changes were observed in the cyclic voltammograms of complexes of group **B** (**8**, **9**) obtained under a CO atmosphere when compared with those under a nitrogen atmosphere. This suggests no interaction between CO and the nickel species, and corroborates further that reduction of group **B** complexes does not involve the metal centre. Contrastingly, the voltammograms of group **A** complexes are slightly different from those in a nitrogen atmosphere: a reduction process is always observed, but (i) the ΔE values are larger; (ii) the values of ΔE increase significantly with increasing scan rates; and (iii) the i_{pa}/i_{pc} ratios are smaller than 1, which suggests a slow reaction between the nickel species and CO [6,7].

In order to get further information on the interaction of CO with reduced complexes of **1**–**7**, electrolysis of the Ni(II) complexes were made in a CO atmosphere. During the electrolysis a change in colour was observed from red to crimson, which differs from the dark blue–green colour of the reduced species in a nitrogen atmosphere, indicating the presence of different species in solution. Cyclic voltammograms obtained after electrolysis show one reduction process with $\Delta E = 60$–70 mV at $v = 50$ mV s^{-1}, and with $i_{pa}/i_{pc} = 1$, but with $E_{1/2}$ at slightly more positive potentials than those observed in a N_2 atmosphere. In Table 3 are summarised the electrochemical data for the complexes in CO atmosphere. The new electrochemical process corresponds to reduction of nickel species with axial coordinated CO; the more positive $E_{1/2}$ values imply that coordination of CO originates more stable Ni(I) species.

The difference between $E_{1/2}(N_2)$ and $E_{1/2}(CO)$ can be taken as a measure of the extent of CO coordination. From data in Tables 1 and 3 it is possible to infer that complexes with large tetrahedral distortions (**6** and **7**) show the weaker interactions with CO, and that complexes with ethylenic bridges, except those with axial substituents (**2**, **3** and **4**), exhibit the strongest interactions. These results suggest that the planarity of the coordination sphere $[(Ni^I)N_2O_2]^-$ plays an important role in the CO interaction with the nickel centre.

2.7. EPR and electronic spectroscopy of reduced species with bound CO

Frozen EPR spectra of nickel species with bound CO have g features similar to those obtained in a N_2 atmosphere, but with larger anisotropy and rhombicity ($g_{av} \approx 2.15$, $\Delta_{xy} \approx 0.06$–0.07). EPR data are summarised in Table 4, and an analysis of data in this table shows that the reduced species are still Ni(I) complexes with a $B_{1g}(d_{xy})^1$ ground state, as $g_z > g_x, g_y$. Furthermore, the observation that g_z and g_x have been shifted to lower magnetic field values and that no hyperfine splitting could be detected in any of the g regions (Fig. 2(a)) suggests that only one CO molecule is bound per nickel centre, leading to a square pyramidal geometry for the Ni(I) complexes, as a six-coordinate complex would have the g_z and g_x shifted to higher magnetic fields [14,22]. EPR spectra of the reduced species that interact less extensively with CO (**6**,**7**) show a sobreposition of the parent Ni(I) complex and the one with bound CO.

Table 3
Electrochemical data for nickel reduced complexes in CO atmosphere [a]

Complex	E_{pc} (V)	E_{pa} (V)	$-\Delta E$ (V)	$E_{1/2}$ (V)	$-i_{pc}$ (μA)	i_{pa} (μA)	$-i_{pc}/i_{pa}$
[Ni(salen)]$^-$	−1.610	−1.540	0.070	−1.575	4.02	3.94	1.02
[Ni(saltMe)]$^-$	−1.672	−1.598	0.075	−1.635	3.85	3.66	1.05
[Ni(Cl_2-saltMe)]$^-$	−1.363	−1.287	0.076	−1.325	4.12	4.03	1.02
[Ni(salhd)]$^-$	−1.639	−1.561	0.078	−1.600	3.75	3.53	1.06
[Ni(α,α′-Me_2salen)]$^-$	−1.698	−1.631	0.067	−1.665	4.32	4.29	1.00
[Ni(salpd)]$^-$	−1.374	−1.296	0.078	−1.335	3.06	2.75	1.11
[Ni(salbd)]$^-$	−1.410	−1.330	0.080	−1.370	2.94	2.68	1.10
[Ni(saloph)]$_2^{2-}$	[b]						
[Ni(saloph-Cl_2)]$_2^{2-}$	[b]						

[a] Data obtained in dmf at 0.050 V s^{-1}.
[b] No changes were observed in the voltammogram obtained under a CO atmosphere.

Electronic spectra of these CO bound Ni(I) complexes are quite different from those of their parent complexes and show one intense electronic band at $\lambda_{max} = 546$ nm ($\varepsilon = 5000$–6900 dm^{-3} mol^{-1} cm^{-1}) and several high intense bands in the UV region (Fig. 3). The new band in the visible region occurs at the same energy for all the complexes and taking in account their extinction coefficient they can be assigned to a M→CO charge transfer band and is indicative of the high π acceptor capacity of CO. The non-observation of any d–d band can be accounted for by a combination of two factors. First, the energy of the d–d bands is increased due to the high ligand field of CO; second, that of the CT bands is decreased due to the high π acceptor capacity of CO. As a consequence the CT bands that occur in the same region mask less intense d–d bands.

3. Concluding remarks

Species generated by one-electron electrochemical reduction of the nickel(II) Schiff base complexes reported in this work were characterised by combining EPR and UV–Vis–NIR spectroscopy and the results obtained allow for unambiguous identification of the electron transfer site. Reduction of nickel complexes was found to be solvent independent, but on the other hand the final reduction product depends largely on the ligand diimine bridge. Complexes with aromatic diimine bridges, (Group **B**), yielded ligand-centred reduced species, whereas those with aliphatic imine bridges, (group **A**), exhibit metal-centred reduction processes. Furthermore, the observation that the $E_{1/2}$ values for all complexes are practically solvent independent implies that the solvent does not participate in the charge transfer process, and indicates that the reduced nickel species must keep their tetracoordinate geometry. This result must be contrasted with the oxidation process of the same complexes, for which the solvent has a marked influence on oxidation site (metal vs. ligand), with good donor solvents favouring formation of Ni(III) complexes [34–39].

As referred above the extent of unsaturation not only is critical in controlling the ultimate reduction site, but influences also the $E_{1/2}$ values, as complexes with greater unsaturation exhibit the more positive values. Furthermore, the size of the imine bridge and the substituents in the ligand were also found to influence $E_{1/2}$ values. There is a pronounced positive shift in $E_{1/2}$ values when the number of carbon atoms in the aliphatic chain of the

Table 4
EPR values and electronic bands in CO atmosphere in dmf

Complex	g_z	g_x	g_y	g_{av} [a]	λ_{max}/nm (ε/M^{-1} cm^{-1}) [b]
[Ni(salen)]$^-$	2.307	2.104	2.044	2.152	546 (6800)
[Ni(saltMe)]$^-$	2.302	2.106	2.039	2.149	546 (6000)
[Ni(Cl_2-saltMe)]$^-$	2.303	2.107	2.040	2.150	546 (6900)
[Ni(salhd)]$^-$	2.305	2.086	2.056	2.149	546 (6200)
[Ni(α,α′-Me_2salen)]$^-$	2.308	2.111	2.035	2.151	546 (6800)
[Ni(salpd)]$^-$	2.295	2.114	2.052	2.154	545 (5000)
[Ni(salbd)]$^-$	2.294	2.121	2.044	2.153	546 (4600)
[Ni(saloph)]$_2^{2-}$				2.006 [c]	
[Ni(saloph-Cl_2)]$_2^{2-}$				2.007 [c]	

[a] g_{av} is calculated as $1/2(g_x + g_y + g_z)$.
[b] The electronic bands have been deconvoluted with the program ORIGIN.
[c] There is no interaction of the reduced species with CO, the signal corresponds to that observed in the absence of CO.

imine bridge is increased. The larger hole sizes and larger tetrahedral distortions of [Ni(salpd)] (**6**) and [Ni(salbd)] (**7**), [23,24] make it easier to accommodate the size increase expected upon reduction of the metal and thus the more positive $E_{1/2}$ values.

The number, ring position and electronic characteristics of the substituents also influence the reductive properties of the complexes: introduction of chloride atoms increases the stability of the reduced state (comparison between **2** and **3**), whereas the introduction of methyl groups decreases the stability of reduced complexes (comparison of **1** and **2** with **7**). This behaviour is attributed to changes in the electronic density in the metal centre induced by the substituents. In the absence of steric effects, electron-withdrawing substituents decrease electron density on the metal making it easier to reduce, whereas electron donating groups will have the opposite effect. The position of the methyl groups in the ligand is also important, as introduction of two methyl groups in the imine carbon fragment, –C=N, shifts the $E_{1/2}$ to more negative values than four methyl groups in the aliphatic imine bridge.

Due to the large π delocalisation between the Ni(I) and thepolydentate ligands (as quantified by σ and π-out-of plane covalency parameters, α^2 and δ'^2), no interaction with monodentate N and P donor Lewis bases could be observed. However, with a stronger π acceptor like CO, a strong interaction was observed and more stable Ni(I) species were formed as proved by their more positive $E_{1/2}$ values and lower energy charge transfer bands.

4. Experimental

4.1. Reagents, solvents and nickel(II) complexes

The solvents for syntheses were of reagent grade (Merck), and those for spectroscopic and electrochemical measurements were of analytical grade (Merck, pro analysi); all were used as received. Tetra-*n*-butylammonium perchlorate (TBAP) was prepared by published procedures from tetrabutylammonium chloride (Aldrich) and perchloric acid (Merck, p.a.) and recrystallised twice from ethanol [40] (CAUTION: perchlorates are hazardous and may explode). Carbon monoxide gas was purchased from Praxair.

The nickel(II) complexes [Ni(salen)] (**1**), [Ni(saltMe)] (**2**), [Ni(salhd)] (**4**), [Ni(salpd)] (**5**) and [Ni(α,α′-Me_2salen)] (**7**), [Ni(saloph)] (**8**), [Ni(saloph-Cl_2)] (**9**) have been prepared and fully characterised in [35,36]. The complexes [Ni(Cl_4saltMe)] (**3**) and [Ni(salbd)] (**6**) have been prepared by standard methods [35,36] and characterised by elemental analysis: [Ni(Cl_4saltMe)], *bis*(3,5-tetrachlorosalicylaldehyde)tetramethylethylenediamine: $NiC_{16}H_{18}N_2O_2Cl_4$. *Anal*. Calc.: C, 40.8; H, 3.9; N, 5.9. Found: C, 40.2; H, 3.8; N, 5.5%.

[Ni(salbd)], *bis*(salicylaldehyde)butylenediamine: $NiC_{18}H_{18}N_2O_2$. *Anal*. Calc.: C, 61.2; H, 5.1; N, 7.9. Found: C, 61.1; H, 5.0; N, 8.1%.

4.2. Physical measurements

Electrochemical measurements were performed using an EG&G PAR 273 potentiostat–galvanostat using solutions 1 mmol dm^{-3} in nickel(II) complex and 0.1 mol dm^{-3} TBAP. Cyclic voltammograms were obtained in a standard one-compartment electrochemical cell using a platinum-disc electrode (area of 0.0314 cm^2) as working electrode, a platinum gauze as the counter electrode and an Ag–AgCl (1 mol dm^{-3} NaCl) reference electrode. All voltammograms were obtained without IR feedback compensation and measured potentials were not corrected for liquid junction potentials. All potentials are reported relative to that of the Ag–AgCl (1 mol dm^{-3} NaCl) reference electrode and to $E_{1/2}$ of the ferrocenium–ferrocene couple. Cyclic voltammetry was performed in Me_2SO, dmf and MeCN in the potential range -1.0– -2.0 V using scan rates 0.02–0.5 V s^{-1}; for complexes of group B scan rates in the range 5–60 V s^{-1} were also used. Under the experimental conditions used and for scan rate 0.05 V s^{-1}, $E_{1/2}$ (ΔE) for Fc^+–Fc couple are 0.50 V (0.09 V) in Me_2SO, 0.50 V (0.10 V) in dmf, and $E_{1/2} = 0.48$ V (0.085 V) in MeCN.

Controlled potential electrolysis was carried out under a N_2 or a CO atmosphere at a potential 0.1 V higher than the cathodic peak potentials. The electrochemical cell has two compartments: one for the platinum-gauze working electrode and the other for the platinum-gauze counter electrode, which are separated by a silica frit. A Ag–AgCl (1 mol dm^{-3} NaCl) reference electrode was used.

Room-temperature (r.t.) electronic spectra of nickel(II)–(I) complexes were recorded with a Schimadzu UV/3101PC spectrometer in the range 1500–200 nm. Solutions of nickel(II)–(I) complexes, under an atmosphere of N_2 or CO, were typically 1 mmol dm^{-3}.

The EPR spectra were obtained with an X-band Bruker ESP 300E spectrometer equipped with Bruker B-VT 2000 temperature accessory controller, in a dual cavity and using diphenylpicrylhydrazyl (dpph; $g = 2.0037$) as standard; the magnetic field was calibrated by use of Mn^{2+} in MgO. Typical experimental conditions used were: microwave power 10–15 mW, modulation amplitude 0.5 mT; modulation frequency 100 kHz. Spectra were recorded at -120 °C, using sealed quartz tubes and the reported EPR parameters were obtained by computer simulation, [41] using a rhombic g tensor. As the spectra in Me_2SO and CH_3CN have lower resolution than in dmf, the values of superhyperfine

splittings obtained for spectra in dmf were used to simulate spectra in the former solvents. Even for spectra in dmf the superhyperfine couplings with the ligand nitrogen atoms had to be obtained from second-derivative EPR spectra, after a Fourier transformation and the subsequent elimination of all high-frequency components with a cut off filter just above the typical frequency components of nitrogen hyperfine coupling. After back-transformation to the magnetic field space, the noise at high frequencies introduced by differentiation is eliminated.

4.3. Reduction of Ni(II) complexes

Nickel(I) species were generated in-situ by electrolysis or chemical reduction of 1 mmol dm^{-3} solutions of the corresponding nickel(II) complexes under strict anaerobic conditions. Electrochemical reduction was performed in all solvents used the procedure outlined above. Chemical reduction was performed in dimethylformamide using an excess of 5% sodium mercury amalgam. The solution–amalgam was stirred for 15 min, and a fast solution colour change was observed. The progress of the reduction was monitored by UV–Vis and EPR spectroscopy and was assumed to be complete (1 mmol dm^{-3} in Ni(I) species, at approximately 15 min), when no changes in intensity of the EPR signals and in the absorbance of electronic bands were detected.

Manipulations of nickel(I) species were carried out in a nitrogen atmosphere, by use of standard Schlenk techniques and/or of a glove box. Addition of pyridine, imidazole and triphenylphosphine to freshly electrolysed or chemically reduced solutions was performed under anaerobic conditions at r.t. The resulting solutions were immediately transferred to EPR tubes and frozen in liquid nitrogen. Adducts with CO were prepared by making the reduction (electrochemically and chemically) under a CO atmosphere.

Acknowledgements

This work was partially supported by the 'Fundação para a Ciência e Tecnologia', Lisboa, Portugal, through Project POCTI/32831/QUI/2000.

References

[1] (a) C. Gosden, K.P. Healy, D. Pletcher, J. Chem Soc. Dalton Trans. (1978) 972;
(b) C. Gosden, D. Pletcher, J. Organomet. Chem. 186 (1980) 401;
(c) K.P. Healey, D. Pletcher, J. Organomet. Chem. 161 (1978) 109;
(d) C. Gosden, J.B. Kerr, D. Pletcher, R. Rosas, J. Electroanal. Chem. 117 (1981) 101;
(e) J.Y. Becker, J.B. Kerr, D. Pletcher, R. Rosas, J. Electroanal. Chem. Interf. Electrochem. 117 (1981) 87.

[2] (a) A. Bakac, J.H. Espenson, J. Am. Chem. Soc. 108 (1986) 713;
(b) A. Bakac, J.H. Espenson, J. Am. Chem. Soc. 108 (1986) 719;
(c) A. Bakac, J.H. Espenson, J. Am. Chem. Soc. 108 (1986) 5353;
(d) M.S. Ram, A. Bakac, J.H. Espenson, Inorg. Chem. 25 (1986) 3267;
(e) N. Sadler, S.L. Scott, A. Bakac, J.H. Espenson, Inorg. Chem. 28 (1989) 3951.

[3] (a) G.K. Lahiri, L.J. Schussel, A.M. Stolzenberg, Inorg. Chem. 31 (1992) 4991;
(b) K.M. Kadish, M.M. Franzen, B.C. Han, C. Araullo-McAdams, D. Sazou, Inorg. Chem. 31 (1992) 4399.

[4] (a) B. Fischer, R. Eisenberg, J. Am. Chem. Soc. 102 (1980) 7361;
(b) M. Beley, J.P. Collin, R. Rupert, J.P. Sauvage, J. Am. Chem. Soc. 108 (1986) 7641;
(c) J.B. Collin, A. Jouaiti, J.P. Sauvage, Inorg. Chem. 27 (1988) 1986.

[5] A.A. Isse, A. Gennaro, E. Vianello, Electrochim. Acta 37 (1992) 113.

[6] A.J. Bard, L.R. Faulkner, Electrochemical Methods. Fundamentals and Applications, 2nd ed., Wiley, New York, 2001.

[7] R.S. Nickolson, Anal. Chem. 37 (1965) 178.

[8] S. Gambarotta, C. Floriani, A. Chiesi-Villa, C. Guastini, J. Chem. Soc., Chem. Commun. (1982) 756.

[9] S. Gambarotta, F. Urso, C. Floriani, A. Chiesi-Villa, C. Guastini, Inorg. Chem. 22 (1983) 3966.

[10] F. Azevedo, M.A.A.F. De, C.T. Carrondo, M. Coney, B. de Castro, D. Domingues, M.T. Duarte, C. Freire, K. Nielsen, I. Santos, Inorg. Chim. Acta 112 (1994) 1634.

[11] G.A. Bowmarker, P.D.W. Boyd, G.K. Campbell, J.H. Hop, Inorg. Chem. 21 (1982) 1152.

[12] G.A. Bowmaker, G.A. Boyd, G.K. Campbell, M. Zvagulis, J. Chem. Soc., Dalton Trans. (1986) 1065.

[13] M. Valente, C. Freire, B. de Castro, J. Chem. Soc., Dalton Trans. (1998) 1557.

[14] J. Maroney, N.J. Rose, Inorg. Chem. 23 (1984) 2252.

[15] A.D. Toy, M.D. Hobday, P.D.W. Boyd, J. Chem. Soc., Dalton Trans. (1973) 1259.

[16] M. Chikira, H. Yokoi, T. Isobe, Bull. Chem. Soc. Jpn. 47 (1974) 2208.

[17] A.H. Maki, N. Edelstein, A. Davison, R.H. Holm, J. Am. Chem. Soc. 86 (1964) 4580.

[18] A.H. Maki, B.R. McGarvey, J. Chem. Phys. 29 (1958) 31.

[19] A.H. Maki, B.R. McGarvey, J. Chem. Phys. 29 (1958) 39.

[20] R. Neiman, D. Kivelson, J. Chem. Phys. 35 (1962) 149.

[21] H.G. Gersmann, J.D. Swalen, J. Chem. Phys. 36 (1962) 3221.

[22] U. Sakaguchi, A.W. Addison, J. Chem. Soc. (1979) 600.

[23] M.G.B. Drew, R.N. Prasad, R.P. Sharma, Acta Crystallogr. Sect. C 41 (1985) 1755.

[24] M. Calligaris, G. Nardin, L. Randaccio, Coord. Chem. Rev. 7 (1972) 385.

[25] A.M. Stolzenberg, M.T. Stershic, J. Am. Chem. Soc. 110 (1988) 5397.

[26] L.R. Furenlid, M.W. Renner, K.M. Smith, J. Fajer, J. Am. Chem. Soc. 112 (1990) 1634.

[27] M.P. Sugh, I.S. Kim, S.J. Cho, W. Shin, J. Chem. Soc., Dalton Trans. (1994) 2765.

[28] M.P. Suh, Adv. Inorg. Chem. 44 (1996) 93.

[29] D.J. Szalda, E. Fijita, R. Sanzenbacher, H. Paulus, H. Elias, Inorg. Chem. 33 (1994) 5855.

[30] Y. Nishida, K. Hayashida, A. Sumita, S. Kida, Inorg. Chim. Acta 31 (1978) 19.

[31] Y. Nishida, K. Hayashida, S. Kida, J. Coord. Chem. 10 (1980) 101.

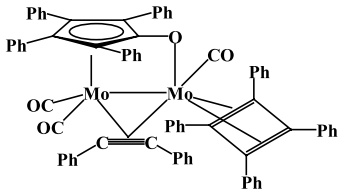
[32] M.C.R. Symmons, D.X. West, J. Chem. Soc., Dalton Trans. (1985) 379.

[33] P.J. Chmielewski, L. Latos-Grazynski, E. Paholska, Inorg. Chem. 33 (1994) 1992.
[34] M. Vilas Boas, C. Freire, B. de Castro, P.A. Christensen, A.R. Hillman, Inorg. Chem. 36 (1997) 4919.
[35] C. Freire, B. de Castro, J. Chem. Soc., Dalton Trans. (1998) 1491.
[36] C. Freire, B. de Castro, Polyhedron 17 (1998) 4227.
[37] M. Vilas-Boas, C. Freire, B. de Castro, A.R. Hillman, J. Phys. Chem. B 102 (1998) 8533.
[38] M. Vilas Boas, M.J. Henderson, C. Freire, A.R. Hillman, E. Vieil, Chem. Eur. J. 6 (2000) 1160.
[39] I.C. Santos, M. Vilas-Boas, F. Piedade, C. Freire, M. Teresa Duarte, B. de Castro, Polyhedron 19 (2000) 655.
[40] S.T. Donald, R.L. Julien, Experimental Electrochemistry for Chemistry, Wiley, New York, 1974.
[41] J.R. Pilbrow, M.E. Winfield, Mol. Phys. 25 (1973) 1073.

$$[Mo(CO_6])\ \text{or}\ [Mo(CO_3(\text{diglyme})] + \text{excess}\ C_2Ph_2 \xrightarrow{16\ \text{atm}/160\ C/\ \text{benzene}} [Mo(C_5Ph_5)_2]$$

$$[Mo(CO_3)(\text{toluene})] + 5\,C_2Ph_2 \xrightarrow{1\ \text{atm}/98\ C/\ \text{heptane}} [Mo(C_5Ph_5)_2]$$

Scheme 1.



(II)

In both syntheses, the yield of decaphenylmolybdenocene is very low (~ 5%). Decaphenylmolybdenocene is quite stable towards air and moisture, and is sparingly soluble in all common solvents. However, it can easily be oxidised by bromine in dichloromethane to a product formulated as decaphenylmolybdenocenium tribromide. This compound can be reduced to decaphenylmolybdenocene by magnesium in a mixture of dichloromethane and methanol. Both molybdenum compounds were characterised only by elemental analyses, magnetic susceptibility and melting point determination [29,30]. The reaction chemistries of decaphenylmolybdenocene and its cation have not been reported.

In contrast, then, to the unknown $[Mo(C_5H_5)_2]$ and to '$[Mo(C_5Me_5)_2]$', the compound formulated as $[Mo(C_5Ph_5)_2]$, decaphenylmolydenocene, although produced only in low yield, is remarkably stable, being indefinitely stable in air [29,30].

Because of their low solubilities, only one of the transition metal decaphenylmetallocenes, $[Fe(\eta^5\text{-}C_5Ph_5)_2]$, has been structurally characterised and even in that case, the structure failed to refine well, although the metallocene structure is clear [32]. However, even the seemingly simple $[Fe(\eta^5\text{-}C_5Ph_5)_2]$ can also exist as its linkage isomer, $[Fe(\eta^5\text{-}C_5Ph_5)_2]$ $[Fe\{(\eta^6\text{-}C_6H_5)C_5Ph_4\}]$ [33], and both $[Fe(C_5Ph_5)_2]$ isomers have been shown to undergo complicated series of isomerisations/protonations/deprotonations in the solid state and in solution [33–35]. We have remarked previously [36] that the $[M(\eta^5\text{-}C_5Ph_5)_2]$ conformation can be distinguished from the isomeric $[M\{(\eta^6\text{-}C_6H_5)C_5Ph_4)\}(\eta^5\text{-}C_5Ph_5)]$ [33] on the basis of a set of strong absorptions at approximately 1500, 741, 713 and 699 cm^{-1} in the infrared spectrum of the former. However, this diagnosis was unknown at the time of the synthesis of $[Mo(C_5Ph_5)_2]$ and in any case, no infrared data were reported. Thus, although there is no reason to suspect that $[Mo(C_5Ph_5)_2]$ has other than a metallocene structure, $[Mo(\eta^5\text{-}C_5Ph_5)_2]$, nor is it obvious that it has. However, clearly the strict analogue of $[Mo(\eta^5\text{-}C_5Me_5)(\eta^6\text{-}C_5Me_4CH_2)H]$ is not possible in the pentaphenylcyclopentadienyl system.

In contrast to $[Mo(\eta^5\text{-}C_5Me_5)(\eta^6\text{-}C_5Me_4CH_2)H]$, $[Mo(C_5Ph_5)_2]$, has been oxidised by bromine to $[Mo(C_5Ph_5)_2]Br_3$, which can be reduced to $[Mo(C_5Ph_5)_2]$ by magnesium turnings [30]. $[Mo(C_5Ph_5)_2]Br_3$ is the first, and is still the only, 'decaphenylmetallocenium' salt of the second and third transition metals. The structures of decaphenylmetallocenium salts of Cr, Fe, Co and Ni have all been determined and the cations shown to adopt the $[M(\eta^5\text{-}C_5Ph_5)_2]^+$ configuration [36–38].

Accordingly, we report here the crystal structure and so preliminary cyclic voltammetric data for 'decaphenylmolybdenocenium' tribromide.

1. Results and discussion

Decaphenylmolybdenocene was prepared by the method of Holtzapple [30]. Although we explored several other possible routes, this synthesis, although low yielding, was still the most convenient preparation of decaphenylmolybdenocene, which was obtained as a red solid, insoluble in all common solvents.

Several unsuccessful attempts were made to find alternative, higher yielding, routes to decaphenylmolybdenocene. For example, reactions of $Mo(OAc)_2$ or $MoCl_5$ with $Li(C_5Ph_5)$, of $Mo(CO)_6$ or $[Mo(CO)_3(CH_3CN)_3]$ with C_5Ph_5Br did not produce the desired decaphenylmolybdenocene.

Decaphenylmolybdenocene was isolated as a bright-red air stable solid identified as $[Mo(C_5Ph_5)_2]$ by conversion to $[Mo(C_5Ph_5)_2]^+$ salts, and by comparison of its infrared and mass spectra with those of other decaphenylmetallocenes. It is sparingly soluble in most solvents. The infrared spectrum of decaphenylmolybdenocene we prepared by the method of Holtzapple [30] contains strong absorptions at 1500, 739 s, 711 vs, and 700 vs cm^{-1}. The presence of these absorptions in the infrared spectrum of $[Mo(C_5Ph_5)_2]$ suggests [36] that $[Mo(C_5Ph_5)_2]$ does indeed have the bis-pentahapto, decaphenylmetallocene, structure, $[Mo(\eta^5\text{-}C_5Ph_5)_2]$, rather than the mixed η^5, η^6 structure of the linkage isomer. In this respect, it represents the first molybdenum metallocene stable under ambient conditions.

The compound previously formulated as $[Mo(C_5Ph_5)_2]Br_3$ was prepared by oxidation of $[Mo(C_5Ph_5)_2]$ with Br_2 in dichloromethane [29]. We have confirmed this synthesis and prepared $[Mo(C_5Ph_5)_2]BF_4$ by a route similar those used for its Cr, Fe, Co and Ni analogues [32,36–38]. Both

$[Mo(C_5Ph_5)_2]Br_3$ and $[Mo(C_5Ph_5)_2]BF_4$ could be reduced reversibly to the neutral species by magnesium turnings or by $NaBH_4$ in a mixture of methanol and dichloromethane. Both decaphenylmolybdenocenium salts are air-stable as solids and stable in dichloromethane, or under ether, hexane or pentane for a week without noticeable degradation. However, they were rapidly reduced to the neutral decaphenylmolybdenocene in solvents such as tetrahydrofuran, acetonitrile and methanol. No analogous reaction was found among other decaphenylmetallocenium complexes. In this respect, $[Mo(C_5Ph_5)_2]^+$ is more reactive than the other decaphenylmetallocenium cations reported to date.

1.1. Cyclic voltammetry

In view of the long standing and general interest in the electron transfer chemistry of metallocenes [39,40], the chemical reversibility of the $[Mo(C_5Ph_5)_2]^{+/0}$ couple, the absence of any data directly obtained from $[Mo(C_5R_5)_2]$ compounds (the datum for $[Mo(C_5H_5)_2]$ was obtained from a cyclic voltammogram of the solution generated by the irreversible two electron coulometric reduction of $[Mo(C_5Ph_5)_2Cl_2]$ [39]), the existence of, albeit very reactive, $[Cr(C_5H_5)_2]^-$, [41] and the synthetic utility of a variety of $[M(C_5R_5)_2]^{n\pm}$ ions, [42,43] it was of interest to examine the electron transfer reactions of $[Mo(C_5Ph_5)_2]^+$. Cyclic voltammograms of $[Mo(C_5Ph_5)_2]BF_4$ were obtained under similar conditions to those used to study other decaphenylmetallocene analogues. Two reversible redox processes at -0.46 and -1.92 V, corresponding to the $[Mo(C_5Ph_5)_2]^{+/0}$ and $[Mo(C_5Ph_5)_2]^{0/1-}$ couples, respectively, were observed.

Strelets et al. reported a value of -1.65 V for the $[Mo(C_5H_5)_2]^{+/0}$ couple which was observed by means of rapid scanning cyclic voltammetry in DMSO and by low-temperature voltammetry techniques in tetrahydrofuran [44]. The '$[Mo(C_5H_5)_2]$' was produced by the irreversible two-electron reduction of $[Mo(C_5H_5)_2Cl_2]$. However, given the generally small difference between the $E_{1/2}$ values of $[M(C_5H_5)_2]^{+/0}$ and $[M(C_5Ph_5)_2]^{+/0}$ couples, confirmation of this value would be useful. Literature values of the $E_{1/2}$ values of selected metallocenes, decamethyl-, nonaphenyl- and decaphenyl-metallocenes (converted to a common scale) are collected in Table 1. The generally more positive oxidation potentials of the $[M(\eta^5\text{-}C_5Ph_5)_2]$ compounds relative to their $[M(\eta^5\text{-}C_5Me_5)_2]$ analogues offers some rationalization for the very high reactivity of $[Mo(\eta^5\text{-}C_5Me_5)_2]$ which might be expected to be very easily oxidised [26].

The decaphenylmolybdenocium cation, $[Mo(C_5Ph_5)_2]^+$ is a moderately good oxidant. The anion, $[Mo(C_5Ph_5)_2]^-$, may be a useful reductant. However, since any synthetic applications of these reagents are likely to require a higher-yielding synthesis, this chemistry was not pursued.

1.2. X-ray diffraction

Air-stable crystals of $[Mo(C_5Ph_5)_2]BF_4$ were obtained as a dichloromethane and water solvate complex, $[Mo(C_5Ph_5)_2]BF_4\cdot 0.5CH_2Cl_2\cdot 0.75H_2O$, similar to those of the chromium and cobalt analogues. The solvated salt crystallises in the space group $P\bar{1}$, isostructural with other decaphenylmetallocenium complexes (Table 2).

The structure and dimensions of $[Mo(C_5Ph_5)_2]^+$ are comparable to those of the known $[M(C_5Ph_5)_2]^+$ (M = Cr, Fe, Co and Ni) cations. The crystallographic data have been deposited.

Selected bond distances and angles for the $[Mo(C_5Ph_5)_2]^+$ cation (Fig. 1) are collected in Table 3.

The C_5 rings of each of the ligands are almost planar to within 0.0094 Å. The two ligand C_5 rings are parallel and adopt the staggered configuration observed for other decaphenylmetallocenium cations. The *ipso* carbon atoms of the phenyl rings are displaced on the opposite side of the C_5 plane (average 0.149 Å, range

Table 1
$[M(C_5R_5)_2]^{n+/(n-1)+}$ redox couples for selected metallocenes (cp = C_5H_5), decamethylmetallocenes (cp* = C_5Me_5), octaphenylmetallocenes and decaphenylmetallocenes (cp** = C_5Ph_5)

Metallocene	2+/+ couple	+/0 couple	0/− couple	Reference
[Vcp_2]	+0.28	−0.86	−3.05	[41]
[$Crcp_2$]		−0.98	−2.61	[3,41]
[$Mncp_2$]				
[$Fecp_2$]	+1.71	0.00	−3.25	[3,41]
[$Cocp_2$]		−1.26	−2.20	[3,41]
[$Nicp_2$]	+0.43	−0.40	−1.97	[3,41]
'[$Mocp_2$]'		−1.57		[39]
[$Rucp_2$]	+0.71	+0.57		[39]
[$Rhcp_2$]		−1.73	−2.50	[39]
'[Wcp_2]'		−1.80		[39]
[$Crcp^*_2$]		−1.35		[3]
[$Mncp^*_2$]		−0.87 (−0.95)		[56]
[$Fecp^*_2$]		−0.43 (−0.51)		[3,57]
[$Cocp^*_2$]		−1.78		[3]
[$Nicp^*_2$]		−0.96	−0.10	[3,56]
[$Rucp^*_2$]		+0.10 (+0.20)		[9,27,56,58]
[$Oscp^*_2$]		+0.08 (+0.15)		[9,56]
[Nicp*cp**]	+0.60	−0.30		[59]
[$Crcp^{**}_2$]		−0.95	−2.30 [b]	[36,60]
[$Fecp^{**}_2$]		−0.04		[34]
[$Cocp^{**}_2$]		−0.88	−1.74	[36,60]
[$Nicp^{**}_2$]	+0.51	−0.24	−1.95 [b]	[38,60]
[$Mocp^{**}_2$]		−0.46	−1.92	This work [a]
[$Cr(C_5HPh_4)_2$]		−0.87		[61]
[$Fe(C_5HPh_4)_2$]		+0.03		[61]
[$Co(C_5HPh_4)_2$]		−1.00		[61]
[$Ni(C_5HPh_4)_2$]	+0.30	−0.31	−1.77	[61]

Potentials (V) converted from literature values to a common scale in which the $[Fe(C_5H_5)_2]^{+/0}$ couple is assigned a potential of 0.00 V.

[a] Measured in CH_2Cl_2 scan rate 100 mV s^{-1}, glassy carbon working electrode, Ag/AgCl (3 M NaCl) reference electrode, 0.1 M tetrabutylammonium tetrafluoroborate, 100% IR compensation.

[b] Not reversible.

Table 2
Crystallographic parameters of the compounds $[M(\eta^5\text{-}C_5Ph_5)_2]X$ (M = Mo, Cr, Co, Ni; X = BF_4; M = Ni Fe; X = Br_3)

Compound	$[Mo(\eta^5\text{-}C_5Ph_5)_2]BF_4\cdot 0.5CH_2Cl_2\cdot 0.75H_2O$	$[Ni(\eta^5\text{-}C_5Ph_5)_2]Br_3$ [38]	$[Ni(\eta^5\text{-}C_5Ph_5)_2]BF_4\cdot CH_2Cl_2$ [38]	$[Fe(\eta^5\text{-}C_5Ph_5)_2]Br_3$ [38]	$[Cr(\eta^5\text{-}C_5Ph_5)_2]BF_4\cdot 0.5CH_2Cl_2\cdot 0.5H_2O$ [36]	$[Co(\eta^5\text{-}C_5Ph_5)_2]BF_4\cdot 0.5CH_2Cl_2\cdot 0.5H_2O$ [36]
Molecular formula of structure model	$C_{70.5}H_{50}BClF_4MoO_{0.75}$	$C_{70}H_{50}Br_3Ni\cdot CH_2Cl_2$	$C_{71}H_{52}BCl_2F_4Ni$	$C_{70}H_{50}Br_3Fe\cdot CH_2Cl_2$	$C_{70.5}H_{52}BCrF_4ClO_{0.5}$	$C_{70.5}H_{52}BF_4CoClO_{0.5}$
M	1127.37	1274.5	1121.6	1271.7	1079.42	1086.36
Crystal system	triclinic	triclinic	triclinic	triclinic	triclinic	triclinic
Space group	$P\bar{1}$	$P\bar{1}$	$P\bar{1}$	$P\bar{1}$	$P\bar{1}$	$P\bar{1}$
a (Å)	13.629(2)	13.597(2)	13.537(2)	13.599(5)	13.634(5)	13.633(2)
b (Å)	17.329(3)	17.682(2)	17.448(2)	17.700(6)	17.424(5)	17.683(3)
c (Å)	13.306(3)	13.254(3)	13.250(1)	13.225(4)	13.298(4)	13.255(3)
α (°)	105.70(2)	107.18(2)	106.88(1)	106.94(2)	106.45(2)	107.95(1)
β (°)	101.70(1)	101.15(2)	101.82(1)	101.22(3)	101.83(3)	102.71(1)
γ (°)	75.23(1)	71.93(2)	74.11(1)	72.06(2)	74.56(2)	73.23(1)
Z	2	2	2	2	2	2
U (Å^3)	2894	2876	2853.5(5)	2878(2)	2892(1)	2880(1)

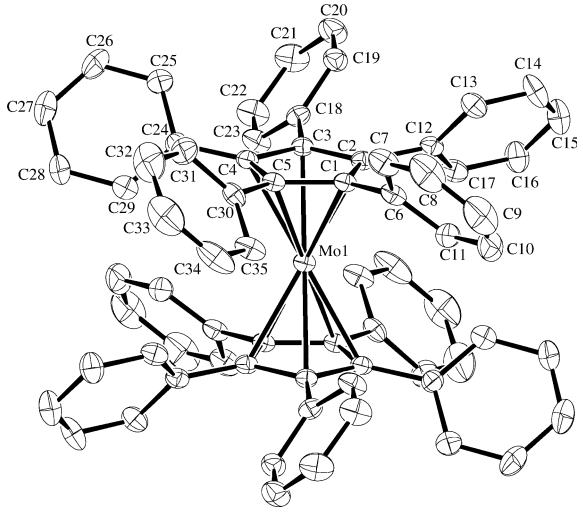


Fig. 1. ORTEP [45] (25% probability) illustration of the molecular structure of one cation of $[Mo(\eta^5\text{-}C_5Ph_5)_2][BF_4]$ showing the numbering scheme.

Table 3
Selected bond and Mo–r_{cent} distances (Å) and angles (°) for the $[(C_5Ph_5)_2Mo]^+$ cation

Bond lengths			
Mo(1)–r_{cent}	2.0414	Mo(2)–r_{cent}	2.0382
Mo(1)–C(1)	2.379(7)	Mo(2)–C(36)	2.370(7)
Mo(1)–C(2)	2.361(7)	Mo(2)–C(37)	2.368(7)
Mo(1)–C(3)	2.370(7)	Mo(2)–C(38)	2.389(7)
Mo(1)–C(4)	2.388(8)	Mo(2)–C(39)	2.379(7)
Mo(1)–C(5)	2.392(7)	Mo(2)–C(40)	2.362(8)
Average Mo–C	2.378(7)	Average Mo–C	2.374(7)
C(1)–C(2)	1.428(9)	C(36)–C(37)	1.419(10)
C(1)–C(5)	1.435(10)	C(36)–C(40)	1.443(10)
C(2)–C(3)	1.429(9)	C(37)–C(38)	1.429(10)
C(3)–C(4)	1.428(10)	C(38)–C(39)	1.428(10)
C(4)–C(5)	1.447(10)	C(39)–C(40)	1.43(1)
Average C–C	1.433(10)	Average C–C	1.430(8)
Bond angles			
C(2)–C(1)–C(5)	107.7(6)	C(37)–C(36)–C(40)	108.3(7)
C(1)–C(2)–C(3)	108.7(7)	C(36)–C(37)–C(38)	108.1(7)
C(2)–C(3)–C(4)	108.0(7)	C(37)–C(38)–C(39)	108.1(7)
C(3)–C(4)–C(5)	107.8(7)	C(38)–C(39)–C(40)	108.2(7)
C(1)–C(5)–C(4)	107.8(6)	C(36)–C(40)–C(39)	107.2(7)

0.132–0.173 Å) from the molybdenum atom. This value is the smallest among the known decaphenylmetallocenium cations due to the longer Mo–r_{cent} distance compared with those of known decaphenylmetallocenium cations (Table 4). The phenyl rings are canted at an average angle of 49.7° (range 44.6°–53.3°) with respect to the C_5 ring and adopt the 'paddle wheel' orientation. The average Mo–C (2.376 Å) and Mo–r_{cent} (2.040 Å) distances are the longest among the known decaphenylmetallocenium cations (Table 4) as expected for a second row metal with few valence electrons to occupy the bonding molecular orbitals. However, the Mo–r_{cent} and average Mo–C distances of the 15 electron $[Mo(C_5Ph_5)_2]^+$ cation are slightly shorter than those reported for the 18 electron half-sandwich complex $[Mo(C_5Ph_5)(CO)_3I]$ (2.042 and 2.378 Å, respectively) [46]. Further comparisons are not possible since no other molybdenocene derivatives or molybdenum complexes containing the (C_5Ph_5) ligand have been structurally characterised. The dimensions of the C_5 rings of the decaphenylmolybdenocenium cation are regular, similar to those observed in other decaphenylmetallocenium cations and the half-sandwich complex, $[Mo(C_5Ph_5)(CO)_3I]$.

Table 4
Comparison of selected average metric data for decaphenylmetallocenium cations of Mo, Cr, Fe, Co and Ni

$[M(\eta^5\text{-}C_5Ph_5)_2]^+$	M–(ring centroid) (Å)	Average M–C (Å)	C–C(C_5) (Å)	Reference
Mo	2.040	2.376	1.432	This work
Cr	1.935	2.282	1.429	[36]
Fe	1.810	2.164		[38]
Co	1.750	2.133	1.43	[36]
Ni	1.837	2.206	1.434	[38]

2. Conclusion

Decaphenylmolybdenocene exists in the solid state with two η^5-ligands, apparently isostructural with $[M(\eta^5\text{-}C_5Ph_5)_2]$ (M = Fe, Cr, Ni, Co) [37]. It undergoes a one electron oxidation and a one electron reduction, both of which are reversible on the cyclic voltammetric timescale and both of which occur at synthetically useful potentials. Oxidation to the decaphenylmolybdenocenium cation with Br_2 or NO^+ is near quantitative. The decaphenylmolybdenocenium cation exists as discrete $[Mo(\eta^5\text{-}C_5Ph_5)_2]^+$ units, with parallel C_5 rings of the two ($\eta^5\text{-}C_5Ph_5^-$) ligands and is thus isostructural with $[Mo(\eta^5\text{-}C_5Ph_5)_2]^+$ (M = Cr, Fe, Co, Ni) [36–38]. The $[Mo(\eta^5\text{-}C_5Ph_5)_2]^{n+}$ ($n = 0$, 1) compounds are unique amongst $[Mo(\eta^5\text{-}C_5R_5)_2]$ (R = H, Me, Ph) in having metallocene structures at r.t. The compounds may be useful as synthetic reagents if a higher yielding synthesis can be developed.

3. Experimental

All reactions were carried out at atmospheric pressure under an inert atmosphere of high purity argon (99.995%, CIG) or nitrogen (99.995%, CIG), unless otherwise stated, and manipulations were performed using conventional Schlenk techniques [47]. All solvents used were Analytical Reagent grade and were distilled under an atmosphere of nitrogen and used within 24 h. All solvents were degassed by bubbling with inert gas for at least 0.5 h before use. Tetrahydrofuran (Merck or Rhône–Poulenc) and diethylether (Merck) were predried over sodium wire, and distilled from sodium benzophenone ketyl. Toluene (BDH), was distilled from sodium wire. Dichloromethane (Rhône–Poulenc), was distilled from calcium hydride. Tetraphenylcyclopentadienone, tetramethylsilane, molybdenum hexacarbonyl, $NOBF_4$ (all Aldrich) were used as received. C_5Ph_5H and C_5Ph_5Br, were prepared as described previously [48]. Melting points were determined using a Gallenkamp Melting Point Apparatus in air and are uncorrected. Elemental analyses were carried out by one of the following departments: the Australian Microanalytical Service in Melbourne, the Microanalytical Service at the Australian National University or at the JEAF in The University of Sydney. Infrared spectra were recorded on a Digilab FTS-40 infrared spectrophotometer either as a solution or as a suspension in a potassium bromide matrix. The resolution used was 4 cm^{-1} and the number of scans was 16. ^1H NMR spectra (200.13 MHz) were recorded on a Bruker AC-200F spectrometer. Spectra were referenced internally to the residual solvent resonances [CD_2Cl_2 (δ 5.31 ppm)] or to tetramethylsilane (δ 0.00 ppm). Mass spectra were performed by Dr. X. Song of the School of Chemistry, University of Sydney. They were obtained via a direct insertion probe using an electron impact ion source at 200 °C (variations as required), 70 eV ionisation voltage and 8 kV acceleration voltage using a Kratos MS 902 double focussing mass spectrometer. Electrochemical experiments were performed using a BAS 100 W Electrochemical Analyser. The sample cell was fitted with a plastic top that could be sealed almost air-tight. A three-electrode configuration was used. The working electrode was a BAS glassy carbon disc (3 mm diameter) which was polished with an alumina (0.25 mm grade) suspension on a velvet polishing cloth, then rinsed with distilled water and acetone, and then dipped in the solvent of use for 1 min before each cyclic voltammogram was recorded. The auxiliary electrode was a platinum wire (0.5 mm diameter, 4 cm length) which did not need cleaning between voltammograms but was cleaned by rinsing with 5 M aqueous HNO_3, distilled water and the solvent used prior to each set of experiments. The reference electrode was a BAS Ag/AgCl/NaCl (3 M) electrode with a vycor frit. All samples were thoroughly degassed with high purity argon (CIG) which was passed through a scrubber and a drying tower to remove any traces of oxygen and water, respectively. All potentials are quoted relative to the ferrocenium/ferrocene redox couple, which was observed at approximately 500 mV against the reference electrode [Ag/AgCl/NaCl (3 M)]. Samples were prepared as approximately 1 mM solutions with tetra(*n*-butyl)-ammonium tetrafluoroborate (TBATFB approximately 0.1 M) as the supporting electrolyte. TBATFB was prepared either from aqueous HBF_4 (35% v/v, Merck) and (n-C_4H_9)NOH (40% w/w, Aldrich) or by recrystallisation of TBATFB (Aldrich) three times from ethyl

acetate/diethyl ether in air, then drying in vacuo. Full IR (100%) compensation was employed in each scan. All measurements were carried out in dichloromethane solution with 0.1 M TBATFB as the supporting electrolyte and a scan rate of 100 mV s^{-1}.

A black prismatic crystal of $[Mo(C_5Ph_5)_2]BF_4 \cdot 0.5CH_2Cl_2 \cdot 0.75H_2O$ having approximate dimensions of $0.38 \times 0.25 \times 0.17$ mm was attached to a thin glass fibre and mounted on an Enraf–Nonius CAD4 diffractometer employing graphite monochromated Mo Kα radiation generated from a sealed tube. Cell constants were obtained from a least-squares refinement using the setting angles of 25 reflections in the range $2\theta = 16.60°$ and 24.00°. Data were collected at a temperature of 21 ± 1 °C using ω–2θ scans to a maximum 2θ value of 49.96°. The intensities of three representative reflections measured every 60 min did not change significantly during the data collection. Lorentz and polarisation corrections were applied to the data. An empirical absorption correction based on azimuthal scans of three suitable reflections was also applied to the data. Processing and calculations were undertaken with the TEXSAN [49] crystallographic software package. Neutral atom scattering factors were taken from Cromer and Waber [50]. Anomalous dispersion effects were included in F_{calc} [51] and the values for $\Delta f'$ and $\Delta f''$ were those of Creagh and McAuley [52]. The values for the mass attenuation coefficients were those of Creagh and Hubbell [53]. The structure was solved in the space group $P\bar{1}$ (#2) by direct methods with SIR92 [54] and expanded with difference Fourier maps generated by DIRDIF [55]. The asymmetric unit contains two crystallographically independent molecules each residing on inversion sites, a disordered BF_4^- counterion, a 0.5 occupancy dichloromethane solvate molecule and two water oxygens sites with occupancies of 0.5 and 0.25. The BF_4^- counterion is rotationally disordered about the B(1)–F(1) axis and five fluorine sites were used to model the disorder. In general, the non-hydrogen atoms were modeled anisotropically, the exceptions being C(71), B(1), F(4), F(5), O(1) and O(2), which were refined with isotropic thermal parameters. The hydrogen atoms included in the model were placed at calculated positions with group thermal parameters. Two sites in the asymmetric unit were treated as partially occupied water oxygen sites and no hydrogens were included for these isotropically refined sites. The BF_4^- ion is disordered and was modeled with five fluorine sites. The asymmetric unit population of a dichloromethane solvate molecule was refined and then fixed at 0.5 and no hydrogens were included for this molecule.

3.1. Synthesis of decaphenylmolybdenocene

Into a 250 ml two neck Schlenk flask fitted with a condenser were charged $Mo(CO)_6$ (1.87 g, 7.08 mmol) and toluene (100 ml). The initially colourless solution was refluxed for 18 h producing a colour change to deep yellow. The reaction was cooled to r.t. and the solvent was removed under reduced pressure to yield pale yellow crystalline $[Mo(toluene)(CO)_3]$ which was used without further purification. Into the same reaction flask was added a solution of diphenylacetylene (6.3 g, 35.4 mmol) in dry heptane (100 ml). The mixture was heated to reflux for 16 h. The deep red precipitate was collected by gravity filtration and washed with dichloromethane in air until the washings became colourless (0.59 g, 8.3%). IR ν_{max} (KBr, cm^{-1}) 3054w, 3036w, 1600m, 1500s, 1444m, 1177w, 1074w, 1026w, 799w, 781m, 739s, 711vs, 700vs, 618w, 555s. MS (EI, *m/e*, %) 988 (M^+, 100%), 543 ($M^+ - C_5Ph_5$, 14), 494 (M^{2+}, 6), 446 ($C_5Ph_5H^+$, 22)

3.2. Synthesis of decaphenylmolybdenocenium tetrafluoroborate

Solid $NOBF_4$ (0.10 g, 0.86 mmol) was added to a well-stirred suspension of $[Mo(C_5Ph_5)_2]$ (0.51 g, 0.52 mmol) in dichloromethane (30 ml). The mixture was stirred for 2 h and filtered to yield a green filtrate. This was mixed with ether (30 ml) to produce a green crystalline precipitate, which was recrystallised from dichloromethane/ether (0.40 g, 72%) m.p. 260 °C. Anal. Calc. for $C_{70}H_{50}MoBF_4$: C 78.29; H, 4.69. Found: C, 78.4; H, 4.7%. ^1H NMR (ppm 200 MHz) δ 13.8 (s, br, Ar–*H*), 7.25–6.79 (m, Ar–*H*), 1.27 (s, Ar–*H*), 0.88 (s, Ar–*H*), 0.13 (s, br, Ar–*H*). IR ν_{max} (KBr, cm^{-1}) 3055w, 1601w, 1502m, 1445m, 1411w, 1184w, 1099m, 1058vs, br, 1028m, 800w, 780m, 741s, 710vs, 699vs, 618w, 556s. MS (EI) (*m/e*, %): 988 (M^+, 100%), 543 ($M^+ - (C_5Ph_5)$, 15), 494 (M^{2+}, 10), 446 ($C_5Ph_5H^+$, 18)

3.3. Crystal data

Formula $C_{70.50}H_{50}BClF_4MoO_{0.75}$, M 1127.37, triclinic, space group $P\bar{1}$(#2), a 13.629(2), b 17.329(3), c 13.306(3) Å, α 105.70(2), β 101.70(1), γ 75.23(1)°, V 2894(1) $Å^3$, D_{calc} 1.293 g cm^{-3}, Z 2, crystal size 0.38 by 0.25 by 0.17 mm, colour black, habit prism, λ(Mo Kα) 0.7107 Å, μ(Mo Kα) 0.328 mm^{-1}, $T(\psi$ scans$)_{min,max}$ 0.648, 0.994, $2\theta_{max}$ 49.96, *hkl* range −16 15, −20 1, −15 15, N 11 275, N_{ind} 10 166(R_{merge} 0.03334), N_{obs} 5829($I > 3.00\sigma(I)$), N_{var} 713, residuals* $R(F)$ 0.0630, $R_w(F)$ 0.0590, GoF(obs) 2.727, GoF(all) 2.727, $\Delta\rho_{min,max}$ −0.67, 0.92 e $Å^{-3}$. $*R = \Sigma\ ||F_o| - |F_c||/\Sigma\ |F_o|$; $R_w = (\Sigma\ w(F_o - F_c)^2/\Sigma\ (wF_c)^2)^{1/2}$. $w = 1/[\sigma^2(F_o)]$.

4. Supplemntary materials

Data have been deposited with the Cambridge Crystallographic Data Centre, 12 Union Road, Cam-

bridge CB2 1EZ, UK (fax: +44-1223-336033; e-mail: deposit@ccdc.cam.ac.uk or www: http://www.ccdc.cam.ac.uk), deposition number CCDC 150280.

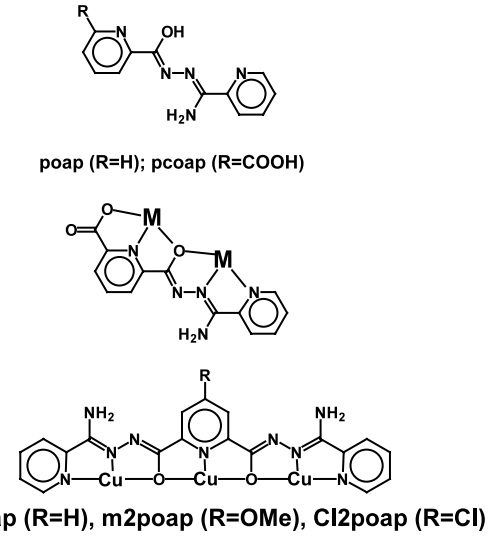
Acknowledgements

We thank the Australian Research Council for financial support and SOCG for time in which to prepare the manuscript. T.H. acknowledges the receipt of an Australian Postgraduate Award.

References

[1] J.E. Bercaw, H.H. Brintzinger, J. Am. Chem. Soc. 93 (1971) 2045.
[2] J.L. Robbins, Energy Res. Abstr. Lawrence Berkely Lab., Abstr. 20584 (1981).
[3] J.L. Robbins, N. Edelstein, B. Spencer, J.C. Smart, J. Am. Chem. Soc. 104 (1982) 1882.
[4] J.C. Smart, J.L. Robbins, J. Am. Chem. Soc. 100 (1978) 3936.
[5] R.B. King, M.B. Bisnette, J. Organomet. Chem. 8 (1967) 287.
[6] F.G.N. Cloke, J.P. Day, J. Chem. Soc., Chem. Commun. (1985) 967.
[7] J.A. Bandy, F.G.N. Cloke, G. Cooper, J.P. Day, R.B. Girling, R.G. Graham, J.C. Green, R. Grinter, R.N. Perutz, J. Am. Chem. Soc. 110 (1988) 5039.
[8] T.D. Tilley, R.H. Grubbs, J.E. Bercaw, Organometallics 3 (1984) 274.
[9] D. O'Hare, J.C. Green, T.P. Chadwick, J.S. Miller, Organometallics 7 (1988) 1335.
[10] O.V. Gusev, L.N. Morozova, T.Y.A. Peganova, P.V. Petrovskii, N.A. Ustynyuk, P.M. Maitlis, J. Organomet. Chem. 472 (1994) 359.
[11] O.V. Gusev, L.N. Morozova, M.G. Peterleitner, S.M. Peregudova, P.V. Petrovskii, N.A. Ustynyuk, P.M. Maitlis, J. Organomet. Chem. 509 (1996) 95.
[12] O.V. Gusev, T.Y.A. Peganova, M.G. Peterleitner, S.M. Peregudova, L.I. Denisovich, N.A. Ustynyuk, P.M. Maitlis, J. Organomet. Chem. 480 (1994) C16.
[13] S. Gambarotta, C. Floriani, A. Chiesi-Villa, C. Guastini, Inorg. Chem. 23 (1984) 1739.
[14] F. Bottomley, J. Chen, S.M. MacIntosh, R.C. Thompson, Organometallics 10 (1991) 906.
[15] D.P. Freyberg, J.L. Robbins, K.N. Raymond, J.C. Smart, J. Am. Chem. Soc. 101 (1979) 892.
[16] Y.T. Struchkov, V.G. Andrianov, T.N. Sal'nikova, I.R. Lyatifov, R.B. Materikova, J. Organomet. Chem. 145 (1978) 213.
[17] D.C. Liles, A. Shaver, E. Singleton, M.B. Wiege, J. Organomet. Chem. 26 (1985) C33.
[18] M.O. Albers, D.C. Liles, D.J. Robinson, A. Shaver, E. Singleton, M.B. Wiege, J.C.A. Boeyens, D.C. Levendis, Organometallics 5 (1986) 2321.
[19] J. Darkwa, J.F. Richardson, T.S. Sorenson, Acta Crystallogr., Sect. C 46 (1990) 745.
[20] W.E. Broderick, J.A. Thompson, B.M. Hoffman, Inorg. Chem. 30 (1991) 2958.
[21] X. Wang, L.M. Liable-Sands, J.L. Manson, A.L. Rheingold, J.S. Miller, J. Chem. Soc., Chem. Commun. (1996) 1979.
[22] D. Buchholz, L. Zsolnai, G. Huttner, D. Astruc, J. Organomet. Chem. 593 (2000) 494.
[23] Y.T. Struchkov, M.Y. Antipin, K.A. Lyssenko, O.V. Gusev, T.A. Peganova, N.A. Ustynyuk, J. Organomet. Chem. 536 (1997) 281.
[24] J.L. Thomas, H.H. Brintzinger, J. Am. Chem. Soc. 94 (1972) 1386.
[25] J.L. Thomas, J. Am. Chem. Soc. 95 (1973) 1838.
[26] F.G.N. Cloke, J.P. Day, J.C. Green, C.P. Morley, A.C. Swain, J. Chem. Soc., Dalton Trans. (1991) 789.
[27] A.Z. Kreindlin, P.V. Petrovskii, M.I. Rybinskaya, A.I. Yanovskii, Y.T. Struchkov, J. Organomet. Chem. 319 (1987) 229.
[28] A.Z. Kreindlin, P.V. Petrovskii, M.I. Rybinskaya, Izv. Akad. Nauk SSSR, Ser. Khim. (1987) 1620.
[29] W. Hübel, R. Merenyi, J. Organomet. Chem. 2 (1964) 213.
[30] G.M. Holtzapple, P.S. Woon, M.F. Farona, Inorg. Nucl. Chem. Lett. 12 (1976) 623.
[31] J.A. Potenza, R.J. Johnson, R. Chirico, A. Efraty, Inorg. Chem. 16 (1977) 2354.
[32] H. Schumann, A. Lentz, R. Weimann, J. Pickardt, Angew. Chem., Int. Ed. Engl. 33 (1994) 1731.
[33] K.N. Brown, L.D. Field, P.A. Lay, C.M. Lindall, A.F. Masters, J. Chem. Soc., Chem. Commun., (1990) 408.
[34] A.M. Bond, R. Colton, D.A. Fiedler, L.D. Field, T. He, P.A. Humphrey, C.M. Lindall, F. Marken, A.F. Masters, H. Schumann, K. Sühring, V. Tedesco, Organometallics 16 (1997) 2787.
[35] A.M. Bond, D.A. Fiedler, A. Lamprecht, V. Tedesco, Organometallics 18 (1999) 642.
[36] L.D. Field, T.W. Hambley, T. He, A.F. Masters, P. Turner, Aust. J. Chem. 50 (1997) 1035.
[37] L.D. Field, G.J. Gainsford, T.W. Hambley, P.A. Humphrey, C.M. Lindall, A.F. Masters, T.G.S. Pierre, J. Webb, Aust. J. Chem. 48 (1995) 851.
[38] L.D. Field, T.W. Hambley, T. He, P.A. Humphrey, C.M. Lindall, A.F. Masters, Aust. J. Chem. 49 (1996) 889.
[39] V.V. Strelets, S.V. Kukharenko, Nouv. J. Chim. 8 (1984) 785.
[40] S. Lu, V.V. Strelets, M.F. Ryan, W.J. Pietro, A.B.P. Lever, Inorg. Chem. 35 (1996) 1013.
[41] J.D.L. Holloway, J.W.E. Geiger, J. Am. Chem. Soc. 101 (1979) 2038.
[42] W.E. Geiger, Jr., J. Am. Chem. Soc. 96 (1974) 2633.
[43] N. El Murr, L. Etienne, Can. J. Chem. 54 (1976) 3350.
[44] V.V. Strelets, Coord. Chem. Rev. 114 (1992) 1.
[45] C.K. Johnson, ORTEP-II, a Thermal Ellipsoid Plotting Program, Report ORNL-5138, Version Oak Ridge National Laboratories, Oak Ridge, TN, 1976.
[46] L.C. Song, Q.M. Hu, J.S. Yang, X.C. Cao, R.J. Wang, T.C.W. Mak, Inorg. Chim. Acta 245 (1996) 109.
[47] D.F. Shriver, M.A. Drezdzon, The Manipulation of Air-sensitive Compounds, Wiley-Interscience, New York, 1986.
[48] L.D. Field, K.M. Ho, C.M. Lindall, A.F. Masters, A.G. Webb, Aust. J. Chem. 43 (1990) 281.
[49] Molecular Structure Corporation, TEXSAN: Single Crystal Structure Analysis Software, Version 1.6, Molecular Structure Corporation, The Woodlands, TX, USA, 1993.
[50] D.T. Cromer, J.T. Waber, in: J.A. Ibers, W.C. Hamilton (Eds.), International Tables for X-Ray Crystallography, vol. IV, Kynock Press, Birmingham, UK, 1974, p. 71.
[51] J.A. Ibers, W.C. Hamilton, Acta Crystallogr. 17 (1964) 781.
[52] D.C. Creagh, W.J. McAuley, in: A.J.C. Wilson (Ed.), International Tables for Crystallography, vol. C, Kluwer Academic Publishers, Boston, 1992, p. 219.
[53] D.C. Creagh, J.H. Hubbell, in: A.J.C. Wilson (Ed.), International Tables for Crystallography, vol. C, Kluwer Academic Publishers, Boston, 1992, p. 200.
[54] A. Altomare, M. Cascarano, C. Giacovazzo, A. Guagliardi, J. Appl. Cryst. 26 (1993) 343.
[55] P.T. Beurskens, G. Admiraal, G. Beurskens, W.P. Bosman, R. de Gelder, R. Israel, J.M.M. Smits, The DIRDIF-94 Program System. Technical Report. Crystallography Laboratory, University of Nijmegen, The Netherlands, DIRDIF-94, Nijmegen, 1994.

[56] M.F. Ryan, D.E. Richardson, D.L. Lichtenberger, N.E. Gruhn, Organometallics 13 (1994) 1190.
[57] U. Koelle, A. Salzer, J. Organomet. Chem. 243 (1983) C27.
[58] P.G. Gassman, C.H. Winter, J. Am. Chem. Soc. 110 (1988) 6130.
[59] W. Kläui, L. Ramacher, Angew. Chem., Int. Ed. Engl. 25 (1986) 97.
[60] T. He, Ph.D. Thesis, The University of Sydney, 1999.
[61] M.P. Castellani, S.J. Geib, A.L. Rheingold, W.C. Trogler, Organometallics 6 (1987) 1703.



Scheme 1.

2. Experimental

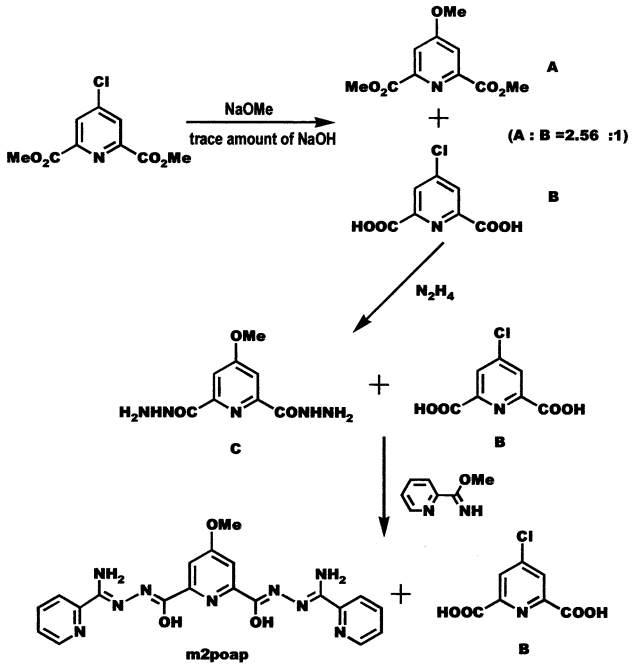
2.1. Physical measurements

Infrared spectra were recorded as Nujol mulls using a Mattson Polaris FT-IR instrument. Mass spectra were obtained with VG Micromass 7070HS instrument. Micro-analyses were carried out by Canadian Microanalytical Service, Delta, Canada. Variable temperature magnetic data (2–300 K) were obtained using a Quantum Design MPMS5S SQUID magnetometer with field strengths in the range of 0.1–5.0 T. Samples were prepared in aluminum pans, and mounted inside straws for attachment to the sample transport rod. Background corrections for the sample holder assembly and diamagnetic components of the complexes were applied.

2.2. Synthesis of ligands and complexes

2.2.1. m2poap

The synthesis route of m2poap is shown in Scheme 2. A methanolic solution of sodium methoxide (2.60 g, 0.130 mol sodium in 100 mL methanol) was mixed with a methanolic solution of 4-chloro-dimethyl-2,6-pyridinedicarboxylate (11.5 g, 0.05 mol in 30 ml methanol). The resulting clean solution was refluxed for 2 h, followed by removing ~100 ml methanol. The white precipitate, which formed was filtered off and washed with methanol then ether. Yield 10.7 g. However, this product proved to be a mixture of 4-methoxy-dimethyl-2,6-pyridinedicarboxylate (**A** in Scheme 2) and 4-chloro-2,6-pyridinedicarboxylic acid (ClpicH$_2$) (**B** in Scheme 2), in a the ratio of **A**:**B** of ~ 2.6:1, which was deduced from the purification result of the final ligand, m2poap.



Scheme 2.

This probably occurred because the methanol used was not dry enough.

The mixture was suspended and stirred with hydrazine hydrate in 60 mL methanol at room temperature. **A** was converted into 4-methoxy-2,6-pyridinedicarboxylic acid dihydrazide (**C** in Scheme 2), but no change apparently occurred to **B**. This impure dihydrazide (**C** with a small amount of **B**) was further reacted under refluxing conditions with the methyl ester of iminopicolinic acid, which was prepared in situ by the reaction of 2-cyanopyridine (15.6 g, 0.150 mol) with sodium methoxide solution, produced by dissolving sodium metal (0.35 g, 0.015 mol) in dry methanol (150 ml). The final ligand m2poap (with a small amount of **B**) with filtered and washed with methanol then ether. Yield 16.7 g. M.p. 245–250 °C. The melting point of the purified sample (purified in hot water) is 258–260 °C. IR: ν_{max}/cm^{-1} (Nujol) 3415, 3315, 3217 (νNH_2, νOH), 1672, 1631($\nu C{=}O$ and $\nu C{=}N$) and 993 (py); *m/z* 411 ($M-H_2O$), 397 ($M-2H_2O$), 369,307,279,253, 223, 194, 162, 105. The complexation reactions were done with the crude sample of the ligand m2poap. Purification of the ligand was carried out subsequent to the structural determination of **1**.

2.2.2. Synthesis of $[Cu_9(m2poap-2H)_4(Clpic)_2(H_2O)_4](NO_3)_6\cdot 22H_2O$ (1)

The crude ligand m2poap (0.43 g, 1.0 mmol) was added to a warm (~60 °C) solution of $Cu(NO_3)_2\cdot 6H_2O$ (0.87g, 3.0 mmole) in 10 ml H_2O and 5 ml methanol. The resulting mixture was stirred for a few minutes at that temperature forming a clear solution,

which was filtered. Dark khaki-green crystals suitable for X-ray diffraction formed from the filtrate after standing for several days at room temperature (r.t.). Yield: 66%. IR (Nujol mull, cm^{-1}), 3550 (w) (νH_2O); 3300 (w), 3152 (w) (νNH_2); 1673 ($\nu C{=}N$); 1613 (νCOO); 1017 (m) (νpy). *Anal.* Found for **1**: C, 31.87; H, 2.92; N, 17.28. Calc. for $(C_{20}H_{17}N_9O_3)_4(C_7H_2NO_4Cl)_2Cu_9(NO_3)_6\cdot 26H_2O$: C, 31.92; H, 3.52; N, 17.42%.

2.2.3. Synthesis of $Cu_3(m2poap{-}2H)(NO_3)_4\cdot 4.5H_2O$ (**2**)

The ligand m2poap (0.43 g, 1.0 mmol) was added to a solution of $Cu(NO_3)_2\cdot 6H_2O$ (0.87 g, 3.0 mmol) in 10 ml acetonitrile and 10 ml methanol at room temperature. The resulting mixture was stirred for a few minutes at r.t. (no heat). A clear deep green solution formed, which was filtered. A green crystalline precipitate formed from the filtrate after standing overnight at room temperature. Yield: 72%. IR (Nujol mull, cm^{-1}), 3502 (w) (νH_2O); 3350 (w), 3187 (w) (νNH_2); 1693, 1676 ($\nu C{=}N$); 1039, 1004 (m) (νpy); 1797(w), 1751(w) (NO_3). *Anal.* Found for **2**: C, 24.99; H, 2.29; N, 19.32. Calc. for $(C_{20}H_{17}N_9O_3)Cu_3(NO_3)_4\cdot 4.5H_2O$: C, 25.26; H, 2.75; N, 19.14%.

2.3. X-ray crystallography

The diffraction intensities of a dark green, almost black prismatic crystal of **1** were collected with graphite monochromatized Mo Kα X-radiation (rotating anode generator) using a Bruker P4/CCD diffractometer at 193(1) K to a maximum 2θ value of 52.8°. The data were corrected for Lorentz and polarization effects. The structure was solved by direct methods [10,11]. All atoms except hydrogens were refined anisotropically. Hydrogen atoms were placed in calculated positions with isotropic thermal parameters set to 20% greater than their bonded partners, and were not refined. Neutral atom scattering factor [12] and anomalous-dispersion terms [13,14] were taken from the usual sources. All other calculations were performed with the TEXSAN [15] crystallographic software package using a PC computer. Crystal data collection and structure refinement details are given in Table 1. Two methanol molecules appear in the X-ray structure, which appear not to be present in the dried analytical sample (vide supra).

Table 1
Crystal data and structure refinement parameters for compound **1**

Empirical formula	$C_{96}H_{112}N_{44}O_{56}Cu_9Cl_2$
Formula weight	3421.02
Temperature (K)	190(1)
Wavelength (Å)	0.71073
Crystal system	monoclinic
Space group	$P2_1/n$ (no. 14)
Unit cell dimensions	
a (Å)	26.612(3)
b (Å)	20.465(3)
c (Å)	26.99293)
β (°)	111.792(2)
V (Å^3)	13650(3)
Z	4
D_{calc} (g cm^{-3})	1.665
μ (cm^{-1})	15.19
R_1	0.071
wR_2	0.249

$R_1 = \Sigma||F_o|-|F_c||/\Sigma|F_o|$, $wR_2 = \{\Sigma[w(|F_o|^2-|F_c|^2)^2]/\Sigma[w(|F_o|^2)^2]\}^{1/2}$.

3. Results and discussion

3.1. Structure of $[Cu_9(m2poap{-}2H)_4(Clpic)_2](NO_3)_6\cdot(CH_3OH)_2\cdot 16H_2O$ (**1**)

The structure of the nona-nuclear cation in **1** is shown in Fig. 1, and selected bond distances and angles are listed in Table 2. Fig. 2 shows a simplified structure with non-donor atoms of the terminal ligand groups removed. The structure is unique within this class of compounds in that it contains two different ligands—deprotonated m2poap and $ClpicH_2$. The $Clpic^{2-}$ results from the batch of ligand being impure ($ClpicH_2$ is a hydrolysis product of the starting material methyl-4-chloro-2,6-pyridine dicarboxylate (Scheme 2), which is present at a level of ~30%). Nine copper(II) ions are arranged in the familiar [3 × 3] grid with oxygen bridges linking each adjacent pair of metals. Three deprotonated m2poap ligands are arranged in parallel on one face of the grid, while on the other two tridentate $Clpic^{2-}$ ligands flank a central m2poap ligand, with the pyridine rings of the three ligands being roughly parallel. Copper atoms Cu(2), Cu(4), Cu(8), Cu(6) and Cu(5) are six-coordinate, while the other coppers at the corners of the square grid are five-coordinate, with a water molecule

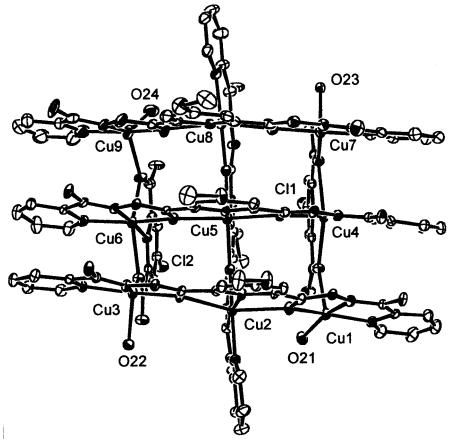


Fig. 1. Structural representation of the cation in **1** (40% thermal ellipsoids) with hydrogen atoms omitted.

Table 2
Selected bond lengths (Å) and bond angles (°) for **1**

Bond lengths			
Cu1–N3	1.907(6)	Cu5–O14	2.125(5)
Cu1–O21	1.952(5)	Cu5–O4	2.212(5)
Cu1–O1	1.960(5)	Cu5–O6	2.226(5)
Cu1–N1	2.023(6)	Cu6–N16	1.909(5)
Cu1–O11	2.244(5)	Cu6–N38	2.010(5)
Cu2–N31	1.900(6)	Cu6–O6	2.013(5)
Cu2–N5	2.001(5)	Cu6–N18	2.073(6)
Cu2–O14	2.051(5)	Cu6–O20	2.291(6)
Cu2–N29	2.068(6)	Cu6–O18	2.359(5)
Cu2–O1	2.299(5)	Cu7–N21	1.893(6)
Cu2–O3	2.327(4)	Cu7–O13	1.957(5)
Cu3–N7	1.884(5)	Cu7–O7	1.992(5)
Cu3–O18	1.958(5)	Cu7–N19	2.039(6)
Cu3–O3	1.980(4)	Cu7–O23	2.243(5)
Cu3–N9	2.030(6)	Cu8–N35	1.899(6)
Cu3–O22	2.215(5)	Cu8–N23	1.996(6)
Cu4–N12	1.904(6)	Cu8–O16	2.072(5)
Cu4–O4	2.016(5)	Cu8–N37	2.083(7)
Cu4–N28	2.035(6)	Cu8–O9	2.343(6)
Cu4–N10	2.067(6)	Cu8–O7	2.348(5)
Cu4–O11	2.333(5)	Cu9–N25	1.880(8)
Cu4–O13	2.390(5)	Cu9–O9	1.969(6)
Cu5–N33	1.902(5)	Cu9–O24	2.012(7)
Cu5–N14	1.928(5)	Cu9–N27	2.051(8)
Cu5–O16	2.112(5)	Cu9–O20	2.106(5)
Bond angles			
Cu1–O1–Cu2	138.8(2)	Cu1–O11–Cu4	124.9(2)
Cu3–O3–Cu2	140.9(2)	Cu7–O13–Cu4	114.8(2)
Cu4–O4–Cu5	140.8(2)	Cu2–O14–Cu5	139.9(2)
Cu6–O6–Cu5	140.0(2)	Cu8–O16–Cu5	141.5(2)
Cu7–O7–Cu8	141.4(2)	Cu3–O18–Cu6	110.1(2)
Cu9–O9–Cu8	139.1(3)	Cu9–O20–Cu6	121.1(2)

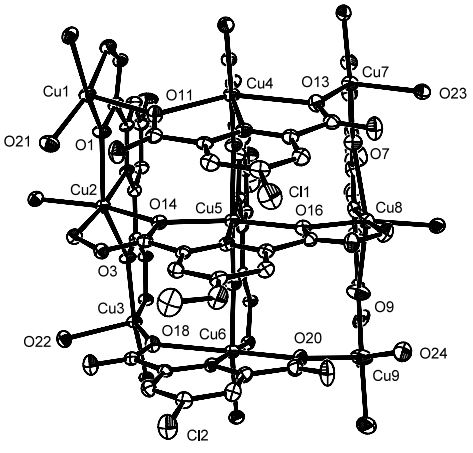


Fig. 2. Simplified structural representation of the core in **1**, highlighting the two pyridine dicarboxylate ligands.

completing the coordination spheres in each case. The corner copper atoms (Cu(1), Cu(3), Cu(7), Cu(9)) have distorted square-pyramidal geometries, while the side coppers have tetragonally elongated octahedral geometries, and the central copper Cu(5) has a tetragonally compressed octahedral geometry. The two $Clpic^{2-}$ ligands bridge three metals within the grid with the carboxylate oxgen donor atoms acting in an unusual bridging capacity. The m2poap ligands act in a heptadenetate fashion in the usual way, filling nine metal coordination sites. Cu–Cu separations fall in the range 3.54–4.10 Å, with three having very short distances (Cu(3)–Cu(6) 3.545(3) Å, Cu(6)–Cu(9) 3.831(4) Å, Cu(4)–Cu(7) 3.670(3) Å). It is no accident that the $Clpic^{2-}$ oxygen atoms bridge these metal atoms and that the angles subtended at the bridging oxygens are also very small (110.1(2)°, 121.1(2)°, 114.8(2)°, respectively). Cu(1)–O(11)–Cu(4) is also small (124.9(2)°), despite a quite long Cu–Cu separation (4.059(4) Å). This leads to a somewhat more distorted grid than those observed previously [5–7].

The inclusion of two 4-chloro-2,6-dipicolinate ligands in the structure may be serendipitous, but it shows that a nominally monotopic, chelating ligand, can have its coordination character completely changed if it is placed in an environment where other related tritopic ligands create a coordination framework into which it can be accommodated by virtue of its similar core dimensions. We are not aware of this coordination mode for a simple ligand of this sort. Within the grid all of the connections between copper centers around the peripheral ring of eight metals are either axial/axial (d_{z^2}/d_{z^2}) or axial/equatorial ($d_{z^2}/d_{x^2-y^2}$), based on the metal ion geometry. This leads to strict magnetic orbital orthogonality (vide infra). The central copper (Cu(5)) has an unusual d_{z^2} ground state, with four long equatorial Cu–O distances in the range 2.112–2.226 Å, and two short axial Cu–N distances (1.902(5) Å, 1.928(5) Å), and so nominally its connections to neighboring copper atoms Cu(2), Cu(4), Cu(6) and Cu(8) are also magnetically orthogonal.

3.2. Structure of $[(m2poap-2H)Cu_3(NO_3)_4]\cdot 4.5H_2O$ (**2**)

Although crystals of **2** have been obtained, a structural solution has not yet been possible. The green color of **2** differs markedly from **1** (almost black), and elemental analysis is consistent with a 1:3 (L:M) trinuclear derivative. Two other examples of linear trinuclear complexes $[Cu_3(2poap-2H)(CH_3CO_2)_4]\cdot 3H_2O$ and $[Cu_3(2poap-2H)\ (H_2O)(DMF)_3(CH_3OH)_2]\cdot(BF_4)_4$ with a closely related ligand [16], involve an almost *trans* (N–N)-bridged linear trinuclear arrangement, resulting in quite strong antiferromagnetic exchange. Such systems are rare with ligands in this class, but appear to form when strong donor solvents or coordinating anions are used and are synthesized without significant heating. Compound **2** is expected to have a similar structure. Preliminary results indicate that recrystallization of some trinuclear Cu(II) derivatives in water, with heat-

ing, converts them to the corresponding nona-nuclear grid complexes [17].

3.3. Magnetic properties

The room temperature magnetic moment for **1** ($5.6\mu_B$) (Fig. 3) is consistent with a nona-nuclear system ($5.2\mu_B$ for the spin only case), and it drops to a minimal value of $5.26\mu_B$ in the range 30–40 K, followed by a sharp rise to $7.18\mu_B$ at 2 K. This behaviour is consistent with the other reported [3 × 3] copper(II) grids [5–8], and indicates a combination of antiferromagnetic and ferromagnetic coupling. The exchange Hamiltonian expression for **1** is given in Eq. (1). The total spin state (S') values, and

$$H = -J1\{S_1\cdot S_2 + S_2\cdot S_3 + S_3\cdot S_6 + S_6\cdot S_9 + S_8\cdot S_9 + S_7\cdot S_8 + S_4\cdot S_7 + S_1\cdot S_4\} - J2\{S_2\cdot S_5 + S_5\cdot S_6 + S_5\cdot S_8 + S_4\cdot S_5\} \quad (1)$$

their energies for all spin vector combinations were evaluated in the normal way [18], and substituted into the Van Vleck equation within the internal structure of the software package MAGMUN-4.0 [19]. The magnetic data were fitted to Eq. (1) within MAGMUN-4.0 to give $g = 2.146(3)$, $J1 = 1.8(3)$ cm^{-1}, $J2 = -27.0(7)$ cm^{-1}, TIP $= 450 \times 10^{-6}$ emu mol^{-1}, $\rho = 0.003$, $\theta = -0.1$ K ($10^2R = 0.97$; $R = [\Sigma(\chi_{obs} - \chi_{calc})^2/\Sigma\ \chi^2_{obs}]^{1/2}$; ρ = fraction paramagnetic impurity, θ = Weiss-like temperature correction), as the best-fit result. The solid line in Fig. 3 was calculated with these parameters. The orthogonal bridging arrangement around the external ring of eight copper atoms leads to the positive ferromagnetic $J1$ (Cu_8 ring) value, while the negative, antiferromagnetic $J2$ is rationalized in terms of a fluxional magnetic ground state associated with the unusual, tetragonally compressed central copper (Fig. 2), typical of these structures [5,6,8]. On the basis of the nominal d_{z^2} ground state one would expect not to have antiferromagnetic exchange involving the central copper, but the clearly defined $J2$ indicates that on average this metal center interacts with one adjacent copper antiferromagnetically, and this can be rationalized in terms of the copper ion undergoing fluxional motion within a hole in which the metal 'd' orbitals have some orientational freedom. $J1$ is somewhat larger than $J1$ for the analogous grid complex $[Cu_9(2poap)_6](NO_3)_{12}\cdot 9H_2O$ (0.52 cm^{-1}) [8], which can reasonably be associated with the closer average Cu–Cu spacing in **1** (3.928 vs. 4.214 Å) [6]. $J2$ is comparable with the previous value (−24.3 cm^{-1}) [8], expected on the basis of the similarities in the coordination spheres of the central copper atoms.

Magnetization data for **1** as a function of field were determined at 2 K, and shown in Fig. 4. The magnetization increases sharply with increasing field and approaches saturation at 5.0 T. The data were fitted to the standard Brillouin function and the best-fit gave $g = 2.10$ for $S = 7/2$ (solid line in Fig. 4). The experimental data fall slightly short of the theoretical line as would perhaps be expected, given the combination of intramolecular ferromagnetic and antiferromagnetic exchange, but clearly indicate an $S = 7/2$ magnetic ground state, consistent with the variable temperature analysis.

The profile of magnetic moment as a function of temperature for **2** is illustrated in Fig. 5, and is completely different from **1**. The general shape of the profile is typical for a trinuclear derivative with strong intramolecular antiferromagnetic exchange. The data were fitted to a simple linear model based on the Hamiltonian expression shown in Eq. (2)

$$H = -J\{S_1\cdot S_2 + S_2\cdot S_3\} \quad (2)$$

which assumes that coupling between the extreme copper centers is insignificant. A reasonable fit was obtained using MAGMUN-4.0 [19] for $g = 2.260(4)$, $J = -159(2)$ cm^{-1}, TIP $= 160 \times 10^{-6}$ emu mol^{-1}, $\rho = 0.044$, $\theta = -0.2$ ($10^2R = 0.93$). The solid line in Fig. 5 was calculated with these parameters. The fairly large $-J$ value is consistent with N–N bridging in a situation where the metal ions are disposed with their magnetic orbitals arranged in a *trans* arrangement around the N–N single bond [6,20,21].

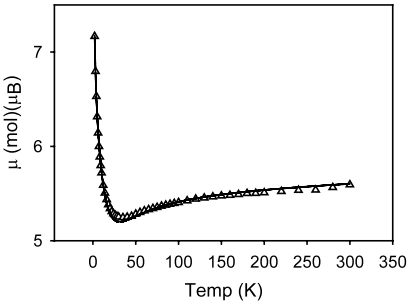


Fig. 3. Variable temperature magnetic data for **1**. The solid line corresponds to the best fit to Eq. (1) with $g = 2.146(3)$, $J1 = 1.8(3)$ cm^{-1}, $J2 = -27.0(7)$ cm^{-1}, TIP $= 450 \times 10^{-6}$ emu mol^{-1}, $\rho = 0.003$, $\theta = -0.1$ K ($10^2R = 0.97$).

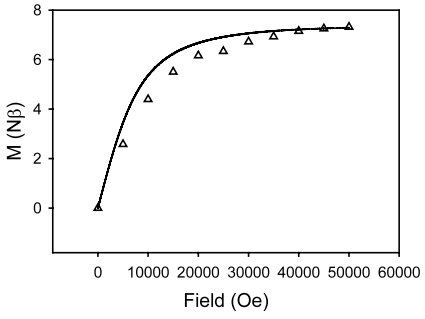


Fig. 4. Magnetization data as a function of field at 2 K for **1**. The solid line represents the best fit to the Brillouin function for $S = 7/2$, $g = 2.10$.

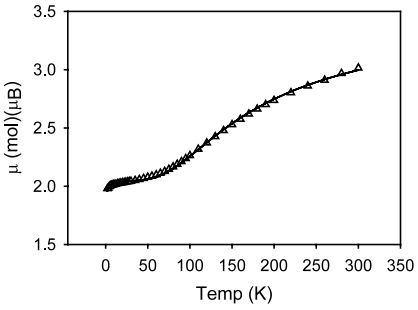


Fig. 5. Variable temperature magnetic data for **2**. The solid line represents the best data fit to Eq. (2), with $g = 2.260(4)$, $J = -159(2)$ cm^{-1}, $TIP = 160 \times 10^{-6}$ emu mol^{-1}, $\rho = 0.044$, $\theta = -0.2$ ($10^2R = 0.93$).

4. Conclusions

The serendipitous presence of a ligand impurity has lead to a most unusual mixed ligand [3 × 3] Cu_9 grid, with substantially different core geometry than in previous examples, and has provided an arrangement of ligands where the pyridine-2,6-dicarboxylate moiety can adopt a most unusual tritopic coordination mode bridging three metal ions. Also a trinuclear derivative is produced under different reaction conditions as the major product. Magnetic data are clearly rationalized, based on the geometrical features of the two structures.

5. Supplementary material

Crystallographic data for the structural analysis have been deposited with the Cambridge Crystallographic Data Centre, CCDC No. 176299 for compound **1**. Copies of this information may be obtained free of charge from The Director, CCDC, 12 Union Road, Cambridge, CB2 1EZ, UK (fax: +44-1223-336033; e-mail: deposit@ccdc.cam.ac.uk or www: http://www.ccdc.cam.ac.uk).

Acknowledgements

This study was supported by the Natural Sciences and Engineering Research Council of Canada (NSERC). We thank Dr. R. McDonald, University of Alberta, for X-ray structural data.

References

[1] C.J. Matthews, K. Avery, Z. Xu, L.K. Thompson, L. Zhao, D.O. Miller, K. Biradha, K. Poirier, M.J. Zaworotko, C. Wilson, A.E. Goeta, J.A.K. Howard, Inorg. Chem. 38 (1999) 5266.
[2] Z. Xu, L.K. Thompson, C.J. Matthews, D.O. Miller, A.E. Goeta, J.A.K. Howard, Inorg. Chem. 40 (2001) 2446.
[3] L.K. Thompson, C.J. Matthews, L. Zhao, Z. Xu, D.O. Miller, C. Wilson, M.A. Leech, J.A.K. Howard, S.L. Heath, A.G. Whittaker, R.E.P. Winpenny, J. Solid State Chem. 159 (2001) 308.
[4] Z. Xu, L.K. Thompson, D.O.Miller, J. Chem. Soc., Dalton Trans. (2002) 2462.
[5] L. Zhao, Z. Xu, L.K. Thompson, D.O. Miller, Polyhedron 20 (2001) 1359.
[6] L. Zhao, Z. Xu, L.K. Thompson, S.L. Heath, D.O. Miller, M. Ohba, Angew. Chem. Int. Ed. 39 (2000) 3114.
[7] L. Zhao, C.J. Matthews, L.K. Thompson, S.L. Heath, J. Chem. Soc., Chem. Commun. (2000) 265.
[8] O. Waldmann, R. Koch, S. Schromm, P. Müller, L. Zhao, L.K. Thompson, Chem. Phys. Lett. 332 (2000) 73.
[9] O. Waldmann, L. Zhao, L.K. Thompson, Phys. Rev. Lett. 88 (2002) 066401.
[10] (a) G.M. Sheldrick, SHELX-97, 1997.;
(b) S.I.R.97: A. Altomare, M. Cascarano, C. Giacovazzo, A. Guagliardi, J. Appl. Crystallogr. 26 (1993) 343.
[11] P.T. Beurskens, G. Admiraal, G. Beurskens, W.P. Bosman, R. de Gelder, R. Israel, J.M.M. Smits, DIRDIF-94, The DIRDIF-94 Program System, Technical Report of the Crystallography Laboratory, University of Nijmegen, The Netherlands, 1994.
[12] D.T. Cromer, J.T. Waber, International Tables for X-ray Crystallography, Table 2.2A, vol. IV, Kynoch Press, Birmingham, UK, 1974.
[13] J.A. Ibers, W.C. Hamilton, Acta Crystallogr. 17 (1964) 781.
[14] D.C. Creagh, W.J. McAuley, in: A.J.C. Wilson (Ed.), International Tables for Crystallography, Table 4.2.6.8, vol. C, Kluwer Academic Publishers, Boston, MA, 1992, pp. 219–222.
[15] TEXSAN for Windows: Crystal Structure Analysis Package, Molecular Structure Corporation, 1997.
[16] L. Zhao, L.K. Thompson, Z. Xu, D.O. Miller, D.R. Stirling, J. Chem. Soc., Dalton Trans. (2001) 1706.
[17] Z. Xu, L.K. Thompson, Unpublished results.
[18] K. Kambe, J. Phys. Soc. Jpn. 5 (1950) 38.
[19] MAGMUN-4.0 is available free of charge. It has been developed by Dr. Zhiqiang Xu (http://www.chem.mun.ca/resinst/) and Kathy He in collaboration with Professor L.K. Thompson (lthomp@mun.ca), and Dr. O. Waldmann (waldmann@physik.uni-erlangen.de). We do not distribute the source codes. The programs may be used only for scientific purposes, and economic utilization is not allowed. If the routine is used to obtain scientific results, which are published, the origin of the programs should be quoted.
[20] Z. Xu, L.K. Thompson, D.O. Miller, Inorg. Chem. 36 (1997) 3985.
[21] L.K. Thompson, Z. Xu, A.E. Goeta, J.A.K. Howard, H.J. Clase, D.O. Miller, Inorg. Chem. 37 (1998) 3217.

procedures [12]. UV-VIS spectra were recorded in dichloromethane solutions on a Systronics 119 spectrometer. IR spectra were recorded with a Perkin–Elmer 597 spectrophotometer as KBr pellets. ^{1}H NMR were recorded in Varian AMX 400 instrument using tetramethylsilane as an internal standard. ^{31}P NMR spectra were recorded on a Varian AMX 400 instrument in $CDCl_3$ with ortho phosphoric acid as a reference. C, H, N and S analysis were carried out with Perkin–Elmer 2400 elemental analyser. Melting points were determined with a Boetius micro heating table and are uncorrected.

2.2. Synthesis of new binuclear ruthenium(II) complexes

All the new complexes were prepared by the following general procedure. To a solution of [RuHCl(CO)(PPh_3)$_3$], [RuHCl(CO)(PPh_3)$_2$(py)], [RuHCl(CO)(PPh_3)$_2$(pip)] or [RuHCl(CO)(PPh_3)$_2$(mor)] (0.1 g; 0.10–0.13 mmol) in benzene (25 cm^3), the appropriate thiobis(β-diketone) (0.012–0.031 g; 0.050–065 mmol) was added and the mixture was heated under reflux for 5 h. The resulting solution was concentrated to approximately 3 cm^3 and cooled. Light petroleum (60–80 °C) (5 cm^3) was then added whereupon the product complex separated. The solid was filtered off, washed and recrystallised from CH_2Cl_2/light petroleum mixture and dried in vacuo.

2.3. Catalytic oxidation of cinnamyl and benzyl alcohol

To a solution of alcohol (1 mmol) in chloroform (20 cm^3), *N*-methylmorpholine-*N*-oxide (3 mmol) and the ruthenium complex (0.01 mmol) were added. The solution was heated under reflux for 3 h. The mixture was filtered and the filtrate was dried over anhydrous sodium sulphate. Then it was evaporated to dryness and extracted with diethyl ether. The ether extract was filtered and evaporated to give the corresponding aldehyde which was then quantified as their 2,4-dinitrophenylhydrazones [12].

2.4. Procedure for antibacterial studies

The nutrient agar medium was prepared by taking 1 L of water in a conical flask followed by the addition of following ingredients one by one (i) beef extract = 3.0 g, (ii) yeast extract = 3.0 g, (iii) peptone = 5.0 g and (iv) sodium hydroxide = 5.0 g. The resulting solution was stirred well to get a clear solution. The pH of the solution was adjusted to 7.5 ± 0.2. After that, 15 mg of agar was added to the solution. The above said set up was sterilized at 120 °C for 15 min. A total of 20 cm^3 of the sterilised medium was poured into the sterilized Petri plates and allowed to solidify. The plates were inoculated with spore suspensions of *Bacillus* sp., *Escherichia coli* and *Pseudomonas* sp. The compounds to be tested were dissolved in DMSO to a final concentration of 0.25 and 0.5% and soaked in filter paper discs of 5-mm diameter and 1-mm thickness. These discs were placed on the already seeded plates and incubated at 35 ± 2 °C for 24 h. The diameter (mm) of inhibition zone around each disc was determined after 24 h and the results are recorded in Table 5. Streptomycin was used as a standard.

3. Results and discussion

The complexes of the general formula {[RuCl(CO)(PPh_3)(B)]$_2$(bis-β-dk)} [where B = PPh_3, pyridine (py), piperidine (pip) or morpholine (mor); bis-β-dk = thiobis(β-diketone)] were synthesised by the reactions of [RuHCl(CO)(PPh_3)$_3$], [RuHCl(CO)(PPh_3)$_2$(py)], [RuHCl(CO)(PPh_3)$_2$(pip)] or [RuHCl(CO)(PPh_3)$_2$(mor)] with the respective thiobis(β-diketones) in a 2:1 molar ratio in benzene as shown below.

$$[RuHCl(CO)(B)(PPh_3)_2] + H_2(\text{bis-}\beta\text{-dk}) \xrightarrow[\text{reflux, 5 h}]{\text{benzene}} \{[RuCl(CO)(B)(PPh_3)]_2(\text{bis-}\beta\text{-dk})\}$$

The analytical data (Table 1) and molecular weight determined (cryoscopic method) for these complexes are in good agreement with the above molecular formula. In all the reactions, it has been observed that the thiobis(β-diketone) behaves as a bifunctional tetradentate bridging ligand by substituting one of the triphenylphosphines and a chloride ion from each mole of the starting complex to form the binuclear complexes.

The new products obtained from the reactions of [RuHCl(CO)(PPh_3)$_3$] with the thiobis(β-diketones) contained two triphenylphosphine on each ruthenium ion, whereas the corresponding reactions of [RuHCl(CO)(PPh_3)$_2$(py)], [RuHCl(CO)(PPh_3)$_2$(pip)] or [RuHCl(CO)(PPh_3)$_2$(mor)] with the thiobis(β-diketone) ligands yielded new complexes with only one triphenylphosphine ligand on each ruthenium ion. These observations do indicate a more labile nature of Ru–P bond compared to the Ru–N bond of the heterocyclic nitrogen bases to the ruthenium ion in these complexes. The difference in the strength of Ru–P and Ru–N bonds may be explained as due to the better σ donating ability of the nitrogen bases [9] compared to that of triphenylphosphine.

3.1. IR spectra

The IR spectrum of (Hacac)$_2$S exhibits a strong band in the 1560 cm^{-1} region, attributable to a strongly conjugated chelated carbonyl group [11]. Absence of a band in the region 780–800 cm^{-1} implies the absence of a hydrogen attached to the carbon joining the two C=O

Table 1
Analytical data, colours, melting points and yields of ruthenium(II) complexes

Complex	Colour	M.p. (°C) [a]	Yield (%)	Found (Calc.) (%)			
				C	H	S	N
{[RuCl(CO)(PPh$_3$)$_2$]$_2$(acac)$_2$S}	yellowish green	155	72	62.80 (62.27)	4.52 (4.07)	1.99 (1.65)	
{[RuCl(CO)(PPh$_3$)(py)]$_2$(acac)$_2$S}	green	136	68	56.17 (55.97)	4.23 (4.07)	2.58 (2.15)	2.26 (1.98)
{[RuCl(CO)(PPh$_3$)(pip)]$_2$(acac)$_2$S}	yellowish green	140	62	58.53 (58.17)	5.93 (5.75)	2.69 (2.35)	2.35 (2.01)
{[RuCl(CO)(PPh$_3$)(mor)]$_2$(acac)$_2$S}	violet	146	64	53.54 (53.15)	4.81 (4.47)	2.55 (2.30)	2.23 (2.01)
{[RuCl(CO)(PPh$_3$)$_2$]$_2$(ba)$_2$S}	brown	122	71	65.24 (64.91)	4.43 (4.10)	1.85 (1.69)	
{[RuCl(CO)(PPh$_3$)(py)]$_2$(ba)$_2$S}	violet	104	62	59.87 (59.40)	4.14 (4.01)	2.35 (1.98)	2.05 (1.91)
{[RuCl(CO)(PPh$_3$)(pip)]$_2$(ba)$_2$S}	green	126	60	59.34 (58.99)	4.98 (4.60)	2.32 (2.06)	2.04 (1.81)
{[RuCl(CO)(PPh$_3$)(mor)]$_2$(ba)$_2$S}	green	156	64	57.43 (57.01)	4.07 (3.80)	2.32 (2.01)	2.03 (1.85)
{[RuCl(CO)(PPh$_3$)$_2$]$_2$(dbm)$_2$S}	green	111	74	67.35 (66.92)	4.35 (4.07)	1.73 (1.50)	
{[RuCl(CO)(PPh$_3$)(py)]$_2$(dbm)$_2$S}	green	102	65	62.94 (62.47)	4.06 (3.75)	2.15 (2.00)	1.88 (1.61)
{[RuCl(CO)(PPh$_3$)(pip)]$_2$(dbm)$_2$S}	green	125	58	62.44 (62.01)	4.84 (4.54)	2.13 (1.98)	1.87 (1.70)
{[RuCl(CO)(PPh$_3$)(mor)]$_2$(dbm)$_2$S}	green	107	60	60.67 (60.11)	4.56 (4.27)	2.13 (2.01)	1.86 (1.64)

[a] Decomposition point.

Table 2
IR and electronic spectral data for ruthenium(II) complexes (ν in cm^{-1} and λ in nm)

Complex	ν(C=O) and ν(C=C)	ν(C≡O)	λ_{max}
{[RuCl(CO)(PPh$_3$)$_2$]$_2$(acac)$_2$S}	1550, 1600	1950	273, 230
{[RuCl(CO)(PPh$_3$)(py)]$_2$(acac)$_2$S}	1570, 1600	1950	273, 229
{[RuCl(CO)(PPh$_3$)(pip)]$_2$(acac)$_2$S}	1560, 1600	1940	274, 231
{[RuCl(CO)(PPh$_3$)(mor)]$_2$(acac)$_2$S}	1560, 1590	1940	274, 230
{[RuCl(CO)(PPh$_3$)$_2$]$_2$(ba)$_2$S}	1560, 1580	1960	271, 231
{[RuCl(CO)(PPh$_3$)(py)]$_2$(ba)$_2$S}	1550, 1590	1950	261, 229
{[RuCl(CO)(PPh$_3$)(pip)]$_2$(ba)$_2$S}	1560, 1890	1950	265, 229
{[RuCl(CO)(PPh$_3$)(mor)]$_2$(ba)$_2$S}	1550, 1610	1950	265, 229
{[RuCl(CO)(PPh$_3$)$_2$]$_2$(dbm)$_2$S}	1570, 1620	1960	261, 229
{[RuCl(CO)(PPh$_3$)(py)]$_2$(dbm)$_2$S}	1560, 1620	1960	261, 225
{[RuCl(CO)(PPh$_3$)(pip)]$_2$(dbm)$_2$S}	1560, 1620	1970	258, 232
{[RuCl(CO)(PPh$_3$)(mor)]$_2$(dbm)$_2$S}	1570, 1610	1960	261, 225

groups. The IR spectra of (Hba)$_2$S and (Hdbm)$_2$S exhibit ν(C=O) at 1650 and 1670 cm^{-1}, respectively, indicating the presence of free carbonyl groups. The presence of a medium intensity band at 780 cm^{-1} in both the ligands is characteristic of CH out-of-plane bending mode [13].

In the IR spectra of all the thiobis(β-diketonato) complexes (Table 2), two bands appeared in the region 1550–1620 cm^{-1}. These bands are characteristic of the mixed modes of vibrations arising from the normal coordinates having contribution from ν(C=O) and ν(C=C) of coordinated β-diketonate groups [14]. From this it is inferred that the thiobis(β-diketones) coordinate to the metal in the conventional O,O bonding mode bridging two [RuCl(CO)(PPh$_3$)(B)] units. A strong band around 1950 cm^{-1} in all the complexes has been assigned to terminally coordinated carbonyl ligand [13]. In the IR spectra of complexes, a medium intensity band is observed in the 1000–1020 cm^{-1} region, characteristic of the coordinated pyridine, piperidine or morpholine [15].

3.2. Electronic spectra

All the ruthenium complexes are found to be diamagnetic which suggests that their geometry ought to be pseudo-octahedral. If the field around Ru^{2+} is assumed as octahedral, the ground state of ruthenium(II) (t_{2g}^6 configuration) should be $^1A_{1g}$. The excited states corresponding to $t_{2g}^5 e_g^1$ configuration are $^3T_{1g}$, $^3T_{2g}$, $^1T_{1g}$ and $^1T_{2g}$ in increasing order of energy. Thus, four bands corresponding to the transitions from $^1A_{1g}$ to $^3T_{1g}$, $^3T_{2g}$, $^1T_{1g}$ and $^1T_{2g}$ should appear in the electronic spectra of the complexes. Regarding charge transfer bands, no band due to L→M transitions is possible in the visible region in the low spin d^6 system [16]. Moreover, the presence of carbonyl and triphenylphosphine as ligands which are capable of producing strong ligand field e_g^* levels place these levels relatively high in energy. As a result, the bands due to charge transfer transitions L$\pi \rightarrow e_g^*$ or L$\sigma_u \rightarrow e_g^*$ should lie in the higher energy region. Therefore, the lowest charge transfer band due to excitation of an electron from metal t_{2g} level to unfilled molecular orbital derived from the π* level of the ligands ($t_{2g} \rightarrow t_{1u}$ or t_{2u}) should appear relatively in high energy region compared to those due to $t_{2g} \rightarrow e_g^*$ transitions [16].

The electronic spectra of all the complexes taken in dichloromethane showed two bands (Fig. 1) in the region 274–225 nm. Based on the values of extinction coefficient ($\varepsilon = 12{,}560$–$18{,}750$ dm^3 mol^{-1} cm^{-1}), both bands have been assigned to charge transfer transitions arising from an excitation of an electron from metal t_{2g} level to unfilled molecular orbitals derived from the π*

level of the ligands [17]. The nature of the observed electronic spectra and the position of absorption bands are consistent with those of other similar octahedral ruthenium(II) complexes [18,19].

3.3. ^{1}H NMR spectra

All the ruthenium(II) complexes exhibit a multiplet at 6.32–8.11 ppm which has been assigned to the protons of phenyl groups present in the triphenylphosphine and thiobis(β-diketone). A singlet observed around 1.21–1.82 ppm in thiobis(acetylacetonato) and thiobis(benzoylacetonato) bridged complexes has been assigned to the methyl protons. The absence of a resonance at approximately 12 ppm in the complexes indicates deprotonation of the enolic group of thiobis(β-diketones) and coordination of the ligand to the metal through O,O donor atoms. The representative spectrum is displayed in Fig. 2.

3.4. ^{31}P NMR spectra

^{31}P NMR spectra were recorded for a few complexes in order to confirm the presence of triphenylphosphine groups and to determine the geometry of the complexes. The observation of six sharp singlets in the spectrum of $\{[RuCl(CO)(PPh_3)_2]_2(acac)_2S\}$ (Fig. 3) and $\{[RuCl(CO)(PPh_3)_2]_2(dbm)_2S\}$ suggests that the compound is a mixture of three possible geometrical isomers (I, II and III). The observation of two singlets around 28 and 45 ppm for the complexes $\{[RuCl(CO)(PPh_3)(pip)]_2(ba)_2S\}$ and $\{[RuCl(CO)(PPh_3)(mor)]_2(dbm)_2S\}$ can be explained as due to a mixture of two geometrical isomers (IV and V). Similar assignment has been made for linkage isomers of diphosphinepalladium nitrite complexes on the basis of ^{31}P NMR [20] Table 3.

In all the complexes, the IR spectrum showed a strong absorption around 1940–1970 cm^{-1}. If the position of CO is *trans* to PPh_3 in the structures II and III, the CO stretching should appear slightly at a higher frequency (ca. 2000 cm^{-1}) due to the presence of π-accepting PPh_3 group *trans* to CO group [21]. In the structures IV and V, the isomers with Cl and CO *trans* to each other are unlikely because of steric hindrance between pyridine and PPh_3 [22].

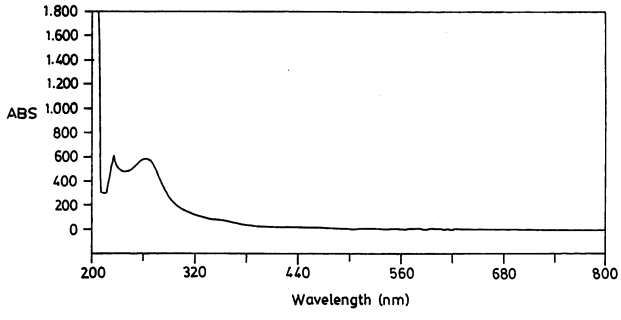
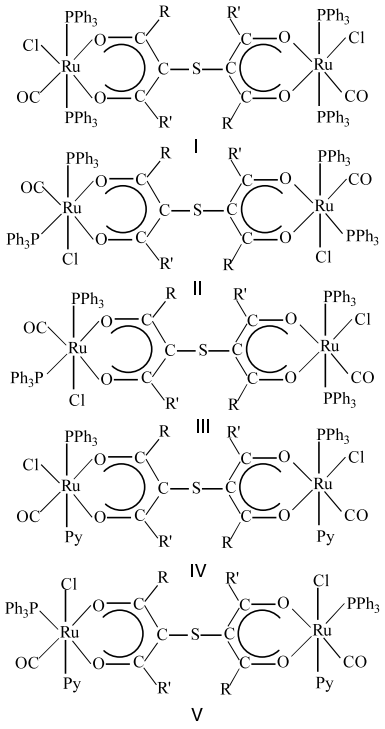


Fig. 1. Electronic spectrum of $\{[RuCl(CO)(PPh_3)(py)]_2(dbm)_2S\}$.



3.5. Catalytic activity

The results of the catalytic oxidation by ruthenium(II) complexes are summarised in Table 4. The oxidation of cinnamyl and benzyl alcohol using the different ruthenium complexes as catalysts in the presence of *N*-methylmorpholine-*N*-oxide (NMO) as co-oxidant were carried out in chloroform. The aldehydes formed after 3 h of reflux were quantified as their 2,4-dinitrophenylhydrazone derivatives. In no case was there any detectable oxidation of alcohols in the presence of *N*-methylmorpholone-*N*-oxide alone without the ruthenium complex. All the synthesised binuclear ruthenium complexes were found to catalyse the oxidation of alcohol to aldehyde but the yields and the turnovers were found to vary with different catalysts.

Complexes that do not contain heterocyclic nitrogen bases exhibit better catalytic activity than the complexes with heterocyclic nitrogen bases. This result is in accord with our observation, taking into account the stronger binding of heterocyclic bases to ruthenium ion, as compared to triphenylphosphine. The formation of the active species is therefore less favoured in the former case than in the latter, resulting in lower catalytic yield [23]. Further, the catalytic activity of binuclear complex, $\{[RuCl(CO)(PPh_3)_2]_2(acac)_2S\}$ has been compared with similar mononuclear complex, $[RuCl(CO)(PPh_3)_2(acac)]$ (VI) and it has been observed that binuclear complex is

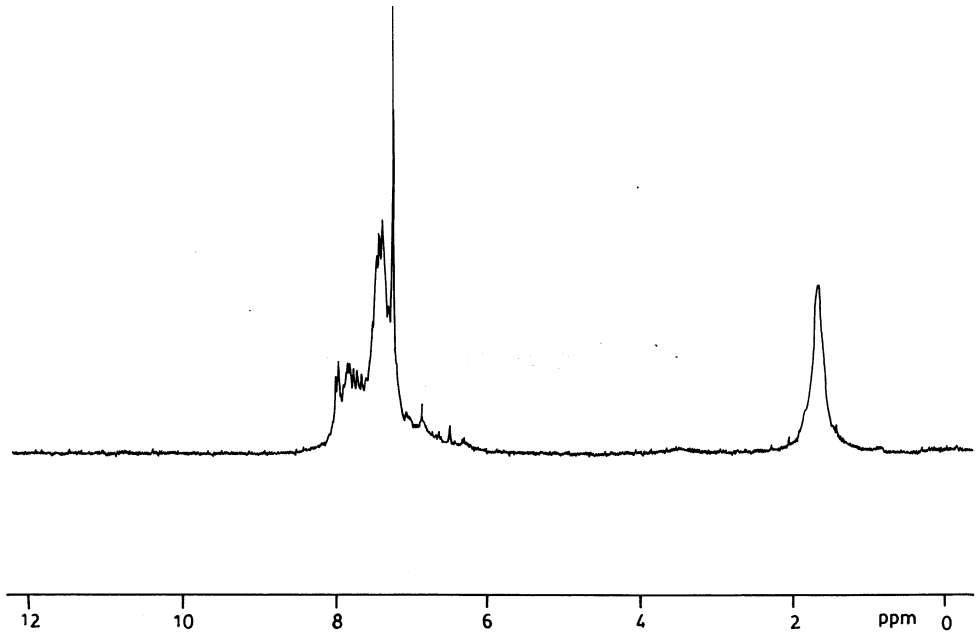
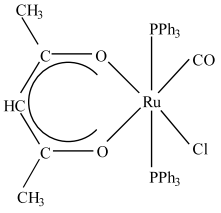


Fig. 2. ^{1}H NMR spectrum of {[RuCl(CO)(PPh$_3$)$_2$](ba)$_2$S}.

better catalyst than the mononuclear complex. This could be because, in binuclear complexes, the catalytically inert M^{n+1}–O–M^{n+1} species formation from possible active species M^{n+2}=O, is less likely than mononuclear complexes, because of its bigger size [24].



VI

3.6. Biocidal studies

The in vitro antibacterial screening of the ligands and some of their ruthenium(II) complexes have been carried out against *Bacillus* sp., *E. coli* and *Pseudomonas* sp. by disc diffusion method [25]. Triplicate plates were maintained in the antibacterial assays. The standard error for each assay is presented in the parenthesis. From the results (Table 5), it has been observed that ruthenium complexes showed better activity than the free ligands. This can be attributed to the Tweedy's chelation theory [26], according to which, chelation reduces the polarity of the central metal atom mainly because of partial

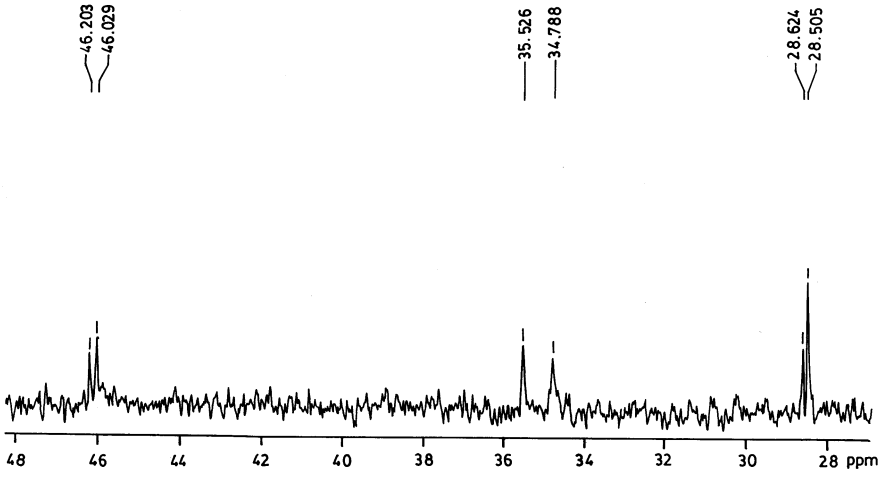


Fig. 3. ^{31}P NMR spectrum of {[RuCl(CO)(PPh$_3$)$_2$]$_2$(acac)$_2$S}.

Table 3
^{1}H and ^{31}P NMR data for ruthenium(II) complexes (δ in ppm)

Complex	^{1}H NMR		^{31}P NMR
	CH_3	Aromatic protons	
{[RuCl(CO)(PPh_3)$_2$]$_2$(acac)$_2$S}	1.21, 1.51	6.87–7.87	28.50, 28.62, 34.79, 35.53, 46.03, 46.20
{[RuCl(CO)(PPh_3)(py)]$_2$(acac)$_2$S}	1.60	6.74–7.72	not recorded
{[RuCl(CO)(PPh_3)(pip)]$_2$(acac)$_2$S}	1.63	6.74–7.91	not recorded
{[RuCl(CO)(PPh_3)(mor)]$_2$(acac)$_2$S}	1.26, 1.69	7.26–7.68	not recorded
{[RuCl(CO)(PPh_3)$_2$]$_2$(ba)$_2$S}	1.65	6.38–8.02	not recorded
{[RuCl(CO)(PPh_3)(py)]$_2$(ba)$_2$S}	1.72	7.67–8.11	not recorded
{[RuCl(CO)(PPh_3)(pip)]$_2$(ba)$_2$S}	1.66	6.32–8.02	28.50, 42.79
{[RuCl(CO)(PPh_3)(mor)]$_2$(ba)$_2$S}	1.82	6.33–8.02	not recorded
{[RuCl(CO)(PPh_3)$_2$]$_2$(dbm)$_2$S}		7.06–8.07	42.11, 42.79, 49.11, 51.83, 51.98, 53.28
{[RuCl(CO)(PPh_3)(py)]$_2$(dbm)$_2$S}		6.75–7.77	not recorded
{[RuCl(CO)(PPh_3)(pip)]$_2$(dbm)$_2$S}		6.74–8.06	not recorded
{[RuCl(CO)(PPh_3)(mor)]$_2$(dbm)$_2$S}		6.33–7.66	28.47, 49.12

Table 4
Catalytic oxidation data of alcohols by ruthenium(II) complexes in the presence of NMO

Complex	Substrate	Product	Yield [a] (%)	Turnover [b]
{[RuCl(CO)(PPh_3)$_2$]$_2$(acac)$_2$S}	cinnamyl alcohol	A	92.5	94
	benzyl alcohol	A	89.9	93
{[RuCl(CO)(PPh_3)(py)]$_2$(acac)$_2$S}	cinnamyl alcohol	A	58.9	60
	benzyl alcohol	A	56.3	58
{[RuCl(CO)(PPh_3)(pip)]$_2$(acac)$_2$S}	cinnamyl alcohol	A	61.8	63
	benzyl alcohol	A	58.9	61
{[RuCl(CO)(PPh_3)(mor)]$_2$(acac)$_2$S}	cinnamyl alcohol	A	60.2	61
	benzyl alcohol	A	49.9	52
{[RuCl(CO)(PPh_3)$_2$]$_2$(ba)$_2$S}	cinnamyl alcohol	A	90.9	93
	benzyl alcohol	A	85.9	89
{[RuCl(CO)(PPh_3)(py)]$_2$(ba)$_2$S}	cinnamyl alcohol	A	58.0	59
	benzyl alcohol	A	50.5	52
{[RuCl(CO)(PPh_3)(pip)]$_2$(ba)$_2$S}	cinnamyl alcohol	A	58.6	60
	benzyl alcohol	A	46.5	48
{[RuCl(CO)(PPh_3)(mor)]$_2$(ba)$_2$S}	cinnamyl alcohol	A	59.6	61
	benzyl alcohol	A	43.5	45
{[RuCl(CO)(PPh_3)$_2$]$_2$(dbm)$_2$S}	cinnamyl alcohol	A	94.1	96
	benzyl alcohol	A	83.5	87
{[RuCl(CO)(PPh_3)(py)]$_2$(dbm)$_2$S}	cinnamyl alcohol	A	56.1	57
	benzyl alcohol	A	44.1	46
{[RuCl(CO)(PPh_3)(pip)]$_2$(dbm)$_2$S}	cinnamyl alcohol	A	60.2	61
	benzyl alcohol	A	57.3	59
{[RuCl(CO)(PPh_3)(mor)]$_2$(dbm)$_2$S}	cinnamyl alcohol	A	53.3	54
	benzyl alcohol	A	38.7	40
[RuCl(CO)(PPh_3)$_2$(acac)] (VI)	cinnamyl alcohol	A	45.5	46
	benzyl alcohol	A	32.3	34

A = corresponding aldehyde.
[a] Yield based on substrate.
[b] Moles of product per mole of catalyst.

sharing of its positive charge with a donor group and possible π-electron delocalisation taking place over the whole ring. This increases the lipophilic character of the metal chelate, which favours the permeation of the complexes through the lipid layer of cell membrane. Though the complexes possess activity, it could not reach the effectiveness of the standard drug, Streptomycin. The inhibition activity of the compounds increases with increase in the concentration of the solution.

Table 5
Antibacterial activity data for selected complexes

Compound	Diameter of inhibition zone (mm)					
	Bacillus sp.		*E. coli*		*Pseudomonas* sp.	
	0.25%	0.5%	0.25%	0.5%	0.25%	0.5%
$(Hacac)_2S$	7 (±0.8)	9 (±1.4)	6 (±0.8)	9 (±1.6)	8 (±1.4)	9 (±0.0)
$\{[RuCl(CO)(PPh_3)_2]_2(acac)_2S\}$	11 (±1.4)	14 (±1.4)	10 (±1.6)	12 (±1.4)	11 (±2.2)	13 (±0.8)
$\{[RuCl(CO)(PPh_3)(py)]_2(acac)_2S\}$	12 (±0.8)	14 (±2.8)	9 (±1.4)	12 (±1.6)	10 (±1.4)	12 (±1.4)
$(Hba)_2S$	8 (±0.8)	10 (±1.6)	7 (±0.8)	10 (±1.4)	7 (±0.8)	9 (±0.8)
$\{[RuCl(CO)(PPh_3)_2]_2(ba)_2S\}$	12 (±1.4)	16 (±2.8)	11 (±0.8)	14 (±0.8)	10 (±1.4)	13 (±1.4)
$\{[RuCl(CO)(PPh_3)(py)]_2(ba)_2S\}$	12 (±1.6)	15 (±2.8)	11 (±0.8)	15 (±1.4)	10 (±0.8)	14 (±1.4)
$(Hdbm)_2S$	6 (±0.0)	10 (±1.6)	7 (±0.8)	9 (±0.8)	6 (±0.0)	9 (±1.4)
$\{[RuCl(CO)(PPh_3)_2]_2(dbm)_2S\}$	11 (±1.4)	13 (±2.2)	11 (±0.8)	14 (±2.8)	10 (±1.4)	15 (±2.8)
$\{[RuCl(CO)(PPh_3)(mor)]_2(dbm)_2S\}$	12 (±1.4)	17 (±2.8)	11 (±1.4)	13 (±2.2)	11 (±1.4)	13 (±0.8)
Streptomycin	21 (±1.4)	25 (±2.8)	20 (±1.4)	23 (±1.4)	19 (±0.8)	21 (±1.6)

Acknowledgements

Financial support received from Council of Scientific and Industrial Research, New Delhi, India, is gratefully acknowledged.

References

[1] H. Sigel (Ed.), Metal Ions in Biological Systems, Copper Proteins, vol. 13, Marcel Dekker, Basel, 1981.
[2] T.G. Spiro (Ed.), Copper Proteins, Wiley Interscience, New York, 1981.
[3] E.I. Solomon, K.W. Penfield, D.E. Wilkox, Struct. Bond. 53 (1983) 1.
[4] A.E. Martell, J. Perutka, D. Kong, Coord. Chem. Rev. 216 (2001) 55.
[5] U. Casellato, P.A. Vigato, D.E. Fenton, M. Vidali, Chem. Soc. Rev. 8 (2) (1979) 199.
[6] D. Fenton, in: A.G. Sykes (Ed.), Adv. Inorg. Bioinorg. Mechanisms, vol. 2, Academic Press, London, 1983, p. 187.
[7] C.J. Cairns, D.H. Busch, Coord. Chem. Rev. 69 (1986) 1.
[8] N. Ahmed, J.J. Levision, S.D. Robinson, M.F. Uttley, Inorg. Synth. 15 (1974) 48.
[9] S. Gopinathan, I.R. Unny, S.S. Deshpande, C. Gopinathan, Indian J. Chem. 25A (1986) 1015.
[10] K. Natarajan, U. Agarwala, Inorg. Nucl. Chem. Lett. 14 (1978) 7.
[11] R.D.J. Jones, L.F. Power, Aust. J. Chem. 24 (1971) 735.
[12] A.I. Vogel, Textbook of Practical Organic Chemistry, 5th ed., Longman, London, 1989.
[13] S. Gopinathan, S.S. Deshpande, C. Gopinathan, Indian J. Chem. 27A (1988) 126.
[14] K. Nakamato, Infrared Spectra of Inorganic and Coordination Compounds, Wiley, New York, 1964.
[15] M. Plytazanopoubs, E. Pnematikakis, N. Hajiliedis, D. Katakia, J. Inorg. Nucl. Chem. 39 (1977) 965.
[16] C.J. Balhausen, H.B. Grey, in: A.E. Martell (Ed.), Coordination Chemistry, vol. 1, Von Nostrand Reinhold, New York, 1971.
[17] A.B.P. Lever, Inorganic Electronic Spectroscopy, 2nd ed., Elsevier, New York, 1984.
[18] R. Karvembu, K. Natarajan, Polyhedron 21 (2002) 219.
[19] V. Chinnusamy, K. Natarajan, Synth. React. Inorg. Met.-Org. Chem. 23 (1993) 745.
[20] J.A. Moser, R.A. Stockland, Jr, G.K. Anderson, Polyhedron 19 (2000) 1329.
[21] J. -Y. Kim, M. -J. Jun, W. -Y. Lee, Polyhedron 15 (1996) 3787.
[22] C. Jayabalakrishnan, K. Natarajan, Transition Met. Chem. 27 (2002) 75.
[23] R.A. Sanchez-Delgado, W.-Y. Lee, S.R. Choi, Y. Cho, M.-J. Jun, Transition Met. Chem. 16 (1991) 241.
[24] P.K. Bhattacharya, Proc. Indian Acad. Sci. (Chem. Sci.) 102 (1990) 247.
[25] C.H. Collins, P.M. Lyne, Microbial Methods, University Park Press, Baltimore, MD, 1970, p. 422.
[26] B.G. Tweedy, Phytopathology 55 (1964) 910.

during which time triethylammonium hydrochloride separated from the colourless solution. This precipitate was removed by suction filtration and the filtrate evaporated to dryness in vacuo to give a white solid product. Yield: 3.92 g, 75%.

2.2. $(C_6H_4O_2)PN(C_2H_4)_2NP(C_6H_4O_2)$ (**2**)

A solution of 1,2-phenylenephosphoro-chloridite (4.65 g, 16.7 mmol) in thf (60.0 cm^3) was added dropwise over a period of 1 h to a stirred solution of piperazine (0.72 g, 8.3 mmol) and triethylamine (1.69 g, 2.3 cm^3, 16.7 mmol) in thf (70.0 cm^3). Stirring was continued for a further 2 h, during which time triethylammonium hydrochloride separated from the colourless solution. This precipitate was removed by suction filtration and the filtrate evaporated to dryness in vacuo to give a white solid product. Yield: 2.15 g, 71%.

2.3. $(C_2H_4O_2)PN(C_2H_4)_2NP(C_2H_4O_2)$ (**3**)

A solution of 2-chloro-1,3,2-dioxaphospholane (5.69 g, 4.0 cm^3, 45.0 mmol) in thf (70.0 cm^3) was added dropwise over a period of 1 h to a stirred solution of piperazine (1.93 g, 22.5 mmol) and triethylamine (4.54 g, 6.2 cm^3, 45.0 mmol) in thf (80.0 cm^3). Stirring was continued for a further 2 h, during which time triethylammonium hydrochloride separated from the colourless solution. This precipitate was removed by suction filtration and the filtrate evaporated to dryness in vacuo to give a white solid product. Yield: 4.31 g, 72%.

2.4. cis-$[PtCl_2\{Ph_2PN(C_2H_4)_2NPPh_2\}]$ (**4**)

To a solution of $[PtCl_2(cod)]$ (0.100 g, 0.26 mmol) in dichloromethane (5.0 cm^3) was added solid $Ph_2PN(C_2H_4)_2NPPh_2$ (0.120 g, 0.26 mmol) and the colourless solution stirred for approximately 2 h. The solution was concentrated under reduced pressure to approximately 1.0 cm^3 and diethyl ether (10.0 cm^3) added. The white product was collected by suction filtration. Yield: 0.152 g, 79%.

2.5. cis-$[PtCl_2\{(C_6H_4O_2)PN(C_2H_4)_2NP(C_6H_4O_2)\}]$ (**5**)

To a solution of $[PtCl_2(cod)]$ (0.100 g, 0.26 mmol) in dichloromethane (15.0 cm^3) was added solid $(C_6H_4O_2)PN(C_2H_4)_2NP(C_6H_4O_2)$ (0.097 g, 0.26 mmol) and the colourless solution stirred for approximately 2 h. The solution was concentrated under reduced pressure to approximately 1.0 cm^3 and diethyl ether (15.0 cm^3) added. The white product was collected by suction filtration. Yield: 0.150 g, 89%.

2.6. cis-$[PtMe_2\{(C_6H_4O_2)PN(C_2H_4)_2NP(C_6H_4O_2)\}]$ (**6**)

To a solution of $[PtMe_2(cod)]$ (0.080 g, 0.24 mmol) in dichloromethane (10.0 cm^3) was added solid $(C_6H_4O_2)PN(C_2H_4)_2NP(C_6H_4O_2)$ (0.087 g, 0.24 mmol) and the colourless solution stirred for approximately 2 h. The solution was concentrated under reduced pressure to approximately 1.0 cm^3 and diethyl ether (40.0 cm^3) added. The white product was collected by suction filtration. Yield: 0.089 g, 63%.

2.7. cis-$[PdCl_2\{Ph_2PN(C_2H_4)_2NPPh_2\}]$ (**7**)

To a solution of $[PdCl_2(cod)]$ (0.100 g, 0.35 mmol) in dichloromethane (5.0 cm^3) was added solid $Ph_2PN(C_2H_4)_2NPPh_2$ (0.160 g, 0.35 mmol) and the yellow solution stirred for approximately 2 h. The solution was concentrated under reduced pressure to approximately 1.0 cm^3 and diethyl ether (10.0 cm^3) added. The yellow product was collected by suction filtration. Yield: 0.137 g, 62%.

2.8. cis-$[Mo(CO)_4\{Ph_2PN(C_2H_4)_2NPPh_2\}]$ (**8**)

To a partially dissolved solution of $[Mo(CO)_4(pip)_2]$ (0.500 g, 1.30 mmol) in dichloromethane (20.0 cm^3) was added solid $Ph_2PN(C_2H_4)_2NPPh_2$ (0.590 g, 1.30 mmol). The solution was heated to reflux for approximately 15 min and allowed to cool to r.t. The solution was concentrated under reduced pressure to approximately 2.0 cm^3 and methanol (15.0 cm^3) added. The yellow product was collected by suction filtration. Yield: 0.635 g, 72%.

2.9. $[Ph_2P(AuCl)N(C_2H_4)_2NP(AuCl)Ph_2]$ (**9**)

To a solution of [AuCl(tht)] (0.071 g, 0.22 mmol) in dichloromethane (5.0 cm^3) was added solid $Ph_2PN(C_2H_4)_2NPPh_2$ (0.050 g, 0.11 mmol) and the colourless solution stirred for approximately 1 h. The solution was concentrated under reduced pressure to approximately 1.0 cm^3 and diethyl ether (5.0 cm^3) added. The white product was collected by suction filtration. Yield: 0.054 g, 53%.

2.10. $[(C_6H_4O_2)P(AuCl)N(C_2H_4)_2NP(AuCl)(C_6H_4O_2)]$ (**10**)

To a solution of [AuCl(tht)] (0.184 g, 0.58 mmol) in dichloromethane (15.0 cm^3) was added solid $(C_6H_4O_2)PN(C_2H_4)_2NP(C_6H_4O_2)$ (0.104 g, 0.29 mmol) and the colourless solution stirred for approximately 1 h. The solution was concentrated under reduced pressure to approximately 1.0 cm^3 and diethyl ether (30.0

cm^3) added. The white product was collected by suction filtration. Yield: 0.205 g, 86%.

2.11. $[(C_2H_4O_2)P(AuCl)N(C_2H_4)_2$-$NP(AuCl)(C_2H_4O_2)]$ (**11**)

To a solution of [AuCl(tht)] (0.160 g, 0.50 mmol) in dichloromethane (15.0 cm^3) was added solid $(C_2H_4O_2)PN(C_2H_4)_2NP(C_2H_4O_2)$ (0.068 g, 0.25 mmol) and the colourless solution stirred for approximately 2 h. The solution was concentrated under reduced pressure to approximately 1.0 cm^3 and diethyl ether (30.0 cm^3) added. The white product was collected by suction filtration. Yield: 0.140 g, 76%.

2.12. $[\{RuCl_2(\eta^6$-p-$MeC_6H_4^iPr)\}_2\{Ph_2PN(C_2H_4)_2NPPh_2\}]$ (**12**)

To a solution of $[\{RuCl(\mu\text{-}Cl)(\eta^6\text{-}p\text{-}MeC_6H_4^iPr)\}_2]$ (0.250 g, 0.40 mmol) in thf (20.0 cm^3) was added solid $Ph_2PN(C_2H_4)_2NPPh_2$ (0.185 g, 0.40 mmol) and the brown solution stirred for approximately 12 h. The solution was concentrated under reduced pressure to approximately 2.0 cm^3 and diethyl ether (10.0 cm^3) added. The red–brown product was collected by suction filtration and washed with diethyl ether (2×10.0 cm^3). Yield: 0.299 g, 69%.

2.13. $Ph_2PN(C_5H_{10})NPPh_2$ (**13**)

A solution of chlorodiphenylphosphine (6.87 g, 5.6 cm^3, 31.2 mmol) in thf (50.0 cm^3) was added dropwise over a period of 1 h to a stirred solution of homopiperazine (1.56 g, 15.6 mmol) and triethylamine (3.13 g, 4.3 cm^3, 31.3 mmol) in thf (75 cm^3) at r.t. Stirring was continued for 2 h, during which time triethylammonium hydrochloride separated from the colourless solution. This precipitate was removed by suction filtration and the filtrate evaporated to dryness in vacuo to give a white solid product. Yield: 4.92 g, 68%.

2.14. $[Ph_2P\{Se\}N(C_5H_{10})N\{Se\}PPh_2]$ (**14**)

To a toluene (20 ml) solution of selenium (0.075 g, 0.904 mmol) was added $Ph_2P\{Se\}N(C_5H_{10})N\{Se\}PPh_2$ (0.207 g, 0.281 mmol). The reaction was stirred and heated to reflux for 2–3 h. The product was collected by suction filtration under nitrogen atmosphere and an off-white product was isolated. Yield: 0.123 g, 70%.

2.15. cis-$[PtCl_2\{Ph_2PN(C_5H_{10})NPPh_2\}]$ (**15**)

To a solution of $[PtCl_2(cod)]$ (0.100 g, 0.26 mmol) in dichloromethane (10.0 cm^3) was added solid $Ph_2PN(C_5H_{10})NPPh_2$ (0.125 g, 0.26 mmol) and the colourless solution stirred for approximately 2 h. The solution was concentrated under reduced pressure to approximately 1.0 cm^3 and diethyl ether (40.0 cm^3) added. The white product was collected by suction filtration. Yield: 0.180 g, 92%.

2.16. cis-$[PtMe_2\{Ph_2PN(C_5H_{10})NPPh_2\}]$ (**16**)

To a solution of $[PtMe_2(cod)]$ (0.100 g, 0.30 mmol) in dichloromethane (10.0 cm^3) was added solid $Ph_2PN(C_5H_{10})NPPh_2$ (0.140 g, 0.30 mmol) and the colourless solution stirred for approximately 2 h. The solution was concentrated under reduced pressure to approximately 1.0 cm^3 and diethyl ether (30.0 cm^3) added. The white product was collected by suction filtration. Yield: 0.130 g, 64%.

2.17. cis-$[PdCl_2\{Ph_2PN(C_5H_{10})NPPh_2\}]$ (**17**)

To a solution of $[PdCl_2(cod)]$ (0.152 g, 0.53 mmol) in dichloromethane (20.0 cm^3) was added solid $Ph_2PN(C_5H_{10})NPPh_2$ (0.250 g, 0.53 mmol) and the yellow solution stirred for approximately 2 h. The solution was concentrated under reduced pressure to approximately 1.0 cm^3 and diethyl ether (40.0 cm^3) added. The yellow product was collected by suction filtration. Yield: 0.300 g, 87%.

2.18. $[Ph_2P(AuCl)N(C_5H_{10})NP(AuCl)Ph_2]$ (**18**)

To a solution of [AuCl(tht)] (0.192 g, 0.60 mmol) in dichloromethane (15.0 cm^3) was added solid $Ph_2PN(C_5H_{10})NPPh_2$ (0.140 g, 0.30 mmol) and the colourless solution stirred for approximately 1 h. The solution was concentrated under reduced pressure to approximately 1.0 cm^3 and diethyl ether (35.0 cm^3) added. The white product was collected by suction filtration. Yield: 0.214 g, 76%.

2.19. $(C_6H_4O_2)PN(C_5H_{10})NP(C_6H_4O_2)$ (**19**)

A solution of 1,2-phenylenephosphoro-chloridite (4.65 g, 16.7 mmol) in thf (55.0 cm^3) was added dropwise over a period of 1 h to a stirred solution of homopiperazine (0.84 g, 8.3 mmol) and triethylamine (1.69 g, 2.3 cm^3, 16.7 mmol) in thf (85.0 cm^3). Stirring was continued for a further 2 h, during which time triethylammonium hydrochloride separated from the colourless solution. This precipitate was removed by suction filtration and the filtrate evaporated to dryness in vacuo to give a white solid product. Yield: 2.58 g, 82%.

2.20. cis-$[PtCl_2\{(C_6H_4O_2)PN(C_5H_{10})NP(C_6H_4O_2)\}]$ (**20**)

To a solution of $[PtCl_2(cod)]$ (0.179 g, 0.48 mmol) in dichloromethane (15.0 cm^3) was added solid

$(C_6H_4O_2)PN(C_2H_4)_2NP(C_6H_4O_2)$ (0.180 g, 0.48 mmol) and the colourless solution stirred for approximately 2 h. The solution was concentrated under reduced pressure to approximately 1.0 cm^3 and diethyl ether (30.0 cm^3) added. The white product was collected by suction filtration. Yield: 0.104 g, 84%.

2.21. *cis-[PtMe$_2${(C$_6$H$_4$O$_2$)PN(C$_5$H$_{10}$)-NP(C$_6$H$_4$O$_2$)}] (**21**)*

To a solution of [$PtMe_2$(cod)] (0.100 g, 0.30 mmol) in dichloromethane (10.0 cm^3) was added solid $(C_6H_4O_2)$-$PN(C_2H_4)_2NP(C_6H_4O_2)$ (0.114 g, 0.30 mmol) and the colourless solution stirred for approximately 2 h. The solution was concentrated under reduced pressure to approximately 1.0 cm^3 and diethyl ether (35.0 cm^3) added. The white product was collected by suction filtration. Yield: 0.120 g, 66%.

2.22. *cis-[PdCl$_2${(C$_6$H$_4$O$_2$)PN(C$_5$H$_{10}$)-NP(C$_6$H$_4$O$_2$)}] (**22**)*

To a solution of [$PdCl_2$(cod)] (0.285 g, 1.00 mmol) in dichloromethane (25.0 cm^3) was added solid $(C_6H_4O_2)$-$PN(C_5H_{10})NP(C_6H_4O_2)$ (0.378 g, 1.0 mmol) and the yellow solution stirred for approximately 2 h. The solution was concentrated under reduced pressure to approximately 1.0 cm^3 and diethyl ether (30.0 cm^3) added. The yellow product was collected by suction filtration. Yield: 0.520 g, 94%.

2.23. *[(C$_6$H$_4$O$_2$)P(AuCl)N(C$_5$H$_{10}$)-NP(AuCl)(C$_6$H$_4$O$_2$)] (**23**)*

To a solution of [AuCl(tht)] (0.140 g, 0.44 mmol) in dichloromethane (15.0 cm^3) was added solid $(C_6H_4O_2)$-$PN(C_5H_{10})NP(C_6H_4O_2)$ (0.083 g, 0.22 mmol) and the colourless solution stirred for approximately 1 h. The solution was concentrated under reduced pressure to approximately 1.0 cm^3 and diethyl ether (30.0 cm^3) added. The white product was collected by suction filtration. Yield: 0.150 g, 81%.

2.24. *(C$_2$H$_4$O$_2$)PN(C$_5$H$_{10}$)NP(C$_2$H$_4$O$_2$) (**24**)*

A solution of 2-chloro-1,3,2-dioxaphospholane (5.69 g, 4.0 cm^3, 45.0 mmol) in thf (55.0 cm^3) was added dropwise over a period of 1 h to a stirred solution of homopiperazine (2.25 g, 22.5 mmol) and triethylamine (4.54 g, 6.2 cm^3, 45.0 mmol) in thf (100.0 cm^3). Stirring was continued for a further 2 h, during which time triethylammonium hydrochloride separated from the colourless solution. This precipitate was removed by suction filtration and the filtrate evaporated to dryness in vacuo to give a white solid product. Yield: 4.91 g, 78%.

2.25. *^{i}Pr$_2$PN(C$_5$H$_{10}$)NP^{i}Pr$_2$ (**25**)*

A solution of diisopropylphosphinechloride (1.61 ml, 0.01 g, 10.0 mmol) in thf (20 cm^3) was added dropwise to a stirred solution of homopiperazine (0.49 g, 4.89 mmol) and degassed Et_3N (1.40 ml, 0.01 g, 10.0 mmol) in thf (20 cm^3) at r.t. The reaction mixture was stirred for a further 2 h, during which time triethylammonium hydrochloride separated from the colourless solution. This precipitate was removed by suction filtration and the filtrate evaporated to dryness in vacuo to give an oily colourless product.

2.26. *[^{i}Pr$_2$P{Se}N(C$_5$H$_{10}$)N{Se}P^{i}Pr$_2$] (**26**)*

To a toluene (10 ml) solution of selenium (0.105 g, 1.330 mmol) was added solid ligand L^3 (0.212 g, 0.638 mmol). The reaction was stirred and heated to reflux for 2–3 h under reflux. The product was collected by suction filtration under nitrogen atmosphere and an off-white product was isolated. Yield: 0.146 g, 47%.

2.27. *cis-[PtCl$_2${^{i}Pr$_2$PN(C$_5$H$_{10}$)NP^{i}Pr$_2$}] (**27**)*

To a solution of [$PtCl_2$(cod)] (0.202 g, 0.541 mmol) in dichloromethane (10 ml) was added solid ligand L^3 (0.180 g, 0.541 mmol). The mixture reaction was stirred for 2 h then diethyl ether (5 ml) was added to solubilise the cod moiety whilst the complex is insoluble and was precipitated as a white solid. After 15 min in the ultrasonic bath, the sample was filtered, the white solid was washed with diethyl ether. Yield: 0.324 g, 50%.

2.28. *Crystallography*

Crystallography was performed using a Bruker SMART diffractometer; full hemisphere of data with 0.3° 'slices', r.t., Mo Kα radiation and empirical absorption corrections. All of the other non-H atoms were refined anisotropically with the hydrogen atoms being refined in idealised geometries. All calculations employed the SHELXTL program system [16].

Compound **7**: $C_{28}H_{28}Cl_2N_2P_2Pd$ $M = 631.8$, monoclinic, space group $P2_1/n$, $a = 11.223(1)$, $b = 27.882(3)$, $c = 17.936(2)$ Å. $\beta = 96.646(3)°$ $U = 5575$ Å^3, $Z = 8$ (two independent molecules), $D_{calc} = 1.51$ g cm^{-3}, $F(000) = 2560$, μ(Mo Kα) = 1.62 mm^{-1}. Of 24 012 measured data, 7949 were unique and observed [$I > 2.0\sigma(I)$] to give $R = 0.080$ and $wR_2 = 0.1421$.

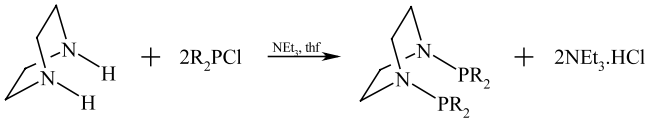
Compound **15**: $C_{47}H_{58}Cl_{10}N_2P_2Pt3$ $M = 1652.7$, orthorhombic, space group $Pca2(1)$, $a = 16.556(1)$, $b = 9.814(1)$, $c = 33.1291(1)$. $U = 5383$ Å^3, $Z = 4$, $D_{calc} = 2.04$ g cm^{-3}, $F(000) = 3152$, μ(Mo Kα) = 8.37 mm^{-1}. Of 21 988 measured data 7523 were unique and observed [$I > 2.0\sigma(I)$] to give $R = 0.0291$ and $wR_2 = 0.0712$. The

H atoms on one of the solvent molecules was not included in the refinement.

$Ph_2(O)PNC_4H_8NP(O)Ph_2 \cdot H_2O$: $C_{28}H_{30}N_2O_3P_2$ $M = 504.5$, monoclinic, space group $P2_1/n$, $a = 9.736(1)$, $b = 12.868(3)$, $c = 10.940(2)$ Å. $\beta = 111.89(1)^\circ$ $U = 1272$ Å^3, $Z = 2$, $D_{calc} = 1.32$ g cm^{-3}, $F(000) = 532$, μ(Mo Kα) = 0.204 mm^{-1} (there was considerable decomposition during data collection and no absorption correction was applied). Of 2560 measured data 1414 were unique and observed [$I > 2.0\sigma(I)$] to give $R = 0.0376$ and $wR_2 = 0.0858$.

3. Results and discussion

Reaction of piperazine with 2 equiv. of the chlorophosphines Ph_2PCl, $R_2 = Ph_2$ (**1**), $C_6H_4O_2$ (**2**) and OC_2H_4O (**3**)



$R_2 = Ph_2$ (**1**), $C_6H_4O_2$ (**2**) and OC_2H_4O (**3**)

(1)

$(C_6H_4O_2)PCl$ and $(C_2H_4O_2)PCl$, in the presence of NEt_3, proceeds in thf to give **1**, **2** and **3** respectively (Eq. (1)).

Addition of the chlorophosphine in thf to a solution of piperazine in thf, at r.t., results in the immediate precipitation of $[Et_3NH]Cl$ as the reaction proceeds. Removal of the ammonium salt by filtration, reduction of the volume of thf in vacuo and addition of diethyl ether gives the new species in 70–80% yield. The $^{31}P\{^1H\}$ NMR spectrum of **1** comprises a singlet at δ(P) 62.9. The possibility of this peak representing the mono-substituted amine was rejected after performing in situ ^{31}P NMR studies. Monitoring of the reaction mixture at regular intervals, immediately after completion of the chlorodiphenylphosphine addition, shows a phosphorus-containing species, with a chemical shift of δ(P) 35.1, to be the initial reaction product. This is assumed to be the mono-substituted amine and gradually decreases in intensity as the reaction proceeds, to leave **1** as the only phosphorus containing compound. The $^{31}P\{^1H\}$ NMR spectrum of **2** and **3** are singlets at δ(P) 144.2 and 137.9 ppm respectively; the large downfield shift when compared with **1** reflecting the close proximity of the phosphorus centre to the strongly electronegative oxygen atoms. Although stable for short periods in the solid state in solution **1**–**3** oxidise readily in solution in air. Crystals of **1O$_2$** were obtained from a CH_2Cl_2 solution of **1** and the structure is shown in Fig. 1

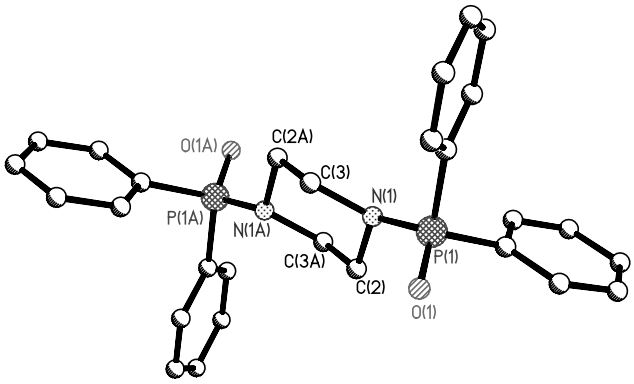
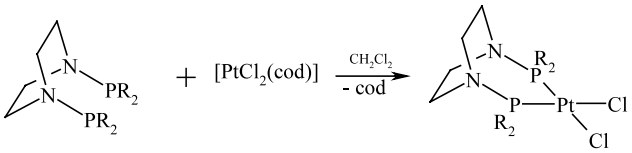


Fig. 1. Solid state structure of $Ph_2P(O)N(C_2H_4)NP(O)Ph_2$.

with selected bond lengths and angles in Table 2. The piperazine ring adopts a chair conformation with the P=O groups being on opposite sides of the molecule.

Reaction of **1** and **2** with equimolar quantities of $[PtCl_2(cod)]$ in dichloromethane (Eq. (2)) to yield the seven-membered, *P,P′* chelates **4** and **5**.



$R_2 = Ph_2$ (**4**), $C_6H_4O_2$ (**5**)

(2)

The $^{31}P\{^1H\}$ NMR spectra of both compounds are singlets with satellites from coupling to ^{195}Pt, the nature of the substituent groups on the phosphorus being reflected in the positions of the chemical shifts (δ(P) 53.5 and 99.6 ppm, respectively) and the magnitude of the $^1J(^{195}Pt-^{31}P)$ coupling constants (3972 and 5480 Hz, respectively) which are in accord with values previously reported for similarly substituted phosphines when *trans* to a chloride in a Pt(II) complex **2** [5,17,18] also reacts with $[PtMe_2(cod)]$, in dichloromethane, to produce the *P,P′* chelate *cis*-$[PtMe_2\{(C_6H_4O_2)PN(C_2H_4)_2NP(C_6H_4O_2)\}]$ (**6**).

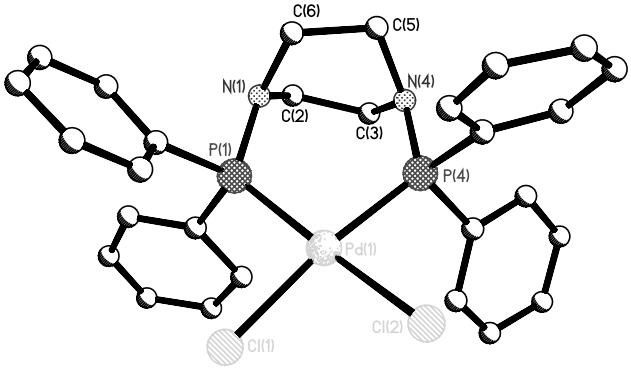


Fig. 2. Solid state structure of *cis*-$[PdCl_2\{Ph_2PN(C_2H_4)_2NPPh_2\}]$ (**7**).

Table 1
Elemental analysis and selected spectroscopic data

	Formula	δ ^{31}P (ppm)/^{1}J(Pt–P) (Hz)	*m/e*	ν(CN)	ν(PN)	C	H	N
1	$Ph_2PN(C_2H_4)_2NPPh_2$	62.9	455	1478	930	73.8(74.0)	6.2(6.2)	5.5(6.2)
2	$(C_6H_4O_2)PN(C_2H_4)_2NP(C_6H_4O_2)$	144.2	362	1479	918	53.2(53.0)	4.3(4.4)	7.3(7.7)
3	$(C_2H_4O_2)PN(C_2H_4)_2NP(C_2H_4O_2)$	137.9	266	1438	952	35.6(36.1)	6.2(6.0)	9.9(10.5)
4	*cis*-$[PtCl_2\{Ph_2PN(C_2H_4)_2NPPh_2]$	53.5/3972	720	1435	960	46.9(46.7)	3.7(3.9)	3.2(3.9)
5	*cis*-$[PtCl_2\{(C_6H_4O_2)_2PN(C_2H_4)_2NP(C_6H_4O_2)_2\}]$	99.6/5480	597[-Cl]	1477	966	30.4(30.6)	2.8(2.6)	4.3(4.5)
6	*cis*-$[PtMe_2\{(C_6H_4O_2)_2PN(C_2H_4)_2NP(C_6H_4O_2)_2\}]$	154.9/2977	587	1480	966	36.3(36.8)	3.9(3.8)	4.6(4.8)
7	*cis*-$[PdCl_2\{Ph_2PN(C_2H_4)_2NPPh_2\}]$	101.7	632	1435	959	52.9(53.3)	4.5(4.5)	4.3(4.4)
8	*cis*-$[Mo(CO)_4\{Ph_2PN(C_2H_4)_2NPPh_2\}]$ [a]	97.2	634	1435	959	57.6(58.0)	3.9(4.3)	3.8(4.2)
9	$[Ph_2P\{AuCl\}N(C_2H_4)_2NP\{AuCl\}Ph_2]$	80.7	883[−Cl]	1434	966	36.4(36.6)	2.8(3.1)	2.4(3.1)
10	$[(C_6H_4O_2)_2P\{AuCl\}N(C_2H_4)_2NP\{AuCl\}(C_6H_4O_2)_2]$	136.4	827	1445	966	23.2(23.2)	1.9(1.9)	3.3(3.4)
11	$[(C_2H_4O_2)_2P\{AuCl\}N(C_2H_4)_2NP\{AuCl\}(C_2H_4O_2)_2]$	131.7	695[−Cl]	1445	967	13.3(13.1)	2.2(2.2)	3.8(3.8)
12	$[\{RuCl_2(\eta^6\text{-}p\text{-}Me\text{-}C_6H_4^iPr)\}_2\{Ph_2PN(C_2H_4)_2NPPh_2\}]$	69.8	1066	1432	953	54.1(54.0)	5.3(5.3)	2.2(2.6)
13	$Ph_2PN(C_5H_{10})NPPh_2$	65.7	468	1431	921	74.4(74.3)	6.1(6.4)	5.8(5.9)
14	$Ph_2P(Se)N(C_5H_{10})NP(Se)Ph_2$	71.9/753	629	1455	912	55.9(55.6)	4.7(4.8)	4.3(4.5)
15	$[PtCl_2\{Ph_2PN(C_5H_{10})NPPh_2\}]$	64.1/4092	734	1436	936	47.4(47.5)	3.9(4.1)	3.4(3.8)
16	$[PtMe_2\{Ph_2PN(C_5H_{10})NPPh_2\}]$	89.1/2231	678[$-CH_3$]	1435	925	53.1(53.6)	4.9(5.2)	3.8(4.0)
17	$[PdCl_2\{Ph_2PN(C_5H_{10})NPPh_2\}]$	92.6	646	1432	953	54.3(54.0)	4.8(4.7)	4.2(4.4)
18	$[Ph_2P\{AuCl\}N(C_5H_{10})NP\{AuCl\}Ph_2]$	78.7	897[−Cl]	1433	903	37.6(37.4)	3.2(3.2)	2.7(3.0)
19	$(C_6H_4O_2)PN(C_5H_{10})NP(C_6H_4O_2)$	148.3	376	1459	916	53.8(54.3)	4.3(4.8)	6.9(7.4)
20	$[PtCl_2\{(C_6H_4O_2)PN(C_5H_{10})NP(C_6H_4O_2)\}]$	102.3/5466	606[-Cl]	1478	951	31.5(31.8)	2.9(2.8)	3.9(4.4)
21	$[PtMe_2\{(C_6H_4O_2)PN(C_5H_{10})NP(C_6H_4O_2)\}]$	156.9/2937	586[$-CH_3$]	1480	919	37.6(37.9)	3.9(4.0)	4.5(4.7)
22	$[PdCl_2\{(C_6H_4O_2)PN(C_5H_{10})NP(C_6H_4O_2)\}]$	125.6	553	1459	916	36.9(36.8)	3.6(3.3)	4.6(5.0)
23	$[(C_6H_4O_2)P\{AuCl\}N(C_5H_{10})NP\{AuCl\}(C_6H_4O_2)]$	139.9	805[−Cl]	1441	908	23.8(24.3)	2.1(2.1)	3.2(3.3)
24	$(C_2H_4O_2)PN(C_5H_{10})NP(C_2H_4O_2)$	143.8	280	1450	931	38.8(38.6)	6.8(6.4)	10.4(10.0)
25	$^iPr_2PN(C_5H_{10})N^iPPr_2$	96.0	215[−Pr2P]	1463	919	60.3(61.4)	12.7(11.6)	8.6(8.4)
26	$^iPr_2P(Se)N(C_5H_{10})N^iP(Se)Pr_2$	101.5/753	629	1455	912	55.9(55.6)	4.71(4.8)	4.3(4.5)
27	*cis*-$PtCl_2[(^iPr_2PN(C_5H_{10})N^iPPr_2)]$	87.6/4020	597	1459	900	34.7(34.1)	6.9(6.4)	4.6(4.7)

NMR in $CDCl_3$. Microanalyses, calculated values in brackets. FAB MS data; values are for parent ions except where indicated otherwise.
[a] ν(CO) 2021, 1917, 1901, 1888 cm^{-1}.

Similarly, the reaction of **1** with an equimolar quantity of $[PdCl_2(cod)]$ in thf results in the bidentate, *P*,*P*′ chelate complex *cis*-$[PdCl_2\{Ph_2PN(C_2H_4)_2NPPh_2]$ (**7**). The X-ray structure of **7** contains two crystallographically independent molecules and shows the product to have the expected square-planar geometry about the Pd centre (Table 2, Fig. 2). The bidentate nature of the co-ordination to the metal results in the formation of two seven-membered Pd–P–N–C–C–N–P ring systems The $N(C_2H_4)_2N$ backbone of the ligand adopts a boat conformation and forms an 'umbrella-like' structure around the Pd centre. The structure also reveals that the square-planar palladium centre is some-

Table 2
Selected comparative bond lengths (Å) and angles (°) in $Ph_2P(O)N(C_2H_4N)P(O)Ph_2$ and $^iPr_2P(Se)N(C_5H_{10})NP(Se)^iPr_2$

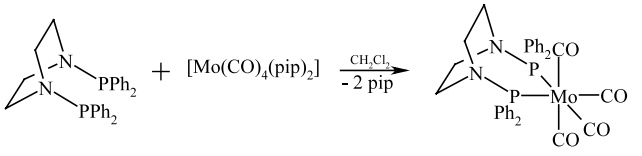
	$Ph_2P(O)N$-$(C_2H_4N)P(O)Ph_2$	$^iPr_2P(Se)N$-$(C_5H_{10})NP(Se)^iPr_2$
Bond lengths		
P(1)–E(1)	1.475(2)	2.115(5)
P(4)–E(4)		2.118(5)
P(1)–N(1)	1.646(3)	1.655(13)
P(4)–N(4)		1.688(14)
Bond angles		
E(1)–P(1)–N(1)	117.4(1)	114.8(5)
E(4)–P(4)–N(4)		111.9(5)

Table 3
Selected comparative bond lengths (Å) and angles (°) in $\{[Pt(cod)Cl_2]_2\cdot[PtCl_2\{Ph_2PN(C_5H_{10})NPPh_2\}]\}$, $[PdCl_2\{Ph_2PN(C_2H_4)_2NPPh_2\}]$ (**7**) and *cis*-$[PtCl_2\{Ph_2PN(C_5H_{10})NPPh_2\}]$ (**15**)

Bond	$[PdCl_2\{Ph_2PN$-$(C_2H_4)_2NPPh_2\}]$ (**7**)	*cis*-$[PtCl_2\{Ph_2PN$-$(C_5H_{10})NPPh_2\}]$ (**15**)
Bond lengths		
M(1)–P(1)	2.246(5) [2.265(5)]	2.255(6)
M(1)–P(4)	2.256 (5) [2.246(5)]	2.215(6)
M(1)–Cl(1)	2.391 (4) [2.363(4)]	2.358(7)
M(1)–Cl(2)	2.381 (5) [2.388(5)]	2.388(5)
P(1)–N(1)	1.697 (13) [1.680(12)]	1.70(2)
P(4)–N(4)	1.666 (13) [1.704(14)]	1.64(2)
Bond angles		
P(1)–M(1)–P(4)	93.9(2) [94.7(2)]	97.3(1)
Cl(1)–M(1)–Cl(2)	92.1(2) [91.9(2)]	89.1(1)
M(1)–P(1)–N(1)	120.1(5) [121.8(6)]	119.0(8)
M(1)–P(4)–N(2)	123.3(5) [121.2(6)]	125.0(8)

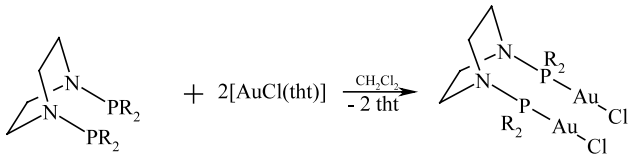
N.B. The values in parentheses are for the second crystallographically independent molecule.

what distorted and in both of the two independent molecules the bite angle of the piperazine is larger than the ideal 90° [94.0 (2°) and 94.7 (2°)] and the Cl–Pd–Cl angles are also greater than 90° [92.1 (2°) and 92.0 (2°)]. The mean deviations of PdP_2Cl_2 from the plane are 0.14 Å for one of the molecules and 0.02 Å for the second. In both molecules the P–N, Pd–P and P–Cl bond lengths are all typical of single bonds.



(3)

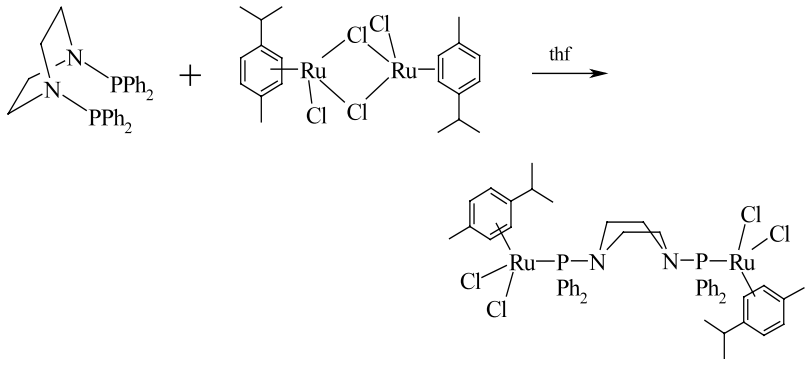
form seven-membered metallacycles. Reactions with compounds containing Au(I) and Ru(II) show that **1**–**3** can also act as a bridging ligands between two metal centres (Eq. (4)).



R = Ph (**9**), $C_6H_4O_2$ (**10**) OC_2H_4O (**11**)

(4)

Analogous ligands to **1**–**3** can be synthesised by reacting the same chlorophosphines with homopiperazine which differs from piperazine by containing an extra CH_2 group, therefore, forming a seven-membered nitrogen–carbon ring system. Reaction of homopiperazine with 2 equiv. of Ph_2PCl, $(C_6H_4O_2)PCl$ and $(C_2H_4O_2)PCl$, in the presence of NEt_3, proceeds in thf to give **13, 19** and **24.** Reaction of $^{i}Pr_2PCl$ with homopiperazine yields the analogous ^{i}Pr derivative **25**. The δ_P values of all three aryl ligands are slightly downfield from the values observed for the analogous piperazine derivatives, **1**–**3**, suggesting that the addition



The reaction of **1** with $[Mo(CO)_4(pip)_2]$ in dichloromethane proceeds, with displacement of the piperidines, to give **8** (Eq. (3)). The $^{31}P\{^{1}H\}$ NMR spectrum of **8** displays a singlet at δ(P) 97.2, a downfield shift of around 35 ppm upon complexation whilst its IR spectrum contains four strong bands due to ν(CO) (2021, 1917, 1901 and 1888 cm^{-1}), confirming the *cis* structure. Compounds **4**–**8** demonstrate the ability of $Ph_2PN(C_2H_4)_2NPPh_2$ and $(C_6H_4O_2)PN(C_2H_4)_2NP(C_6H_4O_2)$ to act as bidentate chelating ligands and

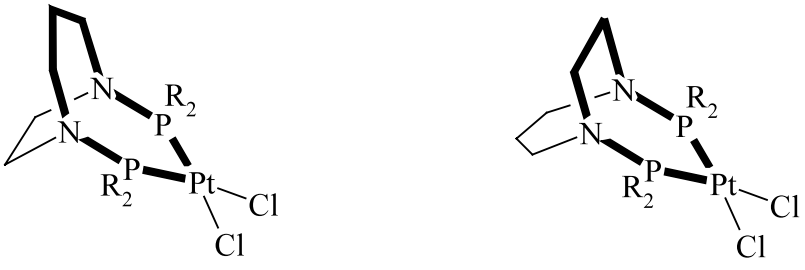


Fig. 3. Different ring sizes in complexes containing the homopiperazine based ligands.

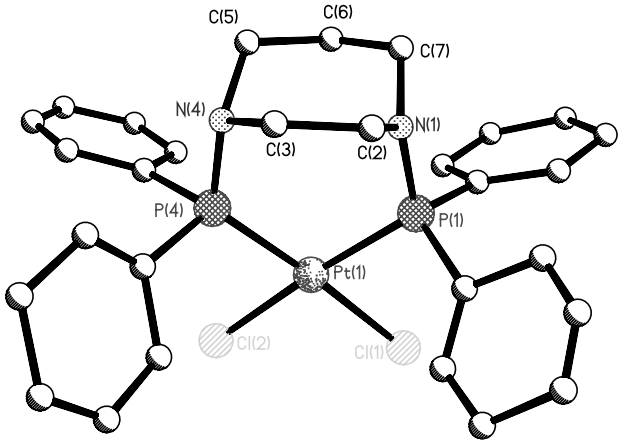


Fig. 4. The structure of $[PtCl_2\{Ph_2PN(C_5H_{10})NPPh_2\}]$ in the crystal structure of $[Pt(cod)Cl_2]_2 \cdot [PtCl_2\{Ph_2PN(C_5H_{10})NPPh_2\}]$.

of an extra CH_2 group into the ligand backbone causes a slight deshielding of the phosphorus centres. The homopiperazine derivatives form complexes in an analogous fashion to their piperazine analogues. Spectroscopic data for the new compounds are summarised in Tables 1–3.

The Pt(II), Pd(II) and Mo(0) complexes of **13**, **19** and **24** contain seven- and eight-membered (Figs. 3 and 4) chelate rings. The spectroscopic data for derivatives of the two amines, which incorporate the same phosphorus substituents, are very similar suggesting that the extra CH_2 in the homopiperazine ligands has little effect on the electronic properties of the ligands and resulting complexes.

The X-ray structure of *cis*-$[PtCl_2\{Ph_2PN(C_5H_{10})NPPh_2\}][PtcodCl_2]_2$ was obtained. It reveals that the P–Pt–P bite angle is expanded to 97° as a consequence of the homopiperazine backbone.

This work clearly demonstrates the usefulness of simple organic nitrogen containing rings in the formation of large bite angle phosphines.

4. Supplementary material

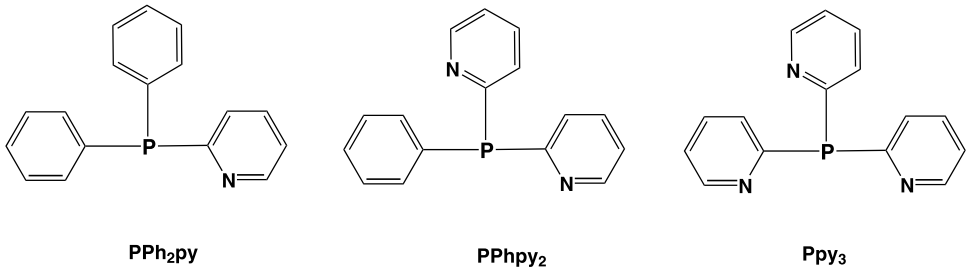
Crystallographic data for the structural analyses has been deposited with the Cambridge Crystallographic data centre, CCDC Nos. 176413–176415. Copies of this information may be obtained free of charge from The Director CCDC, 12 Union Road, Cambridge, CB2 1EZ, UK. (fax: +44-1223-336-033; email: deposit@ccdc.cam.ac.uk or www: http://www.ccdc.cam.ac.uk.

Acknowledgements

We are grateful to the EPSRC for support, to Johnson Matthey for loans of precious metals and to the JREI for an equipment grant.

References

[1] P. Bhattacharyya, J.D. Woollins, Polyhedron 14 (1995) 3367.
[2] T.Q. Ly, J.D. Woollins, Coord. Chem. Rev. 176 (1998) 451.
[3] J.D. Woollins, J. Chem. Soc., Dalton Trans. (1996) 2893.
[4] A.M.Z. Slawin, M.B. Smith, J.D. Woollins, J. Chem. Soc., Dalton Trans. (1996) 4575.
[5] P. Bhattacharyya, A.M.Z. Slawin, M.B. Smith, D.J. Williams, J.D. Woollins, J. Chem. Soc., Dalton Trans. (1996) 3647.
[6] T.Q. Ly, A.M.Z. Slawin, J.D. Woollins, Angew. Chem., Int. Ed. Engl. 37 (1998) 2501.
[7] M.L. Clarke, D.J. Cole-Hamilton, A.M.Z. Slawin, J.D. Woollins, J. Chem. Soc., Chem. Commun. (2000) 2065.
[8] M. Rodriguez i Zubiri, M.L. Clarke, D.F. Foster, D.J. Cole-Hamilton, A.M.Z. Slawin, J.D. Woollins, J. Chem. Soc., Dalton Trans. (2001) 969.
[9] S.M. Aucott, A.M.Z. Slawin, J.D. Woollins, J. Organomet. Chem. 582 (1999) 83.
[10] S.M. Aucott, A.M.Z. Slawin, J.D. Woollins, J. Chem. Soc., Dalton Trans. (2000) 2559.
[11] T.Q. Ly, A.M.Z. Slawin, J.D. Woollins, Polyhedron 18 (1999) 1761.
[12] Q. Zhang, A.M.Z. Slawin, J.D. Woollins, J. Chem. Soc., Dalton Trans. (2001) 3598.
[13] A.M.Z. Slawin, J.D. Woollins, Q. Zhang, J. Chem. Soc., Dalton Trans. (2001) 621.
[14] G.J.P. Britovsek, V.C. Gibson, D.F. Wass, Angew. Chem., Int. Ed. Engl. 38 (1999) 428.
[15] M.A. Bennett, T.N. Huang, T.W. Matheson, A.R. Smith, Inorg. Synth. 21 (1982) 74.
[16] SHELXTL, Bruker AXS, Madison, WI, 1999.
[17] A. Sen, Acc. Chem. Res. 26 (1993) 303.
[18] V.S. Reddy, K.V. Katti, C.L. Barnes, Chem. Ber. 127 (1994) 1355.



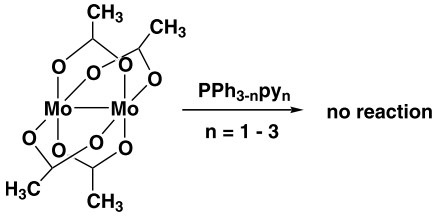
Scheme 1.

tion process while the pyridine ligand would otherwise protect the potential coordination site, thus enhancing the initiator stability. In this work, we report the syntheses and characterization of dimolybdenum and dirhodium compounds bridged and/or axially coordinated by PPh_2py, $PPhpy_2$ and Ppy_3 ligands. The X-ray crystal structures of selected complexes are described as well.

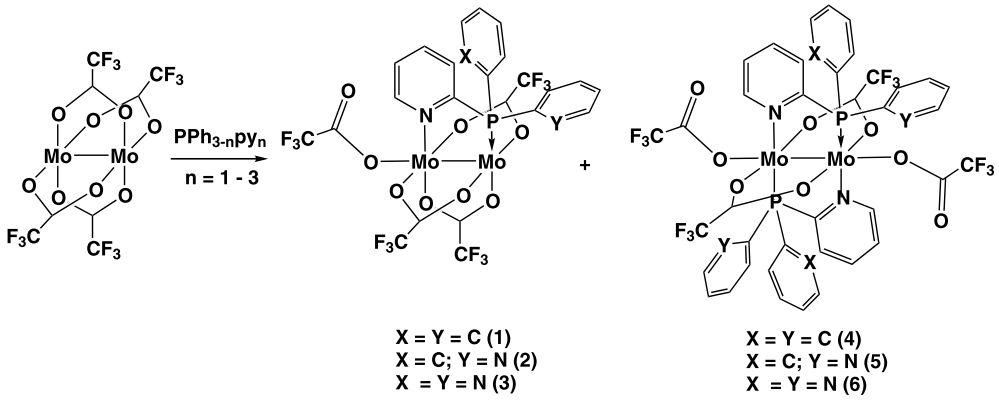
2. Results and discussion

2.1. Synthesis

The reaction of $Mo_2(\mu\text{-}O_2CCF_3)_4$ with 2 equiv. of the corresponding ligand at room temperature yields the complexes **1**–**3**, respectively, with only one $CF_3CO_2^-$ group in the axial position according to Eq. (1). When excess of ligand (fourfold in these cases) is used at room temperature, complexes **4**–**6** (complex **6** is always contaminated with derivative **3**), with two axial $CF_3CO_2^-$ groups are formed according to Eq. (2). Even under reflux conditions a mixture of **3** and **6** is isolated after 4 h, containing only approximately 73% of complex **6**. Reaction of a much higher excess of Ppy_3 with $Mo_2(\mu\text{-}O_2CCF_3)_4$ leads to a mixture of products as well. The reason for this behavior might be that a coordination of Ppy_3 disfavors the coordination of a second ligand of this type in *trans* position, due to the more pronounced *trans* effect of Ppy_3 in comparison to $PPhpy_2$. The *cis* position is probably not available for a second Ppy_3 ligand because of steric reasons. The compounds **1**–**6** are insoluble in CH_2Cl_2, CH_3CN, diethyl ether, and decompose in methanol, DMF and DMSO. This decomposition could be due to an opening of the pyridine–N bond to the metal center in the presence of donor solvents with subsequent cleavage of the metal–metal bond.



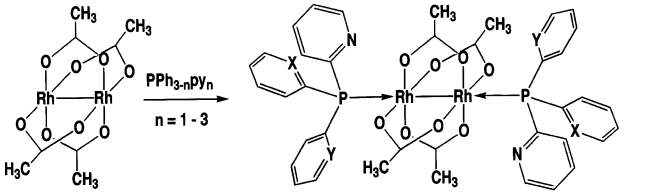
(1)



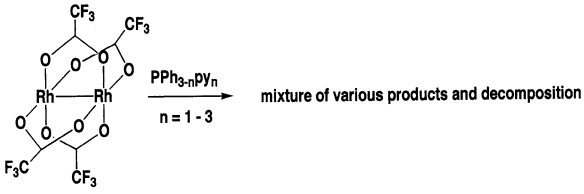
(2)

The orange–red complexes **7**–**9** can be prepared by reacting excess of ligand with $Rh_2(\mu\text{-}O_2CCH_3)_4$ at room temperature (Eq. (3)). The same products **7**–**9**, however, are also formed when $Rh_2(\mu\text{-}O_2CCH_3)_4$ and the ligands are reacted in a 1:1 stoichiometric relationship. Half of

the Rh_2 starting complex remains unchanged, but no product with only one axial ligand is formed. Heating or even refluxing the reaction mixture also does not influence the outcome to our experience (i.e. no equatorial substitution products are formed). The rhodium complexes **7**–**9** are soluble in CH_2Cl_2, but insoluble in THF, acetone and CH_3CN. It is noteworthy in this context that $Mo_2(\mu\text{-}O_2CCH_3)_4$ does not react with PPh_2py, $PPhpy_2$ and PPy_3 (see Eq. (1)). The interaction of $Rh_2(\mu\text{-}O_2CCF_3)_4$ with PPh_2Py, $PPhPy_2$ and PPy_3 leads to a mixture of different products and decomposition products (Eq. (4)). It was, unfortunately, not possible to separate the compounds and characterize them properly.



(3)



(4)

The explanation for the different reaction behavior of the Mo_2 and Rh_2 complexes seems to be that the stronger Mo–O interactions (in contrast to the weaker Rh–O interactions) in the tetra acetato derivatives cannot be easily cleaved by the pyridylphosphines under the reaction conditions applied. The weaker Mo–O bonds to the electron withdrawing tetrakis(trifluoroacetato) ligands are easier to break. In both cases, however, an attack on the axial positions is not observed, probably due to the generally weak interactions of $Mo(II)_2$ units with ligands in this position. In the case of the Rh_2 complex, the tetra acetato complex reacts with the pyridylphosphines, since the interactions with ligands in the axial positions of the Rh–Rh unit are stronger and lead to more stable products. Equatorial bonds, however, are also not cleaved in the Rh_2 complexes. In the case of the more reactive $Rh_2(O(O)C\text{–}CF_3)_4$ derivative, the axial and equatorial positions are available to an attack and the reaction leads to a product mixture. Some of the products are probably not stable and undergo further reactions, thus leading to an inseparable mixture of product compounds.

We found no indication for the formation of orthometallated triaryl phosphines bridging the M–M bonds in any of our reactions. Despite the fact that there are several related compounds forming orthometallated products, this was not observed in our case since our reaction conditions obviously do not favor the abstraction of aryl ring protons. With appropriately changed reaction conditions, however, it might be possible to generate orthometallated derivatives [4j] [11]. The geometry of the examined compounds (see X-ray part) would—at least in principle—allow such reactions.

2.2. Thermogravimmetry

The complexes **1**, **4** and **7** as well as the pyridylphosphine PPh_2py and the starting materials $Mo_2(O(O)CCF_3)_4$ and $Rh_2(O(O)CCH_3)_4$ have been examined by thermogravimmetry (TGA). PPh_2py starts subliming at approximately 179 °C and sublimes completely, not leaving any residue. $Rh_2(O(O)CCH_3)_4$ has a decomposition onset at 278 °C and $Mo_2(O(O)CCF_3)_4$ starts subliming at 226 °C. The compound **7** displays a decomposition onset at 296 °C, being about 20 °C higher than that of the Rh_2 starting material, while compound **4** starts decomposing at approximately 220 °C, slightly below the sublimation point of the Mo_2 starting material. The same is true for compound **1**, which starts decomposing at 211 °C. In the case of compound **1** only one pronounced decomposition step is observed. It starts decomposing slowly with an onset at approximately 211 °C, continues (beginning at 290 °C) with a sharper decline and then keeps loosing mass until the end of the measurement at 650 °C. The total mass loss until the end of the more pronounced step is about 40% of the original mass, which would be the sum of one trifluoro acetate ligand and the PPh_2py ligand. The total mass loss until the end of the measurement at 650 °C is about 68% of the original mass. In the case of compound **7**, one clear decomposition step is observed. It accounts for 30% of the original mass and leads to an unspecific further decomposition, which reaches a total mass loss of 45% at 650 °C.

The observed curve shapes and mass losses indicate that in all three cases (complexes **1**, **4** and **7**) the decomposition starts-as expected-with a loss of an axial ligand. Then the complexes start losing equatorial ligands. A sublimation of the complexes without decomposition is not observed.

2.3. X-ray crystallography

The molecular structures of compounds **5** and **6** have been determined by single crystal X-ray crystallography. PLATON representations of compounds **5** and **6** are

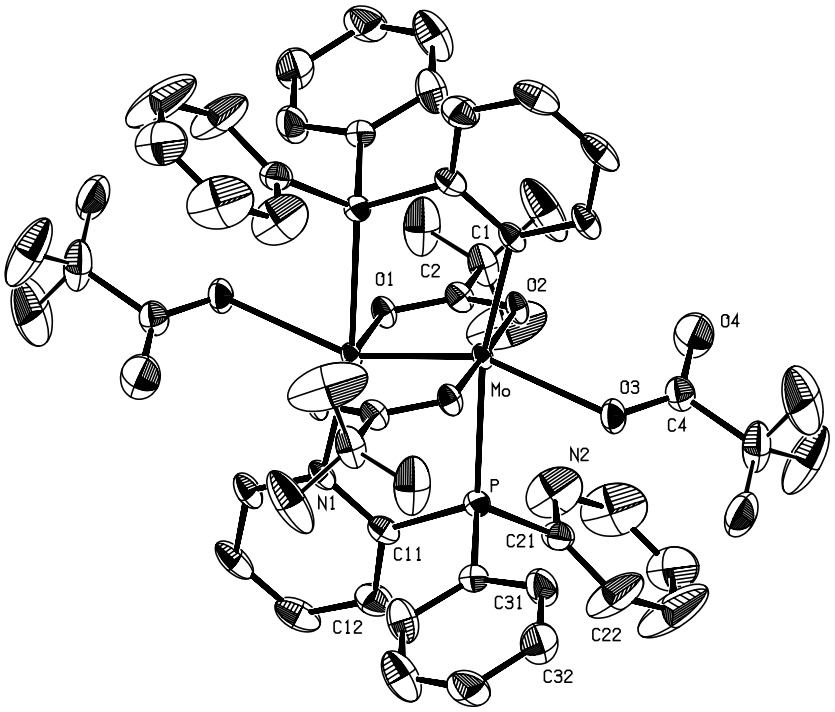


Fig. 1. ORTEP [15] drawing of the molecular structure of the major form of **5** in the solid state; thermal ellipsoids are at the 50% probability level and hydrogens omitted for clarity.

shown in Figs. 1 and 2, respectively. Selected bond distances and angles are listed in Table 1 for the compounds **5** and **6**.

The dimolybdenum centers are coordinated by two bridging CF_3COO^- ligands, which are *trans* positioned to each other. The complex resides on a crystallographic

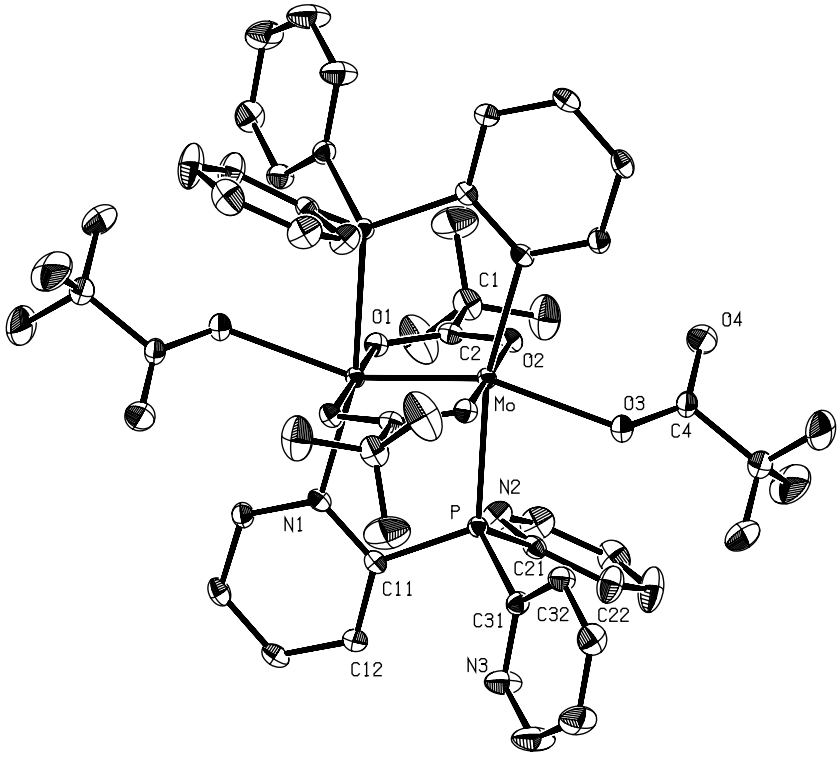


Fig. 2. ORTEP [15a] drawing of the molecular structure of **6** in the solid state; thermal ellipsoids are at the 50% probability level and hydrogens omitted for clarity.

Table 1
Comparison of selected structural data for complexes **5** and **6**. Mo and Mo′ are connected via the symmetry operation (−x, −y, 1−z) for **5** and (−x, −y, −z) for **6**, respectively

	5	**6**
Bond distances (Å)		
Mo–P	2.5085(8)	2.5254(5)
Mo–O2	2.105(2)	2.1265(13)
Mo–O3	2.399(2)	2.3492(13)
Mo–Mo′	2.1901(3)	2.1884(2)
Mo′–O1	2.118(2)	2.1123(13)
Mo′–N1	2.212(2)	2.2056(16)
O1–C2	1.261(4)	1.265(2)
O2–C2	1.254(4)	1.254(2)
O3–C4	1.253(4)	1.259(2)
O4–C4	1.206(5)	1.219(3)
Bond angles (°)		
P–Mo–O2	94.36(6)	91.57(4)
P–Mo–O3	74.75(5)	73.18(4)
Mo′–Mo–P	83.48(2)	83.96(1)
P–Mo–O1′	88.39(6)	90.96(4)
P–Mo–N1′	166.93(6)	167.46(4)
O2–Mo–O3	98.52(7)	84.17(5)
Mo′–Mo–O2	91.23(5)	89.74(4)
O1′–Mo–O2	177.11(8)	177.15(5)
O2–Mo–N1′	90.70(8)	89.79(5)
Mo′–Mo–O3	156.69(5)	156.11(4)
O1′–Mo–O3	81.32(7)	95.33(5)
O3–Mo–N1′	92.60(7)	94.57(5)
Mo′–Mo–O1′	89.98(5)	91.81(4)
Mo′–Mo–N1′	108.49(6)	108.51(4)
O1′–Mo–N1′	86.42(8)	87.46(5)
O1–C2–O2	125.6(3)	126.33(17)
O1–C2–C1	117.0(3)	116.48(16)
O2–C2–C1	117.4(3)	117.09(17)
O3–C4–O4	129.1(3)	130.10(19)
O3–C4–C3	115.3(3)	114.76(17)
O4–C4–C3	115.6(3)	115.09(18)

center of inversion. The other two CF_3COO^- groups coordinate to one of the metal centers in the axial position. The two 2-pyridylphosphine ligands are in a head-to-tail (HT) relationship and are *trans* to each other. A similar structure has been reported for $Mo_2(\mu\text{-}PPh_2Py)_2(\mu\text{-}CH_3COO)_2Cl_2$ by Cotton and Matusz [3h,3i]. In our case and in that of Cotton's compound the thermodynamically more favored HT relationship and not the generally more common head-to-head (HH) arrangement is observed. The reason for the formation of the HT product might in our case be the stepwise formation of **4**–**6** from the in-situ precursors **1**–**3**, which display only one bridging ligand. The first $P(Ar)_3$ ligand probably directs the second $P(Ar)_2$ ligand to the thermodynamically more favored HT arrangement, assisted by the long reaction time at high temperature and the steric bulk of the ligands. As can be seen in Fig. 1, the short Mo–N distance, close to the region of axial coordination, together with the long Mo–P distance and the other two uncoordinated pyridyl groups directed away from the axial region cause a displacement of the axial CF_3COO^- group away from the 'linear' axial site by 156.69(5)° (compound **5**) or 156.11(4)° (complex **6**), respectively.

Similar observations are reported for other dimolybdenum(II) compounds in the literature [3h]. Due to the strong interaction of axial CF_3COO^- group with the Mo_2^{4+} moiety, the Mo–Mo distances, 2.1901(3) Å for **5** and 2.1884(2) Å for **6**, respectively, are approximately 0.1 Å longer than in the precursor complex $Mo_2(\mu\text{-}O_2CCF_3)_4$ (Mo–Mo: 2.090(4) Å) [12]. The Mo–Mo bond lengths observed in the compounds **5** and **6** are among the longest Mo–Mo quadruple bond distances reported to date. [13,14] This lengthening in comparison to the starting material is due to the weakening of the Mo–Mo bond by the axial ligand coordination.

2.4. Vibrational spectroscopy

The solid-state IR spectra of complexes **1**–**6** show strong absorption bands in the range of 1650–1700 cm^{-1}, indicating the presence of monocoordinated carboxylate group(s) [3f]. The vibrations observed at 1687 (**4**), 1690 (**5**) and 1684 cm^{-1} (**6**) are assigned to terminal carboxylate groups. The vibrations at 1650 (**1**), 1654 (**2**) and 1647 cm^{-1}(**3**) are also assigned to the terminal carboxylate group. The vibrations located at approximately 1600 cm^{-1} represent the asymmetric stretching vibration of the bridging trifluoroacetates. The Raman active ν(Mo–Mo) band shows that in the case of **4**, **5** and **6** the Mo–Mo bond strength is significantly weakened by the change of the coordination mode (**4** (305 cm^{-1}), **5** (307 cm^{-1}), **6** (308 cm^{-1})) in comparison to the axially uncoordinated precursor $Mo_2(\mu\text{-}O_2CCF_3)_4$ (397 cm^{-1}) [8]. The Mo–Mo stretching modes of the complexes **1**, **2** and **3**, observed at 375 cm^{-1} for **1**, 376 cm^{-1} for **2** and at 378 cm^{-1} for **3** indicate a much less pronounced influence on the strength of the Mo–Mo quadruple bond, since only one axial ligand is present. The influence of exchanging a Ph group in the ligand by a py ligand, however, has seemingly very little influence on the Mo–Mo bond strength and is of the same order of magnitude as the error range of the measurement.

The vibrations of the bidentate acetato groups are located at 1600, 1423, 623, 507 cm^{-1} for **7**, 1596, 1434, 650, 542 cm^{-1} for **8** and at 1594, 1422, 695, 561, 525 cm^{-1} for **9**, respectively. These vibrations indicate that only one type of carboxylate exists; the strong Raman band at 335 cm^{-1} (**7**), 337 cm^{-1} (**8**) and 338 cm^{-1} (**9**) refers to the complete symmetric Rh–O vibrations of RhO_4 square-planar fragments. Its asymmetric vibrations can appear as IR active mode. In addition, the very intensive Raman band at 285 cm^{-1} (**7**), 287 cm^{-1} (**8**) and 289 cm^{-1} (**9**) can be assigned to the Rh–Rh stretching mode. The Rh–Rh vibration of $Rh_2(Ac)_4$ is

located at 351 cm^{-1}. Unlike equatorial coordination patterns of these pyridylphosphine ligands to the $Mo_2(\mu\text{-}O_2CCF_3)_4$ moiety, these pyridylphoshpines prefer axial interaction with $Rh_2(\mu\text{-}O_2CCH_3)_4$ under the conditions applied. The compounds $Rh_2(\mu\text{-}O_2CR)_4L_n$ ($n = 1$ or 2) are the largest class of dirhodium(II) compounds known to date [14].

2.5. NMR spectroscopy

The ^1H NMR signals of the pyridyl groups in complexes **7**, **8** and **9** display only a slight downfield shift in comparison to the free ligand. Complexes **7** and **8** display seven signals in the aromatic region and one singlet for the acetate $-CH_3$-group, while complex **9** shows four signals in the aromatic region and one singlet for the acetate CH_3-group. All observed ^1H NMR signals are very sharp and the signals in the aromatic region display the expected J-couplings. This is in accord with the postulated structures of the complexes **7**–**9**. Temperature-dependent ^1H NMR spectroscopy was performed to examine fluxionality of the acetates, i.e. exchange of axial and equatorial ligands in solution. However, no broadening or splitting in the temperature range of -90 to 30 °C was observed.

The $^{13}C\{^1H\}$ NMR spectra of the complexes **7** and **8** show nine signals in the aromatic region, the spectrum of compound **9** displays five signals in the aromatic region. These signals as well as the signals of the $-CH_3$ groups and the C(O)O moieties are in accord with the expectations for the suggested structures of the complexes **7**–**9**.

The $^{31}P\{^1H\}$ NMR signals, located at -15.26 (compound **7**) -8.99 (complex **8**) and -2.64 ppm (complex **9**), are broad triplets (half widths ca. 150–160 Hz) in all three cases at room temperature. At -75 °C the signals get significantly sharper. The signals appear to be a doublet of doublets with $^1J_{P-Rh} \approx 45$ Hz, $^2J_{P-Rh} \approx 35$ Hz. The ligand signals are shifted almost 11 ppm upfield for complex **7** and about 6 ppm upfield in the case of complex **8** in comparison to free ligand. The shift change in comparison to the free ligand in the case of complex **9** is smaller, only approximately 1.5 ppm. These observations indicate that the Ppy_3 ligands do not exchange so readily electron density with the metal centers as the PPh_2py and the $PPhpy_2$ ligands. The ability to act as electron acceptor is less pronounced in the electron rich Ppy_3 ligand.

Since the complexes **1**–**6** are insoluble in all common organic solvents, ^{31}P solid-state NMR spectra were measured of all complexes described in this work. Only complex **4** shows sufficient solubility in CH_2Cl_2 to receive a $^{31}P\{^1H\}$ solution NMR spectrum. In the case of the Mo_2 derivatives the solid-state ^{31}P NMR signals are slightly more low field shifted in the row $PPh_2py > PPhpy_2 > Ppy_3$. The opposite trend is observed for the free ligands in solution. The shift difference between coordinated and free ligands is $>$ 30 ppm. Shift differences of this order of magnitude are not uncommon for equatorially coordinated phoshine ligands. The shift differences between the complexes with one or two axial ligands observed here, however, are in quite small, only in the order of 1 ppm. In the case of the axially coordinated phoshine ligands in the compounds **7**–**9** the trend observed in solution (see above) also holds for the solid state. The shift difference between solid state and solution is in all three cases < 2 ppm. The splitting of the solid-state ^{31}P NMR signals due to a P–Rh coupling cannot be observed. The solid state signal are in general very broad.

2.6. Electronic absorption spectroscopy

The electronic absorption spectra of the soluble complexes **7**, **8** and **9** were measured in methylene chloride at room temperature. The lowest energy absorptions centered at 486 nm ($\varepsilon = 350$ M^{-1} cm^{-1}) for compound **7**, at 496 nm ($\varepsilon = 600$ M^{-1} cm^{-1}) for compound **8** and at 568 nm ($\varepsilon = 250$ M^{-1} cm^{-1}) for compound **9** are tentatively assigned to $\pi^*(Rh_2) \rightarrow \sigma^*(Rh_2)$ transitions [14].

3. Conclusions

Compounds of the formula $M_2(\mu\text{-}O_2CCR_3)_n(O_2CCR_3)_4\text{–}(PPh_mPy_{3-m})_x$ (M = Mo or Rh; R = H or F; $n = 2$ or 3; $m = 1$ or 0; $x = 1$, or 2) can be synthesized depending on the starting material and the reaction conditions. The *trans*-$Mo_2(\mu\text{-}O_2CCF_3)_2(O_2CCF_3)_2\text{–}(PPhPy_2)_2$ (**5**) and *trans*-$Mo_2(\mu\text{-}O_2CCF_3)_2(O_2CCF_3)_2(PPy_3)_2$ (**6**) are among the first complexes of this general type characterized by X-ray crystallography. While the Mo_2-complexes displaying two phosphine ligands in equatorial positions and one or two trifluoroacetato ligands in axial positions are insoluble or instable in all common organic solvents, the Rh_2-complexes with two 2-pyridylphosphine ligands in axial positions as bridging ligands are soluble. These latter complexes could, in principle, act as model initiators/catalysts for the polymerization/hydrogenation of cyclopentadiene, and are currently under investigation with regard to this aspect in our laboratory.

4. Experimental

All preparation and manipulation were carried out under an oxygen- and water-free argon atmosphere using standard Schlenk techniques. Methylene chloride was distilled over calcium hydride and diethyl ether over sodium–benzophenone, and kept over 4 Å molecular

sieves. Acetone was dried over 4 Å molecular sieves, too. Anhydrous THF, $Mo_2(\mu\text{-}O_2CCF_3)_4$, $Rh_2(\mu\text{-}O_2CCH_3)_4$, bisphenyl-(2-pyridyl)phosphine (PPh_2py), phenyl-bis-(2-pyridyl)phosphine ($PPhpy_2$) and tri-(2-pyridyl)phosphine (Ppy_3) were prepared according to literature procedures [14,2g].

Elemental analyses were performed in the Mikroanalytisches Labor of the TU München in Garching (M. Barth). Solution ^1H, ^{13}C and $^{31}P\{^1H\}$ NMR were measured with a Bruker Avance DPX-400 spectrometer. The solid-state ^{31}P NMR spectra were recorded at room temperature (298 K) on a Bruker MSL 300 NMR spectrometer using a 4 mm double bearing MAS probehead and ZrO_2 rotators. A spinning speed of 8000 Hz was applied. Chemical shifts are reported on the scale with respect to δ (H_3PO_4(concentration)) = 0 ppm and were referenced to the second, external standard [$NH_4(H_2PO_4)$]; δ ($NH_4H_2PO_4$) = 1.1 ppm. IR spectra were obtained on a Perkin–Elmer FT IR spectrometer using KBr pellets as IR matrix. Electronic absorption spectra were run using a Perkin–Elmer Lambda 2UV–Vis spectrometer. TGA data were obtained by a Perkin–Elmer TGA 7 thermobalance. Each 3–10 mg sample was heated in a dynamic He atmosphere (purity 5.0, flow 45 sccm) using a 50–650 temperature program at a rate of 10 K min^{-1}.

4.1. Preparation of $Mo_2(\mu\text{-}O_2CCF_3)_3(O_2CCF_3)(PPh_2Py)$ (1)

To a stirred solution of $Mo_2(\mu\text{-}O_2CCF_3)_4$ (0.322 g, 0.5 mmol) in 15 ml of CH_2Cl_2 was added an equimolar amount of $PPhPy_2$ (0.132 g, 0.5 mmol) in 10 ml of CH_2Cl_2. An immediate reaction took place with the formation of a bright red precipitate, which was collected after 2 h stirring, washed with portions of CH_2Cl_2 and dried under oil pump vacuum. Yield: 90%. *Anal*. Calc. for $C_{25}H_{14}F_{12}Mo_2NO_8P$ (907.23): C 33.10, H 1.56, N 1.54. Found: C 32.82, H 1.52, N 1.48%. Selected IR data (ν, cm^{-1}): 1650s, 1606vs, 1436m, 1192vs, 1166vs, 1094m, 987m, 856m, 730s, 600w, 547w, 518m. ^{31}P MAS NMR (δ, ppm): 32.28.

4.2. Preparation of $Mo_2(\mu\text{-}O_2CCF_3)_3(O_2CCF_3)(PPhPy_2)$ (2)

To a stirred solution of $Mo_2(\mu\text{-}O_2CCF_3)_4$ (0.322 g, 0.5 mmol) in 15 ml of CH_2Cl_2 was added an equimolar amount of $PPhPy_2$ (0.132 g, 0.5 mmol) in 10 ml of CH_2Cl_2. An immediate reaction took place with the formation of a bright red precipitate, which was collected after 2 h stirring, washed with portions of CH_2Cl_2 and dried under oil pump vacuum. Yield: 90%. *Anal*. Calc. for $C_{24}H_{13}F_{12}Mo_2N_2O_8P$ (908.21): C 31.74, H 1.44, N 3.08. Found: C 31.82, H 1.42, N 2.98%. Selected IR data (ν, cm^{-1}): 1654s, 1608vs, 1431m, 1192vs, 1161vs, 984m, 854m, 723s, 597w, 543w, 518m. ^{31}P MAS NMR (δ, ppm): 30.48.

4.3. Preparation of $Mo_2(\mu\text{-}O_2CCF_3)_3(O_2CCF_3)(PPy_3)$ (3)

The synthetic procedure applied was similar to that used for compound **1a**. PPy_3 was employed instead of $PPhPy_2$. Yield: 87%. *Anal*. Calc. for $C_{23}H_{12}F_{12}Mo_2N_3O_8P$ (909.20): C 30.38, H 1.33, N 4.62; Found: C 29.95, H 1.45, N 4.60%. Selected IR data (ν, cm^{-1}): 1647s, 1608s, 1452m, 1426s, 1193vs, 1164sh, 990w, 856m, 803m, 777w, 730s, 520m. ^{31}P MAS NMR (δ, ppm): 29.19.

4.4. Preparation of trans-$Mo_2(\mu\text{-}O_2CCF_3)_2(O_2CCF_3)_2(PPh_2Py)_2$ (4)

The same procedure was applied as described for compound **1**, only the molar ratio of the $Mo_2(\mu\text{-}O_2CCF_3)_4$: PPh_2Py being 1:2. The resulting compound was of purple color and partial soluble in CH_2Cl_2. The product was, therefore, extracted with portions of cold CH_2Cl_2. Yield: 60%. *Anal*. Calc. for $C_{42}H_{28}F_{12}Mo_2N_2O_8P_2$ (1170.50): C 43.10, H 2.41, N 2.39. Found: C 43.26, H 2.64, N 2.12%. Selected IR data (ν, cm^{-1}): 1687s, 1650vs, 1606vs, 1436m, 1192vs, 1166s, 1094m, 856m, 838m, 793m, 730s, 696m, 528m, 425w; Selected Raman data (ν, cm^{-1}): 1690s, 1199vs, 860w, 836m, 429w, 305s; UV–Vis (CH_2Cl_2 solution): λ_{max} = 276 nm (sh), λ_{max} = 339 nm, (ε = 50 900 $M^{-1}cm^{-1}$), 548 nm (ε = 500 M^{-1} cm^{-1}), ^{31}P MAS NMR (δ, ppm): 31.04.

4.5. Preparation of trans-$Mo_2(\mu\text{-}O_2CCF_3)_2(O_2CCF_3)_2(PPhPy_2)_2$ (5)

The same procedure was applied as described for compound **1a**, only the molar ratio of the $Mo_2(\mu\text{-}O_2CCF_3)_4$: $PPhPy_2$ being 1:4. The resulting compound was of purple color. Yield: 85%. Crystals suitable for X-ray crystallography were obtained by layering a solution of $Mo_2(\mu\text{-}O_2CCF_3)_4$ in CH_2Cl_2 with $PPhPy_2$, dissolved in diethyl ether. *Anal*. Calc. for $C_{40}H_{26}F_{12}Mo_2N_4O_8P_2$ (1172.47): C 40.98, H 2.24, N 4.78. Found: C 40.46, H 2.10, N 4.62%. Selected IR data (ν, cm^{-1}): 1690vs, 1650sh, 1607m, 1192vs, 1166s, 856m, 831m, 791m, 597w, 425w, 379w, 331w, 223w, 137vw. Selected Raman data (ν, cm^{-1}): 1693vw, 1670vw, 1589vs, 1203w, 1144m, 865w, 831w, 772w, 619w, 430w, 376w, 344s, 307vs. ^{31}P MAS NMR (δ, ppm): 30.99.

4.6. Preparation of trans-$Mo_2(\mu\text{-}O_2CCF_3)_2(O_2CCF_3)_2(PPy_3)_2$ (6)

The procedure was similar to that described for compound **1** with the following exceptions: the molar

ratio of starting materials used was $Mo_2(\mu\text{-}O_2CCF_3)_4$:$PPy_3 = 1{:}4$. And the reaction mixture was refluxed for 4 h. The resulting product was purple. The product yield is 63%, however, the obtained material is mixed with complex **1** (27% based on elementary analysis). Attempts to isolate clean complex **6** were not successful due to its insoluble in all common organic solvents. *Anal*. Calc. for $C_{38}H_{24}F_{12}Mo_2N_6O_8P_2$ (1174.45): C 38.86, H 2.06, N 7.16. Found: C 38.38, H 1.94, N 7.50%. Selected IR data (ν, cm^{-1}): 1684sh, 1647s, 1608vs, 1194vs, 1164s, 857m, 836w, 795w, 509m, 382w. selected Raman data (ν, cm^{-1}): 1685vw, 1648vs, 1608vs, 1592m, 1209vw, 867w, 839w, m, 798s, 523vvs, 510s, 388vs, 354s, 308vs. ^{31}P MAS NMR (δ, ppm): 29.45.

4.7. Preparation of trans-$Rh_2(\mu\text{-}O_2CCH_3)_4(PPh_2Py)_2$ (7)

$Rh_2(\mu\text{-}O_2CCH_3)_4$ (0.111 g, 0.25 mmol) and twofold stoichiometric amount of PPh_2Py (0.133 g, 0.50 mmol) was put into a Schlenk tube and 10 ml CH_2Cl_2 was added. A red-brownish solution was immediately formed and the solution was stirred for 2 h. Then the volume of the solution was reduced to 5 ml and layered by *n*-hexane. After 4 days red-brownish tiny crystals were collected. The yield is 65% based on $Rh_2(\mu\text{-}O_2CCH_3)_4$. *Anal*. Calc. for $C_{42}H_{40}N_2O_8P_2Rh_2$ (968.55): C 52.06, H 4.16 N 2.89. Found: C 52.23, H 4.12, N 2.61%. Selected IR data (ν, cm^{-1}): 1600vs, 1585s, 1423s, 1346m, 1192vs, 1154s, 1020w, 854m, 777w, 731s, 623w, 507m; Selected Raman data (ν, cm^{-1}): 1590m, 1425m, 1352w, 1120s, 285s; ^1H NMR(CD_2Cl_2, δ, ppm): 1.63(s, 12H, C**H**$_3$C), 7.21(d, 2H), 7.33(m, 12H), 7.55(dt, 8H), 7.69(d, 2H), 7.84(d, 2H), 8.66(d, 2H); ^{13}C NMR(CD_2Cl_2, δ ppm): 30.05 (**C**H_3C), 123.8, 128.8, 129.0, 129.1, 133.0, 135.3, 136.0, 150.3, 159.5 (aromatic *C*–H signals), 193.3(**C**O_2). $^{31}P\{^1H\}$ NMR (CD_2Cl_2, δ, ppm): −15. 67(t). ^{31}P MAS NMR (δ, ppm): −17.44. UV–Vis (CH_2Cl_2 solution): $\lambda_{max} = 332$ nm (sh), $\lambda_{max} =$ 363 nm, ($\varepsilon = 14\,400$ M^{-1} cm^{-1}), 486 nm ($\varepsilon = 350$ M^{-1} cm^{-1}).

4.8. Preparation of trans-$Rh_2(\mu\text{-}O_2CCH_3)_4(PPhPy_2)_2$ (8)

$Rh_2(\mu\text{-}O_2CCH_3)_4$ (0.111 g, 0.25 mmol) was dissolved in 10 ml of THF to produce a bright green solution. The fourfold stoichiometric amount of $PPhPy_2$ (0.264 g, 1.00 mmol) in 10 ml of acetone was then added. The red-brownish precipitate was gradually formed and the suspension was stirred for 2 h. The crude product was washed several times with THF (3 × 5 ml), acetone (3 × 5 ml), and then dried in oil pump vacuum. The yield is 83% based on $Rh_2(\mu\text{-}O_2CCH_3)_4$. *Anal*. Calc. for $C_{40}H_{38}N_4O_8P_2Rh_2$ (970.53): C 49.50, H 3.95, N 5.77. Found C 49.42, H 4.03, N 5.58%. Selected IR data (ν, cm^{-1}): 1596vs, 1434vs, 1422vs, 1374s, 1320m, 1128w, 1015w, 650w, 542s, 380w, 289w. Selected Raman data (ν, cm^{-1}): 1587m, 1438w, 1386vw, 1327w, 1128s, 580vw, 337s, 287vvs, 240sh. ^1H NMR(CD_2Cl_2, δ, ppm): 1.63(s, 12H, C**H**$_3$C), 7.26(dd, 4H), 7.47(m, 6H), 7.62(dt, 4H), 7.88(d, 4H), 8.02(d, 4H), 8.70(d, 4H). ^{13}C NMR(CD_2Cl_2, δ ppm): 24.2(**C**H_3C), 123.6, 128.4, 130.4, 131.8, 133.3, 135.3, 136.5, 150.2, 159.5 (aromatic *C*–H signals), 193.0(**C**O_2). $^{31}P\{^1H\}$ NMR (CD_2Cl_2, δ, ppm): −8.99(t). ^{31}P MAS NMR (δ, ppm): −9.45. UV–Vis (CH_2Cl_2 solution): $\lambda_{max} = 496$ nm ($\varepsilon = 600$ M^{-1} cm^{-1}), $\lambda_{max} = 318$ nm, ($\varepsilon = 36\,500$ M^{-1} cm^{-1}), $\lambda = 356$ nm (sh).

4.9. Preparation of trans-$Rh_2(\mu\text{-}O_2CCH_3)_4(PPy_3)_2$ (9)

The procedure applied was analogous as described for complex **3.** PPy_3 was used instead of $PPhPy_2$ as a ligand. The yield based on $Rh_2(\mu\text{-}O_2CCH_3)_4$ is 92%. *Anal*. Calc. for $C_{38}H_{36}N_6O_8P_2Rh_2$ (972.50): C 46.93, H 3.73, N 8.64. Found: C 46.96, H 3.70, N 8.53%. Selected IR data (ν,

Table 2
Summary of crystallographic data and details of data collection and structure refinement for **5** and **6**

	5	**6**
Empirical formula	$C_{40}H_{26}F_{12}Mo_2N_4O_8P_2$	$C_{38}H_{24}F_{12}Mo_2N_6O_8P_2$
Molecular weight	1172.47	1174.45
Crystal system	triclinic	Triclinic
Space group	$P\bar{1}$ (Number 2)	$P\bar{1}$ (Number 2)
a (Å)	9.6660(3)	9.1327(2)
b (Å)	10.4678(3)	9.8729(2)
c (Å)	12.0317(3)	12.8791(4)
α (°)	110.453(1)	111.895(1)
β (°)	91.656(2)	91.209(1)
γ (°)	105.882(1)	100.520(1)
V (Å^3)	1086.58(5)	1054.31(5)
Z	1	1
D_{calcd} (g cm^{-3})	1.792	1.850
μ (mm^{-1})	0.760	0.784
Reflections collected	7202	7909
Independent reflections [$I > 2\sigma(I)$/all data]	3541/3797	4467/4821
R_{int}	0.0172	0.0196
Data/restraints/parameter	3797/0/348	4821/0/355
R_1 [a] [$I > 2\sigma(I)$/all data]	0.0300/0.0331	0.0240/0.0273
wR_2 [b] [$I > 2\sigma(I)$/all data]	0.0720/0.0737	0.0548/0.0561
Goodness-of-fit [c]	1.029	1.049
Weights a/b [d]	0.0241/1.8741	0.0087/0.9617
$\Delta\rho_{max/min}$ (e Å^{-3})	0.91/−0.55	0.66/−0.45

[a] $R_1 = \Sigma\,(||F_o| - |F_c||)/\Sigma|F_o|$.
[b] $wR_2 = [\Sigma\, w(F_o^2 - F_c^2)^2/\Sigma\, w(F_o^2)^2]^{1/2}$.
[c] Goodness-of-fit = $[\Sigma\, w(F_o^2 - F_c^2)^2/(NO - NV)]^{1/2}$.
[d] $w = 1/[\sigma^2(F_o^2) + (aP)^2 + bP]$, with $P = [\max(0 \text{ or } F_o^2) + 2F_c^2]/3$.

cm^{-1}): 1594vs, 1422vs, 1284m, 1129vw, 1086m, 1066vvw, 695s, 561w, 525w, 382m, 303vw, 278w. Selected Raman data (ν, cm^{-1}): 1421s, 1278m, 581vw, 527m, 338s, 289vvs. ^1H NMR (CD_2Cl_2, δ, ppm): 1.63 (s, 12H, C**H**$_3$C), 7.28 (dt, 6H), 7.67 (dt, 6H), 7.98 (d, 6H), 8.68 (d, 6H). ^{13}C NMR (CD_2Cl_2, δ ppm): 24.0 (**C**H$_3$C), 123.6, 132.0, 135.2, 150.2, 158.3 (aromatic *C*–H signals), 192.7 (**C**O$_2$). $^{31}P\{^1H\}$ NMR (CD_2Cl_2, δ, ppm): −2.64 (t). ^{31}P MAS NMR (δ, ppm): −3.27. UV–Vis (CH_2Cl_2 solution): $\lambda_{max} = 568$ nm ($\varepsilon = 250\ M^{-1}\ cm^{-1}$), $\lambda_{max} = 318$ nm ($\varepsilon = 28100\ M^{-1}\ cm^{-1}$), $\lambda = 370$ nm (sh).

4.10. X-ray crystal structure determination

Crystallographic data for **5** and **6** are summarized in Table 2. Data were collected at low temperature (123 K) on a Nonius KappaCCD device at the window of a rotating anode (**5:** *theta range*: 1.82–26.07°, *index ranges*: $-11 \le h \le 11$, $-12 \le k \le 12$, $-14 \le l \le 14$, *crystal dimensions*: $0.13 \times 0.15 \times 0.20$ mm; **6:** *theta range*: 2.26 to 27.50°, *index ranges*: $-11 \le h \le 11$, $-12 \le k \le 12$, $-16 \le l \le 16$, *crystal dimensions*: $0.24 \times 0.28 \times 0.33$ mm) [15b]. Absorption correction and decay correction were applied during the scaling procedure [15c]. Both structures were solved by direct methods [15d] and refined anisotropically by full-matrix least-squares on F^2 [15e]. Neutral atom scattering factors for all atoms and anomalous dispersion corrections for the non-hydrogen atoms were taken from the International Tables for Crystallography [15f]. All non-hydrogen atoms of the two complexes where refined anisotropically. All hydrogen atoms were placed in calculated positions riding on the parent carbon atom (**5**). All hydrogen atoms were found in the difference Fourier map and refined with individual isotropic thermal displacement parameters (**6**). Both molecules reside on a crystallographic center of inversion. In **5** both trifluormethyl groups are disordered over two positions in the bridging $(O_2C)CF_3$ ligand (91:9) and in the monodentate $(O_2C)CF_3$ ligand (71:29).

5. Supplementary material

Crystallographic data (excluding structure factors) for the structures reported in this paper have been deposited with the Cambridge Crystallographic Data Center as supplementary publication numbers CCDC-175526 (**5**) and -175527 (**6**). Copies of the data can be obtained free of charge on application to CCDC, 12 Union Road, Cambridge CB2 1EZ, UK (fax: +44-1223-336-033; e-mail: deposit@ccdc.cam.ac.uk or www: http://www.ccdc.cam.ac.uk].

Acknowledgements

G.Z. thanks the *Katholischer Akademischer Ausländer-Dienst* (KAAD) for a Ph.D. stipend. J.Z. is grateful to the *Deutscher Akademischer Austauschdienst* (DAAD) for a Ph.D. grant. Professor Dr. W.A. Herrmann is acknowledged for continuous support of our work, the Fonds der Chemischen Industrie (FCI) for financial support and Dr. É. Bencze for helpful discussions and experimental assistance in vibrational spectroscopy.

References

[1] (a) Z.Z. Zhang, H. Cheng, Coord. Chem. Rev. 147 (1996) 1;
(b) G.R. Newcomer, Chem. Rev. 93 (1993) 2067.
[2] (a) C.Y. Kuo, Y.S. Fuh, J.Y. Shiue, S.J. Yu, G.H. Lee, S.M. Peng, J. Organomet. Chem. 588 (1999) 260;
(b) N.D. Jones, K.S. MacFarlane, M.B. Smith, R.P. Schutte, S.J. Rettig, B.R. James, Inorg. Chem. 38 (1999) 3956;
(c) T. Nicholson, M. Hirsch-Kuchma, A. Shellenbarger-Jones, A. Davison, A. Jones, Inorg. Chim. Acta 267 (1998) 319;
(d) R.P. Schutte, S.J. Rettig, A.M. Joshi, B.R. James, Inorg. Chem. 36 (1997) 5809;
(e) I.R. Baird, M.B. Smith, B.R. James, Inorg. Chim. Acta 235 (1995) 291;
(f) P. Braunstein, D.G. Kelly, A. Tiripicchio, F. Ugozzoli, Bull. Soc. Chim. Fr. 123 (1995) 1083;
(g) H. Schmidbaur, Y. Inoguchi, Z. Naturforsch. 35b (1980) 1329.
[3] (a) G. Franciò, R. Scopelliti, C.G. Arena, G. Bruno, D. Drommi, F. Faraone, Organometallics 17 (1998) 338;
(b) W.H. Chan, Z.Z. Zhang, T.C. Mak, C.M. Che, J. Chem. Soc., Dalton Trans. (1998) 803;
(c) S.M. Kuang, F. Xue, Z.Z. Zhang, W.M. Xue, C.M. Che, T.C.W. Mak, J. Chem. Soc., Dalton Trans. (1997) 3409;
(d) S.M. Kuang, H. Cheng, L.J. Sun, Z.Z. Zhang, Z.Y. Zhou, B.M. Wu, T.C.W. Mak, Polyhedron 15 (1996) 3417;
(e) L.Y. Xie, B.R. James, Inorg. Chim. Acta 217 (1994) 209;
(f) E. Rotondo, G. Bruno, F. Nicolò, S. Lo Schiavo, P. Piraino, Inorg. Chem. 30 (1991) 1195;
(g) P.W. Schrier, D.R. Derringer, P.E. Fanwick, R.A. Walton, Inorg. Chem. 29 (1990) 1290;
(h) F.A. Cotton, M. Matusz, Inorg. Chim. Acta 143 (1988) 45;
(i) F.A. Cotton, M. Matusz, Polyhedron 7 (1988) 2201;
(j) T.J. Barder, F.A. Cotton, G.L. Powell, S.M. Tetrick, R.A. Walton, J. Am. Chem. Soc. 106 (1984) 1323;
(k) R.H. Cayton, M.H. Cisholm, E.F. Putilina, K. Folting, J.C. Huffman, K.G. Moodley, Inorg. Chem. 31 (1992) 2928;
(l) P. Lahuerta, M.A. Ubeda, J. Paya, S. Garciagranda, F. Gomezbeltran, A. Anillo, Inorg. Chim. Acta 205 (1993) 91;
(m) F. Estevan, P. Lahuerta, E. Peris, M.A. Ubeda, S. Graciagranda, F. Gomezbeltran, E. Perezcarreno, G. Gonzalez, Inorg. Chim. Acta 218 (1994) 189.
[4] (a) R. Gobetto, C.G. Arena, D. Drommi, F. Faraone, Inorg. Chim. Acta 248 (1996) 257;
(b) A.J. Deeming, M.B. Smith, J. Chem. Soc., Chem. Commun. (1993) 844 and references therein.
[5] P. Braustein, M. Knorr, M. Strampfer, A. De Cian, J. Fischer, J. Chem. Soc., Dalton Trans. (1994) 117.
[6] N.W. Alcock, P. Moore, P.A. Lampe, K.F. Mok, J. Chem. Soc., Dalton Trans. (1982) 207.
[7] (a) W.J. Zao, T.Q. Fang, S.Q. Zhang, Z.Z. Zhang, L.M. Yang, J. Chem. Eng. Natural Gas 17 (1992) 3;

(b) CA: 119, P 202967;
(c) Y. Xie, C.L. Lee, Y. Yang, S.J. Rettig, B.R. James, Can. J. Chem. 70 (1992) 751;
(d) Z. Galdeki, A. Kowalski, F.P. Pruchnik, K. Wajda-Hermanowicz, R. Starosta, Pol. J. Chem. 73 (1999) 859.

[8] (a) F.E. Kühn, J.R. Ismeier, D. Schön, W.M. Xue, G. Zhang, O. Nuyken, Macromol. Rapid Commun. 20 (1999) 555;
(b) F.E. Kühn, D. Schön, G. Zhang, G.O. Nuyken, J. Macromol. Sci. Chem. A37 (2000) 971;
(c) M. Pillinger, I.S. Gonçalves, A.A. Valente, P. Ferreira, D. Schön, O. Nuyken, F.E. Kühn, Design. Monomers Polym. 4 (2001) 269;
(d) P. Ferreira, F.E. Kühn, Trends Inorg. Chem. 7 (2001) 89;
(e) M. Pillinger, I.S. Gonçalves, P. Ferreira, J. Rocha, M. Schäfer, D. Schön, O. Nuyken, F.E. Kühn, Macromol. Rapid Commun. 22 (2001) 1306.

[9] (a) W. Risse, C. Mehler, E. Connor, Ger. Patent 19729817, 1999, BASF AG;
(b) G. Heublein, W. Freitag, East Ger. Patent 126837, 1976, Chem. Abstract 88 (1978) 74896;
(c) C. Aso, K. Ito, T. Kunitake, Makromol. Chem. 97 (1966) 40;
(d) G. Heublein, W. Freitag, W. Mock, Makromol. Chem. 181 (1980) 267;
(e) G. Heublein, G. Knöppel, D. Stadermann, Polym. Bull. 20 (1988) 109;
(f) G. Heublein, W. Freitag, J. Prakt. Chem. 321 (1979) 544;
(g) G. Heublein, W. Barth, J. Prakt. Chem. 316 (1974) 649;
(h) G. Heublein, G. Albrecht, Acta Polym. 33 (1982) 505.

[10] (a) P. Legzdins, G.L. Rempel, G. Wilkinson, J. Chem. Soc., Chem. Comm. (1969) 825;
(b) J. Telser, R.S. Drago, Inorg. Chem. (23) (1984) 1798;
(c) F.A. Cotton, A.H. Reid, W. Schwotzer, Inorg. Chem. 24 (1985) 3965;
(d) W. Clegg, G. Pimblett, C.D. Garner, Polyhedron 5 (1986) 31;
(e) G. Pimblett, C.G. Garner, W. Clegg, J. Chem. Soc., Dalton Trans. (1986) 1257;
(f) F.A. Cotton, F.E. Kühn, Inorg. Chim. Acta 252 (1996) 257;
(g) F.A. Cotton, F.E. Kühn, A. Yokochi, Inorg. Chim. Acta 252 (1996) 251.

[11] (a) T.J. Barder, S.M. Tetrick, R.A. Walton, F.A. Cotton, G.L. Powell, J. Am. Chem. Soc. 105 (1983) 4090;
(b) F.A. Cotton, K.R. Dunbar, J. Am. Chem. Soc. 109 (1987) 2199;
(c) E.C. Morrison, D.A. Tocher, Inorg. Chim. Acta 157 (1989) 139;
(d) E.C. Morrison, D.A. Tocher, J. Organomet. Chem. 408 (1991) 105;
(e) P. Lahuerta, R. Martinez-Manez, J. Paya, E. Peris, W. Diaz, Inorg. Chim. Acta 173 (1990) 99.

[12] K. Teramoto, Y. Sasaki, K. Migita, M. Iwaizumi, K. Saito, Bull. Chem. Soc. Jpn. 61 (1988) 83.

[13] (a) E.B. Boyar, S.D. Robinson, Coord. Chem. Rev. 50 (1983) 109;
(b) T. Kawamura, H. Katayama, H. Nishikawa, T. Yamabe, J. Am. Chem. Soc. 111 (1989) 8156;
(c) H. Kitamura, T. Ozawa, K. Titsukawa, H. Masuda, H. Einago, Chem. Lett. (1999) 1225.

[14] (a) F.A. Cotton, J.G. Norman, J. Coord. Chem. 1 (1971) 161;
(b) G. Winkhaus, P. Ziegler, Z. Anorg. All. Chem. 350 (1967) 51;
(c) K. Kurtev, D. Ribola, R.A. Jones, D.J. Cole-Hamulton, G. Wilkinson, J. Chem. Soc., Dalton Trans. (1980) 55;
(d) F.A. Cotton, R.A. Walton, Multiple Bonds between Metal Atoms, second ed. (Chapter 10), Wiley, New York, 1993, p. 705.

[15] (a) A.L. Spek, PLATON, A Multipurpose Crystallographic Tool, Utrecht University, Utrecht, The Netherlands, 2001;
(b) Data Collection Software for Nonius KappaCCD Devices, Delft, The Netherlands (1997);
(c) Z. Otwinowski, W. Minor, in: W.C. Carter, Jr., R.M. Sweet (Eds.), Methods in Enzymology, vol. 276, Academic Press, New York, USA, 1997, p. 307;
(d) A. Altomare, G. Cascarano, C. Giacovazzo, A. Guagliardi, M.C. Burla, G. Polidori, M. Camalli, J. Appl. Cryst. 27 (1994) 435;
(e) G.M. Sheldrick, SHELXL-97, University of Göttingen, Göttingen, Germany, 1997;
(f) In: A.J.C. Wilson (ed.), International Tables for Crystallography, vol. C, Kluwer Academic Publishers, Dordrecht, The Netherlands, 1992, Tables 6.1.1.4 (pp. 500–502), 4.2.6.8 (pp. 219–222), and 4.2.4.2 (pp. 193–199).

unusual nature of the reactivity of the dibenzylamine ligand with Me_3Al and Me_3Ga, where orthometalation occurs at higher temperatures, and to observe the influence of the nature of R on the planarity of the central Al_2N_2 ring.

Herein we report the synthesis, ^1H and ^{13}C NMR, and mass spectral characterization of $[Pr^n_2AlN(CH_2Ph)_2]_2$ (**3**), $[Bu^n_2AlN(CH_2Ph)_2]_2$ (**4**), and $[Bu^i_2AlN(CH_2Ph)_2]_2$ (**5**). The ^{13}C and ^1H NMR data of $[R_2AlN(CH_2Ph)_2]_2$ where R = Me, Et, Pr^n, Bu^n and Bu^i are compared in terms of the R group and with data for the previously reported $[R_2AlNMe_2]_2$ series [33]. X-ray molecular structure data for $[Et_2AlN(CH_2Ph)_2]_2$ (**2**) and $[Bu^n_2AlN(CH_2Ph)_2]_2$ are reported and are contrasted with that of $[Me_2AlN(CH_2Ph)_2]_2$ [27]. The structural data for these three aminoalanes are also compared with data for $[MeAlN(H)CH_2Ph]_2$ [34] and $[RAlN(CH_2Ph)$-μ-$(CH_2C_6H_4)]_2$ [26,27] in terms of the Al_2N_2 ring geometry and with $Me_3Al{\cdot}HN(CH_2Ph)_2$ [35]. The ^1H and ^{13}C NMR and molecular structure data for the series $[Me_2AlN(CH_2Ph)_2]_2$ (**1**) [27], $[Me_2GaN(CH_2Ph)_2]_2$ [31], and $[Me_2InN(CH_2Ph)_2]_2$ [36] are discussed in terms of the nature of the Group 13 metal and related to trends in the NMR and molecular structure data for their respective adducts $Me_3M{\cdot}HN(CH_2Ph)_2$ [28,35,37,38].

2. Experimental

2.1. General procedures

Standard inert atmosphere techniques were used for the synthesis and handling of all compounds. Hexane and toluene were distilled over calcium hydride and under an atmosphere of nitrogen. Dibenzylamine, Aldrich, was stored over molecular sieves. The trialkylaluminum compounds, Texas Alkyls, Inc., were used as obtained. Benzene-d_6, Aldrich, was deoxygenated by bubbling with dry nitrogen and stored over molecular sieves. The synthesis and characterization of **1** [28] and **2** [29] have been previously reported. ^1H and ^{13}C NMR data for **1**–**5** were collected on 0.20 M benzene-d_6 solutions of the compounds using a Bruker DRX 400 NMR spectrometer. ^{13}C DEPT, 2-D ^1H–^1H COSY, and 2-D $^{13}C\{^1H\}$ HETCOR NMR spectra were obtained using standard Bruker software. Chemical shifts for all spectra were referenced to those of the solvent. The ^1H and ^{13}C NMR data for **1** and **2** were collected to complete the ^1H NMR assignments for **1** and to have a set of comparable NMR data collected under the same experimental conditions. IR data were collected using a Bruker Vector 22 FT IR spectrometer. Samples were prepared as split mulls in Kel-F and Nujol on KBr plates. EI MS data for **1**–**5** were obtained on a Finnigan MAT95Q spectrometer with an electron energy of 70 eV. The samples were introduced using a direct insertion probe under inert atmosphere conditions. Elemental analyses were performed by E&R Microanalytical Laboratory, Inc., Parsippany, NJ. Melting points were obtained in sealed capillaries and are uncorrected.

2.2. Synthesis of $[Pr^n_2AlN(CH_2Ph)_2]_2$ (3), $[Bu^n_2AlN(CH_2Ph)_2]_2$ (4), and $[Bu^i_2AlN(CH_2Ph)_2]_2$ (5)

Each aminoalane dimer was synthesized by mixing $HN(CH_2Ph)_2$ and the respective trialkylaluminum in a 1:1 mol ratio in pentane solution (For **3**, 5.12 mmol (0.800 g) Pr^n_3 Al with 5.22 mmol (1.03 g) $HN(CH_2Ph)_2$; for **4**, 5.14 mmol (1.02 g) Bu^n_3 Al with 5.07 mmol (1.00 g) $HN(CH_2Ph)_2$; for **5**, 5.09 mmol (1.01 g) Bu^i_3 Al with 5.07 mmol (1.00 g) $HN(CH_2Ph)_2$). The pentane was then removed under vacuum and the neat adduct heated at about 110 °C until gas evolution ceased. Compounds **3** and **4** were recrystallized from hexane solutions at −15 °C. Compound **5** is an oil and was purified by vacuum distillation.

2.3. Characterization of 1–5

2.3.1. $[Me_2AlN(CH_2Ph)_2]_2$ (1) [28]

^1H NMR: δ_H −0.081 (s, 12H, H1), 4.16 (s, 8H, H10), 6.98 (m, 4H, H12), 7.01 (m, 4H, H13), 6.995 (m, 2H, H14). ^{13}C NMR: δ_C −7.57 (C1), 52.65 (C10), 136.63 (C11), 129.31 (C12), 128.08 (C13), 127.25 (C14). MS (EI): *m*/*z* 491 (M^+ −Me), 310 (M^+ −$N(CH_2Ph)_2$), 295 (M^+ −$N(CH_2Ph)_2$−Me), 254 ($M^+/2+H$), 238 (100, $M^+/2$−Me), 160 ($M^+/2-C_7H_9$), 65 ($C_5H_5^+$), 57 (Me_2Al^+).

2.3.2. $[Et_2AlN(CH_2Ph)_2]_2$ (2) [29]

^1H NMR: δ_H 0.56 (q, 8H, H1), 1.49 (t, 12H, H2), 4.25 (s, 8H, H10), 7.01 (m, 8H, H12), 7.05 (m, 8H, H13), 7.00 (m, 4H, H14). ^{13}C NMR: δ_C 2.00 (C1), 10.60 (C2), 52.40 (C10), 136.63 (C11), 129.24 (C12), 128.1 (C13), 127.30 (C14). MS (EI): *m*/*z* 533 (M^+ −Et), 503 (M^+ −Et−EtH), 252 ($M^+/2$−Et), 222 ($M^+/2$−Et−EtH), 196 ($(C_6H_5CH_2)_2N^+$), 120 ($C_6H_5CH_2NHCH_2^+$), 106 ($C_6H_5CH_2NH^+$), 91 (100, $C_7H_7^+$), 65 ($C_5H_5^+$).

2.3.3. $[Pr^n_2AlN(CH_2Ph)_2]_2$ (3)

M.p. 145–146 °C. ^1H NMR: δ_H 0.61 (m, 8H, H1), 1.90 (m, 8H, H2), 1.21 (t, 12H, H3), 4.29 (s, 8H, H10), 7.01 (m, 8H, H12), 7.04 (m, 8H, H13), 7.00 (m, 4H, H14). ^{13}C NMR: δ_C 14.86 (C1), 20.66 (C2), 21.68 (C3), 52.54 (C10), 136.63 (C11), 129.23 (C12), 128.07 (C13), 127.30 (C14). IR (cm^{-1}): 3087 (w), 3061 (w), 2915 (m), 2859 (s), 1168 (m), 1045 (s), 976 (w), 874 (m), 734 (s), 696 (s), 615 (m). Calc. MW: 618.86 g mol^{-1}. Cryo. MW: 613 ± 15 g mol^{-1} (0.050–0.055 m in benzene). MS (EI): *m*/*z* 575 (M^+ −Pr^n), 531 (M^+ −Pr^n −Pr^nH), 378

($M^+ - N(CH_2Ph)_2 - Pr^n$), 266 ($M^+/2 - Pr^n$), 197 ($(C_6H_5CH_2)_2NH^+$), 196 ($(C_6H_5CH_2)_2N^+$), 120 ($C_6H_5CH_2NHCH_2^+$), 106 ($C_6H_5CH_2NH^+$), 91 (100, $C_7H_7^+$), 65 ($C_5H_5^+$). *Anal.* Calc. (Found) for $C_{40}H_{56}Al_2N_2$: C, 77.63 (77.57); H, 9.12 (9.04); N, 4.53 (4.74)%. Yield 62%.

2.3.4. $[Bu^n_2AlN(CH_2Ph)_2]_2$ (4)

M.p. 113–116 °C. ^{1}H NMR: δ_H 0.63 (m, 8H, H1), 1.885 (m, 8H, H2), 1.54 (h, 8H, H3), 1.035 (t, 12H, H4), 4.34 (s, 8H, H10), 7.047 (m, 8H, H12), 7.052 (m, 8H, H13), 7.00 (m, 4H, H14). ^{13}C NMR: δ_C 11.17 (C1), 29.33 (C2), 29.62 (C3), 14.01 (C4), 52.58 (C10), 136.68 (C11), 129.30 (C12), 128.09 (C13), 127.34 (C14). IR (cm^{-1}): 3085 (w), 3062 (w), 3028 (m), 2953 (s), 2919 (s), 2889 (m), 1163 (m), 1051 (s), 906 (m), 874 (s), 850 (m), 731 (s), 699 (s), 681 (m), 635 (s). MS (EI): *m/z* 617 ($M^+ - Bu^n$), 559 ($M^+ - Bu^n - Bu^nH$), 280 (100, $M^+/2 - Bu^n$), 222 ($M^+/2 - Bu^n - Bu^nH$), 132 ($AlNCH_2$-$C_6H_5^+$), 106 ($C_6H_5CH_2NH^+$), 105 ($C_6H_5CH_2N^+$), 91 ($C_7H_7^+$). *Anal.* Calc. (Found) for $C_{44}H_{64}Al_2N_2$: C, 77.98 (77.98); H, 9.35 (9.36); N, 4.33 (3.99)%. Yield 95%.

2.3.5. $[Bu^i_2AlN(CH_2Ph)_2]_2$ (5)

^{1}H NMR: δ_H 0.65 (d, 8H, H1), 2.35 (n, 4H, H2), 1.254 (d, 24H, H3), 4.33 (s, 8H, H10), 7.067 (m, 8H, H12), 7.064 (m, 8H, H13), 7.013 (m, 4H, H14). ^{13}C NMR: δ_C 23.37 (C1), 26.76 (C2), 28.96 (C3), 52.94 (C10), 136.66 (C11), 129.43 (C12), 128.03 (C13), 127.31 (C14). IR (cm^{-1}): 3088 (w), 3062 (w), 3031 (m), 2948 (s), 2862 (s), 1496 (m), 1187 (m), 1049 (s), 954 (m), 872 (s), 740 (s), 698 (s). Calc. MW: 674.96 g mol^{-1}. Cryo. MW: 647 ± 32 g mol^{-1} (0.050–0.055 m in benzene). MS (EI): *m/z* 659 ($M^+ - Me$), 560 ($M^+ - 2Bu^i$), 559 ($M^+ - Bu^i - Bu^iH$), 494 ($M^+ - 2C_7H_9$), 436 ($M^+ - 2C_7H_7 - Bu^iH$), 280 ($M^+/2 - Bu^i$), 224 ($M^+/2 + H - 2Bu^i$), 222 ($M^+/2 - Bu^i - Bu^iH$), 197 ($(C_6H_5CH_2)_2NH^+$), 196 ($(C_6H_5CH_2)_2N^+$), 141 ($Bu^i_2Al^+$), 119 ($C_6H_5CH_2NCH_2^+$), 106 ($C_6H_5CH_2NH^+$), 91 (100, $C_7H_7^+$), 65 ($C_5H_5^+$). *Anal.* Calc. (Found) for $C_{44}H_{64}Al_2N_2$: C, 78.30 (77.98); H, 9.56 (9.85); N, 4.15 (4.30)%. Yield 86%.

2.4. Structural studies for 2 and 4

In the structural studies, an X-ray quality crystal was sealed into a thin-walled glass capillary under anaerobic conditions. The crystal was then mounted and aligned upon an Enraf Nonius CAD4 single-crystal diffractometer. Intensity data (Mo Kα, $\lambda = 0.71073$ Å) were collected at room temperature using graphite-monochromatized radiation. All data were corrected for Lorentz and polarization effects as well as for absorption. Details of each data collection are given in Table 1. The crystallographic calculations were carried out on an IBM-PC with the use of the Siemens SHELXTL-PC program package [39]. The analytical scattering factors for neutral atoms were corrected for both $\Delta f'$ and $i\Delta f''$ components of anomalous dispersion [40]. Each structure was solved by the use of direct methods. Positional and anisotropic thermal parameters of all non-hydrogen atoms were refined. Hydrogen atoms were not located directly, but were input in calculated positions with $d(C–H) = 0.96$ Å and with the appropriate staggered-tetrahedral geometry [41]. The isotropic thermal parameter of each hydrogen atom was then verified by means of a final difference-Fourier synthesis in which no chemically meaningful residuals were found. Selected bond distances and angles for structures **2** and **4** are tabulated in Table 2.

Table 1
Crystallographic data for **2** and **4**

	2	**4**
Formula	$C_{36}H_{48}Al_2N_2$	$C_{44}H_{64}Al_2N_2$
Space group	$P2_1/n$	$P\bar{1}$
Crystal system	monoclinic	triclinic
Temperature (K)	298	298
a (Å)	10.7383(12)	7.7171(10)
b (Å)	12.3652(12)	11.6946(15)
c (Å)	12.6621(13)	12.7760(27)
α (°)		64.791(15)
β (°)	103.354(9)	84.578(14)
γ (°)		84.406(10)
V (Å^3)	1635.8(8)	1036.4(5)
Z	2	1
Crystal size (mm)	0.40 × 0.10 × 0.10	0.25 × 0.20 × 0.10
Habit	colorless plate	colorless block
Absolute coefficient (mm^{-1})	0.115	0.101
Radiation, λ (Å)	Mo Kα, 0.71073	Mo Kα, 0.71073
2θ Range (°)	4.0–45.0	2.0–45.0
Scan type	ω–2θ	ω–2θ
Index ranges	$0 \le h \le 11$, $-13 \le k \le 13$, $-13 \le l \le 13$	$-8 \le h \le 8$, $-12 \le k \le 12$, $-13 \le l \le 13$
Reflections collected	4389	5428
Independent reflections	2126 [$R_{int} = 2.69\%$]	2714 [$R_{int} = 2.51\%$]
Number of parameters refined	182	218
Observed reflections	1205 ($F > 6.0\sigma(F)$)	1684 ($F > 6.0\sigma(F)$)
R indices (3σ data)	$R = 4.98\%$, $R_w = 5.49\%$	$R = 3.95\%$, $R_w = 4.32\%$
R indices (6σ data)	$R = 8.09\%$, $R_w = 9.78\%$	$R = 7.94\%$, $R_w = 6.09\%$
Largest difference peak/hole (e Å^{-3})	0.77/−0.35	0.25/−0.28

$[Et_2AlN(CH_2Ph)_2]_2$ **(2)** crystallizes in the monoclinic crystal system. The systematic absences $h0l$ for $h+l = 2n+1$ define the centrosymmetric space group $P2_1/n$ (No. 14). The structure refined to convergence with $R = 4.98\%$ and $R_w = 5.49\%$ for those 1205 reflections with $|F_o| > 6.0\sigma|F_o|$ and $R = 8.09\%$ for all data.

$[Bu^n_2AlN(CH_2Ph)_2]_2$ **(4)** belongs to the triclinic crystal system with the space group being determined to be the

Table 2
Selected bond distances (Å) and angles (°) for **1**, **2** and **4**

	1[27]	**2**	**4**
Bond lengths			
Al(1)–N(1)	1.982(4)	1.988(3)	1.984(3)
Al(1)–N(1A)	1.982(4)	1.991(3)	1.997(2)
Al(1)–C(1)	1.962(7)	1.990(4)	1.976(3)
Al(1)–C(2)	1.981(10)		
Al(1)–C(3)		1.972(4)	
Al(1)–C(5)			1.976(3)
Al(1A)–N(1)	1.984(4)	1.991(3)	1.997(2)
Al(1)···Al(1A)	2.783(3)	2.820(2)	2.823(1)
N(1)–C(10)	1.512(7)	1.509(4)	1.503(4)
N(1)–C(20)	1.498(7)	1.485(4)	1.503(3)
Bond angles			
N(1)–Al(1)–N(1A)	90.9(2)	89.7(1)	89.6(1)
C(1)–Al(1)–C(2)	118.0(4)		
C(1)–Al(1)–C(3)		118.7(2)	
C(1)–Al(1)–C(5)			117.7(1)
Al(1)–N(1)–Al(1A)	89.1(1)	90.3(1)	90.4(1)
C(10)–N(1)–C(20)	110.8(3)	110.3(3)	110.7(2)
C(10)–N(1)–Al(1A)	114.2(4)	114.0(2)	114.9(1)
C(20)–N(1)–Al(1A)	113.0(3)	113.5(2)	113.0(1)
N(1)–Al(1)–C(1)	111.4(2)	110.8(2)	112.7(1)

centrosymmetric space group $P\bar{1}$ (No. 2). This was verified by successful solution and refinement of the crystal structure. The structure refined to convergence with $R = 3.95\%$ and $R_w = 4.32\%$ for those 1684 reflections with $|F_o| > 6.0\sigma|F_o|$ and $R = 7.94\%$ for all data.

3. Results and discussion

3.1. ^1H and ^{13}C NMR data and chemical shift analysis

The ^1H and ^{13}C NMR chemical shifts for compounds **1**–**5** were obtained using several 1-D and 2-D NMR techniques. The determination of the ^1H NMR chemical shifts for the hydrogens of the alkyl groups are straightforward. The ^1H NMR spectra of the methyl, ethyl, and the *iso*-butyl groups are first-order. The ^1H NMR spectra for *n*-propyl and *n*-butyl groups are more complicated due to restricted conformational averaging about the C(1)–C(2) bond. The initial assignments were verified by ^1H 2-D COSY NMR experiments. Due to the low electronegativity of the aluminum atom, the chemical shifts of the C(1) CH_2 groups are to higher field than the chemical shifts of the other alkyl group protons. For example, for the ethyl group in **2**, the CH_2 group chemical shift is $\delta_H = 0.56$ ppm, whereas that of the CH_3 group is $\delta_H = 1.49$ ppm. The ^{13}C NMR chemical shifts of the alkyl group carbons for **1**–**5** were obtained from simple decoupled 1-D ^{13}C NMR spectra, ^{13}C NMR spectral editing (DEPT-135) experiments, and from $^{13}C\{^1H\}$ 2-D HETCOR experiments. The ^{13}C NMR chemical shifts for the alkyl groups in **1**–**5** are typical of those for R bound to aluminum. The ^{13}C NMR methyl group resonance in **1** consists of a broad singlet at −7.57 ppm, as a result of the low electronegativity and quadrupole moment of the aluminum atom. The C(1) methylene group resonances in **2**–**5** are also broadened. The ^1H NMR resonances for the CH_2 portion of the benzyl group consist of a singlet in each case and are in the range of 4.15–4.34 ppm. The corresponding ^{13}C NMR resonances are in the range of 52.36–52.94 ppm for **1**–**5**.

The ^1H and ^{13}C NMR chemical shift assignments for the aromatic part of the benzyl group are more challenging. The ^1H NMR spectra are non-first order, with the resonances occurring in a narrow range about 7.00 ppm. The *ipso* ^{13}C and tentative *ortho*, *meta*, and *para* ^{13}C NMR assignments were made by comparison of the ^{13}C proton decoupled, ^{13}C proton coupled, and ^{13}C DEPT-45 NMR spectra. The *ortho*, *meta,* and *para* assignments were then verified on the basis of high-resolution 2-D $^{13}C\{^1H\}$ HETCOR experiments.

The benzyl CH_2 group and *ortho* ring protons become more deshielded as the steric bulk of the alkyl group bound to the aluminum atom increases. For example, the CH_2 δ_H data are: R = Me, 4.16 ppm; R = Et, 4.25 ppm; R = Pr^n, 4.29 ppm; R = Bu^n, 4.34 ppm; and R = Bu^i, 4.33 ppm. This trend is similar to that for the ^1H NMR chemical shift data for the three aminoalane series, $[R_2AlR']_2$, where R = Me [28], Et [29] and Bu^i [30] and R′H is a secondary amine. Here, as the steric bulk of R increases, the protons of the C(1) and C(2) carbons of the amine shift to more positive chemical shift values (ppm). This effect is well documented for the ^1H NMR chemical shifts of aluminum–nitrogen compounds in aromatic solvents [15] and is attributed to the more sterically demanding alkyl groups on the aluminum atom disrupting the formation of solvent collision complexes, preventing the influence of the ring current of the solvent on the chemical shifts. A similar trend is noted in a comparison of the ^{13}C NMR chemical shifts for the C(1) and C(2) amine carbons for the $[Me_2AlR']_2$ and $[Et_2AlR']_2$ series versus that of the analogous $[Bu^i_2\ AlR']_2$ series. The amine group also influences the ^1H and ^{13}C NMR chemical shifts of the alkyl groups on the aluminum atom. The δ_H values for the C(1) and C(2) protons of R for **1**–**5** are, on the average, 0.48 ppm and 0.30 ppm, more positive, respectively, for the $[R_2AlN(CH_2Ph)_2]_2$ series compared with the $[R_2AlNMe_2]_2$ series [33]. Similar trends are noted for the ^{13}C NMR chemical shifts for the two series.

The ^{13}C and ^1H NMR chemical shifts for the methyl group in the adducts, $Me_3M{\cdot}HN(CH_2Ph)_2$, where M = Al [28], Ga [37] and In [37] are dependent upon the metal present with $\delta_H = -0.38$, −0.10 and −0.11 ppm, and $\delta_C = -8.06$, −5.10 and −6.68 ppm, respectively. For the $[Me_2MN(CH_2Ph)_2]_2$ dimers, $\delta_H = -0.081$, 0.21, and 0.13 ppm for $[Me_2AlN(CH_2Ph)_2]_2$ (**1**) [28],

$[Me_2GaN(CH_2Ph)_2]_2$ (**6**) [31] and $[Me_2InN(CH_2Ph)_2]_2$ (**7**) [34,36], respectively. The methyl group δ_C values are also dependent on the metal present with $\delta_C = -7.57$, -5.91 and -6.80 ppm, for **1**, **6**, and **7**. The benzyl CH_2 and *ipso* carbon ^{13}C chemical shifts move downfield significantly upon substitution of In or Ga for Al where the ordering is (most downfield shift) In > Ga > Al. These chemical shift effects have been generally attributed to the different electronegativities of the metals (Al, 1.5; Ga, 1.6; In, 1.7) [42].

3.2. Mass spectral data for compounds 1–5

The EI MS for **1**–**5** do not show the existence of molecular ion peaks (M^+). Instead for **1**–**4**, $[M^+ - R]$ ion peaks are observed, indicative of the loss of one alkyl group bound to the aluminum atom. This observation is consistent with the results of mass spectral data on other aminoalane dimers [15,28,30,33,43,44], including the series $[Me_2AlR']_2$ [28], $[Bu^i_2AlR']_2$ [30] and $[R_2AlNMe_2]_2$ [33]. A $[M^+ - Me]$, and not a $[M^+ - Bu^i]$ ion peak is present in **5**. This effect, of cleaving a methyl group off an *iso*-butyl group attached to an aluminum atom, has been observed in the mass spectra of aminoalanes [15]. Also, methyl loss is characteristic for methyl side chains in the EI MS of hydrocarbons [45]. A prominent feature of each mass spectrum is the presence of the monomer peak minus an alkyl group $[R_2AlN(CH_2Ph)_2{}^+ - R]$. This ion peak serves as the base peak for **1** and **4**. The decomposition of the dibenzylamino group is the dominant feature of the mass spectra for **2**, **3**, and **5**, where the base peak is observed at an *m*/*z* ratio of 91 ($C_6H_5CH_2{}^+$, $C_7H_7{}^+$) with related peaks at 65 ($C_5H_5{}^+$), 106 ($C_6H_5CH_2NH^+$), and 120 ($C_6H_5CH_2NHCH_2{}^+$) [43,45]. These mass values are prominent in the EI mass spectrum of dibenzylamine [46]. Selected fragment ion peaks are listed in the Section 2.

3.3. X-ray crystallographic studies

The X-ray crystal data for **2** and **4** are given in Table 1. The ORTEP representations of the two molecular structures for **2** and **4** are shown in Figs. 1 and 2. Selected bond lengths (Å) and angles (°) from the X-ray data are summarized for **1** [27], **2**, and **4** in Table 2. For each of the structures, the Al–N and Al–C bond distances are within the expected range of values for dimeric aminoalanes [15,29,30,47–49]. The C–Al–C, N–Al–N and Al–N–Al angles in the three compounds are highly distorted from tetrahedral, as expected for four-membered rings [15,47]. The internal Al–N–Al and N–Al–N angles are smaller than the external C–Al–C and C–N–C angles, consistent with previously reported values [15,29,30,47–49].

The molecular geometry of the Al_2N_2 ring has been investigated in terms of the influence of different substituent groups on the aluminum and nitrogen atoms. [15,29,30,47–49]. In general, the influence of the substituent bound to the nitrogen has a more pronounced effect on ring geometry than that of the substituent on aluminum. As the steric bulk of the alkyl group attached to the aluminum atom increases, several trends have been observed in a homologous series: an increase in the Al–C bond length; lengthening of the Al···Al non-bonded distance; and a decrease in the N–Al–N bond angle [15,30,47]. Comparison of these parameters for R = Me (**1**), Et (**2**), and Bu^n (**4**) (Table 2) suggests that as the steric bulk of the alkyl group on aluminum is increased from Me to Et or Bu^n, there are only small changes in these parameters. Compounds **2** and **4** have a planar molecular structure with respect to the Al_2N_2 ring, while **1** has a slight deviation from planarity with a fold angle about the N(1)···N(1A) axis of 4.0°. Substitution of a hydrogen atom for a benzyl group on the nitrogen atom in **1** to form $[Me_2AlN(H)CH_2Ph]_2$ (**8**) [34,50] leads to a molecular structure for **8** with a planar Al_2N_2 ring and the benzyl groups in a *trans* orientation. On the average, the molecular structure for **8** has a shorter Al–N bond length than **1** (0.028(6) Å); there is a decrease in the Al–C bond length (0.029(11) Å); and a 2.4(3)° decrease in the N–Al–N bond angle [34]. The molecular structure data for **1**, **2**, and **4** can also be compared with the data for the orthometalated dimer series $[RAlN(CH_2Ph)\text{-}\mu\text{-}(CH_2C_6H_4)]_2$ [26,27] where R = Me, Et, Pr^n, Bu^n and Bu^i. All five molecular structures in the series exhibit planar Al_2N_2 rings. Varying the R group on the aluminum atom in this series has only a minor influence on the Al_2N_2 ring geometry.

The molecular structures of $[Me_2MN(CH_2Ph)_2]_2$ (Al (**1**), Ga (**6**), In (**7**)) are similar in that all three structures belong to the space group, $Cmc2_1$. Each M_2N_2 ring is slightly puckered with angles of fold about the N(1)···N(1A) axis of 4.0, 2.7, and 4.6° for **1**, **6**, and **7**, respectively. The average M–N bond distances for **1**, **6**, and **7** are 1.983(4), 2.044(6), and 2.248(7) Å and the C–M–C angles for **1**, **6**, and **7** are 118.0(4)°, 121.6(7)°, and 129.1(7)°. These bond distances and angles vary with the metal as observed in comparable amino-alanes, gallanes, and indanes [34]. The molecular structures of **1**, **6**, and **7** can also be compared with those of the corresponding adducts, $Me_3M\cdot HN(CH_2Ph)_2$, where M = Al [35], Ga [38], and In [38]. These three adducts crystallize in the same space group $P\bar{1}$, so comparisons of molecular geometry are meaningful. For the adducts as compared with **1**, **6** and **7**, the average C–M–C angles increase in the same order Al < Ga < In with values of 114.2(1)°, 115.5(2)°, and 117.3(4)° and the M–N bond distances also increase in the order Al < Ga < In with values of 2.058(2), 2.151(3), and 2.382(5) Å, respectively. The

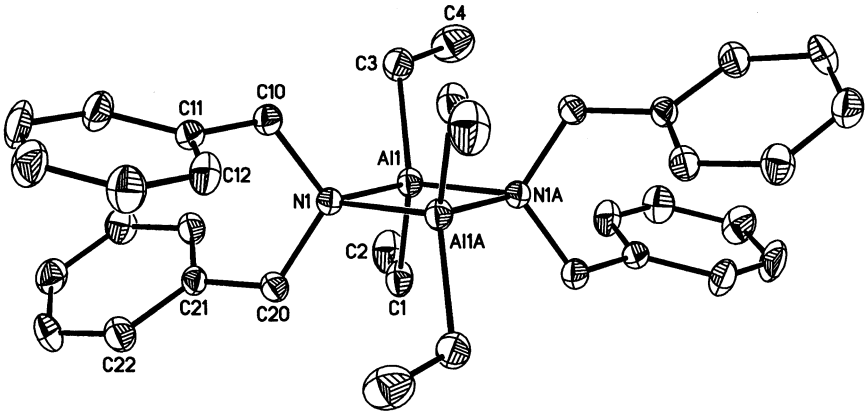


Fig. 1. Molecular structure and atom numbering scheme for $[Et_2AlN(CH_2Ph)_2]_2$ **(2)**. Hydrogen atoms omitted for clarity and thermal ellipsoids at 30% probability.

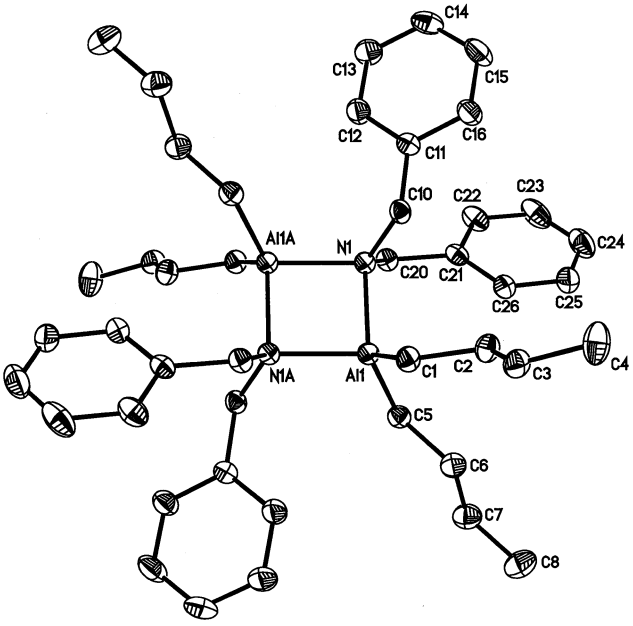


Fig. 2. Molecular structure and atom numbering scheme for $[Bu^n_2AlN(CH_2Ph)_2]_2$ **(4)**. Hydrogen atoms omitted for clarity and thermal ellipsoids at 30% probability.

longer M–N bond lengths for the adducts, as compared with the corresponding dimers, are typical for the two different types of bonding in these main group compounds [51].

4. Supplementary material

Tables of crystallographic data and data collection and structure refinement details have been deposited with the Cambridge Crystallographic Data Center. The CCDC codes are 132622 for $[Et_2AlN(CH_2Ph)_2]_2$ and 132623 for $[Bu^n_2AlN(CH_2Ph)_2]_2$. Copies of this information may be obtained free of charge from The Director, CCDC, 12 Union Road, Cambridge CB2 1EZ, UK (fax: +44-1223-336-033; e-mail: deposit@ccdc.cam.ac.uk or www: http://www.ccdc.cam.ac.uk).

Acknowledgements

This work was supported partially by a US Department of Education GAANN Fellowship to E.K.S.

References

[1] J.J. Eisch, in: G. Wilkinson, F.G.A. Stone, E.W. Abel (Eds.), Comprehensive Organometallic Chemistry, vol. 1, Pergamon Press, Oxford, 1982.
[2] T. Mole, E. Jeffery, Organoaluminium Compounds (Chapter 4), Elsevier, Amsterdam, 1972.
[3] G.E. Coates, M.L.H. Green, K. Wade, Organometallic Compounds, vol. 1, 3rd ed. (Chapter 3), Methuen, London, 1967.
[4] A. McKillop, J.D. Smith, I.J. Worrall, Organometallic Compounds of Aluminum, Gallium, Indium and Thallium, Chapman and Hall, London, 1985.
[5] M.F. Lappert, P.P. Power, A.R. Sanger, R.C. Srivastava, Metal and Metalloid Amides (Chapter 4), Ellis Horwood/Wiley, New York, 1980.
[6] M. Cesari, S. Cucinella, in: I. Haiduc, D.B. Sowerby (Eds.), The Chemistry of Inorganic Homo- and Heterocycles, vol. 1 (Chapter 6), Academic Press, London, 1987.
[7] F.C. Sauls, L.V. Interrante, Coord. Chem. Rev. 128 (1993) 193.
[8] D.C. Bradley, Polyhedron 13 (1994) 1111.
[9] M.G. Gardiner, C.L. Raston, Coord. Chem. Rev. 166 (1997) 1.
[10] (a) J. Pinkas, T. Wang, R.A. Jacobson, J.G. Verkade, Inorg. Chem. 33 (1994) 4202;
(b) J. Pinkas, T. Wang, R.A. Jacobson, J.G. Verkade, Inorg. Chem. 33 (1994) 5244.
[11] C. Jones, G.A. Koutsantonis, C.L. Raston, Polyhedron 12 (1993) 1829.
[12] A.C. Jones, J. Cryst. Growth 129 (1993) 728.
[13] D.C. Bertolet, H. Liu, J.W. Rogers, Jr., J. Appl. Phys. 75 (1994) 5385.
[14] J.F. Janik, E.N. Duesler, R.T. Paine, J. Organomet. Chem. 539 (1997) 19.
[15] D.C. Bradley, I.S. Harding, I.A. Maia, M. Motevalli, J. Chem. Soc., Dalton Trans. (1997) 2969.

[16] S. Amirkhalili, P.B. Hitchcock, J.D. Smith, J. Chem. Soc., Dalton Trans. (1979) 1206.
[17] A.-A.I. Al-Wassil, P.B. Hitchcock, S. Sarisaban, J.D. Smith, C.L. Wilson, J. Chem. Soc., Dalton Trans. (1985) 1929.
[18] K.M. Waggoner, P.P. Power, J. Am. Chem. Soc. 113 (1991) 3385.
[19] A. Haaland, in: G.H. Robinson (Ed.), Coordination Chemistry of Aluminum (Chapter 1), VCH, New York, 1993.
[20] G.H. Robinson, in: G.H. Robinson (Ed.), Coordination Chemistry of Aluminum (Chapter 4), VCH, New York, 1993.
[21] R.J. Wehmschulte, P.P. Power, Inorg. Chem. 33 (1994) 5611.
[22] R.J. Wehmschulte, P.P. Power, J. Am Chem. Soc. 118 (1996) 791.
[23] P.B. Hitchcock, H.A. Jasim, M.F. Lappert, H.D. Williams, Polyhedron 9 (1990) 245.
[24] K.M. Waggoner, M.M. Olmstead, P.P. Power, Polyhedron 9 (1990) 257.
[25] B. Lee, W.T. Pennington, G.H. Robinson, Inorg. Chim. Acta 190 (1991) 173.
[26] E.K. Styron, C.H. Lake, C.L. Watkins, L.K. Krannich, Organometallics 19 (2000) 3253.
[27] E.K. Styron, C.H. Lake, C.L. Watkins, L.K. Krannich, Organometallics 17 (1998) 4319.
[28] C.J. Thomas, L.K. Krannich, C.L. Watkins, Polyhedron 12 (1993) 389.
[29] E.K. Styron, C.H. Lake, S.J. Schauer, C.L. Watkins, L.K. Krannich, Polyhedron 18 (1999) 1595.
[30] C.B. Lagrone, S.J. Schauer, C.J. Thomas, G.M. Gray, C.L. Watkins, L.K. Krannich, Organometallics 15 (1996) 2458.
[31] S.J. Schauer, C.H. Lake, C.L. Watkins, L.K. Krannich, D.H. Powell, J. Organomet. Chem. 549 (1997) 31.
[32] S.J. Schauer, C.H. Lake, C.L. Watkins, L.K. Krannich, Organometallics 15 (1996) 5641.
[33] C.J. Thomas, L.K. Krannich, C.L. Watkins, Polyhedron 12 (1993) 89.
[34] E.K. Styron, C.H. Lake, D.H. Powell, L.K. Krannich, C.L. Watkins, J. Organomet. Chem. 649 (2002) 112.
[35] D.R. Armstrong, F.J. Craig, A.R. Kennedy, R.E. Mulvey, Chem. Ber. 129 (1996) 1293.
[36] E.K. Styron, Ph.D. Dissertation, University of Alabama at Birmingham, March 1999. The crystallographic data for $[Me_2InN(CH_2Ph)_2]_2$ have been deposited with the Cambridge Crystallographic Data Center as CCDC-113675.
[37] S.J. Schauer, C.L. Watkins, L.K. Krannich, R.B. Gala, E.M. Gundy, C.B. Lagrone, Polyhedron 14 (1995) 3505.
[38] C.H. Lake, S.J. Schauer, L.K. Krannich, C.L. Watkins, Polyhedron 18 (1999) 879.
[39] Siemens SHELXTL-PC Manual, Release 4.1. Siemens Analytical Instruments, Madison, WI, 1990.
[40] International Tables for X-Ray Crystallography, vol. 4, Kynoch Press, Birmingham, England, 1974, pp. 99–101, 149–150.
[41] M.R. Churchill, Inorg. Chem. 12 (1973) 1213.
[42] N.N. Greenwood, A. Earnshaw, Chemistry of the Elements, Pergamon, Oxford, 1984, p. 252.
[43] A. Storr, B.S. Thomas, J. Chem. Soc. A (1971) 3850.
[44] K. Gosling, J.D. Smith, D.H.W. Wharmby, J. Chem. Soc. A (1969) 1738.
[45] F.G. Kitson, B.S. Larsen, C.N. McEwen, Gas Chromatography and Mass Spectrometry: A Practical Guide, Academic Press, San Diego, CA, 1996.
[46] S.J. Heller, G.W.A. Milne, EPA/NIH Mass Spectral Data Base Supplement 1, US Government Printing Office, Washington, DC, 1980, p. 4410.
[47] S.J. Schauer, G.H. Robinson, J. Coord. Chem. 30 (1993) 197.
[48] T.Y. Her, C.C. Chang, J.O. Tsai, Y.Y. Lai, L.K. Liu, H.C. Chang, J.H. Chen, Polyhedron 12 (1993) 731.
[49] T. Belgardt, J. Storre, A. Klemp, H. Gornitzka, L. Haming, H.-G. Schmidt, H.W. Roesky, J. Chem. Soc., Dalton Trans. (1995) 3748.
[50] O.T. Beachley, Jr., Inorg. Chem. 20 (1981) 2825.
[51] A. Haaland, Angew. Chem., Int. Ed. Engl. 28 (1989) 992.

chemical shifts are reported with respect to 85% H_3PO_4, with downfield shifts considered positive. The SwaN-MR software package [9] was used to treat NMR data. The conductivity of 10^{-3} mol dm^{-3} solutions of the complexes in $MeNO_2$ at 25 °C was measured with a CDM 83 Radiometer.

2.2. Synthesis of complexes

2.2.1. [Fe(=C=C=CPh$_2$){P(OEt)$_3$}$_5$](BPh$_4$)$_2$ (1) and [Fe{C≡CCPh$_2$(OH)}{P(OEt)$_3$}$_5$]BPh$_4$ (3a)

Anhydrous $FeCl_2$ (0.126 g, 1 mmol) and an excess of $P(OEt)_3$ (1 cm^3, 6 mmol) were placed in a three-necked flask (25 cm^3). The suspension was stirred for 1 h and then 10 cm^3 of EtOH and a solution of HC≡CCPh$_2$(OH) (0.208 g, 1 mmol) in 2 cm^3 of EtOH were added. The reaction mixture was stirred for 2 h, treated with an excess of NEt_3 (0.28 cm^3, 2 mmol), and stirred for a further 2 h. The solvent was removed under reduced pressure, giving an oil which was treated with EtOH (4 cm^3) containing an excess of $NaBPh_4$ (0.68 g, 2 mmol). A dark-pink solid, containing both compounds **1** and **3a**, slowly separated out, and was filtered and crystallised fractionally. Typical separation involved the slow cooling to −25 °C of a saturated solution of the mixture of compounds in EtOH (5 cm^3) and enough CH_2Cl_2 to dissolve the solid at room temperature (r.t.). The first solid separated was acetylide **3a**, with yield: ≥ 15%; propadienylidene **1** was obtained with yield: ≥ 40%.

Anal. Calc. for $C_{93}H_{125}B_2FeO_{15}P_5$ (**1**): C, 65.1; H, 7.3. Found: C, 65.2; H, 7.2%. $\Lambda_M = 121.4$ S cm^2 mol^{-1}.

Anal. Calc. for $C_{69}H_{106}BFeO_{16}P_5$ (**3a**): C, 58.7; H, 7.6. Found: C, 58.9; H, 7.5%. $\Lambda_M = 56.7$ S cm^2 mol^{-1}.

2.2.2. [FeCl(=C=C=CPh$_2$){PPh(OEt)$_2$}$_4$]BPh$_4$ (2)

A suspension of anhydrous $FeCl_2$ (0.126 g, 1 mmol) in an excess of $PPh(OEt)_2$ (1.2 cm^3, 6 mmol) was stirred for 1 h and then a solution of HC≡CCPh$_2$(OH) (0.208 g, 1 mmol) in 10 cm^3 of EtOH was added. The reaction mixture was stirred for 2 h and then an excess of NEt_3 (0.28 cm^3, 2 mmol) was added. After 2 h of stirring, the solvent was evaporated to dryness, giving an oil which was treated with EtOH (4 cm^3) containing an excess of $NaBPh_4$ (0.68 g, 2 mmol). A dark-pink solid separated out, and was filtered and crystallised from CH_2Cl_2 (2 cm^3) and EtOH (5 cm^3); yield: ≥ 55%.

Anal. Calc. for $C_{79}H_{90}BFeClO_8P_4$: C, 68.1; H, 6.5; Cl, 2.5. Found: C, 68.0; H, 6.3; Cl, 2.7%. $\Lambda_M = 51.3$ S cm^2 mol^{-1}.

2.2.3. [Fe{C≡CCMePh(OH)}{P(OEt)$_3$}$_5$]BPh$_4$ (3b)

Anhydrous $FeCl_2$ (0.126 g, 1 mmol) and an excess of $P(OEt)_3$ (1 cm^3, 6 mmol) were placed in a three-necked flask (25 cm^3). The suspension was stirred for 1 h and then EtOH (10 cm^3) and HC≡CCMePh(OH) (0.15 g, 1 mmol) were added. The reaction mixture was stirred for 2 h and an excess of NEt_3 (1.4 cm^3, 10 mmol) was added. After 2 h of stirring at r.t., the solvent was removed under reduced pressure, giving a brown oil which was treated with EtOH containing an excess of $NaBPh_4$ (0.68 g, 2 mmol). A brown solid slowly separated out from the resulting solution, which was filtered and crystallised from CH_2Cl_2 (2 cm^3) and EtOH (5 cm^3); yield: ≥ 30%.

Anal. Calc. for $C_{64}H_{104}BFeO_{16}P_5$: C, 56.9; H, 7.8. Found: C, 57.2; H, 8.0%. $\Lambda_M = 50.4$ S cm^2 mol^{-1}.

2.2.4. [Fe(C≡CPh){P(OEt)$_3$}$_5$]BPh$_4$ (3c)

Anhydrous $FeCl_2$ (0.63 g, 5 mmol) and an excess of $P(OEt)_3$ (5.0 cm^3, 30 mmol) were placed in a three-necked flask (50 cm^3), and the resulting suspension was stirred for about 1 h. EtOH (15 cm^3) and then an excess of the appropriate alkyne (15 mmol) were added and the reaction mixture refluxed for 15 min. The solvent was removed under reduced pressure, giving an oil which was treated with EtOH (4 cm^3) containing an excess of $NaBPh_4$ (3.42 g, 10 mmol). A yellow solid slowly separated out, and was filtered and crystallised from CH_2Cl_2 (2 cm^3) and EtOH (5 cm^3); yield: ≥ 35%.

Anal. Calc. for $C_{62}H_{100}BFeO_{15}P_5$: C, 57.0; H, 7.7. Found: C, 56.8; H, 7.8%. $\Lambda_M = 58.5$ S cm^2 mol^{-1}.

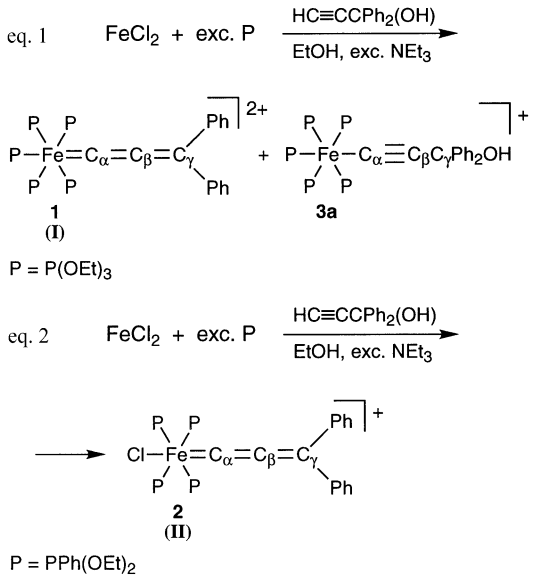
2.2.5. [{Fe[P(OEt)$_3$]$_5$}$_2$(μ-1,4-C≡CC$_6$H$_4$C≡C)](BPh$_4$)$_2$ (4)

An excess of $P(OEt)_3$ (1.0 cm^3, 6 mmol) was added to 0.126 g (1 mmol) of anhydrous $FeCl_2$ in a 25-cm^3 three-necked flask and the resulting suspension stirred for 1 h. Tetrahydrofurane (10 cm^3) and a solution of 1,4-HC≡CC$_6$H$_4$C≡CH (63 mg, 0.5 mmol) in 3 cm^3 in THF were added and, after 2 h of stirring, an excess of NEt_3 (1.4 cm^3, 10 mmol) was further added. The reaction mixture was stirred for 3 h and then the solvent evaporated to dryness under reduced pressure, giving a brown oil which was treated with 4 cm^3 of EtOH. The addition to the resulting solution of an excess of $NaBPh_4$ (0.68 g, 2 mmol) in 2 cm^3 of EtOH caused the separation of an orange–brown solid, which was filtered and crystallised from CH_2Cl_2 (2 cm^3) and EtOH (5 cm^3); yield: ≥ 25%.

Anal. Calc. for $C_{118}H_{194}B_2Fe_2O_{30}P_{10}$: C, 55.9; H, 7.7. Found: C, 56.1; H, 7.8%. $\Lambda_M = 124.5$ S cm^2 mol^{-1}.

3. Results and discussion

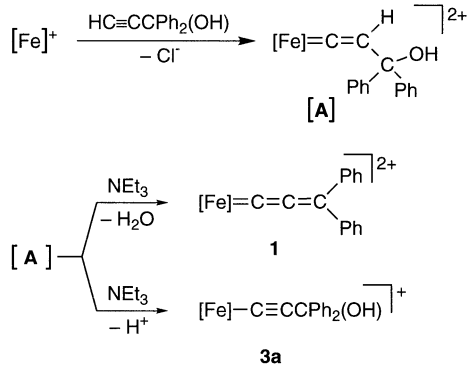
Propadienylidene complexes [Fe(=C=C=CPh$_2$)-{P(OEt)$_3$}$_5$](BPh$_4$)$_2$ (**1**) and [FeCl(=C=C=CPh$_2$)-{PPh(OEt)$_2$}$_4$]BPh$_4$ (**2**) were prepared by allowing iron(II) chloride solutions containing an excess of phosphite to react with propargylic alcohol, as shown in Scheme 1.



Scheme 1.

The reaction depends on the nature of the phosphite, affording pentakis complex **1** with $P(OEt)_3$, or chloro-derivative **2** with $PPh(OEt)_2$. Furthermore, a mixture of propadienylidene **1** and acetylide **3a** (ratio 2.7:1) forms in the case of Eq. (1), and these were separated by fractional crystallisation. The formation of both complexes **1** and **3a** is not surprising, as propargylic alcohol probably tautomerises on the iron centre (Scheme 2), giving a hydroxy-vinylidene [**A**] which, in the presence of NEt_3, can either lose H_2O to give propadienylidene **1** or undergo deprotonation, affording the new acetylide **3a** (Scheme 2).

Phosphite-containing $FeCl_2$ solutions in ethanol probably contain a mixture of phosphite complexes of the type $[FeClP_5]^+$, $FeCl_2P_4$ and $[FeP_6]^{2+}$, analogous to those observed in THF as solvent [10], with the pentakis species predominating in the case of $P(OEt)_3$. Treatment of these solutions with $HC{\equiv}CCPh_2OH$ may afford intermediates of type [**A**], whose reaction with NEt_3 gives final species **1** and **3a**. In contrast, in the case of $PPh(OEt)_2$, a hydroxy-vinylidene of the type $[FeCl\{PPh(OEt)_2\}_4\{{=}C{=}C(H)C(OH)Ph_2\}]^+$ may form, yielding chloropropadienylidene **2** by treatment with NEt_3. However, an acetylide complex of the type $[FeCl\{C{\equiv}CCPh_2(OH)\}\{PPh(OEt)_2\}_4]$ may also form by treatment with NEt_3, but in this case probably in low yield, and this prevents its separation as a solid.



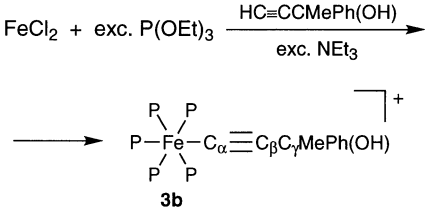
Scheme 2. $[Fe]^+ = [FeClP_5]^+$.

The reactions with $HC{\equiv}CPh_2(OH)$ were also studied in the presence of Brønsted acid (HBF_4, CF_3SO_3H), but no evidence of formatione of propadienylidene complexes was detected. This result is rather surprising, because an acid is generally used to promote the loss of H_2O in hydroxy-vinylidene species to give the $=C=C=CPh_2$ ligand while, in our case, only in the presence of NEt_3 the propadienylidene species **1**, **2** were isolated. Probably, the hydroxy-vinylidene bound to an iron fragment containing phosphites as ancillary ligands requires NEt_3 to give propadienylidene, and the results show as both acid and basic media can promote the loss of H_2O in the reaction of propargylic alcohol.

Propargylic alcohols different from $HC{\equiv}CCPh_2(OH)$, of the type $HC{\equiv}CCPhMe(OH)$, $HC{\equiv}CCH_2(OH)$, or $HC{\equiv}CCHPh(OH)$, also react with phosphite-containing $FeCl_2$ solutions, but afford mixtures of products whose IR spectra exclude the presence of propadienylidene ligands. However, in the case of $HC{\equiv}CCMePh(OH)$, a pale-yellow solid was isolated, which was characterised as the acetylide $[Fe\{C{\equiv}CCMePh(OH)\}\{P(OEt)_3\}_5]BPh_4$ (**3b**) derivative (Scheme 3).

These results on the reactivity of propargylic alcohols with phosphite-containing iron(II) solutions indicate that the nature of both the phosphite ligand and the acetylene play an important role in determining the reaction course and the stoichiometry of the final products. In fact, only with the diphenyl $HC{\equiv}CCPh_2(OH)$ species can propadienylidene complexes **1** and **2** be prepared, containing the pentakis(phosphite) FeP_5 fragment in the case of $P(OEt)_3$ (**1**); with the bulkier $PPh(OEt)_2$ ligand, chloro-species $[FeClP_4(=C=C=CPh_2)]^+$ (**2**) was obtained. Acetylide species **3** can also be prepared, but only in the case of the compound with $P(OEt)_3$ ligand do solid samples result.

Good analytical data were obtained for propadienylidene complexes **1** and **2**, which are purple solids stable in air and in solution of polar organic solvents, where they behave as 2:1 (**1**) or 1:1 (**2**) electrolytes [11].



Scheme 3.

Table 1
IR and NMR data for iron complexes

	Compound	IR [a]		^{1}H NMR [b,c]		Spin system	^{31}P{^{1}H} NMR [b,d]	^{13}C{^{1}H} NMR [b,e]	
		$\bar{\nu}$ (cm^{-1})	Assgnt	δ	Assgnt		δ (J Hz)	δ (J Hz)	Assgnt
1	[Fe(=C=C=CPh$_2$){P(OEt)$_3$}$_5$]-(BPh$_4$)$_2$	1950 m	ν(C=C=C)	4.04 (m) 1.40 (t) 1.24 (t)	POCH_2CH$_3$ POCH$_2$CH_3	AB$_4$	δ_A 139.9 δ_B 138.4 J_{AB} = 119.3	320.0 (m, br) 230.3 (m, br) 148.4 (s) 63.2 (s, br) 16.1 (s, br)	C$_\alpha$ C$_\beta$ C$_\gamma$ POCH_2CH$_3$ POCH$_2$CH_3
2	[FeCl(=C=C=CPh$_2$){PPh(OEt)$_2$}$_4$]-BPh$_4$	1918 m	ν(C=C=C)	3.62 (br) 1.12 (br)	POCH_2CH$_3$ POCH$_2$CH_3	A$_4$ A$_2$B$_2$ [f]	156 (br) δ_A 169.3 δ_B 157.6 J_{AB} = 73.0	319.7 (qnt) J_{CP} = 27 239.7 (s, br) 152.5 (s) 64.9 (s, br) 16.1 (s, br)	C$_\alpha$ C$_\beta$ C$_\gamma$ POCH_2CH$_3$ POCH$_2$CH_3
3a	[Fe{C≡CCPh$_2$(OH)}{P(OEt)$_3$}$_5$]-BPh$_4$	2091 m	ν(C≡C)	4.20 (m) 1.40 (t) 1.37 (t)	POCH_2CH$_3$ POCH$_2$CH_3	AB$_4$	δ_A 154.8 δ_B 152.3 J_{AB} = 107.2	120.1 (m) 103.1 (m) 75.5 (s) 63.2 (s, br) 62.4 (d) 16.1 (s, br)	C$_\beta$ C$_\alpha$ C$_\gamma$ POCH_2CH$_3$ POCH$_2$CH_3
3b	Fe{C≡CCMePh(OH)}{P(OEt)$_3$}$_5$]-BPh$_4$	2074 m	ν(C≡C)	8.65 (br) [g] 4.26 (m) 4.14 (m) 1.34 (t) 1.29 (t)	OH POCH_2CH$_3$ POCH$_2$CH_3	AB$_4$ [g]	δ_A 155.5 δ_B 152.7 J_{AB} = 106.5	119.2 (m) [g] 110.3 (m) 63.0 (s, br) 62.1 (d) 46.9 (s) 16.2 (s) 8.87 (s)	C$_\beta$ C$_\alpha$ POCH_2CH$_3$ C$_\gamma$ POCH$_2$CH_3 C(CH$_3$)
3c	[Fe(C≡CPh){P(OEt)$_3$}$_5$]BPh$_4$	2089 m	ν(C≡C)	4.31 (br) [g] 4.16 (br) 1.34 (t, br)	POCH_2CH$_3$ POCH$_2$CH_3	AB$_4$ [g]	δ_A 154.8 δ_B 151.5 J_{AB} = 105.8	119.0 (m) 108.7 (m) [AB$_4$X system: δ_X 108.7 J_{AX} = −22.25 J_{BX} = 47.3] 62.7 (s, br) 61.6 (d) 15.9 (s, br)	C$_\beta$ C$_\alpha$ POCH_2CH$_3$ POCH$_2$CH_3
4	[{Fe[P(OEt)$_3$]$_5$}$_2$(μ-1,4-C≡CC$_6$H$_4$C≡C)](BPh$_4$)$_2$	2085 m	ν(C≡C)	4.29 (m) 1.33 (t, br)	POCH_2CH$_3$ POCH$_2$CH_3	AB$_4$	δ_A 155.2 δ_B 152.3 J_{AB} = 106.5		

[a] In KBr pellets.
[b] In CD_2Cl_2 at 25 °C.
[c] Phenyl proton resonances are omitted.
[d] Positive shift downfield from 85% H_3PO_4.
[e] Phenyl carbon resonances are omitted.
[f] At −70 °C.
[g] In $(CD_3)_2CO$.

The IR and NMR data (Table 1) support the proposed formulation and allow a geometry in solution to be established. The IR spectra show a medium-intensity band at 1950 cm^{-1} for **1** and 1918 cm^{-1} for **2**, attributed to the $\nu_{(C=C=C)}$ of the propadienylidene ligand. However, support for the presence of the =C$_\alpha$=C$_\beta$=C$_\gamma$Ph$_2$ group in the complexes comes from the ^{13}C{^{1}H} NMR spectra, which show the characteristic highly deshielded C$_\alpha$ carbon resonance at 320.0 ppm for **1** and 319.7 ppm for **2**. The spectra also reveal the signals due to the C$_\beta$ and C$_\gamma$ of the propadienylidene ligand at 239.7–230.3 and 152.5–148.4 ppm, respectively.

In the temperature range +20 to −80 °C, the ^{31}P{^{1}H} NMR spectrum of the [Fe(=C=C=CPh$_2$)P$_5$]$^{2+}$ cation **1** appears as an AB$_4$ multiplet, in agreement with geometry (**I**). In contrast, the ^{31}P spectrum of the related complex [FeCl(=C=C=CPh$_2$)P$_4$]$^+$ (**2**) is temperature-

dependent and the sharp singlet which appears at + 20 °C changes as temperature falls and resolves into an A_2B_2 multiplet at −50 °C.

These results are difficult to interpret, because octahedral geometry with the halogenide and propadienylidene ligands in a mutually *cis* position should give an ABC_2- or AB_2C-type multiplet, whereas, in *trans* geometry, a sharp singlet is expected. However, the presence of inequivalent phosphorus *nuclei* at low temperature for **2** may also be interpreted on the basis of *trans* geometry (**II**), in which the four $PPh(OEt)_2$ phosphite ligands are made inequivalent by the different arrangement of the phenyl and ethoxy groups of one phosphite with respect to the other.

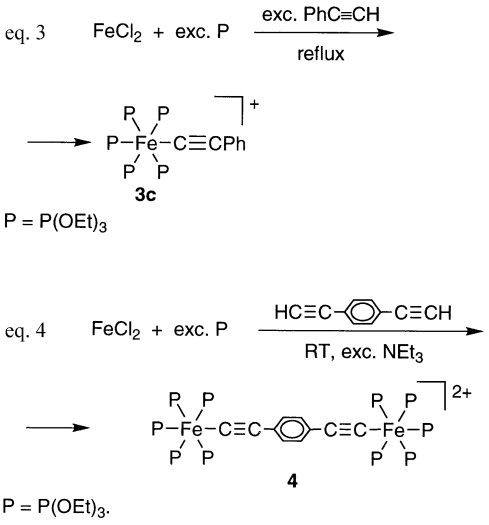
Examples of inequivalent phosphorus *nuclei* in octahedral complexes containing four $PPh(OEt)_2$ ligands in a plane have recently been reported for $FeHCl[PPh(OEt)_2]_4$ [6c], $MnH(CO)[PPh(OEt)_2]_4$ [12] and $[ReCl(ArN_2)\{PPh(OEt)_2\}_4]^+$ [13]. These precedents support the hypothesis of the existence, for **2**, of *trans* geometry in which restricted rotation around the Fe–P bond at low temperature makes the phosphite ligands 'two-by-two' inequivalent in the complex.

The IR spectra of acetylide complexes **3a** and **3b** show the $\nu_{(C\equiv C)}$ of the acetylide ligand as a medium-intensity band at 2091 cm^{-1} for **3a** and 2074 cm^{-1} for **3b**. The $^{13}C\{^1H\}$ NMR spectra also confirm the presence of the acetylide ligand in both complexes showing the characteristic C_α and C_β carbon signals at 110.3–103.1 and 120.1–119.2 ppm, respectively (Table 1). They also show the signals of the C_γ carbon atoms at 46.9 (**3b**) and 75.5 ppm (**3a**), and the proton NMR spectrum of **3b** displays a broad signal at 8.65 ppm, attributed to the OH group of the C≡CCMePh(OH) ligand. Lastly, an AB_4 multiplet is present for both complexes in the ^{31}P spectra, in agreement with the proposed formulation.

The results obtained with propargylic alcohols prompted us to extend study to other terminal alkynes. The results are summarised in Scheme 4 and show the formation of pentakis(phosphite) acetylide complexes **3c** and **4**. However, while the mononuclear complexes **3** had previously been prepared by us (except **3c**) following a different method [6], the dinuclear $[\{FeP_5\}_2(\mu\text{-}4,4'\text{-}C\equiv CC_6H_4C\equiv C)]^{2+}$ (**4**) is new, and was isolated as a pale-yellow solid and characterised.

The formation of acetylide in these reactions is not surprising, and probably involves deprotonation of a vinylidene =C=C(H)R intermediate of the type $[Fe\{=C=C(H)R\}P_4]^{2+}$. Such a vinylidene ligand probably formes by a 1,2-hydrogen shift of a coordinate η^2-alkyne group [14–16]. Deprotonation by NEt_3 or an excess of phosphite of the vinylidene intermediate gives the final acetylide derivative.

Analytical and spectroscopic data (Table 1) support the formulation of acetylide complexes **3c** and **4**.



Scheme 4.

The IR spectra of both mononuclear (**3c**) and binuclear (**4**) acetylide complexes show only one medium intensity band, at 2089 and 2085 cm^{-1}, respectively, due to the $\nu_{C\equiv C}$ of the acetylide ligand. The $^{13}C\{^1H\}$ NMR spectra of **3c** also confirm the presence of the RC≡C group, showing the characteristic signals of the C_α and C_β carbon atoms. Lastly, in the temperature range +30 to −80 °C, the ^{31}P spectra of both complexes **3c** and **4** appear as AB_4 multiplets, in agreement with the presence of a pentakis(phosphite) fragment in these acetylide derivatives.

Acknowledgements

The financial support of MIUR (Rome)—Programmi di Ricerca Scientifica di Rilevante Interesse Nazionale, Cofinanziamento 2000–2001—is gratefully acknowledged. We thank Daniela Baldan for technical assistance.

References

[1] (a) M.I. Bruce, Chem. Rev. 98 (1998) 2797;
(b) V. Cadierno, M.P. Gamasa, J. Gimeno, Eur. J. Inorg. Chem. (2001) 571.
[2] (a) H. Werner, M. Laubender, R. Wiedemann, B. Windmüller, Angew. Chem., Int. Ed. Engl. 35 (1996) 1237;
(b) R. Wiedemann, P. Steinert, O. Gevert, H. Werner, J. Am. Chem. Soc. 118 (1996) 2495;
(c) A. Fürstner, M. Picquet, C. Bruneau, P.H. Dixneuf, J. Chem. Soc., Chem. Commun. (1998) 1315;
(d) M. Picquet, D. Touchard, C. Bruneau, P.H. Dixneuf, New J. Chem. (1999) 141;
(e) K.J. Harlow, A.F. Hill, J.D.E.T. Wilton-Ely, J. Chem. Soc., Dalton. Trans. (1999) 285;
(f) Y. Nishibayashi, I. Wakiji, Y. Ishii, S. Uemura, M. Hidai, J. Am. Chem. Soc. 123 (2001) 3393 (and references therein).

[3] (a) M.A. Esteruelas, A.V. Gómez, A.M. López, J. Modrego, E. Oñate, Organometallics 17 (1998) 5434;
(b) C. Bianchini, N. Mantovani, A. Marchi, L. Marvelli, D. Masi, M. Peruzzini, R. Rossi, A. Romerosa, Organometallics 18 (1999) 4501;
(c) E. Bustelo, M. Jiménez-Tenorio, M.C. Puerta, P. Valerga, Organometallics 18 (1999) 4563;
(d) V. Cadierno, M.P. Gamasa, J. Gimeno, E. Pérez-Carreño, A. Ienco, Organometallics 17 (1998) 5216;
(e) C. Bohanna, B. Callejas, A.J. Edwards, M.A. Esteruelas, F.J. Lahoz, L.A. Oro, N. Ruiz, C. Valero, Organometallics 17 (1998) 373.

[4] (a) S. Nakanishi, K. Goda, S. Uchiyama, Y. Otsuji, Bull. Chem. Soc. Jpn. 65 (1992) 2560;
(b) V. Guillaume, P. Thominot, F. Coat, A. Mari, C. Lapinte, J. Organomet. Chem. 565 (1998) 75.

[5] (a) C. Gauss, D. Veghini, O. Orama, H. Berke, J. Organomet. Chem. 541 (1997) 19;
(b) H. Berke, V. Grössmann, G. Huttner, L. Zsolnai, Chem. Ber. 117 (1984) 3432.

[6] (a) G. Albertin, S. Antoniutti, E. Del Ministro, E. Bordignon, J. Chem. Soc., Dalton. Trans. (1992) 3203;
(b) G. Albertin, S. Antoniutti, E. Bordignon, E. Del Ministro, S. Iannelli, G. Pelizzi, J. Chem. Soc., Dalton. Trans. (1995) 1783;
(c) G. Albertin, S. Antoniutti, E. Bordignon, J. Organomet. Chem. 513 (1996) 147.

[7] R. Rabinowitz, J. Pellon, J. Org. Chem. 26 (1961) 4623.

[8] A.S. Hay, J. Org. Chem. 25 (1960) 637.

[9] G. Balacco, J. Chem. Inf. Comput. Sci. 34 (1994) 1235 (Upgrades via the Internet at: http://qobrue.usc.es/jsgroup/swan/index.html).

[10] S.D. Ittel, A.D. English, C.A. Tolman, J.P. Jesson, Inorg. Chim. Acta 33 (1979) 101.

[11] W.J. Geary, Coord. Chem. Rev. 7 (1971) 81.

[12] G. Albertin, S. Antoniutti, M. Bettiol, E. Bordignon, F. Busatto, Organometallics 16 (1997) 4959.

[13] G. Albertin, S. Antoniutti, A. Bacchi, E. Bordignon, F. Miani, G. Pelizzi, Inorg. Chem. 39 (2000) 3283.

[14] (a) M.I. Bruce, Chem. Rev. 91 (1991) 197;
(b) M.I. Bruce, B.C. Hall, N.N. Zaitseva, B.W. Skelton, A.H. White, J. Chem. Soc., Dalton. Trans. (1998) 1793.

[15] (a) J. Silvestre, R. Hoffmann, Helv. Chim. Acta 68 (1985) 1461;
(b) Y. Wakatsuki, N. Koga, H. Yamazaki, K. Morokuma, J. Am. Chem. Soc. 116 (1994) 8105.

[16] (a) M.D. Fryzuk, L. Huang, N.T. McManus, P. Paglia, S.J. Rettig, G.S. White, Organometallics 11 (1992) 2979;
(b) J.R. Lumphrey, J.P. Selegue, J. Am. Chem. Soc. 114 (1992) 5518;
(c) C. Bianchini, M. Peruzzini, A. Vacca, F. Zanobini, Organometallics 10 (1991) 3697.

2.1. Synthesis of Cu(II) hinokitiol (1)

Hinokitiol (0.30 g, 1.83 mmol) was dissolved in aq. EtOH (50:50, 50 ml) with stirring. Once dissolved, a solution of copper acetate (0.19 g, 0.95 mmol) was added and the stirring continued. After stirring and gentle heating for 2 h, the green/blue solution was allowed to stand for 1 week after which time the product crystallised from solution as green/blue plate-like crystals. *Anal*. Found (Calc. for $C_{20}H_{22}CuO_4$): C, 61.6 (61.6); H, 5.64 (5.69)%. Selected IR data (cm^{-1}): 1600, 1574 ν(C=O); 1512 ν(C=C); 1286–1228 ν(C–O).

2.2. Synthesis of (hinokitiol)$_2$Cu·(pyridine) (2)

Pyridine (5 ml) was added to a solution of **1** (0.30 g, 0.77 mmol) in $C_6H_5CH_3$ (30 ml). After stirring for 20 min, the solution was cooled to −15 °C whereupon a green solid appeared (0.06 g; 17%). Some crystals suitable for X-ray crystallography were obtained from the filtrate. *Anal*. Found (Calc. for $C_{25}H_{27}CuNO_4$): C, 63.7 (64.0); H, 5.79 (5.76); N, 2.85 (2.98)%. Selected IR data (cm^{-1}): 1583, 1569, 1496 ν(C=O) and ν(C=C); 1261, 1231 ν(C–O).

2.3. Synthesis of (hinokitiol)$_2$Cu·(bipyridine) (3)

Bipyridine (1.00 g, 6.25 mmol) was dissolved in $C_6H_5CH_3$ (30 ml) and then added to a solution of **1** (0.40 g, 1.03 mmol) in $C_6H_5CH_3$ (50 ml). The mixture was stirred for 20 min and then left at room temperature for few days, yielding a brown solid (0.44 g, 78%). *Anal*. Found (Calc. for $C_{30}H_{30}CuN_2O_4$): C, 65.5 (65.9); H, 5.48 (5.49); N, 5.83 (5.13)%. Selected IR data (cm^{-1}): 1594, 1554, 1511 ν(C=O) and ν(C=C); 1278, 1199 ν(C–O).

2.4. Crystallography

Suitable crystals of **1** were obtained either from EtOH (modification 1) or from $C_6H_5CH_3$ in the presence of urea (modification 2). Crystals of **2** were obtained from a dilute solution in $C_6H_5CH_3$ (Table 1).

For modification 1 of **1**, crystallographic measurements were made at 293(2) K on a CAD4 automatic four-circle diffractometer in the range $2.40° < \theta < 23.92°$. Data (1685 reflections) were corrected for Lp and 10% decay of the crystal in the X-ray beam. An absorption correction was not applied. In the final least-squares cycles all atoms were allowed to vibrate anisotropically. Hydrogen atoms were included at calculated positions where relevant except for H3, H4, H5 and H7 which were easily located in the penultimate difference Fourier map and refined at a distance of 0.93 Å from the carbon atoms to which they are attached.

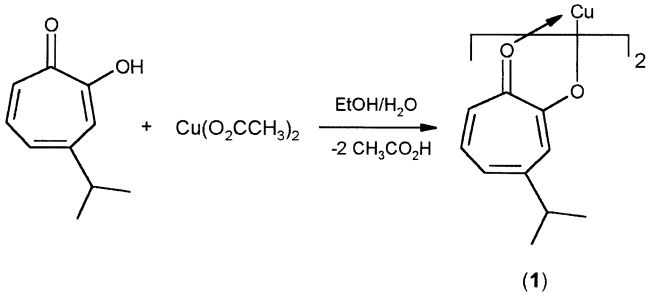
For modification 2 of **1**, crystallographic measurements were made at 150 K on a Nonius Kappa CCD diffractometer in the range $3.80° < \theta < 27.48°$. Data (54 148 reflections) were corrected for Lp, extinction and absorption (max. and min. transmission factors: 1.030 and 0.974, respectively). The asymmetric unit consisted of 2.5 independent molecules. The two full molecules are located proximate to inversion centres and hence dimerise with nearby lattice neighbours. The central copper atom [Cu(3)] in the remaining independent half-molecule is seated on an inversion centre which serves to generate the full molecule in this case. Disorder in one of the isopropyl groups [C(39)/C(40)] was successfully modelled as a 55:45 occupancy ratio. In the final least-squares cycles, all atoms were allowed to vibrate anisotropically and hydrogen atoms were included at calculated positions throughout.

Crystallographic measurements for **2** were made at 293(2) K on a CAD4 automatic four-circle diffractometer in the range $2.24° < \theta < 24.98°$. Data (4337 reflections) were corrected for Lp but not for absorption. In the final least-squares cycles, all atoms were allowed to vibrate anisotropically. Hydrogen atoms were included at calculated positions where relevant.

In all three cases, refinement was based on F_o^2. Software used: SHELXS-86 [19], SHELXL-97 [20], ORTEX [21]. The asymmetric units of **1** (two modifications) and **2** are displayed in Figs. 1–3 along with the atomic numbering scheme. Selected metric data for modification 1 of **1** and **2** are given in the figure captions, while that for modification 2 of **1** are given in Table 2.

3. Results and discussion

Cu(II) hinokitiol (**1**) was synthesised using the method detailed in Eq. (1). After 1 week, a large number of blue plate-like crystals had formed in the solution. Microanalysis of these crystals showed the complex to be anhydrous.



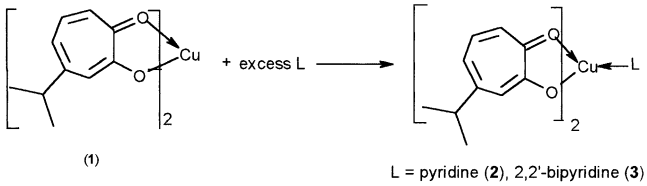
(1)

We have previously noted that copper derivatives of α-hydroxyketones (maltol, hinokitiol etc.) in which the copper is four-coordinate, square-planar geometry are notably anti-bacterially and/or -microbially active, whereas the analogous zinc species, in which the zinc is either five- or six-coordinate, are markedly less so [18].

Table 1
Crystallographic data for **1** and **2**

	1 (modification 1)	**1** (modification 2)	**2**
Empirical formula	$C_{20}H_{22}CuO_4$	$C_{20}H_{22}CuO_4$	$C_{25}H_{27}CuNO_4$
Formula weight	389.92	389.92	469.02
Temperature (K)	293(2)	150(2)	293(2)
λ (Mo Kα) (Å)	0.71069	0.71069	0.71069
Crystal system	monoclinic	monoclinic	monoclinic
Space group	$P2_1/c$	$P2_1/n$	$P2_1/n$
a (Å)	9.254(2)	16.7420(2)	8.616(2)
b (Å)	9.997(2)	15.5370(2)	26.848(4)
c (Å)	11.124(3)	18.3010(3)	9.910(2)
β (°)	113.86(2)	99.4000(6)	102.56(2)
V (Å^3)	941.2(4)	4696.54(11)	2237.5(8)
Z	2	10	4
ρ_{calc} (Mg m^{-3})	1.376	1.379	1.392
μ (mm^{-1})	1.180	1.183	1.007
Crystal size (mm)	0.3 × 0.3 × 0.5	0.25 × 0.10 × 0.10	0.25 × 0.20 × 0.20
θ Range (°)	2.40–23.92	3.80–27.48	2.24–24.98
Reflections collected	1685	54 148	4337
Independent reflections	1475 [$R_{int} = 0.0396$]	10 712 [$R_{int} = 0.0471$]	3928 [$R_{int} = 0.0326$]
Final R indices [$I > 2\sigma(I)$]	$R_1 = 0.0430$, $wR_2 = 0.0704$	$R_1 = 0.0384$, $wR_2 = 0.1000$	$R_1 = 0.0441$, $wR_2 = 0.1232$
R indices (all data)	$R_1 = 0.1066$, $wR_2 = 0.0921$	$R_1 = 0.0558$, $wR_2 = 0.1139$	$R_1 = 0.1271$, $wR_2 = 0.1681$

In order to assess the importance of metal coordination number on activity, we have prepared complexes of **1** by reaction with N-donor Lewis bases (Eq. (2)). 1:1 adducts with pyridine (**2**) and 2,2′-bipyridine (**3**) have been isolated, which presumably contain five- or six-coordinate copper, respectively.



(1)

L = pyridine (**2**), 2,2'-bipyridine (**3**)

(2)

3.1. The structure of Cu(II) hinokitiol (*1*)

Cu(II) hinokitiol, prepared as in Eq. (1), was recrystallised from aqueous ethanol, yielding a crystal of approximate dimensions 0.3 × 0.3 × 0.5 mm which was used for data collection. Selected structural data are included in the caption to Fig. 1. This structure will be discussed as modification 1. An attempt to prepare an adduct of **1** with urea in toluene failed, and green crystals of **1** were recovered but whose cell parameters [$a = 16.7420(2)$; $b = 15.5370(2)$; $c = 18.3010(3)$ Å; $\beta = 99.4000(6)°$] were different to those of modification 1 [$a = 9.254(2)$; $b = 9.997(2)$; $c = 11.124(3)$ Å; $\beta = 113.86(2)°$]. This second crystal structure will be dis-

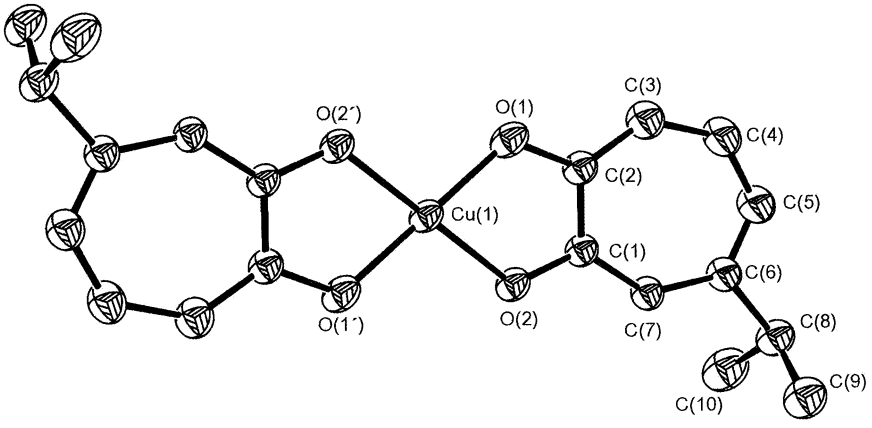


Fig. 1. The asymmetric unit of modification 1 of compound **1** showing the labelling scheme used in the text. Thermal ellipsoids are at the 30% probability level. Selected metrical data: Cu(1)–O(1) 1.904(3), Cu(1)–O(2) 1.900(2), O(1)–C(2) 1.293(5), O(2)–C(1) 1.296(5) Å; O(1)–Cu(1)–O(1′) 180.0, O(2)–Cu(1)–O(2′) 180.0, O(1)–Cu(1)–O(2) 83.84(13), O(1)–Cu(1)–O(2′) 96.16(13), C(2)–O(1)–Cu(1) 113.5(3), C(1)–O(2)–Cu(1) 113.5(3)°. Symmetry related atoms are generated using $-x$, $-y$, $-z$.

cussed as modification 2. Both forms adopt monoclinic $P2_1/c$ (or $P2_1/n$) symmetries.

In modification 1 (Fig. 1), the asymmetric unit comprises half of a molecule, the remaining portion being generated via an inversion centre at the origin on which the copper is sited. The Cu(II) is four-coordinate and in a square-planar environment. The molecule as a whole is essentially planar [maximum deviation from mean plane: 0.029 Å for O(2)]. The Cu–O bonds are equivalent [Cu–O(1), 1.904(3); Cu–O(2), 1.900(2) Å] and the $<$O(1)–Cu–O(2) bond angle is 83.8(1)°. The Cu–O bond lengths are in agreement with other Cu(II) complexes, e.g. Cu(II) erythritol [Cu–O: 1.912(4), 1.922(4) Å] [22]. Both of the C–O bond lengths in **1** compare well with those found in a number of other metal tropolonates, i.e. 1.27–1.30 Å and Zn(II) hinokitiol [1.277(2)–1.306(2) Å] [16]. Furthermore, upon coordination to the Cu(II) the C–O bond lengths become equal [1.293(5), 1.296(3) Å], indicating a similar bond order in both. This is a more symmetric arrangement than the equivalent bonds in hinokitiol itself (C–O: 1.349; C=O: 1.261 Å) [23]. The lengths of the C–C bonds in the hinokitiol ring of **1** are approximately equal (approximately 1.38 Å) with one notable exception. The C(1)–C(2) bond is significantly longer than the others in the ring, indicating that it is not involved to the same extent in the π-electron delocalisation within the C_7 unit. The value of 1.464(6) Å observed for the C(1)–C(2) bond in **1** is closer to that expected for a C(sp^3)–C(sp^3) single bond. For comparison, the π-electron system in hinokitiol is also partially delocalised, though the formal double bonds [C(1)–C(7), C(6)–C(5) and C(4)–C(3); 1.367, 1.355 and 1.364 Å, respectively] are more clearly distinguishable from the formal single bonds [C(7)–C(6), C(5)–C(4) and C(3)–C(2); 1.422, 1.413 and 1.413 Å, respectively] than in **1**. The C(1)–C(2) bond in the ligand (1.469 Å) is, however, significantly longer than the other carbon–carbon bonds and is comparable with that in **1** [23].

In modification 2 of **1**, obtained from toluene in an attempt to prepare a urea adduct, there are two and half molecules in the asymmetric unit; two molecules are in general positions, while half molecule has the copper atom seated on an inversion centre (Fig. 2), as with modification 1. For each molecule, the copper is nominally four-coordinate and in a square-planar environment. The molecule generated by the inversion centre [molecule A, containing Cu(3)] has the isopropyl groups adopting a *trans* configuration and this is also the case for one of the two other molecules [molecule B containing Cu(2)]; in this respect, both molecules replicate the structure of modification 1. However, in the remaining molecule [molecule C containing Cu(1)] the isopropyl groups are *cis* to each other. This is unusual, as for previous structures of α-hydroxyketones, the alkyl groups are *trans* to each other e.g. Zn(hino)$_2$·EtOH [16], Zn(maltol)$_2$ [24], and **2** (*see below*).

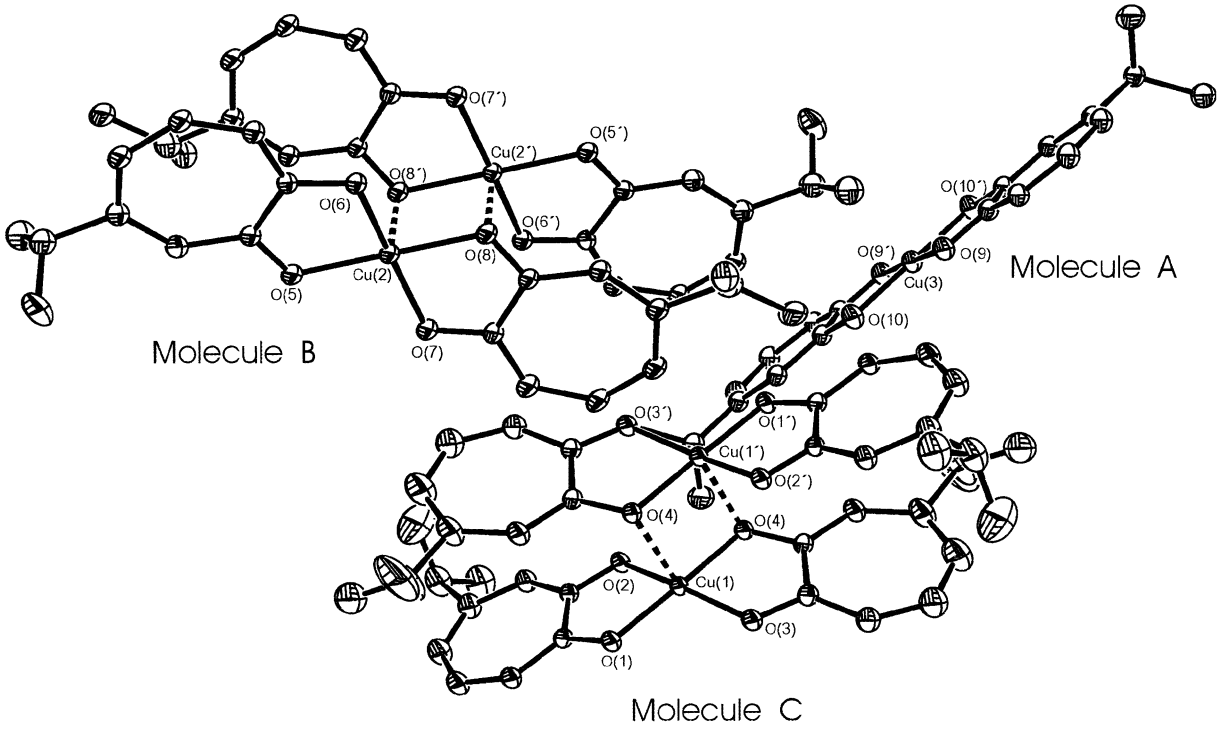


Fig. 2. The asymmetric unit of modification 2 of compound **1** showing the labelling scheme used in the text. Thermal ellipsoids are at the 30% probability level.

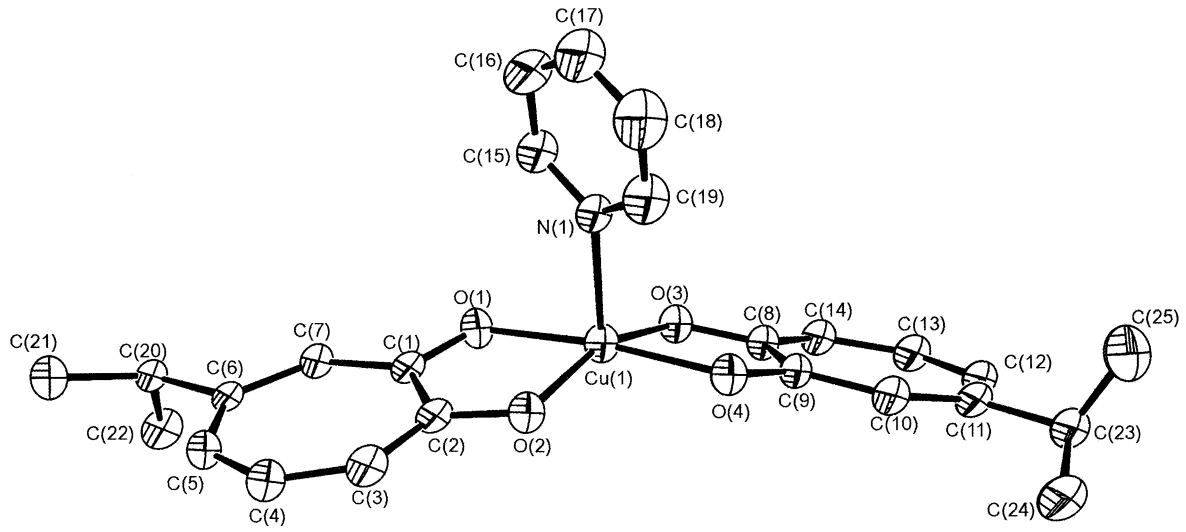


Fig. 3. The asymmetric unit of **2** showing the labelling scheme used in the text. Thermal ellipsoids are at the 30% probability level. Selected metrical data: Cu(1)–O(1) 1.940(3), Cu(1)–O(2) 1.945(3), Cu(1)–O(3) 1.965(3), Cu(1)–O(4) 1.933(3), Cu(1)–N(1) 2.311(5), O(1)–C(1) 1.287(5), O(2)–C(2) 1.278(6), O(3)–C(8) 1.287(5), O(4)–C(9) 1.277(6) Å; O(1)–Cu(1)–O(2) 82.73(14), O(1)–Cu(1)–O(3) 97.28(14), O(1)–Cu(1)–O(4) 172.2(2), O(2)–Cu(1)–O(3) 155.2(2), O(2)–Cu(1)–O(4) 94.3(2), O(3)–Cu(1)–O(4) 82.34(14), O(1)–Cu(1)–N(1) 92.3(2), O(2)–Cu(1)–N(1) 99.0(2), O(3)–Cu(1)–N(1) 105.8(2), O(4)–Cu(1)–N(1) 95.3(2)°.

The two full molecules in modification 2 (B and C) are proximate to inversion centres and hence dimerise with nearby lattice neighbours (Fig. 2). In the dimer based on B, the isopropyl groups sit above each other (eclipsed conformation), while in the dimer of C, they are on opposite sides of the stacked seven-membered rings (staggered conformation). Thus, molecule B minimises repulsions between isopropyl groups within the monomer but maximises it between molecules on dimer formation, while the reverse is true for molecule C.

Table 2
Selected bond lengths (Å) and angles (°) for modification 2 of **1** [a]

	Molecule A	Molecule B	Molecule C
Bond lengths			
trans-Monomer			
Cu(3)–O(9)	1.910(2)		
Cu(3)–O(10)	1.901(2)		
trans-Dimer			
Cu(1)–O(1)			1.919(2)
Cu(1)–O(2)			1.920(2)
Cu(1)–O(3)			1.932(2)
Cu(1)–O(4)			1.933(2)
cis-Dimer			
Cu(2)–O(5)		1.915(2)	
Cu(2)–O(6)		1.921(2)	
Cu(2)–O(7)		1.939(2)	
Cu(2)–O(8)		1.922(2)	
Intermolecular			
Cu(1)···O(4′)			2.476(2)
Cu (2)···O(8′)		2.511(2)	
Bond angles [b]			
O(1)–Cu(1)–O(2)	84.53(8)	84.27(7)	83.86(7)
O(1)–Cu(1)–O(3)	95.47(8)	97.95(7)	99.15(7)
O(1)–Cu(1)–O(4)	180.0	174.64(7)	177.40(7)
O(2)–Cu(1)–O(3)	180.0	166.88(7)	165.00(8)
O(2)–Cu(1)–O(4)	95.47(8)	93.36(7)	93.55(7)
O(3)–Cu(1)–O(4)	84.53(8)	83.29(7)	83.26(7)

[a] Symmetry transformation used to generate equivalent atoms: $-x, -y, -z$.
[b] Atomic labels refer to molecule C; for molecules A [Cu(3)] and B [Cu(2)], oxygens are O(9, 10) and O(5–8), respectively.

In the non-dimerised molecule A, the Cu–O bond lengths [1.901(2), 1.909(2) Å] are similar than those observed in modification 1 [1.900(2), 1.904(3) Å]. For dimers based on molecules B and C, the intramolecular Cu–O bond lengths [1.915(2)–1.939(2) Å] are longer than those in modification 1 and thus the effect of the dimerisation is similar to the effect of the pyridine coordination, as in **2** (*see below*). The intermolecular interactions [Cu(1)–O(4): 2.476(2); Cu(2)–O(8): 2.511(2) Å] are clearly longer and weaker than the analogous intramolecular bonds, with the eclipsed dimerisation in molecule B manifesting itself in the longer of these two contacts. The intermolecular interactions in both cases do, however, generate almost perfect Cu_2O_2 squares [< Cu(1)–O(4)–Cu(1′): 93.09(6)°; < Cu(2)–O(8)–Cu(2′): 94.80(6)°] at the heart of each dimer.

The coordination chemistry of **1** is thus exceedingly flexible, as both *cis* and *trans* ligand arrangements are possible, as are both monomers and dimers.

3.2. The structure of Cu(II) hinokitiol·pyridine adduct 2

Compound **2** crystallises in the monoclinic space group $P2_1/n$. The copper adopts a square pyramidal geometry with the pyridine in the axial position (Fig. 3),

the copper lies 0.125 Å above the plane of the four oxygen atoms. The Cu–O bond lengths [1.940(3), 1.933(3), 1.945(3), 1.985(3) Å] are longer than those observed in isolated molecules of **1** [1.900(2)–1.909(2) Å]. The structure is similar to the one obtained for $Cu(acrp)_2 \cdot$pyridine (Hacrp: 4-hydroxy-6-methyl-3-[3-dimethylaminoacryloyl]-2*H*-pyran-2-one), and the Cu–N bond [2.311(5) Å] is equivalent with the Cu–N bond of this species [2.310(10) Å] [25].

The electronic spectra of Ni(II) and Cu(II) species incorporating both amines and hinokitiol i.e. $[M(hino)(diamine)]^+$ have been studied [26,27] and such compounds exploited in the extraction of unprotected amino acids [26].

4. Supplementary material

Crystallographic data for the structural analysis have been deposited with the Cambridge Crystallographic Data Centre, CCDC Nos. 181131–181133 for compounds **1** (two modifications) and **2**. Copies of this information may be obtained free of charge from The Director, CCDC, 12 Union Road, Cambridge, CB2 1EZ, UK (fax: +44-1223-336033; e-mail: deposit@ccdc.cam.uk or www: http://www.ccdc.cam.ac.uk).

References

[1] T. Okabe, K. Saito, T. Fukui, K. Iinuma, Mokuzai Gakkaishi 40 (1994) 1233.
[2] D. Miyamoto, Y. Kusagaya, N. Endo, A. Sometani, S. Takeo, T. Suzuki, Y. Arima, K. Nakajima, Y. Suzuki, Antiviral Res. 39 (1998) 89.
[3] D. Miyamoto, N. Endo, N. Oku, Y. Arima, T. Suzuki, Y. Suzuki, Biol. Pharmacol. Bull. 21 (1998) 1258.
[4] Y. Inamori, S. Shinohara, H. Tsujibo, T. Okabe, Y. Morita, Y. Sakagami, Y. Kumeda, N. Ishida, Biol. Pharmacol. Bull. 22 (1999) 990.
[5] Y. Inamori, Y. Sakagami, Y. Morita, M. Shibata, M. Sugiura, Y. Kumeda, T. Okabe, H. Tsujibo, N. Ishida, Biol. Pharmacol. Bull. 23 (2000) 995.
[6] E. Matsumura, Y. Morita, T. Date, H. Tsujibo, M. Yasuda, T. Okabe, N. Ishida, Y. Inamori, Biol. Pharmacol. Bull. 24 (2001) 299.
[7] H. Erdtmann, J. Gripenberg, Nature 161 (1948) 719.
[8] R.J. Irving, M.L. Post, D.C. Povey, J. Chem. Soc., Dalton Trans. (1973) 697.
[9] J.-E. Berg, A.-M. Pilotti, A.-C. Söderholm, B. Karlsson, Acta Crystallogr., Sect. B 34 (1978) 3071.
[10] W.P. Griffith, C.A. Pumphrey, A.C. Skapski, Polyhedron 6 (1987) 891.
[11] A. Avdeef, J.A. Costamanga, J.P. Fackler, Jr., Inorg. Chem. 13 (1974) 1854.
[12] A.R. Davis, F.W.B. Einstein, Inorg. Chem. 13 (1974) 1880.
[13] T.P. Lockhart, F. Davidson, Organometallics 6 (1987) 2471.
[14] T. Nozoe, Bull. Chem. Soc. Jpn. 11 (1936) 295.
[15] M.C. Barret, M.F. Mahon, K.C. Molloy, P. Wright, Main Group Met. Chem. 23 (2000) 663.
[16] M.C. Barret, M.F. Mahon, K.C. Molloy, J.W. Steed, P. Wright, Inorg. Chem. 40 (2001) 4384.
[17] I. Abrahams, N. Choi, K. Henrick, H. Joyce, R.W. Matthews, M. McPartlin, F. Brady, S.L. Waters, Polyhedron 13 (1994) 513.
[18] J. Creeth, K.C. Molloy, P. Wright, Oral Care Compositions, PCT Int. Appn. WO 00/16736, 2000.
[19] G.M. Sheldrick, SHELX-86S, A Computer Program for Crystal Structure Determination, University of Göttingen, Göttingen, 1986.
[20] G.M. Sheldrick, SHELX-97L, A Computer Program for Crystal Structure Refinement, University of Göttingen, Göttingen, 1997.
[21] P. McArdle, J. Appl. Cryst. 28 (1995) 65.
[22] P. Klüfers, J. Schuhmacher, Angew. Chem., Int. Ed. Engl. 33 (1994) 1742.
[23] J.E. Derry, T.A. Hamor, J. Chem. Soc., Perkin Trans. 2 (1972) 694.
[24] S.I. Ahmed, J. Burgess, J. Fawcett, S.A. Parsons, D.R. Russell, S.H. Laurie, Polyhedron 19 (2000) 129.
[25] O. Carugo, C.B. Castellani, M. Rizzi, Polyhedron 9 (1990) 2061.
[26] Y. Ihara, M. Yoshizakiya, R. Yoshiyama, K. Sone, Polyhedron 15 (1996) 3643.
[27] Y. Ihara, K. Teranishi, N. Hirose, K. Sone, Polyhedron 17 (1998) 3247.

and to obtain information about the simultaneous photoisomerization of both ions we have undertaken an FT IR study of the photoexcited salt that joins both ions. An additional bonus should be the information about the effect of the rather big cation on the IR and thermal behavior (decay) of the anion excited states (c.f. [22] referred to tetrabutylammonium nitroprusside (TBANP)).

2. Experimental

2.1. Preparative

Nitropentaamminecobalt(III) chloride was prepared according to literature [23]. To obtain the title compound (**I**, from now on), the common procedure of mixing equimolar aqueous solutions of silver nitroprusside and of nitropentaamminecobalt(III) chloride was followed. After separation of AgCl, the solution was concentrated in a rotavapor until beginning of crystallization and then it was left at the open air at room temperature to give place to the slow evaporation of enough solvent water to obtain a good crop of crystals.

2.2. X-ray diffraction

Small enough fragments of the crystals were used for X-ray diffraction. Data collection procedure and structure determination methods are summarized in Table 1. Crystal data is also included in the table.

2.3. Irradiation and FT IR spectra

The FT IR spectra of the crystals were recorded with a Bruker IFS 113v spectrophotometer at 2 cm^{-1} resolution. A variable temperature Oxford OX8ITL optical cell was used to cool with liquid nitrogen Nujol mulls of powdered samples spreaded between CsI disks. After recording the low temperature spectra, the samples were irradiated in the cryostat during 3 h with the 488 nm line of an Ar^+ laser (Spectra Physics #166) operated at approximately 100 mW cm^{-2}. Difference spectra allowed the detection of weak new bands. The decay temperatures of the excited species were obtained by heating slowly the samples and monitoring the corresponding NO stretching bands until disappearance.

3. Results and discussion

3.1. Diffraction data and structure solution and refinement

Crystal data and refinement of results are presented in Table 1.

Table 1
Crystal data, structure solution methods and refinement results for $[Co(NH_3)_5NO_2][Fe(CN)_5NO]\cdot 1.5H_2O$

Empirical formula	$C_5H_{18}CoFeN_{12}O_{4.5}$
Formula weight	433.09
Temperature (K)	293(2)
Crystal system	monoclinic
Space group	$C2/c$
Unit cell dimensions [a]	
a (Å)	28.398(3)
b (Å)	6.418(1)
c (Å)	22.397(3)
β (°)	123.53(1)
V (Å^3)	3402.7(8)
Z	8
Density (calculated) (Mg m^{-3})	1.691
Absorption coefficient (mm^{-1})	1.869
$F(000)$	1768
Crystal size (mm)	$0.32 \times 0.40 \times 0.40$
Crystal color/shape	red/prismatic
Diffractometer/scan	Enraf–Nonius CAD-4/$\omega-2\theta$
Radiation, graphite monochromat.	Mo Kα
λ (Å)	0.71069
Scan width	$0.8+0.35\tan\theta$
Standard reflection	(−7, 5, 3)
Decay of standard	±2%
θ Range for data collection (°)	1.72–28.00
Index ranges	$0 \le h \le 37$, $0 \le k \le 8$, $-29 \le l \le 24$
Reflections collected/unique	4569/4119 [$R_{int} = 0.0194$]
Absorption correction	Gaussian integration [24]
Max/min transmission	0.4879, 0.6062
Observed reflections [$I > 2\sigma(I)$]	3368
Data reduction and correction [b]	XCAD4 [25]
Structure solution [c]	SHELXS-97 [26]
Refinement programs [d]	SHELXL-97 [27]
Refinement method [e]	full-matrix least-squares on F^2
Weights, w	$w = 1/[\sigma^2(F_o^2)+(0.0414P)^2+5.18P]$, $P = [\max(F_o^2,0)+2F_c^2]/3$
Data/restraints/parameters	4119/5/228
Goodness-of-fit on F^2	1.091
Final R indices [$I > 2\sigma(I)$] [f]	$R_1 = 0.0297$, $wR_2 = 0.0827$
R indices (all data)	$R_1 = 0.0416$, $wR_2 = 0.0884$
Largest difference peak and hole (e Å^{-3})	0.58 and −0.52

[a] Least-squares refinement of $[(\sin\theta)/\lambda]^2$ values for 25 reflections in the $26.24 < 2\theta < 49.40°$ range.
[b] Corrections: Lorentz, polarization and numerical absorption correction.
[c] Neutral scattering factors and anomalous dispersion corrections.
[d] Structure solved by direct and Fourier methods
[e] Final molecular model obtained by anisotropic full-matrix least-squares refinement of non-hydrogen atoms.
[f] R indices defined as: $R_1 = \Sigma||F_o|-|F_c||/\Sigma|F_o|$, $wR_2 = [\Sigma\, w(F_o^2-F_c^2)^2/\Sigma\, w(F_o^2)^2]^{1/2}$.

All water and most ammonia H-atoms were located in a difference Fourier map. The water H-atoms were refined with Ow–H and H···H distances restrained to 0.82(1) and 1.31(1) Å, respectively, with a common isotropic displacement parameter that converged to $U =$ 0.079(8) Å^2. The ammonia hydrogen atoms were posi-

tioned stereo-chemically and refined with the riding model. During the refinement, the NH_3 hydrogen atoms were allowed to rotate as a rigid group around the Co–NH_3 bond so as to maximize the sum of the electron densities at the three calculated hydrogen positions.

3.2. Crystallographic structural results and discussion

The crystal consists of distinct $[Co(NH_3)_5NO_2]^{2+}$ and nitroprusside units sited at general positions. Atomic fractional coordinates and equivalent isotropic displacement parameters are given in Table 2. Bond distances and angles are included in Table 3. Fig. 1 is an ORTEP [28] drawing of the $[Co(NH_3)_5NO_2]^{2+}$ cation showing the labeling of the non-hydrogen atoms and their displacement ellipsoids.

The cobalt ion is in a distorted octahedral environment, equatorially coordinated with four ammonia ligands [average $d(Co–N) = 1.958(3)$ Å] and axially, with another NH_3 group [$d(Co–N) = 1.975(2)$ Å]; the other axial position is occupied by the NO_2 group, N-bonded to Co at the slightly shorter Co–N bond distance of 1.936(2) Å. The $CoNO_2$ group is practically planar and Y-shaped. This plane is an approximate bisector of the angles formed by opposite couples of adjacent equatorial Co–NH_3 bonds.

Table 2
Atomic coordinates ($\times 10^4$) and equivalent isotropic displacement parameters (Å$^2 \times 10^3$) for $[Co(NH_3)_5NO_2][Fe(CN)_5NO]\cdot 1.5H_2O$

Atom	X	Y	Z	U_{eq}
Fe	5796(1)	−5241(1)	4652(1)	22(1)
N	5525(1)	−7345(3)	4773(1)	35(1)
O	5349(1)	−8809(4)	4854(2)	75(1)
C(1)	5968(1)	−3820(4)	5514(1)	35(1)
N(1)	6067(1)	−2939(5)	6013(1)	62(1)
C(2)	5093(1)	−3729(4)	4104(1)	36(1)
N(2)	4685(1)	−2812(5)	3772(1)	61(1)
C(3)	5684(1)	−6154(4)	3761(1)	37(1)
N(3)	5637(1)	−6631(5)	3240(1)	62(1)
C(4)	6553(1)	−6364(4)	5152(1)	36(1)
N(4)	7001(1)	−6996(4)	5434(2)	59(1)
C(5)	6125(1)	−2838(4)	4500(2)	39(1)
N(5)	6323(2)	−1464(4)	4396(2)	72(1)
Co	3401(1)	−31(1)	2219(1)	20(1)
N(6)	3278(1)	1173(3)	1342(1)	29(1)
N(7)	2676(1)	−1477(3)	1646(1)	33(1)
N(8)	3503(1)	−1151(3)	3098(1)	31(1)
N(9)	4131(1)	1373(3)	2823(1)	30(1)
N(10)	3788(1)	−2438(3)	2124(1)	35(1)
N(11)	3019(1)	2364(3)	2288(1)	29(1)
O(1)	3163(1)	4086(3)	2254(1)	50(1)
O(2)	2627(1)	2021(3)	2353(1)	52(1)
O(1W)	7716(1)	−10801(5)	5625(1)	67(1)
O(2W)	5000	−11403(14)	2500	166(3)

U_{eq} is defined as one third of the trace of the orthogonalized U_{ij} tensor.

Table 3
Bond distances (Å) and angles (°) in $[Co(NH_3)_5NO_2]$-$[Fe(CN)_5NO]\cdot 1.5H_2O$

Bond distances	
Fe–N	1.649(2)
Fe–C(5)	1.929(3)
Fe–C(2)	1.930(2)
Fe–C(3)	1.932(2)
Fe–C(4)	1.934(2)
Fe–C(1)	1.938(2)
N–O	1.125(3)
C(1)–N(1)	1.139(3)
C(2)–N(2)	1.137(3)
C(3)–N(3)	1.140(3)
C(4)–N(4)	1.138(3)
C(5)–N(5)	1.137(3)
Co–N(11)	1.936(2)
Co–N(6)	1.954(2)
Co–N(7)	1.956(2)
Co–N(9)	1.961(2)
Co–N(8)	1.961(2)
Co–N(10)	1.975(2)
N(11)–O(1)	1.197(3)
N(11)–O(2)	1.218(2)
Bond angles	
N–Fe–C(5)	178.1(1)
N–Fe–C(2)	95.9(1)
C(5)–Fe–C(2)	85.2(1)
N–Fe–C(3)	95.5(1)
C(5)–Fe–C(3)	83.0(1)
C(2)–Fe–C(3)	88.4(1)
N–Fe–C(4)	94.1(1)
C(5)–Fe–C(4)	84.7(1)
C(2)–Fe–C(4)	169.8(1)
C(3)–Fe–C(4)	88.9(1)
N–Fe–C(1)	96.1(1)
C(5)–Fe–C(1)	85.4(1)
C(2)–Fe–C(1)	90.0(1)
C(3)–Fe–C(1)	168.4(1)
C(4)–Fe–C(1)	90.6(1)
O–N–Fe	178.3(2)
N(1)–C(1)–Fe	178.3(3)
N(2)–C(2)–Fe	178.2(2)
N(3)–C(3)–Fe	176.9(3)
N(4)–C(4)–Fe	178.2(3)
N(5)–C(5)–Fe	177.6(3)
N(11)–Co–N(6)	88.29(8)
N(11)–Co–N(7)	89.79(8)
N(6)–Co–N(7)	89.37(8)
N(11)–Co–N(9)	90.34(8)
N(6)–Co–N(9)	92.62(8)
N(7)–Co–N(9)	178.01(8)
N(11)–Co–N(8)	89.38(8)
N(6)–Co–N(8)	177.63(8)
N(7)–Co–N(8)	90.25(8)
N(9)–Co–N(8)	87.77(8)
N(11)–Co–N(10)	178.38(8)
N(6)–Co–N(10)	90.10(8)
N(7)–Co–N(10)	90.27(9)
N(9)–Co–N(10)	89.66(8)
N(8)–Co–N(10)	92.24(9)
O(1)–N(11)–O(2)	122.9(2)
O(1)–N(11)–Co	120.0(2)
O(2)–N(11)–Co	117.1(2)

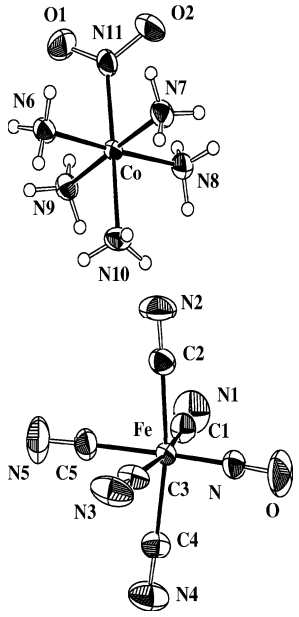


Fig. 1. Molecular plot showing the content of the asymmetric unit of $[Co(NH_3)_5NO_2][Fe(CN)_5NO]\cdot 1.5H_2O$, the labels of the non-H atoms and their displacement ellipsoids at 50% probability level. Metal–ligand bonds are indicated by full lines. The crystallization water molecules are not included in the plot.

The nitroprusside ion has the usual distorted octahedral, pagoda-like, conformation with average Fe–C bond distances of 1.933(3) Å and d(Fe–N) = 1.649(2) Å, in agreement with literature values. [[1,2] and references therein].

One of the water molecules (W1) is at a general crystal position while the other (W2) is sited on a crystallographic twofold axis and exhibits positional disorder.

The solid is stabilized by a network of N–H···N, N–H···O and N–H···Ow bonds, involving as donors the $[Co(NH_3)_5NO_2]^{2+}$ ammonia ligands and as acceptors, nitroprusside cyanide nitrogen atoms [the strongest with d(N6···N5′) = 2.991 Å, ∠(N6–H6B···N5′) = 170.8°], one nitro oxygen atom of a symmetry related $[Co(NH_3)_5NO_2]^{2+}$ complex [the strongest with d(N7···O2′) = 2.972 Å, ∠(N7–H7A···O2′) = 168.3°] and one water oxygen atom [d(N7···O1w′) = 2.928 Å, ∠(N7–H7B···O1w′) = 170.8°]. Further H-bond distances and angles are detailed in the supplementary Table S7.

3.3. Infrared spectra

Infrared spectra of ground state (GS) **I** were recorded at room and at boiling nitrogen temperature. The spectra of the photo-excited compound were run at this later temperature. The main features of the spectra can be immediately assigned to the internal vibrations of the hydration water molecules, the nitroprusside anion and the nitropentaamminecobalt(III) cation.

Wavenumbers of the IR absorption bands and their assignments, based on results of a normal coordinate analysis and Density Functional Theory calculations reported for the nitroprusside anion [8] are presented in Table 4.

Fig. 2 shows the spectra of **I** cooled at 77 K, before and after irradiation with the 488.0 nm line of the Ar^+ laser. After irradiation, new IR bands appear as expected from previous results obtained for the anion [6] and from the isomerization of the cation [29].

Low temperature IR wavenumbers are used in the following discussion of bands.

Bands located at 3644 and 3608 cm^{-1} can be assigned to the anti-symmetric H_2O stretching modes of the two water molecules while the band at 3453 cm^{-1} is probably due to the symmetric mode of one of them. Other bands surely overlap the corresponding band of the other molecule. The single band appearing at 1607 cm^{-1} may be assigned to the bending mode of one of the molecules. For the other one, the same mode, is perhaps overlapped by the NH_3 bending bands.

The water libration bands appear between 790 and 300 cm^{-1} in the IR spectra of other nitroprussides, often overlapped with bands of the anion and in this case with bands of the cation as well. The typical behavior of bands due to these modes are the increase in the intensity and the decrease in half-widths upon cooling, but in the present case it was possible to observe these effects only for the bands located at 433 and 365 cm^{-1}, which can be assigned to these modes. The other bands corresponding to the libration modes may be masked by cation and anion bands.

3.4. Anion bands

3.4.1. CN stretchings

Five features are observed in the low temperature IR spectrum, at 2186 (w), 2165 (sh), 2150 (vs), 2142 (sh) and 2131 (m) cm^{-1}. The weak band at 2186 cm^{-1} could be due to the axial mode of A_1 species under ideal C_{4v} symmetry. As the anions are sited at general C_1 positions in the lattice, the shoulder observed at 2165 cm^{-1} is probably due to the B_1 (under C_{4v} symmetry) equatorial mode activated by the low symmetry of the anions. The strongest band at 2150 cm^{-1} and the shoulder at 2142 cm^{-1} could be due to the doubly degenerated C_{4v} E mode split under C_1 symmetry, originated in the equatorial CN groups, while the medium intense bands at 2131 cm^{-1} could be assigned to the A_1 equatorial mode.

3.4.2. NO and FeNO vibrational bands

Two features are seen in the IR low temperature spectrum in the fundamental NO stretching region, at 1949 and 1912 cm^{-1}, as expected from factor group

Table 4
Observed FT IR bands and assignments for $[Co(NH_3)_5NO_2][Fe(CN)_5NO]\cdot 1.5H_2O$

Ground state		Nitrite isomer [a]	MSI [a,b]	Assignment [c]	Reference
300 K	77 K	77 K	77 K		
3833 w	3842 vw			$2\nu NO$	
3816 sh	3829 sh			$2\nu NO$	
3646 w	3644 m			νOH	
3608 w	3608 w			νOH	
3458 w	3453 m			νOH	
3274 s	3258 s			$\nu_s NH_3$	[29]
3176 s	3176 s			$\nu_a NH_3$	[29]
2173 w	2177 sh		2171 vw	νCN_{ax}	[19]
2159 w	2166 sh		2162 vw	νCN	[19]
2155 w	2160 w		2157 vw	νCN	
2149 sh	2153 vs		2151 vw	νCN	[19]
2142 vs	2145 sh		2138 m	νCN	[19]
2130 m	2131 m			νCN	[19]
1947 vs	1949 vs		1814 s (MSI) 1647vw(MSII)	νNO	[19]
1909 m	1912 m			νNO	[19]
1628 m	1631 m			δNH_3	[29]
1611 m	1607 m			δH_2O	
1553 sh	1550 sh			δNH	[29]
1428 s	1429 s			$\nu_a NO_2$	[29]
1386 m	1385 sh				
1365 w	1364 w			$\nu_s NO_2$	[29]
1332 w	1332 w	1338 w		$\delta_s NH_3$	[29]
1315 sh	1315 sh				
1306 s	1309 s	1316 w		$\delta_s NH_3$	[29]
1286 sh	1284 w				
1181 w	1184 w			$2\times\delta_w NO_2$	
			1140 [d]	CoONO (η)	[21]
		1068 w		νONO	[29]
844 m	842 s	850 w		$\delta_r NH_3$	[29]
823 m	822 m			$\delta_s ONO$	[29]
661 m	663 m			$\delta FeNO$	[19]
646 w	648 w		550 vw	νFeN	[19]
593 m	595 m			$\delta_w NO_2$	[29]
505 w	508 w			$\nu CoNH_3$	[29]
494 w	497 w		492 w	$\nu FeCN$	[19]
481 vw	484 vw			$\nu CoNH_3$	[29]
460 w	462 w		458 w	$\delta FeCN\parallel$	[19]
436 sh	439 sh			$\delta FeCN\parallel$	[19]
428 sh	433 m		424 vw	$\nu FeC+L_{H_2O}$	[19]
415 m	417 m		407 vw	νFeC_{ax}	[19]
363 w	365 w			L_{H_2O}	[19]
337 w	339 w				[19]
318 sh	326 sh			$\delta NCoN$	[29]
311 m	319 sh		308 vw	$\delta FeCN\perp$	[19]
294 m	295 m			$\delta_r NO_2$	[29]

[a] After irradiation.
[b] Metastable states. MSI (nitroprusside) unless otherwise stated.
[c] s: symmetric; a: asymmetric; δ_s: scissoring; δ_w: wagging; δ_r: rocking; a: axial; $\perp$: perpendicular to molecular axis; $\parallel$: parallel to molecular axis; η: lateral (T) bonded; L: libration.
[d] Intermediate cation.

splitting (66Au, 66Bu under factor group C_{2h} symmetry).

IR bands at 663 and 648 cm^{-1} are assigned to the FeNO bending and FeN stretching modes, respectively. No splitting is observed for these modes.

3.4.3. FeC stretchings and FeCN deformations

Table 4 shows the assignments of bands supposedly due to FeC stretchings, FeCN, CFeC and CFeN deformations. They were made following reference [8].

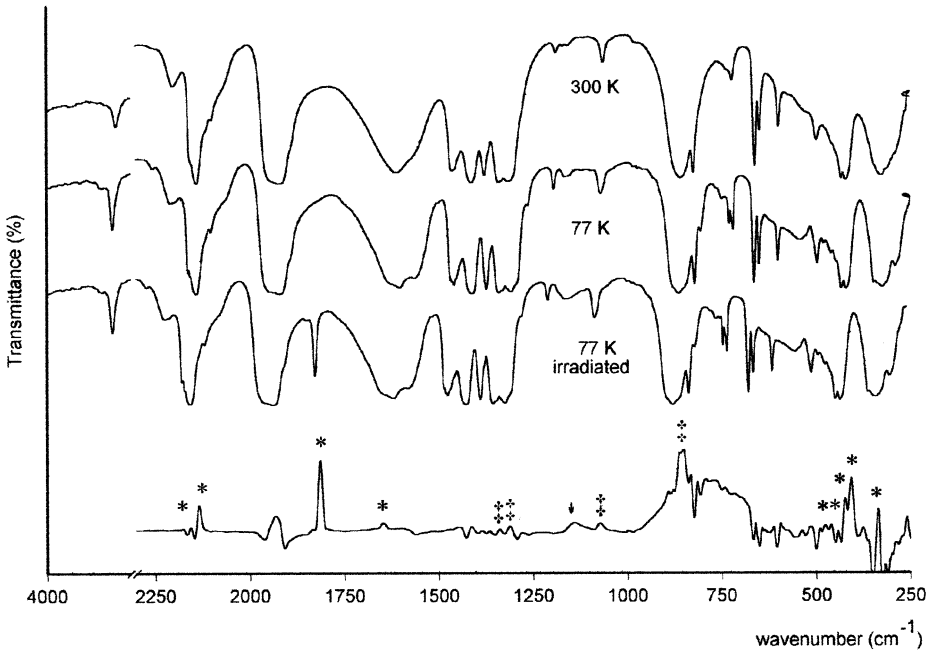


Fig. 2. Infrared spectra of $[Co(NH_3)_5NO_2][Fe(CN)_5NO]\cdot 1.5H_2O$ in the ground state at 300 and 77 K and photoexcited, at 77 K. The difference spectrum between the two last spectra is also included. Features due to MSI and MSII are marked with stars (*) and double crosses (‡), respectively.

3.5. Excited states

3.5.1. Anion

Due to the low concentration of excited states achieved, difference spectra were useful to detect very weak bands. As mentioned above, Fig. 2 shows also the infrared spectrum after irradiation. The irradiation generates two metastable reversible states, MSI and MSII, which can be most easily detected by new bands due to the NO groups. The NO stretching bands of the excited states are shifted to lower wavenumbers in comparison with the ground state band. In general, these bands show downshifts of approximately 110 cm^{-1} for MSI and 300 cm^{-1} for MSII [22].

Three bands due to CN stretchings of the excited states were observed also at lower wavenumbers comparing with the ground sates bands. The average downshift was nearly 8 cm^{-1}.

The new νNO bands due to MSI and MSII of **I** appear at 1814 and 1647 cm^{-1}, respectively, shifted 135 and 302 cm^{-1} with respect to the ground state band located at 1949 cm^{-1} and the decay temperatures are 190 K for MSI and 141 K, for MSII. These values are in agreement with the reported values for other nitroprussides ([22] and references therein) but the MSI νNO downshift is larger than the observed in the other nitroprussides with the exception of the barium salt, for which $\Delta\tilde{\nu}$ is 149 cm^{-1} [30], while the corresponding shift for MSII is the smallest.

It is to be noted that in TBANP, with a big cation, [22] the low decay temperatures of both excited sates (170, 180 and 100, 120 K for MSI and MSII of the dihydrated (DH) and the anhydrous salt, respectively) and the large νNO shifts (118, 122 and 318, 312 cm^{-1}, respectively), were explained by the softness of the structures. In the present case, decay temperatures are larger as well as the MSI νNO shift pointing to a tighter structure as expected from the respective unit cell volumes and Z number (3622.60 $Å^3$ and 3, respectively, for TBANPDH, [22] and 3402.76 $Å^3$ and 8, for **I**). The lower $\Delta\tilde{\nu}$(NO) for MSII remains to be explained.

In the IR spectrum of MSI the δ(FeON) and ν(FeO) modes appear at 573 and 550 cm^{-1}, respectively. The bands expected for the other MSI modes and for MSII are extremely weak, excepting the νFeC_{ax} mode of MSI, which appears as a weak band at 407 cm^{-1}.

3.5.2. Cation

It is known that the photoreaction of the $[Co(NH_3)_5NO_2]^{2+}$ cation in the solid dichloride produces the stable isomeric nitrito species which can be identified by the presence of the IR band at 1055 cm^{-1} due to ν_sNO [29]. Spectral evidence for this isomer in the present cases is the new band located at 1068 cm^{-1}. It was reported that the $(NH_3)_5CoNO_2 \rightarrow (NH_3)_5CoONO$ photoisomerization could probably be an intramolecular process proceeding via a seven-coordinated transition state giving rise to a nitrito compound but with slightly different geometrical parameters from that of the fresh chemically prepared nitrito compound [21]. In another paper about the photochemical nitro–nitrito linkage isomerization [31] the ν_sNO band of a metastable species is reported at 1105 cm^{-1}. In this case, the band due to this species appears at 1140 cm^{-1}. The shift

to higher wavenumbers is perhaps due to the shortening of the N–O distances of the NO_2 group (average: 1.23 Å in [32] and 1.21 Å, in the present case).

3.5.3. TGA, DTA

Thermograms of **I** run under flowing nitrogen show that the dehydration process begins at a relatively low temperature, producing a DTA peak located at 74 °C. The weight loss in this endothermic step corresponds to one and a half water molecules per formula weight (theoretical: 6.4%, measured: 5.8%, mean value).

The following decomposition steps produce two close exothermic DTA peaks at 168.5 and 178.7 °C. The total weight loss is 27.9% (expected: 28.2%) which is due, perhaps, to the evolution of four NH_3 molecules and one of C_2N_2 (the IR spectrum of the residue at this stage showed weak NH_3 bands and bands due to the NO, NO_2 and CN groups). The next steps up to 500 °C occur with a weight change of 27.5% and DTA peaks at 236 °C (endothermic) and at 302.7, 347.4 and 390.9 °C (exothermic).

The infrared spectrum and the X-ray diffractogram of the residue at 500 °C suggest the presence of the mixed oxide $CoFe_2O_4$. The total weight change is in fairly good accordance with the change expected from the following equation (found: 61.0, theoretical: 64.0%), $[Co(NH_3)_5NO_2][Fe(CN)_5NO]\cdot 1.5\ H_2O = 1.5H_2O + 5NH_3 + 5/2C_2N_2 + N_2 + 1/2CoFe_2O_4 + 1/2CoO$. It is to be noted that the composition of the solid residue is speculative.

The solid was further heated up to 900 °C but there was no additional weight change and also, the IR spectrum and the X-ray diffractogram of the residue did not show any modification.

4. Conclusions

$[Co(NH_3)_5NO_2][Fe(CN)_5NO]\cdot 1.5H_2O$ crystallizes in the monoclinic $C2/c$ space group (C_{2h}^6). The anions occupy C_1 sites in the lattice and present the usual distorted octahedral structure and the geometrical parameters (bond distances and angles) as in several nitroprussides. The cation, which has also a distorted octahedral structure, and one water molecule also occupy C_1 sites while the other water molecule is at a C_2 site. The structure of the cation is similar as found in the chloride but the average N–O distance (1.21 Å) seems to be somewhat shorter than reported in [32] (1.23 Å), the difference reflects in the ν_sNO wave numbers (1140 and 1105 cm^{-1}, respectively).

The irradiation of the compound generates the excited states MSI and MSII in the anion. The $\Delta\tilde{\nu}$(NO) wave numbers (difference between the NO stretching of GS and MSI) and the decay temperatures of MSI and MSII are among the greatest measured so far, facts which are assigned to the relatively open structure of the crystal, as done before in the case of tetrabutylammonium nitroprusside dihydrate and anhydrate, which showed a similar behavior [22].

With respect to the cation, irradiation generates the nitrito isomer and the metastable species.

The thermogravimetric results obtained under flowing nitrogen atmospheres pointed to the existence of 1.5 water molecules per formula in the original substance and to the formation of the mixed oxide $CoFe_2O_4$ and of CoO as final solid products. XRD and IRS of the residue seem to confirm the presence of the mixed oxide.

5. Supplementary material

Listings of atomic anisotropic thermal parameters (Table S5), hydrogen atoms positions (Table S6), H-bond distance and angles (Table S7), and calculated and observed structure factor amplitudes (Table S8) are available on request.

Acknowledgements

This work was supported by the Consejo Nacional de Investigaciones Científicas y Técnicas (CONICET), through CEQUINOR and PIP # 4752, Comisión de Investigaciones Científicas de la Provincia de Buenos Aires (CICPBA), also through CEQUINOR, Agencia de Promoción Científica y Tecnológica (PICT # 06-0005-00118) and Universidad Nacional de La Plata (research supporting grant). IR and Raman measurements were performed at the Laboratorio Nacional de Espectrofotometría Optica (LANEFO) and the X-ray diffraction measurements were carried out at the Laboratorio Nacional de Difracción (LANADI), La Plata.

References

[1] D.B. Soria, J.I. Amalvy, O.E. Piro, E.E. Castellano, P.J. Aymonino, J. Chem. Crystallogr. 26 (1996) 315.
[2] D.B. Soria, O.E. Piro, E.E. Castellano, P.J. Aymonino, J. Chem. Crystallogr. 29 (1999) 75.
[3] D.B. Soria, P.J. Aymonino, Spectrochim. Acta, Part A 55 (1999) 1243.
[4] D.B. Soria, J.I. Amalvy, P.J. Aymonino, J. Cryst. Spectrosc. Res. 17 (1987) 139.
[5] L. Tosi, Comput. Rend. 277C (1973) 335.
[6] J.A. Güida, P.J. Aymonino, O.E. Piro, E.E. Castellano, Spectrochim. Acta, Part A 49 (1993) 535.
[7] J.I. Amalvy, E.L. Varetti, E.E. Castellano, O.E. Piro, G. Punte, P.J. Aymonino, J. Cryst. Spectrosc. Res. 16 (1986) 537.
[8] M.E. Chacón Villalba, E.L. Varetti, P.J. Aymonino, Vibrat. Spectrosc. 14 (1997) 275.
[9] D.B. Soria, P.J. Aymonino, Spectrochim. Acta, Part A 51 (1995) 677.

[10] S.R. González, P.J. Aymonino, O.E. Piro, J. Chem. Phys. 81 (1984) 625.
[11] S.R. González, P.J. Aymonino, R. Mercader, O.E. Piro, J. Phys. Chem. Solids 47 (1986) 239.
[12] (a) T. Woike, S. Haussühl, Solid State Commun. 86 (1993) 333;
(b) T. Woike, H Zöllner, W. Krasser, S. Haussühl, Solid State Commun. 73 (1990) 149.
[13] H Zöllner, T. Woike, W. Krasser, S. Haussühl, Z. Kristallogr. 188 (1989) 139.
[14] J.A. Güida, O.E. Piro, P.S. Schaiquevich, P.J. Aymonino, Solid State Commun. 101 (1997) 471.
[15] P.S. Schaiquevich, J.A. Güida, P.J Aymonino, Inorg. Chim. Acta 303 (2000) 277.
[16] (a) U. Hauser, V. Ostreich, H.D. Rohrweck, Z. Phys. A280 (1977) 17;
(b) U. Hauser, V. Ostreich, H.D. Rohrweck, Z. Phys. A280 (1977) 125;
(c) U. Hauser, V. Ostreich, H.D. Rohrweck, Z. Phys. A284 (1978) 9.
[17] (a) T. Woike, W. Krasser, P.S. Betchthold, S. Haussühl, Solid State Commun. 45 (1983) 499;
(b) T. Woike, W. Krasser, P.S. Betchthold, S. Haussühl, Solid State Commun. 45 (1983) 503.
[18] M.D. Carducci, M.R. Pressprich, P. Coppens, J. Am. Chem. Soc. 119 (1997) 2669.
[19] M.E. Chacón Villalba, J.A. Güida, P.J. Aymonino, Spectrochim. Acta, Part A 57 (2001) 367.
[20] I Grenthe, E. Nordin, Inorg. Chem. 18 (1979) 1869.
[21] M. Kubota, S. Ohba, Acta Crystallogr., Sect. B 48 (1992) 627.
[22] M.E. Chacón Villalba, J.A. Güida, P.J. Aymonino, J. Chem. Crystallogr. 31 (2001) 155.
[23] G. Schlessinger, Inorganic Laboratory Preparations, Chemical Publishing Company, New York, 1962, p. 220.
[24] A.L. Spek, PLATON, A Multipurpose Crystallographic Tool, Utrecht University, Utrecht, The Netherlands, 1998.
[25] K. Harms, S. Wocadlo, CAD4 Data Reduction, University of Marburg, Marburg, Germany, 1995.
[26] G.M. Sheldrick, SHELXS-97. Program for Crystal Structure Resolution, University of Göttingen, Göttingen, Germany, 1997.
[27] G.M. Sheldrick, SHELXL-97. Program for Crystal Structures Analysis, University of Göttingen, Göttingen, Germany, 1997.
[28] C.K. Johnson, ORTEP-II. A Fortran Thermal-Ellipsoid Plot Program. Report ORNL-5138, Oak Ridge National Laboratory, Oak Ridge, TN, 1976.
[29] A.M. Heynes, D. De Waal, Spectrochim. Acta, Part A 45 (1989) 905.
[30] J.A. Güida, O.E. Piro, P.J. Aymonino, Solid State Commun. 66 (1988) 1007.
[31] A. Dale, D. Johnson, K. Pashman, Inorg. Nucl. Chem. Lett. 11 (1975) 23.
[32] O. Börtin, Acta Chem. Scand. 22 (1968) 2890.

under a nitrogen atmosphere: the following step was performed in air. The powder was dissolved in dichloromethane (4 ml), filtered to remove a small amount of insoluble material, treated with hexane and allowed to stand for 1 day at r.t. to give red–brown crystals. The product was found to be insoluble in chloroform, dichloromethane, toluene and dimethylsulphoxide (even with warming). Yield: 0.015 g (22%). IR (KBr) ν(CN) 2160 (s), ν(XCN) 2116 (s), $\nu(O_2)$ 863 (m). *Anal*. Calc. for $C_{47}H_{41}Cl_2N_2O_2P_2Rh$ C, 62.61; H, 4.58; N, 3.11. Found: C, 62.27; H, 4.57; N, 3.13%. The last step (crystallisation in air) could not be relied upon to give a product on every occasion.

2.2. X-ray structure determination

Intensity data were collected on a Bruker SMART 1K CCD area detector diffractometer with graphite monochromated Mo Kα radiation (50 kV, 30 mA). The collection method involved ω-scans of width 0.3°. Data reduction was carried out using the program SAINT+ [19] and absorption corrections were made using the program SADABS [20]. The crystal structure was solved by direct methods using SHELXTL [21]. Non-hydrogen atoms were first refined isotropically followed by anistropic refinement by full matrix least-squares calculation based on F^2 using SHELXTL. All hydrogen atoms were placed geometrically and allowed to ride on their respective parent atoms. The structure contains a disordered dichloromethane molecule; the disorder was resolved by applying a treatment involving three differently orientated molecules as rigid bodies and summing their contributions to unity. Diagrams were generated using SHELXTL and PLATON [22]. Structure and refinement data are given in Table 1.

Table 1
Crystal data and structure refinement for $[Rh(CN)(O_2)(PPh_3)_2(XNC)](CH_2Cl_2)$

Empirical formula	$C_{47}H_{41}Cl_2N_2O_2P_2Rh$
Formula weight	901.57
Temperature (K)	293(2)
Wavelength (Å)	0.71073
Crystal system	monoclinic
Space group	$P2_1/c$
Unit cell dimensions	
a (Å)	16.569(3)
b (Å)	11.3593 (17)
c (Å)	23.050(4)
α (°)	90
β (°)	99.947(3)
γ (°)	90
V (Å^3)	4273.1(11)
Z	4
D_{calc} (Mg m^{-3})	1.401
Absorption coefficient (mm^{-1})	0.640
$F(000)$	1848
Crystal size (mm)	0.44 × 0.15 × 0.11
Range for data collection	1.25–28.33°
Index ranges	$-21 \le h \le 22$, $-15 \le k \le 14$, $-22 \le l \le 30$
Reflections collected	29 130
Independent reflections	10 538 [$R_{int} = 0.0323$]
Completeness to θ_{max}	98.8%
Max/min transmission	0.9329, 0.7660
Data/restraints/parameters	10 538/1/498
Goodness-of-fit on F^2	1.046
Final R indices [$I > 2\sigma(I)$]	$R_1 = 0.0476$, $wR_2 = 0.1333$
R indices (all data)	$R_1 = 0.0979$, $wR_2 = 0.1589$
Largest difference peaks (e Å^{-3})	1.238 and −1.004

3. Results and discussion

The complex $[Rh(CN)(O_2)(PPh_3)_2(XNC)]$ Fig. 1 has octahedral geometry with distortions arising from the presence of the O–O bond, which restricts the O–Rh–O angle to 41.77(11)°. The Rh–O and O–O bond lengths (Table 2) are not significantly different from those reported for $[Rh(O_2)\{PPh_2(2\text{-}C_6H_4CHN^iPr)\}_2]BPh_4$ [9] and fall towards the middle of the ranges observed for $Rh(O_2)$ complexes [3–15]. The principal intermolecular interactions are a close contact (2.518 Å) between a phenyl hydrogen (attached to C54) and oxygen O1 (of an adjacent molecule) and several C–H···π [23] interactions.

From the series $[Rh(Y)(PPh_3)_2(XNC)]$ (Y = Cl, N_3, NCO, NCS, $N(CN)_2$, $NCBPh_3$, $CNBPh_3$, CN) the only complex to form an adduct with O_2 is the cyano derivative. The formation of an O_2 adduct involves the transfer of electron density from rhodium to oxygen (to give an Rh(III) peroxo complex [24]), a process favoured by electron-donating ligands on Rh. The CN^- ion, while carrying a negative charge, is not normally considered to be strongly electron-donating, certainly not more so than Cl^- or N_3^-. On two different scales of electron-donating ability (those of Vaska [25], based on carbonyl stretching frequencies of complexes $[M(Y)(PPh_3)_2(CO)]$ (M = Rh, Ir) and Chatt [26], based on the reversible one-electron oxidation potential of $[Cr(CO)_5(Y)]$) the CN^- ligand is rated as less electron-donating than Cl^-, N_3^- and NCO^-. The ability of CN^- to activate the complex *trans*-$[Rh(CN)(PPh_3)_2(XNC)]$ towards reaction with O_2 must, therefore, reside elsewhere, most probably in its polarisability.

The cyano ligand differs from Cl^-, N_3^-, NCO^-, NCS^-, $N(CN)_2^-$ and $NCBPh_3^-$ which, according to Pearson's classification [27], are either hard or borderline, while CN^- is soft, i.e. more polarisable. Although $CNBPh_3$ is also soft it is, in effect, a CN^- modified by attachment of a strong Lewis acid, and its electron-donating ability and polarisability will consequently be reduced. From this perspective the four soft ligands of *trans*-$[Rh(CN)(PPh_3)_2(XNC)]$ can be regarded as con-

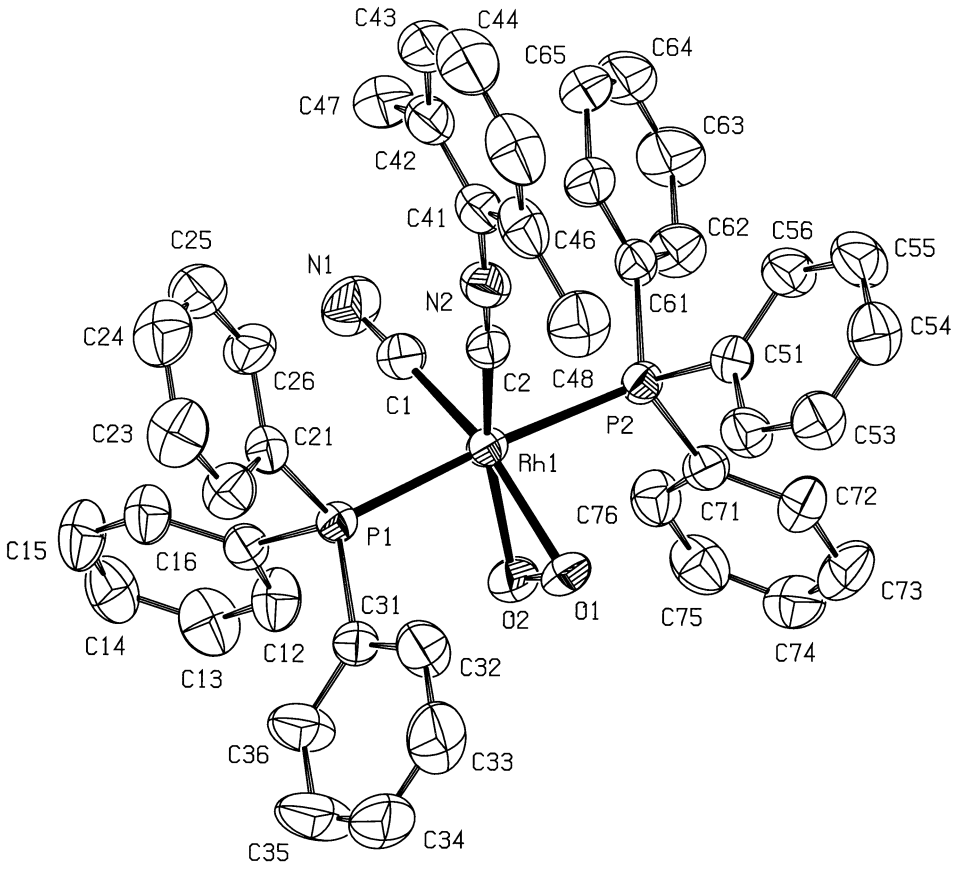


Fig. 1. ORTEP diagram of $[Rh(CN)(O_2)(PPh_3)_2(XNC)](CH_2Cl_2)$; thermal ellipsoids are shown at the 50% probability level; hydrogens and CH_2Cl_2 are omitted.

Table 2
Selected bond lengths (Å) and angles (°) for $[Rh(CN)(O_2)(PPh_3)_2(XNC)](CH_2Cl_2)$

Bond lengths			
Rh–C(1)	2.023(4)	Rh–P(2)	2.3630(10)
Rh–C(2)	1.935(4)	N(1)–C(1)	1.134(5)
Rh–O(1)	2.023(2)	N(2)–C(2)	1.159(5)
Rh–O(2)	2.013(3)	N(2)–C(41)	1.394(5)
Rh–P(1)	2.3574(10)	O(1)–O(2)	1.439(4)
Bond angles			
C(1)–Rh–O(1)	153.11(15)	C(1)–Rh–C(2)	90.09(16)
C(1)–Rh–O(2)	111.48(14)	O(1)–Rh–O(2)	41.77(11)
C(2)–Rh–O(1)	116.75(14)	P(1)–Rh–P(2)	176.18(3)
C(2)–Rh–O(2)	158.34(14)	P(1)–Rh–O(1)	91.42(8)
C(1)–Rh–P(1)	87.99(11)	P(1)–Rh–O(2)	85.21(8)
C(1)–Rh–P(2)	94.59(11)	P(2)–Rh–O(1)	85.00(8)
C(2)–Rh–P(1)	94.03(11)	P(2)–Rh–O(2)	91.22(8)
C(2)–Rh–P(2)	88.79(11)		

ferring enhanced polarisability on rhodium, altering its reactivity so as more to resemble that of iridium, and crossing the threshold at which reaction with O_2 becomes possible. In this context it has been noted by Valentine [28] that the reactivity of Rh(I) towards O_2 is enhanced by strong σ-donor ligands and by polarisable ligands and inhibited by strong π-acceptor ligands (factors which, with important differences, also influence the binding of H_2 by Ir(I) [29]). The carbonyl analogue *trans*-$[Rh(CN)(PPh_3)_2(CO)]$ is unreactive towards oxygen (under ambient conditions) indicating that differences in the σ-donor ability of CO and XNC (CO is a poorer σ-donor) are also important.

4. Supplementary material

Crystallographic data have been deposited with the Cambridge Crystallographic Data Centre, CCDC No. 175286. Copies of this information may be obtained free of charge from The Director, CCDC, 12 Union Road, Cambridge CB2 1EZ, UK (fax: +44-1223-336-033; e-mail: deposit@ccdc.cam.ac.uk or www: http://www.ccdc.cam.ac.uk).

Acknowledgements

We thank the University of the Witwatersrand for financial support.

References

[1] P.D. Morran, S.B. Duckett, P.R. Howe, J.E. McGrady, S.A. Colebrooke, R. Eisenberg, M.G. Partridge, J.A.B. Lohman, J. Chem. Soc., Dalton Trans. (1999) 3949.
[2] L. Vaska, Acc. Chem. Res. 1 (1968) 335.
[3] J.A. McGinnetty, N.C. Payne, J.A. Ibers, J. Am. Chem. Soc. 91 (1969) 6301.
[4] M.J. Nolte, E. Singleton, Acta Crystallogr., Sect B 31 (1975) 2223.
[5] M.J. Nolte, E. Singleton, Acta Crystallogr., Sect. B 32 (1976) 1410.
[6] M.J. Bennett, P.B. Donaldson, Inorg. Chem. 16 (1977) 1581.
[7] M.J. Bennett, P.B. Donaldson, Inorg. Chem. 16 (1977) 1585.
[8] C. Bianchini, C. Mealli, A. Meli, D.M. Proserpio, M. Peruzzini, F. Vizza, J. Organomet. Chem. 369 (1989) C6.
[9] C.A. Ghilardi, S. Midollini, S. Moneti, A. Orlandini, G. Scapacci, J. Chem. Soc., Dalton Trans. (1992) 3371.
[10] E. Lindner, Q. Wang, H.A. Mayer, R. Fawzi, M. Steimann, J. Organomet. Chem. 453 (1993) 289.
[11] K. Osakada, K. Hataya, T. Yamamoto, Inorg. Chem. 32 (1993) 2360.
[12] A. Vigalok, L.J.W. Shimon, D. Milstein, J. Chem. Soc., Chem. Commun. (1996) 1673.
[13] Y. Takahashi, M. Hashimoto, S. Hikichi, M. Akita, Y. Moro-oka, Angew. Chem., Int. Ed. Engl. 38 (1999) 3074.
[14] M.C. Nicasio, M. Paneque, P.J. Pérez, A. Pizzano, M.L. Poveda, L. Rey, S. Sirol, S. Taboada, M. Trujillo, A. Monge, C. Ruiz, E. Carmona, Inorg. Chem. 39 (2000) 180.
[15] G. Argouarch, O. Samuel, O. Riant, J.-C. Daran, H.B. Kagan, Eur. J. Org. Chem. (2000) 2893.
[16] L. Carlton, V. Cîrcu, paper in preparation.
[17] G. Favero, P. Rigo, Gazz. Chim. Ital. 102 (1972) 597.
[18] M. Fernandes, V. Cîrcu, R. Weber, T. Varnali, L. Carlton, J. Chem. Crystallogr. (in press).
[19] SAINT+, Version 6.02, Bruker AXS Inc., Madison, WI, USA, 1999.
[20] G.M. Sheldrick, SADABS, University of Göttingen, Germany, 1996.
[21] SHELXTL, Version 5.1, Bruker AXS Inc., Madison, WI, USA, 1999.
[22] A.L. Spek, Acta Crystallogr., Sect. A 46 (1990) C34.
[23] C. Janiak, J. Chem. Soc., Dalton Trans. (2000) 3885.
[24] L. Vaska, Acc. Chem. Res. 9 (1976) 175.
[25] L. Vaska, J. Peone, J. Chem. Soc., Chem. Commun. (1971) 418.
[26] J. Chatt, C.T. Kan, G.J. Leigh, C.J. Pickett, D.R. Stanley, J. Chem. Soc., Dalton Trans. (1980) 2032.
[27] R.G. Pearson, J. Chem. Ed. 45 (1968) 581.
[28] J.S. Valentine, Chem. Rev. 73 (1973) 235.
[29] F. Abu-Hasanayn, K. Krogh-Jespersen, A.S. Goldman, Inorg. Chem. 32 (1993) 495.

2. Experimental

2.1. Materials and methods

All manipulations were performed under aerobic conditions using materials as received, except where indicated otherwise. $NBu^n_4MnO_4$ was prepared as described elsewhere [46], $[Mn_3O(O_2CEt)_6(py)_3](ClO_4)$ was available from previous work [47].

2.2. Syntheses

2.2.1. $Mn(O_2CEt)_2\cdot 0.35H_2O$

To a slurry of $MnCO_3$ (30 g, 0.26 mol) in water (200 mL) was added dropwise propionic acid (25 ml, 0.33 mol). The mixture was stirred for a few days and the unreacted $MnCO_3$ was removed by filtration. The pale brown filtrate was roto-evaporated to dryness to yield a pink solid. The yield was 79%. *Anal.* Calc. (Found) for $Mn(O_2CEt)_2\cdot 0.35H_2O$: C, 34.75 (34.51); H, 5.20 (4.89); N, 0.00 (0.00)%.

2.2.2. $[Mn_4O_2(O_2CEt)_7(bpya)_2](ClO_4)\cdot 2EtCO_2H$ (**1**)

A solution of $Mn(O_2CEt)_2\cdot 0.35H_2O$ (757 mg, 3.65 mmol) in water (6 ml) was added to a solution of bpya (356 mg, 2.08 mmol) and NBu_4ClO_4 (520 mg, 1.52 mmol) in propionic acid (25 ml). To the resulting yellow solution was added dropwise a solution of $NBu^n_4MnO_4$ (0.27 g, 0.70 mmol) in MeCN (2 ml) to yield a red solution, which was stirred for ~ 3 h. Addition of Et_2O (200 ml) led to precipitation of a microcrystalline red product that was collected by filtration, washed with Et_2O and dried in vacuo. The yield was 68% based on total available Mn. *Anal.* Calc. (Found) for **1**·2Et-CO_2H: C, 41.72 (41.71); H, 4.84 (4.84); N, 6.21 (6.14)%. To a saturated solution of **1** in MeCN was added toluene (approximately one-fourth of the solution volume) and the mixture left to slowly evaporate at room temperature (r.t.). Crystals suitable for X-ray crystallography deposited over two weeks.

2.3. Crystal structure of *1*

Data were collected on a Bruker Smart 6000 CCD system with a sealed molybdenum source and graphite monochromator. Small crystals were selected from the bulk sample and transferred to the goniostat where they were cooled to −160 °C for data collection and characterization. The data were collected using 10 s frames with an omega scan of 0.30° and corrected for Lorentz and polarization effects. Equivalent reflections were averaged using the Bruker SAINT software, as well as utility programs from the XTEL library ($R_{av} = 0.076$). The space group was *Pbca*. The structure was readily solved using SHELXTL and Fourier techniques. Many of the hydrogen atoms were visible in a difference Fourier map phased on the non-hydrogen atoms. All hydrogen atoms were placed in idealized, calculated positions and treated as fixed atom contributors in the final cycles of refinement. The structure was well ordered with the exception of one $EtCO_2^-$ ligand in which the methyl group was disordered (C47). The MeCN solvent was also found to be in 50% occupancy. A final difference Fourier map was essentially featureless, the largest peak being 0.83 e A^{-3}. The final $R(R_w)$ indices were 3.72(3.92) using 5341 independent reflections with $I > 2.33\sigma(I)$. Crystallographic data are summarized in Table 1.

2.4. Other measurements

^1H NMR spectra were collected on a 300 MHz Varian Gemini 2000 spectrometer and a 500 MHz Varian Inova spectrometer with the protio-solvent signal used as reference. Chemical shifts are quoted on the δ scale (downfield shifts are positive). Cyclic voltammetry was performed in MeCN solution using 0.1 M NBu_4PF_6 as supporting electrolyte using a BAS CV-50 voltammetric analyzer. Electrodes were a glassy carbon working electrode, a platinum wire auxiliary electrode, and a silver wire in a 1 M $AgNO_3$ MeCN solution, connected to the cell solution through a saline bridge, as reference electrode. Dc magnetic susceptibility data were collected on powdered, microcrystalline samples (restrained in eicosane to prevent torquing) with a Quantum Design MPMS-XL SQUID magnetometer equipped with a 5.5 T (55 kG) magnet. A diamagnetic correction to the observed susceptibilities was applied using Pascal's constants. Elemental analyses were performed by Atlantic Microlab.

Table 1
Crystallographic data for $[Mn_4O_2(O_2CEt)_7(bpya)_2](ClO_4)\cdot MeCN$ (**1**)

Formula [a]	$C_{43}H_{56}ClMn_4N_7O_{20}$
F_W (g mol^{-1})	1234.15
Space group	*Pbca*
Unit cell dimensions	
a (Å)	23.880(3)
b (Å)	18.019(2)
c (Å)	25.191(3)
V (Å^3)	10839.58
Z	8
T (°C)	−160
Radiation [b] (Å)	0.71069
ρ_{calc} (g cm^{-3})	1.513
μ (cm^{-1})	10.376
R [c] (%)	3.72
R_w [d] (%)	3.92

[a] Including solvate molecules.
[b] Mo Kα, graphite monochromator.
[c] $R = 100\ \Sigma\ ||F_o| - |F_c||/\Sigma\ |F_o|$.
[d] $R_w = 100\ [\Sigma\ w(|F_o| - |F_c|)^2/\Sigma\ w|F_o|^2]^{1/2}$ where $w = 1/\sigma^2(|F_o|)$.

3. Results and discussion

3.1. Synthesis and reactivity

We have recently prepared a number of $Mn_x/O/RCO_2$ aggregates using comproportionation reactions between $Mn(O_2CR)_2$ (R = Me, Et) and MnO_4^- in the presence of a chelating ligand and the corresponding carboxylic acid. This route has provided convenient access to various tetranuclear Mn complexes with trigonal pyramidal or butterfly-like Mn_4 topologies [40]. When $NBu^n_4MnO_4$ in MeCN was added to $Mn(O_2CEt)_2$ in $EtCO_2H/H_2O$ (5:1 v/v) in the presence of bpya and $NBu^n_4ClO_4$, a dark red solution was obtained from which $[Mn_4O_2(O_2CEt)_7(bpya)_2](ClO_4)$ (**1**) was obtained in high yield as a red microcrystalline solid upon addition of Et_2O. The reaction is summarized in Eq. (1).

$$16Mn(O_2CEt)_2 + 4MnO_4^- + 10bpya + 12EtCO_2H \rightarrow 5[Mn_4O_2(O_2CEt)_7(bpya)_2]^+ + 9EtCO_2^- + 6H_2O \quad (1)$$

The crystal structure of **1** (vide infra) shows that bpya is bound in its neutral form, consistent with the acidic conditions of the reaction medium. Since this ligand has been found chelating as a deprotonated anion in a few cases [43,44], the question arose whether under different conditions lacking added acid the ligand would appear in a deprotonated form. The reaction of preformed trinuclear complexes $[Mn_3O(O_2CR)_6(L)_3]^{0,+}$ (L = py, H_2O) with chelating ligands has been used extensively in the past to trigger structural rearrangements leading to higher nuclearity products [45]. With this in mind, the reaction of $[Mn_3O(O_2CEt)_6(py)_3](ClO_4)$ with bpya was investigated. A dark brown solution of the trinuclear complex in MeCN was treated with 1.5 equiv. of bpya, and a red-brown precipitate started to form within minutes. This product was identified as predominantly complex **1** by IR and ^1H NMR spectroscopy.

3.2. Description of the structure of *1*

Crystallographic data for $[Mn_4O_2(O_2CEt)_7(bpya)_2](ClO_4)$ (**1**) are listed in Table 1. A labeled ORTEP representation of the cation of complex **1** is presented in Fig. 1, and selected interatomic distances and bond angles are listed in Table 2. The core consists of four Mn ions bridged by two μ_3-oxide ions, the ensemble having a butterfly-like topology. Approximately octahedral coordination around each Mn(III) is completed by the peripheral ligation, comprising seven μ_2-O_2CEt^- groups and two bpya ligands. One carboxylate is bound only to 'body' Mn ions, Mn2 and Mn3, while each of the other six is bridging a body-wingtip Mn_2 pair. The bpya groups chelate the two wingtip Mn ions Mn1 and Mn4. The cluster possesses virtual C_2 symmetry. Charge considerations indicate the oxidation state +3 for all four metals, as confirmed by the presence of a Jahn–Teller elongation of two *trans* bonds (av. 2.138 Å) at each Mn center, although the equatorial bond distances span a wide range (1.833–2.087 Å). The Mn_4O_2 core contains four different types of Mn···Mn vectors: Mn2 and Mn3 are 2.871(2) Å apart, the body Mn ions are separated from the wingtip ions by averages of 3.307 Å (two carboxylate bridges) and 3.444 Å (one carboxylate bridge), and the Mn1···Mn4 distance is 5.834 Å. The overall structure of this molecule is similar to that of other previously reported clusters with the $[Mn_4O_2]^{8+}$ core [36–40,47] (vide infra), but is the first with a six-membered N-based chelate ring. These six-membered chelate rings are in a boat conformation, as commonly seen for bpya although the extent of the folding varies greatly from compound to compound. The factors determining the exact shape of the chelate ring seem to be mainly steric and possibly involve crystal packing forces as well. The folding of the boat is gauged by the angles between the least-squares plane defined by N_a, N_b, C_b and C_a, and the planes C_a–N_c–C_b and N_a–Mn–N_b, averaging 23.79 and 28.97°, respectively, for complex **1**.

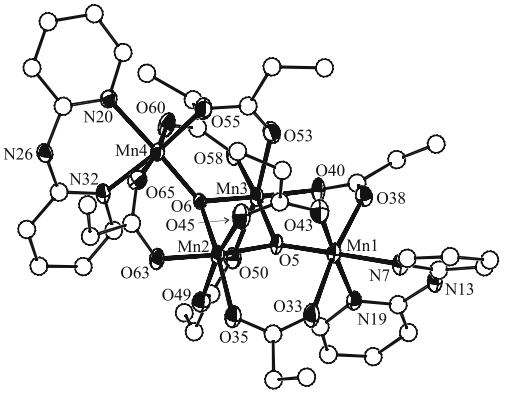
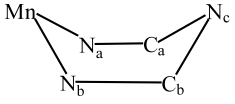


Fig. 1. ORTEP representation of the cation of $[Mn_4O_2(O_2CEt)_7(bpya)_2](ClO_4)$ at the 50% probability level (carbons represented isotropically).



3.2.1. Comparison of *1* with other $[Mn_4O_2]^{8+}$ complexes

As stated above, complex **1** is a new addition to the family of Mn clusters with the butterfly-like $[Mn_4O_2]^{8+}$ core, enlarging the available database of such complexes for identifying correlations between structure and physico-chemical properties. In Table 3 is presented a comparison between the core parameters of **1** and those of $[Mn_4O_2(NO_3)(O_2CEt)_6(bpy)_2](ClO_4)$ (**2**) [40], $[Mn_4O_2(O_2CMe)_7(bpy)_2](ClO_4)$ (**3**) [39] (bpy = 2,2′-bipyridyl), $(NBu^n_4)[Mn_4O_2(O_2CMe)_7(pic)_2]$ (**4**) [36]

Table 2
Selected interatomic distances (Å) and bond angles (°) for $[Mn_4O_2(O_2CEt)_7(bpya)_2](ClO_4)$ (**1**)

Bond lengths			
Mn(2)···Mn(3)	2.871(2)	Mn(3)–O(5)	1.957(3)
Mn(1)–O(5)	1.833(3)	Mn(3)–O(6)	1.876(3)
Mn(1)–O(33)	2.136(3)	Mn(3)–O(40)	1.941(3)
Mn(1)–O(38)	2.107(3)	Mn(3)–O(50)	2.186(3)
Mn(1)–O(43)	1.953(3)	Mn(3)–O(53)	2.134(3)
Mn(1)–N(7)	2.058(4)	Mn(3)–O(58)	2.051(3)
Mn(1)–N(19)	2.087(4)	Mn(4)–O(6)	1.838(3)
Mn(2)–O(5)	1.873(3)	Mn(4)–O(55)	1.948(3)
Mn(2)–O(6)	1.949(3)	Mn(4)–O(60)	2.130(3)
Mn(2)–O(35)	2.047(3)	Mn(4)–O(65)	2.137(3)
Mn(2)–O(45)	2.128(3)	Mn(4)–N(20)	2.035(4)
Mn(2)–O(48)	2.142(3)	Mn(4)–N(32)	2.081(4)
Mn(2)–O(63)	1.937(3)		
Bond angles			
O(33)–Mn(1)–O(38)	93.52(12)	O(5)–Mn(3)–O(53)	99.16(12)
O(33)–Mn(1)–O(43)	92.01(12)	O(5)–Mn(3)–O(58)	172.62(13)
O(5)–Mn(1)–O(33)	93.97(13)	O(6)–Mn(3)–O(40)	173.83(13)
O(5)–Mn(1)–O(38)	175.14(14)	O(6)–Mn(3)–O(50)	87.15(12)
O(5)–Mn(1)–O(43)	90.66(14)	O(6)–Mn(3)–O(53)	88.51(13)
O(5)–Mn(1)–N(7)	173.07(13)	O(6)–Mn(3)–O(58)	99.08(13)
O(5)–Mn(1)–N(19)	91.22(14)	O(40)–Mn(3)–O(50)	98.05(13)
O(33)–Mn(1)–N(7)	88.58(14)	O(40)–Mn(3)–O(53)	86.68(13)
O(33)–Mn(1)–N(19)	86.84(14)	O(40)–Mn(3)–O(58)	84.63(13)
O(38)–Mn(1)–O(43)	92.57(13)	O(50)–Mn(3)–O(53)	172.40(12)
O(38)–Mn(1)–N(7)	85.60(13)	O(50)–Mn(3)–O(58)	86.38(12)
O(38)–Mn(1)–N(19)	88.92(13)	O(53)–Mn(3)–O(58)	88.15(13)
O(43)–Mn(1)–N(7)	90.37(14)	O(6)–Mn(4)–O(55)	94.10(13)
O(43)–Mn(1)–N(19)	175.09(14)	O(6)–Mn(4)–O(60)	93.76(13)
N(7)–Mn(1)–N(19)	85.07(15)	O(6)–Mn(4)–O(65)	91.05(12)
O(5)–Mn(2)–O(6)	82.54(12)	O(6)–Mn(4)–N(20)	176.12(14)
O(5)–Mn(2)–O(35)	98.34(13)	O(6)–Mn(4)–N(32)	91.79(14)
O(5)–Mn(2)–O(45)	88.47(13)	O(55)–Mn(4)–O(60)	94.99(14)
O(5)–Mn(2)–O(48)	88.56(13)	O(55)–Mn(4)–O(65)	92.18(13)
O(5)–Mn(2)–O(63)	174.48(14)	O(55)–Mn(4)–N(20)	89.22(14)
O(6)–Mn(2)–O(35)	172.37(12)	O(55)–Mn(4)–N(32)	173.74(15)
O(6)–Mn(2)–O(45)	100.64(13)	O(60)–Mn(4)–O(65)	171.06(13)
O(6)–Mn(2)–O(48)	87.16(12)	O(60)–Mn(4)–N(20)	83.94(14)
O(6)–Mn(2)–O(63)	94.40(13)	O(60)–Mn(4)–N(32)	86.74(14)
O(35)–Mn(2)–O(45)	86.97(13)	O(65)–Mn(4)–N(20)	90.83(14)
O(35)–Mn(2)–O(48)	85.29(12)	O(65)–Mn(4)–N(32)	85.57(14)
O(35)–Mn(2)–O(63)	85.31(13)	N(20)–Mn(4)–N(32)	84.98(15)
O(45)–Mn(2)–O(48)	171.22(13)	Mn(1)–O(5)–Mn(2)	126.82(16)
O(45)–Mn(2)–O(63)	87.58(13)	Mn(1)–O(5)–Mn(3)	130.10(16)
O(48)–Mn(2)–O(63)	95.90(13)	Mn(2)–O(5)–Mn(3)	97.07(13)
O(5)–Mn(3)–O(6)	82.24(12)	Mn(2)–O(6)–Mn(3)	97.25(13)
O(5)–Mn(3)–O(40)	94.71(12)	Mn(2)–O(6)–Mn(4)	131.38(16)
O(5)–Mn(3)–O(50)	86.43(12)	Mn(3)–O(6)–Mn(4)	125.29(15)

(picH = picolinic acid), $[Mn_4O_2(py)_2(O_2CMe)_6(dbm)_2]$ (**5**) [38] (dbmH = dibenzoylmethane) and $[Mn_4O_2(O_2CPh)_6(dpm)_2]$ (**6**) [47] (dpmH = dipivaloylmethane). All these complexes have idealized C_2 symmetry except for **5**, which possesses a crystallographic inversion center and a planar rather than butterfly Mn_4 topology. The main conclusion to be drawn is that core structures of the C_2 molecules are insignificantly affected by the nature of the chelate ligands and are thus all essentially superimposable, with only minor differences between corresponding structural parameters.

3.3. Magnetochemistry

The molar magnetic susceptibility, χ_m, of complex **1** in the solid state was measured under a constant magnetic field of 1 Tesla in the 5–300 K range. A plot of the effective magnetic moment, μ_{eff}, of complex **1** versus temperature is shown in Fig. 2. The value of μ_{eff} is $8.30\mu_B$ at 300 K and gradually diminishes as the temperature is decreased. A sharp increase of the slope is observed at 50 K, below which μ_{eff} decreases much more rapidly to a value of $4.12\mu_B$ at 5 K.

The Heisenberg spin Hamiltonian for complex **1** is given in Eq. (2), where the numbering in Fig. 1 has been employed.

$$\hat{H} = -2(J_{12}\hat{S}_1\hat{S}_2 + J_{13}\hat{S}_1\hat{S}_3 + J_{23}\hat{S}_2\hat{S}_3 + J_{24}\hat{S}_2\hat{S}_4 + J_{34}\hat{S}_3\hat{S}_4 + J_{14}\hat{S}_1\hat{S}_4) \quad (2)$$

From the virtual C_2 symmetry of **1**, it follows that there are two types of 'body-to-wingtip' Mn–Mn interactions. These can be assumed to be equivalent on the basis of the structural parameters, as was done with previous butterfly complexes, and the spin Hamiltonian then simplifies to that in Eq. (3), where J_{wb} is the wingtip-body interaction, J_{bb} is the body–body interaction,

$$\hat{H} = -2J_{wb}(\hat{S}_1\hat{S}_2 + \hat{S}_1\hat{S}_3 + \hat{S}_2\hat{S}_4 + \hat{S}_3\hat{S}_4) - 2J_{bb}\hat{S}_2\hat{S}_3 - 2J_{ww}\hat{S}_1\hat{S}_4 \quad (3)$$

and J_{ww} refers to the wingtip–wingtip interaction. By use of the Kambe vector coupling method [41,42], and the definitions $\hat{S}_A = \hat{S}_2 + \hat{S}_3$, $\hat{S}_B = \hat{S}_1 + \hat{S}_4$ and $\hat{S}_T = \hat{S}_A + \hat{S}_B$, the spin Hamiltonian can be transformed into that in Eq. (4).

$$\hat{H} = -J_{wb}(\hat{S}_T^2 - \hat{S}_A^2 - \hat{S}_B^2) - J_{bb}\hat{S}_A^2 - J_{ww}\hat{S}_B^2 \quad (4)$$

The corresponding expression of the energy of the spin microstates $|S_T, S_A, S_B\rangle$ is given in Eq. (5). There are a total of 85 S_T states, ranging from $S_T = 0$ to 8.

$$E(S_T, S_A, S_B) = -J_{wb}[S_T(S_T+1) - S_A(S_A+1) - S_B(S_B+1)] - J_{bb}[S_A(S_A+1)] - J_{ww}[S_B(S_B+1)] \quad (5)$$

The solid line in Fig. 2 represents the best fit of the experimental data to the theoretical χ_m versus T equation obtained using the energy values in Eq. (5) and the Van Vleck equation. A temperature independent paramagnetism (TIP) term was held constant at 900×10^{-6} cm^3 mol^{-1}. The fitting parameters were $J_{wb} = -3.27$ cm^{-1}, $J_{bb} = -25.66$ cm^{-1} and $J_{ww} = -0.77$ cm^{-1}, with g held constant at $g = 1.99$. These parameters yield a spin ground state of $S_T = 0$, corresponding to $|0,0,0\rangle$. There is a group of five states, including

Table 3
Comparison of the average core parameters of several $[Mn_4O_2]^{8+}$ complexes (Å, °)

Complex	$Mn_b\cdots Mn_b$	$Mn_b\cdots Mn_w$ [a]	Mn_b–O	Mn_w–O	Mn_b–O–Mn_b	Mn_b–O–Mn_w [a]	O–Mn–O	Dihedral [b]	Ref.
$[Mn_4O_2(NO_3)(O_2CEt)_6(bpy)_2]^+$	2.847	3.258	1.898	1.841	97.2	121.8	82.2	51.80	[40]
		3.344				126.4			
$[Mn_4O_2(O_2CEt)_7(bpya)_2]^+$	2.871	3.307	1.939	1.836	97.16	126.06	82.39	34.69	this work
		3.444				130.74			
$[Mn_4O_2(O_2CMe)_7(bpy)_2]^+$	2.848	3.301	1.912	1.824	96.25	123.7	83.0	44.81	[39]
		3.378				130.2			
$[Mn_4O_2(O_2CMe)_7(pic)_2]^-$	2.842	3.311	1.899	1.844	96.9	125.0	82.1	45.02	[36]
		3.396				129.7			
$[Mn_4O_2(py)_2(O_2CMe)_6(dbm)_2]$	2.875	3.308	1.890	1.877	99.07	123.2	80.93	0.02 [c]	[38]
		3.398				128.6			
$[Mn_4O_2(O_2CPh)_6(dpm)_2]$	2.841	3.255	1.874	1.890	98.53	120.1	81.46	42.0	[47]
		3.362				126.0			

[a] Top and bottom entries refer to Mn pairs bridged by two and one carboxylate, respectively.
[b] Dihedral angle between the two planes formed by the $2Mn_b$ ions with each Mn_w ion.
[c] Planar Mn_4 core.

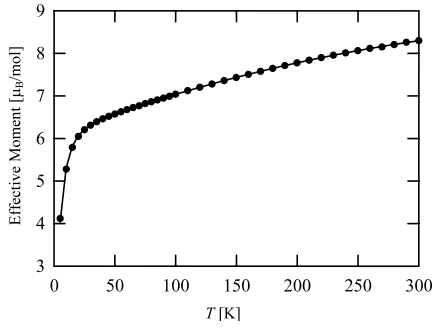


Fig. 2. Plot of effective magnetic moment (μ_{eff}) per molecule vs. T for $[Mn_4O_2(O_2CEt)_7(bpya)_2](ClO_4)$ in a 10.0 kG field. The solid line is a fit of the data to the appropriate theoretical equation; see the text for the fitting parameters.

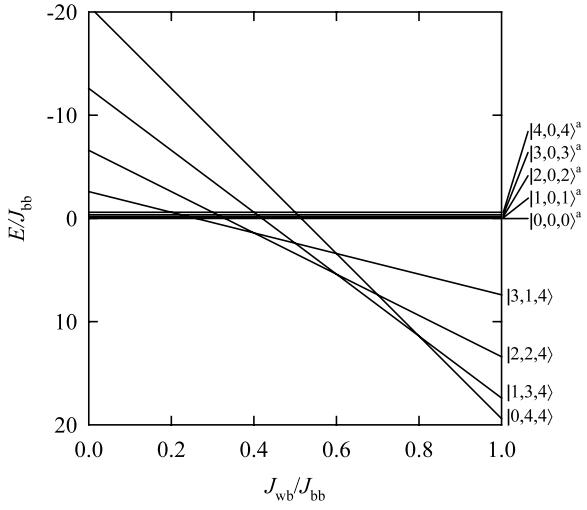


Fig. 3. Relative energy normalized to J_{bb} of the spin-ground state of a $[Mn_4O_2]^{8+}$ system as a function of the ratio J_{wb}/J_{bb} with $J_{ww} = -0.77$ cm^{-1}. For $J_{ww} = 0$, these states would belong to a fivefold degenerate set.

the ground state, within a narrow energy band of 15.3 cm^{-1}, the others being the $|1,0,1\rangle$, $|2,0,2\rangle$, $|3,0,3\rangle$ and $|4,0,4\rangle$ states. This collection of five closely lying spin states becomes degenerate if the weak magnetic coupling between the wing manganese ions (Mn1 and Mn4) is neglected. Although this interaction is very small ($J_{ww} = -0.77$ cm^{-1}), taking it into consideration resulted in a significant improvement of the fit. The introduction of this term results in very small changes to the energies of the different spin states and in the splitting of some groups of states that otherwise would be degenerate, but it strongly influences the behavior of μ_{eff} at very low temperature. The splitting of the ground state caused by this small wing–wing antiferromagnetic interaction leads to a sharp drop of the magnetic moment below 50 K because a diamagnetic state is being populated. Fig. 3 shows the relative energy (normalized to J_{bb}) of the spin ground state for this system as a function of the ratio J_{wb}/J_{bb}, with J_{ww} constant at -0.77 cm^{-1}. This plot shows that the ground-state spin is governed by the J_{wb}/J_{bb} ratio. The value of J_{ww} is assumed to be always very small and it only can affect the ground state when J_{wb}/J_{bb} is sufficiently low, by determining the relative energies of the group of states $|0,0,0\rangle$, $|1,0,1\rangle$, $|2,0,2\rangle$, $|3,0,3\rangle$ and $|4,0,4\rangle$. This is the case in complex **1** ($J_{wb}/J_{bb} = 0.13$), where the drop of μ_{eff} at low temperatures is explained by the existence of the diamagnetic ground state ($|0,0,0\rangle$) that results from the negative value of J_{ww}. A summary of the J_{wb} and J_{bb} parameters found for previously characterized $[Mn_4O_2]^{8+}$ complexes is given in Table 4.

In order to address the question of whether the global rather than a local fitting had been obtained, and to

Table 4
Exchange interaction constants in $[Mn_4O_2]^{8+}$ complexes

Complex	J_{wb} (cm^{-1})	J_{bb} (cm^{-1})	Ref.
$[Mn_4O_2(NO_3)(O_2CEt)_6(bpy)_2]^+$	−1.7	−16.5	[40]
$[Mn_4O_2(O_2CEt)_7(bpya)_2]^+$	−3.3	−25.7	this work
$[Mn_4O_2(O_2CMe)_7(bpy)_2]^+$	−7.8	−23.5	[39]
$[Mn_4O_2(O_2CMe)_7(pic)_2]^-$	−5.3	−24.6	[36]
$[Mn_4O_2(py)_2(O_2CMe)_6(dbm)_2]$	−5.0	−24.9	[38]
$[Mn_4O_2(O_2CPh)_6(dpm)_2]$	−0.4	−27.5	[47]

assess the reliability of the conclusion regarding the ground state of **1**, the relative error surface diagram for this fit was examined. The error surface was generated as a function of J_{wb} (−30.0 to 10.0 cm^{-1}) and J_{bb} (−50.0 to 25.0 cm^{-1}), with J_{ww} and g fixed at −0.77 cm^{-1} and 1.99, respectively. For this, the expression in Eq. (6) was used as the root-mean-square error, where n is the number of data points.

$$\sigma = \sqrt{\frac{\sum(\chi_{calc} - \chi_{exp})^2}{n}} \quad (6)$$

Fig. 4 shows a two-dimensional contour projection of the error surface, showing that the point of minimum error is poorly defined and located within a shallow 'valley'. The area with $\sigma \leq 0.002$ spans approximately the ranges −2 to −4 and −21 to −32 cm^{-1} for J_{wb} and J_{bb}, respectively. Superimposed on top of the contour diagram of Fig. 4 are the lines dividing the {J_{wb}, J_{bb}} space into regions of different ground states. Although the minimum of the error is not very well defined in the surface, it is clear from this plot that the assignment of the spin-ground state is reliable, since the entire region that would contain all reasonable fits is confined within

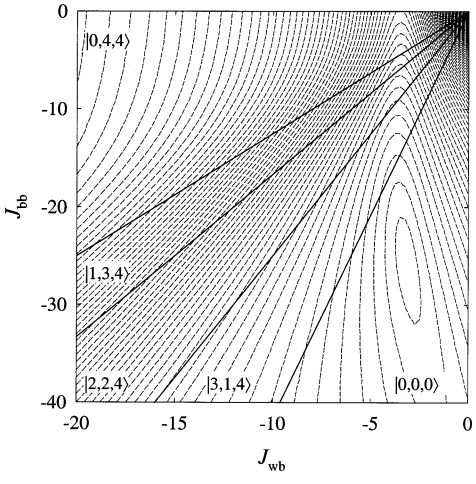


Fig. 4. Error surface of the magnetic susceptibility fit for $[Mn_4O_2(O_2CEt)_7(bpya)_2](ClO_4)$ as a function of J_{wb} and J_{bb}, represented as a contour projection (dashed lines) of the relative error calculated with g and J_{ww} constant at 1.99 and −0.77 cm^{-1}, respectively. Superimposed on the contour diagram are the lines dividing the {J_{wb}, J_{bb}} space into regions of different ground states.

the zone for $S_T = 0$ (or the area where the group of closely lying states |0,0,0⟩, |1,0,1⟩, |2,0,2⟩, |3,0,3⟩, and |4,0,4⟩ have the lowest energy).

The ground state of **1** is in contrast to that of most other $[Mn_4O_2]^{8+}$ complexes [36,38,39] for which the ground state is $S_T = 3$. This emphasizes the importance of the J_{wb}/J_{bb} ratio in determining the ground state of these molecules (Fig. 3). With such a small J_{wb}/J_{bb} ratio (0.13), i.e. $J_{bb} \gg J_{wb}$, the spins of the body Mn ions will be antiparallel-aligned, i.e. $S_A = 0$, and the ground state will then be determined by the interaction of the wingtip Mn ions via the J_{ww} exchange, giving a $S_T = 0$ ground state since J_{ww} is antiferromagnetic. In effect, this |0,0,0⟩ ground state can be described as the result of a weak long-range J_{ww} interaction between the wingtip Mn ions through a strongly coupled, diamagnetic (S_A = 0) central unit. If $J_{ww} = 0$, the ground state is the group of closely spaced states |0,0,0⟩, |1,0,1⟩, |2,0,2⟩, |3,0,3⟩ and |4,0,4⟩, corresponding to two non-interacting Mn(III) ions. The latter situation is approximated in the related complex $[Mn_4O_2(O_2CPh)_6(dpm)_2]$ where the J_{wb}/J_{bb} ratio is only 0.01, J_{ww} is negligible, and the ground state is best described as fivefold degenerate (non-interacting wingtip Mn ions) [47].

3.4. ^1H NMR spectroscopy

Complex **1** is moderately soluble in MeCN and is thus amenable to solution spectroscopic studies. The 500 MHz ^1H NMR spectrum (Fig. 5) was obtained in order to ascertain whether the structure is retained in solution. The spectral data are collected in Table 5. The interpretation of the ^1H NMR spectrum of complex **1** has

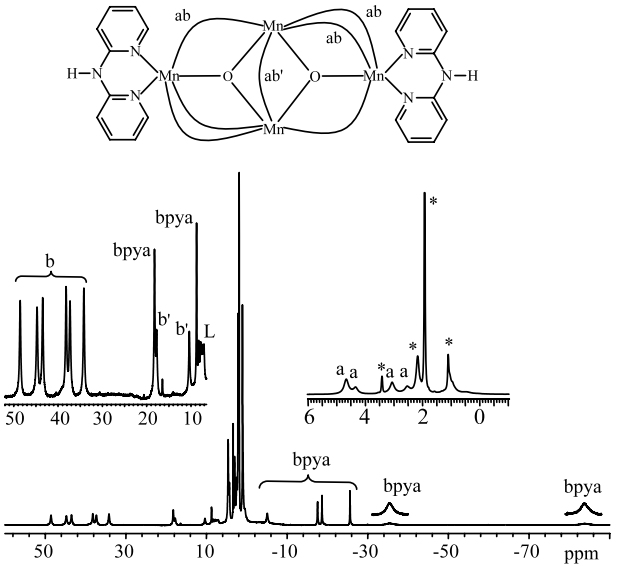


Fig. 5. 500 MHz ^1H NMR spectrum of $[Mn_4O_2(O_2CEt)_7(bpya)_2](ClO_4)$ in CD_3CN; * = $EtCO_2H$, H_2O and MeCN impurities, L = free ligand. Labels a and b refer to propionate CH_3 and CH_2 resonances, respectively.

Table 5
500 MHz ^{1}H NMR data [a] for $[Mn_4O_2(O_2CEt)_7(bpya)_2](ClO_4)$ (**1**) in CD_3CN

a	4.6	bpya	18.3
a	4.3	bpya	8.8
a	3.1	bpya	−5.0
a	2.5	bpya	−17.5
b	48.6(44.7)	bpya	−18.6
b	43.5(38.2)	bpya	−25.5
b	37.3(34.2)	bpya	−35.6
b′	17.8(10.4)	bpya	−83.8

[a] At approximately 23 °C, ppm; *b′* refers to the unique carboxylate bridging the body Mn ions.

benefited from previous spectroscopic studies on the analogous butterfly-like clusters **2**, **3** and **4** [36,39,40].

The ^{1}H NMR spectrum in Fig. 5 exhibits 20 different resonances in addition to the signals from solvent and ligand impurities. This is the number expected if the complex exhibits effective C_2 symmetry in solution. These resonances span a wide range of chemical shifts (−90 to 50 ppm). Four sets of signals in a 2:2:2:1 ratio are observed for the μ_2-O_2CEt groups, according to the scheme shown in Fig. 5. Each of these sets features two peaks from the CH_2 protons, which are diastereotopic, in the 10–50 ppm region, and a singlet from the CH_3 group between 2 and 5 ppm. The two chelating ligands are symmetry-related but all the protons within each bpya group are inequivalent. Accordingly, eight bpya signals are observed, and these display great disparity of linewidths as a result of their different separations from the Mn ions (broadness $\propto r^{-6}$, where r is the Mn···H distance). In addition, these eight resonances are subject to strong paramagnetic shifts to either side of the diamagnetic region, indicating that a π spin-delocalization mechanism is contributing to the coupling of the nuclear and electronic magnetic moments. All these results indicate that the structure of **1** in the solid state is retained in MeCN solution. In contrast, when the cluster is dissolved in DMSO, decomposition takes place, as is evident from the complete loss of the ^{1}H NMR spectral features in this solvent.

3.5. Electrochemistry

Complex **1** was investigated by cyclic voltammetry in MeCN solution with 0.1 M $N^nBu_4PF_6$. The voltammogram of this compound at a scan rate of 100 mV s^{-1} is displayed in Fig. 6. This complex shows a quasi-reversible oxidation process and an irreversible reduction process at 0.71 and −0.20 V versus Fc/Fc^+, respectively. The quasi-reversible oxidation has a peak-to-peak separation of 130 mV and is likely metal-based (Eq. (7)).

$$[Mn_4^{III}O_2]^{8+} - e^- \rightarrow [Mn_3^{III}Mn^{IV}O_2]^{9+} \quad (7)$$

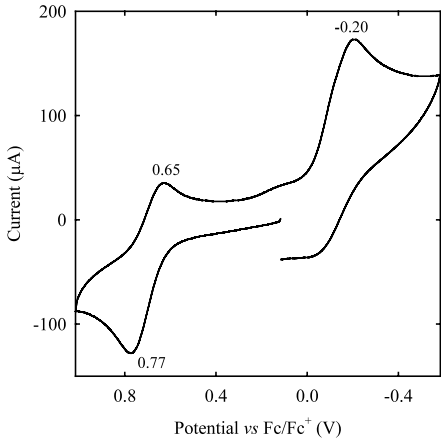


Fig. 6. Cyclic voltammogram at 100 mV s^{-1} for $[Mn_4O_2(O_2CEt)_7(bpya)_2](ClO_4)$ in MeCN containing 0.1 M $NBu^n_4PF_6$.

These values are similar to what has been observed previously for the $[Mn_4O_2(O_2CR)_7(L–L)]^+$ (R = Me, Ph; L–L = bpy, phen, 4-4′-Me_2-bpy) complexes reported previously by our group. Thus the non-ligation to Mn of the NH group of bpya results in **1** exhibiting very similar redox properties to the corresponding bpy and phen complexes.

4. Conclusions

The new tetranuclear complex $[Mn_4O_2(O_2CEt)_7(bpya)_2](ClO_4)$ (**1**) forms from the comproportionation reaction between Mn^{II} and Mn^{VII} in propionic acid in the presence of bpya. The title compound is the first crystallographically characterized species containing the ligand bpya bound to manganese. Unlike the majority of previously characterized Mn clusters with a butterfly core, complex **1** possesses a spin ground state of $S_T = 0$. This result emphasizes that only small changes in the relative strength of competing exchange interactions are necessary in a $[Mn_4O_2]^{8+}$ butterfly system for a change of the ground state spin value to occur. ^{1}H NMR spectroscopy has shown that the new complex retains its structure in MeCN solution. Complex **1** is a new addition to the list of crystallographically characterized clusters with the $[Mn_4O_2]^{8+}$ core.

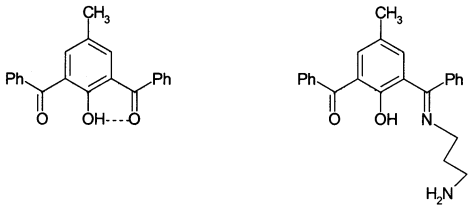
5. Supplementary material

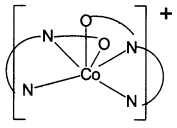
Crystallographic data for the structural analysis have been deposited with the Cambridge Crystallographic Data Centre, CCDC No. 175700 for compound **1**. Copies of this information may be obtained free of charge from The Director, CCDC, 12 Union Road, Cambridge, CB2 1EZ, UK (fax: +44-1223-336033; e-

mail: deposit@ccdc.cam.ac.uk or www: http://www.ccdc.cam.ac.uk) [48].

References

[1] V.L. Pecoraro (Ed.), Manganese Redox Enzymes, VCH Publishers, New York, 1992.
[2] H.J. Eppley, H.-L. Tsai, N. de Vries, K. Folting, G. Christou, D.N. Hendrickson, J. Am. Chem. Soc. 117 (1995) 301.
[3] G. Aromí, S.M.J. Aubin, M.A. Bolcar, G. Christou, H.J. Eppley, K. Folting, D.N. Hendrickson, J.C. Huffman, R.C. Squire, H.-L. Tsai, S. Wang, M.W. Wemple, Polyhedron 17 (1998) 3005.
[4] S.M.J. Aubin, M.W. Wemple, D.M. Adams, H. -L. Tsai, G. Christou, D.N. Hendrickson, J. Am Chem. Soc. 118 (1996) 7746.
[5] S.M.J. Aubin, N.R. Dilley, M.W. Wemple, M.B. Maple, G. Christou, D.N. Hendrickson, J. Am Chem. Soc. 120 (1998) 839.
[6] S.M.J. Aubin, S. Spagna, H.J. Eppley, R.E. Sager, K. Folting, G. Christou, D.N. Hendrickson, Mol. Cryst. Liq. Cryst. 305 (1997) 181.
[7] H. -L. Tsai, S. Wang, K. Folting, W.E. Streib, G. Christou, D.N. Hendrickson, J. Am. Chem. Soc. 117 (1995) 2503.
[8] H.J. Eppley, S. Wang, H. -L. Tsai, S.M.J. Aubin, K. Folting, W.E. Streib, G. Christou, D.N. Hendrickson, Mol. Cryst. Liq. Cryst. 274 (1995) 159.
[9] G. Christou, in: O. Kahn (Ed.), Magnetism: a Supramolecular Function, NATO ASI Series, Kluwer, Dordrecht, 1996.
[10] M.A. Bolcar, S.M.J. Aubin, K. Folting, D.N. Hendrickson, G. Christou, J. Chem. Soc., Chem. Commun. (1997) 1485.
[11] G. Aromí, M.J. Knapp, J.-P. Claude, J.C. Huffman, D.N. Hendrickson, G. Christou, J. Am. Chem. Soc. 121 (1999) 5489.
[12] R. Sessoli, H. -L. Tsai, A.R. Shake, S. Wang, J.B. Vincent, K. Folting, D. Gatteschi, G. Christou, D.N. Hendrickson, J. Am. Chem. Soc. 115 (1993) 1804.
[13] R. Sessoli, D. Gatteschi, A. Caneschi, M.A. Novak, Nature 365 (1993) 141.
[14] J.R. Friedman, M.P. Sarachik, J. Tejada, J. Maciejewski, R. Ziolo, J. Appl. Phys. 79 (1996) 6031.
[15] J. Tejada, R.F. Ziolo, X.X. Zang, Chem. Mater. 8 (1996) 1784.
[16] J.M. Hernádez, X.X. Zang, F. Luis, J. Bartolomé, J. Tejada, R. Ziolo, Europhys. Lett. 35 (1996) 301.
[17] A.L. Barra, P. Debrunner, D. Gateschi, C.E. Shultz, R. Sessoli, Europhys. Lett. 35 (1996) 133.
[18] H.J. Eppley, N. de Vries, S. Wang, S.M.J. Aubin, K. Folting, D.N. Hendrickson, G. Christou, Inorg. Chim. Acta 263 (1997) 323.
[19] M.W. Wemple, H. -L. Tsai, S. Wang, J. -P. Claude, W.E. Streib, K. Folting, G. Christou, Inorg. Chem. 35 (1996) 6437.
[20] H.J. Eppley, S.M.J. Aubin, W.E. Streib, J.C. Bollinger, D.N. Hendrickson, G. Christou, Inorg. Chem. 36 (1997) 109.
[21] R.C. Squire, S.M.J. Aubin, K. Folting, W.E. Streib, G. Christou, D.N. Hendrickson, Inorg. Chem. 34 (1995) 6463.
[22] M.A. Halcrow, W.E. Streib, K. Folting, G. Christou, Acta Crystallogr., Sect.C C51 (1995) 1263.
[23] S. Wang, H. -L. Tsai, K.S. Hagen, D.N. Hendrickson, G. Christou, J. Am. Chem. Soc. 116 (1994) 9339.
[24] D. Luneau, J. -M. Savarinult, J. -P. Tuchagues, Inorg. Chem. 27 (1988) 3912.
[25] R. Bhula, D.C. Weatherburn, Angew. Chem., Int. Ed. Engl. 30 (1991) 688.
[26] D.W. Low, D.M. Eichhorn, A. Draganescu, W.H. Armstrong, Inorg. Chem. 30 (1991) 877.
[27] G.A. Bowmaker, P.C. Healy, D.L. Kepert, J.D. Kildea. B.W. Skelton, A.H. White, J. Chem. Soc., Dalton Trans. (1989) 1639.
[28] O.R. Rodig, T. Brueckner, B.H. Hurlburt, R.K. Schlatzer, T.L. Venable, E. Sinn, J. Chem. Soc., Dalton Trans. (1981) 196.
[29] N.J. Ray, L. Hulett, R. Sheahan, B.J. Hathaway, J. Chem. Soc., Dalton Trans. (1981) 1463.
[30] N. Marsich, A. Camus, F. Ugozzoli, A.M.M. Lanfredi, Inorg. Chim. Acta 236 (1995) 117.
[31] L.-P. Wu, M.E. Keniry, B. Hathaway, Acta Crystallogr., Sect. C. (Cr. Str. Commun.) 48 (1992) 35.
[32] L.-P. Wu, P. Field, T. Morrissey, C. Murphy, P. Nagle, B. Hathaway, C. Simmons, P. Thornton, J. Chem. Soc., Dalton Trans. (1990) 3835.
[33] F.A. Cotton, L.M. Daniels, C.A. Murillo, I. Pascual, Inorg. Chem. Commun. 1 (1998) 1.
[34] E-C. Yang, M.-C. Cheng, M.-S. Tsai, S.-M. Peng, J. Chem. Soc., Chem. Commun. (1994) 2377.
[35] S. Wang, H.-L. Tsai, W.E. Streib, G. Christou, D.N. Hendrickson, J. Chem. Soc., Chem. Commun. (1992) 677.
[36] E. Libby, J.K. McCusker, E.A. Schmitt, K. Folting, D.N. Hendrickson, G. Christou, Inorg. Chem. 30 (1991) 3486.
[37] E. Bowman, M.A. Bolcar, E. Libby, J.C. Huffman, K. Folting, G. Christou, Inorg. Chem. 31 (1992) 5185.
[38] S. Wang, K. Folting, W.E. Streib, E.A. Schmitt, J.K. McCusker, D.N. Hendrickson, G. Christou, Angew. Chem., Int. Ed. Engl. 30 (1991) 305.
[39] J.B. Vincent, C. Christmas, H. -R. Chang, Q. Li, P.D.W. Boyd, J.C. Huffman, D.N. Hendrickson, G. Christou, J. Am. Chem. Soc. 111 (1989) 2086.
[40] G. Aromí, S. Bhaduri, P. Artús, K. Folting, G. Christou, Inorg. Chem. 41 (2002) 805.
[41] K. Kambe, J. Phys. Soc. Jpn. 5 (1950) 8.
[42] A. Cornia, D. Gatteschi, K. Hegetschweiler, Inorg. Chem. 33 (1994) 1559.
[43] A.J. Blake, S. Parsons, J.M. Rawson, R.E.P. Winpenny, Polyhedron 14 (1995) 1895.
[44] F.A. Cotton, L.M. Daniels, G.T Jordan, IV, C.A. Murillo, J. Am. Chem. Soc. 119 (1997) 10377.
[45] G. Christou, Acc. Chem. Res. 22 (1989) 328.
[46] (a) J.B. Vincent, K Folting, J.C. Huffman, G. Christou, Inorg. Chem. 24 (1986) 996;
(b) J.B. Vincent, H. -R Chang, K. Folting, J.C. Huffman, G. Christou, D.N. Hendrickson, J. Am. Chem. Soc. 109 (1987) 5703.
[47] C. Cañada- Vilalta, J.C. Huffman, G. Christou, Polyhedron 20 (2001) 1785.
[48] F.H. Allen, O. Kennard, Chem. Des. Automation News 8 (1993) 131 (The Cambridge Structural Database).





2. Experimental

All the chemicals were of reagent grade and were used as received. Propane-1,3-diamine and $CoCl_2 \cdot 6H_2O$ were obtained from Aldrich. Solvents were purified by standard methods [14].

2.1. Physical measurements

Elemental analysis was carried out by the University of North London, London, UK. Thermogravimetric analysis was carried out on a DuPont TGA 2950 analyzer in the synthetic air atmosphere with a heating rate of 10 °C min^{-1}. The molar conductance in 10^{-3} mol dm^{-3} MeOH solution was measured using a Global DCM-900 digital conductivity meter. The IR spectra were recorded on a Perkin–Elmer 1720 FT spectrometer in Nujol mulls. The EI and FAB mass spectra (recorded in a 3-nitrophenylmethanol matrix) by use of a VG Autospec spectrometer. The electronic spectra in 10^{-4} mol dm^{-3} MeOH solution were obtained using a Shimadzu UV-160A recording spectrophotometer. The ^1H and $^{13}C\{^1H\}$ NMR spectra were recorded on a 500 MHz Bruker NMR instrument and chemical shifts are relative to $SiMe_4$. Assignments were made using selective decoupling, saturation transfer experiments, 2D double quantum filtered (DQF)-COSY and Nuclear Overhauser effect (NOE) experiments. The signals of phenyl CH carbons were assigned by the DEPT 90° pulse technique. Cyclic voltammograms were run in a nitrogen atmosphere in 10^{-4} M MeOH solution of the complex on an EG & G Versastat II system using platinum as working electrode, Pt wire as auxiliary electrode and SCE as the reference electrode. Tetraethylammonium–perchlorate (TEAP) (0.1 M solution in MeOH) was used as the supporting electrolyte. Scan speeds of 50–200 mV s^{-1} were employed.

2.2. Preparation of 4-methyl-2,6-dibenzoylphenol(mdbp) (*I*)

The precursor (mdbp) **I** was prepared by a literature method [15] (m.p. 159 °C, lit. [15] 160 °C). Crystals suitable for an X-ray study were grown as yellow needles by slow evaporation from the ethanol solution. MS (EI) (*m*/*z*) 316 (100, M), 301 (5, $M-CH_3$), 287 (10, $M-HCO$), 239 (40, $M-Ph$), 211 (15, $M-PhCO$), 161 (40, $M-Ph-PhH$), 105 (65, PhCO), 77 (80). IR (cm^{-1}): 3425 [ν(OH)]; 1658, 1620 [ν(CO)]; 1604 [ν(C–C)ring]; 1575 [ν(C–O)]. UV–Vis (nm) (ε, M^{-1} cm^{-1}) (MeOH): 352 (6000); 255 (24 700). ^1H NMR ($CDCl_3$): δ 2.33 (s, 3H, CH_3); 7.3–7.9 (m, 12H, Ph); 12.02 (s, 1H, OH).

2.3. Template synthesis of $[Co(L)_2](Cl) \cdot NH_2(CH_2)_3NH_2 \cdot 2EtOH$ (*1*)

To a boiling solution of $CoCl_2 \cdot 6H_2O$ (0.952 g, 4.00 mmol) and 4-methyl-2,6-dibenzoylphenol (2.53 g, 8.00 mmol) in ethanol (30 cm^3), an ethanolic solution of the propane-1,3-diamine (0.592 g, 8.00 mmol) was added slowly with constant stirring and the mixture was boiled under reflux for 4 h. The resulting brown solution was cooled to room temperature and allowed to stand for 1 week during which brown crystals formed. The crystals were filtered off, washed with cold ethanol and dried in air. Yield 2.60 g (65%), m.p. 240 °C. *Anal*. Calc. for $C_{55}H_{68}ClCoN_6O_6$: C, 65.84; H, 6.78; N, 8.38. Found: C, 66.00; H, 6.86; N, 8.56%. MS (FAB^+) (*m*/*z*): 801 (CoL_2^+). IR (cm^{-1}): 3448 [ν(OH)]; 3177, 3137 [ν(N–H)]; 1650 [ν(CO)]; 1594 [ν(C=N)]; 1529 [ν(C–O)]. UV–Vis (nm) (ε, M^{-1} cm^{-1}) (MeOH): 634 (250), 411 (13 500), 243 (76 500). ^1H NMR (MeOH-d_4, 298 K, atoms numbered as in Fig. 3): δ 1.17 (3H, t, EtOH), 1.55 and 1.86 (1H, m, C^2H_2), 1.94 (2H, m, C^1H_2), 1.97 (3H, s, $C^{24}H_3$), 2.99 and 3.25 (1H, m, C^3H_2), 3.59 (2H, q, EtOH), 6.30 (1H, dq, $^4J = 2.1$ and 0.6 Hz, C^6H), 6.92 (1H, dq, $^4J = 1.9$ and 0.5 Hz, C^8H), 7.06 (1H, d, $^3J = 7.6$ Hz $C^{12}H$), 7.19 (1H, d, $J = 7.3$ Hz, $C^{16}H$), 7.43 (2H, m, $C^{21}H$), 7.46 (^1H, m, $C^{13}H$), 7.50 (1H, m, $C^{20,22}H$), 7.52 (1H, m, $C^{14}H$), 7.55 (1H, m, $C^{15}H$), 7.65 (2H, d, $C^{19,23}H$). ^1H NMR (C_6D_6, 298 K): δ 12.6 (2H, s, NH_2). ^{13}C NMR (MeOH-d_4): δ 21.0 (C^{24}), 27.7 (C^2), 35.8 (C^1), 51.3 (C^3), eight quaternary signals at δ 124.5 (C^{11}), 128.1, (C^{18}), 133.5 (C^7), 138.0 (C^5), 140.9 (C^9), (assignments uncertain), 164.6 (C^{10}), 177.7 (C^4), 199.0 (C^{17}), and ten CH signals at 131.2, 129.7 ($C^{19,23}$, $C^{20,22}$), 128.7, 129.6, 129.9, 130.4, 131.3, 133.6, 138.0, 140.0 ($C^{6,8,12-16,21}$, assignments uncertain). CV data (V): $E_{pc} = -0.67$, $E_{pa} = +0.88$. Λ_M (10^{-3} M, MeOH, 298 K): 85 *S* cm^2 mol^{-1}.

2.4. X-ray structure determination

Yellow needles of the precursor mdbp **I** and brown crystals of complex **1** were grown by slow evaporation from their ethanol solutions. Data were obtained on a Nonius Kappa CCD diffractometer with Mo Kα radiation. Data collection parameters are given in Table 1. No absorption corrections were applied. The structures were solved and refined using SHELXL-97 [16]. The non-hydrogen atoms were refined anisotropically and H atoms in riding mode. Selected bond lengths and angles are listed in Table 2.

3. Results and discussion

3.1. Synthesis and properties

The template condensation of 4-methyl-2,6-dibenzoylphenol (mdbp) **I** with propane-1,3-diamine in the presence of $CoCl_2 \cdot 6H_2O$ in ethanol yields a diamagnetic brown Co(III) complex of composition $[Co(L)_2]Cl \cdot NH_2(CH_2)_3NH_2 \cdot 2EtOH$ (**1**). Presumably an initially formed Co^{II} complex is oxidized by accidentally admitted air.

Table 1
Crystal data and structure refinement for mdbp **I** and Cobalt complex **1**

Empirical formula	$C_{21}H_{16}O_3$	$C_{55}H_{68}ClCoN_6O_6$
Formula weight	316.34	1003.5
Temperature (K)	173(2)	173(2)
Crystal system	orthorhombic	monoclinic
Space group	*Pbca* (No. 61)	$P2_1/c$ (No. 14)
Unit cell dimensions		
a (Å)	11.4728(8)	18.7976(11)
b (Å)	12.5813(6)	23.2938(15)
c (Å)	21.8498(15)	11.9533(6)
α (°)	90	90
β (°)	90	105.409(3)
γ (°)	90	90
V (Å^3)	3153.9(3)	5045.8(5)
Z	8	4
Absorption coefficient (mm^{-1})	0.09	0.45
Reflections collected	14 278	20 282
Independent reflections	2184 [$R_{int} = 0.145$]	6113 [$R_{int} = 0.115$]
Reflections with $I > 2\sigma(I)$	1430	3775
Data/restraints/parameters	2184/0/222	6113/6/568
Goodness-of-fit on F^2	1.035	1.007
Final R indices [$I > 2\sigma(I)$]	$R_1 = 0.055$, $wR_2 = 0.103$	$R_1 = 0.076$, $wR_2 = 0.174$
R indices (all data)	$R_1 = 0.0996$, $wR_2 = 0.1197$	$R_1 = 0.131$, $wR_2 = 0.204$
Largest difference peak and hole (e Å^{-3})	0.21 and −0.24	0.62 and −0.52

Table 2
Bond lengths (Å) and bond angles (°)

I (4-Methyl-2,6-dibenzoylphenol), mdbp

Bond lengths	
O(1)–C(1)	1.360(4)
O(2)–C(8)	1.235(3)
O(3)–C(15)	1.225(3)
C(1)–C(6)	1.394(4)
C(1)–C(2)	1.418(4)
C(2)–C(8)	1.475(4)
C(6)–C(15)	1.497(4)
Bond angles	
O(1)–C(1)–C(6)	118.2(3)
O(1)–C(1)–C(2)	122.0(3)
C(1)–C(2)–C(8)	119.5(3)
C(3)–C(4)–C(7)	121.9(3)
O(3)–C(15)–C(6)	118.4(3)
O(2)–C(8)–C(2)	121.1(3)
O(2)–C(8)–C(9)	119.5(3)

1 $[Co(L)_2]Cl \cdot 2EtOH \cdot NH_2(CH_2)_3NH_2$

Bond lengths			
Co–O(3)	1.878(5)	C(5)–C(10)	1.419(9)
Co–O(1)	1.886(4)	C(9)–C(10)	1.420(10)
Co–N(1)	1.929(5)	C(28)–C(29)	1.474(9)
Co–N(3)	1.932(5)	C(29)–C(34)	1.420(9)
Co–N(2)	1.969(5)	C(33)–C(34)	1.413(9)
Co–N(4)	1.970(5)	C(33)–C(41)	1.496(9)
O(1)–C(10)	1.305(8)		
O(2)–C(17)	1.243(9)		
O(3)–C(34)	1.317(8)		
O(4)–C(41)	1.231(8)		
N(1)–C(4)	1.315(8)		
N(3)–C(28)	1.292(8)		
C(4)–C(5)	1.467(10)		
Bond angles			
O(3)–Co–O(1)	92.57(19)	N(1)–Co–N(2)	89.4(2)
O(3)–Co–N(1)	88.8(2)	N(3)–Co–N(2)	90.7(2)
O(1)–Co–N(1)	89.7(2)	O(3)–Co–N(4)	179.4(2)
O(3)–Co–N(3)	89.9(2)	O(1)–Co–N(4)	86.9(2)
O(1)–Co–N(3)	90.2(2)	N(1)–Co–N(4)	91.3(2)
N(1)–Co–N(3)	178.7(2)	N(3)–Co–N(4)	90.0(2)
O(3)–Co–N(2)	85.1(2)	N(2)–Co–N(4)	95.5(2)
O(1)–Co–N(2)	177.5(2)		
C(34)–C(33)–C(41)	121.4(6)		
O(3)–C(34)–C(33)	119.2(6)		
O(2)–C(17)–C(9)	119.1(7)		
O(3)–C(34)–C(29)	122.9(6)		
N(1)–C(4)–C(5)	122.4(6)		
C(10)–C(5)–C(4)	120.6(6)		
O(4)–C(41)–C(33)	120.9(7)		
N(3)–C(28)–C(29)	121.1(6)		
C(10)–C(9)–C(17)	122.9(9)		
O(1)–C(10)–C(5)	123.0(6)		
O(1)–C(10)–C(9)	120.6(6)		
C(34)–C(29)–C(28)	120.5(6)		

The molar conductance value in MeOH suggests that it is a 1:1 electrolyte. Elemental analysis is found to be in good agreement with this formulation.

3.2. Thermal study

The presence of chloride ion and a molecule of diamine solvate outside the coordination sphere of the complex is confirmed by dynamic TGA studies. Complex **1** is stable up to 198.3 °C and thereafter it registers a mass loss of 3.3% at 261 °C compared with the theoretical value of 3.54%, which corresponds to the loss of half molecule of chlorine. From 260.6 to 333.4 °C a mass loss of 17.0%, compared with the theoretical value of 16.5% is attributed to the combined loss of two moles of ethanol and one mole of propane-1,3-diamine. After 400 °C the complex starts to decompose and a mass loss of 37% at 441.7 °C corresponds to the loss of one ligand (theoretical value 37.1%). The total mass loss up to 551.6 °C is found to be 90.3%, which shows the formation of cobalt oxide. The high mass of the residue (theory 7.5%) is attributed to carbonaceous matter. Thus the decomposition pattern obtained from TGA curve confirms the proposed formulation of the complex.

3.3. Mass spectrum

The FAB mass spectrum shows the presence of the cationic species $[Co(L)_2]^+$ at *m*/*z* 801.

3.4. IR and electronic spectra

The IR spectrum of the precursor mdbp **I** displays two ν(CO) bands at 1658 and 1620 cm^{-1}, the latter being hydrogen bonded. Complex **1** displays a ν(CO) band at 1650 and a ν(CN) vibration at 1594 cm^{-1}. The bands at 3177 and 3137 cm^{-1} are assigned to ν(N–H) vibrations. The low value of ν(N–H) is attributed to the fact that the NH_2 group is coordinated to the metal. The band at 1530 cm^{-1} has been assigned to the ν(C···O) vibration of the phenol [15] as a consequence of the delocalization of double bond in the chelate ring that has increased the bond order of the phenolic C–O. This is confirmed by the crystal structure determination. A broad band at 3448 cm^{-1} is due to ν(OH) in ethanol molecules occluded in the lattice.

Complex **1** is diamagnetic. The electronic spectrum has three bands at 634, 411 and 243 nm. The first band seems to include a major contribution from the $^1A_{1g} \rightarrow {}^1T_{1g}$ transition, suggesting a distorted octahedral geometry [17]. The other two bands are charge transfer and intraligand transitions, respectively. Strong absorption at higher frequencies precludes observation of other possible ligand field transitions.

3.5. Crystal structure of mdbp *I* and complex *1*

An ORTEP view of the mdbp **I** with the atom numbering scheme is shown in Fig. 1. Selected bond lengths and angles are given in Table 2. The phenolic hydrogen forms a hydrogen bond of length 2.58 Å with atom O(2) of the carbonyl group, essentially similar to that, 2.566(3) Å, in $[(PhCO)_2C_6H_2(OH)_2]$ [10]. The 4-methyl substituent in **I** is unable to participate in intermolecular hydrogen bonding so that the molecules in the lattice are isolated, instead of built into an infinite network like those of the hydroquinone. The C(1)–O(1) [1.360(4) Å] is significantly longer than the C(8)–O(2) [1.235(3) Å] and C(15)–O(3) [1.225(3) Å] distances. Similar distances, mean 1.357(3) Å and 1.232(3) Å are also observed in $[(PhCO)_2C_6H_2(OH)_2]$ [10]. The central carbon C(1) is perfectly planar (sum of bond angles 360.0(3)°). Other features of bond lengths and angles are as expected.

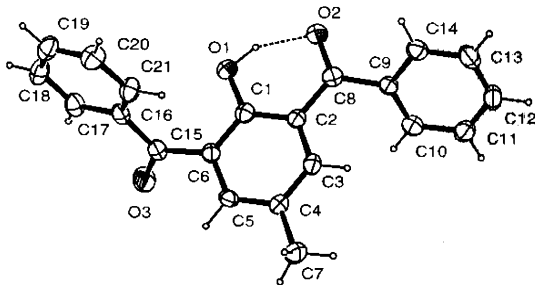


Fig. 1. Molecular structure of 4-methyl-2,6-dibenzoylphenol, mdbp **I**.

The molecular structure of complex **1** is shown in Fig. 2 and another view is given in Fig. 3. The two monoanionic ligands are tridentate, coordinating through amine N, imine N and phenolic O atoms to give a *mer*-CoN_4O_2 octahedral configuration. The two phenolic groups are nearly parallel. The ethanol molecule and the propane-1,3-diamine are disordered and poorly defined, and do not form part of the Co coordination sphere. The phenolic C–O distances in the complex [1.305(8) and 1.317(8) Å] are significantly shorter than that in the ligand **I** [1.360(4) Å] consistent with the infrared data. The average Co–N [1.950(5) Å] and Co–O [1.882(5) Å] bond lengths are in the same range as corresponding values in similar octahedral Co(III) systems [18,19], and significantly shorter than Co^{II}–N and Co^{II}–O bond lengths. For example, the Co–N (peptide) distances range from 2.12 to 2.14 Å and Co–O distances from 2.07 to 2.15 Å in bis-L-histidinate $Co^{II}\cdot H_2O$ [20] and $LCo^{II}_2Br_2\cdot CH_3OH$, in which the N_4O_2 donor set of the macrocyclic ligand L coordinates to two Co atoms [21]. A Co–O distance of 1.98 Å (longer than that in **1**) and Co–N distances from 1.91 to 1.94 Å (similar to those in **1**) have been reported for the *mer*-bis(glycylglycinato)cobalt(III) cation [22]. In general, bite distances of five-membered and six-membered chelate rings are approximately 2.6–2.7 and 2.8–2.9 Å, respectively, and bite angles 84°–88° and 92°–96°,

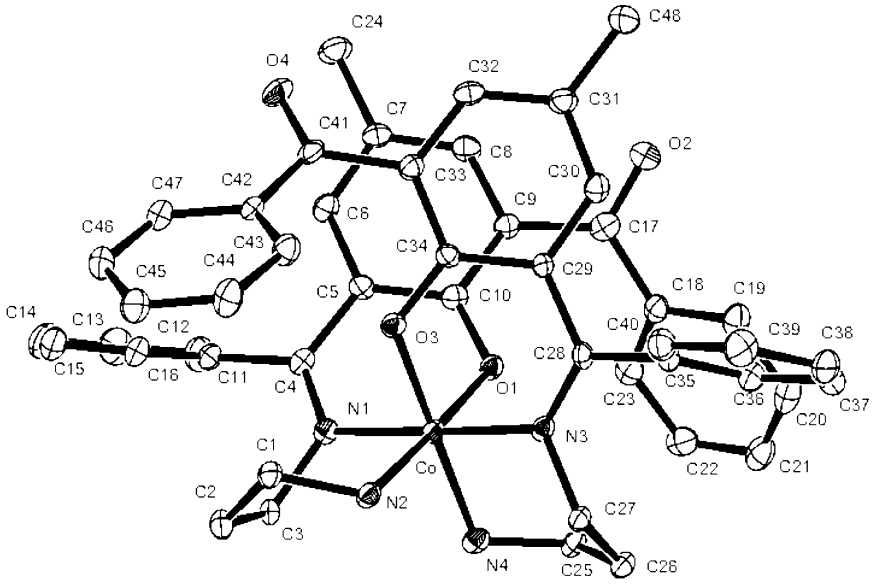


Fig. 2. Molecular structure of the complex $[Co(L)_2]^+$.

respectively [23]. In the present investigation the N···N bite distances (2.74 and 2.76 Å) and the N–Co–N and O–Co–O bite angle, ca. 90°) are in the normal range for six-membered chelate rings and octahedral coordination at the metal. The dihedral angles between the central ring of the Schiff's base and the phenyl rings are 59° and 71° on one side of the complex and 53° and 85° on the other side. There is thus no conjugation between the three aromatic rings with each ligand unit.

3.6. NMR spectra

The ^1H and ^{13}C NMR spectra of **1**, obtained from a sample dissolved in MeOH-d_4, confirmed the presence

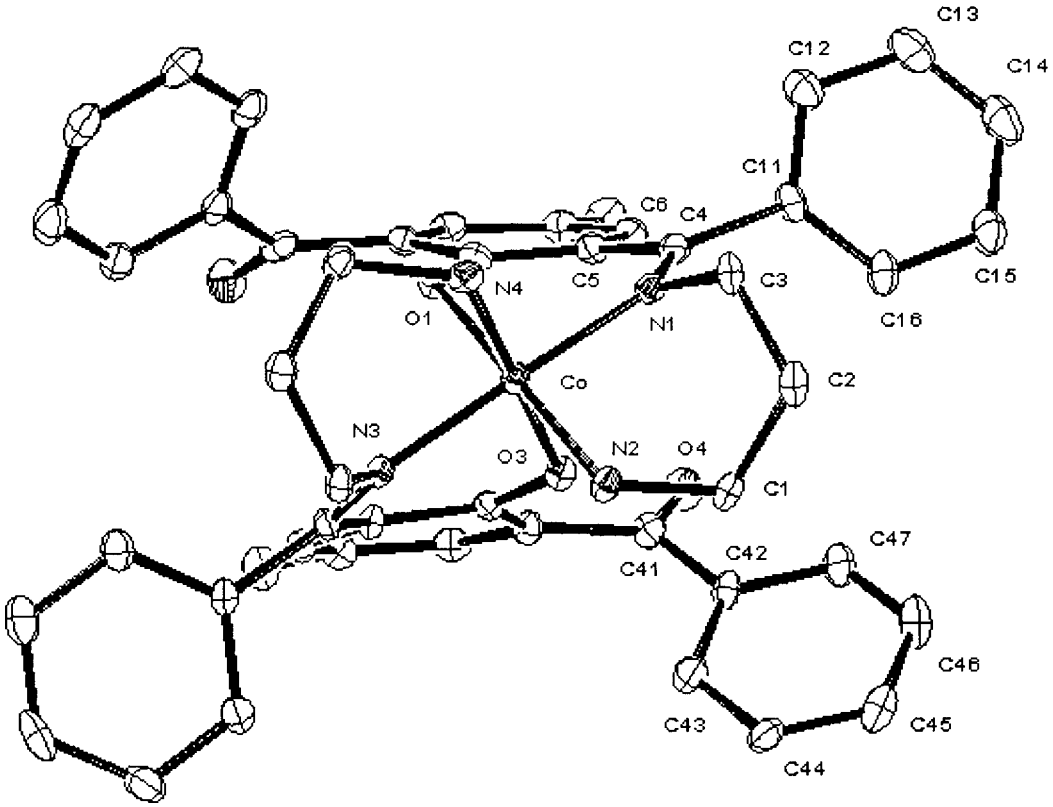


Fig. 3. Another view of the molecular structure of the complex **1**.

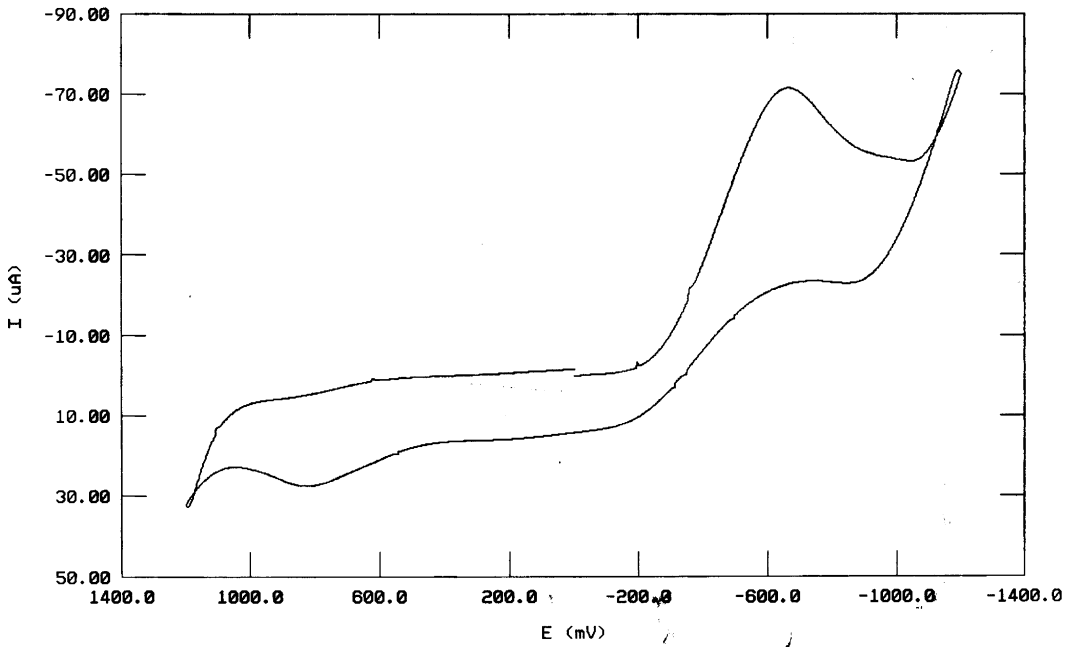


Fig. 4. Cyclic voltammogram of complex **1** (0.1 mM) in MeOH at 200 mV s^{-1}.

of the ion $[CoL_2]^+$. The two ligand fragments, not quite identical in the crystal, appeared to be so in solution, as the ion is freed from packing forces. However, at 298 K, separate signals are obtained for the protons attached to the five carbon atoms of the C^{11}–C^{16} phenyl ring, and separate signals from the six carbon atoms, indicating that rotation of the ring about the C^4–C^{11} bond is slow on the NMR time scale. In contrast, the C^{18}–C^{23} phenyl ring is able to rotate freely. Selective decoupling showed that the signals at δ 7.06 and 7.19 arose from *ortho*-protons at C^{12} and C^{16} attached to the same phenyl ring. A saturation transfer experiment at the highest accessible temperature (336 K) showed that exchange between these protons was beginning to occur on the 1 s^{-1} timescale. As expected, irradiation at the frequency of the protons attached to C^2 caused changes in the signals associated with those attached to C^1 and C^3. Other assignments were made from a 2D double quantum filtered (DQF)-COSY experiment.

Nuclear Overhauser effect (NOE) experiments showed that both the protons attached to C^{12} and those attached to C^{16} are close to the protons on C^6, indicating that the C^{11}–C^{16} and C^5–C^{10} rings are, on average, not far from orthogonal in solution. Further, the protons attached to C^{16} show an NOE at C^2 in the methylene chain and at the *ortho*- protons of the freely rotating ring. These must be those attached to C^{43} and C^{47} in the ligand fragment on the opposite side of the complex. This further confirms that the integrity of the crystal structure is maintained in solution and that rotation of the C^{11}–C^{16} phenyl group is slowed down by the puckering of the $CH_2CH_2CH_2NH_2$ chain. The results suggests that Schiff's bases of the general type discussed here may be sufficiently crowded to make it possible by careful ligand design to fine-tune accessibility to and reducibility of the Co^{III} centre.

3.7. Cyclic voltammetry

The cyclic voltammogram of complex **1** (Fig. 4) shows one irreversible wave at $E_{pc} = -0.66$ to -0.71 V versus the SCE, with the 50–200 mV s^{-1} scan rates. This is attributed to Co(III) to Co(II) reduction. No anodic peak could be observed even after applying a 200 mV s^{-1} scan rate indicating the irreversible nature of the electrode process. The linear plot of the cathodic peak current (I_{pc}) versus the square root of the scan rate ($v^{1/2}$) passes close to the origin, indicating that the electrode reaction is mainly diffusion controlled. An irreversible anodic peak at $E_{pa} = +0.83$–0.97 V could be assigned to the oxidation of the ligand on the electrode surface.

4. Conclusion

The reaction of cobalt(II) chloride with the unsymmetrical Schiff's base, HL (generated in situ) in the presence of traces of air gave a diamagnetic mononuclear cobalt(III) complex. The structure of $[Co(L)_2]^+$ revealed that the NNO-donor sets of two ligand fragments form a distorted octahedral configuration at Co. The dihedral angles between the central ring of the Schiff base and the phenyl rings showed no conjugation, and NMR experiments indicate that rotation of the phenyl ring adjacent to nitrogen is restricted in solution as well as in the solid state. The values of E_{pc} for the

Co(III)/Co(II) couple range from −0.66 to −0.71 V (vs. SCE).

5. Supplementary material

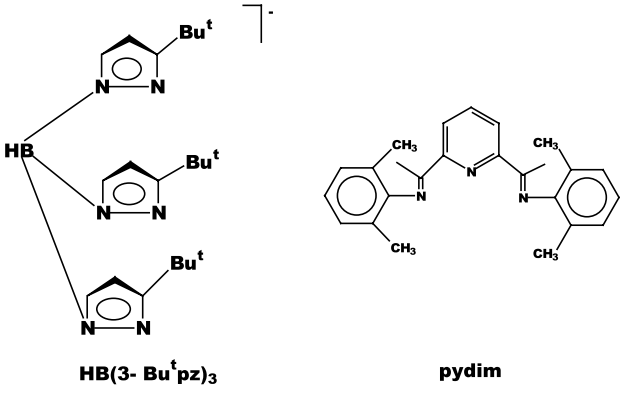
Tables of atomic coordinates and equivalent isotropic displacement parameters, anisotropic displacement parameters for non-hydrogen atoms, hydrogen coordinates and isotropic displacement parameters have been deposited with the Cambridge Crystallographic Data Centre, CCDC Nos. 176395 for $C_{21}H_{16}O_3$ and 176396 for $C_{55}H_{68}ClCoN_6O_6$. Copies of this information may be obtained free of charge from The Director, CCDC, 12 Union Road, Cambridge, CB2 1EZ, UK (fax: +44-1223-336033; e-mail: deposit@ccdc.cam.ac.uk or www: http://www.ccdc.cam.ac.uk).

Acknowledgements

We thank Dr. J.D. Smith, University of Sussex, UK for discussion and Dr. A.G. Avent, University of Sussex, UK, for recording NMR spectra, the Department of Science and Technology, New Delhi, India for financial assistance, the Royal Society of Chemistry, UK, for the award of a JWT Jones Travelling Fellowship to S.K.G., and referees for constructive comments.

References

[1] For reviews see: (a) H. Okawa, H. Furutachi, D.E. Fenton, Coord. Chem. Rev. 174 (1998) 51; (b) J. Nelson, V. Mckee, G. Mckee, G. Morgan, Prog. Inorg. Chem. 47 (1998) 167.
[2] S.A. Komachi, G.A. van Albada, J.G. Haasnoot, H. Kooijman, A.L. Spek, J. Reedijk, Inorg. Chim. Acta 286 (1999) 24.
[3] M. Yammi, H. Furutachi, T. Yokoyama, H. Okawa, Inorg. Chem. 37 (1998) 6832.
[4] C. Fraser, R. Ostrander, A.L. Rheingold, C. White, B. Bosnich, Inorg. Chem. 33 (1994) 324.
[5] C. Svensson, I. Ymen, Cryst. Struct. Commun. 10 (1981) 423.
[6] T. Ama, H. Kawaguchi, T. Yasui, K. Matsumoto, S. Ooi, Bull. Chem. Soc. Jpn. 58 (1985) 2561.
[7] M.S. Bilton, Cryst. Struct. Commun. 11 (1982) 101–109.
[8] S.T. Mandal, L.K. Thomson, M.J. Newlands, A.K. Biswas, B. Adhikari, K. Nag, E.J. Gabe, F.L. Lee, Can. J. Chem. 67 (1989) 662.
[9] B. Adhikari, K.K. Nanda, R. Das, K. Venkatasubramanian, P. Paul, K. Nag, J. Chem. Res. (1992) 2755.
[10] K. Biradha, G.R. Disiraju, H.L. Carrel, A.K. Katz, Acta Crystallogr., Sect. C 52 (1996) 2839.
[11] S.K. Gupta, Y.S. Kushwah, Polyhedron 20 (2001) 2021.
[12] S.K. Gupta, K. Jain, Y.S. Kushwah, Ind. J. Chem. 38A (1999) 506.
[13] S.K. Gupta, P.B. Hitchcock, Y.S. Kushwah, J. Coord. Chem., in press.
[14] W.L.F. Armarego, D.D. Perrin, Purification of Laboratory Chemical, 4th ed., Butterworth–Heinemann, Oxford, 1997.
[15] S.K. Mandal, K. Nag, J. Chem. Soc., Dalton Trans. (1983) 2429.
[16] G.M. Sheldrick, SHELX-97, Program for Solution and Refinement of Crystal Structures, University of Göttingen, Göttingen, Germany, 1997.
[17] A.B.P. Lever, Inorganic Electronic Spectroscopy, 2nd ed., Elsevier, Amsterdam, 1984.
[18] (a) D.C. Ware, W.A. Denny, G.R. Clark, Acta Crystallogr., Sect. C 53 (1997) 1058;
(b) D.C. Ware, W.R. Wilson, W.A. Denny, C.E.F. Rickard, J. Chem. Soc., Chem. Commun. (1991) 1171.
[19] M.C. Weiss, B.B. Bursten, S.-M Peng, V.L. Goedken, J. Am. Chem. Soc. 98 (1976) 8021.
[20] M.M. Harding, H.A. Long, J. Chem. Soc. A (1968) 2554.
[21] B.F. Hoskins, G.A. Williams, Aust. J. Chem. 28 (1975) 2607.
[22] M.J. Barnet, H.C. Freeman, D.A. Buckingham, I-N. Hsu, D. van der Helm, Chem. Commun. (1970) 367.
[23] M.P. Suh, Adv. Inorg. Chem. 44 (1997) 93.



Scheme 1.

with terminal thiocyanate ligands. The planar bonding substituted pyridine ligand pydim was chosen to contrast the tripodal, facial coordination of pyrazolylborate ligands [12]. We also report the syntheses of two lead thiocyanate complexes of less bulky tris(pyrazolyl)borate ligands. Specifically, the syntheses and solid state structure determinations of the following will be discussed: [HB(3-Bu^{t}pz)$_3$]Cd(NCS), [(Bu^{t}Hpz)$_2$Cd(μ-NCS-*N*,*S*)$_2$]$_n$, {[HB(3,5-Me$_2$pz)$_3$]Pb(μ-NCS)}$_2$, {[HB(pz)$_3$]Pb(μ-NCS)}$_n$, [(pydim)Cd(μ-NCS,*N*,*S*)]$_2$[BF$_4$]$_2$, and [(pydim)Pb(NCS)][BF$_4$]. In the two complexes that are monomeric, the terminal thiocyanate ligands are N-bound.

2. Experimental

2.1. General procedure

All operations were carried out under a nitrogen atmosphere using standard Schlenk techniques and a Vacuum Atmospheres HE-493 dry box. All solvents were dried, degassed, and distilled prior to use. The ^{1}H NMR spectra were recorded on a Varian AM300 or AM400 spectrometer using a broad-band probe. Proton chemical shifts are reported in ppm versus internal Me$_4$Si. Mass spectral data were recorded on a VG 70SQ mass spectrometer. Clusters assigned to specific ions show appropriate isotopic patterns as calculated for the atoms present. Infrared spectra were recorded on a Perkin–Elmer 781 spectophotometer. Anhydrous CdCl$_2$ and KSCN were purchased from Aldrich Chemicals. The compounds 2,6-bis[(2,6-dimethylphenylimino)-methyl] pyridine (pydim), 2,6-bis[1-(2,6-dimethylphenyliimno)ethyl]pyridine (pydimMe$_2$) [14], K[HB(pz)$_3$] [1c], K[HB(3,5-Me$_2$pz)$_3$] [1d], Tl[HB(Bu^{t}pz)$_3$] [1g], [Cd$_2$(thf)$_5$][BF$_4$]$_4$ [2b] and [HB(pz)$_3$]PbCl [3a] were prepared according to published methods.

Note! Cadmium and lead compounds and their wastes are extremely toxic and must be handled carefully!!

2.2. {[HB(3-Bu^{t}pz)$_3$]Cd(II)}[BF$_4$]

[Cd$_2$(thf)$_5$][BF$_4$]$_4$ (0.43 g, 0.50 mmol) and Tl[(HB(3-Bu^{t}pz)$_3$] (0.58 g, 1.0 mmol) were dissolved in thf (20 ml) and allowed to stir for 2 h at ambient temperature. The mixture was filtered and the filtrate was evaporated to leave a white solid (0.25 g, 0.43 mmol, 43%); m.p. = 98–103 °C. ^{1}H NMR (acetone-d_6) δ: 7.68, 6.11 (d, d; 3, 3; J = 2.2 Hz; 4,5-H pz); 1.38 (27, s, Bu^t). FAB$^+$ MS: m/z Calc. for {[HB(3-Bu^{t}pz)$_3$]^{113}Cd}$^+$: 495.1966. Found: 495.1980.

2.3. [HB(3-Bu^{t}pz)$_3$]Cd(NCS) (**1**)

[Cd$_2$(thf)$_5$](BF$_4$)$_4$ (0.43 g, 0.50 mmol) and Tl[HB(3-Bu^{t}pz)$_3$] (0.58 g, 1.0 mmol) were charged into a round bottom Schlenk flask and thf (35 ml) was added to the flask via syringe. A white precipitate immediately formed, the mixture was allowed to stir for 2 h at room temperature (r.t.) and then filtered. The volatiles were removed in vacuo leaving a white solid. This solid and KSCN (0.080 g, 1.0 mmol) were dissolved in thf (20 ml). Immediately, a white precipitate formed, this mixture was allowed to stir for 3 h at r.t. then filtered. The solvent was removed in vacuo to leave a white solid (0.10 g, 0.17 mmol, 17%); m.p. = 135–142 °C. X-ray quality crystals were obtained from hot (50°)/cold(0°) toluene. ^{1}H NMR (acetone-d_6) δ: 7.78, 6.22 (3, 3; d, d; J = 2.2 Hz; 4,5-H pz); 1.39 (27, s, Bu^t). IR (νC≡N, Nujol mull, cm^{-1}): 2103. MS, direct ionization: m/z for M^+ Calc. for {[HB(3-Bu^{t}pz)$_3$]^{113}CdNCS}, 549.1732. Found: 549.1739.

2.4. [(3-Bu^{t}Hpz)$_2$Cd(μ-NCS-S,N)$_2$]$_n$ (**2**)

X-ray quality crystals were obtained from an attempted crystallization, from a layered solution of acetone and hexane, of the product produced in the [HB(3-Bu^{t}pz)$_3$]Cd(NCS) preparation. ^{1}H NMR (acetone-d_6), δ: 7.51 (2, br, 5-H pz); 6.09 (2, br, 4-H pz); 1.35 (18, s, Bu^t).

2.5. {[HB(3,5-Me$_2$pz)$_3$]Pb(μ-NCS)}$_2$ (**3**)

PbCl$_2$ (0.25 g, 0.90 mmol) was dissolved in H$_2$O (15 ml) and added to a thf (15 ml) solution of K[HB(3,5-Me$_2$pz)$_3$] (0.30 g, 0.90 mmol). The mixture was stirred for 0.5 h at which time a white precipitate was formed. The mixture was filtered to leave a white solid. KSCN (0.050 g, 0.50 mmol) was added to the filtrate. This solution was allowed to stir for 6 h at r.t. A white precipitate formed and the mixture was filtered. The solvent was removed in vacuo to leave a white solid, (0.16 g, 31%); m.p. = 296–301 °C (dec). X-ray quality crystals were obtained from a layered solution of CH$_2$Cl$_2$ and hexane. ^{1}H NMR (CDCl$_3$) δ: 5.81 (s, 3,

4-H pz); 2.44 (s, 9, CH_3); 2.30 (s, 9, CH_3). IR: (νC≡N, Nujol mull, cm^{-1}): 2060 and 2020. ES^+/MS: Calc. for $\{[HB(3,5\text{-}Me_2pz)_3]^{207}Pb\}^+$, 505.1770. Found: 505.1776. Calc. for $C_{32}H_{44}B_2N_{14}Pb_2S_2$: C, 34.17; H, 3.94. Found: C, 33.85; H, 4.55%.

2.6. $\{[HB(pz)_3]Pb(\mu\text{-}NCS)\}_n$ (**4**)

$[HB(pz)_3]PbCl$ (0.13 g, 0.30 mmol) was dissolved in thf (10 ml) and KSCN (0.030 g, 0.30 mmol) added to this solution. A white precipitate formed as this mixture was stirred for 6 h at r.t. and the solution was filtered. The solvent was removed in vacuo to leave a white solid, (0.080 g, 57%); m.p. = 222–225 °C. Suitable crystals were obtained from a layered solution of CH_2Cl_2 and hexane. ^1H NMR (acetone-d_6) δ: 7.76, 7.53 (3, 3; s, br; 3,5-H pz); 6.12 (3, s, 4-H pz) IR: (νC≡N, Nujol mull, cm^{-1}): 2084, 2045, 2030, 2004. FAB^+ MS: *m/z* Calc. for $\{[HB(pz)_3]^{207}Pb\}^+$, 419.0805. Found: 419.0796.

2.7. $[(pydim)Cd(\mu\text{-}NCS\text{-}S,N)]_2[BF_4]_2$ (**5**)

$[Cd_2(thf)_5](BF_4)_4$ (0.24 g, 0.25 mmol) and pydim (0.18 g, 0.50 mmol) were charged into a round bottom Schlenk flask and thf (20 ml) was added via syringe. The mixture was allowed to stir for 1 h at r.t. and the solvent was removed to leave a yellow solid. This solid (0.15 g) and KSCN (0.050 g, 0.50 mmol) were dissolved in thf (20 ml) and allowed to stir for 3 h at r.t. This mixture was filtered and the volatiles were removed in vacuo to leave a yellow solid (0.18 g, 55%); m.p. = 260–262 °C (dec). Crystals suitable for X-ray analysis were grown from a layered solution of CH_2Cl_2 and hexane. ^1H NMR (acetone-d_6), δ: 9.03 (2, s, H-imino); 8.81 (1, m, 4-H py); 8.56 (2, d, $J = 7.8$, 3,5-H py); 7.14 (6, m, 3,4,5-H ph); 2.26 (12, s, CH_3). IR (νC≡N, Nujol mull, cm^{-1}): 2110, 2079. FAB^+ MS: *m/z* Calc. for $[(pydim)^{113}Cd]^+$ 509.0674. Found: 509.0668.

2.8. $[(pydimMe_2)Pb(NCS)][BF_4]$ (**6**)

$Pb(acac)_2$ (0.10 g, 0.25 mmol) was suspended in thf (10 ml). The mixture was treated with 54% $HBF_4 \cdot Et_2O$ (0.10 ml, 0.50 mmol) and was allowed to stir for 30 min followed by addition of a thf (10 ml) solution of the $pydimMe_2$ ligand (0.090 g, 0.25 mmol) by cannula transfer. The yellow reaction mixture was heated to 70 °C for 1 h. A solution of KSCN (0.040 g, 0.41 mmol) in thf (10 ml) was added to the reaction mixture and allowed to stir for 12 h at r.t. The mixture was filtered and the solvent evaporated to dryness providing a yellow powder (0.14 g, 0.18 mmol, 72%); m.p. = 224–227 °C. Crystals suitable for X-ray analysis were grown from a layered solution of CH_2Cl_2 and hexane. ^1H NMR (acetone-d_6), δ: 8.91 (3, br, 3,4,5-H py); 7.20 (6, br, 3,4,5-H ph); 2.60 (6, s, (CH_3-imino), 2.24 (12, s, CH_3). IR (νC≡N, Nujol mull, cm^{-1}): 2040 br. FAB^+ MS: Calc. for $[(pydimMe_2)^{207}Pb]^+$ 635.1725. Found: 635.1744.

2.9. X-ray crystal determination for **1**, **2**, **3**, **4**, **5** and **6**

Crystal, data collection, and refinement parameters are collected in Table 1. Colorless crystals of **1**, **2**, **3** and **4** and small yellow crystals of **5** and **6** were epoxied onto the end of a thin glass fiber. X-ray intensity data were measured using a Bruker SMART APEX CCD-based diffractometer system using Mo Kα radiation (λ = 0.71073 Å). All unit cells were initially determined based on reflections harvested from a set of three scans measured in orthogonal wedges of reciprocal space. Subsequently, a hemisphere of data was collected with a scan width of 0.3° in ω and an exposure time of 60 s per frame. The first 50 frames were re-collected at the end of data set to monitor crystal decay. The structures were solved by a combination of direct methods and difference Fourier syntheses, and refined by full-matrix least-squares against F^2, using the SHELXTL software package. The final unit cell constants are based upon the refinement of the XYZ centroids. In all structures, hydrogen atoms were placed in calculated positions and refined using a riding model and an empirical absorption correction based on the multiple measurement of equivalent reflections was applied with the program SADABS.

Systematic absences in the data for **1** were consistent with the space groups *Pnma* and $Pna2_1$. After several unsuccessful initial trials in the centrosymmetric space group *Pnma*, the non-centrosymmetric space group $Pna2_1$ was chosen and confirmed by the successful solution and refinement of the structure. Upon successful solution in $Pna2_1$, a check for missing symmetry was performed with the ADDSYM routine in PLATON, which verified the space group choice with a refined absolute structure (Flack) parameter of −0.003(19). All non-hydrogen atoms were refined with anisotropic displacement parameters including the toluene solvent molecule present in the cell. Crystals of **2** were determined to belong to the monoclinic crystal system. Systematic absences in the diffraction data determined that the space group was $P2_1/n$. Compound **3**, $\{[HB(3,5\text{-}Me_2pz)_3]Pb(\mu\text{-}NCS)\}_2 \cdot 1.5CH_2Cl_2$, crystallizes in the orthorhombic crystal system. Examination of the systematic absences in the data set indicated the space groups *Pnma* or $Pna2_1$. A good solution and refinement was obtained in the space group *Pnma*, revealing two $\{[HB(3,5\text{-}Me_2pz)_3]Pb\}^+$ cations related by mirror symmetry, and bridged by 2 inequiv. SCN^- groups. One SCN^- lies in the mirror plane; the second SCN^- is roughly perpendicular to the intervening plane, with the central carbon (C2) in the mirror plane. Due to the incompatibility of the SCN^- anion with a horizontal

Table 1
Crystallographic data for [HB(3-Bu^{t}pz)$_3$]Cd(NCS)·C$_6$H$_5$CH$_3$ (**1**), [(3-Bu^{t}Hpz)$_2$Cd(μ-NCS-*N*,*S*)$_2$]$_n$ (**2**), {[HB(3,5-Me$_2$pz)$_3$]Pb(μ-NCS)}$_2$·1.5CH$_2$Cl$_2$ (**3**), {[HB(pz)$_3$]Pb(μ-NCS)}$_n$ (**4**), [(pydim)Cd(μ-NCS-*N*,*S*)]$_2$[BF$_4$]$_2$ (**5**), and [(pydimMe$_2$)Pb(NCS)][BF$_4$]·2CH$_2$Cl$_2$ (**6**)

	1	**2**	**3**	**4**	**5**	**6**
Empirical formula	$C_{29}H_{42}BCdN_7S$	$C_{16}H_{22}CdN_6S_2$	$C_{33.50}H_{47}B_2Cl_3N_{14}Pb_2S_2$	$C_{10}H_{10}BN_7PbS$	$C_{48}H_{46}B_2Cd_2F_8S_2$	$C_{27}H_{29}BCl_2F_4N_4PbS$
Formula weight (g mol^{-1})	643.97	474.92	1252.32	478.31	1197.47	806.50
Temperature (K)	293(2)	298(2)	293(2)	173(2)	173(2)	293(2)
Crystal system	orthorhombic	monoclinic	orthorhombic	monoclinic	monoclinic	triclinic
Space group	*Pna*2$_1$	*P*2$_1$/*n*	*Pnma*	*P*2$_1$/*c*	*P*2$_1$/*c*	*P*$\bar{1}$
a (Å)	19.684(3)	6.0016(2)	13.971(3)	15.0687(9)	14.884(3)	13.177(4)
b (Å)	16.029(2)	10.2759(3)	22.218(4)	23.3079(14)	11.465(2)	14.677(4)
c (Å)	10.3224(15)	17.4673(5)	14.969(3)	13.4082(8)	15.911(3)	18.478(6)
α (°)	90	90	90	90	90	103.762(6)
β (°)	90	92.2898(16)	90	116.0440(10)	107.843(4)	95.980(6)
γ (°)	90	90	90	90	90	110.748(6)
Volume (Å^3)	3256.9(8)	1076.38(6)	4646.5(14)	4231.0(4)	2584.4(9)	3175.4(17)
Z	4	2	4	12	2	4
Density (Mg m^{-3})	1.313	1.45	1.790	2.253	1.539	1.687
F(000)	1336	480	2412	2664	8556	1568
Crystal size (mm)	0.30 × 0.24 × 0.14	0.10 × 0.10 × 0.5	0.40 × 0.11 × 0.03	0.20 × 0.16 × 0.01	0.40 × 0.40 × 0.04	0.42 × 0.30 × 0.10
Final *R* indices [$I > 2\sigma(I)$] [a]	$R_1 = 0.0318$, $R_2 = 0.0654$	$R_1 = 0.0549$, $wR_2 = 0.1200$	$R_1 = 0.0340$, $wR_2 = 0.0677$	$R_1 = 0.0507$, $wR_2 = 0.1206$	$R_1 = 0.0549$, $wR_2 = 0.1200$	$R_1 = 0.0408$, $wR_2 = 0.0927$

[a] $R_1 = \Sigma||F_o|-|F_c||/\Sigma|F_o|$. $wR_2 = \{\Sigma[w(F_o^2-F_c^2)^2]/\Sigma[w(F_o^2)^2]\}^{1/2}$.
$w = 1/[\sigma^2(F_o^2)+(aP)^2+bP]$, where P is $[2F_c^2+\max(F_o^2, 0)]/3$.

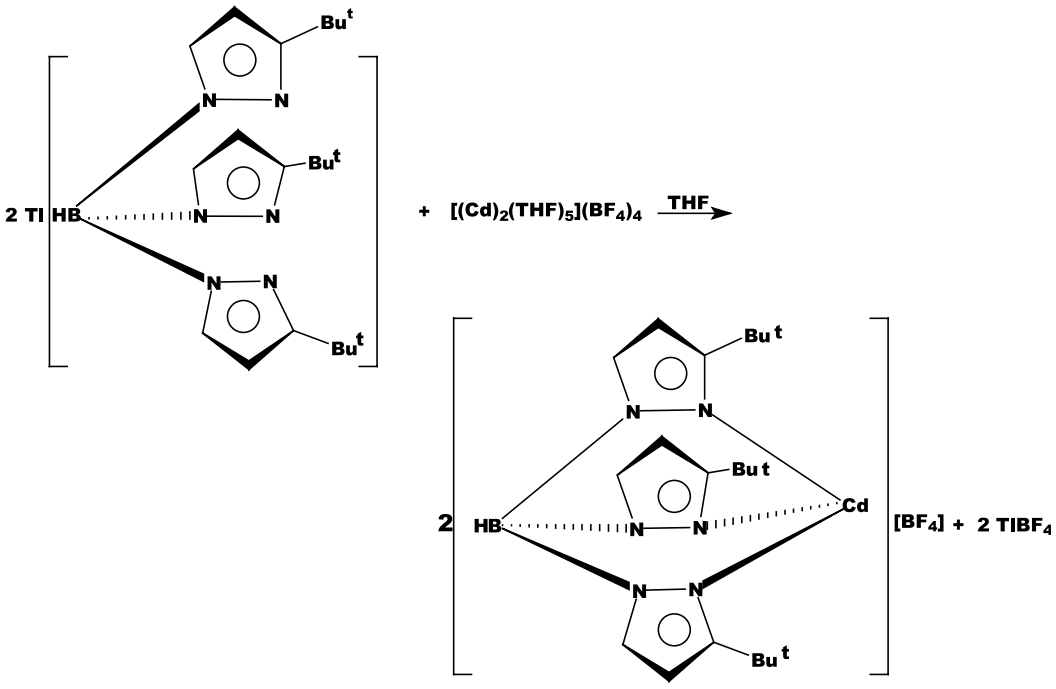
mirror plane, this arrangement results in this perpendicular SCN$^-$ apparently half-occupying two orientations related through the mirror plane, with similar S–C and C–N distances. However, removing the mirror plane relating the two halves of the molecule and refining the structure in *Pna*2$_1$ yielded the same disorder, as well as chemically unreasonable [HB(3,5-Me$_2$pz)$_3$]$^-$ ligand geometry and large correlations between atoms related by symmetry in *Pnma*. Further attempts to remove the disorder by reducing the symmetry even further to monoclinic or triclinic symmetry gave identical results. Therefore, *Pnma* was selected as the correct space group. The similar S2–C2 and C2–N2 distances within the perpendicular SCN$^-$ are an artifact of the disorder. While the displacement ellipsoid of C2 shows elongation along the bond directions, no satisfactory model with C2 off the mirror plane could be found. A total of 1.5 methylene chloride molecules disordered over three positions were located and refined with the aid of three geometrical restraints. Compound **4** crystallizes in the space group *P*2$_1$/*c* as determined from the systematic absences in the intensity data. The asymmetric unit contains three crystallographically inequivalent {[HB(pz)$_3$]Pb}$^+$ cations and three SCN$^-$ counterions and all atoms are on general positions. Crystals of **5** were determined to belong to the monoclinic crystal system. Systematic absences in the diffraction data determined that the space group was *P*2$_1$/c. Compound **6** crystallizes in the triclinic space group *P*$\bar{1}$. The asymmetric unit consists of two [Pb(C$_{25}$H$_{27}$N$_3$)]$^{2+}$ cations, two SCN$^-$ and two BF_4^- counterions, and two CH_2Cl_2 molecules. Comparison of identical reflections measured at the beginning and at the end of the data collection showed an average loss of intensity of 4.1%; a linear decay correction was applied.

All computations were made using SHELXTL NT 5.10 and SADABS software (G. Sheldrick, Bruker AXS, Madison, WI).

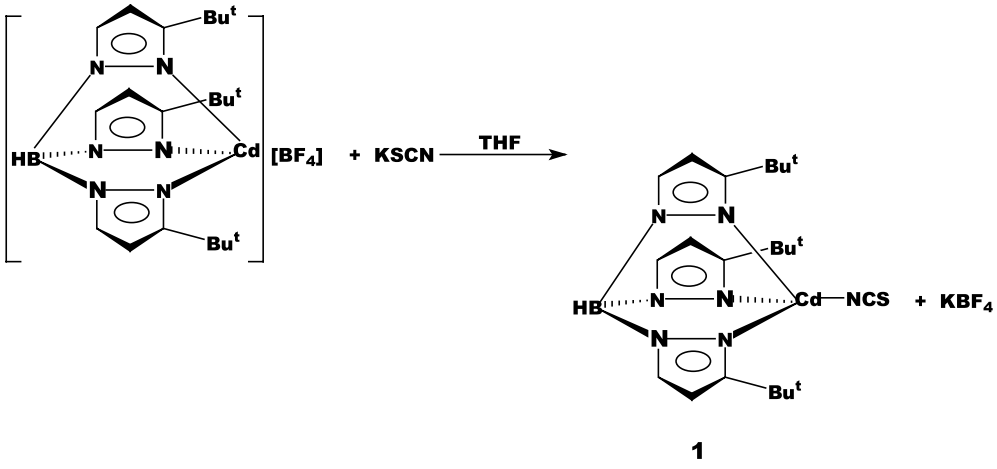
3. Results and discussion

3.1. tris(pyrazolyl)borate chemistry

The direct reaction of $CdCl_2$ with 1 equiv. of Tl[HB(3-Bu^{t}pz)$_3$] and KSCN did not produce the desired [HB(3-Bu^{t}pz)$_3$]Cd(NCS) (**1**) complex. The complex was produced in a two step procedure, starting with the reactive compound [Cd$_2$(thf)$_5$](BF$_4$)$_4$ [2b]. Mixing this compound with two equiv. of Tl[HB(3-Bu^{t}pz)$_3$] produces the intermediate {[HB(3-Bu^{t}pz)$_3$]Cd}[BF$_4$].



This intermediate reacts with potassium thiocyanate to yield [HB(3-Bu^{t}pz)$_3$]Cd(NCS) (**1**).



1

Complex **1** is air stable and is soluble in most common solvents. Infrared analysis shows a strong band at 2103 cm^{-1}, indicating the presence of a N-bound, terminal isothiocyante ligand. Reported CN stretching frequencies for terminal cadmium(II) isothiocyanate are in the range of 2059–2108 cm^{-1} [4b,5].

This arrangement was confirmed by a single crystal X-ray analysis. An ORTEP drawing is shown in Fig. 1 and selected bond angles and distances are shown in Table 2. The cadmium(II) site has a N_4 coordination arrangement in a pseudotetrahedral geometry. The chelate rings restrict the intraligand N–Cd–N angles to an average of 88.6°, with interligand N–Cd–N bond angles averaging 126.2°. The Cd–N–C bond angle of the isothiocyanate ligand is significantly bent at 150.7(3)° and the N–C–S bond angle is nearly linear at 178.9(4)°. The Cd–NCS bond distance is 2.107(3) Å, on the short end of the published ranges of analogous

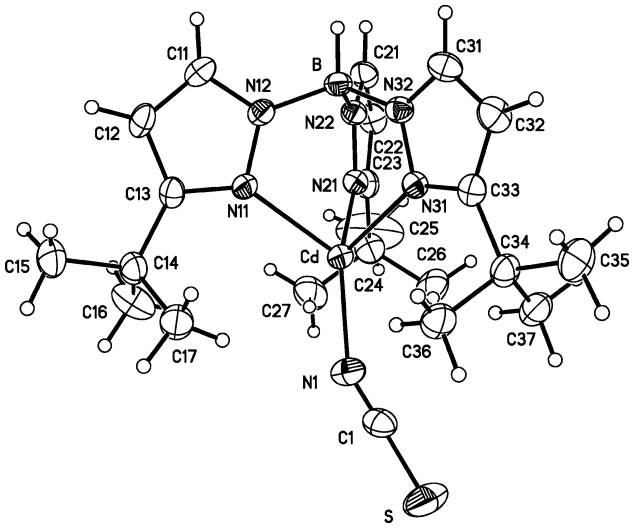


Fig. 1. ORTEP diagram of $[HB(3\text{-}Bu^tpz)_3]Cd(NCS)$ (50% ellipsoids).

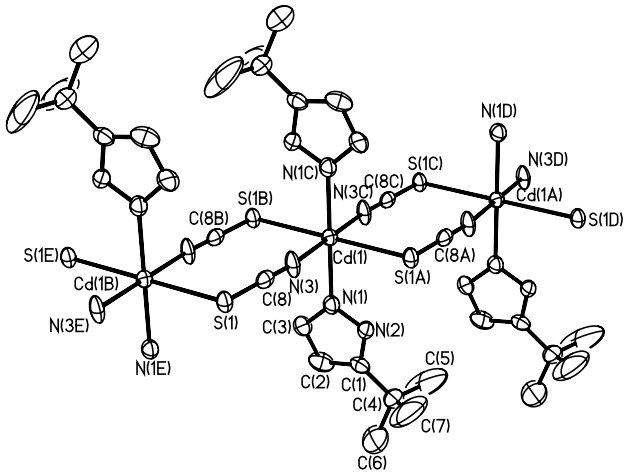


Fig. 2. ORTEP diagram of $[(3\text{-}Bu^tHpz)Cd(\mu\text{-}NCS\text{-}N,S)]_n$ (50% ellipsoids).

Table 2
Selected bond distances (Å) and bond angles (°) for $[HB(3\text{-}Bu^tpz)_3]Cd(NCS)$ (**1**)

Bond distances			
Cd–N(1)	2.107(3)	N(21)–N(22)	1.360(3)
Cd–N(11)	2.2234(19)	N(31)–N(32)	1.364(4)
Cd–N(21)	2.219(2)	N(1)–C(1)	1.093(4)
Cd–N(31)	2.2302(18)	C(1)–S	1.612(4)
N(11)–N(12)	1.364(3)		
Bond angles			
N(1)–Cd–N(11)	128.87(12)	N(11)–Cd–N(21)	87.82(11)
N(1)–Cd–N(21)	126.57(11)	N(21)–Cd–N(31)	90.10(12)
N(1)–Cd–N(31)	123.22(13)	C(1)–N(1)–Cd	150.7(3)
N(11)–Cd–N(31)	87.97(7)	N(1)–C(1)–S	178.9(4)

Table 3
Selected bond distances (Å) and bond angles (°) for $[(3\text{-}Bu^tHpz)Cd(\mu\text{-}NCS\text{-}N,S)]_n$ (**2**)

Bond distances			
Cd(1)–N(1)	2.286(9)	N(3)–C(8)	1.131(13)
Cd(1)–N(3)	2.309(10)	C(8)–S(1)	1.650(13)
Cd(1)–S(1A)	2.762(2)		
Bond angles			
N(1)–Cd(1)–N(1C)	180.0(4)	N(3)–Cd(1)–S(1B)	88.4(2)
N(1)–Cd(1)–S(1A)	92.4(2)	N(3)–Cd(1)–N(3C)	180.0(4)
N(1)–Cd(1)–S(1B)	87.5(2)	S(1A)–Cd(1)–S(1B)	180.0(9)
N(3)–Cd(1)–N(1)	88.5(4)	Cd(1)–N(1)–C(3)	132.1(8)
N(3)–Cd(1)–N(1C)	91.5(4)	Cd(1)–S(1)–C(8)	101.6(3)
N(3)–Cd(1)–(S1A)	91.5(4)	N(3)–C(8)–S(1)	177.5(9)

distances for terminal CdNCS groups [4,5,13]. The Cd–N bond distances for the $[HB(3\text{-}Bu^tpz)_3]^-$ ligand are all very similar and average 2.22 Å.

As expected, the sterically demanding 3-*tert*-butyl groups enforce the formation of a tetrahedral, monomeric complex, the first 4-coordinate cadmium(II)-thiocyanate complex to be structurally characterized. In contrast, many cadmium(II)-thiocyanate complexes form intricate networks with bridging thiocyante ligands coordinated to cadmium forming polymeric chains, 2-D sheets and 3-D extended lattices [4,7,14–16].

In our first attempt to crystallize compound **1** from a layered solution of acetone and hexane, the compound we obtained was a decomposition product that was shown by X-ray crystallography to be a polymer, $[(3\text{-}Bu^tHpz)_2Cd(\mu\text{-}NCS)_2]_n$ (**2**). Fig. 2 shows the ORTEP diagram and bond distances and angles are shown in Table 3. The cadmium(II) is six-coordinate, bonding to two *tert*-butyl pyrazole rings located in the axial positions and four doubly bridging thiocyanate ligands in equatorial positions forming a CdN_4S_2 octahedral arrangement. The cadmium(II) is located on an inversion center. The two pyrazole groups coordinate to cadmium with a Cd–N bond distance of 2.286(9) Å, while the N-coordinated SCN^- groups have a Cd–N distance 0.02 Å longer at 2.309(10) Å. The Cd–S distance is normal at 2.762(2) Å. The SCN^- groups are nearly linear at 177.5(9)°. The atoms of the doubly bridging $(\mu\text{-}NCS\text{-}N,S)^-$ groups and the two cadmium(II) form an eight member ring that closely resembles that observed in $[Cd(NCS)_2(CH_3C_5H_4N)_2]_n$ [17], $Cd(NCS)_2\{(C_6H_5CH_2)_2NH\}_2$ [18], and $[Cd(NCS)_2(\text{iso-nicotinamide})_2]$ [19].

Multiple attempts were made to synthesize the tetrahedral lead(II) compound analogous to **1** with the bulky $[HB(3\text{-}Bu^tpz)_3]^-$ ligand, but this complex could not be prepared. The tetrahedral enforcer character of this ligand apparently prevents the formation of a four-coordinate lead(II) complex with a stereochemically active lone pair. The failure to prepare the lead(II) analog of **1** clearly shows the influence of the lone pair.

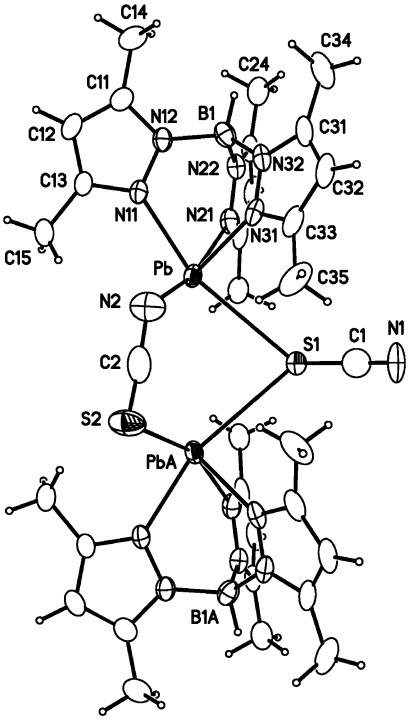
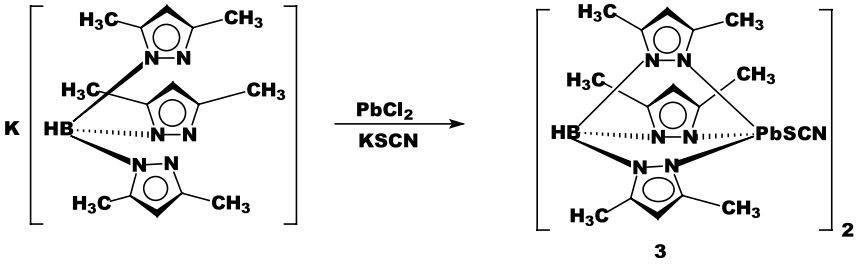


Fig. 3. ORTEP diagram of $\{[HB(3,5\text{-}Me_2pz)_3]Pb(\mu\text{-}NCS)\}_2$ (50% ellipsoids).

In contrast, two new lead(II) compounds with less sterically hindered ligands were prepared. The reaction of equimolar amounts of $PbCl_2$, $K[HB(3,5\text{-}Me_2pz)_3]$ and KSCN in thf yields $\{[HB(3,5\text{-}Me_2pz)_3]Pb(\mu\text{-}NCS)\}_2$ (**3**).

Table 4
Selected bond distances (Å) and bond angles (°) for $\{[HB(3,5\text{-}Me_2pz)_3]Pb(\mu\text{-}NCS)\}_2$ (**3**)

Bond distances			
Pb–S(1)	3.3277(16)	PbA–S(2)	3.326(5)
Pb–N(2)	2.540(14)	S(1)–C(1)	1.673(11)
Pb–N(11)	2.386(4)	S(2)–C(2)	1.394(5)
Pb–N(21)	2.436(5)	C(1)–N(1)	1.079(11)
Pb–N(31)	2.381(5)	C(2)–N(2)	1.378(15)
Pb···Pb(A)	4.2361(9)		
Bond angles			
N(11)–Pb–N(2)	89.2(4)	N(2)–Pb–S(1)	105.2(3)
N(21)–Pb–N(2)	162.5(4)	C(2)–N(2)–Pb	124.2(10)
N(31)–Pb–N(2)	89.6(4)	C(1)–S(1)–Pb	121.3(2)
N(11)–Pb–N(21)	76.30(15)	C(1)–S(1)–Pb(A)	121.3(2)
N(11)–Pb–N(31)	77.79(14)	C(2)–S(2)–Pb(A)	85.5(4)
N(21)–Pb–N(31)	78.08(15)	Pb–S(1)–Pb(A)	79.06(5)
N(11)–Pb–S(1)	161.79(11)	S(2)–Pb(A)–S(1)	109.98(9)
N(21)–Pb–S(1)	87.50(11)	N(1)–C(1)–S(1)	180.0(9)
N(31)–Pb–S(1)	90.93(10)	N(2)–C(2)–S(2)	176.9(11)



3

This compound is air-stable and soluble in halocarbons, thf, and slightly soluble in aromatic solvents. It has CN stretching frequencies at 2060 and 2020 cm^{-1} indicating bridging SCN^- groups.

Fig. 3 shows the ORTEP diagram of the cation in **3** and selected bond distances and angles are shown in Table 4. The solid state structure of **3** is dimeric with an unusual structure containing both μ-NCS-*S*,*N* and μ-NCS-*S*,*S* bridging SCN^- ligands. The μ-NCS-*S*,*S* ligand is in the mirror plane located between the two metal centers and bridges them through sulfur with relatively long Pb–S bond distance of 3.3277(16) Å [4c,11,20]. The other is in a normal bridging μ-NCS-*S*,*N* bonding one metal through nitrogen and the other through sulfur, but due to the incompatibility of this orientation of the SCN^- anion with a horizontal mirror plane, this perpendicular SCN^- half-occupies two orientations related through the mirror plane. The Cd–N bond distances for the $[HB(3,5\text{-}Me_2pz)_3]^-$ ligand are all similar with a range of 2.381(5)–2.436(5) (average 2.40 Å). Overall, the structure about each lead(II) can be considered octahedral with three sites occupied by nitrogen donor atoms from the $[HB(3,5\text{-}Me_2pz)_3]^-$ ligand with N–Pb–N bond angles restricted by the chelate rings to an average of 77.4°. The sulfur of the symmetrically bridged SCN^- occupies a fourth site while the N and S from the disordered SCN^- share the fifth site.

The remaining octahedral site is generally attributed to a stereoactive lone pair on the lead(II) center. In

Table 5
Selected bond distances (Å) and bond angles (°) for $[HB(pz)_3]Pb(\mu\text{-}NCS)]_n$ (**4**)

Bond distances			
Pb(1)–N(111)	2.486(10)	Pb(3)–N(331)	2.410(11)
Pb(1)–N(121)	2.494(11)	Pb(3)–N(311)	2.421(11)
Pb(1)–N(131)	2.524(10)	Pb(3)–N(321)	2.455(10)
Pb(1)–N(1)	2.793(13)	Pb(3)–N(3)	2.802(12)
Pb(1)–N(2)	2.798(13)	Pb(3)–S(3A)	3.251(4)
Pb(1)–S(1)A	3.134(4)	C(1)–N(1)	1.178(18)
Pb(2)–N(211)	2.508(10)	S(1)–C(1)	1.588(16)
Pb(2)–N(221)	2.448(9)	C(2)–N(2)	1.108(16)
Pb(2)–N(231)	2.460(10)	S(2)–C(2)	1.650(16)
Pb(2)–S(1)	3.015(4)	C(3)–N(3)	1.137(15)
S(3)–C(3)	1.644(13)		
Bond angles			
N(111)–Pb(1)–N(121)	73.0(3)	N(211)–Pb(2)–N(221)	78.8(3)
N(111)–Pb(1)–N(131)	78.6(3)	N(211)–Pb(2)–N(231)	75.9(3)
N(121)–Pb(1)–N(131)	74.7(3)	N(221)–Pb(2)–N(231)	74.8(3)
N(111)–Pb(1)–N(1)	84.1(4)	N(211)–Pb(2)–S(1)	157.6(2)
N(121)–Pb(1)–N(1)	145.2(4)	N(221)–Pb(2)–S(1)	97.2(2)
N(131)–Pb(1)–N(1)	126.6(4)	N(231)–Pb(2)–S(1)	81.8(3)
N(111)–Pb(1)–N(2)	97.5(3)	N(311)–Pb(3)–N(321)	75.3(3)
N(121)–Pb(1)–N(2)	78.5(3)	N(311)–Pb(3)–N(331)	77.6(4)
N(131)–Pb(1)–N(2)	152.9(3)	N(321)–Pb(3)–N(331)	78.5(3)
N(111)–Pb(1)–S(1A)	160.4(3)	N(311)–Pb(3)–S(3A)	88.9(2)
N(121)–Pb(1)–S(1A)	94.9(3)	N(321)–Pb(3)–S(3A)	162.0(2)
N(131)–Pb(1)–S(1A)	83.3(2)	N(331)–Pb(3)–S(3A)	90.0(3)
N(1)–Pb(1)–S(1A)	113.3(3)	N(311)–Pb(3)–N(3)	87.6(3)
N(2)–Pb(1)–S(1A)	95.1(2)	N(321)–Pb(3)–N(3)	94.2(3)
Pb(1)–S(1A)–Pb(2A)	152.24(14)	N(331)–Pb(3)–N(3)	164.6(4)

general, it is well known that in higher coordinate lead structures, bonds adjacent to the presumed location of the lead(II) lone pair are longer than bonds remote from the lone pair [21]. The structure of **3** is very unique in that the Pb–N bonds of the $[HB(3,5\text{-}Me_2pz)_3]^-$ ligand adjacent to the open site are only 0.03 Å longer, on average, than the *trans* Pb–N bond. For comparison, the three Pb–N bonds adjacent to the open site in the

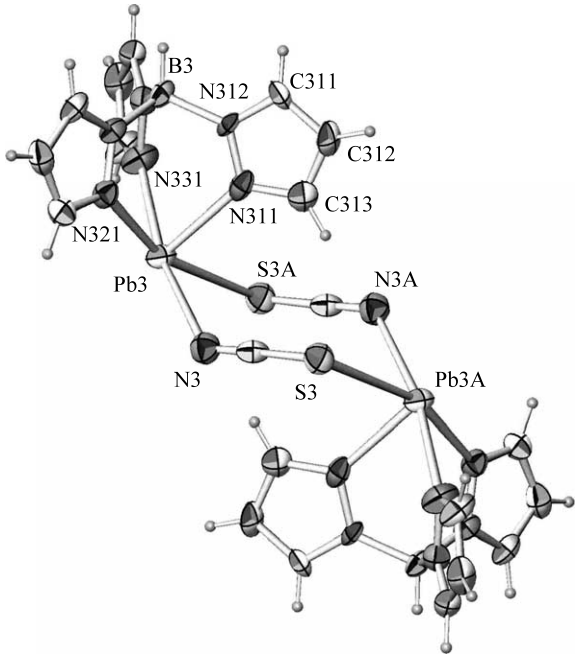


Fig. 5. $\{[HB(pz)_3]Pb(3)(\mu\text{-}NCS\text{-}N,S)\}_2$ units in $\{[HB(pz)_3]Pb(\mu\text{-}NCS)\}_n$.

distorted structure of $[HB(pz)_3]_2Pb$ are 0.24 Å longer, on average, than the *trans* Pb–N bonds [3a]. In addition, the nitrogen atom of the SCN^- ligand in the mirror plane has long range interactions at 3.161(5) Å with both lead(II) centers of an adjacent dimeric unit in the area of this open, sixth site, an unlikely interaction if substantial electron density from the lone pair on lead(II) were present. These results support calculations that indicate that in distorted structures of lead(II) the amount of mixing of the p orbital into the lone pair orbital is small [3g].

The reaction of $[HB(pz)_3]PbCl$ and KSCN in equimolar amounts in thf yields $\{[HB(pz)_3]Pb(\mu\text{-}NCS)\}_n$ (**4**).

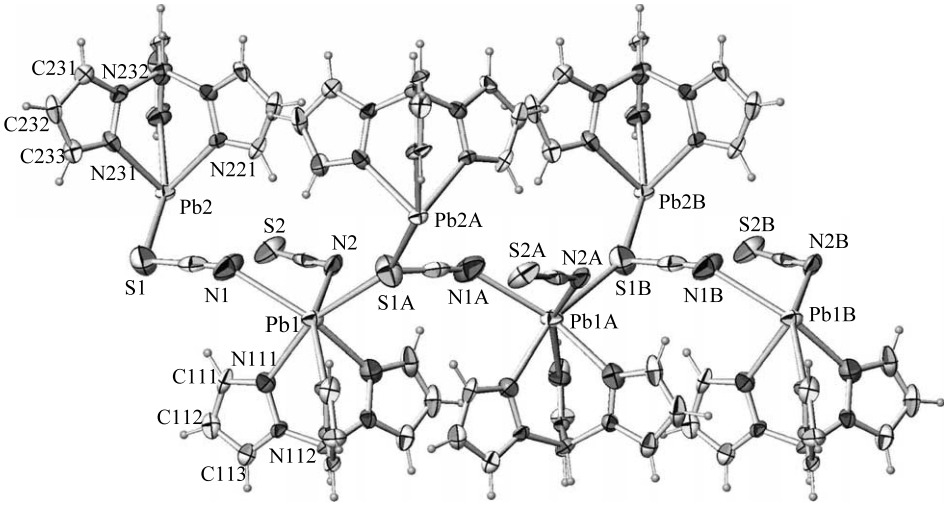


Fig. 4. Diagram of the polymer chain formed by Pb(1) and Pb(2) in $\{[HB(pz)_3]Pb(\mu\text{-}NCS)\}_n$.

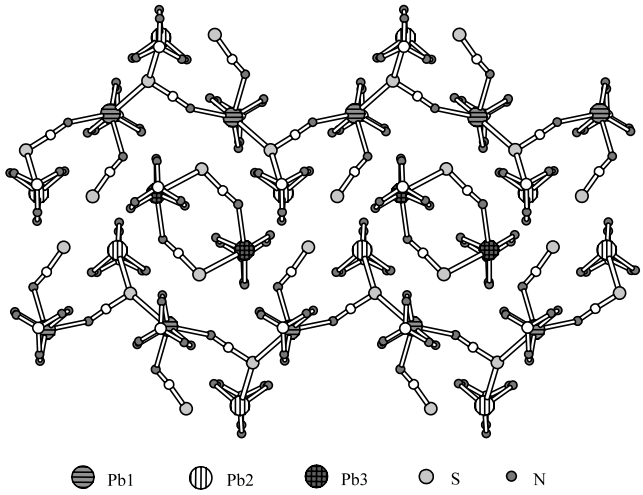


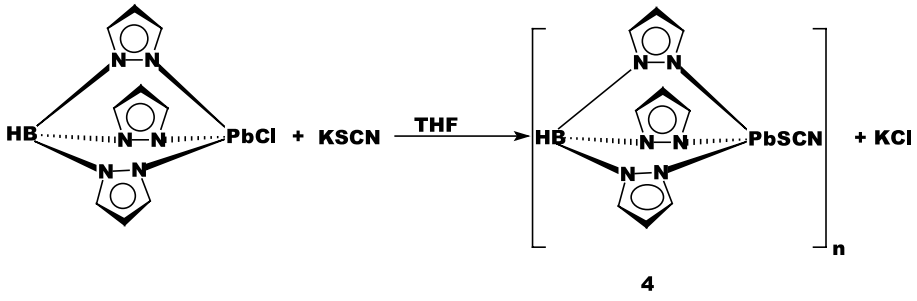
Fig. 6. Total arrangement of the three types of lead(II) in $\{[HB(pz)_3]Pb(\mu\text{-}NCS)\}_n$ viewed perpendicular to the view in Figs. 4 and 5. Hydrogen atoms have been omitted for clarity.

rings, Fig. 5, with the two lead units on each side of the sandwich array.

Shown in Fig. 6 is a combined view perpendicular to the view in Figs. 4 and 5. The $\{[HB(pz)_3]Pb(3)(NCS)\}_2$ units are surrounded by two of the infinite chains formed by Pb(1) and Pb(2). There are secondary interactions between the two units, most notably between the bridging N(3) of the dimeric Pb(3) units and Pb(2) at 2.996 Å. There are also π–π stacking interactions between the pyrazolyl groups attached to Pb(1) along the chain and between alternate Pb(2) and Pb(3) pyrazolyl groups attached parallel to this chain ranging from 3.50 to 3.69 Å. Typical interplanar distances for π–π interactions of aromatic groups range from 3.3 to 3.8 Å [22].

3.2. 2,6-bis(imino)pyridine chemistry

Using a method similar to the preparation of the tris(pyrazolyl)borate compound **1**, a new thiocyanate complex of the pydim ligand is prepared starting with



4

This compound is air-stable and soluble in halocarbons, thf, and slightly soluble in some aromatic solvents. It has CN stretching frequencies at 2084, 2045, 2030, 2004 cm^{-1} indicating a complicated bridging arrangement of the SCN^- groups.

The solid state structure was solved crystallgraphically and selected bond distances and angles are shown in Table 5. The structure of this complex is a complicated infinite 2-D layered array in which $\{[HB(pz)_3]Pb\}^+$ groups sandwich a layer of SCN^- ligands with the lead(II) centers oriented toward them. There are three independent $\{[HB(pz)_3]Pb(NCS)\}^+$ units. As shown in the lower part of Fig. 4, $\{[HB(pz)_3]Pb(1)\}^+$ units form a chain connected by $(\mu\text{-}SCN\text{-}S,N)^-$ ligands. There is also a terminal N-bound SCN^- making Pb(1) six-coordinate. The bridging SCN^- groups are also linked through sulfur to the $\{[HB(pz)_3]Pb(2)\}^+$ units on the other side of the sandwich array. The $\{[HB(pz)_3]Pb(3)\}^+$ units are in a centrosymmetric dimeric arrangement with end-on bridging $(\mu\text{-}SCN\text{-}N,S)^-$ ligands forming eight member

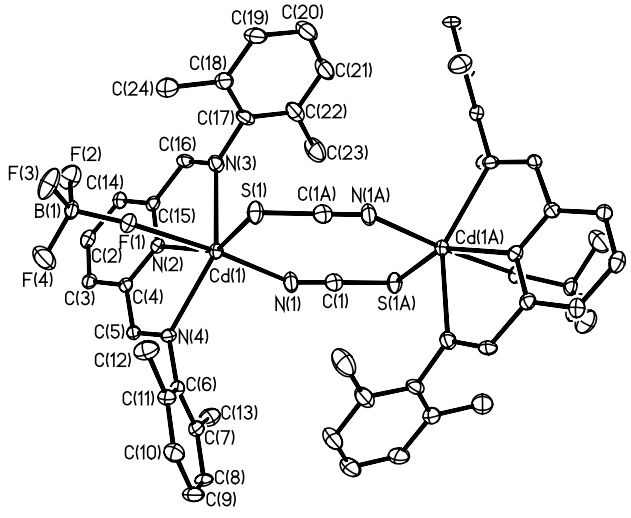


Fig. 7. ORTEP diagram of $[(pydim)Cd(\mu\text{-}NCS\text{-}N,S)]_2[BF_4]_2$ (50% ellipsoids)

Table 6
Selected bond distances (Å) and bond angles (°) for [(pydim)Cd(μ-NCS-*N*,*S*)]$_2$[BF$_4$]$_2$ (**5**)

Bond distances			
Cd(1)–N(1)	2.246(6)	N(1)–C(1)	1.155(8)
Cd(1)–N(2)	2.256(5)	C(1)–S(1)	1.667(7)
Cd(1)–N(3)	2.452(5)	Cd(1)–F(1)	2.544(4)
Cd(1)–N(4)	2.448(5)	Cd(1)–S(1)	2.5551(17)
Bond angles			
N(1)–Cd(1)–N(2)	108.92(19)	N(4)–Cd(1)–S(1)	123.55(12)
N(1)–Cd(1)–N(3)	100.4(2)	S(1)–Cd(1)–F(1)	78.0(9)
N(1)–Cd(1)–N(4)	94.51(19)	N(1)–Cd(1)–F(1)	171.71(18)
N(2)–Cd(1)–N(3)	69.6(17)	N(2)–Cd(1)–F(1)	77.07(15)
N(2)–Cd(1)–N(4)	70.63(17)	N(3)–Cd(1)–F(1)	86.95(15)
N(3)–Cd–N(4)	140.15(16)	N(4)–Cd(1)–F(1)	81.94(15)
N(1)–Cd(1)–S(1)	98.0(15)	N(1)–C(1)–S(1)	178.9(6)
N(2)–Cd(1)–S(1)	148.87(13)	Cd(1)–S(1)–C(1)	99.2(2)
N(3)–Cd(1)–S(1)	90.78(13)	Cd(1)–N(1)–C(1)	156.35(5)

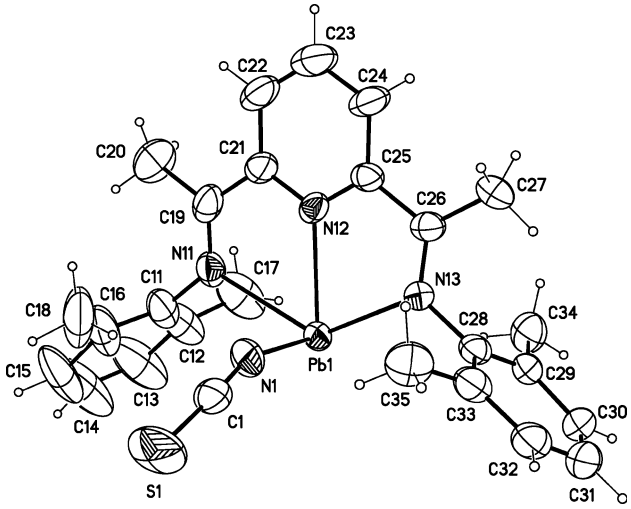
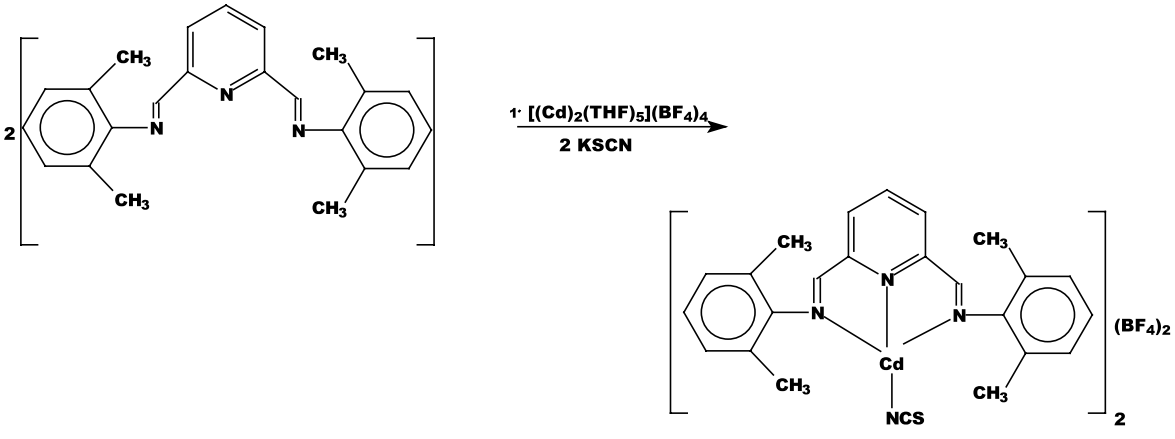


Fig. 8. ORTEP diagram of [(pydimMe$_2$)Pb(1)(NCS)][BF$_4$] (50% ellipsoids).

[Cd$_2$(thf)$_5$][BF$_4$]$_4$. This starting material is treated first with the pydim ligand followed by potassium thiocyanate resulting in the formation of [(pydim)Cd(μ-NCS-*S*,*N*)]$_2$[BF$_4$]$_2$ (**5**).

making the overall structure a dimer. The three nitrogen atoms of the planar pyridine ligand occupy three sites in a meridional arrangement, but the intrinsic bite angle of



5

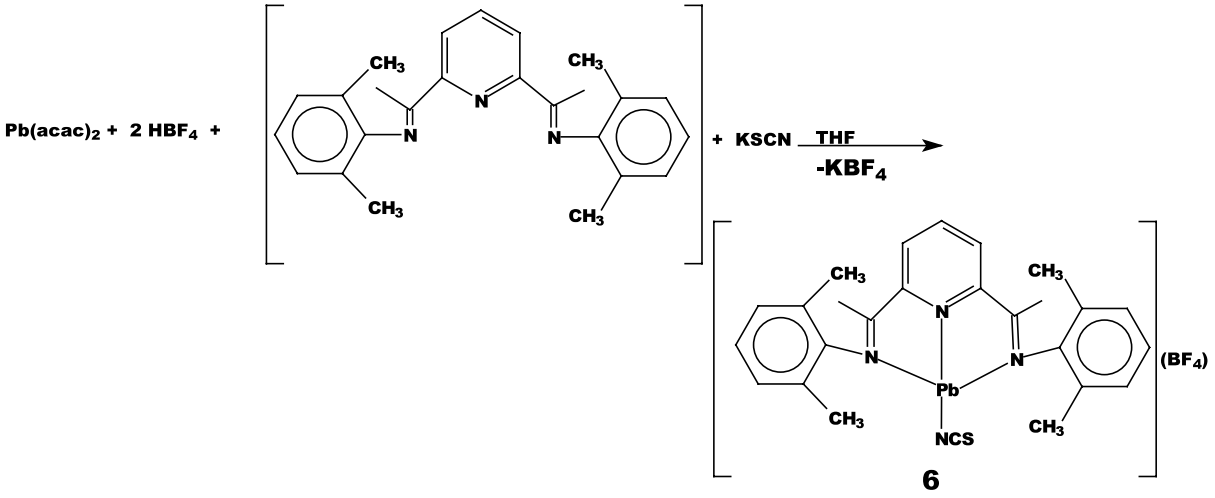
This complex is air-stable in the solution and solid states. It is soluble in acetone, CH_2Cl_2, and chloroform. The infrared spectrum shows CN stretching frequencies of 2078 and 2110 cm^{-1}, indicating that the SCN$^-$ ligands are in bridging positions [5,11].

X-ray crystallography shows that the complex is a dimer. Fig. 7 shows an ORTEP drawing of **5**, and selected bond distances and angles are shown in Table 6. The environment about the cadmium(II) is best described as a distorted octahedron. It is strongly bonded by five donor atoms, with the two bridging thiocyanate groups

the ligand coupled with the large size of the cadmium(II) force a significant distortion from an octahedral arrangement with the *trans* N–Cd–N bond angle of 140.15(16)°. The Cd–N(py) bond (2.256(5) Å) is significantly shorter than the Cd–N(imino) bonds (average 2.45 Å). The bridging SCN$^-$ groups form a N–Cd–S angle much greater than 90° at 123.55(12)° and the SCN$^-$ ligands are nearly linear at 178.9(6)°. The Cd–NCS bond distance is 2.246(6) Å and the Cd–SCN bond distance is 2.5551(17) Å, both typical for this bridging ligand forming an eight membered ring with the two

cadmium(II) [10,14–16]. Within the ring, the Cd(1)–N(1)–C(1) bond angle of 156.35(5)° is much larger than the Cd(1)–S(1)–C(1) bond angle of 99.2(2)°. The sixth coordination site is occupied by a weak interaction from a fluorine of the BF_4^- group.

An analogous lead(II) isothiocyanide complex was synthesized using similar chemistry as outlined in the cadmium synthesis using the pydimMe_2 ligand. In this reaction, $Pb(acac)_2$ was treated with two equiv. of tetrafluorohydroboric acid followed by one equiv. of pydimMe_2 and KSCN to yield a tetra-coordinate lead(II) complex [(pydimMe_2)Pb(NCS)][BF_4] (**6**).



6

This moderately high melting solid compound is air-stable and soluble in halocarbons and acetone. The CN stretching frequency is a broad band centered at 2040 cm^{-1}.

The solid state structure was determined by X-ray crystallography. There are two independent cations in the structure, Fig. 8 shows an ORTEP drawing for one of those, Pb(1), and Table 7 shows the bond angles and distances for both. The primary structures of both cations are similar and are four-coordinate monomeric arrangements. The geometry about lead(II) is irregular, with the N-bound SCN^- ligand oriented basically perpendicular to the N_3Pb plane formed by the donor atoms of the pydimMe_2 ligand and lead(II). The planes of the phenyl rings are also oriented essentially orthogonal to this plane. The Pb–NCS bond distances are short, as would be expected for the low coordinate number for lead(II) of four, at 2.275(7) Å for Pb(1) and 2.333(7) Å for Pb(2). Published Pb–NCS bond distances range from 2.4 to 2.8 Å [11]. The Pb–N–C bond angles are 152.6(7)° and 156.0(7)° while the N–C–S bond angles are nearly linear. In contrast to the cadmium complex **5** and other structures of the pydim ligand [12b], the Cd–N(py) bond (2.466 (6) Å) for Pb(1) is actually longer than one of the Cd–N(imino) bond distances (2.456(6) Å) and only slightly shorter than the other (2.522(6) Å). While the Cd–N(py) bond distance (2.466(5) Å) for Pb(2) is shorter than the average of the Cd–N(imino) bond distances (2.54 Å), the difference is much less than the 0.2 Å distance commonly observed [12]. As expected for the larger size of lead(II) compared with cadmium(II), the three nitrogen atoms of the planar pyridine ligand form even smaller N–Pb–N bond angles with the *trans* N(11)–Pb(1)–N(13) bond angles of only 129.1(2)° for Pb1 and 129.6(2)° for Pb(2).

4. Conclusions

We have prepared and characterized several cadmium(II) and lead(II) thiocyanate complexes containing either tris(pyrazolyl)borate ligands or neutral 2,6-pyridyl-diimine ligands and one thiocyanate ligand per metal. Complex **1**, [HB(3-Bu^{t}pz)$_3$]Cd(NCS), is the first 4-coordinate cadmium(II) isothiocyanate complex to be structurally characterized and contains a short Cd–NCS bond distance (2.107(3) Å). An analogous complex of lead(II) could not be synthesized. It appears that the tetrahedral enforcer character of this ligand prevents the formation of a four-coordinate lead(II) complex with a stereochemically active lone pair and, apparently, a tetrahedral complex isostructural with **1** is energetically unfavorable. The use of less sterically demanding tris(pyrazolyl)borate ligands allowed the preparation

Table 7
Selected bond distances (Å) and bond angles (°) for [(pydim-Me_2)Pb(NCS)][BF_4] (**6**)

Bond distances (*molecule 1*)			
Pb(1)–N(1)	2.275(7)	N(11)–C(19)	1.269(11)
Pb(1)–N(11)	2.456(6)	N(12)–C(21)	1.342(9)
Pb(1)–N(12)	2.466(6)	N(12)–C(25)	1.330(9)
Pb(1)–N(13)	2.522(6)	N(13)–C(26)	1.275(8)
N(1)–C(1)	1.110(9)	N(13)–C(28)	1.436(9)
N(11)–C(11)	1.455(13)	C(1)–S(1)	1.623(9)
Bond angles			
N(1)–Pb(1)–N(11)	83.9(2)	C(1)–N(1)–Pb(1)	152.6(7)
N(1)–Pb(1)–N(12)	86.0(2)	C(11)–N(11)–Pb(1)	116.7(6)
N(1)–Pb(1)–N(13)	86.2(2)	C(19)–N(11)–Pb(1)	119.5(6)
N(11)–Pb(1)–N(12)	64.7(2)	C(21)–N(12)–Pb(1)	119.5(6)
N(11)–Pb(1)–N(13)	129.1(2)	C(25)–N(12)–Pb(1)	119.8(4)
N(12)–Pb(1)–N(13)	64.96(19)	C(26)–N(13)–Pb(1)	120.0(5)
C(28)–N(13)–Pb(1)	119.3(4)	N(1)–C(1)–S(1)	176.4(9)
Bond distances (*molecule 2*)			
Pb(2)–N(2)	2.333(7)	Pb(2)–N(22)	2.466(5)
Pb(2)–N(23)	2.509(5)	Pb(2)–N(21)	2.577(6)
C(2)–N(2)	1.150(9)	C(2)–S(2)	1.604(8)
C(41)–N(21)	1.432(10)	C(49)–N(21)	1.266(9)
C(51)–N(22)	1.345(9)	C(55)–N(22)	1.325(9)
C(56)–N(23)	1.291(8)	C(58)–N(23)	1.430(10)
Bond angles			
N(2)–Pb(2)–N(21)	90.8(2)	C(49)–N(21)–Pb(2)	119.9(5)
N(2)–Pb(2)–N(22)	91.2(2)	C(51)–N(22)–Pb(2)	119.5(6)
N(2)–Pb(2)–N(23)	85.8(2)	C(55)–N(22)–Pb(2)	118.6(5)
N(22)–Pb(2)–N(21)	64.0(2)	C(56)–N(23)–Pb(2)	118.7(5)
N(22)–Pb(2)–N(23)	65.8(2)	C(58)–N(23)–Pb(2)	121.3(5)
C(2)–N(2)–Pb(2)	156.0(7)	N(23)–Pb(2)–N(21)	129.6(2)
C(41)–N(21)–Pb(2)	119.7(4)	N(2)–C(2)–S(2)	178.0(7)

of two interesting new [tris(pyrazolyl)borate]Pb(NCS) complexes. The use of the 3,5-dimethyl substituted ligand produces {[$HB(3,5\text{-}Me_2pz)_3$]Pb(μ-NCS)}$_2$ that has a dimeric structure with both μ-NCS-*S*,*N* and μ-NCS-*S*,*S* bridging SCN^- ligands. The parent ligand produces {[$HB(pz)_3$]Pb(μ-NCS)}$_n$, having an unusual infinite 2-D layered array in which three nonequiv. {[$HB(pz)_3$}Pb}$^+$ groups sandwich a layer of SCN^- ligands, where the overall structure is supported by π–π stacking interaction.

It was possible to prepare parallel complexes of both metals using the bulky pydim ligands. However, for cadmium(II) the ligand was not bulky enough to prevent formation of dimeric **5**, [(pydim)Cd (μ-NCS-*N*,*S*)]$_2$[BF_4]$_2$, that has a conventional bridging mode where the two cadmium(II) and two (μ-NCS-*N*,*S*)$^-$ groups form an eight membered ring. It is interesting that compound **1** with a bulky tripodal ligand is monomeric, whereas **5** with a bulky tridentate planar ligand is dimeric. For lead(II), the monomeric complex **6**, [(pydimMe_2)Pb(NCS)][BF_4], formed in which the isothiocyanate ligand is N-bound and the lead(II) has the low coordination number of four. The structure of **6** is very different from **5**, presumably because of the stereoactive lone pair on lead(II).

5. Supplementary material

Crystallographic data for the structures reported in this paper have been deposited at the Cambridge Crystallographic Data Center, CCDC 177361–177366. Copies of the information may be obtained free of charge from the Director, CCDC, 12 Union Road, Cambridge, CB2 1EZ, UK (fax: +44-1223-336-033; e-mail: deposit@ccdc.cam.ac.uk or www: http://www.ccdc.cam.ac.uk).

Acknowledgements

The authors thank the National Institute of Health (GM-26295 for D.L.R) and the National Science Foundation (CHE-0110493 for D.L.R) for support. The Bruker CCD Single Crystal Diffractometer (at the University of South Carolina) was purchased using funds provided by the NSF Instrumentation for Materials Research Program through Grant DMR: 9975623. The NSF (Grants CHE-8904942 and CHE-9601723) and NIH (Grant RR-02425) have supplied funds to support NMR equipment and the NIH (Grant RR-02849) has supplied funds to support mass spectrometry equipment at the University of South Carolina.

References

[1] (a) S. Trofimenko, Scorpionates—The Coordination Chemistry of Poly(pyrazolyl)borate Ligands, Imperial College Press, London, 1999;
(b) S. Trofimenko, Acc. Chem. Res. 4 (1971) 17;
(c) S. Trofimenko, J. Am. Chem. Soc. 89 (1967) 3170;
(d) S. Trofimenko, J. Am. Chem. Soc. 89 (1967) 6288;
(e) A.J. Shaver, Organomet. Chem. Lib. 3 (1976) 157;
(f) S. Trofimenko, Prog. Inorg. Chem. 34 (1988) 115;
(g) S. Trofimenko, Chem. Rev. 93 (1993) 943.
[2] (a) D.L. Reger, S.M. Myers, S.S. Mason, A.L. Rheingold, B.S. Haggerty, P.D. Ellis, Inorg. Chem. 34 (1995) 4996;
(b) D.L. Reger, J.E. Collins, S.M. Myers, A.L. Rheingold, L.M. Liable-Sands, Inorg. Chem. 35 (1996) 4904;
(c) D.L. Reger, S.S. Mason, A.L. Rheingold, Inorg. Chim. Acta 240 (1995) 669.
[3] (a) D.L. Reger, M.F. Huff, A.L. Rheingold, B.S. Haggerty, J. Am. Chem. Soc. 114 (1992) 579;
(b) D.L Reger, Synlett. (1992) 469.;
(c) D.L. Reger, T.D. Wright, C.A. Little, J.J.S. Lamba, M.D. Smith, Inorg. Chem. 40 (2001) 3810;
(d) D.L. Reger, Y. Ding, A.L. Rheingold, R.L. Ostrander, Inorg. Chem. 33 (1994) 4226;
(e) S.P. Constantine, H. Cox, P.B. Hitchcock, G.A. Lawless, Organometallics 19 (2000) 317 (and references therein);
(f) D.R. Armstrong, M.J. Duer, M.G. Davidson, D. Moncrieff, C.A. Russell, C. Stourton, A. Steiner, D. Stalke, D.S. Wright,

Organometallics 16 (1997) 3340;
(g) L. Shimoni-Livny, J.P. Glusker, C.W. Bock, Inorg. Chem. 37 (1998) 1853 (and reference therein).
[4] (a) C. Pariya, N.R. Chaudhuri, S. Seth, A. Das, Acta Crystallogr., Sect. C 52 (1996) 358;
(b) J. Dillen, T.H. Lentra, J.G. Haasnoot, J. Reedijk, Polyhedron 2 (1983) 195;
(c) D.J. Williams, D.L. VanDerveer, A. Lipscomb, R.L. Jones, Inorg. Chim. Acta 192 (1992) 51.
[5] (a) A. Diaz, M. Massaesi, G.J. Ponticelli, Inorg. Nucl. Chem. 37 (1975) 2469;
(b) R. Baggio, A. Frigerio, E.B. Halac, D. Vega, M.J. Perec, J. Chem. Soc., Dalton Trans. (1992) 549.
[6] L.M. Engelhardt, B.M. Furphy, J.M. Harrowfield, J.M. Patrick, B.W. Skelton, A.H. White, J. Chem. Soc., Dalton Trans. (1989) 595.
[7] (a) N. Mondal, M.K. Saha, S. Mitra, V.J. Gramlich, Chem. Soc., Dalton Trans (2000) 3218.;
(b) I.W. Nowell, Acta Crystallogr., Sect. B 35 (1979) 1891.
[8] A.E. Shvelashvili, M.A. Porai-Koshits, A.I. Kvitashvili, B.M. Shchedrin, L.P. Sarishvili, Zh. Strukt. Khim. 15 (1974) 315.
[9] L. Cavalca, M. Nardelli, G. Fava, Acta Crystallogr. 13 (1960) 125.
[10] (a) P.F. Rodesiler, R.W. Turner, N.G. Charles, A.H. Griffith, E.L. Amma, Inorg. Chem. 23 (1984) 999;
(b) H. Zhang, X. Wang, K. Zhang, B.K. Teo, Coord. Chem. Rev. 183 (1999) 157.
[11] (a) N.A. Bailey, D.E. Fenton, I.T. Jackson, R. Moody, L.R. Barbarin, J. Chem. Soc., Chem. Commun. (1983) 1463.;
(b) L.M. Engelhardt, J.M. Patrick, A.H. White, Aust. J. Chem. 42 (1989) 335;
(c) M.G.B. Drew, S.M. Nelson, Acta Crystallogr. 35 (1979) 1594;
(d) J.M. Harrowfield, H. Miyamae, B.W. Skelton, A.A. Soudi, A.H. White, Aust. J. Chem. 49 (1996) 1051;
(e) A.Y. Nazarenko, E.B. Rusanov, J. Coord. Chem. 34 (1995) 265;
(f) I.O. Cabral, M.F. Cabral, W.J. Cummins, G.B. Drew, A. Rodgers, S.M. Nelson, Inorg. Chim. Acta 30 (1978) L313.
[12] (a) B. Cetinkaya, E. Cetinkaya, M. Brookhart, P.S. White, J. Mol. Catal. 142 (1999) 101;
(b) G.J.P. Britovsek, M. Bruce, V.C. Gibson, B.S. Kimberley, P.J. Maddox, S. Mastoianni, S.J. McTavish, C. Redshaw, G.A. Solan, S. Stromberg, A.J.P. White, D.J. Williams, J. Am. Chem. Soc. 121 (1999) 8728;
(c) B.L. Small, M. Brookhard, Polym. Prepr. (Am. Chem. Soc. Div. Polym. Chem.) 39 (1998) 213;
(d) P. Merrell, E. Alyea, L. Ecott, Inorg. Chim. Acta 59 (1982) 25;
(e) D.A. Edward, M.F. Mahon, W.R. Martina, K.C. Molloy, J. Chem. Soc., Dalton Trans. (1990) 3161.
[13] (a) S.M. Kuang, Z.Z. Zhang, B.M. Wu, T.C.W. Mak, J. Organomet. Chem. 540 (1997) 55;
(b) S.L. Li, Z.Z. Zhang, T.C.W. Mak, Inorg. Chim. Acta 268 (1998) 177;
(c) Chow, M.Y. Chen, X.M. Mak, T.C.W., J. Chem. Soc., Dalton Trans. (1993) 3413.
[14] M. Taniguchi, A. Ouchi, Bull. Chem. Soc. Jpn. 62 (1989) 424.
[15] M. Cannas, G. Carta, A. Cristini, G.J. Marongiu, Inorg. Chem. 16 (1977) 228.
[16] M. Cannas, G. Carta, A. Cristini, G.J. Marongiu, J. Chem. Soc., Dalton Trans. (1976) 210.
[17] M. Taniguchi, S. Mamoru, A. Ouchi, Bull. Chem. Soc. Jpn. 59 (1986) 2299.
[18] M. Taniguchi, S. Mamoru, A. Ouchi, Bull. Chem. Soc. Jpn. 60 (1987) 1192.
[19] G. Yang, H.G. Zhu, B.H. Liang, X.M. Chen, J. Chem. Soc., Dalton Trans. (2001) 580.
[20] (a) G.A. Bowmaker, J.M. Harrowfield, H. Miyamae, T.M. Shand, B.W. Skelton, A.A. Soudi, A.H. White, Aust. J. Chem. 49 (1996) 1081;
(b) G.A. Bowmaker, J.M. Harrowfield, H. Miyamae, T.M. Shand, B.W. Skelton, A.A. Soudi, A.H. White, Aust. J. Chem. 49 (1996) 1121;
(c) L.M. Engelhardt, B.M. Furphy, J.M. Harrowfield, J.M. Patrick, A.H. White, Inorg. Chem. 28 (1989) 1410.
[21] (a) P.G. Harrison, in: G. Wilkinson, R.D. Gillard, J.A. McCleverty (Eds.), Comprehensive Coordination Chemistry, vol. 3, Permagon, Oxford, 1987, p. 183;
(b) S.L. Lawton, G.T. Kokotailo, Inorg. Chem. 11 (1972) 363.
[22] C. Janiak, J. Chem. Soc., Dalton Trans (2000) 3885.

the application of Re compounds and development of radiopharmaceuticals [13]. Therefore, we decided to prepare more suitable S-bridged polynuclear complexes for apparent investigation of the Re^{III} ion.

Generally, *fac*(*S*)-[Ir(aet)$_3$] can be used as a building block for construction of the S-bridged polynuclear structures and has some advantages over *fac*(*S*)-[Rh(aet)$_3$]. For example, electrochemical properties of the Re^{III} ion incorporated into the S-bridged polynuclear structure using spectroelectrochemical techniques can be investigated clearly, since *fac*(*S*)-[Ir(aet)$_3$] shows little absorption in the visible region [8–11]. Moreover, the Ir^{III} complexes tend to indicate shorter metal–metal distances and lower magnetic moments than the corresponding Rh^{III} complexes [9–11], and these characteristic properties seem to be interesting. In this work, a reducing reaction of an acidic mixture of Re^{VII} and *fac*(*S*)-[Ir(aet)$_3$] was attempted. Moreover, a substitution reaction using Re^{III} was applied. The crystal structures of two isomers of $[Re\{Ir(aet)_3\}_2]^{3+}$ were determined by X-ray crystallography. The obtained complexes were characterized on the basis of elemental analysis, ICP, UV–Vis absorption, diffuse reflectance, CD, IR, NMR spectra, molar conductivities and magnetic susceptibilities. Furthermore, the electrochemical behavior for the Re^{III} ion incorporated into S-bridged trinuclear complexes was also investigated.

2. Results and discussion

2.1. Syntheses

The reaction of *fac*(*S*)-[Ir(aet)$_3$] with NH_4ReO_4 in acidic solution (HCl or HBr) using $SnCl_2\cdot 2H_2O$ as a reducing agent at room temperature in the molar ratio of 1:1:2 gave a dark reddish brown solution. The solution was separated into two yellow bands and a purple band using a SP-Sephadex C-25 column. The first two yellow bands were *meso* (**1a**) and racemic (*rac*, **1b**) isomers of $[Re\{Ir(aet)_3\}_2]^{3+}$, whose structures were determined by X-ray diffraction method (vide infra). The purple band was unidentified and it may contain certain Re^{V} species. Of the two yellow bands separated, the crystallization of only the *meso*-isomer was successful. The *rac*-isomer could not be isolated, since a dinuclear Ir^{III} complex, which was confirmed by X-ray crystallography [14], was obtained during this isolation procedure. This means that the Re–S bonds are cleaved, followed by rearrangement during the desaltation, although the *rac*-isomer is relatively stable in water at room temperature.

A more convenient method was developed to isolate *rac*-$[Re\{Ir(aet)_3\}_2]^{3+}$ (**1b**), namely, *fac*(*S*)-[Ir(aet)$_3$] reacts with the Re^{III} complex $[Re(Metu)_6]Cl_3$ (Metu = *N*-methylthiourea) [15] in aqueous solution at room temperature in the molar ratio of 1:1. Although both isomers are formed in the reaction mixture (from the column chromatography), as is the case in the reaction using the Re^{VII} ion, the *rac*-isomer could be selectively crystallized as dark brown rod crystals by adding bromide ion to the reaction mixture. Consequently, we could investigate stereochemical, spectrochemical and electrochemical properties of both the *meso*- and *rac*-isomers.

2.2. Structures of complexes

It has been revealed by the X-ray structural analysis that each of the crystals for **1a** and **1b** consists of a complex cation and three bromide anions. Further, the crystals for **1b** contain a water molecule. The total number of anions implies that the entire complex cations are trivalent. This is compatible with the observed molar conductivities in water (420 S cm^2 mol^{-1} for **1a**Br_3 and 384 S cm^2 mol^{-1} for **1b**$Br_3\cdot H_2O$), which are in agreement with those of 1:3 electrolytes, for example *meso*-$[Cr\{Ir(aet)_3\}_2](NO_3)_3\cdot 3H_2O$ (355 S cm^2 mol^{-1}) and *rac*-$[Cr\{Ir(aet)_3\}_2]Br_3\cdot 1.5H_2O$ (369 S cm^2 mol^{-1}) [10].

Perspective views of the complex cations **1a** and **1b** are given in Figs. 1 and 2, and their selected bond distances and angles are listed in Tables 1 and 2, respectively. **1a** and **1b** consist of two approximately octahedral *fac*(*S*)-[Ir(aet)$_3$] units and one Re atom, being complete linear-type S-bridged trinuclear structures, $[Re\{Ir(aet)_3\}_2]^{3+}$. These results are consistent with the plasma emission spectral analysis that gave a value of Re:Ir as 1:2. From the formal charge of the coordinated ligands, it is reasonable to assume that the central Re ions are in oxidation state +3 (d^4-electronic configuration) and situated in an octahedral environment with a $Re^{III}S_6$ chromophore. Considering the absolute configurations (Δ and Λ) of the two terminal *fac*(*S*)-[Ir(aet)$_3$] units, three isomers ($\Delta\Delta$, $\Lambda\Lambda$ and $\Delta\Lambda$) are possible for $[Re\{Ir(aet)_3\}_2]^{3+}$. As shown in Fig. 1, **1a** is the *meso*-isomer with a $\Delta\Lambda$ configuration, having an inversion

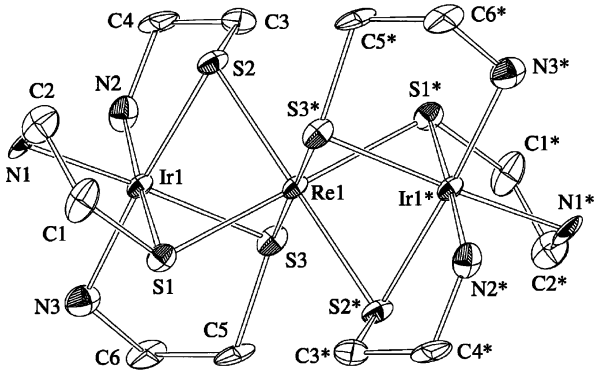


Fig. 1. Perspective view of $\Delta\Lambda$-$[Re\{Ir(aet)_3\}_2]^{3+}$ (**1a**) with the atomic labelling scheme (50% probability ellipsoids).

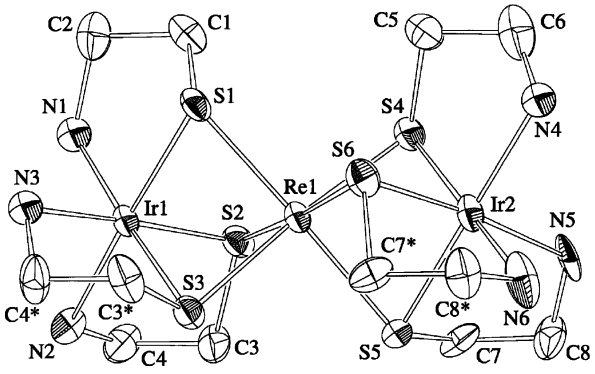


Fig. 2. Perspective view of ΔΛ/ΛΛ-$[Re\{Ir(aet)_3\}_2]^{3+}$ (**1b**) with the atomic labelling scheme (30% probability ellipsoids). The overlapped ΛΛ isomer is omitted for clarity.

Table 1
Selected bond distances (Å) and angles (°) for ΔΛ-$[Re\{Ir(aet)_3\}_2]^{3+}$ (**1a**)

Bond lengths			
Ir(1)···Re(1)	2.7961(4)	Ir(1)–N(2)	2.129(10)
Ir(1)–S(1)	2.324(3)	Ir(1)–N(3)	2.11(1)
Ir(1)–S(2)	2.328(3)	Re(1)–S(1)	2.389(3)
Ir(1)–S(3)	2.338(3)	Re(1)–S(2)	2.394(3)
Ir(1)–N(1)	2.133(10)	Re(1)–S(3)	2.408(3)
Bond angles			
S(1)–Ir(1)–S(2)	91.68(10)	S(1)–Re(1)–S(2)	88.49(9)
S(1)–Ir(1)–S(3)	89.58(10)	S(1)–Re(1)–S(3)	86.41(10)
S(2)–Ir(1)–S(3)	89.17(10)	S(2)–Re(1)–S(3)	86.01(10)
N(1)–Ir(1)–N(2)	96.4(4)	Ir(1)–S(1)–Re(1)	72.77(8)
N(1)–Ir(1)–N(3)	93.6(4)	Ir(1)–S(2)–Re(1)	72.61(8)
N(2)–Ir(1)–N(3)	94.3(4)	Ir(1)–S(3)–Re(1)	72.19(8)

Table 2
Selected bond distances (Å) and angles (°) for ΔΔ/ΛΛ-$[Re\{Ir(aet)_3\}_2]^{3+}$ (**1b**)

Bond lengths			
Ir(1)···Re(1)	2.801(2)	Ir(2)···Re(1)	2.819(2)
Ir(1)–S(1)	2.352(10)	Ir(2)–S(4)	2.39(1)
Ir(1)–S(2)	2.30(1)	Ir(2)–S(5)	2.36(1)
Ir(1)–S(3)	2.35(1)	Ir(2)–S(6)	2.21(1)
Ir(1)–N(1)	2.03(3)	Ir(2)–N(4)	2.10(4)
Ir(1)–N(2)	2.10(3)	Ir(2)–N(5)	2.25(4)
Ir(1)–N(3)	2.11(4)	Ir(2)–N(6)	2.06(5)
Re(1)–S(1)	2.40(1)	Re(1)–S(4)	2.42(1)
Re(1)–S(2)	2.42(1)	Re(1)–S(5)	2.41(1)
Re(1)–S(3)	2.40(1)	Re(1)–S(6)	2.40(1)
Bond angles			
S(1)–Ir(1)–S(2)	91.2(4)	S(4)–Ir(2)–S(5)	88.0(4)
S(1)–Ir(1)–S(3)	89.6(4)	S(4)–Ir(2)–S(6)	90.8(5)
S(2)–Ir(1)–S(3)	90.4(4)	S(5)–Ir(2)–S(6)	91.9(4)
N(1)–Ir(1)–N(2)	94(1)	N(4)–Ir(2)–N(5)	91(2)
N(1)–Ir(1)–N(3)	92(1)	N(4)–Ir(2)–N(6)	95(1)
N(2)–Ir(1)–N(3)	93(1)	N(5)–Ir(2)–N(6)	94(1)
S(1)–Re(1)–S(2)	87.2(4)	S(4)–Re(1)–S(5)	86.1(4)
S(1)–Re(1)–S(3)	87.3(4)	S(4)–Re(1)–S(6)	85.5(4)
S(2)–Re(1)–S(3)	86.4(4)	S(5)–Re(1)–S(6)	86.1(4)
Ir(1)–S(1)–Re(1)	72.2(3)	Ir(2)–S(4)–Re(1)	71.8(4)
Ir(1)–S(2)–Re(1)	72.7(4)	Ir(2)–S(5)–Re(1)	72.4(3)
Ir(1)–S(3)–Re(1)	72.1(3)	Ir(2)–S(6)–Re(1)	75.3(4)

center on the Re atom. While **1b** is the *rac*-isomer with ΔΔ and ΛΛ configurations (Fig. 2). The O atom of the water molecule in **1b**$Br_3 \cdot H_2O$ seems to participate in hydrogen bonds (N(2)···O(1) = 3.18 Å and Br(2)···O(1) = 3.22 Å). These intermolecular interactions may be related to the selective crystallization of the *rac*-isomer. All of the bridging sulfur atoms in **1a** and **1b** are fixed to the *R* configuration for the Δ unit and the *S* configuration for the Λ unit, which corresponds to the results in all of the reported trinuclear structures [7–12,16].

The bond distances and angles in **1a** and **1b** are similar to each other, suggesting that they are almost independent of the absolute configuration of the two terminal *fac*(*S*)-[Ir(aet)$_3$] units (Tables 1 and 2). The Re–S distances (average 2.401(3) Å in **1a** and average 2.406(1) Å in **1b**) for ΔΛ- and ΔΔ/ΛΛ-$[Re\{Ir(aet)_3\}_2]^{3+}$ are slightly longer than those (average 2.383(6) and average 2.386(9) Å) for ΔΛ- and ΔΔ/ΛΛ-$[Re\{Rh(aet)_3\}_2]^{3+}$ [12], reflecting the electron donating ability of the thiolato sulfur atoms of the terminal *fac*(*S*)-[M(aet)$_3$] (M = Ir^{III}, Rh^{III}) units. On the other hand, the Re···Ir distances (2.7961(4) Å for **1a** and average 2.810(2) Å for **1b**) are shorter than the Re···Rh distances (2.8248(9) and average 2.840(2) Å) for the corresponding Rh^{III} isomers [12]. Similar results were observed in the M′–S and M′···M distances for $[M'\{M(aet)_3\}_2]^{3+}$ (M′ = V^{III}, Cr^{III}), whose structures were previously reported for both Ir^{III} and Rh^{III} complexes [9,10].

The Re–S distances in **1a** and **1b** are approximately 0.1 Å longer than the Co–S distances (average 2.297(2) Å) in $[Co\{Ir(aet)_3\}_2]^{3+}$ [8]. However, the Re···Ir distances in **1a** and **1b** are approximately 0.1 Å shorter than the Co···Ir distances (2.906(1) Å) [10] in the Co^{III} complexes. Namely, the *fac*(*S*)-[Ir(aet)$_3$] units are attracted by the Re^{III} ion, and this is obviously apparent in the M′–S–Ir angles (averages 72.52(8)° for **1a**, 72.8(4)° for **1b**, 78.3(1)° for the Co^{III} complex) [10]. The corresponding complexes containing the V^{III} or Mo^{IV} ion, which has an unsaturated t_{2g}-orbital, also indicate acute M′–S–Ir angles (71.12(10)° for V^{III} complex and 69.8(2)° for Mo^{IV} complex) [10,11] than that containing the Co^{III} ion, which has a saturated t_{2g}-orbital. Accordingly, the differences of the distances and angles in the complexes may be related to the electronic state of the central metal ions. Since the bond distances and angles around the Ir^{III} ions indicate no significant differences for all reported trinuclear complexes which have the *fac*(*S*)-[Ir(aet)$_3$] units [8–11], it can be understood that the character of the incorporated metal ion is apparent in the structures.

2.3. Spectrochemical characterization

The UV–Vis absorption, diffuse reflectance and CD spectra of $[Re\{Ir(aet)_3\}_2]^{3+}$ are shown in Fig. 3. The absorption bands of **1b** in water are observed in approximately the same region as the diffuse reflectance bands in the solid state. Further, the absorption spectral patterns of **1a** and **1b** are similar to each other over the whole region, although the intensities of some bands are slightly different. These facts indicate that **1a** and **1b** retain the trinuclear structure in solution.

The most intense band above 45×10^3 cm^{-1} in the UV region corresponds well to the sulfur to Ir^{III} CT band and the bands between 30 and 35×10^3 cm^{-1} to the d–d transition bands due to the terminal *fac*(*S*)-[Ir(aet)$_3$] units, as similar bands were observed in complexes which contain the *fac*(*S*)-[Ir(aet)$_3$] units [8–11]. The bands at approximately 40×10^3 cm^{-1} for **1a** and **1b** are assigned to the sulfur to Re^{III} CT band, as in the case of $[Re\{Rh(aet)_3\}_2]^{3+}$ [12]. The characteristic intense three absorption bands in the region of 12–29 $\times$ 10^3 cm^{-1} are assigned to be arising from the central $Re^{III}S_6$ chromophore. Since the Re^{III} ion belongs to the group of 5d ions known to occur in a strong crystal field octahedral coordination, these bands are thought to depend upon $(t_{2g})^4$ ground state configurations.

The CD spectrum of $(-)^{CD}_{460}$-**1b**, which was optically resolved by the SP-Sephadex C-25 column, shows negative bands at 33.50 and above 45×10^3 cm^{-1}. These CD bands correspond well to the d–d and CT bands for the *fac*(*S*)-[Ir(aet)$_3$] units in the absorption spectra. Although these absorption and CD bands of $(-)^{CD}_{460}$-**1b** are shifted by approximately 5×10^3 cm^{-1} to higher energy than those for the *fac*(*S*)-[Rh(aet)$_3$] units of $[Re\{Rh(aet)_3\}_2]^{3+}$, the CD spectral pattern of $(-)^{CD}_{460}$-**1b** is in agreement with that of ΛΛ-$[Re\{Rh(aet)_3\}_2]^{3+}$ [12]. Accordingly, it seems that the $(-)^{CD}_{460}$-**1b** isomer is ΛΛ-$[Re\{Ir(aet)_3\}_2]^{3+}$ and $(+)^{CD}_{460}$-**1b** isomer is ΔΔ-$[Re\{Ir(aet)_3\}_2]^{3+}$. On the other hand, the CD bands, which are observed in the absorption band regions depending on the Re^{III} ion, of $(-)^{CD}_{460}$-**1b** imply that the absolute configuration of the asymmetric sulfur atoms of all *S* configurations from the Λ-*fac*(*S*)-[Ir(aet)$_3$] units affects the environment around the central Re^{III} ion. These bands are shifted by approximately 5×10^3 cm^{-1} to lower energy than those for the Re^{III} ion in the $[Re\{Rh(aet)_3\}_2]^{3+}$ [12], contrary to the case of the bands due to the Ir^{III} ion. Consequently, most absorption and CD bands due to the $Re^{III}S_6$ chromophore in the present Ir^{III} complexes are displayed more clearly than those in the Rh^{III} complexes [12]. For the UV–Vis absorption and CD spectra of **1a** and **1b**, no significant changes with time were observed at least for several hours. This illustrates that the trinuclear structures are fairly stable even under aerobic condition, retaining the oxidation state.

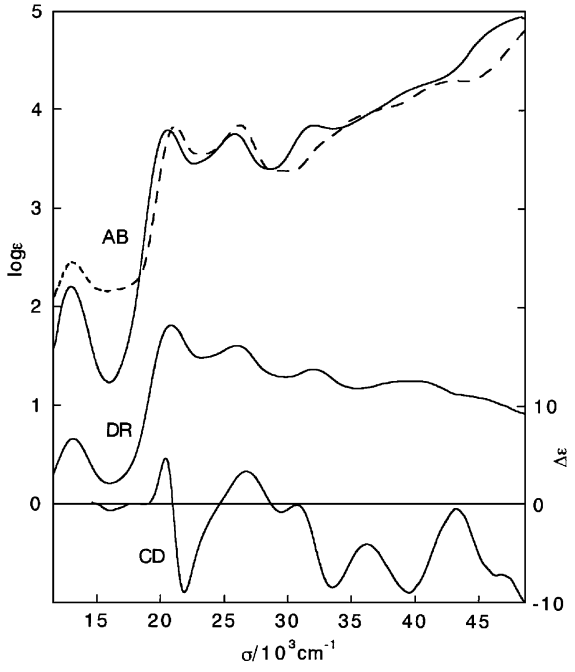


Fig. 3. UV–Vis absorption (AB, log ε), diffuse reflectance (DR, arbitrary scale) and CD (Δε) spectra of ΔΔ-$[Re\{Ir(aet)_3\}_2]^{3+}$ (**1a**; ----) and ΛΛ-$[Re\{Ir(aet)_3\}_2]^{3+}$ ($(-)^{CD}_{460}$-**1b**; —).

The complexes **1a**Br_3 and **1b**$Br_3 \cdot H_2O$ indicated the typical IR spectral pattern for linear-type S-bridged trinuclear complexes in the range of 4000–400 cm^{-1} [9,11,12]. Namely, the bands due to the vibration mode of the NH_2 group appear between 3500 and 3400 cm^{-1} and those of the CH_2 group between 3200–2900 cm^{-1}. The bands due to the bending mode of NH_2 group are observed around 1600 cm^{-1} and those of the CH_2 group around 1400 cm^{-1}. The fact that these bands in **1a** and **1b** are similar to those in the starting *fac*(*S*)-[Ir(aet)$_3$] support that the terminal units retain their structure during the formation of the S-bridged complexes. On the other hand, the bands in the range of 650–100 cm^{-1} are complicated as observed in $[Re\{Rh(aet)_3\}_2]^{3+}$ [12]. Therefore, it was difficult to assign the bands from the shifts depending upon the Re–S bonds.

2.4. Magnetic properties

The effective magnetic moment for the Re^{III} ion in *rac*-$[Re\{Ir(aet)_3\}_2]^{3+}$ (**1b**) is 1.11μ_B, considering a diamagnetic correction (magnetic susceptibility at 296 K is -0.585×10^{-6} cm^3 mol^{-1}) [17]. This value is significantly lower than the spin only value for the $(t_{2g})^4$ configuration. Further, its value is somewhat lower than that (1.32μ_B) in the corresponding Rh^{III} complex *rac*-$[Re\{Rh(aet)_3\}_2]^{3+}$ (**1b**) [12], and similar trend was observed in the effective magnetic moment for the V^{III} ion in $[V\{M(aet)_3\}_2]^{3+}$ (M = Rh^{III}, Ir^{III}) [9]. Mononuclear Re^{III} complexes with a distorted octahedral

coordination often show similar magnetic moments (1.6–2.1μ_B) [18,19]. $[Re(S_2CC_6H_5)_2(S_3CC_6H_5)_2]$, which has a significantly distorted octahedral structure, is diamagnetic and its NMR spectrum showed no paramagnetic shift [20]. Since a similar diamagnetism was also observed for some five coordinate [21] and seven coordinate [19,22] Re^{III} d^4 systems, the consequent distortion as compared with octahedral symmetry could explain the pairing of electrons. In the S-bridged polynuclear structure, however, it is noted that the relatively less distorted octahedral Re^{III} ion (from the X-ray diffraction study) shows lower magnetic moments. These magnetic properties are reflected in the NMR spectral behavior.

In D_2O, each of **1a** and **1b** exhibits six sets of sharp ^1H NMR signals and two ^{13}C NMR signals due to the six aet ligands. This means that the S_6 or D_3 symmetrical S-bridged trinuclear structures observed in the crystals are retained in their aqueous solution. In the ^{13}C–^1H heteronuclear multiple-bond correlation (HMBC) of **1b**, the proton signals at δ 4.47 and 3.05 are coupled with carbon signals at δ 56.58, while the signals at δ 2.60 and 1.45 are coupled with the carbon signals at δ 46.92. Moreover, the signals at δ 4.47 and 3.05 indicate coupling with those of NH_2 protons in ^1H–^1H correlation spectroscopy (COSY). A similar coupling pattern was observed in the HMBC and COSY spectra of **1a**. Accordingly, it can be assigned that the carbon signals at δ 57.62 (**1a**) and 56.58 (**1b**) are due to the CH_2 group neighboring the N atom in the aet ligands, while the signals at δ 44.72 (**1a**) and 46.92 (**1b**) are due to CH_2 group neighboring its S atom. As summarized in Table 3, the chemical shifts of CH_2 groups in the ^{13}C NMR spectra of **1a** and **1b** show some paramagnetic shifts to lower field in comparison with those of diamagnetic $[Co\{Ir(aet)_3\}_2]^{3+}$ [8]. The carbon neighboring sulfur atoms, which coordinate to the Re^{III} ion, indicate especially significant lower shifts (10.98 ppm for ΔΛ isomer and 13.00 ppm for ΔΔ/ΛΛ isomer). However, the degree of paramagnetic shifts in **1a** and **1b** seems to be smaller than those in $[Re\{Rh(aet)_3\}_2]^{3+}$ [12]. A similar trend was also observed in the ^1H NMR chemical shifts.

Table 3
^{13}C NMR chemical shifts (δ (ppm) from DSS in D_2O) for $[M'\{M(aet)_3\}_2]^{3+}$ (M = Ir^{III}, Rh^{III}; M′ = Re^{III}, Co^{III})

Complex	NCH_2	SCH_2	References
ΔΛ-$[Re\{Ir(aet)_3\}_2]^{3+}$ (**1a**)	57.62	44.72	This work
ΔΔ/ΛΛ-$[Re\{Ir(aet)_3\}_2]^{3+}$ (**1b**)	56.58	46.92	This work
ΔΛ-$[Re\{Rh(aet)_3\}_2]^{3+}$	57.61	52.16	[12]
ΔΔ/ΛΛ-$[Re\{Rh(aet)_3\}_2]^{3+}$	57.10	55.04	[12]
ΔΛ-$[Co\{Ir(aet)_3\}_2]^{3+}$	51.46	33.74	[8]
ΔΔ/ΛΛ-$[Co\{Ir(aet)_3\}_2]^{3+}$	51.96	33.92	[8]
ΔΛ-$[Co\{Rh(aet)_3\}_2]^{3+}$	49.89	34.40	[6]
ΔΔ/ΛΛ-$[Co\{Rh(aet)_3\}_2]^{3+}$	50.11	34.62	[6]

Accordingly, it can be considered that the NMR spectral behavior depends upon the effective magnetic moments of the Re^{III} ion in the S-bridged polynuclear structures.

2.5. Electrochemistry

Cyclic voltammetry experiments were performed for the bromide salts of the present $Ir^{III}Re^{III}Ir^{III}$ complexes *meso*- and *rac*-$[Re^{III}\{Ir^{III}(aet)_3\}_2]^{3+}$ (**1a** and **1b**) together with *rac*-$[Re^{III}\{Rh^{III}(aet)_3\}_2]^{3+}$. As summarized in Table 4, each of the voltammograms displays a redox couple in a positive potential region. The observed peak separation (E_{pa}–E_{pc} = 0.07 V) establish that all redox processes are almost reversible, therefore, the complexes retain their trinuclear structure during the redox process. In the $Ir^{III}Re^{III}Ir^{III}$ complexes **1a** and **1b**, the redox wave appeared at a similar position, indicating that the redox potentials are almost independent of the absolute configuration of the terminal *fac*(*S*)-$[Ir(aet)_3]$ units. On the other hand, the $Rh^{III}Re^{III}Rh^{III}$ complex exhibits the redox wave at more positive potential depending on the terminal units. Since the previous trinuclear complexes have shown no waves due to the aet ligands [8–10], all waves given in Table 4 are probably due to the metals. Indeed, the $Ir^{III}Cr^{III}Ir^{III}$ and $Ir^{III}Co^{III}Ir^{III}$ complexes $[M'\{Ir^{III}(aet)_3\}_2]^{3+}$ (M′ = Cr^{III}, Co^{III}) show the redox wave ($E^{0\prime}$ = +0.64 V for Cr^{III} and +0.73 V for Co^{III}) due to the one-electron $Ir^{IV/III}M'Ir^{III}$ redox process, while the corresponding $Rh^{III}Cr^{III}Rh^{III}$ and Rh^{III}-$Co^{III}Rh^{III}$ complexes exhibit a redox wave at +1.01 V due to the one-electron $Rh^{IV/III}M'Rh^{III}$ redox process [8,10]. However, the potentials of the waves observed for the present $Ir^{III}Re^{III}Ir^{III}$ and $Rh^{III}Re^{III}Rh^{III}$ complexes (Table 4) are approximately 0.4 V more negative than those of $Ir^{IV/III}$ (or $Rh^{IV/III}$) redox processes for the previous complexes. Therefore, it is difficult to assign the waves for the present complexes from only the electrochemical measurements.

In order to elucidate the origin of the redox waves for the trinuclear complexes containing the Re^{III} ion, spectroelectrochemical experiments using a thin-layer quartz cell and a platinum mesh electrode were carried out. The absorption spectral change of the representative isomer **1b** of the $Ir^{III}Re^{III}Ir^{III}$ complex in visible region is shown in Fig. 4. The characteristic band at 476 nm, which is assigned as arising from the central $Re^{III}S_6$

Table 4
Redox potentials (E/V vs. Ag/AgCl with scan rate 100 mV s^{-1}) for $[Re^{III}\{M(aet)_3\}_2]^{3+}$ (M = Ir^{III}, Rh^{III})

Complex	$E^{0\prime}$	E_{pa}	E_{pc}
ΔΛ-$[Re\{Ir(aet)_3\}_2]^{3+}$ (**1a**)	+0.34	+0.37	+0.30
ΔΔ/ΛΛ-$[Re\{Ir(aet)_3\}_2]^{3+}$ (**1b**)	+0.37	+0.40	+0.33
ΔΔ/ΛΛ-$[Re\{Rh(aet)_3\}_2]^{3+}$	+0.60	+0.63	+0.56

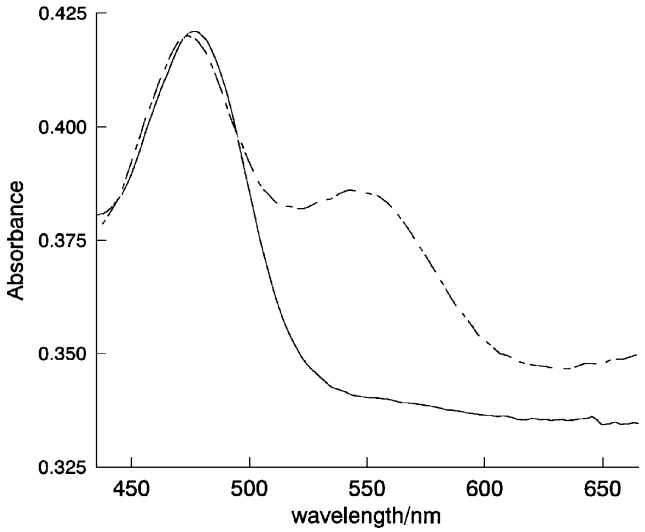


Fig. 4. UV–Vis absorption spectra of ΔΔ/ΛΛ-$[Re\{Ir(aet)_3\}_2]^{3+}$ (**1b**) obtained during spectroelectrochemical experiments. Applied potentials vs. Ag/AgCl are: original (—) and +0.75 V for 5 min (–·–·–).

chromophore (vide supra), is observed before electrochemical oxidation. At a potential of +0.75 V, a new absorption band appeared at 542 nm, whereas the band at 476 nm showed no significant changes. Therefore, it is reasonable to assume that the new band at 542 nm is due to an $Ir^{IV}N_3S_3$ chromophore rather than a $Re^{IV}S_6$ one. When the potential was back to 0 V, the new band disappeared and the spectrum coincided well with the original spectrum. This spectroelectrochemical result also confirms the reversibility of the redox processes. Accordingly, it can be assigned that the wave of the cyclic voltammogram for **1a** and **1b** is due to the one-electron $Ir^{IV/III}Re^{III}Ir^{III}$ redox process (Table 4). Namely, the Ir^{III} ions in the present $Ir^{III}Re^{III}Ir^{III}$ complexes are more easily oxidized than those in the corresponding $Ir^{III}Cr^{III}Ir^{III}$ and $Ir^{III}Co^{III}Ir^{III}$ complexes, $[M'\{Ir^{III}(aet)_3\}_2]^{3+}$ [8,10]. This behavior may be related to the fact that the relatively low oxidation state of the Re^{III} ion is stabilized by the terminal *fac*(*S*)-$[Ir(aet)_3]$ units. Similarly, the wave for the $Rh^{III}Re^{III}$-Rh^{III} complex is thought to be dominated by the one-electron $Rh^{IV/III}Re^{III}Rh^{III}$ redox process (Table 4). The difference of the redox potential ($\Delta E^{0\prime} = 0.23$ V) between the $Ir^{IV/III}$ and $Rh^{IV/III}$ processes for the $MRe^{III}M$ complexes is comparable to those for the $MCr^{III}M$ and $MCo^{III}M$ complexes [8,10]. These facts also support the assignment of the redox waves, and the different positions of the $Ir^{IV/III}$ or $Rh^{IV/III}$ process seem to depend on the central Re^{III} ion. On the other hand, the wave due to the $Re^{IV/III}$ redox process could not be observed. Accordingly, it was elucidated that the oxidation state of Re^{III} is highly stabilized in the S-bridged trinuclear structures, $[Re\{M(aet)_3\}_2]^{3+}$ ($M = Ir^{III}$, Rh^{III}).

3. Experimental

3.1. Materials

2-Aminoethanethiolate (Haet) and *N*-methylthiourea (Metu) were purchased from Tokyo Kasei Kogyo Co. Ltd. NH_4ReO_4 was purchased from Soekawa Chemical Co. Ltd. $Na_2[Sb_2(R,R\text{-tart})_2]\cdot 5H_2O$ (H_4tart = tartaric acid) was prepared by the general procedure from $Na_2(R,R\text{-}H_3tart)_2\cdot H_2O$ and Sb_2O_3 (Kanto Chemical Co. Inc). *fac*(*S*)-$[Ir(aet)_3]$ [8,10] and $[Re(Metu)_6]Cl_3$ [15] were prepared by procedures similar to those in the literature. $IrCl_3$, $SnCl_2\cdot 2H_2O$ and the other reagents used were purchased from Wako Pure Chemical Ind. Ltd. All the chemicals were of reagent grade and were used without further purification.

3.2. Preparation of complexes

3.2.1. ΔΛ-$[Re\{Ir(aet)_3\}_2]^{3+}$ (**1a**)

To the colorless solution of NH_4ReO_4 (0.305 g, 1.14 mmol) in 20 cm^3 of 1 mol dm^{-3} (M) HBr or 1 M HCl were added *fac*(*S*)-$[Ir(aet)_3]$ (0.500 g, 1.14 mmol) and $SnCl_2\cdot 2H_2O$ (0.515 g, 2.28 mmol). The dark reddish brown mixture was stirred at room temperature (r.t.) for 1 h. The reaction mixture was subjected to SP-Sephadex C-25 column (Na^+ form) and eluted by 0.5 M NaCl aqueous solution, where upon two yellow bands, *meso* (**1a**) and *rac* (**1b**) isomers and an unidentified purple band were eluted in this order. The *meso* and *rac* bands separated were concentrated by rotary evaporator and partially desalted by the addition of methanol. After the solution was concentrated again, an orange powder of the iodide salt was obtained by the addition of saturated NaI solution. The powder was dissolved in a small amount of water and subjected to QAE-Sephadex A-25 column (Br^- form). The eluate was concentrated by rotary evaporator and kept in the refrigerator after the addition of a few drops of saturated NaBr solution. The *meso*-isomer was separated as dark orange crystals (**1a**), filtered, washed with acetone and dried. Yield: 0.095 g (6.4%). *Anal*. Found: C, 11.13; H, 2.84; Ir, 32.0, N, 6.50; Re, 14.8%. $[Re\{Ir(NH_2CH_2CH_2S)_3\}_2]Br_3\cdot H_2O$ requires C, 11.22; H, 2.98; Ir, 29.9, N, 6.54; Re, 14.5%. Absorption maxima [σ (10^3 cm^{-1}) (log ε (M^{-1} cm^{-1}))]: 12.94 (2.45), 20.97 (3.83), 26.11 (3.84), 32.3sh (3.6), 36.2sh (4.0), 42.84 (4.30). The sh label denotes a shoulder. ^1H NMR spectrum in D_2O (δ (ppm) from DSS): 5.77 (dd, $J = 10.6$ and 5.3 Hz, NH_2), 5.61 (d, $J = 7.0$ Hz, NH_2), 4.69 (d, $J = 12.5$ Hz, NCH_2), 3.12 (dd, $J = 23.3$ and 10.3 Hz, NCH_2), 2.61 (d, $J = 12.0$ Hz, SCH_2), 1.67 (td, $J = 13.6$ and 3.3 Hz, SCH_2). ^{13}C NMR spectrum in D_2O (δ (ppm) from DSS): 57.62 (NCH_2), 44.72 (SCH_2). The *rac*-isomer could not be isolated due to rearrangement to a dinuclear Ir^{III} complex during this procedure (vide supra).

3.2.2. $\Delta\Delta/\Lambda\Lambda$-[Re{Ir(aet)$_3$}$_2$]$^{3+}$ (**1b**)

To a clear bright yellow solution of [Re(Metu)$_6$]Cl$_3$ (1.350 g, 1.625 mmol) in 30 cm^3 of H_2O was added *fac*(*S*)-[Ir(aet)$_3$] (0.675 g, 1.625 mmol). The reddish brown mixture was stirred at r.t. for 1 h. After unreacted materials were filtered off, 2.5 cm^3 of saturated NaBr was added to the filtrate and then kept in a refrigerator overnight. The dark brown rod crystals (**1b**) that appeared, were collected by filtration, washed with acetone and dried. Yield: 0.129 g (16.4%). *Anal*. Found: C, 10.70; H, 3.11; Ir, 26.0, N, 6.32; Re, 13.6%. [Re{Ir($NH_2CH_2CH_2S)_3$}$_2$]$Br_3\cdot 2.5H_2O$ requires C, 10.98; H, 3.15; Ir, 29.3; N, 6.40; Re, 14.2%. Absorption maxima [σ (10^3 cm^{-1}) (log ε (M^{-1} cm^{-1}))]: 12.90 (2.25), 20.42 (3.80), 25.69 (3.76), 31.88 (3.84), 38.5sh (4.1), 45.5sh (4.8). Reflectance maxima (σ (10^3 cm^{-1})): 13.02, 20.70, 26.01, 31.75, 40.32, 45.8sh. The sh label denotes a shoulder. ^{1}H NMR spectrum in D_2O (δ (ppm) from DSS): 5.86 (dd, $J = 10.5$ and 5.3 Hz, NH_2), 5.65 (d, $J = 6.6$ Hz, NH_2), 4.47 (d, $J = 12.7$ Hz, NCH_2), 3.05 (dd, $J = 24.8$ and 13.9 Hz, NCH_2), 2.60 (d, $J = 11.5$ Hz, SCH_2), 1.45 (td, $J = 13.6$ and 3.6 Hz, SCH_2). ^{13}C NMR spectrum in D_2O (δ (ppm) from DSS): 56.58 (NCH_2), 46.92 (SCH_2).

1b was optically resolved by SP-Sephadex C-25 column chromatography, which was eluted with 0.15 M $Na_2[Sb_2(R,R\text{-tartrato})_2]\cdot 5H_2O$ aqueous solution. The bands, which were partially separated, were further eluted with 0.5 M NaCl aqueous solution. Several portions from the lower and upper parts of the band were collected and their CD spectra were measured, which showed the positive or negative CD sign at 460 nm (21.83×10^3 cm^{-1}). The $\Delta\varepsilon$-values of each eluate containing the $(+)^{CD}_{460}$ and $(-)^{CD}_{460}$-**1b** isomers were evaluated on the basis of the absorption spectral data of **1b**$Br_3\cdot 2.5H_2O$. CD extrema for $(-)^{CD}_{460}$ isomer [σ (10^3 cm^{-1}) ($\Delta\varepsilon$ (M^{-1} cm^{-1}))]: 16.20 (−0.74), 20.37 (+5.25), 21.83 (−9.45), 26.75 (+3.39), 29.38 (−0.85), 33.50 (−8.52), 38.97 (−8.64), 45.74 (−6.67).

3.3. Measurements

The elemental analysis (C, H and N) was performed by the Chemical Analysis Center of the University of Tsukuba. The concentrations of Re and Ir in the complexes were determined with a NIPPON Jarell-Ash ICPA-575 spectrophotometer. The UV–Vis absorption spectra were recorded with a JASCO V-560 spectrophotometer and the CD spectra were recorded with a JASCO J-600 spectropolarimeter in aqueous solution. The diffuse reflectance spectrum was recorded by a JASCO V-570 spectrophotometer equipped with an integrating sphere apparatus. The IR spectra were recorded on a JASCO FT IR-550 spectrometer using KBr disks in the range of 4000–400 cm^{-1} and polyethylene pellets in the range of 650–100 cm^{-1}. The ^{1}H and ^{13}C NMR spectra were recorded with BRUKER AM-500 or AM-600 NMR spectrometers in D_2O and the sodium 4,4-dimethyl-4-silapentane-1-sulfonate (DSS) was used as an internal reference. The molar conductance of the complexes was measured with a HORIBA conductivity meter DS-14 in aqueous solution. The magnetic measurement was performed by using a Sherwood Scientific MSB-AUTO susceptibility balance. Electrochemical experiments were performed by a CV-50W apparatus, Bioanalytical Systems, Inc. (BAS) using a platinum-working electrode (BAS, Pt). Spectroelectrochemical experiments were performed by a JASCO CT-10TP multichannel spectrophotometer and a CV-1B apparatus (BAS) using a thin-layer quartz cell and a platinum mesh working electrode. In both electrochemical and spectroelectrochemical experiments, an aqueous (aq.) Ag/AgCl/NaCl (3 M; BAS, RE-1B) and platinum wire were used as reference and auxiliary electrodes. The experiments were conducted in 0.1 M aqueous solution of Na_2SO_4 as a supporting electrolyte. All the measurements were carried out at r.t.

3.4. X-ray crystallography

Red prismatic crystals of **1a**Br_3 were obtained by recrystallization of the isomer from water containing few drops of saturated NaBr solution at r.t. Brown rod crystals of **1b**$Br_3\cdot H_2O$ were obtained from the reaction mixture containing saturated NaBr solution at r.t. or by keeping in a refrigerator. Single crystal X-ray diffraction experiments were performed on a Rigaku AFC-7S four-circle diffractometer with Mo Kα (0.71069 Å) radiation. The intensity data were collected by the ω (**1a**Br_3) or ω–2θ (**1b**$Br_3\cdot H_2O$) scan technique up to 55° (2θ) at 296 K. The crystallographic data and experimental parameters are summarized in Table 5. The structures were determined by a direct method (SIR-92) [23], and refined by full-matrix least-squares techniques. All of the non-hydrogen atoms were refined anisotropically, and all the hydrogen atoms except for those of amino group in **1b**$Br_3\cdot H_2O$ were included in the refinement but restrained to ride on attached atoms [C–H=N–H = 0.95 Å, U(H) = 1.2U(C, N)]. In **1a**Br_3 only Re(1) and Br(2) atoms were constrained to special positions and refined with a site occupancy factor of 0.5. On the other hand, in **1b**$Br_3\cdot H_2O$ two sets of atom peaks corresponding to a pair of enantiomers co-exist in each of four sites in the unit cell. This behavior is often observed in the *rac* isomer of the S-bridged $\Delta\Delta/\Lambda\Lambda$-[M$'_3${M(aet)$_3$}$_2$]$^{3+}$ (M = Co^{III}, Rh^{III}; M$'$ = Ag^I, Au^I) [2,24]. Ir(1, 2), Re(1), Br(1), O(1) and C(1, 2, 5, 6) atoms were constrained to special positions. The site-occupancy factor of each atom except for the Br(2) and C(3, 4, 7, 8) atoms was fixed to 0.5. All of the calculations were performed on an Indigo II computer using the TEXSAN crystallographic software package [25].

Table 5
Crystallographic data for ΔΛ-[Re{Ir(aet)$_3$}$_2$]Br$_3$ (**1a**Br$_3$) and ΔΔ/ΛΛ-[Re{Ir(aet)$_3$}$_2$]Br$_3$·H$_2$O (**1b**Br$_3$·H$_2$O)

	1aBr_3	**1b**$Br_3 \cdot H_2O$
Chemical formula	$C_{12}H_{36}Br_3Ir_2N_6ReS_6$	$C_{12}H_{38}Br_3Ir_2N_6ORES_6$
Formula weight	1267.18	1285.19
Crystal system	monoclinic	orthorhombic
Space group	*C*2/*c* (number 15)	*Pnma* (number 62)
a (Å)	15.147(3)	17.296(4)
b (Å)	8.993(1)	12.413(2)
c (Å)	20.891(4)	14.020(2)
β (°)	96.56(2)	
V (Å^3)	2827.0(9)	3009(1)
Z	4	4
D_{calc} (g cm^{-3})	2.977	2.836
μ(Mo Kα) (cm^{-1})	184.02	172.89
Reflections measured, unique, R_{int}	3649, 1087, 0.039	4060, 3616, 0.024
Reflections used ($>1.5\sigma I_0$)	2790	1933
Parameters	138	208
Final $R(F^2)$, $wR(F^2)$	0.096, 0.113	0.075, 0.134
Goodness-of-fit	1.47	1.50

4. Supplementary material

Crystallographic data for the structural analysis have been deposited with the Cambridge Crystallographic Data Center, CCDC numbers 173446 and 173447. Copies of the information may be obtained free of charge from the Director, CCDC, 12 Union Road, Cambridge, CB2 1EZ, UK (fax: +44-1223-336-033; e-mail: deposit@ccdc.cam.ac.uk or www: http://www.ccdc.cam.ac.uk).

Acknowledgements

This work was supported by a Grant-in-Aid for Scientific Research from the Ministry of Education, Science, Sports and Culture.

References

[1] (a) T. Konno, K. Okamoto, J. Hidaka, Chem. Lett. (1990) 1043;
(b) T. Konno, K. Okamoto, J. Hidaka, Inorg. Chem. 30 (1991) 2253;
(c) T. Konno, K. Okamoto, J. Hidaka, Bull. Chem. Soc. Jpn. 67 (1994) 101;
(d) T. Konno, K. Okamoto, J. Hidaka, Inorg. Chem. 33 (1994) 538;
(e) K. Okamoto, T. Konno, J. Hidaka, J. Chem. Soc., Dalton Trans. (1994) 533;
(f) T. Konno, Y. Kageyama, K. Okamoto, Bull. Chem. Soc. Jpn. 67 (1994) 1957;
(g) Y. Kageyama, T. Konno, K. Okamoto, J. Hidaka, Inorg. Chim. Acta 239 (1995) 19.

[2] (a) T. Konno, K. Okamoto, Inorg. Chem. 36 (1997) 1403;
(b) T. Konno, K. Tokuda, T. Abe, M. Hirotsu, Mol. Cryst. Liq. Cryst. 342 (2000) 45.

[3] (a) K. Okamoto, T. Konno, Y. Kageyama, J. Hidaka, Chem. Lett. (1992) 1105;
(b) K. Okamoto, Y. Kageyama, T. Konno, Bull. Chem. Soc. Jpn. 68 (1995) 2573.

[4] (a) T. Konno, K. Okamoto, J. Hidaka, Inorg. Chem. 31 (1992) 3875;
(b) T. Konno, C. Sasaki, K. Okamoto, Chem. Lett. (1996) 977;
(c) K. Okamoto, C. Sasaki, Y. Yamada, T. Konno, Bull. Chem. Soc. Jpn. 72 (1999) 1685;
(d) Y. Yamada, M. Uchida, Y. Miyashita, K. Fujisawa, T. Konno, K. Okamoto, Bull. Chem. Soc Jpn. 73 (2000) 913.

[5] (a) S. Aizawa, Y. Sone, S. Yamada, M. Nakamura, Chem. Lett. (1998) 775.;
(b) S. Aizawa, Y. Sone, S. Khajar, Y. Ohishi, S. Yamada, M. Nakamura, Bull. Chem. Soc. Jpn. 73 (2000) 2043.

[6] T. Konno, S. Aizawa, K. Okamoto, J. Hidaka, Bull. Chem. Soc. Jpn. 63 (1990) 792.

[7] T. Konno, K. Okamoto, Bull. Chem. Soc. Jpn. 68 (1995) 610.

[8] T. Konno, K. Nakamura, K. Okamoto, J. Hidaka, Bull. Chem. Soc. Jpn. 66 (1993) 2582.

[9] Y. Miyashita, M. Hamajima, Y. Yamada, K. Fujisawa, K. Okamoto, J. Chem. Soc., Dalton Trans. (2001) 2089.

[10] Y. Miyashita, N. Sakagami, Y. Yamada, T. Konno, J. Hidaka, K. Okamoto, Bull. Chem. Soc. Jpn. 71 (1998) 661.

[11] Y. Miyashita, Y. Yamada, K. Fujisawa, T. Konno, K. Kanamori, K. Okamoto, J. Chem. Soc., Dalton Trans. (2000) 981.

[12] Y. Miyashita, N. Mahboob, S. Tsuboi, Y. Yamada, K. Fujisawa, K. Okamoto, Bull. Chem. Soc. Jpn. 74 (2001) 1295.

[13] (a) E. Deutsch, K. Libson, J.L. Vanderheyden, A. Ketring, H.R. Maxon, Nucl. Med. Biol. 13 (1986) 465;
(b) S. Jurisson, D. Berning, W. Jia, D. Ma, Chem. Rev. 93 (1993) 1137;
(c) W.A. Volkert, T.J. Hoffman, Chem. Rev. 99 (1999) 2269.

[14] Unpublished work.

[15] D. Gambino, J. Benítez, L. Otero, E. Kremer, E.J. Baran, O.E. Piro, Polyhedron 18 (1999) 2099.

[16] (a) M.J. Heeg, E.L. Blinn, E. Deutsch, Inorg. Chem. 24 (1985) 1118;
(b) T. Konno, K. Okamoto, J. Hidaka, Acta Crystallogr., Sect. C 49 (1993) 222;
(c) K. Okamoto, M. Matsumoto, Y. Miyashita, N. Sakagami, J. Hidaka, T. Konno, Inorg. Chim. Acta 260 (1997) 17.

[17] C.J. O'Connor, Prog. Inorg. Chem. 29 (1982) 203.

[18] (a) H.P. Gunz, G.J. Leigh, J. Chem. Soc. A (1971) 2229;
(b) S. Bhattacharyya, S. Banerjee, B.K. Dirghangi, M. Menon, A. Chakravorty, J. Chem. Soc., Dalton Trans. (1999) 155;
(c) I. Chakraborty, S. Bhattacharyya, S. Banerjee, B.K. Dirghangi, A. Chakravorty, J. Chem. Soc., Dalton Trans. (1999) 3747.

[19] G. Battistuzzi, M. Cannio, R. Battistuzzi, Polyhedron 19 (2000) 2163.

[20] (a) C.A. McConnachie, E.I. Stiefel, Inorg. Chem. 36 (1997) 6144;
(b) C.A. McConnachie, E.I. Stiefel, Inorg. Chem. 38 (1999) 964.

[21] H. Spies, M. Glaser, H. Pietzsch, F.E. Hahn, T. Lügger, Inorg. Chim. Acta 240 (1995) 465.

[22] D.J. Rose, K.P. Maresca, P.B. Kettler, Y.D. Chang, V. Soghomomian, Q. Chen, M.J. Abrams, S.K. Larsen, J. Zubieta, Inorg. Chem. 35 (1996) 3548.

[23] A. Altomare, M.C. Burla, M. Camalli, M. Cascarano, C. Giacovazzo, A. Guagliardi, G. Polidori, J. Appl. Cryst. 27 (1994) 435.

[24] T. Konno, K. Tokuda, T. Suzuki, K. Okamoto, Bull. Chem. Soc. Jpn. 71 (1998) 1049.

[25] Single Crystal Structure Analysis Software, Version 1.10b, Molecular Structure Corporation, The Woodlands, TX, 1999.

2. Results and discussion

2.1. Synthesis and spectroscopic characterization

Reaction of $[W(CO)_4(NCMe)(PPh_3)]$ with an equimolar quantity of $SnCl_4$ in CH_3CN produced a mixture of oxidative addition products, i.e. tungsten(II) compounds, as observed by $^{31}P\{^1H\}$ NMR spectra (Fig. 1). Four signals at δ_P about 30 ppm indicate the formation of four tungsten(II) compounds containing triphenylphosphine ligands. The intensity ratio of these signals changes slowly during the 1 week NMR measurement, indicating some transformation processes in solution. Two signals at δ_P 30.16 and 32.44, due to the presence of ^{117}Sn ($I = 1/2$, 7.6%) and ^{119}Sn ($I = 1/2$, 8.6%) satellites, and characteristic $^2J_{PSn}$ coupling constants in the range 308–348 Hz [13,14] can be assigned to tungsten(II) compounds containing a W–Sn bond. The intensity of these two signals decreases much faster in time than others. Two other signals at δ_P 30.70 and 32.77 are due to compounds without a W–Sn bond, being the products of the elimination of $SnCl_2$ species from the trichlorostannyl ligand. It is interesting that for the compounds without of a W–Sn bond the value of $^1J_{PW}$ −150 and 170 Hz, respectively—is much smaller than the value of $^1J_{PW}$ for signals due to W–Sn compounds ($^1J_{PW} = 222$ and 235 Hz). This suggests stronger W–P interactions in compounds containing trichlorostannyl ligands than in analogues with chlorine ligands only. Three broad bands in the ν(CO) region (2030–1840 cm^{-1}) of the IR spectra of these compounds suggest the presence of compounds with two and three carbonyl groups [11,13–16]. $^{13}C\{^1H\}$ NMR spectra of these compounds show three groups of carbonyl carbon signals in the region 232–227 ppm. The very narrow ranges of δ_P suggest a similar mutually *cis* position of the CO and PPh_3 ligands in the above tungsten(II) compounds.

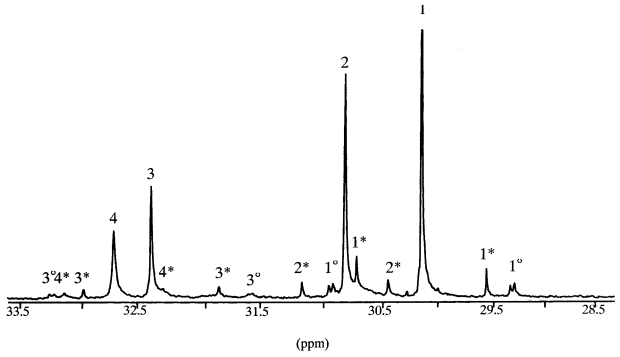


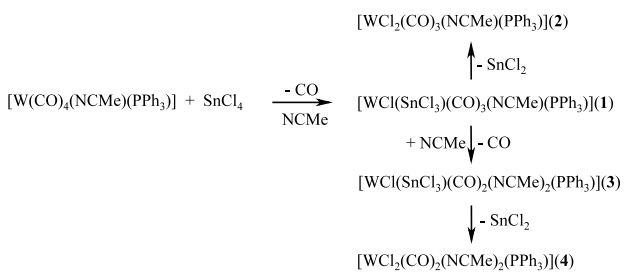
Fig. 1. $^{31}P\{^1H\}$ NMR spectrum showing the mixture of four seven-coordinate tungsten(II) compounds: $[WCl(SnCl_3)(CO)_3(NCMe)(PPh_3)]$(**1**), $[WCl_2(CO)_3(NCMe)(PPh_3)]$ (**2**), $[WCl(SnCl_3)(CO)_2(NCMe)_2(PPh_3)]$(**3**), and $[WCl_2(CO)_2(NCMe)_2(PPh_3)]$(**4**) formed during the reaction of $[W(CO)_4(NCMe)(PPh_3)]$ and $SnCl_4$ in acetonitrile. The signals denoted by an asterisk (*) are due to ^{183}W satellites and by circle (○) are due to ^{117}Sn and ^{119}Sn satellites.

Based on these spectral data, the formation of four seven-coordinate tungsten(II) compounds: $[WCl(SnCl_3)(CO)_3(NCMe)(PPh_3)]$ (**1**), $[WCl_2(CO)_3(NCMe)(PPh_3)]$ (**2**), $[WCl(SnCl_3)(CO)_2(NCMe)_2(PPh_3)]$ (**3**), and $[WCl_2(CO)_2(NCMe)_2(PPh_3)]$ (**4**), can be proposed (Scheme 1).

In reactions carried out in a coordinating solvent, such as acetonitrile, we considered the oxidative addition of $SnCl_4$ to $[W(CO)_4(NCMe)(PPh_3)]$ followed by the dissociation of $SnCl_2$ and the displacement of the CO ligands by the solvent (CH_3CN) molecules. However, during the reaction of $[WCl(SnCl_3)(CO)_3(NCMe)_2]$ with 1 equiv. of PPh_3 in CH_3CN, the formation of a mixture of compounds **3** and **4** was detected due to the presence of ν(CO) bands characteristic for bis(carbonyl) compounds [11,13–16]. Two pairs of ν(CO) bands: 1913(m), 1840(vs) and 1935(m), 1864(vs) cm^{-1}, deriving from compounds **3** and **4**, respectively, were observed in IR spectrum of a solid sample.

Treatment of $[W(CO)_4(NCMe)(PPh_3)]$ with 1 equiv. of $SnCl_4$ in CH_2Cl_2 solution besides compounds **1** and **2** also gave ionic species such as $[HPPh_3]^+$, $[SnCl_6]^{2-}$, and cationic complexes of tungsten(II). One of the cationic complex of tungsten(II) was isolated in crystalline form and X-ray analysis showed it to be $[WH(CO)_3(NCMe)(PPh_3)_2][SnCl_5\cdot MeOH]$ (**5**). The IR spectra (KBr disc) of compound **5** exhibit two sharp ν(CO) bands at 2040(w) and 1939(vs) cm^{-1}; this is fully consistent with the unusual *mer* configuration of the CO groups observed crystallographically. To our knowledge, a similar arrangement of three carbonyl groups has previously been detected only for $[WCl(SnCl_3)(CO)_3(\eta^4\text{-NBD})]$ [17].

The appearance of two carbonyl resonances in the $^{13}C\{^1H\}$ NMR spectrum (125.8 MHz, 293 K) of **5** at an intensity ratio of 2:1, at $\delta_C = 212.09$ and $\delta_C = 208.48$, respectively, conforms with the solid state structure of the distorted capped octahedron and *mer* geometry of the carbonyl groups. The $^{31}P\{^1H\}$ NMR spectrum (121.5 MHz, 293 K) of **5** shows a broad resonance due to 2 equiv. triphenylphosphine ligands at δ_P 25.04 ($^1J_{PW} = 131$ Hz). The ^1H spectra (500 MHz, 293 K) of **5** exhibit a three-line resonance due to a hydride ligand



Scheme 1.

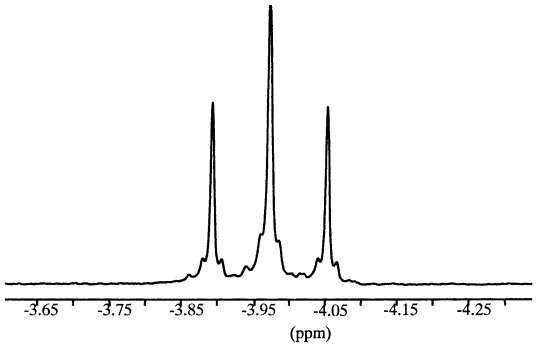


Fig. 2. High field ^{1}H NMR spectrum of the $[WH(CO)_3(NCMe)(PPh_3)_2][SnCl_5\cdot MeOH]$ (**5**) complex obtained at 293 K in CD_2Cl_2, showing the hydride signal at $\delta_H = -3.98$.

at $\delta_H = -3.98$ ($^2J_{PH} = 40$ Hz), which is further split due to a coupling to the tungsten atom ($^1J_{WH} = 13$ Hz) and to the carbonyl carbon atom ($^1J_{CH} = 32$ Hz) (Fig. 2). The $^1J_{WH} = 13$ Hz observed here is much smaller than that for $[^nPr_4N]_4[H_4W_4(CO)_{12}]$ (44.5 Hz [18]), $[Et_4N]_4[W_2(CO)_8(PMe_2Ph)_2]$ (44 Hz [19]), $[Et_4N][(\mu\text{-}H)(\mu\text{-}Ph_2P(CH_2)_4PPh_2)W_2(CO)_8]$ (46.1 Hz [20]), and $[PPN][HW(CO)_4(PMe_3)]$ (54 Hz [21]). In contrast, the $^2J_{PH} = 40$ Hz is about two times higher than observed in those tungsten(0) compounds [18–21], but very close to that found for tungsten(II) compounds such as $[WH(CO)_3(PMe_2Ph)_3]^+$ (47 Hz [22]) and $[WH(SPh)(CO)_3(PCy_3)_2]$ (43 Hz [23]). This suggests that the electronic configuration of the metal atom (d^6 or d^4) can exert influence on W–H interactions. The ^{13}C satellites ($I = 1/2$, 1%) observed on the hydride signal suggest a C–H interaction. The small hydrogen–carbon coupling constant indicates a three-center W–H···C agostic interaction [24,25], which was additionally proved by X-ray structure investigations (see next paragraph).

Similar spectral characteristic to those of compound **5** were shown by the product formed in the reaction of *trans*-$[W(CO)_4(PPh_3)_2]$ and $SnCl_4$ in CH_2Cl_2. Two broad ν(CO) bands at 2030(w) and 1937(vs) in the IR spectrum, a signal at $\delta_P = 25.92$ ($^1J_{PW} = 138$ Hz) in the $^{31}P\{^1H\}$ NMR spectrum and two doublets at $\delta_C = 218.36$ ($^2J_{CP} = 32$ Hz) and $\delta_C = 213.75$ ($^2J_{CP} = 9$ Hz) in the $^{13}C\{^1H\}$ NMR spectrum were observed. These spectral data suggest the formation of the cationic compound of tungsten(II) analogues to **5**. This compound has never been isolated in pure crystalline form, so the counter-ion is unknown. However, during the reaction of *trans*-$[W(CO)_4(PPh_3)_2]$ and $SnCl_4$ in CH_3CN solution, the formation of $[WCl_2(CO)_3(PPh_3)_2]$ as the main product was observed by IR spectra, due to characteristic ν(CO) bands at 2014(s), 1936(vs), and 1894(s) cm^{-1} [11]. In the $^{31}P\{^1H\}$ NMR spectra (CD_3CN, 293 K) of the reaction products, only very low-intensity signals in the range $\delta_P = 32.77–30.16$, assigned to compounds **1**–**4**, were observed. The solubility of $[WCl_2(CO)_3(PPh_3)_2]$ in CD_3CN is probably extremely low.

The oxidative addition reaction of phosphine complexes of tungsten(0) with $SnCl_4$ carried out in dichloromethane is always accompanied by the formation of $[HPPh_3]^+$ cations. The latter species gives a ν(PH) band at 2430 cm^{-1} and other characteristic bands [26–29] at 1114 and 721 cm^{-1} in IR spectra. In ^{1}H NMR spectra of the reaction products containing $[HPPh_3]^+$ cations, a doublet at $\delta_H = 9.36$ with $^1J_{HP} = 526$ Hz can be detected.

From the experimental results we deduce that the reaction course strongly depends on the solvent. When the reaction is carried out in acetonitrile solution, the elimination of $SnCl_2$ from the coordination sphere of tungsten occurs to give neutral compounds. In dichloromethane solution, the elimination of $SnCl_3^-$ anionic ligands takes place yielding cationic compounds of tungsten(II). The $SnCl_3^-$ anion should be oxidized by CH_2Cl_2 [30,31] producing the counterpart anion $[SnCl_5]^-$ or $[SnCl_6]^{2-}$.

2.2. Structure of $[WH(CO)_3(NCMe)(PPh_3)_2][SnCl_5\cdot MeOH]$ (5)

Fig. 3 shows an ORTEP perspective view of compound **5** that includes the atom numbering scheme. Selected interatomic bond distances and angles are summarized in Table 2. The crystal structure of **5** consists of well separated $[WH(CO)_3(NCMe)(PPh_3)_2]^+$ cations and $[SnCl_5\cdot MeOH]^-$ anions. The tungsten atom is in a

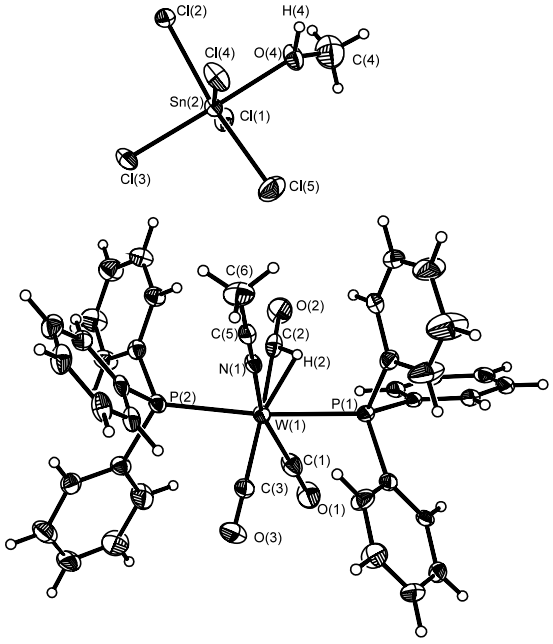


Fig. 3. The crystal structure of $[WH(CO)_3(NCMe)(PPh_3)_2][SnCl_5\cdot MeOH]$ (**5**).

seven-coordinate environment that can be approximately described [32,33] as capped octahedral, with the hydride ligand H(2) capping the triangular face formed by the carbon, nitrogen, and phosphorus atoms (Fig. 4). Within the distorted octahedral description, the two carbon atoms, two phosphorus atoms, and the nitrogen and the carbon atoms are mutually *trans* with C(2)–W–C(3), P(1)–W–P(2), and N(1)–W–C(1) angles of 175.31(18)°, 164.90(4)°, and 160.57(17)°, respectively. The capped octahedral face defined by the angles C(2)–W–N(1) = 90.29(16)°, P(1)–W–C(2) = 88.13(3)°, and P(1)–W–N(1) = 83.16(9)° is a little larger than the opposite face defined by P(2)–W–C(3) = 83.81(13)°, C(3)–W–C(1) = 81.65(19)°, and P(1)–W–C(1) = 78.79(14)°.

The bond lengths from tungsten are not unusual and are of the same order of magnitude as those reported in the literature for related complexes. For example, the average W–P bond length of 2.54 Å is only a little shorter than the values of 2.58 Å (av.) found in the complexes $[WCl(CO)(^tBuC{\equiv}CH)(NCMe)(PPh_3)_2]_2$-$[SnCl_6]\cdot 4NCMe$ [12] and $[WI_2(CO)_3(PEt_3)_2]$ [34]. The average W–C bond length of 2.035 Å, found for the two mutually *trans* carbonyl ligands, is a little longer than a W–C bond length of 1.971(5) Å for a carbonyl ligand in the *trans* position to an acetonitrile ligand. This is in accord with the higher *trans* influence of the CO group as compared with the nitrile ligand. The W–N bond distance of 2.159(3) Å is a little shorter than found in the complexes $[WCl(CO)(^tBuC{\equiv}CH)(NCMe)(PPh_3)_2]_2$-$[SnCl_6]\cdot 4NCMe$ (2.186(6) Å [12]) and $[WCl(SnCl_3)$-$(CO)_3(NCMe)_2]$ (2.18(1) Å [4]). The W–H distance of 1.713 Å in **5** is a little shorter than the W–H distances previously reported for the other tungsten(II) hydrides, e.g. 1.78 Å in $[WH(Cl)(CO)_2(PMe_3)_3]$ [35] and 1.835(36) Å in $[WCl_2(CHCMe_3)(CO)(PMe_3)_2]$ [24]. The H(2)–C(2) distance in **5** is only 0.9992 Å, indicative of a three-centre W–H···C agostic interaction [24,25]. The H(2)–C(2)–W angle is 57.1° and the H(2)–W–C(2) angle is 29.3°. Similar agostic interactions, but involving the α-H of the neopentylidene ligand, have been detected in $[WCl_2(CHCMe_3)(CO)(PMe_3)_2]$, where a C–H distance of 1.053(36) Å, an H–C–W angle of 72.2(20)°, and an H–W–C angle of 33.1(11)° were observed [24]. Interestingly, the carbonyl carbon atom adjacent to the hydride ligand is associated with a little shorter C–O length (1.128(5) Å) than in the other two CO ligands (1.161(5) and 1.143(5) Å).

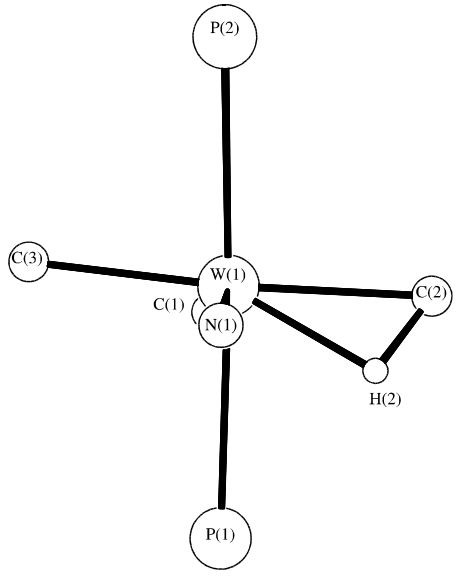


Fig. 4. The coordination sphere of tungsten(II) in $[WH(CO)_3$-$(NCMe)(PPh_3)_2]^+$ cation.

The $[SnCl_5(MeOH)]^-$ anion has irregular octahedral geometry. The *cis* Cl–Sn–Cl angles fall in the range 87.65(4)°–96.25(4)°, while the *cis* Cl–Sn–O angles are smaller (81.66(9)°–86.70(10)°), which is consistent with chlorine having a greater van der Waals radius than oxygen. The Sn(2)–Cl(2) distance of 2.442(1) Å is significantly longer than the remaining four Sn–Cl distances of 2.384 Å (av.). This difference is readily explained in terms of Cl···H interactions. The Cl(2) atom is involved in an intermolecular contact of 3.090(4) Å to H(4). Thus, an alcohol ligand coordinated through the oxygen atom to the tin atom is also hydrogen-bonded to a Cl(2) atom of the $SnCl_5$ counter-ion.

3. Experimental

3.1. General data

All reactions were carried out under nitrogen by standard Schlenk line techniques. The solvents and reagents applied were dried, distilled, and deoxygenated. Solution IR spectra were obtained using KBr or NaCl plates, while solid samples were recorded using KBr pellets on an FT IR model-400 Nicolet instrument. Far-IR spectra were recorded (600–100 cm^{-1}) with a Bruker IFSv instrument in a Nujol mull on a polyethylene film. ^1H, $^{13}C\{^1H\}$, and $^{31}P\{^1H\}$ NMR spectra were recorded on an AMX 300 and 500 MHz Bruker spectrometer. Chemical shifts were referenced against solvent resonance as the internal standard. In ^1H NMR spectra $\delta_H = 1.98$ for CD_3CN and $\delta_H = 5.32$ for CD_2Cl_2 and in ^{13}C NMR spectra $\delta_C = 118.00$ for CD_3CN and $\delta_C = 54.00$ for CD_2Cl_2. ^{31}P NMR spectra were referenced to external 85% H_3PO_4.

3.2. Synthesis of $[W(CO)_4(NCMe)(PPh_3)]$ [8]

$[W(CO)_5(PPh_3)]$ (1.05 g, 1.79 mmol), prepared according to the published procedure [36], was dissolved in acetonitrile (50 cm^3) with continuous stirring under a nitrogen atmosphere in a 100 cm^3 round-bottomed flask

equipped with a quartz window through which the solution was irradiated with an HBO 200 Hg lamp. The course of the reaction was monitored by IR measurements, and photolysis was stopped when the IR band of $[W(CO)_5(PPh_3)]$ at 2073 cm^{-1} had decayed (about 3 h). The solvent was evaporated in vacuum to yield a yellow residue containing $[W(CO)_4(NCMe)(PPh_3)]$ (90%), $[W(CO)_3(NCMe)_2(PPh_3)]$, and $[W(CO)_5(PPh_3)]$ identified by $^{31}P\{^1H\}$ NMR spectra in CD_3CN due to respective signals at $\delta_P = 28.77$, $^1J_{PW} = 240$ Hz [8], $\delta_P = 32.42$, $^1J_{PW} = 222$ Hz, and $\delta_P = 21.24$, $^1J_{PW} = 242$ Hz. Unreacted $[W(CO)_5(PPh_3)]$ was removed from the mixture by extraction to heptane.

3.3. Oxidative addition of $SnCl_4$ to $[W(CO)_4(NCMe)(PPh_3)]$

3.3.1. Reaction in CH_3CN solution

To $[W(CO)_4(NCMe)(PPh_3)]$ (0.83 g, 1.38 mmol) dissolved in 50 cm^3 of acetonitrile was added $SnCl_4$ (0.36 g, 1.38 mmol) by means of a syringe. The mixture was stirred for 4 h, during which time the yellow solution gradually changed to an orange color, while the ν(CO) frequency of the starting tungsten compound disappeared. After the completion of the reaction, the solution was evaporated to dryness and the residue washed with heptane.

IR (KBr disc): ν(CN) 2318(vw), 2287(vw) cm^{-1}, ν(CO) 2031(w), 1935(vs), 1913(sh), 1859(sh), 1840(sh) cm^{-1}; (Nujol): ν(SnCl) broad 330(w) cm^{-1}. ^1H NMR, (CD_3CN, 293 K): $\delta_H = 7.80–7.28$ m (PPh_3), $\delta_H = 2.17$ (CH_3CN). $^{13}C\{^1H\}$ NMR, (CD_3CN, 293 K): δ_C 231.9, 230.69, 226.72 (CO), $\delta_C = 135.14–129.93$d (PPh_3). $^{31}P\{^1H\}$ NMR (CD_3CN, 293 K): $\delta_P = 32.77$, $^1J_{PW} = 170$ Hz, $\delta_P = 32.44$, $^1J_{PW} = 235$ Hz, $^2J_{PC} = 57$ Hz, $^2J_{PSn} = 341$ and 348 Hz, $\delta_P = 30.70$, $^1J_{PW} = 150$ Hz and $\delta_P = 30.16$, $^1J_{PW} = 222$ Hz, $^2J_{PC} = 57$ Hz, $^2J_{PSn} = 308$ and 320 Hz. These spectral data were assigned to the following tungsten(II) compounds: $[WCl(SnCl_3)(CO)_3(NCMe)(PPh_3)]$ (**1**), $[WCl_2(CO)_3(NCMe)(PPh_3)]$ (**2**), $[WCl(SnCl_3)(CO)_2(NCMe)_2(PPh_3)]$ (**3**), and $[WCl_2(CO)_2(NCMe)_2(PPh_3)]$ (**4**).

3.3.2. Reaction in CH_2Cl_2 solution

To $[W(CO)_4(NCMe)(PPh_3)]$ (0.9 g, 1.5 mmol) dissolved in 5 cm^3 of CH_2Cl_2 was added $SnCl_4$ (0.39 g, 1.5 mmol). After 2 h stirring, IR spectroscopy confirmed the reaction to be complete. Volatiles were removed in vacuum to yield an orange solid, which was washed with heptane and dried. The IR spectrum in a KBr disc showed two broad carbonyl bands at 2030(m) and 1930(vs) cm^{-1}, and a shoulder on the former band. The $^{31}P\{^1H\}$ NMR spectra in CD_2Cl_2 showed the formation of a mixture of compounds; very low-intensity ^{31}P signals, decaying over time, were observed at δ_P about 30 ppm and intense signals at δ_P about 25 ppm. Slow crystallization from CH_2Cl_2–CH_3OH–toluene–heptane solution at approximately 273 K gave yellow crystals, which were isolated and fully characterized as $[WH(CO)_3(NCMe)(PPh_3)_2][SnCl_5 \cdot MeOH]$ (**5**). Simultaneously precipitated colorless crystals were identified by X-ray analysis as $[HPPh_3]_2[SnCl_6]$ and *cis*-$[SnCl_4(OPPh_3)_2]$ [37].

Anal. Calc. for $C_{42}H_{38}Cl_5NO_4P_2SnW$: C, 43.39; H, 3.29; N, 1.20. Found: C, 43.30; H, 3.45; N, 1.28%. IR (KBr disc): ν(CN) 2287(vw), ν(CO) 2040(w), 1939(vs) cm^{-1}. ^1H NMR (CD_2Cl_2, 293 K): $\delta_H = 7.90–7.70$d (PPh_3), $\delta_H = 5.85$ (broad) ($HOMe$), $\delta_H = 3.87$ (broad) ($HOMe$), $\delta_H = -3.97$t, $^1J_{HW} = 13$ Hz, $^2J_{PH} = 40$ Hz, $^1J_{HC} = 32$ Hz. $^{13}C\{^1H\}$ NMR, (CD_2Cl_2, 293 K): $\delta_C = 212.09$ (2 CO), $\delta_C = 208.48$ (1 CO), $\delta_C = 127.7$ (CH_3CN), $\delta_C = 35.81$ ($HOMe$), $\delta_C = 5.11$ (CH_3CN). $^{31}P\{^1H\}$ NMR (CD_2Cl_2, 293 K): $\delta_P = 25.04$, $^1J_{PW} = 131$ Hz.

3.4. Reaction of $[W(CO)_4(PPh_3)_2]$ with $SnCl_4$

To $[W(CO)_4(PPh_3)_2]$, prepared in photochemical reaction of $[W(CO)_5PPh_3]$ with PPh_3 [38], (0.18 g, 0.22 mmol) in 25 cm^3 of CH_2Cl_2, 2 equiv. of $SnCl_4$ were added (0.12 g, 0.46 mmol). After 48 h stirring, IR spectroscopy confirmed the reaction to be complete. Volatiles were removed in vacuum to yield an orange solid, which was washed with heptane and dried. The IR spectrum in a KBr disc showed two broad carbonyl bands at 2030(m) and 1937(vs) cm^{-1}. The $^{31}P\{^1H\}$ NMR spectra in CD_2Cl_2 showed the formation of a mixture of new tungsten(II) compounds characterized by ^{31}P signals at $\delta_P = 28.94$ (15%), 25.92, $^1J_{PW} = 138$ Hz (50%) and 25.63 (10%). Signal at $\delta_P = 20.95$, $^1J_{PW} = 244$ Hz (25%) indicates the formation of $[W(CO)_5(PPh_3)]$. In the $^{13}C\{^1H\}$ spectrum, two (2:1) doublets at $\delta_C = 218.36$, $^2J_{CP} = 32$ Hz and $\delta_C = 213.75$, $^2J_{CP} = 9$ Hz were observed. Two additional doublets (1:4) at $\delta_C = 199.19$, $^2J_{CP} = 22$ Hz and $\delta_C = 197.22$, $^2J_{CP} = 7$ Hz proved the presence of $[W(CO)_5(PPh_3)]$. From a CH_2Cl_2 solution of these compounds the colorless crystals of $[HPPh_3]_2[SnCl_6]$ salts always precipitate. IR spectra (KBr, disc): ν(PH) 2430 cm^{-1} and other characteristic bands at 1114, 869, and 721 cm^{-1} [26–29].

3.5. Reaction of $[WCl(SnCl_3)(CO)_3(NCMe)_2]$ with PPh_3 in CH_3CN

To $[WCl(SnCl_3)(CO)_3(NCMe)_2]$ [4] (0.16 g, 0.3 mmol) dissolved in 10 cm^3 of acetonitrile was added PPh_3 (0.7 g, 0.3 mmol) in 5 cm^3 of acetonitrile. The mixture was stirred for 25 min, during which time the ν(CO) frequency of the starting tungsten compound disappeared. After that time the solution was evaporated to dryness and the orange residue washed with heptane. *Anal*. Calc. for $C_{24}H_{21}Cl_4N_2O_2PSnW$ (**3**): C, 34.12; H,

2.51; N, 3.32. Found: C, 34.13; H, 2.68; N, 3.68%. IR (KBr disc): ν(CN) 2339(vw), 2295(vw); ν(CO) 1935(m), 1864(vs) cm^{-1}; $^{31}P\{^{1}H\}$ NMR (CD_3CN): $\delta_P = 32.44$, $^{1}J_{PW} = 235$ Hz, $^{2}J_{PSn} = 341$ and 348 Hz. After prolonged reaction time in acetonitrile the purple crystals of another bis(carbonyl) compound (**4**) were precipitated. IR (KBr disc): ν(CN) 2290(vw), ν(CO) 1914(m), 1840(vs) cm^{-1}.

3.6. Crystal and refinement data for compound 5

Crystal data and relevant refinement details for **5** are presented in Table 1. The yellow crystals of **5** were grown from a CH_2Cl_2–CH_3OH–toluene–heptane (5:0.1:1:10) solution. The crystals were stable enough when handled in an inert atmosphere or coated with a light hydrocarbon oil to protect them from the atmosphere.

Crystal data for **5** were collected on a Kuma KM4CCD κ-axis diffractometer with graphite-monochromated Mo Kα radiation ($\lambda = 0.71073$ Å), μ(Mo Kα) = 3.467 mm^{-1}. The data were corrected for Lorentz and polarization effects. After refinement with isotropic displacement parameters for all atoms, an absorption correction based on the least-squares filled against $|F_c| - |F_o|$ differences was also applied [39].

Table 1
Crystal data and structure refinement for $[WH(CO)_3(NCMe)(PPh_3)_2][SnCl_5 \cdot MeOH]$ (**5**)

Chemical formula	$C_{42}H_{38}Cl_5NO_4P_2SnW$
Molecular weight	1162.46
Crystal system	triclinic
Space group	$P\bar{1}$
Unit cell dimensions	
a (Å)	10.166(2)
b (Å)	12.254(2)
c (Å)	18.424(4)
α (°)	93.31(3)
β (°)	92.35(3)
γ (°)	94.18(3)
V (Å^3)	2282.9(8)
Z	2
T (K)	100
Crystal size (mm)	0.10 × 0.13 × 0.15
D_{calc} (g cm^{-3})	1.691
λ (Mo Kα) (Å)	0.71073
μ (Mo Kα) (mm^{-1})	3.467
F(000)	1136
Method of collection	ω–2θ scan
2θ Range for data collection (°)	$6.7 < 2\theta < 52.0$
Index ranges	$-6 \le h \le 12$, $-15 \le k \le 15$, $-22 \le l \le 22$
Number of unique data	8639
Number of data with $[I \le 2\sigma(I)]$	7392/511
Refinement method	Full-matrix least-squares on F^2
Residuals R_1, wR_2	0.0305, 0.0691
Final ($\Delta\rho$)(e Å^{-3})	1.87/−1.19
Goodness-of-fit on F^2	1.063
Absorption correction factors, min, max	0.726, 1.495

Table 2
Selected bond lengths (Å) and angles (°) for $[WH(CO)_3(NCMe)(PPh_3)_2][SnCl_5 \cdot MeOH]$ (**5**)

Bond lengths	
W(1)–C(1)	1.971(5)
W(1)–C(3)	2.033(5)
W(1)–C(2)	2.037(5)
W(1)–N(1)	2.159(3)
W(1)–P(2)	2.525(1)
W(1)–P(1)	2.550(1)
W(1)–H(2)	1.7132
C(2)–H(2)	0.9992
O(1)–C(1)	1.161(5)
O(2)–C(2)	1.128(5)
O(3)–C(3)	1.143(5)
Sn(2)–O(4)	2.220(3)
Sn(2)–Cl(5)	2.380(1)
Sn(2)–Cl(3)	2.380(1)
Sn(2)–Cl(1)	2.384(1)
Sn(2)–Cl(4)	2.395(1)
Sn(2)–Cl(2)	2.442(1)
O(4)–C(4)	1.391(7)
O(4)–H(4)	0.92(6)
Bond angles	
C(1)–W(1)–C(3)	81.65(19)
C(1)–W(1)–C(2)	96.45(19)
C(3)–W(1)–C(2)	175.31(18)
C(1)–W(1)–N(1)	160.57(17)
C(3)–W(1)–N(1)	92.88(15)
C(2)–W(1)–N(1)	90.29(16)
C(1)–W(1)–P(2)	115.74(14)
C(3)–W(1)–P(2)	83.81(13)
C(2)–W(1)–P(2)	93.23(12)
N(1)–W(1)–P(2)	81.89(9)
C(1)–W(1)–P(1)	78.79(14)
C(3)–W(1)–P(1)	94.87(13)
C(2)–W(1)–P(1)	88.93(13)
N(1)–W(1)–P(1)	83.16(9)
P(2)–W(1)–P(1)	164.90(4)
C(1)–W(1)–H(2)	103.4
C(3)–W(1)–H(2)	155.3
C(2)–W(1)–H(2)	29.3
N(1)–W(1)–H(2)	74.3
P(2)–W(1)–H(2)	114.2
P(1)–W(1)–H(2)	63.2
O(2)–C(2)–H(2)	126.1
W(1)–C(2)–H(2)	57.1
O(4)–Sn(2)–Cl(5)	86.7(1)
O(4)–Sn(2)–Cl(3)	177.81(9)
Cl(5)–Sn(2)–Cl(3)	94.08(5)
O(4)–Sn(2)–Cl(1)	86.74(9)
Cl(5)–Sn(2)–Cl(1)	90.34(5)
Cl(3)–Sn(2)–Cl(1)	95.30(4)
O(4)–Sn(2)–Cl(4)	81.66(9)
Cl(5)–Sn(2)–Cl(4)	92.41(5)
Cl(3)–Sn(2)–Cl(4)	96.25(4)
Cl(1)–Sn(2)–Cl(4)	167.91(4)
O(4)–Sn(2)–Cl(2)	86.3(1)
Cl(5)–Sn(2)–Cl(2)	172.84(4)
Cl(3)–Sn(2)–Cl(2)	92.95(5)

Minimum and maximum value of the absorption correction factors ranging between 0.726 and 1.495. Data reduction and analysis were carried out with Kuma Diffraction (Wrocław) programs. The structure was solved by heavy-atom methods using the SHELXS-97 program [40] and refined by a full-matrix least-squares method on all F^2 data using the SHELXL-97 program [41] to $R_1 = 0.0305$ and $wR_2 = 0.0691$. Non-hydrogen atoms were refined with anisotropic thermal parameters. The hydrogen atoms were located according to HFIX procedure using the SHELXL-97 program [41].

4. Supplementary material

Crystallographic data have been deposited at the Cambridge Crystallographic Data Centre with deposition no. 174363. Copies of this information may be obtained free of charge from The Director, CCDC, 12 Union Road, Cambridge CB2 1EZ UK (fax: +44-1223-336033; e-mail: deposit@ccdc.cam.ac.uk or www: http://www.ccdc.cam.ac.uk).

Acknowledgements

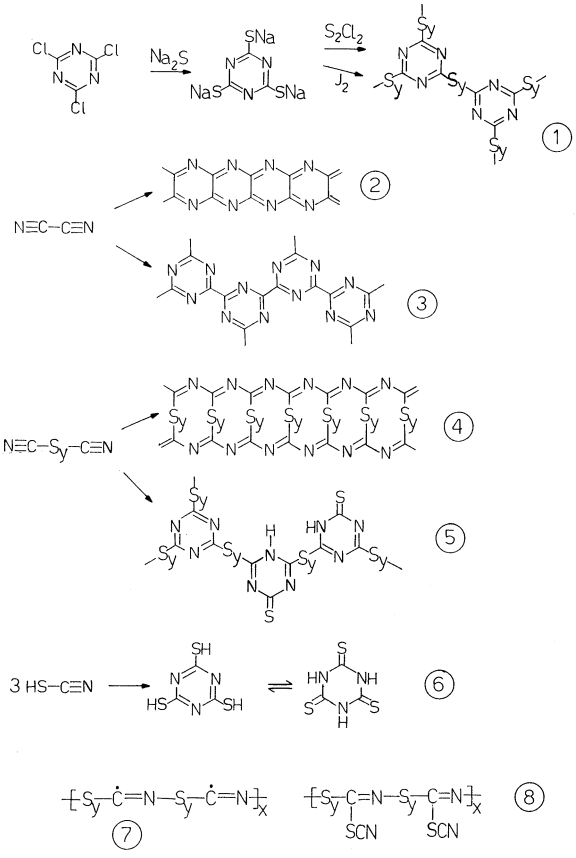
Financial support from the Polish State Committee for Scientific Research (grant No. 3 T09A 059 17) is gratefully acknowledged. The authors thank to A. Gądek for synthesis and M. Kowalska and S. Baczyński for recording the NMR spectra.

References

[1] P.K. Baker, Adv. Organomet. Chem. 40 (1996) 45.
[2] P.K. Baker, Chem. Soc. Rev. 27 (1998) 125.
[3] M.A. Jahdali, P.K. Baker, A.J. Lavery, M.M. Meehan, D.J. Muldoon, J. Mol. Catal. A: Chem. 159 (2000) 51.
[4] T. Szymańska-Buzar, T. Głowiak, Polyhedron 17 (1998) 3419.
[5] T. Szymańska-Buzar, T. Głowiak, J. Organomet. Chem. 564 (1998) 143.
[6] T. Szymańska-Buzar, T. Głowiak, J. Organomet. Chem. 575 (1999) 98.
[7] T. Szymańska-Buzar, T. Głowiak, I. Czeluśniak, J. Organomet. Chem. 585 (1999) 215.
[8] R.D. Adams, J.L. Perrin, J. Am. Chem. Soc. 121 (1999) 3984.
[9] P.K. Baker, S.G. Fraser, Transition Met. Chem. 12 (1987) 560.
[10] P.K. Baker, S.J. Coles, M.C. Durrant, S.D. Harris, D.L. Hughes, M.B. Hursthouse, R.L. Richards, J. Chem. Soc., Dalton Trans. (1996) 4003.
[11] T. Szymańska-Buzar, T. Głowiak, J. Organomet. Chem. 492 (1995) 241.
[12] I. Czeluśniak, T. Głowiak, T. Szymańska-Buzar, Inorg. Chem. Commun. 316 (2000) 285.
[13] D. Miguel, J.A. Pérez-Martínez, V. Riera, S. Garcia-Granda, Polyhedron 14 (1991) 1717.
[14] D. Miguel, J.A. Pérez-Martínez, V. Riera, S. Garcia-Granda, J. Organomet. Chem. 455 (1993) 121.
[15] F.A. Cotton, J.H. Meadows, Inorg. Chem. 23 (1984) 4688.
[16] B.J. Brisdon, A.G. Hodson, Inorg. Chim. Acta 128 (1987) 51.
[17] T. Szymańska-Buzar, T. Głowiak, Polyhedron 16 (1997) 1599.
[18] J.T. Lin, J.E. Ellis, J. Am. Chem. Soc. 105 (1983) 6252.
[19] J.T. Lin, G.P. Hagen, J.E. Ellis, J. Am. Chem. Soc. 105 (1983) 2296.
[20] J.T. Lin, Y.M. Shiao, J. Organomet. Chem. 334 (1987) C31.
[21] S.G. Slater, R. Lusk, B.F. Schumann, M. Darensbourg, Organometallics 1 (1982) 1662.
[22] V. Zannotti, V. Rutar, R.J. Angelici, J. Organomet. Chem. 414 (1991) 177.
[23] R.F. Lang, T.D. Ju, G. Kiss, C.D. Hoff, J.C. Bryan, G.J. Kubas, Inorg. Chim. Acta 259 (1997) 317.
[24] J.H. Wengrovius, R.R. Schrock, M.R. Churchill, H.J. Wasserman, J. Am. Chem. Soc. 104 (1982) 1739.
[25] M. Brookhart, M.L.H. Green, L.L. Wong, Prog. Inorg. Chem. 36 (1988) 1.
[26] J.C. Sheldon, S.Y. Tyree, J. Am. Chem. Soc. 80 (1958) 2117.
[27] J. Lewis, R. Whyman, J. Chem. Soc. (A) (1967) 77.
[28] P.K. Baker, S.G. Fraser, Inorg. Chim. Acta 116 (1986) L1.
[29] P.K. Baker, S.G. Fraser, J. Chem. Soc., Dalton Trans. (1988) 2729.
[30] W.L. Olson, D.A. Nagaki, L.F. Dahl, Organometallics 5 (1986) 630.
[31] A.S. Goldman, D.R. Tyler, Inorg. Chem. 26 (1987) 253.
[32] M.G.B. Drew, Prog. Inorg. Chem. 23 (1977) 67.
[33] M. Melnik, P. Sharrock, Coord. Chem. Rev. 65 (1985) 49.
[34] P.K. Baker, A.I. Clark, M.M. Meehan, E.E. Parker, A.E. Underhill, M.G.B. Drew, M.C. Durrant, R.L. Richards, Transition Met. Chem. 23 (1998) 155.
[35] L. Contreras, A. Monge, A. Pizzana, C. Ruiz, L. Sánchez, E. Carmona, Organometallics 12 (1993) 4228.
[36] R.J. Angelici, M.D. Malone, Inorg. Chem. 6 (1967) 1731.
[37] T. Szymańska-Buzar, T. Głowiak, I. Czeluśniak, Main Group Met. Chem. 24 (2001) 821.
[38] D.J. Darensbourg, M.A. Murphy, J. Am. Chem. Soc. 100 (1978) 463.
[39] P. Starynowicz, COSABS99, Program for Absorption Correction, University of Wrocław, Wrocław, Poland, 1999.
[40] G.M. Sheldrick, SHELXS-97, Program for Solution of Crystal Structures, University of Göttingen, Göttingen, Germany, 1997.
[41] G.M. Sheldrick, SHELXS-97, Program for Crystal Structure Refinement, University of Göttingen, Göttingen, Germany, 1997.

2. Experimental

All the equipment and procedures used have already been described in the previous papers [3–8]. In particular the synthesis of thiocyanogen and sulfur dicyanide has already been detailed in Refs. [5,6]. The chemical synthesis of polythiocyanogen $[S_2(CN)_2]_x$ has already been reported in Refs. [3,5]. The electrochemical synthesis of polythiocyanogen $[S_2(CN)_2]_x$ has been described both in Refs. [4,7]. The synthesis of all the series of polythiocyanogens $[S_y(CN)_2]_x$ with $y = 1$, 2, 3 and 4 is detailed in the patent of Ref. [8] and/or will be reported in another future work. In the reaction of polythiocyanogens with NaCN or Na_2S we have followed the procedure already described in Ref. [5]. The triazine-based monomeric model compounds trithiocyanuric acid sodium salt has been prepared by reacting trichlorotriazine with sodium sulfide (see Refs. [3–5]). The polymerisation of trithiocyanuric acid with iodine to produce compound **1** of Scheme 1 has been described in Ref. [5]. The procedure to follow the polymerisation of thiocyanogen on a KBr plate described in Ref. [5] has been applied in the present work to follow also the polymerisation of tetrasulfur dicyanide $S_4(CN)_2$.



Scheme 1.

2.1. Preparation of $S_4(CN)_2$ and study of its polymerisation over a KBr plate

In a two necked round bottomed flask with condenser and magnetic stirrer, S_2Cl_2 (2.0 g) was added dropwise to a stirred suspension of $Pb(SCN)_2$ (5.0 g) in CH_2Cl_2 (80 ml) at r.t. For the addition of S_2Cl_2 use was made of a dropping funnel. The reaction is slightly exothermic since CH_2Cl_2 is refluxing at the end of the addition. After having stirred for 1.5 h at r.t. the resulting $PbCl_2$ formed was decanted from the solution. The $S_4(CN)_2$ solution in CH_2Cl_2 shows a maximum at 253 nm followed by a shoulder at about 300 nm. $S_2(CN)_2$ in the same conditions show a maximum at about 250 nm followed by another maximum at 294 nm.

The solution of $S_4(CN)_2$ is reasonably stable for about 1 week if kept in a cool place in a tightly closed flask in the dark. However, if a few drops of the solution are put over a substrate, as soon as almost all the CH_2Cl_2 evaporates a quick polymerisation reaction takes place with the formation of a brick-red–orange solid. Thus a few drops of the solution were placed on a KBr plate and the polymerisation was followed immediately after the almost complete evaporation of CH_2Cl_2. The IR spectral changes are reported in Figs. 1 and 3. A similar procedure has been adopted to follow the polymerisation of $S_2(CN)_2$ after its preparation according to the method reported in Ref. [5]. The spectra of polymerising $S_2(CN)_2$ are reported in Fig. 2.

2.2. Preparation of $S(CN)_2$ and its thermal polymerisation in refluxing acetic acid

AgCN (9.1 g) was suspended in 70 ml of CH_2Cl_2 in the same apparatus described above. Sulfur dichloride SCl_2 (3.3 g) was added dropwise and then the mixture was stirred at r.t. for 1.5 h before the decantation of the AgCl formed. The evaporation of all the solvent at reduced pressure in a water bath leaves a residue of white crystals mixed with orange–red polythiocyanogen. Sublimation of this crude residue gives white tabular crystals on the top of the flask. The FT-IR spectrum of these crystals is perfectly coincident with that reported in Ref. [5] for $S(CN)_2$. The solution of these crystals in acetonitrile shows a maximum at 224 nm and another maximum at 235 nm. A shoulder appears at 324 nm. The residual matter remained in the bottom of the flask after the sublimation appears as a rusty-brown solid. The yield was 1.34 g. The spectrum of this polymeric mass is shown in Fig. 4(D) and it corresponds to that of a polythocyanogen.

The white sublimed crystals (abut 500 mg) were dissolved in 5 ml of acetic acid and refluxed for 15 h. At the end of the thermal treatment the mixture appeared as orange–red. The polymer was insoluble in acetic acid and was recovered by filtration, washed with

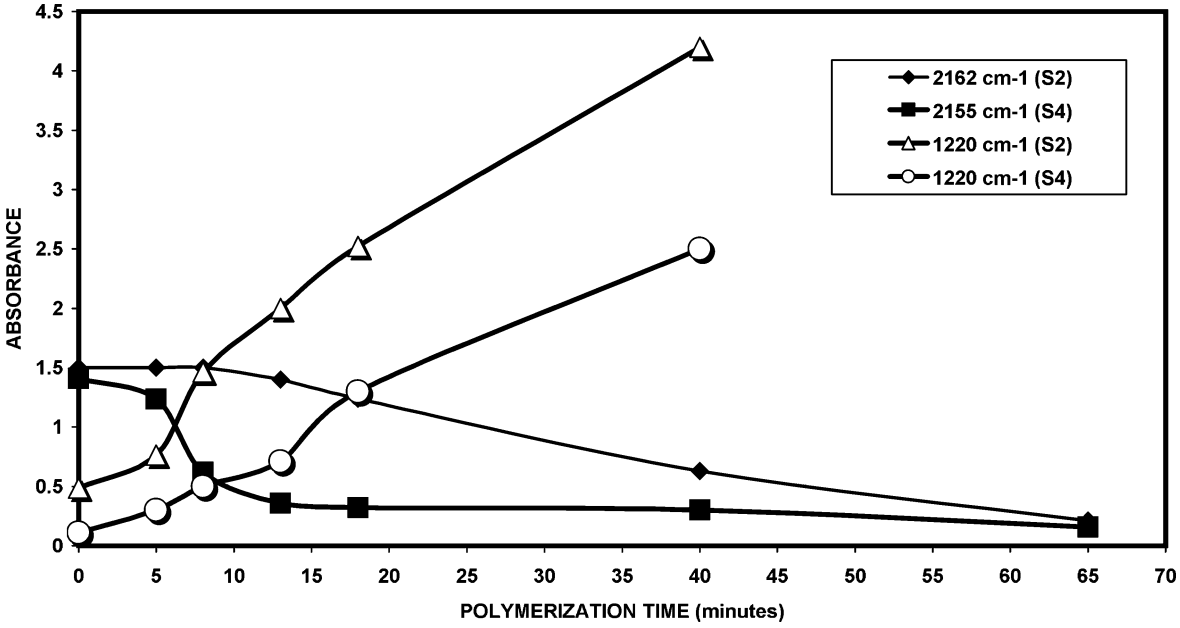


Fig. 1. Kinetics of $S_2(CN)_2$ and $S_4(CN)_2$ polymerisation followed by FT-IR spectroscopy.

abundant water and acetone and left to dry. The yield was almost quantitative. The spectrum of this $[S(CN)_2]_x$ is shown in Fig. 4(C) and corresponds to that of a polythiocyanogen.

2.3. Preparation of the triazine-based model compound **1** (Scheme 1) by the action of S_2Cl_2 over trithiocyanuric acid sodium salt

Trithiocyanuric acid (1.0 g) is dissolved in 20 g of dimethyl sulfoxide (DMSO) and 0.68 g of NaOH are added. The mixture is heated and stirred and becomes bluish-green. On cooling the mass solidifies and a small volume of water (5 ml) was added to re-dissolve the mass. A rapid precipitation of a yellow mass occurred on dropwise addition of S_2Cl_2 (4.0 g) under stirring. The mixture was left overnight and the following day was diluted with acetone and filtered under reduced pressure. The filtrate was washed repeatedly with acetone and dried in air. The yield of recovered bright yellow material was 0.92 g. The FT-IR spectrum of this material is reported in Fig. 6(C) and agrees reasonably with the spectrum of polymeric trithiocyanuric acid prepared by the action of I_2 over $(SH)_3(CN)_3$ Fig. 6(B), Ref. [5].

2.4. Thermal treatments of polythiocyanogens $[S_2(CN)_2]_x$ and $[S_4(CN)_2]_x$ as well as model compound **1** of Scheme 1

The thermal treatment involved the use of 200 mg of each compound, respectively $[S_2(CN)_2]_x$ and $[S_4(CN)_2]_x$ as well as model compound **1** of Scheme 1. Each compound was put into a porcelain crucible with a cap and heated in a muffle at 300 °C for 1 h. After cooling the FT-IR spectra shown in Figs. 6(E) and 7(E and F) have been recorded.

3. Results and discussion

In the previous works [3–8] which were limited only to the study of the structure of parathiocyanogen the polythiocyanogen with $y = 2$ derived from the polymerisation of $S_2(CN)_2$, we have shown that parathiocyanogen does not possess a 1,3,5-triazine-based structure 1 (Scheme 1) as reasonably proposed by other researchers for a number of experimental facts.

i) The FT-IR spectrum of $[S_2(CN)_2]_x$ does not match the spectrum of a 1,3,5-triazine-based polymer prepared through a sure route which has the chemical structure 1 (see Scheme 1) originally expected for parathiocyanogen [3–5].
ii) The ^{13}C NMR spectrum of parathiocyanogen has a relatively broad signal at 186 ppm while trithiocyanuric acid $(SH)_3(CN)_3$ shows a narrow signal at about 145 ppm [4,5].
iii) The electronic spectrum of parathiocyanogen shows a maximum at 267 nm followed by another maximum at 440 nm while the 1,3,5-triazine-based model compound shows a maximum at 275 nm and another peak at about 350 nm [4,5].
iv) The X-ray powder diffraction pattern of $[S_2(CN)_2]_x$ is very peculiar showing only a relatively broad peak at $2\theta = 26$ (Cu Kα) while the triazine-based model compound is dominated by a series of reflections which are similar to those of cyclooctasulfur [5].

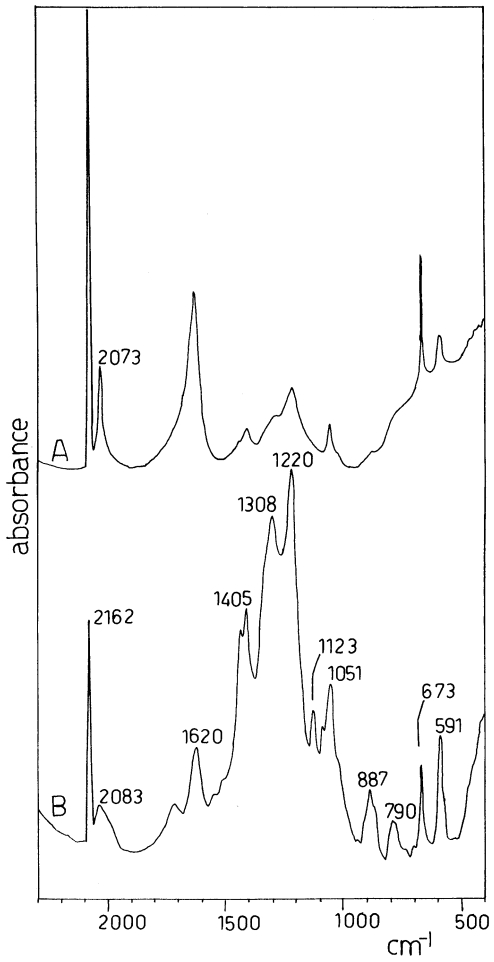


Fig. 2. (A) FT-IR of $S_2(CN)_2$ polymerisation: spectrum taken 7 min after the evaporation of the CH_2Cl_2 solvent from a KBr plate. This is the spectrum of the monomeric thiocyanogen and the incipient polymerisation product (band at 1220 cm^{-1}). (B) FT-IR of $S_2(CN)_2$ polymerisation product 21 min after solvent evaporation.

3.1. Aspects of the polymerisation of sulfur dicyanides (thiocyanogens)

In the present work, we have followed the $S_2(CN)_2$ and the $S_4(CN)_2$ polymerisation by leaving few drops of a fresh solution in CH_2Cl_2 of each pseudohalogen to evaporate spontaneously on a KBr plate and recording by FT-IR the spectral changes as function of time. When almost all the CH_2Cl_2 has been evaporated the polymerisation of the non-volatile pseudohalogen started ($t = 0$) immediately. The spectral changes are summarised in Fig. 1 and show two main trends: the decay in the optical density of the bands associated to the –CN stretching at 2162 and 2073 cm^{-1}, and the concomitant increase of a new main band at about 1220 cm^{-1}. Almost the same trend has been observed for both $S_2(CN)_2$ and $S_4(CN)_2$ as shown in Fig. 1 suggesting that in both cases the –CN groups were the reaction sites and the polymer is deriving just from the reaction of these groups. Visually, the polymerisation can be observed from the fact that the pseudohalogen thin film on the KBr plate becomes yellow, then yellow–orange, orange and red at the end of the reaction. At this final stage the film is hard and brittle.

The details of the spectral evolution during the polymerisation of $S_2(CN)_2$ are illustrated in Fig. 2(A and B). Fig. 2(A) refers to the early polymerisation stages and is dominated by the -CN stretching bands at 2162 and 2073 cm^{-1} as well as the C–S stretching at 670 cm^{-1} [6]. The incipient polymerisation is suggested in Fig. 2(A) by the weak bands at 1405, 1220 and 1051 cm^{-1}. The mentioned bands develop greatly their intensity (see Fig. 2(B)) as the polymerisation goes to completion with the simultaneous decay in intensity of the –CN stretching bands. These new bands are not associated to the 1,3,5-triazine ring formation as will be discussed in the next section.

Of extreme interest are the spectra shown in Fig. 3(A–D) and recorded on $S_4(CN)_2$ at increasing degrees of polymerisation. In fact these spectra show for the first time that also the superior homologue of thiocyanogen $S_2(CN)_2$, namely tetrasulfur dicyanide $S_4(CN)_2$, polymerises exactly as its inferior homologue, suggesting that all the family of the thiocyanogen or sulfur cyanides polymerise in the same fashion. In detail, Fig. 3(A) shows the spectrum of $S_4(CN)_2$ at the beginning of the polymerisation. Again the spectrum is dominated by the asymmetric and symmetric stretching of the –CN group, respectively, at 2155 and 2068 cm^{-1} and by the C–S stretching band at 668 cm^{-1}. The polymerisation involves the gradual development of a band at 1220 cm^{-1} (see Fig. 3(B–D)) which is accompanied by weak bands at 1405 and 1060 cm^{-1}. Simultaneously a decay on the –CN stretching band is observed. The new bands of the polymeric $[S_4(CN)_2]_x$ are located at the same wavenumbers as polymeric $[S_2(CN)_2]_x$ previously discussed. A comparison between the polymerisation kinetics of $S_4(CN)_2$ in comparison to $S_2(CN)_2$ is illustrated in Fig. 1.

Sulfur dicyanide is the most stable molecule of the series of thiocyanogens: it can be isolated as stable crystals. Elsewhere [6] we have discussed the reasons of this unusual stability. However, $S(CN)_2$ is not stable indefinitely. Even at r.t., under the action of moisture, light and heat it is converted into a brick-red polymeric material $[S(CN)_2]_x$. Fig. 4(A) shows the FT-IR spectrum of aged crystals of $S(CN)_2$: they are mixed with the polymeric derivative as suggested by the presence of the broad band at 1242 cm^{-1} together with the –CN band at 2186 cm^{-1} and the C–S band at 678 cm^{-1} due to the monomer. The progression of the polymerisation at r.t. is shown in Fig. 4(B) where, as usual, a reduction of the intensity of the band at 2186 cm^{-1} (–CN stretching) corresponds to the development of the broad band at 1240–1220 cm^{-1}. $S(CN)_2$ can be completely poly-

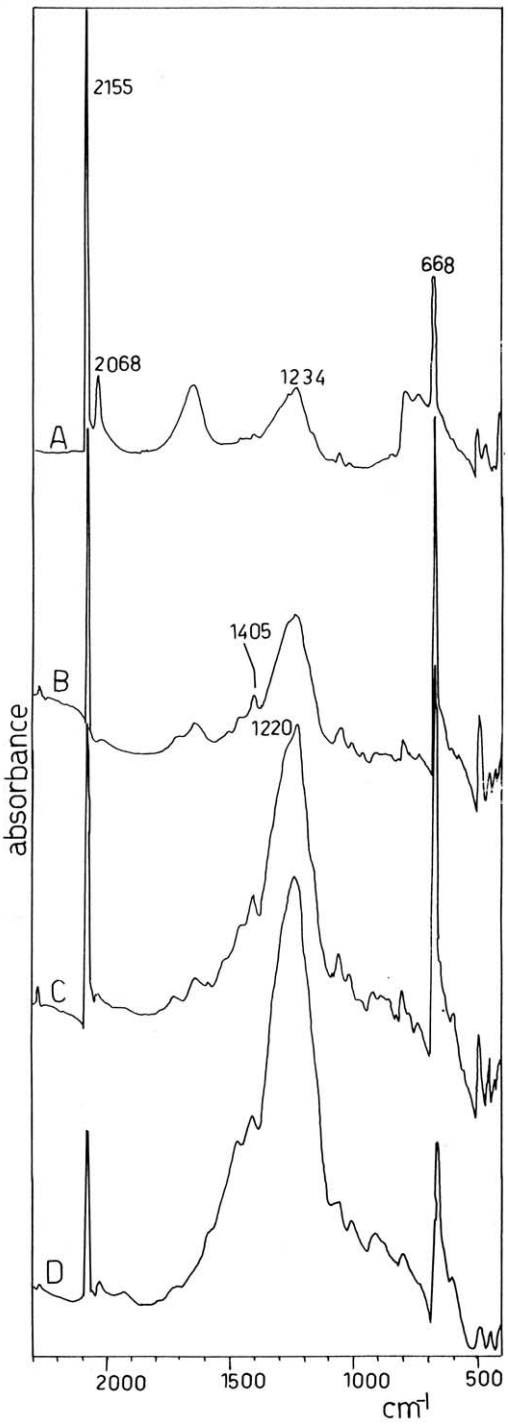


Fig. 3. (A) FT-IR of $S_4(CN)_2$ polymerisation: spectrum taken 5 min after the evaporation of the CH_2Cl_2 solvent from a KBr plate. This is the spectrum of the monomeric tetrasulfur dicyanide and the incipient polymerisation product (band at 1220 cm^{-1}). (B) FT-IR of $S_4(CN)_2$ polymerisation product 10 min after solvent evaporation. (C) FT-IR of $S_4(CN)_2$ polymerisation product 15 min after solvent evaporation. (D) FT-IR of $S_4(CN)_2$ polymerisation product 45 min after solvent evaporation.

merised when heated in refluxing acetic acid; the spectrum of the corresponding $[S(CN)_2]_x$ is shown in Fig. 4(C).

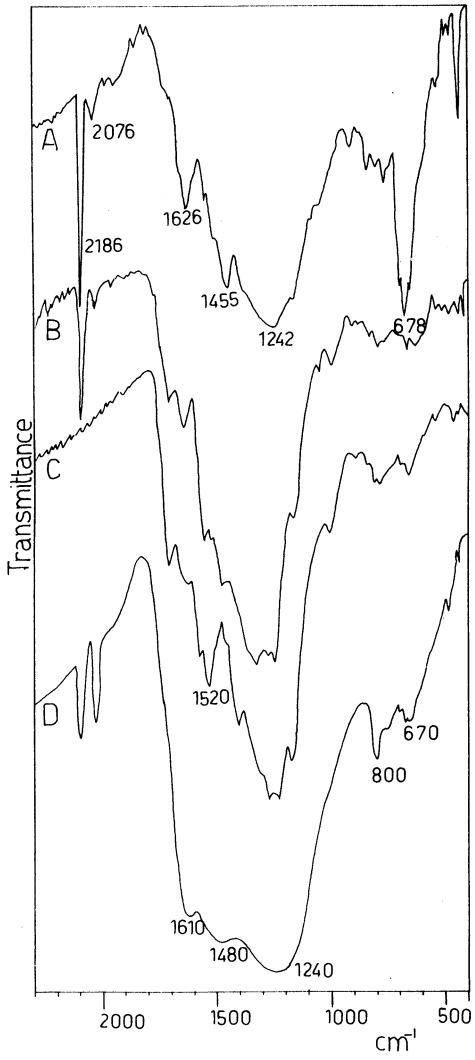


Fig. 4. (A) FT-IR of partially polymerised $S(CN)_2$. (B) FT-IR of polymerised $S(CN)_2$ at r.t. after several weeks. (C) FT-IR of polymerised $S(CN)_2$ after refluxing in acetic acid for 15 h. (D) FT-IR of polymerised $S(CN)_2$ formed in the bottom of the flask after the thermal treatment for the sublimation recovery of pure $S(CN)_2$.

The experimental evidences are now sufficient to affirm that all the sulfur cyanide family $S_y(CN)_2$ polymerise in the same way yielding polymers whose general structure may be described by the general formula:

$[S_y(CN)_2]_x$ with y and integer 1, 2, 3, 4, ...

and x an high number but unknown

All the polythiocyanogens show the same spectrum essentially characterised by a very strong and broad band centred at about 1220 cm^{-1} and by several other minor bands. Fig. 5 illustrates the concept by comparing the spectra of $[S_2(CN)_2]_x$, $[S_3(CN)_2]_x$ and $[S_4(CN)_2]_x$: it is clear the spectral identity and thus the structural identity of these polymers.

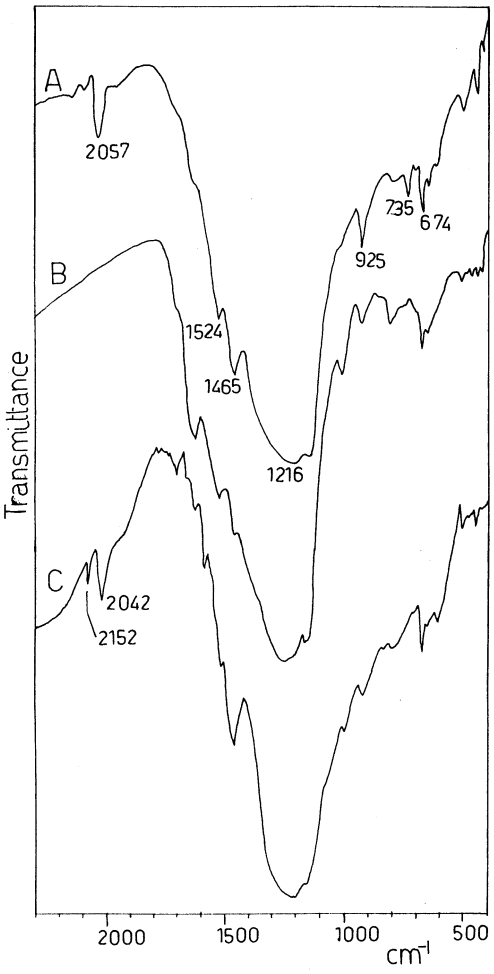


Fig. 5. (A) FT-IR of polymerised $S_2(CN)_2$: polythiocyanogen $[S_2(CN)_2]_x$. (B) FT-IR of polymerised $S_3(CN)_2$: polythiocyanogen $[S_3(CN)_2]_x$. (C) FT-IR of polymerised $S_4(CN)_2$: polythiocyanogen $[S_4(CN)_2]_x$.

Thus the provisory conclusions we can draw at this stage is that despite the different length of the sulfur bridges connecting the –CN end groups, the latter polymerise in the same way. Therefore, it appears that the –CN groups are transformed into derivatives having the same chemical structure. Since nitrile groups are prone to trimerise into 1,3,5-triazine rings, the simplest explanation for the polymerisation of all sulfur dicyanides is the formation of 1,3,5-triazine rings connected together by sulfur bridges. The length of the sulfur bridges depends on the original chain length of the starting monomeric sulfur dicyanide. This interpretation has been proposed by Feher et al. in 1956 [9].

3.2. The FT-IR spectra of the 1,3,5-triazine-based polymers with sulfur bridges do not match the spectra of polythiocyanogens

As illustrated in Scheme 1 we have prepared trithiocyanuric acid by reacting trichlorotriazine with disodium sulfide and we have polymerised the trithiocyanuric acid by the action of iodine or by reacting the sodium salt of trithiocyanuric acid with sulfur monochloride (Scheme 1, structure 1). In the last two cases we have obtained through two different sure routes the chemical structures expected from the polymerisation of sulfur cyanides or thiocyanogens, supposing that they trimerise into triazine rings. Fig. 6(A–C) illustrate the FT-IR spectra of both trithiocyanuric acid (Fig. 6(A)) and its polymers with S_2 (Fig. 6(B)) and polysulfide bridges (Fig. 6(C)): if we compare these spectra with those of $[S_y(CN)_2]_x$ for instance shown in Fig. 5, it appears immediately evident that the polythiocyanogens cannot have the triazine-based structure. First of all the triazine-based structure is characterised by the out-of plane bending of the triazine ring which is located at 783 and 751 cm^{-1} in the monomeric trithiocyanuric acid (Fig. 6(A)) and is shifted to higher wavenumbers after the polymerisation. In fact the triazine ring bending appears at about 823 cm^{-1} in Fig. 6(B and C) both referring to the polymeric triazine structure 1 (Scheme 1). This characteristic band is weak or completely absent in the case of the $[S_y(CN)_2]_x$ (see Fig. 5). Other characteristic triazine bands present in the spectrum of Fig. 6(A) are the very strong bands at 1540 and 1362 cm^{-1} respectively due to quadrant and semicircle triazine ring stretch [10]. After polymerisation these two bands are still detectable at 1480 and 1242 cm^{-1}, shifted to shorter wavenumbers (see Fig. 6(B and C)). In any case these spectra cannot be compared with those of polythiocyanogens of Fig. 5. Thus, once again structure 1 is not the structure of polythiocyanogen.

3.3. Some chemical aspects of polythiocyanogens: their reaction with sodium sulphide and sodium cyanide

Although polythiocyanogens do not display the same FT-IR spectra of the triazine-based polymer, they are reduced to polymeric trithiocyanuric acid (Structure 1, Scheme 1) when they are treated with sodium sulfide in water solution (see Ref. [5]). This is evident by comparing Fig. 7(A) and especially Fig. 7(B) with the spectra of Fig. 6(C and B). This is the first indication that polythiocyanogens undergo a structural isomerisation to a triazine-based polymer. Thus the Na_2S treatment causes the passage from structure 4 to 1.

Another interesting reaction, which can be observed on the polythiocyanogens, involves their treatment with NaCN. Sodium cyanide is able to abstract sulfur from the polysulfide bridges of structure 4, with the consequent formation of NaSCN, causing the passage from structure 4 to 2 of paracyanogen (see Scheme 1). This is documented by the spectra of Fig. 7(D and E) which should be compared with the IR spectra of the pristine samples shown in Fig. 5. The formation of paracyanogen $(CN)_x$ by sulfur abstraction from polythiocyano-

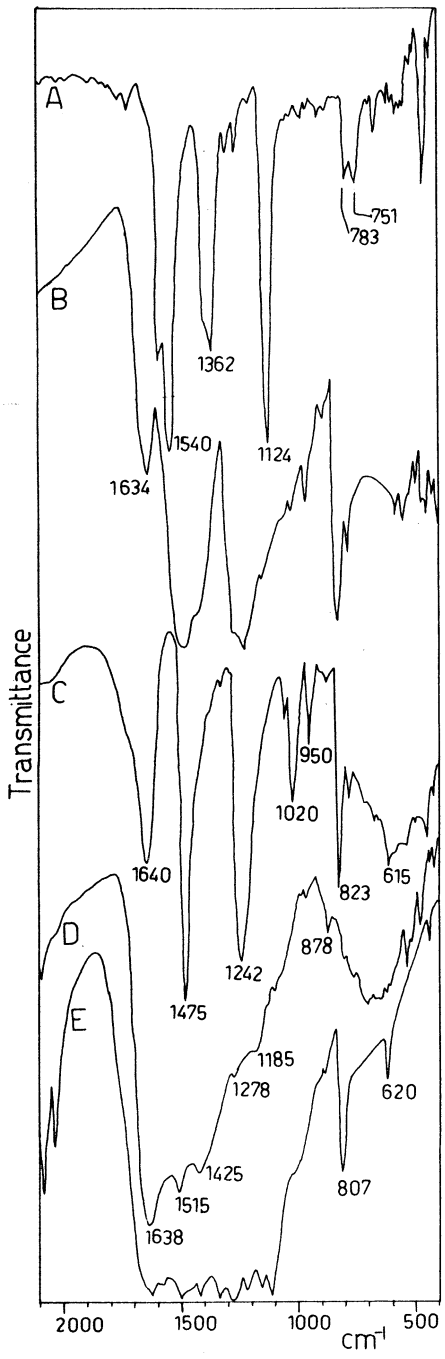


Fig. 6. (A) FT-IR of trithiocyanuric acid sodium salt (1,3,5-triazine-based model compound). (B) FT-IR of polymerised trithiocyanuric acid with iodine catalyst according to Ref. [5] (1,3,5-triazine-based model compound **1** of Scheme 1). (C) FT-IR of polymerised trithiocyanuric acid with S_2Cl_2 according to Ref. [5] (1,3,5-triazine-based model compound **1** of Scheme 1). (D) FT-IR of 1,3,5-triazine-based model compound **1** of Scheme 1 after treatment with NaCN. The spectrum is now that of paracyanogen (structure 3, Scheme 1) see Refs. [11,13,17]. (E) FT-IR of 1,3,5-triazine-based model compound **1** of Scheme 1 after a thermal treatment at 300 °C. The spectrum is now that of paracyanogen (structure 3, Scheme 1).

gens $[S_y(CN)_2]_x$ is suggested by the development of new bands at 1630–1640 and at about 1500 cm^{-1} which

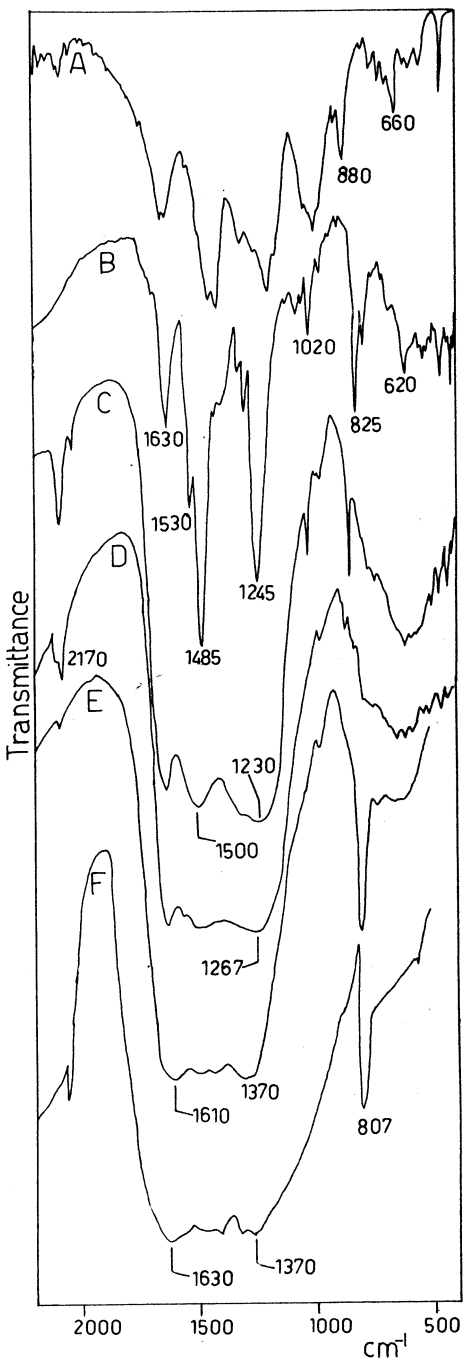


Fig. 7. (A) FT-IR of polythiocyanogen $[S_2(CN)_2]_x$ after the treatment with Na_2S according to Ref. [5]. The spectrum is now that of 1,3,5-triazine-based model compound **1** of Scheme 1; compare with Fig. 6(B and C). (B) FT-IR of polythiocyanogen $[S_4(CN)_2]_x$ after the treatment with Na_2S according to Ref. [5]. The spectrum is now that of 1,3,5-triazine-based model compound 1 of Scheme 1; compare with Fig. 6(B and C). (C) FT-IR of polythiocyanogen $[S_2(CN)_2]_x$ after the treatment with NaCN according to Ref. [5]. The spectrum is now that of paracyanogen structure 2, Scheme 1. (D) FT-IR of polythiocyanogen $[S_4(CN)_2]_x$ after the treatment with NaCN according to Ref. [5]. The spectrum is now that of paracyanogen structure 2, Scheme 1. (E) FT-IR of polythiocyanogen $[S_2(CN)_2]_x$ after thermal treatment at 300 °C. The spectrum is now that of paracyanogen structure 3, Scheme 1. (F) FT-IR of polythiocyanogen $[S_4(CN)_2]_x$ after thermal treatment at 300 °C. The spectrum is now that of paracyanogen structure 3, Scheme 1.

reach the same intensity as the band at 1220 cm^{-1} as shown in the spectra of Fig. 7(C and D).

The other aspect, which links again (by chemical behaviour) the triazine, based polymer and the polythiocyanogens is the treatment with sodium cyanide of the former (according to Ref. [5]). In fact when the polymeric triazine compound (structure 1, Scheme 1) is treated with NaCN, sulfur abstraction occurs as well because of the formation of NaSCN and the IR spectrum changes into that of paracyanogen $(CN)_x$ as illustrated in Fig. 6(D). This spectrum is characterised by the intense and broad band at 1640–1450 cm^{-1} and by the triazine ring band at 878 cm^{-1} but by the absence of the intense band at 1230–1260 cm^{-1} observed in the paracyanogen obtained from polythiocyanogens. Therefore, the triazine-based polymer of structure 1 is transformed into the triazine isomer of paracyanogen (structure 3 of Scheme 1) when treated with NaCN. Conversely, the polythiocyanogens with structure 4 are converted into ladder paracyanogen of structure 2 upon NaCN treatment.

Elsewhere [11–13] we have already discussed about paracyanogen $(CN)_x$ and about its formation from the photopolymerisation of dicyanogen $(CN)_2$ and about the synthesis and the existence of a triazine-based isomer of paracyanogen having structure 3, in addition to the well known ladder paracyanogen of structure 2 (Scheme 1). The spectrum of Fig. 6(D) is analogous to the IR spectrum of the triazine-based isomer of paracyanogen $(CN)_x$ with structure 3 of Scheme 1 which we have prepared through a sure route [11–13].

Furthermore, the thermal treatment at 300 °C of both the polythiocyanogens and the triazine-based polymer transform both these macromolecules into paracyanogen as clearly suggested by the spectra of Figs. 6(E) and 7(E and F), with release of detectable free sulfur vapours. After this thermal treatment there are no doubts about the fact that both the polythiocyanogens having structure 4 and the triazine polymer of structure 1 have been transformed into paracyanogen. In fact the spectra of Figs. 6(E) and 7(E and F) are completely comparable with those of the paracyanogen prepared by Bircumshaw et al. [14]. It is of particular interest that all the spectra just mentioned show an intense band at 807 cm^{-1} which could be assigned also to a triazine ring and hence the paracyanogen formed from both the model compound and the polythiocyanogens may be the triazine isomer of Scheme 1 structure 3.

3.4. Further reflections and discussions about the structure of polythiocyanogens

Among the data discussed in the preceding paragraph, these are still some puzzling result concerning the structure assignment of the polythiocyanogens. In fact the treatment with sodium sulfide of $[S_y(CN)_2]_x$ favours the idea that polythiocyanogens may have structure 5 instead of structure 4 (Scheme 1) where we have represented a polymer with triazine rings having both possible tautomers (thioketo and sulfidic form). In this context it is useful to recall that thiocyanic acid is an unstable molecule and trimerises to trithiocyanuric acid which is in tautomeric equilibrium with its trithioketo form (isothiocyanuric acid trimer) as illustrated in Scheme 1 structure 6.

Structure 5 reported in Scheme 1 is in fact able to justify why the polythiocyanogens show an FT-IR spectrum different from that of triazine polymers with structure 1. The strong band at 1220 cm^{-1} in fact could reasonably be assigned to the thioketo group C=S which absorb just in this spectral region [15]; additionally the spectrum of 1,3,5-triazine-2,4,6-trithione shows a strong band at 1140 cm^{-1} which is shifted to 1210 cm^{-1} in the parent compound 1,3,5-triazine-2,4-amino-6-thione [15]. Moreover in these compounds the triazine ring bending is weak or absent, as in the case of polythiocyanogens spectra of Fig. 5. Structure 5 for polythiocyanogens may also be able to explain their orange and red colour since the chromophore will be just the C=S group and the quinoid structures associated (see structure 5). Of course, with structure 1 it is almost impossible to explain the orange–red colour of polythiocyanogens.

Thus it appears reasonable to think that when the sulfur dicyanides polymerise, they form triazine rings containing also thioketonic groups as shown in Scheme 1 structure 5. The treatment of these polymers with sodium sulfide causes the rearrangement of the structure 5 to the structure 1 (Scheme 1). The treatment with NaCN, being an alkaline agent probably causes the passage from structure 5 to 1 and simultaneously causes the partial abstraction of sulfur from the polysulphidic bridges connecting the triazine rings leading to both structure 1 with $y = 1$ or directly to structure 3 (see Scheme 1) which is the structure of the triazine-isomer paracyanogen. However, in the previous paragraph we have already shown that the treatment of polytiocyanogens with NaCN is leading to paracyanogen with the ladder structure 2 and not with the triazine isomer with structure 3. Thus this fact strongly supports structure 4 for polythiocyanogens rather than structure 5.

Furthermore, the strong heating of both polythiocyanogens and also the triazine-based model polymer (structure 1) causes the extrusion of sulfur and the passage to structure 3 in both cases. This fact does not necessarily support structure 5 for polythiocyanogens since one can expect a rather easy decomposition and thermal depolymerisation from structure 5 rather than its rearrangement to structure 3.

Additional data, which are against structure 5 for polythiocyanogens, are provided by ^{13}C NMR spectroscopy. We have already excluded that the polythiocyanogens have a triazine-based structure 1 because the

trithiocyanuric acid shows a peak at 145 ppm while $[S_2(CN)_2]_x$ shows a broad peak at 186 ppm [4,5]. Thus the newly proposed structure 5 is not correct because it requires at least two ^{13}C NMR signals: one for the C=S group which is expected at about 200 ppm or at lower field and the triazine signal at 145 ppm. Since we have recorded only a unique peak at 186 ppm [5], it is now allowed to drop the structure 5 as the corrected structure for polythiocyanogens.

In our previous works we have proposed a linear structure for polythiocyanogen $[S_2(CN)_2]_x$. The possible linear structures are 7 and 8 (see Scheme 1) and have also been proposed by Skorobogatova et al. [16]. However structure 8 can be phased out because the ^{13}C NMR of $[S_2(CN)_2]_x$ shows only one peak at 186 ppm while from structure 8 two different ^{13}C signals are expected but have not been observed [4,5]. Furthermore, the –SCN stretching band is not always present in the IR spectra of polythiocyanogens and if present is always weak while for structure 8 it is expected to be strong.

Structure 7 is coherent with the ^{13}C NMR spectrum of $[S_2(CN)_2]_x$ but it appears to be not extremely stable. The criticism against this structure is that it could easily undergo a crosslinking reaction with adjacent chains so that it cannot survive for long time under the form of 7 but other more complex networked structures should be derived easily from 7.

The discovery that all polythiocyanogens $[S_y(CN)_2]_x$ have essentially the same IR spectrum and hence the same chemical structure also creates problems with structure 7 since it becomes difficult to explain why the introduction of a different number of sulfur atoms in the polymer backbone does not alter at all either the FT-IR spectrum or the UV spectra of the series.

In fact, the introduction of more than one sulfur atom in the chain structure 7 must necessarily reduce the conjugation along the chain and the electronic spectra should change abruptly by passing from $y = 1$ to 2 and then to $y > 2$ but this is not observed experimentally for all the polythiocyanogen series as outlined in Fig. 8, where the electronic spectra in DMSO are very similar to each other from $y = 1$ to 4 showing essentially two absorption bands in all series. One of the absorption bands is located at about 270 nm and other one in the range of 375–410 nm. Moreover the colour of all the polythiocyanogen series is invariably orange to brick-red but if structure 7 is correct we should expect a gradual shift from red to orange, to yellow, to pale yellow as the length of the sulfur bridge increases for $y \to \infty$.

3.5. Attempt to interpret the spectral data and the chemical data in a unique coherent model

All the discussion in the previous paragraphs has shown that structure 5 is not satisfactorily describing the structure of polythiocyanogens, although it has some merit. Conversely, structure 8 and especially structure 7 which were originally proposed by us [3–5] and by

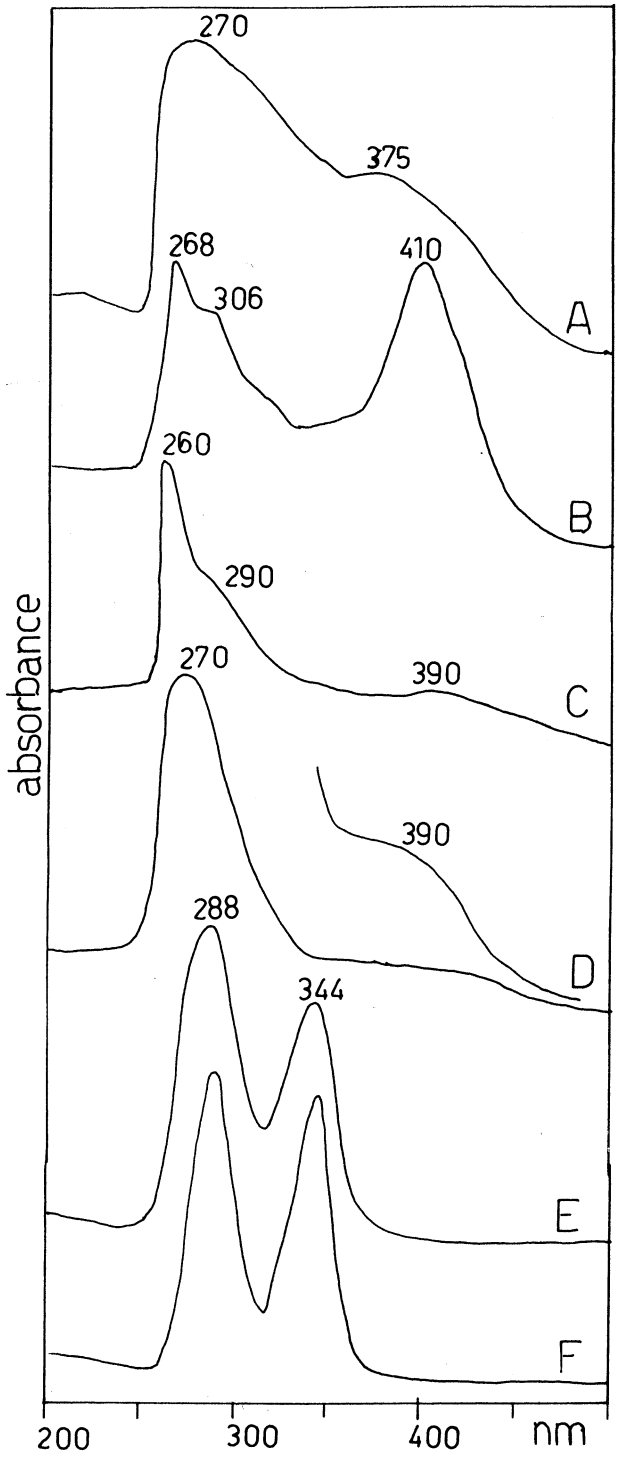


Fig. 8. (A) Electronic spectrum of $[S(CN)_2]_x$ in DMSO solvent. (B) Electronic spectrum of $[S_2(CN)_2]_x$ in DMSO solvent. (C) Electronic spectrum of $[S_3(CN)_2]_x$ in DMSO solvent. (D) Electronic spectrum of $[S_4(CN)_2]_x$ in DMSO solvent. (E) Electronic spectrum of trithiocyanuric acid in DMF solvent. (F) Electronic spectrum of compound **1** of Scheme 1 in DMF solvent.

others [16] present too many flaws in front of the experimental data available. Thus the structure of polythiocyanogens can be represented as structure 4 of Scheme 1. Let us summarise the reason for this choice and proposal:

i) dicyanogen NC–CN can be considered the most inferior homologue of the polythiocyanogen series of $[S_y(CN)_2]_x$; in fact when $y = 0$ we get $[(CN)_2]_x$. It polymerise thermally [14] and under the action of the UV light [11–13] into a polymer having essentially a polypyrazino–pyrazine ladder structure 2 (see Scheme 1). The ladder structure 2 is a little bit of an idealised structure because recently ourselves [11,13] and other authors [17,18] have proposed a more disordered structure derived from structure 2. However, in the frame of our discussion here we can utilise the structure 2. In normal conditions dicyanogen does not polymerise into the polytriazine structure 3 [11,13,17,18].

ii) Therefore, it is reasonable to think that also the superior homologues of dicyanogen, those containing S (so that when $y > 0$ the general formula is $[S_y(CN)_2]_x$) should polymerise in the same fashion of dicyanogen giving polyazomethine chains connected together by sulfur bridges (structure 4, Scheme 1) rather than the triazine rings of structure 1. Many experimental facts can be explained with this model.

iii) First of all, the structure 4 proposed for polythiocyanogens explains well both the FT-IR spectra and the electronic spectra of the series and the fact that these spectra appear exactly the same for all the polythiocyanogen series. Concerning the strong infrared band at about 1220 cm^{-1} we should not anymore advocate the thioketonic C=S stretching band which has been postulated in the case of structure 5. Instead the band at 1220 is due to the polyazomethine chain which, due to the tight sulfur crosslink of structure 4, causes the shift of this band from 1600 to 1450 cm^{-1} (typical paracyanogen band, see Refs. [11–14]) to about 1250–1220 cm^{-1}. Furthermore, structure 4 explains well the electronic spectra of polythiocyanogens of Fig. 8 and the colour of these polymeric compounds which does not change as function of the sulfur chain length. The polyazomethyne chain of structure 4 is a sequence of single and double bonds and this explains well the long wavelength transition at 380–410 nm observed in the electronic spectra of Fig. 8(A–D) for all the polythiocyanogen series. Thus, the polyazomethyne chain is the chromophore for all the polythiocyanogen series. As expected, the triazine-based structure 1 cannot display any transition at so long wavelengths due to the lack of conjugated chains. In fact, both the compound having structure 1 and the parent compound trithiocyanuric acid (structure 6) show the longest transition at only 344 nm (see Fig. 8(E and F)). In the case of the alternative structure 5 for polythiocyanogen series we were forced to introduce the ad hoc hypothesis of the presence of the thioketo (C=S) groups which should cause the transition at 400 nm or even at longer wavelength.

iv) The ^{13}C NMR spectrum of polythiocyanogen $[S_2(CN)_2]_x$ shows a unique broad band at 186 ppm [5]. The paracyanogen ^{13}C MAS NMR spectrum appears at about 158–150 ppm [17] while the spectrum of triazine ring shows just one unique sharp carbon signal at 145 ppm [4]. Initially we have thought that the signal at 186 ppm was the proof for the linearity of $[S_2(CN)_2]_x$ but in the preceding section we have explained the reasons which have led us to abandon the linear structure 7: the intrinsic instability of that structure together with the fact that it cannot explain many properties of all $[S_y(CN)_2]_x$. At this point, the peculiar peak at 186 ppm is assigned to the carbon atoms present in the azomethine chains connected with sulfur bridges of structure 4 (Scheme 1). The connection of the azomethine chains with sulfur bridges causes a deshielding of the carbon atoms which appear at 20 ppm downfield in comparison to the usual chemical shift of an azomethine chain not connected with sulfur. In fact the azomethine chain is expected to give a ^{13}C NMR signal at about 167 ppm in imines, oximes and hydrazones [19] and it is reported to appear at 158–150 ppm in the solid state spectra of paracyanogen. Thus a shift of 20 ppm downfield is expected for sulfur substitution [19] and leads to a value just at about 186 ppm as experimentally found.

v) The treatment of the polythiocyanogen series with NaCN causes the formation of ladder parathiocyanogen as suggested by the FT-IR spectra of Fig. 7(C and D) confirming that the correct structure of polythiocyanogen is 4 of Scheme 1. Conversely, the triazine-based polymer with structure 1 is transformed into the triazine-isomer of paracyanogen with structure 3 when treated with NaCN. The thermal treatment of both polythiocyanogens with structure 4 and the triazine polymer with structure 1 involves the elimination of sulfur and causes their transformation into paracyanogen with presumable structure 3 as documented by FT-IR spectroscopy (Figs. 6(E) and 7(E–F)). There is no clear mechanism for the passage from structure 2 to 3, but the FT-IR of the thermally processed polythiocyanogens suggest that the final structure is structure 3, the same obtained by thermal processing of the triazine-based structure 1 (see discussion in the

preceding sections). The sodium sulfide treatment of the polythiocyanogen series converts structure 4 into 1. This is again the passage from a ladder structure to a triazine structure and is documented by the FT-IR spectra of Fig. 7(A and B). Sulfur abstraction may cause the direct isomerisation and cyclisation from structure 4 to 3 although the mechanism is not yet clear.

4. Conclusions

On the basis of a considerable body of experimental facts which have been reviewed step-by-step the conclusion has finally been reached that polythiocyanogens of $[S_y(CN)_2]_x$, the red–orange polymeric materials derived from the polymerisation of the thiocyanogens or sulfur cyanides of $S_y(CN)_2$ (with y an integer 1, 2, 3, 4...) have the structure 4 of Scheme 1. This structure is characterised by two long polyazomethine chains connected together by sulfur bridges of different length. The linear structure originally proposed has now been rejected due to various reasons including the experimental evidences.

Acknowledgements

We are deeply indebted with Agenzia Spaziale Italiana (ASI), Viale Liegi 26, Rome, Italy for the financial support of the present work.

References

[1] Gmellins Handbuch der Anorganischen Chemie, vol.14/11, System C14, TL D5, Springer-Verlag, Berlin, 1978, pp. 161–237.
[2] P. Brun, A. Fontaine, P. Pascal, Nouveau Traitè de Chimie Minerale, vol. 8, Masson, Paris, 1961, p. 973.
[3] F. Cataldo, Polyhedron 11 (1992) 79.
[4] F. Cataldo, P. Fiordiponti, Polyhedron 12 (1993) 279.
[5] F. Cataldo, J. Inorg. Organomet. Polymer 7 (1997) 35.
[6] F. Cataldo, Polyhedron 19 (2000) 681.
[7] F. Cataldo, Italian Patent No. 1273004, originally filed 30 June, 1994.
[8] F. Cataldo, Italian Patent No. 1231927, originally filed 19 June, 1989.
[9] F. Feher, D. Hirschfeld, K.H. Linke, Z. Naturfosch. B17 (1962) 624.
[10] D. Lin-Vien, N.B. Colthup, W.G. Fateley, J.G. Grasselli, The Handbook of Infrared and Raman Characteristic Frequencies of Organic Molecules, Academic Press, San Diego, CA, 1991, pp. 295–300.
[11] F. Cataldo, Eur. Polymer J. 35 (1999) 571.
[12] F. Cataldo, Meteoritics Planetary Sci. (2001) A38.
[13] F.Cataldo Intern., J. Astrobiol. 1 (2002) 25.
[14] L.L. Bircumshaw, F.M. Tayler, D.H. Whiffen, J. Chem. Soc. (1954) 931.
[15] N.B. Colthup, L.H. Daly, S.E. Wiberley, Introduction to Infrared and Raman Spectroscopy, 3rd ed. (see also the spectra No. 412 and 415 at page 452), Academic Press, San Diego, CA, 1990, pp. 377–379.
[16] E.V. Skorobogatova, V.R. Karthashov, Russian Chem. Rev. 67 (1998) 423.
[17] L. Maya, J. Polymer Sci. Polymer Chem. 31 (1993) 2595.
[18] R.P. Subrayan, P.G. Rasmussen, Trends Polymer Sci. 3 (1995) 165.
[19] E. Pretsch, W. Simon, J. Seibl, T. Clerc, Tables of Spectral Data for Structure Determination of Organic Compounds, 2nd ed., Springer-Verlag, Berlin, 1989, pp. C201–C203.

scopic properties of perchlorate complexes containing trivalent rare earth ions. The perchlorate anion (ClO_4^-) has been chosen due to its poor ability to coordinate to metal ions; this is useful for the investigation of the influence of ligands on metal ions in solution in the absence of anionic interference. However, in some compounds [13–15] vibrational spectroscopy and conductance data have shown that some perchlorate groups are coordinated to the rare earth ion as monodentate or chelating bidentate ligands. The formation of the complexes between the perchlorate group and RE^{3+} ions has been explained in terms of hard acid–base interactions, which are predominantly electrostatic. Furthermore, the coordination sphere of the rare earth ions is large enough to accept several bonds, which favour the competition between the perchlorate anion and water or organic solvents. A detailed study on the perchlorate anion and its coordination modes in complexes was reported by Pascal and Favier [16].

N-(2-Pyridyl)acetamide and some related amides serve as model compounds for the study of polypeptides and proteins conformation, their vanadium(III) and oxovanadium(IV/V) complexes also have been used to investigate the interaction between vanadium and proteins in biological systems [17]. Some complexes between transition metals and trivalent rare earth ions with *N*-(2-pyridyl)acetamide and derived ligands were previously characterized and studied, showing that this ligand is chelating bidentate to the metal ions by using heterocyclic pyridinic nitrogen and oxygen amide atoms [18–20]. Recently, theoretical studies [21] of the complexes containing trivalent rare earth ions and pyridine and amide as ligands indicate that the metal–ligand interaction increases with the electron donating character of the substituent.

Perchlorate complexes of Eu with *N*-(2-pyridyl)acetamide ligand [20] showed high luminescence and it was observed by vibrational spectroscopy and conductance data that the ClO_4^- anions were not coordinated to the metal.

This work describes the synthesis, characterization and study of the influence of the methyl group in the 3, 4 and 6 positions on the pyridine ring of the *N*-(2-pyridyl)acetamide ligand in the luminescent properties of the Eu(III)-complexes with these ligands.

2. Experimental

2.1. Synthesis of the ligands and Eu(III)-perchlorate complexes

The *x*-mpa ligands (where mpa = *N*-[methylpyridyl]acetamide and $x = 3$, 4 and 6) were synthesized by the method described by Bould and Brisdon [19]. A mixture of 0.048 mol of 2-amino *x*-methylpyridine and 0.06 mol of Ac_2O was heated on a steam bath and remained under stirring. After 30 min, water ($\sim$100 ml) was added to the mixture to hydrolyze the excess of Ac_2O. The resulting solution was maintained under stirring for 1 h. The AcOH formed in the mixture was neutralized with $NaHCO_3$ and the ligand was extracted from the solution with $CHCl_3$ solvent. The solid product was recrystallized from ether to give large colorless crystals with efficiency of 70% and dried under in a desiccator vacuum over anhydrous $CaCl_2$.

The Eu(III)-perchlorate complexes were prepared by direct reaction between ethanolic solutions of the ligand and Eu(III)-perchlorate, in the molar ratio ligand–metal of 3:1, at room temperature (r.t.) and under stirring. The complexes precipitated immediately after addition of the Eu(III)-perchlorate solution, which were filtered, washed with EtOH and dried in vacuum in a desiccator. The complexes are not hygroscopes, except for the one with the 6-mpa ligand.

2.2. Measurements

The ^1H NMR spectra of the ligands were recorded on a Varian Unit 300 MHz spectrometer in $CDCl_3$ at r.t. with TMS as an internal standard.

The IR absorption spectra of solid samples were recorded in the range of 400 up to 4000 cm^{-1} in KBr plates using a Perkin–Elmer model 180 spectrophotometer. The Raman spectra of the complexes were obtained using a Renishaw Raman spectrometer. The laser power was approximately 7 mW.

The carbon, hydrogen and nitrogen percentages were obtained from elemental analyses. The Eu(III) content was determined by complexometric titration with EDTA (0.01 mol l^{-1}) using xylenol orange as indicator.

The conductance measurements of the complexes were carried out in methanolic millimolar solution at r.t. using an equipment composed of a Leeds and Northrup 4760 resistance box, a 2370 a.c. pointer galvanometer and a cell with $K_C = 0.00962$ cm.

The thermogravimetric curves were recorded on a Shimatzu model TGA thermobalance at a heating rate of 10 °C min^{-1} in a nitrogen dynamic atmosphere of 10 ml min^{-1} from r.t. to 900 °C.

The luminescence spectra were obtained using a spectrofluorimeter Spex 212L with a 450 W xenon lamp. The signal was detected using a water-cooled Hammamatsu R928 photomultiplier. The excitation spectra were obtained using both monochromator and lamp corrections. The luminescence spectra were obtained at room and liquid nitrogen temperature using a detector mode correction. This apparatus was fully controlled by a DM3000F spectroscopic computer.

3. Results and discussions

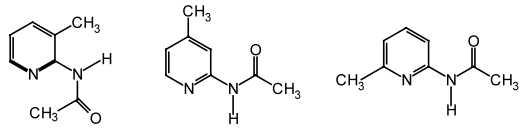
3.1. Characterization

The ^{1}H NMR data for the free ligands are summarized in Table 1. The 4- and 6-mpa ligands data have been interpreted in terms of a planar structure where the pyridine ring is trans to the methyl of the amide group (*Z* configuration), this is shown in Fig. 1(b and c), respectively. These configurations are stabilized due to strong dipole–dipole interactions between the pyridine ring and the acetamide group [22]. This supposition is in agreement with the presence of three protons at downfield ($\sim$8.25 ppm) due to the deshielding by larger anisotropic effects from the carbonyl group on these protons. On the other hand, for the 3-mpa ligand, the presence of a substituent on the aromatic ring may produce a deviation from the planarity between the aromatic ring and the amide group to relieve the steric hindrance between 3-methyl pyridine ring and amide group.

The chemical shift of the acetyl methyl protons observed for the 3-mpa ligand (2.27 ppm) compared to those 4- (2.36 ppm) and 6-mpa (2.44 ppm) ligands is indicative that the acetyl methyl protons are situated in a region close to the plane of the pyridine ring where the shielding effect is operative [22]. These results indicate that the 3-mpa ligand has a conformation close to that illustrated in Fig. 1(a).

The rare earth percentages in the complexes were determined by complexometric titration with ethylenediaminetetraacetic acid disodium salt (EDTA) in aqueous solution. Whereas carbon, hydrogen and nitrogen contents were determined by microanalytical procedures. C, H, N and Eu(III) percentages (found/calculated) for $Eu(ClO_4)_3(x\text{-mpa})_n$ with the respective ligands are: 3-mpa (C, 31.93/32.01; H, 3.90/4.03; N, 9.42/9.33; Eu(III), 16.76/16.87%), 4-mpa (C, 32.46/32.01; H, 3.78/4.03; N, 9.82/9.33; Eu(III), 16.80/16.87%) and 6-mpa (C, 25.61/25.42; H, 2.68/3.53; N, 7.46/7.27; Eu(III), 20.24/20.34%). These data are consistent with the stoichiometries suggested.

According to the results of molar conductivities of a 10^{-3} M methanol solution, all complexes be have as 2:1 electrolytes, suggesting the coordination of only one perchlorate group to the Eu(III) ion. These results indicate that these complexes present two general formulae $[Eu(ClO_4)(x\text{-mpa})_3](ClO_4)_2$ (where $x = 3$ and 4) and $[Eu(ClO_4)\ (6\text{-mpa})_2](ClO_4)_2$.



(a) (b) (c)

Fig. 1. Molecular conformation of the *N*-[*x*-methylpyridyl]acetamide ligands: (a) 3-mpa; (b) 4-mpa; and (c) 6-mpa.

The IR (infrared) absorption spectral data of the free ligands and Eu(III)-perchlorate complexes are summarized in Table 2. It was observed the absence of broad bands around 3500 cm^{-1} (νOH) indicating that the coordination compounds with *x*-mpa ligands are anhydrous. The bands in the IR region used to diagnose the coordination of the ligands to the Eu(III) ion were those the amide I band (mainly of νC=O), amide II band (νC–N and δN–H), νC=C, νC=N and deformation modes of pyridine ring. If coordination occurs through the oxygen of the amide group, a shift of the amide I band to lower frequency is expected and, consequently, the amide II band will shift to a higher frequency, as compared with the spectrum of the free ligand. If coordination occurs through the nitrogen of the pyridine ring, a shift to higher frequencies of the νC=C and νC=N stretching and deformation bands of the pyridine ring is expected [19].

The amide I band in the complexes compared to the bands of the free ligands shows a displacement to lower frequencies, suggesting that the amide group is coordinated in all the complexes through the carbonyl oxygen atom. The νC=C and νC=N stretching and one deformation band of the pyridine ring around 620 cm^{-1} are shifted to higher frequencies upon coordination with the Eu(III) ion indicating that coordination also occurs through the pyridine nitrogen. Thus the *N*-(*x*-methyl 2-pyridyl)acetamide ligands have acted as chelating agents coordinating to the metal ion through both nitrogen pyridine and oxygen atoms.

The IR and Raman vibrational spectroscopies offer precious information about bonding modes of the perchlorate anion [16]. The ClO_4^- group in the ionic form has T_d symmetry and in the of IR spectral region

Table 1
^{1}H NMR chemical shifts of the free *N*-[methyl 2-pyridyl]acetamide ligands in $CDCl_3$

Ligands	δ (ppm)						
	Py–CH_3	CH_3–(C=O)	3-proton	4-proton	5-proton	6-proton	N–H
3-mpa	2.21	2.28		7.57	7.11	8.22	9.57
4-mpa	2.19	2.36	6.88		8.11	8.14	10.22
6-mpa	2.16	2.44	6.89	7.59	8.01		8.84

Table 2
Assignments in the IR spectra of the amide group and pyridine ring of the free and coordinated ligand in the Eu(III)-perchlorate complexes

Compounds	Amide I ν(C=O) [a]	Amide II	νC=C and νC=N (ring) [b]	δC=C and δC=N (ring) [c]
3-mpa	1669	1549	1592, 1457	620
$[Eu(3\text{-mpa})_3(ClO_4)](ClO_4)_2$	1658	1576	1617, 1466	637
4-mpa	1668	1550	1613, 1568	617
$[Eu(4\text{-mpa})_3(ClO_4)](ClO_4)_2$	1657	1533	1622, 1479	630
6-mpa	1661	1549	1600, 1458	619
$[Eu(6\text{-mpa})_2(ClO_4)](ClO_4)_2$	1653	1553	1630, 1458	629

[a] Very strong.
[b] Strong.
[c] Weak.

between 1200 and 1000 cm^{-1}, a strong broad band is generally observed, corresponding to the triply degenerate frequency ν_3. Under coordination to the metal ion the ClO_4^- ion is expected to undergo a lowering in the symmetry. If one or two of oxygen atoms are coordinated its T_d symmetry is lowered to C_{3V} or C_{2V} splitting the ν_3 band in the IR spectrum to give a doublet or triplet, respectively.

The IR spectra of the complexes with the 3- and 4-mpa ligands showed two strong bands well defined around 1088 and 1115 cm^{-1}, while in the Raman spectra these bands appear around 1077 and 1126 cm^{-1}. This can be assigned to the splitting of the frequency ν_3 of the ClO_4^- group, i.e. this group is acting as a monodentate ligand. On the other hand, the IR spectrum of complex with the 6-mpa ligand presented an additional band around 1174 cm^{-1} that is assigned to the lowering of the symmetry (C_{2V}) of the ClO_4^- group due to coordination to the rare earth ion through two oxygen atoms. These data are agreement with the molar conductance data indicating that in all complexes only one perchlorate group is coordinated to the Eu(III) ion.

The TG curves were obtained for the complexes $[Eu(ClO_4)(x\text{-mpa})_3](ClO_4)_2$ (where $x = 3$ and 4). The curves do not present weight loss in the temperature interval 25–180 °C, indicating that the complexes containing the 3- and 4-mpa ligands are anhydrous corroborating the IR data. On the other hand for the range 180–400 °C weight loss occurs in three consecutive stages, where the quantitative analyze on this interval show a good correlation between the experimental and calculated values considering releases of the all three ligands, it is in concordance with data of elemental analyses. In the next stage, in the temperature range from 400 to 900 °C, the thermal decomposition of the Eu(III)-perchlorate is observed. However, the TG curves are very complex in this interval, making it difficult to assign on the reaction that the perchlorate group undergoes. The thermogravimetric study on the complex containing the 6-mpa ligand is not possible due to its high hygroscopicity.

3.2. Photoluminescence study

Fig. 2 presents the excitation spectra of the complexes in the range of 250–500 nm at 77 K monitored at 612 nm. These spectral data present narrow absorption bands originated from f^6-configuration of the Eu(III) ion corresponding to the $^7F_0 \rightarrow {}^5H_4$ ($\sim$360 nm), $^7F_0 \rightarrow {}^5G_6$ ($\sim$375 nm), $^7F_0 \rightarrow {}^5L_6$ ($\sim$394 nm), and $^7F_0 \rightarrow {}^5D_2$ ($\sim$462 nm) transitions, while the broad absorption bands refer to the ligands. The spectra (Fig. 2(a and b)) corresponding to the $[Eu(ClO_4)(3\text{-mpa})_3](ClO_4)_2$ and $[Eu(ClO_4)(4\text{-mpa})_3](ClO_4)_2$ complexes are similar, but they are different from the one with the 6-mpa ligand (Fig. 2(c)). It is observed that the complexes with 3- and 4-mpa ligands present their maxima around 290 nm while the complex containing the 6-mpa ligand present a maximum around 320 nm.

The emission spectra recorded at 77 K in the region of the $^5D_0 \rightarrow {}^7F_J$ transitions (where $J = 0$–4) in the range 560–720 nm by exciting at the $^7F_0 \rightarrow {}^5L_6$ transition around 394 nm are shown in Fig. 3. The profiles of the

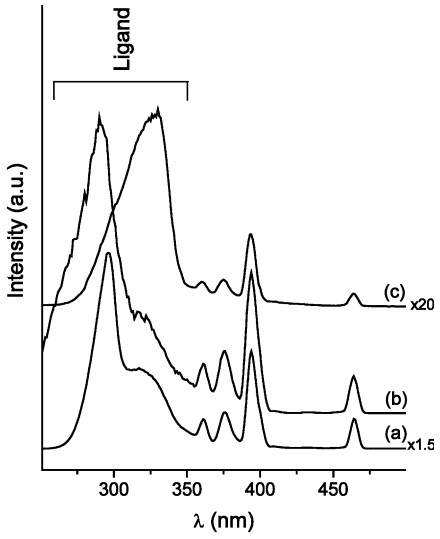


Fig. 2. Excitation spectra of the $[Eu(ClO_4)(x\text{-mpa})_3](ClO_4)_2$ complexes with ligands: (a) 3-mpa; (b) 4-mpa; and (c) $[Eu(ClO_4)(6\text{-mpa})_2](ClO_4)_2$.

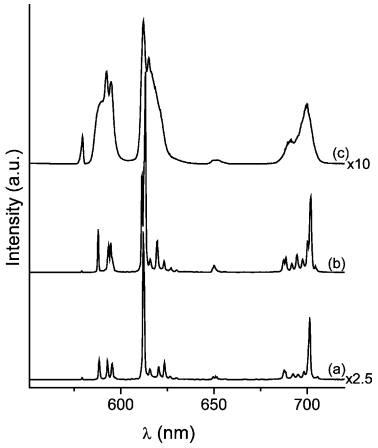


Fig. 3. Emission spectra of the complexes $[Eu(ClO_4)(x\text{-mpa})_3](ClO_4)_2$ with: (a) 3-mpa; (b) 4-mpa; and (c) 6-mpa with general formula $[Eu(ClO_4)(6\text{-mpa})_2](ClO_4)_2$.

spectra of the complexes with the 3- and 4-mpa ligands consist of sharp and defined bands. In contrast, the emission spectrum of the complex with the 6-mpa ligand shows broadened bands.

As shown in Fig. 3, the emission spectra of the complexes with the 3- and 4-mpa ligands present only one sharp peak in the region of the $^5D_0 \rightarrow {}^7F_0$ transition indicating the presence of a single chemical environment around the Eu(III) ion. The presence of three components assigned to the magnetic dipole allowed $^5D_0 \rightarrow {}^7F_1$ transition is consistent with a ligand field perturbation of low symmetry. All the electronic $^5D_0 \rightarrow {}^7F_J$ transitions are split in the maximum of $(2J+1)$-components, $J = 0$ (one band), 1 (three bands) and 4 (nine bands), but in the case of $J = 2$ there are seven bands more than $(2J+1 = 5)$ components (Fig. 3).

Fig. 3 shows two satellite bands in region of the $^5D_0 \rightarrow {}^7F_2$ hypersensitive transition (around 626 and 630 nm) for the complexes with the 3- and 4-mpa ligands (Table 3). The Eu-complexes present two additional low intensity bands at 1301 and 1387 cm^{-1}, for the 3-mpa ligand, and at 1322 and 1398 cm^{-1} for the 4-mpa ligand where the $^5D_0 \rightarrow {}^7F_0$ transition was taken as reference. They are assigned to vibronic transitions due to the coupling between the electronic and vibrational transitions from the $^7F_2$ and ν(C–N–CO) and ν(C–C) stretching, respectively, even though they could also be interpreted in terms of an electronic Raman effect as in Ref. [4]. The vibrational (IR and Raman) and electronic (emission) spectra of the $[Eu(ClO_4)(4\text{-mpa})_3](ClO_4)_2$ complex are presented in Fig. 4.

The Ω_2 and Ω_4 experimental intensity parameters were determined from the emission spectra (Fig. 3) based on the $^5D_0 \rightarrow {}^7F_2$ and $^5D_0 \rightarrow {}^7F_4$ electronic transitions of the Eu(III) ion, and they are estimated according to equation [23,24]

Table 3
Energies of the $^5D_0 \rightarrow {}^7F_J$ transitions ($J = 0$–4) (in cm^{-1}) observed in the emission spectra of the complexes $[Eu(ClO_4)(x\text{-mpa})_3](ClO_4)_2$ ($x = 3$ and 4) and $[Eu(ClO_4)(6\text{-mpa})_2](ClO_4)_2$, at 77 K

Transition	3-mpa	4-mpa	6-mpa
$^5D_0 \rightarrow {}^7F_0$	17 265	17 271	17 259
$^5D_0 \rightarrow {}^7F_1$	16 995	17 012	16 984
	16 869	16 852	16 880
	16 795	16 818	16 812
$^5D_0 \rightarrow {}^7F_2$	16 339	16 356	16 335
	16 286	16 308	16 260
	16 244	16 239	16 103
	16 119	16 139	
	16 041	16 046	
	15 964 [a]	15 949 [a]	
	15 878 [a]	15 873 [a]	
$^5D_0 \rightarrow {}^7F_4$	14 543	14 548	14 505
	14 526	14 522	14 463
	14 443	14 455	14 302
	14 384	14 397	14 282
	14 323	14 335	
	14 257	14 282	
		14 245	
	14 172	14 196	

[a] Vibronic transitions. The $^5D_0 \rightarrow {}^7F_3$ transition was not assigned in this study due to its very low intensity.

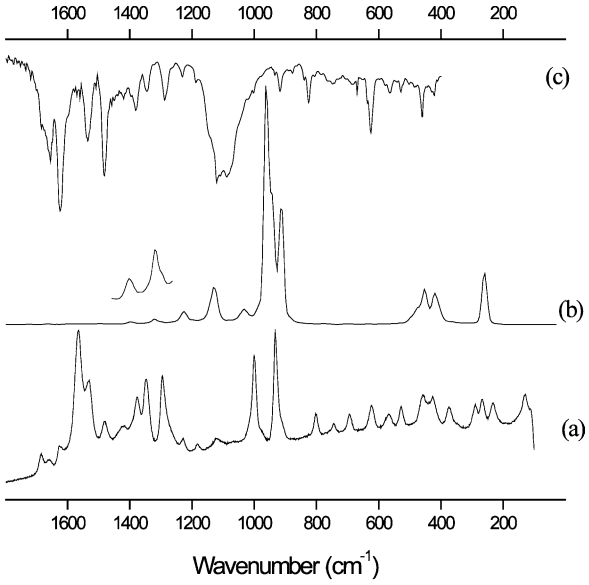


Fig. 4. IR (top) and Raman (bottom) spectra of the $[Eu(ClO_4)(4\text{-mpa})_3](ClO_4)_2$ complex and comparison with the emission spectrum (middle) recorded at 77 K. The energy of the $^7F_0$ level of the Eu(III) ion was taken as the origin.

$$A_{0J} = \frac{4e^2\omega^3}{3\hbar c^3}\,\chi \sum_{\lambda}\,\Omega_{\lambda}\langle {}^7F_J||U^{(\lambda)}||{}^5D_0\rangle^2 \qquad (1)$$

where, $\lambda = 2$ and 4, A_{0J} is the coefficient of spontaneous emission, χ is the Lorentz local field correction term that is given by $n(n^2+2)^2/9$ with the refraction index $n = 1.5$ and $\langle {}^7F_J||U^{(\lambda)}||{}^5D_0\rangle^2$ are the square reduced matrix

elements whose values are 0.0032 and 0.0023 for $J=2$ and 4, respectively. Since the intensity of a magnetic dipole transition ($^5D_0 \rightarrow {}^7F_1$) is relatively insensitive to the ligand field around of the Eu(III) ion, so that it may be used as internal standard to avoid the difficulty in experimental measurement of absolute emission intensities. The experimental coefficients of spontaneous emission, A, to be used in Eq. (1) are obtained according to the relation

$$A_{0J} = A_{01}\left(\frac{I_{0J}}{I_{01}}\right)\left(\frac{\nu_{01}}{\nu_{0J}}\right) \quad (2)$$

where I_{01} and I_{0J} are the integrated intensities of the $^5D_0 \rightarrow {}^7F_1$ and $^5D_0 \rightarrow {}^7F_J$ transitions ($J=2$ and 4) with ν_{01} and ν_{0J} energy baricenters, respectively. The coefficient of emission spontaneous, A_{01} in Eq. (2) is given by the expression $A_{01} = 0.31 \times 10^{-11}(n)^3(\nu_{01})^3$, and its value is estimated to be around 50 s^{-1} [25].

The Ω_2 and Ω_4 intensity parameters for the three complexes are presented in Table 4. The values of the Ω_2 parameters ($\sim 6.5 \times 10^{-20}$ cm^2) and the band profiles for the compounds with 3- and 4-mpa ligands are very similar, suggesting a similar chemical environment around the Eu(III) ion in these complexes.

When we compare the value of the Ω_2 parameter for the x-mpa complexes it is observed that in the compound with the 6-mpa ligand it is smaller than in the compounds containing the 3- and 4-mpa ligands. This might be expected on the basis of a steric effect of the methyl group on the pyridyl ring, decreasing the interaction between the N-pyridyl and the Eu(III) ion. Besides, the presence of only two 6-mpa ligands and one perchlorate group acting as bidentate ligands leads to a six-coordination complex, conferring a smaller electric dipole character to the $^5D_0 \rightarrow {}^7F_2$ transition. The hydrated salt presents the smallest value of the Ω_2 parameter compared with the complexes containing the 3-, 4- and 6-mpa ligands (Table 4) because the $^5D_0 \rightarrow {}^7F_2$ transition in octahedral complexes is formally forbidden owing to the electric dipole selection rules in centrosymmetric compounds.

From the luminescence decay curves for all the complexes (Fig. 5) we have determined the lifetime values (Table 4) of the emitting $^5D_0$ level of Eu(III) at room temperature as described in Ref. [24]. The short lifetime ($\tau = 0.078$ ms) of the emitting $^5D_0$ level in the salt precursor $[Eu(H_2O)_6](ClO_4)_3$ compared with the Eu-complexes (around $\tau = 0.270$ ms), presented in Table 4, is associated with the non-radiative decay channel due to vibronic coupling with the vibrations of the H_2O molecules.

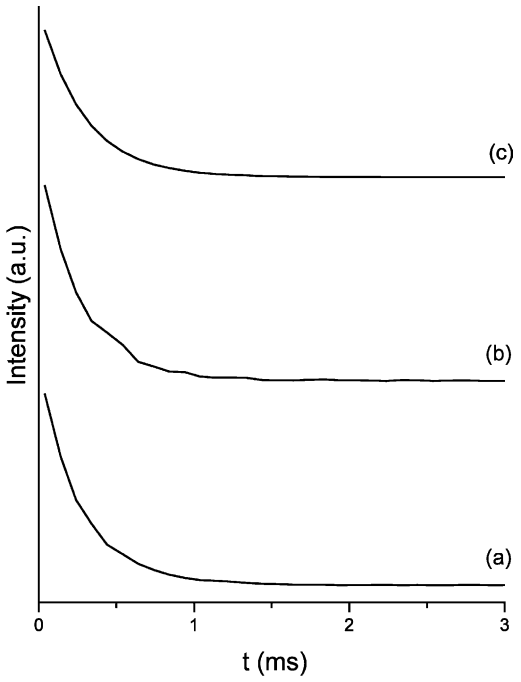


Fig. 5. Luminescence decay curves at room temperature of the emitting $^5D_0$ level of the Eu(III)-perchlorate complexes with ligands: (a) 3-mpa; (b) 4-mpa; and (c) 6-mpa.

The lifetime, non-radiative (A_{nrad}) and radiative (A_{rad}) rates are related through the following equation

$$A_{tot} = \frac{1}{\tau} = A_{rad} + A_{nrad} \quad (3)$$

where A_{rad} rates were obtained by summing over the radiative rates A_{0J} for each $^5D_0 \rightarrow {}^7F_J$ transitions ($A_{rad} = \Sigma_J\, A_{0J}$).

The quantum efficiency of the emitting $^5D_0$ level can be defined by

Table 4
Photoluminescent data of the complexes of the Eu(III)-perchlorate with acetamide ligands in solid state

Compounds	Ω_2	Ω_4	R_{02}	A_{rad}	A_{nrad}	A_{tot}	τ	η
$[Eu(H_2O)_6](ClO_4)_3$	1.1	4.7	0.003	155	12 573	12 728	0.078	1.2
$[Eu(ClO_4)(3\text{-mpa})_3](ClO_4)_2$	6.6	8.8	0.005	381	3364	3745	0.267	10.2
$[Eu(ClO_4)(4\text{-mpa})_3](ClO_4)_2$	6.5	9.1	0.002	382	3281	3663	0.273	10.4
$[Eu(ClO_4)(6\text{-mpa})_2](ClO_4)_2$	2.6	3.0	0.036	174	3322	3496	0.286	5.0
$[Eu(TTA)_3(DBSO)_2]$ [a]	29.0	3.5	0.005	980	420	1400	0.714	70

The experimental intensity parameters Ω_λ (10^{-20} cm^2), R_{02}, lifetimes τ (ms), radiative emission coefficient A_{rad} (s^{-1}), non-radiative emission coefficient A_{nrad} (s^{-1}), and quantum efficiency η (%) were obtained at room temperature (around 298 °C).

[a] Refs. [25,26].

$$\eta = \frac{A_{rad}}{A_{rad} + A_{nrad}} \quad (4)$$

We made a comparison between the 3-, 4- and 6-mpa complexes by considering that these three ligands are very similar. Table 4 shows that the complexes with 3- and 4-mpa ligands exhibit quantum efficiencies twice higher than the complex with 6-mpa, which is due to the higher radiative decay rates in the former case. As mentioned above, the smallest value of the quantum efficiency, which corresponds to the hydrated Eu(III)-perchlorate salt, is due to multiphonon relaxation by coupling to the OH vibration, quenching considerably its luminescence. For the sake of comparison the complexes in solid state bis(dibenzylsulfoxide)trithenoyltrifluoacetonateeuropium(III) has highest quantum efficiency ($\eta = 70\%$) that those with 3-, 4- and 6-mpa complexes indicating that non-radiative processes are operative [26–28].

Table 4 shows also the R_{02} intensity parameter, which is the ratio between the intensities of the $^5D_0 \rightarrow {}^7F_0$ and $^5D_0 \rightarrow {}^7F_2$ transitions. The R_{02} parameter may give information on the J-mixing effect associated with the $^5D_0 \rightarrow {}^7F_0$ transition as described in detail in Refs. [29,30]. In this case, this effect is mainly due to the mixing between the $^7F_2$ manifold and the $^7F_0$ level though the rank-two components of the ligand field. By comparison between the three Eu(III)-perchlorate complexes, the following order for the magnitude of the J-mixing effect is proposed: 6-mpa $\gg$ 3-mpa $>$ 4-mpa.

4. Conclusion

In this work we synthesized new Eu(III)-perchlorate complexes with 3-, 4- and 6-methyl substituted ligands derived from N-[2-pyridyl]acetamide. The elemental analyses, TG and molar conductivities data suggested that the complexes present the formula $Eu[(ClO_4)(x\text{-mpa})_3](ClO_4)_2$, with $x = 3$ or 4, and $Eu[(ClO_4)(6\text{-mpa})_2](ClO_4)_2$. The IR spectra showed that the amide ligands are coordinated to the Eu(III) ion by the oxygen atom of the amide group and the nitrogen atom of the pyridyl ring and that one perchlorate group coordinates to the Eu(III) ion as a monodentate ligand in the complexes with the 3- and 4-mpa ligands and as a bidentate ligand in the complex with the 6-mpa ligand. The emission spectra show only one peak for the $^5D_0 \rightarrow {}^7F_0$ transition indicating the presence of a single chemical environment around the Eu(III) ion. The detailed analysis in the region corresponding the $^5D_0 \rightarrow {}^7F_2$ transition showed the presence of satellite bands that were attributed to vibronic transitions due to the resonance between the energies of the νC–N–CO and νC–C stretching and the electronic $^7F_2$ level of the Eu(III) ion. This result was confirmed by the IR and Raman spectra of the compounds.

The Ω_2 intensity parameter for the $[Eu(ClO_4)(6\text{-mpa})_2](ClO_4)_2$ compound is smaller than for the complexes with the 3- and 4-mpa ligands. This was interpreted in terms of steric effect of the methyl group on the pyridyl ring, which decreases the interaction between the N-pyridyl and the Eu(III) ion. The $[Eu(H_2O)_6](ClO_4)_3$ precursor salt shows the smallest value of the Ω_2 parameter compared with all the complexes (Table 4) due to the fact the $^5D_0 \rightarrow {}^7F_2$ transition occurs in a chemical environment with point symmetry very close to (O_h).

The complexes obtained exhibit small values of the quantum efficiencies, η, indicating that energy transfer from (ClO_4^-) group and x-mpa ligands (where $x = 3$, 4 and 6) to Eu(III) ion is not very efficient compared with $[Eu(TTA)_3(DBSO)_2]$ complex suggesting that non-radiative processes are operative possibly due to vibronic coupling with the vibrations of the N–H on the amide group.

Acknowledgements

The authors are grateful to the Coordenação de Aperfeiçoamento de Pessoal de nível Superior (CAPES), Fundação de Amparo à Pesquisa do Estado de São Paulo (FAPESP) and Conselho Nacional de Desenvolvimento Científico e Tecnológico (CNPq-RENAMI) for financial support.

References

[1] N. Sabbatini, M. Guardigli, J.M. Lehn, Coord. Chem. Rev. 123 (1993) 201.
[2] G.F. Buono-Core, H. Li, B. Marciniak, Coord. Chem. Rev. 99 (1990) 55.
[3] G.F. de Sá, O.L. Malta, C.M. Donegá, A.M. Simas, R.L. Longo, P.A. Santa-Cruz, E.F.da Silva, Jr., Coord. Chem. Rev. 196 (2000) 165.
[4] J.-C.G. Bünzli, G.R. Choppin (Eds.), Lanthanide Probes in Life, Chemical and Earth Sciences—Theory and Practice, Elsevier, Amsterdam, 1989, pp. 219–293.
[5] L.C. Thompson, in: K.A. Gschneider, L. Eyring (Eds.), Handbook on the Physics and Chemistry of Rare Earths, vol. 3, North-Holland, Amsterdam, 1979, pp. 209–297.
[6] G. Blasse, B.C. Grabmaier, Luminescente Materials, Springer-Verlag, Heidelberg, 1994, pp. 210–219.
[7] I.A. Hemmilä, Application of Fluorescence in Immunoassays, Wiley, New York, 1991, pp. 84–119.
[8] A.O. Yoshimasa, in: Hiap L. Ong (Ed.), Eletroluminescent Display, vol. 1, World Scientific, Singapore, 1995, pp. 1–17.
[9] M.A. Bizeto, V.R.L. Constantino, H.F. Brito, J. Alloys Compd. 311 (2000) 159.
[10] J.H. Forsberg, T. Moeller, Inorg. Chem. 8 (1969) 883.
[11] J.H. Forsberg, T. Moeller, Inorg. Chem. 8 (1969) 889.
[12] E. Galdecka, Z. Galdecki, E. Huskiwska, V. Amirkhanov, J. Legendziewicz, J. Alloys Compd. 257 (1997) 182.

[13] A.A. Khan, K. Iftikhar, Polyhedron 16 (1997) 4153.
[14] S. Joseph, P.K. Radhakrishnan, Synth. React. Inorg. Met. 28 (1998) 423.
[15] C.Y. Su, B.S. Kang, H.Q. Liu, Q.G. Wang, Z.N. Chen, Z.L. Lu, Y.X. Tong, T.C.W. Mak, Inorg. Chem. 8 (1999) 1374.
[16] J.L. Pascal, F. Favier, Coord. Chem. Rev. 178 (1998) 865.
[17] K.D. Soulti, A. Troganis, A. Papaioannou, T.A. Kabanos, A.D. Keramidas, Y.G. Deligiannakis, C.P. Raptopoulo, A. Terzis, Inorg. Chem. 37 (1998) 6785.
[18] M. Nonoyama, S. Tomita, K. Yamasaki, Inorg. Chim. Acta 12 (1975) 33.
[19] J. Bould, D. Brisdon, Inorg. Chim. Acta 19 (1976) 159.
[20] C. Airoldi, F.S. Dias, J.G.P. Espinola, G.S. de Sá, J. Chem. Res. 4 (1980) 142.
[21] M. Baaden, F. Berny, C. Boehme, N. Muzet, R. Schurhammer, G. Wipff, J. Alloys Comp. 303 (2000) 104.
[22] R.F.C. Brown, L. Radom, S. Sternhel, I.D. Rae, Can. J. Chem. 46 (1968) 2578.
[23] B.R. Judd, Phys. Rev. 127 (1962) 750.
[24] G.S. Ofelt, Phys. Rev. 37 (1962) 511.
[25] W.T. Carnall, H. Crosswhite, H.M. Crosswhite, Energy Level Structure and Transition Probabilities of the Trivalent Lanthanides in LaF_3, Argonne National Laboratory Report, unnumbered, 1977.
[26] O.L. Malta, H.F. Brito, J.F.S. Menezes, F.R.G. Silva, S. Alves, Jr., F.S. Farias, Jr., A.V.M. de Andrade, J. Lumin. 75 (1997) 255.
[27] O.L. Malta, H.F. Brito, J.F.S. Menezes, F.R.G. Silva, C.M. Donegá, S. Alves, Jr., Chem. Phys. Lett. 282 (1998) 233.
[28] H.F. Brito, O.L. Malta, J.F.S. Menezes, J. Alloys Comp. 303 (2000) 336.
[29] O.L. Malta, Mol. Phys. 42 (1981) 65.
[30] O.L. Malta, W.M. de Azevedo, E.G. de Araújo, G.F. de Sá, J. Lumin. 26 (1982) 337.

about the co-ordination chemistry of the Group 12 elements with this ligand. We have earlier reported [15] that DMPP does not form 2:1 complexes with mercury(II) halides due to the steric bulk of the phosphine ligand. The structures of the 1:1 complexes vary from weakly linked dimers for the chloride and bromide to a distorted trigonal planar monomer for the iodide, the latter being the first example of the monomeric 1:1 tertiary phosphine mercury(II) iodide complex. All three complexes have secondary interactions with one of the *ortho*-methoxy oxygen atoms on each ring [15].

Bowmaker and coworkers [21] have formed complexes of unusual stoichiometries with TMPP and mercury(II) halides. ^{31}P NMR studies of 1:1 solutions of the phosphine and the metal salts in acetonitrile showed the presence of $[(TMPP)HgX]^+$ and $[(TMPP)_2Hg]^{2+}$ cations, both with $[Hg_2X_6]^{2-}$ counterions, and with the amount of the first relative to the second increasing from chloride to iodide. These complexes thus have empirical formulae $TMPP(HgX_2)_2$ and $(TMPP)_2Hg_3X_6$, respectively, both having a P:Hg ratio <1:1. In an attempt to isolate the former complexes, solid complexes for X-ray structural and vibrational spectroscopic studies were obtained by adding a solution of the phosphine ligand in acetonitrile to a *suspension* of HgX_2 in the same solvent in a 1:2 molar ratio. For the chloride and bromide, complexes were isolated which analysed for $(TMPP)_4Hg_7X_{14}$ and which were shown by vibration spectroscopy to be essentially equimolar mixtures of $[TMPPHgX^+]_2[Hg_2X_6]^{2-}$ and $[(TMPP)_2Hg]^{2+}[HgX_6]^{2-}$. X-ray structural determination of a crystal obtained from the solid product from the chloride reaction confirmed the formulation as $[(TMPP)_2Hg][Hg_2Cl_6]$ having a slightly different crystal structure [21] to that found for $(Me_3P)_2(HgI_2)_3$ [16]. The cation was significantly distorted from linearity (P–Hg–P, 166.51(9)°) due to interactions with the *ortho*-methoxy oxygen atoms. For the iodide $[TMPPHgI^+]_2[Hg_2I_6]^{2-}$ was isolated, its formulation being confirmed spectroscopically [21].

Herein we report the results of our studies of the reactions of ethanolic solutions of HgX_2 (X = Cl, Br, I) and TMPP in a variety of proportions and the crystal structures of monomeric $(TMPP)HgX_2$ (X = Br, I) and $(TMPP)(HgI_2)_2$.

2. Experimental

Mercury(II) chloride, bromide and iodide, reagent grade, were used without further purification. The ligand, tris(2,4,6-trimethoxyphenyl)phosphine, was prepared as described previously [22] by reaction of 1,3,5-trimethoxybenzene with butyllithium, followed by the addition of triphenylphosphite in diethyl ether. After hydrolysis a white crystalline solid was obtained on recrystallisation from hot ethanol; m.p. 159–162, lit. 158–160 °C [17].

Melting points were obtained using an electrothermal melting point apparatus and are uncorrected. Elemental analyses were carried out by the Sheffield University Centre for Chemical Instrumental Analytical Services. ^{31}P NMR spectra were recorded as solutions in dimethylsulfoxide-d_6 using a Bruker AMX 400 spectrometer at 161.97 MHz with chemical shifts referenced to 85% H_3PO_4. Raman spectra were acquired by excitation with at 785 nm (300 mW) solid-state laser using a Renishaw Raman System 1000 spectrometer which comprised an integral Raman microscope (Olympus BH2 system), a stigmatic single spectrograph and a Peltier-cooled CCD detector (400 × 600) pixels. The holographic notch filters allowed a lower spectral limit of ~ 120 cm^{-1}.

2.1. Preparation of complexes

The complexes were prepared using solutions of the phosphine ligand and the mercury(II) halide, both separately dissolved in hot ethanol. Precipitation occurred almost immediately and the complexes were filtered off and dried in vacuo. A typical synthesis is described below. For 1:1, 1:2 and 2:3 (P:Hg) ratios of reactants used, the ligand was added to the metal salt whereas for the 2:1 ratio of reactants, the reverse order of addition was used. However, in the case of chloride it was found to be necessary for the formation of the 1:1 complex to add the mercury salt to the phosphine. Quantities of materials used and ratio of reactants, together with analytical data for the products isolated, their appearance and melting points are reported in Table 1.

2.1.1. Tris(2,4,6-trimethoxyphenyl)phosphine–dibromomercury(II)

Tris(2,4,6-trimethoxyphenyl)phosphine (0.399 g, 0.75 mmol) dissolved in warm ethanol (50 cm^3) was added with stirring to mercury(II)bromide (0.270 g, 0.75 mmol) also dissolved in warm ethanol (50 cm^3) with stirring. The white precipitate which formed almost immediately was filtered off and dried in vacuo as white needles; m.p. 250–251 °C. *Anal.* Found: C, 36.38; H, 3.87. Calc. for $C_{33}H_{27}OPHgBr_2$: C, 36.32; H, 3.72%.

2.2. X-ray crystallography

Crystals suitable for X-ray study were grown by slow evaporation of ethanolic solutions of the complexes, mounted on glass fibres and intensity data collected. A summary of crystal data, data collection strategy and model refinement parameters are given in Table 2. The structures of $TMPPHgX_2$ (X = Br (**I**), I (**II**)) and $TMPP(HgI_2)_2$ (**III**) were solved by direct methods

Table 1
Quantities of reactants, analytical data and physical properties of products

Ratio of reactants [a]	Mass HgX_2/g (mmoles)	Mass TMPP/g (mmoles)	Analyses [b]		Melting point (°C)	Appearance
			Carbon	Hydrogen		
1:1 ratio						
$HgCl_2$ [c]	0.271 (0.99)	0.534 (1.00)	34.77(40.33) [c]	3.62 (4.13) [c]	246–248	white crystals
$HgCl_2$ [d]	0.270 (0.99)	0.532 (1.00)	39.14 (40.33)	4.10 (4.13)	215–216	white powder
$HgBr_2$	0.270 (0.75)	0.399 (0.75)	36.38 (36.32)	3.87 (3.72)	250–251	white needles
HgI_2	0.454 (1.00)	0.532 (1:00)	32.52 (32.85)	3.32 (3.37)	240–242	pale yellow needles
2:1 ratio						
$HgCl_2$	0.350 (1.29)	1.39 (2.61)	47.89 (48.52)	5.07 (4.97)	179–182	white powder
HgBr	0.434 (1.20)	1.31 (2.46)	45.22 (45.50)	4.76 (4.67)	176–179	white powder
HgI_2	0.520) (1.14)	1.23 (2.31)	41.09 (42.68)	4.23 (4.38)	189–193	pale yellow powder
1:2 ratio						
$HgCl_2$	0.820(3.02)	0.82(1.54)	34.19(30.15) [c]	3.50(3.09) [c]	244–246	white powder
$HgBr_2$	0.721(2.00)	0.54(1.01)	29.45(25.87) [e]	3.03(2.65) [e]	245–247	white powder
HgI_2	0.923(2.02)	0.55(1.03)	22.59(22.50)	2.32(2.31)	238–240	pale yellow powder
2:3 ratio						
$HgBr_2$	0.722(2.00)	0.48(1.33)	29.32(30.22)	2.98(3.10)	250–252	white powder
HgI_2	1.37(3.01)	1.07(2.00)	25.91(26.70)	2.66(2.74)	232–234	pale yellow powder

[a] TMPP:HgX_2.
[b] Theoretical values for the stated ratio of reactants are shown in parentheses.
[c] Addition of TMPP to $HgCl_2$ produces $(TMPP)_2(HgCl_2)_3$, theoretical values: C, 34.50; H, 3.54%.
[d] Addition of $HgCl_2$ to TMPP produces $TMPPHgCl_2$, theoretical values as shown in table.
[e] Theoretical value for $(TMPP)_2(HgBr_2)_3$: C, 30.22; H, 3.10%.

Table 2
Crystal data and model refinement parameters for $[TMPPHgBr_2]$ (**I**), $[TMPPHgI_2]$ (**II**) and $[TMPP(HgI_2)_2]_2$ (**III**)

	I	**II**	**III**
Empirical formula	$C_{27}H_{33}Br_2HgO_9P$	$C_{27}H_{33}HgI_2O_9P$	$C_{27}H_{33}Hg_2I_4O_9P$
Formula weight	892.91	986.89	1441.28
Crystal system	orthorhombic	monoclinic	triclinic
Space group	$Pna2_1$	$P2_1/n$	$P\bar{1}$
Unit cell dimensions			
a (Å)	14.936 (3)	11.399 (2) Å	11.8284(2)
b (Å)	11.632 (2)	23.599 (5) Å	12.5518(2)
c (Å)	18.380 (4)	12.137 (4) Å	14.7798(3)
α (°)			68.8760(10)
β (°)	90.0	91.77 (3)	69.3090(10)
γ (°)			66.304(2)
V (Å^3)	3193.3 (11)	3263.2 (11)	1817.61(6)
Z	4	4	2
Diffractometer	Nonius CAD4	Bruker–Nonius κCCD	Bruker–Nonius κCCD
Temperature (K)	293	120	120
Wavelength (Å)	1.54178	0.71073	0.71073
Absorption correction	psi scans	semi-empirical	semi-empirical
D_{calc} (Mg m^{-3})	1.857	2.009	2.633
Absorption coefficient (mm^{-1})	12.459	6.704	11.923
$F(000)$	1728	1872	1308
Crystal size (mm)	0.8 × 0.6 × 0.4	0.30 × 0.02 × 0.01	0.10 × 0.02 × 0.02
$2\theta_{max}$ (°)	67.06	54.98	50.06
Reflections collected	5421	33669	11866
Independent reflections	5421	7421	6238
R_{int}	0.0	0.1048	0.0269
Final R indices [$I > 2\sigma(I)$]	$R_1 = 0.0842$, $wR_2 = 0.2082$	$R_1 = 0.0433$, $wR_2 = 0.0745$	$R_1 = 0.0496$, $wR_2 = 0.1260$
Final R indices (all data)	$R_1 = 0.0969$, $wR_2 = 0.2198$	$R_1 = 0.0880$, $wR_2 = 0.0870$	$R_1 = 0.0571$, $wR_2 = 0.1311$
ρ max/min (e Å^{-3})	1.692 and −2.199	0.851 and −1.003	4.364 and −2.820

(SHELXS-97 [23]) and refined using SHELXL-97 [23]. Non hydrogen atoms were refined anisotropically, whilst hydrogens were refined isotropically in idealised positions with temperature factors tied to the values of their parent atom. Large residual peaks are observed approximately 1 Å from the mercury centres in **III** and are attributed to absorption effects.

3. Results and discussion

The results described herein both complement and contrast with those reported by Bowmaker and coworkers [21] for reactions of TMPP solutions with *suspensions* of mercury(II) halides, both in acetonitrile. We have examined reactions of TMPP on the metal halide in a variety of ratios (Table 1) in ethanol solutions. All complexes were only sparingly soluble and readily precipitated out. For reactions involving the ligand and HgX_2 in 1:1, 1:2 and 2:3 molar ratios the ligand solution was added to the halide solution (except in one case for the chloride, vide infra), while for reactions involving the phosphine in a greater molar ratio than the metal halide, the reverse order of addition was used.

When the solutions of the ligand and mercury(II) halides were mixed in 1:1 ratio, the 1:1 complexes were readily isolated for the bromide and iodide which have been shown herein to be monomeric due to the steric bulk of the tertiary phosphine ligand. Despite repeated attempts for the chloride, when the ligand ethanolic solution was added to metal halide solution, in every case the known [21] 2:3 complex, $(TMPP)_2(HgCl_2)_3$ was isolated. This latter complex was structurally characterised by Bowmaker and co-workers [21], a crystal having been obtained from the reaction of TMPP and a suspension of $HgCl_2$ in MeCN in a 1:2 molar ratio, though the bulk material appeared to be an equimolar mixture of the above compound and $(TMPP)(HgCl_2)_2$. However when an equimolar solution of $HgCl_2$ was added to the phosphine, also in ethanol, the 1:1 complex precipitated from solution as a white powder which was characterised by carbon and hydrogen analyses (Table 1). Unfortunately, recrystallisation of this material, in an attempt to obtain crystals suitable for X-ray study, resulted in isolation of the known complex [21] $(TMPP)_2(HgCl_2)_3$. The other 2:3 complexes $(TMPP)_2(HgX_2)_3$ (X = Br, I), which may be formulated as $[(TMPP)_2Hg][Hg_2X_6]$ like the chloride [21], were obtained readily by reaction of the phosphine and metal halide in a 2:3 ratio (Table 1). Recrystallisation of the bromide and iodide from hot ethanol resulted in isolation of the 1:1 complexes.

When TMPP and HgX_2 were mixed in a 3:2 ratio no analogues of $(Me_2EtP)_3(HgCl_2)_2$ [24] were obtained, due to the steric bulk of the ligand, and only the previously described $(TMPP)HgX_2$ (X = Br, I) and $(TMPP)_2(HgCl_2)_3$ were isolated. The reaction between the tertiary phosphine and mercury(II) halides in a 1:2 ratio in ethanol resulted in the isolation of $(TMPP)_2(HgX_2)_3$ (X = Cl, Br), whereas for the iodide, $(TMPP)(HgI_2)_2$ was isolated (Table 1). This complements Bowmaker's NMR findings [21] that 1:1 solutions of the phosphine and mercury (II) halides in MeCN contain $TMPP(HgX_2)_2$ and $(TMPP)_2(HgX_2)_3$, both given an ionic formulation, with the amount of the former to the latter increasing from chloride to iodide. They were also able to isolate this particular complex and formulated it as the ionic compound $[TMPPHgI]_2[Hg_2I_6]$ from spectroscopic data. However our X-ray structural analysis shows that these units are linked together via a single bridging iodine between two mercury atoms.

In contrast to reactions with DMPP [15] we were readily able to isolate the 2:1 complex $(TMPP)_2HgX_2$ (X = Cl, Br, I) (Table 1), presumably due to the stronger basicity of TMPP (pK_a, 11.02) compared to DMPP (pK_a, 9.33) [18] as the two phosphines have similar steric requirements. However, the second ligand must be weakly held as recrystallisation, to obtain suitable crystals for X-ray structural examination, yielded the 1:1 complexes for the bromide and iodide, and $(TMPP)_2(HgCl_2)_3$ for the chloride.

The X-ray crystal structures of $(DMPP)HgX_2$ (X = Cl, Br, I) showed a trend from very weakly linked halogen-bridged dimeric structures (X = Cl, Br) to a monomeric trigonal planar arrangement for the iodide. All three show additional interactions between mercury and one of the *ortho*-methoxy oxygen atoms on each ring [15]. An attempt to compare this series with the corresponding TMPP complexes were unsuccessful as unfortunately recrystallisation of $(TMPP)HgCl_2$ resulted in the formation of $(TMPP)_2(HgCl_2)_3$ whose structure has been reported [21]. However, recrystallisation of the corresponding bromide (**I**) and iodide (**II**) yielded crystals suitable for X-ray study. Crystallographic data for **I** and **II** are shown in Table 2 and selected bond lengths and angles in Table 3. The structures of **I** and **II** (Figs. 1 and 2, respectively) are both highly distorted trigonal planar monomeric molecules with a shorter Hg–P distance (2.420(4) (**I**), 2.437(2) (**II**) Å) than in the corresponding DMPP complexes (2.4490 (12), 2.4656(16) Å, respectively [15], reflecting the stronger donor capacity of TMPP, larger size of iodide and also the better donor capability of iodide to mercury compared to bromide. These are however longer than in the corresponding triphenylphosphine complex [6,13], despite the much higher pK_a of TMPP (11.02) [18] compared to Ph_3P (2.73) [19], due to the buttressing effect of the *ortho*-methoxy groups.

In contrast to its DMPP analogue [15], a weakly linked halogen-bridged dimer, in which the two bridging distances differ somewhat (2.6272(6), 2.9195(6) Å) with

Table 3
Selected bond lengths (Å) and bond angles (°) for **I**, **II** and **III**

	I	**II**	**III**	$[Hg_2I_6]$
Bond lengths				
Hg–P	2.420(4)	2.437(2)	2.408(2)	
Hg–X_{term}	2.637(3)	2.675(1)	2.6192(7)	
	2.528(3)	2.758(1)		
Hg–O	2.773(4)	2.904(4)	2.667(6)	
	2.953(3)	2.939(4)	2.869(5)	
	3.153(4)	3.247(5)	3.207(6)	
Hg–X				2.7562(8)
				2.6862(7)
				2.8637(8)
				2.9787(7)
Bond angles				
P–Hg–X	138.47(14)	133.35(4)	161.47(6)	
	117.48(14)	113.92(4)	95.20(6)	
X–Hg–X	103.79(10)	111.37(2)	103.31(2)	119.28(3)
				113.16(2)
				97.42(2)
				119.17(3)
				92.45(2)
				108.53(2)
P–Hg–O	71.04(6)	67.85(5)	73.96(1)	
	61.77(5)	57.28(6)	56.85(3)	
	59.27(6)	61.23(5)	63.72(2)	
X–Hg–O	117.69(4)	118.18(8)	83.27(2)	
	87.28(5)	95.61(6)	91.32(3)	
	82.06(5)	81.39(8)	104.56(2)	
	164.67(7)	162.73(7)	156.92(1)	
	113.37(6)	105.06(9)	125.54(2)	
	93.73(7)	94.48(5)	97.89(2)	

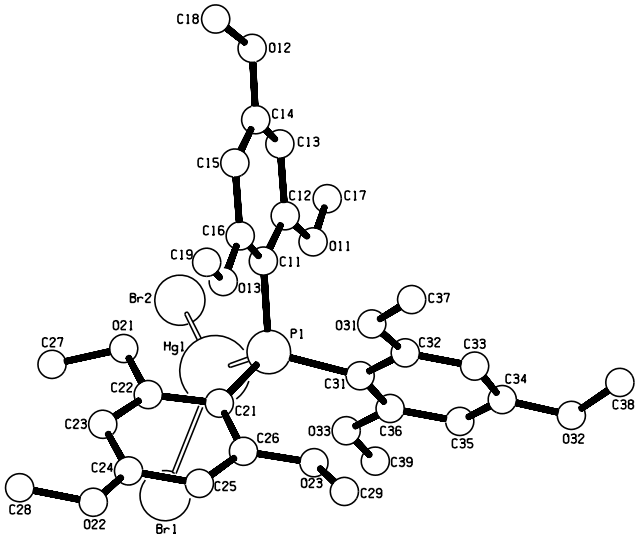


Fig. 1. The molecular structure of monomeric $TMPPHgBr_2$.

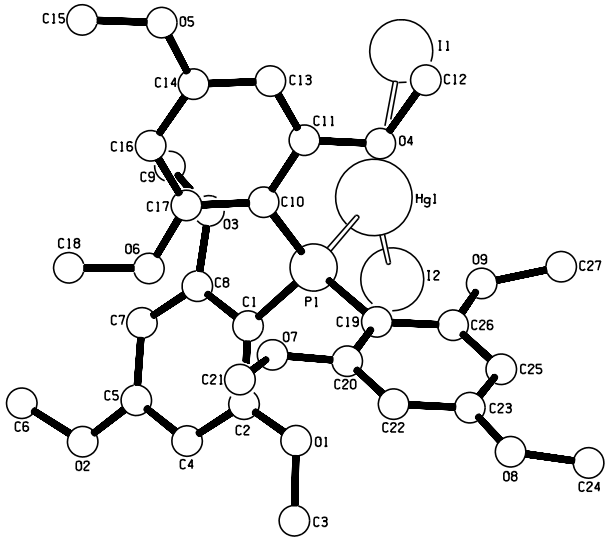


Fig. 2. The molecular structure of monomeric $TMPPHgI_2$.

one of these similar to the terminal Hg–Br bond length (2.6129(6) Å), $TMPPHgBr_2$ is monomeric (Fig. 1). The only other structurally characterised monomeric tertiary phosphine–mercury(II) bromide complex, bis(triphenylphosphonio)isophosphindolide–$HgBr_2$ [25], contains a shorter Hg–P bond still (2.399(2) Å). There are however other marked differences in the structures of these two monomeric complexes. In the phosphindolide complex the mercury atom displays almost T-shaped co-ordination geometry with the two Br–Hg–P angles differing significantly (157.7(1)°, 96.4(1)°) as also do the two Hg–

Br distances (2.491(1), 2.737(1) Å) and thus the complex could almost be formulated as $[R_3PHgBr]^+Br^-$. In contrast the TMPP complex described herein, whilst also showing planarity round mercury, contains much more similar Hg–Br distances (2.528(3), 2.637(3) Å). Additionally, whilst the two P–Hg–Br angles are somewhat different (138.47(14)°, 117.48(14)°) and larger than the Br–Hg–Br angle (103.79(10)°) they are more akin to trigonal planarity around mercury, albeit somewhat distorted due to the bulk of the phosphine ligand. There are no intermolecular Hg–Br distances less than 4 Å.

In $TMPPHgI_2$ the I–Hg–I angle (111.37(2)°) is approximately 8° greater than the corresponding angle in the bromide (103.79(10)°) reflecting the greater steric bulk of iodide and is ~4° smaller than in monomeric $DMPPHgI_2$ due to the stronger basicity of TMPP compared to DMPP resulting in a shorter Hg–P bond distance. This results in a reduction of both P–Hg–I angles of ~4° so that the P–Hg–I angles are still very asymmetric (113.92(4)°, 133.35(4)°), as in the bromide, due to strong interactions with the central mercury and one of the oxygens of the *ortho*-methoxy groups on each phenyl ring. These contacts (Table 3) are within the sum of the van der Waals radii for mercury and oxygen and can thus be considered as bonding interactions. Hence the co-ordination round mercury is raised to six although the overall geometry is significantly distorted from a regular octahedral arrangement.

The structure (Fig. 3) of complex **III** of empirical formula $(TMPP)(HgI_2)_2$ is somewhat different from that suggested previously [21] from spectroscopic data. In contrast to $[(TMPP)_2Hg]^{2+}[Hg_2Cl_6]^{2-}$, in which the presence of the two bulky phosphine ligands forces approximate linearity about the attached mercury atom and also precludes any interaction with neighbouring halogens, the presence of only one phosphine bonded to mercury in **III** does allow such an interaction to occur. Thus we have shown that **III**, rather than being described as the discrete ions $[(TMPP)HgI^+]_2[Hg_2I_6]^{2-}$ suggested from ^{31}P NMR and vibrational spectroscopic data [21], consists of the discrete molecular unit (TMPP)HgI(μ-I)HgI(μ-I)$_2$HgI(μ-I)HgI(TMPP). There are no Hg–I interactions between these units of less than 4 Å. Thus the centrosymmetric structure contains a double halogen bridge between mercury atoms in the central Hg_2I_6 core with one of the two terminal iodines on each mercury linked via a single bridge to a (TMPP)HgI unit. This single bridge (3.0705(7) Å) is slightly longer than the terminal Hg(1)–I(2) (2.6192(7) Å) and Hg(2)–I(3) (2.6862(7) Å) distances and is much shorter than the single iodine bridge (3.417(2) Å) linking $(Me_3P)_2Hg^{2+}$ cations to $Hg_2I_6^{2-}$ in $(Me_3P)_2(HgI_2)_3$ [16] but it is much closer to the bridging distances in the asymmetric Hg_2I_6 core (2.8037(8), 2.9787(7) Å). Such asymmetry in HgX_2Hg bridges has been noted previously in 1:1 dimers $(R_3PHgX_2)_2$ [6,7,10,13,14] and in $(Ph_4P)_2Hg_2I_6$ (2.864(1), 2.962(1) Å) [26]. The Hg–P distance (2.408(2) Å) is shorter than in (II) resulting from less steric crowding round mercury because of Hg1–I1 being longer than both of the Hg–I distances in (II). The angles in the Hg_2I_2 bridge are similar to those found in $(Ph_4P)_2Hg_2I_6$ [26] but the external angles around Hg2 are ~5° more distorted from tetrahedral due to the additional bonding to Hg1. Atoms P, Hg1, I1 and I2 are coplanar (deviation from least squares mean plane = 0.0055(10) Å) though there is considerable distortion of these atoms from trigonal planar geometry both due to bonding to Hg2 and also strong interactions of Hg1 with one of the *ortho*-methoxy oxygen atoms on each of the phenyl rings (2.667(6), 2.869(5), 3.207(6) Å). In all three complexes the geometry of the phosphine is not significantly altered from that of the free ligand [22].

3.1. Vibrational spectra

Important Raman bands in the 600–100 cm^{-1} region are summarized in Table 4 and displayed in Figs. 4–7. The assignment of the vibrational spectral features of a range of R_3PHgX_2 complexes has previously been correlated with their full crystal and molecular structures [6,27]. The structural variety found for the TMPP complexes described herein gives rise to differences in Raman spectra. There are several bands that are common to all spectra which are assigned to the skeletal vibrations of the phosphine ligand. However, there are clear differences, especially in the 300–100 cm^{-1} region, which may be assigned to terminal and bridging ν(HgX) modes, sym and anti-sym ν(HgX) and ν(HgP) stretching vibrations. For the 1:1 centrosymmetric dimer $[(R_3P)_2Hg_2X_4]$ (X = Cl, R = Ph, Pr, 1,2,5-triphenylphosphole; X = Br, R = Ph_3P; X = I, R = Bu_3P, 1-phenyl,3,4-dimethylphosphole), whose structures have been crystallographically determined [6,13,27], group theory predicts one ν(HgP), one $\nu(HgX_t)$ and two $\nu(HgX_b)$ vibrations and when the inversion centre is lost the number of possible bands is doubled. However these are not always all observed, so that vibrational spectral data do not give a very clear indication of the exact symmetry of the dimer [27]. The terminal and bridging ν(Hg–Cl) stretching modes (Fig. 4, Table 4) for the 1:1 $HgCl_2$ complex described herein may be assigned at 283 and 253 cm^{-1} respectively with ν(HgP) either below the cut off of the notch filters or hidden beneath the multicomponent band observed between 100 and 300 cm^{-1}. Thus this indicates that this is a halogen bridged dimer with the closeness of the bridging and terminal modes being ascribed to very weak bridging, as found in the DMPP complexes [15]. A different pattern and intensity of bands arises for the bromide and iodide species, which have Raman bands of much higher intensity than for the chloride. Bromide and iodide have diminished ability as bridging groups and the X-ray structure of

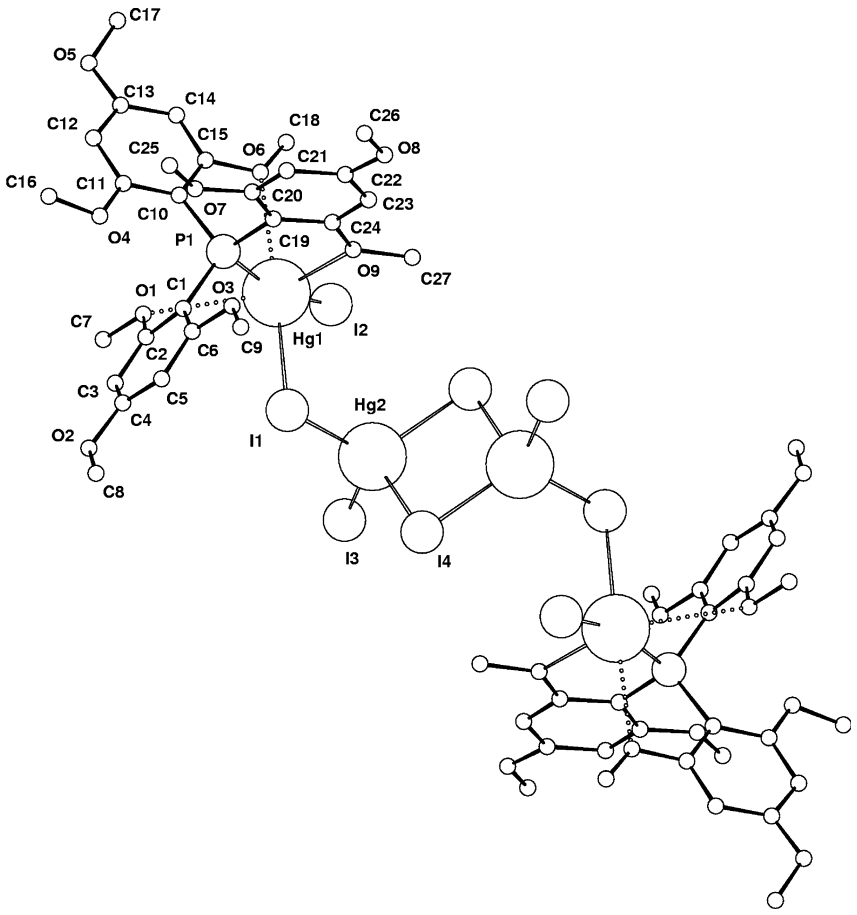


Fig. 3. The molecular structure of $(TMPP)_2(HgI_2)_4$.

these has shown them to be monomeric. Thus, for $TMPPHgX_2$ (X = Br, I) only a symmetric and anti-symmetric ν(Hg–X) stretching vibration are predicted which should have very similar band positions with the possibility of these bands overlapping. A single band was observed for both these complexes found at 176 (bromide) and 140 cm^{-1} (iodide). The iodo complex ν(Hg–I) mode is very asymmetric indicating that further bands are probably beneath the overall band structure. The ν(Hg–P) band was not observed for these complexes probably due to the cut-off of the notch filter.

Table 4
Raman spectral data for $TMPPHgX_2$: 1:1, 2:1, 1:2 and 2:3 complexes

X	TMPP	Cl	Br	I
1:1	122(m), 138(m), 151(m,b), 189(m,b), 222(m,b), 287(w,b), 370(s), 464(m), 529(m), 578(m)	122(w), 138(w), 154(m), 172(m,b), 188(m,b), 218(m,b), 253(m)*, 283(s)*, 329(w), 372(m), 443(m), 470(m), 520(m), 528(m,sh), 580(m)	122(w), 137(w), 150(m), 176(s)*, 378(m), 426(m), 436(m), 468(m), 479(m), 523(m), 581(w)	122(w), 140(s,b)*, 187(w,b), 224(w,b), 376(m), 423(m), 434(m), 466(m), 486(w), 522(m), 580(w)
2:1		123–300(MCB), 321(w), 375(s), 435(s), 470(m), 486(w), 519(m), 570(w), 589(w)	123(w), 138(m), 157(s)*, 219(MCB), 373(s), 437(m), 471(m), 519(m), 589(m)	122(m), 137(m), 150(s)*, 371(m), 421(w), 467(w), 520(w), 583(m)
1:2				120(m), 146(s)*, 171(s)*, 244(w), 370(m), 445(w), 469(w), 516(w), 529(w)
2:3		121(w), 138(m), 154(m), 176(m,b), 217(m,b), 258(m)*, 285(s)*, 330(w), 370(m), 445(m), 470(m), 518(m), 527(m,sh),	122(w), 138(m), 153(m), 178(s)*, 215(w), 370(m), 445(m), 469(m), 518(m)	122(m), 140(s,sh)*, 147(s)*, 172(s)*,190(m,b), 218(w,b), 244(w,b), 373(m), 428(m), 444(m), 468(m), 479(w,sh), 517(m), 528(m), 583(m)

w, weak intensity band; m, medium intensity band; s, strong intensity band, sh, shoulder; b, broader than expected band; MCB, multicomponent band; *, assigned bands.

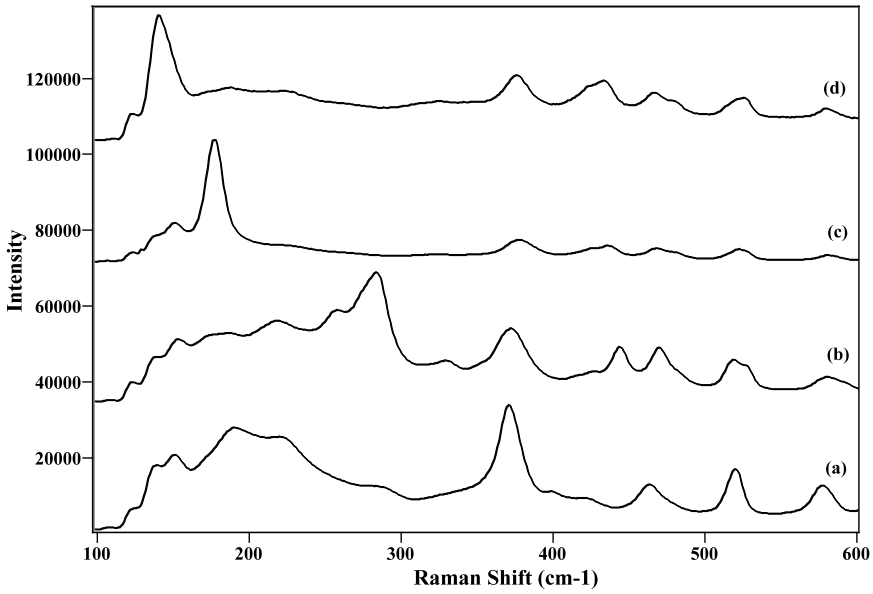


Fig. 4. Raman spectra of the 1:1 complexes ((a) TMPP, (b) chloride (c) bromide and (d) iodide).

The 2:1 complexes $[L_2HgX_2]$ in principle should give one ν(Hg–X) symmetric and one anti-symmetric mode and two ν(Hg–P) modes. However this was not observed for all of the complexes (Fig. 5). The chloride did not give well resolved bands which could be ascribed to ν(Hg–Cl) and it seems likely that it has decomposed in the laser beam like 1-phenyl –3,4-dimethylphosphole-mercury(II)chloride [27]. The bromide complex shows only one clearly visible ν(Hg–Br) mode at 157 cm^{-1}, however there is spectral intensity seen as a shoulder which may be obscuring further bands. The iodo complex shows only a single very intense band at 150 cm^{-1} which can clearly be ascribed to ν(Hg–I) as also found in a range of other tertiary phosphine–mercury(II)iodide complexes [27]. In the spectra of all three complexes no clear ν(Hg–P) band can again be observed.

The spectra of the 2:3 complexes $(TMPP)_2(HgX_2)_3$ which may be formulated as $[Hg(TMPP)_2][Hg_2X_6]$ on the basis of the crystal structure of X = Cl [21] are shown in Fig. 6 and assignments listed in Table 4. The spectra do not contain bands ascribed to $[TMPPHgX]^+$ which was found to be present in products crystallised from 2:1 solutions of HgX_2 and TMPP in MeCN. For the iodide the main component in such mixtures was described as $[TMPPHgI]_2[Hg_2I_6]$ whereas the chloride and bromide systems were believed to consist of mixtures of analogues of the above and $[Hg(TMPP)_2]$-

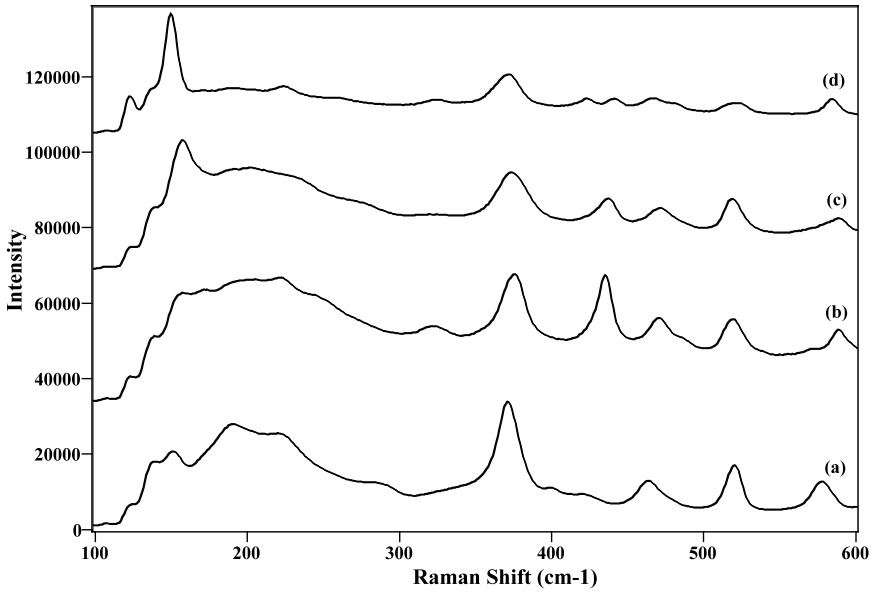


Fig. 5. Raman spectra of the 2:1 complexes ((a) TMPP, (b) chloride (c) bromide and (d) iodide).

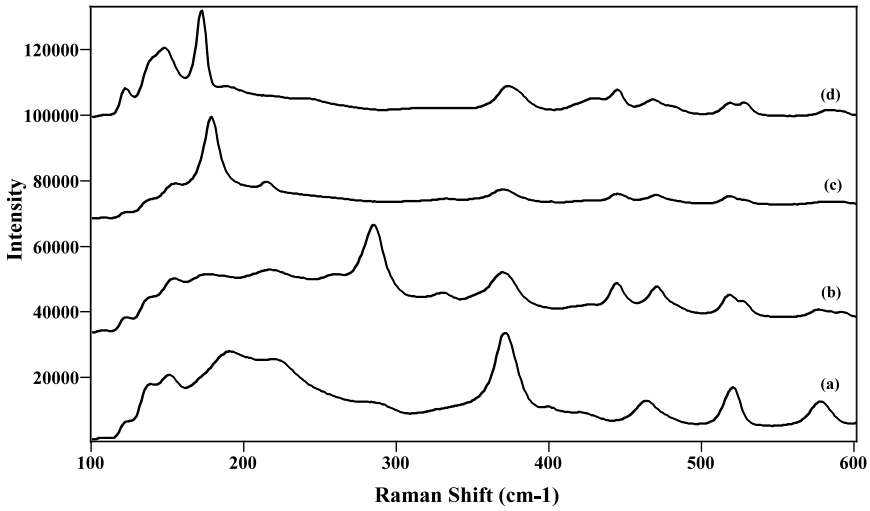


Fig. 6. Raman spectra of the 3:2 complexes ((a) TMPP, (b) chloride (c) bromide and (d) iodide).

$[Hg_2X_6]$ (X = Cl, Br) [21]. The solid 2:3 chloro complex isolated here contains bands due to terminal and bridging Hg–Cl vibrations at 285 and 258 cm^{-1}(Table 4). Only a single intense band was observed for the bromide complex at 178 cm^{-1}. The corresponding iodo complex showed three bands at 172 cm^{-1} (terminal) and 147 and 140 cm^{-1} (bridging) which are close to the assignments for one of the components $[Hg(TMPP)_2]$-$[Hg_2X_6]$ (X = Br, I) in the mixed complexes [21] and can thus be ascribed to the $[Hg_2X_6]^{2-}$ ion. Thus the vibrational spectra of all three 2:3 complexes confirm their formulation as $[Hg(TMPP)_2][Hg_2X_6]$.

The spectrum of the 1:2 iodo complex and assignments agree well with those discussed for this complex previously although formulated as $[TMPPHgI]_2[Hg_2I_6]$ [21]. Thus, the terminal Hg1–I1 vibration is found as a strong band at 171 $cm^{-1}$and the terminal Hg–I vibration of the central Hg_2I_6 core at 146 cm^{-1} although, due to its asymmetry, there is the possibility of further bands beneath the 147 cm^{-1} mode. The bridging Hg–I vibrations occur below the cut off point of the instrument.

3.2. Solution ^{31}P NMR spectra

^{31}P NMR spectral data for $TMPPHgX_2$, $(TMPP)_2(HgX_2)_3$ (X = Cl, Br, I) and $TMPP(HgI_2)_2$ as solutions in DMSO are listed in Table 5. All were only sparingly soluble but showed two central peaks due to components containing the non-magnetic isotopes of mercury, indicating the presence of two species in solution. Also present were small satellites from coupling of ^{31}P to ^{199}Hg which has nuclear spin, $I = 1/2$ and natural abundance of 16.8%. The parameters are non-halogen dependent and remain essentially constant for one of the species in solutions of all seven compounds and must be ascribed to $[(TMPP)_2Hg]^{2+}$ as found for 1:1 solutions of the ligand and mercury(II) halides in

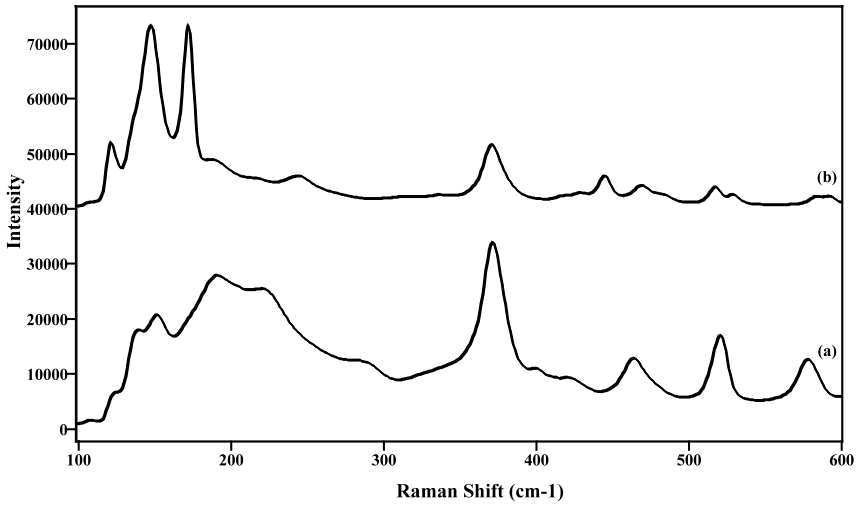


Fig. 7. Raman spectrum of the 1:2 iodo complex ((a) TMPP (b) iodide).

Table 5
^{31}P NMR spectral data

	δ/ppm	^1J (^{31}P^{199}Hg)/Hz	δ/ppm	^1J (^{31}P^{199}Hg)/Hz
$TMPPHgCl_2$	−35.54	5087	−33.54	9278
$TMPPHgBr_2$	−35.55	5149	−30.12	8486
$TMPPHgI_2$	−35.49	5251	−28.00	6939
$(TMPP)_2(HgCl_2)_3$	−35.43	5180	−34.36	9295
$(TMPP)_2(HgBr_2)_3$	−35.39	5168	−32.16	8580
$(TMPP)_2(HgI_2)_3$	−35.39	5239	−28.22	7631
$TMPP(HgI_2)_2$	−35.47	5282	−28.20	7656

MeCN solutions [21]. The other species present are halogen dependent and show the expected trend of chemical shift with $J(^{199}Hg-^{31}P)$ decreasing from chloride to iodide.

For the 1:1 complexes all of the chemical shifts and coupling constants are much greater than for other R_3PHgX_2 complexes [27,28] due to the much greater basicity of TMPP. Although others [21] have ascribed the halogen dependent peaks as due to $[TMPPHgX]^+$, in view of our crystallographic data, we believe that they are simply due to $[TMPPHgX_2]$. The ratio of the non-halogen to the halogen dependent peaks is ~2:1 for X = Cl, 1:1 (Br) and 1.6:1 (I).

For $(TMPP)_2(HgX_2)_3$ the dominant species (ratio ~2.2:1) for the chloride was $[(TMPP)_2Hg]^{2+}$ while for the bromide and iodide the non-halogen: halogen ratio of peaks was ~3.2:1 and 1:1, respectively. The chemical shifts and coupling constants for the chloride and bromide were very close to those of the corresponding 1:1 complexes and, as the vibrational spectra do not contain bands due to $[TMPPHgX]^+$ [21] this indicates the presence of $[TMPPHgX_2]$ (X = Cl, Br) as the halogen containing species. The chemical shift and coupling constant for the iodide were very similar to those of $TMPP(HgI_2)_2$ indicating the presence in both cases of the same species in solution which is likely to be the covalent dimer, $(TMPP)HgI(\mu\text{-}I)HgI(\mu\text{-}I)_2HgI(\mu\text{-}I)HgI(TMPP)$, determined crystallograpically.

4. Conclusion

Reaction of TMPP with mercury(II) halides in varying molar ratio in ethanol solutions produces complexes with a variety of stoichiometries. Crystal structure determinations has proved the uncommon monomeric nature for the 1:1 complexes containing bromide and iodide while ^{31}P NMR studies have shown the presence of significant amounts of both halogen dependent and non-halogen dependent species in DMSO solution.

5. Supplementary material

Crystallographic data for the structural analysis have been deposited with the Cambridge Crystallographic Data Centre, CCDC Nos. 169399 for compound **I**, 169400 for compound **II** and 178058 for compound **III**. Copies of this information may be obtained free of charge from The Director, CCDC, 12 Union Road, Cambridge, CB2 1EZ, UK (fax: +44-1223-336033; e-mail: deposit@ccdc.cam.ac.uk or www: http://www.ccdc.cam.ac.uk).

References

[1] N.A. Bell, T.D. Dee, P.L. Goggin, M. Goldstein, R.J. Goodfellow, T. Jones, K. Kessler, D.M. McEwan, I.W. Nowell, J. Chem. Res. (S) (1981) 2; (M) (1981) 0201.
[2] N.A. Bell, T.D. Dee, M. Goldstein, P.J. McKenna, I.W. Nowell, Inorg. Chim. Acta 71 (1983) 135.
[3] D.W. Allen, N.A. Bell, S.T. Fong, L.A. March, I.W. Nowell, Inorg. Chim. Acta 99 (1985) 157.
[4] N.A. Bell, L.A. March, I.W. Nowell, Inorg. Chim. Acta 156 (1989) 195.
[5] N.A. Bell, M. Goldstein, L.A. March, I.W. Nowell, J. Chem. Soc., Dalton Trans., (1984) 1621.
[6] N.A. Bell, M. Goldstein, T. Jones, I.W. Nowell, Inorg. Chim. Acta 43 (1980) 87.
[7] N.A. Bell, M. Goldstein, T. Jones, I.W. Nowell, Inorg. Chim. Acta 48 (1981) 185.
[8] N.A. Bell, M. Goldstein, T. Jones, L.A. March, I.W. Nowell, Inorg. Chim. Acta 61 (1982) 83.
[9] N.A. Bell, M. Goldstein, T. Jones, I.W. Nowell, Inorg. Chim. Acta 69 (1983) 155.
[10] N.A. Bell, T.D. Dee, M. Goldstein, I.W. Nowell, Inorg. Chim. Acta 70 (1983) 215.
[11] N.A. Bell, M. Goldstein, T. Jones, I.W. Nowell, Inorg.Chim. Acta 75 (1983) 21.
[12] N.A. Bell, N.A. Chudley, L.A. March, I.W. Nowell, Inorg. Chim. Acta 141 (1988) 155.
[13] N.A. Bell, L.A. March, I.W. Nowell, Inorg. Chim. Acta 156 (1989) 201.
[14] N.A. Bell, L.A. March, I.W. Nowell, Inorg.Chim. Acta 162 (1989) 57.
[15] N.A. Bell, S.J. Coles, M.B. Hursthouse, M.E. Light, K.A. Malik, R. Mansor, Polyhedron 19 (2000) 1719.
[16] N.A. Bell, L.A. March, I.W. Nowell, Inorg. Chim. Acta 179 (1991) 73.
[17] M.S. Wade, S. Higashizaka, A. Tsubo, J. Chem Res (S) (1985) 38; (M) (1985) 0467.
[18] Y. Yamashoji, T. Matsushita, M. Tanaka, T. Shono, M. Wade, Polyhedron 8 (1989) 1053.
[19] C.A. Streuli, Analyt. Chem. 32 (1960) 985.
[20] K.R. Dunbar, S.C. Haefner, C.E. Uzelmeier, A. Howard, Inorg. Chim. Acta 240 (1995) 527.
[21] L.-J. Baker, G.A. Bowmaker, B.W. Skelton, A.H. White, J. Chem. Soc., Dalton Trans. (1993) 3235.
[22] K.R. Dunbar, S.C. Haefner, Polyhedron 13 (1994) 727.
[23] G.M. Sheldrick, Programs for Crystal Structure Solution and Refinement, University of Göttingen, Germany, 1997.
[24] N.A. Bell, M. Goldstein, T. Jones, I.W. Nowell, Acta Crystallogr., Sect. B 36 (1980) 708.

[25] D. Gudat, M. Nieger, M. Schrott, Inorg. Chem. 36 (1997) 1476.
[26] B. Zacharie, J.D. Wuest, M.J. Oliver, A.L. Beauchamp, Acta Crystallogr., Sect. C 41 (1985) 369.
[27] G.A. Bowmaker, H.J. Clase, N.W. Alcock, J.M. Kessler, J.H. Nelson, J.S. Frye, Inorg. Chim. Acta 210 (1993) 107.
[28] (a) S.O. Grim, D.P. Shah, C.K. Haas, J.M. Ressner, P.H. Smith, Inorg. Chim. Acta 36 (1979) 139;
(b) T. Allman, R.G. Goel, Can. J. Chem. 62 (1984) 615;
(c) E.C. Alyea, S.A. Dias, R.G. Goel, W.O. Ogini, P. Pilon, D.W. Meek, Inorg. Chem. 17 (1978) 1697.

2. Experimental

2.1. Investigation in the solid state

2.1.1. Preparation of the complexes

The hydrochloride 5-hydroxymethyl-4-methylimidazole (Aldrich Europe) was alkalized with a $KHCO_3$ solution. The free imidazole base was extracted with 1-BuOH.

The Cu(II) and Ni(II) complexes of 4-CH_2OH–5-CH_3im were prepared in aq. solution. Thus, to a solution of 8 mmol of the imidazole base, a solution containing 2 mmol of the particular metal nitrate was added. The crystals of the Cu(II) complex were navy-blue, while those of the Ni(II) complex were dark-violet. Results of the elemental analyses are as follows: Cu(II) complex: C, 37.9; H, 5.0; N, 22.2. Calc. for $CuL_4(NO_3)_2$: C, 37.76; H, 5.07; N, 22.02%. Ni(II) complex: C, 38.0; H, 5.0; N, 22.4. Calc. for $NiL_4(NO_3)_2$: C, 38.05; H, 5.11; N, 22.19%.

2.1.2. Physical measurements

Elemental analyses were run on a Model 240 Perkin–Elmer CHN analyser. The IR spectra were recorded on a Perkin–Elmer 180 (spectral range 50–4000 cm^{-1}) spectrophotometer in Nujol and in KBr pellets. The far-IR spectra were obtained in Nujol mulls sandwiched between polyethylene plates. The electronic spectra (5000–30 000 cm^{-1}) were recorded on a Cary 5 UV–Vis–NIR spectrophotometer in Nujol mulls.

The EPR spectra were recorded on a Bruker ESP 300E (Bruker, Germany) spectrometer operating at X-band and equipped with the Bruker NMR gaussmeter ER 035M and the Hewlett-Packard microwave frequency counter HP 5350B. EPR parameters were calculated by computer simulation of the experimental spectra using Bruker's WIN-EPR SimFonia Software Version 1.25.

2.1.3. Crystal data

X-ray measurements were performed on a Kuma KM4 diffractometer. The structures were solved by direct methods using the SHELXS-86 [11] and SHELXS-97 [12] programs and refined by full-matrix least-squares methods using the SHELXL-93 [13] and SHELXL-97 [14] programs (respectively for the Cu(II) and Ni(II) complexes). Details of the crystal data and refinement for the studied compounds are collected in Table 1.

Table 1
Crystal data and structure refinement for $[CuL_4](NO_3)_2$ and $[NiL_4](NO_3)_2$ complexes

	$[CuL_4](NO_3)_2$	$[NiL_4](NO_3)_2$
Empirical formula	$C_{20}H_{32}CuN_{10}O_{10}$	$C_{20}H_{32}N_{10}NiO_{10}$
Molecular weight	636.10	631.27
Temperature (K)	293(2)	100(1)
Radiation	Mo Kα ($\lambda = 0.71073$ Å)	
Crystal system	monoclinic	monoclinic
Space group	$P2_1/c$	$P2_1/c$
Unit cell dimensions		
a (Å)	7.238(2)	7.236(2)
b (Å)	18.784(4)	18.537(4)
c (Å)	10.064(3)	10.064(2)
β (°)	100.86(3)	101.37(3)
V (Å^3)	1343.8(6)	1323.4(5)
Z	2	2
D_{calc} (g cm^{-3})	1.572	1.584
Absorption coefficient (cm^{-1})	8.86	8.07
$F(000)$	662	660
Crystal size (mm)	0.15 × 0.15 × 0.20	0.15 × 0.15 × 0.18
2θ Range (°)	2.99–26.00	3.62–28.40
Index ranges	$-7 \le h \le 8$, $-23 \le k \le 23$, $-12 \le l \le 12$	$-7 \le h \le 9$, $-24 \le k \le 24$, $-12 \le l \le 13$
Reflections collected	7245/2620 [$R_{int} = 0.0285$]	8570/3107 [$R_{int} = 0.0236$]
Data [$I > 2\sigma(I)$]/parameters	2196/252	2697/252
Final R indices [$I > 2\sigma(I)$]	$R_1 = 0.0539$, $wR_2 = 0.1479$	$R_1 = 0.0287$, $wR_2 = 0.0650$
R indices (all data)	$R_1 = 0.0613$, $wR_2 = 0.1565$	$R_1 = 0.0372$, $wR_2 = 0.0683$
Goodness-of-fit	1.120	1.070
Largest difference peak and hole (e Å^{-3})	1.249 and −0.533	0.326 and −0.481

2.2. Solution studies

2.2.1. Potentiometric measurements

Potentiometric measurements of the metal-ion systems were carried out using a PHM-84 pH meter (Radiometer) and a GK 24001 C combination electrode placed in a glass vessel thermostatted at 298 K in a solution of a constant ionic strength $I = 0.5$ mol dm^{-3} maintained with KNO_3. The electrode was calibrated by means of a HCl solution of known titre with a KOH solution. The concentration of the protonated ligand (HL^+) in stock solutions used in potentiometric titrations was 0.20 mol dm^{-3}.

In the three series of measurements the metal–HL^+ molar ratios were 1:4, 1:8 and 1:10. The titration with the base was conducted in triplicate, over the pH range 2.5–7.1. The dissociation constants of the conjugate acid and stability constants, β_n, of the complexes were refined by the SUPERQUAD program.

2.2.2. Spectroscopic measurements

The visible-range absorption spectra of the Cu(II) and Ni(II) complexes in aq. solutions were recorded on a Specord M-500 (Carl Zeiss, Jena) spectrophotometer. The solutions were prepared in an analogous manner to those for the potentiometric titrations. The initial metal concentrations were 0.05 mol dm^{-3}. The highest concentration of the protonated ligand was 0.20 mol dm^{-3}.

3. Results and discussion

3.1. Investigation in the solid state

3.1.1. Molecular structure of the Cu(II) and Ni(II) complexes

The molecular structure of the Ni(II) complex together with the atom labelling is shown in Fig. 1. The molecular packing of $[Ni(4\text{-}CH_2OH\text{–}5\text{-}CH_3im)_4](NO_3)_2$ in the unit cell is presented in Fig. 2. The angles and bond lengths for both complexes are collected in Tables 2 and 3.

On account of the tautomeric transformation of the hydrogen atom, which is bonding with the pyrrole nitrogen atom >NH in the heterocyclic ring, imidazole substituted at positions 4 and 5 occur in two forms, 5(4)-CH_2OH–4(5)-CH_3im. The determined molecular structure of the Cu(II) and Ni(II) complexes reveals that the 4-CH_2OH–5-CH_3im tautomer is involved in complexation. In the co-ordination compounds, this ligand has a dual nature. Namely, two molecules act as monodentate ligands co-ordinating through the 'pyridynic' atom of the imidazole ring, whereas the remaining two are bidentate ligands, where the oxygen atom of the hydroxymethyl group acts as another electron donor. Consequently, the immediate surrounding of the central ion is made up of four nitrogen atoms of the imidazole rings and two oxygen atoms of the hydroxymethyl groups (CuN_4O_2 and NiN_4O_2 chromophores).

The shape of the co-ordination polyhedron of the Cu(II) ion is that of a slightly distorted tetragonal bipyramid. The copper–nitrogen bond lengths are 1.981(2) and 2.050(2) Å, and the angles between bonds lying in this plane are 90.3(1)° and 89.7(1)°, thus differing from a right angle by ±0.3°. The elongated copper–oxygen bonds are 2.496(2) Å long each. The O(11)–Cu–N(21) and O(11)–Cu–N(21a) angles are, respectively 93.6(1)° and 86.4(1)°. On account of chelation, the O(11)–Cu–N(11) and O(11)–Cu–N(11a) angles are deformed to 75.8(1)° and 104.2(1)°, respectively.

In the Ni(II) complex, the bonds between the central ion and the nitrogen atoms are slightly longer than those in the Cu(II) complex, namely 2.046(1)° and 2.108(1) Å. The bonds with the oxygen atoms are 0.385 Å shorter, being 2.141 Å each.

In the *xy* co-ordination plane, the nitrogen–nickel–nitrogen angles are 89.4(1)° and 90.6(1)°, whereas those of N(21a)–Ni–O(11) and N(21)–Ni–O(11) are, respectively 87.7(1)° and 92.3(1)°. The largest distortion of the octahedral environment of the Ni(II) ion is caused by the N(11)–Ni–O(11) and N(11a)–Co–O(11) angles being equal to 80.2(1)° and 99.8(1)°, respectively.

In the aforementioned complexes the non-co-ordinating $-CH_2OH$ group is involved in two intramolecular hydrogen bonds, one with the oxygen atom of the

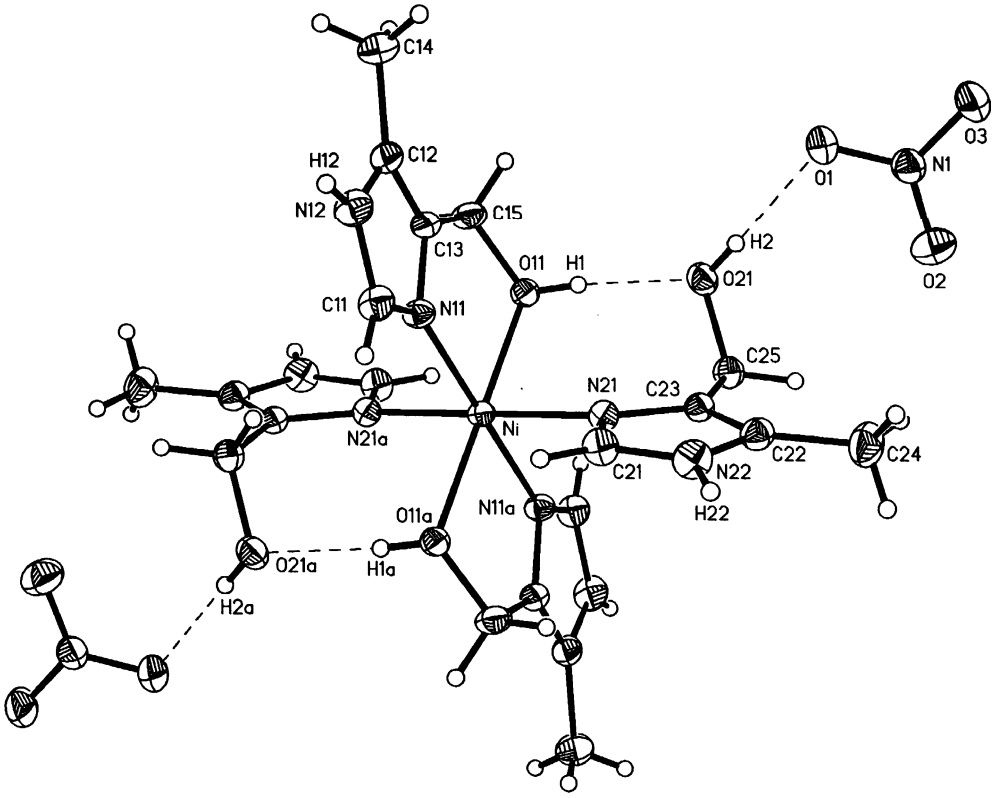


Fig. 1. The molecular structure of the Ni(II) complex with 4-hydroxymethyl-5-methylimidazole, $[M(4\text{-}CH_2OH\text{–}5\text{-}CH_3im)_4](NO_3)_2$.

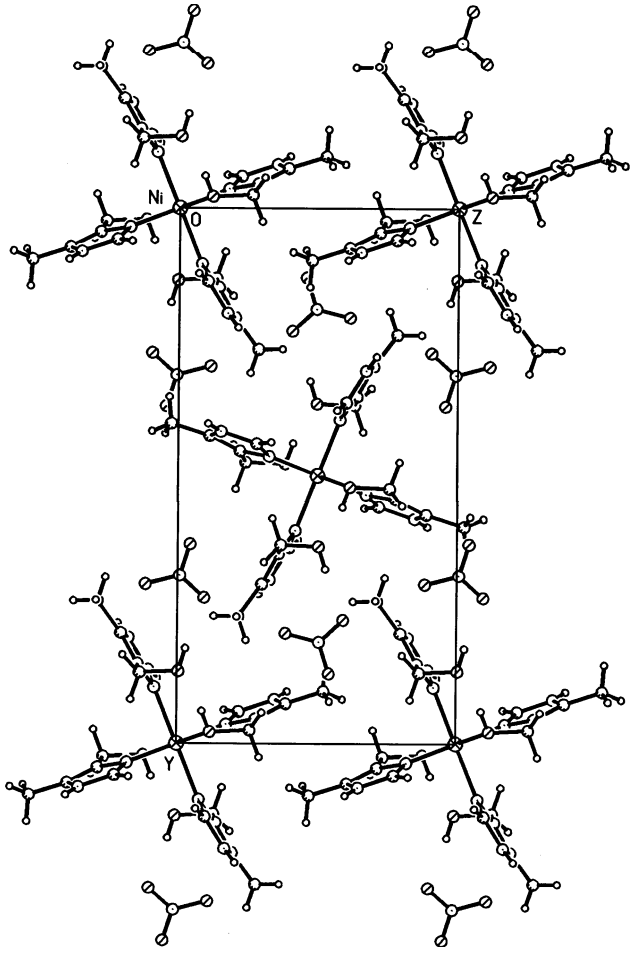


Fig. 2. Molecular packing of $[Ni(4\text{-}CH_2OH\text{–}5\text{-}CH_3im)_4](NO_3)_2$ in the unit cell.

nitrate group and the other with the hydrogen atom of the hydroxyl group of the bidentate azole ligand. Both the lengths and angles between the bonds are shown in Tables 4 and 5.

3.1.2. The IR spectra

Interpretation of the IR and far-IR spectra was based on changes in the spectra of the complexes relative to that of non-complexed 4-CH_2OH–5-CH_3im. Those of both studied complexes are in accord with their structure. Involvement of the 'pyridine' nitrogen atom of the imidazole ring in co-ordination is highlighted by displacement of the band assigned to ν(C=C) conjugated with ν(C=N) from 1499 (free ligand) to 1510 cm^{-1} for the Cu(II) complex and to 1506 cm^{-1} for the Ni(II) complex. The metal–nitrogen bond was identified on the basis of the far-IR spectra in which double bands at 302, 279 and 298, 283 cm^{-1} for the Cu(II) and Ni(II) complexes, respectively, have been assigned to ν(M–N). Co-ordination through the oxygen atom of the hydroxymethyl group shifts the ν(OH) band from 3415 cm^{-1} (free base) down to 3327 cm^{-1} in the Cu(II) complex

Table 2
Selected bond lengths (Å) for studied complexes

	$[CuL_4](NO_3)_2$	$[NiL_4](NO_3)_2$
M–N(11a)	1.981(2)	2.046(1)
M–N(11)	1.981(2)	2.046(1)
M–N(21a)	2.050(2)	2.108(1)
M–N(21)	2.050(2)	2.108(1)
M–O(11)	2.496(2)	2.141(1)
M–O(11a)	2.496(2)	2.141(1)
O(11)–C(15)	1.420(4)	1.443(2)
O(21)–C(25)	1.436(4)	1.447(2)
N(11)–C(11)	1.310(4)	1.322(2)
N(11)–C(13)	1.385(4)	1.387(2)
N(12)–C(11)	1.339(4)	1.350(2)
N(12)–C(12)	1.364(5)	1.384(2)
N(21)–C(21)	1.315(4)	1.326(2)
N(21)–C(23)	1.397(4)	1.396(2)
N(22)–C(21)	1.333(5)	1.344(2)
N(22)–C(22)	1.369(4)	1.382(2)
C(12)–C(13)	1.349(4)	1.365(2)
C(12)–C(14)	1.491(5)	1.488(2)
C(13)–C(15)	1.496(5)	1.501(2)
C(22)–C(23)	1.354(4)	1.368(2)
C(22)–C(24)	1.494(5)	1.492(2)
C(23)–C(25)	1.480(4)	1.492(2)
O(1)–N(1)	1.251(4)	1.267(2)
O(2)–N(1)	1.224(4)	1.244(2)
O(3)–N(1)	1.240(4)	1.256(2)

Symmetry transformations used to generate equivalent atoms: $a = -x, -y, -z$.

and 3337 cm^{-1} in the Ni(II) complex. Again, a strong sharp ν(C–O) peak in the spectrum of the free base at 1004 cm^{-1} is split in that of the Cu(II) complex into two bands emerging at 993 and 1024 cm^{-1} due to the dual nature of the hydroxymethyl group in this complex. One of the split bands can be assigned to the hydroxymethyl group co-ordinated to the central ion, while the other to the non-co-ordinated group. In the spectra of the Ni(II) complex, this band is not displaced.

In the IR spectra of both complexes, there are two new bands which are missing in the spectrum of the free base. One of these, at 1385 cm^{-1}, is very strong and sharp, and the other, at 812 cm^{-1} is weak. Both the shape and position of the latter is typical for the nitrate group non-co-ordinated to the central ion [15].

3.1.3. EPR spectra of $[Cu(4\text{-}CH_2OH\text{–}5\text{-}CH_3im)_4](NO_3)_2$ complex

The EPR spectrum of polycrystalline $[Cu(4\text{-}CH_2OH\text{–}5\text{-}CH_3im)_4](NO_3)_2$ presents a slightly anisotropic line (Fig. 3(a)). A very weak resolution of the parallel orientation peak and the lack of copper hyperfine splitting is most likely caused by spin–spin interaction between Cu(II) paramagnetic centres at a relatively small distance (7.238 Å). In the case of the Cu(II) complex with the analogous ligand donor set from four 1-benzyl-2-hydroxymethylimidazoles this distance is 9.580 Å and distinctly resolved copper hyperfine struc-

Table 3
Selected bond angles (°) for studied complexes

	$[CuL_4](NO_3)_2$	$[NiL_4](NO_3)_2$
N(11a)–M–N(11)	180.0	180.0
N(11a)–M–N(21a)	90.3(1)	90.3(1)
N(11)–M–N(21a)	89.7(1)	89.7(1)
N(21a)–M–N(21)	180.0	180.0
N(11a)–M–O(11)	104.2(1)	99.8(1)
N(11)–M–O(11)	75.8(1)	80.2(1)
N(21a)–M–O(11)	86.4(1)	87.7(1)
N(21)–M–O(11)	93.6(1)	92.3(1)
O(11)–M–O(11a)	180.0	180.0
C(11)–N(11)–C(13)	105.8(3)	106.0(1)
C(11)–N(11)–M	133.6(2)	140.2(1)
C(13)–N(11)–M	120.5(2)	113.8(1)
C(11)–N(12)–C(12)	108.4(3)	108.4(1)
C(21)–N(21)–C(23)	105.5(3)	105.4(1)
C(21)–N(21)–M	120.0(2)	119.9(1)
C(23)–N(21)–M	133.5(2)	133.3(1)
C(21)–N(22)–C(22)	108.5(3)	108.4(1)
N(11)–C(11)–N(12)	110.7(3)	110.7(1)
C(13)–C(12)–N(12)	105.6(3)	105.0(1)
C(13)–C(12)–C(14)	132.2(4)	132.0(1)
N(12)–C(12)–C(14)	122.1(3)	122.9(1)
C(12)–C(13)–N(11)	109.5(3)	110.0(1)
C(12)–C(13)–C(15)	130.3(3)	131.2(1)
N(11)–C(13)–C(15)	120.1(3)	118.8(1)
O(11)–C(15)–C(13)	112.3(3)	109.6(1)
N(21)–C(21)–N(22)	111.1(3)	111.2(1)
C(23)–C(22)–N(22)	105.7(3)	105.2(1)
C(23)–C(22)–C(24)	131.8(3)	132.4(1)
N(22)–C(22)–C(24)	122.6(3)	122.3(1)
C(22)–C(23)–N(21)	109.2(3)	109.8(1)
C(22)–C(23)–C(25)	127.9(3)	128.3(1)
N(21)–C(23)–C(25)	122.8(3)	121.9(1)
O(21)–C(25)–C(23)	112.8(3)	112.1(1)
O(2)–N(1)–O(3)	120.6(3)	120.5(1)
O(2)–N(1)–O(1)	120.5(3)	120.4(1)
O(3)–N(1)–O(1)	118.9(3)	119.0(1)

Symmetry transformations used to generate equivalent atoms: $a = -x, -y, -z$.

Table 4
Hydrogen bond lengths (Å) and bond angles (°) for complex $[CuL_4](NO_3)_2$

D–H···A	d(D–H)	d(H···A)	d(D···A)	<(DHA)
O(11)–H(1)···O(21)	0.79(4)	1.93(5)	2.673(4)	157(4)
N(12)–H(12)···O(3b)	0.82(4)	2.03(4)	2.834(4)	167(4)
O(21)–H(2)···O(1)	0.84(4)	1.97(4)	2.776(4)	162(4)
N(22)–H(22)···O(2c)	0.96(5)	2.16(5)	3.009(4)	146(4)
N(22)–H(22)···O(1d)	0.96(5)	2.42(4)	3.076(4)	125(3)

Symmetry transformations used to generate equivalent atoms: $a = -x, -y, -z$; $b = x-1, -y-1/2, z+1/2$; $c = x-1, y, z$; $d = x-1, -y-1/2, z-1/2$.

ture has been observed in the EPR spectrum of the complex polycrystalline sample [8]. After dilution of the paramagnetic $[Cu(4\text{-}CH_2OH\text{–}5\text{-}CH_3im)_4](NO_3)_2$ centres by diamagnetic solvent molecules (ethanol or methanol)

Table 5
Hydrogen bond lengths (Å) and bond angles (°) for complex $[NiL_4](NO_3)_2$

D–H···A	d(D–H)	d(H···A)	d(D···A)	<(DHA)
O(11)–H(1)···O(21)	0.80(2)	1.85(2)	2.643(2)	167(2)
N(12)–H(12)···O(3b)	0.83(2)	2.01(2)	2.828(2)	171(2)
O(21)–H(2)···O(1)	0.90(3)	1.86(3)	2.741(2)	168(2)
N(22)–H(22)···O(2c)	0.84(2)	2.39(2)	3.030(2)	133(2)
N(22)–H(22)···O(1d)	0.82(2)	2.31(2)	3.004(2)	140(2)

Symmetry transformations used to generate equivalent atoms: $a = -x, -y, -z$; $b = x-1, -y-1/2, z+1/2$; $c = x-1, y, z$; $d = x-1, -y-1/2, z-1/2$.

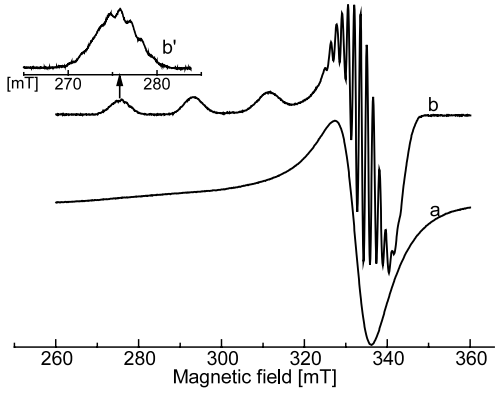


Fig. 3. EPR spectra of $[Cu(4\text{-}CH_2OH\text{–}5\text{-}CH_3im)_4](NO_3)_2$: (a) polycrystalline; (b) in methanolic frozen solution at 77 K (b′ is an amplified peak of copper hyperfine coupling).

the EPR spectrum at 77 K exhibits hyperfine splittings due to interaction with both copper and nitrogen nuclei (Fig. 3(b and b′)). The values of EPR parameters ($g_\parallel = 2.263$ and $A_\parallel = 185 \times 10^{-4}$ cm^{-1}) are characteristic of tetragonally elongated octahedral geometry of the complex, in agreement with the Cu(II) environment determined by crystal structure analysis. The ^{14}N hyperfine splittings at the peaks due to copper hyperfine coupling of parallel orientation (Fig. 3(b′)) and at the high field peak of perpendicular orientation (Fig. 3(b)) result from strong interaction between four nitrogen donors and Cu(II). The EPR parameters of the complex characteristically differ from those found for the complex with similar chelate rings around Cu(II) provided by four 1-benzyl-2-hydroxymethylimidazole ligands (with $g_\parallel = 2.277$ and $A_\parallel = 175 \times 10^{-4}$ cm^{-1}) [8]. A decrease of $g_\parallel$ and an increase of $A_\parallel$ values may be assigned to higher donor properties of 4-hydroxymethyl-5-methylimidazole ($pK_a = 7.14$) as compared to 1-benzyl-2-hydroxymethylimidazole ($pK_a = 6.58$) [8] taking into account that the axial positions are occupied in a similar way in both complexes.

3.1.4. d–d Electronic spectra

The previously described spatial configuration of the CuN_4O_2 chromophore is closely related to the shape and

position of the visible absorption spectrum. The absorption band at 18 100 cm^{-1} is broad, diffuse and asymmetric. With tetragonal Cu(II) complexes such a shape of the spectrum results from superposition of three component bands. Their exact positions established by means of the Gaussian distribution are at 11 600, 14 400 and 18 900 cm^{-1} In addition, the EPR survey shows that the ground state of the Cu(II) ion in the complex is within the $d_{x^2-y^2}$ orbital (spectroscopic state $^2B_{1g}$). Consequently, the identified absorption bands can be assigned as the $^2B_{1g} \rightarrow {}^2A_{1g}$, $^2B_{1g} \rightarrow 2B_{2g}$ and $^2B_{1g} \rightarrow {}^2E_g$ transitions, respectively [16].

For the octahedral Ni(II) complexes the crystal field theory predicts three spin permissible electronic transitions, namely $^3A_{2g}(F) \rightarrow {}^3T_{2g}(F)$ (ν_1), $^3A_{2g}(F) \rightarrow {}^3T_{1g}$ (ν_2) and $^3A_{2g}(F) \rightarrow {}^3T_{1g}(P)$ (ν_3) [17]. In the d–d spectra of the Ni(II) complex, the low-energy absorption due to the first transition appears in the near-IR at $\nu_1 = 11\,700$ cm^{-1}. The next two bands appear in the visible range, at $\nu_2 = 18\,100$ and $\nu_3 = 28\,600$ cm^{-1}.

3.2. Investigation in aqueous solution

Under the adopted experimental conditions, the dissociation constant of protonated 4-CH_2OH–5-CH_3im is 8.08×10^{-8} (pK_a 7.09). The base is thus a one order of magnitude weaker base than its alkyl counterpart, 4,5-dimethylimidazole (pK_a 8.19).

The complexation of the Cu(II) and Ni(II) ions was studied over the pH range 2.5–7.1. The determined stability constants of consecutive complexes are collected in Table 6. Percent molar contributions of particular complexes in aqueous solution, calculated on the basis of β_n, are presented in Fig. 4. As seen in Table 6, despite the fact that 4-CH_2OH–5-CH_3im is a weaker Brönsted base than 4,5-dimethylimidazole, it forms complexes of higher stability (missing β_n constants for the Ni(II)—4,5-dimethylimidazole complexes precludes making similar comparison for this central ion). In order to identify factors affecting stability of the hydroxymethylimidazole complexes, substitution constants, $\log {}^*\beta_1 = \log \beta_1 - pK_a$ have been determined. These constants represent the tendency of the ligand towards complexation after elimination of the basicity effect. For the Cu(II) complexes of 4-CH_2OH–5-CH_3im, the $\log {}^*\beta_1$ value is a respective 1.28 units

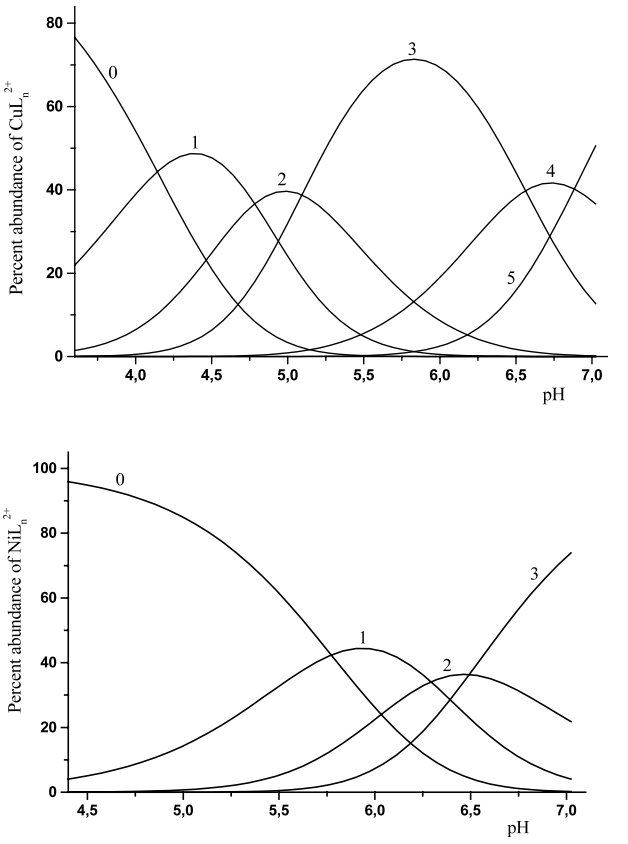


Fig. 4. Distribution diagrams of complexes formed in the M^{2+}-4-hydroxymethyl-5-methylimi-dazole (M^{2+}=Cu^{2+} and Ni^{2+}) systems as a function of pH at 298 K and $I = 0.5$ mol dm^{-3}. The number in the diagrams mean n in ML_n^{2+}.

higher than for their 4,5-dimethylmidazole counterparts. The enhanced stability of the complexes due to substitution of the methyl group for the hydroxymethyl ones can be explained in terms of an additional participation of the oxygen atom in the co-ordination bond. Consequently, the enhanced stability of the 4-CH_2OH–5-CH_3im complexes is an outcome of the possibility of formation of five-member chelate rings under involvement of both the nitrogen and oxygen atoms. Quantitative analysis of $\log(K_1/K_2)$ does not indicate the existence of typical, strong chelates in solution because the metal–oxygen bond is weak and easily broken. Formation of this chelate is not accompanied by loss of a proton from the hydroxymethyl group. This interpretation is in accord with studies of

Table 6
Stability and substitution constants $\log {}^*\beta_1$ of the 4,5-dimethylimidazole and 4-hydroxymethyl-5-methylimidazole complexes in aqueous solution [a]

Ligand	Central ion	$\log \beta_1$	$\log \beta_2$	$\log \beta_3$	$\log \beta_4$	$\log \beta_5$	$\log \beta_1^*$	Reference
4,5-Dimethyl imidazole ($pK_a = 8.19$)	Cu^{2+}	3.72	6.92	9.55	10.78		−4.47	[18]
4-Hydroxymethyl-5-methylimidazole ($pK_a = 7.14$)	Ni^{2+}	2.32(1)	4.12(1)	5.72(2)				this work
	Cu^{2+}	3.95(1)	7.26(2)	10.26(2)	11.79(3)	13.00(2)	−3.19	

[a] At 298 K, ionic strength $I = 0.5$ mol dm^{-3} (KNO_3).

Table 7
Position of absorption bands of Cu(II) and Ni(II) complexes with 4-hydroxymethyl-5-methylimidazole in aqueous solution

Ligand	Absorption band position (cm^{-1})		
	Ni(II)		Cu(II)
	$^3A_{2g}(F) \rightarrow {}^3T_{1g}(F)$	$^3A_{2g}(F) \rightarrow {}^3T_{1g}(P)$	$^2E_g \rightarrow {}^2T_{2g}$
H_2O	15 200	25 300	12 600
4-Hydroxymethyl-5-methylimidazole	16 000 ($e = 6.1$)	26 800	15 900 ($e = 69$)

these complexes in the solid state. It was shown that Cu(II) and Ni(II) were bonded to four molecules of the ligand, two of which are unidentate and the remaining two are bidentate (chelate). With the Cu(II)–4-CH_2OH–5CH_3im complexes, remarkable is the enhanced stability of the first three complexes and a distinct weakening of the fourth complex. One might thus speculate that the metal–oxygen bonds are weak and, after inclusion of four ligand molecules into the coordination sphere of the central ion, they are broken. Similar variations in the consecutive stability constants have been noted with the 1-alkyl-2-hydroxymethylimidazole complexes [1–3,8].

The structure of the Cu(II) and Ni(II) complexes with 4-CH_2OH–5-CH_3im in aqueous solution was established on the basis of their visible spectra. Formation of the Cu(II) and Ni(II) complexes is accompanied by an increase in the mean molar absorptivity and a hypsochromic shift of the maximum. Both the shape and position of the absorption bands as well as the magnitude of the mean molar absorptivity (Table 7) indicate the presence of hexacoordinate tetragonal Cu(II) as well as pseudo-octahedral Ni(II) complexes in aqueous solution [17].

4. Supplementary material

Crystallographic data for the structural analysis have been deposited with the Cambridge Crystallographic Data Centre, CCDC Nos. 179897 and 179898 for compounds $[Cu(4\text{-}CH_2OH\text{–}5\text{-}CH_3im)_4](NO_3)_2$ and $[Ni(4\text{-}CH_2OH\text{–}5\text{-}CH_3im)_4](NO_3)_2$, respectively. Copies of this information may be obtained free of charge from The Director, CCDC, 12 Union Road, Cambridge, CB2 1EZ, UK (fax: +44-1223-336033; e-mail: deposit@ccdc.cam.ac.uk or www: http://www.ccdc.cam.ac.uk).

References

[1] J. Kulig, K. Kurdziel, B. Barszcz, B. Lenarcik, Pol. J. Chem. 65 (1991) 2159.
[2] J. Kulig, B. Barszcz, B. Lenarcik, Pol. J. Chem. 66 (1992) 79.
[3] B. Barszcz, J. Kulig, J. Chem. Soc., Dalton Trans. (1993) 1559.
[4] T.J. Lane, C.S.C. Quinlan, K.P. Quinlan, J. Am. Chem. Soc. 82 (1960) 2994.
[5] K.S. Patel, I.M. Bhatt, D.P. Dani, Indian Chem. Soc. LIV (1977) 1007.
[6] M. Rzepka, W. Surga, Pol. J. Chem. 67 (1993) 2121.
[7] V.I. Sokol, M.A. Porai-Koshic, V.P. Nikolaev, E.S. Domnina, L.V. Baikalova, G.G. Skvorcova, L.A. Butman, Koord. Khim. 5 (1979) 1725.
[8] B. Barszcz, J. Jezierska, T. Głowiak, Polyhedron 18 (1999) 3713.
[9] B. Piggott, M.B. Hursthouse, L. Short, Polyhedron 8 (1989) 769.
[10] L. Alagna, S.S. Hasnain, B. Piggott, D.J. Williams, Biochem. 220 (1984) 591.
[11] G.M. Sheldrick, Acta Crystallgr. Sect. A46 (1990) 467.
[12] G.M. Sheldrick, SHELXS-97, Program for Solution of Crystal Structure, University of Göttingen, Göttingen, Germany.
[13] G.M. Sheldrick, SHELX-93, Program for the Refinement of Crystal Structure, University of Göttingen, Göttingen, Germany.
[14] G.M. Sheldrick, SHELXL-97, Program for the Refinement of Crystal Structure, University of Göttingen, Göttingen, Germany.
[15] K. Nakamoto, Infrared and Raman Spectra of Inorganic and Coordination Compounds, 4th ed., Wiley, New York, 1986, p. 254.
[16] B.J. Hathaway, D.E. Billing, Coord. Chem. Rev. 5 (1970) 143.
[17] A.B.P. Lever, Inorganic Electronic Spectroscopy, Elsevier, Amsterdam, 1984, p. 479.
[18] B. Lenarcik, K. Kurdziel, Pol. J. Chem. 55 (1981) 737.

2. Experimental

2.1. Materials and measurements

All solvents were reagent grade and purified according to the standard procedure [7]. All chemicals used in syntheses were of reagent grade and used without further purification. The dithiadiazamacrocycle [8], cyanogen-di-*N*-oxide [9], $[Cu(CH_3CN)_4]$ PF_6^- [10] and 1,2-bis(2-chloroethoxy)benzene [11] were prepared as described previously. ^1H, ^{13}C NMR and IR spectra were recorded on a Varian XL-200 and on a Perkin–Elmer 1600 FT IR spectrometer, respectively. Fast atom bombardment mass spectra were recorded on a Varian MAT 711 and VG Zapspec spectrometers using *m*-nitrobenyl alcohol as the matrix. The elemental analysis and metal contents of the complexes were determined on a Hewlett-Packard 185 CHN analyzer and on a Unicam 929 AA spectrometer.

2.2. Synthesis of 1,2-dinitro-4,5-bis(2-chloroethoxy)benzene (**2**)

Concentrated HNO_3 (13.5 ml, 70%) was added dropwise to a solution of **1** (5.0 g, 21 mmol) at room temperature (r.t.) over 1 h, then the mixture was stirred for 7 h at 60 °C. After the end of this period, the reaction mixture was cooled to r.t., filtered off, washed with water and cold ethanol, and then dried in vacuo. The crude product was recrystallized from methanol to yield pale yellow crystals. Yield: 6.0 g, 86.8%, melting point (m.p.) 102 °C. Found (Calc. for $C_{10}H_{10}N_2O_6Cl_2$): C, 37.14 (36.93); H, 3.29 (3.07); N, 8.40 (8.61)%. ^1H NMR (DMSO-d_6, ppm): δ 7.81 (s, 2H, Ar–H), 4.52 (t, 4H, CH_2O), 4.05 (t, 4H, CH_2Cl). IR (KBr, cm^{-1}); 3031 (Ar–H), 2978 (C–H), 1337 (NO_2), 1288–1223 (Ar–O–C), 678 (C–C1). EI MS (*m*/*z*): 324 $[M]^+$.

2.3. Synthesis of 1,2-dinitro-4,5-bis(2-iodoethoxy)benzene (**3**)

Compound **2** (4.5 g, 13.8 mmol) was dissolved in dry acetone (100 ml) containing anhydrous NaI (8.29 g, 55.2 mmol) under an argon atmosphere and refluxed for 29 h. After a while, the solution turned cloudy and then solid product precipitated. Then the reaction mixture was cooled to r.t. and the precipitate was filtered off and washed with dry acetone. The mother liquor and the washing solvents were combined and evaporated to dryness under reduced pressure. The crude product was purified by column chromatography using silica gel. The elution was carried out successively with petroleum–ether–ethyl acetate [(6:1), $R_f = 0.58$] to yield yellow needle crystals. Yield: 5.77 g, 84.4%, m.p. 112 °C. Found (Calc. for $C_{10}H_{10}N_2O_6I_2$); C, 23.38 (23.63); H, 2.17 (1.96); N, 5.35 (5.51)%. ^1H NMR (DMSO-d_6, ppm): δ 7.67 (s, 2H, Ar–H), 4.41 (t, 4H, CH_2O), 3.52 (t, 4H, CH_2I). IR (KBr, cm^{-1}): 3055 (Ar–H), 2883 (C–H), 1369 (NO_2), 1291–1224 (Ar–G–C), 662 (C–I), FAB MS (*m*/*z*): 507 $[M+1]^+$.

2.4. Synthesis of dinitro substituted dioxadithiadiazamacrobicycle (**5**)

A 500 ml round-bottom flask containing dry acetonitrile–DMF mixture (3:1) (200 ml) and fitted with a condenser was evacuated, refilled several times with argon and connected to a vacuum-line. Under argon, the flask was charged with **4** (1.32 g, 4 mmol) and finely ground anhydrous Cs_2CO_3 (3.24 g, 9.92 mmol) and the mixture was stirred at r.t. A solution of **3** (2.03 g, 4 mmol) in dry acetonitrile (80 ml) was added to this mixture and the reaction mixture was stirred at r.t. for 94 h. The reaction was monitored by TLC [chloroform–acetone–petroleum ether (4:6:1), $R_f = 0.51$]. At the end of this period, the reaction mixture was filtered and washed with dry chloroform and then the combined solution was evaporated to dryness under reduced pressure. The crude product was crystallized from chloroform–ethyl ether to yield yellow crystals. Yield: 1.36 g, 58.36%, m.p. 239 °C. Found (Calc. for $C_{28}H_{30}N_4O_6S_2$): C, 57.94 (57.73); H, 4.94(5.15); N, 9.39 (9.39)%. ^1H NMR (DMSO-d_6, ppm): δ 7.62 (s, 2H, Ar–H), 7.15–7.03 (m, 8H, Ar–H), 4.20 (t, 4H, CH_2O), 4.14 (s, 4H, $ArCH_2$), 3.47 (m, 8H, NCH_2), 2.69 (t, 4H, SCH_2). ^{13}C NMR (DMSO-d_6): δ 151.38, 139.27, 135.92, 132.71, 131.67, 128.59, 127.87, 126.23, 107.44, 66.94, 60.01, 52.74, 32.85. IR (KBr, cm^{-1}): 3055 (Ar–H), 2923–2786 (C–H), 1375 (NO_2), 1288–1218 (Ar–O–C). FAB MS (*m*/*z*): 583 $[M+1]^+$.

2.5. Synthesis of diamine substituted dioxadithiadiazamacrobicycle (**6**)

Palladium (10%)–activated carbon (1.25 g) was added to a solution of **5** (1.7 g, 2.92 mmol) in dry dioxane (100 ml) at 60 °C and 5.2 ml of anhydrous hydrazine was then added dropwise at reflux temperature. The reaction mixture was refluxed and stirred for 15 h. The extent of the reaction was monitored by using TLC [petroleum–ether–acetone (1:2), $R_f = 0.88$]. The reaction mixture was filtered through Celite as an extraction agent and concentrated to 15 ml under reduced pressure and then was allowed to stand in a refrigerator at −18 °C overnight. The colorless crystalline product was collected by filtration and washed with cold ethanol and diethyl ether and then dried in vacuo. Yield: 1.0 g, 65.78%, m.p. 181 °C. Found (Calc. for $C_{28}H_{34}N_4O_2S2$): C, 64.53 (64.36); H, 6.36 (6.51); N, 10.89 (10.72)%. ^1H NMR ($CDCl_3$, ppm): δ 7.22 (s, 2H, Ar–H), 7.04–6.97 (m, 6H, Ar–H), 6.31 (s, 2H, Ar–H), 4.30 (m, 4H, Ar–OCH_2), 3.88 (m, 4H, Ar–CH_2), 3.58 (s, 4H, NH_2), 3.27

(m, 8H, CH_2–N), 2.61 (m, 4H, CH_2–S). ^{13}C NMR ($CDCl_3$, ppm): δ 148.15, 146.67; 129.88, 128.21, 128.12, 127.83, 125.93, 122.89, 103.87, 65.82, 59.54, 53.41, 33.92. IR (KBr, cm^{-1}): 3349 (NH_2), 3053 (Ar–H), 2958–2852 (C–H), 1605 (N–H), 1234–1199 (Ar–O–C). FAB MS (m/z): 522.1 $[M]^+$.

Caution: Anhydrous hydrazine is potentially hazardous. While working with this chemical, half-mask respirators should be used and the reaction should be performed in a very well ventilated system. The system should be handled with caution.

2.6. Synthesis of dioxime (*H_2L*)

A solution of cyanogen-di-*N*-oxide (**7**) prepared from (*E*,*E*)-dichloroglyoxime (0.31 g, 2 mmol) in dichloromethane (20 ml) and an aqueous solution of Na_2CO_3 (10 ml, 0.5 M), was added to a cold solution (−15 °C) of **6** (1.44 g, 2 mmol) in dichloromethane (40 ml) under argon atmosphere. The reaction was continued for 12 h at the above mentioned temperature and the pale brown product formed separated by filtration, washed with dichloromethane and diethyl ether, and then dried in vacuo. The purification of this compound was performed by using column chromatography with chloroform as the eluent ($R_f = 0.62$). Yield: 0.83 g, 68.9%, m.p. 282 °C (dec.). Found (Calc. $C_{30}H_{34}N_6O_4S_2$): C, 59.24 (59.40); H, 5.40 (5.61); N, 14.05 (13.86)%. ^1H NMR (DMSO-d_6, ppm); δ 10.22 (s, 2H, OH), 9.30 (s, 2H, NH), 732–7.03 (m, 10H, Ar–H), 4.29 (m, 4H, Ar–O–CH_2), 3.83 (m, 4H, Ar–CH_2), 3.39 (m, 8H, CH_2–N), 2.62 (m, 4H, CH_2–S). ^{13}C NMR (DMSO-d_6, ppm): δ 145.28, 143.92, 133.53, 131.36, 129.61, 128.46, 127.83, 123.25, 114.97, 104.37, 67.45, 60.08, 54.32, 35.11. IR (KBr, cm^{-1}): 3318 (N–H), 3245 (O–H), 3043 (Ar–H), 2922–2793 (C–H), 1639 (C=N), 1601 (N–H), 1265–1153 (Ar–O–C), 948 (N–O), FAB MS (m/z): 607.2 $[M+1]^+$.

2.7. Synthesis of [Ni(HL)$_2$] (*8*)

A solution of $NiCl_2 \cdot 6H_2O$ (0.15 g, 0.625 mmol) in ethanol (10 ml) was added to a solution of **H_2L** (0.75 g, 1.25 mmol) in ethanol (75 ml) at 60 °C, a distinct change in color from pale brown to orange and a decrease in the pH of the solution was observed. While heating and stirring at the above mentioned temperature, an equivalent amount of ethanolic solution of triethylaminc (0.1 M) was added and an orange precipitate of **8** formed. After heating the mixture for 2 h in a water-bath, the precipitate was filtered off, washed several times with water, ethanol and diethyl ether and then dried in vacuo. Yield: 0.68 g, 86%, m.p. 274 °C (dec.). Found (Calc. for $C_{60}H_{66}N_{12}O_8S_4Ni$): C, 56.92 (56.75); H, 5.37 (5.20); N, 13.01 (13.24); Ni, 4.38 (4.62)%. ^1H NMR (DMSO-d_6, ppm): δ 16.97 (s, 2H, O–H–O), 9.37 (s, 4H, NH), 7.43–7.11 (m, 20H, Ar–H), 4.36 (m, 8H, Ar–O–CH_2), 3.89 (m, 8H, Ar–CH_2), 3.46 (m, 16H, CH_2–N), 2.78 (m, 8H, CH_2–S). IR (KBr, cm^{-1}): 3334 (N–H), 3054 (Ar–H), 2917–2823 (C–H), 1709 (O–H–O), 1625 (C=N), 1605 (N–H), 1252–1138 (Ar–O–CH_2), 936 (N–O). FAB MS (m/z): 1269.2 $[M+1]^+$.

2.8. Synthesis of [Ni(LBF$_2$)$_2$ (*9*)

A suspension of **8** (0.63 g, 0.5 mmol) in 50 ml of freshly distilled dry acetonitrile was brought to reflux temperature in an argon atmosphere. An equivalent amount of boron–trifluoride etherat complex (0.41 ml) was added with continuous stirring to this suspension, which changed its color to red immediately. After refluxing for 30 min., the solvent was evaporated to dryness. Then the dark red crude product was dissolved in 10 ml dry acetonitrile and allowed to stand in a refrigerator at −18 °C overnight, whereupon the compound crystallized from the solution. The red crystallized product was collected by filtration, washed with cold acetonitrile and diethyl ether and then dried in vacuo. Yield: 0.32 g, 47%, m.p. 253 °C. Found (Calc. for $C_{60}H_{64}N_{12}O_8S_4\ B_2F_4Ni$); C, 52.58 (52.77); H, 4.87 (4.69); N, 12.12 (12.31); Ni, 4.46 (4.30)%. ^1H NMR (DMSO-d_6, ppm): δ 9.25 (m, 4H, NH), 7.34–6.79 (m, 20H, Ar–H), 4.52 (m, 8H, Ar–O–CH_2), 3.98 (m, SH, Ar–CH_2), 3.44 (m, 16H, CH_2–N), 2.74 (m, 8H, CH_2–S). IR (KBr, cm^{-1}): 3419 (N–H), 3059 (Ar–H), 2935–2827 (C–H), 1654 (C=N), 1258–1141 (Ar–O–C), 940 (N–O), 1112 (B–O), 885 (B–F). FAB MS (m/z); 1362.3 $[M]^+$.

2.9. Synthesis of [Cu$_2$Ni(LBF$_2$)$_2$](PF$_6$)$_4$ (*10*)

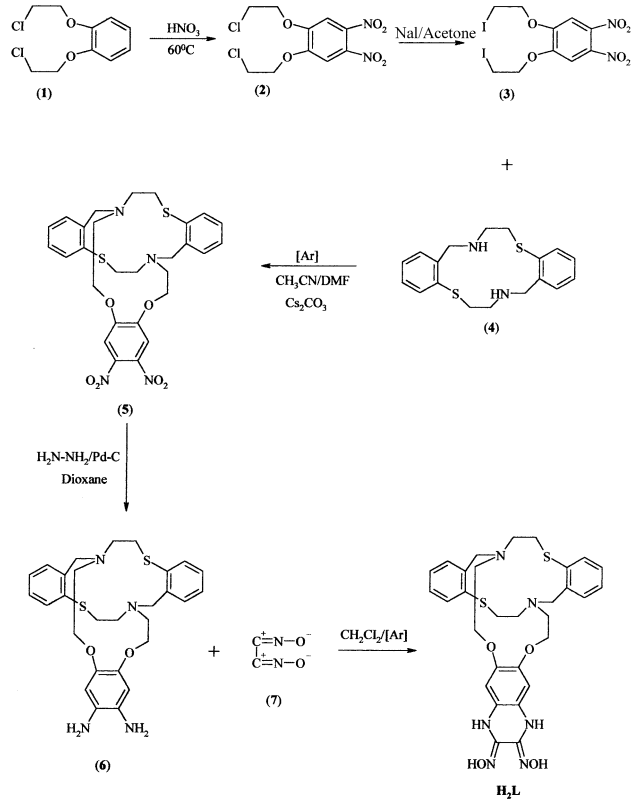
A solution of $[Cu(CH_3CN)_4]PF_6$ (0.11 g, 0.29 mmol) in dry acetonitrile (20 ml) was added to a solution of **9** (0.24 g, 0.15 mmol) in dry acetonitrile (80 ml) under an oxygen-free nitrogen atmosphere at 45 °C. Then the reaction was refluxed and stirred under nitrogen for 4 h. The end of the reaction was determined by TLC [*n*-butanol–acetic acid–water (4:1:5), $R_f = 0.33$]. After cooling to r.t. the reaction mixture was concentrated to 10 ml under reduced pressure. The reaction mixture was allowed to stand at −18 °C overnight whereupon the product crystallized from the solution. The reddish brown crystallized product was collected by filtration, washed with cold ethanol, acetonitrile and diethyl ether and then dried in vacuo. Yield: 0.19 g, 61.5%, m.p. 144 °C Found (Calc. for $C_{60}H_{64}N_{12}O_8S_4B_2P_2F_{16}NiCu_2$): C, 40.57 (40.41); H, 3.41 (3.59); N, 9.29 (9.41); Ni, 3.59 (3.29); Cu, 6.94 (7.13)%. ^1H NMR (DMSO-d_6, ppm): δ 8.29 (m, 4H, NH), 7.38–6.81 (m, 20H, Ar–H), 4.63 (m, 8H, Ar–O–CH_2), 4.12 (m, 8H, Ar–CH_2), 3.55 (m, 16H, CH_2–N), 2.91 (m, 8H, CH_2–S). IR (KBr,

cm^{-1}): 3365 (N–H), 3059 (Ar–H), 2919–2825 (C–H), 1653 (C=N), 1607 (N–H), 1272–1142 (Ar–O–C), 1085 (B–O), 897 (B–F), 845 $(PF_6)^-$, FAB MS (*m*/*z*); 1777 $[M+1]^+$.

3. Results and discussion

The preparation of the target heterotrinuclear complex **9** was synthesized in a seven-step (Scheme 1) sequence from 1,2-bis(2-chloroethoxy)benzene [11]. The conversion of **1** to the dinitro derivative (**2**) was accomplished in 86.8% yield. In the ^{1}H NMR spectrum of **2**, the presence of the singlet at $\delta = 7.81$ ppm showed that dinitration had occurred. The mass spectrum (EI) of this compound showed a dominant peak at $m/z =$ 324, which corresponds to $[M]^+$. This compound was easily converted to the diiodo derivative **3** by reaction with NaI in dry acetone and the yield of the conversion reaction was very high (84.4%). The ^{1}H NMR resonances of **3** are very similar to those of the precursor compound **2** except the proton resonances connected to iodo atoms. The fast atom bombardment EI of **3** also supports the replacement of chlorine by iodide, with the peak at $m/z = 507$ $[M+1]^+$.

The macrobicyclization reaction **5** was performed by starting from the 14-membered macrocycle **4** [8] and **3** using Cs^+ as a promoter [12] and in acetonitrile–DMF



Scheme 1.

mixture at r.t. in a Schlenk system connected vacuum-line under argon. The macro-bicycle compound was isolated in 58.36% yield, crystallized a mixture of chloroform–ethyl ether and characterized. Analytical and spectroscopic data of **5** clearly confirm the success of the macrobicyclization reaction. The new signals due to methylene and aromatic protons at $\delta = 4.20$ and 7.62 ppm, respectively, confirm the formation of **5.** The disappearance of NH chemical shifts and N–H stretching vibration in the IR spectrum of this compound also suggests the desired macrobicycle. Proton-decoupled ^{13}C NMR spectral data are also in good agreement with the proposed structure (Scheme 1). The new resonances belonging to dinitro substituted phenyl and methylene carbons at $\delta = 151.38$, 139.27, 135.92 and 66.94 ppm, respectively, that can be attributed to the macro-cyclization have occurred. The value of the molecular ion observed shows good agreement with the calculated value for **5** ($m/z = 583$ $[M+1]^+$).

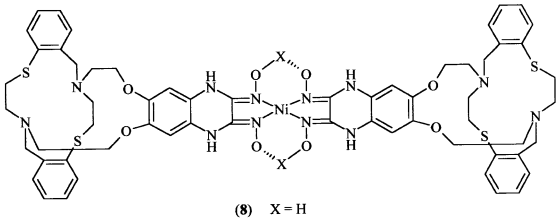
The diamine compound **6** was prepared in 65.78% yield by reduction [13] of the corresponding dintro compound **5** with palladium-activated charcoal and anhydrous hydrazine, which was sufficiently stable to make characterization. The amine **6**, apparently sensitive to both light and air, is colorless and darkens as expected when it is left to standing at r.t. In the ^{1}H NMR spectrum of **6**, there is a broad signal at $\delta = 3.58$ ppm due to the aromatic amine protons. A comparison of the proton resonances of **5** and **6** resulted in an upfield shift of the aromatic proton. The ^{13}C NMR spectrum for **6** also supported this situation and was consistent with the proposed formulation. The disappearance of the Ar–NO_2 (1375 cm^{-1}) stretching and appearance of Ar–NH_2 stretching (3349 cm^{-1}) and bending vibrations (1605 cm^{-1}) indicate completion of the reduction. On the other hand, the EI (FAB) of **6**, which shows a molecular ion peak at $m/z = 522.1$ $[M]^+$, confirms the proposed structure.

The preparation **H_2L** has been accomplished as described [14] in 68.9% yield by the reaction of **6** with cyanogen-di-*N*-oxide (**7**) at -15 °C in dichloromethane media. In the ^{1}H NMR spectrum of **H_2L**, the deuterium exchangeable protons of the OH and NH groups appear as two singlets at $\delta = 10.22$ and 9.30 ppm, respectively. More detailed information about the structure of **H_2L** is provided by its ^{13}C NMR spectrum. The carbon resonance of amidoxime is found to be at the higher field value of $\delta = 143.92$ ppm compared with the values for the aldo- and ketooximes [15]. The equivalent carbon and proton signals of the azomethine and hydroxyimino groups confirm the (*E*,*E*) form of *vic*-odioxime [16].

The FAB EI of this ligand exhibited an intense peak at $m/z = 607.2$ $[M+1]^+$, which is in accord with the expected formulation.

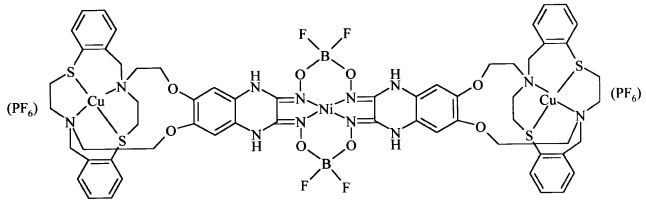
It was found that when on equivalent amount of nickel(II) chloride hexahydrate is used as the Ni(II) salt, the mononuclear Ni(II) complex **8** of **H_2L** is obtainable in a good yield (86.0%) (Scheme 2). It is interesting to note that this complexation reaction does not occur in the macrobicyclic moieties under the same conditions, which we attributed to greater affinity of the Ni(II) oxime promoting oxime nucleophile formation. In the ^{1}H NMR spectrum of **8**, only slight differences between those of the ligand and its Ni(II) complex were observed. While the chemical shifts of deuterium exchangeable NH protons were observed at $\delta = 9.37$ ppm, the intramolecular hydrogen bridging O–H–O protons have been shifted to a lower field at $\delta = 16.97$ ppm as expected [17]. Since a distinct decrease in the pH of the solution was observed during complex formation, deprotonation of the ligand with subsequent *N*,*N*′-chelation with the (*E*,*E*)-dioxime groups occurs **8**. The weak band at 1709 cm^{-1} assigned to the intramolecular hydrogen bonded bending vibrations in the IR spectrum also indicates the same formation [18], The FAB EI of this complex showed the expected molecular ion peak at $m/z = 1269.2$ $[M+1]^+$.

The template synthesis of the BF_2^+-capped nickel(II) complex **9** was performed in 47% yield by adding borontrifluoride ethyl ether complex to a refluxing suspension of **8** in acetonitrile media. The hydrogen bridging protons were replaced by BF_2^+ groups. In the ^{1}H NMR spectrum of **9**, the hydrogen bonding protons disappeared after the replacement with $BF_2'^+$. This new group causes the resonances of **9** to shift down-field relative to those of the precursor nickel(II) complex. The disappearance of the characteristic O–H–O bending vibrations when substituting the hydrogen bonds with BF_2^+ also confirm the formation of **9**. On the other hand, an upward shift of the C=N stretching vibration was observed due to the strong electron-withdrawing influence of the difluoroboron-linked group incorporated in this macrocycle [19]. The molecular ion peak at $m/z = 1362.3$ $[M]^+$ in the FAB EI of this compound also supports the proposed formulation.



(8) X = H

(9) X = BF_2



(10)

Scheme 2.

In order to synthesize the heterotrinuclear complex $[Cu_2Ni(LBF_2)_2](PF_6)_2$ (**10**), the reaction of mononuclear complex **9** with a solution of $[CucCH_3CN)_4]PF_6$ was carried out in 61.5% yield. In this product Ni(II) is still coordinated to the dioxime groups, and the two Cu(I) ions are coordinated to two dithiadiaza hetero atoms of macrobicycles [20] according to the analytical and spectroscopic data. The ^{1}H NMR spectrum of **10** is largely similar to those of the precursor compound **9**, but the expected shifts due to complexation with Cu(I) cations belonging to macrobicyclic units such as CH_2–N and CH_2–S are significant. In the IR spectrum of **10**, the resonances at 845 and 563 cm^{-1}, assigned to $[PF_6]^-$, support a structure in which the PF_6^- ions are not coordinated to the Cu(I) cations [21]. The EI of **10** was obtained by the FAB technique using a matrix (matrix: *m*-nitrobenzyl alcohol) in the region of the molecular ion peak at $m/z = 1777$ $[M+1]^+$.

4. Conclusions

We have presented a novel *o*-dinitrobenzene containing macrobicyclic unit as a starting material and its conversion to macrobicycle substituted *o*-phenylenediamine and also to the quinoxaline substituted (*E*,*E*)-dioxime. Starting form **H_2L** and $NiCl_2 \cdot 6H_2O$, the mono-nuclear nickel(II) complex was prepared. We succeeded in other transition metal binding to the macrobicyclic cavities of $N_2S_2O_2$ macrocycles by Cu(I) cations, causing a distinct change in the spectral data compared with those of the diazadithiadioxamacrobicycle substituted compounds. The approach described here allows the preparation of a wide number of homo or hcterotrinuclear complexes whose properties will be a subject of heavy metal extraction from aqueous media to organic solvents.

Acknowledgements

This work was supported by the Research Fund of Karadeniz Technical University (Trabzon, Turkey). We are also indebted to Professor M. Hanack (Tübingen University, Germany) for his assistance with MS spectral data. Y.G. thanks the Deutsche Akademischc Austauschdienst (DAAD) commision for an invitation to Germany for 2 months in Tübingen University.

References

[1] (a) T.I. Meade, D.H. Busch, Prog. Inorg. Chem. 33 (1985) 59;
(b) J.J. Christensen, J.O. Hill, R.M. Izatt, Science 174 (1971) 459;
(c) J.-M. Lehn, Pure Appl. Chem. 52 (1980) 2441;
(d) J.-M. Lehn, Pure Appl. Chem. 52 (1980) 2303;
(e) H. An, J.S. Bradshaw, R.M. Izatt, Chem. Rev. 92 (1992) 543;
(f) J.-M. Lehn, Acc. Chem. Res. 11 (1978) 49;
(g) J.-M. Lehn, Pure Appl. Chem. 50 (1978) 871;
(h) L.F. Lindoy, The Chemistry of Macrocyclic Complexes, Cambridge University Press, Cambridge, 1990;
(i) G.A. Melson (Ed.), Coordination Chemistry of Macrocyclic Compounds, Plenum Press, New York, 1879;
(j) J.-M. Lehn, Structure Bonding 16 (1973) 1.

[2] (a) B. Dietrich, J.-M. Lehn, J.P. Sauvage, Tetrahedron Lett. 34 (1969) 2885;
(b) B. Dietrich, J.-M. Lehn, J.P. Sauvage, J. Chem. Soc., Chem. Commun. (1970) 1055.;
(c) B. Dietrich, J.-M. Lehn, J.P. Sauvage, J. Blanzat. Tetrahedron 29 (1973) 1629.

[3] (a) E. Kaufmann, J.L. Dye, J.-M. Lehn, A.J. Pope, J. Am. Chem. Soc. 102 (1980) 2274;
(b) R.M. Tzatt, J.J. Christensen (Eds.), Synthesis of Macrocycles, vol. 1–3, Wiley-Interscience, New York, 1979–1987;
(c) J.-M. Lehn, Supramolecular Chemistry, VCH, Weinheim, 1995.

[4] L. Tschugaeff, Chem. Ber. 38 (1905) 2520.

[5] (a) E. Uhlig, M. Friedrich, Z. Anorg. Allg. Chem. 343 (1966) 299;
(b) A.W. Addison, M. Carpenter, L.K.-M. Lau, M. Wicholas, Inorg. Chem. 17 (1978) 1545;
(c) A.W. Addison, C.P. Landee, R.D. Willett, M. Wicholas, Inorg. Chem. 19 (1980) 1921;
(d) Y. Gök, New J. Chem. 20 (1996) 971.

[6] (a) M.J. Prushan, A.W. Addison, R.J. Butcher, Inorg. Chim. Acta 300–302 (2000) 992;
(b) J.P. Leonard, D.P. Novotnik, R.D. Neirickx, J. Nucl. Med. 27 (1986) 1819;
(c) M.A. Green, Adv. Met. Med. 1 (1993) 75;
(d) E.K. John, A.J. Bott, M.A. Green, J. Pharm. Sci. 83 (1994) 587.

[7] D.D. Perrin, W.L.F. Armarego, D.R. Perrin, Purification of Laboratory Chemicals, 2nd ed., Pergamon Press, New York, 1985.

[8] J.W.L. Martin, G.J. Organ, K.P. Wainwright, K.D.V. Weerasuria, A.C. Willis, S.B. Wild, Inorg. Chem. 26 (1987) 2963.

[9] C. Grundman, V. Mini, S.M. Dean, H.D. Frommeld, Ann. Chem. 687 (1965) 191.

[10] A.L. Crumbliss, P.L. Gaus, Inorg. Chem. 14 (1975) 486.

[11] D. Landin, F. Montanari, F. Rolla, Synthesis 3 (1978) 223.

[12] (a) S. Kulstad, L.A. Malmsten, Tetrahedron Lett. (1980) 643.;
(b) S.Z. Yildiz, Y. Gök, New J. Chem. (1998) 1365.

[13] Y. Gök, Org. Prep. Proc. Int. 22 (1990) 641.

[14] (a) Y. Gök, S. Serin, Synth. React. Inorg. Met.-Org. Chem. 18 (1988) 975;
(b) Y. Gök, B. Ozcan, Trans. Met. Chem. 16 (1991) 393;
(c) Y. Gök, H. Ertepmar, M. Küçükislamoglu, Eur. Polym. J. 31 (1995) 603;
(d) Y. Gök, H. Kantekin, H. Alp, M. Özdemir, Z. Anorg. Allg. Chem. 621 (1995) 1237.

[15] (a) M.S. Gordon, S.A. Sojka, J.G. Krause, J. Organomet. Chem. 49 (1984) 97;
(b) G.C. Levy, G.L. Nelson, Carbon-13 Nuclear Magnetic Resonance for Organic Chemists, Wiley-Interscience, New York, 1972.

[16] (a) Y. Gök, H. Kantekin, New J. Chem. 19 (1995) 461;
(b) Y. Gök, H. Kantekin, Chem. Ber. 123 (1990) 1479;
(c) H. Kantekin, Ö. Hasançebi, R. Abbasoglu, Y. Gök, New J. Chem. 25 (2001) 879.

[17] (a) S.B. Pedersen, E. Larsen, Acta Chem. Scand. 27 (1973) 3294;
(b) A. Gül, Ö. Bekaroglu, J. Chem. Soc., Dalton Trans. (1983) 2537.;
(c) A. Gül, A.I. Okur, A. Cihan, N. Tan, Ö. Bekaroglu, J. Chem. Res. S (1986) 90.

[18] (a) Y. Gök, Ö. Bekaroglu, Synth. React. Inorg. Met. -Org. Chem. 11 (1981) 621;
(b) Y. Gök, H. Kantekin, Synth. React. Inorg. Met. -Org. Chem. 20 (1990) 1085;
(c) Y. Gök, H. Kantekin, I. Degirmencioglu, Polyhedron 12 (1993) 2097;
(d) Y. Gök, Polyhedron 13 (1994) 1793;
(e) Y. Gök, S.Z. Yildiz, M. Tüfekçi, J. Coord. Chem. 28 (1994) 237.

[19] (a) M.S. Hussain, H.M. Al-Mohdar, A.R. Al-Arfaj, J. Coord. Chem. 18 (1988) 339;
(b) Y. Gök, H. Kantekin, Polyhedron 16 (1997) 2413;
(c) Y. Gök, Z. Anorg. Allg. Chem. 621 (1995) 1243;
(d) H. Kantekin, Ü. Ocak, Y. Gök, Z. Anorg. Allg. Chem. 627 (2001) 1095.

[20] Y. Gök, Ö. Ocak, H.B. Senturk, New J. Chem. 25 (2001) 364.

[21] (a) G.L. Kubas, B. Monza, A.L. Crubles, Inorg. Synth. 19 (1971) 90;
(b) Y. Gök, H. Kantekin, Acta Chem. Scand. 51 (1997) 664.

compound in the 2–300 K region have been studied as well.

2. Experimental

Pyridine derivative ligands were purchased from the Aldrich or BDH companies and other chemicals are of analytical grade quality.

Abbreviations for the pyridine ligands are given as a footnote under Table 1.

2.1. Preparation of complexes

2.1.1. $[Ni(4\text{-}Etpy)_4(N_3)]PF_6$ (**1**)

This complex was prepared by mixing an aqueous solution of $Ni(NO_3)_2\cdot 6H_2O$ (2.0 mmol) dissolved in 10 cm^3 water and 4-Etpy (5.0 mmol) in approximately 15 cm^3 ethanol followed by KPF_6 (2.0 mmol, 3 cm^3 water) and NaN_3 (1.5 mmol, in ca. 3 cm^3 water). The final clear solution mixture was allowed to stand in an open beaker over several days until good quality blue crystals of the complex deposited.

2.1.2. $[Ni(py)_4(N_3)]PF_6$

This complex was prepared by mixing $Ni(NO_3)_2\cdot 6H_2O$, pyridine, KPF_6 and NaN_3 in the molar ratio of 1:6:1.5:1, respectively, in approximately 30 cm^3 aqueous-ethanol medium. The final clear solution mixture was allowed to stand over several days to produce the complex as a blue microcrystalline powder.

2.1.3. $[Ni(4\text{-}Mepy)_4(N_3)]PF_6$

This complex was prepared in a crystalline form by adding an ethanol solution (10 cm^3) of 4-Mepy (4.0 mmol) to an aqueous solution (10 cm^3) of $Ni(NO_3)_2\cdot 6H_2O$ (1.5 mmol), followed by addition of KPF_6 (2.0 mmol, in ca. 2 cm^3 water) and NaN_3 (1.0 mmol, in ca. 2 cm^3 water). The final clear solution mixture was heated for several minutes and then allowed to stand over several days.

2.1.4. $[NiL_4(N_3)]PF_6$; for L = 3-Clpy and 3-Brpy

These complexes were prepared in powder form by mixing 3-Clpy or 3-Brpy, $Ni(NO_3)_2\cdot 6H_2O$, KPF_6 and NaN_3 in a molar ratio of 6:1:1.5:1, respectively, in approximately 30 cm^3 water–ethanol medium, and the final mixture allowed to stand over several days in the open air. Trials to crystallize the powder products from water or ethanol, failed to produce crystalline complexes.

2.1.5. $[Ni(3\text{-}hydpy)_4(N_3)]PF_6$

This complex was prepared by mixing $Ni(NO_3)_2\cdot 6H_2O$,3-hydpy, KPF_6 and NaN_3 in the molar ratio of 2:3:4:1.5, respectively, in approximately 30 cm^3 aqueous-ethanol medium and allowing the final mixture to stand over several days to produce a micro-crystalline powder of the complex. Molar ratios of the components other than that given above produce a mixture of the desired complex with the 1:4 nickel(II) azide complex. The elemental analyses of the isolated complexes are given in Table 1.

2.2. Physical measurements

The experimental procedures and instruments used for physical measurements were described previously [16].

2.3. X-ray crystallography

A modified STOE four-circle diffractometer was used for the single X-ray measurement. Orientation matrix and lattice parameters were obtained by least-squares refinement of 42 reflections ($9.3^\circ < \theta < 14.8^\circ$). Data were collected at 293(2) K, using graphite-monochromatized Mo Kα radiation ($\lambda = 0.71069$ Å) and the ω-scan technique. The data were corrected for Lorentz-polarization and intensity decay (16% observed intensity decay of three control reflections). The structure was solved by direct methods and subsequent Fourier analysis. Anisotropic displacement parameters were applied to non-hydrogen atoms in full-matrix least-

Table 1
Analytical data and electronic spectra of the complexes

Complex	Color	*Anal*. Found(%)/(Calc.)				Electronic spectra (nm)
		C	H	N	Ni	
$[Ni(py)_4(N_3)]PF_6$	sky blue micro-crystals	42.5 (42.7)	3.6 (3.6)	17.7 (17.4)	10.0 (10.4)	420wm, 605s
$[Ni(4\text{-}Mepy)_4(N_3)]PF_6$	sky blue crystals	46.6 (46.1)	4.7 (4.5)	15.2 (15.7)	9.8 (9.4)	464w, 591vs, br
$[Ni(4\text{-}Etpy)_4(N_3)]PF_6$	sky blue crystals	50.1 (49.9)	5.2 (5.4)	14.4 (14.5)	8.8 (8.7)	455sh, 600s
$[Ni(3\text{-}Clpy)_4(N_3)]PF_6$	pale blue powder	34.9 (34.3)	2.6 (2.3)	13.5 (14.0)	8.0 (8.4)	395m, 600s
$[Ni(3\text{-}Brpy)_4(N_3)]PF_6$	pale blue powder	28.0 (27.4)	1.9 (1.8)	13.5 (13.0)	6.5 (6.7)	395m, 600s
$[Ni(3\text{-}hydpy)_4(N_3)]PF_6$	sky blue powder	38.7 (38.4)	3.6 (3.2)	15.8 (15.6)	9.8 (9.4)	376sh, 600s

Abbreviations: py, pyridine; 4-Mepy, 4-methylpyridine; 4-Etpy, 4-ethylpyridine; 3-Clpy, 3-chloropyridine; 3-Brpy, 3-bromopyridine; 3-hydpy, 3-hydroxypyridine.

squares refinement based on F^2. The hydrogen atoms were assigned with common isotropic displacement factors and included in the final refinement cycles by use of geometrical restraints. Analytical expressions of neutral atom scattering factors were employed and anomalous dispersion corrections were incorporated. The program DIFABS [17] and the SHELXTL/PC-V 5.03 [18] program package were used for computations. Crystal data: empirical formula: $C_{28}H_{36}F_6N_7NiP$, formula weight = 674.32; triclinic; space group: $P\bar{1}$, a = 11.600(3), b = 15.188(6), c = 20.496(6) Å; α = 95.22(3)°, β = 106.35(2)°, γ = 107.04(3)°; V = 3253.1(18) Å^3; Z = 4; D_{calc} = 1.377 g cm^{-3}, μ (Mo Kα) = 0.710 mm^{-1} crystal size = 0.35 × 0.22 × 0.17 mm; 1153 reflections, 786 parameters; R_1 = 0.0777, R_{int} = 0.0290.

3. Results and discussion

3.1. Preparation of the complexes

Nickel(II) nitrate hexahydrate interacts with pyridine derivative ligands in the presence of sodium azide and potassium hexafluoro phosphate in aqueous-ethanol media giving the nickel(II) azido complexes collected in Table 1. Such reactions are very sensitive to the ratio between azide and PF_6^- ions. A small amount of the azide ion higher than PF_6^- ion, leads to the isolation of nickel(II) azido complexes, usually 1:4, rather than the desired complex containing the PF_6^- ion. Our trials to prepare such cationic complexes with pyridine derivative ligands other than those mentioned in Table 1, resulted in the isolation of 1:4, nickel(II) azide: ligand complexes. Crystals of the cationic complex in case of L = 4-Mepy were found to be twins rather than single crystals.

All the isolated complexes are soluble in one or more of the following solvents; water, MeOH, EtOH, acetone, DMF and DMSO. Aqueous solutions of these complexes behave as 1:1 electrolytes (molar conductance in the range of 105–128), a result which is suggestive of the ionic nature of these complexes in aqueous solutions.

3.2. IR and electronic spectra

The IR spectral results for these complexes are collected in Table 2. These spectra show bands that can be assigned to the PF_6^- anions [19] as follows: 550–560 (ν4), 740–750 wm (ν1) and 845–850 vs, br (ν3) (all values are in cm^{-1}). These results meet the criteria for non- coordinated PF_6^- anions, as described previously [19] and are consistent with the structure of complex (**1**) (see later). The spectra of all complexes show a single or slightly split very strong band in the 2070–2090 cm^{-1} range due to the ν_{as} (N_3) mode. We could not locate any absorption band in the 1360–1270 cm^{-1} range, associated with the ν_s (N_3) mode in these complexes. The disappearance of the latter band is a strong evidence of the symmetric nature of the azido bridges [20,21] not only in complex (**1**) as shown by the X-ray structure analysis described later but also for all other complexes. In the far IR region we tentatively assigned the bands in the 300–250 and 240–210 cm^{-1} ranges [22,23] to νNi–N(azide) and νNi–N(L), respectively.

The electronic spectral data given in Table 1, for solid complexes mulled in Nujol are consistent with six-coordination around nickel(II) atoms. All these spectra exhibit a weak band or shoulder in the region of 376–465 nm, and a strong band in the vicinity of 590–610 nm, associated with $^3A_{2g}(F) \rightarrow {}^3T_{2g}(P)$ and $^3A_{2g}(F) \rightarrow {}^3T_{1g}(F)$ transitions, respectively, as found for other six-coordinated complexes involving substituted pyridines [24,25].

3.3. Structure of [Ni(4-Etpy)$_4$(N$_3$)](PF$_6$) complex (1)

Figs. 1 and 2 illustrate the principal structural features of complex (**1**), and selected bond distances and angles are collected in Table 3. The structure of **1** consists of 1D nickel-azido chains, isolated by PF_6^- anions, which are found in the interchain space. In the chain structure each nickel(II) atom is coordinated by four nitrogen atoms from the four pyridine ligands and two nitrogen atoms from two μ-1,3-azide bridges in an octahedral trans arrangement. The four nitrogen atoms of the

Table 2
IR spectral data

Compound	Azide vibrations			PF_6^- vibrations	νNi–N_3	νNi–N(L)
	ν_{as} N_3	ν_s N_3	δ N_3			
[Ni(py)$_4$(N$_3$)]PF$_6$	2075vs		620w	845vs, 733wm, 558m	295wm	250m
[Ni(4-Mepy)$_4$(N$_3$)]PF$_6$	2065vs, b		615w	845vs, 745m, 556m	290wm	240m
[Ni(4-Etpy)$_4$(N$_3$)]PF$_6$	2090sh, 2077vs		610wm	842ms, 740w, 558m	275wm	235w
[Ni(3-Clpy)$_4$(N$_3$)]PF$_6$	2080vs			846ms, 745m, 561w	265wm	230w
[Ni(3-Brpy)$_4$(N$_3$)]PF$_6$	2077vs		610w	844s, 735m, 561w	270wm	225w
[Ni(3-hydpy)$_4$(N$_3$)]PF$_6$	2070vs		605vw	846s, 742m, 555wm	285wm	230w

w, weak; m, medium; s, strong; b, broad; v, very.

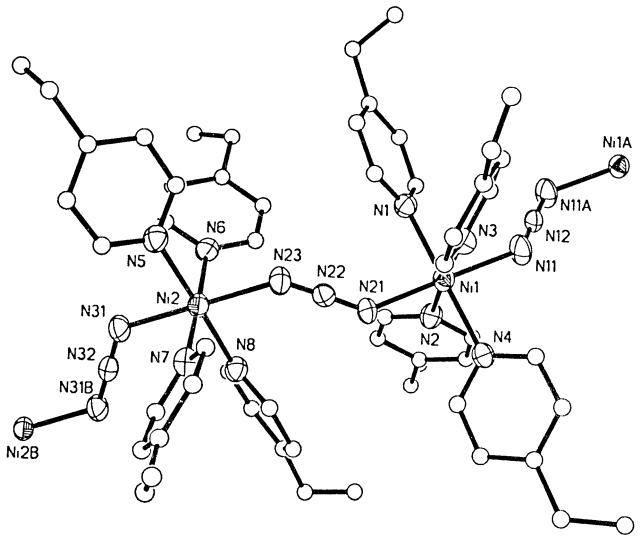


Fig. 1. Perspective view of the $[Ni(4\text{-ethylpyridine})_4(N_3)]^+$ chain in compound (**1**).

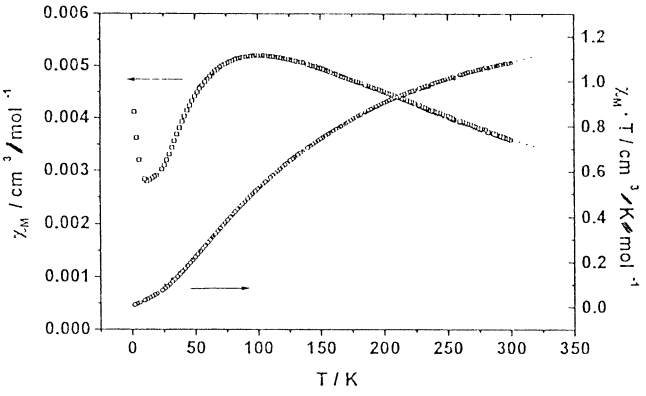


Fig. 2. Susceptibility data for compound **1**. Dotted lines show the best fit using a single average J parameter. Solid line show the best fit obtained using a ring of nine Ni(II) centers and three J superexchange parameters (see text).

pyridine ligands are in the same plane (maximum deviation from the plane = 0.03 Å); the coordination of the μ(1,3) azide bridge is slightly asymmetric; the Ni–N–N angles are 135.6(4)° and 140.3(4)°. The torsion angles are: Ni(2B)–N(31B)···N(31)–Ni(2) = 180.0°, Ni(1)–N(11)···N(11A)–Ni(1A) = 180.0° and Ni(1)–N(21)···N(23)–Ni(2) = 133.4°. The first two are a consequence of the inversion centers which are occupied by central azido atoms N(12), N(32). The four Ni–N (L) distances are almost equal [2.117–2.132 Å] as well as the Ni–N(N_3) bond lengths [2.096–2.124 Å]. The azido ligand itself is symmetrical and linear (Table 3) within the experimental error. This structure is very close to the corresponding structure of $[Co(4\text{-Mepy})_4(N_3)]PF_6$, although the latter crystallizes in the monoclinic, space group, $P2_1/c$ and the Co–N–N angles are symmetrical [135.3(3)° and 133.0(3)°] [16].

Table 3
Selected bond lengths (Å) and angles (°) for (**1**)

Bond lengths			
Ni(1)–Ni(2)	5.950(3)	Ni(1)–Ni(1a)	6.113(3)
Ni(2)–Ni(2b)	5.950(3)	Ni(1)–N(21)	2.096(5)
Ni(1)–N(1)	2.117(5)	Ni(1)–N(4)	2.122(5)
Ni(1)–N(11)	2.124(5)	Ni(1)–N(3)	2.126(5)
Ni(1)–N(2)	2.132(5)	Ni(2)–N(31)	2.101(5)
Ni(2)–N(5)	2.101(5)	Ni(2)–N(8)	2.122(5)
Ni(2)–N(7)	2.127(5)	Ni(2)–N(6)	2.125(5)
Ni(2)–N(23)	2.127(5)	N(11)–N(12)	1.152(5)
N(12)–N(11a)	1.152(5)	N(21)–N(22)	1.164(6)
N(22)–N(23)	1.162(6)	N(31)–N(32)	1.169(6)
N(32)–N(31b)	1.169(6)		
Bond angles			
N(21)–Ni(1)–N(1)	91.3(2)	N(21)–Ni(1)–N(4)	88.5(2)
N(1)–Ni(1)–N(4)	179.3(2)	N(21)–Ni(1)–N(11)	178.3(2)
N(1)–Ni(1)–N(11)	90.4(2)	N(4)–Ni(1)–N(11)	89.8(2)
N(21)–Ni(1)–N(3)	91.5(2)	N(1)–Ni(1)–N(3)	89.9(2)
N(4)–Ni(1)–N(3)	89.5(2)	N(11)–Ni(1)–N(3)	88.1(2)
N(21)–Ni(1)–N(2)	91.0(2)	N(1)–Ni(1)–N(2)	92.2(2)
N(4)–Ni(1)–N(2)	88.5(2)	N(11)–Ni(1)–N(2)	89.4(2)
N(3)–Ni(1)–N(2)	176.8(2)	N(31)–Ni(2)–N(5)	88.2(2)
N(31)–Ni(2)–N(8)	89.4(2)	N(5)–Ni(2)–N(8)	177.2(2)
N(31)–Ni(2)–N(7)	91.2(2)	N(5)–Ni(2)–N(7)	89.3(2)
N(8)–Ni(2)–N(7)	92.4(2)	N(31)–Ni(2)–N(6)	88.7(2)
N(5)–Ni(2)–N(6)	87.7(2)	N(8)–Ni(2)–N(6)	90.7(2)
N(7)–Ni(2)–N(6)	176.9(2)	N(31)–Ni(2)–N(23)	179.4(2)
N(5)–Ni(2)–N(23)	91.5(2)	N(8)–Ni(2)–N(23)	90.8(2)
N(7)–Ni(2)–N(23)	89.3(2)	N(6)–Ni(2)–N(23)	90.8(2)
N(12)–N(11)–Ni(1)	135.6(4)	N(11)–N(12)–N(11a)	180.0
N(22)–N(21)–Ni(1)	140.3(4)	N(23)–N(22)–N(21)	178.0(6)
N(22)–N(23)–Ni(2)	128.7(4)	N(32)–N(31)–Ni(2)	128.7(4)
N(31)–N(32)–N(31b)	180.0		

Symmetry codes; (a) $-x+1, -y+2, -z+1$ (b) $-x, -y+1, -z$.

A single μ(1,3) bridging azide has previously been found in the cation in $[Ni_2(Me_4Cyclam)_2(N_3)_3]I$ [26]. Furthermore, X-ray analysis of $Mn(acac)_2N_3$ has established the presence of single μ(1,3) azide bridge which links adjacent metal atoms to form polymeric chains of six-coordinate Mn(II) polyhedra [27]. The structure of the present complex resembles that of catena-μ(N_3)–[Ni(Cyclam)]$ClO_4 \cdot H_2O$ (Cyclam = 1,4,8,11-tetraazo-cyclotetradecano) (**2**) [28] which features six-coordinate Ni(II), trans arrangement, 1D nickel azide chains and ClO_4^- anions. Complex (**2**) differs in the asymmetric arrangement of the azido bridges: the two Ni–N–N angles are 140.7(3)° and 128.2(3)°. The azide ligand itself is asymmetric [N_1–N_2 = 1.178(5), N_2–N_3 = 1.138(5) Å], as well as the bond lengths of the two Ni–N(azide) distances being longer [2.165 and 2.172 Å] than the four Ni–(Cyclam) distances [2.059–2.073 Å].

3.4. Magnetic data for complex (*1*)

The magnetic behavior of compound **1** plotted as $\chi_M T$ versus T is shown in Fig. 2 (the data represent duplicated values from two separate preparations). As

suggested by the presence of end-to-end (EE) azido bridges between the Ni(II) centers, the magnetic behavior of compound **1** indicates overall antiferromagnetic superexchange interactions: $\chi_M T$ at room temperature is 1.03 cm^3 K mol^{-1} and on cooling $\chi_M T$ tends to zero at low temperature. The susceptibility plot shows a well-defined maximum at 102 K.

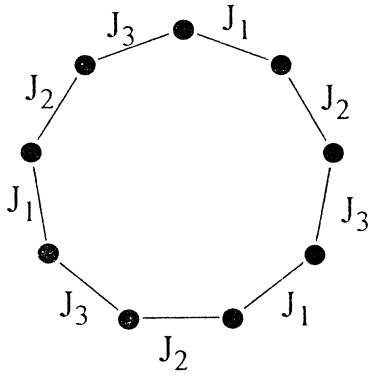
Structural data show a set of three different azido bridges in a regular alternating arrangement along the chain and so same kind of alternating superexchange parameters J_1, J_2 and J_3 should be assumed as a starting point for the analysis of the magnetic behavior. As was previously published [29] the J value is highly sensitive to the bond parameters involving the bridging region: the antiferromagnetic contribution to the superexchange parameter J increases for lower Ni–N–N bond angles, giving the maximum contribution at 108°, and simultaneously shows a strong dependence on the Ni–N–N–N–Ni torsion angle, giving the maximum J values for the planar arrangement (torsion 180°). Deviation from these optimal bond parameters implies a decrease in the overlap between the e_g atomic orbitals and the non-bonding MOs of the bridge and a decrease in the antiferromagnetic component of J. MO extended-Huckel calculations performed with the CACAO program [30] on the previously described model and using the experimental bond angles shows a semi-quantitative approach to this assumption following the Hoffmann model [31], Table 4, in which it is assumed that the antiferromagnetic contribution to the J parameter is proportional to Δ^2, Δ being the gap between the pairs of symmetric and antisymmetric MOs built from the e_g atomic orbitals and the adequate orbitals of the bridge. In Table 4 the relevant structural parameters in the bonding region together with the calculated Δ and Δ^2 values for the three kinds of bridges present along the chain.

Following the above rules, the greater J_3 value should be expected for the bridge Ni(2′)–N(31′)–N(32)–N(31)–Ni(2), an intermediate J_1 value for the bridge Ni(1)–N(11)–N(12)–N(11′)–Ni(1′) and the lower J_2 value is expected for the bridge Ni(1)–N(21)–N(22)–N(23)–Ni(2) on the bases of the bond parameters summarized in Table 4.

Several expressions have been proposed for the analytical fit of alternating 1-D systems with local spin $S = 1$, but all cases are limited to only two J parameters [32]. As a first approach to the J superexchange parameters, a fit using the analytical expression for a homogeneous system with local spin $S = 1$ on the Hamiltonian $H = -JS_1S_2$ in the range 75–300 K, gave an average value of $-55.2(1)$ cm^{-1} and $g = 2.42$, Fig. 2. A more detailed approach may be performed by using the full-matrix diagonalization procedure applied to a ring of nine Ni atoms with the alternance of J_3- J_2- J_1 superexchange parameters [33], Scheme 1. This procedure may be applied only up to the maximum region because the number of chosen paramagnetic centers is odd. The best fit parameters were $J_3 = -65.0$, $J_1 = -35.0$ and $J_2 = -52.7$ cm^{-1}, R agreement factor 3.4×10^{-4} ($R = \Sigma (\chi_M^{calc} - \chi_M^{exp})^2 / \Sigma (\chi_M^{exp})^2$), in good accordance with the expected J values gradation. Therefore, it should be noted that the accurate calculation of the J superexchange parameters for a system of this kind implies a large degree of vagueness. The accurate fit should be performed by using larger rings of 12 or 15 paramagnetic centers, but the size of the matrix and the time of calculation make this not possible to apply to these models.

4. Supplementary data

Further details of the crystal structure investigation are available from the Cambridge Crystallographic Data Centre, 12 Union Road, Cambridge CB2 IEZ, UK (fax: +44-1223-336033; e-mail: deposit@ccdc.cam.ac.uk or



Scheme 1.

Table 4
Relevant structural parameters for the three different bridges of compound **1**

Ni–N–N (°)	Ni–N_3–Ni torsion (°)	Δ	Gap	Δ^2	Gap
Ni(2′)–N(31′)–N(32)–N(31)–Ni(2)	128.7	180	0.497	0.247	128.7
Ni(1)–N(11)–N(12)–N(11′)–Ni(1′)	135.6	180	0.399	0.159	135.6
Ni(1)–N(21)–N(22)–N(23)–Ni(2)	128.6	133.4	0.279	0.078	140.3

Δ^2 Parameter is equal to the gap $(E\phi(z^2_{(s)}) - E\phi(z^2_{(d)})^2$ which is directly related to the antiferromagnetic component of J in the Hoffmann model.

www: http://www.ccdc.cam.ac.uk) on request, quoting the deposition number CCDC 163777.

Acknowledgements

This research work was partially supported by OENB (grant 6630) and CICYT (grant PB96/0163). F.A.M. thanks Professor C. Kratky and Dr. Belaj (University of Graz) for use of the 4-circle diffractometer.

References

[1] N.A. Baily, D.E. Fenton, C.H. McLean, Inorg. Chim. Acta 179 (1991) 1.
[2] (a) M.A.S. Goher, T.C.W. Mak, Inorg. Chim. Acta 85 (1984) 117;
(b) M.A.S. Goher, T.C.W. Mak, Inorg. Chim. Acta 89 (1984) 119.
[3] (a) T.C.W. Mak, M.A.S. Goher, Inorg. Chim. Acta 115 (1986) 17;
(b) M.A.S. Goher, R.-J. Wang, T.C.W. Mak, J. Mol. Struct. 243 (1991) 179.
[4] (a) M.A.S. Goher, F.A. Mautner, Z. Naturforsch., Teil. B 46 (1991) 687;
(b) F.A. Mautner, M.A.S. Goher, Polyhedron 12 (1993) 2823.
[5] (a) M.A.S. Goher, F.A. Mautner, Crystallogr. Res. Technol. 27 (1992) 817;
(b) F.A. Mautner, M.A.S. Goher, A.E.H. Abdou, Polyhedron 12 (1993) 2815.
[6] (a) M.A.S. Goher, N.A. Al-Salem, F.A. Mautner, Polyhedron 15 (1996) 4513;
(b) M.A.S. Goher, F.A. Mautner, N.A. Al-salem, Polyhedron 16 (1997) 2239.
[7] (a) M.A.S. Goher, F.A. Mautner, Polyhedron 15 (1996) 5;
(b) F.A. Mautner, M.A.S. Goher, Polyhedron 15 (1996) 1133.
[8] M.A.S. Goher, N.A. Al-Salem, F.A. Mautner, J. Coord. Chem. 44 (1998) 119.
[9] (a) A. Escuer, R. Vicente, M.A.S. Goher, F.A. Mautner, Inorg. Chem. 36 (1997) 1233;
(b) A. Escuer, R. Vicente, M.A.S. Goher, F.A. Mautner, Inorg. Chem. 36 (1997) 3440.
[10] (a) A. Escuer, R. Vicente, F.A. Mautner, M.A.S. Goher, Inorg. Chem. 37 (1998) 782;
(b) M.A.M. Abu-Youssef, A. Escuer, M.A.S. Goher, F.A. Mautner, G.J. ReiB, R. Vicente, Angew. Chem., Int. Ed. 39 (2000) 1624.
[11] J. Ribas, A. Escuer, M. Monfort, R. Vicente, R. Corties, L. Lezama, T. Rojo, Coord. Chem. Rev. 193–195 (1999) 1027.
[12] (a) M.A.S. Goher, A. Escuer, M.A.M. Abu-Youssef, F.A. Mautner, Polyhedron 17 (1998) 4265;
(b) A. Escuer, M.A.S. Goher, F.A. Mautner, R. Vicente, Inorg. Chem. 39 (2000) 2107.
[13] M.A.S. Goher, A.A. Hasanein, S.M. Soliman, Bull. Soc. Chim. Fr. I (1982) 221.
[14] M.A.S. Goher, A.A. Hasanein, G.M. El-Subruiti, Polish J. Chem. 57 (1983) 1169.
[15] (a) M.A.S. Goher, A.A. Hasanein, S.M. Soliman, Bull. Soc. Chim. Fr. I (1984) 169;
(b) M.A.S. Goher, Acta Chim. Hung. 117 (1984) 215.
[16] M.A.S. Goher, F.A. Mautner, Polyhedron 18 (1999) 2339.
[17] N. Walker, D. Stuart, Acta Crystallogr., Sect. A 39 (1983) 158.
[18] SHELXTL/PC-V. 5.03, Simens Analytical Automation, Madison, WI, 1995.
[19] F. Wagner, M.T. Mocella, M.J. D'Aneillo, A.H.J. Wang, E.K. Barefield, J. Am. Chem. Soc. 96 (1974) 2625.
[20] A. Agrell, Acta Chem. Scand. 25 (1971) 2865.
[21] M.A.S. Goher, Acta Chim. Hung. 127 (1990) 213.
[22] R.M. Morrison, R.C. Thompson, Can. J. Chem. 56 (1978) 985.
[23] B.N. Figgis, J. Lewis, Progr. Inorg. Chem. 4 (1964) 37.
[24] R.A. Walton, J. Inorg. Nucl. Chem. 28 (1966) 2239.
[25] A.B.P. Lever, Inorganic Electronic Spectroscopy, Elsevier, Amsterdam, 1968.
[26] F. Wagner, M.T. Mocella, M.J. D'Aniello, A.H.J. Wang, A.K. Barefield, J. Am. Chem. Soc. 96 (1974) 2625.
[27] V.W. Day, B.R. Status, E.L. Tasset, R.O. Day, R.S. Marianelli, J. Am. Chem. Soc. 96 (1974) 2650.
[28] A. Escuer, R. Vicente, J. Ribas, M.S. El Fallah, X. Solans, Inorg. Chem. 32 (1993) 1033.
[29] A. Escuer, R. Vicente, J. Ribas, M.S. El Fallah, X. Solans, M. Font-bardia, Inorg. Chem. 33 (1994) 1842.
[30] C. Mealli, D.M. Proserpio, J. Chem. Educ. 67 (1990) 399.
[31] P.J. Hay, J.C. Thibeault, R. Hoffmann, J. Am. Chem. Soc. 97 (1975) 4884.
[32] J.J. Borras-Almenar, E. Coronado, J. Curely, R. Georges, Inorg. Chem. 34 (1995) 2699.
[33] D. Gatteschi, P. Luca, Gazz. Chim. Ital. 123 (1993) 231.

2.1. $Ga(^tBu)_2(OPh)(pyz)\cdot(PhOH)$ (1)

Solid $[(^tBu)_2Ga(\mu\text{-}OPh)]_2$ (0.10 g, 0.18 mmol) and, as received, pyrazine (35 mg, 0.43 mmol) were combined in a round bottom flask. The combined powders changed color from white to yellow over a few minutes. Toluene (15 ml) was added to the flask and the resulting solution stirred for 12 h. Pentane (10 ml) was layered on to the solution, and upon cooling to −30 °C white crystals along with a small quantity of yellow crystals were deposited. ^{1}H NMR characterization of the white crystals showed it to be unreacted $[(^tBu)_2Ga(\mu\text{-}OPh)]_2$ [5]. The yellow crystals were suitable for X-ray analysis.

2.2. $[(^tBu)_2Ga(H_2O)(\mu\text{-}OH)Ga(^tBu)_2]_2(\mu\text{-}OC_6H_4O)\cdot 4(2\text{-}Mepy)$ (2)

A solution of $[\{(^tBu)_2Ga\}_2(\mu\text{-}OC_6H_4O)]_8$ (0.25 g, 0.53 mmol) in degassed wet 2-picoline (30 ml) was allowed to stir for a day. The solution was cooled to −30 °C overnight yielding colorless crystals suitable for single crystal X-ray analysis. Yield: 0.406 g, 37%. m.p. 98 °C (dec.). MS (EI, %): *m/z* 1229 ($M^+ - {}^t$Bu, 60). IR (cm^{-1}): 3349 (br m), 2952 (m), 2937 (m), 2867 (m), 2828(s), 2753 (w), 2694 (w), 1601(w), 1492 (s), 1457 (m), 1388 (w), 1298 (w), 1214 (s), 1199 (s), 1005 (w), 841 (m), 812 (m), 787 (m), 752 (m). ^{1}H NMR ($CDCl_3$): δ 8.51 [1H, d, J(H–H) = 4.0 Hz, NC*H*], 7.59 [1H, t, J(H–H) = 6.5 Hz, *p*-C*H*], 7.16 [1H, d, J(H–H) = 5.5 Hz, *m*-C*H*], 7.11 [1H, t, J(H–H) = 7.5 Hz, *m*-C*H*], 6.7 (1H, s, OCC*H*), 2.57 (3H, s, CH_3), 1.13 [9H, s, C(CH_3)$_3$], 1.11 [9H, s, C(CH_3)$_3$]. ^{13}C NMR ($CDCl_3$): δ 158.6 (O*C*), 149.2 (N*C*H), 136.6 (*p*-*C*H), 123.6 (*m*-*C*H), 120.8 (OC*C*H), 31.1 [C(*C*H$_3$)$_3$], 24.6 (*C*H$_3$), 24.5 [C(*C*H$_3$)$_2$].

2.3. X-ray data collection, solution and refinement

Data for compounds **1** and **2** were collected at 298 K on a Bruker CCD SMART system, equipped with graphite monochromated Mo Kα radiation (λ = 0.71073 Å) and corrected for Lp effects. The structures were solved using the direct methods program xs [6] and difference Fourier maps and refined by using full-matrix least-squares methods. All non-hydrogen atoms were refined with anisotropic thermal parameters. Hydrogen atoms involved in hydrogen bonding were located in the electron difference map. Hydrogen atoms bound to carbon were introduced in calculated positions and allowed to ride on the attached carbon atoms [d(C–H) = 0.95 Å]. Refinement of positional and anisotropic thermal parameters led to convergence (see Table 1).

Table 1
Summary of X-ray diffraction data for $Ga(^tBu)_2(OPh)(pyz)\cdot(PhOH)$ (**1**) and $[(^tBu)_2Ga(H_2O)(\mu\text{-}OH)Ga(^tBu)_2]_2(\mu\text{-}OC_6H_4O)\cdot 4(2\text{-}Mepy)$ (**2**)

Compound	**1**	**2**
Empirical formula	$C_{24}H_{33}GaN_2O_2$	$C_{62}H_{110}Ga_4N_4O_6$
Molecular weight	451.24	1286.42
Crystal system	triclinic	triclinic
Space group	$P\bar{1}$	$P\bar{1}$
a (Å)	9.467(2)	9.237(2)
b (Å)	10.435(2)	11.548(2)
c (Å)	13.526(3)	17.727(3)
α (°)	93.17(3)	97.12(3)
β (°)	110.05(3)	91.12(3(3)
γ (°)	93.26(3)	107.48(3)
V (Å^3)	1249.3(4)	1786.5(6)
Z	2	1
D_{calc} (g cm^{-3})	1.200	1.196
μ_{calc} (mm^{-1})	1.12	1.54
Reflections collected	5603	8309
Reflections observed	3198 ($\|F_o\| > 4.0\sigma \|F_o\|$)	2820 ($\|F_o\| > 4.0\sigma \|F_o\|$)
Independent reflections	3535 [R_{int} = 0.0568]	5150 [R_{int} = 0.086]
Weighting scheme SHELXTL parameters	0.0577, 0.1068	0.592, 0
R	0.0321	0.0589
R_w	0.0890	0.1290

3. Results and discussion

Reaction of $[(^tBu)_2Ga(\mu\text{-}OPh)]_2$ with wet pyrazine ($N_2C_4H_4$, pyz), followed by crystallization from toluene–pentane, results in the isolation of small quantity of yellow crystals of $Ga(^tBu)_2(OPh)(pyz)\cdot(PhOH)$ (**1**). The formation of compound **1** may be rationalized by assuming that the pyrazine cleaves the Ga_2O_2 core and allows for the formation of the monomeric Lewis acid–base complex, $Ga(^tBu)_2(OPh)(pyz)$. Subsequent, hydrolysis, or direct hydrolysis of $[(^tBu)_2Ga(\mu\text{-}OPh)]_2$ yields PhOH and presumably the ubiquitous hydroxide compound, $[(^tBu)_2Ga(\mu\text{-}OH)]_3$ [7,8]. The phenol thus formed, hydrogen bonds to the most basic ligand in the system, the terminal aryloxide in $Ga(^tBu)_2(OPh)(pyz)$.

The structure of $Ga(^tBu)_2(OPh)(pyz)\cdot(PhOH)$ (**1**) is shown in Fig. 1; selected bond lengths and angles are given in Table 2. The bond lengths and angles about gallium are within the ranges observed for related compounds [5,9]. The geometry about the phenoxide oxygen [O(1)], as measured by the N(1)–Ga(1)–O(1)–C(1) torsion angle (131.2°), is significantly different from $Ga(^tBu)_2(OPh)(py)$ (180°) [2], as a result of an O···H–O hydrogen bond to the phenol. The O(1)···O(30) distance of 2.64 Å is comparable to the typical range observed for such interactions (2.57–2.69 Å) [10].

If the synthesis of $[(^tBu)_2Ga(2\text{-}Mepy)]_2(\mu\text{-}OC_6H_4O)$ is attempted without sufficiently drying the 2-Mepy,

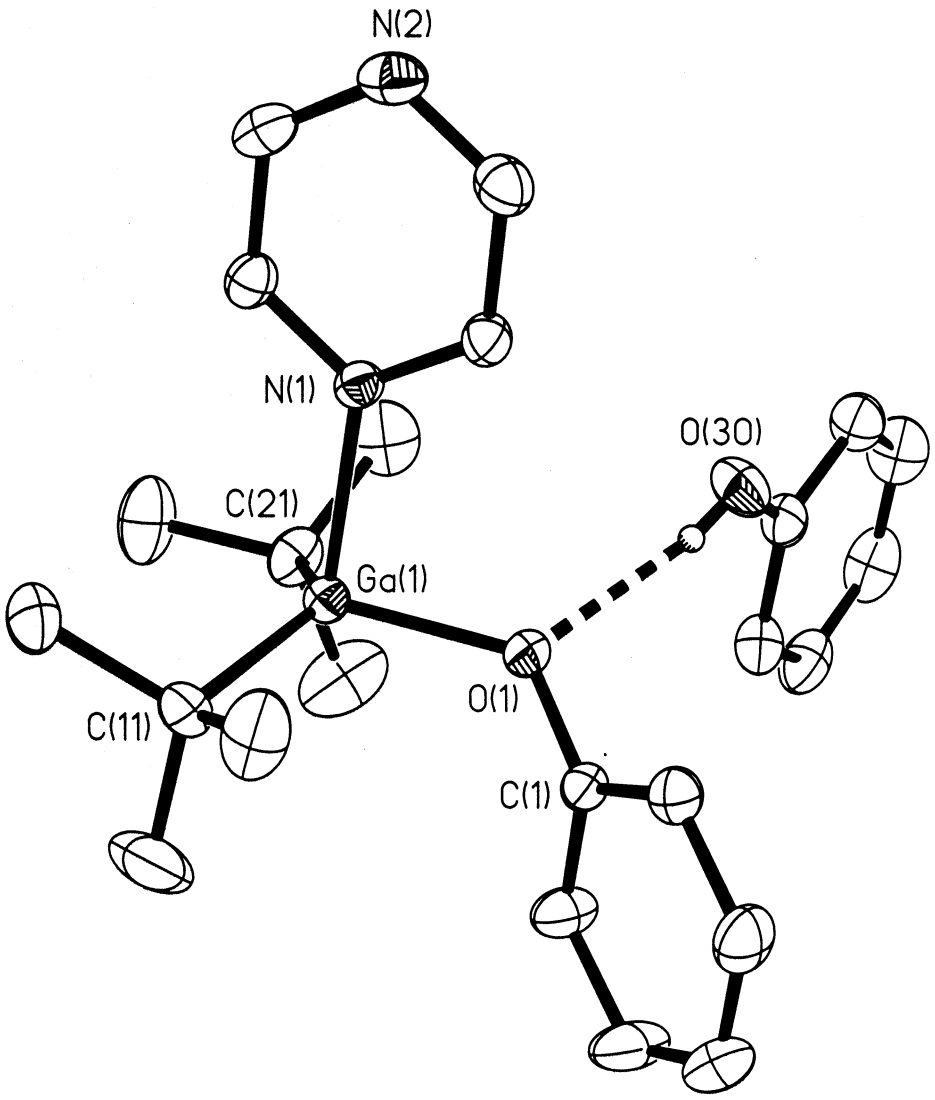


Fig. 1. Molecular structure of $Ga(^tBu)_2(OPh)(pyz)\cdot(PhOH)$ (**1**) showing the intra-molecular hydrogen bond. Thermal ellipsoids shown at the 20% level, and hydrogen atoms bound to carbon are omitted for clarity.

partial hydrolysis occurs, yielding the tetra-gallium compound, $[(^tBu)_2Ga(H_2O)(\mu\text{-}OH)Ga(^tBu)_2]_2(\mu\text{-}OC_6H_4O)\cdot 4(2\text{-Mepy})$ (**2**). The IR spectrum of compound **2** indicates the presence of hydrogen bonding with a very broad signal at 3350 cm^{-1} and an N–H stretch at 3050 cm^{-1}. Unfortunately, no signals could be assigned to the hydroxide and/or water ligands in the ^1H NMR spectrum, presumably due to H-bonding effects [11].

The solid state structure of compound **2** is shown in Fig. 2; selected bond lengths and angles are given in Table 3. The centrosymmetric structure of compound **2**

Table 2
Selected bond lengths (Å) and angles (°) for $Ga(^tBu)_2(OPh)(pyz)\cdot(PhOH)$ (**1**)

Bond lengths			
Ga(1)–O(1)	1.897(2)	Ga(1)–N(1)	2.123(2)
Ga(1)–C(11)	2.007(3)	Ga(1)–C(21)	2.010(3)
Bond angles			
O(1)–Ga(1)–N(1)	93.08(8)	O(1)–Ga(1)–C(21)	106.9(1)
O(1)–Ga(1)–C(11)	114.3(1)	N(1)–Ga(1)–C(11)	103.9(1)
N(1)–Ga(1)–C(21)	104.3(1)	C(11)–Ga(1)–C(21)	127.8(1)
Ga(1)–O(1)–C(1)	126.3(2)		

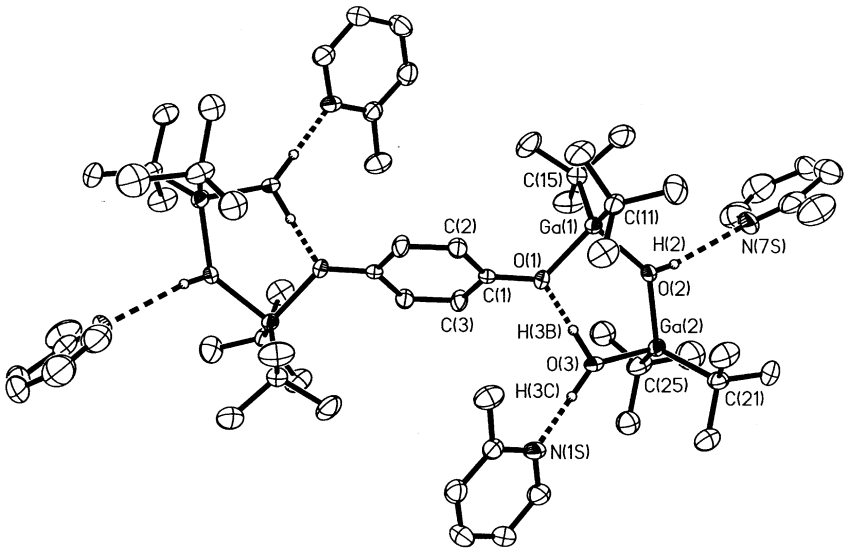


Fig. 2. Structure of $[(^tBu)_2Ga(H_2O)(\mu\text{-}OH)Ga(^tBu)_2]_2(\mu\text{-}OC_6H_4O)\cdot 4(2\text{-Mepy})$ (**2**). Thermal ellipsoids shown at the 30% level, and hydrogen atoms are omitted for clarity.

Table 3
Selected bond lengths (Å) and angles (°) for $[(^tBu)_2Ga(H_2O)(\mu\text{-}OH)Ga(^tBu)_2]_2(\mu\text{-}OC_6H_4O)\cdot 4(2\text{-Mepy})$ (**2**)

Bond lengths			
Ga(1)–O(1)	1.885(4)	Ga(1)–O(2)	1.963(4)
Ga(1)–C(11)	1.982(7)	Ga(1)–C(15)	1.975(7)
Ga(2)–O(2)	1.945(4)	Ga(2)–O(3)	1.946(4)
Ga(2)–C(21)	1.974(7)	Ga(2)–C(25)	1.960(7)
Bond angles			
O(1)–Ga(1)–O(2)	92.0(2)	O(1)–Ga(1)–C(11)	110.9(3)
O(1)–Ga(1)–C(15)	108.8(2)	O(2)–Ga(1)–C(11)	106.6(2)
O(2)–Ga(1)–C(15)	108.7(2)	C(11)–Ga(1)–C(15)	124.9(3)
O(2)–Ga(2)–O(3)	91.4(2)	O(2)–Ga(2)–C(21)	113.3(2)
O(2)–Ga(2)–C(25)	112.3(3)	O(3)–Ga(2)–C(21)	104.4(3)
O(3)–Ga(2)–C(25)	106.8(3)	C(21)–Ga(2)–C(25)	123.0(3)
Ga(1)–O(1)–C(1)	129.8(4)	Ga(1)–O(2)–Ga(2)	137.0(2)

consists of a $[(^tBu)_2Ga]_2(\mu\text{-}OC_6H_4O)$ core to which two $Ga(^tBu)_2(H_2O)(OH)$ moieties are coordinated via bridging hydroxides. Each of the terminal water ligands is hydrogen bonded to an aryloxide's oxygen, resulting in a six-membered O–Ga–O–Ga–O–H cycle. Each water ligand is also hydrogen bonded to a 2-Mepy ligand of crystallization. As a result, the molecule is stabilized through both intra- and inter-molecular hydrogen bonding, see Fig. 2.

The O(1)···O(3) distance (2.50 Å) associated with the intra-molecular hydrogen bond is significantly shorter than typical O–H···O hydrogen bonds (2.57–2.69 Å), and close to the values found for a strong H-bond [10]. The O(3)···N(1S) distance (2.65 Å) is shorter than observed for transition metal aqua complexes (2.71–2.72 Å) [12]. This observation is in line with the known acidity of the coordinated water ligands in $[Ga(H_2O)_6]^{3+}$. There have been several recent examples of coordinated water molecules undertaking two intra-molecular hydrogen bonds [13], two inter-molecular hydrogen bonds [14], or one intra- and one inter-molecular hydrogen bonding interaction [12,15].

The Ga(1)–O(2) and Ga(2)–O(2) distances [1.963(4) and 1.945(4) Å, respectively] are typical for a gallium hydroxide (approximately 2.00 Å), rather than a gallium oxide (1.87–1.89 Å) [16], suggesting that there is negligible contribution from the Zwitter ionic ($O^-\cdots H\text{–}N^+$) form. The Ga(1)–O(2)–Ga(2) angle associated with the bridging hydroxide [137.0(2)°] is within the range previously observed for similar six-membered cyclic systems [132.0(3)°–143.0(2)°] [7,17]. The hydrogen bond between 2-Mepy and the bridging hydroxide [O(2)···N(7S) = 2.95 Å] is significantly longer than for the water ligand (2.65 Å). Furthermore, the O(2)···N(7S) interaction appears to be weaker than the intra-molecular gallium hydroxide···amine interaction in $(^tBu)_2Ga(o\text{-}C_6H_4NMe_2)(\mu\text{-}OH)Ga(^tBu)[o\text{-}C_6H_4N(O)Me_2]$ (2.80 Å) for which a significant Zwitter ionic contribution is proposed [13].

As illustrated in the crystal packing diagram of compound **2**, the orientation of the 2-Mepy ligand hydrogen bonded to the water ligands allows for a series of π-stacking interactions between adjacent molecules, see Fig. 3. The result of this hydrogen bonding is the formation of a series of molecular 'S's' along the crystallographic *a*-axis. On the basis of the hierarchical levels of crystal architecture [18], the structure of compound **2** may be described as a series of head-to-tail (*primary* level) interactions, creating a series of corrugations (*secondary* level) which are coplanar but contain no inter-layer contacts (*tertiary* level). A sche-

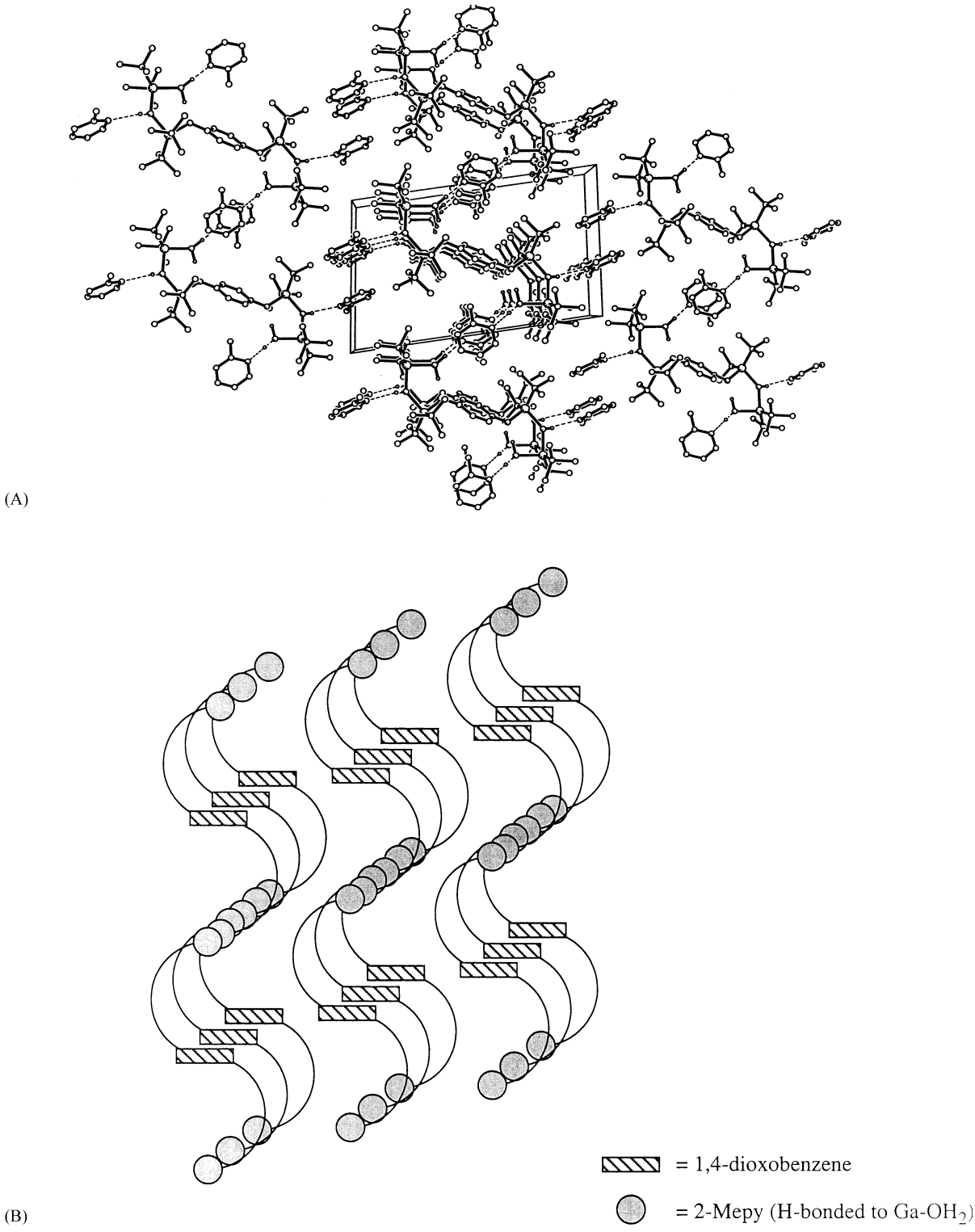
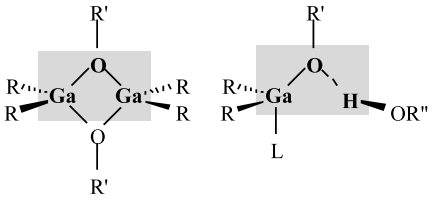


Fig. 3. Crystal packing of $[(^tBu)_2Ga(H_2O)(\mu\text{-}OH)Ga(^tBu)_2]_2(\mu\text{-}OC_6H_4O)\cdot 4(2\text{-Mepy})$: (**2**), (a) as viewed along the crystallographic *a*-axis; and (b) a schematic representation, demonstrating the series of molecular 'S's' created by a combination of hydrogen bonding and π-stacking.

matic representation of the crystal packing is shown in Fig. 3(b).

Both compounds **1** and **2** show examples of strong hydrogen bonding to the oxygen atom of a terminal aryloxide ligand. We have previously observed that the basicity of terminal Group 13 aryloxides is sufficient to enolize ketones [19]. It is possible to consider the hydrogen bonding to the aryloxides in compounds **1**

and **2** as an isolobal analog [20] of a bridging alkoxide compound. In particular, the Ga(1)–O(1)···H(30) unit (see **I**) may be considered analogous to a bridging alkoxide unit, Ga(μ-OR)Ga (**II**). This analogy has some precedent since we have previously shown by ^{17}O NMR spectroscopy that Group 13 metals and a proton have similar electronegativities with regard to oxygen [21].



4. Supplementary material

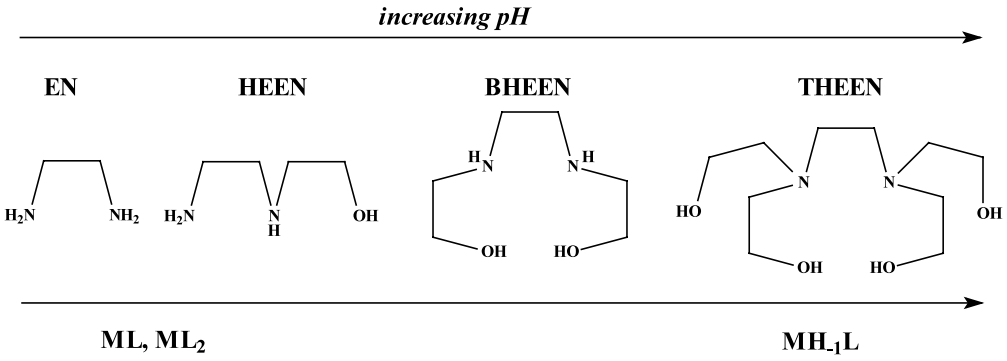
Crystallographic data for the structural analyses have been deposited with the Cambridge Crystallographic Data Center, CCDC Nos. 178641 and 178642 for compounds **1** and **2**. Copies of this information may be obtained free of charge from The Director, CCDC, 12 Union Road, Cambridge, CB2 1EZ, UK (fax: +44-1223-336033; e-mail: deposit@ccdc.cam.ac.uk or www: http://www.ccdc.cam.ac.uk).

Acknowledgements

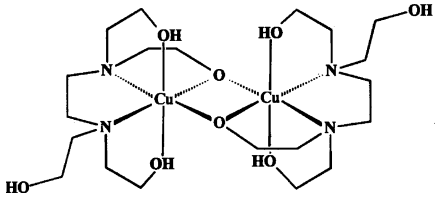
Financial support for this work is provided by the Robert A. Welch Foundation.

References

[1] A.R. Barron, M.B. Power, Gallium: organometallic chemistry, in: R.B. King (Ed.), Encyclopedia of Inorganic Chemistry, Wiley, Chichester, 1994.
[2] L.H. van Poppel, S.G. Bott, A.R. Barron, submitted for publication.
[3] C.N. McMahon, A.R. Barron, J. Chem. Soc., Dalton Trans. (1998) 3703.
[4] L.G. van Poppel, S.G. Bott, A.R. Barron, J. Chem. Crystallogr. (2002), in press.
[5] W.M. Cleaver, A.R. Barron, A.R. McGuffey, S.G. Bott, Polyhedron 13 (1994) 2831.
[6] G.M. Sheldrick, SHELXTL. Bruker AXS, Inc., Madison, WI, 1997.
[7] D.A. Atwood, A.H. Cowley, P.J. Harris, R.A. Jones, S.U. Koshmieder, C.M. Nunn, Organometallics 12 (1993) 24.
[8] M.B. Power, W.M. Cleaver, A.W. Apblett, A.R. Barron, J.W. Ziller, Polyhedron 11 (1992) 477.
[9] D.G. Tuck, in: G. Wilkinson, F.G.A. Stone, E.W. Abel (Eds.), Comprehensive Organometallic Chemistry, vol. 1 (Chapter 7), Pergamon Press, Oxford, 1982.
[10] R. Taylor, O. Kennard, Acc. Chem. Res. 17 (1984) 320.
[11] K.Z. Malik, S.D. Robinson, J.W. Steel, Polyhedron 19 (2000) 1589.
[12] C.A. Johns, G.M.G. Hossain, K.M.A. Malik, S.Z. Haider, U.K.R. Romman, Polyhedron 20 (2001) 721.
[13] N.C. McMahon, S.G. Bott, A.R. Barron, J. Chem. Soc., Dalton Trans. (1997) 3129.
[14] D. Miklos, P. Segl'a, M. Palicová, M. Kopcová, M. Melník, M. Valko, T. Glowiak, M. Korabik, J. Mrozinski, Polyhedron 20 (2001) 1867.
[15] R.P. Hughes, D.C. Linder, J.M. Smith, D. Zhang, C.D. Incarvito, K.-C. Lam, L.M. Liable-Sands, R.D. Sommer, A.L. Rheingold, J. Chem. Soc., Dalton Trans. 1 (2001) 2270.
[16] C.C. Landry, C.J. Harlan, S.G. Bott, A.R. Barron, Angew. Chem., Int. Ed. Engl. 34 (1995) 1202.
[17] Y. Koide, J.A. Francis, S.G. Bott, A.R. Barron, Polyhedron 17 (1998) 983.
[18] J.A. Zerkowski, J.C. MacDonald, G.M. Whitesides, Chem. Mater. 6 (1994) 1250.
[19] M.B. Power, A.W. Apblett, S.G. Bott, J.L. Atwood, A.R. Barron, Organometallics 9 (1990) 2529.
[20] R. Hoffmann, Angew. Chem., Int. Ed. Engl. 21 (1982) 711.
[21] A.W. Apblett, A.C. Warren, A.R. Barron, Can. J. Chem. 70 (1992) 771.



Scheme 1. Increased substitution of ethylenediamine and the predominant complexes that are present.



Scheme 2. Copper complex of THEEN.

Table 1
Crystal data

Empirical formula	$C_{20}H_{46}Cl_2Cu_2N_4O_{16}$
Formula weight	796.59
Temperature (K)	173(2)
Wavelength (Å)	0.71073
Crystal system	Monoclinic
Space group	$P2_1/c$
Unit cell dimensions	
a (Å)	11.9072(2)
b (Å)	8.1114(1)
c (Å)	19.531(2)
α (°)	90
β (°)	123.839(6)
γ (°)	90
V (Å^3)	1566.8(3)
Z	2
D_{calc} (Mg m^{-3})	1.688
Absorption coefficient (mm^{-1})	1.605
$F(000)$	828
Crystal size (mm)	0.44 × 0.38 × 0.24
Theta range for data collection	2.06°–28.29°
Index ranges	$-15 \le h \le 15$, $-10 \le k \le 10$, $-26 \le l \le 22$
Reflections collected	10 429
Independent reflections	3839 [R(int) = 0.0143]
Completeness to theta = 28.29°	98.6%
Absorption correction	Empirical
Max/min transmission	0.6993 and 0.5386
Refinement method	Full-matrix least-squares on F^2
Data/restraints/parameters	3839/3/211
Final R indices [$I > 2\sigma(I)$]	$R_1 = 0.0257$, $wR_2 = 0.0671$
R indices (all data)	$R_1 = 0.0305$, $wR_2 = 0.0696$
Goodness-of-fit on F_2	1.042
Largest difference peak and hole (e Å^{-3})	0.660 and −0.445

Table 2
Selected bond lengths (Å) and angles (°) with e.s.d.s in parentheses

Bond lengths	
Cu(1)–O(1)	1.9404(1)
Cu(1)–O(1A)	1.9588(1)
Cu(1)–N(1)	2.0218(1)
Cu(1)–N(2)	2.0384(1)
Cu(1)–O(3)	2.3324(1)
Cu(1)–O(4)	2.6743(1)
Cu(1)–Cu(1A)	2.9584(5)
Cl(1)–O(13)	1.406(2)
Cl(1)–O(11)	1.432(2)
Cl(1)–O(10)	1.434(2)
Cl(1)–O(12)	1.451(2)
Bond angles	
O(1)–Cu(1)–O(1A)	81.30(5)
O(1)–Cu(1)–N(1)	84.85(5)
N(1)–Cu(1)–N(2)	88.04(6)
N(2)–Cu(1)–O(4)	74.85(5)
C(4)–O(1)–Cu(1)	113.26(1)
Cu(1)–O(1)–Cu(1A)	98.71(5)
C(8)–O(3)–Cu(1)	106.81(1)
C(10)–O(4)–Cu(1)	102.62(1)
C(1)–N(1)–Cu(1)	105.23(1)
C(3)–N(1)–Cu(1)	100.50(9)
C(7)–N(2)–Cu(1)	109.24(1)
C(9)–N(2)–Cu(1)	112.02(1)
C(2)–N(2)–Cu(1)	106.24(1)
O(13)–Cl(1)–O(1)	112.33(1)
O(13)–Cl(1)–O(1)	110.34(2)
O(11)–Cl(1)–O(1)	110.11(1)
O(13)–Cl(1)–O(1)	109.49(1)
O(11)–Cl(1)–O(1)	109.06(1)
O(10)–Cl(1)–O(1)	105.25(1)

Table 3
Torsion angles (°) with e.s.d.s in parentheses

N(1)–C(1)–C(2)–N(2)	−46.8(2)
N(1)–C(3)–C(4)–O(1)	41.4(2)
N(2)–C(7)–C(8)–O(3)	−55.0(2)
N(2)–C(9)–C(10)–O(4)	52.4(2)

mine was obtained as a free ligand from Fluka.

$$2Cu(ClO_4)_2 6H_2O + 2H_4THEEN + 2OH^- \rightarrow [Cu(H_3THEEN)ClO_4]_2 + 8H_2O$$

An aqueous 20 ml solution of $(CuClO_4)_2 \cdot 6H_2O$ (0.02 mol) and NaOH (0.02 mol) was prepared. To this was added a mixture of *N*,*N*,*N*′,*N*′-tetrakis(2-hydroxyethyl)ethylenediamine (0.01 mol) and 15 ml deionised water at 60 °C. The solution was stirred for a further 2 h at 60 °C and then left to cool down to room temperature. Slow evaporation yielded blue crystals after 4 days. The crystals were collected by filtration and air-dried.

Anal. Calc. for $C_{10}H_{23}ClCuN_2O_8$: C, 30.16; H, 5.82; N, 7.03. Observed: C, 30.14; H, 5.97; N, 6.92%.

3. Data collection

Intensity data were collected at −100 °C on a Bruker SMART [5] 1K CCD area detector diffractometer with graphite monochromated Mo Kα radiation (50 kV, 30 mA). The collection method involved ω-scans of width 0.3°. Data reduction was carried out using the program SAINT+ [6] and absorption corrections were made using the program SADABS [7]. The crystal structure was solved by direct methods using SHELXTL [8]. Non-hydrogen atoms were first refined isotropically followed by anisotropic refinement by full matrix least-squares calculation based on F^2 using SHELXTL. Hydrogen atoms were positioned geometrically and allowed to ride on their respective parent atoms. All the CH_2 hydrogen positions were calculated while the hydroxyl hydrogens (H_{200}, H_{300} and H_{400}) were placed from the Difference Fourier map and refined isotropically. These hydrogen atoms are all involved in extensive hydrogen bonding. Diagrams and publication material were generated using SHELXTL and PLATON [8,9]. No disorder models were required for the ClO_4^- ion (Fig. 1).

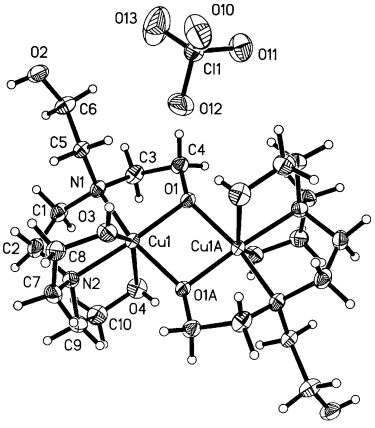


Fig. 1. The molecular structure of the copper complex of THEEN, showing the atom-labeling scheme and 50% probability displacement ellipsoids.

The X-ray structure is that of a dimer comprising two $[CuH_3THEEN]^+$ monomers bonded by the formation of a Cu_2O_2 ring across an inversion centre. The complex utilizes the hydroxylate oxygens to form two Cu–O–Cu bridges. Oxygen O(1) is binucleating serving to bridge between the copper centers. The Cu(1)–Cu(1A) and O(1)–O(1A) transannular distances are 2.958 and 2.540 Å and the O(1)–Cu(1)–O(1A) and Cu(1)–O(1)–Cu(1A) angles are 81.30° and 98.71°, respectively. Coordination to the copper center occurs via two amine nitrogen atoms (N(1) and N(2)) and three oxygen atoms (O(1), O(3) and O(4)). The coordination polyhedron is best interpreted as a distorted octahedron rather than the distorted square-pyramidal coordination reported for $[CuH_3THPED]^+$ [4]. The sixth coordination site completing the octahedral coordination geometry includes the oxygen donor O(1A) of the symmetry related $[CuH_3THEEN]^+$ monomer that forms the second of the two metal–oxygen–metal bridges (Fig. 2).

Oxygen atoms in the Cu_2O_2 ring have shortened bond lengths of 1.940 and 1.959 Å to the Cu(II) ion in comparison to the oxygen atoms (O(3) and O(4)) that occupy the axial positions defining the principal axis. These longer bond lengths of 2.332 and 2.674 Å are associated with characteristic Jahn–Teller distortions observed for copper coordination compounds. The shorter Cu(1)–O(1) and Cu(1)–O(1A) bonds imply deprotonation of the oxygen atoms of the hydroxyethyl moieties and compare favourably with copper to oxygen bond lengths of negatively charged oxygen donors reported for the Cu(II) complex of EDTA [11]. Chelation of the Cu(II) ion by THEEN forms four chelate rings as one of the hydroxyethyl pendant donor moeities does not form part of the coordination sphere. This may be due to steric influences arising from H–H non-bonded interactions of adjacent chelate rings [12].

Early studies of the stereochemistry of five-membered chelate rings were based on metal complexes of ethylenediamine. These studies established geometric requirements necessary for the metal–ethylenediamine chelate ring that would afford a strain-free structure [13]. In these calculations ideal bond lengths were used and the

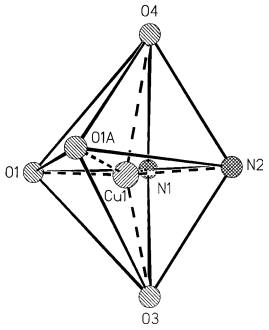
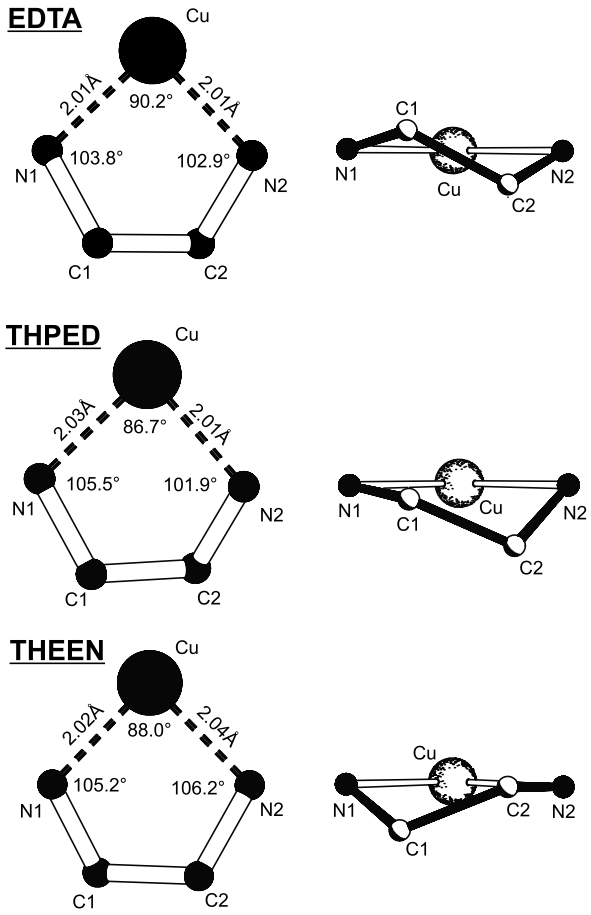


Fig. 2. Distorted octahedral coordination sphere of Cu(II) on complexation to THEEN.

M–N–C bond angle was selected to be 109.5°, comparable to the value observed in the chair conformation of cyclohexane, which minimizes H–H non-bonded interactions on adjacent carbon atoms. An N–M–N angle of 86.2° and a dihedral angle of 48.8° was calculated if the M–N distance is taken as 2.00 Å. The above parameters determined by Corey and Bailar [13] essentially defined a strain-free, five-membered metal–ethylenediamine chelate ring. Orama et al. [4] reported a N–Cu–N angle of 86.8° in their structure of the Cu(II) complex of THPED that is comparable to the calculated value above, however, it must be noted that their Cu–N(1)–C(1) and Cu–N(2)–C(2) angles are 105.5° and 101.9°, respectively. These angle deviations are accompanied by a similar difference in the dihedral angle of 50.6° as compared to the calculated 48.8°. The deviations arise as a result of the geometric inability of the ethylenediamine ring to accommodate the N–M–N and M–N–C angles simultaneously at their required values, but minimizes the angle strain by altering the dihedral angle as a function of M–N bond length, thereby changing the bite size [13,14]. This phenomenon has been used to explain why larger metal ions prefer five-membered chelate rings while smaller metal ions prefer six-membered chelate rings [14,15]. The 'asymmetric envelope' conformation observed for $[CuH_3THPED]^+$ due to deviations of the carbon atoms towards the same side of the N–Cu–N plane [4] is not observed for the $[CuH_3THEEN]^+$ monomer. Carbon C(2) however is nearly contained within the N(1)–Cu(1)–N(2) plane and its deviation is only 0.04 Å. The effect of this conformation is to flatten the ethylenediamine chelate ring as can be concluded from the dihedral angle of 46.8° compared to 55.9° for [CuEDTA] where the carbon atoms C(1) and C(2) of the ethylenediamine chelate ring distinctly deviate to opposite sides of the plane of the metal ion and the two nitrogen donors by 0.25 and 0.45 Å, respectively (Scheme 3).

The decreased puckering of the ethylenediamine chelate ring has been explained as a function of M–N length were the ring flattens for short M–N values, decreasing the bite size [12–14]. The bite sizes of the ethylenediamine chelate ring for the Cu(II) structures of EDTA, THPED and THEEN are 2.848, 2.787 and 2.821 Å, respectively. The Cu–N bond lengths for the same structures are also comparable which reinforces the idea that the ring flattening can in this case be attributed in principal to the conformations adopted by the ethylenediamine ring in the THPED and THEEN structures of the copper complexes.

An analogous analysis of the three ethanolamine–metal chelate rings in $[CuH_3THEEN]^+$ reveals similar results although differences between C–N and C–O bond lengths and coordination geometries of nitrogen and oxygen donors must be appreciated [16,17,19]. The chelate ring formed by the hydroxyethyl pendant arm



Scheme 3. Comparison N–M–N and M–N–C angles and M–N bond lengths of the ethylenediamine chelate ring in the copper complexes of EDTA, THPED and THEEN. Orientations of the carbon atoms of the ethylenediamine chelate ring relative to the N–M–N plane.

containing the O(1) donor adopts a conformation that strongly resembles that of the ethylenediamine chelate ring in $[CuH_3THPED]^+$. Carbon atoms C(3) and C(4) both deviate to the same side of the N(1)–Cu(1)–O(1) plane by 0.85 and 0.34 Å, respectively. Similarly the Cu(1)–N(1)–C(3) and Cu(1)–O(1)–C(4) angles deviate significantly from the strain-free value and are 100.51° and 113.25°, respectively, compressing the N(1)–Cu(1)–N(2) angle to 84.9°. The fact that O(1) is a binucleating donor in the Cu_2O_2 ring influences the geometric requirements of the chelate ring. The Cu(1)–O(1) bond length (1.940 Å) is significantly smaller than that of Cu(1)–O(3) (2.332 Å) or Cu(1)–O(4) (2.674 Å). Decreased puckering of the chelate ring, as seen from a dihedral angle of 41.39°, accommodates the shorter bond length adjusting the bite size to 2.674 Å which is the smallest in $[CuH_3THEEN]^+$. The reduced bite size forces the opening of the Cu(1)–O(1)–C(4) angle to 113.25°. Chelate rings including the larger Cu–O bonds are more open and puckered to facilitate the larger bite size requirements. The Cu(1)–O(3) and Cu(1)–O(4)

Table 4
Hydrogen bonds for $[Cu(H_3THEEN)ClO_4]_2$ (Å and °)

D–H	d(D–H)	d(H···A)	DHA	D(D···A)	A	Symmetry
O(3)–H(300)	0.780	1.990	174.28	2.766	O(2)	$[-x, y+\frac{1}{2}, -z+\frac{1}{2}]$
O(4)–H(400)	0.770	2.282	142.95	2.934	O(12)	$[-x+1, -y+1, -z+1]$
O(4)–H(400)	0.770	2.338	127.40	2.872	O(1)	$[-x+1, -y+1, -z+1]$
O(2)–H(200)	0.798	2.039	162.42	2.810	O(12)	$[-x, y-\frac{1}{2}, -z+\frac{1}{2}]$

bonds along the axial positions contribute to the bite sizes of 2.831 and 2.908 Å for their chelate rings with dihedral angles of 54.97° and 52.48°, respectively. Different conformations are adopted by these rings and atoms C(9) and C(10) are oriented towards a single side of the O(4)–Cu(1)–N(2) plane that mimics the asymmetric envelope conformation, however atoms C(7) and C(8) deviate to opposite sides of the N(2)–Cu(1)–O(3) plane and more closely resemble the conformation of the ethylenediamine bridge in the Cu(II) complex of EDTA. Both intermolecular and intramolecular hydrogen-bonding occurs in the $[Cu(H_3THEEN)ClO_4]_2$ structure. Intermolecular hydrogen-bonding clarifies the observed orientation of the uncoordinated hydroxyethyl pendant arm and the involvement of the perchlorate anions with coordinated O(4) hydroxyethyl moiety. Intramolecular hydrogen-bonding occurs between O(1) in the Cu_2O_2 ring and H(400) on the O(4) donor forming the longest Cu–O bond length in this structure (Table 4; Fig. 3).

Thermodynamic data for THPED [2,18] and THEEN [18] shows a marked increase in stability of THPED complexes compared to complexes of THEEN. Increasing the number of hydroxypropyl groups over hydroxyethyl groups results in an increased stability. Inductive effects of the additional electron releasing methyl groups makes the O-donor a better nucleophile and more attracted to an electron deficient metal ion (Table 5).

The $[CuH_3THPED]^+$ complex has an average Cu–O bond length of 2.058 Å, substantially shorter than that for $[CuH_3THEEN]^+$ at 2.316 Å; for their respective coordination geometries. The bite sizes of the chelate rings adjust accordingly and chelate rings are generally flatter for $[CuH_3THPED]^+$. The architectural difference between the ligands lies in the C-alkyl substituents adjacent to the oxygen pendant donors of THPED. Effects on complex stability by the addition of alkyl

Table 5
Formation constant for complexes of THEEN and THPED [18]

Metal	THEEN (log K)	THPED (log K)
Co(II)	5.40	6.33
Ni(II)	6.50	7.65
Cu(II)	8.49	9.75
Zn(II)	4.74	6.09
Cd(II)	7.04	7.80

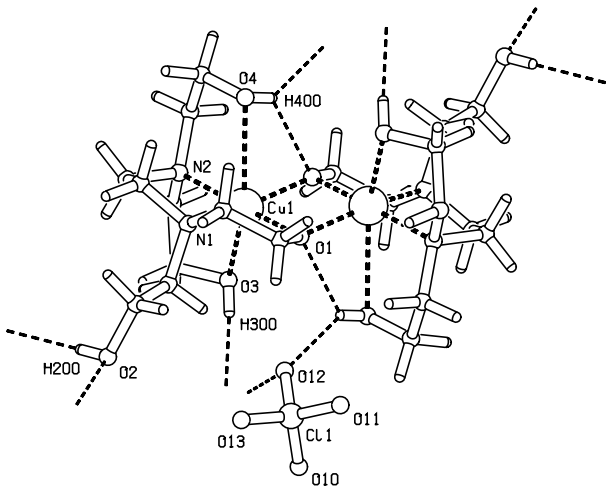


Fig. 3. Hydrogen bonding in the structure of $[Cu(H_3THEEN)ClO_4]_2$.

groups to ligands, has been documented [19,20] as has their ability to affect metal ion selectivity. Steric destabilization derived from alkyl substitution may outweigh favourable contributions to complex stability by inductive effects. Unfavourable steric contributions in the coordination polyhedron of THPED arising from the bulkier 2-hydroxypropyl pendant groups are absent in the THEEN complex that may facilitate dimerisation for complexes of smaller metal ions. A dimeric structure observed for Ti^{IV}THPED suggests that larger metal ions are more readily able to tolerate steric crowding produced by bulky pendant donors, and multinuclear complexes of the type observed for the open-chain β-amino alcohols such as THEEN and THPED are feasible. The ligands THEEN and THPED however, have identical donor sets and the Cu(II) complexes indicate that metal ion size may not be the only factor contributing towards dimerisation. The effects of steric crowding due to pendant donors need to be understood for successful syntheses of multinuclear complexes of open-chain ligands bearing 2-hydroxyalkyl pendant groups.

4. Supplementary material

Crystallographic data for the structure analysis has been deposited with the Cambridge Crystallographic

Data Centre, CCDC No. 175807 for compound ($Cu(H_3THEEN)ClO_4]_2$). Copies of this information may be obtained free of charge from The Director, CCDC, 12 Union Road, Cambridge, CB2 1EZ, UK (fax: +44-1223-336033; e-mail: deposit@ccdc.cam.ac.uk or www: http://www.ccdc.cam.ac.uk).

Acknowledgements

The authors are grateful to the University of the Witwatersrand and the H.E. Griffin Trust for their financial support in carrying out this research. We also thank the Jan Boeyens Structural Chemistry laboratory at the University of the Witwatersrand for the use of their computational facilities.

References

[1] J.L. Hall, W.E. Dean, J. Am. Chem. Soc. 82 (1960) 3300.
[2] J.L. Hall, W.E. Dean, E.A. Pacofsky, J. Am. Chem. Soc. 82 (1960) 3303.
[3] M. Orama, H. Saarinen, L. Kaila, Finn. Chem. Lett. (1979) 182.
[4] O. Orama, M. Orama, U. Schubert, Finn. Chem. Lett. 1 (1979) 136.
[5] Bruker, SMART-NT, Version 5.050, Bruker AXS Inc., Madison, WI, USA, 1998.
[6] Bruker, SAINT+, Version 6.02 (includes XPREP and SADABS), Bruker AXS Inc., Madison, WI, USA, 1999.
[7] G.M. Sheldrick, SADABS, University of Göttingen, Germany, 1996.
[8] Bruker, SHELXTL, Version 5.1, (includes XS, XL, XP, XSHELL) Bruker AXS Inc., Madison, WI, USA, 1999.
[9] A.L. Spek, Acta Crystallogr., Sect. A 46 (1990) C-34.
[10] D.F. Evans, J. Parr, S. Rahman, A.M.Z. Slawin, D.J. Williams, C.Y. Wong, J.D. Wollins, Polyhedron 12 (1993) 337.
[11] I.N. Polykova, A.L. Poznyak, V.S. Sergienko, Crystallogr. Rep. 45 (2000) 35.
[12] G.J. McDougall, R.D. Hancock, J. Chem. Soc., Dalton Trans. (1980) 654.
[13] E.J. Corey, J.C. Bailar, J. Am. Chem. Soc. 81 (1959) 2620.
[14] R.D. Hancock, Prog. Inorg. Chem. 37 (1990) 187.
[15] R.D. Hancock, P.W. Wade, M.P. Ngwenya, A.S. de Sousa, K.V. Damu, Inorg. Chem. 39 (1990) 1968.
[16] B.P. Hay, J.R. Rustad, C. Hostetler, J. Am. Chem. Soc. 115 (1993) 11158.
[17] A.E. Martell, R.D. Hancock, Metal Complexes in Aqueous Solution, Plenum Press, New York, 1996, p. 77.
[18] A.E. Martell, R.M. Smith, Critical Stability Constants, vol. 1–6, Plenum Press, New York, 1974–1988.
[19] R.D. Hancock, H. Maumela, A.S. de Sousa, Coord. Chem. Rev. 148 (1996) 315.
[20] R.D. Hancock, Analyst 122 (1997) 51R.

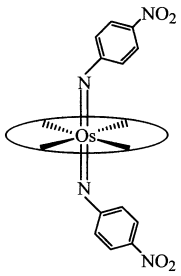


Fig. 1. Drawing of $Os(TTP)(NC_6H_4NO_2)_2$. For clarity, the porphyrin ring is depicted as an ellipse.

received. The alkenes were distilled under nitrogen or recrystallized prior to use. Ultraviolet–Visible (UV–Vis) spectra were recorded with a Hewlett Packard 8452A diode array spectrophotometer. The temperature of the cell compartment was maintained to ± 0.2 °C using a constant temperature bath. Gas chromatography/mass spectrometry (GC–MS) data was obtained with a Hewlett Packard 5890 Series II gas chromatograph.

2.1. Reaction with phosphines, PY_3

Toluene solutions of $Os(TTP)(NC_6H_4NO_2)_2$ and $PMe_{3-x}Ph_x$ ($x = 0$, 1, 2, 3) or $P(OMe)_2Ph$ were allowed to reach thermal equilibrium in a constant temperature bath prior to each run. After equilibration to the desired temperature, the solutions were combined in a cuvette that had also been thermally equilibrated. The rate of the reaction was followed by monitoring the decrease in absorbance of $Os(TTP)(NC_6H_4NO_2)_2$ at 576 nm. The initial concentration of $Os(TTP)(NC_6H_4NO_2)_2$ was 7.5×10^{-5} M. The reactions were run under pseudo first order conditions with $[PY_3] \gg Os(TTP)(NC_6H_4NO_2)_2$. The initial concentration of phosphine was varied between 0.01 and 0.29 M. Although the solutions were typically prepared in a glovebag under 1 atm. of N_2, the same kinetic data was obtained if the solutions were prepared under 1 atm. of air.

2.2. Reaction with alkenes

All reactions were performed under nitrogen. The alkenes studied were dimethyl fumarate, styrene, *cis*-cyclooctene, and 2,3-dimethylbutene. Three reaction conditions were examined. In each case, approximately 500 equiv. of alkene were used. The first set of conditions involved the combination of alkene and $Os(TTP)(NC_6H_4NO_2)_2$ in C_6H_{14} or $C_6H_5CH_3$ at room temperature. Since no reaction was observed by thin layer chromatography or by UV–Vis spectroscopy after 4 h, the solutions were heated to reflux and the reactions were monitored for an additional 2 h. The third set of conditions involved the combination of alkene and $Os(TTP)(NC_6H_4NO_2)_2$ in C_6H_6 or $C_6H_5CH_3$ followed by irradiation with a 450 W Hanovia lamp for 1 h.

3. Results and discussion

Reactivity studies of $Os(TTP)(NC_6H_4NO_2)_2$ suggest the two *p*-nitrophenyl imido ligands coordinated to the osmium porphyrin are mildly electrophilic in character. Treatment of $Os(TTP)(NC_6H_4NO_2)_2$ with excess phosphine, PY_3, yields $Os(TTP)(PY_3)_2$ [17] and the corresponding phosphinimine identified by GC–MS.

$$Os(TTP)(NC_6H_4NO_2)_2 + \text{excess } PY_3 \rightarrow Os(TTP)(PY_3)_2 + 2O_2NC_6H_4N{=}PY_3$$

Clean isosbestic points at 419 and 431 nm indicate the absence of any long-lived intermediate.

The kinetics of the reaction were studied by monitoring the decrease in absorbance of $Os(TTP)(NC_6H_4NO_2)_2$ at 576 nm. At this wavelength, $Os(TTP)(NC_6H_4NO_2)_2$ has a modest absorption ($\log \varepsilon = 4.4$) [16] whereas $Os(TTP)(PY_3)_2$ does not absorb. The reaction was performed under pseudo first order conditions with $[PY_3] \gg Os(TTP)(NC_6H_4NO_2)_2$. Plots of $\ln|A_t - A_\infty|$ versus time were linear over four half lives with slopes equal to the pseudo first order rate constant, k_{obs}, where A_t is the absorbance at time t and A_∞ is the absorbance once the reaction has reached completion. Under the reaction conditions described, no loss in absorbance of $Os(TTP)(NC_6H_4NO_2)_2$ was observed in the absence of PY_3. At each concentration of PY_3, two or three independent runs were performed and the average k_{obs} was calculated. Plots of average k_{obs} versus $[PY_3]$ were linear with slopes equal to the second-order rate constants, k_2, Table 1. Saturation kinetics was not observed even at high PY_3 concentrations, $[PY_3] = 0.20$ M. The lack of saturation kinetics suggests an initial equilibrium to form an adduct between $Os(TTP)(NC_6H_4NO_2)_2$ and PY_3 does not occur, or if it does, reactants are highly favored and the equilibrium constant is small.

The enthalpies, $\Delta H^\ddagger$, and entropies, $\Delta S^\ddagger$, of activation for PMe_2Ph and $PMePh_2$ were determined by measuring k_2 at three different temperatures and using the Eyring equation. A plot of $\ln(k_2/T)$ versus $1/T$ yields a slope equal to $-\Delta H^\ddagger/R$, where R is the universal gas constant, and a y-intercept equal to the sum of $\ln(k'/$

Table 1

PY_3	$10^4\ k_2$ ($M^{-1}\ s^{-1}$) [a]	θ (°) [b]	pK_a [c]	pK_a' [d]
PMe_3	253 ± 7	118	8.65	6.45
$P(OMe)_2Ph$	7 ± 1	120	2.64	1.48
PMe_2Ph	198 ± 4	122	6.50	5.07
$PMePh_2$	24 ± 2	136	4.57	4.06
PPh_3	2.5 ± 0.3	145	2.73	3.28

[a] At 298 K.
[b] Ref. [19].
[c] Ref. [21].
[d] Ref. [22].

h) and $\Delta S^{\ddagger}/R$ where k' is Boltzmann's constant and h is Planck's constant. The enthalpies of activation were 42 ± 1 and 25 ± 1 kJ mol^{-1} and the entropies of activation were -135 ± 20 and -210 ± 20 J mol^{-1} K^{-1} for PMe_2Ph and $PMePh_2$, respectively. Due to experimental difficulties such as the high volatility of PMe_3 and the slowness of reaction for PPh_3 and $P(OMe)_2Ph$, activation parameters were not determined for the other phosphines. The negative values for the entropies of activation are consistent with an associative mechanism [18].

Several authors have examined the relationship between rate constants for associative reactions involving phosphine nucleophiles and the stereoelectronic properties of phosphines [19–22]. In general, data for these reactions give a good fit to the following relationship:

$$\log k_2 = \alpha + \beta X + \gamma\theta$$

The first term, α, is related to the intrinsic reactivity of the metal complex. The second term, βX, is related to the electronic properties of the incoming phosphine, and the third term, $\gamma\theta$, where θ is Tolman's cone angle [19], is related to the steric properties of the phosphine. In early studies, pK_a values were used for X [19,20]. However, the use of this term as a measure of basicity was found insufficient [21,22]. More recent analyses have used values of χ [21] or pK_a' [22] for X. χ values are derived from infrared data whereas pK_a' values are derived from pK_a values, corrected for hydration effects. In all cases, the protocol for stereoelectronic analysis involves plotting log k_2 versus X (where $X = pK_a$, χ, or pK_a') for isosteric or nearly isosteric phosphines. The resulting plot is called an electronic profile and since the nucleophiles used have identical or nearly identical cone angles, γ can be assumed to be zero and the slope equals β. A subsequent plot of (log $k_2-\beta X$) versus θ yields a steric profile. In systems where steric effects are important, the steric profile has a horizontal region at low values of θ for nucleophiles small enough not to show any steric effects, i.e. phosphines with cone angle below some threshold cone angle, $\theta < \theta_{th}$, followed by a region with a linear downward slope for phosphines with cone angles above the threshold angle, $\theta > \theta_{th}$ [21,22].

Using the analysis suggested by Chen and Poë [22], an electronic profile was prepared by plotting log k_2 versus pK_a' (Fig. 2), for the nearly isosteric phosphines, PMe_3, $P(OMe)_2Ph$, and PMe_2Ph. The non-zero slope in Fig. 2 indicates the basicity of PY_3 affects the rate of imido ligand transfer. $P(OMe)_2Ph$, the least basic of the three isosteric phosphines, exhibits a much smaller k_2 than PMe_3 or PMe_2Ph. The slope of this line equals β. Deviations from linearity may be due to experimental design. All of the PY_3 solutions were prepared from neat reagents except for the PMe_3 solutions, which were prepared from a purchased 1.0 M solution. The true concentration of this solution was not confirmed and

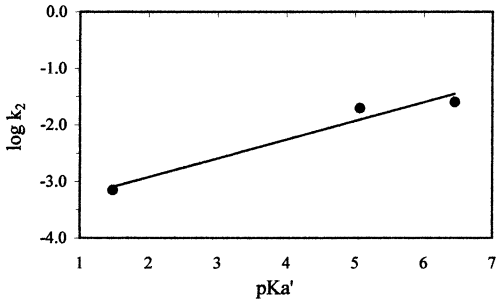


Fig. 2. Electronic profile, plot of log k_2 versus pK_a'.

may have been less than 1.0 M due to the high volatility of PMe_3. In this case, a smaller than expected k_2 value would be observed.

A subsequent plot of log k_2^{o} [22] versus θ was prepared (Fig. 3). The shape of this steric profile indicates the steric properties of the incoming nucleophile affect the rate of imido ligand transfer. If steric properties were not important, all of the data points would lie on a horizontal line. An estimate for the threshold cone angle (125°) is the intersection of the horizontal and downward sloping parts of the steric profile [22].

Similar stereoelectronic analyses have been reported for oxo ligand transfer to PY_3 from an oxorhenium(VII) complex [23], a molybdenum dithiolene species [24], and *trans*-$Ru(TMP)O_2$ [25] where TMP is the dianion of 5,10,15,20-tetramesitylporphyrin. However, this type of stereoelectronic analysis has not been reported for imido ligand transfer to PY_3. Although osmium imido complexes are relatively common and several are known to transfer their imido ligands to phosphines [11,14], no kinetic studies have been reported. A kinetic study has been reported for the reaction of PMe_2Ph and a ruthenium porphyrin complex possessing one imido ligand, Ru(tbpp)(NR) where tbpp is the dianion of 5,10,15,20-tetrakis(p-*tert*-butylphenyl)porphyrin [10]. Using similar concentrations of complex as used in this study, the reaction demonstrates saturation kinetics at relatively low phosphine concentrations, [PMe_2Ph] < 0.002 M. The proposed mechanism for the ruthenium system involves reversible binding of the phosphine to

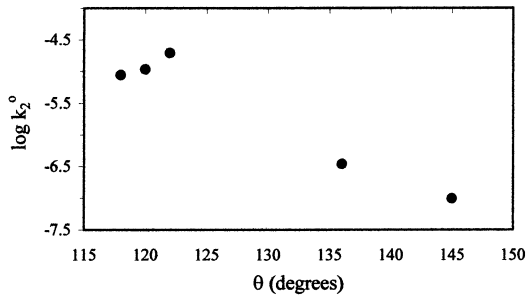


Fig. 3. Steric profile, plot of log k_2^{o} versus θ where log k_2^{o} equals log $k_2-\beta$ (p$K_a'+4$) [22].

the nitrogen of the imido ligand followed by a rate-limiting irreversible intramolecular imido-group transfer. Since only one phosphine was examined, a stereoelectronic analysis could not be performed.

Although $Os(TTP)(NC_6H_4NO_2)_2$ transferred the *p*-nitrophenyl imido ligands to phosphines, no reaction was observed with a variety of alkenes. Four alkenes were studied and varied from electron poor dimethyl fumarate to electron rich 2,3-dimethylbutene. No reaction was observed with 500 equiv. of alkenes at room temperature, at refluxing hexane or toluene, or photolysis with an ultraviolet lamp.

These results suggest the two *p*-nitrophenyl imido ligands coordinated to the osmium(VI) porphyrin are mildly electrophilic in character. Upon addition of a good nucleophile such as PY_3, imido ligand transfer occurs to form a phosphinimine and $Os(TTP)(PY_3)_2$. Both the basicity and the steric properties of PY_3 affect the rate of reaction with the most basic, least sterically hindered phosphines yielding the fastest rates of reaction. Imido ligand transfer does not occur to alkenes. This reactivity is similar to the reactivity of other osmium imido [11,14] complexes whereby reactions only occur with good nucleophiles. In contrast, ruthenium imido complexes are known to react with both phosphines [10] and alkenes [12].

Acknowledgements

This research was supported by the Petroleum Research Fund of the American Chemical Society (Grants 28303-B3 and 33991-B3).

References

[1] W.A. Nugent, J.M. Mayer, Metal-Ligand Multiple Bonds, Wiley-Interscience, New York, 1988, p. 21.
[2] P. Müller, Advances in Catalytic Processes 2 (1997) 113.
[3] J.P. Mahy, G. Bedi, P. Battioni, D. Mansuy, J. Chem. Soc., Perkin Trans II (1988) 1517.
[4] T.S. Lai, H.L. Kwong, C.M. Che, S.M. Peng, J. Chem. Soc., Chem. Commun. (1997) 2373.
[5] S. Cenini, S. Tollari, A. Penoni, C. Cereda, J. Mol. Catal. A: Chem. 137 (1999) 135.
[6] P. Müller, C. Baud, Y. Jacquier, Can. J. Chem. 76 (1998) 738.
[7] M.M. Díaz-Requejo, P.J. Pérez, M. Brookhart, J.L. Templeton, Organometallics 16 (1997) 4399.
[8] Z. Li, R.W. Quan, E.N. Jacobsen, J. Am. Chem. Soc. 117 (1995) 5889.
[9] D.A. Evans, M.M. Faul, M.T. Bilodeau, J. Am. Chem. Soc. 116 (1994) 2742.
[10] W.H. Leung, T.S.M. Hun, H.W. Hou, K.Y. Wong, J. Chem. Soc., Dalton Trans. (1997) 237.
[11] S.M. Au, W.H. Fung, J.S. Huang, K.K. Cheung, C.M. Che, Inorg. Chem. 37 (1998) 6564.
[12] S.M. Au, J.S. Huang, W.Y. Yu, W.H. Fung, C.M. Che, J. Am. Chem. Soc. 121 (1999) 9120.
[13] B. Moubaraki, K.S. Murray, P.J. Nichols, S. Thomson, B.O. West, Polyhedron 13 (1994) 485.
[14] (a) P.A. Shapley, J.M. Shusta, J.L. Hunt, Organometallics 15 (1996) 1622;
(b) R.I. Michelman, R.G. Bergman, R.A. Andersen, Organometallics 12 (1993) 2741;
(c) J.T. Anhaus, T.P. Kee, M.H. Schofield, R.R. Schrock, J. Am. Chem. Soc. 112 (1990) 1642.
[15] (a) W.H. Leung, M.C. Wu, T.C. Lau, W.T. Wong, Inorg. Chem. 34 (1995) 4271;
(b) D.A. Dobbs, R.G. Bergman, Organometallics 13 (1994) 4594;
(c) E.W. Harlan, R.H. Holm, J. Am. Chem. Soc. 112 (1990) 186;
(d) H.F. Sleiman, S. Mercer, L. McElwee-White, J. Am. Chem. Soc. 111 (1989) 8007.
[16] J.A. Smieja, K.M. Omberg, G.L. Breneman, Inorg. Chem. 33 (1994) 614.
[17] C.M. Che, T.F. Lai, W.C. Chung, W.P. Schaefer, H.B. Gray, Inorg. Chem. 26 (1987) 3907.
[18] J.D. Atwood, Inorganic and Organometallic Reaction Mechanisms, Brooks/Cole, Pacific Grove, CA, 1985, p. 17.
[19] C.A. Tolman, Chem. Rev. 77 (1977) 313.
[20] P.M. Zizelman, C. Amatore, J.K. Kochi, J. Am. Chem. Soc. 106 (1984) 3771.
[21] (a) H.Y. Liu, K. Eriks, A. Prock, W.P. Giering, Organometallics 9 (1990) 1758;
(b) M.N. Golovin, M.M. Rahman, J.E. Belmonte, W.P. Giering, Organometallics 4 (1985) 1981.
[22] L. Chen, A.J. Poë, Coord. Chem. Rev. 143 (1995) 265.
[23] W.D. Wang, I.A. Guzei, J.H. Espenson, Organometallics 20 (2001) 148.
[24] C. Lorber, M.R. Plutino, L.I. Elding, E. Norglander, J. Chem. Soc., Dalton Trans. (1997) 3997.
[25] S.Y.S. Cheng, B.R. James, J. Mol. Catal. A: Chem. 117 (1997) 91.

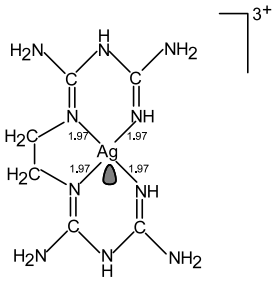


Fig. 1. Structure of $[Ag(enbbg)]^{3+}$. Bond lengths are in Å. ● is weakly bonded ClO_4^- ion at the axial site.

sulfate (G.R., E. Merck) with barium nitrate (G.R., E. Merck) and standardised by oxidation with $KBrO_3$ in presence of dilute H_2SO_4 [19]. We found this solution to be stable for at least 6 months when kept at low temperature ($\sim$5–10 °C) and in dark. Aqueous solutions of $NaNO_3$ (G.R., E. Merck) was standardised by passing through a Dowex 50W X-8 strong cation exchange resin in the H^+ form and titrating the liberated acid with standard NaOH to a phenolphthalein end-point. All measurements were made at 25 °C and $I = 1.0$ mol dm^{-3} ($NaNO_3$). All solutions were prepared in water which was deionised and then double distilled.

2.2. Physical measurements and kinetics

All absorbance versus time data were recorded with a Shimadzu (1601 PC) spectrophotometer using 1.00 cm quartz cells. The kinetics was monitored in situ in the 'kinetic mode' of the instrument at 420 nm in the electrically controlled thermostated (25.0 ± 0.1 °C) cell-housing (CPS-240A). In this mode the change in absorbance is automatically and continuously recorded. Hydroxylamine solution (adjusted to the desired pH) was directly injected in to the spectrophotometer cell containing other components of the reaction mixture kept at the same pH. The desired concentration of the complex and reducing agent was achieved after mixing. The ionic strength (I) was maintained at 1.0 mol dm^{-3} ($NaNO_3$). The solution pH values were adjusted with $HClO_4$ or NaOH. Although the measured pH is usually defined in terms of the activity of hydrogen ions, we used the hydrogen ion concentration by calibrating the pH electrode with analytically prepared solutions as described earlier [20].

2.3. Stoichiometric measurements

The stoichiometry was measured under kinetic conditions by estimating excess hydroxylamine spectrophotometrically. Excess hydroxylamine was mixed with the complex in the pH range 4.0–6.0. After the reaction mixtures turned colourless indicating complete reduction of Ag(III) to Ag(I), pH of the mixtures were made to $\sim$2. A solution of $Fe_2(SO_4)_3$ at pH $\sim$ 2 was then added in each set and after a few minutes excess 2,2′-bipyridyl solution (at pH $\sim$ 2) was added. The resulting red $[Fe(bipy)_3]^{2+}$, generated by the quantitative reduction of excess Fe(III) by hydroxylamine was measured [21] at 523 nm ($\varepsilon = 8500$ dm^3 mol^{-1} cm^{-1}) after proper dilution.

3. Results and discussions

3.1. Preliminary observations

Within the time span of the reactions the autodecomposition [22] of the silver(III) complex is insignificant. No silver(I) catalysis was found in the reactions below pH $\sim$ 5.0. Above this pH, addition of $AgNO_3$ in the reaction mixture produces a faint blackish suspension probably due to metallic silver and/or silver oxide and thus Ag^+ catalysis, if any, was examined below pH $\sim$ 5.0. No external buffer was used in the kinetic measurements since buffering (by acetate for example) affects the spectra of the complex; specific interaction of buffer with the complex was thus indicated. Even in the absence of an external buffer, the media pH before and after the reactions did not change by more than 0.05 units.

3.2. Stoichiometry and reaction products

Stoichiometric experiments under kinetic conditions indicate 1:1 reaction between the redox partners (Table 1). The principal conversion may then be represented by Eq. (1).

$$2Ag(III) + 2NH_2OH \rightarrow 2Ag(I) + N_2O + H_2O + 4H^+ \quad (1)$$

Immediately after completion of reaction (absorbance < 0.01 at 380 nm), all Ag^+ was precipitated as AgCl and removed by filtration. From the filtrate, the free ligand, ethylenebis(biguanide), was quantitatively isolated [23] as the sparingly soluble [ethylenebis(biguanide)]copper(II) sulfate, and the amount of Cu(II) thus held was estimated iodometrically after decomposing the Cu(II) complex. The results showed that more than 95% of the free ligand (H_2L) was recovered.

The complicated redox chemistry of hydroxylamine in solution has been studied extensively [15]. It was observed that hydroxylamine is most commonly oxidised to N_2O [24–26]. Oxidation to N_2, NO_2^-, NO_3^- and NO are relatively rare [16,24–26]. ESR spectroscopy has established the formation of the $H_2NO^\bullet$ radical in the oxidation of NH_2OH with one-electron oxidants [27]. The ultimate oxidation product varies depending on the mode of decay (Eq. (3)) of $H_2NO^\bullet$

Table 1
Stoichiometric results for the oxidation of N(−I) by the silver (III) complex [a]

$[Ag(III)]_T$ (mmol dm^{-3})	$[N(-I)]_T$ (mmol dm^{-3})	pH	$[N(-I)]_{left}$ (mmol dm^{-3})	$\Delta[N(-I)]_T/\Delta[Ag(III)]_T$
0.15	0.30	3.8	0.17	0.87
	0.40	4.0	0.26	0.93
	0.50	4.9	0.34	1.07
0.30	0.80	5.0	0.48	1.07
	1.20	4.6	0.94	0.87
0.50	1.00	4.9	0.52	0.96
	1.50	3.9	1.05	0.90
				Average = 0.97 ± 0.10.

[a] $T = 25.0$ °C; $I = 1.0$ mol dm^{-3} ($NaNO_3$).

radical under different conditions [15]. Thus $H_2NO^{\bullet}$ may decay to N_2 (Eq. (2)) or may be further oxidised (Eq. (3)) to HNO, which dimerises to *cis*- and *trans*-hyponitrous acid [28]. The *trans* form is more stable than the *cis*- form, decomposes into N_2O [29]. With strong oxidants such as Mn^{3+}(aq) or Ag^{2+}(aq), present in excess, the free radical is further oxidised to NO_3^- [30].

$$H_2NO^{\bullet} \rightarrow 0.5N_2 + H_2O \quad (2)$$

$$H_2NO^{\bullet} \rightarrow HNO + H^+ + e^- \quad (3)$$

$$2HNO \rightarrow H_2N_2O_2 \rightarrow N_2O + H_2O \quad (4)$$

Thermodynamic oxidising strength of the title complex under investigation is moderate [4,11]. Hence N(III) or N(V) is not an expected oxidation product.

3.3. Kinetics

No immediate spectral change was observed on mixing hydroxylamine with the Ag(III) complex over the entire range of experimental pH. However, the absorbance at $\lambda \geq 380$ nm gradually decreases to less than 0.01. Trace metal ions [31] in solution strongly catalyse the oxidation of hydroxylamine and affects both rate and the oxidation product. Ambient light sometime also plays a definite role [32]. We measured some k_0 values in presence of added ethylenebis(biguanide) [1.0 mmol dm^{-3}] and found to be identical with its absence within experimental uncertainties, and we observed no effect of diffused light in our system. The $\log_{10}$(absorbance) versus time plots were found to be linear for more than 90% of reactions and the pseudo first-order rate constants, k_0, defined by Eq. (5) were obtained from the least-squares slopes of these plots.

$$-d[Ag(III)]/dt = k_0[Ag(III)] \quad (5)$$

Any initial drop in absorbance for faster reactions can be computed from the time of mixing of solutions (~ 4 s) and the observed first-order rate constants. Averages of the k_0 values from at least three runs were taken and individual runs were reproducible within 3%. Detailed data of the kinetics of the process were obtained as a function of pH and total NH_2OH (defined as $[N(-I)]_T$, which is $[NH_2OH]+[NH_3OH^+]$) and some representative data are summarised in Table 2. Over the entire pH range studied the reaction shows a clear first-order dependence on $[N(-I)]_T$ and there is no $[N(-I)]_T$ independent term. The following changes in the reaction conditions had, within the limits of experimental uncertainties, no influence on the values of k_0: a fivefold variation in [Ag(III)] from 0.1 to 0.5 mmol dm^{-3}, addition of $AgNO_3$ (studied up to 0.01 mol dm^{-3}), variation of ionic strength maintained by $NaNO_3$ or $NaClO_4$ in the range 0.1–1.0 mol dm^{-3}, the occasional shaking of the spectrophotometer cell, presence or

Table 2
First-order rate constants for the oxidation of N(−I) by the Ag(III) complex [a]

pH	$[N(-I)]_T$ (mmol dm^{-3})	$10^4\ k_0$ (s^{-1})
3.00	3.0	0.57
3.10		0.71
3.25		0.98
3.45		1.49
3.73		2.65
4.00		4.58
4.35		9.25
4.60		15.4
4.93		29.9
5.21		51.0
5.55		89.0
5.85		129
6.05		152
6.30		169
6.65		168
6.92		159
7.15		150
7.30		145
3.10	6.0	1.40
3.25	12.0	4.05
4.00	6.0	9.25
4.00	12.0	18.0
4.00	18.0	26.8
4.00	30.0	47.0
6.65	1.5	82.2

[a] $T = 25.0$ °C, $I = 1.0$ mol dm^{-3}; [complex] = 0.15 mmol dm^{-3}.

absence of dissolved oxygen, and a variation in the monitoring wavelength in the range 380–480 nm.

No polymer is formed when 6% (v/v) acrylonitrile is added to the reaction mixture and whole reaction course is epr silent. There is thus no evidence for the formation of detectable amounts of free radicals or other paramagnetic species during the reaction. However, one can not conclude from these observations as to whether the reactions of Ag(III) with hydroxylamine are one or two electron processes, because the radicals produced from one-electron oxidation of hydroxylamine may react in a very fast manner with Ag(III) before they can escape into the bulk solvent, thus evading detection.

A plot of k_0 versus pH has a bell shape (Fig. 2). Such a pH dependence indicates the involvement of two or more acid–base equilibria [33]. Considering the values for the acid dissociation constants of the complex in aqueous solution [34] (K_{a_1} and K_{a_2}, which are 1.58×10^{-4} and 5.01×10^{-7} mol dm^{-3}, respectively) and K_a ($= 1.0 \times 10^{-6}$ mol dm^{-3}), the acid dissociation constant [35] of NH_3OH^+, the scheme in Eqs. (3)–(8) provide a reasonable explanation for the kinetic observations.

$$[Ag(H_2L)]^{3+} \overset{K_{a_1}}{\rightleftharpoons} [Ag(HL)^{2+} + H^+ \quad (6)$$

$$[Ag(HL)]^{2+} \overset{K_{a_2}}{\rightleftharpoons} [AgL]^+ + H^+ \quad (7)$$

$$NH_3OH^+ \overset{K_a}{\rightleftharpoons} NH_2OH + H^+ \quad (8)$$

$$[Ag(H_2L)]^{3+} + NH_2OH \overset{k_1}{\rightarrow} \text{Products} \quad (9)$$

$$[Ag(HL)]^{2+} + NH_2OH \overset{k_2}{\rightarrow} \text{Products} \quad (10)$$

$$[AgL]^+ + NH_2OH \overset{k_3}{\rightarrow} \text{Products} \quad (11)$$

From these, expression (12) can be derived where the fraction of the complex present as $[Ag(H_2L)]^{3+}$ is given by Eq. (13) and the fraction of $[N(-I)]_T$ present as NH_2OH is given by Eq. (14).

$$k_0[H^+]^2/([N(-I)]_T\alpha_1\alpha_2) = k_1[H^+]^2 + k_2K_{a_1}[H^+] + k_3K_{a_1}K_{a_2} \quad (12)$$

$$\alpha_1 = [H^+]^2/([H^+]^2 + K_{a_1}[H^+] + K_{a_1}K_{a_2} \quad (13)$$

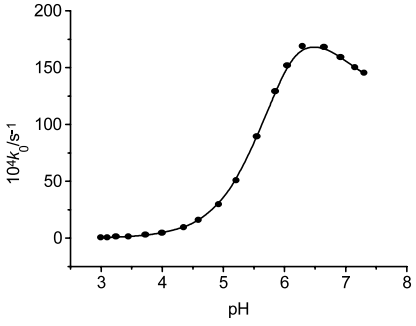


Fig. 2. Dependence of k_0 on pH at 25.0 °C, $[Ag(III)]_T = 0.15$ mmol dm^{-3}, $[N(-I)]_T = 3.0$ mmol dm^{-3}, $I = 1.0$ mol dm^{-3} ($NaNO_3$). The solid line represents the fit of Eq. (12).

$$\alpha_2 = K_a/(K_a + [H^+]) \quad (14)$$

Non-linear fitting of left-hand-side of Eq. (12) with $[H^+]$ yielded k_1, $k_2K_{a_1}$ and $k_3K_{a_1}K_{a_2}$. Using known values of K_{a_1} and K_{a_2}, the rate constants k_2 and k_3 were evaluated. All these second-order rate constants are presented in Table 3 which reproduced all k_0 within 5%.

It may also be noted that in the pH interval 3.00–4.60, the second dissociation of the Ag(III) complex (K_{a_2}) can be neglected and Eqs. (9) and (10) are sufficient to represent the observed first-order rate constants. On the other hand, in the higher pH range 6.30–7.30 the first dissociation of the Ag(III) complex (K_{a_1}) can be neglected and only Eqs. (10) and (11) may account for the observed situation. The second-order rate constants evaluated in this manner agreed nicely with the values represented in Table 3 within 7%.

3.4. Mechanism

The observed sequence $k_1 > k_2 > k_3$ indicates that protonation of the oxidant increases its kinetic reactivity whereas the opposite is true for protonation of the reductant. Majority of the other known redox systems also follow a similar trend [36,37]. The trend was observed earlier for the oxidation [12] of N(III) with the title Ag(III) complex. In the present investigation we found that the conjugate acid NH_3OH^+ is kinetically inactive towards the Ag(III) complexes under investigation and its conjugate bases, whereas HNO_2 was active, though to a much lesser extent than NO_2^- towards the reduction of the Ag(III) complex. We anticipate that an unfavourable charge interaction between the cationic silver(III) complexes with NH_3OH^+ makes the situation a different one. A molecule with a free electron pair should have a greater affinity for cation than would another positively charged ion.

One may use Marcus cross relation [38], $k_{12} = (k_{11}k_{22}K)^{1/2}$ to identify the nature of electron transfer. The equilibrium constant K of the one-electron transfer between $[Ag(H_2L)]^{3+}$ and NH_2OH may be calculated from the known redox potentials of $[Ag(H_2L)]^{3+/2+}$ couple (0.43 V) [4,11] and NH_2OH–NH_2OH^+ (−0.42 V) [39]. The self-exchange rate constant for the couple NH_2OH–NH_2OH^+ is 5×10^{-13} dm^3 mol^{-1} s^{-1} [39] and the maximum possible self-exchange rate for

Table 3
Second-order rate constants (in dm^3 mol^{-1} s^{-1}) for the oxidation of N(−I) by the Ag(III) complex [a]

Reaction	Rate constant
$[Ag(H_2L)]^{3+} + NH_2OH$	$k_1 = 20.1 \pm 1.0$
$[Ag(HL)]^{2+} + NH_2OH$	$k_2 = 12.5 \pm 0.60$
$[AgL]^+ + NH_2OH$	$k_3 = 4.35 \pm 0.50$

[a] [Complex] = 0.15 mmol dm^{-3}, $I = 1.0$ mol dm^{-3} ($NaNO_3$), $T = 25.0$ °C.

$[Ag(H_2L)]^{3+/2+}$ couple is $10^{6.6}$ [13]. Using these values, the calculated maximum value of k_{12} becomes $\sim 1.7 \times 10^{-3}$ dm^3 mol^{-1} s^{-1}, much lower than the experimentally observed value (20.1 dm^3 mol^{-1} s^{-1}), which refutes one-electron outer sphere pathway as the rate-determining step. This is not unexpected in light of the remarkably low NH_2OH–NH_2OH^+ self-exchange rate coupled with a near zero E° value for the one electron reaction.

It is well documented that hydroxylamine (NH_2OH) can co-ordinate to higher valent metal ions [40–42]. The electron affinity of the Ag(III) in the present complex is high [43] as established by X-ray photoelectron spectroscopic measurements that the Ag(III) centre has a high degree of positive charge and it is known from structural [44–46] and kinetic [6,7] studies that the complex undergoes axial co-ordination with alcohols, H_2O_2, SO_4^{2-}, NO_3^- or even ClO_4^-. We thus anticipate a similar co-ordination of NH_2OH to the Ag(III) centre and subsequent electron transfer.

4. Conclusions

Reduction of the complex cation $[Ag(H_2L)]^{3+}$ may proceed via a Ag^+- catalysed path and/or an uncatalysed path depending on the nature of the reductant. Only the uncatalysed path is detectable in the oxidation of N(−I), N(III) [12], alcohols [6], ascorbic acid [10] and Fe^{2+}(aq) [11] by this complex. The catalysed path involves a Ag^+–Ag^0 cycle (for HCO_2H [5], $N_2H_5^+$ [8] and H_3PO_2 [9]) or a Ag(I)–Ag(II) cycle (for H_2O_2 [7]). Predominance of the uncatalysed or catalysed path depends on a critical balance of thermodynamic and also on kinetic factors, but grossly speaking when the reductant is powerful [47] like HCO_2H, $N_2H_5^+$ or H_3PO_2 or a good ligand for Ag(III), then catalysed path dominates. We observed that below pH $\sim$ 5.0 hydroxylamine does not react with Ag^+ over a long period and we observed no Ag^+ catalysis in our reactions. Below pH 3.0, hydroxylamine was found to be kinetically inactive towards the reduction of the title complex which indicates absence of any possible $[Ag(H_2L)]^{3+}$–NH_3OH^+ path. We found that NH_3OH^+ is kinetically inactive but the conjugate base, NH_2OH, a neutral species reacts with the charged Ag(III) complexes. An indirect outcome of these types of reacting species may be the innocent influence of media ionic strength on the rate of reactions. All the reaction paths k_1, k_2 and k_3 possibly involve inner-sphere processes. It cannot be concluded at this stage whether the reaction involves one- or two-electron changes.

Acknowledgements

We are grateful to Professor L.J. Kirschenbaum, University of Rhode Island, Kingston RI 02881, for many suggestions. Financial assistance from Departmental Special Assistance (DSA) Programme in Chemistry, Jadavpur University from University Grants Commission (New Delhi) is thankfully acknowledged.

References

[1] P. Ray, Nature (London) 151 (1943) 643.
[2] P.J. Blower, J.R. Dilworth, Coord. Chem. Rev. 76 (1987) 121.
[3] D. Sen, N.N. Ghosh, P. Ray, J. Indian Chem. Soc. 27 (1950) 619.
[4] K. Das, R. Banerjee, A. Das, S. Dasgupta, Bull. Electrochem. 5 (1989) 477.
[5] R. Banerjee, K. Das, A. Das, S. Dasgupta, Inorg. Chem. 28 (1989) 585.
[6] R. Banerjee, A. Das, S. Dasgupta, J. Chem. Soc., Dalton Trans. (1990) 1207.
[7] R. Banerjee, A. Das, S. Dasgupta, J. Chem. Soc., Dalton Trans. (1989) 1645.
[8] R. Banerjee, A. Das, S. Dasgupta, J. Chem. Soc., Dalton Trans. (1990) 2271.
[9] R. Banerjee, R. Das, S. Mukhopadhyay, J. Chem. Soc., Dalton Trans. (1992) 1317.
[10] S. Dasgupta, E. Herlinger, W. Linert, J. Chem. Soc., Dalton Trans. (1993) 567.
[11] R. Banerjee, Proc. Indian Acad. Sci. (Chem. Sci.) 106 (1994) 655.
[12] S. Mukhopadhyay, R. Banerjee, J. Chem. Soc., Dalton Trans. (1994) 1349.
[13] S.P. Ghosh, M.C. Ghosh, E.S. Gould, Inorg. Chim. Acta 225 (1994) 83.
[14] S. Mukhopadhyay, S. Kundu, R. Banerjee, Proc. Indian Acad. Sci. (Chem. Sci.) 107 (1995) 403.
[15] K. Wieghardt, Advances in Inorganic and Bioinorganic Mechanisms, vol. 3, Academic Press, New York, 1984, p. 213.
[16] R.A. Scott, G.P. Haight, Jr., J.N. Cooper, J. Am. Chem. Soc. 96 (1974) 4136.
[17] L.J. Kirschenbaum, Personal communication.
[18] (a) P. Ray, K. Chakravarty, J. Indian Chem. Soc. 21 (1944) 47; (b) P. Ray, Inorg. Synth. 6 (1960) 74.
[19] A.I. Vogel, A Text Book of Quantitative Inorganic Analysis including Elementary Instrumental Analysis, 3rd ed., The English Language Book Society and Longmans, Green & Co, London, 1961, p. 391.
[20] S. Banerjee, U. Roy Choudhury, B.C. Ray, R. Banerjee, S. Mukhopadhyay, Anal. Lett. 34 (2001) 2797.
[21] R.L. Davies, K.W. Dunning, J. Chem. Soc. (1965) 4168.
[22] R. Banerjee, D. Banerjea, Indian J. Chem. 17A (1979) 246.
[23] P. Ray, Chem. Rev. 61 (1961) 313.
[24] F.T. Bonner, N.Y. Wang, Inorg. Chem. 25 (1986) 1858.
[25] (a) R.M. Liu, M.R. McDonaldand, D.W. Margerum, Inorg. Chem. 34 (1995) 6093; (b) O.P. Strausz, H.F. Gunning, Trans. Faraday Soc. 60 (1964) 347; (c) D. Behar, D. Shapira, A. Treinin, J. Phys. Chem. 76 (1972) 180.
[26] (a) W.A. Waters, I.R. Wilson, J. Chem. Soc. A (1966) 534.; (b) R. Swaroop, Y.K. Gupta, J. Inorg. Nucl. Chem. 36 (1974) 169; (c) G. Rabai, M.T. Beck, J. Chem. Soc., Dalton Trans. (1982) 573.
[27] (a) J.Q. Adams, J.R. Thomas, J. Chem. Phys. 39 (1963) 1904; (b) J.Q. Adams, S.W. Nicksic, J.R. Thomas, J. Chem. Phys. 45

(1965) 654;
(c) R. Stone, W.A. Waters, Proc. Chem. Soc., London (1962) 253.;
(d) C.J.W. Gutch, W.A. Waters, J. Chem. Soc. (1965) 751.
[28] M.N. Hughes, G. Stedman, J. Chem. Soc. (1963) 2824.
[29] (a) J.R. Buchholz, R.E. Powell, J. Am. Chem. Soc. 85 (1963) 509;
(b) J.R. Buchholz, R.E. Powell, J. Am. Chem. Soc. 87 (1965) 2350.
[30] D.S. Honig, K. Kustin, J.F. Martin, Inorg. Chem. 11 (1972) 1895.
[31] G. Bengtson, Acta Chem. Scand., Ser. A 37A (1983) 639.
[32] (a) J.H. Butler, L.T. Gordon, Inorg. Chem. 25 (1986) 4573;
(b) K. Arora, P. Bhatnagar, A.P. Bhargava, Y.K. Gupta, J. Chem. Soc., Dalton Trans. (1991) 1081.
[33] R.G. Wilkins, The Study of Kinetics and Mechanism of Reactions of Transition Metal Complexes (Ch. 1), Allyn and Bacon, Boston, 1974, p. 460.
[34] S. Mukhopadhyay, R. Banerjee, Polyhedron 13 (1994) 53.
[35] R.M. Smith, A.E. Martell, Critical Stability Constants, vol. 4, Plenum Press, New York, 1976, p. 44.
[36] S.K. Ghosh, R.N. Bose, E.S. Gould, Inorg. Chem. 26 (1987) 2688.
[37] K.D. Asmus, M. Bonifacie, P. Toffel, P. O'Neill, D.S. Frohlinde, S. Steenken, J. Chem. Soc., Faraday Trans. 1 (1978) 1820.
[38] (a) R.A. Marcus, Annu. Rev. Phys. Chem. 15 (1964) 155;
(b) R.A. Marcus, N. Sutin, Inorg. Chem. 14 (1975) 213.
[39] M.L. Hung, M.L. McKee, D.M. Stanbury, Inorg. Chem. 33 (1994) 5108.
[40] S.K. Ghosh, E.S. Gould, Inorg. Chem. 27 (1988) 4228.
[41] Ms. Rekha, A. Prakash, R.N. Mehrotra, Can. J. Chem. 71 (1993) 2164.
[42] N. Rajasekar, R. Subramaniam, E.S. Gould, Inorg. Chem. 22 (1983) 971.
[43] D.A. Zatko, J.P. Prather, J. Electron Spectrosc. Relat. Phenom. 2 (1973) 191.
[44] N.R. Kunchur, Nature (London) 217 (1968) 539.
[45] M.L. Simms, J.L. Atwood, D.A. Zatko, J. Chem. Soc., Chem. Commun. (1973) 46.
[46] L. Coghi, G. Pelizzi, Acta Crystallogr., Sect. B 31 (1975) 131.
[47] W.M. Latimer, The Oxidation States of the Elements and their Potentials in Aqueous Solutions, 2nd ed., Prentice-Hall, Englewood Cliffs, NJ, 1952.

Table 1
Elemental analyses [a] for the copper complexes (%)

Complex	C	H	N	Cu
1 $Ba[Cu(dtc\text{-}asn)]_2 \cdot 4H_2O$	15.8(16.0)	2.6(2.7)	7.3(7.5)	17.3(17.0)
2 $Ba[Cu(dtc\text{-}gln)]_2 \cdot 4H_2O$	18.2(18.5)	2.9(3.1)	7.0(7.2)	16.7(16.4)
3 $Ba[Cu_2(dtc\text{-}ser)]_2 \cdot 2H_2O$	12.2(12.2)	1.4(1.5)	3.4(3.6)	31.3(32.4)
4 $Ba[Cu_2(dtc\text{-}thr)]_2 \cdot 3H_2O$	14.8(14.5)	1.9(2.2)	3.3(3.4)	29.1(30.6)
5 $Ba[Cu_2(dtc\text{-}tyr)]_2 \cdot 3H_2O$	24.0(25.1)	2.2(2.3)	2.7(2.9)	25.5(26.6)
6 $Ba[Cu(dtc\text{-}pro)_2] \cdot 3H_2O$	21.1(22.2)	2.9(3.2)	4.1(4.4)	10.8(10.1)
7 $[Cu(dtc\text{-}pro)_2][Cu(en)(EtOH)(H_2O)_3]$	28.6(28.8)	4.8(5.1)	9.5(8.4)	19.8(19.1)

[a] Calculated values in parentheses.

allowing determination of its structure by X-ray diffraction.

2. Experimental

2.1. Materials and methods

All amino acids were used in the L form and were purchased from Fluka. Other reagents (i.e. $Ba(OH)_2$, CS_2, $Cu(NO_3)_2 \cdot 3H_2O$, $CuCl_2 \cdot 2H_2O$) and the organic solvents were from Fluka (pa) as well. Chemical analyses for carbon, hydrogen and nitrogen were performed on a 2400 elemental analyser from Perkin–Elmer. Barium and copper were determined on an ICP spectrometer Perkin–Elmer model 2380 Plasma 2. IR spectra were recorded using KBr mulls and a Perkin–Elmer instrument. Electronic spectra were recorded in aqueous solution on Shimadzu UV-240 double beam and Hewlett–Packard 8452A diode spectrophotometers. The room temperature (r.t.) magnetic moment was measured by the Faraday method on a AZTEC DSM8 pendulum-type susceptometer and electron paramagnetic resonance spectra were recorded at X-band frequencies with a Bruker ER200D. The water content in the complexes was determined by thermal analysis using a Perkin–Elemer TGA-7 thermobalance and a DTA-7 differential thermal analysis apparatus, both operating at a heating rate of 5 $^{\circ}C\ min^{-1}$ and under oxygen as the reaction atmosphere.

2.2. Preparation of the barium dithiocarbamates

The dithiocarbamate ligands have been prepared in the form of the barium salts through reaction of the corresponding amino acid with CS_2 in a basic medium ($Ba(OH)_2$), following the method described elsewhere [3]. The use of the barium salts permits larger yields (ca. 85%) than if sodium salts are used, due to their low solubility in ethanol. The general formula of the salts is $Ba(dtc\text{-}a.a.) \cdot H_2O$, where a.a. stands for the amino acid; the existence of the crystallisation water molecule has been checked by thermogravimetric and differential thermal analysis of the barium salts. These salts are very soluble in water, but insoluble in organic solvents.

2.3. Preparation of the copper complexes

The copper complexes have been prepared by direct reaction between the dithiocarbamate barium salts and soluble Cu(II) salts (nitrate or chloride), results being different depending on the precise nature of the amino acid (with an alcohol or an amide group, or proline). The method was as follows: 0.8 mmol of the dithiocarbamate are dissolved in 25 ml H_2O and dropwise added to a magnetically stirred solution containing 0.4 mmol Cu(II) soluble salt in 25 ml H_2O. For compounds **1**–**5** (see Table 1) the solution immediately darkens when addition starts, finally giving a dark brown precipitate, which is separated by filtration. Elemental chemical analysis results are given in Table 1; yields ranged between 40 and 45% in all cases.

The proline derived compound (**6**) behaves differently. The solution changes to a dark green colour and precipitation only takes place after strong concentration, by slow evaporation of water or in a vacuum dessicator; the yield was 70–75% in this case. Unfortunately, we failed to crystallise this compound, despite its solubility in water. However, well defined crystals were obtained upon addition of a second ligand, ethylenediamine (en), leading to formation of a mixed, more stable complex. This was obtained as follows: 2.2 mmol of the barium salt of the proline derived dithiocarabamate are dissolved in 25 ml H_2O; the solution is strongly magnetically stirred and 2.2 mol Cu, dissolved in 25 ml H_2O, and 2.2 mmol ethylenediamine are added. After completing the addition, a green precipitate is formed (compound **7**), which is separated by filtration. After standing for 3 days at r.t., the supernatant liquid forms green, needle-like, crystals whose elemental chemical analysis data and FTIR spectrum coincide with those of the precipitate. It is worth noting the presence of an ethanol molecule in the composition of this compound as evidenced by X-ray diffraction (see below), which probably was present in the starting barium salt (precipitated in ethanol medium). The presence of crystal-

lisation water molecules has been checked in all cases by thermogravimetric and differential thermal analyses.

2.4. Crystal structure determination

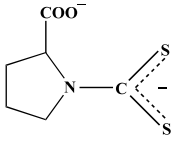
A dark green prismatic crystal of [Cu(en)(EtOH)$(H_2O)_3$][Cu(dtc-pro)$_2$] was mounted on a glass fiber and used for data collection. Crystal data were collected at 291(2) K, using a Bruker SMART CCD 1000 diffractometer. Graphite monochromated Mo Kα radiation ($\lambda = 0.71073$ Å) was used throughout. The data were processed with SAINT [11] and corrected for absorption using SADABS (transmissions factors: 1.000–0.573) [12]. The structure was solved by direct methods using the program SHELXS-97 [13] and refined by full-matrix least-squares techniques against F^2 using SHELXL-97 [14]. Positional and anisotropic atomic displacement parameters were refined for all non-hydrogen atoms of the anion and the copper atom of the cation, and isotropic displacement parameters for the other cation atoms. The cation atoms are disordered over two positions; the occupancy factor for each was initially refined, resulting in a value of 0.50(6) for each. Hydrogen atoms, except those bonded to oxygen atoms, were placed geometrically and positional parameters were refined using a riding model. Isotropic atomic displacement parameters for hydrogen atoms were constrained to be 1.2 (1.5 for methyl groups). Atomic scattering factors were obtained from 'International Tables for X-ray Crystallography' [15]. Molecular graphics were obtained from PLATON [16] and SCHAKAL [17]. A summary of the crystal data, experimental details and refinement results are listed in Table 2.

Table 2
Crystal data and structure refinement for [Cu(en)(EtOH)$(H_2O)_3$][Cu(dtc-pro)$_2$]

Empirical formula	$C_{16}H_{34}Cu_2N_4O_8S_4$
Formula weight	665.79
Temperature (K)	293(2)
Wavelength (Å)	0.71073
Crystal system	orthorhombic
Space group	$C222_1$ (No. 20)
Unit cell dimensions	
a (Å)	6.560(2)
b (Å)	28.384(9)
c (Å)	14.927(4)
α (°)	90
β (°)	90
γ (°)	90
V (Å^3)	2779.3(14)
Z	4
Calculated density (Mg m^{-3})	1.591
Absorption coefficient (mm^{-1})	1.875
$F(000)$	1376
Crystal size (mm)	0.43 × 0.10 × 0.03
Theta range for data collection (°)	1.98–28.08
Limiting indices	$-8 \le h \le 8$, $-36 \le k \le 26$, $-17 \le l \le 19$
Reflections collected/unique	8276/3243 [$R_{int} = 0.0945$]
Completeness to θ	28.08(%) 48.9
Absorption correction	SADABS
Max/min transmission	0.9459, 0.4993
Refinement method	full-matrix least-squares on F^2
Data/restraints/parameters	3243/0/154
Goodness-of-fit on F^2	0.974
Final R indices [$I > 2\sigma(I)$]	$R_1 = 0.0914$, $wR_2 = 0.2032$
R indices (all data)	$R_1 = 0.1607$, $wR_2 = 0.2322$
Largest difference peak and hole (e Å^{-3})	1.638 and −1.346

3. Results and discussion

Reaction of Cu(II) salts with dithiocarbamates derived from α-amino acids possessing alcohol or amide groups leads to reduction of the metal cation to Cu(I), probably through oxidation of the dithiocarbamate to the corresponding disulfide. An additional feature of the compounds prepared with serine, threonine and tyrosine arises from the presence of an alcohol group in their structures, which becomes deprotonated, thus providing a total formal charge of −3 to the corresponding ligands. However, such a reduction does not takes place with the proline compound, a Cu(II) complex being formed. This results further confirms that the reduction ability of dithiocarbamates depends on the nature of the organic chain linked to the NCS_2^- moiety, as previously observed for some dithiocarbamate complexes of Mo [8,10]. Probably, the fact that the nitrogen atom belongs to the organic ring (Scheme 1) decreases its electron donor ability towards the sulfur atoms, thus decreasing their reducing ability.



Scheme 1. Schematic representation of proline dithiocarbamate.

3.1. IR spectra

The positions of the main FT-IR bands recorded for all seven complexes synthesised are given in Table 3. The band close to 1490 cm^{-1} is due to the stretching of the C–N group of the NCS_2^- moiety; its position corresponds to a partial double bond character, and is recorded in the range previously reported for similar compounds [18,19]. The band designated as ν(N–C′) in the table corresponds to the vibration of the two N–C bonds within the five members ring, and corresponds to single N–C bonds. The additional band at 1044 cm^{-1} in complex **7** is due to the ethylenediamine ligand.

The bands recorded in the region corresponding to the C–S vibrations are typical of a bidentate bonding of the dithiocarbamate unit to the metal cation [18,19], and

Table 3
Vibrational frequencies (cm^{-1}) for selected absorption bands in the IR spectra

Complex	ν(C–N)	ν(N–C′)	ν_{as}(C–S)	ν_s(C–S)	$\nu_{as}(COO^-)$	$\nu_s(COO^-)$	$\rho(COO^-)$	ν(S–Cu)
1 $Ba[Cu(dtc\text{-}asn)]_2\cdot 4H_2O$	1484	1112	927	622	1589	1396	548	337
2 $Ba[Cu(dtc\text{-}gln)]_2\cdot 4H_2O$	1488	1107	939	614	1577	1396	541	328
3 $Ba[Cu_2(dtc\text{-}ser)]_2\cdot 2H_2O$	1499	1172	928	609	1602	1385	556	326
4 $Ba[Cu_2(dtc\text{-}thr)]_2\cdot 3H_2O$	1498	1177	936	608	1606	1383	556	328
5 $Ba[Cu_2(dtc\text{-}tyr)]_2\cdot 3H_2O$	1513	1233	901	612	1609	1373	538	327
6 $Ba[Cu(dtc\text{-}pro)_2]\cdot 3H_2O$	1472	1164 1139	940	659	1598	1382	487	345
7 $[Cu(en)(EtOH)(H_2O)_3][Cu(dtc\text{-}pro)_2]$	1489	1173 1152 1044	952	661	1598	1381	487	339

the vibration of the sulfur–copper bond gives rise to a band close to 330 cm^{-1} in all complexes synthesised [18–20]. The bands close to 1600 and 1390 cm^{-1} are due to the antisymmetric and symmetric vibrations of the carboxylate groups.

3.2. Crystal structure of $[Cu(en)(EtOH)(H_2O)_3][Cu(dtc\text{-}pro)_2]$

In addition to the other experimental data described above, X-ray diffraction for this complex shows both the cation and the anion are coordination compounds. Most significant structural parameters are given in Table 4 and the molecular structure of both ions are shown in Fig. 1(a and b).

As shown in this figure, the copper is coordinated by four sulfur atoms in the anion $[Cu(dtc\text{-}pro)_2]^{2-}$, giving rise to a local symmetry of D_{2h} around the metallic site, as the SCS angles are lower than 90° (otherwise the local geometry would approach D_{4h}). The four Cu–S distances are almost coincident, as well as the C–S distances, thus confirming the bidentate nature of the dithiocarbamate ligand; actually, the C–S distances are close to 1.71 Å, similar to the values previously reported for other dithiocarbamates [21], including the barium salt of glycine dithiocarbamate [22]. The C–N distance, 1.312 Å, is also similar and in agreement with a marked double bond character. However, the –SCS– angle is about 6° smaller in the copper complex than in the glycine dithiocarbamate (as the barium salt), i.e. the angles become somewhat closed upon coordination to copper. Overall, the bond angles and bond distances are rather similar to those reported for Cu complexes with alkyldithiocarbamates [23].

In the other complex subunit, $[Cu(en)(EtOH)(H_2O)_3]^{2+}$, Cu(II) is hexacoordinated, with a distorted octahedral symmetry. The aquo ligands stand in a *fac* symmetry, and two of the three water molecules are in the same plane as the nitrogen atoms of the ethylenediamine ligand; the oxygen atom of the third water molecule is 0.27 Å further out than the other two, and that of the ethanol molecule is even further out, probably because of the tetragonal distortion favoured for this configuration (d^9), according to the Jahn–Teller

Table 4
Selected bond lengths (Å) and angles (°) for $[Cu(en)(EtOH)(H_2O)_3][Cu(dtc\text{-}pro)_2]$

Bond lengths	
Cu(1)–S(12)	2.293(2)
Cu(1)–S(12)#1	2.293(2)
Cu(1)–S(11)#1	2.308(3)
Cu(1)–S(11)	2.308(3)
Cu(2)–N(21)	1.795(15)
Cu(2)–O(22)	2.011(17)
Cu(2)–O(21)	2.024(17)
Cu(2)–N(22)	2.060(18)
Cu(2)–O(23)	2.392(16)
Cu(2)–O(31)	2.571(16)
S(11)–C(5)	1.724(9)
S(12)–C(5)	1.721(10)
N(1)–C(5)	1.312(11)
Bond angles	
S(12)–Cu(1)–S(12)#1	163.22(18)
S(12)–Cu(1)–S(11)#1	103.84(10)
S(12)#1–Cu(1)–S(11)#1	78.10(10)
S(12)–Cu(1)–S(11)	78.10(10)
S(12)#1–Cu(1)–S(11)	103.84(10)
S(11)#1–Cu(1)–S(11)	167.0(2)
N(21)–Cu(2)–O(22)	91.1(7)
N(21)–Cu(2)–O(21)	170.3(7)
O(22)–Cu(2)–O(21)	81.8(7)
N(21)–Cu(2)–N(22)	88.5(7)
O(22)–Cu(2)–N(22)	175.6(8)
O(21)–Cu(2)–N(22)	99.0(7)
N(21)–Cu(2)–O(23)	95.1(6)
O(22)–Cu(2)–O(23)	91.5(7)
O(21)–Cu(2)–O(23)	91.8(6)
N(22)–Cu(2)–O(23)	84.2(7)
N(21)–Cu(2)–O(31)	79.6(6)
O(22)–Cu(2)–O(31)	95.8(7)
O(21)–Cu(2)–O(31)	94.4(6)
N(22)–Cu(2)–O(31)	88.4(6)
O(23)–Cu(2)–O(31)	171.0(6)
S(12)–C(5)–S(11)	114.6(5)

Symmetry transformations used to generate equivalent atoms: #1 $-x+2, y, -z+1/2$.

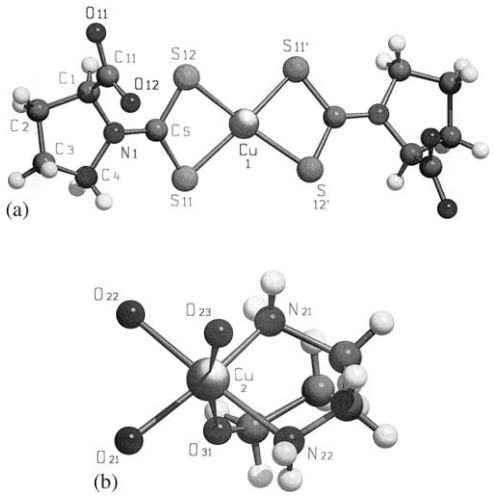


Fig. 1. Atomic structure and labelling scheme for (a) $[Cu(dtc\text{-}pro)_2]^{2-}$ and (b) $[Cu(en)(EtOH)(H_2O)_3]^{2+}$.

effect. The two Cu–N (from ethylenediamine) distances are also different, probably because of packing effects in the crystalline state and/or in order to minimise repulsions with the other ligands.

3.3. Electronic and ESR spectra

Compounds **1**–**5** are diamagnetic and do not show well defined bands in the visible region, but the absorption extends almost in all the visible range. On the contrary, the proline complexes show a broad, ill defined, absorption band centred at about 630 nm for compound **6** and at 615 nm for compound **7**, with an extinction coefficient of 100 M^{-1} cm^{-1}, that should correspond to transits from lower energy levels to dx^2-y^2 [24]. An additional band at 430 nm ($\varepsilon = 3500$ M^{-1} cm^{-1}) is recorded for both complexes and can be assigned to a S→Cu charge transfer process. These two compounds are paramagnetic, the effective magnetic moments being 1.78 and 1.76 BM for complexes **6** and **7**, respectively, very close to the value calculated for the spin-only moment, 1.73 BM, thus suggesting only weak, if any, spin-orbit coupling [25]. Cu^{2+} possesses an orbitally non-degenerate ground state in the Jahn–Teller distorted polyhedra and hence essentially a spin-only magnetic moment; deviations are due to admixtures of very small orbital contributions of excited states via spin-orbit coupling.

The ESR spectra for both proline complexes are included in Fig. 2; no fine structure was observed in either case. That for compound **6** is axial, with ESR parameters deduced from simulation [26] of $g_{\parallel} = 2.09$, $g_{\perp} = 2.03$ and $g_o = 2.07$. The spectrum corresponding to compound **7** corresponds to a mixture of two Cu(II) ions (d^9 configuration) under two different surroundings, as it can be considered as being formed by two

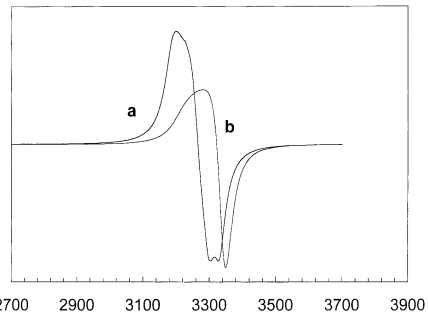


Fig. 2. Experimental polycrystalline X-band ESR spectra at 298 K of the copper complexes: (a) $[Cu(en)(EtOH)(H_2O)_3][Cu(dtc\text{-}pro)_2]$, (b) $Ba[Cu(dtc\text{-}pro)_2]\cdot 3H_2O$.

axial quasi-isotropic spectra, unable to be simulated, with average values of $g_o = 2.08$ and 2.06 for both Cu atoms [25].

4. Supplementary material

Complete lists with atomic coordinates, anisotropic displacement parameters, bond lengths and angles have been deposited at the Cambridge Crystallographic Data Centre [CCDC 178510], 12 Union Road, Cambridge, CB2 1EZ, UK (fax: +44-1223-336033; e-mail: deposit@ccdc.cam.ac.uk or www: http://www.ccdc.cam.ac.uk).

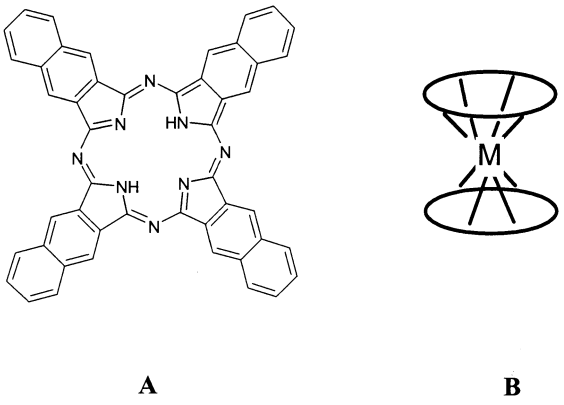
Acknowledgements

The authors thank CICYT (grant PM97-0105-C02-02) for financial support and critical reading of the manuscript by Professor V. Rives is also acknowledged.

References

[1] D. Coucouvanis, Prog. Inorg. Chem. 26 (1979) 301.
[2] A.M. Bond, R.L. Martin, Coord. Chem. Rev. 54 (1984) 23.
[3] M.A. Stalteri, S.J. Parrot, V.A. Griffiths, J.R. Dilworth, S.J. Mather, Nucl. Med. Commun. 18 (1997) 870.
[4] V. Scarcia, A. Furlani, D. Fregona, G. Faraglia, S. Sitran, Polyhedron 18 (1999) 2827.
[5] M. Castillo, J.J. Criado, B. Macías, M.V. Vaquero, Inorg. Chim. Acta 124 (1986) 127.
[6] J.J. Criado, I. Fernández, B. Macías, J.M. Salas, M. Medarde, Inorg. Chim. Acta 42 (1991) 17.
[7] B. Macías, J.J. Criado, M.V. Vaquero, M.V. Villa, M. Castillo, J. Inorg. Biochem. 42 (1991) 17.
[8] B. Macías, P. Malet, R. Paradinas, V. Rives, M.V. Villa, Inorg. Chim. Acta 288 (1999) 127.
[9] B. Macías, J.J. Criado, M.V. Villa, M.R. Iglesias, M. Castillo, Polyhedron 12 (1993) 501.
[10] B. Macías, J.J. Criado, M.V. Villa, L.J. Rodriguez, M. Castillo, Polyhedron 12 (1993) 2791.

[11] Smart, Saint, Area Detector Control and Integration Software, Bruker Analytical X-ray Instruments Inc, Madison, WI, USA, 1997.
[12] G.M. Sheldrick, SADABS. Program for Empirical Absorption Correction of Area Detector Data, University of Göttingen, Germany, 1997.
[13] G.M. Sheldrick, Acta Crystallogr., Sect. A 46 (1990) 467.
[14] G.M. Sheldrick, SHELXL-97. Program for the Refinement of Crystal Structures, University of Göttingen, Germany, 1997.
[15] International Tables for X-ray Crystallography, vol. C, Kluwer Academic Publishers, Dordrecht, 1995.
[16] A.L. Spek, PLATON. A Multipurpose Crystallographic Tool, Utrecht University, Utrecht, The Netherlands, 2000.
[17] E. Keller, SCHAKAL-97. A Computer Program for the Graphic Representation of Molecular Crystallographic Models, University of Freiburg, Germany, 1997.
[18] H.S. Sangari, G.S. Sodhi, J. Kaur. Chem. Papers 51 (1997) 282.
[19] M. Lalia-Kantouri, M. Uddin, C.C. Hadjikostas, H. Papanikolas, G. Palios, S. Anagnostis, V. Anesti, Z. Anorg. Allg. Chem. 623 (1997) 1983.
[20] A.C. Fabreti, F. Forghieri, A. Giusti, C. Preti, G. Tosi, Inorg. Chim. Acta 86 (1984) 127.
[21] K. Unoura, A. Yamazaki, A. Nagasawa, Y. Kato, H. Itoh, H. Kudo, Y. Fukuda, Inorg. Chim. Acta 269 (1998) 260.
[22] C.F. Conde, M. Millan, A. Conde, R. Marquez, Acta Crystallogr., Sect. C 42 (1986) 286.
[23] J. Willemse, J.A. Cras, J.J. Steggerda, C.P. Keijzers, Structure and Bonding, vol. 28, Springer-Verlag, Berlin, 1976, p. 83.
[24] A.B.P. Lever, Inorganic Electronic Spectroscopy, 2nd ed., Elsevier, Amsterdam, 1984, p. 558.
[25] B.J. Hathaway, Comprehensive coordination chemistry, in: G. Wilkinson, J.A. McCleverty, R.D. Gillard (Eds.), Late Transition Elements, vol. 5, Pergamon Press, Oxford, 1987, p. 656.
[26] WINEPR-Simfonia 1.25, Bruker Analytik GmbH, Kalsruhe, Germany, 1994–1996.



A B

Fig. 1. (A) Structural formula of naphthalocyanine; and (B) skeletal representation of bis(naphthalocyaninato) rare earth sandwich complexes $M(2,3\text{-}Nc)_2$.

iono-electronics [5,6]. By the continuous efforts of Jiang and co-workers to develop new examples of sandwich compounds, a series of homoleptic and heteroleptic sandwich rare earth complexes containing naphthalocyanine ligands have been reported based on newly developed methodology [7–12].

Although naphthalocyanine derivatives have been known for a long time, relatively little is known of their vibrational spectroscopic properties. In 1984, Kaplan et al. reported the IR characteristics of the most intense absorptions of some Nc metal complexes [13]. Yanagi et al. investigated the IR spectra of various Nc complexes of Zn, Al, Ga, and V in 1992 and 1993 [14]. Aroca and co-workers also studied the vibrational spectra (IR, Raman, resonance Raman, surface enhanced resonance Raman) for free base $H_2(2,3\text{-}Nc)$ and copper complex Cu(2,3-Nc) following their intensive work on phthalocyanine counterparts [15]. Very recently, the group of Campos-Vallette tried to interpret the structure of free base naphthalocyanine and a series of naphthalocyaninato metal complexes on the basis of their FT-IR and Raman spectroscopic investigation [16]. Before the report on IR spectroscopic characterization of some bis(naphthalocyaninato) rare earth compounds [17], the sole relevant report concerning the vibrational properties is that of L'Her who attributed a strong band at approximately 1330 cm^{-1} to the stretching vibration of the pyrrole rings of naphthalocyanine in $Lu(2,3\text{-}Nc)_2$ and Lu(Pc)(2,3-Nc) [18]. Since 1999, Jiang, Arnold, and Homborg have started to pay attention to the vibrational spectroscopic characterization of Nc rare earth sandwich complexes and have briefly reported the Raman spectra for several bis(naphthalocyaninato) rare earth complexes [19,20]. The aim of the present paper is not only to add more information on the Raman spectroscopy of naphthalocyanine but also to give insight into the influence of the rare earth ionic size on the Raman spectra of naphthalocyanine in the sandwich compounds. Herein we describe the Raman spectroscopic characteristics of naphthalocyanine anions in the bis(naphthalocyaninato) rare earth compounds $M(2,3\text{-}Nc^*)_2$ [$M = Ce\cdots Lu$ except Nd and Pm, Y; $Nc^* = Nc(t\text{Bu})_4$] by means of excitation by laser sources at 632.8 and 785 nm. It is worth noting that the Raman spectra of several bis(naphthalocyaninato) rare earth compounds under excitation by 632.8 nm radiation have been recorded previously [19]. For the purpose of systematic comparison with those under 785 nm laser excitation and re-assignment of some vibrational modes, the spectra of the complete set of compounds discussed in this paper were re-measured under 632.8 nm excitation and their spectra are in good accordance with the previous measurements [19,20].

2. Experimental

Bis(naphthalocyaninato) rare earth complexes $M(2,3\text{-}Nc^*)_2$ [$M = La\cdots Lu$ except Nd and Pm, Y; Nc^* = 3(4),12(13),21(22),30(31)-tetra(t-butyl)-2,3-naphthalocyanine, $Nc(t\text{Bu})_4$] were prepared according to the reported procedures [8]. Raman spectra were recorded on a few grains of the solid samples with approximately 4 cm^{-1} resolution using a Renishaw Raman Microprobe, equipped with a Spectra Physics Model 127 He–Ne laser excitation source emitting at a wavelength of 632.8 nm and a Renishaw diode laser emitting at 785 nm, and a cooled charge-coupled device (CCD) camera. An Olympus BHZ-UHA microscope was attached and was fitted with three objective lenses ($\times 10$, $\times 20$, $\times 50$). For these experiments, the $\times 10$ objective was employed giving a spot size on the sample of about 5 μm. Laser power at the sample was approximately 0.08 mW. Spectra of excellent quality were obtained in approximately 3 min.

3. Results

In bis(phthalocyaninato) rare earth complexes $M(Pc)_2$, the single crystal X-ray diffraction structural data have shown that the rare earth cation is at the centre of two Pc ligands facing each other in a staggered arrangement. In the solid state, these compounds can be assumed to belong to the D_4 or D_{4d} point-groups depending on the skew angle between the two macrocyclic rings. There has been no crystallographic report on the molecular structure of bis(naphthalocyaninato) metal complexes as systematic research on these complexes has not been pursued until the recent work of Jiang and co-workers [7]. However, according to the recently reported molecular structures of mixed (octaethylporphyrinato)(naphthalocyaninato) rare earth double-deckers M(OEP)(2,3-Nc) (M = Pr, Nd, Sm, Eu,

Gd, Y, Tm, Lu), the skew angles between OEP and 2,3-Nc macrocyclic ligands in the whole series of rare earth compounds remain unchanged at 45° in order to minimize the non-bonding interactions between the fused benzene rings of Nc and the β-ethyl groups of OEP [8,21]. Therefore, it is reasonable to assume that the skew angle between two Nc rings in M(2,3-Nc)$_2$ is near 45° due to the same reason. The equilibrium geometry of M(2,3-Nc)$_2$ should be D_{4d} group symmetry when the skew angle is 45° or D_4 when the skew angle is not 45°. This needs direct confirmation from X-ray molecular structure analysis in future. The actual materials M(2,3-Nc*)$_2$ [Nc* = Nc(tBu)$_4$] contain more than one isomer due to the alternative locations of the *tert*-butyl groups. However, for each substituted Nc ring and the central rare earth metal atom, a local C_{4v} symmetry should be seen and the interpretation of the observed vibrational spectra could be assisted by this approximation. In the Raman spectra of Zr[Pc(tBu)$_4$]$_2$, only frequencies corresponding to the characteristic fingerprint vibrations of the Pc macrocycle were observed and *tert*-butyl vibrations were very weak or absent [22]. Moreover, because both laser lines used in our experiments appear to enhance modes associated with the aromatic macrocycles (see below), the *tert*-butyl groups will be ignored in our subsequent analysis. Even the unsubstituted naphthalocyaninato metal fragment with 81 atoms and 237 normal vibrational modes is a tremendous challenge for the vibrational spectroscopist. For a C_{4v} M(2,3-Nc) fragment there will be only 31 A_1 totally symmetric modes that dominate the spontaneous Raman spectra. The other Raman active modes include $30B_1+30B_2+118E$, which will show a number of new frequencies in the resonance Raman scattering in view of the Herzberg–Teller mechanism. Despite the large number of fundamental vibrational modes, the Raman spectra of these double-decker complexes are composed of a small number of bands, as shown in Figs. 2 and 3.

Based on their intensive research on the vibrational spectra of both phthalocyanine and naphthalocyanine compounds, Aroca and co-workers found that the following three groups of characteristic phthalocyanine or naphthalocyanine vibrations dominate their IR and Raman spectra [15,23,24]. In the spectral region from 400 to 1000 cm^{-1}, the vibrations are mainly composed of the dihedral plane deformations involving the aromatic C–H groups (wagging and torsion vibration) which are normally seen in the IR spectra, and ring radial vibrations of the isoindole moieties and the macrocycle which show strong Raman signals. Aromatic in-plane C–H vibrations are responsible for the IR and resonance Raman spectra of phthalocyanine molecules in the region of 1000–1300 cm^{-1}, with the exception of the pyrrole ring vibration at about 1140 cm^{-1}. Vibrational frequencies in the range of 1320–1650 cm^{-1} are derived from isoindole ring stretches and the aza group stretch, for which the pyrrole stretching vibrations at approximately 1330 and 1510 cm^{-1}, and *ortho*-substituted benzene (or naphthalene) stretchings at approximately 1560, 1590, and 1610 cm^{-1} or above can be distinguished by frequency and relative intensity.

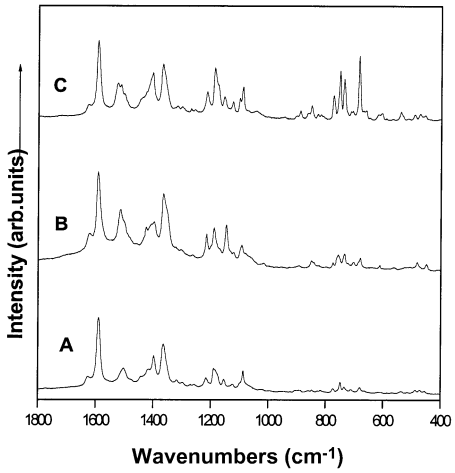


Fig. 2. Raman spectra of M(2,3-Nc*)$_2$ [Nc* = Nc(tBu)$_4$]: (A) M = Ce; (B) Gd; (C) Lu with excitation at 632.8 nm.

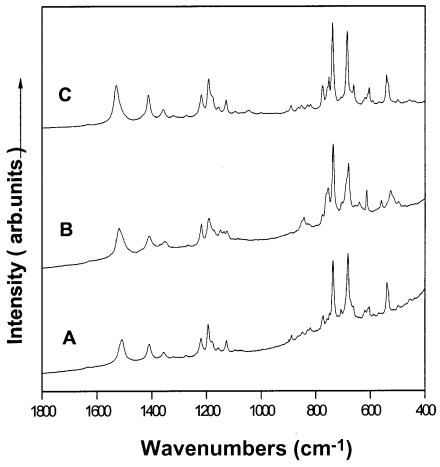


Fig. 3. Raman spectra of M(2,3-Nc*)$_2$ [Nc* = Nc(tBu)$_4$]: (A) M = Ce; (B) Gd; (C) Lu with excitation at 785 nm.

3.1. Raman characteristics of M(2,3-Nc)$_2$ [M = Ce···Lu except Nd and Pm, Y; Nc* = Nc(tBu)$_4$] with excitation by laser line at 632.8 nm*

Fig. 2 compares the Raman spectra obtained with laser excitation at 632.8 nm of three compounds M(2,3-Nc*)$_2$ [M = Ce, Gd, Lu; Nc* = Nc(tBu)$_4$], typical for the light, middle, and heavy rare earths, respectively. The observed Raman spectroscopic frequencies of naphthalocyanine for M(2,3-Nc*)$_2$ were partially assigned by analogy with the Raman characteristics of

bis(phthalocyaninato) rare earth counterparts [19,20] and naphthalocyanine derivatives [13–16]. Due to the similar electronic structure and electronic absorption properties among the whole series of bis(naphthalocyaninato) rare earth compounds, all these compounds show similar Raman characteristics, so the results have been summarized in the shortened form given in the Table 1. The naphthalene stretchings around 1592 cm^{-1} appear as the most intense band. The Nc breathing mode in M(2,3-Nc*)$_2$ appears as a weak band at approximately 681–684 cm^{-1}, which gains intensity gradually from M = Ce to Lu and shows a trend to blue-shift slightly along with the decrease of rare earth radius. The pyrrole stretching gives two peaks at approximately 1154 and 1500 cm^{-1}. The former one remains unchanged at approximately 1154 cm^{-1} as a single weak peak whereas the latter one seems to be blue-shifted along with the rare earth contraction. It must be pointed out that this latter peak overlaps with the aza stretch vibration at approximately 1520 cm^{-1} and thus appears as a shoulder for M(2,3-Nc*)$_2$ from M = Ce to M = Tm. Only in the spectra of the smallest rare earth bis(naphthalocyaninato) compounds M(2,3-Nc*)$_2$ (M = Yb, Lu) is this vibration apparent as a well-separated band at 1512 and 1513 cm^{-1}, respectively. The sensitivity of this vibrational mode to the central metal radius in the complexes suggests that it must contain significant C=N aza character and therefore is assigned to the coupling of pyrrole C=C and aza C=N stretches, which is consistent with the point of Melendres on the same vibrational mode of phthalocyanine derivatives [25]. The weak bands in the region from 400 to 1000 cm^{-1} are assigned to the ring radial vibrations of the isoindole moieties and the naphthalocyanine macrocycle. One of these at 750 cm^{-1} is due to the aromatic naphthalocyanine C–H wagging, which also gains intensity along with the decrease of rare earth size from Ce to Lu just as does that at 684 cm^{-1} due to the Nc ring breathing. The frequencies with weak and medium intensity observed in the spectral region of 1050–1280 cm^{-1} are attributed to the in-plane naphthalocyanine C–H bending vibrations. The remaining vibrations in 1320–1650 cm^{-1} range are isoindole stretch, aza group, and naphthalene stretch as organized in Table 1. In this group, except for the above-mentioned frequency at 1503–1513 cm^{-1} derived from the coupling of pyrrole C=C and aza C=N stretches, the C=N aza group stretch exhibits a weak shoulder band at approximately 1515 cm^{-1} for Ce(2,3-Nc*)$_2$ and a weak separated band at 1524 cm^{-1} for Lu(2,3-Nc*)$_2$. The most intense vibration at approximately 1592 cm^{-1} and a very weak shoulder at approximately 1625 cm^{-1} are assigned to the naphthalene stretches in M(2,3-Nc*)$_2$ (M = Ce···Lu except Nd and Pm, Y) by analogy with those of bis(phthalocyaninato) rare earths and monomeric naphthalocyaninato metal compounds [19,20,23]. In our preliminary report on the Raman spectra of M(2,3-Nc*)$_2$, we tentatively assigned the intense band at approximately 1370 cm^{-1} to the pyrrole vibration [19]. However, according to its appearance with a shoulder at approximately 1340 cm^{-1} and the sensitivity of this frequency to the nature of the rare earth ion, we now revise our assignment of the broad band centred at 1364–1369 cm^{-1}, and attribute it to the overlapped vibrations of the naphthalene stretching with some contributions from the pyrrole stretchings. This has been verified by the corresponding characteristics of the same band in M(OEP)(2,3-Nc). For the early rare earth double-deckers in the series M(OEP)(2,3-Nc) (M = La···Gd except for Ce and Pm), with excitation at 632.8 nm, a broad band locating at 1363–1364 cm^{-1} was attributed to the naphthalene stretching vibrations, whose shoulder at approximately 1340 cm^{-1} was assigned to the pyrrole stretchings. For late rare earth compounds M(OEP)(2,3-Nc) (M = Tb···Lu, Y), the two well-separated bands respectively at 1346–1350 and 1361–1364 cm^{-1} were undoubtedly assigned to pyrrole stretchings and naphthalene stretchings, respectively [26].

Under excitation by the laser line at 632.8 nm, the vibrations at 681–684 cm^{-1} assigned to the Nc breathing, 1357–1361 cm^{-1} due to the naphthalene stretchings, 1409–1415 cm^{-1} attributed to the isoindole stretchings, and 1517–1530 cm^{-1} contributed from the aza stretchings in the Raman spectra of M(2,3-Nc*)$_2$ shift slightly to higher energy along with the decrease of rare earth radius, clearly showing the rare earth size effect. A weak vibrational band at 878–886 cm^{-1} in the IR spectra of bis(phthalocyaninato) rare earths M(Pc)$_2$ has also been found to be sensitive to the central rare earth metal size and was thus attributed to the metal–

Table 1
Major Raman bands [a] (cm^{-1}) for M(2,3-Nc*)$_2$ [Nc* = Nc(tBu)$_4$] under excitation by different laser lines

λ_{ex} = 632.8 nm	λ_{ex} = 785 nm	Assignment
	539m–541m (526m)	
681m–684s (679w)	681s–685s (680s)	Nc breathing
735w–738m	737s–739s (736s)	
749m–752s (756m)		C–H wag
1086m–1089m (1093m)		C–H bend
1154m–1155m (1146m)		pyrrole breathing
1188m–1189m	1192m–1194m (1191m)	C–H bend
1215m	1220m	C–H bend
1364s–1369s		naphthalene stretch (see text)
1397m–1404m	1409m–1415m	isoindole stretch
1512m–1524m	1515m–1531m	aza stretch
1587s–1592s		naphthalene stretch

[a] Extremes of observed frequencies for medium or strong bands over the series M = Ce···Lu (except Nd, Pm); Y, values in parentheses are for the Gd complex where its frequency lies outside the quoted range.

nitrogen vibration by Isago and Shimoda [27]. This seems to be in line with the assignment of the same vibration at 886 cm^{-1} to the metal–nitrogen bond in the IR spectra of monomeric phthalocyaninato metal complexes according to Kobayashi [28] and Kenn [29]. However, in the present work, the frequency near 890 cm^{-1} shows no dependence on size (this is also true when recording the Raman spectra with excitation by the laser line at 785 nm). A vibration in the range of 849–854 cm^{-1} does seem to show such a trend, shifting slightly from 849 for Ce(2,3-Nc*)$_2$ to 853 cm^{-1} for Lu(2,3-Nc*)$_2$. It seems that the present results support the points of Shurvell [30] and Janczak [31] who associated the band in the range of 810–830 cm^{-1} with the metal–ligand vibration. Anyway, more theoretical and experimental efforts are necessary to make clear assignment of the frequencies in the region from 800 to 900 cm^{-1} to the metal–nitrogen vibration.

As noted previously, strong fluorescence occurred when trying to measure the Raman spectrum of La(2,3-Nc*)$_2$ using excitation at 632.8 nm.

3.2. *Raman characteristics of M(2,3-Nc*)$_2$ [M = Ce···Lu except Nd and Pm, Y; Nc* = Nc(t Bu)$_4$] with excitation by laser line at 785 nm*

Using the excitation laser line at 785 nm, as shown in Fig. 3 and summarized in the Table 1, the macrocyclic ring deformation and ring radial vibrations between 400 and 900 cm^{-1} in the Raman spectra of M(2,3-Nc*)$_2$ are selectively intensified. This is in good accordance with the Raman characteristics of bis(phthalocyaninato) rare earth analogues [19,20]. The Nc breathing at approximately 682 cm^{-1} and the aromatic C–H wagging at approximately 738 cm^{-1} are the most intense bands. The intense band due to the naphthalene stretches around 1592 cm^{-1} under 632.8 nm excitation is absent whereas the vibration at approximately 1637 cm^{-1} remains as a very weak band. Similar to those excited with 632.8 nm laser line, the frequencies of the coupling of pyrrole C=C and aza C=N stretches at 1508 cm^{-1} and the aza stretch in the region above 1520 cm^{-1} overlap to form a broad band. For the bis(naphthalocyaninato) complexes of larger rare earths such as Ce and Pr, the contribution from coupling of pyrrole C=C and aza C=N stretches dominates the frequencies and the two overlapped vibrations show a broad weak band at 1508 and 1507 cm^{-1}, respectively. For metals heavier than Sm, the frequency of the two overlapped vibrations is dominated by the contribution of the aza stretches and a relatively intense and broad band shifts from 1512 for Sm(2,3-Nc*)$_2$ to 1524 cm^{-1} for Lu(2,3-Nc*)$_2$. Obviously, the application of the 785 nm laser line adds intensity to this vibration and its frequency is clearly also dependent on the size of the metal ion. The broad, weak band locating at 1357–1361 cm^{-1} is assigned to the overlapped vibrations of pyrrole and naphthalene stretchings by analogy with those under 632.8 nm excitation.

Under 785 nm laser line excitation, the vibrations at 681–685 cm^{-1} assigned to the Nc breathings, 1357–1361 cm^{-1} due to the naphthalene stretchings, 1409–1413 cm^{-1} attributed to the isoindole stretchings, and 1517–1530 cm^{-1} contributed from the aza stretch in the Raman spectra of M^{III}(2,3-Nc*)$_2$ [Nc* = Nc(t Bu)$_4$] are shifted to higher energy along with the ionic radius contraction. For instance, a linear correlation exists between the frequency of the aza stretchings at approximately 1530 cm^{-1} and the tervalent rare earth ionic radii, as shown in Fig. 4.

4. Discussion

The Raman spectra of this series of compounds are clearly quite sensitive to the frequency of the exciting radiation, and in particular there are dramatic changes in relative intensities of various bands. The electronic absorption spectra of M(2,3-Nc*)$_2$ [M = Ce, Gd, Lu; Nc* = Nc(t Bu)$_4$] which are typical representatives of the UV–Vis spectra of the light, middle, and heavy rare earth complexes, respectively, are shown in Fig. 5 [7]. The spectral features resemble those of bis(phthalocyaninato) rare earth complexes except that all absorption bands are significantly red-shifted in the Nc series due to the extended conjugation. It is worthwhile to describe briefly the assignments of these electronic absorption bands [7]. The spectra consist of a broad Soret region peaking at 328–334 nm, an intense band in the region 767–799 nm described as the $Nc^{\bullet -}$ Q(0, 0) band (i.e. a transition from the singly-occupied orbital to the LUMO), and the intermediate region which includes the Q(1, 0) band and the 'π-radical anion band' (593–648 nm), representing transitions from lower levels to the SOMO. As the ionic radius of the tervalent metal decreases from La to Lu, the Soret band of M(2,3-Nc*)$_2$

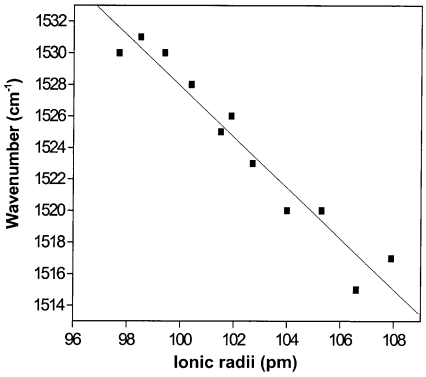


Fig. 4. Plot of wavenumber of the aza stretching scattering of M(2,3-Nc*)$_2$ [Nc* = Nc(t Bu)$_4$] at approximately 1530 cm^{-1} with excitation at 785 nm as a function of the ionic radius of M^{III}.

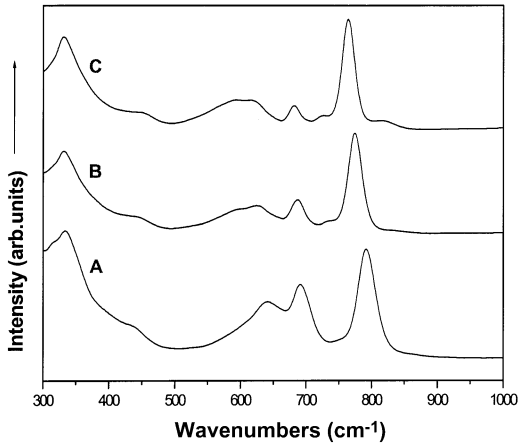


Fig. 5. Electronic absorption spectra of M(2,3-Nc*)$_2$ [Nc* = Nc(tBu)$_4$] (A) M = Ce, (B) Gd, (C) Lu in $CHCl_3$.

remains almost unchanged but the Q band and π-radical anion band are shifted to the blue [7]. As indicated from the electronic absorption, IR, and ^{1}H NMR spectra, bis(naphthalocyaninato) cerium exists in the form Ce^{III}(2,3-Nc*$^{2-}$)(2,3-Nc*$^{\bullet -}$) [Nc* = Nc(tBu)$_4$], the same as other analogues in the rare earth series [7,32]. It must be noted that in either bis(phthalocyaninato) double-deckers Ce(Pc′)$_2$ (Pc′ = Pc, Pc*) or mixed (porphyrinato)[(na)phthalocyaninato) double-deckers Ce(Por)(P) (P = Pc, 2,3-Nc) the cerium appears to exist in a mixed III/IV valency according to the recent work of Jiang, Ng, and Homborg [32,33].

The 632.8 nm laser line is far away from resonance with the most intense Q band at 767–799 nm of M(2,3-Nc*)$_2$, but is in near-resonance with the π-radical anion band and therefore would be expected to enhance particular vibrational modes. On the other hand, the 785 nm laser line is apparently in closer resonance with the intense Q band. According to the IR investigation, the unpaired electron in M(2,3-Nc*)$_2$ does delocalize over both naphthalocyanine macrocyclic ligands at a rate faster than the vibrational time scale [3,4,7,17,34]. Similarly, the Raman spectra of bis(naphthalocyaninato) rare earth(III) complexes can be attributed solely to the naphthalocyanine monoanion radical Nc*$^{\bullet -}$. This conclusion is in line with that of Tran-Thi from the Raman spectroscopic study of Gd(Pc)$_2$ [35]. When the laser excitation (632.8 nm) is well away from resonance with the Q band absorption, the strongly enhanced Raman band at approximately 1592 cm^{-1}, which is assigned to the naphthalene stretch of Nc ring, is a typical feature of naphthalocyanine monoanion radical Nc*$^{\bullet -}$, in M(2,3-Nc*)$_2$ [Nc* = Nc(tBu)$_4$]. On the other hand, when using excitation by the laser line at 785 nm, the band at approximately 1520 cm^{-1} with contributions from the aza C=N stretches, is a prominent Raman marker band for the naphthalocyanine anion Nc*$^{\bullet -}$. Moreover, the most intense band under 632.8 nm excitation (approximately 1592 cm^{-1}) is absent from these spectra.

Under excitation by either frequency, the vibrations at approximately 680 cm^{-1} assigned to the Nc breathings, approximately 1360 cm^{-1} derived from naphthalene stretchings, 1400 cm^{-1} contributed from isoindole stretchings, 1503 cm^{-1} due to the coupling of pyrrole C=C ring and aza C=N stretches, and 1515–1524 cm^{-1} contributed from the aza stretches, are sensitive to the central metal size, and are all slightly blue-shifted along with the decrease of rare earth radius. According to the recent theoretical work of Smith [36] on the IR and Raman spectra of ZnPc, the 'naphthalene stretching' band near 1360 cm^{-1} is actually from the out-of-phase indole ring expansions and the naphthalene ring deformations. Based on their theoretical investigations into the vibrational spectra of ZnPc, among the Raman active A_1 and B_1 modes, the scatterings at 1417, 1483 and 1517 cm^{-1} have been assigned to vibrations involving the aza C=N stretches. The strengths of these bonds could be easily affected by the ionic radius of the central metal and their frequencies are thus dependent on metal ionic size in the Raman spectra of phthalocyaninato metal complexes. In the sandwich-type bis(phthalocyaninato) metal complexes, X-ray single crystal molecular structure analyses have demonstrated that the degree of distortion of the Pc rings in the double-decker molecules containing different sized metal ions arises mainly from the extent of tilting of the isoindole sub-units using the bridging aza N atom as hinge [37]. Therefore, not only the scatterings at 1503 and 1515–1524 cm^{-1} but also that around 1400 cm^{-1} should be overlapped vibrations containing some contribution also from aza C=N stretches. Any modes involving the pyrrole ring nitrogens which are coordinated to the central metal ion could potentially be size-sensitive, such as the peak at approximately 1360 cm^{-1}, if it is a vibration involving pyrrole stretches coupled with the out-of-phase indole ring expansions and the naphthalene ring deformations. In view of the above, the reassignment of this band is reinforced.

Under both laser line excitations, the Raman characteristics of naphthalocyanine in Ce(2,3-Nc*)$_2$ correspond well with those of its tervalent rare earth analogues, confirming the tervalent nature of cerium in Ce(2,3-Nc*)$_2$ which is also implied by other spectroscopic techniques.

From a simplistic viewpoint, the trends in frequency of the electronic absorption bands seem to be largely responsible for the gradual changes seen in the relative intensities of some of the Raman lines, as the laser frequency more or less coincides with the most intensely absorbing region of the electronic spectrum. In order to understand and generalize the effects of changing excitation frequencies on the individual vibrational modes, we require a deeper knowledge of the electronic

structure of these complexes as well as more comparative data on other series of compounds. In a subsequent paper, we will describe the Raman characteristics of two sets of heteroleptic naphthalocyanine/porphyrin double-deckers [26].

Finally, it is worth noting that examination of our data indicates that several of the Raman bands for $Gd(2,3\text{-}Nc^*)_2$ do not correspond with those of other rare earth counterparts. This spectroscopic anomaly, however, has also been revealed in the electronic [7a] and IR [34a] absorption characteristics of the same compound compared with its analogues of the remaining rare earths in the lanthanide series. The reason might be related to the special $4f^7$ electronic configuration of Gd^{3+} but actually is not clear at this stage.

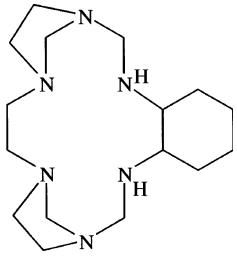
Acknowledgements

The authors thank the National Natural Science Foundation of China (Grant No. 20171028), National Ministry of Science and Technology of China (Grant No. 2001CB6105-04, 2001CB6105-06), Natural Science Foundation of Shandong Province (Grant No. Z99B03), National Educational Ministry of China, The Science Committee of Shandong Province, Shandong University, and the Centre for Instrumental and Developmental Chemistry, Queensland University of Technology for financial support.

References

[1] C.C. Leznoff, A.B.P. Lever (Eds.), Phthalocyanines—Properties and Applications, vol. 1–4, VCH, New York, 1989–1996.
[2] N.B. McKeown, Phthalocyanine Materials—Synthesis, Structure and Function, Cambridge University Press, New York, 1998.
[3] J. Jiang, K. Kasuga, D.P. Arnold, in: H.S. Nalwa (Ed.), Supramolecular Photo-sensitive and Electro-active Materials (Chapter 2), Academic Press, New York, 2001, pp. 113–210.
[4] D.K.P. Ng, J. Jiang, Chem. Soc. Rev. 26 (1997) 433.
[5] (a) J.-J. Andre, K. Holczer, P. Petit, M.-T. Riou, C. Clarisse, R. Even, M. Fourmigue, J. Simon, Chem. Phys. Lett. 115 (1985) 463;
(b) D. Markovitsi, T.-H. Tran-Thi, R. Even, J. Simon, Chem. Phys. Lett. 137 (1987) 107;
(c) M. Mardru, G. Guillaud, M. Al Sadoun, M. Maitrot, C. Clarisse, M. Le Contellec, M.J.-J. Andre, J. Simon, Chem. Phys. Lett. 142 (1987) 103;
(d) P. Turek, P. Petit, J.-J. Andre, J. Simon, R. Even, B. Boudjema, G. Guillaud, M. Maitrot, J. Am. Chem. Soc. 109 (1987) 5119;
(e) J. Simon, F. Tournilhac, J.-J. Andre, J. Appl. Phys. 62 (1987) 3304.
[6] (a) M. Maitrot, G. Guillaud, B. Boudjema, J.-J. Andre, H. Strzelecka, J. Simon, R. Even, Chem. Phys. Lett. 133 (1987) 59;
(b) H.-H. Tran-Thi, D. Markovtsi, R. Even, J. Simon, Chem. Phys. Lett. 139 (1987) 207;
(c) Z. Belarbi, M. Maitrot, K. Ohta, J. Simon, J.-J. Andre, P. Petit, Chem. Phys. Lett. 143 (1988) 400;
(d) R. Madru, G. Guillaud, M. Al Sadoun, M. Maitrot, J.-J. Andre, J. Simon, R. Even, Chem. Phys. Lett. 145 (1988) 343.
[7] (a) J. Jiang, W. Liu, K.-W. Poon, D.P. Arnold, D.K.P. Ng, Eur. J. Inorg. Chem. (2000) 205;
(b) T. Nyokong, F. Furuya, N. Kobayashi, W. Liu, D. Du, J. Jiang, Inorg. Chem. 39 (2000) 128.
[8] (a) J. Jiang, Y. Bian, F. Furuya, W. Liu, M.T.M. Choi, N. Kobayashi, H.-W. Li, Q. Yang, T.C.W. Mak, D.K.P. Ng, Chem. Eur. J. 7 (2001) 5059;
(b) J. Jiang, W. Liu, K.-L. Cheng, K.-W. Poon, D.K.P. Ng, Eur. J. Inorg. Chem. (2001) 413;
(c) F. Furuya, N. Kobayashi, Y. Bian, J. Jiang, Chem. Lett. (2001) 944;
(d) J. Jiang, D. Du, M.T.M. Choi, J. Xie, D.K.P. Ng, Chem. Lett. (1999) 261.
[9] (a) J. Jiang, W. Liu, W.-F. Law, J. Lin, D.K.P. Ng, Inorg. Chim. Acta 268 (1998) 49;
(b) J. Jiang, R.C.W. Liu, T.C.W. Mak, T.D.W. Chan, D.K.P. Ng, Polyhedron 16 (1997) 515;
(c) J. Jiang, T.C.W. Mak, D.K.P. Ng, Chem. Ber. 129 (1996) 933.
[10] (a) J. Jiang, R.L.C. Lau, T.W.D. Chan, T.C.W. Mak, D.K.P. Ng, Inorg. Chim. Acta 255 (1997) 59;
(b) R.L.C. Lau, J. Jiang, D.K.P. Ng, T.W.D. Chan, J. Am. Soc. Mass Spectrosc. 8 (1997) 161;
(c) J. Jiang, W. Liu, W.-F. Law, D.K.P. Ng, Inorg. Chim. Acta 268 (1998) 141.
[11] (a) J. Jiang, M.T.M. Choi, W.-F. Law, J. Chen, D.K.P. Ng, Polyhedron 17 (1998) 3903;
(b) J. Jiang, J. Xie, M.T.M. Choi, S. Sun, D.K.P. Ng, J. Porphyrins Phthalocyanines 3 (1999) 322.
[12] D. Chabach, M. Tahiri, A. De Cian, J. Fischer, R. Weiss, M. El Malouli Bibout, J. Am. Chem. Soc. 117 (1995) 8548.
[13] M.L. Kaplan, A.J. Lovinger, W.D. Reents, Jr., P.H. Schmidt, Mol. Cryst. Liq. Cryst. 12 (1984) 345.
[14] (a) H. Yanagi, T. Kouzeki, M. Ashida, T. Noguchi, A. Manivannan, K. Hashimoto, A. Fujishima, J. Appl. Phys. 71 (1992) 5146;
(b) H. Yanagi, T. Kouzeki, M. Ashida, J. Appl. Phys. 73 (1993) 3812.
[15] C. Jennings, R. Aroca, A.M. Hor, J.A. DeSaja, Chem. Mater. 7 (1995) 118.
[16] (a) R.E. Clavijo, C., M.M. Campos-Vallette, M. Saavedra, S., A. Alvarado, G. Diaz, F., Vib. Spectrosc. 14 (1997) 79;
(b) M. Saavedra, S., F. Mendizabal, M.M. Campos-Vallette, R.E. Clavijo, C., G. Diaz, F., Vib. Spectrosc. 18 (1998) 25;
(c) E.A. Carrasco, F., M.M. Campos-Vallette, M. Saavedra, S., G. Diaz, F., R.E. Clavijo, C., J.V. Garcia-Ramos, S. Sanchez-Cortes, Vib. Spectrosc. 26 (2001) 201.
[17] J. Jiang, D.P. Arnold, H. Yu, Polyhedron 18 (1999) 2129.
[18] (a) F. Guyon, A. Pondaven, P. Guenot, M. L'Her, Inorg. Chem. 33 (1994) 4787;
(b) F. Guyon, A. Pondaven, J.-M. Kerbaol, M. L'Her, Inorg. Chem. 37 (1998) 569.
[19] J. Jiang, L. Rintoul, D.P. Arnold, Polyhedron 19 (2000) 1381.
[20] J. Jiang, U. Cornelisson, D.P. Arnold, X. Sun, H. Homborg, Polyhedron 20 (2001) 557.
[21] Y. Bian, L. Wong, D. Zhao, J. Jiang, manuscript in preparation.
[22] (a) R. Aroca, E. Johnson, Langmuir 8 (1992) 3137;
(b) R.E. Clavijo, D. Battisti, R. Aroca, G.J. Kovacs, C.A. Jennings, Langmuir 8 (1992) 113;
(c) M.L.R. Mendez, Y. Khoussed, J. Souto, J. Sarabia, R. Aroca, J.A. de Saja, Sens. Actuators B 18–19 (1994) 89.
[23] A. Aroca, R.E. Clavijo, C.A. Jennings, G.J. Kovacs, J.M. Duff, R.O. Loutfy, Spectrochim. Acta 45A (1989) 957.
[24] (a) C.A. Jennings, A. Aroca, A.M. Hor, R.O. Loutfy, Spectrochim. Acta 41A (1985) 1095;

(b) C.A. Jennings, A. Aroca, A.M. Hor, R.O. Loutfy, Spectrochim. Acta 42A (1986) 991.
[25] C.A. Melendres, V.A. Maroni, J. Raman Spectrosc. 15 (1984) 319.
[26] Y. Bian, L. Rintoul, D.P. Arnold, N. Pan, J. Jiang, manuscript in preparation.
[27] H. Isago, M. Shimoda, Chem. Lett. (1992) 147.
[28] T. Kobayashi, F. Kurosawa, N. Uyeda, E. Suito, Spectrochim. Acta 26A (1970) 1305.
[29] I.M. Kenn, B.W. Malerbi, J. Inorg. Nucl. Chem. 27 (1965) 1311.
[30] H.F. Shurvell, L. Pinzuti, Can. J. Chem. 44 (1966) 125.
[31] J. Janczak, Polish J. Chem. 72 (1998) 1871.
[32] Y. Bian, Y. Tao, M.T.M. Choi, N. Pan, X. Sun, D.K.P. Ng, J. Jiang, manuscript in preparation.
[33] H. Homborg, personal communications.
[34] (a) X. Sun, M. Bao, N. Pan, X. Cui, D.P. Arnold, J. Jiang, Aust. J. Chem., accepted;
(b) M. Bao, Y. Bian, N. Pan, X. Cui, D.P. Arnold, J. Jiang, manuscript in preparation.
[35] T.-H. Tran-Thi, T.A. Mattioli, J. Phys. Chem. 98 (1994) 8279.
[36] D.R. Tackley, G. Dent, W.E. Smith, Phys. Chem. Chem. Phys. 2 (2000) 3949.
[37] H. Huckstadt, A. Tutab, U. Cornelissen, M. Goldner, H. Homborg, Z. Anorg. Allg. Chem. 627 (2001) 485.



L

2. Experimental

2.1. Materials and physical measurements

All chemicals and solvents used in the syntheses were of reagent grade and were used without further purification. Distilled water was used for all procedures. IR spectra were recorded on a Perkin–Elmer Paragon 1000 FT-IR spectrophotometer as KBr pellets. Solution electronic spectra were obtained on a JASCO Uvidec 610 spectrophotometer. Solid-state spectra were measured by diffuse reflectance method on a Shimadzu UV2401 PC/DRS spectrophotometer. Room temperature (r.t.) magnetic susceptibilities were measured with a Johnson Matthey MK-II magnetic balance, and the variable temperature magnetic susceptibility data on powder samples were obtained in the range 5–300 K by using a Quantum Design MPMS-7 SQUID magnetometer with 0.5 T external magnetic field. The diamagnetic corrections were evaluated from Pascal's constants. Electrochemical measurements were accomplished with a three electrode potentiostat BAS-100BW system. A hanging mercury dropping electrode was used as the working electrode. The counter electrode was a coiled Pt wire and a Ag/AgCl electrode was used as a reference electrode. Cyclic voltammetric data were obtained in dimethylformamide (DMF) solution with 0.10 M tetraethylammonium perchlorate (TEAP) as supporting electrolyte at 20.0 ± 0.1 °C. The solution was degassed with high purity nitrogen prior to carrying out the electrochemical measurements. Elemental analyses (C, H, N) were performed on a Perkin–Elmer CHN-2400 analyzer.

2.2. Preparation of $[Ni(H_2L)Cl_2]Cl_2 \cdot 2H_2O$ (2)

Compound **1** was obtained in a manner similar to the procedure described in Ref. [12]. To a MeOH solution (100 ml) of $NiCl_2 \cdot 6H_2O$ (11.9 g, 0.05 mol) was added *N*,*N*′-bis(2-aminoethyl)ethylenediamine (7.3 g, 0.05 mol), 1,2-diaminocyclohexane (5.7 g, 0.05 mol) and 37% HCHO (16.2 g, 0.2 mol). The mixture was heated to reflux for 1 day and then cooled to r.t. After an excess amount of HCl has been added, the mixture was placed in a refrigerator to complete the crystallization. The violet crystals were filtered off, washed with MeOH, and dried in air. Yield: 8.5 g (31%). *Anal*. Found: C, 35.22; H, 7.04; N, 15.28. Calc. for $C_{16}H_{38}Cl_4N_6NiO_2$: C, 35.13; H, 7.00; N, 15.36%. IR (KBr, cm^{-1}): 3212 (νNH). Magnetic moment (μ_{eff}): 2.94 μ_B at 20.0 ± 0.1 °C.

2.3. Preparation of $[Ni_2(L)_2(N_3)_4] \cdot 5H_2O$ (3)

To a MeCN solution (20 ml) of **2** (274 mg, 0.5 mmol) was added NaN_3 (65 mg, 1 mmol) and the mixture refluxed for 1 h. The solution was filtered to remove the KCl. The filtrate was allowed to stand for a few days, a quantity of violet crystals precipitated. These were collected by filtration and dried in air. Yield: 105 mg (73%). *Anal*. Found: C, 38.85; H, 7.64; N, 33.72. Calc. for $C_{32}H_{74}N_{24}Ni_2O_5$: C, 38.73; H, 7.52; N, 33.87%. IR (KBr, cm^{-1}): 3242 (νNH), 2037 (νN_3). Magnetic moment (μ_{eff}): 2.95 μ_B at 20 ± 0.1 °C.

2.4. Preparation of $[Ni(L)(tp)] \cdot 2H_2O$ (4)

A $CHCl_3$ solution (20 ml) of **2** (274 mg, 0.5 mmol) was allowed to diffuse into an aq. solution (5 ml) of sodium terephthalate (186 mg, 1 mmol) in a tube for several days. Pink crystals formed at the water | $CHCl_3$ interface. Crystals were collected by filtration and dried in air. Yield: 0.3 g (72%). *Anal*. Found: C, 50.68; H, 7.03; N, 14.67. Calc. for $C_{24}H_{40}N_6NiO_6$: C, 50.81; H, 7.11; N, 14.81%. IR (KBr, cm^{-1}): 3203 (νNH), 1569 (νCOO).

2.5. X-ray crystallography

Single-crystals of **2**, **3** and **4** were mounted at 293 K on an Enraf–Nonius CAD4 diffractometer using graphite-monochromated Mo Kα radiation ($\lambda = 0.71069$ Å) and operating the ω–2θ scan mode. Unit cell parameters and orientation matrix were determined by least-squares treatment of the setting angles of 25 reflections. The intensity data were corrected for Lp effects. Empirical absorption corrections were carried out using φ-scan. The structures were solved by direct methods [13] and refined by full-matrix least-squares on F^2 [14]. All non-hydrogen atoms were anisotropically refined. For **2**, four H aoms bound to N(1), N(2), N(5) and N(6) atoms were found from the difference Fourier and they were refined isotropically, but the H atoms of two water molecules were not located. For **3**, positional parameters of all H atoms except for Ow(1), Ow(2), Ow(3) and Ow(4) atoms were calculated geometrically and constrained to ride on their attached atoms with $U_{iso}(H) = 1.2U_{eq}$(C or N), but the H atoms of Ow(5) were not located. For **4**, all H atoms were placed in calculated positions allowing to ride on their attached atoms with

Table 1
Crysatallographic data

	2	3	4
Empirical formula	$C_{16}H_{38}Cl_4N_6NiO_2$	$C_{32}H_{74}N_{24}Ni_2O_5$	$C_{24}H_{40}N_6NiO_6$
Formula weight	547.03	992.57	567.33
Temperature (K)	293(2)	293(2)	293(2)
Wavelength (Å)	0.71069	0.71069	0.71069
Crystal system	triclinic	triclinic	monoclinic
Space group	$P\bar{1}$	P	C_2/c
Unit cell dimensions			
a (Å)	8.195(1)	8.688(5)	34.475(5)
b (Å)	11.153(1)	15.700(2)	11.230(1)
c (Å)	14.483(2)	17.457(2)	14.497(3)
α (°)	106.42(1)	109.27(1)	
β (°)	97.49(1)	90.85(2)	91.10(2)
γ (°)	103.45(1)	93.59(2)	
V (Å^3)	1207.3(2)	2241.7(14)	5611.5(16)
Z	2	2	8
D_{calc} (Mg m^{-3})	1.505	1.470	1.343
Absorption coefficient (mm^{-1})	1.271	0.909	0.739
$F(000)$	576	1060	2416
Crystal size (mm)	0.36 × 0.30 × 0.17	0.53 × 0.33 × 0.13	0.36 × 0.33 × 0.23
θ Range for data collection (°)	2.06–24.97	2.13–25.04	2.36–24.98
Index ranges	$-9 \le h \le 9$, $-13 \le k \le 12$, $0 \le l \le 17$	$-10 \le h \le 10$, $-18 \le k \le 17$, $0 \le l \le 20$	$-40 \le h \le 12$, $-13 \le k \le 12$, $-17 \le l \le 17$
Reflection collected/unique	4429/4246 [$R_{int} = 0.0158$]	8163/7878 [$R_{int} = 0.0225$]	9885/4934 [$R_{int} = 0.1240$]
Absorption correction	φ-scan	φ-scan	φ-scan
Max./min. transmission	0.994 and 0.885	1.000 and 0.744	0.842 and 0.084
Data/restraints/parameters	4246/0/292	7878/0/568	4934/0/328
Final R indices [$I > 2\sigma(I)$]	R_1[a] = 0.048, wR_2[b] = 0.136	$R_1 = 0.044$, $wR_2 = 0.093$	$R_1 = 0.096$, $wR_2 = 0.272$
R indices (all data)	$R_1 = 0.061$, $wR_2 = 0.145$	$R_1 = 0.072$, $wR_2 = 0.104$	$R_1 = 0.144$, $wR_2 = 0.321$
Goodness-of-fit on F^2	1.06	1.03	1.07
Largest difference peak and hole (e Å^{-3})	1.99 and −0.93	0.39 and −0.41	2.48 and −0.86

[a] $R_1 = \Sigma\ ||F_o| - |F_c||/\Sigma|F_o|$.
[b] $wR_2 = [\Sigma\ [w(F_o{}^2 - F_c{}^2)^2]/\Sigma\ [w(F_o{}^2)^2]]^{1/2}$.

$U_{iso}(H) = 1.2U_{eq}$(C or N). The water hydrogen atoms were not located. Crystallographic data and refinement results for the compounds are summarized in Table 1.

3. Results and discussion

3.1. Description of the structures

An ORTEP drawing of $[Ni(H_2L)Cl_2]Cl_2 \cdot 2H_2O$ (**2**) with the atomic numbering scheme is shown in Fig. 1. Selected bond distances and angles are listed in Table 2. The complex cation contains one cyclohexane subunit in the five-membered chelate ring and two 1,3-diazacyclopentane subunits in the six-membered chelate rings. The water molecules are disorderd. The complex has a distorted octahedral coordination geometry with two secondary and two tertiary amines of the macrocycle and two axial chloride ions. The macrocyclic ligand takes the most stable *trans*-III configuration. The 1,3-diazacyclopentane ring moiety assumes an envelope conformation with the N–C–C–N torsion angles of −18.2(4)° and −18.9(4)°, respectively. The 1,3-diazacyclopentane subunits of the complex are also protonated toward the uncoordinated tertiary N(5) and N(6). The Ni–N bond distances range from 2.060(3) to 2.121(3) Å, and the average of the four distances is 2.092(2) Å. These values are comparable to those of other octahedral nickel(II) complexes of 14-membered polyaza macrocyclic ligands [15–17]. The average Ni–N (secondary) distance of 2.065(2) Å is significantly shorter than the average Ni–N (tertiary) distance of 2.119(2) Å, indicating comparatively strong coordination. The N–Ni–N angles (93.8(1)° and 94.5(1)°) of six-membered chelate ring are much larger than the N–Ni–N angles (86.2(1)° and 85.8(1)°) of the five-membered chelate rings. The axial Ni–Cl distances of 2.490(1) and 2.512(1) Å can be compared to that found in $[Ni(cyclam)Cl_2]$ (2.510(1) Å) [18]. Furthermore, the axial Ni–Cl linkage is bent slightly off the perpendicular to the NiN_4 plane by 0.4°–7.1°. It is also interesting to observed that the average N(5)–C (1.503(3) Å) and N(6)–C (1.508(3) Å) distance involving the uncoordinated tertiary nitrogens is approximately 0.03 Å longer than the average N(3)–C

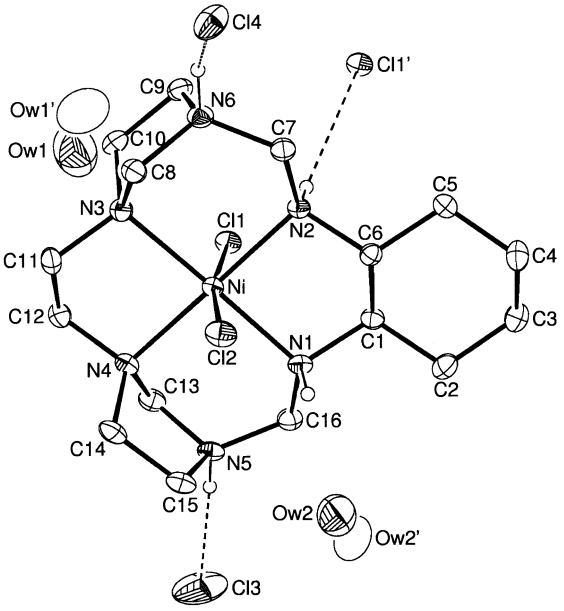


Fig. 1. An ORTEP diagram of $[Ni(H_2L)Cl_2]Cl_2\cdot 2H_2O$ (**2**) with the atom-numbering scheme (30% probability ellipsoids shown). The dotted lines indicate the hydrogen bonds.

(1.484(3) Å) and N(4)–C (1.478(3) Å) distance involving the coordinated tertiary nitrogens. This result may be attributed to the sp^3 hybridization by protonation of the uncoordinated tertiary nitrogen atoms. Interestingly, the coordinated chloride forms hydrogen bond with the secondary amine of the macrocycle ($Cl(1)^{i}\cdots N(2)$ 3.506(4) Å, 152(4)°; symmetry code: (i) $-x, -y, -z$). Furthermore, the non-coordinated chlorides form hydrogen bonds with the uncoordinated tertiary nitrogens ($Cl(3)\cdots N(5)$ 2.999(4) Å, 171(5)° and $Cl(4)\cdots N(6)$ 2.967(4) Å, 145(5)°) and with the water molecules ($Cl(3)^{ii}\cdots Ow(1)$ 3.213 Å, $Cl(4)\cdots Ow(1)'$ 3.118 Å, $Cl(3)^{iii}\cdots Ow(2)$ 2.949 Å and $Cl(3)^{iii}\cdots Ow(2)'$ 3.307 Å; symmetry codes: (ii) $-x, -y, 1-z$; (iii) $-1+x, y, z$).

An ORTEP drawing of $[Ni_2(L)_2(N_3)_4]\cdot 5H_2O$ (**3**) with the atomic numbering scheme is shown in Fig. 2. Selected bond distances and angles are listed in Table 3. There are two crystallographically independent complexes, in each of which revels an asymmetric unit. The structure of **3** shows that the nickel atom is coordinated by the two secondary and two tertiary amines of the macrocycle and that the axial positions are bonded by two nitrogen atoms of the azide ligands. The average bond distance of two axial Ni(1)–N and Ni(2)–N is similar (2.179(2) and 2.185(2) Å) and longer than the average distance of $Ni(1)N_4$ and $Ni(2)N_4$ plane (2.078(2) and 2.074(2) Å), giving an axially elongated octahedral geometry. The average Ni–N (tertiary) distance of

Table 2
Selected bond lengths (Å) and angles (°) of $[Ni(H_2L)Cl_2]Cl_2\cdot 2H_2O$ (**2**)

Bond lengths			
Ni–N(1)	2.070(3)	N(3)–C(10)	1.494(5)
Ni–N(2)	2.060(3)	N(3)–C(11)	1.496(5)
Ni–N(3)	2.116(3)	N(4)–C(12)	1.481(6)
Ni–N(4)	2.121(3)	N(4)–C(13)	1.468(6)
Ni–Cl(1)	2.512(1)	N(4)–C(14)	1.486(5)
Ni–Cl(2)	2.490(1)	N(5)–C(13)	1.482(6)
N(1)–C(1)	1.505(5)	N(5)–C(15)	1.514(6)
N(1)–C(16)	1.455(5)	N(5)–C(16)	1.514(6)
N(2)–C(6)	1.498(5)	N(6)–C(7)	1.511(5)
N(2)–C(7)	1.464(5)	N(6)–C(8)	1.500(5)
N(3)–C(8)	1.461(5)	N(6)–C(9)	1.512(6)
Bond angles			
N(1)–Ni–N(2)	86.2(1)	Ni–N(3)–C(10)	117.2(3)
N(1)–Ni–N(3)	175.6(1)	Ni–N(3)–C(11)	103.8(3)
N(1)–Ni–N(4)	93.8(1)	C(1)–N(1)–C(16)	114.4(3)
N(2)–Ni–N(3)	94.5(1)	C(6)–N(2)–C(7)	113.6(3)
N(2)–Ni–N(4)	175.7(1)	C(8)–N(3)–C(10)	100.7(3)
N(3)–Ni–N(4)	85.8(1)	C(8)–N(3)–C(11)	113.0(3)
N(1)–Ni–Cl(1)	90.4(1)	C(10)–N(3)–C(11)	113.6(3)
N(1)–Ni–Cl(2)	82.9(1)	C(12)–N(4)–C(13)	113.9(4)
N(2)–Ni–Cl(1)	84.6(1)	C(12)–N(4)–C(14)	113.8(3)
N(2)–Ni–Cl(2)	88.1(1)	C(13)–N(4)–C(14)	101.2(3)
N(3)–Ni–Cl(1)	93.9(1)	C(13)–N(5)–C(15)	104.2(3)
N(3)–Ni–Cl(2)	92.9(1)	C(13)–N(5)–C(16)	116.2(3)
N(4)–Ni–Cl(1)	91.1(1)	C(15)–N(5)–C(16)	115.5(4)
N(4)–Ni–Cl(2)	96.2(1)	C(7)–N(6)–C(8)	116.1(3)
Ni–N(1)–C(1)	106.2(2)	C(7)–N(6)–C(9)	114.8(3)
Ni–N(1)–C(16)	118.0(3)	C(8)–N(6)–C(9)	104.1(3)
Ni–N(3)–(8)	108.7(3)		

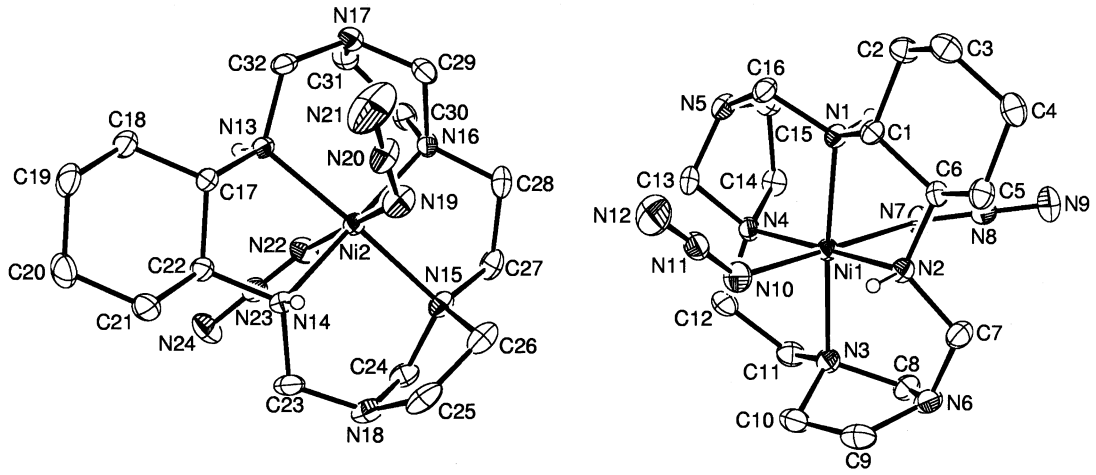


Fig. 2. An ORTEP diagram of $[Ni_2(L)_2(N_3)_4]\cdot 5H_2O$ (**3**) with the atom-numbering scheme (30% probability ellipsoids shown). Five water molecules are omitted for clarity.

Table 3
Selected bond lengths (Å) and angles (°) of $[Ni_2(L)_2(L)_2(N_3)_4]\cdot 5H_2O$

Bond lengths			
Ni(1)–N(1)	2.063(3)	Ni(2)–N(13)	2.062(3)
Ni(1)–N(2)	2.056(3)	Ni(2)–N(14)	2.052(3)
Ni(1)–N(3)	2.098(3)	Ni(2)–N(15)	2.099(3)
Ni(1)–N(4)	2.093(3)	Ni(2)–N(16)	2.081(3)
Ni(1)–N(7)	2.213(3)	Ni(2)–N(19)	2.175(3)
Ni(1)–N(10)	2.145(3)	Ni(2)–N(22)	2.195(3)
N(7)–N(8)	1.167(4)	N(19)–N(20)	1.167(4)
N(8)–N(9)	1.176(4)	N(20)–N(21)	1.147(5)
N(10)–N(11)	1.164(4)	N(22)–N(23)	1.179(4)
N(11)–N(12)	1.150(4)	N(23)–N(24)	1.171(4)
Bond angles			
N(1)–Ni(1)–N(2)	85.5(1)	N(13)–Ni(2)–N(14)	85.9(1)
N(1)–Ni(1)–N(3)	173.9(1)	N(13)–Ni(2)–N(15)	174.6(1)
N(1)–Ni(1)–N(4)	93.8(1)	N(13)–Ni(2)–N(16)	94.1(1)
N(2)–Ni(1)–N(3)	94.7(1)	N(14)–Ni(2)–N(15)	94.0(1)
N(2)–Ni(1)–N(4)	176.8(1)	N(14)–Ni(2)–N(16)	176.0(1)
N(3)–Ni(1)–N(4)	86.3(1)	N(15)–Ni(2)–N(16)	86.3(1)
N(1)–Ni(1)–N(7)	83.7(1)	N(13)–Ni(2)–N(19)	94.6(1)
N(2)–Ni(1)–N(7)	92.3(1)	N(14)–Ni(2)–N(19)	83.5(1)
N(3)–Ni(1)–N(7)	90.3(1)	N(15)–Ni(2)–N(19)	90.7(1)
N(4)–Ni(1)–N(7)	90.8(1)	N(16)–Ni(2)–N(19)	92.5(1)
N(1)–Ni(1)–N(10)	95.0(1)	N(13)–Ni(2)–N(22)	84.1(1)
N(2)–Ni(1)–N(10)	85.6(1)	N(14)–Ni(2)–N(22)	92.1(1)
N(3)–Ni(1)–N(10)	91.0(1)	N(15)–Ni(2)–N(22)	90.6(1)
N(4)–Ni(1)–N(10)	91.4(1)	N(16)–Ni(2)–N(22)	91.9(1)
N(7)–Ni(1)–N(10)	177.5(1)	N(19)–Ni(2)–N(22)	175.5(1)
Ni(1)–N(7)–N(8)	135.4(3)	Ni(2)–N(19)–N(20)	135.5(3)
N(7)–N(8)–N(9)	179.3(4)	N(19)–N(20)–N(21)	177.6(5)
Ni(1)–N(10)–N(11)	139.6(3)	Ni(2)–N(22)–N(23)	133.1(2)
N(10)–N(11)–N(12)	179.2(4)	N(22)–N(23)–N(24)	178.8(4)

2.093(2) Å is significantly longer than that of Ni–N (secondary) (2.058(2) Å). The axial Ni(1)–N and Ni(2)–N linkages are bent slightly off the perpendicular to the NiN_4 planes by 0.3°–6.3° and 0.6°–6.5°, respectively. The apical Ni–N bond distance and Ni–N–N angles related to the azide ligands are similar to the observed for $[Ni(dttd)(N_3)_2]$ (dttd = 3,14-dimethyl-2,6,13,17-tetraazatricyclo-[14,4,$0^{1.18}$,$0^{7.12}$]docosane) [15] and $[Ni(tmtt)(N_3)_2]$ (tmtt = 2,5,9,12-tetramethyl-1,4,8,11-tetraazacyclo-tetradecane) [16]. Both azide groups which act monodentate ligands are slightly asymmetric and linear within the experimental error. In contrast to **1**, the N–C bond distances of the uncoordinated tertiary amines are significantly shorter than other N–C single bond distances. This result supports an sp^2-like hybridization of the uncoordinated nitrogen atoms [11,19].

An ORTEP diagram of $[Ni(L)(tp)]\cdot 2H_2O$ (**4**) with the atomic numbering scheme is shown in Fig. 3. Selected bond distances and angles are listed in Table 4. The nickel atom occupies a distorted octahedral coordination geometry in which the macrocycle, two water molecules and two *trans* tp ligands have assembled around each nickel center. The average Ni–N (tertiary) distance of 2.094(4) Å is much longer than the average Ni–N (secondary) distance (2.028(5) Å). The average NiN_4 distance of 2.061(3) Å is similar to that found **3** and shorter than the average Ni–O (carboxylate oxygen) distance (2.152(4) Å), indicating an axially elongated octahedron in the one-dimensional chain direction. The axial Ni–O linkage is bent slightly off the perpendicular to the NiN_4 plane by 0.5°–4.5°. The coordination of the benzenedicarboxylato bridge is slightly asymmetrical; the two Ni–O(1)–C(17) and Ni–O(3)–C(21) angles are 135.8(5)° and 139.3(5)°, respectively. The Ni···Ni′ distance across the polymer backbone is 11.526 Å. The dihedral angles (α) between the plane of the benzene ring and carboxylate group are 5.1° and 11.2°. Moreover, the dihedral angles (β) between the plane of the carboxylate group and NiN_2O_2 plane are 6.0° and 15.0°, respectively. Furthermore, the average N(5)–C (1.477(6) Å) and N(6)–C (1.463(6) Å) distance involving the uncoordinated tertiary nitrogen atoms is significantly shorter than

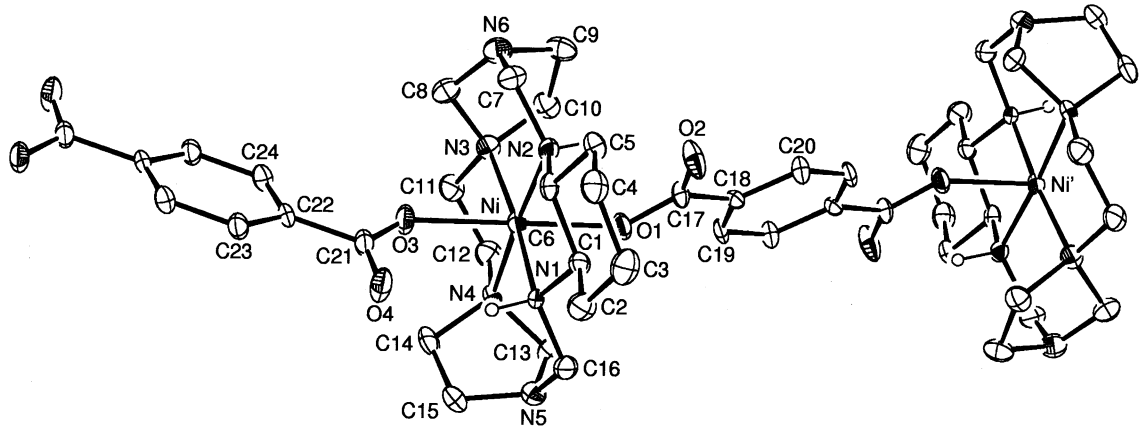


Fig. 3. An ORTEP diagram of $[Ni(L)(tp)]\cdot 2H_2O$ (**4**) with the atom-numbering scheme (30% probability ellipsoids shown). Two water molecules are omitted for clarity.

Table 4
Selected bond lengths (Å) and angles (°) of $[Ni(L)(tp)]\cdot 2H_2O$ (**4**)

Bond lengths			
Ni–N(1)	2.025(7)	Ni–O(3)	2.179(5)
Ni–N(2)	2.030(6)	O(1)–C(17)	1.282(8)
Ni–N(3)	2.084(6)	O(2)–C(17)	1.229(9)
Ni–N(4)	2.103(6)	O(3)–C(21)	1.253(9)
Ni–O(1)	2.125(5)	O(4)–C(21)	1.236(9)
Bond angles			
N(1)–Ni–N(2)	86.3(3)	N(1)–Ni–O(3)	89.3(2)
N(1)–Ni–N(3)	174.8(2)	N(2)–Ni–O(3)	93.4(2)
N(1)–Ni–N(4)	93.5(3)	N(3)–Ni–O(3)	85.5(2)
N(2)–Ni–N(3)	93.9(2)	N(4)–Ni–O(3)	90.5(2)
N(2)–Ni–N(4)	176.0(2)	O(1)–Ni–O(3)	177.2(2)
N(3)–Ni–N(4)	86.6(2)	Ni–O(1)–C(17)	135.8(5)
N(1)–Ni–O(1)	92.7(2)	O(1)–C(17)–O(2)	125.6(7)
N(2)–Ni–O(1)	88.7(2)	Ni–O(3)–C(21)	139.3(5)
N(3)–Ni–O(1)	92.5(2)	O(3)–C(21)–O(4)	126.5(7)
N(4)–Ni–O(1)	87.3(2)		

other N–C single bond distances, which indicate the sp^2-like hybridization of the uncoordinated N(5) and N(6) atoms [11,19].

3.2. Characterization of the nickel(II) complexes

The spectroscopic data of the complexes are listed in Table 5. The visible spectra of the complexes **2**–**4** in acetonitrile, DMF and the solid state show two bands at 542–556 and 845–859 nm which assigned to the spin-allowed d–d transitions $^3A_{2g}\rightarrow{}^3T_{1g}$ and $^3A_{2g}\rightarrow{}^3T_{2g}$, respectively [20]. The IR spectrum of **2** shows ν(NH) band at 3212 cm^{-1} associated with secondary amines of the macrocycle. Visible absorptions are found at 554 nm in the solid state, and at 556 and 554 nm respectively in acetonitrile and DMF solution, consistent with a distorted octahedral nickel center. However, a visible band in water shows at 458 nm, indicative of a square-planar geometry. Compound **3** reveals ν(NH) band at 3242 cm^{-1} associated with secondary amines and a strong band at 2037 cm^{-1} due to the azide stretching mode. Complex **3** exhibits a broad visible band in the solid state (547 nm), acetonitrile (551 nm) and DMF (548 nm), again consistent with a distorted octahedral environment. However, this band shifts to higher energy (463 nm) in water, indicative of a significantly structural change (square-planar geometry) in solution. The IR spectrum of **4** reveals ν(NH) of the secondary amines and ν(COO) of the carboxylate at 3203 and 1569 cm^{-1}, respectively. The diffuse reflectance absorption spectrum of **4** reveals a broad band at 540 nm, which is the characteristic spectrum expected for a high-spin d^8 nickel(II) ion in an octahedral environment [21]. However, it dissolves in water (456 nm) and decomposes into the building block, consistent with the square-planar complex $[Ni(L)](ClO_4)_2$ [12].

Table 5
Electronic spectral data [a]

Complex	State	λ_{max} nm ($\varepsilon = M^{-1}\ cm^{-1}$)
$[Ni(L)](ClO_4)_2$ (**1**) [b]	H_2O	456 (121)
	CH_3CN	459 (116)
	DMF	458 (113)
$[Ni(H_2L)Cl_2]Cl_2\cdot 2H_2O$ (**2**)	H_2O	458 (109)
	CH_3CN	556 (12), 857 (sh)
	DMF	554 (12), 859 (sh)
	Solid	554, 852
$[Ni_2(L)_2(N_3)_4]\cdot 5H_2O$ (**3**)	H_2O	463 (98)
	CH_3CN	551 (11), 849 (sh)
	DMF	548 (11), 847 (sh)
	Solid	547, 848
$[Ni(L)(tp)]\cdot 2H_2O$ (**4**)	H_2O	457 (110)
	CH_3CN	542 (12), 850 (sh)
	DMF	542 (11), 848 (sh)
	Solid	540, 845

[a] Solutions = water, acetonitrile and DMF; solid = diffuse reflectance.
[b] Ref. [12].

Cyclic voltammetric data for the nickel(II) macrotetracyclic complexes in DMF solution are given in Table

Table 6
Cyclic voltammetric data [a]

Complex	Potentials (V) vs. Ag/AgCl	
	M(II)/M(III)	M(II)/M(I)
$[Ni(L)](ClO_4)_2$ (**1**)	+0.955(i) [b]	−0.789(i) [b]
$[Ni(H_2L)Cl_2]Cl_2\cdot 2H_2O$ (**2**)	+0.739	−0.524(i) [b]
$[Ni_2(L)_2(N_3)_4]\cdot 5H_2O$ (**3**)	+0.742(i) [b]	−1.083(i) [b]
$[Ni(L)(tp)]\cdot 2H_2O$ (**4**)	+0.815(i) [b]	−0.460(i) [b]

[a] Measured in 0.10 M TEAP–DMF solution at 20.0±0.1 °C.
[b] i, irreversible.

6. A typical cyclic voltammogram of **2** is shown in Fig. 4. The complexes exhibit two one-electron waves corresponding to Ni(II)/Ni(III) and Ni(II)/Ni(I) processes. It is of interest to compare the redox potentials for the nickel(II) complexes containing the organic ligands. The oxidation potentials for **2**, **3** and **4** are considerably less positive than that for the square-planar $[Ni(L)](ClO_4)_2$ (**1**). This fact can be attributed to the coordination of the organic ligands. It has been noted that when the organic ligands of the macrotetracyclic nickel(II) complexes are coordinated to the metal ion the attainment of Ni(III) is made easier. Meanwhile, although the complexes **2**, **3** and **4** have a similar average NiN_4 bond distance, the reduction potential for **3** is much more negative than that for **2** and **4**. This result may be due to the π-donor ability of the coordinated organic ligands. The above results, together with the crystal structures and the electronic spectra, clearly show that the organic ligands are coordinated to the metal ion.

The effective magnetic moments (μ_{eff}) of **2** and **3** in the solid state are 2.94 and 2.95 μ_B at room temperature, which are consistent with a d^8 electronic configuration in an octahedral geometry. The magnetic susceptibility (χ_m) of **4** was measured from 5 to 300 K. The magnetic

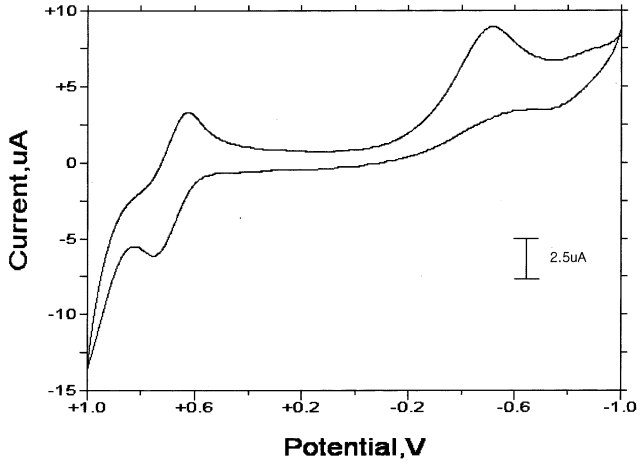


Fig. 4. Cyclic voltammogram of $[Ni(H_2L)Cl_2]Cl_2\cdot 2H_2O$ (**2**) in 0.10 M TEAP–DMF solution at 20.0±0.1 °C. The scan rate is 100 mV s^{-1}.

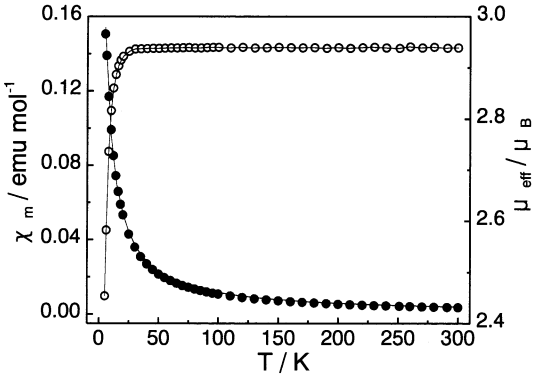


Fig. 5. Plots of χ_m vs. T (●) and μ_{eff} vs. T (○) for **4**. The solid line represents the best fit of the experimental data.

properties of the complex are given in Fig. 5 in the form of χ_m and μ_{eff} versus T show a very weak antiferromagnetic behavior. Compound **4** has a room-temperature magnetic moment ($\mu_{eff} = 2.94\ \mu_B$) close to the spin-only value for nickel(II). However, the magnetic moments gradually decrease with decreasing temperature, suggesting the presence of an antiferromagnetic coupling between the nickel(II) centers, which are clearly bridged by the carboxylate group. The magnetic susceptibility data are analyzed by Fisher's model for the classical spin chain system ($S = 1$ and $H_{chain} = -J\ \Sigma\ S_i \cdot S_{i+1}$) [22].

$$\chi_m = \{N\beta^2 g^2 S(S+1)/3kT\}\{(1+u)/(1-u)\}$$

with

$$u = \coth[JS(S+1)/kT] - [kT/JS(S+1)]$$

The parameters giving the best-fit were obtained using a nonlinear regression analysis with $g = 2.19(1)$, $J = -1.18(3)$ cm^{-1} and $R = 5.2 \times 10^{-3}$ ($R = [\Sigma\ (\chi_{obs} - \chi_{calc})^2/\Sigma\ \chi^2_{obs}]^{1/2}$). The value of the weak antiferromagnetic coupling observed in compound **4** is similar to those previously reported through bridging carboxylato in the nickel(II) chains $[Ni(dttd)(tp)]\cdot 2H_2O$ ($J = -1.37$ cm^{-1}) [23] and $[Ni(dttd)(PDC)]\cdot 2H_2O$ (PDC = 2,5-pyridinedicarboxylate) ($J = -1.47$ cm^{-1}) [23]. This fact can be understood in terms of the large intramolecular Ni···Ni′ distance and dihedral angles.

4. Supplementary material

Crystallographic data for the structural analysis have been deposited with the Cambridge Crystallographic Data Center, CCDC Nos. 179227–179229 for compounds **2**–**4**. Copies of this information may be obtained free of charge from The Director, CCDC, 12 Union Road, Cambridge, CB2 1EZ, UK (fax: +44-1223-336033; e-mail: deposit@ccdc.cam.ac.uk or www: http://www.ccdc.cam.ac.uk).

Acknowledgements

This work was supported by grant No. (R05-2001-000-00206-0) from the Basic Research Program of the Korea Science and Engineering Foundation. J. Kim also acknowledges the financial support from the Ministry of Science and Technology (NRL), Korea.

References

[1] R.M. Izatt, J.J. Christensen, Synthesis of Macrocycles, The Design of Selective Complexing Agents, Wiley, New York, 1987, pp. 1–51.
[2] L.F. Lindoy, The Chemistry of Macrocyclic Ligand Chemistry, Cambridge University Press, Cambridge, 1989.
[3] R.M. Clay, M. Micheloni, P. Paoketti, W.V. Steele, J. Am. Chem. Soc. 101 (1979) 4119.
[4] L. Fabbrizzi, A. Poggi, P. Zanello, J. Chem. Soc., Dalton Trans. (1983) 2191.
[5] M.P. Suh, W. Shin, S.-G. Kang, M.S. Lah, Inorg. Chem. 28 (1989) 1602.
[6] R.W. Hay, A. Danby, P. Lightfoot, Y.D. Lampeka, Polyhedron 16 (1997) 2777.
[7] M.R. Suissa, C. Romming, J. Dale, Chem. Commun. (1997) 113.
[8] S.V. Rosokha, Y.D. Lampeka, I.M. Maloshtan, J. Chem. Soc., Dalton Trans. (1993) 631.
[9] L. Fabbrizzi, M. Licchelli, A.M.M. Lanfredi, O. Vassalli, F. Ugozzoli, Inorg. Chem. 35 (1996) 1582.
[10] P.V. Barnhardt, E.J. Hays, Inorg. Chem. 37 (1998) 4241.
[11] S.-G. Kang, K. Ryu, S.-K. Jung, J.H. Jeong, Inorg. Chim. Acta 317 (2001) 314.
[12] S.-G. Kang, S.-K. Jung, J. Korean Chem. Soc. 35 (1991) 527.
[13] G.M. Sheldrick, Acta Crystallogr., Sect. A 46 (1990) 467.
[14] G.M. Sheldrick, SHELXL-97. Program for the Refinement of Crystal Structures, University of Göttingen, Germany, 1997.
[15] K.-Y. Choi, H. Ryu, I.-H. Suh, Polyhedron 17 (1998) 1241.
[16] K.-Y. Choi, S.N. Choi, I-H. Suh, Polyhedron 17 (1998) 1415.
[17] I.A. Fallis, L.J. Farrugia, N.M. Macdonald, R.D. Peacock, J. Chem. Soc., Dalton Trans. (1993) 2759.
[18] T. Ito, M. Kato, H. Ito, Bull. Chem. Soc. Jpn. 57 (1984) 2641.
[19] M.P. Suh, J. Choi, S.-G. Kang, W. Shin, Inorg. Chem. 28 (1989) 1763.
[20] E. Konig, Structure and Bonding, Springer, New York, 1971.
[21] G.A. Melson (Ed.), Coordination Chemistry of Macrocyclic Compounds, Plenum Press, New York, 1979, p. 534.
[22] M.E. Fisher, Am. J. Phys. 32 (1964) 343.
[23] K.-Y. Choi, K.M. Chun, I.-H. Suh, Polyhedron 20 (2001) 57.

2. Experimental

2.1. General

The following chemicals were purchased from commercial sources and used without further purification: $Na_2MoO_4{\cdot}2H_2O$ (Fluka), $NaAsO_2$ (Fluka), pyridine (Fluka), $Co(acac)_2$ (Fluka) and H_2O_2 (Fluka). All reactions and manipulations were carried out in air. The infrared spectra (4000–400 cm^{-1}) were recorded from KBr pellets on a Perkin–Elmer FT IR 1720 X spectrophotometer. Micro-analytical data were obtained from the Laboratoire de Chimie Pharmaceutique et Organique Propédeutique de l'Université de Genève, Switzerland.

2.2. Preparations

2.2.1. $[NC_5H_6]_5[Mo_8^{VI}O_{26}(OH)]{\cdot}3H_2O$ (anion **1**)

$Na_2MoO_4{\cdot}2H_2O$ (1.48 g, 6×10^{-3} mol) and pyridine (1 ml, 1.2×10^{-2} mol) were dissolved in water (8 ml), and the pH of the solution was adjusted to 5.0 by dropwise addition of diluted hydrochloric acid (2 M). The solution was heated to 130 °C in a pressure Schlenk tube (250 ml) for 2 days. Then the solution was filtered and cooled to 4 °C. The colourless crystals of the product, obtained after some days, were filtered off, washed with water and acetone and dried in vacuo. Yield: 60%. Found: C, 18.44; H, 2.54; N, 4.28. Calc. for $C_{25}H_{42}N_5Mo_8O_{30}$: C, 18.14; H, 2.25; N, 4.23%. IR (KBr): ν (cm^{-1}) 1635(m), 1605(m), 1539(m), 1487(s), 889(vs), 823(vs), 797(s), 749(m), 678(s), 608(w).

2.2.2. $[C_5H_6N]_6[HAs^{III}As^{V}Mo^{V}Mo_8^{VI}O_{34}]{\cdot}3H_2O$ (anion **2**)

$Na_2MoO_4{\cdot}2H_2O$ (1.48 g, 6×10^{-3} mol), $NaAsO_2$ (1.56 g, 1.2×10^{-2} mol) and pyridine (1 ml, 1.2×10^{-2} mol) were dissolved in water (15 ml), and the pH of the solution was adjusted to 5.0 by dropwise addition of diluted hydrochloric acid (2 M). Then the solution was heated at 130 °C in a pressure Schlenk tube for 2 days. After this period, the deep-blue solution was filtered hot and cooled to 4 °C. The resulting light-blue crystals (obtained overnight) were filtered off, washed with water and acetone and dried in vacuo. Yield: 38% (based on Na_2MoO_4). Found: C, 16.84; H, 2.15; N, 3.78. Calc. for $C_{31}H_{42}N_6As_2Mo_9O_{37}$: C, 17.22; H, 2.07; N, 4.02%. IR (KBr): ν (cm^{-1}) 2084(w, br), 1633(m), 1605(m), 1530(m), 1485(s), 931(s), 858(vs), 845(vs), 748(m), 676(s), 649(s), 607(s).

2.2.3. $[C_5H_6N]_{10}[HAs^{III}As^{V}Mo^{V}Mo_8^{VI}O_{34}\{Co(C_5H_5N)_2(H_2O)_3\}][HAs^{III}As^{V}Mo^{V}Mo_8^{VI}O_{34}]{\cdot}8H_2O$ (anions **3** and **2**)

A solution of $Co(acac)_2$ (38.65 mg, 0.147 mmol) in 4 ml of water was added to 10 ml of an aqueous solution of $[C_5H_6N]_6$**2** (300 mg, 0.147 mmol). The resulting pink solution was refluxed for 3 h. Then the solution was filtered hot and cooled to 4 °C. After several weeks light brown crystals of the product were isolated by filtration and dried in vacuo. Yield: 70% (based on **2**). Found: C, 16.77; H, 2.07; N, 3.89. Calc. for $C_{60}H_{78}N_{12}CoAs_4Mo_{18}O_{71}$: C, 16.63; H, 2.19; N, 3.88%. IR (KBr): ν (cm^{-1}) 2079(w, br), 1634(m), 1603(m), 1531(m), 1485(s), 932(s), 860(vs), 780(w), 750(m), 704(w), 680(m), 645(s), 607(m).

2.2.4. $[NBu_4]_3[As^{V}Mo_{12}^{VI}O_{40}]{\cdot}0.5H_2O_2$ (anion **4**)

A solution of NBu_4Br (316 mg, 0.98 mmol) in 5 ml of water was added to a well stirred aqueous solution (8 ml) of $[NC_5H_6]_6$**2** (200 mg, 0.098 mmol). Immediate precipitation of a light blue solid was observed. After stirring the mixture for 10 min, the precipitate, which is the tetrabutylammonium salt of **2**, was isolated on a medium-porosity filter, washed successively with 5 ml of water, 5 ml of acetone and 5 ml of diethylether and dried in vacuo. Then the isolated $[NBu_4]_6$**2** (230 mg, 0.078 mmol) was dissolved in acetonitrile (5 ml); to this solution aqueous H_2O_2 (35%, 0.05 ml, 1.56 mmol) was added dropwise. The colour changed immediately from light green to yellow. After stirring this solution for 16 h at room temperature (r.t.), 5 ml of ether were added, which caused the crystallisation of the product over several hours at r.t. The yellow crystals were isolated, washed with ether and dried in vacuo. Yield: 63% (based on **2**). Found: C, 22.01; H, 4.35; N, 3.89. Calc. for $C_{96}H_{217}N_6As_2Mo_{24}O_{85}$: C, 21.89; H, 4.15; N, 1.60%. IR (KBr): ν (cm^{-1}) 2962(m), 2933(w), 2873(w), 963(s), 898(vs), 856(m), 792(vs), 619(w).

2.3. X-ray crystallography

Relevant crystallographic data for compounds **1**, **2**, **3** and **4** are summarized in Table 1. The intensity data were collected at −120 °C on a Stoe Image Plate Diffraction system using Mo Kα graphite monochromated radiation ($\lambda = 0.71073$). The structures were solved by direct methods using the program SHELXS-97 [25] and refined by full-matrix least-squares on F^2 with SHELXL-97 [26]. The compound **1** crystallises with five pyridinium cations and three water molecules. The compound **2** crystallises with six pyridinium cations and three water molecules (four positions, two of them being half occupied). The position of the arsene hydrogen atom is derived from difference Fourier maps and freely refined while the remaining hydrogen atoms are fixed in their theoretical positions and refined as riding atoms using SHELXL-97 default parameters. An absorption correction was applied using DIFABS ($T_{min} = 0.331$, $T_{max} = 0.759$). The measured crystal of compound **3** contains co-crystallised $[(HAs_2Mo_9O_{34})\{Co(NC_5H_5)_2(H_2O)_3\}]^{4-}$ and $[HAs_2Mo_9O_{34}]^{6-}$ anions, ten pyridi-

Table 1
Crystal data for compounds **1**, **2**, **3** and **4**

	1	**2**	**3**	**4**
Empirical formula	$C_{25}H_{37}Mo_8N_5O_{30}$	$C_{30}H_{43}As_2Mo_9O_{37}N_6$	$C_{60}H_{94}As_4CoMo_{18}N_{12}O_{79}$	$C_{96}H_{217}As_2Mo_{24}N_6O_{85}$
Crystal habit	colourless block	light blue block	light brown block	yellow plate
Crystal size (mm)	0.50 × 0.40 × 0.40	0.40 × 0.40 × 0.30	0.25 × 0.20 × 0.10	0.25 × 0.20 × 0.10
M (g mol^{-1})	1655.12	2093.00	4333.00	5268.16
Temperature (K)	153(2)	153(2)	153(2)	153(2)
Crystal system	orthorhombic	monoclinic	triclinic	monoclinic
Space group	$P2_12_12_1$	$P21/n$	$P\bar{1}$	$C2/c$
a (Å)	13.1469(11)	10.0156(8)	10.0590(7)	45.343(4)
b (Å)	17.902(2)	26.1552(14)	12.6714(9)	14.1355(8)
c (Å)	18.9482(16)	20.5935(17)	25.4951(19)	26.258(2)
U (Å^3)	4459.6(7)	5307.6(7)	2978.8(4)	16714(2)
Z	4	4	1	4
D_{calc} (g cm^{-3})	2.465	2.619	2.415	2.094
$F(000)$	3192	4020	2085	10356
θ limits (°)	2.15–26.10	2.13–25.90	2.88–25.85	1.81–25.94
Reflections collected	34 981	39 747	23 221	64 026
Independent reflections	8698	9783	10793	16173
Reflections observed [$I = 2\sigma(I)$]	8198	8297	8563	8545
Goodness-of-fit on F^2 [a]	1.082	1.019	1.034	0.883
R_1, R_w [$I = 2\sigma(I)$] [b]	0.0386, 0.1085	0.0263, 0.0644	0.0476, 0.1146	0.0513, 0.1068
R_1, R_w (all data)	0.0419, 0.1121	0.0333, 0.0690	0.0609, 0.1200	0.1101, 0.1190

[a] $S = [\Sigma w(F_o^2 - F_c^2)^2/(n-p)]^{1/2}$ (n, number of reflections; p, number of parameters).
[b] $R_1 = \Sigma||F^o| - |F_c||/\Sigma|F^o|$. $wR_2 = [\Sigma w(F_o^2 - F_c^2)^2/\Sigma w(F^o)^4]^{1/2}$.

nium cations and eight water molecules. The two clusters anions occupy the same space in the crystal structure which is realised by a half occupation of the attached $Co(NC_5H_5)_2(H_2O)_3$ fragment to the cluster framework. At the same time, a pyridinium cation and two water molecules (disordered over three position), also being half occupied, use the same space than the $[Co(NC_5H_5)_2(H_2O)_3]^{2+}$ fragment. The position of the arsene hydrogen atom is derived from difference Fourier maps and fixed while the remaining hydrogen atoms are fixed in their theoretical positions and refined as riding atoms using SHELXL-97 default parameters. An absorption correction was applied using DIFABS ($T_{min} = 0.454$, $T_{max} = 0.821$). For $[NBu_4]_3$**4** there are two highly symmetrical positively charged complex molecules in the unit cell [molecule 1 (As1, Mo1-6) possessing C_2 symmetry and molecule 2 (As11, Mo11-16) possessing C_i symmetry] together with six $[NBu_4]^+$ cations. It was also possible to locate, what we assume to be, half a molecule of H_2O_2 in the unit cell. Selected bond lengths for **1**, **2**, **3** and **4** are given in Table 2.

3. Results and discussion

The metamolybdate anion $[MoO_4]^{2-}$ is known to undergo condensation in acidic media to give a variety of isopolyoxomolybdates(VI), the major species being $[Mo_7O_{24}]^{6-}$ at pH below 6 [27]. Careful adjustment of acidity, concentration and temperature, often coupled with slow crystallisation, can lead other polyoxomolybdates(VI) based on fused MoO_6 octahedra. In particular, three different octamolybdate isomers (α, β, γ), $[Mo_8O_{26}]^{4-}$, have been isolated and structurally characterised [28]. Surprisingly, we now found the anion $[MoO_4]^{2-}$ to react in aqueous solution at pH 5 with pyridine under hydrothermal conditions to give a new hydroxo octamolybdate anion, $[Mo_8^{VI}O_{26}(OH)]^{5-}$ (**1**), which crystallises as pyridinium salt. The structure of **1** derives from that of the α-isomer of $[Mo_8^{VI}O_{26}]^{4-}$ by replacing two oxygen–molybdenum bonds by a additional hydroxo bridge (Fig. 1).

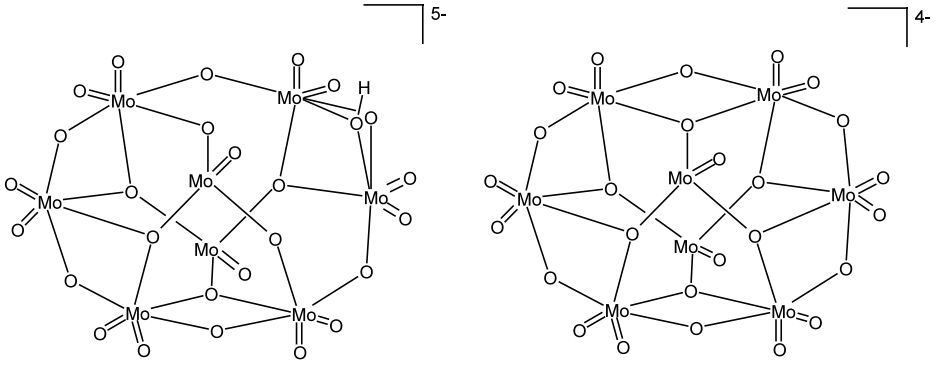
Selected bond distances of the new isopolyoxomolybdate are shown in Table 2. The structure of **1** consists of a ring of six octahedra capped by two tetrahedra (Fig. 2). Each octahedron has Mo–O bonds in the range of 1.898–1.914 Å for short, 1.916–1.998 Å for medium and 2.205–2.473 Å for long bonds. All molybdenum atoms in the ring have two terminal Mo–O(t) bonds in the short range (1.694–1.723 Å) indicating the double bond character. The capping MoO_4 units have two kinds of Mo–O bonds: Mo–O(t) (1.651–1.730 Å) and Mo–O(μ_3) (1.668–1.707 Å), and in the case of Mo(4) there are two Mo–O(μ_2) bond (1.665 and 1.668 Å), because with respect to the parent α-octamolybdate anion, two Mo(4)–O bond are opened and replaced by a new hydroxo bridge bewteen Mo(1) and Mo(2). Both ring and capping MoO_4 tetrahedral units have O–Mo–O angles in the ranges of 70.6–168.8 and 107.8–111.9°, respectively. Anion **1** can be regarded as an association of a barely perturbed α-$[Mo_8^{VI}O_{26}]^{4-}$ anion and an OH^- anion, the resulting bonds Mo(1)–O(5) and

Table 2
Selected bond lengths (Å) for compounds **1**, **2**, **3** and **4**

1		**2**		**3**		**4**	
Mo(1)–O(2)	1.698(7)	As(1)–O(2)	1.687(2)	As(1)–O(2)	1.682(4)	As(11)–O(22)	1.613(11)
Mo(1)–O(1)	1.898(6)	As(1)–O(29)	1.710(2)	As(1)–O(31)	1.717(4)	As(11)–O(40)	1.652.(12)
Mo(1)–O(5)	2.473(6)	As(2)–O(16)	1.810(2)	As(2)–O(16)	1.802(5)	As(11)–O(41)	1.673(12)
Mo(1)–O(6)	2.247(5)	As(2)–O(21)	1.802(2)	As(2)–O(21)	1.802(2)	As(11)–O(42)	1.691(11)
Mo(1)–O(4)	1.937(6)	As(2)–O(31)	1.897(2)	As(2)–O(29)	1.888(5)	Mo(11)–O(22)	2.436(10)
Mo(2)–O(6)	2.296(5)	Mo(1)–O(6)	1.702(2)	Mo(1)–O(6)	1.708(5)	Mo(11)–O(30)	1.650(6)
Mo(2)–O(7)	1.705(6)	Mo(1)–O(1)	1.956(2)	Mo(1)–O(1)	1.965(5)	Mo(11)–O(34)	1.817(8)
Mo(2)–O(8)	1.703(6)	Mo(1)–O(3)	2.226(2)	Mo(1)–O(3)	2.240(5)	Mo(11)–O(41)	2.387(11)
Mo(2)–O(9)	1.896(6)	Mo(1)–O(5)	1.727(2)	Mo(1)–O(5)	1.733(5)	Mo(12)–O(27)	1.801(8)
Mo(2)–O(4)	1.905(6)	Mo(2)–O(9)	1.932(3)	Mo(2)–O(9)	1.966(5)	Mo(12)–O(31)	1.650(6)
Mo(2)–O(5)	2.430(6)	Mo(2)–O(7)	2.263(2)	Mo(2)–O(7)	2.283(5)	Mo(12)–O(40)	2.430(12)
Mo(3)–O(10)	1.704(6)	Mo(2)–O(8)	2.289(2)	Mo(2)–O(8)	2.271(4)	Mo(12)–O(41)	2.403(11)
Mo(3)–O(12)	1.706(6)	Mo(3)–O(12)	2.252(2)	Mo(3)–O(12)	2.293(5)	Mo(13)–O(22)	2.477(12)
Mo(3)–O(16)	2.205(6)	Mo(3)–O(8)	2.331(3)	Mo(3)–O(8)	2.306(4)	Mo(13)–O(23)	1.795(7)
Mo(3)–O(9)	1.901(6)	Mo(4)–O(17)	2.342(2)	Mo(4)–O(17)	2.320(5)	Mo(13)–O(32)	1.650(6)
Mo(3)–O(14)	1.978(6)	Mo(4)–O(13)	1.885(2)	Mo(4)–O(13)	1.865(5)	Mo(13)–O(42)	2.387(11)
Mo(4)–O(22)	1.655(6)	Mo(4)–O(16)	2.259(2)	Mo(4)–O(16)	2.257(5)	Mo(14)–O(21)	1.643(6)
Mo(4)–O(18)	1.692(5)	Mo(5)–O(23)	1.711(3)	Mo(5)–O(23)	1.724(6)	Mo(14)–O(38)	2.001(7)
Mo(4)–O(16)	1.668(6)	Mo(5)–O(17)	2.331(2)	Mo(5)–O(17)	2.298(5)	Mo(14)–O(40)	2.449(11)
Mo(4)–O(17)	1.730(6)	Mo(5)–O(21)	2.309(2)	Mo(5)–O(21)	2.300(5)	Mo(14)–O(42)	2.411(11)
Mo(5)–O(19)	1.916(6)	Mo(6)–O(33)	2.231(2)	Mo(6)–O(33)	2.248(5)	Mo(15)–O(35)	1.639(6)
Mo(5)–O(14)	1.914(6)	Mo(6)–O(1)	1.957(2)	Mo(6)–O(1)	1.910(5)	Mo(15)–O(39)	1.797(8)
Mo(5)–O(18)	2.333(6)	Mo(7)–O(27)	2.119(2)	Mo(7)–O(27)	2.148(5)	Mo(15)–O(41)	2.414(11)
Mo(5)–O(20)	1.694(6)	Mo(7)–O(3)	1.772(3)	Mo(7)–O(3)	1.794(5)	Mo(15)–O(42)	2.393(10)
Mo(6)–O(22)	2.190(6)	Mo(8)–O(31)	2.196(2)	Mo(8)–O(29)	2.192(5)	Mo(16)–O(22)	2.399(10)
Mo(6)–O(27)	2.308(5)	Mo(8)–O(16)	2.031(2)	Mo(8)–O(16)	2.045(5)	Mo(16)–O(29)	2.006(8)
Mo(7)–O(18)	2.352(5)	Mo(8)–O(29)	2.368(2)	Mo(8)–O(31)	2.392(4)	Mo(16)–O(37)	1.657(6)
Mo(7)–O(27)	2.256(5)	Mo(9)–O(31)	2.148(2)	Mo(9)–O(29)	2.129(5)	Mo(16)–O(40)	2.379(12)
Mo(8)–O(6)	1.699(5)	Mo(9)–O(21)	2.057(2)	Mo(9)–O(21)	2.061(5)		
Mo(8)–O(11)	1.707(5)	Mo(9)–O(29)	2.430(2)	Mo(9)–O(31)	2.379(5)		
Mo(8)–O(15)	1.651(5)			Co(1)–O(23)	2.291(7)		
				Co(1)–O(37)	2.195(11)		
				Co(1)–N(1)	2.127(14)		
				Co(1)–N(2)	2.141(15)		

Mo(2)–O(5) are longer (2.473 and 2.430 Å) than those of the Mo(1)–O(4) and Mo(2)–O(4) bonds (1.905 and 1.937 Å) of the neighbouring oxo bridge. In the unit cell of **1**, the five pyridinium cations are crystallographically independent and have no bonding interaction with the $[Mo_8^{VI}O_{26}(OH)]^{5-}$ anion. The hydroxyl H-atom of atom O(5) was located from a difference Fourier map and held fixed with $U_{iso} = 1.5U_{eq}(05)$ Å^2.

The thermal reaction of sodium metaarsenite with sodium molybdate in pyridine and water at 130 °C



$[Mo^{VI}{}_8O_{26}(OH)]^{5-}$ (**1**) α-$[Mo^{VI}{}_8O_{26}]^{4-}$

Fig. 1. Comparison of anion **1** with the known α-octamolybdate.

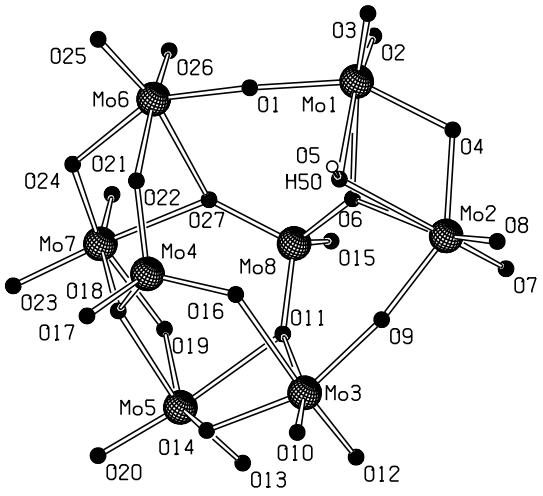


Fig. 2. ORTEP plot of $[Mo_8^{VI}O_{26}(OH)]^{5-}$ (**1**).

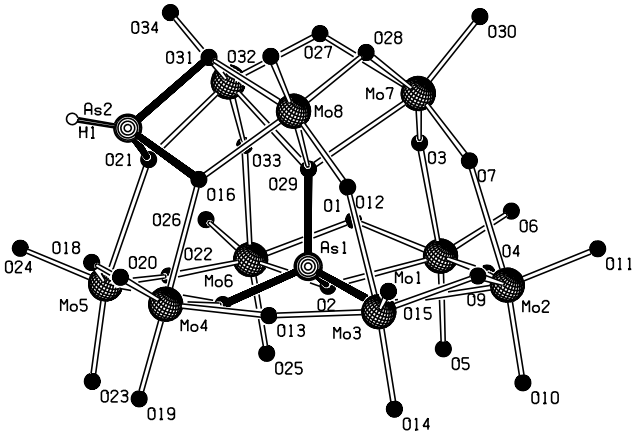
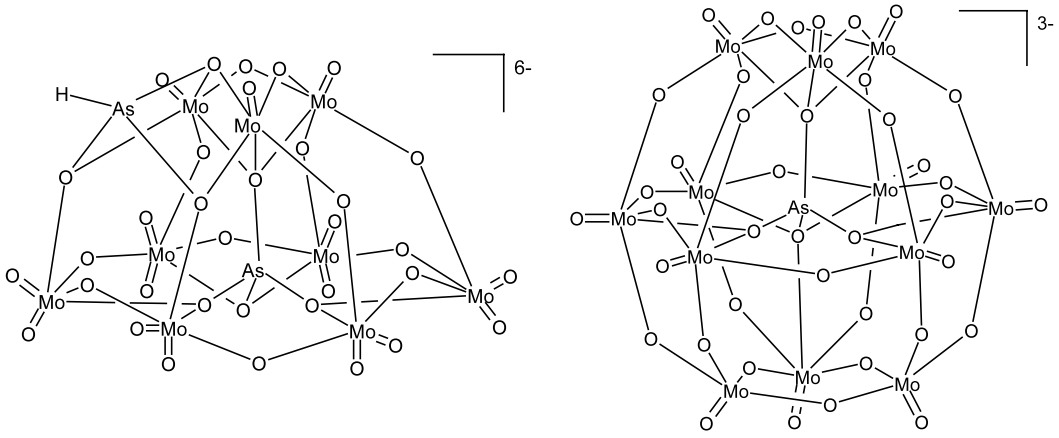


Fig. 3. ORTEP plot of $[HAs^{III}As^{V}Mo^{V}Mo_8^{VI}O_{34}]^{6-}$ (**2**).

gives after 48 h a clear blue solution. When this solution is allowed to stand for 12–16 h at 4 °C, colourless crystals of the pyridinium salt of $[HAs^{III}As^{V}Mo^{V}Mo_8^{VI}O_{34}]^{6-}$ (**2**) are obtained. The infrared spectrum of **2** exhibits characteristic ν(Mo–O), ν(Mo–O–Mo) and ν(As–O–Mo) absorptions in the region between 950 and 600 cm^{-1}. A weak absorption of 2084 cm^{-1} is assigned to the ν(As–H) vibration. In accordance with the presence of a Mo(V) centre, the ^1H NMR spectrum shows **2** to be paramagnetic.

A single-crystal X-ray structure analysis of $[C_5H_6N]_6$**2** reveals the presence of crystal water (3 equiv.). The molecular anion $[HAs^{III}As^{V}Mo^{V}Mo_8^{VI}O_{34}]^{6-}$ (**2**) shown in Fig. 3, is the second example of a monocapped trivacant 1:9 Keggin species. Its structure derives from the trivacant α-Keggin anion by removing three edge-sharing MoO_6 octahedra and by capping a trioxygen face of three remaning MoO_6 octahedra with an AsH group (Fig. 4), while the anion $[As^{III}As^{V}Mo_9^{VI}O_{34}]^{6-}$ published recently [20] derives from the β-Keggin structure.

The anion structure reveals the presence of a central AsO_4 tetrahedron which shares its four oxygen atoms with one Mo_3O_{13} group and three Mo_2O_{10} groups. These Mo_3O_{13} and Mo_2O_{10} groups are in turn joined to each other by corner-sharing, three Mo_2O_{10} groups form a 12-membered Mo_6O_6 ring, each Mo_2O_{10} group of this ring shares two oxygen atoms with a MoO_6 octahedron of the Mo_3O_{13} group. The anion is capped by a HAs group, and this group shares its oxygen atoms with four MoO_6 octahedra. The central AsO_4 tetrahedron has As(1)–O bond distances in the range of 1.675–1.710 Å. The triply bridging oxo group O(29) exhibits angles with the Mo_3O_{13} group of As(1)–O(29)–Mo(7) 122.14(11), As(1)–O(29)–Mo(8) 122.18(12) and As(1)–



$[HAs^{III}As^{V}Mo^{V}Mo^{VI}{}_8O_{34}]^{6-}$ (**2**) α-$[As^{V}Mo^{VI}{}_{12}O_{40}]^{3-}$

Fig. 4. Comparison of **2** with the α-Keggin anion.

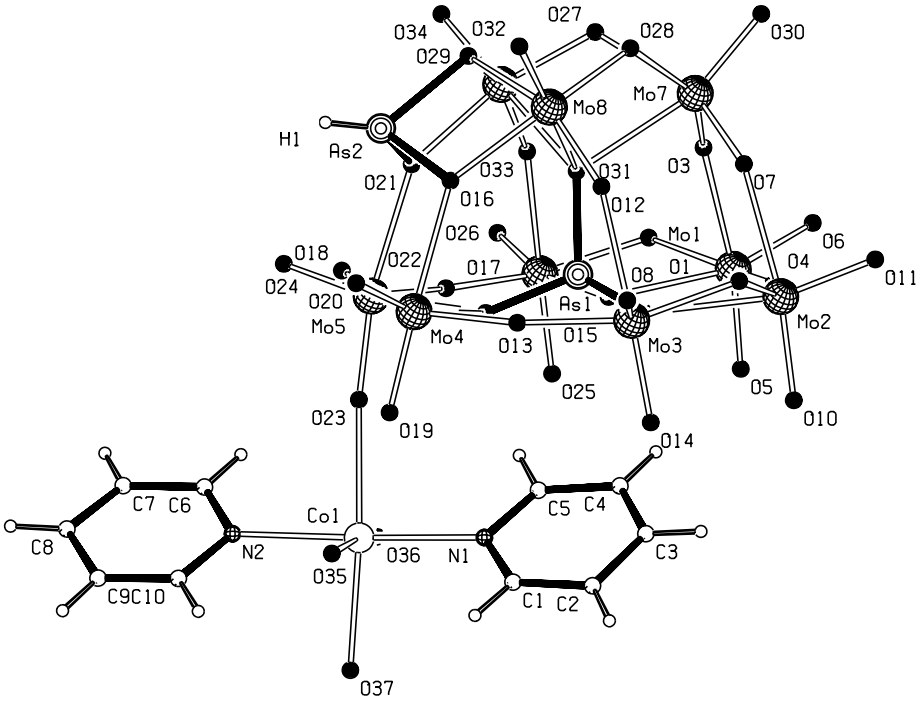


Fig. 5. ORTEP plot of $[HAs^{III}As^{V}Mo^{V}Mo_8^{VI}\ O_{34}\{Co(C_5H_5N)_2(H_2O)_3\}]^{4-}$ (**3**).

O(29)–Mo(9) 123.49°. The AsH group has two short As–O bond distances of 1.802(2) Å [As(2)–O(21)] and 1.810(2) Å [As(2)–(O16)] and one long As–O bond distance of 1.897(2) Å [As(2)–O(31)]. The O(31) associated with the long As–O bond is bonding two MoO_6 octahedra with bond angles: As(2)–O(31)–Mo(9) [97.95(11)°], As(2)–O(31)–Mo(8) [97.24(10)°] and Mo(9)–As(2)–Mo(8) [113.58(10)°]. The other oxygen atoms O(16) and O(21) associated with the short As–O distances are bonding one Mo_2O_{10} group with bond angles of: As(2)–O(16)–Mo(8) [106.34(12)°], As(2)–O(16)–Mo(4) [111.12(11)°], Mo(8)–O(16)–Mo(4) [139.93(12)], As(2)–O(21)–Mo(9) [104.58(11)°], As(2)–O(21)–Mo(8) [109.61(11)°] and Mo(9)–O(21)–Mo(8) [142.39(11)°].

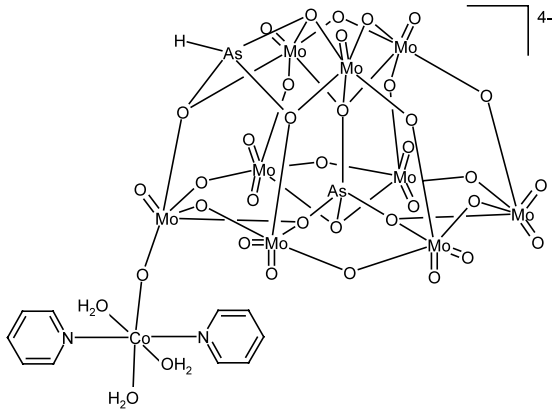


Fig. 6. Anion $[HAs^{III}As^{V}Mo^{V}Mo_8^{VI}\ O_{34}\{Co(C_5H_5N)_2(H_2O)_3\}]^{4-}$ (**3**).

The charge of **2**, determinated by valence sum calculations based on the bond distances associated with the Mo centres [29], confirmed that the electrons are effectively delocalised throughout the cluster. The oxidation state of eight of the nine Mo atoms is +6 ($\Sigma s = 5.8$–5.9) while one Mo atom is the oxydation state of +5 ($\Sigma s = 5.5$). The As (1) atom associated with the AsO_4 tetrahedron is in the oxidation state of +5, while

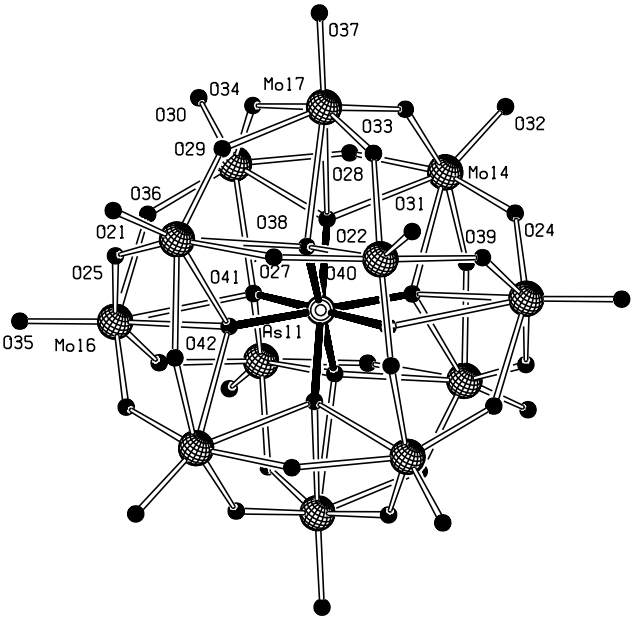


Fig. 7. ORTEP plot of $[As^{V}Mo_{12}^{VI}\ O_{40}]^{3-}$ (**4**). The central arsenic atom is coordinated to four disordered oxygen atoms; the eight positions of which are occupied to 50%.

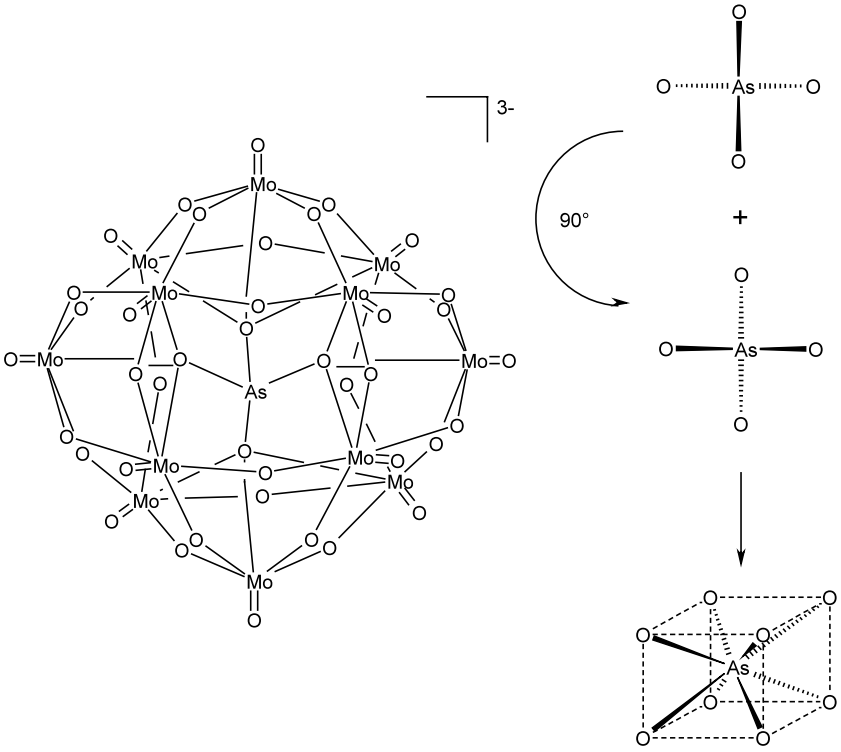


Fig. 8. Disorder in anion **4** (two of the three independent anions of the unit cell).

As(2) is in the oxidation state of +3, which explains the six negative charges of **2**.

$[C_5H_6N]_6$**2** reacts in aqueous solution with Co^{2+} (in variable amounts) at 100 °C to give the new arsenomolybdate anion $[HAs^{III}As^{V}Mo^{V}Mo_8^{VI}O_{34}\{Co(C_5H_5N)_2(H_2O)_3\}]^{4-}$ (**3**) (Fig. 5) which crystallises together with **2** as pyridinium salt. The ν(As–H) vibration is found as a weak, broad absorption at 2079 cm^{-1}. Because of the paramagnetism of **2** and **3**, a well-resolved ^1H NMR spectrum could not be recorded.

The molecular structure of **3**, solved by a single-crystal X-ray structure analysis of the pyridinium salt, is shown in Fig. 6; selected bond distances are given in Table 2. The structure of **3** derives from that of **2** by attaching a $Co(C_5H_5N)_2(H_2O)_3$ fragment to a terminal oxo ligand. The Mo(5)–O(23) distance is 1.724(6) Å, which is longer than the Mo(5)–O(23) distance found in **2** [1.711(3) Å]. In **3** the cobalt atom Co has an octahedral environment with the bond angles: O(36)–Co(1)–O(23) [84.6(3)°], N(1)–Co(1)–O(23) [91.2(4)°], N(2)–Co(1)–O(23) [87.1(5)°] and N(1)–Co(1)–O(37) [94.5(4)°], the Co–O(23) distance being 2.291(7) Å. In general, the Mo–O(t) and the Mo–O bond distances in **3** remain unaffected in relation to **2**. The charge of **3** is determinated by valence sum calculations [29] which explains the four negative charges of the anion.

The anion $[As^{V}Mo_{12}^{VI}O_{40}]^{3-}$ (**4**) is obtained by adding an excess of aqueous H_2O_2 to acetonitrile solution of $[NBu_4]_6$**2** at 20 °C. It crystallises after several hours at 4 °C as the tetrabutylammonium double-salt. A single-crystal of the tetrabutylammonium salt was analysed by X-ray crystallography; it turned out to contain the known [30] α-Keggin anion with three independent anionic molecules in the unit cell two of which being disordered. The structure of **4** is shown in Fig. 7; selected bond distances are given in Table 2. The structure is disordered because of the location of the As atom on a center of inversion, incompatible with the tetrahedral symmetry of the α-Keggin unit. This disorder leads to the apparent presence of eight oxygen atoms (50% occupancy) surrounding the central arsenic atom at the vertices of a cube, which is composed of two inverted AsO_4 tetrahedron (Fig. 8). This type of disorder has already been encountered a few times for heteropolyoxomolybdates [31] and was first described by Evans and Pope [32].

Chemically identical bond distances and angles vary only slighty with the exception of Mo–O(As) and As–O(Mo) bonds. For the α-Keggin anion structure reported [30], these distances are in the range of 2.356–2.369 and 1.658–1.666 Å, respectively. In comparasion to these values, the distances in **4** (Mo–O(As) (2.387–2.449 Å), As–O(Mo) (1.613–1.691 Å) are slightly larger. The Mo–O(t) bonds remains unaffected. The Mo–O–Mo angles are in the range of 139.8(5)–140.5(5)° which are sligthly smaller than the Mo–O–Mo angle for the α-Keggin structure. The charge of the anion is deduced from the number of tetrabutylammonium cations,

together with an examination of the Mo–O bond lengths and a calculation of bond valence sums [29].

4. Supplementary material

The crystallographic data for compounds **1**, **2**, **3** and **4** have been deposited with the Cambrigde Crystallographic Data Centre as supplementary publication: No. CCDC 166546 (**1**), CCDC 166547 (**2**), CCDC 166548 (**3**) and CCDC 166549 (**4**). Copies of this information may be obtained free of charge from The Director, CCDC, 12 Union Road, Cambridge, CB2 1EZ, UK (fax: +44-1223-336033; e-mail: deposit@ccdc.cam.ac.uk or www: http://www.ccdc.cam.ac.uk).

Acknowledgements

Financial support from the Swiss National Science Foundation (grant no. 20-61'227.00) is gratefully acknowledged.

References

[1] M.J. Morris, Coord. Chem. Rev. 146 (1985) 43.
[2] M.J. Morris, Coord. Chem. Rev. 152 (1996) 309.
[3] A. Müller, H. Reuter, S. Dillinger, Angew. Chem., Int. Ed. Eng. 34 (1995) 2328.
[4] M.T. Pope, A. Müller, Angew. Chem., Int. Ed. Eng. 30 (1991) 34.
[5] M.T. Pope, Heteropoly and Isopoly Oxometalates, Springer, New York, 1983.
[6] A. Müller, F. Reters, M.T. Pope, D. Gatteschi, Chem. Rev. 98 (1998) 23.
[7] R.C. Haushalter, L.A. Mundi, Chem. Mater. 4 (1992) 31.
[8] K.H. Lii, R.C. Haushalter, Angew. Chem., Int. Ed. Engl. 69 (1987) 320.
[9] R.C. Haushalter, K.G. Strohmaier, F.W. Lai, Science 246 (1989) 1289.
[10] K.H. Lii, J.J. Chen, S.L. Wang, Solid State Chem. 78 (1989) 178.
[11] L.A. Mundi, K.G. Strohmaier, R.C. Haushalter, Inorg. Chem. 30 (1991) 153.
[12] G. Costentin, A. Leclaire, M.M. Borel, A. Grandin, B. Raveau, Rev. Inorg. Chem. 13 (1993) 77.
[13] A. Guesdon, M.M. Borel, A. Leclaire, A. Grandin, B.J. Raveau, Solid State Chem. 111 (1994) 315.
[14] W.T.A. Harrison, L.L. Dussack, A.J. Jacobson, Inorg. Chem. 34 (1995) 4774.
[15] P. Lightfoot, D. Masson, Mater. Res. Bull. 30 (1995) 1005.
[16] S. Ledain, A. Leclaire, M.M. Borel, J. Provost, B.J. Raveau, J. Solid State Chem. 124 (1996) 24.
[17] K.F. Hsu, S.L. Wang, Inorg. Chem. 36 (1997) 3049.
[18] M.I. Khan, Q. Chen, J. Zubieta, J. Chem. Soc., Chem. Commun. (1993) 356.
[19] H. Kondo, A. Kobayashi, Y. Sasaki, Acta Crystallogr., Sect. B 36 (1980) 661.
[20] Q. He, E. Wang, W. You, C. Hu, J. Mol. Struct. 508 (1999) 217.
[21] J. Martin-Frère, Y. Jeannin, F. Robert, J. Vaissermann, Inorg. Chem. 30 (1991) 3635.
[22] A. Müller, E. Krickemeyer, M. Penk, V. Wittneben, J. Doring, Angew. Chem. 102 (1990) 84.
[23] (a) K.M. Barkigia, L.M. Rajkovic, M.T. Pope, C.O.J. Quicksall, J. Am. Chem. Soc. 97 (1975) 4146;
(b) K.M. Barkigia, L.M. Rajkovic-Blazer, M.T. Pope, E. Prince, C.O.J. Quicksall, Inorg. Chem. 19 (1980) 2531.
[24] K.F. Hsu, S.L. Wang, Inorg. Chem. 37 (1998) 3230.
[25] G.M. Sheldrick, Acta Crystallogr., Sect. A 46 (1990) 467.
[26] G.M. Sheldrick, SHELXL-97, Program for crystal structure refinement, University of Göttingen, Germany, 1997.
[27] P. Roman, A. Luque, A. Aranzabe, J.M. Gutierrez-Zorrilla, Polyhedron 11 (1992) 2027.
[28] M.L. Niven, J.J. Cruywagen, J.B.B. Heyns, J. Chem. Soc., Dalton Trans. (1991) 2007.
[29] I.D. Brown, R.D. Shannon, Acta Crystallogr., Sect. A 29 (1973) 266.
[30] L.C. Baker, J.S. Figgis, J. Am. Chem. Soc. 92 (1970) 3794.
[31] (a) J.-C.P. Gabriel, R. Nagarajan, S. Natarajan, A.K. Cheetham, C.N.R.J. Rao, J. Solid State Chem. 129 (1997) 257;
(b) R. Neier, C. Trojanowski, R.J. Mattes, J. Chem. Soc., Dalton Trans. (1995) 2521;
(c) Y. Xu, J.-Q. Xu, G.-Y Yang, G.-D Yang, Y. Ying, Y.-H Lin, Acta Crystallogr., Sect. C 54 (1998) 9;
(d) J. Fuchs, A. Thiele, R. Palm, Angew. Chem., Int. Ed. Engl. 23 (1982) 789;
(e) A. Dolbecq, E. Cadot, D. Eisner, F. Sécheresse, Inorg. Chem. 38 (1999) 4217.
[32] H.T. Evans, Jr., M.T. Pope, Inorg. Chem. 23 (1984) 501.

2. Experimental

2.1. Materials and methods

Reactions were carried out in dry solvents under a dinitrogen atmosphere using Schlenk techniques. Chemicals were obtained from commercial sources. The precursor complex $[(\eta^6\text{-}p\text{-cymene})RuCl_2]_2$ was prepared by a literature method [19]. The chiral Schiff base (HL*) was prepared by condensation of 3,5-di-*t*-butyl-2-hydroxybenzaldehyde (Aldrich) and (*S*)-α-methylbenzylamine (Fluka) using a method reported for the preparation of (*S*)-(α-methylbenzyl)salicylaldimine [20]. Solvents were purified by standard procedures [21]. Elemental analysis was performed on a Perkin–Elmer model 2400 CHN analyzer. NMR measurements were carried out using a Bruker AMX 400 MHz spectrometer.

2.2. Preparation of *[(η⁶-p-cymene)Ru{2-O-(3,5-di-t-Bu)C₆H₂CH=NCH(Me)Ph}Cl] (1)*

A 200 mg (0.33 mmol) quantity of $[(\eta^6\text{-}p\text{-cymene})RuCl_2]_2$ was reacted with 225 mg (0.66 mmol) of the Schiff base (HL*) and 0.14 cm^3 (1.0 mmol) of NEt_3 in 15 cm^3 CH_2Cl_2 under stirring for 3 h at 0 °C. The orange–red solution was filtered and the filtrate was reduced to a volume of ~2 cm^3. *n*-Hexane (10 cm^3) was added to the solution to precipitate the complex which was isolated and thoroughly washed with *n*-hexane and finally dried in vacuum. Yield: 360 mg (0.59 mmol, 90%). *Anal.* Found: C, 65.41; H, 7.05; N, 2.42. Calc. for $C_{33}H_{44}ClNORu$: C, 65.24; H, 7.25; N, 2.31%. ^{1}H NMR data for the major diastereomer (88%) in $CDCl_3$ at 293 K (δ, ppm; multiplicity; $^3J_{HH}$, Hz): *p*-cymene ligand, 1.05, 1.16 (d, 7.2, CH*Me*$_2$); 2.16 (s, Me); 2.75 (sp, 6.0, *CH*Me$_2$); 4.84, 4.88, 5.06, 5.24 (d, 6.0, ring H); Chiral Schiff base, 1.21, 1.42 (s, CMe_3); 1.82 (d, 6.8, C*–Me); 5.82 (q, 6.0, C*–H); 6.68, 7.24 (s, ring C_6H_2); 7.45 (m, C*–Ph); 7.84 [s, N=CH (imine)]. ^{1}H NMR data for the minor diastereomer (12%) in $CDCl_3$: 0.82, 0.84 (d, 7.2, CH*Me*$_2$); 2.36 (s, Me); 2.90 (sp, 6, *CH*Me$_2$); 5.02, 5.19, 5.41, 5.44 (d, 6.0, ring H); Chiral Schiff base, 1.18, 1.21 (s, CMe_3); 1.96 (d, 6.8, C*–Me); 5.65 (q, 6.0, C*–H); 6.48, 7.35 (s, ring C_6H_2); 7.40 (m, C*–Ph); 7.58 (s, imine H) [s, singlet; d, doublet; q, quartet; sp, septet; m, multiplet]. The ^{1}H NMR spectrum at 233 K in $CDCl_3$ showed a shift only for the *p*-cymene ring protons. The data for the cymene ring protons of the major isomer at 233 K are: 4.75, 4.90 (d, $^3J_{HH} = 4.1$ Hz); 5.11, 5.33 (d, $^3J_{HH} = 5.2$ Hz).

2.3. Crystallographic analysis for *[(η⁶-p-cymene)Ru{2-O-(3,5-di-t-Bu)C₆H₂CH=NCH(Me)Ph}Cl] (1)*

Single crystals suitable for X-ray diffraction were grown by a slow diffusion technique in which *n*-hexane was layered above the CH_2Cl_2 solution of **1** at −5 °C under a dinitrogen atmosphere. A crystal of approximate size $0.41 \times 0.53 \times 0.56$ mm was mounted on a glass fiber with epoxy cement. Unit cell dimensions were obtained using twenty centered reflections in the θ range 8.16–17.77 on an Enraf–Nonius CAD4 diffractometer equipped with graphite monochromated Mo Kα radiation ($\lambda = 0.71073$ Å). The intensity data were collected by ω–2θ scan mode within $2^\circ \le 2\theta \le 50^\circ$ for $0 \le h \le 11$, $-10 \le k \le 12$, $-20 \le l \le 20$ in the triclinic crystal system. Out of 5696 unique reflections, 5317 with $I > 2\sigma(I)$ were used for structure solution and refinement. Data were corrected for Lorentz and polarization effects.

The structure was solved in the triclinic space group $P1$ by the combination of Patterson and Fourier techniques and refined by full-matrix least-squares. The PLATON checks on the $P1$ structure suggested that it could be described in the centrosymmetric space group $P\bar{1}$, where there was an almost perfect match for all the non-hydrogen atoms except the methyl carbons C19 and C52 that are attached to the chiral C18 and C51 atoms, respectively. This ruled out the $P\bar{1}$ space group. All non-hydrogen atoms were refined anisotropically. The hydrogen atom positions were generated and assigned isotropic thermal parameters using a riding model. The hydrogen atoms' numbering was same as the carbon they are attached to. An absorption correction was made to the data using DIFABS after obtaining the complete structural model [22]. In the final cycle of refinement, each ruthenium atom was found to have a residual peak of ~1.2 e Å^{-3} situated ~1.0 Å from the metal center. These two residual peaks had no significant effect on the structural parameters and were left as such. The final refinement was converged to $R_1 = 0.0408$ and $wR_2 = [\Sigma\, w\{(F_o^2 - F_c^2)^2/\Sigma\, w(F_o^2)^2\}]^{1/2} = 0.1097$ with a weighting scheme: $w = 1/[\sigma^2(F_o^2) + (0.0963P)^2 + 0.0711P]$, where $P = (F_o^2 + 2F_c^2)/3$ [*R* indices (all data): $R = 0.0433$, $wR = 0.1124$] using 667 parameters and 5696 data. The goodness-of-fit on F^2 was 1.066 and the maximum shift/e.s.d. was 0.001. The highest peak in the final ΔF map, other than those two residual peaks near ruthenium, was 0.96 e Å^{-3}. All calculations were done using PC versions of the SHELX system of programs [23]. The perspective view of the molecules were obtained using ORTEP [24].

2.3.1. Crystal data

$C_{33}H_{44}ClNORu$ **1** (**1a**, **1b**), $M = 607.2$, triclinic, space group $P1$ (no. 1), $a = 9.638(4)$, $b = 10.138(3)$, $c = 17.599(6)$ Å, $\alpha = 84.13(1)^\circ$, $\beta = 80.89(1)^\circ$, $\gamma = 63.87(4)^\circ$,

$U = 1523.4(9)$ Å^3, $F(000) = 636$, $Z = 2$, $D_{calc} = 1.324$ g cm^{-3}, Mo Kα radiation, $\lambda = 0.71073$ Å, μ (Mo Kα) = 6.27 cm^{-1}, $T = 293(2)$ K.

3. Results and discussion

3.1. Synthesis and ^{1}H NMR spectra

The complex [(η^6-*p*-cymene)Ru(L*)Cl] (**1**) has been prepared as a diastereomeric mixture of two species **1a** and **1b** from a reaction of [(η^6-*p*-cymene)$RuCl_2]_2$ with the N,O-donor chiral Schiff base (*S*)-HO-2-(3,5-di-*t*-Bu)C_6H_2CH=NCH(Me)Ph and NEt_3 in CH_2Cl_2 at 0 °C. The complex is moderately stable in the solid state but unstable in a solution phase. The ^{1}H NMR spectral data in $CDCl_3$ suggest a 1:1 molar ratio of the *p*-cymene and the Schiff base ligand in **1**. The spectral features indicate the presence of two diastereomers in a 88:12 ratio (Fig. 1). The *p*-cymene ring protons appear as doublets in the range δ 4.8–5.4 ppm. The methyl and isopropyl methyl protons of *p*-cymene are observed as singlet and doublets in the δ range 2.2–2.4 and 1.7–2.0 ppm, respectively. The septet corresponding to the isopropyl proton appears at ~2.8 ppm. The *t*-butyl, C*–Me and C*–H protons of the Schiff base display signals in the respective δ ranges 1.2–1.6, 1.7–1.9 and 5.6–5.8 ppm. The peaks in the aromatic region are assignable to the imine proton and the phenyl ring protons of the Schiff base. The diastereomeric ratio remains the same in the spectra recorded at 233 K with a minor shift of the *p*-cymene ring protons along with a minor broadening of the signals.

3.2. Crystal structure

The crystals of complex **1** belong to the triclinic space group $P\bar{1}$ (no. 1) with two molecules in the unit cell. The structure was refined with the expected S_C-configuration of the chiral carbon of the Schiff base ligand. The ruthenium atom configuration is obtained using a priority sequence: η^6-*p*-cymene > Cl > O(L*) > N(L*) [25]. The structure consists of two diastereomers in a 1:1 molar ratio having (R_{Ru}, S_C)- and (S_{Ru}, S_C)-configurations. The ORTEP views of the molecules differing in metal configuration are shown in Fig. 2. Selected bond distances and angles are given in Table 1. The molecular species (R_{Ru}, S_C)-**1a** and (S_{Ru}, S_C)-**1b** consist of a *p*-cymene ligand showing η^6-mode of bonding, a terminal chloride and a bidentate N,O-donor chelating chiral Schiff base ligand.

A general observation in the molecular structures of the diastereomers **1a** and **1b** is the presence of non-covalent CH–π attractive interaction involving the phenyl group attached to the chiral carbon and two *p*-cymene ring protons [10,26–28]. While the distances from H(6) and H(7) to the centroid of the phenyl group (C^0_{Ph}) attached to the chiral carbon are 3.183 and 3.859

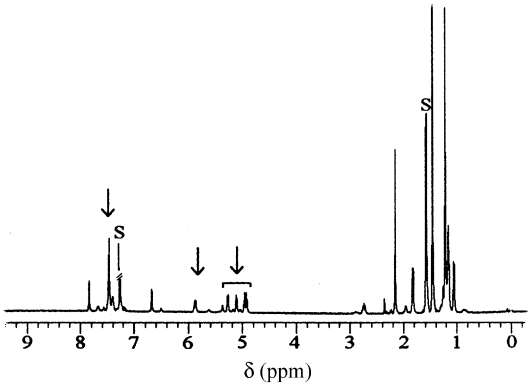


Fig. 1. ^{1}H NMR spectrum of complex **1** in $CDCl_3$ at 293 K displaying a diastereomeric ratio of 88:12. Arrows in the spectrum indicate diagnostic signals used for the 2D measurements (S, solvent peaks).

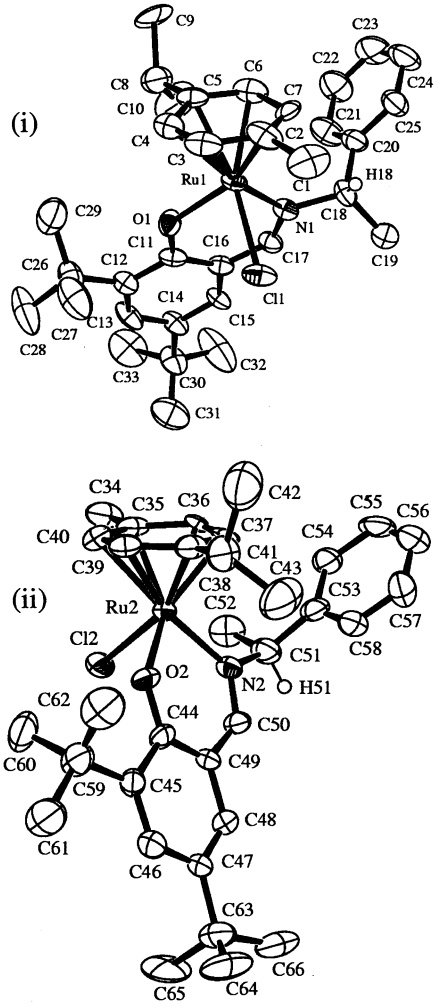


Fig. 2. ORTEP view of the two diastereomers (R_{Ru}, S_C)-**1a** (i) and (S_{Ru}, S_C)-**1b** (ii) showing thermal ellipsoids at the 50% probability level along with the atom numbering scheme.

Table 1
Selected bond lengths (Å) and angles (°) for [(η^6-*p*-cymene)Ru{2-*O*-(3,5-di-*t*-Bu)C_6H_2CH=NCH(Me)Ph}Cl] [(R_{Ru}, S_C)-**1a**, (S_{Ru}, S_C)-**1b**] [a]

Molecule **1a**		Molecule **1b**	
Bond lengths			
Ru(1)–Cl(1)	2.424(3)	Ru(2)–Cl(2)	2.414(3)
Ru(1)–O(1)	2.069(6)	Ru(2)–O(2)	2.044(7)
Ru(1)–N(1)	2.100(8)	Ru(2)–N(2)	2.110(8)
Ru(1)–C(2)	2.226(9)	Ru(2)–C(35)	2.223(9)
Ru(1)–C(3)	2.201(11)	Ru(2)–C(36)	2.225(8)
Ru(1)–C(4)	2.153(9)	Ru(2)–C(37)	2.160(8)
Ru(1)–C(5)	2.221(10)	Ru(2)–C(38)	2.155(10)
Ru(1)–C(6)	2.198(10)	Ru(2)–C(39)	2.197(9)
Ru(1)–C(7)	2.177(9)	Ru(2)–C(40)	2.186(11)
Ru(1)–C^0_{1a}	1.684(12)	Ru(2)–C^0_{1b}	1.673(10)
Bond angles			
O(1)–Ru(1)–N(1)	88.0(3)	O(2)–Ru(2)–N(2)	88.4(3)
O(1)–Ru(1)–Cl(1)	86.3(2)	O(2)–Ru(2)–Cl(2)	85.7(3)
O(1)–Ru(1)–C^0_{1a}	125.1(1)	O(2)–Ru(2)–C^0_{1b}	123.5(6)
N(1)–Ru(1)–Cl(1)	82.0(2)	N(2)–Ru(2)–Cl(2)	82.8(2)
N(1)–Ru(1)–C^0_{1a}	132.8(9)	N(2)–Ru(2)–C^0_{1b}	134.1(9)
Cl(1)–Ru(1)–C^0_{1a}	127.2(9)	Cl(2)–Ru(2)–C^0_{1b}	126.9(3)

[a] C^0_{1a} and C^0_{1b} are the centroids of the η^6-*p*-cymene rings in molecules **1a** and **1b**, respectively.

Å, the separation between the C^0_{Ph} and the cymene ring protons H(3), H(4) is ~7 Å. In **1a**, the H(6) and H(7) atoms are likely to be involved in CH–π interaction. In **1b**, the H(36) and H(37) atoms are involved in CH–π interaction [$C^0_{Ph}\cdots$H(36), 3.584; $C^0_{Ph}\cdots$H(37), 2.922; $C^0_{Ph}\cdots$H(39), H(40), ~7 Å]. Such an interaction restricts the number of diastereomers to two with the methyl group (C*–Me) or the proton (C*–H) attached to the chiral carbon orienting themselves differently with respect to the cymene group.

In the (R_{Ru}, S_C)-diastereomer, the distances from the centroid of the *p*-cymene ring to the H and Me attached to the chiral carbon are 3.627 and 5.419 Å, respectively. The H atom attached to C* has a 'proximal' geometry with respect to the *p*-cymene ring. In the (S_{Ru}, S_C)-diastereomer, the $C^0_{1b}\cdots$H(51) and $C^0_{1b}\cdots$C(52) spatial separations are 5.124 and 4.387 Å. Another structural feature is the proximity of H(18) to the Cl atom in **1a** [Cl(1)···H(18), 3.431; Cl(1)···C(19), 4.252 Å], while the methyl group in the other diastereomer lies in the proximity of the chloride [Cl(2)···C(52), 3.496; Cl(2)···H(51), 4.360 Å]. From the steric point of view, the diastereomer with a (R_{Ru}, S_C)-configuration having H(18) in proximity to the chloride atom is expected to be the thermodynamically more stable species compared with the (S_{Ru}, S_C)-diastereomer having C*–Me near the Cl atom [10].

3.3. 2D NMR spectra

The crystal structure of **1** shows the presence of two diastereomers having (R_{Ru}, S_C)- and (S_{Ru}, S_C)-configurations in a 1:1 ratio. The solution ^{1}H NMR spectrum of the crystalline sample in $CDCl_3$ displays the presence of two diastereomers in a 88:12 ratio. The ^{1}H NMR data are not adequate enough for an unequivocal determination of the metal configuration of the diastereomers in the solution phase. We have thus made investigations using 2D NMR spectroscopy, which has enabled us to analyze the diastereomeric mixture of **1** in solution.

The presence of a rapid inter-conversion between the diastereomers in **1** is observed in the 2D ROESY spectra at 293 K showing exchange cross peaks. Such an exchange, however, reduces considerably at 233 K. The NOE cross peaks involving the C*–Ph and two *p*-cymene ring protons suggest the presence of CH–π interaction in the solution phase (Fig. 3(a)). This interaction imposes restriction of rotation around the C*–N single bond. It is again observed that the C*–H proton in the major isomer which appears as a quartet at δ 5.8 ppm displays cross peaks with the cymene ring protons (Fig. 3(b)). The C*–Me protons of the major isomer do not show any such cross peaks with the cymene ring protons. This is indicative of a close proximity of the C*–H moiety to the cymene ring while the C*–Me is away from the same in the major diastereomer. The 2D NMR spectral features suggest a (R_{Ru}, S_C)-configuration for the major diastereomer in solution.

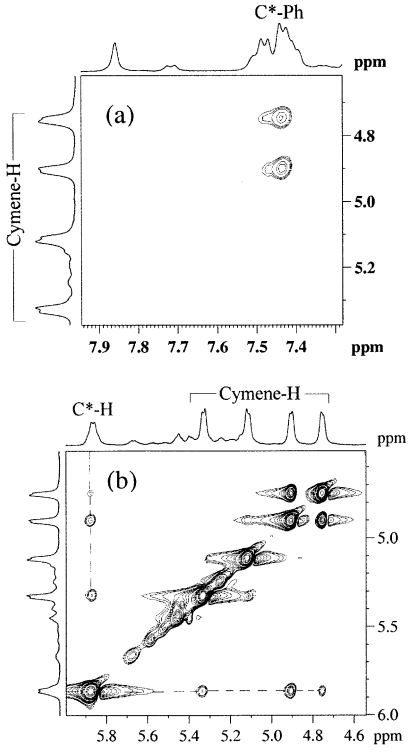


Fig. 3. The 400 MHz ^{1}H ROESY spectrum of **1** in $CDCl_3$ at 233 K for the major diastereomer showing (a) CH–π interaction and (b) the cross peaks involving the C*–H and the *p*-cymene ring protons.

The crystal structure shows the separations of the hydrogen atoms H(3), H(4), H(6) and H(7) of the *p*-cymene ring from the H(18) atom attached to the chiral carbon in the (R_{Ru}, S_C)-diastereomer as 5.071, 5.602, 3.413 and 2.235 Å, respectively. It is likely that the H(7) atom because of its proximity would interact strongly with H(18). The intensity of the NOE cross peaks helps us to assign the protons involved in this interaction. The peak, observed at δ 4.90 ppm in the ^{1}H NMR spectrum at 233 K in $CDCl_3$, is assignable to H(7). The atoms H(6) and H(7) show NOE cross peaks with the phenyl group attached to C* due to the CH–π interaction (Fig. 3(a)). The signal at δ 4.75 ppm is assignable to the H(6) atom of the cymene ring. The up-field shift of the H(6) and H(7) protons is possibly due to the shielding effect caused by the phenyl group involved in the CH–π interaction. Interestingly, the H(6) proton having a distance of 3.4 Å from H(18) shows only a weak interaction while the H(3) atom which appears at δ 5.33 ppm displays a relatively stronger interaction with H(18). This suggests a dynamic process to be operative in solution by which the H(3) proton may come closer to H(18). The peak at δ 5.11 ppm is assignable to the H(4) proton as it shows NOE cross peaks to the methyl protons [H(1A)–H(1C)] of the *p*-cymene ligand. The 2D NMR spectral studies have been done with only the major diastereomer as the proton signals of the minor species (12%) are not found to be suitable for the NOE measurements.

4. Conclusions

We have prepared and structurally characterized a new diastereomeric (η^6-arene)ruthenium(II) complex [(η^6-*p*-cymene)Ru{2-O-(3,5-di-*t*-Bu)C_6H_2CH=NCH(Me)Ph}Cl] (**1**). The complex crystallizes in the triclinic space group *P*1 with two diastereomers (R_{Ru}, S_C)-**1a** and (S_{Ru}, S_C)-**1b** in a 1:1 ratio in the unit cell. Complex **1**, however, shows the presence of two diastereomers in a 88:12 ratio in $CDCl_3$ as evidenced from the ^{1}H NMR spectrum. Both the diastereomers are stabilized by non-covalent CH–π attractive interaction involving the phenyl group attached to the chiral carbon and two hydrogen atoms of the *p*-cymene ring. The di-*t*-butyl group on the chiral ligand has caused a marginal enrichment of the d.e. to 76 from the 70% d.e. reported for its salicylaldimine analogue [7].

The 2D NMR spectra of the complex displays spatial interaction of the *p*-cymene ring protons with the proton(s) of either the C*–H of (R_{Ru}, S_C)-**1a** or the C*–Me of (S_{Ru}, S_C)-**1b**. The major diastereomer shows NOE cross peaks that are indicative of a 'proximal' arrangement of the C*–H proton to the cymene ring. This suggests a (R_{Ru}, S_C)-configuration for the major diastereomer in solution. The 2D NMR spectroscopic results along with the single crystal X-ray structural data have enabled us to unequivocally determine the metal configuration in the major diastereomer of **1** in solution.

5. Supplementary material

Crystallographic data for the structural analysis have been deposited with the Cambridge Crystallographic Data Centre (CCDC), CCDC No. 178110 for complex **1**. Copies of the information may be obtained free of charge from The Director, CCDC, 12 Union Road, Cambridge, CB2 1EZ, UK (fax: +44-1223-336033; e-mail: deposit@ccdc.cam.ac.uk or www: http://www.ccdc.cam.ac.uk).

Acknowledgements

We thank the Council of Scientific and Industrial Research (CSIR), New Delhi, for funding and the Sophisticated Instruments Facility, Indian Institute of Science, Bangalore, for providing the NMR facility.

References

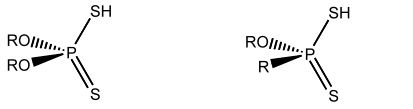
[1] (a) R. Noyori, Asymmetric Catalysis in Organic Synthesis, Wiley-Interscience, New York, 1994;
(b) R. Noyori, S. Hashiguchi, Acc. Chem. Res. 30 (1997) 97;
(c) T. Ohkuma, R. Noyori, in: E.N. Jacobsen, A. Pfaltz, H. Yamamoto (Eds.), Comprehensive Asymmetric Catalysis, Springer Press, New York, 1999, p. 1;
(d) K. Mikami, T. Korenaga, M. Terada, T. Ohkuma, T. Pham, R. Noyori, Angew. Chem., Int. Ed. 38 (1999) 495.

[2] (a) H. Brunner, Angew. Chem., Int. Ed. 38 (1999) 1194;
(b) H. Brunner, Acc. Chem. Res. 12 (1979) 251;
(c) H. Brunner, Adv. Organomet. Chem. 18 (1980) 151;
(d) H. Brunner, M. Prommesberger, Tetrahedron Asymm. 9 (1998) 3231.

[3] (a) D.G.I. Petra, P.C.J. Kamer, P.W.N.M. van Leeuwen, K. Goulbitz, A.M.V. Loon, J.G.D. Vries, H.E. Schoemaker, Eur. J. Inorg. Chem. (1999) 2335;
(b) P. Braunstein, M.D. Fryzuk, F. Naud, S.J. Rettig, J. Chem. Soc., Dalton Trans. (1999) 589;
(c) K. Everaere, J.F. Carpentier, A. Mortreux, M. Bulliard, Tetrahedron Asymm. 10 (1999) 4663;
(d) J. Harlow, A.F. Hill, J.D.E.T. Wilton-Ely, J. Chem. Soc., Dalton. Trans. (1999) 285.

[4] (a) D.G.I. Petra, J.N.H. Reek, J.W. Handgraff, E.J. Meijer, P. Dierkes, P.C.J. Kamer, J. Brussee, H.E. Schoemaker, P.W.N.M. van Leeuwen, Chem. Eur. J. 6 (2000) 2818;
(b) Y.R.S. Laxmi, J.E. Backvall, Chem. Commun. (2000) 611;
(c) A. Katho, D. Carmona, F. Viguri, C.D. Remacha, J. Kovacs, F. Joo, L.A. Oro, J. Organomet. Chem. 593–594 (2000) 299;
(d) M. Bernard, F. Delbecq, P. Sautet, F. Fache, M. Lemaire, Organometallics 19 (2000) 5715;
(e) A.J. Davenport, D.L. Davies, J. Fawcett, S.A. Garratt, D.R. Russell, J. Chem. Soc., Dalton Trans. (2000) 4432;
(f) J.W. Faller, J. Parr. Organometallics 19 (2000) 1829;

(g) V. Ritleng, J.P. Sutter, M. Pfeffer, C. Sirlin, Chem. Commun. (2000) 129.
[5] (a) D.L. Davies, J. Fawcett, S.A. Garratt, D.R. Russell, Organometallics 20 (2001) 3029;
(b) J.W. Faller, A. Lavoie, J. Organomet. Chem. 630 (2001) 17;
(c) J.W. Faller, B.J. Grimmond, D.J. D'Alliessi, J. Am. Chem. Soc. 123 (2001) 2525;
(d) C.S. Hauser, C. Slugovc, K. Mereiter, R. Schmid, K. Kirchner, L. Xiao, W. Weissensteiner, J. Chem. Soc., Dalton Trans. (2001) 2989.
[6] S.K. Mandal, A.R. Chakravarty, J. Organomet. Chem. 417 (1991) C59.
[7] S.K. Mandal, A.R. Chakravarty, J. Chem. Soc., Dalton Trans. (1992) 1627.
[8] S.K. Mandal, A.R. Chakravarty, Inorg. Chem. 32 (1993) 3851.
[9] H. Brunner, R. Oeschey, B. Nuber, Inorg. Chem. 34 (1995) 3349.
[10] H. Brunner, R. Oeschey, B. Nuber, J. Chem. Soc., Dalton Trans. (1996) 1499.
[11] H. Brunner, C. Valério, M. Zabel, New J. Chem. 24 (2000) 275.
[12] H. Brunner, Eur. J. Inorg. Chem. (2001) 905.
[13] (a) H. Brunner, T. Neuhierl, B. Nuber, Eur. J. Inorg. Chem. (1998) 1877.;
(b) H. Brunner, B. Nuber, M. Prommesberger, Tetrahedron Asymm. 9 (1998) 3223.
[14] H. Brunner, T. Zwack, Organometallics 19 (2000) 2423.
[15] H. Brunner, A. Köllnberger, T. Burgemeister, M. Zabel, Polyhedron 19 (2000) 1519.
[16] (a) S. Attar, J.H. Nelson, J. Fischer, A. de Cian, J.-P. Sutter, M. Pfeffer, Organometallics 14 (1995) 4559;
(b) S. Attar, V.J. Catalano, J.H. Nelson, Organometallics 15 (1996) 2932;
(c) H.D. Hansen, J.H. Nelson, Organometallics 20 (2001) 5257.
[17] (a) M.R. Manneghetti, M. Grellier, M. Pfeffer, J. Dupont, J. Fischer, Organometallics 18 (1999) 5560;
(b) V. Ritleng, P. Bertani, M. Pfeffer, C. Sirlin, J. Hirschinger, Inorg. Chem. 40 (2001) 5117.
[18] M.L. Loza, J. Parr, A.M.Z. Slawin, Polyhedron 16 (1997) 2321.
[19] M.A. Bennett, T.N. Huang, T.W. Matheson, A.K. Smith, Inorg. Synth. 21 (1985) 75.
[20] E.S. Howard, L.C. Susan, Jr., E.W. Mitchum, J. Org. Chem. 29 (1964) 2265.
[21] D.D. Perrin, W.L.F. Armaregg, Purification of Laboratory Chemicals, 3rd ed., Pergamon Press, New York, 1988.
[22] N. Walker, D. Stuart, DIFABS, program for applying empirical absorption corrections, Acta. Crystallogr., Sect. A 39 (1983) 158.
[23] G.M. Sheldrick, SHELX-97, Programs for X-ray Crystal Structure Solution and Refinement, University of Göttingen, Germany, 1997.
[24] C.K. Johnson, ORTEP II. Report ORNL-5138, Oak Ridge National Laboratory, Oak Ridge, TN, 1976.
[25] K. Stanley, M.C. Baird, J. Am. Chem. Soc. 97 (1975) 6598.
[26] (a) M. Yamakawa, I. Yamada, R. Noyori, Angew. Chem., Int. Ed. 40 (2001) 2818;
(b) R. Noyori, M. Yamakawa, S. Hashiguchi, J. Org. Chem. 66 (2001) 7931.
[27] H. Brunner, Angew. Chem., Int. Ed. Engl. 22 (1983) 897.
[28] (a) W.S. Sheldrick, S. Heeb, Inorg. Chim. Acta 168 (1990) 93;
(b) R. Krämer, K. Polborn, H. Wanjek, I. Zahn, W. Beck, Chem. Ber. 123 (1990) 767.



Scheme 1.

These Ni(II) dithiophosphate can coordinate one or two additional donor molecules forming five- and six-coordinate adducts, respectively [12–15]. *Trans*-octahedral complexes [16–19], e.g. $Ni\{S_2P(OR)_2\}_2{\cdot}2Py$ and *cis*-octahedral complexes [20–26], e.g. $Ni\{S_2P(OR)_2\}_2{\cdot}$bipy have also been structurally characterized. The ring-opening of the Laweson's reagent $(ArP(S)S)_2$ ($Ar = p$-$MeOC_6H_4$) [27] has been induced by reaction with alcohols and sylanols [28] generating dithiophosphonic acids and under appropriate conditions a new route to obtain dithiophosphonate complexes. Although, the reactivity of the Laweson's reagent has received much attention, the reactions of these substrates with transition metal ions have been explored scarcely [29,30]. In this paper we describe the simple 'one-pot' synthesis, as well as their spectroscopic and structural characterization, of novel dithiophosphate and dithiophosphonate complexes of pentacoordinate Ni(II) containing the $[Ni([12]aneN_3)]^{2+}$ fragment ([12]aneN$_3$ = 2,4,4-trimethyl-1,5,9-triazacyclododec-1-ene ([12]aneN$_3$-mc1) and its 9-methyl derivative ([12]aneN$_3$-mc2)) the first pentacoordinate derivatives with these ligands and a different ancillary ligand.

2. Experimental

2.1. General methods

C, H, N and S analyses were carried out with a microanalyzer Carlo Erba model EA 1108. Infrared (IR) spectra were recorded on a Perkin–Elmer 16F PC FT-IR spectrophotometer using Nujol mulls between polyethylene sheets. The UV–Vis spectra (in C_3H_6O) were recorded on a Hitachi 2000V spectrophotometer for 300–800 nm range. The ^1H NMR spectra of $(CD_3)_2CO$ solutions were recorded on a Bruker model AC 200E or a Varian Unity 300 spectrometer. Fast atom bombardment (FAB) mass spectra were run on a Fisons VG Autospec spectrometer operating in the FAB$^+$ mode. Conductance measurements were performed with a Crison 525 conductimeter (in C_3H_6O solution, $c \approx 10^{-3}$ mol dm^{-3}). All chemicals were purchased from Aldrich and were used without further purification. Solvents were dried and distilled by general methods before use. The complexes $[Ni([12]aneN_3)(\mu\text{-}OH)]_2(PF_6)_2{\cdot}$([12]aneN$_3$ = 2,4,4-trimethyl-1,5,9-triazacyclododec-1-ene ([12]aneN$_3$-mc1) and its 9-methyl derivative ([12]aneN$_3$-mc2) were prepared by procedures previously described [31,32]. The *O*,*O*′-dialkyldithiophosphoric acids [33], $HS(S)P(OR)_2$ and (4-methoxyphenyl)-*O*-alkyldithiophosphonic acids [28], $HS(S)P(p\text{-}CH_3OPh)(OR)$ were prepared according reported methods, with slight modifications.

2.2. Syntheses

2.2.1. [Ni([12]aneN$_3$-mc1){S$_2$P(OR)$_2$}][PF$_6$] (R = Me (1), Et (2), ^{i}Pr (3))

$[Ni([12]aneN_3\text{-}mc1)(\mu\text{-}OH)]_2(PF_6)_2$ (0.15 g, 0.17 mmol) was added to a solution of *O*,*O*′-dialkyldithiophosphoric acid (0.34 mmol) in the corresponding alcohol (20 ml), and the mixture was stirred at room temperature (r.t.) for 24 h. The solvent was removed under reduced pressure to approximately 10 ml and Et_2O (20 ml) was added to the solution which was then cooled to −18 °C for 24 h. The resulting green solid was filtered off, washed with Et_2O and air-dried.

Complex **1**: Yield: 74%. *Anal*. Found: C, 29.2; H, 5.6; N, 7.4; S, 11.0. Calc. for $C_{14}H_{31}F_6N_3NiO_2P_2S_2$: C, 29.4; H, 5.5; N, 7.3; S, 11.2%. Λ_M: 109 S cm^2 mol^{-1}. FAB: *m*/*z* 426 $[M]^+$. UV–Vis in C_3H_6O: λ (nm) (ε, M^{-1} cm^{-1}): 635 (78), 395 (174). IR (cm^{-1}): ν 3278, 3264, 1654, 1164, 1142, 1076, 1018, 838, 672, 656, 558, 452. ^1H NMR ($(CD_3)_2CO$, ppm): δ 340.3 (H_α), 306.6 (H_α), 244.8 (H_α), 217.2 (H_α), 74.3 (H_α), 42.7 (4-Me, 3H), 34.1 (H_α), 30.1 (H_α, 2H), 22.9 (4-Me, 3H), 3.5 (O–CH_3, 3H), −7.6 (H_β), −12.8 (H_β, 2H), −17.4 (2-Me, 3H), −28.7 (H_β), −36.3 (H_β, 2H).

Complex **2**: Yield: 77%. *Anal*. Found: C, 31.9; H, 6.0; N, 7.2; S, 10.5. Calc. for $C_{16}H_{35}F_6N_3NiO_2P_2S_2$: C, 32.0; H, 5.9; N, 7.0; S, 10.7%. Λ_M: 139 S cm^2 mol^{-1}. FAB: *m*/*z* 454 $[M]^+$. UV–Vis in C_3H_6O: λ (nm), (ε, M^{-1} cm^{-1}): 630 (159), 394 (375). IR (cm^{-1}): ν 3284, 3214, 1652, 1162, 1144, 1010, 964, 838, 652, 558, 452. ^1H NMR ($(CD_3)_2CO$, ppm): δ 340.8 (H_α), 309.3 (H_α), 243.0 (H_α), 213.6 (H_α), 73.8 (H_α), 41.8 (4-Me, 3H), 33.8 (H_α), 29.1 (H_α, 2H), 22.8 (4-Me, 3H), 3.0 (O–CH_2, 2H), 1.1 (–CH_3, 3H), −7.5 (H_β), −12.7 (H_β, 2H), −17.3 (2-Me, 3H), −28.6 (H_β), −36.3 (H_β, 2H).

Complex **3**: Yield: 65%. *Anal*. Found: C, 34.1; H, 6.3; N, 6.9; S, 9.9. Calc. for $C_{18}H_{39}F_6N_3NiO_2P_2S_2$: C, 34.4; H, 6.2; N, 6.7; S, 10.2%. Λ_M: 123 S cm^2 mol^{-1}. FAB: *m*/*z* 482 $[M]^+$. UV–Vis in C_3H_6O: λ (nm), (ε, M^{-1} cm^{-1}): 630 (145), 393 (308). IR (cm^{-1}): ν 3282, 3260, 1656, 1164, 1142, 994, 968, 838, 666, 558, 452. ^1H NMR ($(CD_3)_2CO$, ppm): δ 348.8 (H_α), 314.8 (H_α), 244.3 (H_α), 213.4 (H_α), 75.5 (H_α), 42.2 (4-Me, 3H), 34.8 (H_α), 29.7 (H_α, 2H), 23.8 (4-Me, 3H), 3.1 (O–CH), 1.0 (–CH_3, 6H), −6.5 (H_β), −11.8 (H_β, 2H), −16.3 (2-Me, 3H), −27.8 (H_β), −35.6 (H_β, 2H).

*2.2.2. [Ni([12]aneN$_3$-mc2){S$_2$P(OR)$_2$}][PF$_6$] (R = Me (**4**), Et (**5**), ^{i}Pr (**6**))*

The experimental procedure was similar to that described above using [Ni([12]aneN$_3$-mc2)(μ-OH)]$_2$(PF$_6$)$_2$ (0.15 g, 0.16 mmol) and *O*,*O*′-dialkyldithiophosphoric acid (0.32 mmol) in the corresponding alcohol (20 ml).

Complex **4**: Yield: 72%. *Anal*. Found: C, 31.0; H, 5.9; N, 7.3; S, 10.6. Calc. for $C_{15}H_{33}F_6N_3NiO_2P_2S_2$: C, 30.7; H, 5.7; N, 7.2; S, 10.9%. Λ_M: 134 S cm^2 mol^{-1}. FAB: *m/z* 440 $[M]^+$. UV–Vis in C_3H_6O: λ (nm), (ε, M^{-1} cm^{-1}): 655 (81), 402 (235). IR (cm^{-1}): ν 3262, 1652, 1168, 1136, 1042, 1022, 838, 672, 558, 438. ^{1}H NMR ((CD$_3$)$_2$CO, ppm): δ 292.1 (H$_\alpha$), 276.8 (H$_\alpha$), 256.1 (H$_\alpha$), 200.1 (H$_\alpha$), 128.5 (H$_\alpha$), 114.8 (9-Me, 3H), 67.1 (H$_\alpha$), 38.0 (4-Me, 3H), 30.4 (H$_\alpha$), 29.2 (H$_\alpha$), 23.5 (4-Me, 3H), 3.3 (O–CH$_3$, 3H), −6.8 (H$_\beta$), −10.7 (H$_\beta$), −17.0 (H$_\beta$), −17.7 (2-Me, 3H), −27.8 (H$_\beta$), −33.5 (H$_\beta$), −37.7 (H$_\beta$).

Complex **5**: Yield: 75%. *Anal*. Found: C, 33.5; H, 6.3; N, 6.9; S, 10.1. Calc. for $C_{17}H_{37}F_6N_3NiO_2P_2S_2$: C, 33.2; H, 6.1; N, 6.8; S, 10.4%. Λ_M: 129 S cm^2 mol^{-1}. FAB: *m/z* 468 $[M]^+$. UV–Vis in C_3H_6O: λ (nm), (ε, M^{-1} cm^{-1}): 654 (102), 402 (295). IR (cm^{-1}): ν 3212, 1652, 1160, 1136, 1016, 964, 838, 658, 558, 442. ^{1}H NMR ((CD$_3$)$_2$CO, ppm): δ 290.3 (H$_\alpha$), 275.7 (H$_\alpha$), 255.4 (H$_\alpha$), 197.2 (H$_\alpha$), 127.1 (H$_\alpha$), 113.3 (9-Me, 3H), 66.7 (H$_\alpha$), 36.8 (4-Me, 3H), 30.3 (H$_\alpha$), 28.8 (H$_\alpha$), 23.5 (4-Me, 3H), 2.5 (O–CH$_2$, 2H), 0.9 (–CH$_3$, 3H), −6.9 (H$_\beta$), −10.7 (H$_\beta$), −17.1 (H$_\beta$), −17.6 (2-Me, 3H), −27.9 (H$_\beta$), −33.4 (H$_\beta$), −37.7 (H$_\beta$).

Complex **6**: Yield: 69%. *Anal*. Found: C, 35.3; H, 6.4; N, 6.4; S, 9.5. Calc. for $C_{19}H_{41}F_6N_3NiO_2P_2S_2$: C, 35.5; H, 6.4; N, 6.5; S, 9.9%. Λ_M: 100 S cm^2 mol^{-1}. FAB: *m/z* 496 $[M]^+$. UV–Vis in C_3H_6O: λ (nm), (ε, M^{-1} cm^{-1}): 648 (104), 402 (265). IR (cm^{-1}): ν 3264, 1656, 1140, 1100, 980, 950, 838, 666, 558, 452. ^{1}H NMR ((CD$_3$)$_2$CO, ppm): δ 286.6 (H$_\alpha$), 273.4 (H$_\alpha$), 252.3 (H$_\alpha$), 192.2 (H$_\alpha$), 137.1 (H$_\alpha$), 111.4 (9-Me, 3H), 66.8 (H$_\alpha$), 37.4 (4-Me, 3H), 31.1 (H$_\alpha$), 29.1 (H$_\alpha$), 24.4 (4-Me, 3H), 3.5 (O–CH), 0.8 (–CH$_3$, 6H), −5.6 (H$_\beta$), −9.6 (H$_\beta$), −16.0 (2-Me, 3H), −16.5 (H$_\beta$), −26.4 (H$_\beta$), −32.1 (H$_\beta$), −35.7 (H$_\beta$).

*2.2.3. [Ni([12]aneN$_3$-mc1){S$_2$P(p-CH$_3$OPh)(OR)}][PF$_6$] (R = Me (**7**), Et (**8**), ^{i}Pr (**9**))*

[Ni([12]aneN$_3$-mc1)(μ-OH)]$_2$(PF$_6$)$_2$ (0.13 g, 0.15 mmol) was added to a solution of (4-methoxyphenyl)-*O*-alkyldithiophosphonic acid (0.30 mmol) in the corresponding alcohol (30 ml) and the mixture was stirred at r.t. for 24 h. The solvent was removed under reduced pressure to approximately 15 ml and Et$_2$O (25 ml) was added to the solution which was then cooled overnight. The resulting green solid was filtered off, washed with Et$_2$O and air-dried.

Complex **7**: Yield: 83%. *Anal*. Found: C, 36.9; H, 5.6; N, 6.7; S, 9.6. Calc. for $C_{20}H_{35}F_6N_3NiO_2P_2S_2$: C, 37.1; H,5.4; N, 6.5; S, 9.9%. Λ_M: 132 S cm^2 mol^{-1}. FAB: *m/z* 502 $[M]^+$. UV–Vis in C_3H_6O: λ (nm), (ε, M^{-1} cm^{-1}): 634 (108), 395 (267). IR (cm^{-1}): ν 3280, 3206, 1656, 1594, 1298, 1260, 1116, 1042, 1026, 838, 664, 632, 558, 544, 440. ^{1}H NMR ((CD$_3$)$_2$CO, ppm): δ 341.8 (H$_\alpha$), 310.8 (H$_\alpha$), 242.9 (H$_\alpha$), 215.3 (H$_\alpha$), 75.9 (H$_\alpha$), 40.9 (4-Me, 3H), 33.4 (H$_\alpha$), 29.7 (H$_\alpha$, 2H), 22.6 (4-Me, 3H), 7.2 (Ph, 2H), 6.4 (Ph, 2H), 3.9 (*p*-CH$_3$O, 3H), 3.4 (O–CH$_3$, 3H), −7.7 (H$_\beta$), −12.7 (H$_\beta$, 2H), −17.3 (2-Me, 3H), −28.7 (H$_\beta$), −36.1 (H$_\beta$, 2H).

Complex **8**: Yield: 61%. *Anal*. Found: C, 38.0; H, 5.8; N, 6.5; S, 9.5. Calc. for $C_{21}H_{37}F_6N_3NiO_2P_2S_2$: C, 38.1; H, 5.6; N, 6.3; S, 9.7%. Λ_M: 130 S cm^2 mol^{-1}. FAB: *m/z* 516 $[M]^+$. UV–Vis in C_3H_6O: λ (nm), (ε, M^{-1} cm^{-1}): 634 (105), 394 (281). IR (cm^{-1}): ν 3264, 3214, 1656, 1116, 1596, 1298, 1260, 1116, 1034, 964, 838, 662, 632, 558, 545, 445. ^{1}H NMR ((CD$_3$)$_2$CO, ppm): δ 338.1 (H$_\alpha$), 319.4 (H$_\alpha$), 243.8 (H$_\alpha$), 214.4 (H$_\alpha$), 76.6 (H$_\alpha$), 40.8 (4-Me, 3H), 33.5 (H$_\alpha$), 29.9 (H$_\alpha$), 29.8 (H$_\alpha$), 22.7 (4-Me, 3H), 7.2 (Ph, 2H), 6.3 (Ph, 2H), 3.9 (*p*-CH$_3$O, 3H), 3.1 (O–CH$_2$, 2H), 1.1 (–CH$_3$, 3H), −7.7 (H$_\beta$), −12.8 (H$_\beta$, 2H), −17.4 (2-Me, 3H), −28.8 (H$_\beta$), −36.4 (H$_\beta$, 2H).

Complex **9**: Yield: 68%. *Anal*. Found: C, 38.9; H, 6.1; N, 6.5; S, 9.1. Calc. for $C_{22}H_{39}F_6N_3NiO_2P_2S_2$: C, 39.1; H, 5.8; N, 6.2; S, 9.5%. Λ_M: 125 S cm^2 mol^{-1}. FAB: *m/z* 530 $[M]^+$. UV–Vis in C_3H_6O: λ (nm), (ε, M^{-1} cm^{-1}): 629 (95), 393 (217). IR (cm^{-1}): ν 3286, 3210, 1654, 1596, 1296, 1256, 1112, 1102, 972, 838, 630, 620, 558, 546, 438. ^{1}H NMR ((CD$_3$)$_2$CO, ppm): δ 342.1 (H$_\alpha$), 314.2 (H$_\alpha$), 241.4 (H$_\alpha$), 211.3 (H$_\alpha$), 75.6 (H$_\alpha$), 39.5 (4-Me, 3H), 33.4 (H$_\alpha$), 29.6 (H$_\alpha$), 28.5 (H$_\alpha$), 22.4 (4-Me, 3H), 7.2 (Ph, 2H), 6.6 (Ph, 2H), 3.9 (*p*-CH$_3$O, 3H), 3.4 (O–CH), 0.9 (–CH$_3$, 6H), −7.6 (H$_\beta$), −11.7 (H$_\beta$), −12.6 (H$_\beta$), −17.2 (2-Me, 3H), −28.5 (H$_\beta$), −36.0 (H$_\beta$, 2H).

*2.2.4. [Ni([12]aneN$_3$-mc2){S$_2$P(p-CH$_3$OPh)(OR)}][PF$_6$] (R = Me (**10**), Et (**11**), ^{i}Pr (**12**))*

The experimental procedure was similar to that described for **7**–**9** but using [Ni([12]aneN$_3$-mc2)(μ-OH)]$_2$(PF$_6$)$_2$ (0.16 g, 0.18 mmol) and (4-methoxyphenyl)-*O*-alkyldithiophosphonic acid (0.36 mmol) in the corresponding alcohol (20 ml).

Complex **10**: Yield: 77%. *Anal*. Found: C, 38.3; H, 5.9; N, 6.2; S, 9.4. Calc. for $C_{21}H_{37}F_6N_3NiO_2P_2S_2$: C, 38.1; H, 5.6; N, 6.3; S, 9.7%. Λ_M: 128 S cm^2 mol^{-1}. FAB: *m/z* 516 $[M]^+$. UV–Vis in C_3H_6O: λ (nm), (ε, M^{-1} cm^{-1}): 660 (100), 404 (320). IR (cm^{-1}): ν 3228, 1650, 1594, 1294, 1268, 1114, 1048, 1024, 838, 646, 622, 558, 544, 438. ^{1}H NMR ((CD$_3$)$_2$CO, ppm): δ 287.5 (H$_\alpha$), 273.5 (H$_\alpha$), 255.3 (H$_\alpha$), 198.8 (H$_\alpha$), 126.0 (H$_\alpha$), 111.2 (9-Me, 3H), 69.5 (H$_\alpha$), 36.7 (4-Me, 3H), 30.1 (H$_\alpha$), 28.8 (H$_\alpha$), 23.2 (4-Me, 3H), 7.9 (Ph, 2H), 7.0 (Ph, 2H), 3.9 (*p*-CH$_3$O, 3H), 3.0 (O–CH$_3$, 3H), −7.2 (H$_\beta$), −10.7 (H$_\beta$), −16.8 (H$_\beta$), −17.6 (2-Me, 3H), −27.7 (H$_\beta$), −33.3 (H$_\beta$), −37.4 (H$_\beta$).

Complex **11**: Yield: 67%. *Anal*. Found: C, 39.5; H, 6.1; N, 6.4; S, 9.1. Calc. for $C_{22}H_{39}F_6N_3NiO_2P_2S_2$: C, 39.1; H, 5.8; N, 6.2; S, 9.5%. Λ_M: 123 S cm^2 mol^{-1}. FAB: *m/z* 530 $[M]^+$. UV–Vis in C_3H_6O: λ (nm), (ε, M^{-1} cm^{-1}): 659 (121), 403 (361). IR (cm^{-1}): ν 3224, 1652, 1594, 1292, 1266, 1114, 1050, 1020, 838, 644, 622, 558, 546, 440. ^{1}H NMR ($(CD_3)_2CO$, ppm): δ 287.5 (H_α), 275.5 (H_α), 256.5 (H_α), 197.5 (H_α), 125.9 (H_α), 110.9 (9-Me, 3H), 69.4 (H_α), 36.8 (4-Me, 3H), 30.2 (H_α), 28.7 (H_α), 23.3 (4-Me, 3H), 7.7 (Ph, 2H), 7.0 (Ph, 2H), 3.9 (*p*-CH_3O, 3H), 2.6 (O–CH_2, 2H), 0.7 (–CH_3, 3H), −7.2 (H_β), −10.8 (H_β), −16.9 (H_β), −17.7 (2-Me, 3H), −27.9 (H_β), −33.5 (H_β), −37.6 (H_β).

Complex **12**: Yield: 65%. *Anal*. Found: C, 39.9; H, 6.3; N, 6.3; S, 9.0. Calc. for $C_{23}H_{41}F_6N_3NiO_2P_2S_2$: C, 40.0; H, 6.0; N, 6.1; S, 9.3%. Λ_M: 128 S cm^2 mol^{-1}. FAB: *m/z* 545 $[M]^+$. UV–Vis in C_3H_6O: λ (nm), (ε, M^{-1} cm^{-1}): 654 (124), 400 (388). IR (cm^{-1}): ν 3256, 1652, 1594, 1304, 1256, 1110, 1054, 1024, 838, 660, 622, 558, 550, 445. ^{1}H NMR ($(CD_3)_2CO$, ppm): δ 286.2 (H_α), 272.1 (H_α), 254.6 (H_α), 194.4 (H_α), 125.1 (H_α), 109.4 (9-Me, 3H), 68.8 (H_α), 36.3 (4-Me, 3H), 29.9 (H_α), 28.3 (H_α), 23.0 (4-Me, 3H), 8.1 (Ph, 2H), 6.9 (Ph, 2H), 3.9 (*p*-CH_3O, 3H), 3.2 (O–CH), 0.4 (–CH_3, 6H), −7.2 (H_β), −10.6 (H_β), −16.8 (H_β), −17.5 (2-Me, 3H), −27.8 (H_β), −33.2 (H_β), −37.2 (H_β).

2.3. Determination of the X-ray crystal structure of compounds 2 and 9

Crystals of [Ni([12]aneN_3-mc1){$S_2P(OEt)_2$}][PF_6] (**2**) suitable for X-ray diffraction studies were grown from C_3H_6O/Et_2O liquid diffusion and crystals of [Ni([12]aneN_3-mc1){S_2P(*p*-CH_3OPh)(O^iPr)}][PF_6] (**9**) were obtained by slow evaporation of an C_3H_6O solution. In both cases, crystals were mounted on glass fibres and transferred to a Siemens P4 diffractometer. The crystallographic data are summarised in Table 1.

Cell constants were refined from 60 (**2**) and 56 (**9**) reflections in the 2θ range 10°–25°. The structures were solved by direct methods and refined anisotropically on F^2 [34]. Hydrogen atoms were included using a riding model.

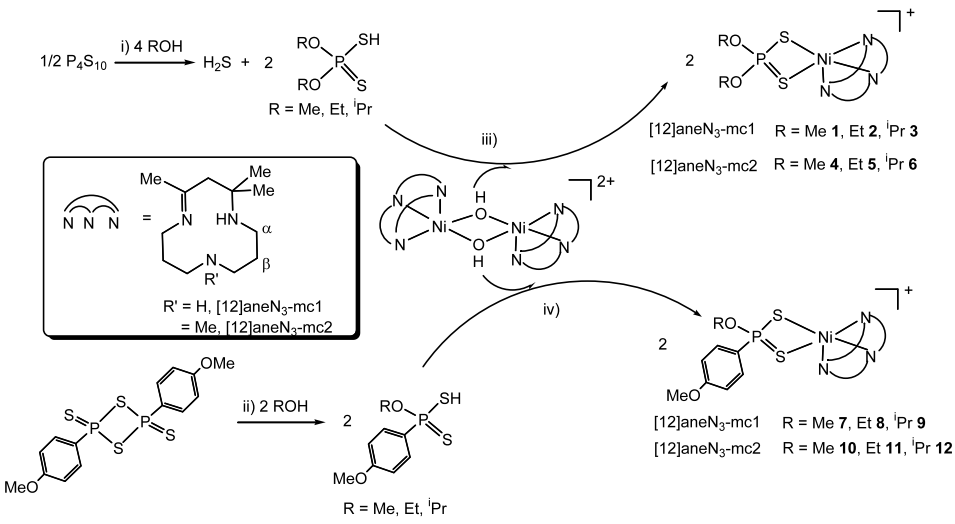
Table 1
Crystal data and structure refinement for complexes **2** and **9**

	2	**9**
Empirical formula	$C_{16}H_{35}F_6N_3NiO_2P_2S_2$	$C_{25}H_{45}F_6N_3NiO_3P_2S_2$
Molecular mass	600.24	734.41
Temperature (K)	173(2)	293(2)
Wavelength (Å)	0.71073	0.71073
Crystal system	triclinic	triclinic
Space group	$P\bar{1}$	$P\bar{1}$
a (Å)	12.7780(10)	11.6733(9)
b (Å)	13.0360(10)	12.7794(12)
c (Å)	15.6040(10)	13.4905(12)
α (°)	87.06	66.453(6)
β (°)	87.65	65.203(5)
γ (°)	86.42	72.676(6)
V (Å^3)	2588.9(3)	1654.2(2)
Z	4	2
D_{calc} (g cm^{-3})	1.540	1.474
Absorption coefficient (mm^{-1})	1.096	0.875
F(000)	1248	768
θ Range (°)	3.01–25.00	3.03–25.00
Reflections collected	10 065	8000
Independent reflections	9101 [R_{int} = 0.0145]	5741 [R_{int} = 0.0197]
Data/restraints/parameters	9101/0/577	5741/0/551
Final *R* indices [$I > 2\sigma(I)$]	R_1 = 0.0372, wR_2 = 0.0905	R_1 = 0.0395, wR_2 = 0.0960
Goodness-of-fit on F^2	0.973	0.905

3. Results and discussion

3.1. Dithiophosphate and dithiophosphonate complexes

The *O*,*O*′-dialkyldithiophosphoric acids, HS(S)P$(OR)_2$, and (4-methoxyphenyl)-*O*-alkyldithiophosphonic acids, HS(S)P(*p*-MeOPh)(OR), are monoprotic acids and their deprotonation gives anions which can be trapped by a metal substrate to form new complexes [2]. On the other hand, previous work demonstrated that $[Ni([12]aneN_3)(\mu\text{-}OH)]_2^{2+}$ ([12]aneN_3 = 2,4,4-trimethyl-1,5,9-triazacyclododec-1-ene ([12]aneN_3-mc1) [31] and its 9-methyl derivative ([12]aneN_3-mc2) [32]) are useful precursors for the preparation of salicylaldiminate [35], β-ketoiminate [36], 2-pyridonate [37] and heterocyclic-2-thionate [38] complexes. Thus, the synthesis of *O*,*O*′-dialkyldithiophosphate and *O*-alkyldithiophosphonate complexes proceeds smoothly via a 'one-pot' method according to equations (i–iv) shown in Scheme 2. Typically, *O*,*O*′-dialkyldithiophosphoric acids were prepared by reaction of the appropriate alcohol with P_4S_{10} eq. (i) followed by the neutralization of the resulting acid with the hydroxo precursor $[Ni([12]aneN_3)(\mu\text{-}OH)]_2(PF_6)_2$ eq. (iii), *O*,*O*′-dialkyldithiophosphate complexes **1**–**6** were obtained. The ring opening of Laweson's reagent used in the formation of the complexes requires a nucleophilic agent that is the same solvent, for example ROH in eq. (ii). Therefore, (4-methoxyphenyl)-*O*-alkylphosphonate derivatives (**7**–**12**) are prepared by the acid–base reaction between the hydroxo complexes and the corresponding (4-methoxyphenyl)-*O*-alkyldithiophosphonic acids in the same alcohol [eq. (iv)]. The new complexes exhibit conductance values corresponding to 1:1 electrolytes in acetone [39].



Scheme 2. Syntheses of nickel complexes and proton labelling.

3.2. IR spectra

The IR spectra show the bands attributable to [12]aneN$_3$-mc1 and [12]aneN$_3$-mc2 ligands and the two strong characteristic bands due to the $[PF_6]^-$ anion, at normal frequencies [38]. The IR spectra of **1**–**6** exhibit two bands the in the regions 1164–1100 and 1076–950 cm^{-1} which could be assigned to the ν[(P)–O–C] and ν[P–O–(C)] vibrations, respectively, whereas for complexes **7**–**12** appear between 1116 and 1034 and around 1020 cm^{-1}, respectively [40,41]. The bands due to ν_{asym}(P–S) and ν_{sym}(P–S) vibrations fall in the range 672–652 and at 558 cm^{-1}, respectively, in the spectra of complexes **1**–**6** and in the range 664–629 and around 545 cm^{-1} for complexes **7**–**12** [40,41]. The bands at 452 cm^{-1} for complexes **1**–**6** and around 445 cm^{-1} for complexes **7**–**12** can be assigned to ν(Ni–S) vibrations.

3.3. Electronic spectra

The electronic spectra of the complexes in acetone solution are all similar and show bands in the 650 and 400 nm regions which could be assigned to $^3B_1(F) \rightarrow {}^3E(F)$ and $^3B_1(F) \rightarrow {}^3A_2, {}^3E(P)$ transitions, respectively [42]. Both λ_{max} values and molar absorptivities are consistent with a pentacoordinate environment around Ni(II) [38].

3.4. ^{1}H NMR spectroscopy

The representative proton NMR spectra for complexes **1** and **11** are shown in Fig. 1. The ^{1}H NMR spectra for complexes **1**–**12** exhibit relatively sharp hyperfine shifted signals spanning from approximately 340 to −40 ppm. The spectra show the resonance line pattern observed for the [12]aneN$_3$-macrocycle ligands that has been assigned on the basis of previous studies of nickel macrocyclic complexes [35–38]. The α-methylene protons shift downfield whereas the β-methylene protons shift upfield with regard to the diamagnetic position probably because of spin polarization mechanisms [43]. Equatorial protons are expected to experience larger contact shifts than axial protons and therefore the most downfield resonances are due to α-CH$_{eq}$ and the most upfield ones to β-CH$_{eq}$ [44]. The isotropically shifted ^{1}H NMR signals observed for methyl groups (2-Me, 4-Me(a, b) and 9-Me–N) can be initially assigned by inspection of their peak areas as well as alkyl groups of *O*,*O*′-dialkyldithiophosphate and *O*-alkyldithiophosphonate ligands. However, the resonances of alkyl and phenyl groups of dithiophosphate and dithiophosphonate ligands farther to the nickel atom have the smaller shift with regard to the diamagnetic position and all these resonances are downfield to TMS.

3.5. Crystal structures of complexes *2* and *9*

The crystal structures of **2** and **9** have been determined by single-crystal X-ray diffraction. ORTEP views of the structures together with atom-numbering schemes are shown in Fig. 2 (**2**) and Fig. 3 (**9**). Selected bond lengths and angles are given in Tables 2 and 3.

The crystal structure determination revealed that green crystals of **2** consist of [Ni([12]aneN$_3$-mc1)-$(S_2P(OEt)_2]^+$ cations and $[PF_6]^-$ anions. The structure shows the presence of two independent molecules. In each one, the nickel atom is pentacoordinate, with a square pyramid arrangement of the chelating atoms. The three nitrogen atoms of the N$_3$-macrocycle occupy the apical position and two adjacent basal ones, whereas the other two basal positions correspond to the *O*,*O*′-dialkyldithiophosphate group. The coordination geometry around the nickel atoms are distorted square pyramidal with the basal plane formed by N1, N2, S1

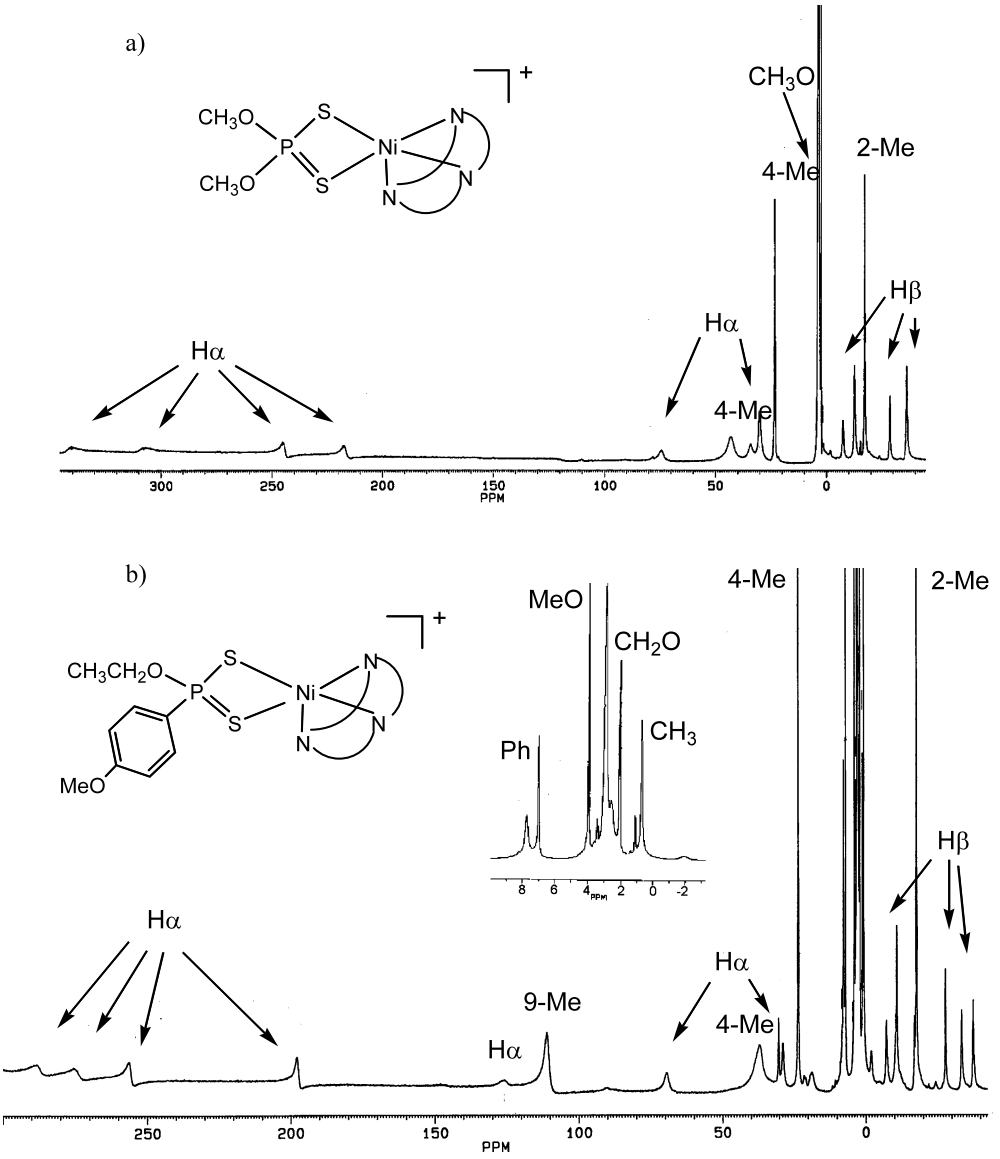


Fig. 1. ^{1}H NMR spectra (in d_6-acetone solution at room temperature) of **1** (a) and **11** (b).

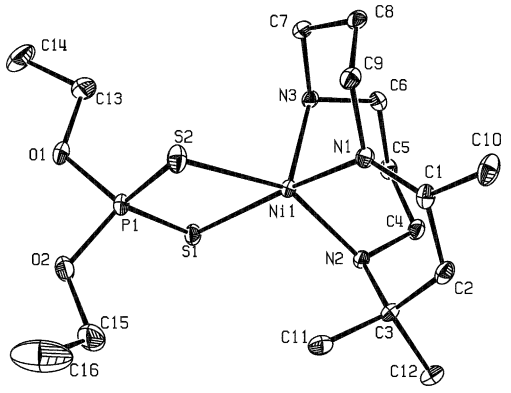


Fig. 2. ORTEP plot of the cation of [Ni([12]aneN$_3$-mc1)-{S$_2$P(OEt)$_2$}][PF$_6$] (**2**).

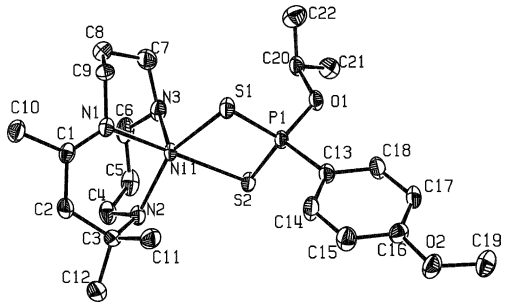


Fig. 3. ORTEP plot of the cation of [Ni([12]aneN$_3$-mc1){S$_2$P(*p*-CH$_3$OPh)(O^{i}Pr)}][PF$_6$] (**9**).

and S2 and N4, N5, S3 and S4 (Table 2). The r.m.s.d. of these planes are 0.171 and 0.181 Å, respectively. The Ni1 and Ni2 atoms are 0.336 and 0.338 Å out of the corresponding basal plane towards the apical N3 or N6 atom. The Ni–[12]aneN$_3$-mc1 distances are not significantly different (2.018–2.059 Å) in contrast with

Table 2
Selected bond lengths (Å) and angles (°) for **2**

Bond lengths			
Ni(1)–N(3)	2.028(3)	Ni(2)–N(6)	2.018(2)
Ni(1)–N(1)	2.030(2)	Ni(2)–N(4)	2.031(2)
Ni(1)–N(2)	2.041(2)	Ni(2)–N(5)	2.059(2)
Ni(1)–S(1)	2.4338(9)	Ni(2)–S(4)	2.4436(9)
Ni(1)–S(2)	2.5005(9)	Ni(2)–S(3)	2.4831(9)
Bond angles			
N(3)–Ni(1)–N(1)	91.66(10)	N(6)–Ni(2)–N(4)	91.39(10)
N(3)–Ni(1)–N(2)	101.21(10)	N(6)–Ni(2)–N(5)	100.30(10)
N(1)–Ni(1)–N(2)	91.18(10)	N(4)–Ni(2)–N(5)	91.59(10)
N(3)–Ni(1)–S(1)	105.60(8)	N(6)–Ni(2)–S(4)	106.88(7)
N(1)–Ni(1)–S(1)	94.48(7)	N(4)–Ni(2)–S(4)	92.89(7)
N(2)–Ni(1)–S(1)	152.39(7)	N(5)–Ni(2)–S(4)	152.32(7)
N(3)–Ni(1)–S(2)	96.92(8)	N(6)–Ni(2)–S(3)	96.94(7)
N(1)–Ni(1)–S(2)	171.21(8)	N(4)–Ni(2)–S(3)	170.88(7)
N(2)–Ni(1)–S(2)	89.03(7)	N(5)–Ni(2)–S(3)	90.56(7)
S(1)–Ni(1)–S(2)	81.40(3)	S(4)–Ni(2)–S(3)	81.17(3)

Table 3
Selected bond lengths (Å) and angles (°) for **9**

Bond lengths	
Ni(1)–N(3)	2.026(3)
Ni(1)–N(2)	2.038(3)
Ni(1)–N(1)	2.055(2)
Ni(1)–S(1)	2.4020(9)
Ni(1)–S(2)	2.5222(8)
Bond angles	
N(3)–Ni(1)–N(2)	102.44(11)
N(3)–Ni(1)–N(1)	90.79(11)
N(2)–Ni(1)–N(1)	90.58(10)
N(3)–Ni(1)–S(1)	108.17(9)
N(2)–Ni(1)–S(1)	148.49(8)
N(1)–Ni(1)–S(1)	96.21(8)
N(3)–Ni(1)–S(2)	92.22(8)
N(2)–Ni(1)–S(2)	90.36(8)
N(1)–Ni(1)–S(2)	176.58(8)
S(1)–Ni(1)–S(2)	81.31(3)

$[Ni([12]aneN_3\text{-mc2})(hp)]^+$ (hp = 2-pyridonate) where there are two Ni–N distances (2.057 and 2.044 Å) longer than the other (2.002 Å) [37]. The two Ni–S bond lengths are similar, 2.4338(9) and 2.5005(9) Å, or 2.4436(9) and 2.4831(9) Å) as previously found for five-coordinate adducts [12–15]. The P–S bond lengths are also similar (1.9765(12) and 1.9913(11) Å or 1.9767(12) and 1.9839(13) Å) suggesting a delocalized P–S π bond. The P–S distances are comparable with those found in the five-coordinate adducts [12–15].

The X-ray structural analysis of compound **9** showed a monomeric nickel complex in which the nickel atom is bonded to three nitrogen atoms of the macrocycle and to two sulfur atoms of the *O*-alkyldithiophosphonate ligand in a distorted square pyramidal geometry (Fig. 3). The nickel atom is 0.319 Å out of the basal plane defined by N1, N2, S1 and S2. The r.m.s.d of this plane is 0.261 Å. The Ni–N distances (2.027–2.055 Å) are similar to those found in **2** as well as the Ni–S distances (2.4020(9) and 2.5222(8) Å). However, the Ni–S bond distances are longer than that observed in homoleptic square-planar complexes [29,30]. The P–S bond lengths are also comparable with those found in **2** (2.0092(11) and 2.0037(11) Å), that is in accordance with delocalization of the P–S π bond over the S–P–S fragment. However, these distances are comparable with those found in *trans*-square-planar homoleptic nickel complexes with similar ligands [29,30]. To our knowledge, this complex is the first pentacoordinate ditiophosphonate Ni(II) derivative crystallographically characterised.

4. Conclusions

This work shows that mononuclear dithiophosphate $[Ni([12]aneN_3)(S_2P(OR)_2]\cdot(PF_6)$ and dithiophosphonate $[Ni([12]aneN_3)\{S_2P(p\text{-}CH_3OPh)(OR)\}](PF_6)$ complexes of pentacoordinate Ni(II) containing the $[Ni([12]aneN_3)]^{2+}$ fragment can be conveniently prepared by acid–base reactions between the a hydroxo precursor and the corresponding *O*,*O*′-dialkyldithiophosphoric acid $HS(S)P(OR)_2$ or (4-methoxyphenyl)-*O*-alkyldithiophosphonic acid in the corresponding alcohol as solvent. All these compounds have been fully characterised by means of spectroscopic and diffractometric techniques. The mild reaction conditions and high yields allows the introduction of dithiophosphate and dithiophosphonate ligands in the five-coordination environment of Ni(II).

5. Supplementary material

Crystallographic data (excluding structure factors) for the structures reported in this paper have been deposited with the Cambridge Crystallographic Data Centre, CCDC Nos. 175301 and 175302 for complexes **2** and **9**, respectively. Copies of this information may be obtained free of charge from The Director, CCDC, 12 Union Road, Cambridge, CB2 1EZ, UK (fax: +44-1223-336033; e-mail: deposit@ccdc.cam.ac.uk or www: http://www.ccdc.cam.ac.uk).

Acknowledgements

This work was supported by the Dirección General de Investigación del Ministerio de Ciencia y Tecnología (Project No. BQU2001-0979-C02), Spain. A.A.L. thanks Fundación Seneca for a grant.

References

[1] V.K. Jain, V.S. Jakkal, J. Organomet. Chem. 515 (1996) 81.
[2] I. Haiduc, J. Organomet. Chem. 623 (2001) 29.
[3] I. Haiduc, D.B. Sowerby, S.-F. Lu, Polyhedron 14 (1995) 3389.
[4] V. Kastalsky, J.F. McConnell, Acta Crystallogr., Sect. B 25 (1969) 909.
[5] E.A. Glinskaya, M.A. Porai-Koshits, Kristallografiya 4 (1960) 241.
[6] Q. Fernando, C.D. Green, J. Inorg. Nucl. Chem. 29 (1967) 647.
[7] J.F. McConnell, V. Kastalsky, Acta Crystallogr. 22 (1967) 853.
[8] N.D. Yordanov, G. Gochev, O. Angelova, J. Macicek, Polyhedron 9 (1990) 2597.
[9] V.V. Tkachev, L.O. Atovmyan, Koord. Khim. 2 (1976) 997.
[10] B.F. Hoskins, E.R.T. Tiekink, Acta Crystallogr., Sect. C 41 (1985) 322.
[11] C.C. Lin, S.X. Liu, Z. Xu, J.H. Lin, X.Z. You, J. Struct. Chem. 6 (1987) 186.
[12] H.W. Chen, J.P. Fackler, Am. Crystallogr. Assoc. Summer Meeting (1974) 229.
[13] S.X. Liu, C.C. Lin, Y.P. Yu, D.L. Zhu, Z. Xu, S.H. Gou, X.Z. You, Acta Crystallogr., Sect. C 47 (1991) 43.
[14] P.S. Shetty, Q. Fernando, J. Am. Chem. Soc. 92 (1970) 3964.
[15] W. Rudzinski, M. Shiro, Q. Fernando, Anal. Chem. 47 (1975) 1194.
[16] S. Ooi, Q. Fernando, Inorg. Chem. 6 (1967) 1558.
[17] S.X. Liu, C.C. Lin, Z. Xu, Y.P. Yu, X.Z. You, J. Org. Chem. (1987) 369.
[18] S.X. Liu, X.C. Lin, Z. Xu, J.H. Lin, Y.P. Yu, X.Z. You, Chem. J. Chin. Univ. 10 (1989) 1225.
[19] X.Z. You, Z. Xu, X. Xu, J.H. Lin, Y.P. Yu, C.C. Lin, S.X. Liu, Chin. Sci. Bull. 37 (1992) 657.
[20] J.S. Huang, Y.P. Yu, Z. Xu, X.X. You, Acta Crystallogr., Sect. C 46 (1990) 991.
[21] S.K. Arora, D.E. Carter, Q. Fernando, K. Seff, Acta Crystallogr., Sect. B 33 (1977) 3230.
[22] X.Z. You, Z. Xu, Y.P. Yu, S.X. Liu, C.C. Lin, J. Struct. Chem. 5 (1986) 154.
[23] M. Shiro, Q. Fernando, J. Chem. Soc., Sect. D (1971) 350.
[24] D.C. Craig, E.T. Pallister, N.C. Stephenson, Acta Crystallogr., Sect. B 27 (1971) 1163.
[25] D.B. Sowerby, I. Haiduc, Inorg. Chim. Acta 17 (1976) L15.
[26] D.B. Sowerby, I. Haiduc, Inorg. Nucl. Chem. Lett. 12 (1976) 791.
[27] B. Yde, N.M. Yuosif, U. Pedersen, I. Thomsen, S.-O. Lawesson, Tetrahedron 40 (1984) 2047.
[28] W.E. van Zyl, R.J. Staplez, J.P. Fackler, Jr., Inorg. Chem. Commun. 1 (1998) 51.
[29] M. Arca, A. Cornia, F.A. Devillanova, A.C. Fabretti, F. Isaia, V. Lippolis, G. Verani, Inorg. Chim. Acta 262 (1997) 81.
[30] M.C. Aragoni, M. Arca, F. Demartin, F.A. Devillanova, C. Graiff, F. Isaia, V. Lippolis, A. Tiripicchio, G. Verani, Eur. J. Inorg. Chem. (2000) 2239.
[31] J.W.L. Martin, J.H. Johnston, N.F. Curtis, J. Chem. Soc., Dalton Trans. (1978) 68.
[32] A. Escuer, R. Vicente, J. Ribas, Polyhedron 11 (1992) 453.
[33] J.L. Lefferts, K.C. Molloy, J.J. Zuckerman, I. Haiduc, C. Guta, D. Ruse, Inorg. Chem. 19 (1980) 1662.
[34] G.M. Sheldrick, SHELX-97. Programs for Crystal Structure Analysis (Release 97-2), University of Göttingen, Germany, 1998.
[35] M.D. Santana, A. Rufete, G. Sánchez, G. García, G. López, J. Casabó, E. Molins, C. Miravitlles, Inorg. Chim. Acta 255 (1997) 21.
[36] M.D. Santana, A. Rufete, G. García, G. López, J. Casabó, A. Cabrero, E. Molins, C. Miravitlles, Polyhedron 16 (1997) 3713.
[37] M.D. Santana, G. García, A. Rufete, G. Sánchez, M.C. Ramírez de Arellano, G. López, Inorg. Chem. Commun. 1 (1998) 267.
[38] M.D. Santana, G. García, A. Rufete, M.C. Ramírez de Arellano, G. López, J. Chem. Soc., Dalton Trans. (2000) 619.
[39] W.J. Geary, Coord. Chem. Rev. 7 (1971) 81.
[40] R.K. Gupta, A.K. Rai, R.C. Mehrotra, V.K. Jain, B.F. Hoskins, E.R.T. Tiekink, Inorg. Chem. 24 (1985) 3280.
[41] P.G. Harrison, M.J. Begley, T. Kikabhai, F. Killer, J. Chem. Soc., Dalton Trans. (1986) 925.
[42] A.B.P. Lever, Inorganic Electronic Spectroscopy, Elsevier, Amsterdam, 1984, pp. 513–520.
[43] A. Dei, M. Wicholas, Inorg. Chim. Acta 166 (1989) 151.
[44] G.N. La Mar, W. Horrocks, Jr., R.H. Holm (Eds.), NMR of Paramagnetic Molecules, Academic Press, New York, 1973, p. 243.

phosphides have received attention as potentially interesting nanomaterials [16]. It is anticipated that such nanomaterials may have interesting mechanical, optical and electrical properties [17]. They are also known to be catalysts of alkylation reactions [18].

Here we report the first instance of a tin phosphide film prepared by dual source atmospheric pressure chemical vapour deposition (APCVD).

2. Experimental

Nitrogen (99.99%) was obtained by BOC and used as supplied. Coatings were obtained on SiO_2 coated float glass. APCVD experiments were conducted on $150 \times 45 \times 3$ mm^3 pieces of glass using a flat bed cold walled APCVD reactor. The glass was cleaned prior to use by washing with petroleum ether (60–80 °C) and isopropanol and then dried in air. A graphite block containing a Whatman cartridge heater was used to heat the glass substrate. The temperature of the substrate was monitored by a Pt–Rh thermocouple. Independent thermocouple measurements indicated that temperature gradients of up to 50 °C were observable at 600 °C across the surface of the glass. The rig was designed so that four independent gas lines could be used. All gas handling lines, regulators and flow valves were made of stainless steel and were $\frac{1}{4}''$ internal diameter except for the inlet to the mixing chamber and the exhaust line from the apparatus that were $\frac{1}{2}''$ in diameter. In these experiments three gas lines were used. Gases came directly from a cylinder and were preheated by passing along 2-m lengths of stainless steel tubing, which were curled and inserted inside a tube furnace. The temperatures of all the gas inlet lines were monitored by Pt–Rh thermocouples and Eurotherm heat controllers.

Tin(IV) chloride (99.99%) was obtained from the Aldrich Chemical Company and used without further purification and was placed into a stainless steel bubbler. The bubbler was heated to 35 °C by a heating jacket and $SnCl_4$ introduced into the gas streams by passing hot nitrogen gas through the liquid. $PCyc^{hex}H_2$, $PCyc^{hex}{}_2H$, $PCyc^{hex}{}_3$ and $PhPH_2$ were purchased from Strem Chemicals and used without further treatment. The two components of the system were mixed by the use of two concentric pipes of $\frac{1}{4}''$ and $\frac{1}{2}''$ diameter, respectively. The inner pipe being 3 cm shorter than the outer pipe. The concentric pipes were attached directly to the mixing chamber of the coater. Gas flows were adjusted using suitable regulators and flow controllers. The exhaust from the reactor was vented directly into the extraction system of a fume cupboard. All of the apparatus was baked out with nitrogen at 150 °C for 30 min before use. Deposition experiments were conducted by heating the horizontal bed reactor and the bubblers to the desired temperatures before diverting the nitrogen line through the bubbler and hence to the reactor. Deposition experiments were timed by use of a stopwatch and were conducted typically for 1 min. At the end of the deposition only nitrogen was allowed to flow over the glass substrate until the substrate was sufficiently cool to handle (approximately 60 °C). Cool, coated samples were handled and stored in air. The large coated glass sample was cut into smaller samples (1×1 cm^2), for analysis by X-ray photoelectron spectroscopy (XPS), energy dispersive X-ray analysis (EDXA), scanning electron microscopy (SEM), electron probe, transmission/reflectance and UV absorption studies. Larger pieces of glass (4×4 cm^2) were used for sheet resistance, X-ray powder diffraction, contact angle and Scotch tape tests.

X-ray powder diffraction patterns were measured on a Siemens D5000 diffractometer using filtered (Cu Kα1, $\lambda = 1.5406$ Å) radiation in the reflection mode using glancing angle incidence (1.5°). SEM was obtained on a Hitachi S570 instrument. EDXA was obtained using a JEOL 35-CF instrument. Electron microprobe analysis was obtained on a JEOL EMA and referenced against Sn and P standards. X-ray photoelectron spectra were recorded with a VG ESCALAB 220I XL instrument using a focused (300 μm spot) monochromatic Al Kα radiation at a pass energy of 20 eV. Scans were acquired with steps of 50 meV. A flood gun was used to control charging and the binding energies were referenced to an adventitious C 1s peak at 284.6 eV. Depth profiling measurements were obtained by using Ar beam sputtering.

UV–Vis spectra were obtained using a Helios double beam instrument. Reflectance and transmission spectra were recorded between 300 and 1150 nm by a Zeiss miniature spectrometer. Measurements were standardised relative to an Rh mirror (reflectance) and air (transmission). Raman spectra were acquired on a Renishaw Raman system 1000 using He–Ne laser of wavelength 632.8 nm. The Raman system was calibrated against the emission lines of Ne. Contact angle experiments were determined by measuring the spread of a 1 μl droplet of water and applying a simple trigonometric program. Electrical properties were determined by using a four-probe device.

3. Results

APCVD of tin phosphide films were achieved on glass substrates from the dual source CVD reaction of $SnCl_4$ or $SnBr_4$ and a substituted phosphine ($PCyc^{hex}H_2$, $PCyc^{hex}{}_2H$, $PCyc^{hex}{}_3$ or $PhPH_2$). The process was studied at different substrate temperatures and flow rates of precursor (Table 1).

No film could be grown at substrate temperatures below 400 °C, uniform films were obtained at 500 °C

Table 1
Experimental conditions and microanalytical results

Substrate temperature (°C)	Nitrogen flow through SnX_4 bubbler (l min^{-1}) (SnX_4) [bubbler temperature (°C)]	Nitrogen flow through R_xPH_{3-x} bubbler (l min^{-1}) (R_xPH_{3-x}) [bubbler temperature (°C)]	Nitrogen flow of make up gas (l min^{-1})	EDAX and electron probe analysis
500	0.5 ($SnCl_4$) [35]	0.5 ($PCyc^{hex}H_2$) [120]	1.4	$SnP_{0.40}$
500	0.5 ($SnCl_4$) [35]	0.5 ($PCyc^{hex}H_2$) [120]	1.8	$SnP_{0.66}$
500	0.2 ($SnCl_4$) [35]	0.8 ($PCyc^{hex}H_2$) [120]	1.0	$SnP_{0.40}$
500	0.3 ($SnCl_4$) [35]	0.3 ($PCyc^{hex}H_2$) [120]	1.0	$SnP_{1.00}$
500	0.8 ($SnCl_4$) [35]	0.2 ($PCyc^{hex}H_2$) [120]	1.0	Sn
550	0.3 ($SnCl_4$) [35]	0.3 ($PCyc^{hex}H_2$) [120]	1.0	$SnP_{1.00}$
600	0.3 ($SnCl_4$) [35]	0.3 ($PCyc^{hex}H_2$) [120]	1.0	$SnP_{1.00}$
500	0.3 ($SnCl_4$) [35]	0.3 ($PhPH_2$) [145]	1.0	$SnP_{0.66}$
500	0.3 ($SnCl_4$) [35]	0.5 ($PhPH_2$) [145]	1.0	$SnP_{1.33}$
600	0.3 ($SnCl_4$) [35]	0.5 ($PhPH_2$) [145]	1.0	$SnP_{1.00}$
600	0.3 ($SnCl_4$) [35]	0.7 ($PCyc_2^{hex}$ H) [250]	0.7	$SnP_{0.66}$
600	0.3 ($SnCl_4$) [35]	1.8 ($PCyc_2^{hex}$ H) [250]	0.2	$SnP_{1.00}$
600	0.5 ($SnBr_4$) [200]	0.3 ($PCyc_3^{hex}$) [120]	0.8	$SnP_{1.00}$
600	0.4 ($SnBr_4$) [200]	0.4 ($PCyc_3^{hex}$) [120]	0.8	$SnP_{1.33}$

and above. The films grown from the dual source CVD reaction of $SnCl_4$ or $SnBr_4$ and a substituted phosphine ($PCyc^{hex}H_2$,$Cyc^{hex}{}_2H$, $PCyc^{hex}{}_3$ or $PhPH_2$) were opaque in colour, although those grown at higher temperatures had a blue tint. The films appeared unreflective. The films prepared at higher temperatures exhibited some birefringence due to thickness effects. All of the films passed the Scotch tape test. They could not be marked with a wet towel but could be marked with a brass stylus or steel scalpel. The films prepared at higher precursor flow rates showed some 'pin holing' due to gas phase nucleation. The films showed no optical change after storage in air for 3 months.

Raman microscopy was used to investigate all of the films. In all cases no Raman scattering due to the films was observed. It is thought that tin phosphides are poor Raman scatters, indeed a sample of Sn_4P_3 purchased form Aldrich gave no Raman spectra. In the samples prepared using $PCyc^{hex}H_2$ and $PhPH_2$ no free carbon was detected by Raman. This was not the case with films prepared using $PCyc^{hex}{}_2H$ and $PCyc^{hex}{}_3$ where free carbon was present in the films. No Raman scattering was observed from the film due to the presence of tin oxides. In previous work we have shown that even trace amounts of tin oxides (SnO_2 or Sn_3O_4) give strong Raman patterns [19].

Compositional analysis of the films was determined by EDXA and electron probe measurements (summarised in Table 1). The results show that the films are free of chlorine (or bromine if $SnBr_4$ was used) and contain only tin and phosphorus. In all cases some breakthrough to the underlying glass was observed. This was corrected for based on a sample of plain glass. These results show that it is possible to create films with a selection of stoichiometries, ranging from $SnP_{1.33}$ to $SnP_{0.40}$. The analysis showed that there was a slight variation in composition across the surface of the glass substrate, for example films with composition $SnP_{1.33}$ had a composition of $SnP_{1.00}$ at the extreme edges, this correlates with the measured temperature gradient across the glass substrate. Area maps indicate that particles containing tin and phosphorus are made (Fig. 1), and that no oxygen is present in these particles.

SEM analysis of the films showed that the deposition reaction proceeded via an island growth mechanism. The majority of samples consisted of microspheres of tin phosphide covering the majority of the surface. Two representative samples are shown in Fig. 2.

The optical properties of the films were studied by reflectance/transmission measurements and UV absorption between 400 and 1100 nm. All samples showed a shift in the absorption edge relative to the plain glass

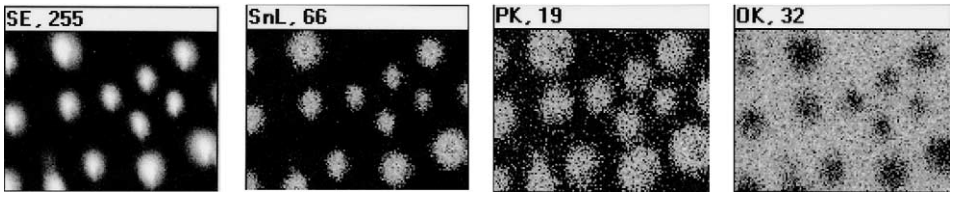


Fig. 1. EDXA area maps of tin phosphide particles. The lighter colours indicate a higher concentration of the specific element. The key on each caption SE, secondary electron image; SnL, tin L X-ray line; PK, phosphorus K X-ray line; OK, oxygen K X-ray line. The numbers 255, 66, 19 and 32 indicate the uncorrected counts per second for each X-ray line.

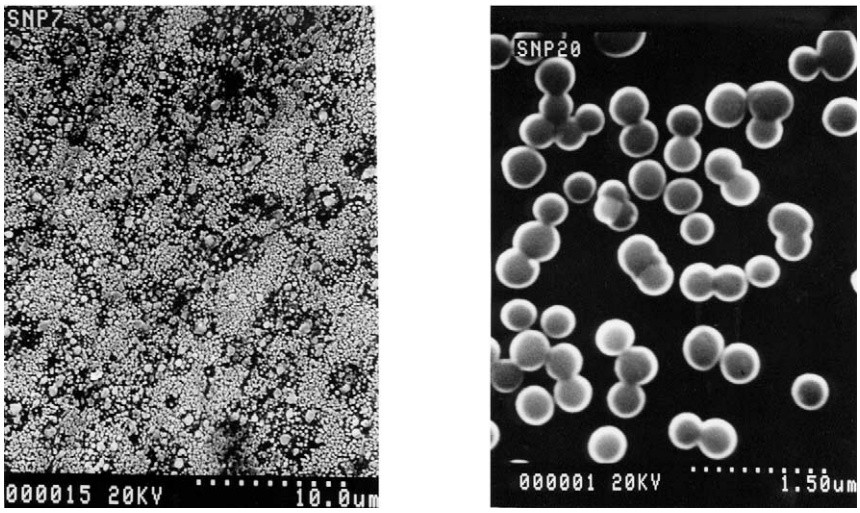


Fig. 2. Scanning electron microscope pictures of tin phosphide films formed from the APCVD reaction of tin tetrachloride and monocyclohexylphosphine at 600 °C.

substrate. The films showed minimal reflectivity (2%), less than the substrate (10%). The transmission spectra were indicative of hazing; this is due to scattering by particles in the film of a similar size to the wavelength of the light.

XPS measurements on a sample of $SnP_{1.00}$ composition, revealed binding energy shifts of 487.2 and 133.6 eV for Sn $3d_{5/2}$ and P $2p_{3/2}$, respectively. These are in reasonable agreement with previous values published in the literature concerning nanoscale Sn_4P_3[6] of 487.6 eV for Sn $3d_{5/2}$ and 134.1 eV for P $2p_{3/2}$. A sample of composition $SnP_{0.40}$ revealed similar binding shifts of 487.2 and 133.8 eV for Sn $3d_{5/2}$ and P $2p_{3/2}$, respectively. The XPS peak profiles for both samples (Fig. 3) are consistent with one environment for both tin and phosphorus. There is no evidence for the presence of tin oxides from the XPS profiles.

The tin phosphide films were X-ray amorphous. Sheet resistance measurements indicated that the films were insulating. The films were shown to have contact angles of 70°–80°. This contact angle did not change significantly after irradiation with 254 nm UV light for 1 h. This contact angle is similar to that of plain glass 50°–75°.

4. Discussion

Reaction of $SnCl_4$ (or $SnBr_4$) and a substituted phosphine ($PCyc^{hex}H_2$, $PCyc^{hex}{}_2H$, $PCyc^{hex}{}_3$ or $PhPH_2$) under APCVD affords opaque films of tin phosphide on glass substrates. The tin phosphide films were shown in most cases to be tin rich, although it was possible to make the stoichiometric compound tin monophosphide when equimolar quantities of precursor were introduced into the gas phase.

The films were found to be insulating. This is because of grain boundary effects due to the island growth mechanism.

The mechanism of this reaction was not determined in this study. It is likely that HCl is produced in the reaction as well as $Cyc^{hex}Cl$ or PhCl (depending on the

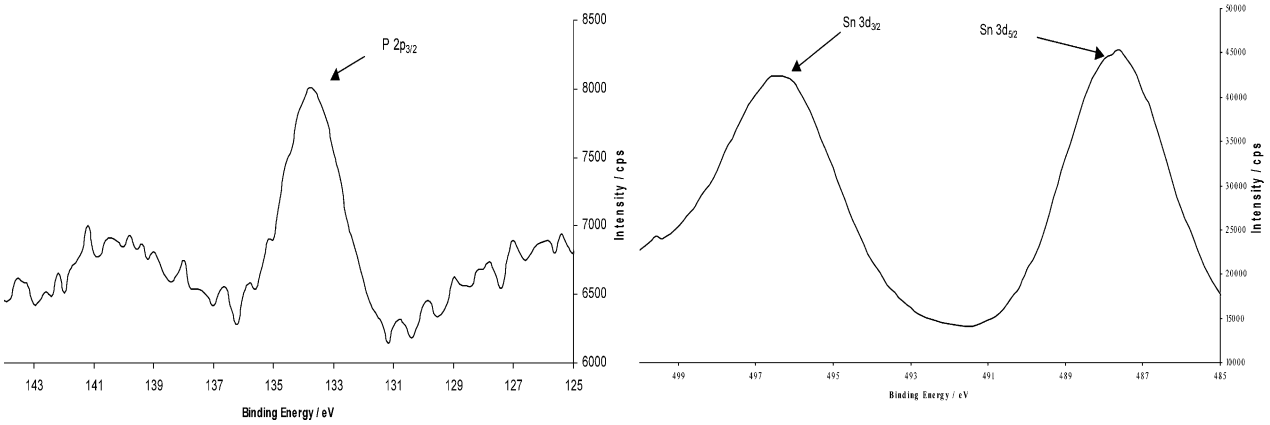


Fig. 3. The XPS peak profiles for a $SnP_{1.00}$ sample showing on the left, the phosphorus $2p_3$ region and on the right, the tin $3d_{5/2}$ and $3d_{3/2}$ region.

phosphine precursor used) [20]. It is plausible that the reaction occurs via the formation of a adduct as some material was recovered from the exhaust which was not starting material. Previous work also suggests that similar deposition process occur via adducts [21].

These films show no Raman spectra. They shift the absorption edge of, and undergo less transmission and reflection than SiO_2 coated glass due to scattering haze. EDAX and electron probe results suggest that the composition over the surface of the glass is similar. SEM shows that whilst various morphologies are possible, one predominates in samples of tin phosphide films.

There is no variation of film stoichiometry with different precursors. It was noted that distinct phases ($SnP_{1.33}$, $SnP_{1.00}$, $SnP_{0.66}$ and $SnP_{0.40}$) were seen and no intermediate phases were observed. Higher nitrogen flow rates had the effect of lowering the phosphorus content of the resultant films. Using di- and tri-substituted phosphines required higher substrate temperatures (600 °C) for films to form. Where films did form at lower substrate temperatures (500 °C) with the di- and tri-substituted phosphines they were lower in phosphorus content than those formed at higher substrate temperatures.

5. Conclusion

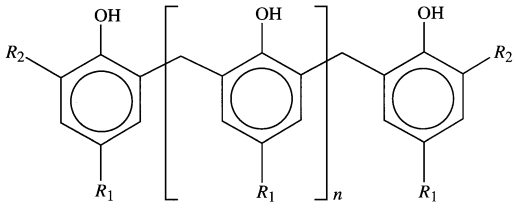
Reaction of $SnCl_4$ (or $SnBr_4$) and a substituted phosphine ($PCyc^{hex}H_2$, $PCyc^{hex}{}_2H$, $PCyc^{hex}{}_3$ or $PhPH_2$) under APCVD affords opaque films of tin phosphide on glass substrates. The films show good surface coverage, adhesion and reasonable uniformity. Tin phosphide films with a range of stoichiometries ($SnP_{0.40}$–$SnP_{1.33}$) could be obtained; these were all opaque in appearance and electrical insulators.

Acknowledgements

The authors wish to thank the EPSRC for funding and Pilkington for a CASE award to RB and for glass. The EPSRC are also thanked for providing financial assistance in the purchasing of the Raman spectrometer.

References

[1] (a) K.A. Gingerich, Nature 200 (1963) 877;
(b) S. Motojima, T. Wakamatsu, K. Sugiyama, Less Common Metals 82 (1981) 379.
[2] K. Komaki, Japan Koka Tokkyo Kokon JP02150067.
[3] H. Su, Y. Xie, B. Li, X. Liu, Y. Qian, J. Solid State Chem. 146 (1999) 110.
[4] (a) J.C. Bailer, H.J. Emeleus, R. Nyholm, A.F. Trotman-Dickenson, Comprehensive Inorganic Chemistry, vol. 2, Pergamon, Oxford, 1973, p. 233;
(b) G.R. Gordon, S.R. Kurtz, Thin Solid Films 140 (1986) 277.
[5] A.N. Gleizes, Chem. Vapour Deposition 6 (2000) 155.
[6] V.B. Chernogorenko, S.V. Muchnik, K.A. Lynchak, Z.A. Klimak, Mater. Res. Bull. 16 (1981) 1.
[7] (a) N. Schonberg, Acta Chem. Scand. 8 (1954) 226;
(b) T. Ludstrom, P.O. Snell, Acta Chem. Scad. 21 (1967) 1343.
[8] J.R. Van Wazer, Phosphorous and its Compounds, vol. 1, Interscience, New York, 1958, p. 123.
[9] (a) R.L. Ripley, Less Common Metals 4 (1962) 496;
(b) W. Blitz, A. Rink, F. Wiechman, Z. Anorg. Chem. 238 (1938) 395.
[10] L.L. Vereikina, G. Samsanov, V. Zh. Neorgkhim. 5 (1960) 1888.
[11] (a) R.B. Kaner, R.E. Treece, J.A. Conklin, Inorg. Chem. 33 (1994) 5701;
(b) R.B. Kaner, R.M. Jacubinas, R.J. Jarvis, Inorg. Chem. 39 (2000) 3242;
(c) I.P. Parkin, A.L. Hector, J. Mater. Chem. 4 (1994) 229;
(d) I.P. Parkin, A.L. Hector, Z. Naturforsch., Teil B 49 (1994) 477;
(e) I.P. Parkin, J.C. Fitzmaurice, A.T. Rowley, J. Mater. Chem. 4 (1994) 285;
(f) I.P. Parkin, A.T. Rowley, J. Mater. Chem. 3 (1993) 689.
[12] A.C. Vivian, J. Inst. Met. 23 (1920) 325.
[13] (a) Vses. Konf. Kntalbkhim Intermet Soedin 2nd, 1974, p. 168;
(b) IZV Akad. Navk. SSSR Serziz 38 (1974) 562.
[14] (a) G. Katz, J.A. Kohn, J.D. Broder, Acta Crystallogr. 10 (1957) 607;
(b) O. Olofsson, Acta Chem. Scand. 21 (1967) 1659;
(c) P.C. Donohue, Inorg. Chem. 9 (1970) 335;
(d) O. Olofsson, Acta Chem. Scand. 24 (1970) 1153;
(e) J. Gullman, O. Olofsson, J. Solid State Chem. 5 (1972) 441.
[15] (a) Yu.B. Kuz'ma, S.I. Chikhrii, V.N. Davydov, Inorg. Mater. 35 (1999) 10;
(b) J. Gullman, J. Solid State Chem. 87 (1990) 202.
[16] Y. Xie, H. Su, B. Li, Y. Qian, Mater. Res. Bull. 35 (2000) 675.
[17] A.M. Rao, E. Richter, S. Bandow, B. Chase, P.C. Eklund, K.A. Williams, S. Fang, K.R. Subbaswamy, M. Menon, A. Thess, R.E. Smalley, G. Dresselhaus, M.S. Dresselhaus, Science 275 (1997) 187.
[18] (a) R.L. Halm, K.M. Chadwick, B.R. Keyes, US Patent 4,946,980;
(b) R.L. Halm, K.M. Chadwick, B.R. Keyes, US Appl. 258,950;
(c) R.L. Halm, K.M. Chadwick, US Patent 4,985580.
[19] (a) L.S. Price, Ph.D. Thesis, University of London, 2001;
(b) T.G. Hibbert, M.F. Mahon, K.C. Molloy, I.P. Parkin, L.S. Price, J. Mater. Chem. 11 (2001) 464.
[20] (a) J.T. Scheper, K.C. Jayaratne, L.M. Liable-Sands, G.P.A. Yap, A.L. Rheingold, C.H. Winter, Inorg. Chem. 38 (1999) 4354;
(b) T.S. Lewkebandara, J.W. Prosica, C.H. Winter, Chem. Mater. 7 (1995) 1053.
[21] C.S. Blackman, C.J. Carmalt, S.A. O'Neill, I.P. Parkin, L. Apostilco, K.C. Molloy, J. Mater. Chem. 11 (2000) 2408.



1 $n=0$ $R_1=H$ $R_2=H$
2 $n=0$ $R_1=CH_3$ $R_2=CH_2OH$
3 $n=0$ $R_1=C(CH_3)_3$ $R_2=CH_2OH$
4 $n=1$ $R_1=C(CH_3)_3$ $R_2=H$
5 $n=1$ $R_1=C(CH_3)_3$ $R_2=CH_3$
6 $n=4$ $R_1=C(CH_3)_3$ $R_2=CH_2OH$

Scheme 1. The polyphenols under study.

CH_3CN, while on recrystallizing **3** from CCl_4 a solvate was obtained, **3**·1/3(CCl_4), denoted **3s** hereafter. The triphenol **4** has been synthesized as previously reported [4c,d] and single crystals were obtained by slow evaporation of a $CHCl_3$–CH_3CN (1:1) solution.

2.1.1. [HDABCO]$_2$[UO_2(**3**–2H)$_2$]·2H_2O (**7**)

The diphenol **3** (32 mg, 0.086 mmol) and a slight excess of DABCO (23 mg, 0.205 mmol) were dissolved in $CHCl_3$ (100 ml). Uranyl nitrate hexahydrate in slight excess with respect to the 1:2 metal–ligand stoichiometry (25 mg, 0.050 mmol) in CH_3OH (30 ml) was then added dropwise, giving immediately an orange solution which was refluxed for 10 min. Orange crystals of low quality but suitable for X-ray crystallography deposited after several recrystallizations from $CHCl_3$, CH_3CN, CH_3OH and mixtures of these solvents.

2.1.2. [HDABCO]$_2$[UO_2(**4**–2H)$_2$]·2CH_3CN (**8**)

The triphenol **4** (350 mg, 0.738 mmol) and a large excess of DABCO (420 mg, 3.75 mmol) were dissolved in $CHCl_3$–CH_3CN (120 ml). Uranyl nitrate hexahydrate in slight excess with respect to the 1:2 metal–ligand stoichiometry (200 mg, 0.40 mmol) in CH_3CN (30 ml) was then added dropwise, giving immediately a dark orange solution, which deposited in a few days orange crystals suitable for X-ray crystallography.

2.2. Crystallography

The data were collected on a Nonius Kappa-CCD area detector diffractometer [5] using graphite-monochromated Mo Kα radiation (0.71073 Å). The crystals were introduced in Lindemann glass capillaries with a protecting 'Paratone' oil (Exxon Chemical Ltd) coating. The unit cell parameters were determined from the reflections collected on ten frames and were then refined on all data. The data were processed with DENZO-SMN [6]. The structures were solved from Patterson map interpretation (compound **7**) or by direct methods (all other compounds) with SHELXS-97 [7] and subsequent Fourier-difference synthesis, and refined by full-matrix least-squares on F^2 with SHELXL-97 [8]. Absorption effects in compounds **3s**, **7** and **8** were empirically corrected with the programs DELABS (**3s**, **7**) and MULABS (**8**) from PLATON [9]. Special details for each compound are as follows:

Compound **2**. All non-hydrogen atoms were refined with anisotropic displacement parameters. All hydroxy protons but one were found on the Fourier-difference map (one of them disordered over two positions, each corresponding to a possible hydrogen bond).
Compounds **3s** and **4**. All non-hydrogen atoms were refined with anisotropic displacement parameters. The hydroxy protons were found on the Fourier-difference map.
Compound **7**. One *tert*-butyl group was found disordered over two positions, which have been refined with occupation parameters constrained to sum to unity. All non-hydrogen atoms were refined with anisotropic displacement parameters, except the disordered ones. Restraints on bond lengths, angles and displacement parameters were applied to the badly resolved HDABCO ions. The hydroxy and ammonium ion protons were not found, nor introduced.
Compound **8**. One *tert*-butyl group was found disordered over two positions, which have been refined with occupation parameters constrained to sum to unity. All non-hydrogen atoms were refined with anisotropic displacement parameters, except the disordered ones. The hydroxy and ammonium ion protons were found on the Fourier-difference map.

All the carbon-bound hydrogen atoms were introduced at calculated positions, except in the disordered parts. All hydrogen atoms were treated as riding atoms with an isotropic displacement parameter equal to 1.2 (OH, NH, CH, and CH_2) or 1.5 (CH_3) times that of the parent atom. Crystal data and refinement details are reported in Table 1. The molecular plots were drawn with SHELXTL [10]. All calculations were performed on a Silicon Graphics R5000 workstation.

3. Discussion

3.1. Uncomplexed polyphenols

Compounds **2** and **3** pertain to the family of *bis*(hydroxymethylated) diphenols (R_2=CH_2OH). The structure of the analogous compound with *iso*-propyl *para*-substituents R_1 has previously been described [11]. Compared with *ortho*-unsubstituted diphenols (R_2=H) [2,12], which crystallize as hydrogen bonded dimers or chains, the hydroxymethyl groups add further possibi-

Table 1
Crystal data and structure refinement details

	2	**3s**	**4**	**7**	**8**
Empirical formula	$C_{17}H_{20}O_4$	$C_{70}H_{96}Cl_4O_{12}$	$C_{32}H_{42}O_3$	$C_{58}H_{90}N_4O_{12}U$	$C_{80}H_{112}N_6O_8U$
M (g mol^{-1})	288.33	1271.27	474.66	1273.37	1523.80
T (K)	100(2)	100(2)	123(2)	100(2)	100(2)
Crystal system	triclinic	Trigonal	triclinic	triclinic	monoclinic
Space group	$P\bar{1}$	$P\bar{3}$	$P\bar{1}$	$P\bar{1}$	$P2_1/c$
a (Å)	9.1209(12)	17.8612(10)	9.710(2)	18.1657(15)	9.1153(5)
b (Å)	11.502(2)	17.8612(10)	9.971(2)	18.2741(14)	13.9305(9)
c (Å)	15.396(2)	12.7537(10)	15.700(3)	18.8974(15)	29.350(2)
α (°)	78.214(7)	90	83.90(3)	79.408(4)	90
β (°)	73.939(9)	90	82.38(3)	86.786(4)	96.112(4)
γ (°)	72.339(9)	120	65.94(3)	76.804(4)	90
V (Å^3)	1466.2(4)	3523.6(4)	1373.5(5)	6002.9(8)	3705.7(4)
Z	4	2	2	4	2
μ (mm^{-1})	0.092	0.225	0.072	2.765	2.249
Reflections collected	10 835	23 889	10 202	36 554	15 949
Independent reflections	5077	4451	5331	19965	4548
Observed reflections [$I > 2\sigma(I)$]	3406	2304	3517	7222	3480
R_{int}	0.063	0.090	0.090	0.065	0.066
Parameters refined	383	265	335	1374	436
R_1	0.064	0.090	0.107	0.100	0.083
wR_2	0.144	0.229	0.279	0.209	0.162

lities of intra- or inter-molecular hydrogen bonding. The asymmetric unit in the crystal structure of **2** contains two independent but nearly identical molecules with intramolecular hydrogen bonds linking three successive oxygen atoms. The intermolecular hydrogen bonding pattern gives rise to double chains or ribbons directed along the *a*-axis, as illustrated in Fig. 1. The asymmetric unit in the trigonal 3:1 tetrachlorocarbon solvate of compound **3**, **3s**, includes one diphenol molecule and a third of a CCl_4 molecule located on a ternary axis. The intramolecular hydrogen-bonding pattern is identical to that in compound **2**. The trigonal arrangement gives rise to layers parallel to the *ab*-plane held by intermolecular hydrogen bonds. The bonds involving one of the terminal oxygen atoms and its symmetry-related counterparts around the $\bar{3}$-axis lead to the formation of a trigonal $(OH)_6$ pattern, as represented in Fig. 2, whereas the CCl_4 molecules are located on the 3-axis and are surrounded, in projection along this axis, by three diphenol molecules linked by hydrogen bonds. The crystal structure of compound **4** has previously been briefly described [11], but to the best of our knowledge, no detailed data have been published. This structure is essentially similar to that of the related triphenol **5** previously published [2], with formation of dimers held by cyclic (isodromic) hydrogen bonds, and it will not be described further herein.

3.2. Uranyl complexes

$[HDABCO]_2[UO_2(\mathbf{3}–2H)_2]\cdot 2H_2O$ (**7**) crystallizes with one complete and two halves complex molecules in the repeat unit of the triclinic cell. The three molecules are quite similar, at least regarding the main features of the complex core, molecule A (represented in Figs. 3 and 4) being pseudo-centrosymmetric and the uranium atom in molecules B and C being located on a symmetry center. The uranium atoms are bound to four deprotonated phenolic groups, which gives the usual slightly distorted square-planar equatorial environment (Table 2). The U–O distances are in the range 2.217(4)–2.285(11) [mean value 2.25(2)] Å and the uranium atom in molecule A is at 0.061(6) Å from the mean plane defined by the four donor atoms. Numerous hydrogen bonds involve the diphenol and water molecules (Table 2). In molecule A, an intramolecular hydrogen bond links the hydroxymethyl oxygen atom O4A and the deprotonated phenolic atom O5A of the other coordinated molecule. As a result, the two ligand molecules are closer one to the other on the side of this bond, which is reflected by an O2A–U1–O5A angle [85.5(4)°] smaller than O1A–U1–O6A [97.8(5)°]. In molecules B and C, where such a bond does not occur, the O–U–O angles involving adjacent phenoxide oxygen atoms deviate little from 90° [89.0(5)°–91.0(5)°]. The dihedral angles between adjacent aromatic rings are 73.3(6)° and 77.6(6)° in molecule A, 79.6(7)° in molecule B and 71.4(6)° in molecule C. These values are larger than that in the compound **1**·0.5DABCO·0.5H_2O, but are in the range usual in diphenols with more or less distorted 'butterfly' conformations [2]. The dihedral angles between the phenolic rings and the mean O_4 plane defined by the coordinating atoms are 52.4(5)°, 49.1(4)°, 48.1(5)° and 36.9(6)° in molecule A, 44.1(7)° and 44.9(6)° in molecule B and

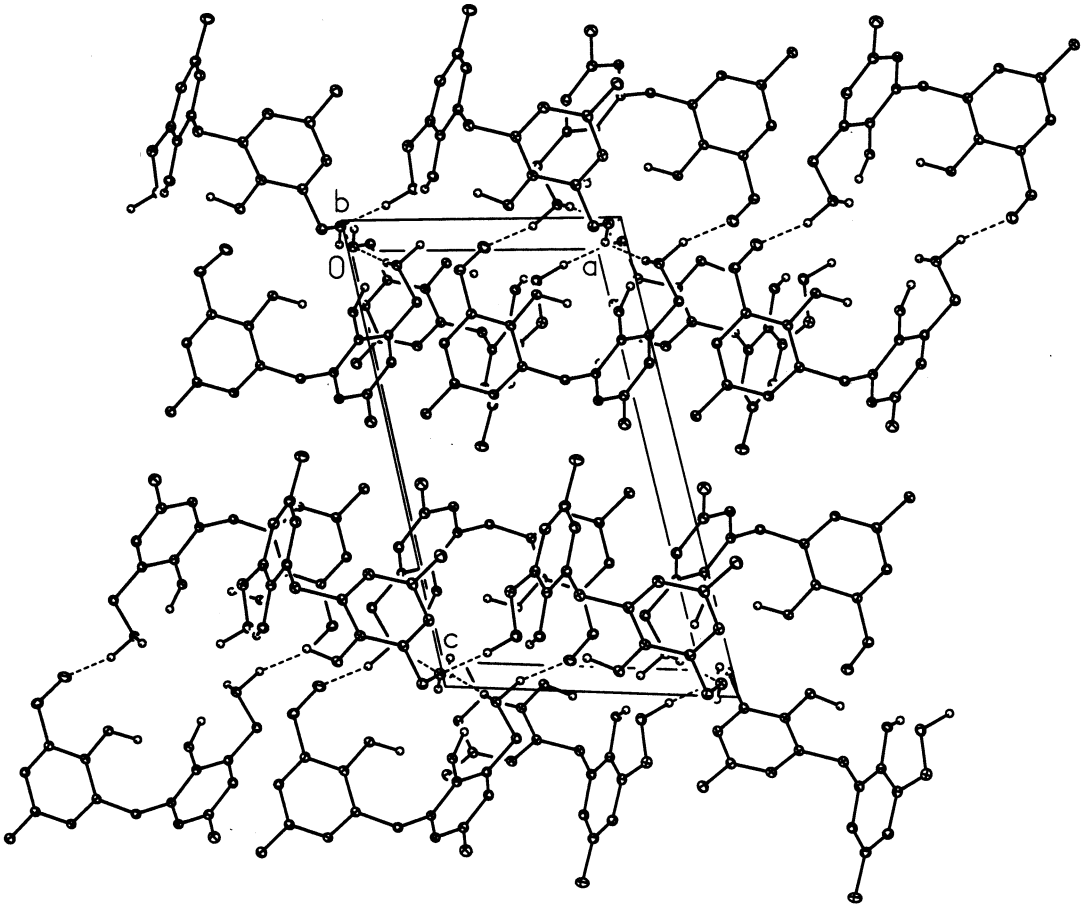


Fig. 1. View of the packing in compound **2**. Hydrogen bonds are represented as dashed lines and hydrogen atoms as small spheres of arbitrary radii (intramolecular hydrogen bonds and carbon-bound hydrogen atoms are omitted for clarity). Hydrogen atoms are omitted for clarity. Ellipsoids are drawn at the 10% probability level.

43.5(6)° and 47.7(5)° in molecule C. In each molecule, the two protonated DABCO counterions are hydrogen bonded to the two oxo atoms of the uranyl ion, each on one side of the equatorial plane. They are further located near the cup built by the two phenolic rings of each ligand and near one other phenolic ring pertaining to a neighboring complex. The interactions involved in this arrangement will be discussed below.

$[HDABCO]_2[UO_2(\mathbf{4}–2H)_2]\cdot 2CH_3CN$ **8** crystallizes in the monoclinic space group $P2_1/c$, with only half a molecule in the repeat unit, the uranium atom being located on the symmetry center (Figs. 5 and 6). Each ligand is bound by two phenoxide oxygen atoms only and is in this way equivalent to a diphenol with regard to complexing properties, as in the previously reported complex $[HDABCO]_2[UO_2(\mathbf{5}–2H)_2]\cdot CH_3OH$ **9** [2]. This behavior has been discussed in relation with the complexing properties of calixarenes, and in particular those of calix[6]arene [2]. An obvious difference with complex **9** is the relative position of the two ligands with respect to the central cation. Complex **9** does not possess any symmetry and the two ligands are such that the two uncomplexed phenolic moieties are surprisingly located on the same side of the complex. On the other hand, these two remaining units are diametrically located in the centrosymmetric complex **8**, which seems a more likely geometry in terms of steric interactions. The uranyl ion in **8** is bound to two phenoxide oxygen atoms and their symmetry-related counterparts, with bond lengths of 2.207(8) and 2.297(7) Å. Such different bond lengths have already been observed in compounds **7** (see above) and **9** [mean values 2.18(1) and 2.27(1) Å], which has been attributed in the latter case to some distortion of the complex core due to the repulsion between the two uncomplexed phenolic units (the usual values for tetra-phenoxide bound uranyl in calixarene complexes are close to 2.23 Å). In the present case, the difference between the two values is the same (with a slight increase of both), but the previous explanation does not hold true any more. A repulsion between O4 and O2′ is also unlikely, the distance between these atoms being 3.61(1) Å [for comparison, the O2···O3 distance is 3.16(1) Å]. The most plausible origin is the presence of the strong hydrogen bond between O3 and

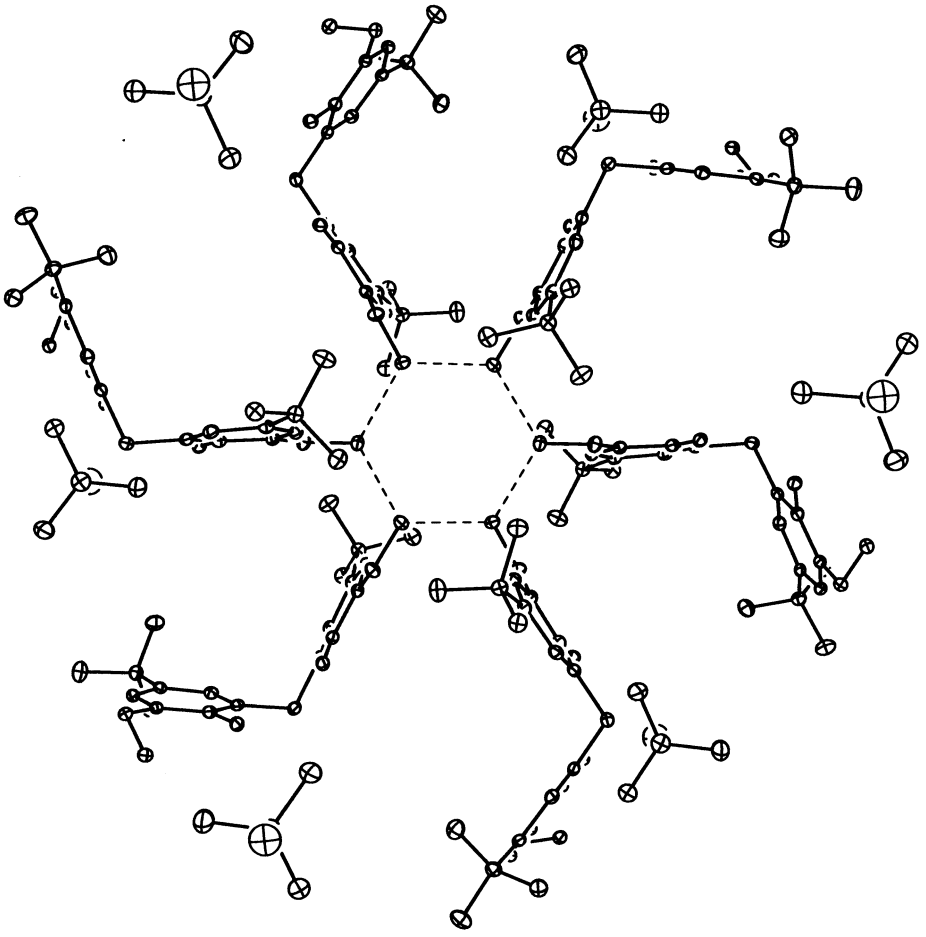


Fig. 2. View of the trigonal arrangement in the *ab*-plane in compound **3s**. Intermolecular hydrogen bonds are represented as dashed lines. Hydrogen atoms are omitted for clarity. Ellipsoids are drawn at the 20% probability level.

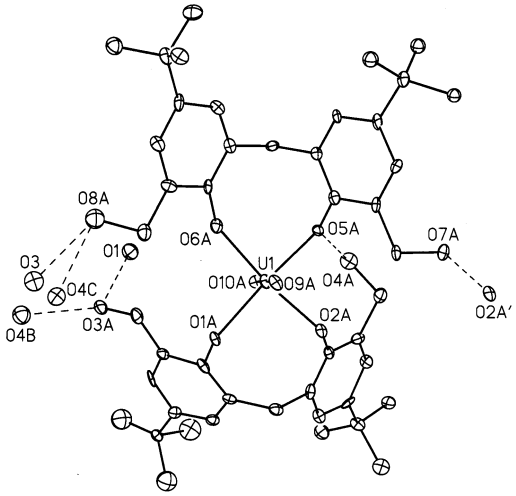


Fig. 3. View of molecule A in the uranyl complex **7**. Hydrogen bonds are represented as dashed lines. HDABCO ions are omitted for clarity. Only one position of the disordered *tert*-butyl group is represented. Ellipsoids are drawn at the 10% probability level.

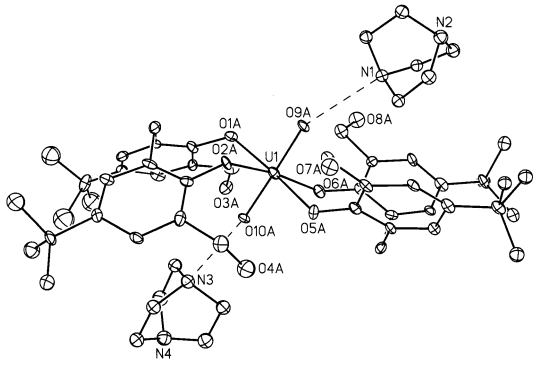


Fig. 4. View of molecule A in the uranyl complex **7** including the counterions. Hydrogen bonds are represented as dashed lines. Only one position of the disordered *tert*-butyl group is represented. Ellipsoids are drawn at the 10% probability level.

O4, which likely diverts some electronic density from the former atom. In comparable calixarene complexes, the U–O bond lengths appear also to be slightly larger when hydrogen bonding is present, in the absence of any other identifiable cause, but this effect is probably often hindered by other effects inducing an asymmetry in the coordination sphere, such as the ligand geometric constraints. The U1–O5A distance in complex **7** is a

Table 2
Selected distances (Å) and angles (°) in complexes **7** and **8**

Uranium environment							
Compound **7** [a]							
U1–O1A	2.285(11)	U2–O1B	2.265(15)	U3–O1C	2.255(13)		
U1–O2A	2.265(12)	U2–O2B	2.229(15)	U3–O2C	2.242(12)		
U1–O5A	2.227(12)	U2–O5B	1.800(14)	U3–O5C	1.811(11)		
U1–O6A	2.217(14)						
U1–O9A	1.798(10)						
U1–O10A	1.792(10)						
O1A–U1–O2A	89.9(4)	O1B–U2–O2B	89.4(5)	O1C–U3–O2C	89.0(5)		
O2A–U1–O5A	85.5(4)	O1B–U2–O2B′	90.6(5)	O1C–U3–O2C″	91.0(5)		
O5A–U1–O6A	86.7(5)						
O6A–U1–O1A	97.8(5)						
O9A–U1–O10A	178.8(6)						
Compound **8** [b]							
U–O1	1.797(8)	U–O2	2.207(8)	U–O3	2.297(7)		
O2–U–O3	89.3(3)	O2–U–O3′	90.7(3)				
Hydrogen bonding geometry							
Compound **7** [c,d]							
N1···O9A	3.06(2)	N3···O10A	2.70(2)	N4···O8A′	2.96(2)		
N5···O5B	2.77(2)	N7···O5C″	2.92(2)				
O3A···O4B	2.65(2)	O3A···O1	2.69(2)	O4A···O5A	2.78(2)		
O7A···O2A‴	2.79(2)	O8A···O4C	2.93(3)	O8A···O3′	2.65(3)		
O4B···O3′	2.72(2)	O3C···O1A″	2.76(2)	O4C···O2	2.83(2)		
O4C···O3′	2.69(2)	O1···O6A′	2.89(2)				
Compound **8**							
O4···O3	2.67(2)	O4–H4	1.19	H4···O3	1.69	O4–H4···O3	136
N1···O1	2.70(2)	N1–H1	1.29	H1···O1	1.56	N1–H1···O1	144

[a] Symmetry codes: ′ = 1−*x*; 1−*y*; 1−*z*, ″ = 1−*x*; −*y*; 1−*z*.
[b] Symmetry code: ′ = −*x*; −*y*; −*z*.
[c] Symmetry codes: ′ = 1−*x*; 1−*y*; −*z*, ″ = 1−*x*; −*y*; 1−*z*, ‴ = 1−*x*; −*y*; −*z*.
[d] Hydrogen atoms not found.

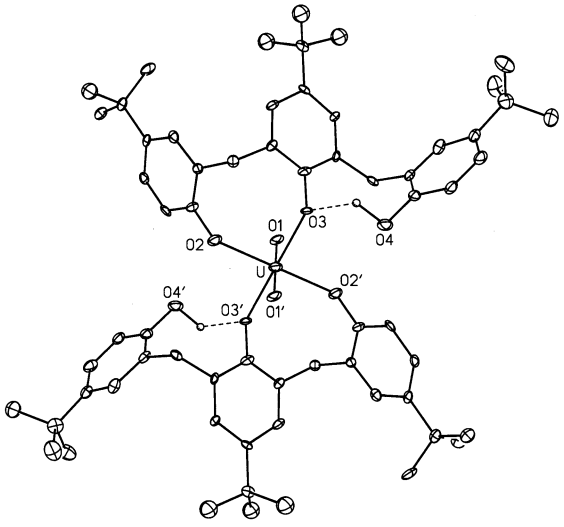


Fig. 5. View of the uranyl complex **8**. The protons involved in hydrogen bonds are represented as small spheres of arbitrary radii. Hydrogen bonds are represented as dashed lines. Other hydrogen atoms, HDABCO ions and solvent molecules are omitted for clarity. Only one position of the disordered *tert*-butyl group is represented. Ellipsoids are drawn at the 30% probability level.

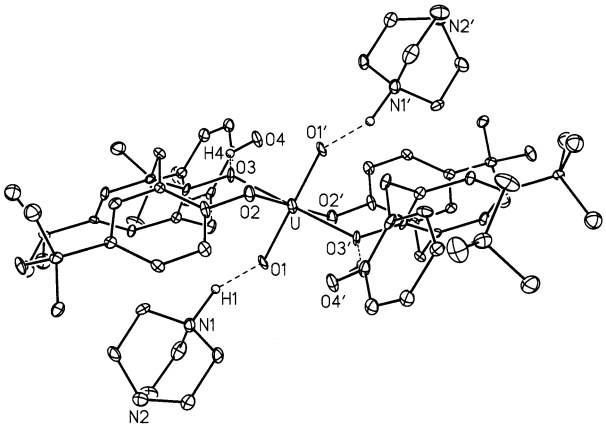


Fig. 6. View of the uranyl complex **8** including the counterions. The protons involved in hydrogen bonds are represented as small spheres of arbitrary radii. Hydrogen bonds are represented as dashed lines. Other hydrogen atoms and solvent molecules are omitted for clarity. Only one position of the disordered *tert*-butyl group is represented. Ellipsoids are drawn at the 30% probability level.

short one, in spite of the involvement of O5A in a strong hydrogen bond. The difference with complex **8** is that, in **7**, the donor atom in the hydrogen bond pertains to the second ligand in the complex molecule, and not to the same one as in **8**, which implies a slightly different geometry (see above). The O–U–O angles involving adjacent phenolic oxygen atoms of the coordination

sphere do not deviate much from 90° in **8**, whereas a strong deviation was observed in compound **9**, one of the angles, involving one oxygen atom from each ligand, being as large as 100.6(4)° as a result of the repulsion between the two uncomplexed phenol units. The four-phenoxide oxygen atoms and the uranium atom in **8** define a plane, the phenolic oxygen atoms O4 and O4′ being at a distance of 1.11(2) Å on each side of it. The conformation of the triphenol is the one that has been termed *trans* or *anti* [11], the first and third aromatic rings being on either side of the plane defined by the central ring. The dihedral angles between adjacent aromatic rings are 80.4(4)° and 75.3(4)°, i.e. larger than in complex **9** (range 62.4°–74.5°) and the dihedral angles between the two bonding phenolic rings and the mean O_4 plane defined by the coordinating atoms are 43.1(3)° and 50.4(3)°. The torsion angles φ and χ, as defined for calixarenes [13], correspond to a sequence of distorted *gauche* angles $-++-$, identical to that in complex **9** or in the uncomplexed ligands **4** and **5**. It may be considered as rather surprising that the conformation of so flexible a molecule does not change much upon uranyl complexation. In this respect, uranyl bonding by two phenoxide groups does not differ much from an intramolecular hydrogen bond from a purely geometric viewpoint. Such a similarity in the geometries of uncomplexed and uranyl-complexed ligands has already been observed in the case of several calixarenes. Some preorganization effects due to hydrogen bonding in cyclic and acyclic polyphenols may be assumed in such cases.

The location of the $HDABCO^+$ cations in **8** is similar to that in complexes **7** and **9**, with the formation of a N–H···O(oxo) hydrogen bond. The counterion is further located in the cup formed by the two bonding phenolic groups. We have discussed in previous papers the interactions involved in the inclusion of ammonium counterions in the cavity of calixarene complexes [14]. In the present cases, the ammonium···oxo hydrogen bond is certainly of a primary importance in the counterion location, but this does not prevent some weak interactions being involved as well. The shortest distances observed between the carbon and nitrogen atoms of the HDABCO ions and the centroids of the aromatic rings may reveal these interactions. In complex **7**, these shortest contacts are 3.56 Å for carbon atoms in α positions with respect to the charged nitrogen and aromatic rings of the cup of the same complex molecule, 3.54 Å for carbon atoms and aromatic rings of neighboring molecules and 3.84 Å for nitrogen atoms and aromatic rings of the cup. In compound **8**, the corresponding values are 3.38, 3.88 and 3.97 Å, respectively. Such distances are in a range indicative of possible cation–π interactions [14,15]. These interactions may be at the origin of the rather strong deviation of the N–H···O(oxo) bond from linearity (144° around H in compound **8**), the HDABCO ion being tilted towards the aromatic rings of the cup. Besides, some weaker CH–π interactions [16,17] may also be present: in compound **8** for example, one of the hydrogen atoms linked to the HDABCO carbon atom more imbedded in the cup is possibly involved in a hydrogen bond with the neighboring aromatic ring, with a H···centroid distance of 2.41 Å and a C–H···centroid angle of 172.5°.

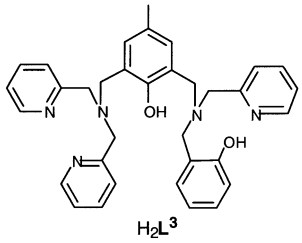
4. Supplementary data

Crystallographic data for the structural analysis have been deposited with the Cambridge Crystallographic Data Centre, CCDC no. 182688 (**2**), 182689 (**3s**), 171000 (**4**), 182690 (**7**) and 171001 (**8**). Copies of the information may be obtained free of charge from the Director, CCDC, 12 Union Road, Cambridge CB2 1EZ, UK (fax: +44-1223-336-033; e-mail: deposit@ccdc.cam.ac.uk or www: http://www.ccdc.cam.ac.uk).

References

[1] P. Thuéry, M. Nierlich, J. Chem. Soc., Dalton Trans. (1997) 1481.
[2] P. Thuéry, M. Nierlich, Z. Asfari, J. Vicens, J. Chem. Soc., Dalton Trans. (2000) 1297.
[3] (a) J. Harrowfield, Gazz. Chim. Ital. 127 (1997) 663;
(b) P. Thuéry, M. Nierlich, J. Harrowfield, M. Ogden, in: Z. Asfari, V. Böhmer, J. Harrowfield, J. Vicens (Eds.), Calixarenes 2001, Kluwer Academic Publishers, Dordrecht, 2001.
[4] (a) T. Haino, K. Matsumura, T. Harano, K. Yamada, Y. Saiyo, Y. Fukazawa, Tetrahedron 54 (1998) 12185;
(b) B. Dhawan, C.D. Gutsche, J. Org. Chem. 48 (1983) 1536;
(c) A. Zinke, R. Ott, H.F. Garrana, Monat. Chem. 89 (1958) 135;
(d) T. Cairns, G. Eglinton, Nature 196 (1962) 535.
[5] KAPPA-CCD Software, Nonius B.V., Delft, 1998.
[6] Z. Otwinowski, W. Minor, Methods Enzymol. 276 (1997) 307.
[7] G.M. Sheldrick, Acta Crystallogr., Sect. A 46 (1990) 467.
[8] G.M. Sheldrick, SHELXL-97, Program for the Refinement of Crystal Structures, University of Göttingen, 1997.
[9] A.L. Spek, PLATON, University of Utrecht, 2000.
[10] G.M. Sheldrick, SHELXTL, Version 5.1, University of Göttingen, distributed by Bruker AXS Inc, Madison, WI, 1999.
[11] M. Perrin, D. Oehler, in: J. Vicens, V. Böhmer (Eds.), Calixarenes: a Versatile Class of Macrocyclic Compounds, Kluwer Academic Publishers, Dordrecht, 1991, pp. 68–71.
[12] (a) See, for example: G. Casiraghi, M. Cornia, G. Sartori, G. Casnati, V. Bocchi, G.D. Andreetti, Makromol. Chem. 183 (1982) 2611;
(b) G. Casiraghi, M. Cornia, G. Ricci, G. Balduzzi, G. Casnati, G.D. Andreetti, Makromol. Chem. 184 (1983) 1363;
(c) G. Ferguson, R. McCrindle, A.J. McAlees, Can. J. Chem. 67 (1989) 779.

[13] F. Ugozzoli, G.D. Andreetti, J. Incl. Phenom. 13 (1992) 337.
[14] (a) B. Masci, M. Nierlich, P. Thuéry, New J. Chem. 26 (2002) 120 (and references therein);
(b) B. Masci, M. Nierlich, P. Thuéry, New J. Chem. 26 (2002) 766;
(c) See also: P. Thuéry, Z. Asfari, M. Nierlich, J. Vicens, Acta Crystallogr., Sect. C 58 (2002) o223.
[15] J.C. Ma, D.A. Dougherty, Chem. Rev. 97 (1997) 1303.
[16] (a) H. Takahashi, S. Tsuboyama, Y. Umezawa, K. Honda, M. Nishio, Tetrahedron 56 (2000) 6185;
(b) H. Suezawa, T. Yoshida, M. Hirota, H. Takahashi, Y. Umezawa, K. Honda, S. Tsuboyama, M. Nishio, J. Chem. Soc., Perkin Trans. 2 (2001) 2053.
[17] T. Steiner, Angew. Chem., Int. Ed. 41 (2002) 48.



H_2L^3

2. Experimental

2.1. Materials and measurements

Elemental analyses were carried out by the University of Sheffield microanalytical service. Infrared spectra were recorded as KBr discs or as liquid films between NaCl plates, using a Perkin–Elmer 297 (4000–600 cm^{-1}) or a Perkin–Elmer 1600 (4000–400 cm^{-1}) infrared spectrophotometer. Positive ion fast atom bombardment (FAB) mass spectra were recorded using a Kratos MS80 or a VG PROSPEC spectrometer (the matrix used was 4-nitrobenzyl alcohol).

The proligand 2,6-bis[((2-pyridylmethyl)-aminomethyl)-6-((2-hydroxybenzyl)(2-pyridylmethyl))-aminomethyl]-4-methylphenol (H_2L^3) was prepared by the method of Neves et al. [4]

2.2. Synthesis of complexes

The complexes were prepared by dissolving H_2L^3 (1 equiv.) in a warm methanolic solution (15 cm^3) and then adding NEt_3 (2 equiv.) and $Zn(OAc)_2\cdot 2H_2O$ (2 equiv.). The solution was refluxed for 60–90 min and 2 equiv. of the requisite alkali metal salt were added ($NaBF_4$, $NaClO_4$ or KPF_6). The solutions were cooled and crystals removed for analysis; the bulk sample was then recovered by filtration, washed and dried in vacuo.

The bulk sample of $[Zn_2L^3(OAc)(OH_2)](BF_4)\cdot 2MeOH\cdot H_2O$ (**1**) was prepared from H_2L^3 (112 mg, 0.2 mmol), $Zn(OAc)_2\cdot 2H_2O$ (88 mg, 0.4 mmol) and $NaBF_4$ (44 mg, 0. 4 mmol). Yield: 96 mg (52%). MS (+veFAB): *m/z*: 732 (100%) $[Zn_2L3(OAc)]^+$, 692 (17%) $[Zn_2L^3(OH)]^+$. IR (KBr disc, ν (cm^{-1})): 1608($C{=}N_{pyr}$), 1581(C=C–Ar), 1565(ν_{as}OAc), 1446(ν_sOAc), 1059(BF_4). *Anal*. Calc. for $C_{38}H_{48}BF_4N_5O_8Zn_2$: C, 49.5; H, 5.4; N, 7.6. Found: C, 49.2; H, 5.2; N, 7.7%.

The bulk sample of $[Zn_2L^3(OAc)(OH_2)](ClO_4)\cdot 2MeOH\cdot H_2O$ (**2**) was prepared from H_2L^3 (347 mg, 0.6 mmol), $Zn(OAc)_2\cdot 2H_2O$ (275 mg, 1.2 mmol) and $NaClO_4$ (176 mg, 1.2 mmol). Yield: 352 mg (63%). MS (+veFAB): *m/z*: 732 (100%) $[Zn_2L3(OAc)]^+$. IR (KBr disc, ν (cm^{-1})): 1608($C{=}N_{pyr}$), 1582(C=C–Ar), 1569(ν_{as}OAc), 1432(ν_sOAc). *Anal*. Calc. for $C_{38}H_{48}ClN_5O_{12}Zn_2$: C, 48.9; H, 5.2; N, 7.5. Found: C, 48.2; H, 5.0; N, 7.8%.).

The bulk sample of $[Zn_2L^3(OAc)(OH_2)](PF_6)\cdot MeOH\cdot 2H_2O$ (**3**) was prepared from H_2L3 (119 mg, 0.22 mmol), $Zn(OAc)_2\cdot 2H_2O$ (97 mg, 0.44 mmol) and KPF_6 (81 mg, 0. 44 mmol). Yield: 135 mg (64%). MS (+veFAB): *m/z*: 732 (24%) $[Zn_2L3(OAc)]^+$, 692 (25%) $[Zn_2L3(OH)]^+$. IR (KBr disc, ν (cm^{-1}))): 1609($C{=}N_{pyr}$), 1582(C=C–Ar), 1568(ν_{as}OAc), 1446(ν_sOAc). *Anal*. Calc. for $C_{37}H_{47}F_6N_5O_8PZn_2$: C, 46.0; H, 4.9; N, 7.3. Found: C, 45.8; H, 4.9; N, 7.2%.

2.3. X-ray crystallography

Crystal data: $C_{38}H_{48}BF_4N_5O_8Zn_2$: $M = 920.36$. Crystallises from CH_3OH as colourless blocks; crystal dimensions $0.24\times0.24\times0.10$ mm. Triclinic, space group $P\bar{1}$, $a = 10.9887(13)$, $b = 13.1778(16)$, $c = 15.7302(19)$ Å, $\alpha = 67.418(2)^\circ$, $\beta = 77.199(2)^\circ$, $\gamma = 83.622(2)^\circ$. $U = 2050.1(4)$ $Å^3$, $Z = 2$, $D_{calc} = 1.491$ Mg m^{-3}, Mo Kα radiation ($\lambda = 0.71073$ Å), μ(Mo Kα) = 1.245 mm^{-1}, $F(000) = 952$. Data collected were measured on a Bruker Smart CCD area detector with an Oxford Cryosystems low temperature system at 150 K. Cell parameters were refined from the setting angles of 72 reflections (θ range 1.43°–28.34°). Reflections were measured from a hemisphere of data collected of frames each covering 0.3° in omega. Of the 13 000 reflections measured, all of which were corrected for Lorentz and polarisation effects and for absorption by semi empirical methods based on symmetry-equivalent and repeated reflections (minimum and maximum transmission coefficients 0.7544 and 0.8856), 7283 independent reflections exceeded the significance level $|F|/\sigma(|F|) > 4.0$. The structure was solved by direct methods and refined by full matrix least-squares methods on F^2. Hydrogen atoms were placed geometrically and refined with a riding model (including torsional freedom for methyl groups) and with U_{iso} constrained to be 1.2 (1.5 for methyl groups) times U_{eq} of the carrier atom. Refinement converged at a final $R_1 = 0.0529$ ($wR_2 = 0.1531$, for all 9274 data, 525 parameters, mean and maximum δ/σ 0.000, 0.000) with allowance for the thermal anisotropy of all non-hydrogen atoms. Minimum and maximum final electron density: −1.096 and 1.108 e $Å^{-3}$. A weighting scheme $w = 1/[\sigma^2(F_o^2)+(0.1000P)^2+0.00P]$ where $P = (F_o^2+2F_c^2)/3$ was used in the latter stages of refinement. Complex scattering factors were taken from the program package SHELXTL as implemented on the Viglen Pentium computer [5].

3. Results and discussion

H_2L^3 was synthesised by the method of Neves et al. [4] and reacted with zinc(II) acetate in methanol. The

dizinc(II) complexes $[Zn_2L^3(OAc)(OH_2)](BF_4)\cdot 2MeOH\cdot H_2O$ (**1**), $[Zn_2L^3(OAc)(OH_2)](ClO_4)\cdot 2MeOH\cdot H_2O$ (**2**) and $[Zn_2L^3(OAc)(OH_2)](PF_6)\cdot MeOH\cdot 2H_2O$ (**3**) were isolated after metathesis with the appropriate alkali metal salt. Colourless crystals of **1** and **2** suitable for X-ray structural determination were obtained on standing. The MS of all the complexes showed peaks at $m/z = 732$ affirming the presence of the dinuclear core $[Zn_2L^3(OAc)]^+$ and those of complexes **1** and **3** showed further peaks at $m/z = 692$ indicating the presence of $[Zn_2L^3(OH)]$. In the IR spectra the difference between the absorption bands for $\nu_{asym}(OAc)$ and $\nu_{sym}(OAc)$ is in the range 119–137cm^{-1} suggesting the presence of an acetato-bridge in all of the complexes [6].

The molecular structure of the monocation from **1** [**A**], is shown in Fig. 1 with selected bond lengths and angles given in the caption to the figure. The structure shows that the complex is donor atom, geometry and co-ordination number asymmetric with one five-co-ordinate zinc atom [Zn(1)] and one six-co-ordinate Zn atom [Zn(2)]. There is an endogenous cresolato bridge and an exogenous *syn–syn* acetato bridge at the dinuclear centre and a water molecule is co-ordinated to Zn(2). Two molecules of methanol and one of water are also present in the structure.

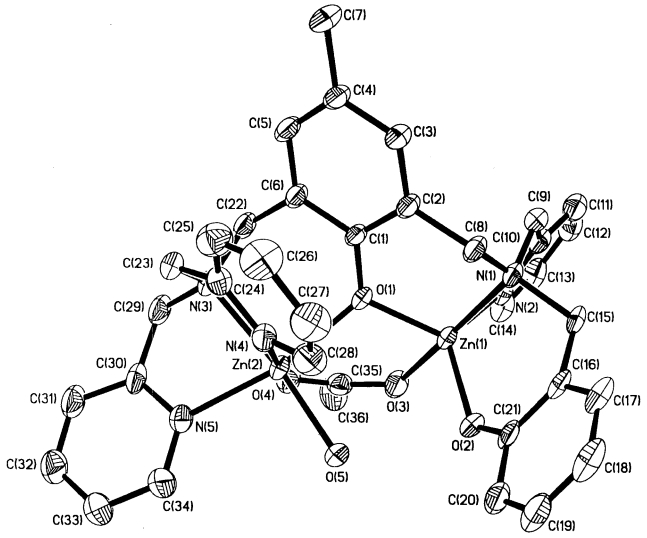
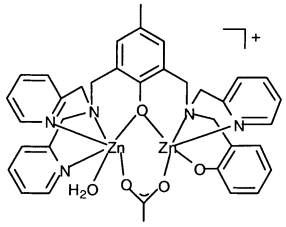


Fig. 1. ORTEP drawing of the molecular structure of the monocation from **1**, $[Zn_2L3(OAc)(OH_2)]^+$. Thermal ellipsoids for the non-hydrogen atoms are drawn at the 50% probability level. Selected bond lengths and angles at the zinc(II) atom. Zn(1)–O(1), 1.975(2); Zn(1)–O(2), 1.971(2); Zn(1)–O(3), 2.034(2); Zn(1)–N(1), 2.164(2); Zn(1)–N(2), 2.069(3); Zn(2)–O(1), 2.103 (2); Zn(2)–O(4), 2.077(2); Zn(2)–O(5), 2.063(2); Zn(2)–N(3), 2.179(2); Zn(2)–N(4), 2.158(3); Zn(2)–N(5), 2.176(3); Zn(1)–Zn(2), 3.4260(6) Å. N(1)–Zn(1)–O(3), 170.28(9)°; O(1)–Zn(1)–N(2), 123.66(9)°; N(2)–Zn(1)–O(2), 125.42(9)°; O(2)–Zn(1)–O(1), 110.64(9)°; Zn(1)–O(1)–Zn(2), 114.25(9)°; N(4)–Zn(2)–O(4), 171.16(9)°; O(1)–Zn(2)–N(5), 166.25(9)°; O(5)–Zn(2)–N(3), 168.43(10)°; O(1)–Zn(2)–O(5), 97.16(8)°; O(5)–Zn(2)–N(5), 96.45(9)°; N(3)–Zn(2)–N(5), 77.11(10)°; N(3)–Zn(1)–O(1), 89.79(9)°.



[A]

Zn(1) is five-co-ordinate with an N_2O_3 co-ordination environment provided by the bridging cresolato-O and acetato-O donor atoms [O(1) and O(3)], a pendant phenolato-O donor atom [O(2)], an articular tertiary aminic-N atom [N(1)] and a pendant pyridinyl-N atom [(N2)]. The degree of trigonality (τ) at Zn(1) is 0.75 and represents a distorted trigonal bipyramidal co-ordination geometry [a perfect geometry has $\tau = 1$ and a perfect square pyramidal geometry has $\tau = 0$] [7]. The cresolato bridge is non-symmetric [Zn(1)–O(1), 1.97; Zn(2)–O(1), 2.10 Å] as is the acetato bridge [Zn(1)–O(3), 2.03; Zn(2)–O(4), 2.08 Å]. The largest angle at Zn(1) is O(3)–Zn(1)–N(1), 170.3°, indicating that a bridging acetato-O atom and the articular aminic-N atom occupy the axial positions. The Zn–N_{pyr} interaction (2.07 Å) is shorter than the The Zn–N_{amine} interaction (2.16 Å). The distribution of bond lengths and angles at Zn(1) is closely similar to that reported for the corresponding Zn atom in the complex $[Zn_2L^2(OAc)(OH_2)]\cdot CH_3CO_2H$ (**4**) derived from the symmetric compartmental ligand H_3L^2 which has pairs of pendant pyridyl and phenolic pendant arms providing two N_2O_2 donor sets [3]. The τ value for the polyhedron at Zn(1) in **4** is 0.63 indicating a larger distortion from ideal geometry than that found in **1**.

Zn(2) is in a distorted octahedral geometry with an N_3O_3 donor set derived from the bridging cresolato-O and acetato-O donor atoms [O(1) and O(4)], an articular tertiary aminic-N atom [N(3)], two pendant pyridinyl-N atoms [N(4) and N(5)] and the O-atom [O(1W)] The three *trans*-axial angles at Zn(2) are 171.2° [O(4)–Zn(2)–N(4)], 166.3° [O(1)–Zn(2)–N(5)], and 168.4° [N(3)–Zn(2)–O(5)]. The co-ordinated water molecule is bound *trans*- to the articular tertiary amine N-atom as was found for the N_2O_4 donor set at the corresponding Zn atom in complex **4** [3]. The Zn–O distances at Zn(2) average 2.08 Å and the Zn–N distances at this Zn atom average 2.17 Å, both are slightly longer than the corresponding distances at Zn(1).

Fig. 2 presents a schematic comparison of the (μ-cresolato)(μ-acetato) cores in complexes **1**, **2** and **4** and clearly shows the similarity between them. In each complex the cresolato bridge is non-symmetric with the acetato bridge being more symmetric. The inter-metallic separations [Zn(1)···Zn(2)] are closely similar being 3.43 (**1**); 3.40 (**2**) and 3.41 Å (**4**).

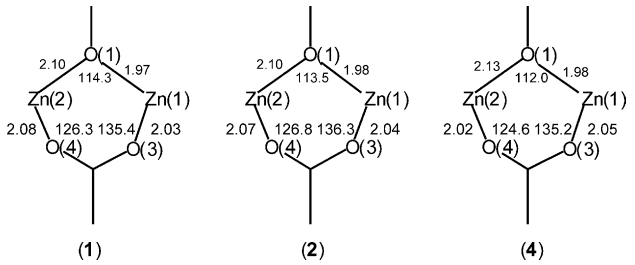


Fig. 2. Comparison of the (μ-cresolato)(μ-acetato) cores in complexes **1**, **2** and **4** (bond lengths are given in Å and bond angles in °).

The crystal structure of complex **2** was also solved. The structure and dimensions of the cation $[Zn_2\mathbf{L}3(OAc)(OH_2)]^+$ were closely similar to those for the cation from **1** and so the crystallographic data has been deposited electronically [8]. No crystals suitable for X-ray analysis were obtained for complex **3** but it is likely the cation in this structure will closely resemble those in complexes **1** and **3**.

4. Conclusions

The formation of co-ordination number asymmetric dinuclear zinc(II) complexes of the unsymmetrical compartmental proligand $H_2\mathbf{L}^3$ follows the reaction pattern observed for dinuclear zinc(II) complexes of the symmetrical proligands $H\mathbf{L}^1$ and $H_3\mathbf{L}^2$. It is interesting to note that the co-ordinated water molecule in complexes **1** and **2** is bound at the Zn atom that resides in the nitrogen-rich binding compartment. This parallels the bound water molecule found at catalytic Zn sites in hydrolytic enzymes where the most common donor is the imidazole N-atom from histidine residues [9]. Although the asymmetric complexes above have the necessary features-a bound, and, therefore, polarisable, water molecule at one zinc atom adjacent to an available co-ordination site at the second zinc [10] to serve as plausible models for hydrolytic enzymes study of this property has been hindered by the relative insolubilities of the complexes after isolation. The most efficient solvent for dissolution is DMSO and as this is a strongly co-ordinating solvent it is likely that the solvent would co-ordinate to the metal at the expense of the water and could also block the vacant co-ordination site at the second zinc atom. Both of these events would severely affect the course of any hydrolysis of substrate, such as phosphate esters and would not necessarily be directly relevant to enzymatic activity, which occurs in aqueous media. If is, therefore, essential that the complexes should be made more soluble in aqueous media and to that end it is suggested that the attachment of polar groups, such as sulphonate, to the ligand perifery should facilitate the solubility of the complexes in aqueous media [11] and permit kinetic studies to be carried out under more enzymatic conditions.

5. Supplementary material

Crystallographic data (excluding structure factors) for the structural analysis have been deposited with the Cambridge Crystallographic Data Centre CCDC No. 173827 [complex **1**]. Copies of this information may be obtained free of charge from The Director, CCDC, 12 Union Road, Cambridge CB2 1EZ, UK (fax: (internat.) +44-1223-336033; e-mail: deposit@ccda.cam.ac.uk or www: http://www.ccdc.cam.ac.uk).

Acknowledgements

We thank the BBSRC for a studentship (to D.B.) and the EPSRC for funds towards the purchase of the diffractometer.

References

[1] J.H. Satcher, Jr., M.W. Droege, T.J.R. Weakley, R.T. Taylor, Inorg. Chem. 34 (1995) 3317.
[2] S. Uhlenbrock, B. Krebs, Angew.Chem., Int. Ed. Engl. 31 (1992) 1647.
[3] H. Adams, D. Bradshaw, D.E. Fenton, Supramolecular Chem. 13 (2001) 513.
[4] A. Neves, M.A. de Brito, V. Drago, K. Griesar, W. Haase, Inorg Chim. Acta 237 (1995) 131.
[5] SHELXTL version, An integrated system for solving and refining crystal structures from diffraction data (Revision 5.1), Bruker AXS Ltd., Madison., WI, USA, 1997.
[6] G.B. Deacon, R.J. Phillips, Coord. Chem. Rev. 23 (1980) 227.
[7] A.W. Addison, T.N. Rao, J. Reedijk, J. van Rijn, G.C. Verschoor, J. Chem. Soc., Dalton Trans. (1984) 1349.
[8] Cambridge Crystallographic Data centre supplementary publication no. CCDC 173826.
[9] B.L. Vallee, D.S. Auld, Proc. Natl. Acad. Sci. USA 87 (1990) 220.
[10] B.L. Vallee, D.S. Auld, Biochemistry 32 (1993) 6493.
[11] (a) D.F. Evans, P.H. Missen, J. Chem.Soc., Dalton Trans. (1987) 1279.;
(b) D.F. Evans, P.H. Missen, J. Chem.Soc., Dalton Trans. (1985) 1471.

$[Cu(DLM)_2(H_2O)_2](ClO_4)_2$ [17], complexes showing the $[M^{II}L_2(H_2O)_2]X_2$ formula display the octahedral cation $[ML_2(H_2O)_2]^{2+}$ in which the ligands are arranged in *trans* positions. In a few compounds, as $[CdL_2(NO_3)_2]$ [14] and halide complexes [15,18,19], the counteranion is coordinated to the metal ion, the relative position of the donor atoms always being *trans*.

Now, the preparation and characterization of a number of perchlorate complex salts with divalent cobalt, nickel, copper, zinc, cadmium and mercury ions are reported. The crystal structures of $[Cu(MLM)_2(H_2O)_2](ClO_4)_2$, $[Zn(MLM)_2(H_2O)_2](ClO_4)_2$ and $[Cu(MLM)(MLMD)(H_2O)(CH_3CN)](ClO_4)_2$ have been determined by X-ray diffraction methods. The presence of a hydrogen in N3-position promotes a different H-bond scheme respect to previous perchlorate complex salts with 1,3-dialkyllumazines [13,17].

2. Experimental

2.1. Synthesis

The ligands MLM and MLMD were obtained according to literature procedures [20] and characterized through analysis, ^{1}H NMR and IR spectroscopy [21]. The coordination compounds were prepared by reaction of metal perchlorate and the pteridine ligand (M/L = 2:1) in MeCN (50 ml) heating at 40–50 °C (CAUTION: perchlorate salts are dangerous and must be handled with care), except to Hg/MLM in which the solvent was water. The mixed Cu(II) complex was obtained adding 1 mmol of copper perchlorate to $\frac{1}{2}$ mmol of MLM and MLMD ligands dissolved in MeCN solution (approximately 50 ml). In some cases, after several hours, a solid was obtained and in the others, after standing at room temperature (r.t.) for several days, the solutions gave different solids. Only the complexes $[Cu(MLM)_2(H_2O)_2](ClO_4)_2$, $[Zn(MLM)_2(H_2O)_2](ClO_4)_2$ and $[Cu(MLM)(MLMD)(H_2O)(CH_3CN)](ClO_4)_2$ were obtained as single crystals suitable for X-ray diffraction. The solids were filtered off, washed with a small amount of EtOH and Et_2O and air-dried.

Analytical data were as follows (%): $Co(ClO_4)_2(MLM)_2\cdot 2H_2O$ (orange): *Anal.* Found: C, 26.05; H, 2.61; N, 18.00. Calc.: C, 25.86; H, 2.48; N, 17.23%. $Ni(ClO_4)_2(MLM)_2\cdot 2H_2O$ (green): *Anal.* Found: C, 25.77; H, 2.76; N, 17.31. Calc.: C, 25.86; H, 2.48; N, 17.24%. $Cu(ClO_4)_2(MLM)_2\cdot 2H_2O$ (green): *Anal.* Found: C, 25.15; H, 2.55; N, 16.75. Calc.: C, 25.67; H, 2.47; N, 17.12%. $Zn(ClO_4)_2(MLM)_2\cdot 2H_2O$ (orange): *Anal*. Found: C, 25.33; H, 2.59; N, 16.83. Calc.: C, 25.60; H, 2.43; N, 17.07%. $Hg(ClO_4)_2(MLM)_2\cdot 3H_2O$ (yellow): *Anal*. Found: C, 20.14; H, 1.73; N, 13.25. Calc.: C, 20.76, H, 2.24; N, 13.83%. $Co(ClO_4)_2(MLMD)_2\cdot 2H_2O$ (yellow): *Anal*. Found: C, 30.34; H, 3.50; N, 16.08. Calc.: C, 30.60; H, 3.43; N, 15.87%. $Ni(ClO_4)_2(MLMD)_2\cdot 3H_2O$ (pale green): *Anal.* Found: C, 29.73; H, 3.50; N, 15.46. Calc.: C, 29.85; H, 3.62; N, 15.47%. $Cu(ClO_4)_2(MLMD)_2\cdot 3H_2O$ (green): *Anal.* Found: C, 29.68; H, 3.53; N, 15.72. Calc.: C, 29.65; H, 3.60; N, 15.37%. $Zn(ClO_4)_2(MLMD)_2\cdot 4H_2O$ (yellow): *Anal.* Found: C, 28.89; H, 3.35; N, 14.94. Calc.: C, 28.87; H, 3.77; N, 14.97%. $Cd(ClO_4)_2(MLMD)_2\cdot 2H_2O$ (yellow): *Anal.* Found: C, 28.39; H, 3.20; N, 14.71. Calc.: C, 28.45; H, 3.19; N, 14.75%. $Cu(ClO_4)_2(MLM)(MLMD)\cdot H_2O\cdot C_2H_3N$ (green): *Anal.* Found: C, 30.41; H, 2.97; N, 17.63. Calc.: C, 30.62; H, 3.00; N, 17.86%.

2.2. Instrumentation

Microanalyses of C, H and N were performed in the Fisons-Instruments EA-1008; the water content of the complexes was determined from the TG plot. TG and DSC studies were carried out under pure air on a SHIMADZU system (TGA-50 thermobalance and DSC-50 differential scanning calorimeter) using approximately 5 mg of sample and a 20 °C min^{-1} heating rate in the TG and 10 °C min^{-1} in the DSC plots. Infrared (IR) spectra were measured on a Perkin–Elmer FT-IR 1760-X (KBr pellets, 4000–400 cm^{-1}) and on a Bruker FT-IR VECTOR 22 spectrophotometer (polyethylene pellets, 600–180 cm^{-1}). ^{13}C and ^{1}H NMR spectra were recorded using a Bruker DPX-300 apparatus (DMSO-d_6 solutions). The ESR spectra were obtained in the X-band at r.t. on a Bruker ESP 300E apparatus, with a microwave frequency of 9.79 GHz and a modulation frequency of 100 kHz. Magnetic measurements were carried out on a Manics DSM-8 system between 77 and 290 K. Reflectance diffuse spectra (200–1200 nm) were recorded on a Perkin–Elmer UV–Vis–NIR Lambda-19 machine using a $BaSO_4$ pellet as reference.

2.3. Crystallography

Crystal data and structure refinement details are given in Table 1. Intensity data were measured at 173 K on a Nonius Kappa CCD diffractometer with graphite monochromated Mo Kα radiation ($\lambda = 0.71070$ Å). The structure was solved by direct methods using the SHELXTL program package [22]. Refinement was carried out using SHELXL employing full-matrix least-squares methods on F^2. All non-hydrogen atoms were refined anisotropically. The hydrogen atoms were placed in their ideal positions.

Table 1
Crystallographic and refinement data

Compound	Cu/MLM	Zn/MLM	Cu/MLM/MLMD
Empirical formula	$C_{14}H_{16}Cl_2CuN_8O_{14}$	$C_{14}H_{16}Cl_2N_8O_{14}Zn$	$C_{18}H_{21}Cl_2CuN_9O_{13}$
Formula weight (g mol^{-1})	654.79	656.62	705.88
Crystal system	monoclinic	monoclinic	monoclinic
Space group	$P2_1/c$	$P2_1/c$	$P2_1/c$
Unit cell dimensions			
a (Å)	6.7340(2)	6.7200(1)	14.1110(2)
b (Å)	12.8290(3)	12.8140(3)	13.1270(2)
c (Å)	13.5250(3)	13.6340(3)	14.1710(3)
β (°)	102.473(1)	102.1830(8)	94.4090(8)
V (Å^3)	1140.85(5)	1147.58(4)	2617.20(8)
Z	2	2	4
D_{calc} (Mg m^{-3})	1.906	1.900	1.791
Absorption coefficient (mm^{-1})	1.283	1.394	1.124
F(000)	662	664	1436
Crystal size (mm)	0.80 × 0.25 × 0.08	0.50 × 0.40 × 0.10	0.80 × 0.25 × 0.08
θ Range for data collection (°)	2.21–33.12	2.20–36.34	2.12–29.57
Index ranges	$0 \le h \le 10$, $-19 \le k \le 19$, $-19 \le l \le 15$	$0 \le h \le 11$, $-21 \le k \le 21$, $-22 \le l \le 22$	$0 \le h \le 19$, $0 \le k \le 18$, $-19 \le l \le 19$
Reflections collected/independent	18 085/3894	21 633/5383	7352/7352
R_{int}	0.0661	0.0628	0.0000
Weighting scheme $w = 1/[\sigma^2(F_o^2)+(xP)^2+yP]$ [a]	$x = 0.0525/y = 0.3399$	$x = 0.0557/y = 0.5524$	$x = 0.0470/y = 7.6200$
Data/restraints/parameters	3892/0/202	5383/0/202	7277/0/451
Final R indices [$I > 2\sigma(I)$] R/wR^2	0.0441/0.1012	0.0451/0.1121	0.0544/0.1287
R indices (all data) R/wR^2	0.0762/0.1176	0.0659/0.1199	0.0751/0.1632
Goodness-of-fit on F^2	1.035	1.043	1.176
Largest difference peak and hole (e Å^{-3})	0.883/−0.556	0.734/−0.659	1.264/−0.658

3. Results and discussion

3.1. X-ray structural study of the complexes

The $[Cu(MLM)_2(H_2O)_2](ClO_4)_2$ and $[Zn(MLM)_2(H_2O)_2](ClO_4)_2$ complexes are isostructural; the molecular unit of Zn/MLM complex with numbering scheme is shown in Fig. 1. Selected bond distances and angles are listed in Table 2. It is readily seen that both complex salts are primarily ionic in nature, consisting on $[ML_2(H_2O)_2]^{2+}$ cations and perchlorate anions. Both metal ions are encircled by six donating centres. Four of these atoms are two N5 and two O4 atoms from the bidentate lumazine derivative ligands, which are linked to the metal ion as usual, producing two chelate rings of five members. The coordination sphere is completed by

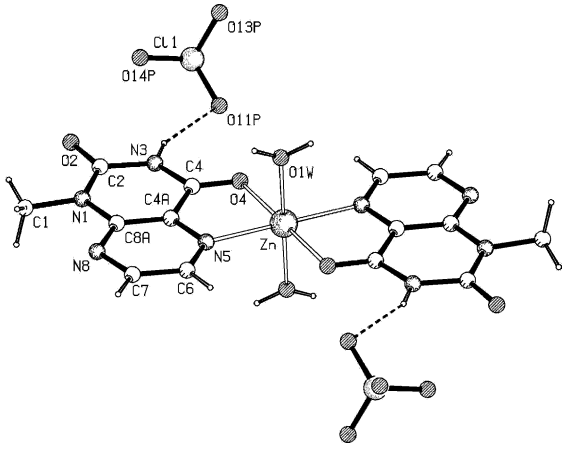


Fig. 1. Molecular unit and numbering scheme of $[Zn(MLM)_2(H_2O)_2](ClO_4)_2$.

Table 2
Selected bond distances (Å) and angles (°) in the coordination sphere in the complexes $[Cu(MLM)_2(H_2O)_2](ClO_4)_2$ and $[Zn(MLMD)_2(H_2O)_2](ClO_4)_2$

	Cu/MLM	Zn/MLM
Bond distances		
M–O(4)	2.246(2)	2.122(1)
M–N(5)	1.992(2)	2.115(1)
M–O(1W)	2.071(2)	2.118(1)
Bond angles		
N(5)–M–O(1W)	91.43(7)	87.59(6)
N(5)–M–O(4)	80.04(6)	80.08(5)
O(1W)–M–O(4)	88.91(7)	90.61(6)
C(4)–O(4)–M	106.8(1)	110.6(1)
C(6)–N(5)–M	128.6(2)	132.8(1)
C(4A)–N(5)–M	113.7(1)	110.0(1)

two water molecules directly bonding to the metal centre.

The six-coordinated copper ion is equatorially bonded to two N5 atoms of MLM ligands and two water oxygens and axially bonded to two O4 MLM atoms. The coordination geometry around the copper ion can be described as an elongated tetragonal octahedral of the CuN_2O_4 chromophore with the tetragonality of 0.91. The observed distortions are due to the Jahn–Teller effect. The complex $[Zn(MLM)_2(H_2O)_2](ClO_4)_2$ exhibits a roughly regular octahedral geometry in which the Zn–N and Zn–O distances (see Table 2) are not significantly different to each other, ranging from 2.115(1) to 2.122(1) Å.

In the Cu/MLM and Zn/MLM complexes, the O4–M–N5 bite angle of the lumazine derivative ligands is similar (see Table 2) and the normalized *bite* is approximately 1.29. Following Kepert [23], the bidentate ligands that form five-membered chelate rings and have relatively large normalized bites ($b \sim 1.2$–1.5) normally form undistorted *trans* structures, like is a familiar pattern in this kind of complexes [12–19].

The bonding parameters for the organic ligands are very close to those found for previously reported bidentate lumazine derivatives [10–19]. The C2–O2 distances are a little shorter than that of C4–O4 because of the involvement of the O4 atom in the coordination. The angle between pyrazine and pyrimidine rings is 1.9° (Cu/MLM) and 1.5° (Zn/MLM), so the lumazine ligands are roughly planar. The greatest deviations from the mean plane in the lumazine derivative occur in the N1 for the endocyclic atom and in the C1 for the exocyclic ones. Each organic ligand and the five-membered chelate ring are quasi-coplanar because the least-squares plane defined by the pteridine skeleton and the chelate rings (M–O4–C4–C4A–N5) define acute angles of 0.7° and 0.5° in the Cu/MLM and Zn/MLM, respectively. Pteridine moieties are parallel but not coplanar being distanced by 0.050 (Cu/MLM) and 0.022 Å (Zn/MLM) to each other.

The geometrical data of hydrogen bonds in the Cu/MLM and Zn/MLM complexes are summarized in Table 3 and a stereoview of the copper complex is shown in Fig. 2. In both complexes, a three-dimensional network is produced by two OW–H···O(ClO_4^-) hydrogen bonds and N3–H3···O(ClO_4^-) ones. The disordered perchlorate anions are located between zig-zag layers of the complexes and are hydrogen bonded to either the water molecules or to the N3 atom of lumazine ligands, as shown in Fig. 2.

In Fig. 3, the molecular drawing and numbering scheme for the monomeric unit of $[Cu(MLM)(MLMD)(H_2O)(CH_3CN)](ClO_4)_2$ is shown and in Table 4, selected bond distances and angles are given. This complex differs from related complexes [14,17] because it contains two different lumazine derivatives and one

Table 3
Hydrogen bonding (D–H···A) in (a) $[Cu(MLM)_2(H_2O)_2](ClO_4)_2$ and (b) $[Zn(MLM)_2(H_2O)_2](ClO_4)_2$

D	A	d(D–A) (Å)	d(H···A) (Å)	∠(D–H···A) (°)
(a)				
N3	O11P	2.071	2.345	151
O1W	O11P [a]	2.908	2.192	163
O1W	O14P [b]	2.806	1.963	173
(b)				
N3	O11P [c]	2.995	2.240	157
O1W	O11P	2.931	2.150	167
O1W	O14P [d]	2.826	1.960	166

[a] $1-x, -y, -z$.
[b] $1-x, -1/2+y, 1/2-z$.
[c] $1+x, y, z$.
[d] $x, -1/2-y, -1/2+z$.

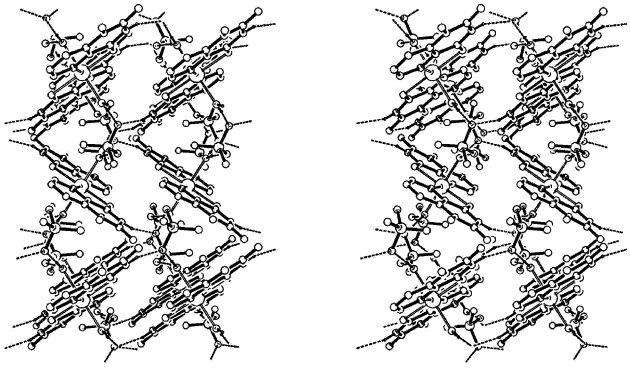


Fig. 2. Stereoview of the three-dimensional network of the complex $[Cu(MLM)_2(H_2O)_2](ClO_4)_2$. Hydrogen atoms of methyl groups are omitted for clarity.

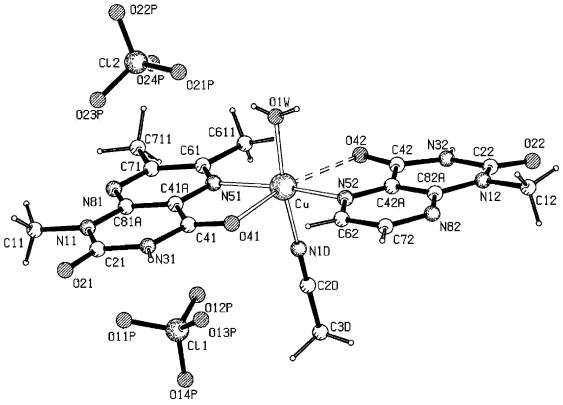


Fig. 3. Molecular unit of complex $[Cu(MLM)(MLMD)(H_2O)(CH_3CN)](ClO_4)_2$. The Cu–O42 bond (2.558(3) Å) is dotted to emphasize the semicoordination.

acetonitrile molecule directly linked to the metal ion. Both lumazine ligands are bonded to the copper ion through the N5 and O4 atoms.

As it is shown in Fig. 3, the metal ion is surrounded at distances of approximately 2.0 Å by two N5 atoms from

Table 4
Selected bond distances (Å) and angles (°) of [Cu(MLM)(MLMD)-(H_2O)(CH_3CN)](ClO_4)$_2$

Bond distances	
Cu–N(1D)	1.955(3)
Cu–O(1W)	1.971(3)
Cu–N(52)	2.026(3)
Cu–N(51)	2.044(3)
Cu–O(41)	2.293(2)
Cu–O(42)	2.558(3)
Bond angles	
N(1D)–Cu–O(1W)	167.2(1)
N(1D)–Cu–N(52)	90.8(1)
O(1W)–Cu–N(52)	90.8(1)
N(1D)–Cu–N(51)	89.4(1)
O(1W)–Cu–N(51)	91.4(1)
N(52)–Cu–N(51)	169.2(1)
N(1D)–Cu–O(41)	97.7(1)
O(1W)–Cu–O(41)	94.9(1)
N(52)–Cu–O(41)	90.6(1)
N(51)–Cu–O(41)	78.7(1)
N(1D)–Cu–O(42)	80.6(1)
O(1W)–Cu–O(42)	87.7(1)
N(52)–Cu–O(42)	73.7(1)
N(51)–Cu–O(42)	117.0(1)
O(41)–Cu–O(42)	164.1(1)

pteridine ligands in a *trans* arrangement, a water molecule and the N-coordinated acetonitrile defining a regular square-plane. In addition to these, in a roughly perpendicular tetragonal axis, two O4 atoms from lumazine ligands are placed at distances-to-metal very different to each other and the four square-plane donor atoms. The apical Cu–O42 and Cu–O41 distances are significantly different with $\Delta O_{42,41} = 0.265$ Å. The ratio between apical and equatorial bond lengths is 1.21, which is smaller than that needed (≥ 1.4) to force a square-planar complex [23].

The larger Cu–O41 distance (2.293(3) Å), if compared with the Cu–L bond lengths in the equatorial plane, must be attributed to the Jahn–Teller effect whereas the larger Cu–O42 distance (2.558(3) Å) must be due, in addition to the Jahn–Teller effect, to the O42 atom cannot be involved in direct bonding along the z-axis, but is close enough to the z direction to involve at least some weak or semi-coordination of the O42 atom to the Cu(II) ion. Consequently, the stereochemistry of the Cu/MLM/MLMD complex should not be considered to involve a five coordination, but six-coordinate elongated octahedral with a 4+1+1* -type coordination [24,25]. If the weak interaction between Cu(II) and O42 is not considered, the copper centre displays a slightly distorted square-pyramidal stereochemistry ($\tau = 0.03$) [26], with atoms N51, N52, N1D and O1W arranged in the basal plane.

The effect of both electronic and steric hindrances of the ligands can be seen in the opening of the L–M–L angles of the respective metallocyclic rings. The five-membered chelate rings, with an angle type O–M–N, have values of 73.1(1)° in the MLM and 78.7(1)° to MLMD ligand. The chelate rings are roughly coplanar (4.4°) and the greatest deviations from the mean plane of the pteridine ligands are in the O2 in both ligands for the exocyclic atoms and C2 (MLM) and N1 (MLMD) for the endocyclic ones.

The Cu–N1D–C2D bond angle 177.5(3)° is slightly distorted from the expected value for a sp hybridised nitrogen atom (180°). The N1D–C2D bond lengths of 1.13(5) Å compare well with the literature values [27] for coordinated acetonitrile and are a little shorter than the value found for the free acetonitrile 1.157 Å.

The monomeric units are connected through the N–H···O and O–H···O hydrogen bonds (see Table 5) in a similar way than the above mentioned Cu(II) and Zn(II) complexes, in which one perchlorate anion is bonded to the N31 and the water molecules and the other is not involved in the hydrogen bonds network. In addition to the N3–H···O(ClO_4^-) hydrogen bond, the crystal structure is packed via the strong involvement of the coordinated water molecule in the H-bond scheme, since it is linked with two perchlorate anions and the O2 oxygen from MLMD moiety through a bifurcated hydrogen bond in which the D–H···A angle (109°) is too smaller than the other ones (approximately 180°). The hydrogen bonds generate two-dimensional networks which are packed by van der Waals interactions following the a-axis as it is shown in Fig. 4.

3.2. Thermal and spectral studies

The study of the thermal decomposition of these compounds in air has been carried out from their TG and DSC plots. These indicate the water molecules are lost in only one clearly defined step in the TG plot, but, in most cases, the corresponding endothermic effect in the DSC plot is splitted, indicating the non-equivalence of all water molecules. In all cases, the weight losses agree well with those expected for the elimination of solvent molecules. The dehydrated intermediates are stable at temperatures up to 300 °C. At this point, an abrupt weight loss occurs as consequence of the

Table 5
Hydrogen bonding interactions in [Cu(MLM)(MLMD)(H_2O)-(CH_3CN)](ClO_4)$_2$

D	A	d(D–A) (Å)	d(H···A) (Å)	∠(D–H···A) (°)
(a)				
N31	O21P [a]	2.972(5)	2.19(4)	155(4)
O1W	O21P	2.805(4)	2.17(6)	178(7)
O1W	O21 [a]	2.884(4)	2.53(6)	109(5)
O1W	O22P [b]	3.006(4)	2.23(6)	171(6)

[a] $-x, -1/2+y, 1/2-z$.
[b] $x, 1/2-y, 1/2+z$.

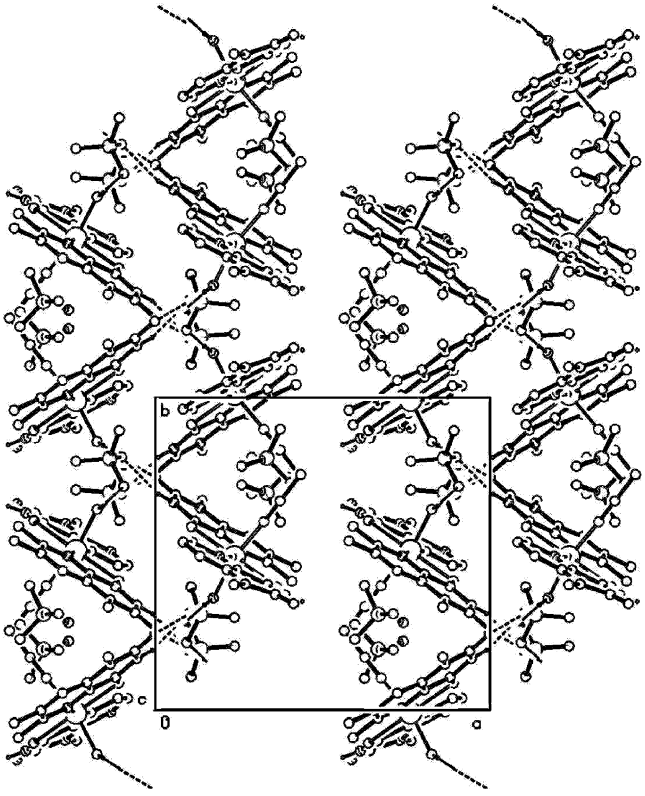


Fig. 4. Packing scheme of the hydrogen-bonded network in the complex $[Cu(MLM)(MLMD)(H_2O)(CH_3CN)](ClO_4)_2$ viewed down the [0 0 1] direction. Hydrogen atoms of methyl groups are omitted for clarity.

combustion of the organic matter and the sharp decomposition of perchlorate anions. The pyrolysis finishes at 400 °C, leaving as final residue the corresponding oxides, as it has been corroborated from the corresponding IR spectrum, but it was not possible to calculate the experimental total weight loss because there are material losses from the crucible.

In the 3500–2800 cm^{-1} region, the IR spectra show the ν(O–H), ν(N–H) and ν(C–H) bands. The $[Cu(MLM)(MLMD)(H_2O)(CH_3CN)](ClO_4)_2$ complex shows a weak ν(C≡N) band at 2330 cm^{-1} due to the presence of coordinated acetonitrile [28] which is shifted to upper wavenumber with respect its position in the free acetonitrile (2255 cm^{-1}), this shift is consistent with the shortening in the C≡N distance upon coordination.

The bands assignable to the C=C, C=N and C=O stretching vibrations are shifted respect to their position in the spectra of uncoordinated MLM and MLMD. The vibrational activity of carbonyl groups is coupled and appears as two bands. The higher (1700–1730 cm^{-1}) is mainly due to ν(C2=O) and the other one (1650–1680 cm^{-1}) must be assigned to ν(C4=O). In all MLM complexes, both bands are strong shifted with respect to their position in the IR spectrum of the free ligand whereas in the MLMD complexes the shifts are weaker. These displacements are due to the different H-bond scheme found in the free MLM and MLMD; thus, in the free MLM, dimeric units are produced via O2···H3–N3 hydrogen bonds, whereas in the MLMD ligand, these H-bonds are established through the O4 atom. Therefore, in the MLMD complexes, the participation of the O4 atom in the coordination sphere induces a weaker shift than in the MLM complexes. The spectra also show a strong ν(Cl–O) band splitted into three peaks between 1150 and 1090 cm^{-1} and the δ(O–Cl–O) band at 626 cm^{-1} assignable to the perchlorate anions [29].

Within experimental error, NMR spectra of zinc, cadmium and mercury complexes display signals at the same values of chemical shift than the free ligands, clearly indicating that these compounds may undergo strong solvolysis. Although, an alternative explanation based on the π-electronic density is unchanged upon coordination cannot be discarded.

The room temperature powder ESR spectra of $[Cu(MLM)_2(H_2O)_2](ClO_4)_2$ and $[Cu(MLM)(MLMD)(H_2O)(CH_3CN)](ClO_4)_2$ are axial with $g_{\parallel} \gg g_{\perp} > 2.0$ [24,30]. The g values of Cu/MLM complex are $g_{\parallel} = 2.38$ and $g_{\perp} = 2.09$, corresponding to elongated tetragonal octahedral CuN_2O_4 chromophore and the $d_{x^2-y^2}$ ground state. The G-parameter, calculated from the relation $G = (g_{\parallel} - 2)/(g_{\perp} - 2)$ in the axial-elongated complex Cu/MLM has a value of 4.3. This indicates the absence of interaction between the copper centres in the solid state and a rhombic symmetry with the local tetragonal axes aligned or slightly misaligned, as it is expected from the structural data. In the $[Cu(MLM)(MLMD)(H_2O)(CH_3CN)](ClO_4)_2$ complex only the $g_{\perp}$ (2.03) value can be measured that it is consistent with an square-pyramidal coordination sphere around Cu(II) ion and the single unpaired electron is located in an essentially $d_{x^2-y^2}$ orbital. In the $Cu(MLMD)_2(ClO_4)_2 \cdot 3H_2O$ complex, the ESR spectrum at room temperature is apparently isotropic with g_i of 2.17 value.

The electronic reflectance spectra (see Table 6) of the Co(II) complexes show two d–d bands assignable to the transitions $^4T_{2g}(F) \leftarrow {}^4T_{1g}$ and $^4T_{1g}(P) \leftarrow {}^4T_{1g}$ in a d^7 (high spin) system in octahedral symmetry. The transition $^4A_{2g}(F) \leftarrow {}^4T_{1g}$ value has been calculated by means of the algebraic Dou's method [31]. The transitions bands, B and Δ_o values are characteristic of Co(II) at the octahedral site. In the Ni(II) complexes, three bands can be observed due to $^3T_{2g}(F) \leftarrow {}^3A_{2g}$, $^3T_{1g}(F) \leftarrow A_{2g}$ and $^3T_{1g}(P) \leftarrow {}^3A_{2g}$ transitions typical from octahedral Ni(II) complexes. The values of B are about 55% respect of those for the free ions, indicating there is a high degree of covalence in the metal–ligand bonds [31,32].

The Cu(II) complex spectrum shows a broad and asymmetric band centred at 13 300 (Cu/MLM), 13 800 (Cu/MLMD) and 14 300 cm^{-1} (Cu/MLM/MLMD). This band is typical for distorted octahedral Cu(II) complexes [32]. In each case, the band was deconvoluted

Table 6
Electronic spectra

Complex	ν (cm^{-1})	Transition	B (cm^{-1})	Δ_o (cm^{-1})
Co/MLM	9200	$^4T_{2g}(F) \leftarrow {}^4T_{1g}$	677	10 200
	19 400 [a]	$^4A_{2g}(F) \leftarrow {}^4T_{1g}$		
	18 200	$^4T_{1g}(P) \leftarrow {}^4T_{1g}$		
Co/MLMD	9500	$^4T_{2g}(F) \leftarrow {}^4T_{1g}$	563	10 400
	19 900 [a]	$^4A_{2g}(F) \leftarrow {}^4T_{1g}$		
	16 900	$^4T_{1g}(P) \leftarrow {}^4T_{1g}$		
Ni/MLM	10 500	$^3T_{2g}(F) \leftarrow {}^3A_{2g}$	602	10 500
	15 900	$^3T_{1g}(F) \leftarrow {}^3A_{2g}$		
	24 700	$^3T_{1g}(P) \leftarrow {}^3A_{2g}$		
Ni/MLMD	9300	$^3T_{2g}(F) \leftarrow {}^3A_{2g}$	489	9300
	13 800	$^3T_{1g}(F) \leftarrow {}^3A_{2g}$		
	21 400	$^3T_{1g}(P) \leftarrow {}^3A_{2g}$		
Cu/MLM	13 300	$^2T_{2g} \leftarrow {}^2E_g$	–	13 300
Cu/MLMD	13 800	$^2T_{2g} \leftarrow {}^2E_g$	–	13 800
Cu/MLM/MLMD	14 300	$^2T_{2g} \leftarrow {}^2E_g$	–	14 300

[a] Calculated by means of algebraic method (from Ref. [31]).

into Gaussian component bands in the visible region. Starting from a set of six peaks, computer iteration processes for experimental curves fitting were carried out to minimize the standard deviation from the calculated ones, reaching a standard deviation of approximately 0.003 absorbance units. Thus, three peaks for all copper spectra were obtained. In the Cu/MLM (15 000, 13 300 and 11 200 cm^{-1}) and Cu/MLMD (14 600, 11 600 and 9300 cm^{-1}) complexes, these bands are assignable to the transitions between the Jahn–Teller splitted t_{2g} and e_g orbitals [24]. The deconvolution of the spectrum of the Cu/MLM/MLMD complex gives four peaks at 15 300, 13 300, 11 400 and 9100 cm^{-1}, which could be assigned to the four d–d transitions expected for the orbital distribution in a tetragonal 4+1+1* geometry.

The molar susceptibility values at different temperatures for the Co/MLM and Co/MLMD complexes have been successfully fitted to the Curie–Weiss law. Whereas the Co/MLMD displays a Curie's behaviour, in the Co/MLM complex, the θ value (−67(5) K) could indicate a slightly antiferromagnetic interaction. The magnetic moments in the Co(II) complexes are 4.9(3) and 4.52(1) MB in the Co/MLM and Co/MLMD, respectively; these values are quite different from the spin-only value due to the orbital contribution expected in the octahedral d^7 (high spin) systems. The molar susceptibility values at room temperature for the Ni(II) and Cu(II) complexes were measured. In these complexes, where no orbital contribution to the magnetic moment must be expected, the μ_{eff} values measured differ only slightly from the spin-only moment (2.83 and 1.73 MB in Ni(II) and Cu(II) complexes, respectively) and are in accordance with the existence of magnetically dilute monomeric units [33].

4. Supplementary material

Supplementary material including all atomic coordinates, anisotropic displacement parameters for non-hydrogen atoms and all interatomic distances and bond angles have been deposited with the Cambridge Crystallographic Data Centre, CCDC Nos. 181136–181138 for compounds $[Cu(MLM)_2(H_2O)_2](ClO_4)$, $[Zn(MLM)_2(H_2O)_2](ClO_4)$ and $[Cu(MLM)(MLMD)(H_2O)(CH_3CN)](ClO_4)_2$, respectively. Copies of this information may be obtained free of charge from The Director, CCDC, 12 Union Road, Cambridge, CB2 1EZ, UK (fax: +44-1233-336033; e-mail: deposit@ccdc.cam.ac.uk or www: http://www.ccdc.cam.ac.uk).

Acknowledgements

This work was supported by the spanish *Ministerio de Ciencia y Tecnología* (projects PB97-0786C0303 and BQU2001-2955-C02-02).

References

[1] (a) R.J.P. Williams, Eur. J. Biochem. 234 (1995) 363;
(b) R.J.P. Williams, Inorg. Chim. Acta 5 (1971) 137.
[2] J.S. Valentine, C.S. Foote, A. Greenberg, J.F. Liebman (Eds.), Active Oxygen in Biochemistry, Search Series, Vol. 3, 1995.
[3] (a) M.J. Clarke, Comments Inorg. Chem. 3 (1984) 133;
(b) M.J. Clarke, Rev. Inorg. Chem. 2 (1980) 27.
[4] W. Kaim, Rev. Chem. Intermed. 8 (1987) 247.
[5] (a) W. Kaim, A. Schulz, F. Hilgers, H.D. Hausen, M. Moscherosch, A. Lichtblau, J. Jordanov, E. Roth, S. Zalis, Res. Chem. Intermed. 19 (1993) 603;
(b) J.E. Ayling, M.G. Nair, C.M. Baugh (Eds.), Chemistry and Biology of Pteridines and Folates, Plenum Press, New York, 1993, pp. 67–68.
[6] W. Kaim, B. Schwederski, Bioinorganic Chemistry, Wiley, Chichester, 1994, pp. 33–40.
[7] (a) W. Pfleiderer, in: S.J. Benkovic, R.L. Blakeley (Eds.), Chemistry and Biochemistry of Pterins, vol. 2, Wiley, Chichester, 1985, pp. 105–109;
(b) W. Pfleiderer, J. Heterocycl. Chem. 29 (1992) 583.
[8] S.P. Greatbanks, I.H. Hillier, C.D. Garner, J.A. Joule, J. Chem. Soc., Perkin Trans. 2 (1997) 1529.
[9] D.W. Young, Chem. Soc. Rev. 23 (1994) 119.
[10] A. Odani, H. Masuda, K. Inukai, O. Yamauchi, J. Am. Chem. Soc. 114 (1992) 6294.
[11] (a) M. Mitsumi, J. Toyoda, K. Nakasuji, Inorg. Chem. 34 (1995) 3367;
(b) M. Mitsumi, J. Toyoda, K. Nakasuji, N. Kanehisa, Y. Kai, Mol. Cryst. Liq. Cryst. Sci. Tec., Sect. A 276 (1996) 229.
[12] F. Hueso-Ureña, S.B. Jiménez-Pulido, M.N. Moreno-Carretero, M. Quirós-Olozábal, J.M. Salas-Peregrín, Polyhedron 16 (1997) 607.
[13] F. Hueso-Ureña, S.B. Jiménez-Pulido, M.N. Moreno-Carretero, M. Quirós-Olozábal, J.M. Salas-Peregrín, Inorg. Chim. Acta 268 (1998) 77.
[14] F. Hueso-Ureña, S.B. Jiménez-Pulido, M.N. Moreno-Carretero, M. Quirós-Olozábal, J.M. Salas-Peregrín, Inorg. Chim. Acta 277 (1998) 103.

[15] F. Hueso-Ureña, S.B. Jiménez-Pulido, M.N. Moreno-Carretero, M. Quirós-Olozábal, J.M. Salas-Peregrín, Polyhedron 17 (1998) 3409.
[16] F. Hueso-Ureña, S.B. Jiménez-Pulido, M.N. Moreno-Carretero, M. Quirós-Olozábal, J.M. Salas-Peregrín, J. Chem. Crystallogr. 28 (1998) 565.
[17] F. Hueso-Ureña, S.B. Jiménez-Pulido, M.N. Moreno-Carretero, M. Quirós-Olozábal, J.M. Salas-Peregrín, J. Chem. Crystallogr. 29 (1999) 571.
[18] F. Hueso-Ureña, S.B. Jiménez-Pulido, M.N. Moreno-Carretero, M. Quirós-Olozábal, J.M. Salas-Peregrín, Polyhedron 18 (1999) 85.
[19] S.B. Jiménez-Pulido, M. Sieger, A. Knödler, O. Heilmann, M. Wanner, B. Schwederski, J. Fiedler, M.N. Moreno-Carretero, W. Kaim, Inorg. Chim. Acta 325 (2001) 65.
[20] D.J. Brown, N.W. Jacobsen, J. Chem. Soc (1961) 4413.
[21] D. Jung, Y. Kim, Y. Kang, D. Baek, Bull. Korean Chem. Soc. 22 (2001) 1.
[22] SHELXTL-5.1, Bruker Analytical X-Ray Systems, Madison, WI, USA, 1998.
[23] D.L. Kepert, Inorganic Stereochemistry, Springer-Verlag, Berlin, 1982, pp. 79–86.
[24] B.J. Hathaway, Comprehensive coordination chemistry, in: G. Wilkinson, R.D. Gillard, J.A. McCleverty (Eds.), The Synthesis, Reactions, Properties and Applications of Coordination Compounds, vol. 5 (Section 53), Pergamon Press, Oxford, 1987, pp. 674–680.
[25] (a) B.J. Hathaway, Struct. Bonding 57 (1984) 55;
(b) B.J. Hathaway, D.E. Billing, Coord. Chem. Rev. 5 (1970) 143.
[26] A.W. Addison, T.N. Rao, J. Reedijk, J. van Rijn, G.C. Verschoor, J. Chem. Soc., Dalton Trans. (1984) 1349.
[27] M.C. Weiss, B. Bursten, S.M. Peng, V.L. Goedken, J. Am. Chem. Soc. 98 (1976) 8021.
[28] P.K. Baker, C.T. Brown, Polyhedron 20 (2001) 2559.
[29] K. Nakamoto, Infrared and Raman Spectra of Inorganic and Coordination Compounds, 4th ed. (Part B), Wiley, New York, 1971, pp. 82–84.
[30] (a) K. Burger, Coordination Chemistry: Experimental Methods, Butterworths, London, 1973, pp. 255–265;
(b) B.J. Hathaway, D.E. Billing, Coord. Chem. Rev. 5 (1970) 143.
[31] Y Dou, J. Chem. Ed. 67 (1990) 134.
[32] A.B.P. Lever, Inorganic Electronic Spectroscopy, Elsevier, New York, 1984, pp. 554–572.
[33] (a) R.L. Carlin, Magnetochemistry, Springer-Verlag, Berlin, 1986;
(b) F.E. Mabbs, D.S. Machin, Magnetism and Transition Metal Complexes, Chapman & Hall, London, 1973, pp. 10–15.

d^5d^5 system $M_2Cl_9^{3-}$ (M = Fe, Ru, Os) to include the heterobimetallic dimers $FeRuCl_9^{3-}$, $FeOsCl_9^{3-}$ and $RuOsCl_9^{3-}$. In addition, we apply methodology developed previously in the context of d^nd^n dimers ($n = 1$–3) to assess trends in metal–metal bonding in terms of three fundamental electronic factors, ligand field splitting, spin polarization energy and overlap of the metal orbitals.

2. Computational details

All calculations described in this work were performed on Linux-based Pentium III computers using the 1999 release of the AMSTERDAM DENSITY FUNCTIONAL (ADF) program developed by Baerends et al. [4]. The local density approximation to the exchange potential was used, along with the correlation potential of Vosko, Wilk and Nusair [5]. The LDA was used throughout as previous work has shown that incorporation of non-local corrections to the exchange-correlation potential leads to generally poorer agreement with experiment, particularly in relation to metal–metal distances [1c]. A double-ζ Slater type orbital basis set extended with a single d-polarization function was used to describe the chlorine atoms, while all metals were modeled with triple-ζ basis sets. Electrons in orbitals up to and including 2p {Cl}, 3p {Fe}, 4p {Ru,}, 5p {Os} were treated in accordance with the frozen-core approximation. Geometries were fully optimized using the algorithm of Versluis and Ziegler [6]. Calculations for the LS $S = 0$, 1 and HS $S = 0$, 5 states, were performed in a spin-unrestricted manner using D_{3h} (homobimetallic) or C_{3v} (heterobimetallic) nuclear symmetry of the molecule. In the BS calculations, all symmetry elements connecting the two metal centers were removed, resulting in overall C_{3v} point group symmetry. In addition, an asymmetry in the initial spin density was introduced using the modifystartpotential key. Potential energy curves for the BS and other spin states were generated by freezing the metal–metal separation and optimizing all other structural parameters independently.

3. Results and discussion

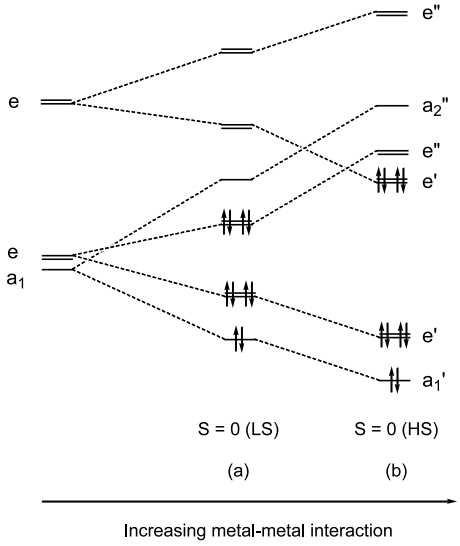
3.1. Modes of electronic coupling in $M_2Cl_9^{3-}$ dimer complexes

In this section, we first present a qualitative description of the various possible coupling schemes for two d^5 metal ions in a confacial array, and establish appropriate single determinant wavefunctions to describe the electronic states involved. The calculated energies of these states are then compared for the homo- ($Fe_2Cl_9^{3-}$, $Ru_2Cl_9^{3-}$ and $Os_2Cl_9^{3-}$) and heterobimetallic ($FeRuCl_9^{3-}$, $FeOsCl_9^{3-}$ and $RuOsCl_9^{3-}$) species. The latter offer an additional degree of complexity, as it is possible for the two metal ions to be in different single-ion spin states ($S = 5/2$ or $S = 1/2$). The various dimer states for the homobimetallic systems have been described elsewhere, but a systematic description is justified here to provide a framework for the subsequent description of dimer states for the heterobimetallic species.

3.2. Homobimetallic dimers

3.2.1. Strongly coupled limit

Where all electrons are delocalized over both sides of the molecule, the metal-based orbitals split as shown in Scheme 1. The local C_{3v} symmetry splits the t_{2g} orbitals on each metal center into a_1 and e subsets having, respectively, σ and δ_π ($^1/_3\pi + {}^2/_3\delta$) symmetry relative to the metal–metal axis. The e_g orbitals do not split and transform as another e subset with $^2/_3\pi + {}^1/_3\delta$ symmetry, denoted π_δ. In a D_{3h}-symmetric confacial array, the t_{2g} orbitals form metal–metal bonding and antibonding molecular-orbitals of $a_1'(\sigma)$, $e'(\delta_\pi)$, $e''(\delta_\pi^*)$ and $a_2''(\sigma^*)$ symmetry, while the higher lying e levels form $e'(\pi_\delta)$ and $e''(\pi_\delta^*)$ bonding and antibonding combinations. Depending on the relative magnitude of the ligand-field splitting and the metal–metal interaction it is possible, in principle, to identify two limiting situations. If the metal–metal interaction is relatively weak, the occupied orbitals (*) bonding and antibonding combinations. Depending on the relative magnitude of the ligand-field splitting and the metal–metal interaction it is possible, in principle, to identify two limiting situations. If the metal–metal interaction is relatively weak, the occupied orbitals (a_1', e' and e'') all originate from the t_{2g} subshell, and the metal–metal bond order is 1. To emphasize its



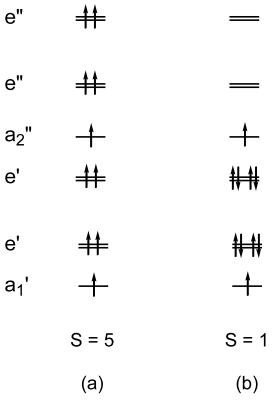
Scheme 1.

descent from the LS configuration of the single ion, it is denoted $S = 0$ (LS) (Scheme 1(a)). In contrast, if the metal–metal interaction is very strong, the metal–metal bonding π_δ orbital may fall below δ_π^*, resulting in a formal metal–metal bond order of 5. This state is denoted $S = 0$ (HS) (Scheme 1(b)) to emphasize the fact that it correlates with a HS single ion configuration.

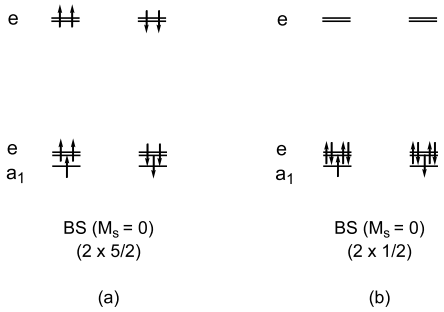
3.2.2. Weakly-coupled limit

In the limit of weak coupling between the single ions, the metal-based electrons remain localized on opposite sides of the dimer. Coupling of two $S = 5/2$ single ions gives rise to dimer states with total spin $S = 5$, 4, 3, 2, 1 and 0, while two $S = 1/2$ single ions combine to give dimer states with $S = 1$ and 0. Only the states with maximum multiplicity for each coupling mode ($S = 5$ and $S = 1$, respectively) can be described by single determinant wavefunctions (see Scheme 2(a) and (b)). In the $S = 1$ case, the determinant with the unpaired electrons in the a_1' and a_2'' orbitals is used because it correlates directly with the M–M σ bonded configuration in the delocalized limit.

In contrast, the singlet state arising from coupling of two $S = 1/2$ single ions is properly described by a linear combination of two single determinant wavefunctions, while its counterpart from coupling of two $S = 5/2$ ions requires a total of 252 single determinants. It has, however, been shown that in either case, a single-determinant BS wavefunction of the type shown in Scheme 3 provides a close approximation, in energetic terms, to the true singlet antiferromagnetic states [3]. To emphasize the fact that this BS wavefunction is an eigenfunction of $\boldsymbol{S_z}$ but not of $\boldsymbol{S^2}$, and, therefore, does not represent a pure singlet spin state, it is denoted BS ($M_s = 0$). Whilst it is possible to obtain an estimate of the true singlet energy by spin projection, we have shown in related cases that the difference between this and BS ($M_s = 0$), in the limit of weak coupling, is not large [1]. In this study, where the emphasis is on qualitative trends, no attempt has, therefore, been made to obtain spin-projected energies. In the context



Scheme 2.

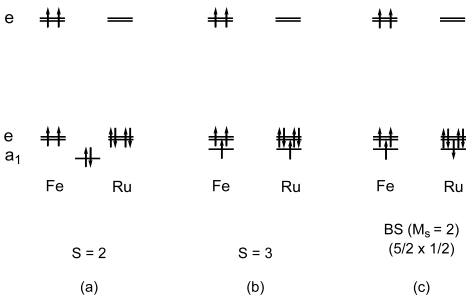


Scheme 3.

of this work, the most important point to note is that the BS wavefunctions for both high-spin (Scheme 3(a)) and low-spin (Scheme 3(b)) limits are represented by the same electronic configuration, $a_1^{1/1}e^{2/2}e^{2/2}$ (the numbers on either side of the '/' indicate the number of electrons of α and β spin). As a consequence, the same BS configuration can encompass both weakly coupled high- and low-spin situations. Moreover, it also correlates with both $S = 0$ (HS) and $S = 0$ (LS) in the delocalized limit, and so can also encompass the complete range of metal–metal interactions, from strong to weak coupling. This extreme flexibility provides a powerful tool in investigating changes in metal–metal interaction, allowing us to define a single electronic configuration that can encompass all possible limiting behaviors of the dimer manifold. The flexibility does, however, present a problem, in that it is often difficult to unambiguously define the precise nature of the coupling at any given point on the BS potential energy surface. In this context, the ferromagnetically coupled states of maximum multiplicity (single-determinants) provide, through their energetic proximity to the BS state, a useful indicator of the precise nature of the coupling. Thus, where the $S = 5$ state, which is derived unambiguously from two $S = 5/2$ single ions, lies close to its BS counterpart, then the latter must be formed from antiferromagnetically coupled $S = 5/2$ single ions. Likewise, where the $S = 1$ state lies close to BS state, the latter is formed by antiferromagnetic coupling of two $S = 1/2$ ions.

3.2.3. Heterobimetallic dimers

Where the two metal centers in a heterobimetallic dimers share a common spin state ($S = 5/2$ or $S = 1/2$), the limiting single-determinant wavefunctions are as described above. In the case where one ion is low-spin and the other high-spin, however, a different series of dimer states arises. In the low-spin $S = 1/2$ state, the t_{2g}-based orbital of e symmetry is fully occupied, and, therefore, cannot participate in any magnetic coupling. As a result, the only coupling pathway is through the orbitals of a_1 symmetry, giving rise, in the strongly coupled limit, to a single metal–metal σ bond. In such circumstances, the molecular ground state will be a



Scheme 4.

quintet ($S = 2$), well described by the single determinant wavefunction shown in Scheme 4(a).

In the weakly coupled limit, the coupling of one $S = 5/2$ single ion with one with $S = 1/2$ results in dimer spin states with $S = 3$ and 2. Once again the state of maximum multiplicity is well described by a single determinant, denoted $S = 3$ in Scheme 4(b), but its ferrimagnetic counterpart, $S = 2$, is not. It is, however, possible to construct a BS wavefunction (Scheme 4(c)) that will closely approximate the energy of the true $S = 2$ state. Unlike the broken symmetry states for the symmetric systems, the inequivalence of the single-ion spin states leaves four residual unpaired electrons. The BS wavefunction illustrated in Scheme 4(c) is, therefore, denoted BS ($M_s = 2$) to distinguish it from the BS states in the symmetric systems, BS ($M_s = 0$). Significantly, the $S = 2$ and BS ($M_s = 2$) states share a common electronic configuration in C_{3v} symmetry, and so the latter has the flexibility to describe both strongly and weakly coupled limits, as well as all intermediate situations. In fact, because the two ends of the dimer are now physically different, it is not possible to enforce electron delocalization through the imposition of the full nuclear symmetry, as it was in the homobimetallic cases. Consequently, it is not possible to unambiguously evaluate the energy of the delocalized $S = 2$ case in the same way as it was possible to evaluate $S = 0$ (HS) and $S = 0$ (LS). As a result, only the energy of the BS ($M_s = 2$) state, and not $S = 2$, is reported in subsequent discussions.

In summary, we have identified a number of electronic states, all of which can be adequately represented by a single determinant, that defines the limiting behavior of a dimer containing two d^5 single ions. In species where the ions share a common spin state, we have identified the BS ($M_s = 0$) state, along with its ferromagnetic counterparts $S = 1$ and $S = 5$ as potentially important in the weakly coupled limit, and $S = 0$ (HS) and $S = 0$ (LS) at the strongly coupled limit. Where the spin states differ we have identified two further states, BS ($M_s = 2$) and its ferromagnetic counterpart, $S = 3$. Any one of these states may constitute the global minimum in a given system, and, in the following section, we report energies for each of them for all possible combinations of metals of the iron triad.

Calculated minima for all states described above are listed in Table 2. In our previous detailed analysis of the potential energy curves for $Ru_2Cl_9^{3-}$ and $Os_2Cl_9^{3-}$, [3] we noted that the BS minimum was identical to that in the $S = 0$ (LS) state, indicating that there was no driving force for electron localization, and, therefore, that the dimers were stabilized by a covalent σ bond between the metal ions. The data contained in Table 2 confirm that the situation is very similar in $RuOsCl_9^{3-}$, the preference for LS configurations on both metal centers ensuring that the $S = 0$ (LS) state lies lowest in energy and, analogous to $Ru_2Cl_9^{3-}$ and $Os_2Cl_9^{3-}$, the ground state geometry corresponds to a metal–metal σ bonded structure.

In contrast, the BS minimum for $Fe_2Cl_9^{3-}$ is almost identical, structurally and energetically, with the $S = 5$ state, confirming that the ground state contains weakly antiferromagnetically coupled $S = 5/2$ single ions. In both $FeRuCl_9^{3-}$ and $FeOsCl_9^{3-}$, the most stable state is $S = 3$, indicating that the Fe center retains an $S = 5/2$ single ion state while the heavier metal ions prefer to adopt a low-spin configuration. The BS ($M_s = 2$) is relatively close in energy, confirming the weak coupling between the two metal ions. In contrast, the BS ($M_s = 0$) state, where both ions are forced to adopt the same spin state (either high or low), lies much higher in energy. Moreover, the energy is identical to that of the $S = 0$ (LS) state, rather than $S = 0$ (HS), indicating that the both adopt a LS, rather than HS, state. This observation is consistent with the greater energy required to promote a Ru^{3+} ion from LS to HS than to promote an Fe^{3+} from HS to LS (see later discussion and also reference [3]).

The greater stability of the $S = 3$ state relative to BS ($M_s = 2$) is, at first sight, somewhat surprising, as the half-filled orbitals of a_1 symmetry on each center should provide an effective superexchange pathway, stabilizing the ferrimagnetic BS ($M_s = 2$) state. The origin of this apparent anomaly can be traced to the very strong spin polarization induced on the bridging chloride ligands by the HS Fe^{3+} ion. The occupation of the Fe–Cl σ antibonding orbitals with spin-α electrons, causes a considerable leakage of spin density onto the bridging ligands, resulting in the net destabilization of the spin-β manifold of π-donor orbitals relative to their spin-α counterparts. Donation of π electron density from the bridging ligand into the vacant orbital in the t_{2g} shell of the LS Ru^{3+} ion is, therefore, most effective when the vacancy is also in the spin-β manifold, as the energy separation between donor and acceptor orbitals is then minimized. The spin polarization of the bridging ligands, therefore, favors ferromagnetic coupling, with the result that the $S = 3$ state is the global minimum.

The calculated energies of the various spin states provide us with an overview of the global minimum in each case, and, therefore, of periodic trends in metal–metal bonding. They do not, however, allow us to evaluate the relative importance of metal–metal interactions, ligand-field splitting and spin polarization in dictating these trends. In the following section, we extend a model previously used to analyze the bonding in $d^n d^n$ dimers ($n = 1$–3) [1b,1e] to evaluate the contributions of these three distinct electronic mechanisms. We begin with review of the factors that determine the ground spin states of the octahedral monomers, MCl_6^{3-} [3], where metal–metal interactions are obviously absent. We then extrapolate to the dimer systems, where metal–metal bonding emerges as a perturbation. Much of the following section rests on the definition of appropriate reference states where one or more of the three electronic factors noted above are effectively removed. It is important to emphasize that these reference states are artificial constructs designed to afford insight into the fundamental nature of the bonding, and are not intended to represent any real electronic state of the molecule.

3.2.4. MCl_6^{3-} complexes

The energetic separation of high-spin ($S = 5/2$) and low-spin ($S = 1/2$) states of $FeCl_6^{3-}$, $RuCl_6^{3-}$ and $OsCl_6^{3-}$ is summarized in Table 2. From these data, it is clear that, consistent with experiment, the iron complex adopts a high-spin ground state, while the Ru and Os analogues are low spin. In the closed energy cycle shown in Fig. 1, we define two additional reference states, where the circles indicate that the electrons are of undefined spin (achieved in a computational sense by performing a spin-restricted calculation). The resulting closed cycle illustrates the fact that the nature of the ground state depends on the relative magnitudes of three terms. The ligand-field energy, denoted LFE, takes into account the energy required to promote two electrons from the t_{2g} orbital to e_g, as well as the difference in coulombic repulsion between the LS and HS configurations. The spin-polarization energies for the LS state, SPE(LS), and HS state, SPE(HS) reflect the difference in energy between unrestricted and restricted energies for the same configuration. From the cycle, we can derive the following relationships:

$$\mathrm{LFE} = E_{\mathrm{ref}}(\mathrm{HS}) - E_{\mathrm{ref}}(\mathrm{LS})$$

$$\mathrm{SPE(LS)} = E_{\mathrm{ref}}(\mathrm{LS}) - E(\mathrm{LS})$$

$$\mathrm{SPE(HS)} = E_{\mathrm{ref}}(\mathrm{HS}) - E(\mathrm{HS})$$

where E(LS) and E(HS) are the calculated energies for the d^5 octahedral MCl_6^{3-} LS and HS states, respectively, using spin-unrestricted density functional theory. Based on the above definitions, the position of the LS/HS equilibrium, i.e. the energetic difference between LS and HS configurations, can be expressed as:

$$\Delta E(\mathrm{HS/LS}) = E(\mathrm{HS}) - E(\mathrm{LS})$$
$$= \mathrm{LFE} + \mathrm{SPE(LS)} - \mathrm{SPE(HS)}$$

As written, the position of the HS/LS equilibrium is defined to be a positive quantity when the LS configuration is favored.

The calculated values of LFE, SPE(LS), SPE(HS) are also collected in Table 2 for the hexachloride complexes. The ligand-field term, LFE, follows the trend anticipated on the basis of the greater radial extent of the 4d and 5d orbitals, increasing dramatically by over 40% from Fe to Ru with only a minor increase of approximately 5% from Ru to Os. The opposite trend is observed in both the spin-polarization terms, corresponding to a 40% reduction from Fe to Ru and a further 10% reduction from Ru to Os. For $FeCl_6^{3-}$, the large SPE(HS) term is clearly responsible for maintaining a HS configuration. For $RuCl_6^{3-}$ and $OsCl_6^{3-}$, the lower spin-polarization energies and significantly larger ligand-field terms result in positive values for ΔE(HS/LS) and thus LS ground states. Based on the data given in Table 2, the trend towards LS ground states in the heavier metals is due to approximately equal changes in the spin-polarization and ligand-field energies.

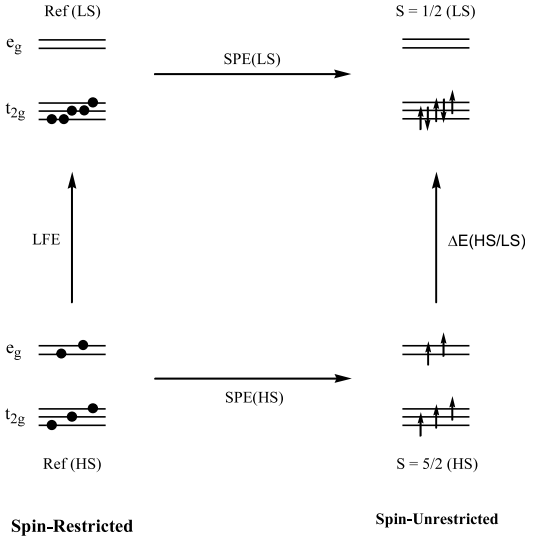


Fig. 1. Closed-energy cycle for HS/LS equilibrium in octahedral d^5 MCl_6^{3-} (M = Fe, Ru, Os) complexes.

3.2.5. Factors effecting electron localization in dimers

In our earlier work involving d^3d^3 dimers, where the single ions are by definition low-spin, we showed that the extent of delocalization of the metal-based electrons is dictated by two terms, namely spin-polarization energy, favoring localization of the metal-based electrons, and the energy associated with metal–metal orbital overlap, favoring delocalization. These two terms are in direct opposition and, therefore, the

position of the localized/delocalized equilibrium depends on their relative magnitudes. The driving force for electron delocalization is determined by the relative energies of the $S = 0$ and $S = S_{max}$ associated states. The depth of the $S = 0$ curve at short metal–metal distances, where the metal-based electrons are delocalized, is a measure of the stabilizing effects of metal–metal orbital overlap. In contrast, the depth of the $S = S_{max}$ curve at large metal–metal distances, where there is the maximum number of unpaired electrons on each metal center, is associated with the stabilizing influence of spin-polarization. Absolute estimates for the energetic contributions of these terms can, however, only be obtained by defining an appropriate reference state, analogous to those shown for MCl_6^{3-}, where both metal–metal bonding and spin polarization were factored out.

For d^5d^5 systems, it is necessary to define two reference states, depicted on the LHS of Figs. 2 and 3, one for low-spin dimer configurations $[(a_1')^1(e')^4(e'')^4(a_2'')^1]$, the other for high-spin $[(a_1')^1(e')^2(e'')^2(a_2'')^1(e')^2(e'')^2]$. In each case, all metal–metal bonding and antibonding orbitals are equally occupied to ensure a formal bond order of zero, and the use of spin-restricted theory ensures that there is no energetic contribution from spin polarization. In the LS case, the ΔE_{ovlp} and ΔE_{spe} terms represent the difference in energy between the LS reference state and the $S = 0$ (LS) and $S = 1$ associated states, respectively. Similarly, for the HS configuration, the ΔE_{ovlp} and ΔE_{spe} terms denote the difference in energy between the HS reference state and the $S = 0$ (HS) and $S = 5$ associated states. In either case, the difference $\Delta E_{ovlp} - \Delta E_{spe}$ quantifies the driving force for delocalization of the metal-based electrons. It only remains then to make a connection between the HS and LS reference states. The dimer ligand field term, ΔE_{LF}, is defined as the difference between the spin-restricted energies of the LS and HS d^5d^5 reference states

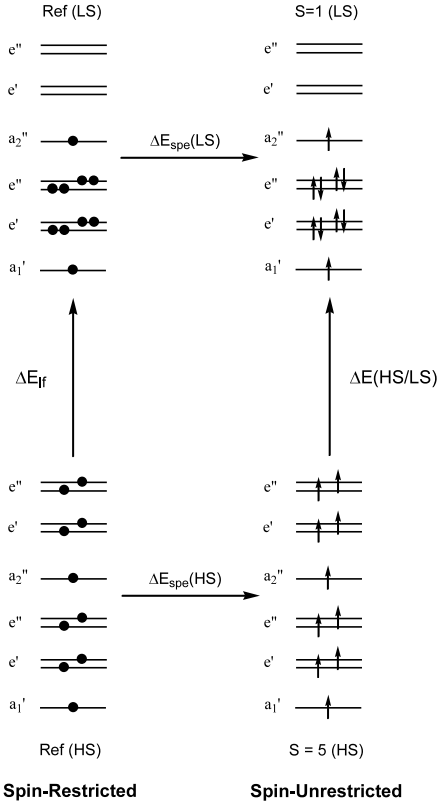


Fig. 2. Closed-energy cycle for the HS/LS equilibrium in d^5d^5 $M_2Cl_9^{3-}$ (M = Fe, Ru, Os) complexes.

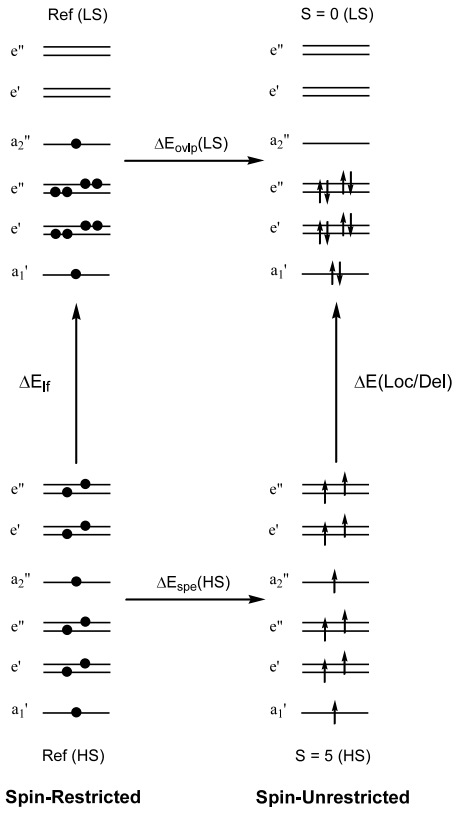


Fig. 3. Closed-energy cycle for the Loc/Del equilibrium in d^5d^5 $M_2Cl_9^{3-}$ (M = Fe, Ru, Os) complexes.

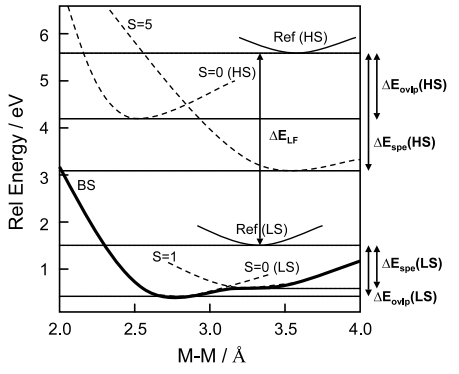


Fig. 4. Schematic representation of the potential energy curves for the BS and $S = 0$ (LS), $S = 1$, $S = 0$ (HS) and $S = 5$ associated states and the energetic terms involved in the HS/LS and Loc/Del equilibria in d^5d^5 $M_2Cl_9^{3-}$ dimers.

and, in the absence of any interaction between the component MCl_6^{3-} fragments, should equal approximately twice the appropriate octahedral ligand field term (Table 2). An appreciation of the energetic terms described above can be gained from Fig. 4 where a schematic representation of the potential energy curves for the LS, HS and reference states are plotted as a function of the metal–metal separation.

The various terms described above, ΔE_{ovlp}, ΔE_{spe} and ΔE_{LF}, along with the difference $\Delta E_{ovlp} - \Delta E_{spe}$, can be simply extracted from the data in Table 1, and are summarized in Table 3 for the LS and HS configurations of all six dimers. For both LS and HS configurations, the progressive reduction in ΔE_{spe} and increase in both ΔE_{ovlp} and ΔE_{LF} going down the group can be rationalized on the basis of the increased dilation of the 4d and 5d metal orbitals relative to 3d. As found in previous studies, the ΔE_{spe} term for the dimer is very close to the sum of the single-ion spin-polarization energies for the constituent metals. A prominent feature of the data given in Table 3 is the large ΔE_{spe} terms compared with ΔE_{ovlp} for the HS complexes. Thus, the $\Delta E_{ovlp} - \Delta E_{spe}$ terms are all negative implying that in the HS state, the metal-based electrons remain strongly localized. In the LS case, the $\Delta E_{ovlp} - \Delta E_{spe}$ terms are much smaller. The negative value for $Fe_2Cl_9^{3-}$ indicates that this complex would prefer to remain localized, even if the Fe^{3+} ions were forced to adopt low-spin configurations. In contrast, the Ru and Os complexes yield positive values for $\Delta E_{ovlp} - \Delta E_{spe}$ corresponding to delocalized electrons and thus metal–metal σ bonded structures.

To quantify both the LS/HS and localized/delocalized equilibria, use is made of the closed-cycle energy diagrams in Figs. 2 and 3 which detail the energetic quantities involved in going from a localized HS ($S = 5$) d^5d^5 dimer to either a localized ($S = 1$) or delocalized ($S = 0$) LS dimer. The alternate energy cycles involving a delocalized HS d^5d^5 dimer are not considered as the data in Table 2 indicate that such a state [$S = 0$ (HS)] is highly unfavorable energetically. On the basis of Fig. 2, the following expression can be written for the energy change, ΔE(HS/LS), associated with conversion from a localized HS to a localized LS d^5d^5 dimer,

$$\Delta E(\mathrm{HS/LS}) = \Delta E_{LF} - \Delta E_{spe}(\mathrm{HS}) + \Delta E_{spe}(\mathrm{LS}) \quad (1)$$

where ΔE(HS/LS) is defined to be positive when a LS localized ground state is favored. In an analogous fashion, the energy change associated with conversion from a localized HS to a delocalized LS d^5d^5 dimer (Fig. 3) can be written as:

Table 2
Spin-polarization, ligand-field and high-spin/low-spin equilibrium energies (eV) for d^5 MCl_6^{3-} (M = Fe, Ru, Os) complexes

Complex	ΔE(HS/LS)	SPE(HS)	SPE(LS)	LFE
$FeCl_6^{3-}$	−0.91	+3.46	+0.21	2.34
$RuCl_6^{3-}$	+1.31	+2.05	+0.11	3.25
$OsCl_6^{3-}$	+1.67	+1.84	+0.09	3.42

Table 1
Metal–metal distances and total energies relative to the BS state, for the associated states of d^5d^5 $M_2Cl_9^{3-}$ (M = Fe, Ru, Os) complexes

Complex	BS ($M_s = 0$)	High-spin (5/2 × 5/2)			Low-spin (1/2 × 1/2)			Intermediate spin (5/2 × 1/2)	
		$S = 0$	$S = 5$	Reference	$S = 0$	$S = 1$	Reference	BS ($M_s = 2$)	$S = 3$
$Fe_2Cl_9^{3-}$									
M–M (Å)	3.45	2.38	3.45	3.50	2.67	3.07	3.08		
E_{rel} (eV)	0.00	6.14	0.01	6.78	1.59	1.29	1.95		
$Ru_2Cl_9^{3-}$									
M–M (Å)	2.74	2.53	3.65	3.73	2.75	3.26	3.27		
E_{rel} (eV)	0.00	6.00	3.47	7.49	0.00	0.48	0.83		
$Os_2Cl_9^{3-}$									
M–M (Å)	2.79	2.64	3.73	3.76	2.80	3.35	3.37		
E_{rel} (eV)	0.00	6.27	4.33	7.96	0.00	0.67	0.98		
$RuOsCl_9^{3-}$									
M–M (Å)	2.76	a	3.76	3.76	2.77	3.31	3.32		
E_{rel} (eV)	0.00	a	3.91	7.74	0.00	0.58	0.92		
$FeRuCl_9^{3-}$									
M–M (Å)	2.76	a	3.58	3.64	2.74	3.18	3.16	3.42	3.41
E_{rel} (eV)	0.00	a	1.00	6.43	0.00	0.03	0.68	−0.61	−0.82
$FeOsCl_9^{3-}$									
M–M (Å)	2.77	a	3.62	3.68	2.74	3.23	3.24	3.49	3.48
E_{rel} (eV)	0.00	a	1.30	6.49	0.00	0.10	0.59	−0.73	−0.81

[a] Unable to be calculated.

Table 3
Overlap, spin-polarization and ligand-field energies (eV) for d^5d^5 $M_2Cl_9^{3-}$ (M = Fe, Ru, Os) complexes

Complex	High-spin			Low-spin			ΔE_{LF}
	ΔE_{ovlp}	ΔE_{spe}	$\Delta E_{ovlp}-\Delta E_{spe}$	ΔE_{ovlp}	ΔE_{spe}	$\Delta E_{ovlp}-\Delta E_{spe}$	
$Fe_2Cl_9^{3-}$	+0.63	+6.77	−6.14	+0.36	+0.67	−0.31	4.83
$Ru_2Cl_9^{3-}$	+1.49	+4.02	−2.53	+0.83	+0.36	+0.47	6.66
$Os_2Cl_9^{3-}$	+1.69	+3.63	−1.94	+0.98	+0.31	+0.67	6.98
$FeRuCl_9^{3-}$		+5.43		+0.68	+0.65	+0.03	5.75
$FeOsCl_9^{3-}$		+5.19		+0.59	+0.49	+0.10	5.90
$RuOsCl_9^{3-}$		+3.83		+0.92	+0.34	+0.58	6.82

$$\Delta E(\mathrm{Loc/Del}) = \Delta E_{LF} - \Delta E_{spe}(\mathrm{HS}) + \Delta E_{ovlp}(\mathrm{LS}) \quad (2)$$

where again ΔE(Loc/Del) is defined to be positive when a LS delocalized ground state is favored. On the basis that Eq. (1) quantifies the tendency to adopt a LS ground state in the absence of any delocalization of the metal-based electrons, it, therefore, defines the pure HS/LS equilibrium of the dimer. Eq. (2) on the other hand, quantifies the influence of metal–metal bonding on the HS to LS transition.

From the data in Table 3, values of ΔE(HS/LS) and ΔE(Loc/Del) can be calculated and are summarized in Table 4. For the Fe complex, both these values are negative indicating that $Fe_2Cl_9^{3-}$ prefers to be HS with the metal-based electrons localized, largely as a consequence of the large spin-polarization energy for this system but also because of a smaller ligand field term. For the Ru and Os analogues and all three heterobimetallic complexes, the calculated values of ΔE(HS/LS) and ΔE(Loc/Del) are positive and, therefore, these complexes are predicted to be LS with the metal-based electrons delocalized in a metal–metal σ bond. The change in ΔE(HS/LS) from $Fe_2Cl_9^{3-}$ to $Ru_2Cl_9^{3-}$ is substantial, just under 4.5 eV, and can be attributed to a 2.74 eV (40%) reduction in spin-polarization energy compared with $Fe_2Cl_9^{3-}$ accompanied by a 1.79 eV (35%) increase in the ligand field energy. An additional but smaller increase in both ΔE(HS/LS) and ΔE(Loc/Del) is observed in passing from $Ru_2Cl_9^{3-}$ to $Os_2Cl_9^{3-}$. This trend is again consistent with the increased radial dilation of the 5d orbitals compared with 4d, which leads to a further reduction in the spin-polarization energy and increases in both orbital overlap and ligand field terms. Not unexpectedly, $FeRuCl_9^{3-}$, $FeOsCl_9^{3-}$ and $RuOsCl_9^{3-}$ are essentially intermediate between their homobimetallic counterparts.

Table 4
High-spin/low-spin and localized/delocalized equilibria data (eV) for d^5d^5 $M_2Cl_9^{3-}$ (M = Fe, Ru, Os) complexes

Complex	ΔE(HS/LS)	ΔE(Loc/Del)
$Fe_2Cl_9^{3-}$	−1.27	−1.58
$Ru_2Cl_9^{3-}$	+3.00	+3.47
$Os_2Cl_9^{3-}$	+3.66	+4.33
$FeRuCl_9^{3-}$	+0.96	+1.00
$FeOsCl_9^{3-}$	+1.20	+1.30
$RuOsCl_9^{3-}$	+3.33	+3.91

In our earlier studies of d^3d^3 $M_2Cl_9^{n-}$ dimers of the Cr and Mn triads, a linear dependence of ΔE_{ovlp} on ΔE_{spe} was observed [1b]. The same trend is also found for the Fe triad. This dependence can be rationalized on the basis that both terms are sensitive to the dilation of the metal-based orbitals. As the orbitals expand going down a group, ΔE_{ovlp} increases due to the greater metal–metal orbital overlap. Conversely, ΔE_{spe} decreases due to the magnetic electrons on each metal being on average further apart. Furthermore, as can be seen from Fig. 5, an almost exact linear relationship is observed between ΔE_{spe}(HS) and ΔE_{LF}. This relationship is analogous to the dependence of ΔE_{ovlp} on ΔE_{spe} in the sense that the ligand-field term is also a measure of the orbital overlap, in this case between the metal-based orbitals and the ligand array.

The interdependence of ΔE_{spe}, ΔE_{ovlp} and ΔE_{LF} and their involvement in the expressions for ΔE(HS/LS) and ΔE(Loc/Del), suggests a possible connection between

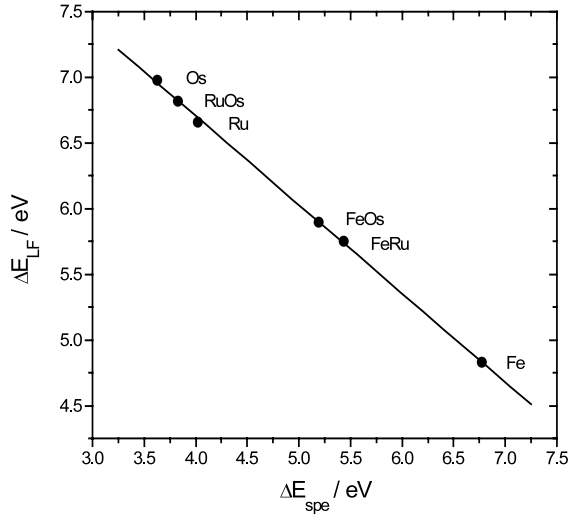


Fig. 5. Plot showing the dependence of the dimer ligand-field energy, ΔE_{lf}, on the spin-polarization energy, ΔE_{spe}, for d^5d^5 $M_2Cl_9^{3-}$ (M = Fe, Ru, Os) complexes.

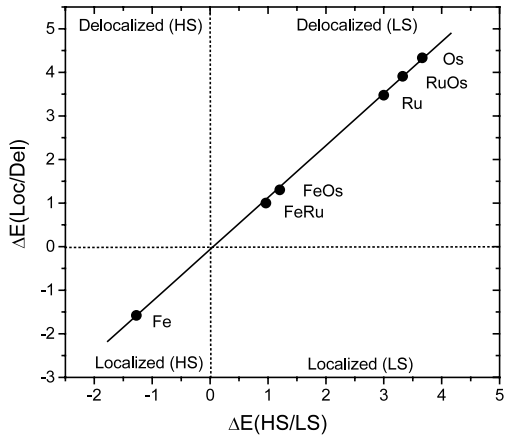


Fig. 6. Plot showing the dependence of the Loc/Del equilibrium, ΔE(Loc/Del), on the HS/LS equilibrium, ΔE(HS/LS), for d^5d^5 $M_2Cl_9^{3-}$ (M = Fe, Ru, Os) complexes.

the HS/LS and localized/delocalized equilibria. Indeed, from Fig. 6, a strong linear correspondence is apparent between these two equilibria with all complexes except $Fe_2Cl_9^{3-}$ falling into the LS-delocalized quadrant. The correlation implies that the onset of metal–metal bonding is intimately linked to the HS/LS crossover in these complexes and that neither delocalized HS or localized LS d^5d^5 dimer structures are likely to occur. Further comment is necessary in relation to the heterobimetallic systems $FeRuCl_9^{3-}$ and $FeOsCl_9^{3-}$. Although these two complexes are located midway between their homobimetallic counterparts, close to the crossover between LS-delocalized and HS-localized regimes, on the basis of Fig. 6, they should still possess LS-delocalized structures. However, as pointed out earlier, our calculations reveal that the global minimum in both complexes corresponds to an intermediate $S = 3$ spin state where the Fe adopts a HS configuration while the Ru or Os centers are LS.

4. Conclusion

The HS/LS and localized/delocalized equilibria in homo- and hetero-bimetallic d^5d^5 face-shared $M_2Cl_9^{3-}$ (M = Fe, Ru, Os) dimers, as defined by the energetic quantities ΔE(HS/LS) and ΔE(Loc/Del), respectively, are found to exhibit a strong linear dependence which can be attributed to their mutual dependence on the single-ion spin-polarization energy. The conclusion drawn from this correlation is that metal–metal bond formation necessitates a crossover from a HS to LS configuration and, therefore, neither delocalized HS or localized LS d^5d^5 structures are likely to occur.

Acknowledgements

The Australian Research Council and the Engineering and Physical Sciences Research Council (UK) are gratefully acknowledged for financial support. T.L. would also like to thank the latter for an overseas scholarship.

References

[1] (a) T. Lovell, J.E. McGrady, R. Stranger, S.A. Macgregor, Inorg. Chem. 35 (1996) 3079;
(b) J.E. McGrady, R. Stranger, T. Lovell, Inorg. Chem. 36 (1997) 3242;
(c) J.E. McGrady, R. Stranger, T. Lovell, J. Phys. Chem., Sect. A 101 (1997) 6265;
(d) J.E. McGrady, R. Stranger, T. Lovell, Inorg. Chem. 37 (1998) 3802;
(e) R. Stranger, J.E. McGrady, T. Lovell, Inorg. Chem. 37 (1998) 6795;
(f) R. Stranger, T. Lovell, J.E. McGrady, Inorg. Chem. 38 (1999) 5510.
[2] (a) L. Noodleman, J.G. Norman, Jr., J. Chem. Phys. 70 (1979) 4903;
(b) L. Noodleman, J. Chem. Phys. 74 (1981) 5737;
(c) L. Noodleman, D.A. Case, Adv. Inorg. Chem. 38 (1992) 423.
[3] R. Stranger, T. Lovell, J.E. McGrady, Inorg. Chem. 40 (2001) 39.
[4] (a) E.J. Baerends, D.E. Ellis, P. Ros, Chem. Phys. 2 (1973) 42;
(b) E.J. Baerends, P. Ros, Int. J. Quantum Chem. S12 (1978) 169;
(c) G. teVelde, E.J. Baerends, J. Comp. Phys. 99 (1992) 84.
[5] S.H. Vosko, L. Wilk, M. Nusair, Can. J. Phys. 58 (1980) 1200.
[6] L. Versluis, T.J. Ziegler, Chem. Phys. 88 (1988) 322.

have isolated one solid complex and characterized it by means of elemental analysis, thermal behavior and IR and diffuse reflectance spectroscopies.

2. Experimental

2.1. Reagents and instrumentation

All chemicals were of analytical grade and were used without further purification. Caffeic acid, $VOSO_4 \cdot 5H_2O$ and $VOCl_2 \cdot 2H_2O$ (50% aqueous solution) were purchased from Sigma, Merck and Carlo Erba, respectively.

IR spectra of powdered samples were measured with a Bruker IFS 66 FTIR-spectrophotometer from 4000 to 400 cm^{-1}, using the KBr pellet technique. Electronic absorption spectra were recorded on a Hewlett–Packard 8453 diode-array spectrophotometer, using 1 cm quartz cells. Diffuse reflectance spectra were recorded with a Shimadzu UV-300 instrument, using MgO as an internal standard. Thermogravimetric (TG) and differential thermal analysis (DTA) were performed on a Shimadzu system (models TG-50 and DTA-50, respectively), working in an oxygen flow (50 ml min^{-1}) and at a heating rate of 10 °C min^{-1}. Sample quantities ranged between 10 and 20 mg. Al_2O_3 were used as a DTA standard.

Vanadium contents were determined by atomic absorption, C and H were determined using a Carlo Erba EA 1108 elemental analyzer, and sodium by flame photometry.

2.2. Potentiometric titrations

The EMF measurements were performed with a Schott Gerate TS165 pH meter and the added volumes were measured using a Techware (Sigma) Digitrate (25 ml). Volume of titrated aliquotes was always 25 ml.

$VOSO_4 \cdot 5H_2O$ was used without further purification and dried at 60 °C until constant weight. The 'formula weight' was re-calculated ($VOSO_4 \cdot 4.84\ H_2O$, 250.12) on the basis of a TG analysis before preparing the solutions. NaCl was dried until constant weight and stored over $CaCl_2$ All solutions were made in freshly boiled tridistilled water cooled under a constant flow of nitrogen. The solutions were freshly prepared prior to their use. Diluted solutions of HCl (Merck p.a.) were standardized against TRISMA-base (hydroxymethyl aminomethane). Diluted NaOH solutions were prepared from a saturated NaOH solution and standardized against the HCl. In order to assess the degree of carbonate contamination the Gran's method [11] was used. Cell compartments were kept at 25 ± 0.1 °C with circulating water from a thermostated bath. The ionic strength was fitted at 0.150 M with NaCl in the solutions. The glass electrode was calibrated separately in a solution with known $[H^+]$ before and after each titration.

2.2.1. L^{3-}–H^+ system

Ligand solutions were titrated in the absence of metal to determine the dissociation constant values (pK_a). Two series of titrations were performed in different conditions:

a) Vessel: 5 mM Caf–5 mM H^+; burette: 20 mM NaOH, pH range: 2.3–11.
b) Vessel: 10 mM Caf–40 mM OH^-, burette: 50 mM HCl, pH range: 12–2.1.

2.2.2. VO^{2+}–L^{3-}–H^+ system

In order to determine the formation constants of the VO^{2+}–Caf^{3-}–H^+ system, further titrations of vanadium–ligand solutions were performed in the pH range 2.3–11.3. Different experimental conditions were used:

a) Vessel: 2.5 mM VO^{2+}–5 mM Caf–5 mM H^+; burette: 20 mM and 40 mM NaOH.
b) Vessel: 5 mM VO^{2+}–5 mM Caf–5 mM H^+, burette: 40 mM NaOH.

The formation constants denoted β_{pqr} correspond to the general notation:

$$pM^{2+} + qL^{3-} + rH^+ \rightleftharpoons (M^{2+})_p(L^{3-})_q(H^+)_r$$

A value of $pK_w = 13.76$ (corresponding to $\log \beta_{00-1} = -13.76$) was assumed for the experimental conditions ($T = 298$ K, $I = 150$ mM).

2.3. Synthesis

All the operations were carried out under high-purity dry argon atmosphere and using standard Schlenk techniques.

2.3.1. Sodium caffeate

To a solution of caffeic acid (0.180 g, 0.999 mmol) in methanol (20 ml), sodium methoxide was added until the pH of the solution raised to 8. Addition of toluene in excess gave a solid precipitate, which was filtered, washed with toluene and dried in air. Yield: 82%.

2.3.2. $Na_3[VOCaf(OH)_2] \cdot 3H_2O$

Caffeic acid (0.180 g, 0.999 mmol) was added to a solution of $VOCl_2 \cdot 2H_2O$ (0.348 ml, 1.00 mmol) in water (10 ml). Solid NaOH was added to the solution until a final pH 12 was reached. Absolute ethanol (50 ml) was added to the stirred solution and a green precipitate was formed. It was filtered off, washed with ether and dried under argon atmosphere.

Yield: 65%. *Anal.* Calc. for $C_9H_{13}O_{10}Na_3V$: C, 26.90; H, 3.24; Na, 17.20; V, 12.72. Found: C, 27.10; H, 3.15; Na, 17.30; V, 12.65%.

3. Results

3.1. Potentiometric titrations

Acidity constants for caffeic acid were determined from titrations using pKas values and BEST calculation programs [12]. In the experimental conditions only the first two deprotonation constants ($pK_{a1} = 4.51$, $pK_{a2} = 8.67$) could be calculated. These results are in accordance with the reported data [9]. The third deprotonation constant was optimized using SUPERQUAD program, taking a starting pK_a value of 13.0, according to the literature [9]. The calculated pK_{a3} value was 12.50. On this basis, L^{3-} has been considered as the proper component of the system. To estimate the formation constants of the ternary system VO^{2+}–L^{3-}–H^+ the data collected from two sets of titrations were analyzed with BEST and SUPERQUAD [13].

The usual criteria for this kind of programs (CHI^2 and R values, standard deviations, etc.) were used to select the equilibrium model of speciation. The results were compared with spectroscopic measurements.

In Table 1 the proposed model for the ternary system and the corresponding β values for the species are shown. The species distribution as a function of pH was obtained with SPECIES program and is depicted in Fig. 1.

Calculation also indicates the presence of some VO^{2+} hydrolysis species: $M(OH)_3^-$ ($\log \beta_{10-3} = -17.90$) and $M_2(OH)_5^-$ ($\log \beta_{20-5} = -21.85$). No precipitation of VO^{2+} hydrolysis products was observed during the experiences. A more complete model, including other monomeric and dimmeric complex species (ML_2H_4, ML_2H_2, MLH_2, MLH, ML, M_2L_3) was considered in a first attempt of calculation. Nevertheless, several species have to be excluded to improve the fitting with experimental data.

Table 1
Composition, notation and formation constants (β) for the VO^{2+}–L^{3-}–H^+ system (0.150 M NaCl, 25 °C) [a]

Species	Formula	log β
011	LH	12.50
012	LH_2	21.17
013	LH_3	25.68
110	ML	16.52
11-1	MLH_{-1}	11.10
11-2	MLH_{-2}	0.79
120	ML_2	29.42
320	M_3L_2	39.67
210	M_2L	20.30

[a] In the final calculation log β for vanadium hydrolysis products were −17.90 and −21.85 for MH_{-3} and M_2H_{-5}, respectively.

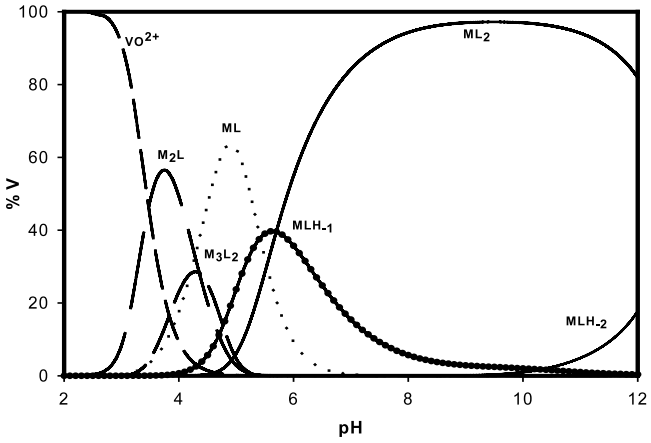


Fig. 1. Species distribution for the vanadyl (IV)–caffeic acid system (2.5/5.0 mM) as a function of pH at 25 °C, $I = 0.150$ M NaCl.

3.2. UV–Vis spectra

The UV–Vis spectrum of the ML_2 species has been calculated on the basis of the spectrum of 4 mM:1 mM L:M solution. In this conditions the species distribution shows a 99.9% of (120) complex at pH 8.3. The resulting bands are located at 800(sh), 728(sh), 620 ($\varepsilon = 168$ M^{-1} cm^{-1}) and 536(sh) nm. Upon consideration of the species distribution model, different solutions with variable total vanadyl concentration, and V:L ratio were prepared at determined pH values. The respective UV–Vis spectra were registered. The percentage of each species present in solution was calculated from the distribution curves and used to estimate the corresponding electronic spectra. The positions of the electronic band maxima of the complexes in solution are listed in Table 2. The extinction coefficient values are not shown because their calculated errors have no statistical significance.

3.3. IR spectrum

Table 3 shows the main characteristic bands of caffeic acid, sodium caffeate and the solid complex. The strong band at 1619 cm^{-1} is assigned to (C=O) stretching of

Table 2
UV–Vis calculated spectra of the VO^{2+}–L^{3-}–H^+ system

Complex	λ (nm)
ML	724, 586
MLH_{-1}	> 820, 716
MLH_{-2}	> 820, 776, 706
ML_2	800(sh), 728(sh), 620, 536(sh)
M_2L	766, 644
M_3L_2	> 800, 722, 524

Table 3
Assignments of some characteristic IR bands (cm^{-1}) of caffeic acid, sodium caffeate and $Na_3[VOCaf(OH)_2]\cdot 3H_2O$

Caffeic acid	Sodium caffeate	$Na_3[VOCaf(OH)_2]\cdot 3H_2O$	Assignments
1644 (vs)	1644 (vs)	1634 (s)	ν(C=C)
1619 (vs)			ν(COOH)
	1572 (vs)	1567 (s)	$\nu_{as}(COO^-)$
1450 (vs)	1444 (vs)	1487 (s)	ν(ring)
	1395 (vs)	1392 (s)	$\nu_s(COO^-)$
1218 (s)	[a]	1260 (s)	ν(CO), phenol
		955 (s)	ν(V=O)

vs: Very strong, s: strong.
[a] Masked.

the –COOH group in the free ligand. In the sodium salt this band disappears and the spectrum shows two new bands located at 1572 cm^{-1} (ν_{as} COO^-) and 1395 cm^{-1} (ν_s COO^-). Similar behavior is observed in the complex spectrum where the bands appear at 1567 and 1392 cm^{-1}, respectively.

The band related to the ring stretching, located at 1450 cm^{-1} (vs) in caffeic acid, remains unaltered in the caffeate anion but is shifted to higher energy values in the vanadyl complex spectrum. A similar shift is observed in the ν(CO, phenol) band, located at 1218 cm^{-1} in the acid and at 1260 cm^{-1} in the vanadyl complex.

The band at 955 cm^{-1} in the solid complex has been assigned to V=O stretching. This value is lower than that of $VOSO_4\cdot 5H_2O$ [14].

3.4. Thermogravimetric behavior

The thermal behavior of the solid complex was investigated by means of TG and DTA measurements under a flowing O_2 atmosphere up to 1100 °C.

The dehydration begins early and covers a temperature range between 18 and 231 °C, with an observed mass loss of 13.96%, in agreement with the calculated value of 13.46%. This process is accompanied by a weak endothermic DTA signal located at 67 °C that corresponds to the loss of three water molecules:

$$Na_3[VOCaf(OH)_2]\cdot 3H_2O \xrightarrow{O_2} Na_3[VOCaf(OH)_2] + 3H_2O$$

After the release of water, a complex degradation process of the remaining material is observed. It shows, at least, five consecutive TG steps:

1) Between 231 and 402 °C (with a weak exothermic DTA signal at 368 °C).
2) Between 402 and 633 °C (exothermic DTA signal at 505 °C).
3) 633 and 737 °C (strong exothermic DTA signal at 677 °C);
4) 737 and 830 °C (exothermic DTA signal at 781 °C).
5) The last pyroliysis step is extended between 830 and 1100 °C and is accompanied by an exothermic DTA peak at 1009 °C. After this last mentioned process, weight constancy is attained. The total observed mass loss is of 54.2%, in very good agreement with the theoretically expected (54.1%) according to the following equation:

$$Na_3[VOCaf(OH)_2]\cdot 3H_2O \xrightarrow{O_2} Na_3VO_4 + \text{volatile products}$$

The generation of the ortovanadate as the final residue was confirmed, unambiguously by IR spectroscopy.

4. Discussion

4.1. Potentiometric titrations

From the potentiometric results, it can be seen that complexation occurs in a wide pH range, depending on the total concentration of the components and the M:L ratio. This observation is in agreement with the spectroscopic results. Even at M:L 1:1 ratio and total concentration 5 mM, potentiometric titration curves of caffeic acid with and without vanadyl(IV) are not superimposable from pH 3, indicating that complex formation starts at low pH values.

The species present in solution in the acidic region involve coordination of the metal to the fully deprotonated ligand. This fact indicates that both carboxylic and phenolic protons are more strongly acidic in the vanadyl complexes than in the free ligand (see pK_a values above). According to Rheder and Rieger [15] this effect can be explained through the delocalization of the electron pair generated by deprotonation in a molecular orbital extended onto the metal.

This model can be compared with the speciation of Cu(II)–L^{-3}–H^+ system, previously reported [9]. In the 3–4 pH range, the $CuLH_2$ complex, which involves only the carboxylate donor groups in the metal coordination, has been identified. The analogous $VOLH_2$ should be discarded from the model in order to improve the fitting parameters. In contrast to other metal-carboxylate complexes, vanadyl(IV)-carboxylate compounds were difficult to be obtained by the usual methods [16,17] due to their tendency to form polymeric species. These complexes show particular magnetic properties as a consequence of anisotropic antiferromagnetic exchange along infinite linear chains of interacting spins [18]. The calculated equilibrium constants denote the preference to form M_3L_2, M_2L, ML_2 and ML complexes in solution in the VO^{2+}–Caf system.

4.2. Spectroscopic Measurements

4.2.1. UV–Vis spectra

The visible spectra of VO^{2+}–caffeate system (see Table 2) show strong similarities with those of vanadyl(IV) linked to catecholate-like ligands (cat) [19,20]. In this type of complexes both species $VO(cat)_2^{2-}$ and $V(cat)_3^{2-}$ exist, but the equilibrium is displaced to the 1:2 species at higher pH [4]. In contrast, for VO^{2+}-Caffeate system in very strongly basic solutions, the involvement of the third ligand in the coordination sphere of vanadium is not observed, probably due to the steric hindrance of the carboxylate group. Moreover, the air oxidation of $V(cat)_3^{2-}$ to $V(cat)_3^{-}$ is not easily detected (the blue color remains unaltered) while the air oxidation of caffeate complexes, either in solution or in solid state, is immediately observed due to the development of a brown color.

However, the system behaves in a similar manner to that of catechol [19]. At pH 4–5 the main species is ML and at higher pH is ML_2 for a ligand to metal ratio of 1:2. The UV–Vis spectrum calculated for ML is similar to that of [VO(cat)]. For ML_2, the spectrum shows additional bands at the red side, probably due to the interaction of the carboxylate moiety of caffeic acid with the sixth position of the coordination sphere of the metal center. This last behavior may have connection with the higher stability of this species in comparison with the copper analogues [9]. In the alkaline region (pH > 10), the hydrolysis of ML_2 takes place generating mixed hydroxo complexes: MLH_{-1}, MLH_{-2}. The bands in the electronic spectra of these complexes appear at low energy (> 820 nm).

The experimental conditions for solid complex precipitation were selected from the species distribution curves Fig. 2. It can be seen that for VO:Caf: 100:100 mM, the main species at pH 12.0 is MLH_{-2}. The position of the bands in the diffuse reflectance spectrum of the solid (> 800, 780, 690 nm) were coincident with the calculated for the UV–Vis spectrum. The elemental analysis, the thermal behavior and the IR characterization (see below) also support the proposed complex composition: $Na_3[VOCaf(OH)_2]\cdot 3H_2O$. The complex is oxygen sensitive either in solution or in solid state, but it is indefinitely stable under inert atmosphere.

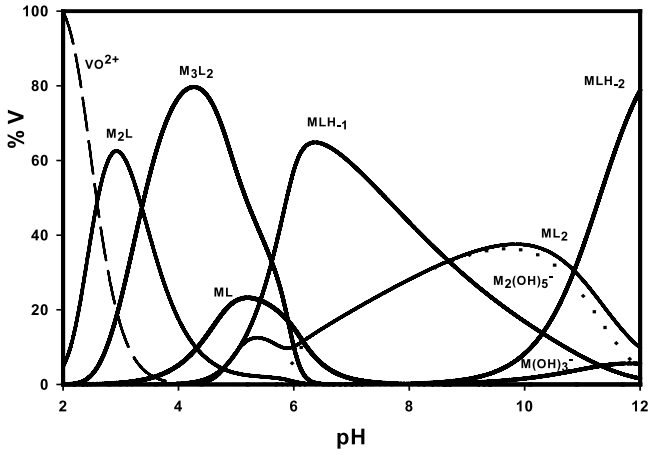


Fig. 2. Species distribution for the vanadyl (IV)–caffeic acid system (100/100 mM) as a function of pH at 25 °C, $I = 0.150$ M NaCl.

4.2.2. IR spectrum

IR spectroscopy has been a powerful tool in the analysis of the purity of the solid samples. When the complex was prepared in the presence of small quantities of oxygen, an additional band located at 1717 cm^{-1} was observed. This band is indicative of the oxidation of the OH groups to ketone of the catechol moiety [21].

Copper et al. [19] has also reported an infrared evidence for quinone formation by oxidation of catechol by atmospheric oxygen. The band located at 892 cm^{-1} is related to ketone formation. We have also detected this band in the experiments described above. Working under Ar atmosphere, ketone formation together with the oxidation of the metal center was avoided.

The frequency difference observed in the sodium caffeate spectrum between the bands ν_{as} COO^- and ν_s COO^- ($\Delta\nu$) is 177 cm^{-1}. This value is in accordance with the presence of an ionic carboxylate group. In the solid complex the $\Delta\nu$ value (175 cm^{-1}) indicates that the carboxylate group remains in an ionic form without coordination to the metal center.

The behavior of the ring stretching bands denotes that deprotonated OH groups of the catecholate-like part of the ligand are involved in the coordination to the vanadium atom.

The shift of the V=O band to lower frequencies compared with vanadyl sulfate spectrum has been observed in other catechol–vanadyl complexes. It implies a weakening of the V=O bond as a consequence of the strong σ electron donation of the ligand to antibonding orbitals of the V=O group [19,20].

Acknowledgements

E.G.F. is member of the Research Career of CONICET. P.A.M.W. is member of the Research Career from CICPBA. This study has been partially supported by CONICET, CICPBA and Agencia Nacional de Promoción Científica y Tecnológica (PICT 06-06148). E.G.F. acknowledges support from Fundación 'Antorchas'.

References

[1] R.A. Olsen, J.C. Brown, J.H. Bennet, D. Blume, J. Plant. Nutr. 5 (1982) 433.

[2] V. Römheld, H. Marschnner, J. Plant. Nutr. 3 (1981) 551.
[3] H. Sigel, A. Sigel (Eds.), Metal Ions in Biological Systems, vol. 31, Marcel Dekker, New York, 1995, 1–43.
[4] J.O. Nriagu (Ed.), Vanadium in the Environment, vol. 30, Wiley, New York, 1998.
[5] D. Rehder, Coord. Chem. Rev. 182 (1999) 297.
[6] K.H. Thompson, J.H.M. Neill, C. Orvig, Chem. Rev. 99 (1999) 2561.
[7] C. Orvig, K.H. Thompson, M. Battel, J.H. Mc. Neill, in: H. Sigel, A. Sigel (Eds.), Metal Ions in Biological Systems, vol. 31, Marcel Dekker, New York, 1995, p. 576.
[8] Y. Allegretti, E.G. Ferrer, A.C. González Baró, P.A.M. Williams, Polyhedron 19 (2000) 2613.
[9] T. Kiss, G. Nagy, M. Pécsi, H. Kozlowski, G. Micera, L.S. Erre, Polyhedron 8 (1989) 2345.
[10] S. Cocks, P.W. Linder, A. Voyé, J. Coord. Chem. 25 (1992) 211.
[11] G. Gran, Analyst 77 (1952) 661.
[12] A.E. Martell, R.J. Motekaitis, Determination and Use of Stability Constants, 2nd ed., VCH Publishers, New York, 1992.
[13] P. Gans, A. Sabatini, A. Vacca, J. Chem. Soc., Dalton Trans. (1985) 1195.
[14] J. Selbin, L.H. Holmes, S.P. Mc. Glym, J. Inorg. Chem. 25 (1963) 1359.
[15] R.R. Redher, P.H. Rieger, Inorg. Chem. 10 (1971) 1258.
[16] V.T. Kalinnikov, V.V. Zelentsov, O.N. Kuz'Micheva, T.G. Aminov, Russ. J. Inorg. Chem. 15 (1970) 341.
[17] B.G. Bennett, D. Nicholles, J. Inorg. Nucl. Chem. 34 (1972) 673.
[18] A.T. Casey, B.S. Morris, E. Sinn, J.R. Thackeray, Aust. J. Chem 25 (1972) 1195.
[19] S.R. Cooper, Y.B. Koh, K.N. Raymona, J. Am. Chem. Soc. 104 (1982) 5092.
[20] T.M. Dewey, J. DuBois, K.N. Raymond, Inorg. Chem. 32 (1993) 1729.
[21] L.J. Bellamy, The Infrared Spectra of Complex Molecules, vol. 2, 2nd ed., Chapman & Hall, London, 1980.

2. Experimental

All manipulations were routinely performed under nitrogen atmosphere using Schlenk tubes and vacuum line techniques with dried and distilled solvents. Hexafluoroisopropanol (hfipH) (Aldrich) was stored over molecular sieves and used as received. The Ce(IV) hexafluoroisopropoxide adducts were obtained as previously reported by us [15]. XPS experiments were performed with an Escalab 200R (VG Scientific) spectrometer using the monochromated Kα Al radiation as excitation source. SEM images were collected on a Hitachi S800 spectrometer. XRD data were collected on a Siemens D 5000 diffractometer using the Cu Kα radiation.

2.1. Crystallography of 1 and of 2

Suitable crystals of **1** were grown directly from the reaction medium, those of **2** were obtained by recrystallization in petroleum ether. The crystals were fixed at a glass fiber with paratone. Data collection was made on a Nonius CCD diffractometer at 123 K. Three thousand seven hundred thirty-eight reflections were measured for **1** and 12 721 reflections of which 8787 were unique were measured for **2**. Cell parameters were refined using DENZO [16]. Compound **1** crystallizes in the monoclinic system (*C*2/*c* group) whereas **2** crystallizes in the triclinic system ($P\bar{1}$ group). The structures were solved by direct methods and refined by least-squares using SHELXTL [17]. All non-H atoms were refined anisotropically giving the values of *R* listed in Table 1. Hydrogen atoms position were calculated at theoretical positions and refined isotropically riding on C. The distribution of the C–F bond lengths is quite large due to disorder phenomena which are also illustrated by high thermal factors and a large residual density.

2.2. Decomposition experiments

Compounds **1** and **2** were sublimed and decomposed in a hot-wall, dynamic vacuum reactor with argon flow. The precursor reservoir was charged with 200–300 mg of compound and maintained at about 150 °C; the furnace temperature was 550 °C and the pressure was 5×10^{-3} bar, the decomposition took place over a 4–8 h period. About 15% in weight of residue remained in the source reservoir after this time. After removing the residue, a flow of water-saturated argon (water bubbler at room temperature) was introduced and the furnace was maintained at 550 °C for over 8 h.

Table 1
Crystal data and structure refinement for Ce(hfip)$_4$(TMEDA) (**1**) and Ce(hfip)$_4$(diglyme) (**2**)

	1	**2**
Chemical formula	$C_{18}H_{20}CeF_{24}N_2O_4$	$C_{18}H_{18}CeF_{24}O_7$
Formula weight	924.48	942.44
Temperature (K)	123(2)	123(2)
Wavelength (Å)	0.71073	0.71073
Crystal system	monoclinic	triclinic
Space group	*C*2/*c*	$P\bar{1}$
a (Å)	10.026(2)	10.003(2)
b (Å)	17.622(4)	10.261(2)
c (Å)	17.563(4)	16.791(3)
α (°)	90	88.39(3)
β (°)	91.22(3)	83.50(3)
γ (°)	90	65.71(3)
V (Å^3)	3102.3(11)	1560.5(5)
Z	4	2
D_{calc} (Mg m^{-3})	1.979	2.006
Absorption coefficient (mm^{-1})	1.641	1.638
Range for data collection (°)	2.31–28.33	1.22–30.09
Refinement method	full-matrix least-squares on F^2	full-matrix least-squares on F^2
Data/restraints/parameters	3738/0/224	8787/0/451
Goodness-of-fit on F^2	1.034	0.765
Final *R* indices [$I > 2\sigma(I)$]	$R_1 = 0.0795$, $wR_2 = 0.1952$	$R_1 = 0.0539$, $wR_2 = 0.1358$
R indices (all data)	$R_1 = 0.1177$, $wR_2 = 0.2178$	$R_1 = 0.1005$, $wR_2 = 0.1748$
Largest difference peak and hole (e Å^{-3})	2.348 and −1.470	0.885 and −1.005

3. Results and discussion

3.1. Synthesis and molecular structures of Ce(hfip)$_4$(TMEDA) (1) and of Ce(hfip)$_4$(diglyme) (2)

The alcohol exchange reaction between cerium isopropoxide $Ce_2(OPr^i)_8(Pr^iOH)_2$ and hexafluoroisopropanol (hfipH = $OHCH(CF_3)_2$) (1:8 stoichiometry) in THF at room temperature afforded a cerium hexafluoropropoxide THF adduct Ce(hfip)$_4$(THF)$_2$. The high Lewis acidity of fluoroalkoxides makes, however, this adduct extremely prone to hydration. Ligand exchange with polydentate Lewis bases such as TMEDA and diglyme $MeO(CH_2CH_2O)_2Me$ provided more stable adducts. Those were characterized (FT-IR, ^{1}H and ^{19}F NMR) by comparison with authentic samples as previously reported [15]. Their FT-IR spectra are characterized by very intense broad absorption bands around 1290–1100 cm^{-1} corresponding to the C–F vibrations. Additional sharp bands due to the coordinated Lewis base are present as well but they are shifted downfield with respect to the free ligand. The absorption bands of the Ce–OR bonds are observed below 600 cm^{-1}.

The ligand exchange reactions between Ce(hfip)$_4$(THF)$_2$ and chelating ligands afforded derivatives

being more air stable, the order of stability being $Ce(hfip)_4(TMEDA) < Ce(hfip)_4(diglyme) \ll Ce(hfip)_4(bipy)_2$. All these compounds are volatile and sublime unchanged (no loss of the Lewis base occurs during volatilization). Compound **1** is more favorable than **2** in terms of melting point (155 vs. 234 °C) whereas their volatility properties are comparable (sublimation around 70 °C under 10^{-4} mm of Hg). Their solubility properties make them suitable as precursors for liquid injection CVD. By contrast to barium and yttrium derivatives with various ligands [4], no rationale and predictive trends could be established by analysis of the relationship between sublimation temperatures and molecular weight data. However, for derivatives having similar formula, the volatility appears to be in favor of the hfac derivatives with the ranking hfac > hfip > fdh > thd > fod. $Ce(hfip)_4$(diglyme) has a volatility comparable to that of $Ce(hfac)_3$(dedg) (dedg = diethyldiglyme) [10].

Compounds **1** and **2** were characterized by low temperature single crystal X-ray diffraction. Their structures are depicted in Figs. 1 and 2 for **1** and **2**, respectively. Selected bond lengths and angles are collected in Tables 2 and 3. The coordination polyhedron of the hexacoordinated cerium atom is quite distorted with angles ranging from 69.6(3)°—the bite angle of the bidentate ligand—to 170.5(3)°. The Ce–O distances have values of 2.115(5) and 2.152(6) Å, the shortest ones being *trans* to the Ce–N coordination bonds of 2.624(7) Å. Data on Ce–N bond distances are scarce. The Ce–N coordination bond observed for **1** are shorter than those reported for $[Ce_2(O^iPr)_6(\mu,\eta^2\text{-}OC_2H_4NMeC_2H_4NMe)_2]$ but where the metal is heptacoordinated [18]. The shortest intramolecular cerium–fluorine distance corresponds to Ce···F(210) with a value of 3.754 Å. Four other Ce···F–C distances are found in the range 4.128–4.332 Å, each of the fluoroisopropoxide ligand providing either one or two

Table 2
Selected bond lengths (Å) and angles (°) for $Ce(hfip)_4$(TMEDA) (**1**)

Bond lengths	
Ce–O(1)	2.115(5)
Ce–O(2)	2.152(6)
Ce–N(1)	2.624(7)
Bond angles	
O(1)–Ce–O(1)#1	108.7(3)
O(1)–Ce–O(2)	92.3(2)
O(1)–Ce–N(1)	90.9(2)
O(2)–Ce–N(1)	87.1(2)
O(2)–Ce–N(1)#1	85.1(2)
O(1)#1–Ce–O(2)	93.2(2)
O(2)#1–Ce–O(2)	170.5(3)
O(1)–Ce–N(1)#1	160.4(2)
O(2)#1–Ce–N(1)	85.1(2)
N(1)#1–Ce–N(1)	69.6(3)
C(1)–O(1)–Ce	166.5(7)
C(2)–O(2)–Ce	156.7(7)

Symmetry transformations used to generate equivalent atoms: #1 $-x+1, y, -z+3/2$.

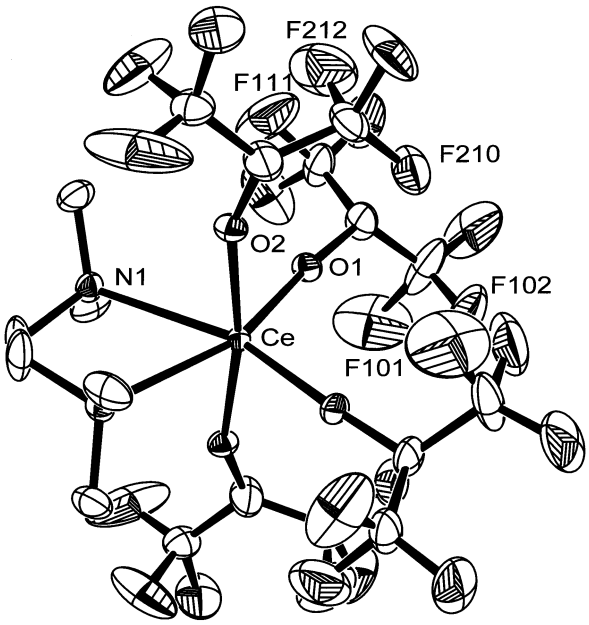


Fig. 1. Molecular structure of $Ce(hfip)_4$(TMEDA) (**1**) showing the atom numbering scheme (thermal ellipsoids at 20% probability). F(210), F(212), F(111), F(102), F(101) have Ce···F interactions in the range 3.745–4.332 Å.

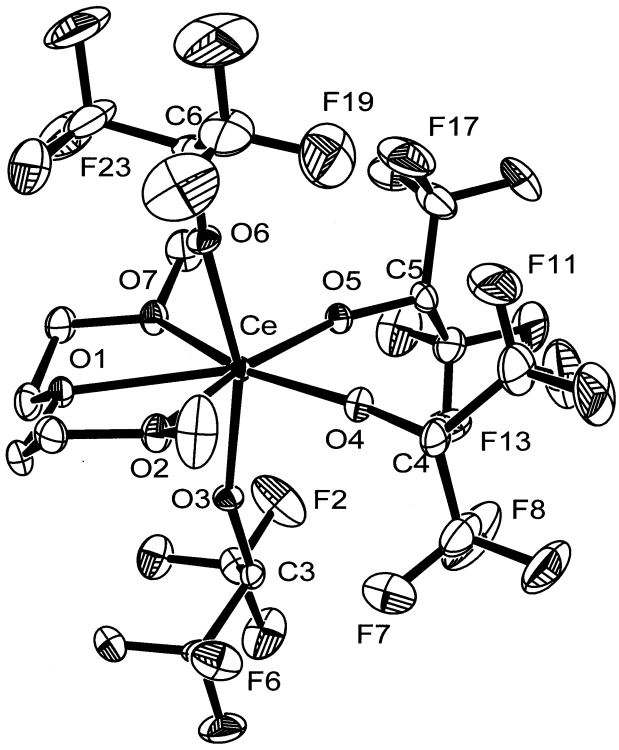


Fig. 2. Molecular structure of $Ce(hfip)_4$(diglyme) (**2**) showing the atom numbering scheme (thermal ellipsoids at 20% probability). F(2), F(6), F(7), F(8), F(11), F(13), F(17), F(19) and F(23) have Ce···F interactions in the range 4.060–4.309 Å.

Table 3
Selected bond lengths (Å) and angles (°) for Ce(hfip)$_4$(diglyme) (**2**)

Bond lengths	
Ce–O(1)	2.580(4)
Ce–O(2)	2.581(5)
Ce–O(7)	2.585(5)
Ce–O(3)	2.132(4)
Ce–O(4)	2.139(5)
Ce–O(5)	2.127(4)
Ce–O(6)	2.122(4)
Bond angles	
O(1)–Ce–O(2)	62.54(16)
O(1)–Ce–O(3)	78.49(16)
O(1)–Ce–O(7)	62.02(15)
O(1)–Ce–O(4)	138.72(17)
O(1)–Ce–O(5)	136.41(17)
O(1)–Ce–O(6)	83.43(18)
O(2)–Ce–O(3)	89.26(17)
O(2)–Ce–O(4)	76.94(17)
O(2)–Ce–O(5)	160.79(18)
O(2)–Ce–O(6)	82.39(18)
O(2)–Ce–O(7)	124.26(16)
O(3)–Ce–O(4)	94.18(19)
O(3)–Ce–O(5)	97.50(18)
O(3)–Ce–O(6)	161.92(19)
O(3)–Ce–O(7)	85.30(18)
O(4)–Ce–O(5)	84.61(18)
O(4)–Ce–O(6)	99.47(19)
O(4)–Ce–O(7)	158.74(17)
O(5)–Ce–O(6)	95.55(19)
O(5)–Ce–O(7)	74.42(17)
O(6)–Ce–O(7)	86.22(18)
C(3)–O(3)–Ce	160.2(4)
C(4)–O(4)–Ce	174.2(5)
C(5)–O(5)–Ce	149.4(5)
C(6)–O(6)–Ce	170.3(5)

fluorine for these interactions. Activation of carbon–fluorine bonds by metallic species has been observed in a number of complexes giving short M···F–C interactions [19]. The shortest distance is much longer than the Ce–O bond lengths or the sum of the van der Waals radii ($\sim$3.20 Å) and than the interactions found for barium derivatives (usually 3–3.20 Å) [12]. The Ce···F(210) interaction might however account for the opening of the O(1)–Ce–O(1)# angle [108.7(3)°]. Some intramolecular F···N interactions involving F(111), F(112), F(200) are also observed (4.137–4.259 Å). These interactions are much longer than the Ce–F bond distances reported for cerium fluoride derivatives such as $NH_4[CeF_2(PO_4)]$ for instance [20].

The molecular structure of the Ce(hfip)$_4$(diglyme) adduct **2** is based on a heptacoordinated metal center since all oxygens of the diglyme are involved in coordination. Such a coordination number was observed for $Ce_4O(OPr^i)_{14}$ [21]. The Ce–O(hfip) bond lengths are similar to those of **1** [2.122(4)–2.139(5) Å] and are much shorter than the Ce–O bond distances involving the diglyme ligand [2.582 Å av.]. The stereochemistry around the metal corresponds to a trigonal prism capped by one of the oxygen O(1) of the glyme. The metric parameters of the diglyme ligand are in agreement with the literature body [9,10]. The shortest Ce···F distance [with F(17)] has a value of 4.060 Å but additional Ce···F distances having values below 4.31 Å are observed with eight other fluorine atoms.

The Ce–OR bond distances are, for both complexes, quite short, although longer than those observed for non-fluorinated terminal Ce–OR alkoxides (2.088 Å av. for $[Ce_2(OPr^i)_8(PriOH)_2]$) [22]. They are shorter than those observed for the $[Ce(hfip)_6]^{2-}$ anion [2.183(5)–2.208(5) Å]. The Ce–O–(hfip) angles display values of [156.7(7)°–166.5(7)°] and [149.4(5)°–174.2(5)°] for **1** and **2**, respectively. Those are large by comparison to most other hexafluoroisopropoxide derivatives [143.3(5)°–156.5(5)° for $[Ce(hfip)_6]^{2-}$] and nearly comparable to those observed for non-fluorinated OR ligands which are considered to be more prone to π-bonding [23]. These large Ce–O–C angles do, however, not prevent interaction of the fluorine atoms with the metal center. These interactions shield the positive charge of the metal and reduce its electrophilic character. Its is noticeable that metal–fluorine interactions are generally absent in the solid state structures of fluorinated β-diketonate complexes in which the coordination number of the metal is usually higher than for fluorinated alkoxide adducts [10].

3.2. CVD experiments

Deposition experiments were achieved at various temperatures using an horizontal cold wall reactor under dynamic vacuum ($4–5 \times 10^{-3}$ bar). Compounds **1** and **2** were transported into the vapor phase at 120–140 °C. No deposits were observed below 500 °C and depositions were thus conducted at a temperature of 550 °C for **1** and **2**. Films were homogeneous, white and displayed poor mechanical properties. They were characterized by XPS in the range 0–1000 eV and gave similar spectra in terms of peak energies and profile for both compounds (Fig. 3(a) and (b)). The Ce3d spectra displayed peaks due to Ce^{4+} and Ce^{3+} atoms namely those of ceria CeO_2 and of fluoride, CeF_3, the latter being predominant. Indeed the F1s spectra showed a peak at 684.5 eV and the O1s spectra displayed a broad peak at 530 eV representing the O^{2-} contributions of Ce^{3+}–O and Ce^{4+}–O bonds. Under similar experimental conditions, the amount of cerium oxide was slightly higher for the diglyme adduct (42%) than for the TMEDA one (33%) by measuring the relative intensity of peak u‴ in the Ce3d$_{3/2}$ region [24]. Subsequent heating at 550 °C under a water-saturated argon atmosphere allowed to convert CeF_3 into CeO_2 as shown by the XPS pattern (Fig. 3(c)). The latter compares with that reported for an authentic CeO_2 sample [25] and no

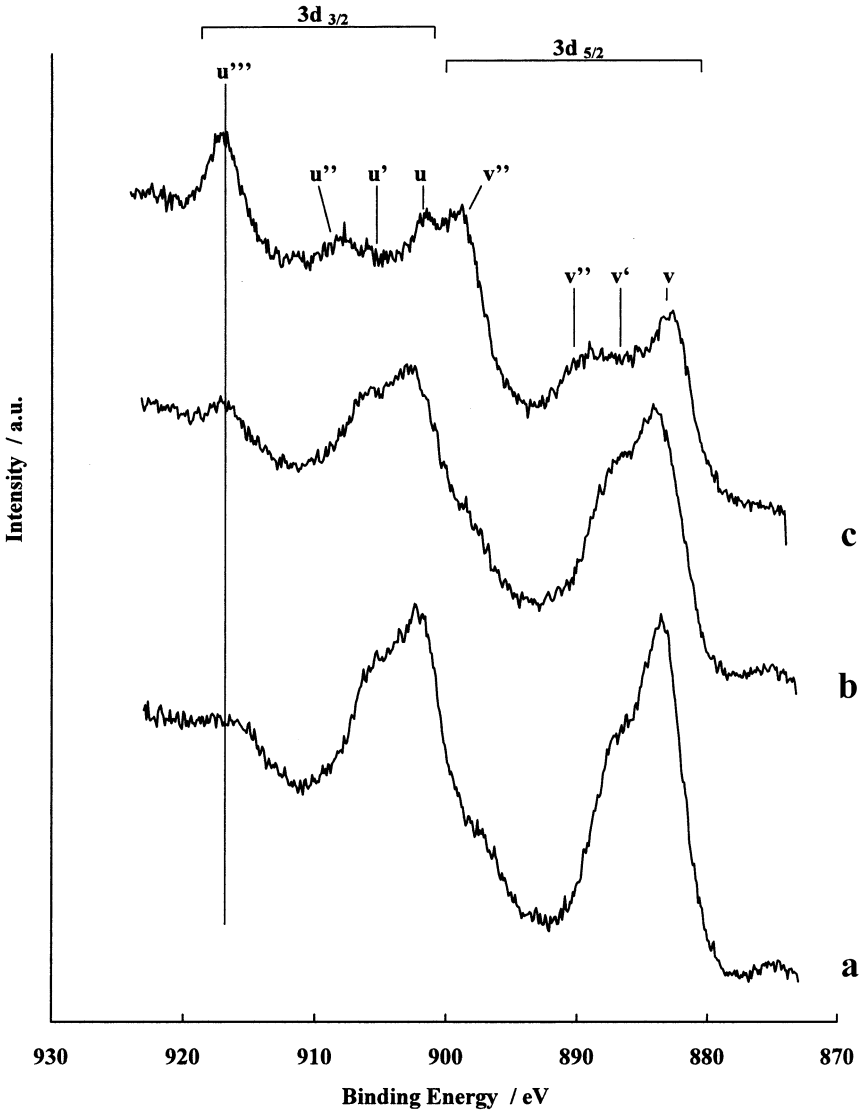


Fig. 3. Ce3d XPS patterns of films obtained from: (a) $Ce(hfip)_4(TMEDA)$ (**1**), (b) $Ce(hfip)_4(diglyme)$ (**2**), (c) **2** with water-saturated argon treatment at 550 °C.

peaks assigned to fluorine could be detected. These films were homogeneous, colorless with very good transparency (transmittance of 90–95% in the range 350–900 nm) and displayed good mechanical properties (tested by applying cellophane tapes to the coated substrate). SEM data featured a smooth film but with small cracks resulting probably from the elimination of the fluorine residues. The thickness was estimated from cross sectional SEM pictures to be around 20 nm and XRD experiments indicated that the films were amorphous.

The formation of cerium(III) fluoride indicates cleavage of the C–F bonds. Although fluorine contamination has been observed for systems without M...F interactions in the ground-state structure, this process is probably assisted here by the metal–fluorine interactions which weaken the C–F bonds but was not further investigated. It should be noted that while fluorine contamination of oxide films is generally undesirable, pure metal fluorides have many desirable properties of their own and cerium fluoride is involved in the formulation of γ-scintillations [26]. Thus production of pure metal fluoride films has its own relevance.

4. Supplementary material

Tables of coordinates, of thermal parameters, of bond lengths and angles have been deposited at the Cambridge Crystallographic Data Base Centre. CCDC reference numbers: 171191 for **1** and 171192 for **2**. Copies of this information may be obtained free of charge from The Director, CCDC, 12 Union Road, Cambridge CB2 IEZ, UK (fax: +44-1223-336033; e-

mail: deposit@ccdc.cam.ac.uk or www: http://www.ccdc.cam.ac.uk).

Acknowledgements

We thank Mr. P. Delichere and Mr. G. Wicker for XPS and SEM experiments, respectively.

References

[1] F. Cerwinski, J.A. Szpunar, J. Sol–Gel Sci. Tech. 9 (1997) 103.
[2] (a) S. Guo, H. Arwin, S.N. Jacobson, K. Järrendahl, V. Helmersson, J. Appl. Phys. 77 (1995) 1829;
(b) C.D. Hogarh, Z.T. Al-Dhhan, Phys. Stat. Sol. 137 (1986) K157;
(c) R. Aguiar, F. Sanches, D. Perro, C. Ferrrater, M. Varela, Physica C 235–240 (1994) 647;
(d) M. Dejneka, R.E. Riman, E. Snitzer, J. Am. Ceram. Soc. 76 (1994) 3147.
[3] (a) M.A.A.M. van Wijck, M.A.J. Verhoeven, E.M.C.M. Reuvekamp, G.J. Gerritsma, D.H.A. Blank, H. Rogalla, Appl. Phys. Lett. 68 (1996) 553;
(b) M. Becht, J.G. Wen, T. Morishita, K. Tanabe, in: M.D. Allendorf, C. Bernard (Eds.), Chemical Vapor Deposition, Proceedings of the XIV International Conference and EuroCVD-11, vols. 97-25, The Electrochemical Society, Pennington, NJ, 1997, p. 756.
[4] (a) L.G. Hubert-Pfalzgraf, New J. Chem. 19 (1995) 727;
(b) L.G. Hubert-Pfalzgraf, H. Guillon, Appl. Organomet. Chem. 12 (1998) 321.
[5] M. Pang, G.Y. Meng, H.W. Xin, C.S. Chen, D.K. Peng, Y.S. Lin, Thin Solid Films 324 (1998) 89.
[6] (a) E. Uhlemann, F. Diandze, Z. Anorg. Allg. Chem. 386 (1971) 329;
(b) M. Becht, T. Gerfin, K.H. Dahmen, Chem. Mater. 5 (1993) 137.
[7] J. McAleese, J.C. Plakatouras, B.C.H. Steele, Thin Solid Films 280 (1996) 152.
[8] M. Becht, K.D. Dahmen, V. Gramlich, A. Mortelli, Inorg. Chim. Acta 248 (1996) 27.
[9] (a) J. McAleese, J.A. Darr, B.C.H. Steele, Chem. Vapor Deposit. 2 (1996) 244;
(b) I. Baxter, J.A. Darr, M.B. Hursthouse, K.M.A. Malik, J. Mc Aleese, D.M.P. Mingos, Polyhedron 17 (1998) 1329.
[10] (a) A. Drozdov, S. Troyanov, Polyhedron 12 (1993) 2973;
(b) G. Malandrino, R. La Nigro, C. Benelli, F. Castelli, I.L. Fragala, Chem. Vapor Deposit. 6 (2000) 233;
(c) K.D. Pollard, H.A. Jenkins, R.J. Puddephatt, Chem. Mater. 12 (2000) 701.
[11] L. Miinea, S. Suh, S.G. Bott, J.R. Liu, W.K. Chu, D.M. Hoffman, J. Mater. Chem. 9 (1999) 929.
[12] (a) F. Labrize, L.G. Hubert-Pfalzgraf, J.C. Daran, J. Chem. Soc., Chem. Commun. (1993) 1556;
(b) F. Labrize, L.G. Hubert-Pfalzgraf, J.C. Daran, P. Tobaly, Polyhedron 14 (1995) 881;
(c) H. Vincent, F. Labrize, L.G. Hubert-Pfalzgraf, Polyhedron 13 (1994) 3223.
[13] D.C. Bradley, H. Chudzynska, M.B. Hursthouse, M. Motevalli, R. Wu, Polyhedron 13 (1994) 1 (and references therein).
[14] J.A. Samuels, E.B. Lobkowsky, W.E. Streib, K. Folting, J.C. Huffman, J.W. Zwanziger, K.G. Caulton, J. Am. Chem. Soc. 115 (1993) 5093.
[15] V. Abada, L.G. Hubert-Pfalzgraf, J. Vaissermann, J. Chem. Soc., Dalton Trans. (1998) 3437.
[16] Z. Otwinowski, W. Minor, in: C.W. Carter, Jr., R.M. Sweet (Eds.), Processing of X-Ray Diffraction Data Collected in Oscillation Mode, Methods in Enzymology. Macromolecular Crystallography, Part A, vol. 276, Academic Press, New York, 1997, pp. 307–326.
[17] G.M. Sheldrick, Program for the refinement of crystal structures, University of Göttingen, Germany (Bruker-AXS, Madison, WI, USA) 1997.
[18] (a) T. Fjelberg, R.A. Andersen, J. Mol. Struct. 129 (1985) 93;
(b) L.G. Hubert-Pfalzgraf, N. El Khokh, J.C. Daran, Polyhedron 11 (1992) 59.
[19] J.L. Kiplinger, T.G. Richmond, C.E. Osterberg, Chem. Rev. 94 (1994) 373.
[20] Y. Ranbo, W. Dan, T. Takahino, K. Hitoshi, K. Nobuhiro, K. Nobukazu, J. Solid State Chem. 1 (2001) 180.
[21] C. Sirio, L.G. Hubert-Pfalzgraf, C. Bois, Polyhedron 16 (1997) 1129.
[22] B.A. Vaarrtstra, J.C. Huffman, P.S. Gradeff, L.G. Hubert-Pfalzgraf, J.C. Daran, S. Parraud, K. Yunlu, K.G. Caulton, Inorg. Chem. 29 (1990) 3126.
[23] L.G. Hubert-Pfalzgraf, Coord. Chem. Rev. 178–180 (1998) 967 (and references therein).
[24] J.Z. Shyu, K. Otto, W.L.H. Watkins, G.W. Graham, R.K. Belitz, H.S. Gandhi, J. Catal. 114 (1988) 23.
[25] (a) P. Burroughs, A. Hammett, A.F. Orchard, G. Thornton, J. Chem.. Soc., Dalton Trans. (1976) 1686;
(b) J.F. Moulder, W.F. Stickle, P.E. Sobal, K.D. Bomben, in: J. Chastain (Ed.), Handbook of X-Ray Photoelectron Spectroscopy: A Reference Book of Standard Spectra for Identification and Interpretation of XPS Data, Imprint Eden Prairie, Minneapolis, MN, USA, 1992.
[26] (a) G. Blasse, Chem. Mater. 6 (1994) 1465;
(b) D.F. Anderson, Nucl. Instrum. Methods Phys. Res. A287 (1990) 606.

2. Experimental

2.1. General

All chemicals and solvents were of AR grade and obtained from commercial sources. Tetrahydrofuran was freshly distilled over sodium under argon before use. Other solvents and liquid reactants were dried by storage over molecular sieves. The complex $[ReBr(CO)_5]$ was prepared according to reported procedures [8]. All reactions were carried out using standard Schlenk techniques under purified nitrogen. Infrared spectra were recorded on a Perkin–Elmer 1600 FT IR Spectrometer or a Bio-Rad FT IR Spectrometer. The reactions were monitored by solution IR spectroscopy, and were considered to be complete when there was no more change in the ν(C–O) pattern. Proton NMR spectra were recorded on a Bruker AMX 500 MHz spectrometer. The ^{1}H chemical shifts are reported in ppm downfield of tetramethylsilane. Elemental analyses were performed by the Microanalytical Laboratory of the Department of Chemistry of the National University of Singapore. The molecular weight analysis of complex **1** was performed by Galbraith Laboratories, Inc. using the three-point vapour pressure osmometry method; the sample was dissolved in dichloromethane at 27 °C. Cytotoxicity tests were carried out as previously reported [7].

2.2. Synthesis of $[Re(\eta^2\text{-}Me_2NCH_2CH_2O)(CO)_3(\mu\text{-}OH)Re(\eta^2\text{-}Me_2NCH_2CH_2OH)(CO)_3]$ (1)

A solution of $[Re_2(CO)_{10}]$ (130 mg, 0.2 mmol) in freshly distilled THF (10 ml) was added at room temperature (r.t.) to a solution of $Me_3NO{\cdot}2H_2O$ (67 mg, 0.6 mmol) and $Me_2NCH_2CH_2OH$ (0.1 cm^3, 89 mg, 1.0 mmol) in THF–MeOH (20 ml, 1:1, v/v). The solution was stirred for 4 h at ambient temperature. Following solvent removal in vacuo, the product was recrystallised from dichloromethane–hexane mixture by slow evaporation at r.t. Yield: 133 mg (90% based on Re). (Found: C, 22.9; H, 3.0; N, 3.8. $C_{14}H_{22}N_2O_9Re_2$ requires C, 22.9; H, 3.0; N, 3.8%); $\tilde{\nu}_{max}$ (cm^{-1}) (CO) 2014s, 1894vs (CH_2Cl_2); δ_H (CD_2Cl_2) 4.33 [1H, dq, H(8B)] (see Fig. 1 for the labelling scheme for the hydrogen atoms), 4.21 [1H, dd, H(12A)], 3.93 [1H, td, H(8A)], 3.68 [1H, td, H(12B)], 3.04 [6H, s, H(10A)–H(10C) and H(13A)–H(13C)], 2.98 [1H, td, H(11B)], 2.85 [3H, s, H(9A)–H(9C)], 2.80 [3H, s, H(14A)–H(14C)], 2.60 [1H, td, H(7A)], 2.23 [2H, tt, H(7B) and H(11A)]; MW found: 1492, calcd. 1470 (for dimer).

When the reaction was carried out in pure THF instead of a THF–MeOH mixture as the solvent, complex **1** was also formed, but in 55% yield (based on Re). Analogous reactions of $[Re_2(CO)_{10}]$ with other ω-aminoalcohols, $Me_2N(CH_2)_nOH$ ($n = 3$, 4, 6), in THF–MeOH mixture were also attempted, but in all these cases intractable oils were obtained.

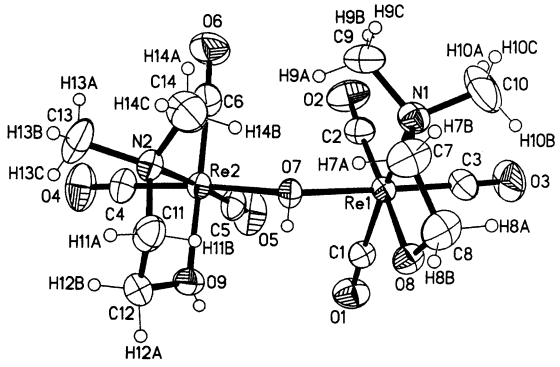


Fig. 1. Crystal structure of $[Re(\eta^2\text{-}Me_2NCH_2CH_2O)(CO)_3(\mu\text{-}OH)Re(\eta^2\text{-}Me_2NCH_2CH_2OH)(CO)_3]$ (**1**).

2.3. Synthesis of $[Re_3(\mu_3\text{-}OH)(\mu\text{-}OH)_2(\mu\text{-}OCH_2CH_2NMe_2H)(CO)_9]$ (2)

2.3.1. Method 1

The procedure was similar to that for the synthesis of complex **1** except that methanol was replaced by water, and that the product was recrystallised from acetone–water mixture by slow evaporation at 0 °C. Yield: 43 mg of **2** (as the acetone solvate) (29% based on Re).

2.3.2. Method 2

A 1 M solution of $Na[OCH_2CH_2NMe_2]$ in THF (0.25 cm^3, 0.25 mmol), prepared by the reaction of $Me_2NCH_2CH_2OH$ with sodium metal, was added to a THF solution (10 cm^3) of $[ReBr(CO)_5]$ (103 mg, 0.25 mmol). The resultant solution was stirred for 18 h, after which the solvent was removed in vacuo. The product was recrystallised from acetone–water mixture as above. Yield: 52 mg (55% based on Re). (Found: C, 23.15; H, 2.62; N, 1.40. $C_{22}H_{32}NO_{16}Re_3$ requires C, 23.49; H, 2.87; N, 1.24%; $\tilde{\nu}_{max}$ (cm^{-1}) (CO) 2026w, 2011m, 1893vs (acetone); δ_H (acetone-d_6) 4.44 (2H, t, OCH_2), 4.03 (1H, br s, NH), 3.32 (2H, t, NCH_2), 3.08 (6H, s, Me_2N).

2.4. X-ray crystallography

Pale yellow crystals of complex **1** were grown from dichloromethane–hexane mixture by slow evaporation at r.t. Colourless crystals of complex **2** were grown from acetone–water mixture by slow evaporation at 0 °C. Crystals of **2** desolvate quite readily on isolation, and were thus sealed in quartz capillaries with the mother liquor during data collection. Data collection was carried out at ambient temperature on a Siemens SMART CCD diffractometer using Mo Kα radiation (λ 0.71073 Å). The data were corrected for absorption effects using the SADABS program [9]. Crystal and

Table 1
Crystal and refinement data for complexes **1** and **2**

	1	**2**
Chemical formula	$C_{14}H_{22}N_2O_9Re_2$	$C_{22}H_{32}NO_{16}Re_3$
Formula weight	734.74	1125.09
Crystal system	monoclinic	triclinic
Space group	$P2_1/c$	$P\bar{1}$
a (Å)	13.9506(1)	9.8316(1)
b (Å)	11.4270(1)	10.5565(2)
c (Å)	14.6124(1)	18.4123(1)
α (°)	90	90.35
β (°)	116.917(1)	105.278(1)
γ (°)	90	114.903(1)
U (Å^3)	2077.05(3)	1656.99(4)
Temperature (K)	296(2)	293(2)
Z	4	2
μ (mm^{-1})	11.691	10.997
F(000)	1368	1048
θ Range for data collection (°)	2.37–29.45	2.15–29.50
Number of reflections collected	12 904	14 817
Number of unique data	5148 ($R_{int} = 0.0293$)	7939 ($R_{int} = 0.0348$)
R_1, wR_2 [$I > 2\sigma(I)$]	0.0237, 0.0504	0.0315, 0.0682
R_1, wR_2 (all data)	0.0302, 0.0526	0.0427, 0.0722
Goodness-of-fit	1.054	0.999

refinement data for complexes **1** and **2** are summarised in Table 1.

The structures of the two complexes were solved by direct methods and difference Fourier maps. Full-matrix least-squares refinements (on F^2) were carried out with anisotropic thermal parameters for all non-hydrogen atoms, using all of the unique data. The hydrogen atoms of the two hydroxyl groups of complex **1** were located in a difference map, and their positional and isotropic thermal parameters were refined independently. All other hydrogen atoms were introduced in calculated positions and refined using the riding model. Computations were carried out using the SHELXTL software package [10]. Selected geometric parameters of the complexes are given in Tables 2 and 3.

2.5. Cytotoxicity tests

Complexes **1** and **2** and the compounds $[NBu^n_4][ReO_4]$ and $[NEt_4]_2[ReBr_3(CO)_3]$ were tested for cytotoxic activity by homogenising the compounds as a 1 mg ml^{-1} solution in 0.05% Tween 80/H_2O. These solutions were sterilised by passing them through an acrodisc (0.45 μm). The cell lines investigated (Table 4) were maintained by literature techniques [11]. The NCI protocol was used to assess the cytotoxicity of the test compounds and standard drugs in each cell line [11]. The number of cells were determined by the trypan blue exclusion technique [11] and the percent inhibition of growth for each concentration of compound was calculated and averaged ($N = 4$). The percent inhibition was plotted against the log of the concentration of compound and the ED_{50} value (concentration of compound in μg ml^{-1} inhibiting 50% of cell growth) estimated. Solid tumour cytotoxicity was determined using crystal violet/MeOH and read at 580 nm (Molecular Devices) [12]. An ED_{50} value of less than 4 μg ml^{-1} was required for significant activity for inhibition of cell growth [11].

Table 2
Selected bond lengths (Å) and angles (°) for complex **1** (including hydrogen-bonding geometry)

Bond lengths			
Re(1)–C(1)	1.906(4)	Re(2)–C(4)	1.897(5)
Re(1)–C(2)	1.895(5)	Re(2)–C(5)	1.900(5)
Re(1)–C(3)	1.889(4)	Re(2)–C(6)	1.909(5)
Re(1)–O(7)	2.164(3)	Re(2)–O(7)	2.157(3)
Re(1)–O(8)	2.137(3)	Re(2)–O(9)	2.123(3)
Re(1)–N(1)	2.251(3)	Re(2)–N(2)	2.301(3)
Bond angles			
C(1)–Re(1)–O(7)	93.00(14)	C(5)–Re(2)–O(7)	95.72(14)
C(2)–Re(1)–O(7)	95.78(15)	C(6)–Re(2)–O(7)	97.11(16)
N(1)–Re(1)–O(7)	84.06(12)	N(2)–Re(2)–O(7)	84.55(11)
O(8)–Re(1)–O(7)	80.13(11)	O(9)–Re(2)–O(7)	79.93(12)
O(8)–Re(1)–N(1)	78.51(12)	O(9)–Re(2)–N(2)	77.34(13)
C(2)–Re(1)–N(1)	98.44(16)	C(4)–Re(2)–N(2)	94.71(17)
C(3)–Re(1)–N(1)	92.69(16)	C(6)–Re(2)–N(2)	95.78(16)
C(1)–Re(1)–O(8)	91.90(14)	C(4)–Re(2)–O(9)	95.78(18)
C(3)–Re(1)–O(8)	98.08(16)	C(5)–Re(2)–O(9)	99.82(18)
C(1)–Re(1)–C(2)	91.03(18)	C(4)–Re(2)–C(5)	84.80(19)
C(1)–Re(1)–C(3)	90.02(18)	C(4)–Re(2)–C(6)	87.2(2)
C(2)–Re(1)–C(3)	85.9(2)	C(5)–Re(2)–C(6)	87.1(2)
C(1)–Re(1)–N(1)	170.31(15)	C(4)–Re(2)–O(7)	175.71(17)
C(2)–Re(1)–O(8)	175.09(15)	C(5)–Re(2)–N(2)	177.07(17)
C(3)–Re(1)–O(7)	176.54(15)	C(6)–Re(2)–O(9)	172.69(17)
Re(1)–O(7)–Re(2)	127.81(13)		

Hydrogen bonding geometry				
D–H···*A*	*D*–H	H···*A*	*D*···*A*	*D*–H···*A*
O(9)–H(9)···O(8A)	0.65(7)	1.81(7)	2.434(4)	161(10)

3. Results and discussion

3.1. Synthesis of $[Re(\eta^2\text{-}Me_2NCH_2CH_2O)(CO)_3(\mu\text{-}OH)Re(\eta^2\text{-}Me_2NCH_2CH_2OH)(CO)_3]$ (**1**)

Complex **1** is easily synthesised in high yield by the reaction of $[Re_2(CO)_{10}]$ with $Me_2NCH_2CH_2OH$ and $Me_3NO{\cdot}2H_2O$ (1:5:3) in a mixture of THF and MeOH at room temperature. This reaction can be described as an oxidative alkoxylation of $[Re_2(CO)_{10}]$, and is analogous to the oxidative methoxylation of $[Re_2(CO)_{10}]$ by methanol in the presence of Me_3NO [13]. Interestingly, no methoxo group is incorporated into complex **1** despite the fact that a large excess of methanol is present in the reaction mixture. The presence of methanol is, however, important, since complex **1** is obtained at a

Table 3
Selected bond lengths (Å) and angles (°) for complex **2** (including hydrogen-bonding geometry)

Bond lengths			
Re(1)–O(1)	2.186(3)	Re(2)–C(8)	1.881(7)
Re(1)–O(2)	2.137(4)	Re(2)–C(9)	1.889(7)
Re(1)–O(4)	2.123(3)	Re(2)–C(10)	1.885(7)
Re(1)–C(5)	1.893(6)	Re(3)–O(1)	2.183(3)
Re(1)–C(6)	1.899(7)	Re(3)–O(3)	2.155(3)
Re(1)–C(7)	1.895(6)	Re(3)–O(4)	2.113(4)
Re(2)–O(1)	2.191(3)	Re(3)–C(11)	1.875(6)
Re(2)–O(2)	2.131(4)	Re(3)–C(12)	1.885(7)
Re(2)–O(3)	2.146(3)	Re(3)–C(13)	1.889(6)
Bond angles			
Re(1)–O(1)–Re(2)	104.76(14)	O(1)–Re(1)–O(2)	72.28(13)
Re(1)–O(1)–Re(3)	102.37(14)	O(1)–Re(1)–O(4)	73.43(13)
Re(2)–O(1)–Re(3)	104.26(14)	O(2)–Re(1)–O(4)	79.42(14)
Re(1)–O(2)–Re(2)	108.65(15)	O(1)–Re(2)–O(2)	72.30(13)
Re(2)–O(3)–Re(3)	106.82(14)	O(1)–Re(2)–O(3)	73.19(13)
Re(1)–O(4)–Re(3)	106.98(15)	O(2)–Re(2)–O(3)	79.81(14)
Re(1)–O(2)–C(1)	123.1(4)	O(1)–Re(3)–O(3)	73.19(13)
Re(2)–O(2)–C(1)	128.2(4)	O(1)–Re(3)–O(4)	73.68(13)
O(2)–C(1)–C(2)	110.9(4)	O(3)–Re(3)–O(4)	78.71(14)
C(1)–C(2)–N(1)	110.9(5)		

Hydrogen bonding geometry				
D–H···*A*	*D*–H	H···*A*	*D*···*A*	*D*–H···*A*
N(1)–H(1A)···O(3)	0.9100	1.93	2.808(6)	162
O(1)–H(1)···O(1S)	0.9800	1.80	2.723(6)	157
O(3)–H(3)···O(3S)	0.9300	2.04	2.828(6)	142
O(4)–H(4)···O(2S)	0.9300	1.97	2.741(6)	139

much lower yield if the reaction is performed in THF instead of a THF–MeOH mixture. The source of the bridging OH group in complex **1** is probably $Me_3NO\cdot 2H_2O$. Increasing the proportion of water in the reaction mixture, however, leads to the formation of complex **2** instead (see below).

The mechanism for the formation of complex **1** is proposed in Scheme 1. This mechanism is analogous to that proposed for the formation of $[Re_2(\mu\text{-}OMe)_2(\mu\text{-}PP)(CO)_6]$ (PP = diphosphine) in the reactions of diphosphines with $[Re_2(CO)_{10}]$ and $Me_3NO\cdot 2H_2O$ in THF–MeOH mixture [13]. The mechanism requires the initial substitution of a CO group by the hydroxyl oxygen, followed by oxidative addition of the coordinated H–$OCH_2CH_2NMe_2$ molecule across the Re–Re bond. Since THF solvates the hydroxyl group but not the amino group, it would favour the coordination of the amino group to rhenium, thereby inhibiting the reaction pathway depicted in Scheme 1. Methanol, on the other hand, can solvate both the hydroxyl group and the amino group; it thus increases the probability of the coordination of the hydroxyl group of $Me_2NCH_2CH_2OH$ to rhenium, thereby facilitating the formation of complex **1**. Methanol may also catalyse an alternative pathway for the formation of the $[Re(\eta^2\text{-}OCH_2CH_2NMe_2)(CO)_4]$ intermediate (Scheme 2).

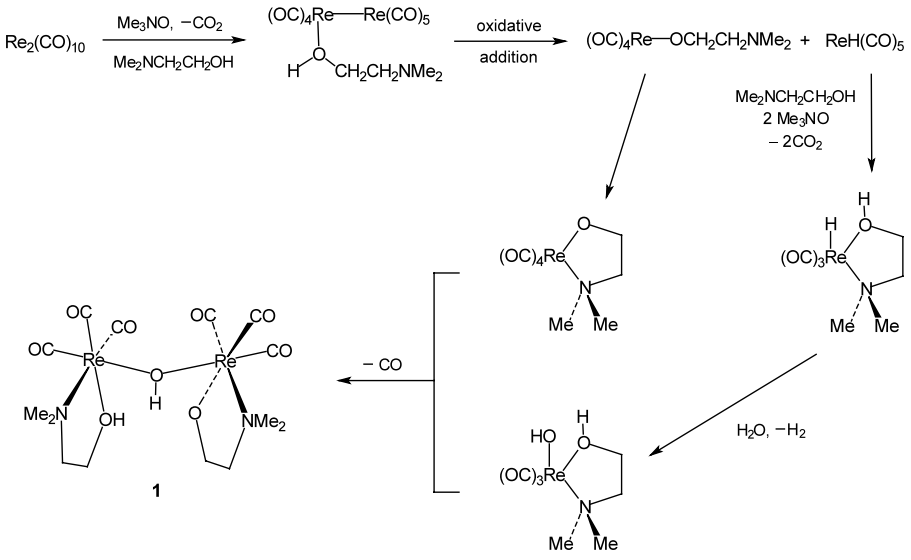
Complex **1** cannot be obtained from the reaction of $Me_2NCH_2CH_2OH$ with aqueous $[NEt_4]_2[ReBr_3(CO)_3]$,

Table 4
Cytotoxicity of rhenium complexes in murine and human cultured tumours (ED_{50} μg ml^{-1}, $n = 4$) [a]

Tumour cell line	Cpx **1**	Cpx **2**	$[NBu^n_4][ReO_4]$	$[NEt_4]_2[ReBr_3(CO)_3]$	Standards [b]	
					6-MP	Ara-C
Suspension cultured cells						
L1210 mouse leukaemia	3.09	3.15	3.65	2.65	2.43	2.07
P388 mouse lymphocytic leukaemia	2.49	2.48	2.69	4.55	2.04	0.79
HL-60 human leukaemia	3.01	5.97	3.56	3.83	3.35	4.00
$Tmolt_3$ T cell leukaemia	3.17	3.74	3.59	3.96	1.62	2.67
T $molt_4$ T cell leukaemia	5.44	5.64	4.96	4.60	2.67	2.36
HuT-78 lymphoma	3.48	3.58	2.54	3.17	1.68	2.50
THP-1 acute monocytic leukaemia	4.93	2.86	2.10	2.85	3.03	2.54
HeLa-S^3 suspended uterine	3.02	2.75	3.12	2.42	2.12	2.13
Solid tumour cultures						
KB Nasopharynx	3.71	6.74	7.79	7.27	11.04	2.84
Lung A549	5.53	5.76	8.87	8.35	4.71	5.62
Ovary 1-A9	6.07	2.48	4.18	5.37	6.64	5.39
Breast MCF-7	3.60	3.11	7.99	2.17	8.84	12.45
Glioma UM 86	4.89	7.28	8.26	8.15	4.46	1.88
Ileum HCT-8	3.51	6.33	8.04	10.92	1.15	2.54
Osteosarcoma HSO	7.11	13.12	12.48	6.74	9.13	0.86
Melanoma SK2	2.85	4.15	3.82	4.46	6.86	10.53
Non-cancerous human cells						
RMPI 1788 fibroblasts	8.50	6.70	7.18	8.00		

[a] ED_{50} values refer to the concentration of the compound inhibiting 50% of cell growth. A value of less than 4 μg ml^{-1} is required for significant activity for inhibition of cell growth [11].

[b] 6-MP, 6-mercaptopurine; Ara-C, cytosine β-D-arabinofuranoside.

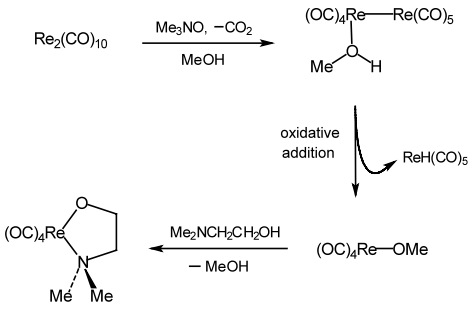


Scheme 1.

which yields the known compounds [2] $[NEt_4][Re_3(\mu_3\text{-}OH)(\mu\text{-}OH)_3(CO)_9]$ (**3**) (when one molar equivalent of aminoalcohol is used) or $[NEt_4][Re_2(\mu\text{-}OH)_3(CO)_6]$ (**4**) (when excess aminoalcohol is used) instead. The complex $[ReBr_3(CO)_3]^{2-}$ is known to react in aqueous solution as $[Re(H_2O)_3(CO)_3]^{+}$, with three labile water ligands [2]. In mildly alkaline medium, the aqua ion reacts to form $[Re_3(\mu_3\text{-}OH)(\mu\text{-}OH)_3(CO)_9]^{-}$, which is in turn converted into the ion $[Re_2(\mu\text{-}OH)_3(CO)_6]^{-}$ in more strongly alkaline medium [2]. The formation of compounds **3** and **4** in the reaction of $Me_2NCH_2CH_2OH$ with aqueous $[NEt_4]_2[ReBr_3(CO)_3]$ can thus be attributed to the basicity of the aminoalcohol.

3.2. Crystal structure of $[Re(\eta^2\text{-}Me_2NCH_2CH_2O)(CO)_3(\mu\text{-}OH)Re(\eta^2\text{-}Me_2NCH_2CH_2OH)(CO)_3]$ (1)

The molecule of **1** (Fig. 1) consists of a $\{Re(\eta^2\text{-}Me_2NCH_2CH_2O)(CO)_3\}$ and a $\{Re(\eta^2\text{-}Me_2NCH_2CH_2OH)(CO)_3\}$ fragment bridged by one OH ligand. To our knowledge, complex **1** is the first structurally characterised singly-bridged dinuclear rhenium hydroxo carbonyl complex. Most other dinuclear rhenium hydroxo–alkoxo carbonyl complexes, e.g. $[Re_2(\mu\text{-}OR)_3(CO)_6]^{-}$ (R = H, Me, Et, Ph) [3a,5,14] $[Re_2(\mu\text{-}OH)(\mu\text{-}OPh)_2(CO)_6]^{-}$ and $[Re_2(\mu\text{-}OR)_2(\mu\text{-}PP)(CO)_6]$ [PP = diphosphine or ethylenebis(phosphino) moiety; R = H, Me, Et, Ph] [3,15] are stabilised by three bridges between the Re(I) centres.



Scheme 2.

Each Re(I) centre is octahedrally coordinated to three *fac*-carbonyl ligands, the (μ-OH) group, and one chelating aminoalkoxide/aminoalcohol ligand. The Re(I) octahedra are staggered, and the Re–(μ-O)–Re angle [127.8(1)°] is much larger than those observed in the triply-bridged complexes $[Re_2(\mu\text{-}OR)_3(CO)_6]^{-}$ (ca. 94°) and $[Re_2(\mu\text{-}OR)_2(\mu\text{-}PP)(CO)_6]$ (ca. 104°) [3,15]. The large Re–O–Re angle of **1** may be attributed to the steric repulsion between the rhenium coordination spheres. It is also noteworthy that the sterically demanding aminoalkoxo moieties are both on the exterior of the V-shaped Re(1)–O(7)–Re(2) unit, i.e. only the *syn*, *exo* conformation is observed. Steric factors probably also account for the preference for a hydroxo-, rather than a methoxo-bridge for the Re atoms in complex **1**. The Re(1)–O(7) and Re(2)–O(7) bond lengths [2.164(3) and 2.157(3) Å, respectively] fall within the range observed in $[Re_2(\mu\text{-}OR)_3(CO)_6]^{-}$ and $[Re_2(\mu\text{-}OR)_2(\mu\text{-}PP)(CO)_6]$ complexes (2.14–2.19 Å) [3,15].

Complex **1** can also be described as a *syn* geometrical isomer with respect to the relative positions of the alkoxo oxygen atoms and those of the amino groups. The two {Re–N–C–C–O} rings are arranged such that N(1) is nearly eclipsed with N(2) and O(8) is nearly eclipsed with O(9). In principle, it is possible for a geometrical isomer with N(1)–O(9) eclipsed and N(2)–O(8) eclipsed to exist. The observed configuration for **1** is probably favoured because it facilitates the formation of cyclic hydrogen-bonded dimers (Fig. 2). Virtually all of the dimers persist in solution at room temperature, as

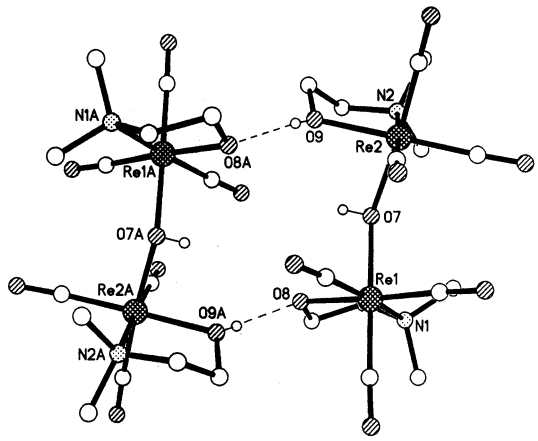


Fig. 2. Hydrogen-bonded dimer of complex **1**.

verified by molecular weight analysis in CH_2Cl_2 solution.

3.3. ^1H NMR spectroscopic studies of complex *1*

The room-temperature ^1H NMR spectrum of **1** shows seven separate signals for the methylene protons and three different signals for the methyl protons. The combination of ^1H–^1H through-bond and through-space interactions, revealed by COSY and NOESY experiments, established that all the above signals are due to protons belonging to the same molecule (Figs. 3 and 4). The NMR results thus indicate, together with the molecular weight measurement results, that the solid-state structure of complex **1** is maintained in solution, and no other stereoisomers of complex **1** are present.

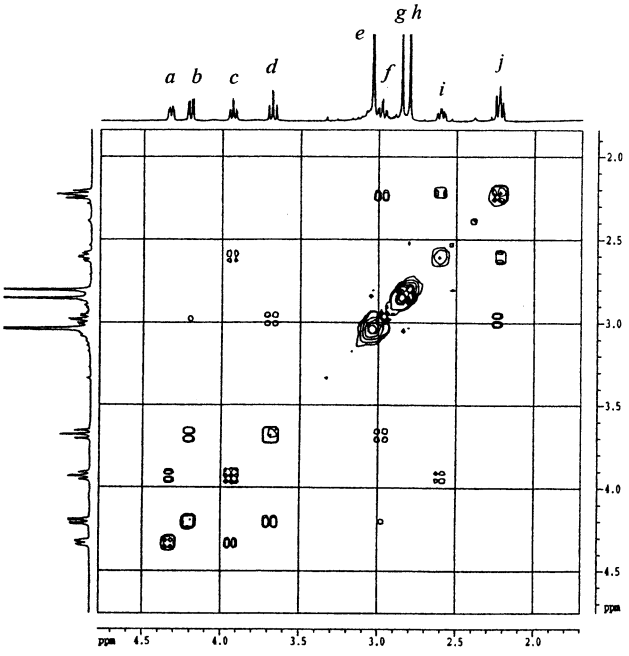


Fig. 3. The ^1H–^1H COSY NMR spectrum (500 MHz, r.t., CD_2Cl_2) of complex **1**. Signal assignments: (a) H(8B), (b) H(12A), (c) H(8A), (d) H(12B), (e) H(10A)–H(10C) and H(13A)–H(13C), (f) H(11B), (g) H(9A)–H(9C), (h) H(14A)–H(14C), (i) H(7A), (j) H(7B) and H(11A).

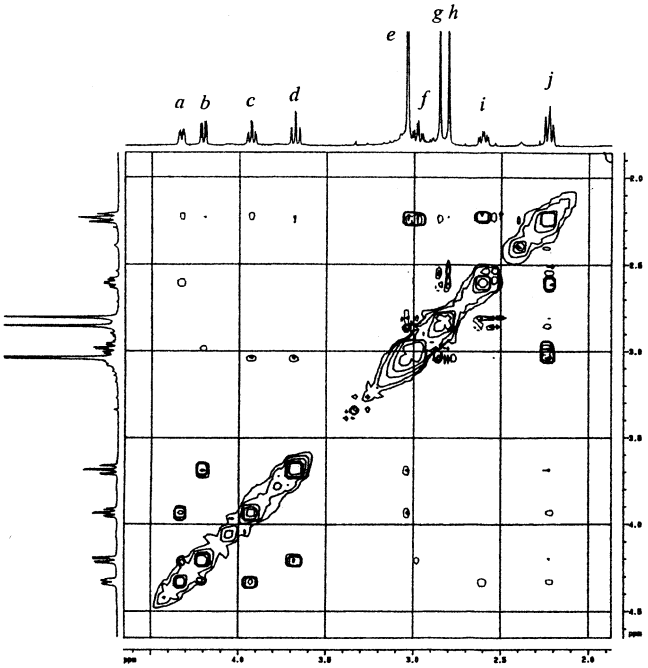
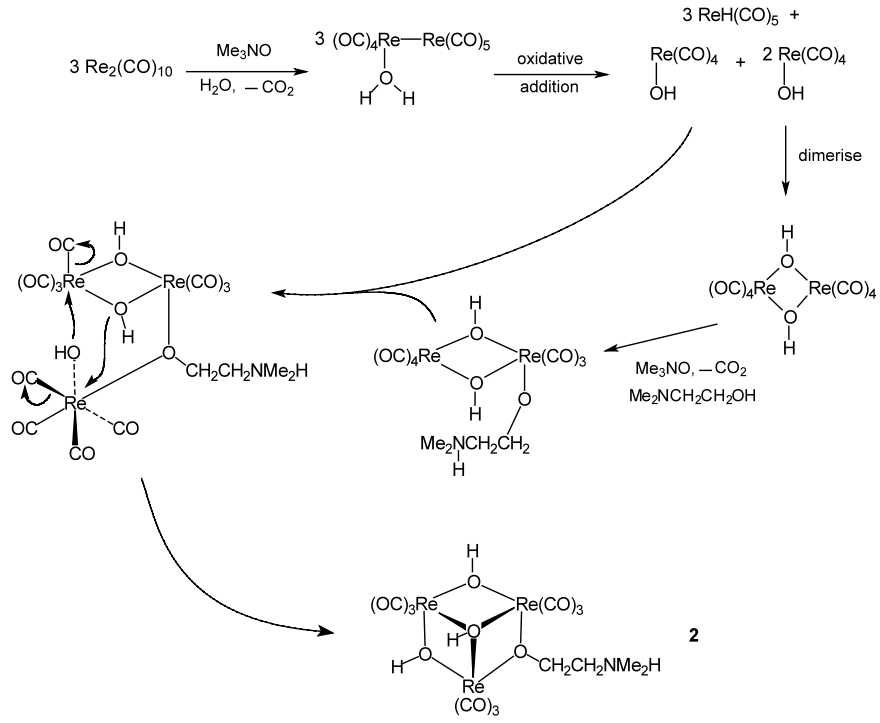


Fig. 4. The ^1H–^1H NOESY NMR spectrum (500 MHz, r.t., CD_2Cl_2) of complex **1**. Signal assignments: (a) H(8B), (b) H(12A), (c) H(8A), (d) H(12B), (e) H(10A)–H(10C) and H(13A)–H(13C), (f) H(11B), (g) H(9A)–H(9C), (h) H(14A)–H(14C), (i) H(7A), (j) H(7B) and H(11A).

3.4. Synthesis of $[Re_3(\mu_3\text{-}OH)(\mu\text{-}OH)_2(\mu\text{-}OCH_2CH_2NMe_2H)(CO)_9]$ (*2*)

Complex **2** was synthesised in similar way as **1**, except MeOH was changed to H_2O. Complex **2** can also be synthesised by the reaction of $[ReBr(CO)_5]$ with $Me_2NCH_2CH_2ONa$ (1:1), followed by recrystallisation from acetone–water mixture. It belongs to the family of $[Re_3(\mu_3\text{-}OR)(\mu\text{-}OR)_3(CO)_9]^-$ complexes (R = H, Me) [2,4]; in this case one of the μ-OR groups is ($OCH_2CH_2NMe_2H$), so the entire molecule is neutral.

The mechanism for the formation of complex **2** by the $[Re_2(CO)_{10}]$ route is proposed in Scheme 3, and is analogous to the mechanism proposed for the formation of the complex $[Re_3(\mu_3\text{-}OMe)(\mu\text{-}OH)_2(\mu\text{-}OMe)(CO)_9]^-$ in the reaction of $[Re_2(CO)_{10}]$ with $Me_3NO\cdot 2H_2O$ and MeOH [4a]. In the reaction of $[ReBr(CO)_5]$ with $Me_2NCH_2CH_2ONa$, displacement of bromide by the aminoalkoxide probably occurs first to generate the intermediate complex $[(OC)_5ReOCH_2CH_2NMe_2]$, which then undergoes hydrolysis and aggregation to form complex **2** during recrystallisation from acetone–water mixture.



Scheme 3.

3.5. Crystal structure of $[Re_3(\mu_3\text{-}OH)(\mu\text{-}OH)_2(\mu\text{-}OCH_2CH_2NMe_2H)(CO)_9]$ (2)

The crystal structure of **2** is depicted in Fig. 5. It contains an Re_3 triangular core held together by one ammonioalkoxo and two hydroxo bridges and face-capped by a hydroxo group. There being no Re–Re bonds, the coordination sphere of each Re atom is completed by three carbonyl ligands.

The hydrogen atom on the ammonio nitrogen (H1A) is involved in intramolecular N–H···O hydrogen-bonding with a bridging OH group. In addition, each of the three OH groups of **2** is hydrogen-bonded to one acetone solvate molecule via an O–H···O linkage.

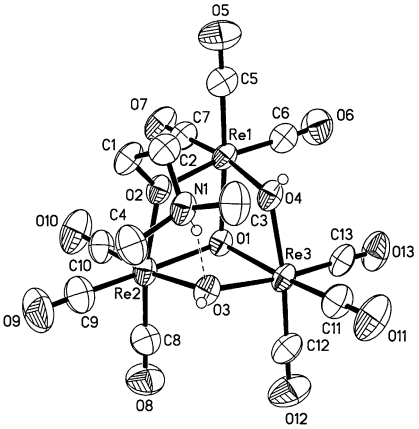


Fig. 5. Crystal structure of $[Re_3(\mu_3\text{-}OH)(\mu\text{-}OH)_2(\mu\text{-}OCH_2CH_2NMe_2H)(CO)_9]$ **2**.

Thus, each molecule of **2** is associated with three acetone solvate molecules exclusive to itself. The structural features of **2** are otherwise similar to those of the analogous $[Re_3(\mu_3\text{-}OR)(\mu\text{-}OR)_3(CO)_9]^-$ complexes (R = H, Me) [2,4].

3.6. Cytotoxicity

Complexes **1** and **2** were generally effective in reducing the growth of the suspended murine and human leukaemias and lymphoma, as well as the HeLa suspended uterine carcinoma cells (Table 4). The compounds were, however, much more selective in inhibiting the growth of tumours derived from human solid cancers. This pattern of cytotoxic activity is similar to that of the rhenium alkoxo complexes $[Re_2(\mu\text{-}OR)_3(CO)_6]^-$ (R = H, Me, Et, Ph), $[Re_2(\mu\text{-}OH)(\mu\text{-}OPh)_2(CO)_6]^-$, $[Re_2(\mu\text{-}OR)_2(\mu\text{-}dppf)(CO)_6]$ [dppf = 1,1′-bis(diphenylphosphino)ferrocene; R = H, Me, Ph] and *fac*-$[Re(OPh)(\eta^2\text{-}dppf)(CO)_3]$ [7]. However, complexes **1** and **2** (average ED_{50} for MCF-7 = 3.36 μg ml^{-1}) show much higher activity against MCF-7 breast cancer cells than the rhenium alkoxo complexes (average ED_{50} for MCF-7 = 9.96 μg ml^{-1}) [7]. Complex **1** is also active against more of the solid tumour cell lines (KB nasopharynx, MCF-7 breast, HCT-8 ileum and SK2 melanoma) than the alkoxo complexes, and complex **2** is especially active against 1-A9 ovary cancer cells.

The compounds $[NBu^n_4][ReO_4]$ and $[NEt_4]_2[ReBr_3(CO)_3]$ were also screened for their cytotoxicity to provide a comparison with complexes **1** and **2**. The

anion $[ReBr_3(CO)_3]^{2-}$ readily hydrolyses in aqueous media [2] to $[Re(H_2O)_3(CO)_3]^+$, which, together with $[ReO_4]^-$, are likely metabolic products of **1** and **2** in cells. It is possible that the cytotoxic activities of **1** and **2** are actually due to their metabolic products rather than the complexes themselves. From Table 4 it can be seen that the compounds $[NBu^n_4][ReO_4]$ and $[NEt_4]_2[ReBr_3(CO)_3]$ were also very active against the suspended cell lines and very selective when it came to the solid tumours. The selectivity patterns of $[NBu^n_4][ReO_4]$ and $[NEt_4]_2[ReBr_3(CO)_3]$ against the solid tumours were, however, quite different from those of **1** and **2**, suggesting that the latter complexes are active on their own.

It is noteworthy that all the compounds tested showed no activity against non-cancerous human fibroblast cells (Table 4). This is an important property for any chemotherapeutic agent since harmful side-effects of the treatment will be minimised.

Whilst it would be premature to draw any definite conclusions on the molecular mechanism responsible for the activity of compounds **1** and **2**, it seems probable that they would bind to DNA bases or side-chains of amino acid residues in peptides and proteins after displacement of the labile ligands, e.g. hydroxide and aminoethanol. It is noteworthy that the related complexes $[Re_2(\mu\text{-}OH)_3(CO)_6]^-$, $[Re_2(\mu\text{-}OH)(\mu\text{-}OPh)_2(CO)_6]^-$, $[Re_2(\mu\text{-}OMe)_2(\mu\text{-}dppf)(CO)_6]$ and $[Re_2(\mu\text{-}OPh)_2(\mu\text{-}dppf)(CO)_6]$ have been shown to interfere with nucleic acid metabolism at multiple enzyme sites in L1210 lymphoid leukaemia cells, and cause DNA strand scission after 60 min incubation [7]. The hydroxo, alkoxo and phenoxo ligands in these complexes have been shown to be labile by electrospray mass spectrometric studies [16]. The lability of the bromide ligands of $[ReBr_3(CO)_3]^{2-}$ is also well-documented [2], and may account for its cytotoxicity by similar arguments.

4. Summary and conclusions

Two new rhenium(I) carbonyl complexes containing the 2-(dimethylamino)ethoxo group, $[Re(\eta^2\text{-}Me_2NCH_2CH_2O)(CO)_3(\mu\text{-}OH)Re(\eta^2\text{-}Me_2NCH_2CH_2OH)(CO)_3]$ (**1**) and $[Re_3(\mu_3\text{-}OH)(\mu\text{-}OH)_2(\mu\text{-}OCH_2CH_2NMe_2H)(CO)_9]$ (**2**), have been synthesised in good yields. The presence of the amino group results in interesting new structural frameworks and hydrogen-bonding motifs exhibited by these complexes. The new complexes also show significant activity against a range of cancer cell lines. Studies on the reactivities of complexes **1** and **2** toward representative Lewis bases, e.g. diphosphines, DNA bases, amino acids, are under way.

5. Supplementary material

Supplementary crystallographic data are available from the CCDC, 12 Union Road, Cambridge CB2 1EZ, UK on request, quoting the deposition numbers 160945 for **1**, and 160946 for **2**. Copies of this information may be obtained free of charge from The Director, CCDC, 12 Union Road, Cambridge, CB2 1EZ, UK (fax: +44-1223-336033; e-mail: deposit@ccdc.cam.ac.uk or www: http://www.ccdc.cam.ac.uk).

Acknowledgements

We thank the National University of Singapore (NUS) and the National Institute of Education, Nanyang Technological University (RP23/98YYK) for financial support. W. W. is grateful to NUS for a scholarship award. We also thank Ms. Geok Kheng Tan for assistance in X-ray crystallography.

References

[1] (a) S.K. Mandal, D.M. Ho, M. Orchin, Organometallics 12 (1993) 1714;
(b) R.G. Bergman, Polyhedron 14 (1995) 3227;
(c) R.D. Simpson, R.G. Bergman, Organometallics 12 (1993) 781;
(d) R.D. Simpson, R.G. Bergman, Organometallics 11 (1992) 4306;
(e) S.K. Mandal, D.M. Ho, M. Orchin, Inorg. Chem. 30 (1991) 2244;
(f) Y.K. Yan, H.S.O. Chan, T.S.A. Hor, K.L. Tan, L.-K. Liu, Y.-S. Wen, J. Chem. Soc., Dalton Trans. (1992) 423;
(g) T.S.A. Hor, C.F. Lam, Y.K. Yan, Bull. Sing. Nat. Inst. Chem. 19 (1991) 115;
(h) S.L. Lam, Y.X. Cui, S.C.F. Au-Yeung, Y.K. Yan, T.S.A. Hor, Inorg. Chem. 33 (1994) 2407;
(i) C.H. Jiang, W. Henderson, T.S.A. Hor, L.J. McCaffrey, Y.K. Yan, J. Chem. Soc., Chem. Commun. (1998) 2029.
[2] R. Alberto, A. Egli, U. Abram, K. Hegetschweiler, V. Gramlich, P.A. Schubiger, J. Chem. Soc., Dalton Trans. (1994) 2815.
[3] (a) C.H. Jiang, Y.-S. Wen, L.-K. Liu, T.S.A. Hor, Y.K. Yan, Organometallics 17 (1998) 173;
(b) P.M.N. Low, Y.L. Yong, Y.K. Yan, T.S.A. Hor, S.-L. Lam, K.K. Chan, C. Wu, S.C.F. Au-Yeung, Y.-S. Wen, L.-K. Liu, Organometallics 15 (1996) 1369.
[4] (a) C.H. Jiang, Y.-S. Wen, L.-K. Liu, T.S.A. Hor, Y.K. Yan, J. Organomet. Chem. 543 (1997) 179;
(b) W.A. Herrmann, D. Mihalios, K. Öfele, P. Kiprof, F. Belmedjahed, Chem. Ber. 125 (1992) 1795.
[5] (a) A.A. Ioganson, B.V. Lokshin, E.E. Kolobova, K.N. Anisimov, J. General Chem. 20 (1974) 20 (translated from Zh. Obshch. Khim. 44 (1974) 23);
(b) A.P. Ginsberg, M.J. Hawkes, J. Am. Chem. Soc. 90 (1968) 5930;
(c) G. Ciani, G. D'Alfonso, M. Freni, P. Romiti, A. Sironi, J. Organomet. Chem. 152 (1978) 85;
(d) M. Freni, P. Romiti, Atti Accad. Naz. Lincei, Mem. Cl. Sci. Fis. Mat. Nat. Rend. 55 (1973) 515;
(e) G. Ciani, A. Sironi, Gazz. Chim. Ital. 109 (1979) 615.

[6] W.A. Herrmann, A. Egli, E. Herdtweck, R. Alberto, F. Baumgärtner, Angew. Chem., Int. Ed. Engl. 35 (1996) 432.
[7] Y.-K. Yan, S.E. Cho, K.A. Shaffer, J.E. Rowell, B.J. Barnes, I.H. Hall, Pharmazie 55 (2000) 307.
[8] (a) V.G. Albano, P.L. Bellon, M. Sansoni, J. Chem. Soc. A (1971) 2420;
(b) R.J. Angelici, A.E. Kruse, J. Organomet. Chem. 22 (1970) 461.
[9] G.M. Sheldrick, SADABS, Program for Siemens Area Detector Absorption Correction, University of Göttingen, Germany, 1996.
[10] G.M. Sheldrick, SHELXTL PC, Version 5.03, Siemens Analytical X-ray Instruments Inc., Madison, WI (USA), 1994.
[11] R.I. Geran, N.H. Greenberg, M.M. MacDonald, A.M. Schumacher, B.J. Abbott, Cancer Chemother. Rep. Part 3, 3 (1972) 7.
[12] A.L. Leibovitz, J.C. Stinson, W.B. McComb, III, C.E. McCoy, K.C. Mazur, N.D. Mabry, Cancer Res. 36 (1976) 4562.
[13] Y.-K. Yan, W. Koh, C. Jiang, W.K. Leong, T.S.A. Hor, Polyhedron 19 (2000) 641.
[14] T. Beringhelli, G. Ciani, G. D'Alfonso, A. Sironi, M. Freni, J. Chem. Soc., Dalton Trans. (1985) 1507.
[15] C. Jiang, Y.-S. Wen, L.-K. Liu, T.S.A. Hor, Y.K. Yan, J. Organomet. Chem. 590 (1999) 138.
[16] (a) C. Jiang, T.S.A. Hor, Y.K. Yan, W. Henderson, L.J. McCaffrey, J. Chem. Soc., Dalton Trans. (2000) 3197;
(b) C. Jiang, T.S.A. Hor, Y.K. Yan, W. Henderson, L.J. McCaffrey, J. Chem. Soc., Dalton Trans. (2000) 3204.

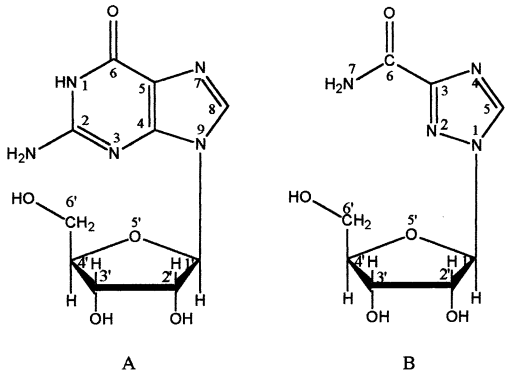


Fig. 1. IUPAC numbering schemes of: (A) guanosine; and (B) ribavirin.

The purpose of the presented work was to isolate new Pt(II) compounds which show similar activity to cisplatin and carboplatin, but have an additional functional group which can be linked to a carrier substances. Therefore, our research was focused on complexes bearing the ribavirin and dmso ligand, which is expected to improve water solubility of the complex and might influence better diffusion through membranes. To the best of our knowledge, it is the first report on mixed Pt(II) complexes with an antiviral agent (1-β-D-ribofuranosyl-1,2,4-triazole-3-carboxamide) and dmso.

2. Experimental

2.1. Chemicals

Dipotassium tetrachloroplatinum(II) and dmso were purchased from Aldrich, and the inorganic salts of analytical grade from POCh Gliwice (Poland). Ribavirin was obtained according to the reported method [13], while *cis*-$[PtCl_2(dmso)_2]$ was prepared from the reaction of K_2PtCl_4 in aq. solution and dmso [22].

2.2. Instrumentation

IR spectra were obtained with a Perkin–Elmer 2000 FTIR spectrometer using KBr discs for the 400–4000 cm^{-1} range and polyethylene ones for 100–400 cm^{-1}. ^1H, ^{13}C, ^{195}Pt and ^{15}N–^1H NMR HETCOR spectra were detected on a Bruker DRX 500 spectrometer, in the latter case by Gradient Heteronuclear Single-Quantum Coherence. Samples were dissolved in dmf-d_7; the concentration of samples were 0.01 M for ^1H, ^{13}C, ^{195}Pt and 0.1 M for ^{15}N, the temperature was 295 K. The reference standard was TMS (internal) for ^1H or ^{13}C and CH_3NO_2 (external) for ^{15}N. ^{195}Pt chemical shifts were referenced relative to an external sample of 0.1 M K_2PtCl_4 in D_2O ($\delta = -1624$ ppm). C, H, N contents were determined by semimicroanalysis, whereas platinum was determined by a spectrophotometric method on a Specord M40 Carl Zeiss Jena ($\lambda = 400$ nm).

2.3. Synthesis

2.3.1. Preparation of Pt(II) complexes

A suspension of *cis*-$[PtCl_2(dmso)_2]$ (0.222 g; 0.53 mmol) in MeOH 15 ml was treated with the stoichiometric amount of ribavirin (0.129 g; 0.53 mmol) dissolved in 20 ml MeOH–water (1:1) solution, stirred at room temperature for 1 day and filtered. The filtrate was left for crystallisation and after 3 days white crystals of the complex precipitates, which were washed with C_3H_6O, Et_2O and dried in vacuum over P_2O_5. The results of elemental analyses for **1** were (% Calc./Found): Pt (34.2/33.9), C (20.7/20.7), N (9.7/9.2), H (3.7/3.7). Yield: 73%.

By slow crystallisation from water–MeOH mixture (1:1) white crystals of **1** and **2** suitable for X-ray structure analysis were obtained.

2.4. Crystal data

Two different crystals of $[PtCl(dmso)(N^4N^7\text{-rib})]\cdot H_2O$ (**1**) and $[PtCl(dmso)(N^4N^7\text{-rib})]\cdot 2H_2O$ (**2**) were selected after examination under a microscope. The X-ray measurements were carried out for a $0.10 \times 0.10 \times 0.15$ mm crystal of **1** with a Kuma KM-4 CCD diffractometer using graphite-monochromated Mo Kα radiation at 293 K. Ten thousand one hundred and twenty-five reflections were collected for the θ range 2.75°–26°. Data reduction and analysis were carried out with the Kuma Diffraction (Wroclaw) programs. The reflection data for **2** were collected in the range 3.23°–25° on the same diffractometer (Mo Kα radiation) at 100 K. No absorption correction was applied. Both structures were solved by heavy-atom methods (program SHELXS-97 [23]) and refined by the full-matrix least-squares method on all F^2 data using the SHELXL-97 programs [24]. Non-hydrogen atoms were refined with anisotropic thermal parameters. The crystallographic data for **1** and **2** are listed in Table 1.

3. Results and discussion

3.1. Discussion of the crystal structure

Selected bond distances and angles for **1** and **2** are listed in Table 2. The molecular geometry of **1** and **2** with the atom numbering scheme are presented in Figs. 2 and 3. Both complexes revealed square-planar coordination geometry for Pt atoms.

The coordination sites in **1** and **2** are occupied by one chloride atom, the sulfur atom of dmso, N(4) nitrogen of the triazole ring and N(7) nitrogen of the deproto-

Table 1
Crystallographic data for compounds **1** and **2**

Formula	$C_{10}H_{17}ClN_4O_6PtS\cdot H_2O$	$C_{10}H_{17}ClN_4O_6PtS\cdot 2H_2O$
Formula weight	569.89	587.91
Crystal system	orthorhombic	orthorhombic
Space group	$P2_12_12_1$	$P2_12_12_1$
a (Å)	7.681(2)	6.593(2)
b (Å)	11.052(2)	12.464(2)
c (Å)	19.960(4)	21.821(4)
V (Å^3)	1694.4(6)	1793.1(7)
Z	4	4
D_{calc} (Mg m^{-3})	2.234	2.178
Index ranges	$-6 \le h \le -9$; $-13 \le k \le -13$; $-24 \le l \le -24$	$-4 \le h \le -7$; $-14 \le k \le -14$; $-25 \le l \le -25$
Reflections measured (total)	10 125	9465
Reflections measured (unique)	3285	3084
Observations [$I > 2\sigma(I)$]	3274	3036
R	0.021	0.038
R_w	0.054	0.092

nated carboxamide group. The structures of **1** and **2** demonstrate distortions from the square geometry with N–Pt–N a chelate angle of 79.2(2)° and 80.0(2)°, respectively. The remaining X–Pt–Y angles are greater than 90°, being of 96.3° (**1**) and 97.3° (**2**) for N(4)–Pt–S due to the bulky dmso ligand. The sulfur atoms in dmso ligands are in an approximate tetrahedral environment. The Pt–S–O angles of 117.0(2)° for **1** and 115.9(3)° for **2** are larger than Pt–S–C (109.1°–111.6°) in comparison to the values observed in other Pt–dmso complexes [26]. The S=O length for **2** 1.493(7) Å is appreciably longer compared to 1.468(4) Å in **1**. It may be supposed that this difference is closely associated with the O(3′)-H(3′)···O(3) = S$^{(i)}$ hydrogen bond in the crystal structure of **2**. The Pt–N(7) bond distance (2.041(4) Å) in **1** appears to be significantly longer than the Pt–N(4) bond distance of 2.009(4) Å. On the other hand in **2** the analogous bond distances are almost the same (2.032(7), 2.2028(7)). This discrepancy can be related to the hydrogen bond interaction N(7)–H(7)···O(1) in **1**. The bond distances and angles of the coordinated 1-β-D-ribofuranosyl-1,2,4-triazole-3-carboxamide are similar to those found in two crystalline forms of ribavirin [27] and in a Cu(II) complex [15], except the internal ring angles centred at N(4), C(3) and C(5). These angles are larger at N(4) and smaller at C(3) and C(5) in both **1** and **2** as compared to the neutral ligand [27], most probably due to the metallation at N(4). The geometry of carboxamide group is also affected by deprotonation

Table 2
Selected bond lengths (Å) and angles (°) for complexes **1** and **2**

Bond lengths		
Pt–N(4)	2.009(4)	2.032(7)
Pt–N(7)	2.041(4)	2.028(7)
Pt–S	2.218(1)	2.212(2)
Pt–Cl	2.304(1)	2.290(2)
S–O	1.468(4)	1.493(7)
S–C(7)	1.768(5)	1.774(9)
S–C(8)	1.776(5)	1.778(8)
O(6)–C(6)	1.250(6)	1.250(11)
O(2′)–C(2′)	1.410(6)	1.417(10)
O(3′)–C(3′)	1.417(5)	1.421(10)
O(5′)–C(1′)	1.411(6)	1.410(10)
O(5′)–C(4′)	1.458(5)	1.452(10)
O(6′)–C(6′)	1.423(6)	1.426(10)
N(1)–C(5)	1.314(6)	1.324(11)
N(1)–N(2)	1.373(6)	1.375(10)
N(2)–C(3)	1.316(7)	1.344(11)
N(2)–C(1′)	1.495(6)	1.460(10)
N(4)–C(3)	1.326(6)	1.319(11)
N(4)–C(5)	1.357(6)	1.357(10)
N(7)–C(6)	1.321(6)	1.334(11)
C(5)–C(6)	1.497(6)	1.494(11)
C(1′)–C(2′)	1.521(6)	1.551(10)
C(2′)–C(3′)	1.536(6)	1.545(11)
C(3′)–C(4′)	1.533(6)	1.535(11)
C(4′)–C(6′)	1.509(7)	1.528(12)
Bond angles		
N(4)–Pt–N(7)	79.2(2)	80.0(2)
N(4)–Pt–S	96.3(1)	97.3(2)
N(7)–Pt–S	175.4(1)	176.7(2)
N(4)–Pt–Cl	172.7(1)	171.2(2)
N(7)–Pt–Cl	93.5(1)	91.2(2)
S–Pt–Cl	91.04(4)	91.47(8)
O–S–C(7)	108.3(2)	108.7(4)
O–S–C(8)	108.9(3)	108.4(4)
C(7)–S–C(8)	101.7(3)	102.2(4)
O–S–Pt	117.0(2)	115.9(3)
C(7)–S–Pt	109.9(2)	111.6(3)
C(8)–S–Pt	110.0(2)	109.1(3)
C(1′)–O(5′)–C(4′)	110.5(3)	110.3(6)
C(5)–N(1)–N(2)	101.6(4)	103.1(6)
C(3)–N(2)–N(1)	112.4(4)	110.4(7)
C(3)–N(2)–C(1′)	128.0(4)	129.7(8)
N(1)–N(2)–C(1′)	119.2(4)	119.8(6)
C(3)–N(4)–C(5)	105.7(4)	106.4(7)
C(3)–N(4)–Pt	140.1(3)	140.6(6)
C(5)–N(4)–Pt	114.1(3)	112.7(5)
C(6)–N(7)–Pt	119.0(3)	118.2(5)
N(1)–C(5)–N(4)	113.2(4)	112.3(7)
N(1)–C(5)–C(6)	129.0(4)	129.1(7)
N(4)–C(5)–C(6)	117.8(4)	118.5(7)
O(6)–C(6)–N(7)	129.1(4)	129.5(8)
O(6)–C(6)–C(5)	120.9(4)	119.9(8)
N(7)–C(6)–C(5)	110.0(4)	110.6(7)
O(5′)–C(1′)–N(2)	106.6(4)	107.7(7)
O(5′)–C(1′)–C(2′)	107.7(4)	107.4(6)
N(2)–C(1′)–C(2′)	112.6(4)	112.8(7)
O(2′)–C(2′)–C(1′)	105.4(4)	107.2(7)
O(2′)–C(2′)–C(3′)	113.9(4)	110.8(6)
C(1′)–C(2′)–C(3′)	100.6(4)	100.7(6)
O(3′)–C(3′)–C(4′)	112.8(4)	113.3(7)
O(3′)–C(3′)–C(2′)	114.6(4)	113.1(7)
C(4′)–C(3′)–C(2′)	103.0(4)	101.3(7)

Table 2 (*Continued*)

Bond angles		
O(5′)–C(4′)–C(6′)	109.1(4)	108.8(7)
O(5′)–C(4′)–C(3′)	104.0(3)	103.3(7)
C(6′)–C(4′)–C(3′)	114.3(4)	114.4(8)
O(6′)–C(6′)–C(4′)	108.8(4)	111.8(7)

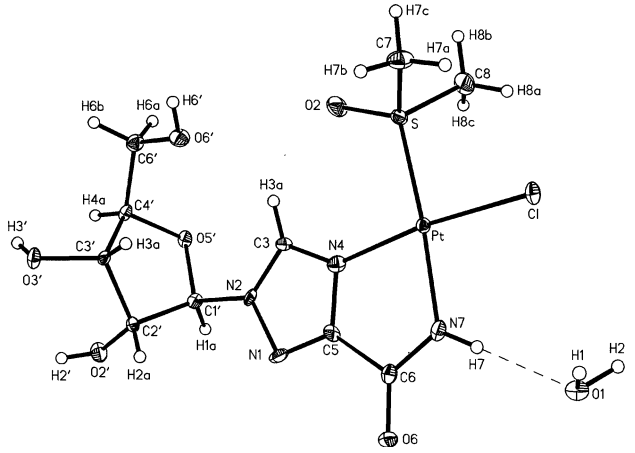


Fig. 2. The ORTEP [25] drawing of [PtCl(dmso)(N^4N^7-rib)]·H_2O (**1**).

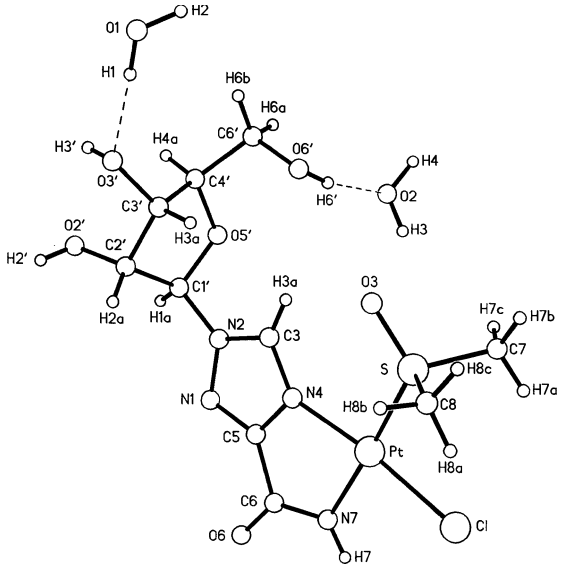


Fig. 3. The ORTEP [25] drawing of [PtCl(dmso)(N^4N^7-rib)]·$2H_2O$ (**2**).

and coordination. While forming the chelate ring, the N(7)–C(6)–C(5) angle decreases from 116.0° and 116.8° for two forms of free ribavirin [27] to 110.0° in **1** and 110.6° in **2**. Similarly, the N(4)–C(5)–C(6) angle decreases from 121.2° and 122.1° in the uncoordinated ligand to 117.8° and 118.5° for **1** and **2**, respectively, whereas the C(5)–C(6)–O(6) angle is almost unaffected. The glycosidic torsion angle χ defined by O(1′)–C(1′)–N(1)–C(5) is 2.0(6)° (**1**) and 39.5(1)° (**2**) compared to 10.4° and 119.0° in ribavirin [27] and −112.6° in the Cu(II) complex [15]. These differences are considered to arise from intermolecular interactions rather than the metal ion influence. The crystal packing is formed through the three-dimensional hydrogen bond network. The intermolecular hydrogen bonding networks in both structures are extensive (Figs. 4 and 5). Specifically in **2** almost all possible sites on the Pt complex are involved in hydrogen bonding, e.g. each of the hydroxy groups of the sugar moiety act both as donor and acceptor. On the other hand in **1** the monohydrate water molecule forms bridges between four symmetry-related complex molecules. A detailed geometry of all hydrogen bonds in the two crystal structures is presented in Table 3.

3.2. NMR results

All the measurements were performed in dmf-d_7, due to the poor solubility or decomposition reaction of the Pt(II) complex in other solvents (dmso-d_6, acetone-d_6, D_2O). When [PtCl(rib)(dmso)] was left for 1 h in dmso-d_6, ribavirin was displaced by the solvent because of the strong trans-labilizing effect of the sulfur ligands. The assignment of signals for both ligand and complex was based on the heteronuclear correlation technique (HETCOR). For NMR analysis we used IUPAC numbering schemes of ribavirin (Fig. 1(B)).

The ^1H, ^{13}C, ^{15}N and ^{195}Pt NMR data of [PtCl(dmso)(N^4N^7-rib)]·H_2O (**1**) are listed in Tables 4–6.

The signal of H(5) was detected at 8.94, whereas $N(7)H_2$ protons in the free ribavirin spectrum appear at 7.86 and 7.60 ppm as singlets due to the interaction with the oxygen atom from carboxy. Ribose protons (H(1′)–H(4′) and H(5′)) in the free ligand have been observed as multiplets in the range 5.95–3.73 ppm (Table 4).

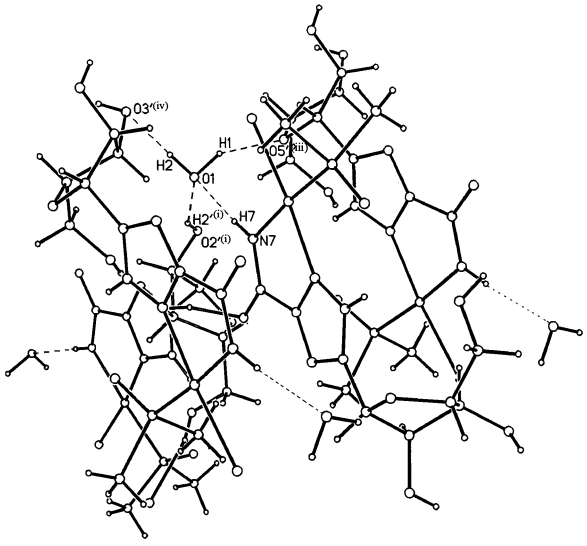


Fig. 4. Drawing of **1** showing hydrogen bonds between H_2O and four neighbouring molecules. Symmetry codes: (i) $-x+0.5, -y+1, z-0.5$; (iii) $x-0.5, -y+0.5, -z+1$; (iv) $x+0.5, -y+0.5, -z+1$.

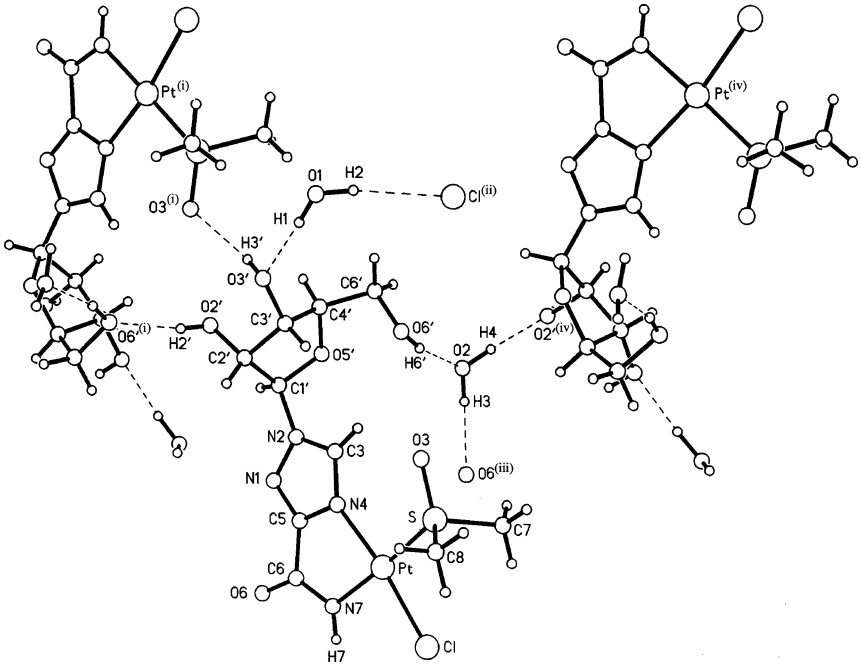


Fig. 5. System of three-dimensional hydrogen bonds in **2**. Symmetry codes: (i) $-x+1,\ y+0.5,\ -z-0.5$; (ii) $-x+0.5,\ -y,\ z-0.5$; (iii) $x-0.5,\ -y+0.5,\ -z$; (iv) $-x,\ y-0.5,\ -z-0.5$.

Table 3
Hydrogen bonds (Å, °) in **1** and **2**

D–H···A	D–H	H···A	D···A	<(D–H···A)
Compound **1**				
O(2′)–H(2′)···O(1)^{i}	0.82	1.99	2.718(5)	146.8
O(3′)–H(3′)···O(6)^{i}	0.82	1.85	2.653(5)	166.5
O(6′)–H(6′)···O(3′)^{ii}	0.82	1.98	2.796(5)	161.2
N(7)–H(7)···O(1)	0.86	2.19	3.047(5)	175.2
O(1)–H(1)···O(5′)^{iii}	1.03	1.85	2.790(5)	149.0
O(1)–H(2)···O(3′)^{iv}	0.98	1.90	2.870(5)	171.6
Compound **2**				
O(2′)–H(2′)···O(6′)^{i}	0.82	1.84	2.636(8)	162.2
O(3′)–H(3′)···O(3)^{i}	0.82	2.06	2.827(9)	156.6
O(6′)–H(6′)···O(2)	0.82	1.87	2.669(9)	165.6
O(1)–H(1)···O(3′)	0.96	1.92	2.879(11)	174.9
O(1)–H(2)···Cl^{ii}	0.93	2.75	3.656(9)	163.8
O(2)–H(3)···O(6)^{iii}	0.86	1.88	2.738(9)	176.8
O(2)–H(4)···O(2′)^{iv}	0.94	1.83	2.767(9)	176.8

Symmetry codes for **1**: (i) $-x+0.5,\ -y+1,\ z+0.5$; (ii) $-x,\ y-0.5,\ z+1.5$; (iii) $x-0.5,\ -y+0.5,\ -z+1$; (iv) $x+0.5,\ -y+0.5,\ -z+1$. Symmetry codes for **2**: (i) $-x+1,\ y+0.5,\ -z-0.5$; (ii) $-x+0.5,\ -y,\ z-0.5$; (iii) $x-0.5,\ -y+0.5,\ -z$; (iv) $-x,\ y-0.5,\ -z-0.5$.

Protons H(5) and N(7)H_2 are sensitive to the nature of the complex, hence coordination of ribavirin caused significant shift of the free ligand signals, H(5) (+0.55 ppm), N(7)H (−1.42 ppm) or (−1.16) (Table 4). The upfield shift of N(7)H can be related to the deprotonation of the carboxamide group and coordination to the Pt(II) ion. The magnitude of N(7)H and H(5) coordination shifts comes out from the close proximity of these protons to the central ion linked via N(4) and N(7). Metallation of ribavirin by Pt(II) ions also results in downfield shifts of the ribose protons signals, which can be related to the lower negative charge on the hydrogen atoms (Table 4). Resonances of CH_3 groups in dmso molecules appeared at 3.56 ppm, which is typical for the sulfur-bonded ligands [28]. It is noteworthy that no $^{195}Pt\{^{1}H\}$ spin–spin interaction has been detected.

Upon coordination, the resonances of C(3) and C(5) are shifted upfield (−0.4, −2.4 ppm) which can be related to the charge increase in the heterocyclic ring. This can be rationalised as a result of π-back donation from the Pt(II) d^8 electron system to the unsaturated heterocyclic ring. The downfield shift (+2.8 ppm) of

Table 4
Selected ^{1}H NMR spectral data (in ppm)

Compound	H(5)	N(7)H_2	H(1′)	H(2′)	H(3′)	H(4′)	H(6′)
Ribavirin	8.94	7.86; 7.60	5.95	4.55	4.35	4.10	3.73
1	9.49	6.44	6.13	4.57	4.36	4.14	3.74
Δ	+0.55	−1.42; −1.16	+0.18	+0.02	+0.01	+0.04	+0.01

$\Delta = \delta_{complex} - \delta_{ribavirin}$.

Table 5
^{13}C NMR data (in ppm)

Compound	C(6)	C(3)	C(5)	C(1′)	C(2′)	C(3′)	C(4′)	dmso
Ribavirin	161.3	158.4	145.5	93.3	76.0	71.3	86.8	
1	164.1	158.0	143.1	94.8	76.0	71.0	87.2	44.0
Δ	+2.8	−0.4	−2.4	+1.5	0	−0.3	+0.4	

$\Delta = \delta_{complex} - \delta_{ribavirin}$.

Table 6
^{15}N NMR data

Compound	N(1)	N(2)	N(4)	N(7)
Ribavirin	−149.7	−85.4	−128.6	−280.4
1	−151.3	−89.8	−221.3	−262.0
Δ	−1.6	−4.4	−92.7	+18.4

$\Delta = \delta_{complex} - \delta_{ribavirin}$.

C(6) can be related to the σ electron withdrawal upon NH coordination. In ^{13}C NMR the largest coordination shifts were observed at carbon atoms which are in close proximity to the coordination centre (Table 5), which is in favour of coordination via N(4), N(7) atoms.

^{15}N resonances are very useful in determination of coordination sites of heterocyclic rings [29–32], however in the case of this ligand, the assignment is not straightforward. In order to determine the coordination sites of ribavirin, we have measured ^{15}N–^{1}H HETCOR spectra of the free ligand and **1**.

The ^{15}N NMR data and assignment for the ligands and complex **1** are collected in Table 6. From the magnitude of the coordination shift (Δ), it is evident that the Pt(II) linkage affects most significantly N(4) and N(7) resonances which are shifted upfield approximately 92.7 ppm and downfield 18.4 ppm, respectively. The downfield shift of the N(7) signal can be caused by two simultaneous effects i.e. coordination and deprotonation of the carboxamide group. Hence we can unambiguously indicate that the complexation occurs via these nitrogen atoms in solution.

The ^{195}Pt resonance of **1** was observed at −3103 ppm. This value is very close to that reported in the literature for *cis*-[PtCl(Xpy)$_2$(dmso)] where Xpy = 2-, 2,5-, 2,6-halogenopyridines, (−2876– −3042 ppm) [33]. This range is characteristic for the square-planar Pt(II) complexes in which two adjacent corners are occupied by two nitrogen atoms and the other positions by dmso and chloride. A spectrum of **1** exhibits ^{195} Pt resonances shifted downfield 373 ppm in relation to the starting platinum complex, *cis*-[PtCl$_2$(dmso)$_2$]. The downfield coordination shift can be explained by the charge displacement from (σ-donation) ribavirin to the metal centre caused by Pt–N bond formation. The ^{195}Pt signals of **1** have been detected as broad singlets, their half-line widths being approximately 460 Hz. Such values are relatively high, compared to those found for $[PtCl_4]^{2-}$ ions (approximately 110 Hz) [34], which most likely can be related to the quadrupolar interactions between ^{195}Pt and ^{14}N nuclei.

3.3. IR spectroscopy

Absorption bands of ribavirin in the spectra of **1** are affected by coordination. The characteristic band of νC=O vibration appeared at 1639 cm^{-1}, whereas NH vibration at 1620 cm^{-1}. In a spectrum of the free ligand the former band was found at 1658 and 1625 cm^{-1}. The frequencies of the ribavirin absorption band is shifted approximately 19 cm^{-1} towards lower frequencies upon coordination in comparison to the spectrum of free ribavirin. The sharp absorption band at 1130 cm^{-1} indicates S-bonded dmso, as reported for this soft coordination centre [35,36]. The spectrum of **1** has exhibited one new strong absorption band at 347 cm^{-1}. A similar frequency was detected in the spectra of Pt(II) with ammonia, pyridine (py) or imidazole (imH) [37], where it was assigned to a Pt–Cl stretching vibration.

4. Conclusion

Presented results of X-ray and spectral analyses revealed the same coordination site (N(4), N(7)) of ribavirin both in the solid state and dmf-d_7 solution. The crystal structure of **1** and **2** indicates that the Pt(II) ions have the square-planar geometry with chelating bonded ribavirin (N(4), N(7)), S-bonded dmso and chloride anion. The way of ribavirin bonding is different from described carboxamide analogs where the majority of the complexes revealed Pt(II) bonded via N, O atoms. An extensive intermolecular hydrogen bond network is evident in both hydrates. The coordination sphere of **1** is stable only in dmf solution which allows NMR studies.

5. Supplementary material

Crystallographic data for the structural analysis have been deposited with the Cambridge Crystallographic

Data Centre, CCDC Nos. 168127 and 168128 for compounds **1** and **2**, respectively. Copies of this information may be obtained free of charge from The Director, CCDC, 12 Union Road, Cambridge, CB2 1EZ, UK (fax: +44-1223-336033; e-mail: deposit@ccdc.cam.ac.uk or www: http://www.ccdc.cam.ac.uk).

Acknowledgements

The support of COST programs (COST action D8; project D8/002/97) is gratefully acknowledged.

References

[1] B. Lippert, Cisplatin, in: Chemistry and Biochemistry of a Leading Anticancer Drug, Wiley-VCH, Weinheim, 1999, pp. 405–428.
[2] F. Reeder, Z. Guo, P. Murdoch, A. Corazza, T.W. Hambley, S.J. Berners-Price, J.C. Chottard, P.J. Sadler, Eur. J. Biochem. 249 (1997) 370.
[3] H. Sigel, Chem. Soc. Rev. (1993) 255.
[4] H. Sigel, S.S. Massand, N.A. Corfu, J. Am. Chem. Soc. 116 (1994) 2958.
[5] B. Lippert, Coord. Chem. Rev. 182 (1999) 263.
[6] P.J. Loeher, L.H. Einhorn, Ann. Intern. Med. 100 (1984) 704.
[7] S.L. Bruhn, J.H. Toney, S.J. Lippard, Bioinorg. Chem. 38 (1991) 478.
[8] S. Shamusuddin, I. Takahashi, Z.H. Siddik, A.R.J. Khokhar, Inorg. Biochem. 61 (1996) 291.
[9] L.S. Hollis, A.R. Amundsen, E.W. Stern, J. Med. Chem. 32 (1989) 128.
[10] P.J. Sadler, Z. Guo, Pure Appl. Chem. 70 (1998) 863.
[11] G.M. Dusheiko, Antiviral Res. 29 (1996) 77.
[12] R. Storer, C.J. Ashton, A.D. Baxter, M.M. Hann, Nucl. Nucl. 18 (1999) 203.
[13] J.T. Witkowski, R.K. Robins, R.W. Sidwell, L.N. Simon, J. Med. Chem. 15 (1972) 1150.
[14] J. Lee, M. Wagner, W.K. Roth, G. Teuber, Ch. Sarrazin, S. Zuuzem, J. Hematol. 29 (1998) 29.
[15] P. Bukovec, L. Golic, B. Orel, J. Kobe, J. Carb. Nucls. Nuclt. 8 (1981) 1.
[16] T. Komorita, J. Hidaka, Y. Shimura, Bull. Chem. Soc. Jpn. 52 (1979) 1832.
[17] Y. Ilan, M. Kapon, Inorg. Chem. 25 (1986) 2350.
[18] T. Komorita, A. Fuyuhiro, K. Tanimoto, K. Yamauchi, K. Fujita, Bull. Chem. Soc. Jpn. 68 (1995) 1593.
[19] T.G. Appleton, J.R. Hall, T.W. Hambley, P.D. Prenzeler, Inorg. Chem. 29 (1990) 3562.
[20] F.D. Rochon, R. Boughzala, R. Melanson, Can. J. Chem. 70 (1992) 2476.
[21] F.D. Rochon, R.C. Kong, R. Melanson, Inorg. Chem 29 (1990) 1352.
[22] Y.N. Kukuszkin, Y.E. Vyaznenskii, L.I. Zorina, Russ. J. Inorg. Chem. 13 (1958) 1573.
[23] G.M. Sheldrick, Acta. Crystallogr., Sect. B 37 (1990) 467.
[24] G.M. Sheldrick, SHELXS-93, Program for Refinement of Crystal Structures, University of Göttingen, Göttingen, Germany, 1994.
[25] C.K. Johnson, ORTEP II, Report ORNL-5138, Oak Ridge National Laboratory, Oak Ridge, TN, 1976.
[26] L.I. Elding, A. Oskarsson, Inorg. Chim. Acta 130 (1987) 209.
[27] P. Prusiner, M. Sundaralingam, Acta Crystallogr., Sect. B 32 (1976) 419.
[28] O. Clement, A.W. Roszak, E. Buncel, Inorg. Chim. Acta 253 (1996) 53.
[29] E. Sz(yk, I. (akomska, A. Surdykowski, T. G(owiak, L. Pazderski, J. Sitkowski, L. Kozerski, Inorg. Chim. Acta 333 (2002) 93.
[30] M.C. Cox, K.J. Barnham, T.A. Frenkiel, J.D. Hoeschele, A.B. Mason, Q. He, R.C. Woodworth, P.J. Sadler, J. Bioinor. Chem. 4 (1999) 621.
[31] M. Galanski, B.K. Keppler, Inorg. Chim. Acta 300–302 (2000) 783.
[32] E. Szłyk, I. Łakomska, Polyhedron 24 (1992) 3147.
[33] L.G. Marzilli, Y. Hayden, M.D. Reily, Inorg. Chem. 25 (1998) 974.
[34] J.J. Pesek, W.R. Mason, J. Magn. Res. 25 (1977) 519.
[35] A. Cornia, A.C. Fabretti, M. Bonivento, L. Cattalini, Inorg. Chim. Acta 255 (1997) 405.
[36] F.A. Cotton, R. Francis, W.D. Horrocks, J. Phys. Chem. 64 (1960) 1534.
[37] K. Nakamoto, Infrared and Raman Spectra of Inorganic and Coordination Chemistry, Wiley, New York, 1997, p. 24.

could be found that present its synthesis by chemical methods, using different precursors. Niobium ammonium oxalate, $(NH_4)H_2[NbO(C_2O_4)_3]\cdot 3H_2O$, was used in the synthesis of fine $NaNbO_3$ powders by the Pechini method [8,9], and by thermal decomposition of a precursor obtained through solvent evaporation [10]. Kinomura et al. have prepared $NaNbO_3$ by hydrothermal reaction of $Na_8[Nb_6O_{19}]\cdot 13H_2O$ with NaOH and found a new metastable phase with ilmenite-type structure, that was obtained pure in a very narrow temperature and concentration region [11]. Also, $NaNbO_3$ has been obtained by evaporation of a solution of $Na_7H[Nb_6O_{19}]$ under a CO_2 atmosphere [12]. An old report states that crystals of $NaNbO_3$ were obtained by boiling a suspension of Nb_2O_5 in NaOH for about 20 min, but no synthetic details were provided [13]. To our knowledge, no report referring the synthesis of $NaNbO_3$ by hydrothermal reaction of Nb_2O_5 with NaOH has been published.

The synthesis of $KNbO_3$ through the hydrothermal reaction of Nb_2O_5 with KOH has already been reported [14,15]. Depending on the KOH concentration and temperature, that reaction may provide $KNbO_3$, $K_4Nb_{16}O_{17}\cdot 3H_2O$ or complete dissolution of the initial niobium oxide [14,15]. These studies were mainly concerned with the synthesis of the oxides and the dissolution of Nb_2O_5 in the alkaline solutions was only briefly mentioned.

Potassium hexaniobates of general formula $K_{8-x}H_x[Nb_6O_{19}]\cdot nH_2O$, $x = 0$–3, have been prepared before and some spectroscopic data has been published [6,16]. They are usually obtained by crystallization or precipitation from aqueous alkaline solutions of Nb(V) with pH 9–14 [16–19].

We report here the hydrothermal synthesis of microcrystalline, single phase $NaNbO_3$ through the reaction of commercial Nb_2O_5 with NaOH, at 200 °C. Different concentrations and NaOH:Nb_2O_5 molar relations were examined. In the conditions used for the synthesis of $NaNbO_3$, the use of KOH in place of NaOH leads to solubilization of the initial Nb_2O_5. From these solutions, solids like $K_6H_2[Nb_6O_{19}]\cdot 13H_2O$ or niobic acid were obtained. This procedure allows, thus, preparation of alkaline solutions of Nb(V) without need of the cumbersome technique of fusion of mixtures of Nb_2O_5 with alkali.

2. Experimental

2.1. Reagents and methods

All chemicals and solvents were used as received. Decarbonated water was used. Nb_2O_5 (99.5%) was purchased from Aldrich. NaOH and KOH were pro analysi grade.

Elemental analysis for Nb, Na and K were performed by ICP spectrometry (University of Aveiro, Central Laboratory of Analysis). Thermogravimetric analyses were carried out in air between 25 and 800 °C at a heating rate of 5 °C min^{-1}, on a Mettler M3 thermobalance equipped with a TC 10A microprocessor.

Infrared absorption spectra were recorded on a Mattson 7000 FTIR spectrometer, using KBr pellets. Raman measurements were performed with solid samples in a Bruker RFS 100/S FT-Raman spectrometer, equipped with a Nd:YAG laser emitting at 1064 nm. The spectra were obtained in the 200–1200 cm^{-1} range, using the following settings: power at the sample, 50 mW; resolution, 4 cm^{-1}. X-ray powder diffraction patterns were measured on a RigakuD–Max III instrument, using Cu Kα, radiation in the range $2\theta = 3°$–$130°$. Powder X-ray diffraction patterns were indexed with the POWDERX package [20] and the unit cells were indicated by the TREOR90 indexing program [21]. Cell parameters were refined using the program RIETICA 1.6.7A, by B.A. Hunter. Scanning electron microscope images (SEM) were recorded on a Hitachi S-4100 microscope.

2.2. General procedure for hydrothermal reaction of Nb_2O_5 with MOH, M = K, Na

Nb_2O_5 (0.1 or 0.2 g) and an aqueous solution of MOH (20 cm^3) with concentration corresponding to molar ratio MOH:Nb_2O_5 between 2 and 75 were placed in a Teflon lined cylindrical autoclave (60 cm^3 capacity), and introduced in an oven pre-heated to 200 °C for a predetermined period of time. After cooling down (under running cold water), any solid residue was separated by filtration or centrifugation, washed with water and ethanol and dried in a desiccator under vacuum. To the filtrate, absolute ethanol was added and any precipitated solid was filtered, washed with very cold ethanol–water (50%) and ethanol and dried under vacuum. Care should be taken to prevent contamination with carbonates.

2.3. Specific synthetic procedures

2.3.1. $NaNbO_3$

The reaction of Nb_2O_5 and NaOH was performed as described in 2.2, using molar ratios NaOH:Nb_2O_5 between 35 and 67 and 6–24 h reaction time. After cooling down, the obtained solid was separated by filtration, washed and dried as described above. *Anal.* Found: (Calc.): Nb, 56.2 (56.7); K, 14.2 (14.0)%.

2.3.2. $K_6H_2[Nb_6O_{19}]\cdot 13H_2O$

The reaction of Nb_2O_5 (0.2 g) and KOH was performed as described in Section 2.2, with a molar ratio KOH:$Nb_2O_5 = 60$ and 24 h reaction time. After cooling down, any insoluble residue was eliminated by

centrifugation. To the obtained solution was added an equal volume of absolute ethanol and the precipitated solid was filtered, washed successively with very cold ethanol–water (50%) and ethanol and dried under vacuum.

Anal. Found: (Calc.): Nb, 39.8 (41.8); K, 17.2 (17.6); H_2O, 17.7 (17.6)%. Infrared spectra (cm^{-1}): ν(Nb–O_t) 859 (vs); ν(Nb–O_b), 788 (m), 670 (s), 528 (s); ν(Nb–O_c) 418 (s), 400 (s). Raman spectra (cm^{-1}): ν(Nb–O_t) 900 (vs), 850 (m), 829 (m); ν(Nb–O_b), 679 (m), 535 (m); δ(O_b–Nb–O_b) 284(s), 217(s).

2.3.3. $Nb_2O_5 \cdot nH_2O$

The reaction of Nb_2O_5 and KOH was performed as described for the previous compound. After filtration of the insoluble residue, HCl 1 mol dm^{-3} was added until complete precipitation of the white solid formed. The solid was separated by centrifugation, washed repeatedly with water, followed by ethanol and left in a desiccator.

3. Results and discussion

Hydrothermal reactions of Nb_2O_5 with aqueous alkali metal hydroxides, MOH, M = Na, K, were performed at 200 °C and autogenic pressure in an autoclave and the obtained solids and solutions studied. Time of reaction and molar ratio mol(MOH):mol(Nb_2O_5) were systematically varied.

3.1. Reactions with NaOH

Experiments were performed with molar ratios NaOH:Nb_2O_5 between 3 and 67 and different time of reaction (6–48 h). After cooling, an abundant white solid material was found inside the autoclave. The composition of these powders varied with reaction conditions. In most cases, the mass of solid obtained suggested that little dissolution had occurred.

Fig. 1 presents the X-ray patterns of reaction products obtained after 6 h. In those solids $NaNbO_3$ was first identified by comparison of the correspondent powder X-ray diffractogram with published data [22]. For the molar ratio NaOH:Nb_2O_5 = 9 the obtained $NaNbO_3$ was contaminated with Nb_2O_5, but synthesis of single phase $NaNbO_3$ was achieved for the higher molar ratio. The same results were observed for 24 h reactions. Further reaction time did not lead to any improvement. The electron micrographs of the powders obtained from the reactions performed with molar ratios NaOH:Nb_2O_5 = 67 and different reaction times are shown in Fig. 2. They show small parallelepiped crystals of different sizes with length smaller than about 1.5 μm. By analysis of the powder X-ray diffraction patterns an orthorhombic unit cell was found, with $a = 5.510(2)$, $b = 5.569(1)$, $c = 15.533(6)$ Å. At room temperature, $NaNbO_3$ crystallizes in a pseudoperovskite phase, frequently referred as phase P [23], that has been indicated as orthorhombic [13,24–27] but also as monoclinic [28].

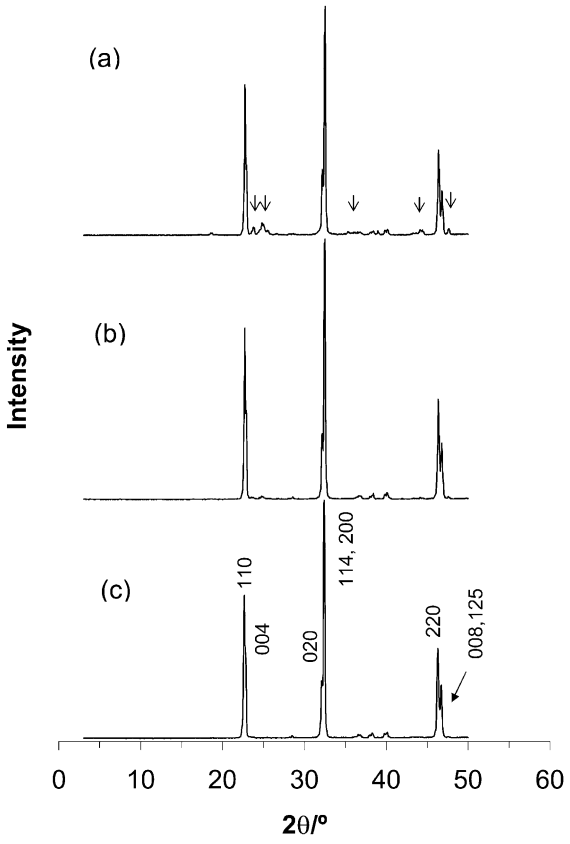


Fig. 1. X-ray powder diffraction patterns of products obtained after 6 h hydrothermal reaction, with different ratio mol(NaOH)–mol(Nb_2O_5): (a) 9; (b) 34; (c) 67. Mass of Nb_2O_5 used: 0.2 g. Main peaks corresponding to $NaNbO_3$ are indexed in (c). Arrows indicate Nb_2O_5 impurity.

The infrared spectrum of $NaNbO_3$ is distinct from that of the initial Nb_2O_5, presenting a broad strong peak at 640 cm^{-1}, with a shoulder near 780 cm^{-1} and one medium band at 372 cm^{-1} with a shoulder at lower frequency. This spectrum compares well with that of powders prepared by other techniques [7,29].

Some experiments were performed using $Nb_2O_5 \cdot nH_2O$ (obtained by the method described in Section 2.2) instead of Nb_2O_5 (NaOH:Nb_2O_5 ratio approximately equal to 60, 24 h). $NaNbO_3$ was also the product obtained.

The direct synthesis of $NaNbO_3$, from Nb_2O_5 and aqueous NaOH, at 200 °C, under hydrothermal conditions, represents thus an easy method of preparation of this compound. This method eliminates the need of using high temperature reactions, calcination steps, or less accessible precursors. It compares well with published procedures starting from $Na_8[Nb_6O_{19}] \cdot 13H_2O$ [11] or $Na_7H[Nb_6O_{19}] \cdot 15H_2O$ [12], as preparation of

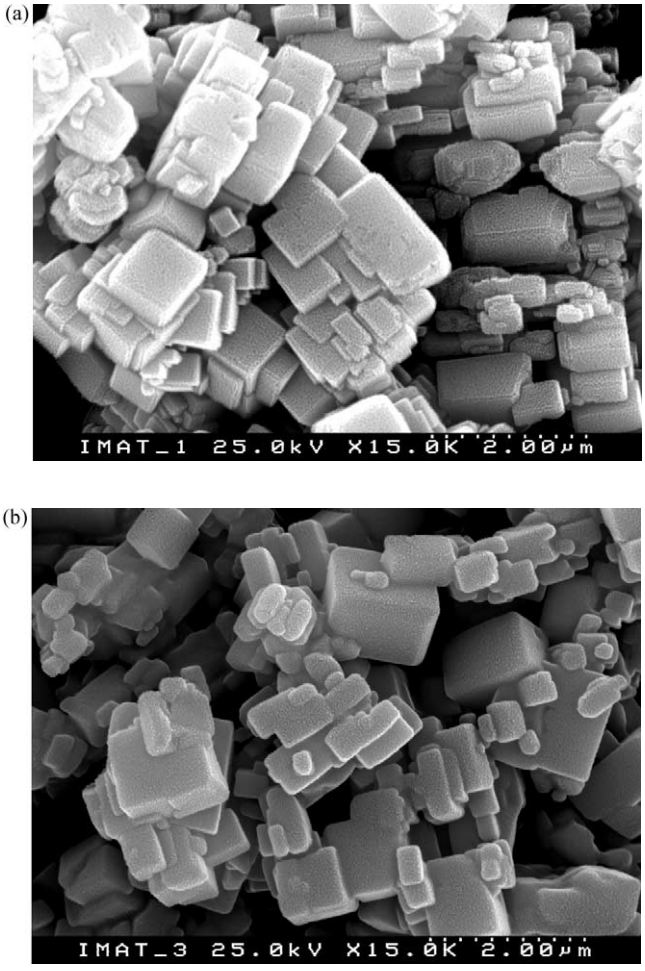


Fig. 2. Electron micrographs of powders obtained from reactions performed with mol(NaOH)–mol(Nb_2O_5) = 67 and different reaction times: (a) 24 h; (b) 48 h.

these starting materials is not necessary. Our work is not in accordance with the only report that claims that crystals of $NaNbO_3$ were obtained by boiling a suspension of Nb_2O_5 in NaOH for about 20 min [13], as longer periods of time at higher temperatures were found to be necessary. It is possible that a hydrated form of niobium pentoxide had been used. $Nb_2O_5{\cdot}nH_2O$ is known for being more reactive than Nb_2O_5. We have confirmed that the hydrothermal reaction of niobic acid with NaOH yields also $NaNbO_3$, but the study of the best reaction conditions was not performed in this work.

We observed that commercial niobium oxide had an insoluble residue that never dissolved in the reactions with KOH (see Section 3.2). It is possible that this residue may not react also with NaOH. However, we could not identify any impurity in the prepared $NaNbO_3$ by any of the used techniques and thus be sure of its presence or absence. This residue was eliminated during the preparation of $Nb_2O_5{\cdot}nH_2O$ and, thus, synthesis starting with niobic acid may lead to purer products. Otherwise, the preparation of $Nb_2O_5{\cdot}nH_2O$ introduces an extra procedure in the synthetic pathway of no particular advantage.

3.2. Reactions with KOH

The reaction of Nb_2O_5 with aqueous KOH under hydrothermal conditions had been previously used to successfully prepare $KNbO_3$ [14,15] and $K_4Nb_6O_{17}{\cdot}3H_2O$ [15]. The work here presented concerns mainly the dissolution of niobium pentoxide in aqueous KOH, as this reaction provides an interesting new process of obtaining alkaline solutions of Nb(V). We were particularly interested in observing if solutions prepared by hydrothermal dissolution of Nb_2O_5 could be used to perform standard niobium chemistry, like preparation of potassium hexaniobates [16,17] or niobic acid [3–5].

In the conditions here reported, it was found that Nb_2O_5 was practically all dissolved after 24 h reaction if the molar ratio KOH:Nb_2O_5 was larger than 35 (molar ratio between 2 and 75 were evaluated). Extra time or increase of the molar ratio did not eliminate a small amount of an insoluble residue always present. That residue could not be obtained in the necessary quantities for identification and was considered as an insoluble phase of the commercial reagent used. When the reaction time was equal or less than 8 h or the molar ratio smaller than 35, a solid was obtained in reasonable amounts, which was found by powder X-ray diffraction to be mostly un-reacted Nb_2O_5. Reaction times between 8 and 24 h were not monitored.

When solubilization was almost complete the solid residue was eliminated and ethanol added to the filtrate. In all cases, the formation of a white precipitate was observed. Elemental analysis of the obtained solids yielded a K:Nb molar ratio near 1.0. The correspondent infrared spectra and Raman showed in the 400–900 cm^{-1} region the characteristic pattern of the hexaniobate anions, $H_xNb_6O_{19}{}^{(8-x)-}$, assigned to Nb=O and Nb–O–Nb stretching vibrations [6,16,30–32]. Reasonably pure $K_6H_2[Nb_6O_{19}]{\cdot}13H_2O$ was obtained from solutions prepared with an initial molar ratio KOH:Nb_2O_5 = 60 (see Section 2). The correspondent infrared and Raman spectra are shown in Fig. 3. Mixtures with other hexaniobates, like $K_7H[Nb_6O_{19}]{\cdot}nH_2O$, could not be ruled out in other conditions. Identification of the degree of protonation cannot be done with certainty by infrared spectroscopy, as the values of the frequencies of hexaniobate anions have been found to depend slightly on protonation and on the degree of hydration of the salts, for a given cation [6,16]. The anions $H_xNb_6O_{19}{}^{(8-x)-}$, $x = 0$–3 are known to exist in aqueous solutions with pH in the 8.5–14 region [5,17]. Studies of the preferential conditions of precipitation of some potassium hexaniobates have been published [16,17] and were not pursued in this work.

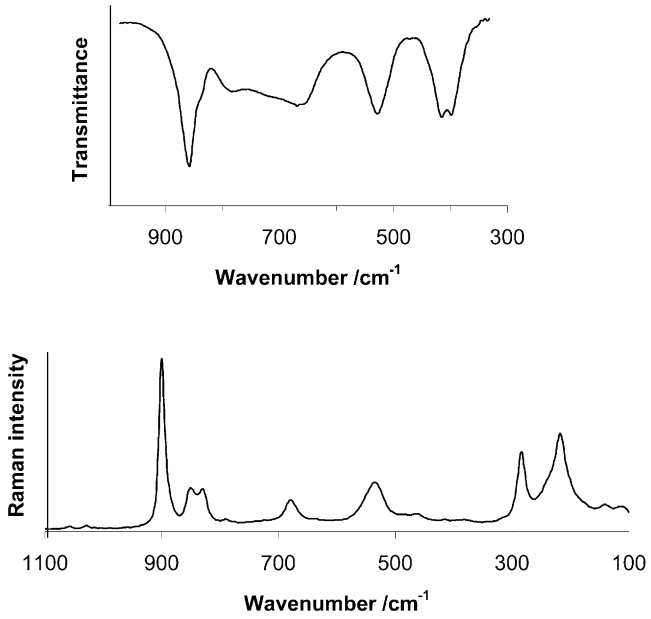


Fig. 3. Vibrational spectra of $K_6H_2[Nb_6O_{19}]\cdot 13H_2O$: (a) infrared spectrum; (b) Raman spectrum.

$K_6H_2[Nb_6O_{19}]\cdot nH_2O$ was obtained in the form of crystalline, slightly agglomerated powders (Fig. 4). The corresponding X-ray powder diffraction pattern is presented in Fig. 5(a). Indexation of this will be presented elsewhere. Of the possible salts $K_{8-x}H_x[Nb_6O_{19}]\cdot nH_2O$, only for $K_8[Nb_6O_{19}]\cdot 10H_2O$ has the powder X-ray diffraction patterns been published [33], but this was never observed for our compounds. Calcinations of $K_6H_2[Nb_6O_{19}]\cdot nH_2O$ at 800 °C yielded $KNbO_3$ as the only product, identified by its X-ray powder diffractogram match with the ICDD database [34] (Fig. 5(b)) and confirmed by elemental analysis (EDAX). This result is in accordance with equation (1), thus confirming the molecular stoichiometry of the prepared potassium hexaniobate.

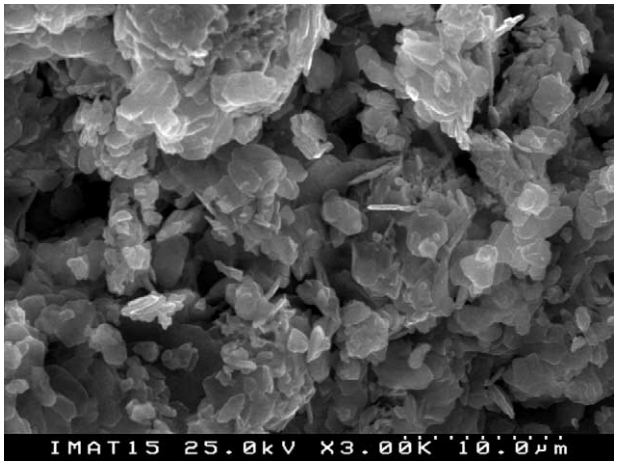


Fig. 4. Electron micrograph of $K_6H_2[Nb_6O_{19}]\cdot 13H_2O$.

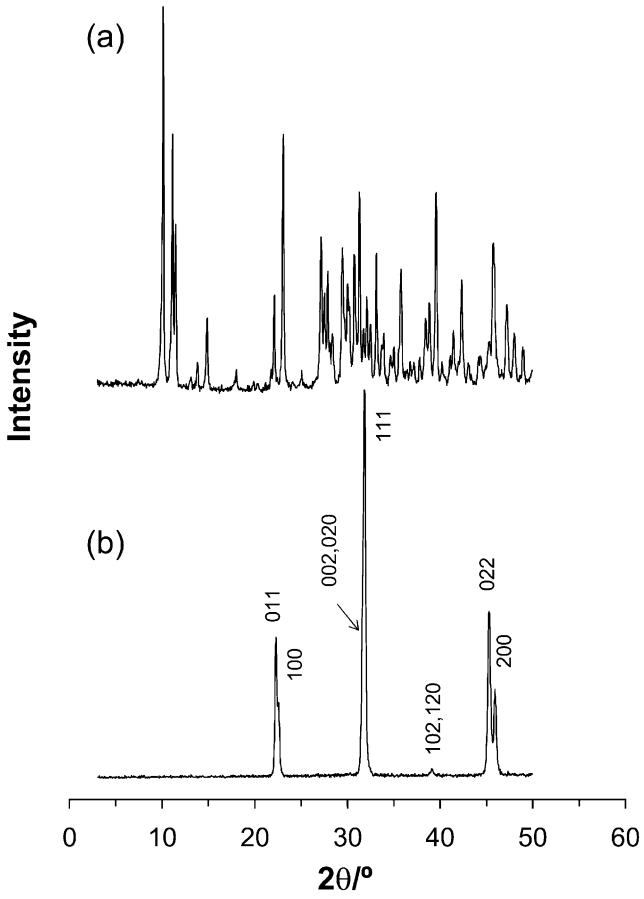


Fig. 5. X-ray powder diffraction patterns of (a) $K_6H_2[Nb_6O_{19}]\cdot 13H_2O$ and (b) $KNbO_3$ (orthorhombic, $a = 3.968(1)$, $b = 5.691(1)$, $c = 5.700(1)$ Å) obtained by calcinations of $K_6H_2[Nb_6O_{19}]\cdot 13H_2O$ at 800 °C.

$$K_6H_2[Nb_6O_{19}]\cdot 13H_2O \rightarrow 6KNbO_3 + 14H_2O \quad (1)$$

Even when Nb_2O_5 did not dissolve extensively, addition of ethanol to the filtrate originated solids with the hexaniobate anions, as determined by infrared spectroscopy. If HCl was added to the filtrate, instead of ethanol, precipitation of hydrated niobium pentoxide was observed, as expected [3,4]. We have used this method to prepare $Nb_2O_5\cdot nH_2O$ used in the reactions with NaOH (see Section 3.1).

The oxide Nb_2O_5 has a complicated structural chemistry and occurs in several polymorphs [35,36]. The commercial solid used was found to be a mixture of forms where the main components were identified by powder X-ray diffraction as being a low-temperature orthorhombic phase and a M-form [37]. The reactivity of the different modifications was not the same and thus the form of Nb_2O_5 identified by X-ray diffraction when the reactions (either with KOH or NaOH) were not complete varied with experimental conditions. The infrared spectra of different samples of un-reacted Nb_2O_5, obtained from the experiments with KOH, were, however, very similar, presenting three broad strong bands centered around 827, 710 and 513 cm^{-1}

with several weak, poorly resolved, peaks on the larger wavenumber side.

The insolubility of the different forms of niobium pentoxide in common aqueous acids and bases has been recognized for many years as a characteristic of these oxides. The solubilization of Nb_2O_5 in KOH solutions, under hydrothermal conditions at 200 °C offers great advantage, as it is experimentally easy and does not need the use of high temperatures. It has been reported that dissolution was obtained with shorter reaction times [14] than those here described, but this was obtained in a stirred reactor with a different range of reagent concentrations. In this work, the conditions used were identical to those in the preparation of $NaNbO_3$ (Section 3.1). Under these conditions, formation of $KNbO_3$ or $K_4Nb_6O_{17}\cdot 3H_2O$ [14,15] was never detected. Comparison of the results here presented with those previously published [14,15] seems to imply that different factors (concentration of KOH solution, KOH:Nb_2O_5 molar ratio and experimental settings) influence the outcome of the studied reactions.

3.3. Final remarks

It is interesting to note that the method and conditions of attack of Nb_2O_5 described in this work provided different results when NaOH or KOH were used. Soluble potassium and sodium hexaniobates, of general formula $M_{8-x}H_x[Nb_6O_{19}]\cdot nH_2O$, are well known [3]. Potassium hexaniobates are, generally, more soluble in water than the corresponding sodium salts and thus sodium hexaniobates are frequently obtained by cation metathesis, starting with solutions of the potassium analogues [3]. Muller et al. have studied a series of sodium hexaniobates prepared by reaction of niobic acid with NaOH [6,38]. Different solubility and thermal stability of these salts may explain the different results observed.

In conclusion, we have found that the hydrothermal reaction of Nb_2O_5 with NaOH at 200 °C can be used in the synthesis of $NaNbO_3$ under milder conditions than by the ceramic method. A low temperature form, described previously as stable up to 365 °C [26,27], was obtained. Under similar conditions, reactions of Nb_2O_5 with KOH allowed the preparation of solutions containing soluble potassium hexaniobates by a more convenient process than the traditional method of fusion of mixtures of the niobium oxide with KOH or other potassium salts.

Acknowledgements

We are grateful to Dr. M.R. Soares for assistance with the X-ray diffraction analysis. Thanks are also due to the University of Aveiro and Center of Inorganic and Materials Chemistry (FCT) for financial support of this work.

References

[1] D. Segal, J. Mat. Chem. 7 (1997) 1297.
[2] W.J. Dawson, Ceram. Bull. 67 (1988) 1673.
[3] F. Fairbrother, The Chemistry of Niobium and Tantalum, Elsevier, Amsterdam, 1967.
[4] D. Brown, in: J.C. Bailar, H.J. Emeleus, R. Nyholm, A.F. Trotman-Dickerson (Eds.), Comprehensive Inorganic Chemistry, vol. 3, Pergamon, Oxford, 1973, p. 553.
[5] I. Nowak, M. Ziolek, Chem. Rev. 99 (1999) 3603.
[6] M. Muller, Rev. Chim. Min. 7 (1970) 359.
[7] B. Vaidhyanathan, P. Raizada, K.J. Rao, J. Mater. Sci. Lett. 16 (1997) 2022.
[8] M.A.L. Nobre, E. Longo, E.R. Leite, J.A. Varela, Mater. Lett. 28 (1996) 215.
[9] E.R. Leite, M.A.L. Nobre, M. Cerqueira, E. Longo, J.A. Varela, J. Am. Ceram. Soc. 80 (1997) 2649.
[10] S. Lanfredi, L. Dessemond, A.C. Martins Rodrigues, J. Eur. Ceram. Soc. 20 (2000) 983.
[11] N. Kinomura, N. Kumata, F. Muto, Mat. Res. Bull. 19 (1984) 299.
[12] P. Sue, Ann. Chim. 7 (1937) 493.
[13] P. Vousden, Acta Crystallogr. 4 (1951) 373.
[14] C.H. Lu, S.Y. Lo, H.C. Lin, Mater. Lett. 34 (1998) 172.
[15] S. Uchida, Y. Inoue, Y. Fujishiro, T. Sato, J. Mater. Sci. 33 (1998) 5125.
[16] R. Rohmer, J.E. Guerchais, Bull. Soc. Chim. France (1961) 324.
[17] B. Spinner, Rev. Chim. Min. 5 (1968) 839.
[18] (a) C.M. Flynn, G.D. Stucky, Inorg. Chem. 8 (1969) 179; (b) C.M. Flynn, G.D. Stucky, Inorg. Chem. 8 (1969) 332.
[19] M. Filowitz, R.K.C. Ho, W.G. Klemperer, W. Shum, Inorg. Chem. 18 (1979) 93.
[20] C. Dong, J. Appl. Cryst. 32 (1999) 838.
[21] P.E. Werner, L. Eriksson, M. Westdahl, J. Appl. Cryst. 18 (1985) 367.
[22] Powder Diffraction File, Swarthmore, ICDD-PDF2, card number 73-0803 (2001).
[23] I. Lefkowitz, K. Lukaszewicz, H.D. Megaw, Acta Crystallogr. 20 (1966) 670.
[24] A.C. Sakowski-Cowley, K. Lukaszewicz, H.D. Megaw, Acta Crystallogr., Sect. B 25 (1969) 851.
[25] M. Ahtee, A.M. Glazer, H.D. Megaw, Phil. Mag. 26 (1972) 995.
[26] H.D. Megaw, Ferroelectrics 7 (1974) 87.
[27] W. Pies, A. Weiss, Landolt–Börnstein numerical data and functional relationships in science and technology, new series, in: K.H. Hellwege (Ed.), Crystal Structure Data of Inorganic Compounds, vol. 7 (Group III, part e), Springer, Berlin, 1976, p. 436.
[28] C.N.W. Darlington, K.S. Knight, Physica B 266 (1999) 368.
[29] E. Housson, Y. Repelin, Spectrochim. Acta 40A (1984) 315.
[30] F.J. Farrell, V.A. Maroni, T.G. Spiro, Inorg. Chem. 8 (1969) 2638.
[31] R. Mattes, H. Bierbusse, J. Fuchs, Z. Anorg. Allg. Chem. 385 (1971) 230.
[32] C. Rocchiccioli-Deltcheff, R. Thouvenot, M. Dabbabi, Spectrochim. Acta 33A (1977) 143.
[33] Powder Diffraction File, ICDD-PDF2, card number 14-0288 (2001).
[34] Powder Diffraction File, ICDD-PDF2, card number 77-1098 (2001).
[35] H. Schafer, R. Gruehn, F. Schulte, Angew. Chem., Int. Ed. 5 (1966) 40.

[36] W. Pies, A. Weiss, Landolt–Börnstein numerical data and functional relationships in science and technology, new series, in: K.H. Hellwege (Ed.), Crystal Structure Data of Inorganic Compounds, vol. 7 (Group III, part b), Springer, Berlin, 1975, p. 439.
[37] Powder Diffraction File, ICDD-PDF2, cards number 30-0873 and 30-0872 (2001).
[38] M. Muller, R. Rohmer, Bull. Soc. Chim. France (1967) 925.

2. Experimental

Methanol (99.8%, anhydrous), copper(II) acetate monohydrate (98+%) and nitric acid (trace metal grade) were obtained from commercial sources and used as received. UV–Vis spectra were recorded using matched quartz cells on a Shimadzu UV2101 PC spectrophotometer. IR spectra were recorded on a Mattson Galaxy 5000 FT-IR spectrometer. GC-MS data were obtained using a Varian Saturn 2100D instrument, and inductively coupled plasma emission data were recorded and analyzed using a Thermo Jarrell Ash Atom Scan 25 instrument and associated software.

2.1. Synthesis of copper(II) methoxide

In a typical experiment, a glass vial was charged with 24.5 mg (0.123 mmol) of copper(II) acetate monohydrate and 5.0 ml of methanol. After stirring, the vial was placed into a Teflon-lined stainless steel autoclave and heated to 110 °C for three days. Upon opening the autoclave, dark purple block-shaped crystals of **1** were observed on the bottom and sides of the vial. No other solid product was evident, and the supernatant liquid was colorless. The vial containing the crystals and mother liquor was capped with a rubber septum and attached to the Schlenk line via a needle. Under argon, the mother liquor was withdrawn and analyzed by UV–Vis and GC-MS. These experiments clearly indicated the presence of methyl acetate in the mother liquor. The crystals remaining in the vial after removal of the mother liquor were washed with several 5 ml portions of methanol under argon. No observable change occurred during the washing or subsequent evacuation of the vial.

2.2. Spectroscopic characterization of copper(II) methoxide

A sample of the washed crystalline material described above was ground under methanol to produce a fine slurry. Several drops of the slurry were placed on a sodium chloride plate in an argon-filled chamber that was subsequently evacuated. When the methanol had evaporated from the slurry, the chamber was filled with argon and brought to the IR spectrometer, the sample cavity of which had been purged with nitrogen gas. The salt plate was mounted in the spectrometer and a spectrum matching that of copper(II) methoxide [1,2] was recorded. The sample cavity was then opened to the air and spectra were recorded at approximately five-minute intervals, during which time the bands ascribed to copper methoxide were replaced by a broad O–H band typical of a hydrogen-bonded O–H stretch and other unidentified signals.

2.3. Inductively coupled plasma emission spectroscopic analysis.

The synthesis of **1** was carried out using a 24.7 mg (0.124 mmol) sample of copper(II) acetate monohydrate. After reaction, the mother liquor was transferred to a Schlenk flask that was then subjected to dynamic vacuum until no solvent was evident. The residue was dissolved in nitric acid and diluted to 50.00 ml with deionized water. Analysis of this solution against a 10.00 ppm Cu standard indicated a Cu concentration of 0.157 ppm with a standard deviation of 0.005 ppm. This corresponds to 1.24×10^{-4} mmol Cu in the entire analyte solution.

2.4. Crystallography

Crystal evaluation and data collection were performed on a Bruker CCD-1000 diffractometer with Mo Kα radiation ($\lambda = 0.71073$ Å). A purple block-shaped crystal with approximate dimensions $0.45 \times 0.14 \times 0.12$ mm, obtained directly from the reaction vial, was mounted under oil on the tip of a glass capillary. The crystal was mounted in a stream of nitrogen gas at 173(2) K and centered in the X-ray beam.

Crystal Data: $C_2H_6CuO_2$ (formula weight = 125.61), tetragonal, space group $P4_2/mbc$, $a = 8.1848(6)$ Å, $c = 5.8770(4)$ Å, $V = 393.71(5)$ Å^3, $Z = 4$, $\rho_{calc} = 2.119$ g cm^{-3}, $F(000) = 252$, μ (Mo Kα) = 5.356 mm^{-1}. Initial cell constants were obtained from three series of ω scans at different starting angles. Each series consisted of 50 frames collected at intervals of 0.3 in a 15° range about ω with an exposure time of 20 s per frame. The final cell constants were calculated from a set of 1084 strong reflections. Data were collected by use of the hemisphere data collection routine. A total of 3205 data were harvested by collecting three sets of 30-s frames with 0.3° scans in ω. Data were corrected for Lorentz and polarization effects. An absorption correction was performed and was based on fitting a function to the empirical transmission surface as sampled by multiple equivalent measurements [5]. Systematic absences in the diffraction data were consistent with the space groups $P4_2bc$ and $P4_2/mbc$. The E-statistics strongly suggested the centrosymmetric space group $P4_2/mbc$ that yielded chemically reasonable and computationally stable refinement results [6]. A solution by direct methods provided most of the non-hydrogen atoms from the E-map. The remaining non-hydrogen atoms were located in an alternating series of least-squares and difference Fourier maps. Non-hydrogen atoms were refined anisotropically. Hydrogen atoms were included in the structure factor calculation at idealized positions and were allowed to ride on the neighboring atoms with relative isotropic displacement coefficients. A total of 3205

reflections were collected, 224 of which were independent [$R_{int} = 0.0300$] in the range $3.52^\circ < \Theta < 26.38^\circ$. The data were 100% complete over this range. The final least squares refinement on F^2 yielded $R_1 = 0.0204$ ($wR_2 = 0.0713$) for 179 reflections having $I > 2\sigma(I)$, where $wR_2 = \Sigma[w(F_o^2 - F_c^2)]/\Sigma[(wF_o^2)^2]^{1/2}$; $R_1 = \Sigma\Delta/\Sigma(F_o)$, $\Delta = |(F_o - F_c)|$. The Cu atom occupies three crystallographic twofold axes while the carbon and oxygen atoms reside on a crystallographic mirror plane.

3. Results and discussion

We have found that treatment of copper(II) acetate monohydrate with methanol for three days at 110 °C produces exceptionally well-formed deep purple block-shaped crystals of copper(II) methoxide with no other solid products. These crystals are indefinitely stable under the mother liquor or pure methanol at room temperature. They also appear to be stable for at least several hours under argon or vacuum. In the air in absence of methanol, the crystals decompose rapidly, undergoing an irreversible color change to light blue. Interestingly, if the amount of copper acetate reacting in 5.0 ml of methanol is raised above 25 mg, the yield of purple crystals is drastically decreased and a large amount of uncharacterized brown/black solid forms. Further, no reaction is observed if the same starting material is left to stand in methanol under argon for 11 days, indicating that solventothermal conditions are necessary for the facile synthesis of **1** by this reaction.

3.1. Description of the crystal structure of copper(II) methoxide

After preliminary identification of the identity of the purple crystalline product as copper(II) methoxide, confirmation was achieved via single crystal X-ray methods. In the structure of **1**, infinite one-dimensional chains of copper atoms with bridging methoxide ligands run parallel to the crystallographic *c*-axis in the tetragonal space group $P4_2/mbc$. The copper atoms in **1** are each coordinated by four oxygen atoms in a distorted square planar fashion. The methyl groups on either side of the one-dimensional chain tip in alternating directions away from the mean copper–oxygen plane in a 'zig–zag' arrangement, and the copper atoms are arranged in a linear fashion with respect to one another. A segment of this coordination polymer is shown in Fig. 1. Fig. 2 is a view down the crystallographic *c*-axis showing the orientation of the chains with respect to one another. Fig. 3 presents a view looking down the crystallographic a axis, illustrating the orientation of the methyl groups in **1** with respect to the linear arrangement of copper atoms. Selected bond distances and angles are reported in Table 1.

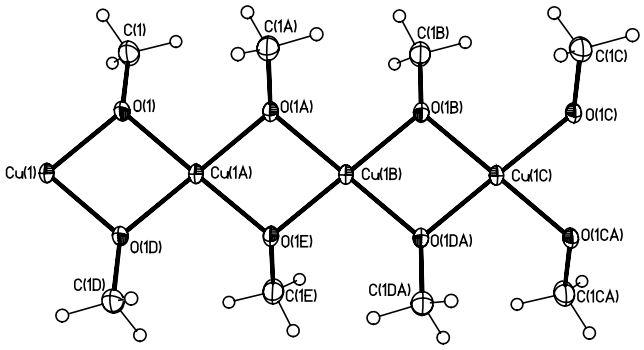


Fig. 1. A section of the infinite one-dimensional chain in **1**, with ellipsoids drawn at the 50% probability level.

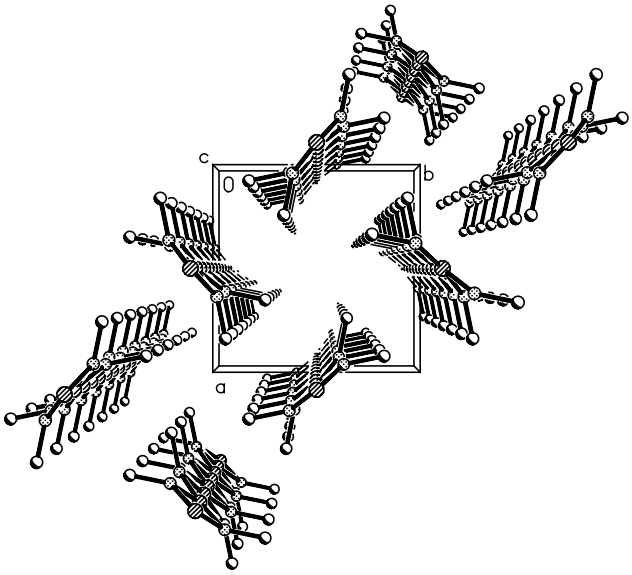


Fig. 2. A view down the crystallographic *c*-axis in the lattice of **1**.

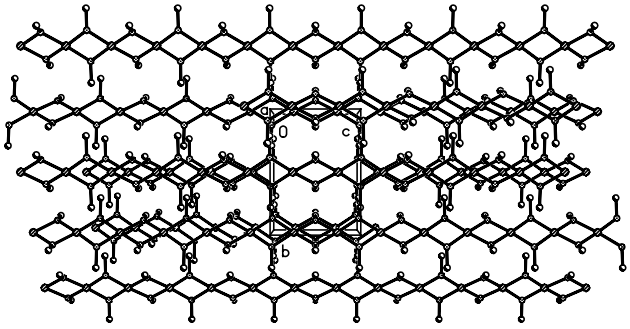


Fig. 3. A view down the crystallographic *a*-axis in the lattice of **1**.

The bridging of copper atoms by methoxide ligands is a common structural motif, but the infinite chain structure determined for **1** is novel. The structure of **1** can be thought of as the most basic of all methoxide-bridged Cu coordination compound structures. A search of the Cambridge Structural Database [7] for compounds containing methoxide ligands bridging copper

Table 1
Selected bond lengths (Å) and bond angles (°) for **1**

Bond lengths			
Cu(1)–O(1)	1.915(1)	O(1)–C(1)	1.417(3)
Bond angles			
O(1)–Cu(1A)–O(1A)	100.5(1)	C(1)–O(1)–Cu(1)	124.22(8)
O(1)–Cu(1A)–O(1D)	79.80(9)		

atoms, limited to structures with final R values of 5% or lower and no disorder yielded 26 hits. Among these structures, the average Cu–O distance was 1.93(2) Å and the average Cu–Cu separation 3.0(1) Å. Both the Cu–O bond distance and Cu–Cu separation in **1**, 1.915(1) and 2.9385(2) Å, respectively, compare well with these parameters.

3.2. Discussion of the synthetic reaction and products

The only solid product of the synthesis is **1**, as confirmed by IR spectroscopy**.** Analysis of the mother liquor by inductively coupled plasma emission spectroscopy showed only a minute trace of copper, corresponding to about 0.1% of the copper in the starting material. This indicates that the conversion of copper(II) acetate to copper(II) methoxide is essentially quantitative, as there are no reasonable volatile copper-containing products. A UV–Vis spectrum of the mother liquor was transparent in the visible region, showing only an absorbance attributable to methyl acetate, the presence of which was confirmed by GC-MS. We believe that the methyl acetate forms via a classical condensation reaction whereby methanol and acetic acid react with elimination of water and concomitant formation of the ester. This observation strongly suggests that acetate ions, present in solution due to the use of copper acetate as the copper source, are responsible for deprotonation of methanol. It is not clear what role, if any, copper atoms may play in this process. Nonetheless, the overall pathway by which **1** and methyl acetate form can be summarized as shown in Scheme 1.

This work has confirmed initial suppositions of a methoxide-bridged polymeric structure for copper(II) methoxide [1], well supported from the beginning by observed physical properties. What is not clear is whether the initial suggestion of a three-dimensional coordination polymer (as opposed to the crystallographically-determined one-dimensional structure) was in fact in error, or rather that the present conditions result in the formation of a different phase of copper methoxide than those that had been prepared and characterized previously. This question will be difficult to answer conclusively, as none of the previously reported synthetic conditions lead to products that are suitable for complete structural characterization by X-ray methods.

$$CH_3OH + CH_3COO^- \leftrightarrows CH_3O^- + CH_3COOH$$
$$n(Cu^{2+}) + 2n(CH_3O^-) \rightarrow [Cu(OCH_3)_2]_n$$
$$CH_3COOH + CH_3OH \rightarrow CH_3COOCH_3 + H_2O$$

Scheme 1.

The observed stability of **1** under methanol, even in the presence of a significant amount of water (present because of the use of hydrated copper acetate as starting material) is somewhat surprising and worthy of note. The observation that a sample of **1** identified in the nitrogen-purged sample cavity of an IR spectrometer decomposes rapidly upon the introduction of air is, however, consistent with the known air sensitivity of copper methoxide in the absence of solvent.

4. Supplementary material

Crystallographic data for the structural analysis have been deposited with the Cambridge Crystallographic Data Centre, CCDC No. 178855. Copies of this information may be obtained free of charge from The Director, CCDC, 12 Union Road, Cambridge, CB2 1EZ, UK (fax: +44-1223-336033; e-mail: deposit@ccdc.cam.ac.uk or www: http://www.ccdc.cam.ac.uk).

Acknowledgements

Acknowledgement is made to the donors of The Petroleum Research Fund, administered by the ACS, for support of this research**.** The authors thank Dr. Paul J. Taylor and Dr. Paul D. Miller of UW-La Crosse for assistance with ICP analysis and GC-MS, respectively.

References

[1] C.H. Brubaker, M. Wicholas, J. Inorg. Nucl. Chem. 27 (1965) 59.
[2] G. Costa, A. Camus, N. Marsich, J. Inorg. Nucl. Chem. 27 (1965) 281.
[3] M. Gargano, N. Ravasio, M. Rossi, A. Tiripicchio, M. Tiripicchio Camellini, J. Chem Soc. Dalton Trans. (1989) 921.
[4] S.T. King, Catal. Today 33 (1997) 173.
[5] R.H. Blessing, Acta Crystallogr. Sect. A 51 (1995) 33.
[6] G. Sheldrick, All software and sources of the scattering factors are contained in the SHELXTL (version 5.1) program library, Bruker Analytical X-ray Systems, Madison, WI.
[7] F.H. Allen, O. Kennard, Chem. Des. Autom. News 8 (1993) 31.

the spectra were obtained at ambient temperature (approximately 24 °C). EPR measurements were taken on a Bruker ESP300 EPR spectrometer with the following settings: modulation amplitude, 1G; modulation frequency, 100 KHz; time constant 163.84 ms; scan time, 83.886 s; receiver gain, 6.32×10^3 unless otherwise noted. The frequency is calibrated using frequency meter. The solvents were purged with nitrogen before use.

3,5-Di-*t*-pentylsalicylaldehyde (**1**) is prepared by modification of a reported method [11] and is reported elsewhere, together with the preparation of ligand **2** [12].

Preparation of vanadyl complex **3**: in dry EtOH (10 cm^3), salen schiff base ligand **2** (1.000 g, 1.66 mmol) and vanadyl(IV) acetylacetonate [$VO(acac)_2$, 0.467 g, 1.76 mmol] were stirred at room temperature for 8 h. The volume of ethanol was reduced and a green solid was filtered and washed with cold EtOH to afford vanadyl complex **3** (1.04 g, 94%). The analytical sample was obtained with recrystallization from a mixture of C_6H_{14} (hexane) and $CHCl_3$, and dried over P_2O_5 for 24 h. *Anal.* Calc. for $C_{40}H_{60}N_2O_3V$: C, 71.93; H, 9.06; N, 4.20; Found: C, 72.00; H, 9.11; N, 4.20%.

2.2. Crystal structure determination

Crystals suitable for X-ray determination were obtained by slow evaporation of a C_6H_{14}–$CHCl_3$ (1:1, v/v) solution. $C_{46}H_{74}N_2O_3V$: $3 \cdot C_6H_{14}$, $M = 710.93$, triclinic, space group P_1, $a = 10.2439(1)$, $b = 14.4771(2)$, $c = 14.8782$ (2) Å, $\alpha = 68.655(1)°$, $\beta = 85.059(1)°$, $\gamma = 87.060(1)°$, crystal size $0.493 \times 0.221 \times 0.136$ mm, λ(Mo Kα) 0.71073 Å, $Z = 2$, $D_c = 1.153$, $F(000) = 772$, μ(Mo Kα) = 2.81 cm^{-1}.

2.2.1. Data collection

Absorption correction calculated using SADABS with maximum and minimum transmission factors of 0.9628 and 0.8740, respectively; intensity data were collected on a Bruker 1K CCD platform diffractometer; A total of 20271 reflections were collected, of which 14809 independent reflections ($R_{int} = 0.03341$) were observed with $1.47° < \theta < 28.24°$ and used in all the calculations. The unit cell dimensions were determined by a least-square fit of 2θ angles for 8192 reflections.

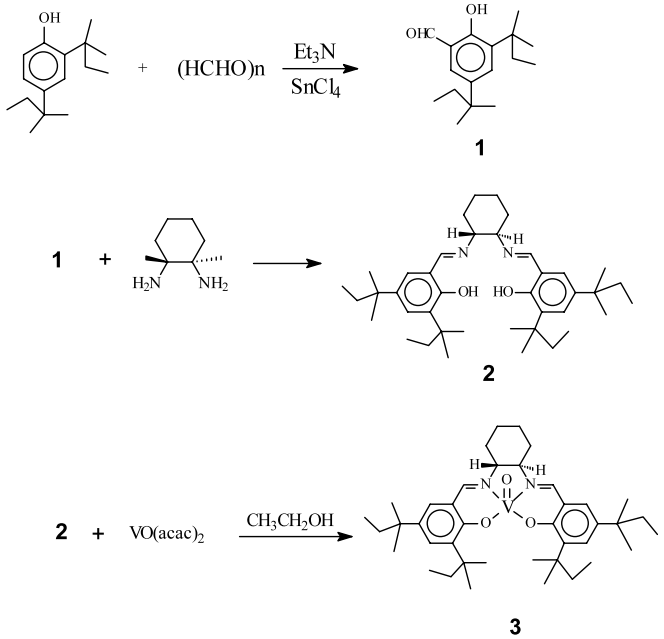
2.2.2. Structure analysis and refinement

The structure was solved by direct methods and subsequent Fourier difference techniques, and refined anisotropically, by full-matrix least-squares, on F^2 using SHELXTL 5.1. Hydrogen atoms were calculated from ideal geometry with coordinates fixed and temperature factors varied. Weights based on counting-statistics were used (based on $w^{-1} = \sigma^2(F_o^2) + (0.0844P)^2 + 0.34P$, where $P = [\mathrm{Max}(F_o^2, 0) + 2 \times F_c^2)/3]$). The last least-square cycle was calculated with 1002 parameters and 14809 reflections. For 10713 reflections with $I > 2\sigma(I)$, $R(F)$ was 0.0596, R_w (F^2) 0.1441 with goodness-of-fit 1.011 where R_w is defined by $R_w(F^2) = [\Sigma(\omega(F_o^2 - F_c^2))^2 / [\Sigma(\omega(F_o^2)^2]^{1/2}$ and GoF defined by $\mathrm{GoF} = [\Sigma(\omega(F_o - F_c))^2/13807]^{1/2}$. For all reflections, $R(F)$ was 0.0919, $Rw(F^2)$ 0.1654. The maximum $\Delta/\sigma = 0.000$, the deepest hole is −0.425 e $Å^{-3}$ and the highest peak is 0.446 e $Å^{-3}$. Full crystallographic data are given in the supporting materials.

3. Results and discussion

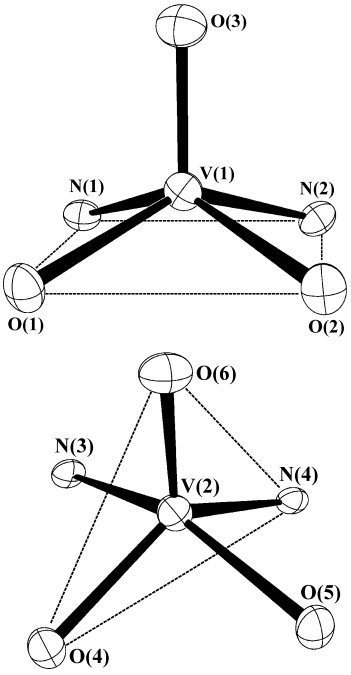
The new vanadyl complex **3** was prepared from the reaction of $VO(acac)_2$ with salen ligand **2** in ethanol (Scheme 1). The important feature of this ligand is to possess *t*-pentyl (Pn) groups at the 3, 5-positions of the aromatic rings. Due to the presence of these bulky components, the vanadyl complex has excellent solubility in most of the commonly used organic solvents such as THF, acetone, chloroform, and methylene chloride. The needle-like crystals of the vanadyl complex were obtained from a mixture of hexane and chloroform solvents.

The crystal structure revealed by X-ray determination showed that there are two independent molecules, referred to as **A** and **B**. Selected bond distances and angles in central metal coordination were listed in Table 1. There is a striking difference in the chromophore coordination geometry in **A** and **B** molecules. Two N–V bonds in **A** are nearly symmetrical with almost equal bond length (~2.06 Å), and so are the two V–O bonds



Scheme 1. Synthesis of salen ligand with *t*-pentyl groups and salen VO complex.

Table 1
Selected bond lengths (Å) and angles (°) in the vanadium geometry



Bond lengths			
V(1) = O(3)	1.610 (4)	V(2) = O(6)	1.595 (4)
V(1)–N(1)	2.056 (4)	V(2)–N(3)	2.058 (4)
V(1)–N(2)	2.067 (5)	V(2)–N(4)	2.090 (4)
V(1)–O(1)	1.930 (4)	V(2)–O(4)	1.903 (4)
V(1)–O(2)	1.937 (4)	V(2)–O(5)	1.944 (4)
Bond angles			
O(3)–V(1)–O(1)	110.27 (18)	O(6)–V(2)–O(4)	115.78 (19)
O(3)–V(1)–O(2)	109.14 (17)	O(6)–V(2)–O(5)	105.36 (19)
N(1)–V(1)–O(3)	105.74 (17)	N(3)–V(2)–O(6)	101.23 (19)
N(2)–V(1)–O(3)	105.85 (19)	N(4)–V(2)–O(6)	112.65 (18)
N(1)–V(1)–O(1)	87.18 (16)	N(3)–V(2)–O(4)	85.88 (16)
N(2)–V(1)–O(2)	85.54 (16)	N(4)–V(2)–O(5)	85.92 (16)
N(1)–V(1)–N(2)	78.49 (17)	N(3)–V(2)–N(4)	78.66 (16)
O(1)–V(1)–O(2)	87.21 (16)	O(4)–V(2)–O(5)	87.65 (15)
N(1)–V(1)–O(2)	144.44 (16)	N(3)–V(2)–O(5)	152.81 (16)
N(2)–V(1)–O(1)	143.56 (17)	N(4)–V(2)–O(4)	131.11 (16)

(~ 1.93 Å). However, they are seriously distorted in **B**. One V–O bond is noticeably longer than the other (1.944 vs. 1.903 Å), and so is the V–N bond (2.09 vs. 2.058 Å). In addition, vanadium is approximately centered in **A**, it is not in **B**. Both shorter N(3)–V(2) and O(4)–V(2) bonds clearly suggest that vanadium is deviated from the center in **B**.

The other significant distortion is bond angles involving basal atoms and V=O in the molecule **B**. There is about 10° deviation between two O=V–O (~ 115° vs. 105°). In addition, the same order of deviation is also found between two O=V–N (~ 101° vs. 112°). In contrast, almost symmetrical angles between two O=V–O (~ 110°) or two O=V–N (~ 105°) are observed in **A** (Fig. 1).

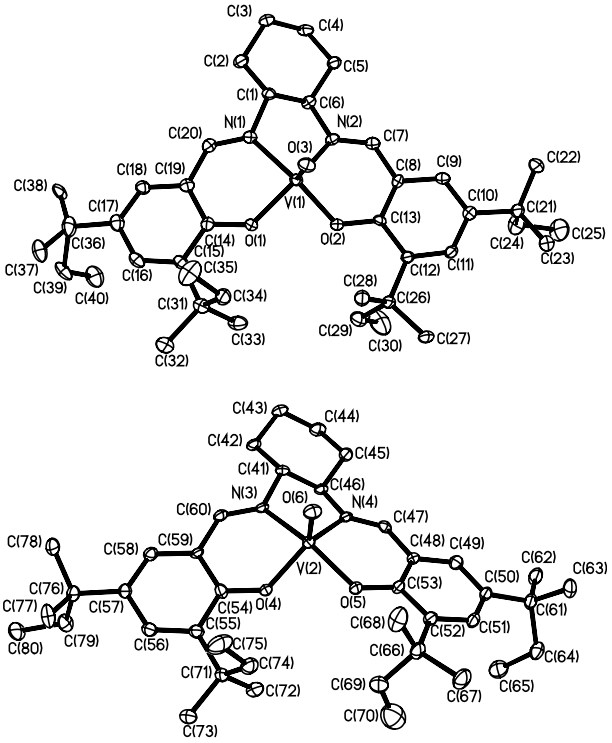


Fig. 1. ORTEP drawings of molecules **A** (top) and **B** (bottom).

It has been suggested that square-pyramidal complex should exhibit apical atom-basal atom in the range of 90°–113° [13], a diagnostics for tbp configuration when the angles exceed the range. The molecule **A** has all the O=V-basal atom angles in this range, fitting into the description of square-pyramidal (sp) geometry. The molecule **B**, on the other hand, has one O=V-basal atom angle beyond this range. Noticeably, the O(6)–V(2)–O(4) is 115.78°, suggesting that the geometry is not exactly square-pyramidal, and may be distorted to tbp, an alternative configuration for a five-coordinated complex.

Another important feature in the molecule **B** is the N(3)–V(2)–O(5) angle. The ideal angle should be 180° for a standard tbp complex with an unconstrained ligand, normally monodentate. When the ligand becomes multidentate, this angle is bent because of the ring restraint upon coordination. For example, in a structurally defined tbp Schiff base vanadyl complex, bis[*N*-(4-chlorophenyl)salicylaldehydeneiminato]oxovanadium (IV) [(Cl-Salim)$_2$VO] where the ligand is a bidentate Schiff base, this value was reported to be 159.1° [14]. It has been speculated that a more restrained ligand should lead to a further decrease in this angle. The salen ligand is an ideal ligand that should offer more restraint due to the tetradentate nature. The smallest value (152.81°) found in this complex appears to provide a direct correlation between ligand restraint and angle distortion with the following deviation trend: tetradentate ligand > bidentate ligand > monodentate.

For practical consideration, it is highly unlikely that a vanadyl complex with a multiple dentate ligand will have a perfect tbp configuration. The extent of such trigonality can be quantitatively described by the τ index, with value of zero for a perfect sp (no trigonality), and a unit for a perfect tbp [15,16]. The τ index is defined by $(\beta-\alpha)/60$ to give molecule **B** a τ value of 0.36 where α (131.11) and β (152.81) are diagonally basal angles. The character of trigonality is obvious when comparison is made against molecule **A** which has a τ value of almost zero. Using the same analysis, the τ value for the tbp-defined $(Cl\text{-}Salim)_2VO$ is 0.43 [17]. This number provides a quantitative insight that more trigonality character is possessed by a complex with bidentate ligands than with a tetradentate ligand, a complimentary description to the diagnosis using O=V-basal atom angles.

The tbp distorted geometry in molecule **B** could be caused by crystal packing although the exact reason is yet to be understood. The lack of two species coexisting in solution strongly suggests the possibility.

The complex in solution clearly shows two bands in the region from 377 to 624 nm due to d–d transition of square-pyramidal vanadyl. The vanadyl complexes can usually accept a sixth ligand to vanadium in the axial position *trans* to the oxygen atom. When this happens, the d–d transition bands will be solvent-dependent. However, some factors can have profound impact on this interaction. We have previously reported that a large displacement of vanadium from the basal plane would make the external ligand more difficult to gain access to the site, leading to weak or no interaction at all [18]. It has been speculated here that the steric effect from the bulky group, in particular, from the 3-position will hamper the approach of the external ligand to the vanadium atom in the sixth position. Fig. 2 shows that in solid state the two ethyl moieties from *t*-pentyl groups in the 3,3′-positions are already opposite to each other due to steric effect. To test this, two solvents, acetonitrile and pyridine, have been chosen. The donating ability of a solvent, defined by $D_{I/II}$ [19], is 2.60 for acetonitrile, a weak donating solvent and 4.40 for pyridine, a strong donating solvent. It has been found that the two bands appear at 377 ($\varepsilon=8151$) and 622 nm ($\varepsilon=162$) in acetonitrile, at 379 (9574) and 623 nm ($\varepsilon=155$) in pyridine, respectively. Clearly, there is no significant shift of absorption bands in both weak and strong donating solvents, suggesting that it is unlikely that there is any strong interaction between vanadium and the donating molecule. The bulky groups indeed appear to have an impact on the approach of the donating solvent to the vanadium.

The A values from EPR also appear to have no significant changes in these two solvents. The $A_{\parallel}$ and $A_{\perp}$ values obtained at -78 °C are also essentially unchanged (Fig. 3, Table 2). It needs to be pointed out that the complex in acetonitrile at low temperature tends to crystallize out, but, both $A_{\parallel}$ and $A_{\perp}$ values can be obtained to be fairly accurate. In addition, more A values from chloroform have been added for comparison. These data are consistent with the suggestion that there is no strong interaction between vanadium and donor molecules, even at low temperature. The anisotropic g values are evidently consistent again. The $g_{\parallel}$ and $g_{\perp}$ values are around 1.96 and 2.00, respectively, in all solvents. The current tensor and g values in solution are consistent with the presence of square-pyramidal configuration. The lack of two sets of peaks in the $A_{\parallel}$ region further suggests that the formation of the tbp geometry is probably a solid state phenomena, and molecule **B** is relaxed into **A** in solution.

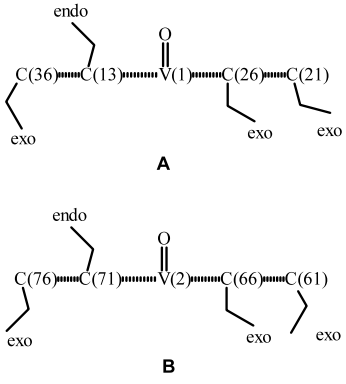


Fig. 2. Schematic representation of orientation of bulky *t*-pentyl groups in both molecules **A** and **B** in solid state.

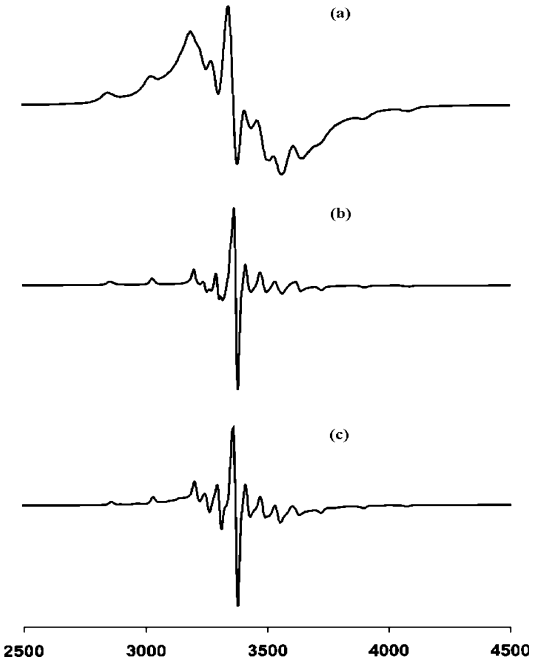


Fig. 3. Low temperature (liquid nitrogen) EPR spectra in various solvents: (a) acetonitrile; (b) pyridine; (c) chloroform.

Table 2
EPR data in various solvents

Solvent	A_o[a]	$A_\parallel$[b]	$A_\perp$[b]	g_0	$g_\perp$	$g_\perp$
Acetonitrile	97.05	171.07	61.58	1.9851	1.9609	1.9973
Pyridine	96.08	171.61	61.06	1.9853	1.9594	1.9983
Chloroform	95.24	172.08	60.61	1.9875	1.9616	2.0004

[a] In Gs, obtained at ambient temperature.
[b] In Gs, obtained at liquid nitrogen temperature.

In conclusion, the two configurations in a chiral vanadyl complex have been identified. One is almost symmetrical regarding coordination chromophore, which leads to square-pyramidal configuration, while the other is unsymmetrical, which leads to distorted tbp configuration. The tetradentate ligand constraint causes significantly large angle deviation between two axial bonds in the tbp configuration. The lack of finding these two species in solution suggests that this may be a solid state phenomena. Square-pyramidal vanadyl complex is only one species found in solution. Steric effect from bulky substituents at the 3-positions prevents donor molecules from interacting with metal centers.

4. Supplementary material

The supplementary material is available from the Cambridge Crystallographic Data Center, CCDC No. 162359 for compound **3**. Copies of this information may be obtained free of charge from The Director, CCDC, 12 Union Road, Cambridge, CB2 1EZ, UK (fax: +44-1223-336033; e-mail: deposit@ccdc.cam.ac.uk or www: http://www.ccdc.cam.ac.uk).

Acknowledgements

Financial support from the National Institute of Health/NIGMS (S06GM08247 and R25GM60414) and NASA (NCC3-552) is gratefully appreciated. We also thank Dr Ron Mason of NIEHS for his support of this work.

References

[1] B.J. Hamstra, A.L.P. Houseman, G.L. Colpas, J.W. Kampf, R. LoBrutto, W.D. Frasch, V.L. Pecoraro, Inorg. Chem. 36 (1997) 4866.
[2] A. Butler, J.V. Walker, Chem. Rev. 93 (1993) 1937.
[3] P. Caravan, L. Gelmini, N. Glover, G.F. Herring, H. Li, J.H. McNeil, S.J. Rettig, I.A. Setyawati, E. Shuter, Y. Sun, A.S. Tracey, V.G. Yuen, C. Orvig, J. Am. Chem. Soc. 117 (1995) 12759.
[4] L.C. Cantley, P. Aisen, J. Biol. Chem. 254 (1979) 1781.
[5] C.J. Chang, J.A. labinger, H.B. Gray, Inorg. Chem. 36 (1997) 5927.
[6] C. Bolm, F. Bienewald, Angew. Chem., Int. Ed. Engl. 34 (1995) 2640.
[7] K. Nakajima, M. Kojima, K. Toriumi, K. Saito, J. Fujita, Bull. Chem. Soc. Jpn. 62 (1989) 760.
[8] D.A. Cogan, G. Liu, K. Kim, B. Backes, J.A. Ellman, J. Am. Chem. Soc. 120 (1998) 8011.
[9] C. Bolm, F. Bienewald, Synlett (1998) 1327.
[10] F.A. Cotton, in: F.A. Cotton, G. Wilkinson (Eds.), Advanced Inorganic Chemistry, 5th ed., Wiley, New York, NY, 1988, p. 673.
[11] G. Casiraghi, G. Casnati, G. Puglia, G. Sartori, G. Terenghi, J. Chem. Soc., Perkin Trans. 1 (1980) 1862.
[12] S. Liang, X.R. Bu, J. Org. Chem. 67 (2002) 2702.
[13] A.L. Beauchamp, M.J. Bennett, F.A. Cotton, J. Am. Chem. Soc. 90 (1968) 6675.
[14] M. Pasquali, F. Marchetti, C. Floriani, S. Merlino, J. Chem. Soc., Dalton Trans. (1976) 139.
[15] A.W. Addison, T.N. Rao, J. Reedijk, J. van Rijn, G.C. Verschoor, J. Chem. Soc., Dalton Trans. (1984) 1349.
[16] Another treatment using dihedral angles, see: E.L. Muetterties, L.J. Guggenberger, J. Am. Chem. Soc. 96 (1974) 1748.
[17] The calculation is based on data provided in Ref. [14].
[18] X.R. Bu, E.A. Mintz, X.Z. You, R.X. Wang, Q.J. Meng, Polyhedron 15 (1996) 4585.
[19] J. Selbin, Chem. Rev. 65 (1965) 168.

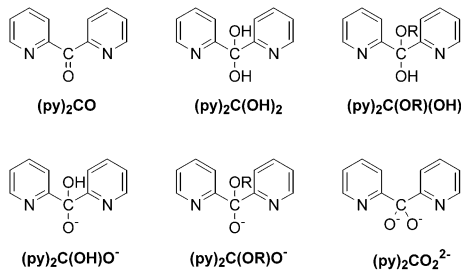


Fig. 1. Some of the ligands discussed in the text; note that $(py)_2C(OH)_2$, $(py)_2C(OR)(OH)$ and all three anions do not exist as free species but exist only in their complexes.

ions are bridged by anionic ligands present in the complexes, e.g. Cl^- or SCN^-.

Completely different and much more interesting (for cluster chemistry) coordination modes are seen when ligands $(py)_2C(OR)(OH)$ and $(py)_2C(OH)_2$ become deprotonated. Upon deprotonation, the former becomes monoanionic, while the latter can function either as monoanion or dianion. The presence of deprotonated hydroxy groups within $(py)_2C(OR)O^-$, $(py)_2C(OH)O^-$ and $(py)_2CO_2^{2-}$ (Fig. 1) leads to a great coordinative flexibility, due to the well known ability of the negatively charged oxygen to bridge two or three metal ions. The monoanionic forms usually bridge two (μ_2) or three (μ_3) metal ions, while the dianionic form can bridge as many as five metal sites. The ability of these forms to adopt a variety of coordination modes has resulted in the isolation of clusters with nuclearities ranging from 4 to 14 [11–13]. It is not known [14] whether the coordination of the oxygen to the metal center occurs *after* the hydration/alcoholysis reaction or *prior* to this reaction; in the former case there is a polarization effect of the metal upon the hydroxy group leading to its deprotonation, while in the latter case there is a direct activation of the carbonyl group towards nucleophilic attack.

Our groups are engaged in developing the polynuclear 3d-metal chemistry of di-2-pyridyl ketone [12,13]. Our main contribution to this area is twofold: firstly, the realisation that $(py)_2C(OH)_2$ can be doubly deprotonated leading to structurally impressive clusters [12] and, secondly, the incorporation of end-on azido ligands into the chemistry of $(py)_2CO_2^{2-}$ and $(py)_2C(OH)O^-$/$(py)_2C(OR)O^-$ as a means to introduce specifically ferromagnetic components in the superexchange schemes, thus increasing the ground-state S values of clusters [12,13].

We recently reported [12] that the reaction of $Co(O_2CMe)_2\cdot 4H_2O$ with $(py)_2CO$ and NaN_3 (9:4:2, 2:1:1 ratios) in DMF under heating led to the nonanuclear cage $[Co_9(N_3)_2(O_2CMe)_8\{(py)_2CO_2\}_4]$ (**1**), in which the nine Co^{II} atoms adopt a topology of two square pyramids sharing a common apex. Salient features of the structure are the unique η^1,μ_4 coordination mode of the azido ligands, the μ_5 coordination mode of $(py)_2CO_2^{2-}$ and the extremely rare coordination number 8 for the Co^{II} atom lying at the common apex of the pyramids. The magnetic study revealed ferromagnetic coupling mediated by the azido bridges giving a total S value of seven times the local spin and leading to a high-spin ferrimagnetic system.

We were interested to study whether and how the nature of the carboxylate ligands affects the structural and magnetic identity of the products resulting from the $Co^{II}/RCO_2^-/N_3^-$ reaction mixtures in DMF. For example, we wondered if replacement of acetates with benzoates in this reaction mixture would give a cluster structurally and magnetically similar to **1**. In this report, we describe the identity, single-crystal X-ray structure and magnetic properties of the product from the $Co^{II}/PhCO_2^-/N_3^-$ reaction mixture in DMF.

2. Experimental

2.1. Preparation of $[Co_4(N_3)_2(O_2CPh)_2\{(py)_2C(OH)O\}_4]\cdot 2DMF$ (2)

DMF (20 ml) was added to a solid mixture containing $Co(O_2CPh)_2$ (0.18 g, 0.60 mmol), $(py)_2CO$ (0.06 g, 0.31 mmol) and NaN_3 (0.02 g, 0.31 mmol). The solid dissolved upon stirring under heating to give a dark blue solution. The solution was allowed to stand undisturbed at room temperature for 3 days. Well-formed, X-ray quality pink crystals of the product appeared within this period. The crystals were collected by filtration, washed with DMF and Et_2O, and dried in vacuo over silica gel. Yield: 40% [based on $(py)_2CO$]. *Anal.* Found: C, 50.8; H, 3.9; N, 14.8. Calc. for $C_{64}H_{60}Co_4N_{16}O_{14}$: C, 50.8; H, 4.0; N, 14.8%. Complex **2** can also be isolated by employing an 1:1:0.5 $Co(O_2CPh)_2$–$(py)_2CO$–NaN_3 molar ratio.

Caution: azide salts are potentially explosive and should be handled in small quantities.

2.2. Physical measurements

Magnetic susceptibility measurements were carried out for a polycrystalline sample of **2** with a SQUID susceptometer working in the range 2–300 K under magnetic fields of approximately 0.1 T. Diamagnetic corrections were estimated from Pascal Tables. IR spectra (4000–400 cm^{-1}) were recorded from KBr pellets on a Nicolet 520 FTIR spectrometer.

2.3. X-ray crystallography

Analyses on pink prismatic single crystal of **2** were carried out with an MAR345 diffractometer with image plate detector. Intensities were collected with graphite

Table 1
Crystallographic data for complex $[Co_4(N_3)_2(O_2CPh)_2\{(py)_2C(OH)O\}_4]\cdot 2DMF$ (**2**)

Parameter	**1**
Empirical formula	$C_{64}H_{60}Co_4N_{16}O_{14}$
Formula weight	1513.02
Colour and habit	pink, prism
T (°C)	20
λ (Mo Kα) (Å)	0.71069
Crystal system	monoclinic
Space group	$C2/c$
a (Å)	14.242(8)
b (Å)	16.075(8)
c (Å)	28.844(3)
α (°)	90.00
β (°)	92.36(4)
γ (°)	90.00
V (Å^3)	6598(5)
Z	4
D_{calc} (Mg m^{-3})	1.523
μ (mm^{-1})	1.066
$F(000)$	3104
Crystal size (mm)	0.10 × 0.10 × 0.20
$2\theta_{max}$ (°)	28.87
Index ranges (°)	$-15 \le h \le 15$, $0 \le k \le 18$, $0 \le l \le 38$
Reflections collected	8219
Independent reflections/R_{int}	5024/0.031
Data with $I > 2\sigma(I)$	3903
Parameters refined	507
R_1 [a]	0.0324
wR_2 [b]	0.0903
Goodness-of-fit (on F^2)	1.073
Residuals (e Å^{-3})	0.508/−0.467

[a] $R_1 = \Sigma\,(|F_o|-|F_c|)/\Sigma\,(|F_o|)$.
[b] $wR_2 = \{\Sigma\,[w((F_o^2-F_c^2)^2]/\Sigma[w(F_o^2)^2]\}^{1/2}$.

monochromatized Mo Kα radiation. A summary of the crystallographic data is reported in Table 1. Unit cell parameters for **2** were determined from automatic centering of 8219 reflections ($3^\circ < \theta < 30^\circ$) and refined by the least-squares method. Five thousand and twenty-four reflections were measured in the range $2.81^\circ < \theta < 28.87^\circ$. Three thousand nine hundred and three reflections were assumed as observed applying the condition $I > 2\sigma(I)$. Lp but no absorption corrections were made.

The structure was solved by direct methods using the SHELXS computer program [15] and refined by full-matrix least-squares method, with the SHELX-97 computer program [16] using 5024 reflections. The function minimized was $\Sigma\, w||F_o|^2-|F_c|^2|^2$, where $w=[\sigma^2(I)+(0.0655P)^2]^{-1}$, and $P=(|F_o|^2+2|F_c|^2)/3$. f, f' and f'' were taken from *International Tables of X-ray Crystallography* [17]. Sixteen hydrogen atoms were located from a difference synthesis and 12 H atoms were computed. All were refined with an isotropic temperature factor equal to 1.2 times the equivalent isotropic temperature factor of the bonded atom. A riding model was used for computed hydrogen atoms. The number of parameters refined was 507. Max. shift/esd = 0.002. Mean shift/esd = 0.000.

3. Results and discussion

3.1. Synthesis

As stated in Section 1, the initial goal of this work was the preparation of a cobalt(II) benzoate cluster with a structure and magnetic properties similar to those of **1**. Our general synthetic approach for the isolation of heteroleptic $RCO_2^-/(py)_2CO_2^{2-}/N_3^-$ metal clusters is to react an excess of the metal carboxylate with $(py)_2CO$ and N_3^- in DMF under heating [12]. Obviously $(py)_2C(OH)_2$ is fully deprotonated by the basic carboxylate groups and polynuclear $M^{II}/RCO_2^-/(py)_2CO_2^{2-}/N_3^-$ complexes result from the reactions [as long as the RCO_2^-–$(py)_2CO$ ratio is high enough to leave an amount of nonprotonated RCO_2^- in the reaction mixture], given the fact that the RCO_2^-, $(py)_2CO_2^{2-}$ and azido ligands can potentially adopt a variety of terminal and bridging modes.

Reaction of $Co(O_2CPh)_2$ with $(py)_2CO$ and NaN_3 (2:1:1 molar ratio) in DMF under heating resulted in a blue solution from which the pink tetranuclear complex $[Co_4(N_3)_2(O_2CPh)_2\{(py)_2C(OH)O\}_4]\cdot 2DMF$ (**2**) was isolated in moderate yield. We did not try to optimize the yield. The low to moderate yield in our experiments is presumably a consequence of the crystallization method (see Section 2.1). The extremely slow evaporation of the solvent (DMF) at room temperature and the relatively short time ($\sim$3 days) of the storage of the open reaction flask before filtration may both be responsible for the obtained yields. The stoichiometric reaction is represented by Eq. (1):

$$4Co(O_2CPh)_2 + 4(py)_2CO + 4H_2O + 2NaN_3 + 2DMF \xrightarrow[T]{DMF} \underset{\mathbf{2}}{[Co_4(N_3)_2(O_2CPh)_2\{(py)_2C(OH)O\}_4]\cdot 2DMF} + 4PhCO_2H + 2NaO_2CPh \quad (1)$$

Surprisingly, a seemingly subtle change in the reaction conditions that gave complex **1** (i.e. changing the acetates with benzoates) led to a dramatic change in the type of complex produced. Complex **1** is a nonanuclear cage containing doubly deprotonated $(py)_2CO_2^{2-}$ ligands, whereas **2** is a tetranuclear cluster containing singly deprotonated $(py)_2C(OH)O^-$ ligands. Further increase in the 'base' ($PhCO_2^-$) to 'acid' ['$(py)_2C(OH)_2$'] ratio, either by increase of the $Co(O_2CPh)_2$–$(py)_2CO$ molar ratio from 2:1 to 3:1 or by employment of external $PhCO_2^-$s, and longer reaction times did not give any evidence for the formation of a complex containing dianions $(py)_2CO_2^{2-}$ as ligands. We strongly believe that the

lower basicity of $PhCO_2^-$ (the pK_a value of its conjugate acid, $PhCO_2H$, is 4.19) compared to $MeCO_2^-$ (pK_a of $MeCO_2H = 4.75$) is responsible for the inability of $PhCO_2^-$s to doubly deprotonate '$(py)_2C(OH)_2$' and the failure to isolate the benzoate analogue of **1**.

Use of external hydroxides (LiOH, Me_4NOH) to help double deprotonation of the *gem*-diol form of $(py)_2CO$ complicates the reaction mixture leading to non-crystalline hydroxo products with poor analytical results.

Looking for an alternative method of preparing the benzoate analogue of **1**, we anticipated that complex **1** would be capable of acetate substitution on treatment with $PhCO_2H$. Such a reactivity pattern is consistent with the known acidities of the RCOOH molecules as reflected in the pK_a values (see above) and the probable mechanism [18] involves protonation of bound acetates by more acidic $PhCO_2H$ molecules, followed by their displacement by generated $PhCO_2^-$s. Such ligand substitution reactions have been widely used in metal carboxylate cluster chemistry [18,19]. Unfortunately, we could not confirm this type of reactivity for **1**. Addition of excess of $PhCO_2H$ to **1** in MeOH or DMF gives a mixture of products (including **2**) depending on the reaction conditions; the separation of these products was impossible.

With the identity of **2** established by single-crystal X-ray crystallography (vide infra), a modified preparative procedure (not reported in detail in Section 2) was devised by adjusting the $Co(O_2CPh)_2$–$(py)_2CO$–NaN_3 reaction ratio in DMF from 2:1:1 to 1:1:0.5 (Eq. (1)). We have also found that heating is not necessary for the preparation of **2**.

3.2. Description of structure

A plot of the structure of the tetranuclear compound $[Co_4(N_3)_2(O_2CPh)_2\{(py)_2C(OH)O\}_4]\cdot 2DMF$ (**2**) is shown in Fig. 2(a). Fig. 2(b) emphasizes the core of the tetranuclear molecule and shows the numbering scheme. Selected distances and angles are listed in Table 2.

The structure consists of centrosymmetric tetranuclear molecules. The four Co^{II} atoms are located at four corners of a defective double cubane (two cubanes sharing one face and each missing one vertex, see Fig. 2(b)) and bridged by means of two end-on (η^1,μ_2) azido ligands and O atoms from the $(py)_2C(OH)O^-$ anions. Peripheral ligation is provided by two O atoms of the terminal benzoate ligands and the N atoms of the eight 2-pyridyl rings. Atoms O(1) of two $(py)_2C(OH)O^-$ ligands are triply bridging with distances to Co^{II} atoms of 2.225(2), 2.155(2) and 2.015(2) Å for Co(1)–O(1), Co(2)–O(1) and Co(2)#1–O(1), respectively. The Co(1)–O(1)–Co(2) and Co(1)–O(1)–Co(2)#1 angles are 97.4(1)° and 96.2(1)°, respectively. Atoms O(3) of the two other $(py)_2C(OH)O^-$ ligands are doubly bridging with distances of 2.012(2) and 2.154(2) Å to Co(1) and Co(2)#1, respectively. The Co(1)–O(3)–Co(2)#1 angle is 98.5(1)°. One O atom of each $(py)_2C(OH)O^-$ ligand remains protonated and unbound to the metals. Therefore, two $(py)_2C(OH)O^-$ ions adopt the η^1:η^3:η^1:μ_3 coordination mode and the other two bind with the η^1:η^2:η^1:μ_2 mode (Fig. 3). Co(1) and Co(2) are also bridged by the N(1) atom of the η^1, μ_2 azido ligand (end-on). The Co(1)–N(1) and Co(2)–N(1) distances are 2.158(2) and 2.103(2) Å, respectively. The Co(1)–N(1)–Co(2) angle is 101.1(1)°. The azido ligand is practically linear with a N(1)–N(2)–N(3) angle of 179.5(3)°.

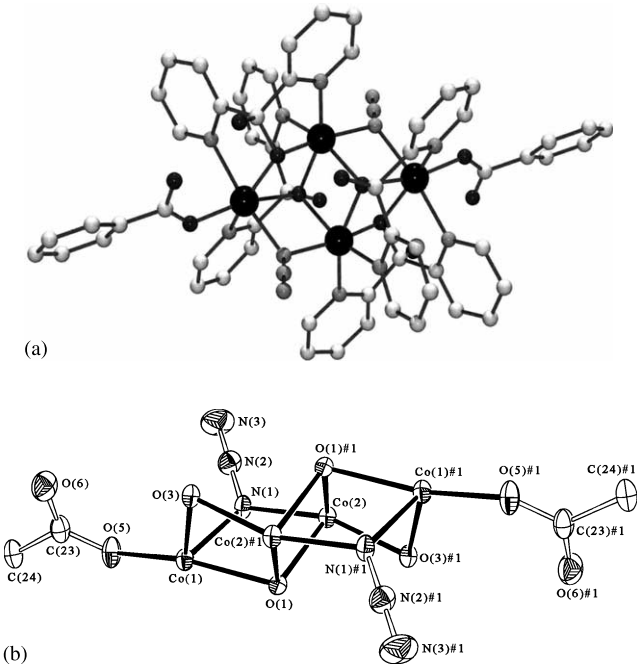


Fig. 2. (a) Plot of $[Co_4(N_3)_2(O_2CPh)_2\{(py)_2C(OH)O\}_4]\cdot 2DMF$ (**2**); the solvate DMF molecules have been omitted. (b) Labelled plot of the defective, double-cubane core present in complex **2**.

The metal ions have distorted octahedral geometries. The Co(1) octahedral coordination is completed by the N(4) and N(6) atoms of two $(py)_2C(OH)O^-$ ligands, and the O(5) atom of the terminal benzoate ligand. The Co(2) octahedral coordination is completed by the N(5)#1 and the N(7)#1 atoms of two $(py)_2C(OH)O^-$ ligands with Co(2)–N(5)#1 and Co(2)–N(7)#1 distances of 2.168(2) and 2.079(2) Å, respectively.

3.3. IR spectroscopy

The presence of DMF in **2** is manifested by a medium-intensity band at 1669 cm^{-1} and a weak band at 645 cm^{-1}, assigned to ν(C=O) and δ(OCN), respectively [20]. The absence of shifts of these bands in the complex, when compared with the corresponding bands in the spectrum of free DMF [21], implies that there is no interaction between DMF and the Co^{II} atoms. The complex exhibits an intense band at 2076 cm^{-1},

Table 2
Selected interatomic distances (Å) and angles (°) for $[Co_4(N_3)_2(O_2CPh)_2\{(py)_2C(OH)O\}_4]\cdot 2DMF$ (**2**)

Bond distances			
Co(1)···Co(2)	3.2897(19)	Co(2)–N(1)	2.103(2)
Co(1)···Co(2)#1	3.1581(18)	Co(2)–O(3)#1	2.154(2)
Co(1)···Co(1)#1	5.631(1)	Co(2)–O(1)	2.155(2)
Co(2)···Co(2)#1	3.1442(1)	Co(2)–N(5)#1	2.168(2)
Co(1)–O(3)	2.012(2)	N(1)–N(2)	1.207(3)
Co(1)–O(5)	2.034(2)	N(2)–N(3)	1.140(4)
Co(1)–N(4)	2.150(2)	O(2)–C(6)	1.420(2)
Co(1)–N(1)	2.158(2)	O(4)–C(17)	1.399(3)
Co(1)–N(6)	2.176(2)	O(6)–C(23)	1.247(3)
Co(1)–O(1)	2.225(2)	O(1)–C(6)	1.372(3)
Co(2)–O(1)#1	2.015(2)	O(3)–C(17)	1.383(2)
Co(2)–N(7)#1	2.079(2)	O(5)–C(23)	1.255(3)
Bond angles			
O(3)–Co(1)–O(5)	115.8(1)	N(7)#1–Co(2)–O(3)#1	76.4(1)
O(3)–Co(1)–N(4)	150.5(1)	N(1)–Co(2)–O(3)#1	162.8(1)
O(5)–Co(1)–N(4)	91.9(1)	O(1)#1–Co(2)–O(1)	82.2(1)
O(3)–Co(1)–N(1)	92.1(1)	N(7)#1–Co(2)–O(1)	105.5(1)
O(5)–Co(1)–N(1)	96.2(1)	N(1)–Co(2)–O(1)	81.4(1)
N(4)–Co(1)–N(1)	94.9(1)	O(3)#1–Co(2)–O(1)	84.3(1)
O(3)–Co(1)–N(6)	75.7(1)	O(1)#1–Co(2)–N(5)#1	76.7(1)
O(5)–Co(1)–N(6)	85.5(1)	N(7)#1–Co(2)–N(5)#1	98.4(1)
N(4)–Co(1)–N(6)	97.8(1)	N(1)–Co(2)–N(5)#1	93.1(1)
N(1)–Co(1)–N(6)	167.1(1)	O(3)#1–Co(2)–N(5)#1	103.8(1)
O(3)–Co(1)–O(1)	80.2(1)	O(1)–Co(2)–N(5)#1	155.9(1)
O(5)–Co(1)–O(1)	163.6(1)	Co(1)–O(3)–Co(2)#1	98.5(1)
N(4)–Co(1)–O(1)	73.2(1)	Co(2)–O(1)–Co(1)	97.4(1)
N(1)–Co(1)–O(1)	78.6(1)	Co(2)#1–O(1)–Co(1)	96.2(1)
N(6)–Co(1)–O(1)	103.1(1)	Co(2)#1–O(1)–Co(2)	97.8(1)
O(1)#1–Co(2)–N(7)#1	155.9(1)	Co(2)–N(1)–Co(1)	101.1(1)
O(1)#1–Co(2)–N(1)	105.4(1)	N(2)–N(1)–Co(1)	126.3(2)
N(7)#1–Co(2)–N(1)	98.4(1)	N(2)–N(1)–Co(2)	122.0(2)
O(1)#1–Co(2)–O(3)#1	81.9(1)	N(1)–N(2)–N(3)	179.6(3)

Symmetry transformations used to generate equivalent atoms: #1 $-x+2$, $-y$, $-z+1$.

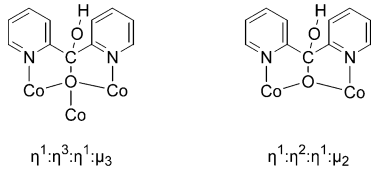


Fig. 3. The crystallographically established coordination modes of the $(py)_2C(OH)O^-$ ligands in complex **2**.

assigned to the asymmetric stretching mode of the azido ligands [13]. The strong bands at 1601 and 1388 cm^{-1} are assigned to the ν_{as}(COO) and ν_s(COO) modes, respectively [22]; the former should also involve a pyridine stretching character. The difference Δ [$\Delta = \nu_{as}(COO) - \nu_s(COO)$] for **2** (213 cm^{-1}) is more than that for NaO_2CPh, as expected for the monodentate mode of carboxylate ligation [22]. The spectrum of **2** also exhibits a strong band at 3445 cm^{-1}, assignable to $\nu(OH)_{(py)_2C(OH)O^-}$. The broadness and relatively low frequency of this band are both indicative of hydrogen bonding.

3.4. Magnetochemistry

The $\chi_M T$ product versus T of **2** in the 300–2 K range is shown in Fig. 4 (χ_M is the corrected molar magnetic susceptibility per tetramer). $\chi_M T$ increases quickly on cooling from 10.8 cm^3 K mol^{-1} at 300 K to a maximum of 16.9 cm^3 K mol^{-1} at 11 K, and then decreases to 14.6 cm^3 K mol^{-1} at 2 K. χ_M increases upon cooling and does not have any maximum in the temperature range studied. The overall behaviour of **2** corresponds to a ferromagnetically coupled system. The strong ferromagnetic interaction in **2** is confirmed by the molar magnetization measurement at 2 K, which shows a quick increase of $M/N\beta$ by increasing the external field, arriving to a final value of 10.37 at 5.0 T (Fig. 5). This strong coupling between Co(2) and Co(1) permits us to assume that the interactions through the η^1,μ_2-N_3^- and the μ-O^- bridge with the Co(1)–O(1)–Co(2) angle of 97.4(1)° are both ferromagnetic, indicating a magnetic behaviour similar to that found for the structurally related Co(II) derivatives $[Co_4(\eta^1,\mu_2\text{-}N_3)_2(N_3)_2\{(py)_2C(OH)O\}_2\{(py)_2C(OMe)O\}_2]\cdot 2H_2O$ (**3**) [13] and $[Co_4(\eta^1,\mu_2\text{-}N_3)_2(H_2O)_2\{(py)_2C(OH)O\}_2\{(py)_2C(OMe)O\}_2](BF_4)_2\cdot 4H_2O$ (**4**) [11]. All three complexes have the same defective double-cubane core. Analysis of the coupling constants for a high-spin rhombic cobalt(II) tetramer is not possible by means of an effective Hamiltonian based on four $S = 3/2$ spins, due to the large anisotropy of this ion [11,13]. At low temperature the local spin of Co^{II} is closer to $\frac{1}{2}$, and then the low temperature data are better defined as an $S_T = 2$ system with a large g_{eff} value.

3.5. Synthetic aspects of the $Co^{II}/(py)_2CO/N_3^-$ reaction system

Complex **2** is structurally related to complexes $[Co_4(\eta^1,\mu_2\text{-}N_3)_2(N_3)_2\{(py)_2C(OH)O\}_2\{(py)_2C(OMe)O\}_2]\cdot 2H_2O$ (**3**) [13] and $[Co_4(\eta^1,\mu_2\text{-}N_3)_2(H_2O)_2\{(py)_2C(OH)O\}_2\{(py)_2C(OMe)O\}_2](BF_4)_2\cdot 4H_2O$ (**4**) [11], prepared from the $Co(O_2CMe)_2\cdot 4H_2O/(py)_2CO/NaN_3$ (1:1:1, 1:2:2, 1:3:3, 1:2:4, 1:4:4) and $CoCl_2\cdot 6H_2O/(py)_2CO/NaN_3/NaBF_4$ (1:1:0.5:0.5) reaction mixtures, respectively, in $MeOH/H_2O$. All three complexes have a defective, double-cubane motif. There are two chemical

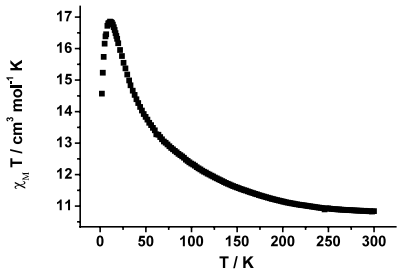


Fig. 4. $\chi_M T$ plot vs. T for compound **2**.

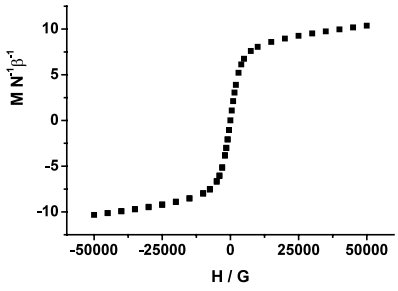


Fig. 5. Plot of the magnetization ($M/N\mu_B$) vs. H for **2** at 2 K.

differences along the series which have no structural effect. First, complexes **3** and **4** have two $(py)_2C(OH)O^-$ and two $(py)_2C(OMe)O^-$ ligands; this is a consequence of MeOH present in the reaction systems that lead to **3** and **4**. Second, the two terminal monodentate ligands differ in the three complexes; these are $PhCO_2^-$ ions in **2**, N_3^- ions in **3** and H_2O molecules in **4** (giving rise to a cationic species). The presence of benzoate ligands in **2** is a result of the high $PhCO_2^-$–N_3^- ratio used (4:1), whereas the presence of the two terminal azide ligands in **3** can be explained by the lower $MeCO_2^-$–N_3^- ratios used (2:1, 1:1, 1:1.5, 1:2) in the reaction mixtures. The existence of aqua ligands in the structure of **4** is certainly due to the presence of BF_4^- ions in the reaction system; the latter favour formation of cationic species.

4. Supplementary material

Further details (excluding structure factors) for the structures reported in this paper have been deposited with the Cambridge Crystallographic Data Centre, CCDC No. 180597 for compound **2**. Copies of the data may be obtained free of charge from The Director, CCDC, 12 Union Road, Cambridge, CB2 1EZ (fax: +44-1223-336033; e-mail: deposit@ccdc.cam.ac.uk or www: http://www.ccd.cam.ac.uk).

Acknowledgements

This research was partially supported by CICYT (Grant BQU2000/0791) and by the Research Committee of the University of Patras (K. CARATHEODORY Program No 1941 to S.P.P.).

References

[1] R.M. Cinco, A. Rompel, H. Visser, G. Aromi, G. Christou, K. Sauer, M.P. Klein, V.K. Yachandra, Inorg. Chem. 38 (1999) 5988.
[2] G. Christou, D. Gatteschi, D.N. Hendrickson, R. Sessoli, MRS Bull. 25 (2000) 1.
[3] D. Gatteschi, R. Sessoli, A. Cornia, Chem. Commun. (2000) 725.
[4] R.E.P. Winpenny, J. Chem. Soc., Dalton Trans. (2002) 1.
[5] G. Yang, S.-L. Zheng, X.-M. Chen, H.K. Lee, Z.-Y. Zhou, T.C.W. Mak, Inorg. Chim. Acta 303 (2000) 86.
[6] A representative reference is: A.C. Devenson, S.L. Heath, C.J. Harding, A.K. Powell, J. Chem. Soc., Dalton Trans. (1996) 3173.
[7] S.O. Sommerer, B.L. Westcott, A.J. Jircitano, K.A. Abboud, Acta Crystallogr. Sect. C 52 (1996) 1426.
[8] A recent representative reference is: O.J. Parker, S.L. Aubol, G.L. Breneman, Polyhedron 19 (2000) 623.
[9] C. Hemmert, M. Renz, H. Gornitzka, S. Soulet, B. Meunier, Chem. Eur. J. 5 (1999) 1766.
[10] Z.E. Serna, R. Cortés, M.K. Urtiaga, M.G. Barandika, L. Lezama, M.I. Arriortua, T. Rojo, Eur. J. Inorg. Chem. (2001) 865.
[11] Z.E. Serna, M.K. Urtiaga, M.G. Barandika, R. Cortés, S. Martin, L. Lezama, M.I. Arriortua, T. Rojo, Inorg. Chem. 40 (2001) 4550 (and references therein).
[12] G.S. Papaefstathiou, S.P. Perlepes, A. Escuer, R. Vicente, M. Font-Bardia, X. Solans, Angew. Chem., Int. Ed. Engl. 40 (2001) 884 (and references therein).
[13] G.S. Papaefstathiou, A. Escuer, C.P. Raptopoulou, A. Terzis, S.P. Perlepes, R. Vicente, Eur. J. Inorg. Chem. (2001) 1567 (and references therein).
[14] E.C. Constable, Metals and Ligand Reactivity, VCH, Weinheim, Germany, 1996, pp. 46, 47, 57–59.
[15] G.M. Sheldrick, A computer program for determination of crystal structure, University of Göttingen, Germany, 1997.
[16] G.M. Sheldrick, A computer program for determination of crystal structure, University of Göttingen, Germany, 1997.
[17] International Tables of X-Ray Crystallography, Kynoch press, vol. IV, 1974, pp. 99–100 and 149.
[18] J.B. Vincent, C. Christmas, H.-R. Chang, Q. Li, P.D.W. Boyd, J.C. Huffman, D.N. Hendrickson, G.C. Christou, J. Am. Chem. Soc. 111 (1989) 2086.
[19] G. Christou, S.P. Perlepes, E. Libby, K. Folting, J.C. Huffman, R.J. Web, D.N. Hendrickson, Inorg. Chem. 29 (1990) 3657.
[20] E. Manessi-Zoupa, S.P. Perlepes, V. Hondrellis, J.M. Tsangaris, J. Inorg. Biochem. 55 (1994) 217.
[21] C. Airoldi, Inorg. Chem. 20 (1981) 998.
[22] G.B. Deacon, R.J. Phillips, Coord. Chem. Rev. 33 (1980) 227.

dinuclear ruthenium terpyridine complexes using the α,α′-diimine based neutral bridging functions NC_5H_4–CH=N–$(C_6H_4)_n$–N=CH–H_4C_5N ($n = 1$, 2), L. Although the bridging functions (L) are stable enough in the free state [28,29], during the reaction with $Ru(trpy)Cl_3$ (trpy = 2,2′:6,2″-terpyridine) one of the imine functions of L has been selectively hydrolyzed. This in turn leads to the formation of ruthenium monoterpyridine complexes of the type $[Ru^{II}(trpy)(L')Cl]^+$ (**1**) where L′ corresponds to NC_5H_4–CH=N–$(C_6H_4)_n$–NH_2 ($n = 1$, 2).

Herein we report the stepwise syntheses of the complexes, $[Ru^{II}(trpy)(L')Cl]^+$ (**1**) → $[Ru^{II}(trpy)(L')H_2O]^{2+}$ (**2**) → $[Ru^{IV}(trpy)(L')O]^{2+}$ (**3**), crystal structures of L^1 and **1a**, and the chemical–electrochemical reactivities of the complexes including the catalytic/electrocatalytic behaviors of the in situ generated oxo species (**3**). The specific role of the electronic nature of L′ in **1**–**3** in comparison with the analogous ancillary functions present in other known ruthenium monoterpyridine complexes have been noted.

2. Experimental

2.1. Materials

The starting complex $Ru(trpy)Cl_3$ and the ligands L^{1-2} were prepared according to the reported procedures [30,28]. 2,2′:6,2″-terpyridine was obtained from Aldrich, USA. Other chemicals and solvents were reagent grade and used as received. Alumina (neutral) was used for column chromatography. For spectroscopic and electrochemical studies HPLC grade solvents were used. Water of high purity was obtained by distillation of the deionized water from $KMnO_4$. Sodium perchlorate for electrochemical work in aqueous medium was recrystallized from water.

2.2. Physical measurements

UV–Vis spectra were recorded by using a Shimadzu-2100 spectrophotometer. FT-IR spectra were taken on a Nicolet spectrophotometer with samples prepared as KBr pellets. Solution electrical conductivity was checked using a Systronic 305 conductivity bridge. Magnetic susceptibility was checked with a PAR vibrating sample magnetometer. NMR spectra were obtained with a 300 MHz Varian FT spectrometer. Cyclic voltammetric, differential pulse voltammetric and coulometric measurements were carried out using a PAR model 273A electrochemistry system. Platinum wire working and auxiliary electrodes and an aqueous saturated calomel reference electrode (SCE) were used in a three-electrode configuration. The supporting electrolyte was $[NEt_4]ClO_4$ and the solute concentration was approximately 10^{-3} M. The half-wave potential E°_{298} was set equal to $0.5(E_{pa}+E_{pc})$, where E_{pa} and E_{pc} are anodic and cathodic cyclic voltammetric peak potentials, respectively. A Pt wire-gauze working electrode was used in coulometric experiments. All experiments were carried out under a dinitrogen atmosphere and were uncorrected for junction potentials. The elemental analyses were carried out with a Carlo–Erba (Italy) elemental analyzer. Solution emission properties were checked using a SPEX-fluorolog spectrofluorometer. X-ray data were collected by using a Nonius MACH 3 four-circle diffractometer with graphite monochromated Mo Kα radiation ($\lambda = 0.71073$ Å).

2.3. Preparation of complexes

The complexes $[Ru(trpy)(L')(Cl)](ClO_4)\cdot 2H_2O$ (**1a** and **1b**) were prepared by following a general procedure. Details are mentioned for the complex **1a**.

2.4. *[Ru(trpy)(L′)(Cl)]$ClO_4\cdot 2H_2O$ (1a)*

The starting complex $Ru(trpy)Cl_3$ (100 mg, 0.227 mmol) was taken in 25 ml of hot EtOH. The preformed bridging ligand L^1 (65 mg, 0.228 mmol) was added to the above solution and the mixture was heated to reflux for 14 h. The solvent was removed under reduced pressure. The residual mass was dissolved in a minimum volume of MeCN and saturated aq. $NaClO_4$ solution was added. The solid product thus obtained on cooling was filtered and washed with ice-cold water followed by cold EtOH. The crude product was purified by using an alumina (neutral) column. Initially the side product, $[Ru(trpy)_2](ClO_4)_2\cdot 2H_2O$ was eluted by CH_2Cl_2–MeCN (5:2) mixture. The pink colored complex, **1a** was eluted by CH_2Cl_2–MeCN (5:3) mixture. Another fraction of the pink solution corresponding to **1a** was eluted later by CH_2Cl_2–MeCN (1:1) from the same column. The complex **1a** thus obtained from the two different batches were further purified separately by following the same above procedures in order to remove any trace of $[Ru(trpy)_2](ClO_4)_2\cdot 2H_2O$ impurity. Similarly the $[Ru(trpy)_2](ClO_4)_2\cdot 2H_2O$ complex obtained from the above column was also purified again in order to make it free from **1a**. The two pink colored solutions thus obtained separately from the same column were found to exhibit identical spectral and electrochemical features. Evaporation of the solvent mixture resulted in pure solid complexes, **1a** and $[Ru(trpy)_2](ClO_4)_2\cdot 2H_2O$. Yield: **1a** (95.0 mg, 61%) and $[Ru(trpy)_2](ClO_4)_2\cdot 2H_2O$ (15 mg, 10%). *Anal*. Calc. for **1a**: C, 46.15; H, 3.73; N, 11.97. Found: C, 46.31; H, 3.45; N, 12.22%. Λ_M/Ω^{-1} ($cm^2\ mol^{-1}$) in MeCN at 298 K: 148. *Anal*. Calc. for **1b**: C, 50.90; H, 3.89; N, 10.80. Found: C, 50.52; H, 3.32; N, 11.02%. Λ_M/Ω^{-1} ($cm^2\ mol^{-1}$) in MeCN at 298 K: 140.

2.5. [Ru(trpy)(L′)(H$_2$O)](ClO$_4$)$_2$·2H$_2$O (2a)

The aqua complexes (**2**) were prepared from the corresponding chloro species using excess $AgNO_3$. Details are mentioned for **2a**.

Silver nitrate (120 mg, 0.70 mmol) was added to the aqueous solution of the chloro complex, [Ru(trpy)(L′)(Cl)]ClO$_4$·2H$_2$O (**1a**) (100 mg, 0.14 mmol in 15 ml water) and the solution was heated to reflux for 2.5 h. It was then cooled and the precipitated AgCl was filtered off through a sintered glass crucible (G-4). The volume of the filtrate was reduced to 5 ml and saturated aq. $NaClO_4$ solution was added to it. The mixture was kept in the refrigerator overnight. The solid product (**2a**) thus obtained was filtered and washed with ice-cold water and dried in vacuo over P_4O_{10}. Yield: 78 mg (70%). *Anal*. Calc. for **2a**: C, 41.34; H, 3.60; N, 10.71. Found: C, 40.92; H, 3.33; N, 10.37%. Λ_M/Ω^{-1} (cm^2 mol^{-1}) in MeCN at 298 K: 230. *Anal*. Calc. for **2b**: C, 46.06; H, 3.75; N, 9.77. Found: C, 46.59; H, 3.43; N, 10.11%. Λ_M/Ω^{-1} (cm^2 mol^{-1}) in MeCN at 298 K: 240.

2.6. X-ray structure determination

The single crystals of L^1 were grown by slow diffusion of a CH_2Cl_2 solution of L^1 in C_6H_{14} followed by slow evaporation. The single crystals of **1a** were obtained by slow diffusion of the MeCN solution of **1a** in C_6H_6 followed by slow evaporation. Significant crystal data and data collection parameters are listed in Table 1. The structures were solved by direct methods using SHELXS-86 and refined by full-matrix least-squares on F^2 using SHELXL-97 [31].

Table 1
Crystallographic data for NC$_5$H$_4$–CH=N–(C$_6$H$_4$)–N=CH–H$_4$C$_5$N (L^1) and [Ru^{II}(trpy){NC$_5$H$_4$–CH=N–C$_6$H$_4$–NH$_2$}Cl]ClO$_4$ (**1a**)

	L^1	**1a**
Empirical formula	$C_9H_7N_2$	$C_{27}H_{22}N_6Cl_2O_4Ru$
M	143.17	666.48
Crystal symmetry	monoclinic	monoclinic
Space group	$P2_1/a$	$P2_1/n$
a (Å)	11.5290 (14)	8.4410 (10)
b (Å)	4.8118 (6)	13.884 (2)
c (Å)	13.7074 (14)	23.673 (4)
β (°)	109.14 (1)	98.710 (10)
V (Å^3)	718.39 (14)	2742.4 (7)
Z	4	4
μ (mm^{-1})	0.082	0.812
R_1	0.0403	0.0877
wR_2	0.0940	0.0999

3. Results and discussion

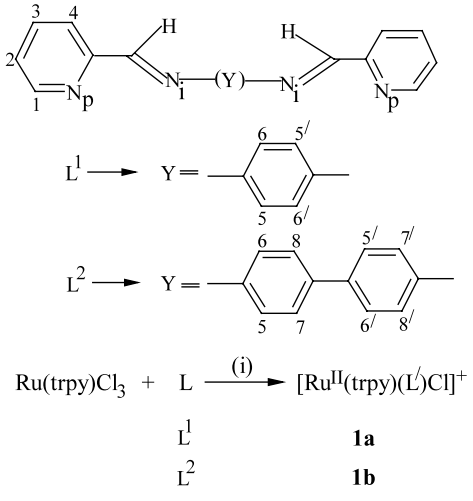
3.1. Synthesis

The bridging ligands L^1–L^2, used for the present study differ primarily with respect to the length of the spacers (Scheme 1). The ligands are designed with the intention of holding two Ru(trpy)Cl units through the terminal N$_p$ (N$_p$ = pyridine nitrogen) and N$_i$ (N$_i$ = imine nitrogen) donor centers of L. However, the reaction of L with the starting complex Ru(trpy)Cl$_3$ in a 1:2 mole ratio in ethanol solvent results in a monomeric species of the type [Ru(trpy)(L′)Cl]$^+$, **1** where L′ corresponds to NC$_5$H$_4$CH=N–(C$_6$H$_4$)$_n$–NH$_2$ ($n = 1$, **1a**; $n = 2$, **1b**) (Scheme 1).

During the course of the reaction one of the imine functions of the preformed bridging ligands (L) has been selectively hydrolyzed and the resulting mononucleating fragment of the bridging moiety (L′) leads to the formation of **1** (Scheme 1). The complexes have been isolated as their dihydrated perchlorate salts, [Ru^{II}(trpy)(L′)Cl]ClO$_4$·2H$_2$O (**1**).

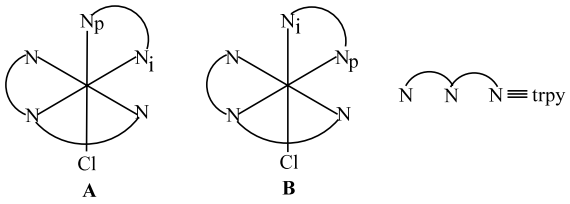
Under identical reaction conditions (Scheme 1) but in the absence of ruthenium precursor Ru(trpy)Cl$_3$, the preformed bridging functions (L) are found to remain intact, implying the effective role of the metal fragment in transforming L → L′ in **1**.

The synthesis of **1** by using a 1:2 mole ratio of L and Ru(trpy)Cl$_3$ is always observed to be accompanied by the formation of a [Ru(trpy)$_2$]$^{2+}$ complex in an approximately 1:1 ratio. However, the use of a 1:1 mole ratio of L and Ru(trpy)Cl$_3$ reduces the yield of [Ru(trpy)$_2$]$^{2+}$ to an appreciable extent {**1**–[Ru(trpy)$_2$]$^{2+}$, 6:1, Section 2}. In order to minimize the perpetual formation of the undesired product [Ru(trpy)$_2$]$^{2+}$, the 1:1 mole ratio of L and Ru(trpy)Cl$_3$ had always been selectively used.



Scheme 1. (i) EtOH, heating, N$_2$.

Although the unsymmetrical nature of L′ in **1** leads to the possibility of the simultaneous formation of two isomers **A** and **B**, here the reaction (Scheme 1) systematically results in one particular isomeric product (see NMR). The existence of the isomeric form **B** has been confirmed by single-crystal X-ray structure for **1a** (see later). Based on the similar spectral features of **1a** and **1b** (see later), we believe that the complex **1b** also exists in same isomeric form **B**.



The aqua complexes $[Ru^{II}(trpy)(L')(H_2O)]^{2+}$ (**2**) have been isolated as their dihydrated perchlorate salts from the corresponding chloro complexes (**1**) in the presence of excess aqueous $AgNO_3$.

The oxo-complexes $[Ru^{IV}(trpy)(L')(O)]^{2+}$ (**3**) can be generated in solution state by chemical oxidation of the aqua species (**2**) using excess ceric solution in 1 (N) H_2SO_4. The isolation of the pure oxo derivative (**3**) in the solid state has not been successful as in the absence of Ce^{IV} ion the oxo-species reduces back to the parent aqua species (see later).

The isolated chloro (**1**) and aqua (**2**) complexes are diamagnetic and show 1:1 and 1:2 conductivities, respectively (Section 2). The complexes exhibit satisfactory elemental analyses (Section 2).

3.2. Crystal structures of $NC_5H_4CH{=}N{-}(C_6H_4){-}N{=}CHC_5H_4N$ (L^1) and $[Ru(trpy)(L')Cl](ClO_4)$ (**1a**)

The single crystal X-ray structure of L^1 is shown in Fig. 1. It shows that each half of the molecule is related to the other half by symmetry. Selective bond distances and angles are listed in Table 2. The bond distances and angles match well with the standard values.

The crystal structure of $[Ru(trpy)(L')Cl](ClO_4)$ (**1a**) is shown in Fig. 2. Selective bond distances and angles are listed in Table 2. The terpyridine group coordinates to the ruthenium center in a meridional fashion with the ligand L′ in a *cis* orientation. The chloride ligand is *trans* to the imine nitrogen (N_i) of L′ (structure **B**). The central Ru–N(1) distance [1.978(9) Å] of terpyridine is shorter than the terminal Ru–N(2)/Ru–N(3) distances, 2.080(9) Å [14–16]. Correspondingly, the geometrical strain of the meridionally disposed terpyridine ligand is reflected in the short *trans* angle, 159.0(4)° [14–16]. The Ru^{II}–N(5) [imine nitrogen, 2.057(10) Å], Ru–N(4) [pyridine nitrogen of L′, 2.097(10) Å] and Ru^{II}–Cl [2.414(3) Å] distances in **1a** are in agreement with those of reported similar complexes [16–20,32,33].

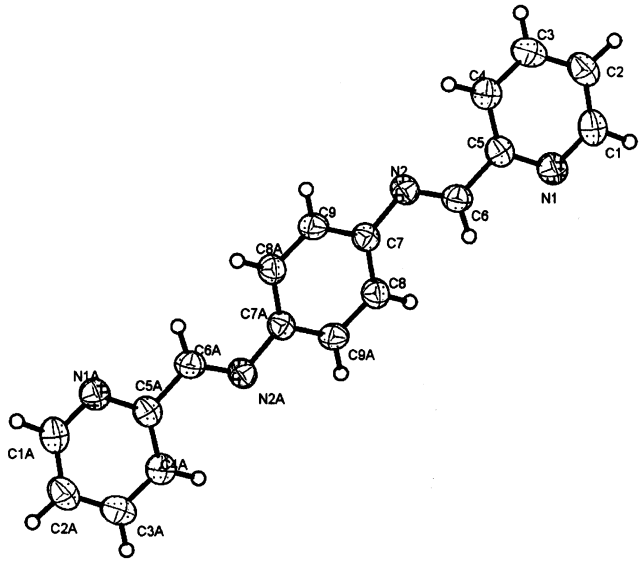


Fig. 1. An ORTEP diagram for $NC_5H_4CH{=}N{-}C_6H_4{-}N{=}CHC_5H_4N$, L^1. Atoms are drawn at 50% probability.

Table 2
Selected bond distances (Å) and angles (°) and their standard deviations for L^1 and **1a**

L^1		**1a**	
Bond distances			
N(1)–C(1)	1.335(2)	Ru–N(1)	1.978(9)
N(1)–C(5)	1.343(2)	Ru–N(2)	2.080(9)
N(2)–C(6)	1.264(2)	Ru–N(3)	2.080(9)
N(2)–C(7)	1.424(2)	Ru–N(4)	2.097(10)
C(4)–C(5)	1.384(2)	Ru–N(5)	2.057(10)
C(5)–C(6)	1.473(2)	Ru–Cl(1)	2.414(3)
		N(5)–C(21)	1.306(12)
Bond angles			
C(6)–N(2)–C(7)	119.90(16)	N(1)–Ru–N(5)	99.5(4)
N(1)–C(5)–C(6)	114.79(16)	N(1)–Ru–N(3)	79.7(5)
C(4)–C(5)–C(6)	122.45(17)	N(5)–Ru–N(3)	89.7(3)
N(2)–C(6)–C(5)	123.16(17)	N(1)–Ru–N(2)	79.4(4)
		N(5)–Ru–N(2)	95.6(3)
		N(3)–Ru–N(2)	159.0(4)
		N(1)–Ru–N(4)	176.1(4)
		N(5)–Ru–N(4)	77.6(4)
		N(2)–Ru–N(4)	103.4(4)
		N(1)–Ru–Cl(1)	89.5(3)
		N(5)–Ru–Cl(1)	170.7(3)
		N(3)–Ru–Cl(1)	89.7(2)
		N(2)–Ru–Cl(1)	88.2(2)
		N(4)–Ru–Cl(1)	93.3(3)

The cationic molecules are packed in a zigzag manner with anions (ClO_4^-) in between the zip when viewed down the *a*-axis (Fig. 3). Both the hydrogens of the pendant amine group are involved in hydrogen bonding. Hydrogen H(6A) forms hydrogen bonds with the chlorine atom Cl(1) $[-x+3/2, y-1/2, -z+1/2]$ of Ru–Cl, N(6)–H(6A)···Cl(1) = 2.543 Å while H(6B) forms hydrogen bonds with the oxygen atom O(2) of

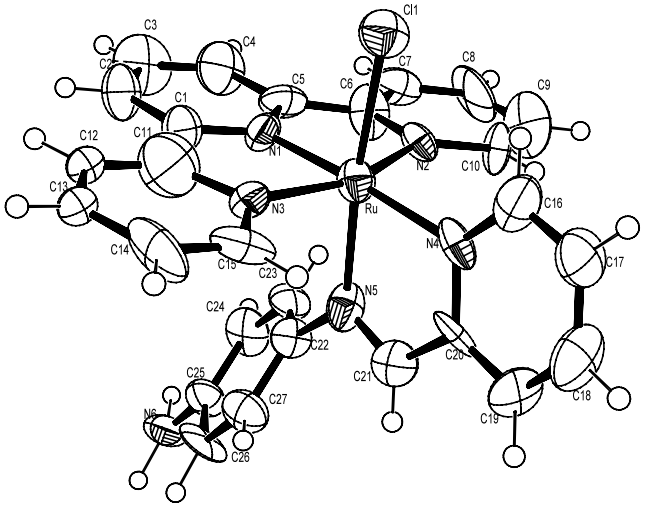


Fig. 2. An ORTEP diagram for $[Ru^{II}(trpy)(L')Cl]ClO_4$ (**1a**). Atoms are drawn at 50% probability.

the translated perchlorate anion moiety, N(6)–H(6B)···O(2) = 2.123 Å (Table 3). The Cl(2)–O(2) distance of 1.372 Å is longer compared to the other Cl–O distances in the ClO_4^- anion which may be due to its involvement in the hydrogen bonding.

3.3. Spectral properties

The ν(C=N) stretching frequency of the coordinated L′ has been observed near 1600 cm^{-1}. The bands due to ionic perchlorate and ν(Ru–Cl) have appeared near 1100/630 and 300 cm^{-1}, respectively.

The ^1H NMR spectra of the free ligands (L) in $CDCl_3$ (Fig. 4(a)) exhibit the signals corresponding to half of the molecule as expected due to the internal symmetry. The complexes (**1a** and **1b**) in DMSO-d^6 solvent display the expected 22 and 26 signals, respectively (Fig. 4(b and c)). The signals due to the NH_2 group [which is absent in the free ligands (Fig. 4(a))], the pendant phenyl ring(s) and the azomethine (–CH=N–) function of L′ appear in isolated regions and are therefore assigned. On the other hand the signals due to the terpyridine ligand and the pyridine fragment of L′ are found to overlap severely which essentially restricts the identification of the individual protons. However, the direct comparison of the intensity of these proton signals with that of the clearly observable NH_2 protons or –CH=N– proton reveals the presence of the calculated number of protons in both the complexes.

Electronic spectral data of the isolated complexes **1a**, **1b**, **2a** and **2b** are listed in Table 4. The complexes display moderately strong MLCT transitions in the visible region ($\lambda_{max} > 500$ nm for **1** and approximately 470 nm for **2**) and strong intra ligand transitions in the UV region (Fig. 5) [34,35]. The observed order of MLCT band energy, **1**(Cl^-) < **2**(H_2O) (Table 4, Fig. 5) is due to relative stabilization of the dπ(Ru) state while moving from $Cl^- \rightarrow H_2O$.

The replacement of one strong π-acidic tridentate trpy ligand from the $[Ru(trpy)_2]^{2+}$core by L′ and Cl^- decreases the MLCT transition energy reasonably {the MLCT transition of $[Ru(trpy)_2]^{2+}$ appears at 478 nm [36]}, however the MLCT transition energy remains almost unaltered when the combination of L′/H_2O is used to replace one trpy group from the $[Ru(trpy)_2]^{2+}$core.

The MLCT transition energy of the aqua derivative, **2a** varies reasonably depending on the nature of the coordinating solvents [37], however little variation has been observed in case of **2b** (Table 4).

The other known ruthenium terpyridine aqua complexes $[Ru(trpy)(L'')(H_2O)]^{2+}$ incorporating analogous

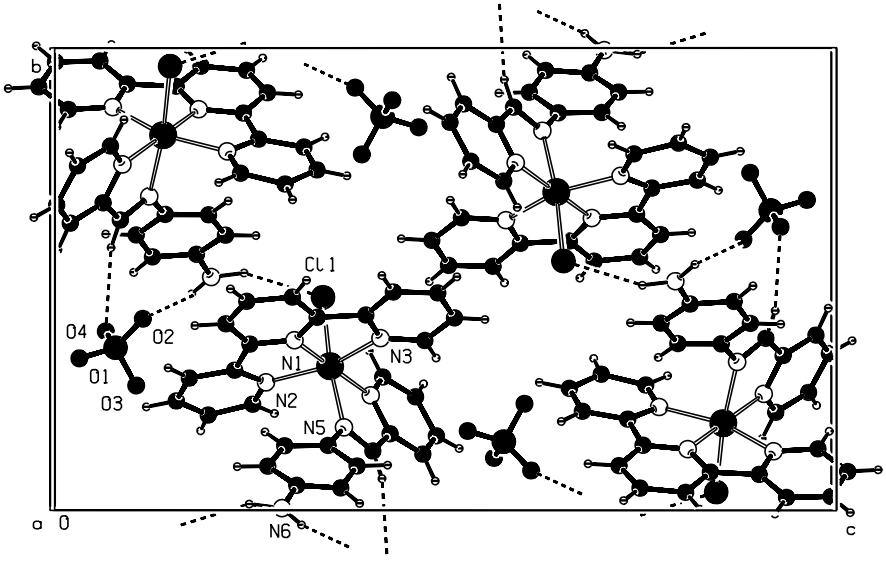


Fig. 3. Packing diagram of the molecule $[Ru^{II}(trpy)(L')Cl]ClO_4$ (**1a**) viewed down the *a*-axis.

Table 3
Hydrogen bonds for **1a** [Å and (°)]

D–H	d(D–H)	d(H···A)	<DHA	d(D···A)	A
N(6)–H(6A)	0.998	2.543	150.65	3.448	Cl(1) [$-x+3/2$, $y-1/2$, $-z+1/2$]
N(6)–H(6B)	0.987	2.123	166.24	3.090	O(2) [$-x+2$, $-y+1$, $-z+1$]

ancillary moieties, L″ = bipyridine [21], bipyrazine [18], azopyridine [15] and 3,6-di(pyrid-2-yl)pyridazine [19] exhibit MLCT transitions at 477, 494, 487–490 and 480–491nm, respectively.

The complexes (**1**) exhibit moderately strong emissions near 590 nm in MeOH–EtOH (1:4 v/v) glass at 77 K from the lowest energy MLCT transitions ($\lambda_{excitation}$: **1a**, 517 nm; **1b**, 520 nm; $\lambda_{emission}$: **1a**, 590 nm; **1b**, 592

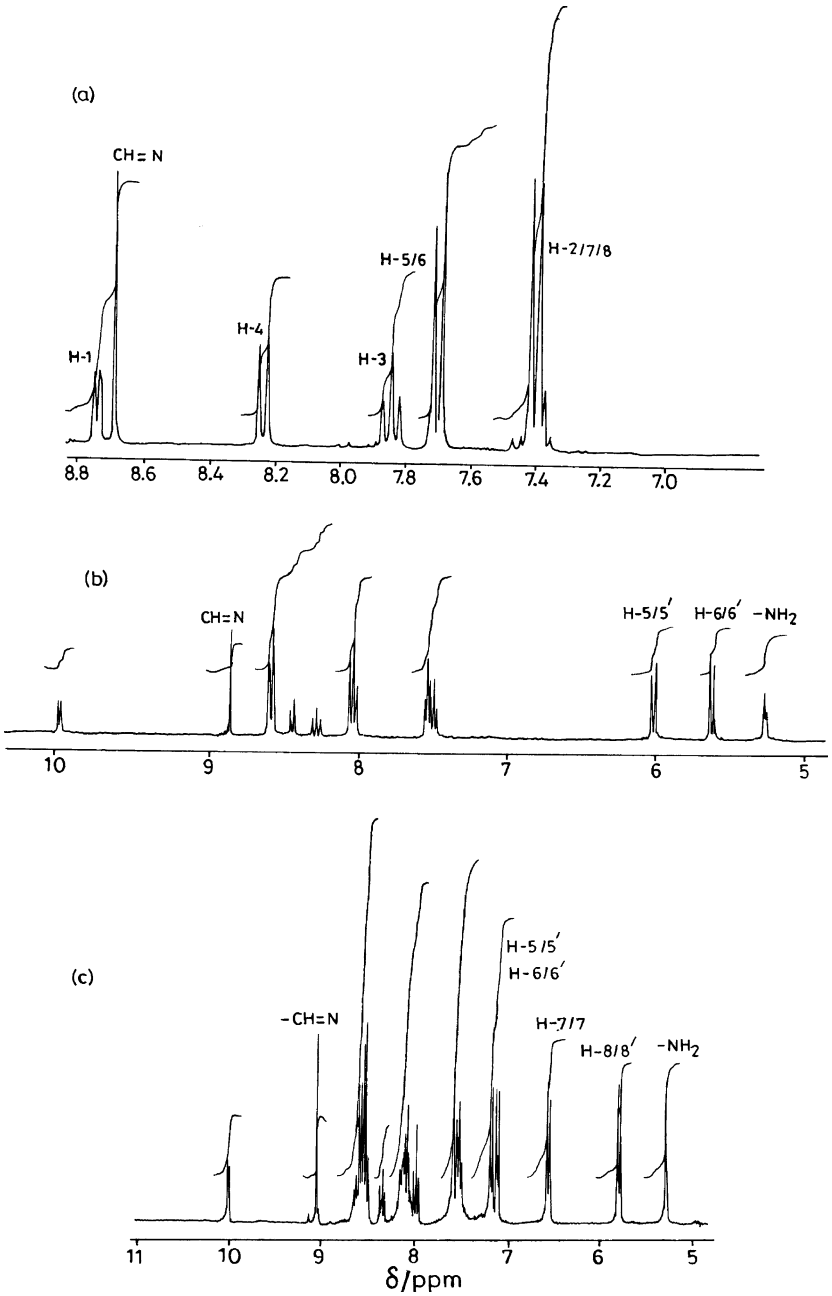


Fig. 4. ^{1}H NMR spectra of: (a) $NC_5H_4CH{=}N{-}C_6H_4{-}C_6H_4{-}N{=}CHC_5H_4N$, L^2 in $CDCl_3$; (b) $[Ru^{II}(trpy)(L')Cl]ClO_4\cdot 2H_2O$ (**1a**); and (c) $[Ru^{II}(trpy)(L')Cl]ClO_4\cdot 2H_2O$ (**1b**) in DMSO-d^6.

Table 4
Electronic spectral data

Complex	UV–Vis λ (nm) (ε, M^{-1} cm^{-1})			
	CH_3CN	CH_3OH	H_2O	DMF
1a	521 (8540) 313 (33 480) 275 (34 090) 234 (35 260) 214 (42 510)			
1b	503 (5890) 314 (41 230) 278 (37 380) 232 (39 970) 213 (47 220)			
2a	471 (6370) 446 (6140) 302 (33 080) 274 (26 310)	475 (6780) 312 (32 000) 274 (25 740)	474 (5590) 310 (26 890) 273 (21 800)	480 (6900) 315 (33 530) 277 (27 510)
2b	473 (7860) 304 (48 870) 280 (32 370)	472 (8430) 304 (50 500) 280 (35 820)	473 (6820) 304 (34 480) 278 (31 800)	474 (9450) 315 (48 870) 285 (36 640)

nm; quantum yield (Φ_{em}): **1a**, 0.03; **1b**, 0.015, Fig. 5, (inset). The observed emissions are believed to have originated from the ^{3}MLCT excited states [38]. The quantum yields (Φ_{em}) of the emission processes were measured in the MeOH–EtOH (1:4 v/v) glass at 77 K relative to $[Ru(bpy)_3]^{2+}$ for which $\Phi_{em} = 0.35$ [39].

3.4. Electron-transfer properties

Redox properties of the complexes **1** and **2** have been studied in acetonitrile and water, respectively using a platinum working electrode at 298 K. Representative voltammograms are shown in Fig. 6. The chloro complexes **1a** and **1b** display reversible ruthenium(III)–ruthenium(II) couples, E°_{298}, V (ΔE_p, mV) at 0.80 (90) and 0.85 (90) versus SCE, respectively. Thus the ruthenium(III)–ruthenium(II) potential increases with the increase in number of phenyl rings in the ligand framework (L′). Although the complexes (**1**) can be coulometrically oxidized to the corresponding ruthenium(III) congeners ($\mathbf{1}^+$), the oxidized species are found to be unstable at room temperature. The observed ruthenium(III)–ruthenium(II) potential of **1** is comparable to that of $[Ru(trpy)(bipyridine)Cl]^+$ (0.81 V) [18] but less anodic compared to those of analogous complexes incorporating other types of *N*,*N*-donors based ancillary functions such as, $[Ru(trpy)\{3,6\text{-di(pyrid-2-yl)pyridazine}\}Cl]^+$ (0.89–1.04 V) [19]; $[Ru(trpy)(azopyridine)Cl]^+$ (1.10–1.24 V) [15] and [Ru(trpy)(2,2′-bipyrazine)Cl] (1.07 V) [18]. Thus the π-acceptor strength of L′ in **1** can be considered to be appreciably closer to that of the bipyridine ligand.

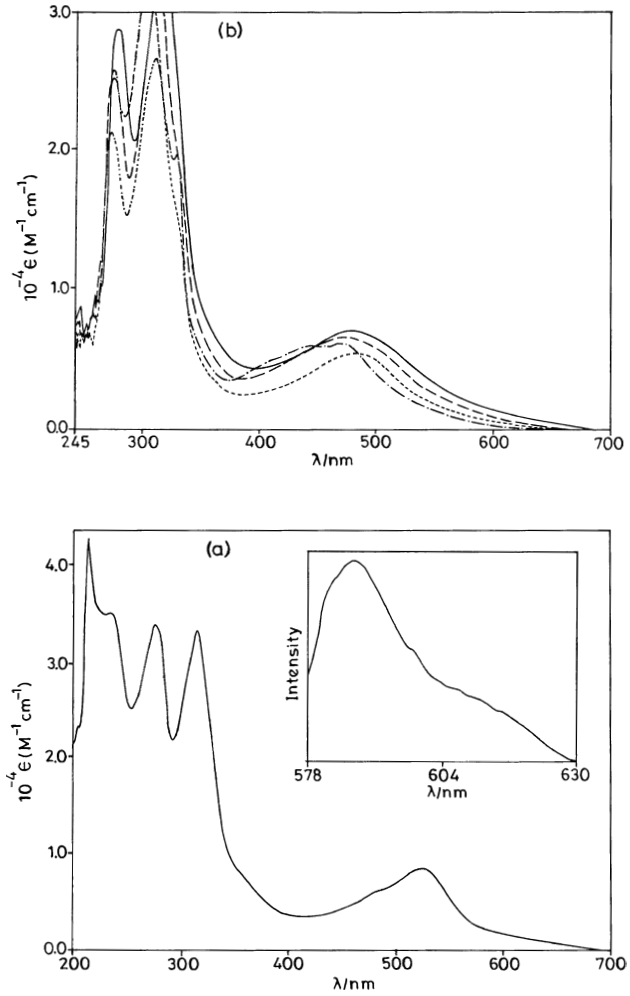


Fig. 5. Electronic spectra of: (a) $[Ru^{II}(trpy)(L')Cl]ClO_4\cdot 2H_2O$ (**1a**) in acetonitrile. Inset shows emission spectrum of $[Ru^{II}(trpy)(L')Cl]ClO_4\cdot 2H_2O$ (**1a**) in EtOH–MeOH 4:1 (v/v) at 77 K; (b) $[Ru^{II}(trpy)(L')(H_2O)](ClO_4)_2\cdot 2H_2O$ (**2a**) in DMF (—), MeOH (----), H_2O (------), CH_3CN (-·-·-).

The complex, **1a** exhibits one irreversible reduction, E_{pc} at −1.09 V and **1b** displays one quasi-reversible reduction, E°_{298}, V (ΔE_p, mV), at −0.96 (190). These are believed to be terpyridine based reductions [40].

Cyclic voltammograms of the aqua species (**2a** and **2b**) have been recorded in aqueous medium in the pH range 1–12. The complexes exhibit one quasi-reversible oxidative response each at the positive side of SCE (Fig. 6(b)). The potentials of the responses are observed to decrease linearly with the increase in pH (Fig. 6(c)). The electron–proton content of the redox processes over the pH range 1–12 have been estimated from the slopes of the experimentally derived potential–pH plots (Fig. 6(c)) [21]. In the pH ranges 1–9 and >9.0, the potentials change at the rate of approximately 60 and 30 mV, respectively per unit change in pH. Therefore, the redox processes in the pH range 1–9 and >9 are associated with $2e^-/2H^+$ and $2e^-/H^+$ oxidation processes, respectively (Eqs. (1) and (2)) [19–21]. The pK_a

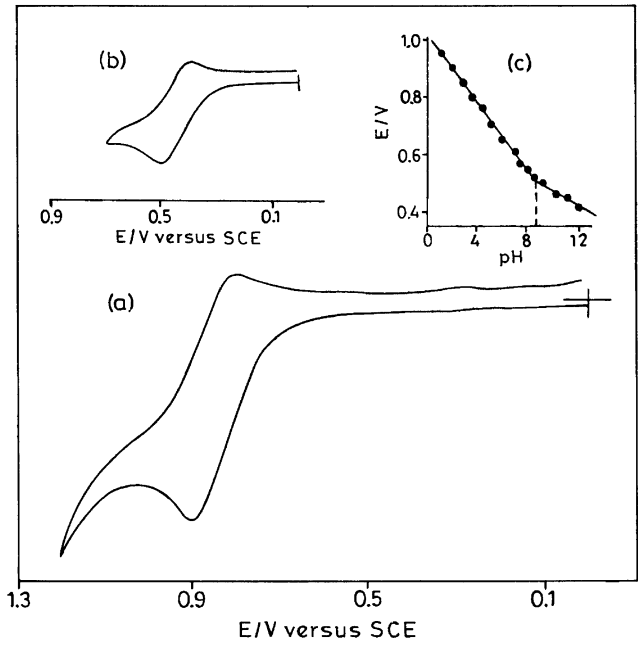


Fig. 6. Cyclic voltammograms of: (a) $[Ru^{II}(trpy)(L')Cl]ClO_4\cdot 2H_2O$ (**1b**) in acetonitrile; (b) $[Ru^{II}(trpy)(L')(H_2O)](ClO_4)_2\cdot 2H_2O$ (**2b**) in water at pH 9.5; and (c) variation of Ru^{IV}/Ru^{II} couple with pH in water for **2b**.

values of the complexes **2a** and **2b**, calculated from the intersection point of the two curves in E versus pH graphs (Fig. 6(c)), are 9.0 and 8.7, respectively. The values are in good agreement with the pK_a data (9.1 for **2a** and 9.0 for **2b**) determined separately by

$$[Ru^{II}(trpy)(L')(H_2O)]^{2+} \rightarrow [Ru^{IV}(trpy)(L')(O)]^{2+} + 2e^- + 2H^+ \quad (1)$$

$$[Ru^{II}(trpy)(L')(OH)]^{+} \rightarrow [Ru^{IV}(trpy)(L')(O)]^{2+} + 2e^- + H^+ \quad (2)$$

spectrophotometric titrations using sodium hydroxide. The pK_a values of the similar monoterpyridine aqua complexes $[Ru(trpy)(L'')(H_2O)]^{2+}$, L″ = 2,2′-bipyridine, 1,10-phenanthroline, 2,2′-bipyrazine, 3,6-di(pyrid-2-yl)pyridazine, tetramethylene diamine, and azopyridine are 9.7, 9.6, 8.8, 10.3, 10.2 and 7.9–8.5, respectively [15,18–20]. Thus, as far as the acidity of the coordinated aqua molecule is concerned, the present set of complexes (**2a** and **2b**) are closest to the bipyrazine derivative.

Similar proton coupled electron-transfer processes have been observed in case of bipyrazine [18] and 3,6-di(pyrid-2-yl)pyridazine [20] complexes. However, the bipyridine analogue shows two step processes in the acidic region, $[Ru^{II}(trpy)(bpy)(H_2O)]^{2+} \rightarrow [Ru^{III}(trpy)(bpy)(OH)]^{2+} + e^- + H^+$ and $[Ru^{III}(trpy)(bpy)(OH)]^{2+} \rightarrow [Ru^{IV}(trpy)(bpy)(O)]^{2+} + e^- + H^+$ [21]. On the other hand the azopyridine analogue exhibits $2e^-/2H^+$-transfer process specifically in the highly acidic region [15]. Therefore, electron-transfer behavior of the ruthenium terpyridine aqua species is primarily controlled by the acidity of the coordinated H_2O molecule or in other words the electronic aspect of the ancillary functions.

3.5. *Chemical oxidation of $[Ru^{II}(trpy)(L')(H_2O)]^{2+}$ (**2**) → $[Ru^{IV}(trpy)(L')(O)]^{2+}$ (**3**): role of **3** in catalyzing the water oxidation process*

Chemical oxidation of the aqua complex (**2**) by excess aqueous ceric solution in 1 (N) H_2SO_4 leads to the spontaneous formation of a yellow colored species. The intensity of the MLCT band of $[Ru(trpy)(L)(H_2O)]^{2+}$ near 470 nm is found to decrease systematically on progressive addition of Ce^{IV} solution with the concomitant development of a new band near 320 nm (Fig. 7). The plots of absorbance versus $[Ce^{IV}]/[\mathbf{2}]$ show that approximately 4.0 mole ratio of Ce^{IV}: **2** is needed for the complete oxidation of the aqua species.

Considering the observed electrochemical concerted $2e^-/2H^+$ oxidation process of the aqua complexes in acidic solution (Eqs. (1) and (2)) it can be assumed that the chemical oxidation of **2** also leads to the formation of the same oxo-species, Eq. (3).

$$[Ru^{II}(trpy)(L')(H_2O)]^{2+} + 2Ce^{4+} \rightarrow [Ru^{IV}(trpy)(L')(O)]^{2+} + 2e^- + 2H^+ + 2Ce^{3+} \quad (3)$$

The oxo-complexes (**3**) thus formed are found to reduce back partially to the parent aqua derivatives (**2**). The MLCT band at 474 nm, characteristic of the aqua species, develops slowly with time but levels off before attaining the calculated intensity of the standard aqua species (Fig. 7, inset). The percent conversion of the oxo (**3**) to aqua (**2**) for **3a** and **3b** are calculated to be 63 and 69%, respectively. The further addition of acidic Ce^{+4} solution into the mixture of **2** and **3** oxidizes the solution completely to the oxo-state and the cycle follows. Therefore, the oxo-species is stable only in presence of excess oxidant. The observed partial conversion of oxo to aqua species possibly can account for the need of excess ceric rather than the 1:2 mole ratio of **2**–Ce^{IV} as expected from the stoichiometric oxidation reaction (Eq. (3)). The partial conversion of oxo to aqua species has essentially precluded the isolation of the oxo-complexes in the pure solid state. The observed conversion of the oxo to aqua species and the subsequent reverse reaction, aqua to oxo on further addition of Ce^{4+} can be best explained on the basis of earlier observations [15,17,41] i.e. the involvement of the chemically generated oxo-species in the catalytic water splitting reaction (Scheme 2). It may be noted that in the case of the azopyridine analogue, the oxo complex was found to transform quantitatively to the aqua species and the backward process, aqua to oxo was observed on further addition of Ce^{4+}. Therefore, as far as water splitting is concerned the present oxo-species (Scheme 2) is much less efficient as compared to the corresponding azopyridine deriva-

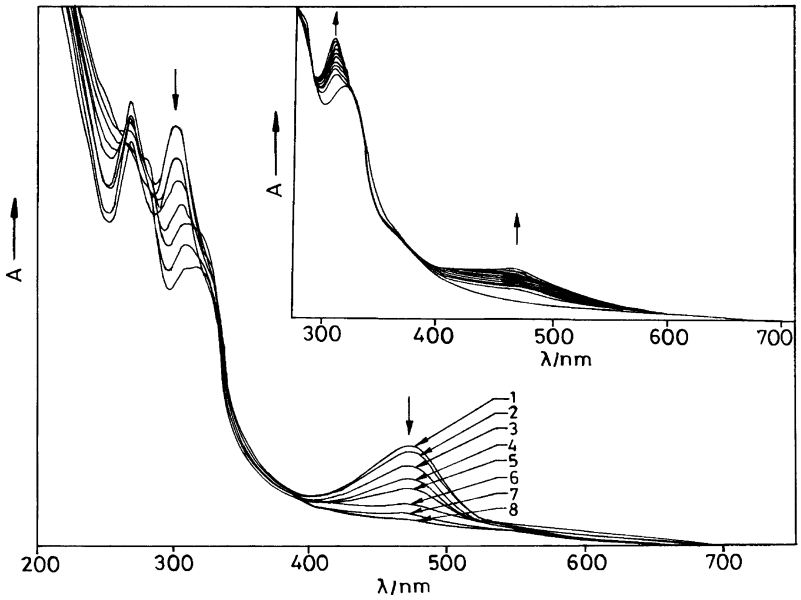
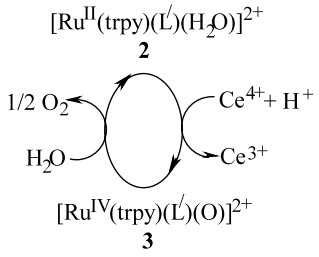


Fig. 7. Change in absorbance of $[Ru^{II}(trpy)(L')(H_2O)](ClO_4)_2\cdot 2H_2O$ (**2a**) as a function of $[Ce^{IV}]$. Ratio of $[Ce^{IV}]$–**2a** = (1) 0:1, (2) 0.5:1, (3) 1:1, (4) 1.5:1, (5) 2:1, (6) 2.5:1, (7) 3:1, (8) 3.5:1. Inset shows time evolution of the electronic spectra of a changing solution of $[Ru^{IV}(trpy)(L')(O)]^{2+}$ (**3a**) → $[Ru^{II}(trpy)(L')(H_2O)]^{2+}$ (**2a**) in water [1 (N) H_2SO_4] at 298 K. The arrows indicate increase or decrease in band intensities as the reaction proceeds.



Scheme 2.

tive, which is certainly due to the greater π-acceptor character of the azopyridine function.

3.6. Electrocatalytic oxidation of benzyl alcohol

The cyclic voltammetric experiments of the aqua species $[Ru(trpy)(L')(H_2O)]^{2+}$ (**2**) in the presence of benzyl alcohol have been studied in order to examine the role of the electrogenerated $[Ru(trpy)(L')(O)]^{2+}$ (**3**) towards the oxidaton of benzyl alcohol [18–20,42–44]. The cyclic voltammogram of **2b** at pH 9.58 is shown in Fig. 8. Under identical experimental conditions the voltammogram of benzyl alcohol does not show any appreciable current (Fig. 8). However, the voltammogram of **2** in the presence of benzyl alcohol displays substantially excess anodic current as compared to that of the standard **2** (Fig. 8). Thus the oxidation of **2** to **3** is followed rapidly by the reaction (Scheme 3) and the regenerated **2** is reoxidized before it can diffuse away from the electrode surface.

Therefore, the electrogenerated **3** is involved in catalyzing the benzyl alcohol oxidation process. A similar electrocatalytic behavior has been reported in case of the corresponding bipyrazine and 3,6-di(4-methylpyrid-2-yl)pyridazine complexes [18–20]. Here catalytic current increases with the increase in ratio of [benzyl alcohol]/[**2**] as expected and maximum catalytic current is observed in case of 25:1 ratio of [benzyl alcohol]/[**2**]. The catalytic effect has been quantifiedly based on the experimentally observed excess current (i_{ex}) with respect to the current only due to the catalyst (i_{ct}) (same catalyst concentration has been used for both the standard and the mixture containing the substrate) at a particular potential (Eq. (4)) (Fig. 8) [45]. Here i_o is the observed current for

$$i_{ex} = i_o + i_d - i_{ct} \quad (4)$$

the mixture and i_d is the difference in current between the catalyst and the catalyst + substrate at the concerned base line potential. The turnover numbers (t) of the processes

$$t = i_{ex}/i_{ct} \quad (5)$$

(Scheme 3; Fig. 8) calculated by using Eq. (5) are found to be 2.7 and 2.3 for **3a** and **3b**, respectively. Further studies on the catalytic aspect of **3** are in progress.

4. Conclusion

The role of α,α′-diimine based ancillary (L′) functions in the ruthenium monoterpyridine [Ru-trpy] core (**1**–**3**) have been scrutinized with special reference to the chemical and electrochemical behaviors of the oxo species $[Ru(trpy)(L')(O)]^{2+}$ (**3**). The ruthenium(III)–

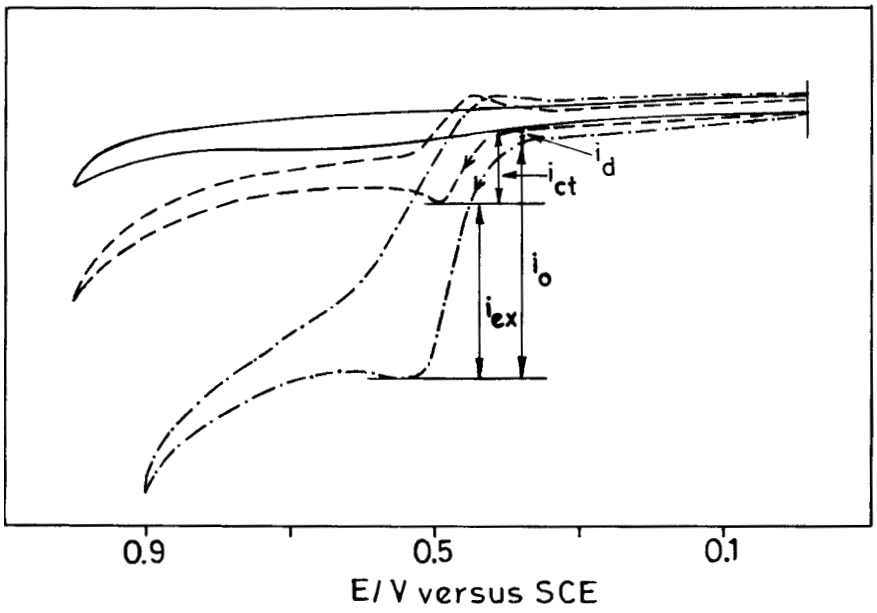
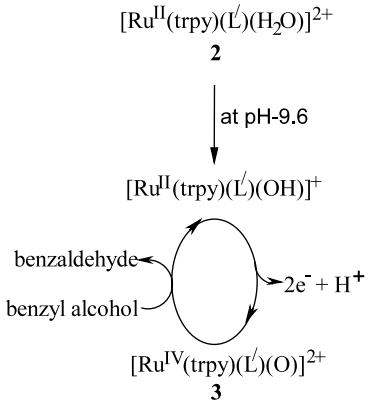


Fig. 8. Cyclic voltammograms of benzyl alcohol in water (20.32×10^{-3} M) (—); $[Ru^{II}(trpy)(L')(H_2O)](ClO_4)_2 \cdot 2H_2O$ (**2b**) in water at pH 9.58 (0.96×10^{-3} M) (----) and the mixture of the two taken at the same concentrations (-·-·-).



Scheme 3.

ruthenium(II) potential of the chloro species $[Ru(trpy)(L')(Cl)]^+$ (**1**) is comparable to that of the corresponding bipyridine complex but less anodic compared to the analogous complexes incorporating 3,6-di(pyrid-2-yl)pyridazine, bipyrazine and azopyridine ancillary functions. The aqua complex $[Ru(trpy)(L')(H_2O)]^{2+}$ (**2**) undergoes one-step-$2e^-/2H^+$ and $2e^-/H^+$ transformations in the acidic and basic regions, respectively to the corresponding oxo-species $[Ru(trpy)(L')(O)]^{2+}$ (**3**) like the bipyrazine and 3,6-di(pyrid-2-yl)pyridazine derivatives. The chemically generated oxo-species (**3**) catalyzes the water oxidation process like the azopyridine derivative but much less efficiently. The electrochemically generated oxo-species (**3**) is found to be effective in catalyzing the oxidation of benzyl alcohol like the bipyrazine and 3,6-di(pyrid-2-yl)pyridazine derivatives. The present study therefore emphasizes the serious impact of the electronic aspect of the ancillary functions in directing the reactivity pattern of the ruthenium monoterpyridine aqua species.

5. Supplementary material

Crystallographic data for the structural analysis have been deposited with the Cambridge Crystallographic Data Center, CCDC Nos. 170396–170397 for compounds **1a** and L^1. Copies of this information may be obtained free of charge from The Director, CCDC, 12 Union Road, Cambridge, CB2 1EZ, UK (fax: +44-1223-336033; e-mail: deposit@ccdc.cam.ac.uk or www: http://www.ccdc.cam.ac.uk).

Acknowledgements

Financial support received from the Council of Scientific and Industrial Research, New Delhi, India, is gratefully acknowledged. The X-ray structural studies were carried out at the National Single Crystal Diffractometer Facility, Indian Institute of Technology, Bombay. Special acknowledgement is made to the Regional Sophisticated Instrumental Center, RSIC, Indian Institute of Technology, Bombay, for providing NMR facility.

References

[1] F. Scandola, C.A. Bignozzi, M.T. Indelli, in: K. Kalyanasundaram, M. Gratzel (Eds.), Photosensitization and Photocatalysis

Using Inorganic and Organometallic Compounds, Kluwer, Dordrecht, 1993, p. 161.
[2] K. Kalyanasundaram, Coord. Chem. Rev. 28 (1989) 2920.
[3] J.P. Sauvage, J.P. Collin, J.C. Chambron, S. Guillerez, C. Coudret, V. Balzani, F. Barigelletti, L. De Cola, L. Flamigni, Chem. Rev. 94 (1994) 993.
[4] C.M. Hartshorn, K.A. Maxwell, P.S. White, J.M. DeSimon, T.J. Meyer, Inorg. Chem. 40 (2001) 601.
[5] B. Gholamkhass, K. Koike, N. Negishi, H. Hori, K. Takeuchi, Inorg. Chem. 40 (2001) 756.
[6] I.V. Yang, H.H. Thorp, Inorg. Chem. 40 (2001) 1690.
[7] V.M. Hultgren, A.M. Bond, A.G. Wedd, J. Chem. Soc., Dalton Trans. (2001) 1076.
[8] H. Sugimoto, K. Tsuge, K. Tanaka, J. Chem. Soc., Dalton Trans. (2001) 57.
[9] B.K. Santra, M. Menon, C.K. Pal, G.K. Lahiri, J. Chem. Soc., Dalton Trans. (1997) 1387.
[10] J. Zadykowicz, P.G. Potvin, Inorg. Chem. 38 (1999) 2434.
[11] M. Kurihara, S. Daniele, K. Tasuge, M. Sugimoto, K. Tanaka, Bull. Chem. Soc. Jpn. 71 (1998) 867.
[12] A. Doveletoglou, S.A. Adeyemi, T.J. Meyer, Inorg. Chem. 35 (1996) 4127.
[13] M. Ebadi, A.B.P. Lever, Inorg. Chem. 38 (1999) 467.
[14] B. Mondal, S. Chakraborty, P. Munshi, M.G. Walawalkar, G.K. Lahiri, J. Chem. Soc., Dalton Trans. (2000) 2327.
[15] B. Mondal, M.G. Walawalkar, G.K. Lahiri, J. Chem. Soc., Dalton Trans. (2000) 4209.
[16] B. Mondal, H. Paul, V.G. Puranik, G.K. Lahiri, J. Chem. Soc., Dalton Trans. (2001) 481.
[17] N.C. Pramanik, K. Pramanik, P. Ghosh, S. Bhattacharya, Polyhedron 17 (1998) 1525.
[18] A. Gerli, J. Reedijk, M.T. Lakin, A.L. Spek, Inorg. Chem. 34 (1995) 1836.
[19] V.J. Catalano, R.A. Heck, C.E. Immoos, A. Ohman, M.G. Hill, Inorg. Chem. 37 (1998) 2150.
[20] V.J. Catalano, R.A. Heck, A. Ohman, M.G. Hill, Polyhedron 19 (2000) 1049.
[21] K.J. Takeuchi, M.S. Thompson, D.W. Pipes, T.J. Meyer, Inorg. Chem. 23 (1984) 1845.
[22] V. Balzani, A. Juris, M. Venturi, S. Campagna, S. Serroni, Chem. Rev. 96 (1996) 759.
[23] M.D. Ward, Chem. Soc. Rev. (1995) 121.
[24] D. Gust, T.A. Moore, L. Moore, Acc. Chem. Res. 115 (1993) 5975.
[25] A.M. Barthram, R.L. Cleary, R. Kowallic, M.D. Ward, Chem. Commun. (1998) 2695.
[26] T. Wada, K. Tsuge, K. Tanaka, Angew. Chem., Int. Ed. Engl. 39 (2000) 1479.
[27] T. Wada, K. Tsuge, K. Tanaka, Inorg. Chem. 40 (2001) 329.
[28] S. Chakraborty, P. Munshi, G.K. Lahiri, Polyhedron 18 (1999) 1437.
[29] W.J. Stratton, D.H. Busch, J. Am. Chem. Soc. 80 (1958) 1286.
[30] B.P. Sullivan, J.M. Calvert, T.J. Meyer, Inorg. Chem. 19 (1980) 1404.
[31] G.M. Sheldrick, SHELXS-97, Program for Crystal Structure Solution and Refinement, University of Göttingen, 1997.
[32] S. Chakraborty, M.G. Walawalkar, G.K. Lahiri, J. Chem. Soc., Dalton Trans. (2000) 2875.
[33] A.E.M. Boelrijk, J. Reedijk, J. Mol. Catal. 89 (1994) 63.
[34] D.A. Bardwell, A.M.W. Cargill Thompson, J.C. Jeffery, J.A. McCleverty, M.D. Ward, J. Chem. Soc., Dalton Trans. (1996) 873.
[35] R.R. Ruminsky, S. Underwood, K. Vallely, S.J. Smith, Inorg. Chem. 37 (1998) 6528.
[36] C.R. Hecker, A.K.I. Gushurst, R.D. McMillin, Inorg. Chem. 30 (1991) 538.
[37] M.D. Ward, Inorg. Chem. 35 (1996) 1712.
[38] L.M. Vogler, K.J. Brewer, Inorg. Chem. 35 (1996) 818.
[39] R. Alsfasser, R.V. Eldik, Inorg. Chem. 35 (1996) 628.
[40] G.B. Deacon, J.M. Patrick, B.W. Skelton, N.C. Thomas, A.H. White, Aust. J. Chem. 37 (1984) 929.
[41] S. Goswami, A.R. Chakravarty, A. Chakravorty, J. Chem. Soc., Chem. Commun. (1982) 1288.
[42] E.L. Lebeau, T.J. Meyer, Inorg. Chem. 38 (1999) 2174.
[43] W. Kutner, T.J. Meyer, R.W. Murray, J. Electroanal. Chem. 195 (1985) 375.
[44] L. Roecker, T.J. Meyer, J. Am. Chem. Soc. 109 (1987) 746.
[45] G.K. Lahiri, S. Bhattacharya, S. Goswami, A. Chakravorty, J. Chem. Soc., Dalton Trans. (1990) 561.

dissociation constant of the ternary complex. Both en and phen are strong coordinated bidentate ligands but en is flexible, having tetrahedral nitrogens whereas phen has rigid, planar nitrogens.

2. Experimental

2.1. Materials

$Ni(NO_3)_2 \cdot 6H_2O$, ethylenediamine, 1,10-phenanthroline and $NaClO_4$ were purchased from Merck. Ethylenediamine was distilled and standarised by a potentiometric titration against standard HCl solution (Merck). 1,10-Phenanthroline was crystallised before use. 2,2′,2″-Triaminotriethylamine was obtained from TCI. The buffers used were *N*-(2-hydroxyethyl)piperazine-*N*′-2-ethanesulfonic acid (HEPES, $pK_a = 7.75$) and {[tris(hydroxymethyl)methyl]amino}propane (TAPS, $pK_a = 8.4$). Sodium perchlorate was used to maintain the ionic strength. All other chemicals and solvents were of reagent grade and used without any purification.

2.2. Synthesis of complexes

2.2.1. Caution

Perchlorate salts of metal complexes with organic ligands are potentially explosive materials and should be handled with care.

The ternary complexes of $[Ni(tren)(H_2O)_2]^{2+}$ with ethylenediamine and 1,10-phenanthroline were prepared in the following way.

2.2.2. Ni(tren)(NO3)2

$Ni(NO_3)_2 \cdot 6H_2O$ (1 g, 3.4 mmol) was dissolved in 100 ml of EtOH and then 0.5 g (3.4 mmol) of tren in 50 ml EtOH was added drop-wise with stirring. During the addition the colour changed from green to blue. The reaction mixture was stirred continuously for 2 h and after that kept in a refrigerator for 5 h. A precipitate was formed and filtered off. The ppt was washed with water, EtOH and Et_2O thoroughly and dried over P_2O_5. The product was recrystallised from hot EtOH. Deep blue crystals were formed. Yield: 68%.

2.2.3. [Ni(tren)(en)](ClO4)2 (**a**)

Ethylenediamine (0.4 g, 2.5 mmol) in 50 ml EtOH was added into a solution of 0.8 g (2.4 mmol) $[Ni(tren)](NO_3)_2$ in 50 ml EtOH with continuous stirring. The colour changed from blue to purple. The reaction mixture was stirred for 2 h at room temperature and then cooled in freezer for complete precipitation. The nitrate salt product was collected by filtration and washed with EtOH and Et_2O. The product was dried over P_2O_5.

The dried product was dissolved in EtOH and 10 ml saturated aq. solution of $NaClO_4$ added. A precipitate was formed immediately and filtered off. The residue was washed with water and EtOH thoroughly and dried over P_2O_5. The product was recrystallised from 1:3 CH_3CN–H_2O mixture. Purple colour crystals were formed. The yield was 55%. Elemental analysis: Found (Calc.): C, 20.62 (20.70); H, 5.53 (5.61); N, 18.22 (18.12)%.

2.2.4. [Ni(tren)(phen)](ClO4)2 (**b**)

$Ni(tren)(NO_3)_2$ (0.8 g, 2.4 mmol) was dissolved in 50 ml EtOH and then added dropwise a solution of 0.5 g (2.5 mmol) 1,10-phenanthroline in 50 ml EtOH. The reaction mixture was stirred continuously for 3 h. The brown crystals of nitrate salts were precipitated out. They were filtered and washed with water and EtOH.

The crystals were dissolved in EtOH and 10 ml saturated aq. solution of $NaClO_4$ was added. The perchlorate salt was precipitated immediately and washed with water and EtOH thoroughly. The product was recrystallised from 1:2 CH_3CN–H_2O. The yield was 48%. Elemental analysis: Found (Calc.): C, 37.11 (37.01); H, 4.44 (4.45); N, 14.48 (14.39)%.

2.3. Physical measurements

Spectral data were obtained using the following instruments: Bomen MB100; UV spectra, Hitachi 3410. The kinetic studies were carried out using a Union Giken RA-401 stopped-flow spectrophotometer equipped with a Union RA-415 rapid-scan attachment at 25.0 ± 0.1 °C. The reactions were monitored at a definite wavelength, 254 nm for en and at 343 nm for the phen reaction path.

2.4. X-ray crystal structure and analysis

X-ray quality crystals were obtained by slow evaporation of an EtOH solution of $[Ni(tren)(en)](ClO_4)_2$ (**a**) and $[Ni(tren)(phen)](ClO_4)_2$ (**b**) at 298 K (crystal size: $[Ni(tren)(en)](ClO_4)_2$, $0.79 \times 0.29 \times 0.20$ mm and $[Ni(tren)(phen)](ClO_4)_2$, $0.60 \times 0.40 \times 0.20$ mm). Data were collected on a Siemens SMART-CCD diffractometer with graphite monochromatised Mo Kα radiation ($\lambda = 0.71073$). The ORTEP of the crystals are shown in Figs. 1 and 2. A summary of the crystallographic data and structure refinement parameters is given in Table 1. The bond lengths and angles within the coordination sphere of the nickel ion are listed in Table 2 for **a** and Table 3 for **b**. The data were corrected for absorption effects by an empirical method. Systematic absences led to the identification of space groups *Pccn* (orthorhombic crystal system) for **a** and *Pbca* (orthorhombic crystal system) for **b**. Of the 45 294 (**a**) and 26 893 (**b**) collected reflections, 9061 and 5441 with $I > 2\sigma(I)$ were used for

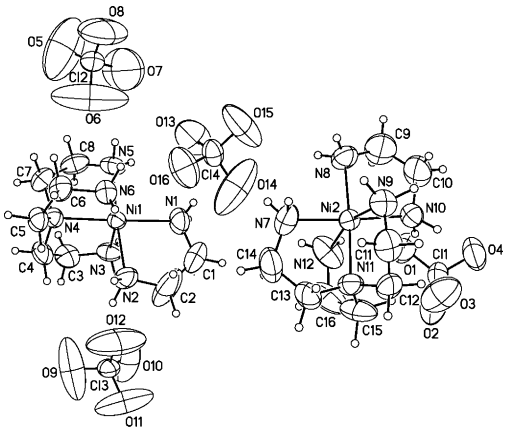


Fig. 1. ORTEP view of $[Ni(tren)(en)](ClO_4)_2$.

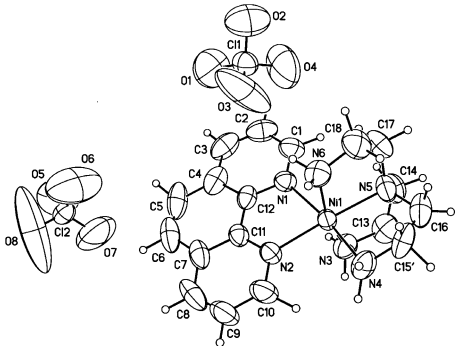


Fig. 2. ORTEP view of $[Ni(tren)(phen)](ClO_4)_2$.

the structure solutions, respectively. In both cases structures were solved by direct method [11]. All non-hydrogen atoms were refined anisotropically. Hydrogen atoms were located in calculated positions and refined isotropically. The final full-matrix least-squares refinements on F^2, including 9061 (**a**) and 5441 (**b**) reflections with $I > 2\sigma(I)$, adjusting 452 (**a**) and 326 (**b**) parameters, converged at R_1 and wR_2 indices of 0.0606 and 0.1788 for **a**, 0.0676 and 0.2232 for **b**. All calculations were carried out using the PC Version SHELXTL [12].

3. Results and discussion

3.1. Synthesis

$Ni(tren)(NO_3)_2$ was prepared by the reaction of $Ni(NO_3)_2 \cdot 6H_2O$ and tren in a 1:1 ratio. In aqueous solution $Ni(tren)(NO_3)_2$ is diaquated. The water molecules are *cis*-oriented. In the presence of bidentated ligands it forms ternary complexes. Ethylenediamine and 1,10-phenanthroline were considered as symmetrical *N*,*N*-bidentate chelating ligands. Thus $[Ni(tren)(en)](ClO_4)_2$ and $[Ni(tren)(phen)](ClO_4)_2$ were prepared when $Ni(tren)(NO_3)_2$ was reacted with en and phen in EtOH solution, followed by the addition of saturated aqueous $NaClO_4$ solution to give the perchlorate salts, respectively. The complexes have been characterised by X-ray crystallographic methods.

Table 1
Crystallographic data for $[Ni(tren)(en)](ClO_4)_2$ (**a**) and $[Ni(tren)(phen)](ClO_4)_2$ (**b**)

	a	**b**
Empirical formula	$C_{16}H_{52}C_{14}N_{12}Ni_2O_{16}$	$C_{18}H_{26}Cl_2N_6NiO_8$
Formula weight	927.92	584.06
Temperature (K)	295	297
λ (Å)	0.71073	0.71073
Crystal system	orthorhombic	orthorhombic
Space group	*Pccn*	*Pbca*
a (Å)	19.7636(9)	14.5386(9)
b (Å)	26.2837(13)	14.1876(8)
c (Å)	14.2689(7)	23.2909(14)
β (°)	90	90
V (Å^3)	7412.1(6)	4804.2(5)
Z	8	8
D_{calc} (Mg m^{-3})	1.663	1.615
Absorption coefficient (mm^{-1})	1.384	1.087
Absorption correction	empirical	empirical
$F(000)$	3872	2416
Crystal size (mm)	$0.79 \times 0.29 \times 0.20$	$0.60 \times 0.40 \times 0.20$
θ Range (°)	1.29–28.32	1.75–28.20
Completeness to theta = 28.2°	98.1%	92.0%
Index ranges	$-26 \le h \le 26$, $-34 \le k \le 34$, $-12 \le l \le 19$	$-14 \le h \le 18$, $-18 \le k \le 18$, $-30 \le l \le 29$
Reflections collected	45 294	26 893
Independent reflections	9061 [$R_{int} = 0.0470$]	5441 [$R_{int} = 0.0339$]
Max/min transmission	0.912/0.744	0.9536/0.8268
Refinement method	full-matrix least-squares on F^2	full-matrix least-squares on F^2
Data/restraints/parameters	9061/1/452	5441/4/326
Final R indices [$I > 2\sigma(I)$]	$R_1 = 0.0606$, $wR_2 = 0.1788$	$R_1 = 0.0676$, $wR_2 = 0.2232$
R indices (all data)	$R_1 = 0.0950$, $wR_2 = 0.2010$	$R_1 = 0.0956$, $wR_2 = 0.2477$
Goodness-of-fit on F^2	1.045	1.073
Largest difference peak/hole (e Å^{-3})	0.919/−0.597	1.074/−0.797

3.2. Molecular structures

The crystal structures of ternary complexes **a** and **b** are shown in Figs. 1 and 2 and bond parameters are listed in Tables 2 and 3, respectively. The coordination around nickel is approximately octahedral.

3.2.1. $[Ni(tren)(en)](ClO_4)_2$ (**a**)

An ORTEP view of the molecular structure of the complex along with the atom-labelling scheme, including the perchlorate ions and H-atoms attached with C- and N-atoms is shown in Fig. 1. The structure consists of two independent units of the $[Ni(tren)(en)]^{2+}$ cation

Table 2
Selected bond lengths (Å) and angles (°) for complex **a**, along with estimated standard deviations

Bond lengths			
Ni(1)–N(1)	2.095(4)	Ni(2)–N(11)	2.095(4)
Ni(1)–N(5)	2.102(4)	Ni(2)–N(8)	2.105(4)
Ni(1)–N(4)	2.103(3)	Ni(2)–N(7)	2.114(5)
Ni(1)–N(2)	2.142(4)	Ni(2)–N(9)	2.139(4)
Ni(1)–N(6)	2.150(4)	Ni(2)–N(12)	2.144(4)
Ni(1)–N(3)	2.158(4)	Ni(2)–N(10)	2.165(4)
Bond angles			
N(1)–Ni(1)–N(5)	93.68(18)	N(11)–Ni(2)–N(8)	176.66(17)
N(1)–Ni(1)–N(4)	176.25(17)	N(11)–Ni(2)–N(7)	81.76(17)
N(5)–Ni(1)–N(4)	83.14(16)	N(8)–Ni(2)–N(7)	95.50(18)
N(1)–Ni(1)–N(2)	82.02(18)	N(11)–Ni(2)–N(9)	83.33(17)
N(5)–Ni(1)–N(2)	175.67(17)	N(8)–Ni(2)–N(9)	98.74(18)
N(4)–Ni(1)–N(2)	101.14(16)	N(7)–Ni(2)–N(9)	92.22(18)
N(1)–Ni(1)–N(6)	100.32(16)	N(11)–Ni(2)–N(12)	82.2(2)
N(5)–Ni(1)–N(6)	92.24(16)	N(8)–Ni(2)–N(12)	96.1(2)
N(4)–Ni(1)–N(6)	81.84(14)	N(7)–Ni(2)–N(12)	94.0(2)
N(2)–Ni(1)–N(6)	89.00(16)	N(9)–Ni(2)–N(12)	163.3(2)
N(1)–Ni(1)–N(3)	95.76(17)	N(11)–Ni(2)–N(10)	101.73(16)
N(5)–Ni(1)–N(3)	92.11(16)	N(8)–Ni(2)–N(10)	81.06(17)
N(4)–Ni(1)–N(3)	82.40(15)	N(7)–Ni(2)–N(10)	176.15(18)
N(2)–Ni(1)–N(3)	87.88(16)	N(9)–Ni(2)–N(10)	86.62(16)
N(6)–Ni(1)–N(3)	163.03(15)	N(12)–Ni(2)–N(10)	88.12(18)

Table 3
Selected bond lengths (Å) and angles (°) for complex **b**, along with estimated standard deviations

Bond lengths			
Ni(1)–N(2)	2.074(4)	Ni(1)–N(4)	2.113(4)
Ni(1)–N(5)	2.109(4)	Ni(1)–N(6)	2.132(5)
Ni(1)–N(3)	2.112(4)	Ni(1)–N(1)	2.194(4)
Bond angles			
N(2)–Ni(1)–N(5)	176.66(2)	N(3)–Ni(1)–N(6)	162.40(2)
N(2)–Ni(1)–N(3)	96.68(2)	N(4)–Ni(1)–N(6)	94.98(2)
N(5)–Ni(1)–N(3)	83.66(2)	N(2)–Ni(1)–N(1)	78.65(2)
N(2)–Ni(1)–N(4)	94.24(2)	N(5)–Ni(1)–N(1)	104.68(2)
N(5)–Ni(1)–N(4)	82.43(2)	N(3)–Ni(1)–N(1)	87.03(2)
N(3)–Ni(1)–N(4)	92.85(2)	N(4)–Ni(1)–N(1)	172.82(2)
N(2)–Ni(1)–N(6)	98.43(2)	N(6)–Ni(1)–N(1)	87.15(2)
N(5)–Ni(1)–N(6)	81.78(2)		

which have also been found in $[Ni(tren)(O_2CCH_3)]^+$ [13]. Selected bond lengths and angles are given in Table 2. The metal centre possesses a distorted octahedral geometry with a NiN_6 chromophore with two en-N, three primary tren-N and one tertiary tren-N. The *trans* bond angles, N(1)–Ni(1)–N(4), 176.25(2)° and N(5)–Ni(1)–N(2) 175.67(2)°, and *cis* bond angles, N(4)–Ni(1)–N(2), 101.14(2)° and N(1)–Ni(1)–N(5), 93.68(2)°, support that N(1), N(2), N(4) and N(5) constitute the equatorial square base of the octahedron. The other *trans* bond angle, N(6)–Ni(1)–N(3), is 163.03(2)°. The Ni–N(tren) bond lengths of $[Ni(tren)(en)]^{2+}$ are normal and essentially equivalent with the reported values [13,14]. The bond lengths of Ni(1)–N(3), 2.158(4) and Ni(1)–N(6), 2.150(4) Å are essentially higher than the other Ni(1)–N bond lengths (Table 2). So it is clear that N(3) and N(6) are in the axial sites of the octahedron. The other two chelate rings, Ni(1), N(3), C(3), C(4), N(4) and Ni(1), N(6), C(6), C(5), N(4) are appreciably orthogonal with respect to the equatorial chelate rings of the square base of the octahedron. The bond angle between en nitrogens is 82.02° which is comparable with the reported bond angle, 81.90° of the $Ni(en)_3^{2+}$ [15] complex. The bond distances Ni(1)–N(1) and Ni(1)–N(2) are 2.095(4) and 2.142(4) Å, respectively. Both are en nitrogens but the later bond distance is longer than former. This is due to the fact that N(2) is *cis*-oriented to a sterically hindered tertiary tren nitrogen.

3.2.2. *[Ni(tren)(phen)](ClO4)2*

A perspective view of the complex cation with the atom numbering scheme, including the perchlorate ions and H-atoms attached to C- and N-atoms is shown in Fig. 2. The structure consists of a $[Ni(tren)(phen)]^{2+}$ cation. The charge of the nickel is satisfied by the perchlorate ions outside of the coordination sphere. Selected bond lengths and angles are listed in Table 3. The structure of the complex is distorted octahedral with a NiN_6 chromophore with two phen-N, three primary tren-N and one tertiary tren-N. The phenanthroline chelate ring, Ni(1), N(1), C(12), C(11), N(2) is planar and it is appreciably orthogonal to the chelate rings, Ni(1), N(6), C(18), C(17), N(5), dihedral angle 95.6° and Ni(1), N(5), C(14), C(13), N(3), dihedral angle 83.4°. The chelate ring, Ni(1), N(5), C(16), C(15), N(4) is inclined to the phenanthroline plane by an angle of 6.9°. The *trans* bond angles, N(2)–Ni(1)–N(5), 176.66(2)° and N(4)–Ni(1)–N(1), 172.82(2)° and *cis* bond angles, N(5)–Ni(1)–N(1), 104.68(2)° and N(2)–Ni(1)–N(4), 94.24(2)° support that N(1), N(2), N(4) and N(5) constitute the equatorial square base of the octahedron. The other *trans* bond angle, N(3)–Ni(1)–N(6), is 162.40(2)°. The Ni–N(tren) bond lengths of this complex are almost equivalent with the reported values [13,14]. The bond lengths of Ni(1)–N(6), 2.132(5) and Ni(1)–N(3), 2.112(4) Å support that N(3) and N(6) of the tren-N are in the axial positions of the octahedron. The N(1) of the phenanthroline ligand suffers some steric effects, created by the tertiary tren-N which is in the *cis*-position, causing the long Ni(1)–N(1) (= 2.194(4) Å) bond distance compared to Ni(1)–N(2) (= 2.074(4) Å). Four chelate angles, N(2)–Ni(1)–N(1), N(5)–Ni(1)–N(3), N(5)–Ni(1)–N(6), N(5)–Ni(1)–N(4) are 78.65(2)°, 83.66(2)°, 81.78(2)° and 82.43(2)°, respectively. Since all tren-N do not face similar environments, the bite angles are so different.

3.3. Kinetic studies

3.3.1. Ethylenediamine

Reactions were carried out with a 10-fold excess of en concentrations than $[Ni(tren)(H_2O)_2]^{2+}$ over a pH range of 7.32–8.26. HEPES and TAPS were used as buffers. The ionic strength was 0.10 ± 0.01 M. Under these conditions, the reaction is first-order in $[Ni(tren)(H_2O)_2]^{2+}$ and is reversible. The observed rate constants are listed in Table 4. The rate equation is expressed as in Eq. (2) with L = en and T = tren. Assuming that L remains constant, Eq. (2)

$$-\frac{d[NiT]}{dt} = k_f[L][NiT] - k_d[NiTL] \quad (2)$$

integrates to Eq. (3) where $[NiT]_e$ and $[NiT]_i$ are the equilibrium and initial concentrations, respectively. The observed pseudo-first-order rate constants (k_{obsd}) at different pH versus en

$$k_{obsd} = k_f[L] + k_d = -\frac{2.303}{t}\log\frac{[NiTL^{2+}]_e - [NiTL^{2+}]}{[NiT^{2+}]_e - [NiT^{2+}]_i} \quad (3)$$

Table 4
Experimental observed rate constants for the reaction of $[Ni(tren)(H_2O)_2]^{2+}$ with ethylenediamine at 25.0 ± 0.1 °C and $\mu = 0.10$ M (NaCl)

pH	10^4 [Ni(tren)$H_2O)_2^{2+}$] (M)	10^2[en] (M)	k_{obsd} (s^{-1})
7.32 [a]	5.10	0.50	16.9
		1.00	30.4
		1.50	43.5
		2.00	57.4
		2.50	70.8
7.51 [a]	5.10	0.50	17.0
		1.00	30.7
		1.50	43.9
		2.00	57.8
		2.50	71.0
7.81 [a]	5.1	0.50	17.2
		1.00	30.9
		1.50	44.2
		2.00	58.3
		2.50	72.0
7.99 [a]	5.10	0.50	17.6
		1.00	31.4
		1.50	44.7
		2.00	58.9
		2.50	73.1
8.26 [b]	5.10	0.50	18.1
		1.00	31.9
		1.50	45.8
		2.00	60.6
		2.50	74.9

[a] 0.01 M HEPES buffer.
[b] 0.01 M TAPS buffer.

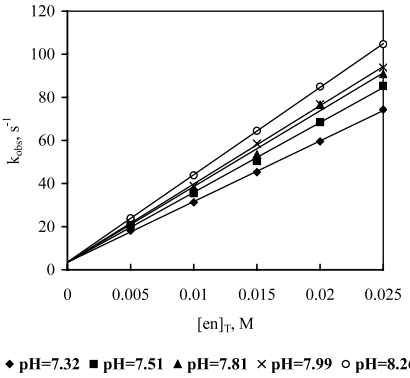


Fig. 3. A plot of k_{obsd} versus $[en]_T$ for the reaction of $[Ni(tren)(H_2O)]^{2+}$ + en ($\mu = 0.10$ M, 25.0 ± 0.1 °C).

concentrations are plotted in Fig. 3 and provide straight line according to Eq. (3) in each case. The k_f and k_d values are obtained from the slope and intercept of straight lines, respectively and the data are given in Table 5.

The en concentration becomes significant at high pH where k_{obsd} depends on both Hen^+ and en concentrations. Reactions of these two species with $[Ni(tren)(H_2O)_2]^{2+}$ to produce the ternary complex are expressed as Eqs. (4) and (5). Eq. (3) can be written as the sum of two

$$NiT(H_2O)_2^{2+} + en \underset{k^{NiT}}{\overset{k^{en}_{NiT}}{\rightleftharpoons}} NiT(en)^{2+} + 2H_2O \quad (4)$$

$$NiT(H_2O)_2^{2+} + Hen^+ \underset{k^{NiT(en)}_{H}}{\overset{k^{Hen}_{NiT}}{\rightleftharpoons}} NiT(en)^{2+} + H^+ + 2H_2O \quad (5)$$

formation terms involving the two reactive forms of the bidentate ligand as well as the reverse terms for each pathway as shown in Eq. (6). Multiple linear regression analysis of Eq. (6)

$$k_{obs} = k^{en}_{NiT}[en] + k^{Hen}_{NiT}[Hen^+] + k^{NiT(en)} + k^{H}_{NiT(en)}[H^+] \quad (6)$$

$$\frac{k_{obs}}{[en]} = k^{en}_{NiT} + k^{Hen}_{NiT}K^{H}_{1}[H^+] + \frac{k^{NiT(en)}}{[en]} + k^{H}_{NiT(en)}\frac{[H^+]}{[en]} \quad (7)$$

cast in the form shown in Eq. (7) with $K_1^H = [Hen^+]/[H^+][en] = 7.76 \times 10^9$ M^{-1} [16]. Regression analysis of Eq. (7) using only the first three terms on the right hand

Table 5
Rate constants for the forward reaction (k_f) and reverse reaction (k_d) of $[Ni(tren)(H_2O)_2]^{2+}$ with en at 25.0 ± 0.1 °C and $\mu = 0.10$ M (NaCl)

PH	10^3 k_f (M^{-1} s^{-1})	k_d (s^{-1})
7.32	2.81	3.52
7.51	3.24	3.52
7.81	3.52	3.42
7.99	3.66	3.47
8.26	4.06	3.54

Table 6
Rate constants for the reaction of $[Ni(tren)(H_2O)_2]^{2+}$ with ethylenediamine at 25.0±0.1 °C and $\mu = 0.10$ M (NaCl)

	Experimental	Predicted
$k^{en}{}_{NiT}$ ($M^{-1}\,s^{-1}$)	1.13×10^5	2.21×10^6 [a]
k^{Hen}_{NiT} ($M^{-1}\,s^{-1}$)	2.67×10^3	3.14×10^3 [b]
$k^{NiT(en)}$ (s^{-1})	3.50	

[a] Predicted from Eq. (7) including ICB effect and steric factor.
[b] Predicted from Eq. (7).

side yielded the values of k^{en}_{NiT}, k^{Hen}_{NiT} and $k^{NiT(en)}$, given in Table 6.

The Eigen–Tamm mechanism (Scheme 1) has been used successfully as a model for predicting complex formation rates for many systems [17]. Differences seen by comparison of experimental formation rate constants to those predicted from the Eigen–Tamm mechanism are used to reveal the presence of other factors which effect the formation rate. The complex formation reactions of $[Ni(tren)(H_2O)_2]^{2+}$ with en and Hen^+ follow the mechanism represented in Scheme 1. If the usual assumptions are made that: (i) the outer-sphere formation and dissociation reactions are rapid; (ii) the steady-state approximation is applied to the singly bonded intermediates B and B′; and (iii) the protonation equilibrium is rapid compared to other steps; the formation rate expression can be written for the two forward pathways as shown in Eqs. (8) and (9). The factor 2/6 is due to

$$k^{L}_{NiT} = \frac{2}{6}\frac{K_{OS}k_1k_2}{k_{-1} + k_2} \tag{8}$$

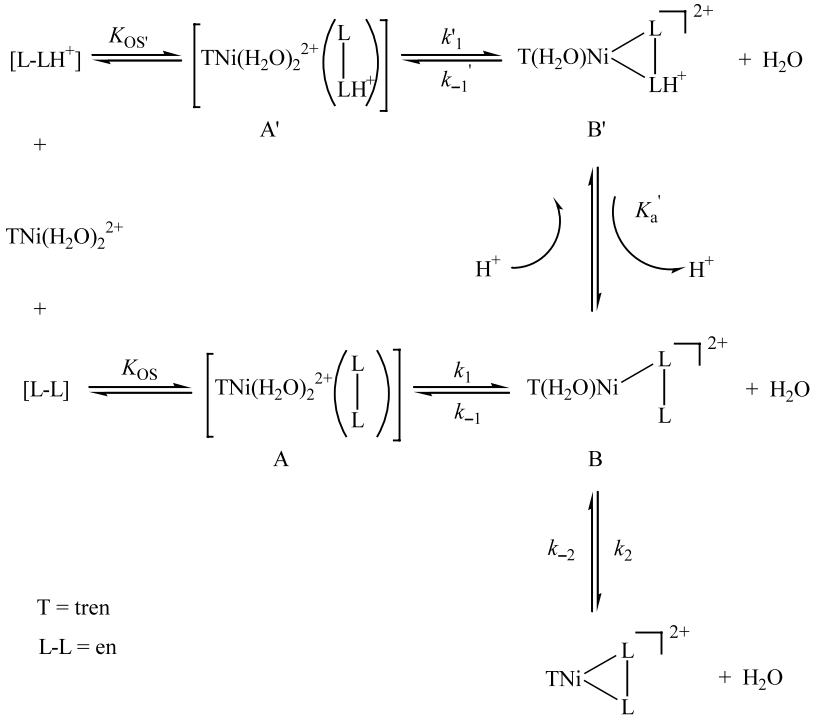
$$k^{HL}_{NiT} = \frac{2}{6}\frac{K_{OS}k'_1k_2}{k'_{-1}K'_H[H^-] + k_2} \tag{9}$$

the number of available coordination sites on $[Ni(tren)(H_2O)_2]^{2+}$ relative to $[Ni(H_2O)_6]^{2+}$.If the ring closure step is fast compared with step A to B, then $k_2 > k_{-1}$ and Eq. (8) simplifies to Eq. (10); the formation rate constants may be predicted from calculated values of K_{OS} and independent measurements of k^{-H_2O} ($= k_1$).

$$k^{L}_{NiT} = \frac{2}{6}K_{OS}k_1 \tag{10}$$

k^{Hen}_{NiT} could be predicted by using either Eq. (9) or Eq. (10), depending upon the relative sizes of k_2 and $k_{-1}K'_H[H^+]$. A plot of $(k_{obsd} - k^{NiT(en)})/[en]$ versus $[H^+]$ (Fig. 4) provides a straight line and the slope of the line give the value of $k^{Hen}_{NiT(en)}$ which is independent of $[H^+]$. Incorporating the steric factor, 14 [18] and intramolecular hydrogen bonding factor, 3 [19], K_{OS}, 0.044 [2] and k^{-H_2O}, 9×10^6 [5] in Eq. (10), the predicted k^{Hen}_{NiT} is corroborated with the experimental value (Table 6). The steric factor value is also applicable for the reaction of en with $[Ni(tren)(H_2O)_2]^{2+}$since the unprotonated end of Hen^+ is the initial reaction site.

To predict the k^{en}_{NiT} value either Eq. (8) or Eq. (10) are useful and this is dependent on k_2 and k_{-1}. In both cases an ICB factor must be incorporated because the reaction proceeds through an internal conjugate base



Scheme 1.

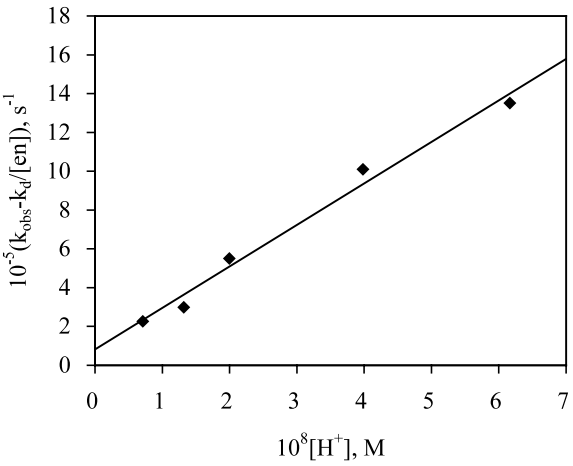


Fig. 4. A plot of $(k_{obsd}-k_d)/[en]$ versus $[H^+]$ for the reaction of $[Ni(tren)(H_2O)]^{2+}$ + en ($\mu = 0.10$ M, 25.0 ± 0.1 °C).

mechanism. Incorporating an ICB factor, 193, a steric factor, 14, K_{OS}, 0.16 [2] and the value of k^{-H_2O}, Eq. (10) predicts a value of k^{en}_{NiT} (Table 6) which is 20 times larger than the experimentally observed value. Thus Eq. (10) is not applicable and the initial bond formation is not the rate-determining step.

If the complex formation path follows as stated in Scheme 1 and the rate-determining step k_2 i.e. the ring closure step, can be calculated from Eq. (8), incorporating $k_{-1} = 1.2 \times 10^5$ [2] and all other parameters are the same as used before in Eq. (10), the found value of k_2 is 3.07×10^3 s^{-1} which is very low compared to the k_2 value 2.2×10^5 s^{-1}, of the en and $Ni(en)_2^{2+}$ reaction [20]. The causes behind the low value of k_2 may be due to: (i) the three en segments are tied on the same nitrogen of tren and ring closure occurs in that side where tertiary tren-N is bonded; (ii) the existence of a conformation-angle-distortion (CAD) effect. The crystal structure of $[Ni(tren)(en)]^{2+}$ reveals that the bond angle formed between the en nitrogens and nickel is 82.02°. The structure also shows that the chelate bite angles between tren nitrogens with nickel varies from 81.84° to 83.14°. Thirdly the crystal structure of $[Ni(tren)(NO_2)_2]\cdot H_2O$ provides a bond angle between the two NO_2^- ligands and nickel of 86.3° [14]. This indicates that the coordinated tren to nickel forces a bite angle 86.3° onto the two open coordination sites. It does not affect the initial bond formation of en but imposes considerable strain when en undergoes ring closure in $Ni(tren)^{2+}$. But this CAD effect is comparatively low compared to those found in the reaction of $[Ni(trien)(H_2O)_2]^{2+}$ with en, because the coordination of trien to nickel forces a bite angle of 92.7° on $Ni(trien)^{2+}$ involving the two open coordination sites. Thus the formation rate constants k^{en}_{NiT} and k^{Hen}_{NiT} for the reaction of $[Ni(tren)(H_2O)_2]^{2+}$ are larger than those of $[Ni(trien)(H_2O)_2]^{2+}$ (Table 7); on the other hand, the dissociation rate constant, $k^{NiT(en)}$, for the reaction of $[Ni(tren)(H_2O)_2]^{2+}$ is smaller than that of $[Ni(trien)(H_2O)_2]^{2+}$ (Table 7).

Table 7
Rate constants values for $[Ni(tren)(H_2O)_2]^{2+}$-en and $[Ni(trien)(H_2O)_2]^{2+}$-en systems at 25.0 ± 0.1 °C and $\mu = 0.10$ M (NaCl)

	$[Ni(tren)(H_2O)_2]^{2+}$-en	$[Ni(trien)(H_2O)_2]^{2+}$-en [a]
k^{en}_{NiT} (M^{-1} s^{-1})	1.13×10^5	2.67×10^4
k^{Hen}_{NiT} (M^{-1} s^{-1})	2.67×10^3	1.77×10^3
$K^{NiT(en)}$ (M^{-1} s^{-1})	3.50	8.62

[a] Values taken from Ref. [2].

3.3.2. 1,10-Phenanthroline

The kinetics of ternary complex formation between $[Ni(tren)(H_2O)_2]^{2+}$ and phen were studied over a pH range from 7.18 to 7.53 both with and without buffer, covering a phen concentration range of $(2.00–5.00) \times 10^{-3}$ M at 25.0 ± 0.1 °C and $\mu = 0.1$ M (NaCl). All reactions were carried out with at least a 10-fold excess of phen to $[Ni(tren)(H_2O)_2]^{2+}$. The observed pseudo-first-order constants are given in Table 8. Under these

Table 8
Experimental observed rate constants for the reaction of $[Ni(tren)(H_2O)_2]^{2+}$ with 1,10-phenanthroline

pH	10^4 $[Ni(tren)(H_2O)_2^{2+}]$ (M)	10^3 [phen] (M)	k_{obsd} (s^{-1})
7.34 [a]	1.02	2.00	31.4
		2.50	37.6
		3.00	44.7
		3.50	50.8
		4.00	58.2
		4.50	63.7
		5.00	70.2
7.45 [a]	1.02	2.00	32.7
		2.50	37.9
		3.00	45.0
		3.50	51.6
		4.00	58.5
		4.50	64.1
		5.00	70.8
7.53 [a]	1.02	2.00	32.4
		2.50	37.7
		3.00	45.2
		3.50	51.8
		4.00	59.2
		4.50	64.6
		5.00	70.9
7.18 [b]	1.02	2.00	32.0
		2.50	37.7
		3.00	44.6
		3.50	51.0
		4.00	57.7
		4.50	53.8
		5.00	70.5

[a] 0.01 M HEPES buffer.
[b] No buffer.

conditions, $[Ni(tren)(phen)]^{2+}$ is formed completely and follows the rate expression in Eq. (11) with L = phen and T = tren. A plot of k_{obsd}, versus phen concentrations follow Eq. (12) and are shown in Fig. 5. The obtained rate constants are listed in Table 9.

$$-\frac{d[NiT]}{dt} = k^{L}_{NiT}[NiT][L] - k_d[NiTL] \quad (11)$$

$$k_{obsd} = k^{L}_{NiT}[L] + k_d \quad (12)$$

In the formation reactions involving Ni(II), the Eigen–Tamm mechanism has been found to hold. As shown in Scheme 2, $NiT(H_2O)_2^{2+}$ is $[Ni(tren)(H_2O)_2]^{2+}$, L–L is phen, species II is an outer-sphere complex, species III is mono-coordinated and species IV is chelated.

Like bipyridine [21], the reaction of phen with $[Ni(tren)(H_2O)_2]^{2+}$ follows the reversible path. Assuming that: (1) the outer-sphere reaction is rapid ($K_{OS} = k_1/k_{-1}$); and that (2) the singly bonded species is a steady-state intermediate, then the formation rate constant can be written as shown in Eq. (13).

$$k^{phen}_{NiT} = \frac{K_{OS}k_2k_3}{k_{-2} + k_3} \quad (13)$$

If the ring closure (k_3) is much faster than the bond rupture (k_{-2}) of species III, then the initial complex formation (k_2) is the rate limiting and the formation rate constant could be predicted as Eq. (14). The statistical factor of 2/6 accounts for the number of available coordination sites of $[Ni(tren)(H_2O)_2]^{2+}$ relative to $[Ni(H_2O)_6]^{2+}$.

$$k^{phen}_{NiT} = \frac{2}{6} K_{OS}k_2 \quad (14)$$

The rate constant values of Ni–polyamine complexes with en, bpy and phen are displayed in Table 10. The effect of coordinated tren on the formation reaction is evaluated by comparing experimental and predicted values. The predicted value is obtained by incorporating $K_{OS} = 0.16$ and $k_2 = 9 \times 10^6$ in Eq. (14). The very low

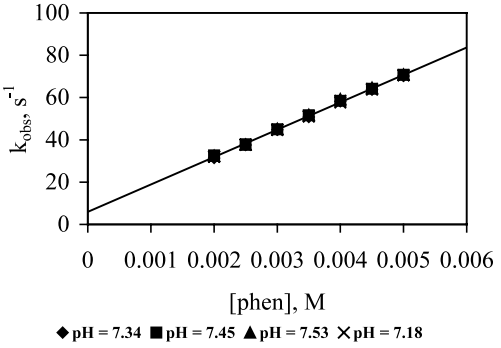


Fig. 5. Dependence of k_{obsd} upon [phen] for reaction of $[Ni(tren)(H_2O)]^{2+}$ + phen ($\mu = 0.10$ M, 25.0 ± 0.1 °C): runs with buffers (◆, ■, △); run without buffer (×). Solid line is least-squares best fit of the points.

Table 9
Rate constants for the forward reaction (k_f) and reverse reaction (k_b) of $[Ni(tren)(H_2O)_2]^{2+}$ with phen at 25.0 ± 0.1 °C and $\mu = 0.10$ M (NaCl)

pH	10^4 k_f (M^{-1} s^{-1})	k_b (s^{-1})
7.18	1.29	5.84
7.34	1.30	5.42
7.45	1.29	6.36
7.53	1.31	5.86

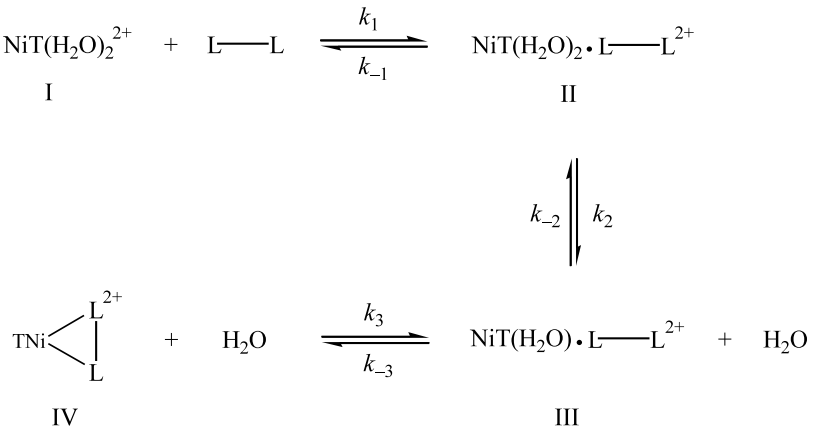
basicity of phen offers a negligibly small ICB contribution to the rate [1]. As listed in Table 10, the predicted value is about 37 times larger than the experimental value of k^{phen}_{NiT}. Further, the experimental rate constant values of phen and bpy reacting with $[Ni(tren)(H_2O)_2]^{2+}$, $[Ni(trien)(H_2O)_2]^{2+}$, $[Ni(cyclen)(H_2O)_2]^{2+}$ are almost identical and 30–84 times less than that of predicted values for all of those reactions. Those differences indicate that the coordinated ligands exert a decelerating effect on the complexation of the attacking bpy or phen and suggest that ring closure contributes to the rate of formation. Thus, the rate-determining step is the formation of the second Ni–N bond. The coordinated tren increases the lability at the remaining coordination sites and increases the monodentate phen dissociation rate constant (k_{-2}). In addition, the steric effect of the coordinated tren blocks the formation of the second Ni–N bond so that ring closure contributes to the rate.

The formation rate constant for the reaction of phen with $[Ni(H_2O)_6]^{2+}$ and the water exchange rate constant of $[Ni(H_2O)_6]^{2+}$ are 1.6×10^3 M^{-1} s^{-1} and 3.2×10^4 s^{-1}, respectively [22,23]. The coordinated tren increases the rate of water loss of Ni(II) by a factor of about 280, but phen reacts only eight times faster with $[Ni(tren)(H_2O)_2]^{2+}$ than with $[Ni(H_2O)_6]^{2+}$. The relatively low rate of reaction between $[Ni(tren)(H_2O)_2]^{2+}$ and phen is due to the steric blocking of coordinated tren.

As shown in Table 10, the rate constants of the phen or bpy reaction with $[Ni(tren)(H_2O)_2]^{2+}$, $[Ni(cyclen)(H_2O)_2]^{2+}$ and $[Ni(trien)(H_2O)_2]^{2+}$ are similar. These results indicate that the steric effect of coordinated tren upon the formation reaction of its Ni(II) complex with phen is very similar to those of coordinated cyclen and trien.

4. Supplementary material

Crystallographic data for the structural analysis have been deposited with the Cambridge Crystallographic Data Centre, CCDC Nos. 176793–176794 for compounds **a** and **b**, respectively. Copies of this information may be obtained free of charge from The Director,



Scheme 2.

Table 10
Rate constants for the reaction of Ni(II)-polyamines with bpy and phen at 25.0±0.1 °C and $\mu = 0.10$ M (NaCl)

	Experimental	Predicted
$k^{bpy}_{Ni(dien)}$ (M^{-1} s^{-1})	1.1×10^4 [a]	8×10^4
$k^{phen}_{Ni(dien)}$ (M^{-1} s^{-1})	2.3×10^4 [a]	8×10^4
$k^{bpy}_{Ni(en)2}$ (M^{-1} s^{-1})	8.4×10^3 [a]	3×10^5
$k^{phen}_{Ni(en)2}$ (M^{-1} s^{-1})	9.3×10^3 [a]	3×10^5
$k^{bpy}_{Ni(trien)}$ (M^{-1} s^{-1})	7.6×10^3 [a]	3×10^5
$k^{phen}_{Ni(trien)}$ (M^{-1} s^{-1})	8.2×10^3 [a]	3×10^5
$k^{bpy}_{Ni(tren)}$ (M^{-1} s^{-1})	1.01×10^4	4.8×10^5
$k^{phen}_{Ni(tren)}$ (M^{-1} s^{-1})	1.30×10^4	4.8×10^5
$K^{bpy}_{Ni(cyclen)}$ (M^{-1} s^{-1})	1.05×10^4	1.1×10^6
$k^{phen}_{Ni(cyclen)}$ (M^{-1} s^{-1})	1.31×10^4 [c]	1.1×10^6
$k^{Ni(tren)(bpy)}$ (s^{-1})	2.9×10^{-1} [b]	
$k^{Ni(tren)(phen)}$ (s^{-1})	5.9 [b]	

[a] Values taken from Ref. [2].
[b] Values taken from Ref. [9].
[c] Values taken from Ref. [10].

CCDC, 12 Union Road, Cambridge, CB2 1EZ, UK (fax: +44-1223-336033; e-mail: deposit@ccdc.cam.ac.uk or www: http://www.ccdc.cam.ac.uk). Additional figures (UV–Vis spectral changes) are available from the authors (C.-S.C.) on request.

Acknowledgements

The authors are thankful to the National Science Council of the Republic of China for financial support under Grants NSC 89-2119-M-007-006. They are also indebted to Yau-Chen Jiang and Fen-Ling Liao for collecting the X-ray diffraction data and crystal structure solutions.

References

[1] R.K. Steinhaus, B.I. Lee, Inorg. Chem. 21 (1982) 1829.
[2] R.K. Steinhaus, L.H. Kolopajlo, Inorg. Chem. 24 (1985) 1839.
[3] S.E. Rasmussen, Acta Chem. Scand. 13 (1959) 2009.
[4] C.J. Jorgenson, Acta. Chem. Scand. 10 (1956) 887.
[5] D.P. Rablen, H.W. Dodgen, J.P. Hunt, J. Am. Chem. Soc. 94 (1972) 1771.
[6] A.D.R. Mark, C.T. William, Inorg. Chem. 29 (1990) 2409.
[7] D.E. Newlin, M.A. Pellack, R. Nakon, J. Am. Chem. Soc. 99 (1977) 1078.
[8] S.A. Bedell, R. Nakon, Inorg. Chem. 16 (1977) 3055.
[9] R.G. Wilkins, Acc. Chem. Res. 3 (1970) 408.
[10] C.-Y. Lai, W.-J. Lan, C. Wang, C.-S. Chung, Polyhedron 17 (1998) 2127.
[11] P. Main, S.J. Fiske, S.E. Hull, L. Lessinger, G. Germain, J.P. DeClercq, W.W. Woolfson, MULTAN-80, A. System of Computer Programs for the Automatic Solutions of Crystal Structures from X-ray Diffraction Data, University of New York, 1980.
[12] G.M. Sheldrick, SHELXTL-PLUS Crystallographic System, 1991, version 5.0, Siemens Analytical International Inc., Madison, WI, USA.
[13] H.-K. Fun, B.-C. Yip, Z.-L. Lu, C.-Y. Duan, Y.-P. Tian, X.-Z. You, Acta Crystallogr., Sect. C 52 (1996) 509.
[14] R. Wen, I. Bernal, F. Somoza, W. Li, F.R. Fronczek, Inorg. Chim. Acta 282 (1998) 96.
[15] Mazhar-UI-Hague, C.N. Caughlin, K. Emerson, Inorg. Chem. 24 (1970) 2811.
[16] A.E. Martel, R.M. Smith, Critical Stability Constants, vol. 2, Plenum, New York, 1979, pp. 36–38.
[17] (a) D.W. Mergerum, C.W. Cayley, D.C. Watherburn, G.K. PagenKopf, Coordination Chemistry, A.E. Martell (Ed.), American Chemical Society, Washington DC, 1978;
(b) ACS Monogr. 174, pp. 26–30.
[18] D.B. Rorabacher, C.A. Melendez-Cepeda, J. Am. Chem. Soc. 93 (1974) 6071.
[19] R.W. Taylor, H.K. Stepien, D.B. Rorabacher, Inorg. Chem. 13 (1974) 1282.
[20] J. Jones, D.W. Margerum, J. Am. Chem. Soc. 92 (1970) 470.
[21] D.N. Hague, A.R. White, J. Chem. Soc., Dalton Trans. (1993) 1337.
[22] R.G. Wilkins, Kinetics and Mechanism of Reaction of Transition Metal Complexes, VCH, New York, 1991, p. 214.
[23] R.H. Holyer, C.D. Hubbard, S.F.A. Kettle, R.G. Wilkins, Inorg. Chem. 4 (1965) 929.

mol) in MeCN (30 ml). Orange needles slowly crystallised.

Analysis for $FeCl_3$(*N*-methylimidazole)$_3$: $C_{12}H_{18}Cl_3FeN_6$ requires C, 35.27; H, 4.44; N, 20.57. Found: C, 34.85; H, 4.27; N, 19.92%.

Mer-[$FeCl_3$(terpy)] (**3**) and [$FeCl_3$(imidazole)$_4$] (**6**) were prepared similarly by adding a warm solution of the ligand (0.10 g; 0.49×10^{-3} mol (terpy) or 1.72×10^{-3} mol (imidazole)) in MeCN (40 ml) to a solution of $FeCl_3$ (0.08 g; 0.49×10^{-3} mol) in MeCN (8 ml); (**3**) formed yellow crystals and (**6**) yellow to orange diamonds.

Analysis for $FeCl_3$(terpy): $C_{15}H_{11}Cl_3FeN_3$ requires C, 45.55; H, 2.81; N, 10.63. Found: C, 45.44; H, 2.76; N, 10.64%.

Analysis for $FeCl_3$(imidazole)$_4$: $C_{12}H_{12}Cl_3FeN_8$ requires C, 35.45; H, 3.96; N, 20.67. Found: C, 34.50; H, 4.26; N, 19.81%.

Mer-[$FeCl_3$(tptz)] (**4**) was obtained as yellow–orange crystals from the addition of a warm solution of the ligand (0.12 g; 0.385×10^{-3} mol) in MeCN (20 ml) to a solution of $FeCl_3$ (0.06 g; 0.37×10^{-3} mol) in MeCN (2 ml). X-ray crystallography confirms the presence of 1 molecule of MeCN and $\frac{1}{2}$ molecule of H_2O in the lattice of the crystal studied.

Analysis for $FeCl_3$(tptz): $C_{18}H_{12}Cl_3FeN_6$ requires C, 45.55; H, 2.55; N, 17.71; $C_{20}H_{16}Cl_3FeN_6O_{0.5}$ ($FeCl_3$(tptz)·MeCN·$\frac{1}{2}H_2O$) requires C, 45.79; H, 3.07; N, 18.69. Found: C, 43.10; H, 2.79; N 16.51%.

[$FeCl_3$(3-methylpyrazole)$_4$] (**5**) was prepared by the addition of 3-methylpyrazole (0.10 g; 1.22×10^{-3} mol) to a solution of $FeCl_3$ (0.08 g; 0.49×10^{-3} mol) in MeCN (8 ml). Well formed orange–red crystals slowly crystallised. Analysis for $FeCl_3$(3-methylpyrazole)$_4$: $C_{16}H_{24}Cl_3FeN_8$ requires C, 39.16; H, 4.93; N, 22.84. Found: C, 38.76; H, 4.76; N, 22.39%.

[$FeCl_3$(3-methylpyrazole)$_3$] was prepared by the literature method [1], by addition of 3-methylpyrazole (0.40 g; 4.88×10^{-3} mol) to a solution of $FeCl_3$ (0.30 g; 1.85×10^{-3} mol) in EtOH (5 ml). An oil initially formed, which changed to an orange solid on scratching the glass.

Analysis for $FeCl_3$(3-methylpyrazole)$_3$: $C_{12}H_{18}Cl_3FeN_6$ requires C, 35.27; H, 4.44; N, 20.57. Found: C, 34.01; H, 4.28; N, 19.76%.

2.2. X-ray crystallography

Full spheres of diffraction data for **1**, **2**, **3** and **4** were collected on a Bruker APEX 2000 CCD diffractometer at 150 K. Data for **5** were measured at 190 K on a Bruker P4 diffractometer. All data sets were collected using graphite monochromated Mo Kα radiation ($\lambda = 0.7107$ Å) and the reflections were corrected for Lp and absorption effects. The structures were solved by Patterson methods using the program SHELXS [8] and refined by full-matrix least squares on F^2 using SHELXTL [9]. All hydrogen atoms were included in calculated positions (C–H = 0.96 Å) with isotropic displacement parameters set to $1.5U_{eq}$(C) for the methyl groups and $1.2U_{eq}$(C) for all other hydrogen atoms. All non-hydrogen atoms were refined with anisotropic displacement parameters.

Crystal data are presented in Table 1, with important bond lengths and angles in the metal's co-ordination sphere listed in Table 2.

3. Results and discussion

3.1. Description of the structures

3.1.1. *mer*-[$FeCl_3$(pyrazole)$_3$] (**1**)

This molecule (Fig. 1) has six co-ordination of iron with bond angles showing slight distortion from a regular octahedral geometry (*cis* N–Fe–N 84.97(5)° and 85.95(5)°; *trans*-N–Fe–N 170.90(5)°; *cis* Cl–Fe–Cl 90.81(2)° and 94.77(2)°; *trans*-Cl–Fe–Cl 174.42(2)°). The mutually *trans*-Fe–N bonds are virtually identical in length at 2.1186(14) and 2.1195(13) Å, shorter than that *trans*-to chlorine, where Fe–N is 2.1721(13) Å. This indicates a greater *trans*-influence for chloride. As far as the Fe–Cl distances are concerned, Fe–Cl (3) (*trans*-to nitrogen) is 2.3053(5) Å, shorter than the mutually *trans*-Fe–Cl bonds of 2.3185(5) and 2.3548(5) Å. A possible explanation for the discrepancy in Fe–Cl bond length between 'equivalent' bonds lies in Cl···H–N hydrogen-bonding. Cl(1), involved in the greater Fe–Cl bond length, has intramolecular hydrogen bonds at 2.461 and 2.628 Å as well as an intermolecular one at 2.555 Å, whilst Cl(2) has an intramolecular hydrogen bond at 2.585 Å and an intermolecular one at 2.686 Å. M–Cl moities have been shown to be good hydrogen-bond acceptors [10] and there is X-ray and neutron-diffraction evidence for intramolecular hydrogen-bonding causing strong N–H···Cl interactions in another pyrazole complex, *trans*-[$NiCl_2$(pyrazole)$_4$], leading to long Ni–Cl distances [11]. Similarly, in $(NH_4)_2$[$FeCl_5(OH_2)$], there is considerable variety in Fe–Cl distances. Apart from a short Fe–Cl bond *trans*-to water (2.323(1) Å), the other Fe–Cl distances are 2.350(1), 2.3838(8), 2.3828(8) and 2.390(1) Å. The first-named is regarded as unperturbed; the others are all lengthened (by up to 0.04 Å) owing to hydrogen-bonding [12].

The only '$FeCl_3$(N-donor)$_3$' complex previously characterised crystallographically is mer-[$FeCl_3$(py)$_3$]·py [3],where the respective Fe–Cl distances were 2.306(2) Å *trans*-to N and 2.326(2) Å *trans*-to Cl; there was a more striking difference in Fe–N distance, at 2.168(5) Å *trans*-to N and 2.274(6) Å *trans*-to Cl.

Table 1
Crystal data

	1	2	3	4	5
Empirical formula	$C_9H_{12}Cl_3FeN_6$	$C_{12}H_{18}Cl_3FeN_6$	$C_{15}H_{11}Cl_3FeN_3$	$C_{20}H_{16}Cl_3FeN_7O_{0.5}$	$C_{16}H_{24}Cl_3FeN_8$
Formula weight (M)	366.45	408.52	395.47	524.60	490.63
T (K)	150	150	160	160	200
Crystal system	monoclinic	monoclinic	monoclinic	triclinic	monoclinic
Space group	$P2_1/n$	$P2_1/c$	$P2_1/n$	$P\bar{1}$	$P2/n$
a (Å)	8.377(1)	7.315(1)	8.256(1)	8.304(1)	10.303(3)
b (Å)	13.866(2)	8.475(1)	14.052(2)	11.899(2)	8.746(3)
c (Å)	12.653(2)	27.906(2)	13.696(2)	12.240(2)	12.731(4)
α (°)	90	90	90	96.28(1)	90
β (°)	107.04(2)	92.81(1)	104.91(1)	102.90(1)	98.44(2)
γ (°)	90	90	90	107.77(1)	90
V (Å^3)	1407.2(4)	1727.95(17)	1535.4(4)	1101.9(2)	1134.8(6)
Z	4	4	4	2	2
μ(Mo Kα) (mm^{-1})	1.635	1.341	1.501	1.074	1.036
Reflections measured	11 134	13 070	12 617	8266	3246
Reflections independent	2923	3383	3343	4048	2464
R_{int}	0.022	0.025	0.031	0.014	0.057
Reflections $\{F > 4\sigma(F)\}$	2587	2942	3044	3703	1659
θ_{max}, % complete	26.50, 99.9	26.0, 100.0	27.0, 99.6	25.5, 98.7	27.0, 99.2
R_1 $\{I > 2\sigma(I)\}$	0.023	0.027	0.027	0.028	0.057
wR_2 (F^2) all data	0.065	0.074	0.074	0.085	0.141

Table 2
Selected bond distances (Å) with esds in parentheses

	1	2	3	4	5 [a]
Fe–Cl (*trans*-Cl)	2.3548(5)	2.3871(5)	2.3150(5)	2.3473(5)	2.3183(13)
	2.3185(5)	2.3527(5)	2.3743(5)	2.3228(6)	
Fe–Cl (*trans*-N)	2.3053(5)	2.3151(5)	2.2526(5)	2.2487(6)	
Fe–N (*trans*-N)	2.1195(13)	2.1247(16)	2.1267(14)	2.1774(15)	2.137(4)
	2.1186(14)	2.1353(15)	2.1335(13)	2.1928(15)	2.140(4)
Fe–N (*trans*-Cl)	2.1721(13)	2.1526(15)	2.1021(13)	2.1104(15)	

[a] The Fe atom of compound **5** is located on a centre of symmetry and therefore there is one unique Fe–Cl1 and two Fe–N distances.

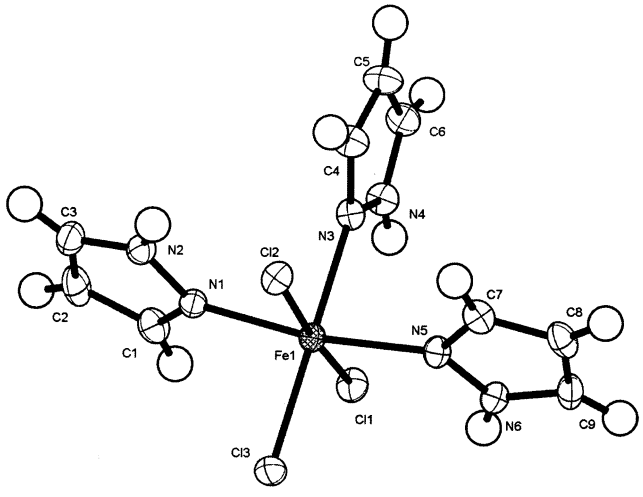


Fig. 1. Molecular structure of **1** showing the atom label scheme. Displacement ellipsoids are shown at the 50% level. H atoms are shown as spheres of arbitary radius.

The Fe–Cl bond lengths in these compounds are substantially shorter than those in $[FeCl_6]^{3-}$ ions, such as in $[Co(NH_3)_6]\cdot[FeCl_6]$ where it is 2.3926(3) Å, where the lengthening, even in comparison with salts of the $[FeCl_5(OH_2)]^{2-}$ ion, has been ascribed to Cl···Cl repulsions in a congested coordination sphere [13].

3.1.2. *mer*-[$FeCl_3$(*N*-methylimidazole)$_3$] (**2**)

The molecule is similar in structure to (**1**) (Fig. 2). Here the *cis* N–Fe–N angles are 85.21(6)° and 88.05(6)°; *trans*-N–Fe–N 172.88(6)°; *cis* Cl–Fe–Cl 91.354(19)° and 93.619 (18)°; trans-Cl–Fe–Cl 174.86(2)°. The mutually *trans*-Fe–N bonds are again very similar in length at 2.1247(16) and 2.1353(15) Å, shorter than that *trans*-to chlorine, where Fe–N is 2.1526(15) Å, again indicating a greater *trans*-influence for chloride. The iron–chlorine distance *trans*-to nitrogen Fe–Cl(1) is 2.3151 (5) Å, shorter than the other two mutually trans-Fe–Cl bonds of 2.3527(5) and 2.3871(5)

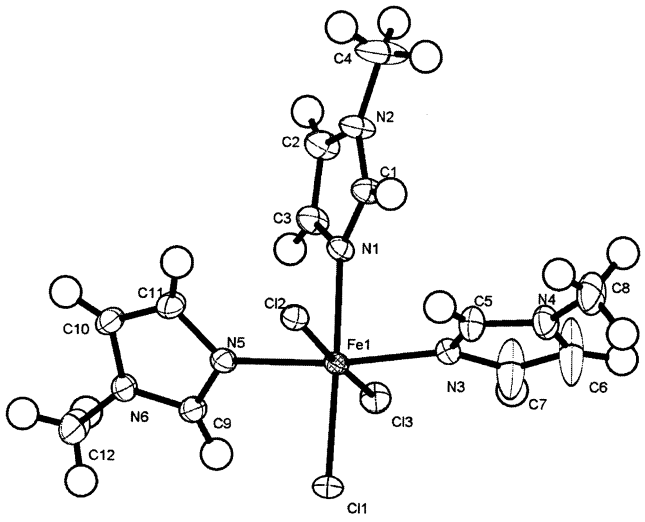


Fig. 2. Molecular structure of **2** showing the atom label scheme. Displacement ellipsoids are shown at the 50% level.

Å. The only H···Cl contact below 2.7 Å is Cl(2)···H(5)–N(5) at 2.641 Å.

3.1.3. *mer*-[$FeCl_3$(terpy)] (**3**)

A mer-geometry is enforced on this complex by the tendency of a co-ordinated terpyridyl ligand to adopt a near-planar geometry when tridentate (Fig. 3). *Mer*-[$FeCl_3$(terpy)] exhibits a greater distortion from regular octahedral geometry than the pyrazole and methylimidazole complexes, due to the steric demands of the terpyridyl ligand. However, the N–Fe–N angles subtended by two neighbouring nitrogens in the same ring, at 74.89° and 75.00(5)°, are very similar to those in the $[FeCl_2(bipy)_2]^+$ cation (74.9(1)° and 75.2(1)°) and in the $[FeCl_4(bipy)]^-$ anion (74.6°) [14]. The presence of the three nitrogen donor atoms in the terpy complex leads to a N(1)–Fe–N(3) angle of 149.84(5)°. The chlorides

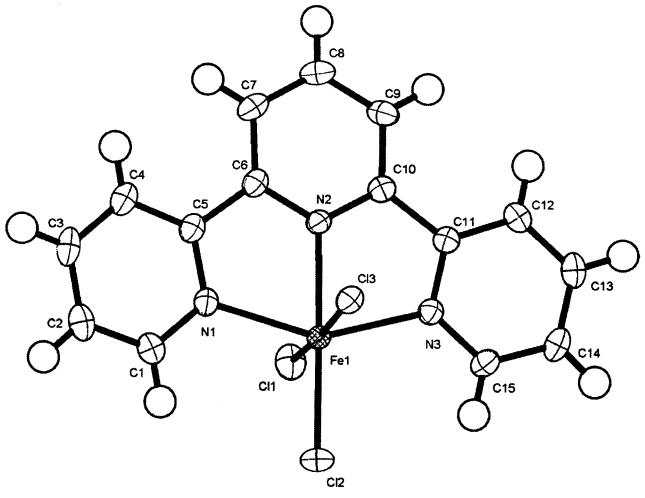


Fig. 3. Molecular structure of **3** showing the atom label scheme. Displacement ellipsoids are shown at the 50% level.

are less constrained, so that in contrast the Cl–Fe–Cl angles are nearer to the regular octahedral angles, at 90.902(19)° and 94.58(2)° (*cis*) and 174.468(17)° (*trans*).

Another consequence of the linkage between the three pyridine rings in *mer*-[$FeCl_3$(terpy)] is the short Fe–N (2) distance trans-to chlorine (2.1021(13) Å) which is shorter than the mutually trans-Fe–N distances (2.1335(13) and 2.1267(14) Å), in the opposite sense to the *trans*-influence observed in the pyrazole complex, but which clearly is an imposed consequence of bringing N(1) and N(3) close enough to iron to bond. In the similarly six co-ordinate *cis*-$[FeCl_2(bipy)_2]^+$ cation, Fe–N distances *trans*-to N lie in the range 2.126–2.144 Å, whilst *trans*-to chlorine they fall into a narrower 2.174–2.178 Å range (2.187–2.199 Å in $[FeCl_4(bipy)]^-$).

The Fe–Cl distances in *mer*-[$FeCl_3$(terpy)], however, observe the expected pattern, with Fe–Cl (2) *trans*-to N (2.2526(5) Å) being shorter than the Fe–Cl(1) and Fe–Cl(3) distances of 2.3150(5) and 2.3743(5) Å, respectively; the range in distances is, however, rather large. The discrepancy between the mutually *trans*-Fe–Cl distances is again noticeable; however, one possible explanation lies in C–H···Cl–Fe interactions, as Cl(3) has 3 C–H··· contacts at <2.8 Å against none for Cl(1).

In the comparable *cis*-$[FeCl_2(bipy)_2]^+$ cation, the Fe–Cl distance *trans*-to N are 2.254–2.282 Å (in the $[FeCl_4]^-$ and $[FeCl_4(bipy)]^-$ salts), whilst in the $[FeCl_4(bipy)]^-$ anion, the Fe–Cl distances are 2.305–2.310(2) Å (*trans*-to N) and 2.371–2.374(2) Å *trans*-to Cl.

The layer structure has a repeat sequence every 4th layer with the shortest C···C contact of 3.421 Å; this may be compared with the interlayer spacing in graphite of 3.35–3.44 Å [15]. The *trans*-Cl atoms fit into holes in the terpy layers above and below.

3.1.4. [$FeCl_3$(tptz)] (**4**)

This compound has a similar co-ordination geometry (Fig. 4) to *mer*-[$FeCl_3$(terpy)], with a 'central' Fe–N distance of 2.1104(15) Å and other Fe–N distances of 2.1774(15) and 2.1928(15) Å. Fe–Cl *trans*-to N is 2.2487(6) Å, with other Fe–Cl distances being 2.3228(6) and 2.3473(5) Å.

The N–Fe–N angles subtended by two neighbouring nitrogen atoms in the same ring, at 72.84(6)° and 73.55(5)°, are very similar to those in [$FeCl_3$(terpy)]. The N(1)–Fe–N(5) angle, at 146.29(6)°, is similar to that in the terpy complex [149.84(5)°] whilst there is a similar pattern in the Cl–Fe–Cl angles at 91.69(2)° and 93.09(2)° (*cis*) and 174.84(2)° (*trans*).

There are a number of short Cl···H contacts, with a notable discrepancy between the intra molecular Cl1···H1 and Cl1···H13 distances of 3.076 and 3.249 Å, respectively, where more similar values might be expected; the discrepancy may be due to the effects of a

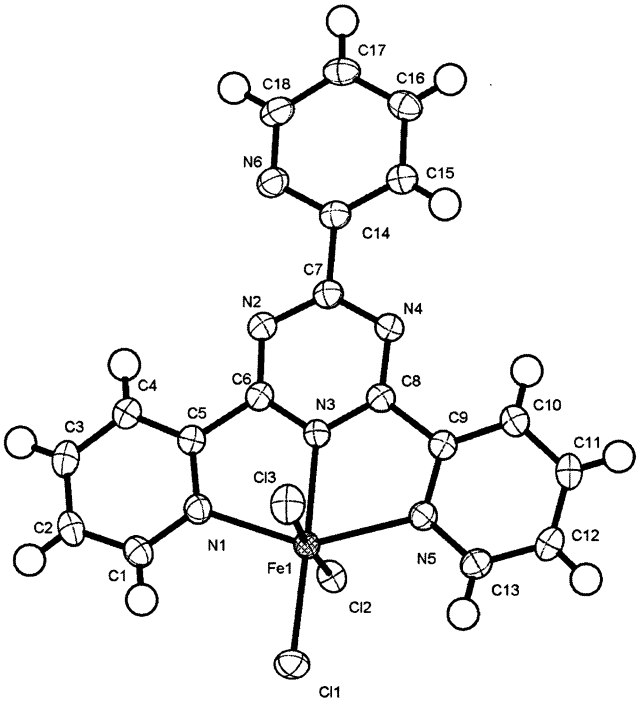


Fig. 4. Molecular structure of **4** showing the atom label scheme. Displacement ellipsoids are shown at the 50% level.

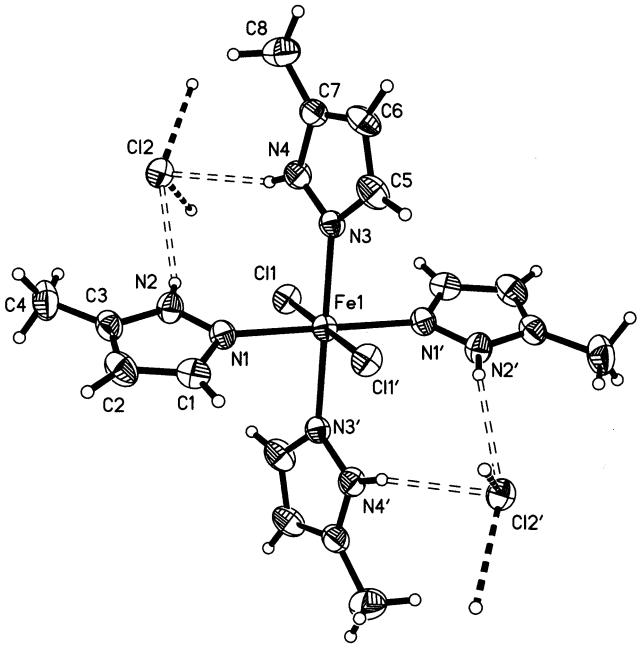


Fig. 5. Molecular structure of **5** showing the atom label scheme. Displacement ellipsoids are shown at the 50% level.

number of intermolecular hydrogen bonds, notably short distances being Cl2···H17′ 2.775; Cl1···H12′ 2.782; Cl2···H2′ 2.905; Cl2···H3′ 2.914; Cl3···H15′ 3.078 and Cl3···H16′ 3.102 Å. There is a molecule of MeCN in the lattice, as well as a half-molecule of water per formula unit; the MeCN is involved in a short N···H contact with $CH_3CN\cdots H(11)$–C(11) at 2.49 Å.

3.1.5. *trans*-[$FeCl_2$(3-methylpyrazole)$_4$]Cl (**5**)

The structure of this compound (Fig. 5) exhibits similarities to the recently reported *trans*-[$FeCl_2$(imidazole)$_4$]Cl·thf·H_2O [5] but there are differences too. The Fe atom is located on a center of symmetry as is Cl(1) and the methylpyrazoles. The Fe–N distances at 2.137–2.140(4) Å and Fe–Cl at 2.3183(13) Å are unsurprising and compare with respective values of 2.125–2.140(5) and 2.355(2) Å, respectively for the *trans*-$[FeCl_2(\text{imidazole})_4]^+$ ion. The mutually *trans*-Fe–Cl distances are rather similar to the corresponding Fe–Cl distances in (**1**–**3**), which fall in the range 2.3150–2.3871 Å, the longer ones being lengthened by Q–H···Cl–Fe interactions (Q = N, C).

The structure is linked by strong N–H···Cl hydrogen bonds. Each chloride ion is involved in two hydrogen bonds (Cl2···H2a = 2.470 and Cl2···H4a = 2.411 Å) to mutually *cis*-3-methylpyrazole ligands (shown as solid dash lines in Fig. 5) and in two further bonds to neighbouring complex cations (shown as open dash lines). In contrast, the imidazole complex is described [5] as 'having no significant cation–anion interactions'. The imidazole groups are aligned nearly parallel to the Cl–Fe–Cl axis, as in the pyrazole complex.

3.1.6. *trans*-[$FeCl_2$(imidazole)$_4$]Cl (**6**)

The poor quality of crystals obtained from this reaction meant that no satisfactory refinement of the data was possible ($R = 0.258$), probably because of unresolved disorder due to solvent molecules in the lattice. It was clear, however, that the structure was *trans*-$[FeCl_2(\text{imidazole})_4]^+\cdot Cl^-$, with dimensions in the cation similar to those in *trans*-[$FeCl_2$(imidazole)$_4$]+ $Cl^-\cdot$thf·H_2O [5].

4. Discussion

We attempted to synthesise new complexes by reaction of the N-donor ligands with a solution of anhydrous $FeCl_3$ in MeCN, reasoning that a labile complex [$FeCl_3(MeCN)_x$] ($x \sim 3$) would be a suitable synthon from which weakly bound nitrile ligands would be readily displaced by N-donors and obviate problems encountered in solvents used hitherto such as ethanol or propanone. Though not successful in every case, this method led to the isolation of complexes with pyrazole, 3-methylpyrazole, imidazole and *N*-methylimidazole; although [$FeCl_3$(pyrazole)$_3$] was synthesised by this route, in the event superior crystals were obtained by recrystallisation from $MeNO_2$. We also observed colour changes indicating complex formation with 4-methylpyrazole and 3,5-dimethylpyrazole, but were unable to isolate crystalline material; we were also able to extend

the method to isolate suitable crystals of the terpyridyl and 2,4,6-tris(2-pyridyl)-1,3,5-triazine complexes.

The complex isolated from the reaction of $FeCl_3$ with 3-methylpyrazole in MeCN was *trans*-[$FeCl_2$(3-methylpyrazole)$_4$]Cl (**5**), in contrast to earlier syntheses carried out in ethanol, when molecular [$FeCl_3$(3-methylpyrazole)$_3$] was formed [1]. The earlier synthesis of [$FeCl_3$(3-methylpyrazole)$_3$] was found to be reproducible, but it is not possible to isolate crystals suitable for X-ray diffraction.

The one-step synthesis of *mer*-[$FeCl_3$(terpy)] by this route represents a considerable improvement over the previously reported three-step method [16], which involved prior preparation of $[Fe(terpy)_2]^{2+}$, its oxidation to $[Fe(terpy)_2]^{3+}$ followed by reaction with Cl^- to afford [$FeCl_3$(terpy)]. Apart from ultimate confirmation of its nature by its crystal structure and microanalyses, our material had a similar peak in the far-IR spectrum [16] due to νFe–Cl at 343 cm^{-1} comparable with the earlier reported value for [$FeCl_3$(terpy)] of 353 cm^{-1}.

Four of the six complexes characterized have structures of the *mer*-[$FeCl_3L_3$] type (L = pyrazole, *N*-methylimidazole, $\frac{1}{3}$terpy, $\frac{1}{3}$tptz), which has hitherto not been well represented. A number of octahedral $FeCl_3$ complexes are known where a *fac*-geometry is enforced by the steric requirements of the ligand making it occupy a face; such systems include *fac*-[$FeCl_3$(L)] (L = 1,3,5-trimethyltriazacyclohexane [17a]; 1,3,5-trithiazacyclononane [17b]; di(2-pyridyl)methylamine (DPMA) [17c]; (bis(pyridin-2-ylmethyl)amine) [17d]; bis(2-pyridylmethyl)amine) (BPA) [17e]. However, meridional systems have been characterized before, such as *mer*-[$FeCl_3(py)_3$]·py [3] and *mer*-[$FeCl_3$L] (L = 2,6-bis(*N*-(2-pyridylethyl)iminomethyl]-4-methylphenolate), which contains a $FeCl_3N_2O$ co-ordination sphere [18]. Whilst the ligands terpy and tptz enforce a *mer*-geometry, in principle either a *fac*- or *mer*-isomer could be obtained for a [$FeCl_3L_3$] complex where L is a monodentate ligand; so far, only the *mer*-isomer has been obtained with these N-donors (L = py, *N*-methylimidazole, pyrazole) and this is presumably due to the desire of the bulky N-donor ligands to mimimise repulsions between them.

Otherwise, there can be a fine balance of forces dictating whether a *fac*- or *mer*-isomer is obtained. Thus, reaction of $FeCl_3$ with phen gives a complex of 1:1 stoichiometry $FeCl_3$(phen). Its recrystallisation from methanol gives *fac*-[$FeCl_3$(phen)(MeOH)], whilst recrystallisation from presumably wet MeCN gives *fac*-[$FeCl_3$(phen)(H_2O)] [14,19a]; in contrast, recrystallisation from DMF affords *mer*-[$FeCl_3$(phen)(DMF)] (DMF = dimethylformamide) [19b]. Even in a relatively non-polar solvent, reaction of $FeCl_3$ with a Lewis base can lead to a number of species in solution, some neutral and some ionic, possibly resulting from self-ionisation. Thus a spectrophotometric study of solutions of $FeCl_3$ in pyridine identified the presence of at least three complexes, neutral [$FeCl_3py_n$] ($n = 3$, presumably), $[FeCl_4]^-$ and (by implication) $[FeCl_2py_n]^+$ ($n \sim 4$) with the first named predominating, as the solution was essentially a non-electrolyte [20]. The choice of solvent can affect the identity of the complex isolated, thus reaction of $FeCl_3$ with pyridine N-oxide (pyO) in ether yielded [$Fe(pyO)_3Cl_3$] whilst in ethanol $[Fe(pyO)_4Cl_2]^+$ $[FeCl_4]^-$ ('$Fe(pyO)_2Cl_3$') was obtained [21].

Ultimately the nature of the complex isolated will depend upon the balance of a number of factors, including the concentration of each species and its solubility, as well as steric requirements of the ligand.

5. Supplementary material

Crystallographic data for the structural analysis have been deposited with the Cambridge Crystallographic Data Centre, CCDC Nos. 183556–183560, for compounds **1**–**5**. Copies of this information may be obtained free of charge from The Director, CCDC, 12 Union Road, Cambridge CB2 1EZ, UK (fax: +44-1223-336033; email: deposit@ccdc.cam.ac.uk or www: http://www.ccdc.cam.ac.uk).

Acknowledgements

We are very grateful to Dr J.C. Anderson of the University of Nottingham for helpful discussions and for assistance with the collection of far-IR data, and to T.F. Spencer of the University of Nottingham for microanalytical data.

References

[1] S.A. Cotton, J.F. Gibson, J. Chem. Soc. Sect. A (1971) 1693.
[2] S.A. Cotton, P.V.H. Pisani, R. Stubbs, Inorg. Nuclear Chem. Lett. 12 (1976) 695.
[3] (a) A. Hoser, Z. Kaluski, M. Januszczyk, J. Pietrzak, T. Glowiak, Acta Crystallogr., Sect. C 39 (1983) 1039;
(b) M. Januszczyk, J. Janicki, H. Wojakowska, R. Krzyminiewski, J. Pietrzak, Inorg. Chim. Acta 186 (1991) 27.
[4] J.-C. Daran, Y. Jeannin, L.M. Martin, Inorg. Chem. 19 (1980) 2934.
[5] S.J. Obrey, S.G. Bott, A.R. Barron, J. Chem. Cryst. 30 (2000) 61.
[6] K.R. Millington, S.R. Wade, G.R. Willey, M.G.B. Drew, Inorg. Chim. Acta 89 (1984) 185.
[7] F. Calderazzo, U. Englert, G. Pampaloni, E. Vanni, C.R. Acad. Sci.Paris, t.2 Sér IIc (1999) 311.
[8] G.M. Sheldrick, SHELXS-86, Program for Crystal Structure Solution, University of Göttingen, Germany, 1986.
[9] G.M. Sheldrick, SHELXTL-pc Release 6.10, Siemens Analytical X-ray Instruments, Madison, WI, 1991.

[10] G. Aullón, D. Bellamy, L. Brammer, E.A. Bruton, A.G. Orpen, Chem. Commun. (1998) 653.
[11] R.B. Helmholdt, W. Hinrichs, J. Reedijk, Acta Crystallogr., Sect. C 43 (1987) 226.
[12] B.N. Figgis, C.L. Raston, R.P. Sharma, A.H. White, Aust. J. Chem. 31 (1978) 2712.
[13] (a) J.K. Beattie, C.J. Moore, Inorg. Chem. 21 (1982) 1292;
(b) M.C. Morón, F. Palacio, J. Pons, J. Casabó, X. Solans, K. Merabit, D. Huang, X. Shi, B.K. Teo, R.L. Carlin, Inorg. Chem. 33 (1994) 746.
[14] B.N. Figgis, J.M. Patrick, P.A. Reynolds, B.W. Skelton, A.H. White, P.C. Healy, Aust. J. Chem. 36 (1983) 2043.
[15] A.F. Wells, Structural Inorganic Chemistry, 4th ed., Clarendon Press, Oxford, 1975, p. 734.
[16] W.M. Reiff, W.A. Baker, N.E. Erickson, J. Am. Chem. Soc. 90 (1968) 4794.
[17] (a) R.D. Köhn, G. Kociok-Köhn, Angew. Chem., Int. Ed. Engl. 33 (1994) 1877;
(b) J. Ballester, O.J. Parker, G.L. Breneman, Acta Crystallogr., Sect. C 50 (1994) 712;
(c) M. Renz, C. Hemmert, H. Gornitzka, B. Meunier, New. J. Chem. 23 (1999) 773;
(d) R. Viswanathan, M. Palaniandavar, T. Balasubramanian, P.T. Muthiah, J. Chem. Soc., Dalton Trans. (1996) 2519;
(e) M.-C. Rodriguez, F. Lambert, I. Morgenstern-Badarau, M. Cesario, J. Guilhem, B. Keita, L. Nadjo, Inorg. Chem. 36 (1997) 3525.
[18] M. Muikuriya, K. Kushida, H. Nakayama, W. Mori, M. Kishita, Inorg. Chim. Acta 165 (1989) 35.
[19] (a) P.C. Healy, J.M. Patrick, B.W. Skelton, A.H. White, Aust. J. Chem. 36 (1983) 2031;
(b) W.M. Reiff, E.H. Whitten, K. Mottle, T.F. Brennan, A.R. Garofolo, Inorg. Chim. Acta 77 (1983) L27.
[20] H. Peterson, R.S. Drago, Inorg. Chim. Acta 3 (1969) 155.
[21] S.A. Cotton, J.F. Gibson, J. Chem. Soc. Sect. A (1970) 2105.

1:2 molar ratio, an untreatable mixture was obtained, instead of the expected intramolecularly bonded complex, whereas reaction in a 1:4 molar ratio gave compounds with the diphosphine acting as a chelating ligand.

2. Experimental

2.1. Safety note: caution

Perchlorate salts of metal complexes with organic ligands are potentially explosive. Only small amounts of these materials should be prepared and handled with great caution.

The synthesis of complexes **1**, **2** and **8** has been reported previously by us [30]. Solvents were purified by standard methods [31]. Chemicals were reagent grade. The phosphines PPh_3, $P(p\text{-}MeOC_6H_4)_3$, $P(p\text{-}NMe_2C_6H_4)Ph_2$ and *cis*-$Ph_2PCH{=}CHPPh_2$ were purchased from Aldrich-Chemie. Microanalyses were carried out using a Carlo Erba Elemental Analyser, Model 1108. IR spectra were recorded as Nujol mulls or polyethylene discs on a Perkin–Elmer 1330 and Mattson spectrophotometer. NMR spectra were obtained as $CDCl_3$ solution and referenced to $SiMe_4$ (^1H, $^{13}C\{^1H\}$) or 85% H_3PO_4 ($^{31}P\{^1H\}$) and were recorded on a Bruker AC-200F spectrometer. All chemical shifts were reported downfield from standards. The FAB-MS were recorded using a VG Quatro mass spectrometer with a Cs ion gun; 3-nitrobenzyl alcohol was used as the matrix. Conductivity measurements were made on a CRISON GLP 32 conductimeter using 10^{-3} mol dm^{-3} solutions in dry MeCN.

2.2. Preparation of [1,3-{Pd[2,3,4-(MeO)$_3$C$_6$HC(H)=NCH$_2$](OAc)(PPh$_3$)}$_2$C$_6$H$_4$] (3)

To a suspension of **1** (50 mg, 0.061 mmol) in C_3H_6O (approximately 15 cm^3), triphenylphosphine (32 mg, 0.122 mmol) was added. The solution was stirred for 24 h at room temperature, after which a yellow precipitate appeared, which was filtered off, washed with cold C_3H_6O, dried in vacuo, and recrystallized from $CHCl_3$/*n*-C_6H_{14}. Yield: 75%. *Anal*. Found: C, 60.3; H, 4.7; N, 2.2. $C_{68}H_{66}N_2O_{10}P_2Pd_2$ requires: C, 60.7; H, 4.9; N, 2.1%. IR: $\nu_{as}(COO) = 1580$s; $\nu_s(COO) = 1380$s; $\nu(C{=}N) = 1610$m cm^{-1}. FAB-MS: *m*/*z* 1024 $[M-PPh_3-OAc]^+$, 765 $[M-2PPh_3-OAc]^+$, 597 $[(L-H)\ Pd]^+$. ^1H NMR (200 MHz, $CDCl_3$, δ ppm, *J* Hz): 8.07 [d, 2H, Hi, *J*(HiP) = 8.3], 5.70 [d, 2H, H5, *J*(H5P) = 5.9], 4.85 [br, 4H, CH_2], 3.75 (s, 6H, MeO), 3.64 (s, 6H, MeO), 2.86 [s, 6H, C(4)–MeO], 1.26 (s, 6H, $MeCO_2$). $^{31}P\{^1H\}$ NMR (80.96 MHz, $CDCl_3$, δ ppm): 41.2s. $^{13}C\{^1H\}$ NMR (50.28 MHz, $CDCl_3$, δ ppm, *J* Hz): 176.9 (CH_3COO), 171.2 [d, C=N, *J*(CP) = 2.8]; 152.1, (C2); 151.5 [d, C6, *J*(CP) = 3.5]; 154.2 [d, C4, *J*(CP) = 5.7]; 137.4, 137.1 (C3, C7); 133.7 (C1); 129.9, 129.2, 128.7 (C8, C9, C10); 118.2 [d, C5, *J*(CP) = 12.0]; 59.9 (CH_2); 61.7, 60.6, 55.3 (MeO), 23.3 (CH_3COO). P–phenyl: C_o 135.4d, *J*(PC) = 12.0; C_i 131.5d, *J*(PC) = 52.5; C_p 130.6; C_m 128.2d, *J*(PC) = 10.6.

Compounds **4**, **5** and **6** were prepared similarly and isolated as white (**4**) or yellow (**5** and **6**) solids.

2.3. [1,3-{Pd[2,3,4-(MeO)$_3$C$_6$HC(H)=NCH$_2$](Cl)(PPh$_3$)}$_2$C$_6$H$_4$] (4)

Yield: 80%. *Anal*. Found: C, 58.7; H, 4.5; N, 2.2. $C_{64}H_{60}Cl_2N_2O_6P_2Pd_2$ requires: C, 59.2; H, 4.7; N, 2.2%. IR: $\nu(C{=}N) = 1610$m cm^{-1}. FAB-MS: *m*/*z* 1037 $[M-PPh_3]^+$, 1000 $[M-PPh_3-Cl]^+$, 739 $[M-2PPh_3-Cl]^+$, 597 $[(L-H)\ Pd]^+$. ^1H NMR (200 MHz, $CDCl_3$, δ ppm, *J* Hz): 8.21 [d, 2H, Hi, *J*(HiP) = 8.3], 5.72 [d, 2H, H5, *J*(H5P) = 6.3], 5.20 [br, 4H, CH_2], 3.77 (s, 6H, MeO), 3.66 (s, 6H, MeO), 2.81 [s, 6H, C(4)–MeO]. $^{31}P\{^1H\}$ NMR (80.96 MHz, $CDCl_3$, δ ppm, *J* Hz): 43.0s. $^{13}C\{^1H\}$ NMR (50.28 MHz, $CDCl_3$, δ ppm): 172.3 [d, C=N, *J*(CP) = 4.3]; 154.4, 152.0, (C2, C6); 154.3 [d, C4, *J*(CP) = 6.4]; 138.2 [d, C3, *J*(CP) = 1.4]; 137.5 (C7); 133.7 [d, C1, *J*(CP) = 1.4]; 130.1, 129.1, 128.8 (C8, C9, C10); 117.8 [d, C5, *J*(CP) = 11.0]; 60.8 (CH_2); 61.9, 60.6, 55.2 (MeO). P–phenyl: C_o 135.4d, *J*(PC) = 12.0; C_i 131.2d, *J*(PC) = 46.8; C_p 130.7d, *J*(PC) = 3.7; C_m 128.1d, *J*(PC) = 10.6.

2.4. [1,3-{Pd[2,3,4-(MeO)$_3$C$_6$HC(H)=NCH$_2$](Cl){P(p-MeOC$_6$H$_4$)$_3$}}$_2$C$_6$H$_4$] (5)

Yield: 70%. *Anal*. Found: C, 56.8; H, 5.0; N, 1.9. $C_{70}H_{72}Cl_2N_2O_{12}P_2Pd_2$ requires: C, 56.9; H, 4.9; N, 1.9%. IR: $\nu(C{=}N) = 1600$m cm^{-1}. FAB-MS: *m*/*z* 1478 $[M]^+$, 1127 $[M-PR_3]^+$, 1091 $[M-PR_3-Cl]^+$, 739 $[M-2PR_3-Cl]^+$, 597 $[(L-H)\ Pd]^+$. ^1H NMR (200 MHz, $CDCl_3$, δ ppm, *J* Hz): 8.20 [d, 2H, Hi, *J*(HiP) = 8.3], 7.40 (m, 3H, H8, H9, H10), 5.79 [d, 2H, H5, *J*(H5P) = 6.3], 5.20 [br, 4H, CH_2], 3.77 (s, 6H, MeO), 3.67 (s, 6H, MeO), 2.87 [s, 6H, C(4)–MeO]; $P(p\text{-}MeOC_6H_4)_3$: 7.63 [dd, 12H, H_o, $J(H_oH_m) = 8.8$, $J(PH_o) = 11.2$], 6.87 [dd, 12H, H_m, $J(PH_m) = 1.5$], 3.80 (s, 18H, MeO–). $^{31}P\{^1H\}$ NMR (80.96 MHz, $CDCl_3$, δ ppm): 39.4s. $^{13}C\{^1H\}$ NMR (50.28 MHz, $CDCl_3$, δ ppm): 171.9 [d, C=N, *J*(CP) = 2.8]; 154.4, 151.9, (C2, C6); 154.1 [d, C4, *J*(CP) = 6.4]; 138.2 [d, C3, *J*(CP) = 1.4]; 137.4 (C7); 133.7 [d, C1, *J*(CP) = 1.4]; 130.2, 129.0, 128.7 (C8, C9, C10); 117.8 [d, C5, *J*(CP) = 12.0]; 60.8 (CH_2); 61.9, 60.6, 55.3 (MeO); 55.2 ($P(MeO\text{–}C_6H_4)_3$). P–phenyl: C_p 161.3d, *J*(PC) = 2.1; C_o 136.8d, *J*(PC) = 13.5; C_i 122.7d, *J*(PC) = 55.4; C_m 113.6d, *J*(PC) = 12.0.

2.5. [1,3-{Pd[2,3,4-(MeO)$_3$C$_6$HC(H)=NCH$_2$](Cl)(P(p-NMe$_2$C$_6$H$_4$)Ph$_2$)}$_2$C$_6$H$_4$] (6)

Yield: 70%. *Anal*. Found: C, 59.1; H, 5.5; N, 4.1. $C_{68}H_{70}Cl_2N_4O_6P_2Pd_2$ requires: C, 59.0; H, 5.1; N, 4.0%. IR: ν(C=N) = 1605m cm^{-1}. FAB-MS: *m*/*z* 1384 $[M]^+$, 1080 $[M-PR_3]^+$, 1044 $[M-PR_3-Cl]^+$, 739 $[M-2PR_3-Cl]^+$, 597 [(L–H) Pd]$^+$. ^{1}H NMR (200 MHz, $CDCl_3$, δ ppm, *J* Hz): 8.20 [d, 2H, Hi, *J*(HiP) = 8.3], 5.83 [d, 2H, H5, *J*(H5P) = 6.3], 5.20 [br, 4H, CH_2], 3.76 (s, 6H, MeO), 3.66 (s, 6H, MeO), 2.86 [s, 6H, C(4)–MeO]; P(*p*-NMe$_2$C$_6$*H*$_4$)Ph$_2$: 6.66 [dd, 4H, H$_m$, *J*(H$_o$H$_m$) = 8.8, *J*(PH$_m$) = 1.5], 2.99 (s, 6H, N*Me*$_2$). ^{31}P{^{1}H} NMR (80.96 MHz, $CDCl_3$, δ ppm): 41.2s. ^{13}C{^{1}H} NMR (50.28 MHz, $CDCl_3$, δ ppm): 171.9 [d, C=N, *J*(CP) = 3.7]; 154.4, 151.8, (C2, C6); 154.1 [d, C4, *J*(CP) = 6.4]; 138.3 [d, C3, *J*(CP) = 1.4]; 137.3 (C7); 133.7 [d, C1, *J*(CP) = 1.4]; 130.1, 129.0, 128.8 (C8, C9, C10); 118.0 [d, C5, *J*(CP) = 12.0]; 60.7 (CH_2); 61.9, 60.6, 55.3 (MeO); 39.9 (P(N*Me*$_2$–C$_6$H$_4$)). P–phenyl: C$_p$ 130.2, 151.8d, *J*(PC) = 2.1, 1.4; C$_o$ 137.6d, 134.9d, *J*(PC) = 13.4, 12.4; C$_i$ 132.9d, 113.4d, *J*(PC) = 51.1; C$_m$ 127.8d, 111.2d, *J*(PC) = 12.0, 10.6.

2.6. Preparation of [1,3-{Pd[2,3,4-(MeO)$_3$C$_6$HC(H)=NCH$_2$](Ph$_2$PCH=CHPPh$_2$-P,P)}$_2$C$_6$H$_4$][ClO$_4$]$_2$ (7)

cis-Ph$_2$PCH=CHPPh$_2$ (25.3 mg, 0.064 mmol) was added to a suspension of **3** (25 mg, 0.016 mmol) in C_3H_6O (15 cm^3). The mixture was stirred for 2 h, after which an excess of sodium perchlorate was added, and the resulting solution stirred for a further 2 h. The complex was then precipitated out by addition of water, filtered off and dried in vacuo. Recrystallization from $CHCl_3/C_6H_{14}$ gave the final compound as a yellow solid. Yield: 85%. *Anal*. Found: C, 56.8; H, 4.7; N, 1.6. $C_{80}H_{74}Cl_2N_2O_{14}P_4Pd_2$ requires: C, 56.7; H, 4.4; N, 1.6%. IR: ν(C=N) = 1605m cm^{-1}. FAB-MS: *m*/*z* 1495 $[M]^+$, 1099 $[M-(cis\text{-}Ph_2PCH=CHPPh_2)]^+$, 993 $[M-(cis\text{-}Ph_2PCH=CHPPh_2)-Pd]^+$. $\Lambda_M = 240\ \Omega^{-1}$ cm^2 mol^{-1} (in MeCN). ^{1}H NMR (200 MHz, $CDCl_3$, δ ppm, *J* Hz): 8.29 [d, 2H, Hi, *J*(HiP) = 8.3], 6.94 [t, 1H, H10, *J*(H9H10) = 7.8], 6.68 (d, 1H, H9), 6.22 (s, 1H, H8), 6.20 [dd, 2H, H5, *J*(H5P) = 8.8, 5.8], 4.52 [br, 4H, CH_2], 3.94 (s, 6H, MeO), 3.72 (s, 6H, MeO), 3.16 [s, 6H, C(4)–MeO]. ^{31}P{^{1}H} NMR (80.96 MHz, $CDCl_3$, δ ppm): 63.2 [d, *J*(PP) = 11.0], 51.5 d. ^{13}C{^{1}H} NMR (50.28 MHz, $CDCl_3$, δ ppm): 179.5m (C=N); 163.1 [d, C6, *J*(CP) = 121.4], 153.9 [d, C2, *J*(CP) = 9.2]; 156.8 [dd, C4, *J*(CP) = 12.1, 5.7]; 139.2, 136.9 (C3, C7); 130.9, 129.0, 129.2 (C8, C9, C10); 117.4 [dd, C5, *J*(CP) = 11.0, 3.2]; 64.3 (CH_2); 62.3, 60.0, 55.8 (MeO). P*C*H=*C*HP: 145.2 [dd, *J*(PC) = 49.7, 34.8], 143.8 [dd, *J*(PC) = 41.2, 22.7]. P–phenyl: C$_p$ 130.4; C$_o$ 133.9d, 133.0, *J*(PC) = 12.8, 12.0; C$_i$ 126.6d, 126.1d, *J*(PC) = 54.6, 41.9; C$_m$ 130.0d, *J*(PC) = 11.4.

Complexes **9**, **10** and **11** were prepared following a similar procedure to the **3** and isolated as white (**9**) or yellow (**10** and **11**) solids.

2.7. [1,4-{Pd[2,3,4-(MeO)$_3$C$_6$HC(H)=NCH$_2$](Cl)(PPh$_3$)}$_2$C$_6$H$_4$] (9)

Yield: 80%. *Anal*. Found: C, 58.9; H, 4.8; N, 2.2. $C_{64}H_{60}Cl_2N_2O_6P_2Pd_2$ requires: C, 59.2; H, 4.7; N, 2.2%. IR: ν(C=N) = 1610s cm^{-1}. FAB-MS: *m*/*z* 1037 $[M-PPh_3]^+$, 1000 $[M-PPh_3-Cl]^+$, 739 $[M-2PPh_3-Cl]^+$. ^{1}H NMR (200 MHz, $CDCl_3$, δ ppm, *J* Hz): 8.24 [d, 2H, Hi, *J*(HiP) = 8.3], 7.48 (s, 4H, H8), 5.72 [d, 2H, H5, *J*(H5P) = 6.3], 5.18 [br, 4H, CH_2], 3.83 (s, 6H, MeO), 3.67 (s, 6H, MeO), 2.81 [s, 6H, C(4)–MeO]. ^{31}P{^{1}H} NMR (80.96 MHz, $CDCl_3$, δ ppm): 42.9s. ^{13}C{^{1}H} NMR (50.28 MHz, $CDCl_3$, δ ppm): 172.2 (C=N); 154.2, 151.9, (C2, C6); 154.3 [d, C4, *J*(CP) = 6.4]; 137.4, 137.1 (C3, C7); 133.6 [d, C1, *J*(CP) = 1.4]; 129.7 (C8); 117.9 [d, C5, *J*(CP) = 12.0]; 60.5 (CH_2); 61.8, 60.6, 55.2 (MeO). P–phenyl: C$_o$ 135.4d, *J*(PC) = 12.0; C$_i$ 131.1d, *J*(PC) = 49.7; C$_p$ 130.8d, *J*(PC) = 2.1; C$_m$ 128.0d, *J*(PC) = 10.6.

2.8. [1,4-{Pd[2,3,4-(MeO)$_3$C$_6$HC(H)=NCH$_2$](Cl){P(p-MeOC$_6$H$_4$)$_3$}}$_2$C$_6$H$_4$] (10)

Yield: 60%. *Anal*. Found: C, 55.5; H, 4.9; N, 1.9. $C_{70}H_{72}Cl_2N_2O_{12}P_2Pd_2$ requires: C, 56.9; H, 4.9; N, 1.9%. IR: ν(C=N) = 1610sh, m cm^{-1}. FAB-MS: *m*/*z* 1478 $[M]^+$, 1091 $[M-PR_3-Cl]^+$, 739 $[M-2PPh_3-Cl]^+$. ^{1}H NMR (200 MHz, $CDCl_3$, δ ppm, *J* Hz): 8.23 [d, 2H, Hi, *J*(HiP) = 8.3], 7.47 (s, 4H, H8), 5.89 [d, 2H, H5, *J*(H5P) = 6.3], 5.17 [br, 4H, CH_2], 3.81 (s, 6H, MeO), 3.68 (s, 6H, MeO), 2.88 [s, 6H, C(4)–MeO]; P(*p*-MeOC$_6$*H*$_4$)$_3$: 7.63 [dd, 12H, H$_o$, *J*(H$_o$H$_m$) = 8.8, *J*(PH$_o$) = 11.2], 6.87 [dd, 12H, H$_m$, *J*(PH$_m$) = 1.5], 3.83 (s, 18H, *Me*O–). ^{31}P{^{1}H} NMR (80.96 MHz, $CDCl_3$, δ ppm): 39.4s. ^{13}C{^{1}H} NMR (50.28 MHz, $CDCl_3$, δ ppm): 172.0 [d, C=N, *J*(CP) = 3.6]; 154.3, 151.8, (C2, C6); 154.2 [d, C4, *J*(CP) = 6.4]; 137.3, 137.1 (C3, C7); 133.6 (C1); 129.7 (C8); 117.8 [d, C5, *J*(CP) = 11.4]; 60.9 (CH_2); 61.9, 60.6, 55.2 (MeO); 55.2 (P(*Me*O–C$_6$H$_4$)$_3$). P–phenyl: C$_p$ 161.3d, *J*(PC) = 2.8; C$_o$ 136.9d, *J*(PC) = 13.5; C$_i$ 123.3d, *J*(PC) = 55.4; C$_m$ 113.5d, *J*(PC) = 12.0.

2.9. [1,4-{Pd[2,3,4-(MeO)$_3$C$_6$HC(H)=NCH$_2$](Cl){P(p-NMe$_2$C$_6$H$_4$)Ph$_2$}}$_2$C$_6$H$_4$] (11)

Yield: 60%. *Anal*. Found: C, 58.7; H, 5.5; N, 4.1. $C_{68}H_{70}Cl_2N_4O_6P_2Pd_2$ requires: C, 59.0; H, 5.1; N, 4.0%. IR: ν(C=N) = 1605sh, m cm^{-1}. FAB-MS: *m*/*z* 1080 $[M-PR_3]^+$, 1044 $[M-PR_3-Cl]^+$, 739 $[M-2PR_3-Cl]^+$. ^{1}H NMR (200 MHz, $CDCl_3$, δ ppm, *J* Hz): 8.22 [d, 2H, Hi, *J*(HiP) = 8.3], 7.47 (s, 4H, H8), 5.83 [d,

2H, H5, J(H5P) = 6.3], 5.18 [br, 4H, CH_2], 3.82 (s, 6H, MeO), 3.68 (s, 6H, MeO), 2.86 [s, 6H, C(4)–MeO]; P(*p*-$NMe_2C_6H_4$)Ph_2: 6.66 [dd, 4H, H_m, $J(H_oH_m)$ = 8.8, $J(PH_m)$ = 1.5], 3.00 (s, 6H, N*Me*$_2$). $^{31}P\{^1H\}$ NMR (80.96 MHz, $CDCl_3$, δ ppm): 41.1s. $^{13}C\{^1H\}$ NMR (50.28 MHz, $CDCl_3$, δ ppm): 171.9 [d, C=N, J(CP) = 4.3]; 154.4, 151.7, (C2, C6); 154.2 [d, C4, J(CP) = 5.7]; 137.3, 137.1 (C3, C7); 133.6 [d, C1, J(CP) = 1.4]; 129.8 (C8); 118.0 [d, C5, J(CP) = 12.0]; 60.5 (CH_2); 61.8, 60.6, 55.3 (MeO); 39.9 (P(N*Me*$_2$–C_6H_4)). P–phenyl: C_p 130.2, 151.8; C_o 137.5d, 134.9d, J(PC) = 14.2, 11.5; C_i 133.9d, 113.4d, J(PC) = 57.5, 50.4; C_m 127.8d, 111.2d, J(PC) = 12.0, 10.6.

Compound **12** was synthesized following a similar method to the **7** as a yellow solid.

2.10. [1,4-{Pd[2,3,4-(MeO)$_3$C$_6$H$_1$C(H)=NCH$_2$](Ph$_2$PCH=CHPPh$_2$-P,P)}$_2$C$_6$H$_4$]-[ClO$_4$]$_2$ (12)

Yield: 95%. *Anal*. Found: C, 56.9; H, 4.8; N, 1.6. $C_{80}H_{74}Cl_2N_2O_{14}P_4Pd_2$ requires: C, 56.7; H, 4.4; N, 1.6%. IR: ν(C=N) = 1605m cm^{-1}. FAB-MS: *m/z* 1495 $[M]^+$, 993 $[M-(cis\text{-}Ph_2PCH{=}CHPPh_2)-Pd]^+$. Λ_M = 290 Ω^{-1} cm^2 mol^{-1} (in MeCN). ^{1}H NMR (200 MHz, $CDCl_3$, δ ppm, J Hz): 8.32 [d, 2H, Hi, J(HiP) = 8.3], 6.67 (s, 4H, H8), 6.19 [dd, 2H, H5, J(H5P) = 9.3, 5.9], 4.62 [br, 4H, CH_2], 3.91 (s, 6H, MeO), 3.72 (s, 6H, MeO), 3.15 [s, 6H, C(4)–MeO]. $^{31}P\{^1H\}$ NMR (80.96 MHz, $CDCl_3$, δ ppm): 63.1 [d, J(PP) = 11.0], 51.5d. $^{13}C\{^1H\}$ NMR (50.28 MHz, $CDCl_3$, δ ppm): 179.1m (C=N); 162.9 [d, C6, J(CP) = 122.0], 153.8 [d, C2, J(CP) = 9.2]; 156.7 [dd, C4, J(CP) = 12.1, 5.7]; 139.1, 135.6 (C3, C7); 128.1 (C8); 117.4 [dd, C5, J(CP) = 11.0, 3.2]; 64.2 (CH_2); 62.2, 60.9, 55.8 (MeO). P*C*H=*C*HP: 145.3 [dd, J(PC) = 49.6, 34.8], 143.7 [dd, J(PC) = 40.4, 22.7]. P–phenyl: C_p 132.5; C_o 134.0d, 133.1, J(PC) = 12.8; C_i 126.7d, 126.1d, J(PC) = 54.6, 41.9; C_m 130.1d, 129.9d, J(PC) = 11.4, 9.9.

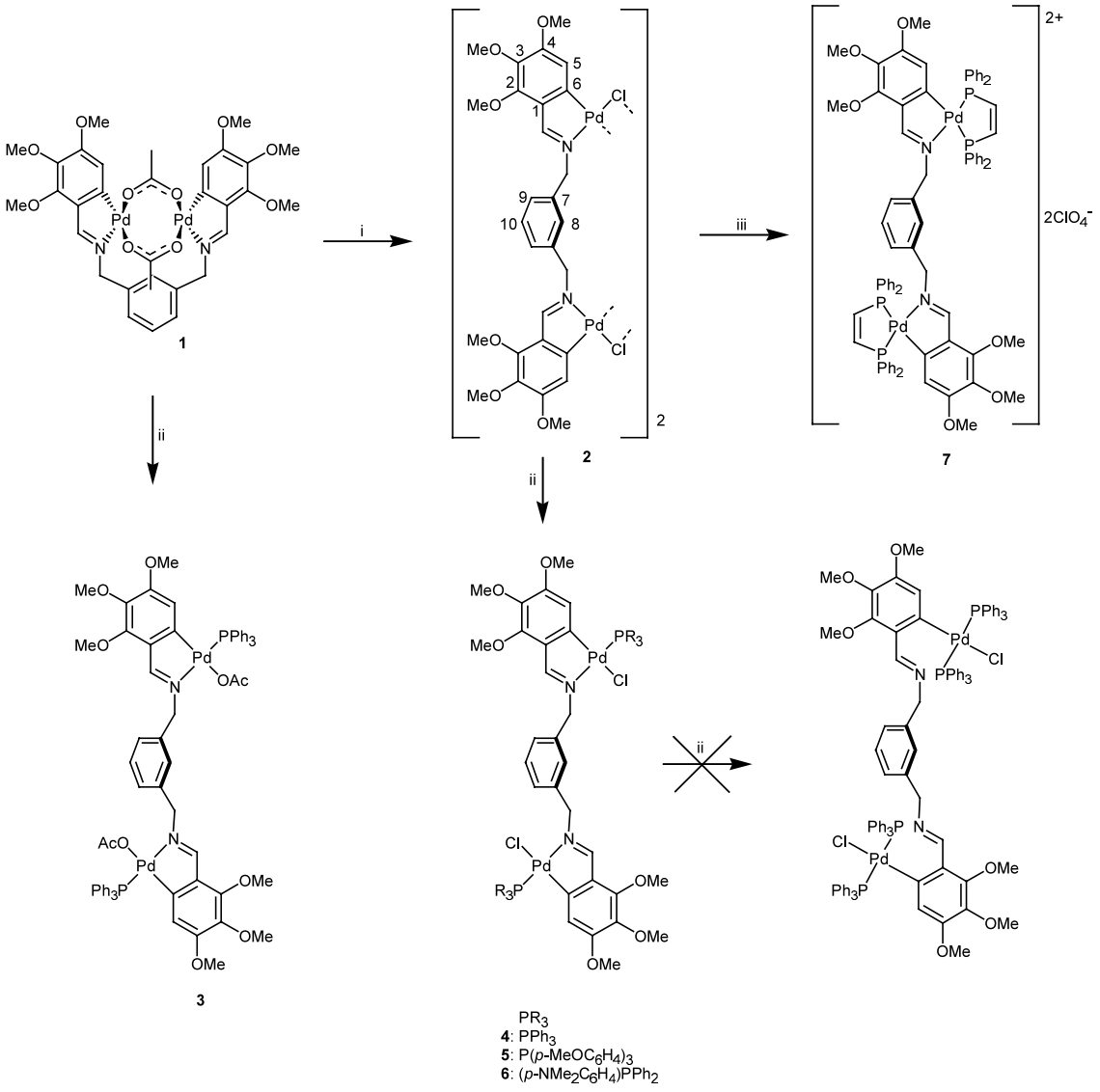
3. Results and discussion

For the convenience of the reader the compounds and reactions are shown in Schemes 1 and 2. The compounds described in this paper were characterized by elemental analysis (C, H, N) and by IR spectroscopy and by ^{1}H, $^{31}P\{^1H\}$ NMR and, in part, $^{13}C\{^1H\}$ NMR spectroscopy and FAB mass spectrometry (data in the Section 2).

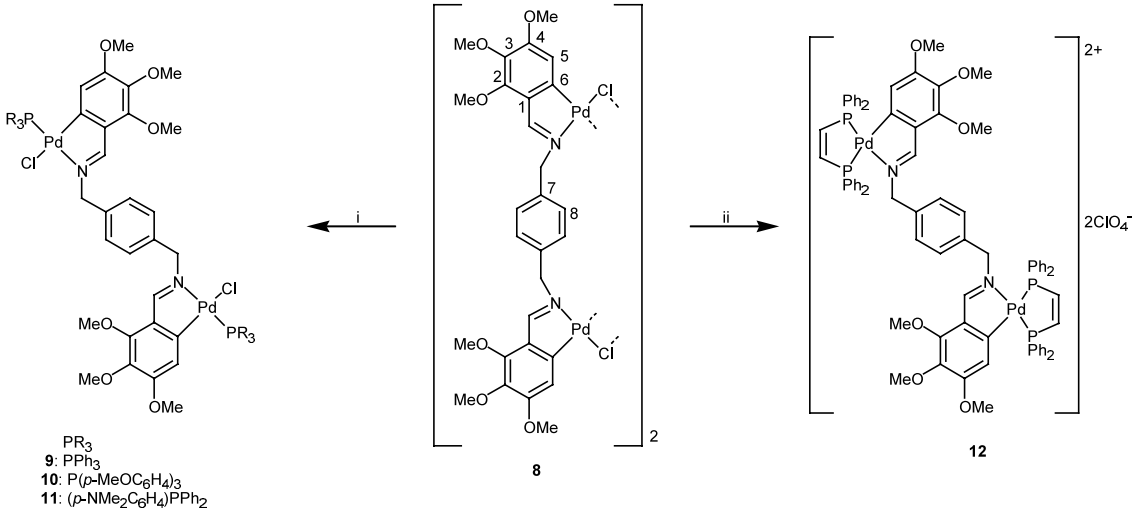
The reaction of complex **1** [30] with triphenylphosphine in a 1:2 molar ratio gave the doubly cyclometallated complex [1,3-{Pd[2,3,4-(MeO)$_3$C$_6$HC(H)=NCH$_2$](OAc)(PPh$_3$)}$_2$C$_6$H$_4$] (**3**), after cleavage of the two acetate-bridging ligands. The IR spectrum of **3** showed the ν(C=N) stretch at 1610 cm^{-1}, shifted to lower wavenumbers (as compared to the free ligand) due to N-coordination of the imine [32,33]. The IR spectrum also showed strong bands assigned to the symmetric and asymmetric ν(COO) vibrations, in agreement with those expected for monodentate acetate ligands [34] (see Section 2). The *H*C=N and H5 resonances in the ^{1}H NMR spectrum were coupled to the phosphorus nucleus [δ 8.07 and 5.70, respectively; J(HP) = 8.3 and 5.9 Hz, also, respectively], and in the $^{31}P\{^1H\}$ NMR spectrum, the phosphorus resonance appeared as a singlet at δ 41.2 in accordance with the symmetric nature of the complex. These data are indicative of a phosphorus *trans* to nitrogen geometry [35–38]. The relative position of the phosphine ligand in the coordination sphere of the palladium atom was confirmed by the highfield shift of the signal corresponding to the C(4)–OMe group, due to shielding by a phenyl ring from the phosphine [35–38]. In complex **1**, the signals assigned to the diastereotopic CH_2 protons in the ^{1}H NMR spectrum appeared as two doublets, due to the hindered rotation of this group. However, only one rather broad resonance at δ 4.85 was assigned to the methylene group in complex **3**, after cleavage of the intramolecular-bridges. The $^{13}C\{^1H\}$ NMR spectrum of **3** showed the high-frequency shift of the resonances corresponding to the HC=N, C6 and C1 carbons, evidencing formation of the cyclometallated ring [39,40].

The synthesis of complexes **2** and **8** has been described previously by us [30]. Reaction of **2** and **8** with the tertiary monophosphines PPh_3, P(*p*-$MeOC_6H_4)_3$ and P(*p*-$NMe_2C_6H_4$)Ph_2 gave the doubly cyclometallated complexes [1,3-{Pd[2,3,4-(MeO)$_3$C$_6$HC(H)=NCH$_2$](Cl)-(PR_3)}$_2$C$_6$H$_4$] (PR_3 = PPh_3, **4**; P(*p*-$MeOC_6H_4)_3$, **5**; P(*p*-$NMe_2C_6H_4$)Ph_2, **6**) and [1,4-{Pd[2,3,4-(MeO)$_3$C$_6$HC(H)=NCH$_2$](Cl)-(PR_3)}$_2$C$_6$H$_4$] (PR_3 = PPh_3, **9**; P(*p*-$MeOC_6H_4)_3$, **10**; P(*p*-$NMe_2C_6H_4$)Ph_2, **11**), respectively, which were fully characterized (see Section 2). The spectroscopic features of these complexes are similar to those described for **3**. Thus, the IR spectra was in accordance with coordination of the HC=N group. The ^{1}H NMR spectra showed the coupling of the HC=N and H5 resonances to the ^{31}P nucleus and the $^{13}C\{^1H\}$ NMR spectra also showed the high-frequency shift of the resonances corresponding to the HC=N, C6 and C1 carbons. In all the cases, the FAB-MS rendered clusters of peaks whose isotopic patterns were in agreement with $[M]^+$ and/or $[M-PR_3]^+$ fragments.

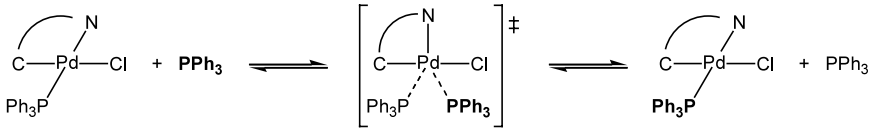
The reaction of the **4** with PPh_3 in a 1:2 molar ratio did not yield the expected non-cyclometallated complex, with two phosphine ligands coordinated to palladium and the Pd–N bond cleaved [37,41]. The ^{1}H NMR spectra of the reaction mixture in $CDCl_3$ showed the resonances corresponding to the HC=N and H5 resonances as singlets (no coupling to the ^{31}P nucleus was observed). This behavior is characteristic of the non-cyclometallated complexes, where in the absence of Pd–



Scheme 1. (i) NaCl (acetone/water); (ii) PR_3 (acetone); (iii) 1: *cis*-dppe; 2: $NaClO_4$ (acetone/water).



Scheme 2. (i) PR_3 (acetone); (ii) 1: *cis*-dppe; 2: $NaClO_4$ (acetone/water).



Scheme 3.

N bond the metallated ring can rotate about the Pd–C vector so that its plane is at 90° to the palladium coordination plane and coupling of the H5 proton to the ^{31}P nucleus is absent [37,41]. Furthermore, the $^{31}P\{^{1}H\}$ spectrum did not show the expected singlet. In order to clarify this controversy the ^{1}H and $^{31}P\{^{1}H\}$ spectra of the reaction mixture were recorded at different temperatures. The $^{31}P\{^{1}H\}$ spectrum at 223 K showed two slightly broad resonances at δ 43.0 and −6.3 corresponding to complex **4** and free PPh_3, respectively. At 298 K the signals coalesced and at 323 K a broad resonance at approximately δ 20 appeared. The ^{1}H NMR spectra showed the progressive broadening of the HC=N and H5 resonances on cooling, however no coupling to phosphorus was observed even at 223 K. These results seem to indicate that although the Pd–N was not cleaved, a fast exchange between coordinated and free PPh_3, which could proceed through the typical substitution reaction mechanism in square-planar d^8 complexes, is responsible for the absence of the PH coupling [42,43] (see Scheme 3).

The reaction of **2** and **8** with the tertiary diphosphine *cis*-$Ph_2PCH{=}CHPPh_2$, in a 1:4 molar ratio yielded the doubly cyclometallated complexes [1,3-{Pd[2,3,4-$(MeO)_3C_6HC(H){=}NCH_2$]($Ph_2PCH{=}CHPPh_2$-*P*,*P*)}$_2C_6H_4$][ClO_4]$_2$ (**7**) and [1,4-{Pd[2,3,4-$(MeO)_3C_6HC(H){=}NCH_2$]($Ph_2PCH{=}CHPPh_2$-*P*,*P*)}$_2C_6H_4$][ClO_4]$_2$ (**12**), respectively, as air-stable solids which were fully characterized (see Section 2). In the ^{1}H NMR spectra of the complexes the resonance corresponding to the HC=N protons appeared as a doublet, showing coupling only to the phosphorus atom *trans* to the imine nitrogen atom [29,44]. However, the H5 resonance showed coupling to both ^{31}P nuclei [29,44]. Only one set of signals appeared for each proton, as proof of the symmetric nature of the complexes. The $^{31}P\{^{1}H\}$ spectra showed two doublets for the 2 non-equivalent phosphorus atoms. In the $^{13}C\{^{1}H\}$ the signal assigned to C6 was a doublet due to coupling to the *trans* ^{31}P nucleus [approximately 122 Hz] [45]. The FAB-MS of the complexes showed a cluster of peaks at 1495 amu corresponding to the $[M]^+$ fragments.

Acknowledgements

We thank the Ministerio de Educación y Cultura (Proyecto PB98-0638-C02-01/02), the Xunta de Galicia (Proyecto PGIDT99PXI20907B) and the Universidad de la Coruña for financial support.

References

[1] M. Pfeffer, J.P. Sutter, M.A. Rottevel, A. de Cian, J. Fischer, Tetrahedron 48 (1992) 2427.
[2] A.D. Ryabov, R. van Eldik, G. Le Borgne, M. Pfeffer, Organometallics 12 (1993) 1386.
[3] C. Navarro-Ranninger, I. López Solera, J. Rodríguez, J. García-Ruano, P.R. Raithby, J.R. Masaguer, C. Alonso, Med. Chem. 36 (1993) 3795.
[4] C. Navarro-Ranninger, I. López Solera, V.M. Gonzalez, J.M. Pérez, A. Alvarez-Valdés, A. Martin, P.R. Raithby, J.R. Masaguer, C. Alonso, Inorg. Chem. 35 (1996) 5181.
[5] P. Espinet, M.A. Esteruelas, L.A. Oro, J.L. Serrano, E. Sola, Coord. Chem. Rev. 17 (1992) 215.
[6] K. Selvakumar, S. Vancheesan, Polyhedron 14 (1995) 2091.
[7] C.R. Baar, S.G. Hill, J.J. Vittal, R.J. Puddephatt, Organometallics 17 (1998) 32.
[8] R.M. Ceder, J. Sales, J. Organomet. Chem. 294 (1985) 389.
[9] R.M. Ceder, J. Sales, X. Solans, M. Font-Altaba, J. Chem. Soc., Dalton Trans. (1986) 1351.
[10] Y.J. Wu, Y.H. Liu, L. Yang, Q. Zhu, Polyhedron 16 (1997) 335.
[11] P.J. Steel, G.B. Caygill, J. Organomet. Chem. 395 (1990) 359.
[12] G.B. Caygill, R.M. Hartshorn, P.J. Steel, J. Organomet. Chem. 382 (1990) 455.
[13] R.F. Carina, A.F. Williams, G. Bernardinelli, J. Organomet. Chem. 548 (1997) 45.
[14] I.G. Phillips, P.J. Steel, J. Organomet. Chem. 410 (1991) 247.
[15] D.P. Lydon, J.P Rourke, J. Chem. Soc., Chem. Commun. (1997) 1741.
[16] K.K. Nanda, K. Nag, K. Venkatsubramanian, P. Paul, Inorg. Chim. Acta 196 (1992) 195.
[17] S. Trofimenko, Inorg. Chem. 12 (1973) 1215.
[18] S. Trofimenko, J. Am. Chem. Soc. 93 (1971) 1808.
[19] S. Chakladar, P. Paul, K. Venkatsubramanian, K. Nag, J. Chem. Soc., Dalton Trans. (1991) 2669.
[20] S. Chakladar, P. Paul, A.K. Mukherjee, S.K. Dutta, K.K. Nanda, D. Podder, K. Nag, J. Chem. Soc., Dalton Trans. (1992) 3119.
[21] B.J. O'Keefe, P.J. Steel, Organometallics 17 (1998) 3621.
[22] J. Vicente, J.A. Abad, B. Rink, F.S. Hernández, M.C. Ramirez de Arellano, Organometallics 16 (1997) 5269.
[23] M.D. Meijer, A.W. Kleij, M. Lutz, A. Speck, G. van Koten, J. Organomet. Chem. 640 (2001) 166.
[24] E.C. Constable, D.G.F. Ress, Polyhedron 17 (1998) 3281.
[25] C. Chan, D.M.P. Mingos, A.J.P White, D.J. Williams, J. Chem. Soc., Chem. Commun. (1996) 81.
[26] M. Sugimoto, M. Nonoyama, Inorg. Nucl. Chem. Lett. 15 (1979) 405.
[27] S. Chattopadhyay, C. Sinha, S.C. Choudhury, A.J. Chakravorty, J. Organomet. Chem. 427 (1992) 111.
[28] J.M. Vila, M. Gayoso, M.T. Pereira, M. Camino-Rodriguez, J.M. Ortigueira, J. Organomet. Chem. 426 (1992) 267.
[29] J.M. Vila, M. Gayoso, M.T. Pereira, M. Camino-Rodriguez, J.M. Ortigueira, J.J. Fernández, M. López-Torres, J. Organomet. Chem. 479 (1994) 37.

[30] M. López-Torres, P. Juanatey, J.J. Fernández, A. Fernández, A. Suárez, R. Mosteiro, J.M. Ortigueira, J.M. Vila, Organometallics, in press.
[31] D.D. Perrin, W.L.F. Armarego, Purification of Laboratory Chemicals, 4th ed., Butterworth-Heinemann, London, 1996, p. 153.
[32] H. Onoue, I. Moritani, J. Organomet. Chem. 43 (1972) 431.
[33] H. Onoue, K. Minami, K. Nakagawa, Bull. Chem. Soc. Jpn. 43 (1970) 3480.
[34] K. Nakamoto, IR and Raman Spectra of Inorganic and Coordination Compounds, 5th ed., Wiley, New York, 1997, Part B, p. 271.
[35] R. Bosque, J. Granell, J. Sales, M. Fon-Bardiá, X. Solans, J. Organomet. Chem. 453 (1994) 147.
[36] J.M. Vila, M. Gayoso, M.T. Pereira, M. López-Torres, G. Alonso, J.J. Fernández, J. Organomet. Chem. 445 (1993) 287.
[37] J.M. Vila, M. Gayoso, M.T. Pereira, A. Romar, J.J. Fernández, M. Thornton-Pett, J. Organomet. Chem. 401 (1991) 385.
[38] R. Bosque, J. Granell, J. Sales, M. Fon-Bardiá, X. Solans, Organometallics 14 (1995) 1393.
[39] J.M. Vila, M. Gayoso, M.T. Pereira, M. López-Torres, J.J. Fernández, A. Fernández, J.M. Ortigueira, J. Organomet. Chem. 532 (1997) 171.
[40] D. Vázquez-García, A. Fernández, J.J. Fernández, M. López-Torres, A. Suárez, J.M. Ortigueira, J.M. Vila, H. Adams, J. Organomet. Chem. 595 (2000) 199.
[41] J.M. Vila, M.T. Pereira, J.M. Ortigueira, M. López-Torres, A. Castiñeiras, D. Lata, J.J. Fernández, A. Fernández, J. Organomet. Chem. 556 (1998) 31.
[42] J. Albert, J. Granell, A. Luque, J. Mínguez, R. Moragas, M. Font-Bardía, X. Solans, J. Organomet. Chem. 522 (1996) 87.
[43] G.K. Anderson, R.J. Cros, S.A. Leaman, F.J. Robertson, D.S. Rycroft, M. Rocamora, J. Organomet. Chem. 388 (1990) 221.
[44] J.M. Vila, M. Gayoso, M. López-Torres, J.J. Fernández, A. Fernández, J.M. Ortigueira, N.A. Bailey, H. Adams, J. Organomet. Chem. 511 (1996) 129.
[45] H. Mizuno, M. Kita, J. Fujita, M. Nonoyama, Inorg. Chim. Acta 202 (1992) 183.

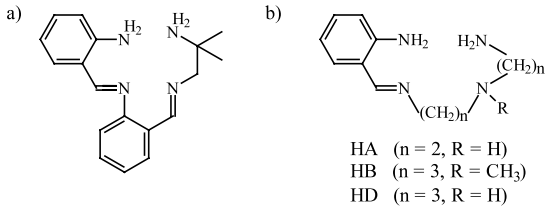


Fig. 1. Structural formulae: (a) for the Cummins ligand [6], (b) for ligands of the present study.

incorporate singly condensed products of 2-aminobenzaldehyde and triamines (Fig. 1(b)).

2. Experimental

2.1. Reagents

1,5-Diamino-3-azapentane, 1,7-diamino-4-azaheptane and 1,7-diamino-4-methyl-4-azaheptane were dried over potassium hydroxide, distilled and fractions boiling in ranges of 206–208, 110–122/6 mm and 105–106 °C/5 mm, respectively, were collected. 2-Aminobenzaldehyde was obtained from 2-nitrobenzaldehyde and purified by the method described elsewhere [7]. Nickel(II) iodide monohydrate has been obtained by recrystallization of anhydrous NiI_2 from water and gentle drying.

2.2. Ligands

2.2.1. 1-(2′-Aminophenyl)-2,5-diaza-7-amino-1-heptene, HA

To a rapidly stirred solution of 1,5-diamino-3-azapentane (3.26 g, 0.031 mol) in MeOH (50 ml) a solution of freshly purified 2-aminobenzaldehyde (3.72 g, 0.031 mol) in MeOH (50 ml) was slowly added over a period of 1 h. The solvent was removed from the mixture in vacuo to give an oily residue. Mass spectrum of the product showed a prominent peak at $m/z = 206$, which may be assigned to the molecular ion. 1-(2′-Aminophenyl)-2,6-diaza-6-methyl-9-amino-1-nonene, HB, and 1-(2′-aminophenyl)-2,6-diaza-9-amino-1-nonene, HD, were obtained in a similar way as HA. Mass spectra of the reaction products revealed molecular ions at $m/z =$ 248 and 234, respectively. Structural formulae of ligands are shown in Fig. 1(b).

2.3. Complexes

Complexes were prepared by the reaction of preformed HA, HB and HD ligands with nickel(II) chloride, nitrate and perchlorate hexahydrates, nickel(II) iodide monohydrate and palladium(II) chloride. The following method was used. To a vigorously stirred solution of the corresponding metal salt (3 mmol) in MeOH (25 ml) was slowly added the HA or HB or HD ligand (3 mmol) in MeOH (25 ml). After 2–3 h of stirring the precipitate was filtered off washed with MeOH and dried over molecular sieves. Crystals of $NiAClO_4$ suitable for X-ray investigations were obtained using a slow diffusion of diisopropylether vapor into acetonitrile solution of the complex, but those of NiBI by slow recrystallization of that compound from acetonitrile solution.

Caution: One of the complexes reported here was isolated as a perchlorate salt. We worked with them dissolved in DMSO and acetonitrile solvents and also as solid without any accident. In spite of this the potentially explosive behavior of perchlorate salts necessitates extreme care in their handling.

2.3.1. 1-(2′-Iminophenyl)-2,5-diaza-7-amino-1-heptenonickel(II) perchlorate, $NiAClO_4$

Black amorphous powder, soluble in DMSO and acetonitrile but sparingly soluble in alcohols. Yield: 40%. *Anal*. Calc. for $C_{11}H_{17}ClN_4NiO_4$: C, 36.6; H, 4.9; N, 15.4. Found: C, 36.5; H, 4.9; N, 15.4%. IR (KBr, cm^{-1}): 3387, 3302, 3205 (ν_{N-H}), 1615 ($\nu_{C=N}+\nu_{C=C}$), 1538 (ν_{C-N}), 1090, 620 (ν_{ClO_4}). DRS, λ_{max} (nm): 425, 550 (the latter with a shoulder extending far to the red). PAS, λ_{max} (nm): 450 (broad band with shoulder extending to the red) (Fig. 2). Absorption spectrum in DMSO, λ_{max} (nm), ε (M^{-1} cm^{-1}): 285 (3200), 318 (1840), 450 (1660). ^1H NMR in DMSO-d_6 [ppm vs. TMS, r.t., s, singlet; d, doublet; t, triplet; m, multiplet; dd, doublet of doublets; dt, doublet of triplets; td, triplet of doublets; tt, triplet of triplets; br, broad; hydrogen atom attached to the ith carbon atom (Ci) is denoted as Hi, but that attached to jth nitrogen atom (Nj) as H_Nj]: H_N1, 4.739 (s, 1H); H_N3, 5.417 (s, 1H); H_N4a, 4.144 (dt, 1H); H_N4b, 3.506 (dd, 1H); H2, 6.636 (d, 1H, $^3J = 8$ Hz); H3, 6.939 (td, 1H, $^3J = 8$ Hz, $^4J = 1.5$ Hz); H4, 6.232 (td, 1H, $^3J = 8$ Hz, $^4J = 1.2$ Hz); H5, 7.159 (dd, 1H, $^3J = 7$ Hz); H7, 7.848 (s, 1H); H8a, 3.676 (td, 1H, $^2J = 13$ Hz, $^3J = 3$ Hz); H8b, 3.625 (dd, 1H); H11b, 2.436 (t, 1H); signals of H9a, H9b, H10a, H10b and H11a overlap

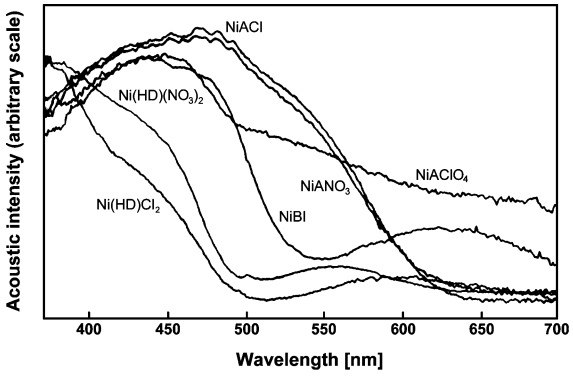


Fig. 2. Photoacoustic spectra for nickel(II) complexes.

giving rise to a 5H multiplet in the 2.58–2.62 ppm region.

2.3.2. 1-(2′-Iminophenyl)-2,5-diaza-7-amino-1-heptenonickel(II) chloride, NiACl

Red plates after recrystallization from MeOH, soluble in DMSO, hot acetonitrile and MeOH. Yield: 34%. *Anal*. Calc. for $C_{11}H_{17}ClN_4Ni$: C, 44.2; H, 5.9; N, 18.7. Found: C, 44.1; H, 5.7; N, 18.7%. IR (KBr, cm^{-1}): 3245, 3185, 3098 (ν_{N-H}), 1613, 1595 ($\nu_{C=N}+\nu_{C=C}$), 1541 (ν_{C-N}). DRS, λ_{max} (nm): 430, 450. PAS, λ_{max} (nm): 470. Absorption spectrum in DMSO, λ_{max} (nm), ε (M^{-1} cm^{-1}): 285 (2950), 319 (1530), 450 (1580). ^{1}H NMR in DMSO-d_6 (ppm, r.t.): H_N1, 4.778 (s, 1H); H_N3, 5.558 (s, 1H); H_N4a, 4.172 (s, 1H); H_N4b, 3.552 (s, 1H); H2, 6.674 (d, 1H, $^3J=8$ Hz); H3, 6.937 (t, 1H, $^3J=7$ Hz); H4, 6.230 (t, 1H, $^3J=7$ Hz); H5, 7.160 (d, 1H); H7, 7.848 (s, 1H); H8a and H8b, 3.62-3.72 (m, 2H); H9a, H9b, H10a, H10b, H11a and H11b overlap giving rise to a 6H multiplet in 2.36–2.78 range.

2.3.3. 1-(2′-Iminophenyl)-2,5-diaza-7-amino-1-heptenonickel(II) nitrate, NiANO$_3$

Red brown plates after recrystallization from methanol, soluble in DMSO, hot acetonitrile and methanol. Yield: 38%. *Anal*. Calc. for $C_{11}H_{17}N_5NiO_3$: C, 40.6; H, 5.2; N, 21.4. Found: C, 40.5; H, 5.3; N, 21.5%. IR (KBr, cm^{-1}): 3261, 3122, 3090 (ν_{N-H}), 1615 ($\nu_{C=N}+\nu_{C=C}$), 1541 (ν_{C-N}), 1380, 1041, 710 ($\nu_3+\nu_1+\nu_{4(NO_3)}$). DRS, λ_{max} (nm): 450. PAS, λ_{max} (nm): 470. Absorption spectrum in DMSO, λ_{max} (nm), ε (M^{-1} cm^{-1}): 285 (3180), 320 (1710), 450 (1640). ^{1}H NMR in DMSO-d_6 (ppm, r.t.): H_N1, 4.750 (s, 1H); H_N3, 5.472 (tt, 1H); H_N4a, 4.177 (dt, 1H, $^2J=10.7$ Hz, $^3J=5.6$ Hz); H_N4b, 3.531 (dd, 1H, $^2J=10.7$ Hz, $^3J=5.3$ Hz); H2, 6.635 (d, 1H, $^3J=8$ Hz); H3, 6.935 (td, 1H, $^3J=8$ Hz, $^4J=1.7$ Hz); H4, 6.228 (td, 1H, $^3J=7.5$ Hz, $^4J=1.3$ Hz); H5, 7.159 (dd, 1H, $^3J=8$ Hz, $^4J=1.7$ Hz); H7, 7.848 (s, 1H); H8a, 3.672 (td, 1H, $^3J=14$ Hz; $^3J=6$ Hz); H8b, 3.628 (dd, 1H); H9a and H10b, 2.55–2.57 (m, 2H); H9b, H10a and H11a, 2.61–2.77 (m, 3H); H11b, 2.418 (tt, 1H). ^{13}C NMR in DMSO-d_6 (ppm vs. TMS): 158.7, 151.5, 131.2, 130.0, 118.8, 115.7, 111.7, 62.1, 50.7, 49.8, 44.8.

2.3.4. 1-(2′-Iminophenyl)-2,5-diaza-7-amino-1-heptenopalladium(II) chloride, PdACl

Golden color needles after recrystallization from MeOH. Yield: 20%. *Anal*. Calc. for $C_{11}H_{17}ClN_4Pd$: C, 38.1; H, 4.9; N 16.1. Found: C, 38.2; H, 5.0; N, 16.3%. IR (KBr, cm^{-1}): 3250, 3187, 3107 (ν_{N-H}), 1617, 1592 ($\nu_{C=N}+\nu_{C=C}$), 1520 (ν_{C-N}). DRS, λ_{max} (nm): 412, 485. Absorption spectrum in DMSO, λ_{max} (nm), ε (M^{-1} cm^{-1}): 448 (3160). ^{1}H NMR in DMSO-d_6 (ppm, r.t.): H_N1, 6.524 (s, 1H); H_N3, 6.679 (br. s., 1H); H_N4a, 4.912 (tt, 1H); H_N4b, 4.607 (td, 1H); H2, 6.727 (d, 1H, $^3J=8$ Hz); H3, 7.001 (t, 1H, $^3J=7$ Hz); H4, 6.190 (t, 1H, $^3J=7$ Hz); H5, 7.206 (d, 1H, $^3J=8$ Hz); H7, 7.982 (s, 1H); H8a and H8b, 4.01–4.10 (m, 2H); H9a, H9b, H10a, H10b, H11a and H11b overlap giving rise to a 6H multiplet in the 2.82–3.00 range. ^{13}C NMR in DMSO-d_6 (ppm vs. TMS): 161.7, 157.3, 133.6, 117.4, 112.6, 110.3, 54.6, 54.2, 51.4, 49.5.

2.3.5. 1-(2′-Iminophenyl)-2,6-diaza-6-methyl-9-amino-1-nonenonickel(II) iodide, NiBI

Greenish black needles after recrystallization from acetonitrile solution. Yield: 37%. *Anal*. Calc. for $C_{14}H_{23}IN_4Ni$: C, 38.8; H, 5.4; N 12.9. Found: C, 38.9; H, 5.4; N, 12.8%. IR (KBr, cm^{-1}): 3267, 3177, 3104 (ν_{N-H}), 1617, 1592 ($\nu_{C=N}+\nu_{C=C}$), 1520 (ν_{C-N}). DRS, λ_{max} (nm): 440, 670sh. PAS, λ_{max} (nm): 450, 650. Absorption spectrum in DMSO, λ_{max} (nm), ε (M^{-1} cm^{-1}): 285 (3180), 439 (1620), 598 (68). ^{1}H NMR data listed in Table 4.

2.3.6. 1-(2′-Aminophenyl)-2,6-diaza-9-amino-1-nonenonickel(II) dichloride, Ni(HD)Cl$_2$

Pale green precipitate. Yield: 35%. *Anal*. Calc. for $C_{13}H_{22}Cl_2N_4Ni$: C, 42.6; H, 6.3; N 15.2. Found: C, 42.4; H, 6.4; N, 15.0%. IR (KBr, cm^{-1}): 3345, 3151, 3072 (ν_{N-H}), 1636 (δ_{NH_2}), 1611, 1593, 1572 ($\nu_{C=N}+\nu_{C=C}$). DRS, λ_{max} (nm): 412. PAS, λ_{max} (nm): 350sh, 430sh, 620. Absorption spectrum in DMSO, λ_{max} (nm), ε (M^{-1} cm^{-1}): 314 (460), 425 (240), 587 (20). The effective magnetic moment measured in MeOH + 1% cyclohexane is 3.17.

2.3.7. 1-(2′-Aminophenyl)-2,5-diaza-9-amino-1-nonenonickel(II) dinitrate, Ni(HD)(NO$_3$)$_2$

Brownish green needles. Yield: 37%. *Anal*. Calc. for $C_{13}H_{22}N_6NiO_6$: C, 37.4; H, 5.4; N, 20.2. Found: C, 37.4; H, 5.3; N, 20.4%. IR (KBr, cm^{-1}): 3329, 3303, 3230, 3223, 3117 (ν_{N-H}), 1637 (δ_{NH_2}), 1614, 1577 ($\nu_{C=N}+\nu_{C=C}$) 1421, 1308, 1044 ($\nu_3+\nu_{1(NO_3)}$). DRS, λ_{max} (nm): 420, 550. PAS, λ_{max} (nm): 440sh, 560. Absorption spectrum in DMSO, λ_{max} (nm), ε (M^{-1} cm^{-1}): 314 (260), 425 (240), 564 (18), 950 (6). The effective magnetic moment in MeOH + 1% cyclohexane determined by the Evans' method is 3.19.

2.4. Measurements

Carbon, hydrogen and nitrogen contents were determined on a Carlo Erba MOD 1106 elemental analyzer. Field desorption mass spectra were recorded with a Mat 711 spectrometer. FT-IR spectra of solid samples (KBr pellets) were run on a Bruker IFS 66, and electronic spectra on the Perkin–Elmer LAMBDA 18 spectrophotometer. ^{1}H and ^{13}C NMR spectra were obtained with a Varian Unity Plus 500 MHz spectrometer. Photoacoustic spectra were measured using a MTEC Model 200 Photoacoustic Detector.

2.5. Magnetic moments

The magnetic moment, μ, of each of Ni(HD)X_2 complexes was determined in methanol solution by the method of Evans [8] using in the experiment co-axial tubes, the outer containing solvent and cyclohexane as indicator and the inner-solvent, cyclohexane and the paramagnetic complex. The difference in proton resonance frequencies of cyclohexane present in the outer and inner tubes, $\Delta\nu$, could be read out accurately from the spectrum and allowed to obtain effective magnetic moments using the relationship $\mu = a(T\Delta\nu/c)^{1/2}$ [9], where T is temperature, c the concentration of the paramagnetic substance and a the proportionality constant obtained from Evans relations [8]. Magnetic moment of NiBI has been obtained in DMSO-d_6 using hexamethyldisiloxane as a reference.

2.6. X-ray investigations

The structures of $NiAClO_4$ and NiBI were determined. Crystal data and refinement details are provided in Table 1. Data for both the complexes were obtained with Mo Kα radiation using the Nonius Kappa CCD diffractometer. Structures were solved using direct methods with SHELXS-97 [10] and refined by full-matrix least-squares using the SHELXL-97 [11] with anisotropic thermal parameters for the non-hydrogen atoms. Hydrogen atoms on the carbon and nitrogen atoms were included in calculated positions and given thermal parameters equivalent to 1.2 times those of the atom to which they were attached.

Table 1
Crystal data and structure refinement for $NiAClO_4$ and NiBI

Compound	$NiAClO_4$	NiBI
Empirical formula	$C_{11}H_{17}ClN_4NiO_4$	$C_{14}H_{23}IN_4Ni$
Formula weight	363.45	432.97
Temperature (K)	293(2)	293(2)
Wavelength (Å)	0.71073	0.71073
Crystal system	monoclinic	orthorhombic
Space group	$P2_1/c$	$Pbca$
Unit cell dimensions		
a (Å)	15.0710(3)	17.1640(2)
b (Å)	11.0280(4)	19.6800(3)
c (Å)	9.3820(7)	19.9420(3)
β (°)	107.295(1)	90
Volume (Å^3)	1488.8(1)	6736.16(16)
Z	4	16
D_{calc} (g cm^{-3})	1.621	1.708
Absorption coefficient (mm^{-1})	1.503	2.982
$F(000)$	752	3456
Crystal size (mm)	0.30 × 0.18 × 0.03	0.35 × 0.30 × 0.15
θ Range for data collection (°)	2.93–27.44	2.04–27.48
Limiting indices	$-19 \le h \le 19$, $-13 \le k \le 14$, $-12 \le l \le 11$	$-22 \le h \le 22$, $-25 \le k \le 25$, $-25 \le l \le 25$
Reflections collected/ unique	6059/3373 [$R_{int} = 0.025$]	14 722/7704 [$R_{int} = 0.0351$]
Completeness to $\theta = 27.44$	99.1%	99.7%
Refinement method	full-matrix least-squares on F^2	full-matrix least-squares on F^2
Data/restraints/parameters	3373/0/207	7704/2/387
Goodness-of-fit on F^2	1.039	0.951
Final R indices [$I > 2\sigma(I)$]	$R_1 = 0.0526$, $wR_2 = 0.1135$	$R_1 = 0.0373$, $wR_2 = 0.0887$
R indices (all data)	$R_1 = 0.0836$, $wR_2 = 0.1232$	$R_1 = 0.0817$, $wR_2 = 0.1123$
Largest difference peak and hole (e Å^{-3})	0.860 and −0.422	0.676 and −0.734

3. Results and discussion

Each of the NiAX (X = Cl, NO_3, ClO_4), Ni(HD)X_2 (X = Cl, NO_3), NiBI and PdACl complexes was obtained after addition of a corresponding metal salt to the preformed product of monocondensation of a diprimary triamine with 2-aminobenzaldehyde in 1:1 mole ratio like in the preparative procedure of the [Cu(HB)I]I complex comprising undeprotonated HB ligand [12]. Microanalytical data showed that HA and HB ligands were coordinated in singly deprotonated forms while the HD ligand reacted intact with Ni(II) retaining all its hydrogen atoms. It is worthy to note a striking difference in color of nickel complexes comprising perchlorate and iodide counterions as compared with those with nitrate and chloride counterions. $NiAClO_4$ and NiBI are black, the latter with a faint green tint, respectively, but NiAX (X = Cl, NO_3) complexes are red brown.

3.1. Infrared and electronic spectra

Separate peaks in the 3050–3350 cm^{-1} region of IR spectra of solid compounds were assigned to N–H stretching vibrations and their number does not exceed the number of NH stretching frequencies characteristic either for non-deprotonated or deprotonated ligand. Five bands in this region for Ni(HD)$(NO_3)_2$ may be attributed to asymmetric and symmetric stretching vibrations of both NH_2 groups and to the NH stretching of the secondary amino group. The approximately 1637 cm^{-1} bands which occur in the spectra of Ni(HD)X complexes has been assigned to deformation (scissoring) vibrations of the aromatic amino group. The 1617–1592 cm^{-1} frequencies may be assigned to C=C and azomethine C=N vibrations. However, single bands in the 1541–1538 cm^{-1} region or 1520 cm^{-1} which occur only in the spectra of Ni and Pd complexes comprising deprotonated ligands may be attributed to C–N stretch-

ing vibrations of the bond connecting deprotonated amino nitrogen with carbon atom of the aromatic ring, since order of that bond evaluated as 1.57 on the basis of Pauling's formula[1] [13], bond length data for single and double C–N bonds [14] and C1–N1 bond length in $NiACIO_4$ is comparable to the order (1.70) of aldimine C=N bond for that compound. A broad band at 1090 and a sharper one at 620 cm^{-1} for $NiACIO_4$ are attributed to the perchlorate v_3 and v_4 vibrations, respectively [15]. A lack of any splitting would be consistent with a non-coordinated, tetrahedral ClO_4 [16]. Broad and intense bands at 1421, 1308 and 1044 cm^{-1} in the spectrum of $Ni(HD)(NO_3)_2$ suggest that both the nitrate anions are coordinated since these bands may be assigned to IR active v_3 (split into two components) and v_1 vibrations which as expected will occur when the symmetry of that anion is lowered to C_{2v} or less [17]. The nitrate group of $NiANO_3$ gives rise to one strong and broad band at 1380 cm^{-1} and low intensity bands at 1041 and 710 cm^{-1} which may be attributed to v_3, v_1, v_4 vibrations of weakly interacting nitrate.

The reflectance (DRS) and photoacoustic (PAS) spectra of solid chelates have been recorded, the latter are presented in Fig. 2. The photoacoustic spectroscopy has been included in the study since it gives a direct information about the optical-absorption bands even when the surface of solid material is not highly reflective [18] as in the case of black complexes obtained in this work. All the complexes show intensive absorptions (285–320 nm) which may be assigned to π–π* transitions of the co-ordinated aldimine group and those which incorporate A or B ligands exhibit also intense bands in the 450–500 nm region. The d–d bands expected for planar complexes in the latter region [19] are not resolved but obscured by charge transfer transitions like the bands occurring at 481 and 495 nm in related complexes: *N*,*N*′-ethylenebis(2′-iminobenzaldimino)nickel(II) [Niamben] and *N*,*N*′-propylenebis(2′-iminobenzaldimino)nickel(II) [Niambtn], respectively [20]. Unexpectedly band of the solid $NiACIO_4$ and NiBI complexes show a much higher absorption above 600 nm than the NiAX (X = Cl, NO_3) complexes. To gain information on structural reasons for the occurrence of unusual spectroscopic properties we determined the crystal and molecular structures of $NiACIO_4$ and NiBI complexes by X-ray diffraction studies. These studies showed (vide infra) a planar for $NiACIO_4$ and planar-to-tetrahedral distorted metal configuration for NiBI, and significantly shorter contacts between Ni(II) and aromatic carbon atoms of a neighboring unit in the former and between two nickel ions in an asymmetric unit in the latter compound. These short contacts may facilitate intermolecular charge transfer transitions which account for the intense absorption above 600 nm in solid $NiACIO_4$ and in NiBI with that difference that absorption overlaps the lowest field d–d band in the latter compound. In spite of different colors of solid $NiACIO_4$ (black) and NiAX (X = Cl, NO_3; red) complexes the spectra of their DMSO solutions are similar and do not show absorption above 600 up to 1000 nm in consistency with planar coordination [21]. However, concentrated solutions of $NiACIO_4$ in acetonitrile are black and became red after dilution, what suggests the presence of associated forms in concentrated solution. In contrast to NiAX, the NiBI and $Ni(HD)X_2$ (X = Cl, NO_3) complexes show weak low-energy bands in the 540–800 nm region. The 598 nm band of NiBI in DMSO solution has been assigned to a metal d–d band shifted to the red in consequence of planar-to-tetrahedral distortion and weakening of the ligand field strength. Two low energy bands and one UV band which occur at 314, 564 and 950 nm for $Ni(HD)(NO_3)_2$ could be assigned to d–d transitions in a octahedral field providing that the magnitude of that field may be approximated as a weighted average of octahedral fields associated with each set of N and O ligands separately, according to the rule of averaged environment [22]. The lowest energy band gives then $10Dq$ (10 504 cm^{-1}) which compares well with the value of that parameter (10 640 cm^{-1}) calculated on the basis of equation:

$$Dq = \{9(v_2 + v_3) - [81(v_2 - v_3)^2 - 16v_2v_3]^{1/2}\}/340$$

The equation was obtained by reduction of Dou's equation [23] to a more convenient form. Wave numbers v_2 and v_3 of 587 and 314 nm bands, respectively, for $Ni(HD)Cl_2$ led to a comparable $10Dq$ value (10 626 cm^{-1}). For octahedral stereochemistry the magnetic moment for Ni(II), μ_{eff} is given by the expression $\mu_{eff} = \mu_{s.o.}(1 - \alpha\lambda/10Dq)$ [24] where λ is the spin–orbit coupling constant and $\mu_{s.o.}$ is the spin only moment. Using μ_{eff} of 3.19, 3.17 and the evaluated Dq values we obtained λ values of approximately −340 and −320 cm^{-1} for $Ni(HD)(NO_3)_2$ and $Ni(HD)Cl_2$, respectively, as compared with the free ion value of −320 cm^{-1}.

3.2. NMR spectra

Diamagnetic NiAX and PdACl complexes have been characterized by ^1H and ^{13}C NMR ($NiANO_3$ and PdACl) spectroscopy. In all cases, the spectra show the simultaneous occurrence of two set of signals which are attributable on the one hand to the substituted benzaldimine entity and on the other hand to the aliphatic part of the ligand. Protons which are bonded to nitrogen atoms give rise to separate bands which were

[1] Fractional bond orders, n, were calculated according to the formula $\log n = [d(1) - d(n)]/c$, where $d(1)$ and $d(n)$ are the distances of single and n-ple bond, respectively, and c is a constant to be determined.

identified by using deuterium exchange and H–H connectivities established by the ^1H–^1H COSY experiment. Splitting of each H3 and H4 signal into two doublets and one triplet shows two unequal *ortho* couplings (9.5 and 7.6 Hz for H3) and one *meta* coupling (ca. 1 Hz for both H3 and H4 atoms) and are consistent with the *ortho* disubstitution of the benzene ring. Resonance frequencies of H2 (ca. 6.65 ppm) and H4 (6.23 ppm) indicate shielding of these protons in NiAX and PdACl complexes affected by mesomeric (+) effect of the deprotonated amino group acting as an electron donor substituent. The complexity of multiplets observed in the aliphatic part of the spectrum *i.a.* due to the chirality of the coordinated secondary amino group provide evidence of rigidity of the MA(II) ionic species in solutions. Resonance signals of primary (H_N4a at ca. 4.16, and H_N4b at ca. 3.53 ppm), deprotonated primary (H_N1 at ca. 4.76 ppm) and secondary amino (H_N3 at ca. 5.48 ppm) protons for NiAX complexes are shifted upfield in the PdACl complex to 4.912 ppm (H_N4a), 4.607 ppm (H_N4b), 6.524 ppm (H_N1) and 6.679 ppm (H_N3). These shifts imply stronger N–Pd interaction and better stabilization of the partial negative charge on the nitrogen by Pd(II) versus Ni(II). The farthest downfield signal and the next one in ^{13}C NMR spectrum (at 158.7 and 151.5 ppm) for $NiANO_3$ and (at 161.7 and 157.3 ppm) for PdACl may be assigned to the chemical shifts of aldimine (C7) and aromatic (C1) carbon atom since these atoms are strongly deshielded on account of polarization of their carbon–nitrogen bonds which like in $NiACLO_4$ (vide infra) may be of comparable order (>1.5).

Chemical shifts of NiB^+ protons are spread over approximately 16 ppm (at 325 K). Resonance signals of protons except those of aromatic ring are broadened relative to the same protons in diamagnetic NiAX complexes. The observed spin–spin coupling between aromatic ring protons made their resonances readily assignable. Disappearance of two singlets at 0.77 ppm (two-proton signal) and at 2.356 ppm (one-proton signal) at 325 K after addition of D_2O to the solution of NiBI allowed assigning these signals to NH_2 and NH protons, respectively. Relative ^1H–^1H connectivities established by the COSY experiment allowed assigning the remaining resonances. The data presented in Table 4 show that NiBI proton resonance frequencies decrease or increase with increasing temperature depending on the position of proton in the molecule. The difference in chemical shift of a NiBI proton relative to the shift of proton occupying the same position in the diamagnetic reference, $NiANO_3$, the ($\delta-\delta'$) value in Table 4, is shown to be positive or negative. Clear downfield or upfield shifts of signals from the diamagnetic reference in addition to the line broadening effects are thought to arise because of a weak paramagnetic properties of NiBI in DMSO-d_6 solution. Weak paramagnetism may be the result of spin equilibrium between low spin, close to square planar and high spin presumably tetrahedral NiB^+ and five-coordinate NiBI forms, in which the high spin forms are in low concentration. A rapid interconversion of the paramagnetic into diamagnetic species will result that the paramagnetic spin density is distributed over a large number of NiB^+ ions and becomes 'diamagnetically diluted'. The differences between the chemical shifts of NiBI protons and those of diamagnetic reference (Table 4) seem to arise mainly due to contact interactions since pseudocontact interactions in paramagnetic Ni(II) complexes are judged to be very small [25a]. The Table 4 data suggest that the unpaired spin density is spread over the whole organic ligand and that contact shifts which cause shielding and deshielding effects alternate in sign by going from H3 to H6 owing to spin correlation effects like contact shifts of succeeding ring protons in paramagnetic bis(*N*,*N*′-diethylaminotroponeimino)nickel(II) [25b]. Molar susceptibility and magnetic moment for NiBI were determined in DMSO-d_6 solution (0.04 M) by the method of Evans. The Table 5 data show that there is an increase in magnetic moment, in the fraction of high spin form ($N_{h.s.}=\mu^2/\mu^2_{h.s.}$, where $\mu_{h.s.}$ is assumed to be 3.3 μ_B) and in the planar⇄tetrahedral equilibrium constant [$K_{eq}=N_{h.s.}/(1-N_{h.s.})$] with the increase in temperature. The thermodynamic parameters of the equilibrium ($\Delta G^\circ=4.7\pm0.1$ kJ mol^{-1}, $\Delta H^\circ=1.8\pm0.2$ kJ mol^{-1}, $\Delta S^\circ=-9\pm2$ J mol^{-1} K) were obtained from standard equations as described previously [26].

3.3. Crystal structures

3.3.1. $NiACLO_4$

A perspective view of the asymmetric unit is shown on Fig. 3, while the selected bond distances are given in Table 2. The crystal structure consists of discrete $Ni(C_{11}H_{17}N_4)^+$ cations and perchlorate anions. The HA is singly deprotonated at the aromatic amino group and binds Ni(II) atom through four nitrogen atoms. The geometry of metal coordination sphere is distorted square planar, the sum of bond angles at the Ni(II) atom is 359.9(5)°. The nitrogen atoms lie exactly in plane (their maximal deviation from least-squares plane

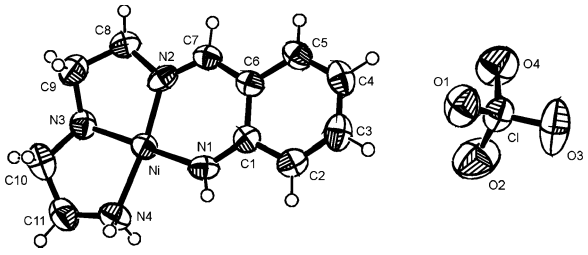


Fig. 3. The structure of the $NiACLO_4$ asymmetric unit with atom numbering scheme. Displacement ellipsoids are drawn at the 30% probability level; H atoms are drawn as spheres of arbitrary radii.

Table 2
Selected geometric parameters (Å, °) for $NiAClO_4$ and NiBI

$NiAClO_4$	
Ni–N1	1.823(3)
Ni–N2	1.812(3)
Ni–N3	1.912(3)
Ni–N4	1.928(3)
N1–Ni–N2	94.18(14)
N1–Ni–N3	178.34(15)
N2–Ni–N3	86.00(13)
N1–Ni–N4	93.74(15)
N2–Ni–N4	171.82(14)
N3–Ni–N4	86.02(14)
NiBI	
Ni–N1	1.848(3)
Ni–N2	1.874(3)
Ni–N3	2.018(3)
Ni–N4	1.932(4)
Ni′–N1’	1.848(4)
Ni′–N2′	1.885(4)
Ni′–N3′	2.014(3)
Ni′–N4′	1.940(4)
N1–Ni–N2	90.87(14)
N1–Ni–N3	167.16(14)
N2–Ni–N3	93.31(14)
N1–Ni–N4	88.17(15)
N2–Ni–N4	168.18(15)
N3–Ni–N4	90.17(15)
N1′–Ni′–N2′	90.92(15)
N1′–Ni′–N3′	166.74(15)
N2′–Ni′–N3′	93.72(15)
N1′–Ni′–N4′	87.80(16)
N2′–Ni′–N4′	167.35(16)
N3′–Ni′–N4′	90.32(15)

The apostrophy sign denotes atoms belonging to the other crystallographically independent molecule.

is 0.002 Å) and are arranged at the corners of an irregular quadrangle reflecting the difficulty of the ligand to span square planar coordinative positions. The Ni(II) atom resides a little out [0.029(2) Å] of the N1–N4 plane. The structure comprises one six and the two five-membered chelate rings. The six-membered metallocycle involving the 2-iminobenzaldimino moiety is practically coplanar with the N1–N4 coordination plane (dihedral angle 1.5°). Both the five membered metallocycles are in envelope conformation one on C9 the other on C10. Both C9 and C10 atoms are on the same side of the least-squares plane defined by the remaining 14 non-hydrogen atoms constituting the cationic unit and are separated from that plane by −0.633(4) and −0.594(4) Å, respectively. The Ni–N1 and Ni–N2 distances (Table 2) are significantly shorter and the N1–Ni–N2 angle a little more obtuse [94.2(2)°] than the corresponding quantities reported for planar Ni(II) complexes comprising deprotonated 2-aminobenzylideneimino ligands being 1.857(6), 1.878(9) Å and 92.5° for Niambpn [*N*,*N*′-2-methylethylenebis(2′-iminobenzaldimino)nickel(II)] [27] and 1.860(7), 1.923(7) Å and 90.1(3)° for Niambtn [*N*,*N*′-propylenebis(2′-iminobenzaldimino)nickel(II)] [28], and 1.81(1), 1.89(1) Å for Cummins’ complex [6], respectively. The Ni–N3 and Ni–N4 distances (Table 2) comparable with the average Ni–N bond length (1.92 Å) found in low spin $Ni(en)_2$ complex [29] are a little below the Ni–N (primary amine) distance in Cummins’ complex [1.94(1) Å] and the averaged values reported recently for four coordinate planar Ni(II) tetraamine complexes (1.95 Å) [30] and (1.94 Å) [31]. Perchlorate anion does not directly interact with Ni(II) (Ni···O distances exceed 4.7 Å) but is involved in hydrogen bonding interactions with amino hydrogens of the aliphatic part of the ligand. Geometric details of these bonds are given in Table 3. The closest intermolecular approaches in the structure excluding pairs of atoms participating in hydrogen bonding interactions, occur between Ni(II) and both the $C4^j$ and $C5^j$ atoms of the aromatic ring [symmetry code in (*j*): $-x$, $-y$, $-z$) and are by 0.62 and 0.52 Å less, respectively, than the corresponding radius sum [32].

3.3.2. *NiBI*

Each asymmetric unit contains two crystallographically independent NiBI moieties related by the pseudo-twofold rotation axis. The molecular structure of one independent ionic pair is shown in Fig. 4. Pairs of crystallographically independent complex cations are linked with crystallographically independent iodide anions by hydrogen bonds to give an $[NiB]_2I_2$ four ion assembly, which may be considered the motif that crystallized (Fig. 5). Geometric details of these bonds are listed in Table 3. Proton donors in that assembly are both the undeprotonated and deprotonated amino groups of the coordinated ligand, and the proton acceptor is only the iodide anion in accordance with the Etter’s rule [33], that best proton donors and best proton acceptors will bind to one another. A shorter separation of nickel atoms (4.125 Å) than the sum of their

Table 3
Hydrogen bonding geometry (Å, °) for $NiAClO_4$ and NiBI

DH···A	D–H	H···A	D···A	DH···A
$NiAClO_4$				
$N3–H_N3\cdots O2^{i}$	0.84(2)	2.56(4)	3.27(3)	142(2)
$N4–H_N4a\cdots O3^{ii}$	0.90(4)	2.26(2)	3.16(3)	171(3)
$N4–H_N4b\cdots O1^{iii}$	0.88(2)	2.60(3)	3.36(2)	145(2)
NiBI				
$N1–H_N1\cdots I$	0.93(2)	2.86(2)	3.789(2)	171(3)
$N1'–H_N1'\cdots I'$	0.95(2)	2.89(3)	3.809(4)	163(5)
$N4–H_N4a\cdots I$	0.84(4)	2.80(4)	3.609(4)	163(3)
$N4–H_N4b\cdots I'$	0.95(5)	2.85(5)	3.748(4)	159(4)
$N4'–H_N4b'\cdots I$	0.91(5)	2.86(5)	3.726(4)	161(4)
$N4'–H_N4a'\cdots I'$	1.02(5)	2.68(5)	3.673(4)	165(4)

Symmetry code in: (i) x, $1/2-y$, $1/2+z$; (ii) x, $1/2-y$, $-1/2+z$; (iii) x, $-1+y$, z. The apostrophy sign denotes atoms belonging to the other crystallographically independent molecule.

Table 4
Chemical shifts for NiBI protons in DMSO-d_6 [a]

		Temperature (K)					
		δ				$\delta-\delta'$	
		295	305	315	325	325	
H_N1	1H, s	2.630	ov [b]	2.437	2.356	−2.39	
H_N4a, H_N4b	2H, br.s.	1.039	0.934	0.825	0.771	−3.41	−2.76
H2	1H, d	5.886	5.839(7)	5.767(7)	5.703(7)	−1.53	
H3, H5	2H, m	7.383	7.411	7.458	7.482	0.55	0.32
H4	1H, t	5.517	5.457(7)	5.391(7)	5.311(7)	−0.92	
H7	1H, s	15.129	15.634	16.233	16.788	8.94	
H8a	1H, s	8.191	8.464	8.737	9.136	5.46	
H8b	1H, s	5.646	5.830	6.059	6.282	3.25	
H9a	1H, s	1.853	1.871	1.885	1.893		
H9b	1H, s	1.761	1.776	1.784	1.791		
H10a	1H, s	5.517	5.631	5.887	6.142		
H10b	1H, s	3.364	3.407	3.455	3.502		
H11	3H, s	4.167	4.315	4.475	4.643		
H12a	1H, s	4.167	4.315	4.475	4.643		
H12b	1H, s	3.931	3.971	4.021	4.076		
H13a, H13b	2H, s	1.395	1.434	1.485	1.522		
H14a	1H, s	7.477	7.761	8.099	8.436		
H14b	1H, s	5.403	5.631	5.765	6.027		

[a] The position of resonance signal measured relative to that of hexamethyldisiloxane (δ) or relative to the proton which occupies the same position in diamagnetic $NiANO_3$ ($\delta-\delta'$).
[b] Overlapped by the solvent signal.

Table 5
Temperature dependence of magnetic moments and of planar–tetrahedral equilibrium constant for NiBI in DMSO-d_6 solution

T (K)	$\Delta\nu$ (Hz) [a]	$10^6\,\chi$ [b]	μ (μ_B) [c]	$N_{h.s.}$ [d]	K_{eq} [e]
295	15.6	619	1.20	0.134	0.155
305	15.1	610	1.22	0.137	0.159
315	14.7	603	1.23	0.140	0.163
325	14.2	594	1.24	0.142	0.166

[a] Chemical shift difference for the reference hexamethyldisiloxane signal obtained in the method of Evans.
[b] Molar susceptibility corrected for diamagnetism and expressed in c.g.s. unit. It should be multiplied by $4\pi \times 10^{-6}$ to be converted into SI unit.
[c] The effective magnetic moment.
[d] Fraction of the high spin form.
[e] Equilibrium constant.

van der Waals radii (4.60 Å) may suggest a weak Ni···Ni interaction within the asymmetric unit. The unit cell contains eight $[NiB]_2I_2$ assemblies. In the structure we find nickel(II) atoms four coordinated by the nitrogen atoms of singly deprotonated Schiff base ligand. The coordination geometry about the nickel atom may be described as planar with significant tetrahedral distortion in contrast to the reported by us earlier square pyramidal coordination in the related [CuBI]I complex [12]. Deviations of the plane defining atoms N1, N2, N3 and N4 from the least-squares plane through these atoms being 0.214, −0.198, 0.187, −0.202 Å, respectively, and the

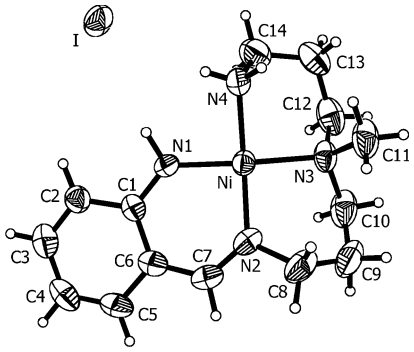


Fig. 4. The structure of one of the independent NiBI complex molecule with atom numbering scheme. Displacement ellipsoids are drawn at the 30% probability level; H atoms are drawn as spheres of arbitrary radii.

acute angle of 41.4° between Ni, N1, N2 and Ni, N3, N4 planes in comparison with that angle anticipated for tetrahedral (90°) and for planar (0°) coordination geometry indicate a marked tetrahedral character of this distortion. The nickel atom is displaced from the N1, N2, N3, N4 plane by 0.046 Å. The distorted arrangement of coordinating atoms results in a twisting of the Schiff base backbone so that least-squares plane through Ni, N1, N2, C1, C6, C7 atoms makes an angle of 39.35° with the least-square plane through Ni, N3, N4, C12, C13, C14. The Ni–N1 and Ni–N2 bond distances fit the ranges of 1.827–1.860 and of 1.812–1.925 Å, respectively, observed in $NiAClO_4$, Niambpn [27] and Niambtn [28] complexes. The Ni–N3 bond distance is markedly longer

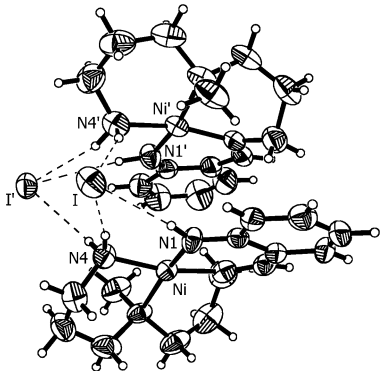


Fig. 5. The structure of the $(NiB)_2I_2$ aggregate showing hydrogen bonding arrangement.

than the nickel tertiary amino nitrogen separation (1.951 Å), whereas the Ni–N4 distance compares well with the nickel primary amino nitrogen bond length in the planar nickel(II) complex with aliphatic tetraamines [30,31]. The NiBI comprises three chelate rings. The ring incorporating N1 and N2 atoms is approximately planar, deviations of plane defining atoms do not exceed 0.134 Å. Cremer and Pople parameters [34] like puckering amplitude 0.789 Å, and $\theta = 91.0^\circ$, $\phi = 87.49^\circ$ angles show that the central chelate ring (with N2 and N3 atoms) is approximately in twist-boat conformation. It is worthy to note the proximity of certain aromatic rings in the crystal. The shortest approach of gravity centers of two aromatic rings of 5.25 Å was found for that ring which occupies equivalent position x, y, z and the other $-x$, $1-y$, $1-z$.

4. Supplementary material

Crystallographic data for the structural analysis have been deposited with the Cambridge Crystallographic Data Centre, CCDC 180372 for 1-(2′-iminophenyl)-2,5-diaza-7-amino-1-heptenonickel(II) perchlorate and CCDC 180373 for 1-(2′-iminophenyl)-2,6-diaza-6-methyl-9-amino-1-nonenonickel(II) iodide. Copies of this information may be obtained free of charge from The Director, CCDC, 12 Union Road, Cambridge, CB2 1EZ, UK (fax: +44-1223-336033; e-mail: deposit@ccdc.cam.ac.uk or www: http://www.ccdc.cam.ac.uk).

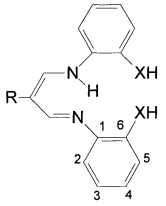
Acknowledgements

This research was supported by the Grant from the Polish State Committee for Scientific Research (KBN 7 T09A 132 20) and partially by the Grant from the University of Gdańsk (BW/8000-5-0300-2).

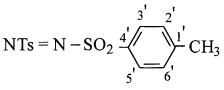
References

[1] U. Bachram, Function of Naturally Occurring Polyamines, Academic Press, New York, 1988.
[2] S. Schultz, Angew. Chem., Int. Ed. Engl. 36 (1997) 314.
[3] L.E. Heyman, R. Cheney, L.E. Blinn, J. Inorg. Nucl. Chem. 35 (1973) 2217.
[4] R.H. Prince, D.A. Stotter, Inorg. Chim. Acta 10 (1974) 69.
[5] G.M. Sheldrick, D.A. Stotter, J. Chem. Soc., Dalton Trans. (1975) 666.
[6] D. Cummins, E.D. McKenzie, I.W. Nowell, J.M. Worthington, Inorg. Chim. Acta 15 (1975) L17.
[7] I.E. Smith, J.W. Opie, Org. Synth. 3 (1956) 56.
[8] (a) D.F. Evans, J. Chem. Soc. (1959) 2003;
(b) D.F. Evans, G.V. Fazakerley, R.F. Phillips, J. Chem. Soc. A (1971) 1931.
[9] J. Loliger, R.J. Sheffold, J. Chem. Educ. 49 (1972) 646.
[10] G.M. Sheldrick, SHELXS-97, Program for Crystal Structure Solution, University of Göttingen, Germany, 1997.
[11] G.M. Sheldrick, SHELXL-97, Program for Crystal Structure Refinement, University of Göttingen, Germany, 1997.
[12] E. Kwiatkowski, M. Kwiatkowski, A. Olechnowicz, T. Ossowski, B. Kościuszko, U. Dettlaff-Węglikowska, J. Crystallogr., Spec. Res. 21 (1991) 75.
[13] L. Pauling, The Nature of the Chemical Bond and the Structure of Molecules and Crystals. An Introduction to Modern Structural Chemistry, 3rd ed., Cornell University Press, Ithaka, NY, 1960.
[14] F.H. Allen, O. Kennard, D.G. Watson, L. Brammer, A.G. Orpen, R. Taylor, J. Chem. Soc., Perkin. Trans. II (1987) S1.
[15] M.G.B. Drew, M. McCann, S.M. Nelson, J. Chem. Soc., Dalton Trans. (1981) 1868.
[16] K. Nakamoto, Infrared Spectra of Inorganic Compounds, Wiley, New York, 1970.
[17] C. Addison, N. Logan, S.C. Wallock, C.D. Gardner, Quart. Rev. 25 (1971) 289.
[18] A. Rosencwaig, Phys. Today, September 1975, 23.
[19] I. Bertini, F. Mani, Inorg. Chem. 6 (1967) 2032.
[20] M. Green, P.A. Tasker, J. Chem Soc. A (1970) 2531.
[21] A.B.P. Lever, Inorganic Electronic Spectroscopy, Elsevier, Amsterdam, 1968, p. 343.
[22] B.N. Figgis, Introduction to Ligand Fields, Interscience Publishers, New York, 1966, p. 292.
[23] Y. Dou, J. Chem. Educ. 67 (1990) 134.
[24] B.N. Figgis, J. Lewis, Prog. Inorg. Chem. 6 (1964) 37.
[25] (a) R.H. Holm, E.H. Abbott, in: A. Martell (Ed.), Coordination Chemistry, vol. 1, Van Norstrand Reinhold, New York, 1971, p. 315;
(b) R.H. Holm, E.H. Abbott, in: A. Martell (Ed.), Coordination Chemistry, vol. 1, Van Norstrand Reinhold, New York, 1971, pp. 308–309.
[26] R.H. Holm, M.J. O'Connor, Prog. Inorg. Chem. 14 (1971) 214.
[27] N.A. Bailey, E.D. McKenzie, Inorg. Chim. Acta 43 (1980) 205.
[28] N.A. Bailey, E.D. McKenzie, J.M. Worthington, J. Chem. Soc., Dalton Trans. (1974) 1363.
[29] R. Stomberg, Acta Chem. Scand. 23 (1969) 3498.
[30] T.-H. Lu, C.-S. Chung, T. Ashida, J. Chin. Chem. Soc. (Taipei) 38 (1991) 147.
[31] T.H. Tahirov, T.H. Lu, K. Shu, C.S. Chung, Acta Crystallogr., Sect. C 50 (1994) 516.
[32] A. Bondi, J. Phys. Chem. 68 (1964) 441.
[33] M.C. Etter, Acc. Chem. Res. 23 (1990) 120.
[34] D. Cremer, J.A. Pople, J. Am. Chem. Soc. 97 (1975) 1534.

Cu(II), Ni(II), Co(II), Zn(II), Cd(II) were isolated and characterized.



VI X=O, R=NO_2; VIa X=O, R=Ph;
VII X=S, R=NO_2; VIIa X=S, R=Ph;
VIII X=NTs, R=NO_2; VIIIa X= NTs, R=Ph;



VI - VIII

Compounds of the types (**VI**, **VIa**–**VIII**, **VIIIa**) possess a potential tetradenticity. On their basis, little known polynuclear metal chelates can be isolated. Variations of different donor centers (–N, –O, –S) and substituents (R = $-NO_2$, –Ph) can be carried out in the frameworks of the same molecule.

It is well known that, in addition to the nature of metal center and ligand, the applied synthetic technique influences considerably the type, structure, and properties of metal complexes [23–26]. In this respect, two methods were used: chemical (metal acetates as source of metal centers) and electrochemical (sacrificial metal anode).

2. Experimental

2.1. Materials and equipment

IR spectra were recorded by the spectrophotometer Specord-71 (the samples were prepared in as nujol mulls). ^{1}H NMR spectra were measured in DMSO-d_6 solutions (TMS standard) using Varian UNITY 300. The EPR spectra of the powders were obtained with the ER-9 (Zeiss) equipment in the temperature interval 77–300 K, and those of the solutions were made in DMF at 77 K (in low-temperature glass). Effective magnetic moments were determined by the Faraday method in the crystalline phase at 77–300 K with equipment made at Rostov State University [27]. Hg[Co(CNS)$_4$] was used as a calibration standard. Calculations of molar magnetic susceptibility were performed by taking into account the diamagnetic properties of ligands and the available theoretic data for organic species [28].

2.2. Synthetic techniques

The bis-[(2-oxy-, mercapto-, *N*-tosylamino)aniles] of nitro- and phenylmalondialdehyde (**VI**, **VIa**–**VIII**, **VIIIa**; X = O, S, NTs; R = NO_2, Ph), used as ligands, were obtained as follows. A solution of *o*-aminophenol hydrochloride or *o*-aminothiophenol hydrochloride or 2-(*p*-toluenesulfamine)aniline hydrochloride (0.02 M in each case) in 10 ml of MeOH was added to a solution of sodiumnitro(phenyl)malonic aldehyde (0.01 M) in MeOH (10 ml). The precipitate formed was treated with a solution of KOH in MeOH to achieve pH 7, filtered, washed with MeOH (3 × 3 ml) and dried in air. Yield was in the range of 70–78%.

A solution of *o*-aminothiophenol hydrochloride (0.02 M) in 10 ml of MeOH and a solution of metal acetate in 15 ml of MeOH was added to a 0.01 M solution of sodium nitromalondialdehyde in 20 ml of the MeOH–dioxane mixture (1:1). The mixture was refluxed for 1 h. The solid formed was filtered, washed (3 × 10 ml) with a hot mixture of MeOH–dioxane (1:1), and dried under vacuum at 150 °C.

Both chemical and electrochemical techniques were applied in order to obtain metal chelates. The chemical synthesis was carried out by refluxing MeOH–dioxane solutions of ligands and acidified MeOH solutions of their corresponding metal acetates (molar ratio metal–ligand 1:2.5). In the case of Ni(II) and Co(II) complexes, a MeOH solution of equimolar quantity of KOH was added to neutralize produced CH_3COOH. The precipitates formed were filtered, washed with MeOH, and dried under vacuum at 120 °C. Yields were in the range of 50–80%.

The electrochemical synthesis of the metal complexes [24,29–31] was carried out in an electrochemical cell containing a MeOH solution of the ligand (10^{-3} mol in 30 ml of MeOH). A copper sheet was used as a sacrificial anode while a platinum wire was used as a cathode. $LiClO_4$ was used as supporting electrolyte. The electrolysis was performed with a current of 20 mA and initial voltage of 20 V during 4 h at room temperature. The precipitates formed were filtered, washed with hot MeOH (3–5 ml) and dried under vacuum at 150 °C. Yield was in the range of 70–80%. The characteristics of the compounds obtained are presented in Table 1.

3. Results and discussion

According to the data of elemental analysis, all metal complexes synthesized with the studied bis-azomethines **VI**, **VIa**–**VIII**, **VIIIa** have the general formula M_3L_2, corresponding to trinuclear structures, independently of the synthetic method applied (Table 1, compounds **5**–**20**). Their IR spectra contain changes indicating chelate formation [32]: disappearance of valent oscillations of acidic protons of –OH and NH groups and a decrease of frequencies of oscillations of the conjugated C=N and C=C bonds (Table 2).

The chelate structure of Zn(II) and Cd(II) trinuclear complexes (Table 1, compounds **19** and **20**) was also confirmed by ^{1}H NMR spectroscopy data. The spectrum of 3 **VIII** (X = NTs, R = NO_2) contain peaks of protons of the methyl groups of tosyl fragments at δ = 2.23 ppm (s, 6H, $2CH_3$). The following peaks are observed: at 7.0–9.4 {aromatic protons δ = 7.0–7.5

Table 1
Elemental analysis and related data for the compounds **VI**, **VIa–VIII**, **VIIIa** and their metal complexes

No.	X	R	M	Composition	Formula	Color	M.p. (°C)	Found/calculated					$\mu_{eff.}$, B.M. (T, K)
								C	H	N	S	M	
1	O	NO_2		H_3L^{VI}	$C_{15}H_{13}N_3O_4$	yellow	229	60.35, 60.12	4.58, 4.38	14.03, 14.06			
2	O	Ph		H_3L^{Via}	$C_{25}H_{18}N_2O_2$	pale yellow	191	76.00, 76.34	5.52, 5.49	8.21, 8.48			
3	NTs	NO_2		H_3L^{VIII}	$C_{29}H_{27}N_5O_6S_6$	pale yellow	198	57.62, 57.61	4.53, 4.49	11.65, 11.56	10.75, 10.59		
4	NTs	Ph		H_3L^{VIIIa}	$C_{35}H_{32}N_4O_4S_2$	pale yellow	255	66.09, 66.02	5.08, 5.07	8.78, 8.80			
5	O	NO_2	Cu	$Cu_3L_2^{VI}$	$C_{30}H_{20}Cu_3N_6O_8$	brown	> 300	46.42, 46.01	2.83, 2.57	10.42, 10.73		24.65, 24.34	1.55 (292)
6	O	Ph	Cu	$Cu_3L_2^{VIa}$	$C_{42}H_{30}Cu_3N_4O_4$	brown	> 300	59.95, 59.68	3.98, 3.58	6.80, 6.63		22.85, 22.55	1.55 (290.7), 1.35 (82.6)
7	O	Ph	Cu [a]	$Cu_3L_2^{VIa} \cdot 3H_2O$	$C_{42}H_{36}Cu_3N_4O_7$	brown	> 300	56.00, 56.09	4.00, 4.04	6.25, 6.23		21.35, 21.19	1.82 (301), 1.55 (122)
8	S	NO_2	Cu	$Cu_3L_2^{VII}$	$C_{30}H_{20}Cu_3N_6S_4$	black	> 300	42.75, 42.52	2.49, 2.38	9.48, 9.92	15.43, 15.13	22.14, 22.50	1.37 (296)
9	S	Ph	Cu	$Cu_3L_2^{VIIa}$	$C_{42}H_{30}Cu_3N_4S_4$	dark brown	206	55.80, 55.46	4.08, 3.32	6.30, 6.16	13.60, 14.10	20.55, 20.96	1.01 (302), 0.98 (257)
10	S	Ph	Cu [a]	$Cu_3L_2^{VIIa} \cdot CH_3OH$	$C_{43}H_{34}Cu_3N_4S_4O$	dark brown	211	54.70, 54.85	3.58, 3.64	6.20, 5.95	13.80, 13.62	20.28, 20.24	1.01 (302), 0.98 (120)
11	NTs	NO_2	Cu	Cu_3L^{VII}	$C_{58}H_{48}Cu_3N_{10}O_{12}S_4$	dark brown	250	50.12, 49.90	3.62, 3.46	9.67, 10.03	9.42, 9.18	14.00, 13.66	1.51 (292)
12	NTs	Ph	Cu	$Cu_3L_2^{VIIa} \cdot 2H_2O$	$C_{70}H_{62}Cu_3N_8O_{10}S_4$	dark brown	> 300	56.46, 56.27	4.53, 4.18	7.64, 7.49	9.15, 8.58	13.10, 12.76	1.55 (304), 1.39 (100)
13	NTs	Ph	Cu [a]	$Cu_3L_2^{VIIa} \cdot 2H_2O$	$C_{70}Cu_3H_{62}N_8O_{10}S_4$	dark brown	> 300	56.12, 56.27	4.41, 4.18	7.84, 7.49	9.10, 8.58	12.85, 12.76	1.00 (304), 0.99 (100)
14	O	Ph	Ni	$Ni_3L_2^{VIa} \cdot 2H_2O$	$C_{42}H_{34}N_4Ni_3O_6$	brown	> 300	58.02, 58.19	4.65, 3.95	6.80, 6.46		20.15, 20.32	3.17 (304)
15	S	Ph	Ni	$Ni_3L_2^{VIIa} \cdot 2H_2O$	$C_{42}H_{38}N_4Ni_3S_4O_4$	brown	> 300	51.80, 52.15	3.82, 3.96	6.27, 5.79	13.82, 13.26	18.94, 18.21	2.88 (302)
16	NTs	NO_2	Ni	$Ni_3L_2^{VIII}$	$C_{58}H_{48}N_{10}Ni_3S_4O_{12}$	black	> 300	50.84, 50.43	3.85, 3.50	9.95, 10.14	9.48, 9.28	12.55, 12.75	
17	NTs	NO_2	Co	$Co_3L_2^{VIII}$	$C_{58}H_{48}Co_3N_{10}S_4O_{12}$	brown	> 300	50.92, 50.40	3.15, 3.50	9.96, 10.13	9.14, 9.28	13.06, 12.79	3.50 (292)
18	NTs	Ph	Co	$Co_3L_2^{VIIIa} \cdot 2H_2O$	$C_{70}H_{62}Co_3N_8O_{10}S_4$	dark brown	> 300	56.12, 56.79	4.69, 4.22	7.75, 7.57	8.43, 8.66	12.25, 11.95	4.15 (296)
19	NTs	NO_2	Zn	$Zn_3L_2^{VIII}$	$C_{58}H_{48}N_{10}O_{12}S_4Zn_3$	orange	> 300	50.12, 49.71	3.05, 3.45	10.12, 9.99	9.42, 9.15	13.87, 14.00	diam.
20	NTs	NO_2	Cd	$Cd_3L_2^{VII}$	$C_{58}H_{48}Cd_3N_{10}O_{12}S_4$	orange	> 300	45.66, 45.16	3.05, 3.14	9.28, 9.08	8.52, 8.31	21.96, 21.86	diam.

[a] Obtained electrochemically.

Table 2
IR spectral data for the compounds **VI**, **VIa**–**VIII**, **VIIIa** and their complexes

No.	X	R	M	ν_{NH}, ν_{OH}, ν_{SH} (cm^{-1})	$\nu_{C=N}$	ν_{as} SO_2, ν_s SO_2 (cm^{-1})
1	O	NO_2		3200–3400 w, 3550 m	1626 s	
2	O	Ph		3240 m, 3364 w	1644 v.s.	
3	NTs	NO_2		3180 m	1620 v.s.	1326 v.s., 1140 v.s.
4	NTs	Ph		3353–3280 w	1633 s	1330 s, 1153 v.s.
5	O	NO_2	Cu		1570 m	
6	O	Ph	Cu		1580 m	
7	O	Ph	Cu [a]	3340 w	1580 m	
8	NTs	NO_2	Cu		1590 s	
9	S	Ph	Cu		1600 m	
10	S	Ph	Cu [a]	3400–3350 w	1607 s	
11	S	NO_2	Cu	3400–3200 w	1575 s	1280 s, 1195 s
12	NTs	Ph	Cu	3400–3200 w	1583 s	1253 s, 1115 v.s.
13	NTs	Ph	Cu [a]	3400–3200 w	1580 s	1260 s, 1120 v.s.
14	O	Ph	Ni	3400–3300 w	1566 s	
15	S	Rh	Ni	3400–3300 w	1600 m	
16	NTs	NO_2	Ni	3400–3250 w	1580 m	1265 s, 1110 v.s.
17	NTs	NO_2	Co	3400–3250 w	1583 m	1273 s, 1125 v.s.
18	NTs	Ph	Co	3400–3200 w	1592 m	1284 s, 1138 v.s.
19	NTs	NO_2	Zn	3400–3250 w	1585 m	1275 s., 1125 v.s.
20	NTs	NO_2	Cd	3400–3250 w	1580 s	1280 s, 1115 v.s.

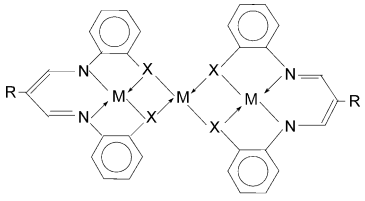
[a] Obtained electrochemically.

ppm (m, 16H, $4C_6H_4$)}, 8.3 (2H, 2NHTs in NH–Ts groups), and 9.4 ppm (s, 2H, =CH–NH–, –CH=N–, singlet peak of methyne protons). The protons of the NH group of the –NH–CH= fragment are revealed at $\delta = 12.0$ ppm (t, 1H, NH, $^3J(-NH-CH=) = 6$ Hz) in the form of a triplet peak with vicinal constant 6 Hz.

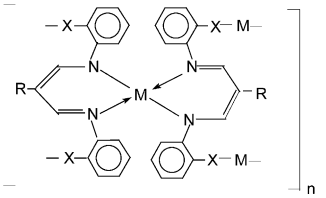
The ^1H NMR spectrum of the bis-azomethine complex (19 **VIII**) Zn_3L_2 does not contain peaks at $\delta = 12$ ppm of N–H protons, as well as the peak at $\delta =$ 8.3 ppm of the protons of the NH–Ts-fragment. This fact testifies for a substitution of the protons in the ligand system by the metal during formation of the complex chelate type. In other respects the spectra of Zn_3L_2 (19 **VIII**) correspond to the ligand's spectrum: δ (ppm) 2.23 (s, 12H, $4CH_3$), 6.76 (t, 4H, $4C_6H_4(3)$, $^3J = 8$ Hz), 6.84 (t, 4H, $4C_6H_4(4)$, $^3J = 8$ Hz), 6.98 (d, 4H, $4C_6H_4(2)$, $^3J = 8$ Hz), 7.12 (d, 8H, $4C_6H_4(2'6')$, $^3J = 8$ Hz), 7.28 (d, 4H, $4C_6H_4(5)$, $^3J = 8$ Hz), 7.8 (d, 8H, $4C_6H_4(3'5')$, $^3J = 8$ Hz), 9.15 (s, 4H, 2(=CH–NH–, –CH=N–).

The complex (20 **VIII**) Cd_3L_2 shows analogous ^1H NMR spectral data, confirming the chelate type of the formation of the complex: δ (ppm) 2.23 (s, 12H, $4CH_3$), 6.76 (t, 4H, $4C_6H_4(3)$, $^3J = 8$ Hz), 6.84 (t, 4H, $4C_6H_4(4)$, $^3J = 8$ Hz), 6.94 (d, 4H, $4C_6H_4(2)$, $^3J = 8$ Hz), 7.2 (d, 12H, $4C_6H_4(5)$, $4C_6H_4(2'6')$), 7.92 (d, 8H, $4C_6H_4(3'5')$, $^3J = 8$ Hz), 9.24 (t, 4H, (=CH–NH–, –CH=N–), $^3J(^{111}Cd-^1H) = 12$ Hz).

The composition M_3L_2 of the products formed may correspond to the chelate structures of any of two types: trinuclear (**IX**) or polymeric (**X**) complexes.



IX



X

The magnetic properties of complexes **IX** and **X** should be considerably different: the trinuclear clusters **IX** have a definite spin–spin exchange interaction of the antiferromagnetic type between the paramagnetic centers, which is impeded in the polymeric structures **X** [33]. In this respect, the study of structures of coordination units, as well as the inner-sphere influence of various heteroatoms (X) and substituents (R) on the physicochemical characteristics of the metal chelates obtained, was carried out using magnetochemical and EPR-spectral data.

Table 3
Magnetochemical data for copper complexes

T (K)	85.7	91.7	100.1	102.9	128.3	162.2	196.2	219.1	244.9	259.2	269.2	277.0	292.0
Compound **5** (X = 0, R = NO_2): $g = 2.09$; $J = -100$ cm^{-1}; $F = 0.2$; $R = 2.5\%$													
$\mu_{eff.exp.}$, B.M.	1.24	1.25	1.27	1.28	1.35	1.42	1.47	1.49	1.50	1.52	1.53	1.53	1.55
$\mu^{T}_{eff.}$, B.M.	1.23	1.24	1.27	1.27	1.35	1.41	1.46	1.49	1.51	1.51	1.52	1.53	1.55
T (K)	83.0	100.0	120.0	1.30	1.54	161.2	180.0	205.5	267.0	245.0	301.0		
Compound **6** (X = 0, R = Ph): $g = 2.15$; $J = -180$ cm^{-1}; $F = 0$; $R = 2.35\%$													
$\mu_{eff.exp.}$, B.M.	1.35	1.35	1.36	1.39	1.42	1.45	1.49	1.53	1.54	1.54	1.55		
$\mu^{T}_{eff.}$, B.M.	1.35	1.35	1.36	1.38	1.42	1.44	1.49	1.52	1.54	1.54	1.55		
T (K)	122.0	130.0	134.0	161.0	180.0	205.0	227.0	245.0	301.0				
Compound **7*** (X = 0, R = Ph): $g = 2.15$; $J = -140$ cm^{-1}; $F = 0$; $R = 2.29\%$													
$\mu_{eff.}$, B.M.	1.55	1.56	1.58	1.63	1.68	1.71	1.74	1.77	1.82				
$\mu^{T}_{eff.}$, B.M.	1.55	1.58	1.59	1.64	1.67	1.70	1.72	1.74	1.78				
T (K)	83.1	84.0	85.2	101.0	129.0	256.0	270.0	295.6					
Compound **8** (X = S, R = NO_2): $g = 2.2$; $J = -181$ cm^{-1}; $F = 0$; $R = 2.71\%$													
$\mu_{eff.exp.}$, B.M.	1.12	1.12	1.12	1.14	1.18	1.31	1.32	1.37					
$\mu^{T}_{eff.}$, B.M.	1.12	1.12	1.12	1.12	1.17	1.31	1.33	1.37					
T (K)	257.0	268.0	279.0	302.0									
Compound **9** (X = S, R = Ph): $g = 2.2$; $J < -300$ cm^{-1}; $F = 0$; $R = 2.25\%$													
$\mu_{eff.exp.}$, B.M.	0.98	0.98	0.99	1.01									
$\mu^{T}_{eff.}$, B.M.	0.98	0.98	0.99	1.01									
T (K)	100.0	252.0	265.0	283.0	301.1								
Compound **10*** (X = S, R = Ph): $g = 2.15$; $J < -300$ cm^{-1}; $F = 0$; $R = 2.20\%$													
$\mu_{eff.exp.}$, B.M.	0.98	0.98	0.99	1.01	1.01								
$\mu^{T}_{eff.}$, B.M.	0.98	0.99	0.99	1.00	1.00								
T (K)	83.6	110	130	146	1.69	188	255	272	300				
Compound **11** (X = NTs, R = NO_2): $g = 2.02$; $J = 355$ cm^{-1}; $F = 0.58$; $R = 2.20\%$													
$\mu_{eff.exp.}$, B.M.	1.51	1.51	1.52	1.51	1.53	1.54	1.53	1.50	1.52				
$\mu^{T}_{eff.}$, B.M.	1.50	1.50	1.51	1.51	1.51	1.51	1.53	1.53	1.54				
T (K)	83	100	119	140	160	182	201	220	260	273	304		
Compound No. **12** (X = NTs, R = Ph): $g = 2.02$; $J = -300$ cm^{-1}; $F = 0$; $R = 2.35\%$													
$\mu_{eff.exp.}$, B.M.	1.40	1.39	1.40	1.41	1.43	1.48	1.48	1.49	1.52	1.53	1.55		
$\mu^{T}_{eff.}$, B.M.	1.40	1.39	1.39	1.41	1.42	1.48	1.49	1.50	1.51	1.53	1.55		

It was established that the experimental effective magnetic moments $\mu_{eff.exp.}$ of all isolated copper complexes (Table 1, compounds **5**–**13**) at room temperature have magnitudes which are slightly lower as compared to the ones of pure spins (1.73 B.M.). The study of temperature dependence of their magnetic properties at 80–300 K revealed a symbiotic decrease of $\mu_{eff.exp.}$ with temperature (Table 3). This fact testifies the presence of a spin–spin exchange interaction of the antiferromagnetic type between Cu(II) ions. Such phenomena are characteristic for bi- and polynuclear structures and correlated with the trinuclear structure **IX** [34].

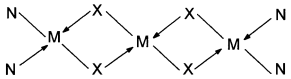
It is well known that magnetic properties of polynuclear complexes are determined by both their electronic structure and the geometric positions of the metal center and the ligands [33]. The presence of three paramagnetic centers in the molecule of a complex compound assumes several variants in their mutual positions, for example: in the tops of the equilateral triangle (D_{3h} symmetry), isosceles triangle (C_{2V} symmetry) or in the straight line ($C_{\infty V}$). A definite character of the spin–spin exchange interaction corresponds to each variant.

Good coincidence of the experimental and theoretical magnetic moments ($\mu_{eff.exp.}$ and $\mu_{eff.theor.}$, Table 3), calculated by using the model of isotropic exchange interaction of Geisenberg–Dirak–van Vlek [34], in approximation of the linear chain ($C_{\infty V}$), testifies that

the selected configuration (**IX**) is optimal for describing the mentioned exchange effects.

Deviation from the trinuclear structure **IX** was noted only for copper complexes with ligands **VI** and **VIII** containing the substituent R = NO_2. The molar ratio of the paramagnetic impurity (F) in these complexes, i.e. the polymeric form **X**, is 0.2 and 0.58, respectively (Table 3).

A considerable part of the polymeric form **X** in the copper complex with the ligand **VIII** is probably caused, additionally to the influence of the electron-acceptor substituent (R = NO_2), by the spatial conditions, created by bulky N–Ts fragments. A comparison of exchange parameters of bis-azomethines **VI**, **VIa**–**VIII**, **VIIIa** represents a peculiarity of magnetic properties of these compounds, caused by the nature of the bridge atoms X.



XI

X=O, S, N–Ts

As it is seen in Table 3, the constant of exchange interaction (J) is practically double on its absolute magnitude for complexes with bridge S atoms in comparison with those with O atoms. Taking into account the isostructural character of these compounds, it is possible to suppose that more considerable exchange interactions occur through the S-bridges due to the existence of free d-orbitals in S-atoms. It is known that the presence of sulfur atoms in a binuclear complex could lead to such strong increase of the exchange antiferromagnetic interaction that the complex becomes practically diamagnetic even at room temperature [33].

It is also necessary to mention the considerable value (conductivity) of spin–spin exchange interactions, occurring through X = N atoms ($J < -300$ cm^{-1}) (Table 3). Evidently, the identity of atoms of chelate and bridge connection in the coordination unit CuN_4 in comparison with the chelate environment in CuN_2O_2, as well as the presence of the sulfur atoms in the tosyl fragment, leads to maximum exchange between copper ions.

The magnitudes of exchange effect depend also on the character of the substituent R in the aldehyde fragment of ligands. They are considerably higher (Table 3) for the chelates with ligands **VIa**, **VIIa**, **VIIIa** (where R = Ph) in comparison with **VI**, **VII**, **VIII** (where R = NO_2). As it is seen, the role of electronic effects, created by R-substituents, is considerable for the existence of structures **IX** or **X**, as for magnetochemical characteristics of the complexes. This emphasizes the good electronic conductivity of the bond system and testifies indirectly for the planarization of trinuclear metal chelates. It was noted [35] that the introduction of a nitro group into the malondialdehyde fragment of bis-aryhydrazones could lead to a ferromagnetic exchange interaction between the copper ions.

The EPR spectral studies of copper complexes, obtained by both methods with all examined ligands at 80–300 K, confirm and complete the magnetochemical data. All EPR spectra of crystalline samples contain peaks of low intensity. The isotropic form of the peaks ($g = 2.117$–2.124), absence of hyperfine structure and anisotropy, typical for $S > 1/2$ state, testify for a composition of complexes having unusual number of copper atoms. This conclusion is also confirmed by the dependence of the intensity and the form of the spectra on the temperature. When the temperature is decreased from 300 to 80 K, the intensity and asymmetry of the peaks is increased. This fact could be related to an increase of occupancy of the spin level $S = 1/2$ and decrease of occupancy of the level $S = 3/2$ in trinuclear copper complexes with antiferromagnetic exchange interaction Cu–Cu–Cu (Fig. 1).

For complexes with even number of copper atoms, the decrease of temperature would lead to a decrease of the intensity of EPR peaks as a result of the increase of occupancy of the level ($S = 0$, in the case of antiferromagnetic exchange Cu–Cu). It is also necessary to mention that for O- and S-containing complexes (Table 1, compounds **7**–**12**) the intensity of EPR peaks of frozen DMF solutions is higher than those of the powders of these compounds. Such an effect is absent in the case of copper complexes with the ligand **VIII** (Table 1, X = NTs, compounds **13**–**15**). This fact could be related with both inner-molecular and inter-molecular exchange interaction of O- and S-containing chelates, taking place in crystals. At 77 K the inter-molecular interaction disappears.

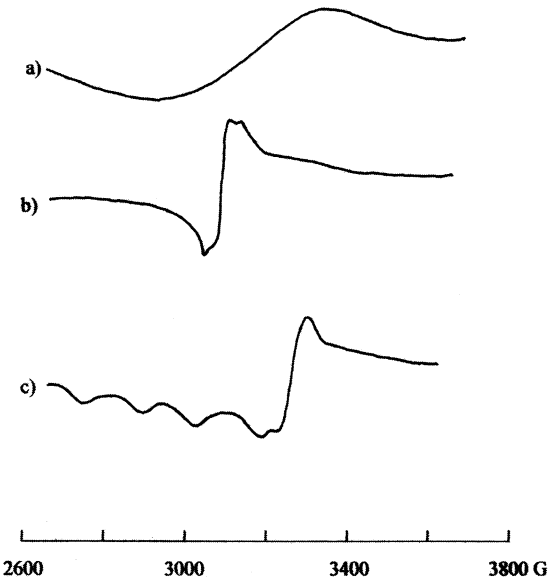


Fig. 1. X-band ESR spectra: a) polycrystalline **7** at room temperature, b) polycrystalline **7** at 80 K, c) **13** in DMF at 80 K

Absence of inter-molecular exchange effects in crystalline copper complexes with the ligands **VIII** and **VIIIa** (X = NTs) is, evidently related with spatial difficulties, caused by bulky tosyl groups. Spatial strains in these complexes leads also to their weak dissociation in DMF solution: in the frozen solutions of the complexes, additionally to intensive peaks of trinuclear metal chelates the anisotropic spectrum of a mononuclear copper complex ($g_{\parallel} = 2.211$, $g_{\perp} = 2.062$, $A_{\parallel} = 138$) with a hyper-fine structure on one copper nucleus ($I = 3/2$) is observed (Fig. 1). The magnitudes of the parameters of anisotropic spectrum of this mononuclear complex testify that the copper atom is in a distorted tetrahedral environment of nitrogen atoms [36]. Evidently, the spatial factor of tosyl groups is also an obstacle for its planarization.

The nickel and cobalt chelates show at room temperature the magnetic moments characteristic for high-spin ions (Table 1, compounds **14**, **15**, **17**, and **18**). Varying the temperature from 80 to 300 K, the magnitudes of $\mu_{\text{eff.exp.}}$ for these compounds are practically unchanged. Such magnetic properties of Ni(II) and Co(II) chelates can be explained taking into account the fact that the metal ions in a trinuclear chain **XI** are non-equivalent and have different electronic configuration. Really, two terminal ions have coordination units NiN_2X_2 and should be low-spin. At the same time, the central ion, arranged in a coordination unit of non-chelating bridge X-atoms (NiX_4), has a distorted high-spin tetrahedral structure. The resulting magnetic moment of complexes should correspond to the normal paramagnetism of one high-spin ion of Ni(II) and should practically not depend on the change of temperature that it is really observed.

Magnetic properties of Co(II) complexes can be interpreted using the same point of view. Taking into account the non-equivalency of three Co(II) ions in metal chelates, their $\mu_{\text{eff.exp.}}$ magnitudes should be 3.5–4.5 B.M., this corresponds to the experimental data (Table 1, compounds **17** and **18**).

4. Conclusions

The trinuclear metal chelates (M_3L_2) containing new tetradentate ligands β-aminovinylketones with aryl substituents with NTs, OH and SH groups at the nitrogen atom were obtained by conventional chemical and direct electrochemical synthesis. Magnetochemical and EPR studies testify for preferential realization of trinuclear structures with a spin–spin interaction of the antiferromagnetic type.

Acknowledgements

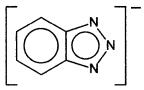
The authors are grateful to *Universidad Autónoma de Nuevo León*, Monterrey, México (project PAICyT CA263-01) and the *Russian Foundation for Fundamental Research* (grants 01-03-32538 and 00-15-97320) for financial support, to Dr G.S. Borodkin (*Rostov State University*, Russia) for preparation of NMR spectra, and to Professor Dr Juan Manuel Barbarín Castillo (U.A.N.L., México) for critical revision of this paper.

References

[1] J.E. Parks, R.H. Holm, Inorg. Chem. 7 (1968) 1408.
[2] H. Hennig, Z. Chem. 11 (1971) 81.
[3] S.V. Serbina, V.P. Kurbatov, O.A. Osipov, Zhurn. Neorg. Khim. 16 (1971) 1089.
[4] V.P. Kurbatov, S.V. Serbina, O.A. Osipov, Zhurn. Org. Khim. 43 (1973) 701.
[5] T.V. Torgova, O.A. Osipov, V.P. Kurbatov, N.A. Belonog, Zhurn. Org. Khim. 47 (1977) 896.
[6] T.V. Torgova, O.A. Osipov, V.P. Kurbatov, B.D. Vysotsky, Zhurn. Org. Khim. 49 (1979) 439.
[7] V.P. Kurbatov, T.V. Torgova, O.A. Osipov, Zhurn. Neorg. Khim. 26 (1981) 120.
[8] A.V. Kirichenko, V.P. Kurbatov, E.S. Kuharicheva, O.A. Osipov, Zhurn. Org. Khim. 55 (1985) 688.
[9] R. Knorr, H. Polzer, E. Bischler, J. Am. Chem. Soc. 97 (1975) 643.
[10] R. Knorr, A. Weiss, H. Polzer, E. Bischler, J. Am. Chem. Soc. 99 (1977) 650.
[11] R. Knorr, F. Ruf, J. Am. Chem. Soc. 101 (1979) 5424.
[12] W.S. Sheldrick, R. Knorr, H. Polzer, Acta Crystallogr., Sect. B 35 (1979) 739.
[13] R. Knorr, A. Weiss, Chem. Ber. 114 (1981) 2104.
[14] R. Knorr, F. Ruf, Angew. Chem. 96 (1984) 350.
[15] G.V. Panova, N.K. Vikulova, V.M. Potapov, Usp. Khim. 39 (1980) 1234.
[16] A.D. Garnovskii, V.P. Kurbatov, G.N. Lipunova, G.N. Sigeikin, Koord. Khim. 17 (1991) 1011.
[17] A.D. Garnovskii, A.L. Nivorozhkin, V.J. Minkin, Coord. Chem. Rev. 126 (1993) 1.
[18] L. Patrik, P.L. Holland, W.P. Tolman, J. Am. Chem. Soc. 121 (1999) 7270.
[19] P.L. Holland, W.P. Tolman, J. Am. Chem. Soc. 122 (2000) 6331.
[20] D.W. Randall, S.D.B. George, P.L. Holland, B. Hedman, K.O. Hodgson, W.B. Tolman, E.L. Solomon, J. Am. Chem. Soc. 122 (2000) 11632.
[21] A.I. Uraev, A.L. Nivorozhkin, V.P. Kurbatov, K.A. Lisenko, M.Yu. Antipin, A.D. Garnovskii, Koord. Khim. 26 (2000) 947.
[22] (a) W.A. Baker, F.T. Helm, J. Am. Chem. Soc. 97 (1975) 2295; (b) C.B. Singh, B. Sahoo, J. Inorg. Nucl. Chem. 36 (1974) 1259; (c) C.B. Singh, H.C. Rai, B. Sahoo, Indian J. Chem. 15 (1977) 691; (d) V.P. Kurbatov, T.V. Torgova, O.A. Osipov, N.A. Belonog, Koord. Khim. 7 (1981) 208.
[23] E.M. Padilla, J.H. Imamato, G.M. Jensen, Inorg. Chim. Acta 174 (1990) 209.
[24] A.D. Garnovskii, B.I. Kharisov, G. Gójon-Zorrilla, D.A. Garnovskii, Russ. Chem. Rev. 64 (1995) 201.
[25] A.D. Garnovskii, D.A. Garnovskii, A.S. Burlov, I.S. Vasilchenko, Mendeleev Chem. J. 40 (1996) 19.

[26] A.S. Burlov, L.I. Kuznetsova, D.A. Garnovskii, B.J. Kharisov, L.M. Blanco, V.V. Lukov, A.D. Garnovskii, J. Coord. Chem. 47 (1999) 467.
[27] V.P. Kurbatov, A.V. Khokhlov, A.D. Garnovskii, O.A. Osipov, L.A. Khulhachieva, Koord. Khim. 5 (1979) 351.
[28] P. Selwood, Magnetochemistry, 2nd ed., Interscience, New York, 1956.
[29] V.V. Skopenko (Ed.), Direct Synthesis of Coordination Compounds, VENTURY, Kiev, 1997, pp. 109–128.
[30] A.D. Garnovskii, B.I. Kharisov (Eds.), Direct Synthesis of Coordination and Organometallic Compounds, Elsevier Science, Amsterdam, 1999, pp. 73–134.
[31] A.D. Garnovskii, I.S. Vasilchenko, D.A. Garnovskii, Modern Aspects of the Synthesis of Metal Complexes, LAPO, Rostov-on-Don, 2000, p. 355.
[32] K. Nakamoto, IR-spectra of Inorganic and Coordination Compounds, Mir, Moscow, 1991, p. 531.
[33] Yu.V. Rakitin, Results of Science and Technology, vol. 10, VINITI, Moscow, 1986, p. 95.
[34] V.T. Kalinnikov, Yu.V. Rakitin, Introduction to Magnetochemistry, Nauka, Moscow, 1980, 240 pp.
[35] V.A. Kogan, V.V. Lukov, Koord. Khim. 19 (1993) 476.
[36] B.C. Tsukerblat, M.I. Belinsky, Magnetochemistry and Radiospectroscopy of Exchange Clusters, Shtiintsa, Kishinev, 1983, pp. 164–168.

dinuclear precursory species was also investigated and reported in this work.



(bta)

2. Experimental

2.1. Syntheses and preparation of compounds

Benzotriazole (btaH) was commercially purchased (1*H*-1,2,3-benzotriazole; 99%) and recrystallized from hot ethanol–water. The lithium benzotriazolate salt was prepared as described previously [6,8]. All other chemicals and organic solvents employed in the syntheses were analytical reagent grade and were used without further purification. Deionized water was used throughout the experiments.

The syntheses of *trans*-$[RuCl_2(NH_3)_4]Cl$ [13], $Ru(Hedta)H_2O$ [14], $Ru(Hedta)(btaH)$ [15] and $Li_n[Ru(edta)(L)]^{n-}$ ($L = btaH$, $n = 1$; $L = bta$, $n = 2$) [8–10] were based on the literature methods. The purity and characterization of the final products were assessed by means of elemental analysis, electronic spectroscopy and electrochemistry.

2.1.1. *trans*-$[Ru^{II}(NH_3)_4(btaH)_2](PF_6)_2$

The preparation of the mononuclear precursor was performed by an adaptation of the procedure published earlier for the pyrazine [16–19] analogue: 55 mg of *trans*-$[RuCl_2(NH_3)_4]Cl$ (0.20 mmol) were dissolved in approximately 5 ml of deionized water and reduced for 30 min with zinc amalgam, under an argon atmosphere. Then, the deep yellow solution of *trans*-$RuCl_2(NH_3)_4$ was anaerobically transferred by syringe techniques to a recipient containing 0.60 g of benzotriazole (5.0 mmol). The final orange solution was treated with approximately 5 ml of a concentrated solution of ammonium hexafluorophosphate, yielding a yellow precipitate. The solid product was collected on a filter, washed with cold ethanol and dried in vacuum for a couple of days in the presence of anhydrous calcium chloride. *Anal.* Found: C, 20.2; H, 3.5; N, 19.5. Required for $[Ru(NH_3)_4(C_6H_5N_3)_2](PF_6)_2\cdot H_2O$ ($MM = 715.4$ g mol^{-1}): C, 20.2; H, 3.4; N, 19.6%.

2.1.2. *trans*-$Na[(bta)(NH_3)_4Ru^{II}(bta)Ru^{III}(edta)]$

The unsymmetrical mixed-valent dinuclear complex was prepared and characterized in aqueous solutions. In the electrochemical experiments, 18 mg of *trans*-$[Ru(NH_3)_4(btaH)_2](PF_6)_2\cdot H_2O$ (2.5×10^{-2} mmol) was added into 5.0 ml of a deaerated, buffered solution (pH 7.0; pipes 5.0×10^{-2} M; where pipes = 1,4-piperazinediethanesulfonic acid) containing 12 mg of $Ru(Hedta)(H_2O)\cdot 4H_2O$ (2.5×10^{-2} mmol). The pH of the solution was adjusted to 9.0 by the controlled addition of 3.0 M sodium hydroxide solution under an argon atmosphere. The initial yellow mixture became brownish immediately and, eventually, deeply red at the completeness of the acid–base titration. In the spectroelectrochemical experiments, the aqueous solutions were also prepared as described above. However, 36 mg of *trans*-$[Ru(NH_3)_4(btaH)_2](PF_6)_2\cdot H_2O$ (5.0×10^{-2} mmol) and 24 mg of $Ru(Hedta)H_2O\cdot 4H_2O$ (5.0×10^{-2} mmol) were used instead.

The complex was also isolated in the solid form, for comparison purposes. The procedure was similar to the method reported for the pyrazine derivative [16] and consisted of mixing stoichiometric amounts of the starting complexes in aqueous solutions and, then, precipitating with the addition of acetone. Further treatment of the solid was carried out as described for the mononuclear precursor. *Anal.* Found: C, 30.2; H, 4.5; N, 19.3. Required for $Na[Ru(NH_3)_4(C_6H_4N_3)_2\text{-}Ru(C_{10}H_{12}N_2O_8)]\cdot 3H_2O$ ($MM = 871.8$ g mol^{-1}): C, 30.3; H, 4.4; N, 19.3%.

2.1.3. *trans*-$Na_2[(NH_3)_4Ru^{II}\{(bta)Ru^{III}(edta)\}_2]$

Analogously to the dinuclear species, the symmetrical mixed-valent trinuclear complex was prepared and characterized in aqueous solutions. All the solutions were generated by mixing the precursors *trans*-$[Ru(NH_3)_4(btaH)_2](PF_6)_2\cdot H_2O$ and $Ru(Hedta)(H_2O)\cdot 4H_2O$, at the 1:2 molar ratio, in 5.0 ml of deoxygenated buffer solution (5.0×10^{-2} M pipes; pH 7.0). Nevertheless, the employed amount of each starting complex for electrochemistry was half the quantity used for spectroelectrochemistry, in order to give solutions of the trinuclear complex with concentrations of 5.0×10^{-3} and 1.0×10^{-2} M, respectively. The pH of the mixture was then adjusted to 9.0 by addition, under argon, of 3.0 M sodium hydroxide, yielding a purple product.

To obtain the compound in the solid form, stoichiometric amounts of the starting species were mixed in aqueous solutions, at pH above 9, and precipitated with acetone after reaction. Further procedure was identical to the above description for the precursory complexes. *Anal.* Found: C, 29.6; H, 4.2; N, 15.0. Required for $Na_2[Ru(NH_3)_4(C_6H_4N_3)_2\{Ru(C_{10}H_{12}N_2O_8)]\cdot 4H_2O$ ($MM = 1302.0$ g mol^{-1}): C, 29.5; H, 4.0; N, 15.1%.

2.1.4. Preparation of solutions

For the physical measurements, 5.0×10^{-3} M (cyclic voltammetry) or 1.0×10^{-2} M solutions (spectroelectrochemistry) of the complexes were prepared in pipes buffer at the required pH (pH 7–10). The final pH was adjusted by adding microvolumes of 3.0 M sodium

hydroxide or hydrochloric acid. Sodium trifluoroacetate (0.10 M) and potassium nitrate (0.25 M) were employed as supporting electrolytes in cyclic voltammetry and spectroelectrochemistry, respectively. Solutions of Na(tfa) (where tfa = trifluoroacetate) were prepared by titration, up to neutrality, of diluted solutions (0.10 M) of trifluoroacetic acid with 3.0 M sodium hydroxide.

2.1.5. General precautions

In order to minimize the absorption by water in the near-infrared (NIR) region of the spectra, D_2O was used as solvent. All measurements at pH above 6.5 were run under an inert atmosphere of argon, to avoid further oxidation processes involving the edta–ruthenium(III) complex [20].

2.2. Physical measurements

Electronic spectra were recorded either on a Hewlett–Packard 8453 diode-array spectrophotometer or on a Guided-Wave 260 fiber-optic instrument.

Cyclic voltammetry measurements were carried out using a PAR 283 potentiostat. A conventional three-electrode arrangement consisting of a glassy carbon working electrode, a Luggin capillary with a Ag/AgCl (1.0 M KCl) reference electrode ($E^\circ = +0.222$ V vs. SHE, standard hydrogen electrode) and a platinum wire as the auxiliary electrode, was used. Cyclic voltammograms were recorded at sweep rates of 10–500 mV s^{-1}. The sample solutions were thoroughly degassed with argon prior to each measurement. $E_{1/2}$ values given in this paper are uncorrected for junction potentials.

Spectroelectrochemical measurements in the UV–Vis region were carried out using a PAR 366 bi-potentiostat in parallel with the diode-array spectrophotometer. A three-electrode system was specially designed for a rectangular quartz cell of 0.25 mm internal optical length. A gold minigrid was used as a transparent working electrode, in the presence of a small Ag/AgCl (1.0 M KCl) reference electrode and a platinum auxiliary electrode. The OTTLE cell was located directly in the spectrophotometer, and the absorption was monitored during the electrolysis.

Spectroelectrochemical measurements in the NIR region were performed by using a fiber-optic probe for in situ monitoring in a quartz, flat bottom, electrochemical cell. The fiber-optic probe was placed perpendicularly to the mirror surface of the platinum electrode, which was kept approximately 0.2 mm from the bottom, providing a constant optical length.

pH measurements were monitored with a Digimed MD21 digital pH meter. Calibration was carried out by using commercial standard buffers.

Elemental analyses were obtained by the Microanalytical Laboratory of the Institute of Chemistry, University of São Paulo.

2.3. Computational calculations

Semiempirical molecular calculations were carried out as described in details elsewhere [21,22], by using Zerner's geometric implementation of the Intermediate Neglect Differential Overlap method (ZINDO/1) [23] within the HYPERCHEM™-5.1 program from Hypercube Inc. [24]. The default resident parameterization was kept. Quantum mechanics geometry optimizations were performed at the RHF (Restricted Hartree–Fock) and UHF (Unrestricted Hartree–Fock) levels for the low-spin, closed-shell (Ru^{II}) and open-shell (Ru^{III}) ground state species, respectively. The starting nuclear coordinates used here were obtained from the geometry optimizations at molecular mechanics level by using the MM+ module, a modified MM2 force field [25] within HYPERCHEM™. A gradient of 1×10^{-2} cal $Å^{-1}$ mol^{-1} was set as a convergence criterion in all the molecular mechanics and quantum calculations, which were processed on a PC WINDOWS® platform with a Pentium® III microprocessor.

3. Results and discussion

Despite the emphasis on the mixed-valence di- and trinuclear systems, the characterization of the mononuclear precursor was found to be necessary in order to understand the properties of the polynuclear complexes.

Note: since herein all derivatives containing the tetraammineruthenium(II/III) fragment are *trans* with regard to their coordination geometry, the *trans* prefix which should appear as a notation along with the formulas was neglected in this section.

3.1. Mononuclear complexes

Analogously to pentaamminechlororuthenium(II) [26], the starting complex $Ru^{II}Cl_2(NH_3)_4$ reacts promptly in an aqueous solution to form $[Ru^{II}(H_2O)_2(NH_3)_4]^{2+}$ (**1**). This aqua complex is labile and easily exchanges the ligand water in the presence of N-heterocyclic ligands, yielding the corresponding disubstituted species Eq. (2).

$$[Ru(H_2O)_2(NH_3)_4]^{2+} + L \rightleftharpoons [Ru(H_2O)(NH_3)_4(L)]^{2+} + H_2O \quad (1)$$

$$[Ru(H_2O)(NH_3)_4(L)]^{2+} + L \rightleftharpoons [Ru(NH_3)_4(L)_2]^{2+} + H_2O \quad (2)$$

In the particular case with L = benzotriazole, the two-step formation reaction of $[Ru(NH_3)_4(btaH)_2]^{2+}$ follows $k_1 = 1.9 \pm 0.2 \times 10^2$ M^{-1} s^{-1} and $k_2 = 0.28 \pm 0.03$ M^{-1} s^{-1} ($T = 25 \pm 1$ °C; $I = 0.10$ M; pH 4.5) [27]. This result shows that the second step is rather slower than

the first substitution, which can be interpreted in terms of the so-called *trans* effect. The reaction mechanism is essentially dissociative, near the S_N1 limit [27].

The cyclic voltammograms of the benzotriazole-disubstituted complex in a slightly acidic solution (pH 4.5) exhibited a single reversible wave couple with $E_{1/2} = 0.20$ V (vs. SHE). In acidic medium, the oxidized species displays a red color, and its absorption spectrum in the Vis region shows a single band at 510 nm (2.1×10^3 M^{-1} cm^{-1}), which was assigned to a ligand-to-metal charge transfer (LMCT) involving the transition $\pi(\text{btaH}) \rightarrow d\pi(Ru^{III})$. The corresponding reduced species absorbs at 425 nm (9.0×10^3 M^{-1} cm^{-1}), whose band was associated with a metal-to-ligand charge transfer (MLCT) related to the $d\pi(Ru^{II}) \rightarrow \pi^*(\text{btaH})$ transition.

If the pH of a solution of $[Ru(NH_3)_4(btaH)_2]^{2+}$ is raised to 8.5–9.0, its color changes from yellow to dark orange. Such variation was ascribed to the deprotonation of the coordinated ligands, as shown in Eqs. (3) and (4).

$$[Ru(NH_3)_4(btaH)_2]^{2+} \rightleftharpoons [Ru(NH_3)_4(btaH)(bta)]^{+} + H^{+} \quad (3)$$

$$[Ru(NH_3)_4(btaH)(bta)]^{+} \rightleftharpoons Ru(NH_3)_4(bta)_2 + H^{+} \quad (4)$$

Both pK_a values for the equations above were determined ($pK_{a1} = 6.0$ and $pK_{a2} = 8.6$) by means of spectrophotometric titrations, whose acid–base equilibrium constants are equivalent to 1.0×10^{-6} and 2.5×10^{-9} M, respectively [27]. The calculations of K_{a1} and K_{a2} followed a method of graphical analysis for successive equilibria [28].

The constants indicate a substantial stabilization of $[Ru(NH_3)_4(btaH)(bta)]^{+}$ ($pK_a = 6.0$) over the uncoordinated anion, since the pK_a of the free ligand is 8.38 ± 0.03 ($T = 25$ °C; $I = 0.0$) [29]. On the other hand, the second deprotonation of the complex reflects no additional stabilization on the involved ligand within $Ru(NH_3)_4(bta)_2$ ($pK_a = 8.6$). Indeed, the latter process occurs with a slight destabilization in comparison with the free benzotriazolate. That is because the extra charge from the first deprotonation is partially transmitted through the $L \rightarrow Ru \rightarrow LH$ axis, increasing significantly the electron density on the LH molecule and, consequently, the nucleophilicity. In addition to the manifestation of *trans* effects, the π-back-donation features of the Ru(II) ion ($4d^6$; low-spin) attenuate the acid character of the complex.

The cyclic voltammograms of the complex are also sensitive to the pH of the solution, with redox potentials ($E_{1/2}$) ranging from 0.20 V at pH 4.5 (protonated complex) to ~0.05 at pH > 9 (deprotonated complex). By using these reduction potentials for the couples $[Ru^{III/II}(NH_3)_4(btaH)_2]^{3+/2+}$ and $[Ru^{III/II}(NH_3)_4(bta)_2]^{+/0}$, respectively, and assuming that $pK_{a1} = 6.0$, the value of pK_{a2} was estimated from the square thermodynamic cycle as 8.5, which is in accordance with the value (8.6) obtained by spectrophotometry. Electronic spectra from spectroelectrochemical measurements at pH 9.5 showed a MLCT absorption band at 410 nm (7.0×10^3 M^{-1} cm^{-1}), associated with the $d\pi(Ru^{II}) \rightarrow \pi^*(\text{bta})$ transition in $Ru^{II}(NH_3)_4(bta)_2$, and a LMCT band at 515 nm (2.2×10^3 M^{-1} cm^{-1}), attributed to the transition $\pi(\text{bta}) \rightarrow d\pi(Ru^{III})$ in the species $[Ru^{III}(NH_3)_4(bta)_2]^{+}$.

For assignment purposes and comparison with the mononuclear $[Ru(NH_3)_4(L)_2]^{n+}$ complexes, the redox potentials for the starting species (L = Cl^- and H_2O) are given: −0.18 and 0.02 V, respectively [18]. In addition, the MLCT lambda and the half-potential for the analogue containing L = pyrazine (pz) are 485 nm [19] and 0.78 V [18].

The set of results shown above point at the same time to the σ/π-donor electronic character of the anion benzotriazolate (comparable with imidazole derivatives [8,9,15]), and the π-acceptor character of neutral benzotriazole (which places it close to pyridine [18,19,30]), as revealed by their redox properties. These features are stressed below in the context of the mixed-valence chemistry and the characteristics of benzotriazolate as a bridging ligand.

Unlike some monosubstituted ruthenium [10,11] and iron [12] complexes with benzotriazole or benzotriazolate (in aqueous solutions), no evidence of linkage isomerism was observed herein for the disubstituted species $[Ru^{III/II}(NH_3)_4(btaH)_2]^{3+/2+}$ or $[Ru^{III/II}(NH_3)_4(bta)_2]^{+/0}$. As a matter of fact, linkage isomers were also recently observed in organic solutions for *cis*-$[Ru^{III/II}Cl(bpy)_2(btaH)]^{2+/+}$ but not for the disubstituted complex, *cis*-$[Ru^{III/II}(bpy)_2(btaH)_2]^{3+/2+}$ [31]. Therefore, the set of systems studied with benzotriazole clearly shows that disubstitution of complexes of both types *cis*- and *trans*-$[MX_4L_2]$ inhibits the expected isomerization reaction: $M-\{\kappa N(1)-L\} \rightleftharpoons M-\{\kappa N(2)-L\}$ (L = btaH or bta) [32]. This particular aspect of such systems will be explored in a separate work.

In the light of theoretical studies [31], the isomer $[(NH_3)_4Ru^{III/II}\{\kappa N(1)\text{bta}\}_2]^{+/0}$ should most likely exist, due to a higher basicity–donicity on the nitrogen atom N(1). Hence, since there is an electrochemical indication on the presence of a single species at both oxidation states (at several pH), only the mentioned $\kappa N(1)$ isomer is to be considered herein.

Prior to advancing to the next sections on polynuclear complexes based on the mononuclear species introduced above, another important issue concerning the structure of this precursor must be addressed. That is because it has two possible molecular geometries: C_{2h} and C_{2v}. In fact, other isomers of lower symmetry can exist, and their presence depend on the reciprocal/relative rotation of both ligands around the *trans* (L–M–L) axis. Based on structural data for similar compounds, which show

that the coplanar conformation prevails in the most electronically stable structures, only the two mentioned major symmetries were taken into account in this consideration.

In order to gain some theoretical insight into the relative stability of the isomers, quantum calculations at the semiempirical level (see Sections 2 and 2.3 for computational details) were carried out by assuming both molecular symmetries: C_{2h} (isomer **A**) and C_{2v} (isomer **B**); see illustration in Fig. 1.

According to ZINDO results for the geometry-optimized molecules, the isomer **A** is about 3 kcal mol^{-1} more stable than isomer **B**. On the basis of this argumentation, only the structure **A** was considered for the assumptions of this work.

3.2. Dinuclear complexes

The mixture of $[(btaH)Ru^{II}(NH_3)_4(bta)]^+$ with $[Ru^{III}(edta)(H_2O)]^-$ at the molar ratio 1:1 in aqueous solution yields, at pH around 7, a deeply brownish species. The reaction was promoted by adding slowly a solution of $[Ru^{III}(edta)(H_2O)]^-$ over another containing $[(btaH)Ru^{II}(NH_3)_4(bta)]^+$ at the same concentration and, then, adjusting the pH of the buffered mixture to 9.0 under an argon atmosphere. At these medium conditions, the cyclic voltammograms exhibited two reversible wave couples of identical intensities, displaying linear response with respect to the square root of the scan rates. The calculated half-potentials ($E_{1/2}$) are $E_1 = 0.15$ V and $E_2 = -0.21$ V versus SHE, both with $\Delta E_p = 60$ mV.

By comparison of these results with the redox potentials for the Ru^{III}/Ru^{II} couple in the reagents $Ru(NH_3)_4(bta)_2$ (0.05 V) and $[Ru(edta)(H_2O)]^-$ (−0.05 V; Section 3.3) under similar conditions, the formation of a new unsymmetrical dinuclear complex, formulated as $[(bta)(NH_3)_4Ru^{II}(bta)Ru^{III}(edta)]^-$, was

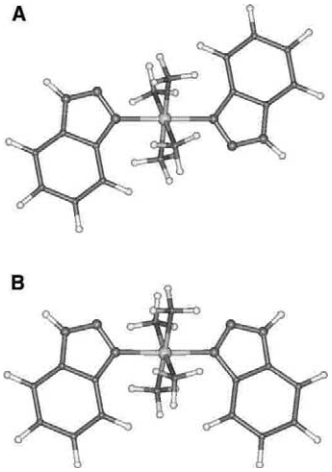


Fig. 1. Theoretical molecular structure for the C_{2h} (**A**) and C_{2v} (**B**) geometric isomers of the complex *trans*-$[Ru(NH_3)_4(btaH)_2]^{2+}$.

electrochemically evidenced. Therefore, the two redox potentials E_1 and E_2, which are separated by $\Delta E_{1/2} = 0.36$ V, refer to the following monoelectronic reduction steps:

$$(bta)Ru_a^{III}(bta)Ru_b^{III} + e^- \rightleftharpoons [(bta)Ru_a^{II}(bta)Ru_b^{III}]^- \quad (5)$$

$$[(bta)Ru_a^{II}(bta)Ru_b^{III}]^- + e^- \rightleftharpoons [(bta)Ru_a^{II}(bta)Ru_b^{II}]^{2-} \quad (6)$$

where $Ru_a = \{Ru(NH_3)_4\}$ and $Ru_b = \{Ru(edta)\}$.

As for the analysis of these potentials, an increase of ~0.2 V on the $E_{1/2}$ value for the couple $[Ru^{III/II}(NH_3)_4(bta)_2]^{+,0}$ was realized following the binding of $[Ru^{III}(edta)]^-$. In contrast, the dimer formation is accompanied by a decrease of more than 0.1 V on the value of $E_{1/2}$ for $[Ru^{III/II}(edta)(bta)]^{2-,3-}$ (−0.09 V; [15]). These observations reflect the influence of the π-backbonding effects through the Ru_a^{II}–bta bonding, induced by the Ru_b^{III} fragment attached to the bridging ligand. The same trend applies to the charge-transfer properties to be discussed below.

Another important indication of the existence of a dinuclear complex comes from the presence of a strong electronic absorption band in the NIR region. Given the redox states of the starting mononuclear and aqua complexes (Ru^{II} and Ru^{III}, respectively), this observation is consistent with the formation of a mixed-valent species, where the NIR band is related to the intervalence charge-transfer (IVCT) transition.

Spectroelectrochemistry in the NIR region confirmed that the band at 1510 nm appears only if the system is submitted to a potential between E_1 and E_2, with the absorption reaching the maximum intensity (1.6×10^3 M^{-1} cm^{-1}) around −0.03 V, the middle point between the two redox potentials (E_1 and E_2) obtained from the cyclic voltammograms. Under potentials above or below that value, the absorptivity decreases gradually up to the complete disappearance of the band at positive (> 0.4 V) and negative (< −0.5 V) regions.

The spectroelectrochemical behavior described above is dependent on the presence of a reduced (Ru_a^{II}) and an oxidized (Ru_b^{III}) redox center, which is coherent with an IVCT process inherent to the mixed-valent species:

$$[(bta)Ru_a^{II}(bta)Ru_b^{III}]^- \xrightarrow{h\nu} [(bta)Ru_a^{III}(bta)Ru_b^{II}]^- \quad (7)$$

Following the photo-induced intervalence transfer, an inverse electron transfer process through a thermal pathway is expected to take place (i.e. $[(bta)Ru_a^{III}(bta)Ru_b^{II}]^- \rightarrow [(bta)Ru_a^{II}(bta)Ru_b^{III}]^-$), since the system is unsymmetrical and there is a driving force, ΔG° or ΔE_0 (see comparison for the reduction potentials of each moiety), favoring the electronic isomer $[(bta)(NH_3)_4Ru^{II}(bta)Ru^{III}(edta)]^-$.

The thermodynamic stability of the mixed-valent complex relative to the isovalent species can be estimated from the comproportionation equilibrium constant (K_c) associated with the reaction:

$$(bta)Ru_a^{III}(bta)Ru_b^{III} + [(bta)Ru_a^{II}(bta)Ru_b^{II}]^{2-} \rightleftharpoons 2\,[(bta)Ru_a^{II}(bta)Ru_b^{III}]^{-} \quad (8)$$

Calculation of K_c [33] by assuming a redox separation ($\Delta E_{1/2}$) of 0.36 V results a value of 1.2×10^6, which corresponds to a comproportionation free energy (ΔG_c) of -8.3 kcal mol^{-1}.

In spite of the high stability of the mixed-valent complex, as shown by the thermodynamic parameters, according to the criteria established by the perturbational formalism of Hush [34] this system features localized oxidation states (class II, within the classical Robin–Day scheme [35]) if one takes into account the fact that (i) the experimental half-bandwidth (5.5×10^3 cm^{-1}) is larger than the theoretical [34,36] value (3.9×10^3 cm^{-1}); (ii) the IVCT band is solvatochromic (even though the solubility of the complex is very poor in organic solvents, preventing a more systematic solvent-dependence study to be performed).

Based on these considerations, the Mulliken–Hush theory [34] applies adequately to the estimation of the electronic coupling energy (H_{ab}) ground state electron delocalization degree (α^2) from the observed IVCT band parameters, through the Eqs. (9) and (10), respectively [34,36].

$$H_{ab} = 2.05 \times 10^{-2} \left(\frac{\varepsilon_{max} \Delta \bar{\nu}_{1/2} \bar{\nu}_{max}}{d^2} \right)^{1/2} \quad (9)$$

$$\alpha^2 = \left(\frac{H_{ab}}{\bar{\nu}_{max}} \right)^2 \quad (10)$$

In these formulas, the energy at the maximum optical absorption (ν_{max}), the molar absorptivity (ε_{max}), and the bandwidth at half-height ($\Delta\nu_{1/2}$) for the IVCT band of the mixed-valent species, $[(bta)(NH_3)_4Ru^{II}$-$(bta)Ru^{III}(edta)]^-$ are 6.6×10^3 cm^{-1}, 1.6×10^3 M^{-1} cm^{-1}, and 5.5×10^3 cm^{-1}, respectively. The electron transfer distance d is roughly assumed to be the metal–metal geometric separation (5.7 Å) and was extracted from the theoretical calculations (see Sections 2 and 2.3 for computational details).

The H_{ab} and α^2 parameters were, in this way, calculated as 870 cm^{-1} and 0.017, respectively. Even though this system exhibits a trapped-valence configuration, the magnitude for the resonance energy, H_{ab} is quite remarkable for this type of complex, surpassing most of similar class II systems and approaching some values previously reported for mixed-valence systems with charge delocalization [9]. In this context, an illustrative comparison is provided below along with the trinuclear species.

In addition to the NIR band, the spectral changes in the UV–Vis region were also monitored by means of spectroelectrochemical experiments. The results can be summarized as follows: if the applied potential corresponds to the fully oxidized species, $Ru_a^{III}Ru_b^{III}$, then two bands are observed at 610 nm (1.2×10^3 M^{-1} cm^{-1}) and $\sim$380 nm (1.0×10^3 M^{-1} cm^{-1}); they were assigned to LMCT bands associated with the chromophores $\{Ru^{III}(NH_3)_4(bta)_2\}$ and $\{Ru^{III}(edta)(bta)\}$, respectively, by analogy with the spectra and the redox potentials of the mononuclear species (Table 1 and Section 3.1). In contrast, for the fully reduced species, $Ru_a^{II}Ru_b^{II}$, a single absorption band is defined at 455 nm (2.3×10^3 M^{-1} cm^{-1}); it arises simultaneously with the disappearance of the band at 610 nm and thus corresponds to the MLCT on the ammine moiety, $\{Ru^{II}(NH_3)_4(bta)_2\}$. The analogous band for the edta moiety occurs below 350 nm and is probably obscured by the intraligand $\pi \rightarrow \pi^*$ transitions.

At potentials applied in the intermediate dominion delimited by E_1 and E_2, i.e. upon electrolytic generation of the mixed-valent state, a rather more complex spectrum is displayed in the range from 350 to 550 nm. By using deconvolution methods, it was shown that one of the bands refers to the shift of the LMCT band for $\{Ru^{III}(edta)(bta)\}$ to 540 nm ($\sim 8.0 \times 10^2$ M^{-1} cm^{-1}) by virtue of the reduction of the ammineruthenium fragment, which in turn promotes the energy raise of the π-HOMO levels of benzotriazolate (L_b) by means of π-backbonding interactions. The same reasoning explains why the MLCT band for $\{Ru(NH_3)_4(bta)_2\}$ appears shifted (with regard to the fully reduced dimer) to the red (500 nm). Such redox behavior in the UV–Vis region is typical of a mixed-valent species with significant electronic coupling [8,9], and is caused by the perturbation of the frontier orbitals/electronic levels at each of the donor–acceptor centers in reference to the isovalent reduced and oxidized species (Table 1).

3.3. Trinuclear complexes

The mixture of $Ru^{II}(NH_3)_4(bta)$ and $[Ru^{III}(edta)(H_2O)]^-$ at the 1:2 molar ratio in basic (pH > 9) aqueous solutions reacts to yield a purple product, which was found to be the trinuclear complex. Like previous procedure [16,17], excess $[Ru(edta)(H_2O)]^-$ (ca. 1 equiv.; 1:3 molar ratio) was added to the solutions to ensure the completeness of the substitution reactions (Eqs. (11) and (12)), although the use of stoichiometric amounts also gives the quantitative formation of the very stable mixed-valent trinuclear species.

$$(bta)Ru_a^{II}(bta) + [Ru_b^{III}(H_2O)]^- \rightleftharpoons [(bta)Ru_a^{II}(bta)Ru_b^{III}]^- + H_2O \quad (11)$$

$$[(bta)Ru_a^{II}(bta)Ru_b^{III}]^- + [Ru_b^{III}(H_2O)]^- \rightleftharpoons [Ru_a^{II}\{(bta)Ru_b^{III}\}_2]^{2-} + H_2O \quad (12)$$

The cyclic voltammograms of a 1:3 mixture, for instance, display three pairs of reversible waves (labeled

Table 1
Electrochemical and spectroscopic parameters for the mono-, di- and trinuclear complexes [a]

Complex [a,b]	$E_{1/2}$ (V) [c]		MLCT (nm) (ε ($dm^3\ mol^{-1}\ cm^{-1}$))		LMCT (nm) (ε ($dm^3\ mol^{-1}\ cm^{-1}$))	
	Ru_a	Ru_b	Ru_a	Ru_b	Ru_a	Ru_b
$[Ru^{II,III}(NH_3)_4(btaH)_2]^{2+,3+}$	0.20		425 (9.0×10^3)		510 (2.1×10^3)	
$[Ru^{II,III}(NH_3)_4(bta)_2]^{0,+}$	0.05		410 (7.0×10^3)		515 (2.2×10^3)	
$[Ru^{II,III}(edta)(btaH)]^{2-,-}$ [d]		0.10		400 (6.5×10^3)		350 (sh) [e]
$[Ru^{II,III}(edta)(bta)]^{3-,2-}$ [d]		−0.09		395 (6.0×10^3)		510 (1.5×10^3)
$[(bta)(NH_3)_4Ru^{II}(bta)Ru^{II}(edta)]^{2-}$	0.15	−0.21	455 (2.3×10^3) [f]	< 350 (sh) [g]		
$[(bta)(NH_3)_4Ru^{II}(bta)Ru^{III}(edta)]^{-}$	0.15	−0.21	500 (~ 2.0×10^3) [g]			540 (~ 8.0×10^2) [h]
$(bta)(NH_3)_4Ru^{III}(bta)Ru^{III}(edta)$	0.15	−0.21			610 (1.2×10^3) [i]	~ 380 (~ 1.0×10^3) [h]
$[(NH_3)_4Ru^{II}\{(bta)Ru^{II}(edta)\}_2]^{4-}$	0.15	−0.22	460 (2.4×10^3)	~ 300 (sh)		
$[(NH_3)_4Ru^{II}\{(bta)Ru^{III}(edta)\}_2]^{2-}$	0.15	−0.22	~ 500 (~ 2.0×10^3)			540 (~ 1.6×10^3) [j]
$[(NH_3)_4Ru^{III}\{(bta)Ru^{III}(edta)\}_2]^{-}$	0.15	−0.22			600 (1.3×10^3)	400 (~ 2.1×10^3) [j]

[a] Abbreviations: Ru_a = *trans*-{$Ru(NH_3)_4$}, Ru_b = {Ru(edta)}, btaH = benzotriazole, bta = benzotriazolate.
[b] While the two benzotriazolate ligands are not equivalent in the dinuclear complex, which is of the type *trans*-$[(L_p)(NH_3)_4Ru(L_b)Ru(edta)]^n$ (with L_p = peripheral ligand and L_b = bridging ligand), they are equivalent in the trinuclear complex, which is of the type *trans*-$[(NH_3)_4Ru\{(L_b)Ru(edta)\}_2]^n$ (with both ligands acting as bridging ligands).
[c] Potential vs. SHE.
[d] Ref. [15].
[e] Ru ($d_\pi \rightarrow d_\sigma$) transition [15].
[f] $Ru(II) \rightarrow L_p$.
[g] $Ru(II) \rightarrow L_b$.
[h] $L_b \rightarrow Ru(III)$.
[i] $L_p \rightarrow Ru(III)$.
[j] It must be taken into account the fact that the absorptivity of this transition is about twice the one of the dinuclear analogue due to the two terminal non-interacting {Ru(edta)(bta)$^-$} moieties.

as **I**, **II**, and **III** in Fig. 2) with half-potentials at 0.15, −0.05 and −0.22 V, respectively. The waves **III** present current intensities twice higher than waves **I** (Fig. 2).

By analogy with the $E_{1/2}$ values for the mono- and dinuclear species (Table 1), the observed potentials were assigned to the following redox couples:

$$\textbf{(I)}\ [Ru_a^{III}\{(bta)Ru_b^{III}\}_2]^- + e^- \rightleftharpoons [Ru_a^{II}\{(bta)Ru_b^{III}\}_2]^{2-} \quad (13)$$

$$\textbf{(II)}\ [Ru_b^{III}(H_2O)]^- + e^- \rightleftharpoons [Ru_b^{II}(H_2O)]^{2-} \quad (14)$$

$$\textbf{(III)}\ [Ru_a^{II}\{(bta)Ru_b^{III}\}_2]^{2-} + 2e^- \rightleftharpoons [Ru_a^{II}\{(bta)Ru_b^{II}\}_2]^{4-} \quad (15)$$

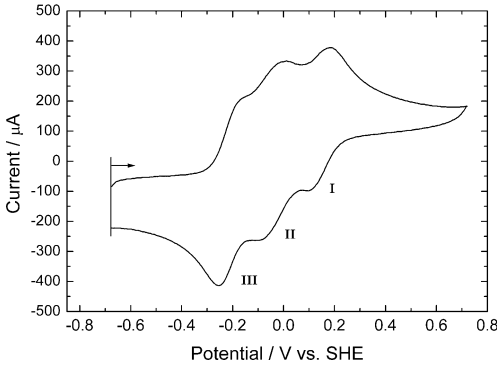


Fig. 2. Cyclic voltammograms of *trans*-$[(NH_3)_4Ru\{(bta)Ru(edta)\}_2]^{n-}$ ($n = 1$, 2, or 4) in aqueous solutions ($c = 2.0 \times 10^{-2}$ M; *I*, KNO_3 0.25 M; pH 9.5).

Despite the quite significant electronic interaction between the adjacent terminal (Ru_b) and central (Ru_a) redox centers (whose potentials are indeed rather similar to the ones for the dinuclear species), the direct communication between the identical peripheral ruthenium–edta units must be negligible, since there is no measurable split in their half-potentials ($\Delta E_{1/2} < 30$ mV) and thus they are both reduced practically at the same redox potential (−0.22 V), as can be deduced from the voltammograms (Fig. 2).

NIR spectroelectrochemistry showed that the IVCT spectral features are also similar to the dinuclear species (Fig. 3), with a strong absorption band at 1530 nm ($1.9 \times 10^3\ M^{-1}\ cm^{-1}$) under application of potentials between **I** and **III** (mixed-valent state; $Ru_b^{III}Ru_a^{II}Ru_b^{III}$). At potentials above **I** or below **III**, the absorptivity vanishes gradually due to the electrolytic generation of the fully oxidized, $Ru_b^{III}Ru_a^{III}Ru_b^{III}$, and fully reduced species, $Ru_b^{II}Ru_a^{II}Ru_b^{II}$, respectively, which do not absorb in the NIR region (Fig. 3).

As mentioned, the electrochemical and NIR spectral properties presented above for the di- and the trinuclear complexes are quite similar. The main changes that arises upon passing from $[(bta)Ru_a^{II}(bta)Ru_b^{III}]^-$ to $[Ru_b^{III}(bta)Ru_a^{II}(bta)Ru_b^{III}]^{2-}$ are basically (i) an increase of 10 mV on the redox separation $\Delta E_{1/2}$ (0.37 V) between E_1 (**I**) and E_2 (**III**), due to a cathodic shift of the half-potential centered on the Ru_b center, (ii) a lower-energy shift of 20 nm and an increase of absorptivity

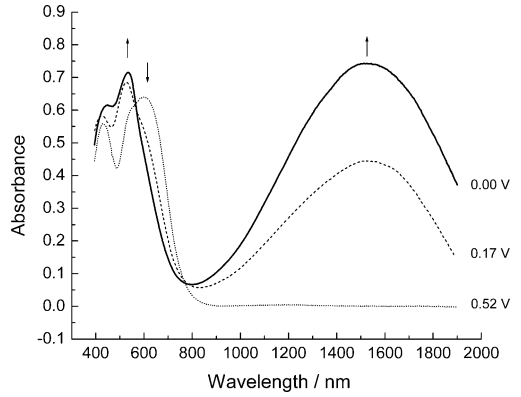


Fig. 3. Electronic spectra of *trans*-$[(NH_3)_4Ru\{(bta)Ru(edta)\}_2]^{n-}$ ($n = 1$, 2, or 4) in D_2O solutions under application of potentials ($c = 2.0 \times 10^{-2}$ M; I, KNO_3 0.25 M; pH 9.5; $l = 0.24$ mm; applied potentials vs. SHE are indicated in the figure).

($\Delta\varepsilon_{max} = 3 \times 10^2$ M^{-1} cm^{-1}) on the IVCT band. These slight differences can be rationalized partially in terms of coordination effects of the additional negatively charged ruthenium–edta unit with regard to the dinuclear precursor, and partially by an enhancement of electron delocalization following the increasing nuclearity of the system.

By taking the properties of the IVCT band ($\nu_{max} = 6.5 \times 10^3$ cm^{-1}, $\varepsilon_{max} = 1.9 \times 10^3$ M^{-1} cm^{-1}, and $\Delta\nu_{1/2} = 5.6 \times 10^3$ cm^{-1}) and the theoretical intermetallic distance ($d = 5.7$ Å; see illustration in Fig. 4) into the Eqs. (9) and (10), the parameters H_{ab} and α^2 were calculated as 945 cm^{-1} and 0.021, respectively. These results are rather interesting because they reveal that the extent of electronic coupling (and so the delocalization) is significantly enlarged in the symmetrical trinuclear system. Its mixed-valence properties are summarized in Table 2 along with the dinuclear species and other literature analogues, for comparison purposes.

As discussed briefly in Section 3.2, although these systems behave consistently with a localized oxidation states description (on the Hush model basis), the magnitude of H_{ab} is remarkable for both mixed-valent di- and trinuclear complexes. An illustrative comparison is provided by the trinuclear analogue with pyrazine as bridging ligand, $[Ru_b^{III}(pz)Ru_a^{II}(pz)Ru_b^{III}]$, whose spectra display no evidence of IVCT band (i.e. with absorption higher than 1×10^2 M^{-1} cm^{-1}) in the NIR region [16], which means that the electronic coupling is negligible in that system (in this case, the large $\Delta E_{1/2}$ of ca. 0.6 V shown in Table 2 comes primarily from the redox asymmetry of the complex). Besides, the systems reported herein are very stable at all the isovalent and mixed-valent states with respect to disproportionation, whereas the literature analogues are electrostatically unstable at some of the oxidation states, as is the case of the pyrazine example given by the replacement of the terminal units Ru_b with pentacyanoferrate ions, i.e. $[(CN)_5Fe^{II}(pz)Ru_a^{III}(pz)Fe^{II}(CN)_5]^{3-}$ [17]. An additional notice within this perspective comes from the fact that the pyrazine-derivatives are symmetrical and linear [39], while the benzotriazolate-bridged systems are symmetrical and nonlinear.

The results of UV–Vis spectroelectrochemistry resemble the ones for the dinuclear species, and were interpreted on the basis of assignments made in the previous section. The redox/charge-transfer data were collected in Table 1 in order to make the comparison easier (the spectra are shown in Fig. 5). Variations in reduction potentials, LMCT and MLCT energies can be plausibly explained as a function of the synergistic charge-transfer and cooperative π-acid–base or π-back-bonding effects on each species, and are compatible with a greater perturbation at the mixed-valent state.

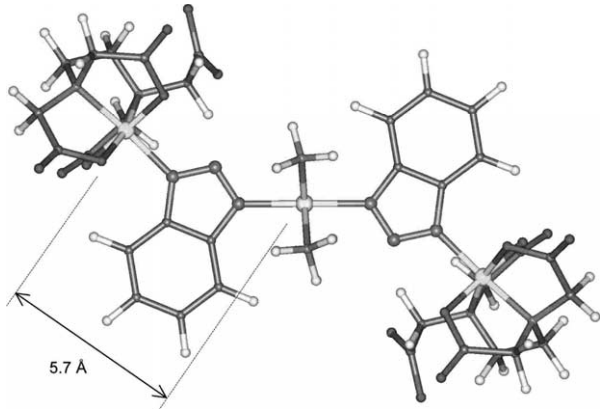


Fig. 4. Theoretical molecular structure of the symmetrical (C_2) trinuclear complex, *trans*-$[(NH_3)_4Ru\{(bta)Ru(edta)\}_2]^{2-}$.

4. Concluding remarks

The current investigation of mono-, di-, and trinuclear complexes with ammine- and edta–ruthenium units leads to the conclusion that polymetalic derivatives

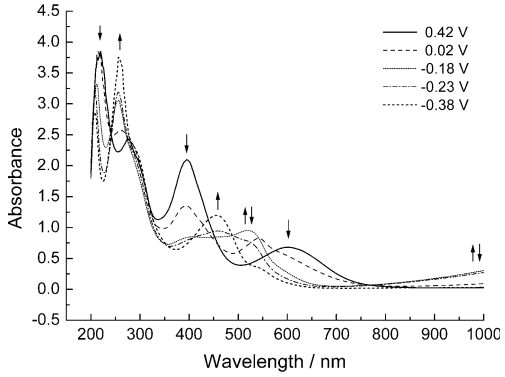


Fig. 5. Electronic spectra of *trans*-$[(NH_3)_4Ru\{(bta)Ru(edta)\}_2]^{n-}$ ($n = 1$, 2, or 4) in aqueous solutions under application of potentials ($c = 2.0 \times 10^{-2}$ M; I, KNO_3 (M); pH 9.5; $l = 0.25$ mm; applied potentials vs. SHE are indicated in the figure).

Table 2
Electrochemical, NIR-spectral, and electronic coupling parameters for a series of related dinuclear and trinuclear complexes [a]

Complex [a]	$E_{1/2}$ (1) [b] (V) [d]	$E_{1/2}$ (2) [c] (V) [d]	$\Delta E_{1/2}$ [e] (V)	ν_{max} (cm^{-1})	ε_{max} ($dm^3\ mol^{-1}\ cm^{-1}$)	$\Delta\nu_{1/2}$ (cm^{-1})	H_{ab} (cm^{-1})	Reference
$(NH_3)Ru_a^{II}(bta)Ru_b^{III}$	0.18	−0.11	0.29	6.8×10^3	2.3×10^3	3.7×10^3	$> 8.7 \times 10^2$	[8]
$[(NH_3)Ru_a^{II}(pz)Ru_b^{III}]^+$	0.56	0.42	0.14	9.8×10^3	3.0×10^2	$\sim 3.7 \times 10^3$	2.8×10^2	[36,37]
$[(NH_3)Ru_a^{III}(bta)Fe^{II}]^-$	−0.09	0.39	0.48	8.3×10^3	3.9×10^3	6.5×10^3	1.7×10^3	[6]
$(NH_3)Ru_a^{III}(pz)Fe^{II}$	0.49	0.72	0.23	6.1×10^3	1.6×10^3	4.3×10^3	6.0×10^2	[38]
$[(bta)Ru_a^{II}(bta)Ru_b^{III}]^-$	0.15	−0.21	0.36	6.6×10^3	1.6×10^3	5.5×10^3	8.7×10^2	This work
$[(pz)Ru_a^{II}(pz)Ru_b^{III}]^+$	0.87	0.27	0.60	[e]	[e]	[e]		[16]
$[Ru_b^{III}(bta)Ru_a^{II}(bta)Ru_b^{III}]^{2-}$	0.15	−0.22	0.37	6.5×10^3	1.9×10^3	5.6×10^3	9.5×10^2	This work
$Ru_b^{III}(pz)Ru_a^{II}(pz)Ru_b^{III}$	0.91	0.29	0.62	[e]	[e]	[e]		[16]
$[Fe^{II}(pz)Ru_a^{II}(pz)Fe^{III}]^{3-}$	0.95	0.65	0.30	9.5×10^3	$\sim 2.7 \times 10^3$	[f]	[f]	[17]
$[Fe^{III}(pz)Ru_a^{II}(pz)Fe^{III}]^{3-}$	0.95	0.65	0.30	7.0×10^3	$\sim 1.5 \times 10^3$	[f]	[f]	[17]

[a] Abbreviations: Ru_a = *trans*-{$Ru(NH_3)_4$}, Ru_b = {Ru(edta)}, Fe = {$Fe(CN)_5$}, bta = benzotriazolate, pz = pyrazine.
[b] Refers to the Ru_a(III/II) couple.
[c] Refers to either the Ru_b(III/II) or the Fe(III/II) couple, as applicable.
[d] Potential vs. SHE.
[e] According to ref. [16], no IVCT band was detected in the NIR region up to 2200 nm.
[f] Not available in the literature.

containing benzotriazolate as a bridging ligand exhibit electronic interactions suitable for the design of multicomponent supramolecular systems with conductor linkers [40].

An interesting feature of the complexes reported herein is that the electron communication between the adjacent (donor–acceptor) centers increases slightly with the nuclearity of the system. In this perspective, molecular wires can be devised via a combination of appropriate metallic units to act as building/ending blocks interconnected by the electron-rich benzotriazolate mediator. Unlike pyrazine-bridged polynuclear complexes [16,17], which afford linear polymer-like chains [39], the extended molecular systems bridged by benzotriazolate can provide a 'zigzag' type of wires.

Acknowledgements

The authors wish to thank Fundação de Amparo à Pesquisa do Estado de São Paulo (FAPESP) and Conselho Nacional de Desenvolvimento Científico e Tecnológico (CNPq) for supporting this research.

References

[1] R.C. Rocha, H.E. Toma, Quim. Nova 25 (2002) 624 (and references cited therein).
[2] M.D. Ward, Chem. Soc. Rev. 24 (1995) 121 (and references cited therein).
[3] H.E. Toma, Ann. Acad. Bras. Cienc. 72 (2000) 5 (and references cited therein).
[4] C. Joachim, J.K. Gimzewski, A. Aviram, Nature 408 (2000) 541 (and references cited therein).
[5] M.A. Reed, J.M. Tour, Sci. Am. 282 (2000) 86.
[6] R.C. Rocha, H.E. Toma, Can. J. Chem. 79 (2001) 145.
[7] R.C. Rocha, H.E. Toma, Inorg. Chem. Commun. 4 (2001) 230.
[8] R.C. Rocha, H.E. Toma, Inorg. Chim. Acta 310 (2000) 65.
[9] R.C. Rocha, K. Araki, H.E. Toma, Inorg. Chim. Acta 285 (1999) 197.
[10] R.C. Rocha, K. Araki, H.E. Toma, Transition Met. Chem. 23 (1998) 13.
[11] H.E. Toma, E. Giesbrecht, R.L.E. Rojas, J. Chem. Soc., Dalton Trans. (1985) 2469.
[12] H.E. Toma, E. Giesbrecht, R.L.E. Rojas, Can. J. Chem. 61 (1983) 2520.
[13] K. Gleu, W. Breuel, Z. Anorg. Allg. Chem. 237 (1938) 197.
[14] M. Mukaida, H. Okuno, T. Ishimori, Nippon Kagaku Zasshi 86 (1965) 589.
[15] R.C. Rocha, F.N. Rein, H.E. Toma, J. Braz. Chem. Soc. 12 (2001) 234.
[16] H.E. Toma, R.L. Sernaglia, Talanta 42 (1995) 1867.
[17] H.E. Toma, J. Coord. Chem. 7 (1978) 231.
[18] H.S. Lim, D.J. Barclay, F.C. Anson, Inorg. Chem. 11 (1972) 1460.
[19] A.M. Zwickel, C. Creutz, Inorg. Chem. 10 (1971) 2395.
[20] D. Chatterjee, Coord. Chem. Rev. 168 (1998) 273.
[21] F.N. Rein, R.C. Rocha, H.E. Toma, J. Coord. Chem. 53 (2001) 99.
[22] M. Franco, K. Araki, R.C. Rocha, H.E. Toma, J. Solution Chem. 29 (2000) 667.
[23] M.C. Zerner, in: D.B. Boyd, K.B. Lipkowitz (Eds.), Reviews in Computational Chemistry, vol. 2, VCH, 1991, p. 313.
[24] HyperChem(TM) [version 5.1, 1998], Hypercube, Inc., 1115 NW 4th Street, Gainesville, FL 32601, USA.
[25] N.L. Allinger, J. Am. Chem. Soc. 99 (1977) 8127.
[26] P. Ford, D.F.P. Rudd, R. Gaunder, H. Taube, J. Am. Chem. Soc. 90 (1968) 1187.
[27] R.L.E. Rojas, Ph.D. thesis, Universidade de São Paulo, São Paulo, 1985.
[28] L.A. Morino, H.E. Toma, Talanta 31 (1984) 224.
[29] L.D. Hansen, B.D. West, E.J. Baca, C.L. Blank, J. Am. Chem. Soc. 90 (1968) 6588.
[30] P.C. Ford, C. Sutton, Inorg. Chem. 8 (1969) 1544.
[31] R.C. Rocha, Ph.D. thesis, Universidade de São Paulo, São Paulo, 2000.
[32] H.E. Toma, R.C. Rocha, Croat. Chem. Acta 74 (2001) 499.
[33] D.E. Richardson, H. Taube, Coord. Chem. Rev. 60 (1984) 107.
[34] N.S. Hush, Prog. Inorg. Chem. 8 (1967) 391.

[35] M.B. Robin, P. Day, Adv. Inorg. Chem. Radiochem. 10 (1967) 247.
[36] C. Creutz, Prog. Inorg. Chem. 30 (1983) 1.
[37] C. Creutz, P. Kroger, T. Matsubara, T.L. Netzel, N. Sutin, J. Am. Chem. Soc. 101 (1979) 5442.
[38] A. Yeh, A. Haim, J. Am. Chem. Soc. 107 (1985) 369.
[39] A. von Kameke, G.M. Tom, H. Taube, Inorg. Chem. 17 (1978) 1790.
[40] H.E. Toma, K. Araki, Coord. Chem. Rev. 196 (2000) 307 (and references cited therein).

integration of the CN^- resonances in the ^{13}C NMR. Although the complexes of thiones with gold(I) have been studied extensively [17–19], there is no known report describing the synthesis of gold(I) complexes of selenones (except that of selenourea) [20]. The complexation of gold(I) with selenium containing ligands is important since selenocysteine is present at the active binding site of the enzyme, Se-glutathione peroxidase and gold(I) is known to be a strong inhibitor for the catalytic activity of Se-glutathione peroxidase [21–23]. The structures of the selenones used in this study and their resonance assignments are described in Scheme 1.

2. Experimental

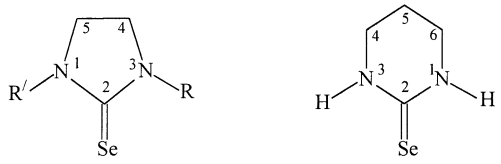
2.1. Chemicals

AuCN, using ^{13}C and ^{15}N labelled KCN (99% enriched) was prepared according to the published procedure [5]. Acetone, MeCN and DMSO-d_6 were obtained from Fluka Chemical Co. All the selenones were synthesized according to the procedure described in the literature [24,25].

2.2. Preparation of complexes

AuCN was suspended in C_3H_6O and an equimolar amount of the selenone in MeCN was added. The mixture was stirred for almost half an hour (in the case of Et_2ImSe, it was stirred for 1 day), after which a colorless solution was obtained. The solution was filtered and kept in a refrigerator for crystallization. As a result, white crystalline products were obtained with 50–60% yield.

The elemental analyses of all the complexes are given in Table 1.



(a) R = R′ = H; Imidazolidine-2-selenone (ImSe)

(b) R = H, R′ = CH_3; N-methylimidazolidine-2-selenone (MeImSe)

(c) R = H, R′ = C_2H_5; N-ethylimidazolidine-2-selenone (EtImSe)

(d) R = H, R′ = *i*-C_3H_7; N-(*i*-propyl)imidazolidine-2-selenone (*i*-PrImSe)

(e) R = H, R′ = C_6H_5; N-phenylimidazolidine-2-selenone (PhImSe)

(f) R = R′ = C_2H_5; N,N′-diethylimidazolidine-2-selenone (Et_2ImSe)

(g) R = H; 1,3-Diazinane-2-selenone (DiazSe)

Scheme 1.

Table 1
Elemental analyses of the [>C=Se–Au–CN] complexes

Complex	Found (Calc.)%			M.p. (°C)
	C	H	N	
ImSeAuCN	13.36 (12.91)	1.70 (1.63)	11.12 (11.30)	168 (dec.)
MeImSeAuCN	15.75 (15.55)	2.19 (2.09)	10.69 (10.89)	172 (dec.)
EtImSeAuCN	18.05 (18.01)	2.65 (2.52)	10.12 (10.50)	140 (dec.)
i-PrImSeAuCN	20.58 (20.30)	2.99 (2.92)	10.46 (10.15)	160 (dec.)
PhImSeAuCN	26.63 (26.74)	2.37 (2.40)	9.85 (9.36)	165 (dec.)
Et_2ImSeAuCN	22.62 (22.44)	3.31 (3.29)	9.89 (9.82)	110–111
DiazSeAuCN	16.17 (15.55)	2.22 (2.09)	10.90 (10.89)	119–121

All the complexes are written in the nonionic form, since on the basis of elemental analysis the ionic and nonionic forms cannot be distinguished.

2.3. Spectroscopic measurements

The solid state IR spectra of the ligands and their cyano gold(I) complexes were recorded on a Perkin–Elmer FTIR 180 spectrophotometer using KBr pellets over the range 4000–400 cm^{-1}.

The ^1H NMR spectra were obtained on a JEOL JNM-LA 500 NMR spectrometer operating at a frequency of 500 MHz. The ^{13}C NMR spectra were obtained at the frequency of 125.65 MHz with ^1H broadband decoupling at 297 K. The spectral conditions were: 32 K data points, 0.967 s acquisition time, 1.00 or 30.00 s pulse delay and 45° pulse angle. ^{13}C chemical shifts (relative to TMS) were assigned according to the references given in the literature for analogous thiones [17,19].

The ^{15}N NMR spectrum was recorded at 50.55 MHz using $NH_4^{15}NO_3$ as an external reference, which lies at 375.11 ppm relative to pure CH_3NO_2, 380.2 ppm [26]. The spectral conditions for ^{15}N NMR were: 32 K data points, 0.721 s acquisition time 2.50 s delay time, 60° pulse angle and approximately 10 000 scans.

T_1 values for the ^{13}C nuclei were measured only for CN^- carbons in [ImSeAuCN] and $[Au(CN)_2]^-$ using the inversion recovery method. The average values obtained are 4.0 and 5.1 s, respectively. Based on these T_1 values, a delay time of 30.0 s was used to record the ^{13}C NMR spectra of all the complexes so that the spectra could be integrated quantitatively.

2.4. Determination of equilibrium constant (K_{eq})

Equilibrium constants (K_{eq}) were calculated using relative intensities (I) of cyanide resonances of [>C=Se–Au^{13}C^{15}N] and $[Au(^{13}C^{15}N)_2]^-$ complexes, in the ^{13}C NMR, which gives the relative concentrations of both species;

$$K_{eq} = (I[Au(^{13}C^{15}N)_2]^-) \times (I[Au(>C{=}Se)_2]^+)/(I[>C{=}Se{-}Au^{13}C^{15}N])^2 \quad (2)$$

Where,

$I[Au(^{13}C^{15}N)_2]^- = I[Au(>C{=}Se)_2]^+$

Each K_{eq} value is the result of at least seven measurements.

3. Results and discussion

3.1. IR Studies

Table 2 lists the significant IR bands of free selenones and their gold(I) complexes. The ν(C=Se) vibration, which occurs around 600 cm^{-1} for the free ligands [27], shifts towards lower frequency upon complexation, in accordance with the data observed for the analogous thione complexes [17]. Another important vibrational band observed in IR spectra of the selenones is the ν(NH), which appears around 3200 cm^{-1}. Upon coordination to AuCN this band shifts to higher wave numbers with some exceptions. The presence of a band around 3200 cm^{-1} in free ligands as well as in the complexes indicates the existence of the selenone form of the ligands in the solid state. One or two bands around 2100 cm^{-1} corresponding to CN^- stretches are observed in IR spectra of all the complexes. For the complexes of ImSe and DiazSe only one ν(CN) mode was observed, which appeared at a lower frequency (by approximately 150 cm^{-1}) compared to free AuCN. For the rest of the complexes, two stretching bands (asymmetric and symmetric) are observed for the CN^- group which are characteristic of $[Au(CN)_2]^-$ (since the NC–Au–CN bond angle in $[Au(CN)_2]^-$ is found to be less than 180°) [7,8].

Several studies on the crystal structures of cyanogold(I) complexes show that these complexes exist as monomers and in the nonionic form in the solid state [2–4]. However, the crystal structures of two of the complexes, [DmTu–Au–CN] [8] and [CEP–Au–CN] [7] show that they exist as ionic complexes, $[Au(DmTu)_2]^+$-$[Au(CN)_2]^-$ and $[Au(CEP)_2]^+[Au(CN)_2]^-$, respectively, in the solid state. We prepared these two complexes in our laboratory and in the IR spectra of these complexes, it was observed that they possess two bands corresponding to the CN^- stretch. For the other cyano(thione)gold(I) complexes only one ν(CN) band was observed [17]. Thus it is established that the complexes which show only one CN^- stretch in IR exist as nonionic complexes (i.e. as [L–Au–CN]), while those which possess two CN^- bands exist in the form (i.e. as $[AuL_2]^+[Au(CN)_2]^-$. The IR spectra of $[Au(CN)_2]^-$ and a representative complex are shown in Fig. 1.

The appearance of one ν(CN) peak for the complexes [ImSeAuCN] and [DiazSeAuCN], indicates that these two complexes exist in the nonionic form. The appearance of two ν(CN) bands for the other five selenone complexes suggests that they exist in the ionic form (i.e. as $[Au(>C{=}Se)_2]^+[Au(CN)_2]^-$) in the solid state, similar to $[Au(CEP)_2]^+[Au(CN)_2]^-$ and $[Au(DmTu)_2]^+[Au(CN)_2]^-$ [7,8].

3.2. NMR studies

In solution, the complexes were characterized by ^1H, ^{13}C and ^{15}N NMR in DMSO-d_6. All the complexes were observed to undergo the ligand scrambling reactions in solution similar to that shown in Eq. (1). In ^1H NMR the N–H signal was broadened upon coordination and a downfield shift of 0.7–1.0 ppm was observed for the N–H proton of all the ligands. The appearance of the N–H signal in ^1H NMR of all ligands after complexation shows that the ligands are coordinating in the selenone form in solution. The ^1H NMR chemical shifts of N–H protons and ^{13}C NMR chemical shifts of all the ligands and their gold(I) complexes are given in Table 3. In ^{13}C NMR, no significant change in the chemical shifts of the ligands upon complexation was observed except in the C-2 resonance (Table 3). A shift of 9–13 ppm for the C-2 resonance indicates that in all the complexes, gold(I) is bonded to the selenone ligands through the selenium atom only. In the case of bonding through nitrogen, a considerable shift of the C-4 resonance would have been observed, but there is only a slight shift in C-4.

Table 2
IR frequencies, ν(cm^{-1}) of the selenones and their cyanogold(I) complexes

Species	ν(C=Se) of ligands	ν(C=Se) of complexes	ν(NH) of ligands	ν(NH) of complexes	ν(CN) of complexes
ImSe	558	520	3254	3310	2048
MeImSe	580	550	3184	3230	2136, 2096
EtImSe	588	582	3198	3200	2144, 2096
i-PrImSe	600	582	3200	3192	2146, 2106
PhImSe	596	584	3190	3186	2146, 2098
Et_2ImSe	628	624			2132, 2090
DiazSe	602	586	3198	3260	2060
AuCN					2220
$K[Au(CN)_2]$					2140, 2068

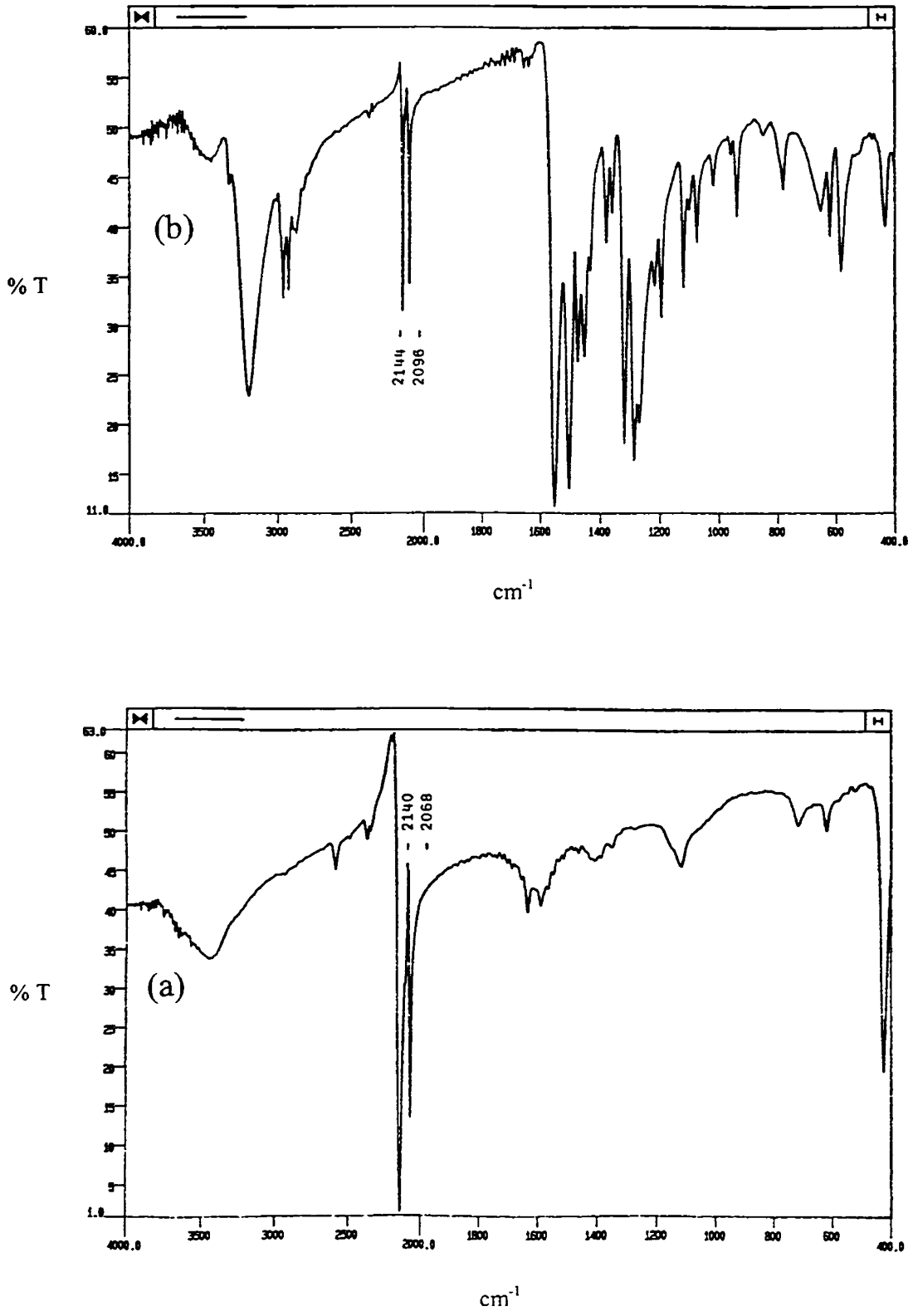


Fig. 1. IR spectra of: (a) $K[Au(CN)_2]$; (b) EtImSeAuCN (existing as $[Au(EtImSe)_2]^+[Au(CN)_2]^-$).

The ligand scrambling reactions of the cyano(selenone)gold(I) complexes were followed by ^{13}C NMR and were further characterized by ^{15}N NMR spectroscopy. Some representative ^{13}C and ^{15}N spectra are shown in Fig. 2. The ^{13}C and ^{15}N NMR shifts of the CN^- group for all the selenone complexes are given in Table 4. In the CN^- region of the ^{13}C spectrum, two intense resonances were observed for all the complexes (Fig.

Table 3
^{1}H and ^{13}C chemical shifts (ppm) of the ligands and their cyanogold(I) complexes [a] in DMSO-d_6

Species	N–H	C-2	C-4	C-5	C-6	N–C1	N–C2
ImSe	8.48	177.09	44.94	44.94			
ImSeAuCN	9.51	166.72	45.39	45.39			
MeImSe	8.47	178.67	42.07	50.35		35.06	
MeImSeAuCN	9.31	167.65	43.10	51.55		35.35	
EtImSe	8.44	177.72	42.17	47.21		42.14	11.93
EtImSeAuCN	9.34	166.64	43.12	48.47		43.08	12.21
i-PrImSe	8.43	177.18	42.28	47.72		42.26	19.10
i-PrImSeAuCN	9.34	165.94	43.56	49.71		42.96	19.41
PhImSe	9.02	177.22	42.61	51.74		140.81	128.20 [b], 125.61 [c], 124.67 [c]
PhImSeAuCN	9.92	168.54	43.93	53.63		138.67	129.43 [b], 128.47 [c], 126.29 [d]
Et_2ImSe		178.57	45.81	45.81		43.07	11.77
Et_2ImSeAuCN		165.68	46.96	46.96		44.06	12.24
DiazSe	8.23	169.14	40.10	18.76	40.10		
DiazSeAuCN	9.15	158.48	40.50	18.01	40.50		

[a] The chemical shifts for [>C=Se–Au–CN] and $[Au(>C=Se)_2]^+$ species could not be distinguished.
[b] N–C2/6.
[c] N–C4.
[d] N–C3/5.

2b). One CN^- resonance at 149.6 ppm is characteristic of $[Au(CN)_2]^-$ [5,6,9] while the other corresponds to [>C=Se–Au–CN] complexes. These two resonances demonstrate that [>C=Se–Au–CN] type complexes undergo the same type of scrambling reaction as given by Eq. (1), i.e.

$$2[>C{=}Se{-}Au{-}CN] \rightleftharpoons [Au(>C{=}Se)_2]^+ + [Au(CN)_2]^- \quad (3)$$

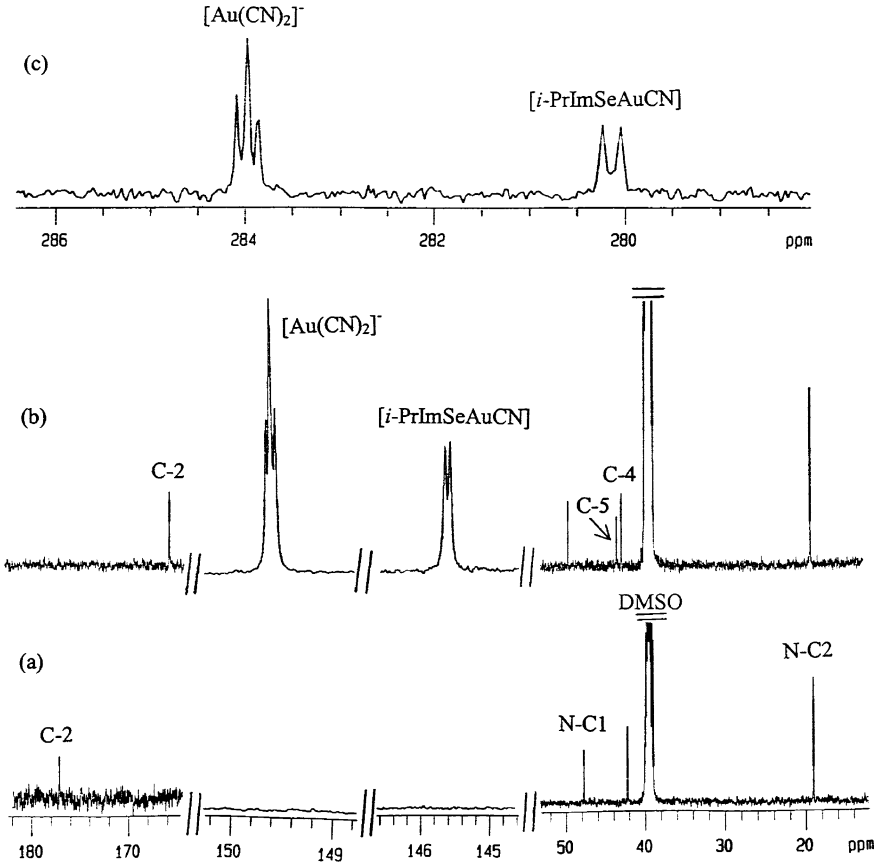


Fig. 2. (a) 125.65 MHz $^{13}C\{^1H\}$ NMR spectrum of *i*-PrImSe in DMSO. (b) ^{13}C NMR spectrum of [*i*-PrImSe–Au–CN]. (c) 50.55 MHz ^{15}N NMR spectrum of [*i*-PrImSe–Au–CN].

Table 4
The ^{13}C and ^{15}N chemical shifts of CN^- (ppm), coupling constants (Hz) and K_{eq} of cyanogold(I) complexes in DMSO-d_6

Species	$\delta^{13}C$	$\delta^{15}N$	$^1J_{C-N}$	K_{eq} (±esd)
ImSeAuCN	146.13	280.26	8.2	2.95±0.05
MeImSeAuCN	145.61	280.32	10.0	2.90±0.08
EtImSeAuCN	145.54	280.32	9.0	2.76±0.06
i-PrImSeAuCN	145.59	280.14	9.4	3.12±0.02
PhImSeAuCN	145.66	279.84	9.4	4.28±0.05
Et_2ImSeAuCN	143.93	280.36	8.9	2.84±0.07
DiazSeAuCN	146.67	279.02	9.4	3.64±0.06
Ph_3PAuCN[5,6]	156.2		6.4	0.112 [a]
Et_3PAuCN[5]	160.4	265.54	6.5	0.24 [a]
$(i\text{-Pr})_3$PAuCN[5]	160.9	264.61	6.2	0.29 [a]
Cy_3PAuCN[5,6]	160.29	264.35	5.5	0.49 [a]
Cy_3PSAuCN[12]	144.85	261.55	11.3	0.147 [a]
Cy_3PSeAuCN[11,12]	146.44	260.65	8.9	1.81 [a]
ImtAuCN[9]	144.40	281.18	9.3	0.630
	147.02	262.23	10.3	0.47 [a]
MeImtAuCN[9]	143.64	281.18	9.0	0.56
EtImtAuCN[9]	143.62	281.36	10.4	0.62
i-PrImtAuCN[9]	143.81	280.99		0.55
DiazAuCN[9]	144.75	281.12	8.2	0.91

[a] In methanol.

The $[Au(CN)_2]^-$ resonance appears as a triplet with an average coupling constant of 5.9 Hz. The triplet appearance of the $[Au(^{13}C^{15}N)_2]^-$ resonance is because the $^{13}C-^{15}N$ coupling in $[Au(^{13}C^{15}N)_2]^-$ follows the AA′XX′ spin system as described in the previous studies [11–13]. The $^{13}C^{15}N$ resonance due to [>C=Se–Au–$^{13}C^{15}N$] complexes is a doublet with the $^1J_{C\text{-}N}$ values given in Table 4. Separate resonances for selenone ligands in [>C=S–Au–CN] and $[Au(>C=S)_2]^+$ species were not observed either due to their rapid exchange or the chemical shifts of the two species are overlapped so that they cannot be resolved.

The results of the ^{15}N NMR studies are consistent with the ^{13}C NMR data. The ^{15}N NMR also showed two resonances for the CN^- nitrogen corresponding to equilibrium (3) (Fig. 2c). The resonance at 284.1 was a triplet of $[Au(^{13}C^{15}N)_2]^-$ (as observed in the ^{13}C spectrum) with an average coupling constant of 5.9 Hz. The other resonance is a doublet due to $^{13}C-^{15}N$ coupling in the [>C=Se–Au–$^{13}C^{15}N$] complexes. The ^{15}N chemical shift is very much affected by the change of solvent. When the ^{15}N spectrum of ImtAuCN, a thione analogue of ImSeAuCN (Imt = imidazolidine-2-thione), was taken in methanol, the $[Au(CN)_2]^-$ resonance was observed at 264.7 ppm [9].

3.3. Evaluation of equilibrium constant (K_{eq})

Equilibrium constants (K_{eq}) were determined for the [>C=Se–Au–CN] complexes at 297 K using 0.025 M concentration of each complex in DMSO-d_6. The average K_{eq} values calculated for the complexes using Eq. (2) are given in Table 4 and for comparison, K_{eq} values of some known cyanogold(I) complexes are also given.

In the scrambling reactions of cyanogold(I) complexes of phosphines, it was observed that the basicity of the phosphine is the most important factor which affects K_{eq} [5], although K_{eq} is also affected by external factors such as ionic strength [5,9]. An increase in K_{eq} was observed with an increase in basicity of the phosphine. As shown in Table 4, the K_{eq} values for the cyanogold(I) complexes of selenones are found to be much larger than for the complexes of other ligands. The larger K_{eq} values indicate that the selenones are more basic towards Au(I) compared to phosphines and thiones. A shift of 9–13 ppm in the C-2 resonance also indicates that they are very strong σ donors. It seems that greater donation of electron density to gold(I) would result in a stronger Au–CN bond. This should lead to an easier formation of $[Au(CN)_2]^-$, resulting in a larger value of K_{eq}. In the case of R_3PAuCN complexes, π accepting ability of phosphines stabilizes the Au–P bond and thus would result in a lower value of K_{eq}. This shows that the selenones are weaker π acceptors compared to phosphines and thiones. A comparison of the K_{eq} value for scrambling of Cy_3PSeAuCN with its sulfur analogue, Cy_3PSAuCN (Table 4) further suggests that the K_{eq} values for the selenones complexes should be greater than the complexes of their sulfur analogues (thiones). Moreover, since five of the eight complexes being reported exist in the solid state as ionic complexes, in solution the ionic form will also be more populated resulting in a larger value of K_{eq}. Thus the order of ability of different L–Au–CN complexes undergoing disproportionation is, [>C=SeAuCN] > [R_3PSeAuCN] > [>C=SAuCN] > [R_3PAuCN] ≥ [R_3PSAuCN].

In the scrambling reactions of cyano(phosphine)gold(I) complexes [5,6], it was observed that with increasing basicity of phosphines, δ ^{13}C for CN^- in R_3PAuCN also increased due the increased π bond character in the Au–C bond, while there was a decrease in δ ^{15}N. However, in the present study, δ ^{13}C and ^{15}N for CN^- and the coupling constants, $^1J_{C-N}$ in all the complexes are very close showing that the difference in their basicity is small. Table 4 shows the highest value of δ ^{13}C for a CN^- resonance DiazSe–AuCN indicating that it is the most basic, while Et_2ImSe–AuCN with the lowest $\delta^{13}C$ is the least basic among the selenones. The least basicity of Et_2ImSe–AuCN is due to its inability to exhibit the selenol–selenone equilibrium. However, the greater δ ^{13}C and smaller ^{15}N of selenone complexes compared to that of thione ones indicate that selenones are comparatively more basic than thiones.

4. Conclusion

In this study we have shown that some of the cyanogold(I) complexes of selenones exist as nonionic complexes and some as the ionic species in the solid state as proved by IR spectroscopy. However, in solution all cyano(selenone)gold(I) complexes undergo dissociation showing an equilibrium between ionic and nonionic species. The equilibrium constants (K_{eq}), measured for the scrambling of selenone complexes, have the highest values compared to those observed for all other reported complexes.

Acknowledgements

This research work was supported by the KFUPM Research Committee under project no. CY/NMR-STUDIES/214.

References

[1] R.D. Hancock, N.P. Finnkelstein, A. Avers, J. Inorg. Nucl. Chem. 34 (1972) 3747.
[2] P.G. Jones, J. Launter, Acta Crystallogr., Sect. C 44 (1988) 2091.
[3] A.R. Al-Arfaj, J.H. Reibenspies, M.S. Hussain, M.Y. Darensbourg, M.N. Akhtar, A.A. Isab, Acta Crystallogr., Sect. C 53 (1997) 1553.
[4] A.L. Hormann, C.F. Shaw, III, D.W. Bennett, W.M. Reiff, Inorg. Chem. 25 (1986) 3953.
[5] A.L. Hormann, C.F. Shaw, III, Inorg. Chem. 29 (1990) 4683.
[6] A.A. Isab, M.S. Hussain, M.N. Akhtar, M.I.M. Wazeer, A.R. Al-Arfaj, Polyhedron 18 (1999) 1401.
[7] M.S. Hussain, A.R. Al-Arfaj, M.N. Akhtar, A.A. Isab, Polyhedron 16 (1996) 2781.
[8] F.B. Stocker, D. Britton, Acta Crystallogr., Sect. C 56 (2000) 798.
[9] S. Ahmad, A.A. Isab, H.P. Perzanowski, Can J. Chem. (2002), accepted for publication.
[10] G. Lewis, C.F. Shaw, III, Inorg. Chem. 25 (1986) 58.
[11] S. Ahmad, A.A. Isab, M.N. Akhtar, A.R. Al-Arfaj, M.S. Hussain, J. Coord. Chem. 51 (2000) 225.
[12] S. Ahmad, A.A. Isab, H.P. Perzanowski, M.S. Hussain, M.N. Akhtar, Transition Met. Chem. 27 (2002) 177.
[13] S. Ahmad, A.A. Isab, Inorg. Chem. Commun. 4 (2001) 362.
[14] G.G. Graham, J.R. Bales, M.C. Grootveld, P.J. Sadler, J. Inorg. Biochem. 25 (1985) 163.
[15] A.A. Isab, A.L. Hormann, M.T. Coffer, C.F. Shaw, III, J. Am. Chem. Soc. 110 (1988) 3278.
[16] A.A. Isab, J. Inorg. Biochem. 45 (1992) 261.
[17] A.A. Isab, M.S. Hussain, J. Coord. Chem. 15 (1986) 125.
[18] A.A. Isab, M.S. Hussain, Polyhedron 4 (1985) 1683.
[19] A.A. Isab, Polyhedron 8 (1989) 2823 (and references therein).
[20] P.G. Jones, C. Thone, Chem. Ber. 124 (1991) 2725.
[21] J. Chaudiere, A.L. Tappel, J. Inorg. Biochem. 20 (1984) 313.
[22] W.C. Hawakws, E.C. Wilhelmsen, A.L. Tappel, J. Inorg. Biochem. 23 (1985) 77.
[23] C.J. Dillard, A.L. Tappel, J. Inorg. Biochem. 28 (1986) 13.
[24] F. Cristiani, F.A. Devillanova, G. Verani, J. Chem. Soc., Perkin Trans. II (1977) 324.
[25] F.A. Devillanova, G. Verani, Aust. J. Chem. 31 (1978) 2609.
[26] M.N. Akhtar, A.A. Isab, A.R. Al-Arfaj, M.S. Hussain, Polyhedron 16 (1997) 125 (and references therein).
[27] F.A. Devillanova, A. Diaz, F. Isaia, G. Verani, Transition Met. Chem. 14 (1989) 153.

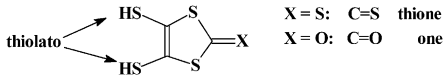


Fig. 1. X = S: H_2dmit; X = O: H_2dmio.

expected, only small structural differences are found between dmit and dmio complexes when these 1,2-dithiolato ligands merely act as chelates, as in [Q][R_2SnX(dmit)] and [Q][R_2SnX(dmio)] [9,10], [Q]$_2$[Sn(dmit)$_3$] and [Q]$_2$[Sn(dmio)$_3$] [11], as well as [Q][Zn(dmit)$_2$] and [Q][Zn(dmio)$_2$] [12]. However, when the chalcogen atoms are involved in secondary bonding, structural differences are realised as is the case with the pair, Me_2Sn(dmit) and Me_2Sn(dmio) [9,13].

A series of bis(1,3-dithiole-2-one-4,5-dithiolato)antimonate(1-) complexes, [Q][Sb(dmio)$_2$] (**3**) have been prepared and the structures of two complexes, (**3**: Q = NEt_4 and DMP), have been determined and are now reported. These are compared with the structures of the previously reported (**1**: Q = NEt_4, DMP and PPh_4) as well as with those of the new compounds, (**1**: Q = NBu_4 and $AsPh_4$).

2. Experimental

2.1. General

NMR spectra were run on Bruker 250 and 300 MHz instruments, IR spectra on Nicolet Magna 760 FTIR, Philips Analytical PU9800 and Nicolet Fourier-transform spectrometers and UV–Vis spectra on a Varian–Cary 1E UV–Vis instrument. Melting points (m.p.) were measured on a Melt–TempII instrument and a Kofler hotstage and are uncorrected. Elemental analyses were obtained using a Perkin–Elmer 2400 Instrument or from Butterworth Laboratories Ltd, Middlesex. The compounds, (ferrocenylmethyl)trimethylammonium iodide, [$FcCH_2NMe_3$]I [14], [Q]$_2$[Zn(dmit)$_2$] (Q = NBu_4 and $AsPh_4$) and [Q]$_2$[Zn(dmio)$_2$] (Q = NEt_4, DMP, $FcCH_2NMe_3$ and PPh_4) [12,15] were prepared by published procedures.

2.1.1. Synthesis of *1* and *3*

These were prepared by a procedure similar to that previously used for (**1**: Q = NEt_4, PPh_4 or DMP) [2,3]. Reactions between $SbBr_3$–NaSCN and [Q]$_2$[Zn(dmit)$_2$] or [Q]$_2$[Zn(dmio$_2$] gave the target products in yields generally greater than 60% after recrystallisation. The procedure used for (**1**: Q = $AsPh_4$) is given as an illustration.

2.1.2. Compound (*1*: *Q* = *AsPh*$_4$) from [*AsPh*$_4$][*Zn*(*dmit*)$_2$]

To a solution of NaSCN·$2H_2O$ (0.351 g, 3 mmol) in acetone (20 cm^3) was successively added a solution of $SbBr_3$ (0.36 g, 1 mmol) in acetone (20 cm^3) and a solution of [$AsPh_4$]$_2$[Zn(dmit)$_2$] (1.22 g, 1 mmol) in acetone (35 cm^3). The reaction mixture was stirred for 30 min after the addition of [$AsPh_4$]$_2$[Zn(dmit)$_2$], the solvent removed by rotary evaporation and the crude product recrystallised from acetone to give dark green–black crystals (blocks), m.p. 185–187 °C. *Anal.* for (**1**: Q = $AsPh_4$). Found: C, 40.2; H, 2.3. $C_{30}H_{20}AsS_{10}Sb$ requires C, 40.1; H, 2.2%. ^{1}H NMR (DMSO-d_6, 300 MHz): δ: 7.8–7.9(m, aryl-H). ^{13}C NMR (DMSO-d_6, 75.5 MHz): δ: 121.5, 131.5, 133.7 and 134.9(aryl-C), 132.7(C=C), 212.2(C=S). IR (KBr, cm^{-1}): 1437 (C=C), 1053, 1014(C=S), 883(C–S). IR (CsI, cm^{-1}): 516, 482, 463, 398, 360, 351, 323, 289, 279, 270, 246, 223.

2.1.3. Compound (*1*: *Q* = *NBu*$_4$) from [*NBu*$_4$]$_2$[*Zn*(*dmit*)$_2$]

The product was recrystallised from DMSO as dark red crystals (needles): m.p. 168–170 °C. *Anal.* for (**1**: Q = NBu_4). Found: C, 34.8; H, 4.9; N, 1.8. $C_{22}H_{36}NS_{10}Sb$ requires C, 34.9; H, 4.8; N, 1.9%. ^{1}H NMR (DMSO-d_6, 300 MHz): δ 0.93(t, 12H, J(^{1}H–^{1}H) = 7.2 Hz, CH_3), 1.30(m, 8H, CH_2), 1.57(m, 8H, CH_2), 3.18(t, 8H, H_2C–N). ^{13}C NMR (DMSO-d_6, 75.5 MHz): δ 13.5(CH_3), 19.2(CH_2), 23.1(CH_2), 57.6(CH_2), 132.4(C=C) and 211.5(C=S). IR (KBr, cm^{-1}): 1437(C=C), 1063, 1016(C=S), 889(C–S). IR (CsI, cm^{-1}): 526, 519, 462, 441, 390, 343, 329, 300, 288, 266, 246, 219.

2.1.4. Compound (*3*: *Q* = *NEt*$_4$) from [*NEt*$_4$]$_2$[*Zn*(*dmio*)$_2$]

The target product was recrystallised from acetone as a dark green–black crystalline solid, m.p. 193–195 °C. Yield: 0.57 g (67%). *Anal.* for (**3**: Q = NEt_4). Found: C, 27.6; H, 3.5. $C_{14}H_{20}NO_2Sb$ requires C, 27.5; H, 3.3%. ^{1}H NMR (DMSO-d_6, 250 MHz): δ: 1.2 (t of t, 12H, J(^{1}H–^{1}H) = 7.2 Hz, Me of cation), 3.2 (q, 8H, J(^{1}H–^{1}H) = 7.5 Hz, CH_2N of cation). ^{13}C NMR (DMSO-d_6, 63 MHz): δ: 8.7(Me), 53.0(CH_2N), 119.9(C=C), 195.4(C=O). IR (CsI, cm^{-1}): 2075, 1660, 1607, 1473, 1391, 1365, 1171, 1000, 883, 786, 755, 545, 462, 365, 338, 321, 280, 257, 172.

2.1.5. Compound (*3*: *Q* = *DMP*) from [*DMP*]$_2$[*Zn*(*dmio*)$_2$]

The target product was recrystallised from acetone as a dark green–black crystalline solid, m.p. 182–183 °C. Yield: 0.58 g (68%). *Anal.* for (**3**: Q = DMP). Found: C, 26.7; H, 1.7; N, 2.5. $C_{13}H_{10}NO_2S_8Sb$ requires C, 26.4; H, 1.7; N, 2.4%. ^{1}H NMR (DMSO-d_6, 250 MHz): δ: 2.6 (s, 3H, Me of cation), 4.3 (s, 3H, MeN of cation), 7.9 (d, 2H, J(^{1}H–^{1}H) = 6.2 Hz, C_3 and C_5), 8.8 (d, 2H, J(^{1}H–^{1}H) = 6.6 Hz, C_2 and C_6). ^{13}C NMR (DMSO-d_6, 63 MHz): δ: 23.1(Me), 48.8(MeN), 120.0(C=C), 129.7, 146.2, 159.9 (aromatic-C), 195.4(C=O). IR (CsI,

cm^{-1}): 1771, 1660, 1641, 1605, 1517, 1471, 1295, 1189, 885, 877, 816, 803, 752, 695, 542, 486, 460, 366, 333, 318, 279, 252, 174, 154.

2.1.6. Compound (3: Q = Ph_4P) from $[PPh_4]_2[Zn(dmio)_2]$

The target molecule was recrystallised from acetone as a black crystalline solid, m.p. 173–175 °C. Yield: 0.88 g (66%). *Anal.* for (**3**: Q = Ph_4P). Found: C, 43.5; H, 2.6. $C_{30}H_{20}O_2PS_8Sb$: requires C, 43.8; H, 2.4%. ^{1}H NMR (DMSO-d_6, 250 MHz): δ: 7.8 (m, 12H, *m*-H + *p*-H), 8.0 (m, 8H, *o*-H). ^{13}C NMR (DMSO-d_6, 63 MHz): δ: 118.6 (C=C), 120.0 ($J(^{31}P-^{13}C) = 88.5$ Hz, C_i), 132.0 [$J(^{31}P-^{13}C) = 12.2$ Hz, C_m], 136.1 ($J(^{31}P-^{13}C) = 11.0$ Hz, C_o), 137.0($^{31}P-^{13}C) = 2.2$ Hz, C_p), 195.3(C=O). IR (KBr, cm^{-1}): 1660, 1610, 1585, 1471, 1434, 1104, 995, 885, 752, 686, 526, 460.

2.1.7. Compound (3: Q = $FcCH_2NMe_3$) from $[FcCH_2NMe_3]_2[Zn(dmio)_2]$

The target molecule was recrystallised from acetone as a dark orange–green solid, m.p. 203–205 °C. Yield: 0.78 g, (60%). *Anal.* for (**3**: Q = $FcCH_2NMe_3$): C, 32.0; H, 3.0; N, 1.7. $C_{20}H_{20}NO_2FeS_8Sb$ requires C, 32.4; H, 2.7; N, 2.0%. ^{1}H NMR (DMSO-d_6, 250 MHz): δ: 2.9 (s, 9H, Me of cation), 4.2 (s, 5H, unsubstituted cp-H), 4.4 (s, 4H, substituted cp-H), 4.5 (s, 2H, CH_2N). ^{13}C NMR (DMSO-d_6, 63 MHz): δ: 53.0(Me), 67.1(CH_2N), 70.6(unsubstituted cp-C), 71.7, 73.6, 74.7(substituted cp-C), 119.9(C=C), 195.3(C=O). IR (KBr, cm^{-1}): 1666, 1610, 1479, 1467, 867, 825, 482, 464.

2.2. Crystallography

2.2.1. Data collection

For (**3**: Q = NEt_4 or DMP) unit cell and intensity data were obtained at 293 and 150 K, respectively, on the Delft Instruments FAST diffractometer of the EPSRC's crystallographic service at Cardiff. Unit cells were determined and the data collected using the routines ENDEX, REFINE and MADONL of the MADNES software [16] and data reduction carried out using ABSMAD [17]. Full procedural details are available elsewhere [18]. The triclinic cell determined initially for (**3**: Q = NEt_4) was found to correspond to a C-centred monoclinic cell and the cell dimensions were adjusted accordingly and the intensity data re-indexed with the row-wise transformation matrix −1 −1 0; −1 1 0; 0 0 −1. In both cases correction for absorption was made using XABS-2 [19].

Unit cell and intensity data for (**1**: Q = NBu_4) and (**1**: Q = $AsPh_4$), both at 150 K, were obtained by means of the Enraf Nonius KappaCCD area detector diffractometer of the EPSRC's crystallographic service at Southampton. The entire process of data collection, cell refinement and data reduction was accomplished by means of the programs DENZO [20] and COLLECT [21]. Correction for absorption was by means of SORTAV [22].

2.2.2. Structure solution and refinement

The direct methods approach of SHELXS-97 [23] provided solutions for the structures of (**1**: Q = NBu_4) and (**3**: Q = NEt_4 or DMP), while the structure of (**1**: Q = $AsPh_4$) was solved by the heavy atom method using SHELXS-86 [23]. Structure refinement in all cases was by means of SHELXL-97 [24]. In the case of (**1**: Q = $AsPh_4$) correction for extinction was applied with k in the formula: $F_c^* = kF_c[1 + 0.001 \times F_c^2\lambda^3/\sin(2\theta)]^{1/4}$ taking the value 0.0035(5). In all four cases, all non-H atoms were refined anisotropically and in the final stages H atoms were introduced in calculated positions and refined with a riding model. Special action was required to deal with disorder in two of the Bu groups of the counter cation of (**1**: Q = NBu_4) and the centrosymmetric symmetry of the cation sites in (**3**: Q = NEt_4) and (**3**: Q = DMP). Further details of data collection and structure refinement are available in Table 1.

3. Results and discussion

3.1. General

The dmit complexes, (**1**: Q = NBu_4 and $AsPh_4$), were prepared from $[Q]_2[Zn(dmit)_2]$ and $SbBr_3$–NaSCN in acetone, using a previously reported procedure [2]. A related procedure was used to obtain (**3**: Q = NEt_4, DMP, PPh_4 or $FcCH_2NMe_3$) from $[Q]_2[Zn(dmio)_2]$ and $SbBr_3$–NaSCN. The complexes have little solubility in non-coordinating solvents: the NMR spectra were run in DMSO-d_6 for this reason. The values of ν(C=C) for **1** and **3** are generally found in the regions 1430–1443 and 1455–1470 cm^{-1}, respectively, while the d^{13}C(C=C) NMR values are between 132.4–133.9 and 118.6–120.0 ppm, respectively. Spectral data for the C=S groups in **1** ν(C=S) 1016–1026 cm^{-1} and δ ^{13}C(C=S) 211.5–213.3 ppm: values for C=O in **3** are ν(C=O) 1660–1667 and 1605–1610 $cm^{-1}$and δ ^{13}C (C=O) 195.3–195.4 ppm.

3.2. Crystal structures

In what follows, the geometry of the previously published structures of (**1**: Q = NEt_4, DMP or PPh_4) [2,3] is described in terms of values obtained by the use of PLATON [25] applied to cif data extracted from the Cambridge Structural Database [26] at the Chemical Database Service of the EPSRC at Daresbury [27] with the atomic coordinates unchanged but with the atoms relabelled for conformity with the new structures presented here.

Complexes **1** and **3** are, in all cases, ionic species exhibiting only electrostatic cation–anion interactions.

Table 1
Crystal data and structure refinement

	1: Q = $AsPh_4$	**1**: Q = Nbu_4	**3**: Q = Net_4	**3**: Q = DMP
Empirical formula	$C_{30}H_{20}AsS_{10}Sb$	$C_{22}H_{36}NS_{10}Sb$	$C_{14}H_{20}NO_2S_8Sb$	$C_{13}H_{10}NO_2S_8Sb$
M	897.73	756.87	612.54	590.45
Temperature (K)	150(2)	150(2)	293(2)	150(2)
Wavelength (Å)	0.71073	0.71073	0.71073	0.71073
Crystal system	triclinic	monoclinic	monoclinic	triclinic
Space group	$P\bar{1}$	$P2_1/n$	$C2/c$	$P\bar{1}$
Unit cell dimension				
a (Å)	9.1083(1)	9.0802(4)	12.579(7)	8.7965(14)
b (Å)	12.0855(2)	19.1957(8)	12.373(7)	10.741(3)
c (Å)	16.4877(3)	18.0213(10)	14.976(7)	11.251(3)
α (°)	95.6559(6)	90	90	89.310(14)
β (°)	96.1007(6)	94.4590(15)	103.15(3)	100.566(10)
γ (°)	111.0647(13)	90	90	109.903(10)
V (Å^3)	1665.67(4)	3131.6(3)	2270(2)	981.1(4)
Z	2	4	4	2
D_{calc} (g cm^{-3})	1.790	1.605	1.792	1.999
Absorption coefficient (mm^{-1})	2.464	1.563	1.962	2.266
$F(000)$	888	1544	1224	580
Crystal colour	dark green–black	dark red	dark green–black	dark green–black
Crystal size (mm)	0.36 × 0.20 × 0.06	0.25 × 0.05 × 0.03	0.2 × 0.2 × 0.2	0.22 × 0.14 × 0.07
θ Range for data collection (°)	3.21–30.54	3.09–27.51	2.34–25.02	1.84–25.52
Index range	$-11 \le h \le 11$, $-15 \le k \le 17$, $-21 \le l \le 23$	$-11 \le h \le 11$, $-24 \le k \le 24$, $-21 \le l \le 23$	$-14 \le h \le 14$, $-9 \le k \le 13$, $-16 \le l < 11$	$-10 \le h \le 9$, $-12 \le k \le 12$, $0 \le l \le 11$
Reflections collected/unique [R_{int}]	25 181/8684 [0.0390]	19 918/7137 [0.1185]	4259/1692 [0.0822]	3753/2752 [0.1443]
Completeness to 2 θ limit (%)	85.2	98.9	84.1	75.2
Absorption correction	semi-empirical from equivalents	semi-empirical from equivalents	empirical (XABS-2.0)	empirical (XABS-2.0)
Max/min transmission	0.864, 0.756	0.959, 0.905	0.641, 0.623	1.000, 0.582
Refinement method	full-matrix least-squares on F^2	full-matrix least-squares on F^2	full-matrix least-squares on F^2	full-matrix least-squares on F^2
Data/restraints/parameters	8684/0/380	7137/0/331	1692/0/138	2752/0/226
Goodness-of-fit on F^2	1.060	0.890	1.065	1.166
Final R indices [$I > 2\sigma(I)$] R_1	0.0366	0.0522	0.0526	0.0712
wR_2	0.0876	0.0782	0.1235	0.1881
R indices (all data) R_1	0.0454	0 1647	0.0591	0.0761
WR_2	0.0922	0.1018	0.1251	0.1898
Extinction coefficient	0.0035(5)			
Largest difference in peak and hole (e Å^{-3})	1.061 and −2.020	0.981 and −0.757	2.733 and −0.604	2.696 and −1.210

The cations have their usual geometries and are not discussed further. The V-shape (Table 2) of the anions in **1** and **3** is shown, along with the numbering scheme used, in Fig. 2. The bond lengths and angles within dmit, in **1**, and dmio, in **3**, vary little from complex to complex. The central C=C bond of each of the ligands and its attached S constitutes a planar entity with Sb and the C=O or C=S atoms displaced from this plane by varying amounts as shown in Table 2. In all complexes each of the two chelating dmit–dmio ligands is asymmetrically bound to Sb (Table 3) with shorter and longer Sb–S bond lengths in the range 2.4679(18)–2.527(3) and 2.529(3)–2.7311(6) Å, respectively, both of which can be compared with the PLATON [25] estimate of the sum of the covalent radii of Sb and S of 2.48 Å. As indicated in the Introduction, the complex, $[NEt_4][Sb(1,2\text{-}S_2C_6H_4)_2]$, has been reported [7] to have non-interacting anions and have a pseudo 5-coordinate Sb centre, if one coordination site is assumed to be occupied by the antimony lone pair. The dithiolato ligands in $[NEt_4][Sb(1,2\text{-}S_2C_6H_4)_2]$ [7] are also asymmetrically bonded to Sb, with Sb–S bond lengths of 2.4400(7) and 2.6093(7), in one chelate, and 2.4450(7) and 2.6266(8) Å, in the other and are, therefore, comparable with those in **1** and **3**.

In all of the complexes **1** and **3** antimony also forms two weaker bonds to chalcogen atoms of neighbouring anions with Sb–S and Sb–O, in the range 3.271(4)–3.4968(16) and 3.131(5)–3.285(3) Å respectively (cf. PLATON [25] estimates of sums of van der Waals radii for Sb and S and Sb and O and of covalent radii of Sb

Table 2
Out of plane displacements [a] and interplanar and anion V-shape angles, Ip and V (Å, °)

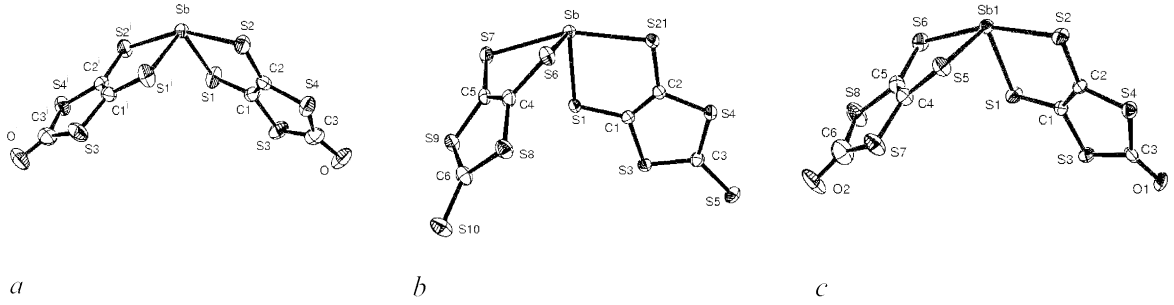
	Sb-oop(Å): Sb out of the ligand plane	C3-oop(Å): C3 out of the ligand plane	X-oop(Å): thione-S or one-O out of the ligand plane	Ip (°): angle between the ligand planes	V (°): angle subtended at Sb by the two thione S in (1) or two one-O in (3)
(**1**: Q = NEt_4) [b]	0.247(2)	0.095(11)	0.292(4)	86.52(12)	105.85(11)
(**3**: Q = NEt_4)	−0.188(3)	0.054(7)	0.100(6)	86.95(5)	107.42(10)
(**1**: Q = PPh_4) [c]	−0.096(1), 1.315(1)	−0.003(5), 0.004(5)	0.003(1), −0.022(2)	67.29(6)	84.5(2)
(**1**: Q = $AsPh_4$)	−0.0819(10), −1.338(9)	0.005(3), 0.004(5)	0.0010(12), 0.0386(14)	66.43(2)	83.39(1)
(**1**: Q = NBu_4)	−0.099(2), 1.208(2)	0.031(5), 0.026(6)	0.103(3), 0.216(3)	63.35(5)	82.50(2)
(**1**: Q = DMP) [b]	0.606(1), 0.141(1)	0.047(10), −0.009(9)	0.091(3), −0.025(3)	66.31(11)	120.8(2)
(**3**: Q = DMP)	0.030(4), 0.711(4)	−0.030(10), −0.087(15)	0.024(9), −0.158(12)	76.41(9)	97.21(11)

[a] Dmit and dmio ligand planes are defined by the C–C double bond and the attached S atoms.
[b] Ref. [2].
[c] Ref. [3].

and O of 4.06, 3.78 and 2.14 Å, respectively). These link the anions into 2D sheets or chains and in some cases, along with S···S or S···O contacts shorter than the sum of van der Waals radii (3.60 or 3.32 Å, respectively), into 3D networks in a manner described in more detail below.

In all of the structures discussed here, the anions are confined to layers whose orientation is indicated compound by compound in Table 3 and which are stacked alternating with parallel layers of counter cations. The simplest case, the anion layer in isostructural (**1** and **3**: Q = NEt_4), is clearly evident in Fig. 3(a). Here the disposition of the anions is entirely due to the C-centred nature of the unit cell so that all the anions within a single layer at $z = 1/4$ or 3/4 point in the same direction along b. Adjacent anion layers are then related to one another by crystallographic centres of symmetry or equivalently by the operation of the c-glide of the space group $C2/c$, thus inverting the orientation of the anions from one layer to the next. Contacts between anion layers as S3···S5^{i} (i: $1/2-x$, $1/2-y$, $-z$) at 3.556(5) Å in (**1**: Q = NEt_4) and S3···S1^{i} (i: $-x$, $-y$, $1-z$) and S3···O1^{ii} (ii: $-1/2-x$, $-1/2-y$, $1-z$) at 3.550(3) and 3.317(5) Å, respectively, in (**3**: Q = NEt_4) complete the connectivity.

In all of the other compounds discussed in this paper the secondary Sb–S and Sb–O bonds interconnect the anions to form chains. This is brought about in two stages leading to three different situations (Fig. 3(b–d), Tables 3 and 4). In the first stage one atom, X′ in Table 3, i.e. a symmetry related equivalent of thione S5 in (**1**: Q = NBu_4, $AsPh_4$, PPh_4 and DMP) or of thiolato S2 in (**3**: Q = DMP), bonds to Sb to form a centrosymmetric dimer in which inevitably a pair of parallel and head to tail ligands overlap to a greater or lesser extent (ring pairs a–a′ in Table 4). The second stage involves further contacts, Sb–X″ where X″ (Table 3) is a second and different symmetry related eqivalent, relative to the original Sb, of the same thione S5 as before for (**1**: Q = NBu_4, $AsPh_4$ and PPh_4), or symmetry equivalent thione S, S10, or one-O, O1, in (**1**: Q = DMP) [2] or (**3**: Q = DMP), respectively. These connect the anions in (**1**: Q = NBu_4, $AsPh_4$ and PPh_4) (Fig. 3(b)) and (**3**: Q = DMP) (Fig. 3(c)), to form linear double chains in which the face to face ligands, including their chelate function, are now μ^3 bridging species while the other ligands, protruding on either side of the spine of the double



a *b* *c*

Fig. 2. Atom arrangements and numbering systems for (a) (**3**: Q = NEt_4) which, with S5 replacing O, applies equally well to (**1**: Q = NEt_4) [2] as relabelled for comparison purposes; (b) (**1**: Q = $AsPh_4$, NBu_4 and relabelled PPh_4 [3] and DMP [2]), $AsPh_4$ salt shown; (c) (**3**: Q = DMP).

Table 3
Bond lengths and angles [a] (Å, °) about Sb in anions of **1** and **3**

	(**1**:Q = NEt_4) [b]	(**3**:Q = NEt_4)	(**1**:Q = NBu_4)	(**1**:Q = $AsPh_4$)	(**1**:Q = PPh_4) [c]	(**1**:Q = DMP) [b]	(**3**:Q = DMP)
S(A)	S1	S1	S1	S1	S1	S1	S1
S(B)	S2	S2	S2	S2	S2	S2	S2
S(C)	S1′ [i]	S1′ [i]	S6	S6	S6	S6	S5
S(D)	S2′ [i]	S2′ [i]	S7	S7	S7	S7	S6
X″	S5′ [ii]	O1′ [iv]	S5′ [vi]	S5′ [vi]	S5′[ix]	S10′ [xi]	O1′ [vi]
X′	S5″ [iii]	O1″ [v]	S5″ [vii]	S5″ [viii]	S5″ [x]	S5′ [xii]	S2′ [viii]
Bond lengths							
Sb–S(A)	2.496(3)	2.4679(18)	2.4883(15)	2.4825(6)	2.4777(12)	2.502(3)	2.527(3)
Sb–S(B)	2.673(3)	2.666(2)	2.6047(15)	2.6146(6)	2.6194(13)	2.696(3)	2.648(3)
Sb–S(C)	2.496(3)	2.4679(18)	2.4854(16)	2.5114(6)	2.5080(15)	2.527(3)	2.478(3)
Sb–S(D)	2.673(3)	2.666(2)	2.7228(16)	2.7311(6)	2.7235(16)	2.661(3)	2.529(3)
Sb–X′	3.271(4)	3.131(5)	3.4968(16)	3.3721(7))	3.4016(17)	3.336(4)	3.285(3)
Sb–X″	3.271(4)	3.131(5)	3.3413(15)	3.4965(7)	3.5495(15)	3.354(4)	3.173(8)
Sb···Sb′	–	–	4.3098(8)	4.0636(3)	4.0785(10)	–	3.6008(15)
Bond angles							
S(A)–Sb–S(B)	83.22(13)	83.12(6)	84.45(5)	84.08(2)	84.1(2)	82.6(2)	83.70(8)
S(C)–Sb–S(D)	83.22(13)	83.12(6)	80.55(5)	80.34(2)	80.3(2)	82.9(2)	83.42(9)
S(A)–Sb–S(C)	101.65(13)	105.26(10)	97.17(6)	95.73(2)	95.7(2)	101.5(2)	96.52(9)
S(B)–Sb–S(D)	158.86(13)	157.47(18)	158.99(5)	158.72(2)	159.5(2)	155.6(2)	162.81(9)
S(A)–Sb–S(D)	83.47(13)	83.27(6)	77.97(5)	76.347(19)	77.2(2)	81.3(2)	82.54(9)
S(B)–Sb–S(C)	83.47(13)	83.27(6)	90.43(5)	93.61(2))	93.5(2)	82.5(2)	87.97(9)
X′–Sb–X″	103.54(13)	100.6(2)	101.90(3)	107.481(14)	108.2(2)	103.4(2)	115.84(15)
X′–Sb–S(A)	82.44(13)	86.16(10)	83.40(4)	83.837(18)	83.2(2)	86.1(2)	82.32(8)
X′–Sb–S(B)	120.55(13)	128.96(11)	78.25(4)	85.946(18)	86.8(2)	123.2(2)	106.15(7)
X′–Sb–S(C)	155.98(13)	147.36(10)	168.58(5)	179.409(19)	178.9(2)	154.1(2)	165.56(8)
X′–Sb–S(D)	73.67(13)	67.71(12)	110.64(3)	99.935(18)	99.1(2)	73.8(2)	82.15(8)
X″–Sb–S(A)	155.98(13)	147.36(10)	148.45(4)	145.204(18)	145.8(2)	156.5(2)	151.94(15)
X″–Sb–S(B)	73.67(13)	67.71(12)	66.67(4)	64.661(17)	65.1(2)	74.2(2)	71.06(14)
X″–Sb–S(C)	82.44(13)	86.16(10)	71.73(5)	72.656(18)	72.9(2)	79.4(2)	71.15(15)
X″–Sb–S(D)	120.55(13)	128.96(11)	126.70(4)	130.899(18)	129.8(2)	121.8(2)	119.47(14)
Direction of chain propagation [d]			*a*	*a*	*c*	*a*	*a*
Orientation of chain [e]	(001)	(001)	(010)	(010)	(100)	(01$\bar{1}$)	(011)

For all but (**1**: Q = NEt_4) and (**3**: Q = NEt_4), X″ is the atom which connects the anions into chains, and X′ is the atom used to connect the anions in centrosymmetric pairs with face to face ligands.

[a] Symmetry operations as designated by roman numerals in square brackets: i: $-x, y, 1/2-z$; ii: $x-1/2, 1/2+y, z$; iii: $1/2-x, 1/2+y, 1/2-z$; iv: $-1/2-x, 1/2+y, 1/2-z$; v: $1/2+x, 1/2+y, z$; vi: $x-1, y, z$; vii: $1-x, 1-y, 1-z$; viii: $1-x, 1-y, -z$; ix: $x, y, z-1$; x: $1-x, -y, 1-z$; xi: $1-x, y, z$; xii: $1-x, 2-y, 2-z$.

[b] Ref. [2].

[c] Ref [3].

[d] Direction of propagation of anion chains.

[e] Form of plane parallel to anion (and cation) layers.

chain, are purely chelating. In (**1**: Q = DMP) [2], on the other hand, the secondary Sb–S10 bond, which was overlooked in the original report of this structure, creates a chain in the form of a succession of loops, Fig. 3(d), and both ligands are now μ^2 bridges while still chelating.

In the case of (**1**: Q = $AsPh_4$) and (**1**: Q = PPh_4) [3], which are isostructural despite the different labelling of the cell edges, there is no significant contact between the linear chains within or between the layers and adjacent layers being related to one another purely by cell translation are all identical. In (**1**: Q = NBu_4), which is isostructural with (**2**: Q = NBu_4) [4], there is likewise no significant contact between the chains but adjacent anion layers are now related by the operation of the *n*-glide of the space group $P2_1/n$. In (**1**: Q = DMP) [2], there is no significant contact between the anion layers, once again related by cell translation and, therefore, all identical, where the looped chains are opposed face to face but within the layers edge to edge contacts between the chains as S5···$S5_i$ (*i*: $1-x, 3-y, 2-z$) and S5···$S9^{ii}$ (ii: $1+x, 1+y, z$) at 3.387(4) and 3.544(4)Å, respectively, are found (Fig. 3(d)). Also present here between the chains within the layer is limited overlap of centrosymmetrically related pairs of loop forming ligands comprising C4–C6 and S6–S10 (ring pair b–b′

Table 4
Ring overlaps in terms of PLATON [25] π–π interaction parameters (Å, °) and lateral displacements, O

	Ring pair [a] [symmetry operation]	A	α	β	β'	B	B'	O [b]
(**1**: Q = NBu_4)	a–a′ [vii]	3.534	0	12.80	12.80	3.447	3.447	0.779
(**1**: Q = $AsPh_4$)	a–a′ [viii]	3.512	0	13.37	13.37	3.417	3.417	0.811
(**1**: Q = PPh_4) [c]	a–a′ [x]	3.541	0	13.02	13.02	3.450	3.450	0.798
(**1**: Q = DMP)	a–a′ [xii]	4.245	0	33.50	33.50	3.540	3.540	2.359
	b–b′ [xiii]	5.571	0	48.99	48.99	3.654	3.654	4.205
	a–c′ [xiv]	3.732	8.88	18.20	24.53	3.395	3.545	1.374
(**3**: Q = DMP) [d]	a–a′ [xv]	4.441	0	32.77	32.77	3.734	3.734	2.404
	d–d′ [x]	4.960	0	51.73	51.73	3.072	3.072	3.894
	e–e′ [vii]	4.068	0	40.14	40.14	3.110	3.110	2.622

[a] Rings defined as: (a) C1, C2, S4, C3, S3; (b) C4, C5, S7, C6, S6; (c) the DMP ring; (d) C4, C5, S8, C6, S7; (e) Sb, S1, C1, C2, S2. Symmetry operations as in Table 3, plus: xiii: $-x, 1-y, 1-z$; xiv: $1-x, 2-y, 1-z$; xv: $2-x, 1-y, -z$.

[b] Calculated as $(A^2-B^2)^{1/2}$ for all except in (1: Q = DMP) for the a–c′ overlap, which was calculated as $[A^2-(B+B')^2/4]^{1/2}$. The overlap of rings x and y with centroids Cg_x and Cg_y and points F_x (or F_y) defined as the foot of the perpendicular from Cg_x (or Cg_y) to the plane of ring y (or x) is defined in the manner used by PLATON [25] in terms of the following: distances Cg_x–Cg_y (A); Cg_x–F_x (B) and Cg_y–F_y (B') and angles between the ring planes (α); Cg_y–Cg_x–F_x (β) and Cg_x–Cg_y–F_y (β'). If the rings are related to one another by the operation of a crystallographic centre of symmetry they are by definition parallel to one another and hence $\alpha = 0$, $\beta = \beta'$ and $B = B'$.

[c] Ref. [3].

[d] Ref. [2].

in Table 4). More significant is π–π overlap between the DMP counter cation and the dimer forming ligand (ring pair a–c′ in Table 4). In (**3**: Q = DMP) there is yet again no significant contact between chains within or between layers. However, in this case the use of thiolato S2 in dimer formation promotes overlaps d–d′ and e–e′ (Table 4) within the essentially linear double chains.

3.3. Geometry at Sb

In all of the complexes **1** and **3**, Sb forms six bonds in two groups as four strong intra- and two weaker inter-anion bonds. Inclusion of the Sb lone pair results in pseudo seven-coordinate geometry probably pentagonal bipyramidal in form (see reference [28]). In contrast, the antimony geometry in $[NEt_4][Sb(1,2\text{-}S_2C_6H_4)_2]$ is reported to be pseudo trigonal bipyramidal [7]. The site of the lone pair in compounds (**1**: Q = NBu_4 or $AsPh_4$) is assumed to be as shown in Fig. 4(b) and is exactly the same, allowing for the changed atom numbering scheme, as that previously reported for (**1**: Q = PPh_4) [3]. In all three complexes, the lone pairs on centrosymmetrically related Sb atoms are directed away from one another on opposite sides of the centrosymmetric Sb_2S_2 rings and are in equatorial sites between S5′ and S7. The S5′–Sb–S7 angles [X″–Sb–S(D) in Table 3] are less than twice the ideal ligand–M–ligand angle of 72° but are perceived as sufficiently large [$>126.70(4)°$] to accommodate the lone pair. The axial atoms are S5″ and S6 with angles at Sb [X′–Sb–S(C)] of 168.58(5)°, 179.409(19)° and 178.9(2)°, respectively.

The situation in (**3**: Q = DMP) is similar with the lone pair between O1′ and S6 (Fig. 4(d)). The angle O1′–Sb–S6 is only 119.47(14)° but still regarded as large enough to accommodate the lone pair. The axial atoms are now S2′ and S5 making an angle of 165.56(8)° at Sb which also shows a greater departure from the ideal than the corresponding angles in the previous cases.

The location of the lone pair in isostructural (**1** and **3**: Q = NEt_4) is not so simply or obviously determined. In the earlier report on the structure of (**1**: Q = NEt_4) [2], it was considered to be in an equatorial site between the two Sb–S5 inter-anion bonds, i.e. directed along the crystallographic twofold axis (Fig. 4(a)). It then bisects an angle of only 103.54(13)° which appears extremely small to accommodate it. However, the estimate of this angle has been increased by positing [2] an increase to that of ϕ (Fig. 5), which is achieved if the inter-anion bonds from Sb are directed toward p-orbitals on S (or O) rather than directly toward the atoms. The equivalent bond angle in (**3**: Q = NEt_4) is still less at 100.6(2)° but the same argument regarding the use of ϕ applies here also. The difference between ϕ and the X–Sb–X bond angle (X = S5 or O1) for the same orbitals increases as the Sb–X bond lengths decrease and the inter-anion bonds Sb–S5 and Sb–O1 are the shortest of all inter-anion bonds found in **1** and **3**. Thus the impact of considering orbital overlap rather than direct atom to atom vectors to determine bond direction and hence bond angles will be greatest for these two complexes. With the lone pairs in equatorial sites directed along the twofold axis as just described the axial sites are then occupied by S2 atoms which form the longest intra-anion bonds in these complexes which is appropriate for their perceived axial status. The angle they form, while only about 158°, is, however, the largest subtended at Sb.

Bearing in mind the twofold axial symmetry of these last two complexes, alternative dispositions of the lone pair can also be envisaged. In (**3**: Q = NEt_4) the bond

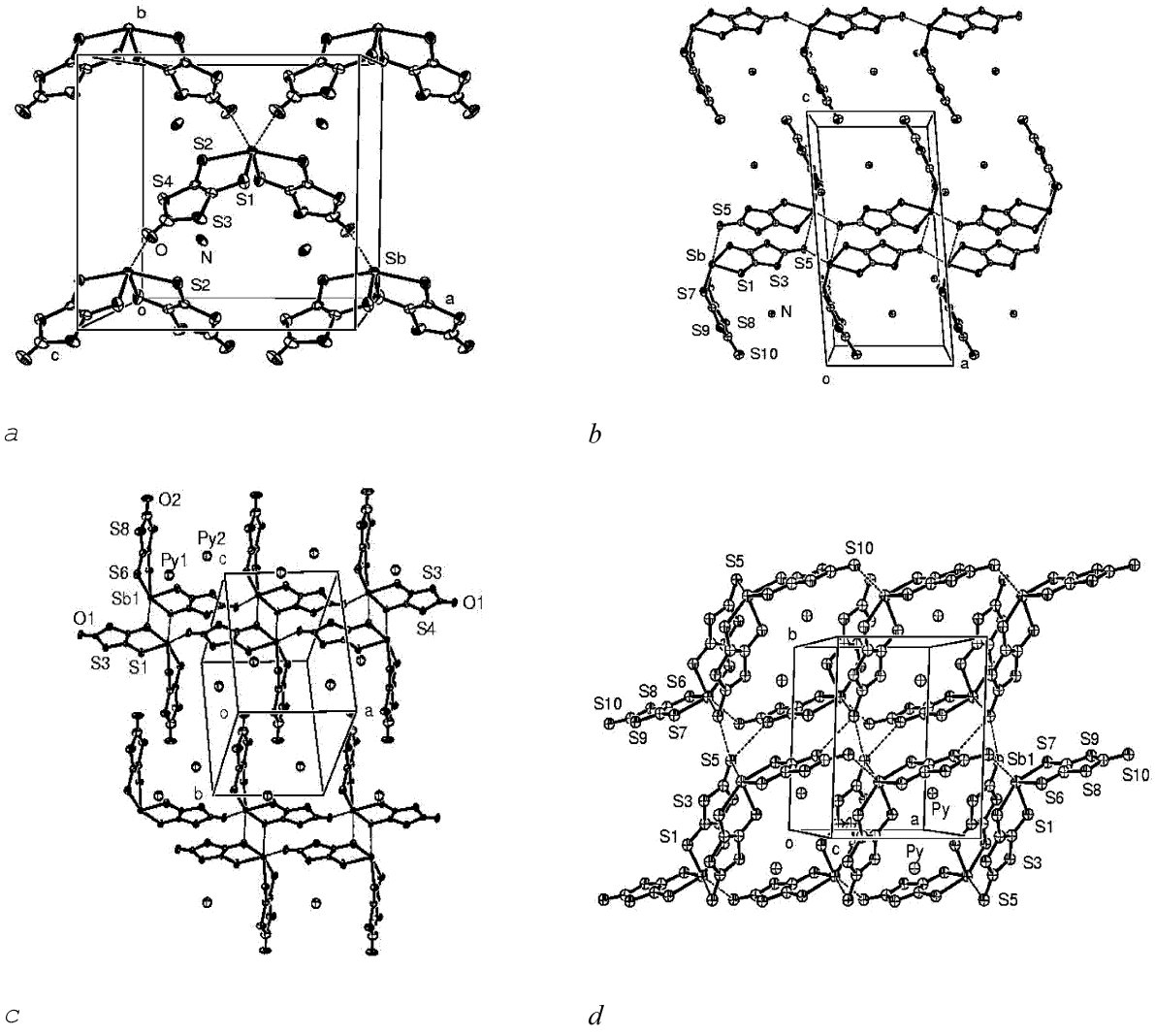


Fig. 3. Anion layers in (a) (**3**: Q = NEt_4], (b) (**1**: Q = NBu_4), (c) (**3**: Q = DMP) and (d) (**1**: Q = DMP) [2]. In all cases only selected atoms are labelled and in a generic manner i.e. lacking symmetry relationships which are instead given in Table 3. Cations are crudely represented either by N or for DMP by the centroid. Atoms are shown as 50% ellipsoids [isotropic atoms for (**1**: Q = DMP)] and the cell edges are labelled. Dashed lines represent Sb–X (X = thione S or one-O) bonds or, in (d), S···S contacts.

angles O1′–Sb1–S2 = O1″–Sb1–S2′ = 128.96(11)°, associated with axial pairs O1″–S1 and O1′–S1′ with *trans*-axial angle 147.36(10)°, are sufficiently large to accommodate the lone pair more easily. If the lone pair occupies only one of these sites the axial symmetry is destroyed but, if the lone pair on Sb occupied an orbital of *d*-type character, it would no longer concentrate electron density towards a single notional coordination site. A similar situation obtains for (**1**: Q = NEt_4) and, see below, (**1**: Q = DMP). Dispersal or smearing out of the lone pair electron density in this way is also consistant with the comparatively short inter-anion Sb–X bonds observed in these complexes.

While crystallographic symmetry does not apply in the case of the remaining complex (**1**: Q = DMP) the atom pairs S1–S6, S2–S7 and S5′–S10′ approximate twofold axial symmetry in their disposition (Fig. 4(c)). On this basis the situation in (**1**: Q = DMP) with angles S10′–Sb–S5′ [103.4(2)°], S2–Sb–S7 [159.5(2)°], S10′–Sb–S7 [121.8(2)°] and S5′–Sb–S2 [123.2(2)°] relates to that in (**3**: Q = NEt_4) and (**1**: Q = NEt_4) with corresponding angles of similar magnitude.

4. Supplementary material

Crystallographic data for the structural analyses have been deposited with the Cambridge Crystallographic Data Centre, CCDC numbers 174409–174412. Copies of this information may be obtained free of charge from

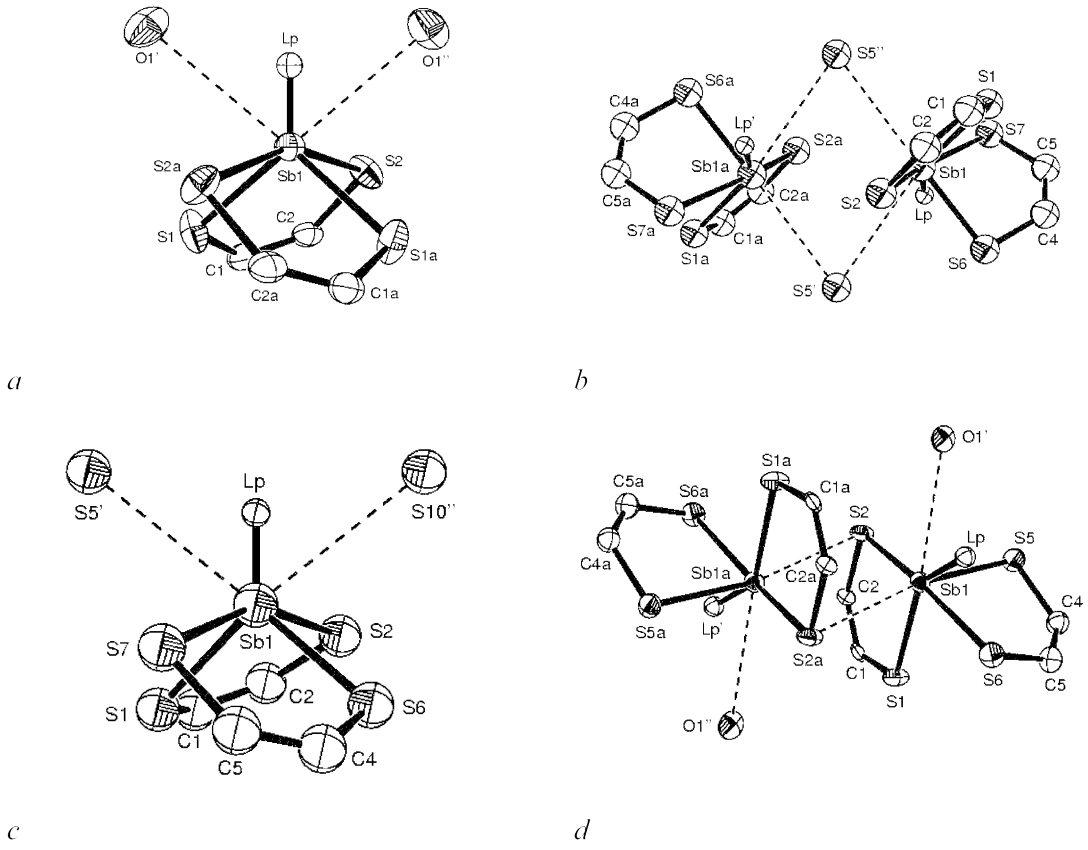


Fig. 4. Representations of the co-ordination of Sb including the stereochemically active lone pair (Lp and where appropriate the centrosymmetrically related Lp′) in (a) (**1**: Q = NEt_4) and (**3**: Q = NEt_4); (b) (**1**: Q = NBu_4, PPh_4 or $AsPh_4$) [the example shown is (**1**: Q = PPh_4)]; (c) (**1**: Q = DMP) and (d) (**3**: Q = DMP). In (a), (b) and (d) the suffix 'a' marks atoms related by symmetry to atoms without suffix. For clarity the ligands providing the primary coordination of Sb are indicated only in terms of the 5-membered chelate rings thus formed.

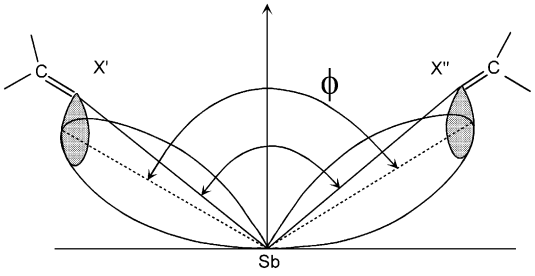


Fig. 5. Comparison of the angle, ϕ, from overlap of Sb and S (or O) orbitals with the S–Sb–S (or O–Sb–O) bond angle.

the Director, CCDC, 12 Union Road, Cambridge CB2 1EZ, UK (fax: +44-1223-336033; e-mail: deposit@ccdc.cam.ac.uk or www: http://www.ccdc.cam.ac.uk).

Acknowledgements

We acknowledge the use of the Chemical Database Service of the EPSRC at Daresbury, UK and the National Data Collection Service of the EPSRC, now at the University of Southampton, previously at the University of Wales, Cardiff, and the expert assistance of the staff there. The financial support of CNPq, FAPERJ and FUJB, Brazil is gratefully acknowledged.

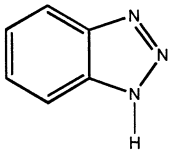
References

[1] (a) P. Cassoux, Coord. Chem. Rev. 186 (1999) 213;
(b) A.E. Pullen, R.M. Olk, Coord. Chem. Rev. 188 (1999) 211.
[2] S.M.S.V. Doidge-Harrison, J.T.S. Irvine, G.M. Spencer, J.L. Wardell, P. Ganis, G. Valle, Inorg. Chem. 34 (1995) 4581.
[3] P. Ganis, D. Marton, G.M. Spencer, J.L. Wardell, S.M.S.V. Wardell, Inorg. Chim. Acta 308 (2000) 139.
[4] N.M. Comerlato, W.T.A. Harrison, R.A. Howie, A.C. Silvino, J.L. Wardell, S.M.S.V. Wardell, Inorg. Chem. Commun. 3 (2000) 572.
[5] T. Sheng, X. Wu, P. Lin, W. Zhang, Q. Wang, L. Chen, Polyhedron 18 (1999) 1049.
[6] N.M. Comerlato, L.A.C. Costa, R.A. Howie, R.P. Pereira, A.M. Rocco, A.C. Silvino, J.L. Wardell, S.M.S.V. Wardell, Polyhedron 20 (2001) 415.
[7] J. Wegener, K. Kirschbaum, D.M. Giolando, J. Chem. Soc., Dalton Trans. (1994) 1213.
[8] (a) J.M. Hough, C.A. Haney, R.D. Bereman, C.E. Keefer, J. Coord. Chem. 51 (2000) 45;

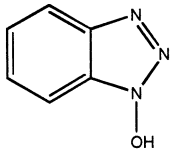
(b) H. Müller, A.P. Molina, B.Z. Narymbetov, L.V. Zorina, S.S. Khasanov, R.P. Shibaeva, Z. Anorg. Allg. Chem. 624 (1998) 1492.
[9] Z.H. Chohan, R.A. Howie, J.L. Wardell, J. Organomet. Chem. 577 (1999) 140.
[10] (a) J.H. Aupers, Z.H. Chohan, P.J. Cox, S.M.S.V. Doidge-Harrison, R.A. Howie, A. Khan, G.M. Spencer, J.L. Wardell, Polyhedron 17 (1998) 4475;
(b) Z.H. Chohan, J.L. Wardell, J.N. Low, P.R. Meehan, G. Ferguson, Acta Crystallogr, Sect. C 54 (1998) 1401.
[11] F. de Assis, Z.H. Chohan, R.A. Howie, A. Khan, J.N. Low, G.M. Spencer, J.L. Wardell, S.M.S.V. Wardell, Polyhedron 18 (1999) 3533.
[12] Z.H. Chohan, R.A. Howie, J.L. Wardell, R. Wilkens, S.M.S.V. Doidge-Harrison, Polyhedron 16 (1997) 2689 (and references therein).
[13] G.M. Allan, R.A. Howie, J.M.S. Skakle, J.L. Wardell, S.M.S.V. Wardell, J. Organomet. Chem. 627 (2001) 189.
[14] D. Lednicer, C.R. Hauser, Org. Synth. 40 (1960) 31.
[15] L. Valade, J.P. Legros, M. Bousseau, P.J. Cassoux, J. Chem. Soc., Dalton Trans. (1985) 783.
[16] J.W. Pflugrath, A. Messerschmidt, MADNES version 11, September, 1989. Distributed by Delft Instruments, Delft, The Netherlands.
[17] A.I. Karaulov, ABSMAD. Program for FAST Data Processing, University of Wales, Cardiff, Wales, 1992.
[18] J.A. Darr, S.R. Drake, M.B. Hursthouse, K.M.A. Malik, Inorg.Chem. 32 (1993) 5704.
[19] S. Parkin, B. Moezzi, H. Hope, J. Appl. Crystallogr. 28 (1995) 53.
[20] Z. Otwinowski, W. Minor, Macromolecular crystallography, Part A, in: C.W. Carter, R.M. Sweet (Eds.), Methods in Enzymology, vol. 276, Academic Press, New York, 1997, pp. 307–326.
[21] R. Hooft, COLLECT, Nonius BV, Delft, The Netherlands, 1998.
[22] (a) R.H. Blessing, Acta Crystallogr., Sect. A 51 (1995) 33–37;
(b) R.H. Blessing, J. Appl. Crystallogr. 30 (1997) 421.
[23] G.M. Sheldrick, Acta Crystallogr., Sect. A 46 (1990) 467.
[24] G.M. Sheldrick, SHELXL-97. Program for Crystal Structure Refinement, University of Göttingen, Germany, 1997.
[25] A.L. Spek, Acta Crystallogr., Sect. A 46 (1990) c-34.
[26] F.H. Allen, O. Kennard, Chem. Des. Autom. News (1993) 1 and 31.
[27] D.A. Fletcher, R.F. McMeeking, D. Parker, J. Chem. Inf. Comput. Sci. 36 (9) (1996) 746.
[28] (a) R.J. Gillespie, Can. J. Chem. 38 (1960) 818;
(b) J.F. Sawyer, R.J. Gillespie, Prog. Inorg. Chem. 34 (1986) 65.

thetic procedures to clusters of middle and late 3d metals in moderate oxidation states with interesting structural and magnetic properties. One of our routes takes advantage of the observation that the 1:1 reactions between metal(II) β-diketonates and benzotriazole (btaH, **I**) or ring-substituted (with non-donor groups) benzotriazoles (RbtaH) lead to incomplete replacement of the β-diketonato ligands by the deprotonated benzotriazoles and large heteroleptic 3d metal cages. Restricting further discussion to nickel(II) chemistry, the systematic investigation of the [Ni(β-diketonate)$_2$L$_2$]–RbtaH reaction mixtures has led to three families of polynuclear complexes: [Ni$_5$(OH)(acac)$_4$(Rbta)$_5$(H$_2$O)$_4$] [18,19], [Ni$_5$(dbm)$_4$(Rbta)$_6$(Me$_2$CO)$_4$] [20] and [Ni$_9$(bzac)$_6$(Rbta)$_{12}$(MeOH)$_6$] [20] (L = H$_2$O, EtOH; acacH = acetylacetone; bzacH = benzoylacetone; dbmH = dibenzoylmethane; RbtaH = 5-methyl-, 6-methyl-, 5,6-dimethyl- and 5-chlorobenzotriazole, or benzotriazole). The families of the Ni$_5$(OH), Ni$_5$ and Ni$_9$ clusters possess the intermediate-spin ground states [$S = 0$, $S = 1$], [$S = 1$, $S = 2$] and [$S = 2$, $S = 3$], respectively. Thus, the benzotriazolate ligands are important players in the field of polynuclear transition metal chemistry.

However, the main reason for which several groups [21–27], involving our group [28–31], have been exploring the coordination chemistry of btaH over the last 25 years is the anticorrosion action of this compound and its benzene ring-substituted derivatives toward certain metals, particularly copper and its alloys [32–37]. Inorganic chemists study the chemical, physical and structural properties of model complexes to probe several aspects of corrosion inhibitors, to understand the complicated surface chemistry that leads to corrosion inhibition and to create new inhibitors more efficient than btaH.



btaH, I



btaOH, II

More recently [38–40], our efforts have turned towards the use of benzotriazoles, substituted on the azole ring with donor groups, to see how incorporation of this ligand type might affect the structures and physical properties of the products. The first ligand employed was 1-hydroxybenzotriazole (btaOH, **II**), a well-known peptide-coupling additive [41], which exhibits corrosion inhibitive properties toward Cu [42,43] and Fe [44]. The synthetic investigation of the [Cu$_2$(O$_2$CMe)$_4$(H$_2$O)$_2$]–btaOH reaction system in MeOH resulted in the isolation of the three-dimensional (3D), diamond-like coordination polymer [Cu(btaO)$_2$(MeOH)]$_n$ (**1**), which is a soft magnet exhibiting two critical temperatures at 6.4 and 4.4 K [38]. Later [39], the reaction of Ni(NO$_3$)$_2$·6H$_2$O with btaOH in aqueous NH$_3$–DMF yielded the trinuclear complex [Ni$_3$(btaO)$_6$(NH$_3$)$_6$] (**2**). Reaction of zerovalent manganese with btaOH and NH$_4$SCN in DMF has recently allowed the isolation of the one-dimensional (1D) polymer [Mn$_3$(btaO)$_2$(SCN)$_4$(DMF)$_8$]$_n$ (**3**) [40].

The flexibility of the 1-hydroxybenzotriazolate ligand (btaO$^-$) observed in the structures of **1**–**3** prompted us to explore further the coordination properties of this anionic ligand with the goal of isolating large clusters. It seemed logical to us that a good starting point of our efforts would be the synthetic investigation of the [Ni(β-diketonate)$_2$L$_2$]–btaOH reaction systems; analogous reaction systems, involving RbtaHs instead of btaOH, had led to the synthesis of the penta- and nonanuclear heteroleptic nickel(II) clusters mentioned above. Here we report the preparation, spectroscopic characterization, X-ray crystal structure and magnetic properties of the structurally novel heptanuclear complex [Ni$_7$(OH)$_2$(acac)$_8$(btaO)$_4$(H$_2$O)$_2$]·MeCN·0.9H$_2$O (**4**·MeCN·0.9H$_2$O), which is the product from the [Ni(acac)$_2$(H$_2$O)$_2$]–btaOH reaction mixture in MeCN.

2. Experimental

2.1. General and physical measurements

All manipulations were performed under aerobic conditions using materials (reagent grade) and solvents as received. Compound [Ni(acac)$_2$(H$_2$O)$_2$] was prepared as described elsewhere [45].

Microanalyses (C, H, N) were performed by the University of Ioannina (Greece) Microanalytical Service using an EA 1108 Carlo Erba analyzer. Nickel analysis was carried out by EDTA titration. IR spectra (4000–500 cm^{-1}) were recorded on a Perkin–Elmer 16 PC FT spectrometer with samples prepared as KBr pellets. Solid-state (diffuse reflectance, 800–300 nm) electronic spectra were recorded on a Varian, Cary 3 instrument. Magnetic susceptibility measurements were carried out on a polycrystalline sample of **4**·H$_2$O in the 300–3 K temperature range using a Quantum Design SQUID susceptometer. The applied magnetic field was 1000 G. The experimental magnetic susceptibilities were corrected for the diamagnetic response using Pascal's constants. The solid-state EPR spectrum of the complex at 4 K was recorded on a Bruker ER 200D-SRC X-band spectrometer, equipped with an Oxford ESR 9 cryostat.

Safety note: Benzotriazoles and benzotriazolate complexes are potentially explosive, and caution should be exercised in handling such compounds. However, the small quantities used in this study were not found to present a hazard.

2.2. Preparation of $[Ni_7(OH)_2(acac)_8(btaO)_4(H_2O)_2]\cdot MeCN\cdot 0.9H_2O$ ($\mathbf{4}\cdot MeCN\cdot 0.9H_2O$)

Solid btaOH·H_2O (0.11 g, 0.7 mmol) was dissolved with stirring in a pale green solution of [Ni(acac)$_2$(H_2O)$_2$] (0.50 g, 1.7 mmol) in MeCN (20 ml) under reflux. The reflux was continued for a further 30 min after dissolution. The resulting deep green solution was layered with an 1:1 mixture (25 ml) of *n*-hexane and Et_2O. Slow mixing yielded light green–blue crystals (some of them were of X-ray quality), which were collected by filtration, washed with cold MeCN and Et_2O, and dried in air. Yields as high as 75% were obtained. The crystals were found to lose solvent readily, and they were kept in the mother liquor until a suitable crystal had been found for X-ray crystallography. The latter established the formulation $\mathbf{4}\cdot MeCN\cdot 0.9H_2O$; the dried analysis sample analyzed for $\mathbf{4}\cdot H_2O$. *Anal.* Found: C, 42.2; H, 4.3; N, 9.3; Ni, 23.2. Calc. for $C_{64}H_{80}N_{12}O_{25}Ni_7$: C, 42.0; H, 4.4; N, 9.2; Ni, 22.5%. IR data (KBr pellet, cm^{-1}): 3390mb, 3074w, 2996w, 2920w, 1598s, 1518s, 1454m, 1398sb, 1262s, 1198m, 1166m, 1140w, 1116m, 1018s, 928s, 852w, 766m, 746s, 670w, 646w, 614sh, 584m, 540sh. Solid-state (diffuse reflectance) electronic spectral data (λ_{max}, nm): 690, 400.

2.3. X-ray crystallography

A light green–blue crystal of $\mathbf{4}\cdot MeCN\cdot 0.9H_2O$ was mounted in a capillary filled with drops of mother liquid. Diffraction measurements were made on a $P2_1$ Nicolet diffractometer upgraded by Crystal Logic using Ni-filtered Cu radiation. Complete crystal data and parameters for data collection and processing are reported in Table 1. Unit cell dimensions were determined and refined by using the angular settings of 25 automatically centred reflections in the range $24° < 2\theta < 54°$. Three standard reflections, monitored every 97 reflections, showed less than 3% intensity fluctuation and no decay. Lorentz, polarization and Ψ-scan absorption corrections were applied using CRYSTAL LOGIC software.

The structure was solved by direct methods using SHELXS-86 [46] and refined by full-matrix least-squares techniques on F^2 with SHELXL-93 [47]. Hydrogen atoms of C(42), C(52) and C(62) of the acac$^-$ ligands were located by difference maps and refined with isotropic thermal parameters. The hydrogen atoms on the hydroxo and aqua ligands were located by difference maps and refined in fixed positions. All the rest hydrogen atoms were introduced at calculated positions as riding on bonded atoms. All non-hydrogen atoms were refined anisotropically, except those of the solvent H_2O molecules which were refined isotropically with occupation factors fixed at 0.30.

Table 1
Crystallographic data for complex $\mathbf{4}\cdot MeCN\cdot 0.9H_2O$

Formula	$C_{66}H_{82.8}N_{13}O_{24.9}Ni_7$
Formula weight	1867.62
Crystal colour, habit	green–blue, prism
Crystal dimensions (mm)	$0.10 \times 0.20 \times 0.70$
Crystal system	monoclinic
Space group	$P2/c$
a (Å)	34.163(7)
b (Å)	11.926(3)
c (Å)	23.515(5)
β (°)	94.44(1)
V (Å^3)	9552(3)
Z	4
D_{calc} (g cm^{-3})	1.299
Radiation, Cu Kα (λ, Å)	1.54180
Temperature (K)	298
Scan mode/speed (° min^{-1})	$\theta-2\theta/1.5$
$2\theta_{max}$ (°)	91.0
Reflections collected	8171
Unique reflections (R_{int})	7883 (0.0362)
Data with $I > 2\sigma(I)$	5642
Parameters refined	1049
$[\Delta/\sigma]_{max}$	0.011
$(\Delta\rho)_{max}$, $(\Delta\rho)_{min}$ (e Å^{-3})	1.157, −0.380
w [a]	$a = 0.1401$, $b = 37.9872$
Goodness-of-fit (on F^2)	1.096
$R1$ [b]	0.0623
$wR2$ [c]	0.1950

[a] $w = 1/[\sigma^2(F_o^2)+(aP)^2+bP]$ and $P = (\max(F_o^2,0)+2F_c^2)/3$.
[b] $R1 = \Sigma(|F_o|-|F_c|)/\Sigma(|F_o|)$.
[c] $wR2 = \{\Sigma[w(F_o^2-F_c^2)^2]/\Sigma[w(F_o^2)^2]\}^{1/2}$.

3. Results and discussion

3.1. Synthesis

The preparation of compound $\mathbf{4}\cdot MeCN\cdot 0.9H_2O$ was achieved via the reaction of [Ni(acac)$_2$(H_2O)$_2$] with btaOH·H_2O in MeCN under reflux. The preparation is summarized in Eq. (1).

$$7[Ni(acac)_2(H_2O)_2] + 4\ btaOH\cdot H_2O + MeCN \xrightarrow[T]{MeCN} \underset{\mathbf{4}\cdot MeCN\cdot 0.9H_2O}{[Ni_7(OH)_2(acac)8(btaO)4(H_2O)_2]\cdot MeCN\cdot 0.9H_2O} + 6\ acacH + 13.1\ H_2O \quad (1)$$

Obviously btaOH is deprotonated by the basic acac$^-$ groups. The excess of [Ni(acac)$_2$(H_2O)$_2$] used in the reaction leaves an amount of nonprotonated acac$^-$ in the mixture and the heptanuclear cluster results from the acac$^-$–btaO$^-$ ligand 'blend'.

The exact metal to ligand molar ratio does not affect the identity of the product in MeCN provided that the

acac$^-$ to btaOH ratio is large; thus complex **4**·MeCN·0.9H_2O is the only product from the 4:1 and 3:1 reactions between [Ni(acac)$_2$(H_2O)$_2$] and btaOH·H_2O in MeCN.

The same product can be isolated from Me_2CO. The 7:4 reaction of [Ni(acac)$_2$(H_2O)$_2$] and btaOH·H_2O in refluxing Me_2CO results in a blue–green solid which, on the basis of microanalytical, IR and UV–Vis data, appears to be [$Ni_7(OH)_2(acac)_8(btaO)_4(H_2O)_2$]·$H_2O$ (**4**·H_2O).

Temperature is a particularly important synthetic parameter for the isolation of **4**. If the reaction mixtures in MeCN or Me_2CO are not refluxed, they yield non-hydroxo species with non-reproducible analytical results.

Complex **4** is moderately soluble in MeOH under heating, but it is readily soluble in DMF and DMSO.

3.2. IR and UV–Vis spectra

In the IR spectrum, the heptanuclear cluster exhibits a broad band of medium intensity at 3390 cm^{-1} assignable [48] to $\nu(OH)_{OH^-H_2O}$. The broadness and relatively low frequency of this band are both indicative of strong hydrogen bonding. A series of four bands is found in the 1600–1390 cm^{-1} region. Contributions from benzotriazolate ν(C=C) and ν(C=N) vibrations would be expected in this region [19], but overlap with the $\nu(C{=}C)_{acac^-}$, $\nu(C{=}O)_{acac^-}$, $\delta(CH)_{acac^-}$ and $\delta_d(CH_3)$ bands [48] renders assignments difficult. The strong band at 1018 cm^{-1} is assigned to the $\rho_r(CH_3)$ mode of the acac$^-$ ligands [48]. The bands in the 1200–1100 cm^{-1} are associated with the ν_{as}(N···N···N), ν_s(N···N···N) and ν(N–O) modes of vibration [26,38–40] but detailed assignments seem impossible. Most probably the band at 1166 cm^{-1} is due to ν(N–O) [38–40]. This band is shifted to lower wavenumbers in **4** compared with its frequency (1224 cm^{-1}) in the IR spectrum of potassium salt of 1-hydroxybenzotriazolate, btaOK. Such a large shift to lower frequencies was also observed [38,40] in the spectra of **1** and **3**, where the deprotonated oxygen is a donor atom.

The solid-state UV–Vis spectrum of **4** exhibits d–d maxima typical [49] of octahedral nickel(II). The bands at 690 and 400 nm are assigned to the spin-allowed transitions $^3A_{2g}\rightarrow{}^3T_{1g}$(F) and $^3A_{2g}\rightarrow{}^3T_{1g}$(P), respectively, under O_h symmetry. The wavelengths are in accord with Ni(II) chromophores rich in O-donors [49].

3.3. Description of structure

A plot of the molecular structure of **4**·MeCN·0.9H_2O is shown in Fig. 1 and selected interatomic distances and angles are collected in Table 2.

The complex crystallizes with a pseudo twofold axis passing through Ni(1) and the middle of the Ni(2)···Ni(3) distance. The heptanuclear assembly is held together by two μ_3-OH$^-$ ions [O(2), O(3)], two terminal H_2O molecules, two η^2:η^1:η^1:μ_4-btaO$^-$ ligands (or 4.211 using Harris notation [50]), two η^1:η^1:μ_2-btaO$^-$ ligands (or 2.011 using Harris notation [50]) which use only their nitrogen atoms for coordination, four chelating η^2-acac$^-$ groups (or 1.11), two η^1:η^2:μ_2-acac$^-$ groups (or 2.21) and two η^2:η^2:μ_3-acac$^-$ groups (or 3.22). According to Harris notation, the binding mode of a ligand is referred to as $X.\ Y_1Y_2Y_3\ldots Y_n$, where X is the overall number of metals bound by the whole ligand and each value of Y refers to the number of metal ions attached to the different donor atoms. The ordering of Y is listed by the Cahn–Ingold–Prelog priority rules, hence here O before N. Therefore, for the 1-hydroxybenzotriazolate ligands of **4**·MeCN·0.9H_2O there will be three values of Y, as there are three donor atoms. Similarly for the acetylacetonate ligands there will be two values of Y, as there are two donor atoms. The notation for the hydroxo and aqua ligands includes one Y value. The seven bonding modes of the ligands, and the Harris notation to describe these modes, are given in Fig. 2.

The btaO$^-$ ligands binding with the 4.211 mode are those involving O(11) and O(21), and they bridge the tetrads Ni(1), Ni(3), Ni(4), Ni(6) and Ni(1), Ni(2), Ni(5), Ni(7), respectively. The btaO$^-$ ligands binding with the 2.011 mode are those involving O(1) and O(31), and they bridge the pairs Ni(2), Ni(4) and Ni(3), Ni(5), respectively. The four chelating acac$^-$ groups are those involving the oxygen atoms O(41), O(42)/O(43), O(44)/O(47), O(48)/O(53), O(54) and they are parts of the coordination spheres of Ni(2), Ni(6), Ni(3) and Ni(7), respectively. The two μ_2 (2.21) acac$^-$ ligands involve the oxygen atoms O(51), O(52)/O(55), O(56) and they bridge the Ni(4), Ni(6)/Ni(5), Ni(7) pairs through O(51) and O(56), respectively. The two acac$^-$ ligands adopting the 3.22 mode are those containing the oxygen atoms O(45), O(46)/O(49), O(50) and they bridge the Ni(1), Ni(4), Ni(6) and Ni(1), Ni(5), Ni(7) triads, respectively. The hydroxo ligands bridge the triads Ni(1), Ni(2), Ni(4) and Ni(1), Ni(3), Ni(5). Thus, the central metal ion of the cluster [Ni(1)] is attached exclusively to six bridging oxygen atoms [O(2), O(3), O(46), O(49), O(11), O(21)].

All terminal, i.e. chelating, acetylacetonate ligands form short Ni–O bonds, with a range of 1.969(9)–2.013(7) Å. For the μ_2 acac$^-$ ligands, the bridging Ni–O bonds [2.036(7)–2.104(6) Å] are longer than the terminal ones [1.988(8) and 2.004(7) Å]. Each of the acac$^-$ ligands adopting the 3.22 mode forms three relatively short Ni–O bonds [2.039(7)–2.084(6) Å], whereas one bridging atom [O(45), O(50)] forms a long bond [2.213(6) and 2.230(7) Å, respectively] to the non-chelated Ni(II) atom [Ni(6) and Ni(7), respectively]. The Ni–O bonds to the bridging hydroxides [average value:

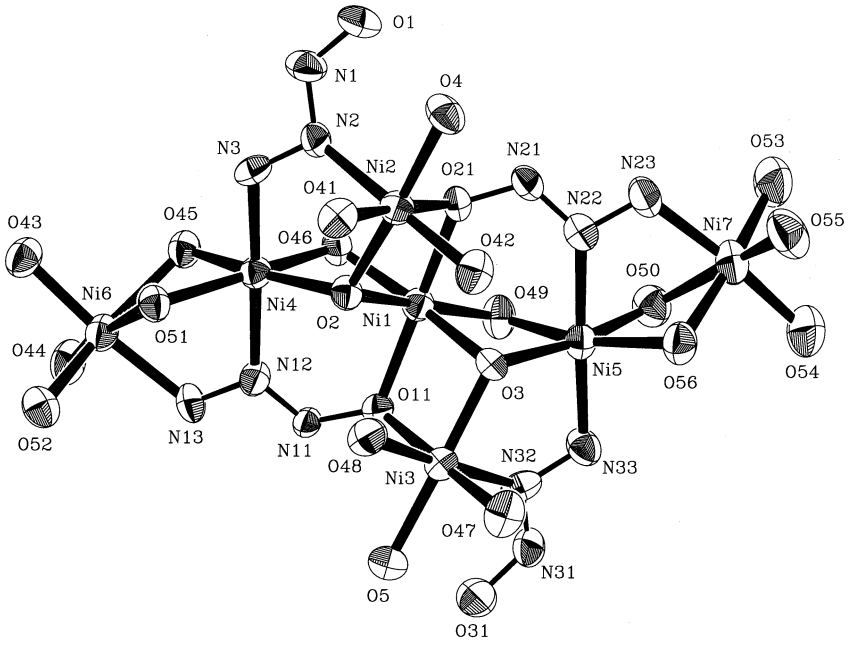


Fig. 1. ORTEP view of **4**·MeCN·0.9H_2O with 50% thermal ellipsoids showing the atom labeling scheme. To avoid congestion, all carbon atoms and the solvate molecules have been omitted. Atoms O(1), O(11), O(21) and O(31) belong to the deprotonated 1-hydroxybenzotriazolate (btaO$^-$ ligands). Atoms O(2) and O(3) belong to the hydroxo ligands, while the coordinated water oxygen atoms are O(4) and O(5). Each of the pairs O(41), O(42)/O(43), O(44)/O(45), O(46)/O(47), O(48)/O(49), O(50)/O(51), O(52)/O(53), O(54)/O(55), O(56) belongs to a different acac$^-$ ligand.

2.033(6) Å] are slightly shorter than those to the terminal aqua ligands [average value: 2.066(7) Å]. The four Ni–$N_{\mu_4\text{-btaO}-}$ bond lengths [2.076(8)–2.097(8) Å] are almost equal, while each μ_2 btaO$^-$ ion forms one strong [2.026(8) and 2.035(9) Å] and one weaker [2.157(8) and 2.171(8) Å] bond to the Ni(II) atoms. The Ni–N distances are generally within the normal range observed for other structurally characterized nickel(II)-benzotriazolate complexes [19,20,39].

The metal centres have distorted octahedral geometries; the chromophores are NiO_6 for Ni(1), NiO_5N for Ni(2), Ni(3), Ni(6) and Ni(7) and *trans*-NiO_4N_2 for Ni(4) and Ni(5).

The crystal structure is stabilized by a strong, intermolecular hydrogen bond involving one coordinated H_2O molecule [O(4)] as donor and the deprotonated 1-hydroxybenzotriazolate oxygen O(31) as acceptor (Table 3). There are also intramolecular hydrogen bonds (Table 3). Of particular interest are the two very strong hydrogen bonds with the coordinated H_2O oxygens O(4) and O(5) as donors and the deprotonated 1-hydroxybenzotriazolate oxygens O(1) and O(31), respectively, as acceptors.

Complex **4** is only the second structurally characterized Ni(II) complex comprising three different types of acac$^-$-ligation, the first example being the well-known trinuclear species $[Ni_3(acac)_6]$ [51].

Complex **4** joins a small family [52–57] of structurally characterized, discrete heptanuclear Ni(II) clusters with O- and/or N-ligation.

The structures displayed by the 3d-metal heptanuclear complexes containing N- or O-donors are mostly irregular [11]. There are a number of 'metallacrowns' [53,58–63], vertex-sharing double cubanes [64–67], oxo-centred vertex-sharing bitetrahedra [68,69], one example where two Mn_4O_2 butterfly units are fused together by sharing of one wing-tip Mn(III) atom [70] and three examples from cobalt chemistry [11] where the metal core can be derived from a square-based pyramid, capped on one edge of the square base and on the neighboring triangular face by two further Co(II) atoms. However, many other heptanuclear compounds [11,71–74] have no easily describable core. Complex **4** is no exception; the seven Ni(II) atoms do not seem to define any established topology.

3.4. Magnetochemistry

The magnetic susceptibility of **4**·H_2O was measured in the 3.0–300 K temperature range. The $\chi_M T$ product (χ_M is the corrected molar magnetic susceptibility per heptamer) decreases from a value of 7.28 $cm^3\ mol^{-1}$ K at 300 K to a value of 2.1 $cm^3\ mol^{-1}$ K at 3.0 K (Fig. 3). The spin-only value for seven uncoupled Ni(II) atoms is 7.66 $cm^3\ mol^{-1}$ K for $g = 2.1$ (this g value is reasonable for polynuclear Ni(II) species [52,75]), close to the experimental value at r.t.

Complex **4** has not any crystallographic symmetry; therefore, in principle, for this cluster there are a large number of independent exchange interactions. This

Table 2
Selected interatomic distances (Å) and bond angles (°) for complex **4**·MeCN·0.9H_2O

Bond lengths					
Ni(1)···Ni(2)	3.111(2)	Ni(2)···Ni(4)	3.519(1)	Ni(3)···Ni(7)	6.546(2)
Ni(1)···Ni(3)	3.125(2)	Ni(2)···Ni(5)	4.916(1)	Ni(4)···Ni(5)	6.085(2)
Ni(1)···Ni(4)	3.054(2)	Ni(2)···Ni(6)	6.563(2)	Ni(4)···Ni(6)	3.141(2)
Ni(1)···Ni(5)	3.041(2)	Ni(2)···Ni(7)	6.740(2)	Ni(4)···Ni(7)	8.721(2)
Ni(1)···Ni(6)	5.798(2)	Ni(3)···Ni(4)	4.930(2)	Ni(5)···Ni(6)	8.726(2)
Ni(1)···Ni(7)	5.790(2)	Ni(3)···Ni(5)	3.544(2)	Ni(5)···Ni(7)	3.133(2)
Ni(2)···Ni(3)	5.018(1)	Ni(3)···Ni(6)	6.810(2)	Ni(6)···Ni(7)	11.573(2)
Ni(1)–O(2)	2.025(6)	Ni(3)–O(47)	1.995(7)	Ni(5)–N(22)	2.097(8)
Ni(1)–O(3)	2.038(6)	Ni(3)–O(48)	2.003(7)	Ni(5)–N(33)	2.035(9)
Ni(1)–O(49)	2.059(6)	Ni(3)–O(11)	2.148(6)	Ni(6)–O(43)	1.989(7)
Ni(1)–O(46)	2.074(6)	Ni(3)–N(32)	2.171(8)	Ni(6)–O(44)	1.983(7)
Ni(1)–O(11)	2.103(6)	Ni(4)–O(2)	2.015(6)	Ni(6)–O(45)	2.213(6)
Ni(1)–O(21)	2.105(6)	Ni(4)–O(45)	2.051(6)	Ni(6)–O(51)	2.052(6)
Ni(2)–O(2)	2.051(6)	Ni(4)–O(46)	2.084(6)	Ni(6)–O(52)	2.004(7)
Ni(2)–O(4)	2.055(7)	Ni(4)–O(51)	2.104(6)	Ni(6)–N(13)	2.076(8)
Ni(2)–O(41)	1.985(7)	Ni(4)–N(3)	2.026(8)	Ni(7)–O(50)	2.230(7)
Ni(2)–O(42)	2.013(7)	Ni(4)–N(12)	2.089(8)	Ni(7)–O(53)	1.975(8)
Ni(2)–O(21)	2.129(7)	Ni(5)–O(3)	2.032(6)	Ni(7)–O(54)	1.969(9)
Ni(2)–N(2)	2.157(8)	Ni(5)–O(49)	2.055(6)	Ni(7)–O(55)	1.988(8)
Ni(3)–O(3)	2.038(6)	Ni(5)–O(50)	2.039(7)	Ni(7)–O(56)	2.036(7)
Ni(3)–O(5)	2.077(7)	Ni(5)–O(56)	2.073(7)	Ni(7)–N(23)	2.083(9)
Bond angles					
O(2)–Ni(1)–O(3)	95.5(3)	O(47)–Ni(3)–O(11)	177.3(3)	O(44)–Ni(6)–O(51)	170.9(3)
O(2)–Ni(1)–O(49)	174.8(3)	O(48)–Ni(3)–N(32)	177.0(3)	O(52)–Ni(6)–N(13)	93.4(3)
O(49)–Ni(1)–O(11)	88.8(3)	N(3)–Ni(4)–O(45)	94.3(3)	O(43)–Ni(6)–N(13)	173.8(3)
O(3)–Ni(1)–O(46)	174.9(3)	O(2)–Ni(4)–O(45)	164.4(3)	O(45)–Ni(6)–O(52)	165.8(3)
O(11)–Ni(1)–O(21)	174.0(3)	O(46)–Ni(4)–N(12)	88.1(3)	O(54)–Ni(7)–O(56)	91.0(3)
O(2)–Ni(2)–O(41)	95.5(3)	O(46)–Ni(4)–O(51)	160.5(3)	O(53)–Ni(7)–O(56)	173.4(3)
O(2)–Ni(2)–O(4)	172.1(3)	N(3)–Ni(4)–N(12)	177.4(3)	O(56)–Ni(7)–N(23)	85.7(3)
O(42)–Ni(2)–O(21)	88.6(3)	O(3)–Ni(5)–O(49)	80.5(3)	O(54)–Ni(7)–N(23)	172.2(4)
O(42)–Ni(2)–N(2)	176.7(3)	O(3)–Ni(5)–O(50)	166.4(3)	O(50)–Ni(7)–O(55)	165.7(3)
O(41)–Ni(2)–O(21)	176.2(3)	O(50)–Ni(5)–O(56)	78.2(3)	Ni(1)–O(2)–Ni(2)	99.5(3)
O(47)–Ni(3)–O(48)	92.0(3)	O(49)–Ni(5)–O(56)	162.8(3)	Ni(1)–O(2)–Ni(4)	98.2(3)
O(3)–Ni(3)–O(5)	172.3(3)	N(22)–Ni(5)–N(33)	177.5(3)	Ni(1)–O(3)–Ni(3)	100.1(3)
O(48)–Ni(3)–O(11)	90.3(3)	O(43)–Ni(6)–O(44)	91.6(3)	Ni(3)–O(3)–Ni(5)	121.1(3)

would lead to the fit being vastly over-parameterized in any computational model. Therefore, we decided to attempt to fit the data using the simplest possible coupling scheme. The best simple model to fit the susceptibility data is a 3-J model. The magnetic model that was used is shown graphically in Fig. 4. Only the monoatomic O bridges (derived from the OH^-, $acac^-$ and $btaO^-$ ligands) have been taken into consideration for more effective coupling, and the exchange interactions are defined mainly according to the Ni–O–Ni angle and the distance between the Ni(II) atoms. Exchange interactions for distances more than 4 Å were excluded. The corresponding zero-field Hamiltonian is given in Eq. (2).

$$H = -2J_1[S_1(S_3 + S_2) + S_7S_5 + S_4S_6] - 2J_2[S_1(S_5 + S_4)] - 2J_3(S_2S_4 + S_3S_5) \quad (2)$$

Due to the low symmetry of the cluster, an efficient procedure [76] was applied using irreducible tensor operators and point symmetry classification of the functions. Following this procedure the exchange matrix, initially of size 2187×2187, is formed by S-block matrices with a maximum size of 105×105. By fixing the value of g to 2.0, the fitting parameters are $J_1 = 0.45$ cm^{-1}, $J_2 = 11.0$ cm^{-1} and $J_3 = -13.7$ cm^{-1}. The theoretical curve is shown in Fig. 3 as a solid line. Table 4 gives selected bond lengths and angles according to Fig. 4.

When we considered a 4-J model using the Hamiltonian given in Eq. (3)

$$H = -2J_1[S_1(S_3 + S_2)] - 2J_2[S_1(S_5 + S_4)] - 2J_3(S_2S_4 + S_3S_5) - 2J_4(S_7S_5 + S_4S_6) \quad (3)$$

no improvement of the fit was succeeded and the values of the J_1, J_4 parameters were almost equal ($J_1 \approx J_4$). For the same reason we did not use zero-field terms in the Hamiltonian, although it seems that they play an important role in the low-temperature limit.

The obtained J values are in agreement with magnetostructural correlations found in nickel(II) clusters [19,77–81]. The negative (antiferromagnetic) value of J_3 is explained by the fact that both Ni(2)–O(2)–Ni(4)

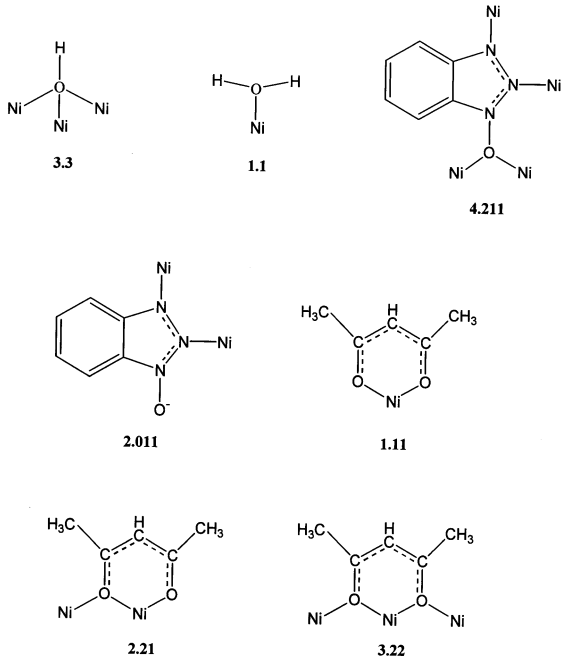


Fig. 2. The seven different coordination modes of the ligands present in the heptanuclear cluster, and the Harris notation [50] to describe these modes.

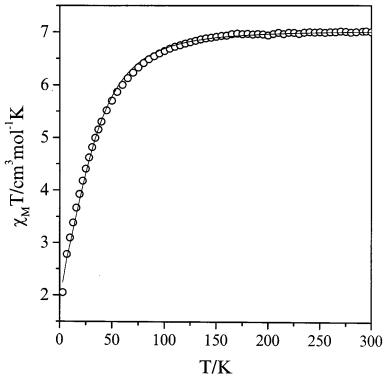


Fig. 3. Plot of $\chi_M T$/Ni(II)$_7$ vs. T for **4**·H_2O. The solid line represents the fit to the theoretical model; see the text for the fitting parameters.

and Ni(3)–O(3)–Ni(5) angles (119.9°, 121.1°) are well above the limit (approximately 100°) from which the Ni–μ_3(OH^-)–Ni interactions become antiferromagnetic [19,75,79–82]. The ferromagnetic values of J_1 and J_3 are in agreement with the relatively small (< 100°) Ni–O–Ni bond angles within the Ni(1)···Ni(3), Ni(1)···Ni(2), Ni(5)···Ni(7), Ni(4)···Ni(6), Ni(1)···Ni(5) and Ni(1)···Ni(4) pairs, see Table 4.

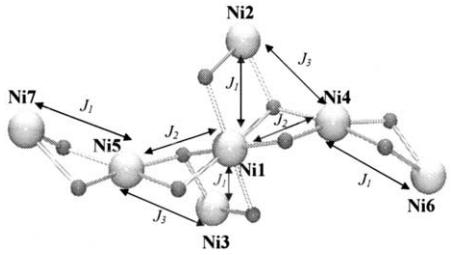


Fig. 4. The simplified magnetic model used for **4** with the monoatomic O bridges and the exchange pathways between the Ni(II) atoms at distances < 4 Å. The numbering scheme used for the Ni(II) atoms is the same with that used in Fig. 1.

According to the J values the ground state of the system is $S = 1$ with two excited states, $S = 0$ and $S = 2$, very close to it (0.57 and 1.19 cm^{-1}, respectively).

In order to validate the correctness of the fit, a simulation of the magnetization data at 4 K was carried out employing the parameters deduced from the fitting of the susceptibility data. As it can be seen in Fig. 5, the model reproduces the behavior of the magnetization versus field quite well.

The presence of a state with an integer spin which is thermally populated at 4 K is confirmed by the EPR spectrum of **4** (Fig. 6), which shows a transition centred at approximately 800 G due to small zero-field splitting effects. A HF-EPR spectrum is needed to resolve the broad line to proceed to a satisfactory interpretation.

4. Conclusions and perspectives

The 3d-metal β-diketonates–benzotriazoles chemistry seems to continue its promise as a source of polynuclear complexes with interesting structures and properties. When the 3d-metal is copper(II) this general reaction system gives pentanuclear clusters of the general formula $[Cu_5(L–L)_4(bta)_6]$, where L–L represents various diketonate ligands [21,22]. When the 3d-metal is nickel(II) the products of this general reaction system are the

Table 3
Hydrogen bonding details for complex **4**·MeCN·0.9 H_2O

D–H···A	D···A (Å)	H···A (Å)	D–H···A (°)	Symmetry equivalence of A
O(2)–H(O2)···O(48)	2.839	2.225	149.6	x, y, z
O(3)–H(O3)···O(42)	2.821	1.951	153.9	x, y, z
O(4)–HA(O4)···O(1)	2.654	1.672	161.3	x, y, z
O(4)–HB(O4)···O(31)	2.781	1.907	166.0	$x, -1+y, z$
O(5)–HA(O5)···O(31)	2.665	1.739	172.3	x, y, z
O(5)–HB(O5)···N_{MeCN}	2.981	2.008	159.4	x, y, z

A = acceptor; D = donor.

Table 4
Structural characteristics of the magnetic model shown in Fig. 4

J values	Interatomic distances (Å)		Ni–O–Ni angles (°)
J_1	Ni(1)···Ni(3)	3.125	94.7/100.1
	Ni(1)···Ni(2)	3.111	94.6/99.5
	Ni(5)···Ni(7)	3.133	94.3/99.4
	Ni(4)···Ni(6)	3.141	94.8/98.2
J_2	Ni(1)···Ni(5)	3.041	96.7/95.3
	Ni(1)···Ni(4)	3.054	98.2/94.5
J_3	Ni(2)···Ni(4)	3.519	119.9
	Ni(3)···Ni(5)	3.544	121.1

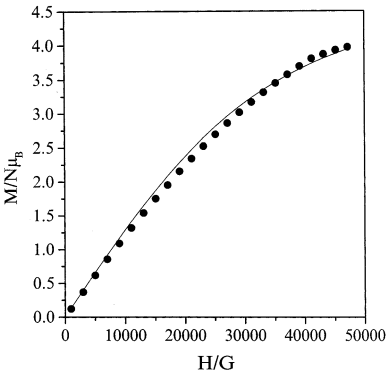


Fig. 5. Magnetization study of **4**·H_2O at 4 K in the field range 0–5 T. The solid line represents the simulation of the magnetization data employing the parameters deduced from the fitting of the susceptibility data.

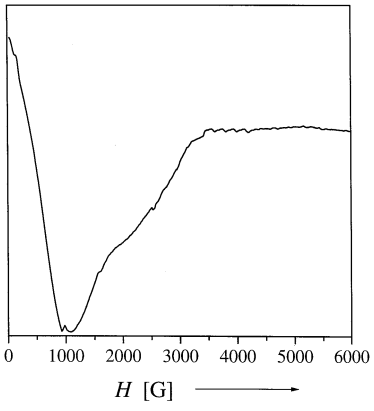


Fig. 6. The X-band EPR spectrum of **4**·H_2O at 4 K.

$Ni_5(OH)$, Ni_5 and Ni_9 clusters [18–20] mentioned in the Introduction; the structures of the products depend mainly on the nature of the β-diketonate ligand. Complex **4** is a new addition in the Ni(II)–β-diketonates–benzotriazoles family of clusters. From a synthetic inorganic viewpoint, the isolation of **4** shows that it is possible to generate Ni(II) clusters with nuclearities significantly different than those known to date (Ni_5, Ni_9) by perturbations to the Ni(II)–β-diketonate–benzotriazole reaction system, in the present case, the introduction of a donor substituent group in the azole ring of benzotriazole. From the magnetic viewpoint, an attempt was made to fit the data of a compound of high nuclearity ($Ni(II)_7$). The ground state is $S = 1$ with $S = 0$ and $S = 2$ low-lying excited states.

Compound **4** is the seventh structurally characterized complex of any metal containing btaO$^-$ ligands. Compounds **1**, **2** and **3** (see Section 1), synthesized by our group [38–40], are coordination complexes (Werner-type). The other three compounds are the organometallic complexes $[Os_3H(CO)_{10}(btaO)]$ (**5**), $[Os_3(C{=}NHPr^n)(CO)_{10}(btaO)]$ (**6**) and $[Os_3(C{=}NHCH_2Ph)(CO)_{10}(btaO)]$ (**7**) containing bridging hydrido (**5**) or bridging aminocarbyne (**6**, **7**) ligands [83]. The 1-hydroxybenzotriazolate(−1) ligand (btaO$^-$) adopts four different coordination modes in the seven compounds, conveniently shown in Fig. 7; for the reader's convenience, we have incorporated in Fig. 7 the bonding modes exhibited by the btaO$^-$ ligands in **4** (although these modes were also shown in Fig. 2). In the 3D coordination polymer **1**, both btaO$^-$ ions adopt the bonding mode 2.101, i.e. they function as bidentate bridging ligands with N(3) and the deprotonated oxygen being the ligating atoms [38]. In the trinuclear complex **2**, all the btaO$^-$ ions bind with the 2.011 mode with the uncoordinated, deprotonated oxygen participating in hydrogen bonding with the ammine ligands [39]. In the 1D coordination polymer **3**, the btaO$^-$ exhibits the coordination mode 3.201. As described in Section 3.3, the btaO$^-$ ligands adopt two different coordination modes in **4**; two bind with the 4.211 mode and two with the 2.011 mode. It is clear that only the 2.011 mode is found in more than one compounds, i.e. in **2** and **4**–**7**. The coordinative flexibility of btaO$^-$ observed in the structures of **1**–**7** makes this ion a versatile new ligand

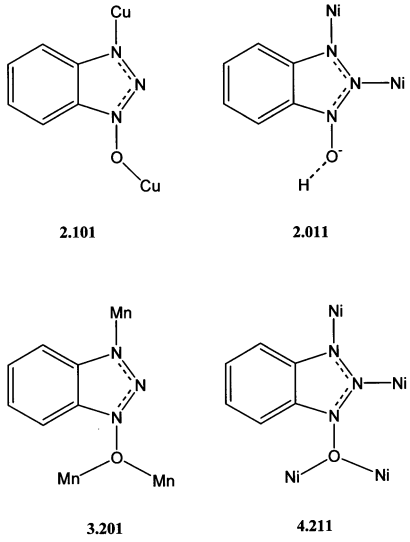


Fig. 7. The crystallographically established coordination modes of the 1-hydroxybenzotriazolate(−1) ligand (btaO$^-$).

for a variety of objectives/advantages, including variable denticity levels, high-nuclearity cluster formation, linking of clusters into 2D, 2D and 3D polymeric arrays, 3d–4f mixed-metal chemistry and ferromagnetic exchange interactions.

Very recently Winpenny reported [1] that the idea of synthesizing polynuclear compounds without strictly designing the final product is an extremely productive means of producing new polymetallic cages. In this approach, termed 'serendipitous assembly' (as a contrast to the designed assembly approach), the element of strict design is absent. In contrast to designed assembly, ligands are used that display several different coordination modes. Much interesting synthetic work can arise where results, originally obtained by chance, are exploited through design. It is clear that the structure of **4** is not a structure we would choose to design. Therefore, the isolation of this complex has been achieved in the context of serendipitous assembly. Since the blend of nickel(II) with $acac^-$ and $btaO^-$ generated an interesting cluster, a rational extension of the work presented here is to look at other 3d-metals, for example manganese(II) and cobalt(II). Another rational extension is to try to find out if the Ni(II)–β-diketonate–$btaO^-$ blend can be extended fruitfully to other β-diketonate ligands, e.g. dbm^-, $bzac^-$.

We wish to do a last comment on the anticorrosion properties of btaOH (**II**). The corrosion inhibitive properties of benzotriazole (btaH, **I**) have been attributed to the 3.111, i.e. μ_3, coordination of its conjugate base, bta^-, that leads to the formation of a tight, close-packed, inert surface polymer [21,26,35–37]. The anticorrosion action of btaOH [42–44] may be associated with the capability of its conjugate base, $btaO^-$, to bridge three (as in **3**) or four (as in **4**) metal ions.

5. Supplementary material

Crystallographic data for the structural analysis have been deposited with the Cambridge Crystallographic Centre, CCDC No. 102274 for complex **4**·MeCN·$0.9H_2O$. Copies of this information may be obtained free of charge from the Director, CCDC, 12 Union Road, Cambridge, CB2 1EZ, UK (fax: +44-1233-336-033; e-mail: deposit@ccdc.cam.ac.uk or www: http://www.ccdc.cam.ac.uk).

References

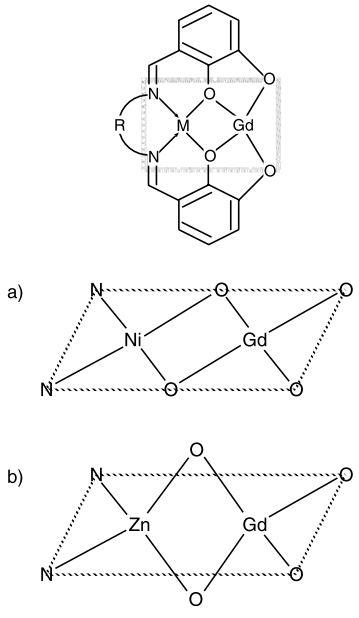
[1] R.E.P. Winpenny, J. Chem. Soc., Dalton Trans. (2002) 1.
[2] E. Libby, K. Folting, C.J. Huffman, J.C. Huffman, G. Christou, Inorg. Chem. 32 (1993) 2549.
[3] G.L. Abbati, A. Cornia, A.C. Fabretti, A. Caneschi, D. Gatteschi, Inorg. Chem. 37 (1998) 1430.
[4] G. Aromi, P.C. Berzal, P. Gamez, O. Roubeau, H. Kooijman, A.L. Spek, W.L. Driessen, J. Reedijk, Angew. Chem., Int. Ed. Engl. 40 (2001) 3444.
[5] S. Herold, S.J. Lippard, Inorg. Chem. 36 (1997) 50.
[6] S.J. Lippard, J.M. Berg, Principles of Bioinorganic Chemistry, University Science Books, Mill Valley, CA, 1994.
[7] R.M. Cinco, A. Rompel, H. Visser, G. Aromi, G. Christou, K. Sauer, M.P. Klein, V.K. Yachandra, Inorg. Chem. 38 (1999) 5988.
[8] D. Gatteschi, R. Sessoli, A. Cornia, Chem. Commun. (2000) 725.
[9] G. Christou, D. Gatteschi, D.N. Hendrickson, R. Sessoli, MRS Bull. 25 (2000) 1.
[10] E. Coronado, C.J. Gómez-Garcia, Chem. Rev. 98 (1998) 273.
[11] E.K. Brechin, A. Graham, A. Parkin, S. Parsons, A.M. Seddon, R.E.P. Winpenny, J. Chem. Soc., Dalton Trans. (2000) 3242 and references therein.
[12] G.S. Paraefstathiou, A. Escuer, R. Vicente, M. Font-Bardia, X. Solans, S.P. Perlepes, Chem. Commun. (2001) 2414.
[13] N. Lalioti, C.P. Raptopoulou, A. Terzis, A.E. Aliev, I.P. Gerothanassis, E. Manessi-Zoupa, S.P. Perlepes, Angew. Chem., Int. Ed. Engl. 40 (2001) 3211.
[14] A.K. Boudalis, N. Lalioti, G.A. Spyroulias, C.P. Raptopoulou, A. Terzis, V. Tangoulis, S.P. Perlepes, J. Chem. Soc., Dalton Trans. (2001) 955.
[15] G.S. Papaefstathiou, A. Escuer, C.P. Raptopoulou, A. Terzis, S.P. Perlepes, R. Vicente, Eur. J. Inorg. Chem. (2001) 1567 and references therein.
[16] G.S. Papaefstathiou, S.P. Perlepes, A. Escuer, R. Vicente, M. Font-Bardia, X. Solans, Angew. Chem., Int. Ed. Engl. 40 (2001) 884.
[17] G.S. Papaefstathiou, C.P. Raptopoulou, A. Tsohos, A. Terzis, E.G. Bakalbassis, S.P. Perlepes, Inorg. Chem. 39 (2000) 4658 (and references therein).
[18] E.G. Bakalbassis, E. Diamantopoulou, S.P. Perlepes, C.P. Raptopoulou, V. Tangoulis, A. Terzis, T.F. Zafiropoulos, J. Chem. Soc., Chem. Commun. (1995) 1347.
[19] V. Tangoulis, C.P. Raptopoulou, A. Terzis, E.G. Bakalbassis, E. Diamantopoulou, S.P. Perlepes, Inorg. Chem. 37 (1998) 3142.
[20] V. Tangoulis, E. Diamantopoulou, E.G. Bakalbassis, C.P. Raptopoulou, A. Terzis, S.P. Perlepes, Mol. Cryst. Liq. Cryst. 335 (1999) 463.
[21] J. Handley, D. Collison, C.D. Garner, M. Helliwell, R. Docherty, J.R. Lawson, P.A. Tasker, Angew. Chem., Int. Ed. Engl. 32 (1993) 1036.
[22] M. Murrie, D. Collison, C.D. Garner, M. Helliwell, P.A. Tasker, S.S. Turner, Polyhedron 17 (1998) 3031.
[23] D.S. Moore, S.D. Robinson, Adv. Inorg. Chem. 32 (1988) 171.
[24] M.B. Hursthouse, R.L. Short, S.D. Robinson, Polyhedron 5 (1986) 1573.
[25] I. Søtofte, K. Nielsen, Acta Chem. Scand. A38 (1984) 257 (and references therein).
[26] J. Reedijk, A.R. Siedle, R.A. Velapoldi, J.A.M. Van Hest, Inorg. Chim. Acta 74 (1983) 109.
[27] J. Reedijk, G. Roelofsen, A.R. Siedle, A.L. Spek, Inorg. Chem. 18 (1979) 1947.
[28] J.C. Plakatouras, S.P. Perlepes, D. Mentzafos, A. Terzis, T. Bakas, V. Papaefthymiou, Polyhedron 11 (1992) 2657.
[29] E. Diamantopoulou, T.F. Zafiropoulos, S.P. Perlepes, C.P. Raptopoulou, A. Terzis, Polyhedron 13 (1994) 1593.
[30] E. Skorda, E.G. Bakalbassis, J. Mrozinski, S.P. Perlepes, C.P. Raptopoulou, A. Terzis, J. Chem. Soc., Dalton Trans. (1995) 2317.
[31] K. Skorda, R. Keuleers, A. Terzis, C.P. Raptopoulou, S.P. Perlepes, J.C. Plakatouras, Polyhedron 18 (1999) 3067.
[32] L.E. Merk, Stud. Conserv. 26 (1981) 73.
[33] J.S. Wu, K. Nobe, Corrosion (NACE) 37 (1981) 223.
[34] G. Schmitt, Br. Corros. J. 19 (1984) 165.

[35] B.-S. Fang, C.G. Olson, D.W. Lynch, Surf. Sci. 176 (1986) 476 (and references therein).
[36] S.L.F.A. Da Costa, S.M.L. Agostinho, Corrosion (NACE) 45 (1989) 472.
[37] D. Sockalingum, M. Fleischmann, M.M. Musiani, Spectrochim. Acta 47A (1991) 1475.
[38] V. Tangoulis, C.P. Raptopoulou, V. Psycharis, A. Terzis, K. Skorda, S.P. Perlepes, O. Cador, O. Kahn, E.G. Bakalbassis, Inorg. Chem. 39 (2000) 2522.
[39] E. Diamantopoulou, S.P. Perlepes, D. Raptis, C.P. Raptopoulou, Transition Met. Chem. 27 (2002) 377.
[40] G.S. Papaefstathiou, A. Escuer, R. Vicente, C.P. Raptopoulou, A. Terzis, S.P. Perlepes, Eur. J. Inorg. Chem., in press.
[41] W. Konig, R. Geiger, Ber. Dtsch. Chem. Ges. 103 (1970) 788, 2024, 2034.
[42] W. Qafsaoui, C. Blanc, J. Roques, N. Pebere, A. Srhiri, C. Mijoule, G. Mankowski, J. Appl. Electrochem. 31 (2001) 223.
[43] R. Youda, H. Nishihara, K. Aramaki, Corros. Sci. 28 (1988) 87.
[44] M.J. Collie (Ed.), Corrosion Inhibitors: Developments Since 1980, Noyes Data Corporation, NJ, USA, 1983, pp. 227, 228.
[45] R.G. Charles, M.A. Pawlikowski, J. Phys. Chem. 62 (1958) 440.
[46] G.M. Sheldrick, SHELXS-86, Structure Solving Program, University of Göttingen, Germany, 1986.
[47] G.M. Sheldrick, SHELXL-93, Crystal Structure Refinement, University of Göttingen, Germany, 1993.
[48] K. Nakamoto, Infrared and Raman Spectra of Inorganic and Coordination Compounds, fourth ed., Wiley, New York, 1986, pp. 227–231, 259–263.
[49] A.B.P. Lever, Inorganic Electronic Spectroscopy, second ed., Elsevier, Amsterdam, 1984, pp. 507–520.
[50] R.A. Coxall, S.G. Harris, D.K. Henderson, S. Parsons, P.A. Tasker, R.E.P. Winpenny, J. Chem. Soc., Dalton Trans. (2000) 2349.
[51] M.B. Hursthouse, M.A. Laffey, P.T. Moore, D.B. New, P.R. Raithby, P. Thornton, J. Chem. Soc., Dalton Trans. (1982) 307.
[52] M.S. El Fallah, E. Rentschler, A. Caneschi, R. Sessoli, D. Gatteschi, Inorg. Chem. 35 (1996) 3723.
[53] E.K. Brechin, S.G. Harris, S. Parsons, R.E.P. Winpenny, Angew. Chem., Int. Ed. Engl. 36 (1997) 1967.
[54] S.-Y. Lai, T.-W. Lin, Y.-H. Chen, C.-C. Wang, G.-H. Lee, M.-H. Yang, M.-K. Leung, S.-M. Peng, J. Am. Chem. Soc. 121 (1999) 250.
[55] S.-Y. Lai, C.-C. Wang, Y.-H. Chen, C.-C. Lee, Y.-H. Liu, S.-M. Peng, J. Chin. Chem. Soc. (Taipei) 46 (1999) 477.
[56] M. Murrie, H. Stoeckli-Evans, H.U. Güdel, Angew. Chem., Int. Ed. Engl. 40 (2001) 1957.
[57] D. Gaynor, Z.A. Starikova, S. Ostrovsky, W. Haase, K.B. Nolan, Chem. Commun. (2002), Advanced Article (DOI: 10.1039/b110799b).
[58] R. Schmid, A. Mosset, J. Galy, J. Chem. Soc., Dalton Trans. (1991) 1999.
[59] A.J. Blake, R.O. Gould, C.M. Grant, P.E.Y. Milne, D. Reed, R.E.P. Winpenny, Angew. Chem., Int. Ed. Engl. 33 (1994) 195.
[60] L. Chen, F.A. Cotton, Inorg. Chim. Acta 267 (1998) 271.
[61] M.A. Bolcar, S.M.J. Aubin, K. Folting, D.N. Hendrickson, G. Christou, Chem. Commun. (1997) 1485.
[62] G.L. Abbati, A. Cornia, A.C. Fabretti, A. Caneschi, D. Gatteschi, Inorg. Chem. 37 (1998) 3759.
[63] M. Tesmer, B. Muller, H. Vahrenkamp, Chem. Commun. (1997) 721.
[64] J.A. Real, G. De Munno, R. Chiappetta, M. Julve, F. Lloret, Y. Journaux, J.-C. Colin, G. Blondin, Angew. Chem., Int. Ed. Engl. 33 (1994) 1184.
[65] V. Tangoulis, C.P. Raptopoulou, S. Paschalidou, E.G. Bakalbassis, S.P. Perlepes, A. Terzis, Angew. Chem., Int. Ed. Engl. 36 (1997) 1083.
[66] M.L. Ziegler, J. Weiss, Angew. Chem., Int. Ed. Engl. 9 (1970) 905.
[67] M. Ishimori, T. Hagiwara, T. Tsuruta, Y. Kai, N. Yasuoka, N. Kasai, Bull. Chem. Soc. Jpn. 49 (1976) 1165.
[68] N. Lalioti, C.P. Raptopoulou, A. Terzis, A.E. Aliev, S.P. Perlepes, I.P. Gerothanassis, E. Manessi-Zoupa, Chem. Commun. (1998) 1513.
[69] D. Attanasio, G. Dessy, V. Fares, J. Chem. Soc., Dalton Trans. (1979) 28.
[70] S. Wang, H.-L. Tsai, W.E. Streib, G. Christou, D.N. Hendrickson, J. Chem. Soc., Chem. Commun. (1992) 677.
[71] D. Christodoulou, C. George, L.K. Keefer, J. Chem. Soc., Chem. Commun. (1993) 937.
[72] U. Bemm, R. Norrestam, M. Nygren, G. Westin, J. Solid State Chem. 134 (1997) 312.
[73] A. Müller, J. Meyer, H. Bögge, A. Stammler, A. Botar, Chem. Eur. J. 4 (1998) 688.
[74] R. Bhula, D.C. Weatherburn, Angew. Chem., Int. Ed. Engl. 30 (1991) 688.
[75] A. Cornia, A.C. Fabretti, D. Gatteschi, G. Palyi, E. Rentschler, O.I. Schegolikhina, A.A. Shdanov, Inorg. Chem. 34 (1995) 5383.
[76] D. Gatteschi, L. Pardi, Gazz. Chim. Ital. 123 (1993) 231.
[77] C. Dendrinou-Samara, G. Psomas, L. Iordanidis, V. Tangoulis, Chem. Eur. J. 7 (2001) 5041.
[78] J.M. Clemente-Juan, E. Coronado, J.R. Galán-Mascarós, C.J. Gómez-Garcia, Inorg. Chem. 38 (1999) 55.
[79] M.A. Halcrow, J.-S. Sun, J.C. Huffman, G. Christou, Inorg. Chem. 34 (1995) 4167and references therein..
[80] F. Paap, E. Bouwman, W.L. Driessen, R.A.G. De Graaf, J. Reedijk, J. Chem. Soc., Dalton Trans. (1985) 737.
[81] K.S. Murray, Adv. Inorg. Chem. 43 (1996) 322.
[82] E.K. Brechin, R.O. Gould, S.G. Harris, S. Parsons, R.E.P. Winpenny, J. Am. Chem. Soc. 118 (1996) 11293.
[83] K.-L. Lu, S. Kumaresan, Y.-S. Wen, J.R. Hwu, Organometallics 13 (1994) 3170.

ture with RE(III) and M(II) ions (RE = rare-earth element, and M = d-block metal) [8–12].

In order to change the flexibility of the ligand, various diamines were used as a bridging chain of ethylene, propylene and *o*-phenylene. When the bridging chain has a π-conjugated system, such as *o*-phenylene, the ligand is considered to have a rigid frame, and the coordinating structure of the ligand must be planar. The d-block ions of Ni(II) and Zn(II) prefer their coordination structure to be square-planar and tetrahedral, respectively. Therefore, the coordination structure of the cavity at the O_4 site of the ligand is affected by the structure of the N_2O_2 site around the M(II) ion in the complex (Scheme 1). In other words, it is assumed to be possible to control the coordinating structure around the RE(III) ion by changing the d-block metal ions, M(II), and the bridging chains. In this paper, please note that the transition metal free structure is referred as 'vacancy', but it is not a real meaning; an H^+ may be placed at that site.

There are cases in which magnetically diluted single crystals are hard to obtain, Gd(III) ions serve as a probe in a biological system or the structure of the complexes in solution are of interest. We are also attempting to develop a method for investigating the properties of the Gd(III) complexes in a disordered system using the EPR technique. Therefore, the frozen solutions of the complexes were used for the investigation.



Scheme 1. The schematic coordination structure around the transition metal ion and the gadolinium ion. The structures are (a) planar for Ni, (b) tetrahedral distortion by Zn.

2. Experimental

2.1. Materials

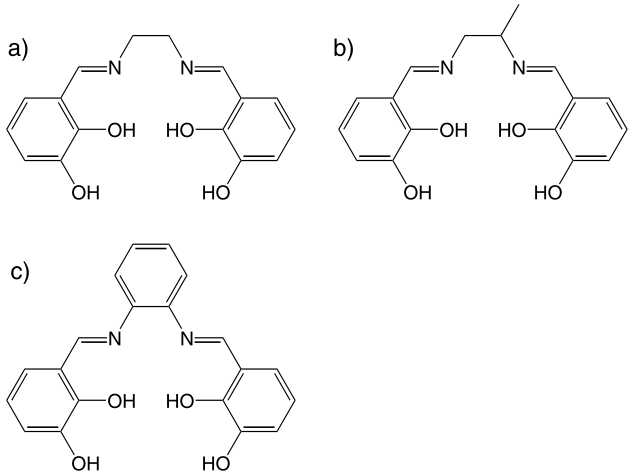
All of the chemicals used were commercially obtained, and no further purifications were performed. The ligands used in this study are shown in Scheme 2. The Gd(III) complexes with the Schiff base ligand were synthesized by the usual method [8–12]. The obtained ligands and the Ni and Zn complexes were examined by IR and NMR spectra [11,15]. Complex formations with the Gd(III) ion were confirmed by the EPR and IR spectra. In order to obtain the complex $[GdNi(osalph)]^+$, both synthetic procedures, a one-pot reaction and a two-step reaction, gave the same product, which was confirmed by the IR spectra.

2.2. UV–Vis absorption spectra

The UV–Vis absorption spectra were measured by a continuous variational method in order to investigate the complex formation between the metal ions and the ligands. The concentrations of the Ni(II) solution and the H_4osalph solution were approximately 10^{-4} mol l^{-1} with methanol as a solvent. The spectra were recorded using a Hitachi U-2001 spectrophotometer at room temperature (r.t.).

2.3. EPR measurement

The EPR spectra were observed using a JEOL RE3X X-band EPR spectrometer with a liquid-nitrogen dewar. Typical measurement conditions involved a temperature of 77 K and a microwave power of 5–20 mW. Frozen dimethylsulfoxide (dmso) solutions of the Gd(III) complexes were used for observing the EPR spectra. This solvent was chosen for the appropriate solubility of the



Scheme 2. The structure of the ligands used in this study. (a) H_4osalen, (b) H_4osalpn, (c) H_4osalph.

complexes, and it was also confirmed to form a glassy matrix by the spectral pattern of EPR. The magnetic fields were measured using a EFM-2000AX field meter (Echo Electronics Co., Ltd.), and the microwave frequencies were determined by a Mn^{2+} marker.

2.4. Molecular orbital calculations

In order to study the structures of the Gd(III) complexes, ab initio molecular orbital (MO) calculations were performed. The model complexes used here were $[YNi(osalen)]^+$, $[YZn(osalen)]^+$ and [YH(osalen)], where the structures were assumed to have C_2 symmetry. The complexes with the osalph ligand were also calculated. It can be mentioned that the ionic radii of Y and Gd are comparable, and that the unpaired electrons of the spin octet system in the Gd will bring an unessential difficulty in the MO calculation. The optimized geometries, where a local energy minimum was achieved, of these model complexes were obtained by the RHF method using a 3-21G basis set. All calculations were done using the GAMESS program package [13] on a CONVEX SPP1000 at the Computer Center of Hirosaki University. PLUTON was used to draw the molecular structures [14].

3. Results and discussion

3.1. Structure of the complexes

The ligands used in this study have two kinds of metal coordination site, an N_2O_2 coordination site and an O_4 site. Sakamoto et al. [9–12] and Casellato et al. [15] reported that the d-block metal ions were coordinated by the N_2O_2 site, while the rare-earth ions were coordinated by the O_4 site. The former group discussed the hardness of the metal ions and the C=N stretching frequencies of the complexes. The latter group showed the crystal structures of $[Cu(H_2osalen)]$ and $[YCu(osalen)](NO_3)$ with IR and NMR data; the structures of these are considered to be similar to those of the corresponding Ni(II) complexes. Here, the structures of the synthesized complexes were confirmed by IR, ^1H and ^{13}C NMR, and the continuous variational method applied for the absorption band at the visible region. The optimized structures of the model complexes obtained by the ab initio MO calculations also give useful information about the structure of the O_4 coordination site.

According to both the hardness and the size of the cavity at the N_2O_2 and O_4 sites of the ligands, it is considered that the rare-earth ion prefers to be coordinated at the latter, while the d-block ion is coordinated in the former. This is suggested by the following experimental data.

Table 1
C=N stretching frequencies of the Gd(III)–M(II)–osalR complexes [a] in cm^{-1}

Ligands	H_4osalen	H_4osalpn	H_4osalph
Metal free	1632.0 (1640 [b], 1632 [c])	1631.2	1617.0
Ni(II)	1618.7 (1626 [b], 1610 [c])	1619.6	1614.0
Zn(II)			1616.0
Gd(III)	1636.0 (1634 [c])	1638.4	1618.0
Gd(III)–Ni(II)	1619.1		1614.4 (1612.3 [d])
Gd(III)–Zn(II)			1613.0

[a] Chloride as a counter anion.
[b] Ref. [15].
[c] Ref. [11].
[d] This work, PF_6^- salt.

Table 1 shows that the C=N stretching frequencies of the ligand were shifted lower when a metal ion was coordinated, and the observed shift in the C=N stretching frequencies was larger in coordinating a d-block metal ion than coordinating a rare-earth ion. These IR data are consistent with the reported results [11,15], and are shown in Table 1, indicating that the d-block ion is coordinated at the N_2O_2 site which neighbors to the C=N bond.

The ^1H and ^{13}C NMR data are summarized in Tables 2 and 3, where those for H_4osalen show good agreement

Table 2
^{13}C and ^1H NMR data (δ in ppm vs. TMS) for some comparmental ligands in dmso-d_6 solution

		H_4osalen	H_4osalpn	H_4osalph
^{13}C	CH=N	167.045	167.1 165.2	164.6
	osal unit	151.1, 145.8 121.8 118.0 117.7, 117.5	151.2, 150.6 145.8, 145.7 121.8, 121.8 118.1, 118.0 117.7, 117.7 117.5	149.4, 148.8 145.6, 142.4, 142.1 127.6, 122.7, 122.3 120.0, 119.9 119.5, 119.1 118.7, 118.6 118.5, 118.2 116.8, 115.3
	bridging -R-	57.9	63.5 63.0 19.8	[a]
^1H	CH=N	8.53 (s, 2H)	8.54 (s, 1H) 8.50 (s, 1H)	8.88 (s, 1H) 8.81 (s, 1H)
	osal unit	6.8–6.9 (m, 4H) 6.64 (t, 2H)	6.8–6.9 (m, 4H) 6.6–6.7 (m, 2H)	6.7–7.4 (m, 10H)
	bridging -R-	3.92 (s, 4H)	3.8 (t, 3H) 1.34 (d, 3H)	[a]
	OH			12.87 (s, 2H) 9.18 (s, 2H)

[a] Signals of the bridging phenylene cannot be separated from those of the osal unit.

Table 3
^{13}C and ^{1}H NMR data (δ in ppm vs. TMS) for some compartmental complexes in dmso-d_6 solution

		[Ni(H_2osalen)]	[Ni(H_2osalph)]	[Zn(H_2osalph)]
^{13}C	CH=N	162.7	156.6	162.7
	osal unit	152.6, 147.6	154.5, 148.1, 142.1	160.1, 139.1, 127.3
		121.9	127.5, 123.3	125.1, 120.1
		119.1	119.1	117.2
		114.5, 114.3	116.2, 115.5, 115.3	116.4, 113.9, 112.8
	bridging -R-	57.9	[a]	[a]
^{1}H	CH=N	7.88 (s, 2H)	9.09 (s, 2H)	9.05 (s, 2H)
	osal unit	6.3–6.8 (m, 6H)	7.09 (d, 2H)	6.94 (d, 2H)
			6.81 (d, 2H)	6.80 (d, 2H)
			6.54 (t, 2H)	6.42 (t, 2H)
	bridging -R-	3.44 (s, 4H)	8.16 (AA′BB′, 2H)	7.93 (AA′BB′, 2H)
			7.34 (AA′BB′, 2H)	7.39 (AA′BB′, 2H)
	OH	8.14 (br, 2H)	8.50 (s, 2H)	8.30 (s, 2H)

[a] Signals of the bridging phenylene cannot separate from those of osal unit.

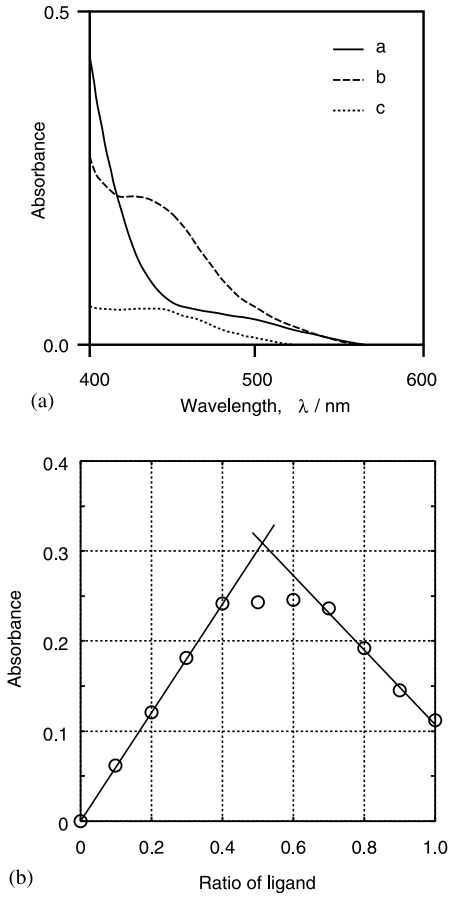


Fig. 1. Plot for the continuous variation method with H_4osalph and Ni(II) ion, and UV–Vis absorption spectra. (a) Absorption spectra at various ligand ratios. The ratio of the ligand is (a)1.0, (b) 0.5, (c) 0.1. (b) Observed wavelength, 437.0 nm; solvent, methanol; concentration, approximately 10^{-4} mol l^{-1}; temperature, r.t.

with the reported values [15]. The chemical-shift values of the metal complexes are different from those of the ligands; for example, the chemical-shift values for [M(H_2osalph)] (M = Ni(II), Zn(II)) have changed from that for H_4osalph, which indicates a complex formation. Furthermore, [M(H_2osalph)] (M = Ni(II), Zn(II)) shows only ten peaks for the ^{13}C NMR spectra; this means that these complexes are symmetric. The chemical-shift values for these Ni(II) and Zn(II) complexes are different. It is also shown that the structures of these complexes are different, assuming that the Ni(II) complex has a planar structure while that of Zn(II) is a tetrahedrally distorted one (vide infra). These NMR results also point out the magnetic properties of the Ni(II) complexes; that these coordination complexes are diamagnetic, i.e. the Ni(II) ions have a low-spin ground state.

A new absorption band at approximately 450 nm appeared for a mixture of the solution of the Ni(II) ion and that of H_4osalph; the band was not seen either in the solution of the Ni(II) ion or in that of the ligand. This band is then thought to arise from the formation of the Ni(II)–H_2osalph complex (Fig. 1(a)). The optical density at 437 nm versus the ratio of the contents of the Ni(II) ion and the H_4osalph ligand is plotted in Fig. 1(b). These results show that the complex formation between the Ni(II) ion and the ligand occurs in a 1:1 molar ratio.

As a conclusion of the above results, it is strongly suggested for the M(II)–H_2osalR system that only a single d-block ion was coordinated to the one site of the compartmental ligand (N_2O_2 site), and that the other binding site remains free for the other rare-earth ion.

In the next step, the three-dimensional structure of the Gd(III)–M(II) complexes and the local environment around the Gd(III) ion were of interest. Ni(II) and Zn(II) were used for the d-block metal ion, M(II), which was introduced to the N_2O_2 site of the complexes; they are considered to take a square-planar and a tetrahedral coordination structure, respectively. The coordination structure around the Gd(III) ions will strongly be affected by these d-block metal ions, where the structures are illustrated in Scheme 1.

We did not think about the bridged dimer reported by Casellato et al. [15]. If the dimeric structure was formed, the line-shape of its EPR spectrum should be different from that of the $S = 7/2$ system, and/or the line-width might be too broad to observe the signals, because of the magnetic interaction between the nearest Gd(III) ions. It is considered enough to rationalize the observed spectra being caused by the Gd(III) complexes (vide infra).

In order to estimate the structure of the Gd(III)–M(II)–osalR complexes, ab initio MO calculations

were carried out, and then the optimized geometry of the model complexes of $[YNi(osalen)]^+$, $[YZn(osalen)]^+$ and $[YH(osalen)]^0$ were obtained, where C_2 symmetry was assumed. Moreover, the complexes with osalph ligand were also calculated. The selected bond lengths, bond angles, and dihedral angles obtained by the MO calculations are listed in Table 4 and the stereo views of $[YM(osalen)]^{n+}$ ($M = Ni^{2+}$, $n = 1$; $M = Zn^{2+}$, $n = 1$; $M = H^+$, $n = 0$) are shown in Fig. 2. The bond lengths of M–N, M–O, and Y–O are essentially same between $[YM(osalen)]^{n+}$ and $[YM(osalph)]^{n+}$, though the bond angles with respect to the metal coordination sphere (both M and Y) are different.

The most remarkable difference between osalen and osalph can be seen in dihedral angles. The dihedral angles are used to measure the distortion of the coordinating structure around the metal ion. The dihedral angles around the d-block metal ion sites show that the angle for (N1–Ni–O1)–(N2–Ni–O2) is 6.0° for the osalen complex and 6.4° for the osalph complex, and that for (N1–Zn–O1)–(N2–Zn–O2) is 30.4° and 23.4°, respectively. These results represent the properties of Ni(II) and Zn(II) well, where the coordination structure around the Ni(II) ion is planar, while that of Zn(II) is tetrahedrally distorted. Furthermore, it is interesting that the distortion around Zn(II) is smaller because of the rigidity of the *o*-phenylene bridge. In addition to that, the dihedral angles around the Y(III) ion in the osalen complex were determined as (O1–Y–O3)–(O2–Y–O4) to be 21.8° for M(II) = Ni(II), 33.2° for M(II) = Zn(II), and 50.1° for $M(II) = H^+$, while in the osalph complex, 12.5°, 33.6°, and 52.6°, respectively (see Table 4). These results indicate that the coordination structure around the Y(III) ion, which is a model of the rare-earth ion, has more distortion in $[YZn(osalR)]^+$ than in $[YNi(osalR)]^+$. It is interesting that the coordination structure around the Y(III) ion for [YH(osalR)] has a greatly distorted structure, too. The

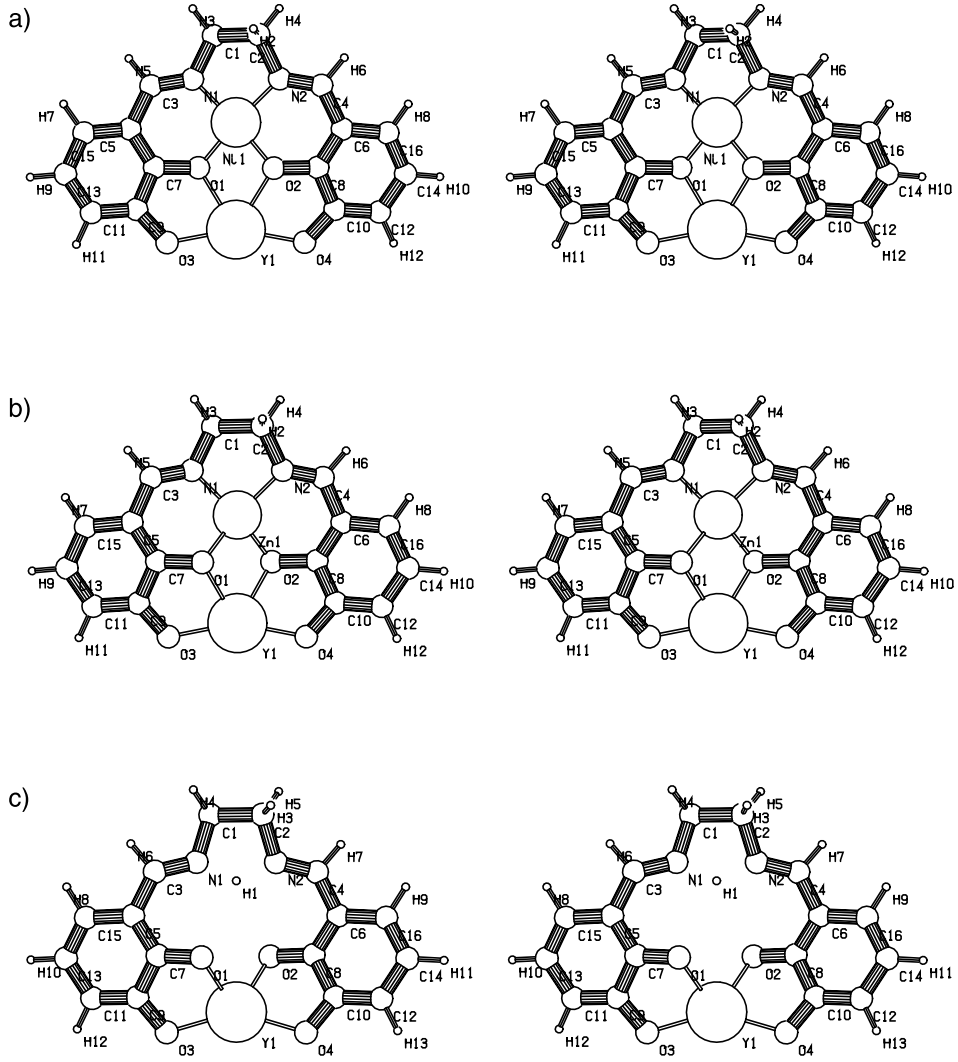


Fig. 2. Stereo views of $[YM(osalen)]^n$ [14]. a) M = N, $n = +1$; b) M = Zn, n = +1; c) M = H, $n = 0$. These structures were obtained from RHF/3-21G MO calculations.

Table 4
Selected bond lengths, bond angles and dihedral angles of Y–M–osalen and Y–M–osalph complexes obtained from MO calculations

	$[YNi(osalen)]^+$	$[YZn(osalen)]^+$	[YH(osalen)]	$[YNi(osalph)]^+$	$[YZn(osalph)]^+$	[YH(osalph)]
Bond lengths (*Å*)						
M–N(1)	1.872	1.921	1.311	1.883	1.931	1.311
M–O(1)	1.811	1.890	2.639	1.852	1.896	2.640
M–Y	3.248	3.256	3.873	3.255	3.277	3.873
Y–O(1)	2.205	2.225	2.137	2.226	2.216	2.137
Y–O(3)	2.130	2.118	2.141	2.102	2.124	2.142
O(1)–C(7)	1.352	1.371	1.328	1.378	1.366	1.327
O(3)–C(9)	1.361	1.360	1.360	1.339	1.359	1.360
Bond angles (°)						
N(1)–M–N(2)	90.489	90.708	129.91	85.546	89.249	129.975
N(1)–M–O(1)	94.584	97.667	88.033	97.666	96.627	88.002
O(1)–M–O(2)	80.683	82.942	63.358	82.408	81.360	63.344
O(1)–Y–O(2)	64.232	68.462	80.854	66.492	67.815	80.875
O(1)–Y–O(3)	70.287	71.205	75.222	73.528	70.888	75.215
O(3)–Y–O(4)	159.061	157.833	147.401	160.062	159.999	147.387
N(1)–C(1)–C(2)	108.101	109.945	129.686	124.787	124.647	129.718
Dihedral angles (°)						
(N(1)–M–O(1))–(N(2)–M–O(2))	6.043	30.380	30.857	6.423	23.429	24.380
(O(1)–Y–O(3))–(O(2)–Y–O(4))	21.846	33.230	50.116	12.519	33.579	52.605
(O(1)–Y–O(2))–(O(3)–Y–O(4))	19.951	29.364	41.144	11.461	29.838	43.171

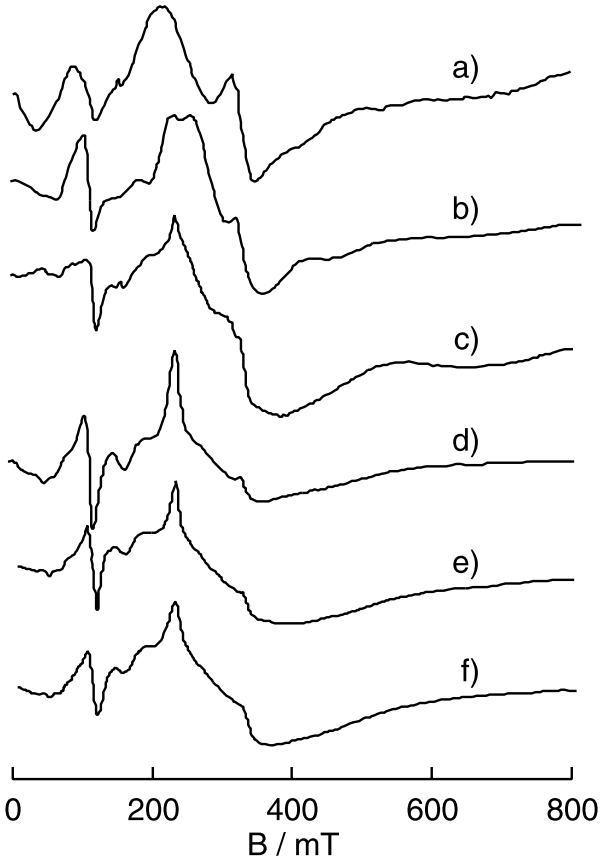


Fig. 3. X-band EPR spectra of Gd(III)–M(II)–osalR complexes. (a) $[GdNi(osalen)]^+$; (b) $[GdNi(osalph)]^+$; (c) [GdZn(osalph)]; (d) [GdH(osalph)]; (e) [GdH(osalen)]; (f) [GdH(osalpn)].

vacant N_2O_2 site (where $M(II) = H^+$) is thought to be a site where it would be possible to arrange the donor atoms around the rare-earth ion with less strain, because the flexibility of the ligand does not restrict the structure of the complex. The effect of the *o*-phenylene bridge is also interesting, that the coordination sphere around M(II) is lesser distorted in osalph ($M(II) = Zn(II)$ and H^+), but it is not around Y(III). While in the Y–Ni–osalph complex, the dihedral angle (O1–Y–O3)–(O2–Y–O4) is smaller than the osalen complex. These results indicate that the rigidity of the bridging R also affects the coordination sphere around the Y(III) ion. It is important to conclude that the coordination structure around the Gd(III) ion is able to be controlled by the d-block metal ion through the structure of the compartmental ligand unit.

It is certainly important that the coordination number of the rare-earth ions is not only four, like some of the d-block ions, but can possibly number in six or more. By those means, it was obvious that the above model calculation did not give the whole coordination sphere of the Gd(III) ion of the Gd(III)–M(II)–osalR complex in solution. The solvent molecules and/or the counter anions may occupy the fifth site and more of the Gd(III) ion. For example, the chloride anion may easily be accessible to the additional fifth and sixth coordination site of the Gd(III) ion in the $[GdNi(osalen)]^+$ complexes, where the osalen-ligand has a more planar structure around the rare-earth ion than that of the Zn-including or the metal-free complex. Because of the rigidity of the osalph-ligand, the dihedral angle (O1–Y–O3)–(O2–Y–O4) of $[YNi(osalph)]^+$ is smaller than others, indicating that the ligand in $[GdNi(osalph)]^+$ is more planar around the coordination sphere of the Gd(III) ion. In any case, it is clear that the coordination structure of these additional donors is also controlled by the d-block metal ions. In addition, the changes in the structure of the compartmental ligands also makes it possible to rearrange the structures of the additional coordinating atoms which come from anions and/or solvents around the Gd(III) ion.

3.2. EPR spectra

The observed X-band EPR spectra are shown in Fig. 3. Strong signals were easily obtained in the wide range of 100–800 mT at 77 K. The properties of the line-shapes of these spectra were essentially similar to those of the Gd(III)-β-diketonate complexes [5]. Furthermore, though the d-block ions were changed in our Gd(III)-M(II) complexes (M(II) = Ni(II), Zn(II) and vacancy), the dominant line-shapes of the spectra were not changed, which means that the Ni(II) ion has a low-spin as a ground state. It was also pointed out that the complexes without the Gd(III) ion, [M(H_2osalR)], show the normal NMR spectra (Tables 2 and 3), which indicates that all the d-block ions used in this study are diamagnetic. These results suggest that the diamagnetic d-block ions play a role as a building block, and the complexes for which we observed the EPR spectra have the electron spin $S = 7/2$.

The X-ray structural analyses and the magnetic properties of some related RE(III)–M(II) complexes with the H_4osalR ligand were reported [15–17]. Casellato et al. said that the mononuclear [Cu(H_2osalen)] complex forms a square-planar configuration around the Cu(II) ion [15]. Costes et al. determined that the ground state of their Gd(III)–Ni(II) complex has $S = 9/2$; in other words, the Ni(II) ion is in a high-spin state [16,17]. So as in the Casellato's Cu(II) case, our Ni(II)-including complexes are expected to have the square-planar coordination structure around the Ni(II) ion. However, in contrast to the Costes' case, the Ni(II) in our complex is diamagnetic, as shown by the NMR and EPR spectra. Consequently, it can be considered that the observed EPR signals are only due to the Gd(III) ion.

As was mentioned above, the observed line-shapes of the EPR spectra of the Gd(III)–M(II) complexes are essentially similar to those of the Gd(III)-β-diketonate complexes [5]. The latter complexes are known to have

some negatively charged β-diketonates as ligands, and the Gd(III) ions are surrounded by the oxygen atoms. Hence the former complexes are supposed to have a similar local environment around the Gd(III) ions as the latter complexes.

In Fig. 3(b–d), the EPR spectra of the [GdM(osalph)]$^{n+}$ complexes with various diamagnetic d-block M(II) ions, such as Ni(II), Zn(II), and a vacancy, are displayed. It can be seen that the detailed line-shape of the spectra differs from each other upon changing the d-block ion M(II). These results indicate that the local environments around the Gd(III) ion are changed, and are controlled by the d-block ion.

Though the accurate spectral line-shapes are varied, the line-shape of [GdZn(osalph)]$^{+}$ and that of [GdH(osalph)]^{0} are essentially similar, whereas that of [GdNi(osalph)]$^{+}$ is different. Both [GdZn(osalph)]$^{+}$ and [GdH(osalph)]^{0} have a single peak at approximately 230 mT in their EPR spectral line-shape (Fig. 3(c–d)), while [GdNi(osalph)]$^{+}$ has a split peak at the corresponding position (Fig. 3(b)). Furthermore, only the latter spectrum has a shoulder at approximately 450 mT. The similarity in the spectral line-shapes of the former two suggests a similarity in the local environment around the Gd(III) ion. The optimized structures of both [GdZn(osalph)]$^{+}$ and [GdH(osalph)]^{0} obtained from the MO calculation have a tetrahedral distorted coordination sphere (Table 4). The EPR data of those complexes can be explained by the MO results.

In Fig. 3(a–b), the EPR spectra of the [GdNi(osalR)]$^{+}$ complexes with various compartmental ligands are shown. The EPR spectron of [GdNi(osalen)]$^{+}$ shows a broad peak at approximately 220 mT (Fig. 3(a)), while that of [GdNi(osalph)]$^{+}$ has a split peak at approximately 250 mT (Fig. 3(b)). The line-shape of the obtained EPR spectra is different, when the bridging chain R is changed. Due to the the rigid π-conjugated system of the phenylene bridge, [GdNi(osalph)]$^{+}$ is expected to have a planar coordination structure around the Gd(III) ion, however, the coordination structure around Gd(III) in the [GdNi(osalen)]$^{+}$ complex, which has an ethylene bridge, may be slightly distorted. This flexibility in the ligand is very interesting. Unfortunately, the complex having a longer alkyl chain, trimethylene, was reported to have a Ni(II) in a high-spin state [16,17]. Consequently, it is suggested that the coordination structure around the Gd(III) ion is able to be governed by the bridging chain in the ligand, through the structure around the Ni(II) ion.

In Fig. 3(d–f), the EPR spectra of the [GdH(osalR)] complexes are shown. The obtained spectra are very similar to each other. These results strongly suggest that the coordination structure of the Gd(III) ion is equivalent in these three complexes, though the bridging chain R is varied. Indeed, when the d-block ion site is vacant, the local environment around the Gd(III) ion is considered to be less restricted. Furthermore, the angle of O(1)–Y–O(2) for the calculated structure of the [YH(osalen)] complex is much larger than that for the others, indicating that the osalen^{4-} ligand is very flexible. This means that the local environment is determined by the nature of the Gd(III) ion itself when the ligand is flexible. The calculated structure for [YH(osalen)] shows that the O_4-donating atoms are arranged in a tetrahedral coordination structure (Fig. 2(c), Table 4) with a large steric distortion at the N_2O_2 vacant site.

EPR spectral simulations are required to determine the EPR parameters and for more precise discussions. However, we have not obtained good results so far, because there was a distribution in the structure of the complexes in solution which causes a distribution in the EPR parameters, or there was a D-strain which causes a m_S-dependent linewidth [5,18–21]. For these reasons, qualitative discussions only were achieved here. A study on the EPR spectral simulations of the Gd(III) complexes for the frozen solution system requires a great deal of computer power, and is in progress.

4. Concluding remarks

The EPR spectra of Gd(III) complexes with the compartmental ligands, osalR^{4-}, and d-block ions M(II), such as Ni(II), Zn(II), and a vacancy, were measured here. It was confirmed by some experimental results and by the optimized structure obtained by MO calculations that the structures of the rare-earth binding site were the O_4 site, and were changed by changing M and R. It is interesting that the obtained EPR spectra clearly reflect the local environment of the Gd(III) ions. In other words, various line shapes of the EPR spectra can be observed when the d-block ion M and the bridging chain R are changed. This means that the coordinating structures around the Gd(III) ions can be controlled by the compartmental ligands and d-block ions, and that the 4f-electrons of the Gd(III) ion are affected by the coordinating ligands and their structures, though the 4f-electrons are shielded by the outer-shell electrons.

Acknowledgements

The present work was partially supported by a Grant-in-Aid for Scientific Research on Priority Areas 'New Development of Rare Earth Complexes' Nos. 06241202, 07230202, and 08220204 from the Ministry of Education, Science and Culture. The authors would like to acknowledge Dr. Jun Kawakami for his useful advice and discussions with us on NMR.

References

[1] For example: R. Sanz-Puche, P. Caro (Eds.), Rare Earths, Editorial Complutense, Madrid, 1998.
[2] P. Caravan, J.J. Ellison, T.J. McMurry, R.B. Lauffer, Chem. Rev. 99 (1999) 2293.
[3] M.B. Yim, M.W. Makinen, J. Magn. Reson. 70 (1986) 89.
[4] R.C. Nicklin, J.K. Johnstone, R.G. Barnes, D.R. Wilder, J. Chem. Phys. 59 (1973) 1652.
[5] R. Miyamoto, S. Sudoh, Bull. Chem. Soc. Jpn. 68 (1995) 3439.
[6] R. Miyamoto, S. Sudoh, in: G. Adachi, T. Yamase, J. Inanaga, M. Komiyama, K. Machida (Eds.), New Development of Studies on Rare Earth Complexes, Report of a Priority Area Research Program Supported by The Ministry of Education, Science, Sports and Culture Japan (Area Code: 251), 1977, p. 227.
[7] R. Miyamoto, S. Sudoh, in: C.Z. Rudowicz, K.N. Yu, H. Hiraoka (Eds.), Modern Applications of EPR/ESR: From Biophysics to Materials Science—Proceedings of first Asia-Pacific EPR/ESR Symposium, Springer-Verlag, Singapore, 1998, p. 256.
[8] M. Sakamoto, private communication, 1994.
[9] M. Sakamoto, Y. Nishida, K. Ohhara, A. Matsumoto, M. Ohba, H. Sakiyama, N. Matsumoto, H. Okawa, Synth. React. Inorg. Met. Org. Chem. 25 (1995) 705.
[10] M. Sakamoto, Y. Nishida, K. Ohhara, Y. Sadaoka, A. Matsumoto, H. Okawa, Polyhedron 14 (1995) 2505.
[11] M. Sakamoto, Y. Nishida, A. Matsumoto, Y. Sadaoka, M. Sakai, Y. Fukuda, M. Ohba, H. Sakiyama, N. Matsumoto, H. Okawa, J. Coord. Chem. 38 (1996) 347.
[12] M. Sakamoto, T. Ishikawa, Y. Nishida, Y. Sadaoka, A. Matsumoto, Y. Fukuda, M. Sakai, M. Ohba, H. Sakiyama, H. Okawa, J. Alloys Compd. 238 (1996) 23.
[13] GAMESS version 11-Sep-1996: M.W. Schmidt, K.K. Baldridge, J.A. Boatz, S.T. Elbert, M.S. Gordon, J.H. Jensen, S. Koseki, N. Matsunaga, K.A. Nguyen, S.J. Su, T.L. Windus, M. Dupuis, J.A. Montgomery, J. Comput. Chem. 14 (1993), 1347.
[14] PLUTON: A.L. Spek, Byvoet Center for Biomolecular Research, University of Utrecht.
[15] U. Casellato, P. Guerriero, S. Tamburini, S. Sitran, P.A. Vigato, J. Chem. Soc. Dalton Trans. 1991, 2145.
[16] J.-P. Costes, F. Dahan, A. Dupuis, J.-P. Laurent, Inorg. Chem. 35 (1996) 2400.
[17] J.-P. Costes, F. Dahan, A. Dupuis, J.-P. Laurent, Inorg. Chem. 36 (1997) 4284.
[18] C.M. Brodbeck, L.E. Iton, J. Chem. Phys. 83 (1985) 4285.
[19] C. Legein, J.Y. Buzaré, G. Silly, C. Jacoboni, J. Phys. Condens. Matter 8 (1996) 4339.
[20] R. Miyamoto, 4th Sendai Symposium on Advanced EPR, 1998, p. 9.
[21] T. Kato, private communication, 2001.

tobenzoxazol. This is an unsaturated heterocycle which exists both in solid and in polar solution in the thione tautomeric form with a protonated N-atom [9a,10]. Bzoxsh is structurally related to biologically important bases and several transition-metal complexes have been described in the literature [9].

2. Experimental

2.1. Physical measurements and instrumentation

Ligand dissociation reactions were followed through conventional kinetics using a Hewlett-Packard Model 8452A diode-array spectrophotometer in MeOH/H_2O (75:25%) thermostated solutions. All experiments were performed under pseudo-first-order conditions and the reactions were monitored for 5–6 half-lives. Dissociation of the substituted pentacyanoferrates takes place to a very small extent at room temperature. The kinetics were investigated in the presence of the compounds L = dimethylsulfoxide (dmso), pyridine (py) for Fe^{III} and *N*-methylpyrazinium for Fe^{II}. These have strong affinities for pentacyanoferrate group, allowing the dissociation reactions to be safely followed [3,5a]. The rates of substitution were studied as a function of 7–10 different concentrations of L at a fixed bzoxsh concentration. First-order rate constants were determined by four different mathematical methods: least-squares or the infinite absorbance method, Guggenheim, Kezdy–Swinbourne and a non-linear fitting [12], with excellent result agreement. Second-order rate constants were calculated from literature data (for Fe^{II}) and from the thermodynamic cycle presented in this work. Temperature dependence of the rate dissociation constants was studied in the range of 10–30 °C.

Cyclic voltammetry measurements were carried out with a Princeton Applied Research Potentiostat model 273A. A Pt disc electrode was employed for the measurements at an ionic concentration of 0.5 mol dm^{-3} kept constant with tetrabutylammonium tetrafluoroborate. A Ag/$AgNO_3$ ($[Ag^+] = 0.01$ mol dm^{-3} in an MeCN solution of $Bu^t_4NBF_4$ 0.1 mol dm^{-3}) along with a Pt wire were used as reference and auxiliary electrodes, respectively. Typical experiments were conducted with a 2.5×10^{-3} mol dm^{-3} complex concentration in MeOH/H_2O (75:25%) solutions at ambient temperature.

2.2. Materials

$Na_3[Fe(CN)_5NH_3]\cdot 3H_2O$ was prepared from sodium nitroprusside as described in the literature [11]. The yellow product was stored in the dark at −15 °C. *Anal*. Calc. for $Na_3[Fe(CN)_5NH_3]\cdot 3H_2O$: C, 18.4; H, 2.8; N, 25.8. Found: C, 18.0; H, 2.1; N, 24.6%.

The purity of the 2-mercaptobenzoxazole (Aldrich) was confirmed by elemental analysis. *Anal*. Calc. for C_7H_5NOS: C, 55.6; H, 3.3; N, 9.3. Found: C, 56.1; H, 3.3; N, 8.9%.

Solutions of the aquapentacyanoferrate(II) complex were always freshly prepared using Schlenk techniques. $Na_3[Fe(CN)_5NH_3]\cdot 3H_2O$ was dissolved in dinitrogen-saturated water, mixed with three parts of MeOH (to give a total iron concentration of $1–5 \times 10^{-4}$ mol dm^{-3}) and enough sodium perchlorate to keep the ionic strength at 1.00 mol dm^{-3}. Solid 2-mercaptobenzoxazole (bzoxsh) was always dissolved in excess (20-fold) to avoid competing reactions with small amounts of free NH_3 coming from the starting material.

Solutions of the aquapentacyanoferrate(III) complex were also freshly prepared by oxidizing $[Fe^{II}(CN)_5(H_2O)]^{3-}$ (obtained by dissolving the ammine complex in water) with PbO_2 in dinitrogen-saturated water. The excess of PbO_2 was filtered off and three volumes of MeOH were added. After correction of the ionic strength, solid bzoxsh was added, resulting in a clear deep-green solution.

3. Results and discussion

Typical spectral changes for the reaction of $[Fe^{III}(CN)_5(bzoxsh)]^{2-}$ with dmso and of $[Fe^{II}(CN)_5(bzoxsh)]^{3-}$ with *N*-methylpyrazinium are illustrated in Fig. 2. The concentrations used gave well-defined and reproducible first-order kinetic plots. Dmso is suitable because it forms a very stable and colorless complex with pentacyanoferrate(III) [3] and the reaction was studied following the decay of the band of the reactant at 706 nm. The same procedure was applied when pyridine was the attacking reagent as the $[Fe^{III}(CN)_5(py)]^{2-}$ complex is faintly yellow and absorbs at 410 nm. For the dissociation reactions involving Fe^{II}, the formation of the blue $[Fe^{II}(CN)_5(N\text{-methylpyrazinium})]^{2-}$ was monitored at 690 nm. The dissociation kinetics exhibited good pseudo-first-order behavior during at least two half-lives, with the attacking L always present in large excess over the iron complex ($10^2–10^3$-fold).

According to the general mechanism for the dissociation reactions in pentacyanoferrate complexes [5a] we can write:

$$[Fe^{III/II}(CN)_5(bzoxsh)]^{2/3-} \underset{k_f}{\overset{k_d}{\rightleftharpoons}} [Fe^{III/II}(CN)_5(H_2O)]^{2/3-} + bzoxsh$$

$$[Fe^{III/II}(CN)_5(H_2O)]^{2/3-} + L \underset{k_{-L}}{\overset{k_L}{\rightleftharpoons}} [Fe^{III/II}(CN)_5(L)]^{2-/3-} + H_2O$$

where the loss of bzoxsh is the rate-determining step.

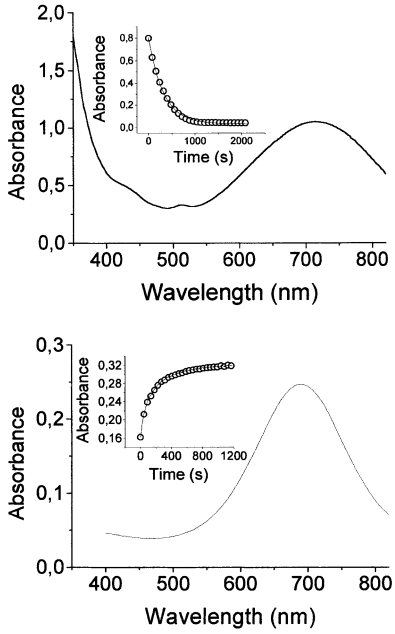


Fig. 2. UV–Vis spectra of $[Fe^{III}(CN)_5(bzoxsh)]^{2-}$ (top) and $[Fe^{II}(CN)_5(N\text{-methylpyrazinium})]^{2-}$ in MeOH/H_2O 75:25 (v/v); Inset shows typical first-order kinetic curves: scatter, experimental data; line, non-linear first-order exponential fit. Top shows the absorbance decay of the 706 nm band typical of $[Fe^{III}(CN)_5(bzoxsh)]^{2-}$ after reaction with dmso; Bottom shows the increase of the 690 nm band when $[Fe^{II}(CN)_5(bzoxsh)]^{3-}$ reacts with *N*-methylpyrazinium.

Assuming a steady-state approximation for $[Fe(CN)_5(H_2O)]^{2/3-}$ the observed rate constant and its reciprocal form (if $k_{-L} \ll k_d$) are given by Eqs. (1) and (2):

$$k_{obs} = \frac{k_f k_{-L}[bzoxsh] + k_L k_d[L]}{k_f[bzoxsh] + k_L[L]} \quad (1)$$

$$\frac{1}{k_{obs}} = \frac{k_f[bzoxsh]}{k_L k_d[L]} + \frac{1}{k_d} \quad (2)$$

The expression (Eq. (1)) is coherent with the saturation curve of k_{obs} versus L and Eq. (2) with the linear behavior of the reciprocal form as seen in Fig. 3. Since the rates of formation of $[Fe(CN)_5L]^{3-}$ are completely independent of the nature of the entering ligand, as expected for a limiting SN_1 mechanism, we calculated a medium value of $k_f^{II} = 290$ dm^3 mol^{-1} s^{-1} from published results for neutral ligands at the same ionic strength. k_f^{II} and (L) used for calculation were: 240 (dmso), 212 (imidazole), 184 (histidine) [6], 354 (4-picoline), 365 (pyridine), 295 (isonicotinamide) and 380 (pyrazine) [3]. The stability constant K_f^{II} was calculated as k_f^{II}/k_d^{II} from the formation and dissociation reactions. K_f^{III} was calculated from the measured electrochemical potentials and the following redox cycle:

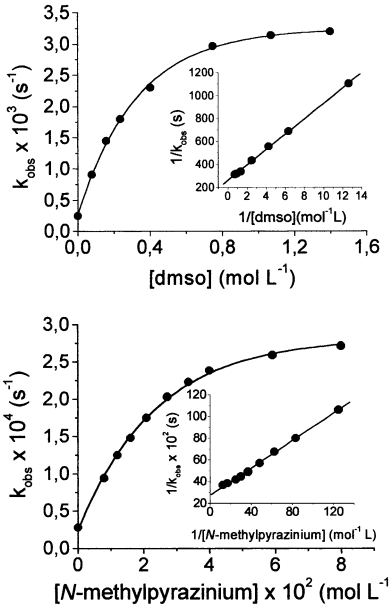
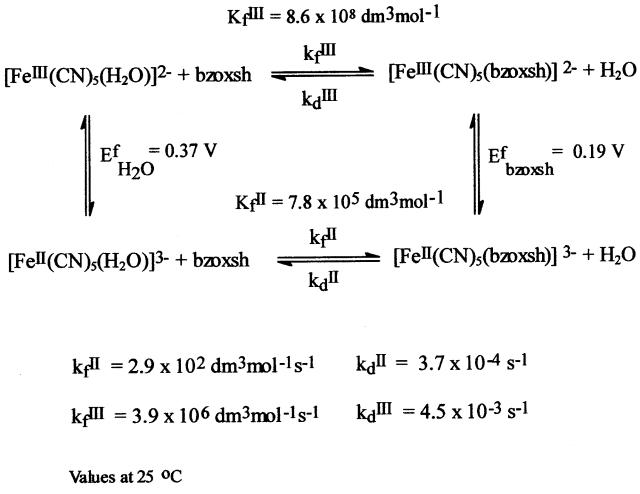


Fig. 3. Plot of k_{obs} versus attacking ligand concentration, showing rate saturation. Top: reaction of $[Fe^{III}(CN)_5(bzoxsh)]^{2-}$ with dmso. Bottom: $[Fe^{II}(CN)_5(bzoxsh)]^{3-}$ reacts with *N*-methylpyrazinium. Inset shows double reciprocals for determination of k_d.



where $K_f^{III} = K_f^{II}\{\exp[(nF/RT)(E^f_{bzoxsh} - E^f_{H_2O})]\}^{-1}$.

The results for bzoxsh are similar to those described for other neutral ligands. This holds for k_f^{II} (240–400 dm^3 mol^{-1} s^{-1}) and K_f^{II} (10^2–10^6 dm^3 mol^{-1}) [3,5a,6]. K_f^{III} is out of the range of 10^{-2}–10^6 dm^3 mol^{-1} and this is consistent with the lower limit of the formal reduction potential, E^f_{bzoxsh} (Table 1). The relative strength of the Fe–L bond can be related with the basicity of L as suggested by Eldik et al. [13]. The higher the sigma-donor capacity of L the lower the lability of the Fe–L bond. However, pK_a values represent only the sigma part of metal–ligand interactions. As can be seen from Table 1, the dissociation constants (k_d) are not much sensitive to large variations of pK_a (compare, for example pyrazine with histidine). This can be explained

Table 1
Kinetic and thermodynamic data for $[Fe(CN)_5L]^{2-/3-}$ complexes. The entries are in order of decreasing formal reduction potentials, E_L^f

L	Donor group	pK_a	k_d^{II} (s^{-1}) at 25 °C	k_d^{III} (s^{-1}) at 25 °C	k_f^{II} (mol^{-1} s^{-1}) at 25 °C	k_f^{III} (mol^{-1} s^{-1}) at 25 °C	I (mol dm^{-3})	K_f^{II} (dm^3 mol^{-1})	K_f^{III} (dm^3 mol^{-1})	E_L^f [a]	Reference
Dmso	*S*=O		7.5×10^{-5}	2.5×10^{-5} [f]	2.4×10^{2}	9.3×10^{-7}	1.00 $LiClO_4$	4.9×10^{6}	3.7×10^{-2}	850	[3,6]
Pyrazinium	C=*N*	0.6	4.2×10^{-4}	[e]	3.80×10^{2}	[e]	1.00 $LiClO_4$	1.9×10^{6} [b]	1.7×10^{3}	550	[3,5] [a][6]
Isonicotinamide	C=*N*	3.7	7.3×10^{-4}	[e]	2.95×10^{2}	[e]	1.00 $LiClO_4$	8.2×10^{5} [b]	5.2×10^{3}	500	[3,5] [a][6]
Pyridinium	C=*N*	5.3	1.1×10^{-3}	1.5×10^{-5} [f]	3.65×10^{2}	1.4×10^{-1}	1.00 $LiClO_4$	4.6×10^{5} [b]	9.4×10^{3}	470	[3,5] [a][6]
Histidine	C=*N*	6.1	5.3×10^{-4}	[e]	3.20×10^{2}	[e]	0.100 $LiClO_4$	5.9×10^{5}	1.1×10^{6}	355	[6]
Imidazole	C=*N*	7.1	1.3×10^{-3}	[e]	2.4×10^{2}	[e]	0.100 $LiClO_4$	1.8×10^{5}	5.8×10^{5}	340	[6]
2-mpy [c]	C=*S*	1.8	1.7×10^{-2}	[e]	2.85×10^{2}	[e]	0.1 KCl	1.6×10^{4}	6.4×10^{5}	272	[5c]
Bzoxsh	C=*S*	5.1	3.7×10^{-4}	4.5×10^{-3}	2.9×10^{2}	3.9×10^{6}	1.00 $NaClO_4$	7.8×10^{5}	8.6×10^{8}	190	[f]
mtr [d]	C=*S*		4.6×10^{-4}	[e]	3.0	[e]	0.100 $NaClO_4$	1.5×10^{4}	[e]	[e]	[14]
1,4-Dithiane	R–*S*–R		5.6×10^{-4}	[e]	[e]	[e]	0.1 $LiClO_4$	[e]	[e]	[e]	[4b]

[a] mV vs EPH, the values refer to the $Fe^{III} + e^- \rightleftharpoons Fe^{II}$ reversible process.
[b] Calculated from K_f^{II} and redox potentials.
[c] 2-Mercaptopyridine.
[d] 3-Mercapto-1,2,4-triazole.
[e] Not determined
[f] This work.

Table 2
Temperature dependence of the rate constant for the dissociation of $[Fe^{III}(CN)_5(bzoxsh)]^{2-}$

Temperature (°C)	$10^4\ k_d$ (s^{-1})
10	5.69
15	11.5
20	22.9
25	45.6
30	81.4

if we consider that both the σ-donor and back-bonding have the same effect on the substitution rate of L in a pentacyanoferrate complex, making it more inert. Back-bonding is bigger for less basic L. The $[Fe^{III}(CN)_5(bzoxsh)]^{2-}$ complex is approximately 10 times more labile than the reduced form, a result consistent with the lack of back-bonding for the Fe^{III} ion. The same argument can be used to explain the higher observed lability of $[Fe^{III}(CN)_5(dmso)]^{2-}$ over $[Fe^{II}(CN)_5(dmso)]^{3-}$ ($k_d^{III} = 2.5 \times 10^{-4}\ s^{-1}$ [this work] versus $7.5 \times 10^{-5}\ s^{-1}$ [3]). In this case preferential π-back-bonding stabilization of the Fe^{II}–dmso complex is an important factor being also probably responsible also for the high value of K_f^{II} (Table 1).

Interestingly, bzoxsh appears to behave as a fair π-acceptor as well as a strong σ-donor ligand, as it stabilizes both oxidation states of pentacyanoferrate complexes. This bonding behavior is also observed for histidine, imidazole and 2-mercaptopyridine (2-mpy). Considering the thermodynamic stability of the complexes, although both the pK_a values of bzoxsh (S–H group) and pyridine are similar, bzoxsh is a weaker π-acceptor, consistent with the significantly lower value of E^f_{bzoxsh} and the high value of K_f^{III}. Conversely, pyridine shows greater stabilization of the pentacyanoferrate(II) ion over the oxidized form (Table 1).

The dissociation constants observed for $[Fe^{III}(CN)_5(py)]^{2-}$ and $[Fe^{II}(CN)_5(py)]^{3-}$ are 1.5×10^{-5} [this work] and $1.1 \times 10^{-3}\ s^{-1}$ [5a], respectively, showing that pyridine prefers the hard Fe^{III} ion, the back-bonding interactions having less importance here.

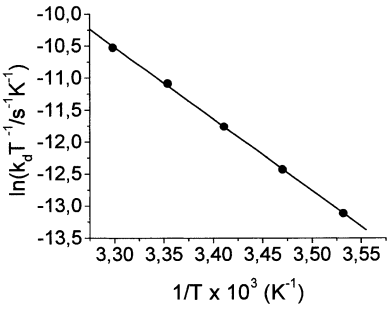


Fig. 4. Eyring plot for the reaction of $[Fe^{III}(CN)_5(bzoxsh)]^{2-}$ with pyridine.

The effect is very pronounced, $[Fe^{III}(CN)_5(py)]^{2-}$ being much more inert than its reduced form.

If we compare the k_d^{III} values for the $[Fe^{III}(CN)_5L]^{2-}$ complexes, we can establish the following order of increasing lability: py ($1.5 \times 10^{-5}\ s^{-1}$) < dmso ($2.5 \times 10^{-4}\ s^{-1}$) < bzoxsh ($4.5 \times 10^{-3}\ s^{-1}$). This result suggests that bzoxsh is bound to Fe^{III} through the soft sulfur atom. If the coordination were through the nitrogen atom, we would expect the complex to be as inert that of pyridine. When k_d^{II} values are compared, the order is dmso ($7.5 \times 10^{-5}\ s^{-1}$) < bzoxsh ($3.7 \times 10^{-4}\ s^{-1}$) < py ($1.1 \times 10^{-3}\ s^{-1}$), emphasizing the importance of back-bonding in the stabilization of these Fe^{II} compounds.

Completing the investigation of the less studied $[Fe^{III}(CN)_5L]^{n-}$ series, activation parameters for the dissociation reaction of $[Fe^{III}(CN)_5(bzoxsh)]^{2-}$ were determined (Fig. 4 and Table 2). They are $\Delta S^{\#} = +11.4\ J\ K^{-1}\ mol^{-1}$ and $\Delta H^{\#} = 93.3\ kJ\ mol^{-1}$, typical of a dissociative type mechanism.

We hope that these results will help fill the gap in the kinetic data available for pentacyanoferrate(III).

Acknowledgements

This work was supported by Brazilian PRONEX Program (Contract Number 41.96.0884.00), whose help we gratefully acknowledge. We thank Professor Henrique Eisi Toma (Institute of Chemistry—USP, Brasil) for the valuable suggestions. J.B.L. and F.S.N. also thank UFPR and Brazilian Research Council (CNPq) for research fellowships.

References

[1] E.I. Stiefel, G.N. George, in: I. Bertini, H.B. Gray, S.J. Lippard, J.S. Valentine (Eds.), Bioinorganic Chemistry, University Science Books, Mill Valley, CA, 1994, p. 365.
[2] (a) L.M. Baraldo, P.F. Forlano, A.R. Parise, L.D. Slep, J.A. Olabe, Coord. Chem. Rev. 219–221 (2001) 881;
(b) B. Sieklucka, Proc. React. Kinet. Mec. 24 (1999) 165;
(c) R.G. Wilkins, Kinetics and Mechanism of Reactions of Transition Metal Complexes, 2nd ed., VCH, New York, 1991, pp. 23 and 31.
[3] H.E. Toma, J.M. Malin, E. Giesbrecht, Inorg. Chem. 12 (1973) 2084.
[4] (a) H.E. Toma, R.M. Serrasqueiro, R.C. Rocha, G.J.F. Demets, H. Winnischofer, K. Araki, P.E.A. Ribeiro, C.L. Donnici, J. Photochem. Photobiol. A: Chem. (2000) 135;
(b) S.S.S. Borges, A.L. Coelho, I.S. Moreira, M.A.B. Araújo, Polyhedron 13 (1994) 1015;
(c) H.E. Toma, M.S. Takasugi, Polyhedron 1 (1982) 429.
[5] (a) H.E. Toma, J.M. Malin, Inorg. Chem. 12 (1973) 1039;
(b) H.E. Toma, J.M. Martins, J. Chem. Soc., Dalton Trans. (1978) 1610;
(c) H.E. Toma, F.S. Nunes, Anais do VI Simp. Bras. Eletroquim. Eletroanal. (1988) 175.

[6] H.E. Toma, A.lzir A. Batista, H.B. Gray, J. Am. Chem. Soc. 104 (1982) 7509.
[7] (a) I. Maciejowska, Z. Stasicka, G. Stochel, R. van Eldik, J. Chem. Soc., Dalton Trans. (1999) 3643;
(b) G. Stochel, R. van Eldik, Inorg. Chim. Acta 190 (1991) 55;
(c) S. Alshehri, J. Burguess, R. van Eldik, C.D. Hubbard, Inorg. Chim. Acta 240 (1995) 305;
(d) C.L. Lin, K. Hung, A. Yeh, Inorg. Chem. 38 (1999) 411;
(e) C.N. Chen, M.C. Wu, A. Yeh, T.Y.R. Tsai, Inorg. Chim. Acta 267 (1998) 81;
(f) H.E. Toma, T.E. Chavez-Gil, Spectrosc. Lett. 32 (1999) 963;
(g) P.R. Norris, P.L.S. Harper, J.M. Pratt, J. Chem. Soc., Dalton Trans. (1997) 2505;
(h) A.E. Almaraz, L.A. Gentil, L.M. Baraldo, J.A. Olabe, Inorg. Chem. 35 (1996) 7718.
[8] (a) D.J. Evans, P.B. Hitchcock, D.L. Hughes, G.J. Leigh, B.H. Nicholson, A.C. Niedwieski, F.S. Nunes, J.F. Soares, Inorg. Chim. Acta 319 (2001) 147;
(b) A.C. Niedwieski, P.B. Hitchcock, G.J. Leigh, J.F. Soares, F.S. Nunes, J.D. da M. Neto, Int. J. Quantum Chem. 88 (2002) 245;
(c) A.C. Raimondi, P.B. Hitchcock, G.J. Leigh, F.S. Nunes, J. Chem. Crystal (2002), in press;
(d) A.C. Niedwieski, P.B. Hitchcock, J.D. da M. Neto, F. Wypych, G.J. Leigh, F.S. Nunes, J. Chem. Soc., Dalton Trans. (2002), submitted;
(e) V. Poulopoulou, H. Taube, F.S. Nunes, Inorg. Chem. 38 (1999) 2844.
[9] (a) C. Preti, G. Tosi, Can. J. Chem. 54 (1976) 85;
(b) C. Preti, G. Tosi, J. Coord. Chem. 8 (1978) 15;
(c) C. Preti, G. Tosi, Spectrochim. Acta 35A (1979) 577;
(d) J. Vicente, M.T. Chicote, P.G. Herrero, P.G. Jones, J. Chem. Soc., Dalton Trans. (1994) 3183;
(e) J. Vicente, M.T. Chicote, D. Rubio, Chem. Ber. 129 (1996) 327;
(f) F.A. Bandbury, M.G. Davidson, P.R. Rai They, D. Stalke, R.J. Snaith, J. Chem. Soc., Dalton Trans. (1995) 3139;
(g) C. Preti, G. Tosi, Can. J. Chem. 55 (1977) 1409.
[10] R.S. Balestrero, D.M. Forkey, J.G. Russell, Magn. Reson. Chem. 24 (1986) 651.
[11] G. Brauer, Handbook of Preparative Inorganic Chemistry, vol. 2, 2nd ed., Academic Press, New York, 1965, p. 1511.
[12] J.H. Espenson, Chemical Kinetics and Reaction Mechanisms, 2nd ed., McGraw-Hill, Highstown, NJ, 1995, p. 15.
[13] S. Alshehri, J. Burgess, R. van Eldik, C.D. Hubbard, Inorg. Chim. Acta 240 (1995) 305.
[14] Y. Baran, A. Ülgen, Intern. J. Chem. Kinet. 30 (1998) 415.

the contributions by the 5,6-disubstitutions in the phen frameworks in more detail, we have determined the crystal structures of $[CuCl(dmphen)_2]PF_6$ (**1**) and $[CuCl(phendione)_2]PF_6 \cdot H_2O$ (**2**) under the regulated condition with the same monodentate co-ligand and counteranion. The crystal structures of **1**, **2** and $[CuCl(phen)_2]PF_6$, in which the structure of $[CuCl(phen)_2]PF_6$ was already determined [10], are discussed in relation to their absorption and reflectance spectral, and electrochemical behaviors.

2. Experimental

2.1. Materials

$CuCl_2 \cdot 2H_2O$, 1,10-phenanthroline monohydrate and NH_4PF_6 were purchased from Wako Pure Chemical Ind. Co., Ltd. 5,6-Dimethyl-1,10-phenanthroline was obtained from Aldrich Chemical Co., Inc. The other chemicals were purchased from Wako Pure Chemical Ind. Co., Ltd., Aldrich Chemical Co., Inc., or Tokyo Chemical Co., Ltd. All of the chemicals were of reagent grade and were used without further purification. 1,10-Phenathroline-5,6-dione was synthesized as described in the literature [15]. $[CuCl(phen)_2]PF_6$, which was used for the comparative studies on spectroscopic and electrochemical properties of the present complexes, was prepared by a modified method from the literature [10].

2.2. Preparations of the complexes

2.2.1. Synthesis of $[CuCl(dmphen)_2]PF_6$ (*1*)

This complex was prepared by a similar method to that for $[CuCl(phen)_2]PF_6$ [10]. To a solution containing dmphen (0.052 g, 0.25 mmol) in 20 ml EtOH was added a solution of $CuCl_2 \cdot 2H_2O$ (0.021 g, 0.13 mmol) in 10 ml EtOH, and the mixture was stirred at room temperature (r.t.) for 20 h. After removing any undissolved materials by filtration, a solution containing NH_4PF_6 (0.41 g, 2.5 mmol) in 10 ml EtOH was added to the filtrate. The whole was stirred for 1 day and the resulting green fine crystals were collected by filtration. The crystals were recrystallized from CH_3CN and a well-formed crystal was used for the X-ray structural analysis. Yield: 0.072 g (88%). *Anal.* Found: C, 50.92; H, 3.66; N, 8.48%. Calc. for $C_{28}H_{24}N_4F_6PClCu$ (**1**): C, 50.73; H, 3.69; N, 8.41%. UV–Vis: ν_{max} (10^3 cm^{-1}) (ε, mol^{-1} dm^3 cm^{-1}) (MeCN): 10.27 (141), 13.72 (190), 29.41 (1775), 36.10 (49 500), 44.05 (48 600). Diffuse reflectance spectrum: ν_{max} (10^3 cm^{-1}): 10.22, 13.35, 28.74, 31.85, 35.09. EPR: $g_{\|} = 2.02$, $g_{\perp} = 2.11$ (solid, 140 K); 2.12 (MeCN solution, 140 K). Cyclic voltammetry (MeCN): $E^{\circ\prime} = -0.39$ V.

2.2.2. Synthesis of $[CuCl(phendione)_2]PF_6$ (*2*)

This complex was prepared by a similar method to that for $[CuCl(dmphen)_2]PF_6$ (**1**). To a solution containing phendione (0.10 g, 0.50 mmol) in 20 ml EtOH was added a solution of $CuCl_2 \cdot 2H_2O$ (0.043 g, 0.25 mmol) in 10 ml EtOH, and the mixture was stirred at r.t. for 20 h. After removing any undissolved materials by filtration, a solution containing NH_4PF_6 (0.82 g, 5.0 mmol) in 10 ml EtOH was added to the filtrate. The whole was stirred for 1 day and the resulting green fine crystals were collected by filtration. Recrystallization was accomplished by slow diffusion of ether into a solution of the compound in CH_3CN. A well-formed crystal was used for the X-ray structural analysis. Yield: 0.16 g (92%). *Anal*. Found: C, 41.16; H, 2.30; N, 8.00%. Calc. for $C_{24}H_{14}N_4O_5F_6PClCu$ (**2**): C, 41.78; H, 2.31; N, 7.97%. UV–Vis: ν_{max} (10^3 cm^{-1}) (ε, mol^{-1} dm^3 cm^{-1}) (MeCN): 10.24 (112), 13.76 (179), 28.65 (2440), 33.22 (15 200), 39.68 (52 000). Diffuse reflectance spectrum: ν_{max} (10^3 cm^{-1}): 10.12, 13.89, 27.40, 31.55, 38.02. EPR: 2.10 (solid, 140 K); 2.11 (MeCN solution, 140 K). Cyclic voltammetry (MeCN): $E^{\circ\prime} = -0.79$, -0.14 V.

2.3. Measurements

Electronic absorption and diffuse reflectance spectra were recorded with JASCO Ubest V-560 and V-570 spectrophotometers, respectively. EPR spectra were measured with a Bruker EMX-T ESR spectrometer. Electrochemical measurements were made with a CV-50W apparatus (Bioanalytical Systems, Inc.; BSI) using a platinum disk as working electrode. The Ag/AgCl/MeCN electrode (BSI) and a platinum wire were used as reference and auxiliary electrodes, respectively. These experiments were conducted at r.t. in a 0.1 mol dm^{-3} MeCN solution of Bu_4N as a supporting electrolyte, and at concentrations of the complexes or ligand with 1.0 mmol dm^{-3}. Elemental analyses (C, H, N) were performed by the Analysis Center of the University of Tsukuba.

2.4. X-ray structure determination

Intensity data for **1** and **2** were collected on the Rigaku RASA-7S four-circle diffractometer with graphite-monochromatized Mo Kα radiation ($\lambda = 0.71069$ Å). The structures were solved by the direct method using SIR92 and refined by the full-matrix least-squares method using a TEXSAN program package [16]. All calculations were performed on an Indigo II computer. Crystal data for **1** = $C_{28}H_{24}N_4F_6PClCu$, F.W. = 660.49, triclinic, space group $P\bar{1}$ (#2), $a = 11.497(3)$, $b = 14.526(4)$, $c = 8.750(2)$ Å, $\alpha = 100.23(2)^\circ$, $\beta = 112.20(2)^\circ$, $\gamma = 88.35(2)^\circ$, $V = 1330.2(5)$ $Å^3$, $Z = 2$, $D_{calc} = 1.649$ g cm^{-3}, $\mu = 1.051$ mm^{-1}, crystal size $0.23 \times 0.33 \times 0.58$ mm, trans. factors 0.88–1.00, 6385

reflections measured ($2\theta_{max} = 55.0°$), 4302 observed reflections [$I > 2.00\sigma(I)$] used in the refinement, $R = 0.053$, $Rw = 0.071$ and GOF = 1.81 for 370 parameters. Crystal data for **2** = $C_{24}H_{14}N_4O_5F_6PClCu$, F.W. = 682.36, monoclinic, space group $P2_1/c$ (#14), $a = 13.167(7)$, $b = 14.225(8)$, $c = 15.171(3)$ Å, $\beta = 114.06(3)°$, $V = 2594(2)$ Å^3, $Z = 4$, $D_{calc} = 1.747$ g cm^{-3}, $\mu = 1.095$ mm^{-1}, crystal size $0.15 \times 0.15 \times 0.20$ mm, trans. factors 0.96–1.00, 6200 reflections measured ($2\theta_{max} = 55.0°$), 1913 observed reflections [$I > 2.00\sigma(I)$] used in the refinement, $R = 0.056$, $Rw = 0.065$ and GOF = 1.41 for 442 parameters.

3. Results and discussion

3.1. Crystal structures

The X-ray structural analyses revealed that each of **1** and **2** consists of a discrete monovalent complex cation and one PF_6^- anion, and that **2** additionally involves one H_2O molecule. As shown in Fig. 1, both of the complex cations in **1** and **2** possess five-coordinated environments with $CuClN_4$ chromophores similar to that in $[CuCl(phen)_2]PF_6$ [10]. Namely, each of the Cu atoms in **1** and **2** is coordinated by four N atoms from two phen frameworks and one Cl atom. As shown in Table 1, however, the Cu–Cl distances in **1** (2.257(1) Å) and **2** (2.250(2) Å), which are almost identical with each other, are significantly shorter than that in $[CuCl(phen)_2]PF_6$ (2.294(2) Å). Furthermore, the values of differences between the longest and shortest Cu–N bond distances, ΔCu–N = 0.188(3) Å for **1** and 0.190(7) Å for **2**, are considerably different from that for $[CuCl(phen)_2]PF_6$ (0.156(4) Å) [17]. These suggest that the geometries around Cu(II) centers in **1** and **2** are fairly distinct from that in $[CuCl(phen)_2]PF_6$. The largest angle around the Cu(II) center (β: N3–Cu–N1 = 170.8(1)° for **1**, 173.7(3)° for **2**) is considerably different from the second-largest one (α: N2–Cu–Cl = 150.13(8)° for **1**, 154.0(2)° for **2**). This implies that the geometries around Cu(II) centers in **1** and **2** are of distorted square-pyramidal or trigonal-bipyramidal one. Since the angular structural index parameter, $\tau = (\beta - \alpha)/60$, is evaluated by the two largest angles ($\alpha < \beta$) in the five-coordinated geometry [18], the value of $\tau = 0.34$

Table 1
Selected bond distances (Å) and angles (°) of **1**, **2** and, $[CuCl(phen)_2]PF_6$ [a]

	1	**2**	$[CuCl(phen)_2]PF_6$
Cu–Cl	2.257(1)	2.250(3)	2.294(2)
Cu–N1	2.016(3)	2.011(6)	2.001(4)
Cu–N2	2.073(3)	2.052(7)	2.076(4)
Co–N3	1.998(3)	1.997(6)	2.003(4)
Co–N4	2.186(3)	2.187(6)	2.157(4)
Cl–Cu–N(1)	95.72(8)	95.6(2)	93.4(1)
Cl–Cu–N(2)	150.13(8)	154.0(2)	131.6(1)
Cl–Cu–N(3)	92.86(8)	90.7(2)	91.0(1)
Cl–Cu–N(4)	107.40(8)	106.2(2)	114.4(1)
N(1)–Cu–N(2)	80.3(1)	79.8(3)	81.0(2)
N(1)–Cu–N(3)	170.8(1)	173.7(3)	175.2(2)
N(1)–Cu–N(4)	95.4(1)	100.1(2)	96.3(2)
N(2)–Cu–N(3)	93.9(1)	94.1(3)	97.5(2)
N(2)–Cu–N(4)	102.4(1)	99.9(2)	114.1(2)
N(3)–Cu–N(4)	78.9(1)	79.0(2)	80.1(2)

[a] Ref. [10].

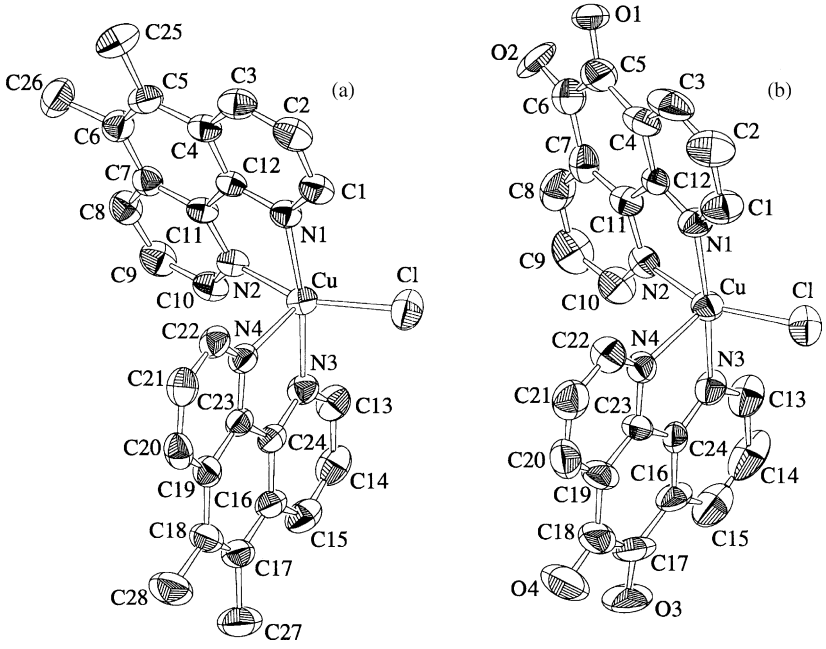


Fig. 1. Perspective views of the complex cations in **1** (a) and **2** (b) with the atomic labeling schemes (ellipsoids at 50% probabilities).

for **1** or 0.33 for **2** seems to indicate a distorted square-pyramid. This is in marked contrast to the unsubstituted phen complex, $[CuCl(phen)_2]PF_6$, with a distorted trigonal-bipyramidal geometry ($\tau = 0.73$) [10].

In both crystals of **1** and **2**, no PF_6^- anions are close enough to interact with the Cu(II) centers in the complex cations, as in the case of $[CuCl(phen)_2]PF_6$ [10]. As shown in Fig. 2(a), however, one dmphen framework in the complex cation in **1** is in close proximity to that in the other complex cation accompanied by the formation of a dimeric unit. Namely, the interplane distance and angle between the neighboring two dmphen frameworks are 3.356(7) Å and 0.000(1)°, respectively, indicating the interaction between the two π-electronic systems of dmphen frameworks. Although slight differences due to the O atoms on the 5- and 6-positions of phen are recognized for the interactions between the π-electronic systems in **2**, the formation of a dimeric unit based on the interaction between the adjacent two phendione frameworks (interplane distance: 3.36(1) Å, interplane angle: 0.000(3)°) occurs as in the case of **1** (Fig. 2(b)). However, the morphology of interactions between the π-frameworks in **1** and **2** is obviously distinguishable from that in $[CuCl(phen)_2]PF_6$, in which each of the two phen frameworks interacts with one phen framework in the adjacent complex cation to form a polymeric chain [10]. Considering these facts, it can be concluded that the five-coordinated geometries of these complexes are appreciably governed by the interactions between the π-frameworks. Since the interactions of π-frameworks are significantly dependent on the steric and electronic natures of the substituents, the five-coordinated geometries of the present complexes seem to be brought by the introductions of the substituents into the phen frameworks.

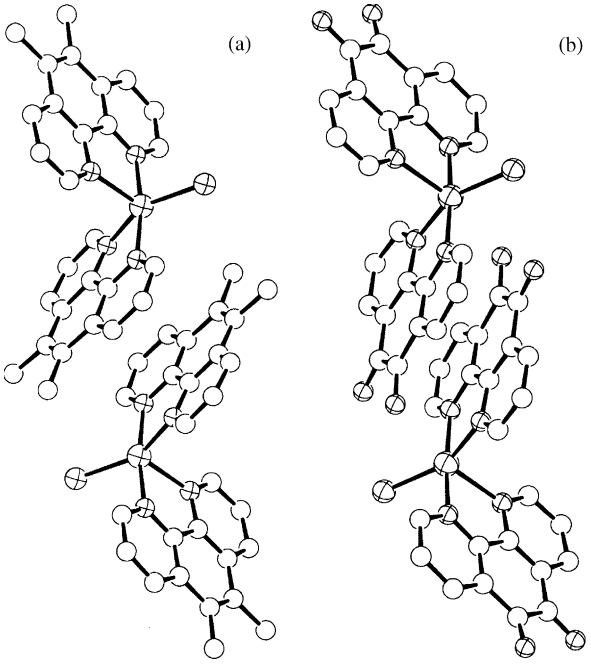


Fig. 2. Dimeric structures in the crystalline state of **1** (a) and **2** (b).

3.2. Electronic absorption and diffuse reflectance spectral behaviors

The reflectance spectrum of $[CuCl(phen)_2]PF_6$ exhibits single peak due to the $d_{xz} \approx d_{yz} \rightarrow d_{z^2}$ transition at 12.10×10^3 cm^{-1} accompanied by a shoulder due to the $d_{x^2-y} \rightarrow d_{z^2}$ transition at 10.50×10^3 cm^{-1} [19], as reported by Hathaway et al. [10]. In the UV region, the complex shows additional four bands at 27.47, 30.40, 33.22, and 35.84×10^3 cm^{-1}. Among these bands, the corresponding band to the 27.47×10^3 cm^{-1} one is also observed for $[CuCl(bpy)_2]Cl$ (bpy = 2,2′-bipyridine) with a different kind of π character [18]. Therefore, the 27.47×10^3 cm^{-1} band of $[CuCl(phen)_2]PF_6$ can be assigned as a Cl-to-Cu CT transition [20,21]. The remaining bands in the UV region seem to be mainly due to the π–π* transitions localized on the phen frameworks. While similar spectral patterns in the UV region are also recognized for **1** and **2**, both complexes exhibit well-resolved two peaks due to the d–d transitions (10.22 and 13.35×10^3 cm^{-1} for **1**, 10.12 and 13.89×10^3 cm^{-1} for **2**) in contrast to $[CuCl(phen)_2]PF_6$. These spectral features seem to reflect differences from $[CuCl(phen)_2]PF_6$ in the geometries around Cu(II) centers and the resulting one-electron ground-state configurations of **1** and **2** [10]. In MeCN, the absorption spectra of **1** and **2** exhibit similar spectral patterns to the reflectance spectra, indicating almost the same geometries around the Cu(II) centers as in the crystalline state. On the other hand, the d-d bands for $[CuCl(phen)_2]PF_6$ are observed as the well-resolved two components, which are appeared at similar energies to those for **1** and **2**. This implies that the geometry around the Cu(II) center of $[CuCl(phen)_2]PF_6$ in solution is distinct from that in the crystalline state and is considered to be rather similar to those of **1** and **2** with a distorted square-pyramid. This is supported by the results of the EPR spectral measurements for the present complexes. Namely, for instance, the anisotropic spectral pattern for the polycrystalline sample of $[CuCl(phen)_2]PF_6$ is slightly different from that in frozen MeCN solution, but seems to be rather similar to that for the polycrystalline sample of **1** with a distorted square-pyramidal geometry [19]. It is suggested therefore that the geometries around the Cu(II) centers of these complexes in the crystalline state are significantly governed by the lattice forces.

3.3. Electrochemical properties

The cyclic voltammogram at platinum disk electrode for $[CuCl(phen)_2]PF_6$ displays only one reversible

Cu(II)/Cu(I) redox couple with $E^{\circ\prime} = -0.37$ V [19]. While **1** also shows the redox couple in a similar potential region, the value of $E^{\circ\prime}$ (-0.39 V) is of slightly negative compared with that for $[CuCl(phen)_2]PF_6$. It is known that the redox potential for Cu(II)/Cu(I) process is shifted to more negative as the electron-donating ability of the substituents on the phen framework becomes higher [14]. Accordingly, it can be regarded that a slight difference in the Cu(II)/Cu(I) redox couple between $[CuCl(phen)_2]PF_6$ and **1** is due to the electron-donating methyl groups on 5- and 6-positions at phen framework. Contrary to the cases of these complexes, **2** shows two reversible redox couples with $E^{\circ\prime} = -0.79$ and -0.14 V in the negative potential region. Among these redox couples, the one with $E^{\circ\prime} = -0.79$ V is also observed for the free phendione ligand [22], and can be assigned as the redox process in the phendione. Although the couple with $E^{\circ\prime} = -0.14$ V of **2** can be regarded as the Cu(II)/Cu(I) redox process, the potential is located on rather positive region than $[CuCl(phen)_2]PF_6$ and **1**. This seems to reflect the characteristic electronic nature of **2** due to the electron-withdrawing substituents on 5- and 6-positions at phen framework. It can be concluded, therefore, that the electrochemical properties of these complexes are significantly influenced by the electronic characters of the substituents on the phen frameworks.

4. Supplementary material

Crystallographic data for the structural analysis have been deposited with the Cambridge Crystallographic Data Centre, CCDC Nos. 181117 and 181118 for **1** and **2**, respectively. Copies of this information may be obtained free of charge from The Director, CCDC, 12 Union Road, Cambridge, CB2 1EZ, UK (fax: +44-1223-336033; e-mail: deposit@ccdc.cam.ac.uk or www: http://www.ccdc.cam.ac.uk).

Acknowledgements

This work was partially supported by a Grant-in-Aid for Scientific Research No. 13555257 from the Ministry of Education, Science, Sports, and Culture.

References

[1] H. Nakai, Y. Deguchi, Bull. Chem. Soc. Jpn. 48 (1975) 2557.
[2] O.P. Anderson, Inorg. Chem. 14 (1975) 730.
[3] H. Nakai, Y. Noda, Bull. Chem. Soc. Jpn. 51 (1978) 1386.
[4] D. Boys, C. Escobar, S. Martínez-Carrera, Acta Crystallogr., Sect. B 37 (1981) 351.
[5] S. Tyagi, B. Hathaway, S. Kremer, H. Stratemeier, D. Reinen, J. Chem. Soc., Dalton Trans. (1984) 2087.
[6] C.J. Simmons, N.W. Alcock, K. Seff, W. Fitzgerald, B.J. Hathaway, Acta Crystallogr., Sect. B 41 (1985) 42.
[7] W.D. Harrison, D.M. Kennedy, M. Power, R. Sheahan, B.J. Hathaway, J. Chem. Soc., Dalton Trans. (1981) 1556.
[8] O. Carugo, C.B. Castellani, J. Chem. Soc., Dalton Trans. (1990) 2895.
[9] P. Nagle, E. O'Sullivan, B.J. Hathaway, E. Muller, J. Chem. Soc., Dalton Trans. (1990) 3399.
[10] G. Murphy, P. Nagle, B. Murphy, B. Hathaway, J. Chem. Soc., Dalton Trans. (1997) 2645 and references therein.
[11] D. Tran, B.W. Skelton, A.H. White, L.E. Laverman, P.C. Ford, Inorg. Chem. 37 (1998) 2505.
[12] M. Brophy, G. Murphy, C. O'Sullivan, B. Hathaway, B. Murphy, Polyhedron 18 (1999) 611.
[13] S.M. Morehouse, H. Suliman, J. Haff, D. Nguyen, Inorg. Chim. Acta 297 (2000) 411.
[14] P.M. Bush, J.P. Whitehead, C.C. Pink, E.C. Gramm, J.L. Eglin, S.P. Watton, L.E. Pence, Inorg. Chem. 40 (2001) 1871 (and references therein).
[15] M. Yamada, Y. Tanaka, Y. Yoshimoto, Bull. Chem. Soc. Jpn. 65 (1992) 1006.
[16] 'TEXSAN. Molecular Structure Corporation. Single Crystal Structure Analysis Software. Version 1.9,' MSC, 3200 Research Forest Drive, The Woodlands, TX77381, USA, 1998.
[17] The ΔCu–N value means a difference between the longest and shortest Cu–N bond distances.
[18] A.W. Addison, T.N. Rao, J. Reedijk, J. Rijn, G.C. Verschoor, J. Chem. Soc., Dalton Trans. (1984) 1349.
[19] Spectral and electrochemical data of $[CuCl(phen)_2]PF_6$ are as follows: UV–Vis: ν_{max} (10^3 cm^{-1}) (ε, mol^{-1} dm^3 cm^{-1}) (MeCN): 10.35 (127), 13.66 (183), 37.04 (57 500), 44.44 (62 900). Diffuse reflectance spectrum: ν_{max} (10^3 cm^{-1}): 10.50, 12.10, 27.47, 30.40, 33.22, 35.84. EPR: $g_{\|} = 2.01$, $g_{\perp} = 2.17$ (solid, 140 K); $g_{\|} = 2.01$, $g_{\perp} = 2.14$ (MeCN solution, 140 K). Cyclic voltammetry (MeCN): $E^{\circ\prime} = -0.37$ V.
[20] F.S. Stephens, P.A. Tucker, J. Chem. Soc., Dalton Trans. (1973) 2293.
[21] A. Altomare, M.C. Burla, M. Camalli, M. Cascarano, C. Giacovazzo, A. Guagliardi, G. Polidori, J. Appl. Crystallogr. 27 (1994) 435.
[22] Cyclic voltammetry (MeCN) for the free 1,10-phenanthroline-5,6-dione: $E^{\circ\prime} = -0.79$ V.

complexes of the most common di- and tripeptides were first recorded more than three decades ago [7–11] and the most important conclusions were reviewed by Sigel and Martin [12]. It was found that these metal ions form stable, tetragonal $[MH_{-2}L]^{-}$ complexes with tripeptides via the coordination of the terminal amino, two deprotonated amide nitrogen and carboxylate oxygen donor functions. The non-coordinating side chains (e.g. Ala or Leu) do not affect the binding modes of these complexes and the CD spectra can be easily explained by the use of a double octant or hexadecant sector rule [7,12]. Donor atoms in the side chains of peptides, however, can alter the coordination modes of complexes and this is reflected in characteristic changes of the CD spectra.

The metal binding of thioether donor functions of methionyl residues is among the most contradictory issues of metallopeptide chemistry. Thioether donor atoms are among the major metal binding sites in blue copper proteins and in some other metalloenzymes, but the thioether donor groups are generally considered as weakly or non-coordinating side chains in the complexes of the first row transition elements [12]. It was found in our previous study on copper(II) and nickel(II) complexes of tripeptides of methionine that coordination of the sulfur atoms depends on both the number and the position of methionyl residues in the peptide sequence [13]. The results were obtained from combined potentiometric, UV–Vis and EPR measurements and indicated a weak, *axial* or *equatorial* coordination of the sulfur atoms. Metal ion coordinations of N-terminal methionyl residues were also reported in copper(II) and nickel(II) complexes of some dipeptides [14–16], and in some cases these observations were supported by CD measurements [16]. Soft metal ions, like palladium(II), have much higher affinity to thioether binding. As a consequence, the sulfur atoms in the di- and tripeptides of methionine are the primary ligating groups towards palladium(II) [17–21]. Complex formation reactions between palladium(II) and peptides are generally monitored by NMR spectroscopy and in the case of methionine and its derivatives, relatively little information has been gained from CD measurements [18–20].

These data on metal complexes of peptides containing methionyl residues revealed that metal ion coordination of the thioether functions depends on several crucial factors, including the nature of the metal ion and location of the thioether donor atoms. The results were generally obtained from potentiometric studies supported by UV–Vis and EPR or NMR measurements. CD spectra have been reported for several dipeptide complexes, but tripeptides or higher oligomers have not been studied yet. In this paper, we report the results of CD spectroscopic measurements on the copper(II), nickel(II) and palladium(II) complexes of tripeptides containing methionine in all possible locations. The measurements were aimed to reveal the high sensitivity and applicability of CD spectroscopy for the structural elucidation of metal ion–peptide complexes and the results provide a significant contribution to the better understanding of metalloenzymes [1].

2. Experimental

2.1. Materials

The optically pure di- and tripeptides Gly-L-Met, L-MetGly, L-AlaGly, L-MetGlyGly, Gly-L-MetGly, Gly-L-AlaGly, GlyGly-L-Met, L-MetGly-L-Met, L-Met-L-Met-L-Ala and L-Met-L-Met-L-Met were purchased from Bachem and used without further purification. The concentrations of the peptide stock solutions were checked by potentiometric titrations and the pK values of the ligands were reported earlier [13,21]. Stock solutions of copper(II) and nickel(II) chlorides were prepared from analytical grade reagents and their concentrations were determined gravimetrically via the precipitation of oxinates. Palladium(II) complexes were prepared from $K_2[PdCl_4]$ obtained from Fluka.

2.2. CD studies

CD spectra were recorded on a JASCO J-810 spectropolarimeter using 1 or 10 mm cells in the 200–800 nm range with metal ion concentration of 3×10^{-4}–1×10^{-2} mol dm^{-3} in aqueous solution. The pH was varied by adding small portions of either 0.2 mol dm^{-3} KOH or 0.2 mol dm^{-3} HNO_3 to the solution of the metal complexes. All CD spectra are reported as the difference in molar absorptivity ($\Delta\varepsilon = \varepsilon_l - \varepsilon_r$). All experiments were performed at room temperature, near 22 °C.

The CD spectra of the individual complexes were calculated by means of a general computational program PSEQUAD [22], using the original spectra and the total concentrations of metal ion, ligand, hydrogen ion and the potentiometrically determined stability constants.

2.3. Determination of stability constants

The stability constants of peptide complexes were defined by Eqs. (1) and (2) and determined from CD spectroscopic measurements.

$$pM + qH + rL \rightleftharpoons M_pH_qL_r \quad (1)$$

$$\beta_{pqr} = \frac{[M_pH_qL_r]}{[M]^p[H]^q[L]^r} \quad (2)$$

The calculation of the stability constants were performed for copper(II)–tripeptide systems by the use of

the general computational program PSEQUAD [22]. The original spectra, the total concentrations of the metal ion and ligand and the pH values or the total hydrogen ion concentrations were used as the primary input parameters for calculations. The CD spectra of the same samples were taken at 7–10 different pH values in the pH range 3.5–9.0 and $\Delta\varepsilon$ values belonging to 50–60 different wavelengths were used for calculation from each spectrum.

3. Results and discussion

3.1. Copper(II) complexes

Stability constants of the copper(II) and nickel(II) complexes of tripeptides containing methionyl residues have already been reported from potentiometric studies [13]. These data show a very close similarity in the complex formation reactions of the six tripeptides and a good correlation with any other tripeptides containing non-coordinating side chains [12,23]. In all cases, the metal ion speciation of the copper(II) complexes was characterised by the successive formation of the species $[CuL]^+$, $[CuH_{-1}L]$ and $[CuH_{-2}L]^-$ (Fig. 1). The metal binding sites of these species were described by the (NH_2, CO), (NH_2, N^-, CO) and (NH_2, N^-, N^-, COO^-)-coordination modes, respectively.

CD spectra of the copper(II)–tripeptide systems were measured in equimolar solutions and Fig. 2 is used to demonstrate the differences in the measured CD spectra obtained by increasing the pH values in the copper(II)–GlyMetGly system. Although the measured CD spectra always corresponded to a mixture of different complexes in accordance with the distribution curves, the CD spectra of the individual species $[CuL]^+$, $[CuH_{-1}L]$ and $[CuH_{-2}L]^-$ could be derived from the recorded CD spectra by using PSEQUAD program (Fig. 3). The CD data from these optimized spectra for all the major species are collected in Table 1. It is evident that the species $[CuL]^+$, $[CuH_{-1}L]$ and $[CuH_{-2}L]^-$ have significantly different chiroptical properties (Fig. 3 and Table 1), and in all cases, the Cotton effects (CEs) observed in the wavelength range 280–800 nm can be assigned to three different types of transitions: d–d (500–800 nm), N^-(amide)→Cu(II) (280–310 nm) and S(thioether)→Cu(II) transitions (320–360 nm). The NH_2→Cu(II) CT bands were generally observed in the range 250–280 nm but they overlapped with intraligand transitions and the corresponding parameters could not be accurately determined. In addition, the amino groups are coordinated in all species in the whole pH range, thus the changes in NH_2→Cu(II) transitions are not characteristic of the different coordination modes of the complexes.

3.1.1. Species $[CuL]^+$

The formation of the species $[CuL]^+$ is accompanied with a low intensity negative CE in the d–d absorption bands (Table 1 and Fig. 3). This is in agreement with the previous findings of Sigel and Martin [12], which states that the ability of metal ions to sense asymmetry on a nearby side chain is transmitted in the decreasing order: N^-(amide) > NHCO(amide) > COO^- > NH_2. The low intensity of the CEs in the visible range and the lack of any N^-→Cu(II) CT transition below 300 nm strongly

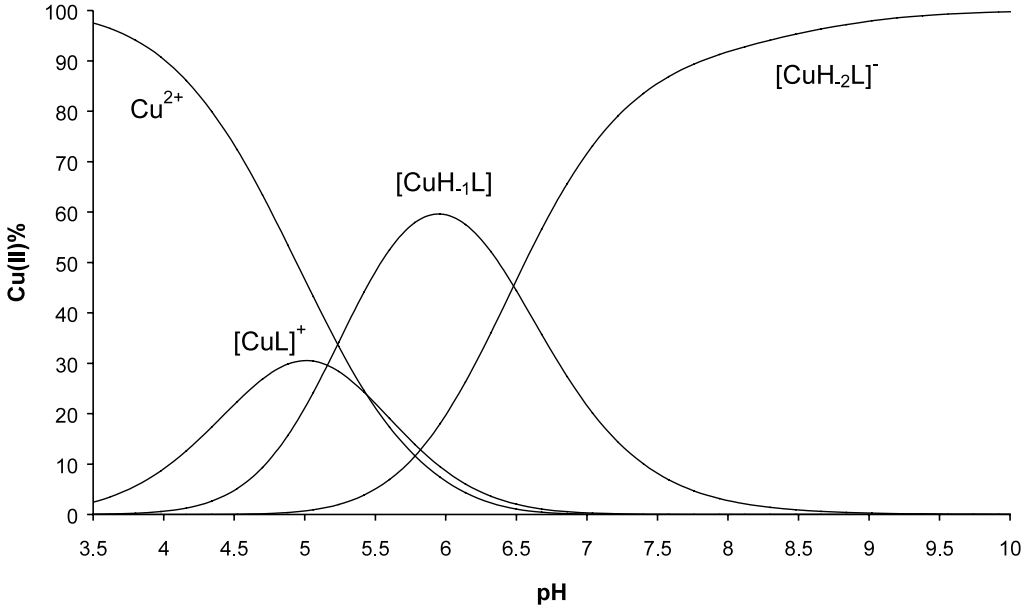


Fig. 1. Concentration distribution of the species formed in copper(II)–GlyMetGly system as a function of pH ($c_{Cu(II)} = c_{GlyMetGly} = 4 \times 10^{-3}$ mol dm^{-3}).

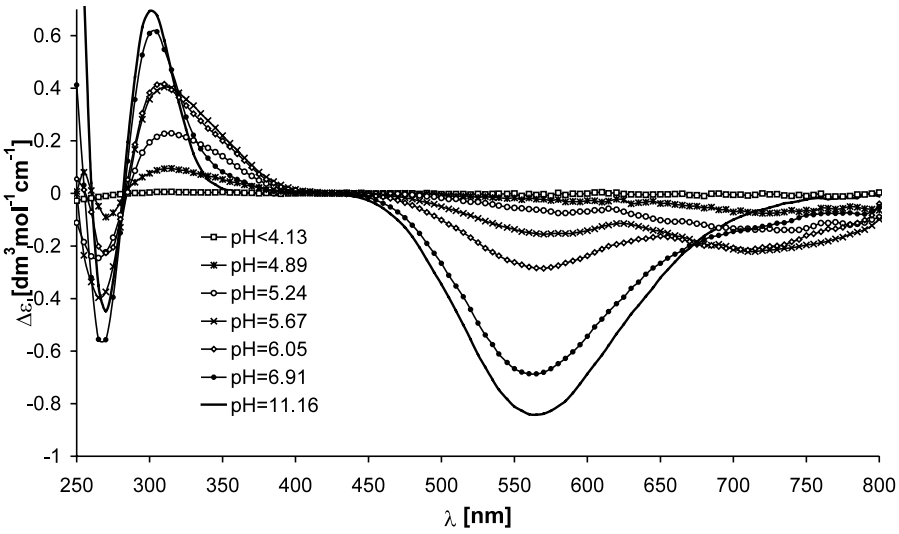


Fig. 2. CD spectra measured in equimolar solutions of copper(II) and GlyMetGly as a function of pH ($c_{Cu(II)} = c_{GlyMetGly} = 1 \times 10^{-2}$ mol dm^{-3}).

support the (NH_2, CO) binding mode in all $[CuL]^+$ species. There are, however, characteristic differences in the CD spectra of $[CuL]^+$ around 330 nm. A moderately intense CT band with a negative CE is developed in all tripeptide complexes containing N-terminal methionyl residues. These CEs can be attributed to the S(thioether)→Cu(II) CT transitions supporting the *axial* coordination of the thioether residues (Scheme 1a). The intensities of these transitions are changing via maximum curves in the function of pH and the locations of the maxima correspond to the highest concentration of $[CuL]^+$.

3.1.2. Species $[CuH_{-1}L]$

The species $[CuH_{-1}L]$ was formed in a medium pH range ($4.5 < pH < 8$) and it was characterised by the coordination of the terminal amino and the deprotonated nitrogen atoms of the subsequent amide groups [13]. The visible absorption spectra of $[CuH_{-1}L]$ exhibit a broad, single absorption band around 630–650 nm in agreement with the coordination of two nitrogen donor atoms [4,5]. In most cases, the CD of the d–d transitions are, however, split into a low intensity negative (700–730 nm) and an even less intense positive (540–570 nm) CE. The highest intensities of these CD extrema were obtained for the copper(II) complexes of tripeptides containing internal methionyl residues, supporting the above mentioned coordination mode and the increased ability of the amide nitrogen to transmit chiral information. The $N^- \rightarrow Cu(II)$ CT transitions were observed in all systems and the intensities followed the same trends. The S(thioether)→Cu(II) CT bands were developed only in the $[CuH_{-1}L]$ species of peptides containing internal methionyl residues. In this case, the

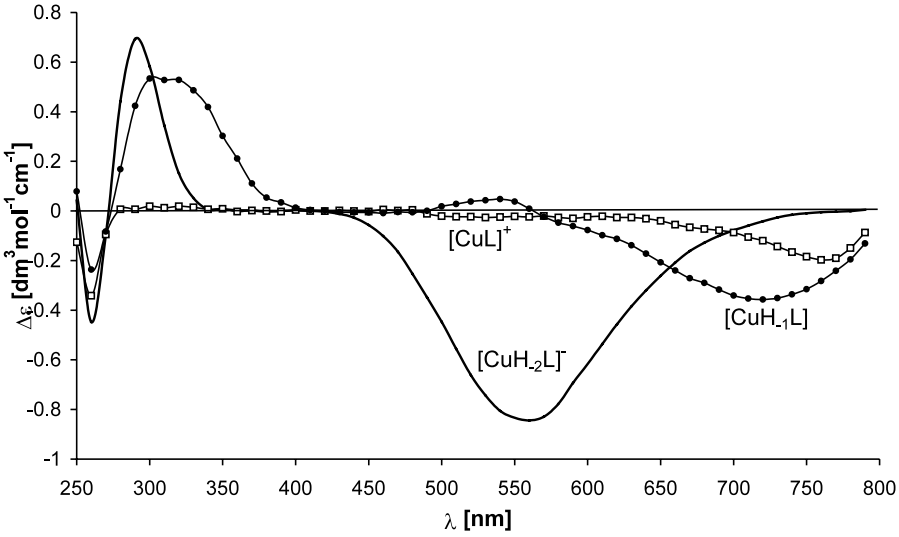
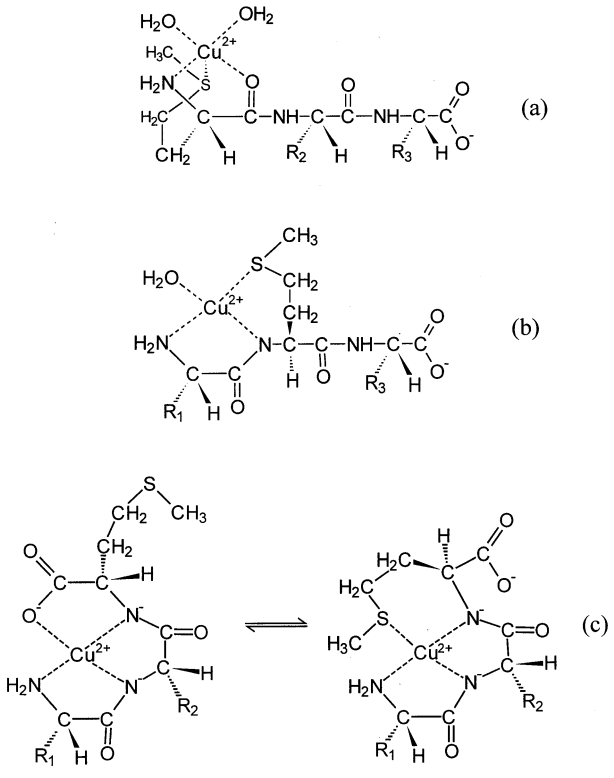


Fig. 3. Optimized CD spectra of the individual species $[CuL]^+$, $[CuH_{-1}L]$ and $[CuH_{-2}L]^-$ formed in the copper(II)–GlyMetGly system and calculated with the program PSEQUAD by using the measured CD spectra and the stability constants.

Table 1
Optimized CD extrema ($\lambda(\Delta\varepsilon)$) of the individual species calculated from the pH dependent CD spectra of copper(II)–tripeptide systems with the program PSEQUAD

Species	Ligand	$N^- \rightarrow Cu(II)$	$S \rightarrow Cu(II)$	d–d
$[CuL]^+$	GlyAlaGly			610 (+0.04); 760 (−0.08)
	GlyMetGly			768 (−0.23)
	GlyGlyMet			590 (−0.12)
	MetGlyGly		331 (−0.77)	720 (−0.26)
	MetGlyMet		330 (−0.98)	540 (+0.10); 710 (−0.27)
	MetMetAla		330 (−0.85)	566 (−0.32); 790 (−0.27)
	MetMetMet		325 (−0.95)	560 (−0.56); 755 (−0.55)
$[CuLH_{-1}]$	GlyAlaGly	305 (+0.72)		560 (−0.11); 730 (−0.27)
	GlyMetGly	310^{sh} (+0.54)	350^{sh} (+0.42)	544 (+0.05); 720 (−0.34)
	GlyGlyMet	290 (+0.29)		569 (+0.19); 722 (−0.13)
	MetGlyGly	302 (+0.09)		560 (−0.03)
	MetGlyMet	310 (+0.12)		556 (+0.07); 720 (−0.09)
	MetMetAla	310^{sh} (+0.47)	340^{sh} (+0.45)	540 (+0.07); 700 (−0.63)
	MetMetMet	310^{sh}	356^{sh} (+0.36)	544 (+0.28); 716 (−0.45)
$[CuLH_{-2}]^-$	GlyAlaGly	302 (+0.50)		559 (−0.85)
	GlyMetGly	301 (+0.69)		562 (−0.86)
	GlyGlyMet	296 (−0.69)	347 (+0.06)	563 (−0.69)
	MetGlyGly	297 (+0.38)		485 (+0.03); 545 (−0.02); 612 (+0.04)
	MetGlyMet	300 (−0.26)	350 (+0.04)	558 (−0.61)
	MetMetAla	304 (+0.52)		557 (−1.28)
	MetMetMet	283 (−0.49)	335 (+0.46)	548 (−1.65)



Scheme 1.

S(thioether) → Cu(II) transitions were, however, observed in the form of a positive CE, appearing as a red-shifted shoulder on the $N^- \rightarrow Cu(II)$ CT transitions. The change in the sign of CE strongly suggests a different binding mode, namely, an *equatorial* coordination of the thioether residue as represented by Scheme 1b. The absence of this transition in the copper(II) complexes of Gly-L-AlaGly provides further support for the thioether coordination of internal Met residues in $[CuH_{-1}L]$ species.

3.1.3. Species $[CuH_{-2}L]^-$

The stability constants, UV–Vis and EPR spectral parameters of $[CuH_{-2}L]^-$ complexes of different tripeptides were reported to be very similar to each other, while CD spectra of these species (Fig. 4) revealed significant differences. The CD data obtained for the complexes of tripeptides with two or three optically active residues make it possible to assess the so-called additivity rule [12]. For instance, the comparison of the data for the d–d transitions of the species $[CuH_{-2}L]^-$ in Table 1 and Fig. 4 reveals that in the case of tripeptides with one methionyl residues, the intensities of the d–d and $N^- \rightarrow Cu(II)$ CT transitions are changing in the following order: GlyMetGly > GlyGlyMet ≫ MetGlyGly. The CD intensities of the studied complexes are collected in Table 2 for both d–d (560 nm) and CT (300 nm) transitions. Table 2 shows that the measured intensities of the d–d transitions for MetGlyMet and MetMetMet complexes gave good agreement with the calculated ones. The additivity is also reasonable for MetMetAla, but in this case the exact comparison would require the consideration of the data for GlyGlyAla. Similar observations on the addi-

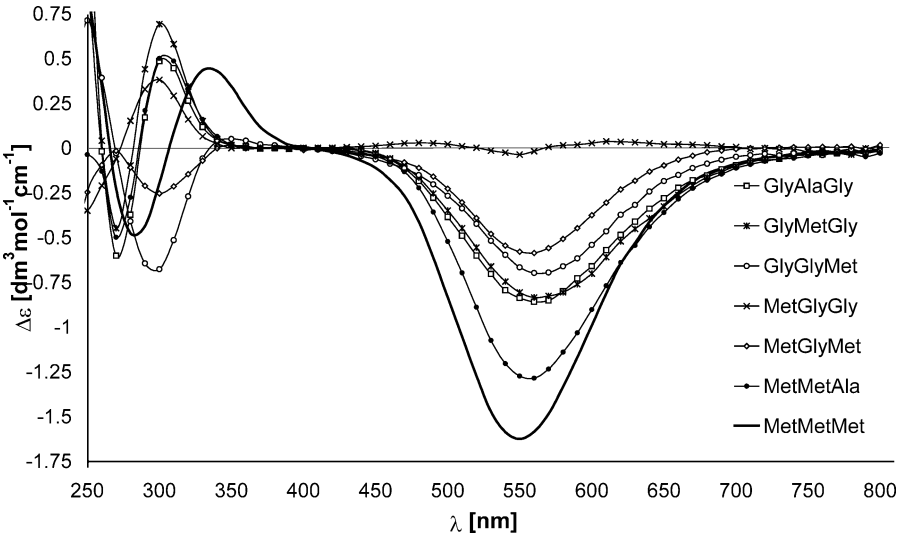


Fig. 4. CD spectra of the species $[CuH_{-2}L]^{-}$ formed in the copper(II)–tripeptide systems.

Table 2
CD intensities measured at 300 and 560 nm for the $[CuH_{-2}L]^{-}$ complexes of tripeptides

Ligand	300 nm		560 nm	
	Measured	Calculated [a]	Measured	Calculated [a]
GlyAlaGly	+0.49		−0.84	
GlyMetGly	+0.69		−0.86	
GlyGlyAla [b]	no data		−0.42	
GlyGlyMet	−0.67		−0.68	
MetGlyGly	+0.37		−0.01	
MetGlyMet	−0.26	−0.30	−0.61	−0.69
MetMetAla	+0.50		−1.27	−1.29
MetMetMet	−0.20	+0.38	−1.60	−1.55

The choosen wavelengths are characteristic of the CT and d–d transitions and are aimed to certify the validity of the additivity rule.
[a] Calculations are based on additivity rule [12].
[b] Data from Ref. [12].

tivity of CD transitions have already been reported for the copper(II) complexes of tripeptides of alanine and leucine [10].

Moreover, the CD spectra recorded in the near UV range show marked differences both in the signs and intensities of CD extrema. In the case of the tripeptides containing N-terminal and/or internal Met residues (GlyMetGly, MetGlyGly and MetMetAla), only the $N^{-}\rightarrow Cu(II)$ CT transitions are observed. These data reflect a significant positive CE and the additivity also holds for these transitions. However, in the case of tripeptides containing C-terminal Met residues (GlyGlyMet, MetGlyMet and MetMetMet), the $N^{-}\rightarrow Cu(II)$ and $S\rightarrow Cu(II)$ transitions overlap, which makes the interpretation of data more complex. Our previous EPR studies on the same systems proved that in the case of C-terminal methionyl residues an *axial/equatorial* equilibrium is possible for the thioether binding (Scheme 1c.). It was also concluded from the EPR data that the *axial* coordination is much favoured for MetMetMet as compared to the other peptides [13]. Previous CD data reported for the copper(II) complexes of tripeptides with C-terminal alanine or leucine residues showed a negative CE in the $N^{-}\rightarrow Cu(II)$ CT transitions upon the coordination of two amide functions and their additivities were also well established [9]. The data in Tables 1 and 2 reveal very similar tendencies for GlyGlyMet and MetGlyMet, whereas MetMetMet exhibits very significant deviation from the additivity. This difference can probably be explained by the differences in the coordination modes of the thioether residues in various complexes. The data in Table 1 unambiguously prove that *axial* coordination of thioether residues are accompanied with a significant negative, whereas *equatorial* coordination with a less intense positive CE.

The measured CD spectra of the Cu(II)–tripeptide systems also allow the calculation of the stability constants. Details of these calculations were given in Section 2, while the final data are collected in Table 3 and compared with the stability constants determined by potentiometric titrations [13]. The agreement of potentiometric and CD spectroscopic data is excellent in almost all the cases, which supports that besides structural characterisation, CD spectroscopy is a very sensitive tool for determination of metal ion speciation of peptide complexes.

3.2. Nickel(II) complexes

Complex formation processes between nickel(II) ions and tripeptides are characterised by the formation of a diamagnetic, square planar $[NiH_{-2}L]^{-}$ complex which exists as the major species in slightly alkaline solutions

Table 3
Stability constants of copper(II) complexes of tripeptides determined by potentiometric and CD spectroscopic methods

Ligand	Species	pH-metric data from Ref. [13]	CD spectra
GlyAlaGly	$[CuL]^+$	5.18	5.2 (1)
	$[CuLH_{-1}]$	−0.14	−0.01 (9)
	$[CuLH_{-2}]^-$	−6.76	−6.67 (9)
GlyMetGly	$[CuL]^+$	5.06	4.8 (1)
	$[CuLH_{-1}]$	−0.10	−0.23 (2)
	$[CuLH_{-2}]^-$	−6.58	−6.51 (2)
GlyGlyMet	$[CuL]^+$	5.09	4.9 (1)
	$[CuLH_{-1}]$	−0.12	−0.13 (7)
	$[CuLH_{-2}]^-$	−6.67	−6.64 (7)
MetGlyGly	$[CuL]^+$	4.42	4.27 (9)
	$[CuLH_{-1}]$	−0.29	−0.32 (2)
	$[CuLH_{-2}]^-$	−7.06	−7.14 (9)
MetGlyMet	$[CuL]^+$	4.18	4.28 (7)
	$[CuLH_{-1}]$	−0.40	−0.38 (2)
	$[CuLH_{-2}]^-$	−7.01	−6.91 (2)
MetMetAla	$[CuL]^+$	4.39	4.57 (5)
	$[CuLH_{-1}]$	0.00	0.05 (3)
	$[CuLH_{-2}]^-$	−6.01	−6.15 (3)
MetMetMet	$[CuL]^+$	3.90	4.1 (2)
	$[CuLH_{-1}]$	−0.26	−0.27 (6)
	$[CuLH_{-2}]^-$	−6.17	−6.34 (4)

Standard deviations of the last digits are in parenthesis.

[12,23]. In the case of tripeptides of methionine, the formation of these species have already been reported, containing (NH_2, N^-, N^-, COO^-)-coordinated central nickel(II) ions without any involvement of the thioether residue in the metal binding [13]. The formation of an octahedral (NH_2, CO)-coordinated species, $[NiL]^+$, was also detected at low pH values in all cases. Thioether coordination was proposed only in these $[NiL]^+$ complexes of tripeptides containing N-terminal methionyl residues.

The evaluation of the CD spectra of the nickel(II)–tripeptide complexes supports the published structures obtained by the combined application of potentiometric and UV–Vis measurements [13]. Moreover, CD investigations provide some additional information on the binding properties of the ligands and reveal significant differences in the spectral behaviour of these tripeptide complexes (Table 4). The S → Ni(II) CT transitions are found only in the $[NiL]^+$ complexes of tripeptides that contain N-terminal methionyl residues. The intensities of these CD transitions are increasing with the increasing number of Met residues (MetMetMet > MetMetAla > MetGlyGly), suggesting that the coordination of the metal ion to the thioether group of the N-terminal methionine may help the subsequent metal binding of the other thioether functions. Considering the high number of free coordination sites in the octahedral

Table 4
Parameters of CD extrema ($\lambda(\Delta\varepsilon)$) calculated from the CD spectra of nickel(II)–tripeptide complexes measured at different pH values

Ligand	Species	$N^- \rightarrow Ni(II)$	S → Ni(II)	d–d
MetGlyGly	$[NiL]^+$		261 (+0.13)	
	$[NiLH_{-2}]^-$	237 (−2.45)		495 (−0.22); 424 (+0.38)
GlyMetGly	$[NiLH_{-2}]^-$	250 (+8.35)		479 (−1.50)
GlyGlyMet	$[NiLH_{-2}]^-$	236 (+1.89)		454 (−1.27)
MetMetAla	$[NiL]^+$		257 (+0.23)	
	$[NiLH_{-2}]^-$	250 (+9.30)		475 (−2.96)
MetMetMet	$[NiL]^+$		253 (+0.60)	
	$[NiLH_{-2}]^-$	248 (+8.77)		474 (−3.06)

$[NiL]^+$ complexes, the coordination of more than one sulfur atom is possible.

The species $[NiH_{-2}L]^-$ is exclusively formed in all the studied nickel(II)–tripeptide systems above pH 9. The UV–Vis spectra of these complexes are almost the same for all tripeptides, exhibiting a rather intense absorption maximum at $\lambda_{max} = 429 \pm 2$ nm. The CD spectra of these species are, however, much more sophisticated, and always contain d–d and $N^- \rightarrow$ Ni(II) CT transitions around 470 and 250 nm, respectively. Moreover, the intensities of these CD extrema reveal quite significant differences depending on the number and location of methionyl residues. The $[NiH_{-2}L]^-$ complexes of tripeptides containing internal methionyl residues show strong CE at around 250 nm due to their $N^- \rightarrow$ Ni(II) CT transitions, while this CE is significantly less intense in the case of tripeptides without internal methionyl residues. This observation agrees with earlier results published on the nickel(II) complexes of tripeptides containing non-coordinating side chains where the highest intensities were always reported for the ligands containing the optically active residue in internal position [9]. However, for the peptides of methionine, the effect of the internal residues is much more enhanced than that of other side chains, which is most likely due to the effect of the non-coordinated thioether residues.

The results obtained for the d–d transitions of the square-planar $[NiH_{-2}L]^-$ complexes show a very high similarity to those of the corresponding tetragonal copper(II) complexes. Thus, the transmission of the asymmetry from the optically active residues is decreasing in the order: GlyMetGly > GlyGlyMet ≫ MetGlyGly, which is manifested in a decrease in the CD intensities of the d–d transitions. The d–d CD intensities of the peptides containing three optically active residues (MetMetAla and MetMetMet) are much stronger which is in accordance with the calculated value [475 nm (+2.81)] assuming the additivity of CD intensities.

3.3. Palladium(II) complexes

Numerous studies have been reported in the literature on the palladium(II) complexes of simple dipeptides of methionine and the results unambiguously prove that the thioether donor functions are the primary metal binding sites [17–21,24–26]. The structures of the palladium(II) complexes of the ligands containing methionine in C-terminal or internal positions were described by the (NH_2, N^-, S)- or (NH_2, N^-, N^-, S)-coordination modes [21]. The coordination chemistry of N-terminal methionine peptides was reported to be more complicated due to the formation of polynuclear species. Most of these observations were based upon ^1H NMR measurements which requires concentrated solutions (at least 10^{-2} mol dm^{-3}). In contrast, CD measurements of these systems can be carried out at a concentration less than 3×10^{-4} mol dm^{-3}. Several CD spectra were reported for the simple dipeptides of methionine and *S*-methyl-L-cysteine [19,20] but a systematic study for the CD characterisation of di- and tripeptides of methionine is not yet available in the literature. In this study, we performed CD measurements on the palladium(II) complexes of the dipeptides GlyMet and MetGly and the tripeptides GlyMetGly and GlyGlyMet with various pHs and metal ion to ligand ratios.

The characteristic CD spectra obtained in equimolar acidic (pH $\approx$ 3) solutions of $K_2[PdCl_4]$ and GlyMet, GlyMetGly or GlyGlyMet are shown in Fig. 5. The CD data of the palladium(II) complexes of GlyMet and GlyMetGly reflect a close similarity to each other below 370 nm, but they are distinctly different from those of MetGly and GlyGlyMet. It is also noteworthy that the CD spectra of the Pd(II)–GlyMet and –GlyMetGly systems are significantly different from Pd(II)–GlyAla (375 nm (−0.80) and 320 nm (+0.25)) reported by Wilson and Martin [11]). These observations clearly indicate the existence of the (NH_2, N^-, S)-coordination mode in the palladium(II) complexes of GlyMet and GlyMetGly in agreement with previous results from NMR studies [21]. The stoichiometric compositions of the corresponding species in solution can be given as $[PdH_{-1}L]$ or $[PdL]^+$ ($=[PdH_{-1}LH]^+$) depending on the pH because the non-coordinating carboxylate group is protonated in acidic solutions. The fourth coordination sites of palladium(II) ions are certainly available for the monodentate binding of any complexing agents present in solution. In equimolar samples, this results in species like $[PdH_{-1}L(H_2O)]$, $[PdH_{-1}LCl]$, $[PdH_{-1}L(OH)]^-$ depending on the chloride concentration and pH of the solutions. In agreement with these expectations, the change of pH or increasing chloride concentration of solutions does not induce substantial shifts of the CD extrema of Pd(II)–GlyMet or –GlyMetGly systems, and there is no change in the shape of the absorption bands at all. Similar observations were obtained with an excess of di- or tripeptide ligands, supporting that the second ligand is coordinated monodentately via the thioether residues in acidic solutions ($[PdL_2]=[Pd(H_{-1}L)(LH)]$ and via the deprotonated amino group at higher pH values ($[PdH_{-1}L_2]^-=[Pd(H_{-1}L)(L)]^-$). Our previous NMR studies on the bis(ligand) complexes of these peptides clearly indicated the existence these (S)- or (N)-bonded isomers [21].

The CD spectra of Pd(II)–GlyGlyMet system is characterised by a relatively intense negative CE ($\Delta\varepsilon = -1.15$) at 290 nm. This is entirely different from those reported for the palladium(II)–GlyGlyAla system: 335 nm (−1.00) and 290 nm (+0.37) [11]. In agreement with the previous findings from NMR measurements [21] these data strongly support the existence of the

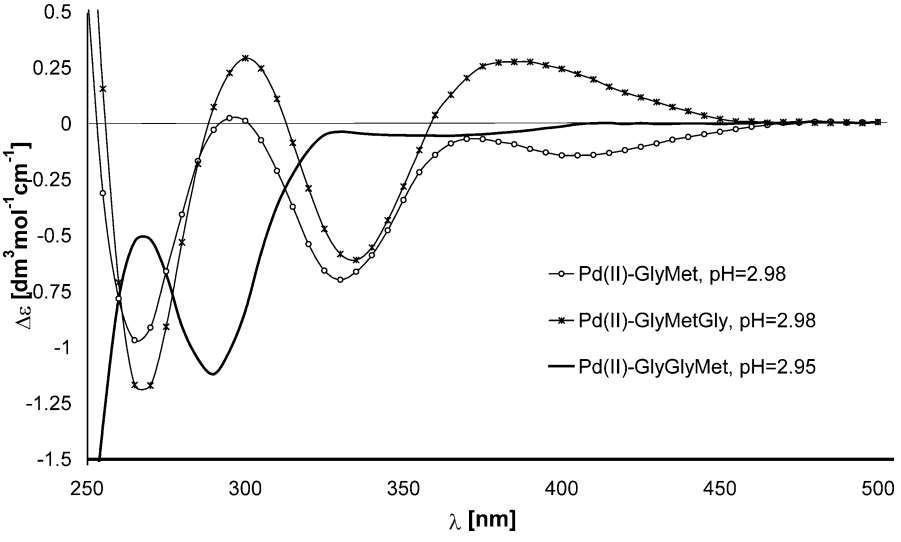


Fig. 5. CD spectra of the palladium(II) complexes of GlyMet, GlyMetGly and GlyGlyMet obtained in equimolar solutions ($c = 4 \times 10^{-4}$ mol dm^{-3}).

(NH_2, N^-, N^-,S)-coordination mode in the $[PdH_{-2}L]^-$ species of GlyGlyMet. It is also important to note that the CD spectrum measured in equimolar solutions at pH 3 and shown in Fig. 5 does not show any change when increasing or decreasing pH or adding an excess of ligand, which provides an unambiguous proof for the outstanding thermodynamic stability of the palladium(II) complexes of peptides containing methionyl residues as the third amino acid in the peptide sequence.

In contrast to the above-mentioned findings, the CD spectra of the palladium(II)–MetGly system exhibit very significant changes in the function of pH values and metal ion to ligand ratios. These spectral changes are best represented by Fig. 6 where the CD spectra of Pd(II)–MetGly = 1:2 samples are plotted in the function of pH. It can be seen from Fig. 6 that the CD spectra obtained in acidic solutions ($2.06 < pH < 6.61$) are the same and the spectral parameters show a good agreement with those of bis(ligand) complexes of palladium(II) with methionine [11]. Namely, the CD transitions occurred at $\lambda = 381$ and 305 nm ($\Delta\varepsilon = +0.62$ and -2.56, respectively) for MetGly in this study and $\lambda =$ 379 and 300 nm ($\Delta\varepsilon = +0.32$ and -1.80, respectively) for L-methionine. In agreement with the previous NMR studies [17], these observations strongly support the bidentate (NH_2, S)-coordination of the N-terminal Met residues in the bis(ligand) complexes of palladium(II). Thermodynamic data for the outstanding stability of this type of coordination have been reported recently [27]. As a consequence, the coordinatively saturated bis(ligand) complexes of palladium(II) are formed under strongly acidic conditions and their CD spectra remains intact because deprotonation of the non-coordinated carboxylic functions do not have any effect on the CD parameters. Characteristic changes of the CD spectra are, however, observed above pH 7, suggesting a significant change in the coordination modes of the ligands. The appearance of an isobestic point at 345 nm strongly supports the presence of two species in the pH range 7–10. It should also be considered that the spectral parameters of Pd(II)–MetGly = 1:2 system at $pH > 10$ are reminiscent of those of Pd(II)–AlaGly [350 and 301 nm ($\Delta\varepsilon = -0.50$ and -0.41) for MetGly and 360 and 279 nm (-0.32 and -0.35) for AlaGly], suggesting the bidentate (NH_2, N^-) binding mode in the palladium(II) complexes of both peptides above pH 10 [21,28].

The changes of the CD spectra in the equimolar solutions of palladium(II) and MetGly are more complicated because of the formation of polynuclear species. The CD spectra obtained in strongly acidic solutions ($pH < 3$) correspond to the bidentate chelation via the amino and thioether donor functions in mononuclear complexes. An increase in pH results in very significant changes both in the locations and intensities of the CD transitions but neither isobestic points nor saturation of spectra can be observed in equimolar samples at the studied pH values. The previous NMR experiments [17] were interpreted by the deprotonation and coordination of amide groups resulting in (NH_2, N^-, COO^-)-coordination with sulfur bridging at the fourth coordination site. A further increase in pH leads to hydroxo complex formation, but these can also be polynuclear via hydroxo and/or thioether bridging.

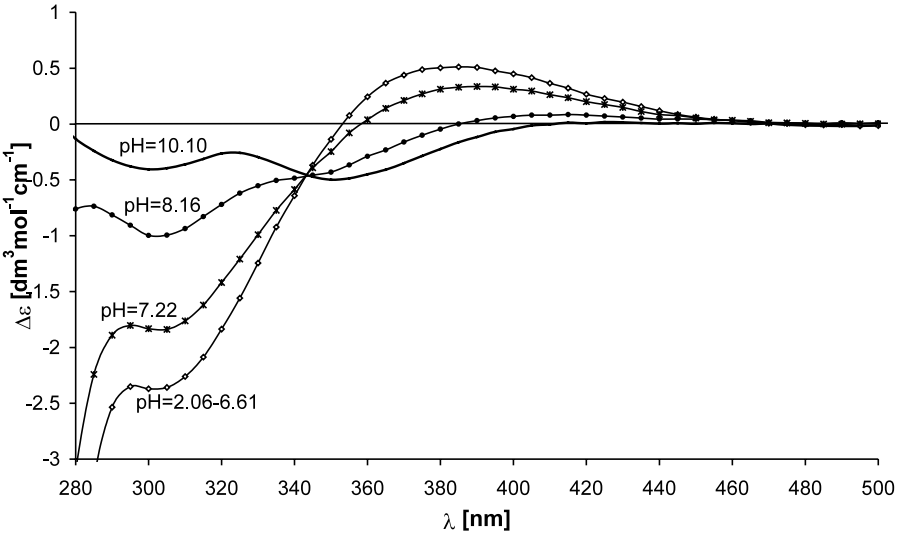


Fig. 6. CD spectra of the palladium(II) complexes of MetGly obtained in 1:2 metal ion to ligand ratio at different pH values ($c_{Pd(II)} = 4 \times 10^{-4}$ mol dm^{-3}).

4. Conclusions

The results presented in this paper provide clear evidence that CD spectroscopy is a valuable, fast and relatively simple experimental technique for the structural characterisation of peptide complexes. In the case of the copper(II) complexes of tripeptides, the results gave an unambiguous proof for the weak metal ion coordination of thioether donor functions depending on the number and location of methionyl residues. Although, similar observations have already been reported on the basis of UV–Vis and EPR measurements [13], CD spectroscopy have three major advantages compared to those techniques: (i) d–d transitions, $S\rightarrow$ Cu(II) and $N^{-}\rightarrow$Cu(II) CT transitions are generally well separated and easily observable; (ii) the intensities of the individual transitions depend on the location of the optically active residue or on the nature of the coordinating donor atoms; (iii) the results obtained for the $S\rightarrow$Cu(II) CT bands indicate that the *axial* and *equatorial* coordination of thioether residues results in the different signs of the CE providing an unambiguous proof for the conformation in solution.

It has been shown for copper(II) complexes that the CD data of metal complexes can be used for the determination of stability constants. In general, this is true for any spectroscopic technique, but the application of UV–Vis spectroscopy is very limited, because of the broad, unresolved absorption bands of copper(II) complexes. The sensitivity of EPR spectroscopy is much better, but it can be applied only for selected metal ions. It is well demonstrated that changes of pH values have a very significant impact on the CD spectra. Moreover, these spectral changes can involve the changes of the sign of CD extrema, which makes CD spectroscopy a very sensitive tool for the characterisation of metal ion speciation and provide a unique possibility for the detection of species present in low concentration. A further advantage of the application of CD spectroscopy comes from the fact that pH-potentiometry can only be applied if complexation is accompanied by a change in pH values. It is not the case for the monodentate coordination of thioether ligands, but CD spectroscopy can be an adequate method even for these systems.

In the case of square-planar, diamagnetic species (e.g. tripeptide complexes of nickel(II) and any palladium(II) complex), the application of NMR spectroscopy is probably as informative as CD spectroscopy. The NMR measurements, however, require the use of relatively high concentrations (≥ 0.01 mol dm^{-3}), while 10–100 times lower concentrations can be used in CD measurements. This makes the investigation of peptide complexes possible, when the ligands are available in very small quantities. On the other hand, the combined application of CD and NMR spectroscopies provides a valuable tool for structural studies in a wide concentration range, e.g. for the detection of different oligomers.

Acknowledgements

This work was supported by the Hungarian Scientific Research Fund (OTKA T034361, TS040685 and T034250). We are indebted to Professor R.B. Martin (University of Virginia) for helpful discussion.

References

[1] E. Farkas, I. Sóvágó, Metal complexes of amino acids and peptides, in: J.S. Davies (Ed.), Specialist Periodical Reports, Amino Acids, Peptides and Proteins, vol. 31, Royal Society of Chemistry, Cambridge, 2000, pp. 336–412.
[2] T. Szabó-Plánka, N. Nagy, A. Rockenbauer, L. Korecz, Polyhedron 19 (2000) 2049.
[3] S. Bruni, F. Cariati, P.G. Daniele, E. Prenesti, Spectrochim. Acta, Part A 56 (2000) 815.
[4] I. Sóvágó, D. Sanna, A. Dessi, K. Várnagy, G. Micera, J. Inorg. Biochem. 63 (1996) 99.
[5] E. Prenesti, P.G. Daniele, M. Prencipe, G. Ostacoli, Polyhedron 18 (1999) 3233.
[6] (a) R.B. Martin, Optical properties of transition metal ion complexes of amino acids and peptides, in: H. Sigel (Ed.), Metal Ions in Biological Systems, vol. 1 (Chapter 4), Marcel Dekker, New York, 1974, pp. 129–156;
(b) H. Kozlowski, G. Micera, Spectroscopic techniques and structural determinations of low-molecular–mass metal complexes in solution, in: G. Berthon (Ed.), Handbook on Metal–Ligand Interactions in Biological Fluids, vol. 1, Marcel Dekker, New York, 1995, pp. 566–582.
[7] (a) C.J. Hawkins, E. Larsen, Acta Chem. Scand. 19 (1965) 185;
(b) R.B. Martin, J.M. Tsangaris, J.W. Chang, J. Am. Chem. Soc. 90 (1968) 821.
[8] J.W. Chang, R.B. Martin, J. Phys. Chem. 73 (1969) 4277.
[9] J.M. Tsangaris, J.W. Chang, R.B. Martin, J. Am. Chem. Soc. 91 (1969) 726.
[10] J.M. Tsangaris, R.B. Martin, J. Am. Chem. Soc. 92 (1970) 4255.
[11] E.W. Wilson, Jr., R.B. Martin, Inorg. Chem. 9 (1970) 528.
[12] H. Sigel, R.B. Martin, Chem. Rev. 82 (1982) 385.
[13] K. Várnagy, B. Bóka, I. Sóvágó, D. Sanna, P. Marras, G. Micera, Inorg. Chim. Acta 275–276 (1998) 440.
[14] I. Sóvágó, G. Petõcz, J. Chem. Soc., Dalton Trans. (1987) 1717.
[15] T. Kowalik-Jankowska, K. Várnagy, C. Bertalan, J. Chem. Res.(S) (1993) 172.
[16] T. Kowalik-Jankowska, A. Kiss, I. Sóvágó, H. Kozlowski, Polish J. Chem. 68 (1994) 1093.
[17] B. Jezowska-Trzebiatowska, T. Kowalik, H. Kozlowski, Bull. Acad. Pol. Sci. 26 (1978) 223.
[18] M. Delporte, B. Decock-Le Reverend, C. Loucheux, H. Kozlowski, Polym. Bull. 10 (1983) 351.
[19] B. Decock-Le Reverend, H. Kozlowski, J. Chim. Phys. 82 (1985) 883.
[20] T. Kowalik, H. Kozlowski, B. Decock-Le Reverend, Inorg. Chim. Acta 67 (1982) L40.
[21] B. Bóka, Z. Nagy, K. Várnagy, I. Sóvágó, J. Inorg. Biochem. 83 (2001) 77.
[22] (a) L. Zékány, I. Nagypál, in: D. Leggett (Ed.), Computational Methods for the Determination of Stability Constants, Plenum Press, New York, 1985, pp. 291–355;

(b) M.T. Beck, I. Nagypál, Chemistry of Complex Equilibria, Ellis Horwood, Chichester, 1990, pp. 243–282.
[23] I. Sóvágó, Metal complexes of peptides and their derivatives, in: K. Burger (Ed.), Biocoordination Chemistry, Ellis Horwood, New York, 1990, pp. 135–184.
[24] L.D. Pettit, M. Bezer, Coord. Chem. Rev. 61 (1985) 97.
[25] A. Iakovidis, N. Hadjiliadis, Coord. Chem. Rev. 135/136 (1994) 17.
[26] T.G. Appleton, Coord. Chem. Rev. 166 (1997) 313.
[27] B. Stypinski-Mis, G. Anderegg, Inorg. Chim. Acta 406 (2000) 325.
[28] C.G. Ágoston, T. Kowalik-Jankowska, I. Sóvágó, J. Chem. Soc., Dalton Trans. (1999) 3295.

complexes have shown interesting cytotoxic activity [9], similar behaviour may be expected by the Zn(II) complexes that we have synthesized and studied also for this purpose. In fact, Zn(II) is recognized to be essential for life, being present in several naturally occurring metalloenzymes; then its metal complexes should be investigated as potential cytotoxic agents.

2. Results and discussion

2.1. Molecular and crystal structure of trichloro(1-methylpiperazin-1-ium-N^4)zinc(II), [$ZnCl_3(H_2Meppz)$] (1)

Selected bond distances and angles of complex **1** are reported in Table 1 and the molecular structure is depicted in Fig. 1. The crystals of [$ZnCl_3(H_2Meppz)$] are isomorphous with those of [$CoCl_3(H_2Meppz)$] [7], in particular they are both zwitterionic (amphiionic) species being the HMeppz ring protonated at the N2 nitrogen atom, both show the piperazine ring in the characteristic chair conformation and both possess the same distorted tetrahedral geometry compressed along the metal–nitrogen bond [7].

The Zn–N(1) distance of 2.078(3) Å is shorter than the Zn–N distance of 2.102(5) Å found in (1,3,5,7-tetraazaadamantane)trichlorozincate(II) anion, $[\{(CH_2)_6N_4\}ZnCl_3]^-$ [10], the only known complex that shows the aminotrichlorozinc(II) group N–$ZnCl_3$ with a N atom of an aliphatic amine. This is probably due to the steric hindrance exerted by the hydrogen atoms bonded to C_1^b atom of the adamantine ring towards the Zn(II)–N bond.

The three Zn(II)–Cl distances [Zn–Cl(1) = 2.257(1), Zn–Cl(2) = 2.264(2) and Zn–Cl(3) = 2.228(1) Å] are in the normal range usually observed in N–$ZnCl_3$ complexes [10–19], but become slightly longer when the corresponding chlorine atom is involved in strong hydrogen bonding [7]. In fact, Zn–Cl(3) is the shortest distance as Cl(3) is not involved in any hydrogen bond.

Table 1
Selected bond distances (Å) and angles (°) in trichloro(1-methylpiperazin-1-ium-N^4)-zinc(II), [$ZnCl_3(H_2Meppz)$] (**1**)

Bond lengths			
Zn–N(1)	2.078(3)		
Zn–Cl(1)	2.257(1)		
Zn–Cl(2)	2.264(1)		
Zn–Cl(3)	2.228(1)		
Bond angles			
N(1)–Zn–Cl(1)	104.18(7)	C(1)–N(1)–Zn	111.3(2)
N(1)–Zn–Cl(2)	104.27(7)	C(4)–N(1)–Zn	114.5(2)
N(1)–Zn–Cl(3)	107.69(8)	Cl(1)–Zn–Cl(3)	112.94(4)
Cl(1)–Zn–Cl(2)	113.56(4)	Cl(2)–Zn–Cl(3)	113.20(4)

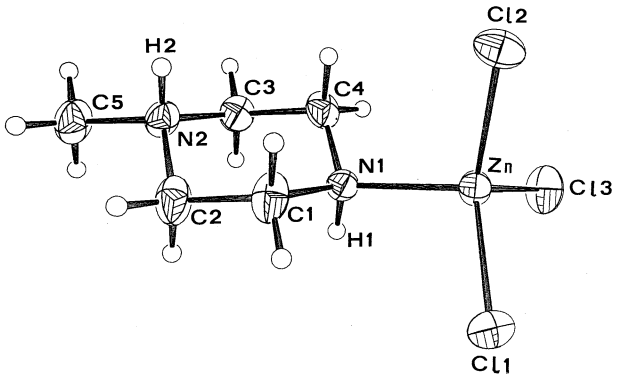


Fig. 1. ORTEP drawing of the [$ZnCl_3(H_2Meppz)$] complex (**1**) showing the atom numbering scheme. For clarity the hydrogen atoms are shown as spheres of arbitrary radius.

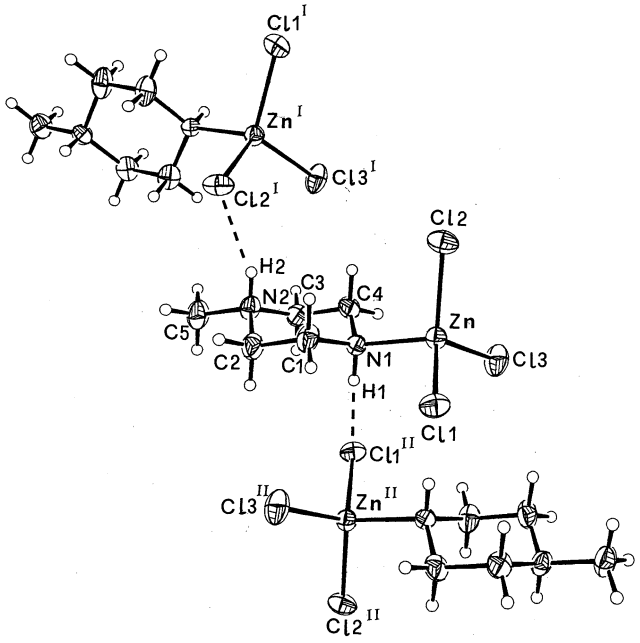


Fig. 2. ORTEP drawing of the [$ZnCl_3(H_2Meppz)$] complex (**1**) showing the two N–H···Cl hydrogen bonds connecting the fundamental molecule (in the middle) with the two molecules at ($I = 1/2+x$; $1/2-y$; $1/2+z$) (top) and at (II = $-x$; $-y$; $2-z$) (bottom).

The structure consists of discrete [$ZnCl_3(H_2Meppz)$] molecules held together by N^+–H···Cl intermolecular hydrogen bonds (Fig. 2), thus giving rise to the same crystal packing of [$CoCl_3(H_2Meppz)$] complex [7]. The parameters of the two very strong N^+–H···Cl intermolecular hydrogen bonds are (prior to calculations the N(2)–H(2) and N(1)–H(1) bond lengths were normalized to 1.033 Å): (i) $H(2)\cdots Cl(2)^I = 2.156(3)$ Å, $N(2)\cdots Cl(2)^I = 3.137(4)$ Å, $N(2)^+–H(2)\cdots Cl(2)^I = 157.8(3)°$; (ii) $H(1)\cdots Cl(1)^{II} = 2.373(3)$ Å, $N(1)\cdots Cl(1)^{II} = 3.361(3)$ Å, $N(1)–H(1)\cdots Cl(1)^{II} = 159.4(2)°$.

Table 2
Selected bond distances (Å) and angles (°) in trichloro(1,4-dimethylpiperazin-1-ium-N^4)-zinc(II), $[ZnCl_3(HMe_2ppz)]$ (**2**) [a]

Bond lengths			
Zn–N(1)	2.117(5)		
Zn–Cl(1)	2.258(1)		
Zn–Cl(2)	2.232(2)		
Bond angles			
N(1)–Zn–Cl(1)	102.45(7)	Cl(1)–Zn–Cl(1)^I	107.77(6)
N(1)–Zn–Cl(2)	116.4 (1)	C(1)–N(1)–Zn	112.9(2)
Cl(1)–Zn–Cl(2)	113.29(4)	C(4)–N(1)–Zn	105.1(3)

[a] Symmetry transformation $I = x, 1/2-y, z$.

2.2. Molecular and crystal structure of trichloro(1,4-dimethylpiperazin-1-ium-N^4)zinc(II), $[ZnCl_3(HMe_2ppz)]$ (2)

Selected bond lengths and angles of complex **2** are reported in Table 2 and the molecular structure is illustrated in Fig. 3. Also the crystals of $[ZnCl_3(HMe_2ppz)]$ are isomorphous with those of $[CoCl_3(HMe_2ppz)]$ [7]; in particular they are both zwitterionic (amphiionic) species being the 1,4-dimethylpiperazine ring protonated at the N2 nitrogen atom, both show the piperazine ring in the characteristic chair conformation and both possess the same distorted tetrahedral geometry but different from that of complex $[ZnCl_3(H_2Meppz)]$ and of course of $[CoCl_3(H_2Meppz)]$. In fact, analogously to $[CoCl_3(HMe_2ppz]$ [7], the bulky $-ZnCl_3$ group is coordinated to the axial position of piperazine ring instead of the less hindered equatorial position. This event produces two short intramolecular non-bonding H···Cl distances: H(2)A···Cl(2) = 2.821(4) Å and H(4)A···Cl(1) = 2.910 (4) Å and, in addition, a very long Zn–N coordination bond, Zn–N(1) = 2.117(5) Å, while that observed in complex **1** is only 2.078(3) Å. Similarly to the $[CoCl_3(HMe_2ppz]$

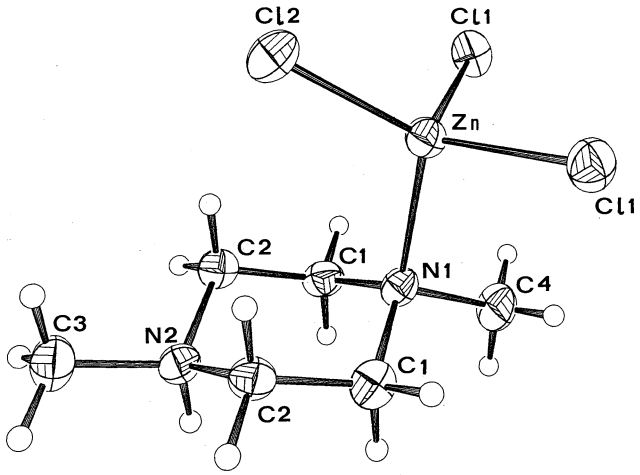


Fig. 3. ORTEP drawing of the $[ZnCl_3(HMe_2ppz)]$ complex (**2**) showing the atom numbering scheme. For clarity the hydrogen atoms are shown as spheres of arbitrary radius.

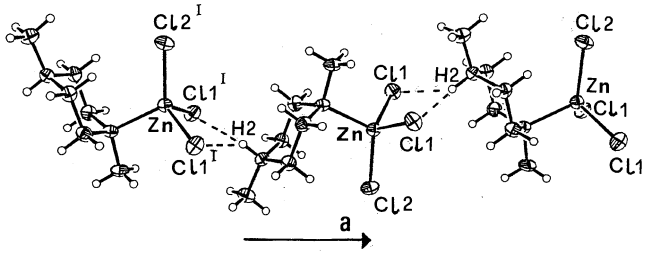


Fig. 4. ORTEP drawing of the $[ZnCl_3(HMe_2ppz)]$ complex (**2**) showing the symmetrical three-centre



hydrogen bond connecting molecules positioned across the mirror plane at $y = 1/4$ and running along the a-axis. Symmetry transformation: ($I = -1/2+x, 1/2-y, 1/2-z$).

complex [7], the crystal packing consists of discrete $[ZnCl_3(HMe_2ppz]$ molecules held together by a strong symmetrical (imposed by the space group symmetry) three-centre hydrogen bond as shown in Fig. 4, with the following parameters (prior to calculations the N(2)–H(2) bond length was normalized to 1.033 Å): H(2)···Cl(1)^I = 2.520(2) Å, N(2)···Cl(1)^I = 3.283(4) Å, N(2)$^+$–H(2)···Cl(1)^I = 130.18(3) Å.

2.3. The N–$ZnCl_3$ group and the Zn–N bond

The tetrahedral or distorted tetrahedral N–$ZnCl_3$ group is very uncommon in literature when N belongs to an aliphatic amine but is more common when N belongs to an aromatic ring. So far the only known aminotrichlorozinc(II) species is the (1,3,5,7-tetraazaadamantane)trichlorozincate(II) anion $[\{(CH_2)_6N_4\}ZnCl_3]^-$ [10]. The Zn–N distances are, on average, shorter when N is aromatic rather than aliphatic, in fact, for example, they are: 2.020(2) Å in [trichloro(7-methyladenine-N^9)zinc(II)]$^-$ anion [11]; 2.040(3) Å in Zn(thiamine)$Cl_3 \cdot 0.4H_2O$ [12]; 2.050 Å in 9-methyladeninium) trichloro(9-methyladenine)-zinc(II) [13]; 2.054(3) Å in trichloro-(purinium)-zinc(II) [14]; 2.055(8) Å in trichloro(*N*-4′-pyridyl)-4-ethoxypyridinium)-zinc(II) [15]; 2.073(11) Å in trichloro(8-aza-adeninium)-zinc(II) [16]; 2.079(2) Å in trichloro-adeninium-zinc(II) form(ii) [17]; 2.091(1) Å in (adeninium-N)-trichloro-zinc(II) [18]; 2.094(2) Å in trichloro-adenium-zinc(II) form(i) [19].

Another interesting aspect of the N–$ZnCl_3$ group is its ability to form hydrogen bonds, usually involving only two chlorine atoms.

Among the numerous [1,4-dimethylpiperazinium]$^{2+}$ $[MX_4]^{2-}$ complexes (M(II) = Fe(II), Co(II), Zn(II); X = Cl^-, Br^-) studied by Kemnitz et al. [20–23], we want to remember the $[H_2Me_2ppz][ZnCl_4]$ [20] and $[H_2Me_2ppz][ZnBr_4]$ [21] complexes; their structures

consist of discrete, slightly distorted, $[MX_4]^{2-}$ tetrahedral and centrosymmetric $[H_2Me_2ppz]^{2+}$ dications, in the chair form, held together by electrostatic forces and hydrogen bonds. They are formed as charged species because the syntheses were carried out in concentrated HCl and HBr solutions, while our complexes are formed at basic pH for the presence of piperazine free bases, thus metal atom may bind the piperazine nitrogen atom instead of the X^- anion. So far, only two complexes, namely *N*,*N*′-bis(6-(2-hydroxymethyl)-pyridylmethyl)-piperazine zinc(II) nitrate and dichloro-*N*,*N*′-bis(6-(2-hydroxy-methyl)pyridylmethyl)piperazine zinc(II), possessing a Zn(II)–N(piperazine) bond of 2.238(4) and 2.232 (4) Å, respectively, are reported in literature [24]. No comparison with our complexes is possible because they differ for coordination geometry, coordination number and donor site. Our complexes are distorted tetrahedral (c.n. = 4) with NCl_3 donor set, and those in Ref. [24] are distorted square-pyramidal (c.n. = 5) with O_3N_2 donor set.

2.4. Formation of isomorphous and isostructural Zn(II) and Co(II) complexes

The formation of isomorphous and isostructural Co(II) and Zn(II) coordination compounds is common enough and occurs in particular with the c.n. = 4, (pseudo)tetrahedral [25] or with c.n. = 6, (pseudo)octahedral [26]. In addition, other geometries with c.n. = 5 are sometimes observed, namely (pseudo)trigonal bipyramidal [27] or (pseudo)square-pyramidal [28].

The factors favouring such a phenomenon are: (i) the similarity of Zn(II) and high spin Co(II) ionic radii in various environments (0.74, 0.72 Å with c.n. = 4, 0.78, 0.79 with c.n. = 5 and 0.88, 0.89 Å with c.n. = 6, respectively); (ii) the easy formation of (pseudo) tetrahedral, octahedral and pentacoordinate compounds for both the ions. On the contrary, the factors contrasting this phenomenon are the easy oxidation of Co(II) to Co(III) complexes and the impossibility of forming Zn(III) complexes. In fact, tetrahedral species containing $Co(II)O_4$, $Co(II)S_4$ or $Co(II)S_xO_{4-x}$ cores oxidize very easily while complexes containing $Co(II)N_4$ and $Co(II)N_2O_2$ cores are more difficult to oxidize.

2.5. Infrared spectra of complexes 1 and 2

Table 3 summarizes the most significant IR absorption frequencies of complexes **1** and **2** compared with those of free HMeppz and Me_2ppz ligands. The attribution of vibrational modes is consistent with that reported in literature [7,14,15,29] and with the molecular structure now determined.

The ν(N–H) frequency, occurring at 3266 cm^{-1} in free HMeppz, decreases to 3188 cm^{-1} in complex **1** ($\Delta = 78$ cm^{-1}). This frequency shift, due to both metal co-ordination and hydrogen bond formation, has been observed also in the isostructural $CoCl_3$(HMeppz) complex ($\Delta = 89$ cm^{-1}) [7] and in the $CuCl_3$(HMeppz) ($\Delta = 121$ cm^{-1}) complex [8].

The modest change observed in both complexes for the skeleton vibrational and deformation modes in respect to those of the free ligands is consistent with a little distortion of the chair conformation upon coordination.

Finally, in the far-IR region, in agreement with other authors [14,15,29] the absorptions at 315ms and 301sh cm^{-1} (complex **1**) and at 312w and 301s cm^{-1} (complex **2**) are assigned to the ν(Zn–Cl) stretching frequencies while the bands at 278s cm^{-1} and at 276m cm^{-1} are assigned to the ν(Zn–N) stretching frequency for complex **1** and complex **2**, respectively. All the other features of infrared spectra are analogous to the isostructural Co(II) complexes [7].

3. Experimental

3.1. Materials and laboratory equipment

Commercial reagent grade chemicals 2-methylpiperazine(HMeppz), 1,4-dimethylpiperazine (Me_2ppz) (98%,

Table 3
Infrared spectra (cm^{-1}) of free HMeppz and Me_2ppz and of $[ZnCl_3(H_2Meppz)]$ (**1**) and $[ZnCl_3(HMe_2ppz)]$ (**2**)

Hmeppz	$[ZnCl_3(H_2Meppz)]$ **1**	Me_2ppz	$[ZnCl_3(HMe_2ppz)]$ **2**	Band assignment
3266m	3188s	–	–	ν(N–H)
–	3006s	–	3100–3020 [a]	$\nu(N^+–H)$
2937s, 2883sh	2957m, 2859w,	2966m, 2936s,	3102s, 3037w	ν(C–H)
2837m, 2789s, 2744sh, 2680m	2827w, 2771ms, 2737sh	2877m, 2840s, 2791s, 2739m, 2688m	3025w, 2929w, 2860m	
1454s	1459s, 1449sh	1456s	1454s	δ(C–H) scissor
1448sh, 1371m	1414m, 1388m, 1338w	1420w, 1370m	1425w, 1369m, 1346sh	δ(C–H)
1300w, 1262s	1279w, 1223w	1292s, 1261s	1277m, 1210w	skeleton vibr.
–	315ms, 301sh	–	312w, 301s	ν(Zn–Cl)
352sh, 327vs	293s	359s, 322m	289s	skeleton deform.
–	278s	–	276m	ν(Zn–N)

[a] $\nu(N^+–H)$ band is overlapped by the large ν(C–H) absorption in the 3100–3020 cm^{-1} region.

Acros) and anhydrous $ZnCl_2$ (Fluka) were used without further purifications.

IR spectra were performed as KBr pellets with a Perkin Elmer 598 spectrometer in the 4000–600 cm^{-1} region and as Nujol mulls with a Nicolet 5Sxc FT-IR (20 far IR) spectrometer in the 600–50 cm^{-1} region.

3.2. X-ray single-crystal studies

Experimental details of crystal structure determinations including crystal data, data collection, structure determination and refinement for complexes **1** and **2** are listed in Table 4. X-ray data were collected on a Philips PW 1100/20 diffractometer equipped with a graphite-monochromated Mo Kα radiation using the θ–2θ scan technique. Cell parameters were determined using 21 reflections. The intensities were corrected for Lorentz, polarization and absorption factors utilizing the program RIFLUP-80 [30]. Absorption measurements were made using a Ψ-rotation method [31]. Structure determinations were performed with SHELXL-86 [32], refinements were carried out with SHELXL-97 [33] and geometrical calculations were performed with PARST [34] set of programs. Molecular graphics were drawn using ORTEX [35] programs.

3.3. Syntheses

3.3.1. Trichloro(1-methylpiperazin-1-ium-N^4)zinc(II), [$ZnCl_3(H_2Meppz)$] (1)

The complex was synthesized by adding dropwise under stirring a solution of anhydrous $ZnCl_2$ (0.136 g, 1 mmol) in 10 ml EtOH to a solution of 1-methylpiperazine (HMeppz) (0.113 ml, 1 mmol) in 10 ml EtOH. A white powder compound precipitates and the solution was stirred for 2 h and then cooled to room temperature. The solid product was filtered, washed with EtOH–Et_2O (1:2 v/v) and dried under vacuum for 2 h and at 70°C for 8 h. Then, complex **1** was nearly quantitatively extracted from the precipitate by refluxing CH_3CN at 80°C for 7 h (solubility in $CH_3CN \sim 0.5$ mg ml^{-1}). After filtration, the solution was allowed to evaporate slowly for 5 days. The uncoloured parallelepiped crystals were filtered off, washed with CH_3CN–EtOH (1:1 v/v) and dried under vacuum. M.p. 262.3–263.5°C (decomp.). Yield: 0.177 g., 0.65 mmol. Found: C, 21.98; H, 4.87; N, 10.22; Cl, 38.95%. Calculated for $C_5H_{13}Cl_3N_2Zn$: C, 22.01; H, 4.80; N, 10.27; Cl, 38.97%. Good quality well-formed single crystals suitable for X-ray structure determination, were obtained after 2 weeks by recrystallization from CH_3CN using the Et_2O vapour diffusion technique.

Table 4
Crystallographic data and structure refinement for zwitterionic pseudotetrahedral complexes [$ZnCl_3(H_2Meppz)$] (**1**) and [$ZnCl_3(HMe_2ppz)$] (**2**)

Complex	[$ZnCl_3(H_2Meppz)$] **1**	[$ZnCl_3(HMe_2ppz)$] **2**
Empirical formula	$C_5H_{13}Cl_3N_2Zn$	$C_6H_{15}Cl_3N_2Zn$
Formula weight	272.91	286.94
Temperature (K)	293(2)	293(2)
Crystal system	monoclinic	orthorhombic
Space group	$P2_1/n$ (no. 14)	*Pnma* (no. 62)
a (Å)	7.390(2)	14.860(3)
b (Å)	17.319(4)	9.715(2)
c (Å)	8.470(2)	8.005(2)
α (°)	90.00(2)	90.00
β (°)	92.20(3)	90.00
γ (°)	90.00(2)	90.00
V (Å^3)	1083.3(5)	1155.6(5)
Z	4	4
D_{calc} (g cm^{-3})	1.673	1.649
λ	0.7107	0.7107
μ(Mo Kα) (mm^{-1})	3.019	2.773
Relative transmission factors	0.75–1.00	0.79–1.00
$F(000)$	552	584
Crystal size (mm)	0.20 × 0.15 × 0.25	0.10 × 0.20 × 0.20
Colour	colourless	colourless
Max 2θ (°)	56.00	52.00
Index ranges	$h(-9/9)$, $k(0/22)$, $l(0/11)$	$h(0/18)$, $k(-11/11)$, $l(0/9)$
Total data collection	2593	2501
Total unique data	2558	1195
Reflections with $F > 4\sigma(F)$	2411	858
Parameters refined	100	62
Final R indices ($[I > 2\sigma(I)]$)	R_1 [a] = 0.0367, wR_2 [b] = 0.0861	R_1 [a] = 0.0373, wR_2 [b] = 0.0947
Goodness-of-fit	1.328	1.369
Largest difference peak and hole (e Å^{-3})	0.39; −0.53	0.73; −0.57

[a] $R_1 = \Sigma(|F_o| - |F_c|)/\Sigma|F_o|$.
[b] $wR_2 = \{\Sigma w[(F_o^2 - F_c^2)^2]/\Sigma\,[w(F_o^2)^2]\}^{1/2}$.

3.3.2. Trichloro(1,4-dimethylpiperazin-1-ium-N4)zinc(II), [$ZnCl_3(HMe_2ppz)$] 2

This complex was prepared and recrystallized following the same procedures used for complex **1** except for 1,4-dimethylpiperazine (Me_2ppz) (0.138 ml, 1 mmole) instead of HMeppz. M.p. 268.1–269.9 °C (dec.). Yield: 0.189 g, 0.66 mmol. Found: C, 25.08; H, 5.31; N, 9.72; Cl, 37.02. Calc. for $C_6H_{15}Cl_3N_2Zn$: C, 25.12; H, 5.27; N, 9.76; Cl, 37.06%.

4. Supplementary data

Crystallographic data for the structural analysis have been deposited with the Cambridge Crystallographic

Data Centre, CCDC Nos. 184085/184086 for compounds **1** and **2**, respectively. Copies of this information may be obtained free of charge from The Director, CCDC, 12 Union Road, Cambridge, CB2 1EZ, UK (fax: +44-1223-336033; e-mail: deposit@ccdc.cam.ac.uk or www: http://www.ccdc.cam.ac.uk).

Acknowledgements

One of the authors (A.M.) thanks the Programma Finalizzato CNR-Rome for financial support.

References

[1] A. Marzotto, D.A. Clemente, G. Valle, Acta Crystallogr., Sect. C 53 (1997) 1580.
[2] A. Ciccarese, D.A. Clemente, F.P. Fanizzi, A. Marzotto, G. Valle, Inorg. Chim. Acta 275–276 (1998) 410.
[3] A. Ciccarese, D.A. Clemente, F.P. Fanizzi, A. Marzotto, G. Valle, Inorg. Chim. Acta 275–276 (1998) 419.
[4] A. Marzotto, D.A. Clemente, G. Valle, Acta Crystallogr., Sect. C 54 (1998) 27.
[5] A. Ciccarese, D.A. Clemente, F.P. Fanizzi, A. Marzotto, G. Valle, Acta Crystallogr., Sect. C 54 (1998) 1779.
[6] A. Marzotto, D.A. Clemente, G. Valle, Acta Crystallogr., Sect. C 55 (1999) 43.
[7] D.A. Clemente, A. Marzotto, G. Valle, C.J. Visona', Polyhedron 18 (1999) 2749.
[8] A. Marzotto, D.A. Clemente, F. Benetollo, G. Valle, Polyhedron 20 (2001) 171.
[9] A. Marzotto, D.A. Clemente, A. Zampiron, M. Carrara, Nucleosides Nucleotides Nucleic Acids 19 (2000) 1311.
[10] T.C.W. Mak, S.-H. Huang, Polyhedron 6 (1987) 1111.
[11] C.L. Price, M.R. Taylor, Acta Crystallogr., Sect. C 52 (1996) 2736.
[12] A. Bencini, E. Borghi, Inorg. Chim. Acta 135 (1987) 85.
[13] M.J. McCall, M.R. Taylor, Biochim. Biophys. Acta 390 (1975) 137.
[14] W.S. Sheldrick, Z. Naturforsch., Teil B 37 (1982) 653.
[15] W.L. Steffen, G.L. Palenik, Inorg. Chem. 17 (1978) 1338.
[16] L.G. Purnell, D.J. Hodgson, J. Am. Chem. Soc. 99 (1977) 3651.
[17] P.T. Muthiah, S.K. Mazumdar, S. Chaudhuri, J. Inorg. Biochem. 19 (1983) 237.
[18] M.R. Taylor, L.M. Vilkins, M.J. McCall, Acta Crystallogr., Sect. C 45 (1989) 1625.
[19] M.R. Taylor, Acta Crystallogr., Sect. B 29 (1973) 884.
[20] M. Feist, S. Trojanov, E. Kemnitz, Z. Anorg. Allg. Chem. 621 (1995) 1775.
[21] M. Feist, S. Trojanov, E. Kemnitz, Z. Naturforsch., Teil B 51 (1996) 9.
[22] M. Feist, S.I. Troyanov, H. Mehner, K. Witke, E. Kemnitz, Z. Anorg. Allg. Chem. 625 (1999) 141.
[23] S.I. Troyanov, M. Feist, E. Kemnitz, Z. Anorg. Allg. Chem. 625 (1999) 806.
[24] S. Loukiala, J. Ratilainen, K. Airola, J. Valkonen, K. Rissanen, Acta Chem. Scand. 52 (1998) 593.
[25] (a) H. Mori, S. Tanaka, T. Mori, A. Kobayashi, H. Kobayashi, Bull. Chem. Soc. Jpn. 71 (1998) 797;
(b) N. Duran, W. Clegg, L. Cucurull-Sánchez, R.A. Coxall, H.R. Jiménez, J.-M. Moratal, F. Lloret, P. Gonzáles-Duarte, Inorg. Chem. 39 (2000) 4821;
(c) P. Sekar, J.A. Ibers, Inorg. Chim. Acta 319 (2001) 117;
(d) A. Bernalte-García, F.J. García-Barros, F.J. Higes-Rolando, F. Luna-Giles, Polyhedron 20 (2001) 3315;
(e) L. Broge, U. Pretzmann, N. Jensen, I. Søtofte, C.E. Olsen, J. Springborg, Inorg. Chem. 40 (2001) 2323.
[26] (a) J.M. González Pérez, J. Niclós Gutiérrez, N.-H. Dung, B. Viossat, A. Busnot, M. Wintenberger, Inorg. Chim. Acta 184 (1991) 243;
(b) O.M. Yaghi, H. Li, T.L. Groy, J. Am. Chem. Soc. 118 (1996) 9096;
(c) E.J. Baran, E.G. Ferrer, C.I. Muglia, B. Krebs, M. Läge, U. Simonis, Z. Anorg. Allg. Chem. 623 (1997) 316;
(d) C.-R. Lee, C.-C. Wang, K.-C. Chen, G.-H. Lee, Y. Wang, J. Phys. Chem. A 103 (1999) 156;
(e) L.A. Gerrard, P.T. Wood, Chem. Commun. (2000) 2107;
(f) R. Murugavel, M. Sathiyendiran, M.G. Walawalkar, Inorg. Chem. 40 (2001) 427;
(g) T.W. Kajdan, P.J. Squattrito, S.N. Dubey, Inorg. Chim. Acta 300–302 (2000) 1082.
[27] M. Ruf, B.C. Noll, M.D. Groner, G.T. Yee, C.G. Pierpont, Inorg. Chem. 36 (1997) 4860.
[28] S. Kita, H. Furutachi, H. Ōkawa, Inorg. Chem. 38 (1999) 4038.
[29] K. Nakamoto, in: Infrared and Raman Spectra of Inorganic and Coordination Compounds, Wiley Interscience, New York, 1986, p. 191.
[30] M. Biagini Cingi, G. Bandoli, D.A. Clemente, A. Tiripicchio, J. Appl. Cryst. 13 (1980) 197.
[31] A.C. North, D.C. Phillips, F.S. Mathews, Acta Crystallogr., Sect. A 24 (1968) 351.
[32] G.M. Sheldrick, Acta Crystallogr., Sect. A 46 (1990) 467.
[33] G.M. Sheldrick, SHELXL-97, Program for the Refinement of Crystal Structures, University of Göttingen, Germany, 1997.
[34] M. Nardelli, Comput. Chem. 7 (1983) 95.
[35] P. McArdle, J. Appl. Cryst. 24 (1991) 972.

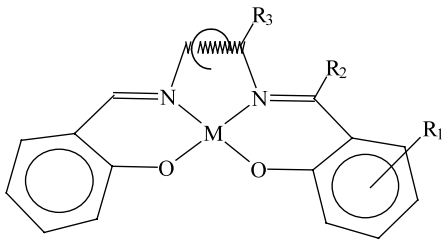


Fig. 1. The simplest symmetric Schiff's base framework. Conformational flexibility is to be induced by the systematic expansion of the alkyl chain between the imine moieties $-(CH_2)_n-$, $n = 2, 3, 4$. To avoid steric and electronic influences from substituent groups around the ligand R_1, R_2 and R_3 will be kept to their simplest protic form.

throughout the process occurring. Once again it is possible that Schiff's base complexes (Fig. 1) could meet the stringent demands on this concept. Due to the multidentate nature of the ligands, the formation constants for their complexes are high thus preventing ligand exchange. As the donor atoms are pre-organised within the ligand detrimental donor atom scrambling cannot occur. Thus, the prospect exists to develop functionally and conformationally active Schiff's base complexes based on the common geometries displayed by many transition metals (Fig. 2).

Although there may be a wealth of prior information on the synthesis of Schiff's base complexes, some of which encompass aspects of the concept being put forward here, many of these reports were designed to serve other needs and consequently many of the key examples, structures or connectivities remain absent [1,16–22]. As such, the important trends required to demonstrate the principles of conformational active complexes remain unclear. Within this study the field of view must be limited to identify the problems and potential of the concept. Thus, to service the conformational changes described in Fig. 2 we need only re-visit the chemistry of nickel, copper and zinc in the first

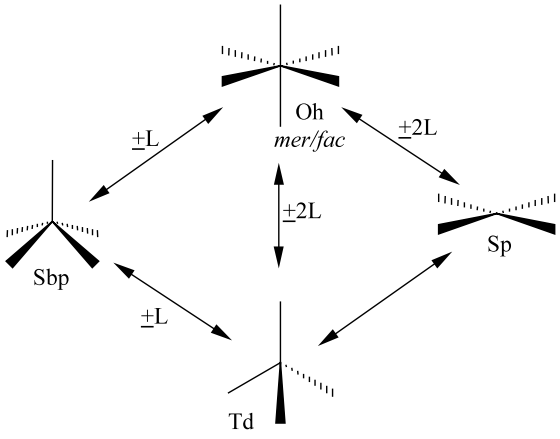


Fig. 2. Conformational geometries available to tetradentate Schiff's base ligands coordinated to late transition metals (Ni, Cu, Zn). Td: tetrahedral; Oh: Octahedral; Sbp: square based pyramid and Sp: square-planar.

instance. To avoid any contribution from additional steric or electronic effects, we have reduced the ligands to their simplest, symmetric, protic forms (Fig. 1; R_1, R_2, $R_3 = H$). Similarly to avoid more complex reorganisation at the metal centre, flexibility has been limited to the alkyl chain between the imine moieties, hence the use of the salicylidene unit. Even here it has been possible to further limit the study to the more inflexible ethylenediamine and the potentially more flexible 1,3-propane and 1,4-butane diamines thus generating a central chelate ring of five, six and seven members, respectively.

The initial survey of the three chosen ligands with the three metal cations identified is best conducted from the perspective of the metal as this allows a clear analysis of the specific co-ordination preferences which occur as the alkyl chain between the imine moieties increases in size. A further factor in this choice is the previous publication [16–21] of the required series of complexes for four coordinate copper(II) requiring us to only complete the fragmentary data sets for six coordinate nickel [20,22–25] and five coordinate zinc [26–28]. This, however, remains a substantive task. As such we have found it necessary to limit the report here to an analysis of the nickel complexes only, principally *N*,*N*′-bis(salicylidene)-1,4-butanediamine nickel (NiSalbu), leaving the analysis of the zinc complexes and the overall comparison for the following report. Thus within this report we focus on the structural analysis of the nickel complexes of Salbu. To fully delineate the structural patterns linking the well established *N*,*N*′-bis(salicylidene)-1,2-ethylenediamine nickel (NiSalen) with the hitherto uncharacterised NiSalbu we have sought to also increase our structural knowledge on the sparsely [20,24,25] studied *N*,*N*′-bis(salicylidene)-1,3-propanediamine nickel (NiSalpr) system.

2. Experimental

Unless otherwise stated, all chemicals were commercially obtained. Magnetic measurements were determined using an MSB1 Magnetic susceptibility balance. *N*,*N*′-bis(salicylidene)-1,3-propanediamine (Salpr), *N*,*N*′-bis(salicylidene)-1,4-butanediamine (Salbu), were prepared by standard methods. Briefly, 2 mol equiv. of salicylaldehyde (20 ml) were mixed with 1 mol equiv. of the required amine in methanol (80 ml). The resulting solution was refluxed for an hour, filtered while hot and allowed to cool, whereupon, copious amounts of yellow crystal began to form. These were collected, washed with diethylether and allowed to air dry. Yields were typically 70% or better.

Found: C, 72.35; H, 6.38; N, 9.90. Salpr $C_{17}H_{18}O_2N_2$ requires: C, 72.32; H, 6.43; N, 9.92%.

^{1}H NMR: δ_H (400.1 MHz; solvent $CDCl_3$) 2.1 (q, 2H, $-CH_2-$), 3.7 (t, 4H, $-CH_2-$), 6.9 (m, 4H, arom), 7.3 (m, 4H, arom), 8.4 (s, 2H, –CH=), 13.5 (br s, 2, OH). Melting point (m.p.): 52 °C (54–55 °C, lit. [29]).

Found: C, 72.76; H, 6.95; N, 9.58. Salbu $C_{18}H_{20}O_2N_2$ requires: C, 72.95; H, 6.80; N, 9.45%.

^{1}H NMR: δ_H (400.1 MHz; solvent $CDCl_3$) 1.8 (q, 4H, $-CH_2-$), 3.6 (t, 4H, $-CH_2-$), 6.9 (m, 4H, arom), 7.3 (m, 4H, arom), 8.4 (s, 2H, –CH=), 13.5 (br s, 2, OH). M.p.: 89 °C (91 °C, lit. [30]).

2.1. Ni(Salbu)

Salbu (0.59 g, 2.0 mmol) was dissolved in methanol (50 ml) to which was added nickel acetate tetrahydrate (0.5 g, 2.0 mmol). The mixture was refluxed for an hour whereupon a green precipitate formed. The solid was collected by filtration. The mother liquor was set aside. The resulting solid was then washed with water, methanol and diethylether. Yield 0.3 g, 41%.

Found: C, 60.75; H, 5.23; N, 7.59. Ni(Salbu) $C_{18}H_{18}O_2N_2Ni_1$ requires: C, 61.23; H, 5.14; N, 7.93%. $\mu_{eff} = 2.3$ BM.

Crystal suitable for X-ray analysis were obtained directly from the methanol mother liquors over a prolonged period as the solution slowly evaporated. However, these were found to be {[Ni(Salbu)$HOCH_3$]$_2$(μOAc)$_2$Ni}.

2.2. {[Ni(Salbu)$HOCH_3$]$_2$(μOAc)$_2$Ni}

Salbu (0.59 g, 2.0 mmol) was dissolved in methanol (50 ml) to which was added nickel acetate tetrahydrate (0.75 g, 3.0 mmol). The mixture was refluxed for an hour whereupon a green precipitate formed. The solid was collected by filtration, washed with water, methanol and diethylether and allowed to air dry. Yield 0.6 g, 62%.

Found: C, 48.04; H, 5.06; N, 5.70. {[Ni(Salbu)$HOCH_3$]$_2$(μOAc)$_2$Ni}·5H_2O· $C_{42}H_{60}O_{15}N_4Ni_3$ requires: C, 48.64; H, 5.83; N, 5.40%. $\mu_{eff} = 5.17$ BM.

The complex was only sparing soluble in methanol and suitable single crystals could not be grown. However, suitable crystals for X-ray analysis were obtained from DMF–methanol 1:5 solution. However, these were found to be consistent with the DMF adduct.

Found: C, 53.44; H, 5.55; N, 8.05. Expected for {[Ni(Salbu)Me_2NCOH]$_2$(μOAc)$_2$Ni}·$C_{42}H_{56}O_{10}N_6Ni_3$: C, 53.69; H, 5.48; N, 8.16. $\mu_{eff} = 5.18$ BM.

2.3. {[Ni(Salpr)$HOCH_3$]$_2$(μOAc)$_2$Ni}

Salpr (0.56 g, 2.0 mmol) was dissolved in methanol (80 ml) to which was added nickel acetate tetrahydrate (0.5 g, 2.0 mmol). The mixture was refluxed for an hour whereupon a green precipitate formed. This was collected, washed with water, methanol and diethylether. Yield 0.3 g, 45%.

Table 1
Experimental details of the crystal structure determination of {[Ni(Salbu)DMF]$_2$(OAc)$_2$Ni}, {[Ni(Salbu)MeOH]$_2$(OAc)$_2$Ni}, {[Ni(Salpr)py]$_2$(OAc)$_2$Ni}·C_5H_5N and {[Ni(Salpr)(py)$_2$]$PbCl_2$}·C_5H_5N

	{[Ni(Salbu)MeOH]$_2$-(OAc)$_2$Ni}	{[Ni(Salbu)DMF]$_2$-(OAc)$_2$Ni}	{[Ni(Salpr)py](OAc)$_2$Ni}·C_5H_5N	{[Ni(Salpr)(py)$_2$]$PbCl_2$}·C_5H_5N
Molecular formula	$C_{42}H_{50}N_4O_{10}Ni_3$	$C_{46}H_{56}N_6O_{10}Ni_3$	$C_{53}H_{53}N_7O_8Ni_3$	$C_{32}H_{31}N_5O_2Cl_2Ni_1Pb_1$
Molecular weight	946.99	1029.10	1092.08	854.41
Crystal system	orthorhombic	triclinic	monoclinic	monoclinic
Space group	*Pbna* (No. 60)	$P\bar{1}$ (No. 2)	$P2_1/n$ (No. 14)	$P2_1/a$ (No. 14)
a (Å)	11.3106(2)	9.5894(2)	10.4009(7)	16.6900(3)
b (Å)	18.6362(3)	10.6165(2)	17.6811(12)	10.2015(2)
c (Å)	19.6118(4)	12.5176(3)	14.0227(11)	19.5331(4)
α (°)	90	111.962(1)	90	90
β (°)	90	101.245(1)	101.142(4)	107.227(1)
γ (°)	90	92.065(1)	90	90
V (Å^3)	4133.91(13)	1150.85(4)	2530.2(3)	3176.57(11)
Z	4	1	2	4
μ (Mo Kα) (mm^{-1})	1.415	1.279	1.165	6.092
Reflections measured	7660	9961	18270	13874
Unique reflections	4066 [$R_{int} = 0.0278$]	5261 [$R_{int} = 0.0331$]	5034 [$R_{int} = 0.1251$]	7283 [$R_{int} = 0.0377$]
Observed reflections	3041	3922	3246	5859
R_1	0.0420	0.0335	0.0662	0.0291
wR_2	0.1032	0.0713	0.1736	0.0633
Number of parameters	343	333	362	388

Found: C, 47.91; H, 4.69; N, 5.26. {[Ni(Salpr)-$HOCH_3]_2(\mu OAc)_2Ni\}\cdot 5H_2O\cdot C_{40}H_{56}O_{15}N_4Ni_3$ requires: C, 47.62; H, 4.60; N, 5.55%. $\mu_{eff} = 5.17$ BM.

A portion of this material was recrystalised from pyridine–diethylether to give yellow–brown crystals suitable for X-ray analysis identified as {[Ni(Salpr)-$NC_5H_3]_2(\mu OAc)_2Ni\}$.

Found: C, 58.04; H, 4.87; N, 8.83. {[Ni(Salpr)-$NC_5H_5]_2(\mu OAc)_2Ni\}\cdot NC_5H_5\cdot C_{53}H_{53}O_8N_7Ni_3$ requires: C, 58.29; H, 4.89; N, 8.98%.

A second portion of $\{[Ni(Salpr)HOCH_3]_2(OAc)_2Ni\}\cdot 5H_2O$ was recrystallised from pyridine saturated with $PbCl_2$ using vapour diffusion from diethylether again affording crystals suitable for X-ray analysis.

Found: C, 44.73; H, 3.64; N, 8.17. {[Ni(Salpr)-$(NC_5H_5)_2]PbCl_2\}\cdot NC_5H_5\cdot C_{32}H_{31}O_2N_5Cl_2Ni_1Pb_1$ requires: C, 45.09; H, 3.66; N, 8.22%.

2.4. X-ray analysis

All measurements were conducted with a Nonius Kappa CCD diffractometer at 123 K using graphite monochromated Mo Kα radiation on suitable crystals mounted on glass fibres. Details of the data collection and refinements are given in Table 1. The structures were solved by direct methods [31]. The non-hydrogen atoms were refined anisotropically except for the disordered carbon sites in the butane backbone of $\{[Ni(Salbu)DMF]_2(\mu OAc)_2Ni\}$, which were treated isotropically. In all cases the refinement converged satisfactorily.

3. Results and discussion

Within the family of ligands under study, complexes of Salbu remain the poorest characterised. Reports of the nickel(II) adducts remain sparse and even those products obtained have yet to be unequivocally characterised structurally. Apart from an early report of a diamagnetic form [32], which will undoubtedly be square-planar, the exact structure of the dominant paramagnetic green form is still open to speculation. These considerations not-withstanding, the early reports [2,32] clearly suggest that our desire to construct *mer* and *fac* confomers[1] of Ni(Salbu) adducts should be attainable. Sadly we were unable to isolate samples of the red diamagnetic form. Furthermore, although we were able to prepare a bulk amorphous sample of Ni(Salbu) consistent with that of Holm [2], we were frustrated by its lack of solubility and were unable to isolate suitable samples for structural analysis. However, from the mother liquors we did retrieve a small number of crystals suitable for analysis by X-ray methods. These were structurally characterised initially in the hope that they were representative of the bulk. Clearly, however, this was not the case, as instead of Ni(Salbu) we obtained the structure of {[Ni(*fac*-Salbu)MeOH]$_2$(μOAc)$_2$Ni} (Fig. 3). Although a somewhat slightly disappointing result, this rogue complex is still the first structurally characterised NiSalbu containing species. As a consequence of this result we were prompted to produce this complex by a more rational route using a 3:2 ratio of nickel acetate and the Schiff's base. Typical of these species, its solubility in common solvents were again found to be poor. We were, however, able to isolate crystalline materials from methanol–DMF (5:1). However, in contrast to the complex obtained from the methanol liquors, that obtained from DMF (Fig. 4) was found to be the *mer* form, i.e. {[Ni(*mer*-Salbu)DMF]$_2$(μOAc)$_2$Ni} indicative that slow ligand exchange and Schiff's base reorganisation (*fac* ⇒ *mer*) had taken place at the metal centre.

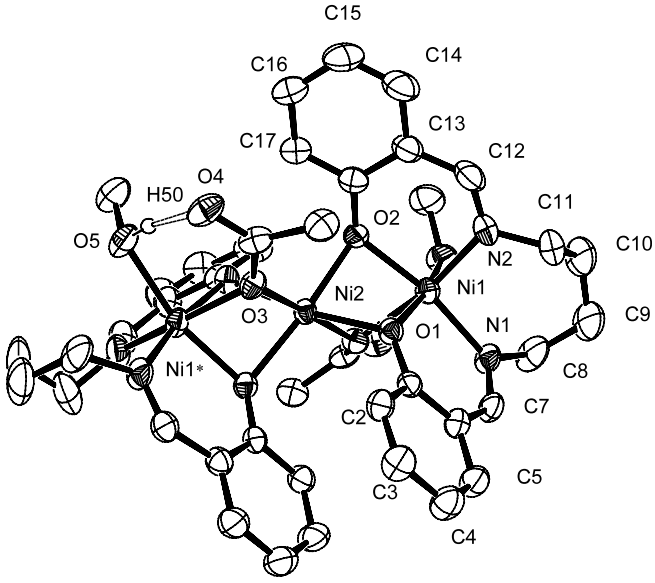


Fig. 3. The structure of {[Ni(Salbu)MeOH]$_2$(μOAc)$_2$Ni}. The key bond lengths and angles for the Salbu regions are given in Table 2. Each of the nickel atoms sit in slightly distorted octahedral geometry ($<$O5–Ni1–O1, 164.9° Salbu; $<$O3–Ni2–O3′, 176.9°; O2–Ni2–O2′, 171.7°). The structure is presented to show the *fac* arrangement of the salicylidene units and the hydrogen bonding between the methanol Hydrogen (H50) and the acetate unit (O4).

[1] The terms *mer* and *fac*, properly used, describe the positions of three identical ligands within an octahedral complex. This nomenclature is employed here to include the relative positions of the four donor atoms of these tetradentate Schiff's base ligands. Thus, *mer* is used to imply a ligand lying meridionally around the metal centre with the other ligands occupying the *trans* positions. *Fac* implies that the four donors occupy one face of the metal allowing the remaining ligands to lie *cis* to one another.

3.1. {Ni(fac-Salbu)MeOH}$_2$(μOAc)$_2$Ni}

The structure of the nickel adduct of Salbu (Fig. 3) roughly follows the reported structure of {[Ni(Salpr)DMSO]$_2$(μOAc)$_2$Ni} [24] and {[Ni(Salpr)DMF]$_2$(OAc)$_2$Ni} [25] insofar as we have a trimetallic complex comprising two Ni(Salbu) moieties bridged by a third nickel bonded to the four oxygens of the two Schiff's base moieties (Fig. 3). The three nickel atoms all sit in slightly distorted octahedral environment. The environment around the Ni(Salbu) moieties is completed by a coordinated methanol and an oxygen from the acetate bridge. In turn the central nickel's coordination sphere is completed by the two bridging acetates. Holding the methanol ligand *cis* to the acetate bridge via hydrogen bonding (O4···H50; 172.6 pm) forces the Salbu moiety to adopt the *fac* configuration. As will be seen below removing the hydrogen-bonding interaction allows the Salbu ligand to adopt the *mer* configuration. This interaction influences the bonding around the acetates such that the acetate bridge is formed using a single oxygen (O3) rather than the entire carboxylate bridge (O=C–O–) as is found in the Salpr complexes [24,25]. The key bond lengths and angles for the Schiff's base motif are given in Table 2 and collectively described below.

3.2. {[Ni(mer-Salbu)DMF]$_2$(μOAc)$_2$Ni}

In contrast to the *fac* complex described above (Fig. 3), the structure obtained for {[Ni(*mer*-Salbu)DMF]$_2$(OAc)$_2$Ni} (Fig. 4) more closely follows that of the previously reported structure of {[Ni(Salpr)DMSO]$_2$(OAc)$_2$Ni} [24] and {[Ni(Salpr)DMF]$_2$(OAc)$_2$Ni} [25]. In this instance the acetate bridge adopts the more familiar μO–C–O form and consequently the distance between the nickel centres increases from 282.8 pm for the *fac* complex (Fig. 3) to 307.6 pm for the *mer* complex. This distance is, however, comparable at 304.8 pm to the homologous Ni(Salpr) adduct [25]. Although it is evident that the ligand exchange process which formed this species is accompanied by a geometric change at the nickel Schiff's base centre, it remains unclear if the DMF adopts the position *trans* to acetate ($<173.5°$) due to the lack of hydrogen bonding or whether it is a simple consequence of the ligand exchange process. That the Salbu ligand is confined to the equatorial plane by the axial nature of the DMF forces the seven membered ring to adopt a flat point chair conformation, with C_9 and C_{10} being juxtaposed to the N–Ni–N unit. The Salbu ligand is more cumbersome than Salen or Salpr and significant disorder is encountered in the alkyl chain between the imines of the structure at these two carbons. Consequently the N–Ni–N angle at nickel is forced wider (103.7°) than that found in the analogous Salpr complex (97.9°) [25].

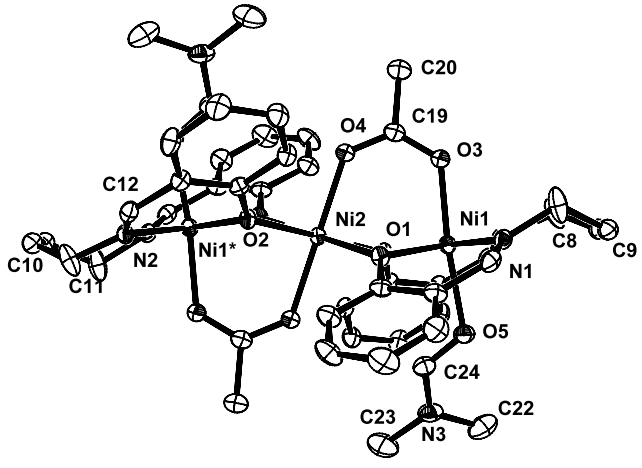


Fig. 4. The structure of {[Ni(Salbu)DMF]$_2$(μOAc)$_2$Ni}. The key bond lengths and angles for the Salbu regions are given in Table 2. Each of the nickel atoms sit in an octahedral geometry ($<$O3–Ni–O5, 173.4°; O4–Ni2–O4′, 180.0°; O1–Ni–O1′, 180.0°). The structure is presented to show the *mer* arrangement of the salicylidene units. In the absence of hydrogen bonding, the acetate unit reverts to its more common bridging mode.

We have been remarkably successful in obtaining two structurally characterised six coordinate NiSalbu complexes which provide a unique view of the Salbu ligand in both the *mer* and *fac* conformations. It is evident that the Ni(OAc)$_2$ bridge unit has an important effect on the *mer*–*fac* conformation via a stablising effect of the hydrogen-bonding between the adjacent axial ligand and itself. Thus there is some concern that the bridge unit may also profoundly affect the bond length and bond angles (Table 2) of the Ni(Salbu) moiety, bearing in mind that it is the behaviour of the Schiff's base environment around the metal cation which is the central theme of this work. It was deemed appropriate, therefore, to look at the effect of the Ni(OAc)$_2$ unit on the adjacent Schiff's base ligand in more detail. As we had been unable to structurally characterise either of the Ni(Salbu) complexes reported [2,32] which are free of the Ni(OAc)$_2$ unit, we moved to the use of Ni(Salpr) where complexes free of Ni(μOAc)$_2$ units were available for comparison with their respective more complex forms.

3.3. {[Ni(Salpr)NC$_5$H$_5$]$_2$(μOAc)$_2$Ni}

A sample of the {[Ni(Salpr)MeOH]$_2$(μOAc)$_2$Ni} complex was prepared and recrystallised from pyridine in an initial attempt to sequester the unwelcome nickel unit. From this system we obtained good quality crystals which, on analysis revealed an identical motif to the parent complex, i.e. a trimetallic systems comprising two Ni(Salpr) units bridged by a nickel acetate (Fig. 5), but with the octahedral geometry around the nickels within the Schiff's base motif now being completed by a

Table 2
The key bond lengths and bond angles for the established structures of Ni(Salen), Ni(Salpr) and Ni(salbu) complexes where the nickel resides in a four or six coordinate environment

Compound	–(CH_2)– units between the imines	N_2O_2 plane angles (°)	M–N distance	M–O distance	< aromatic planes (°)	< CN–NC torsion angle (°)
NiSalen [22]	2	178.6	184.3	185.4	0.4	20.8
		178.4	185.3	185.0		
{(NiSalen)(Ni$(OH_2)_2$}·2ClO_4 [23]	2	176.5	182.4	185.9	2.8	14.1
		177.5	183.2	185.9		
Ni(Salpr) [20]	3	169.1	190.1	184.6	0	0
		169.1	190.1	184.6		
{Ni(Salpr)DMSO(μOAc)$_2$Ni} [24]	3	172.7	201.3	202.0	4.0	1.3
		172.5	201.8	200.9		
{Ni(Salpr)DMF(μOAc)$_2$Ni} [25]	3	171.7	203.5	202.0	0.4	0.8
		170.9	201.1	199.8		
{Ni(Salpr)NC_5H_5(μOAc)$_2$Ni}	3	174.8	201.9	202.2	3.1	2.6
		172.0	200.2	200.8		
{Ni(Salpr)$(NC_5H_5)_2$}$PbCl_2$	3	173.5	201.8	202.2	1.6	3.5
		173.6	203.4	202.7		
{Ni(Salbu)MeOH}$_2$(μOAc)$_2$Ni	4	98.9	202.8	200.8	69.5	57.9
		169.1	202.7	203.0		
{Ni(Salbu)DMF}$_2$(μOAc)$_2$Ni	4	168.9	206.6	205.3	1.2	7.9
		167.3	205.5	202.3		

The < O–M–N angles are used to depict the geometry within the metal ligand plane. The M–N and M–O distances are presented to indicate that there is minimal change in the metal to ligand bond nature. The torsion angles associated with the di-imine backbone and aromatic planes are used to show how the ligand contorts to accommodate the desired geometry at the nickel centre.

coordinating pyridine. The acetate units in this complex are observed to bridge via the carboxylate unit in a manner similar to that discussed above for {[Ni(*mer*-Salbu)DMF]$_2$(μOAc)$_2$Ni}. Sadly the association of the central nickel at the Schiff's base oxygen's is maintained. However, it would seem that the presence strong donors (DMSO, DMF or pyridine) and the additional nickel acetate unit (cf. Ni(Salpr) [20,24,25], Table 2) although inducing an increase in the M–O distances as expected has minimal effect on the bond angles at the nickel centres within the Schiff's base complex. The small

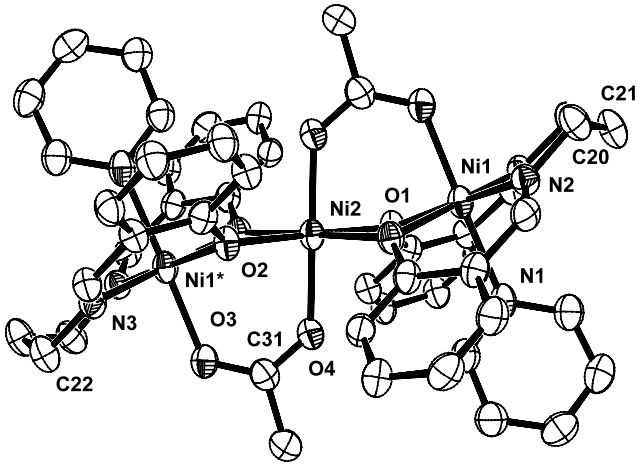


Fig. 5. The structure of {[Ni(Salpr)NC_5H_5]$_2$(μOAc)$_2$Ni}. The key bond lengths and angles for the Salpr regions are given in Table 2. Each of the nickel atoms sit in an octahedral geometry (< N1–Ni–O3, 175.8°; O4–Ni–O4′, 180.0°; O1–Ni–O2, 180.0°).

increase in the bond lengths (M–O; M–N; Table 2) within the Ni(Salpr) motif due to the presence of the included nickel, allows the metal within the Schiff's base moiety to adopt a slightly greater degree of planarity by approximately 3°–4° (Table 2). Consequently we believe that the bond angles and distances found for the *mer* and *fac* Ni(Salbu) complexes above will only have been increased to a similar but small extent (~2%) by the presence of the bridging $Ni(OAc)_2$ unit.

It is noteworthy that the homologous {[Ni(Salpr)MeOH]$_2$(μOAc)$_2$Ni} does not adopt the *fac* configuration via the formation of hydrogen bonds but remains in the *mer* form. At this juncture this behaviour is ascribed to the Salpr unit which will preferentially wish to be in the chair conformation. Thus it can be suggested that whereas hydrogen bonding does stabilise the structure of {[Ni(Salbu)MeOH]$_2$(μOAc)$_2$Ni} (Fig. 3), there remains some contribution to this conformation from the ligand and its need to accommodate a seven membered ring at the nickel centre.

3.4. {Ni(Salpr)$(NC_5H_5)_2$}$PbCl_2$

We remain perplexed by the stability of the central nickel acetate and reasoned that our choice of competing ligand (pyridine) may not have been suitable for the task envisaged. Thus rather than remove the nickel acetate an attempt was made to replace it within the motif using lead(II) chloride. Remarkably introducing lead chloride into the re-crystallising solvent we were

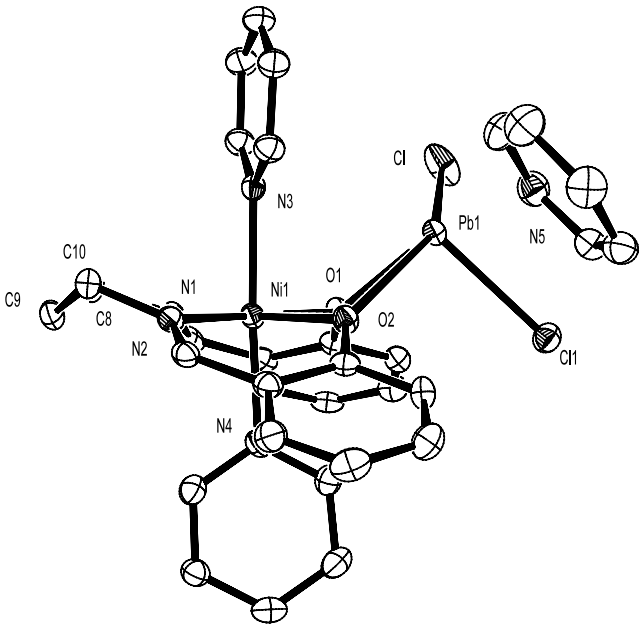


Fig. 6. The structure of $\{[Ni(Salbu)(NC_5H_5)_2]PdCl_2\}.NC_5H_5$. The key bond lengths and angles for the Salbu regions are given in Table 2. The lead atom sits in a heavily distorted tetrahedral environment (Pb–O1, 236.3 pm; Pb–O2, 267.7 pm; O1–Pb–O2, 64.52°). There is a long-range interaction to the pyridine solvent (Pb–N5 300.6 pm).

successful in removing the nickel acetate moiety. However, as a consequence of this action the Ni(Salpr) moiety was transferred to the lead centre forming $\{Ni(Salpr)(NC_5H_5)_2\}PbCl_2$ (Fig. 6). This is an intriguing result, which suggests that Schiff's base complexes can be considered to be neutral ligands, which are capable of undergoing exchange processes. The data presented in Table 2 indicates that the presence of the larger cation again does not profoundly affect the bond distances or angels around the metal Schiff's base moiety. Significantly the O–Ni–O angle at the Schiff's base centre (83.8°) is not significantly larger than that found in the absence of a metal (78.4°) and is curiously smaller than found in the parent nickel (85.0°) complexes discussed above. This result further confirms that although the nickel acetate unit is present in the solid state structures of Salpr and Salbu complexes (Table 2), there remains significant freedom within the key Schiff's base complex. Should the ligand wish to adopt a specific conformation i.e. *mer*–*fac*, the presence of the internal metal cation will be unlikely to prevent this from occurring.

4. Concluding remarks

The isolation of the two Ni(Salbu) complexes completes the matrix of motifs which can be constructed between Salen, Salpr and Salbu and nickel. To highlight the effect of the increasing size of the alkyl chain between the imine moieties we have focused on a small selection of structural elements within these species (Table 2). These are the geometry at the metal centre (M–N and M–O distance; O–M–N angles), the dihedral angle around the imines of the central chelate (N–C···C–N) and the orientation of the aromatic rings with respect to one another. These factors demonstrate how the local environment around the metal distorts to accommodate the increasing internal chelate ring and how the ligand itself adjusts should the metal centre maintain is preferred geometry.

The popular Salen motif has limited conformational flexibility and is confined to the equatorial plane. The N_2O_2 plane about the nickel is distorted only to a minimal extent with the major strain being taken up by the torsion in the ethylene bridge unit ($<$CN–NC of 20.8° and 14.1°, respectively [22,23]). Although the Salpr ligand may be expected to have slightly greater flexibility the propensity of the central chelate ring to adopt a chair conformation generates a motif with less distortion than the Salen system. Consequently, in the five examples cited in Table 2, the torsion angles have fallen to values very close to 0°. As anticipated, extending the di-imine chelate to a seven membered ring does re-introduces strain. In one instance $\{[Ni(Salbu)MeOH]_2(\mu OAc)_2Ni\}$, the Salbu ligand flips into a facial orientation which has a concomitant impact on the torsion angles and the aromatic planes (Fig. 3). For the alternative meridial species the strain is transferred to the tetramethylene backbone manifesting itself as disorder at C_9 and C_{10} (Fig. 4). However, in all cases (Salen, Salpr and Salbu) the planar geometry around the nickel centre is conserved at the expense of the ligand most notably for the *mer* and *fac* Ni(Salbu) complexes.

From the data above it is obvious that within the nickel family of complexes it is possible to obtain a variety of coordination geometries. However, it would seem that Salbu is capable of supporting the broadest range and furthermore that the potential exists for interconversion (Fig. 7) between motifs. The missing element in the scheme is a structurally characterised five coordinate species similar to $[Ni(Salpr)OH_2]$ [33] which is inferred to exists as the intermediate in the *mer*–*fac* re-organisation. However, that Salbu is content to support five coordinate geometries of this type will become clearer in the following study on zinc complexes which have a marked preference for this geometry.

Schiff's base complexes have been in the literature for over 150 years. Most workers rely on them to provide a stable, rigid chelating environment for metals and consequently workers have kept faith with Salen and five membered rings. The realisation that Salbu has the potential to move between conformations illicits the prospect of conformationally active complexes which should have an rich, interesting and independent chemistry worthy of greater exploration.

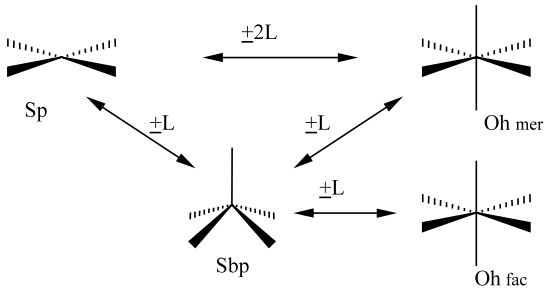


Fig. 7. Conformational geometries available to the Salbu complexes of Nickel. Sp: square-planar, Sbp: square based pyramid and Oh: Octahedral.

5. Supplementary material

Supplementary information are available form The Director, CCDC, 12 Union Road, Cambridge, CB2 1EZ, UK (fax: +44-1223-336033; e-mail: deposit@ccdc.cam.ac.uk or www: http://www.ccdc.cam.ac.uk) on request quoting the deposition numbers 182534–182537.

Acknowledgements

D.S. would like to thank the Wellcome trust and Nuffield foundation for financial support. J.R. would like to thank Alan Kennedy and Mark D. Spicer for their assistance with the X-ray analysis.

References

[1] S. Yamada, Coord. Chem. Rev. 192 (1999) 537.
[2] R.H. Holm, J. Am. Chem. Soc. 82 (1960) 5632.
[3] E.C. Niederhoffer, J.H. Timmons, A.E. Martell, Chem. Rev. 84 (1984) 137.
[4] K. Srinivasan, P. Michaud, J.K. Kochi, J. Am. Chem. Soc. 108 (1986) 2309.
[5] W. Zhang, J.L. Loebach, S.R. Wilson, E.N. Jacobsen, J. Am. Chem. Soc. 112 (1990) 2801.
[6] J. Tisato, F. Refosco, F. Bandoli, Coord. Chem. Rev. 135 (1994) 325.
[7] J. Lacroix, Eur. J. Inorg. Chem. 2 (2001) 339.
[8] J. Nagel, U. Oertel, P. Friedel, H. Komber, D. Mobius, Langmuir 13 (1997) 4698.
[9] S.S. Sundari, A. Dhathathreyan, M. Kanthimathi, U.N. Balachandran, Langmuir 13 (1997) 4923.
[10] A.M. Brouwer, C. Frochot, F.G. Gatti, D.A. Leigh, L. Mottier, F. Paolucci, S. Roffia, G.W.H. Wurpel, Science 291 (2001) 2124.
[11] J.K. Gimzewski, C. Joachim, R.R. Schlittler, V. Langlais, H. Tang, I. Johannsen, Science 281 (1998) 531.
[12] T.R. Kelly, H. De Silva, R.A. Silva, Nature 401 (1999) 150.
[13] R.G. Hayter, F.S. Humiec, Inorg. Chem. 4 (1965) 1701.
[14] S.J. LaPlaca, J.A. Ibers, J. Am. Chem. Soc. 87 (1965) 2581.
[15] N.N. Greewood, A. Earnshaw (Eds.), Chemistry of the Elements, Pergamon, Oxford, 1984, p. 1313.
[16] E.N. Baker, D. Hall, T.N. Waters, J. Chem. Soc. A (1970) 400.
[17] A. Bencini, C. Benelli, A. Caneschi, R.L. Carlin, A. Dei, D. Gatteschi, J. Am. Chem. Soc. 107 (1985) 8128.
[18] M.B. Ferrari, G.G. Fava, C. Pelizzi, Acta Crystallogr., Sect. B 32 (1976) 901.
[19] N. Matsumato, M. Mimura, Y. Sunatsuki, S. Eguchi, Y. Mizuguchi, H. Miiyasaka, T. Nakashima, Bull. Chem. Soc. Jpn. 70 (1997) 2461.
[20] M.G.B. Drew, R.N. Prasad, R.P. Sharma, Acta Crystallogr., Sect. C 41 (1985) 1755.
[21] H.H. Vao, J.M. Lo, B.H. Chem, T.H. Lu, Acta Crystallogr., Sect. C 53 (1997) 1012.
[22] A.G. Manfredotti, C. Guatini, Acta Crystallogr., Sect. C 39 (1983) 863.
[23] L. Carbonaro, M. Isola, P. LaPegna, L. Senatore, F. Marchetti, Inorg. Chem. 38 (1999) 5519.
[24] D. Ulku, F. Ercan, O. Atakol, F.N. Dincer, Acta Crystallogr., Sect. C 53 (1997) 1056.
[25] A. Elmali, V. Elerman, I. Svoboda, H. Feuss, K. Griesar, W. Haase, Z. Naturforsch., Teil B 51 (1996) 665.
[26] D. Hall F.H. Moore, J. Chem. Soc., A (1966) 1822.
[27] O. Atakol, L. Tata, M.A. Akay, D. Ulku, Anal. Sci. 15 (1999) 199.
[28] D. Ulku, L. Tatar, O. Atakol, M. Aksu, Acta Crystallogr., Sect. C 57 (2001) 273.
[29] A.E. Frost, H.H. Freedman, J. Org. Chem. 24 (1959) 1905.
[30] P. Pfeiffer, T. Hesse, H. Pflitzner, W. Scholl, H. Thiellert, J. Prakt. Chem. 149 (1937) 217.
[31] G.M. Sheldrick, SHELXL-97, University of Göttingen, Germany, 1997.
[32] R.W. Asmussen, Ph.D., Kopenhagen, in: R.H. Holm (ed.) Beilstein, p. 230, 1944 as reported. J. Am. Chem. Soc., 82 (1960) 5632.
[33] Y. Elerman, M. Kabak, O. Atakol, Acta Crystallogr., Sect. C 49 (1993) 1905.

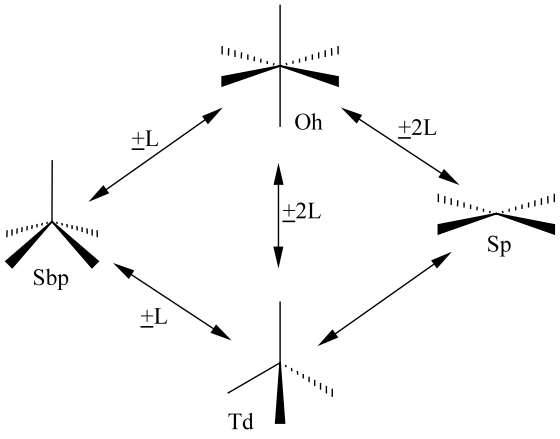


Fig. 1. Conformational geometries available to tetradentate Schiff's base ligands coordinated to late transition metals (Ni, Cu, Zn). Td: tetrahedral; Oh: Octahedral; Sbp: square based pyramid and Sp: square-planar.

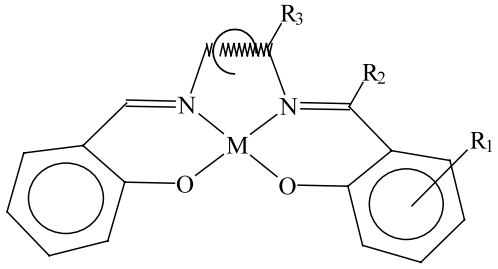


Fig. 2. The simplest symmetric Schiff' base framework. Conformational flexibility is induced by the systematic expansion of the alkyl chain between the two imine moieties; $-(CH_2)_n-$, $n = 2, 3, 4$. To avoid steric and electronic influences from substituent groups around the ligand R_1, R_2 and R_3 will be kept to their simplest protic form.

the preferred octahedral geometry of the metal cation coupled with the stability of the chair conformation of the six membered Ni(Salpr) chelate. This limited structural variety contrasts markedly with that of Salbu, which formed both *mer* and *fac* octahedral complexes[1] (Eq. (1)).

$$\{[Ni(fac-Salbu)HOCH_3]_2(\mu OAc)_2Ni\} \xrightarrow{DMF} \{[Ni(mer-Salbu)Me_2NCOH]_2\text{-}(\mu OAc)_2Ni\} \quad (1)$$

Coupled with the structural preference of Salbu for octahedral geometries with nickel, it is also reported to support a planar four coordinate geometry [7] similar to Salen [2] and Salpr [4]. However, a more complete picture of the structure of these Salbu moieties within a four coordinate environment can be obtained by extending the remit to include the established structures of divalent copper [4,8–12]. Here a definite trend from planar (Salen, Salpr) to a distorted tetrahedral environment (Salbu) was observed as the alkyl chain between the two imine moieties increases in length (Fig. 1). Thus it is clear that Salbu is also capable of adopting either a square-planar (nickel) or a tetrahedral (copper) motif at the behest of the metal centre.

Thus, we have a complete picture of the chosen ligand system within a four and six coordinate environment (Figs. 1 and 3). Consequently, the missing element in the concept put forward is a clear understanding of the chosen ligand's behaviour in a five coordinate environment. Since Zinc demonstrates a marked preference for this geometry, its complexes with the ligand set have been identified as the third important structural motif (Fig. 1) for our initial studies. Although Schiff's base complexes of zinc have been known for many years [13–15], surprising they still remain very poorly characterised structurally. In a comparable earlier study to that presented here Batley and Graddon [15] attempted to delineate the structural preferences of these complexes using spectroscopic methods. Their early study suggested that as the alkyl chain between the two imine moieties increases in length ($n \geq 3$, Fig. 2) the complexes change structural preference from a five coordinate configuration (e.g. $[Zn(salen)OH_2]$ [16]) to a more complex polymeric form. However, more recently two structural reports on Zn(salpr) complexes have appeared [17,18] in which the zinc atom adopts a five coordinate environment.

These recent conflicting studies suggest that the structural patterns available to zinc may be more complex and divergent than previously thought. Consequently, this study seeks to characterise the key parent zinc complexes derived from Salen, Salpr and Salbu such that the structural preferences of zinc can be clearly identified. Combining this information with that derived from the previous study [1] on nickel and copper should make it possible to generate a complete picture of the behaviour of the chosen ligands within a four, five and six coordinate environment.

2. Experimental

Unless otherwise stated, all chemicals were commercially obtained.

N,*N*′-bis(salicylidene)-1,2-ethylenediamine (Salen), *N*,*N*′-bis(salicylidene)-1,3-propane-diamine (Salpr), *N*,*N*′-bis(salicylidene)-1,4-butanediamine (Salbu), were prepared by standard methods. Briefly: 2 mol equiv. of salicylaldehyde (20 ml) were mixed with 1 mol equiv. of the required diamine in methanol (80 ml). The resulting

[1] The terms *mer* and *fac*, properly used, describe the positions of three identical ligands within an octahedral complex. This nomenclature is employed here to include the relative positions of the four donor atoms of these tetradentate Schiffs base ligands. Thus, *mer* is used to imply a ligand lying meridionally around the metal centre with the other ligands occupying the *trans* positions. *Fac* implies that the four donors occupy one face of the metal allowing the remaining ligands to lie *cis* to one another.

solution was refluxed for an hour, filtered while hot and allowed to cool, whereupon copious amounts of yellow crystal began to form. These were collected, washed with diethyl-ether and allowed to air dry. Yields were typically 70% or better.

Expected for Salen $C_{16}H_{16}O_2N_2$: C, 71.62; H, 6.01; N, 10.44. Found: C, 71.19; H, 6.02; N, 10.43%. Melting point (m.p.): 124 °C (124 °C, lit [19]).

^{1}H NMR (400.1 MHz, $CDCl_3$) δ 4.0 (s, 4H, CH_2), 6.9 (m, 4H, arom), 7.3 (m, 4H, arom), 8.4 (s, 2H, –CH=), 13.2 (br s, 2H –OH).

Expected for Salpr $C_{17}H_{18}O_2N_2$: C, 72.32; H, 6.43; N, 9.92. Found: C, 72.35; H, 6.38; N, 9.90%. M.p.: 52 °C (54–55 °C, lit [20]).

^{1}H NMR (400.1 MHz, $CDCl_3$) δ 2.1 (q, 2H, CH_2), 3.7 (t, 4H, CH_2), 6.9 (m, 4H, arom), 7.3 (m, 4H, arom), 8.4 (s, 2H, –CH=), 13.5 (br s, 2H, OH).

Expected for Salbut $C_{18}H_{20}O_2N_2$: C, 72.95; H, 6.80; N, 9.45. Found: C, 72.76; H, 6.95; N, 9.58%. M.p.: 89 °C (91 °C, lit [13]).

^{1}H NMR (400.1 MHz, $CDCl_3$) δ 1.8 (q, 4H, CH_2), 3.6 (t, 4H, CH_2), 6.9 (m, 4H, arom), 7.3 (m, 4H, arom), 8.4 (s, 2H, –CH=), 13.5 (br s, 2H, OH).

2.1. Zn(Salen)

Zinc acetate dihydrate (0.44 g, 2.0 mmol) were dissolved in methanol (50 ml). Salen (0.54 g, 2.0 mmol) was added and the solution brought to reflux. The mixture was heated for 2 h during which time a lemon yellow precipitate formed. The solid was recovered from the hot liquor by filtration. Yield 0.5 g; 75%.

Expected for $Zn(Salen)\cdot C_{16}H_{14}O_2N_2Zn_1$: C, 58.26; H, 4.28; N, 8.49. Found: C, 57.89; H, 4.09; N, 8.28%.

A small amount of this material was recrystallised from pyridine–diethylether by vapour diffusion, affording crystals suitable for X-ray analysis.

Expected for $[Zn(Salen)NC_5H_5]\cdot C_{21}H_{19}O_2N_3Zn_1$: C, 61.40; H, 4.66; N, 10.23. Found: C, 60.97; H, 4.61; N, 10.21%.

2.2. Zn(Salpr)

Zinc acetate dihydrate (0.44 g, 2.0 mmol) were dissolved in pyridine (25 ml). Salpr (0.56 g, 2.0 mmol) was added and the solution allowed to stir for 24 h during which time a very pale yellow precipitate formed. The solid was recovered by filtration and recrystalised from dichloromethane–diethylether by vapour diffusion. Yield 0.3 g; 43%.

Expected for $Zn(Salpr)\cdot 0.5CH_2Cl_2\cdot C_{17.5}H_{17}O_2N_2Cl_1Zn_1$: C, 54.15; H, 4.41; N, 7.22. Found: C, 54.45; H, 4.84; N, 7.15%.

2.3. Zn(Salbu)

Zinc acetate dihydrate (0.44 g, 2.0 mmol) were dissolved in pyridine (25 ml). Salbu (0.59 g, 2.0 mmol) was added and the solution allowed to stir for 48 h. The mixture was treated with diethylether to produce a pale lemon yellow powder, which was recovered by filtration. Yield 0.3 g; 42%.

Expected for $Zn(Salbu)\cdot C_{18}H_{14}O_2N_2Zn_1$: C, 60.10; H, 5.04; N, 7.79. Found: C, 60.45; H, 5.15; N, 7.85%.

Crystals suitable for X-ray analysis were obtained by treating the dichloromethane extract with THF using vapour diffusion methods. However, the sample isolated in this manner was identified as $\{[Zn(Salbu)]_2(OAc)_2Zn\}$.

Expected for $\{[Zn(Salbu)]_2(OAc)_2Zn\}\cdot C_{40}H_{42}O_8N_4Zn_3\cdot H_2O$: C, 52.60; H, 4.82; N, 6.08. Found: C, 52.21; H, 4.88; N, 5.77%.

2.4. {[Zn(Salbu)]$_2$(OAc)$_2$Zn}

Salbu (0.59 g, 2.0 mmol) was dissolved in methanol (50 ml) to which was added zinc acetate dihydrate (0.66 g, 3.0 mmol). The mixture was refluxed for 2 h, allowed to cool and the solvent removed. The resulting white powder was recrystallised from dichloromethane–THF by vapour diffusion. Yield 0.34 g, 38%.

Expected for $\{[Zn(Salbu)]_2(OAc)_2Zn\}$ $C_{40}H_{42}O_8N_4Zn_3$: C, 53.21; H, 4.66; N, 6.20. Found: C, 52.97; H, 4.77; N, 6.10%.

2.5. X-ray analysis

All measurements were conducted with a Nonius Kappa CCD diffractometer at 123 K, using graphite monochromated Mo Kα radiation, on suitable crystals mounted on glass fibres. Details of the data collection and refinements are given in Table 1. The structures were solved by direct methods [21]. The non-hydrogen atoms were refined anisotropically. In all cases the refinement converged satisfactorily.

3. Results and discussion

Similarly to many other workers the synthesis of zinc complexes of Salen, Salpr and Salbu was relatively straightforward to prepare. The complexes forthcoming from solution were essentially pure amorphous solids. Typically, however, their solubility remained poor and great difficulty was encountered in their re-crystallisation. Although Zn(Salen) could be re-crystallised from pyridine to form the desired five coordinate $[Zn(Salen)NC_5H_5]$ complex, the corresponding Salpr and Salbu complexes refused to behave in a similar manner. Resorting to the synthesis of Salpr and Salbu in pyridine

Table 1
Experimental details for the crystal structure determination of $[Zn(Salen)NC_5H_5]$, $[Zn(Salpr)]_2$ and $\{[Zn(Salbu)]_2(OAc)_2Zn\}$

	$\{Zn(Salen)NC_5H_5\}$	$[Zn(Salpr)]_2 \cdot 1.5CH_2Cl_2$	$\{[Zn(Salbu)]_2(OAc)_2Zn\}$
Molecular formula	$C_{21}H_{19}O_2N_3Zn_1$	$C_{35.5}H_{35}O_4N_4Zn_2Cl_3$	$C_{40}H_{42}O_8N_4Zn_3$
Molecular weight	410.78	818.76	902.88
Crystal system	orthorhombic	monoclinic	monoclinic
Space group	*Cmc*21	*C*2	$P2_1/c$
a (Å)	20.2949(6)	19.1735(6)	9.1046(3)
b (Å)	12.7075(4)	9.9447(3)	13.2815(4)
c (Å)	7.1240(5))	14.8067(5)	15.5559(6)
α (°)	90	90	90
β (°)	90	137.801(2)	96.606(1)
γ (°)	90	90	90
V (Å^3)	1837.26	1896.41	1868.57(2)
Z	4	2	2
μ (Mo Kα) (cm^{-1})	1.358	1.518	1.970
Reflections measured	2994	3313	7099
Unique reflections	1112	3313	3678
Observed reflections	897	3103	2943
R_1	0.060	0.051	0.035
WR_2	0.120	0.149	0.076
Number of parameters	127	227	322

in an attempt to force the donor solvent into the fifth coordination site still generated complexes devoid of pyridine (consistent with Batley et al. [15]). Curiously, however, the material derived from this reaction lead to the formation of a dichloromethane soluble [Zn(Salpr)] complex which could be crystallised and fully characterised. Once again, the Salbu species refused to mirror the behaviour of its lower homologue. However, as a consequence of our aggressive behaviour towards this material we were able to isolate suitable crystals of a minor product $\{[Zn(Salbu)]_2(OAc)_2Zn\}$ which we were subsequently able to prepared by more rational means. Thus although we were capable of synthesising a series of five coordinate zinc complexes, the structural homology between them is somewhat more complex than initially anticipated.

3.1. $[Zn(Salen)NC_5H_5]$

The structure obtained for $[Zn(Salen)NC_5H_5]$ (Fig. 3) was the expected square based pyramidal configuration isostructrual with the monohydrate of Hall et al. [16]. In both compounds association occurs alternately between the bases of adjacent Salen units and the apical substituents (H_2O, pyridine). However, unlike the monohydrate the distance between the co-planar pyridine rings (330 pm) in $[Zn(Salen)NC_5H_5]$ support the view that the pyridine ligands are π-stacked in the bulk solid. For $[Zn(Salen)NC_5H_5]$ the zinc sits within the body of the pyramid approximately 33 pm from the base as defined by the Salen ligand donor atoms. The N_{py}–Zn distance at 208.8 pm is commensurate with the nitrogen donors (208.7 pm) in the chelate. At the apex of the pyramid the pyridine ligand lies at an angle of 172.1°

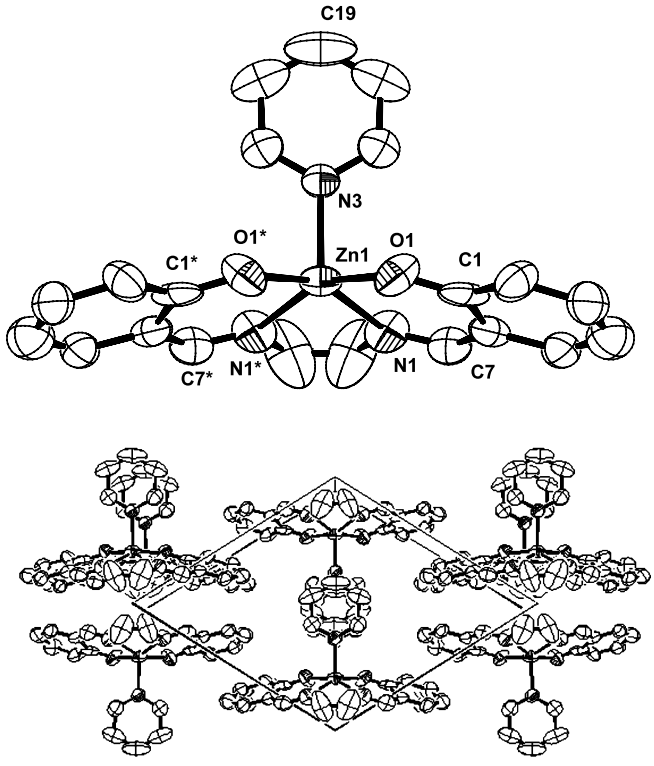


Fig. 3. (Above): The pyramidal structure of $[Zn(Salen)NC_5H_5]$. The key bond lengths are given in Table 2. The large displacement ellipsoids of C13 and C14 indicate their relative freedom of movement. Attempts to model this motion as disorder over a number of sites failed. (Below): The arrangement of the molecules in the unit cell showing the base to base orientation of the Salen and π-stacking of the pyridine ligands.

to the N_{py}–Zn axis and is tilted in the direction of and parallel to the oxygen donor atoms. The orientation of

the pyridine is again reflected by the angles at the N_{py}–zinc which are 105.2° (∠ N_{py}–Zn–N) and 99.8° (∠ N_{py}–Zn–O), respectively. The torsion angles around the aromatic planes and the di-imine chelate ring (Table 2) confirm that the structure of the pyridine adduct is generally more regular than the monohydrate. Selected bond distances and angles within the Salen framework are shown in Table 2 and discussed collectively below.

3.2. {Zn(Salpr)}$_2$

Extending the alkyl chain between the two imine moieties by one methylene unit induces a profound change in the structure of the complex isolated. The material synthesised in pyridine and recrystallised from dichloromethane was found to be devoid of pyridine instead favouring a dimeric arrangement. However, the structure obtained for Zn(Salpr) can still be described in a manner which is consistent with a five coordinate environment. The dimeric structure (Fig. 4) contains three distinct Zn–O distances (195.5, 204.1 and 209.2 pm). As expected the shortest of these is found for the bond between the zinc and the unbridged oxygen (Zn1–O1). However, of some surprise is that the Zn–O distance to the oxygen derived from the adjacent ligand is shorter than to the oxygen within the chelating Salpr unit. This observation substantiates the view of this complex as a five coordinate dimer. This finding in itself was surprising not just because the complex was prepared deliberately in pyridine but also because the analogous copper and nickel complexes have been

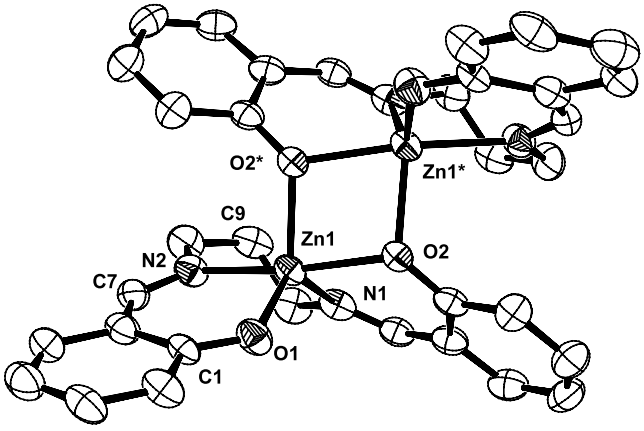


Fig. 4. The dimeric structure of [Zn(Salpr)] showing the Zn_2O_2 core. The key bond lengths are given in Table 2.

reported, where the fifth coordination site is filled by a bridging oxygen [22] or a water ligand [23,24] (Table 2). The facial arrangement of the Zn(Salpr) units and formation of oxygen bridges significantly distorts the pyramidal shape (c.f. [Ni(Salpr)OH_2] and [Cu(Salpr)OH_2]) and consequently the ∠ O2–Zn–O2* is highly constrained (77°).

The motif retrieved here for Zn(Salpr) closely follows that predicted by Batley and Graddon [15]. However, the system characterised by us is dimeric rather than polymeric and there is a far stronger association between the zinc units than might have been predicted. Considering the lack of solubility of the bulk material it is thought that the species structurally characterised here

Table 2
The key bond lengths and bond angles for the established structures of Zn(Salen), Zn(Salpr) and Zn(Salbu) complexes and those of five coordinate {[Ni(Salpr)]$_2$O} [22], [Ni(Salpr)OH_2] [23] and [Cu(Salpr)OH_2] [24]

Compound	–(CH_2)– units between the imines	N_2O_2 plane angles (°)	M–N distance	M–O distance	Aromatic planes (°)	∠ CN–NC torsion angle (°)
{Zn(Salen)OH_2} [16]	2	154.7 153.4	219.7 202.0	190.7 202.0	53.1	31.2
{Zn(Salen)py}	2	154.2 154.2	208.7 208.7	195.5 195.5	0	0
{Ni(Salen)}$_2$O [22]	2	155.0 135.0	210.8 211.6	194.9 191.7	20.2	25.2
{(ZnSalpr)$_2$}	3	170.8 123.4	208.1 208.5	195.5 209.2	58.8	29.0
[(ZnSalpr)HOMe]$ZnCl_2$ [17]	3	148.2 159.7	202.8 204.0	207.5 202.2	10.8	4.9
{[(ZnSalpr)$_2$](Oac)$_2$Zn} [18]	3	155.0 150.9	207.1 206.0	205.8 203.4	3.5	6.8
{Ni(Salpr)OH_2)} [23]	3	172.7 172.5	203.4 203.4	202.9 202.9	0	0
{(Cu(Salpr)OH_2} [24]	3	168.9 168.9	200.5 200.5	193.9 193.9	0	0
{[(ZnSalbu)$_2$](Oac)$_2$Zn}	4	135.0 168.4	204.4 210.2	209.1 200.8	32.1	39.8

The ∠ O–M–N angles are used to depict the geometry within the metal–ligand plane. The M–N and M–O distances are presented as a measure of the change in the ligand to metal bond nature. The torsion angles associated with the region adjacent to the two imine moieties and aromatic planes are used to show how the ligand contorts to accommodate the desired geometry of the metal centre.

is the simplest homologue of a series of polymers, i.e. $[Zn(Salpr)]_n$, $n = 2$, which has been preferentially extracted from the bulk material. The structure of Zn(Salpr) displayed here contrasts markedly with the two other reported Zn(Salpr) species namely [(ZnSalpr)HOMe]$ZnCl_2$ [17] and {[(ZnSalpr)$_2$](OAc)$_2$Zn} [18] which are bi and tri metallic (c.f. Zn(Salbu) below). The contrast between these two motifs again [1] indicates that structural divergence occurs at this juncture i.e. where the alkyl chain between the two imine moieties contains three or more methylene units.

3.3. ZnSalbu

Unfortunately the structural progression was interrupted at Salbu as no simple complex could be structurally characterised. However, from the mixture it was possible to isolate crystals of an important minor component, {[Zn(Salbu)]$_2$(OAc)$_2$Zn}, which could be prepared by a more rational route. Intriguingly, this species follows the reported structures of ({[ZnSalpr]$_2$[OAc]$_2$Zn}) [18] and ({[Ni(Salbu)DMF]$_2$[OAc]$_2$Ni}) [1] in that we obtain a trimetallic complex (Fig. 5). The motif in the vicinity of the Salbu ligand is a typical five coordinate zinc environment with a slight saddle shape in the 'plane' defined by the Schiff's base donors (Table 2) and the zinc atom. The increased size of the chelate ring demands that the ligand alters certain characteristics to accommodate the additional ring methylene unit. Thus we observe an large increase (c.f. {[ZnSalpr]$_2$[OAc]$_2$Zn}; 3.5°) in the torsion angles associated with the aromatic planes (32.1°) and imine regions (39.8°) and a divergence of the M–N and M–O bond distances to values greater and smaller than the respective Salpr complex (Table 2). The effect of the buckling in the Salbu ligand also affects the geometry at the apical acetate ligand (∠ OAc–Zn–N, 96.1° and 117.0°; ∠ OAc–Zn–O, 90.5° and 106.7°) which moves away from the more regular pyramidal values observed for the ZnSalpr complex [18] (∠ OAc–Zn–N, 102.9° and 104.9°; ∠ OAc–Zn–O 101.2° and 103.7°).

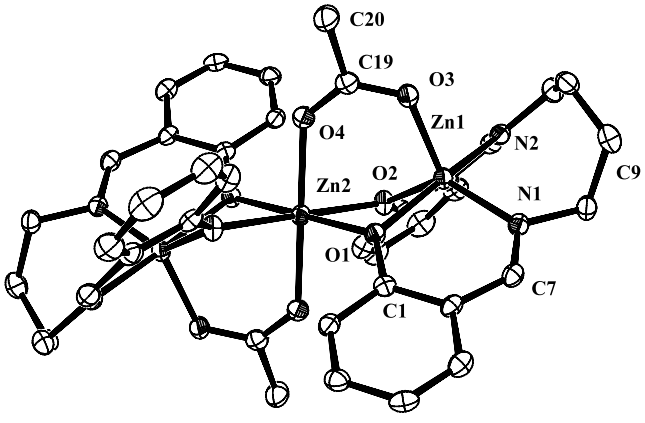


Fig. 5. The structure of {[Zn(Salbu)]$_2$(OAc)$_2$Zn}. The key bond lengths within the Zn(Salbu) unit are given in Table 2. The central zinc sits in an octahedral position. Although the *trans* ∠ O–Zn2–O angles are 180° the *cis* ∠ O–Zn–O angles are more variable with the somewhat tighter internal ∠ O1–Zn1–O2 angle (76.9°) being compensated by the more obtuse cross Salbu ∠ O1–Zn2–O1 angle (103.1°).

3.4. Structural homology

The structural homology of zinc Schiff's base complexes has been unclear for many years. Our ability to crystallise additional representative species offers us an opportunity to identify and clarify certain key patterns available to zinc. It has been known for some time that the simple Salen complexes of zinc can have two interchangeable forms, a five coordinate motif (viz. Zn(Salen)L, L = Pyridine, H_2O) and an anhydrous form. In the absence of any substantive structural data Bately resorted to spectroscopic measurements to suggest a structure for the anhydrous forms of Zn(Salen) and Zn(Salpr). Notably the motif isolated for Zn(Salpr) is not vastly different to that suggested and consequently it is proposed that this motif is representative of Zn(Salen) also. Batley formed the opinion that since Zn(Salbu) would not form a pyridine adduct that it must be four coordinate. However, their supporting IR infrared evidence (phenolic νC–O at 1530 cm^{-1}) is at odds with current band assignments. Furthermore, we now know that five coordinate complexes do form when suitable ligands such as acetate are involved (Fig. 5). Thus with the realisation that Salbu affords greater flexibility and thus less strain and that with suitable ligands and environments five coordinate species are highly favoured, we believe that Zn(Salbu) structurally follows Salpr and Salen and is an oxygen bridged polymer in its simplest form.

Although ZnSalen is content to adopt a five coordinate environment as yet no complexes have been clearly identified which include a second metal complexed to the oxygen donor atoms (c.f. Salen complexes of nickel [3] and copper [25]). In contrast to Salen, zinc complexes of Salpr and Salbu would seem to readily accept a second guest metal cation thus forming bi and tri metallic complexes. This behaviour is a common feature for Salpr and Salbu complexes of late transition metals [1] (Tables 2 and 3). The contrast between the ligand sets here is marked. However, there is little evidence to suggest that Salpr and Salbu have more favourable donor characteristics than Salen. The propensity of these complexes to accept a guest metal in this manner most probably arises from the greater degree of flexibility afforded to the Salpr and Salbu ligands, allowing them to cantilever into a more accommodating orientation for complexation. Indeed a narrowing of the

Table 3
The key bond lengths and bond angles for the established structures of Cu(Salen) [8–10], Cu(Salpr) [4,11] and Cu(Salbu) [12] complexes

Compound	$-(CH_2)-$ units between the imines	N_2O_2 plane angles (°)	M–N distance	M–O distance	Aromatic planes (°)	∠ CN–NC torsion angle
Cu(Salen) [8]	2	176.5	192.8	190.5	2.9	18.0
		174.5	190.3	188.5		
Cu(Salen) [9]	2	176.5	196.6	192.5	11	16.7
		174.8	193.8	190.4		
Cu(Salen) [10]	2	167.4	194.4	188.9	22.8	23.9
		164.5	191.8	189.1		
Cu(Salpr) [11]	3	164.1	199.4	191.0	7.7	7.1
		172.7	200.0	193.3		
Cu(Salpr) [4]	3	174.1	193.8	187.8	32.0	20.3
		159.9	195.8	185.7		
Cu(Salbu) [18]	4	153.3	200.0	189.7	56.6	49.4
		143.9	194.0	190.3		

The ∠ O–M–N angles are used to depict the geometry within the metal–ligand plane. The M–N and M–O distances are presented as a measure of the change in the ligand to metal bond nature. The torsion angles associated with the region adjacent to the two imine moieties and aromatic planes are used to show how the ligand contorts to accommodate the desired geometry of the metal centre.

internal ∠ O–Zn–O angle is observed between Zn(Salen)NC_5H_5 (93.3°) and {$[Zn(Salbu)]_2(OAc)_2Zn$} (79.9°).

3.5. Comparative analysis

The isolation of the three zinc complexes above completes the matrix of motifs, which can be constructed between Salen, Salpr and Salbut with nickel [1], copper [4,8–11,18] (Table 3) and zinc. By combining the data above with the existing data it is possible to demonstrate clearly the structural geometry available to these ligands [1] (Tables 2 and 3) with these metals. Unsurprisingly the Salen ligand remains conformationally restricted to planar and square-pyramid geometries at the metal centre. Within these planar geometries any strain would seem to be transmitted into the alkyl chain between the two imine moieties where –CN–NC torsion angles of 20° are commonly observed. By virtue of the stability of the chair conformation six membered rings, Salpr also demonstrate a preference for a meridial arrangement (e.g. planar and pyrimidal geometry). However, in contrast to Salen, Salpr also supports *mer*-octahedral configurations. Unlike Salen the increased freedom afforded by the extra methylene unit would seem to be able to offset the torsional strain in the di-imine region with angles falling to negligible values (Table 2). At this juncture the incorporation of additional metals at the phenolic oxygen's becomes highly favoured and we observed a trend towards bi and tri metallic systems.

The greatest geometric variation is found for the Salbu ligand which can be seen to support five different geometries; namely distorted tetrahedral (CuSalbu) [18], planar (NiSalbu) [7], square based pyramid (Zn(Salbu), *mer*-Oh (NiSalbu) [1] and *fac*-Oh (NiSalbu) [1]. In all examples of Salbu complexes the formation of the seven membered ring creates some strain in the backbone. The M–O and M–N distances are in general longer [1] (Tables 2 and 3). This strain is sufficient to facilitate the adoption of a *fac*-octahedral geometries with nickel. In the structural chemistry of copper (Table 2) it manifests itself as clear shift from a planar to a heavily distorted tetrahedral motif. Our inability to isolate a regular tetrahedral motif with this ligand set probably stems simply from the geometric preferences of the metal cations studied (e.g. Ni(II) and Cu(II)) each of which will prefer either a planar or a more distorted conformation. Studies currently being conducted clearly show that a butanediamine based ligand system coupled to copper(I) can move to a tetrahedral motif once the electronic factors are accommodated.

Overall the Salbu ligand offers the widest possible conformational flexibility (Fig. 2) which suggests that a generic system could be designed which could support metal cations during chemistry which operate at the extremes of conformational change. The preponderance of the complexes themselves to act as ligands via the formation of bridging oxygen's could be considered as both an advantage or disadvantage and will need great consideration during any refinement of this concept.

4. Supplementary material

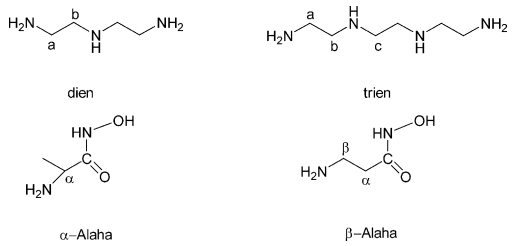
Supplementary information are available from The Director, CCDC, 12 Union Road, Cambridge, CB2 1EZ, UK (fax: +44-1223-336033; e-mail: deposit@ccdc.cam.ac.uk or www: http://www.ccdc.cam.ac.uk) on request quoting the deposition numbers 182539–182541.

Acknowledgements

D.S. would like to thank the Wellcome Trust and the Nuffield Foundation for financial support. J.R. would like to thank Alan Kennedy and Mark D. Spicer for their assistance with the X-ray analysis.

References

[1] J. Reglinski, S. Morris, D.E. Stevenson, Polyhedron 21 (2002) 2167.
[2] A.G. Manfredotti, C. Guatini, Acta Crystallogr., Sect. C 39 (1983) 863.
[3] L. Carbonaro, M. Isola, P. LaPegna, L. Senatore, F. Marchetti, Inorg. Chem. 38 (1999) 5519.
[4] M.G.B. Drew, R.N. Prasad, R.P. Sharma, Acta Crystallogr., Sect. C 41 (1985) 1755.
[5] D. Ulku, F. Ercan, O. Atakol, F.N. Dincer, Acta Crystallogr., Sect. C 53 (1997) 1056.
[6] A. Elmali, V. Elerman, I. Svoboda, H. Feuss, K. Griesar, W. Haase, Z. Naturforsch., Teil B 51 (1996) 665.
[7] R.W. Asmussen, Ph.D., Copenhagen, in: R.H. Holm (ed.) Beilstein, p. 230, 1944 as reported. J. Am. Chem. Soc. 82 (1960) 5632.
[8] E.N. Baker, D. Hall, T.N. Waters, J. Chem. Soc. A (1970) 400.
[9] A. Bencini, C. Benelli, A. Caneschi, R.L. Carlin, A. Dei, D. Gatteschi, J. Am. Chem. Soc. 107 (1985) 8128.
[10] M.B. Ferrari, G.G. Fava, C. Pelizzi, Acta Crystallogr., Sect. B 32 (1976) 901.
[11] N. Matsumato, M. Mimura, Y. Sunatsuki, S. Eguchi, Y. Mizuguchi, H. Miiyasaka, T. Nakashima, Bull. Chem. Soc. Jpn. 70 (1997) 2461.
[12] H.H. Vao, J.M. Lo, B.H. Chem, T.H. Lu, Acta Crystallogr., Sect. C 53 (1997) 1012.
[13] P. Pfeiffer, T. Hesse, H. Pflitzner, W. Scholl, H. Thiellert, J. Prakt. Chem. 149 (1937) 217.
[14] C.S. Marvel, S.A. Asprey, E.A. Dudley, J. Am. Chem. Soc. 78 (1956) 4905.
[15] G.E. Batley, D.P. Graddon, Aust. J. Chem. 20 (1967) 885.
[16] D. Hall, F.H. Moore, J. Chem. Soc. A (1966) 1822.
[17] O. Atakol, L. Tatar, M.A. Akay, D. Ulku, Anal. Sci. 15 (1999) 199.
[18] D. Ulku, L. Tatar, O. Atakol, M. Aksu, Acta Crystallogr., Sect. C 57 (2001) 273.
[19] J. Beretka, B.O. West, M.J. O'Connor, Aust. J. Chem. 17 (1964) 192.
[20] A.E. Frost, H.H. Freedman, J. Org. Chem. 24 (1959) 1905.
[21] G.M. Sheldrick, SHELXL-97, University of Göttingen, Germany, 1997.
[22] B. Bag, N. Mondal, G. Rosair, S. Mitra, Chem.Commun. (2000) 1729.
[23] C. Arici, F. Ercan, O. Atakol, O. Cakirer, Acta Crystallogr., Sect. C 55 (1999) 1654.
[24] Y. Elerman, M. Kabak, O. Atakol, Acta Crystallogr., Sect. C 49 (1993) 1905.
[25] J.M. Epstein, B.N. Figgis, A.H. White, A.C. Willis, J. Chem. Soc., Dalton Trans. (1974) 1954.



Scheme 1.

line acids Zn^{II}, Cu^{II} and Ni^{II} [14–16] to softer Cd^{II} [17]. Both donor sets (O,O) and (N,N) of α-alaninehydroxamic acid form, when co-ordinated, very stable five-membered chelate rings, β-alaninehydroxamic acid forms less stable six-membered chelate ring when co-ordinated via N_{amino}, $N_{hydroxamate}$ donor atoms.

The aim of the study in this paper was to obtain information on preferred sets of donor atoms of α- and β-alaninehydroxamic acids in mixed-ligand complexes, as well as to collect information about their spectroscopic data. The co-ordination tendencies of studied ligands towards zinc(II) ions in aqueous solution were studied by potentiometry and NMR spectroscopy.

2. Experimental

2.1. Materials

α- and β-Alaha were prepared by us via the methyl ester of the respective amino acid as described in [18]. Dien and trien were from Aldrich (Germany) used without further purification and its purity was greater than 99%.

The exact concentrations of the stock solutions of the hydroxamic acids and polyamines were determined by Gran's method [19]. Zinc(II) chloride solution was purchased from Titrisol ampoule (Merck). Zinc(II) nitrate (Aldrich) was used as a source of Zn^{II} in the NMR studies.

2.2. Methods

2.2.1. Potentiometric measurements

The potentiometric measurements were carried out at 25.0±0.1 °C. A summary of the experimental details is given in Table 1.

The data for the Zn^{II}–α-Alaha and Zn^{II}–β-Alaha binary systems can be found in our early papers [14,20] and some of them are included in Table 2. Data for the Zn^{II}–dien binary system can be found in the literature [21], but for a comparison we had to determine stability constants under identical conditions to those of the ternary systems, i.e. at 25.0 °C and ionic strength of 0.2 M (KCl). For the binary system 1:1, 1:2 and 1:4 metal to ligand ratios were used. For the determination of the stability constants of the mixed ligand complexes the concentration ratios of metal–dien/trien–α-Alaha/β-Alaha were 1:1:1, 1:1:2, 1:2:1 and 1:2:2. All the pH-metric titrations were carried out with carbonate-free KOH solution of known concentration (ca. 0.2 M). Titration emf data were used to calculate the hydrogen ion concentration, $[H^+]$. Stability constants $\beta_{pqrs} = [M_pA_qL_rH_s]/[M]^p[A]^q[L]^r[H]^s$ were calculated with the aid of the SUPERQUAD computer program [22].

Table 1
Summary of experimental parameters for the potentiometric measurements

Systems	Binary:dien, trien, α-Alaha or β-Alaha with H^+ or Zn^{II} in water solution; ternary–dien/trien and α-Alaha/β-Alaha with Zn^{II} in water solution
Solution composition	[dien], [trien], [α-Alaha] and [β-Alaha] range—0.002–0.004 M, $[Zn^{II}]$ range—0.001–0.004 M; ionic strength—0.200 M; electrolyte KCl
Experimental method	pH-metric titration of 5 cm^3 samples in the range of pH 2–11; $pK_w = 13.73$
Instruments	Microburette ABU-80 (Radiometer), Radelkis OP-208/1 pH-meter, micro combination pH electrode (Mettler-Toledo, Type 2)
Calibration	By periodic titrations of a HCl solution (5×10^{-2} M KCl) against standard KOH soution
T (°C)	25.0±0.1
n_{tot} [a]	50–70
n_{tit} [b]	6–8
Method of calculation	SUPERQUAD [22]

[a] Number fo titration points per titration.
[b] Number of titration per metal–ligand (or metal–ligand A–ligand L) systems.

For clarity, the charges of the complexes have been omitted in the tables. It has to be mentioned, however, that the fully deprotonated forms of aminohydroxamic acids are negative (L^-) while the polyamines are neutral (A).

2.2.2. NMR spectra

NMR spectra were recorded on a Bruker DRX spectrometer operating at 300.13 MHz for ^1H and 75.46 MHz for ^{13}C at 300 K, unless otherwise noted. The chemical shifts are given in relation to $SiMe_4$. All downfield shifts are denoted as positive.

The assignments for carbon atoms of dien and trien (Scheme 1) follow those presented in ref. [23]. In order to correlate the ^1H and ^{13}C chemical shift assignments for the studied ligands inverse detected [^1H–^{13}C] HMQC NMR experiments were performed using STANDARD BRUKER program.

The samples for NMR studies were prepared in deuteriated water. The measurements were performed only for freshly prepared solutions. In the Zn^{II}–hydroxamate binary systems the metal to ligand molar ratios were 1:1 and 1:2, the ligand concentration was 2×10^{-2} M. The binary Zn^{II}–polyamine and ternary Zn^{II}–

Table 2
Overall stability constants (log β) and stepwise formation contants (log K) for H^+ and Zn^{II} complexes formed with dien/trien (A) and α-Alaha/β-Alaha (L) in binary systems at 25 °C and $I = 0.2$ M (KCl) in water solutions (the ion charges are omitted)

Assignments	A = dien	A = trien	Assignments	L = α-Alaha	L = β-Alaha
log β[HA]	9.97(1)	9.83(1)	log β[HL]	9.20(0)	9.89(1)
log β[H_2A]	19.05(1)	19.30(1)	log β[H_2L]	16.54(1)	18.38(1)
log β[H_3A]	23.40(1)	26.19(1)	pK_1^{micro} (NH_3^+)	7.48(2) [a]	8.85(2) [a]
log β[H_4A]		29.64(1)	pK_2^{micro}(CONHOH)	7.90(3) [a]	8.47(2) [a]
pK_1	4.35	3.45			
pK_2		6.89	log β[ZnHL]	12.27(1)	14.66(5)
pK_3	9.08	9.47	log β[ZnL]	5.29(1)	
pK_4	9.97	9.83	log β[Zn_2L_3]	18.77(2)	
			log β[$ZnLH_{-1}$]	−2.26(2)	
log β[ZnAH]		17.43(6)	log β[$Zn(HL)_2$]		28.51(3)
log β[ZnA]	8.94(2)		log β[$ZnHL_2$]		20.36(4)
log β[$Zn(AH)_2$]		35.38(2)	log β[ZnL_2]	9.32(4)	11.19(4)
log β[ZnA_2H]	22.26(5)	26.51(4)	log β[ZnL_2H_{-1}]		1.16(4)
log β[ZnA_2]	13.96(5)	17.02(5)			
log K[ZnA]	8.94		log K[ZnL]	5.29	
[ZnA] + A ⇌ [ZnA_2]			[ZnL] + L ⇌ [ZnL_2]		
log K[ZnA_2]	5.02		log K[ZnL_2]	4.03	
[ZnA] + HA ⇌ [ZnA_2H]			pK[ZnHL]	6.98	
log K[ZnA_2H]	3.35		pK[ZnL]	7.55	
			pK[$Zn(HL)_2$]		8.15
pK[$Zn(AH)_2$]		8.87	pK[$ZnHL_2$]		9.17
pK[ZnA_2H]	8.30	9.49	pK[ZnL_2]		10.03
log(K_{ZnA}/K_{ZnA_2})	3.92		log(K_{ZnL}/K_{ZnL_2})	1.26	

[a] E. Farkas, T. Kiss, B. Kurzak, J. Chem. Soc., Perkin trans. 2 (1990) 1255.

polyamine–hydroxamate systems were prepared with a zinc(II) concentration of 1×10^{-1} M at the 1:1 or 1:1:1 metal to ligand A to ligand L molar ratios, respectively.

The pH of the samples was measured using a Radiometer pHM83 instrument equipped with a 2401c combined electrode and given as meter readings without correction for pD.

3. Results and discussion

3.1. Solution equilibria

The acid dissociation constants of the studied ligands are given in Table 2, together with the values previously published by us for dien, trien, α- and β-Alaha. The values of the stability constants obtained for the complexes in the studied systems are listed in the same Table 2.

The general four-component equilibria can be written as:

$$pZn + qA + rL + sH \rightleftharpoons Zn_pA_qL_rH_s$$

where p, q, r and s are the stoichiometric coefficients corresponding to the zinc(II) metal ion, A = dien or trien, L = α-Alaha or β-Alaha, and H, respectively; charges are omitted for simplicity.

The overall formation constants are defined as:

$$\beta_{pqrs} = [Zn_pA_qL_rH_s]/[Zn]^p[A]^q[L]^r[H]^s$$

The β_{pqrs} constant expresses the stability of the $[ZnAL]^+$ mixed-ligand species.

3.1.1. Zn^{II}–dien–α-Alaha/β-Alaha systems

The equilibrium constant, K_{ZnAL}, evaluated from the computed values of the related β_{pqrs} values according to equation: $\log K_{ZnAL} = \log \beta_{ZnAL} - \log \beta_{ZnA}$, shows how tightly L (aminohydroxamic anion) is bound to the simple $[ZnA]^{2+}$ complex.

The log $K_{Zn(dien)L}$ values are 4.65 and 5.09 for L = α-Alaha or β-Alaha, respectively. These values should be compared with log β_{ZnL}. For L = β-Alaha this comparison cannot be done, since the complex with 1:1 ratio is not formed in measurable concentrations in the Zn^{II}–β-Alaha system. The log β_{ZnL} value describing the reaction Zn^{2+} + α-Alaha ⇌ $[Zn(\alpha\text{-Alaha})]^+$ gives 5.29. The difference of these two values (4.65 − 5.29), $\Delta \log K$, describes the difference between the affinities of α-Alaha to Zn^{II} and to $[Zn(dien)]^{2+}$. Since it is similar to that expected on a statistical basis [24,25], it indicates that α-Alaha binds to the $[Zn(dien)]^{2+}$ complex as easily as to Zn^{II}.

Sigel's log $X_{Zn(dien)L}$ value (the constant due to the equilibrium $[Zn(dien)_2]^{2+} + [ZnL_2] \rightleftharpoons 2[Zn(dien)L]^+$) for L = α- or β-Alaha are 3.92 and 3.22, respectively, and are abnormally high (expected on a statistical basis is 0.6

Table 3
Overall stability constants (log β), deprotonation constants (pK) and characteristic parameters for Zn^{II} complexes formed with diethylenetriamine–triethylenetetramine (A) and α-Alaha/β-Alaha (L) in ternary systems at 25 °C and $I = 0.2$ M (KCl) in wayter solutions (the ion charges are omitted)

No	Assignment	A = dien		A = trien	
		α-Alaha	β-Alaha	α-Alaha	β-Alaha
1	log β[ZnALH$_2$]				32.12(8)
2	log β[ZnALH]		22.77(3)	24.88(7)	27.04(3)
3	log β[ZnAL]	13.60(2)	14.04(4)	17.32(9)	17.75(4)
4	log β[ZnALH$_{-1}$]	2.89(3)		6.69(6)	
5	log β[ZnALH] − p$K^{micro}_{NH_3^+}$		13.92	17.40	18.19
6	log β[ZnAL] − pK^{micro}_{NHOH}	5.70	5.57	9.42	9.28
7	pK[ZnALH$_2$]				5.08
8	pK[ZnALH]		8.73	7.56	9.19
9	pK[ZnAL]	10.71		10.63	
10	[ZnAL] + L ⇌ [ZnAL]				
	log K[ZnAL]	4.65	5.09		
11	[ZnA] + A ⇌ [ZnA$_2$]				
	log K[ZnA$_2$]	5.02	5.02		
12	Δ log K	−0.63			
13	log X	3.92	3.22	8.31	7.30
14	χ^2	5.04	8.13	11.07	10.30
15	σ	2.86	2.92	5.08	6.41

[24,25]), which means that the formation of the mixed complexes is strongly favoured in these systems (Table 3) and there are some special causes to stabilise them. It is notable that the denticity of the amines is certainly different in the ternary and binary systems. This is clearly demonstrated by the derived equilibrium constant, representing the binding ability of dien to their 1:1 complex and to the 1:1 complex of α-Alaha:

$$Zn(dien) + dien \rightleftharpoons Zn(dien)_2 \quad \log K = 5.02$$

$$Zn(\alpha\text{-Alaha}) + dien \rightleftharpoons Zn(\alpha\text{-Alaha})(dien) \quad \log K = 8.31$$

In the second case, the derived equilibrium constant is significantly higher, indicating that dien has a higher denticity in the ternary complex, than in the binary one.

From Table 3, it can be seen that for the Zn^{II}–dien–α-Alaha system the speciation model contains six simple species an two mixed-ligand ones: [Zn(dien)(α-Alaha)]$^+$ and [Zn(dien)(α-Alaha)H$_{-1}$]. For this system concentration distribution curves are presented in Fig. 1.

The Zn^{II}–dien 1:1 and 1:2 complexes are formed at high concentrations at zinc(II)–dien–α-Alaha ratio of 1:2:2. Under these conditions the mixed-ligand complexes are of approximately 30% of the total zinc content, but at 1:1:2 ratio the mixed-ligand complex reaches of approximately 90% (Fig. 1(c)). Additionally, Fig. 1(c) shows that the presence of dien suppresses the formation of polymeric [Zn$_2$(α-Alaha)$_3$]$^+$ species in the ternary system.

The calculated concentrations of these eight zinc(II) complex species, as a function of pH (shown in Fig. 1(c)) indicate that under these conditions the [Zn(dien)(H–dien)]$^{3+}$, [Zn(α-Alaha)$_2$], [Zn(dien)$_2$]$^{2+}$ species are the minor ones, so can be regarded as negligible. The first mixed-ligand species, [Zn(dien)(α-Alaha)]$^+$, is seen above pH 7 whereas above pH 9.5 [Zn(dien)(α-Alaha)H$_{-1}$] appears.

In the Zn^{II}–dien–β-Alaha system, the titration data fit satisfactorily to the assumption of the presence of the four simple species: [Zn(dien)]$^+$, [Zn(H–β-Alaha)$_2$]$^+$, [Zn(dien)$_2$]$^{2+}$, [Zn(dien)(H–dien)]$^{3+}$, and two mixed-ligand ones: [Zn(dien)(H–β-Alaha)]$^{2+}$ and [Zn(dien)(β-Alaha)]$^+$. The stability constants obtained for the complexes in the binary and ternary systems are given in Tables 2 and 3, together with the values for the simple complexes taken from the previous studies [14].

Concentration distribution curves are presented in Fig. 2.

The calculated concentrations of these six zinc(II) complex species, as a function of pH, for Zn^{II}–dien–β-Alaha 1:1:2 ratio system (shown in Fig. 2(c)) indicate that under these conditions the first mixed-ligand species, [Zn(dien)(H–β-Alaha)]$^{2+}$, appears above pH 6 and reaches a maximum concentration of approximately 65% at pH 8. The next mixed-ligand species [Zn(dien)(β-Alaha)]$^+$, is a major one (ca. 100% at pH 11). The [Zn(dien)$_2$]$^{2+}$ and [Zn(dien)(H–dien)]$^{3+}$ species were found in the ternary system with a very low ($<4\%$) concentrations. However, when these species were not included in the model the goodness of fit tests was much worse.

The deprotonation process of [Zn(dien)(H–β-Alaha)]$^{2+}$ leading to the formation of [Zn(dien)(β-Alaha)]$^+$ above pH 7 corresponds to the liberation of the proton from the $-NH_3^+$ group of β-Alaha, which is hardly likely, since the p$K_{Zn(dien)(H-\beta\text{-Alaha})}$ value equal to 8.73 (Table 3 number 8) is characteristic for the pK_{β}-

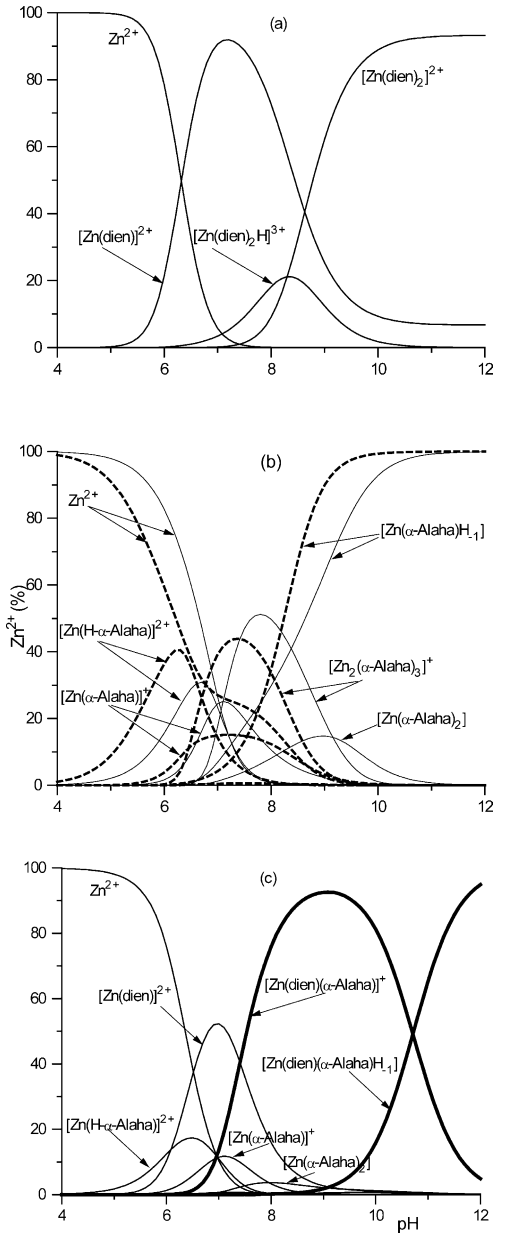


Fig. 1. Species distribution patterns of Zn^{II} complexes in the binary and ternary systems: (a) Zn^{II}–dien at 1:2 molar ratio; $c_{Zn^{II}} = 4 \times 10^{-3}$ M; (b) Zn^{II}–α-Alaha at 1:2 molar ratio; $c_{Zn^{II}} = 4 \times 10^{-3}$ M (solid lines) and Zn^{II}–α-Alaha at 1:1 molar ratio; $c_{Zn^{II}} = 2 \times 10^{-2}$ M (dashed lines; simulated for conditions used in NMR studies); (c) Zn^{II}–dien–α-Alaha at 1:1:2 molar ratio; $c_{Zn^{II}} = 4 \times 10^{-3}$ M.

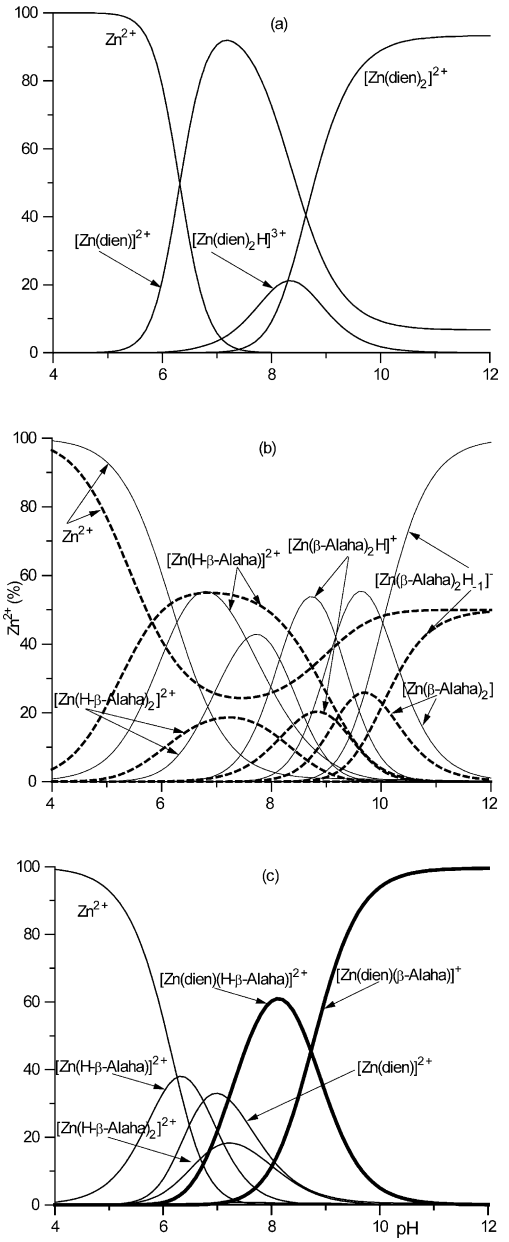


Fig. 2. Species distribution patterns of Zn^{II} complexes in the binary and ternary systems: (a) Zn^{II}–dien at 1:2 molar ratio; $c_{Zn^{II}} = 4 \times 10^{-3}$ M; (b) Zn^{II}–β-Alaha at 1:2 molar ratio; $c_{Zn^{II}} = 4 \times 10^{-3}$ M (solid lines) and Zn^{II}–β-Alaha at 1:1 molar ratio; $c_{Zn^{II}} = 2 \times 10^{-2}$ M (dashed lines; simulated for conditions used in NMR studies); (c) Zn^{II}–dien–β-Alaha at 1:1:2 molar ratio; $c_{Zn^{II}} = 4 \times 10^{-3}$ M.

$_{Alaha}{}^{micro}$ (NH_3^+) microconstant (8.85) (see Table 2). Taking into account these protonation constants, hydroxamate type (O,O) co-ordination of H–β-Alaha can be supposed for the $[Zn(dien)(H\text{–}\beta\text{-Alaha})]^{2+}$ species.

Comparing both Zn^{II}–dien–L ternary systems, it can be seen that α-Alaha is the same effective chelating ligand as β-Alaha. This is reflected in almost identical basicity-adjusted stability constants, $\log K_{Zn(dien)(\alpha\text{-Alaha})/(\beta\text{-Alaha})} - pK^{micro}_{\beta\text{-Alaha}}$. These values are −3.25 and −3.38 for $[Zn(dien)(\alpha\text{-Alaha})]^+$ and $[Zn(dien)(\beta\text{-Alaha})]^+$, respectively (Table 4). Taking into account these basicity-adjusted stability constants, hydroxamate type (O,O) co-ordination of α-Alaha and β-Alaha can be supposed for these species.

Owing to the larger space requirement and neutral charge of dien (the fully deprotonated hydroxamate group has a charge of −1), the chelating ability of this ligand to the $[Zn(dien)]^{2+}$ species is lower than that of the hydroxamate anion. So, the mixed-ligand species are more stable than the simple, $[Zn(dien)_2]^{2+}$.

Table 4
Overall stability constants (log β), stepwise formation constants (log K) and basicity-adjusted stability constants for Zn^{II} mixed-ligand complexes formed with amines (A) and α-alaninehydorxamic acid–β-alaninehydroxamic acid (L) at 25 °C and $I = 0.2$ M (KCl) in water solutions (the ion charges are omitted)

	A = en		A = en		A = trien	
	α-Alaha [a]	β-Alaha [b]	α-Alaha	β-Alaha	α-Alaha	β-Alaha
log β_{ZnALH}		20.11(0)		22.77(3)	24.88(7)	27.04(3)
log β_{ZnAL}	11.15(2)	11.65(0)	13.60(2)	14.04(4)	17.32(9)	17.75(4)
$ZnA + L \rightleftharpoons ZnAL$						
log K_{ZnAL}	5.55	6.05	4.65	5.09		
log $K_{ZnAL} - pK^{micro}_{NHOH}$	−2.35	−2.42	−3.25	−3.38		

[a] Ref. [33].
[b] Ref. [34].

3.1.2. Zn^{II}–trien–α-Alaha/β-Alaha systems

For the determination of the stability constants of the mixed complexes formed in the Zn^{II}–trien–α-Alaha/β-Alaha systems (presented in Table 3), potentiometric measurements were carried out with at least twofold excess of the total amount of moles of aminohydroxamic ligands relative to the number of moles of trien and the metal ion. Within the whole studied pH range (i.e. from ca. 5 to 11) no precipitate was observed. The mixed complexes start to be formed from pH of about 5 and above pH 6.5 only mixed-ligand species exist in both systems (Fig. 3(b and c)).

The $[Zn(H–α\text{-Alaha})]^{2+}$ and $[Zn(α\text{-Alaha})]^{+}$ species are minor ones, so may be regarded as negligible (Fig. 3(b)).

The deprotonation process of $[Zn(trien)(H–α\text{-Alaha})]^{2+}$ leading to the formation of $[Zn(trien)(α\text{-Alaha})]^{+}$ above pH 6.5 corresponds to the liberation of the proton from the $–NH_3^+$ group of α-Alaha, the $pK_{Zn(trien)(H–α\text{-Alaha})}$ value equal to 7.56 (Table 3 number 8) is characteristic for the $pK^{micro}_{β\text{-Alaha}}$ (NH_3^+) microconstant (7.48) (see Table 2). Thus, hydroxamate type (O,O) co-ordination of H–α-Alaha ligand can be supposed for the $[Zn(trien)(H–α\text{-Alaha})]^{2+}$ species.

The final deprotonation of $[Zn(trien)(α\text{-Alaha})]^{+}$ leading to the $[Zn(trien)(α\text{-Alaha})H_{-1}]$ species at pH ≈ 9 corresponds to the ionisation of a metal-bound water molecule.

In the Zn^{II}–trien–β-Alaha system all pH-metric titration curves were consistent with the formation of $[Zn(trien)(H–β\text{-Alaha})]^{2+}$ and $[Zn(trien)(β\text{-Alaha})]^{+}$ as main complexes (ca. 98%). Optimisation using the SUPERQUAD software necessitated the introduction of $[Zn(H–trien)]^{3+}$, $[Zn(H–β\text{-Alaha})]^{2+}$ and $[Zn(H–trien)(H–β\text{-Alaha})]^{3+}$ as the additional complex species in the complexation set. The stability constants obtained for the complexes in the binary and ternary systems are given in Tables 2 and 3. Concentration distribution curves are presented in Fig. 3(c).

The deprotonation process of $[Zn(trien)(H–β\text{-Alaha})]^{2+}$ leading to the formation of $[Zn(trien)(β\text{-Alaha})]^{+}$ above pH 8 may correspond to the liberation of the proton from the $–NH_3^+$ group of β-Alaha, as it was in the system with α-Alaha, but it is not univocal (see deprotonation constants of trien in Table 2). However, the basicity-adjusted stability constants, $\log \beta_{Zn(trien)(H–α\text{-Alaha})/(H–β\text{-Alaha})} - pK^{micro}_{NH_3^+}$, are almost identical with $\log \beta_{Zn(trien)(α\text{-Alaha})/(β\text{-Alaha})}$ (Table 3). Therefore, we suggest that the amino group of either α-Alaha or β-Alaha is out of the co-ordination sphere in the ternary systems.

Sigel's log $X_{Zn(trien)L}$ value (the constant due to the equilibrium $[Zn(trien)_2]^{2+} + [ZnL_2] \rightleftharpoons 2[Zn(trien)L]^{+}$) for L = α-Alaha or β-Alaha are 8.31 and 7.30, respectively, and are abnormally high. This means that the formation of mixed complexes is even more strongly favoured in these systems (Table 3) than in those discussed in Section 3.1.1. So, the statistical effects are more important in the systems with trien than with dien. The larger space requirement for trien, compared with dien, is the reason that the chelating ability of trien to the $[Zn(trien)]^{2+}$ species is lower than of dien to $[Zn(dien)]^{2+}$ and the hydroxamate anion (which is smaller from both polyamines) is preferred as a secondary ligand in these systems.

In the Zn^{II}–trien–L ternary systems α-Alaha is as effective chelating ligand as is β-Alaha. This is reflected in almost identical basicity-adjusted stability constants, $\log \beta_{Zn(trien)(α\text{-Alaha})/(β\text{-Alaha})} - pK^{micro}_{NHOH}$ (the same situation was observed in the systems with dien). These values are 9.42 and 9.28 for $[Zn(trien)(α\text{-Alaha})]^{+}$ and $[Zn(trien)(β\text{-Alaha})]^{+}$, respectively (Table 3). Taking into account these basicity-adjusted stability constants, hydroxamate type (O,O) co-ordination of α- and β-Alaha ligand can be supposed for these species.

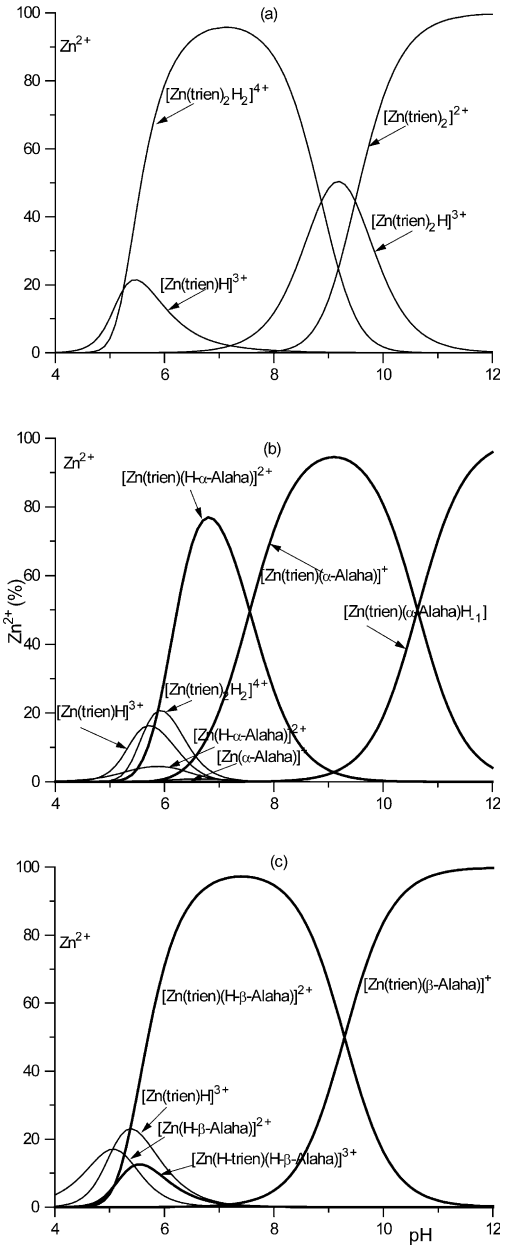


Fig. 3. Species distribution patterns of Zn^{II} complexes of trien: (a) at 1:2 molar ratio and trien–α-Alaha (b) and trien–β-Alaha (c) at 1:1:2 molar ratio; $c_{Zn^{II}} = 4 \times 10^{-3}$ M.

3.2. NMR studies

In order to obtain supporting evidence for the interpretation of the potentiometric data and to get some structural information of the species in solution, we undertook the ^{1}H and ^{13}C NMR studies. The spectra were measured as a function of pH and compared with those obtained for free ligand alone and for the respective Zn^{II}–hydroxamate and Zn^{II}–polyamine binary systems. Finally, we compared the NMR titration

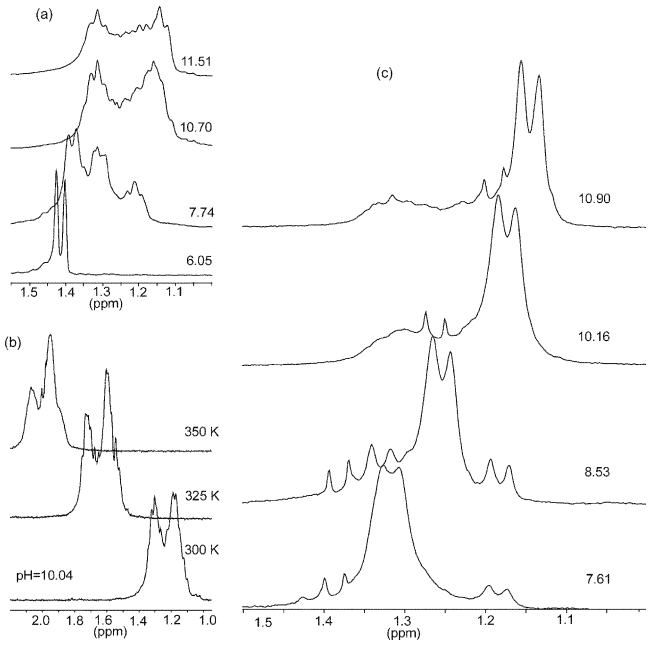


Fig. 4. ^{1}H MNR spectra (CH_3 region) for the Zn^{II}–α-Alaha binary systems at different molar ratios and pH values: (a), (b) 1:1 solutions, (c) 1:2 solutions; $c_{\alpha\text{-Alaha}} = 2 \times 10^{-2}$ M.

data with the species distribution curves recalculated for the conditions used in NMR experiments.

3.2.1. Zn^{II}–α-Alaha and Zn^{II}–β-Alaha binary systems

There are significant differences between the spectra of the Zn^{II}–α-Alaha solutions depending on the metal to ligand stoichiometric ratio. Specifically, the zinc(II) equimolar mixture exhibits rather complex pattern of the resonances in the pH range ~7–12. As an illustration, the number of doublets for the CH_3 group in the proton spectra is presented in Fig. 4(a).

As seen, most of the peaks are almost intact versus pH, whereas their intensities change when pH is varied. The spectra are temperature sensitive. The signals move gradually downfield with increasing temperature and some coalescence above 330 K. Finally, at 350 K two broad features are observed (Fig. 4(b)). Interesting is, that under the same conditions the spectra of the 1:2 molar ratio system are significantly simplified. The intensities of the most resonances roughly decrease with resultant one set of signals predominating in an evident manner in the studied range of pH (Fig. 4(c)). Accordingly, the zinc(II) system with sarcosine hydroxamic acid (not discussed here) exhibits similar behaviour, whereas comparative study with harder magnesium(II) ion revealed only one set of resonances in the whole range of pH. All these facts demonstrate that aminohydroxamic acids are capable of binding zinc(II) not only through the (O,O) hydroxamate function but also through the *N*-amino donor, which, in turn, can enhance the (N,N) chelate binding mode

involving N_{amino} and $N_{hydroxamate}$ donor set. The evidences for facilitating such co-ordination in the case, when the amino group is in adjacent (α or β) position in relation to the nitrogen of the hydroxamate group are provided from both X-ray and solution studies for Cu^{II}, Ni^{II} and Mo^{VI} [15,26–30].

Unfortunately, the character of the spectra precludes the detailed assignments. We can only speculate that the observed phenomena are due to a slow on the NMR time scale equilibria for complexation reactions. A noteworthy feature of the 1:1 molar ratio system is that all ligand is consumed to form $[Zn_2(\alpha\text{-Alaha})_3]^+$ and $[Zn(\alpha\text{-Alaha})H_{-1}]$ as the two major species at $pH > 7$. In the former complex, the only way of co-ordination is that one molecule serves as a bridge between the two zinc(II) ions, involving both pairs of available donor sets, (O,O) and (N,N), whereas the two others bind to the dinuclear core in the chelate modes ((O,O) or (N,N)). Such co-ordination enables the formation of four different co-ordination isomers of this complex that could give rise to the separate set of signals in the NMR spectra. In the latter complex, the most likely co-ordination mode is via the *N*-amino and *N*-hydroxamic functions. Therefore, a kinetic inertness of both complexes may be either due to a strained structure of $[Zn_2(\alpha\text{-Alaha})_3]^+$ imposed by the planar disposed hydroxamate (O,O) and N-donors or due to inert, long-lived in respect of the NMR time scale, zinc(II)–nitrogen bonds. Consequently, the behaviour of the 1:2 molar ratio system may be associated with the metal-free ligand, proved from the potentiometric data to remain in solution over the whole range of pH. In particular, $[Zn_2(\alpha\text{-Alaha})_3]^+$ and free ligand are the major species contributing the spectrum at pH 8.53, whereas $[Zn(\alpha\text{-Alaha})H_{-1}]$ and free ligand, appearing in nearly the same concentrations, contribute the spectrum at pH 10.90 (Fig. 4(b)). Both these complexes are shown to be capable of a slow on the NMR time-scale complex-formation kinetics. Therefore, may be considered as exchanging slow with the ligand present in the system.

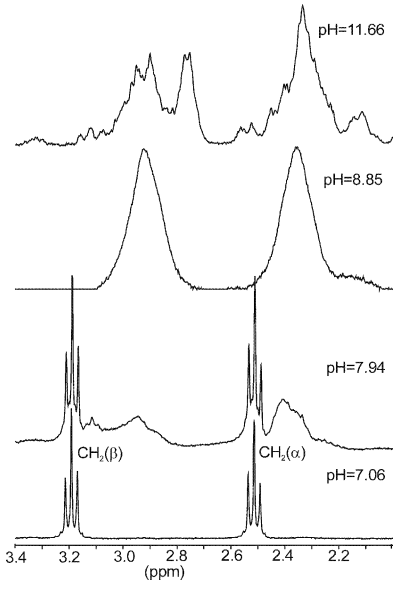


Fig. 5. ^1H NMR spectra for the Zn^{II}–β-Alaha 1:1 solutions at different pH values, $c_{\beta\text{-Alaha}} = 2 \times 10^{-2}$ M.

The comparative studies with β-Alaha having reversed, with respect to α-Alaha, acidity sequence for the $-NH_3^+$ and –CONHOH groups (Table 2) reveal differences between both Zn^{II}–β-Alaha and Zn^{II}–α-Alaha systems. One most important is the lack of the dinuclear complex, besides 1:2 molar ratio complexes are formed. In addition, due to increased basicity of the $-NH_3^+$ group the protonated complexes dominate over a wider range of pH (up to ~8.5) (Fig. 2(b)). As long as the amino group remains protonated, the ligand is capable of co-ordinating via the oxygens of the hydroxamate group. Accordingly, the only effects of co-ordination are little changes in chemical shifts of the major CH_2 signals, with respect to the metal-free ligand (Fig. 5).

However, the spectra show that the relatively inert (N,N) bonded species may also be formed under

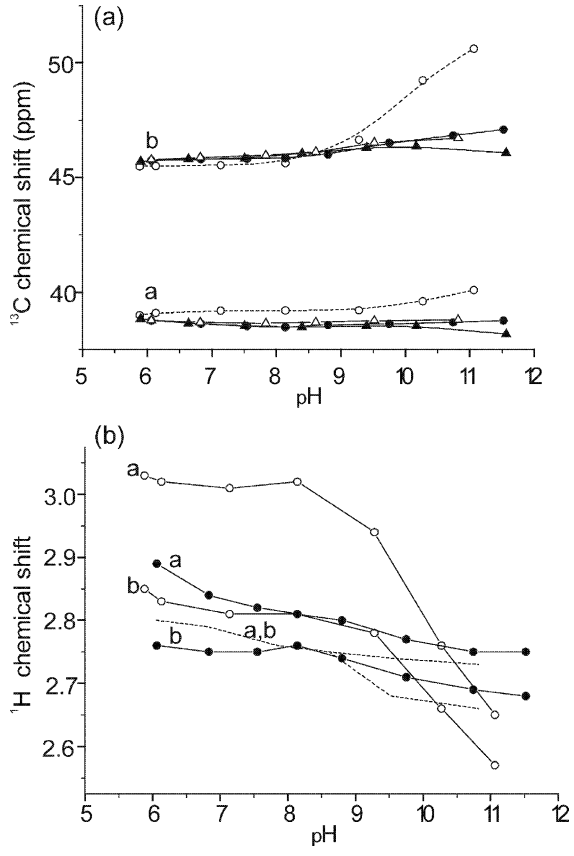


Fig. 6. ^{13}C and ^1H chemical shifts for C carbons (a) and CH_2 protons (b) of dien as a function of pH:free dien (○); Zn^{II}–dien 1:1 (Δ, …); Zn^{II}–dien–α-Alaha 1:1:1 (●) and Zn^{II}–dien–β-Alaha 1:1:1 (▲) ternary solutions. The assignments for C and CH_2 are consistent with those in Scheme 1.

conditions where the amino nitrogen is capable of competing with the hydroxamate oxygens for co-ordination. This is accompanied with a significant broadening of the resonance signals and their upfield shifts with respect to free β-Alaha. Thus, we suggest that formation of [Zn(β-Alaha)$_2$] and further [Zn(β-Alaha)$_2$H$_{-1}$]$^-$ is somehow accompanied with a change in the co-ordination modes from (O,O) towards the (N,N).

3.3. Ternary systems

The set of pH profiles of the ^{13}C chemical shifts for metal-free dien, dien in 1:1 molar ratio solutions with zinc(II) and of equimolar mixtures of zinc(II) and dien with α- or β-Alaha in the 1:1:1 molar ratio is presented in Fig. 6(a).

It is generally accepted for aliphatic polyamines that the change in chemical shift for a particular C atom on forming a zinc(II) chelate is typically about half that seen on fully protonating free ligand (A) [30–32]. The chemical shifts for both C_a and C_b in the Zn^{II}–dien system are nearly constant at pH > 6 and fulfill the above requirement. Thus, clearly show that dien apparently acts as a tridentate ligand involving all available nitrogen donors. The same is confirmed if consider the methylene protons of dien in the ^{1}H NMR spectra (Fig. 6(b)). Taking into account that under conditions studied the chemical shifts for the corresponding C and CH_2 of dien in the Zn^{II}–dien–α-Alaha/β-Alaha ternary systems are almost unchanged with respect to those of Zn^{II}–dien at pH > 6 (Fig. 6(a and b)) it is clear that, the arrangement adopted by amine in the [Zn(dien)]$^{2+}$ complex is retained on formation of the mixed-ligand species with either α- or β-Alaha. A similar conclusion holds in the case of the ternary systems with trien. (Fig. 7(a and b)).

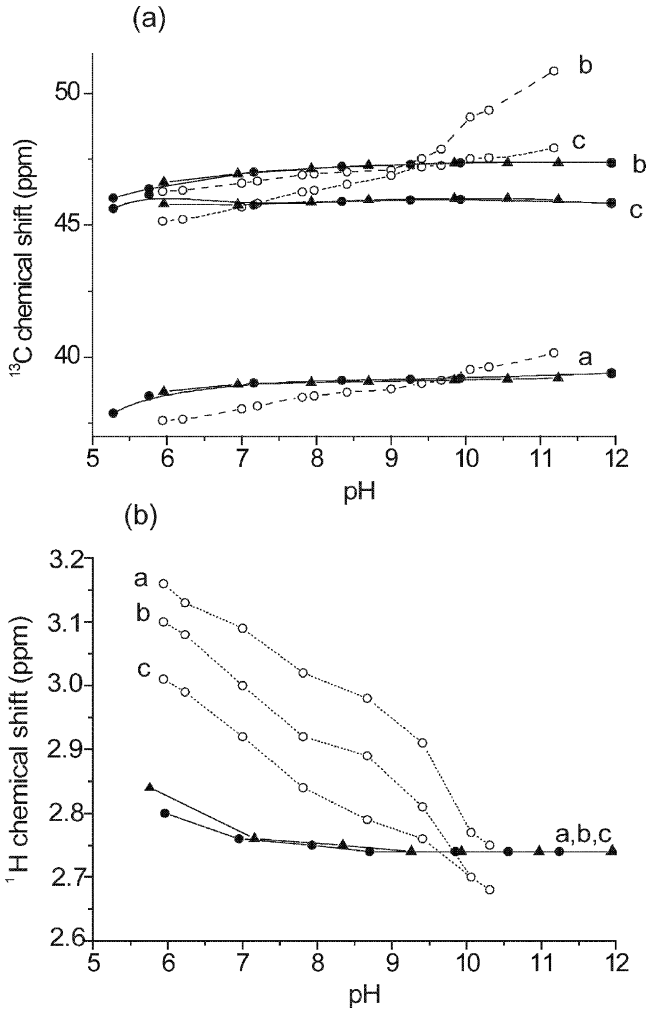


Fig. 7. ^{13}C and ^{1}H chemical shifts for C carbons (a) and CH_2 protons (b) of trien as a function of pH: free trien (○); Zn^{II}–trien–α-Alaha 1:1:1 (●) and Zn^{II}–trien–β-Alaha 1:1:1 (▲) ternary solutions. The assignments for C and CH_2 are consistent with those in Scheme 1.

The general invariance of the chemical shifts on pH in the appropriate ^{1}H and ^{13}C NMR spectra above pH 7 shows that a tetradentate co-ordination of trien is a common feature of either [Zn(trien)(α-Alaha)]$^+$ and [Zn(trien)(α-Alaha)H$_{-1}$] or [Zn(trien)(H–β-Alaha)]$^{2+}$ and [Zn(trien)(β-Alaha)]$^+$, respectively.

Interestingly, co-ordination exerts relatively small effect on the chemical shifts of bound α- and β-Alaha (Fig. 8).

Moreover, in contrast to the binary Zn^{II}–α-Alaha and Zn^{II}–β-Alaha systems both ^{1}H and ^{13}C NMR spectra comprise a single set of sharp signals indicating that exchange of hydroxamate between complex species is fast throughout. Under conditions where the mixed-ligand complexes emerge as the major species the resonance attributed to $C_\alpha H$ of α-Alaha in the ^{1}H spectra shifts downfield ($\Delta\delta \sim 0.15$ ppm) with respect to the fully deprotonated free ligand form (L^-) (Fig. 8(a)). A comparative study with β-Alaha reveal little differences in the ^{1}H NMR behaviour between both acids (Fig. 8(b)). All these facts demonstrate that there is no binding to the amino group in the mixed-ligand species, thus confirm, that in principal complexes ([ZnAL]$^+$ with α-Alaha and [ZnA(LH)]$^{2+}$ with β-Alaha) hydroxamic acids coordinate zinc(II) exclusively through the (O,O) hydroxamate donor set. The same evidence is provided from the ^{13}C NMR experiments where upfield shifts due to zinc(II) complexation are detected for either $C_\alpha H$ of α-Alaha or $C_\alpha H_2$ of β-Alaha (Fig. 8(c and d)).

The above results are fully consistent with the previous studies on zinc(II) mixed-ligand complexes of aliphatic polyamines with a range of small potentially bidentate O- and N-binding ligands (L) [30–32]. The noteworthy feature of all these complexes is a little transmission of inductive effects from ligand L to the polyamine moiety through the zinc(II) ion resulting in apparent similarities of the chemical shifts for respective

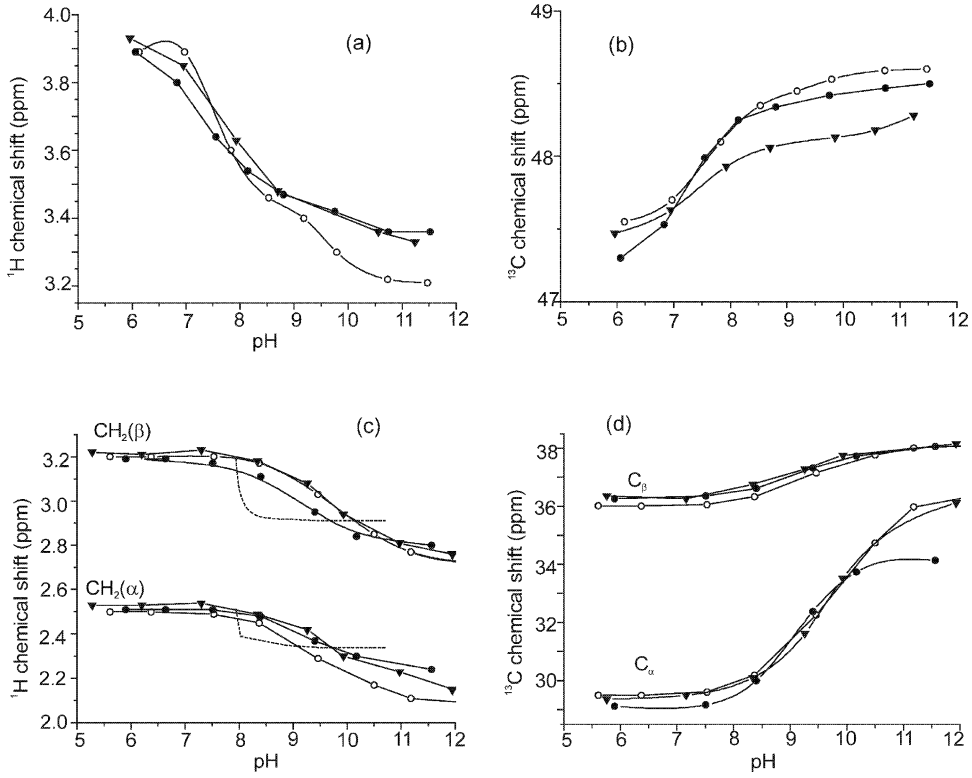


Fig. 8. ^{1}H and ^{13}C chemical shifts for $C_\alpha H$ (a) C_α (b) of α-Alaha and $CH_2(\alpha)$, $CH_2(\beta)$ (c), C_α, C_β (d) of β-Alaha as a function of pH:free ligand (○) and Zn^{II}–dien-hydroximate 1:1:1 (●), Zn^{II}–trien-hydroxamate 1:1:1 (▼) ternary solutions. The assignments for C, CH and CH_2 are consistent with those in Scheme 1. For comparison the ^{1}H NMR titration curves for the major peaks of the Zn^{II}–β-Alaha 1:1 solutions, $c_L = 2 \times 10^{-2}$ M (dashed lines).

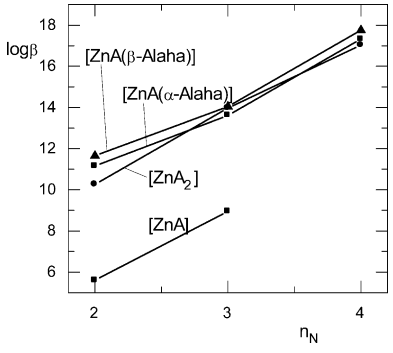


Fig. 9. Plot of log $\beta_{[ZnA(\beta\text{-Alaha})]}$ as a function of log $\beta_{[ZnA(\alpha\text{-Alaha})]}$.

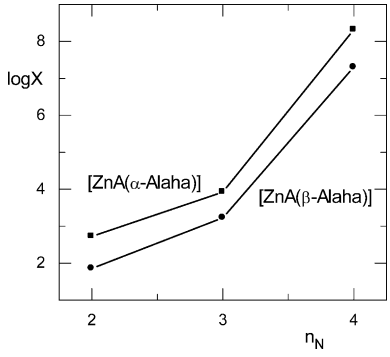


Fig. 11. Plot of log X as a function of number of nitrogen donors in polyamine.

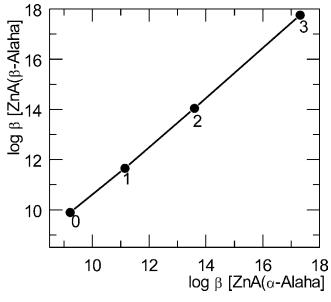


Fig. 10. Plot of log β_{ZnAL} as a function of a number of nitrogen donors in polyamine.

carbons of polyamines between the simple Zn^{II}–polyamine and mixed-ligand complexes (Figs. 9–11).

4. Conclusion

A comparison of the stability constants of the mixed-ligand complexes obtained from the studied ternary systems: Zn^{II}–en–α-Alaha/β-Alaha [33,34], Zn^{II}–dien–α-Alaha/β-Alaha and Zn^{II}–trien–α-Alaha/β-Alaha reveals that the stability constants of mixed-ligand species

with α-Alaha are lower than those with β-Alaha. This can probably be explained by the higher basicity of the hydroxamic oxygen of β-Alaha. There is a strong evidence from our pH-metric and NMR results that two oxygen donors of the aminohydroxamic anion are involved in the zinc(II) co-ordination sphere. Besides, we found a linear correlation between stability constants of the mixed-ligand complexes. Plot of log $\beta_{[ZnA(\beta\text{-Alaha})]}$ as a function of log $\beta_{[ZnA(\alpha\text{-Alaha})]}$ (A = en, dien or trien) is presented in Fig. 9. Taking into account that 'A' represents polyamine that forms a very stable complex and aminohydroxamic anions are compounds of the same type this plot, to a first approximation, can be interpreted as reflecting the same type of co-ordination in these complexes.

Plotting log β of the mixed-ligand species as a function of the number of nitrogen donors in polyamine (Fig. 10) we found that the correlation between these two parameters is a function of the number of the co-ordinated nitrogens in the mixed-ligand species. As the log K values of [ZnA_2] and [ZnAL] are very close, one can conclude that sterical hindrance is the major factor, which determinates a formation of the mixed-ligand complexes. Accordingly, the smaller α- or β-Alaha are bound preferentially over second dien or trien to form the mixed-ligand [ZnAL] species. Plot of log X as a function of a number of nitrogen donors in polyamines (Fig. 11) shows that the formation of mixed complexes is more favoured if polyamine has more nitrogen donors.

References

[1] B. Kurzak, D. Kroczewska, J. Jezierska, Polyhedron 17 (1998) 1831.
[2] B. Kurzak, K. Bogusz, D. Kroczewska, J. Jezierska, Polyhedron 20 (2001) 2627.
[3] E. Kimura, T. Koike, M. Shionoya, in: H.A.O. Hill, P.J. Sadler, A.J. Thomson (Eds.), Metal Sites in Proteins and Models. Phosphatases, Lewis Acids and Vanadium, vol. 89, Springer, Berlin, 1997, p. 1.
[4] T. Koike, M. Inoue, E. Kimura, M. Shiro, J. Am. Chem. Soc. 118 (1996) 3091.
[5] T. Koike, S. Kajitani, I. Nakamura, E. Kimura, M. Shiro, J. Am. Chem. Soc. 117 (1995) 1210.
[6] E. Kimura, Pure Appl. Chem. 65 (1993) 355.
[7] E. Kimura, T. Koike, T. Shiota, Y. Iitaka, Inorg. Chem. 29 (1990) 4622.
[8] X. Zhang, R. Van Eldick, Inorg. Chem. 34 (1995) 5606.
[9] E. Kimura, in: K.K. Karlin (Ed.), Progress in Inorganic Chemistry, vol. 41, Wiley, 1994, p. 443.
[10] E. Kimura, I. Nakamara, T. Koike, M. Shionoya, Y. Kodama, T. Ikeda, M. Shiro, J. Am. Chem. Soc. 116 (1994) 4764.
[11] E. Kimura, M. Shionoya, A. Hoshino, T. Ikeda, Y. Yamada, J. Am. Chem. Soc. 114 (1992) 10134.
[12] B. Kurzak, H. Kozłowski, E. Farkas, Coord. Chem. Rev. 114 (1992) 169.
[13] E. Farkas, E. Kozma, T. Kiss, I. Toth, B. Kurzak, J. Chem. Soc., Dalton Trans. (1995) 477.
[14] B. Kurzak, E. Farkas, J. Coord. Chem. 28 (1993) 203.
[15] B. Kurzak, E. Farkas, T. Glowiak, H. Kozłowski, J. Chem. Soc., Dalton Trans. (1991) 163.
[16] T. Glowiak, B. Kurzak, J. Crystallogr. Spectr. Res. 22 (1992) 341.
[17] B. Kurzak, J. Spychała, J. Świątek, J. Coord. Chem. 25 (1992) 95.
[18] B. Kurzak, K. Kurzak, J. Jezierska, Inorg. Chim. Acta 125 (1986) 77.
[19] G. Gran, Acta Chem. Scand. 4 (1950) 599.
[20] B. Kurzak, H. Kozłowski, P. Decock, J. Inorg. Biochem. 41 (1991) 71.
[21] Stability Constants of Metal-ion complexes: Part B. Organic ligands, IUPAC Chemical Data Series, No 22, compiled by D.D. Perrin, Pergamon, Oxford, Wheaton & Co Ltd., Exeter, 1983.
[22] P. Gans, A. Sabatini, A. Vacca, J. Chem. Soc., Dalton Trans. (1985) 1195.
[23] S.P. Dagnall, D.N. Hague, M.E. McAdams, J. Chem. Soc. Perkin Trans. 2 (1984) 435.
[24] H. Sigel, Metal Ions in Biological Systems, vol. 2, Marcel Dekker, New York, 1973.
[25] (a) H. Sigel, Angew. Chem., Int. Ed. Engl. 87 (1975) 391;
(b) H. Sigel, Angew. Chem., Int. Ed. Engl. 14 (1975) 394.
[26] C.O.B. de Miranda-Pinto, E.B. Paniago, S. Carvalho, A.M. Tabak, Y.P. Mascarenhas, Inorg. Chim. Acta 137 (1987) 145.
[27] T.T. Pakkanen, T.A. Pakkanen, K. Smolander, D.A. Brown, W.K. Glass, A.L. Roche, J. Mol. Struct. 162 (1987) 313.
[28] M. Julien-Pouzon, S. Jaulmes, P. Laruelle, S. Carvalho, E.D. Paniago, Acta Crystallogr., Sect. C 41 (1985) 712.
[29] E. Farkas, H. Csóka, G. Bell, D.A. Brown, L.P. Cuffe, N.J. Fitzpatrick, W.K. Glass, W. Errington, T.J. Kemp, J. Chem. Soc., Dalton Trans. (1999) 2789.
[30] D.N. Hague, A.D. Moreton, J. Chem. Soc., Dalton Trans. (1987) 2889.
[31] (a) S.P. Dagnall, D.N. Hague, A.D. Moreton, J. Chem. Soc., Dalton Trans. (1986) 1499;
(b) S.P. Dagnall, D.N. Hague, A.D. Moreton, J. Chem. Soc., Dalton Trans. (1987) 2897;
(c) S.P. Dagnall, D.N. Hague, A.D. Moreton, J. Chem. Soc., Dalton Trans. (1988) 1989.
[32] D.N. Hague, A.D. Moreton, J. Chem. Soc., Dalton Trans. (1989) 1171.
[33] B. Kurzak, D. Kroczewska, J. Coord. Chem. 34 (1995) 67.
[34] B. Kurzak, D. Kroczewska, Transit. Metal Chem. 18 (1993) 295.

vides the first example of a dien-bridged dinuclear complex.

2. Experimental

2.1. Materials and physical measurements

All the chemicals were purchased from Aldrich and used without further purification. Microanalyses were performed by Perkin–Elmer 2400II elemental analyzer and CE instruments. IR spectra (4000–400 cm^{-1}) were recorded from KBr disks with a Nicolet Magna-IR spectrophotometer (Series II), UV–Vis spectra on a Shimadzu UV-160A spectrophotometer, ^1H NMR and ^{13}C NMR spectra by a Bruker DPX200 spectrometer. FAB mass spectra (3-nitrobenzyl alcohol as a matrix in DMF as solvent) were carried out on a VG Autospec M-250 instrument. Cyclic voltammetry was performed at a planar EG&G PARC G0229 glassy carbon milli electrode using EG&G PARC electrochemical analysis system (model 250/5/0) in purified and anhydrous DMF under dry nitrogen atmosphere in conventional three electrode configurations. Under the experimental conditions employed here and scan rate of 50 mV s^{-1}, the reference ferrocene–ferrocenium couple appears at 0.468 V versus SCE with ΔE_p of 114 mV.

2.2. Preparations

2.2.1. $[Hg_2(dien)_3](ClO_4)_4$ (1)

Pulverized $Hg(CH_3COO)_2$ (0.320 g, 1 mmol) was dissolved in 50 ml of 80% ethanol. To this solution 0.11 ml (1 mmol) of dien was added drop-wise with constant stirring. The colorless reaction mixture was stirred at room temperature (r.t.) for 1 h, after which it was filtered. To the filtrate, 0.146 g (1.2 mmol) of sodium perchlorate dissolved in 5 ml of water was added drop-wise with constant stirring. This reaction mixture was left in the air for 3 days. Colorless crystals suitable for X-ray analysis were deposited. Then, they were filtered, washed with few drops of 80% ethanol and dried in air. Yield: 0.185 g, 33%. ^1H NMR (200 MHz, $(CD_3)_2SO$, TMS): δ_H: 2.64 (d, methylene protons). ^{13}C NMR (200 MHz, $(CD_3)_2SO$, TMS): δ 47.8. Main IR bands (KBr, ν, cm^{-1}): 3323(vs), 3255(s), 2930(m), 2880(m), 1570(s), 1490(s), 1435(m), 1147(vs), 1114(vs), 1090(vs), 627(s, split). *Anal.* Found: C, 12.83; H, 3.64; N, 11.32. Calc. for $C_{12}H_{39}N_9O_{16}Cl_4Hg_2$: C, 12.99; H, 3.55; N, 11.37%.

2.2.2. $[Hg(dien)(H_2O)](PF_6)_2$ (2)

This compound was prepared by a procedure exactly the same as used for **1**, by reacting 0.320 g (1 mmol) of pulverized $Hg(CH_3COO)_2$ and 0.11 ml (1 mmol) of dien in 50 ml of 80% ethanol, and then adding 5 ml water solution of 0.200 g (1.2 mmol) of sodium hexafluorophosphate. Colorless crystals suitable for X-ray analysis were obtained by keeping the reaction mixture in air for 4 days. They were filtered out, washed with few drops of 80% ethanol and dried in air. Yield: 0.330 g, 54%. ^1H NMR (200 MHz, $(CD_3)_2SO$, TMS): δ_H: 2.66 (d, methylene protons). ^{13}C NMR (200 MHz, $(CD_3)_2SO$, TMS): δ 46.7. Main IR bands (KBr, ν, cm^{-1}): 3323(vs), 3256(vs), 3145 (w), 2927(m), 2880(m), 1579 (vs), 1434(s, split), 1129(s), 1060(s), 835(vs), 561(vs). *Anal*. Found: C, 7.96; H, 3.38; N, 6.82. Calc. for $C_4H_{15}N_3OP_2F_{12}Hg$: C, 7.85; H, 2.47; N, 6.87%.

Caution! Perchlorate salts with organic ligands are potentially explosive and mercury salts are expected to be toxic. These materials should be handled with the necessary precautions.

2.3. Crystallography

The X-ray diffraction measurements were carried out at approximately 110 K on a Nonius KappaCCD diffractometer, using Mo Kα ($\lambda = 0.7107$ Å) radiation and 1.0° ϕ scans. The intensity data were integrated and scaled by the programs DENZO-SMN and SCALEPACK [14]. The analyzed crystals were coated with a layer of hydrocarbon oil (in order to avoid deterioration) and mounted on a glass fiber. The intensity data were corrected empirically for absorption effects. The structures were solved by Patterson and Fourier methods (DIRDIF-96, [15]), and refined by full-matrix least-squares based on F^2 for all reflections (SHELXL-97, [16]). All non-hydrogen atoms were refined with anisotropic displacement parameters. The hydrogen atoms were located in calculated positions to correspond to standard bond lengths and angles, and were included in the refinement with isotropic displacement parameters using a riding model. The crystal and experimental data are summarized in Table 1. The two compounds crystallized in non-centrosymmetric space groups (as confirmed by the corresponding intensity statistics and structure solution) as racemic twins. Furthermore, in structure **2** there are two mirror-related $[Hg(H_2O)(dien)]$ molecules in the asymmetric unit. One of the perchlorates in **1** is rotationally disordered.

3. Results and discussion

3.1. Syntheses and spectral characterization

The nuclearity of the product (P) in reaction (1) between $Hg(CH_3COO)_2$ and dien in the presence of NaX ($X^- = ClO_4^-$ and PF_6^-) in 80% of EtOH, appears to depend on the nature of the anion. When X^- is ClO_4^-, the product is a dimer, bridged by one dien, while when X^- is PF_6^- the product is only a monomer

Table 1
Crystal and experimental data for **1** and **2**

	1	**2**
Formula	$C_{12}H_{39}Hg_2N_9\cdot(ClO_4)_4$	$C_4H_{15}HgN_3O\cdot(PF_6)_2$
Formula weight	1108.50	611.72
Habit	prisms	prisms
Color	colorless	colorless
Temperature (K)	110(2)	110(2)
Radiation	Mo Kα	Mo Kα
Crystal size (mm)	0.30 × 0.20 × 0.20	0.25 × 0.20 × 0.20
Crystal system	orthorhombic	orthorhombic
Space group	$Pna2_1$	$P2_12_12_1$
a (Å)	29.1720 (10)	10.1860 (2)
b (Å)	13.5900 (3)	11.8410 (2)
c (Å)	7.9030 (2)	25.203 (5)
V (Å^3)	3133.1 (4)	3039.8 (1)
Z	4	8
D_{calc} (g cm^{-3})	2.350	2.673
$F(000)$	2120	2288
μ (mm^{-1})	10.21	10.47
2θ Range (°)	2.6–50.7	2.1–50.7
Number of unique reflections	2927	3143
hkl Limits	0, 35/0, 16/0, 8	0, 12/0, 14/0, 30
Number of variables	392	418
Number of reflections with $[I > 2\sigma(I)]$	2705	2364
Flack parameter	0.58 (3)	0.46 (1)
Final R indices [a] $[I > 2\sigma(I)]$/ all data		
R_1	0.034/0.039	0.029/0.045
wR_2	0.080/0.083	0.072/0.079
$\|\Delta\rho\|$ (e Å^{-3})	≤ 1.2	≤ 0.75, except for one strong diffraction ripple of 2.9 e Å^{-3} near each Hg
Goodness-of-fit	1.00	1.05

[a] $R_1 = \Sigma\ ||F_o|-|F_c||/\Sigma\ |F_o|$. $wR_2 = \{\Sigma[w(F_o^2-F_c^2)^2]/\Sigma[w(F_o^2)^2]\}^{1/2}$.

(comfirmed by elemental analysis, FAB mass spectra and X-ray crystal structure). In both cases the acetate residues are excluded from the resulting complexes. This phenomena is an example of 'unproliferating effect' exerted by larger non-coordinating anion [17,3i]. The volumes of ClO_4^- and PF_6^- are 51.3 and 69.7 Å^3, respectively [17]. When the anion is smaller the product is a dimer, but when the anion is larger, the product is only a monomer.

$$Hg(CH_3COO)_2 + Dien + NaX \xrightarrow[80\%\ \ EtOH]{1:1:1.2} Product\ (P) \quad (1)$$

The solution behavior of complexes **1** and **2** was analyzed by fast atom bombardment mass spectrometry (FAB MS) and cyclic voltammetry. From FAB MS of **1**, it is clear that the dimeric structure of **1** is preserved in solution too. Its FAB MS is little bit complicated but still informative, indicating successive loss of ClO_4^- and dien fragment. The peaks at $m/z = 1009.0$, 909.5, 810, 710.5 and 607.5 could be assigned as (**1**–ClO_4), (**1**–$2ClO_4$), (**1**–$3ClO_4$), (**1**–$4ClO_4$) and [**1**–($4ClO_4$ + $C_4H_{13}N_3$)], respectively. FAB MS of **2** displays three characteristic peaks at $m/z = 467.0$ (**2**–PF_6), 322.1 (**2**–$2PF_6$) and 304.1 [**2**–($2PF_6 + H_2O$)], respectively. The complexes **1** and **2** do not show any absorption in their electronic spectra in the 900–200 nm region.

In the NMR spectra of **1**, $(CD_3)_2SO$, all the methylene protons appear at, 2.64 ppm, and all the methylene carbons are also characterized by the same chemical shift of 47.8 ppm. In **2**, these protons appear at 2.66 ppm, and the carbon atoms at 46.7 ppm. The NH protons of the two compounds could not be observed.

There are only slight differences between the IR spectra of **1** and **2**, when the characteristic bands due to the anions are not taken into account. In the IR spectra of **1**, the peaks at 3323 and 3255 cm^{-1} may be attributed to ν(N–H) vibrations. Then, the sharp peak at 1570 cm^{-1} is due the $\delta(NH_2)$ bending vibration [13], two close peaks at 2930 and 2880 cm^{-1} are due to the ν(C–H) vibrations [18], and three very well resolved and strong bands at 1147, 1114 and 1090 cm^{-1} along with a very strong doublet at 627 cm^{-1} were assigned to the non-coordinated $\nu(ClO_4^-)$ vibrations in a distorted geometry [19]. For the complex **2**, the ν(N–H) vibrations appear at 3323 and 3256 cm^{-1}, the ν(C–H) vibrations appear at 2927 and 2880 cm^{-1}, and $\delta(NH_2)$ bending vibration appears at 1579 cm^{-1}. The non-coordinated $\nu(PF_6^-)$ vibrations appear at 1060, 835 and 561 cm^{-1} [20].

3.2. Cyclic voltammetry

The electrochemical behavior of the complexes **1** and **2** has been examined by cyclic voltammetry in DMF (0.1 M tetraethyl ammonium perchlorate as supporting electrolyte) under dry N_2 atmosphere at a glassy carbon electrode in the voltage range −0.5 to 0.7 V versus SCE. For both complexes, somewhat irreversible cyclic responses are obtained. Complexes **1** and **2** show Hg(II)–Hg(III) couple with half-wave potential ($E_{1/2}$) of 0.030 and 0.026 V versus SCE with ΔE_p, 0.400 and 0.410 V at a scan rate of 50 mV s^{-1} (Fig. 1).

3.3. Structural description

The molecular structures of **1** and **2** are illustrated in Figs. 2 and 3, respectively. Selected structural parameters are summarized in Table 2. All the nitrogen coordinate to the Hg ions (within Hg–N = 2.2–2.4 Å) in the two structures. The N–Hg–N angles of five-membered chelate ring formed by the tridentate dien ligand are less than 90° due to the inherent geometric constraints in this ligand. All the N–C–C–N conformations are gauche to facilitate of the N-sites to the metal

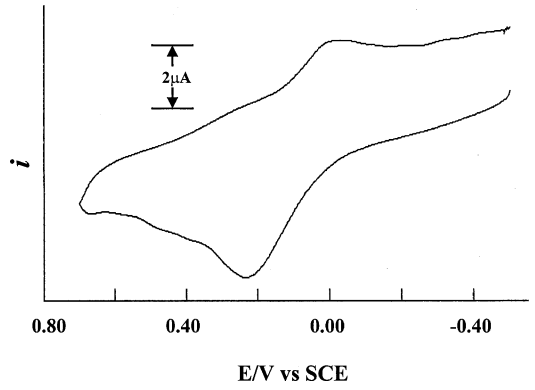


Fig. 1. The cyclic voltammogram of **1** in DMF (0.1 M in tetra-ethylammonium perchlorate) at a glassy electrode (scan rate = 50 mV s^{-1}).

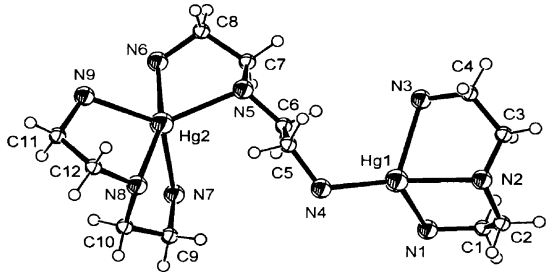


Fig. 2. Perspective view of the molecular structure of oligomer **1**, in which one of the dien species coordinates to two different mercury ions, showing the atom labeling scheme. Hydrogen atoms on N and the perchlorate anions are omitted for clarity.

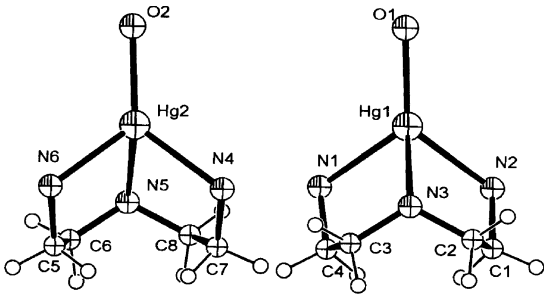


Fig. 3. The two crystallographically independent [Hg(dien)(H_2O)] complexes in structure **2**, showing the atom labeling scheme. Hydrogen atoms on N and O and the PF_6 anions are omitted for clarity.

ions, with the exception of the N4–C5–C6–N5 torsion angle in the conformationally stretched bridging ligand in **1**, which is anti (Table 2). Noteworthy also is the unusual penta Hg–N coordination around Hg2 in **1**, as opposed to the more common tetrahedral coordination environment in other parts of the two structures. The perchlorate and hexa-fluorophosphate anions are not bonded to the Hg atoms.

Table 2
Selected bond lengths (Å), bond angles (°) and torsion angles (°)

*Compound **1***	
Bond lengths	
Hg1–N1	2.285(13)
Hg1–N2	2.319(12)
Hg1–N3	2.379(13)
Hg1–N4	2.174(10)
Hg2–N5	2.353(10)
Hg2–N6	2.388(12)
Hg2–N7	2.336(11)
Hg2–N8	2.371(9)
Hg2–N9	2.336(10)
Bond angles	
N1–Hg1–N2	78.2(5)
N1–Hg1–N3	108.5(5)
N2–Hg1–N3	76.2(4)
N1–Hg1–N4	123.9(5)
N2–Hg1–N4	145.2(5)
N3–Hg1–N4	114.5(4)
N5–Hg2–N6	76.5(4)
N5–Hg2–N7	102.5(4)
N5–Hg2–N8	121.7(4)
N5–Hg2–N9	131.8(4)
N6–Hg2–N7	104.8(4)
N6–Hg2–N8	161.3(4)
N6–Hg2–N9	89.0(4)
N7–Hg2–N8	76.7(4)
N7–Hg2–N9	125.6(4)
N8–Hg2–N9	75.6(4)
N1–C1–C2–N2	−57.4(17)
N2–C3–C4–N3	−56.0(20)
N4–C5–C6–N5	168.4(11)
N5–C7–C8–N6	−65.0(15)
N7–C9–C10–N8	−65.7(16)
N9–C11–C12–N8	−54.7(19)
*Compound **2***	
Bond lengths	
Hg1–N1	2.310(5)
Hg1–N2	2.310(5)
Hg1–N3	2.350(5)
Hg1–O1	2.141(5)
Hg2–N4	2.318(6)
Hg2–N5	2.363(5)
Hg2–N6	2.294(6)
Hg2–O2	2.141(5)
Bond angles	
N1–Hg1–N2	99.3(2)
N1–Hg1–N3	77.4(2)
N2–Hg1–N3	77.1(1)
O1–Hg1–N1	124.6(2)
O2–Hg2–N4	128.7(2)
O2–Hg2–N5	133.0(2)
N4–Hg2–N5	77.2(2)
N4–Hg2–N6	99.0(2)
N5–Hg2–N6	77.3(2)
O1–Hg1–N2	128.0(2)
O1–Hg1–N3	133.8(2)
O2–Hg2–N6	124.6(2)
N1–C3–C4–N3	−52.9(8)
N2–C1–C2–N3	53.2(8)
N4–C7–C8–N5	−54.2(8)
N5–C6–C5–N6	53.0(8)

4. Supplementary material

Crystallographic data for the structural analysis have been deposited with the Cambridge Crystallographic Data Centre, CCDC Nos. 185110 (**1**) and 185111 (**2**). Copies of this information may be obtained free of charge from The Director, CCDC, 12 Union Road, Cambridge, CB2 1EZ, UK (fax: +44-1223-336033; e-mail: deposit@ccdc.cam.ac.uk or www: http://www.ccdc.cam.ac.uk).

Acknowledgements

The authors thank the Israeli Science Foundation for their support for this work.

References

[1] M. Ciampolini, N. Nardi, G.P. Speroni, Coord. Chem. Rev. 1 (1966) 222.
[2] Z. Dori, R. Eisenberg, H.B. Gray, Inorg. Chem. 6 (1967) 483.
[3] (a) N.F. Curtis, H.K.J. Powell, J. Chem. Soc. A (1968) 3069.;
(b) F.S. Stephens, J. Chem. Soc. A (1969) 883.;
(c) F.S. Stephens, J. Chem. Soc. A (1969) 2233.;
(d) G. Nardin, L. Randaccio, G. Annibale, G. Natile, B. Pitteri, J. Chem. Soc., Dalton Trans. (1980) 220.;
(e) D.A. House, V. Mckee, W.T. Robinson, Inorg. Chim. Acta 157 (1989) 15;
(f) R.M. Chin, J. Barrera, R.H. Dubois, L.E. Helberg, M. Sabat, T.Y. Bartucz, A.J. Lough, R.H. Morris, W.D. Harman, Inorg. Chem. 36 (1997) 3553;
(g) C. Meiser, B. Song, E. Freisinger, M. Peilert, H. Sigel, B. Lippert, Chem. Eur. J. 3 (1997) 388;
(h) L. Ballester, A. Gutierrez, M.F. Perpinan, U. Amador, M.T. Azcondo, A.E. Sanchez, C. Bellitto, Inorg. Chem. 36 (1997) 6390;
(i) G.K. Patra, G. Mostafa, M.G.B. Drew, D. Datta, Cryst. Eng. Commun. (2000) 19.
[4] F. Miller, J. Simplicio, R. Wilkins, J. Am. Chem. Soc. 91 (1969) 1962.
[5] D.C. Bebout, D.E. Ehmann, J.C. Trinidad, K.K. Crahan, M.E. Kastner, D.A. Parrish, Inorg. Chem. 36 (1997) 4257.
[6] F.A. Cotton, G. Wilkinson, Advanced Inorganic Chemistry, fifth ed., Wiley, New York, 1998.
[7] (a) N.L. Brown, Trends Biol. Sci. (1985) 400.;
(b) R.A. Steele, S.J. Opella, Biochemistry 36 (1997) 6885;
(c) G. Veglia, F. Porcelli, T. Desilva, A. Prantner, S.J. Opella, J. Am. Chem. Soc. 122 (2000) 2389.
[8] M.J. Stillman, C.F. Shaw, III, K.T. Suzuki (Eds.), Metallothioneins, VCH Publishers, New York, 1992.
[9] Z. Kyklenyik, L.G. Marzilli, Inorg. Chem. 35 (1996) 5654.
[10] B.V. Chessman, A.P. Arnold, D.L. Rabenstein, J. Am. Chem. Soc. 110 (1988) 6359.
[11] R.C. Mehrotra, R. Bhora, Metal Carboxylates, Academic Press, London, 1983.
[12] J. Yau, D.M.P. Mingos, S. Menzer, D.J. Willams, J. Chem. Soc., Dalton Trans. (1995) 2575.
[13] E.C. Plappert, D.M.P. Mingos, S.E. Lawrence, D.J. Willams, J. Chem. Soc., Dalton Trans. (1997) 2119.
[14] Z. Otwinowski, W. Minor, SCALEPACK, Nonius B.V., The Netherlands, 1998. Methods Enzymol. 276 (1996) 307.
[15] P.T. Beurskens, G. Admiraal, G. Beurskens, W.P. Bosman, S. Garcia-Granda, R.O. Gould, J.M.M. Smits, C. Smykalla, The DIRDIF-96 Program System. Technical Report of the Crystallography Laboratory, University of Nijmegen, The Netherlands, 1996.
[16] G.M. Sheldrick, SHELXL-97. Program for the Refinement of Crystal Structures from Diffraction Data, University of Göttingen, Germany, 1997.
[17] G.K. Patra, G. Mostafa, D.A. Tocher, D. Datta, Inorg. Chem. Commun. 3 (2000) 56.
[18] C.A. Johns, K.M.A. Malik, Polyhedron 21 (2002) 395.
[19] K. Nakamato, Infrared and Raman Spectra of Inorganic and Coordination Compounds, fourth ed., Sect. II, 8, Wiley, New York, 1986.
[20] F. Wagner, M.T. Mocella, M.J. D'Aneillo, A.H.K. Wang, E.K. Barefield, J. Am. Chem. Soc. 96 (1974) 2625.

trans configuration with respect to terminal bonds, an argument that seems to be based on the fact that individual *trans*-to-*oxo* bonds in polyanions are considerably weaker than *cis*-to-*oxo* (bridging) bonds.

In a recent comparative investigation of W complexes and polyanions containing tri-*oxo* groups [32], we have found that the fact that these species are rarely observed does not appear to be a direct consequence of the individually weak *trans*-to-*oxo* bonds. Valency and bonding-energy analyses have indicated that the bonding capacity of the high-coordinate bridging centres can be similar to that of the unshared terminal sites. This article is focused on the chemical bonding in the isolated $[W_4O_{16}]^{8-}$ anions, and contains a detailed description of the electronic structures of the T_d and C_{2h} forms, which reveals that closed-loop orbital interactions are possible in these polyanions.

2. Computational approach

All density–functional calculations reported in this work were performed with the ADF (2000.02) [33–37] program. Functionals based on the Vosko–Wilk–Nusair (VWN) [38] form of the local density approximation (LDA) [39], and on a combination (labelled BP86) of Becke's 1988 exchange [40] and Perdew's 1986 correlation [41] corrections to the LDA were employed. Slater-type-orbital (STO) basis sets of triple-zeta quality incorporating frozen cores and the ZORA relativistic approach (ADF O.1s and W.4f type IV) [37] were utilised.

The functional and basis-set choices were based on the results of tests performed on several $[MO_4]$ and $[M_2O_7]$ species [42,43]. Geometry optimisations were carried out using LDA methods, whereas data on thermochemistry and energetics were extracted from single-point BP86 calculations. Graphics of molecular orbitals were generated with the MOLEKEL [44] program.

3. Results and discussion

Structural and atom-labelling schemes for the $[W_4O_{16}]^{8-}$ isomers are shown in Fig. 1. In the T_d form there are two types of oxygen sites, terminal (O_t) and three-coordinate bridging (O_b) atoms. The C_{2h} form contains a mixture of *cis* di-*oxo* (W2–O_t) and tri-*oxo* (W3–O_t) terminal moieties, and two classes of bridging sites, the two-coordinate O2 and the three-coordinate O3 atoms. A detailed report of calculated structural and bonding parameters for the T_d and C_{2h} isomers, and a comparison with experimental results have been presented in a previous publications [32]. A summary of computational W–O distances and bond orders is given in Table 1.

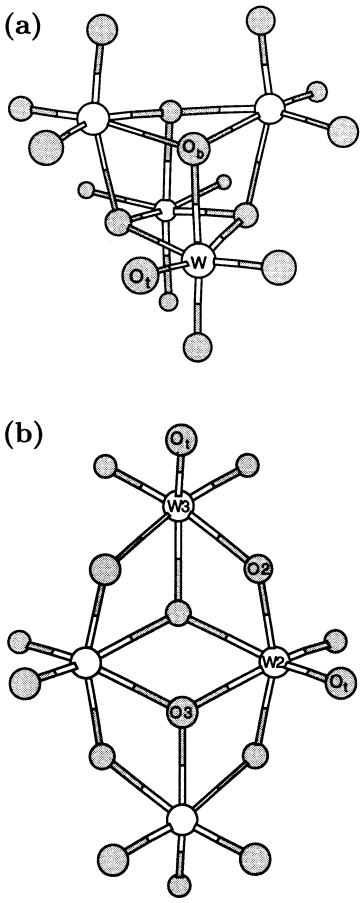


Fig. 1. Structural and atom-labelling schemes for (a) T_d and (b) C_{2h} isomers of $[W_4O_{16}]^{8-}$.

Table 1
Calculated W–O distances (in pm) and bond orders for the $[W_4O_{16}]^{8-}$ anions

Isomer	Parameter	Bond distance	Bond order
T_d	W–O_t	185	1.44
	W–O_b	223	0.47
C_{2h}	W2–O_t	185	1.43
	W3–O_t	188	1.38
	W2–O2	195	0.92
	W3–O2	214	0.52
	W2–O3	227	0.43
	W3–O3	219	0.52

3.1. Molecular-orbital description

Qualitative molecular-orbital schemes showing predominant metal and oxygen contributions to the valence levels of the T_d and C_{2h} isomers are given in Fig. 2. These diagrams are entirely qualitative in the sense that no accurate quantitative correlation exists amongst the

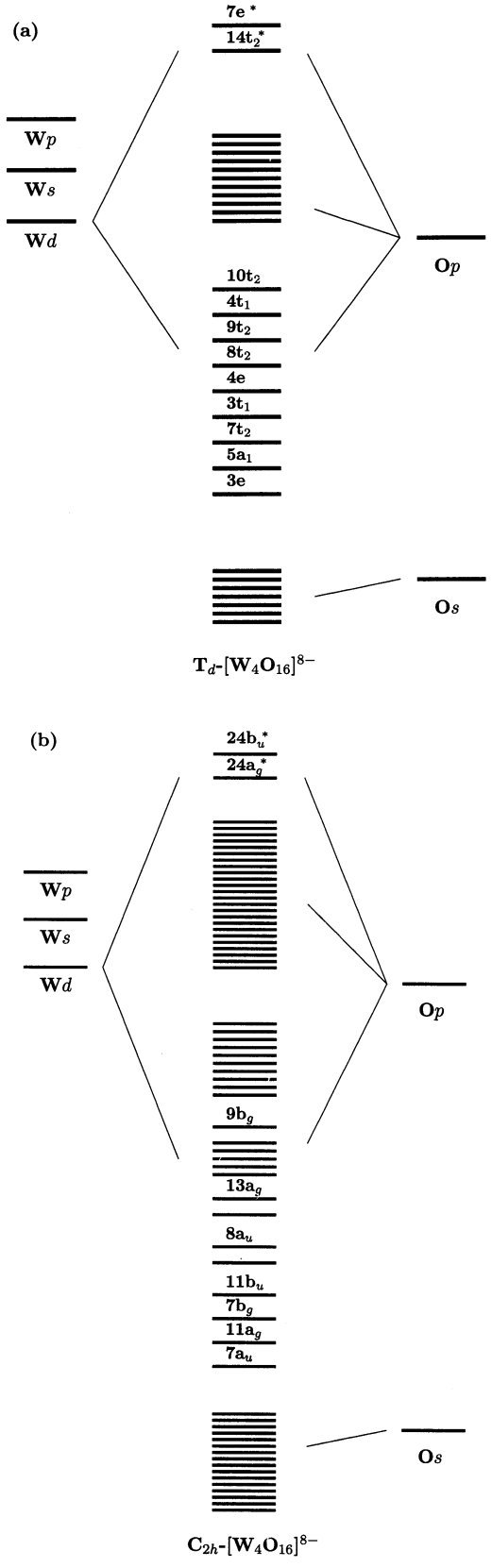


Fig. 2. Qualitative molecular-orbital schemes showing predominant W and O contributions to the valence levels of (a) T_d and (b) C_{2h} isomers of $[W_4O_{16}]^{8-}$.

positions of the atomic and molecular energy levels. They are intended to summarise the most general and representative characteristics of the electronic structure of the polyanions by highlighting the major atomic contributions to the molecular orbitals.

The schemes in Fig. 2 are characterised by the presence of two distinct sets of molecular energy levels, separated by a gap of approximately 10 eV. The low-lying orbitals comprise a predominantly nonbonding Os band. The high-lying set can be further divided into two bands. The higher-energy levels ('Op band') correspond to nonbonding combinations of Op-type functions, whereas the lower-energy levels ('Wd–Op band') are composed of orbitals that incorporate significant contributions from both the metal and oxygen atoms, and represent W–O bonding interactions of largely Wd–Op character.

All W–O bonding orbitals in the T_d form have been identified with their symmetry labels in the diagram of Fig. 2. The four lowest (3e, $5a_1$, $7t_2$, $3t_1$) levels incorporate both W–O_b and W–O_t interactions, but the remaining (higher) levels involve, primarily, W–O_t bonds. A similar pattern is observed in the C_{2h} form. All W–O bonding orbitals possess W–O_t character, but only the lower-lying levels incorporate substantial contributions from the various W–O2 and W–O3 interactions. Some of the highest-lying levels involve the relatively short W2–O2 bonds (in addition to W–O_t bonds).

It has been mentioned that Nomiya and Miwa have concluded that there are no closed loops in the T_d-$[W_4O_{16}]^{8-}$ anion. This is not supported by the present calculations. In this isomer, although all bridging-oxygen atoms occupy *trans*-to-*oxo* sites, they participate in the formation of delocalised bonds along $[W_2O_2]$ rings (representing the faces of the central $[WO_b]$ cube) that possess both σ and π character. Spatial plots (for the 3e orbitals) describing these multicentred bonding modes are shown in Fig. 3.

In C_{2h}-$[W_4O_{16}]^{8-}$, the bridging sites are in partial or total *trans* configuration with respect to the terminal bonds and, as in the T_d form, these oxygen atoms are involved in closed loops. An example of a $[W_2O_2]$ ring is given in Fig. 4, where the spatial plots of the σ and π components ($7b_g$ and $11b_u$ orbitals, respectively) of a four-membered loop comprising the W2 and O3 atoms are displayed.

In addition to $[W_2O_2]$ loops, eight-membered $[W_4O_4]$ rings are also found in the C_{2h} isomer. Spatial representations of σ and π interactions involving the W2 and W3 sites and all four O2 atoms are given in Fig. 5. These plots correspond to the $7a_u$, and $9b_g$ orbitals (and similar closed loops occur in the $11a_g$, $13a_g$, and $8a_u$, orbitals).

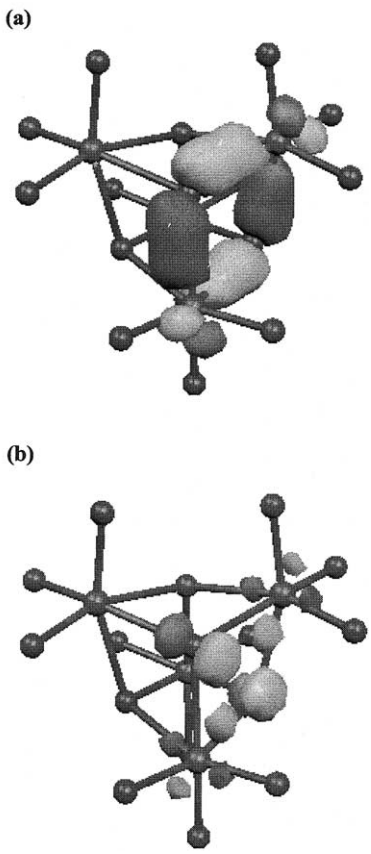


Fig. 3. Spatial molecular-orbital representation of (a) σ and (b) π $[W_2O_2]$ closed loops in the T_d-$[W_4O_{16}]^{8-}$ anion.

3.2. Bonding energetics

The molecular bonding energy (E_B) can be decomposed as:

$$E_B = E_O + E_P + E_E \quad (1)$$

where E_O, E_P, and E_E are, respectively, orbital-mixing, Pauli-repulsion, and electrostatic-interaction terms. Descriptions of the physical significance of these properties have been given by Landrum, Goldberg, and Hoffmann [45], and by Baerends and coworkers [37,46]. Both E_O and E_P represent orbital-interaction effects, but the former is stabilising whereas the latter is destabilising. The E_E contribution is primarily dominated by the nucleus-electron attractions and, therefore, has a stabilising influence.

Calculations on the $[W_4O_{16}]^{8-}$ anions, performed at the BP86 level of theory, indicate that the C_{2h} form is more stable than the T_d form by 223 kJ mol^{-1} (2.31 eV). Table 2 provides a summary of the contributions (to the individual bonding energies) associated with orbital-mixing, Pauli-repulsion, and electrostatic effects.

The orbital-mixing and electrostatic interactions are more favourable in the C_{2h} isomer, whereas Pauli repulsion is somewhat less destabilising in the T_d isomer. These results correlate with the W–O distances and

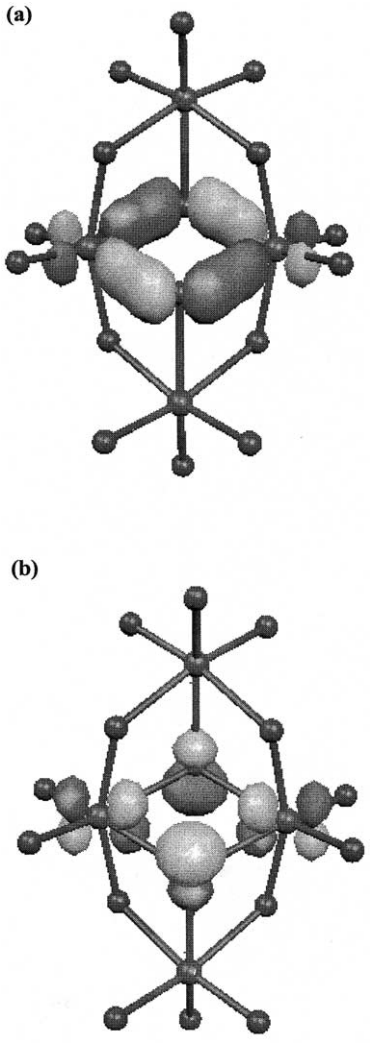


Fig. 4. Spatial molecular-orbital representation of (a) σ and (b) π $[W_2O_2]$ closed loops in the C_{2h}-$[W_4O_{16}]^{8-}$ anion.

indexes observed in the two $[W_4O_{16}]^{8-}$ anions. The terminal bonds show largely similar parameters, but the average bond lengths and orders of the bridging bonds suggest that, these are stronger in the C_{2h} (with respect to the T_d) form. The shorter distances and higher indexes of the W–O bridging interactions in C_{2h} $[W_4O_{16}]^{8-}$ should be associated with greater orbital and charge-distribution overlap, which can be related with the larger E_O, E_E, and E_P values obtained for this isomer [46].

The results of the present calculations are in agreement with some of the original ideas presented by Nomiya and Miwa [23], in the sense that the stabilising effects of orbital mixing are involved in making the C_{2h} isomer more stable than the T_d isomer. This is, however, not a general result. In the case of the α and β isomers of $[Mo_8O_{26}]^{4-}$ [47], the latter has a larger orbital-mixing contribution but a smaller total bonding energy than the former.

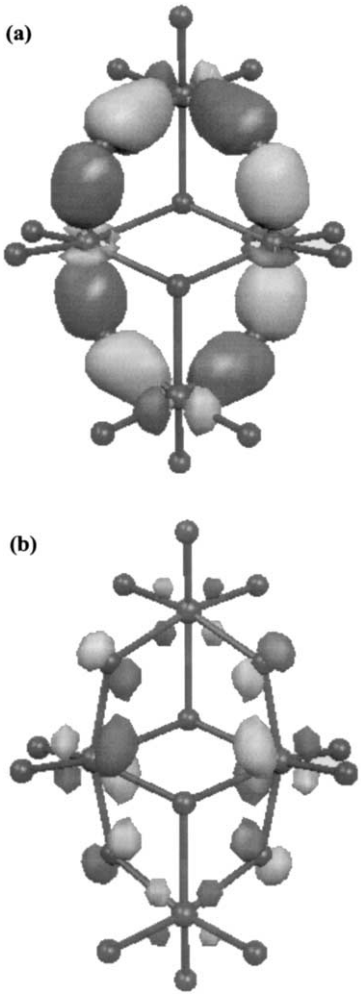


Fig. 5. Spatial molecular-orbital representation of (a) σ and (b) π $[W_4O_4]$ closed loops in the C_{2h}-$[W_4O_{16}]^{8-}$ anion.

Table 2
Orbital (E_O), Pauli (E_P), and electrostatic (E_E) contributions (in eV) to the bonding energy (E_B) of the T_d and C_{2h} isomers of $[W_4O_{16}]^{8-}$

Term	Isomer	
	T_d	C_{2h}
E_O	−273.98	−277.78
E_P	+297.49	+299.56
E_E	−110.61	−111.19
E_B	−87.10	−89.41

A fragment approach to the molecular structures of the polyanions can provide further insight into the relative effects of terminal and bridging W–O interactions on the bonding stability. In the present work, we have utilised the following decomposition scheme:

$$[W_4O_{15}]^{(6-)} + [O]^{(2-)} = [W_4O_{16}]^{(8-)} \quad (2)$$

for a comparison of all types of oxygen atoms in each $[W_4O_{16}]^{8-}$ isomer. The total molecular bonding energy relative to the fragments—described by Eq. (2)—is given by:

$$\Delta E_B = \Delta E_O + \Delta E_P + \Delta E_E \quad (3)$$

The results of the application of Eqs. (2) and (3) are shown in Table 3. It is observed that the orbital-mixing contributions from the various oxygen atoms are comparable despite the individual coordination environments and W–O interactions of the terminal and bridging sites being rather different. The *trans*-to-*oxo* configuration of the latter does not appear to lead to weaker overall bonding, neither does their participation in closed-loop delocalised interactions seem to generate a distinctively stronger contribution. The structural stability derived from the orbital interactions in the polyanions appears to be the result of the combined effect of all bonding modes involving the various oxygen types.

The molecular-orbital analysis has indicated that bonding to the metal atoms in the $[W_4O_{16}]^{8-}$ isomers is predominantly realised through participation of W d-type functions, the contributions from W s and p orbitals being minor or not significant. This phenomenon can be quantitatively characterised if the polyanions are described as:

$$4[W]^{(6+)} + 16[O]^{(2-)} = [W_4O_{16}]^{(8-)} \quad (4)$$

and calculations are carried out both with and without metal s and p valence orbitals. The relative effect of removing these orbitals can be measured as:

$$\delta(\Delta E_{B/O}) = \frac{\Delta E_{B/O}(d) - \Delta E_{B/O}(dsp)}{\Delta E_{B/O}(dsp)} \quad (5)$$

The results are summarised in Table 4 and support the general description of the W–O bonds as predominantly Wd–Op in character. The contributions from metal s and p orbitals are less that 1% if the total bonding energy is considered, and approximately 3% in the case of the orbital-mixing term.

4. Conclusion

The electronic structures of the T_d and C_{2h} isomers of $[W_4O_{16}]^{8-}$ have been calculated using density–

Table 3
Fragment analysis (ΔE_O in eV) for the isomers of $[W_4O_{16}]^{8-}$

Isomer	Atom	ΔE_O
T_d	O_t	−13.73
	O_b	−12.67
C_{2h}	O_t	−13.13
	O2	−13.72
	O3	−12.66

Results are based on Eq. (2).

Table 4
Changes (percentage) to the bonding (ΔE_B) and orbital-mixing (ΔE_O) energies caused by removal of metal s and p valence functions

Isomer	$\delta(\Delta E_B)$	$\delta(\Delta E_O)$
T_d	−0.5	−2.6
C_{2h}	−0.5	−2.5

Results are based on Eqs. (4) and (5).

functional methods, and analysed on the basis of molecular-orbital theory and bonding-energy approaches. In both anions, the W–O bonds have been found to be of predominantly Wd–Op character, and the greater stability (as isolated species) of the C_{2h} (with respect to the T_d) form has been observed to be, primarily, the consequence of somewhat stronger W–O orbital interactions.

As in the case of larger polyanions, some molecular orbitals are delocalised along closed loops, with $[W_2O_2]$ (T_d and C_{2h}) or $[W_4O_4]$ (C_{2h}) structures, which can involve all bridging sites. The results obtained from orbital and fragment analyses have suggested that these multicentred interactions are an important bonding mode and that bonding to the bridging-oxygen atoms should make a significant contribution to the stability of the $[W_4O_{16}]^{8-}$ clusters.

It should be noted that in the $[W_4O_{16}]^{8-}$ polyanions, as in the larger clusters, the presence of closed loops is not exclusively a consequence of the relatively high symmetry of these species. The calculations suggest that the (extensively) delocalised orbital interactions along the structural rings are possible due to the significant covalent character of metal–oxygen bridging bonds.

Acknowledgements

The authors would like to thank EPSRC, the Cambridge Overseas Trust, Selwyn College (Cambridge), and the University of Hull for financial support, and the Computational Chemistry Working Party for access to computational facilities in the Rutherford Appleton Laboratory.

References

[1] M.T. Pope, Heteropoly and Isopoly Oxometalates, Springer-Verlag, Heidelberg, 1983.
[2] M.T. Pope, A. Müller, Angew. Chem., Int. Ed. Engl. 30 (1991) 34.
[3] L.C.W. Baker, D.C. Glick, Chem. Rev. 98 (1998) 3.
[4] M.T. Pope, A. Müller (Eds.), Polyoxomeltalates: from Platonic Solids to Anti-retroviral Activity, Kluwer Academic Publishers, Dordrecht, 1994.
[5] K. Eguchi, T. Seiyama, N. Yamazoe, S. Katsuki, H. Taketa, J. Catal. 111 (1988) 336.
[6] H. Taketa, S. Katsuki, K. Eguchi, T. Seiyama, N. Yamazoe, J. Phys. Chem. 90 (1986) 2959.
[7] S.X. Xiao, J. Ji, T.L. Chen, T.X. Cai, G.S. Yan, Theochem. 63 (1990) 33.
[8] T.L. Chen, J. Ji, S.X. Xiao, T.X. Cai, G.S. Yan, Int. J. Quant. Chem. 44 (1992) 1015.
[9] T. Cai, Z.D. Chen, X.Z. Wang, L.M. Li, J.X. Lu, Prog. Nat. Sci. 7 (1997) 554.
[10] M.-M. Rohmer, R. Ernenwein, M. Ulmschneider, R. Wiest, M. Bénard, Int. J. Quant. Chem. 40 (1991) 723.
[11] J.Y. Kempf, M.-M. Rohmer, J.-M. Poblet, C. Bo, M. Bénard, J. Am. Chem. Soc. 114 (1992) 1136.
[12] M.-M. Rohmer, M. Bénard, J. Am. Chem. Soc. 116 (1994) 6959.
[13] J. Devémy, M.-M. Rohmer, M. Bénard, R. Ernenwein, Int. J. Quant. Chem. 58 (1996) 267.
[14] M.-M. Rohmer, J. Devémy, R. Wiest, M. Bénard, J. Am. Chem. Soc. 118 (1996) 13007.
[15] J.M. Maestre, J.P. Sarasa, C. Bo, J.M. Poblet, Inorg. Chem. 37 (1998) 3071.
[16] J.M. Maestre, J.M. Poblet, C. Bo, N. Casañ-Pustor, P. Gomez-Romero, Inorg. Chem. 37 (1998) 3444.
[17] A. Dolbecq, A. Guirauden, M. Fourmigué, K. Boubekeur, P. Batail, M.-M. Rohmer, M. Bénard, C. Coulon, M. Sallé, P. Blanchard, J. Chem. Soc., Dalton Trans. (1999) 1241.
[18] J.M. Maestre, X. López, C. Bo, J.M. Poblet, N. Casañ-Pastor, J. Am. Chem. Soc. 123 (2001) 3749.
[19] X. López, J.M. Maestre, C. Bo, J.-M. Poblet, J. Am. Chem. Soc. 123 (2001) 9571.
[20] J.M. Maestre, X. López, C. Bo, J.-M. Poblet, C. Daul, Inorg. Chem. 41 (2002) 1883.
[21] M.-M. Rohmer, M. Bénard, J.-P. Blaudeau, J.-M. Maestre, J.-M. Poblet, Coord. Chem. Rev. 178–180 (1998) 1019.
[22] H. Duclusaud, S.A. Borshch, J. Am. Chem. Soc. 123 (2001) 2825.
[23] K. Nomiya, M. Miwa, Polyhedron 3 (1984) 341.
[24] K. Nomiya, M. Miwa, Polyhedron 4 (1985) 89.
[25] K. Nomiya, M. Miwa, Polyhedron 4 (1985) 675.
[26] K. Nomiya, M. Miwa, Polyhedron 4 (1985) 1407.
[27] K. Nomiya, Polyhedron 6 (1987) 309.
[28] R.B. King, Inorg. Chem. 30 (1991) 4437.
[29] A. Hüllen, Ber. Bunsenges. Phys. Chem. 70 (1966) 598.
[30] P.M. Skarstad, S. Geller, Mater. Res. Bull. 10 (1975) 791.
[31] L.Y.Y. Chan, S. Geller, J. Solid State Chem. 21 (1977) 331.
[32] A.J. Bridgeman, G. Cavigliasso, Polyhedron 20 (2001) 3101.
[33] E.J. Baerends, D.E. Ellis, P. Ros, Chem. Phys. 2 (1973) 41.
[34] L. Versluis, T. Ziegler, J. Chem. Phys. 88 (1988) 322.
[35] G. te Velde, E.J. Baerends, J. Comput. Phys. 99 (1992) 84.
[36] C. Fonseca Guerra, J.G. Snijders, G. te Velde, E.J. Baerends, Theor. Chem. Acc. 99 (1998) 391.
[37] G. te Velde, F.M. Bickelhaupt, E.J. Baerends, C. Fonseca Guerra, S.J.A. van Gisbergen, J.G. Snijders, T. Ziegler, J. Comput. Chem. 22 (2001) 931.
[38] S.H. Vosko, L. Wilk, M. Nusair, Can. J. Phys. 58 (1980) 1200.
[39] W. Kohn, L.J. Sham, Phys. Rev. 140 (1965) A1133.
[40] A.D. Becke, Phys. Rev. A 38 (1988) 3098.
[41] J.P. Perdew, Phys. Rev. B 33 (1986) 8822.
[42] A.J. Bridgeman, G. Cavigliasso, Polyhedron 20 (2001) 2269.
[43] A.J. Bridgeman, G. Cavigliasso, J. Phys. Chem. A 105 (2001) 7111.
[44] S. Portmann, H.P. Lüthi, CHIMIA 54 (2000) 766.
[45] G.A. Landrum, N. Goldberg, R. Hoffmann, J. Chem. Soc., Dalton Trans. (1997) 3605.
[46] F.M. Bickelhaupt, E.J. Baerends, Rev. Comp. Chem. 15 (2000) 1.
[47] A.J. Bridgeman, G. Cavigliasso, J. Chem. Soc., Dalton Trans. (2002) 2244.

2. Experimental

2.1. Synthesis

Bis(triphenylarsine oxide)hydrogen(I) tetrachloroaurate(III), $[(Ph_3AsO)_2H][AuCl_4]$, and bis(pyridine *N*-oxide)hydrogen(I) tetrachloroaurate(III), $[(PyO)_2H][AuCl_4]$, were prepared by the slow evaporation of a solution containing the respective oxo-ligand and $HAuCl_4$ in a 2:1 molar ratio, according to [6,2], respectively. $DAuCl_4$ was obtained by dissolving Au_2O_3 in a DCl solution in D_2O and was used for the preparation of deuterated compounds. The extent of deuteration was not determined for the partially deuterated compounds except for $[(PyO)_2D][AuCl_4]$. In the following, we tentatively use the chemical formula with deuterium for the sake of convenience to distinguish the partially deuterated compound from the normal compound. $[Ph_3AsOD][AuCl_4]$ and $[PyOD][AuCl_4]$ were obtained accidentally using the oxo ligand and $DAuCl_4$ in a 2:1 molar ratio. For the synthesis of $[(PyO)_2D][AuCl_4]$ a large excess (ca. 2.5 equiv.) of the ligand was employed. A single crystal suitable for X-ray analysis was obtained by the slow evaporation of the solution of PyO and $DAuCl_4$ in a 5:1 molar ratio. $[PyOH][AuCl_4]$ was prepared from the solution of PyO and $HAuCl_4$ in a 1:2 molar ratio. This ratio was selected since $[(PyO)_{1.5}H][AuCl_4]$ had been obtained from the 1:1 solution.

$[(Ph_3AsO)_2H][AuCl_4]$ and $[(PyO)_2H][AuCl_4]$ were identified by comparing X-ray powder diffraction patterns with the expected ones from the reported crystal data [2,3]. Elemental analysis was made by Center for Organic Elemental Microanalysis, Kyoto University for the following compounds. *Anal*. Calc. for $[(Ph_3AsO)_2H][AuCl_4]$: C, 43.9; H, 3.2; Cl, 14.4. Found: C, 44.1; H, 3.4; Cl, 14.4%. Calc. for $[Ph_3AsOD][AuCl_4]$: C, 32.6; H/D, 2.6; Cl, 21.4. Found: C, 32.7; H/D, 2.6; Cl, 21.4%. Calc. for $[PyOH][AuCl_4]$: C, 13.8; H, 1.4; Cl, 32.6. Found: C, 13.8; H, 1.4; Cl, 32.4%. Calc. for $[(PyO)_2D][AuCl_4]$: C, 22.6; H/D, 2.3; Cl, 26.7; N, 5.3; O, 6.0. Found: C, 23.0; H/D, 2.3; Cl, 26.8; N, 5.3; O, 6.2%. Calc. for $[PyOD][AuCl_4]$: C, 13.8; H/D, 1.6; Cl, 32.5; N, 3.2; O, 3.7. Found: C, 13.7; H/D, 1.4; Cl, 32.3; N, 3.0; O, 3.5%. Calc. for $[(PyO)_{1.5}H][AuCl_4]$: C, 18.7; H, 1.8; Cl, 29.4. Found: C, 18.8; H, 1.7; Cl, 29.1%.

2.2. Physical measurements

A pulsed spectrometer based on the Matec gated amplifier 515A was used for the nuclear quadrupole resonance (NQR) measurements. The sample temperature was controlled using an electronic controller LakeShore 331 and measured with an accuracy of ± 0.5 K by use of gold +0.07% iron versus chromel thermocouple.

Powder diffraction experiments were performed using a Rigaku RINT 2100S diffractometer with Cu Kα radiation. Silicon powder was used as an internal standard of the diffraction angle.

IR spectra in the region 4000–400 cm^{-1} were recorded on a Bio-Rad FTS-7 FT IR spectrometer using KBr pellets.

For the ^2H NMR measurements of the solution, a JEOL JNM-EX270 NMR spectrometer was employed.

The density of the crystal at room temperature (r.t.) was determined by a floating method by using a mixture of *o*-xylene and bromoform.

2.3. Crystal structure determination of $[(PyO)_2D][AuCl_4]$

A SMART 1000/CCD diffractometer (Bruker) was employed for the diffraction measurements using graphite monochromated Mo Kα radiations (2θ range 3.2°–55.0°). Data collections were carried out at 289 K. Crystal data and the details of the experiments and refinements are given in Table 1.

Table 1
Crystal data and details of the experiments and refinements

Formula	$C_{10}H_{10}N_2O_2DAuCl_4$
Formula weight	530.97
X-ray radiation	Mo Kα
Wavelength (Å)	0.71073
Crystal system	Orthorhombic
Space group	*Pbca*
a (Å)	7.139(1)
b (Å)	15.631(2)
c (Å)	27.888(4)
Cell volume (Å^3)	3112.2(7)
Z	8
D_{calc} (g cm^{-3})	2.262
D_m (g cm^{-3})	2.27(1)
μ(Mo Kα) (mm^{-1})	10.138
F(000)	1984
Temperature (K)	289
Crystal color	Orange
Crystal size (mm)	0.17 × 0.07 × 0.04
Theta range (°)	2.61–27.50
Index range	$-6 \le h \le 9;\ -20 \le k \le 20;\ -32 \le l \le 33$
Reflections collected	16498
Reflections unique	3270
R_{int}	0.1010
Reflections ($I > 2\sigma(I)$)	1638
$R_1(F)$ ($I > 2\sigma(I)$)	0.0446
$wR_2(F^2)$ for all reflection	0.0860
Number of parameters	175
Goodness-of-fit for all reflections (F^2)	0.839
Weighting scheme	$w^{-1} = [\sigma^2(F_2^2) + (0.0293p)^2 + 0.00p]$, $p = (F_o^2 + 2F_o^2)/3$
Maximum shift/e.s.d.	0.001
ρ_{max} (e Å^{-3})	2.173
ρ_{min}(e Å^{-3})	−0.859

The structure was solved by the direct method and refined by full-matrix least-squares calculations based on F_o^2 with absorption correction (SADABS) using SHELXL-97 [7]. Non-hydrogen atoms were included in the least-squares calculations with anisotropic displacement parameters. The positions of the hydrogen atoms on the six-membered rings were calculated and they were included in the refinement under constraints with isotropic displacement parameters. To account for the H (or D) atom attached to the O atom, we applied two models. In the first one, a hydrogen atom (H(11)) was fixed at the midpoint between the two oxygen atoms of the $(PyO)_2$ group (final R values: $R_1 = 0.0447$ and $wR_2 = 0.0862$). In the second model, starting from the first one, the positional parameters were included in the refinement. The hydrogen atom converged to a point apart from the O(1) and O(2) by 1.36(10) and 1.35(10) Å, respectively (final R values: $R_1 = 0.0446$ and $wR_2 = 0.0860$). In each model, the maximum residual electron density (peak) was approximately 2.2 e $Å^{-3}$ on the final difference Fourier map. The position of the peak is too close to Cl(4) (ca. 1.68 Å) to assign any atom to it. The observed density of the crystal (2.27 ± 0.01 g cm^{-3}) was in good agreement with the calculated one (2.262 g cm^{-3}). The IR spectrum indicated that the crystal was free of the water of crystallization.

3. Results and discussion

3.1. Isotope dependent synthetic feature and new phases of the complexes between pyridine N-oxide and tetrachloroauric acid

Yuqiu and Shihua [6] reported for the compound with Ph_3AsO that the 2:1 compound of $[(Ph_3AsO)_2H][AuCl_4]$ crystallized even from the aqueous solution of Ph_3AsO–$HAuCl_4 = 1{:}1$, and the 1:1 compound was obtained only by the extraction method using 1,2-dichloroethane as an extraction solvent. These results suggest the stability of the diadduct of proton in the non-deuterated aqueous system. Similarly, for the complexes between PyO and tetrachloroauric acid, the stability of the diadduct of proton was suggested by the following observations in the present work. (1) The 2:1 compound of $[(PyO)_2H][AuCl_4]$ was obtained from the aqueous solution of PyO–$HAuCl_4 = 5{:}1$ as well as 2:1. (2) The 3:2 compound of $[(PyO)_{1.5}H][AuCl_4]$ and the 1:1 compound of $[PyOH][AuCl_4]$ were obtained from the solution of PyO–$HAuCl_4 = 1{:}1$ and 1:2, respectively.

In the course of the present study, on the other hand, we have found the tendency that the dimeric cation was less stable in the deuterated solvent system as compared with that in the non-deuterated one. To prepare the compound with the base-to-acid molar ratio of 2:1 in the deuterated system, we had to employ the solution with the much higher ratio of the base. In other words, the monoadduct of deuteron, instead of the diadduct, seems to be more stable in the deuterated system.

$[PyOH][AuCl_4]$ and $[(PyO)_{1.5}H][AuCl_4]$ are new compounds reported here for the first time. The X-ray powder diffraction of the latter was completely different from the superposition of those of $[(PyO)_2H][AuCl_4]$ and $[PyOH][AuCl_4]$, indicating the presence of a 3:2 compound as an independent crystalline phase.

3.2. ^{35}Cl NQR spectrum

In accordance with the reported crystal structure, two ^{35}Cl NQR frequencies were observed at 29.056 and 28.863 MHz at 77 K in $[(Ph_3AsO)_2H][AuCl_4]$, and at 28.295 and 27.799 MHz at 77 K in $[(PyO)_2H][AuCl_4]$. The temperature dependences of the resonance frequencies are shown in Fig. 1. The temperature dependence curves are smooth in the whole temperature range studied indicating no structural phase transition takes place down to 4.2 K. This means the symmetric hydrogen bond is retained even at 4.2 K presumably due to a tunneling motion of hydrogen atom in these compounds.

At 77 K, ^{35}Cl NQR frequencies were observed at 28.822 and 28.600 MHz in $[Ph_3AsOD][AuCl_4]$ and at 29.164, 28.727, 28.625, 28.272 and 27.618 MHz in $[PyOD][AuCl_4]$. As for $[PyOH][AuCl_4]$, $[(PyO)_2D][AuCl_4]$ and $[(PyO)_{1.5}H][AuCl_4]$, NQR measurements have not been undertaken since we have not yet obtained enough crystals for the measurements.

3.3. Infrared spectrum and ^2H NMR

In $[Ph_3AsOD][AuCl_4]$ and $[PyOD][AuCl_4]$, an IR band which can be assigned to the O–D stretching

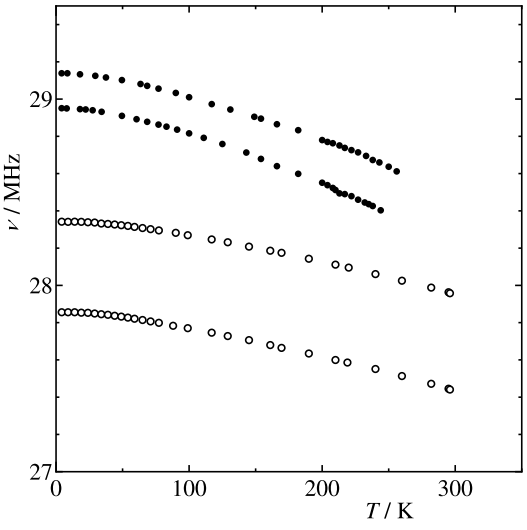


Fig. 1. Temperature dependence of ^{35}Cl NQR frequencies of $[(Ph_3AsO)_2H][AuCl_4]$ (●) and $[(PyO)_2H][AuCl_4]$ (○).

vibration was clearly observed at 2470 and 2378 cm^{-1}, respectively, without overlapping with the other bands. However, the bands observed at 3316 and 3179 cm^{-1} in $[Ph_3AsOD][AuCl_4]$ and [PyOD][$AuCl_4$], respectively, suggest an occurrence of isotope exchange with a proton. The strong broad IR bands which are assignable to vibrations corresponding to a symmetric O···H···O hydrogen bond were observed in the region 1500–400 cm^{-1} [8,9] in $[(RO)_2H][AuCl_4]$ type compounds. Similar broad bands were observed also in $[(RO)_{1.5}H][AuCl_4]$, although weakened, suggesting the presence of a symmetric O···H···O hydrogen bond. The IR spectra of $[(PyO)_2D][AuCl_4]$ also showed broad bands in the same region. Therefore, the partial isotope exchange with proton is suggested. The extent of the deuteration of $[(PyO)_2D][AuCl_4]$ has been estimated to be H/D = approximately 30/70 by use of ^2H NMR measurements of the aqueous solution.

3.4. Characterization of $[(PyO)_nH/D][AuCl_4]$ ($n = 1, 2$) by X-ray powder diffraction

The effect of hydrogen isotope substitution on the crystal structure was investigated both on the 2:1 and 1:1 compounds of PyO by use of X-ray powder diffraction measurements. The crystal structures of the 1:1 compounds, i.e. [PyOH][$AuCl_4$] and [PyOD][$AuCl_4$], are considered to be independent of the hydrogen isotope substitution, because they gave diffraction patterns similar to each other. In the case of the 2:1 compound, on the other hand, the diffraction patterns of $[(PyO)_2H][AuCl_4]$ and $[(PyO)_2D][AuCl_4]$ were found to exhibit a drastic difference as can be seen in Fig. 2. The unit cell parameters obtained by the single crystal X-ray study (Table 1) completely reproduced the positions of the peaks in the powder X-ray diffraction pattern of $[(PyO)_2D][AuCl_4]$. Thus the crystal structure of $[(PyO)_2D][AuCl_4]$ was expected to be remarkably different from that of $[(PyO)_2H][AuCl_4]$. Since the solution from which the $[(PyO)_2D][AuCl_4]$ crystal was obtained had not the same composition as that used in the preparation of the non-deuterated compound, one may propose the difference of the condition of the preparation as a cause of the structural change. Then, we have prepared $[(PyO)_2H][AuCl_4]$ repeatedly from a solution of PyO–$HAuCl_4$ = 5:1, the composition of which is the same as that used for $[(PyO)_2D][AuCl_4]$ preparation. By powder X-ray measurements, we have found a case in which the reflection peaks characteristic of 'the $[(PyO)_2D][AuCl_4]$ type crystal' are coexisting together with the peaks of the normal $[(PyO)_2H][AuCl_4]$ crystal. Therefore, the present phenomenon will be recognized as a polymorphism depending on the isotope concentration of the solvent used for crystallization. The phenomenon was interesting enough to lead to the single crystal X-ray study on the deuterate, the results of which will be discussed in the next section.

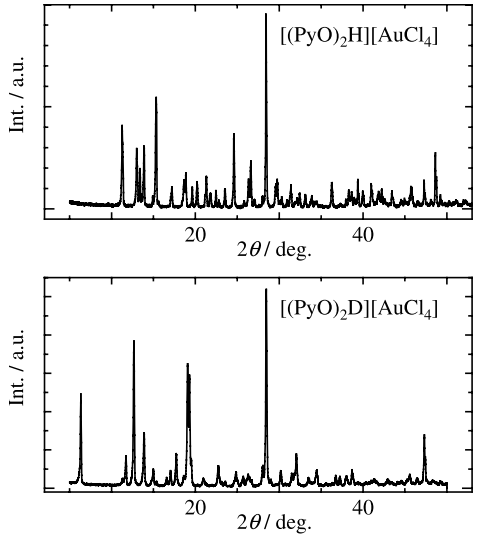


Fig. 2. X-ray powder diffraction patterns of $[(PyO)_2H][AuCl_4]$ and $[(PyO)_2D][AuCl_4]$. Strong diffraction at 28.46° and 47.34° are from silicon powder used as an internal standard. The pattern of $[(PyO)_2H][AuCl_4]$ can be explained by the reported crystal data in ref. [2]: $P\bar{1}$, $a = 7.276$, $b = 8.631$, $c = 6.799$ Å, $\alpha = 105.4$, $\beta = 96.4$, $\gamma = 67.9°$.

3.5. Crystal structure of $[(PyO)_2D][AuCl_4]$

The structures of the anion and cation in $[(PyO)_2D][AuCl_4]$ (D-salt) are shown in Fig. 3. For the sake of convenience, the corresponding structures of

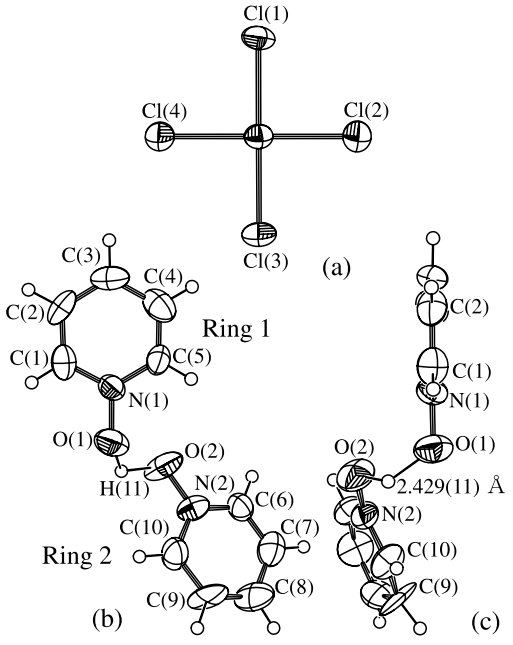


Fig. 3. Structure of the anion and cation in the D-salt with atom labelling. (a) the anion; (b) and (c) the cation viewed perpendicular and parallel to the pyridine ring having N1 (Ring 1), respectively. The distance 2.429(11) Å given in (c) is the O(1)···O(2) distance.

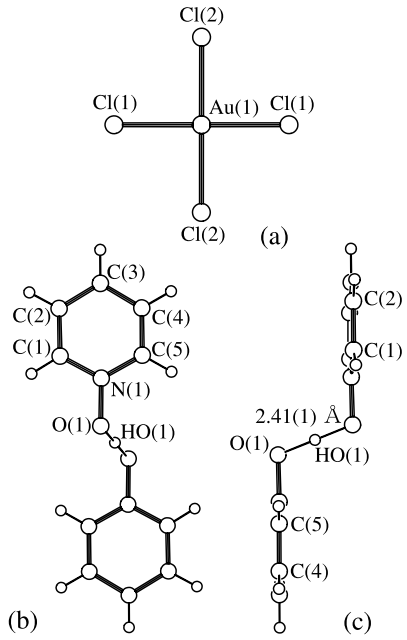


Fig. 4. Structure of the anion and cation in the H-salt with atom labelling. (a) the anion; (b) and (c) the cation viewed perpendicular and parallel to the pyridine ring, respectively. The distance 2.41(1) Å given in (c) is the O···O distance.

$[(PyO)_2H][AuCl_4]$ (H-salt) [2] are given in Fig. 4. The relevant bond lengths and angles are summarized in Table 2. We will tentatively describe the $(PyO)_2H$ group in the D-salt as $[PyO–D–PyO]^+$. The anion in the D-salt is almost planar: the maximum deviation from the mean plane of the anion is 0.024 Å for Cl(2). The average of the Au–Cl bond lengths of the D-salt is only by approximately 0.01 Å longer than that of the H-salt. The structure of the PyO moiety also agrees between the two salts (see Table 2). Thus, one can conclude that the structures of the $[AuCl_4]$ unit and the PyO moiety of the two salts are very close to each other except for the slight reduction in the C(8)–C(9) bond length of the D-salt, for which a certain thermal motion would be responsible.

Contrary to the case of the PyO moiety, the three-dimensional structure of $[PyO–H–PyO]^+$ in the H-salt is completely different from that of $[PyO–D–PyO]^+$ in the D-salt (Fig. 3 (b and c) and Fig. 4 (b and c)). As can be seen in Fig. 4 (b and c), the former cation has center of symmetry. In the case of the latter, however, the magnitude of the torsion angle χ around the O···O axis is 142.8° and the two pyridine planes make an angle of approximately 29.2°. Thus, the cation in the D-salt is asymmetric (C_1 point symmetry). The $[(PyO)_2H]$ cation is able to have another symmetry in a different crystal: i.e. it has twofold symmetry in the crystal of $[(PyO)_2H][ClO_4]$ [9]. The observation that the structure of the cation differs from compound to compound is considered to be a consequence of the fact that its three-

Table 2
Bond lengths (L (Å)) and angles (θ (°)) for D-salt (Ref. for H-salt from [2])

L (in anion)		Ref.	θ (in anion)		Ref.
Au(1)–Cl(1)	2.272(2)	2.270(2)	Cl(1)–Au(1)–Cl(2)	90.15(9)	89.94(8)
Au(1)–Cl(2)	2.279(2)	2.271(2)	Cl(2)–Au(1)–Cl(3)	89.70(9)	
Au(1)–Cl(3)	2.279(2)		Cl(1)–Au(1)–Cl(4)	89.92(9)	
Au(1)–Cl(4)	2.295(2)		Cl(3)–Au(1)–Cl(4)	90.25(9)	
			Cl(1)–Au(1)–Cl(3)	179.11(10)	
			Cl(2)–Au(1)–Cl(4)	178.61(10)	
L (in Ring 1 of cation)		L (in Ring 2 of cation)			Ref.
O(1)–N(1)	1.354(9)	O(2)–N(2)	1.314(9)		1.362(8)
C(1)–N(1)	1.329(12)	C(6)–N(2)	1.323(13)		1.33(1)
C(5)–N(1)	1.331(11)	C(10)–N(2)	1.325(11)		1.34(1)
C(1)–C(2)	1.345(13)	C(6)–C(7)	1.333(13)		1.35(1)
C(2)–C(3)	1.389(14)	C(7)–C(8)	1.372(14)		1.38(2)
C(3)–C(4)	1.384(15)	C(8)–C(9)	1.326(15)		1.38(2)
C(4)–C(5)	1.335(13)	C(9)–C(10)	1.352(13)		1.34(1)
θ (in Ring 1 of cation)		θ (in Ring 2 of cation)			
C(1)–N(1)–O(1)	117.6(8)	C(6)–N(2)–O(2)	120.0(9)		117.7(7)
C(5)–N(1)–O(1)	120.6(8)	C(10)–N(2)–O(2)	120.8(9)		119.9(7)
C(1)–N(1)–C(5)	121.8(8)	C(6)–N(2)–C(10)	119.2(9)		122.4(7)
N(1)–C(1)–C(2)	119.8(9)	N(2)–C(6)–C(7)	122.0(10)		119.7(8)
C(1)–C(2)–C(3)	119.3(9)	C(6)–C(7)–C(8)	119.5(11)		119.9(9)
C(2)–C(3)–C(4)	119.4(9)	C(7)–C(8)–C(9)	117.0(10)		117.8(8)
C(3)–C(4)–C(5)	118.2(10)	C(8)–C(9)–C(10)	121.9(10)		121.6(8)
C(4)–C(5)–N(1)	121.4(10)	C(9)–C(10)–N(2)	119.2(10)		118.6(8)

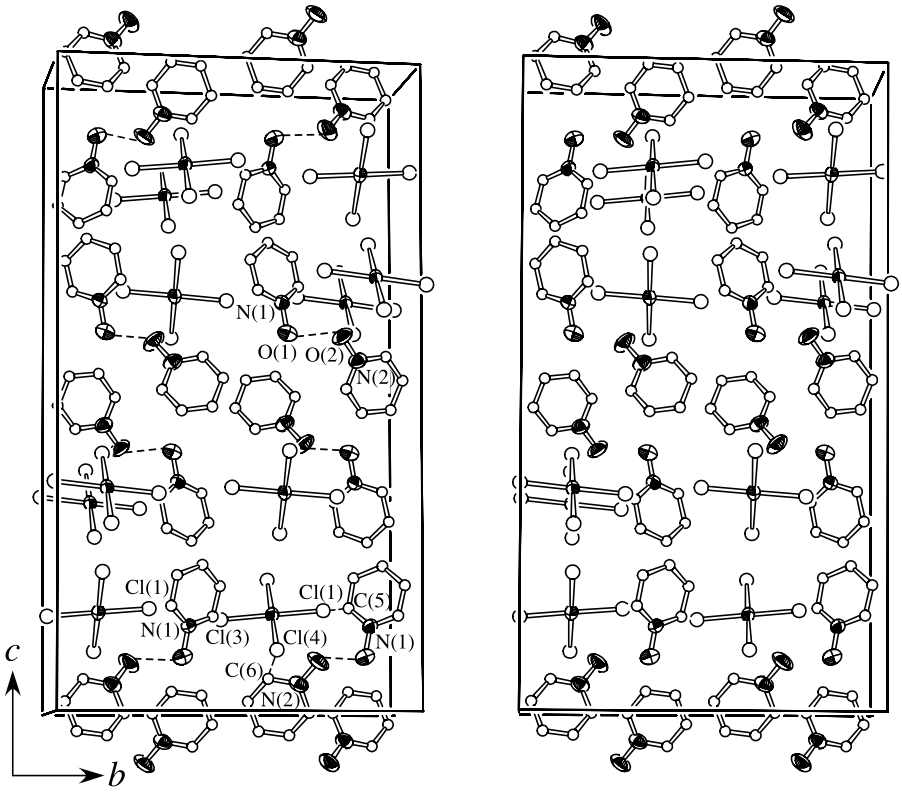


Fig. 5. Stereo drawing of the crystal structure of the D-salt viewed along the *a*-axis. Light broken lines indicate short Cl···C contacts (Cl(4)···C(6) and Cl(1)···C(5): 3.448(11) and 3.476(11) Å, respectively).

dimensional structure is flexible owing to the possibility of the two kinds internal rotations around the O···O and N–O axes.

Besides the fact that the overall structure of the cation in the D-salt is asymmetric, it should be noted that the two N–O bond lengths in the D-salt are not equivalent: N(1)–O(1) and N(2)–O(2) are 1.354(9) and 1.314(9) Å, respectively, the former value being closer to the N–O distances in the H-salt (1.362(8) Å) and that in $[(PyO)_2H][ClO_4]$ (1.353(3) Å). The O···O distance in the D-salt (2.429(11) Å) would differ from that of the H-salt (2.41(1) Å). These observations suggest the difference in the nature of the hydrogen bond between H- and D-salts. The position of the D atom in $[(PyO)_2D]^+$ may deviate from the mid-point between the two O atoms to result in a hydrogen bond with an asymmetric potential well.

The crystal structures of the D- and the H-salts are shown in Figs. 5 and 6, respectively. In the H-salt, the anion and the cation pack alternately parallel to the (100) plane to result in a layer structure. In the D-salt, however, there exists no such simple layer structure. As can be seen from a comparison of the figures, the D-salt adopts a crystal structure completely different from that of the H-salt. This phenomenon is interesting, but not necessarily unusual because the structure of the cation is also totally different in the two salts as mentioned above.

The isotope effect on the crystal structure is a rather rare phenomenon, but it has been observed, for instance, in the following compounds. The fully deuterated oxalic acid dihydrate has been reported to crystallize with a structure (β-form) different from that of the non-deuterated one (α-form) [10–12]. Since the fully deuterated crystal with an α-form was also obtained [13,14], these forms are regarded as crystalline polymorphs. For trifluoroacetic acid tetrahydrate, a change from an ionic to a molecular structure on deuteration has been reported [15]. As to the structural change of $Rb_3H(SeO_4)_2$ due to deuteration, the symmetry-breaking of the symmetric hydrogen bond or the reduction of tunneling motion has been proposed as the possible cause [4].

The structural difference between the D- and H-salts presented in this paper may be explained as a result of polymorphism. But, the present phenomenon is not a usual one, where the structure of the component is expected to be identical in the polymorphs.

A slight difference in the intermolecular interaction due to the isotope difference will determine which structure is more stable as in the case of $Rb_3H(SeO_4)_2$. It should be mentioned, however, that the effect of hydrogen isotope substitution in the present case might include not only a pure isotope effect, but also an effect of the condition of the preparation, because it was different between the preparations of the normal and

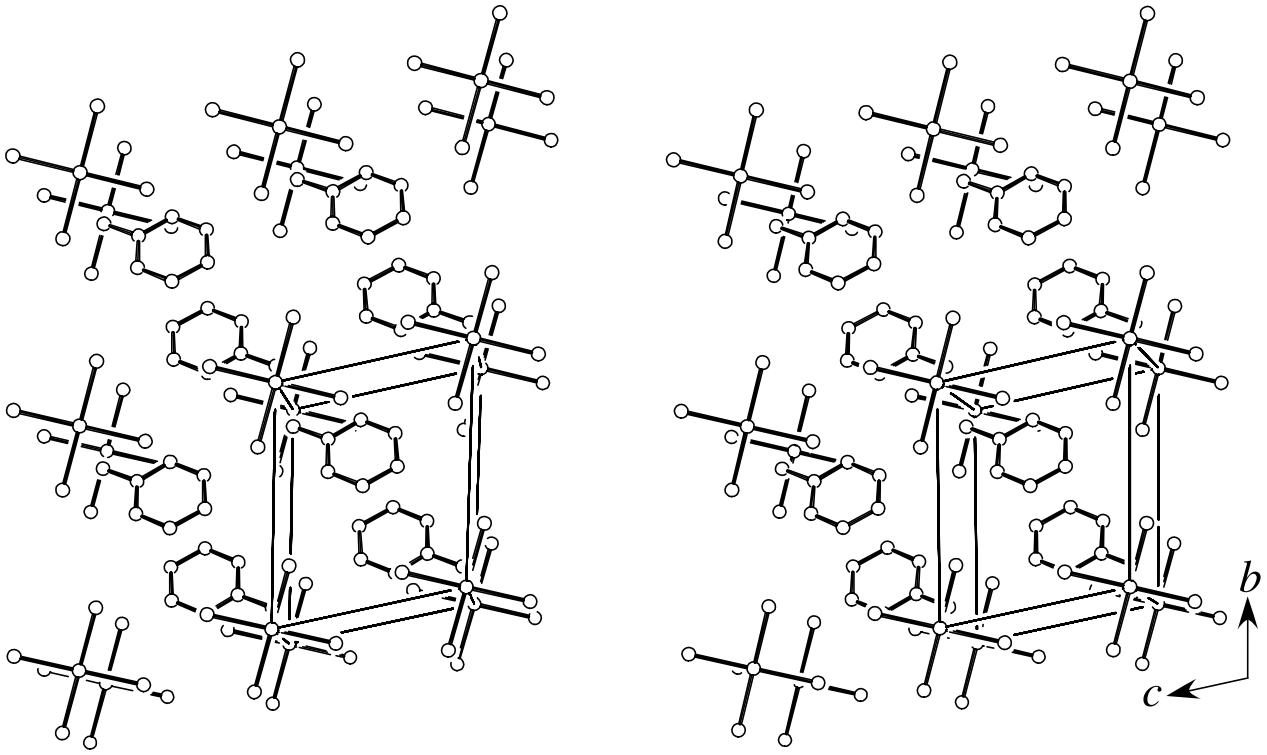


Fig. 6. Stereo drawing of the crystal structure of the H-salt viewed along the *a*-axis.

deuterated compounds as described in the earlier section. It is ambiguous, therefore, that the change in the structure of the cation and hence that of the crystal can be ascribed to mere isotope effect.

4. Supplementary material

Crystallographic data for the structural analysis have been deposited with the Cambridge Crystallographic Data Centre, CCDC No. 184567. Copies of this information may be obtained free of charge from The Director, CCDC, 12 Union Road, Cambridge, CB2 1EZ, UK (fax: +44-1223-336033; e-mail: deposit@ccdc.cam.ac.uk or www: http://www.ccdc.cam.ac.uk).

Acknowledgements

Miss M. Kenmotsu (Nagoya University), Miss S. Hisamatsu, Miss H. Sugawara, Miss K. Nakajima, Miss T. Nishioka, Mr T. Ishimaru and Mr E. Akiyama (Nihon University) are thanked for collaboration in this investigation. This work was partially supported by a Grant for 2001 from the College of Humanities and Sciences, Nihon University and by a Grant from the Ministry of Education, Culture, Sports, Science and Technology to promote advanced scientific research.

References

[1] M.S. Hussain, E.O. Schlemper, J. Chem. Soc., Dalton Trans., (1980) 750.
[2] M.S. Hussain, E.O. Schlemper, J. Chem. Soc., Dalton Trans., (1982) 751.
[3] P.G. Jones, A. Olbrich, R. Schelbach, E. Schwarzmann, Acta Crystallogr., Sect. C 44 (1988) 2201.
[4] T. Matsuo, A. Inaba, O. Yamamuro, N. Onoda-Yamamuro, J. Phys. Condens. Matter 12 (2000) 8595.
[5] T. Gustafsson, M. Ichikawa, I. Olovsson, Solid State Commun. 115 (2000) 473.
[6] G. Yuqiu, X. Shihua, Polyhedron 6 (1987) 2077.
[7] G.M. Sheldrick, SHELXL-97 Program for the Solution and the Refinement of Crystal Structures, University of Göttingen, Germany, 1997.
[8] R.A. Potts, Inorg. Chem. 9 (1970) 1284.
[9] J. Wasicki, M. Jaskolski, Z. Pajak, M. Szafran, Z. Dega-Szafran, M.A. Adams, S.F. Parker, J. Mol. Struct. 476 (1999) 81.
[10] T. Chiba, J. Chem. Phys. 41 (1964) 1352.
[11] F.F. Iwasaki, Y. Saito, Acta Crystallogr. 23 (1967) 56.
[12] F.F. Iwasaki, H. Iwasaki, Y. Saito, Acta Crystallogr. 23 (1967) 64.
[13] P. Coppens, T.M. Sabine, Acta Crystallogr., Sect. B 25 (1969) 2442.
[14] A. Lehmann, P. Luger, C.W. Lehmann, R.M. Ibberson, Acta Crystallogr., Sect. B 50 (1994) 344.
[15] D. Mootz, M. Schilling, J. Am. Chem. Soc. 114 (1992) 7435.

position, and examination of the ^{1}H NMR signals of this complex in the aromatic region should provide evidence on orientations of the two phenanthrolines with respect to the sugar. The conformation of crystalline sucrose [11] is such that complexation at an octahedral center does not markedly distort the sugar residue [10].

The ^{1}H NMR signals of the sucrose moiety showed that the face of one phenanthroline is sufficiently close to the glucose residue to allow observation of a nuclear overhauser effect (NOE) between H-2(g) and one phenanthroline hydrogen, and there was a second NOE involving OH-1(f) of the fructose residue and a hydrogen of the other phenanthroline ligand. Both aromatic hydrogens are at positions adjacent to nitrogens, and the phenanthrolines are in different environments relative to the sugar [10b], but there was no information on the other ^{1}H NMR signals. These conclusions were consistent with structural optimization of the Δ-complex with semi-empirical PM3(tm) parameters [12,13], which gives the structure shown in Fig. 1. This structure was obtained by a slightly different optimization procedure from that used earlier [10b], and it is described later. Structures from the two procedures are superimposable. We designate phenanthroline A as *trans*- to O-2(g), phenanthroline B as *trans*- to HO-1(f) [10b], and phenanthroline positions are numbered 1–10 with N-1(A) and N-1(B) in a trans-relationship. The linkage of the fructose residue to Co(III) through a hydroxymethyl group ensures that the fructose ring is not in close contact with a phenanthroline group, but the linkage through O-2(g) brings the glucose residue very close to phenanthroline B.

The ^{1}H NMR signals of the mixed sucrose complex in the aromatic region and other spectral evidence showed that this complex is sufficiently stable in solution to allow examination of all the ^{1}H signals of the two

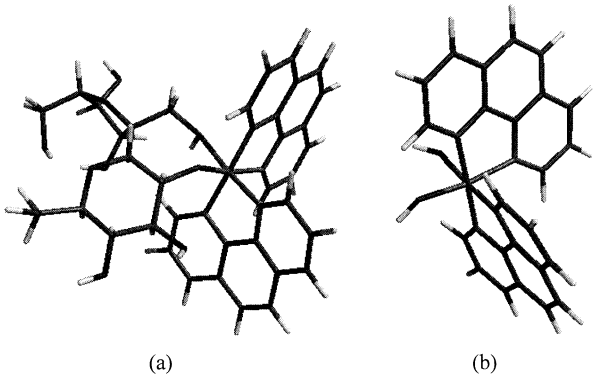


Fig. 1. Reoptimized geometry of the Δ-complex. Phenanthroline ring A is attached to the upper coordination site of Co(III) with the sucrose residue on the left and ligated glucose at the front, B is attached to the lower site of Co(III): (a) complex; (b) with sucrose ligand removed for clarity.

phenanthroline ligands and their interactions with the sugar residue, which had not been feasible with monosaccharide complexes [3,8,10]. Ito et al. had assigned the aromatic ^{1}H signals in a mixed complex of Co(phen)$_2$ with ethylenediamine, where the phenanthrolines are identical [14]. They showed that hydrogens in one part of a phenanthroline are close to the face of the other phenanthroline with consequent π-shielding and chemical shifts at position 9 are lower than at position 2 by approximately 2 ppm.

The ^{1}H signals of OH groups of the sugar residue had been examined in DMSO, where there was less overlap of the aromatic ^{1}H NMR signals than in D_2O, which simplifies assignment. Aliphatic ^{1}H signals were similar in the two solvents, and we assumed that the structure did not change, but we planned to confirm that assumption by comparing the CD spectra in H_2O and DMSO [10b]. We were also interested in comparison of the absorption and CD spectra of the sucrose complex and other mixed monosaccharide complexes, because positions of the CD extrema seemed to be insensitive to monosaccharide structure [3,8]. We have been unable as yet to obtain crystals of these mixed complexes suitable for X-ray crystallography and, therefore, rely on evidence from CD and NMR spectroscopy [6,8,10], and use semi-empirical treatments to predict overall structures consistent with spectral and other data.

2. Results and discussion

2.1. NMR spectroscopy

The ^{1}H NMR spectrum in the aromatic region in either D_2O or DMSO-d_6 shows signals of 16 hydrogens, with some overlap (Table 1). Signals of H-2 (A) and H-2(B), which had been assigned [10b], have the highest chemical shifts [14], and their $H_{2,3}$ coupling constants (Table 1) show that they are adjacent to phenanthroline nitrogens [15]. Following the Rules of Ito et al. [14] we conclude that signals with the lowest chemical shifts are of H-9 (A, B), consistent with their coupling constants [14,15], but these observations do not distinguish between signals of phenanthrolines A or B.

Hydrogens 3(A) and 4(A), and 3(B) and 4(B), are assigned from the COSY spectrum and decoupling in both DMSO-d_6 and D_2O. We applied a similar approach to hydrogens at positions 7, 8 and 9 in each phenanthroline, but to assign them to phenanthroline A or B we had to establish connectivities through positions 5 and 6 for each phenanthroline.

Signals in DMSO-d_6 are sufficiently separated that we could use NOE to establish connectivities within each phenanthroline. We irradiated one H-5, which could be in either ring, and saw an NOE in one, but not the other, H-4 signal, and then irradiated the other H-5 and saw

Table 1
^{1}H NMR spectra of the phenanthroline groups [a]

	Position							
	2	3	4	5	6	7	8	9
In DMSO-d_6								
δ, (ppm), A	9.86	8.51	9.18	8.45	8.34	8.82	7.72	7.62–7.65
B	10.18	8.31	9.13	8.42	8.27	8.87	7.62–7.65	7.48
T1, s, A	1.6	2.1	2.4	2.3	2.0	2.4	2.1	
B	1.1	2.1	2.3	2.2	1.7	2.3		2.2
Coupling	2.3	3.4	5.6	7.8	8.9			
J, (Hz), A	5.0	8.0	9.0	8.0	5.0			
B	5.5	8.5	9.0	8.0	5.0			
In D_2O								
δ, (ppm), A	9.78	8.43	9.10	8.31–8.36	8.19–8.24	8.68	7.59	7.48
B	10.01	8.31–8.36	9.08	8.31–8.36	8.19–8.24	8.66	7.55	7.38
Coupling	2.3	2.4	3.4	5.6	7.8	7.9	8.9	
J, (Hz), A	5.5	1.0	8.0	9.0	8.0	0.8	5.5	
B	5.5	1.0	7.0	9.0	8.0	0.8	5.5	

[a] At 500 MHz, referred to DMSO or TSP in D_2O.

the NOE in the other H-4 signal, thus assigning H-5 (A and B). Connectivities between H-5 and -6 (A and B) where then assigned by the COSY spectrum and decoupling. Connectivities between H-6 and -7 of rings A or B were similarly established by observing the appropriate NOE after irradiating H-7 of either ring A or B. This procedure gives assignments of all the ^{1}H phenanthroline signals and chemical shifts, coupling constants and T_1 values are in Table 1.

Assignments of the ^{1}H NMR signals in D_2O are based on the COSY spectrum, values of coupling constants [15], and decoupling at positions 2–4, 5–6, 7–9, the rules given by Ito et al. [14], and the assumption that sequences of chemical shifts will be the same in DMSO-d_6 and D_2O (Table 1). We saw long-range coupling for some phenanthroline signals in D_2O, but not in DMSO-d_6, probably because its higher viscosity broadens signals sufficiently to obscure weak coupling.

For a given phenanthroline ^{1}H chemical shifts vary qualitatively as predicted [14], and differences between values in rings A and B (Table 1) are governed by mutual interactions between the phenanthrolines and those with the glucose and fructose residues of the sugar. Differences in the ^{1}H NMR chemical shifts for a given phenanthroline, and between hydrogens at similar positions in the two rings, are largest for H-2 and -3 which are nearest to the sugar residues but are in different environments (Fig. 1 and Table 1).

2.2. Absorption and CD spectra

Spectra of the Δ-complex in the UV and visible regions are in Table 2. Positions of the CD extrema and shoulders are similar in H_2O and DMSO, although solvent absorbance by DMSO limits the low wavelength range. Positions and signs of the CD signals are similar to those of Δ-complexes of $Co(phen)_2$ with α-D-galactose and β-D-arabinose [8], where the sugar is bonded to Co(III) in a five-membered ring as compared with the eight-membered ring in the sucrose complex, i.e. they depend on the atoms bound to Co(III) rather than on the ring size. Following classical work on the electronic spectra of mixed complexes with $Co(phen)_2$ [9], as applied to the galactose and arabinose complexes [8], assignments in water are: λ, (nm), and ν, (cm^{-1}) in parentheses: phenanthroline transitions: 229, 241 (4.37×10^4, 4.15×10^4); β; 267, 281 (3.75×10^4, 3.56×10^4), p; 297 (3.37×10^4), α. Co(III), d–d transitions: 323, 363 (3.01×10^4, 2.75×10^4), ^1T_2g; 413, 513 (2.42×10^4, 1.95×10^4), ^1T_1g; approximately 610 (1.64×10^4), ^3T_2g. Assignments in DMSO are as in H_2O, within the wavelength range that can be examined, and there is a positive CD signal at < 260 nm (Table 2), although we cannot specify its location. In both solvents excitonic effects confirm that two phenanthrolines are bound to Co(III) and the sign sequence establishes the Δ-configuration [6,8]. The CD signals at 332 and 363 nm assigned to the ^1T_2g state represent forbidden transitions for a complex with strict octahedral symmetry, but in these mixed complexes there is distortion of the octahedral Co(III).

The CD signals in the UV are at similar wavelengths in H_2O and DMSO, confirming that there is no solvent effect on configuration, but those in the visible are red-shifted in DMSO, and apparently solvent effects upon energies associated with the d–d transitions are larger than those with the phenanthrolines. There is a shoulder at 413–436 nm in the absorption spectrum in DMSO, which was not seen in H_2O [10b].

Table 2
Absorption and CD spectra of Δ-[Co(III)(phen)$_2$(sucrose)]Cl$_2$

H_2O [a]				DMSO			
Absorption		CD		Absorption		CD	
λ (nm)	log ε	λ (nm)	$\Delta\varepsilon$	λ (nm)	log ε	λ (nm)	$\Delta\varepsilon$
227	5.03	229	−5.5				
		241	+8.6				
		267	+11.3	271	4.63	260	+10.9
270	4.67	281	−15.4			284	−14.2
		297sh	−5.7	298sh	4.32	297sh	−6.5
295sh	4.31	323	+3.3	329sh	3.78	346	+3.6
329sh	3.67	363	−1.8			389	−0.32
		413	+3.6			436	+4.3
519	2.15	513	−6.8	515	2.25	518	−6.7
		610sh	−0.27			620sh	−0.52

[a] From ref. [10b].

The quantitative treatment applied to electronic transitions of mixed complexes of Co(phen)$_2$ with α-galactose or β-arabinose [8] applies to spectra of the sucrose complex in terms of similar energy levels on the basis of similar wavelengths of extrema and shoulders in the CD spectra.

2.3. Geometrical optimization

The structure of the Δ-sucrose complex had been treated by using semi-empirical PM3(tm) parameters (PC Spartan Plus 2.0, Wavefunction) [13] which had been parameterized for transition metal ions, including Co(III), but only the geometry of the sucrose-Co(III) residue had been discussed [10b]. The predicted O-2(g)–Co–O-1(f) bond angle of 92.8° was higher than in a strictly octahedral complex. We, therefore, repeated the optimization with this angle constrained to 90°, which gave a less favorable heat of formation by approximately 10 kcal mol^{-1}, but removal of the constraint and re-optimization gave the structure (Fig. 1) which is indistinguishable from the original and has the original bond angle at Co(III) indicating that the optimized structure was not in a false minimum. The heat of formation, rounded off to the fourth significant figure, is −1684 kcal mol^{-1} as found earlier [10b].

Predicted bond lengths and angles at Co(III) are given in Table 3 and [10b] for the Δ- and the hypothetical Λ-complex, which was not detected and whose formation is predicted to be disfavored, relative to the Δ- complex, by approximately 9 kcal mol^{-1} [10b].

2.4. Factors that control structure of the complex

The ^{1}H NMR and CD spectra of Δ-Co(phen)$_2$(sucrose) identify the configuration at Co(III) and the ligating groups of the sugar. The NMR spectra show

Table 3
Predicted bond lengths and angles of the Δ-complex

Bond distances (Å)	
O^--2(g)–Co	1.89 (1.85)
HO-1(f)–Co	2.03 (2.03)
N-1(A)–Co	1.93 (1.93)
N-10(A)–Co	1.96 (1.96)
N-1(B)–Co	1.93 (1.93)
N–10(B)–Co	1.90 (1.90)
Bond angles (°)	
O^--2(g)–Co–HO-1(f)	92.8 (82.2)
HO-1(f)–Co–N-1(A)	84.4 (97.4)
N-1(A)–Co–N-10(A)	89.9 (90.0)
N-10(A)–Co–N-10(B)	91.9 (92.3)
N-10(B)–Co–N-1(B)	89.7 (90.5)
N-1(B)–Co–O^-2(g)	99.4 (80.9)

Values for a hypothetical Λ-complex are in parentheses.

that the phenanthrolines are in different environments [10b] and we need to rationalize these observations.

Predicted values of the torsional angles ϕ (O-5(g)–C-1(g)–O-1(g) –C-2(f)) of 114.5° and Ψ (C-1(g)–O-1(g)–C-2(f)–O-5(f)) of −51.2° are not very different from those of crystalline sucrose, 107.8° and −44.8°, respectively, indicating that ligation does not markedly perturb the conformation of sucrose [10b,11]. However, it forces the glucose moiety into close proximity with phenanthroline B, as shown by the strong upfield shift of O*H*-3(g) (by ca. 1.4 ppm) [10b]. There is not room for H_2O to hydrogen-bond to OH-3 (g), but there may be hydrogen bonding to the π-system [16]. We note that geometrical optimization orients OH-3 (g) away from the face of phenanthroline B (Fig. 1), which does not agree with the NMR evidence [10b]. It appears that the semi-empirical PM3(tm) treatment does not take into account O–H–π hydrogen bonding. In a Λ-complex the sucrose conformation would be perturbed relative to

that of the free sugar [11], with $\phi = 131.1$ and $\psi = -22.5°$, consistent with the relatively low stability of this hypothetical complex [10b].

The multiplicity of the ^{1}H NMR signal of H-3 (g) in the Δ-complex confirms that HO-3 (g) is oriented towards the face of phenanthroline B [10]b and the computed distance from O-3(g) to the phenanthroline face is approximately 2.7 Å. Accomodation of the glucose moiety with respect to phenanthroline B affects bond angles at Co(III) and optimization indicates that the N-1(A)–Co–N-1(B) axis is approximately linear, but not strictly orthogonal to the O^--2(g)–Co–HO-1(f) plane. This deviation from octahedral symmetry is consistent with the large predicted N-1(B)–Co–O^--2(g) angle, which reflects congestion between the glucose moiety and phenanthroline B, and the correspondingly smaller HO-1(f)–Co–N-1(A) angle (Table 2). In the optimized structure the fructose ring is not close to phenanthroline A because ligation is through the hydroxymethyl group, HO-1(f), whereas for the glucose residue it involves O^--2(g) [10b].

Deviations from strict octahedral symmetry place the phenanthrolines in different environments with respect to both the sugar residue and themselves, in accord with their different NMR signals (Table 1). These interactions may bow the phenanthroline rings. In a Co(III) bis-phenanthroline complex each phenanthroline rear face is close to H-9 of the other phenanthroline [14] consistent with variations in the ^{1}H chemical shifts (Table 1). In the Δ-sucrose complex H-9(B) is predicted to be approximately 2.7 Å from positions 1(A) and 2(A), and H-9(A) is a similar distance from positions 1(B) and 2(B). However, H-9(A) and H-9(B) are further from other positions of phenanthrolines B and A, respectively. These interactions between the phenanthrolines are, in general, opposed by those with the third bidentate ligand, e.g. sucrose, whose glucose moiety is very close to the front face of phenanthroline B [10b]. These opposing interactions can cause a phenanthroline to bow towards, or away from, sucrose and tilt in either direction. The magnitude of the bowing, or curvature, is indicated by the absolute sum of the torsional angles indicated by the heavy lines in Fig. 2(a). The tilt, with respect to the O–Co–O plane, is given by the absolute mean of the torsional angles indicated by the heavy lines in Fig. 2(b). The magnitude and direction of these distortions in a given phenanthroline depend on the balance between opposing effects of interactions with the sugar ligand and the second phenanthroline. Therefore, in the Δ-complex, where phenanthroline B is very close to the glucose moiety, predicted curvature is towards the sugar by 19°, and phenanthroline A, which is distant from the fructose ring, is curved away from the sugar by 15°, and is tilted modestly towards the sugar by approximately 6°, while ring B is tilted away by a similar extent. Thus phenanthroline A presents a convex, and B

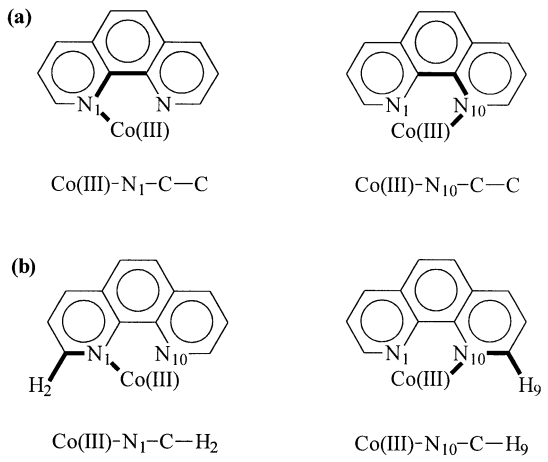


Fig. 2. Illustrations of estimated distortions of the phenanthroline group, c.f. Fig. 1. (a) Curvature of a group, the heavy lines indicate the noncoplanarities of Co(III)–N_1–C–C and Co(III)–N_{10}–C–C. (b) Tilt of a group, indicated by the torsional angles of Co(III)–N_1–C–H_2 and Co(III)–N_{10}–C–H_9.

a concave face towards sucrose, representing the balance between the interactions. Congestion between the glucose moiety and phenanthroline B more than offsets interactions from the rear with phenanthroline A. Predicted distortions for a hypothetical Λ-complex are similar in magnitude to those given above, except that curvatures are in the opposite sense.

These predicted deviations from planarity are responsible for differences between ^{1}H chemical shifts in the two phenanthroline rings (Table 1), even for hydrogens, which are distant from the sucrose moiety or the other phenanthroline (Fig. 1). These differences are more evident in DMSO-d_6 than in D_2O. The structure around Co(III) is very congested, as shown by examination of space-filling models, data not shown. Several distances between non-bonded atoms are within, or close to, the sum of the van der Waals radii.

So far as we are aware there is little information on structures of mixed bis-phenanthrolineCo(III) complexes from X-ray crystallography. There is distortion of octahedral symmetry in the carbonato complex [17] where the O–Co–O bond angle is low (ca. 69°), and Niederhoffer et al. report only modest bowing of the phenanthrolines, although Hennig et al. report deviations from planarity [18].

3. Experimental

Preparation and isolation of the mixed completes with Cl^- or I_3^- as counterion have been described, but the I_3^- salt was not used in the present work [10]. The ^{1}H NMR spectra were monitored on a Bruker DRX instrument, (300 MHz for ^{1}H) at 25 °C, or on a Varian Unity instrument (500 MHz for ^{1}H) at 21 or 25 °C for

the COSY spectrum and are referred to TSP (sodium 3-(trimethylsilyl)propanesulfonate) in D_2O ($\delta = 0$ ppm), or to DMSO ($\delta = 2.50$ ppm). Signals of the sucrose residue had been assigned [10]. There are uncertainties in chemical shifts of some of the phenanthroline signals in D_2O due to overlap (Table 1) but they do not affect the sequence of the chemical shifts.

The CD and absorption spectra in water are from [10], and those in DMSO were monitored at 25 °C on a Jobin–Yvon CD6 spectrometer, or, for the absorption spectrum, on a Unicam UV3 spectrometer, with freshly prepared solutions. With some monosaccharides the less stable diastereomer is formed initially and is gradually converted into the thermodynamically preferred complex [7,8], but only the Δ-complex was detected with sucrose.

4. Conclusions

The CD spectrum of $[Co(III)(phen)_2(sucrose)]Cl_2$ shows that it has the Δ-configuration in H_2O and DMSO and allows assignment of the electronic transitions. Differences in the ^1H NMR signals in the aromatic region show that the nonequivalent phenanthrolines differ in their non-bonding interactions with the sucrose moiety. The glucose residue is very close to one phenanthroline and structural optimization with the semi-empirical PM3 (tm) parameters indicates that there should be deviations from strict octahedral symmetry and planarity of the phenanthrolines consistent with differences in the ^1H NMR signals.

Acknowledgements

We acknowledge instrumental support from CEPEDEQ, Facultad de Ciencias Quimicas y Farmaceuticas, Universidad de Chile and Professor Ines Ahumada. J.P. Acknowledges support from FONDECYT Project 2970036.

References

[1] (a) D.W. Whitfield, S. Stojkovski, B. Sarkar, Coord. Chem. Rev. 122 (1993) 171;
(b) M. Zimmer, Chem. Rev. 95 (1995) 2629.
[2] (a) K. Hegetschweiler, Chem. Soc. Rev. 28 (1999) 239;
(b) B. Gyuresik, L. Nagy, Coord. Chem. Rev. 203 (2000) 81;
(c) S.J. Angyal, Adv. Carbohydr. Chem. Biochem. 47 (1989) 1;
(d) V. Piarulli, A.J. Rogers, C. Floriani, G. Gervasio, D. Viterbo, Inorg. Chem. 16 (1997) 6127.
[3] S. Bunel, C. Ibarra, E. Moraga, J. Parada, A. Blasko, C. Whiddon, C.A. Bunton, Carbohydr. Res. 312 (1998) 191 (and references cited therein).
[4] C.H. du Penhoat, A. Imberty, N. Roques, V. Michon, J. Mentech, G. Descotes, S. Perez, J. Am. Chem. Soc. 113 (1991) 3720.
[5] (a) K. Bock, R.U. Lemieux, Carbohydr. Res. 100 (1982) 63;
(b) B. Adams, L. Lerner, J. Am. Chem. Soc. 114 (1992) 4827;
(c) L. Poppe, H. van Halbeck, J. Am. Chem. 114 (1992) 1092.
[6] (a) B. Bosnich, Acc. Chem. Res. 2 (1969) 266;
(b) L.J. Katzin, J. Eliezer, Coord. Chem. Rev. 7 (1972) 331;
(c) K. Nakanishi, N. Berova, R.W. Woody (Eds.), Circular Dichroism, Principles and Applications, VCH, Cambridge, 1994.
[7] S. Bunel, C. Ibarra, E. Moraga, V. Calvo, A. Blasko, C.A. Bunton, Carbohydr. Res. 239 (1993) 185.
[8] J. Parada, S. Bunel, E. Moraga, C. Ibarra, N.D. Gillitt, C.A. Bunton, Polyhedron 20 (2001) 2223.
[9] (a) S.F. Mason, Inorg. Chem. Acta Rev. 2 (1968) 89;
(b) S.F. Mason, B.J. Peart, J. Chem. Soc., Dalton Trans., (1973) 949.;
(c) T. Yasui, B.E. Douglas, Inorg. Chem. 10 (1971) 97.
[10] (a) J. Parada, S. Bunel, C. Ibarra, G. Larrazabal, E. Moraga, N.D. Gillitt, C.A. Bunton, Carbohydr. Res. 329 (2000) 195;
(b) J. Parada, S. Bunel, C. Ibarra, G. Larrazabal, E. Moraga, N.D. Gillitt, C.A. Bunton, Carbohydr. Res. 333 (2001) 185.
[11] (a) S.M. Brown, H.A. Levy, Acta Crystallogr., Sect. B 29 (1973) 790;
(b) J.C. Hanson, L.C. Sieker, L.H. Jensen, Acta Crystallogr., Sect. B 29 (1973) 797.
[12] I.N. Levine, Quantum Chemistry, fifth ed. (chapter 17), Prentice Hall, Upper Saddle River, NJ, 2000.
[13] (a) J.J.P. Stewart, J. Comput. Chem. 10 (1989) 209;
(b) J.J.P. Stewart, J. Comput. Chem. 111 (1990) 543;
(c) W.J. Hehre, J. Yu, Abstracts of the 221st ACS National Meeting, New Orleans, LA, March, 1996.
[14] H. Ito, J. Fujita, T. Ito, Bull. Chem. Soc. Jpn. 44 (1971) 723.
[15] L.M. Jackman, S. Sternhell, Applications of Nuclear Magnetic Resonance Spectroscopy in Organic Chemistry, second ed. (chapter 3–6c), Pergamon, New York, 1969.
[16] I. Alkorta, I. Rozas, J. Elquero, J. Chem. Soc. Rev. 27 (1998) 163.
[17] E.C. Niederhoffer, A.E. Martell, R. Rudolf, A. Clearfield, Inorg. Chem. 27 (1982) 3734.
[18] H. Hennig, J. Sieler, R. Benedix, J. Kaiser, L. Sjoelin, O. Lindquist, Z. Anorg. Allg. Chem. 464 (1980) 151.

reflections were performed with the HKL Denzo–Scalepack system of programs [8]. Absorption corrections were carried out using the integration method [9] for compound **I** and multi-scan method [10] for **II**.

The structures were solved by direct methods with SHELXS-97 [11]. The model was refined by full-matrix least-squares on F^2 by means of SHELXL-97 [12]. All the hydrogen atoms were stereochemically positioned and refined with the riding model [12]. All H atoms were located on stereochemical grounds. Hydrogen atoms of the aromatic rings and CH_2 were set isotropic with a thermal parameter 20% greater than the equivalent isotropic displacement parameter of the atom to which each one is bonded; this percentage was set to 50% for the hydrogen atoms of the methyl groups.

Data collection and experimental details for complexes **I** and **II** are summarized in Table 1. Relevant interatomic bond lengths and angles are listed in Table 4.

2.2. Measurements

The infrared spectra of the complexes were measured from powder samples diluted in CsI on a FTIR Bomem–Michelson 102 spectrometer in the 4000–200 cm^{-1} region. Cyclic voltammetry (CV) experiments were carried out at room temperature (r.t.) in CH_2Cl_2 containing 0.10 M $Bu_4N^+ClO_4^-$ (TBAP) (Fluka Purum) using a BAS-100B/W Bioanalytical Systems Instrument; the working and auxiliary electrodes were stationary Pt foils, and the reference electrode was Ag/AgCl, 0.10 M TBAP in CH_2Cl_2, a medium in which ferrocene is oxidized at 0.43 V (Fc^+/Fc).

All the NMR experiments were running in a Bruker, DRX400 9.4 Tesla equipment, in a BBO 5 mm probe at 298 K. For the compounds **I** and **II** CH_2Cl_2 was used as solvent while for the compound **III** $CDCl_3$ was utilized. TMS and H_3PO_4 85% were used for internal and external reference for ^1H, ^{13}C and ^{31}P, respectively.

For complex **III** the completely ^1H, ^{13}C and ^{31}P attribution were done using 1D $^1H\{^{31}P\}$, $^{31}P\{^1H\}$ and 2D g^1H-^1H COSY45, $^1H-^{13}C$ gHMQC, $^1H-^{13}C$ gHMBC, $^{31}P-^1H$ HETCORR NMR experiments.

Table 1
Crystal data, data collection details and structure refinement results for *fac*-[$RuCl_3NO$(dppb)] and *mer*-[$RuCl_3NO$(diop)]

	fac-[$RuCl_3NO$(dppb)]	*mer*-[$RuCl_3NO$(diop)]
Molecular formula	$C_{28}H_{28}Cl_3NOP_2Ru$	$C_{31}H_{32}Cl_3NO_3P_2Ru$
Molecular weight	663.87	735.94
Crystal system	monoclinic	orthorhombic
Space group	$P2_1/n$	$P2_12_12_1$
a (Å)	11.4530(7)	12.0210(3)
b (Å)	14.787(1)	14.4160(3)
c (Å)	17.2260(8)	18.6640(5)
β (°)	103.394(4)	90.0
V (Å^3)	2838.0(3)	3234.4(1)
Z	4	4
D_{calc} (Mg m^{-3})	1.554	1.511
Absorption coefficient (mm^{-1})	0.970	0.864
Reflections collected	8555	48 157
Unique reflections	4996 [$R_{int} = 0.0695$]	7436 [$R_{int} = 0.0676$]
Absorption correction	Integration	multiscan
Maximum and minimum transmission	0.992 and 0.926	0.956 and 0.878
Data/parameters	4996/325	7436/372
Goodness-of-fit on F^2	1.088	1.204
Final R indices [$I > 2\sigma(I)$]	$R_1 = 0.0595$, $wR_2 = 0.1585$	$R_1 = 0.0384$, $wR_2 = 0.0965$

2.3. Material and methods

All manipulations involving solutions of the complexes were performed under argon. Solvents were purified by standard methods. All chemicals used were of reagent grade or comparable purity. The $RuCl_3 \cdot 3H_2O$ was purchased from Degussa and the ligands dppb and diop were purchased from Aldrich. The $RuCl_3(NO)$, *mer*-[$RuCl_3$(diop)H_2O] and *mer*-[$RuCl_3$-(NO)(dppb)] were prepared according to the literature [6,13] Yields are based on the metal. Microanalyses were performed by Microanalytical Laboratory of Universidade Federal de São Carlos, São Carlos (SP) or by Universidade de São Paulo, São Paulo (SP).

2.4. Preparation of compounds

2.4.1. *fac*-Trichloronitrosyl-1,4-bis-(diphenylphosphino)butaneruthenium(II) (*I*)

A methanol solution of *mer*-[$RuCl_3$(NO)(dppb)] (0.15 g, 0.226 mmol) was refluxed for 4 h under Ar. The yellow precipitate was collected, washed with ether and methanol, and dried under vacuum. Re-crystallization from dichloromethane–ether yielded orange crystals. Yield: 0.14 g (95%). *Anal*. Calc. for $C_{28}H_{28}Cl_3NORuP_2$: C, 50.7; H, 4.2; N 2.1. Found: C, 51.3; H, 4.4; N, 2.2%. Selected IR (cm^{-1}): 1868 (NO), 310, 289 (Ru–Cl). $^{31}P\{^1H\}$ NMR: 22.8 ppm.

2.4.2. *mer*-Trichloronitrosyl-2S,3S-O-isopropylidene-2,3-dihydroxy-1,4-bis(diphenylphosphino)-butaneruthenium(II) (*II*)

mer-[$RuCl_3NO$(diop)] was synthesized by bubbling NO [generated by reaction of dilute nitric acid (ca. 33%) over copper metal and dried passing it through a column containing anhydrous $CaCl_2$] in a dichloromethane solution of the *mer*-[$RuCl_3$(diop)(H_2O)] (0.07 g, 0.0967 mmol) for 1 h. After this time the red solution initially formed gradually changed to yellow. The dichloromethane was removed by evaporation and CCl_4 was added (10 cm^3). A small amount of green solid was separated from the yellow solution. After removing the

green solid by filtration, the yellow filtrate was reduced in volume to approximately 5 cm^3 and hexane (15 cm^3) added. The yellow precipitate formed was filtered off, and dried under vacuum. Re-crystallization from dichloromethane yielded yellow crystals. Yield: 0.05 g (70%). *Anal*. Calc. for $C_{31}H_{32}Cl_3NO_3RuP_2$: C, 50.6; H, 4.4; N, 1.9. Found: C, 50.9; H, 4.3; N, 1.9%. Selected IR (cm^{-1}): 1879 (NO), 339, 292 (Ru–Cl). $^{31}P\{^1H\}$ NMR: −2.1(d) and 5.5(d) ppm, $^2J(P–P) = 40.0$ Hz.

3. Results and discussion

In both complexes studied in this work, the NO stretching band (νNO) in the infrared spectra were close to 1870 cm^{-1} corresponding to the $\{Ru^{II}–NO^+\}$ type [14,15]. The $^{31}P\{^1H\}$ NMR spectra obtained for **I** and **II** indicate different geometries for these complexes. The *fac* isomer of the dppb species **I** presents a singlet signal (22.8 ppm) while the diop complex **II** shows two doublets (5.5 and −2.1 ppm, $^2J(P–P) = 40.0$ Hz) that can be assigned to the *mer* configuration. It is interesting to mention that the isomerization process from the *fac* to the *mer*-[$RuCl_3$(NO)(dppb)] was observed through $^{31}P\{^1H\}$ NMR experiments. This was noticed by the appearance of two doublets ($\delta = 13.65$(d) and 10.10(d) ppm, $^2J(P–P) = 36.6$ Hz) and also by the lower intensity of the singlet at 22.8 ppm of a solution maintained at room temperature. After 3 h of the compound solubilization the doublets can be identified and after 24 h approximately 50% of the *fac*-isomer was converted to the *mer*-isomer. Under longer periods of time the conversion was not completed. From this observation and from our previous report [5] it follows that these two isomers are likely to coexist in a CH_2Cl_2 solution at room temperature but at high one (temperature of boiling methanol) the *fac* isomer is the only species present in the solution. Complex **II** does not isomerize at room temperature, as indicated by the fact that its $^{31}P\{^1H\}$ NMR spectrum in dichloromethane solution remains unchanged over several days. A suggestion for this lack of isomerization in the diop complex could be the steric effect or rigidity caused by the additional ring in this ligand compared with dppb. The difference in the structures of these two ligands probably is also responsible by the better solubility of the *mer*-[$RuCl_3$(NO)(diop)] complex in common organic solvents when compared with its similar isomer with dppb, the same behavior is observed in the precursors *mer*-[$RuCl_3$(dppb)(H_2O)] and *mer*-[$RuCl_3$(diop)(H_2O)]. This can be advantageous in using this diop complex in catalytic processes.

In the $^{31}P\{^1H\}$ NMR spectrum of the *mer*-[$RuCl_3$(NO)(dppb)] complex **III**, two doublets are observed (Table 2) and we assume that the more shielded phosphorous is *trans* positioned to NO group (P_d), because the competitive effect between two strong acceptors ligands (P and NO group). In Table 3 there is the complete assignment of carbon and hydrogen signals of the coordinated diphosphine for the *mer*-isomer **III**. This assignment was based on two-dimension $^{31}P–^1H$ HETCORR spectrum, COSY $^1H–^1H$ spectrum and an HMQC $^1H–^{13}C$ experiment. The HMBC $^1H–^{13}C$ spectrum, was used to correct the attribution of the quaternary aromatic carbon.

Table 2
$^{31}P\{^1H\}$ chemical shifts in $CDCl_3$ of the *mer*-[$RuCl_3$(NO)(dppb)] complex

	δ (ppm)	$^2J_{^{31}P–^{13}P}$ (Hz)
P_a	12.80	37.3
P_d	9.96	37.3

Table 3
^1H and ^{13}C chemical shifts in $CDCl_3$ of the *mer*-[$RuCl_3$(NO)(dppb)] complex

Groups	Hydrogen	Carbon 13
CH_2a	3.24 t $J_{^1H–^1H} = 5.94$	26.5 d $^1J_{^{13}C–^{31}P} = 28.0$
CH_2c	1.81–1.92 m	24.9 t(AB) $^2J_{^{13}C–^{31}P} = 3.3$
CH_2d	2.70 t $J_{^1H–^1H} = 5.94$	27.7 dd $^1J_{^{13}C–^{31}P} = 24.7$; $^2J_{^{13}C–^{31}P} = 3.3$
CH_2b	1.96–2.08 m	20.3 d $^2J_{^{13}C–^{31}P} = 3.3$
Ring A		
1′		132.4 d $^1J_{^{13}C–^{31}P} = 49.5$
2′	7.78–7.83 m 4H	133.1 d $^2J_{^{13}C–^{31}P} = 8.2$
3′	7.40–7.47 m 4H	128.7 d $^3J_{^{13}C–^{31}P} = 9.9$
4′	7.47–7.54 m 2H	131.5 d $^4J_{^{13}C–^{31}P} = 2.5$
Ring D		
1″		130.5 d $^1J_{^{13}C–^{31}P} = 50.3$
2″	7.86–7.91 m 4H	134.5 d $^2J_{^{13}C–^{31}P} = 7.4$
3″	7.34–7.40 m 4H	127.7 d $^3J_{^{13}C–^{31}P} = 10.7$
4″	7.40–7.47 m 2H	130.7 d $^4J_{^{13}C–^{31}P} = 3.3$

The numbering scheme of the hydrogen and carbon atoms in compound **III** is shown in Fig. 1.

The limited solubility of the *fac* isomer **I** in most of the usual solvents do not permitted the realization of NMR experiments for the attribution of ^1H and ^{13}C signals.

The proposed structures for complexes **I** and **II** based upon $^{31}P\{^1H\}$ NMR data have been confirmed by X-ray structure measurements. The molecular structures of **I** and **II** are shown in Fig. 2(a) and (b), respectively, together with the numbering scheme of the atoms.

In the *fac*-[$RuCl_3$(NO)(dppb)] isomer **I** the NO is essentially linear with the ruthenium atom [Ru–N–O = 171.8(8)°] and the Ru–Cl [2.418(2), 2.434(3) and 2.355(3) Å, for Cl(1), Cl(2) and Cl(3), respectively]. Ru–N (1.731(8) Å) and Ru–P (2.405(2) and 2.420(2) Å) bond lengths in this nitrosyl complex are comparable to those found for the similar complex *fac*-[$RuCl_3$(NO)(dppm)] [6]. It is interesting to point out

Table 4
Selected bond distances (Å) and selected bond angles (°) for *fac*-[$RuCl_3$(NO)(dppb)] (**I**) and *mer*-[$RuCl_3$(NO)(diop)] (**II**)

fac-[$RuCl_3$(NO)-(dppb)] (**I**)		*mer*-[$RuCl_3$(NO)-(diop)] (**II**)	
Bond distances			
Ru–Cl(1)	2.418(2)	Ru–Cl(1)	2.3810(11)
Ru–Cl(2)	2.434(3)	Ru–Cl(2)	2.4159(12)
Ru–Cl(3)	2.355(3)	Ru–Cl(3)	2.3700(13)
Ru–N	1.731(8)	Ru–N	1.816(5)
Ru–P(1)	2.405(2)	Ru–P(1)	2.5124(11)
Ru–P(2)	2.420(2)	Ru–P(2)	2.3887(11)
N–O	1.124(10)	N–O	1.022(6)
P(1)–C(1)	1.868(10)	P(1)–C(4)	1.842(5)
P(2)–C(4)	1.850(9)	P(2)–C(1)	1.844(4)
P(1)–C(11)	1.817(9)	P(1)–C(111)	1.846(4)
P(1)–C(21)	1.820(10)	P(1)–C(121)	1.827(4)
P(2)–C(31)	1.831(11)	P(2)–C(211)	1.821(4)
P(2)–C(41)	1.831(10)	P(2)–C(221)	1.822(4)
Bond angles			
Cl(1)–Ru–*Cl*(2)	88.99(9)	*Cl*(1)–Ru–*Cl*(2)	91.00(5)
Cl(1)–Ru–*Cl*(3)	88.65(9)	*Cl*(1)–Ru–*Cl*(3)	177.50(5)
Cl(2)–Ru–*Cl*(3)	86.67(10)	*Cl*(2)–Ru–*Cl*(3)	90.10(5)
Cl(1)–Ru–N	86.5(3)	*Cl*(1)–Ru–N	88.51(16)
Cl(2)–Ru–N	86.4(3)	*Cl*(2)–Ru–N	88.68(14)
Cl(3)–Ru–N	171.7(3)	*Cl*(3)–Ru–N	89.27(16)
Cl(1)–Ru–P(1)	174.94(10)	*Cl*(1)–Ru–P(1)	90.86(4)
Cl(1)–Ru–P(2)	87.02(9)	*Cl*(1)–Ru–P(2)	86.89(4)
Cl(2)–Ru–P(1)	91.98(9)	*Cl*(2)–Ru–P(1)	84.83(5)
Cl(2)–Ru–P(2)	174.34(9)	*Cl*(2)–Ru–P(2)	177.90(5)
Cl(3)–Ru–P(1)	86.45(9)	*Cl*(3)–Ru–P(1)	91.48(5)
Cl(3)–Ru–P(2)	97.24(9)	*Cl*(3)–Ru–P(2)	92.00(5)
P(1)–Ru–P(2)	92.36(8)	P(1)–Ru–P(2)	95.13(3)
P(1)–Ru–N	98.5(3)	P(1)–Ru–N	173.47(14)
P(2)–Ru–N	89.3(3)	P(2)–Ru–N	91.33(14)
Ru–N–O	171.8(8)	Ru–N–O	176.0(6)
Ru–P(1)–C(1)	113.9(4)	Ru–P(1)–C(4)	117.02(14)
Ru–P(1)–C(11)	113.9(3)	Ru–P(1)–C(111)	117.40(14)
Ru–P(1)–C(21)	114.8(3)	Ru–P(1)–C(121)	113.35(15)
Ru–P(2)–C(4)	117.2(4)	Ru–P(2)–C(1)	116.62(14)
Ru–P(2)–C(31)	106.7(3)	Ru–P(2)–C(211)	108.72(14)
Ru–P(2)–C(41)	121.6(3)	Ru–P(2)–C(221)	120.28(14)

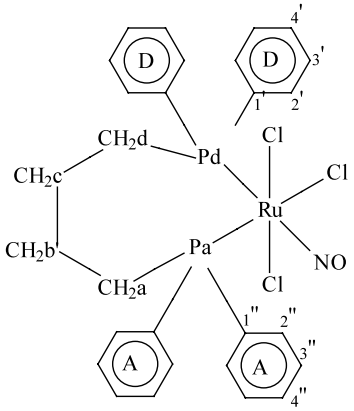


Fig. 1. Scheme of *mer*-[$RuCl_3$(NO)(dppb)], showing proton and carbon numbering.

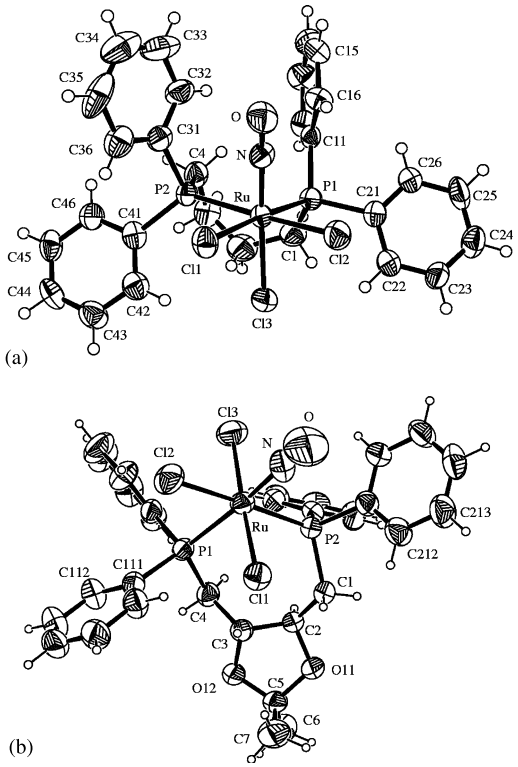


Fig. 2. ORTEP [16] view of *fac*-[$RuCl_3NO$(dppb)] (a) and *mer*-[$RuCl_3NO$(diop)] (b) with 50% probability thermal ellipsoids.

that the distance Ru–Cl(3), the chloride *trans* to NO, is shorter than the distances Ru–Cl(1) and Ru–Cl(2). Here, like in our *fac*-[$RuCl_3$(NO)(dppm)] complex [6] the *trans* influence of the NO group is observed. In the *mer*-[$RuCl_3$(NO)(diop)] isomer **II** the NO is also linear with the ruthenium atom [Ru–N–O = 176.0(6)°] and the Ru–Cl [2.3810(11), 2.4159(12) and 2.3700(13) Å, for Cl(1), Cl(2) and Cl(3), respectively]. Ru–N [1.816(5) Å) and Ru–P (2.5124(11) and 2.3887(11) Å] bond lengths are also comparable to those found for the similar complex *mer*-[$RuCl_3$(NO)(dppp)] [5]. The distance Ru–P(1), P(1) *trans* to the NO in the *mer*-[$RuCl_3$(NO)-(diop)], is much longer than the Ru–P(2) in the same complex. This observation can be ascribed as a consequence to the competition between two good coordinating species (NO group and phosphorus atom) for the electrons of the ruthenium atom. This same situation is found in the *ttt*-[$RuCl_2(CO)_2(PPh_3)_2$] isomer where the CO's *trans* to each other show a longer Ru–C separation than the corresponding separation when the CO is *trans* to the chlorine [17,18]. The NO bond length for complex **I** [1.124(10) Å] is a little longer than the distance 1.06 Å of the free NO^+ group [19] and practically the same NO distance [(1.151(9) Å] was found for the complex *mer*-[$RuCl_3(NO)(AsPh_3)_2$] [5].

The observed Ru–N–O bond angle for the *fac*-[$RuCl_3$(NO)(dppb)] isomer [171.8(8)°] is bigger than the angle of approximately 160.0° for the *mer*-

[$RuCl_3(NO)(dppb)$] isomer [6]. This probably happens because in the *fac* complex the axial NO group is symmetrically surrounded by the phenyl rings and two chloride ligands present in the equatorial plane, such a way the NO group tends to assume an almost linear configuration. In contrast, in the *mer* complex, three chloride ligands and the phenyl rings of the dppb ligand asymmetrically surround the NO ligand. This asymmetry, coupled with the big repulsion between the extensive molecular orbital of NO and the phenyl rings of the dppb ligand, tends to distort the NO group away from the phenyl groups. The bond lengths and bond angles for *mer*-[$RuCl_3(NO)(dppb)$] and for the *mer*-[$RuCl_3(NO)(diop)$] complex are essentially the same except only for the Ru–NO angles. This difference is probably due to the different rigidities of the chains in the dppb and diop ligands since the lengths between the two phosphorus atoms in these biphosphines are practically the same.

In a previous paper [6], we suggested that the faster isomerization process in the *mer*-[$RuCl_3(NO)(dppp)$] compared with the *mer*-[$RuCl_3(NO)(dppb)$] is due to the stronger strain caused by the shorter carbon chain between the phosphorus atoms in the dppp ligand when compared with the dppb molecule. Here we could suggest that the rigidity introduced by the ring present in diop ligand is the principal cause of the absence of the isomerization process in the *mer*-[$RuCl_3(NO)(diop)$], a process that is present in both *fac*- and *mer*-[$RuCl_3(NO)(dppb)$] isomers [6]. The silent EPR of the *fac*-[$RuCl_3(NO)(dppb)$] and the *mer*-[$RuCl_3(NO)(diop)$] complexes confirm the diamagnetic character of them, and consequently the presence of the $\{Ru^{II}–NO^{+}\}$ unit.

Both **I** and **II** complexes exhibit irreversible electrochemical processes. The cathodic waves at -900 and -650 mV, respectively, for the complex **I** and **II** are attributed to the $Ru–NO^{+} \rightarrow Ru–NO^{\circ}$ reduction. No waves corresponding to the metal centers were observed until $+1.4$ V what is consequency of the high stabilization of Ru(II) by the nitrosyl group.

4. Conclusions

The *fac* and *mer*-[$RuCl_3(NO)(dppb)$] isomers coexist in a CH_2Cl_2 solution at room temperature while in refluxing methanol only the *fac* isomer is present. The *mer*-[$RuCl_3(NO)(diop)$] complex does not isomerize at room temperature in CH_2Cl_2. The grater rigidity of the diop ligand, as compared with that of dppb, is probably the principal cause for the absence of the isomerization process of the *mer*-[$RuCl_3(NO)(diop)$] isomer and its high solubility in common organic solvents.

5. Supplementary data

Crystallographic data for structural analysis have been deposited with Cambridge Crystallographic Centre, CCDC No. 171904 for complex **I** and 171905 for complex **II**. Copies of this information may be obtained free of charge from The Director, CCDC, 12 Union Road, Cambidge, CB2 1EZ, UK (fax: +44-1223-336033; e-mail: deposit@ccdc.cam.ac.uk or www: http://ccdc.cam.ac.uk).

Acknowledgements

We thank CNPq, CAPES, FINEP, PRONEX and FAPESP for financial support.

References

[1] P.L. Feldman, O.W. Griffith, D.J. Stuehr, Chem. Eng. 20 (1993) 26.
[2] E. Cullota, D.E. Koshland, Jr., Science 258 (1992) 18.
[3] E.I. Ochiai, J. Chem. Ed. 73 (1996) 130.
[4] G.B. Richter-Addo, P. Ledzdins, Metal Nitrosyls, Oxford University Press, Oxford, 1992.
[5] D.H.F. Souza, G. Oliva, A. Teixeira, A.A. Batista, Polyhedron 14 (1995) 1031.
[6] A.A. Batista, C. Pereira, K. Wohnrath, S.L. Queiroz, R.H. de A. Santos, M.T.P. Gambarella, Polyhedron 18 (1999) 2079.
[7] Enraf-Nonius, COLLECT. Nonius BV, Delft, The Netherlands, 1997–2000.
[8] Z. Otwinowski, W. Minor, H.K.L. Denzo, H.K.L. Scalepack, in: C.W. Carter, Jr., R.M. Sweet (Eds.), Methods in Enzymology, vol. 276, Academic Press, New York, 1997, pp. 307–326.
[9] P. Coppens, in: F.R. Ahmed, S.R. Hall, C.P. Huber (Eds.), Crystallographic Computing, Munksgaard, Copenhagen, 1970, pp. 255–270.
[10] R.H. Blessing, Acta Crystallogr., Sect. A 51 (1995) 33.
[11] G.M. Sheldrick, SHELXS-97. Program for Crystal Structure Resolution, University of Göttingen, Göttingen, Germany, 1997.
[12] G.M. Sheldrick, SHELXL-97, Program for Crystal Structures Analysis, University of Göttingen, Göttingen, Germany, 1997.
[13] L.R. Dinelli, A.A. Batista, K. Wohnrath, M.P. de Araujo, S.L. Queiroz, M.R. Bonfadini, G. Oliva, O.R. Nascimento, P. Cyr, K. MacFarlane, B.R. James, Inorg. Chem. 38 (1999) 5341.
[14] F. Bottomley, Coord. Chem. Rev. 26 (1978) 7.
[15] J.H. Enemark, R.D. Feltham, Coord. Chem. Rev. 13 (1974) 339.
[16] L.J. Farrugia, ORTEP3 for Windows. J. Appl. Cryst., 30 (1997) 565.
[17] M.P. de Araujo, O.M. Porcu, A.A. Batista, G. Oliva, D.H.F. Souza, M. Bonfadini, O.R. Nascimento, J. Coord. Chem. 54 (2001) 81.
[18] L.M. Wilkes, J.H. Nelson, J.P. Mitchener, M.W. Babich, W.C. Riley, B.J. Helland, R.A. Jacobson, M.Y. Cheng, K. Seff, L.B. McCusker, Inorg. Chem. 21 (1982) 1376.
[19] J.E. Huheey, E.A. Keiter, R.L. Keiter, Inorganic Chemistry: Principles of Structure and Reactivity, 4th ed., HarperCollins College Publishers, New York, 1993.

2. Experimental

2.1. General comments

All operations were carried out under nitrogen using Schlenk and vacuum techniques. Nitrogen was dried over molecular sieves. Hexane, tetrahydrofuran and $C_6H_5CH_3$ were distilled over sodium/benzophenone. Acetonitrile was distilled over phosphorus pentoxide. All the solvents were used immediately after distillation or stored under nitrogen over molecular sieves. Ethane-1,2-dithiol ($EDTH_2$), propane-1,3-dithiol ($PDTH_2$) from Aldrich and [$NbCl_2Cp_2$] from Fluka, were used as supplied. Infrared spectra in the 4000–200 cm^{-1} region were recorded on a Perkin–Elmer 283 spectrometer, as a Nujol mull, in CsI plates. C, H, N elemental analyses were performed using a Perkin–Elmer PE-2400 CHN microanalyser. Cyclic voltammetry studies were performed on a Bioanalytical Systems 200 A voltamograph. The potentials were referred to a Ag^0/AgCl electrode with Pt metal as the working electrode. The auxiliary electrode was Pt wire. Solutions were 1 mM in solute and 0.1 M in supporting electrolyte [Bu_4N][PF_6]. The niobium samples and the supporting electrolyte were weighed inside the glovebox. Purified solvents were syringed into the cell containing the supporting electrolyte under a flow of N_2 at the electrochemical instrument bench. Fast atom bombardment mass spectra were recorded on a VG analytical 70-S mass spectrometer. ESR spectra were recorded on a spectrometer built at the Physics Department of Federal University of Minas Gerais, Brazil, utilizing a Varian magneton, a Hewlett-Packard microwave source, a Bruker resonance cavity and as locking EG&G.

2.2. Syntheses

2.2.1. Dithiolate salts

These were prepared by reacting 2 mol of CH_3ONa with 1 mol of the appropriate dithiolate compound ($EDTH_2$, $PDTH_2$) in THF, at room temperature for 2 h. After this time a precipitate was obtained that was separated from the solution and dried in vacuum. The salts (Na_2EDT, Na_2PDT) were characterized as described before [3].

2.2.2. [$NbCp_2PDT$] (**1**)

In a Schlenk flask were loaded 0.13 g (0.85 mmol) of Na_2PDT and 0.25 g (0.85 mmol) of [$NbCl_2Cp_2$], together with 50 ml of $C_6H_5CH_3$. The reaction mixture was left under reflux for 2 h, after which a violet solution was obtained. This was let to cool to room temperature and filtered over neutral alumina and then over celite. Upon addition of C_6H_{14} [$NbCp_2PDT$] was obtained in 71% yield. IR (cm^{-1}, Nujol): $\nu_{Nb-S} = 330$. ^1H NMR (δ, C_3H_6O-d_6): 6.22 (s, C_5H_5), 2.11 and 2.00 (t, 4H, $SCH_2CH_2CH_2S$), 1.59 (m, $SCH_2CH_2CH_2S$). ^{13}C NMR (δ, C_3H_6O-d_6): 112.04 (C_5H_5), 28.37 ($SCH_2CH_2CH_2S$), 18.48 ($SCH_2CH_2CH_2S$). EPR: $\langle A\rangle iso = 90.5$ G, $g = 1.948$, 10 lines. *Anal*. Calc. for $C_{13}H_{16}NbS_2$ (Found): C, 47.41 (47.44); H, (4.85) 4.89%. FAB mass spectrum: $m/z = 328.9$ (100%) [M^+, $C_{13}H_{16}NbS_2$].

2.3. Crystallographic studies

Dark violet crystals of [$NbCp_2PDT$] were mounted at room temperature, in mineral oil, on a glass fiber, and quickly cooled to −95 °C. Preliminary examination and data collection were performed on a Siemens P4 diffractometer using Mo Kα ($\lambda = 0.71073$ Å) radiation, a graphite crystal monochromator, employing ω–2θ scanning techniques with a variable scan rate (2.27°–25.00° min^{-1}). Details of the crystallographic data collection and refinement are summarized in Table 1. The molecular structure was solved by direct methods and was refined employing the SHELXS-97 [6] and SHELXL-97 programs, respectively [7]. Complex **1** crystallizes in space group $P2(1)/n$. A total of 2439 reflections were collected of which 2267 were independent and 1994 were flagged as observed. Cell constants were obtained from the refinement of 146 reflections. The structure was refined on F^2, against all reflections, by full-matrix least-square calculations. The weighted R-factors wR and GOF are based on F^2 and conventional R-factors are based on F, with F set to zero for negative F^2.

Table 1
Summary of crystallographic data of complex **1**

Empirical formula	$C_{13}H_{16}NbS_2$
Formula weight	329.29
Temperature (°C)	−80
Crystal system	monoclinic
Space group	$P2(1)/n$
a (Å)	7.9072(16)
b (Å)	13.873(3)
c (Å)	11.7673(15)
α (°)	90
β (°)	93.78
γ (°)	90
Z	4
V (Å^3)	1288.0(4)
Radiation	Mo Kα (0.71073)
D_{calc} (g cm^{-3})	1.698
μ (cm^{-1})	12.28
θ_{max} (°)	25
R, R_w	0.0274, 0.0680
Reflections (collected/independent)	2439/2267
Parameters refined	146
Goodness-of-fit	1.184

2.4. Computational details

All quantum chemistry calculations were performed at Hartree-Fock level employing an effective core potentials (ECP) [8] to describe the average eletrostatic potential, due to the core electrons of C, S, and Nb atoms. The GAMESS [9] program, working in a direct SCF mode [10] was used for all computations. The need for using ECPs comes from, on one hand, the large computational demands for an all electron evaluation of the electronic charge density and the corresponding molecular geometry optimization thereof for the size of molecules reported in this work and, on the other hand, for an effective inclusion of some relativistic correction on the total electronic energy required by the heavy niobium atom [8a]. The SBKJ effective core potentials [8a] were used throughout for C, S and Nb atoms, and the respective atomic basis set were taken as the ECP/SBK(d) sp(4-21G+)d(3-1G+) splitted valence plus diffuse basis for niobium [8b] and sp(4G) plus d polarization function for sulphur ($\alpha d(\mathrm{S}) = 0.65$) and carbon ($\alpha d(\mathrm{C}) = 0.8$) atoms. For the hydrogens a 3-1G* set of Pople [11] plus polarization was used.

A doublet spin ground state electronic configuration is expected for both [$NbCp_2EDT$] and [$NbCp_2PDT$], due the odd number of electrons and the +4 formal oxidation state of the niobium metallic center. Stable molecular conformations were sought using restricted open shell Hartree-Fock (ROHF) [12a] energies and wave functions, analytic molecular gradients and numeric hessians.

The ROHF method was chosen because it warrants the correct spectroscopic doublet state of the molecules for all stationary and distorted molecular geometries, although an unrestricted Hartree-Fock (UHF) [12b] spin polarized electronic density will give a lower electronic energy for this doublet electronic state and might induce some change on the optimized ROF geometries. However, based on the considerations and results presented in what follows, keeping the calculations at an uncorrelated Hartree-Fock level, the ROF/ECP appears to be a safer method for computing the electronic structure and molecular equilibrium geometries obtained thereof, since this wave function displays the expected correct qualitative valence orbital space structure, including there the SOMO (single occupied molecular orbital) molecular orbital, for the present class of cyclopentadienyl dithiolate bent metallocenes. For bent metallocenes compounds it has been shown [13] that the occupation of the metal d_{xy} SOMO drives the extent of the L–M–L′ bond angle: the ionized (or oxidized) HOMO$\{-1\}$ molecular state is expected to tight the L–M–L′ bond angle to values close to 80° [13], a reduction of about 10°–20° as compared with the parent neutral (or non-oxidized) species. Any resulting ROHF/UHF change on the metal d_{xy} SOMO orbital electronic occupation may then produce slightly different molecular equilibrium geometries, if this effect is not fully or partially compensated by equivalent changes on other key occupied molecular orbitals. In order to access possible resulting changes induced on the issued optimized ROHF stable molecular structure, induced by relaxing the electronic orbital doubly occupation restriction, we have computed their UHF energies, charge and spin densities, at their respective found stable ROHF molecular conformations. The net spin densities may qualitatively be used to estimate the atomic metallic and non-metallic center contribution. The results showed a ROHF/ECP SOMO orbital displaying the expected correct qualitative feature of a major content of Nb d_{xy} atomic orbital whereas within the UHF/ECP SOMO, unexpectedly, a large amount of the ligand atomic sulfur p_x and p_y has been built in. Actually, the UHF/ECP solution moves the molecular orbital which has the largest Nb d_{xy} contribution downward in energy leaving it as a doubly occupied molecular orbital instead. It should be noticed that, in spite of this qualitative contradicting results, quantitatively, the UHF SOMO Koopmans ionization potential is found to be much better in agreement with the experimental result than the ROHF SOMO Koopmans ionization potential (vide infra). These results point out the need of inclusion of some correction for the correlation energy, a point which has not been further pursuit in this work [14]. Here, the role of the electronic correlation energy was only partially accounted for through a simple restricted and unrestricted open-shell MP2 [15] energies and natural orbitals analysis, obtained at the ROHF stable molecular geometries.

Stable geometric unconstrained optimization searches were performed for molecular structures; a C_1 symmetry point group symmetry was used throughout. The starting geometries were guessed for a distorted tetrahedron environment around the Nb atom bounded to the two dithiolate ligands and two Cp rings. These were initially disposed in a more symmetric C_s or C_2 arrangement. After locating the equilibrium geometries, the potential energy profile along the relative internal Cp–Cp ring rotation were evaluated for fixed Nb–EDT/PDT metallocene stable ring fragment in order to ascertain that no other minimum energy molecular structure along this path could be found. Indeed, no such structure could be found (Fig. 8), a result that indicates that the final optimized geometries most certainly were not propensitly caused by the initial guess. The [$NbCp_2EDT$] five member ring was refined for a starting twisted conformation, whereas the chair, boat and twisted [$NbCp_2PDT$] six member ring conformations were initially guessed and optimized. A tight gradient geometry convergency criterion of 10^{-7} was requested, and all stable conformations were confirmed as being true relative minima at the respective electronic

potential energy hypersurfaces, by their vibrational normal mode analysis. The vibrational frequencies for all found structures were computed as real numbers.

3. Results and discussion

The complexes that were studied in the present work are shown in Fig. 1.

The solution EPR spectrum of complex **1**, at room temperature, showed the expected ten lines for a niobium paramagnetic species, $I = 9/2$, with $g_{iso} = 1.9483$ and $A_{iso} = 90.5$ G (Fig. 2). The spectrum that was taken at 14 K (Fig. 3), has a much more intense central line than the other ones. A solid solution of a Nb(IV) paramagnetic ion, d^1 configuration, is formed, and the spectrum becomes the sum of several EPR resonances, due to the various directions of the anisotropic spin magnetic momentum, having different $g_\perp$ and $g_\parallel$ factor components. This behavior has been observed before, for instance for complexes [Nb(O_2C-NEt)$_4$] [16], [Nb(hfacac)$_4$] [16] and [YTc_2Cl_8]·$9H_2O$ [17].

In Table 2 are listed some related complexes to **1** with the g_{iso} and A_{iso} values, obtained from the EPR spectra. As can be observed the g_{iso} values for complex **1** is smaller than the other ones. Smaller values of g are related to the unpaired electron be more tightly bound to the metal [19]. In the other complexes the electron is expected to be more delocalized over the ligands. For example, if one compares complexes **1** and [$NbCp_2(SPh)_2$] [4], it is expected for the first a g value lager then the former as the PDT^{2-} ligand is a better electron donor than SPh. Indeed, this is the observed tendency.

3.1. X-ray diffraction analysis

Crystals of complex **1** suitable for X-ray analysis were obtained from a dichloromethane/ether 3:1 solution, at 5 °C. In Fig. 4 is shown a ZORTEP for **1**, in the chair form, and in Table 3 is shown selected bond angles and distances.

The geometry around niobium is tetrahedral with minor distortions, S–Nb–Cp(1) = 104.2° (mean value) and S–Nb–Cp(2) = 108.85° (mean value). The bond angle Cp(1)–Nb–Cp(2) = 133.5° is in the range normally observed for related niobium bent metallocenes [4,20,21]. The S(1)–Nb–S(2) bond angle of 87.86° is within the range of S–M–S angles for related d^1 complexes, that is, bigger than 80° [13,21–23], and is close to the one found in complex [VCp_2PDT], 86.91° [24]. The Nb–S bond distances were determined to be 2.487 and 2.478 Å, and are smaller than the values found for niobium metallocenes complexes containing non-chelating ligands [21,22]. The same was observed for the [VCp_2PDT] complex and was attributed to the greater basicity of the chelating ligand.

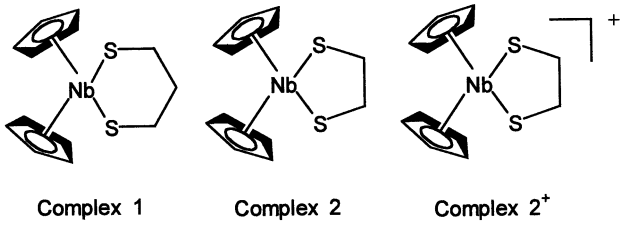


Fig. 1. Complexes studied in the present work.

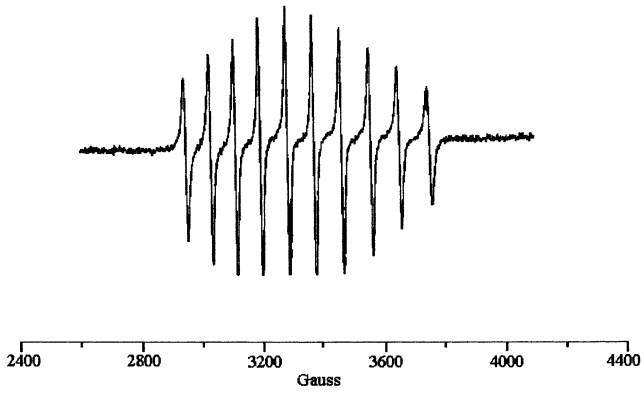


Fig. 2. EPR spectrum of complex **1** at room temperature.

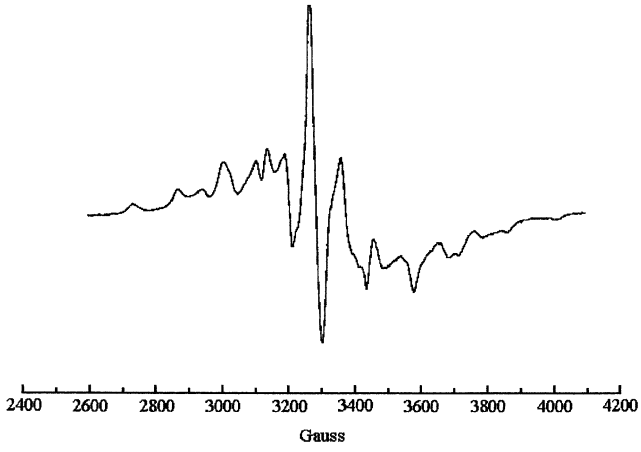


Fig. 3. EPR spectrum of complex **1** at 14 K.

Table 2
g and A (G) values for selected compounds

Complex	g	A	Reference
$Cp_2Nb(SPh)_2$	1.990	85.0	[4]
Cp_2Nbdmit [a]	1.988	83.5	[16]
Cp_2Nbdmio [b]	1.988	83.2	[16]
Cp_2Nbddt [c]	1.999	79.5	[16]
Cp_2NbPDT	1.948	90.5	this work

[a] dmit = 1,3-dithiol-2-thiona-4,5-dithiolate;
[b] dmio = 1,3-dithiol-2-ona-4,5-dithiolate;
[c] ddt = 5,6-dihydrido-1,4-dithiin-2,3-dithiolate.

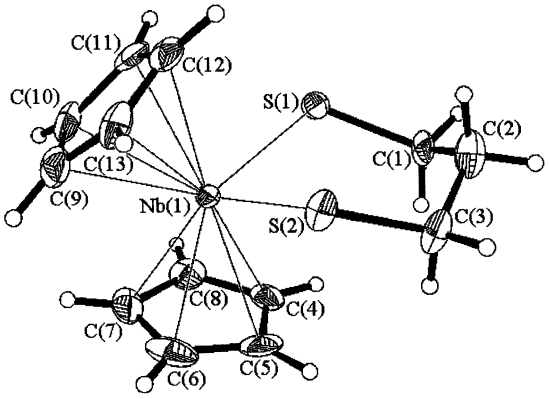


Fig. 4. ZORTEP for complex **1** with ellipsoids at 30% probability.

Table 3
X-ray selected bond distances (Å) and angles (°) for complex **1**

Bond distances	
Nb–S(1)	2.4785(11)
Nb–S(2)	2.4876(11)
C(1)–S(1)	1.827(4)
C(3)–S(2)	1.821(4)
C(1)–C(2)	1.524(6)
C(2)–C(3)	1.516(7)
Bond angles	
S(1)–Nb–S(2)	87.86(4)
Cp(1)–Nb–Cp(2)	133.10(1)
Cp(1)–Nb–S(1)	104.7(4)
Cp(1)–Nb–S(2)	103.7(3)
Cp(2)–Nb–S(1)	108.8(5)
Cp(2)–Nb–S(2)	108.9(3)
Nb–S(1)–C(1)	111.33(14)
Nb–S(2)–C(2)	109.85(15)

3.2. ECP quantum results

Theoretical calculations were performed in order to determine an equilibrium molecular geometry for the hypothetical complex **2** and for complex **1**, to allow a comparison of the data for these two complexes according to this technique, and with the experimental data obtained from the X-ray investigation, for the latter. Also, theoretical calculations were performed for the hypothetical cationic analog of **2**, complex $\mathbf{2}^+$. This was done in order to verify the variation of the S–Nb–S angle in these complexes. According to theoretical calculations and as observed experimentally for a number of complexes, the X–M–X angle opens up, as a result of less electronic repulsion, on going from a d^1 to a d^0 complex [13]. In Table 4 are shown the data obtained and in Fig. 5 the optimized geometry of **2**.

At the end of the optimization process, whereby no other symmetry constraints but C_1 has been required, the minimal energy molecular structure was found to have a C_2 symmetry, with the symmetry axis lying along the line connecting the niobium atom and midway of the C–C bond. The L1–Nb–L2 bond angles average to 107.8° for L1 = S and L2 = Ctr(Cp) (Ctr is the Cp's

Table 4
Selected theoretical calculations bond distances (Å) and angles (°) for complexes **1**, **2** and $\mathbf{2}^+$

	1	**2**	$\mathbf{2}^+$
Bond distances			
Nb(1)–S(1)	2.548	2.550	2.492
Nb(1)–S(2)	2.547	2.549	2.489
Nb(1)–Ctr–Cp(1′)	2.170	2.170	2.137
Nb(1)–Ctr–Cp(2′)	2.163	2.171	2.137
S(1)–S(2)	3.577	3.348	3.386
S(2)–C(1)	1.827	1.827	1.837
S(1)–C(2)	1.827	1.827	1.837
C(1)–C(2)		1.531	1.539
C(1)–C(3)	1.539		
Bond angles			
Nb(1)–S(1)–C(4)	111.4	104.2	100.6
CtrCp(1′)–Nb(1)–CtrCp(2′)	132.4	132.0	133.3
S(1)–C(2)–C(1)		111.9	110.2
S(1)–C(2)–C(3)	116.8		
S(1)–Nb(1)–S(2)	89.2	82.1	85.6
S(1)–Nb(1)–CtrCp(1′)	108.6	108.6	111.0
S(1)–Nb(1)–CtrCp(2′)	104.8	107.1	102.8
S(2)–Nb(1)–CtrCp(1′)	108.6	107.1	102.7
S(2)–Nb(1)–CtrCp(2′)	104.8	108.6	111.1
Nb(1)–S(2)–C(1)	111.2	104.1	100.6
S(2)–C(1)–C(3)	116.8		
S(2)–C(1)–C(2)		111.9	110.1
Torsion angles			
S(1)S(2)C(3)–H(31)	86.9		
S(1)S(2)C(3)–H(32)	−19.3		
H(26)C(2)C(1)–H(29)	359.6	174.2	179.7
H(27)C(2)C(1)–H(29)	359.4	296.8	299.2
CtrCp(1′)Nb(1)CtrCp(2′)–C(6)	179.9		
Offset C–CtrCp(1′):CtrCp(2′)–C	39.4	−22.5	18.8
C(2)–CtrCp(1′):CtrCp(2′)–C(12)	0.82	16.6	57.6

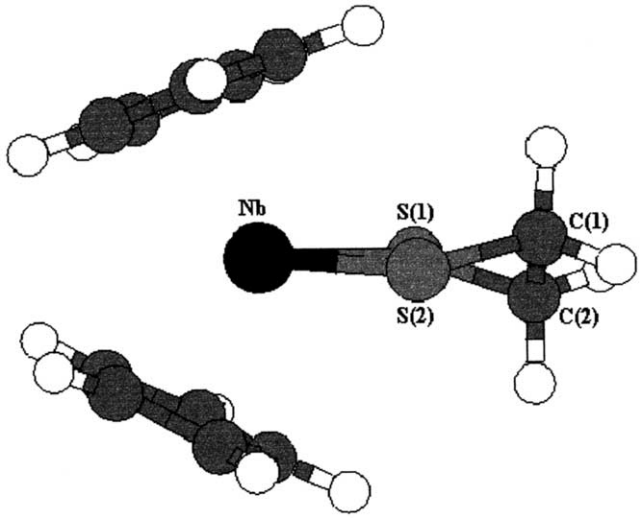


Fig. 5. Proposed molecular structure for complex **2** according to theoretical calculations.

centroid), and for L1 = L2 = S it was found to be 82.1°, according to the smaller size of the chelate ring. The Ctr(Cp)–Nb–Ctr(Cp) bond angle of 132.0° is in the range normally observed for related niobium bent metallocene complexes [4,20,21]. The calculated Nb–S and Nb–Ctr(Cp) equilibrium bond distances are 2.55 and 2.17 Å, figures that are in the range observed for other compounds [4,20,21]. The metal ethanedithiol five member ring adopts a twisted conformation, with the two carbon atoms lying out the S–Nb–S plane by ± 12.5°, respectively, and typical values are obtained for the included interatomic distances, 1.83 (S–C), 1.53 (C–C) and 1.09 Å (C–H). Actually, a pair of interconverting stable twisted conformations are possible, λ and Δ [25]. Fig. 5 represents the λ conformation. These two minima are separated by a ROHF/ECP barrier of 2997 cm^{-1}, as can be seen in Fig. 6.

This value should be taken as an upper limit for the correct inversion barrier energy since it has been evaluated for fixed Cps ligands spatial arrangement: as λ/Δ interconverting pseudo-rotation angle, θ, was swept, a semi-empirical (PM3 hamiltonian) re-optimization for the bond and torsion angles at the Nb(SCH_2CH_2S) ring was allowed. Besides, a differential contribution from the correlation energy may reduce the quoted interconvertion energy barrier by about 10%. The harmonic vibrational distortion mode around the λ or Δ equilibrium geometry has a ROHF/ECP frequency of 280 cm^{-1}. Combined, these data thus indicate a fairly slow interconversion rate between the two conformers at room temperature; the thermal energy KT is about 190 cm^{-1}. There are two rigid Cp pseudo-rotation modes with respect to a frozen Nb(SCH_2CH_2S) equilibrium

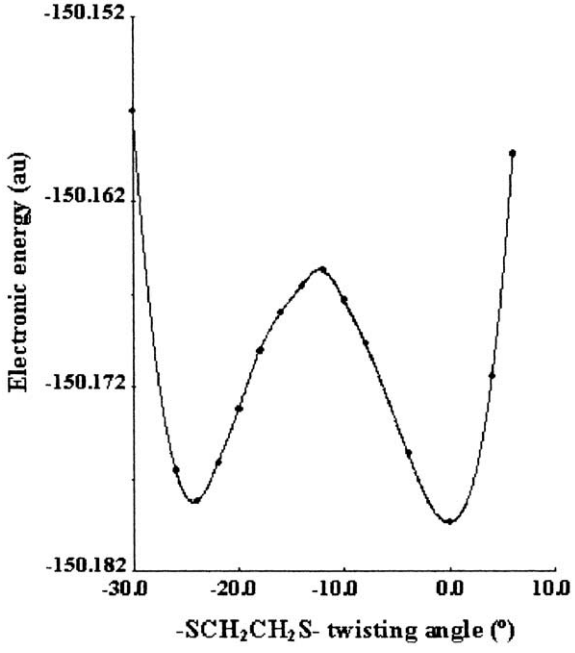


Fig. 6. Complex **2** ROHF/ECP ring puckering energy.

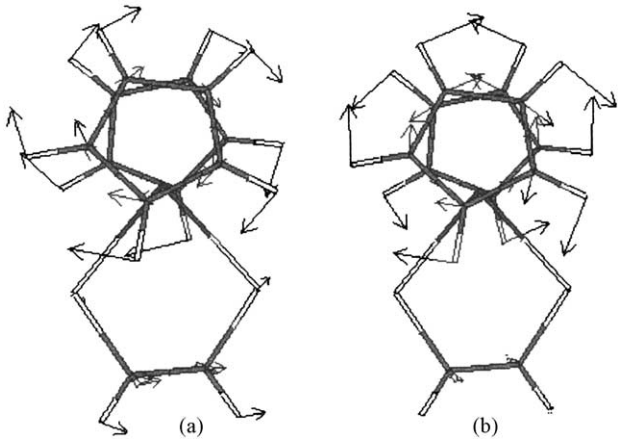


Fig. 7. Cp pseudo-rotation modes: (a) in phase clockwise rotation; (b) out of phase clockwise rotation.

conformation. The first corresponds to an in phase clockwise rotation mode with an harmonic frequency as low as 30 cm^{-1} (Fig. 7(a)), whereas the second corresponds to an out-of-phase clockwise-counter rotation with a harmonic frequency of 32 cm^{-1} (Fig. 7(b)).

The in-phase Cp–Cp pseudo-rotation leads to a breakdown of the overall C_2 molecular symmetry. The ROHF/ECP energy barrier along the out-of-phase Cp–Cp pseudo-rotation was computed to be only 1049 cm^{-1} (Fig. 8).

The maximum in Fig. 8 corresponds to the [$NbCp_2(SCH_2CH_2S)$] conformation with the two Cp–Cp rings aligning each other such that each sulphur atom is surrounded by only two equidistant Cp's

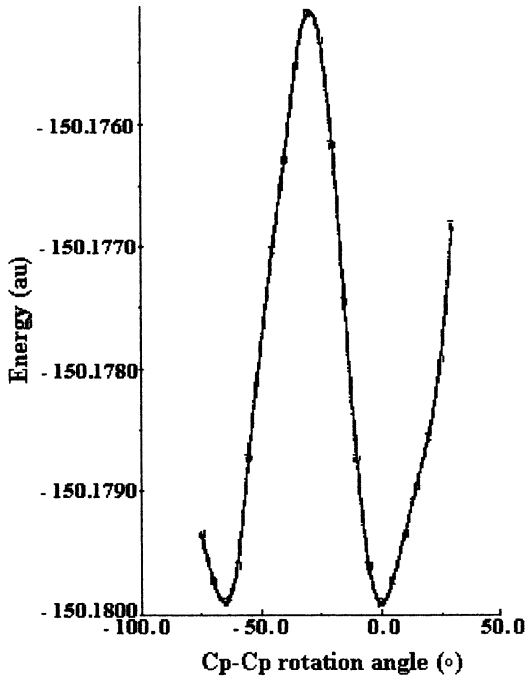


Fig. 8. Complex **2** ROHF/ECP electronic energy along a Cp–Cp pseudo-rotation motion.

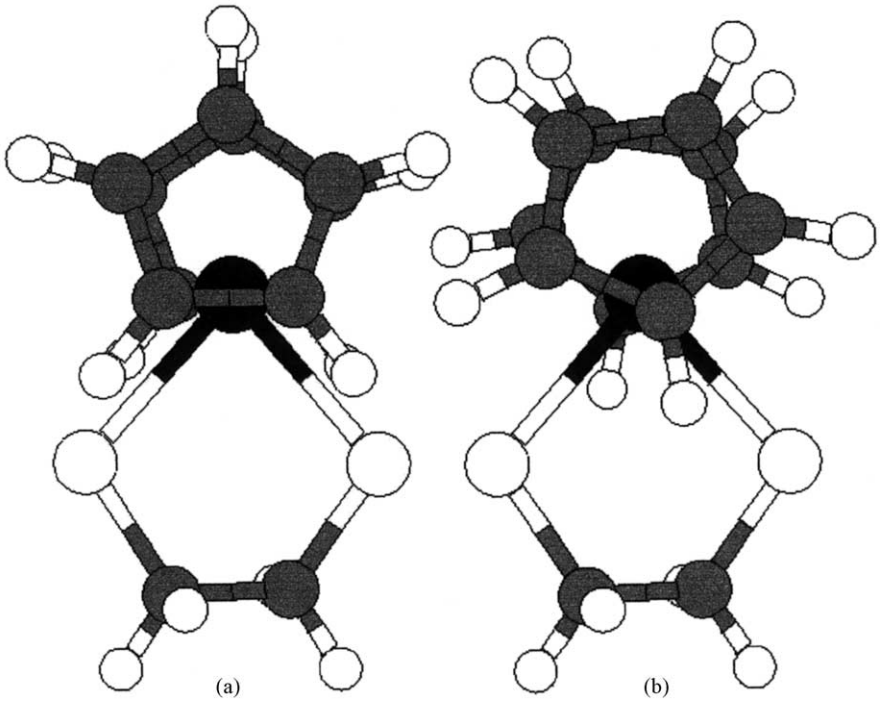


Fig. 9. (a) Conformation adopted by complex **2** at the maximum Cp–Cp rotation angle shown in Fig. 8; (b) 180° Cp–Cp ring in phase rotation of the structure shown in Fig. 8.

hydrogen atoms (Fig. 9(a)). The 180° Cp–Cp ring in phase rotation of the previous molecular structure (Fig. 9(b)), corresponds to the +10° pseudo-rotation angle in Fig. 8, and the asymmetry of the potential energy curve seen at about 20°, would correspond to the mirror [$NbCp_2(SCH_2CH_2S)$] equilibrium structure except for the restriction that the Nb(SCH_2CH_2S) five member rings has been kept frozen.

A molecular dipole moment of 4.94 D is calculated for [$NbCp_2(SCH_2CH_2S)$], where the partial negative charge is distributed over the Cp rings. The outermost single occupied molecular orbital (SOMO) has a restricted Hartree-Fock orbital energy of -3140 cm^{-1} whereas the spin polarized unrestricted solution sum up $-62\,370$ cm^{-1}. This gives a fairly large 4.2 eV of spin correlation energy for the UHF result. The adiabatic ΛSCF first ionization potential energy of [$NbCp_2(SCH_2CH_2S)$] is computed as being 6.4 eV which favours the UHF Koopmans ionization energy of 7.7 eV, as above. Despite of the bad performance of the ROHF calculation for describing the SOMO energy orbital, the UHF spin contamination is only 0.034 ($\langle S^2\rangle$UHF) = 0.784 to be compared with the spectroscopic ($\langle S^2\rangle$ROHF = 0.7) of an electronic doublet state), an indication that the total ROHF and UHF wave functions have about the same quality. The Mulliken atomic net spin population over niobium is +0.95 and +1.45 for the ROHF and UHF wave functions, respectively, where an electronic density withdrawing, mostly from the sulphur atoms, is responsible by the large UHF spin density.

The ECP/Hartree-Fock 50–4000 cm^{-1} calculated infrared spectrum for complex **2**, showed two groups of strong bands at 925 and 3230 cm^{-1} and a few groups of medium intensity bands. The two bands that are seen lying around 273 and 370 cm^{-1} that are formed by individual vibrational excitations on mainly six normal modes that contain, each, Cp ring tilting, ethylenic HCH wagging, the five member Nb(SCH_2CH_2S) ring deformation and distortion due to S–Nb–S symmetric (351 cm^{-1}) and antisymmetric (267, 283 cm^{-1}) stretching and in-plane S–Nb–S bending (270, 318 cm^{-1}) modes. At 366 cm^{-1} a vibrational transition occurs that can be assigned to an antisymmetric stretching mode for pseudo-triatomic Cp–Nb–Cp. The strong band around 925 cm^{-1} is composed of four peaks due to Cp's CCH out-of-plane angular deformation. The weak band about 1120 cm^{-1} contains excitations on Cp's in-plane CHH bending, rocking and HCCH scissoring modes. At 1443 cm^{-1} a week band is seen for the HCH ethylenic wagging mode, at 1590 cm^{-1}, a weak one, for the ethylenic HCH in-plane bending modes and at 1600 cm^{-1} Cp's C=C stretching and HCC. At higher energy, the CH stretching modes can be found: the ethylenic CH vibration modes gives the strong and medium intense bands lying between 3204 and 3287 cm^{-1} and the weak band around 3427 and 3478 cm^{-1} corresponds to Cp's CH stretching modes. For the [$NbCp_2$PDT] complex the following bands were observed: $\nu_{Nb-S} = 330$ cm^{-1}; $\delta_{C-H} = 1010$ cm^{-1} (in plane); $\delta_{C-H} = 870$ and 735 cm^{-1} (out of plane); $\nu_{C=C} = 1430$ cm^{-1}; $\nu_{C-H} = 3080$

cm^{-1}. It can be observed that there is a good agreement between the experimental IR data for complex **1** with the theoretical ones for complex **2**.

The determined geometry around niobium in complex **1** was in good agreement with the results obtained from the X-ray experiment. As can be observed, the bond distances and angles determined by this technique differed only slightly from the values obtained from the X-ray diffraction studies (Table 4). A comparison of the data for complexes **1** and **2**, according to the theoretical calculations, showed that, as expected, the S–Nb–S angle decreased from 89.1° to 82.1°, due to the smaller size of the chelate ligand. However, the bond distances did not differ at all.

For complex $\mathbf{2}^{+}$, the geometry is more distorted from the tetrahedral as the angles S(22)–Nb–Cp(2) and S(23)–Nb–Cp(1) were found to be 102.8° and 102.7°, respectively. The S–Nb–S angle was found to be bigger, 85.6°, than in **2**, as predicted [22], and the bond distances, smaller.

3.3. Cyclic voltammetric studies

The voltammogram for complex **1** showed two reversible waves with defined anodic and cathodic peaks with $E_{1/2} = -0.29$ and $E_{1/2} = -1.48$ V that were attributed to the redox process shown below:

$$Cp_2Nb(SCH_2CH_2CH_2S)^{+}_{d^0} \overset{-0.29\ V}{\rightleftharpoons} Cp_2Nb(SCH_2CH_2CH_2S)_{d^1} \overset{-1.48\ V}{\rightleftharpoons} Cp_2Nb(SCH_2CH_2CH_2S)^{-}_{d^2}$$

The potential of −1.48 V for the process Nb(IV)⇔Nb(III) is much higher than the values described in the literature for other bismetallocene complexes such as $[NbCp_2(SPh)_2]$ [4], $[NbCp_2dmit]$ [17] and $[NbCp_2ddt]$ [18]. This difference can be ascribed to the fact that in complex **1** the electron is more tightly bound to the metal, in agreement with the results obtained from the EPR data.

4. Conclusions

The six member niobium metallacycle complex $[NbCp_2PDT]$ is reported for the first time and although we have tried to obtain the five member analog, $[NbCp_2EDT]$, we were unsuccessful, as it was always obtained as a mixture together with the alkoxide complex. Semi-empirical calculations for **2** showed that the five member ring adopts a twisted conformation, with the carbon atoms lying above and below the S–Nb–S plane by ±12.5°, leading to the conformers λ and Δ, that are separated by an energy potential barrier of 8.6 kcal mol^{-1}. According to the g values obtained from the EPR spectra and confirmed by the results obtained from cyclic voltammetric studies, in niobium (IV) complexes, paramagnetic species, that have good electron donors as ligands, the unpaired electron is more tightly bound to the metal. As observed by others [18] and confirmed by this work, niobium complexes that have aliphatic thiolate ligands are very susceptible to hydrolysis originating the alkoxo analog complex very easily, being very difficult to handle and to be obtained in a pure form.

5. Supplementary material

A table of complete crystallographic data, tables of fractional atomic coordinates for all atoms, complete list of bond distances and angles and tables of anisotropic displacement parameters, have been deposited with the Cambridge Crystallographic Data Centre, CCDC No. 150217 for complex **1**. Copies of this information are available, free of charge, from The Director, CCDC, 12 Union Road, Cambridge, CB2 1EZ, UK (fax: +44-1223-336033; e-mail: deposit@ccdc.cam.ac.uk or www: http://www.ccdc.cam.ac.uk). Table of complete theoretical calculations data for complexes **1**, **2** and $\mathbf{2}^{+}$ can be obtained from the authors upon request.

Acknowledgements

The agencies Fapemig, CAPES, CNPq and CENAPAD/MGCO are thanked for their support.

References

[1] (a) J.A. Kovacs, R.H. Holm, Inorg. Chem. 26 (1987) 711; (b) J.R. Rambo, J.C. Huffman, G. Christou, J. Am. Chem. Soc. 111 (1987) 8027.
[2] N.P. Azevedo, A.R.G. Lopes, R.M. Silva, N.L. Spezilai, A. Abras, M. Hörner, R.A. Burrow, J. Braz. Chem. Soc. 9 (1998) 279.
[3] A.P.G. Sousa, R.M. Silva, A. Cesar, J.L. Wardell, J.C. Huffman, A. Abras, J. Organomet. Chem. 605 (2000) 82.
[4] M.Y. Darensbourg, R. Silva, J. Reibenspies, C.K. Prout, Organometallics 8 (1989) 1315.
[5] R.M. Silva, J.C. Huffman, Polyhedron 18 (1999) 2823.
[6] G.M. Sheldrick, SHELXS-97, program for the solution of crystal structures, Universität Göttingen, 1997.
[7] G.M. Sheldrick, SHELXL-97, program for the solution of crystal structures Universität Göttingen, 1997.
[8] M.W. Schmidt, K.K. Baldridge, J.A. Boatz, S.T. Elbert, M.S. Gordon, J.J. Jensen, S. Koseki, N. Matsunaga, K.A. Nguyen, S. Su, T.L. Windus, M. Dupuis, J.A. Montgomery, J. Compt. Chem. 14 (1993) 1347.
[9] J. Almlof, K. Faegri, J. Compt. Chem. 3 (1982) 385.

[10] (a) W.J. Stevens, H. Basch, M. Krauss, P. Jasien, Can. J. Chem. 70 (1992) 612;
(b) W.J. Stevens, H. Basch, M. Krauss, J. Chem. Phys. 81 (1984) 6026.
[11] W.J. Hehre, R. Ditchfield, R.F. Stewart, J.A. Pople, J. Chem. Phys. 52 (1970) 2769.
[12] (a) C.C. Roothaan, Rev. Mod. Phys. 23 (1951) 69;
(b) J.A. Pople, R.K. Nesbet, J. Chem. Phys. 22 (1954) 571.
[13] (a) R. Hoffman, J.W. Lauher, J. Am. Chem. Soc. 98 (1976) 1729;
(b) J.L. Petersen, L.F. Dahl, J. Am. Chem. Soc. 197 (1975) 6416;
(c) L.F. Dahl, J.L. Petersen, D.L. Lichtenberger, R.F. Fenske, J. Am. Chem. Soc. 97 (1975) 6433.
[14] For instance, DFT/B3LYP settle these difficulties, as we have seen through the calculations we are currently developing for an ab-initio evaluation of the [$NbCp_2PDT$] and [$NbCp_2EDT$] g and A hyperfine coupling constants ESR parameters.
[15] (a) T.J. Lee, D. Jayatilaka, Chem. Phys. Lett. 201 (1993) 1;
(b) T.J. Lee, A.P. Rendell, K.G. Dyall, D. Jayatilaka, J. Chem. Phys. 100 (1994) 7400.
[16] F. Calderazzo, U. Englert, C. Maichle-Mössmer, F. Marchetti, G. Pampaloni, D. Petroni, C. Pinzino, J. Sträle, G. Tripepi, Inorg. Chim. Acta 270 (1998) 177.
[17] F.A. Cotton, E. Pedersen, Inorg. Chem. 14 (1975) 383.
[18] W.E. Lindsell, G.M. Rosair, M.A. Spence, J. Chem. Soc., Dalton Trans. (1998) 3281.
[19] F. Guyon, J. Amaudrut, M.-F. Mercier, J. Organomet. Chem. 465 (1994) 187.
[20] M.Y. Darensbourg, C.J. Bischoff, S.A. Housliston, M. Pala, J. Reibenspies, J. Am. Chem. Soc. 112 (1990) 6905.
[21] O.M. Kekia, A.A.L. Rheingold, Organometallics 16 (1997) 5142.
[22] K.C. Prout, S.T. Cameron, R.A. Forder, R.S.R. Critchley, B. Denton, G.V. Rees, Acta Crystallogr., Sect. B 30 (1974) 2290.
[23] E.G. Muller, S.F. Watkins, L.F. Dahl, J. Organomet. Chem. 11 (1976) 73.
[24] D.W. Stephan, Inorg. Chem. 31 (1992) 4218.
[25] F.A. Cotton, G. Wilkinson, Advanced Inorganic Chemistry, 6th ed., Wiley, New York, 1988, p. 54.

2. Experimental

2.1. Physical measurements and materials

Elemental analyses were carried out using a Perkin–Elmer 2400 II elemental analyser. Infrared spectrum was recorded on a Perkin–Elmer 883-Infrared spectrophotometer in the range 4000–200 cm^{-1} as KBr pellets. $Ca(NO_3)_2 \cdot 2H_2O$ (Lancaster), 1,10-phenanthroline and $K_3[Fe(CN)_6]$ (Loba Chemie. India) were obtained commercially and used as received.

2.2. Synthesis of $[(Phen)_2(H_2O)_2CaNC(NC)_4FeCN\text{-}Ca(OH_2)(Phen)_2NO_3] \cdot H_2O$

An aqueous solution (10 ml) of $K_3[Fe(CN)_6]$ (0.33 gm, 1 mmol) was added to a stirred mixture of 10 ml aqueous solution of $Ca(NO_3)_2 \cdot 2H_2O$ (0.40 gm, 2 mmol) and 15 ml methanolic solution of 1,10-phenanthroline (0.79 gm, 4 mmol). On slow evaporation of the solution, at r.t., the orange crystals appeared. The crystals were washed with water and dried in air and used for X-ray analysis. *Anal.* Found: C, 56.39; H, 3.32; N, 18.11.Calc. for $C_{54}H_{40}Ca_2FeN_{15}O_7$: C, 56.54; H, 3.51; N, 18.30%.

2.3. X-ray crystallography

Intensity data for an orange block ($0.29 \times 0.32 \times 0.36$ mm) were collected at 173 K on a Rigaku AFC7R diffractometer employing Mo Kα radiation (λ 0.71073 Å) and the ω–2θ scan technique such that θ_{max} was 27.5°. Corrections were made for Lorentz and polarisation effects [22], and for absorption [23]. Of the 12 241 reflections measured, 11 705 were unique and of these, 8157 satisfied $I > 2.0\sigma(I)$ criterion of observability. Crystal data and refinement details are given in Table 1.

Table 1
Crystallographic data for **1**

Empirical formula	$C_{54}H_{40}Ca_2FeN_{15}O_7$
Formula weight	1147.02
Temperature (K)	173
Wavelength (Å)	0.71073
Crystal system	Triclinic
Space group	$P\bar{1}$
Unit cell dimensions	
a (Å)	12.400(2)
b (Å)	19.757(6)
c (Å)	10.902(1)
α (°)	96.86(2)
β (°)	98.04(1)
γ (°)	75.89(2)
Volume (Å^3)	2555(1)
Z	2
μ (Mo Kα) (cm^{-1})	5.67
$F(000)$	1182
Crystal size (mm)	$0.29 \times 0.32 \times 0.36$
θ_{max} (°)	27.5
Refinement method	Full-matrix least-squares on F^2
R (observed data)	0.036
R_w (all data)	0.112
Maximum residual e.d.p (e $Å^{-3}$)	1.23

The structure was solved by heavy-atom methods [24] and refined by a full-matrix least-squares procedure based on F^2 [25]. Non-hydrogen atoms were refined employing anisotropic displacement parameters, carbon-bound hydrogen atoms were included in the model at their calculated positions and the O–H atoms were located from a difference map. The nitrate anion was found to be disordered over two positions. From refinement these were assigned 0.52% and 0.48% site occupancy factors. A weighting scheme of the form $w = 1/[\sigma^2 (F_o^2) + (0.0467P)^2 + 1.5976P]$ where $P = (F_o^2 + 2F_c^2)/3$ was employed and at convergence, final $R = 0.036$ (obs. data) and $R_w = 0.112$ (all data). The maximum residual electron density peak (1.23 e $Å^{-3}$) was located in the vicinity of the disordered nitrate anion. Fig. 1, showing the crystallographic numbering scheme, was drawn with ORTEP at the 50% probability level [26].

3. Results and discussion

3.1. IR spectra

The IR spectrum of the complex is consistent with the structural data presented in this paper. The broad absorption band for ν(O–H) appeared in the region 3316 cm^{-1}, indicating the presence of water molecules in the crystal. For ν(C≡N) mode of $[Fe(CN)_6]^{3-}$ two main band systems of comparable intensity are observed. The band at 2118 cm^{-1} is assigned to the intermetallic C≡N stretching, and the band appeared at 2055 cm^{-1} due to the terminal C≡N stretching mode [19]. The bands at 1538, 1140, 1099, 718 cm^{-1} are the characteristic absorptions of 1,10-phenanthroline [27].

3.2. Description of structure

The molecular structure of **1** is illustrated in Fig. 1 and selected geometric parameters are collected in Table 2. The structure features a central $[Fe(CN)_6]^{3-}$ unit that links a $[Ca(phen)_2(OH_2)_2]^{2+}$ dication and a $[Ca(phen)_2(OH_2)(NO_3)]^{+}$ cation via two *trans*-cyanide bridges. The asymmetric unit is completed by a solvent water molecule of crystallisation, which is associated with the anion, and there is no molecular symmetry owing to the presence of different calcium coordination geometries. The coordination geometry about iron is almost regular octahedral with the greatest deviation from the ideal being found in the C50–Fe–C53 angle of 84.42(9)°. There is evidence that the Fe–C distances fall into two classes with the longer distances, i.e. involving C49, C50 and C52, participating in links to calcium or water. By

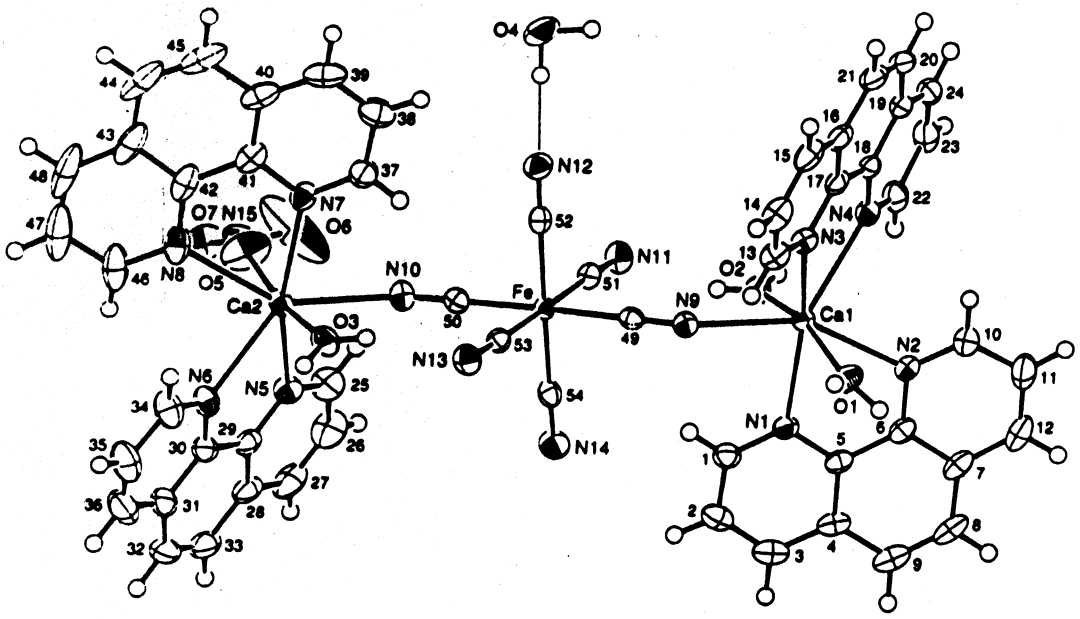


Fig. 1. Molecular structure and crystallographic numbering scheme for **1**. Atoms otherwise not indicated are carbons. Only one component of the disordered nitrate anion in the monodentate orientation is shown.

contrast to the regular geometry found for iron, the geometries about calcium are irregular. The Ca1 atom exists within a N_5O_2 donor set with the water molecules subtending an angle of 163.56(6)° at Ca1. If the five nitrogen atoms defined an approximate plane, the geometry might be described as being based on a pentagonal bipyramidal arrangement. However, the dihedral angle between the two effectively planar five-membered CaN_2C_2 chelate rings (respective mean deviations: 0.056 and 0.006 Å) is large at 53.4° suggesting that this is not an appropriate description. An examination of the Ca–N bond distances revealed that the Ca–N4 bond length is significantly longer than the others and that Ca–N2, N3 are longer than Ca–N1, N9. A capped octahedral geometry for Ca1 may be thus envisaged where the two octahedral faces are defined by O1, N1 and N9; N2, N3 and O2 with a dihedral angle of 9.8° between them. The N4 atom may be thought to protrude through the later face, thereby elongating the Ca1–N2, N3 bonds. However, it is noted that (i) there is no significant difference between the Ca1–O bonds and, (ii) that the Ca1 atom lies 1.4 Å from the first face and 0.7 Å from the larger octahedral face in this decription. The situation is even more complicated for the Ca2 atom as the nitrate is disordered so that approximately 50% of the time it functions as a unidentate ligand and 50% of the time it is bidentate, (see Section 2 for details). On the basis that the Ca2–O chelating distances are longer than the Ca2–O monodentate distance and the O8–Ca2–O9 chelate angle is very acute (Table 2), this ligand is assumed to occupy a single position in the coordination geometry about the Ca2 atom. The average Ca2–O chelating distance of 2.672 Å is slightly longer than the values given in the literature [28,29] whereas the Ca2–O monodentate distance of 2.236(5) Å is slightly shorter than that of the reported complexes [29,30]. The Ca2 atom also exists in a seven coordinate geometry defined by a N_5O_2 donor set as for the Ca1 centre and the description of the coordination geometry follows that given above for Ca1. Seven coordination is very uncommon [31,32], whereas the eight coordination is very common [28–30,33] for Ca complexes. There are significant distortions away from a pentagonal bipyramidal geometry in that while the O–Ca2–O axial angle is 170.9(2)°, the dihedral angle between the two CaN_2C_2 five-membered chelates (respective mean deviations of 0.025 and 0.057 Å) is 48.4°. In the capped octahedral description, the dihedral angle between the smaller O5, N7 and N10 and larger O3, N5 and N8 octahedral faces is 14.2° with the Ca2 atom 1.4 and 0.7 Å from these faces, respectively. The N6 atom caps the larger face and the trends in the interatomic parameters match those seen for Ca1. The Ca–O_{water} bond distances [2.379(2)–2.382(2) Å] are comparable with the other seven co-ordinated calciun complexes [31,32,34]. The Ca–N–C angle is 147.74(17)° for Ca1 and 151.01(17)° for Ca2, which give the arrangement of a slightly asymmetric 'bowed' disposition [20] rather than an exclusively linear arrangement.

As can be seen from Fig. 1, the O4 water molecule forms a hydrogen bond with a coordinated cyanide group. Indeed, the structure is stabilised by a complicated network of hydrogen bonds as well as π···π and O–H···π interactions. Table 3 summarises key hydrogen bonding contacts for **1**. The coordinated water molecule, O1, forms a bifurcated interaction with two

Table 2
Selected interatomic parameters (Å, °) for the coordination geometries in **1** [a]

Bond lengths			
Fe–C49	1.948(2)	Fe–C50	1.943(2)
Fe–C51	1.938(2)	Fe–C52	1.953(2)
Fe–C53	1.938(2)	Fe–C54	1.938(2)
Ca1–O1	2.379(2)	Ca1–O2	2.382(2)
Ca1–N1	2.512(2)	Ca1–N2	2.540(2)
Ca1–N3	2.519(2)	Ca1–N4	2.586(2)
Ca1–N9	2.489(2)	Ca2–O3	2.382(2)
Ca2–O5^{i}	2.236(5)	Ca2–N5	2.531(2)
Ca2–N6	2.571(2)	Ca2–N7	2.547(2)
Ca2–N8	2.562(2)	Ca2–N10	2.510(2)
Ca2–O8^{ii}	2.624(7)	Ca2–O9^{ii}	2.719(4)
Bond angles			
C49–Fe–C50	178.81(9)	C49–Fe–C51	85.56(9)
C49–Fe–C52	91.81(8)	C49–Fe–C53	95.03(9)
C49–Fe–C54	87.95(9)	C50–Fe–C51	94.98(9)
C50–Fe–C52	89.26(9)	C50–Fe–C53	84.42(9)
C50–Fe–C54	90.99(9)	C51–Fe–C52	88.93(9)
C51–Fe–C53	179.28(8)	C51–Fe–C54	89.30(9)
C52–Fe–C53	91.45(9)	C52–Fe–C54	178.23(9)
C53–Fe–C54	90.32(9)		
O1–Ca1–O2	163.56(6)	O1–Ca1–N1	83.98(6)
O1–Ca1–N2	74.47(6)	O1–Ca1–N3	76.62(6)
O1–Ca1–N4	112.85(6)	O1–Ca1–N9	98.84(7)
O2–Ca1–N1	79.61(6)	O2–Ca1–N2	97.85(6)
O2–Ca1–N3	119.33(6)	O2–Ca1–N4	79.86(6)
O2–Ca1–N9	81.31(6)	N1–Ca1–N2	65.85(6)
N1–Ca1–N3	154.90(6)	N1–Ca1–N4	139.40(6)
N1–Ca1–N9	87.48(6)	N2–Ca1–N3	122.27(6)
N2–Ca1–N4	82.83(6)	N2–Ca1–N9	152.86(6)
N3–Ca1–N4	64.41(6)	N3–Ca1–N9	80.04(6)
N4–Ca1–N9	123.24(6)		
O3–Ca2–O5^{i}	170.9(2)	O3–Ca2–N5	107.98(7)
O3–Ca2–N6	78.08(6)	O3–Ca2–N7	79.249(6)
O3–Ca2–N8	102.26(6)	O3–Ca2–N10	79.85(6)
O5^{i}–Ca2–N5	79.7(2)	O5^{i}–Ca2–N6	110.2(2)
O5^{i}–Ca2–N7	91.9(2)	O5^{i}–Ca2–N8	75.7(2)
O5^{i}–Ca2–N10	97.1(2)	N5–Ca2–N6	64.40(7)
N5–Ca2–N7	160.97(7)	N5–Ca2–N8	128.01(7)
N5–Ca2–N10	80.09(6)	N6–Ca2–N7	134.59(7)
N6–Ca2–N8	82.35(7)	N6–Ca2–N10	129.07(7)
N7–Ca2–N8	64.85(7)	N7–Ca2–N10	84.05(6)
N8–Ca2–N10	147.44(7)	O3–Ca2–O8^{ii}	157.9(1)
O3–Ca2–O9^{ii}	155.35(9)	O8^{ii}–Ca2–O9^{ii}	46.7(1)

[a] Atoms indicated with a superscript i have a site occupancy factor (sof) = 0.52 and those with ii have sof = 0.48.

non-coordinating oxygen atoms of the nitrate coordinating in the monodentate mode and forms a donor interaction to the water molecule of solvation, i.e. O4. The O2 water molecule forms two donor interactions and bridges two cyanide nitrogen atoms, one intramolecularly to N11 and another intermolecularly to N11 that results in the formation of a centrosymmetric eight-membered $(H–O–H\cdots N\cdots)_2$ ring. The O3 water molecule behaves in the same way, forming a similar eight-membered ring but involving two N13 atoms. The interaction between the solvent water molecule and the iron-bound cyanide ligand has already been mentioned. The second hydrogen atom of the O4 water forms an interaction of the type O–H···π so that the H···ring centroid of the N4–C22 ring is 2.55 Å and the angle subtended at H is 151° (symmetry operation: $-x$, $-y$, $-z$). The most significant π···π interaction occurs between a centrosymmetrically related pair of C28–C33 rings such that the separation between the centroids is 3.51 Å (symmetry operation: $1-x$, $-y$, $-z$). In terms of the overall crystal structure, the hydrogen bonding interactions described above involving the coordinated O1, O2 and O3 water molecules leads to the formation of a two-dimensional (layer) structure. This arises as the water molecules concerned along with the key N11 and N13 acceptor atoms are, to a first approximation, coplanar. Successive layers are linked via the O–H···π and π···π interactions resulting in the formation of a cohesive three-dimensional network.

4. Supplementary material

Crystallographic data has been deposited at the Cambridge Crystallographic Data Centre with deposition number 166280. Copies of the information may be obtained free of charge from The Director, CCDC, 12 Union Road, Cambridge, CB2 1EZ, UK (fax: +44-1223-336033; e-mail: deposit@ccdc.cam.ac.uk or www: http://www.ccdc.cam.ac.uk).

Table 3
Key hydrogen bonding contacts (Å, °) in **1** [a]

AHB	A–H	H···B	A···B	A–H···B	Symmetry operation
O1 H11w O6^{i}	0.93	1.99	2.785(6)	142	$1+x$, y, $1+z$
O1 H11w O7^{i}	0.93	1.95	2.85(1)	161	$1+x$, y, $1+z$
O1 H12w O4	0.95	1.81	2.755(3)	177	$1+x$, y, z
O2 H21w N11	0.84	2.23	3.041(3)	163	intra
O2 H22w N11	0.88	1.93	2.812(3)	174	$1-x$, $1-y$, $1-z$
O3 H31w N13	0.86	2.23	3.066(3)	163	intra
O3 H32w N13	0.99	1.83	2.817(3)	177	$1-x$, $-y$, $1-z$
O4 H41w N12	0.93	1.95	2.882(3)	178	intra

[a] Atoms indicated with a superscript i have a site occupancy factor (sof) = 0.52.

Acknowledgements

This work is supported by the grants from DST, UGC, CSIR and AICTE, New Delhi, India. The Australian Research Council is also thanked for support of the crystallographic facility.

References

[1] N.W. Alcock, A. Samotus, J. Szklarzewicz, J. Chem. Soc., Dalton Trans. (1993) 885.
[2] S. Das, S. Ganguli, M. Bhattacharya, J. Phys. Chem. Solids 46 (1985) 143.
[3] Y.Y. Yang, J.I. Zink, J. Am. Chem. Soc. 107 (1985) 4799.
[4] M.R. Pressprich, M.A. White, Y. Vekhter, P. Coppens, J. Am. Chem. Soc. 116 (1994) 5233.
[5] V. Gadet, M. Bujoli-Doeuff, L. Force, M. Verdaguer, K. El Malkhi, A. Deroy, J.P. Besse, in: D. Gatteschi, et al. (Eds.), Molecular Magnetic Material, NATO ASI Series198, Kluwer Academic Publishers, Dordrecht, 1990, p. 281.
[6] V. Gadet, T. Mallah, I. Castro, M. Verdaguer, J. Am. Chem. Soc. 114 (1992) 9213.
[7] W.R. Entley, G.S. Girolomi, Inorg. Chem. 33 (1994) 5165.
[8] M. Verdaguer, A. Bleuzen, V. Marvaud, J. Vaissermann, M. Seuleiman, C. Desplanches, A. Scuiller, C. Train, R. Garde, G. Gelly, C. Lomenech, I. Rosenman, P. Veillet, C. Cartier, F. Villain, Coord. Chem. Rev. 192 (1999) 1023 (and references therein).
[9] P. Braunstein, B. Oswald, A. Tiripicchio, M.T. Camellini, Angew. Chem., Int. Ed. Engl. 29 (1990) 1140.
[10] G. Boxhoorn, J. Moolhuysen, J.G.F. Coolegem R.A. VanSanten, J. Chem. Soc., Chem. Commun. (1985) 1305.
[11] M. Kaneko, N. Takabayashi, Y. Yamauchi, A. Yamada, Bull. Chem. Soc. Jpn. 57 (1984) 156.
[12] S.M. Morehouse, Inorg. Chim. Acta 243 (1996) 327.
[13] G. Murphy, C. O' Sullivan, B. Murphy, B. Hathaway, Inorg. Chem. 37 (1998) 240.
[14] S. Zhan, X. Chen, A. Vij, D. Guo, Q. Meng, Inorg. Chim. Acta 292 (1999) 157.
[15] T. Yi, S. Gao, X.W. Chen, C.H. Yan, B.G. Li, Acta Crystallogr., Sect. C 54 (1998) 41.
[16] N. Mondal, M.K. Saha, B. Bag, S. Mitra, V. Gramlich, J. Ribas, M.S. El fallah, Polyhedron 19 (2000) 1935.
[17] P. Kundu, M.K. Saha, S. Sen, S. Mitra, S. Kumar, D. Banerjee, R. Bhattacharya, Polyhedron 15 (1990) 3353 (and references therein).
[18] N. Mondal, S. Mitra, G. Rosair, Polyhedron 20 (2001) 2473.
[19] N. Mondal, M.K. Saha, B. Bag, S. Mitra, V. Gramlich, J. Ribas, M.S. El Fallah, J. Chem. Soc., Dalton Trans. (2000) 1601.
[20] N.K. Karan, S. Mitra, G. Rosair, D.J. Jenkins, K.M. Abdul Malik, Inorg. Chem. Commun. 4 (2001) 712.
[21] N.K. Karan, S. Mitra, G.M.G. Hossain K.M. Abdul Malik, Z. Naturforsch. (Teil. B), 57 (2002) 736.
[22] Programs used for X-ray analysis: TEXSAN, Structure Analysis Package, Molecular Structure Corporation, TX, 1992.
[23] N. Walker, D. Stuart, Acta Crystallogr., Sect. A 39 (1983) 158.
[24] P.T. Beurskens, G. Admiraal, G. Beurskens, W.P. Bosman, S. García-Granda, J.M.M. Smits C. Smykalla, The DIRDIF program system, Technical Report of the Crystallography Laboratory, University of Nijmegen, 1992.
[25] G.M. Sheldrick, SHELXL-97, University of Göttingen, Germany, 1997.
[26] C.K. Johnson, ORTEP II, Report ORNL-5136, Oak Ridge National Laboratory, Oak Ridge, TN, 1976.
[27] S. Sen, S. Mitra, P. Kundu, M.K. Saha, C. Kruger, J. Bruckmann, Polyhedron 16 (1997) 2475.
[28] X.M. Chen, T.C.W. Mak, Inorg. Chem. 33 (1994) 2444.
[29] X.M. Chen, T.C.W. Mak, Polyhedron 13 (1994) 1087.
[30] G. Smith, E.J. O'Reilly, C.H.L. Kennard, A.H. White, J. Chem. Soc., Dalton Trans. 243 (1985).
[31] B.L. Barnet, N.A. Wchtman, Inorg. Chem. 18 (1979) 2674.
[32] S.H. Whitlow, Acta Crystallogr., Sect. B 28 (1972) 1914.
[33] G. Hundal, M.S. Hundal, S. Obrai, N.S. Poonia, S. Kumar, Inorg. Chem. 41 (2002) 2077.
[34] G.H. Cohen, J.L. Hoard, J. Am. Chem. Soc. 88 (1966) 3228.

$[Ni(NO_2)(R'NHCS_2)(PR_3)]$ or $[NiBr(R'NHCS_2)(PR_3)]$ with Lewis bases such as $(CH_3)_3N$ and NH_3 [12]. However, their structures were not determined by X-ray diffraction techniques.

Herein we investigate the three new bis(triphenylphosphine)*N*-R-sulfonyldithio-carbimatenickel(II) complexes (R = 2-$CH_3C_6H_4$, 4-$CH_3C_6H_4$, 4-BrC_6H_4) that were obtained in the crystalline form by the reaction of $NiCl_2 \cdot 6H_2O$ with triphenylphosphine and dithiocarbimate anions derived from sulfonamides. These complexes were characterized by UV–Vis, IR, ^1H, ^{13}C and ^{31}P NMR, elemental analyses for C, H, N, Ni and by single crystal X-ray diffraction techniques.

2. Experimental

2.1. Methods and materials

The solvents were purchased from Merck and used without further purification. The sulfonamides, 4-bromophenylsulphonyl chloride, nickel(II) chloride hexahydrate and triphenylphosphine were purchased from Aldrich. Carbon disulfide and potassium hydroxide were purchased from Vetec. The 4-bromobenzenesulphonamide was prepared from the 4-bromobenzenesulphonyl chloride as described elsewhere [13]. The *N*-R-sulfonyldithiocarbimate potassium salts dihydrate were prepared in dimethylformamide from sulfonamides analogously as described in the literature [14,15]. These salts, which are soluble in water and insoluble in most of the organic solvents, were re-crystallized from hot ethanol–water. Melting points (m.p.) were determined with a Mettler FP5 equipment. Microanalyses for C, H and N were obtained from a Perkin–Elmer 2400 CHN. Nickel was analyzed by atomic absorption with a Hitachi Z-8200 Atomic Absorption Spectrophotometer. The IR spectra were recorded with a Perkin–Elmer 283 B infrared spectrophotometer using CsI pellets. The UV–Vis spectra were recorded with a Beckman DU 640 spectrometer using nujol mull suspension. The ^1H (400 MHz), ^{13}C (100 MHz) and ^{31}P (162 MHz) NMR spectra of the complexes were recorded on a Bruker Advance RX-400 spectrophotometer in $CDCl_3$ with TMS (H_3PO_4 for ^{31}P NMR spectra) as internal standard.

2.2. Syntheses

The syntheses of the nickel(II) complexes were performed according to the Scheme 1. A solution of *N*-R-sulfonyldithiocarbimate dihydrate (1.0 mmol) in water (10 ml) was added to a solution of triphenylphosphine (2.0 mmol) in ethanol (40 ml). Nickel(II) chloride hexahydrate (1.0 mmol) was added to the suspension and the reaction mixture was stirred for 6 h at room temperature (r.t.). The color of the suspension changed from green to pink/red. The solid product of the reaction was filtered, washed with distilled water and ethanol, and dried under reduced pressure for 1 day yielding $[Ni(PPh_3)_2(RSO_2N{=}CS_2)]$ (ca. 70%). Suitable crystals for X-ray structure analysis were obtained after slow evaporation of solutions of the compounds in dichloromethane–methanol and few drops of water.

$$RSO_2N{=}CS_2K_2.2H_2O \xrightarrow[-8H_2O,\ -2KCl]{NiCl_2.6H_2O,\ 2PPh_3,\ EtOH/H_2O} [Ni(PPh_3)_2(RSO_2N{=}CS_2)]$$

1, **2**, **3**

1 (R = 2-$CH_3C_6H_4$), **2** (R = 4-$CH_3C_6H_4$), **3** (R = 4-BrC_6H_4)

Scheme 1.

2.2.1. Bis(triphenylphosphine)2-methylphenyldithiocarbimatenickel(II) (*1*)

Elemental analysis: Found (Calc.): C, 63.39 (63.78); H, 4.37 (4.50); N, 1.70 (1.69); Ni, 7.01 (7.08)%. M.p. (°C): 165.5–166.0. UV–Vis (nm): 197; 236; 320; 426 and 557. IR (most intense bands) (cm^{-1}): 1440 ν(C=N); 1300 $\nu_{ass}(SO_2)$; 1120 $\nu_{sym}(SO_2)$; 920 $\nu_{ass}(CS_2)$ and 345 ν(NiS). ^1H NMR (δ): 7.88–7.79 (m, 1H, H2′ (R group)); 7.42–7.05 (m, 33H, H3′, H4′, H5′, R group and triphenylphosphine signals) and 2.63 (s, 3H, CH_3). $^{13}C\{^1H\}$ NMR (δ): 197.35 (N=CS_2); 140.77 (C1′); 137.98 (C2′); 131.49 (C3′); 129.02 (C5′); 127.94 (C6′); 125.09 (C4′) and 20.84 (CH_3). Triphenylphosphine signals: 134.39 (t, $J = 7$, C2″ and C6″); 130.89 (s, C4″); 129.35 (d, $J = 31$, C1″); 128.45 (t, $J = 7$, C3″ and C5″). ^{31}P NMR (δ): 31.69 (s).

2.2.2. Bis(triphenylphosphine)4-methylphenyldithiocarbimatenickel(II) (*2*)

Elemental analysis: Found (Calc.): C, 63.91 (63.78); H, 4.39 (4.50) N, 1.72 (1.69); Ni, 7.11 (7.08)%. M.p. (°C): 166.5–167.0. UV–Vis (nm): 197; 234; 320; 429 and 557. IR (most intense bands) (cm^{-1}): 1445 ν(C=N); 1300 $\nu_{ass}(SO_2)$; 1135 $\nu_{sym}(SO_2)$; 910 $\nu_{ass}(CS_2)$ and 344 ν(NiS). ^1H NMR (δ): 7.69–7.57 (m, 2H, H2′ and H6′ (R group)); 7.44–7.20 (m, 30H triphenylphosphine signals); 7.17–7.15 (m, 2H, H3′ and H5′ (R group)) and 2.39 (s, 3H, CH3). $^{13}C\{^1H\}$ NMR (δ): 197.37 (N=CS2); 142.58 (C1′); 139.42 (C4′); 128.94 (C3′ and C5′); 127.49 (C2′ and C6′); 21.78 (CH_3). Triphenylphosphine signals: 134.29 (t, $J = 6$, C2″ and C6″); 130.64 (s, C4″); 129.25 (d, $J = 46$, C1″); 128.27 (t, $J = 5$, C3″ and C5″). ^{31}P NMR (δ): 30.47 (s).

2.2.3. Bis(triphenylphosphine)4-bromophenyldithiocarbimatenickel(II) (*3*)

Found (Calc.): C, 57.29 (57.80); H, 3.79 (3.84); N, 1.60 (1.57); Ni, 6.61 (6.57)%. M.p. (°C): 169.0–170.5. UV–Vis (nm): 193; 247; 308; 426 and 557. IR (most intense bands) (cm^{-1}): 1435 ν(C=N); 1310 $\nu_{ass}(SO_2)$; 1135 $\nu_{sym}(SO_2)$; 915 $\nu_{ass}(CS_2)$ and 335 ν(NiS). ^1H NMR (δ): 7.68–7.65 (m, 2H, H2′ and H6′ (R group)); 7.45–

7.19 (m, 32H, H3′, H5′ R group and triphenylphosphine signals). $^{13}C\{^1H\}$ NMR (δ): 145.00 (C1′); 131.93 (C3′ and C5′); 128.88 (C2′ and C6′); 127.50 (C4′). Triphenylphosphine signals: 134.29 (t, $J = 6$, C2″ and C6″); 130.75 (s, C4″); 129.33 (d, $J = 54$, C1″); 128.33 (t, $J = 5$, C3″ and C5″). ^{31}P NMR (δ): 31.75 (s).

2.3. X-ray crystallography

X-ray intensity data for all crystals were collected using graphite monochromatic Mo Kα radiation on a four circle KUMA KM-4 diffractometer with a two-dimensional area CCD detector. The ω-scan technique with $\Delta\omega = 0.75^\circ$ for each image was used for data collection. The 960 images for six different runs covered over 90% of the Ewald sphere were performed. Initially the lattice parameters were refined on about 200 reflections obtained from 40 images for eight runs with different orientation in the reciprocal space. Finally the lattice parameters were refined by least-squares method based on the all reflection with $I > 4\sigma(F^2)$. One image was used as standard for monitoring the data collection after every 40 images, and no correction on the relative intensity variation was necessary. Integration of the intensities, correction for Lorenz and polarization effects were performed using a KUMA KM-4 CCD program system [16]. Total of 18 419 (9819 independent, $R_{int} = 0.0294$), 27 613 (10 354 independent, $R_{int} = 0.0750$) and 55 811 (9891 independent, $R_{int} = 0.0773$) reflections were collected for the complexes **1**–**3**, respectively. The face-indexed analytical absorption was calculated using the SHELXTL program [17].

The structures were solved by a Patterson heavy-atom method using the SHELXL-97 program [18]. The Patterson map revealed the positions of the nickel, sulfur, bromide (**3**) and some of the P and C atoms. The remaining non-hydrogen atoms were located from difference Fourier synthesis. The structures were refined with anisotropic thermal parameters. Difference Fourier maps gave electron density concentrations approximately located for all hydrogen atom positions; these positions were idealized (HFIX 43 for all hydrogen atoms of the phenyl rings with isotropic thermal parameters of 1.2 U_{eq} of the carbon atoms joined directly to the hydrogen atoms, and HFIX 137 for the CH_3 group in the complexes **1** and **2** with isotropic thermal parameters of 1.5 U_{eq} of the methyl carbon atom). Final differences Fourier maps showed no peaks of chemically significance. Details of data collection parameters and final agreement factors are collected in Table 1. Selected bond lengths and angles are listed in Table 2.

3. Results and discussion

The compounds are quite stables at the ambient conditions. In contrast to the dithiocarbamate Ni-complexes with the general formula of $[Ni(PR_3)_2(RN{=}CS_2)]$ which are soluble in THF, benzene and dichloromethane [12], these *N*-R-sulfonyldithiocarbimate Ni-complexes characterized in this paper are insoluble in most organic solvents and are slightly soluble in chloroform and dichloromethane. These complexes are stable up to the melting point without decomposition. Attempted to prepare the monotriphenylphosphine Ni-complexes like $K[NiCl(PPh_3)(N\text{-}RSO_2N{=}CS_2)]$ in the same conditions described above, with 1 equiv. of triphenylphosphine was unsuccessful.

The electronic spectra of the complexes show two shoulders (ca. 426 and 557) that are typical for square-planar nickel complexes and are assigned to d–d transitions [9]. The 190–300 nm region in the spectra of the complexes is dominated by three very intense bands of the triphenylphosphine and the dithiocarbimate ligands.

There are no strong or medium bands in the 1400–1600 cm^{-1} region in the IR spectra of the potassium dithiocarbimates related to the complexes **1**–**3**, the ν(CN) band being observed around 1260 cm^{-1} [14,19]. This low value indicates a great contribution of the canonical forms (a) and (b) for the resonance hybrid (Fig. 1). A strong band observed around 1455 cm^{-1} in the spectra of the complexes was assigned to the ν(CN). In the spectrum of the complex $[Ni(PPh_3)_2(4\text{-}CH_3C_6H_4N{=}CS_2)]$ that has no SO_2 group linked to the nitrogen atom, this band is located at 1500 cm^{-1} [12]. In the case of the complex $[Ni(4\text{-}CH_3C_6H_4SO_2N{=}CS_2)_2]^{2-}$ this band is observed around 1345 cm^{-1} [20]. This fact is probably due to a major negative charge on the Ni atom in this anionic complex in comparison to the complexes here synthesized. The substitution of one dithiocarbimate ion by two triphenylphosphine molecules is expected to result in a greater drift of electrons from the remainder dithiocarbimate ion to the metal. This effect is also observed, for example when the spectrum of the complex $[Ni(dtc)_2]$ (dtc = *N*,*N*-diethyldithiocarbamate) (ν(CN) band is observed in 1518 cm^{-1}) is compared with the spectrum of $[Ni(dtc)(PPh_3)_2]^+$ (ν(CN) band is observed in 1530 cm^{-1}) [8]. The $\nu_{ass}(CS_2)$ were observed at higher frequency in the spectra of the potassium salts of dithiocarbimates (ca. 955 cm^{-1}) [19] than that in the spectra of the complexes here studied (ca. 915 cm^{-1}). The shifts observed in the ν_{ass}(CS2) and ν(CN) in the spectra of the complexes when compared with the spectra of the ligands, are consistent with the increased importance of the canonical form (c) after complexation (Fig. 1). The spectra of the complexes also show the expected medium band in the 300–400 cm^{-1} range

Table 1
Crystallographic data

Complex	1	2	3
Chemical formula	$C_{44}H_{37}NNiO_2P_2S_3$	$C_{44}H_{37}NNiO_2P_2S_3$	$C_{43}H_{34}BrNNiO_2P_2S_3$
Formula weight	828.61	828.61	893.48
Crystal dimensions (mm)	0.30 × 0.28 × 0.14	0.24 × 0.18 × 0.14	0.36 × 0.16 × 0.06
Crystal system	triclinic	orthorhombic	orthorhombic
Space group	$P\bar{1}$	*Pbcn*	*Pbcn*
a (Å)	10.000(2)	16.556(3)	16.497(3)
b (Å)	13.923(3)	18.333(4)	18.556(4)
c (Å)	14.953(3)	25.412(5)	25.364(5)
α (°)	100.16(3)		
β (°)	103.28(3)		
γ (°)	95.20(3)		
V (Å^3)	1975.7(7)	7713(3)	7764(3)
Z	2	8	8
D_{obsd} (g cm^{-3})	1.39	1.42	1.52
D_{calc} (g cm^{-3})	1.393	1.427	1.529
T (°C)	295	295	295
λ (Å)	0.71073	0.71073	0.71073
μ (cm^{-1})	0.769	0.788	1.812
Transmission factors: min, max	0.8020, 0.8999	0.8334, 0.8977	0.5616, 0.8991
$R(F^2)$	0.0433	0.0540	0.0449
$R_w(F^2)$	0.1104	0.1385	0.0639
S	1.015	1.140	1.004
Residual electron density (e Å^{-3})	+0.524 and −0.552	+0.656 and −0.611	+0.819 and −1.454

[a]Function minimized: $\Sigma\, w(|F_o|-|F_c|)^2$, where $w = 4F_o^2/\sigma^2(F_o^2)$; $[\Sigma\, w(|F_o|-|F_c|)^2/(N_o-N_v)]^{1/2}$, where N_o, number of observations, N_v, number of variables. The final discrepancy factors: $R = \Sigma||F_o|-|F_c||/\Sigma|F_o|$ and $R_w = [\Sigma\, w(|F_o|-|F_c|)^2/\Sigma\, wF_o^2]^{1/2}$.

assigned to the NiS vibrations [21]. The ν(NiP) band was not observed above 200 cm^{-1}.

The NMR spectra of **1**–**3** were typical for diamagnetic species. The ^{1}H NMR spectra of the complexes showed the signals for the hydrogen atoms of the triphenylphosphine. The remaining signals could be assigned to the CH_3 group of the aromatic moiety and the other aromatic hydrogen atoms. The integration curves on the ^{1}H NMR spectra were consistent with a 2:1 proportion between the triphenylphosphine ligands and the dithiocarbimate anion. The signals in the spectra of the free dithiocarbimates [19] and in the complexes show approximate the same chemical shifts. The chemical shifts of the aromatic carbon atoms of the dithiocarbimate anions in the complexes are similar to those of the corresponding sulfonamides [22]. The N=CS_2 (C1) signal is shifted in the spectra of the complexes to higher field if compared with the spectra of the ligands (this signal is too weak and was not observed for **3**). Although the solvents are, necessarily different, this shift is expected. If the canonical form (c) (Fig. 1) is more important for the complexes than for the ligands, then the C1 carbon atom is expected to be more shielded in the complexes. The C1 signal for the complex **2** is also shifted to higher field when compared with the spectrum of the correspondent anionic complex $[Ni(4\text{-}CH_3C_6H_4SO_2N{=}CS_2)_2]^{2-}$ [20]. Most of the triphenylphosphine signals in the ^{13}C NMR spectra appeared as pseudo triplets or doublets. This is consistent with square-planar geometry for the complexes. Doublets or pseudo triplets are commonly observed in the ^{13}C NMR spectra of bis-phosphine transition metal *cis*-complexes [23]. As expected, the ^{31}P NMR spectra exhibited only one signal (ca. 30 δ) indicating that all phosphorus atoms in the molecules are magnetically equivalent.

The X-ray molecular structures of the **1**–**3** complexes are illustrated in Fig. 2(a–c), respectively. In all complexes, the nickel cation is coordinated by two triphenylphosphine ligands and chelated by two sulfur atoms of the *N*-R-sulfonyldithiocarbimate anion into a similarly distorted square-planar configuration. The P(1)–Ni(1)–S(1) and P(2)–Ni(1)–S(2) angles are less distorted from 90° than the P(1)–Ni(1)–P(2) and S(1)–Ni(1)–S(2) angles. The P(1)–Ni(1)–P(2) angle is significantly greater than 90° in all complexes due to the steric effect of the large triphenylphosphine ligands and the S(1)–Ni(1)–S(2) angle is smaller than 90° due to the chelation of the *N*-R-sulfonyldithiocarbimate ligand. The *N*-R-sulfonyldithiocarbimate anion $(RSO_2N{=}CS_2)^{2-}$ as an asymmetric didentate ligand forms a stable four membered ring by chelation through the two sulfur atoms (NiS_2C). The Ni(1)–S(1) bond lengths of 2.190(1) in **1**, 2.179(1) in **2** and 2.178(1) in **3** Å are shorter than the Ni(1)–S(2) [2.220(1), 2.219(1) and 2.224(1) Å in **1**, **2** and **3**, respectively]. These deviations are more obvious than those found in the $[Ni(CH_3SO_2N{=}CS_2)_2]^{2-}$ [24]. This fact may be ex-

Table 2
Selected bond lengths (Å) and angles (°)

	1	2	3
Bond lengths			
Ni(1)–S(1)	2.190(1)	2.179(1)	2.178(1)
Ni(1)–S(2)	2.220(1)	2.219(1)	2.224(1)
Ni(1)–P(1)	2.206(1)	2.134(1)	2.227(1)
Ni(1)–P(2)	2.224(1)	2.230(1)	2.184(1)
P(1)–C(11)	1.833(3)	1.846(4)	1.840(4)
P(1)–C(21)	1.837(3)	1.805(3)	1.808(3)
P(1)–C(31)	1.825(3)	1.829(4)	1.823(4)
P(2)–C(41)	1.838(3)	1.821(4)	1.820(3)
P(2)–C(51)	1.852(3)	1.812(4)	1.837(3)
P(2)–C(61)	1.834(3)	1.830(4)	1.834(4)
C(1)–S(1)	1.751(3)	1.739(4)	1.764(3)
C(1)–S(2)	1.740(3)	1.743(4)	1.725(3)
C(1)–N(1)	1.279(3)	1.288(5)	1.296(4)
N(1)–S(3)	1.631(2)	1.655(3)	1.626(3)
O(1)–S(3)	1.441(2)	1.435(3)	1.430(2)
O(2)–S(3)	1.431(2)	1.441(3)	1.422(2)
C(2)–S(3)	1.783(3)	1.767(4)	1.776(4)
C(3)–C(8)	1.497(4)		
C(5)–C(8)		1.505(7)	
C(5)–Br(1)			1.890(5)
Bond angles			
P(1)–Ni(1)–P(2)	98.48(4)	98.84(4)	98.92(4)
S(1)–Ni(1)–S(2)	77.87(4)	78.18(4)	78.14(3)
S(1)–Ni(1)–P(1)	92.31(4)	90.76(4)	91.16(4)
S(1)–Ni(1)–P(2)	168.21(3)	168.58(4)	167.95(4)
S(2)–Ni(1)–P(1)	167.92(3)	167.01(4)	167.42(4)
S(2)–Ni(1)–P(2)	91.96(4)	92.94(4)	92.53(4)
S(1)–C(1)–S(2)	105.1(2)	105.6(2)	105.3(2)
S(1)–C(1)–N(1)	132.0(2)	132.2(3)	131.0(3)
S(2)–C(1)–N(1)	122.9(2)	122.1(3)	123.6(3)
C(1)–N(1)–S(3)	120.7(2)	120.6(3)	121.5(2)
N(1)–S(3)–O(1)	111.9(1)	111.6(2)	111.5(2)
N(1)–S(3)–O(2)	106.0(1)	104.2(2)	105.8(2)
O(1)–S(3)–O(2)	116.9(1)	118.7(2)	117.7(2)
N(1)–S(3)–C(2)	105.7(1)	107.3(2)	107.7(2)
O(1)–S(3)–C(2)	108.2(1)	108.0(2)	106.9(2)
O(2)–S(3)–C(2)	107.5(1)	106.5(2)	106.8(2)

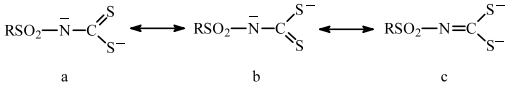


Fig. 1. Some possible canonical forms for the *N*-R-sulfonildithiocarbimate anion.

plained by the stereochemistry affecting the phenyl ring of the *N*-R-sulfonyldithiocarbimate ligand, which is located in *cis* position to the S1 atom. The C1–N1 bond lengths of 1.279(3), 1.288(3) and 1.296(4) in **1**–**3**, respectively, are shorter than the normal single C(sp^2)–N(sp^2) bond length (ca. 1.35 Å), and similar to that of the double bond C=N (1.275–1.295 Å) [25,26]. The C(1)–S(1) and C(1)–S(2) averaged bond lengths (1.745 Å) are slightly shorter than the typical C–S single bond length (ca. 1.81 Å) due to partial π-delocalization in the S–C–S group. The S(1)–C(1)–N(1) angles of 132.0(2)°,

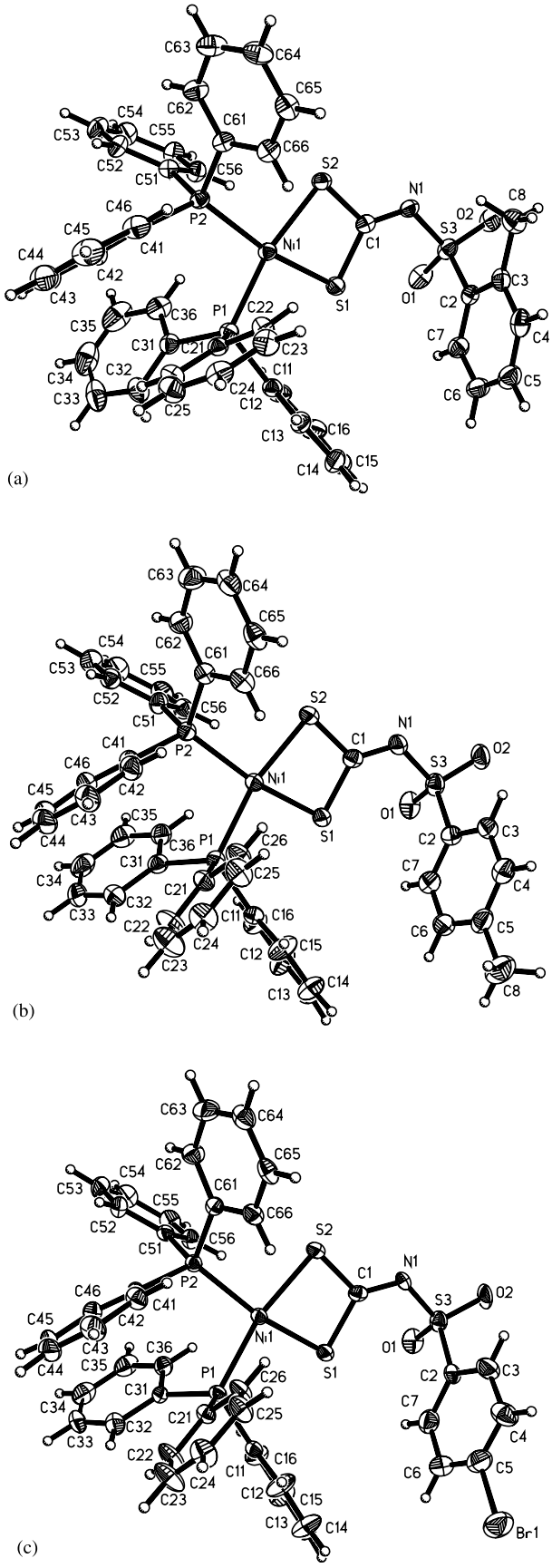


Fig. 2. View of the molecular structure of the complexes **1** (a), **2** (b) and **3** (c).

132.2(3)° and 131.0(3)° in the complexes **1**–**3**, respectively, are significantly greater than S(2)–C(1)–N(1) [122.9(2) in **1**, 122.1(3)° in **2** and 123.6(3)° in **3**] due to the interaction between the SO_2R group and the S(1) atom, which are joined in *cis* position in relation to the C(1)–N(1) bond. The steric effect of the R-sulfonyl group is greater than the effect of the lone-pair of electron at the N(1) atom, since the C(1)–N(1)–S(3) angle is greater than 120° in all complexes. If R is a small group such as $-SO_2CH_3$ [24] or –C≡N [27] the repulsive interaction predicted by the valence-shell electron pair repulsion theory (VSEPR) [28] between the lone-pair of electron at the N(1) atom and the S(2) atom is greater than the steric effect and the angle S(2)–C(1)–N(1) is greater than the angle S(1)–C(1)–N(1). In other dithiocarbimate complexes with larger R groups, the steric effect between S(1) and R group is more important and similarly as in the **1**–**3** complexes the angle S(1)–C(1)–N(1) is greater than S(2)–C(1)–N(1) [29].

The C(1)–N(1)–S(3) fragment of the *N*-R-sulfonyldithiocarbimate ligand (Fig. 2(a–c)) is coplanar with the NiS_2P_2 fragment, thus the P(1)P(2)Ni(1)S(1)S(2)C(1)-N(1)S(3) atoms lie in plane. The phenyl ring of the *N*-R-sulfonyldithiocarbimate ligand is inclined by about

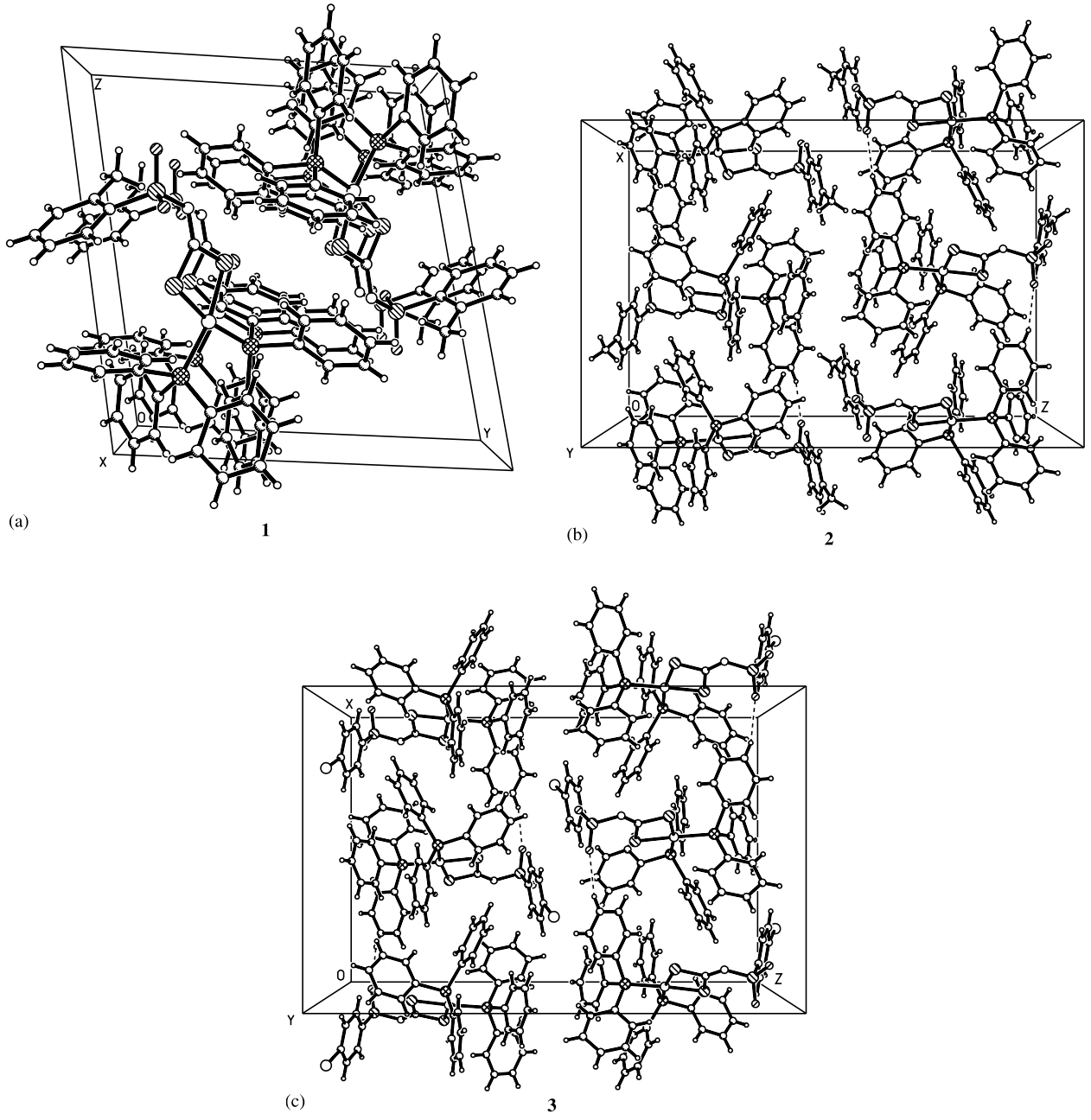


Fig. 3. Molecular arrangements of the complexes **1** (a), **2** (b) and **3** (c) in the unit cells.

Table 3
Comparison between selected crystallographic and spectroscopic data for the CN bond in compound **2** and related compounds

Parameters	**2**	$[Ni(4\text{-}CH_3C_6H_4SO_2N{=}CS_2)]^{2-}$ [b]	$(4\text{-}CH_3C_6H_4SO_2N{=}CS_2)^{2-}$ [a]
CN length (Å)	1.288(5)	1.35(2)	
ν(CN) (cm^{-1})	1445	1390	1260
^{13}C chemical shift (NCS_2) (ppm)	197.37	210.07	225.19

[a] Ref. [19].
[b] Ref. [20].

88.6(2)° in the complex **1**, and 78.1(2)° and 79.1(2)° in the isostructural crystals of the **2** and **3** complexes, respectively. The torsion angle of C(1)–N(1)–S(3)–C(2) describing the conformation of the ligand along the N(1)–S(3) bond is more similar in the complexes **1** and **2** [−65.2(2)° and −65.0(1)°], since both have a methyl group in the phenyl ring, than in **3** [−61.4(2)°], containing a Br-substituted aromatic ring. The S(3) atom has an expected slightly distorted tetrahedral geometry. The S(3)–O(1) and S(3)–O(2) bond lengths indicate their double bond character (S=O); a typical distance of the double S=O bond ranging from 1.431 to 1.442 Å [27]. The S(3)–C(2) bond with a distance ranging from 1.767(4) to 1.783(3) Å is well correlated with the C_{Ar}–S bond length in the related complexes which comprise the C_{Ar}–SO_2–N fragment [26]. The S(3)–N(1) bond length with a value ranging from 1.626(3) to 1.655(3) Å indicates a single bond nature; the typical value of the N(sp^2)–S bond distance is 1.623–1.659 Å [26]. Both P atoms of the triphenylphosphine ligands have similar tetragonal geometry. The phenyl ring C(21)–C(26) of the P(1) triphenylphosphine is almost parallel to the phenyl ring C(41)–C(46) of the P(2) triphenylphosphine, the dihedral angle being equal to 9.3(2)° in the complex **1**, and 15.2(2)° and 15.8(2)° in isostructural **2** and **3** complexes. Although the crystal of the complex **1**, is not isostructural with the crystals of **2** and **3** the structure analysis clearly shows that the geometry of the molecules of the compound **1** is quite similar to that of **2** and **3**. The differences between the **1** and **2** and/or **3** may be found in the molecular arrangement and the crystal packing. The complexes **1** and **2** differ only in the position of the methyl group substituted in the aromatic ring of the *N*-R-sulfonyldithiocarbimate ligands (**1** in *ortho* and **2** in *para* position). The crystal of the isomer **2** is more compacted since the molecules interact more effectively than in compound **1**. The arrangement of molecules in both **2** and **3** crystals is quite similar since both have *para*-substituents. These structures are slightly stabilized by weak C–H···O intermolecular hydrogen interactions of neighbouring molecules to form a polymeric structure. The C–H···O interactions with C···O of approximately 3.37 and 3.36 Å distances in **2** and **3** compounds, respectively, lead to the formation of the pseudo mono-dimensional columns aligned along the *a*-axis in the crystal (Fig. 3(b–c)). Although the intermolecular C–H···O are weak, we suppose that they are important for the crystal packing, since this can be the reason for the more compacted arrangement of the molecules in **2** and in **3** in relation to the crystal of **1**, in which the C–H···O interactions were not observed.

4. Conclusion

Three novel bis(triphenylphosphine)*N*-R-sulfonyldithiocarbimatenickel(II) complexes were prepared and characterized by UV–Vis, IR, ^1H, ^{13}C and ^{31}P NMR, elemental analyses for C, H, N, Ni and by single crystal X-ray diffraction techniques.

The spectroscopic and X-ray data for the complex $[Ni(4\text{-}CH_3C_6H_4SO_2]^{2-}$ [20] show an interesting relation with the data obtained for compound **2** (Table 3). The C(1)–N(1) bond length in **2** is shorter than in $[Ni(4\text{-}CH_3C_6H_4SO_2N{=}CS_2)_2]^{2-}$ [20]. The wavenumber for the ν(CN) in the IR spectrum of **2** is greater than that in the spectrum of the related anionic complex and this band is observed in smaller wavenumber in the spectrum of the parent dithiocarbimate ligand [19]. The NMR spectra show that the carbon atom of the dithiocarbimate group of **2** is more shielded than that of the anionic complex and in the parent ligand. These facts are in accord with an increase of the contribution of the (c) canonical form (Fig. 1) to the resonance hybrid from the ligands to the complexes, with a consequent increase of the CN double bond character.

5. Supplementary material

Crystallographic data for the structural analysis have been deposited with the Cambridge Crystallographic Data Centre, CCDC Nos. 181695, 181696 and 181697 for the compounds **1**–**3**, respectively. Copies of this information may be obtained free of charge from The Director, CCDC, 12 Union Road, Cambridge, CB2 1EZ, UK (fax: +44-1223-336033; e-mail: deposit@ccdc.cam.ac.uk or www: http://www.ccdc.cam.ac.uk).

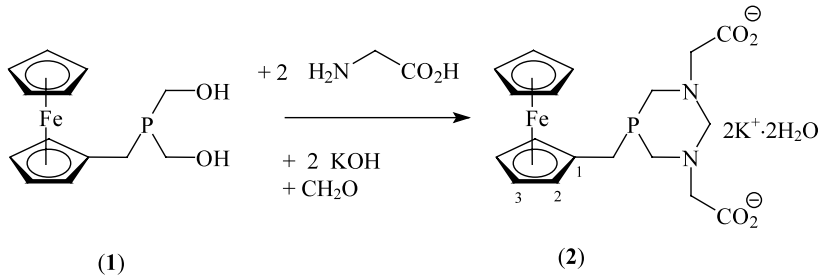
Acknowledgements

This work has been supported by CNPq, CAPES and FAPEMIG (Brazil).

References

[1] P.J. Nieuwenhuizen, J. Reedijk, M. van Duin, W.J. McGill, Ruber Chem. Technol. 70 (1997) 368.
[2] D. Coucouvanis, Prog. Inorg. Chem. 11 (1969) 233.
[3] S. Thiumaran, K. Ramalingan, Transition Met. Chem. 25 (2000) 60.
[4] A. Manohar, L. Righi, K. Ramalingan, G. Bocelli, Inorg. Chim. Acta 314 (2001) 172.
[5] R.G. Cavell, B. Creed, L. Gelmini, D.J. Law, R. McDonald, A.R. Sanger, A. Somogyvari, Inorg. Chem. 37 (1998) 757.
[6] A.M.A. Bennet, D.A. Thorton, Spectroscopy 10 (1992) 85.
[7] G.A. Foulds, A.M.A. Bennet, M.I. Niven, D.A. Thorton, K.J. Cavell, S. Desjardins, E.J.J. Peacock, Mol. Catal. 87 (1994) 117.
[8] K. Ramalingan, G. Avaramudan, M. Seshasayee, Inorg. Chim. Acta 128 (1987) 231.
[9] R. Pastorek, Z. Trávníček, J. Marek, D. Dastych, Z. Šidelár, Polyhedron 19 (2000) 1713.
[10] G.A. Katsoulos, C.A. Tsipis, Inorg. Chim. Acta 84 (1984) 89.
[11] J. Ahmed, K. Itoh, I. Matsuda, F. Veda, Y. Ishii, J.A. Ibers, Inorg. Chem. 16 (1977) 620.
[12] C.A. Tsipis, I.P. Meleziadis, D.P. Kessissoglou, G.A. Katsoulos, Inorg. Chim. Acta 90 (1984) L19.
[13] A.I. Vogel, A Textbook of Practical Organic Chemistry Including Qualitative Organic Analysis, Longmans, Green, London, 1966.
[14] K. Hartke, Arch. Pharm. 299 (1966) 164.
[15] H.U. Hummel, U.Z. Korn, Z. Naturforsch., Teil. B 44 (1989) 24.
[16] Kuma Diffraction. KM-4 CCD Software, Ver. 163, Wroclaw, Poland, 1999.
[17] G.M. Sheldrick, SHELXTL. Program System, Siemens Analytical X-ray Instruments, Madison, WI, 1990.
[18] G.M. Sheldrick, SHELXL97: Program for the Solution and Refinement of Crystal Structures, Univesity of Göttingen, Germany, 1997.
[19] M.R.L. Oliveira, V.M. De Bellis, Transition Met. Chem. 24 (1999) 127.
[20] M.R.L. Oliveira, J.E.J.C. Graúdo, N.L. Speziali, V.M. De Bellis, Struct. Chem. 10 (1999) 41.
[21] K. Nakamoto, Infrared and Raman of Inorganic and Coordination Compounds, 3rd ed., Wiley, New York, 1978, p. 339.
[22] M. Pomerantz, W.N. Chou, M.K. Witczak, C.G. Smith, J. Org. Chem. 52 (1987) 159.
[23] D.A. Redfield, L.W. Cary, J.H. Nelson, Inorg. Chem. 14 (1975) 50.
[24] M.R.L. Oliveira, V.M. De Bellis, N.G. Fernandes, Struct. Chem. 8 (1997) 205.
[25] D. Coucouvanis, J.P. Frackler, Jr., Inorg. Chem. 6 (1967) 2047.
[26] F.H. Allen, O. Kennard, D.G. Watson, L. Brammer, A.G.J. Orpen, Chem. Soc., Perkin Trans. 2 (1987) S1.
[27] F.A. Cotton, C.B. Harris, Inorg. Chem. 7 (1968) 2140.
[28] R.J.J. Gillespie, Chem. Educ. 40 (1963) 295.
[29] H.U. Hummel, U.Z. Korn, Z. Naturforsch., Teil. B 44 (1989) 29.

anes [14]. Reaction of bis(hydroxymethyl)(ferrocenylmethyl)phosphine (**1**) [3] with 2 equiv. of glycine in the presence of 2 equiv. of KOH and 1 equiv. of paraformaldehyde gives the corresponding 1,3-diaza-5-phosphacyclohexane **2** (Eq. (1)).



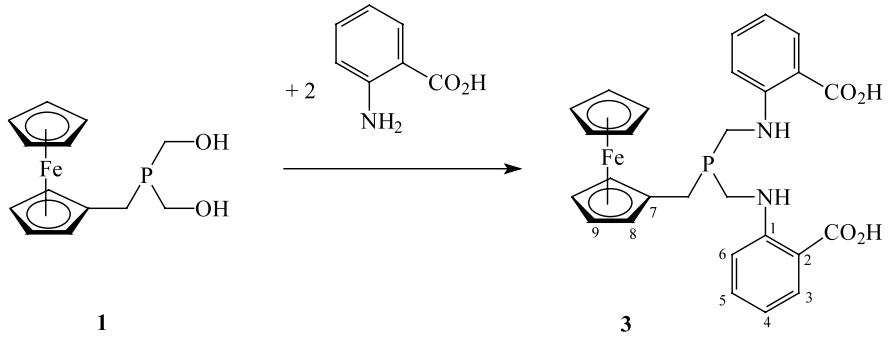
(1)

Although the ^{31}P chemical shift of **2** (in CD_3OD) is to lower field than expected for diazaphosphacyclohexanes [14], the presence of this type of heterocycle was established on the basis of the ^{1}H and ^{13}C NMR spectra. Well-identified signals of the protons and the carbon atom of the N–CH_2–N fragment and signals for all other groups confirmed the structure of **2**.

In the ^{31}P NMR spectrum in 10% aqueous solution of NaOH only a very broad signal at about −55 ppm was observed together with sharp, intense signals at 35.6 and 1.7 ppm, which probably correspond to products of hydrolysis of the C–N bond and oxidation, and thus indicate some instability of **2** in water.

Oxidation in the course of a Mannich-type reaction of **1** was observed earlier with dimethylamine [3] and by us with optically active (*S*)-α-phenylglycine and (*S*)-1-methylbenzylamine. In the ^{31}P NMR spectra of the reaction mixtures and products isolated as powders the signals of the desired products were accompanied by those of the phosphine oxides.

The stability of aminobenzoic acid derivatives is usually higher than that of α-amino acids [14–16]. It was recently established that the type of amino acid used in the condensation reaction with primary phosphines and formaldehyde determines the type of phosphino amino acid that is formed regardless of the stoichiometry of the reagents, i.e. primary phosphine, formaldehyde and amino acid [15,16]. For example, for *o*-aminobenzoic acid bis(*o*-carboxyphenylaminomethyl)phosphines are the predominant products, even when an excess of formaldehyde is employed in the reaction [9,10,15]. Thus, the reaction of **1** with 2 equiv. of *o*-aminobenzoic acid leads as expected to the open-chain product **3**, even when an excess of CH_2O is employed in the formation of **1** from (ferrocenylmethyl)phosphine (Eq. (2)).



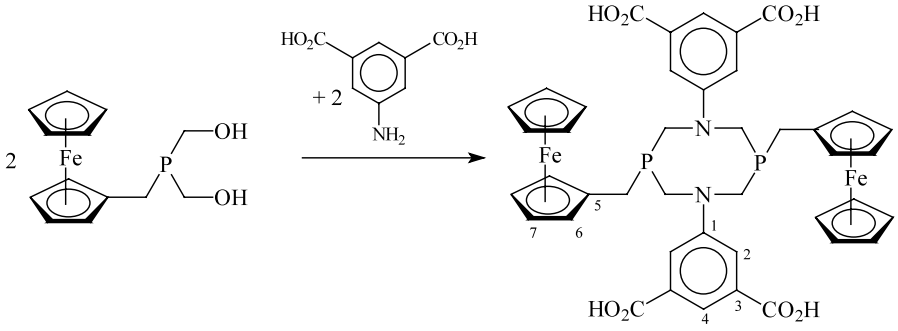
(2)

Compound **3** was isolated as a yellow microcrystalline solid. The ^{31}P NMR chemical shifts of **3** in methanol and DMF are similar and comparable to those of previously reported bis(arylaminomethyl)phenylphosphines [9,15]. The ^{1}H and ^{13}C NMR spectra of **3** are in accordance with the open-chain structure. The

protons of the P–CH_2–N and P–CH_2–Fc fragments give rise to broad singlets, in contrast to the P–CH_2–N groups of the previously obtained analogues, for which two doublets of doublets were observed due to inequivalence of the two prochiral hydrogen atoms [15].

In the presence of at least 2 equiv. of potassium or sodium hydroxide, **3** is soluble in water (up to 1 M). The ^{31}P NMR signal of the salt solution is broadened and slightly shifted upfield relative to neutral **3** in DMF solution. ^{1}H NMR signals in D_2O/NaOD are also broad, but are generally similar to those in DMF solution.

It was shown previously that bis(hydroxymethyl)-phosphines react with primary aryl- and benzylamines (2:2) with the formation of crystalline, air- and moisture-stable 1,5-diaza-3,7-diphosphacyclooctanes [17–19], which can be used as bidentate chelate diphosphine ligands for various transition metals [20–22]. However, water-soluble derivatives were obtained only with *p*-aminobenzoic acid as primary amine and oxymethyl derivatives of *o*-phosphinophenols [15]. Therefore, a more hydrophilic amine should be used to obtain water-soluble 3,7-bis(ferrocenylmethyl)-1,5-diaza-3,7-diphosphacyclooctane ligands. Heating of **1** with 5-aminoisophthalic acid in boiling ethanol resulted in the formation of yellow, microcrystalline, air-stable 1,5-bis(*meta*-dicarboxyphenyl)-3,7-bis(ferrocenylmethyl)-1,5-diaza-3,7-diphosphacyclooctane (**4**) (Eq. (3)).



1 **4** (3)

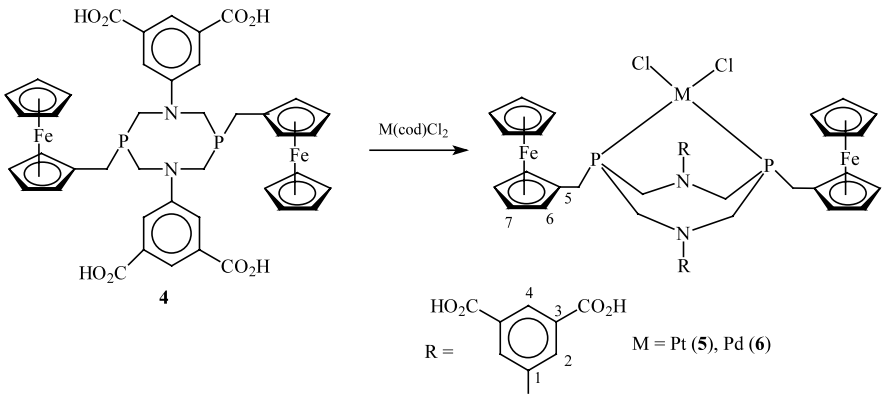
The IR spectrum of **4** exhibits strong absorptions for the carboxyl groups (1596, 1698, and 3440 cm^{-1}). In the ^{31}P NMR spectrum only one signal is observed in the characteristic region for 1,5-diaza-3,7-diphosphacyclooctanes [15,17–19]. The ^{13}C and ^{1}H NMR spectra of **4** are consistent with the heterocyclic phosphine structure [15,17–19]. The ^{13}C NMR spectrum shows signals for the P–CH_2–N and P–CH_2–Fc methylene groups, one signal for the cyclopentadienyl rings, three signals for the substituted cyclopentadienyl rings, four signals for the aryl carbon atoms and a singlet for the carboxyl groups. ^{1}H NMR data provide additional information about the conformational behavior of heterocyclic phosphines. The protons of the P–CH_2–N methylene group form an ABX spin system (two doublets of doublets) with a notable difference in the values of the P–H coupling constants ($^{2}J(PH^{A})$ approximately 5 Hz, $^{2}J(PH^{B})$ approximately 9 Hz). This pattern is typical of diazadiphosphacyclooctanes in a crown conformation with diaxial orientation of the phosphorus lone pairs [17–19], that is, the ferrocenylmethyl substituents on the phosphorus atoms and the *meta*-dicarboxyphenyl groups on the nitrogen atoms do not change the conformational behavior of diazadiphosphacyclooctanes.

The NMR data of **4** in 10% aqueous solutions of NaOH are quite similar to those of **4** in DMF. Deprotonation of the carboxyl groups results in a high-field shift of the aryl and P–CH_2–N signals in the ^{1}H NMR spectrum. No evidence of oxidation or hydrolysis was observed in aqueous solutions.

When **4** is treated with [MCl_2(cod)] (M = Pt, Pd; cod = cyclooctadiene) in DMF, the ^{31}P NMR spectrum of the reaction mixture shows a signal downfield relative to **4** ($\Delta\delta = 44.1$ (M = Pt) and 61.1 ppm (M = Pd)) with satellites due to coupling with ^{195}Pt nuclei. The Pt–P coupling constant of 3064 Hz indicates the formation of the *cis*-*P*,*P* chelate trinuclear complexes **5** and **6** [22] (Eq. (4)).

The IR spectra of **5** and **6** exhibit strong absorptions for carboxyl groups (1590–1720 and 3430 cm^{-1}) and also absorption bands of the backbone vibrations of heterocycles.

The ^{13}C and ^{1}H NMR spectra are consistent with the structure and are in general similar to that of **4**. In the ^{1}H NMR spectra only the signal of the P–CH_2–Fc



4

(4)

methylene groups of **5** and **6** change dramatically. These signals are shifted downfield ($\Delta\delta \sim 1.2$–1.5 ppm) and overlap with those of the P–CH_2–N fragment. Due to this overlap it is impossible to establish the conformation of **5** and **6** in solution. In the ^{13}C NMR spectra, the signal of the P–CH_2–Fc methylene group is situated in the usual region.

The trinuclear complexes **5** and **6** are readily soluble in water in the presence of at least 4 equiv. of base (NaOH). The deprotonation and change of solvent cause a high-field shift of the ^{13}P NMR signal ($\Delta\delta = -6.2$ ppm) and a decrease in the Pt–P coupling constant for **5** ($\Delta = 85$ Hz). High-field shifts in aqueous solution were previously observed for tertiary phosphino amino acids [15], including **4**. The ^1H NMR signals of the P–CH_2–N methylene groups are slightly shifted to low-field relative to **4**.

Studies on the coordination chemistry of **2**, **3** and **4** are in progress.

3. Conclusions

A number of water-soluble open-chain and cyclic phosphino amino acids containing ferrocenylmethyl moieties was obtained via a Mannich-type condensation reaction of bis(hydroxymethyl)ferrocenylmethylphosphine with potassium glycinate, *o*-aminobenzoic acid and 5-aminoisophthalic acid. The water-soluble trinuclear Fe_2Pt and Fe_2Pd complexes were synthesized and characterized spectroscopically.

4. Experimental

4.1. General considerations

All manipulations were carried out with standard high-vacuum and dry-nitrogen techniques. NMR spectra: Avance DRX 400 (Bruker), standards: ^1H NMR (400 MHz): internal solvent; ^{13}C NMR (100.6 MHz): internal solvent; ^{31}P NMR (162 MHz): external 85% H_3PO_4. The IR spectra were recorded as KBr mulls on a Perkin–Elmer FT-IR spectrometer System 2000 in the range 350–4000 cm^{-1}. The m.p. were determined in sealed capillaries and are uncorrected.

Bis(hydroxymethyl)(ferrocenylmethyl)phosphine (**1**) was obtained according to a literature procedure [3].

4.1.1. 1,3-Bis(carboxymethyl)-5-(ferrocenylmethyl)-1,3-diaza-5-phosphacyclohexane (**2**)

To a suspension of **1** (0.75 g, 2.6 mmol) were added glycine (0.39 g, 5.2 mmol) and paraformaldehyde (0.08 g, 2.7 mmol) in 3 ml of MeOH and 2.8 ml of 10% KOH (5.3 mmol) in MeOH, and the reaction mixture was stirred for 24 h. The yellow microcrystalline solid which formed was filtered off, washed with MeOH and dried under vacuum. Yield: 0.62 g (38%); m.p. >250 °C (dec.). *Anal*. Calc. for $C_{18}H_{25}FeK_2N_2O_6P$ [530.42]: C, 40.8; H, 4.8; N, 5.3; P, 5.9. Found: C, 40.3; H, 4.5; N, 5.4; P, 6.1%.

^1H NMR (MeOH-d_4): δ 2.99 (s, br, 2H, P–CH_2–Fc), 3.28–3.30 (m, 4H, P–CH_2–N), 3.41 (s, 4H, N–CH_2–CO_2), 4.05 (d, $J_{HH} = 12.0$ Hz, 1H, N–CH_2^B–N), 4.06 (s, br, 2H, C_5H_4–H3 (for numbering scheme see Eq. (1))), 4.12 (s, 5H, C_5H_5), 4.16 (d, $J_{HH} = 12.0$ Hz, 1H, N–CH_2^A–N), 4.19 (s, 2H, C_5H_4–H2), 4.83 (s, 4H, H_2O). $^{13}C\{^1H\}$ NMR (MeOH-d_4): δ 18.7 (s, br, P–CH_2–Fc), 60.7 (s, br, P–CH_2–N), 68.8 (s, C_5H_4–C3), 69.9 (s, C_5H_5), 70.0 (s, C_5H_4–C2), 76.4 (s, N–CH_2–N), 84.7 (s, br, C_5H_4–C1), 174.1 (s, CO_2H). $^{31}P\{^1H\}$ NMR (MeOH-d_4): δ -50.0; $^{31}P\{^1H\}$ NMR (10% NaOH in D_2O): δ -55 (s, br). IR ($\tilde{\nu}/cm^{-1}$, KBr): 1599, 1630 (CO + H_2O), 3424 (HO).

4.1.2. Bis(o-carboxyphenylaminomethyl)-ferrocenylmethylphosphine (3)

A solution of **1** (0.77 g, 2.6 mmol) and anthranilic acid (0.72 g, 5.2 mmol) in 15 ml of MeOH was stirred for 24 h. The solvent was removed under vacuum, and the yellow powder was washed with Et_2O, collected by filtration and dried under vacuum. Yield: 1.00 g (72%); m.p. >250 °C (dec.). *Anal*. Calc. for $C_{27}H_{27}FeN_2O_4P$ [530.34]: C, 61.1; H, 5.1; N, 5.3; P, 5.8. Found: C, 60.9; H, 5.3; N, 5.1; P, 5.6%.

^{1}H NMR (DMF-d_7): δ 3.04 (s, br, 2H, P–CH_2–Fc), 3.71 (s, br, 4H, P–CH_2–N), 4.24 (s, br, 2H, C_5H_4–H9 (for numbering scheme see Eq. (2))), 4.29 (s, 5H, C_5H_5), 4.34 (s, br, 2H, C_5H_4–H8), 6.76 (dd, $^3J_{HH}=7.8$, $^3J_{HH}=7.3$ Hz, 2H, C_6H_4–H4) 7.04 (d, $^2J_{HH}=8.3$ Hz, 2H, C_6H_4–H6), 7.52 (m, $^3J_{HH}=8.3$, $^3J_{HH}=7.3$ Hz, 2H, C_6H_4–H5), 8.07 (d, $^3J_{HH}=7.83$ Hz, 2H, C_6H_4–H3), 13.0 (s, br, 2H, CO_2H). ^{13}C{^{1}H} NMR (DMF-d_7): 24.8 (d, $^1J_{PC}=16.5$ Hz, P–CH_2–Fc), 39.6 (d, $^1J_{PC}=14.5$ Hz, P–CH_2–N), 68.1 (s, C_5H_4–C9), 69.4 (s, $C_5H_5+C_5H_4$–C8), 84.4 (s, br, C_5H_4–C7), 111.4 (s, C_6H_4–C6), 112.5 (s, C_6H_4–C2), 115.2 (s, C_6H_4–C4), 132.5 (s, C_6H_4–C3), 135.0 (s, C_6H_4–C5), 152.1 (s, br, C_6H_4–C1), 171.1 (s, CO_2H). ^{31}P{^{1}H} NMR (DMF-d_7): δ −30.0 (s); ^{31}P{^{1}H} NMR (10% NaOH in D_2O): δ −35.4 (s, br). IR ($\tilde{\nu}$/cm^{-1}, KBr): 1590–1720 (CO+aryl), 3500 (HO, NH).

4.1.3. 1,5-Bis(meta-dicarboxyphenyl)-3,7-bis(ferrocenylmethyl)-1,5-diaza-3,7-diphosphacyclooctane (4)

A solution of **1** (1.42 g, 5 mmol) and 5-aminoisophthalic acid (0.88 g, 5 mmol) in 40 ml of EtOH was refluxed for 6 h. The resulting yellow crystals were collected by filtration, washed with EtOH, and dried under vacuum. Yield: 1.21 g (57%); m.p. >250 °C (dec.). *Anal*. Calc. for $C_{42}H_{40}Fe_2N_2O_8P_2$ [874.43]: C, 57.7; H, 4.6; N, 3.2; P, 7.1. Found: C, 56.9; H, 4.4; N, 3.4; P, 7.4%.

^{1}H NMR (DMF-d_7): δ 2.81 (s, 4H, P–CH_2–Fc), 3.96 (dd, $^2J_{HH}=14$, $^2J_{PH}=6.0$ Hz, 4H, P–CH_2^A–N), 4.14 (s, 4H, C_5H_4–H7 (for numbering scheme see Eq. (3))), 4.15 (s, 4H, C_5H_4–H6), 4.19 (s, 10H, C_5H_5), 4.27 (dd, $^2J_{HH}=14.0$, $^2J_{PH}=13.0$ Hz, 4H, P–CH_2^B–N), 7.54 (s, 4H, C_6H_3–H2), 7.89 (s, 2H, C_6H_3–H4), 13.3 (s, br, 4H, CO_2H); ^{1}H NMR (10% NaOH in D_2O): 2.78 (s, 4H, P–CH_2–Fc), 3.6 (dd, $^2J_{HH}=12.0$, $^2J_{PH}=12.0$ Hz, 4H, P–CH_2^A–N), 3.8 (dd, $^2J_{HH}=12.0$, $^2J_{PH}=2.0$ Hz, 4H, P–CH_2^B–N), 4.01 (s, 4H, C_5H_4–H7), 4.03 (s, 10H, C_5H_5), 4.07 (s, 4H, C_5H_4–H6), 7.12 (s, 4H, C_6H_5–H2), 7.48 (s, 2H, C_6H_5–H4). ^{13}C{^{1}H} NMR (DMF-d_7): δ 25.7 (s, br, P–CH_2–Fc), 56.2 (d, $^1J_{PC}=18.3$ Hz, P–CH_2–N), 68.1 (s, C_5H_4–C7), 69.4 (s, C_5H_5), 69.5 (s, C_5H_4–C6), 84.4 (s, br, C_5H_4–C5), 117.6 (s, C_6H_3–C2), 118.0 (s, C_6H_3–C4), 132.4 (s, C_6H_3–C3), 146.6 (s, C_6H_3–C1), 168.0 (s, CO_2H). ^{31}P{^{1}H} NMR (DMF-d_7): δ −53.9 (s); ^{31}P{^{1}H} NMR (10% NaOH in D_2O): δ −54.6 (s). IR ($\tilde{\nu}$/cm^{-1}, KBr): 1596, 1698 (CO+aryl), 3440 (HO).

4.1.4. cis-{P,P-1,5-Bis(meta-dicarboxyphenyl)-3,7-bis(ferrocenylmethyl)-1,5-diaza-3,7-diphosphacyclooctane}dichloroplatinum(II) (5)

[$PtCl_2$(cod)] (0.18 g, 0.5 mmol) was added to a solution of **4** (0.41 g, 0.5 mmol) in 15 ml of DMF, and the reaction mixture was stirred for 24 h. The solvent was removed in vacuum, and the yellow microcrystalline solid was washed with Et_2O, collected by filtration and dried under vacuum. Yield: 0.30 g (52%); m.p. >250 °C (dec.). *Anal*. Calc. for $C_{42}H_{40}Cl_2Fe_2N_2O_8P_2Pt$ [1140.42]: C, 44.2; H, 3.5; N, 2.4; P, 5.4. Found: C, 43.8; H, 3.8; N, 2.3; P, 5.2%.

^{1}H NMR (DMF-d_7): δ 3.99–4.04 (m, 8H, P–CH_2–Fc+P–CH_2^A–N), 4.17 (d, $^2J_{HH}=15.6$ Hz, 4H, P–CH_2^B–N) 4.23 (s, 10H, C_5H_5), 4.26 (s, 4H, C_5H_4–H7 (for numbering scheme see Eq. (4))), 4.68 (s, 4H, C_5H_4–H6), 7.74 (s, 4H, C_6H_3–H2), 8.17 (s, 2H, C_6H_3–H4), 13.5 (s, br, 4H, CO_2H); ^{1}H NMR (10% NaOH in D_2O): δ 2.04 (s, 4H, P–CH_2–Fc), 3.31 (m, 4H, P–CH_2^A–N), 3.64 (d, $^2J_{HH}=14.4$, 4H, P–CH_2^B–N), 3.88 (s, 4H, C_5H_4–H7), 4.06 (s, 10H, C_5H_5), 4.19 (s, 4H, C_5H_4–H6), 7.18 (s, 4H, C_6H_5–H2), 7.66 (s, 2H, C_6H_5–H4). ^{13}C{^{1}H} NMR (DMF-d_7): δ 22.5 (d, $^1J_{PC}=24.8$ Hz, P–CH_2–Fc), 46.7 (d, $^1J_{PC}=36.0$ Hz, P–CH_2–N), 69.4 (s, C_5H_4–C7), 69.7 (s, C_5H_5), 70.2 (s, C_5H_4–C6), 80.2 (s, br, C_5H_4–C5), 122.1 (s, C_6H_3–C2), 122.7 (s, C_6H_3–C4), 133.1 (s, C_6H_3–C3), 150.9 (s, C_6H_3–C1), 167.4 (s, CO_2H). ^{31}P{^{1}H} NMR (DMF-d_7): δ −9.8 (s with Pt satellites, $^1J_{PPt}=3064$ Hz); ^{31}P{^{1}H} NMR (10% NaOH in D_2O): δ −16.0 ($^1J_{PPt}=2979$ Hz). IR ($\tilde{\nu}$/cm^{-1}, KBr): 1595, 1644, 1715 (CO+aryl), 3426 (HO).

4.1.5. cis-{P,P-1,5-Bis(meta-dicarboxyphenyl)-3,7-bis(ferrocenylmethyl)-1,5-diaza-3,7-diphosphacyclooctane}dichloropalladium(II) (6)

[$PdCl_2$(cod)] (0.13 g, 0.5 mmol) was added to a solution of **4** (0.39 g, 0.5 mmol) in 15 ml of DMF, and the reaction mixture was stirred for 24 h. The solvent was removed in vacuum, and the yellow microcrystalline solid was washed with acetone collected by filtration and dried under vacuum. Yield: 0.20 g (42%); m.p. >250 °C (dec.). *Anal*. Calc. for $C_{42}H_{40}Cl_2Fe_2N_2O_8P_2Pd$ [1051.73]: C, 47.9; H, 3.8; N, 2.7; P, 5.9. Found: C, 47.3; H, 4.0; N, 2.4; P, 5.6%.

^{1}H NMR (DMF-d_7): δ 4.11 (d, $^2J_{HH}=15.6$ Hz, 4H, P–CH_2^A–N), 4.23 (s, br, 4H, P–CH_2–Fc), 4.40–4.45 (m, 14H, C_5H_5+P–CH_2^B–N), 4.47 (s, 4H, C_5H_4–H7 (for numbering scheme see Eq. (4))), 4.90 (s, br, 4H, C_5H_4–H6), 7.94 (s, 4H, C_6H_3–H2), 8.21 (s, 2H, C_6H_3–H4), 13.6 (s, br, 4H, CO_2H). ^{13}C{^{1}H} NMR (DMF-d_7): δ 25.2 (s, br, P–CH_2–Fc), 47.4 (d, $^1J_{PC}=31.3$ Hz, P–CH_2–N), 69.5 (s, C_5H_4–C7), 69.7 (s, C_5H_5), 70.2 (s, C_5H_4–C6), 80.5 (s, br, C_5H_4–C5), 122.2 (s, C_6H_3–C2),

122.9 (s, C_6H_3–C4), 133.4 (s, C_6H_3–C3), 150.1 (s, C_6H_3–C1), 167.3 (s, CO_2H). $^{31}P\{^1H\}$ NMR (DMF-d_7): δ 7.2 (s). IR ($\tilde{\nu}$/cm^{-1}, KBr): 1598, 1650, 1715 (CO + aryl), 3430 (HO).

Acknowledgements

Financial support from INTAS (N 00-00677) is gratefully acknowledged. K.A.A. thanks the Sächsisches Ministerium für Wissenschaft und Kunst (SMWK, Az.: 4-7531.50-04-0361-01/11) and DFG (Az.: 436 RUS 17/60/01) for financial support.

References

[1] N.J. Goodwin, W. Henderson, B.K. Nicholson, J. Chem. Soc., Chem. Commun. (1997) 31.
[2] N.J. Goodwin, W. Henderson, B.K. Nicholson, J. Fawcett, D.R. Russel, J. Chem. Soc., Dalton Trans. (1999) 1785.
[3] N.J. Goodwin, W. Henderson, B.K. Nicholson, J.K. Sarfo, J. Fawcett, D.R. Russel, J. Chem. Soc., Dalton Trans. (1997) 4377.
[4] Y. Yamamoto, T. Tanase, I. Mori, Y.J. Nakamura, J. Chem. Soc., Dalton Trans. (1994) 3191.
[5] N.C. Zanetti, F. Spindler, J. Spencer, A. Togni, G. Rihs, Organometallics 15 (1996) 860.
[6] H.C.L. Abbenhuis, U. Burckhard, V. Gramlich, A. Martelletti, J. Spencer, I. Steiner, A. Togni, Organometallics 15 (1996) 1614.
[7] (a) P. Barbaro, C. Bianchini, A. Togni, Organometallics 16 (1997) 3004;
(b) M. Ogasawara, K. Yoshida, T. Hayashi, Organometallics 20 (2001) 3913.
[8] R. Sommer, P. Lönnecke, P.K. Baker, E. Hey-Hawkins, Inorg. Chem. Commun. 5 (2002) 115.
[9] I.O. Georgiev, A.A. Karasik, F.F. Nigmadzyanov, G.N. Nikonov, Russ. J. Coord. Chem. 21 (1995) 222.
[10] I.O. Georgiev, A.A. Karasik, G.N. Nikonov, Phosphorus Sulfur Silicon 111 (1996) 133.
[11] A.A. Karasik, I.O. Georgiev, R.I. Vasiliev, O.G. Sinyashin, Mendeleev Commun. (1998) 140.
[12] D.E. Berning, K.V. Katty, C.L. Barnes, W.A. Volkert, J. Am. Chem. Soc. 121 (1999) 1658.
[13] J.G.E. Krauter, M. Beller, Tetrahedron 56 (2000) 771.
[14] A.A. Karasik, I.O. Georgiev, O.G. Sinyashin, E. Hey-Hawkins, Polyhedron 19 (2000) 1455.
[15] A.A. Karasik, I.O. Georgiev, E.I. Musina, O.G. Sinyashin, J. Heinicke, Polyhedron 20 (2001) 3321.
[16] O.G. Sinyashin, A.A. Karasik, I.O. Georgiev, S.V. Bobrov, J. Heinicke, E. Hey-Hawkins, Phosphorus Sulfur 177 (2002), in press.
[17] B.A. Arbuzov, O.A. Erastov, G.N. Nikonov, I.A. Litvinov, D.S. Yufit, Yu.T. Struchkov, Dokl. AN SSSR 257 (1981) 127.
[18] B.A. Arbuzov, O.A. Erastov, G.N. Nikonov, Izv. AN SSSR, Ser. Khim. (1983) 1846.
[19] A.A. Karasik, G.N. Nikonov, Zh. Obsch. Khim. 63 (1993) 2775.
[20] B.A. Arbuzov, A.A. Karasik, G.N. Nikonov, E.V. Malova, R.S.h. Khadiullin, A.Kh. Plyamovatyi, K.M. Enikeev, Izv. AN SSSR, Ser. Khim. (1992) 335.
[21] A.A. Karasik, G.N. Nikonov, A.S. Dokuchaev, I.A. Litvinov, Russ. J. Coord. Chem. 20 (1994) 300.
[22] A.A. Karasik, S.V. Bobrov, G.N. Nikonov, A.P. Pisarevskii, I.A. Litvinov, A.S. Dokuchaev, Yu.T. Struchkov, K.M. Enikeev, Russ. J. Coord. Chem. 21 (1995) 574.

Table 1
Summary of crystallographic data and parameters for $[Cu(L)(oxalato)(H_2O)]\cdot H_2O$ and $[Cu(L)_2(H_2O)_2](NO_3)_2$

	$[Cu(L)(oxalato)(H_2O)]\cdot H_2O$	$[Cu(L)_2(H_2O)_2](NO_3)_2$
Formula	$C_{10}H_{12}CuN_4O_7$	$C_{16}H_{20}CuN_{10}O_{10}$
Colour, habit	blue, prismatic	green, prismatic
Crystal size (mm)	$0.25 \times 0.15 \times 0.15$	$0.50 \times 0.20 \times 0.15$
Molecular weight (g)	363.78	575.96
System	triclinic	triclinic
Space group	$P\bar{1}$	$P\bar{1}$
a (Å)	8.3611(5)	7.0898(7)
b (Å)	8.9493(6)	7.3727(7)
c (Å)	10.7891(7)	11.429(1)
α (°)	112.438(1)	72.418(2)
β (°)	93.797(1)	82.321(2)
γ (°)	115.046(1)	86.878(2)
V (Å^3)	650.52(7)	564.35(9)
Z	2	1
$F(000)$	370	295
ρ_{calc} (g cm^{-3})	1.857	1.695
μ (Mo Kα) (mm^{-1})	1.724	1.045
Temperature (K)	298 ± 2	298 ± 2
Measurements		
Radiation λ Mo Kα (Å)	0.71073	0.71073
θ Range (°)	2–28	2–26
Number collected reflections	4655	3499
Interval h, k, l	$-11 \le h \le 11$; $-11 \le k \le 10$, $-8 \le l \le 14$	$-7 \le h \le 8$, $-9 \le k \le 8$, $-14 \le l \le 14$
Independent reflections	3159	2265
R_{int}	0.0186	0.0330
Absorption correction	empirical	semi-empirical
Max/min transmission	0.7820 and 0.6724	0.8590 and 0.6231
Refinements		
Refinement method	full-matrix least-squares on F^2	full-matrix least-squares on F^2
Data/restraints/parameters	3159/0/200	2265/0/209
Goodness-of-fit on F^2	1.020	1.138
W	$1/[\sigma^2(F_o)^2+(0.0607P)^2+(0.2175P)]$	$1/[\sigma^2(F_o)^2+(0.1057P)^2+(0.5919P)]$
P	$[(F_o)^2+2(F_c)^2]/3$	$[(F_o)^2+2\ (F_c)^2]/3$
R_1 $[I \ge 2\sigma(I)]$	0.0370	0.0535
WR_2 $[I \ge 2\sigma(I)]$	0.0948	0.1422
R_1 [all data]	0.0501	0.0579
WR_2 [all data]	0.1012	0.1641
Largest difference peak and hole (e Å^{-3})	0.550, −0.673	0.620, −1.211

and angles are listed in Table 2. The stereochemistry of the copper(II) ion can be described as a distorted square-pyramid with a geometrical factor $\tau = 0.06$ (where $\tau = (\beta - \alpha)/60$; β is the greatest of the basal angles and α the second in magnitude) [9]. The basal plane is formed by two oxalato oxygen, the pyridine N(1) and the oxadiazole N(2) nitrogen atoms, with bond lengths of 1.929(2), 1.931(2), 2.023(2) and 2.012(2) Å, respectively. A water oxygen is placed in the apical position [Cu–O(1S) 2.414(2) Å]. The metal ion sits at 0.141 Å above the basal plane.

The oxadiazole ligand may be considered as quasi-planar. The maximum deviation from the pyridine plane corresponds to the C(8) atom, 0.167(4) Å.

The structure of **1** can be viewed as an alternating sequence of monomeric units (up-and-down with respect to the coordinated water molecule) forming double sheets parallel to the (1,−1,1) plane (Fig. 2). The crystallization water molecules reside between these sheets, but their arrangement is better described as planes parallel to (1,−1,2). The $[Cu(L)(oxalato)(H_2O)]$ entities are interconnected by strong hydrogen bonds in which the oxalato and water oxygen atoms play an important role (see Table 2).

It is worth mentioning that the shortest C···C distance between the pyridine and oxadiazole from different monomers is 3.22 Å. This fact suggests the existence of π–π stacking interactions between the aromatic rings. The stacking does not necessarily exhibits a perfect face-to-face alignment of the atoms as shown in Fig. 3, but can be described as a slipped packing [10]. These types of interactions have been evaluated [11,12], and the results are shown in Table 3. The coordination of a metal ion to the nitrogen

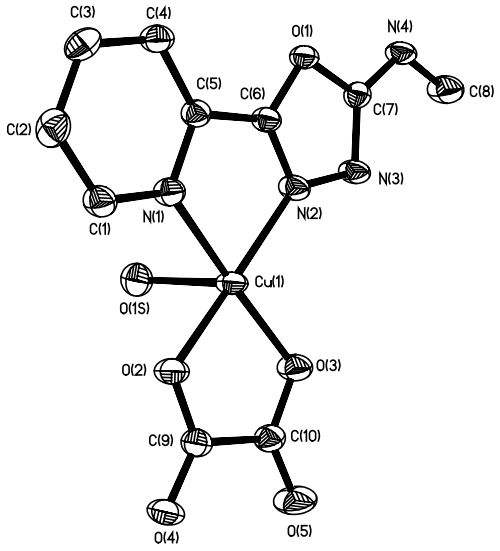


Fig. 1. Molecular structure of the [Cu(L)(oxalato)(H_2O)] entity with thermal ellipsoids at 30% probability level.

heteroatom from pyridines and other heterocycles enhances the electron-withdrawing effect through its positive charge, so that the stability of the π–π interaction increases [13,14]. In our case, the existence of further π–π interactions between the oxadiazole rings and the carboxylato groups with a shortest C(7)···C(10) distance of 3.27 Å cannot be excluded.

The crystal structure of complex **2** consists of $[Cu(L)_2(H_2O)_2]^{2+}$ cationic discrete entities and nitrate groups acting as counterions. A perspective view of the molecular structure of the centrosymmetric cationic entity is shown in Fig. 4. Selected interatomic dimensions are given in Table 4. The metal ion exhibits an elongated *trans*-octahedral geometry. It is coordinated by four nitrogen atoms at the equatorial plane: the pyridine N(1) and the oxadiazole N(2) atoms belonging to each ligand, at distances 2.033(3) and 2.040(3) Å, respectively. The axial positions are occupied by the oxygen atoms from both water molecules [Cu–O(2) 2.319(3) Å].

The oxadiazole ligand exhibits high planarity, the maximum deviation from the pyridine plane corresponding to the C(8) atom (0.163(6) Å).

Several hydrogen bonds are established in the lattice in which the nitrate ions, the water molecules, the amino N(4) and the oxadiazole N(3) nitrogen atoms and some of the pyridine carbon atoms are involved (Table 4). It is interesting to note the existence of an intramolecular hydrogen bond between the C(1) and N(3) atoms from the two different ligands.

The shortest interplanar atom···atom distance is 3.42 Å. The results of the structural analysis shown in Table 3 are in good agreement with the presence of π–π stacking interactions in compound **2**.

To evaluate some geometrical features in this 1,3,4-oxadiazole system, a comparative study on complexes containing the L ligand has been carried out. The ligand in compounds **1** and **2** shows a *syn* conformation with respect to both the C(5)–C(6) and C(7)–N(4) bonds, as in the free L molecule [8]. However, in the case of the $[\{Cu(L)(H_2O)_2(SO_4)\}_2]\cdot 2H_2O$ dimeric compound [8], the C(8) and N(3) atoms are anti with respect to the C(7)–N(4) bond. This conformational change can be attributed to the presence of a steric hindrance between the methyl and sulfato groups in the dimer. There is not

Table 2
Selected bond distances (Å) and angles (°) for [Cu(L)(oxalato)(H_2O)]·H_2O

Bond lengths					
Cu(1)–O(2)	1.929(2)	Cu(1)–N(2)	2.012(2)	Cu(1)–O(1S)	2.414(2)
Cu(1)–O(3)	1.931(2)	Cu(1)–N(1)	2.023(2)		
Bond angles					
O(2)–Cu(1)–O(3)	85.74(8)	O(2)–Cu(1)–O(1S)	91.82(8)	C(10)–O(3)–Cu(1)	112.0(2)
O(2)–Cu(1)–N(2)	168.85(9)	O(3)–Cu(1)–O(1S)	96.57(8)	C(1)–N(1)–Cu(1)	126.1(2)
O(3)–Cu(1)–N(2)	100.36(8)	N(2)–Cu(1)–O(1S)	96.70(9)	C(5)–N(1)–Cu(1)	115.0(2)
O(2)–Cu(1)–N(1)	91.82(8)	N(1)–Cu(1)–O(1S)	90.85(8)	C(6)–N(2)–Cu(1)	111.5(2)
O(3)–Cu(1)–N(1)	172.25(9)	C(9)–O(2)–Cu(1)	112.6(2)	N(3)–N(2)–Cu(1)	140.2(2)
N(2)–Cu(1)–N(1)	80.91(9)				

	A–H (Å)	H···B (Å)	A···B (Å)	A–H···B (°)
Hydrogen bonding contacts A–H···B				
N(4)–H(4A)···O(4)^{I}	0.86	2.11	2.899(3)	152.4
N(4)–H(4A)···O(5)^{I}	0.86	2.55	3.116(3)	124.6
O(1S)–H(1SA)···O(4)^{ii}	0.82	1.95	2.766(3)	174.9
O(1S)–H(1SB)···O(2S)^{iii}	0.86	1.98	2.817(3)	163.0
O(2S)–H(2SA)···O(5)	0.87	1.86	2.719(3)	168.3
O(2S)–H(2SB)···O(1S)^{iv}	0.95	2.13	3.071(3)	172.6

Symmetry transformations used to generate equivalent atoms: i, $x, y-1, z-1$; ii, $-x+1, -y+2, -z+2$; iii, $-x+2, -y+3, -z+2$; iv, $x, y+1, z$.

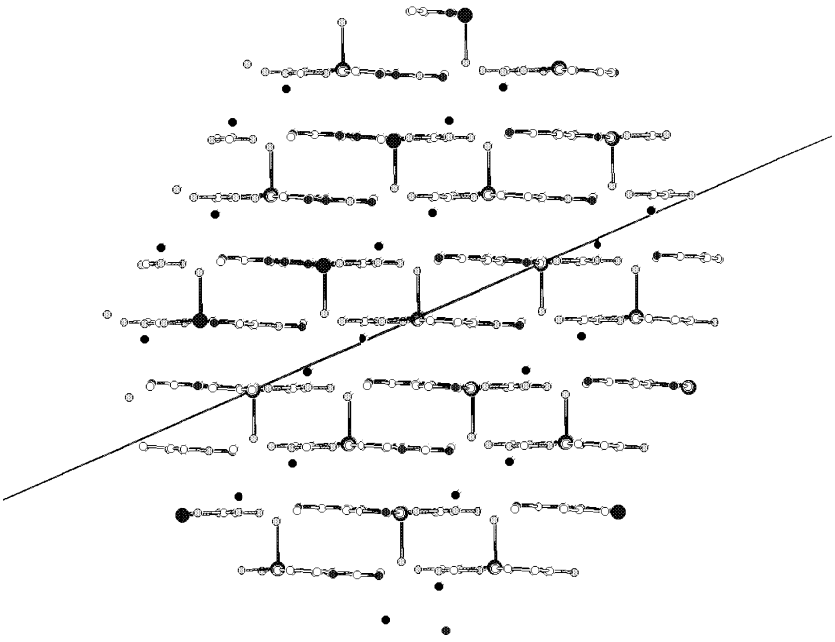


Fig. 2. View of the planar arrangement in **1**. The line in the drawing represents the (1, −1, 2) plane.

a significant variation in the bond lengths of L with complexation to the copper(II) ions. The main divergences for some selected parameters are given in Table 5. As can be seen, the value of the N(1)–C(5)–C(6)–N(2) dihedral angle between the pyridine and the oxadiazole rings decreases for the coordinated ligand. The C(5)–C(6)–N(2) angle also decreases with complexation. Complexes **1** and **2** exhibit the smallest values for both mentioned angles. This fact correlates well with the increase of the N(1)–Cu–N(2) bite angle for the monomer compounds, indicating that (i) the metal ion induces a higher planarity in the ligand, and (ii) the monomeric systems are less stressed than the dimer one.

The existence of different infrared absorption corresponding to the methylamino substituent, the pyridine and the oxadiazole rings, together with the electron delocalization along the whole oxadiazole molecule, make the unambiguous assignation of the bands difficult in these compounds. Moreover, the infrared spectra of 2-methylamino-5-pyridin-2-yl-1,3,4-oxadiazolecopper(II) derivatives show many important differences with respect to that of the free ligand. The intense band observed at 1653 cm^{-1} in the free ligand can be attributed to the $\nu(C{=}N)_{oxadiazolic}$, $\nu(C{=}N)_{pyridinic}$ and $\delta(NH)$ modes. This absorption shows a slight shift to

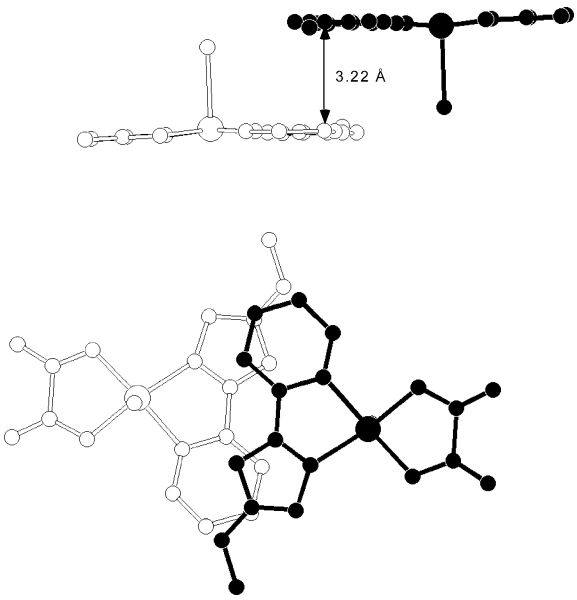


Fig. 3. Details of π–π stacking in compound **1**.

Table 3
Interactions between aromatic rings

I	*j*	DC	ANG	DZ	DXY	DZ′	DXY′	DS
1	2	3.72	0.9	3.25	1.70	3.30	1.70	3.34
3	4^{iv}	3.50	1.8	3.32	1.31	3.29	1.31	3.43

The symmetry transformations follow the nomenclature used in Tables 2 and 4; iv, $-x+1, -y, -z+2$. Ring 1: N(1), C(1), C(2), C(3), C(4), C(5) in compound **1**. Ring 2: C(6), N(2), N(3), C(7), O(1) in compound **1**. Ring 3: N(1), C(1), C(2), C(3), C(4), C(5) in compound **2**. Ring 4: C(6), N(2), N(3), C(7), O(1) in compound **2**. DC, distance between the centroids of the aromatic rings i and j; ANG, angle between the least-squares planes; DZ, distance between the centroid of j ring and the least-squares plane of i ring; DZ′, distance between the centroid of i ring and the least-squares plane of j ring; DXY, distance between the centroids of i and j projected onto the least-squares plane of i; DXY′, distance between the centroids of i and j projected onto the least-squares plane of j; DS, distance from the centroid of j to the nearest hydrogen atom of i ring.

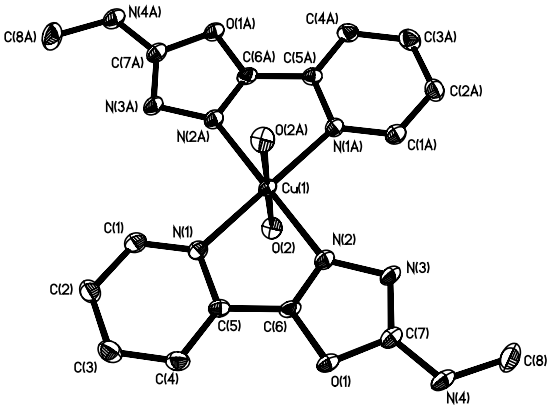


Fig. 4. Molecular structure of the $[Cu(L)_2(H_2O)_2]^{2+}$ entity with thermal ellipsoids at 30% probability level.

1656 and 1658 cm^{-1} for compounds **1** and **2**, respectively.

The absorptions at 1683 (vs), 1411 (s), 1273 (m) and 810 cm^{-1} in complex **1** have been attributed to the $\nu_a(C{=}O)$, $[\nu_s(C{=}O)+\nu(CC)]$, $[\nu_s(CO)+\delta(O{-}C{=}O)]$ and $[\nu(MO)+\delta(O{-}C{=}O)]$ modes of the oxalato ligand, respectively. Nevertheless, some of these absorptions are overlapped with those corresponding to the oxadiazole ligand. The spectrum of compound **2** shows a strong absorption at 1385 cm^{-1} and a weak band at 826 cm^{-1}, which can be assigned to the free nitrate groups, in good agreement with the structural results.

The reflectance spectra show bands in the 225–275, 345–405 and 650–1040 nm regions (see Table 6). They are attributed to intraligand, LMCT N/O → d and d → d transitions, respectively.

In order to make a good assignment of these bands a study in solution for the free ligand and compound **2** was carried out. Complex **1** is practically insoluble in all common solvents. The absorption at 226 nm in the reflectance spectrum of **2** is shifted towards higher energies in solution, and its maximum is only observed in the spectrum recorded on a methanolic solution. The strong band at 272 nm in the solid UV–Vis spectrum of **2** shows a shift to 297–304 nm in solution (see Table 6). A very small dependence of this band with respect to the polarity of the solvents is detected. These absorptions correspond to those observed in the free ligand at 204 and 298–300 nm, respectively, corroborating the intraligand character in both complexes. These bands have been assigned to the $(\pi\rightarrow\pi^*)_{pyridine/oxadiazole}$ and $(n\rightarrow\pi^*)_{pyridine/oxadiazole}$ transitions, respectively [15].

Table 4
Selected bond distances (Å) and angles (°) for $[Cu(L)_2(H_2O)_2](NO_3)_2$

Bond lengths					
Cu(1)–N(1)	2.033(3)	Cu(1)–N(2)	2.040(3)	Cu(1)–O(2)	2.319(3)
Bond angles					
$N(1)^i$–Cu(1)–$N(1)^{ii}$	180.0(2)	$N(1)^i$–Cu(1)–$O(2)^{ii}$	89.2(1)	C(1)–N(1)–Cu(1)	127.6(2)
$N(1)^i$–Cu(1)–$N(2)^{ii}$	81.1(1)	$N(2)^i$–Cu(1)–$O(2)^i$	90.3(1)	C(5)–N(1)–Cu(1)	114.1(2)
$N(1)^i$–Cu(1)–$N(2)^{ii}$	98.9(1)	$N(2)^i$–Cu(1)–$O(2)^{ii}$	89.7(1)	C(6)–N(2)–Cu(1)	110.2(2)
$N(2)^i$–Cu(1)–$N(2)^{ii}$	180.0(2)	$O(2)^i$–Cu(1)–$O(2)^{ii}$	180.0(2)	N(3)–N(2)––Cu(1)	140.3(2)
$N(1)^i$–Cu(1)–$O(2)^i$	90.8(1)				
	A–H (Å)	H···B (Å)	A···B (Å)	A–H···B (°)	
Hydrogen bonding contacts A–H···B					
O(2)–H(2A)···O(3S)	0.80(6)	2.08(6)	2.807(5)	152(5)	
O(2)–H(2A)···O(2S)	0.80(6)	2.61(6)	3.344(5)	154(5)	
$N(4)–H(4A)\cdots O(2S)^{iii}$	0.75(6)	2.23(6)	2.942(5)	160(6)	
$O(2)–H(2B)\cdots O(2S)^{iv}$	0.75(6)	2.05(6)	2.786(5)	165(6)	
$C(1)^i–H(1)^i\cdots N(3)^{ii}$	0.93(6)	2.43(6)	3.262(5)	149(6)	
$C(4)–H(4)\cdots O(2)^{iv}$	0.92(6)	2.45(6)	3.310(5)	161(6)	

Symmetry transformations used to generate equivalent atoms: i, x, y, $z-1$; ii, $-x$, $-y$, $-z+1$; iii, $-x+1$, $-y-1$, $-z+2$; iv, $-x+1$, $-y$, $-z+2$.

Table 5
Selected angles (°) for L containing compounds

Compound	C(5)–C(6)–N(2)	α	N(1)–Cu–N(2)	Reference
$L\cdot 3H_2O$	128.9(1)	7.0(2)		[8]
$[\{Cu(L)(H_2O)_2(SO_4)\}_2]\cdot 2H_2O$	125.8(2)	5.9(3)	77.23(6)	[8]
$[Cu(L)_2(H_2O)_2](NO_3)_2$	123.2(3)	1.0(5)	81.1(1)	This work
$[Cu(L)(oxalato)(H_2O)]\cdot H_2O$	122.0(2)	1.1(4)	80.91(9)	This work

α = N(1)–C(5)–C(6)–N(2) dihedral angle.

Table 6
UV–Vis spectral data

1 [a]	227, 268, 352 (sh), 654 (b)
2 [a]	226, 272, 347 (sh), 402 (sh), 670 (b), 1037 (vb)
2 [b]	297 (28935), 736 (13)
2 [c]	302 (30083), 774 (41)
2 [d]	304 (30667), 827 (35)
2 [e]	208 (39083), 302 (24300), 328 (sh, 12500), 684 (45.2)
L [e]	204 (23517), 298 (40783)
L [f]	300 (11150)

Values of λ in nm. In brackets, the molar extinction coefficient ε in $M^{-1}\,cm^{-1}$.
[a] In solid.
[b] In water solution 6×10^{-5} M.
[c] In DMF solution 6×10^{-5} M.
[d] In DMSO solution 6×10^{-5} M.
[e] In methanol solution 6×10^{-5} M.
[f] In ethanol solution 6×10^{-5} M.

The shoulders observed at 345–405 nm in the reflectance spectra are attributed to the N→Cu(II) and O→Cu(II) charge transfer transitions. Unfortunately, these bands do not appear in the solution spectra because they are obscured by the tail of the intense intraligand absorption. A shoulder at around 328 nm was only observed for compound **2** in methanol, which does not appear in the spectrum of the free ligand. This fact is consistent with a decrease in the intensity of the intraligand band at around 300 nm observed in the methanol solution of **2** with respect to other solutions of this complex (see Table 6). These results suggest that the charge transfer bands shift to higher energies in solution overlapping with the intraligand absorption.

The reflectance spectrum of **1** shows a band at 654 nm characteristic of d→d transitions for compounds exhibiting a square-pyramidal geometry with a $d_{x^2-y^2}$ ground state. Compound **2** shows a broad band at 670 nm and a less intense absorption at around 1037 nm. This spectrum is typical of octahedral tetragonally distorted copper(II) complexes. These bands could be assigned to the $^2E_g \leftarrow {}^2B_{1g}$ and $^2A_{1g} \leftarrow {}^2B_{1g}$ transitions, respectively, in good agreement with the results reported for analogous triazole systems [16]. The band at 670 nm is shifted to lower energies in solution suggesting the replacement of the axially coordinated aquo ligands by the solvent molecules.

The X-band EPR spectrum of compound **1** at r.t. exhibits axial symmetry with $g_{\parallel}=2.269$ and $g_{\perp}=2.063$. These g-values are typical of complexes containing copper(II) ions in distorted square-pyramidal topologies with $d_{x^2-y^2}$ ground state. The value of $G=(g_{\parallel}-2)/(g_{\perp}-2)=4.3$, suggests that exchange coupling interactions are negligible in this complex [17]. This fact allows us to calculate the mixing coefficient c between the $d_{x^2-y^2}$ and d_{z^2} orbitals using the vibrational model proposed by Reinen and Atanasov [18]. The obtained c value is 0.577, which corresponds to a perfect square-pyramidal geometry, in good agreement with the structural results.

In the case of compound **2**, the EPR spectrum at r.t. shows an axial signal with $g_{\parallel}=2.235$ and $g_{\perp}=2.080$. These values are characteristic of octahedral copper(II) complexes with $d_{x^2-y^2}$ ground state.

It is worth mentioning that the title complexes are stable for months at r.t., while the free oxadiazole ligand decomposes with time. The addition of ferrocyanide removes easily the copper(II) ions from the ligand [8]. In this sense, the coordination represents a good route to stabilise and store the free ligand, in particular as the biscomplex **2**.

On the other hand, the presence of uncoordinated potential chelating centers in compounds **1** and **2**, as the oxadiazole N(3) and the oxalato O(4) and O(5) atoms, and/or a further substitution of the water molecules by ligands acting as bridges between the metal ions suggest that these compounds can be used as precursors of systems with a higher dimensionality (polynuclear complexes, chains, sheets, ...). In this sense, a simple preparative protocol as that reported in this work could be of importance to synthesize biologically active molecules, as well as active site models, which are bridged by histidine moieties.

3. Experimental

3.1. Preparation of the complexes

Potassium oxalato and copper(II) nitrate were purchased from Fluka. 2-Methylamino-5-pyridin-2-yl-1,3,4-oxadiazole (L) and $[\{Cu(L)(H_2O)_2(SO_4)\}_2]\cdot 2H_2O$ were synthesized following a published method [8].

3.2. Synthesis of $[Cu(L)(oxalato)(H_2O)]\cdot H_2O$ (1)

An aqueous solution of potassium oxalato (0.024 g, 0.13 mmol) was added dropwise to a solution of $[\{Cu(L)(H_2O)_2(SO_4)\}_2]\cdot 2H_2O$ (0.051 g, 0.06 mmol) in 40 ml of water. The mixture was stirred at room temperature (r.t.) overnight. The resulting precipitate was filtered off and washed with water. The yield was 48%. *Anal.* Calc.: C, 33.02; H, 3.32; N, 15.40; Found: C, 32.75; H, 3.44; N, 15.25%. Turquoise-blue crystals suitable for X-ray studies were grown by slow evaporation of the mother liquor at r.t. The compound is insoluble in water, methanol, ethanol, dimethylformamide, dimethylsulfoxide and acetone.

3.3. Synthesis of $[Cu(L)_2(H_2O)_2](NO_3)_2$ (2)

Copper(II) nitrate dissolved in 20 ml of water was allowed to react with solid, crystalline L (0.070 g, 0.3 mmol) suspended in 10 ml of water to give a green

solution. The yield was 43%. *Anal*. Calc.: C, 33.36; H, 3.50; N, 24.32; Found: C, 33.18; H, 3.33; N, 24.07%. Bright green crystals of **2** suitable for X-ray analysis were separated from the mother liquor by slow evaporation at r.t. This complex could also be synthesized starting from **1**: an aqueous solution of $Cu(NO_3)_2 \cdot 3H_2O$ (0.070 g, 0.3 mmol) was added to a suspension of $[Cu(L)(oxalato)(H_2O)] \cdot H_2O$ (0.054 g, 0.15 mmol) in water. The compound is soluble in water, methanol, dimethylformamide and dimethylsulfoxide, slightly soluble in ethanol and not soluble in acetone. Molar conductivity of 5×10^{-4} M solutions in water (dimethylformamide) at 25 °C: $\Lambda_M = 281$ (139) Ω^{-1} cm^2 mol^{-1}.

3.4. Physical measurements

Microanalyses were performed with a LECO CHNS-932 analyzer. Conductivity measurements were made by a CRISON-522 conductimeter. Infrared spectra were obtained with samples prepared as KBr pellets in the 400–4000 region on a Nicolett Impact 410 FTIR spectrophotometer. Reflectance spectra were carried out on a Cary 2415 spectrometer in the range 5000–50 000 cm^{-1}. For UV–Vis solution measurements, a Varian UV–Vis–NIR spectrophotometer was employed. X-band EPR spectra were recorded on a Bruker EMX spectrometer, equipped with a standard Oxford continuous flow cryostat.

3.5. X-ray crystallographic studies

Crystal data collections were carried out on an Bruker Smart CCD area detector equipped single crystal diffractometer. Absorption corrections were made using the SADABS program [19]. Direct methods (SHELXS-97) [20] were employed to solve the structures and then they were refined by a full-matrix least-squares method, using the SHELXL-97 computer program [21]. All non-hydrogen atoms were assigned anisotropic thermal parameters. Hydrogen positions were determined by difference Fourier syntheses and introduced in calculations with a riding model. The scattering factors and anomalous dispersion coefficients were taken from International Tables of X-ray Crystallography [22]. Refinements were made on F_o^2 for all reflections.

4. Supplementary material

Crystallographic data (excluding structure factors) for the structures reported in this paper have been deposited with the Cambridge Crystallographic Data Center. The deposition numbers are CCDC-182346, and -182347 for compounds **1** and **2**, respectively. Copies of the data can be obtained free of charge on application to The Director, CCDC, 12 Union Road, Cambridge CB2 1EZ, UK (fax: +44-1223-336033; e-mail: deposit@ccdc.cam.ac.uk or http://www.ccdc.cam.ac.uk).

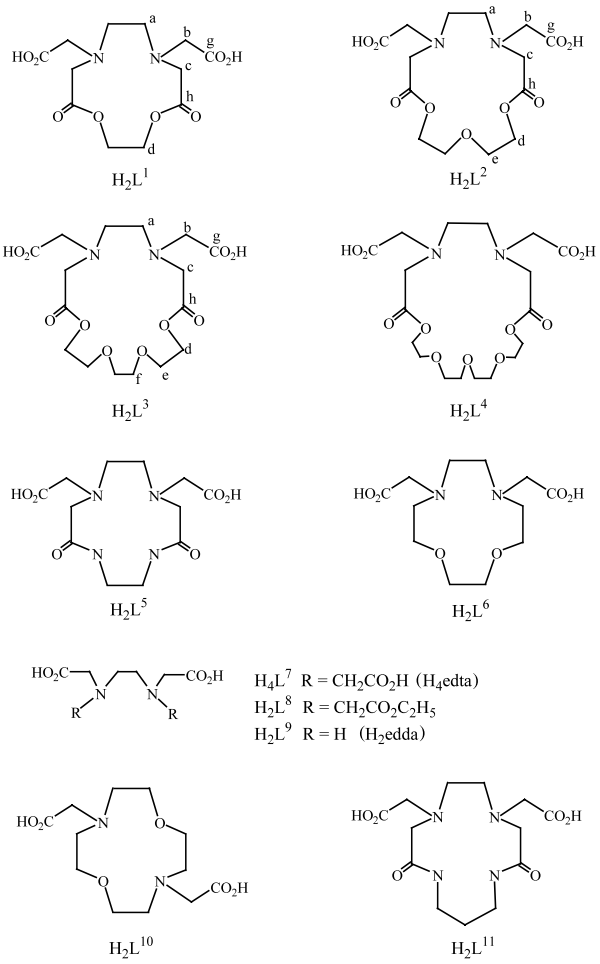
Acknowledgements

We thank Dr. J.J. Delgado (SCAI, Universidad de Burgos, Spain) for the elemental analysis and Professor R. Olazcuaga and Dr. F. Guillen (CNRS, Pessac, France) for the reflectance measurements. This work has been carried out with the financial support of the Basque Government (PI99/53). P.G.-S. thanks to the Universidad de Burgos for her Doctoral Fellowship.

References

[1] B.L. Sharma, S.K. Tandon, Pharmazie 39 (1984) 858.
[2] J.P. Wignacourt, S. Sueur, M. Lagrenée, Acta Crystallogr., Sect. C 46 (1990) 394.
[3] M. Lagrenée, S. Sueur, J.P. Wignacourt, B. Mernari, A. Boukhan, J. Chim. Phys. 88 (1991) 2075.
[4] C. Incarvito, A.L. Rheingold, C.J. Qin, A.L. Gavrilova, B. Bosnich, Inorg. Chem. 40 (2001) 1386.
[5] A. Gueddi, B. Mernari, M. Giorgi, M. Pierrot, Acta Crystallogr., Sect. C 56 (2000) e426.
[6] X.-H. Bu, H. Liu, M. Du, L. Zhang, Y.-M. Guo, M. Shionoya, J. Ribas, Inorg. Chem. 41 (2002) 1855.
[7] M. Lagrenee, S. Sueur, J.P. Wignacourt, Acta Crystallogr., Sect. C 47 (1991) 1158.
[8] P. Gómez-Saiz, J. García-Tojal, M.A. Maestro, F.J. Arnáiz, T. Rojo, Inorg. Chem. 41 (2002) 1345.
[9] A.W. Addison, T.N. Rao, J. Reedijk, J. van Rijn, G.C. Verschoor, J. Chem. Soc., Dalton Trans. (1984) 1349.
[10] C. Janiak, J. Chem. Soc., Dalton Trans. (2000) 3885.
[11] A. Albert, F.H. Cano, Cristalografia, Publicaciones CSIC, Madrid, 1995.
[12] I. Unamuno, J.M. Gutiérrez-Zorrilla, A. Luque, P. Román, L. Lezama, R. Calvo, T. Rojo, Inorg. Chem. 37 (1998) 6452.
[13] C.A. Hunter, J.K.M. Sanders, J. Am. Chem. Soc. 112 (1990) 5525.
[14] F. Cozzi, M. Cinquini, R. Annunziata, J.S. Siegel, J. Am. Chem. Soc. 115 (1993) 5330.
[15] E.S. Stern, C.J. Timmons, Electronic Absorption Spectroscopy in Organic Chemistry, Edward Arnold, London, 1970.
[16] W.M.E. Koomen-van Oudenniel, R.A.G. de Graaf, J.G. Haasnoot, R. Prins, J. Reedijk, Inorg. Chem. 28 (1989) 1128.
[17] B.J. Hathaway, J. Chem. Soc., Dalton Trans. (1972) 1196.
[18] D. Reinen, M. Atanasov, Chem. Phys. 136 (1989) 27.
[19] R.H. Blessing, Acta Crystallogr., Sect. A 51 (1995) 33.
[20] G.M. Sheldrick, SHELXS-97, Program for Crystal Structure Solution, University of Göttingen, Göttingen, Germany, 1997.
[21] G.M. Sheldrick, SHELXL-97, Program for the Refinement of Crystal Structures from Diffraction Data, University of Göttingen, Göttingen, Germany, 1997.
[22] International Tables for Crystallography, Kluwer Academic Publishers, Dordrecht, The Netherlands, 1992.

received much attention [27–32]. The cyclic diamides as well as the corresponding cyclic diesters derived from edta dianhydride cannot be useful for applications such as those mentioned above, because of the low stability constants of their metal complexes [13,14,28,30]. However, the diester macrocyclic compounds combine two moieties of contrasting metal complexes preferences. The edta-moiety, which contains two amines, two ester functions incorporated into the macrocyclic backbone and two appended *N*-acetate groups, and the crown-ether moiety, consisting of an increasing number of ether oxygen atoms. The length of the crown-ether pocket can be tuned for the selective complexation of an alkali or an alkaline-earth metal ion, while the edta-moiety is more appropriate for the co-ordination of transition or post-transition metal ions. Thus the latter metal ion complexes formed in the edta moiety can behave as a molecular sensor for the recognition of alkali or alkaline-earth metal ions. With this in mind, we synthesised a series of macrocyclic compounds of the diester type derived of edta, H_2L^1–H_2L^4, as shown in Scheme 1. The protonation reactions of the ligands and their thermodynamic stability constants with a series of divalent metal ions were undertaken. However, the easy hydrolysis of those ligands and especially of some of their metal complexes, with the consequent rupture of the macrocyclic backbone, never mentioned before [27–31], restricts their possible applications. The hydrolysis reaction observed was studied with the objective of understanding the metal catalysis involved in the procedure.



Scheme 1.

2. Results and discussion

2.1. Synthesis of compounds

Reaction of the ethylenediamine tetracetic dianhydride with polyethyleneglycols $HO(CH_2CH_2O)_nH$ ($n = 1$–4) leads to the macrocyclic diesters H_2L^1–H_2L^4 [27]. The original procedure and published modifications [28] led to materials, which still contained edta. We, therefore, modified the reaction conditions and the work up to obtain products free from this impurity, albeit in lower yield. The compound H_2L^2 was obtained in such small amount that only NMR and EPR spectroscopic studies could be performed. The ^1H and ^{13}C spectra in D_2O and d_6-DMSO for all compounds and some of their zinc(II) and lead(II) complexes are summarised in Table 1. We also checked the published assignment [29,30] of the ^1H and ^{13}C b and c resonances, of the $-NCH_2COO^-$ groups, as well as the ^{13}C g and h signals, of the $-NCH_2COO^-$ groups, see NMR studies.

2.2. Acid-base behaviour of H_2L^1–H_2L^4

The protonation constants of H_2L^1–H_2L^4 are collected in Table 2. For each compound only two values were determined, the other two are very low to be obtained by the technique used. Both values for all compounds have similar magnitude, although slightly smaller ones for the 12-membered macrocycle H_2L^1. The latter and the corresponding diamide compound, H_2L^5, present practically the same values, indicating that it is the presence of the carbonyl function that matters. In agreement with this, both protonation constant values are higher for H_4edta [33], and for H_2L^6 [34], while the diester derivative of edta, H_2L^8 [28], has values similar to those of the cyclic derivatives (see Table 2). This is due to the greater electron-withdrawing ability of the carbonyl over that of the carboxylate group. Thus the introduction of the carbonyl group in the cyclic backbone of H_2L^1–H_2L^4 leads to a significant decrease of the overall basicity of these compounds when compared with H_4edta or H_2L^6 (of about 5–6 log units), which will have important implications upon its metal complexing behaviour.

On the other hand, although no doubts exist about the site where the first protonation occurs, which is in

Table 1
NMR data for compounds H_2L^1–H_2L^3 and some of their Zn^{2+} and Pb^{2+} complexes

Compound	Solvent	pD [a]	Nucl.	a	b	c	d	e	f	g	h
H_2L^1	D_2O	3.0	^1H	3.18	3.61	3.79	4.43				
H_2L^1	D_2O	3.0	^{13}C	53.4	57.9	58.5	63.7			173.7	170.7
H_2L^1	DMSO		^1H	2.70	3.46	3.46	4.38				
H_2L^1	DMSO		^{13}C	53.4	58.0	58.0	62.7			174.3	172.8
$[L^1Zn]$	DMSO		^1H	3.15	3.83	3.79	4.45				
$[L^1Zn]$	DMSO		^{13}C	53.4	57.4	57.4	63.3			172.5	170.9
$[L^1Pb]$	DMSO		^1H	3.08	3.75	3.75	4.48				
$[L^1Pb]$	DMSO		^{13}C	54.0	58.2	58.4	63.2			173.8	170.8
H_2L^2	D_2O	2.4	^1H	3.37 (s)	3.84 (s)	4.08 (s)	4.45 (m)	3.83 (m)			
H_2L^2	D_2O	2.4	^{13}C	53.8	59.5	56.9	65.9	70.0		176.3	172.2
$(HL^2)^-$	D_2O	4.4	^1H	3.33	3.66	4.04	4.45	3.83			
$(L^2)^{2-}$	D_2O	7.4	^1H	2.97	3.36	3.73	4.45	3.84			
$[L^2Pb]$	D_2O	1.6	^1H	3.13 (s)	3.86 (s)	3.83 (s)	3.98	3.66, 3.75			
$[L^2Pb]$	D_2O	1.6	^{13}C	57.4	62.4	60.2	68.4	71.4		182.3	177.8
H_2L^3	D_2O	3.2	^1H	3.17 (s)	3.53 (s)	3.92 (s)	4.26 (m)	3.62 (m)	3.64 (s)		
H_2L^3	D_2O	3.2	^{13}C	54.7	57.8	60.0	67.6	71.4	72.7	176.8	173.0
H_2L^3	DMSO		^1H	2.64 (s)	3.48 (s)	3.34 (s)	4.20 (s, br)	3.65 (s, br)	3.57 (s)		
H_2L^3	DMSO		^{13}C	53.6	57.0	57.0	65.0	69.9	71.7	174.8	172.6
$[L^3Zn]$	DMSO		^1H	3.21 (s, br)	4.00 (s, br)	3.85 (s, br)	4.29 (s)	3.64 (s)	3.54 (s)		
$[L^3Zn]$	DMSO		^{13}C	52.9	56.6	56.6	65.9	69.7	71.9	176.4	172.2
$[L^3Pb]$	DMSO		^1H	2.97 (s)	3.84 (s)	3.79 (s)	4.27 (s, br)	3.67 (s, br)	3.58 (s)		
$[L^3Pb]$	DMSO		^{13}C	54.7	57.6	59.4	66.1	69.5	71.6	176.8	172.2

For numbering of the atoms see Scheme 1.
[a] When the pD is not quoted, the compound was dissolved in pure solvent without any additional pD adjustment.

the amine nitrogen, the same cannot be said about the second protonation, that can be attributed to the second amine or to a carboxylate group. If it occurs in the other amine, which is at short distance from that already protonated, a net decrease of basicity would be observed due to the strong repulsion of positive charged ammonium ions formed, as happens in H_4edta [33] and in H_2L^6 [34]. The value obtained for the second protonation is also in agreement with the protonation of an *N*-acetate group appended to a non-protonated amine, as found for many *N*-polyacetate polyaza-macrocycles [34–36]. A titration followed by NMR spectroscopy can elucidate this problem [34–36]. In fact, the observed deshielding of the methylene hydrogen atoms due to the protonation of basic centres of the ligands located in their vicinity can be correlated with the percentage of protonation of the amine and carboxylate groups [34–36]. The ^1H NMR obtained at three distinguishable pD values of H_2L^2 in D_2O, corresponding to the formation of H_2L, HL^- and L^{2-} species, gave the following results, see Table 1: at $pD \geq 7$ the main species in solution is completely deprotonated corresponding to a high shielding of the protons. A single protonation can be achieved by lowering the pH to 4.4, which is accompanied by a deshielding of the protons of the CH_2 groups attached to nitrogen (for compound H_2L^2: $\Delta\delta$ (a) = 0.36 ppm, $\Delta\delta$ (b) = $\Delta\delta$ (c) = 0.31 ppm, see Scheme 1 for labelling of compounds). This suggests that the first protonation occurs at the nitrogen atoms, which will be 50% protonated. Further lowering of the

Table 2
Protonation (log K_i^H) constants of H_2L^1–H_2L^4 and of other ligands for comparison

Equilibrium quotient	H_2L^1	H_2L^{2a}	H_2L^3	H_2L^4	H_2L^5 [a]	H_2L^6 [b]	H_4L^7 [c] (H_4edta)	H_2L^8 [d]
[HL]/[H] × [L]	6.48(1) 6.44 [a]	6.82	7.12(1), 6.97 [a]	7.20(1), 7.20 [a]	6.50	10.54	10.37	7.33
$[H_2L]/[HL] \times [H]$	3.72(1), 3.49 [a]	3.84	3.81(1), 3.75 [a]	3.80(1), 3.91 [a]	3.54	4.84	6.13	3.66
$[H_2L]/[L] \times [H]^2$	10.20	10.66	10.93	11.00	10.04	15.38	16.50	10.99

$T = 298.0$ K; $I = 0.10$ mol dm^{-3} in NMe_4NO_3. Values in parenthesis are S.D. in the last significant figures.
[a] $I = 0.1$ mol dm^{-3} KCl, Ref. [14].
[b] Ref. [34].
[c] $I = 0.10$ mol dm^{-3}, Ref. [33].
[d] Ref. [28].

pD to 2.4, results in a second protonation. At this pD value only the b signal shifts downfield ($\Delta\delta$ (b) = 0.18 ppm), all the other resonances remain basically unchanged, implying the assignment of protons b to the methylene group of CH_2COOH and testifying that the second protonation occurs in a carboxylate group. The lower shift observed for protons b by the protonation of the nearby carboxylate when compared with the shift caused by the protonation of amine centres is due to the lower shielding constant of the carboxylate compared with that of an amine [35].

2.3. Stability constants of some complexes and metal-catalysed hydrolysis of the ligands

The stability constants of H_2L^1, H_2L^3 and H_2L^4 with alkaline-earth metal ions, Cu^{2+}, Ni^{2+}, Cd^{2+} and Pb^{2+} are collected in Table 3, together with the corresponding constants for complexes of other ligands taken from the literature for comparison. Only mononuclear complexes, ML and MHL, were found in solution for all the compounds with the studied metal ions. Hydroxocomplexes, $ML(OH)_i$, could not be determined due to decomposition of the complexes in aqueous solution at higher pH values, as explained below. Dinuclear or other species, such as M_2L, M_2HL, M_3L_2 or ML_2, were expected to form with the larger membered rings, but were either not accepted by the HYPERQUAD program [37] or accepted with worse statistical parameters.

Aqueous solutions of the ligands decompose slowly with time, especially at pH $\geq$ 7. Minor increases of the rate of decomposition were observed in presence of alkaline-earth metal ions, while for the other complexes studied the decomposition rate depends of the metal ion following the order: Cu(II) > Pb(II) > Cd(II) > Zn(II) for H_2L^1 and Pb(II) $\gg$ Cd(II) > Cu(II) > Zn(II) for H_2L^2–H_2L^4. Even so, it was possible to determine the equilibrium constants by dissolution of the ligand immediately before starting the titration. It was observed that the rate of the decomposition reaction is lower than that of the formation of the complex, and in all the studied cases the equilibrium was attained in a pH range sufficient for calculations. Some of the constants were determined with few data points, due to the critical compromise between equilibration and decomposition rates, although with larger standard deviations.

The solutions resulting from complete decomposition of ligands, or of their complexes, needed 1 equiv. more of strong base for total neutralisation. The reason for this is obviously hydrolysis of the ester bonds, which liberates a carboxylic acid that is neutralised by the strong base. The 18- and 21-membered macrocycles are more stable in water, probably because of less strained conformations. On the other hand, the edta- or dtpa-derived diamides studied by Q. Fernando et al. [7,9–26] and C.A. Chang et al. [8] are also stable due to the greater stability of amide bonds compared with ester ones.

Table 3
Stability constants (log units) for metal complexes of H_2L^1, H_2L^3, and H_2L^4 and other similar ligands with several divalent metal ions

Ion	Equilibrium quotient	H_2L^1	H_2L^3	H_2L^4	H_2L^5	H_2L^6 [d]	H_2L^7 [e] (H_4edta)
Mg^{2+}	[ML]/[M] × [L]	3.67(4)	3.02(2)		0 [a]	4.79	8.96
	[MHL]/[ML] × [H]	5.18(3)	5.67(8)				4.0
Ca^{2+}	[ML]/[M] × [L]	4.50(2)	5.34(1)	5.36(1)	3.51 [a]	8.12	10.81
	[MHL]/[ML] × [H]	4.30(5)					3.1
Sr^{2+}	[ML]/[M] × [L]	3.58(3)	4.62(1)	4.56(1)		7.19	8.72
	[MHL]/[ML] × [H]	5.16(4)					3.93
Ba^{2+}	[ML]/[M] × [L]	3.66(3)	4.68(1)	4.69(1)		6.68	7.88
	[MHL]/[ML] × [H]	5.06(3)	4.35(2)				
Cu^{2+}	[ML]/[M] × [L]	> 10.1	> 11.0	10.5	11.34 [b]	14.33	18.78
	[MHL]/[ML] × [H]				1.29 [b]		3.1
Zn^{2+}	[ML]/[M] × [L]	8.57(4)	9.91(2)		8.98 [b]	12.52	16.5
	[MHL]/[ML] × [H]				1.47 [b]		3.1
Cd^{2+}	[ML]/[M] × [L]	7.0(1)	10.0(1)	9.71(1)	7.3 [c]	13.58	16.5
	[MHL]/[ML] × [H]				2.6 [c]		2.9
Pb^{2+}	[ML]/[M] × [L]	8.8(1)	> 11.5	> 10.5		14.63	18.0
	[MHL]/[ML] × [H]						2.8

T = 298.0 K; I = 0.10 mol dm^{-3} NMe_4NO_3. Values in parenthesis are S.D. in the last significant figures.
[a] I = 0.10 mol dm^{-3} KCl, Ref. [14].
[b] I = 0.10 mol dm^{-3} KCl, Ref. [13].
[c] I = 0.10 mol dm^{-3} KCl, Ref. [16].
[d] Ref. [34].
[e] I = 0.10 mol dm^{-3}, Ref. [33].

Surprisingly, the metal-catalysed hydrolysis of H_2L^1–H_2L^4 has only mentioned before by us [32]. One can understand that the alkali metal ions should be the least efficient catalysts, however, lanthanides should even be more effective than the cations studied by us, but the authors did not mention it [28,30].

The self-destruction of the studied macrocycles by hydrolysis reactions excludes their use as analytical reagents, namely as molecular sensors or as catalysts for other reactions.

The thermodynamic stability of the alkaline-earth metal complexes of H_2L^1, H_2L^3 and H_2L^4 decreases from Ca^{2+} to Sr^{2+} but slightly increases from Sr^{2+} to Ba^{2+}. For each metal ion, the complexes of the 12-membered ligand present the lower values and a plateau of stability is observed for the 18- and 21-membered ligands. Thus, the charge density on the metal mainly govern the complexation, as the Ca^{2+} complexes of all ligands are the most stable (except for the Mg^{2+} complexes due to it small size), and that the complexes of all ligands present the same stability trend independently of its cavity size. These conclusions allow to infer that (1) the complexation with the rigid 12-membered macrocyclic compound is only possible with severe steric strain, and (2) the co-ordination sphere should be the same for all the complexes, implying that the ether oxygen atoms do not directly co-ordinate to these metal ions. In other words, all the studied metal ions are co-ordinated to the edta-moiety of the ligands.

For the complexes formed with the other metal ions studied, Cu^{2+}, Zn^{2+}, Cd^{2+} and Pb^{2+}, roughly the same conclusions are applied, in spite of the more covalent character of their interactions with ligands, and the strict stereochemical demands of co-ordination geometry and the limited co-ordination number of the Cu^{2+} complexes. The highest thermodynamic stability values of the Pb^{2+} complexes worth to be emphasised, and once more the size of this metal ion is the important factor. Also, the stability constants of the complexes with the 12-membered ligand are lower than with the 18- and 21-membered ligands, H_2L^3 and H_2L^4, the values for the latter ligands being practically identical.

The comparison of stability constants of complexes of the three 12-membered ligands (H_2L^1, H_2L^5 and H_2L^6) compiled in Table 3 for all the metal ions allows to conclude that: (1) the values for the diester (H_2L^1) and the diamide (H_2L^5) macrocycles are practically identical indicating the same co-ordination sphere for the complexes of both ligands (see below) and (2) the differences of values between complexes of H_2L^1 and the corresponding complexes with the compound without ester bonds (H_2L^6) are mainly due to differences on overall basicity of both ligands, as indicated by pM values determined at pH 7 (not shown).

The comparison of linear ligands, such as H_4edta (unfortunately values for H_2L^8, which would be more adequate for comparison, were not found), with H_2L^1 is not straightforward because besides the large differences in the overall basicity of both ligands, differences in entropic changes and of solvating effect of complexes with both ligands should also be taken into account as H_4edta has two additional carboxylate groups with their respective negative charges.

2.4. Structural studies in solution

2.4.1. NMR spectroscopic data

^1H and ^{13}C spectra of all the compounds were studied before [28–32]. We agree with the assignment of the resonances made by those authors except for b and c of the ^1H NMR and g and h in the ^{13}C NMR spectra of all compounds (for labelling see Scheme 1). In fact as mentioned in the acid-base discussion, only resonance b and also g (in the ^{13}C NMR spectra) shift to lower field when the pD is decreased from 4.4 to 2.4, as at this pD range only the acetate group is being protonated the assignment is unambiguous. For the cyclic amides derivatives of edta, Q. Fernando et al. [14] reached the same conclusion in another way. These authors consider that the internal fluctuation of the CH_2 protons close to the carbonyl in the macrocyclic backbone is significantly slower than that of the CH_2 protons in the acetate arm, thus the taller signal of the spectra is assigned to b (acetate arm) and the shorter to protons c in the ring, due to the rigid macrocyclic ring resulting from the planarity of the $CH_2NHCOCH_2$ moiety (confirmed by X-ray crystal analysis) [14]. This argument is also valid for the assignment of g and h resonances of the ^{13}C NMR spectra, the taller signal was assigned to g (carboxylate of the arm). In Table 1 we compiled the ^1H and ^{13}C NMR resonances for H_2L^1–H_2L^3 and also for their Zn^{2+} and Pb^{2+} complexes. The spectra of the free ligands were performed in D_2O and in d_6-DMSO, but most of the complexes were studied only in d_6-DMSO due to their decomposition in the first solvent.

Compound H_2L^1 shows only singlet resonances in the ^1H NMR spectrum due to its symmetric structure. The signals d and e of the $-CO-OCH_2CH_2O-$ units in compounds H_2L^2 and H_2L^3 in d_6-DMSO appear as broad singlets where one might expect triplets for a symmetric compound. This points to conformational equilibria in the macrocycles with coalescence about room temperature. In D_2O, each of the corresponding signals consists of a superposition of two multiplets of the AA′XX′ type, indicating a single conformation with slightly different environments for the two protons of each CH_2 group.

^1H NMR resonances corresponding to the edta-derived part (protons a, b and c) of the Zn^{2+} and Pb^{2+} complexes of H_2L^1 and H_2L^3 shift considerably ($\Delta\delta$ 0.3–0.57 ppm) but the shifts are negligible for the glycol-derived part ($\Delta\delta < 0.09$ ppm for the resonance d

of H_2L^1 complexes and for d, e and f of H_2L^3 complexes), see Table 1. This means that the oxygen atoms of the ether units do not participate in the metal complexation. The same was observed for the corresponding alkali [31] and Y^{3+} complexes [30]. However, the ^1H NMR data of Y^{3+} complexes indicate that the acetate protons (a) and the methylene ester protons (c) become indistinguishable upon metal co-ordination, both exhibiting an AB splitting pattern indicative of long-lived metal–nitrogen bonds, and short-lived metal–oxygen bonds as also found in $[Y(edta)]^-$ [30,38]. In the case of our complexes the edta-derived part exhibit only singlets indicating short lifetimes for both the metal–oxygen (of acetate or ester) and the metal–nitrogen bonds [38].

The 15-membered ligand, which we obtained in minute amount, was used to study the ligand as well as its Pb^{2+} complex in D_2O, the latter at low pD value. Even at that pD value the complex is completely formed, as the signals of the free ligand are not present on the NMR spectra. After complexation all ^1H resonances shift to upfield except b, see Fig. 1. This

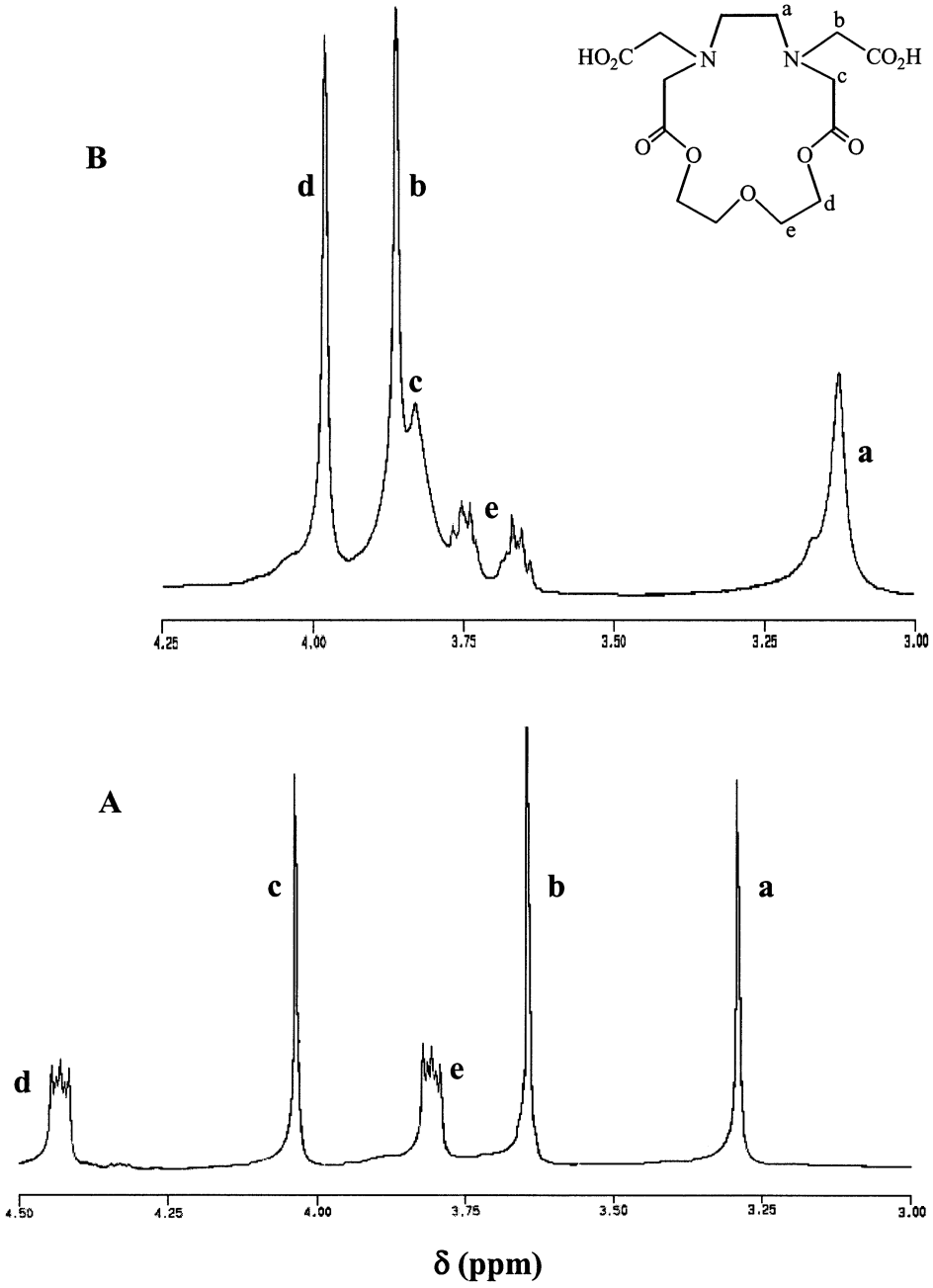


Fig. 1. ^1H NMR spectra of H_2L^2 at pD 4.4 (A) and of its Pb^{2+} complex at pD 1.6 (B) in D_2O (δ ppm vs. 3-(trimethylsilyl)-propanoic acid-d_4-sodium salt) at probe temperature and assignments of resonances.

apparent contradiction is due to the lower pH value of the solution after complexation and to the fact that at this pH range only the b protons shift downfield by acid addition, thus for a correct comparison a spectrum of the free ligand at pD 1.6 would be necessary. The ^{1}H NMR spectrum exhibits three singlets assigned to a, b and c, a broad signal corresponding to d and a ABX_2 pattern assigned to protons e. Nuclear Overhauser effect (NOE) experiments point to close proximity of d and a protons. The spectra and the NOE experiments clearly show that, in this case, the oxygen atom of the ether moiety is involved on the direct co-ordination to Pb^{2+}, as protons and carbon d and e significantly shift after complexation (see Table 1). CPK models also show that the folding of the macrocycle approaches the ether oxygen at a co-ordinated distance to a metal such as Pb^{2+}. The large size of the Pb^{2+} and its no strict stereochemical demands strongly contribute to the folding of the ligand.

On the other hand, the ^{13}C NMR spectra of the Y^{3+} complexes of H_2L^1–H_2L^4 exhibited only one resonance for g and h carbon atoms of the carboxylate and ester groups, at about 180 ppm, pointing to similar chemical environments of both oxygen atoms on complexation [30]. Otherwise, the ^{13}C NMR spectra of the Zn^{2+} and Pb^{2+} complexes of H_2L^1–H_2L^3 exhibit two downfield resonances, in the range 170–182 ppm, which indicate a dissimilar environment for the carboxylate and ester moieties upon co-ordination or different co-ordination of both oxygen of the ester groups or of the carboxylate groups. The last hypotheses seem more likely according to the behaviour of similar bisamide derivatives. Indeed, in spite of the unsymmetrical molecules formed, the simple ^{1}H NMR spectra obtained can be interpreted by an alternately co-ordination of the two ester oxygen atoms, or of the two carboxylate oxygen, or both, to the metal in an exchange rate higher than the NMR frequency, which indicate a high degree of lability of the of the metal carbonyl bonds. Similarly the ^{1}H NMR of the Ca^{2+} complexes of the 12- and 13-membered macrocycles of the amide derivatives of edta (H_2L^5 and H_2L^{11}, respectively) showed only four and five resonances, respectively, indicative of symmetrical molecules, but the X-ray crystal structure of the Ca^{2+} complex of H_2L^{11} revealed that a dimer was formed $[Ca_2(L^{11})_2(H_2O)_4]$, where each calcium atom is co-ordinated to only one amide oxygen and both oxygen atoms of the acetate groups of one molecule but also to one carboxylate oxygen of the neighbouring molecule, besides two nitrogen atoms, and two oxygen atoms from water molecules. This means that eight donor atoms form a distorted square antiprism around each calcium atom, one carboxylate oxygen of each molecule being simultaneously co-ordinated to two calcium atoms forming a binuclear structure with a double bridge of carboxylate oxygen atoms [16].

No X-ray crystal structures exist of the studied macrocycles or their metal complexes [39], because its hydrolysis prevents the slow evaporation of solutions to obtain good crystals. However, some crystal structures of several divalent metal complexes of 12- to 14-membered macrocycles of cyclic amides derived of edta [7,11,13,16,21], Ca^{2+}, Mn^{2+}, Ni^{2+}, Cu^{2+}, Zn^{2+}, Cd^{2+} and Pb^{2+} complexes, have shown that most of them co-ordinate to all the donor atoms of the ligands but only one amide oxygen, plus one water molecule. Dinuclear complexes of the type M_2L_2 are also frequent [13,16]. Only one complex is known where both amide oxygen atoms are directly co-ordinated to the metal; it is the case of $[Pb(L^{11})(H_2O)]\cdot 2H_2O$, thus in this complex all the donor atoms of the ligand are co-ordinated to the metal [11]. This means that the 12-membered ring, being too rigid and small, force the metal out of the plane formed by the donor atoms of the macrocycle, preferring to co-ordinate one water molecule rather than leading to the fold of the macrocycle, to achieve the most stable conformation. The arms of this molecule, with additional donor atoms, are not passive agents and also contribute to the final adopted configuration. Similar structures should be adopted by $[ZnL^1]$ and $[PbL^1]$ to explain our NMR spectra, in particular the two downfield resonances of the ^{13}C NMR spectra.

The cavity size of the 18-membered macrocycle, H_2L^3, is too large for the co-ordination of the studied metal ions, and, also, it prefers to accommodate the metal ion in one side of the molecule (the edta moiety) than to fold to co-ordinate both ether oxygen atoms. As shown by the NMR spectra, the protons and carbons of the ethylene groups of the ether moiety (d, e and f) remain unchanged upon co-ordination to zinc(II) and lead(II). The two signals at lower field of the ^{13}C spectra point also to one co-ordinated and the other uncoordinated ester oxygen atoms similar to what happens with the 12-membered complexes. These observations are indicative that the configurational energy necessary to fold the macrocycle is too much to compensate the gain with the ether oxygen interactions.

2.4.2. *UV–Vis and EPR spectra of the copper(II) complexes*

The copper(II) complexes of H_2L^1–H_2L^4 exhibit a broad band in the visible region with the maximum centred about 740 nm, but 667 nm for $[CuL^2]$, see Table 4. The X-band EPR spectra of the four complexes, in 1:1 rates and low concentrations ($\approx 4\times10^{-3}$ mol dm^{-3}) in water glasses at 165 K are shown in Fig. 2 and the simulated parameters [40] compiled in the Table 4, together with some of other complexes from the literature for comparison. All the studied complexes present the same g_i parameters and hyperfine coupling constants (A_i) and the presence of two species although in different proportions for each complex, as can be seen

Table 4
Spectroscopic X-band EPR data for the Cu^{2+} complexes of H_2L^1–H_2L^4, and other similar complexes

Complex	Visible band λ_{max} (nm) (ε_{molar} dm^3 mol^{-1} cm^{-1})	EPR $A_i \times 10^4$ (cm^{-1})						Reference
		g_x	g_y	g_z	A_x	A_y	A_z	
[CuL^1]	741(40.5)							
[CuL^2]	667 (59.0)	2.043	2.078	2.322	8.1	4.2	156.4	This work
[CuL^3]	739 (49.5)	2.045	2.093	2.280	14.0	8.1	157.9	This work
[CuL^4]	728 (51.7)							
[CuL^{10}]	685	2.056	2.080	2.284	1.0	8.7	168.7	[43]
[CuL^9]	671	2.049	2.049	2.237			187.0	[44]
[$Cu(H_2L^7)(H_2O)$]	764	2.065	2.070	2.330	10	10	155.0	[45,46]
[$Cu(L^7)$]$^{2-}$	735	2.071	2.071	2.295			166.0	[44]

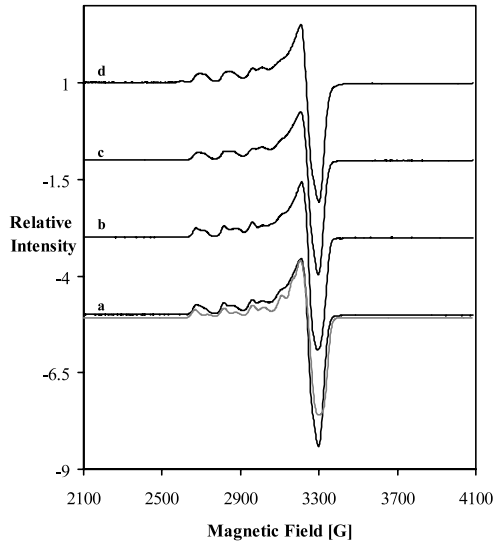


Fig. 2. EPR X-band spectra of the Cu^{2+} complexes of H_2L^1–H_2L^4 in 1:1 ratio at pH 3.0 in 1.0 M $NaClO_4$ (black lines) and the simulated spectrum of the first one (grey line): (a) [CuL^1], 3.93×10^{-3} mol dm^{-3}; (b) [CuL^2], 3.70×10^{-3} mol dm^{-3} (c) [CuL^3], 5.91×10^{-3} mol dm^{-3}, and (d) [CuL^4], 3.55×10^{-3} mol dm^{-3}, recorded at 165 K, microwave power of 2.4 mW, modulation amplitude of 1.0 mT. The frequency (ν) were of 9.405, 9.408, 9.404 and 9.409 GHz for a, b, c and d, respectively. All the spectra show the presence of two species in different proportions.

by the splitting of the bands at low field. As our potentiometric studies, in the same solvent, have not revealed the presence of protonated or other complexes, the two species formed in glass water are probably different isomers. Both species exhibit three well resolved lines of the four expected at low field, due to the interaction of the unpaired electron spin with the copper nucleus, and no superhyperfine splitting due to the coupling with the two nitrogen atoms of the macrocycle has been observed. The fourth copper line is completely overlapped by the much stronger and not resolved band of the high field part of the spectra. The simulation of the spectra indicated three different g values, showing that the Cu^{2+} ion is in a rhombically-distorted ligand field. Both species show $g_z > (g_x + g_y)/2$ and the lowest $g \geq 2.04$, which is characteristic of mononuclear copper(II) complexes having rhombic symmetry with elongation of the axial bonds and a $d_{x^2-y^2}$ ground state. Trigonal–bipyramidal or tetragonal geometries involving compression of axial bonds are not compatible with those data [41].

All the complexes reported in Table 4 have g_z and A_z parameters consistent with N_2O_2 donor atoms closelying the metal [42]. The differences between them can be visualised in the diagram g_z versus A_z of the Fig. 3, and rationalised in terms of different axial field of each complex. Indeed, the g_i and A_i values are related to the electronic transitions by the factors derived from the ligand field theory [47,48]: the g_i values increase and the A_i values decrease as the axial ligand field becomes stronger and this occurs with the simultaneous red-shift of the d–d absorption bands in the electronic spectra [48–50]. Thus, the position of each complex in the diagram of Fig. 3 can be analysed in this way. The complex of H_2edda([CuL^9]) fits to a square plane structure formed by two amine nitrogen and two carboxylate oxygen atoms [42]. According to the structures of [CuL^{10}] [51] and [$Cu(L^7)$]$^{2-}$ [52] both complexes are octahedral having the equatorial plane identical to that of the edda complex and the axial positions occupied by the two ether oxygen atoms of the macro-

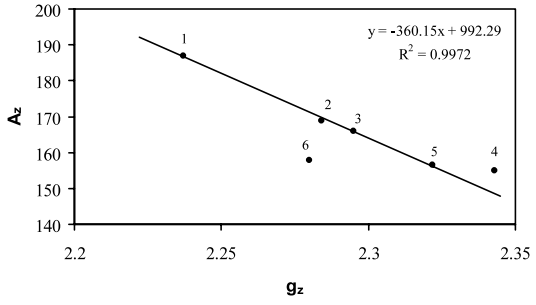


Fig. 3. Diagram of the EPR parameters A_z vs. g_z for a series of copper(II) complexes in 1:1 ratio, the ligands being, respectively: (1) H_2L^9 (edda); (2) H_2L^{10}; (3) H_4L^7 (edta); (4) H_4L^7 (edta), diprotonated complex; (5) H_2L^1–H_2L^4, first isomer; (6) H_2L^1–H_2L^4, second isomer.

cycle of H_2L^{10} and the other oxygen of the remaining two acetate groups of H_4edta, respectively. The parameters of the first isomer of the copper(II) complexes of H_2L^1–H_2L^4 fall in the straight-line g_z versus A_z (Fig. 3) pointing to stronger axial field, as indicated by larger g_z and smaller A_z values and a slight red shift. On the other hand, two complexes exhibit parameters which do not fit into the mentioned straight line: the protonated complex of edta, $[Cu(H_2L^7)\cdot(H_2O)]$, and the second isomer of the complexes studied in this work, H_2L^1–H_2L^4. The first one, has EPR parameters in agreement to the crystal structure [53], the stronger axial field derived from the co-ordination of one amine nitrogen and one carboxylate oxygen in axial positions. The equatorial plane is formed by the other nitrogen, two other carboxylate oxygens and one oxygen from a water molecule, and the last carboxylate group protonated and not co-ordinated to the copper. The second isomer of the complexes studied in this work, although having g_z higher than that of $[CuL^9]$, have lower A_z values when compared with those of edta, $[CuL^7]^{2-}$, and a noticeable anisotropy of the $g_\perp$ values, all these factors giving a clear indication of a geometrical distortion from the planar to tetrahedral geometry in the case of our complexes [54].

The increase of the concentrations of copper(II) complexes of H_2L^1–H_2L^4 to $\approx 3.5 \times 10^{-2}$ mol dm^{-3} in the 1:1 ratio or the amount of copper(II) to the ratio 1.8:1 lead to spectra with the typical features of a triplet-state dinuclear copper(II) species, see Fig. 4, a well-defined hyperfine structure consisting of seven peaks observed in the $\Delta M_s = 1$ transition and the signal in

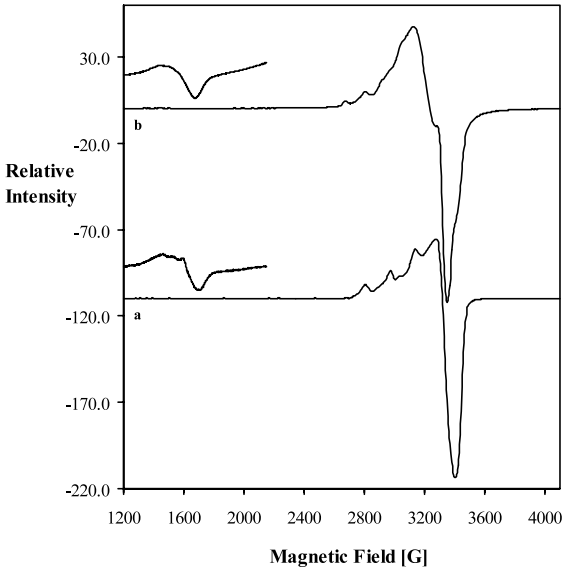


Fig. 4. EPR X-band spectra of the Cu^{2+} complexes of H_2L^4 in 1.0 M $NaClO_4$ recorded at 5 K: (a) at 1:1 ratio, concentration 3.41×10^{-2} mol dm^{-3} and at pH 3.95, and (b) at 1.8:1 ratio, concentration 2.00×10^{-2} mol dm^{-3} and at pH 3.50. Microwave power of 2.4 mW, modulation amplitude of 1.0 mT, and frequency (ν) 9.642 GHz.

$\Delta M_s = 2$ transition suggesting the proximity of two copper atoms. The spectra for all complexes are similar, but the solutions at 1.8:1 ratio show slightly different spectra. The $\Delta M_s = 2$ signal, which lies in the 1620 G range ($g = 4.3$) reveals a spin exchange interaction between the two copper atoms. However, the singlet-triplet transition could not be observed, presumably is obscured by the $\Delta M_s = 1$ absorption. If assumed that two unpaired electrons, each located on a Cu^{2+}, are exchanged with an energy larger than the hyperfine coupling energy, each unpaired electron ($S = 1/2$) couples with two copper nuclei ($I_{Cu} = 3/2$) in an equivalent manner, the hyperfine structure consists of seven lines. In our spectra the seven hyperfine lines can be observed in the $\Delta M_s = 1$ region with an average hyperfine spacing of 90.4 G and $g_\parallel = 2.26$ and $g_\perp = 2.07$. The hyperfine constant is approximately half the value found in mononuclear copper(II) complexes having the same donor atoms and geometry. In the $\Delta M_s = 2$ region the signal is very broad but even so some hyperfine lines can be observed, but it is impossible to confirm the hyperfine spacing. In practice, $\Delta M_s = 2$ transitions are expected mainly for dinuclear complexes with Cu–Cu distances between ~ 3 and 5 Å, because when the Cu–Cu distance is small the $\Delta M_s = 2$ signal is not observed due to the overlap zero-field split components of the $\Delta M_s = 1$ and $\Delta M_s = 2$ transitions. When the Cu–Cu distance is large the zero-field parameter D (dipolar term which depends on d^{-3}, d being the distance between the two copper atoms) and the intensity of the $\Delta M_s = 2$ signal is very low [55–57].

3. Conclusions

Compounds H_2L^1–H_2L^4 were prepared by one step synthetic way although with low yield. The critical point of them and their complexes is the hydrolysis of the ester bonds, which is metal-catalysed.

However, in spite of the low yield of the synthesis of these compounds and of the hydrolysis reaction that prevented a complete study of them, it was possible to achieve some interesting conclusions. (1) In the complexes formed with these ligands the metal atom is accommodated close to the edta-moiety of the ligand. This conclusion was supported by our potentiometric studies of alkaline-earth, Cu^{2+}, Zn^{2+}, Cd^{2+} and Pb^{2+} complexes of H_2L^1, H_2L^3 and H_2L^4, by the ^1H and ^{13}C NMR spectroscopic studies of the Zn^{2+} and Pb^{2+} complexes of H_2L^1 and H_2L^3 and the EPR spectroscopic studies of the copper(II) complexes of all ligands. (2) In most complexes the metal prefer to co-ordinate to one water molecule and only one ester oxygen then to both ester oxygen atoms of the molecule, as shown by the NMR studies. (3) The ether oxygen atoms seems to be involved directly on the co-ordination to the metal in

only one complex, among all studied by us, which was the case of the Pb^{2+} complex of the 15-membered macrocycle, H_2L^2. Unhappily, we had not enough compound for the determination of stability constants of metal complexes, as a peak of stability for the Pb^{2+} and Ba^{2+} complexes of this ligand and a normal trend for metals such as Cu^{2+} and Zn^{2+} will be expected. Indeed the EPR spectroscopy of the copper(II) complex of H_2L^2 did not show any particular difference from the others in agreement to the last prediction. (4) EPR studies of the copper(II) complexes revealed the presence of dinuclear species with the two copper atoms at short distance (between 3 and 5 Å). The fact that these species were not observed by the NMR experiments point to the formation of dinuclear complexes involving donors of the edta-moiety and only one amide oxygen atom, similarly to $[Ca_2(L^{11})_2(H_2O)_4]$, where the distance Ca–Ca is 4.019 Å [16]. This type of dinuclear structure, which can dissociate in solution to form two mononuclear molecules, are also in agreement with our potentiometric studies, as M_2L_2 complexes cannot be distinguished from the ML species in the solution studies.

4. Experimental

4.1. Materials

Dioxane was dried with sodium–benzophenone, distilled and stored under nitrogen. Ethyleneglycols were dried by storage over molecular sieves. All the other chemicals were of reagent grade and used as supplied.

4.2. Equipment for ligands and metal complexes characterisation

^1H and ^{13}C NMR spectra were recorded with a Bruker AMX-300 spectrometer at probe temperature in D_2O and d_6-DMSO, using 3-(trimethylsilyl)-propanoic acid-d_4-sodium salt as standard. Solutions of the ligands and respective complexes for the measurements (≈ 0.01 mol dm^{-3}) in D_2O were made up and the pD was adjusted by addition of DCl or CO_2-free KOD with an Orion 420A instrument fitted with a combined Ingold 405M3 microelectrode. The $-\log[D^+]$ was measured directly in the NMR tube, after the calibration of the microelectrode with buffered aqueous solutions. The final pD was calculated from $pD = pH^* + 0.40$ [58]. The value of pH* corresponds to the reading of the pH meter previously calibrated with two standard aqueous buffers at pH 4 and 7 [58]. Electronic spectra were measured with a UNICAM UV4 spectrophotometer using aqueous solutions of the complexes. EPR spectroscopic measurements of the Cu^{2+} complexes were recorded with a Bruker ESP 380 spectrometer equipped with continuous-flow cryostats for liquid helium or for liquid nitrogen, operating at X-band. The complexes were prepared at $(3.6–5.91) \times 10^{-3}$ mol dm^{-3} and $(2.0–3.8) \times 10^{-2}$ mol dm^{-3} in 1.0 mol dm^{-3} $NaClO_4$ at pH ≈ 3 and were recorded at 165 K (lower concentrations) and 5 K (higher concentrations). C, H, and N analysis were performed by the Analytical Laboratory at ITQB (Oeiras, Portugal).

4.3. Synthesis of ligands (H_2L^1–H_2L^4)

The ligands were prepared by the reaction between ethylenediamine tetracetic dianhydride and the corresponding mono- or polyethyleneglycol $[HO(CH_2CH_2O)_nH$, $n = 1$, 2, 3 and 4] as described before [27–30]. A typical procedure is as following: ethylenediamine tetracetic dianhydride (1.00 g, 3.90 mmol) was added to dioxane (300 cm^{-3}) under nitrogen and the temperature adjusted to 90–95 °C. When the entire solid had dissolved, a solution of the corresponding polyethyleneglycol (39.2 mmol for mono- and diethyleneglycol, 19.5 mmol for tri- and tetraethyleneglycol) in dioxane (150 cm^{-3} for the monoethyleneglycol and 100 cm^{-3} for the others) was added during 6 h at the same temperature. The mixture was heated to reflux for 24 h (for the monoethyleneglycol) and 40 h (for the others). After cooling to 0 °C, the product precipitated within a few minutes and was filtered off, washed with acetone (3×5 cm^{-3}) and dried under vacuum.

H_2L^1: yield. 9%, m.p. 182–4 °C. Found: C, 44.3; H, 5.9; N, 8.6. Calc. for $C_{12}H_{18}N_2O_8 \cdot 5H_2O$: C, 44.6; H, 6.1; N, 8.4%. For NMR data, see Table 1.

H_2L^2: 40 mg (3%), m.p. 161–2 °C. Found: C, 45.3; H, 6.2; N, 7.5. Calc. for $C_{14}H_{22}N_2O_9 \cdot 0.5H_2O$: C, 45.4; H, 6.5; N, 7.2%. For NMR data, see Table 1.

H_2L^3: 12%, m.p. 155–6 °C. Found: C, 45.3; H, 6.7; N, 6.6. Calc. for $C_{16}H_{26}N_2O_{10}.H_2O$: C, 45.6; H, 6.7; N, 6.3%. For NMR data see Table 1.

H_2L^4: 17%, m.p. 136–8 °C. Found: C, 47.9; H, 6.6; N, 6.0. Calc. for $C_{18}H_{30}N_2O_{11}$, 48.0; H, 6.7; N, 6.2%. NMR in D_2O δ (ppm), ^1H: 3.19 (s, 4H, NCH_2CH_2), 3.55 (s, 8H, OCH_2CH_2O), 3.66 (br, 4H, $COOCH_2CH_2O$), 3.70 (s, 4H, NCH_2COOH)), 3.91 (s, 4H, NCH_2COOCH_2), 4.27 (m, 4H, $COOCH_2CH_2$). ^{13}C: 53.8, 57.0, 58.5, 67.3, 70.7, 72.2, 172.3, 174.9.

4.4. Potentiometric measurements

4.4.1. Reagents and solutions

Metal ion solutions were prepared at about 0.025 mol dm^{-3} from the nitrate salts of the metals, of analytical grade with demineralised water obtained by a Millipore/Milli-Q system, and were standardised as described [57]. Carbonate-free solutions of the titrant, tetramethylammonium hydroxide, were prepared by reaction of a

tetramethylammonium iodide solution with Ag_2O, maintained and discarded as described [57].

4.4.2. Equipment

For the potentiometric measurements an Orion 720A instrument was used together with a 91-01 glass electrode, 90-05 Ag/AgCl reference electrode and a Wilhelm-type salt bridge containing a 0.10 mol dm^{-3} NMe_4NO_3 solution; a glass-jacketed titration cell (50 cm^3) completely sealed from the atmosphere was used and the temperature was controlled by a Grant W6 thermostat coupled with a cryostat by circulation of thermostatted water through the jacketed cell; and the standard base (or acid) was added through a capillary tip at the surface of the solution by a Metrohom Dosimat 665 burette.

4.4.3. Work conditions

The temperature was kept at 298.0 ± 0.1 K; atmospheric CO_2 was excluded from the cell during the titration by passing purified argon across the top of the experimental solution in the reaction cell. The ionic strength of the solutions was kept at 0.10 mol dm^{-3} with NMe_4NO_3.

4.4.4. Measurements

The $[H^+]$ of the solutions was determined by the measurement of the electromotive force of the cell, $E = E'^0 + Q \log[H^+] + E_j$. E'^0, Q, E_j and $K_w = ([H^+][OH])$ were obtained as described previously [57]. The term pH is defined as $-\log [H^+]$. The value of K_w was found equal to $10^{-13.80}$ mol^2 dm^{-6}.

The potentiometric equilibrium measurements were made on 20.00 cm^3 of $\cong 2.50 \times 10^{-3}$ mol dm^{-3} ligand solutions diluted to a final volume of 30.00 cm^3, in the absence of metal ions and in the presence of each metal ion for which the C_M:C_L ratios were 1:1 and 2:1. A minimum of two replicates was made.

4.4.5. Calculation of equilibrium constants

Protonation constants ($K_i^H = [H_iL]/([H_{i-1}L] \times [H^+])$) were calculated by fitting the potentiometric data obtained for the free ligand to the HYPERQUAD program and listed in Table 2 [37]. Stability constants of the various species formed in solution were obtained from the experimental data corresponding to the titration of solutions of different metal ions to ligand ratios, also using the HYPERQUAD program. The initial computations were obtained in the form of overall stability constants, $\beta_{M_mH_hL_l}$ values,

$$\beta_{M_mH_hL_l} = M_mH_hL_l/([M]^m \times [H]^h \times [L]^l)$$

Only mononuclear species, ML and MHL were found. Differences, in log units, between the values β_{MHL} and β_{ML} provide the stepwise protonation reaction constants, shown in Table 3. The errors quoted are the standard deviations of the overall stability constants given directly by the program for the input data, which include all the experimental points of all titration curves. The standard deviations of the stepwise constants were determined by the normal propagation rules.

5. Supplementary material

The data on the ^1H NMR spectrum of H_2L^2at pD 2.4 in D_2O at probe temperature and assignments of resonances (δ ppm vs. 3-(trimethylsilyl)-propanoic acid-d_4-sodium salt) is available on request from the authors.

Acknowledgements

The authors acknowledge J.R. Ascenso for the help in the assignment of NMR spectra and the helpful discussions and M. Teixeira for the help in EPR measurements. The authors also acknowledge the financial support from Fundação para a Ciência e Tecnologia (FCT) and POCTI, with coparticipation of the European Community fund FEDER (Project n. POCTI/1999/QUIM/35396).

References

[1] C.J. Anderson, M.J. Welch, Chem. Rev. 99 (1999) 2219.
[2] W.A. Volkert, T.J. Hoffman, Chem. Rev. 99 (1999) 2269.
[3] S. Liu, D.S. Edwards, Bioconjug. Chem. 12 (2001) 7.
[4] P. Caravan, J.E. Ellison, T.J. McMurry, R.B. Lauffer, Chem. Rev. 99 (1999) 2293.
[5] A. Bianchi, L. Calabi, F. Corana, S. Fontana, P. Losi, A. Maiocchi, L. Paleari, B. Valtancoli, Coord. Chem. Rev. 204 (2000) 309.
[6] V. Alexander, Chem. Rev. 95 (1995) 273.
[7] M.B. Inoue, C.A. Villegas, K. Asano, M. Nakamura, M. Inoue, Q. Fernando, Inorg. Chem. 31 (1992) 2480.
[8] J.F. Carvalho, S.-H. Kim, C.A. Chang, Inorg. Chem. 31 (1992) 4065.
[9] M.B. Inoue, M. Inoue, I.C. Muñoz, M.A. Bruck, Q. Fernando, Inorg. Chim. Acta 209 (1993) 29.
[10] M.B. Inoue, M. Inoue, Q. Fernando, Inorg. Chim. Acta 209 (1993) 35.
[11] M.B. Inoue, Q. Fernando, C.A. Villegas, M. Inoue, Acta Crystallogr., Sect. C 49 (1993) 875.
[12] M.B. Inoue, M. Inoue, Q. Fernando, Acta Crystallogr., Sect. C 50 (1994) 1037.
[13] M.B. Inoue, P. Oram, G. Andreu-de-Riquer, M. Inoue, P. Borbat, A. Raitsimring, Q. Fernando, Inorg. Chem. 34 (1995) 3528.
[14] M.B. Inoue, P. Oram, M. Inoue, Q. Fernando, Inorg. Chim. Acta 232 (1995) 91.
[15] M.B. Inoue, R.E. Navarro, M. Inoue, Q. Fernando, Inorg. Chem. 34 (1995) 6074.
[16] M.B. Inoue, P. Oram, M. Inoue, Q. Fernando, Inorg. Chim. Acta 246 (1996) 401.

[17] M.B. Inoue, P. Oram, M. Inoue, Q. Fernando, Inorg. Chim. Acta 248 (1996) 231.
[18] M.B. Inoue, F. Medrano, M. Inoue, A. Raitsimring, Q. Fernando, Inorg. Chem. 36 (1997) 2335.
[19] M.B. Inoue, E.F. Velasquez, M. Inoue, Q. Fernando, J. Chem. Soc., Perkin Trans. 2 (1997) 2113.
[20] M.B. Inoue, L. Machi, M. Inoue, Q. Fernando, Inorg. Chim. Acta 261 (1997) 59.
[21] M.B. Inoue, R.E. Navarro, I.O. Landín, D.M. López, M. Inoue, Q. Fernando, Inorg. Chim. Acta 269 (1998) 224.
[22] M.B. Inoue, F. Medrano, M. Inoue, Q. Fernando, J. Chem. Soc., Perkin Trans. 2 (1998) 2275.
[23] M.B. Inoue, M. Inoue, Q. Fernando, Inorg. Chim. Acta 271 (1998) 207.
[24] M.B. Inoue, E.F. Velasquez, F. Medrano, K.L. Ochoa, J.C. Galvez, M. Inoue, Q. Fernando, Inorg. Chem. 37 (1998) 4070.
[25] M.B. Inoue, E.F. Velazquez, A. Ruiz-Lucero, M. Inoue, A. Raitsimring, Q. Fernando, Inorg. Chem. 38 (1999) 834.
[26] M.B. Inoue, H. Santacruz, M. Inoue, Q. Fernando, Inorg. Chem. 38 (1999) 1596.
[27] S.-Y. Qin, Org. Chem. (Shangai) 4 (1984) 290.
[28] C.A. Chang, P.H.-L. Chang, S.-Y. Qin, Inorg. Chem. 27 (1988) 944.
[29] A. Zhang, S. Wang, S. Huang, S. Qing, Chin. J. Magn. Res. 7 (1990) 225.
[30] R.C. Holz, C.A. Chang, W. DeW Horrocks, Jr., Inorg. Chem. 30 (1991) 3270.
[31] A. Zhang, S. Wang, S.-Y. Qin, Acta Chim. Sin. 49 (1991) 164.
[32] A. Zhang, J. Zhou, S. Wang, R. Delgado, Chin. J. Magn. Res. 15 (1998) 291.
[33] (a) R.M. Smith, A.E. Martell, R.J. Motekaitis, Nist Critical Stability Constants of Metal Complexes Database, US Department of Commerce, Gaithersburg, MD, 1993;
(b) L.D. Pettit, H.K.J. Powell, IUPAC Stability Constants Database, Academic Software, Timble, UK, 1993.
[34] M.T.S. Amorim, R. Delgado, J.J.R. Fraústo da Silva, Polyhedron 11 (1992) 1891.
[35] J.R. Ascenso, R. Delgado, J.J.R. Fraústo da Silva, J. Chem. Soc., Perkin Trans. 2 (1985) 781.
[36] M.T.S. Amorim, J.R. Ascenso, R. Delgado, J.J.R. Fraústo da Silva, J. Chem. Soc., Dalton Trans. (1990) 3449.
[37] P. Gans, A. Sabatini, A. Vacca, Talanta 43 (1996) 1739.
[38] P.A. Baisden, G.R. Choppin, B.B. Garrett, Inorg. Chem. 16 (1977) 1367.
[39] F.H. Allen, J.E. Davies, J.J. Galloy, O. Johnson, O. Kennard, C.F. Macrae, D.G. Watson, J. Chem. Inf. Comp. Sci. 31 (1991) 204.
[40] F. Neese, Diploma thesis, University of Konstanz, Germany, June 1993.
[41] B.J. Hathaway, Coord. Chem. Rev. 52 (1983) 87.
[42] J. Peisach, W.E. Blumberg, Arch. Biochem. Biophys. 165 (1974) 691.
[43] S. Chaves, A. Cerva, R. Delgado, Polyhedron 17 (1998) 93.
[44] R. Delgado, J.J.R. Fraústo da Silva, M.C.T.A. Vaz, Talanta 33 (1986) 285.
[45] B.J. Hathaway, B.J. Bew, D.E. Billing, R.J. Dudley, P. Nicholls, J. Chem. Soc. (A) (1969) 2312.
[46] K.M. More, G.R. Eaton, S.S. Eaton, Inorg. Chem. 25 (1986) 2638.
[47] H.R. Gersmann, J.D. Swalen, J. Chem. Phys. 36 (1962) 3221.
[48] P.W. Lau, W.C. Lin, J. Inorg. Nucl. Chem. 37 (1975) 2389.
[49] A.W. Addison, M. Carpenter, L.K.-M. Lau, M. Wicholas, Inorg. Chem. 17 (1978) 1545.
[50] M.J. Maroney, N.J. Rose, Inorg. Chem. 23 (1984) 2252.
[51] Z. Urbanczyk-Lipkowska, J.W. Krajewski, P. Gluzinki, R.A. Kolinski, J. Crystallogr. Spectrosc. Res. 18 (1988) 157.
[52] X. Solans, M. Font-Altaba, J. Oliva, J. Herrera, Acta Crystallogr., Sect. C 39 (1983) 435.
[53] F.S. Stephens, J. Chem. Soc. (A) (1969) 1723.
[54] I. Bertini, G. Canti, R. Grassi, A. Scozzafava, Inorg. Chem. 19 (1980) 2198.
[55] T.D. Smith, J.R. Pilbrow, Coord. Chem. Rev. 13 (1974) 173.
[56] D.M. Duggan, D.N. Hendrickson, Inorg. Chem. 13 (1974) 2929.
[57] M.F. Cabral, R. Delgado, M.T. Duarte, M. Teixeira, Helv. Chim. Acta 83 (2000) 702.
[58] R. Delgado, J.J.R. Fraústo da Silva, M.T.S. Amorim, M.F. Cabral, S. Chaves, J. Costa, Anal. Chim. Acta 245 (1991) 271.

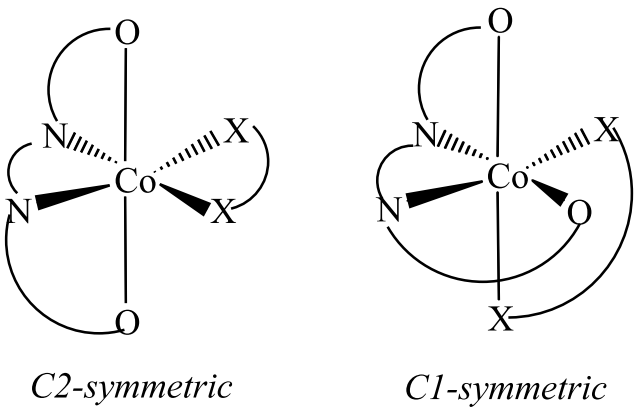


Fig. 1. Possible geometric isomers of the $[Co(eddp)XX]^+$ complexes, $XX = R_2eddp$.

2. Experimental

Reagents were obtained commercially and used without further purification.

Infrared spectra were recorded on a Perkin–Elmer FTIR 31725-X spectrophotometer using the KBr pellet technique. Electronic absorption spectra were recorded on a Varian GBC 911A spectrophotometer. Aqueous 1×10^{-3} molar solutions of the complexes were used for these measurements. ^1H and ^{13}C NMR spectra were recorded on a Varian Gemini-200 NMR spectrometer using DSS [sodium salt of 3-(trimethylsilyl)propanesulfonic acid] as internal reference in D_2O. Elemental analyses for C, H and N were performed by standard methods.

2.1. Preparation of ethylenediamine-N,N′-di-3-propanoic acid dihydrochloride ($H_2eddp \cdot 2HCl$)

This substance was prepared by the reported method [10].

2.2. Preparation of ethylenediamine-N,N′-di-3-propanoate dimethyl ester dihydrochloride (dmeddp·2HCl)

This substance was prepared by the modificated method reported from Haydock and Mulholland [11]. Thionyl chloride (1.95 cm^3; 26.9 mmol) was added dropwise to ice-cold absolute MeOH (30.00 cm^3). The acid (2.500 g; 9.0 mmol) was then added and the suspension was refluxed for 16 h. The resulting suspension was filtered off from the $H_2eddp \cdot 2HCl$, and left to crystallize. The product was recrystallized from boiling MeOH. M.p. 208 °C.

2.3. Preparation of ethylenediamine-N,N′-di-3-propanoate diethyl ester dihydrochloride (deeddp·2HCl)

This was prepared by the same method as that used to prepare the dmeddp·2HCl using an equal volume of absolute EtOH in place of absolute MeOH. The crude products were recrystallized from boiling EtOH. M.p. 209 °C. Yield: 2.52 g (75.5%). *Anal.* Found: C, 42.95; H, 7.97; N, 8.39. Calc. for $C_{12}H_{26}Cl_2N_2O_4$: C, 43.25; H, 7.86; N, 8.40%.

2.4. Preparation of ethylenediamine-N,N′-di-3-propanoate dipropyl ester dihydrochloride (dpeddp·2HCl)

This was prepared by the same method as that used to prepare the dmeddp·2HCl using an equal volume of absolute C_3H_7OH in place of absolute MeOH. M.p. 200 °C. Yield: 2.30 g (63.7%). *Anal.* Found: C, 46.39; H, 8.82; N, 7.88. Calc. for $C_{14}H_{30}Cl_2N_2O_4$: C, 46.54; H, 8.37; N, 7.75%.

2.5. Preparation of ethylenediamine-N,N′-di-3-propanoate dibutyl ester dihydrochloride (dbeddp·2HCl)

This was prepared by the same method as that used to prepare the dmeddp·2HCl using an equal volume of absolute C_4H_9OH in place of absolute MeOH. M.p. 185 °C. Yield: 2.34 g (60.1%). *Anal.* Found: C, 49.07; H, 8.58; N, 7.49. Calc. for $C_{16}H_{34}Cl_2N_2O_4$: C, 49.35; H, 8.80; N, 7.19%.

2.6. Preparation of ethylenediamine-N,N′-di-3-propanoate dipentyl ester dihydrochloride (dveddp·2HCl)

This was prepared by the same method as that used to prepare the dmeddp·2HCl using an equal volume of absolute pentanol in place of absolute MeOH. M.p. 176 °C. Yield: 1.80 g (43.1%). *Anal.* Found: C, 51.64; H, 8.82; N, 6.85. Calc. for $C_{18}H_{38}Cl_2N_2O_4$: C, 51.79; H, 9.17; N, 6.71%.

2.7. Preparation of C_1-symmetric-(ethylenediamine-N,N′-di-3-propanoato)(O,O-dimethyl-ethylenediamine-N,N′-di-3-propanoate)cobalt(III)chloride, C_1-symmetric-[Co(eddp)dmeddp]Cl

To a solution of $CoCl_2 \cdot 6H_2O$ (0.048 g; 0.2 mmol) in 10.0 cm^3 of water, dmeddp·2HCl (0.152 g; 0.5 mmol) and charcoal (0.01 g) were added. The pH of the solution was adjusted to 8.5 with KOH (0.1 mol dm^{-3}) and was accompanied by oxidation of Co(II) to Co(III) with atmospheric oxygen during 4 h. The solution was filtered, then concentrated to 5.0 cm^3 and placed onto a 2.5×30 cm column containing Sephadex G-10. The violet eluate was then poured onto a 2.5×32

cm column containing SP-Sephadex C-25. The column was washed with water to remove the non-adsorbed by-product and then eluted with 0.2 molar KCl. The adsorbed complex was violet. The violet eluate was concentrated under reduced pressure, then MeOH was added in order to remove KCl. From the desalted solution the C_1-symmetric-[Co(eddp)dmeddp]Cl complex was obtained. Yield: 0.046 g (42.59%). *Anal.* Found: C, 40.28; H, 6.05; N, 10.16. Calc. for $CoC_{18}H_{34}ClN_4O_8 \cdot 0.5H_2O$: C, 40.19; H, 6.55; N, 10.41%.

2.8. Preparation of C_1-symmetric-(ethylenediamine-*N,N′*-di-3-propanoato)(*O,O*-diethyl-ethylenediamine-*N,N′*-di-3-propanoate)cobalt(III)chloride, C_1-symmetric-[Co(eddp)deeddp]Cl

This was prepared by the same method as that used to prepare C_1-symmetric-[Co(eddp)dmeddp]Cl, using deeddp·2HCl (0.167 g; 0.5 mmol) in place of dmeddp·2HCl. Yield: 0.050 g (40.65%). *Anal.* Found: C, 39.36; H, 6.72; N, 9.23. Calc. for $CoC_{20}H_{38}ClN_4O_8 \cdot 3H_2O$: C, 39.31; H, 7.26; N, 9.17%.

2.9. Preparation of C_1-symmetric-(ethylenediamine-*N,N′*-di-3-propanoato)(*O,O*-dipropyl-ethylenediamine-*N,N′*-di-3-propanoate)cobalt(III)chloride, C_1-symmetric-[Co(eddp)dpeddp]Cl

This was prepared by the same method as that used to prepare C_1-symmetric-[Co(eddp)dmeddp]Cl, using dpeddp·2HCl (0.181 g; 0.5 mmol) in place of dmeddp·2HCl. Yield: 0.048 g (38.88%). *Anal.* Found: C, 43.26; H, 7.84; N, 9.82. Calc. for $CoC_{22}H_{42}ClN_4O_8 \cdot 1.5H_2O$: C, 43.17; H, 7.41; N, 9.16%.

2.10. Preparation of C_1-symmetric-(ethylenediamine-*N,N′*-di-3-propanoato)(*O,O*-dibutyl-ethylenediamine-*N,N′*-di-3-propanoate)cobalt(III)chloride, C_1-symmetric-[Co(eddp)dbeddp]Cl

This was prepared by the same method as that used to prepare C_1-symmetric-[Co(eddp)dmeddp]Cl, using dbeddp·2HCl (0.195 g; 0.5 mmol) in place of dmeddp·2HCl. Yield: 0.055 g (38.73%). *Anal*. Found: C, 40.62; H, 8.02; N, 8.37. Calc. for $CoC_{24}H_{46}ClN_4O_8 \cdot 5H_2O$: C, 40.99; H, 8.03; N, 8.07%.

2.11. Preparation of C_1-symmetric-(ethylenediamine-*N,N′*-di-3-propanoato)(*O,O*-dipentyl-ethylenediamine-*N,N′*-di-3-propanoate)cobalt(III)chloride, C_1-symmetric-[Co(eddp)dveddp]Cl

This was prepared by the same method as that used to prepare C_1-symmetric-[Co(eddp)dmeddp]Cl, using dveddp·2HCl (0.209 g; 0.5 mmol) in place of dmeddp·2HCl. Yield: 0.051 g (36.37%). *Anal.* Found: C, 44.80; H, 8.10; N, 7.72. Calc. for $CoC_{26}H_{50}ClN_4O_8 \cdot 3H_2O$: C, 44.91; H, 8.11; N, 8.06%.

3. Results and discussion

The *O,O*-dialkyl-ethylenediamine-*N,N′*-di-3-propanoate, R_2eddp·2HCl, ligands have been obtained from the reaction between H_2eddp·2HCl, the corresponding absolute alcohol and thionyl chloride. All the ligands show a strong band for the ester group around 1730 cm^{-1} in their IR spectra. The ^{1}H NMR spectra of the ligands show the methylene protons between two nitrogen donor atoms, and between the carbonyl group and nitrogen donor atom, at around 2.9 ppm, as a triplet, and 3.4 ppm, as a triplet, respectively. All ligands show in the ^{13}C NMR spectra resonances at around 33 ppm for the carbons from ethylenediamine, 46 ppm for the carbons between the ester group and nitrogen donor atom, and 174 ppm for the ester carbon. The isolated esters crystallized as thin and flimsy crystals, and because of that we were unable to obtain a single crystal.

The reaction of $CoCl_2$ with ester in aqueous solutions using an air oxidation method has yielded only one isomer. During the preparation of these complexes, one part of the ester coordinated as a bidentate ligand and the other part hydrolyzed and coordinated as a tetradentate ONNO ligand. The isolated complexes are very hygroscopic and because of that we were unable to obtain single crystals. Each of the IR spectra of these complexes shows an antisymmetric CO_2 vibration at around 1600 cm^{-1}, which is of lower energy than that of H_2eddp·2HCl, indicating bond formation between the metal and the ligand carboxylate oxygen donor atoms [12]. C_1- and C_2-symmetric isomers can differ in the shape of the carboxylate region. The presence of one broad shape or two shapes is characteristic for C_1-symmetric and a strait shape for the C_2-symmetric isomers [8,9]. IR spectra of isolated complexes showed a broad shape in this region, from which we assigned the configuration as C_1-symmetric. All of the complexes show an antisymmetric CO_2 absorption at around 1730 cm^{-1}, like the free ligand ester, which indicate that ester groups are present in the complexes. The symmetric stretching bands of the coordinated carboxylate groups lie in the expected region (about 1400 cm^{-1}). The stretching bands of the amino groups are also summarized in Table 1.

The electronic absorption spectra of [Co(eddp)-R_2eddp]$^+$ (Fig. 2) are related to those of [Co(edda)X_2] species [13–15], a *symmetric*-CoN_4O_2 system [1,8], and suggest that these complexes prepared in this work have the *symmetric* configuration. Since the C_1-symmetric isomer has a bigger $^1T_{tg}$ splitting than the C_2-symmetric isomer, the electronic absorption spectra of the C_1-

Table 1
Selected frequencies of R_2eddp·2HCl and the C_1-symmetric-[Co(eddp)R_2eddp]Cl complexes

Compound	ν(NH)	ν_{as}(COOR)	ν_{as}(COO$^-$)	ν_r(COO$^-$)
dmeddp·2HCl	3439 s	1730 vs	–	–
deeddp·2HCl	3455 s	1736 vs	–	–
dpeddp·2HCl	3465 s	1732 vs	–	–
dbeddp·2HCl	3474 s	1742 s	–	–
dveddp·2HCl	3474 s	1743 s	–	–
C_1-symmetric-[Co(eddp)dmeddp]$^+$	3426 vs	1729 s	1582 vs	1402 vs
C_1-symmetric-[Co(eddp)deeddp]$^+$	3416 s	1729 vs	1598 vs	1398 vs
C_1-symmetric-[Co(eddp)dpeddp]$^+$	3418 v	1730 vs	1600 vs	1401 s
C_1-symmetric-[Co(eddp)dbeddp]$^+$	3427 s	1729 s	1603 s	1405 s
C_1-symmetric-[Co(eddp)dveddp]$^+$	3412 s	1733 s	1593 vs	1403 s

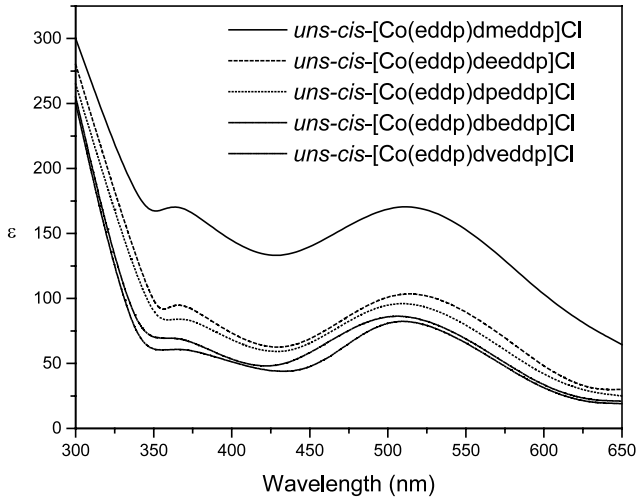


Fig. 2. Electronic absorption spectra of C_1-symmetric-[Co(eddp)R_2eddp]Cl.

symmetric isomer may have a very broad and non-symmetrical absorption band, while the C_2-symmetric isomer have a more Gaussian shape [1,13,16,17]. The C_1-symmetric geometry of [Co(eddp)en]Cl assigned by crystal structure [7] was investigated with an electronic absorption spectrum [8]. From the absorption spectrum (Fig. 2, Table 2) of [Co(eddp)R_2eddp]$^+$ very broad bands are found at $\lambda_{max} \approx 505$ nm, like C_1-symmetric-[Co(eddp)en]Cl, which suggests the compounds are the C_1-symmetric isomers. The second bands at $\lambda_{max} \approx 360$ nm, are assigned to the transition $^1A_{1g}$ to $^1B_{2g}+{}^1E_g$ [1,16].

^{1}H NMR has been used extensively in the characterization of metal chelates containing aminocarboxylate ligands [8,15,18,19]. The $C1$- and C_2-symmetric geometry of [Co(eddp)en]Cl assigned by crystal structures [7] was investigated with ^{1}H NMR spectra [8]. Consistent

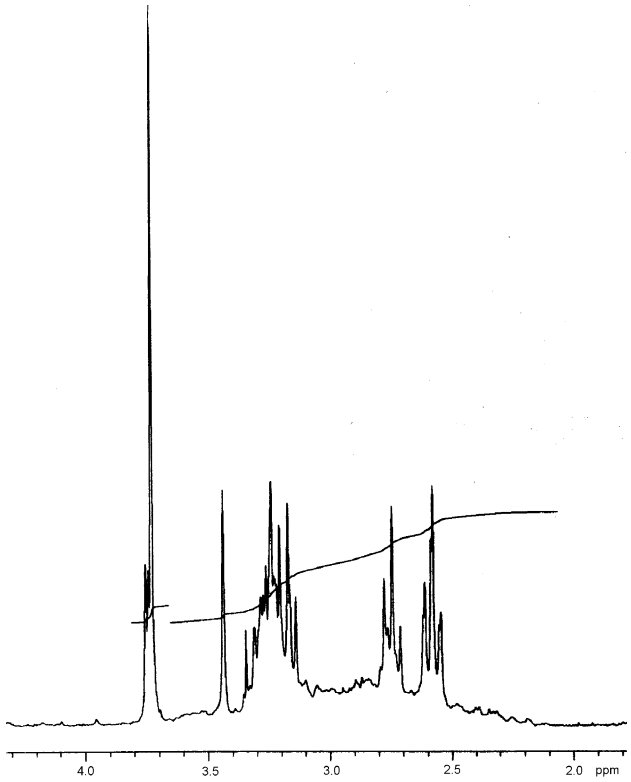


Fig. 3. ^{1}H NMR spectrum of the C_1-symmetric-[Co(eddp)dmeddp]Cl complex.

Table 2
Electronic absorption spectral data for the cobalt(III) complexes with edda-type ligands[a]

Complex	$\lambda_1(\varepsilon_1)$	$\lambda_2(\varepsilon_2)$	$\lambda_3(\varepsilon_3)$	Reference
C_2-symmetric-[Co(edda)en]$^+$	528(87.3)	449(sh)	364(113)	[9]
C_1-symmetric-[Co(edda)en]$^+$	493(170)		359(169)	[9]
C_2-symmetric-[Co(eddp)en]$^+$	542(93)	455(33)	362(81)	[8]
C_1-symmetric-[Co(eddp)en]$^+$	508(218)		367(120)	[8]
C_1-symmetric-[Co(eddp)dmeddp]$^+$	511(206.5)		360.5(193.1)	
C_1-symmetric-[Co(eddp)deeddp]$^+$	510(140.5)		358(118.5)	This work
C_1-symmetric-[Co(eddp)dpeddp]$^+$	505(128)		363(101.5)	
C_1-symmetric-[Co(eddp)dbeddp]$^+$	502(118)		361.5(84)	
C_1-symmetric-[Co(eddp)dveddp]$^+$	502(113)		361(75)	

[a] Wavelength (λ) in nm. Extinction coefficient (ε) in mol^{-1} dm^3 cm^{-1}.

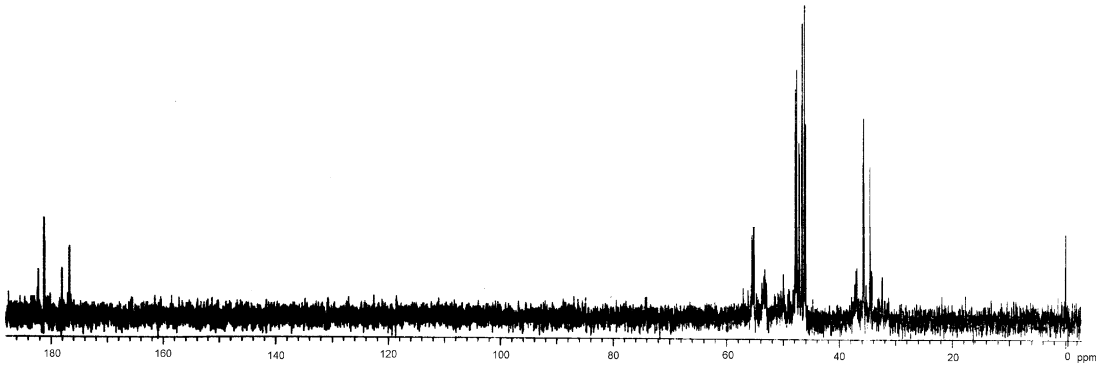


Fig. 4. ^{13}C NMR spectrum of the C_1-symmetric-[Co(eddp)dmeddp]Cl complex.

with above papers, our complex (Fig. 3) showed an AA′BB′ pattern at δ 3.0–3.4 due to the protons of the β-alaninato ring of eddp ligand. Protons associated with the N–CH_2–CH_2–N ring of both eddp and esters are found between δ 2.5 and 3.0. These protons exhibit an AA′BB′ pattern owing to the different chemical shifts of axial and equatorial protons. Because of the highly collapsed nature and overlap of the patterns, a complete analysis is very difficult. The C_1-symmetric isomers exhibit complex spectra in asymmetry introduced by changing one of the R β-alaninato rings [20] (oxygen above the plane containing Co and eddp nitrogens) to a G ring (oxygen in Co-eddp nitrogen plane) which should result in two different patterns observed at δ 2.75 and 3.22. Similarities of ^1H NMR spectra of the isolated complexes with the C_1-symmetric-[Co(eddp)en]Cl complex suggest C_1-symmetric geometry of our compounds. While the proton spectra of these complexes have had definite usefulness in the study of molecular geometry of these complexes, collapsed nature and overlapping of peaks have placed limits upon their utility.

The ^{13}C NMR spectra of the [Co(eddp)dmeddp]$^+$ complex (Fig. 4) exhibits shifts at 183 and 181 ppm, which correspond with shifts from the carbon atoms of coordinated carboxyl groups. Shifts found at 178 and 177 ppm are assigned to the ester carbons [21]. All methylene resonances occur within the range 50–32 ppm, and the methyl carbons resonate at 55.5 and 55.3 ppm. For the other complexes methyl carbons resonate from 16.0 to 12.2 ppm, α-methylene (ester) carbons resonate from 70.7 to 65.0 ppm, carboxyl carbons resonate from 183 to 181 ppm and ester carbons resonate from 178 to 177 ppm. As expected these spectra exhibit twice as many peaks in the methylene and carboxyl regions as are observed for the free ligand. Finally, as expected from electronic absorption, infra red and ^1H NMR spectra, differences in shifts indicate that these are C_1-symmetric isomers. Selected ^1H and ^{13}C NMR shifts for esters and the corresponding complexes are given in Table 3.

Table 3
Characteristic ^1H and ^{13}C NMR shifts of R_2eddp·2HCl and the C_1-symmetric-[Co(eddp)R_2eddp]Cl complexes

Compound	^1H		^{13}C	
	CH_3	COO^-	COO–R	CH_3
dmeddp·2HCl	3.75s[a]	–	175.3	55.5
[Co(eddp)dmeddp]Cl	3.75s	183.1	178.0	55.5
		181.2	176.7	55.2
deeddp·2HCl	1.26t[b]	–	174.9	15.9
[Co(eddp)deeddp]Cl	1.26t	183.0	177.5	16.0
		181.1	175.6	
dpeddp·2HCl	0.91t	–	175.0	12.2
[Co(eddp)dpeddp]Cl	0.91t	183.0	177.6	12.5
		181.0	175.8	
dbeddp·2HCl	0.90t	–	175.0	15.6
[Co(eddp)dbeddp]Cl	0.90t	183.4	177.5	15.6
		181.2	175.5	
dveddp·2HCl	0.87t	–	171.7	12.6
[Co(eddp)dveddp]Cl	0.88t	183.0	177.5	13.2
		181.1	175.3	

[a] Singlet.
[b] Triplet.

Acknowledgements

The authors are grateful to the Ministry of Science, Technology and Development of the Republic of Serbia for financial support, (Project 1253-Synthesis and structure of potentially antitumor platinum(IV) complexes and similar coordination compounds as precursor for nanophased materials).

References

[1] D.J. Radanović, Coord. Chem. Rev. 54 (1984) 159.
[2] S.R. Trifunović, J.M. Dišić, T.J. Sabo, Synth. React. Inorg. Met-Org. Chem. 29 (1999) 1673.
[3] T.J. Sabo, S.R. Grgurić, D.M. Minić, S.R. Trifunović, J. Coord. Chem. 44 (1998) 173.
[4] Ž.Lj. Tešić, S.R. Grgurić, S.R. Trifunović, D. Milojković-Opsenica, T.J. Sabo, J. Planar Chromatogr. 10 (1997) 457.

[5] G.N. Kaluđerović, G.A. Bogdanović, T.J. Sabo, J. Coord. Chem. 55 (2002) 817.
[6] H. Kawaguchi, N. Maruyama, T. Ama, T. Yasui, Bull. Chem. Soc. Jpn. 65 (1992) 175.
[7] N. Sakagami, T. Yasui, H. Kawaguchi, T. Ama, S. Kaizaki, Bull. Chem. Soc. Jpn. 67 (1994) 680.
[8] S.R. Grgurić, T.J. Sabo, Synth. React. Inorg. Met.-Org. Chem. 29 (1999) 1567.
[9] T.J. Sabo, S.R. Grgurić, J. Serb. Chem. Soc. 65 (2000) 167.
[10] S. Chabarek, Jr., A.E. Martell, J. Am. Chem. Soc. 74 (1952) 6228.
[11] D.B. Haydock, T.P.C. Mulholland, J. Chem. Soc. C (1971) 2389.
[12] K. Nakamoto, Infrared and Raman Spectra of Inorganic and Coordination Compounds, Wiley, New York, 1986, p. 62.
[13] M. Strasak, F.J. Bachraty, Coord. Chem. 13 (1984) 105.
[14] T. Woon, M. O'Connor, Aust. J. Chem. 32 (1979) 1661.
[15] G. Hawn, C. Maricondi, B.E. Douglas, Inorg. Chem. 18 (1979) 2542.
[16] P.F. Coleman, J.I. Legg, J. Steele, Inorg. Chem. 9 (1970) 937.
[17] R.S. Drago, Physical Methods in Chemistry, W.B. Saunders, Philadelphia, 1977, pp. 107–122.
[18] P.J. Garnett, D.W. Watts, Inorg. Chim. Acta 8 (1974) 293.
[19] J.L. Sudmeier, G. Occupati, Inorg. Chem. 7 (1968) 2524.
[20] H.A. Weakliem, J.L. Hoard, J. Am. Chem. Soc. 81 (1959) 549.
[21] K.D. Gailey, K. Igi, B.E. Douglas, Inorg. Chem. 14 (1975) 2956.

amine to give the conjugate amido species [Pt(bpmaH$_{-1}$)Cl]. Following on these observations and considering the paucity of kinetic data on amine deprotonation of Pt(II) systems and the effect of amine deprotonation on associatively activated substitution reactions, we thought of interest to carry out a kinetic study on the base hydrolysis of $[Pt(bpma)Cl]^+$. An investigation on the acid–base behaviour of the aqua species $[Pt(bpma)(OH_2)]^{2+}$ has also been performed in order to elucidate the nature and the distribution of the species formed in solution.

The crystal structures of $[Pt(bpma)Cl]Cl\cdot H_2O$ and $[Pt(bpma)(OH_2)](ClO_4)_2\cdot 2H_2O$ are also included.

2. Experimental

2.1. Materials

Pure reagent grade NaBr, $LiClO_4$, $NaCH_3SO_3$, $AgClO_4$ and $AgCF_3SO_3$ (Fluka and Aldrich) were dried over P_2O_5 in a vacuum desiccator and used without further purification. Deuterated solvents were furnished by Euriso-top. Bis(2-pyridylmethyl)amine was prepared according to a published method [8] and its identity confirmed by ^{1}H NMR.

2.2. Instruments

Infrared spectra (4000–250 cm^{-1}, KBr discs and Nujol mulls; 400–150 cm^{-1}, polyethylene pellets) were recorded on a Nicolet Magna FT IR 750 spectrometer. Electronic spectra and kinetics measurements were obtained on a Perkin–Elmer Lambda 15 spectrophotometer. Proton NMR spectra were taken on a Bruker AC 200 F spectrometer. pH measurements were obtained using an Amel combined glass electrode on an Amel 334-B instrument. Conductivity measurements were carried out with a CDM 83 Radiometer Copenhagen conductivity meter and a CDC 334 immersion cell. Elemental analyses were performed by the Microanalytical Laboratory of the University of Padua.

2.3. Preparation of complexes

2.3.1. Chloro[bis(2-pyridylmethyl)amine]platinum(II)-chloride monohydrate, [Pt(bpma)Cl]Cl·H$_2$O (1)

It was prepared as previously reported [7]. Crystals suitable for X-ray structure determination was grown from a hot concentrated aqueous solution of the compound by slow cooling.

2.3.2. Aqua[bis(2-pyridylmethyl)amine]platinum(II)-trifluoromethanesulfonate, [Pt(bpma)(OH$_2$)](CF$_3$SO$_3$)$_2$ (2)

Silver trifluoromethanesulfonate (0.257 g, 1 mmol) was added to a warm solution (70 °C) of $[Pt(bpma)Cl]Cl\cdot H_2O$ (0.241 g, 0.5 mmol) in water (20 cm^3) and the mixture stirred in the dark for 15 min. The AgCl formed was filtered off and the solution evaporated to dryness. The title compound was obtained as a white powder in almost quantitative yield. (*Anal*. Found: C, 23.6; H, 1.96; N, 5.95. $C_{14}H_{15}F_6N_3O_7PtS_2$ requires: C, 23.7; H, 2.13; N, 5.91%). Λ_M (dmf = dimethylformamide) = 139 Ω^{-1} cm^2 mol^{-1}; λ_{max}/nm (water) 267, 274 (sh) (ε/dm^3 mol^{-1} cm^{-1} = 14 100); δ_H (200 MHz; solvent D_2O; protonated signals of the solvent downfield from $SiMe_4$ as reference) 8.20 [2H, d, J = 5.3 Hz, J(Pt–H) = 28 Hz, H_6], 7.99 (2H, t, J = 7.8 Hz, H_4), 7.45 (2H, d, J = 7.7 Hz, H_3), 7.38 (2H, t, J = 7.5, 5.3 Hz, H_5), 4.45 (4H, m, 2CH_2, partially masked by solvent peak).

2.3.3. Aqua[bis(2-pyridylmethyl)amine]platinum(II)-perchlorate dihydrate, [Pt(bpma)(OH$_2$)](ClO$_4$)$_2$·2H$_2$O

The complex was obtained by dissolving **2** (50 mg) in hot water (80 °C, 10 cm^3) containing an excess of $LiClO_4$ (100 mg). Slow cooling of the solution at room temperature resulted in the formation of colourless crystals, which were filtered off, washed with cold water (2–3 cm^3) and dried in vacuo. Yield: > 80%.

2.4. Kinetics

The reactions were followed spectrophotometrically by measuring the changing absorbance at a suitable wavelength (296 nm) as a function of time. They were initiated by adding 2–20 μl of a 0.015 mol dm^{-3} water solution of the substrate, $[Pt(bpma)Cl]Cl\cdot H_2O$, to 3 cm^3 of the required NaOH or NaBr solution previously brought to the reaction temperature (25 °C) in a thermostated cell in the spectrophotometer. The ionic strength was kept constant at 0.2 mol dm^{-3} with $NaCH_3SO_3$. Pseudo first-order rate constants (k_{obs}/s^{-1}) were obtained either from the gradients of plots of $\log(D_t - D_\infty)$ versus time or from a non-linear least-squares fit of experimental data to the equation $D_t = D_\infty + (D_o - D_\infty)\exp(-k_{obs}t)$, where D_o, D_∞ and k_{obs} are the parameters to be optimized (D_o, absorbance after mixing of reactants; D_∞, absorbance at completion of reaction).

2.5. Determination of the pK$_a$'s values of the complex [Pt(bpma)(OH$_2$)](CF$_3$SO$_3$)$_2$

Aliquots of a 0.01 mol dm^{-3} aq. solution of $[Pt(bpma)(OH_2)](CF_3SO_3)_2$ (I = 0.2 mol dm^{-3},

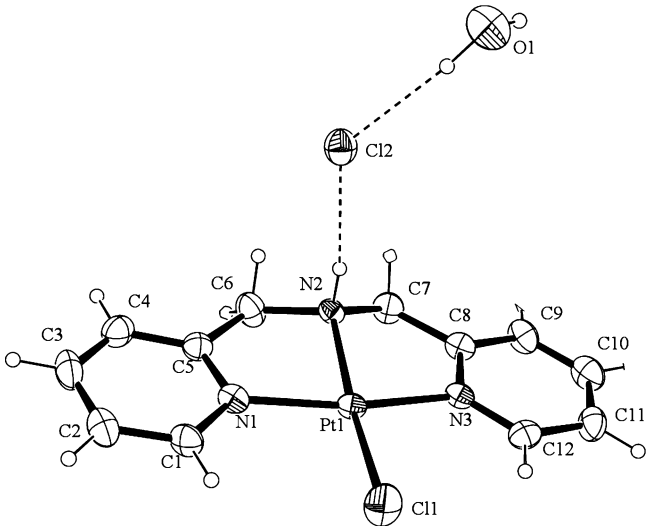


Fig. 1. ORTEP view and atom numbering of the asymmetric unit of **1** showing the thermal ellipsoids at 30% probability level.

$NaCH_3SO_3$) thermostated at 25 °C were titrated with standard CO_2-free 0.1 mol dm^{-3} NaOH solution (I = 0.2 mol dm^{-3}, $NaCH_3SO_3$). The electrode was calibrated with buffer solutions of the same ionic strength prepared according to Ref. [9]. The ionization constants pK_1 and pK_2 have been computed by a non-linear regression of the titration data by means of the Marquardt algorithm.

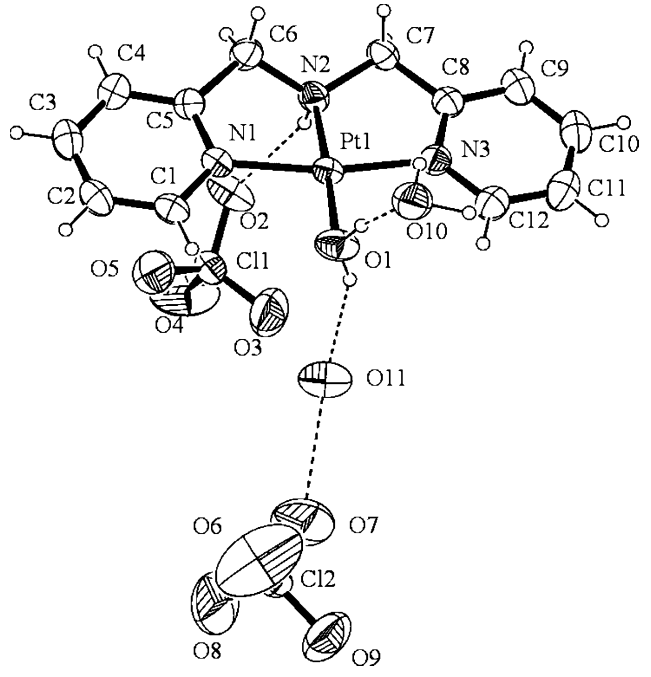


Fig. 2. ORTEP view and atom numbering of the asymmetric unit of **2** showing the thermal ellipsoids at 30% probability level.

2.6. X-ray crystallography

The data for both structures **1** and **2** were collected on a Nonius Kappa CCD area detector diffractometer using graphite monochromated Mo Kα radiation (λ = 0.7107 Å). The reflections were corrected for Lp and absorption [10] effects. The crystal parameters and other experimental details of the data collections are summarized in Table 3. The structures were solved by direct and Fourier methods. Full-matrix least-squares refinement was performed with all non-hydrogen atoms anisotropic and hydrogens in calculated positions. For structure **1**, the positions of both hydrogens belonging to the water molecule were found in the difference-Fourier map and kept fixed during the refinement. The N2 atom of the secondary amine group was found to be disordered over two positions with occupancy factors of 0.62(4) and 0.38(4), respectively. For structure **2**, the hydrogens belonging to the water molecules O1 and O10 were found in the difference-Fourier map and refined isotropically, while the positions of those linked to the water oxygen O11 were not determined. Programs used and sources of scattering factor data are given in Ref. [11].

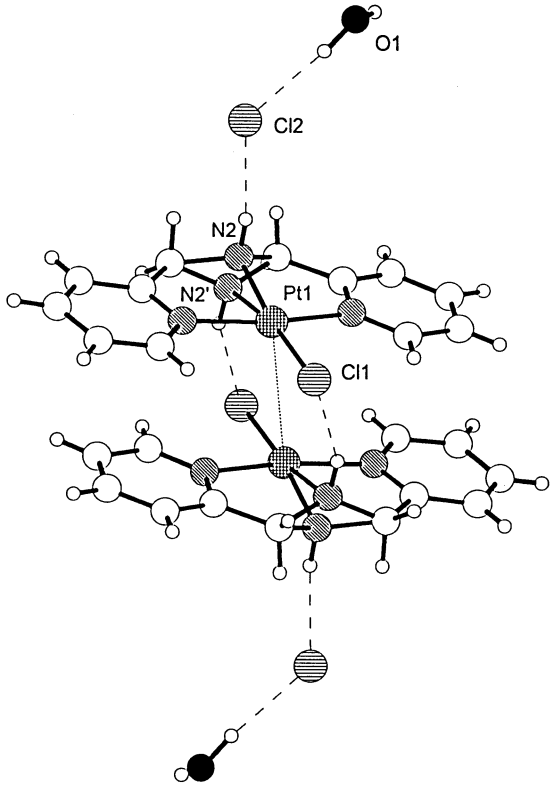


Fig. 3. The dimeric arrangement in the crystal of **1** showing the N2 atom disordered over two positions and the interactions between two square-planar Pt(II) complexes.

3. Results and discussion

3.1. Structures of $[Pt(bpma)Cl]Cl\cdot H_2O$ and $[Pt(bpma)(OH_2)](ClO_4)_2\cdot 2H_2O$

ORTEP [12] views of the asymmetric units of **1** and **2** are shown in Figs. 1 and 2, respectively. Selected bond distances and angles are reported in Table 4.

The asymmetric unit of compound **1** consists of a square-planar $[Pt(bpma)Cl]^+$ cation, a Cl^- anion and a water molecule. The bpma molecule binds the central metal with its three N atoms; the coordination around Pt is completed by a Cl atom in *trans* position with respect to N2 atom, which is found to be disordered over two positions, N2 and N2′, below and above the mean coordination plane with deviations of −0.45(2) and +0.34(5) Å, respectively. Pt–N and Pt–Cl distances (Table 4) compare well with the mean values of 2.01 [4] and 2.29 [1] Å, respectively, obtained from a systematic analysis of several $PtCl_2L_2$ complexes (L = N-donor ligand) [13]. Due to the strain induced by the small bite of the chelate ligand both the N–Pt–N(*cis*) angles have a value of 83.3°, rather smaller than 90°.

The Cl^- counterion acts as a bridge between the cation and the water molecule being involved in two hydrogen bonds with O1 and N2 atoms (Table 5). The square-planar cations are assembled in dimeric units, through a crystallographic centre of symmetry, by means of Pt···Pt interactions of 3.7467(4) Å and N2–H···Cl1 hydrogen bonds. This arrangement is shown in Fig. 3 and the intra- and intermolecular H-bonds are listed in Table 5. Intermolecular short contacts between Pt atoms are not infrequent in crystals. Taken as reference-value the van der Waals radius given by Bondi [14] for Pt atom of 1.80 Å, a search has been made on the Cambridge Crystallographic Database [15] of all structures of Pt(II) complexes containing at least a pyridine ligand, where the Pt metal is involved in Pt···Pt contacts less than 4.0 Å. Thirty-eight structures have been retrieved, giving a mean Pt–Pt distance of 3.5 Å [2]. A list of CSD refcodes and Pt···Pt distances is available in Section 4. The mutual orientation of the complexes joined by means of Pt···Pt contacts has been evaluated by calculating the angle ϕ formed by the least-squares coordination plane and the line connecting the two central metal. The shortest Pt···Pt distances of 3.235, 3.237 and 3.244 Å [16] are associated with angles of 85.2°, 80.6° and 85.7°, very close to 90°, while longer distances, similar to that found in the present compound, of 3.755, 3.787 and 3.852 Å [17] are associated with smaller angles of 64.0°, 67.0° and 61.7°, respectively. In the present compound the ϕ angle is 73.0(1)°. It can be concluded that the Pt···Pt interaction is as stronger as the ϕ angle is closer to 90°, in agreement with the presence of an interaction between two filled d_z^2 and two empty p_z orbitals of the two adjacent Pt atoms [18].

The asymmetric unit of compound **2** is built up by a square-planar $[Pt(bpma)H_2O]^{2+}$ cation, two ClO_4^- anions and two water molecules. Pt1, the three N coordinated atoms and O1 lie almost perfectly on a plane; the deviations from the best plane are as follows: Pt1, 0.024(1); N1, −0.001(6); N2, −0.011(6); N3, −0.002(6); O1, −0.011(6) Å. Pt1–N (pyridine) distances of 2.010(5) and 2.014(6) are in agreement with those observed in compound **1**, in $[Pt(bpma)pyridine]^{2+}$ [7] and in other Pt(II) square-planar complexes [13,19]. Pt–N2(sp^3) distance of 1.952(7) Å, however, is remarkably shorter than those found both in [Pt(II)bpma] complexes [2.009(12) in **1**, 2.008(5) [7], 2.11(2) [19] Å] and in square-planar Pt(II) complexes where an N(sp^3) atom is in *trans* position to a water molecule [Pt–N in the range 2.01–2.02 Å] [20]. From a search on CSD files [15], a number of structures containing a water molecule directly co-ordinated to Pt(II) has been retrieved. From these structural data it is possible to determine the *trans* influence exerted by different atoms on the water oxygens. For instance, in structures where the water molecule is in *trans* position with respect to a nitrogen atoms [Pt–OH_2 distances from 2.05 to 2.10 Å [20], in

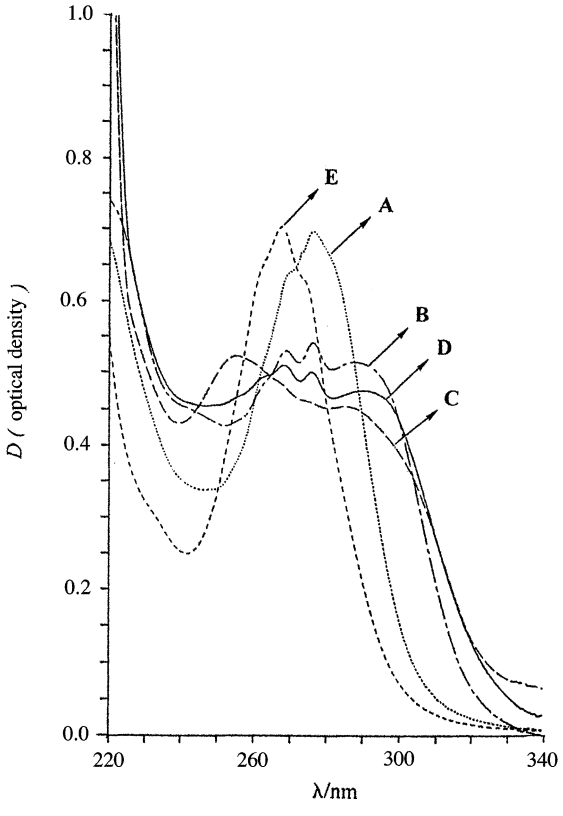


Fig. 4. Absorption spectra of 5×10^{-5} mol dm^{-3} $[Pt(bpma)Cl]^+$ (25 °C, $I = 0.2$ mol dm^{-3}): in water solution (A); aged with $[OH^-] = 5\times10^{-4}$ mol dm^{-3} (B); immediately after dissolution in the presence of $[OH^-] = 10^{-1}$ mol dm^{-3} (C); aged in the presence of $[OH^-] = 10^{-1}$ mol dm^{-3} (D). Absorption spectrum of 5×10^{-5} mol dm^{-3} $[Pt(bpma)(OH_2)](CF_3SO3)_2$ (25 °C, $I = 0.2$ mol dm^{-3}) at pH 4 ($HClO_4$) (E).

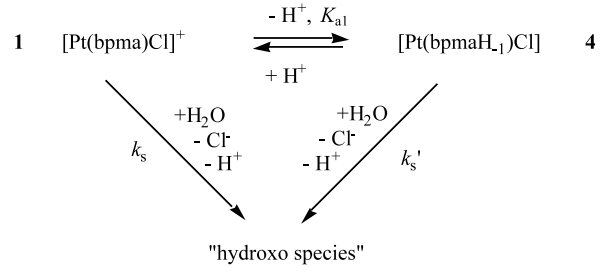
agreement with the value of 2.048(7) Å reported for the present structure], the *trans* influence exerted by the nitrogen can be evaluated by comparing these distances with those of 2.015 Å observed in a *trans*-diaqua Pt(II) complex [21] where the *trans* influences on Pt–O bonds are mutually balanced. The maximum lengthening is observed in Pt(II) complexes where the water molecule is in *trans* position to a carbon atom [22] [Pt–O distances from 2.17 to 2.27 Å] while similar effects to that observed for nitrogen are found for P–Pt(II)–OH_2 [23] and Cl–Pt(II)–OH_2 [24] systems where Pt–O lengths are in the range 2.08–2.12 Å.

The analysis of the crystal packing of complex **2** shows that all the water molecules, the perchlorate anions and the N2–H amine group are involved in the formation of a complex network of hydrogen bonds listed in Table 3, and that no Pt···Pt contacts less than 7.5 Å are present in the crystal.

3.2. Solution chemistry

The UV–Vis spectrum of an aqueous solution of [Pt(bpma)Cl]Cl (curve A in Fig. 4) does not change appreciably even after a long period of time. Addition of NaOH to this solution leads to an immediate change in the spectrum. The new spectrum depends to some extent on $[OH^-]$, but for $[OH^-] \geq 0.16$ mol dm^{-3} it becomes pH independent (curve C). Immediate reacidification of the basic solutions leads to a spectrum which is identical with that of the starting chloro species. Without reacidification, subsequent slow spectral changes are observed which is pH dependent. The final spectra for $[OH^-] = 5 \times 10^{-4}$ and 0.1 mol dm^{-3} are shown as curves B and D, respectively. Addition of NaCl up to 0.1 mol dm^{-3} has no effect on these spectra.

The above observations can be accounted for by the reactions shown in Scheme 1. The amino species **1** undergoes reversible deprotonation of the secondary amino group to give the conjugate amido species **4**. This rapid process (spectral changes from A to C) is followed by slow solvolysis of **1** and **4** to give the corresponding aqua complexes which, under our experimental conditions, are fully converted to hydroxo species which are known to be inert toward nucleophilic substitution [25].



Scheme 1.

Table 1
Pseudo first-order rate constants, k_{obs}, for the overall process (Scheme 1) in water at 25 °C

$10^2[OH^-]$ (mol dm^{-3})	$10^3 k_{obs}$ [a] (s^{-1})
0.05	0.354 ± 0.001
0.08	0.399 ± 0.002
0.10	0.434 ± 0.004
0.15	0.517 ± 0.003
0.20	0.594 ± 0.004
0.25	0.654 ± 0.006
0.30	0.72 ± 0.01
0.40	0.83 ± 0.01
0.50	0.96 ± 0.02
0.60	1.10 ± 0.04
0.80	1.32 ± 0.03
1.00	1.47 ± 0.03
1.50	1.80 ± 0.01
2.00	1.96 ± 0.04
2.50	2.16 ± 0.05
3.00	2.24 ± 0.06
4.00	2.44 ± 0.06
5.00	2.57 ± 0.05
7.00	2.79 ± 0.05
8.00	2.88 ± 0.04
9.00	2.96 ± 0.03
10.00	3.07 ± 0.05
12.00	3.14 ± 0.05
14.00	3.21 ± 0.04
15.00	3.23 ± 0.05
16.00	3.25 ± 0.07
18.00	3.27 ± 0.05
19.00	3.26 ± 0.07
20.00	3.27 ± 0.06

[a] $I = 0.2$ mol dm^{-3} $NaCH_3SO_3$ + NaOH.

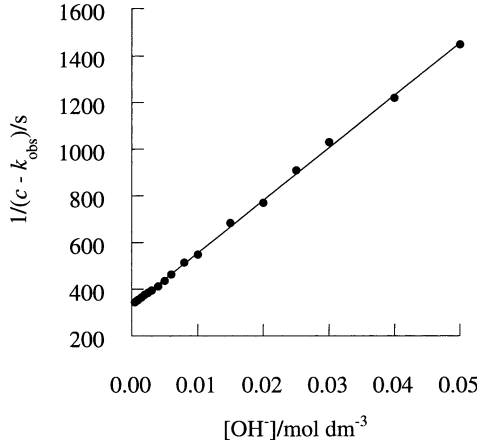


Fig. 5. Plot of $1/(c - k_{obs})$ against $[OH^-]$ for the base hydrolysis of $[Pt(bpma)Cl]^+$.

3.3. Kinetics of the base hydrolysis

The kinetics of the base hydrolysis were carried out in presence of at least 10-fold excess of sodium hydroxide ($5 \times 10^{-4} \leq [OH^-] \leq 0.2$ mol dm^{-3}) with respect to the concentration of the substrate. The individual runs gave

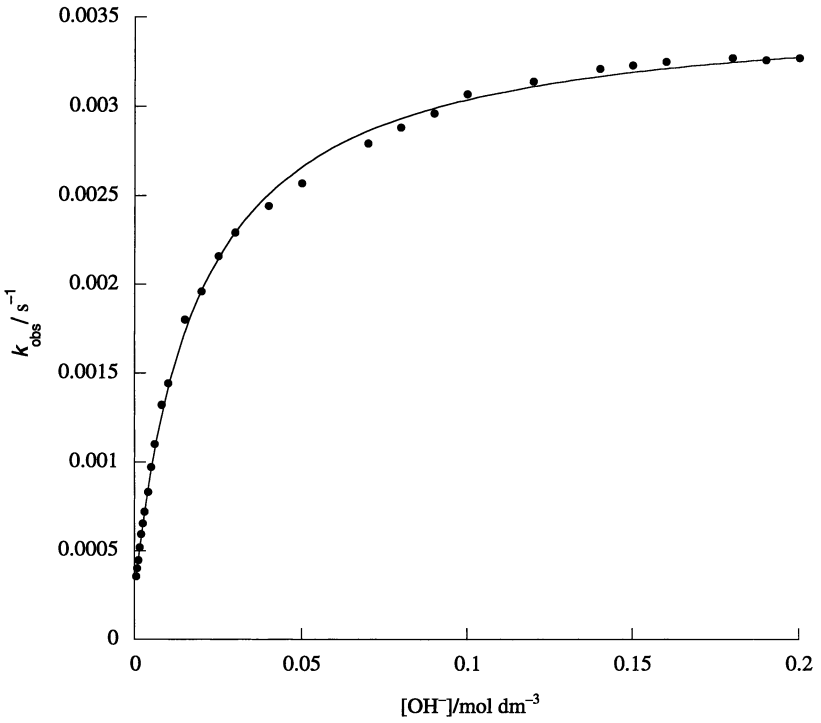


Fig. 6. Plot of pseudo first-order rate constants k_{obs} against $[OH^-]$ for the base hydrolysis of $[Pt(bpma)Cl]^+$.

first-order plots. The pseudo first-order rate constants, k_{obs}, has been reported in Table 1.

k_{obs} increases with increasing $[OH^-]$, but for $[OH^-] \geq 0.16$ mol dm^{-3} it is independent of $[OH^-]$, the mean value of four determinations being $c = (3.26 \pm 0.01) \times 10^{-3}$ s^{-1}. A plot of $1/(c - k_{obs})$ against $[OH^-]$ is linear up to $[OH^-] = 0.05$ mol dm^{-3} (Fig. 5), with finite intercept $a = (330 \pm 3)$ s and slope $b = (2.26 \pm 0.02) \times 10^4$ s mol^{-1} dm^3 according to Eq. (1)

$$1/(c - k_{obs}) = a + b[OH^-] \quad (1)$$

Eq. (1) can be rearranged to Eq. (2) to give the explicit dependance of k_{obs} from $[OH^-]$

$$k_{obs} = (c - 1/a + [OH^-]bc/a)/(1 + [OH^-]b/a) \quad (2)$$

From reaction Scheme 1, assuming the preequilibrium condition between **1** and **4**, and for $[OH^-] \gg$ [substrate], the following expression for k_{obs} is derived

$$k_{obs} = (k_s + [OH^-]k_s'K_{a1}/K_w)/(1 + [OH^-]K_{a1}/K_w) \quad (3)$$

where k_s and k_s' are the rate constants for the solvolysis of **1** and **4**, respectively, K_{a1} the protolysis constant of **1**, and $K_w = [H^+][OH^-]$. Eq. (3) is in complete agreement with the observed kinetics, the equilibrium and kinetic constants being related to those extracted from the empirical rate law (2) through the expressions $c = k_s'$, $a = 1/(k_s' - k_s)$, and $b/a = K_{a1}/K_w$. From a non-linear best fit of all the experimental data to Eq. (3) with k_s, k_s' and K_{a1} the parameters to be optimized ($K_w = 10^{-14}$ mol^2 dm^{-6}) the values $k_s = (2.8 \pm 0.2) \times 10^{-4}$ s^{-1}, $k_s' = (3.28 \pm 0.02) \times 10^{-3}$ s^{-1}, $pK_{a1} = 12.3$ have been computed (Fig. 6). An independent determination of the solvolytic rate constant k_s has been achieved by carrying out the kinetics of the reaction $[Pt(bpma)Cl]^+ + Br^- \rightarrow [Pt(bpma)Br]^+ + Cl^-$ in water solution at 25 °C and $I = 0.2$ mol dm^{-3} under pseudo first-order conditions. The two terms rate law $k_{obs} = k_s + k_{Br}[Br^-]$, usually found in nucleophilic substitution in square-planar complexes [25], is obeyed (Fig. 7) with $k_{Br} = (4.1 \pm 0.1) \times 10^{-2}$ s^{-1} mol^{-1} dm^3 and $k_s = (2.6 \pm 0.3) \times 10^{-4}$ s^{-1}, in close agreement with the value obtained from the kinetics of the base hydrolysis. The pseudo first-order rate constants, k_{obs}, has been reported in Table 2.

The higher reactivity of the amido species **4** with respect to the amino species **1** ($k_s'/k_s = 11.7$) is in

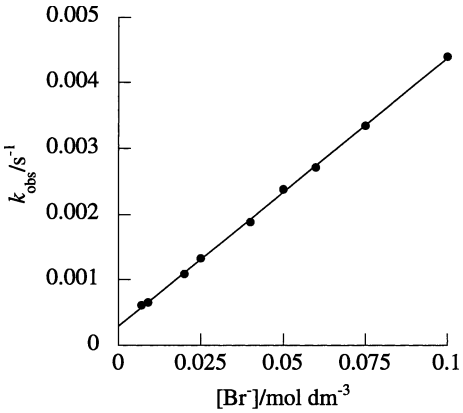


Fig. 7. Plot of pseudo first-order rate constants k_{obs} against $[Br^-]$ for the reaction $[Pt(bpma)Cl]^+ + Br^- \rightarrow [Pt(bpma)Br]^+ + Cl^-$.

Table 2
Pseudo first-order rate constants, k_{obs}, for the reaction: $[Pt(bpma)Cl]^+ + Br^- \rightarrow [Pt(bpma)Br]^+ + Cl^-$ in water at 25 °C

10^2[Br] (mol dm^{-3})	$10^3 k_{obs}$ (s^{-1})
0.7	0.60 ± 0.01
0.9	0.66 ± 0.01
2.0	1.04 ± 0.01
2.5	1.33 ± 0.02
4.0	1.89 ± 0.01
5.0	2.38 ± 0.07
6.0	2.71 ± 0.02
7.5	3.34 ± 0.02
10	4.50 ± 0.04

$I = 0.2$ mol dm^{-3} $NaCH_3SO_3$.

Table 3
Crystallography data for $[Pt(bpma)Cl]Cl\cdot H_2O$ (**1**) and $[Pt(bpma)(OH_2)](ClO_4)_2\cdot 2H_2O$ (**2**)

Complex	**1**	**2**
Empirical formula	$C_{12}H_{15}Cl_2N_3OPt$	$C_{12}H_{19}Cl_2N_3O_{11}Pt$
M	483.26	647.29
Temperature (K)	295	295
Crystal system	monoclinic	monoclinic
Space group	$P2_1/c$	$P2_1/c$
a (Å)	8.4991(2)	7.7675(3)
b (Å)	12.7963(3)	14.9477(3)
c (Å)	13.5678(3)	17.2872(5)
β (°)	103.359(1)	100.755(1)
U (Å^3)	1435.67(6)	1971.9(1)
Z	4	4
D_{calc} (g cm^{-3})	2.24	2.18
μ(Mo Kα) (cm^{-1})	101.40	74.49
F(000)	912	1248
Crystal size (mm)	0.26 × 0.23 × 0.15	0.33 × 0.17 × 0.14
θ_{min}–θ_{max} (°)	2.93–25	3–30
Unique reflections	2516	5715
Refined parameters	183	278
Observed reflections [$I \geq 2\sigma(I)$]	2481	4652
R on F^2 (observed reflections)	0.0291	0.0456
wR on F^2 (all reflections)	0.0741	0.1133
Goodness-of-fit on F^2	1.285	1.165

keeping with the results found by Romeo et al. [5] in the study of the system $[Pt(enH_{-1})(dmso)_2]^+$/$[Pt(en)(dmso)_2]^{2+}$ ($k_s'/k_s \simeq 10$). If one assumes that the different charge on the substrates has no a significative effect on the rate of hydrolysis, as found by Martin and coworkers [26] for a number of Pt(II) chloroammine complexes, the difference in reactivity could be ascribed to the greater *trans* effect of the amido group. Unfortunately, no study has been performed on other comparable systems and a comparison with data relative to substitution reactions with anionic nucleophiles in other amino–amido systems [2,5], for which a reversal of behaviour with the conjugate base becoming less labile than the amine species was observed, cannot be properly done as charge neutralization, absent in the hydrolysis reactions, could overcome the effect of the deprotonation. Therefore, further investigations are necessary before any reasonable conclusion can be drawn.

Table 4
Selected bond distances (Å) and angles (°) with estimated standard deviations (e.s.d.s) in parentheses

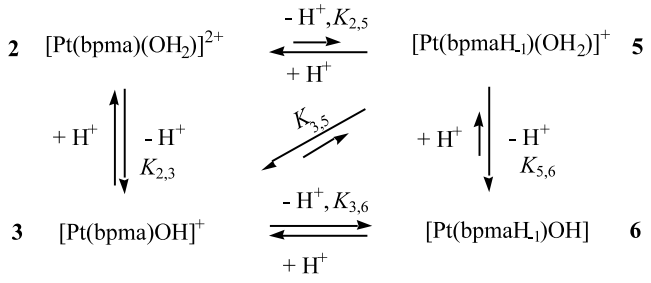
	1	**2**
Bond distances		
Pt1–N1	2.008(6)	2.010(5)
Pt1–N2	2.009(12)	1.952(7)
Pt1–N3	2.011(5)	2.014(6)
Pt1–Cl1	2.301(2)	
Pt1–O1		2.048(7)
N1–C5	1.349(10)	1.338(9)
C5–C6	1.529(11)	1.511(10)
N2–C6	1.472(15)	1.475(9)
N2–C7	1.458(13)	1.484(9)
C7–C8	1.497(11)	1.491(10)
N3–C8	1.356(9)	1.351(9)
Bond angles		
N1–Pt1–N2	83.3(3)	83.6(2)
N1–Pt1–N3	166.0(2)	166.7(2)
N1–Pt1–Cl1	97.2(2)	
N1–Pt1–O1		93.4(3)
N2–ZPt1–N3	83.3(3)	83.2(2)
N2–Pt1–Cl1	168.7(6)	
N2–Pt1–O1		176.4(3)
N3–Pt1–Cl1	97.8(2)	
N3–Pt1–O1		99.8(3)

Table 5
Hydrogen bond distances (Å)

Donor···acceptor	Symmetry operation	Distance (on acceptor atom)
1		
O1···Cl2		3.202(7)
N2···Cl2		3.16(2)
O1···Cl2	$-x-1, -y, -z-1$	3.237(8)
N2′···Cl1	$-x, -y, -z$	3.38(5)
2		
O1···O10		2.547(11)
O1···O11		2.550(11)
N2···O2		3.003(9)
O11···O7		2.715(16)
O10···O4	$-x, y-1/2, -1/2-z$	2.748(12)
O10···O5	$x, 1/2-y, 1/2+z$	2.892(12)
O11···O9	$-x, 1-y, -z$	2.890(15)

The nature and the distribution of the species formed in solution have been elucidated on investigating the acid–base behaviour of the aqua species $[Pt(bpma)(OH_2)]^{2+}$.

In Fig. 4, the UV spectrum of the aqua-complex $[Pt(bpma)(OH_2)](CF_3SO_3)_2$ (**2**) in perchloric acid solution (pH 4) is shown as curve E. When titrated with NaOH, **2** behaves as a dibasic acid and two acid



Scheme 2.

dissociation constants, $pK_1 = 5.4 \pm 0.1$ and $pK_2 = 11.5 \pm 0.1$, are obtained which can be discussed on considering the acid–base equilibria occurring in solution, as depicted in Scheme 2.

Not all of the microscopic equilibrium constants in Scheme 2 can be derived from the two experimentally determined K_1 and K_2 constants unless at least one piece of additional information is available. Literature data on similar systems indicate that the dissociation constant of a –NH– group ($K_{2,5}$ in the present case) is always some six order of magnitude smaller than the acid dissociation constant of a coordinated water molecule ($K_{2,3}$ in the present case). For instance, the pK_a values for the deprotonation of the secondary amino group in the cationic species $[Pt(dien)(Me_2SO)]^{2+}$ [5] and $[PtMe(dpa)(Me_2SO)]^{+}$ [6] are 11.94 ± 0.02 and 12.1 ± 0.2, respectively, while a $pK_a = 6.13$ for the protolysis of co-ordinated water in the aquo-cation $[Pt(dien)(OH_2)]^{2+}$ has been reported [27].

It is therefore reasonable to assume $K_{2,3} \gg K_{2,5}$ and since [28] $K_1 = K_{2,3} + K_{2,5}$ and $K_2 = (K_{3,6} \times K_{5,6})/(K_{3,6} + K_{5,6})$, it follows that $K_1 \cong K_{2,3}$ and $K_2 \cong K_{3,6}$. Consequently, it can be concluded that the reaction products formed in the base hydrolysis of **1** are the hydroxo species **3** and **6**, the anpholite **5** being completely dismutated. Up to $[OH^-] \cong 3 \times 10^{-4}$ mol dm^{-3}, the prevailing product is the amino-hydroxo species **3**, whose spectrum is shown as curve B in Fig. 4.

4. Supplementary material

Crystallographic data of the structural analysis have been deposited with the Cambridge Crystallographic Data Centre, CCDC Nos. 168846–168847 for the compounds $[Pt(bpma)Cl]Cl \cdot H_2O$ and $[Pt(bpma)(OH_2)](ClO_4)_2 \cdot 2H_2O$. Copies of this information may be obtained free of charge from The Director, CCDC, 12 Union Road, Cambridge, CB2 1EZ, UK (fax: +44-1223-336033; e-mail: deposit@ccdc.cam.ac.uk or www: http://www.ccdc.cam.ac.uk).

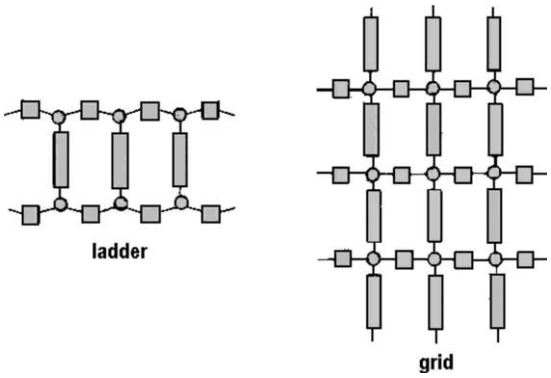
Acknowledgements

We thank the Italian Ministry of University for financial support and Tatiana Bobbo for technical assistance.

References

[1] M.L. Tobe, Adv. Inorg. Bioinorg. Mech. 2 (1984) 1 (and references therein).
[2] W.H. Baddley, F. Basolo, Inorg. Chem. 3 (1964) 1087.
[3] C.F. Weick, F. Basolo, Inorg. Chem. 5 (1966) 576.
[4] W.H. Baddley, F. Basolo, J. Am. Chem. Soc. 88 (1966) 2944.
[5] R. Romeo, D. Minniti, G. Alibrandi, L. De Cola, M.L. Tobe, Inorg. Chem. 25 (1986) 1944.
[6] R. Romeo, N. Nastasi, L. Monsù Scolaro, M.R. Plutino, A. Albinati, A. Macchioni, Inorg. Chem. 37 (1998) 5460.
[7] L. Cattalini, G. Marangoni, B. Pitteri, F. Visentin, V. Bertolasi, P. Gilli, Polyhedron 20 (2001) 869.
[8] H.J. Hoorn, P. de Joode, W.L. Driessen, J. Reediik, Recl. Trav. Chim. Pais-Bas 115 (1996) 191.
[9] International Critical Tables, vol. 1, The Maple Press Company, York, PA, 1926, p. 82.
[10] R.H. Blessing, Acta Crystallogr., Sect. A 51 (1995) 33.
[11] (a) D.T. Cromer, J.T. Waber, International Tables for X-ray Crystallography, vol. 4, Kynoch Press, Birmingham, 1974, pp. 149–150;
(b) A. Altomare, G. Cascarano, C. Giacovazzo, A. Guagliardi, M.C. Burla, G. Polidori, M. Camalli, SIR92, J. Appl. Crystallogr. 27 (1994) 435;
(c) G.M. Sheldrick, SHELXL-97, Program for Crystal Structure Refinement, University of Göttingen, Germany, 1997.
[12] C.K. Johnson, ORTEP-II, Report ORNL-5138, Oak Ridge National Laboratory, Oak Ridge, TN, 1976.
[13] G.J. Palenik, T.J. Giordano, J. Chem. Soc., Dalton Trans. (1987) 1175.
[14] A. Bondi, J. Phys. Chem. 68 (1964) 441.
[15] F.H. Allen, S. Bellard, M.D. Brice, B.A. Cartwright, A. Doubleday, H. Higgs, T. Hummelink, B.G. Hummelink-Peters, O. Kennard, W.D.S. Motherwell, J.R. Rodgers, D.G. Watson, Acta Crystallogr., Sect. B 35 (1979) 2331.
[16] (a) M.J. Coyer, R.H. Herber, S. Cohen, Inorg. Chim. Acta 175 (1990) 47;
(b) A.D.Q. Ferreira, A. Bino, D. Gibson, Inorg. Chim. Acta 265 (1997) 155;
(c) T.K. Aldridge, E.M. Stacy, D.R. McMillin, Inorg. Chem. 33 (1994) 722.
[17] (a) J. Breu, K.-J. Range, A. von Zelewsky, H. Yersin, Acta Crystallogr., Sect. C 53 (1997) 562;
(b) A. Benedetti, A.C. Fabretti, C. Preti, G. Tosi, P. Zannini, J. Crystallogr. Spectrosc. Res. 17 (1987) 771;
(c) D.M.L. Goodgame, T.E. Muller, D.J. Williams, Polyhedron 14 (1995) 2557.
[18] D.M. Roundhill, H.B. Hill, C.-M. Che, Acc. Chem. Res. 22 (1989) 55.
[19] H.J. Jenkins, G.P.A. Yap, R.J. Puddephatt, Organometallics 16 (1997) 1946.
[20] (a) F.D. Rochon, R. Melanson, Inorg. Chem. 26 (1987) 989;
(b) J.F. Britten, B. Lippert, C.J.L. Lock, P. Pilon, Inorg. Chem. 21 (1982) 1936;
(c) H.A. Meinema, F. Verbeek, J.W. Marsman, E.J. Bulten, J.C. Dobrowiak, B.S. Krishnan, A.L. Spek, Inorg. Chim. Acta 114 (1986) 127;

(d) H. Rauter, E.C. Hillgeris, A. Erxleben, B. Lippert, J. Am. Chem. Soc. 116 (1994) 616.
[21] F.P. Intini, M. Lanfranchi, G. Natile, C. Pacifico, A. Tiripicchio, Inorg. Chem. 35 (1996) 1715.
[22] (a) A.R. Siedle, W.B. Gleason, R.A. Newmark, L.H. Pignolet, Organometallics 5 (1986) 1969;
(b) J.-T. Chen, Y.-S. Yeh, G.-H. Lee, Y. Wang, J. Organomet. Chem. 414 (1991) C64;
(c) M. Ito, M. Ebihara, T. Kawamura, Inorg. Chim. Acta 218 (1994) 199;
(d) A.C. Dema, C.M. Lukehart, A.T. McPhail, D.R. McPhail, J. Am. Chem. Soc. 111 (1989) 7615;
(e) M. Schmulling, D.M. Grove, G. van Koten, R. van Eldik, N. Veldman, A.L. Spek, Organometallics 15 (1996) 1384.
[23] (a) A. Varshney, M.L. Webster, G.M. Gray, Inorg. Chem. 31 (1992) 2580;
(b) A. Crispini, K.N. Harrison, A.G. Orpen, P.G. Pringle, J.R. Wheatcroft, J. Chem. Soc., Dalton Trans. (1996) 1069;
(c) S. Fallis, G.K. Anderson, N.P. Rath, Organometallics 10 (1991) 3180;
(d) N.P. Rath, K.A. Fallis, G.K. Anderson, Acta Crystallogr., Sect. C 49 (1993) 2079.
[24] F.D. Rochon, P.C. Kong, R. Melanson, Inorg. Chem. 29 (1990) 2708.
[25] F. Basolo, R.G. Pearson, Mechanism of Inorganic Reactions, 2nd ed., Wiley, New York, 1967, p. 384.
[26] M.A. Tucher, C.B. Colvin, D.S. Martin, Jr., Inorg. Chem. 3 (1964) 1373.
[27] R.M. Alcoch, F.R. Hartley, D.E. Rogers, J. Chem. Soc., Dalton Trans. (1973) 1070.
[28] A. Albert, E.P. Serjeant, The Determination of Ionization Constants, Chapman and Hall, London, 1975, p. 79.



Scheme 1.

$[Cd_2(ibn)(SeCN)_4]_n$ **(1)** (ibn = 1, 2-diamino-2-methyl propane) and $[Cd(pyz)(SeCN)_2]_n$ **(2)** (pyz = pyrazine). Compound **1** shows the unique symbiotic phenomena [25] with alternating octahedral (CdN_6) and tetrahedral ($CdSe_4$) centre.

2. Experimental

2.1. Reagents

High purity (98%) 1,2-diamino-2-methylpropane, pyrazine and potassium selenocyanate were purchased from Aldrich Chemical Company Inc. and used as received. All other chemicals used were of AR grade.

2.2. Physical measurements

Elemental analyses (carbon, hydrogen and nitrogen) were performed using a Perkin–Elmer 240C elemental analyser and cadmium(II) content was estimated gravimetrically [26]. Infrared spectra (4000–400 cm^{-1}) were taken using Nicolet Magna-IR 750 spectrometer series-II where KBr was used as medium.

2.3. Synthesis of complexes

Complex $[Cd_2(ibn)(SeCN)_4]_n$ (**1**): an aqueous solution (5 cm^3) of potassium selenocyanate (2 mmol, 0.288 g) was added to an aqueous solution (10 cm^3) of cadmium perchlorate hexahydrate (1 mmol, 0.419 g) with constant stirring. After 10 min 1,2-diamino-2-methylpropane (ibn) (1 mmol, 0.088 g) was added slowly to the reaction mixture and stirred for 30 min. The resulting solution was filtered and the filtrate was kept in a $CaCl_2$ desiccator. After a few days shiny crystals suitable for X-ray determination were obtained. Yield: 80%. *Anal.* Found: C, 13.15; H, 1.66; N, 11.47; Cd, 30.41. Calc. for $C_8H_{12}Cd_2N_6Se_4$: C, 13.10; H, 1.63; N, 11.46; Cd, 30.67%.

Complex $[Cd(pyz)(SeCN)_2]_n$ (**2**): An aqueous solution (5 cm^3) of potassium selenocyanate (2 mmol, 0.288 g) was added to an aqueous solution (10 cm^3) of cadmium nitrate tetrahydrate (1 mmol, 0.308 g) with vigorous stirring for about 10 min. A methanolic solution (5 cm^3) of pyrazine was (1 mmol, 0.080 g) added to it very slowly with constant stirring. The resulting mixture was filtered and the filtrate was kept in a $CaCl_2$ desiccator. After a few days shiny single crystals suitable for X-ray structural analysis were obtained. Yield: 75%. *Anal.* Found: C, 17.83; H, 0.98; N, 13.87; Cd, 27.87. Calc. for $C_6H_4CdN_4Se_2$: C, 17.80; H, 0.99; N, 13.85; Cd, 27.79%.

2.4. X-ray data collection and structure determination

Suitable single crystals of complex **1** was mounted on a Siemens SMART CCD diffractometer whereas complex **2** was mounted on Rigaku/AFC 7S diffractometer equipped with a graphite monochromated Mo Kα (λ = 0.71069 Å) radiation. The intensity data were corrected for Lp [27] and an empirical absorption corrections were also employed using SAINT program [28] for complex **1** and using ψ scan for complex **2**. For **1** a total of 3329 reflections were measured and 2775 were assumed observed applying the condition $I > 2\sigma(I)$, and 471 reflections were measured and 418 were assumed observed applying the condition $I > 2\sigma(I)$ for complex **2**. Both the structures were solved by Patterson syntheses and followed by successive Fourier and difference Fourier syntheses. Full matrix least-squares refinements on F^2 were carried out using SHELXL-97 with anisotropic displacement parameters for all non-hydrogen atoms. Hydrogen atoms were constrained to ride on the respective carbon or nitrogen atoms with an isotropic displacement parameter equal to 1.2 times the equivalent isotropic displacement parameter of their parent atom. The refinement converged to residual indices R = 0.0352 and 0.0197; wR_2 = 0.0953 and 0.0550 with $I > 2\sigma(I)$ for complexes **1** and **2**, respectively. Complex neutral atomic scattering factors [29] were used throughout. The final difference Fourier map showed the minimum and maximum peak heights of −1.55 and 0.95 e $Å^{-3}$ for complex **1** and −0.45 and 0.53 e $Å^{-3}$ for complex **2**. All calculations were carried out using SHELXS-97 [30], SHELXL-97 [31], PLATON-99 [32] and ORTEP-3 [33] programs. All crystallographic data for complexes **1** and **2** are summarized in Table 1. Selected bond lengths and angles are given in Table 2 and H-bonding parameters in Table 3 for complex **1**. For complex **2** the selected bond lengths and angles are displayed in Table 4.

Table 1
Crystal data and structure refinements for complexes **1** and **2**

	1	**2**
Empirical formula	$C_8H_{12}Cd_2N_6Se_4$	$C_6H_4CdN_4Se_2$
Formula weight	732.90	402.46
Crystal system	Triclinic	monoclinic
T (K)	297	293
Space group	$P\bar{1}$ (No. 2)	$C2/m$ (No. 12)
a (Å)	8.4609(17)	10.9700(10)
b (Å)	10.5221(13)	7.647(2)
c (Å)	11.9200(15)	6.0070(10)
α (°)	107.050(11)	90
β (°)	102.203(15)	95.945(12)
γ (°)	101.848(13)	90
V (Å^3)	950.2(3)	501.2(2)
Z	2	2
D_{calc} (g cm^{-3})	2.562	2.667
λ (Mo Kα) (Å)	0.71069	0.71069
μ (Mo Kα) (mm^{-1})	9.896	9.397
Total data	3329	471
Unique data (R_{int})	3329	471
Observed data [$I > 2\sigma(I)$]	2775	418
R	0.0352	0.0197
wR_2	0.0953	0.0550

Table 2
Selected bond lengths (Å) and angles (°) for complex **1**

Bond lengths			
Cd1–N1	2.374(6)	Cd1–N2	2.355(6)
Cd1–N3	2.258(6)	Cd1–N4	2.376(6)
Cd1–N5	2.336(6)	Cd1–N6	2.334(6)
Cd2–Se1	2.6646(9)	Cd2–Se2	2.6756(10)
Cd2–Se3	2.6110(10)	Cd2–Se4	2.6378(11)
N1–C1	1.136(8)	N2–C2	1.142(8)
N5–C5	1.484(8)		
Bond angles			
N1–Cd1–N2	82.8(2)	N1–Cd1–N3	86.5(2)
N1–Cd1–N4	169.1(2)	N1–Cd1–N5	102.8(2)
N1–Cd1–N6	87.2(2)	N2–Cd1–N3	95.9(2)
N2–Cd1–N4	86.3(2)	N2–Cd1–N5	168.7(2)
N2–Cd1–N6	95.8(2)	N3–Cd1–N4	94.3(2)
N3–Cd1–N5	94.2(2)	N3–Cd1–N6	165.9(2)
N4–Cd1–N5	88.0(2)	N4–Cd1–N6	94.2(2)
N5–Cd1–N6	74.9(2)	Se1–Cd2–Se2	109.63(3)
Se1–Cd2–Se3	103.09(3)	Se1–Cd2–Se4	110.71(3)
Se2–Cd2–Se3	108.31(3)	Se2–Cd2–Se4	108.56(3)
Se3–Cd2–Se4	116.33(3)	Cd2–Se1–C1	93.9(2)
Cd2–Se2–C2	94.4(2)	Cd2–Se3–C3	93.3(2)
Cd2–Se4–C4	99.8(2)	Cd1–N1–C1	152.6(6)
Cd1–N2–C2	148.5(5)	Cd1–N3–C3	169.4(5)

3. Results and discussion

3.1. IR spectra

The complex **1** shows several split strong bands in the range 3270–3356 cm^{-1}, which can be assigned to the ν(NH) stretching frequency of the corresponding diamine ligand. Several bands in the range 2869–2950 cm^{-1} are assigned to the aliphatic ν(CH) stretching vibrations for complex **1**. The free SeCN ligand shows one sharp band corresponding to ν(CN) at 2070 cm^{-1}. The most intense split band is observed assigned to ν(CN) at 2113, 2134 cm^{-1} for complex **1** and only one sharp band at 2133 cm^{-1} for complex **2**. The higher frequency correlates that all the selenocyanato groups in both the complexes are involved in bridging with same environment [34]. All other bands appear at their usual positions.

Table 3
Hydrogen bonds (Å/°) for complex **1**

D–H···A	D–H	H···A	D···A	D–H···A
N5–H5B···Se1$^{(I)}$	0.90	2.9014	3.791(7)	169.78
N6–H6B···N2$^{(II)}$	0.90	2.5706	3.369(8)	148.15

Symmetry code: (I), $-x$, $2-y$, $2-z$; (II), x, $2-y$, $1-z$.

Table 4
Selected bond lengths (Å) and angles (°) for complex **2**

Bond lengths			
Cd–Se	2.7987(9)	Cd–N1	2.429(5)
Cd–N^a	2.296(5)		
Bond angles			
Se–Cd–N1	90.00(1)	Se–Cd–N^a	86.17(11)
Se–Cd–Se^g	180.0	Se–Cd–N^I	93.83(11)
Se–Cd–N1^h	90.00(1)	N^a–Cd–N1	90.00(1)
Se^g–Cd–N1	90.00(1)	N^i–Cd–N1	90.00(1)
N1–Cd–N1^h	180.0	Se^g–Cd–N^a	93.83(11)
N^a–Cd–N^i	180.0	N^a–Cd–N1^h	90.00(1)
Se^g–Cd–N^i	86.17(11)	Se^g–Cd–N1^h	90.00(1)
N^i–Cd–N1^h	90.00(1)	Cd–Se–C	96.23(18)
Cd^e–N–C	169.1(4)	Cd–N1–C1	122.1(2)
Cd–N1–C1^g	122.1(2)	C1–N1–C1^g	115.9(4)

Symmetry code: a = x, y, $-1+z$; e = x, y, $1+z$; g = $1-x$, y, $1-z$; i = $1-x$, y, $2-z$; h = $1-x$, $1-y$, $1-z$.

3.2. Description of structure $[Cd_2(ibn)(SeCN)_4]_n$ (**1**)

An ORTEP drawing with atom numbering scheme of complex **1** is shown in Fig. 1. X-ray structure determination reveals that it is a neutral infinite molecular ladder in which selenocyanate anions function both as support and rung. According to Fig. 1, two adjacent racemic chains are interlinked by selenocyanate anions to form a one-dimensional ladder like chain. Every chain running parallel to b-axis comprises of alternating octahedral and tetrahedral cadmium(II) centres bridging through selenocyanate anions. Tetrahedral and octahedral centres possess the chromophores $CdSe_4$ and CdN_6, respectively. The supports are alternatively singly and doubly bridged evident from the extended structure shown in Fig. 2. Although there was only one observation of alternating tetrahedral and octahedral array in cadmium(II) system [18], it is to be remembered that no

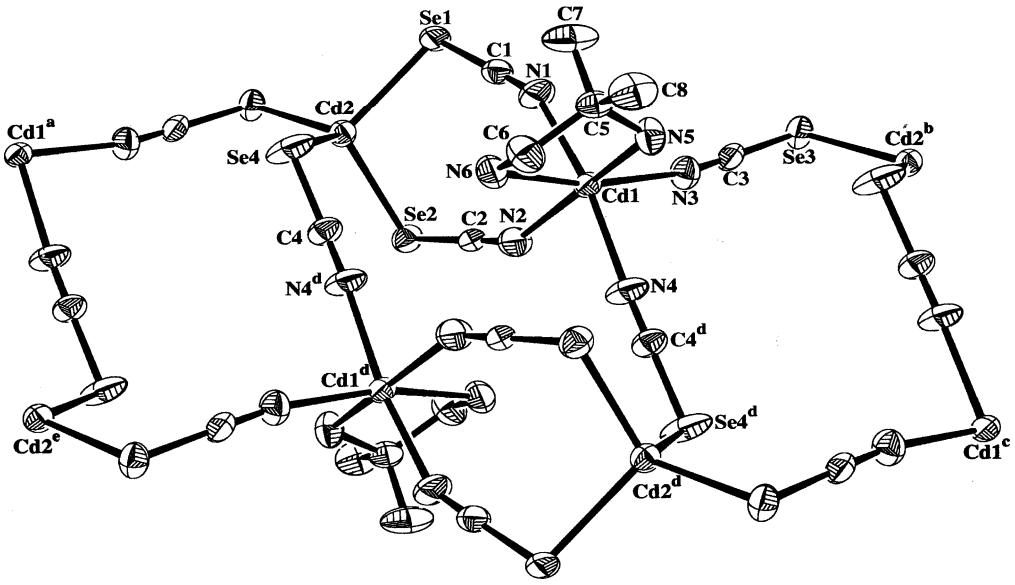


Fig. 1. ORTEP diagram of $[Cd_2(ibn)(SeCN)_4]_n$, **1** with atom numbering scheme. Ellipsoids are drawn at 50% probability. (Symmetry code: a = x, $1+y$, z; b = x, $-1+y$, z; c = $-x$, $2-y$, $1-z$; d = $-x$, $2-y$, $1-z$; e = $-x$, $3-y$, $1+z$.)

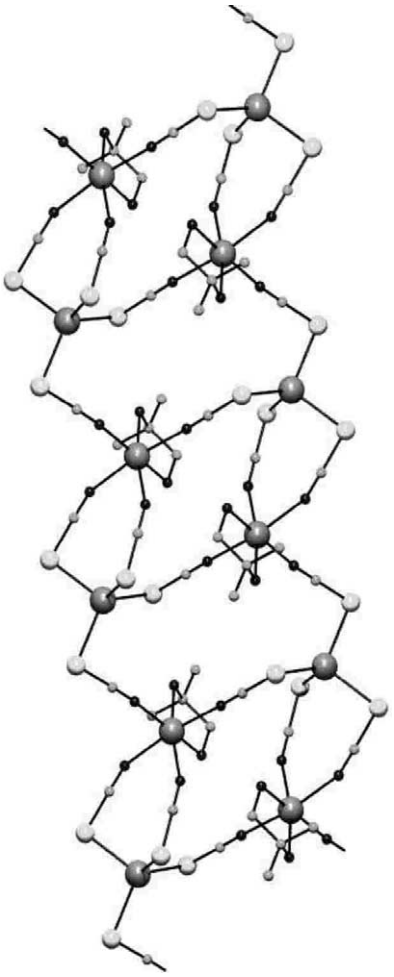


Fig. 2. Extended ladder like view of complex **1** having alternatively octahedral and tetrahedral cadmium(II) centres with singly and doubly bridged SeCN ligand.

analogous ladder structure has yet been reported previously in the cadmium(II)–selenocyanate system.

The Cd1 atom exists in a distorted octahedral environment. The nitrogen atoms, N3 and N6 (Cd1–N3, 2.258(6); Cd1–N6, 2.334(6) Å) of the diamine ligand (ibn) and two nitrogen atoms, N2 and N5, (Cd1–N2, 2.355(6); Cd1–N5, 2.336(6) Å) from two different bridging as well as supporting selenocyanate anions describe the equatorial plane around Cd1 atom. The axial positions are occupied by N4 atom (Cd1–N4, 2.375(6) Å) of the rung selenocyanate anion and N1 atom (Cd1–N1, 2.374(6) Å) of another bridging as well as support selenocyanate anion. The deviation of Cd1 from the mean plane formed by the four equatorial nitrogen atoms is 0.025(1) Å and the maximum deviation of N5 atom from plane among all the equatorial nitrogen atoms is 0.156(7) Å. The Cd2 atom is in distorted tetrahedral environment, being coordinated by four selenocyanato Se donors (Cd2–Se1, 2.6646(9); Cd2–Se2, 2.6756(10); Cd2–Se3, 2.6110(10); Cd2–Se4, 2.6378(11) Å). The degrees of distortion from an ideal octahedral geometry are reflected in the cisoid [74.9(2)°–102.8(2)°] and transoid angles [165.9(2)°–169.1(2)°]. It is interesting to note that only nitrogen atoms surround the octahedral centres (Cd1) whereas only selenium atoms surround the tetrahedral centers (Cd2). The nitrogen atoms of the diamine ligand 'harden' Cd1, so the selenocyanate anions are bonded to it preferentially through N atoms. Conversely the soft ends (Se atoms) of the selenocyanate anions are coordinated to tetrahedral Cd2 making it 'soft'. Thus all the selenium atoms of selenocyanate ligand are clubbed together around Cd2. The bridging Cd1–N–C and Cd2–Se–C are in the range 148.5(5)°–172.7(6)° and 93.3(2)°–99.8(2)°, respec-

tively. The selenocyanate ligands are quasi linear [range 175.8(7)°–178(6)°]. The bond distances and angles are comparable to other similar selenocyanato bridging systems [18,23c]. The linkage forming the rungs of the ladder has a Cd1···Cd2 distance of 6.523 Å and the bridges forming the side of the ladder have Cd1···Cd2 distances of 5.468 Å for double selenocyanate bridge and of 6.035 Å for single selenocyanate bridge. It is worth noting that there are two types of hydrogen bonding due to N6 donor of diamine ligand forming an intra-ladder hydrogen bonds with N2 atom of a selenocyanate (H6B···N2, 2.5706; N6···N2, 3.369(8) Å; <N6–H6B···N2, 148.15°) and due to N5 atom of diamine ligand forming one hydrogen bond with Se1 atom of adjacent ladder (H5B···Se1, 2.9014; N5–Se1, 3.791(7) Å; <N5–H5B···Se1, 169.78°). As shown in Fig. 3, this arrangement results in a supramolecular 2D sheet in *bc*-plane.

3.3. Description of structure $[Cd(pyz)(SeCN)_2]_n$ (2)

Complex **2** is made up of a 2D neutral rectangular-grid layer (Fig. 4). The pyrazine ligand is in μ-mode and forms [Cd(μ-pyrazine)]$_n$ chain running along parallel to *b*-axis. The SeCN anion is also in μ-mode and bridges two Cd atoms in adjacent chains, resulting in a rectangular-grid coordination layer in *bc*-plane. The principal structural features of the present complex with atom labelling scheme are shown in Fig. 4. The structure determination reveals that the cadmium atom, Cd, occupies 2/*m* site [1/2, 1/2, 1/2]. Se, C and N atoms of selenocyanate ligand are located on a mirror plane [*x*, 1/2, *z*] and N1 atom of pyrazine ligand lies on a twofold axis [1/2, *y*, 1/2]. The geometry around Cd atom is a distorted octahedron. The two nitrogens (N^a and N^i, a = *x*, *y*, −1+*z*; i = 1−*x*, *y*, 2−*z*) of the selenocyanate anion are in the equatorial plane [Cd–N^a/N^i 2.296(5) Å] together with two nitrogens (N1 and $N1^h$, h = 1−*x*, 1−*y*, 1−*z*) of pyrazine ligand [Cd–N1/$N1^h$

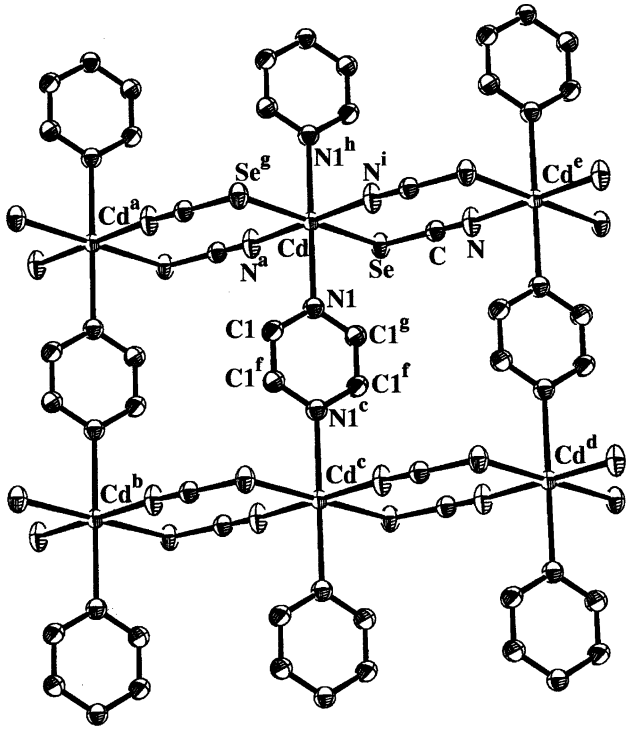


Fig. 4. ORTEP diagram of $[Cd(pyz)(SeCN)_2]_n$, **2** with atom numbering scheme showing the rectangular grid like structure. Ellipsoids are drawn at 50% probability. (Symmetry code: a = *x*, *y*, −1+*z*; b = *x*, −*y*, −1+*z*; c = *x*, −*y*, *z*; d = *x*, −*y*, 1+*z*; e = *x*, *y*, 1+*z*; f = 1−*x*, −*y*, 1−*z*; g = 1−*x*, *y*, 1−*z*.)

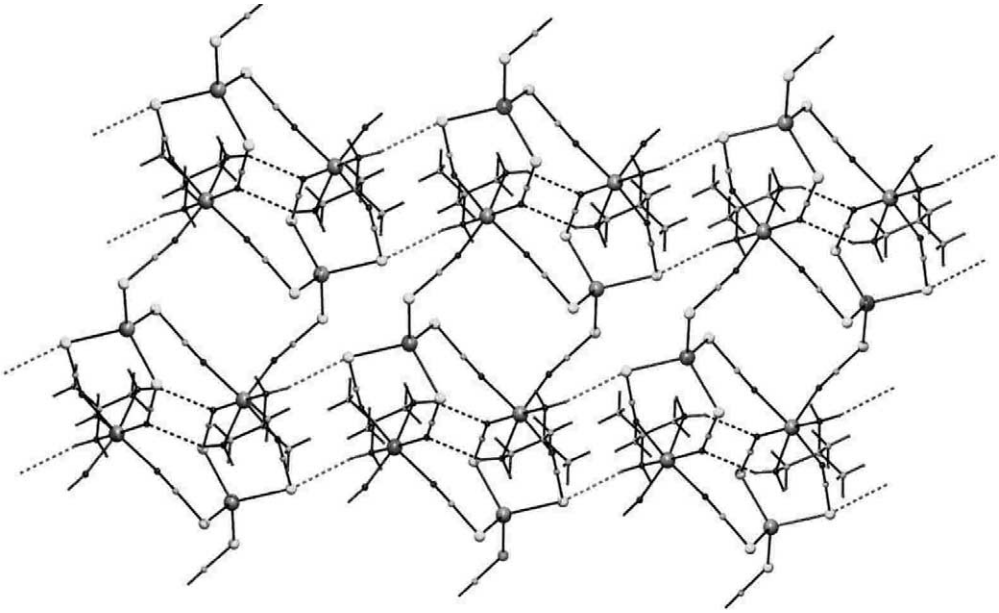


Fig. 3. 2D supramolecular sheet of complex **1** lying on the *bc*-plane.

2.429(5) Å]. The Se atoms (Se and Se^{g}, g = 1 − *x*, *y*, 1 − *z*) of selenocyanate anion occupy *trans*-axial sites [Cd–Se/Se^{g} 2.7987(9) Å]. The axial distance is larger than the Cd–Se distances of complex **1**. The cisoid angles are in the range 86.11(11)°–93.83(11)° and the transoid angles are 180°. The equatorial plane is essentially planar with Cd atom. The bridging Cd–Se–C angles [96.23(18)°] and Cd–N–C (SeCN) [169.1(4)°] are comparable with those found in other similar complexes [18,23c]. The pyrazine moieties of alternate layers are found to shift towards the SeCN moieties (Fig. 5). The Cd···Cd distance of pyrazine linkage is 7.647 Å and that of SeCN linkage is 6.007 Å. The distance between the two adjacent layers is 5.485 Å.

4. Conclusions

Two new coordination polymers of selenocynato-bridged cadmium(II) complexes are synthesized in combination of two organic (ibn and pyz) ligands. Single crystal X-ray diffractions are carried out to determine the structures of complexes. In complex **1**, reaction of cadmium selenocyanate with ibn results in two 1D parallel chains of cadmium(II), each having alternate tetrahedral ($CdSe_4$) and octahedral (CdN_6) centres bridged through selenocyanate exhibiting symbiotic phenomena, whereas in complex **2**, reaction of cadmium selenocyanate with pyrazine generates a 2D network in which doubly selenocyanato bridged 1D coordination polymeric chains are linked through the pyrazine ligand forming rectangular grid in *bc* plane. In our recent work [18], $[Cd(medien)(SeCN)_2]_n$ **1a** is 1D polymeric chain with CdN_4Se_2 octahedra and $[Cd(iprdien)(SeCN)_2]_n$ **1b** is 2D network with alternating CdN_6 octahedra and $CdSe_4$ tetrahedra. In the synthesis of the compounds **1**, **1a** of **1b** we have taken three different amines keeping other reagents and synthetic procedure the same. The complex **1a** showed usual structural features that each cadmium atom was coordinated by both N and Se atoms, but the generation of two types of Cd environments in complexes **1** and **1b** are rather unique. The 'ibn' (contains two methyl group at one C atom) and 'iprdien' (contains one isopropyl group at one end of primary N-atom) are asymmetric ligands in comparison to 'medien' (contains one methyl group at central N-atom) and exert greater steric forces which may be the responsible for the formation of the alternating octahedral (CdN_6) and tetrahedral ($CdSe_4$) centres as tetrahedral geometry occupies less space than the octahedral geometry. On the other hand, tetrahedral cadmium centres have sp^3 hybridization and the octahedral centres have sp^3d^2 hybridization leading to tetrahedral centre more electronegative than the octahedral centre. Thus, according to the Jørgenson symbiotic theory, [25] the hard species will tend to increase the hardness of the atom to which they are bound and thus increase its tendency to attract more hard species, i.e. 'ibn' and 'iprdien' ligands increase the hardness of octahedral cadmium(II) which preferably bind the N-atoms of the ambidentate SeCN ligand. And in case of thiocyanate ligand we reported the symbiotic phenomena between two octahedral cadmium centres (CdN_6 and CdS_6) [17]. The occurrence of such phenomenon in between octahedral and tetrahedral cadmium(II) centres in title complex **1** is probably due to the large size of Se (more soft) in comparison to small size S atom (less soft). For complex **2** the molar ratio of metal–selenocyanate–pyz (1:1:1) is very much important and the use 'organic-rod' pyrazine enhances the formation of grid-like structure. The above facts indicate the utility and reliability of the selenocyanate moiety as spacer in forming coordination polymer and also reveal that the variation of organic spacer profoundly influences the packing of the polymeric complexes.

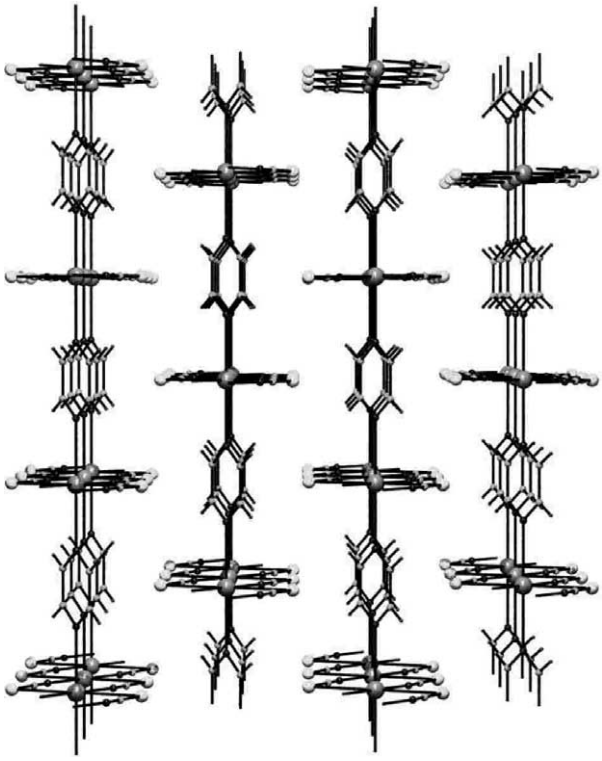


Fig. 5. Packing diagram of complex **2** showing the layers along the *z*-axis.

5. Supplementary data

Crystallographic data for the structural analysis have been deposited with the Cambridge Crystallographic Data Centre, CCDC Nos. 177056 and 177057 for complexes **1** and **2**. Copies of this information can be obtained free of charge from The Director, CCDC, 12

Union Road, Cambridge, CB2 1EZ, UK (fax: +44-1223-336033; e-mail: deposit@ccdc.cam.ac.uk or www: http://www.ccdc.cam.ac.uk).

Acknowledgements

We thank National Science Council, ROC (grant no. NSC 90-2112-M-007-063 and NSC 90-2811-M-007-007) (T.H.L and G.M.) and Council of Scientific and Industrial Research, New Delhi (N.R.C.) for financial support.

References

[1] J.M. Lehn, Supramolecular Chemistry, VCH, Weinheim, 1995.
[2] P.J. Hagrman, D. Hagraman, J. Zubieta, Angew. Chem., Int. Ed. Engl. 38 (1999) 2638.
[3] T.K. Maji, G. Mostafa, S. Sain, J. Shashidhara Prasad, N. Ray Chaudhuri, Cryst. Eng. Comm. (2001) 37.
[4] A.K. Powell, P.T. Wood, J. Chem. Soc., Dalton Trans. (2000) 3566.
[5] S.L. Zheng, M.L. Tong, X.L Yu, X.M. Chen, J. Chem. Soc., Dalton Trans. (2001) 586.
[6] K. Biradha, M. Fujita, Chem. Commun. (2001) 15.
[7] L.R. Macgillivary, R.H. Groeneman, J.L. Atwood, J. Am. Chem. Soc. 120 (1998) 2676.
[8] L. Carlucci, G. Ciani, D.M. Proserpio, J. Chem. Soc., Dalton Trans. (1999) 1799.
[9] A.J. Blake, S.J. Hill, P. Hubberstey, W.S. Li, J. Chem. Soc., Dalton Trans. (1997) 913.
[10] M.L. Tong, X.M. Chen, X.L Yu, T.C.W. Mak, J. Chem. Soc., Dalton Trans. (1998) 5.
[11] X. Hao, Y. Wei, S. Zhang, Chem. Commun. (2000) 2274.
[12] J.L. Manson, A.M. Arif, J.S. Miller, Chem. Commun. (1999) 1479.
[13] R.D. Bailey, W.T. Pennington, Polyhedron 16 (1997) 417.
[14] M.X. Li, G.Y. Xie, Y.D. Gu, J. Chen, P.J. Zheng, Polyhedron 14 (1995) 1235.
[15] G. Mostafa, A. Mondal, I.R. Laskar, A.J. Welch, N. Ray Chaudhuri, Acta Crystallogr., Sect. C 56 (2000) 146.
[16] A. Mondal, G. Mostafa, A. Ghosh, N. Ray Chaudhuri, J. Chem. Res. (S) (1998) 570.
[17] A. Mondal, G. Mostafa, A. Ghosh, I.R. Laskar, N. Ray Chaudhuri, J. Chem. Soc., Dalton Trans. (1999) 9.
[18] T.K. Maji, S. Sain, G. Mostafa, D. Das, T.H. Lu, N. Ray Chaudhuri, J. Chem. Soc., Dalton Trans. (2001) 3149.
[19] H. Zhang, X. Wang, K. Zhang, B.K. Teo, Coord. Chem. Rev. 183 (1999) 157 (and references therein).
[20] H. Zhang, D.E. Zelmon, G.E. Price, B.K. Teo, Inorg. Chem. 39 (2000) 1868.
[21] (a) V. Vrabel, J. Garaj, L. Kutschabsky, Acta Crystallogr., Sect. B 35 (1979) 357;
(b) K. Brodersen, M. Cygan, H.-U. Hummel, Z. Naturforsch., Teil B 39 (1984) 582;
(c) V. Vrabel, J. Garaj, Acta Crystallogr., Sect. A 34 (1978) S131.
[22] L.J. Farrugia, C.J. Carmalt, N.C. Norman, Inorg. Chim. Acta 248 (1996) 263.
[23] (a) U. Turpeinen, Finn. Chem. Lett. (1977) 75;
(b) A. Crispini, R.J. Errington, G.A. Fisher, F.J. Funke, N.C. Norman, A.G. Orpen, S.E. Stratford, O. Struve, J. Chem. Soc., Dalton Trans. (1994) 1327;
(c) R. Vicente, A. Escuer, J. Ribas, X. Solans, M. Font-Bardia, Inorg. Chem. 32 (1993) 6117.
[24] (a) R.P. Shibaeva, L.P. Rozenberg, N.D. Kushch, E.B. Yagubskii, Kristallografiya 39 (1994) 825;
(b) M. Rowley, J.W. Steed, D.A. Tocher, Polyhedron 14 (1995) 1415;
(c) P.M. Secondo, J.M. Land, R.G. Baughman, H.L. Collier, Inorg. Chim. Acta 309 (2000) 13.
[25] C.K. Jørgenson, Inorg. Chem. 3 (1964) 1201.
[26] A.I. Vogel, Textbook of Quantitative Inorganic Analysis., 4th ed., E.L.B.S and Longman, London, 1978. p. 393.
[27] A.C.T. North, D.C. Philips, F.S. Mathews, Acta Crystallogr., Sect. A 24 (1968) 351.
[28] G.M. Sheldrick, SAINT, 1995, Ver5, Siemens Analytical X-ray Instrument Inc. Madison WI, USA.
[29] International Tables for Crystallography, Kluwer Academic Publishers, Boston, MA.
[30] G.M. Sheldrick, SHELXS-97, Program for the Solution of Crystal Structure, University of Göttingen, Germany, 1997.
[31] G.M. Sheldrick, SHELXL-97, Program for the Solution of Crystal Structure, University of Göttingen, Germany, 1997.
[32] A.L. Spek, PLATON, Molecular Geometry Program, University of Utrecht, The Netherlands, 1999.
[33] L.J. Farrugia, ORTEP-3 for Windows Version 1.07, J. Appl. Crystallogr. 30 (1997) 565.
[34] K. Nakamoto, Infrared and Raman Spectra of Inorganic and Coordination Compounds, Wiley-Interscience, New York, 3rd edn., 1978, pp. 227 and 275.

2. Experimental

2.1. General procedures

All the reagents used in this research were purchased from commercial sources and used as they were required. The starting materials used in this research namely, $[MI_2(CO)_3\{MeC(CH_2PPh_2)_3\text{-}P,P'\}]$ (M = Mo or W) [30], $[MoX(CO)_2(NCMe)_2(\eta^3\text{-}C_3H_4R)]$ (X = Cl, R = H or Me; X = Br, R = H) [31] and $[FeI(CO)_2(Cp \text{ or } Cp')]$ (Cp = C_5H_5; Cp′ = C_5H_5Me) [32] were prepared by published procedures.

Elemental analyses (C, H and N) were determined using a Carlo Erba Elemental Analyser MOD 1108 (using helium as the carrier gas). IR spectra were obtained using a Perkin–Elmer 1600 series FT IR spectrophotometer. ^1H and $^{31}P\{^1H\}$ spectra were recorded on a Bruker AC250 MHz NMR spectrometer; ^1H NMR spectra were referenced to $SiMe_4$, $^{31}P\{^1H\}$ NMR spectra were referenced to 85% H_3PO_4. Molecular weight measurements were made using Rast's method [33], using camphor as the standard.

2.2. $[\{Mo(\mu\text{-}Cl)(CO)_2(L^{Mo})(\eta^3\text{-}C_3H_5)\}_2]$ (1)

To a stirred solution of $[MoCl(CO)_2(NCMe)_2(\eta^3\text{-}C_3H_5)]$ (0.08 g, 0.32 mmol) in CH_2Cl_2 (25 cm^3) was added $[MoI_2(CO)_3\{MeC(CH_2PPh_2)_3\text{-}P,P'\}](L^{Mo})$ (0.3 g, 0.26 mmol). Filtration and removal of solvent in vacuo after 24 h, gave the green crystalline powder $[\{Mo(\mu\text{-}Cl)(CO)_2(L^{Mo})(\eta^3\text{-}C_3H_5)\}_2]$ (**1**), which was recrystallized from CH_2Cl_2–Et_2O at −17 °C. Yield of pure product = 0.22 g (54%).

Similar reactions of $[MoX(CO)_2(NCMe)_2(\eta^3\text{-}C_3H_4R)]$ (X = Cl and Br) with 1 equiv. of L^{Mo} or L^W {L^{Mo} or $L^W = [MI_2(CO)_3\{MeC(CH_2PPh_2)_3\text{-}P,P'\}]$ in CH_2Cl_2 at room temperature (r.t.) gave the complexes $[\{Mo(\mu\text{-}X)(CO)_2(L^{Mo} \text{ or } L^W)(\eta^3\text{-}C_3H_4R)\}_2]$ {X = Cl, R = H, L^W (**2**); R = Me, L^{Mo} (**3**); L^W (**4**)}; {X = Br, R = H, L^{Mo} (**5**), L^W (**6**)}. For physical and analytical data see Table 1.

2.3. $[MoCl(CO)_2(L^{Mo})_2(\eta^3\text{-}C_3H_5)]$ (7)

To a stirred solution of $[MoCl(CO)_2(NCMe)_2(\eta^3\text{-}C_3H_5)]$ (0.05 g, 0.16 mmol) in CH_2Cl_2 (25 cm^3) was added $[MoI_2(CO)_3\{MeC(CH_2PPh_2)_3\text{-}P,P'\}]$ (0.34 g, 0.32 mmol). Filtration and removal of solvent in vacuo after 24 h, gave the green crystalline powder $[MoCl(CO)_2(L^{Mo})_2(\eta^3\text{-}C_3H_5)]$ (**7**), which was recrystallized from CH_2Cl_2–Et_2O at −17 °C. Yield of pure product = 0.24 g (64%).

Similar reactions of $[MoX(CO)_2(NCMe)_2(\eta^3\text{-}C_3H_4R)]$ (X = Cl and Br) with 2 equiv. of L^{Mo} or L^W {L^{Mo} or $L^W = [MI_2(CO)_3\{MeC(CH_2PPh_2)_3\text{-}P,P'\}]$} in CH_2Cl_2 at r.t. gave the complexes, $[MoX(CO)_2$ (L^{Mo} or $L^W)_2(\eta^3\text{-}C_3H_4R)]$ {X = Cl, R = H, L^W (**8**); R = Me, L^{Mo} (**9**); L^W (**10**)}; {X = Br, R = H, L^{Mo} (**11**), L^W (**12**)}. For physical and analytical data see Table 1.

Table 1
Physical [a] and analytical data [b] for the multimetallic complexes **1**–**19**

1	$[\{Mo(\mu\text{-}Cl)(CO)_2(L^{Mo})(\eta^3\text{-}C_3H_5)\}_2]\cdot CH_2Cl_2$	54	43.5 (43.8)	3.6 (3.4)
2	$[\{Mo(\mu\text{-}Cl)(CO)_2(L^W)(\eta^3\text{-}C_3H_5)\}_2]$	54	42.8 (42.8)	3.6 (3.2)
3	$[\{Mo(\mu\text{-}Cl)(CO)_2(L^{Mo})(\eta^3\text{-}C_3H_4Me\text{-}2)\}_2]$	28	46.5 (46.2)	3.8 (3.6)
4	$[\{Mo(\mu\text{-}Cl)(CO)_2(L^W)(\eta^3\text{-}C_3H_4CH_3\text{-}2)\}_2]$	21	43.1 (43.2)	3.6 (3.3)
5	$[\{Mo(\mu\text{-}Br)(CO)_2(L^{Mo})(\eta^3\text{-}C_3H_5)\}_2]$	22	44.3 (44.2)	3.7 (3.3)
6	$[\{Mo(\mu\text{-}Br)(CO)_2(L^W)(\eta^3\text{-}C_3H_5)\}_2]$	50	41.8 (41.5)	3.5 (3.1)
7	$[MoCl(CO)_2(L^{Mo})_2(\eta^3\text{-}C_3H_5)]$	64	47.2 (47.6)	4.2 (3.6)
8	$[MoCl(CO)_2(L^W)_2(\eta^3\text{-}C_3H_5)]$	49	44.2 (44.3)	3.6 (3.3)
9	$[MoCl(CO)_2(L^{Mo})_2(\eta^3\text{-}C_3H_4Me\text{-}2)]$	75	48.5 (47.9)	4.1 (3.6)
10	$[MoCl(CO)_2(L^W)_2(\eta^3\text{-}C_3H_4Me\text{-}2)]$	39	44.7 (44.5)	3.6 (3.4)
11	$[MoBr(CO)_2(L^{Mo})_2(\eta^3\text{-}C_3H_5)]\cdot Et_2O$	48	47.8 (47.3)	3.9 (3.8)
13	$[Fe(CO)_4(L^{Mo})]\cdot CH_2Cl_2$	45	45.8 (44.9)	4.5 (3.2)
14	$[Fe(CO)_4(L^W)]$	48	47.3 (46.7)	3.7 (4.1)
15	$[Fe(CO)_2(L^{Mo})Cp]I$	32	45.4 (45.0)	3.8 (3.3)
16	$[Fe(CO)_2(L^W)Cp]I$	55	42.4 (42.2)	3.3 (3.1)
17	$[Fe(CO)_2(L^{Mo})Cp']I$	37	44.7 (45.3)	3.5 (3.4)
18	$[Fe(CO)_2(L^W)Cp']I$	30	42.3 (42.6)	3.3 (3.2)
19	$[Fe(CO)_2(L^W)Cp][BPh_4]$	35	54.3 (54.8)	5.7 (3.9)

[a] All complexes **1** to **19** are green.
[b] Calculated values in parenthesis.

2.4. $[Fe(CO)_4(L^{Mo})]$ (13)

To a stirred solution of $[Fe_2(CO)_9]$ (0.05 g, 0.13 mmol) in CH_2Cl_2 (25 cm^3) was added $[MoI_2(CO)_3\{MeC(CH_2PPh_2)_3\text{-}P,P'\}]$ (0.3 g, 0.28 mmol). Filtration and removal of solvent in vacuo after 24 h, gave the green powder $[Fe(CO)_4(L^{Mo})]$ (**13**), which was recrystallized from CH_2Cl_2–Et_2O at −17°C. Yield of pure product = 0.08 g (45%).

A similar reaction of $[Fe_2(CO)_9]$ with 2 equiv. of L^W in CH_2Cl_2 at r.t. gave the complex, $[Fe(CO)_4(L^W)]$ (**14**). For physical and analytical data see Table 1.

2.5. $[Fe(CO)_2(L^{Mo})(Cp]I$ (15)

To a stirred solution of $[FeI(CO)_2(\eta^5\text{-}C_5H_5)]$ (0.05 g, 0.16 mmol) in warm CH_2Cl_2 (25 cm^3) was added $[MoI_2(CO)_3\{MeC(CH_2PPh_2)_3\text{-}P,P'\}]$ (0.17 g, 0.16 mmol). Filtration and removal of solvent in vacuo after 2 h gave $[Fe(CO)_2(L^{Mo})(\eta^5\text{-}C_5H_5)]I$ (**15**), which was recrystallized from CH_2Cl_2–Et_2O. Yield of pure product = 0.07 g (32%).

A similar reaction of $[FeI(CO)_2(\eta^5\text{-}C_5H_4R)]$ (R = H or Me) with 1 equiv. of L {L = $[MI_2(CO)_3\{MeC(CH_2PPh_2)_3\text{-}P,P'\}]$ (M = Mo or W)} in warm CH_2Cl_2 at r.t. gave the complexes $[Fe(CO)_2(L^{Mo} \text{ or } L^W)(\eta^5\text{-}C_5H_4R)]I$, {R = H, L^W (**16**); R = Me, L^{Mo} (**17**), L^W (**18**)}. For physical and analytical data see Table 1.

2.6. [Fe(CO)$_2$(L^W)(η^5-C$_5$H$_5$)][BPh$_4$] (19)

To a stirred solution of [Fe(CO)$_2$(L^W)(η^5-C$_5$H$_5$)]I (0.05 g, 0.43 mmol) in CH_2Cl_2 (25 cm^3) was added Na[BPh$_4$] (0.012 g, 0.42 mmol). Filtration and removal of solvent in vacuo after 24 h, gave the green complex, [Fe(CO)$_2$(L^W)(η^5-C$_5$H$_5$)][BPh$_4$] (**19**), which was recrystallized from CH_2Cl_2–Et_2O at −17 °C. Yield of pure product = 0.02 g (35%).

3. Results and discussion

3.1. Preparation and characterization of the tetrametallic complexes [{Mo(μ-X)(CO)$_2$(L^{Mo} or L^W)(η^3-C$_3$H$_4$R)}$_2$] (1–6)

The starting materials used in this research, [MI$_2$(CO)$_3${MeC(CH$_2$PPh$_2$)$_3$-*P*,*P*′}] (M = Mo or W) were prepared by reacting the bis(acetonitrile) complexes [MI$_2$(CO)$_3$(NCMe)$_2$] [24], with 1 equiv. of tripodal triphos, MeC(CH$_2$PPh$_2$)$_3$, in CH_2Cl_2 for 15 min at room temperature [30]. Equimolar amounts of [MoX(CO)$_2$(NCMe)$_2$(η^3-C$_3$H$_4$R)] (X = Cl, R = H or Me; X = Br, R = H) and [MI$_2$(CO)$_3${MeC(CH$_2$PPh$_2$)$_3$-*P*,*P*′}] (M = Mo, L^{Mo}; M = W, L^W) react in CH_2Cl_2 at room temperature to eventually give the halo-bridged and tripodal triphos-bridged tetrametallic complexes, [{Mo(μ-X)(CO)$_2$(L^{Mo} or L^W)(η^3-C$_3$H$_4$R)}$_2$] (**1**–**6**) in moderate yield, via displacement of both of the acetonitrile ligands. All the complexes **1**–**6** were characterised by elemental analysis (C, H and N) (Table 1), IR (Table 2), ^{1}H and ^{31}P{^{1}H} NMR spectroscopy (Tables 3 and 4). Molecular weight measurements of selected complexes were determined using Rast's method [33]. These measurements confirmed the tetrametallic nature of these complexes. Complex **1** (X = Cl, R = H, L^{Mo}) was confirmed as a CH_2Cl_2 solvate by repeated elemental analyses and ^{1}H NMR spectroscopy. The new complexes **1**–**6** are moderately stable in the solid-state when stored under dinitrogen, but they all readily decompose in solution when exposed to air. Complexes **1**–**6** are soluble in $CHCl_3$ and CH_2Cl_2, but only slightly soluble in diethyl ether.

The IR spectra of complexes **1**–**6** (Table 2) as expected all show a number of carbonyl bands due to both the [MI$_2$(CO)$_3${MeC(CH$_2$PPh$_2$)$_3$-*P*,*P*′}] unit, and the π-allyl molybdenum fragment. For example, complex **1** showed bands at 2015, 1941, 1933 and 1842 cm^{-1}. It is highly likely that the bands at 1933 and 1842 cm^{-1} are due to the *cis*-carbonyl groups on the π-allyl molybdenum part of the molecule. {The complex, [MoCl(CO)$_2$(NCMe)$_2$(η^3-C$_3$H$_5$)] has carbonyl bands at ν(CO)($CHCl_3$) = 1955 and 1848 cm^{-1} [31].} The broad band at 1933 cm^{-1}, together with the bands at 2015 and 1941 cm^{-1} are very likely to be due to the [MoI$_2$(CO)$_3${MeC(CH$_2$PPh$_2$)$_3$-*P*,*P*′}] part of the molecule. The complex [MoI$_2$(CO)$_3${MeC(CH$_2$PPh$_2$)$_3$-*P*,*P*′}] [30], has ν(CO)($CHCl_3$) = 2041, 1938 and 1917 cm^{-1}. The molecular structures of several π-allyl complexes of the type [MoX(CO)$_2$L$_2$(η^3-allyl)] (L$_2$ = nitrogen donor ligands) have been crystallographically determined [34–43], and all show a *cis*-carbonyl geometry in an equivalent plane with the nitrogen donor ligands. The axial sites have the halide and π-allyl groups. However, the only monodentate bis(phosphorus) donor ligand π-allyl complex of this type to be crystallographically characterised is [MoCl(CO)$_2${P(OMe)$_3$}$_2$(η^3-C$_3$H$_5$)] [44]. This complex has a distorted pentagonal bipyramidal geometry, with a carbonyl ligand and a chloride group in axial positions, and the π-allyl group occupying two adjacent sites. In view of the IR carbonyl pattern for the complexes **1**–**6**, it is likely the *pseudo*-octahedral geometry will be described for the mono(phosphine) complexes **1**–**6**, rather than the pentagonal bipyramidal geometry shown for [MoCl(CO)$_2${P(OMe)$_3$}$_2$(η^3-C$_3$H$_5$)] [44]. The two halides of the halo-bridged dimers are identical, as only two *cis*-carbonyl groups were observed.

The ^{31}P{^{1}H} NMR spectra (Table 4) show resonances for the 2 equiv. phosphorus atoms attached to the molybdenum and tungsten centres in the units, [MI$_2$(CO)$_3${MeC(CH$_2$PPh$_2$)$_3$-*P*,*P*′}]. Tungsten satellites were not observed, due to the poor solubility of the complexes in a range of NMR solvents. For example, the ^{31}P{^{1}H} NMR spectrum of **2** has a resonance at δ = −17.7 ppm (due to the fluxional seven-coordinate L^W fragment), and δ = 27.3 ppm due to the phosphorus

Table 2
Infrared data [a] for the multimetallic complexes **1**–**19**

Complex	ν(C≡O) (cm^{-1})
1	2015(s), 1941(s), 1933(br,s), 1842(m)
2	2031(s), 1956(br,s), 1938(s), 1901(m)
3	2040(s), 1981(s), 1938(br,s), 1846(m)
4	2036(s), 1957(br,s), 1935(s), 1904(s), 1844(m)
5	2021(s), 1948(s), 1939(br,s), 1849(m)
6	2039(s), 1961(br,s), 1945(s), 1906(m)
7	2041(s), 1959(s), 1939(br,s), 1846(m)
8	2038(s), 1960(br,s), 1932(s), 1905(m)
9	2044(s), 1974(s), 1938(br,s), 1841(m)
10	2033(s), 1957(br,s), 1933(s), 1903(m), 1840(m)
11	2037(s), 1968(s), 1931(br,s), 1839(m)
12	2034(s), 1957(br,s), 1904(s), 1843(m)
13	2044(s), 2019(s), 1976(br,s), 1928(s), 1939(m)
14	2030(s), 1955(s), 1928(br,s), 1912(m), 1901(m)
15	2043(s), 2019(s), 1998(s), 1938(br,s), 1906(m)
16	2038(s), 1996(s), 1958(br,s), 1903(m)
17	2039(s), 1993(s), 1940(br,s), 1918(s), 1909(m)
18	2038(s), 1994(s), 1960(br,s), 1906(m)
19	2038(s), 2000(s), 1958(br,s), 1908(m)

[a] Spectra recorded in $CHCl_3$ as thin films between NaCl plates. s, strong; m, medium.

Table 3
^{1}H NMR data [a] (δ) for the multimetallic complexes **1**–**19**

Complex	^{1}H NMR data (δ/ppm)
1	8.4–7.5 (m, 60H, Ph); 5.3 (s, 2H, CH_2Cl_2); 3.6 (m, 2H, CH of allyl); 2.2 (m, 8H, CH of allyl); 1.9 (m, 12H, CH_2 of triphos); 1.3 (s, 6H, CH_3, triphos)
2	8.0–7.2 (m, 60H, Ph); 3.6 (m, 2H, CH of allyl); 2.5–2.2 (m, 8H, CH_2 of allyl); 1.8–1.5 (m, 12H, CH_2 of triphos); 1.3 (s, 6H, CH_3 of triphos)
3	7.9–7.0 (m, 60H, Ph); 3.1 (m, 2H, CH, allyl); 2.4–2.2 (m, 6H, CH_2, allyl); 1.5 (s, 6H, CH_3, allyl); 1.4 (br,s, 12H, CH_2, triphos); 1.1 (s, 6H, CH_3, triphos)
4	7.8–7.1 (m, 60H, Ph); 3.7–3.4 (m, 2H, CH_2, allyl); 2.5–2.1 (m, 6H, CH_2, allyl); 1.6 (s, 6H, CH_3, allyl); 1.7–1.4 (m, 12H, CH_2, triphos); 1.2 (s, 6H, CH_3, triphos)
5	7.8–7.1 (m, 60H, Ph); 3.7–3.5 (m, 2H, CH, allyl); 2.5–2.2 (m, 8H, CH_2, allyl); 1.8–1.4 (m, 12H, CH_2, triphos); 1.3 (s, 6H, CH_3, triphos)
6	7.8–7.2 (m, 60H, Ph); 3.8–3.6 (m, 2H, CH, allyl); 2.4–2.2 (m, 8H, CH_2, allyl); 1.9–1.4 (m, 12H, CH_2, triphos); 1.3 (s, 6H, CH_3, triphos)
7	7.8–7.0 (m, 60H, Ph); 3.65 (m, 1H, CH, allyl); 2.3 (dd, 4H, CH_2, allyl); 2.0 (s, 12H, CH_2, triphos); 1.3 (s, 6H, CH_3, triphos)
8	8.1–7.1 (m, 60H, Ph); 3.5 (m, 1H, CH, allyl); 2.5–2.2 (m, 4H, CH_2, allyl); 1.8–1.5 (m, 12H, CH_2, triphos); 1.3 (s, 6H, CH_3, triphos)
9	7.9–7.0 (m, 60H, Ph); 3.2 (m, 1H, CH, allyl); 2.6–2.2 (m, 3H, CH_2, allyl); 1.5 (s, 3H, CH_3, allyl); 1.3 (s, 12H, CH_2, triphos); 0.9 (s, 6H, CH_3, triphos)
10	7.9–7.0 (m, 60H, Ph); 3.7 (br,s, 1H, CH, allyl); 2.5–2.1 (m, 3H, CH_2, allyl); 1.6 (m, 3H, CH_3, allyl); 1.3 (br,s, 12H, CH_2, triphos); 0.9 (s, 6H, CH_3, triphos)
11	7.8–7.0 (m, 60H, Ph); 3.6 (br,s, 1H, CH, allyl); 3.5 (q, 4H, CH_2, diethyl ether); 2.5 (t, 6H, CH_3, diethyl ether); 2.3–2.1 (m, 15H, CH_2, allyl, CH_2 triphos); 1.6 (m, 3H, CH_3, allyl); 0.9 (s, 6H, CH_3, triphos)
12	7.9–7.1 (m, 60H, Ph); 3.8–3.6 (m, 1H, CH, allyl); 2.6–2.2 (br.m, 15H, CH_2, allyl, CH_2, triphos); 1.3 (s, 6H, CH_3, triphos)
13	7.8–7.0 (m, 30H, Ph); 5.3 (s, 2H, CH_2Cl_2); 2.3 (br,s, 6H, CH_2, triphos); 0.9 (s, 3H, CH_3, triphos)
14	7.7–6.8 (m, 30H, Ph); 2.4 (br,s, 6H, CH_2, triphos); 0.9 (s, 3H, CH_3, triphos)
15	7.7–7.0 (m, 30H, Ph); 5.1 (s, 5H, Cp); 2.3 (s, 6H, CH_2, triphos); 0.9 (s, 3H, CH_3, triphos)
16	7.7–7.2 (m, 30H, Ph); 5.1 (s, 5H, Cp); 2.7 (br,s, 6H, CH_2, triphos); 1.3 (s, 3H, CH_3, triphos)
17	7.7–7.0 (m, 30H, Ph); 4.9 (d, 4H, Cp); 2.4 (br,s, 6H, CH_2, triphos); 2.2 (s, 3H, *Me*Cp); 0.9 (s, 3H, CH_3, triphos)
18	7.8–7.0 (m, 30H Ph); 4.9 (d, 4H, Cp); 2.5 (br,s, 6H, CH_2, triphos); 2.2 (s, 3H, *Me*Cp); 0.9 (s, 3H, CH_3, triphos)
19	7.9–7.1 (m, 50H, Ph); 5.1 (m, 5H, Cp); 2.3 (s, 6H, CH_2, triphos); 0.9 (s, 3H, CH_3, triphos)

[a] Spectra recorded in $CDCl_3$ (+25 °C) and referenced to $SiMe_4$. s, singlet; br, broad; d, doublet; m, multiplet; t, triplet.

Table 4
$^{31}P\{^{1}H\}$ NMR data [a] (δ) for the multimetallic complexes **1**–**18**

Complex	^{31}P data (δ/ppm)
1	17.6 (s, 4P, L^{Mo}); 31.8 (s, 2P, Ph_2P–Mo)
2	−17.7 (s, 4P, L^{W}); 27.3 (s, 2P, Ph_2P–Mo)
3	17.6 (s, 4P, L^{Mo}); 29.0 (s, 2P, Ph_2P–Mo)
4	−12.2 (s, 4P, L^{W}); 32.0 (s, 2P, Ph_2P–Mo)
5	17.6 (s, 4P, L^{Mo}); 34.6 (s, 2P, Ph_2P–Mo)
6	−11.8 (s, 4P, L^{W}); 25.0 (s, 2P, Ph_2P–Mo)
7	17.6 (s, 4P, L^{Mo}); 32.9 (s, 2P, Ph_2P–Mo)
8	−12.8 (s, 4P, L^{W}); 25.3 (s, 2P, Ph_2P–Mo)
9	17.6 (s, 4P, L^{Mo}); 29.5 (s, 2P, Ph_2P–Mo)
10	−14.4 (s, 4P, L^{W}); 25.1 (s, 2P, Ph_2P–Mo)
11	17.6 (s, 4P, L^{Mo}); 27.5 (s, 2P, Ph_2P–Mo)
12	−14.2 (s, 4P, L^{W}); 25.1 (s, 2P, Ph_2P–Mo)
13	17.6 (s, 2P, L^{Mo}); 27.9 (s, 1P, Ph_2P–Fe)
14	−16.4 (s, 2P, L^{W}); 39.3 (s, 1P, Ph_2P–Fe)
15	17.6 (s, 2P, L^{Mo}); 52.7 (s, 1P, Ph_2P–Fe)
16	−12.2 (s, 2P, L^{W}); 52.7 (s, 1P, Ph_2P–Fe)
17	17.6 (s, 2P, L^{Mo}); 52.3 (s, 1P, Ph_2P–Fe)
18	−14.0 (s, 2P, L^{W}); 52.0 (s, 1P, Ph_2P–Fe)

[a] Spectra recorded in $CDCl_3$ (+25 °C) and referenced to 85% H_3PO_4.

atoms attached to the π-allyl fragment in an approximately 2:1 intensity ratio. The assignments of resonances in the $^{31}P\{^{1}H\}$ NMR spectra were due to the expected resonances of the phosphine ligands, $[MI_2(CO)_3\{MeC(CH_2PPh_2)_3\text{-}P,P'\}]$ [30], and the generally lower field and less intense resonance due to the phosphorus atom attached to the π-allyl molybdenum moiety. The geometry of one isomer of complexes **1**–**6** is shown in Fig. 1, which shows that the L^{Mo} or L^{W} are coordinated in a *trans* configuration to each other, with a bulky phosphine group and π-allyl group *trans* to the other one.

Complexes **1**–**6** are most likely to be obtained from the bimetallic complexes, $[MoX(CO)_2(NCMe)(L^{Mo}$ or $L^{W})(\eta^3\text{-}C_3H_4R)]$, which could not be isolated even with short reaction times, and the tetrametallic nature of the products was confirmed by the lack of nitrogen in the elemental analysis results and no acetonitrile resonances observed in the ^{1}H NMR spectra. Also molecular weight studies using Rast's method [33] confirmed the tetrametallic nature of **1**–**6**. Several unsuccessful attempts were made to obtain FAB mass spectra of the complexes, although fragment peaks were obtained the parent ions could not be observed for these complexes.

3.2. Synthesis and characterization of the trimetallic complexes, $[MoX(CO)_2(L^{Mo}$ or $L^{W})_2(\eta^3\text{-}C_3H_4R)]$ (7–12)

Reaction of $[MoX(CO)_2(NCMe)_2(\eta^3\text{-}C_3H_4R)]$ (X = Cl, R = H or Me; X = Br, R = H) with 2 equiv. of L^{Mo} or L^{W} in CH_2Cl_2 at room temperature affords the trimetallic, tripodal triphos-bridged complexes, $[MoX(CO)_2(L^{Mo}$ or $L^{W})_2(\eta^3\text{-}C_3H_4R)]$ (**7**–**12**) in moderate yield, by displacement of both of the acetonitrile ligands. The complexes **7**–**12** have been fully characterised by elemental analysis (C and H), (Table 1), IR (Table 2), ^{1}H and $^{31}P\{^{1}H\}$ NMR spectroscopy. The complex $[MoBr(CO)_2(L^{Mo})_2(\eta^3\text{-}C_3H_5)]\cdot Et_2O$ (**11**) was confirmed as a diethyl ether solvate by repeated

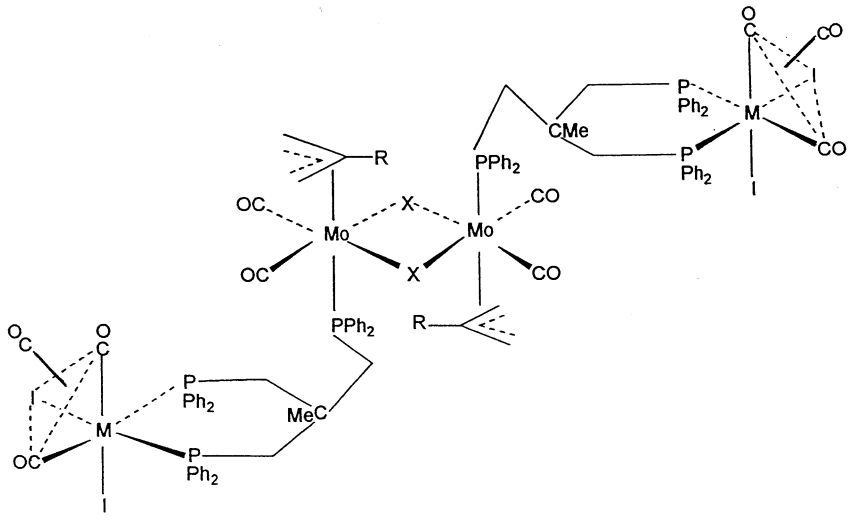


Fig. 1. Proposed structure of [{Mo(μ-X)(CO)$_2$(L^{Mo} or L^{W})(η^3-C$_3$H$_4$R)}$_2$] (M = Mo or W) (**1**–**6**).

elemental analyses and ^{1}H NMR spectroscopy. FAB mass spectra were attempted without success, as no parent ions were observed. However, molecular weight studies by Rast's method [33] suggest the trimetallic nature of these complexes (see Table 5). Generally, complexes **7**–**12** are more stable and less soluble than the tetrametallic complexes **1**–**6** described earlier. Complexes **7**–**12** have to be stored under dinitrogen in the solid-state.

The IR spectra of the trimetallic complexes, **7**–**12** are all relatively simple and show the expected bands for the π-allyl molybdenum *cis*-dicarbonyl unit, and the diiodo tricarbonyl molybdenum and tungsten moieties. For example, complex **7** has bands at ν(CO) = 2041, 1959, 1939 and 1846 cm^{-1}. It is very likely the bands at 1939 and 1846 cm^{-1} are due to the *cis*-dicarbonyl π-allyl unit, and the bands at 2041, 1959 and 1939 cm^{-1} (and probably a masked band due to MI$_2$(CO)$_3$ unit), are due to the L^{Mo} part of the molecule. The room temperature ^{31}P{^{1}H} NMR spectrum for complex **7** shows a resonance due to the equivalent phosphine atoms attached to the fluxional [MoI$_2$(CO)$_3${MeC(CH$_2$-PPh$_2$)$_3$-*P*,*P*′}] units at δ = 17.6 ppm. The resonance at δ = 32.9 ppm is due to the 2 equiv. phosphorus atoms attached to the molybdenum π-allyl unit. The intensity ratio of the resonances at δ = 17.6 and 32.9 ppm is approximately 2:1, which was expected. Although the only crystal structure of a bis(monodentate) phosphorus donor complex [MoCl(CO)$_2${P(OMe)$_3$}$_2$(η^3-C$_3$H$_5$)] [44], has a distorted pentagonal bipyramidal structure with carbonyl and a chloro group in the axial position, the two phosphite ligands are in different environments in the equatorial plane. In view of the IR and ^{31}P{^{1}H} NMR spectral data (Tables 2 and 4), it is more likely the structure of **7**–**12** has distorted pentagonal bipyramidal arrangement with the two organometallic phosphine units *trans* to each other, with the carbonyl groups, chloro group and π-allyl unit occupying the five equatorial sites, (the π-allyl group occupying two sites). The proposed structure for **7**–**12** is shown in Fig. 2. The structure of the seven-coordinate halocarbonyl part of the molecule most likely has a distorted capped octahedral structure as many structures of [MX$_2$(CO)$_3$L$_2$] have distorted capped octahedral geometries [25,26,45–47].

Table 5
Molecular weight studies [a] using Rast's method [33] for selected multimetallic complexes

Complex	Molecular weight {Found (Calc.)}
3	1429 (1300)
9	2667 (2358)
10	2667 (2534)
11	2222 (2389)
12	2667 (2565)
13	1333 (1282)
14	1429 (1370)
15	1429 (1362)
16	1482 (1450)
17	1333 (1376)
18	1379 (1464)

[a] Camphor was used as the solvent in these measurements.

3.3. Synthesis and characterization of the bimetallic complexes, [Fe(CO)$_4$(L^{Mo} or L^{W})] (**13** and **14**)

Reaction of [Fe$_2$(CO)$_9$] with 2 equiv. of L^{Mo} or L^{W} in CH$_2$Cl$_2$ at room temperature affords the bimetallic, tripodal triphos-bridged complexes, [Fe(CO)$_4$(L^{Mo} or L^{W})] (**13** and **14**) in moderate yield. Complexes **13** and **14** have been characterised by elemental analysis (Table 1), IR (Table 2) and ^{1}H and ^{31}P{^{1}H} NMR spectroscopy (Tables 3 and 4). Molecular weight studies by Rast's method [46] on both complexes (Table 5), confirmed the bimetallic nature of these complexes.

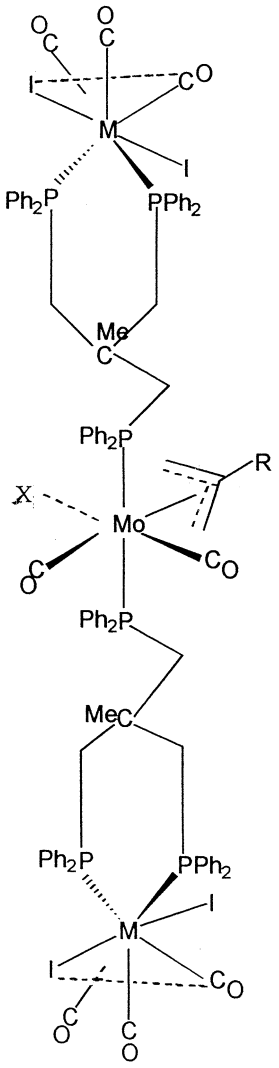


Fig. 2. Proposed structure of $[MoX(CO)_2(L^{Mo}$ or $L^{W})_2(\eta^3\text{-}C_3H_4R)]$ (M = Mo or W) (**7**–**12**).

Complexes **13** and **14** are soluble in CH_2Cl_2, less soluble in $CHCl_3$, and only sparingly soluble in diethyl ether and hydrocarbon solvents. The complexes are air-sensitive in solution, but can be stored in the solid-state under an inert atmosphere.

The IR spectra of **13** and **14** have as expected a number of carbonyl bands, there are four carbonyl ligands on the iron centre and three carbonyl groups on the molybdenum or tungsten centres. For example, complex **14** has carbonyl bands ($CHCl_3$) at 2030, 1955, 1928, 1912 and 1901 cm^{-1}. It is likely the bands at 2030, 1955 and 1901 cm^{-1} are due to the $[WI_2(CO)_3\{MeC(CH_2PPh_2)_3\text{-}P,P'\}]$ fragment [30], but for the $[Fe(CO)_4]$ part of complex **14**, may have three carbonyl bands at 2030, 1928 and 1912 cm^{-1}. It should be noted that the tungsten phosphine ligand, $[WI_2(CO)_3\{MeC(CH_2PPh_2)_3\text{-}P,P'\}]$ has bands at $\nu(CO)(CHCl_3) = 2036$, 1958 and 1904 cm^{-1} [30], and a related simple monodentate phosphine complex, $[Fe(CO)_4\{P(o\text{-tolyl})_3\}]$ has carbonyl bands at $\nu(CO)(Hexane) = 2043$, 1975 and 1947 cm^{-1} [48]. Hence, the bands are similar for the two complexes, which agrees with the broad overlapping carbonyl region of the IR spectra of **13** and **14**.

The $^{31}P\{^1H\}$ NMR spectra of **14** shows one signal due to the fluxional $[WI_2(CO)_3\{MeC(CH_2PPh_2)_3\text{-}P,P'\}]$ unit at $\delta = -16.4$ ppm, and another signal at $\delta = 39.3$ ppm due to the phosphorus atom which is coordinated to the iron centre, in an approximately 2:1 intensity ratio. The X-ray crystal structures of the complexes $[Fe(CO)_4L]$ {L = P(*p*-tolyl)$_3$ [48] and PPh_3 [49]} have been reported, and both have a very similar trigonal bipyramidal geometry, with the phosphine ligand in the axial position. In view of these studies, and the IR and $^{31}P\{^1H\}$ NMR spectral data of complexes **13** and **14**, the most likely structure for **13** and **14** is shown in Fig. 3.

3.4. Synthesis and characterization of the cationic bimetallic complexes, $[Fe(CO)_2(L^{Mo}$ or $L^{W})(Cp$ or $Cp')]X$ (15–19)

Equimolar quantities of $[FeI(CO)_2(Cp$ or $Cp')]$ and L^{Mo} or L^{W} react in warm CH_2Cl_2 to give the cationic iodide displaced bimetallic complexes $[Fe(CO)_2(L^{Mo}$ or $L^{W})(Cp$ or $Cp')]I$ (**15**–**18**) in moderate yield. The cationic nature of these complexes was confirmed by an iodide exchange reaction with $Na[BPh_4]$. Reaction of $[Fe(CO)_2(L^{W})Cp]I$ (**16**) with 1 equiv. of $Na[BPh_4]$ in CH_2Cl_2 at room temperature furnished the iodide-exchanged complex, $[Fe(CO)_2(L^{W})Cp][BPh_4]$ (**19**) in 35% yield. The cationic complexes **15**–**19** were characterised in the normal manner (Tables 1–5). Complexes **15**–**19** are soluble in polar solvents such as CH_2Cl_2, $CHCl_3$ and acetone, but as expected completely insoluble in diethyl ether and hydrocarbon solvents. The complexes are stable in the solid-state if stored under an

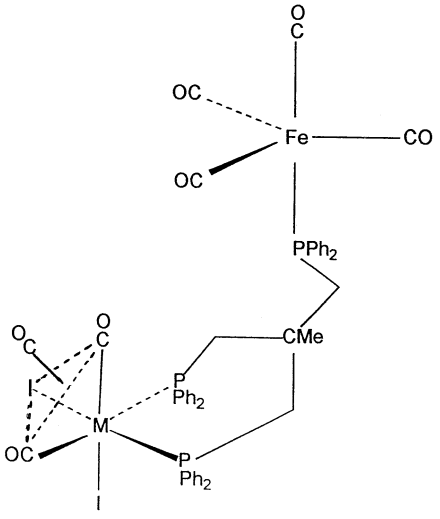


Fig. 3. Proposed structure of $[Fe(CO)_4(L^{Mo}$ or $L^{W})]$ (M = Mo or W) (**13** and **14**).

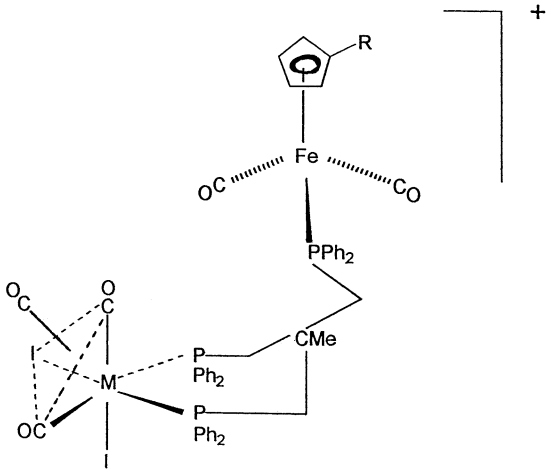


Fig. 4. Proposed structure of the cationic complexes, $[Fe(CO)_2(L^{Mo}$ or $L^{W})(Cp$ or $Cp')]X$ (M = Mo or W) (**15**–**19**).

inert atmosphere, but decompose in solution when exposed to air.

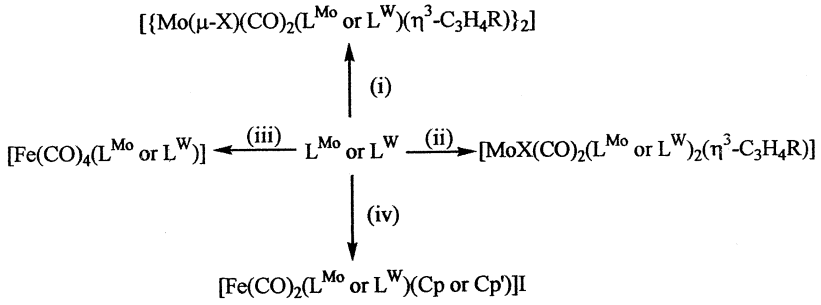
The IR spectra of **15**–**19** show the overlapping carbonyl bands expected for the *cis*-$Fe(CO)_2$-units, and the $[MI_2(CO)_3]$ unit. For example, the IR spectrum for $[Fe(CO)_2(L^{Mo})Cp]I$ (**15**) has bands at $\nu(CO) = 2043$, 2019, 1998, 1938 and 1906 cm^{-1}. The two bands at 2043 and 1998 cm^{-1} are similar to the closely related monodentate phosphine complex, $[Fe(CO)_2(PPh_3)Cp]I$, which has carbonyl stretching bands at $\nu(CO) = 2045$ and 1995 cm^{-1} [50]. The bands at 2019, 1938 and 1906 cm^{-1} are due to L^{Mo} [30]. The $^{31}P\{^1H\}$ NMR spectra of complexes **15**–**19** show two resonances, and suggest a single isomer for the complexes in solution. For example, complex **15** has a single resonance at $\delta = 52.7$ ppm due to $[Ph_2P–Fe]$ unit and at $\delta = 17.6$ ppm for L^{Mo} in an approximately 1:2 intensity ratio. The likely structure of complexes **15**–**19** is as shown in Fig. 4. A number of unsuccessful attempts were made to grow suitable single crystals for X-ray crystallography of complexes **15**–**19** is as shown in Fig. 4.

4. Conclusions

In conclusion, the preparation and characterization of a range of new multimetallic complexes (nineteen) containing bridging-tripodal triphos, attached with two phosphorus atoms on $[MI_2(CO)_3\{MeC(CH_2PPh_2)_3$-$P,P'\}]$, and one phosphorus atom attached to a molybdenum(II) π-allyl unit, an iron(0) unit or an iron(II) moiety. These results are summarised in Scheme 1.

Acknowledgements

M. Al-Jahdali thanks the Saudi Arabian government for supporting him on a PhD studentship.



$L^{Mo} = [MoI_2(CO)_3\{MeC(CH_2PPh_2)_3$-$P,P'\}]$

$L^{W} = [WI_2(CO)_3\{MeC(CH_2PPh_2)_3$-$P,P'\}]$

Reagents:-

(i) One equivalent of $[MoX(CO)_2(NCMe)_2(\eta^3$-$C_3H_4R)]$ (X = Cl, R = H or Me; X = Br, R = H) in CH_2Cl_2

(ii) Half an equivalent of $[MoX(CO)_2(NCMe)_2(\eta^3$-$C_3H_4R)]$

(iii) Half an equivalent of $[Fe_2(CO)_9]$

(iv) One equivalent of $[FeI(CO)_2(Cp$ or $Cp')]$

Scheme 1. Reactions of L^{Mo} and L^{W} with $[MoX(CO)_2(NCMe)_2(\eta^3$-$C_3H_4R)]$, $[Fe_2(CO)_9]$ or $[FeI(CO)_2(Cp$ or $Cp')]$.

References

[1] A.T. Hutton, P.G. Pringle, B.L. Shaw, J. Chem. Soc., Dalton Trans. (1985) 1677.
[2] C.-M. Che, V.W.-W. Yam, W.-T. Wong, T.-F. Lai, Inorg. Chem. 28 (1989) 2908.
[3] P.G. Pringle, B.L. Shaw, J. Chem. Soc., Chem. Commun. (1982) 956.
[4] B. Mohr, E.E. Brooks, N. Rath, E. Deutsch, Inorg. Chem. 30 (1991) 4541.
[5] N. Marsich, A. Camus, G. Nardin, J. Organomet. Chem. 239 (1982) 429.
[6] A.M.M. Lanfredi, F. Ugozzoli, A. Camus, N. Marsich, R. Capellett, Inorg. Chim. Acta 206 (1993) 173.
[7] S. Kitagawa, H. Maruyama, S. Wada, M. Munakata, M. Nakamura, H. Masuda, Bull. Chem. Soc. Jpn. 64 (1991) 2809.
[8] T.A. Annan, J.E. Kickham, D.G. Tuck, Can. J. Chem. 69 (1991) 251.
[9] D.M. Ho, R. Bau, Inorg. Chem. 22 (1983) 4073.
[10] X. Hong, K.-K. Cheung, C.-X. Guo, C.-M. Che, J. Chem. Soc., Dalton Trans. (1994) 1867.
[11] F.A. Cotton, B. Hong, Prog. Inorg. Chem. 40 (1992) 179 (and references cited therein).
[12] A.P. Gaughan, R.F. Ziolo, Z. Dori, Inorg. Chem. 10 (1971) 2776.
[13] D.-N. Horng, S.-T. Jeng, C.-H. Ueng, J. Chin. Chem. Soc. 41 (1994) 53.
[14] D.-N. Horng, C.-H. Ueng, J. Organomet. Chem. 505 (1995) 53.
[15] R.B. King, P.N. Kapoor, R.N. Kapoor, Inorg. Chem. 10 (1971) 1841.
[16] A.R. Khan, S.M. Socol, D.W. Meek, Inorg. Chim. Acta 221 (1994) 187.
[17] F.A. Cotton, L.R. Favello, R.C. Najjar, Organometallics 1 (1982) 1640.
[18] F.R. Askham, G.G. Stanley, E.C. Marques, J. Am. Chem. Soc. 107 (1985) 7423.
[19] S.A. Laneman, F.R. Fronczek, G.G. Stanley, Inorg. Chem. 28 (1989) 1872.
[20] S.E. Saum, S.A. Laneman, G.G. Stanley, Inorg. Chem. 29 (1990) 5065.
[21] A.L. Balch, E.Y. Fung, Inorg. Chem. 29 (1990) 4764.
[22] M.K. Cooper, L.E. Mitchell, K. Henrick, M. McPartlin, A. Scott, Inorg. Chim. Acta 84 (1984) L9.
[23] H. El-Amouri, A.A. Bahsoun, J. Fischer, J.A. Osborn, M.-T. Youinon, Organometallics 10 (1991) 3582.
[24] P.K. Baker, S.G. Fraser, E.M. Keys, J. Organomet. Chem. 309 (1986) 319.
[25] P.K. Baker, Adv. Organomet. Chem. 40 (1996) 45 (and references cited therein).
[26] P.K. Baker, Chem. Soc. Rev. 27 (1998) 125 (and references cited therein).
[27] P.K. Baker, D.J. Sherlock, Polyhedron 13 (1994) 525.
[28] P.K. Baker, S.J. Coles, D.E. Evans, M.M. Meehan, M.B. Hursthouse, J. Chem. Soc., Dalton Trans. (1996) 3995.
[29] P.K. Baker, M.G.B. Drew, M.M. Meehan, J. Szewczyk, J. Organomet. Chem. 580 (1999) 265.
[30] P.K. Baker, M. Al-Jahdali, M.M. Meehan, J. Organomet. Chem. 648 (2002) 99.
[31] R.G. Hayter, J. Organomet. Chem. 13 (1968) P1.
[32] T.S. Piper, G. Wilkinson, J. Inorg. Nucl. Chem. 3 (1956) 104.
[33] F.G. Mann, B.C. Saunders, Practical Organic Chemistry, Longmans Green, London, 1954, pp. 342–344.
[34] A.J. Graham, R.H. Fenn, J. Organomet. Chem. 17 (1969) 405.
[35] A.J. Graham, R.H. Fenn, J. Organomet. Chem. 25 (1970) 173.
[36] A.J. Graham, D. Akrigg, B. Sheldrick, Cryst. Struct. Commun. 5 (1976) 891.
[37] A.J. Graham, D. Akrigg, B. Sheldrick, Cryst. Struct. Commun. 6 (1977) 253.
[38] M.G.B. Drew, B.J. Brisdon, B.J. Cartwright, Inorg. Chim. Acta 36 (1979) 127.
[39] A.J. Graham, D. Akrigg, B. Sheldrick, Acta Crystallogr., Sect. C 39 (1983) 192.
[40] A.J. Graham, D. Akrigg, B. Sheldrick, Acta Crystallogr., Sect. C 41 (1985) 995.
[41] G.D. Gracey, S.J. Rettig, A. Storr, J. Trotter, Can. J. Chem. 65 (1987) 2469.
[42] F.A. Cotton, R.L. Luck, Acta Crystallogr., Sect. C 46 (1990) 138.
[43] J. Jordanov, H. Behm, P.T. Beurskens, J. Crystallogr. Spectrosc. Res. 21 (1991) 657.
[44] B.J. Brisdon, D.A. Edwards, K.E. Paddick, M.G.B. Drew, J. Chem. Soc., Dalton Trans. (1980) 1317.
[45] M.G.B. Drew, Prog. Inorg. Chem. 23 (1977) 67 (and references cited therein).
[46] M. Melńik, P. Sharrock, Coord. Chem. Rev. 65 (1985) 49 (and references cited therein).
[47] C.W. Haigh, P.K. Baker, Polyhedron 13 (1994) 417 (and references cited therein).
[48] J.A.S. Howell, M.G. Palin, P. McArdle, D. Cunningham, Z. Goldschmidt, H.E. Gottlieb, D.H. Langerman, Inorg. Chem. 19 (1980) 159.
[49] P.E. Riley, R.E. Davis, Inorg. Chem. 32 (1993) 3493.
[50] N.J. Coville, E.A. Darling, A.W. Hearn, P. Johnston, J. Organomet. Chem. 328 (1987) 375.

metallated phenyl ring. In the present paper, we report the synthesis and characterization of new examples of mono- and polynuclear cyclometallated compounds of palladium(II) derived from terephthalbenzylidenimines with diphosphine ligands.

2. Experimental

2.1. Materials and instrumentation

All solvents were distilled prior to use from appropriate drying agents [15]. Chemicals were used as supplied from commercial sources. Elemental analyses (C, H, N) were carried out in a Carlo-Erba 1108 elemental analyser. IR spectra were recorded as KBr pellets or Nujol mulls on a Perkin–Elmer 1330 spectrophotometer. NMR spectra were obtained as $CDCl_3$ solutions and referenced to $SiMe_4$ (^1H, $^{13}C-\{^1H\}$) or 85% H_3PO_4 ($^{31}P-\{^1H\}$), and were recorded on a Bruker AC-200F spectrometer (200.0 MHz for ^1H, 50.3 MHz for $^{13}C-\{^1H\}$, 81.0 MHz for $^{31}P-\{^1H\}$). Mass spectra were obtained in a QUATRO mass spectrometer with Cs ion-gun and 3-NBA matrix. Conductivity measurements were made on a Crison GLP 32 conductivimeter using 10^{-3} M solutions in dry acetonitrile at room temperature (r.t., 298 K). The synthesis of [Pd{4-(COH)C_6H_3C(H)=N(Cy)-*C2,N*}(μ-Cl)]$_2$ (**1**) was reported in a recent paper from this laboratory [13].

2.2. Synthesis of the complexes

2.2.1. Syntheses of [{Pd[4-(COH)C_6H_3C(H)=N(Cy)-C2,N](Cl)}$_2$(μ-$Ph_2PCH_2PPh_2$)] (**2**)

To a solution of **1** (25.00 mg, 0.035 mmol) in acetone (ca. 10 cm^3), $Ph_2PCH_2PPh_2$ (dppm, 12.13 mg, 0.032 mmol) was added. The mixture was stirred for 12 h at r.t., after which the precipitate formed was filtered off, dried in vacuo, and recrystallized from chloroform/*n*-hexane to yield the desired product as pale yellow microcrystals. Yield: 42% (14.68 mg). *Anal.* Found: C, 57.9; H, 4.9; N, 2.7. $C_{53}H_{54}Cl_2N_2O_2P_2Pd_2$ requires: C, 58.0; H, 5.0; N, 2.6%. IR: ν(C=O): 1692s, ν(C=N): 1621m. FAB Mass: 1061 $[M-Cl]^+$, 1033 $[M-Cl-COH]^+$, 704, $[LPd(PP)]^+$, 676 $[LPdCl]^+$. NMR ^1H: 9.07 (s, Ha), 7.38 (dd, H5, ^3J(H5H6) = 7.9 Hz, ^4J(H3H5) = 1.2 Hz), 6.88 (dd, H3, ^4J(PH3) = 4.9 Hz), 5.03 (t, CH_2P, ^{2}J(PH) = 13.4 Hz). NMR $^{31}P-\{^1H\}$: 30.90 (s).

Compounds **3**–**8** were prepared similarly, using the corresponding diphosphine ligand as appropriate.

2.2.1.1. [{Pd[4-(COH)C_6H_3C(H)=N(Cy)-C2,N](Cl)}$_2$(μ-$Ph_2PCH_2CH_2PPh_2$)] (**3**).

Yield: 85%. *Anal.* Found: C, 58.7; H, 4.8; N, 2.4. $C_{54}H_{56}Cl_2N_2O_2P_2Pd_2$ requires: C, 58.4; H, 5.1; N, 2.5%. IR: ν(C=O): 1692s, ν(C=N): 1622m. FAB Mass: 1075 $[M-Cl]^+$, 718 $[LPd(PP)]^+$. NMR ^1H: 9.20 (s, Ha), 4.51 (t, CH_2P, ^2J(PH) = 10.8 Hz). NMR $^{31}P-\{^1H\}$: 36.98 (s).

2.2.1.2. [{Pd[4-(COH)C_6H_3C(H)=N(Cy)-C2,N](Cl)}$_2${μ-$Ph_2P(CH_2)_4PPh_2$}] (**4**).

Yield: 91%. *Anal.* Found: C, 58.3; H, 5.0; N, 2.3. $C_{56}H_{60}Cl_2N_2O_2P_2Pd_2\cdot(CHCl_3)_{0.15}$ requires: C, 58.3; H, 5.2; N, 2.4%. IR: ν(C=O): 1695s, ν(C=N): 1622m. FAB Mass: 1103 $[M-Cl]^+$, 746 $[LPd(PP)]^+$, 718 $[(L-COH)Pd(PP)]^+$. NMR ^1H: 9.20 (s, Ha), 8.14 (dd, Hi, ^4J(PHi) = 8.3 Hz, ^5J(HiH7) = 1.0 Hz), 6.79 (dd, H3, ^4J(PH3) = 5.6 Hz, ^4J(H3H5) = 1.2 Hz), 4.52 (m, CH_2P). NMR $^{31}P-\{^1H\}$: 33.78 (s). NMR $^{13}C-\{^1H\}$: 192.2 (s, COH), 170.0 (d, C=N, ^4J(PC) = 4.3 Hz), 157.9 (s, C1), 154.4 (s, C2), 135.7 (d, C4, ^4J(PC) = 5.0 Hz), 135.3 (d, C3, ^3J(PC) = 9.9 Hz), 133.9 (d, C_o, ^2J(PC) = 11.4 Hz), 130.0 (d, C_i, ^1J(PC) = 46.1 Hz), 128.6 (d, C_m, ^3J(PC) = 10.6 Hz), 127.4 (s, C5), 124.3 (s, C6), 62.8 (s, C7), 33.5 (s, C8, C12), 29.7 (d, *C*H_2P, ^1J(PC) = 33.4 Hz), 26.4 (d, *C*H_2CH_2P, ^2J(PC) = 17.8 Hz), 25.8 (s, C10), 25.4 (s, C9, C11).

2.2.1.3. [{Pd[4-(COH)C_6H_3C(H)=N(Cy)-C2,N](Cl)}$_2${μ-$Ph_2P(CH_2)_6PPh_2$}] (**5**).

Yield: 64%. *Anal.* Found: C, 60.5; H, 5.0; N, 1.2. $C_{58}H_{64}Cl_2N_2O_2P_2Pd_2\cdot(Me_2CO)_{0.15}$ requires: C, 60.4; H, 5.6; N, 1.2%. IR: ν(C=O): 1687s, ν(C=N): 1622m. FAB Mass: 1166 $[M]^+$, 1130 $[M-Cl]^+$, 774 $[LPd(PP)]^+$. NMR ^1H: 9.22 (s, Ha), 8.15 (dd, Hi, ^4J(PHi) = 8.3 Hz, ^5J(HiH7) = 1.0 Hz), 6.83 (dd, H3, ^4J(PH3) = 5.2 Hz, ^4J(H3H5) = 1.5 Hz), 4.50 (m, CH_2P). NMR $^{31}P-\{^1H\}$: 33.69(s).

2.2.1.4. [{Pd[4-(COH)C_6H_3C(H)=N(Cy)-C2,N](Cl)}$_2${μ-($Ph_2PC_5H_4$)$_2$Fe}] (**6**).

Yield: 58%. *Anal.* Found: C, 50.2; H, 4.3; N, 1.9. $C_{62}H_{58}Cl_2FeN_2O_2P_2Pd_2\cdot(CHCl_3)_{2.75}$ requires: C, 50.6; H, 4.0; N, 1.8%. IR: ν(C=O): 1698s, ν(C=N): 1622m. FAB Mass: 1229 $[M-Cl]^+$, 874 $[LPd(PP)]^+$, 845 $[(L-COH)Pd(PP)]^+$. NMR ^1H: 9.12 (s, Ha), 8.17 (dd, Hi, ^4J(PHi) = 8.8 Hz, ^5J(HiH7) = 1.0 Hz), 6.59 (dd, H3, ^4J(PH3) = 5.9 Hz, ^4J(H3H5) = 1.0 Hz), 5.00, 4.60 (m, $H_{ferrocene}$). NMR $^{31}P-\{^1H\}$: 31.40 (s).

2.2.1.5. [{Pd[4-(COH)C_6H_3C(H)=N(Cy)-C2,N](Cl)}$_2${μ-trans(Ph_2PCH=$CHPPh_2$)}] (**7**).

Yield: 20%. *Anal.* Found: C, 54.2; H, 4.7; N, 2.6. $C_{54}H_{54}Cl_2N_2O_2P_2Pd_2\cdot(Me_2CO)_{0.85}$ requires: C, 54.4; H, 4.6; N, 2.3%. IR: ν(C=O): 1697m, ν(C=N): 1619m. FAB Mass: 1073 $[M-Cl]^+$, 1045 $[M-Cl-COH]^+$, 716 $[LPd(PP)]^+$, 687[(L-COH)Pd(PP)]$^+$. NMR ^1H: 9.20 (s, Ha), 8.18 (dd, Hi, ^4J(PHi) = 8.3 Hz, ^5J(HiH7) = 1.0 Hz), 7.00 (at, CH=C*H*, *N* = 39.5 Hz), 6.81 (dd, H3, ^4J(PH3) = 4.8 Hz, ^4J(H3H5) = 1.0 Hz). NMR $^{31}P-\{^1H\}$: 34.59 (s).

*2.2.1.6. [{Pd[4-(COH)C$_6$H$_3$C(H)=N(Cy)-C2,N](Cl)}$_2$(μ-Ph$_2$PCCPPh$_2$)] (**8**).* Yield: 50%. *Anal.* Found: C, 58.7; H, 4.6; N, 2.4. $C_{54}H_{52}Cl_2N_2O_2P_2Pd_2$ requires: C, 58.6; H, 4.7; N, 2.5%. IR: ν(C=O): 1698s, ν(C=N): 1626m. FAB Mass: 1106 $[M]^+$, 714 $[LPd(PP)]^+$. NMR ^{1}H: 9.24 (s, Ha), 8.12 (dd, Hi, $^4J(PHi) = 8.9$ Hz, $^5J(HiH7) = 1.0$ Hz), 6.92 (dd, H3, $^4J(PH3) = 7.3$ Hz, $^4J(H3H5) = 1.0$ Hz). NMR ^{31}P–{^{1}H}: 14.46(s).

*2.2.2. Syntheses of [Pd{4-(COH)C$_6$H$_3$C(H)=N(Cy)-C2,N}(Ph$_2$PCH$_2$PPh$_2$-P,P)][PF$_6$] (**9**)*

To a solution of **1** (20.00 mg, 0.028 mmol) in acetone (ca. 15 cm^3), dppm (21.56 mg, 0.056 mmol) was added. The mixture was stirred for 2 h at r.t., after which ammonium hexafluorophosphate (13.69 mg, 0.084 mmol) was added, the resultant solution was stirred for a further 1 h, water (ca. 40 cm^3) was added dropwise and the resulting mixture stirred for 2 h. The precipitate formed was filtered off, washed with water (2×5 cm^3) and dried in vacuo. The desired complex was recrystallized from chloroform/*n*-hexane as pale yellow microcrystals. Yield: 92% (43.72 mg). *Anal.* Found: C, 56.3; H, 3.7; N, 1.4. $C_{39}H_{38}F_6NOP_3Pd\cdot(Me_2CO)_2$ requires: C, 56.0; H, 5.2; N, 1.5%. IR: ν(C=O): 1689s, ν(C=N): 1620m. FAB Mass: 704 $[M]^+$, 676 $[M-COH]^+$. NMR ^{1}H: 9.51 (s, Ha), 8.41 (d, Hi, $^4J(P_\alpha Hi) = 7.3$ Hz), 7.09 (m, H3, $^4J(P_\beta H3) = 9.5$ Hz, $^4J(P_\alpha H3) = 7.3$ Hz, $^4J(H3H5) = 1.2$ Hz), 4.31 (dd, CH_2P, $^2J(PH) = 11.8$, 11.2 Hz). NMR ^{31}P–{^{1}H}: −4.98 (d, P$_\alpha$, $^2J(PP) = 65.7$ Hz), −28.16 (d, P$_\beta$). NMR ^{13}C–{^{1}H}: 191.6 (s, COH), 175.4 (m, C=N), 161.6 (dd, C2, $^2J(P_\beta C) = 127.8$ Hz, $^2J(P_\alpha C) = 9.4$ Hz), 154.0 (d, C1, $^3J(P_\beta C) = 2.1$ Hz), 137.0 (dd, C4, $^4J(P_\beta C) = 8.5$ Hz, $^4J(P_\alpha C) = 6.3$ Hz), 136.6 (dd, C3, $^3J(P_\beta C) = 12.7$ Hz, $^3J(P_\alpha C) = 3.5$ Hz), 133.9 (d, C$_o$, $^2J(PC) = 13.5$ Hz), 133.5 (d, C$_o$, $^2J(PC) = 12.8$ Hz), 133.0 (d, C$_p$, $^4J(PC) = 2.8$ Hz), 132.3 (d, C$_p$, $^4J(PC) = 2.8$ Hz),129.8 (d, C$_m$, $^3J(PC) = 12.1$ Hz), 129.5 (s, C5), 128.8 (d, C$_m$, $^3J(PC) = 10.6$ Hz), 128.3 (b, C6), 70.0 (s, C7), 127.5 (dd, C$_i$, $^1J(PC) = 31.6$ Hz, $^2J(PC) = 4.9$ Hz), 124.8 (dd, C$_i$, $^1J(PC) = 50.3$ Hz, $^2J(PC) = 4.9$ Hz), 41.4 (dd, CH_2P, $^1J(P_\alpha C) = 27.7$ Hz, $^1J(P_\beta C) = 20.4$ Hz), 33.2 (s, C8, C12), 24.9 (s, C10), 24.7 (s, C9, C11).

Compounds **10**–**16** were prepared similarly, but using the corresponding diphosphine ligand as appropriate, in a **1**/diphosphine 1:2 molar ratio.

*2.2.2.1. [Pd{4-(COH)C$_6$H$_3$C(H)=N(Cy)-C2,N}{Ph$_2$P(CH$_2$)$_2$PPh$_2$-P,P}][PF$_6$] (**10**).* Yield: 56%. *Anal.* Found: C, 55.7; H, 4.8; N, 1.5. $C_{40}H_{40}F_6NOP_3Pd\cdot(Me_2CO)$ requires: C, 55.9; H, 4.9; N, 1.5%. IR: ν(C=O): 1695s, ν(C=N): 1614m. FAB Mass: 718 $[M]^+$, 690 $[M-COH]^+$, 383[LPd]$^+$. NMR ^{1}H: 9.42 (s, Ha), 8.48 (d, Hi, $^4J(P_\alpha Hi) = 7.8$ Hz), 7.85 (dd, H5, $^3J(H5H6) = 7.4$ Hz, $^4J(H3H5) = 1.0$ Hz), 7.09 (m, H3, $^4J(P_\beta H3) = 7.8$ Hz, $^4J(P_\alpha H3) = 5.4$ Hz). NMR ^{31}P–{^{1}H}: 61.24 (d, P$_\alpha$, $^2J(PP) = 26.3$ Hz), 45.23(d, P$_\beta$).

*2.2.2.2. [Pd{4-(COH)C$_6$H$_3$C(H)=N(Cy)-C2,N}{Ph$_2$P(CH$_2$)$_4$PPh$_2$-P,P}][PF$_6$] (**11**).* Yield: 49%. *Anal.* Found: C, 56.3; H, 4.9; N, 1.7. $C_{42}H_{44}F_6NOP_3Pd$ requires: C, 56.5; H, 5.0; N, 1.6%. IR: ν(C=O): 1696s, ν(C=N): 1622m. FAB Mass: 746 $[M]^+$, 663 $[M-Cy]^+$. NMR ^{1}H: 9.33 (s, Ha), 8.48 (d, Hi, $^4J(P_\alpha Hi) = 7.5$ Hz). NMR ^{31}P–{^{1}H}: 32.19 (d, P$_\alpha$, $^2J(PP) = 29.1$ Hz), 19.87(d, P$_\beta$).

*2.2.2.3. [Pd{4-(COH)C$_6$H$_3$C(H)=N(Cy)-C2,N}{Ph$_2$P(CH$_2$)$_6$PPh$_2$-P,P}][PF$_6$] (**12**).* Yield: 74%. *Anal.* Found: C, 53.2; H, 5.2; N, 1.6. $C_{44}H_{48}F_6NOP_3Pd$ requires: C, 53.4; H, 5.3; N, 1.5%. IR: ν(C=O): 1694s, ν(C=N): 1624m. FAB Mass: 774 $[M]^+$, 663 $[M-COH-Cy]^+$. NMR ^{1}H: 9.28 (s, Ha), 8.40 (b, Hi). NMR ^{31}P–{^{1}H}: 33.12 (b, P$_\alpha$), 18.37 (b, P$_\beta$).

*2.2.2.4. [Pd{4-(COH)C$_6$H$_3$C(H)=N(Cy)-C2,N}{(Ph$_2$PC$_5$H$_4$)$_2$Fe-P,P}][PF$_6$] (**13**).* Yield: 34%. *Anal.* Found: C, 56.5; H, 3.9; N, 1.2. $C_{48}H_{42}F_6FeNOP_3Pd$ requires: C, 56.6; H, 4.2; N, 1.4%. IR: ν(C=O): 1697s, ν(C=N): 1609m. FAB Mass: 790 $[M-Cy]^+$, 291 [(L-COH)Pd]$^+$. NMR ^{1}H: 9.26 (s, Ha), 6.88 (m, H3), 4.78, 4.65, 4.31, 3.59 (d, H$_{ferrocene}$). NMR ^{31}P–{^{1}H}: 39.93 (d, P$_\alpha$, $^2J(PP) = 30.9$ Hz), 23.15(d, P$_\beta$).

*2.2.2.5. [Pd{4-(COH)C$_6$H$_3$C(H)=N(Cy)-C2,N}{1,2-(Ph$_2$P)$_2$C$_6$H$_4$-P,P}][PF$_6$] (**14**).* Yield: 48%. *Anal.* Found: C, 57.9; H, 4.1; N, 1.4. $C_{44}H_{40}F_6NOP_3Pd$ requires: C, 57.9; H, 4.4; N, 1.5%. IR: ν(C=O): 1694m, ν(C=N): 1615m. FAB Mass: 766 $[M]^+$, 738 $[M-COH]^+$, 684 $[M-COH-Cy]^+$, 291 [(L−COH)Pd]$^+$. NMR ^{1}H: 9.45 (s, Ha), 8.56 (d, Hi, $^4J(P_\alpha Hi) = 8.8$ Hz), 7.74 (dd, H5, $^3J(H5H6) = 7.5$ Hz, $^4J(H3H5) = 1.5$ Hz), 7.15 (m, H3, $^4J(P_\beta H3) = 8.1$ Hz, $^4J(P_\alpha H3) = 6.0$ Hz). NMR ^{31}P–{^{1}H}: 55.89 (d, P$_\alpha$, $^2J(PP) = 25.4$ Hz), 42.95(d, P$_\beta$).

*2.2.2.6. [Pd{4-(COH)C$_6$H$_3$C(H)=N(Cy)-C2,N}(cis-Ph$_2$PCH=CHPPh$_2$-P,P)][PF$_6$] (**15**).* Yield: 51%. *Anal.* Found: C, 55.5; H, 4.1; N, 2.0. $C_{40}H_{38}F_6NOP_3Pd$ requires: C, 55.7; H, 4.4; N, 1.6%. IR: ν(C=O): 1694m, ν(C=N): 1609m. FAB Mass: 716 $[M]^+$, 688 $[M-COH]^+$, 291 [(L−COH)Pd]$^+$. NMR ^{1}H: 9.59 (s, Ha), 8.54 (d, Hi, $^4J(P_\alpha Hi) = 8.8$ Hz). NMR ^{31}P–{^{1}H}: 63.85 (d, P$_\alpha$, $^2J(PP) = 11.0$ Hz), 55.02(d, P$_\beta$).

*2.2.2.7. [Pd{4-(COH)C$_6$H$_3$C(H)=N(Cy)-C2,N}(Ph$_2$PNHPPh$_2$-P,P)][PF$_6$] (**16**).* Yield: 86%. *Anal.* Found: C, 53.8; H, 4.7; N, 3.2. $C_{38}H_{37}F_6N_2OP_3Pd$ requires: C, 53.6; H, 4.4; N, 3.3%. IR: ν(C=O): 1694m, ν(C=N): 1612m. FAB Mass: 705 $[M]^+$, 677 $[M-COH]^+$. NMR ^{1}H: 9.68 (s, Ha), 8.33 (d, Hi,

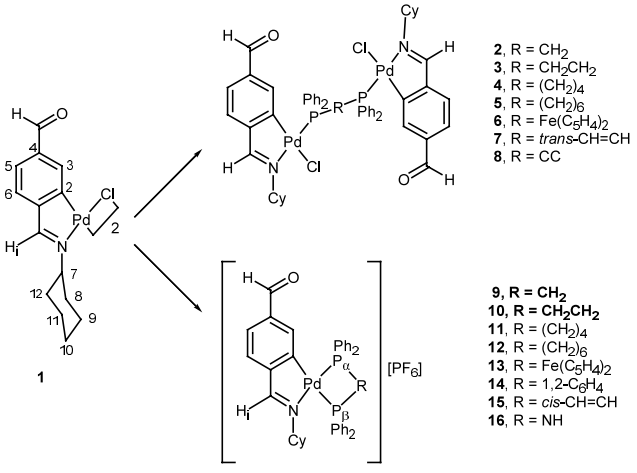
$^4J(P_\alpha Hi) = 7.3$ Hz), 6.14 (m, H3). NMR $^{31}P-\{^1H\}$: 44.40 (d, P_α, $^2J(PP) = 67.8$ Hz), 33.30 (d, P_β). NMR $^{13}C-\{^1H\}$: 191.6 (s, COH), 174.5 (m, C=N), 153.7 (d, C1, $^3J(P_\beta C) = 2.2$ Hz), 137.1 (dd, C4, $^4J(P_\beta C) = 13.5$ Hz, $^4J(P_\alpha C4) = 2.1$ Hz), 133.1 (d, C_o, $^2J(PC) = 13.5$ Hz), 132.5 (d, C_o, $^2J(PC) = 14.9$ Hz), 129.5 (d, C_m, $^3J(PC) = 11.4$ Hz), 127.9 (d, C_m, $^3J(PC) = 12.1$ Hz), 70.1 (s, C7), 33.5 (s, C8, C12), 25.0 (s, C10), 24.7 (s, C9, C11)

2.3. X-ray crystallographic study

Three-dimensional, room temperature X-ray data were collected on a Siemens SMART CCD diffractometer by the omega scan method. Reflections were measured from a hemisphere of data collected of frames each covering 0.3 degrees in omega. Of the 18879 reflections measured, all of which were corrected from Lorentz and polarisation effects and for absorption by semi-empirical methods based on symmetry-equivalent and repeated reflections (max./min. transmissions; 0.87,0.80), 3263 independent reflections exceeded the significance level $|F|/\sigma|F| > 4.0$. The structure was solved by direct methods and refined by full matrix least squares on F^2. Hydrogen atoms were included in calculated positions and refined in riding mode. Refinement converged at a final $R = 0.0588$ ($wR_2 = 0.1310$, for all 7131 unique data; 285 parameters, mean and maximum δ/σ 0.000, 0.000), with allowance for the thermal anisotropy of all non-hydrogen atoms. Minimum and maximum final electron density -0.458 and 1.440 e A^{-3} The structure solution and refinement were carried out using the program package SHELX-97 [16].

3. Results and discussion

For the convenience of the reader the compounds and reactions are shown in Scheme 1. The compounds



Scheme 1.

described in this paper were characterized by elemental analysis (C, H, N), mass spectrometry, and by IR and ^1H, $^{31}P-\{^1H\}$ and (in part) $^{13}C-\{^1H\}$ NMR spectroscopy (data in Section 2).

Reaction of [Pd{4-(COH)C_6H_3C(H)=N(Cy)-*C2*,*N*}-(μ-Cl)]$_2$ (**1**) [13] with bis(diphenylphosphino)methane (dppm), 1,2-bis(diphenylphosphino)ethane (dppe), 1,4-bis(diphenylphosphino)butane (dppb), 1,6-bis(diphenylphosphino)hexane (dpph), 1,1′-bis(diphenylphosphino)ferrocene (dppf), *trans*-bis(diphenylphosphino)-ethene (*trans*-dppe), or bis(diphenylphosphino)acetylene (dppac) in a 1:1 molar ratio, in acetone at room temperature afforded the polinuclear complexes [{Pd[4-(COH)C_6H_3C(H)=N(Cy)-*C2*,*N*](Cl)}$_2$(μ-Ph_2PRPPh_2)] (R: CH_2, **2**; CH_2CH_2, **3**; $(CH_2)_4$, **4**; $(CH_2)_6$, **5**; Fe$(C_5H_4)_2$, **6**; *trans*-CH=CH, **7**; C≡C, **8**) in which the diphosphine is acting as a bridging ligand. The new compounds were air-stable and soluble in the more common solvents, such as toluene, chloroform, acetone or ethanol, and gave satisfactory elemental analysis (see Experimental section). The MS FAB spectra showed similar fragmentation patterns, containing peaks assigned to, among others, $[M]^+$, $[M-Cl]^+$, $[M-Cl-COH]^+$ and $[LPd(PP)]^+$, after consideration of the palladium isotopes [17], thereby confirming the dinuclear (**2**–**5**, **7**, **8**) and trinuclear (**6**) nature of these complexes. The IR spectra showed the shift of the C=N stretch towards lower wavenumbers, as compared to the free Schiff base ligand (1638 vs. ca. 1620 cm^{-1}), indicating N-coordination of the C=N group [18]. A ν(C=O) band in the range 1698–1687 cm^{-1} was assigned to the free formyl group [19]. The $^{31}P-\{^1H\}$ NMR spectra showed a singlet in the range δ 38–30, shifted to higher frequency from the spectrum of the free phosphine, in agreement with phosphorus coordination to the metal center and indicated that the two phosphorus nuclei are equivalent [20].

In the ^1H NMR spectrum for complexes **3**–**8** the COH group gave rise to a singlet ca. δ 9.20, shifted to lower field from the starting product, ca. 0.8 ppm, due to the shielding effect of the phosphine phenyl rings, in agreement with a phosphorus *trans* to nitrogen arrangement [21]. The HC=N resonance ca. δ 8.10 appeared as a doublet of doublets due to coupling to the ^{31}P nucleus [^4J(PHi) ca. 8.5 Hz] and with the NC*H* proton atom of the cyclohexyl ring [$^5J(HiH7) = 1.0$ Hz]. The H6 and H5 proton resonances were overlapped and could not be adequately assigned, but in compound **2** the latter could be clearly distinguished as a doublet of doublets at δ 7.38 by coupling to H3 and H4. A doublet of doublets at δ 6.92–6.59 was assigned to H3, with coupling to the phosphorus nucleus [$^4J(PH3) = 4.8$–7.3 Hz]. This resonance was shifted to lower field from the starting product ca. 1.2 ppm, due to the shielding effect of the phosphine phenyl rings. The non-phenyl proton resonances of the diphosphine ligands could be unambigu-

ously assigned: the CH_2P resonances appeared as a triplet at δ 5.03 and δ 4.51 in compounds **2** and **3**, respectively [^2J(PH) = 13.4, 10.8 Hz, also respectively], and as a multiplet ca. δ 4.50 in compounds **4** and **5**. For complex **6** two multiplets at δ 5.00 and δ 4.60 were assigned to the ferrocene protons, and in complex **7** the AA′XX′ spin system of the PCH=C*H*P group gave rise to an apparent triplet at δ 7.00 [N = 39.5 Hz].

The ^{13}C–{^{1}H} NMR spectrum of compound **4** showed a doublet at δ 170.0 and two singlets at δ 157.9 and δ 154.4 assignable to the HC=N, C1 and C2 carbons, respectively, downfield shifted from the spectrum of the free ligand (ca. 12, 20 and 26 ppm, also respectively) [22], thereby confirming that cyclometallation was maintained [13,23]. The C3 and C4 resonances appeared as doublets at δ 135.7 and δ 135.3, respectively, by coupling to the phosphorus nuclei [^3J(PC3) = 9.9 Hz, ^4J(PC4) = 5.0 Hz]. Two doublets at δ 29.7 and δ 26.4 were assigned to the *C*H$_2$P and *C*H$_2$CH$_2$P carbon atoms, respectively [^1J(PC) = 33.4 Hz, ^2J(PC) = 17.8 Hz, respectively]. The X-ray crystal structure determination of compound **2** (see below) confirmed the spectroscopic data.

Treatment of the chloro-bridged complex **1** with dppm, dppe, dppb, dpph, dppf, *cis*-dppe, 1,2-bis(diphenylphosphino)benzene (1,2-dppb) or bis(diphenylphosphine)amine (dppa) in a 1:2 molar ratio in the presence of NH_4PF_6 yielded the cyclometallated compounds [Pd{4-(COH)C$_6$H$_3$C(H)=N(Cy)-*C2*,*N*}(Ph$_2$PRPPh$_2$-*P*,*P*)][PF$_6$] (R: CH$_2$, **9**; CH$_2$CH$_2$, **10**; (CH$_2$)$_4$, **11**; (CH$_2$)$_6$, **12**; Fe(C$_5$H$_4$)$_2$, **13**; 1,2-C$_6$H$_4$, **14**; *cis*-CH=CH, **15**; NH, **16**). The new compounds were air-stable and soluble in the more common solvents. The conductivity data (125–150 Ω^{-1} cm^2 mol^{-1} in 10^{-3} mol dm^{-3} solutions in dry acetonitrile) showed them to be 1:1 electrolytes [24]. The MS FAB spectra showed, among others, the corresponding peaks assigned to $[M]^+$, $[M-\mathrm{COH}]^+$ and/or $[M-\mathrm{Cy}]^+$ (see Section 2). In the IR spectrum a broad and strong band at 850 cm^{-1} arising from the PF_6^- counterion [19] was observed.

The ^{31}P–{^{1}H} NMR spectra showed two doublets, suggesting the two phosphorus atoms to be non-equivalent. The assignment of the doublets was made on the assumption that a ligand of greater *trans* influence shifts the resonance of the phosphorus atoms *trans* to it to lower frequency [20]. The ^{31}P chemical shifts were clearly influenced by ring size [25], and the corresponding data for compounds **10**–**16** are summarized in Table 1. The four-membered ring compound **9** gave a negative Δ_R, as well as the larger ring compounds **11** and **12**. The five-membered ring compounds **10**, **14** and **15** gave a positive Δ_R. In the case of compounds **13** and **16** the effect of the ferrocene moiety and the heteroatom in the phosphine backbone gave a slightly positive Δ_R.

Table 1
^{31}P NMR parameters

	$\delta(P_\alpha)$	Δ_R [a]
9	−4.98	−44.28
10	61.24	+21.94
11	32.19	−7.11
12	33.12	−6.18
13	39.93	+0.63
14	55.89	+16.69
15	63.85	+24.55
16	44.40	+5.10

[a] Difference respect to an equivalent phosphorus in a non-chelated analogue, [(C–N)Pd(PPh$_3$)(Cl)] (PPh$_3$ *trans* to nitrogen, δ 39.30 ppm), Ref. [13].

The singlet signal of the CO*H* resonance was shifted to lower field from the starting product by 0.3–0.7 ppm due to the shielding effect of the P*Ph*$_2$ groups *cis* to carbon. This was most noteworthy in compounds **11**–**13**, due to larger chelate ring size. The HC=N resonance in the ^{1}H NMR spectra ca. 8.40 ppm appeared as a doublet due to coupling with the ^{31}P nucleus *trans* to nitrogen. The H6 resonance was overlapped and could not be assigned, but the H5 and H3 resonances were clearly distinguished in some complexes (see Section 2). Thus, a doublet of doublets at δ 7.85 (**10**) and δ 7.74(**14**) was assigned to the H5 proton, and a multiplet at δ 7.15–6.14 was assigned to H3, coupled to both phosphorus nuclei. Selective decoupling experiments allowed the correct assignment of the corresponding coupling constants, e.g. for compound **9**, *trans*-^4J(PH3) = 9.5 Hz, *cis*-^4J(PH3) = 7.3 Hz.

For complexes **9** and **16** the ^{13}C–{^{1}H} NMR data were consistent with the proposed structure (see Section 2). A multiplet, a doublet of doublets and a doublet ca. δ 175, δ 161 and δ 154 were assigned to the C=N, C2 and C1 carbon atoms, respectively, coupled to phosphorus. These resonances were shifted downfield from the starting product ca. 17, 33 and 16 ppm, also respectively. In the case of the C2 resonance, a large coupling constant to the phosphorus nucleus *trans* to carbon was observed ($^3J(P_\beta C)$ = 127.8 Hz). The diphosphine phenyl carbon resonances, as well as those of the cyclohexyl ring, could also be unambiguously assigned (see Experimental Section).

4. Molecular structure of complex 2

Suitable crystals of the title compound were grown by slowly evaporating a chloroform/*n*-hexane solution. The labeling scheme for the compound is shown in Fig. 1. The crystals consist of discrete molecules, separated by normal van der Waals distances. Crystallographic data and selected interatomic distances and angles are listed in Tables 2 and 3.

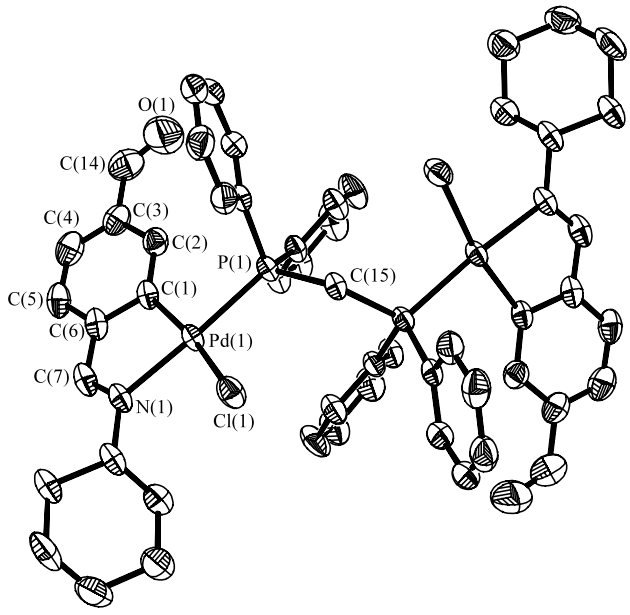


Fig. 1. Molecular structure of [{Pd[4-(COH)C_6H_3C(H)=N(Cy)-*C2,N*](Cl)}$_2$(μ-$Ph_2PCH_2PPh_2$)] (**2**), with labeling scheme. Hydrogen atoms have been omitted for clarity.

The crystal structure of **2** comprises a half molecule per asymmetric unit, and exhibits C_2 symmetry about the central methylene PCH_2P group. The four-coordinated palladium(II) is bonded to an adjacent *ortho*-carbon atom and to the nitrogen atom of the imine group of the deprotonated Schiff base ligand and to a chlorine atom (*trans* to C2). A phosphorus atom from the diphosphine ligand which bridges the two metal centers, completes the metal coordination sphere. The sum of angles about palladium is 360.26°, with the distortion most noticeable in the somewhat reduced 'bite' angle of the cyclometallated moiety consequent upon chelation. The requirements of the five-membered ring forces the bond angle N(1)–Pd(1)–C(1) to 80.43(17)°. The geometry around the palladium atom is slightly distorted square-planar, the mean deviation from the least squares plane (plane 1: Pd1, C1, N1, P1, Cl1) is 0.0916 Å.

Table 2
Crystal and structure refinement data for complex **2**

Formula	$C_{53}H_{54}Cl_2N_2O_2P_2Pd_2$
M_r	1096.62
Temperature (K)	293(2)
Wavelength (A)	0.71073
Crystal system	monoclinic
Space group	*C*2/*c*
Unit cell dimensions	
a (A)	24.474(4)
b (A)	10.424(2)
c (A)	20.531(4)
β (°)	111.302(4)
V (A^3)	4880.0(15)
Z	4
Crystal size (mm)	0.25 × 0.15 × 0.15
μ (mm^{-1})	0.954
$2\theta_{max}$ (°)	71.22
Reflections collected	18879
Reflections independent	7131 (R_{int} = 0.0869)
R [*F*, $I > 2\sigma(I)$]	0.0588
wR [F^2, all data]	0.1310
Max. *ρ* (e A^3)	1.440

Table 3
Selected bond lengths (A) and bond angles (°) for complex **2**

Bond lengths			
Pd(1)–C(1)	2.014(5)	C(6)–C(7)	1.431(7)
Pd(1)–N(1)	2.111(3)	N(1)–C(7)	1.271(6)
Pd(1)–P(1)	2.268(1)	O(1)–C(14)	1.166(8)
Pd(1)–Cl(1)	2.393(1)	P(1)–C(15)	1.844(3)
C(1)–C(6)	1.414(6)		
Bond angles			
C(1)–Pd(1)–N(1)	80.43(17)	N(1)–C(7)–C(6)	119.3(4)
C(1)–Pd(1)–P(1)	93.52(13)	C(1)–C(6)–C(7)	115.3(5)
P(1)–Pd(1)–Cl(1)	93.35(4)	C(6)–C(1)–Pd(1)	112.4(4)
N(1)–Pd(1)–Cl(1)	92.96(12)	C(15)–P(1)–Pd(1)	115.63(6)
C(7)–N(1)–Pd(1)	112.5(3)	P(1)–C(15)–P(1)#1	121.6(3)

The palladium–nitrogen bond length in the metallacycle, 2.111(3) Å, is longer than the predicted single bond value of 2.011 Å, based on the sum of covalent radii for nitrogen(sp^2) and palladium, 0.701 and 1.31 Å, respectively [26], and reflects the *trans* influence of the phosphorus atom [27]. The palladium–carbon bond length, 2.014(5) Å, is within the expected value of 2.081 Å (based on the sum of the covalent radii for carbon(sp^2) and palladium, 0.771 and 1.31 Å, respectively), but longer than those found in related complexes where partial multiple-bond character of the Pd–C bond was proposed [11,28]. The Pd–P bond distance, 2.268(1) Å, is shorter than the sum of the single bond radii for palladium and phosphorus (2.41 Å), suggesting partial double bond character similar to others reported earlier [29,30]. The Pd–Cl bond length, 2.393(1) Å, is consistent with Pd–Cl distances found in related species [30,31] but longer than the sum of the covalent radii (2.30 Å) as a consequence of the *trans* influence of the C(phenyl) carbon.

The mean deviations from the least squares planes determined for the metallacycle (plane 2: Pd1, C1, C6, C7, N1) and the metallated phenyl ring (plane 3: C1, C2, C3, C4, C5, C6) are 0.0122 and 0.0027 Å, respectively. The angle between these planes is 5.3°. The angles between plane 1 and the previous planes are: plane 1/plane 2: 6.2°, and plane 1/plane 3: 11.4°.

5. Supplementary material

Crystallographic data for the structural analysis have been deposited with the Cambridge Crystallographic

Data Centre, CCDC No. 185113 for compound **2**. Copies of this information may be obtained free of charge from The Director, CCDC, 12 Union Road, Cambridge, CB2 1EZ, UK (fax: +44-1223-336033; e-mail: mailto: deposit@ccdc.cam.ac.uk or www: http://www.ccdc.cam.ac.uk).

Acknowledgements

We thank the DGES (Proyecto PB98-0638-C02-01/02) and the Xunta de Galicia (Proyecto PGIDT99PXI20907B) for financial support.

References

[1] (a) L. Main, B.K. Nicholson, Adv. Met. Org. Chem. 3 (1994) 1;
(b) J. Spencer, M. Pfeffer, Adv. Met. Org. Chem. 6 (1998) 103.
[2] (a) J. Dupont, M. Pfeffer, J. Spencer, Eur. J. Inorg. Chem. (2001) 1917.;
(b) L. Botella, C. Najera, Angew. Chem. Int. Ed. Engl. 41 (2002) 179.
[3] M. Marcos, in: J.L. Serrano (Ed.), Metallomesogens. Synthesis, Properties and Applications, VCH, Weinheim, 1996.
[4] (a) O. Cantin, C. Cativiela, M.D. Diaz-de-Villegas, R. Navarro, E.P. Urriolabeitia, Tetrahedron Asymmetry 7 (1996) 2695;
(b) E.P. Urriolabeitia, M.D. Diaz-de-Villegas, J. Chem. Educ. 76 (1999) 77.
[5] (a) S.B. Wild, Coord. Chem. Rev. 166 (1997) 291;
(b) J. Albert, J.M. Cadena, J.R. Granell, X. Solans, M. Font-Bardia, Tetrahedron Asymmetry 11 (2000) 1943.
[6] (a) A. von Zelewski, P. Belser, P. Hayos, R. Dux, X. Hua, A. Suckling, H. Stoeckli-Evans, Coord. Chem. Rev. 132 (1994) 75;
(b) D. Song, Q. Wu, A. Hook, I. Kozin, S. Wang, Organometallics 20 (2000) 4683.
[7] A.G. Quiroga, J.M. Perez, I. Lopez-Solera, J.R. Masaguer, A. Luque, P. Roman, A. Edwards, C. Alonso, C. Navarro-Ranninger, J. Med. Chem. 41 (1998) 1399.
[8] (a) E.C. Constable, Polyhedron 3 (1984) 1037;
(b) O.A. Dunina, V.M. Zalewskaya, V.M. Potapov, Russ. Chem. Rev. 57 (1988) 250;
(c) I. Omae, Organometallic intramolecular-coordination compounds, in: Journal of Organometallic Chemistry Library, Elsevier, Amterdam, 1986.
[9] (a) J.M. Vila, M. Gayoso, M. López Torres, J.J. Fernández, A. Fernández, J.M. Ortigueira, N.A. Bailey, H. Adams, J. Organomet. Chem. 511 (1996) 129;
(b) J.M. Vila, M.T. Pereira, J.M. Ortigueira, J.J. Fernández, A. Fernández, M. López-Torres, H. Adams, Organometallics 18 (1999) 5484;
(c) B. Teijido, A. Fernández, M. López-Torres, S. Castro-Juiz, A. Suárez, J.M. Ortigueira, J.M. Vila, J.J. Fernández, J. Organomet. Chem. 598 (2000) 71;
(d) M. López-Torres, A. Fernández, J.J. Fernández, A. Suárez, S. Castro-Juiz, J.M. Vila, M.T. Pereira, Organometallics 20 (2001) 1350;
(e) B. Teijido, A. Fernández, M. López-Torres, A. Suárez, J.M. Vila, R. Mosteiro, J.J. Fernández, Organometallics 21 (2002) 1304.
[10] J.M. Vila, E. Gayoso, M.T. Pereira, M. Mariño, J. Martínez, J.J. Fernández, A. Fernández, M. López-Torres, J. Organomet. Chem. 637–639 (2001) 577.
[11] M. Lousame, A. Fernández, M. López-Torres, D. Vázquez-García, J.M. Vila, A. Suárez, J.M. Ortigueira, J.J. Fernández, Eur. J. Inorg. Chem. (2000) 2055.
[12] (a) A. Fernández, P. Uría, J.J. Fernández, M. López-Torres, A. Suárez, D. Vázquez-García, M.T. Pereira, J.M. Vila, J. Organomet. Chem. 620 (2001) 8;
(b) A. Fernández, D. Vázquez-García, J.J. Fernández, M. López-Torres, A. Suárez, S. Castro-Juiz, J.M. Vila, New J. Chem. 26 (2002) 398;
(c) A. Amoedo, M. Graña, J. Martínez, M.T. Pereira, M. López-Torres, A. Fernández, J.J. Fernández, J.M. Vila, Eur. J. Inorg. Chem. (2002) 613.
[13] J.M. Vila, M. Gayoso, M.T. Pereira, M. López, G. Alonso, J.J. Fernández, J. Organomet. Chem. 445 (1993) 287.
[14] J.M. Vila, M. Gayoso, M.T. Pereira, M. López-torres, J.J. Fernández, A. Fernández, J.M. Ortigueira, Z. Anorg. Allg. Chem. 623 (1997) 844.
[15] W.L.F. Armarego, D.D. Perrin, Purification of Laboratory Chemicals, 4th ed., Butterworth-Heinemann, Oxford, 1997.
[16] G.M. Sheldrick, SHELX-97, University of Göttingen, Germany, 1997.
[17] (a) L. Tusek-Bozic, M. Curic, P. Traldi, Inorg. Chim. Acta 254 (1997) 49;
(b) L. Tusek-Bozic, M. Komac, M. Curic, A. Lycka, M. Dálpaos, V. Scarcia, A. Furlani, Polyhedron 19 (2000) 937.
[18] H. Onoue, I. Moritani, J. Organomet. Chem. 43 (1972) 431.
[19] K. Nakamoto, Infrared and Raman Spectra of Inorganic and Coordination Compounds, 5th ed., Wiley, New York, 1997.
[20] P.S. Pregosin, R.W. Kuntz, ^{31}P and ^{13}C NMR of transition metal phosphine complexes, in: P. Diehl, E. Fluck, R. Kosfeld (Eds.), NMR Basic Principles and Progress, vol. 16, Springer, Berlin, 1979.
[21] J. Vicente, J.A. Abad, A. Frankland, M.C. Ramirez de Arellano, Chem. Eur. J. 5 (1999) 3066 (and references therein).
[22] J.M. Vila, M. Gayoso, M.T. Pereira, M. López-Torres, J.J. Fernández, A. Fernández, J.M. Ortigueira, J. Organomet. Chem. 506 (1996) 165.
[23] J. Granell, D. Sáinz, J. Sales, X. Soláns and, M. Font-Altaba, J. Chem. Soc., Dalton Trans. (1986) 1785.
[24] W.J. Geary, Coord. Chem. Rev. 7 (1971) 81.
[25] P.E. Garrou, Chem. Rev. 81 (1981) 229.
[26] F.H. Allen, O. Kennard, D.G.Watson, R. Taylor, J. Chem. Soc., Dalton Trans. (1989) S1.
[27] (a) T. Suzuki, A. Morikawa, K. Kashiwabara, Bull. Chem. Soc. Jpn. 69 (1996) 2539;
(b) A. Habtemariam, B. Watchman, B.S. Potter, R. Palmer, S. Parsons, A. Parkin, P.J. Sadler, J. Chem. Soc., Dalton Trans. (2001) 1306.
[28] J.M. Vila, M.T. Pereira, J.M. Ortigueira, M. López-Torres, A. Castiñeiras, D. Lata, J.J. Fernández, A. Fernández, J. Organomet. Chem. 556 (1998) 31.
[29] A. Suarez, J.M. Vila, E. Gayoso, M. Gayoso, W. Hiller, A. Castiñeiras, J. Strähle, Z. Inorg. Allg. Chem. 535 (1986) 213.
[30] R. Bosque, C. López, X. Solans, M. Font-Bardiá, Organometallics 18 (1999) 1267.
[31] J.M. Vila, M. Gayoso, A. Fernández, H. Adams, N.A. Bailey, J. Organomet. Chem. 448 (1993) 233.

sium methoxide with subsequent distillation. Toluene (Merck, *p.a.*) was distilled after refluxing with $LiAlH_4$.

IR spectra of Nujol mulls were obtained with a Perkin–Elmer FT-IR 1720 X spectrometer. Metal ratio in the samples was determined at the Arrhenius Laboratory, Stockholm University using a JEOL JSM-820 scanning microscope (SEM), supplied with a Link AN-10000 energy dispersive spectrometer (EDS). Mass spectra (electron beam ionization, direct probe introduction) were recorded using JEOL JMS-SX/SX-102A mass-spectrometer. The determination of carbon and hydrogen contents was carried out by Mikrokemi AB, Uppsala, Sweden, using the conventional organic microanalysis technique.

The alkoxides, $Nb_2(OMe)_{10}$ and $Ta_2(OMe)_{10}$, used in this work as starting materials for the synthesis of bimetallic complexes, were prepared by anodic oxidation of the corresponding metals in methanol and purified according to conventional techniques [9]. Rhenium(VII) oxide (99.9+%) was purchased from Aldrich.

2.1. Synthesis of $(Nb,Ta)_2(OMe)_8(ReO_4)_2$ (*I*)

Solutions of $Nb(OMe)_5$ (0.131 g, 0.529 mmol) in 3.5 ml of $C_6H_5CH_3$ and $Ta(OMe)_5$ (0.182, 0.543 mmol) in 2.5 ml of $C_6H_5CH_3$ were mixed. Re_2O_7 (0.273 g, 0.564 mmol) was added to the obtained solution upon stirring. No color changes at the initial stage were observed. Slow dissolution of Re_2O_7 occurred and the solution gradually became brownish-pink. Slight brownish coloration of Re_2O_7 particles and the formation of a small amount of nearly colorless crystals were observed. At the end of the process, after dissolution of almost all the Re_2O_7 (40 min), the mixture was heated to 60 °C for 10 min. The solution was cooled to room temperature (r.t.), then to −30 °C for crystallization. After 3 days the solution was decanted and the crystalline product (light pink prismatic platelets) was dried in vacuum. Yield: 0.411 g (76%). IR, cm^{-1}: 1138 s br, 998 m, 945 sh, 935 s (ν-Re=O), 896 sh, 818 s br (ν-Re=O···Nb(Ta), compare [6,8]), 723 w, 618 w, 569 m, 514 s. MS, *m/z* (I,%), interpretation: 641(1.0), $Ta_2(OMe)_9^+$, 595(1.0), $Ta_2O(OMe)_7^+$, 553(1.0), $TaNb(OMe)_9^+$, 522(0.5), $TaNb(OMe)_8^+$, 507(1.1), $TaNbO(OMe)_7^+$, 476(0.5), $TaNbO(OMe)_6^+$, 461(0.6), $TaNbO_2(OMe)_5^+$, 305(19.3), $Ta(OMe)_4^+$, 281(1.7), $ReO_2(OMe)_2^+$, 274(3.6), $Ta(OMe)_3^+$, 266(61.4), $ReO_3(OMe)^+$, 265(51.5), $ReO_3(OCH_2)^+$, 251(2.7), ReO_4^+, 249(2.1), $Re(OMe)_2^+$, 248(1.6), $Re(OCH_2)(OMe)^+$ and $Nb(OMe)_5^+$, 247(1.8), $Nb(OMe)_4(OCH_2)^+$, 238(6.5), $Re(OH)_3^+$, 237(7.5), $ReO(OH)_2^+$, 236(100), $ReO_2(OH)^+$, 235(32.9), ReO_3^+, 234(59.3), $ReO(OMe)^+$, 233(17.3), $ReO(OCH_2)^+$, 231(1.9), $TaO(OH)_2^+$, 220(17.0), $ReO(OH)^+$, 219(61.6), ReO_2^+, 217(50.8), $Nb(OMe)_4^+$, 204(4.8), $Re(OH)^+$, 203(22.0), ReO^+ and $Nb(OMe)_3(OH)^+$, 187(10.5), Re^+, 186(1.8), $Nb(OMe)_3^+$, 172(10.1), $Nb(OMe)_2(OH)^+$, 171(8.4), $NbO(OMe)_2^+$, 157(2.9), $NbO(OH)(OMe)^+$, 155(2.4), $Nb(OMe)_2^+$, 141(1.8), $Nb(OMe)(OH)^+$, 140(1.5), $NbO(OMe)^+$, 139(2.5), $NbO(OCH_2)^+$, 125(2.6), NbO_2^+.

2.2. Synthesis of $(Nb,Ta)_4O_2(OMe)_{14}(ReO_4)_2$ (*II*)

Solutions of $Nb(OMe)_5$ (0.140 g, 0.565 mmol) in 3.5 ml of $C_6H_5CH_3$ and $Ta(OMe)_5$ (0.194, 0.577 mmol) in 2.5 ml of $C_6H_5CH_3$ were mixed. Re_2O_7 (0.276 g, 0.570 mmol) was added to the obtained solution upon stirring. No color changes at the initial stage were observed. Upon slow dissolution of Re_2O_7, the solution became light pink. After 10 min of stirring, the mixture was heated. The solution became reddish-brown and Re_2O_7 changed color to black. The mixture was refluxed for 15 min. The formation of a black non-crystalline residue as a by-product was observed (EDS analysis showed the by-product to comprise of Re as the major component, and Nb and Ta in minor quantities, 5–7% atom). The solution was cooled to r.t., then to −30 °C for crystallization. After 3 days the solution was decanted and a crystalline product (thick needle shaped crystals brownish-pink in color) was dried in vacuum. Yield: 0.306 g (71% on $M(OMe)_5$ and 35% on Re_2O_7). IR, cm^{-1}: 1124 s br, 998 m w, 978 w, 931 s (ν-Re=O), 893 w, 808 s (ν-Re=O···Nb(Ta), compare [5]), 735 sh, 722 m, 569 m, 512 s. MS, *m/z* (I,%), interpretation: 641(2.8), $Ta_2(OMe)_9^+$, 595(4.2), $Ta_2O(OMe)_7^+$, 553(1.7), $TaNb(OMe)_9^+$, 549(1.4), $Ta_2O_2(OMe)_5^+$, 522(0.9), $TaNb(OMe)_8^+$, 517(0.4), $Ta_2(OMe)_5^+$, 508(0.5), $TaNb(OH)(OMe)_7^+$, 507(4.4), $TaNbO(OMe)_7^+$, 503(0.5), $Ta_2(OMe)_4(OH)^+$, 476(2.0), $TaNbO(OMe)_6^+$, 461(2.3), $TaNbO_2(OMe)_5^+$, 446(0.5), $TaNb(OH)(OMe)_5^+$, 429(0.7), $TaNb(OMe)_5^+$, 419(0.9), $Nb_2O(OMe)_7^+$, 415(0.7), $TaNb(OH)(OMe)_4^+$, 399(0.7), $TaNbO_2(OMe)_3^+$, 385(0.6), $TaNbO_2(OH)(OMe)_2^+$, 373(0.6), $Nb_2O_2(OMe)_5^+$, 305(19.0), $Ta(OMe)_4^+$, 281(5.3), $ReO_2(OMe)_2^+$, 275(4.6), $TaO(OH)(OMe)(OCH_2)^+$, 274(1.1), $Ta(OMe)_3^+$, 267(3.2), $ReO_2(OH)(OMe)^+$, 266(92.1), $ReO_3(OMe)^+$, 265(86.8), $ReO_3(OCH_2)^+$, 259(2.4), $TaO(OMe)_2^+$, 251(6.0), ReO_4^+, 249(4.6), $Re(OMe)_2^+$, 248(3.0), $Re(OCH_2)(OMe)^+$ and $Nb(OMe)_5^+$, 247(3.0), $Nb(OMe)_4(OCH_2)^+$, 238(9.4), $Re(OH)_3^+$, 237(12.4), $ReO(OH)_2^+$, , 236(100), $ReO_2(OH)^+$, 235(51.8), ReO_3^+, 234(96.8), $ReO(OMe)^+$, 233(27.3), $ReO(OCH_2)^+$, 231(2.4), $TaO(OH)_2^+$, 221(3.2), $Re(OH)_2^+$, 220(26.8), $ReO(OH)^+$, 219(95.7), ReO_2^+, 217(72.4), $Nb(OMe)_4^+$, 204(8.0), $Re(OH)^+$, 203(32.3), ReO^+ and $Nb(OMe)_3(OH)^+$, 187(15.3), Re^+, 186(2.3), $Nb(OMe)_3^+$, 172(22.9), $Nb(OMe)_2(OH)^+$, 171(15.1), $NbO(OMe)_2^+$, 157(5.5), $NbO(OH)(OMe)^+$, 155(4.1), $Nb(OMe)_2^+$, 141(3.3), $Nb(OMe)(OH)^+$, 140(2.9), $NbO(OMe)^+$, 139(4.4), $NbO(OCH_2)^+$, 125(5.7), NbO_2^+.

2.3. Alternative technique for the synthesis of $(Nb,Ta)_4O_2(OMe)_{14}(ReO_4)_2$ (II)

Solutions of $Nb(OMe)_5$ (0.132 g, 0.532 mmol) in 3.5 ml of $C_6H_5CH_3$ and $Ta(OMe)_5$ (0.178, 0.531 mmol) in 2.5 ml of $C_6H_5CH_3$ were mixed. Re_2O_7 (0.139 g, 0.288 mmol) was added to the obtained solution upon stirring. No color changes at the initial stage were observed. Upon slow dissolution of Re_2O_7, a brownish-violet color of the latter and precipitation of a small amount of lightly colored pink fine crystals were observed. After approximately 20 min of stirring, the solution was light pink in color. After 40 min of stirring most of the Re_2O_7 was dissolved and further formation of fine crystalline precipitate occurred. After 70 min the color of the solution was light orange–pink and almost all of the Re_2O_7 was dissolved. After 80 min the mixture was heated and the solution became brownish–pink. The mixture was refluxed for 15 min. In the course of the heating the dissolution of the initially formed crystals occurred. At the end of refluxing the solution became dark reddish-brown. The solution was cooled to r.t., then to −30 °C for crystallization. After 3 days the solution was decanted and the crystalline product (thick needle shaped crystals brownish-pink in color) was dried in vacuum. Yield: 0.258 g (64%). IR and MS data were identical to those reported above.

2.4. Crystallography

The crystal data and experimental conditions are shown in Table 1. The data were collected using a SMART CCD 1K diffractometer at 22 °C. All calculations were performed on an IBM PC using the SHELXTL-NT [10] program package. The absorption correction has been introduced for both experiments using Bruker SADABS program. Both structures were solved by direct methods. The positions of metal atoms were obtained from the initial solution and refined first in isotropic and then anisotropic approximation. The occupancy factors for all the metal atom positions in the structures of compounds **I** and **II** were refined in supposition that they can be occupied with equal opportunity by both niobium and tantalum atoms; the total occupancy for each position being 1.0. The values obtained are within experimental errors in agreement with those obtained by EDS-analysis. The positions of all other non-hydrogen atoms were obtained from difference Fourier syntheses and refined first in isotropic and then anisotropic approximation. The positions of hydrogen atoms were calculated geometrically and included into the final refinement in isotropic approximation; the thermal parameters for H-atoms were taken as $U_{iso} = 1.50U_{eq}(C)$, where $U_{eq}(C)$ is the equivalent parameter for the carbon atom to which the hydrogen atom is attached.

Table 1
Crystal data and details of diffraction experiments for compounds **I** and **II**

	I	**II**
Chemical formula	$C_8H_{24}NbO_{16}Re_2Ta$	$C_{14}H_{42}Nb_2O_{24}Re_2Ta_2$
Formula weight	1022.53	1514.60
Crystal system	monoclinic	monoclinic
Space group	$P2_1/c$	$P2_1/c$
a (Å)	8.564(2)	9.745(9)
b (Å)	12.982(3)	15.882(14)
c (Å)	10.597(2)	12.204(10)
α (°)	90	90
β (°)	97.279(4)	100.98(2)
γ (°)	90	90
V (Å^3)	1168.7(5)	1854(3)
Z	2	2
μ (mm^{-1})	15.532	13.054
Independent reflections	794 [R(int) = 0.1204]	2402 [R(int) = 0.0977]
Observed reflections	586 [$I > 2\sigma(I)$]	998 [$I > 2\sigma(I)$]
R_1	0.0677	0.0591
wR_2	0.1765	0.1134

3. Results and discussion

3.1. Reaction pathways

The reaction of the alkoxylation of rhenium heptoxide, Re_2O_7, has recently been proved to provide a facile access to bimetallic oxoalkoxide derivatives of rhenium [5,6] and it appeared attractive to investigate its potential for the preparation of trimetallic compounds, applying a bimetallic alkoxide as reactant. We have chosen in this purpose the bimetallic methoxide of niobium and tantalum formed easily on mixing the two homometallic species in hydrocarbon media [7] and existing due to the extraordinary likeness of the coordination geometries of the two metals, which permits to consider it as a product of isomorphous substitution of one metal in the structure with the other.

Carrying out of this reaction at ambient temperature was found to lead practically exclusively to compound **I**, independently of the ratio of the reactants:

$$Re_2O_7 + NbTa(OMe)_{10} \rightarrow (Nb,Ta)_2(OMe)_8(ReO_4)_2\ (\mathbf{I}) + \ldots$$

It may be supposed that the reaction pathway includes in this case, first, some partial oxidation of the methoxide ligands producing water that leads to formation of perrhenic acid, which produces compound **I** via the chemical modification of the bimetallic alkoxide:

$$Re_2O_7 + H_2O \rightarrow 2HReO_4$$

$$2HReO_4 + NbTa(OMe)_{10} \rightarrow (Nb,Ta)_2(OMe)_8(ReO_4)_2 + 2MeOH$$

In favor of this pathway speaks the quite high, but far not quantitative, yield of compound **I**, and the absence of the intensive coloration, indicating otherwise the formation of low-valent rhenium alkoxides in the course of the alkoxylation [5,6].

The processes occurring on heating follow evidently the mechanism proposed earlier [5,6] for the alkoxylation of rhenium heptoxide, but the elevated temperature leads to deeper condensation of the products resulting in formation of a more oxo-substituted tetranuclear core of compound **II**. It is to be noted also that compound **I** formed in the reaction mixture at low temperature can on further heating undergo an almost quantitative thermal condensation in solution with an excess of $NbTa(OMe)_{10}$ and provide **II** with a significantly increased yield in relation to Re_2O_7. The condensation occurs supposedly via partial oxidation of the methoxide ligand by the perrhenate ligand present, which provides the water necessary for this process.

It is important to note that the metal atom content in the product corresponds perfectly to that in the reaction media and the Nb:Ta = 1:1 ratio is conserved in the trimetallic products obtained opening the prospect of the application of these precursors in the preparation of trimetallic oxide and alloy materials.

3.2. Molecular structures

Unfortunately, both **I** and **II** are almost insoluble in common organic solvents at room temperature. On heating, they remain unchanged in hydrocarbons (toluene, hexane), while in methanol the crystals turn slowly dark, supposedly because of the reduction of rhenium(VII) by the alcohol, but still no transfer into solution of the metal-containing species could be observed. This precluded the application of NMR for the estimation of the possible molecular structures in solution (*in statu nascendi*) and those discussed below are the solid state ones obtained by the X-ray single crystal studies.

The structure of **I** (Fig. 1) turned out to be very close to the structures of its bimetallic analogues, $M_2(OMe)_8(ReO_4)_2$, M = Nb, Ta [6]. Its centrosymmetric molecules are pairs of octahedra sharing a common (μ-OR)$_2$ edge, the perrhenate substituents being situated in the axial positions. The oxo-bridging bond to the rhenium atom is as long M(1)–O(2) 2.12(2) Å as that in the structure of the tantalum-only derivative (Ta(1)–O(5) 2.115(16) Å) and has evidently also a decreased multiplicity. The terminal alkoxide ligand situated in the *trans*-position to it has quite logically a significantly shortened M(1)–O(7) 1.78(3) distance (compared to (Ta(1)–O(4) 1.814(19) Å in the tantalum-only analogue) with the multiplicity increased due to the p_π–d_π interaction. The bridging M–O distances are noticeably asymmetric and significantly longer than the terminal

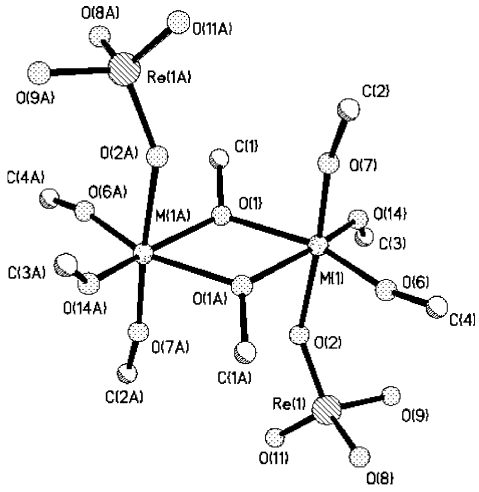


Fig. 1. Molecular structure of $(Nb,Ta)_2(OMe)_8(ReO_4)_2$ (**I**).

M–O bonds (M(1)–O(1) 2.13(2), M(1)–O(1)# 2.02(2) Å in **I** compared to Ta(1)–O(1) 2.08(2), Ta(1)–O(1)# 2.10(2) Å in $Ta_2(OMe)_8(ReO_4)_2$ [6]. The structure of **I** contains only one symmetrically independent position for the quinquevalent metal present, and its unit occupancy is achieved by 50% of niobium and by 50% by tantalum atoms within the standard deviations for this determination (Tables 2 and 3).

The structure of compound **II** (see Fig. 2) is built up of centrosymmetric molecules that contain a planar tetranuclear $M_4(\mu\text{-}O)_2(\mu\text{-}OMe)_4$ core, where M = Nb or Ta, coordinating 10 methoxo and 2 perrhenate ligands. The M–O(Me) distances fall into the range usually observed and are very close to those observed in the structures of the bimetallic analogues based on niobium- or tantalum-only cores [5]. The most interesting feature of this structure is the non-uniform distribution of niobium and tantalum between the two symmetrically

Table 2
Selected bond lengths and angles in the structure of **I**

Bond lengths			
Re(1)–O(11)	1.63(3)	M(1)–O(7)	1.78(3)
Re(1)–O(8)	1.65(3)	M(1)–O(14)	1.88(3)
Re(1)–O(9)	1.75(3)	M(1)–O(1)#1	2.02(2)
Re(1)–O(2)	1.74(2)	M(1)–O(1)	2.13(2)
M(1)–O(6)	1.76(2)	M(1)–O(2)	2.12(2)
Bond angles			
O(11)–Re(1)–O(8)	122.0(2)	O(14)–M(1)–O(1)#1	157.6(9)
O(11)–Re(1)–O(9)	102.0(2)	O(6)–M(1)–O(1)	161.1(10)
O(8)–Re(1)–O(9)	104.0(2)	O(7)–M(1)–O(1)	89.8(9)
O(11)–Re(1)–O(2)	110.5(14)	O(14)–M(1)–O(1)	93.0(9)
O(8)–Re(1)–O(2)	108.9(17)	O(1)#1–M(1)–O(1)	69.1(9)
O(9)–Re(1)–O(2)	109.5(17)	O(6)–M(1)–O(2)	88.0(11)
O(6)–M(1)–O(7)	96.0(12)	O(7)–M(1)–O(2)	175.7(10)
O(6)–M(1)–O(14)	104.2(10)	O(14)–M(1)–O(2)	84.6(9)
O(7)–M(1)–O(14)	96.0(10)	O(1)#1–M(1)–O(2)	80.9(9)
O(6)–M(1)–O(1)#1	92.3(10)	O(1)–M(1)–O(2)	85.9(9)

M(1) = (0.46 ± 0.05)Nb + (0.54 ± 0.05)Ta. Symmetry transformations used to generate equivalent atoms: #1 $-x+1, -y, -z$.

Table 3
Selected bond lengths and angles in the structure of **II**

Bond lengths			
M(1)–O(7)	1.772(16)	M(2)–O(2)	1.855(14)
M(1)–O(9)	1.878(14)	M(2)–O(4)#1	2.066(12)
M(1)–O(1)	1.888(14)	M(2)–O(6)#1	2.080(11)
M(1)–O(3)	2.043(11)	M(2)–O(5)	2.197(13)
M(1)–O(6)	2.056(13)	Re(3)–O(13)	1.53(2)
M(1)–O(4)	2.098(13)	Re(3)–O(11)	1.656(19)
M(2)–O(3)	1.791(11)	Re(3)–O(12)	1.67(3)
M(2)–O(8)	1.830(15)	Re(3)–O(5)	1.727(13)
Bond angles			
O(7)–M(1)–O(9)	101.0(7)	O(3)–M(2)–O(8)	98.8(6)
O(7)–M(1)–O(1)	95.5(7)	O(3)–M(2)–O(2)	97.7(5)
O(9)–M(1)–O(1)	96.9(6)	O(8)–M(2)–O(2)	101.4(6)
O(7)–M(1)–O(3)	87.4(6)	O(3)–M(2)–O(4)#1	93.7(5)
O(9)–M(1)–O(3)	88.6(5)	O(8)–M(2)–O(4)#1	160.2(5)
O(1)–M(1)–O(3)	173.1(6)	O(2)–M(2)–O(6)#1	157.1(6)
O(7)–M(1)–O(6)	163.3(6)	O(4)#1–M(2)–O(6)#1	69.6(5)
O(6)–M(1)–O(4)	69.5(5)	O(3)–M(2)–O(5)	175.7(6)
O(3)–M(1)–O(6)	85.4(5)	O(2)–M(2)–O(5)	83.4(6)
O(13)–Re(3)–O(11)	109.4(11)	O(13)–Re(3)–O(5)	110.4(11)
O(13)–Re(3)–O(12)	105.3(14)	O(11)–Re(3)–O(5)	111.5(9)
O(11)–Re(3)–O(12)	108.0(13)	O(12)–Re(3)–O(5)	112.1(11)
M(2)#1–O(4)–M(1)	109.6(6)	M(2)–O(3)–M(1)	173.2(7)
M(1)–O(6)–M(2)#1	110.7(5)	Re(3)–O(5)–M(2)	145.4(9)

M(1) = (0.29 ± 0.05)Nb + (0.71 ± 0.05)Ta,
M(2) = (0.70 ± 0.05)Nb + (0.30 ± 0.05)Ta. Symmetry transformations used to generate equivalent atoms: #1 $-x+1$, $-y$, $-z$.

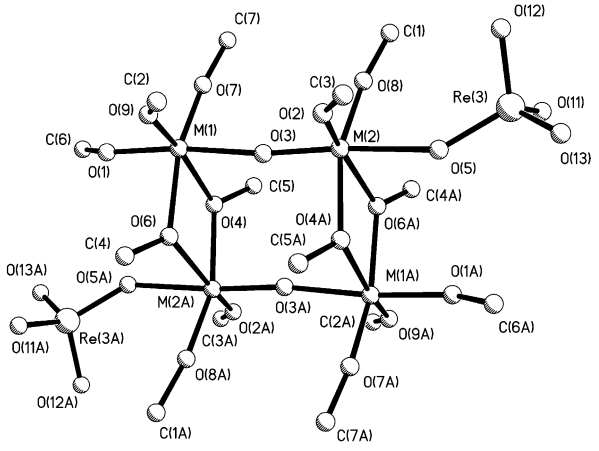


Fig. 2. Molecular structure of $(Nb,Ta)_4O_2(OMe)_{14}(ReO_4)_2$ (**II**).

independent positions: the M(1) position, surrounded by five alkoxide and one bridging oxoligand, turns out to be occupied by tantalum to 70% and niobium by 30% within the accuracy of the experiment, while the M(2) one, connected to four alkoxide, one bridging oxo- and one terminal perrhenate ligand, is in contrast richer in niobium (70%) and poorer in tantalum (30%). This difference can be explained by the difference in the chemical bonding for the atoms occupying these positions: the metal atom in M(1) is involved in the bonding of predominantly σ-character—even the bond to the oxoligand is a strongly elongated one (M(1)–O(3) 2.043(11) Å), which is thermodynamically preferential for the heavier tantalum atom. The metal atom in the M(2) position has a very much shorter distance to the bridging oxo-ligand (M(2)–O(3) 1.791(11) Å), which indicates a considerable π-input in its nature that can easier be made by a light niobium atom.

The difference in composition and molecular structures between compounds **I** and **II** is reflected also in the differences between their mass-spectra. Both compounds undergo a complete decomposition on evaporation. The preparative investigation of the thermal properties of **I** and **II** in vacuum showed the deposition of two different products on the cool parts of the glass vessel at the initial stage (135 °C, 10^{-2} mm Hg) of the sublimation process, namely the white film of a less volatile product and the reddish purple one of a more volatile product. The latter became dark on further heating and resembled the sublimation product of the $Re_4O_6(OMe)_{12}$ [5]. The formation of two different sublimation products should have occurred through the separation of rhenium- and niobium and tantalum-containing volatile methoxide species upon the decomposition of the complex compound. The mass-spectral investigation confirmed this observation as no heterometallic species containing rhenium together with niobium or tantalum could be observed in the spectra. The 'volatility' (total of intensities of different ions in the spectra) appears generally to be higher for **II**, containing a smaller number of oxidizing perrhenate ligands. It is also to be noted that the intensity of the tantalum-containing ions is relatively slightly but noticeably higher for **II** compared to **I**, reflecting thus the placement of predominantly tantalum atoms in the position not connected directly to the perrhenate ligands hindering volatility.

4. Supplementary material

Crystallographic data for the structural analysis have been deposited with the Cambridge Crystallographic Data Center, CCDC Nos. 185852 and 185853 for compounds **I** and **II**, respectively. Copies of this information may be obtained free of charge from The Director, 12 Union Road, Cambridge, CB2 1EZ, UK (fax: +44-1223-336033; e-mail: deposit@ccdc.cam.ac.uk or www: http://www.ccdc.cam.ac.uk).

Acknowledgements

The authors would like to express their gratitude for financial support of this work to the Swedish Council for the Scientific Research (Vetenskapsrådet), the Swed-

ish Royal Academy of Sciences (KVA), the Russian Foundation for Basic Research (project No. 0-03-32527) and the Ministry of Education of Russian Federation (project No. 1 "V"-27-871).

References

[1] R.C. Mehrotra, J. Sol-Gel Sci. Tech. 2 (1994) 1.
[2] N.Ya. Turova, E.P. Turevskaya, V.G. Kessler, M.I. Yanovskaya, The Chemistry of Metal Alkoxides, Kluwer Academic Publishers, London, 2002, p. 104.
[3] M. Veith, S. Mathur, C. Mathur, Polyhedron 17 (1998) 1005.
[4] A. Johansson, V.G. Kessler, Polyhedron 19 (2000) 1791.
[5] G.A. Seisenbaeva, A.V. Shevelkov, L. Kloo, S. Gohil, J. Tegenfeldt, V.G. Kessler, Dalton Trans. (2001) 2762.
[6] G.A. Seisenbaeva, V.G. Kessler, Inorg. Chem. Commun. 4 (2001) 534.
[7] L.G. Hubert-Pfalzgraf, A.A. Pinkerton, J.G. Riess, Inorg. Chem. 17 (1978) 663.
[8] P.A. Shcheglov, D.V. Drobot, G.A. Seisenbaeva, S. Gohil, V.G. Kessler, Chem. Mater. 14 (2002) 2378.
[9] E.P. Turevskaya, N.Ya. Turova, A.V. Korolev, A.I. Yanovsky, Yu.T. Struchkov, Polyhedron 14 (1995) 1531.
[10] SHELXTL-NT Reference Manual, Bruker AXS, 1998.

2. Experimental

2.1. Material and procedures

Experimental work was carried out under an atmosphere of dry nitrogen. All manipulations were conducted using Schlenk techniques, employing a vacuum/nitrogen line or using a glove box under an atmosphere of nitrogen. Solvents were distilled from K or Na suspension and kept in Schlenk flasks with K or Na mirror or else dry molecular sieves. NMR spectra were recorded at 100.62 MHz (^{13}C) and 148.97 MHz (^{119}Sn) using a Bruker DPX-400 spectrometer equipped with an 89 mm wide-bore magnet. ^{13}C shifts are reported relative to $SiMe_4$ and ^{119}Sn shifts relative to $SnMe_4$. ^{119}Sn Mössbauer spectra were collected with samples kept at 77 K using a $CaSnO_3$ source kept at room temperature. All spectra were fitted by means of Lorentzian line shapes. The infrared spectra were recorded with samples pressed as CsI pellets on a Perkin–Elmer 283B spectrometer in the 4.000–200 cm^{-1} range. Carbon, nitrogen and hydrogen analyses were performed on a Perkin–Elmer PE-2400 CHN-analyses using tin sample-tubes. Chlorine and bromine analyses were performed by means of X-ray fluorescence in Rigaku-Geigerflex spectrophotometer with samples pressed as borax plates. Tin analysis was carried out using a Hitachi Z-8200 atomic absorption spectrophotometer (Sn lamp, $\lambda_{max} = 224.6$ nm, N_2O/acetylene flame).

2.2. X-ray structure determination of **1**, **2**, **3** and **6**

The data were collected using a Siemens P4 diffractometer equipped with a SMART CCD area detector; graphite-monochromated Mo Kα. The structures were solved by direct methods with SHELXTL version 5.0 [10] and the refinements were carried out using SHELXTL96 software [11]. Further details are given in Table 1. Tables of atom positions and thermal parameters have been deposited with the CCDC. All non-H atoms were anisotropic. Methyl groups were fixed at idealised geometry but with the torsion angle defining the H atom positions refined and U_{iso}(H) equal to $1.5U_{eq}$(C). The ORTEP drawing shows the non-H atoms as 50% thermal vibration ellipsoids.

2.3. Synthesis of [Ru(η-C_5H_5)(PPh_3)$_2N_3$]

To a Schlenk flask containing [Ru(η-C_5H_5)(PPh_3)$_2$Cl] (0.5 g, 0.69 mmol), under an atmosphere of dry N_2, dissolved in 100 ml of ethanol, was added at once NaN_3 (0.67 g, 10.33 mmol). The resultant mixture was stirred and refluxed for 6 h. Thus, the solvent was partially removed under vacuum to 40 ml and an orange precipitate was obtained. After filtration the solid was washed with *n*-hexane and re-crystallised in a mixture of dichloromethane and *n*-hexane. Yield 85%. M.p. (dec.) 118–120. ^{1}H NMR ($CDCl_3$, 400.13 MHz), δ 4.2 (s, C_5H_5), 6.7–7.4 (m, C_6H_5); ^{13}C{^{1}H} NMR ($CDCl_3$, 100.61 MHz), δ 81.3 (s, C_5H_5), 127.6–131.2 (m, C_6H_5); ^{31}P{^{1}H} ($CDCl_3$, 161,98 MHz), δ 42.4 (s, PPh_3). IR (CsI) ν(N_3) 2005, δ(N_3) 675 ν(Ru–N) 390 cm^{-1}. Elemental analysis for $C_{41}H_{35}N_3P_2Ru$, calc. (found): C, 66.18 (67.20); H, 4.65 (4.81); N, 5.77 (5.73)%.

2.4. Synthesis of [Ru(η-C_5H_5)(dppe)N_3]

To a solution of [Ru(η-C_5H_5)(dppe)Cl] (0.25 g, 0.42 mmol) and 50 ml of ethanol in a Schlenk flask, under an atmosphere of dry N_2, was added at once NaN_3 (0.25 g, 2.5 mmol). After 6 h of stirring and reflux the solvent was partially removed under vacuum to 20 ml and an orange precipitate was obtained. Following filtration, the solid was washed with *n*-hexane and recrystallised in a mixture of CH_2Cl_2 and *n*-hexane. Yield 92%. M.p. (dec.) 245–255. ^{1}H NMR ($CDCl_3$, 400.13 MHz), δ 2.2 (m, CH_2), 4.5 (s, C_5H_5), 7,4–7.8 (m, C_6H_5); ^{13}C{^{1}H} NMR ($CDCl_3$, 100.61 MHz), δ 31.0 (m, CH_2), 81.9 (s, C_5H_5), 127.8–135.8 (m, C_6H_5); ^{31}P{^{1}H} ($CDCl_3$, 161.98 MHz), δ 81.5 (s, dppe). IR (CsI) ν(N_3) 2000, δ(N_3) 680 ν(Ru–N) 393 cm^{-1}. Elemental analysis for $C_{31}H_{29}N_3P_2Ru$, calc. (found): C, 59.62 (61.28); H, 4.10 (4.18); N, 6.59 (6.62)%.

2.5. Synthesis of [Ru(η-C_5H_5)(PPh_3)$_2SnF_3$]

To a Schlenk flask containing [Ru(η-C_5H_5)-(PPh_3)$_2N_3$] (0.47 g, 0.64 mmol), under an atmosphere of dry N_2, dissolved in 100 ml of ethanol, was added at once SnF_2 (0.20 g, 1.28 mmol). The resultant mixture was stirred and refluxed for 6 h. Thus, a yellow solution was separated by filtration from a colourless solid. Then the yellow solid was washed with *n*-hexane and recrystallised in a mixture of CH_2Cl_2 and *n*-hexane. Yield 70%. M.p. 199–202. ^{1}H NMR ($CDCl_3$, 400.13 MHz), δ 4.5 (s, C_5H_5), 7.1–7.4 (m, C_6H_5); ^{13}C{^{1}H} NMR ($CDCl_3$, 100.61 MHz), δ 81.3 (s, C_5H_5), 128.2–138.5 (m, C_6H_5); ^{31}P{^{1}H} ($CDCl_3$, 161.98 MHz), δ 48 (s, PPh_3) {$^2J_{(^{31}P-^{117}Sn)} = 480$ Hz, $^2J_{(^{31}P-^{119}Sn)} = 500$ Hz}, ^{119}Sn{^{1}H} ($CDCl_3$, 149.21 MHz), δ −357 (qt, SnF_3) {$^1J_{(^{19}F-^{119}Sn)} = 3714$ Hz, $^2J_{(^{31}P-^{119}Sn)} = 500$ Hz}. ^{119}Sn Mössbauer: isomer shift (IS) 1.53 mm s^{-1}, QS 2.17 mm s^{-1}. IR (CsI): ν(Sn–F) 490 cm^{-1}. Elemental analysis for $C_{41}H_{35}F_3P_2RuSn$, calc. (found): C, 54.22 (54.86); H, 3.44 (3.57); Sn, 13.18 (13.70)%.

2.6. Synthesis of [Ru(η-C_5H_5)(PPh_3)$_2SnCl_3$]

Was similarly prepared employing [Ru(η-C_5H_5)-(PPh_3)$_2$Cl] (0.35 g, 0.52 mmol) and $SnCl_2$ (0.09 g, 0.52

Table 1
Crystal data and structure refinement for **1**, **2**, **3** and **6**

	[Ru(η-C_5H_5)(PPh_3)$_2SnF_3$] (**1**)	[Ru(η-C_5H_5)(PPh_3)$_2SnCl_3$] (**2**)	[Ru(η-C_5H_5)(PPh_3)$_2SnBr_3$] (**3**)	[Ru(η-C_5H_5)(dppe)$SnBr_3$] (**6**)
Empirical formula	$C_{41}H_{35}F_3P_2RuSn$	$C_{41}H_{35}Cl_3P_2RuSn$	$C_{41}H_{35}Br_3P_2RuSn$	$C_{31}H_{29}Cl_3P_2SnRu$
Formula weight	908.85	1035.11	1668.49	1042.34
Temperature (K)	227(2)	293(2)	293(2)	193(2)
Wavelength (Å)	0.71073	0.71073	0.71073	0.71073
Crystal system	orthorhombic	monoclinic	monoclinic	monoclinic
Space group	*Pbca*	$P2_1/c$	$P2_1/c$	$P2_1/n$
Unit cell dimensions				
a (Å)	21.1767(3)	11.8421(10)	12.0346(10)	11.63290(10)
b (Å)	20.5368(3)	15.7095(10)	15.6844(10)	15.65340(10)
c (Å)	33.9725(3)	22.6490(10)	22.9077(10)	19.41120(10)
α (°)	90			
β (°)	90	95.615	95.620(10)	99.2030(10)
γ (°)	90			
V (Å^3)	1474.7(3)	4193.3(4)	4303.2(4)	3489.17(4)
Z	16	4	4	4
D_{calc} (Mg m^{-3})	1.634	1.640	1.804	1.984
Crystal size (mm)	0.26 × 0.26 × 0.15	0.43 × 0.33 × 0.16	0.43 × 0.33 × 0.16	0.26 × 0.25 × 0.18
Reflections collected/unique	18 006 [$R_{int} = 0.0949$]	6397/7439 [$R_{int} = 0.0182$]	8381/7983 [$R_{int} = 0.0486$]	37264/8419 [$R_{int} = 0.0460$]
Refinement method	semi-empirical from equivalents	full-matrix least-squares on F^2	full-matrix least-squares on F^2	full-matrix least-squares on F^2
Data/restraints/parameters	18 006/0/892	7439/0/478	7983/0/478	8419/0/499
Goodness-of-fit on F^2	1.064	1.048	0.986	1.160
Final R indices [$I > 2\sigma(I)$]	$R_1 = 0.0561$, $wR_2 = 0.12134$	$R_1 = 0.0322$, $wR_2 = 0.0882$	$R_1 = 0.0400$, $wR_2 = 0.0723$	$R_1 = 0.0388$, $wR_2 = 0.0654$
R indices (all data)	$R_1 = 0.1110$, $wR_2 = 0.1547$	$R_1 = 0.0564$, $wR_2 = 0.0969$	$R_1 = 0.1516$, $wR_2 = 0.0909$	$R_1 = 0.0585$, $wR_2 = 0.0723$
Largest difference peak and hole (e Å^{-3})	0.973 and −1.413	0.888 and −0.844	0.883 and −0.807	1.311 and −0.905
CCDC reference	166690	166691	166692	166693

mmol). Yield 85%. M.p. 188–189. ^{1}H NMR ($CDCl_3$, 400.13 MHz), δ 4.5 (s, C_5H_5), 7.0–7.4 (m, C_6H_5); $^{13}C\{^1H\}$ NMR ($CDCl_3$, 100.61 MHz), δ 81.3 (s, C_5H_5), 128.0–138.6 (m, C_6H_5); $^{31}P\{^1H\}$ ($CDCl_3$, 161.98 MHz), δ 45.4 (s, PPh_3) $\{^2J_{(^{31}P-^{119}Sn)} = 437$ Hz$\}$, $^{119}Sn\{^1H\}$ ($CDCl_3$, 149.21 MHz), δ −67.7 (t, $SnCl_3$) $\{^2J_{(^{119}Sn-^{31}P)} = 443$ Hz$\}$. ^{119}Sn Mössbauer: IS 1.98 mm s^{-1}, QS 1.93 mm s^{-1}. IR (CsI): ν(Sn–Cl) 272 and 290 cm^{-1}. Elemental analysis for $C_{41}H_{35}Cl_3P_2RuSn$, calc. (found): C, 53.77 (54.31); H, 3.85 (3.85); Cl, 11.61 (11.20); Sn, 12.96 (13.23)%.

2.7. Synthesis of [Ru(η-C_5H_5)(PPh_3)$_2SnBr_3$]

Was similarly prepared employing [Ru(η-C_5H_5)-(PPh_3)$_2N_3$] (0.26 g, 0.36 mmol) and $SnBr_2$ (0.20 g, 0,72 mmol). Yield 82%. M.p. 181–182. ^{1}H NMR ($CDCl_3$, 400.13 MHz), δ 4.5 (s, C_5H_5), 7.1–7.5 (m, C_6H_5); $^{13}C\{^1H\}$ NMR ($CDCl_3$, 100.61 MHz), δ 83.3 (s, C_5H_5), 128.0–137.5 (m, C_6H_5); $^{31}P\{^1H\}$ ($CDCl_3$, 161.98 MHz), δ 45.80 (s, PPh_3) $\{^2J_{(^{31}P-^{119}Sn)} = 409$ Hz$\}$, $^{119}Sn\{^1H\}$ ($CDCl_3$, 149.21 MHz), δ −139.2 (t, $SnBr_3$) $\{^2J_{(^{119}Sn-^{31}P)} = 417$ Hz$\}$. ^{119}Sn Mössbauer: IS 2.85 mm s^{-1}, QS 1.80 mm s^{-1}. IR (CsI): ν(Sn–Br) 260 and 265 cm^{-1}. Elemental analysis for $C_{41}H_{35}Br_3P_2RuSn$, calc. (found): C, 46.94 (46.90); H, 3.36 (3.37); Br, 22.85 (22.71); Sn, 11.31 (11.56)%.

2.8. Synthesis of [Ru(η-C_5H_5)(dppe)SnF_3]

Similarly prepared using [Ru(η-C_5H_5)(dppe)N_3] (0.39 g, 0.64 mmol) and SnF_2 (0.20 g, 1.27 mmol). Yield 70%. M.p. 271–273. ^{1}H NMR ($CDCl_3$, 400.13 MHz), δ 2.4–2.9 (m, CH_2), 4.9 (s, C_5H_5), 7.0–7.7 (m, C_6H_5); $^{13}C\{^1H\}$ NMR ($CDCl_3$, 100.61 MHz), δ 28.1 (s, CH_2), 81.1 (s, C_5H_5), 128.0–133.2 (m, C_6H_5); $^{31}P\{^1H\}$ ($CDCl_3$, 161.98 MHz), δ 79.7 (s, PPh_3) $\{^2J_{(^{31}P-^{119}Sn)} = 452$ Hz$\}$, $^{119}Sn\{^1H\}$ ($CDCl_3$, 149.21 MHz), δ −345 (qt, $SnCl_3$) $\{^1J_{(^{19}F-^{119}Sn)} = 3714$ Hz, $^2J_{(^{119}Sn-^{31}P)} = 443$ Hz$\}$. ^{119}Sn Mössbauer: IS 1.59 mm s^{-1}, QS 2.19 mm s^{-1}. IR (CsI): ν(Sn–F) 493 cm^{-1}. Elemental analysis for $C_{31}H_{29}F_3P_2RuSn$, calc. (found): C, 50.30 (51.15); H, 3.95 (3.65); Sn, 16.03 (15.05)%.

2.9. Synthesis of [Ru(η-C_5H_5)(dppe)$SnCl_3$]

Prepared similarly reacting [Ru(η-C_5H_5)(dppe)Cl] (0.35 g, 0.52 mmol) with $SnCl_2$ (0.09 g, 0,52 mmol). Yield 85%. M.p. 255–257. ^{1}H NMR ($CDCl_3$, 400.13 MHz), δ 2.3–3.0 (m, CH_2), 4.9 (s, C_5H_5), 7.0–8.0 (m, C_6H_5); $^{13}C\{^1H\}$ NMR ($CDCl_3$, 100.61 MHz), δ 27.7 (s,

CH_2), 80.4 (s, C_5H_5), 128.3–133.1 (m, C_6H_5); $^{31}P\{^1H\}$ ($CDCl_3$, 161.98 MHz), δ 77.8 (s, PPh_3) $\{^2J_{(^{31}P-^{119}Sn)} = 389$ Hz$\}$, $^{119}Sn\{^1H\}$ ($CDCl_3$, 149.21 MHz), δ −22.3 (t, $SnCl_3$) $\{^2J_{(^{119}Sn-^{31}P)} = 389$ Hz$\}$. ^{119}Sn Mössbauer: IS 1.92 mm s^{-1}, QS 1.94 mm s^{-1}. IR (CsI): ν(Sn–Cl) 276 and 291 cm^{-1}. Elemental analysis for $C_{31}H_{29}Cl_3P_2RuSn$, calc. (found): C, 47.15 (46.39); H, 3.70 (3.65); Cl, 13.46 (13.38); Sn, 15.03 (15.15)%.

2.10. Synthesis of [Ru(η-C_5H_5)(dppe)$SnBr_3$]

Synthesised in a similar way using [Ru(η-C_5H_5)(dppe)N_3] (0.22 g, 0.36 mmol) and $SnBr_2$ (0.20 g, 0,72 mmol). Yield 82%. M.p. 253–255. ^{1}H NMR ($CDCl_3$, 400.13 MHz), δ 2.2–3.3 (m, CH_2), 4.9 (s, C_5H_5), 7.2–7.8 (m, C_6H_5); $^{13}C\{^1H\}$ NMR ($CDCl_3$, 100.61 MHz), δ 28.1 (s, CH_2), 81.1 (s, C_5H_5), 128.4–133.2 (m, C_6H_5); $^{31}P\{^1H\}$ ($CDCl_3$, 161.98 MHz), δ 77.4 (s, PPh_3) $\{^2J_{(^{31}P-^{117}Sn)} = 355$ Hz, $^2J_{(^{31}P-^{119}Sn)} = 370$ Hz$\}$, $^{119}Sn\{^1H\}$ ($CDCl_3$, 149.21 MHz), δ −110.8 (t, $SnCl_3$) $\{^2J_{(^{119}Sn-^{31}P)} = 373$ Hz$\}$. ^{119}Sn Mössbauer: IS 2.05 mm s^{-1}, QS 1.80 mm s^{-1}. IR (CsI): ν(Sn–Cl) 256 and 263 cm^{-1}. Elemental analysis for $C_{31}H_{29}Cl_3P_2RuSn$, calc. (found): C, 40.30 (41.10); H, 3.17 (3.05); Br, 26.00 (25.02); Sn, 12.86 (12.85)%.

3. Results and discussion

The starting material [Ru(η-C_5H_5)$(PPh_3)_2$Cl] was prepared as follows (Eq. (1)):

$$RuCl_3 \cdot xH_2O + C_5H_6 + 2PPh_3 \xrightarrow{EtOH} [Ru(\eta\text{-}C_5H_5)(PPh_3)_2Cl] + \text{other products} \quad (1)$$

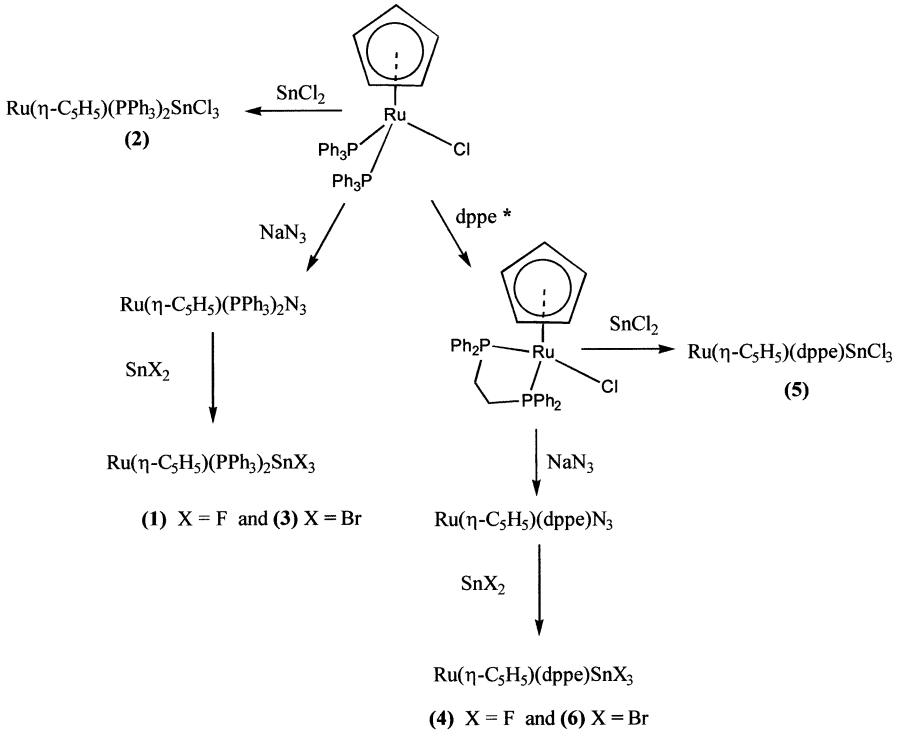
The authentication was carried out by experiments of multinuclear NMR, which showed the expected resonances for ^{1}H at δ 4.1 (C_5H_5) and 6.7–7.5 (C_6H_5); for $^{13}C\{^1H\}$ at δ 81 (C_5H_5) and 127–139 (C_6H_5); and $^{31}P\{^1H\}$ at δ 39.6. Its identity was confirmed by infrared spectroscopic studies as well as by melting point and carbon and hydrogen elemental analysis.

The insertion of SnX_2 into the Ru–X bond was conducted by reacting [Ru(η-C_5H_5)$(PPh_3)_2$Cl] or [Ru(η-C_5H_5)(dppe)Cl] with NaN_3 and following equimolar addition of SnX_2 (Scheme 1).

In all experiments the starting materials were refluxed with SnX_2 {X = F, Cl, Br} in EtOH for 6 h. After removing part of the solvent a precipitate was isolated and filtrated.

3.1. Reactions of [Ru(η-C_5H_5)$(PPh_3)_2N_3$] with SnX_2 (X = F, Cl and Br)

The reaction of [Ru(η-C_5H_5)$(PPh_3)_2$Cl] with NaN_3 yielded [Ru(η-C_5H_5)$(PPh_3)_2N_3$] which was treated with



Scheme 1. Reactions of [Ru(η-C_5H_5)$(PPh_3)_2$X] where X = F, Cl and Br. * The exchanging reaction of PPh_3 by dppe also yielded the boat and chair conformer of [{Ru(η-C_5H_5)Cl}$_2$(μ-dppe)$_2$]. However, for the insertion of $SnCl_2$ or the reaction with NaN_3 only the major product [Ru(η-C_5H_5)(dppe)Cl] was employed [12,13].

equimolar amounts of SnX_2. [Ru(η-C_5H_5)(PPh_3)$_2SnF_3$] (**1**), [Ru(η-C_5H_5)(PPh_3)$_2SnCl_3$] (**2**) and [Ru(η-C_5H_5)(PPh_3)$_2SnBr_3$] (**3**) were isolated as mixture-free derivatives. They were obtained as air- and moisture-stable orange crystalline solids, readily soluble in polar organic solvents. After recrystallisation from a mixture of CH_2Cl_2/*n*-hexane compounds **1**, **2** and **3** showed acceptable melting points at 199–202, 188–189 and 181–182 °C, respectively, as well as satisfactory elemental analysis.

All three compounds were studied by X-ray crystallography (Table 1). Apart from the Ru–Sn and Sn–X distances, the other structural results revealed similar angles and bond lengths for all three compounds. The X-ray study of **1** showed the presence of two unique molecules in the unit cell, not related one to another by symmetry but linked by an intermolecular F···H bond, 2.43 Å at the Cp ring. Such interactions are observed only in the solid state since no splitting of the hydrogen atoms or coupling with the fluorine was observed in the solution-state ^{1}H NMR spectrum (Figs. 1 and 2).

The $RuCp(PPh_3)_2$ fragment remains almost unchanged when the Cl is replaced by the SnX_3^- anion. The geometry at the Sn(II) centre is pyramidal trigonal with the Sn–X bond of 1.956 Å (av.), X = F, 2.394 Å (av.), X = Cl and 2.549 Å (av.) X = Br. The Ru–Sn distance, 2.5375 (av.) Å in the fluorine compound is a bit shorter than in the other two derivatives, implying a stronger interaction of the Ru fragment with the Sn moiety. The Sn–Cl bond in **2** is comparable with other known results and lies in the range of bond lengths which should be expected for such complexes [8,9]. All the molecules present a quasi-symmetry plane through Sn, Ru and the centroid of the Cp ring (Table 2).

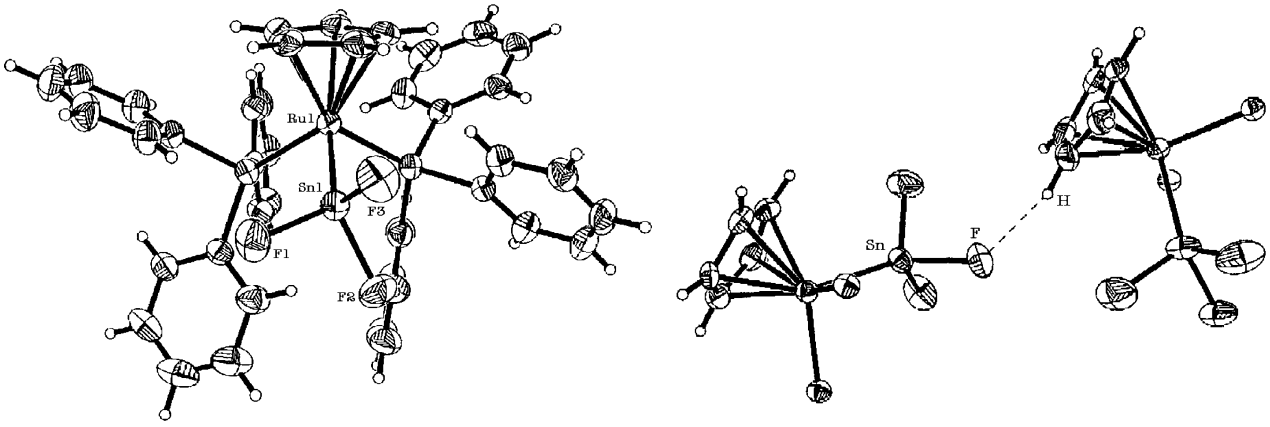


Fig. 1. The molecular structure of **1** and atom numbering scheme. For clarity the hydrogen atoms have been omitted in (A) and in (B) also the phenyl groups.

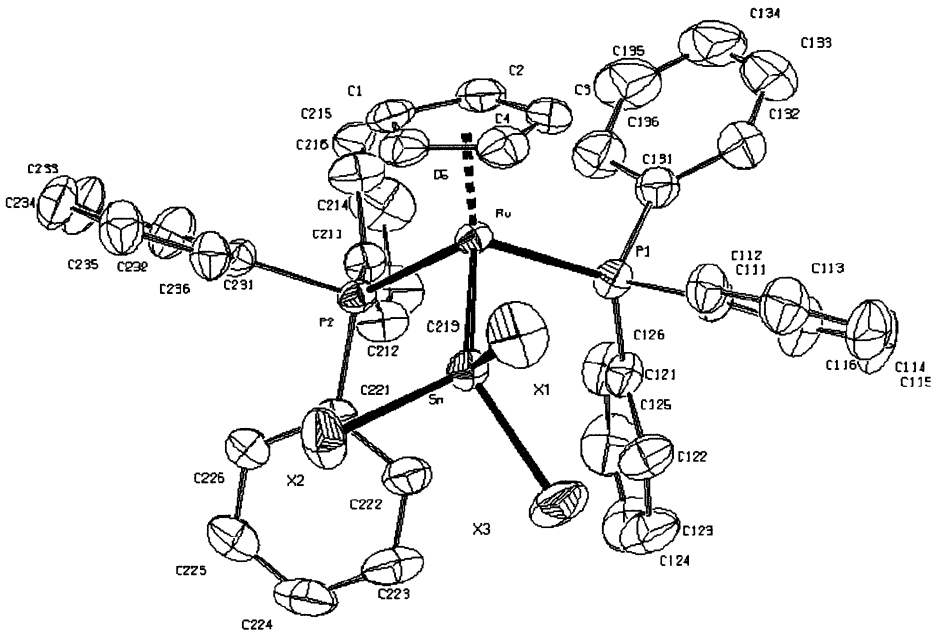


Fig. 2. The molecular structure of **2**, X = Cl, and **3**, X = Br, and atom numbering scheme. Hydrogen atoms have been omitted for clarity.

Table 2
Selected bond lengths (Å) and angles (°) for **1**, **2**, **3** and **6**

1				**2**		**3**		**6**	
Bond lengths									
Ru(1)–Sn(1)	2.5392(5)	Ru(1)–P(1)	2.3499(14)	Ru–Sn	2.5720(4)	Ru–Sn	2.5854(7)	Ru–Sn	2.5649(4)
Ru(1)–P(2)	2.3306(14)	Sn(1)–F(1)	1.949(4)	Ru–P(2)	2.3475(10)	Ru–P(2)	2.3533(17)	Ru–P(2)	2.2907(10)
Sn(1)–F(2)	1.954(4)	Sn(1)–F(4)	1.965(4)	Sn–Cl(2)	2.3790(12)	Sn–Br(2)	2.5600(9)	Sn–Br(2)	2.5639(5)
Ru(1)–M	2.229(5)	Ru(2)–P(3)	2.3226(14)	Ru–M	2.210(9)	Ru–M	2.2136(6)	Ru–M	2.2238(4)
Ru(2)–Sn(2)	2.5357(6)	Sn(2)–F(4)	1.952(4)	Ru–P(1)	2.3461(10)	Ru–P(1)	2.3504(17)	Ru–P(1)	2.2871(10)
Ru(2)–P(4)	2.3243(14)	Sn(2)–F(6)	1.961(4)	Sn–Cl(1)	2.4019(12)	Sn–Br(1)	2.5579(9)	Sn–Br(1)	2.5478(5)
Sn(2)–F(5)	1.956(4)	Ru(2)–M	2.2254(6)	Sn–Cl(3)	2.4012(12)	Sn–Br(3)	2.5298(8)	Sn–Br(3)	2.5408(5)
Bond angles									
P(1)–Ru(1)–Sn(1)	96.28(4)	P(2)–Ru(1)–Sn(1)	94.79(4)	P(1)–Ru–Sn	93.75(3)	P(1)–Ru–Sn	94.26(3)	P(1)–Ru–Sn	89.48(3)
F(1)–Sn(1)–F(2)	93.88(17)	F(1)–Sn(1)–F(3)	93.09(17)	Cl(1)–Sn–Cl(2)	94.68(5)	Br(1)–Sn–Br(2)	92.56(3)	Br(1)–Sn–Br(2)	95.26(2)
F(2)–Sn(1)–F(3)	94.21(17)	F(1)–Sn(1)–Ru(1)	120.47(12)	Cl(2)–Sn–Cl(3)	95.73(5)	Br(2)–Sn–Br(3)	95.47(7)	Br(2)–Sn–Br(3)	94.32(2)
F(2)–Sn(1)–Ru(1)	127.21(12)	F(3)–Sn(1)–Ru(1)	119.21(12)	Cl(2)–Sn–Ru	122.69(3)	Br(2)–Sn–Ru	128.72(3)	Br(2)–Sn–Ru	122.77(3)
P(3)–Ru(2)–Sn(2)	94.52(4)	P(2)–Ru(2)–Sn(2)	94.37(4)	P(2)–Ru–Sn	93.75(5)	P(2)–Ru–Sn	97.25(3)	P(2)–Ru–Sn	100.20(3)
F(4)–Sn(2)–F(5)	93.96(17)	F(4)–Sn(2)–F(6)	93.38(17)	Cl(1)–Sn–Cl(3)	92.88(5)	Br(1)–Sn–Br(3)	94.98(3)	Br(1)–Sn–Br(3)	101.07(2)
F(5)–Sn(2)–F(6)	93.8(17)	F(4)–Sn(2)–Ru(2)	94.37(4)	Cl(1)–Sn–Ru	114.02(4)	Br(1)–Sn–Ru	114.02(2)	Br(1)–Sn–Ru	112.31(3)
F(5)–Sn(2)–Ru(2)	117.79(13)	F(6)–Sn(2)–Ru(2)	121.59(13)	Cl(3)–Sn–Ru	108.90(4)	Br(3)–Sn–Ru	122.85(3)	Br(3)–Sn–Ru	125.34(3)

The results of ^{1}H, ^{13}C and ^{31}P NMR spectroscopy were unexceptional since no great differences were observed in the chemical shifts comparing with other reported results [5,6]. On the other hand, the ^{119}Sn NMR chemical shifts revealed interesting aspects of the bonding scheme in the compounds described here.

It was expected, the greater the halogen electronegativity, the lesser the shielding effect at the Sn centre. For the Cl and Br containing derivatives the chemical shifts, δ −68 (t) for **2** and −139 (t) for **3** are in accordance with the deshielding effect caused for the electronegativity of the halogens. However, compound **1** shows an abnormal value for the ^{119}Sn resonance, δ −357. In our opinion the ^{119}Sn chemical shift in this compound is heavily affected by an anomalous π contribution in the bonding scheme at the Sn(II) centre. In order to counterbalance the strong electronic withdraw inductive effect of the fluorine atom, the Sn centre forms a π-back bond with the Ru atom, stronger than in the other derivatives, which increases the shielding effect on the ^{119}Sn nucleus. Another indication for this is the higher $^{2}J_{(^{31}P-^{119}Sn)}$ coupling constant, 500 Hz, which indicates a closer approach of Sn and P in **1** in the P–Ru–Sn system. In fact the Ru–Sn bond is a bit shorter in **1** compared to the others.

Concerning the infrared spectroscopic studies, the most important signals observed in the spectra were the $\nu_{(Sn-X)}$, 490 cm^{-1} {X = F}, 290 and 272 cm^{-1} {X = Cl} and 265 and 260 cm^{-1} {X = Br}.

In contrast to the ^{119}Sn NMR chemical shifts, the IS obtained from studies of ^{119}Sn Mössbauer spectroscopy revealed an increasing in the IS values with the decreasing of the halogen electronegativity, 1.53 mm s^{-1} (**1**), 1.98 mm s^{-1} (**2**) and 2.10 mm s^{-1}(**3**). The Mössbauer experiments revealed that the π-bond contribution to the bonding scheme does not cause a great change in the Mössbauer spectroscopic data, as expected, since the IS parameters depends only of the *s*-electrons density. The second set of data, QS 2.17 mm s^{-1} (**1**), 1.93 mm s^{-1} (**2**) and 1.79 mm s^{-1} (**3**) showed differences in the symmetry of charge distribution.

3.2. Reactions of $[Ru(\eta\text{-}C_5H_5)(dppe)N_3]$ with SnX_2 (X = F, Cl and Br)

The compound $[Ru(\eta\text{-}C_5H_5)(dppe)N_3]$ was prepared by reacting $[Ru(\eta\text{-}C_5H_5)(dppe)Cl]$ [12] with NaN_3 [13].

Similar reactions with equimolar amounts of SnX_2 {X = F, Cl, Br} afforded $[Ru(\eta\text{-}C_5H_5)(dppe)SnF_3]$ (**4**), $[Ru(\eta\text{-}C_5H_5)(dppe)SnCl_3]$ (**5**) and $[Ru(\eta\text{-}C_5H_5)(dppe)SnBr_3]$ (**6**). These compounds were also isolated as air- and moisture-stable crystalline solids and gave satisfactory elemental analysis and melting points 270–272, 255–257 and 252–254 °C.

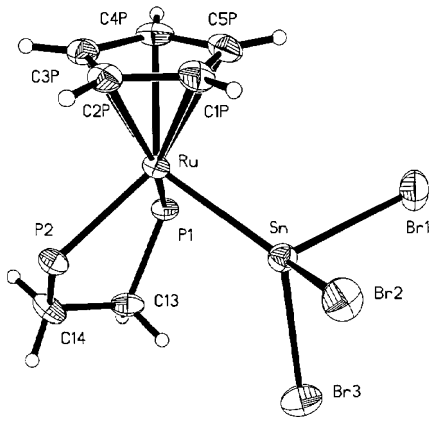


Fig. 3. The molecular structure of **6** and atom numbering scheme. Phenyl rings have been omitted for clarity.

The X-ray crystallographic determination of compound **6** served to compare structural features of compounds **6** with **3** (Fig. 3).

Compound **6** displays shorter Ru–P and Ru–Sn bonds, 2.2889 (av.) and 2.5649(4) Å versus 2.3519 (av.) 2.5854(7) observed for **3**, respectively. Also a smaller P–Ru–P angle, 82.91(4)°, is revealed for **6** compared to the same angle in **3**, 102.00(4)°. It is tentatively explained considering that the two phenyl groups bonded to the phosphorous and the bidentate nature of dppe renders it a less hindered ligand than PPh_3. It causes smaller P–Ru–P angles in **6**, as pointed to by the structural determination. The decrease in the steric effect permits a closer approach of the groups effecting shorter Ru–P and Ru–Sn bonds.

The ^{119}Sn NMR results show that in all the dppe containing derivatives the ^{119}Sn chemical shifts, (**4**) δ −345 (q), (**5**) δ −22 (t) and (**6**) δ −111 (t), locates in higher frequency indicating a decrease in the electronic density at the Sn atom. It is also reflected in the smaller $^{119}Sn-^{31}P$ coupling constants, 444, 390 and 373 Hz, respectively.

The Sn(II) chemical shift in **1**–**6** is not far from the signal exhibited by other Ru–Sn based compounds, such as $[Ru(SnCl_3)_6]^{4-}$, δ −34.6 [14], $[Ru(SnCl_3)_5Cl]^{4-}$, δ −167.9 (equatorial), −149.2 (axial), $[Ru(SnCl_3)_5(MeCN)]^{3-}$, δ −70.6 (equatorial), −103.9 (axial) [15] and *cis*-$[Ru(CO)_4(SnMe_3)_2]$, δ −207.

The changing of ligands caused no differences in the infrared data since in each compound the signals corresponding to $\nu_{(Sn-X)}$, were observed at 493 cm^{-1} {X = F}, 291 and 276 cm^{-1} {X = Cl} and 256 and 257 cm^{-1} {X = Br}, which are coincident with the previous results.

Also no great changes were observed in the ^{119}Sn Mössbauer spectroscopic data. The IS values, 1.59, 1.98 and 2.05 mm s^{-1} and QS data, 2.19, 1.94, 1.80 mm s^{-1} obtained for the dppe derivatives are very close to the

Table 3
Methanol conversion into methyl acetate catalysed by compounds **1**–**6**

[Catalyst] (10^{-3} mol l^{-1})	Rate of methyl acetate formation (10^{-4} mol l^{-1} h^{-1})					
	1	**2**	**3**	**4**	**5**	**6**
1.00	4.4	6.7	4.4	2.4	1.2	1.1
0.50	2.5	3.6	2.0	2.3	1.0	1.0
0.25	1.2	2.3	1.2	2.0	0.6	0.5
0.10	0.6	1.7	0.6	1.3	0.6	0.6

PPh_3 derivatives, indicating little change in the *s*-electronic density at the Sn centre.

3.3. Catalysis reactions

Compounds **1**–**6** showed to be active in the catalytic process of obtaining acetic acid from methanol. The catalytic cycle described here can be more interesting than Monsanto's because it needs only methanol as starting material and uses less expensive material (Ru + Sn vs. Rh) without a corrosive iodide promoter [16]. The only product observed was acetic acid detected as methyl acetate. Neither formaldehyde, which is supposed to be the intermediate in methanol conversion to acetic acid [14], nor methyl formate, possible product of formaldehyde dimerisation, was detected in all cases. We believe that the nature of the phosphorus-containing ligand, the nature of the halogen as well as the presence of the Ru–Sn bond exerts a strong influence on the catalytic activity of complexes (Table 3).

The order of catalytic activity of the complexes follows the halogen electronegativity, the SnF_3 bearing derivatives being far more efficient than the others. It seems to be related to the more efficient π-back donation from the Ru fragment to the Sn centre in the SnF_3^- containing products. It is possible that such a bonding scheme generates an extra positive density of charge in the Ru atom, which could facilitate a coordination to the oxygen atom of the methanol.

4. Supplementary material

Tables of atom positions and thermal parameters have been deposited with the Cambridge Crystallographic Data Centre, CCDC Nos. 166690, 166691, 166692 and 166693 for compounds **1**, **2**, **3** and **6**, respectively. Copies of this information may be obtained free of charge from The Director, CCDC, 12 Union Road, Cambridge, CB2 1EZ, UK (fax: +44-1223-336033; e-mail: deposit@ccdc.cam.ac.uk or www: http://www.ccdc.cam.ac.uk).

Acknowledgements

The authors are grateful to CNPq and Fapemig for financial support.

References

[1] T. Blackmore, M.I. Bruce, F.G.A. Stone, J. Chem. Soc. A (1971) 2376.
[2] (a) G. Domazetis, B. Tarpez, D. Dolphim, B.R. James, J. Chem. Soc., Chem. Commun. (1980) 939;
(b) G. Domazetis, B.R. James, B. Tarpez, D. Dolphim, ACS Symp. Ser. 78 (1981) 152.
[3] (a) G. Stedman, J. Chem. Soc. (1960) 1702;
(b) A. Haim, H. Taube, Inorg. Chem. 2 (1963) 1199.
[4] (a) R.F. Ziolo, Z. Dori, J. Am. Chem. Soc. 90 (1968) 6560;
(b) A.P. Gaughan, K.S. Bowman, Z. Dori, Inorg. Chem. 11 (1972) 601.
[5] M.I. Bruce, M.G. Humphrey, A.G. Swincer, R.C. Wallis, Aust. J. Chem. 37 (1984) 1747.
[6] E.M. Moura, M.H. Dickman, H.G.L. Siebald, G.J. Gama, Polyhedron 18 (1999) 2899.
[7] (a) O.V. Gusev, T.A. Peganova, M.A. Ievlev, A.G. Kropotova, K.A. Lyssenko, P.V. Petrovskii, Y.F. Oprunenko, N.A. Ustynyuk, J. Organomet. Chem. 622 (2001) 221;
(b) T. Lee, S.W. Lee, H.G. Jang, S.O. Kang, J. Ko, Organometallics 20 (2001) 741;
(c) Y. Ishikawa, M.S. Liao, C.R. Cabrera, Surf. Sci. 463 (2000) 66;
(d) W.M. Teles, N.L. Speziali, C.A.L. Filgueiras, Polyhedron 19 (2000) 739;
(e) E.V. Gusevskaya, E.N. dos Santos, R. Augusti, J. Mol. Catal. A Chem. 152 (2000) 15;
(f) R.D. Hoffmann, D. Kussmann, U.C. Rodewald, Z. Naturforsch., Teil B 54 (1999) 709;
(g) W.M. Teles, N.G. Fernandes, A. Abras, C.A.L. Filgueiras, Transition Met. Chem. 24 (1999) 321;
(h) M.C. Janzen, H.A. Jenkins, L.M. Rendina, Inorg. Chem. 38 (1999) 2123.
[8] (a) R.O. Gould, W.J. Sime, T.A. Stephenson, J. Chem. Soc., Dalton Trans. (1978) 76;
(b) J.D. Korp, I. Bernal, Inorg. Chem. 20 (1961) 4065;
(c) L.J. Farrugia, B.R. James, C.R. Lassigne, E.J. Wells, Inorg. Chim. Acta 53 (1981) L261;
(d) L.J. Farrugia, B.R. James, C.R. Lassigne, E.J. Wells, Can. J. Chem. 60 (1982) 1304;
(e) B. Moreno, S. Sabo-Etienne, F. Dahan, B. Chaudret, J. Organomet. Chem. 498 (1995) 139;
(f) M. Akita, R. Hua, T. Oku, M. Tanaka, Y. Moro-oka, Organometallics 15 (1996) 4162;

(g) R.D. Adams, D.A. Katahira, Organometallics 1 (1982) 53;
(h) M. Elder, D. Hall, J. Chem. Soc. A (1970) 245.
[9] G. Consiglio, F. Morandini, G. Ciani, M.K. Kretschmer, J. Am. Chem. Soc. 105 (1983) 1391.
[10] G.M. Sheldrick, SHELXL 5.0, Siemens Analytical Instruments, Madison, WI, 1994.
[11] G.M. Sheldrick, SHELXL 96, University of Göttingen, Göttingen, Germany, 1996.
[12] In the synthesis of [Ru(η-C_5H_5)(dppe)Cl], another species, [{Ru(η-C_5H_5)Cl}$_2$(μ-dppe)$_2$], in the chair and boat conformation was also obtained. However, only the first one was employed in the synthesis of **4**, **5** and **6**.
[13] (a) In the exchange of Cl^- for N_3^-, using the chair and boat conformers, we observed the formation of only the chair conformer which was fully characterised by elemental analysis, multinuclear NMR spectroscopy as well as by X-ray crystallography;
(b) Ref. [4b];
(c) E.M. Moura, H.G.L. Siebald, G.M. de Lima, unpublished results.
[14] H. Moriyama, T. Aoki, S. Shimoda, Y. Saito, J. Chem. Soc., Chem. Commun. (1982) 500.
[15] N.W. Alcock, J.H. Nelson, J. Chem. Soc., Dalton Trans. (1982) 2415.
[16] (a) T. Yamakawa, M. Hiroi, S. Shinoda, J. Chem. Soc., Dalton Trans. (1994) 2265;
(b) S. Shinoda, T. Ohnishi, T. Yamakawa, Catal. Surv. Jpn. 1 (1997) 25;
(c) T. Blackmore, M.I. Bruce, F.G.A. Stone, J. Chem. Soc. A (1971) 2376.

the carboxylic acid [HORc = HO_2CH, HO_2CCH_3, HO_2CCHMe_2, HO_2CCMe_3 (HOBc), $HO_2CCH_2CMe_3$(HONc)], control over the final structures of these ORc-modified $Ti(OR)_4$ complexes was realized. A demonstration of this synthetic control was illustrated through the reaction of HOBc and [Ti(μ-ONep)(ONep)$_3$]$_2$ which, due to steric constraints, yielded the first simple-metathesis, unesterified species, [Ti(μ-OBc)(μ-ONep)(ONep)$_2$]$_2$. One general trend that was noted from this study, and has been shown for other metal systems [10,14–20], was that the ONep ligated species yielded alternative arrangements that were typically lower in nuclearity in comparison to other OR derivatives.

Group 5 $M(OR)_5$ (M = Nb, Ta) are also widely used to prepare a variety of materials; however, little work has been presented concerning the products of HORc-modified Group V compounds. One exception is the report by Hubert-Pfalzgraf and co-workers [21] which detailed the formation of [Nb$_2$(μ-O)$_2$(OMc)$_2$(OCHMe$_2$)$_4$]$_2$, where OMc = $O_2CCMeCH_2$, from the reaction of $Nb(OCHMe_2)_5$ and HOMc (higher yields were realized through the stoichiometric addition of water). In the same report, the acetate (OAc) derivative, [Nb$_2$(μ-O)$_2$(OAc)$_2$(OCHMe$_2$)$_4$]$_2$ was formed from a mixture of $Nb(OCHMe_2)_5$ and $La(OAc)_3\cdot 2HOAc$. Fig. 1 shows the schematic representation of the central core of these compounds.

We were interested in the effects that could be induced using the ONep ligand and sterically hindered ORc with Group 5 cations. Therefore, we investigated the reactions between [M(μ-OEt)(ONep)$_4$]$_2$ (M = Nb (**1**) [15] and Ta (**2**) [17] (see Fig. 2), and HORc where ORc = OBc, ONc to determine the esterification products that were formed (Eq. (1)). The products isolated from the room temperature reactions (Eqs. (2)–(5)) were characterized as [Nb(μ-OBc)(ONep)$_3$]$_2$(μ-O) (**3**), [Nb(μ-O)(μ-ONc)(ONep)$_2$]$_4$ (**4**), [Ta(μ-OBc)(ONep)$_3$]$_2$(μ-O) (**5**), and [Ta(μ-ONc)(ONep)$_4$]$_2$ (**6**). Upon heating of identical reaction mixtures (Eqs. (6) and (7)), only the Ta system yielded additional structural species: [Ta(μ-O)(OBc)(ONep)$_4$]$_2$, (**7**), [Ta(μ-ONc)(ONep)$_3$]$_2$(μ-O) (**8**), and [Ta(μ-O)(μ-ONc)(ONep)$_2$]$_4$ (**9**). Collectively, these compounds lend structural insights into the esterification pathway of Group V alkoxides (see Scheme 1). This work presents the details of the syntheses, characterizations, solid and solution state behaviors of **3**–**8** and a comparison to other HORc modified Group V compounds available in the literature.

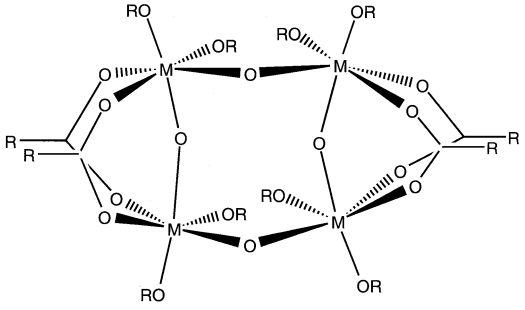


Fig. 1. Schematic representation of the central core of fully esterified carboxylic acid modified Group V complexes.

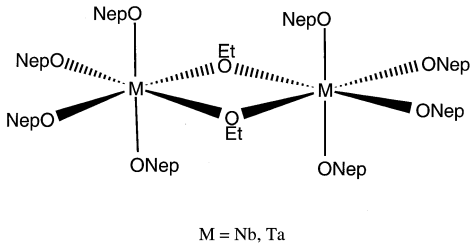


Fig. 2. Schematic representation of [M(μ-OEt)(ONep)$_4$]$_2$ where M = Nb (**1**) or Ta (**2**).

$$[M(OEt)(ONep)_4]_2 + 2HORc \xrightarrow[ORc=OBc,\ ONc]{M=Ta,\ Nb} \rightarrow M_w(O)_x(ORc)_y(ONep)_z \quad (1)$$

$$[Nb(OEt)(ONep)_4]_2 + 2HOBc \rightarrow [Nb(OBc)(ONep)_3]_2(O) \quad (2)$$

$$[Nb(OEt)(ONep)_4]_2 + 2HONc \rightarrow [Nb_2(O)(ONc)_2(ONep)_4]_2 \quad (3)$$

$$[Ta(OEt)(ONep)_4]_2 + 2HOBc \rightarrow [Ta(OBc)(ONep)_3]_2(O) \quad (4)$$

$$[Ta(OEt)(ONep)_4]_2 + 2HONc \rightarrow [Ta(ONc)(ONep)_4]_2 \quad (5)$$

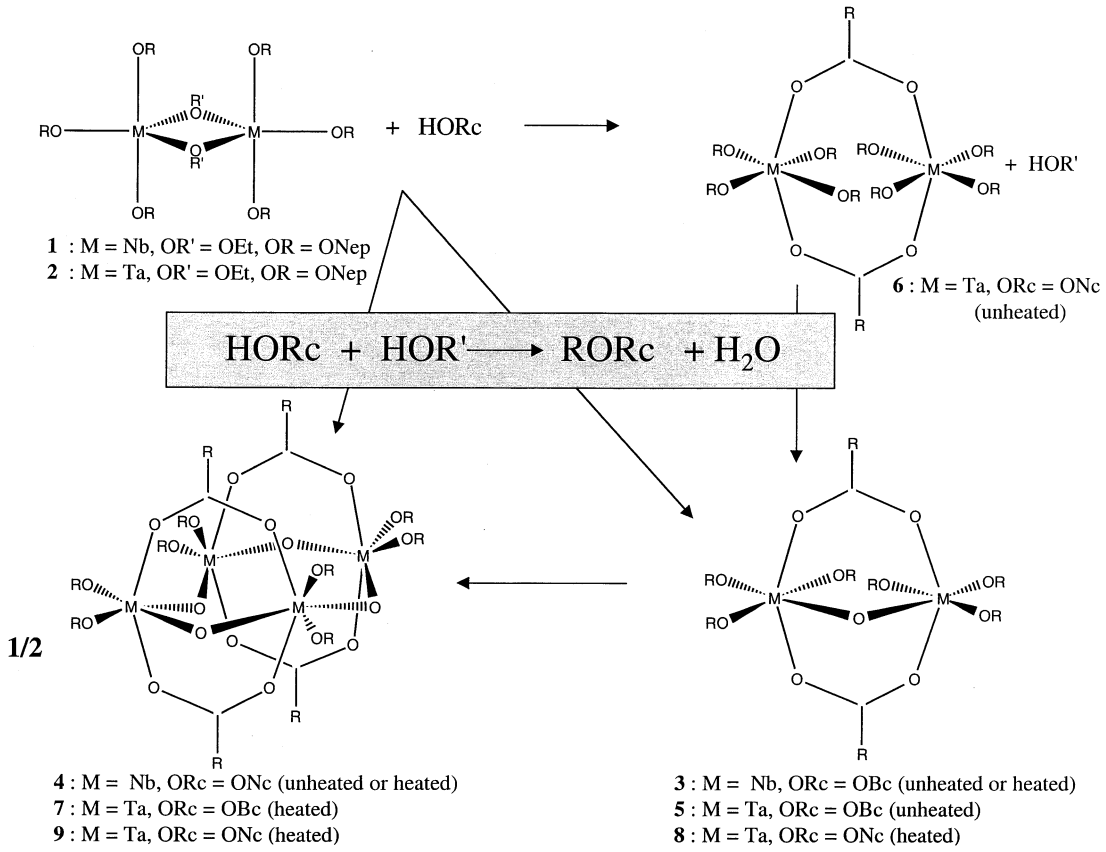
$$[Ta(OEt)(ONep)_4]_2 + 2HOBc \xrightarrow{\Delta} [Ta_2(O)(OBc)_2(ONep)_4]_2 \quad (6)$$

$$[Ta(OEt)(ONep)_4]_2 + 2HONc \xrightarrow{\Delta} [Ta(ONc)(ONep)_3]_2(O) \quad (7)$$

2. Experimental

All compounds described below were handled with rigorous exclusion of air and water using standard Schlenk line and glove box techniques. All solvents were freshly distilled from the appropriate drying agents immediately prior to use [22]. The following chemicals were used as received: $Nb(OEt)_5$, $Ta(OEt)_5$, HONep, HOBc, and HONc. The [M(μ-OEt)(ONep)$_4$]$_2$ (M = Nb (**1**) [15] and Ta (**2**) [17]) compounds were synthesized according to literature reports.

FT-IR data were obtained on a Bruker Vector 22 Instrument using KBr pellets under an atmosphere of flowing nitrogen. Elemental analysis was performed on a Perkin–Elmer 2400 CHN-S/O Elemental Analyzer. All NMR samples were prepared from dried crystalline materials that were handled and stored under an argon



Scheme 1. Schematic representation of the structurally verified (numbered compounds shown in bold bock) esterification pathway of HORc-modified Group V compounds.

atmosphere. All $^{13}C\{^{1}H\}$ solid-state NMR spectra were obtained on a Bruker AMX400 spectrometer, at a frequency of 100.63 MHz using a 4 mm broadband magic angle spinning (MAS) probe spinning at 4 kHz. For all of the $^{13}C\{^{1}H\}$ cross-polarized (CP) MAS spectra acquired, a standard CP sequence with high power ^{1}H decoupling, and a 1 ms contact time and 64-256 scans were utilized. For solution spectra, each sample was redissolved in toluene-d_8 at saturated solution concentrations. All solution spectra were obtained on a Bruker DMX400 spectrometer at 399.87 and 100.54 MHz for ^{1}H and ^{13}C experiments, respectively. A 5 mm broadband probe was used for all experiments. ^{1}H NMR spectra were obtained using a direct single pulse excitation, with a 10 s recycle delay and 8 scan average. The $^{13}C\{^{1}H\}$ NMR spectra were obtained using a WALTZ-16 composite pulse ^{1}H decoupling, a 5 s recycle delay and a $\pi/4$ pulse excitation.

2.1. General synthesis

Due to the similarity of synthetic procedures, a general description is presented for the unheated and heated reaction conditions.

2.1.1. Unheated. Compounds 3–6

$[M(\mu\text{-OEt})(ONep)_4]_2$ (**1** or **2**) was dissolved in toluene followed by addition, via pipette, of the appropriate HORc in toluene at glovebox temperatures. After 12 h, the reaction mixture was allowed to sit at glove box temperature with slow evaporation of any volatile material until crystals formed. If after an extended period of time no crystals were formed, additional volatile materials were removed by rotary evaporation. The reaction mixture was then allowed to again sit at glovebox temperatures or placed at −40 °C until crystals formed.

2.1.2. Heated. Compounds 3–4, 7–8

An identical setup as above was used. After mixing the two reagents, the reaction mixture was heated at reflux temperatures for 12 h and then allowed to cool to room temperature. Crystals were grown as described above.

2.1.3. $[Nb(\mu\text{-OBc})(ONep)_3]_2(\mu\text{-O})$ (3)

Used (unheated): **1** (0.622 g, 1.28 mmol) and HOBc (0.136 g, 1.33 mmol). Crystalline yield: 0.808 g (68.1%). Used (heated): **1** (0.602 g, 1.24 mmol) and HOBc (0.152 g, 1.49 mmol). Crystalline yield: 0.652 g (56.8%). FT-IR (KBr pellet, cm^{-1}) 2952(s), 2906(m), 2866(m), 2687(w),

1573(s), 1540(sh, s), 1480(s), 1420(s), 1361(s), 1235(w), 1089(br, s), 1029(sh, m), 937(w), 904(w), 777(s), 672(s), 480(m), 460(m). ^{1}H NMR (400 MHz, tol-d_8) δ 4.27, 4.26 (2.0H, s, OCH_2CMe$_3$), 4.23 (1.0H, s, OCH_2CMe$_3$), 1.29 (3.8H, s, O$_2$CCMe_3), 1.09, 1.02 (11.2H, s, OCH$_2$CMe_3). ^{13}C{^{1}H} (100 MHz, tol-d_8) δ 182.2 (O$_2C$CMe$_3$) 82.0, 77.3 (OCH$_2$CMe$_3$), 36.1 (O$_2$CCMe$_3$) 29.6, 29.1 (OCH$_2C$Me$_3$), 23.7 (O$_2$CCMe_3), 23.0, 22.2 (OCH$_2$CMe_3). Elemental *Anal*. for $C_{40}H_{84}Nb_2O_{11}$: Calc. C, 51.83; H, 9.13. Found: C, 51.72; H, 8.76%.

2.1.4. [Nb(μ-O)(μ-ONc)(ONep)$_2$]$_4$ (4)

Used (unheated): **1** (0.618 g, 1.27 mmol) and HOBc (0.150 g, 1.29 mmol). Crystalline yield: 0.902 g (44.5%). Used (heated): **1** (0.624 g, 1.28 mmol) and HOBc (0.152 g, 1.31 mmol). Crystalline yield: 0.673 g (32.9%). FT-IR (KBr pellet, cm^{-1}) 2952(s), 2899(m), 2866(m), 2693(m), 1586(s), 1474(w), 1454(w), 1414(w), 1368(w), 1129(br, s), 1096(bs), 1023(sh, m), 785(br, s), 645(br, s). ^{1}H NMR (400 MHz, tol-d_8) δ 4.22 (2H, s, OCH_2CMe$_3$), 4.18 (1.1H, d, OCH_2CMe$_3$), 4.00 (1.1H, d, OCH_2CMe$_3$), 2.66 (0.74H, s, O$_2$CCH$_2$CMe$_3$), 2.37 (0.74H, s, O$_2$CCH$_2$CMe$_3$), 1.23 (4.8H, s, O$_2$CCH$_2$CMe_3), 0.87 (10.6H, mult., OCH$_2$CMe_3). ^{13}C{^{1}H} (100 MHz, tol-d_8) δ 181.4 (O$_2$CCH$_2$CMe$_3$), 88.0, 83.4 (OCH$_2$CMe$_3$), 52.9, 52.3 (O$_2$CCH$_2$CMe$_3$), 34.9 (OCH$_2$CMe$_3$), 30.5, 30.2 (O$_2$CCH$_2$CMe_3), 27.4, 27.2 (OCH$_2$CMe_3). Elemental *Anal*. for $C_{64}H_{132}Nb_4O_{20}$: Calc. C, 48.24; H, 8.35. Found C, 47.87; H, 8.17%.

2.1.5. [Ta(μ-OBc)(ONep)$_3$]$_2$(μ-O) (5)

Used (unheated): **2** (0.616 g, 1.07 mmol) and HOBc (0.114 g, 1.12 mmol). Crystalline yield 0.634 g (53.6%). FT-IR (KBr pellet, cm^{-1}) 2955(s), 2868(m, sh), 1578(s), 1485(m), 1461(w, sh), 1431(m), 1394(m), 1381(w, sh), 1363(m), 1261(w, sh), 1232(m, sh), 1109(s), 1026(m, sh), 936(w), 905(w), 787(s), 751(m, sh), 650(s), 603(w, sh), 456(m). ^{1}H NMR (400 MHz, tol-d_8) δ 4.27, 4.26 (2H, s, OCH_2CMe$_3$), 4.23 (1H, s, OCH_2CMe$_3$), 1.29 (3.6H, s, O$_2$CCH_2CMe$_3$), 1.09, 1.02 (17.1H, s, OCH$_2$CMe_3). ^{13}C{^{1}H} (100 MHz, tol-d_8) δ 188.0 (O$_2C$CMe$_3$), 84.8, 80.7 (OCH$_2$CMe$_3$), 41.0 (O$_2$CCMe$_3$), 34.6, 34.3 (OCH$_2C$Me$_3$), 28.2 (O$_2$CCMe_3), 27.3, 27.0 (OCH$_2$CMe_3). Elemental *Anal*. for $C_{40}H_{84}O_{11}Ta_2$: Calc. C, 43.56; H, 7.68. Found: C, 43.78; H, 7.44%.

2.1.6. [Ta(μ-ONc)(ONep)$_4$]$_2$ (6)

Used (unheated): **2** (0.602 g, 1.05 mmol) and HONc (0.122 g, 1.05 mmol). Crystalline yield 0.839 g (62.0%). FT-IR (KBr pellet, cm^{-1}) 2954(s), 2868(m, sh), 1583(s), 1478(m, sh), 1460(m), 1414(m), 1395(m), 1364(m), 1234(w, sh), 1108(s), 1026(m, sh), 784(m), 651(s). ^{1}H NMR (400 MHz, tol-d_8) δ 4.37 (2H, s, OCH_2CMe$_3$), 4.27 (0.88H, s, OCH_2CMe$_3$), 2.31 (1.4H, s, O$_2$CCH_2CMe$_3$), 1.13, 1.07 (23.2H, s, OCH$_2$CMe_3). ^{13}C NMR (100 MHz, tol-d_8) 181 (O$_2C$CH$_2$CMe$_3$), 83.8, 80.8 (OCH$_2$CMe$_3$), 50.9, 49.2 (O$_2$CCH$_2$CMe$_3$), 33.4, 33.1 (OCH$_2C$Me$_3$), 30.1, 28.9 (O$_2$CCH$_2C$Me$_3$), 26.1, 25.8 (OCH$_2$CMe_3). Elemental *Anal*. for $C_{26}H_{55}O_6Ta_1$: Calc. C, 48.44; H, 8.59. Found: C, 44.50; H, 7.69%.

2.1.7. [Ta(μ-O)(μ-OBc)(ONep)$_2$]$_4$ (7)

Used (heated): **2** (0.588 g, 1.02 mmol) and HOBc (0.106 g, 1.04 mmol). Crystalline yield 1.28 g (66.3%). FT-IR (KBr pellet, cm^{-1}) 2952(s), 2893(m), 2860(m), 1587(s), 1481(m), 1428(m), 1354(w), 1262(w), 1229(w), 1162(br, s), 1109(br, s), 1029(sh, m), 824(s), 804(s), 645(s). ^{1}H NMR (400 MHz, tol-d_8) δ 4.32 (1H, dd, OCH_2CMe$_3$), 4.24 (1H, s, OCH_2CMe$_3$), 1.28 (3.3H, s, O$_2$CCMe_3), 1.10 (3.2H, s, O$_2$CCMe_3), 1.02 (H, s, OCH$_2$CMe_3). ^{13}C{^{1}H} (100 MHz, tol-d_8) δ 187.1 (O$_2C$CMe$_3$), 87.0, 82.3 (OCH$_2$CMe$_3$), 41.0 (O$_2$CCMe$_3$), 34.5, 34.1 (OCH$_2C$Me$_3$), 28.6, 28.4 (O$_2$CCMe_3), 27.1 (OCH$_2$CMe_3). Elemental *Anal*. for $C_{15}H_{31}O_5Ta$: Calc. C, 38.14; H, 6.61. Found: C, 40.78; H, 6.53%.

2.1.8. [Ta(μ-ONc)(ONep)$_3$]$_2$(μ-O) (8)

Used (heated): **2** (0.622 g, 1.08 mmol) and HONc (0.130 g, 1.12 mmol). Crystalline yield: 0.789 g (37.4%). FT-IR (KBr pellet, cm^{-1}) 2959(s), 2899(m), 2853(m), 2700(w), 1580(s), 1474(m), 1414(m), 1387(m), 1354(m), 1255(w), 1096(br, s), 1029(sh, m), 785(br, s), 652(br, s). ^{1}H NMR (400 MHz, tol-d_8) δ 4.33 (2.0H, dd, OCH_2CMe$_3$), 4.20 (0.98H, s, OCH_2CMe$_3$), 2.30 (1.0H, s, O$_2$CCH_2CMe$_3$), 1.11 (5.4H, s, O$_2$CCH$_2$CMe_3), 1.07 (5.4H, s, O$_2$CCH$_2$CMe_3), 1.05 (10.7 H, s, OCH$_2$CMe_3). ^{13}C{^{1}H} (100 MHz, tol-d_8) δ 181.9 (O$_2C$CH$_2$CMe$_3$), 84.6, 80.9 (OCH$_2$CMe$_3$), 51.7 (O$_2$CCH$_2$CMe$_3$), 34.3, 34.1 (O$_2$CCH$_2C$Me$_3$), 31.0, 30.2 (OCH$_2C$Me$_3$), 27.5, 26.7, 26.5, 25.7 (O$_2$CCH$_2C$Me$_3$, OCH$_2$CMe_3). Elemental *Anal*. for $C_{42}H_{88}O_{11}Ta_2$: Calc. C, 44.60; H, 7.84. Found: C, 44.39; H, 7.46%.

2.2. General X-ray crystal structure information [23]

Each crystal was mounted onto a thin glass fiber from a pool of Fluorolube™ and immediately placed under a liquid N_2 stream on a Bruker AXS diffractometer. The radiation used was graphite monochromatized Mo Kα radiation ($\lambda = 0.7107$ Å). The lattice parameters were optimized from a least-squares calculation on carefully centered reflections. Lattice determination and data collection were carried out using SMART Version 5.054 software. Data reduction was performed using SAINT Version 6.01 software. The structure refinement was performed using XSHELL 3.0 software. The data were corrected for absorption using the SADABS program within the SAINT software package.

Each structure was solved using direct methods. This procedure yielded the heavy atoms, along with a number of the C atoms. Subsequent Fourier synthesis yielded

the remaining C atom positions. The hydrogen atoms were fixed in positions of ideal geometry and refined within the XSHELL software. These idealized hydrogen atoms had their isotropic temperature factors fixed at 1.2 or 1.5 times the equivalent isotropic U of the C atoms for which they were bonded. The final refinement of each compound included anisotropic thermal parameters on all non-hydrogen atoms. Additional information concerning the data collection and final structural solutions of **3**–**9** can be found in the supplemental information. Data collection parameters for **3**–**9** are given in Table 1.

2.2.1. $Nb_2(O)(OBc)_2(ONep)_6$ (**3**)

Many of the methyl carbon atoms of the ONep and OBc ligands appeared to be disordered over several sites. These included the methyl carbon positions C(4), C(5), C(10), C(19), C(20), C(23), C(25), and C(30) which were refined as two one-half occupancy sites. The anisotropic refinement of several of the one-half occupancy methyl sites was problematic, which necessitated their subsequent isotropic refinement. Additionally, attempts to model the disorder in the methylene carbon atoms C(16) and C(26) were not successful, and these atom positions were refined isotropically. Finally, C(29) also displayed unrealistic atom positions when attempts were made to split the density over two sites. This carbon was also refined as isotropic. Hydrogen atoms were not refined on split-site carbons, however, the proper number of hydrogens was entered into the formula upon refinement to obtain correct structural parameters.

2.2.2. $[Nb(O)(ONc)(ONep)_2]_4$ (**4**) [23]

A colorless, irregular shaped crystal was attached to a glass fiber using silicone grease and was mounted from a matrix of mineral oil. The crystal was immediately placed on a Bruker P4/CCD/PC diffractometer, and cooled to 203 K using a Bruker LT-2 temperature device. The data were collected using a sealed, graphite monochromatized Mo Kα X-ray source. A hemisphere of data was collected using a combination of φ and ω scans, with 30 s frame exposures and 0.3° frame widths. Data collection and initial indexing and cell refinement were handled using SMART 4.210 software. Frame integration and final cell parameter calculation were carried out using SAINT V 4.05 software. The data were corrected for absorption using the DIFABS program. Decay of reflection intensity was not observed. The structure was solved in space group $C2/c$ using direct methods and difference Fourier techniques. The initial solution revealed the niobium–oxygen framework atomic positions. Subsequent Fourier synthesis revealed the carbon atom positions, including a disordered toluene solvent molecule. Attempts to model the lattice toluene were largely unsuccessful, and the program PLATON/SQUEEZE was used to remove the corresponding solvent electron density. (The solvent volume modeled was 1053 Å^3, and 144 electrons per unit cell were removed. The solvent void was centered at 0, 0.213, 0.25 in the unit cell.) The hydrogen atom positions were fixed (C–H = 0.96 Å for methyl, and 0.97 Å for methylene). The hydrogen atoms were refined using the riding model, with isotropic temperature factors fixed to 1.2 (methylene) or 1.5 (methyl) times the

Table 1
Data collection parameters for **3**–**9**

Compound	**3**	**4**	**5**	**6**	**7**	**8**	**9**
Empirical formula	$C_{40}H_{84}Nb_2O_{11}$	$C_{70}H_{138}Nb_4O_{20}$	$C_{40}H_{84}O_{11}Ta_2$	$C_{52}H_{110}O_{12}Ta_2$	$C_{67}H_{132}O_{20}Ta_4$	$C_{42}H_{88}O_{11}Ta_2$	$C_{68}H_{140}O_{20}Ta_4$
Formula weight	926.89	1671.44	1102.97	1289.30	1981.53	1131.02	2001.60
Temperature (K)	168(2)	203(2)	168(2)	168(2)	168(2)	168(2)	168(2)
Crystal system	orthorhombic	monoclinic	orthorhombic	triclinic	monoclinic	monoclinic	monoclinic
Space group	*Pna*2(1)	*C*2/*c*	*Pna*2(1)	$P\bar{1}$	*C*2/*c*	*P*2(1)/*m*	*C*2/*c*
a (Å)	19.765(8)	26.800(2)	19.748(6)	10.6981(6)	26.7464(15)	10.5894(16)	26.788(8)
b (Å)	12.004(5)	15.2903(12)	12.046(4)	12.0398(7)	14.4506(6)	21.231(3)	15.181(5)
c (Å)	21.598(9)	23.9766(17)	21.655(7)	26.179(16)	23.6841(12)	12.5859(19)	23.833(7)
α (°)				83.437(1)			
β (°)		112.578(2)		82.150(1)	112.698(2)	106.196(3)	112.345(5)
γ (°)				74.267(1)			
V (Å^3)	5124(4)	9072.0(12)	5151(3)	3204.6(3)	8445.0(7)	2717.3(7)	8964(5)
Z	4	4	4	2	4	2	4
D_{calc} (Mg m^{-3})	1.201	1.224	1.422	1.336	1.559	1.382	1.483
μ (mm^{-1}) (Mo Kα)	0.494	0.549	4.292	3.461	5.225	4.070	4.923
R_1 [a] (%)	6.99	9.09	5.73	3.50	8.08	15.94	10.72
wR_2 [b] (%) [$I > 2\sigma(I)$]	14.85	24.59	9.41	8.42	22.39	40.23	30.13
R_1 [a] (%, all data)	15.10	14.20	11.50	5.54	8.73	25.85	13.88
wR_2 [b] (%, all data)	17.96	28.20	10.82	9.24	23.10	46.12	33.10

[a] $R_1 = \Sigma||F_o| - |F_c||/\Sigma|F_o| \times 100$.
[b] $wR_2 = [\Sigma w(F_o^2 - F_c^2)^2/\Sigma(w|F_o|^2)^2]^{1/2} \times 100$.

equivalent isotropic U of the carbon atom they were bound to. Three of the *t*-Bu groups were severely disordered and were modeled using a rigid-body refinement. The final refinement included anisotropic temperature factors on all non-hydrogen atoms. Structure solution, refinement, graphics, and preparation of publication materials were performed using SHELXTL V. 5.10.

2.2.3. $Ta_2(O)(OBc)_2(ONep)_6$ (**5**)

Significant disordering of the O(4) ONep group was observed which resulted in large anisotropic thermal parameters for the methylene carbon C(11) and the methyl carbons C(13), C(14), and C(15). Attempts to refine these carbon atoms anisotropically as shared occupancy resulted in non-positive definite thermal parameters for one or both of the sites. Therefore, after all attempts to model the disordered ONep failed, carbons C(11), C(13), C(14) and C(15) were refined with only isotropic temperature factors. The refinement also indicated racemic twinning. This was accommodated by adding the twin law $(-h, -k, -l)$ to the refinement.

2.2.4. $Ta_2(ONc)_2(ONep)_8$ (**6**)

The ONep groups that displayed significant positional disordering were modeled with partially occupied C sites, namely the ONep ligands off of the O(3), O(9), and O(11) atoms. The disordered carbon sites did not have hydrogen atoms added, however, the correct number of hydrogens were added to the overall composition in the final refinement cycle to obtain accurate calculated structural parameters.

2.2.5. $[Ta(O)(OBc)(ONep)_2]_4\cdot(toluene)$ (**7**)

A disordered toluene solvent molecule was located within the lattice and was modeled using the PLATON/SQUEEZE program (Ver. 01-11-99). (The solvent volume modeled was 1053 $Å^3$, and 218 electrons per unit cell. The solvent void was centered at 0.5, 0.228, 0.25 in the unit cell.) Four toluene molecules were added to the contents of the unit cell during the final refinement series so that the proper structural parameters could be calculated. Many of the methyl carbon atoms appeared to be disordered over two sites, including C(8), C(9), C(10), C(19), C(20), C(29), and C(30). Subsequent refinements of these split sites yielded reasonable positions for rotational disordering of ONep and OBc ligands. Additionally, the bridging O(2) atom was difficult to refine as anisotropic (displayed very elongated ellipsoids) and was fixed as isotropic during refinement.

2.2.6. $[Ta(ONc)(ONep)_3]_2(O)$ (**8**)

Due to difficulty refining some oxygen and carbon atom positions (resulting from disorder of ONep ligands) all carbon and oxygen atoms were refined with a single isotropic temperature factor. Significant bond length restraints were required to achieve convergence of the model. All like bonds within the structure were restrained to be equivalent ($\sigma = 0.04$ Å) resulting in a total of 95 bond length restraints. Due to the poor quality of the high-angle data and structural disorder, the overall refinement was substandard. However, it was possible to discern the central core connectivity of the molecule from the observed data.

2.2.7. $Ta_4(O)_4(ONc)_4(ONep)_8\cdot(THF)$ (**9**)

A disordered THF solvent molecule was observed and modeled using the PLATON/SQUEEZE program (Ver. 01-11-99). The SQUEEZE program located the solvent center to be at (1/2, 0.203, 1/4), with a potential volume of 1040.6 $Å^3$ and electron count of 168 electrons/cell, consistent with four THF molecules/unit cell. Four THF molecules were added to the contents of the unit cell during the final refinement series so that the proper structural parameters could be calculated. Due to difficulty refining some of the carbon atom positions (resulting from disorder of ONep ligands) 12 of the carbon atoms were refined with a single isotropic temperature factor as follows: methylene carbon atoms C(18) and C(23); methyl carbons C(4), C(5), C(15), C(16), C(17), C(20), C(21), C(25, C(26), and C(27). Attempts made to model the disorder by splitting the site occupancy over two sites were largely unsuccessful, hence these carbons were refined isotropically. Additionally, O(5) and O(9) were also fixed as isotropic during refinement. A few bond length restraints were employed to achieve convergence of the model. The quaternary-methyl bonds for the O(8) ONep ligand were restrained to be equivalent ($\sigma = 0.04$ Å). Additionally, the Ta–O bond lengths for the bridging oxygens O(1) and O(9) were also restrained to be equivalent ($\sigma = 0.04$ Å). This resulted in a total of 6 bond length restraints for the refinement.

3. Results and discussion

Previously, the crystallographically characterized ORc-modified Group V metal alkoxides were all found to adopt the general structure $[Nb_2(\mu\text{-}O)_2(ORc)_2(OCHMe_2)_4]_2$ (ORc = OAc, OMc) [21]. Due to the unique structures characterized for the ORc-modified $Ti(OR)_4$ family using the ONep ligand [9], we decided to investigate the reaction between **1** [15] or **2** [17] and HORc (ORc = OBc or ONc). The larger ORc ligands were chosen since it was observed in the titanium system that the OBc ligand yielded species without esterification (i.e., simple exchange) and the ONc ligand formed structures similar to the OAc products [9]. The final products of Eqs. (2)–(7) were characterized in both the

solid and solution state. A schematic representation of the structural variations noted in this study showing the progression of the esterification process for Group V alkoxides is presented in Scheme 1.

3.1. Synthesis

The room temperature reaction between the appropriate Group V metal alkoxides (**1**-or **2**, Fig. 2) and HORc in toluene (Eq. (1)) yielded **3**–**6** which are shown in Figs. 3–6 and Eqs. (2)–(5), respectively. Identical reaction mixtures were also heated at reflux temperatures overnight, to investigate the degree of esterification that could be wrought from these compounds. The concentration of the reactions was held relatively at the same level but was not rigorously controlled. For the Nb system, there was no change in the structures isolated; however, for the Ta system **7**–**8** were isolated upon heating (Eqs. (6) and (7)). Compound **9** was isolated in small yield in an identical synthesis noted for **8** except that the solution was substantially more concentrated which may have played a large role in dictating the structure of the final species obtained. Plots of **7**–**9** are shown in Figs. 7–9, respectively. Interestingly, it appears that the OEt are preferentially reacted for all scenarios and are most likely the main source of the oxide ligands; however, as noted by Hubert-Pfalzgraf [21], the carboxylic acids may also contribute to oxide formation.

3.2. Solid-state

3.2.1. Structure

Plots of **3**–**9** are shown in Figs. 3–9, respectively. Table 1 lists the data collection parameters for **3**–**9**. Tables 2 and 3 are the tabulation of the metrical data for **3**–**4** and **5**–**7** and **9**, respectively. The quality of the crystal structure isolated for **8** precludes discussion of

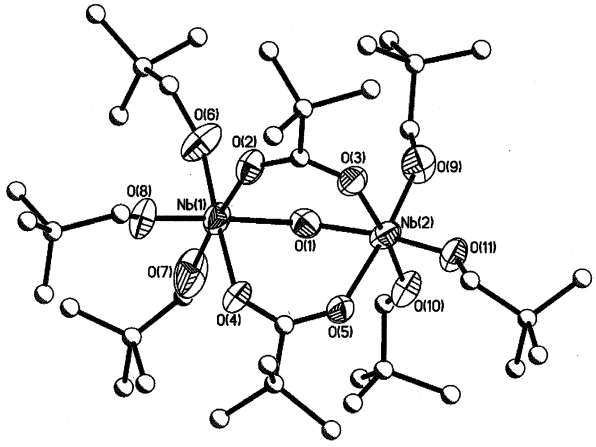


Fig. 3. Thermal ellipsoid plot of **3**. Ellipsoids are drawn at the 30% level.

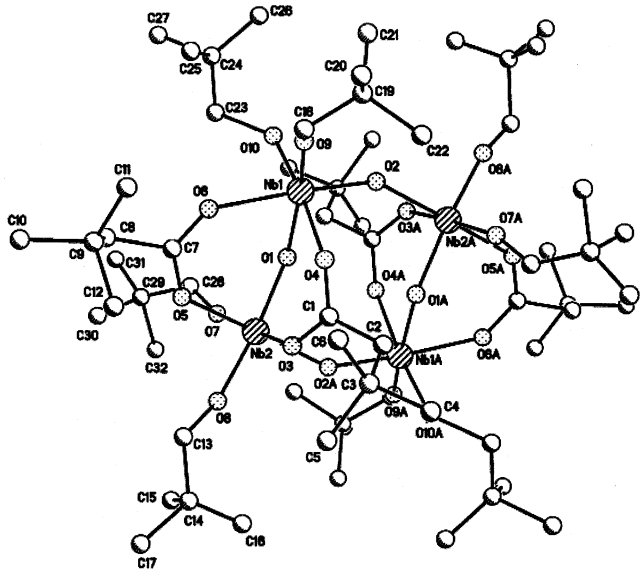


Fig. 4. Ball and stick plot of **4**. Ellipsoids are drawn at the 30% level.

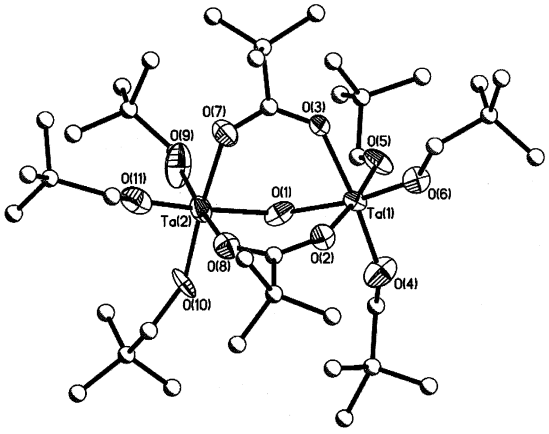


Fig. 5. Thermal ellipsoid plot of **5**. Ellipsoids are drawn at the 30% level.

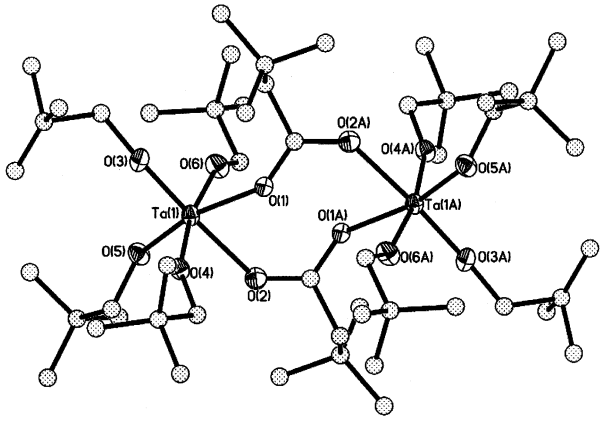


Fig. 6. Thermal ellipsoid plot of **6**. Ellipsoids are drawn at the 30% level.

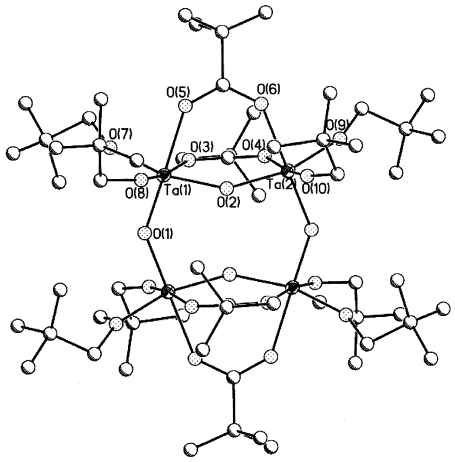


Fig. 7. Thermal ellipsoid plot of **7**. Ellipsoids are drawn at the 30% level.

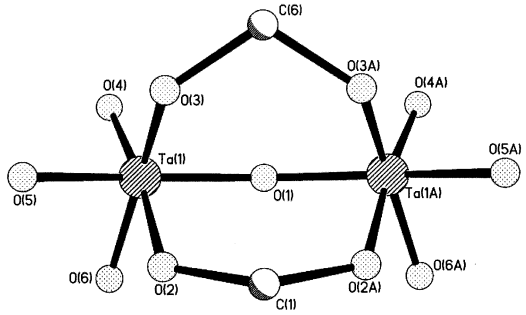


Fig. 8. Ball and stick plot of **8**. Ellipsoids are drawn at the 30% level.

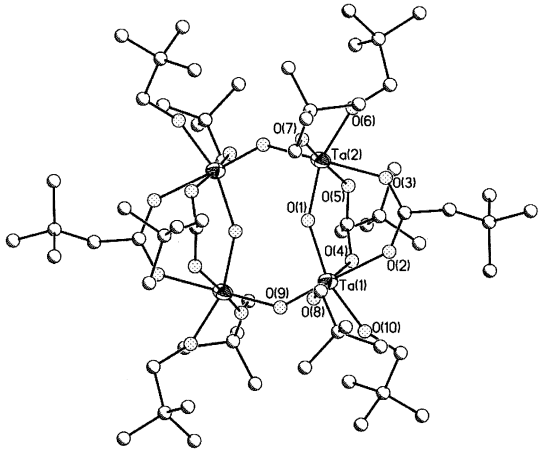


Fig. 9. Ball and stick plot of **9**. Ellipsoids are drawn at the 30% level.

the metrical data for this compound; however, the connectivity of the molecule's central core was unequivocally observed. Additional information pertaining to the full crystal structure can be found in the supplementary information. Notably, the μ-OEt ligands were absent from the final structures, indicating these ligands are preferentially esterified during the syntheses of **3**–**9**.

Compounds **3**, **5**, **6**, and **8** were dinuclear with octahedral (Oh) metal centers. For **3**, **5**, and **8** an oxo atom and two ORc ligands bridge the metal centers with three ONep ligands filling the remainder of the coordination sphere (the metrical data for **8** is omitted from the following discussions). In contrast, compound **6** is the first example of the simple exchange Group V species, surprisingly void of esterification-generated oxo ligands. The Oh coordination spheres of the Ta metal centers are formed by the two bridging ONc ligands and four terminal ONep ligands. The metrical data for **3**, **5**, and **6** are self-consistent and are in agreement with observed literature values [21]. The Nb–O and Ta–O distances aggrandize with increased bonding and reduced electron density (ONep < μ-O < ORc). The Nb···Nb distances for **3** were 3.62 Å and are similar to the Ta···Ta distance of 3.64 Å noted for **5**. For **6**, due to the absence of an oxo ligand, the Ta···Ta distance is substantially longer at av. 5.13 Å. The ORc ligands possess bite angles that range from 122 to 127° for **3**, **5**, and **6**.

Compounds **4**, **7**, and **9** were isolated in the same general centrosymmetric structural arrangement that consists of two "$M_2(\mu\text{-}O)_2(\mu\text{-}ORc)_2(ONep)_4$" moieties which are linked by μ-O ligands. This results in the formation of an eight-member ring of $[M–O]_4$ as the central core. The acetate ligands do not bridge between moieties but instead each pair of metals is bridged by two ORc ligands, independent of the steric bulk of the pendant hydrocarbon chain. This is the same structure as was noted for the ORc/$OCHMe_2$ (ORc = OAc or OMc, Fig. 1) system and the metrical data are in agreement [21]. The shortest M···M distances were av. 3.66 Å wherein substantially longer distances were noted for the diagonally located M···M distances (av. 5.18 Å).

Compounds **1**–**9** structurally reveal the step-wise esterification pathway (see Scheme 1) that Group V species undergo. Initially, the HORc reagent exchanges with the weakest bound and most sterically accessible OR (in this system the OEt) to generate dinuclear bridged species (**6**). Once generated, one of the free HOR (HOEt) reacts with HORc to generate the ester and H_2O. The H_2O reacts with the terminal OR (HONep) to generate an oxo species; however, due to the bite angle of the ORc ligands, linking to the other molecules is unlikely and therefore binding to the second metal in the molecule occurs (**3**, **5**, and **8**). The next step would be to repeat this hydrolysis, however, now the steric hindrance around the metal centers of the molecule prevents further oxo linkages within the molecule and M–O–M bonds are formed externally to form the fully hydrolyzed species (**4**, **7**, and **9**).

While detailed computational investigations are required to fully understand the structures that were preferentially formed, some general trends can be stated for this family of compounds. In the titanium system [9],

Table 2
Selected bond distances (Å) and angles (°) for **3**–**4**

	3		**4**	
Bond distances				
Nb···Nb	Nb(1)···Nb(2)	3.623		
Nb–(ONep)	Nb(1)–O(6)	1.909(11)	Nb(1)–O(9)	1.873(7)
	Nb(1)–O(7)	1.843(11)	Nb(1)–O(10)	1.859(7)
	Nb(1)–O(8)	1.857(12)	Nb(2)–O(7)	1.853(8)
	Nb(2)–O(9)	1.853(10)	Nb(2)–O(8)	1.857(8)
	Nb(2)–O(10)	1.824(11)		
	Nb(2)–O(11)	1.920(11)		
Nb–(μ-ORc)	Nb(1)–O(2)	2.099(11)	Nb(1)–O(4)	2.155(8)
	Nb(2)–O(3)	2.139(10)	Nb(1)–O(6)	2.161(6)
	Nb(1)–O(4)	2.099(12)	Nb(2)–O(3)	2.046(9)
	Nb(2)–O(5)	2.174(10)	Nb(2)–O(5)	2.188(7)
Nb–(μ-O)	Nb(1)–O(1)	1.960(11)	Nb(1)–O(1)	1.917(6)
	Nb(2)–O(1)	1.847(12)	Nb(1)–O(2)	1.801(7)
			Nb(2)–O(1)	1.890(6)
			Nb(2)–O(2′)	2.032(8)
Bond angles				
Nb–(μ-O)–Nb	Nb(2)–O(1)–Nb(1)	144.0(4)	Nb(1)–O(1)–Nb(2)	146.4(3)
(μ-O)–Nb–(μ-O)			O(1)–Nb(1)–O(2)	96.2(3)
(μ-O)–Nb–ORc	O(1)–Nb(1)–O(4)	83.8(4)	O(4)–Nb(1)–O(1)	82.1(3)
	O(1)–Nb(1)–O(2)	84.7(4)	O(4)–Nb(1)–O(2)	91.3(3)
			O(6)–Nb(1)–O(1)	82.7(3)
			O(6)–Nb(1)–O(2)	175.7(3)
(μ-O)–Nb–ONep	O(6)–Nb(1)–O(1)	97.3(5)	O(1)–Nb(1)–O(9)	160.0(3)
	O(7)–Nb(1)–O(1)	94.2(5)	O(1)–Nb(1)–O(10)	97.9(3)
	O(8)–Nb(1)–O(1)	160.9(4)	O(2)–Nb(1)–O(9)	95.5(3)
			O(2)–Nb(1)–O(10)	94.5(4)
(ONep)–Nb–(ONep)	O(7)–Nb(1)–O(6)	98.9(6)	O(10)–Nb(1)–O(9)	97.2(3)
	O(7)–Nb(1)–O(8)	98.6(5)		
	O(8)–Nb(1)–O(6)	94.5(5)		
(ONep)–Nb–(ORc)	O(7)–Nb(1)–O(2)	173.6(5)	O(9)–Nb(1)–O(6)	84.4(3)
	O(8)–Nb(1)–O(2)	80.8(5)	O(9)–Nb(1)–O(4)	81.5(3)
	O(6)–Nb(1)–O(2)	87.8(4)	O(10)–Nb(1)–O(4)	174.1(3)
	O(7)–Nb(1)–O(4)	88.9(6)	O(10)–Nb(1)–O(6)	89.8(3)
	O(8)–Nb(1)–O(4)	82.6(5)		
	O(6)–Nb(1)–O(4)	172.3(5)		
(ORc)–Nb–(ORc)	O(4)–Nb(1)–O(2)	84.7(5)	O(4)–Nb(1)–O(6)	84.4(3)
O–C–O	O(2)–C(1)–O(3)	127.7(14)	O(3)–C(1)–O(4)	122.2(12)
	O(4)–C(6)–O(5)	127.9(15)	O(5)–C(7)–O(6)	127.4(9)

the size and shape of the pendant hydrocarbon chain of the HORc ligands played a vital role in determining nuclearity and shape of the molecules isolated. For the Nb species (**3**, **4**) the ORc ligands also appear to dictate the nuclearity of the product isolated wherein the more sterically hindering OBc ligand led to the smaller, dinuclear species **3**, in comparison to the tetranuclear ONc-ligated species **4**. These are the most kinetically and thermodynamically stable species since the same structures were isolated, independent of the temperature of the reaction. In contrast, the Ta species follow the reverse trend concerning the ORc ligands (the smaller the steric bulk of the carboxylate the less esterification observed). Further, the Ta species appear to be less susceptible to hydrolysis than the Nb complexes as evidenced by the isolation of less condensed species for the former system under identical conditions. Since the ionic radii of Nb^{5+} or Ta^{5+} are the same (0.78 Å [24]) and identically ligated precursors and modifiers were used, the stabilization of the Ta intermediates over the Nb species must be based on the subtle electronic variations between these congeners.

3.2.2. Elemental analysis

Elemental analyses of the bulk powders for the Nb system were consistent with the solved solid-state structures. For the Ta systems, **5** and **8** were found to be consistent with their respective solid-state structures. For **6**, the analyses obtained were in agreement with the oxo species (**8**), which may be due to the rapidity that **6** undergoes hydrolysis under the conditions used for analyses. For **7**, the analyses were consistently higher

Table 3
Selected bond distances (Å) and angles (°) for **5**–**7** and **9**

	5		**6**		**7**		**9**	
Bond distances								
M···M	Ta(1)···Ta(2)	3.635	Ta(1)···Ta(1a)	5.124	Ta(1)···Ta(2)	3.647		
			Ta(2)···Ta(2a)	5.144	Ta(1)···Ta(2a)	3.685		
					Ta(1)···Ta(1a)	5.178		
					Ta(2)–Ta(2a)	5.192		
M–(ONep)	Ta(1)–O(4)	1.876(12)	Ta(1)–O(3)	1.892(3)	Ta(1)–O(7)	1.893(7)	Ta(2)–O(6)	1.873(15)
	Ta(1)–O(5)	1.831(12)	Ta(1)–O(4)	1.880(3)	Ta(1)–O(8)	1.884(8)	Ta(2)–O(7)	1.887(18)
	Ta(1)–O(6)	1.859(13)	Ta(1)–O(5)	1.886(3)	Ta(2)–O(9)	1.888(7)	Ta(1)–O(8)	1.892(14)
	Ta(2)–O(9)	1.889(14)	Ta(1)–O(6)	1.885(3)	Ta(2)–O(10)	1.868(8)	Ta(1)–O(10)	1.902(17)
	Ta(2)–O(10)	1.908(12)						
	Ta(2)–O(11)	1.817(16)						
M–(μ-ORc)	Ta(1)–O(2)	2.112(12)	Ta(1)–O(1)	2.122(3)	Ta(1)–O(3)	2.177(7)	Ta(1)–O(2)	2.144(14)
	Ta(1)–O(3)	2.151(11)	Ta(1)–O(2)	2.179(3)	Ta(1)–O(5)	2.169(7)	Ta(2)–O(3)	2.203(15)
	Ta(2)–O(7)	2.094(16)			Ta(2)–O(4)	2.162(7)	Ta(1)–O(4)	2.126(15)
	Ta(2)–O(8)	2.114(13)			Ta(2)–O(6)	2.143(7)	Ta(2)–O(5)	2.004(18)
M–(μ-O)	Ta(1)–O(1)	1.899(13)			Ta(1)–O(1)	1.841(5)	Ta(1)–O(9)	1.739(10)
	Ta(2)–O(1)	1.916(14)			Ta(1)–O(2)	1.921(7)	Ta(1)–O(1)	1.912(9)
					Ta(2)–O(2)	1.911(7)	Ta(2)–O(1)	1.886(9)
					Ta(2)–O(1′)	2.079(6)	Ta(2)–O(9′)	2.177(11)
Bond angles								
M–(μ-O)–M	Ta(2)–O(1)–Ta(1)	144.7(5)			Ta(1)–O(2)–Ta(2)	144.3(4)		
					Ta(1)–O(1)–Ta(2′)	140.1(3)		
(μ-O)–M–(μ-O)					O(1)–Ta(1)–O(2)	98.5(3)	O(9)–Ta(1)–O(1)	99.2(6)
(μ-O)–M–ORc	O(1)–Ta(1)–O(2)	84.3(5)			O(3)–Ta(1)–O(1)	95.3(3)	O(1)–Ta(1)–O(2)	82.8(6)
	O(1)–Ta(1)–O(3)	84.5(5)			O(3)–Ta(1)–O(2)	85.5(3)	O(1)–Ta(1)–O(4)	81.1(5)
					O(5)–Ta(1)–O(1)	175.3(3)	O(9)–Ta(1)–O(2)	177.7(6)
					O(5)–Ta(1)–O(2)	83.6(3)	O(9)–Ta(1)–O(4)	95.2(56)
(μ-O)–M–ONep	O(4)–Ta(1)–O(1)	94.5(5)			O(1)–Ta(1)–O(7)	94.0(3)	O(8)–Ta(1)–O(1)	98.9(6)
	O(5)–Ta(1)–O(1)	93.7(5)			O(1)–Ta(1)–O(8)	91.9(4)	O(10)–Ta(1)–O(1)	159.2(7)
	O(6)–Ta(1)–O(1)	162.2(5)			O(2)–Ta(1)–O(7)	162.8(3)	O(9)–Ta(1)–O(8)	90.8(7)
					O(2)–Ta(1)–O(8)	97.1(4)	O(9)–Ta(1)–O(10)	94.2(7)
ORc–Ta–ORc	O(2)–Ta(1)–O(3)	82.4(5)	O(1)–Ta(1)–O(2)	80.47(14)	O(5)–Ta(1)–O(3)	80.6(3)	O(4)–Ta(1)–O(2)	84.9(6)
ORc–Ta–ONep	O(4)–Ta(1)–O(2)	89.1(5)	O(4)–Ta(1)–O(1)	84.90(12)	O(7)–Ta(1)–O(5)	83.1(3)	O(8)–Ta(1)–O(4)	173.9(7)
	O(5)–Ta(1)–O(2)	172.8(5)	O(6)–Ta(1)–O(1)	86.93(13)	O(8)–Ta(1)–O(5)	92.0(4)	O(10)–Ta(1)–O(4)	82.1(7)
	O(6)–Ta(1)–O(2)	84.8(5)	O(5)–Ta(1)–O(1)	166.31(13)	O(8)–Ta(1)–O(3)	171.8(3)	O(8)–Ta(1)–O(2)	89.1(7)
	O(4)–Ta(1)–O(3)	171.5(5)	O(3)–Ta(1)–O(1)	93.76(13)	O(7)–Ta(1)–O(3)	81.5(3)	O(10)–Ta(1)–O(2)	83.6(8)
	O(5)–Ta(1)–O(3)	90.6(5)	O(4)–Ta(1)–O(2)	82.91(13)				
	O(6)–Ta(1)–O(3)	80.2(5)	O(6)–Ta(1)–O(2)	88.25(14)				
			O(5)–Ta(1)–O(2)	85.63(13)				
			O(3)–Ta(1)–O(2)	174.01(13)				
ONep–Ta–ONep	O(4)–Ta(1)–O(5)	97.9(6)	O(4)–Ta(1)–O(6)	168.81(14)	O(8)–Ta(1)–O(7)	94.3(4)	O(8)–Ta(1)–O(10)	96.5(8)
	O(4)–Ta(1)–O(6)	99.3(5)	O(4)–Ta(1)–O(5)	94.28(13)				
	O(5)–Ta(1)–O(6)	95.4(5)	O(4)–Ta(1)–O(3)	94.38(14)				
			O(5)–Ta(1)–O(3)	99.93(14)				
			O(6)–Ta(1)–O(3)	93.76(15)				
			O(6)–Ta(1)–O(5)	91.85(14)				
O–C–O	O(8)–C(1)–O(2)	125.9(16)	O(2′)–C(1)–O(1)	123.4(4)	O(3)–C(1)–O(4)	127.3(10)	O(4)–C(1)–O(5)	126.5(19)
	O(7)–C(6)–O(3)	125.3(17)			O(5)–C(6)–O(6)	124.3(9)	O(3)–C(7)–O(2)	125.8(18)

than the calculated values which may be a reflection of residual solvent or incomplete esterification. Due to the limited amount of **9** isolated and the similarity to **4** and **7**, full characterization was not undertaken.

3.2.3. FT-IR spectroscopy

Due to the similarity in ligand constructs of **3**–**8**, it is not surprising that the FT-IR spectra of dried crystalline powders are comparable. Standard aliphatic stretches and corresponding methyl bends for the ONep ligands were observed in each spectrum with no stretches present for OH in any of the spectra. The C=O stretches of the precursor acids, HOBc and HONc, are both located at 1706 cm^{-1}. The $\sim$200 cm^{-1} shift of the C=O stretch was observed when reacted (1573, **3**; 1586, **4**; 1578, **5**; 1583, **6**; 1577, **7**; 1583 cm^{-1}, **8**) indicating the acids are bound to a metal in a chelating manner. These changes are in agreement with the OMc derivative [21].

Table 4
Solid state MAS ^{13}C NMR data for **3**–**8**

Compound	δ ppm (assignment)	Compound	δ ppm (assignment)
3	29.0, 28.1, 27.8, 27.0 (OCH_2CMe_3, O_2CCMe_3)	**6**	27.0 (OCH_2CMe_3)
	35.6, 33.9 (OCH_2CMe_3)		31.1 ($O_2CCH_2CMe_3$)
	41.0 (O_2CCMe_3)		34.1 (OCH_2CMe_3)
	86.3, 81.1 (OCH_2CMe_3)		51.7 ($O_2CCH_2CMe_3$)
	188.0 (O_2CCMe_3)		81.1 (OCH_2CMe_3)
			83.7, 83.3 (OCH_2CMe_3)
			182.9 ($O_2CCH_2CMe_3$)
4	27.1 (OCH_2CMe_3)	**7**	27.3, 26.9 (OCH_2CMe_3)
	31.1 ($O_2CCH_2CMe_3$)		27.9 (O_2CCMe_3)
	33.9 (OCH_2CMe_3)		33.9 (OCH_2CMe_3)
	51.6 ($O_2CCH_2CMe_3$)		40.4 (O_2CCMe_3)
	85.7, 82.6 (OCH_2CMe_3)		83.9, 80.0 (OCH_2CMe)
	181.8 ($O_2CCH_2CMe_3$)		187.3 (O_2CCMe_3)
5	27.1 (OCH_2CMe_3)	**8**	26.9 (OCH_2CMe_3)
	28.6 ($O_2CCH_2CMe_3$)		30.3 ($O_2CCH_2CMe_3$)
	33.6 (OCH_2CMe_3)		34.0 (OCH_2CMe_3)
	40.1 (O_2CCMe_3)		51.5 ($O_2CCH_2CMe_3$)
	83.7, 80.3 (OCH_2CMe_3)		84.2, 80.4 (OCH_2CMe_3)
	187.8 (O_2CCMe_3)		181.3 ($O_2CCH_2CMe_3$)

The M–O–M stretches for the OMc derivative were assigned at 998 and 733 cm^{-1}; however, a shoulder at 605 was also reported. The $[Nb_2(\mu\text{-}O)(OEt)_3(BHMP)]_2$ complex reportedly had an M–O–M stretch at 700 cm^{-1} [15]. For all of the oxo containing species in this study, the two peaks were observed around 650 and 675 cm^{-1}. Only the 650 cm^{-1} peak was noted for the non-oxo species **6**. For every sample, a stretch was noted around 1000 cm^{-1}. Therefore, the stretch around 675 cm^{-1} was assigned to the Nb–O–Nb moieties with the remaining stretches due to the Nb–O of the various ligands.

3.2.4. ^{13}C MAS NMR spectroscopy

To further characterize the bulk powder of these reactions, ^{13}C CP-MAS NMR data were collected on samples that were packed and handled under an argon atmosphere. Compounds **3**, **5**, and **6** are symmetric molecules and it is expected that one type of ORc and one type of terminal ONep resonance would be observed. The centrosymmetric nature of **4**, **7**, and **8** should also generate one type of ONep and one ORc resonances. The collected data were tabulated in Table 4.

The spectra for **3**, **5**, and **8** are very similar and show one set of resonances for the ORc ligands and two sets of resonances for the ONep ligands in what appears to be a 2:1 ratio. This is in agreement with the symmetry of the molecule in the solid-state crystal structure. For **6**, one set of resonances for the ONc and ONep ligands were observed but the observed peaks were broad and fine splitting may be observed on some of these resonances. The spectrum for **7** has one set of OBc resonances and two sets of ONep resonances. Again, packing inequivalencies can be postulated to explain the numerous ONep resonances that were unexpectantly observed. The spectrum of **4** is nearly identical and as was noted for **7**, two ONep and one ONc resonance set were observed; however, the quaternary carbons were not observed. For these compounds, it appears that the solid-state spectra are in agreement with the crystal structures.

3.3. Solution state NMR

Dried crystals of **3**–**8** were redissolved in toluene-d_8 and then sealed in an NMR tube to determine if the solid-state structures were retained in solution. The chemical shifts of the ORc ligands and lack of OH peak in the ^1H NMR spectra are indicative of the bidentate nature of the ORc ligands. Since a number of structural similarities exist between metal and ligand sets, the compounds of identical central cores are discussed collectively. Variable temperature NMR data were collected on selected species (**4**, **5**, **6** were chosen since they represent all of the various structure types observed) to further investigate any dynamic behavior. While there was sharpening of several peaks for the samples studied, there were no significant variations in the NMR spectra observed from -30 to $+60\,^{\circ}C$, demonstrating that there was no ligand exchange that could be observed at this temperature.

The solution state ^1H and ^{13}C NMR spectra of **3**, **5**, and **8** display two ONep resonances in a 2:1 ratio and one ORc methyl resonance. The larger ONep resonance displays multiple J_{H-H} splittings consistent with locked out methylene protons of two ONep ligands. These ONep ligands are most likely hindered from rotating by

the OBc ligands and the *t*-butyl groups of the other ONep ligands. The other methyl is located adjacent to the oxo ligand and is free to rotate. Based on these data, it is apparent that the solid-state structure is maintained in solution for these compounds.

For the unesterified complex **6**, two types of ONep in a 2:1 ratio and one ONc ligand were noted in the ^{1}H NMR toluene-d_8. One of the methylene resonances was present as a multiplet. The ^{13}C NMR spectrum has peaks similar to that observed in the ^{13}C MAS NMR solid-state but hyperfine splitting revealed two complete ONc and two ONep resonance sets. It appears that the solid-state structure is maintained in solution but the fine splitting was observed.

Based on the symmetry of the solid-state structures and assuming averaging of the ligands of **4** and **7** there should be one set of resonances noted for the ONep and ORc ligands. For **7**, two ONep resonances in a 1:2 ratio are observed with only one ORc resonance. Again as noted previously, hindered rotation about one of the ONep ligands and free rotation of the others would explain the observed spectrum.

4. Summary and conclusion

We have successfully isolated and characterized several carboxylic acid derivatives of the Group V congeners (**3**–**9**). The resulting products range from simple exchange through partially hydrolyzed to fully hydrolyzed species, which were found to be dependent *not* only on the pendant hydrocarbon chain of the carboxylic acid, but also on the reactivity of the metal center. Three interesting phenomena were noted for this family of compounds which may be exploitable in controlling the amount of esterification that occurs in a sol–gel system. First, the OEt ligands are completely absent in all of the structures observed indicating preferential substitution/hydrolysis of these ligands over the ONep ligands. Second, the Nb species appear to be more susceptible to the esterification process than the Ta system as evidenced by the increased oxolation in the isolated products. Third, for the Ta system, the ONc ligated species appear to offer more stabilization (protection) against esterification in comparison to the OBc ligated species, again based on the degree of oxolation observed. Combined, these structures lend insight into the esterification pathway which begins with an exchange of an acetate for an alkoxide ligand (**6**). This is then followed by formation of an oxo bond between the metal centers (**3**, **5**, and **8**). Further induced esterification by heating leads to a coupling of these partially hydrolyzed species to yield what appears to be the favored $M_4(O)_4(ORc)_4(ONep)_8$ (**4**, **7**, and **9**). The solution state NMR indicates that these compounds are stable in solution.

5. Supplementary material

X-ray crystallographic files in CIF format for the structures **3**–**9** have been deposited with the Cambridge Crystallographic Data Centre, CCDC Nos. 179216–179221. Copies of this information may be obtained free of charge from The Director, CCDC, 12 Union Road, Cambridge, CB2 1EZ, UK (fax: +44-1223-336033; e-mail: deposit@ccd.cam.ac.uk or www: http://www.ccdc.cam.ac.uk).

Acknowledgements

For support of this research, the authors would like to thank the Office of Basic Energy Science of the Department of Energy and the United States Department of Energy under contract DE-AC04-94AL85000. Sandia is a multiprogram laboratory operated by Sandia Corporation, a Lockheed Martin Company, for the United States Department of Energy.

References

[1] D.C. Bradley, R.C. Mehrotra, I.P. Rothwell, A. Singh, Alkoxo and Aryloxo Derivatives of Metals, Academic Press, San Diego, CA, 2001.
[2] D.C. Bradley, Chem. Rev. 89 (1989) 1317.
[3] D.C. Bradley, R.C. Mehrotra, D.P. Gaur, Metal Alkoxides, Academic Press, New York, 1978.
[4] C.D. Chandler, C. Roger, M.J. Hampden-Smith, Chem. Rev. 93 (1993) 1205.
[5] L.G. Hubert-Pfalzgraf, New J. Chem. 11 (1987) 663.
[6] I. Gautier-Luneau, A. Mosset, J. Galy, Z. Kristallogr. 180 (1987) 83.
[7] S. Doeuff, Y. Dromzee, F. Taulelle, C. Sanchez, Inorg. Chem. 28 (1989) 4439.
[8] S. Doeuff, Y. Dromzee, C. Sanchez, C.R. Acad. Sci. Paris 308 (1989) 1409.
[9] T.J. Boyle, R.P. Tyner, T.M. Alam, B.L. Scott, J.W. Ziller, B.G. Potter, Jr., J. Am. Chem. Soc. 121 (1999) 12104.
[10] T.J. Boyle, T.M. Alam, C.J. Tafoya, B.L. Scott, Inorg. Chem. 37 (1998) 5588.
[11] U. Schubert, E. Arpac, W. Glaubitt, A. Helmerich, C. Chau, Chem. Mater. 4 (1992) 291.
[12] I. Laaziz, A. Larbot, C. Guizard, J. Durand, L. Cot, J. Joffre, Acta Crystallogr., Sect. C 46 (1990) 2332.
[13] X. Lei, M. Shang, T.P. Fehlner, Organometallics 15 (1996) 3779.
[14] T.J. Boyle, T.M. Alam, E.R. Mechenbeir, B. Scott, J.W. Ziller, Inorg. Chem. 36 (1997) 3293.
[15] T.J. Boyle, T.M. Alam, D. Dimos, G.J. Moore, C.D. Buchheit, H.N. Al-Shareef, E.R. Mechenbier, B.R. Bear, Chem. Mater. 9 (1997) 3187.
[16] T.J. Boyle, D.M. Pedrotty, B. Scott, J.W. Ziller, Polyhedron 17 (1997) 1959.
[17] T.J. Boyle, J.J. Gallegos, III, D.M. Pedrotty, E.R. Mechenbier, B.L. Scott, J. Coord. Chem. 47 (1999) 155.
[18] T.J. Boyle, T.M. Alam, C.J. Tafoya, E.R. Mechenbeir, J.W. Ziller, Inorg. Chem. 38 (1999) 2422.
[19] T.J. Boyle, T.M. Alam, M.A. Rodriguez, C.A. Zechmann, Inorg. Chem. 91 (2002) 2574.

[20] T.J. Boyle, T.M. Alam, K.P. Peters, M.A. Rodriguez, Inorg. Chem. 40 (2002) 6281.
[21] L.G. Hubert-Pfalzgraf, V. Abada, S. Halut, J. Roziere, Polyhedron 16 (1997) 581.
[22] D.D. Perrin, W.L.F. Armarego, Purification of Laboratory Chemicals, Pergamon Press, New York, 1988.
[23] The listed versions of SAINT, SMART, XSHELL, and SADABS Software from Bruker Analytical X-Ray Systems Inc., 6300 Enterprise Lane, Madison, WI 53719 were used in analysis.
[24] R.D. Shannon, Acta Crystallogr., Sect. A A32 (1976) 751.

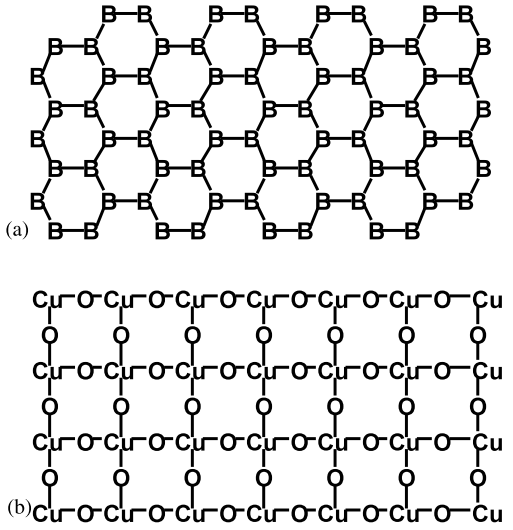


Fig. 1. (a) Part of a hexagonal boron layer in MgB_2; (b) part of a square Cu–O layer in the superconducting cuprate structures.

conductivity in MgB_2 analogous to similar models for the superconducting cuprates. The possible role of the magnesium counterions in doping the conducting boron skeleton of MgB_2 is then examined by comparison of MgB_2 with other inorganic solid state structures in which the magnesium counterions appear to be subvalent, i.e. have an effective formal oxidation state below +2. Such solid state structures include certain ternary magnesium transition metal hydrides [13]. Of particular significance is the observation that the magnesium counterions in some solid state hydrides, such as Mg_2RuH_4, Mg_3RuH_3, and Mg_4IrH_5, appear not to function as simple monomeric Mg^{2+} units expected from the position of magnesium in the periodic table as an alkaline earth. Instead when the solid state geometry forces the magnesium atoms to be relatively close together (i.e. ~3.0 Å or less), the magnesium ions can couple to form Mg_2^{2+} leading to a lower negative charge on the anionic portion of the solid state structure than would be expected with Mg^{2+} counterions. A similar coupling of the magnesium ions in MgB_2 leading to incomplete oxidation to Mg^{2+} provides a mechanism for generating the experimentally observed hole superconductivity [14].

2. Subvalent magnesium in solid state structures: examples in ternary magnesium transition metal hydrides

The prototypical form of subvalent magnesium is the dimeric ion Mg_2^{2+} with an Mg–Mg bond analogous to the well-known mercurous ion, Hg_2^{2+} and a formal magnesium oxidation state of +1. Density functional calculations indicate an Mg–Mg bond distance of 2.928 Å [15,16] in the hypothetical isolated ion Mg_2^{2+} (Table 1). A Mg–Mg bond distance (2.930 Å) similar to that

Table 1
Some Mg–Mg distances

Compound	Formulation	Mg–Mg (Å) [a]	Ref.
Mg_4IrH_5	$[Mg_2^{2+}]_2[Ir^{I}H_3^{2-}][H^-]_2$	2.754	[21]
Mg_2^{2+}	from DFT calculations	2.928	[15,16]
Mg_2RuH_4	$[Mg_2^{2+}][Ru^{II}H_4^{2-}]$ or $[Mg^{2+}]_2[Ru^0H_4^{4-}]$	2.930	[17]
Mg_3RuH_3	$[Mg_2^{2+}]_3[Ru^0H_3^{3-}]_2$	3.034	[20]
MgB_2	$[Mg^{2+}]_\infty[B^-]_{2\infty}$	3.083	[22]
Mg_2CoH_5	$[Mg^{2+}]_2[Co^{I}H_5^{4-}]$		[23]
Mg_2FeD_6	$[Mg^{2+}]_2[Fe^{II}D_6^{4-}]$	3.216	[24]
Mg_2NiD_4	$[Mg^{2+}]_2[Ni^0H_4^{4-}]$	3.254	[25]

[a] For compounds with more than one type of Mg atom, only the smallest Mg–Mg distance is listed.

calculated for Mg_2^{2+} is found in Mg_2RuH_4 [17]. This suggests formulation of Mg_2RuH_4 as $[Mg_2^{2+}][Ru^{II}H_4^{2-}]$ with Ru(II) rather than $[Mg^{2+}]_2[Ru^0H_4^{4-}]$ with Ru(0) [18]. In the former formulation the $Ru^{II}H_4^{2-}$ anion is isoelectronic with the $Rh^{III}H_4^-$ anion found in Li_3RhH_4 [19]. Similarly the Mg–Mg bond distances in Mg_3RuH_3 [20] and Mg_4IrH_5 [21] are also rather short (Table 1). Considering the magnesium counterions as the subvalent Mg_2^{2+} in these ternary hydrides leads to the formulations $[Mg_2^{2+}]_3[RuH_3^{3-}]_2$ and $[Mg_2^{2+}]_2[IrH_3^{2-}][H^-]_2$, respectively, with the central metal atoms in the fairly typical low, but reasonable oxidation states Ru(0) and Ir(I). The special role of magnesium in Mg_2RuH_4, Mg_3RuH_3, and Mg_4IrH_5, possibly through functioning as Mg_2^{2+} rather than the more usual Mg^{2+}, is also suggested by the observations that analogous ternary hydrides are unknown with electropositive metals other than magnesium as counterions. For comparison Table 1 also shows some Mg–Mg distances in other ternary magnesium transition metal hydrides (or the corresponding deuterides) not believed to contain subvalent magnesium such as Mg_2NiD_4, Mg_2CoH_5, and Mg_2FeD_6. These latter three compounds, which all have minimum Mg···Mg distances greater than 3.15 Å, can be formulated with fully oxidized Mg^{2+} cations and NiD_4^{4-}, CoH_5^{4-}, and FeD_6^{4-} anions, respectively. All three of these anions have the favored 18-electron rare gas configurations and are isoelectronic with known cyanometalates and/or metal carbonyls.

Further details of the structure and bonding in the hydrometallate anions in these solid state materials are discussed elsewhere [13,16]. The important point in the context of this paper is that the relatively short Mg–Mg distances in Mg_2RuH_4, Mg_3RuH_3, and Mg_4IrH_5 all provide evidence for subvalent magnesium in these structures. If the subvalent magnesium in these ternary magnesium transition metal hydrides is assumed to be Mg_2^{2+}, then the corresponding hydrometallate counter-

anions have reasonable metal oxidation states, electron counts, and chemical bonding models.

3. A comparison of the chemical bonding topology of magnesium diboride with that of the cuprate superconductors

All of the cuprate superconductors [26–28] appear to consist of layers of two-dimensional Cu–O conducting skeletons separated by layers of positive counterions. The following points are of interest concerning the chemical bonding topology of the cuprate superconductors [3,29]:

1) The conducting skeleton consists of Cu–O layers constructed from Cu–O–Cu bonds rather than direct Cu–Cu bonds (Fig. 1(b)). The much higher ionic character and thus much lower polarizability of metal–oxygen bonds relative to direct metal–metal bonds has been related to the persistence of superconductivity in cuprates to much higher temperatures than that in metals and metal clusters with direct metal–metal bonds.
2) The required metal–metal interactions are antiferromagnetic interactions between the single unpaired electrons in suitable d-orbitals of two d^9Cu(II) ions separated by an oxygen bridge similar to antiferromagnetic Cu(II)–Cu(II) interactions [30,31] in discrete binuclear complexes (the resonating valence bond model of Anderson and co-workers [32,33]).
3) The positive counterions in the cuprate superconductors control the negative charge in the Cu–O layers and thus the oxidation states of the copper atoms.
4) Partial oxidation of some of the Cu(II) to Cu(III) in the cuprate superconductors generates the holes in the valence band required for conductivity in accord with Hall effect measurements [34].

A model for the chemical bonding topology of MgB_2 can be developed which is closely related to that of the cuprates discussed above. In this connection note that the Mg–Mg distance in MgB_2 is 3.083 Å, which is comparable to that in some of the ternary magnesium transition metal hydrides discussed above (Table 1). This suggests the presence of subvalent magnesium of some type in MgB_2 leading to the following chemical bonding topology:

1) The conducting skeleton of MgB_2 consists of the hexagonal boron layers (Fig. 1(a)).
2) Electron transport occurs through the boron–boron σ bonds in the boron layers [6,8].
3) Electron transfer from the magnesium counterions to the boron layers controls the negative charge on the boron layers. If the magnesium ionizes fully to Mg^{2+}, then the boron layers are isoelectronic with graphite.
4) Partial reduction of some of the Mg^{2+} to Mg_2^{2+} (i.e. the formation of subvalent magnesium) generates the holes in the valence band required for conductivity in accord with the positive Hall effect measurements [14].

In this model the magnesium counterions in MgB_2 play an active role in controlling electron transport in the hexagonal boron layers (Fig. 1(a)) thereby affecting conducting and superconducting properties. It is therefore not surprising that substitution of other bivalent metals for MgB_2 leads to materials without comparable superconducting properties.

References

[1] R.B. King, J. Solid State Chem. 131 (1997) 394.
[2] J. Nagamatsu, N. Nakagawa, T. Muranaka, Y. Zenitani, J. Akimitsu, Nature (London) 401 (2001) 63.
[3] R.B. King, J. Chem. Inf. Comput. Sci. 39 (1999) 180.
[4] C.P. Poole, Jr., T. Datta, H.A. Farach, Copper Oxide Superconductors, Wiley, New York, 1988.
[5] J.E. Hirsch, Phys. Lett. A A282 (2001) 392.
[6] K.D. Belashchenko, M. van Schilfgaarde, V.P. Antropov, Phys. Rev. B 64 (2001) 092503(R).
[7] N.I. Medvedeva, J.E. Medvedeva, A.L. Ivanovskiĭ, V.G. Zubkov, A.J. Freeman, JETP Lett. 73 (2001) 336.
[8] Y. Kong, O.V. Dolgov, O. Jepsen, O.K. Andersen, Phys. Rev. B 64 (2001) 020501(R).
[9] A.Y. Liu, I.I. Mazin, J. Kortus, Phys. Rev. Lett. 87 (2001) 087005-1.
[10] X.L. Chen, Q.Y. Tu, M. He, L. Dai, L. Wu, J. Phys. Condens. Matter 13 (2001) L723.
[11] N.I. Medvedeva, A.L. Ivanovskiĭ, J.E. Medvedeva, A.J. Freeman, Phys. Rev. B 64 (2001) 020502(R).
[12] S. Xu, Y. Moritomo, K. Kato, A. Nakamura, J. Phys. Soc. Jpn. 70 (1889) 2001.
[13] R.B. King, Coord. Chem. Rev. 200–202 (2000) 813.
[14] W.N. Kang, C.U. Jung, K.H.P. Kim, M.-S. Park, S.Y. Lee, H.J. King, E.M. Choi, K.H. Kim, M.-S. Kim, S.I. Lee, Appl. Phys. Lett. 79 (2001) 982.
[15] A.S. Dworkin, H.R. Bronstein, M.A. Bredig, J. Phys. Chem. 70 (1966) 2384.
[16] T.K. Firman, C.R. Landis, J. Am. Chem. Soc. 120 (1998) 12650.
[17] F. Bonhomme, K. Yvon, G. Triscone, K. Jansen, G. Auffermann, P. Müller, W. Bronger, P. Fischer, J. Alloys Compounds 178 (1992) 161.
[18] G.J. Miller, H.B. Deng, R. Hoffmann, Inorg. Chem. 33 (1994) 1330.
[19] P. Zolliker, K. Yvon, C. Baerlocher, J.D. Jorgensen, F. Rotella, J. Less Common Metals 129 (1987) 208.
[20] F. Bonhomme, K. Yvon, P. Fischer, J. Alloys Compounds 186 (1992) 309.
[21] F. Bonhomme, N.T. Stetson, K. Yvon, P. Fischer, A.W. Hewat, J. Alloys Compounds 200 (1993) 65.
[22] M.E. Jones, R.E. Marsh, J. Am. Chem. Soc. 76 (1954) 1434.
[23] P. Zolliker, K. Yvon, P. Fischer, J. Schefer, Inorg. Chem. 24 (1985) 4177.

[24] J.-J. Didisheim, P. Zolliker, K. Yvon, P. Fischer, J. Schefer, M. Gubelmann, A.F. Williams, Inorg. Chem. 23 (1953) 1984.
[25] K. Yvon, J. Schefer, F. Stucki, Inorg. Chem. 20 (1981) 2776.
[26] J.M. Williams, M.B. Beno, K.D. Carlson, U. Geiser, H.C. Ivy Kao, A.M. Kini, L.C. Porter, A.J. Schultz, R.J. Thorn, H.H. Wang, M.-H. Whangbo, M. Evain, Acc. Chem. Res. 21 (1988) 1.
[27] C.P. Poole, T. Datta, H.A. Farach, Copper Oxide Superconductors, Wiley, New York, 1988.
[28] P.W. Anderson, The Theory of Superconductivity in the High T_c Cuprates, Princeton University Press, Princeton, NJ, 1997.
[29] R.B. King, in: D.L. Nelson, T.F. George (Eds.), Chemistry of High-Temperature Superconductors II, American Chemical Society, Washington, DC, 1988 (ACS Symposium Series, No. 377), pp. 54–63.
[30] R.J. Doedens, Progr. Inorg. Chem. 21 (1976) 209.
[31] C.J. Cairns, D.H. Busch, Coord. Chem. Rev. 69 (1986) 1.
[32] P.W. Anderson, Science 235 (1987) 1196.
[33] P.W. Anderson, G. Baskaran, Z. Zou, T. Hsu, Phys. Rev. Lett. 58 (1987) 2790.
[34] N.P. Ong, Z.Z. Wang, J. Clayhold, J.M. Tarascon, L.H. Greene, W.R. McKinnon, Phys. Rev. B 35 (1987) 8807.

2. Experimental

2.1. Instrumental

IR spectra were recorded on a BOMEM FT-IR model BM 100 spectrometer. ^{1}H NMR spectra were measured on a BRUKER AC250 instrument with TMS as internal standard. Elemental analyses (CHN) were determined with a FISONS EA-1108 equipment. Enraf–Nonius CAD4 diffractometers were used for the diffraction measurements. Routine FAB$^-$ mass spectra have been recorded on a TSQ spectrometer (Finnigan) with nitrobenzylalcohol as matrix.

2.2. Preparation of the boron complexes

The hydroximatoborates were prepared as described previously [14], with slight modifications. Solvents and commercially available chemicals (H_3BO_3, benzohydroxamic acid, di-*n*-butylamine, dicyclohexylamine, tetra-*n*-butylammonium bromide, tetra-*n*-propylammonium bromide and silver oxide) were used as purchased.

2.2.1. Dicyclohexylammonium bis(benzohydroximato)borate (*1*)

A mixture of 0.068 g H_3BO_3 (1.10 mmol), 0.302 g benzohydroxamic acid (2.20 mmol) and 0.200 g dicyclohexylamine (1.1 mmol) in 25 ml C_6H_6 was heated under reflux for 8 h, using a Dean-Stark trap for azeotropic elimination of water. After evaporation of the C_6H_6, the solid residue was dissolved in 15 ml CH_2Cl_2, 15 ml *n*-C_6H_{14} was added and the mixture was kept at −15 °C. After 48 h the crystals were filtered off and washed with *n*-C_6H_{14} yielding 0.474 g of **1** (yield: 91%). M.p. 226–229 °C. *Anal*. Found: C, 67.12; H, 6.93; N, 9.12. Calc. for $C_{26}H_{34}BN_3O_4$: C, 67.39; H, 7.40; N, 9.07%. NMR (25 °C): ^{1}H (250 MHz, $CDCl_3$): δ 1.02 (m, 6H, CH_2), 1.47 (m, 4H, CH_2), 1.56 (m, 6H, CH_2), 1.95 (m, 4H, CH_2), 3.10 (m, 2H, CH), 7.26 (m, 6H, C_6H_5), 7.78 (m, 4H, C_6H_5). FTIR (KBr): 3035m (ν NH), 2934s (ν CH_2), 2856s (ν CH_2), 1597ms (C_6H_5), 1562ms (C_6H_5), 1499m, 1447m (δ CH_2), 1388vs (ν OCN), 1125s (ν_{as} $^{10}BO_4$), 1085vs (ν_{as} $^{11}BO_4$), 987s, 942m (δ_{as} BO_4), 792m (ν ONC), 742m (ν ONC), 691m (C_6H_5) (IR data: vs, very strong; s, strong; ms, medium strong; m, medium).

2.2.2. Di-n-butylammonium bis(benzohydroximato)borate (*2*)

Compound **2** was prepared from 0.080 g H_3BO_3 (1.30 mmol), 0.357 g benzohydroxamic acid (2.60 mmol) and 0.170 g di-*n*-butylamine (1.31 mmol) as described above. Yield: 0.450 g (84%). M.p. 113–114 °C. *Anal*. Found: C, 64.06; H, 6.45; N, 10.28. Calc. for $C_{22}H_{30}BN_3O_4$: C, 64.24; H, 7.35; N, 10.22%. NMR (25 °C): ^{1}H (250 MHz, $CDCl_3$): δ 0.80 (t, 6H, CH_3), 1.3 (m, 4H, CH_2–CH_3), 1.79 (m, 4H, CH_2–CH_2–CH_2), 3.10 (t, 4H, N–CH_2) 7.49 (m, 6H, C_6H_5), 7.91 (m, 4H, C_6H_5). FTIR (KBr): 3122m (ν NH), 2956ms (ν CH_2/CH_3), 1594ms (C_6H_5), 1563s (C_6H_5), 1498m, 1470m, 1446m (δ CH_2), 1380s (ν OCN), 1124s (ν_{as} $^{10}BO_4$), 1086vs (ν_{as} $^{11}BO_4$), 993s, 942m (δ_{as} BO_4), 773m (ν ONC), 738m (ν ONC), 703m (C_6H_5), 690m (C_6H_5).

2.2.3. Tetra-n-propylammonium bis(benzohydroximato)borate (*3*)

A mixture of 0.031 g H_3BO_3 (0.50 mmol), 0.058 g Ag_2O (0.25 mmol), 0.137 g benzohydroxamic acid (1.00 mmol), 0.133 g tetra-*n*-propylammonium bromide (0.50 mmol) in 25 ml C_6H_6 was heated to reflux for 8 h as described above. The solid was filtered off and extracted with 15 ml CH_2Cl_2. After vacuum evaporation 0.201 g of **3** (yield 86%) were obtained as colorless crystals (m.p. 136 °C). *Anal*. Found: C, 66.41; H, 8.10; N, 8.88. Calc. for $C_{26}H_{38}BN_3O_4$: C, 66.81; H, 8.19; N, 8.99%. NMR (25 °C): ^{1}H (250 MHz, $CDCl_3$): δ 0.84 (t, 12H, CH_3), 1.50 (m, 8H, CH_2–CH_3), 3.03 (t, 8H, CH_2–N), 7.32 (m, 6H, C_6H_5), 7.86 (m, 4H, C_6H_5). FTIR (KBr): 2975ms (ν CH_2/CH_3), 2945m (ν CH_2/CH_3), 1592ms (C_6H_5), 1558ms (C_6H_5), 1488ms, 1461m, 1447m (δ CH_2), 1377vs (ν OCN/δ CH_3), 1114s (ν_{as} $^{10}BO_4$), 1078s (ν_{as} $^{11}BO_4$), 981s, 944m (δ_{as} BO_4), 780m (ν ONC), 736m (ν ONC), 701ms (C_6H_5), 674m. FAB$^-$ MS; *m*/*z*: 281.2, 162.1.

2.2.4. Tetra-n-butylammonium bis(benzohydroximato)borate (*4*)

Compound **4** has been prepared from 0.062 g H_3BO_3 (1.00 mmol), 0.274 g benzohydroxamic acid (2.00 mmol), 0.240 g tetra-*n*-butylammonium bromide (1.00 mmol) and 0.116 g Ag_2O (0.50 mmol) as described for **3**, yielding 0.470 g (90%). M.p. 165 °C. *Anal*. Found: C, 67.64; H, 8.79; N, 8.07. Calc. for $C_{30}H_{46}BN_3O_4$: C, 68.83; H, 8.86; N, 8.03%. NMR (25 °C): ^{1}H (250 MHz, $CDCl_3$): δ 0.84 (t, 12H, CH_3), 1.40 (m, 16H, CH_2–CH_3), 3.14 (t, 8H, N–CH_2), 7.32 (m, 6H, C_6H_5), 7.86 (m, 4H, C_6H_5). FTIR (KBr): 2966ms (ν CH_2/CH_3), 2929m (ν CH_2/CH_3), 1594m (C_6H_5), 1558m (C_6H_5), 1490m, 1382vs (ν OCN), 1118s (ν_{as} $^{10}BO_4$), 1083vs (ν_{as} $^{11}BO_4$), 981 s, 944m (δ_{as} BO_4), 770m (ν ONC), 737m (ν ONC), 695s (C_6H_5), 670m (C_6H_5).

2.3. X-ray crystal structure determinations

Crystals of the chloroform solvate **1**·$CHCl_3$ and of **3** suitable for structure analysis were obtained from $CHCl_3$–*n*-C_6H_{14} solutions (1:1) of the complexes. The cell constants were calculated from 25 reflexes with a wide range of 2θ. The program HELENA [16] was used for the data reduction. Both complexes crystallize monoclinic. The space groups were assigned using the criterion of choosing the setting which corresponds to the lowest monoclinic β angle. The structures were solved by direct methods with SHELXS-97 [17] and

refined with SHELXL-97 [18]. A ψ-scans [16] absorption correction was performed and all non-hydrogen atoms were refined with anisotropic displacement parameters in both structures. The hydrogen atoms were found in the Fourier-map in **1**·$CHCl_3$ and calculated at idealized positions and refined using the riding model in **3**. Crystal data and more detailed information about the structure determinations are given in Table 1. Labeled diagrams of the structures of **1**·$CHCl_3$ and **3** are shown in Figs. 1 and 2, respectively. Selected bond lengths and angles are given in Table 2.

3. Results and discussion

3.1. Synthesis of the bis(benzohydroximato)borates

Bis(benzohydroximato)borates were obtained in high yield in simple one-step reactions according to:

$$H_3BO_3 + 2C_6H_5CONHOH + R_2NH \rightarrow [R_2NH_2][B(C_6H_5CONO)_2] + 3H_2O$$

for **1** and **2**, or:

$$2H_3BO_3 + 4C_6H_5CONHOH + 2[R_4N]Br + Ag_2O \rightarrow 2[R_4N][B(C_6H_5CONO)_2] + 2AgBr + 7H_2O$$

for **3** and **4**.

The use of silver oxide and a quaternary ammonium bromide, which resulted in the formation of insoluble silver bromide and easily removable water as byproducts, proved to be a favorable synthetic route for tetraalkylammonium bis(benzohydroximato)borates.

These quaternary ammonium cations acted efficiently, as expected due to their favorable size, as counter ions for the crystallographic study also in absence of the N–H···O and N–H···N hydrogen bonds between the anionic complex and the counter ion, normally present in the lower alkylammonium salts, as in **1**·$CHCl_3$. Good quality crystals of **3**, additionally

Table 1
Crystal data and structure refinement for **1** $CHCl_3$ and **3**

Compound	**1**·$CHCl_3$	**3**
Empirical formula	$C_{27}H_{35}BCl_3N_3O_4$	$C_{26}H_{38}BN_3O_4$
Formula weight	582.74	467.40
Temperature (°C)	−65(2)	20(2)
Wavelength (pm)	154.056	71.073
Radiation	Cu Kα	Mo Kα
Crystal system	monoclinic	monoclinic
Space group	$P2_1/c$	Pn
Unit cell parameters		
a (pm)	1302.88(9)	1118.7(3)
b (pm)	1127.18(17)	967.64(8)
c (pm)	1987.55(10)	1278.8(3)
β (°)	91.484(8)	108.89(2)
V (pm^3)	$2917.9(5) \times 10^6$	$1309.7(5) \times 10^6$
Z	4	2
Absorption coefficient (mm^{-1})	3.146	0.079
Crystal size (mm)	0.5 × 0.4 × 0.1	0.40 × 0.20 × 0.20
Method	ω scans	ω scans
θ range (°)	5–65	3–25
Index ranges (h, k, l)	−1 → 15, 0 → 13, −23 → 20	−13 → 13, 0 → 11, −15 → 15
Collected reflections	5511	4606
Unique reflections	4843	4606
R_{int}	0.0930	0.0000
Observed data [$I > 2\sigma(I)$]	2774	2518
Absorption correction	ψ-scans [16]	ψ-scans [16]
Min/max transmission	0.76443/0.95645	0.84812/0.94824
Structure refinement	full-matrix least-squares on F^2	full-matrix least-squares on F^2
Weighting scheme	$w = 1/[\sigma 2(F_o^2) + (0.0810P)^2 + 1.8367P]$, $P = (F_o^2 + 2F_c^2)/3$	$w = 1/[\sigma^2(F_o^2) + (0.1097P)^2 + 0.0139P]$, $P = (F_o^2 + 2F_c^2)/3$
Hydrogen treatment	Fourier-map	riding model
Refined parameters	483	308
Structure factors [$I > 2\sigma(I)$]	$R_1 = 0.0647$, $wR_2 = 0.1583$	$R_1 = 0.0758$, $wR_2 = 0.1712$
Goodness-of-fit, S	1.039	1.049
Extinction coefficient	not refined	0.056(7)
Absolute structure parameter	none	0.00001
Programs used	HELENA, PLATON [16], SHELXS-97 [17], SHELXL-97 [18]	HELENA, PLATON [16], SHELXS-97 [17], SHELXL-97 [18]

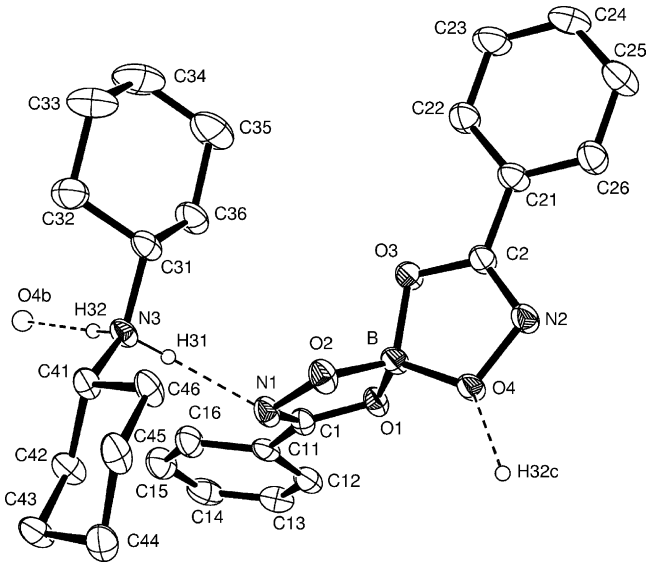


Fig. 1. ORTEP plot (30% probability) of **1** in **1**·$CHCl_3$. The H-atoms are omitted for clarity, except H(31) and H(32). The dashed lines indicate the H-bonds.

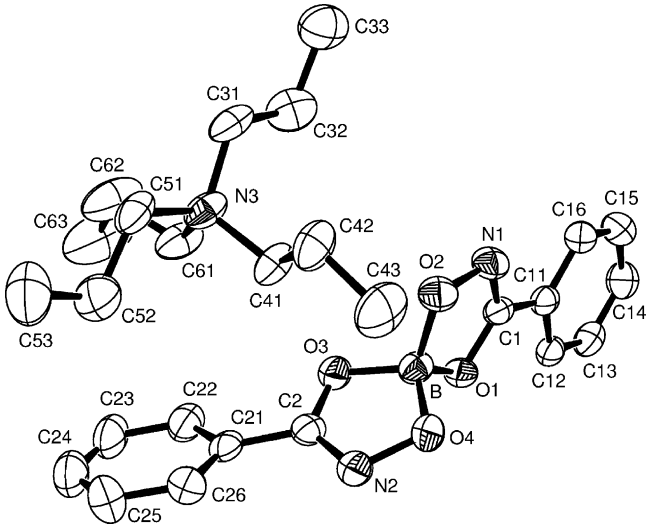


Fig. 2. ORTEP plot (30% probability) of **3**. The H-atoms are omitted for clarity.

without solvent of crystallization, could be obtained for this purpose.

3.2. Spectroscopic characterization

The infrared spectra of the presented compounds (KBr pellets) exhibit the expected characteristic features of the bis(hydroximato)borate moiety [14]. The strongest absorption at about 1080 cm^{-1} corresponds to ν_{as} $^{11}BO_4$, showing the component for ν_{as} $^{10}BO_4$ at about 1120 cm^{-1}. Another strong absorption band at approximately 985 cm^{-1} can be attributed to a deformation mode δ_{as} BO_4. The strong absorption band at about 1380 cm^{-1} most probably involves a stretching vibration of the OCN group (ν OCN) within the hydroximato chelate. The N–H stretching vibration of the dialkylammonium salts **1** and **2** appears as multicomponent absorption pattern in the range 3050–2400 cm^{-1}, characteristic for strong hydrogen bonds.

Table 2
Selected bond lengths (pm) and angles (°) for **1**·$CHCl_3$ and **3**

	1·$CHCl_3$	**3**
Bond lengths		
B–O(1)/B–O(3) [a]	147.0(6)/147.3(5)	146.7(8)/147.9(8)
B–O(2)/B–O(4) [a]	146.8(6)/147.2(5)	146.4(8)/146.9(8)
O(1)–C(1)/O(3)–C(2) [a]	132.6(4)/133.6(5)	133.4(6)/132.7(7)
C(1)–N(1)/C(2)–N(2) [a]	128.1(5)/128.9(5)	126.5(7)/126.9(7)
N(1)–O(2)/N(2)–O(4) [a]	142.0(4)/144.6(4)	141.6(6)/142.6(6)
C(1)–C(11)/C(2)–C(21) [a]	146.6(6)/147.2(5)	147.2(8)/147.6(8)
N(3)–H(31)···N(1)	286.7(6)	
N(3)–H(31)	88.0(6)	
H(31)···N(1)	199(6)	
(N3)–H(32)···O(4) [b]	283.6(4)	
N(3)–H(32)	88.0(5)	
H(32)···O(4) [b]	196(6)	
Bond angles		
O(1)–B–O(2)/O(3)–B–O(4) [a]	102.3(3)/101.9(3)	102.7(5)/101.6(5)
O(1)–B–O(3)	113.3(3)	113.9(5)
O(1)–B–O(4)	113.6(4)	112.8(4)
O(2)–B–O(3)	112.6(4)	112.5(4)
O(2)–B–O(4)	113.6(3)	113.8(5)
O(1)–C(1)–N(1)/ O(3)–C(2)–N(2) [a]	116.0(4)/117.7(3)	117.5(5)/118.5(5)
C(1)–N(1)–O(2)/ C(2)–N(2)–O(4) [a]	107.2(3)/104.7(3)	106.5(4)/105.1(4)
N(1)–O(2)–B/N(2)–O(4)–B [a]	107.0(3)/109.0(3)	107.8(4)/108.9(4)
O(1)–C(1)–C(11)/ O(3)–C(2)–C(21) [a]	120.3(4)/119.9(3)	118.7(4)/118.7(5)
N(1)–C(1)–C(11)/ N(2)–C(2)–C(21) [a]	123.7(4)/122.5(4)	123.8(5)/122.8(6)
N(3)–H(31)–N(1)	178.0(6)	
N(3)–H(32)–O(4) [b]	175.0(5)	

[a] Values for two non equivalent chelate rings, respectively.
[b] Symmetry operation: $-x+1$, $y+1/2$, $-z+1/2$.

The ^1H NMR spectra of the described hydroximatoborates in $CDCl_3$ show the expected patterns.

The FAB^- MS-Spectrum of **3** (nitrobenzylalcohol matrix) shows m/z peaks at 281.2 and 162.1, corresponding to $[B(C_6H_5CONO)_2]^-$ (281) and $[OB(C_6H_5CONO)]^-$ (162), respectively.

3.3. Crystal structures

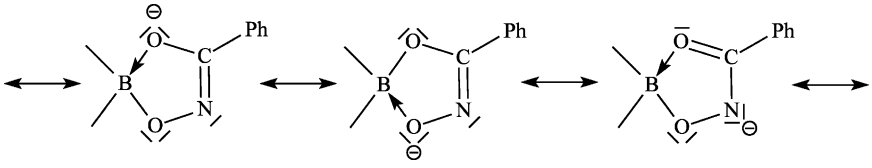
The crystal structures show the expected spirochelate structure of the bis(benzohydroximato)borate anions with slightly distorted tetahedral BO_4 coordination. The B–O distances (mean value 147.0 pm) are in good agreement with the mean value of 146.8 pm for compounds containing the BO_4^- moiety [19]. The endocyclic O–B–O-angles lie between 101.6° and 102.7°, the exocyclic O–B–O-angles (112.5°–113.9°) are slightly larger compared to the ideal tetrahedral angle. The C–N bond lengths (126.5–128.9 pm) are

close to the standard value of a double bond. The C–O bonds (132.6–133.6 pm) are considerably shortened with respect to a single bond [19]. The N–O bond lengths (141.6–144.6 pm) correspond to a single bond and are longer compared to the mean N–O distance of 139.4 pm in oximes [19].

The chelate rings are essentially planar with maximum atomic displacements from the mean plane between 0.80 and 6.1 pm. The phenyl groups are slightly distorted with respect to the adjacent chelate rings, showing torsion angles from 4.80° to 27.18°.

Bond lengths and angles of the BONCO heterocyles in **1** and **3** show only slight variations and are in fairly good agreement with those observed in difluoro-*N*-methylacetohydroxamatoboron (**5**) [1]. The B–O distances in **1** and **3** (mean value 147.0 pm) are slightly shorter compared to **5** (mean value 148.3 pm) while the N–O bonds are considerably longer (mean value 142.7 for **1** and **3**, and 134.2 pm for **5**).

The structural data indicate a considerable delocalization of π electrons in the boron chelates **1** and **3**, as well as in the hydroxamatoboron complexes [1,2]. We propose the following resonance structures having major contribution to the bonding hybrid in the benzohydroximatoborates:



Strong hydrogen bonds between the dicyclohexylammonium nitrogen N(3) and the atoms N(1) and O(4), from different complex molecules, occur in **1**·$CHCl_3$, forming a chain like arrangement, as shown in Fig. 1. The distances N(3)–H(31)···N(1) = 286.7(6) and N(3)–H(31)···O(4b) = 283.6(4) pm are considerably shorter compared to the mean values for these types of H-bond, 307 and 293 pm [20], respectively. The corresponding bond angles are N(3)–H(31)–N(1) = 178(6)° and N(3)–H(31)–O(4b) = 175(5)°.

4. Conclusions

The comparison of crystallographic data shows that the bond lengths among the chelate ring in hydroximate(2−)- and in N-substituted hydroxamate(1−) boron complexes do not differ significantly, suggesting that the presence of an additional negative charge in the hydroximate anion does not change substantially the electron density distribution in the chelate ring, as it could be expected. Thus, the bonds among the rings are not affected due to the presence of the lone electron pair at the hydroximate's nitrogen atom in the bis(benzohydroximato)borate complex. Also the involvement of chelate's atoms in strong hydrogen bonds between the complex and the counter ion do not promote any substantial changes in the ring's bonds in **1**·$CHCl_3$, in comparison with the values found in **3**.

5. Supplementary material

Crystallographic data (excluding structure factors) have been deposited with the Cambridge Crystallographic Data Centre, CCDC Nos. 178861 and 178862 for compounds **1**·$CHCl_3$ and **3**. Copies of the data can be obtained free of charge on application to The Director, CCDC, 12 Union Road, Cambridge CB2, 1EZ, UK (fax: +44-1223-336033; e-mail: deposit@ccdc.cam.ac.uk or www: http://www.ccdc.cam.ac.uk).

Acknowledgements

The authors are grateful to Professor J. Strähle (Tübingen) for the use of the X-ray diffractometer and acknowledge the Federal District Foundation for the Support of Research (FAPDF) for financial support and the National Council for Research and Development (CNPq) for providing a scholarship to V.M.D.

References

[1] S.J. Rettig, J. Trotter, W. Kliegel, D. Nanniga, Can. J. Chem. 55 (1977) 1.
[2] S.J. Rettig, J. Trotter, W. Kliegel, D. Nanniga, Can. J. Chem. 56 (1978) 1676.
[3] B. Chatterjee, Coord. Chem. Rev. 26 (1978) 281.
[4] B. Kurzak, H. Kozlowski, E. Farkas, Coord. Chem. Rev. 114 (1992) 169.
[5] F. Umland, C. Schleyerbach, Angew. Chem. 77 (1965) 151.

[6] F. Umland, E. Hohaus, K. Brodte, Chem. Ber. 106 (1973) 2427.
[7] W. Kliegel, D. Nanniga, Chem. Ber. 116 (1983) 2616.
[8] M.K. Das, B. Biswas, S. Chakraborty, Synth. React. Inorg. Met.-Org. Chem. 16 (1986) 77.
[9] M.K. Das, S. Chakraborty, Indian J. Chem., Sect. A 29 (1990) 352.
[10] M.K. Das, S. Chakraborty, Z. Naturforsch., Teil. B 45 (1990) 1123.
[11] W. Kliegel, U. Schumacher, M. Tajerbashi, S.J. Rettig, J. Trotter, Can. J. Chem. 69 (1991) 545.
[12] M.K. Das, S. Chakraborty, Synth. React. Inorg. Met.-Org. Chem. 16 (1988) 225.
[13] L. Lamandé, D. Boyer, A. Muñoz, J. Organomet. Chem. 328 (1987) 1.
[14] E. Bessler, V.M. Deflon, J. Weidlein, Z. Naturforsch., Teil. B 48 (1993) 1275.
[15] P. Denis, O.N. Ventura, J. Mol. Struct.-Theochem 537 (2001) 173.
[16] A.L. Spek, HELENA, PLATON, Programs for the treatment of crystallographic data, University of Utrecht, The Netherlands, 1996.
[17] G.M. Sheldrick, SHELXS-97, Program for the solution of crystal structures, University of Göttingen, Germany, 1997.
[18] G.M. Sheldrick, SHELXL-97, Program for the refinement of crystal structures, University of Göttingen, Germany, 1997.
[19] F.H. Allen, O. Kennard, D.G. Watson, L. Brammer, A.G. Orpen, J. Chem. Soc., Perkin Trans. II, 1987, p. S1.
[20] S.N. Vinogradov, R.H. Linnell, Hydrogen Bonding, Van Nostrand Reinhold, New York, 1971, p. 178.

could not be isolated in the cases of larger primary and secondary perfluoroalkyl iodides. We have now reinvestigated the reaction of $(COD)PtMe_2$ with a higher fluoroalkyl iodide, $^nC_4F_9I$, and find that selective formation of a single fluoroalkyl product can be achieved under suitable reaction conditions.

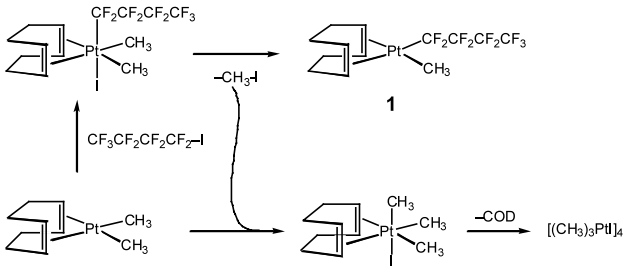
2. Results and discussion

Modifications to the originally described procedures were made. Both previous reports describe syntheses using an excess of CF_3I, making the production of a mixture of compounds understandable. In contrast, we found that when a hexane suspension of $(COD)PtMe_2$ was allowed to react with only one molar equivalent of $^nC_4F_9I$, the ^{19}F NMR spectrum of the crude product indicated that only one fluorinated species was formed. However, the ^1H NMR spectrum showed the presence of two Pt species by virtue of two singlets corresponding to CH_3 groups with Pt satellites at δ 1.73 ($J = 77.1$ Hz) and 1.18 ($J = 79.2$ Hz), though there were only peaks arising from the presence of a single diolefin ligand. The two compounds were easily separated using hexane extraction.

The fluorinated organometallic complex was determined to be $(COD)PtMe(C_4F_9)$ (**1**). The ^{19}F NMR spectrum showed large Pt–F couplings for the α and β CF_2 groups (404, 102 Hz, respectively). The compound exhibited air and moisture stability and was soluble in all common organic solvents. Compound **1** is presumably formed by oxidative addition of the fluoroalkyl iodide to $(COD)PtMe_2$, followed by reductive elimination of CH_3I.

Indeed, the second platinum product giving rise to the ^1H NMR singlet at δ 1.73 was determined to be $[PtMe_3I]_4$, as previously observed [11]. Formation of this product is clearly the result of the oxidative addition of CH_3I (formed in the reductive elimination step that affords **1**) to the starting material $(COD)PtMe_2$, followed by loss of the diolefin from the putative Pt(IV) intermediate $(COD)PtMe_3I$, as shown in Scheme 1.

No bis(perfluoroalkyl) platinum species were formed using these conditions, even though there must be a slight excess of iodoperfluorocarbon due to the consumption of some $(COD)PtMe_2$ that instead reacts with



Scheme 1.

MeI. Presumably the absence of a large excess of iodoperfluorocarbon precludes subsequent oxidative addition reaction with **1** followed by a second elimination of CH_3I. However, we have not attempted to assess the role of the solvent. Previous reports used dichloromethane, and solvent effects have been shown to be important in such oxidative addition/reductive elimination reactions at platinum centers [13,14].

During the course of this work, we were fortuitously able to obtain single crystals of the starting material $(COD)PtMe_2$, the molecular structure of which has not been reported. As this compound would be a benchmark structure for other (COD)Pt compounds, we determined its solid state structure by means of a single crystal X-ray diffraction experiment. An ORTEP diagram is shown in Fig. 1. The Pt–C distances to the diolefin ligand fall in a narrow range [2.204(11)–2.255(12) Å, $\Delta = 0.051$ Å] as do the two Pt–CH_3 distances (2.040(11), 2.072(11) Å). These distances compare favorably with other bond lengths in similar bis(alkyl) or bis(aryl) COD complexes. There is a slightly larger range for the Pt–C bond distances involving the diene than in those observed in $(COD)Pt(Ph)_2$ which range from 2.249(5) to 2.278(6) Å ($\Delta = 0.029$ Å) [15], but they mirror those in $(COD)Pt(CH_2SiMe_3)_2$ where the range is 2.212(8)–2.268(9) Å ($\Delta = 0.056$ Å) [16]. Likewise, the Pt–CH_3 distances correspond well to those in $(COD)Pt(CH_2SiMe_3)_2$ (2.069(7), 2.070(8) Å) whereas the higher s-character in the carbon orbital of the phenyl groups in $(COD)Pt(Ph)_2$ understandably results in shorter Pt–C distances of 2.013(5) and 2.022(5) Å (Table 2).

In conclusion, we have described a controlled synthesis of a perfluoroalkyl platinum compound by the oxidative addition of C_4F_9I to the convenient starting material $(COD)PtMe_2$. By employing only one molar equivalent of iodoperfluorocarbon and using hexanes as the reaction solvent, the selective formation of only one fluorinated species could be achieved. The known Pt(IV) compound $[PtMe_3I]_4$ was isolated as well. An X-ray

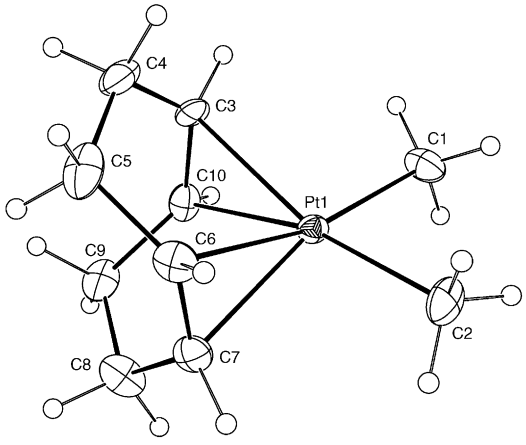


Fig. 1. ORTEP diagram of $(COD)PtMe_2$ (**2**), showing the atom labeling scheme. Thermal ellipsoids are shown at the 30% level.

Table 1
Crystal data and structure refinement for **2**

Empirical formula	$C_{10}H_{18}Pt$
Formula weight	333.33
Diffractometer	Siemens P4
Temperature (K)	235(2)
Wavelength (Å)	0.71073
Crystal system	monoclinic
Space group	$P2(1)/c$
Unit cell dimensions	
a (Å)	8.129(2)
b (Å)	18.217(4)
c (Å)	7.339(2)
α (°)	90
β (°)	115.899(16)
γ (°)	90
Crystal color, habit	colorless block
Crystal size (mm)	0.40 × 0.30 × 0.20
Volume (Å^3)	977.7(5)
Z	4
$R(F)$ (%) [a]	3.86
$R(wF^2)$ (%) [a]	9.90

[a] Quantity minimized $= R(wF^2) = [\Sigma[w(F_o^2 - F_c^2)^2]/\Sigma[(wF_o^2)^2]]^{1/2}$; $R(F) = \Sigma\Delta/\Sigma(F_o)$, $\Delta = |(F_o - F_c)|$.

crystallographic study of (COD)PtMe(C_4F_9) established the bond connectivity within the molecule, though detailed bond distances and angles could not be determined due to poorly diffracting crystals. In addition, we have determined the solid state structure of (COD)$PtMe_2$, which serves as a benchmark structure for COD containing Pt compounds. Future work will focus on the oxidative addition of other perfluoroalkyl iodides to Pt(II) species containing different ligand sets to control the electronic environment at the metal center as well as investigating the effect of solvent in such reactions.

3. Experimental

3.1. General considerations

All reactions were performed in oven-dried glassware, using standard Schlenk techniques, under an atmosphere of dinitrogen that had been deoxygenated over BASF catalyst and dried over Aquasorb®. Hexanes were distilled from sodium immediately before use. NMR spectra were recorded on a Varian Unity Plus 300 FT spectrometer. ^{1}H NMR spectra are referenced as ppm downfield from TMS. ^{19}F NMR spectra were referenced to $CFCl_3$ (0.00 ppm). Microanalyses were performed by Schwarzkopf Microanalytical Laboratory, Woodside, NY. $I(CF_2)_3CF_3$ (Aldrich) was purified by washing with a solution of sodium thiosulfate to remove iodine, followed by washing with water and then drying over magnesium sulfate and deoxygenation by several cycles of freeze–evacuate–thaw.

3.2. Reaction of (COD)$PtMe_2$ and n-C_4F_9I

(COD)$PtMe_2$ (0.10 g, 0.30 mmol) was suspended in hexanes (25 ml) in a 125 ml Schlenk flask and stirred vigorously. Neat n-C_4F_9I (78 μl) was added and the resulting mixture was allowed to stir for 12 h. The resultant yellow solid was filtered and washed twice with hexanes (10 ml). The combined filtrate and washings were evaporated under vacuum to give pale yellow (COD)PtMe(C_4F_9) (0.086 g, 0.16 mmol) in 53% yield. ^{1}H NMR (C_6D_6): δ 5.14 (br s, CH, $J_{PtH} = 34$ Hz); 4.44 (br s, CH, $J_{PtH} = 46$ Hz); 1.53 (br m, CH_2); 1.18 (s, CH_3, $J_{PtH} = 79$ Hz). ^{19}F NMR (C_6D_6): δ −81.2 (s, CF_3); −94.3 (br s, α-CF_2, $J_{PtF} = 404$ Hz); −115.3 (br s, β-CF_2, $J_{PtF} = 102$ Hz); −125.5 (br s, γ-CF_2). ^{19}F NMR (acetone-d_6): δ −82.2 (s, CF_3); −95.5 (br s, α-CF_2, $J_{PtF} = 404$ Hz); −116.4 (br s, β-CF_2, $J_{PtF} = 102$ Hz); −126.4 (br s, γ-CF_2). *Anal*. Calc. for $C_{13}H_{15}F_9Pt$: C, 29.06; H, 2.81. Found: C, 29.65; H, 2.70%.

The hexane-insoluble material was determined to be $[PtMe_3I]_4$ (0.044 g, 0.12 mmol) in 40% yield by comparison of its ^{1}H NMR spectrum to that previously obtained [17,18].

3.3. Crystallographic structural determination

Crystal, data collection, and refinement parameters are given in Table 1. The systematic absences in the diffraction data are uniquely consistent for the reported space group. The structure was solved using direct

Table 2
Bond lengths (Å) and angles (°) for **2**

Bond lengths			
Pt(1)–C(2)	2.040(11)	Pt(1)–C(1)	2.072(11)
Pt(1)–C(7)	2.204(11)	Pt(1)–C(3)	2.224(11)
Pt(1)–C(10)	2.230(11)	Pt(1)–C(6)	2.255(12)
C(3)–C(10)	1.361(17)	C(3)–C(4)	1.495(17)
C(4)–C(5)	1.526(19)	C(5)–C(6)	1.489(17)
C(6)–C(7)	1.348(17)	C(7)–C(8)	1.539(17)
C(8)–C(9)	1.523(19)	C(9)–C(10)	1.498(16)
Bond angles			
C(2)–Pt(1)–C(1)	87.0(6)	C(2)–Pt(1)–C(7)	90.8(5)
C(1)–Pt(1)–C(7)	159.7(5)	C(2)–Pt(1)–C(3)	160.4(5)
C(1)–Pt(1)–C(3)	92.1(5)	C(7)–Pt(1)–C(3)	96.6(5)
C(2)–Pt(1)–C(10)	164.0(5)	C(1)–Pt(1)–C(10)	94.9(5)
C(7)–Pt(1)–C(10)	82.0(5)	C(3)–Pt(1)–C(10)	35.6(4)
C(2)–Pt(1)–C(6)	95.0(5)	C(1)–Pt(1)–C(6)	165.2(5)
C(7)–Pt(1)–C(6)	35.2(4)	C(3)–Pt(1)–C(6)	81.2(5)
C(10)–Pt(1)–C(6)	87.3(5)	C(10)–C(3)–C(4)	125.7(11)
C(10)–C(3)–Pt(1)	72.4(7)	C(4)–C(3)–Pt(1)	105.8(8)
C(3)–C(4)–C(5)	115.7(10)	C(6)–C(5)–C(4)	114.9(10)
C(7)–C(6)–C(5)	127.6(14)	C(7)–C(6)–Pt(1)	70.3(7)
C(5)–C(6)–Pt(1)	109.7(8)	C(6)–C(7)–C(8)	123.0(13)
C(6)–C(7)–Pt(1)	74.5(7)	C(8)–C(7)–Pt(1)	106.0(8)
C(9)–C(8)–C(7)	115.2(11)	C(10)–C(9)–C(8)	114.4(10)
C(3)–C(10)–C(9)	125.0(11)	C(3)–C(10)–Pt(1)	72.0(7)
C(9)–C(10)–Pt(1)	110.8(8)		

methods, completed by subsequent difference Fourier syntheses and refined by full-matrix least-squares procedures. Empirical DIFABS [19] absorption corrections were applied to the data set. All non-hydrogen atoms were refined with anisotropic displacement coefficients and hydrogen atoms were treated as idealized contributions.

All software and sources of the scattering factors are contained in the SHELXTL (5.10) program library.

4. Supplementary material

Crystallographic data have been deposited with the Cambridge Crystallographic Data Centre, CCDC No. 181705. Copies of this information may be obtained free of charge from The Director, CCDC, 12 Union Road, Cambridge, CB2 1EZ, UK (fax: +44-1223-336033; e-mail: deposit@ccdc.cam.ac.uk or www: http://www.ccdc.cam.ac.uk).

Acknowledgements

R.P.H. is grateful to the National Science Foundation for generous financial support.

References

[1] J.A. McCleverty, G. Wilkinson, J. Chem. Soc. (1964) 4200.
[2] D.T. Rosevear, F.G.A. Stone, J. Chem. Soc. A (1968) 164.
[3] A.J. Mukhedkar, M. Green, F.G.A. Stone, J. Chem. Soc. A (1969) 3023.
[4] F.G.A. Stone, Endeavour 25 (1966) 33.
[5] D. Huang, K.G. Caulton, J. Am. Chem. Soc. 119 (1997) 3185.
[6] R.P. Hughes, D.C. Lindner, A.L. Rheingold, L.M. Liable-Sands, J. Am. Chem. Soc. 119 (1997) 11544.
[7] R.P. Hughes, J.M. Smith, J. Am. Chem. Soc. 121 (1999) 6084.
[8] R.P. Hughes, T. Le Husebo, B.J. Holliday, A.L. Rheingold, L.M. Liable-Sands, J. Organomet. Chem. 548 (1997) 109.
[9] R.P. Hughes, S.M. Maddock, A.L. Rheingold, L.M. Liable-Sands, J. Am. Chem. Soc. 119 (1997) 5988.
[10] R.P. Hughes, T.L. Husebo, A.L. Rheingold, L.M. Liable-Sands, G.P.A. Yap, Organometallics 16 (1997) 5.
[11] H.C. Clark, L.E. Manzer, J. Organomet. Chem. 59 (1973) 411.
[12] T.G. Appleton, J.R. Hall, C.H.L. Kennard, M.T. Mathieson, D.W. Neale, G. Smith, T.C.W. Mak, J. Organomet. Chem. 453 (1993) 299.
[13] K.I. Goldberg, J.Y. Yan, E.L. Winter, J. Am. Chem. Soc. 116 (1994) 1573.
[14] K.I. Goldberg, J. Yan, E.M. Breitung, J. Am. Chem. Soc. 117 (1995) 6889.
[15] G.B. Deacon, E.A. Hildebrand, E.R.T. Tiekink, Z. Kristall. 205 (1993) 340.
[16] R. Wyrwa, W. Poppitz, H. Görls, Z. Anorg. Allgem. Chem. 623 (1997) 649.
[17] K. Kite, J.A.S. Smith, E.J. Wilkins, J. Chem. Soc. (1966) 1744.
[18] J.M. Homan, J.M. Kawamoto, G.L. Morgan, Inorg. Chem. 9 (1970) 2533.
[19] N. Walker, D. Stuart, Acta Crystallogr., Sect. A 39 (1983) 158.

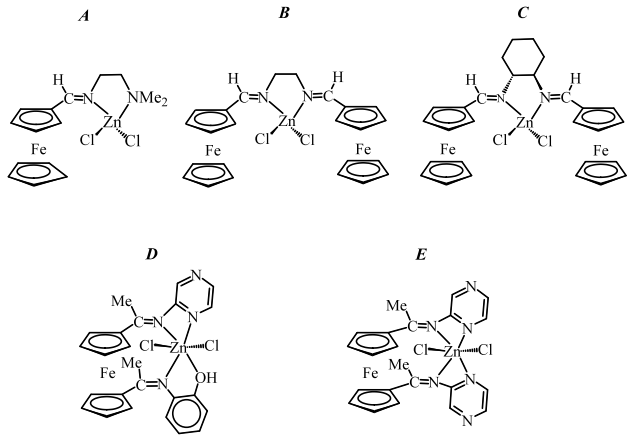


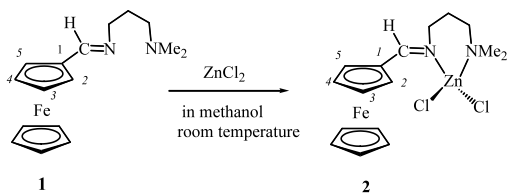
Fig. 1. Schematic view of some Zn(II) compounds containing ferrocenyl Schiff bases described so far.

preparation of several Pd(II) and Pt(II) complexes [11]. On this basis it seemed interesting to test its reactivity towards Zn(II) salts. In this manuscript we describe the synthesis and characterisation of *cis*-[Zn{(η^5-C_5H_5)Fe{(η^5-C_5H_4)–CH=N–$(CH_2)_3$–NMe_2}Cl_2] (**2**) as well as its behaviour in solution.

2. Results and discussion

When ligand **1** was treated with the equimolar amount of $ZnCl_2$ in methanol at room temperature, an orange solid was obtained (Scheme 1). Its elemental analyses (see Section 3) agreed with those expected for [Zn{(η^5-C_5H_5)Fe[(η^5-C_5H_4)–CH=N–$(CH_2)_3$–NMe_2]}Cl_2] (**2**), which arises from the binding of the two nitrogen atoms of the ligand to the '$ZnCl_2$' unit. The band due to the asymmetric stretching of the functional >C=N– group appeared at lower energies ($\nu = 1629$ cm^{-1}) than for the free ligand ($\nu = 1640$ cm^{-1}) [11]. This finding suggests, according to the literature [12], that the ligand binds to the Zn(II) through the imine nitrogen. Compound **2** has also been characterised by X-ray diffraction. Its molecular structure together with the atom numbering scheme is presented in Fig. 2, and a selection of bond lengths and angles are summarised in Table 1.

The structure consists of discrete molecules of [Zn{(η^5-C_5H_5)Fe[(η^5-C_5H_4)–CH=N–$(CH_2)_3$–NMe_2]}Cl_2], separated by van der Waals contacts. The



Scheme 1.

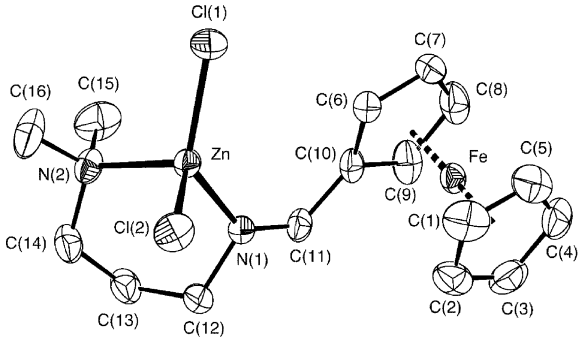


Fig. 2. Molecular structure and atom numbering scheme for compound **2**.

Table 1
Selected bond lengths (in Å) and angles (in °) for compound **2**

Bond lengths			
Zn–N(1)	2.053(2)	Zn–N(2)	2.090(2)
Zn–Cl(1)	2.2140(8)	Zn–Cl(2)	2.2348(8)
N(1)–C(11)	1.286(3)	N(1)–C(12)	1.477(3)
N(2)–C(14)	1.486(4)	N(2)–C(15)	1.480(4)
N(2)–C(16)	1.480(4)	C(10)–C(11)	1.438(3)
C(12)–C(13)	1.518(4)	C(13)–C(14)	1.518(4)
Fe–C [a]	2.047(11)	C–C [a]	1.417(14)
Bond angles			
N(1)–Zn–N(2)	93.60(8)	Cl(1)–N–Cl(2)	114.93(4)
N(1)–Zn–Cl(1)	126.49(6)	N(1)–Zn–Cl(2)	104.98(6)
N(2)–Zn–Cl(1)	105.28(7)	N(2)–Zn–Cl(2)	108.45(7)
C(11)–N–C(12)	115.5(2)	C(15)–N(2)–C(14)	110.9(2)
C(15)–N(2)–C(16)	109.0(3)	C(16)–N(2)–C(14)	108.4(3)
N(1)–C(11)–C(10)	127.8(2)	N(1)–C(12)–C(13)	112.5(2)

Standard deviation parameters are given in parenthesis.
[a] Average value for the ferrocenyl moiety.

zinc atom is tetracoordinated, bound to two chlorines {Cl(1) and Cl(2)} and the two nitrogen atoms of the ferrocenyl Schiff base {N(1) and N(2)} in a slightly distorted tetrahedral environment.

The variations observed in the Zn–Cl(1) and Zn–Cl(2) bond lengths may be attributed to the different *trans*-influence of the two nitrogen atoms {N(imine) vs. N(amine)} [13]. The N(1)–Zn–N(2) angle [93.60(9)°] is drastically reduced from the ideal tetrahedral value and the opposite Cl(1)–Zn–Cl(2) angle is 114.93(4)°.

The six-membered chelate ring has a chair-conformation in which the atoms N(1) and C(14) are out of the main plane defined by the Zn, N(2), C(12) and C(13) atoms.

The >C=N– bond length [1.286(3) Å] is similar to the values reported for related Schiff bases of general formula [(η^5-C_5H_5)Fe{(η^5-C_5H_4)–C(R)=N–R′}], derived from formyl-, acetyl- or benzoylferrocene [14]. The substituents at the imine group: C_5H_4 and the '–$(CH_2)_3$–NMe_2' moiety are in a *trans*-arrangement [the torsion angle defined by: C(10)–C(11)–N(1)–C(12) is 179.5°] thus confirming the *anti*-conformation of the ligand. This arrangement is consistent with the results

obtained from X-ray studies for a wide variety of Schiff bases containing ferrocenyl fragments [14,15].

The distance between the Cl(1) ligand and the H(6) atom is clearly smaller [2.60 Å] than the sum of the van der Waals radii of Cl (1.75 Å) and H (1.20 Å) [16], thus suggesting a weak C(6)···H(6)···Cl(1) intramolecular interaction. Similar types of interactions have also been recently described for a wide variety of transition metal complexes containing N-donor ferrocenyl groups [17].

The Fe–C and C–C bond lengths as well as bond angles of the ferrocenyl unit are similar to those reported for related complexes [18]. The two pentagonal rings are planar, nearly parallel [*tilt angle*: 2.54(19)°] and they deviate by approximately 0.42° from the ideal staggered conformation. The separation between the two metals {Fe and Zn} is 5.0218 Å, which implies that there is no direct interaction.

2.1. Solution studies

Despite the simplicity of the molecular structure of **2**, ^{1}H and $^{13}C\{^{1}H\}$ NMR spectra of **2** in acetone-d_6 or in $CDCl_3$ registered at room temperature (25 °C) were more complex than expected. In all cases, two superimposed sets of signals of relative intensities 1:0.6 in acetone-d_6, (Fig. 3) and in $CDCl_3$ were observed in the ^{1}H NMR spectra (Table 2), thus, suggesting that at least two species coexisted in solution. Besides that, the comparison of the ^{1}H NMR spectra of freshly prepared solutions of **2** and after 24 h of storage at room temperature revealed that neither the positions of the signals or their relative intensities changed with time. The similarity between the molar ratios of the two species in $CDCl_3$ and acetone-d_6, suggested that the relative abundance was not dependent of the solvent.

All these observations are in contrast with the NMR studies reported for related Zn(II) complexes containing a five-membered chelate ring and a ferrocenyl- or a bis(ferrocenyl) Schiff base, such as $[Zn\{(\eta^5\text{-}C_5H_5)Fe[(\eta^5\text{-}C_5H_4)\text{–}CH\text{=}N\text{–}(CH_2)_2NMe_2]\}Cl_2]$ (**3**) [8] and $[Zn\{(\eta^5\text{-}C_5H_5)Fe[(\eta^5\text{-}C_5H_4)\text{–}CH\text{=}N\text{–}CH_2\text{–}]\}_2Cl_2]$ [6], for which only one set of signals was detected in the NMR spectra.

Molar conductivity measurements of 10^{-3} M solutions of **2** in acetone or in $CHCl_3$ (see Section 3) suggested a non-electrolyte nature [19] of the two species present in solution. Variable temperature ^{1}H NMR experiments of **2** in acetone-d_6 were also carried out in the range 220–320 K; however, coalescence was not observed.

The two-dimensional $\{^{1}H\text{–}^{1}H\}$ NMR experiments (NOESY and 2D-phase sensitive ROESY experiments) suggested that the two species did not interchange in solution. For the two species present in solution the signal due to the imine proton showed a cross-peak with that due to the H^5 proton (Fig. 4). Thus suggesting that these two protons are proximal in the two species. In addition, for the major component, the presence of an additional cross-peak between the imine proton and that belonging to the '–N–CH_2–' fragment was also observed (Fig. 4). This is only possible if the ligand adopts the *E*(*anti*-) form. These results suggested that the two species present in solution may differ in the conformation of the ligand *E*(*anti*-) or *Z*(*syn*-) (Fig. 5).

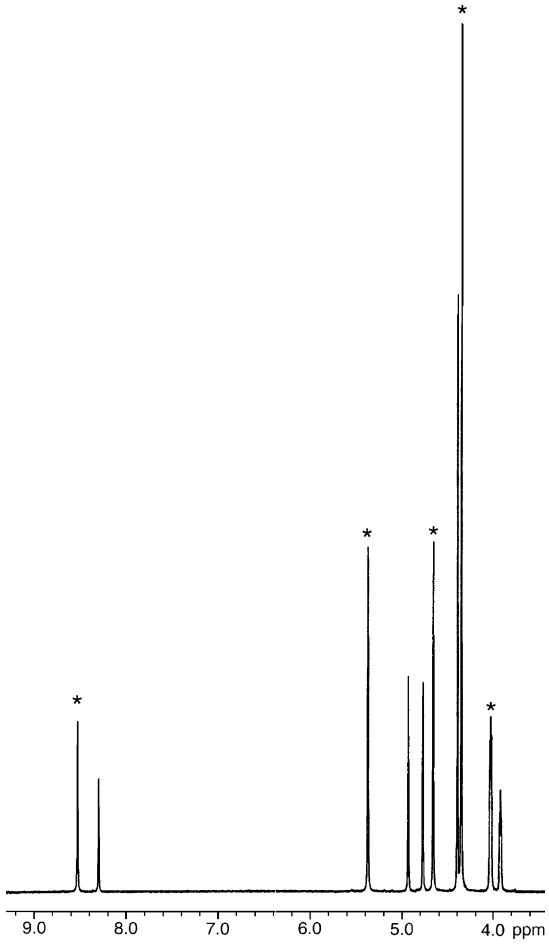


Fig. 3. Partial view of the ^{1}H NMR spectrum (500 MHz) of **2** in acetone-d_6 at room temperature (20 °C), in the range 3.70–9.30 ppm. The signals marked with an asterisk correspond to the major species present in the solution.

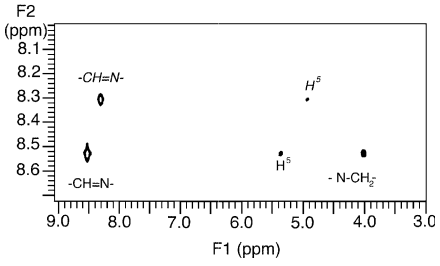


Fig. 4. Partial view of the $\{^{1}H\text{–}^{1}H\}$ NOESY spectrum of **2** in acetone-d_6 at 20 °C. Labels in italics correspond to the protons of the minor component.

Table 2
Proton and $^{13}C\{^1H\}$ NMR data for compound: $[Zn\{(\eta^5\text{-}C_5H_5)Fe[(\eta^5\text{-}C_5H_4)\text{–}CH\text{=}N\text{–}(CH_2)_3NMe_2]\}Cl_2]$ (**2**), in acetone-d_6 or $CDCl_3$ [a]

Compound	C_5H_5	H^2, H^5	H^3, H^4	–CH=N–	=N–CH_2–	–CH_2–	–CH_2–N–	Me
^1H NMR data								
2 (in acetone-d_6)	4.33	5.36	4.65	8.53	4.01	2.85	2.05	2.49
	4.38	4.92	4.76	8.30	3.90	2.98 [b]	2.17 [c]	2.51
2 (in $CDCl_3$)	4.31	5.25	4.67	8.26	3.80	2.90	1.90	2.55
	4.33	4.78	4.65	8.37	4.05	2.82	[d]	2.58
	C_5H_5	C^2, C^5	C^3, C^4	–CH=N–	=N–CH_2–	–CH_2–	–CH_2–N–	Me
$^{13}C\{^1H\}$ NMR data								
2 (in acetone-d_6) [e]	70.2	73.4	72.3	172.3	60.9	30.3	52.5	46.1
	70.4	74.0	73.0	169.1	63.4	[c]	52.2	46.7
2 (in $CDCl_3$) [e,f]	69.9	73.7	71.9	169.3	63.3	26.8	51.9	47.2
	70.2	73.6	71.2	171.2	60.7	25.7	52.0	46.6

[a] Labelling of the atoms refers to that shown in Scheme 1 (see text). The chemical shifts presented in the upper row correspond to the major component, and data given in the second row to the minor component.
[b] Partially overlapped by the signal due to the water present in the commercial acetone-d_6.
[c] Partially masked by the signal due to the solvent used in the experiment.
[d] Partially overlapped by the signal at $\delta = 1.90$ ppm due to the protons of the –N–CH_2– fragment of the major component.
[e] The signal due to the *ipso* carbon atom of the C_5H_4 ring (C^1), appeared at 74.9 ppm for the major component and at 74.0 ppm for the other component, in acetone-d_6 and at 72.1 ppm for the major component present in the $CDCl_3$ solution of **2**.
[f] The resonance due to the C^1 carbon of the minor component of the mixture was not observed.

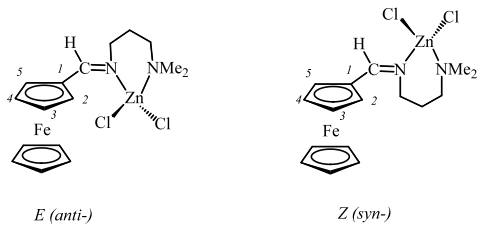


Fig. 5. Schematic view of the two isomeric forms of compound **2** which differ in the conformation of the ligand: *E*(*anti*-) and *Z*(*syn*-).

In order to ascertain if the duplicity of peaks observed in the NMR spectra could be ascribed to the existence in solution of a mixture of these two isomers, a theoretical study was undertaken based in DFT methodology. In a first step, the geometries of both isomers were fully optimised. The comparison of the corresponding energies reveals that the *E*(*anti*-) isomer is 2.78 kcal mol^{-1} more stable than the *Z*(*syn*-) isomer. The results agree with the fact that the *E*(*anti*-) isomer is more abundant in solution. However, the difference in energy is small enough as to allow the co-existence of the two isomers. In a second stage, and in order to perform a thermochemical analyses, a frequency calculation was carried out. In this case the difference in free energies (calculated at 298.15 K) was 2.97 kcal mol^{-1}, again being the *E*(*anti*-) isomer the most stable. Also the values of the corresponding entropies {168.6 cal K^{-1} mol^{-1} for the *Z*(*syn*-) isomer and 168.1 cal K^{-1} mol^{-1} for the *E*(*anti*-) isomer} are very similar. These results suggest that the difference in free energies between both isomers should change very little upon varying the temperature, thus supporting the results obtained from variable temperature ^1H NMR experiments.

Finally, in order to take into account the effects due to the solvent, calculations for the two isomers in chloroform have been performed using the Polarised Continuum Model [20]. The comparison of energies corresponding to the optimised geometries shows that also in this case the *E*(*anti*-) isomer is more stable, although the energy difference is (2.16 kcal mol^{-1}) slightly smaller than in the gas phase calculations.

In conclusion, the results presented here show how tiny changes on the backbone of the ligand such as the incorporation of a –CH_2– group could be important in determining the relative proportion of the two isomeric forms of compounds $[Zn\{(\eta^5\text{-}C_5H_5)Fe[(\eta^5\text{-}C_5H_4)\text{–}CH\text{=}N\text{–}(CH_2)_n\text{–}NMe_2]\}Cl_2]$ with $n = 2$ or 3.

3. Experimental

Elemental analyses (C, H and N) were carried out at the *Serveis Cientifico-Tècnics* de la *Universitat de Barcelona*. The IR spectrum was obtained with a Nicolet 520-FTIR spectrophotometer using KBr pellets. Routine ^1H and $^{13}C\{^1H\}$ NMR spectra were registered with a Gemini-200 MHz instrument at room temperature (r.t.). High resolution ^1H NMR spectra and the two-dimensional NMR experiments {heteronuclear single quantum coherence (HSQC) and heteronuclear multiple bond coherence (HMBC), NOESY and ROESY} were obtained with either a Bruker-DMX 500 MHz or a Varian-500 spectrophotometer using

C_3H_6O-d_6 (99.9%) or $CDCl_3$ (99.9%) as solvents and $SiMe_4$ as internal reference. The $\{^1H-^1H\}$ NOESY spectra of **2** were recorded at 20 °C using different mixing times (t) and the best results were obtained for $t = 0.65$ s. Variable temperature NMR experiments (in the range 220–320 K) were performed with a Bruker-DMX 500 MHz instrument using C_3H_6O-d_6 as solvent. Molar conductivity of 10^{-3} M solutions of **2** in C_3H_6O or $CHCl_3$ were measured at r.t. (25 °C) using a Crison-Micro-MC 2200 conductivity-meter.

3.1. Materials and synthesis

The ligand **1**, was prepared as described previously and $ZnCl_2$ was obtained from standard sources and used as received. The MeOH used for the preparation of **2** was HPLC grade [21], and the remaining solvents were dried and distilled before use.

3.1.1. Preparation of $[Zn\{(\eta^5\text{-}C_5H_5)Fe[(\eta^5\text{-}C_5H_4)\text{–}CH{=}N\text{–}(CH_2)_3\text{–}NMe_2]\}Cl_2]$ (2)

The ferrocenyl Schiff base **1**, (0.261 g, 9.5×10^{-4} mol) was dissolved in the minimum amount of MeOH (approximately 2 ml) [21]. Then a solution formed by 0.130 g (9.5×10^{-4} mol) of $ZnCl_2$ and 5 ml of MeOH was added. The reaction mixture was stirred at r.t. approximately 20 °C for 1 h. The orange solid formed was collected by filtration air-dried and then dried in vacuum for 2 days. (Yield: 0.338 g, 82%.) Good quality X-ray crystals were obtained by slow evaporation of a $CHCl_3$ solution of **2** at 20 °C. *Anal*. % Calc. for $C_{16}H_{22}Cl_2FeN_2Zn$ (Found): C, 44.23 (44.05); H, 5.10 (5.20); N, 6.45 (6.35). IR: $\nu(>C{=}N-) = 1629$ cm^{-1}. $\Lambda_M = 13$ (in C_3H_6O) and 8 (in $CHCl_3$) Ω^{-1} cm^2 M^{-1}.

3.2. Crystallography

3.2.1. Crystal data for 2

$C_{16}H_{22}Cl_2FeN_2Zn$, $M = 434.48$; monoclinic, space group: $P2_1/c$, $a = 10.3650(10)$, $b = 14.5620(10)$, $c = 12.7400(10)$ Å, $\alpha = \gamma = 90$ and $\beta = 111.7130(10)°$; $U = 1786.5(3)$ Å^3; $Z = 4$; $D_{calc} = 1.615$ mg m^{-3}; $\lambda = 0.71069$ Å, μ(Mo Kα) = 2.450 mm^{-1}; $F(000) = 888$, crystal dimensions: $0.1 \times 0.1 \times 0.2$ mm and $T = 293(2)$ K.

3.2.2. Data collection and refinement

A prismatic red crystal of compound **2** was selected and mounted on a MAR345 diffractometer with a image plate detector. Unit cell parameters were determined from automatic centring of 9359 reflections in the range $3 < \Theta < 31°$ and refined by least-squares method. Intensities were collected with a graphite monochromatized Mo Kα radiation. The number of reflections measured was 11 619, of which 5091 were non-equivalent by symmetry {R_{int} (on I) = 0.026} and 4210 reflections were assumed as observed applying the condition $I > 2\sigma(I)$. Lp and absorption corrections were performed. The structure was solved by direct methods, using SHELXS computer program [22] and refined by full-matrix least-squares method using SHELX-97 computer program [23] using 5091 reflections (very negative intensities were not assumed). The function minimized was $\Sigma\, w||F_o|^2 - |F_c|^2|^2$, where $w = [\sigma(I) + (0.0607P)^2 + 1.6746P]^{-1}$ and $P = (|F_o|^2 + 2|F_c|^2)/3$. f, f' and f'' were taken from the literature [24]. All hydrogen atoms were located from a difference synthesis and refined with an overall isotropic temperature factor. The final R (on F) factor was 0.040, wR (on $F^2 = 0.108$) and the goodness-of-fit was 1.099 for all observed reflections. Final R indices were $R_1 = 0.0405$, $wR_2 = 0.1080$ for [$I > 2\sigma(I)$]; and $R_1 = 0.0503$, $wR_2 = 0.1165$ for all data.

3.3. Computational details

DFT calculations were performed using the GAUSSIAN-98 software [25], using B3LYP functional [26]. The basis set has been chosen as follows: 6-31G [27] for hydrogen, 6-31G with polarisation [28] for carbon and nitrogen and LANL2DZ [29] for Fe, Zn and Cl. In the later case, polarisation functions [30] have been added. PCM calculations have been carried out using the polarisable conductor calculation model [20b]. In all cases, geometries have been optimised without imposing any symmetry restriction.

4. Supplementary material

Crystallographic data for the structural analysis have been deposited with the Cambridge Crystallographic Data Centre, CCDC No. 180588 for compound **2**. Copies of this information may be obtained free of charge from The Director, CCDC, 12 Union Road, Cambridge, CB2 1EZ, UK (fax: +44-1233-336-033; e-mail: deposit@ccdc.cam.ac.uk or www: http://www.ccdc.cam.ac.uk).

Acknowledgements

We are indebted to the *Ministerio de Ciencia y Tecnología* of Spain and to the *Generalitat de Catalunya* for financial support (grants no. BQU2000-0652 and SRG-2001-0054, respectively). S.P. is also grateful to the *Generalitat de Catalunya* for a predoctoral fellowship.

References

[1] A. Togni, T. Hayashi (Eds.), Ferrocenes Homogeneous Catalysis. Organic Synthesis and Materials Science, VCH, Weinheim, Germany, 1995, and references therein.

[2] W.R. Cullen, J.D. Woolins, Coord. Chem. Rev. 39 (1981) 1.

[3] For recent publications in this area see for instance the following articles appeared in the special issue of Journal of Organometallic Chemistry dedicated to ferrocene (a): E. Rüba, K. Mereiter, R. Schmid, K. Kirchner, H. Schöttenberger, J. Organomet. Chem. 637–639 (2001) 70;
(b) Y. Yamada, J. Mitzutani, M. Kurihara, H. Nishihara, J. Organomet. Chem. 637–639 (2001) 80;
(c) S.W. Lai, M.G.B. Drew, P.D. Beer, J. Organomet. Chem. 637–639 (2001) 89;
(d) A. González, J.R. Granell, C. López, J. Organomet. Chem. 637–639 (2001) 116;
(e) O. Olt, M.O. Wolf, G.P. Yap, J. Organomet. Chem. 637–639 (2001) 145;
(f) L.F. Tang, W.L. Jia, Z.H. Wang, J.F. Chai, J.T. Wang, J. Organomet. Chem. 637–639 (2001) 209;
(g) K. Bushell, C. Gialou, C.H. Goh, N.J. Long, J. Martin, C.K. Williams, D.J. Williams, M. Fontani, P. Zanello, J. Organomet. Chem. 637–639 (2001) 418;
(h) E.N.M. Ho, B.K.M. Hui, W.T. Wong, J. Organomet. Chem. 637–639 (2001) 276;
(i) J. Gimeno, E. Lastra, C. Madrigal, C. Graiff, A. Tiripicchio, J. Organomet. Chem. 637–639 (2001) 463;
(j) M.I. Bruce, M.E. Smith, B.W. Skelton, A.H. White, J. Organomet. Chem. 637–639 (2001) 483;
(k) R.D. Adams, B. Qu, M.D. Smith, J. Organomet. Chem. 637–639 (2001) 514;
(l) F.F. de Bioni, C. Graiff, G. Oppromolla, G. Predieri, A. Tiripicchio, P. Zanello, J. Organomet. Chem. 637–639 (2001) 586;
(m) Y. Yuan, Z. Cao, N. Fu, J. Wang, L. Wang, A. Bezerra de Carvalho, C. Peppe, J. Organomet. Chem. 637–639 (2001) 631;
(n) J. Diez, M.P. Gomasa, J. Gimeno, M. Lanfranchi, A. Tiripiccio, J. Organomet. Chem. 637–639 (2001) 677;
(o) G.J. Grant, S.M. Carter, A. LeBon Russell, I.M. Poullon, D.G. van der Veer, J. Organomet. Chem. 637–639 (2001) 683;
(p) T.J. Colacot, H. Quan, M. Cea-Olivares, S. Hernández Ortega, J. Organomet. Chem. 637–639 (2001) 691;
(q) B. Longato, R. Cappo, G. Pilloni, C. Corraja, A. Toffoletti, G. Bandoli, J. Organomet. Chem. 637–639 (2001) 710;
(r) Y.C. Neo, J.J. Vittal, T.S. Hor, J. Organomet. Chem. 637–639 (2001) 757;
(s) V. Cardiero, S.E. García-Granda, J. Gimeno, J. Organomet. Chem. 637–639 (2001) 767;
(t) F. Tisato, F. Refosco, M. Porchia, G. Bandoli, G. Pilloni, L. Uccedi, A. Branchi, A. Duatti, J. Organomet. Chem. 637–639 (2001) 772;
(u) Y. Wu, J. Hou, H. Yun, X. Cui, R. Yuan, J. Organomet. Chem. 637–639 (2001) 773;
(v) M.A. Zuideveld, B.H. Swennehuri, P.C.J. Kaman, P.W.N.M. van Leuwen, J. Organomet. Chem. 637–639 (2001) 805;
(w) Z.R. Ratkovia, L. Somoki, K. Mieshei, C. Zucchi, G. Palyi, J. Organomet. Chem. 637–639 (2001) 813.

[4] (a) A. Caubet, C. López, R. Bosque, X. Solans, M. Font-Bardía, J. Organomet. Chem. 577 (1999) 292;
(b) J. Silver, G.R. Fern, J.R. Miller, E. Slade, M. Ahmet, A. Houlton, D.J. Evand, G.J. Leigh, J. Organomet. Chem. 637–639 (2001) 311;
(c) Y. Wu, S. Huo, J. Gang, X. Cui, L. Ding, K. Ding, C. Du, Y. Liu, M. Song, J. Organomet. Chem. 637–639 (2001) 27.

[5] P. Li, I.J. Scowen, J.E. Davies, M.A. Halcrow, J. Chem. Soc., Dalton Trans. (1998) 3791.

[6] O.B. Sutcliffe, A. Cheney, M. Bryce, J. Organomet. Chem. 637–639 (2001) 134.

[7] (a) Z.H. Chohan, M. Pravee, Appl. Organomet. Chem. 15 (2001) 617;
(b) Z.H. Chohan, M. Pravee, Appl. Organomet. Chem. 14 (2000) 376.

[8] R. Bosque, A. Caubet, C. López, E. Espinosa, E. Molins, J. Organomet. Chem. 544 (1997) 233.

[9] (a) T. Kawamoto, Y. Kushi, J. Chem. Soc., Dalton Trans. (1992) 3137;
(b) I. Nagasawa, T. Kawamoto, H. Kuma, Y. Kushi, Bull. Chem. Soc. Jpn. 71 (1998) 1337;
(c) P.J. Palmer, R.B. Trigg, J.V. Warrington, J. Med. Chem. 14 (1971) 248.

[10] (a) E.W. Nause, M.G. Meirim, N.F. Blom, Organometallics 7 (1988) 2562;
(b) A. Benito, J. Cano, R. Martínez-Mañes, J. Soto, J. Payá, F. Lloret, M. Julve, J. Faus, M.D. Marcos, Inorg. Chem. 32 (1993) 1197;
(c) A. Benito, R. Martínez-Máñez, J. Payá, J. Soto, M.J. Tendero, E. Sinn, J. Organomet. Chem. 231 (1995) 45.

[11] C. López, A. Caubet, S. Pérez, X. Solans, M. Font-Bardía, J. Organomet. Chem. 651 (2002) 105.

[12] (a) H. Onue, I. Moritani, J. Organomet. Chem. 43 (1972) 431;
(b) H. Onue, K. Minami, I. Moritani, Bull. Chem. Soc. Jpn. 43 (1970) 3480;
(c) S.Q. Huo, Y.J. Wu, Y. Zhu, L. Yang, J. Organomet. Chem. 470 (1994) 17;
(d) J.M. Vila, E. Gayoso, T. Pereira, M. Mariño, J. Martínez, J.J. Fernández, A. Fernández, M. López-Torres, J. Organomet. Chem. 637–639 (2001) 577.

[13] (a) G. Wilkinson, D.R. Gillard, J. McCleverty (Eds.), Comprehensive Coordination Chemistry. The Synthesis, Reactions, Properties and Applications of Coordination Compounds, vol. 1, Pergamon Press, Exeter, 1987, p. 38;
(b) G. Wilkinson, F.G.A. Stone, W.E. Abel (Eds.), Comprehensive Organometallic Chemistry. The Synthesis, Reactions and Structure of Organometallic Compounds, vol. 6, Pergamon Press, New York, 1982, p. 236.

[14] H.Q. Huo, C.X. Du, Y. Zhu, H.Z. Yuan, X.A. Mao, J. Organomet. Chem. 483 (1994) 139.

[15] (a) C. López, J. Sales, X. Solans, R. Zquiak, J. Chem. Soc., Dalton Trans. (1992) 2321;
(b) R. Bosque, C. López, J. Sales, X. Solans, M. Font-Bardia, J. Chem. Soc., Dalton Trans. (1994) 735;
(c) C. López, R. Bosque, M. Font-Bardía, X. Solans, New J. Chem. 20 (1996) 1285.

[16] (a) A. Bondi, J. Phys. Chem. 63 (1964) 441;
(b) A.I. Kitaigorodskii, Molecular Crystals and Molecules, Academic Press, London, 1973, p. 186.

[17] (a) X. Riera, A. Caubet, C. López, V. Moreno, E. Freisinger, M. Willermann, B. Lippert, J. Organomet. Chem. 629 (2001) 97;
(b) S. Pérez, R. Bosque, C. López, X. Solans, M. Font-Bardía, J. Organomet. Chem. 625 (2001) 67;
(c) C. López, R. Bosque, X. Solans, M. Font-Bardía, Polyhedron 20 (2001) 987.

[18] T.H. Allen, O. Kennard, Chem. Design. Automat. News 8 (1993) 146.

[19] W.J. Geary, Coord. Chem. Rev. 7 (1971) 81.

[20] (a) S. Miertus, S. Scrocco, J. Tomasi, J. Chem. Phys. 55 (1981) 117;
(b) V. Barone, M. Cossi, J. Phys. Chem., Sect. A 102 (1998) 1995.

[21] The use of high quality methanol (HPLC) is strongly recommended for the synthesis of **2**. The success of the preparation of **2** is strongly dependent on the quality of the methanol used since the presence of small amounts of water, reduces considerably the yield of the synthesis and produces the formation of large

amounts of ferrocenecarboxaldehyde due to the hydrolysis of the ligand.

[22] G.M. Sheldrick, SHELXS A Computer Program for Determination of Crystal Structures, University of Göttingen, Germany, 1997.

[23] G.M. Sheldrick, SHELX-97 A Computer Program for Determination of Crystal Structures, University of Göttingen, Germany, 1997.

[24] International Tables of X-ray Crystallography, vol. IV, Kynoch Press, Birmingham, 1974, pp. 99–100.

[25] M.J. Frisch, G.M. Trucks, H.B. Schlegel, G.E. Scuseria, M.A. Robb, J.R. Cheeseman, V.G. Zakrewski, J.A. Montgomery, Jr., R.E. Stratmann, J.C. Burant, S. Dapprich, J.M. Millam, A.D. Daniels, K.N. Kudin, M.C. Strain, O. Farkas, J. Tomasi, V. Barone, M. Cossi, R. Cammi, B. Menucci, C. Pomelli, C. Adamo, S. Cliford, J. Ochterski, G.A. Petersson, P.Y. Ayala, Q. Cui, K. Morokuma, P. Salvador, J.J. Dannenberg, D.K. Malick, A.D. Rabuck, K. Raghacvachari, J.B. Foresman, J. Cioslowski, J.V. Ortiz, A.G. Baboul, B.B. Stefanov, G. Liu, A. Liashenko, P. Piskorz, I. Komaromi, R. Gomperts, R.J. Martin, D.J. Fox, T. Keith, M.A. Al.Laham, C.Y. Peng, A. Nanayakkara, M. Challacombe, P.M.W. Gilli, B. Johnson, M. Chen, M.W. Wong, J.L. Andres, C. Gonzalez, M. Head-Gordon, E.S. Replogle, J.A. Pope, GAUSSIAN-98, Revision A.11, Gaussian, Inc., Pittsburg, PA (USA), 2001.

[26] (a) A.D. Becke, J. Chem. Phys. 98 (1993) 5648;
(b) C. Lee, W. Yang, R. Parr, Phys. Rev. 37 (1998) 785;
(c) P.J. Stephens, F.J. Devlin, C.F. Chabalowski, M. Frisch, J. Phys. Chem. 98 (1994) 11623.

[27] W.J. Hehre, R. Ditchfiels, J.A. Pope, J. Chem. Phys. 56 (1972) 2257.

[28] M.J. Frisch, J.A. Pope, J.S. Binkley, J. Chem. Phys. 80 (1984) 3265.

[29] (a) P.J. Hay, W.R. Wadt, J. Chem. Phys. 82 (1985) 270;
(b) P.J. Hay, W.R. Wadt, J. Chem. Phys. 82 (1985) 284;
(c) P.J. Hay, W.R. Wadt, J. Chem. Phys. 82 (1985) 299.

[30] A. Höllwarth, M. Böhme, S. Dapprich, A.W. Ehlers, A. Gobbi, V. Jonas, K.F. Köhler, R. Vedkamp, G. Frenking, Chem. Phys. Lett. 208 (1993) 237.

carrier ligands (such as cisplatin and carboplatin) [15]. Oxaliplatin and JM216 are in clinical trials and show promise for the treatment of cisplatin-resistant tumors. Another platinum-based drug called L-NDDP (liposome-entrapped *cis*-bis(neodecanoato)(*trans*-diaminocyclohexane)platinum(II), which was developed in our laboratory, is also currently in clinical trials [16].

In our continuing efforts to develop new platinum-based antitumor agents, we have reported platinum(II) and platinum(IV) complexes with various isomers of 1,2-diaminocyclohexane (1,2-DACH) [17–21] and *cis*-1,4-DACH [22–26] as carrier ligands. Here we report the synthesis and characterization of a series of platinum complexes containing heptamethyleneimine as a non-leaving ligand and dicarboxylate as leaving group. We also report the X-ray crystal structure of *cis*-[Pt(heptamethyleneimine)$_2$(malonate)]·H_2O.

2. Experimental

2.1. Chemicals

K_2PtCl_4 was purchased from Johnson Mathey (Seabrook, NH). Heptamethyleneimine, 1,1-cyclobutanedicarboxylic acid, malonic acid, methylmalonic acid, dimethylmalonic acid, ethylmalonic acid, and diethylmalonic acid were obtained from Aldrich Chemical Co. (Milwaukee, WI). Silver nitrate, sodium hydroxide, sodium oxalate, sodium chloride, and potassium iodide were purchased from Fisher Scientific Co. (Houston, TX).

2.2. Physical measurements

Elemental analyses of the complexes were performed by Robertson Microlit Laboratories, Inc. (Madison, NJ). IR spectra in the range of 600–4000 and 100–600 cm^{-1} were recorded for complexes in KBr and polyethylene pellets, respectively, using a Perkin–Elmer 2000 spectrophotometer. ^{195}Pt NMR spectra were recorded at 43.055 MHz in D_2O using a Bruker Advance 300 spectrometer. The chemical shifts were referenced to an external standard of 2.2 M Na_2PtCl_6 in D_2O, which was set to 0.0 ppm.

2.3. Synthesis of platinum complexes

2.3.1. [$Pt^{II}(L)_2(CBDCA)$] (complex **1**)

The desired compound was synthesized using a slight modification of a previously described procedure [23,24]. K_2PtCl_4 (10.00 g, 24.09 mmol) was dissolved in 30 ml of deionized water and filtered. KI (31.99 g, 192.72 mmol) was dissolved in 150 ml of water and added to this solution. The reaction mixture was stirred for 15 min after which a solution of heptamethyleneimine (**L**) (5.46 g, 48.23 mmol) in 30 ml of methanol was added dropwise to the reaction mixture with stirring. After 2 h, a brown precipitate was obtained. The compound was separated by filtration and redissolved in DMF. This solution was filtered, evaporated to 10 ml under reduced pressure, and finally the product was precipitated with water to obtain a yellow crystalline compound, [$Pt(L)_2I_2$]. The solid was isolated by filtration and dried in vacuo. A solution of silver nitrate (0.245 g, 1.44 mmol) in 80 ml water was treated with [$Pt(L)_2I_2$] (0.500 g, 0.74 mmol) in the dark at room temperature. The reaction was allowed to proceed for 24 h before the precipitate of AgI was removed by filtration. The filtrate was reacted with an aqueous solution of the sodium salt of CBDCA (0.123 g, 0.74 mmol). The mixture was stirred for 24 h and concentrated to 15 ml under reduced pressure, then cooled to 6 °C for 24 h to afford a white crystalline precipitate. The product was collected by filtration, washed with small amount of cold water, and dried in vacuo (yield 72%).

Complexes **2**–**8** were prepared using a method similar to that described for preparing complex **1**, except that corresponding sodium salts of dicarboxylic acids were used.

2.4. Single crystal X-ray crystallographic study

The experimental details of the X-ray data collection, the structure solution, and refinement of the title compound are compiled in Table 1. A single crystal of [Pt(heptamethyleneimine)$_2$(malonate)]·H_2O was coated with a thin layer of epoxy cement and glued to the end of a glass fiber mounted on the goniometer of a Bruker SMART 1K diffractometer equipped with a CCD area detector. The data was corrected for Lorentz and polarization effects. Absorption correction was applied using the program SADABS [27]. No appreciable decay of the crystal was detected during data collection.

The structure was solved using direct methods with the SHELXTL software package [27]. Scattering factors were taken from the literature [28]. Heavy atoms were located initially in structure solution. All other atoms were located by successive Fourier maps and were refined using the full-matrix least-squares method on F^2. All non-hydrogen atoms were refined anisotropically. Hydrogen atoms were placed in calculated positions ($d_{C-H} = 0.96$ Å, $d_{N-H} = 0.90$ Å) and allowed to ride on the adjacent carbon atom. Toward the end of the structure solution, it became apparent that one of the heptamethyleneimine ligands was disordered over two positions in the crystal lattice. The disorder was modeled by allowing for partial occupancy of each of the potential atomic locations. Refinement of positional and anisotropic parameters of the resulting model, led to convergence.

Table 1
Crystal data and structure refinement for [Pt(heptamethyleneimine)$_2$(malonate)]·H_2O

Empirical formula	$C_{17}H_{32}N_2O_4Pt \cdot H_2O$
Formula weight	541.54
Temperature (K)	293(2)
Wavelength (Å)	0.71073
Crystal system	monoclinic
Space group	$P2(1)/c$
Unit cell dimensions	
a (Å)	9.781(2)
b (Å)	14.184(3)
c (Å)	14.401(3)
β (°)	93.11(3)
Volume (Å^3)	1995.1(7)
Z	4
Density calculated (Mg m^{-3})	1.796
Absorption coefficient (mm^{-1})	7.061
$F(000)$	1064
Crystal size (mm)	0.32 × 0.31 × 0.25
θ Range for data collection (°)	2.02–23.27
Limiting indices	$-10 \le h \le 10$, $-15 \le k \le 14$, $-9 \le l \le 15$
Reflections collected	8451
Independent reflections	2861 [$R_{int} = 0.0221$]
Completeness to θ (°)	23.27 (99.8%)
Refinement method	full-matrix least-squares on F^2
Data/restraints/parameters	2861/12/240
Goodness-of-fit on F^2	1.048
Final R indices [$I > 2\sigma(I)$]	$R_1 = 0.0207$, $wR_2 = 0.0549$
R indices (all data)	$R_1 = 0.0225$, $wR_2 = 0.0557$
Largest difference peak and hole (e Å^{-3})	0.892 and −1.055

3. Results and discussion

3.1. Synthesis of platinum complexes

The procedure used in the synthesis of complexes is shown in Scheme 1. The desired compound was synthesized using a slight modification of previously described work [23,24]. K_2PtI_4 was prepared in situ according to Dhara's method through the reaction of K_2PtCl_4 with an excess of KI [29]. Addition of 2 equiv. of heptamethyleneimine (**L**) resulted in the precipitation of $[Pt(L)_2I_2]$. Reaction of $[Pt(L)_2I_2]$ with $AgNO_3$ produced $[Pt(L)_2(H_2O)_2](NO_3)_2$ in solution, which was directly reacted with 1 equiv. of the disodium salts of a dicarboxylic acids or an oxalate molecule (Na_2X) to form the white crystalline compound $[Pt(L)_2(X)]$.

$$K_2PtCl_4 + 8KI \longrightarrow K_2PtI_4 + 4KI + 4KCl$$
$$K_2PtI_4 + 2L \longrightarrow [Pt(L)_2I_2] + 2KI$$
$$[Pt(L)_2I_2] + 2AgNO_3 + 2H_2O \longrightarrow [Pt(L)_2(H_2O)_2](NO_3)_2 + 2AgI$$
$$[Pt(L)_2(H_2O)_2](NO_3)_2 + Na_2X \longrightarrow [Pt(L)_2(X)] + 2NaNO_3$$

Scheme 1.

3.2. Characterization of platinum complexes

The complexes were characterized by elemental analysis and IR, ^{13}C and ^{195}Pt NMR spectroscopy. The composition of each complex as determined by elemental analysis showed good agreement between the theoretical and actual values. The analytical results are summarized in Table 2. The results of characterization by IR and ^{195}Pt spectroscopy are shown in Table 3. In the IR spectra of all complexes, prominent changes were observed [30]. Broad absorption between 3120 and 3189 cm^{-1} in the IR spectra of all the complexes was attributed to the coordinated N–H bond of ligand L. The carboxyl groups in all the complexes displayed a band in the range of 1600–1674 cm^{-1} corresponding to the ν(C=O) band. The ν(C–O) band appeared in the range of 1347–1384 cm^{-1}. The Pt–N and Pt–O stretching frequencies in all the complexes showed peaks in the range of 549–609 and 457–483 cm^{-1}, respectively.

The proton-decoupled ^{13}C NMR spectra showed a signal in the range of 175–190 ppm for the carbonyl carbon of coordinated carboxylate ligands. This suggests that the two carboxylate carbons are magnetically equivalent in these complexes. These values are also close to the values for carboxylate carbons reported for other platinum carboxylate complexes [17,31,32]. In all

Table 2
Elemental analysis of platinum(II) complexes

Complex	Complex name	Observed (calculated)		
		C (%)	H (%)	N (%)
1	[Pt(L)$_2$(CBDCA)]·2.5H_2O	42.51 (42.63)	6.53 (6.39)	5.18 (4.97)
2	[Pt(L)$_2$(oxalate)]	37.57 (37.72)	5.70 (5.89)	5.68 (5.50)
3	[Pt(L)$_2$(malonate)]·H_2O	37.48 (37.67)	5.72 (5.91)	5.32 (5.17)
4	[Pt(L)$_2$(methylmalonate)]	40.03 (40.22)	6.58 (6.33)	5.35 (5.21)
5	[Pt(L)$_2$(dimethylmalonate)]	41.14 (41.38)	6.78 (6.53)	5.29 (5.08)
6	[Pt(L)$_2$(ethylmalonate)]	41.52 (41.38)	6.42 (6.38)	5.22 (5.08)
7	[Pt(L)$_2$(diethylmalonate)]	43.49 (43.52)	6.80 (6.91)	4.61 (4.84)

L, heptamethyleneimine.

Table 3
IR, ^{13}C, and ^{195}Pt NMR spectroscopic data for platinum(II) complexes [a]

Number	IR (cm^{-1})					NMR (ppm)	
	ν(N–H)	ν(C=O)	ν(C–O)	ν(Pt–N)	ν(Pt–O)	^{13}C(C=O)	^{195}Pt
1	3143	1674	1371	583	476	183	−2033
2	3151	1656	1357	549	470	173	−2041
3	3056	1620	1384	597	461	182	−2001
4	3120	1673	1381	553	477	180	−1996
5	3168	1612	1381	609	457	182	−1943
6	3189	1600	1384	553	472	184	−1976
7	3135	1623	1376	577	478	182	−1932

[a] NMR data were recorded in D_2O.

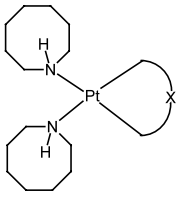


Fig. 1. Chemical structure of [Pt(heptamethyleneimine)$_2$(X)], where X = CBDCA, oxalate, malonate, methylmalonate, dimethylmalonate, ethylmalonate, or diethylmalonate.

cases, the ^{13}C NMR shifts of the free acids and platinum complexes ($\Delta C = \delta$[complex] − δ[ligand]) fell between 1.6 and 2.2 ppm.

In the ^{195}Pt NMR spectra, the singlet observed in the range of −1932 to −2041 ppm was assignable to the PtN_2O_2 system and this value was close to the related square-planar platinum(II) complexes having two nitrogen and two oxygen atoms as donor ligands [33–35], (Fig. 1).

3.3. Crystal structure

The complex [Pt(heptamethyleneimine)$_2$(malonate)] gave crystals suitable for single crystal X-ray diffraction studies. The crystals were obtained by slow evaporation in air of a concentrated aqueous solution of the complex. A representative view of [Pt(heptamethyleneimine)$_2$(malonate)]·H_2O including the numbering scheme employed in this work is provided in Fig. 2. Selected bond lengths and bond angles of the molecule are given in Table 4.

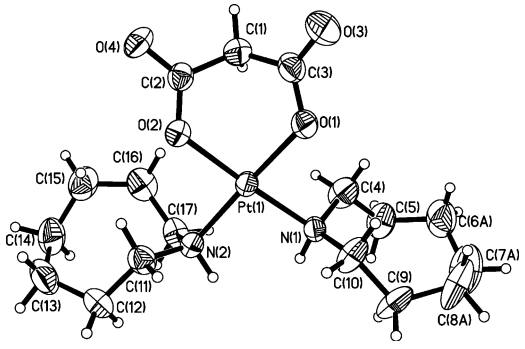


Fig. 2. ORTEP representation of the structure of [Pt(heptamethyleneimine)$_2$(malonate)]. Thermal ellipsoids are drawn at the 50% probability level. Only one orientation of the disordered ligand is shown.

Table 4
Selected bond lengths (Å) and angles (°) for [Pt^{II}(heptamethyleneimine)$_2$ (malonate)]·H_2O

Bond lengths	
Pt(1)–O(1)	2.026(3)
Pt(1)–O(2)	2.036(3)
Pt(1)–N(1)	2.048(3)
Pt(1)–N(2)	2.056(3)
Bond angles	
O(1)–Pt(1)–O(2)	89.27(12)
O(1)–Pt(1)–N(1)	88.46(12)
O(2)–Pt(1)–N(1)	177.35(11)
C(10)–N(1)–Pt(1)	110.6(3)
C(4)–N(1)–Pt(1)	108.6(3)
C(17)–N(2)–Pt(1)	114.2(3)
O(1)–Pt(1)–N(2)	175.92(13)
O(2)–Pt(1)–N(2)	91.39(12)
N(1)–Pt(1)–N(2)	90.96(12)
C(11)–N(2)–Pt(1)	111.6(3)
C(3)–O(1)–Pt(1)	120.3(3)
C(2)–O(2)–Pt(1)	119.9(3)

The platinum center exists in a slightly distorted square-planar coordination environment. The Pt–O bond distances are 2.026(3) and 2.036(3) Å, while the Pt–N bond distances are 2.048(3) and 2.056(3) Å. These distances are in agreement with similar complexes (Pt–N and Pt–O bond distances in compound $Pt(NH_3)_2$(CBDCA) are 2.017 and 2.031 Å) [17,36–40]. An eight-membered cyclic amine acts as a monodentate ligand coordinated with platinum atoms in the *cis* positions. The remaining positions in the metal coordination sphere are occupied by two oxygen atoms of the malonate ligand. The bond angles of O(1)–Pt–O(2) and O(1)–Pt–N(1) are 89.27(12)° and 88.46(12)°, respectively, for the *cis* coordination, where as O(2)–Pt–N(1) and O(1)–Pt–N(2) are 177.35(11)° and 175.92(13)°, respectively, for the *trans* coordination. The Pt–N–C

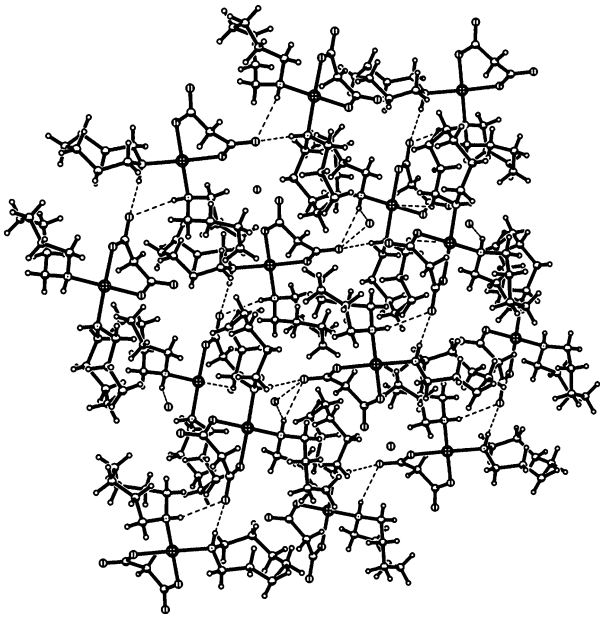


Fig. 3. Packing diagram of [Pt(heptamethyleneimine)$_2$(malonate)]·H_2O. Hydrogen bonds are indicated by dashed lines.

angles are comparable (108.6(3)°, 110.6(3)° and 111.6(3)°, 114.2(3)°), with tetrahedral value as observed in other Pt–amine compounds. The Pt–O–C angles are comparable with (120.3(3)° and 119.9(3)°) $Pt(NH_3)_2$(CBDCA) (Pt–O–C angles are 121.3(3)°) [36,37].

The title complex was found to cocrystallize with a molecule of water in the solid-state. Analysis of the single crystal X-ray diffraction data revealed that there were hydrogen bonds present between the heptamethyleneimine ligand and the malonate ligand ($d_{O\cdots N}$ = ~2.97 Å) and between the solvent water and the malonate ligand ($d_{O\cdots O}$ = ~2.87 Å). A packing diagram including a representation of the hydrogen bonding network is presented in Fig. 3.

In conclusion, we have synthesized and characterized a series of new cisplatin analogs containing heptamethyleneimine as nonleaving ligand and oxalate, malonate, methylmalonate, ethylmalonate, dimethylmalonate, diethylmalonate, or CBDCA as leaving ligand. The structure of *cis*-[Pt(L)$_2$(malonate)]·H_2O was determined by X-ray crystallography.

4. Supplementary material

Crystallographic data for the structural analysis have been deposited with the Cambridge Crystallographic Data Centre, CCDC 182935. Copies of this information may be obtained free of charge from The Director, CCDC, 12 Union Road, Cambridge, CB2 1EZ, UK (fax: +44-1233-336033; e-mail: deposit@ccdc.cam.ac.uk or www: http://www.ccdc.cam.ac.uk).

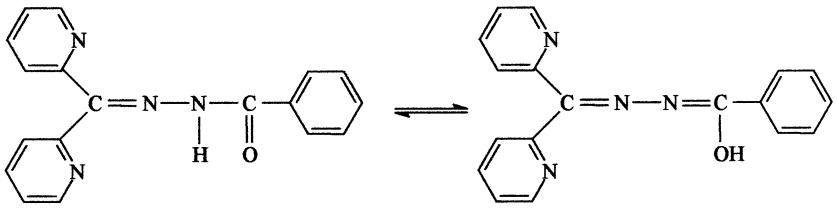
Acknowledgements

This work was supported by grants CA-77332 and CA-82361 from the National Cancer Institute and by grant C0976 from the Robert A. Welch Foundation.

References

[1] P.J. Loehrer, L.H. Einhorn, Ann. Intern. Med. 100 (1984) 704.
[2] W.B. Pratt, R.W. Rudden, W.D. Ensminger, J. Maybaum, The Anticancer Drugs, Oxford University Press, New York, 1994, p. 133.
[3] I.H. Krakoff, Cancer Treat. Rep. 63 (1979) 1523.
[4] J.B. Vermorken, H.M. Pinedo, Neth. J. Med. 25 (1982) 270.
[5] D.D. Vonhoff, R. Schilsky, C.M. Reichart, Cancer Treat. Rep. 63 (1979) 1527.
[6] I.H. Krakoff, in: M. Nicolini (Ed.), Platinum and Other Metal Coordination Compounds in Cancer Chemotherapy: Clinical Application of Platinum Complexes, Martinus Nijhoff, Boston, MA, 1988, p. 351.
[7] P.J. Loehrer, S.D. Williams, Sr., L.H. Einhorn, J. Natl. Cancer Inst. 80 (1988) 1373.
[8] A. Gelasko, S.J. Lippard, Anticancer activity of cisplatin and related complexes: metallopharmaceuticals I: DNA interactions, in: M.J. Clarke, P.J. Sadler (Eds.), Topics in Biological Inorganic Chemistry Series, vol. 1, Springer, Heidelberg, Germany, 1999, p. 1.
[9] L.R. Kelland, Platinum complexes, in: B.A. Teicher (Ed.), Cancer Therapeutics, Human Press, New York, 1997, p. 93.
[10] P. Pil, S.J. Lippard, Cisplatin and related drugs, in: J.R. Bertino (Ed.), Encyclopedia of Cancer, Academic Press, New York, 1997, p. 392.
[11] A.H. Calvert, S.J. Harland, D.R. Newell, Z.H. Siddik, K.R. Harrap, Cancer Treat. Rev. 12 (1985) 51.
[12] B.W. Booth, W.C. Weiss, A.H. Korzun, W.C. Wood, R.W. Carey, L.P. Panasci, Cancer Treat. Rep. 69 (1985) 919.
[13] M.J. Pekham, A. Horwich, M. Barda, A. Drury, W.F. Hendry, Cancer Treat. Rev. Suppl. A 12 (1991) 101.
[14] P.M. Takahar, C.A. Frederick, S.J. Lippard, J. Am. Chem. Soc. 118 (1996) 12309.
[15] A. Vaisman, S.E. Lim, S.M. Patrick, W.C. Copeland, D.C. Hinkle, J.J. Turchi, S.G. Chaney, Biochemistry 38 (1999) 11206.
[16] R. Perez-Soler, G. Lopez-Berestein, J. Lautersztain, S. Al-Baker, K. Francis, D. Macias-Kiger, M.N. Raber, A.R. Khokhar, Cancer Res. 50 (1990) 4254.
[17] A.R. Khokhar, S. Al-Baker, T. Brown, R. Perez-Soler, J. Med. Chem. 34 (1991) 325.
[18] S. Al-Baker, Z.H. Siddik, A.R. Khokhar, J. Coord. Chem. 31 (1994) 109.
[19] A.R. Khokhar, S. Shamsuddin, S. Al-Baker, S. Shah, J. Coord. Chem. 36 (1995) 7.
[20] S. Shamsuddin, S. Al-Baker, Z.H. Siddik, A.R. Khokhar, Inorg. Chim. Acta 241 (1996) 101.
[21] A.R. Khokhar, S. Al-Baker, S. Shamsuddin, Z.H. Siddik, J. Med. Chem. 40 (1997) 112.
[22] S. Shamsuddin, A.R. Khokhar, J. Coord. Chem. 33 (1994) 83.
[23] S. Shamsuddin, I. Takahashi, Z.H. Siddik, A.R. Khokhar, J. Inorg. Biochem. 61 (1996) 291.
[24] S.R. Ali Khan, I. Guzman-Jimenez, K.H. Whitmire, A.R. Khokhar, Polyhedron 19 (2000) 975.
[25] M.S. Ali, U. Mukhopadhyay, S.M. Shirvani, J. Thurston, K.H. Whitmire, A.R. Khokhar, Polyhedron 21 (2002) 125.
[26] U. Mukhopadhyay, A.R. Khokhar, J. Coord. Chem., in press.
[27] SHELXTL 6.10, Bruker AXS, Madison, WI, 2001.

[28] The scattering factors are part of the SHELXTL package and can be found in the International Tables for X-ray Crystallography, vol. C, Kluwer Academic Publishers, Dordrecht, The Netherlands, 1992.
[29] S.C. Dhara, Indian J. Chem. 8 (1970) 193.
[30] K. Nakamoto, Infrared and Raman Spectra of Inorganic Coordination Compounds, fourth ed., Wiley, New York, 1986, p. 383.
[31] S. Al-Baker, R. Perez-Soler, A.R. Khokhar, J. Inorg. Biochem. 47 (1992) 99.
[32] S. Al-Baker, R. Perez-Soler, A.R. Khokhar, J. Coord. Chem. 29 (1993) 1.
[33] J.H. Price, A.N. Williamson, R.F. Schramm, B.B. Wayland, Inorg. Chem. 11 (1972) 1280.
[34] P. Bita, G.O. Morton, T.S. Dunne, E.F. De los Santos, Y. Lin, S.R. Boone, R.C. Haltiwanger, C.G. Pierpont, Inorg. Chem. 29 (1990) 645.
[35] A.R. Khokhar, S. Al-Baker, I.H. Krakoff, R. Perez-Soler, Cancer Chemother. Pharmacol. 23 (1989) 219.
[36] S. Neidle, I.M. Ismail, P.J. Sadler, J. Inorg. Biochem. 13 (1980) 205.
[37] B. Beagley, D.W.J. Cruickshank, C.A. McAuliffe, R.G. Pritchard, A.M. Zaki, R.L. Beddoes, R.J. Cernik, O.S. Mills, J. Mol. Struct. 130 (1985) 97.
[38] F.D. Rochon, R. Melanson, J.-P. Macquet, F. Belanger-Gariepy, A.L. Beauchamp, Inorg. Chim. Acta 108 (1985) 1.
[39] F.D. Rochon, R. Melanson, J.-P. Macquet, F. Belanger-Gariepy, A.L. Beauchamp, Inorg. Chim. Acta 108 (1985) 17.
[40] S.D. Cutbush, R. Kuroda, S. Neidle, A.B. Robins, J. Inorg. Biochem. 18 (1983) 213.



(I) cetonic form (II) enolic form

the knowledge of some spectroscopic, thermal and conductimetric properties, a report of the experiments and results obtained with DPKBH and DPKBH/Ni(II) complex is to follow.

2. Experimental

2.1. Reagents and solutions

All reagents and solvents were of analytical-reagent grade. The synthesis of DPKBH was performed as previously reported by Garcia-Vargas et al. [8]. The ligand was obtained from the reaction of stoichiometric amounts of di-2-pyridyl ketone and benzoylhydrazide mixed in EtOH, when few drops of concd. HCl were added. The mixture was refluxed for 1 h, and after cooling, distilled water was added to a 1:3 volume ratio (EtOH–water). Several drops of NaOH solution were added to the refluxed solution to increase the pH to approximately 5. The resulting precipitate was collected on a Büchner funnel and recrystallized twice from an EtOH–water solution. After synthesis, the m.p. of the product was verified to be (137 ± 1) °C and it is in excellent agreement with the literature [8]. DPKBH solutions were prepared by dissolving the reagent in EtOH; $NiSO_4 \cdot 6H_2O$ was dissolved in water and the respective concentration was determined with standard EDTA solution titration.

The complex was prepared by reaction between the corresponding Ni hydrated salt and the ligand (molar ratio 1:2) in EtOH. This molar ratio was achieved by mixing 30 ml of each solution: 2×10^{-2} mol l^{-1} Ni(II) and 4×10^{-2} mol l^{-1} DPKBH. After a slow evaporation of the solvent, the complex was dried under vacuum over anhydrous $CaCl_2$ and purple crystals were obtained.

The experimental data necessary to apply the continuous variations [13–17] or Job's method are the absorbances relatives to solutions with different ligand molar fraction, varying both from the concentrations (Ni(II) and DPKBH) but maintaining constant the sum of the ligand and metal ion concentrations, 5×10^{-5} mol l^{-1}. These solutions are obtained with complementary volumes of equimolar solutions when the total volume is constant. The stoichiometry of the Ni(II)/DPKBH complexes was determined using a series of solutions having a constant sum of the DPKBH and Ni(II) concentrations, in 50% EtOH–water and pH 6 adjusted with 3.2×10^{-2} mol l^{-1} CH_3COONH_4. The molar ratio was varied from 0 to 1 and the absorbances values were measured at $\lambda = 390$ nm, using pathlength of 1.0 cm.

2.2. Apparatus

The UV–Vis spectra were registered on an Hewlett-Packard (HP) 8452A diode-array spectrophotometer using 1.00 cm quartz cells. The pH measurements were performed with a Metrohm 654 pHmeter equipped with a Metrohm glass electrode of which the Ag/AgCl reference was filled with 3 mol l^{-1} NaCl. FTIR spectra (4000–500 cm^{-1}; KBr pellets) were recorded on a Perkin–Elmer 1750 Series FTIR spectrophotometer. The mass spectra were obtained with a Mat-90 of the Finnigan-Mat. A CHN Elemental Analyzer instrument from Perkin–Elmer model 2400 was used to determine the C, H and N percentages both in DPKBH and Ni(II)/DPKBH complex. The percentage of oxygen in the ligand was calculated by difference and the Ni(II) percentage present in the complex was obtained from TG experiments. The conductance measurements were obtained on a Micronal conductometer model B 330 and using the Analyzer 7A04 conductivity cell. TG/DTG curves were obtained on a Model TGA50 thermogravimetric Analyzer (Shimadzu) in the range of 25–900 °C with 10 °C min^{-1} heating rate, under dynamic nitrogen atmosphere (approximately 50 ml min^{-1}) and samples weighing between 3.5 and 4.3 mg, in Pt crucible. DSC curves were registered on a model DSC50 (Shimadzu) in the temperature range of 25–600 °C, with a heating rate of 10 °C min^{-1}, under dynamic nitrogen atmosphere (approximately 50 ml min^{-1}) with sample masses in the range of 1–2.3 mg, in aluminum crucibles. DSC system was calibrated with indium (m.p. = 156.6 °C; $\Delta H_{fus} = 28.54$ J g^{-1}) and Zn (m.p. = 419.6 °C).

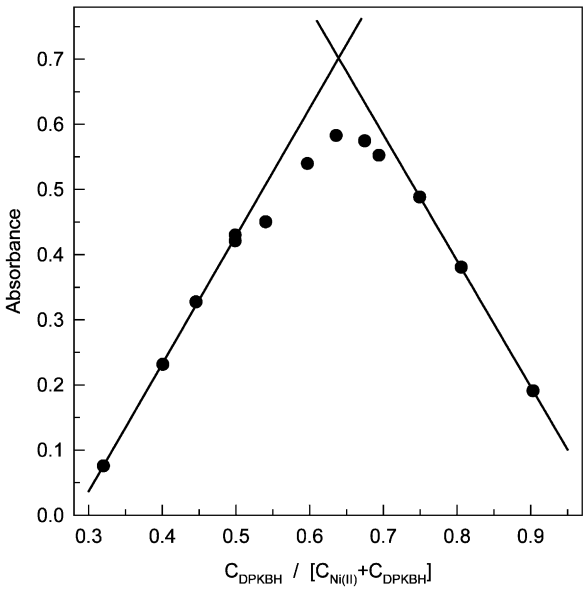


Fig. 1. Values of absorbance vs. molar fraction of the ligand, $C_{DPKBH}/(C_{Ni(II)}+C_{DPKBH})$. Pathlength = 1 cm, $\lambda = 390$ nm, pH 6. $C_{DPKBH}+C_{Ni(II)} = 5.00 \times 10^{-5}$ mol l^{-1} in ethanol/water 50% (v/v).

3. Results and discussion

The molar ratio relative to the maximum of the Job's curve [17] corresponds to the more favorable species present in the equilibrium and it is obtained from the intersection between the tangents of the curves. Fig. 1 shows the absorbances at $\lambda = 390$ nm for several solutions with different molar (DPKBH: [Ni(II)+DPKBH]) ratios. The maximum absorbance was found at a molar ratio equal to 0.64 which corresponds to a 1:2 metal–ligand molar ratio or the coordination of two molecules of DPKBH to Ni(II).

In aqueous–ethanolic–acid solutions, DPKBH exhibits an acid equilibrium between the neutral and the protonated forms. Considering the protonation of a pyridine nitrogen atom, the extension of this equilibrium is given by the respective ionization constant ($pK_1 = 3.362$) [18]. The dissociation of a proton from the neutral DPKBH molecule (from COH group) is not favorable under the conditions of our experiments (pH 6) but, the interaction between DPKBH and the metal cation promotes an enhancement in the ligand acidity and it can change to an anionic form. In order to check this assumption, molar conductances were followed during the complexation of Ni(II) by DPKBH in a titration mode. The very low initial conductance of a DPKBH/ethanol/water solution varied significantly when a solution of Ni(II) was added. The known acidity of the Ni(II) stock solution necessary to avoid its hydrolysis was considered in the calculations.

Molar conductances were determined in a titration of 1.00×10^{-3} mol l^{-1} DPKBH solution with 9.90×10^{-3} mol l^{-1} $Ni(SO_4)\cdot 6H_2O$ (pH 3.1), both of them in ethanol/water 50% (v/v). The conductance values plotted versus Ni(II) volumes showed two linear segments with very different slopes with an intersection that corresponds to 1:2 molar ratio for Ni(II)–DPKBH. The first linear segment, which is in a range of concentration of DPKBH higher than the Ni(II) one, has a slope higher than the second segment showing that the coordination of DPKBH to Ni(II) is via an anionic form with H^+ releasing.

The opposite titration, i.e. 9.90×10^{-4} mol l^{-1} Ni(II) solution (pH 3.1) with 1.00×10^{-2} mol l^{-1} DPKBH showed a similar behavior for the conductance measurements as a function of the DPKBH volume. The intersection between the segments was observed on a 1:2 ratio of Ni(II)–DPKBH, in an excellent agreement with the first titration. The first segment showed a high slope and in the second part the conductance was almost constant due to the presence of excess of ligand, DPKBH, which is a very weak acid.

Mass spectra of the ligand and the complex Ni(II)/DPKBH were recorded in a range of *m/e* ratio between 0 and 800. For the Ni(II)/DPKBH complexes, the more intensive peak or the base peak was found at *m/e* = 169.1. The molecular peak ion was observed at *m/e* = 662.6; corresponding to the formula weight of the complex, $[Ni(DPKBH)_2]$. The base peak for the ligand

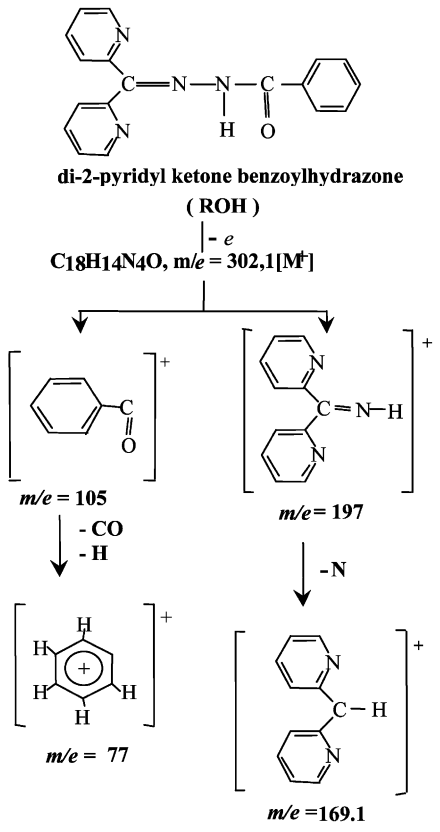
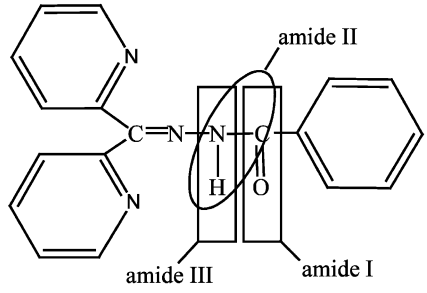


Fig. 2. Main DPKBH fragments relatives to the main peaks registered in the mass spectra.

Table 1
Important IR frequencies (cm^{-1}) of DPKBH and Ni(II)/DPKBH complex and their assignments [a]

Ni(II)/DPKBH λ (cm^{-1})	DPKBH λ (cm^{-1})	Assignment
3055 w	3063 w	=C–H phenolic, N–H
	1686 vs	amide I (C=O)
1587 m	1581 m	(C–C and C–N) phenolic
	1533 m	(CN, δ NH) amide II
1495 s		C–C and C–N pyridyn
1465 m	1464 s	C–C and C–N pyridyn
1357 s		phenolic
1320 s	1322 m	phenolic
1290 s	1265 m	amide III (δ NH)
1087 s	1081 m	C–H phenolic
746 w	746 m	C–H phenolic
714 m	706 s	δ (OH) out-of-plane



[a] s, strong; m, medium; w, weak; and vs, very strong.

was found also at $m/e = 169.1$ and the molecular ion peak at $m/e = 302.1$ which corresponds to the formula weight of the ligand. The peaks lower than 200 (77.0, 105.0, 169.1 and 197.0) were the same for the ligand and the complex. The main fragments found for the DPKBH are indicated in Fig. 2.

Table 1 presents the main IR data for the ligand and the complex. Since DPKBH exhibits a keto-enol tautomerism [8], the IR spectra were used to determine which forms predominate in the nickel complex formation. IR spectrum of the complex differs significantly from that of the free ligand. The ν(N–H) band almost disappears in the 3000 cm^{-1} region, as a consequence of the deprotonation of the CONH system [19]. The high intensity band due to the C=O stretch [19–21] in 1686 cm^{-1} observed for the ligand is also suppressed in the spectrum of the complex. The shift of the carbonyl stretching mode to lower frequencies is in accordance with coordination through oxygen [20]. The bands due to phenolic group C–O in 1322 and 1265 cm^{-1} are shifted to a higher frequency [22] in the complex, to 1357 and 1290 cm^{-1}, respectively, with a higher intensity.

All these observations suggest that, in the complex, DPKBH exists in the enol form and exhibits a tridentate behavior. This result confirms the conductance data that indicated a coordination of DPKBH via an anionic form.

Table 2 shows the elemental analysis data for DPKBH and its complex with Ni(II). These results are in an excellent agreement with the calculated C, H and N percentages for the ligand and the respective complex of Ni(II) considering a 1:2 stoichiometry: $[Ni(DPKBH)_2]$. The calculated oxygen percentage and the complement of (C+H+N) experimental percentage are 5.29 and 5.06, respectively, showing also a good agreement. The calculation was realized considering the formula weight of the DPKBH equal to 302.34 g mol^{-1}.

The thermal behavior of the compounds under investigation was studied using the thermogravimetry/derivative thermogravimetry (TG/DTG) and the DSC techniques. Fig. 3 shows TG/DTG curves for the ligand and the Ni(II) complex. Thermal decomposition of DPKBH occurs abruptly in a single step, with a DTG peak at 315 °C. Several thermal events for the Ni(II)/DPKBH complex appear between 359 and 900 °C. The first and fastest mass loss observed between 359 and 375 °C, with a DTG peak at 365 °C and $\Delta m = 45.4\%$ corresponds to the elimination of one molecule of DPKBH (calculated value = 45.7%). At higher temperatures (375–730 °C), a gradual mass loss totalizes 43.1%. The total mass loss was found to be 88.5% and the color of the residue was green. This evidence led to consider that nickel oxide is the final product of the thermal decomposition.

Considering the total decomposition of the $[Ni(DPKBH)_2]$ complex and NiO as the residue at

Table 2
Elementary analysis of the DPKBH ligand and Ni(II)/DPKBH complex

%	DPKBH (MM = 302.34 Da)			$[Ni(DPKBH)_2]$ (MM = 661.36 Da)		
	Calculated	Experimental	Error (%)	Calculated	Experimental	Error (%)
C	71.51	71.51	0	65.38	65.23	0.2
H	4.67	4.73	1.3	3.96	4.11	−3.8
N	18.53	18.70	−0.92	16.94	16.74	1.2
Ni(II)				8.87	9.04 [a]	−1.9

[a] Calculated from TG/DTG.

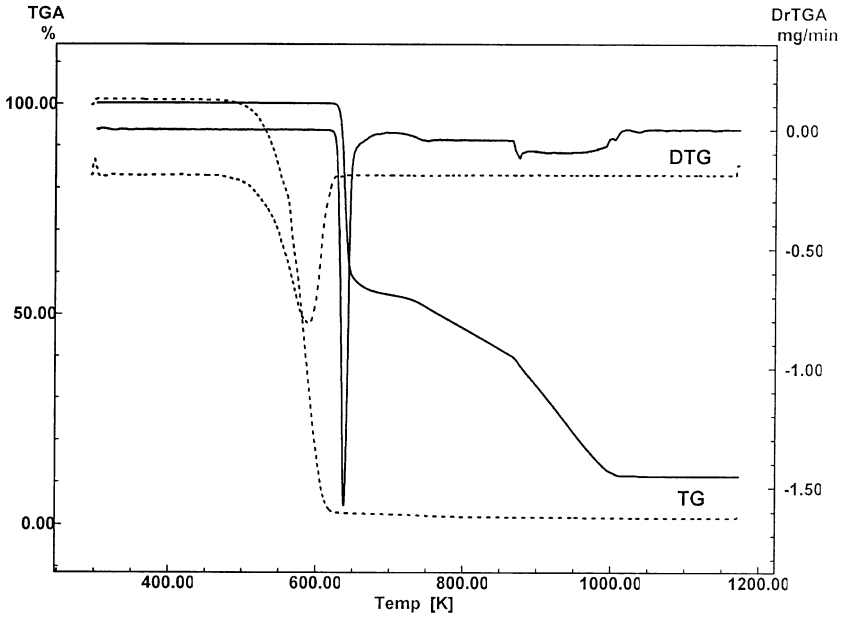


Fig. 3. TG/DTG curves: for (---) DPKBH ($m = 3.577$ mg) and (—) [Ni(DPKBH)$_2$] ($m = 4.285$ mg). Both of the curves were obtained in dynamic nitrogen atmosphere (approximately 50.0 ml min^{-1}) and heating rate of 10 °C min^{-1}.

730 °C, the experimental value (11.5%) is in accordance with the calculated percentage (11.3%) of the residue. This good agreement is another evidence about the coordination of two molecules of DPKBH to Ni(II) cations and confirms the proposed stoichiometry for this complex.

A comparison between TG/DTG curves of the ligand and the complex shows a higher thermal stability for this last because the mass losses begin at 359 and 246 °C for the complex and the ligand, respectively. This higher stability of the ligand when it is coordinated to Ni(II) is owing to the ligand–metal interaction.

DSC curves of DPKBH and [Ni(DPKBH)$_2$] are shown in Fig. 4. DSC curve profiles are quite different for the ligand and the complex. The ligand shows an intense sharp endothermic peak between 137 and 147 °C and, $\Delta H = 122.5$ kJ mol^{-1} that corresponds to the melting of DPKBH; TG/DTG curves do not present mass loss in that temperature range. The onset temperature, 137.9 °C, is in an excellent agreement with the

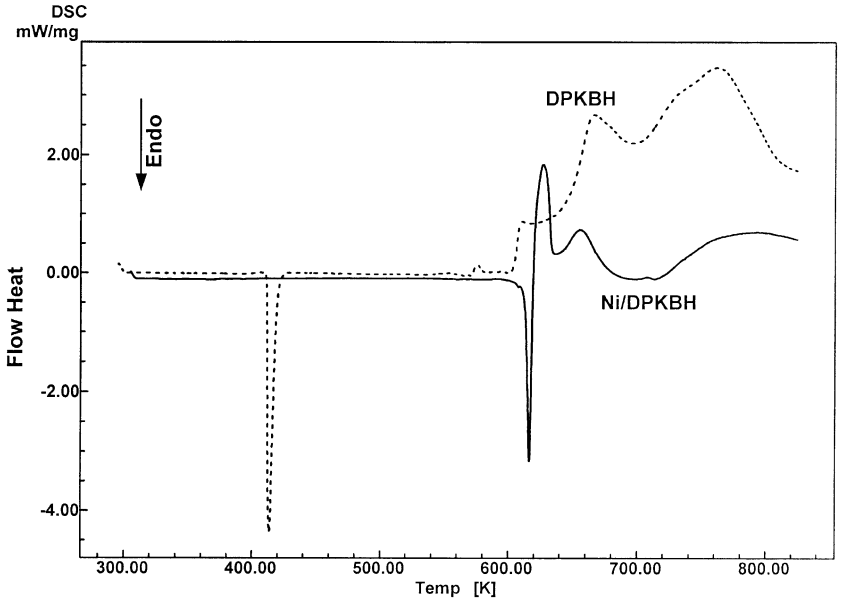


Fig. 4. DSC curves of the ligand and [Ni(DPKBH)$_2$] obtained in dynamic nitrogen atmosphere (approximately 50.0 ml min^{-1}) and heating rate of 10 °C min^{-1}, respectively, with mass 2.305 and 1.128 mg.

temperature range of melting indicated in Section 2. Above 300 °C, several exothermic peaks can be seen and they are related to thermal decomposition processes. DSC curve of the complex shows a sharp endothermic peak which characterizes the melting process at 343 °C with $\Delta H = 72$ kJ mol^{-1}. After the complex melting, a fast thermal decomposition indicated by exothermic peaks is observed and such peaks are associated with a gradual mass loss process.

4. Supplementary material

The material is available from the authors on request.

Acknowledgements

The authors gratefully acknowledge financial support from FAPESP (Fundação de Amparo à Pesquisa do Estado de São Paulo) and CNPq (Conselho Nacional de Desenvolvimento Científico e Tecnológico).

References

[1] T. Nakanishi, M. Otomo, Microchem. J. 33 (1986) 172.
[2] M.M. Kamal, A.Z. Abu Zuhri, M.M. Hannoun, Fresenius J. Anal. Chem. 344 (1992) 275.
[3] M.A. Al-Nuri, M. Abu-Eid, N.A. Zatar, S. Khalaf, M. Hannoun, Anal. Chim. Acta 259 (1992) 175.
[4] N.A. Zatar, A.Z. Abu-Zuhri, M.A. Al-Nuri, F.M. Mahmoud, A.A. Abu-Obai, Spectrosc. Lett. 22 (1989) 1203.
[5] T. Nakanishi, M. Otomo, Anal. Sci. 1 (1985) 161.
[6] S.O. Pehkonen, Y. Erel, M.R. Hoffmann, Environ. Sci. Technol. 26 (1992) 1731.
[7] M.E.V. Suárez-Iha, S.O. Pehkonen, M.R. Hoffmann, Environ. Sci. Technol. 28 (1994) 2080.
[8] M. Garcia-Vargas, M. Belizón, M.P. Hernández-Artiga, C. Martinez, J.A. Pérez-Bustamante, Appl. Spectrosc. 40 (1986) 1058.
[9] M. Katyal, Y. Dutt, Talanta 22 (1975) 151.
[10] R.B. Singh, P. Jain, Talanta 29 (1982) 77.
[11] L.H.S.A. Terra, M.E.V. Suárez-Iha, Spectrosc. Lett. 30 (1997) 625.
[12] L.H.S.A. Terra, M.C.C. Areias, I. Gaubeur, M.E.V. Suárez-Iha, Spectrosc. Lett. 32 (1999) 257.
[13] P. Job, Anal. Chem. 9 (1928) 113.
[14] F. Woldbye, Acta Chem. Scand. 9 (1955) 299.
[15] K.S. Klausen, F.J. Langmyhr, Chim. Acta 28 (1962) 335.
[16] W.C. Vosburgh, G.R. Cooper, J. Am. Chem. Soc. 63 (1941) 437.
[17] L. Sommer, M. Langová, CRC Crit. Rev. Anal. Chem. 19 (1988) 225.
[18] I. Gaubeur, M.V. Rossi, K. Iha, M.E.V. Suárez-Iha, Ecl. Quím. 25 (2000) 63.
[19] R.T. Conley, Infrared Spectroscopy, 2nd ed., Allyn and Bacon, Boston, MA, 1972, pp. 97–201.
[20] L.J. Bellammy, The Infrared Spectra of Complex Molecules, 1st ed., Wiley, New York, 1954, p. 72.
[21] N.S. Biradar, B.R. Havinale, Inorg. Chim. Acta 17 (1976) 157.
[22] R.M. Silverstein, G.C. Bassler, T.C. Morril, Spectrometric Identification of Organic Compounds, 5th ed., Wiley, New York, 1991, ch. 3, pp. 91–164.

After 2 days violet–grey crystals were obtained. The CMANa compound was prepared by a published method [9].

Anal. Calc. for: $C_{36}O_{10}N_6H_{34}Cu$: C, 55.85; H, 4.43; N, 10.85; Cu 8.21. Found: C, 55.12; H, 4.65; N, 10.46; Cu, 8.45%.

2.2. Physical measurements

The solid state spectrum of a powdered sample was measured in the diffuse reflectance mode on a Carry 500 Scan (Varian) UV–Vis–NIR spectrophotometer. Variable temperature magnetic susceptibility data were measured using a Cahn RH electrobalance by the Faraday method. The magnetic field applied was 4.28 kOe, and the temperature range was 4.2–300 K.

The EPR spectrum was recorded on a Bruker ESP 300E (Bruker, Germany) spectrometer operating at X-band and equipped with a Bruker NMR gaussmeter ER 035M and a Hewlett–Packard microwave frequency counter HP 5350B. EPR parameters were calculated by computer simulation of the experimental spectrum using Bruker WIN–EPR SIMFONIA Software Version 1.25.

IR spectra were recorded as KBr pellets or nujol mulls by using Perkin–Elmer 1600 and Perkin–Elmer 180 spectrophotometers. The Raman spectrum of the solid sample was recorded on a Magna (Nicolet) instrument with 1064 nm excitation.

2.3. Crystal data

The crystal was mounted on a glass fiber and then flash-frozen to 100 K (Oxford Cryosystem-Cryostream Cooler). Preliminary examination and intensity data collections were carried out on a Kuma KM4 CCD κ-axis diffractometer with graphite-monochromated Mo Kα radiation. Crystals were positioned at 65 mm from the KM4CCD camera. Six hundred and twelve frames were measured at 0.75° intervals with a counting time of 25 s. The data were corrected for Lorentz and polarization effects. An absorption correction was also applied. Data reduction and analysis were carried out with the Kuma Diffraction (Wrocław) programs. The structure was solved by direct methods [13] (program SHELXS-97) and refined by the full-matrix least-squares method on all F^2 data using the SHELXL-97 [14] programs. All hydrogen atoms were found by Fourier synthesis. Crystal data and the details of data collection and the refinement procedure are given in Table 1.

3. Results and discussion

The direct reaction of Him, CMANa and $CuCl_2$ in water or ethanol solution yields the violet–grey crystals of the title compound. The structure of the molecule of $Cu(CMA)_2(Him)_2\cdot 4H_2O$ is shown in Fig. 1, the packing of the complex in the crystal along with the hydrogen bond system is shown in Fig. 2. Selected bond distances and angles are listed in the Table 2.

Table 1
Experimental data of the X-ray diffraction studies for $Cu(CMA)_2(Him)_2\cdot 4H_2O$

Empirical formula	$C_{36}H_{28}CuN_6O_6\cdot 4(H_2O)$
M	776.26
Crystal system	monoclinic
Space group symbol	$P2_1/c$
a (Å)	9.220(2)
b (Å)	13.153(3)
c (Å)	13.970(3)
β (°)	100.76(3)
V (Å^3)	1664.4(6)
T (K)	100.0(5)
Z	2
μ (mm^{-1})	0.728
Number of reflections measured	10 714
Number of independent reflections	3095
Final R indices [$I > 2\sigma(I)$]	$R_1 = 0.0341$ [a], $wR_2 = 0.0859$ [b]
R indices (all data)	$R_1 = 0.0494$ [a], $wR_2 = 0.0895$ [b]

[a] $R_1 = \Sigma||F_o|-|F_c||/\Sigma|F_o|$.
[b] $wR_2 = \{\Sigma[w(F_o^2-F_c^2)^2]/\Sigma[w(F_o^2)^2]\}^{1/2}$.

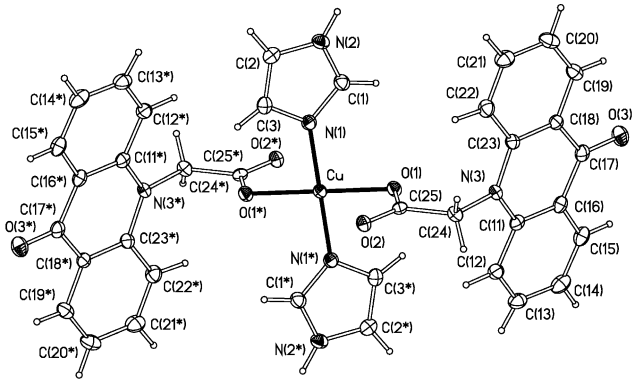


Fig. 1. ORTEP drawing for the $Cu(CMA)_2(Him)_2$ molecule. Ellipsoids at 50% probability level. Symmetry transformations used to generate equivalent atoms: *, $-x$, $-y+1$, $-z$.

The crystal of $Cu(CMA)_2(Him)_2\cdot 4H_2O$ consists of neutral monomers of the complex and water molecules. The copper ion, located in the center of symmetry, is coordinated via two imidazole nitrogen atoms (N1) and two carboxylic oxygen atoms (O1) from the CMA^- ligands. Moreover, short non-bonding Cu–O contacts are observed, the length of Cu–O(2) is 2.790(1) Å. Therefore, the title compound can be regarded as a pseudo-six-coordinated complex. This geometry around the copper is typical of ternary complexes of Cu(II) with carboxylates and aromatic amines or imidazole [4,15–24]. The length of Cu–O(1) bond equals 1.977(2) Å and is in the normal range for a carboxylate group monodentately coordinated to copper, whereas the Cu–N(1)

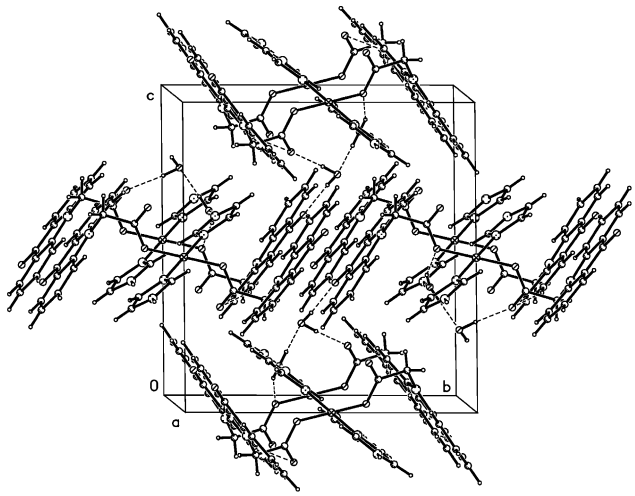


Fig. 2. The crystal packing of $Cu(CMA)_2(Him)_2\cdot 4H_2O$. Hydrogen bonds are indicated by dashed lines.

Table 2
Selected bond lengths (Å) and angles (°) for $Cu(CMA)_2(Him)_2\cdot 4H_2O$

Cu–N(1)	1.953(2)
Cu–O(1)	1.977(2)
Cu–O(2)	2.790(1)
O(1)–Cu–O(2)	52.50(5)
N(1)–Cu–O(1)	90.12(5)
N(1)–Cu–O(2)	88.39(5)
N(1*)–Cu–O(1)	89.88(5)
N(1*)–Cu–O(1*)	90.12(5)
O(1)–Cu–O(1*)	180.00(7)

Symmetry transformations used to generate equivalent atoms: *, $-x$, $-y+1$, $-z$.

distance of 1.953(2) Å is very short as compared with those observed for imidazole coordinated to copper(II) [2–4,7,8,15–17,24,25,27]. The distance between the copper ion and O(2) oxygen atom is very long and corresponds well with those found in similar copper-carboxylate-imidazole systems [2,4,15–17,24,25]. The mean $Cu–O_{axial}$ distance estimated for 136 monomeric hexacoordinate copper(II) compounds with the O_4N_2 chromophore equals 2.56 Å [26]. The group of 15 copper(II) complexes with carboxylate and imidazole or aromatic amine ligands ([4–8,16–25] and this work), shows the largest elongation of the coordination octahedron (tetragonal distortion) among all CuO_4N_2 compounds [26] and the mean value of the $Cu–O_{axial}$ bond length found for this group reaches 2.74(1) Å.

The geometry of carboxylate group of the CMA^- ligand is characteristic of a monodentate bonding mode [28]. The bond distances and angles of the acridine part of 9,10-dihydro-9-oxo-10-acridineacetate ion are in good agreement with those of other CMA^- complexes [10–12] and CMAH [29], differences between average and individual values are insignificant. The geometrical parameters of imidazole correspond to those reported for the neutral ligand in other complexes [27]. The dihedral angle between the imidazole plane and the equatorial plane of the complex equals 88.8(1)°. The acridine ring systems in the molecule are almost parallel, the interplane angle is 0.5(1)°, whereas the imidazole ring is twisted by 16.7(1)° with respect to the acridine plane. The crystal is further stabilized by O–H···O and N–H···O hydrogen bonds involving water and imidazole molecules (Table 3). There are five independent hard hydrogen bonds in the structure, four O–H···O and one N–H···O. Each water molecule acts as a double donor in O–H···O hydrogen bonds and as a single acceptor. The imidazole N(2) atom acts as a single donor in the hydrogen bond network. In addition to hydrogen bonds of the classical type, a weak C–H···O interaction is also observed. The intermolecular C(20)–H(20)···O(2) distances: C···O of 3.326(3) Å and H···O of 2.50(3) Å, and the C–H···O angle of 151(2)° satisfy the criteria for hydrogen bonds of this type [30]. Moreover, stacking interaction is observed between CMA^- ligands. The angle between the interacting rings is 0.52(1)° and the shortest distance equals 3.216(3) Å.

The magnetic moment calculated from the susceptibility data for $\Theta = -9.8$o K equals 1.96 μ_B, which gives the average g value 2.26, and is in the range expected for similarly distorted octahedral complexes of copper (II) [31–33].

The EPR spectrum of finely ground polycrystalline $Cu(CMA)_2(Him)_2\cdot 4H_2O$ complex exhibits axial character with well resolved copper hyperfine splitting of parallel orientation. The spectrum with $g_{zz} = g_{\|} \gg g_{xx} \approx g_{yy} = g_{\perp} > 2.0023$ and $A_{zz} = A_{\|} \gg A_{xx} \approx A_{yy} = A_{\perp}$ is typical of a tetragonal geometry of the Cu(II) environment indicating that the ground state is essentially $d_{x^2-y^2}$. The values of the EPR parameters ($A_{\|} = 180 \times 10^{-4}$ cm^{-1} and $g_{\perp} = 2.058$, $g_{\|} = 2.260$) correspond to the N_2O_2 donor set in Cu(II) coordination plane determined by the crystal structure analysis, although $A_{\|}$ is apparently higher and $g_{\|}$ smaller than usually observed for Cu(II) complexes with two imidazole and two water molecules [34]. This effect should be assigned to stronger donor properties of the negatively

Table 3
Hydrogen bonds for $Cu(CMA)_2(Him)_2\cdot 4H_2O$ (Å and °)

D–H···A	d(D–H)	d(H···A)	d(D···A)	<(DHA)
N(2)–H(2N)···O(12)$^{(ii)}$	0.88(3)	1.85(3)	2.730(3)	174(3)
O(11)–H(111)···O(2)$^{(iii)}$	0.85(3)	1.99(3)	2.830(2)	170(3)
O(11)–H(112)···O(3)$^{(iv)}$	0.77(3)	2.00(3)	2.762(3)	175(3)
O(12)–H(121)···O(11)	0.90(4)	1.83(4)	2.732(2)	178(3)
O(12)–H(122)···O(1)$^{(v)}$	0.81(3)	2.08(3)	2.836(3)	156(3)
C(20)–H(20)···O(2)$^{(vi)}$	0.91(2)	2.50(3)	3.326(3)	151(2)

Symmetry transformations used to generate equivalent atoms (ii) $-x+1$, $y-1/2$, $-z+1/2$ (iii) $-x$, $y+1/2$, $-z+1/2$ (iv) $-x+1$, $-y+1$, $-z+1$ (v) x, $-y-1/2$, $z-3/2$ (vi) $x-1$, y, z.

charged carboxylate oxygen than those associated with water oxygen. On the other hand, the differences displayed by $g_{\|}$ as compared with that found for solid 2-methyl-vinylimidazoles and two nitrato ligands ($g_{\|} = 2.325$) [34] is most likely consistent with stronger in-plane interactions in the $Cu(CMA)_2(Him)_2\cdot 4H_2O$ complex due to a longer axial Cu–O(carboxy) (2.79 Å) than in the case of the Cu–O(nitrato) (2.42 Å) bond. The same tendency to decrease $g_{\|}$ (to 2.249) and increase $A_{\|}$ (to 189×10^{-4} cm^{-1}) as a result of very weak interactions with two carboxylic oxygens at axial positions was found for bis(*N*-tosylglicinato)bis(*N*-methylimidazole) copper(II) [16] where square-planar coordination is realized in the same way by two carboxylic and two imidazole groups.

The diffuse reflectance spectrum of $Cu(CMA)_2(Him)_2\cdot 4H_2O$ exhibits a maximum at 18.2 kK ($d_{xz(yz)} \rightarrow d_{x^2-y^2}$) with a well discernible shoulder at 15.0 kK ($d_{xy} \rightarrow d_{x^2-y^2}$), and is consistent with the presence of a strongly elongated tetragonal ligand field around the copper(II) ion [31]. The position of the former band fits the correlation between the d–d band maximum and $Cu\cdots O_{axial}$ distance for several copper(II)-carboxylate-imidazole systems, proposed by Battaglia [16], (Table 4).

The assignment of the electronic spectra may be correlated with the EPR data. Assuming the ground state as almost pure $d_{x^2-y^2}$ orbital, one can calculate the principal values of the g tensor [35]:

$$g_x = 2.0023 + 2k_x^2\zeta/(E_{GS} - E_{yz}) \quad (1)$$

$$g_y = 2.0023 + 2k_y^2\zeta/(E_{GS} - E_{xz}) \quad (2)$$

$$g_z = 2.0023 + 8k_z^2\zeta/(E_{GS} - E_{xy}) \quad (3)$$

where k is the orbital reduction factor, ζ, the spin-orbit coupling constant (830 cm^{-1}) and E_{GS} is the ground state energy. The EPR and electronic spectra do not show a considerable separation of d_{xz} and d_{yz} orbitals.

Table 4
Correlation between the d–d band maximum and the $Cu\cdots O_{axial}$ distance for copper(II)–carboxylate–imidazole systems

Compound	d–d Band maximum (10^{-3} cm^{-1})	$Cu\cdots O_{axial}$ distance (Å) [a]
$Cu(Ac\text{-}\alpha\text{-}ala)_2(N\text{-}MeIm)_2\cdot H_2O$ [32]	18.2	2.907(4)
$Cu(CMA)_2(Him)_2$ this work	18.2	2.790(2)
$Cu(TsglyH)_2(N\text{-}MeIm)_2$ [16]	17.9	2.758(4)
$Cu(Zala)_2(N\text{-}MeIm)_2$E-tOH [15]	17.6	2.731(4)
$Cu(Hippu)_2(Him)_2$ [4]	17.5	2.736(4)

Hippu, hippurato; Him, imidazole; Zala, *N*-benzyloxycarbonyl-alanilato; *N*-MeIm, *N*-methylimidazole; TsglyH, *N*-tosylglicinato; Ac-α-ala, *N*-acetyl-α-alanilato.

[a] Oxygen atom from carboxylate group.

Therefore, it is reasonable to assume $g_x \approx g_y = g_{\perp}$, $g_z = g_{\|}$ and from (1)–(3) we obtain $k_x \approx k_y = 0.78$ and $k_z = 0.76$. The orbital reduction factors are comparable in magnitude to the k-values of other tetragonal copper(II) complexes [36].

The ν_{as}(COO) and ν_s(COO) bands of $Cu(CMA)_2(Him)_2\cdot 4H_2O$ are found at 1608 and 1381 cm^{-1} in the IR spectrum and at 1609 and 1386 cm^{-1} in the Raman spectrum. The values of $\Delta = \nu_{as}(COO) - \nu_s(COO)$ equal 227 cm^{-1} (IR) and 223 cm^{-1} (R), and correspond well to those estimated for bis(*N*-tosylglycinato)bis(*N*-methylimidazole)copper(II) [16] and are characteristic for a monodentate mode of carboxylate coordination [28]. On the basis of the detailed comparison of the low frequency IR and Raman spectra of $Cu(CMA)_2(Him)_2\cdot 4H_2O$ and $Cu(CMA)_2\cdot 2H_2O$ [10] and other literature data [37,38], the frequencies of stretching vibrations of coordination bonds are assigned as follows: 337 cm^{-1} for ν_{as}(Cu–O), 300 cm^{-1} for ν_s(Cu–O), 269 cm^{-1} for ν_{as}(Cu–N) and 244 cm^{-1} for ν_s(Cu–N). In spite of the very high complexity of the studied compound several characteristic bands of imidazole are very distinctly observed in the IR and Raman spectra. Their wavenumbers are very similar to those assigned in the spectra of the free ligand [39] and of neutral imidazole complexes [40]. In the spectra of $Cu(CMA)_2(Him)_2\cdot 4H_2O$ the $\nu(C\text{–}H)_{im}$ vibrations give rise to the weak bands located at 3138, 3100 cm^{-1} (IR) and at 3162, 3141 cm^{-1} (R). Also the out of plane deformations of $(C\text{–}H)_{im}$ groups are observed as the strong bands in the IR spectrum at 938 and 843 cm^{-1}, and as a weak band at 935 cm^{-1} in the Raman spectrum. Vibrations of the N–H group are assigned to the following bands: ν(N–H) at 3233 cm^{-1} (IR), δ(N–H) at 1314 cm^{-1} (IR, R) and γ(N–H) at 1074 cm^{-1} (IR), 1071 cm^{-1} (R). Imidazole ring stretching and deformation modes generate strong IR and weak Raman bands located at the frequencies: IR—1546, 1450, 1331, 1150, 915, 673, 644 cm^{-1}. Raman, 1331, 643 cm^{-1}.

The results of our work show a preference for monomer formation over dimer formation in copper(II)–carboxylate–imidazole systems and are consistent with other studies. Although the electronic effects play the more important role in adoption of the structure of these compounds than the steric effect, the results of our study demonstrates that steric demand of the CMA^- ligand and strong interligand interactions affect the composition and structure of $Cu(CMA)_2(Him)_2\cdot 4H_2O$. The single crystal X-ray study shows that the structure of the presented compound is very similar to those of known antitumor complexes $Co(O_2CMe)_2(Him)_2$ [6] and $Cu(O_2CMe)_2$(1-methyl-4,5-diphenyloimidazole)$_2$ [7]. The solid state far IR, FT Raman, UV–Vis, EPR and magnetic susceptibility data are consistent with the structure of the complex.

4. Supplementary material

Supplementary data on $Cu(CMA)_2(Him)_2 \cdot 4H_2O$ are available from The Director, CCDC, 12 Union Road, Cambridge, CB2 1EZ, UK (fax: +44-1223-336033; e-mail: deposit@ccdc.cam.ac.uk or www: http://www.ccdc.cam.ac.uk) on request, quoting the deposition number 176220.

References

[1] J.P. Kilnman, Chem. Rev. 96 (1996) 2541.
[2] Y. Akhriff, J. Server-Carrió, A. Sancho, J. Garcia-Lozano, E. Escrivá, J.V. Folgado, L. Soto, Inorg. Chem. 38 (1999) 1174.
[3] R. Bhalla, M. Helliwell, C.D. Garner, Inorg. Chem. 36 (1997) 2944.
[4] L. Antolini, L.P. Battaglia, A.B. Corradi, G. Marcotrigiano, L. Menabue, G.C. Pellacani, M. Saladini, Inorg. Chem. 21 (1982) 1391.
[5] H.A. Henricksson, Acta Crystallogr., Sect. B 33 (1977) 1947.
[6] H. Tamura, H. Imai, J. Kuwahara, Y. Sugiura, J. Am. Chem. Soc. 109 (1987) 6870.
[7] C.P. Raptopoulu, S. Paschalidou, A.A. Pantazaki, A. Terzis, S.P. Perlepes, T. Lialiaris, E.G. Bakalbassis, J. Mroziński, D.A. Kyriakidis, J. Inorg. Biochem. 71 (1998) 15.
[8] J. Fangfang, W. Zuoxiang, W. Chen, B. Zhiping, Y. Xiaozeng, Acta. Crystallogr., Sect. C 55 (1999) 1228.
[9] A.D. Inglot, J. Młochowski, Z. Szulc, O. Inglot, M. Albin, Arch. Immun. Ther. Exp. 33 (1985) 275.
[10] D. Miernik, T. Lis, J. Palus, J. Reedijk, Inorg. Chim. Acta 205 (1993) 231.
[11] D. Miernik, T. Lis, Acta Crystallogr., Sect. C 52 (1996) 1171.
[12] D. Miernik, T. Lis, J. Chem. Crystallogr. 24 (1994) 731.
[13] G.M. Sheldrick, SHELXS-97, Program for Solution of Crystal Structures, University of Göttingen, Göttingen, Germany, 1997.
[14] G.M. Sheldrick, SHELXL-97, Program for Crystal Structure Refinement, University of Göttingen, Göttingen, Germany, 1997.
[15] L. Antolini, L. Menabue, M. Saladini, M. Sola, L.P. Battaglia, A.B. Corradi, Inorg. Chim. Acta 93 (1984) 61.
[16] L.P. Battaglia, A. Corradi, G. Marcotrigiano, L. Menabue, G.C. Pellacani, Inorg. Chem. 22 (1983) 1902.
[17] F.T. Greenaway, A. Pereshk, W.A. Cordes, M.C. Noble, J.R.J. Sorenson, Inorg. Chim. Acta 93 (1984) 67.
[18] M.M. Borel, A. Busnot, F. Busnot, A. Leclaire, M.A. Bernard, Rev. Chim. Miner. 18 (1981) 370.
[19] M.M. Borel, A. Busnot, F. Busnot, A. Leclaire, M.A. Brenard, Rev. Chim. Miner. 18 (1981) 74.
[20] A. Busnot, F. Busnot, A. Leclaire, M.A. Bernard, Z. Anorg. Allg. Chem. 503 (1983) 207.
[21] A.S. Ancyshkina, M.A. Poraj-Koshits, V.N. Ostrinkova, D.A. Garmovskij, A.I. Sadimenko, O.A. Osipov, Koord. Khim. 13 (1987) 1422.
[22] L.P. Battaglia, A. Bonamartini Corradi, C. Grasselli Palmieri, Cryst. Struct. Commun. 3 (1973) 523.
[23] N.N. Hoang, F. Valach, M. Melnik, Z. Kristallogr. 208 (1993) 27.
[24] T.S. Schilperoort, F.J. Rietmeyer, R.A.G. de Graaff, J. Reedijk, Acta Crystallogr., Sect. C 42 (1986) 1491.
[25] A. Bonamartini Corradi, S. Bruni, F. Cariati, A.P. Battaglia, G. Pelosi, Inorg. Chim. Acta 205 (1993) 99.
[26] M. Melnik, M. Kabesová, L. Macásková, C.E. Holloway, J. Coord. Chem. 45 (1998) 31.
[27] A.G. Orpen, L.Brammer, F.H. Allen, O. Kennard, O.G. Watson, R.Taylor, J. Chem. Soc., Dalton Trans. (1989) Supplement.
[28] G. Smith, E.J. O'Reilly, C.H.L. Kennard, K. Stadnicka, B. Oleksyn, Inorg. Chim. Acta 47 (1981) 111.
[29] D. Dobrzyńska, I. Turowska-Tyrk, Acta Crystallogr., Sect. C 53 (1997) 238.
[30] G.R. Desiraju, Acc. Chem. Res. 24 (1991) 290.
[31] G. Willkinson, R.D. Gillard, J.A. McCleverty, Comprehensive Coordination Chemistry, vol. 5, Pergamon Press, Oxford, 1987.
[32] L.P. Battaglia, A.B. Coradi, L. Menabue, G.C. Pellacani, D. Prampolini, M. Saladini, J. Chem. Soc., Dalton Trans. (1982) 781.
[33] M. Melnik, Coord. Chem. Rev. 36 (1981) 1.
[34] K. Kurdziel, T. Glowiak, J. Jezierska, J. Chem. Soc., Dalton Trans. (2000) 1095.
[35] I. Bertini, D. Gatteschi, A. Scozzafava, Coord. Chem. Rev. 29 (1979) 67.
[36] B.N. Figgis, M.A. Hitchman, Ligand Field Theory and its Applications, Wiley-VCH, 2000.
[37] B.C. Cornilsen, K. Nakamoto, J. Inorg. Nucl. Chem. 36 (1974) 2467.
[38] A.L. Abuhijleh, C. Woods, Inorg. Chim. Acta 194 (1992) 9.
[39] D. Garfinkel, J.T. Edsall, J. Am. Chem. Soc. 80 (1958) 3807.
[40] J.B. Hodgson, G.C. Percy, D.A. Thornton, J. Mol. Struct. 66 (1980) 81.

2. Experimental

The starting materials used in the present investigations were prepared by literature methods: Ph_3SbBr_2 [23], and internally functionalized oximes HON=C(R)Ar (R = H, CH_3; Ar = C_5H_4N-2, C_4H_3S-2, C_4H_3O-2 [24,25]). All the preparative reactions were performed under anhydrous conditions. IR spectra were recorded as Nujol mulls using a Perkin–Elmer 577 spectrophotometer. ^1H (in $CDCl_3$) and $^{13}C\{^1H\}$ (in $CHCl_3$ using D_2O lock) NMR spectra were obtained on a JEOL FX 90Q spectrometer using TMS as an internal reference.

2.1. Preparation of $[Ph_3Sb\{ON{=}C(Me)C_5H_4N\text{-}2\}_2]$

To a methanolic solution of sodium salt of 2-acetylpyridyl oxime [prepared in situ from sodium metal (109 mg, 4.74 mmol) dissolved in methanol (15 ml) and 2-acetylpyridine oxime (648 mg, 4.75 mmol)], a benzene solution (20 ml) of Ph_3SbBr_2 (1.218 g, 2.37 mmol) was added with constant stirring. The reactants were refluxed for 4 h. The solvent was evaporated under vacuum and the residue was extracted with benzene (2 × 15 ml) and filtered and dried under vacuum to give light pink solid which was recyrstallized from benzene–hexane mixture at −10 °C as colorless crystals (yield 1.29 g, 87%). All other complexes of the type $[Ph_3Sb\{ON{=}C(R)Ar\}_2]$ were prepared in a similar manner and the corresponding data are summarized in Table 1.

2.2. Preparation of $[Ph_3Sb(Br)\{ON{=}C(H)C_5H_4N\text{-}2\}]$

To a stirred benzene solution (15 ml) of $[Ph_3Sb\{ON{=}C(H)C_5H_4N\text{-}2\}_2]$ (484 mg, 0.81 mmol), a solution of Ph_3SbBr_2 in benzene (410 mg, 0.80 mmol) was added and then mixture was stirred for 30 min. The solvent was stripped off in vacuo to give the title compound in quantitative yield (876 mg, 98%). Similarly $[Ph_3Sb(Br)\{ON{=}C(Me)C_5H_4N\text{-}2\}]$ was prepared from $[Ph_3Sb\{ON{=}C(Me)C_5H_4N\text{-}2\}_2]$ and Ph_3SbBr_2.

2.3. Controlled hydrolysis of $[Ph_3Sb\{ON{=}C(H)C_5H_4N\text{-}2\}_2]$

A methanolic solution (5 ml) of sodium methoxide [prepared from sodium metal (17 mg, 0.76 mmol) in methanol] was added to a benzene solution (15 ml) of $[Ph_3Sb\{ON{=}C(H)C_5H_4N\text{-}2\}_2]$ (451 mg, 0.76 mmol), and refluxed for 2 h. After cooling to room temperature, 0.2 ml of distilled water was added and stirred for 30 min. The solvents were evaporated in vacuo and the residue was extracted with benzene and filtered. The filtrate was concentrated and recrystallized from hexane at −10 °C to give colorless crystals of $[Ph_3Sb(OH)\{ON{=}C(H)C_5H_4N\text{-}2\}]$ (328 mg, 88%).

2.4. X-ray structure determination

Crystals of $[Ph_3Sb\{ON{=}C(Me)C_5H_4N\text{-}2\}_2]$ (**1**) were colorless blocks. A suitable specimen was mounted on a glass fibre and cell dimensions and intensity data were recorded on an Enraf Nonius KCCD diffractometer with ϕ scans and ω scans chosen to give a complete asymmetric unit. Data collection and cell refinement [26] gave cell constants corresponding to a monoclinic cell whose dimensions are given in Table 2 along with other experimental parameters. An absorption correction was applied [27], which resulted in transmission factors ranging from 0.0497 to 0.0263.

The structure was solved by direct methods [28], and the structure was refined using the WINGX version [29] of SHELX-97 [30]. All of the non-hydrogen atoms were treated anisotropically. All hydrogen atoms were included in idealized positions with C–H set at 0.95 Å and with isotropic thermal parameters set at 1.2 times that of the carbon atom to which they were attached. The final cycle of full-matrix least-square refinement [30] was based on 3297 observed reflections (2537 for $F^2 > 4\sigma F^2$))

Table 1
Physical and analytical data of triphenylantimony(V) complexes

Complexes	Recrystallization solvent (%yield)	M.p. (°C)	*Anal*. Found (Calc.) (%)				
			C	H	N	Sb	Br
$[Ph_3Sb\{ON{=}C(Me)C_5H_4N\text{-}2\}_2]$	hexane (87)	142	61.2 (61.2)	4.6 (4.7)	8.7 (8.9)	19.3 (19.5)	
$[Ph_3Sb(Br)\{ON{=}C(Me)C_5H_4N\text{-}2\}]$	(99)	132	52.7 (52.9)	3.7 (3.9)	4.6 (49)	21.1 (21.4)	14.3 (14.1)
$[Ph_3Sb(OH)\{ON{=}C(Me)C_5H_4N\text{-}2\}]$	dichloromethane (83)		59.3 (59.4)	4.7 (4.6)	5.6 (5.5)	23.8 (24.1)	
$[Ph_3Sb\{ON{=}C(Me)C_4H_3O\text{-}2\}_2]$	benzene–hexane (97)	138	59.6 (59.9)	4.6 (4.5)	4.9 (4.7)	20.0 (20.2)	
$[Ph_3Sb\{ON{=}C(Me)C_4H_3S\text{-}2\}_2]$	benzene–hexane (97)	118	56.3 (56.9)	4.1 (4.3)	4.1 (4.4)	19.1 (19.2)	
$[Ph_3Sb\{ON{=}C(H)C_5H_4N\text{-}2\}_2]$	benzene–hexane (98)	145	60.3 (60.5)	4.0 (4.2)	9.6 (9.4)	20.3 (20.4)	
$[Ph_3Sb(Br)\{ON{=}C(H)C_5H_4N\text{-}2\}]$	(97)	186	51.8 (52.0)	3.3 (3.6)	5.0 (5.1)	29.7 (30.0)	14.2 (14.4)
$[Ph_3Sb(OH)\{ON{=}C(H)C_5H_4N\text{-}2\}]$	dichloromethane (88)	54	58.4 (58.7)	4.0 (4.3)	5.7 (5.7)	24.3 (24.8)	
$[Ph_3Sb\{ON{=}C(H)C_4H_3O\text{-}2\}_2]$	benzene–hexane (98)	142	58.3 (58.7)	4.2 (4.0)	4.4 (4.9)	20.9 (21.2)	
$[Ph_3Sb\{ON{=}C(H)C_4H_3S\text{-}2\}_2]$	benzene–hexane (98)	82	55.3 (55.6)	3.4 (3.8)	4.5 (4.6)	20.0 (20.1)	

Table 2
Crystal data and structure refinement for $[Ph_3Sb\{ON{=}C(Me)C_5H_4N\text{-}2\}_2]$

Empirical formula	$C_{32}H_{29}N_4O_2Sb$
Formula weight	1246.68
Temperature (°C)	−153(2)
Wavelength (Å)	0.71073
Crystal system	monoclinic
Space group	*C*2/*c*
Unit cell dimensions	
a (Å)	19.398(4)
b (Å)	10.093(2)
c (Å)	16.542(3)
β (°)	116.57(3)
V (Å^3)	2896.6(10)
Z	4
D_{calc} (g cm^{-3})	1.429
Absorption coefficient (mm^{-1})	0.987
F(000)	1264
Crystal size (mm)	0.10 × 0.10 × 0.10
θ Range for data collection (°)	3.18–27.50
Index ranges	$-19 \le h \le 25$, $-13 \le k \le 12$, $-21 \le l \le 21$
Reflections collected	11 258
Independent reflections	3297 [$R_{int} = 0.0385$]
Max/min transmission	0.0497, 0.0263
Refinement method	full-matrix least-squares on F^2
Data/restraints/parameters	3297/0/237
Goodness-of-fit on F^2	1.010
Final *R* indices [$F^2 > 4\sigma(F^2)$]	$R_1 = 0.0268$, $wR_2 = 0.0530$
R indices (all data)	$R_1 = 0.0440$, $wR_2 = 0.0582$
Extinction coefficient	0.00041(11)
Largest difference peak and hole (e Å^{-3})	0.324 and −0.434

and 237 variable parameters and converged (largest parameter shift was 0.001 times its e.s.d.). Selected bond distances and angles are given in Table 3 and the molecule is displayed in the ORTEP diagram in Fig. 1.

3. Results and discussion

3.1. Preparation

All the preparative reactions were performed under anhydrous conditions and are summarized in Scheme 1. The reaction of Ph_3SbBr_2 with the sodium salt of internally functionalized oximes in 1:2 stoichiometry in refluxing anhydrous benzene afforded $[Ph_3Sb\{ON{=}C(R)Ar\}_2]$ [R = CH_3, Ar = C_5H_4N-2(**1**), C_4H_3S-2(**2**) C_4H_3O-2(**3**); R = H, Ar = C_5H_4N-2(**4**), C_4H_3S-2(**5**) and C_4H_3O-2(**6**)]. Further the reaction of (**1**) and (**4**) with 1 equiv. of Ph_3SbBr_2, yielded the redistribution products $[Ph_3Sb(Br)\{ON{=}C(R)C_5H_4N\text{-}2\}]$ [R = CH_3(**7**), H(**8**)]. The reaction was instantaneous and completed at room temperature. $[Ph_3Sb(OH)\{ON{=}C(R)C_5H_4N\text{-}2\}]$ were prepared by partial hydrolysis of $[Ph_3Sb\{ON{=}C(R)C_5H_4N\text{-}2\}_2]$. All these complexes are pinkish to white solids and are soluble in common organic solvents.

Table 3
Selected bond lengths (Å) and angles (°) for $[Ph_3Sb\{ON{=}C(Me)C_5H_4N\text{-}2\}_2]$ (**1**) [a]

Bond lengths			
Sb(1)–O(1)	2.068(1)	Sb(1)–O(1)′	2.068(1)
Sb(1)–C(1)	2.098(2)	Sb(1)–C(1)′	2.098(2)
Sb(1)–C(7)	2.120(3)	Sb(1)–N(2)	2.817(1)
O(1)–N(1)	1.403(2)	N(1)–C(11)	1.277(3)
C(11)–C(12)	1.498(3)	C(11)–C(13)	1.484(3)
C(13)–C(14)	1.383(3)	C(14)–C(15)	1.382(3)
C(15)–C(16)	1.368(4)	C(16)–C(17)	1.366(4)
N(2)–C(13)	1.334(3)	N(2)–C(17)	1.340(3)
Bond angles			
O(1)–Sb(1)–O(1)′	172.78(7)	C(1)–Sb(1)–C(1)′	118.1(1)
C(1)–Sb(1)–C(7)	120.94(6)	C(1)=Sb(1)–C(7)	120.94(6)
O(1)–Sb(1)–C(1)′	90.38(7)	O(1)=Sb(1)–C(1)	90.38(7)
O(1)–Sb(1)–C(1)	85.91(7)	O(1)=Sb(1)–C(1)′	85.91(7)
O(1)–Sb(1)–C(7)	93.61(4)	O(1)=Sb(1)–C(7)	93.61(4)
Sb(1)–O(1)–N(1)	106.9(1)	O(1)–N(1)–C(11)	114.7(2)
N(1)–C(11)–C(12)	125.6(2)	N(1)–C(11)–C(13)	114.7(2)
C(12)–C(11)–C(13)	119.7(2)	C(11)–C(13)–C(14)	122.0(2)
C(13)–C(14)–C(15)	118.9(2)	C(14)–C(15)–C(16)	119.2(2)
C(15)–C(16)–C(17)	118.3(3)	N(2)–C(17)–C(16)	123.8(3)
N(2)–C(13)–C(11)	115.9(2)	N(2)–C(13)–C(14)	122.1(2)
C(13)–N(2)–C(17)	117.7(2)		

[a] Symmetry equivalent position (−*x*+1, *y*, −*z*+2) given by a prime.

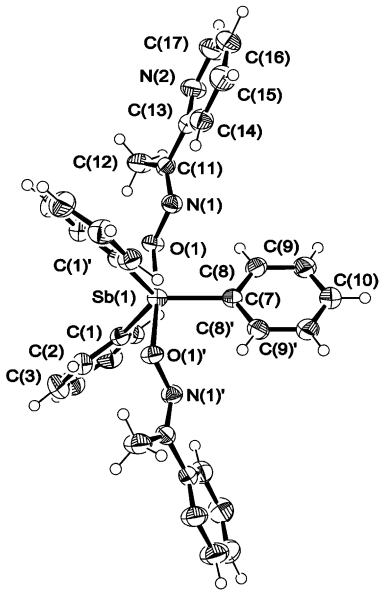
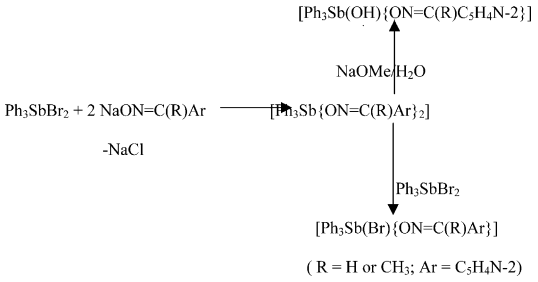


Fig. 1. ORTEP plot of the molecule $[Ph_3Sb\{ON{=}C(Me)C_5H_4N\text{-}2\}_2]$ (**1**). The atoms are drawn with 50% probability ellipsoids.

3.2. IR spectra

The IR spectra of these complexes were interpreted by comparing these with those of the free oximes and other related complexes [12–14,31]. Broad stretching vibra-



Scheme 1.

tions at ~3300 cm^{-1} due to –OH group of the free oximes disappeared in the IR spectra of (**1**)–(**6**), suggesting the deprotonation of –OH group and formation of Sb–O bond. The formation of Sb–O bond is further supported by the appearance to a weak to medium intensity band in the region 410–460 cm^{-1} and is assigned to ν Sb–O [32]. The ν C=N and ν N–O stretching vibrations appear at lower wavenumbers (~45 cm^{-1}) than those of the free ligands [33].

3.3. NMR spectra

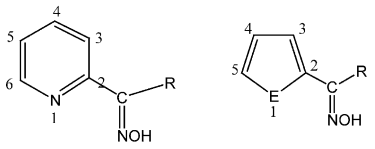
The ^{1}H and $^{13}C\{^{1}H\}$ NMR spectra of these complexes showed characteristic peaks and peak multiplicities for Ph–Sb. The data are summarized in Table 4. The Ph–Sb carbon resonances of complexes are slightly shielded on substituting bromine with oximate in Ph_3SbBr_2. The shielding of these resonances increases in the order: $Ph_3SbBr_2 < Ph_3SbBrL < Ph_3SbL_2$ and are

Table 4
^{1}H and ^{13}C NMR data for oximes and their triphenylantimony(V) complexes in CDCl3

Complexes	13C{1H} NMR in δ (ppm)	1H NMR δ (ppm)
Ph_3SbBr_2	129.5, 131.5, 133.5, 140.9 (Ph [a]–Sb)	7.61–8.40 (m, Ph–Sb)
2N–$C_5H_4C(CH_3)$=NOH	10.7(Me); 120.6(C-5); 123.4(C-3); 136.3(C-4); 148.8(C-6); 154.6(C-2); 156.5(C=N)	2.44(s, Me); 7.25(t, H-4); 7.68(t, H-5); 7.83(d, H-3); 8.63(m, H-6), 9.08(br, S, OH)
[Ph_3Sb{ONC(Me)C_5H_4N-2}$_2$]	10.9(oxime-Me); 120.2(C-5); 122.4(C-3); 136.1(C-4); 148.1(C-6); 154.8(C-2); 156.4(C=N); 128.8, 130.7, 135.7, 139.4 (Ph [a]–Sb)	2.45(s, Me); 7.13(d, H-4); 7.60(t, H-5); 8.16(d, H-3); 8.64(d, H-6), 7.45–8.21 (m, Ph–Sb)
[Ph_3Sb(Br){ON=C(Me)C_5H_4N-2}]	10.9(oxime-Me); 120.2(C-5); 122.9(C-3); 136.1(C-4); 148.2(C-6); 155.0(C-2); 157.5(C=N); 129.2, 131.3, 134.5, 138.0 (Ph [a]–Sb)	2.38(s, Me-oxime); 7.21(t, H-4); 7.40(t, H-5); 8.30(d, H-3); 8.68(m, H-6); 7.48–8.43 (m, Ph–Sb)
[Ph_3Sb(OH){ON=C(Me)C_5H_4N-2}]	10.8(oxime-Me); 120.1(C-5); 122.3(C-3); 135.2(C-4); 148.0(C-6); 156.3(C-2); 156.5(C=N); 128.8, 130.7, 135.6, 138.7 (Ph [a]–Sb)	1.27(br, OH); 2.47(s, Me-oxime); 7.16(t, H-4); 7.37(t, H-5); 8.18(d, H-3); 8.65(d, H-6); 7.15–8.24(m, Ph–Sb)
2-OC_4H_3C(Me)=NOH	11.0(C-Me); 109.6(C-4); 111.2(C-3); 143.5(C-5); 147.6(C-2); 150.3(C=N)	2.21(s, Me); 6.42(d, H-4); 6.62(d, H-3); 7.45(br, H-5); 9.82(br, s, OH)
[Ph_3Sb{ON=C(Me)C_4H_3O-2}$_2$]	11.5(oxime-Me); 106.6(C-4); 111.2(C-3); 143.4(C-5); 148.2(C-2); 152.3(C=N); 128.7, 130.7, 135.8, 142.0 (Ph [a]–Sb)	2.23(s, oxime-Me); 6.37(d, H-4); 6.77(d, H-3); 7.42(br, H-5); 7.52–8.24 (m, Ph–s)
2-SC_4H_3C(Me)=NOH	12.3(C-Me); 126.3(C-4); 126.7(C-3); 127.0(C-5); 140.4(C-2); 151.8(C=N)	2.38(s, Me); 7.13(m, H-4); 7.35(d, H-3); 7.64(d, H-5); 8.01(b, OH)
[Ph_3Sb{ON=C(Me)C_4H_3S-2}$_2$]	12.6(C-Me); 125.9(C-4); 126.6(C-3); 126.9(C-5); 139.7(C-2); 152.0(C=N); 128.7, 130.6, 135.7, 139.8 (Ph [a]–Sb)	2.25(s, oxime-Me); 7.10(d, H-4); 7.39(d, H-3); 7.59(d, H-5); 7.48–8.24 (Ph–Sb)
2-N-C_5H_4C(H)=NOH	120.5(C-5); 123.8(C-3); 136.5(C-4); 149.2(C-6); 150.6(C-2); 153.5(C=N)	7.42(t, H-4); 7.85(t, H-5); 7.89(t, H-3); 8.48(s, CH); 8.76(d, H-6), 9.57(br, OH)
[Ph_3Sb{ON=C(H)C_5H_4N-2}$_2$]	119.9(C-5); 122.9(C-3); 136.0(C-4); 148.8(C-6); 150.9(C-2); 153.5(C=N); 129.0, 131.0, 134.5, 135.7 (Ph [a]–Sb)	7.42(d, H-4); 7.59(t, H-5); 8.18(t, H-3); 8.45(s, CH); 8.65(d, H-6); 7.38–8.31 (Ph–Sb)
[Ph_3Sb(Br){ON=C(H)C_5H_4N-2}]	119.8(C-5); 122.9(C-3); 136.1(C-4); 149.8(C-6); 151.2(C-2); 153.4(C=N); 129.0, 131.4, 133.6, 137.5 (Ph [a]–Sb)	7.40(d, H-4); 7.50(t, H-5); 8.27(d, H-3); 8.38(s, CH); 8.64(d, H-6); 7.52–8.35 (m, Ph–Sb)
[Ph_3Sb(OH){ON=C(H)C_5H_4N-2}]	119.7(C-5); 122.0(C-3); 136.1(C-4); 148.7(C-6); 50.8(C-2); 153.4(C=N); 129.0, 131.0, 134.5, 138.2 (Ph [a]–Sb)	1.73(br, OH); 7.27(d, H-4), 7.80(t, H-5); 7.80(d, H-3); 8.40(s, CH); 8.65(d, H-6); 7.13–8.36 (m, Ph–Sb)
2-OC_4H_3C(H)=NOH	111.9(C-4); 112.2(C-3); 144.5(C-2); 145.8(C-2); 158.2(C=N)	6.62(d, H-4); 7.45(d, H-3); 7.58(t, H-5); 7.67(s, CH); 9.76(br, OH)
[Ph_3Sb{ON=C(H)C_4H_3O-2}$_2$]	111.7(C-4); 112.1(C-3); 144.3(C-5); 146.6(C-2), 160.2(C=N); 129.0, 131.1, 135.1, 137.8 (Ph [a]–Sb)	6.59(d, H-4); 7.26(d, H-3); 7.59(t, H-5); 7.35(s, CH); 7.35–8.29 (m, Ph–Sb)
2-SC_4H_3C(H)=NOH	126.2(C-4); 131.5(C-3); 131.7(C-5); 138.0(C-2); 150.2(C=N)	7.26(t, H-4); 7.56(d, H-3); 7.70(d, H-5); 7.92(s, CH), 9.60(br, OH)
[Ph_3Sb{ON=C(H)C_4H_3S-2}$_2$]	125.7(C-4); 131.6(C-3); 131.4(C-5); 139.9(C-2); 151.8(C=N); 128.9, 131.3, 134.2, 138.9 (Ph [a]–Sb)	7.16(t, H-4); 7.48(d, H-3); 7.60(d, H-5); 7.78(s, CH); 7.35–8.24 (m, Ph–Sb)

[a] Antimony–phenyl (Ph–Sb) carbon values are given in the order C(p), C(o), C(m) and C(i), respectively.

unaffected by the nature of oxime. No significant changes in chemical shifts have been observed for the ligand proton resonances on complexation, except for the methyl and CH signals which, in general, appear at higher field than that for the corresponding free oxime.



(R=H, CH_3; E=O,S)

In the ^{13}C NMR spectra of triphenylantimony(V) complexes C-2 and C=N, in general, are deshielded as compared with their positions with the corresponding free oximes. The carbon signals of the heterocyclic ring of the functionalized oximes were observed at their expected positions and do not show any appreciable shifts indicating that the heteroatom of the aryl group is not coordinated to antimony. This is further substantiated by the X-ray structure of (**1**).

3.4. Crystal and molecular structure of $[Ph_3Sb\{ON=C(Me)C_5H_4N\text{-}2\}_2]$ (*1*)

Important bond distances and angles for $[Ph_3Sb\{ON=C(Me)C_5H_4N\text{-}2\}_2]$ (**1**) are listed in Table 3 and the molecular structure is displayed as an ORTEP diagram in Fig. 1. The structure consists of discrete monomeric $[Ph_3Sb\{ON=C(Me)C_5H_4N\text{-}2\}_2]$ units with both 2-acetylpyridineoxime ligands bound to the antimony atom through oxygen [Sb(1)–O(1) 2.0680(14) Å]. The molecule sites a twofold axis and the coordination environment around the antimony can be described as slightly distorted trigonal bipyramidal with equatorial Sb–C bonds and axial oxygen atoms [O(1)–Sb(1)–O(1)′ angles of 172.78(7)°]. The SbC_3 unit is planer (the sum of the C–Sb–C angle is 359.99°) and O–Sb–C angles lie in the range 85.91°–93.61°. The average Sb–O bond of 2.068(14) Å is approximately equal to the sum of the covalent radii of Sb and O (2.07 Å), while the average Sb–C bond of 2.098(2) Å is slightly shorter than the sum of the covalent radii of Sb and C (2.18 Å), as expected for the axial and equatorial positions of a trigonal bipyramid. The interatomic distances from antimony to the nitrogen [Sb(1)–N(2) 2.817 (1) Å] of the 2-NC_5H_4 moiety is well outside the sum of the van der Waals radii of Sb and N (2.11 Å), thus confirming unidentate linkage of the oximate ligand to antimony.

4. Supplementary material

The crystal code for $[Ph_3Sb\{ON=C(Me)C_5H_4N\text{-}2\}_2]$ is CCDC 181239. Supplementary data are available from The Director, CCDC, 12 Union Road, Cambridge, CB2 1EZ, UK (fax: +44-1223-336033; e-mail: deposit@ccdc.cam.ac.uk or www: http://www.ccdc.cam.ac.uk) on request, quoting the deposition number 181239. Additional material available from the Cambridge Crystallographic Data Centre comprises the final atomic coordinates for all atoms, thermal parameters, and a complete listing of bond distances and angles.

Acknowledgements

Two of the authors (A.G. and R.K.S.) are grateful to DAE, Mumbai for the award of a Senior Research Fellowship and a Research Associateship to them through a BRNS project No. 98/37/33. M.B.H. thanks the UK Engineering and Physical Sciences Research Council for support of the X-ray facilities at Southampton and J.E.D. the Natural Sciences and Engineering Research Council of Canada for financial support. We are also thankful to Mr. Suman Kumar Gupta (Sr. Tech. FT-NMR) for recording the NMR spectra and kind cooperation.

References

[1] V.K. Jain, R. Bohra, R.C. Mehrotra, Struct. Bonding (Berlin) 52 (1982) 147.
[2] M.N Gibbons, D.B. Sowerby, Phosphorus, Sulfur Silicon 93/94 (1994) 305.
[3] I. Haiduc, D.B. Sowerby, S.-F. Lu, Polyhedron 14 (1995) 3389.
[4] M.A. Said, K.C. Kumara Swamy, D.M. Poojary, A. Clearfield, M. Veith, V. Huch, Inorg. Chem. 35 (1996) 3235.
[5] H.J. Breunig, T. Krüger, E. Lork, Angew. Chem., Int. Ed. Engl. 36 (1996) 615.
[6] C. Silvestru, A. Silvestru, I. Haiduc, D.B. Sowerby, K.H. Ebert, H.J. Breunig, Polyhedron 16 (1997) 2643.
[7] S.S. Garje, V.K. Jain, Main Group Met. Chem. 22 (1999) 45.
[8] H. Mahalakshmi, V.K. Jain, E.R.T. Tiekink, Main Group Met. Chem. 23 (2000) 519.
[9] C. Silvestru, L. Silaghi-Dumitrescu, I. Haiduc, M.J. Begley, M. Nunn, D.B. Sowerby, J. Chem. Soc., Dalton Trans. (1986) 1031.
[10] C. Silvestru, M. Curtui, I. Haiduc, M.J. Begley, D.B. Sowerby, J. Organomet. Chem. 426 (1992) 49.
[11] C. Silvestru, C. Socaciu, A. Baba, I. Haiduc, Anticancer Res. 10 (1990) 803.
[12] K.V. Domasevitch, N.N. Gerasimchuk, A. Mokhir, Inorg. Chem. 39 (2000) 1227.
[13] A. Gupta, R.K. Sharma, R. Bohra, V.K. Jain, J.E. Drake, M.B. Hursthouse, M.E. Light, J. Organomet. Chem. 645 (2002) 118.
[14] V. Sharma, R.K. Sharma, R. Bohra, V.K. Jain, R. Ratnani, J.E. Drake, M.B. Hursthouse, M.E. Light, J. Organomet. Chem. 651 (2002) 98.
[15] N.N. Gerasimchuk, E. Kuzmann, A. Buki, A. Vertes, L. Nagy, K. Burger, Inorg. Chim. Acta 188 (1991) 45.
[16] K.V. Domasevich, N.N. Gerasimchuk, Russ. J. Inorg. Chem. 37 (1992) 3207.
[17] A. Hubele, M. Kuehne, Swiss 579 867, 1972, Chem. Abstr. 86 (1977) 38616u.
[18] A. Hubele, A.G. Ciba–Geigy, Patent of US# 3 941 832, 1976, Chem. Abstr. 86 (1977) 5159u.

[19] H. Nakamura, Y. Iitaka, H. Sakakibara, H. Umezawa, J. Antibiot. 27 (1974) 894.
[20] H.A. Kirst, E.F. Szymanski, D.E. Doman, J.L. Occolowitz, N.D. Jones, M.O. Chaney, R.L. Hamill, M.M. Hoehn, J. Antibiot. 28 (1975) 286.
[21] V.K. Jain, R. Bohra, R.C. Mehrotra, Inorg. Chim. Acta 51 (1981) 191.
[22] V.K. Jain, R. Bohra, R.C. Mehrotra, J. Indian Chem. Soc. 57 (1980) 408.
[23] G.O. Doak, G.G. Long, L.D. Freedman, J. Organomet. Chem. 4 (1965) 82.
[24] W. Hückel, M. Sachs, Ann. Chem. 498 (1932) 176.
[25] F. Nerdel, I. Huldschinsky, Chem. Ber. 86 (1953) 1005.
[26] Z. Denzo Otwinowski, W. Minor, Macromolecular crystallography part A, in: C.W. Carter Jr., R.M. Sweet (Eds.), Methods in Enzymology, vol. 276, Academic Press, New York, 1997, pp. 307.
[27] (a) SORTAV, R.H. Blessing, Acta Crystallogr., Sect. A 51 (1995) 33.;
(b) R.H. Blessing, J. Appl. Crystallogr. 30 (1997) 421.
[28] G.M. Sheldrick, Acta Crystallogr., Sect. A 46 (1990) 467.
[29] L.J. Farrugia, J. Appl. Crystallogr. 32 (1999) 837.
[30] G.M. Sheldrick, SHELXL-97, University of Göttingen, Germany, 1997.
[31] E. Maslowsky, Jr., J. Organomet. Chem. 70 (1974) 153.
[32] S.S. Garje, V.K. Jain, Main Group Met. Chem. 18 (1995) 387.
[33] N. Sharma, R.K. Sharma, R. Bohra, Main Group Met. Chem. 24 (2001) 781.

nol)bis(saccharinato)cobalt(II), nickel(II), copper(II) and mercury(II) complexes are also reported.

2. Experimental

2.1. Materials and instrumentation

2-Pyridylmethanol (also named 2-pyridinemethanol, 2-hydroxymethylpyridyl or 2-pyridylcarbinol), sodium saccharinate dihydrate, and all metal salts were purchased from Merck. All other analytical grade chemicals and solvents were purchased commercially and used as received.

IR spectra were recorded on a Mattson FTIR spectrophotometer as KBr pellets. Room temperature (r.t.) magnetic susceptibility measurements were carried out using a Sherwood Scientific MXI model Evans magnetic balance. The elemental analyses (C, H and N contents) were carried out at the TUBITAK Marmara Research Centre, using a Carlo Erba 1106 microanalyser. Thermal analysis curves (TG, DTA and DTG) were obtained using a Rigaku TG8110 thermal analyser in a static air atmosphere. A sample size of 5–10 mg and a heating rate of 10 °C min^{-1} were used.

2.2. Synthesis of the metal complexes

The starting metal complexes of sac, $[M(sac)_2(H_2O)_4]\cdot 2H_2O$ (M = Mn, Fe, Co, Ni, Cu, Zn, Cd and Hg), were prepared by literature methods [4,6].

$[Mn(sac)_2(mpy)_2]$ (**1**): the mpy ligand (0.218 g, 2.0 mmol) dissolved in MeOH (15 cm^3) was added dropwise to a solution of the tetraaquabis(saccharinato)manganese(II) dihydrate (0.527 g, 1 mmol) dissolved in a MeOH–isopropanol mixture (v:v, 1:1) (30 cm^3) with continuous stirring at r.t. The complex **1** precipitated as a white polycrystalline solid, which was filtered off, washed with C_3H_6O and dried in air. Yield: 80%. *Anal.* Calc. for $C_{26}H_{22}MnN_4O_8S_2$: C, 49.0; H, 3.5; N, 8.8. Found: C, 48.7; H, 3.2; N, 8.7%. Main IR features (cm^{-1}, KBr pellet): 3500–3300sbr for ν(OH); 2812w, 2933w for ν(CH); 1620vs for ν(C=O); 1286vs for $\nu_{asym}(SO_2)$; 1158vs for $\nu_{sym}(SO_2)$. $\mu_{eff} = 5.59$ BM.

The preparation of $[Fe(sac)_2(mpy)_2]$ (**2**) is analogous to that described for **1**. Yellow polycrystalline powder of **2** was obtained within 1 day. Yield: 85%. *Anal.* Calc. for $C_{26}H_{22}FeN_4O_8S_2$: C, 48.9; H, 3.5; N, 8.8. Found: C, 48.5; H, 3.2; N, 8.7%. Main IR features (cm^{-1}, KBr pellet): 3500–3100sbr for ν(OH); 2804w, 2963w for ν(CH); 1621vs for ν(C=O); 1304vs for $\nu_{asym}(SO_2)$; 1161vs for $\nu_{sym}(SO_2)$. $\mu_{eff} = 4.74$ BM.

The preparation of $[Co(sac)_2(mpy)_2]$ (**3**) is analogous to that described for **1**, but the starting tetraaquabis(saccharinato)cobalt(II) dihydrate (0.531 g, 1 mmol) was dissolved in MeOH and mixed with a solution of mpy ligand (0.218 g, 2.0 mmol) dissolved in MeOH (15 cm^3) with stirring. The resulting solution was left to stand at r.t. and allowed to evaporate slowly over a night for crystallization. Well-formed plate purple crystals of **3** were collected by suction filtration, washed with C_3H_6O and dried in air. Yield: 94%. *Anal.* Calc. for $C_{26}H_{22}CoN_4O_8S_2$: C, 48.7; H, 3.5; N, 8.7. Found: C, 48.5; H, 3.4; N, 8.3%. Main IR features (cm^{-1}, KBr pellet): 3500–3200sbr for ν(OH); 2963w, 2816w for ν(CH); 1621vs for ν(C=O); 1301vs for $\nu_{asym}(SO_2)$; 1162vs for $\nu_{sym}(SO_2)$. $\mu_{eff} = 4.52$ BM.

The preparation method used for $[Ni(sac)_2(mpy)_2]$ (**4**) was the same as that for **1**, using 0531 g (1 mmol) of tetraaquabis(saccharinato)nickel(II) dihydrate and 0.218 g (2 mmol) of mpy. Pale blue-plate crystals of compound **4** were obtained after 2 days. Yield: 94%. *Anal.* Calc. for $C_{26}H_{22}N_4NiO_8S_2$: C, 48.7; H, 3.5; N, 8.7. Found: C, 48.7; H, 3.5; N, 8.3%. Main IR features (cm^{-1}, KBr pellet): 3550–3200sbr for ν(OH); 2828w, 2963w for ν(CH); 1621vs for ν(C=O); 1301vs for $\nu_{asym}(SO_2)$; 1162vs for $\nu_{sym}(SO_2)$. $\mu_{eff} = 2.85$ BM.

Single crystals of $[Cu(sac)_2(mpy)_2]$ (**5**) were prepared by the same procedure as that used for **4**. Well-shaped blue crystals were obtained after 1 day. Yield: 93%. *Anal.* Calc. for $C_{26}H_{22}CuN_4O_8S_2$: C, 48.3; H, 3.4; N, 8.7. Found: C, 48.0; H, 3.4; N, 8.4%. Main IR features (cm^{-1}, KBr pellet): 3550–3300sbr for ν(OH); 2928w, 2806w for ν(CH); 1621vs for ν(C=O); 1307vs for $\nu_{asym}(SO_2)$; 1172vs for $\nu_{sym}(SO_2)$. $\mu_{eff} = 1.64$ BM.

$[Zn(sac)_2(mpy)_2]$ (**6**) was prepared by following an analogous procedure to that for **4** and obtained as a white polycrystalline solid. Yield: 95%. *Anal.* Calc. for $C_{26}H_{22}N_4O_8S_2Zn$: C, 48.2; H, 3.4; N, 8.6. Found: C, 48.1; H, 3.3; N, 8.4%. Main IR features (cm^{-1}, KBr pellet): 3550–3200sbr for ν(OH); 2938w, 2825w for ν(CH); 1636vs for ν(C=O); 1301vs for $\nu_{asym}(SO_2)$; 1162vs for $\nu_{sym}(SO_2)$.

Single crystals of $[Cd(sac)_2(mpy)_2]$ (**7**) is analogous to that described for **4**. The solid was collected as a polycrystalline solid. Yield: 95%. *Anal*. Calc. for $C_{26}H_{22}CdN_4O_8S_2$: C, 44.9; H, 3.2; N, 8.1. Found: C, 45.0; H, 3.3; N, 7.8%. Main IR features (cm^{-1}, KBr pellet): 3400–3200sbr for ν(OH); 2900w, 2962w for ν(CH); 1626vs for ν(C=O); 1256vs for $\nu_{asym}(SO_2)$; 1151vs for $\nu_{sym}(SO_2)$.

Single crystals of $[Hg(sac)_4(mpy)_2]$ (**8**) were prepared by the same procedure as that used for **4**. Colourless crystals of **8** were obtained after 2 days. Yield: 90%. *Anal.* Calc. for $C_{20}H_{15}HgN_3O_7S_2$: C, 35.5; H, 2.2; N, 6.2. Found: C, 35.5; H, 2.3; N, 6.2%. Main IR features (cm^{-1}, KBr pellet): 3500–3200sbr for ν(OH); 2825w, 2962w for ν(CH); 1635vs for ν(C=O); 1254vs for $\nu_{asym}(SO_2)$; 1152vs for $\nu_{sym}(SO_2)$.

2.3. X-ray crystallography

Suitable crystals of the complexes **3**, **4**, **5** and **8** were glued to a thin glass fibre and mounted on a BRUKER SMART 1000 CCD area detector diffractometer with Mo Kα radiation, $\lambda = 0.71073$ Å. The intensity data were collected at $T = 298 \pm 2$ K and processed with the aid of the SMART, SAINT and SADABS software packages [13]. Absorption corrections were made with SADABS [13]. The structures were solved by direct methods using SIR-97 [14] and refined by a full-matrix least-squares procedure (SHELXL-97) [15]. Molecular drawings were obtained using ORTEP-III [16]. Hydroxyl hydrogen atoms of the complexes **3** and **5** were found in difference maps and refined with geometric restraints [d(O–H) = 0.82 Å)]. All hydrogen atoms of the complexes **4** and **8**, and other H atoms of the phases **3** and **5** were positioned geometrically and refined by riding on their appropriate carbon atoms [d(O–H) = 0.82 Å for the hydroxyl hydrogens and d(C–H) = 0.93 and 0.96 Å for phenyl and methylene hydrogens, respectively]. The details of data collection, refinement and crystallographic data are summarized in Table 1.

3. Results and discussion

3.1. Synthesis

The aim of the work is to prepare new mixed-ligand sac complexes with mpy as a co-ligand, since the mpy ligand offers two different donor atoms to metal centres, namely N and O (hydroxyl). For the synthesis of mixed-ligand metal complexes of sac it became a common practice to apply $[M(sac)_2(H_2O)_4]\cdot 2H_2O$ as synthetic precursors, since the aqua ligands in these metal

Table 1
Crystallographic data and structure refinement details

Complex	**3**	**4**	**5**	**8**
Empirical formula	$C_{26}H_{22}N_4O_8S_2$ Co	$C_{26}H_{22}N_4O_8S_2$ Ni	$C_{26}H_{22}N_4O_8S_2$ Cu	$C_{20}H_{15}N_3O_7S_2Hg$
Formula weight	641.53	641.31	646.14	674.06
Crystal colour, habit	purple, plate	pale blue, plate	blue, block	colourless, chunk
T (K)	298(2)	298(2)	298(2)	298(2)
λ (Å)	0.71073	0.71073	0.71073	0.71073
Crystal system	triclinic	triclinic	orthorhombic	monoclinic
Space group	$P\bar{1}$	$P\bar{1}$	$Pbca$	$P2_1/n$
a (Å)	9.0206(4)	9.0813(9)	9.0428(4)	9.9704(5)
b (Å)	11.1512(5)	11.184(1)	14.2792(6)	11.1978(5)
c (Å)	13.5082(6)	13.634(1)	21.5289(8)	19.9430(9)
α (°)	99.250(1)	98.909(2)	90	90
β (°)	95.131(1)	95.144(2)	90	92.220(1)
γ (°)	95.803(1)	95.906(2)	90	90
V (Å^3)	1326.5(1)	1352.9(2)	2779.9(2)	2224.90(18)
Z	2	2	4	4
D_{calcd} (g cm^{-3})	1.606	1.574	1.544	2.012
F_{000}	658	660	1324	1296
μ (mm^{-1})	0.863	0.929	0.992	7.154
θ Range (°)	1.86–30.04	2.27–27.72	2.83–30.02	2.08–30.05
Crystal dimensions (mm)	0.13 × 0.40 × 0.42	0.02 × 0.16 × 0.27	0.20 × 0.20 × 0.46	0.20 × 0.22 × 0.35
Index ranges	$-12 \le h \le 8$; $-15 \le k \le +15$; $-19 \le l \le +19$	$-11 \le h \le +11$; $-14 \le k \le 13$; $-17 \le l \le 13$	$-10 \le h \le 12$; $-18 \le k \le 20$; $-30 \le l \le +30$	$-14 \le h \le 13$; $-15 \le k \le 13$; $-25 \le l \le 28$
Reflections collected	13 889	8640	22 132	20 934
Independent reflections (R_{int})	7592, 0.020	4935, 0.082	4057, 0.034	6500, 0.0283
Independent reflections with [$I > 2\sigma(I)$]	5665	2417	2829	5083
Min/max transmission	0.703, 0.894	0.837, 0.982	0.788, 0.820	0.165, 0.239
Data/restraints/parameters	7592/2/376	4935/0/370	4057/1/190	6500/0/298
Goodness-of-fit	0.965	0.925	0.963	0.910
R (F)	0.0341	0.0843	0.0327	0.0217
wR (F)	0.0827	0.1892	0.0777	0.0417
Largest difference peak and hole (e Å^{-3})	−0.279, +0.365	−1.169, +1.284	−0.385, +0.370	−0.785, −1.178

complexes are labile and readily displaced by neutral ligands. The new complexes were simply prepared by the direct reaction of mpy with the respective tetraaquabis(saccharinato)M(II) dihydrate in solution. The addition of the mpy ligand to the solutions of the aqua complexes resulted in the substitution of all the four aqua ligands, and the formation of the air-stable complexes of $[M(sac)_2(mpy)_2]$ where M is manganese(II), iron(II), cobalt(II), nickel(II), copper(II), zinc(II), cadmium(II). The complexes **1**, **2**, **6** and **7** were precipitated as polycrystalline solids, while all the other complexes were crystallized from the reaction solutions. All the complexes, except **8** complex are monomeric with a M:mpy molar ratio of 1:2 and show an octahedral coordination geometry around the metal ions, whereas the complex **8** is a coordination polymer. All the complexes do not exhibit melting points, but decompose at the temperatures given in Table 5. All the complexes were obtained in good yields (over 80%) and the analytical data are consistent with the proposed formulation of the complexes, and also confirmed by X-ray crystallography as reported in this paper. All the complexes are soluble in methanol and DMSO, and all the complexes, except the mercury(II) complex are also soluble in warm water and ethanol.

3.2. Spectral and magnetic properties

The most significant frequencies in the IR spectra of the metal complexes are given in Table 3. The IR spectra of all the complexes are resemble each other indicating a similar structural relationship. The strong and broad absorption bands in the range 3200–3500 cm^{-1} are attributed to the ν(OH) vibrations of mpy. The relatively weak two close bands at 2800–2900 cm^{-1} are due to the ν(CH) vibrations. The stretching vibration of C=N of the py ring at approximately 1600 cm^{-1} was not clearly observed because of the overlap of the ν(C=O) vibration of the sac ions. However, the N-coordination of the mpy ligand is confirmed by the absorption bands at around 680 cm^{-1} due to γ(py) [17]. The bands for the carbonyl group appear characteristically at approximately 1620 cm^{-1} as very strong bands for all complexes, while the stretching vibrations of $\nu_{asym.}(SO_2)$ and $\nu_{sym.}(SO_2)$ occur at approximately 1300 and 1160 cm^{-1}, respectively. The asymmetric stretching vibrations of the sulfonyl group in the IR spectra of **8** significantly shift to the low frequency region due to involving in coordination with mercury(II) ion. Furthermore, the carbonyl vibration frequencies of the carbonyl O-bonded sac ligands in the corresponding sac complexes with mpy shifted to the low frequency region by 10–55 cm^{-1} compared to the starting complexes with only N-bonded sac ligands, indicating the coordination of the carbonyl group of sac. The shift value for the copper(II) complex was zero. Additional peaks at approximately 1360 and 960 cm^{-1} may be assigned to the symmetric and asymmetric stretchings of the CNS moiety of the sac ligands, respectively as proposed previously [8,9]. The medium peaks at around 1555 and 1450 cm^{-1} correspond to the ring ν(C–C) vibrations. The weak bands below 500 cm^{-1} may be attributed to both M–N and M–O vibrations.

The room temperature magnetic moments indicate that the metal complexes exhibit high-spin configuration. The effective magnetic moments are consistent with the calculated values of the spin-only magnetic moments of the octahedral coordination geometry around the metal ions.

3.3. Description of the crystal structures

3.3.1. $[M(sac)_2(mpy)_2]$ ($M = Co$ (**3**) and Ni (**4**))

Compounds **3** and **4** are isomorphous and crystallize in the triclinic space group $P\bar{1}$. Molecular structures of the both complexes are given in Figs. 1 and 2, while the selected geometrical data and hydrogen bonding geometry are presented in Table 2. The crystal structures consist of neutral molecules of $[M(sac)_2(mpy)_2]$. Each metal ion is octahedrally coordinated by two mpy and two sac ligands forming a MN_3O_3 core. The mpy ligand acts as a bidentate donor through the amine nitrogen and the methanol oxygen atoms forming a five-membered chelate ring. The nitrogen atoms of the two mpy ligands are placed at *trans* positions, while the hydroxyl oxygen atoms occupy the *cis* positions of the coordination octahedron in **3** and **4**.

Sac usually interacts with transition metal ions through its deprotonated nitrogen atom, whereas O-bonding occurs in the case of alkaline, alkaline earth and p-block metals [20–23]. The coordination of sac to the transition metal ions using the donor groups other than the amine nitrogen atom is unusual and the only examples of O-coordination reported previously in mononuclear complexes are in $[V(sac)_2(py)_4]\cdot 2py$ [6], $[Ni(sac)_2(py)_4]\cdot 2py$ [9], $[Cu(sac)_2(dipyr)_2]$ [24] (py and dipyr are pyridine and dipyridylamine, respectively), $[Cu(sac)(PPh_3)_2]$ [25] and $[Cu(sac)(PPh_3)]_2$ [25] as reported recently. Therefore, the most interesting aspect of the complexes **3** and **4** is the coordination of the sac ligands, which occur in two distinct manners. Both sac ligands behaves as an ambidentate ligand: one of them is N-bonded, while the other one is O-coordinated. The $Ni–O_{sac}$ bond distance of 2.066(6) is significantly longer than 2.070(3) Å found in $[Ni(sac)_2(py)_4]\cdot 2Py$ [9]. Large distortions in the coordination polyhedra from ideal octahedral geometry are also clearly evident from the N–M–N, N–M–O and O–M–O interbond angles. The *cis* and *trans* angles, respectively, range from 76.96(5) to 101.87(5)° and 158.43(5)° to 175.10(5)° in the compound **3**, and 79.3(2)° to 98.5(3)° and 163.2(2)° to 175.9(2)° in

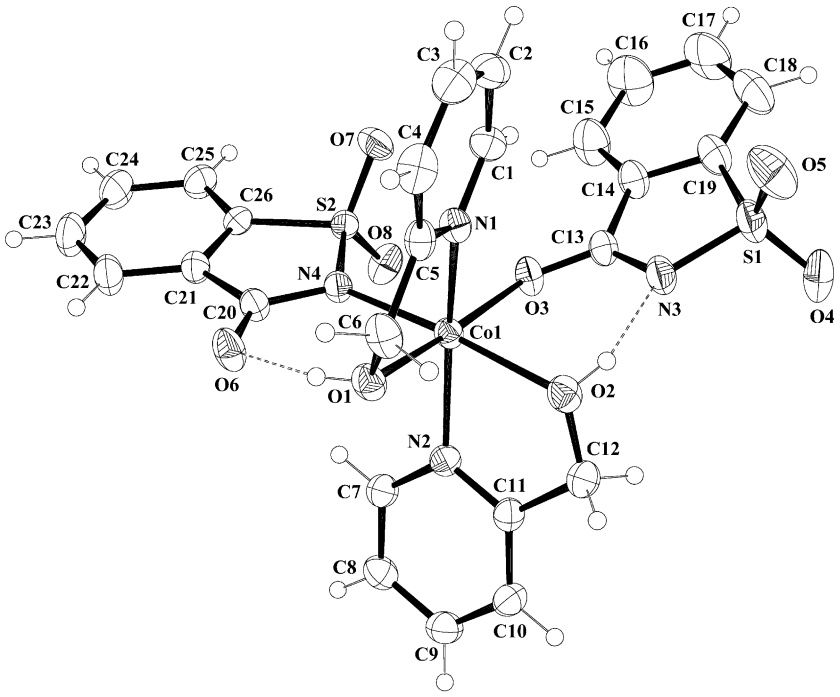


Fig. 1. Molecular structure of **3** showing the atom numbering scheme (40% thermal ellipsoids).

Table 2
Selected bond lengths (Å), angles (°) and hydrogen bond geometrical data in $[Co(sac)_2(mpy)_2]$ (**3**), $[Ni(sac)_2(mpy)_2]$ (**4**) [a]

	3	**4**		**3**	**4**
Bond lengths					
M(1)–N(1)	2.1338(14)	2.114(7)	M(1)–N(2)	2.1058(14)	2.064(6)
M(1)–N(4)	2.1441(14)	2.131(5)	M(1)–O(1)	2.1356(12)	2.077(6)
M(1)–O(2)	2.1813(13)	2.127(5)	M(1)–O(3)	2.0640(11)	2.066(6)
Bond angles					
N(1)–M(1)–O(1)	76.96(5)	79.8(2)	N(1)–M(1)–O(2)	89.24(5)	89.8(2)
N(1)–M(1)–N(4)	95.43(5)	94.2(2)	N(2)–M(1)–O(1)	85.85(5)	86.8(2)
N(2)–M(1)–N(4)	98.03(5)	96.6(2)	N(2)–M(1)–O(2)	77.07(5)	79.3(2)
N(2)–M(1)–N(1)	158.43(5)	163.2(2)	N(4)–M(1)–O(2)	175.10(5)	175.9(2)
O(1)–M(1)–O(2)	87.89(5)	87.0(2)	O(1)–M(1)–N(4)	91.70(5)	92.8(2)
O(3)–M(1)–N(1)	94.31(5)	94.1(2)	O(3)–M(1)–N(2)	101.87(5)	98.5(3)
O(3)–M(1)–N(4)	92.37(5)	90.9(2)	O(3)–M(1)–O(1)	170.68(5)	173.1(2)
O(3)–M(1)–O(2)	88.76(5)	89.6(2)			
D–H···A	D–H (Å)	H···A (Å)	D···A (Å)	<DHA (°)	
3					
O(1)–H(1)···O(6)	0.81(2)	1.82(2)	2.585(2)	156(2)	
O(2)–H(2)···N(3)	0.79(2)	1.94(2)	2.653(2)	151(2)	
C(3)–H(3)···O(2)^{i}	0.93	2.59	3.313(2)	135	
C(8)–H(8)···O(4)^{ii}	0.93	2.42	3.277(2)	153	
C(9)–H(9)···O(8)^{iii}	0.93	2.47	3.157(2)	131	
C(25)–H(25)···O(1)^{iv}	0.93	2.60	3.247(2)	127	
4					
O(1)–H(1)···O(6)	0.82	1.83	2.595(7)	155	
O(2)–H(2)···N(3)	0.82	1.92	2.658(9)	149	
C(3)–H(3)···(O2)^{i}	0.93	2.65	3.355(10)	133	
C(8)–H(8)···O(4)^{ii}	0.93	2.43	3.294(9)	155	
C(9)–H(9)···O(8)^{iii}	0.93	2.50	3.194(10)	131	
C(25)–CH(25)···O(1)^{iv}	0.93	2.62	3.267(9)	127	

[a] Symmetry code: (i) $1-x, -y, -z$; (ii) $x, 1+y, z$; (iii) $1-x, 1-y, 1-z$; (iv) $-1+x, y, z$.

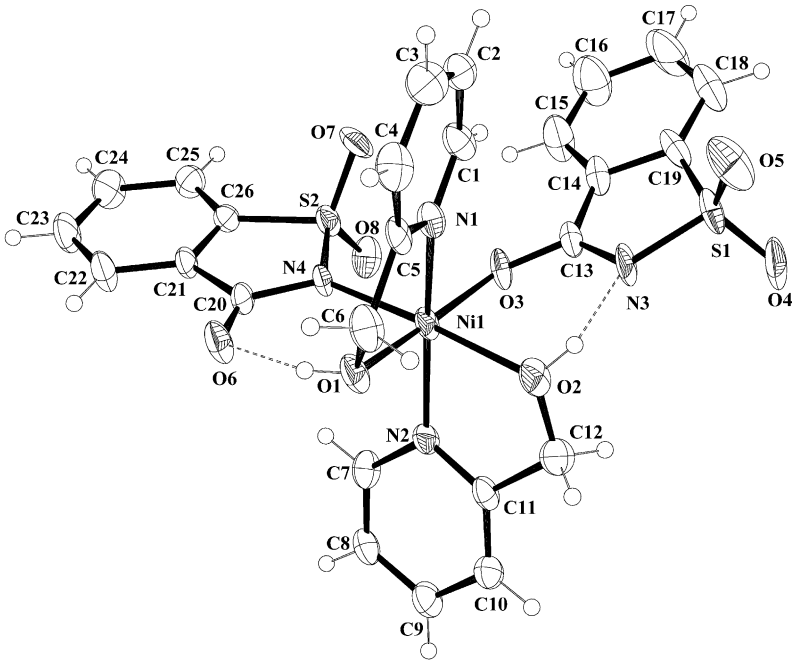


Fig. 2. Molecular structure of **4** showing the atom numbering scheme (40% thermal ellipsoids).

the compound **4**. As a result, these complexes may be regarded as having a distorted octahedral structure.

The sac ligands present in the two complexes are essentially planar with an r.m.s. deviation of approximately 0.02 Å. The py rings of the mpy ligands are also planar and both hydroxyl O and methylene C atoms slightly deviate from the py planes by approximately 0.14(4) Å in the compounds **3** and **4**. The mpy ligands in **3** and **4** are almost perpendicular to each other with the dihedral angles of 82.32(5)° and 79.9(2)°, respectively. The hydrogen atoms of the hydroxyl groups of the mpy ligands form strong intramolecular hydrogen bonds with the carbonyl O and the negatively charged N atoms of the sac ligands (Table 2). The methylene and phenyl hydrogen atoms are involved in weak intermolecular C–H···O interactions with the hydroxyl and sulfonyl O atoms in **3** and **4**. The molecules are held together by the weak hydrogen bonds and van der Waals' interactions by forming a 3D lattice.

3.3.2. *[Cu(sac)$_2$(mpy)$_2$] (**5**)*

The compound **5** crystallizes in orthorhombic system with a space group of *Pbca*. Table 3 presents selected distances and angles about the metal centre together with the hydrogen bonding geometry, while the molecular view of **5** is shown in Fig. 3. The copper(II) ion lies on a centre of symmetry and is coordinated by two neutral mpy and two anionic sac ligands. The sac ligands occupy the *trans* positions, while the two bidentate mpy ligands form the equatorial plane of the coordination octahedron around the copper(II) ion. The Cu–N_{mpy} and Cu–O_{mpy} bond distances are 1.9667(13) and 2.1394(13) Å, respectively and similar to the corresponding values found in [Cu(sal)$_2$(mpy)$_2$] [26] where sal is salicylate. In contrast to complexes **3** and **4**, both sac ligands in **5** are N-coordinated. The Cu–N_{sac} bond distance of 2.3345(15) Å is significantly longer than those reported for [Cu(sac)$_2$(H$_2$O)(py)$_2$] [19], [Cu(sac)$_2$(dipyr)$_2$]·0.5H$_2$O [24], [Cu(sac)$_2$(dea)$_2$] [27], [Cu$_2$(μ-dea)$_2$(sac)$_2$] [28], [Cu(sal)$_2$(NH$_3$)$_4$] [29] and [Cu$_2$(μ-tea)$_2$(sac)$_2$]·2CH$_3$OH [30] (dea and tea = di- and triethanolamine, respectively). The larger deviations from regular octahedral geometry for the complex **5** are characteristic of the Jahn–Teller effect. The Cu–N_{sac} bonds occupying the axial positions are much longer than the Cu–N_{mpy} and Cu–O_{mpy} bonds forming the

Table 3
Selected bond lengths (Å), angles (°) and hydrogen bond geometrical data in [Cu(sac)$_2$(mpy)$_2$] (**5**) [a]

Bond lengths				
Cu(1)–N(1)	1.9667(13)			
Cu(1)–N(2)	2.3345(15)			
Cu(1)–O(1)	2.1394(13)			
Bond angles				
N(1)–Cu(1)–O(1)	80.66(5)			
N(2)–Cu(1)–O(1)	92.65(5)			
N(2)–Cu(1)–N(1)	88.86(5)			
D–H···A	D–H (Å)	H···A (Å)	D···A (Å)	<DHA (°)
O(1)–H(1)···O(2)	0.79(2)	1.82(2)	2.592(2)	167(3)
C(1)–H(1)···O(4)^{i}	0.93	2.38	3.205(2)	148
C(12)–H(12)···O(2)^{ii}	0.93	2.47	3.326(2)	153

[a] Symmetry code: (i) $x-1/2$, $1/2-y$, $1-z$; (ii) $3/2-x$, $1/2+y$, z.

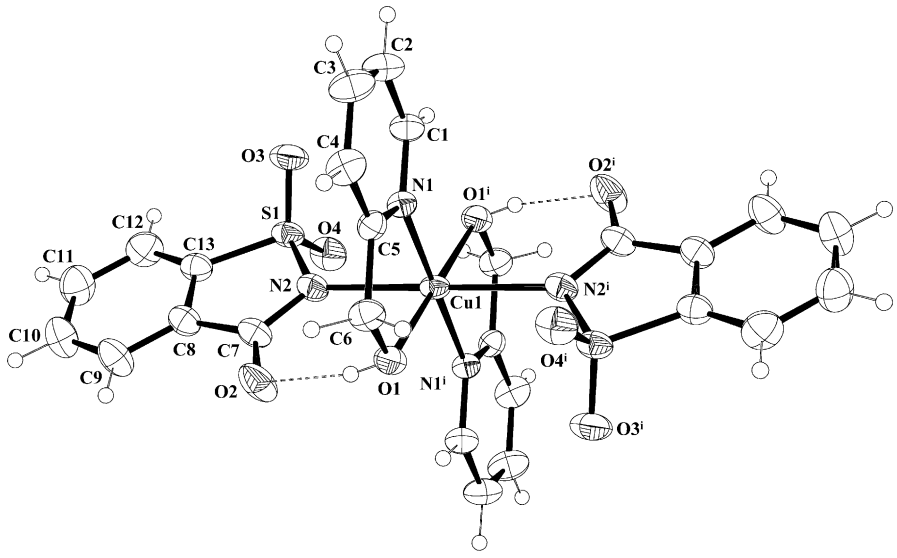


Fig. 3. Molecular structure of **5** showing the atom numbering scheme (40% thermal ellipsoids), (i) = $1-x, -y, 1-z$.

Table 4
Selected bond lengths (Å), angles (°) and hydrogen bond geometrical data in $[Hg_2(sac)_4(mpy)_2]$ (**8**) [a]

Bond lengths				
Hg(1)–N(1)	2.475(2)	Hg(1)–N(2)	2.106(2)	
Hg(1)–N(3)	2.094(2)	Hg(1)–O(1)	2.655(2)	
Hg(1)–O(1)^{i}	2.757(2)	Hg(1)–O(4)^{ii}	2.767(2)	
Bond angles				
N(1)–Hg(1)–O(1)	64.38(7)	N(1)–Hg(1)–O(1)^{i}	132.09(6)	
N(2)–Hg(1)–O(1)	94.95(7)	N(1)–Hg(1)–O(4)^{ii}	102.24(8)	
N(2)–Hg(1)–O(1)^{i}	85.07(7)	N(2)–Hg(1)–O(4)^{ii}	88.91(7)	
N(3)–Hg(1)–O(1)	98.55(7)	N(3)–Hg(1)–O(1a)^{i}	89.22(7)	
N(3)–Hg(1)–O(4)^{ii}	80.65(7)	N(1)–Hg(1)–N(2)	101.13(8)	
N(1)–Hg(1)–N3	95.27(8)	N(2)–Hg(1)–N(3)	162.12(8)	
O(1)–Hg(1)–O(1)^{i}	67.78(7)	O(1)–Hg(1)–O(4)^{ii}	166.54(7)	
O(1)–Hg(1)–O(4)^{i}	125.49(7)			
D–H···A	D–H (Å)	H···A (Å)	D···A (Å)	<DHA (°)
O(1)···H(1)···O(2)	0.82	1.87	2.688(3)	172
C(1)–H(1)···O(3)^{ii}	0.93	2.57	3.487(4)	171
C(3)–H(3)···O(6)^{iii}	0.93	2.39	3.124(4)	136
C(16)–H(16)···O(7)^{iv}	0.93	2.54	3.368(4)	149

[a] Symmetry code: (i) $1-x, -y, -z$; (ii) $-x, -y, -z$; (iii) $1-x, 1-y, -z$; (iv) $1/2-x, -1/2+y, 1/2-z$.

equatorial plane of the CuN_4O_2 chromophore, resulting in an usual elongated tetragonal octahedron around the copper(II) ion. The *cis* bond angles in the complex **5** are in the range 80.66(5)°–92.65(5)°. The individual molecules of **5** are connected by the strong O–H···$O_{carbonyl}$ and weak C–H···$O_{carbonyl\ and\ sulfonyl}$ hydrogen bonds, which stabilize the crystal structure creating a 3D network.

3.3.3. $[Hg_2(sac)_4(mpy)_2]$ (**8**)

The coordination around the mercury atom and a fragment of the polymeric structure of this complex together with the atom-numbering scheme is shown in Fig. 4, while selected bond distances and angles are tabulated in Table 4. The structure consists mainly of the dimeric $[Hg_2(sac)_4(mpy)_2]$ units in which the mercury atoms have a HgN_3O_2 environment by three nitrogen atoms, two from the sac ligands and the other from the mpy ligand, and two oxygen atoms of the neutral mpy ligands. Two methanol oxygen atoms of two mpy ligands bridge two mercury atoms and each methanol oxygen atom serves as a bifurcate bridge between the mercury centers. The dimeric units are sequentially linked by the sulfonyl oxygens of the sac ligands of the adjacent units forming a 1D polymeric chain as shown in Fig. 4. Consequently, the mercury atoms in the coordination polymer are six-coordinate. The most significant difference between the other structures reported in this paper is the bidentate coordination behavior of the sac ligands in **8**.

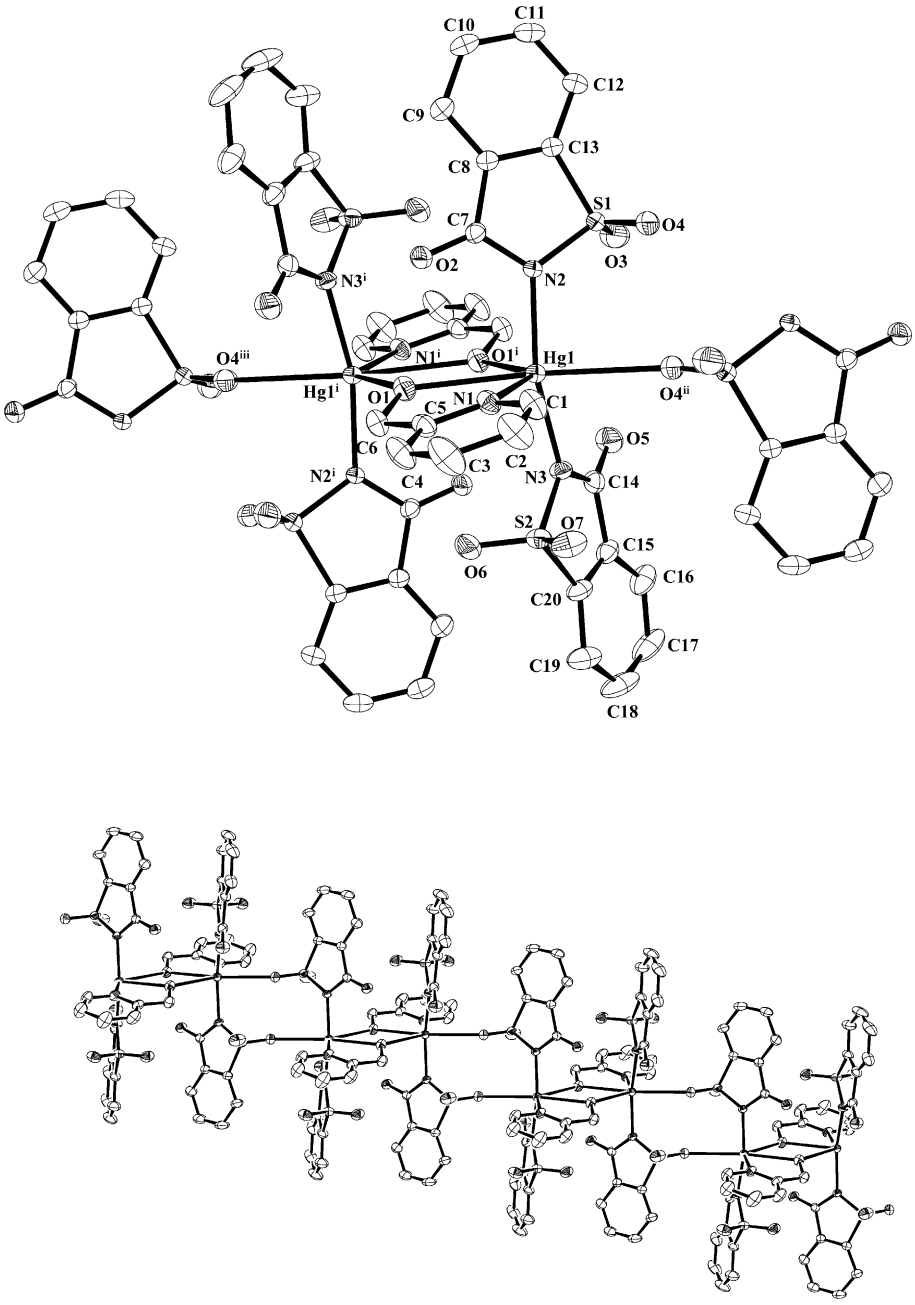


Fig. 4. Coordinartion environment of the mercury atom (30% thermal ellipsoids) and a view of a fragment of the chain in **8**. Hydrogen atoms were omitted for clarity.

The Hg···Hg separation is 4.4927(3) Å. The –Hg–O–Hg–O– bridging group is planar and the bridging angles Hg–O1–Hg(a) and O1–Hg–O1(a) are 112.21(7)° and 67.78(6)°, respectively. Both sac and mpy ligands are essentially planar and dihedral angles between the best planes of sac and mpy ligands are 76.32(6)° and 88.88(7)°. The hydroxyl oxygen atom (O(1)) of the bridging mpy ligand form a very strong intramolecular hydrogen bond with the carbonyl oxygen atom (O(2)) of the sac ligand. The polymeric chains are held together by weak C–H···$O_{sulfonyl}$ interactions. Additionally, some of the phenyl hydrogens (C(9)–H(9) and C(10)–H(10)) of the sac ligands are involved in H···π type interactions with the aromatic rings of the sac and mpy ligands, respectively.

3.4. Thermal analysis

Thermoanalytical data (decomposition stages, temperature ranges, peak maxima and mass losses) for the metal complexes are summarised in Table 5. From the thermal decomposition behaviour of the complexes in the air atmosphere the following general features can be recognized:

Table 5
Thermoanalytical data for the metal complexes

Complex	Stage	Temperature range (°C)	DTG_{max} (°C) [a]	Mass loss (%) [b]	Solid residue
1	1	178–360	204(−), 250(+)	33.7 (34.1)	$[Mn(sac)_2]$
	2	395–775	413(+), 532(−), 546(−)	57.3 (57.2)	MnO
2	1	178–358	203(−)	34.0 (34.1)	$[Fe(sac)_2]$
	2	358–521	497(−)	57.5 (57.2)	FeO
3	1	195–336	262(+)	33.5 (33.9)	$[Co(sac)_2]$
	2		400(+), 543(−)	56.5 (56.9)	CoO
4	1	215–283	265(+)	34.5 (33.9)	$[Ni(sac)_2]$
	2	273–661	417(−), 443(−), 472(−)	55.8 (57.0)	NiO
5	1	168–284	200(+), 278(+)	34.1 (33.7)	$[Cu(sac)_2]$
	2	284–754	420(+), 454(−), 474(−)	55.7 (56.5)	CuO
6	1	148–389	217(+), 247(+)	32.6 (33.6)	$[Zn(sac)_2]$
	2	389–632	412(+), 563(−)	55.6 (56.4)	ZnO
7	1	167–308	213(+), 250(+), 298(+)	31.5 (31.3)	$[Cd(sac)_2]$
	2	348–585	397(+), 573(−)	52.5 (52.6)	CdO
8	1	168–220	200(+)	16.6 (16.2)	$[Hg(sac)_2]$
	2	220–550	273(+), 508(−)	– [c]	– [c]

[a] (+) and (−) donate endothermic and exothermic processes, respectively.
[b] Required values are given in parentheses.
[c] Sublimation above 550 °C.

The complexes exhibit a continuous mass loss in the temperature range 160–715 °C. The low initial decomposition temperatures of the complexes suggest that they are monomeric species. The first decomposition stages correspond to the elimination of the two mpy ligands. This stage are observed as a single peak in the DTA and DTG curves of **2**–**4** and **8**, while **1** and **5**–**7** lose their mpy ligands in two steps, which are associated with the degradation of the mpy ligand. A similar behaviour was observed for the metal complexes of sac with ligands containing ethanol groups [18]. The experimental mass losses are in agreement with the calculated values (Table 5). The removal of the mpy ligand results in the formation of the respective metal saccharinates as stable intermediates, which were identified by the characteristic IR absorption bands of the sac ligand. The metal saccharinates decompose exothermically at higher temperatures to give the corresponding metal oxides, similar to the tetraaquabis(saccharinato)M(II) complexes [19], although the Hg(II) complex sublimes at approximately 550 °C leaving an empty crucible.

4. Conclusions

The results in this paper clearly show that the sac ligand exhibits different modes of coordination in the presence of mpy. Although the conditions for the synthesis and crystallization of the metal complexes are almost the same, the reasons for the occurrence of the different coordination modes are not readily understandable and need further research. However, it may be suggested that some factors such as the electron density or steric effects of the ligands, intermolecular forces and the most favourable crystallization kinetics may determine the coordination type of sac.

5. Supplementary data

Crystallographic data for the structures reported in the paper have been deposited with the Cambridge Crystallographic Data Centre, CCDC nos. 174133, 174134, 174135, 183285 for complexes **3**, **4**, **5** and **8**. Copies of the data can be obtained free of charge from The Director, CCDC, 12 Union Road, Cambridge, CB2 1EZ, UK (fax: +44-1233-336-033; e-mail: deposit@ccdc.cam.ac.uk or www: http://www.ccdc.cam.ac.uk).

Acknowledgements

The authors are thankful to Ondokuz Mayis University for the financial support given to the research project (F-242).

References

[1] D.J. Ager, D.P. Pantaleone, S.A. Henderson, A.L. Katritzky, I. Prakash, D.E. Walters, Angew. Chem., Int. Ed. Engl. 37 (1998) 1802.
[2] K.J. Ahmed, A. Habib, S.Z. Haider, K.M.A. Malik, M.B. Hursthouse, Inorg. Chim. Acta 56 (1981) L37.
[3] Z. Haider, K.M.A. Malik, K.J. Ahmed, H. Hess, H. Riffel, M.B. Hursthouse, Inorg. Chim. Acta 72 (1983) 21.
[4] Z. Haider, K.M.A. Malik, K.J. Ahmed, Inorg. Synth. 23 (1985) 47.

[5] F.A. Cotton, G.E. Lewis, C.A. Murillo, W. Schwotzer, G. Valle, Inorg. Chem. 23 (1984) 4038.
[6] F.A. Cotton, L.R. Falvello, R. Llusar, E. Libby, C.A. Murillo, W. Schwotzer, Inorg. Chem. 25 (1986) 3423.
[7] F.A. Cotton, E. Libby, C.A. Murillo, G. Valle, Inorg. Synth. 27 (1990) 306.
[8] O.V. Quinzani, S. Tarulli, O.E. Piro, E.J. Baran, E.E. Castellano, Z. Naturforsch., Teil B 52 (1997) 183.
[9] O.V. Quinzani, S. Tarulli, C. Marcos, S.G. Granda, E.J. Baran, Z. Anorg. Allg. Chem. 625 (1999) 1848.
[10] G. Jovanovski, P. Naumov, O. Grupce, B. Kaitner, Eur. J. Solid State Inorg. Chem. 35 (1998) 231.
[11] G. Jovanovski, P. Naumov, O. Grupce, Eur. J. Solid State Inorg. Chem. 35 (1998) 579.
[12] P. Naumov, G. Jovanovski, O. Grupce, J. Mol. Struct. 483 (1999) 121.
[13] Software for SMART diffractometers, Bruker Inc. Madison, WI, USA, 1999.
[14] A. Altomare, M.C. Burla, M. Camalli, G.L. Cascarano, C. Giacovazzo, A. Guagliardi, A.G.G. Moliterni, G. Polidori, R. Spagna, J. Appl. Crystallogr. 32 (1999) 115.
[15] G.M. Sheldrick, SHELXL-97, Program for the Refinement of Crystal Structures, University of Göttingen, Germany, 1997.
[16] L.J.J. Farrugia, Appl. Cryst. 30 (1997) 565.
[17] K. Nakamoto, Infrared and Raman Spectra of Inorganic and Coordination Compounds, Part B, 5th ed., Wiley, New York, 1997, p. 23.
[18] V.T. Yilmaz, Y. Topcu, A. Karadag, Thermochim. Acta 383 (2002) 129.
[19] H. Icbudak, V.T. Yilmaz, H. Olmez, J. Thermal. Anal. 53 (1998) 843.
[20] C. Nather, T. Hauck, H. Bock, Acta Crystallogr., Sect. C 53 (1997) 1244.
[21] G. Jovanovski, A. Hergold-Brundic, O. Grupce, D. Matkovic-Calogovic, J. Chem. Crystallogr. 29 (1999) 233.
[22] E.J. Baran, C.C. Wagner, M. Rossi, F. Caruso, Z. Anorg. Allg. Chem. 626 (2000) 701.
[23] E.J. Baran, C.C. Wagner, M. Rossi, F. Caruso, Z. Anorg. Allg. Chem. 627 (2001) 85.
[24] R.M.K. Deng, K.B. Dillon, A.E. Goeta, M. Mapolelo, Inorg. Chim. Acta 315 (2001) 245.
[25] L.R. Falvello, J. Gomez, I. Pascual, M. Thomas, E.P. Urriolabeitia, A.J. Schultz, Inorg. Chem. 40 (2001) 4455.
[26] N.N. Hoang, F. Valach, M. Dunaj-Jurco, M. Melnik, Acta Crystallogr., Sect. C 48 (1992) 443.
[27] V.T. Yilmaz, O. Andac, Y. Topcu, W.T.A. Harrison, Acta Crystallogr., Sect. C 57 (2001) 271.
[28] V.T. Yilmaz, Y. Topcu, F. Yilmaz, C. Thoene, Polyhedron 20 (2001) 3209.
[29] I. Pascual, Acta Crystallogr., Sect. C 51 (1995) 2028.
[30] Y. Topcu, O. Andac, V.T. Yilmaz, W.T.A. Harrison, J. Coord. Chem. 55 (2002) 805.

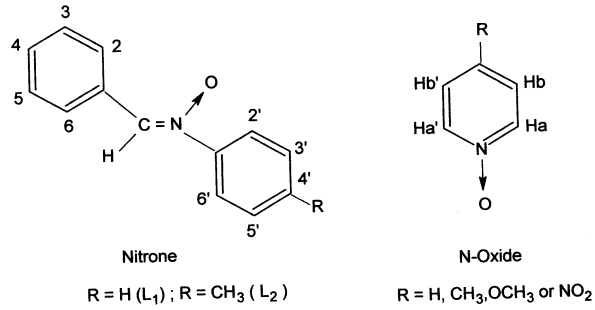


Fig. 1. A view of the ligands nitrone and N-oxide.

were prepared in similar fashion and the pertinent data is given in Table 1.

2.2. Synthesis of $[UO_2(TTA)_2 \cdot p\text{-}NO_2\text{–}C_5H_4NO]$

This compound was synthesized according to the reported method [4a] and the crystals suitable for X-ray analyses were obtained from $CHCl_3$–$C_6H_5CH_3$ mixture.

2.3. Physical methods

^{1}H NMR spectra of free ligands and compounds were recorded in Varian-300 NMR instrument operating at 300 MHz. The chemical shifts are relative to the internal $CHCl_3$ peak (7.21 ppm).

2.4. X-ray crystallography

The X-ray diffraction data for the compound $[UO_2(TTA)_2 \cdot p\text{-}NO_2\text{–}C_5H_4NO]$ was collected on a Siemens SMART CCD diffractometer fitted with graphite monochromated Mo Kα radiation ($\lambda = 0.71073$ Å) at 213(2) K with a detector distance of 4 cm and swing angle of $-35°$. A hemisphere of reciprocal space covered by a combination of three sets of exposures; each set had a different ϕ angle (0°, 88°, 180°) and each exposure of 30 s covered 0.3° in ω. Data collection, indexing and initial cell refinement were handled using SMART software [6a]. Frame integration and final cell refinement were carried out using SAINT software [6b]. The SADABS software [6c] package was used to perform the absorption corrections. The atomic scattering factors are from the International Tables for Crystallography [6d]. The summary of crystallographic data, structural parameters and refinement details is given in Table 2.

Table 2
Crystal and structure refinement details for compounds $[UO_2(TTA)_2 \cdot p\text{-}NO_2\text{–}C_5H_4NO]$

Empirical formula	$C_{21}H_{12}F_6O_9N_2S_2U$
Formula weight	852.48
Temperature (K)	213(2)
Wavelength (Mo Kα) (Å)	0.71073
Crystal system	monoclinic
Space group	$P2_1/c$
a (Å)	15.1900(3)
b (Å)	10.7420(2)
c (Å)	16.4285(1)
β (°)	95.386 (1)
V (Å^3)	2668.82(7)
Z (formula unit)	4
D_{calc} (g cm^{-3})	2.122
μ(Mo Kα) (m^{-1})	6.333
$F(000)$	1608
θ Range for data collection (°)	2.6–28.3
Total reflections collected	15 594
Unique reflections	6286 [$R_{int} = 0.095$]
Absorption correction	empirical
Max./min. transmission	0.3117 and 0.2089
Refinement method	full-matrix least-square on F^2
Data/restraints/parameters	6286/0/372
Final R indices [$I > 2\sigma(I)$]	$R_1 = 0.0434$, $wR_2 = 0.1088$
R indices (all data)	$R_1 = 0.0633$, $wR_2 = 0.1147$
Goodness-of-fit on F^2	0.94
Largest difference peak and hole (e Å^{-3})	1.58, −1.91

$W = 1/[\sigma^2(F_o^2) + (0.0330P)^2]$; $P = (F_o^2 + 2F_c^2)/3$.

2.5. Solution and refinement of the structure

The structure was solved by direct methods, completed by subsequent difference Fourier syntheses and refined by full-matrix least-squares procedures on F^2 using SHELXTL [7] version 5.1. The non-hydrogen atoms were refined anisotropically. The hydrogen atoms were refined with geometrical constraints with ideal bond lengths and angles were treated as riding atoms. All

Table 1
Analytical data for the compounds $[UO_2(OO)_2 \cdot L]$

Complexes	M.p (°C)	Solvents of crystallization	Analysis (%) Found/(Calc.)		
			C	H	N
$[UO_2(TTA)_2 \cdot L_1]$	160	benzene/dodecane	38.0 (38.3)	2.2 (2.1)	1.6 (1.5)
$[UO_2(TTA)_2 \cdot L_2]$	190	benzene/dodecane	38.7 (39.0)	2.2 (2.3)	1.7 (1.5)
$[UO_2(DBM)_2 \cdot L_1]$	165	chloroform/dodecane	56.0 (56.5)	3.5 (3.6)	1.4 (1.5)
$[UO_2(DBM)_2 \cdot L_2]$	205	chloroform/dodecane	56.7 (57.0)	3.7 (3.8)	1.7 (1.5)
$[UO_2(BTA)_2 \cdot L_1]$	191	benzene/dodecane	43.5 (43.7)	3.8 (3.7)	1.6 (1.5)
$[UO_2(BTA)_2 \cdot L_2]$	201	benzene/dodecane	45.0 (44.8)	2.7 (2.7)	1.5 (1.5)
$[UO_2(BA)_2 \cdot L_1]$	222	chloroform/dodecane	49.9 (50.2)	3.5 (3.7)	1.7 (1.6)

computation was carried out on a PC using the SHELXTL-PC program package.

3. Results and discussion

The reaction of $[UO_2(OO)_2\cdot 2H_2O]$ (OO = TTA, DBM, BTA or BA) with 1 equiv. of nitrone in benzene yielded yellow or orange colored products of the type $[UO_2(OO)_2\cdot L]$ (where L = nitrone). IR spectra of all compounds show (Table 3) that the broad peak observed for the H_2O molecules ($\nu_{OH} = 3200–3500$ cm^{-1}) of starting compound $[UO_2(OO)\cdot 2H_2O]$ has been completely disappeared. It indicates clearly that the water molecules from the starting compound $[UO_2(OO)\cdot 2H_2O]$ have been replaced completely by the nitrone ligand. The spectra further show that the ν_{N-O} in compounds has been shifted to lower frequencies compared to the free ligand, indicating the coordination of nitroxyl oxygen atom of nitrone to the uranyl group. The observed frequency differences $\Delta\nu_{(N-O)}$ ($\nu_{free} - \nu_{complex}$) (20–30 cm^{-1}) agree well with the earlier

Table 3
IR and NMR data for the compounds $[UO_2(OO)_2\cdot L]$

Complexes	IR (ν cm^{-1})	^{19}F NMR (δ ppm)	^{1}H NMR (δ ppm)
L_1	1548 [C=N]; 1088 [N–O]		8.43–8.39 (m), 2H, [$H_{2,6}$]; 7.92 (s), 1H, [CH=N]; 7.8–7.74 (m), 2H, [$H_{2',6'}$]; 7.5–7.45, 6H, [$H_{3,4,5}$, $H_{3',4',5'}$]
L_2	1548 [C=N]; 1088 [N–O]		8.42–8.36 (m), 2H, [$H_{2,6}$]; 7.90 (s), 1H, [CH=N]; 7.65 (d), J(HH) 9 Hz, 2H [$H_{2',6'}$]; 7.46 (m), 3H, [$H_{3,4,5}$]; 7.25 (d), J(HH) 9 Hz, 2H, [$H_{3',5'}$]; 2.41 (s), 3H, [CH_3]
$[UO_2(TTA)_2\cdot L_1]$	1615–1575 [C=O, TTA]; 1535 [C=N]; 1315 [C–O···M, TTA]; 1055 [N–O, L_1]; 920 [O=U=O]	−74.99	8.62 (d), J(HH) 9 Hz, [$H_{2,6}$]; 8.32 (s), 1H, [CH=N]; 8.18 (m), 4H, [C_4H_3S]; 7.76 (t), J(HH) 6 Hz, 2H, [$H_{2',6'}$]; 7.52 (t), J(HH) 9 Hz, 1H, [H_4]; 7.44(t), J(HH) 9 Hz, 2H, [$H_{3,5}$]; 7.3–7.2 (m), 5H, [$C_4H_3S + H_{3',4',5'}$]; 6.71 (s), 2H, [CO–CH–CO, TTA]
$[UO_2(TTA)_2\cdot L_2]$	1620–1580 [C=O, TTA]; 1535 [C=N]; 1315 [C–O···M, TTA]; 1055 [N–O, L_2]; 920 [O=U=O]	−74.98	8.6 (d), J(HH) 9 Hz, 2H, [$H_{2,6}$]; 8.28 (s), 1H, [CH=N]; 8.2–8.0 (m), 4H, [C_4H_3S]; 7.76 (d), J(HH) 6 Hz, 2H, [$H_{2',6'}$]; 7.5 (t), J(HH) 8 Hz, 1H, [H_4]; 7.41 (t), J(HH) 8 Hz, 2H, [$H_{3,5}$]; 7.30 (d), J(HH) 9 Hz, 2H, [$H_{3',5'}$]; 7.25 (t), J(HH) 3 Hz, 2H, [C_4H_3S]; 6.71 (s), 2H, [CO–CH–CO, TTA]; 2.18 (s), 3H, [CH_3]
$[UO_2(DBM)_2\cdot L_1]$	1590 [C=O, DBM]; 1535 [C=N]; 1310 [C–O···M, DBM]; 1060 [N–O, L_1]; 910 [O=U=O]		8.61 (d), J(HH) 8 Hz, 2H, [$H_{2,6}$]; 8.4–8.3 (m), 8H, [C_6H_5]; 8.10, 1H, [CH=N]; 7.78 (d), J(HH) 7 Hz, 2H, [$H_{2',6'}$]; 7.6–7.4 (m), 18H, [$H_{3',4',5'}$, $H_{3,4,5}$ and C_6H_5]; 7.1 (s), 2H, [CO–CH–CO, DBM]
$[UO_2(DBM)_2\cdot L_2]$	1590 [C=O, DBM]; 1535 [C=N]; 1310 [C–O···M, TTA]; 1060 [N–O, L_2]; 910 [O=U=O]		8.62 (d), J(HH) 8 Hz, 2H, [$H_{2,6}$]; 8.4–8.3 (m), 8H, [C_6H_5]; 8.10 (s), 1H, [CH=N]; 7.67 (d), J(HH) 9 Hz, [$H_{2',6'}$]; 7.6–7.4 (m) 17H, [$H_{3',5'}$, $H_{3,4,5}$ and C_6H_5]; 7.13 (s), 2H, [CO–CH–CO]; 2.18, 3H, [CH_3]
$[UO_2(BTA)_2\cdot L_1]$	1630–1580 [C=O, BTA]; 1530 [C=N]; 1320 [C–O···M, BTA]; 1060 [N–O, L_1]; 925 [O=U=O]	−75.06	8.63 (d), J(HH) 7 Hz, 2H, [$H_{2,6}$]; 8.43 (d), J(HH) 7 Hz, 4H, [C_6H_5, BTA]; 8.31 (s), 1H, [CH=N]; 8.15 (d), J(HH) 7 Hz, 2H, [$H_{2',6'}$]; 7.7–7.4 (m), 12H, [$H_{3',4',5'}$, $H_{3,4,5}$ and C_6H_5]; 6.87 (s), 2H, [CO–CH–CO, BTA]
$[UO_2(BTA)_2\cdot L_2]$	1630–1580 [C=O, BTA]; 1530 [C=N]; 1320 [C–O···M, BTA]; 1060 [N–O, L_2]; 925 [O=U=O]	−75.08	8.63 (d), J(HH) 7 Hz, 2H, [$H_{2,6}$]; 8.43 (d), J(HH) 7 Hz, 4H, [C_6H_5, BTA]; 8.30 (s) 1H, [CH=N]; 7.95 (d), J(HH) 7 Hz, 2H, [$H_{2',6'}$]; 7.7–7.4 (m), 11H, [$H_{3',5'}$, $H_{3,4,5}$ and C_6H_5]; 6.88 (s), 2H, [CO–CH–CO]; 2.16 (s), 3H, [CH_3]
$[UO_2(BA)_2\cdot L_1]$	1590 [C=O, BA]; 1535 [C=N]; 1315 [C–O···M, BA]; 1055 [N–O, L_1]; 910 [O=U=O]		8.61 (d), J(HH) 8 Hz, 2H, [$H_{2,6}$]; 8.41 (d), 4H, [C_6H_5, BA]; 8.15 (s), 1H, [CH=N]; 8.0 (d), J(HH) 7 Hz, 2H, [$H_{2',6'}$]; 7.7–7.4 (m), 12H, [$H_{3',4',5'}$, $H_{3,4,5}$ and C_6H_5]; 7.15 (s), 2H, [CO–CH–CO]; 2.13 (s), 3H, [CH_3]

$L_1 = C_6H_5CH{=}N(O)C_6H_5$; $L_2 = C_6H_5CH{=}N(O)C_6H_4\cdot CH_3$-*p*; s, singlet; d, doublet; t, triplet; m, multiplet.

reported [bis(β-diketonato)uranium(VI)] N-oxide adduct compounds [4a]. The observed frequencies $\nu_{(C=O\cdots M)}$ and $\nu_{(C-O\cdots M)}$ show that the β-diketonates act as bidentate chelating ligand [5].

The ^{1}H NMR spectra of all the compounds show (Table 3) the expected peaks and multiplicities. The –CH=N(O) and $H_{2,6}$ protons of nitrone ligands are deshielded by about approximately 0.3–0.5 ppm with respect to free ligands, supporting the coordination of nitroxyl oxygen atom of nitrone with uranyl group. The –CH– proton of the β-diketonate part gave only one resonance for all compounds, indicating that the compounds are existing exclusively in one isomeric form [5c]. The ^{19}F NMR spectrum supports this observation by showing only one resonance for the CF_3 group of TTA and BTA ligands. We could not get suitable crystals for all nitrone compounds to carry out single crystal X-ray diffraction studies to support our spectral observations similar to one that is reported in literature [8] viz: [Cu(TTA)$_2$·NIT*p*Py], in which the TTA acts as bidentate chelate ligand and the NIT*p*Py coordinates through its nitroxyl oxygen to copper atom.

In order to confirm our observation the spectral data of all nitrone compounds were compared [4a] with the analogous pyridine N-oxide compounds and which have shown similar spectral results [$\Delta\nu_{N-O} = 25–35$ cm^{-1}; H_a and H_b protons of pyridine N-oxides are deshielded about approximately 0.4–0.8 ppm with respect to the free ligands]. It indicates clearly that the nitrone and pyridine N-oxide ligands have similar type of bonding with uranyl bis(β-diketonates). The structure of the compound [$UO_2(TTA)_2$·*p*-NO_2–C_5H_4NO] was determined by using single crystal X-ray diffraction methods and which is confirming our spectroscopic observations.

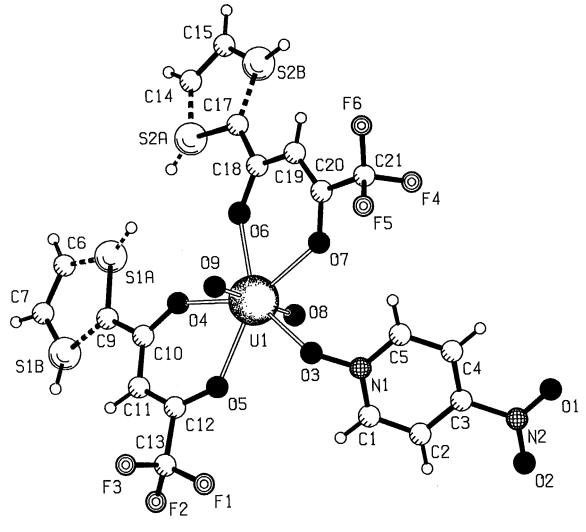


Fig. 2. The molecular structure of [$UO_2(TTA)_2$·*p*-NO_2–C_5H_4NO].

Table 4
Selected interatomic bond distances (Å) and angles (°) for the compound [$UO_2(TTA)_2$·*p*-NO_2–C_5H_4NO]

Bond distances			
U1–O3	2.361(4)	U1–O4	2.358(4)
U1–O5	2.372(4)	U1–O6	2.361(4)
U1–O7	2.377(4)	U1–O8	1.762(4)
U1–O9	1.757(4)	N1–O3	1.330(6)
Bond angles			
O6–U1–O7	69.74(16)	O7–U1–O4	142.86(16)
O6–U1–O4	73.12(12)	O6–U1–O8	91.0(2)
O7–U1–O8	90.1(2)	O9–U1–O8	177.9(2)
O4–U1–O9	91.4(2)	O8–U1–O4	90.4(2)
O9–U1–O5	86.6(3)	O3–N1–C1	119.5(5)
O8–U1–O5	92.8(2)	O3–N1–C5	117.7(5)

3.1. Structure of [$UO_2(TTA)_2$·*p*-NO_2–C_5H_4NO]

The molecular structure of the compound [$UO_2(TTA)_2$·*p*-NO_2–C_5H_4NO] with numbering scheme is given in Fig. 2. The inter atomic bond distances and angles are given in Table 4. The structure of the molecule shows that the uranium atom is surrounded by seven oxygen atoms in a distorted pentagonal bi-pyramidal geometry. Four oxygen atoms of the TTA and one oxygen atom of N-oxide forms a planar pentagon and two uranyl oxygen atoms occupy the apices. The average U–$O_{(uranyl)}$ (1.759(5) Å) and U–$O_{(TTA)}$ (2.367(4) Å) [5a–h] distances are within the accepted values. The U–O(N) N-oxide distance (2.361(4) Å) is comparable with the earlier reported uranyl bis(β-diketonates) neutral ligand adduct compounds [5a–h]. The overall bond lengths and angles show that the uranium atom has a distorted pentagonal bi-pyramidal geometry. The whole molecule is stabilized in solid state by the intermolecular hydrogen bonding interactions to give a polymeric arrangement [C15–H15···O9; 3.241(10) Å, 164.56°]. There is a disorder seen in the thiophene ring and this disorder is due to the 180° rotation of this ring about C17–C18 and C9–C10 bonds. A hybrid scattering factor consisting of 66% sulfur and 34% carbon was used to model this disorder.

4. Conclusion

The IR and ^{1}H NMR spectral studies show that the nitrone forms adduct compounds with the uranyl bis(β-diketonates) and coordinates through its nitrosyl oxygen atom to the uranyl group. The structure of the compound [$UO_2(TTA)_2$·*p*-NO_2–C_5H_4NO] confirms our spectroscopic observations.

5. Supplementary material

Crystallographic data for structural analysis have been deposited with the Cambridge Crystallographic Data Centre, CCDC no. 180472. Copies of this information may be obtained free of charge from The Director, CCDC, 12 Union Road, Cambridge, CB2 1EZ, UK (fax: +44-1223-336033; e-mail: deposit @ccdc.cam.ac.uk or www: http://www.ccdc.cam.ac.uk).

Acknowledgements

S.K wish to thank V. Venugopal, Head, Fuel Chemistry Division, BARC for his support, Professor S. Sivasubramanian, School of Chemistry, Madurai Kamaraj University, Madurai for the donation of ligands L_1 and L_2, the Head, Analytical Chemistry Division, BARC, for carbon, hydrogen and nitrogen analysis and the Head, RSIC, IIT, Mumbai for NMR spectra. H.K.F would like to thank the Malaysian Government and Universiti Sains Malaysia for research grant R&D No. 305/pfizik/610961. A.U. thanks the Universiti Sains Malaysia for a visiting Post-Doctoral Fellowship.

References

[1] (a) N.M. Karayannis, L.L. Pytlewski, C.M. Mikulski, Coord. Chem. Rev. 11 (1973) 93;
(b) N.M. Karayannis, A.N. Speca, D.E. Chasan, L.L. Pytlewski, Coord. Chem. Rev. 20 (1976) 37;
(c) U. Casellato, P.A. Vigato, M. Vidali, Coord. Chem. Rev. 36 (1981) 233.

[2] (a) S. Sivasubramanian, P. Manisankar, M. Palaniandavar, N. Arumugam, Transition Met. Chem. 7 (1982) 346;
(b) D.X. West, S. Sivasubramanian, P. Manisankar, M. Palaniandavar, N. Arumugam, Transition Met. Chem. 8 (1983) 317;
(c) M. Thirumalaikumar, S. Sivakolunthu, S. Muthusubramanian, S. Sivasubramanian, Bull. Chim. Farm. 138 (1999) 207;
(d) M. Thirumalaikumar, S. Sivakolunthu, A. Ponnusamy, S. Sivasubramanian, Indian J. Chem., Sect. A 38 (1999) 720;
(e) G. Valli, S. Sivakolunthu, M. Thirumalaikumar, S. Muthusubramanian, S. Sivasubramanian, J. Indian Chem. Soc. 79 (2002) 79.

[3] (a) V.K. Manchanda, J.P. Sukla, M.S. Subramanian, J. Inorg. Nucl. Chem. 36 (1974) 2595;
(b) V.K. Manchanda, J.P. Shukla, M.S. Subramanian, J. Radioanal. Chem. 29 (1976) 69.

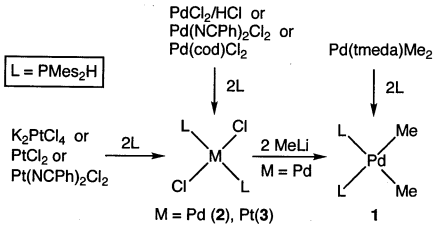
[4] (a) M.S. Subramanian, V.K. Manchanda, J. Inorg. Nucl. Chem. 22 (1971) 3001;
(b) V.K. Manchanda, M.S. Subramanian, Aust. J. Chem. 27 (1974) 1573.

[5] (a) S. Kannan, V. Venugopal, Polyhedron 14 (1995) 2349;
(b) S. Kannan, V. Venugopal, M.R.A. Pillai, P.A. Droege, C.L. Barnes, Polyhedron 15 (1996) 97;
(c) S. Kannan, V. Venugopal, M.R.A. Pillai, P.A. Droege, C.L. Barnes, E.O. Schlember, Polyhedron 15 (1996) 465;
(d) S. Kannan, M.R.A. Pillai, V. Venugopal, P.A. Droege, C.L. Barnes, Inorg. Chim. Acta 254 (1997) 113;
(e) S. Kannan, G. Ferguson, Inorg. Chem. 36 (1997) 1724;
(f) S. Kannan, J. Chem. Res(s). (2000) 344;
(g) S. Kannan, S. Shanmuga Sundara Raj, H.K. Fun, J. Chem. Res(s). (2001) 50;
(h) S. Kannan, S. Shanmuga Sundara Raj, H.K. Fun, Polyhedron 20 (2001) 2157.

[6] (a) SMART, Siemens Analytical X-Ray System, Madison, WI, USA, 1996;
(b) SAINT, Siemens Analytical X-Ray System, Madison, WI, USA, 1996;
(c) George Sheldrick, SADABS, University of Göttingen, Germany, 1996;
(d) International Tables for X-ray Crystallography, vol. C, Tables 4.2.6.8 and 6.1.1.4, 1992

[7] SHELXTL Version 5.1, Software Reference Manual, Brucker Analytical X-ray Systems, Madison, WI, USA, 1997.

[8] I. Yeltsov, V. Ovcharenko, V. Ikorskii, G. Romanenko, S. Vasilevsky, Polyhedron 20 (2001) 1215.



Scheme 1.

highly colored impurity were present. Complex **1** was thermally stable, decomposing slowly in toluene at 105 °C over several days to give unidentified products [8].

Addition of 2 equiv. of $PMes_2H$ to $PdCl_2$ in acidic ethanol gave *trans*-PdL_2Cl_2 (**2**) [9]. This complex could also be prepared by addition of 2 equiv. of $PMes_2H$ to either $Pd(cod)Cl_2$ (cod = 1,5-cyclooctadiene) or $Pd(NCPh)_2Cl_2$ (Scheme 1). The *trans* stereochemistry of **2** and its Pt analogue **3** (see below) was established by NMR. Analysis of the $PMes_2H$ AA′XX′ patterns in the ^1H and ^{31}P NMR spectra [7] and simulation using gNMR [10] gave the coupling constants shown in Table 2. The large J_{PP} values (598 and 523 Hz, respectively) are consistent with the *trans* geometry [11].

Interestingly, treatment of **2** with 2 equiv. of MeLi gave partial conversion to the dimethyl complex **1** (Scheme 1). The steric bulk of $PMes_2H$ would seem to contraindicate the observed *trans*–*cis* isomerization, but similar results have been observed previously. For example, *trans*-$Pd(PPh_3)_2Me_2$ isomerizes on heating in DMSO to the *cis* complex [8a]. Electronic arguments based on the strong *trans* influence of the methyl group

Table 1
Selected NMR and IR data for *cis*-dimesitylphosphine complexes [a]

Complex	δ(P)	$^1J_{PH}$	$^1J_{Pt-P}$	δ(PH)	ν(PH)
PdL_2Me_2 (**1**)	−46.6	339		5.97	2388
PtL_2Cl_2 (**4**) [b]	−48.1	414	3444	6.34	2422
PtL_2Cl_2 (**4A**) [c]	−44.2	408	3631	5.55 [d]	
PtL_2Cl_2 (**4B**) [c]	−51.1	430	3302	6.77 [e]	
PtL_2Cl_2 (**4C**) [c]	−41.6	414	[f]	5.16 [g]	
$PtL(PPh_3)Cl_2$ (**5**) [h]	−39.6 [i]	408	3538	4.89 [j]	2413
$PtL_2(Me)(Cl)$ (**6**)	−38.1	372	1505	[f]	2400
	−49.2	403	4189		
$PtL_2(Me)(Cl)$ (**6A**) [k]	−31.8	[m]	1777	[m]	
	−47.3		3996		
$PtL_2(Me)(Cl)$ (**6B**) [k]	−33.7	[m]	1726	[m]	
	−48.1		4016		
$PtL_2(Me)(Cl)$ (**6C**) [k]	−34.9	[m]	1341	[m]	
	−43.2		4207		
$PtL_2(Me)(Cl)$ (**6D**) [k]	−36.4	[m]	1444	[m]	
	−44.1		4234		
$PtL_2(Et)(I)$ (**7**)	−43.5	388	4315	[f]	2402
	−46.9	368	1350		
$PtL_2(Et)(I)$ (**7A**) [l]	−41.7	386	4355	[m]	
	−46.3	382	1325		
$PtL_2(Et)(I)$ (**7B**) [l]	−40.1	401	4309	[m]	
	−44.0	375	1248		
$PtL_2(Et)(I)$ (**7C**) [l]	−37.1	389	4166	[m]	
	−41.2	361	1627		
$PtL_2(Et)(I)$ (**7D**) [l]	−35.8	409	4132		
	−39.4	362	1563	[m]	

[a] Temperature: 21 °C unless noted; solvents: C_6D_6 for **1**, **6**, $CDCl_3$ for **5**, **7**. ^{31}P NMR chemical shift reference: external 85% H_3PO_4; coupling constants in Hz; IR data in cm^{-1} for KBr pellets.
[b] C_6D_5Cl, 100 °C.
[c] CD_2Cl_2, −70 °C. Two major species (A, B) and a minor one (C) in ca. 1:1:0.15 ratio were observed.
[d] Apparent dd, $J = 408$, 10.
[e] Apparent d, $J = 430$.
[f] Not observed.
[g] Apparent dd, $J = 414$, 10. In addition, another apparent d ($J = 428$) at δ 6.89 was observed.
[h] Additional ^{31}P NMR data: δ 14.5 (d, $J = 14$, $J_{Pt-P} = 3589$, PPh_3).
[i] d, $J = 14$.
[j] dd, $J = 408$, 12.
[k] CD_2Cl_2, −70 °C. Four isomers A–D (ratio 2.9:2.6:1.7:1) were observed; for isomers B–D, $J_{PP} = 8$.
[l] CD_2Cl_2, −40 °C. Four isomers A–D (ratio 7.3:4.4:5.6:1) were observed.
[m] See the text and Section 4 for further discussion and low-temperature ^1H NMR results.

Table 2
Selected NMR and IR data for *trans*-dimesitylphosphine complexes [a]

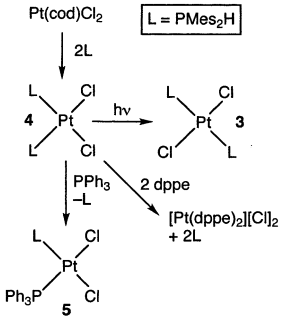
Complex	δ(P)	$^1J_{Pt-P}$	$^2J_{PP}$	$^1J_{PH}$	$^3J_{PH}$	δ(PH)	ν(PH)
PdL_2Cl_2 (**2**)	−38.3		598	386	−2	6.52	2400
PtL_2Cl_2 (**3**)	−37.9	2506	523	396	−2	6.66	2404
$PtL_2(Et)(I)$ (**8**) [b,c]	−37.1	3123	492	389	−3	7.24 [d]	2395

[a] Temperature: 21 °C unless noted; solvents: $CDCl_3$ for **2**, **3**, C_6D_5Cl for **8**; ^{31}P NMR chemical shift reference: external 85% H_3PO_4; coupling constants in Hz; IR data in cm^{-1} for KBr pellets.
[b] 80 °C.
[c] Additional $^{31}P\{^1H\}$ NMR data for **8** (CD_2Cl_2, −70 °C): Four isomers (A–D) with approximate ratio 4.8:2.7:1:1 were observed; δ −39.4 (J_{Pt-P} = 3069, A), −29.0 (J_{Pt-P} = 3153, B), −37.3 (J_{Pt-P} = 3006, C), −26.7 (J_{Pt-P} = 3153, D). See the text and Section 4 for additional discussion of these and related low-temperature ^1H NMR spectra.
[d] Apparent d, J = 384, J_{Pt-H} = 26, perhaps the most intense two peaks of an AA′XX′ pattern.

have been advanced to explain this behavior (''anti-symbiotic effect'' [12], ''transphobia'' [13]).

Reaction of 2 equiv. of L with three different platinum sources [K_2PtCl_4, $PtCl_2$, and $PtCl_2(NCPh)_2$] yielded *trans*-$Pt(PMes_2H)_2Cl_2$ (**3**) as a yellow powder (Scheme 1, Table 2). In contrast, treatment of $Pt(cod)Cl_2$ with L gave *cis*-$Pt(PMes_2H)_2Cl_2$ (**4**) as shown in Scheme 2. Its room temperature NMR spectra contain very broad peaks, attributed to restricted rotation about the P–C and/or Pt–P bonds (see below). At high temperature (100 °C, C_6D_5Cl) a sharp average spectrum consistent with the *cis* geometry is observed (Table 1).

The reactivity of **4** was briefly examined (Scheme 2). Irradiation of a CD_2Cl_2 solution of **4** with a mercury lamp caused slow conversion to the *trans* isomer **3**, consistent with literature reports of related photochemical *cis*–*trans* isomerizations in PtL_2X_2 complexes (L = PPh_3, pyridine, isoquinoline, X = Cl, Br) [9,14]. Treatment of $Pt(cod)Cl_2$ with 3 equiv. of $PMes_2H$ gave a mixture of **4** and $PMes_2H$, which did not undergo exchange on the NMR time scale, while 1 equiv. of $PMes_2H$ gave a mixture of **4** and unreacted $Pt(cod)Cl_2$, as shown by the ^1H NMR spectrum. Addition of more phosphine completed the conversion to **4**. $PMes_2H$ was readily displaced from **4** by 2 equiv. of dppe (dppe = $Ph_2PCH_2CH_2PPh_2$) to yield $[Pt(dppe)_2][Cl]_2$ [15]. Heating **4** at 45 °C in CH_2Cl_2 with 2 equiv. of PPh_3 gave *cis*-$Pt(PMes_2H)(PPh_3)Cl_2$ (**5**). Consistent with the stoichiometry, ^{31}P NMR monitoring of the reaction mixture showed formation of $PMes_2H$ and the presence of unreacted PPh_3. Recrystallization from CH_2Cl_2/petroleum ether gave white crystals, identified by NMR as the *cis* isomer (J_{PP} = 14 Hz, Table 1).



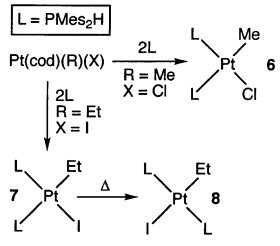
Scheme 2.

Reaction of Pt(cod)(Me)(Cl) with 2 equiv. of L yielded *cis*-$Pt(PMes_2H)_2(Me)(Cl)$ (**6**, Scheme 3). The *cis* geometry was established by ^{31}P NMR (see Table 1) and by the Pt–Me ^{13}C NMR signal (δ 3.5, dd, J = 96, 6 Hz, CD_2Cl_2). Similarly, treatment of Pt(cod)(Et)(I) with 2 equiv. of L gave white *cis*-$Pt(PMes_2H)_2(Et)(I)$ (**7**, Table 1), which readily isomerized on standing or gentle heating to the yellow *trans* isomer (**8**, Scheme 3). The room temperature NMR spectra of complex **8** were very broad, indicative of a dynamic process (see Section 2.2), but at 80 °C in C_6D_5Cl, it showed the expected AA′XX′ ^{31}P NMR spectrum (Table 2).

2.1. Solid-state structures

The X-ray crystal structures of *trans*-PdL_2Cl_2 (**2**·$2CH_2Cl_2$), *cis*-PtL_2Cl_2 (**4**·CH_2Cl_2), *cis*-$PtL(PPh_3)Cl_2$ (**5**·$2CH_2Cl_2$), *cis*-$PtL_2(Me)(Cl)$ (**6**) and the phosphine–borane L-BH_3 (**9**, see Section 4) were determined to investigate the effect of the bulky phosphine on the structures of its simple coordination complexes. For thermal ellipsoid plots, see Figs. 1–5; crystal data is summarized in Table 3, and additional details are included in Sections 4 and 5. See the figure captions and Tables 4 and 5 for selected bond lengths and angles.

The structure of **2** shows a minor distortion from ideal square planar geometry, and Pd–P and Pd–Cl bond



Scheme 3.

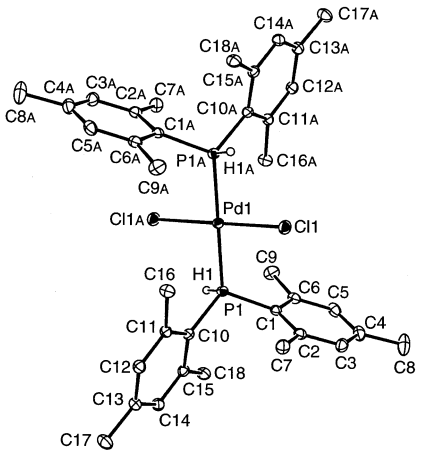


Fig. 1. ORTEP diagram of *trans*-$Pd(PMes_2H)_2Cl_2$ (**2**·$2CH_2Cl_2$), with thermal ellipsoids at 30% probability. The solvent molecules and hydrogen atoms, except those on P, have been removed for clarity. Selected bond lengths (Å) and angles (°): Pd–Cl(1) 2.3028(7), Pd–Cl(1A) 2.3028(7), Pd–P(1) 2.3057(7), Pd–P(1A) 2.3057(7), P(1)–C(10) 1.819(3), P(1)–C(1) 1.822(3), Cl(1)–Pd–Cl(1A) 180.0, Cl(1)–Pd–P(1) 93.91(2), Cl(1A)–Pd–P(1) 86.09(2), Cl(1)–Pd–P(1A) 86.09(2), Cl(1)–Pd–P(1) 93.91(2), P(1)–Pd–P(1A) 180.0, C(10)–P(1A)–C(1) 110.45(12).

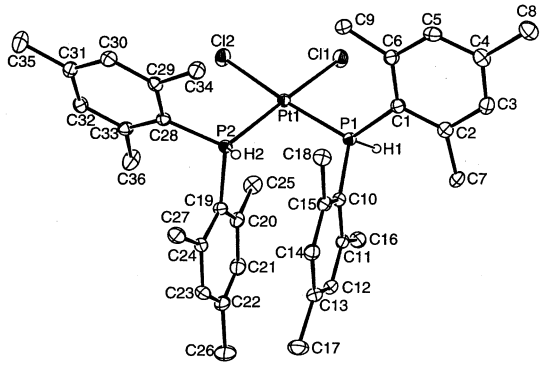


Fig. 2. ORTEP diagram of *cis*-$Pt(PMes_2H)_2Cl_2$ (**4**·CH_2Cl_2), with thermal ellipsoids at 30% probability. The solvent molecule and hydrogen atoms, except those on P, have been removed for clarity.

lengths typical of those in square planar phosphine complexes [16]. The *cis*-Pt complexes **4**–**6** (see Table 4) all show slight distortions from square planar geometry. As might be expected, the P–Pt–P bond angles, which range from 95.65(7)° to 97.07(7)° are larger than the ideal value, presumably due to steric hindrance between the bulky phosphines, as previously observed in *cis*-$Pt(PPh_3)_2Cl_2$ (Table 4) and related structures [17]. The close similarity between the structures of **4**, **5** and *cis*-$Pt(PPh_3)_2Cl_2$ suggests that L and PPh_3 have comparable steric and electronic properties. This is consistent with the similar J_{Pt-P} values found for these phosphines in **5** (3538 Hz for L, 3589 Hz for PPh_3, $CDCl_3$). As expected from *trans* influence trends, the Pt–P bond *trans* to the methyl group in **6** is longer [2.3311(17) Å] than the one *trans* to chloride [2.214(2) Å] [18].

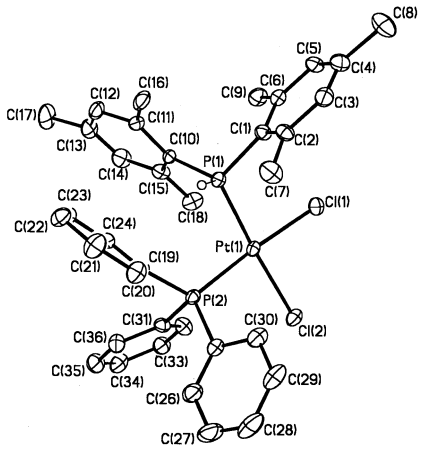


Fig. 3. Thermal ellipsoid plot (25% probability) of *cis*-$Pt(PMes_2H)(PPh_3)Cl_2$ (**5**·$2CH_2Cl_2$). The solvent molecule and hydrogen atoms, except the one on P, have been removed for clarity.

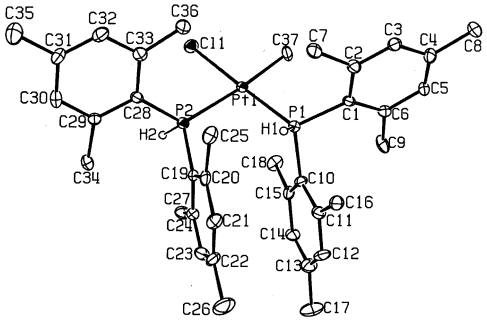


Fig. 4. ORTEP diagram of *cis*-$Pt(PMes_2H)_2(Me)(Cl)$ (**6**), with thermal ellipsoids at 30% probability. The hydrogen atoms, except those on P, have been removed for clarity.

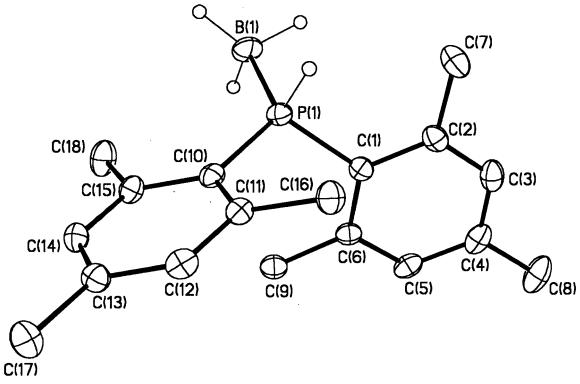


Fig. 5. Thermal ellipsoid plot (25% probability) of $PMes_2H{\cdot}BH_3$ (**9**). Hydrogen atoms, except those on P and B, have been removed for clarity. Selected bond lengths (Å) and angles (°): P–H(1) 1.35(3), P–C(1) 1.824(3), P–C(10) 1.829(3), P–B(1) 1.938(4), H(1)–P–C(10) 97.3(11), H(1)–P–C(1) 104.0(11), H(1)–P–B(1) 108.3(12), C(10)–P–C(1) 110.71(12), C(10)–P–B(1) 124.41(15), C(1)–P–B(1) 109.62(15).

In the structure of phosphine–borane **9**, the PH and BH_3 hydrogens were found and refined freely. The geometry around phosphorus is tetrahedral as expected, though the C(10)–P–B bond angle is somewhat larger

Table 3
Crystallographic data for *trans*-PdL_2Cl_2 (**2**·$2CH_2Cl_2$), *cis*-PtL_2Cl_2 (**4**·CH_2Cl_2), *cis*-$PtL(PPh_3)Cl_2$ (**5**·$2CH_2Cl_2$), *cis*-$PtL_2(Me)(Cl)$ (**6**), and L·BH_3 (**9**)

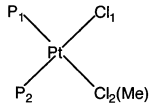
Complex	**2**·$2CH_2Cl_2$	**4**·CH_2Cl_2	**5**·$2CH_2Cl_2$	**6**	**9**
Empirical formula	$C_{38}H_{50}Cl_6P_2Pd$	$C_{37}H_{48}Cl_4P_2Pt$	$C_{38}H_{42}Cl_6P_2Pt$	$C_{37}H_{49}ClP_2Pt$	$C_{18}H_{26}BP$
Formula weight	887.82	891.58	968.45	786.24	284.17
Space group	$P2_1/n$	$P2_1/n$	$P2_1/n$	$P2_1/n$	$P2_1/c$
Temperature (K)	173(2)	173(2)	173(2)	173(2)	173(2)
a (Å)	11.3321(6)	12.4534(10)	11.6372(13)	14.2510(9)	8.1454(14)
b (Å)	11.8745(7)	19.3221(15)	22.830(3)	15.1847(11)	11.3460(19)
c (Å)	15.9474(8)	16.1326(12)	15.2546(18)	16.2727(11)	19.258(3)
α (°)	90	90	90	90	90
β (°)	107.6950(10)	106.418(2)	98.820(3)	97.257(2)	98.973(4)
γ (°)	90	90	90	90	90
V (Å^3)	2044.40(19)	3723.6(5)	4004.9(8)	3493.2(4)	1758.0(5)
Z	2	4	4	4	4
λ (Å)	0.71073	0.71073	0.71073	0.71073	0.71073
D_{calc} (g cm^{-3})	1.442	1.590	1.606	1.495	1.074
μ (mm^{-1})	0.951	4.167	4.010	4.209	0.146
$R(F)$ (%) [a]	3.59	2.98	4.02	4.79	5.53
$R(wF^2)$ (%) [a]	8.44	6.52	8.91	7.87	13.50

[a] Quantity minimized = $R(wF^2) = [\Sigma[w(F_o^2 - F_c^2)^2]/\Sigma[w(F_o^2)^2]]^{1/2}$; $R = \Sigma\Delta/\Sigma(F_o)$, $\Delta = I|(F_o - F_c)|I$.

than the ideal angle at 124.41(15)°. The P–B bond length (1.938(4) Å) is typical of those in phosphine–boranes, for which a recently reported range is 1.832–1.983 Å [19]. Comparison to the structure of $PMes_2H$ [20] (Table 5) shows that borane complexation has little effect on the structure of the phosphine. The P–C bonds become slightly shorter and the C(1)–P–C(10) bond angle is increased.

The program STERIC [21] was used to determine the cone angle of L from the crystal structure data, setting a P–B distance of 2.28 Å in the case of **9** [22]. Although this is longer than the experimental distance, this choice allows comparison to the results for the metal complexes. As shown in Table 6, the cone angle falls in a narrow range in this series of complexes, although significant differences can be seen even within a single compound containing two phosphines, such as **4**. The average cone angle is approximately 149°. Consistent with the discussion above, the crystallographically determined cone angles for L and PPh_3 in **5** are similar;

Table 4
Selected bond lengths (Å) and angles (°) for *cis*-Pt dimesitylphosphine complexes **4**–**6** [a]



Complex	PtL_2Cl_2 (**4**·CH_2Cl_2)	$PtL(PPh_3)Cl_2$ (**5**·$2CH_2Cl_2$)	$PtL_2(Me)(Cl)$ (**6**)	$Pt(PPh_3)_2Cl_2·C_3H_6O$ [b]
Bond lengths				
Pt–P_1	2.2481(9)	2.2438(19)	2.3311(17)	2.251(2)
Pt–P_2	2.2315(9)	2.2444(19)	2.214(2)	2.265(2)
Pt–Cl_1	2.3445(10)	2.3519(19)	2.3591(19)	2.333(2)
Pt–Cl_2 (Me)	2.3385(9)	2.3478(19)	2.084(6)	2.356(2)
Bond angles				
P_1–Pt–P_2	96.93(3)	95.65(7)	97.07(7)	97.8(1)
P_1–Pt–Cl_1	84.13(3)	89.63(7)	85.29(7)	89.8(1)
P_1–Pt–Cl_2 (Me)	173.90(3)	175.02(6)	172.0(2)	176.9(1)
Cl_1–Pt–Cl_2 (Me)	89.79(4)	88.15(7)	87.3(2)	87.1(1)
Cl_1–Pt–P_2	174.46(4)	174.61(6)	177.19(7)	172.4(1)
P_2–Pt–Cl_2 (Me)	89.10(3)	86.68(7)	90.3(2)	85.3(1)

[a] For **4**·CH_2Cl_2, $P_1 = P_2 = L$; for **5**·$2CH_2Cl_2$, $P_1 = L$, $P_2 = PPh_3$; for **6**, $P_1 = P_2 = L$, P_1 *trans* to Me, P_2 *trans* to Cl. Note that the atom numbering in Fig. 5 for **6** is slightly different than the convention used here.
[b] Ref. [17].

Table 5
Selected bond lengths (Å) and angles (°) in $PMes_2H$ [a] and $PMes_2H \cdot BH_3$ (**9**)

Complex	$PMes_2H$	$PMes_2H \cdot BH_3$ (**9**)
Bond lengths		
P–C(1)	1.862(7)	1.824(3)
P–C(10)	1.864(7)	1.829(3)
P–H(1)	1.36(7)	1.35(3)
Bond angles		
C(1)–P–C(10)	107.0(3)	110.71(12)
C(1)–P–H(1)	109(3)	104.0(11)
C(10)–P–H(1)	107(3)	97.3(11)

[a] Ref. [20].

Table 6
Cone angle data for dimesitylphosphine complexes [a]

Complex	Cone angle (°)
trans-PdL_2Cl_2 (**2**·$2CH_2Cl_2$)	147
cis-PtL_2Cl_2 (**4**·CH_2Cl_2)	152, 142
cis-$PtL(PPh_3)Cl_2$ (**5**·$2CH_2Cl_2$)	148 [b]
cis-$PtL_2(Me)(Cl)$ (**6**)	156, 154
$L \cdot BH_3$ (**9**)	146
cis-$Pt(PPh_3)_2Cl_2 \cdot C_3H_6O$ [c]	143, 150

[a] See Section 4 for details of the calculations.
[b] PPh_3 cone angle = 154°.
[c] Ref. [17].

compare to Tolman's reported cone angle of 145° for PPh_3 [22].

2.2. Solution structures: fluxional processes

Conformational isomerism due to restricted rotation has often been observed in metal complexes of bulky secondary phosphines. For example, Shaw reported that room-temperature solutions of *trans*-$Pt[P(t\text{-}Bu)_2H]_2Cl_2$ contained two conformational isomers; this complex has recently been studied in more detail by Mastrorilli et al. [23]. Similarly, Bushweller's detailed investigation of *trans*-$Rh[P(t\text{-}Bu)_2H]_2(CO)(X)$ (X = halide) revealed several conformations as a result of restricted rotation about the Rh–P bonds [24], and analogous behavior was observed for $Ir[P(t\text{-}Bu)_2H]_3(Cl)$ [2c]. We observed similar phenomena in Pt dimesitylphosphine complexes **4**–**8** by low-temperature NMR spectroscopy.

Although the room-temperature ^{31}P NMR spectrum of *cis*-PtL_2Cl_2 (**4**) was very broad, three different signals in about a 1:1:0.15 ratio were observed at −70 °C in CD_2Cl_2 (Table 1). We assign these to two major isomers (A and B) and one minor one (C), although we cannot rule out the possibility that the A and B signals are in fact due to a single conformer which contains two inequivalent dimesitylphosphine ligands [24].

Low-temperature ^1H NMR studies (−70 °C, CD_2Cl_2) provided additional information on the dynamic processes in **4**. As detailed in Section 4, 12 aryl proton signals (8 from the major and 4 from the minor isomers) and 18 methyl signals (12 major, 6 minor) were observed. These observations can be explained if, in the two major isomers, rotation about the P–C and Pt–P bonds is slow on the NMR time scale. If rotation about the P–C bond is slow, the *o*-Me and *m*-aryl protons are inequivalent in a given Mes group; if rotation about the Pt–P bond is slow, then there are two types of mesityl groups in a given $PMes_2H$. The crystal structure (Fig. 2), if maintained in solution at low temperature, would be consistent with these observations. The two major isomers might then be *syn* and *anti* conformers, as reported for *trans*-$Pt[P(t\text{-}Bu)_2H]_2Cl_2$ [23].

Four P–H resonances were also observed (Table 1). Three of these are easily assigned, one each to the major and minor isomers, from matching the P–H couplings in the low temperature ^1H NMR spectrum with those obtained in the low temperature ^{31}P NMR spectrum, but the origin of the fourth signal is not clear. These P–H resonances are expected to show an AA′XX′ pattern, but either simple doublets or doublet of doublets patterns were observed. If the $^2J_{PP}$ and $^3J_{PH}$ couplings are small, then the signals would appear as a doublet. The doublet of doublets patterns could arise if $^2J_{PP}$ is small. Alternatively, the observed resonances could be due to the inner lines of an AA′XX′ pattern, if the low intensity outer peaks are not observed [7].

Similarly, at −20 °C in CD_2Cl_2, the rotation about the P–C and Pt–P bonds in **5** is slow on the NMR time scale, so each of the Mes *m*-aryl protons and *o*-Me groups is inequivalent, consistent with the conformation found in the crystal structure (Fig. 3). Thus, four sharp peaks for the Mes *m*-aryl protons were observed from 6.92 to 6.63 ppm, and four *o*-Me signals appeared at δ 3.38, 2.50, 1.85, and 1.20. Because the two Mes groups are inequivalent, two separate *p*-Me resonances were observed at δ 2.25 and 2.23.

The related complexes **6** and **7** showed similar fluxional behavior, again ascribed to restricted rotation about the Pt–P and P–C bonds, giving rise to four different isomers in each case at low temperature. This could be observed most clearly by ^{31}P NMR (Table 1). Five and six of the expected eight P–H resonances could also be observed by low-temperature ^1H NMR for **6** and **7**, respectively (see Section 4 for details).

trans-$PtL_2(Et)(I)$ (**8**) also showed broad peaks in the room temperature NMR spectra. As for the *cis* isomer **7**, four isomers were observed by low-temperature ^{31}P NMR (Table 2). However, the lines in the expected AA′XX′ patterns could not all be resolved because of weak, overlapping signals. Similarly, the ^1H NMR spectrum (CD_2Cl_2, −70 °C) revealed the most intense

signals of the four expected PH AA′XX′ patterns; however, two of these peaks were obscured by Mes resonances (see Table 2 and Section 4).

3. Conclusion

We prepared several simple coordination complexes of the bulky secondary phosphine $PMes_2H$. Its crystallographically determined cone angle of approximately 149° is comparable to that of PPh_3, and comparison of the structures of *cis*-PtL_2Cl_2 (**4**), *cis*-$PtL(PPh_3)Cl_2$ (**5**), and *cis*-$Pt(PPh_3)_2Cl_2$ shows these ligands to have similar steric and electronic properties. The bulk of dimesitylphosphine is reflected in the dynamic properties of its complexes in solution at low temperature, where restricted rotation about Pt–P and P–C(Mes) bonds was frequently observed.

4. Experimental

4.1. General

Unless otherwise noted, all reactions and manipulations were performed in dry glassware under a nitrogen atmosphere at 20 °C in a dry box or using standard Schlenk techniques. Petroleum ether (b.p. 38–53 °C), ether, THF, CH_2Cl_2 and toluene were dried and degassed using columns with activated alumina [25].

NMR spectra were recorded (at 21 °C unless otherwise noted) with Varian 300 or 500 MHz spectrometers; the latter was used for variable temperature studies. ^1H or ^{13}C NMR chemical shifts are reported versus Me_4Si and were determined by reference to the residual ^1H or ^{13}C solvent peaks. ^{31}P NMR chemical shifts are reported versus H_3PO_4 (85%) used as an external reference. Coupling constants are reported in Hz, as absolute values unless noted otherwise. Unless indicated, peaks in NMR spectra are singlets. Infrared spectra were recorded using KBr pellets on a Perkin Elmer 1600 series FTIR machine and are reported in cm^{-1}. Elemental analyses were provided by Schwarzkopf Microanalytical Laboratory. Low resolution FAB Mass Spectroscopy was performed on a VG ZAB-SE instrument at the University of Illinois.

Unless otherwise noted, reagents were from commercial suppliers. The following compounds were made by the literature methods: $Pd(tmeda)Me_2$ [6], $PMes_2H$ [20], $Pd(cod)Cl_2$ [26], $Pd(NCPh)_2Cl_2$ [27], $Pt(NCPh)_2Cl_2$ [27], $Pt(cod)Cl_2$ [28], Pt(cod)(Me)(Cl) [29], and Pt(cod)(Et)(I) [30].

4.2. *cis*-$Pd(PMes_2H)_2Me_2$ (**1**). Method 1

$Pd(tmeda)Me_2$ (80 mg, 0.32 mmol) and $PMes_2H$ (165 mg, 0.610 mmol) were dissolved in 10 ml of THF to give a pink–red solution. The THF was removed under vacuum to give a brownish white solid, which was washed with petroleum ether (4 ml). The resulting blood-red solution was removed using a pipet to give a pink solid, which was dried under vacuum to yield 189 mg (88%) of the product.

Anal. Calc. for $C_{44}H_{52}P_2Pd$: C, 67.40; H, 7.74. Found: C, 67.23; H, 7.32%. ^1H NMR (C_6D_6): δ 6.55 (8H, Mes), 5.97 (d, $J_{PH} = 339$, 2H, PH), 2.33 (broad, 24H, *o*-Me), 2.01 (12H, *p*-Me), 1.00 (m, 6H, Pd–Me). $^{13}C\{^1H\}$ NMR (C_6D_6): δ 142.7 (Mes), 139.1 (Mes), 130.2 (t, $J = 3$, Mes), 126.3 (d, $J = 26$, Mes), 23.7 (Me), 21.2 (Me), 5.0 (dd, $J = 105$, 10, Pd–Me). IR: 3433, 2922, 2388, 1727, 1600, 1450, 1377, 1133, 1027, 844, 694, 616, 550.

4.3. Method 2

A pale yellow solution of *trans*-$Pd(PMes_2H)_2Cl_2$ (26 mg, 3.6×10^{-2} mmol, **2**, see below) in 10 ml of THF was cooled to −78 °C and treated with methyllithium (106 μl of 1.4 M solution in ether, 0.15 mmol). The resulting golden solution was stirred for 1 h at −78 °C, then quenched by the addition of one drop of water, which turned the solution orange. The solution was concentrated under vacuum and transferred to a NMR tube. The ^{31}P NMR spectrum showed partial conversion (73%) of the dichloro complex **2** to the dimethyl complex **1**. ^{31}P NMR (THF/ether): δ −34.8 (AA′XX′, **2**), −48.3 (d, $J = 339$, **1**).

4.4. *trans*-$Pd(PMes_2H)_2Cl_2$ (**2**). Method 1

$PdCl_2$ (57 mg, 0.32 mmol) was treated with concentrated HCl (4 ml) and the brown solution was stirred for 10 min. After addition of 8 ml of absolute ethanol, the solution was stirred for an additional 5 min. A solution of $PMes_2H$ (174 mg, 0.643 mmol) in 4 ml of ether was added, causing a yellow precipitate to form immediately. The mixture was allowed to stir for another 5 min, and then filtered on a frit. The solid was washed with water (1×10 ml) and ether (2×20 ml) and dried on the frit to give 230 mg, 99%. The yellow solid was recrystallized from methylene chloride/petroleum ether to give yellow crystals of a methylene chloride solvate, as quantified by ^1H NMR integration.

Anal. Calc. for $C_{36}H_{46}Cl_2P_2Pd \cdot 0.6CH_2Cl_2$: C, 57.17; H, 6.19. Found: C, 57.06; H, 6.12%. ^1H NMR ($CDCl_3$): δ 6.85 (8H, Mes), 6.52 (m, $J_{PP} = 598$, $J_{PH} = 386$, $J_{PH'} = -2$, 2H, P–H, AA′XX′), 2.52 (24H, *o*-Me), 2.25 (12H, *p*-Me). $^{13}C\{^1H\}$ NMR ($CDCl_3$, 21 °C): δ 142.5 (t, $J = 5$, Mes), 140.9 (Mes), 130.1 (t, $J = 4$, Mes), 122.1 (t, $J = 24$,

Mes), 23.7 (t, $J = 4$, *o*-Me), 21.3 (*p*-Me). IR: 2956, 2922, 2400, 1600, 1556, 1449, 1405, 1374, 1264, 1029, 837.

4.5. Method 2

A yellow solution of $Pd(cod)Cl_2$ (22 mg, 0.11 mmol) in methylene chloride was treated with $PMes_2H$ (86 mg, 0.32 mmol), causing the solution to turn orange. ^{31}P NMR (CH_2Cl_2): δ −41.0 (AA′XX′, $J_{PP} = 597$, $J_{PH} = 386$, $J_{PH'} = -0.07$). Recrystallization from methylene chloride and petroleum ether gave yellow crystals of compound **2**.

4.6. Method 3

A brown slurry of $Pd(NCPh)_2Cl_2$ (22 mg, 5.7×10^{-2} mmol) in 10 ml of CH_2Cl_2 was treated with $PMes_2H$ (46.5 mg, 0.173 mmol), which gave a homogeneous yellow solution. $^{31}P\{^1H\}$ NMR (CH_2Cl_2): δ −41.0.

4.7. *trans*-$Pt(PMes_2H)_2Cl_2$ (**3**). Method 1

$PMes_2H$ (50 mg, 0.19 mmol) was dissolved in 10 ml of ethanol with gentle heating, then cooled to room temperature. A red–orange solution of K_2PtCl_4 (38 mg, 9.1×10^{-2} mmol) in 14 ml of water was added to the phosphine solution, and a fine white precipitate immediately formed. The mixture was filtered through a fine frit, and the solid was air dried to give 38 mg (51%) of the product as a very fine white powder. Recrystallization from methylene chloride/petroleum ether gave yellow crystals of a methylene chloride solvate. These crystals desolvated under vacuum to give an analytically pure sample.

Anal. Calc. for $C_{36}H_{46}Cl_2P_2Pt$: C, 53.60; H, 5.75. Found: C, 53.58; H, 5.91%. ^1H NMR ($CDCl_3$): δ 6.85 (8H, Mes), 6.66 (m, $J_{PP} = 523$, $J_{PH} = 396$, $J_{P'H} = -2$, 2H, P-H, AA′XX′), 2.53 (24H, *o*-Me), 2.25 (12H, *p*-Me). $^{13}C\{^1H\}$ NMR ($CDCl_3$): δ 142.6 (t, $J = 6$, Mes), 140.7 (Mes), 130.2 (t, $J = 4$, Mes), 121.5 (t, $J = 28$, Mes), 23.5 (t, $J = 4$, *o*-Me), 21.3 (*p*-Me). IR: 2956, 2731, 2404, 1599, 1559, 1446, 1407, 1373, 1289, 1243, 1029, 962, 933, 905, 849, 708, 623, 550, 420.

4.8. Method 2

A CH_2Cl_2 solution of $PtCl_2(NCPh)_2$ (10 mg, 2.2×10^{-2} mmol) was treated with $PMes_2H$ (15 mg, 4.2×10^{-2} mmol). The $^{31}P\{^1H\}$ NMR spectrum of the reaction mixture showed that **3** had formed: δ −37.9 ($J_{Pt-P} = 2506$).

4.9. Method 3

A NMR tube containing a clear solution of *cis*-$PtCl_2(PMes_2H)_2$ (**4**) (20 mg, 2.5×10^{-2} mmol, **4**, see below) in 1 ml of CH_2Cl_2 was suspended about 3 cm from an Ace-Hanovia Photochemical Lamp with a mercury bulb. The tube was irradiated and monitored by $^{31}P\{^1H\}$ NMR. After 9 h the solution was pale yellow and the ^{31}P NMR spectrum showed about 10% conversion of **4** to **3**.

4.10. *cis*-$PtCl_2(PMes_2H)_2$ (**4**)

A solution of $Pt(cod)Cl_2$ (100 mg, 0.267 mmol) in CH_2Cl_2 (4 ml) was treated with $PMes_2H$ (145 mg, 0.535 mmol). Petroleum ether (10 ml) was layered on the methylene chloride and the clear solution was cooled to −20 °C, yielding white crystals after several days. The mother liquor was removed and the crystals dried under vacuum to give 151 mg (70%) of product. ^1H NMR integration and elemental analysis showed that these crystals contained CH_2Cl_2.

Anal. Calc. for $C_{36}H_{46}Cl_2P_2Pt \cdot 0.8CH_2Cl_2$: C, 50.54; H, 5.49. Found: C, 50.12; H, 5.25%. $^{31}P\{^1H\}$ NMR (CD_2Cl_2, 21 °C): δ −47.5 (very broad, $J_{Pt-P} = 3508$). ^1H NMR (CD_2Cl_2, 21 °C): δ 6.78 (broad), 2.39 (very broad), 2.26 (broad). $^{13}C\{^1H\}$ NMR (CD_2Cl_2, 21 °C): δ 142.5 (broad), 141.7, 130.6, 23.7 (broad), 21.1. IR: 3444, 2955, 2911, 2722, 2422, 1600, 1555, 1444, 1405, 1377, 1288, 1255, 1027, 950, 900, 877, 850, 727, 616, 550, 444. FAB mass spectrum (Magic Bullet): *m*/*z* 870, 734 $(PtPMes_2H)(PMes_2)^+$), 600, 463, 343, 271 ($PMes_2H$), 234, 135, 119 (Mes).

^1H NMR (CD_2Cl_2, −70 °C): Three isomers A–C were observed; unless otherwise noted, the ^1H NMR signals are assigned to A and B, with specific assignments given where possible. δ 7.02 (C), 6.98 (d, $J = 3$, 2H, Mes), 6.94 (2H, Mes), 6.91 (C), 6.89 (d, $J = 428$, PH, C), 6.88 (d, $J = 3$, 2H, Mes), 6.86 (C), 6.82 (2H, Mes), 6.78 (C), 6.77 (d, $J = 430$, 2H, PH, B), 6.73 (2H, Mes), 6.68 (2H, Mes), 6.52 (2H, Mes), 6.48 (C), 6.11 (2H, Mes), 5.55 (apparent dd, $J = 408$, 10, 2H, PH, A), 5.16 (apparent dd, $J = 414$, 10, PH, C), 3.41 (6H), 3.37 (6H), 3.33 (C), 3.20 (C), 2.65 (6H), 2.42 (C), 2.26 (6H), 2.23 (6H), 2.22 (6H), 2.08 (6H), 2.07 (6H), 2.03 (C), 1.99 (6H), 1.98 (6H), 1.89 (6H), 1.39 (6H), 1.20 (C), 0.90 (C). $^{13}C\{^1H\}$ NMR (CD_2Cl_2, −60 °C): δ 143.9 (d, $J = 15$), 143.4 (d, $J = 14$), 143.0 (d, $J = 8$), 142.0 (m), 141.5 (m), 141.3 (d, $J = 6$), 141.1 (m), 140.9 (m), 139.9 (m), 139.7 (m), 139.4 (m), 131.0–130.8 (m), 130.3 (d, $J = 10$), 129.7 (m), 129.4 (d, $J = 8$), 129.2 (m), 121.7, 121.2, 118.2, 118.0, 117.9, 117.4, 117.1, 116.7 (m), 27.1 (d, $J = 9$), 26.4 (d, $J = 10$), 22.6–22.2 (m), 21.7 (m), 20.9–20.5 (m).

^1H NMR (C_6D_5Cl, 21 °C): δ 6.53 (broad, Mes), 2.31 (broad, *o*-Me), 2.05 (*p*-Me). ^1H NMR (C_6D_5Cl, 100 °C): δ 6.57 (8H, Mes), 6.34 (d, $J = 414$, 2H, PH), 2.38 (24H, *o*-Me), 2.06 (12H, *p*-Me). $^{31}P\{^1H\}$ NMR (C_6D_5Cl, 21 °C): δ −48.7 (very broad).

4.11. *cis*-Pt(PMes$_2$H)(PPh$_3$)Cl$_2$ (**5**)

PPh_3 (49 mg, 0.19 mmol) was dissolved in methylene chloride (6 ml) to give a clear solution. *cis*-$PtCl_2(PMes_2H)_2$ (100 mg, 0.124 mmol) was added. No color change occurred, and the solid did not dissolve completely. The solution was filtered through Celite to give a yellow filtrate. After the solution was left standing at room temperature overnight, it turned clear. The solution was heated to 45 °C for 5 h using a water bath. The solvent was then removed under vacuum to give white crystals, which were recrystallized from methylene chloride/petroleum ether to give 51 mg (52%) of white solid which was a CH_2Cl_2 solvate, according to the ^{1}H NMR spectrum in $CDCl_3$. Recrystallization from THF/ether gave analytically pure material.

Anal. Calc. for $C_{36}H_{38}Cl_2P_2Pt$: C, 54.14; H, 4.80. Found: C, 54.45; H, 4.60%. ^{1}H NMR (CD_2Cl_2, 21 °C): δ 7.66–7.62 (m, 6H, Ph), 7.47 (m, 3H, Ph), 7.36–7.32 (m, 6H, Ph), 6.89–6.62 (broad, 4H, Mes), 4.89 (dd, J = 409, 12, 1H, PH), 3.42 (broad, 3H, *o*-Me), 2.54 (broad, 3H, *o*-Me), 2.26 (6H, *p*-Me), 1.87 (broad, 3H, *o*-Me), 1.26 (broad, 3H, *o*-Me). ^{1}H NMR (CD_2Cl_2, −20 °C): δ 7.61 (broad, 6H, Ph), 7.48–7.46 (m, 3H, Ph), 7.35–7.32 (m, 6H, Ph), 6.92 (1H, Mes), 6.86 (1H, Mes), 6.75 (1H, Mes), 6.63 (1H, Mes), 4.82 (dd, J = 414, 13, 1H, PH), 3.38 (3H, *o*-Me), 2.50 (3H, *o*-Me), 2.25 (3H, *p*-Me), 2.23 (3H, *p*-Me), 1.85 (3H, *o*-Me), 1.20 (3H, *o*-Me). IR: 3436, 3025, 2919, 2731, 2413, 1601, 1431, 1378, 1096, 1025, 943, 902, 849, 743, 690, 620, 532.

4.12. *cis*-Pt(PMes$_2$H)$_2$(Me)(Cl) (**6**)

A light brown solution of Pt(cod)(Me)(Cl) (100 mg, 0.283 mmol) in CH_2Cl_2 (6 ml) was treated with $PMes_2H$ (153 mg, 0.565 mmol). Petroleum ether (11 ml) was layered on the solution and the mixture was cooled to −20 °C to give 109 mg (49%) of white crystals in two crops.

Anal. Calc. for $C_{37}H_{49}ClP_2Pt$: C, 56.52; H, 6.28. Found: C, 56.43; H, 6.25%. ^{31}P{^{1}H} NMR (CD_2Cl_2, 21 °C): δ −33.9 (J_{Pt-P} = 1492), −45.1 (J_{Pt-P} = 4344). ^{1}H NMR (CD_2Cl_2, 21 °C): δ 6.74 (broad, Mes), 2.34 (broad, *o*-Me), 2.23 (*p*-Me), 0.60 (m, J_{Pt-P} = 50, Pt–Me). ^{1}H NMR (CD_2Cl_2, −70 °C): δ 6.97–6.79 (m, Mes), 6.72–6.67 (m, Mes), 6.59–6.58 (m, Mes), 6.51–6.48 (m, Mes), 6.42 (Mes), 6.37 (apparent dd, J = 449, 5, 1H, PH), 6.10–6.08 (m), 6.03 (Mes), 6.00 (Mes), 5.71 (d, J = 434, 1H, PH), 5.26 (apparent dd, J = 403, 17, 1H, PH), 5.13 (apparent dd, J = 360, 5, 1H, PH), 4.56 (apparent dd, J = 366, 7, 1H, PH), 3.26–3.20 (m, Me), 3.16 (Me), 3.00 (Me), 2.65–2.58 (m, Me), 2.52 (Me), 2.38 (Me), 2.22–2.18 (m, Me), 2.06–2.01 (m, Me), 1.95–1.93 (m, Me), 1.77 (Me), 1.66 (Me), 1.52 (Me), 1.47 (Me), 1.30 (Me), 0.86 (Me), 0.51–0.37 (Pt–Me). ^{13}C{^{1}H} NMR (CD_2Cl_2, 21 °C): δ 142.7 (m), 142.4 (very broad), 140.8 (Mes), 140.6 (Mes), 140.0 (Mes), 130.2 (m, Mes), 123.5 (broad), 122.5, 121.5 (broad), 23.6–22.5 (very broad), 23.1 (m, *o*-Me), 21.1 (*p*-Me), 21.0 (*p*-Me), 3.5 (dd, J = 96, 6, Pt–Me). IR: 3444, 2955, 2911, 2722, 2400, 1600, 1555, 1444, 1405, 1377, 1255, 1200, 1027, 944, 900, 850, 805, 700, 611, 550, 461.

4.13. *cis*-Pt(PMes$_2$H)$_2$(Et)(I) (**7**)

Pt(cod)(Et)(I) (418 mg, 0.910 mmol) was dissolved in methylene chloride (5 ml). $PMes_2H$ (492 mg, 1.82 mmol) was added. Petroleum ether (3 ml) was layered on top of the yellow solution. The solution was refrigerated at 3 °C to give off-white crystals (480 mg, 60%, in two crops).

Anal. Calc. for $C_{38}H_{51}IP_2Pt$: C, 51.18; H, 5.76. Found: C, 51.07; H, 5.85%. ^{1}H NMR ($CDCl_3$): δ 6.71 (broad, 8H, Mes), 2.23 (broad m, 36H, Me), 1.07 (broad, 5H, Et). The PH peaks were not observed. ^{13}C{^{1}H} NMR ($CDCl_3$): δ 143.0 (very broad, Mes), 140.9 (Mes), 140.7 (Mes), 140.0 (Mes), 130.4 (broad m, Mes), 125.4 (Mes), 124.9 (Mes), 121.5 (Mes), 24.1–22.6 (very broad, *o*-Me), 21.8 (*p*-Me), 21.7 (*p*-Me), 21.6 (*p*-Me), 18.8 (CH_2CH_3), 10.4 (d, J = 93, CH_2CH_3). IR: 2915, 2844, 2402, 1603, 1556, 1447, 1407, 1374, 1292, 1263, 1186, 1030, 946, 905, 848, 734, 612, 572, 552, 506, 457, 426, 408. ^{1}H NMR (CD_2Cl_2, 21 °C): δ 6.77 (broad, 8H, Mes) 2.6–2.0 (broad m, *o*-Me), 2.22 (*p*-Me), 1.02 (broad, 5H, Et). The PH signals were not observed. ^{31}P{^{1}H} NMR (CD_2Cl_2, 21 °C): δ −39.9 (very broad, $J_{Pt-P} \approx 4500$) −43.5 (very broad, $J_{Pt-P} \approx 1310$).

^{1}H NMR (CD_2Cl_2, −60 °C): Six different PH groups were observed, confirmed by ^{1}H{^{31}P} NMR: δ 6.82 (obscured by Mes, d, J = 353, 1H, PH), 6.75 (obscured by Mes, d, J = 324, 1H, PH), 5.86 (apparent dd, J = 395, 16, 1H, PH), 5.41 (apparent dd, J = 400, 17, 1H, PH), 5.18 (apparent dd, J = 354, 6, 1H, PH), 4.71 (apparent dd, J = 361, 8, 1H, PH). Additional signals: δ 6.95–6.88 (m, Mes), 6.81–6.79 (m, Mes), 6.69–6.67 (m, Mes), 6.57 (Mes), 6.46 (Mes), 6.35–6.32 (m, Mes), 6.02–5.99 (m, Mes), 3.18–3.17 (m, Me), 3.12–3.11 (m, Me), 3.01 (Me), 2.89 (Me), 2.64 (Me), 2.59 (Me), 2.54 (Me), 2.50 (Me), 2.32–2.27 (m, Me), 2.23–2.18 (broad m, Me), 2.08–2.01 (broad m, Me), 1.99 (Me), 1.91 (Me), 1.88 (Me), 1.85 (Me), 1.80 (Me), 1.76 (Me), 1.66 (Me), 1.50–1.48 (m, Me), 1.33–1.26 (m, Me), 1.16–1.12 (m, Me), 0.94 (Me), 0.83 (Me), 0.71–0.66 (m, Pt–Et), 0.59–0.54 (m, Pt–Et).

4.14. *trans*-Pt(PMes$_2$H)$_2$(Et)(I) (**8**)

cis-PtL_2(Et)(I) (91 mg, 0.10 mmol) was dissolved in approximately 1 ml of $CDCl_3$ to give a yellow solution, which was heated for 4 days at 40 °C and monitored by ^{1}H NMR. When the isomerization to the *trans* compound was complete, the contents of the NMR tube were poured into a vial and petroleum ether was layered

on top. After 3 days, 72 mg (80%) of a bright yellow precipitate formed. Recrystallization from CH_2Cl_2/ether gave analytically pure light yellow crystals.

Anal. Calc. for $C_{38}H_{51}IP_2Pt$: C, 51.18; H, 5.76. Found: C, 50.81; H, 5.80. $^{31}P\{^1H\}$ NMR ($CDCl_3$): δ −39.5 (broad, J_{Pt-P} = ca. 3350). ^1H NMR ($CDCl_3$): δ 6.88 (8H, Mes), 2.48 (broad, Me), 2.30 (broad, Me), 1.10 (q, $J_{H-H}=7$, $J_{Pt-H}=114$, 2H, CH_2CH_3), 0.68 (t, $J_{H-H}=7$, $J_{Pt-H}=70$, 3H, CH_2CH_3). The PH peaks were not observed. $^{13}C\{^1H\}$ NMR (CD_2Cl_2): δ 143.1 (Mes), 140.9 (Mes), 130.6 (Mes), 124.1 (broad, Mes), 23.8 (broad, *o*-Me), 21.5 (*p*-Me), 17.6 (CH_2CH_3), 6.0 ($J_{Pt-C}=671$, CH_2CH_3). IR: 3440, 2953, 2906, 2846, 2728, 2395, 1604, 1556, 1443, 1408, 1378, 1289, 1259, 1200, 1063, 1028, 850, 802, 612, 553, 422.

^1H NMR (CD_2Cl_2, 21 °C): δ 6.96 (8H, Mes), 2.51 (24H, *o*-Mes), 2.42 (12H, *p*-Mes), 1.16 (q, $J_{H-H}=7$, $J_{Pt-H}=83$, CH_2CH_3), 0.73 (t, $J_{H-H}=7$, $J_{Pt-H}=70$, CH_2CH_3). $^{31}P\{^1H\}$ NMR (CD_2Cl_2, 21 °C): δ −39.0 ($J_{Pt-P}=3099$). ^1H NMR (CD_2Cl_2, −70 °C): The four expected PH signals were observed by ^1H and $^1H\{^{31}P\}$ NMR, but their low intensity and the presence of Mes signals precluded detailed analysis of the AA′XX′ patterns. Instead we report the separation between the two most intense lines of these patterns for a given resonance. δ 7.35 (apparent d, J = ca. 400), 7.1 (obscured by Mes), 6.8 (apparent d, $J=355$), 6.15 (apparent d, $J=375$). Additional signals: δ 7.15–6.70 (broad m, Mes), 3.23 (Me), 3.22 (Me), 3.17 (Me), 3.03 (Me), 2.62 (Me), 2.34 (Me), 2.29 (Me), 2.27 (Me), 2.08 (Me), 2.04 (Me), 1.87 (Me), 1.75 (Me), 1.67 (Me), 1.51 (Me), 1.50 (Me), 1.16–1.11 (m, Me), 0.89–0.87 (m, Me), 0.80–0.60 (broad m, Me), 0.45 (m, Pt–Et), 0.29 (m, Pt–Et).

^1H NMR (C_6D_5Cl, 21 °C): δ 6.72 (Mes), 2.52 (*o*-Me), 2.07 (p-Me), 1.35 (m, Pt–Et), 0.84 (m, Pt–Et). The PH resonances were not observed. $^{31}P\{^1H\}$ NMR (C_6D_5Cl, 21 °C): δ −36.8 (very broad, J_{Pt-P} = ca. 3300). ^1H NMR (C_6D_5Cl, 80 °C): δ 7.24 (apparent d, $J=384$, $J_{Pt-H}=26$, perhaps the most intense two peaks of an AA′XX′ pattern), 6.72 (Mes), 2.51 (*o*-Me), 2.08 (*p*-Me), 1.33 (q, $J_{HH}=8$, $J_{Pt-H}=84$, CH_2CH_3), 0.84 (t, $J_{HH}=8$, $J_{Pt-H}=72$, CH_2CH_3).

4.15. $PMes_2H\cdot BH_3$ (**9**)

A clear solution of $PMes_2H$ (300 mg, 1.11 mmol) in THF (6 ml) was cooled to 0 °C and treated with 834 μl of $BH_3\cdot SMe_2$ (1.67 mmol). The solution was warmed to room temperature with stirring. The solvent was removed under vacuum to give a white solid, which was recrystallized from petroleum ether at 0 °C to give large white crystals (297 mg, 95%, in four crops). *Anal.* Calc. for $C_{18}H_{26}BP$: C, 76.08; H, 9.22. Found: C, 75.73; H, 9.37%. $^{31}P\{^1H\}$ NMR (C_6D_6): δ −27.3 (broad). ^{31}P NMR (C_6D_6): δ −27.3 (broad d, $J_{PH}=383$). ^1H NMR (C_6D_6): δ 6.53 (d, $J=3$, 4H, Mes), 6.42 (dq, $J=382$, 8, PH), 2.29 (12H, *o*-Me), 1.96 (6H, *p*-Me). The BH_3 protons were not observed. $^{13}C\{^1H\}$ NMR (C_6D_6): δ 143.0 (d, $J=9$, Mes), 141.1 (d, $J=2$, Mes), 130.8 (d, $J=8$, Mes), 123.4 (d, $J=50$, Mes), 22.3 (d, $J=6$, *o*-Me), 21.2 (*p*-Me). IR: 3445, 3026, 2952, 2732, 2406, 2376, 2338, 2255, 2115, 1725, 1633, 1602, 1446, 1384, 1135, 1061, 1030, 967, 943, 893, 849, 756, 694, 626, 545.

4.16. Crystallographic structural determination

Crystal, data collection, and refinement parameters are given in Table 3. A Siemens P4 diffractometer equipped with a CCD detector was used. The structures were solved using direct methods, completed by subsequent difference Fourier syntheses and refined by full-matrix least-squares procedures. All non-hydrogen atoms were refined anisotropically. The P–H hydrogens were located from the electron difference map and allowed to refine isotropically. All software and sources of the scattering factors are contained in the SHELXTL (5.10) program library (G. Sheldrick, Siemens XRD, Madison, WI). The figures were prepared using either SHELXTL or ORTEP-3 for Windows [31].

4.17. Cone angle calculations

Cone angles were calculated using the program STERIC [21], as previously reported [32]. Hydrogen atoms, as placed in the crystallographic determination, were fixed at a C–H distance of 1.1 Å, and a P–H distance of 1.42 Å [33]. Calculations on **5**·$2CH_2Cl_2$ showed that changing the P–H distance from 1.22 to 1.50 Å had minimal effect (change from 147° to 149°) on the cone angle. The M–P bond distances were fixed at 2.28 Å [22]. The CPK van der Waals radii set was used for all cone angle calculations.

5. Supplementary material

Crystallographic data for the structures reported in this paper have been deposited with the Cambridge Crystallographic Data Centre, CCDC Nos. 181084–181086 and 181088–181089. Copies of this information may be obtained free of charge from The Director, CCDC, 12 Union Road, Cambridge, CB2 1EZ, UK (fax: +44-1223-336033; e-mail: deposit@ccdc.cam.ac.uk or www: http://www.ccdc.cam.ac.uk).

Acknowledgements

We thank the NSF Career Program, DuPont, and Union Carbide (Innovation Recognition Award) for support, and the Department of Education for a GAANN fellowship for M.A.Z. The University of

Delaware acknowledges the NSF (Grant CHE-9628768) for their support of the purchase of the CCD-based diffractometer.

References

[1] W. Levason, in: F.R. Hartley (Ed.), The Chemistry of Organophosphorus Compounds, vol. 1, Wiley, Chichester, England, 1990, pp. 567–641.
[2] For selected examples of secondary phosphine complexes, see: (a) C. Masters, B.L. Shaw, J. Chem. Soc. (A) (1971) 3679; (b) P. Leoni, Organometallics 12 (1993) 2432; (c) H.-C. Bottcher, M. Graf, K. Merzweiler, Polyhedron 16 (1997) 341; (d) R.G. Hayter, J. Am. Chem. Soc. 84 (1962) 3046; (e) R.J. Forder, I.S. Mitchell, G. Reid, R.H. Simpson, Polyhedron 13 (1994) 2129; (f) R. Giannandrea, P. Mastrorilli, C.F. Nobile, Inorg. Chim. Acta 284 (1999) 116; (g) T. Campbell, A.M. Gibson, R. Hart, S.D. Orchard, S.J.A. Pope, G. Reid, J. Organomet. Chem. 592 (1999) 296; (h) M.L. Buil, M.A. Esteruelas, E. Onate, N. Ruiz, Organometallics 17 (1998) 3346; (i) P. Leoni, G. Chiaradonna, M. Pasquali, F. Marchetti, A. Fortunelli, G. Germano, Inorg. Chim. Acta 264 (1997) 185; (j) A. Albinati, F. Lianza, M. Pasquali, M. Sommovigo, P. Leoni, P.S. Pregosin, H. Ruegger, Inorg. Chem. 30 (1991) 4690.
[3] I.V. Kourkine, M.D. Sargent, D.S. Glueck, Organometallics 17 (1998) 125.
[4] M.A. Zhuravel, N.S. Grewal, D.S. Glueck, K.-C. Lam, A.L. Rheingold, Organometallics 19 (2000) 2882.
[5] For complementary studies of mesitylphosphine ($PMesH_2$), see: I.V. Kourkine, S.V. Maslennikov, R. Ditchfield, D.S. Glueck, G.P.A. Yap, L.M. Liable-Sands, A.L. Rheingold, Inorg. Chem. 35 (1996) 6708.
[6] W. de Graaf, J. Boersma, W.J.J. Smeets, A.L. Spek, G. van Koten, Organometallics 8 (1989) 2907.
[7] R.K. Harris, Can. J. Chem. 42 (1964) 2275.
[8] (a) A. Gillie, J.K. Stille, J. Am. Chem. Soc. 102 (1980) 4933; (b) J. Krause, G. Cestaric, K.-J. Haack, K. Seevogel, W. Storm, K.-R. Pörschke, J. Am. Chem. Soc. 121 (1999) 9807.
[9] F.R. Hartley, The Chemistry of Platinum and Palladium, Wiley, New York, 1973.
[10] P. Budzelaar, gNMR, V3.6.5, Cherwell Scientific Publishing, Oxford, 1996.
[11] P.S. Pregosin, R.W. Kunz, ^{31}P and ^{13}C NMR of Transition Metal Phosphine Complexes, Springer-Verlag, New York, 1979.
[12] R.G. Pearson, Inorg. Chem. 12 (1973) 712.
[13] J. Vicente, A. Arcas, D. Bautista, P.G. Jones, Organometallics 16 (1997) 2127.
[14] S.H. Mastin, P. Haake, J. Chem. Soc., Chem. Commun. (1970) 202.
[15] G.K. Anderson, J.A. Davies, D.J. Schoeck, Inorg. Chim. Acta 76 (1983) L251.
[16] A.G. Orpen, L. Brammer, F.H. Allen, O. Kennard, D.G. Watson, R. Taylor, J. Chem. Soc., Dalton Trans. (1989) S1.
[17] G.K. Anderson, H.C. Clark, J.A. Davies, G. Ferguson, M. Parvez, J. Cryst. Spectr. Res. 12 (1982) 449.
[18] F.R. Hartley, Chem. Soc. Rev. 2 (1973) 163.
[19] J.M. Brunel, B. Faure, M. Maffei, Coord. Chem. Rev. 178–180 (1998) 665.
[20] R.A. Bartlett, M.M. Olmstead, P.P. Power, G.A. Sigel, Inorg. Chem. 26 (1987) 1941.
[21] (a) B.C. Taverner, J. Comput. Chem. 17 (1996) 1612; (b) B.C. Taverner, STERIC 1.12B, 1997. Available on the Internet at http://www.gh.wits.ac.za.
[22] C.A. Tolman, Chem. Rev. 77 (1977) 313.
[23] (a) A. Bright, B.E. Mann, C. Masters, B.L. Shaw, R.M. Slade, R.E. Stainbank, J. Chem. Soc. (A) (1971) 1826; (b) R. Giannandrea, P. Mastrorilli, M. Palma, F.P. Fanizzi, U. Englert, C.F. Nobile, Eur. J. Inorg. Chem. (2000) 2573.
[24] C.H. Bushweller, C.D. Rithner, D.J. Butcher, Inorg. Chem. 25 (1986) 1610.
[25] A.B. Pangborn, M.A. Giardello, R.H. Grubbs, R.K. Rosen, F.J. Timmers, Organometallics 15 (1996) 1518.
[26] D. Drew, J.R. Doyle, Inorg. Synth. 28 (1990) 346.
[27] G.K. Anderson, M. Lin, Inorg. Synth. 28 (1990) 60.
[28] J.X. McDermott, J.F. White, G.M. Whitesides, J. Am. Chem. Soc. 98 (1976) 6521.
[29] H.C. Clark, L.E. Manzer, J. Organomet. Chem. 59 (1973) 411.
[30] T.G. Appleton, M.A. Bennett, Inorg. Chem. 17 (1978) 738.
[31] L.J. Farrugia, J. Appl. Cryst. 30 (1997) 565.
[32] J.M. Smith, N.J. Coville, L.M. Cook, J.C.A. Boeyens, Organometallics 19 (2000) 5273.
[33] CRC Handbook of Chemistry and Physics, 71st ed., CRC Press, Boca Raton, FL, 1990.

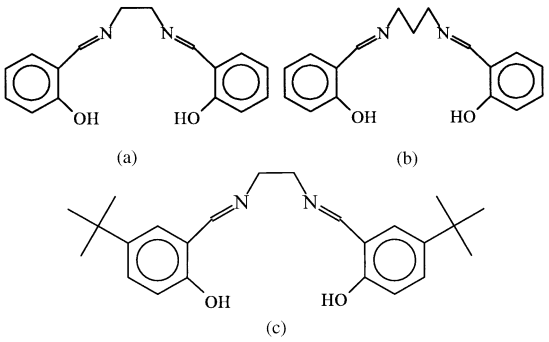


Fig. 1. The ligands: (a) salen; (b) salpn; and (c) *t*-butylsalen.

this steric freedom that makes them an ideal class of ligands for both transition metals and the *f*-block elements. Ligand field effects in most *d*-transition elements favour an arrangement where the equatorial ligands are arranged in an approximately square-planar geometry, whereas the much smaller ligand field effects in the *f*-block elements in combination with a much larger ionic size results in a significantly different coordination geometry for lanthanoid and actinoid elements [6,7,20]. This is further enhanced by the presence of the particularly strong, *trans* O–U–O apical bonds. Hence the ability of the salen type ligands to 'flex' and accommodate both types of geometric requirements impart a degree of stabilization to these systems [21].

Only a limited amount of work has been performed in this area. Early studies investigated the co-crystallisation of UO_2Cl_2 or $UO_2(NO_3)_2$ from methanol in the presence of the salen ligand, and the ethanol adduct of the more sterically rigid [*N*,*N*′-*o*-phenylenebis(salicylideneimine)](phenylsalen) (Fig. 2) [21].

The uranyl ion can also be used as a template ion, and the two constituents of salen (salicylaldehyde and ethylendiamine) were combined in the presence of the metal salt, with the metal facilitating the Schiff base reaction. This yielded complexes of the formula $[UO_2(salen)(X)]$, (where X = ethanol or methanol). The general structural motif involves the salen ligand bound in a tetradentate fashion surrounding the equatorial axis of the uranyl coordination sphere, while a solvent molecule occupies a fifth equatorial position, resulting in distorted pentagonal bipyramidal geometry. This conformation was observed for both the basic salen ligand and the phenyl derivative [14]. Studies involving the more sterically flexible salpn ligand have not revealed any recorded uranyl complexes [22–25].

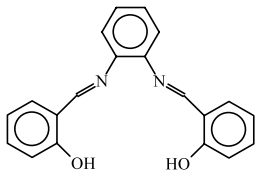


Fig. 2. The phenylsalen ligand, containing the aromatic linker group rather than the ethylene or propylene group.

These studies were undertaken some time ago, hence they were unable to make a detailed study of the crystal packing of the molecule. Modern advancements in X-ray diffraction technology have enabled a more detailed characterization to be undertaken in an effort to elucidate how incorporated solvent molecules may affect the molecular geometry and crystal packing as a whole. We report here-in the synthesis and X-ray crystal characterization of $[UO_2(salen)H_2O]$ (**1**), $[UO_2(salen)EtOH]$ (**2**), $[UO_2(salen)DMSO]$ (**3**), $[UO_2(t\text{-butylsalen})py]$ (**4**), $[UO_2(salpn)MeOH]$ (**5**), $[UO_2(salpn)EtOH]$ (**6**), $[UO_2(salpn)py]$ (**7**), and $[UO_2(NO_3)_2(salpn)]$ (**8**).

2. Experimental

$UO_2(NO_3)_2\cdot 6H_2O$, was purchased from Aldrich and used without purification. Salen and salpn were all synthesised according to literature methods [19,26]. Dimethyl sulfoxide, Py, EtOH and MeOH were purchased from Aldrich and freshly distilled prior to use. IR spectra were recorded in the range of 4000–400 cm^{-1} on KBr plates as Nujol mulls on a Nicolet Nexus FTIR spectrophotometer. Microanalyses were carried out at James Cook University on a Carlo Erba EA 1109 C, H, N by Brian Foster.

2.1. $[UO_2(salen)H_2O]$ (1)

Uranyl nitrate (0.05 g, 0.0996 mmol), was dissolved in a minimum of water, then added to an equimolar solution (0.027 g, 0.1007 mmol) of salen in water (10–20 cm^3). Vigorous heating was used to affect dissolution. The solution was filtered and left open to the atmosphere at ambient conditions, upon which yellow X-ray quality crystals formed after several days. *Anal*. Calc. for $C_{16}H_{16}N_2O_5U$: H, 2.91; C, 34.67; N, 5.05. Found: H, 2.40; C, 33.89; N, 5.39%; IR (Nujol): 1625(m), 1594(m), 1305(w), 1035(w), 904(m), 427(s) cm^{-1}.

2.2. $[UO_2(salen)EtOH]$ (2)

Uranyl nitrate (0.05 g, 0.0996 mmol), was dissolved in a minimum of water, then added to an equimolar solution (0.027 g, 0.1007 mmol) of salen in EtOH (10–20 cm^3). Vigorous heating was used to affect dissolution. The solution was filtered and left open to the atmosphere at ambient conditions, upon which deep yellow, X-ray quality crystals formed after several days. Complex analysed similar to the values reported in the literature [27]. IR (Nujol): 1622(s), 1604(w), 1308(s), 1274(m), 911(s), 663(m) cm^{-1}.

2.3. [UO_2(salen)DMSO] (**3**)

Uranyl nitrate (0.05 g, 0.0996 mmol), was dissolved in a minimum of DMSO, then added to an equimolar solution (0.027 g, 0.1007 mmol) of salen in DMSO (5–10 cm^3). Vigorous heating was used to affect dissolution. The solution was left open to the atmosphere at ambient conditions, upon which deep orange X-ray quality crystals formed after several weeks. *Anal*. Calc. for $C_{18}H_{20}N_2O_5SU$: H, 3.28; C, 35.19; N, 4.56. Found: H, 3.48; C, 35.65, N, 4.43%; IR (Nujol): 1598(w), 1300(m), 1185(m), 891(s), 743(w) cm^{-1}.

2.4. [UO_2(*t*-butylsalen)py] (**4**)

Uranyl nitrate (0.05 g, 0.0996 mmol), was dissolved in a minimum of Py, then added to an equimolar solution of *t*-butyl(salen) (0.03625 g, 0.0857 mmol) in Py (10–20 cm^3). Vigorous heating was used to affect dissolution. The solution was filtered and left open to the atmosphere at ambient conditions, upon which blood red X-ray quality crystals formed after several days. *Anal*. Calc. for $C_{29}H_{35}N_3O_4U_1$: H, 4.85; C, 47.87; N, 5.77. Found: H, 4.92; C, 47.84; N, 5.82%; IR (Nujol): 1625(s), 1547(w), 1299(m), 894(s), 751(w) cm^{-1}.

2.5. [UO_2(salpn)MeOH] (**5**)

Uranyl nitrate (0.05 g, 0.0996 mmol), was dissolved in a minimum of MeOH, then added to an equimolar solution of (salpn) (0.02808 g, 0.0996 mmol) in MeOH (10–20 cm^3). Vigorous heating was used to affect dissolution. The solution was filtered and left open to the atmosphere at ambient conditions, upon which deep yellow X-ray quality crystals formed after several days. *Anal*. Calc. for $C_{18}H_{20}N_2O_5U$: H, 3.46; C, 37.12; N, 4.81. Found: H, 3.45; C, 36.65; N, 5.05%; IR (Nujol): 1650(s), 1605(s), 1308(m), 1272(m), 1022(s), 918(s), 722(m) cm^{-1}.

2.6. [UO_2(salpn)EtOH] (**6**)

Uranyl nitrate (0.05 g, 0.0996 mmol), was dissolved in a minimum of EtOH, then added to an equimolar solution of (salpn) (0.028 g, 0.0993 mmol) in EtOH (10–20 cm^3). Vigorous heating was needed to effect dissolution. The solution was filtered and left open to the atmosphere at ambient conditions, upon which yellow X-ray quality crystals formed after several days. *Anal*. Calc. for $C_{19}H_{22}N_2O_5U$: H, 3.72; C, 38.26; N, 4.70. Found: H, 3.47; C, 38.55; N, 4.85%; IR (Nujol): 1654(s), 1605(s), 1280(m), 1049(s), 902(m), 762(m) cm^{-1}.

2.7. [UO_2(salpn)py] (**7**)

Uranyl nitrate (0.05 g, 0.0996 mmol), was dissolved in a minimum of Py, then added to an equimolar solution of (salpn) (0.02808 g, 0.0996 mmol) in Py (10–20 cm^3). Vigorous heating was used to affect dissolution. The solution was filtered and left open to the atmosphere at ambient conditions, upon which dark orange X-ray quality crystals formed after several days. Repeated attempts to obtain meaningful microanalysis were prevented due to the apparent loss of solvent from the crystalline material. IR (Nujol): 1625(s), 1598(s), 894(s), 662(m), 743(m), 529(s) cm^{-1}.

2.8. [$UO_2(NO_3)_2$(salpn)] (**8**)

Uranyl nitrate (0.05 g, 0.0996 mmol), was dissolved in a minimum of water, then added to an equimolar solution of (salpn) (0.02808 g, 0.0996 mmol) in water (10–20 cm^3). Vigorous heating was used to affect dissolution. The solution was filtered and left open to the atmosphere at ambient conditions, upon which dark red X-ray quality crystals formed after several days. *Anal*. Calc. for $C_{17}H_{18}N_4O_{10}U$: H, 2.10; C, 30.37; N, 8.33. Found: H, 2.46; C, 30.80; N, 9.77%; IR (Nujol): 3385(m), 1650(s), 1605(s), 1308(m), 1274(m), 1022(s), 918(s), 863(w), 757(m) cm^{-1}.

2.9. X-ray determinations

For compounds **1**–**8** hemispheres of data were collected (capillary sealed specimens) at room temperature on a Bruker SMART CCD diffractometer using the omega scan mode with total reflections and unique data listed below. Data sets were corrected for absorption using the program SADABS [28]. The structures were solved using the Patterson method for heavy atoms and refined on F^2 using SHELXL-97-2 [29] with X-SEED as the graphic interface [30]. All non-hydrogen atoms were located and were refined with anisotropic thermal parameters. Hydrogen atoms were placed in calculated positions (riding model) and were not refined. Crystal data and a summary of data collection appear below, while selected bond distances and angles appear in Tables 1–3; hydrogen bonding tables for compounds **1**, **2**, **5** and **6** are found in Table 4.

2.10. [UO_2(salen)H_2O] (**1**)

$C_{16}H_{16}N_2O_5U$, $M = 554.34$, triclinic, space group $P\bar{1}$ (No. 2), $a = 8.237(3)$, $b = 9.335(4)$, $c = 11.562(5)$ Å, $\alpha = 77.830(7)^\circ$, $\beta = 75.638(6)^\circ$, $\gamma = 75.964(6)^\circ$, $V = 824.7(6)$ $Å^3$, $Z = 2$, $D_{calc} = 2.232$ g cm^{-3}, yellow prismatic, $0.20 \times 0.20 \times 0.18$ mm, $F(000) = 516$, $2\theta_{max} = 46.5^\circ$, 3695 reflections collected, 2330 unique ($R_{int} = 0.0536$). Final goodness-of-fit = 1.023, $R_1 = 0.0330$, $wR_2 =$

Table 1
The uranium environment in uranyl salen complexes **1**–**4**

Atoms	*r*	O(2)	O(3)	O(4)	O(5) [a]	N(1)	N(2)
O(1)	2.277(5)	157.5(2)	90.6(2)	88.4(2)	78.91(18)	69.76(18)	132.79(18)
	2.238(6)	155.5(2)	90.2(3)	91.2(4)	78.7(2)	70.0(2)	135.2(2)
	2.256(6)	153.7(3)	91.2(4)	89.3(3)	77.3(3)	70.3(3)	136.1(32)
	2.252(6)	153.2(2)	90.8(3)	90.0(3)	76.0(2)	69.8(2)	136.8(2)
O(2)	2.286(5)		85.3(2)	95.7(2)	79.11(17)	131.58(18)	69.68(17)
	2.296(5)		87.5(2)	90.6(4)	76.9(2)	134.1(2)	69.3(2)
	2.241(7)		89.7(4)	92.2(3)	76.4(3)	136.0(3)	70.3(3)
	2.231(6)		90.0(3)	90.6(3)	77.1(2)	137.0(2)	70.0(2)
O(3)	1.769(5)			178.98(19)	91.1(2)	85.2(2)	97.2(2)
	1.770(6)			177.7(4)	91.8(2)	87.0(2)	92.9(2)
	1.750(6)			176.8(3)	92.1(3)	88.7(3)	89.8(4)
	1.760(6)			177.1(3)	91.6(2)	88.0(2)	89.7(2)
O(4)	1.764(5)				88.7(2)	94.5(2)	83.0(2)
	1.766(7)				89.1(3)	93.3(3)	85.2(3)
	1.758(7)				91.0(3)	88.6(3)	87.6(3)
	1.760(5)				91.3(2)	89.6(2)	87.8(2)
O(5) [a]	2.430(5)					148.39(18)	146.57(17)
	2.420(6)					148.7(2)	145.7(2)
	2.414(6)					147.6(3)	146.5(3)
	2.640(6)					145.8(2)	147.1(2)
N(1)	2.548(6)						64.84(18)
	2.558(7)						65.2(2)
	2.545(9)						65.8(3)
	2.560(7)						67.1(2)
N(2)	2.563(6)						
	2.567(7)						
	2.584(8)						
	2.580(7)						

r is the metal–ligand distance (Å); other entries in the matrices are the angles subtended by the relevant atoms at the head of the rows and columns. Values are listed in the order water, ethanol, DMSO, pyridine adducts.
[a] O(5) becomes N(3) for the pyridine adduct.

0.0821, *R* indices based on 2210 reflections with $I > 2\sigma(I)$ (refinement on F^2), 226 parameters, 3 restraints.

2.11. [UO_2(salen)EtOH] (**2**)

$C_{18}H_{20}N_2O_5U$, $M = 582.39$, monoclinic, space group $P2_1/c$ (No. 14), $a = 11.4563(13)$, $b = 8.3041(10)$, $c = 21.053(2)$ Å, $\beta = 102.417(2)^\circ$, $V = 1956.0(4)$ Å^3, $Z = 4$, $D_{calc} = 1.978$ g cm^{-3}, yellow prismatic, $0.45 \times 0.40 \times 0.20$ mm, $F(000) = 1096$, $2\theta_{max} = 46.5^\circ$, 3695 reflections collected, 2330 unique ($R_{int} = 0.0536$). Final goodness-of-fit = 0.949, $R_1 = 0.0526$, $wR_2 = 0.1147$, *R* indices based on 2210 reflections with $I > 2\sigma(I)$ (refinement on F^2), 248 parameters, 0 restraints.

2.12. [UO_2(salen)DMSO] (**3**)

$C_{18}H_{20}N_2O_5SU$, $M = 614.45$, orthorhombic, space group $P2_12_12_1$ (No. 19), $a = 8.1834(6)$, $b = 13.4278(10)$, $c = 18.1953(13)$ Å, $V = 1999.4(3)$ Å^3, $Z = 4$, $D_{calc} = 2.041$ g cm^{-3}, orange prismatic, $0.14 \times 0.12 \times 0.10$ mm, $F(000) = 1160$, $2\theta_{max} = 46.5^\circ$, 3695 reflections collected, 2330 unique ($R_{int} = 0.0536$). Final goodness-of-fit = 1.196, $R_1 = 0.0365$, $wR_2 = 0.0667$, *R* indices based on 2210 reflections with $I > 2\sigma(I)$ (refinement on F^2), 246 parameters, 0 restraints.

2.13. [UO_2(*t*-butylsalen)py] (**4**)

$C_{29}H_{35}N_3O_4U$, $M = 727.63$, trigonal, space group *R*-3 (No. 148), $a = b = 47.160(2)$, $c = 7.2087(5)$ Å, $V = 13884.8(14)$ Å^3, $Z = 18$, $D_{calc} = 1.566$ g cm^{-3}, red prismatic, $0.10 \times 0.08 \times 0.05$ mm, $F(000) = 6372$, $2\theta_{max} = 46.5^\circ$, 3695 reflections collected, 2330 unique ($R_{int} = 0.0536$). Final goodness-of-fit = 0.885, $R_1 = 0.0408$, $wR_2 = 0.0780$, *R* indices based on 2210 reflections with $I > 2\sigma(I)$ (refinement on F^2), 369 parameters, 48 restraints.

2.14. [UO_2(salpn)MeOH] (**5**)

$C_{18}H_{20}N_2O_5U$, $M = 582.39$, monoclinic, space group $P2_1/n$ (No. 14), $a = 10.3813(10)$, $b = 9.1780(9)$, $c = 20.298(2)$ Å, $\beta = 98.548(2)^\circ$, $V = 1912.5(3)$ Å^3, $Z = 4$,

Table 2
The uranium environment in uranyl salpen solvent adduct complexes **5**–**7**

Atoms	*r*	O(2)	O(3)	O(4)	O(5) [a]	N(1)	N(2)
O(1)	2.301(3)	151.29(13)	91.06(14)	87.97(15)	75.14(13)	68.75(12)	138.88(13)
	2.237(13)	151.5(5)	93.1(5)	88.4(5)	77.3(5)	68.8(5)	138.9(5)
	2.230(9)	150.5(3)	90.7(4)	89.8(4)	76.0(3)	70.2(3)	139.9(3)
O(2)	2.237(3)		93.63(15)	88.01(15)	76.57(13)	139.41(12)	69.65(12)
	2.279(14)		90.7(5)	88.5(5)	74.4(5)	139.6(5)	69.2(5)
	2.243(8)		93.0(4)	87.8(4)	75.1(3)	138.8(3)	69.5(3)
O(3)	1.782(4)			178.08(17)	89.69(17)	90.45(15)	88.19(14)
	1.771(12)			178.2(6)	90.2(6)	89.1(5)	90.5(6)
	1.765(8)			177.6(4)	86.3(3)	91.8(3)	84.0(3)
O(4)	1.766(4)				91.67(17)	87.66(16)	91.45(14)
	1.756(11)				91.2(6)	90.4(5)	87.7(5)
	1.781(7)				96.1(4)	86.2(3)	94.2(4)
O(5) [a]	2.463(4)					143.89(12)	145.94(13)
	2.475(15)					146.1(5)	143.6(5)
	2.632(11)					146.1(4)	142.7(3)
N(1)	2.588(4)						70.14(12)
	2.556(15)						70.3(5)
	2.565(9)						70.3(3)
N(2)	2.565(4)						
	2.611(16)						
	2.587(9)						

r is the metal–ligand distance (Å); other entries in the matrices are the angles subtended by the relevant atoms at the head of the rows and columns. Values are listed in the order methanol, ethanol, pyridine adducts.
[a] O(5) becomes N(3) for the pyridine adduct.

$D_{calc} = 2.023$ g cm^{-3}, yellow prismatic, $0.40 \times 0.40 \times 0.35$ mm, $F(000) = 1096$, $2\theta_{max} = 46.5°$, 3695 reflections collected, 2330 unique ($R_{int} = 0.0536$). Final goodness-of-fit = 1.048, $R_1 = 0.0243$, $wR_2 = 0.0607$, R indices based on 2210 reflections with $I > 2\sigma(I)$ (refinement on F^2), 241 parameters, 0 restraints.

2.15. [UO_2(salpn)EtOH] (**6**)

$C_{19}H_{22}N_2O_5U$, $M = 554.34$, monoclinic, space group $P2_1/n$ (No. 14), $a = 8.237(3)$, $b = 9.335(4)$, $c = 11.562(5)$ Å, $\beta = 75.638(6)°$, $V = 824.7(6)$ Å^3, $Z = 2$, $D_{calc} = 2.232$ g cm^{-3}, yellow prismatic, $0.20 \times 0.20 \times 0.18$ mm, $F(000) = 516$, $2\theta_{max} = 46.5°$, 3695 reflections collected, 2330 unique ($R_{int} = 0.0536$). Final goodness-of-fit = 1.024, $R_1 = 0.0330$, $wR_2 = 0.0822$, R indices based on 2210 reflections with $I > 2\sigma(I)$ (refinement on F^2), 226 parameters, 3 restraints.

2.16. [UO_2(salpn)py] (**7**)

$C_{22}H_{21}N_3O_4U$, $M = 629.45$, orthorhombic, space group *Pbca* (No. 61), $a = 12.2140(7)$, $b = 9.7057(6)$, $c = 35.618(2)$ Å, $V = 4222.4(4)$ Å^3, $Z = 8$, $D_{calc} = 1.980$ g cm^{-3}, orange prismatic, $0.15 \times 0.15 \times 0.12$ mm, $F(000) = 2384$, $2\theta_{max} = 46.5°$, 3695 reflections collected, 2330 unique ($R_{int} = 0.0536$). Final goodness-of-fit = 1.017, $R_1 = 0.0483$, $wR_2 = 0.1228$, R indices based on 2210 reflections with $I > 2\sigma(I)$ (refinement on F^2), 272 parameters, 0 restraints.

Table 3
The uranium environment in uranyl salpen nitrate adduct complex **8**

Atoms	*r*	O(2)	O(3)	O(4)	O(5)	O(6)	(O8)	O(9)
O(1)	2.321(6)	71.5(2)	93.9(3)	85.8(2)	66.6(2)	115.9(2)	169.3(2)	136.8(2)
O(2)	2.300(5)		92.1(2)	87.9(2)	137.9(2)	171.88(18)	113.8(2)	65.5(2)
O(3)	1.769(5)			179.7(2)	86.9(2)	84.2(3)	95.2(3)	91.6(3)
O(4)	1.773(5)				93.0(2)	95.9(3)	85.1(3)	88.7(3)
O(5)	2.574(6)					49.3(2)	59.6(2)	107.3(2)
O(6)	2.566(6)						59.6(2)	48.6(2)
O(8)	2.565(4)							
O(9)	2.543(6)							

r is the metal–ligand distance (Å); other entries in the matrices are the angles subtended by the relevant atoms at the head of the rows and columns.

Table 4
Hydrogen bonding for complexes **1**, **2**, **5** and **6**

Complex	D–H···A	d(D–H)	d(H···A)	d(D···A)	<(DHA)
1	O(5)–H(5A)···O(2)#1	0.996(10)	1.81(3)	2.760(7)	159(8)
	O(5)–H(5B)···O(1)#2	0.996(10)	1.80(2)	2.780(7)	166(8)
2 [a]	O(5)–H(5A)···O(2)#1	0.93	1.70	2.593(8)	161.2
5	O(5)–H(5A)···O(1)#1	0.65(4)	1.99(5)	2.629(6)	168(6)
6	O(5)–H(5E)···O(2)#1	0.99(19)	1.77(19)	2.66(2)	149(17)

D is the donor atom, A is acceptor atom. Distances given in Å, angles in °. #, signifies atoms generated through symmetry.
[a] No e.s.d.'s given due to hydrogen atom being fixed.

2.17. $[UO_2(NO_3)_2(salpn)]$ (**8**)

$C_{17}H_{18}N_4O_{10}U$, $M = 676.38$, triclinic, space group $P\bar{1}$ (No. 2), $a = 9.7300(9)$, $b = 9.7786(9)$, $c = 13.4225(12)$ Å, $\alpha = 83.658(2)^\circ$, $\beta = 72.088(2)^\circ$, $\gamma = 61.6390(10)^\circ$, $V = 1068.37(17)$ Å^3, $Z = 2$, $D_{calc} = 2.103$ g cm^{-3}, red prismatic, $0.30 \times 0.30 \times 0.20$ mm, $F(000) = 640$, $2\theta_{max} = 46.5^\circ$, 3695 reflections collected, 2330 unique ($R_{int} = 0.0536$). Final goodness-of-fit = 1.055, $R_1 = 0.0335$, $wR_2 = 0.0879$, R indices based on 2210 reflections with $I > 2\sigma(I)$ (refinement on F^2), 297 parameters, 0 restraints.

3. Results and discussion

This study was undertaken in an effort to establish what effect the supporting solvent exerts upon the modes of crystallisation of uranyl Schiff base complexes. The synthesis of these complexes involved the mixing of uranyl nitrate and the salen species in the appropriate solvent. In most cases, these ligands displayed only partial solubility, hence vigorous heating was generally required to affect dissolution. The resulting solutions were then filtered and left to crystallise by gradual evaporation. The crystals were intensely coloured, either red or yellow, as would be expected from the highly conjugated nature of these ligands. The IR spectra all contained (C=N) stretches at approximately 1625 and 1594 cm^{-1}.

All the complexes adopt a similar morphology about the uranium centre, in which the Schiff base ligands are tetradentate and adopt a stepped conformation when viewed along the equatorial plane. This is very similar to the [UO_2(salen)MeOH] adduct obtained in a previous study [14]. The angle between the planes of the two aromatic rings deviates slightly from coplanar for the salen ligands, however they are close-to-coplanar for the salpn ligands. In all solvent adducts, pentagonal bipyramidal geometry about U is observed, with four of the equatorial sites about the uranium centre occupied by the Schiff base ligand, while the remaining available area is occupied by a solvent molecule. Oxo ligands occupy the axial sites and the uranyl nitrate species (**8**) contains no solvent molecules, and the salpn ligand acts in a bidentate fashion, with the remainder of the coordination sphere occupied by the bidentate nitrate ions. These compounds exist as monomers unless the coordinated solvent molecules contain hydrogen bond donors, in which case dimers are formed through hydrogen bonding.

3.1. Salen complexes

The eight uranyl complexes will be grouped together according to the salen type involved in the complex, and discussed together so a comparison can be made between these similar complexes. The four salen complexes all crystallise in different space groups, but possess similar asymmetric units. The water adduct [UO_2(salen)H_2O] (**1**) (Fig. 3 crystallises in the centrosymmetric space group $P\bar{1}$, while the ethanol adduct [UO_2(salen)EtOH] (**2**) (Fig. 4) crystallises in $P2_1/c$.

In both these complexes, the coordinated solvent molecules possess hydrogen bonding donor species, and this results in the formation of a hydrogen bonded dimer about an inversion centre through a $O_{(solvent)}$–H···$O_{(salen)}$ interaction (Figs. 3 and 4). These hydrogen

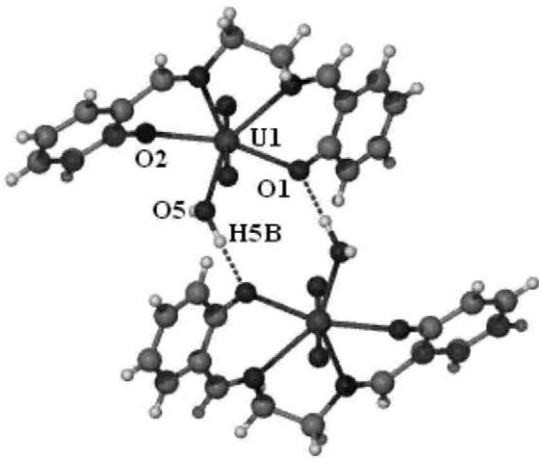


Fig. 3. X-ray crystal structure of the hydrogen-bonded dimer [UO_2(salen)H_2O] (**1**).

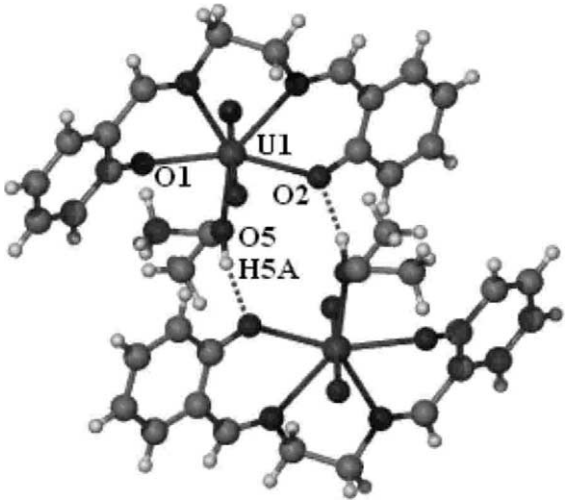


Fig. 4. X-ray crystal structure of the hydrogen-bonded dimer [UO_2(salen)EtOH] (**2**). The methyl group of ethanol molecule is disordered over two sites.

bonding interactions result in the complex packing in rows of zigzagging, polymeric chains where each molecule is linked to an adjacent molecule via the solvent ligand.

In contrast, the DMSO adduct [UO_2(salen)DMSO] (**3**) (Fig. 5) crystallises in the acentric space group $P2_12_12_1$, while the pyridine adduct [UO_2(*t*-butylsalen)py] (**4**) (Fig. 6) crystallises in the space group R-3. Neither of these two latter species contain hydrogen bonding, hence they both crystallise as discrete monomeric units, and are less ordered in terms of crystal packing.

The equatorial geometry surrounding the uranyl centres for all four compounds is distorted pentagonal bipyramidal. The average lengths of the apical uranyl oxygen bonds U1–O3 and U1–O4 (both average 1.76 Å) are in close agreement with other uranyl complexes of this type (average 1.77 Å) [14,21], illustrating how the coordination environment surrounding the uranyl cation has very little effect on the apical bond lengths. The

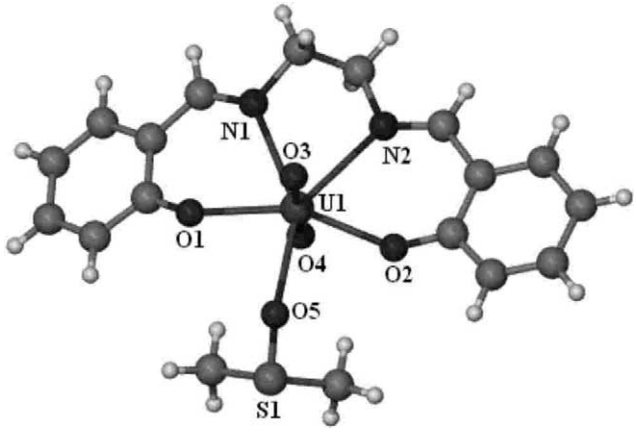


Fig. 5. X-ray crystal structure of monomeric [UO_2(salen)DMSO] (**3**).

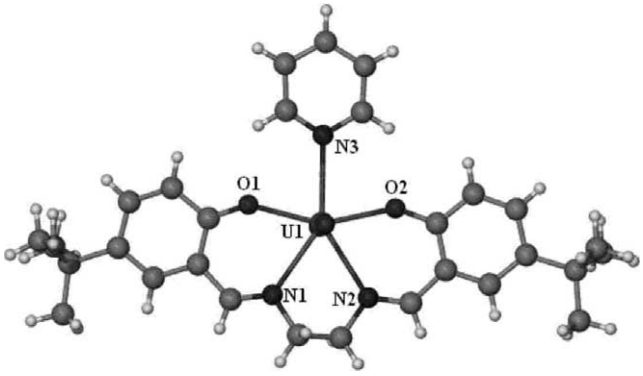


Fig. 6. X-ray crystal structure of monomeric [UO_2(*t*-butylsalen)py] (**4**).

imino–uranium bonds are asymmetric, and the bond lengths of U1–N1 (range of 2.545(9)–2.560(7) Å), U1–N2 (range of 2.563(6)–2.584(8) Å) all fall within the range expected for these types of compounds [14,21].

Previous work by Bandoli et al. investigated both the salen methanol and ethanol adducts, as well as the ethanol adduct of the more sterically rigid [*N*,*N*′-*o*-phenylenebis(salicylideneiminato)UO_2] (phenylsalen) [14,21] and found that all three species crystallised in the dimeric form and contained distorted pentagonal bipyramidal geometry around the uranium metal centre, and the U–$O_{(salen)}$ (range of 2.245(14)–2.330(32) Å) and U–N (range of 2.542(47)–2.572(24) Å) bond lengths were very similar to those reported here. In the case of the ethanol adduct, we discovered disorder in the coordinated ethanol molecule of the salen adduct which was overlooked in the previous study, but they did have extraordinarily large thermal parameters on these C-atoms. This has been included in this study.

The salen ligand has an advantage over cyclic ligands of a polydentate nature in that free rotation between the aromatic planes allow the ligand freedom to orientate the two donor oxygens for favourable U–$O_{(salen)}$ interactions, hence alleviating excess steric repulsions around the uranyl centre. This steric freedom can be influenced by the solvent ligand, illustrated by comparing the plane of the salen phenol rings between the four different compounds.

For **1** and **2**, there is a distinct difference between the planes of opposing phenol rings whereas the corresponding angle deviations for **3** and **4** are far less pronounced. This difference in conformation may be attributed to the hydrogen bonding of the dimeric species anchoring the two monomers together, slightly decreasing the steric freedom. As a result the angles between the apical uranyl–oxygen bond and the five equatorial atoms of **1** and **2** (83.0(2)°–97.2(2)°) show a greater deviation from perpendicular than those of **3** and **4** (87.6(3)°–92.1(3)°), in which hydrogen bonding is absent. The torsion angle between the two nitrogen donor atoms is also narrower for complexes **1** and **2**

(50.06(85)° and 56.62(93)°, respectively), than **3** and **4** (61.41(120)° and 58.95(100)°, respectively) suggesting that the latter are less sterically strained. This is further exemplified by the position of the pyridine ligand in **4**, the plane of which resides almost parallel to the aromatic planes of the phenols. The presence of any significant steric repulsions between the salen ligand the solvent molecule would result in rotation of the pyridine around the $C_{(salen)}$–$N_{(pyridine)}$ bond and this is not observed.

Closer examination of **1** and **2** show the *trans* phenol rings of opposing uranyl units in both dimers align in the same plane, that extends throughout the entire crystal lattice, suggesting π–π stacking may be influencing the crystal packing, however the degree of separation of the aromatic groups precludes this, hence is probably a result of the separation of molecules enforced by the uranyl oxygens. Therefore, the alignment of the aromatic groups must simply be a result of the crystal packing at close to van der Waal separations.

For complexes **3** and **4**, the lack of hydrogen bonding results in the packing of the crystal lattice being solely dependent on the geometry of the uranyl molecule. This is especially true for the DMSO species and demonstrates how the DMSO molecule causes this species to crystallise in repeating helical rows containing a 2_1 screw that extends through the lattice. The resulting crystal displays chirality as a whole, even though the monomeric unit does not.

Even though the aromatic planes of adjacent molecules are coplanar, the distance between aromatic moieties is too great for any significant π–π interactions within the crystal lattice. This coplanarity must therefore again simply be a result of the crystal packing.

Solvent effects again dominate the crystal packing of **4**, although in a significantly different way. This species is a trigonal crystal system, containing a threefold rotational axis. The large steric bulk of the pyridine ligand, along with the presence of the *t*-butyl groups imposes steric limitations on the packing of this molecule. As such there appears to be no significant interactions between rows, rather they are arranged such as steric limitations allow.

There is surprisingly little difference in the U–$O_{(solvent)}$ bond lengths in all three X-ray crystal structures (2.430(5), 2.420(6) and 2.414(6) Å in compounds **1**, **2** and **3**, respectively). Considering the difference in donor strength between these ligands, these distances do not vary significantly and may be dominated by the macrocyclic ligand. The U–$O_{(pyridyl)}$ bond length in **4** (2.640(6) Å) is significantly longer, as expected, than the U–O lengths above.

These four cases demonstrate clearly how, even though the geometry of several closely related uranyl species do not appear to be significantly different, the coordinated solvent can impart a great influence on the overall morphology of the crystal.

3.2. Salpn complexes

The solvent adducts of the uranyl–salpn complexes possess similar geometry directly adjacent to the uranyl centre, however the extended propyl carbon bridge linking the amino units allows them greater steric freedom to orientate favourably around the uranyl moiety and reduce steric interference.

These solvent adducts adopt an asymmetric unit consisting of a single uranyl cation surrounded by a single doubly deprotonated salpn ligand and a single coordinated solvent molecule. The methanol adduct $[UO_2(salpn)MeOH]$ (**5**) (Fig. 7) and the ethanol adduct $[UO_2(salpn)EtOH]$ (**6**) (Fig. 8) crystallise in the monoclinic space group $P2_1/n$ and are structurally very similar to **1** and **2**, again forming a hydrogen bonded dimeric unit. The pyridine adduct $[UO_2(salpn)py]$ (**7**) crystallises in the orthorhombic space group *Pbca*, exists as the discrete monomer and contains no hydrogen bonding (Fig. 9).

The nitrate analogue **8**, however, contains a completely separate morphology in that no solvent is incorporated into the coordination sphere of the uranyl cation, hence the two *bidentate* nitrate anions occupy the four additional coordination sites. This restricts the available coordination sites for the ligand and distorts the salpn ligand into a bidentate, cupped U-shape, illustrating clearly the conformational freedom this ligand possesses (Fig. 10). This has ramifications when considering the packing of the crystal lattice (see below). However, the reason that the nitrates remain coordinated in this case,

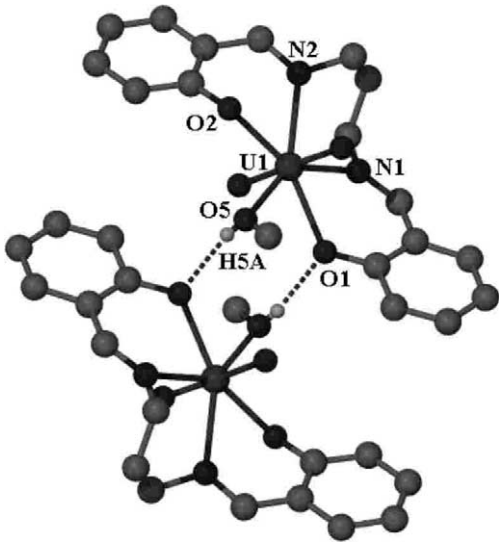


Fig. 7. X-ray crystal structure of the hydrogen-bonded dimer $[UO_2(salpn)MeOH]$ (**5**). Hydrogen atoms except those on the solvent have been omitted for clarity.

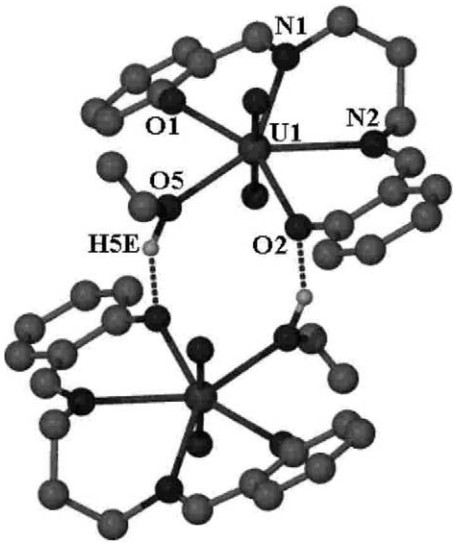


Fig. 8. X-ray crystal structure of the hydrogen-bonded dimer $[UO_2(salpn)EtOH]$ (**6**). Hydrogen atoms except those on the solvent have been omitted for clarity.

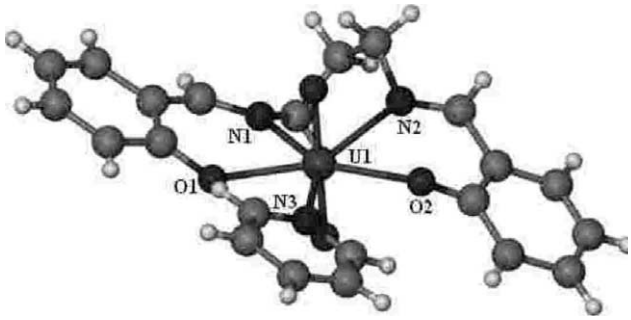


Fig. 9. The X-ray crystal structure of monomeric $[UO_2(salpn)py]$ (**7**).

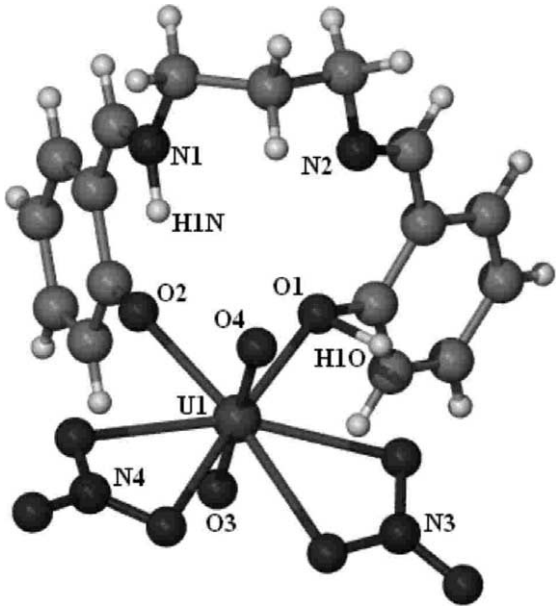


Fig. 10. The X-ray crystal structure of $[UO_2(NO_3)_2(salpn)]$ (**8**).

even though the complex was synthesised in water remains unclear but presumably arose from pH dependency.

The geometry surrounding the uranyl centre for the solvent adducts is again distorted pentagonal bipyramidal, and the U1–O1 and U1–O2 bond lengths of the uranyl cation are in close agreement with those reported [14,21,27], as are U1–N1 (range of 2.556(15)–2.588(4) Å), U1–N2, (range of 2.565(4)–2.661(116) Å), U1–O3 (range of 1.76(8)–1.782(4) Å) and U1–O4 (range of 1.756(11)–1.781(7) Å).

The geometry of unsolvated compound **8** is distorted hexagonal bipyramidal, or octahedral if the nitrate anions are considered as one coordination site, with the plane of the two nitrate ions deviating from coplanar as a result of the steric repulsions of the ligand. The U–$O_{(salpn)}$ bonds are asymmetric since one of the donor oxygens remains protonated, as does one of the imino groups, resulting in a Zwitterion and increasing the distortion of the geometry around the uranyl moiety. This unusual bidentate salpn coordination results in a 13-membered chelate ring, and has not been observed previously for any other metal system. The protonation of the imino group and the retention of a phenolic proton imparts a neutral overall charge on the ligand, allowing the nitrate anions to remain coordinated to the uranyl cation without disturbing the charge balance.

The major conformational differences between the salen complexes and those involving salpn are that the salpn adopts a more 'twisted' conformation in relation to the uranyl cation, with the difference between the planes of the aromatic phenols in the asymmetric unit being very small. The relief of steric repulsions in this exaggerated 'chair' orientation allows can be illustrated by examining the geometry of the five equatorial bonds relative to the apical oxygens. For the dimeric salpn compounds, the deviation of these angles from perpendicular is small (87.97(15)°–93.63(15)°), even in the presence of hydrogen bonding distortions, contrasting with the analogous salen species, in which the deviations from perpendicular are relatively large (83.0(2)°–95.7(2)°).

The geometry of the pyridine analogue deviates slightly from this, however, with the O1–U1–N3 angle distorted up to 6° from perpendicular. Slight rotation is also observed around the U1–$N_{(pyridine)}$ bond, and these two effects probably indicate the greater 'bite diameter' of the salpn is pushing the aromatic rings in closer proximity to the pyridine, hence increasing the repulsions about the pyridine molecule.

Another example of how the salpn ligand encompasses the uranyl coordination sphere more efficiently than salen is illustrated by comparing the respective N1–U1–N2 angles of the complexes **1**–**7**. The N1–U1–N2 angle for compounds **1**–**4** (64.84(18)°–67.1(2)°) is markedly less than that of the salpn complexes which all

display a N1–U1–N2 angle in the range of 70.14(12)°–70.3(5)°.

As stated above, **5** and **6** are structurally similar, and so pack in an identical fashion as alternating rows of dimeric units. In contrast, the crystal packing of the monomeric pyridine adduct (**7**) is relatively simple and consists of rows in which each consecutive monomer is rotated on its horizontal axis by 180°.

The crystal packing in **8** is influenced mainly by the folded orientation of the two aromatic groups in respect to the equatorial plane, and consists of repeating rows of interlocking monomeric units. The planes of opposing aromatic units on each partnered molecule are coplanar, however the degree of separation of these molecules prevents π–π stacking. This particular geometry illustrates clearly how the salpn ligand easily conforms to fill the unique coordination environment of the parent metal ion.

As in the salen complexes above, there is little difference in the $U–O_{(solvent)}$ bond lengths in the salpn structures (2.463(4) and 2.475(15) for **5** and **6**, respectively). These U–O lengths are perhaps surpisingly slightly longer than the salen complexes above given the greater steric freedom associated with the salpn ligand. The $U–O_{(pyridyl)}$ bond length in **7** (2.632(11) Å) is significantly longer, as expected, than the U–O lengths but very similar to that in the salen complex **4**.

4. Conclusions

This study involved the synthesis of a range of solvent adducts of uranyl nitrate with both the salen and salpn ligands, and illustrated how the solvent used in the synthesis of uranyl-salen and uranyl-salpn complexes can influence the morphology of the resulting crystal structures. The geometry immediately surrounding the uranyl cation is quite similar in all cases, with only slight differences observed in the bond lengths and angles of the uranyl salen bonds. These subtle differences, however, are sufficient to drastically alter the packing of each crystal and produce a unique lattice.

The water adduct (**1**) and the ethanol adduct (**2**) exist as hydrogen bonded dimers linked via the two solvent molecules. This hydrogen bonding extends axially from each ligand, resulting in one-dimensional rows extending throughout the lattice. The DMSO adduct (**3**) and the pyridine adduct (**4**) both contain more complicated lattice packing, and lack hydrogen bonding.

The salpn compounds display somewhat more similarity between adducts, with the methanol (**5**) and ethanol (**6**) adducts crystallizing as hydrogen bonded dimers, while the pyridine adduct crystallises as a distinct monomeric unit.

Compound **8** differs from these solvent adducts in that it contains the original uranyl nitrate salt bound to a neutral salpn ligand. The hexagonal bipyramidal geometry surrounding the uranyl centre differs significantly from that of the previous examples, and this is the first example of a structurally characterised complex containing a mononuclear, bidentate salpn ligand with any metal. The 13-membered chelate ring produced by this mode of binding is also unique. The presence of the nitrate anions severely restricts the number of available coordination sites around the uranyl centre, resulting in bidentate coordination. This has the effect of 'folding' the two aromatic units together like the pages of a book, giving a 'cupped' appearance. This added steric freedom of the salpn ligand that results from the elongated propyl linkage causes a slightly larger separation of the aromatic planes, thus preventing the possibility of π–π stacking.

5. Supplementary material

Crystallographic data for the structural analysis have been deposited with the Cambridge Crystallographic Data Centre, CCDC Nos. 184610, 184611, 184612, 184613, 184614, 184860, 184615, 184616 for compounds **1**–**8**, respectively. Copies of this information may be obtained free of charge from The Director, CCDC, 12 Union Road, Cambridge CB2 1EZ, UK (fax: +44-1223-336033; e-mail: deposit@ccdc.cam.ac.uk or www: http://www.ccdc.cam.ac.uk).

References

[1] P. Pietikainen, Tetrahedron Lett. 36 (1995) 319.
[2] I. Ramade, O. Kahn, Y. Jeannin, F. Robert, Inorg. Chem. 36 (1997) 930.
[3] P.C. Junk, S.M. Lynch, B.J. McCool, Supra. Chem. 9 (1998) 151.
[4] H. Hassaballa, J.W. Steed, P.C. Junk, Chem. Commun. (1998) 577.
[5] R.M. Fabicon, M. Parvez, H.G. Richey, Organometallics 18 (1999) 5163.
[6] B.B. Hughes, R.C. Haltiwanger, Inorg. Chem. 19 (1980) 1801.
[7] E.M. Holt, N.M. Alcock, R.R. Hendrixson, G.D. Malpass, R.G. Ghirardelli, R.A. Palmer, Acta Crystallogr., Sect. B 37 (1981) 1080.
[8] P.G. Eller, R.A. Penneman, Inorg. Chem. 15 (1976) 2439.
[9] P. Thuery, N. Keller, M. Lance, J.D. Vigner, M. Nierlich, New J. Chem. 19 (1995) 619.
[10] M.I. Salen, A. Salhin, B. Saad, S.M. Zain, N.A. Rahman, Z. Arifin, J. Mol. Struct. 448 (1998) 63.
[11] J.D.J. Baker-Dirks, J.E. Cook, A.M.R. Galas, J.S. Ghotra, C.J. Gray, F.A. Hart, J. Chem. Soc., Dalton Trans. (1980) 2191.
[12] L. Lee, D.J. Berg, G.W. Bushnell, Inorg. Chem. 33 (1994) 5302.
[13] M. Nierlich, J.M. Sabattie, N. Keller, M.L.J.D. Vigner, Acta Crystallogr., Sect. C: Cryst. Struct. Commun. 50 (1994) 52.
[14] G. Bandoli, D.A. Clemente, U. Croatto, M. Vidali, P.A. Vigato, J. Chem. Soc., Dalton Trans. (1973) 2331.
[15] R.J. Hill, C.E.F. Rickard, J. Inorg. Nucl. Chem 40 (1978) 793.
[16] A. Bencini, C. Benelli, A. Caneschi, R.L. Carlin, A. Dei, D. Gatteschi, J. Am. Chem. Soc. 107 (1985) 8128.

[17] S. Mangani, A. Takeuchi, S. Yamada, P. Orioli, Inorg. Chim. Acta 155 (1989) 149.
[18] L.W. Yang, S. Liu, E. Wong, S.J. Rettig, C. Orvig, Inorg. Chem. 34 (1995) 2164.
[19] S.J. Gruber, C.M. Harris, E. Sinn, Inorg. Chem. 7 (1968) 268.
[20] G.R. Willey, M.D. Rudd, N.W. Alcock, J. Chem. Soc., Dalton Trans. (1993) 2359.
[21] G. Bandoli, U. Croatto, D.A. Clemente, M. Vidali, P.A. Vigato, Chem. Commun. (1971) 1330.
[22] Y. Nishida, K. Kino, S. Kida, J. Chem. Soc., Dalton Trans. (1987) 1957.
[23] S. Sitran, D. Fregona, U. Casellato, P.A. Vigato, Inorg. Chim. Acta 132 (1987) 279.
[24] F. Corazza, C. Floriani, A. Chiesi-Villa, C. Gustini, S. Curli, J. Chem. Soc., Dalton Trans. (1988) 2341.
[25] S.W. Harrison, J.-C.G. Bunzli, Inorg. Chim. Acta 109 (1985) 185.
[26] M. Green, J. Smith, P.A. Tasker, Inorg. Chim. Acta 5 (1971) 17.
[27] N.J. Irons, A.J. Smith, Acta Crystallogr., Sect. C 47 (1991) 2345.
[28] R.H. Blessing, Acta Crystallogr., Sect. A 51 (1995) 33.
[29] G.M. Sheldrick, University of Göttingen, 1997.
[30] L.J. Barbour, X-SEED Crystallographic Interface, 1999.

We have been exploring the possibility of using copper(I) complexes of tertiary aryl phosphines to design systems suitable for sensing anions [8]. While most transition metal ions form rather rigid complexes due to crystal field stabilization effects, closed shell systems like Cu(I) have a plastic coordination sphere [9]. This allows for considerable deviations from the ideal geometry required for stability in partly filled d orbitals. The Cu(I) complex of diphenylphosphinohexane (dpph) reported by Kitagawa et al. [10] hosts oxoanions of different shapes and sizes between two copper centers bridged by the ligand. Our recent studies have demonstrated the efficiency of non-covalent interactions with anions in modulating the conformation of phenyl rings on the ligand such as bis diphenylphosphinomethane (dppm) [8b]. The nuclearity of the Cu(I) dppm complexes is controlled by the nature of anions. Oxoanions form dimers having short contacts or weak interactions between the anion and aromatic hydrogen atoms. However, halides, hydroxide and pseudohalides lead to very strong interactions of the anion with copper and result in the formation of trinuclear copper clusters bridged on the edges by dppm [8a]. Strong interactions are a limitation when sensor applications are envisaged due to possible deactivation on binding. Hence, alternative aryl phoshpines are being explored in our laboratory. Here we report our studies on 1,2-bis(diphenylphosphino)ethane (dppe).

Dppe is one of the most versatile phosphine ligands, capable of stabilizing copper in its +1 state [11]. Unlike dppm, this ligand can chelate as well as bridge copper centers. We have earlier demonstrated the possibility of obtaining both coordination modes upon altering the ratio of the phosphine with respect to the amount of Cu(I) [12]. A survey of Cu(I) dppe complexes indicates repeated occurrence of a family of complexes with the general stoichiometry $Cu_2(dppe)_3X_2$ (X = various mono anions/guest) [13]. In all these structurally characterized complexes, two Cu centers are bridged by a dppe ligand and each metal center possesses one chelating dppe, with the fourth coordination site available for the anion/guest (X). It is found that $[Cu_2(dppe)_3]^{2+}$ forms a cavity capable of accommodating a wide variety of anions of different shapes and sizes. X ranges from chloride to bulky thiolates. In one system, a neutral ligand acetonitrile, is present in the place of X [14]. This prompted us to prepare and study three new complexes with potentially bidentate/bridging anions [15], CN^-, SCN^- and NO_3^-. The complexes have been structurally characterized and their solution behavior examined. A critical examination of the cavity to accommodate guests with diverse steric demands has been made. Surprisingly, copper complexes of phosphines with cyanide or thiocyanate in the monodentate mode are very few and the complexes we have synthesized represent some of the first examples with the anions in this environment. Encapsulation of these anions in a hydrophobic sheath prevents bidentate interactions and introduces new solution behavior.

2. Results

2.1. Molecular composition and characterization

The composition of Cu(I) phosphine complexes is not always determined by the stoichiometry of the reactants. In several cases, it has been shown that halides and phosphines form complexes with very different formulae from those dictated by the reaction stoichiometry [13g,13h]. In the current study, we found that starting with ratios of dppe/Cu equal to 1.5 always gave copper complexes with the same stoichiometry. Single crystal X-ray crystallographic analysis confirmed the structures proposed on the basis of spectroscopic data. The complexes chosen for crystallographic examination have anions that are potentially bidentate and are predominantly found in bridging environments [15]. These compounds join the group of rare examples of Cu(I) complexes where cyanide and thiocyanate anions are found in a monodentate binding mode [16].

2.2. General description of the structures

X-ray diffraction studies of single crystals of the compounds made in this study confirm the formation of molecular structures expected in this series [13,14]. Selected bond angles and lengths are given in Table 1. A representative structure showing the molecular structure of **2** is given in Fig. 1. There are two types of dppe

Table 1
Selected bond lengths and bond angles for **1**, **2** and **3**.

	Bond lengths (Å)		Bond angles (°)	
1	Cu(1)–C(3)	1.964(4)	C(3)–Cu(1)–P(1)	107.05(9)
	Cu(1)–P(1)	2.2808(8)	P(1)–Cu(1)–P(2)	112.76(3)
	Cu(1)–P(2)	2.3040(9)	P(1)–Cu(1)–P(3)	115.16(3)
	Cu(1)–P(3)	2.3276(8)	C(3)–Cu(1)–P(2)	120.73(9)
			C(3)–Cu(1)-P(3)	111.43(8)
			P(2)–Cu(1)-P(3)	89.22(3)
2	Cu(1)–N(1)	1.985(3)	N(1)–Cu(1)–P(1)	108.79(9)
	Cu(1)–P(1)	2.2707(9)	P(1)–Cu(1)–P(3)	115.24(3)
	Cu(1)–P(3)	2.2998(9)	P(1)–Cu(1)–P(2)	117.01(3)
	Cu(1)–P(2)	2.3058(10)	N(1)–Cu(1)–P(3)	113.75(9)
			N(1)–Cu(1)-P(2)	111.44(9)
			P(3)–Cu(1)-P(2)	89.72(4)
3	Cu(1)–O(3)	2.070(3)	O(3)–Cu(1)–P(1)	109.87(8)
	Cu(1)–P(2)	2.2697(10)	P(1)–Cu(1)–P(2)	121.04(4)
	Cu(1)–P(1)	2.2684(10)	P(1)–Cu(1)–P(3)	112.79(4)
	Cu(1)–P(3)	2.3285(10)	O(3)–Cu(1)–P(2)	116.25(8)
			O(3)–Cu(1)-P(3)	104.01(9)
			P(2)–Cu(1)-P(3)	89.84(4)

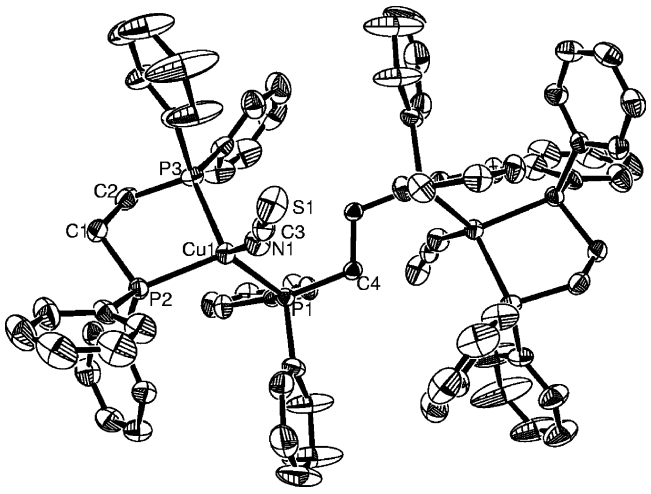


Fig. 1. The molecular structure of **2** at the 30% probability level. (Hydrogen atoms and labels for phenyl rings are omitted for clarity. Structure for **1** and **3** are given in supporting information.)

ligands in each of the three molecules. A bridging dppe holds two metal centers together and both metal centers posses a second chelating dppe. All are centrosymmetric molecules and the center of symmetry is located between the methylene carbons of the bridging dppe. Thus both metal centers are crystallographically equivalent. In all these complexes, the copper atom adopts a distorted tetrahedral geometry due to the constraint imposed by a chelating dppe. The bite angles of the chelating dppe are comparable to what has been observed in other structures [13,14]. They are remarkably constant (89.2°, 89.7°, 89.8° for anions CN^-, SCN^-, NO_3^-, respectively) and hence an invariant feature of the complex. The Cu–P distances range from 2.27 to 2.33 Å. The fourth coordination site is occupied by the anion. In the case of complex **1** the C of CN^- coordinated to the copper makes an angle of 107.05° with respect to the P1 atom of the bridging dppe and 120.71°, 111.44°, respectively to the P2 and P3 atoms of the chelating dppe. Similarly, the N1 atom of the thiocyanate complex **2** and the O3 atom in the nitrate complex **3** coordinate to the copper in a near tetrahedral environment. In the case of the cyanide complex, the Cu–C distance (1.96 Å) is comparable to the value found in a similar complex [16] (1.95 Å, $(PPh_2N(H)PPh_2)Cu(PPh_3)CN$). The Cu–N (1.98 Å) bond distance observed in the thiocyanate structure is in good agreement with the typical length of a Cu–N bond [17]. In the structure containing nitrate, the Cu–O bond distance is 2.07 Å and slightly shorter than other copper complexes where nitrate is coordinated to Cu (2.174(2) Å for $[Cu(PPh_3)_3NO_3]$ [18] and 2.206 Å for $[Cu(PPh_2Me)_3NO_3]$ [19]. Thus no unusual features are observed in these systems other than the slightly shorter bond length in the case of the nitrate ion. The predominantly bridging character of these anions is inhibited as they are encapsulated within the $[Cu_2(dppe)_3]^{2+}$ core.

It is interesting to note that there is a significant relationship between the bending of the anion at the coordinating atom and the dihedral angle of the bridging dppe. The Cu–CN bond is almost linear with the angle of 174.3°, where as the angle of Cu–N–C in the case of thiocyanate, and Cu–O–N bond of the nitrate are 167° and 121.7°, respectively. Similarly, the torsion angles about C–C in chelating dppe is almost similar in these three cases (CN^- 55°, SCN^- 56°, NO_3^- 57°), but the torsion angles of Cu–P–C–C (bridging dppe) vary significantly for the anions CN^- (56.3°), SCN^- (54.9°), and NO_3^- (64.8°). The relevance of these differences to the steric requirements of the anion will be evaluated later after discussing the solution state behavior.

2.3. Spectroscopic characterization

2.3.1. IR spectroscopy

In the solid state, the IR spectra of all these complexes show characteristic bands for the host framework and the guest anions. The preferences of the host for different anions are reflected in the lability of the complexes in solution. A comparison of the solid state spectra with the solution IR spectra offers useful information in this regard. The stretching frequency $\nu_{(C\equiv N)}$ of the cyanide ion in complex **1** occurs at 2100 cm^{-1} in the solid state and at 2105 cm^{-1} in chloroform solution. Compared to the value of the ionic or uncomplexed cyanide [20] (which occurs at 2076 cm^{-1}), the complexed form shows an increase of 30 cm^{-1}. Similarly in complex **2**, the $\nu_{(C\equiv N)}$ mode of the thiocyanate group is very intense and offers information about the nature of anion binding. The thiocyanate group can bind to the metal through sulfur (M–SCN), or nitrogen (M–NCS), or bridge through N and S (M–NCS–M). The mode of coordination can be distinguished from the vibrational frequencies of the SCN group. Although the exact frequency is dependent on the metal center, its oxidation state, and the ancillary ligands [20], the S-bound or bridging thiocyanate groups exhibit $\nu_{(C\equiv N)}$ at higher frequencies than the N-bound thiocyanate [21]. In the structurally characterized complex **2**, the SCN group binds through nitrogen. As expected, in the solid state the value of $\nu_{(C\equiv N)}$ stretch in the present complex is observed at 2070 cm^{-1}. This is lower in energy in comparison with other Cu(I) phosphine complexes possessing a bridging SCN [17] group. This value is also higher than the stretching frequency of the uncomplexed SCN^- ion (which occurs at 2053 cm^{-1}). In chloroform solution, the same complex exhibits a band at 2080 cm^{-1} and free thiocyanate group is not detected (Fig. 2). Significant differences between **1**, **2** and **3** (vide infra) prompted us to examine

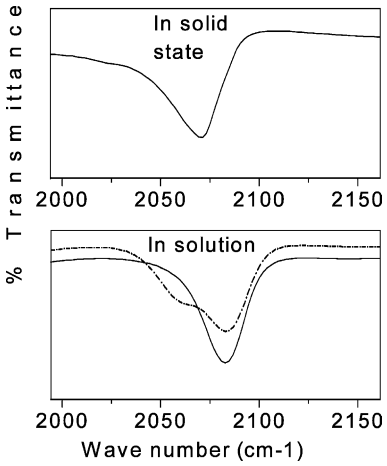


Fig. 2. The IR of complex **2** showing the $\nu_{(C\equiv N)}$ vibrations. The broken trace (in the bottom spectrum) indicates the effect of added dppe ligand. Other IR spectra are given in supporting information.

the analogous complex with azide $Cu_2(dppe)_3(N_3)_2$ (**4**). The IR spectrum of complex **4** indicates a characteristic band at 2033 cm^{-1} in the solid state indicative of the azide ion. In chloroform solution the band shifts to 2041 cm^{-1}. As in the case of the thiocyanate complex, no band corresponding to the presence of free azide anion could be seen.

The behavior of complex **3** is distinctly different from that of complexes, **1**, **2**, and **4**. In the solid state, the nitrate group in complex **3** shows a band at 1287 cm^{-1} close to the value reported for a monodentate nitrate ion [20,21]. Other bands corresponding to this ion could not be observed as they are obscured by bands of the phosphine ligand in the same region. In chloroform solution, however, the nitrate ion remains uncoordinated. In solution, a stretching frequency of 1378 cm^{-1} is observed for this complex very close to that of free nitrate ions. This dissociation in solution is quite surprising since the nitrate–Cu bond should be quite strong if the short Cu–O bond, shorter than other comparable complexes, is any indication of bond strength.

The ability of the host $[Cu_2(dppe)_3]^{2+}$ to retain the anion in its cavity is reflected by its reaction with dppe. This was probed using IR spectroscopy. Excess dppe (2.2 equiv.) was added to a chloroform solution of the respective complex and the solution IR spectrum was recorded. In the case of complex **1** the C≡N stretch remains unaffected and no band corresponding to ionic CN^- ion was observed. In contrast, solutions of **2** and **4** indicate observable dissociation to give the free anion when excess dppe is added. The C≡N stretch of free thiocyanate (Fig. 2), and N≡N stretch of the free azide ions are observed in addition to those of the complexed species. Since the nitrate is uncomplexed in solution in the absence of added dppe, one expects no change on addition of dppe. Indeed this is exactly what is observed.

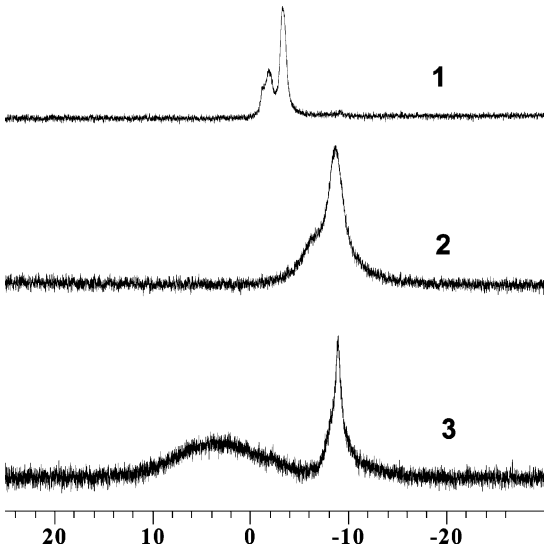


Fig. 3. ^{31}P NMR of complexes: (1) **1**; (2) **2**; and (3) **3** in $CDCl_3$ at 293 K. Other NMR spectra are given in Section 6.

2.4. ^{31}P NMR spectroscopy

The compounds prepared in this study differ only in their counterions and so one would not have expected the ^{31}P NMR of these complexes to be very different. The solution ^{31}P NMR of complex **3** (with NO_3^-), in $CDCl_3$ at room temperature consists of two sets of peaks; a broad resonance at 5.0 ppm and a relatively sharp peak at −9.6 ppm (Fig. 3(3)). At 223 K the broad peak becomes narrower and the peak at −9.6 ppm splits further. The observation of a temperature dependent broad peak is consistent with the presence of a bis chelated intermediate ($[Cu(dppe)_2]^+$) which has been previously observed in the family of $Cu_2(dppe)_3X_2$ complexes, as well as in some other Cu(I) dppe complexes [13a,13f,14].

However, the room temperature ^{31}P NMR of compound **1** in $CDCl_3$ consists of two broad signals at −1.5 and −3.5 ppm (Fig. 3(1)). Surprisingly, there is no peak between 0 and 10 ppm, indicating the absence of the bis chelated form. On lowering the temperature to 223 K, the intensity of the peak at −1.5 ppm increases at the expense of the other peak at −3.5 ppm. Addition of excess dppe (2.5 equiv.) at room temperature results in a new set of peaks with a major peak at −3.4 ppm and a smaller peak at −0.5 ppm. Interestingly, the intensity changes are reversed when the sample is cooled to 223 K and only the peak at −0.5 ppm is observed. The free dppe signal at 223 K undergoes an upfield shift similar to what was observed for dpph by Kitagawa et al. [10].

The room temperature ^{31}P NMR in $CDCl_3$ of thiocyanate (Fig. 3(2)), and azide compounds show two broad signals merged together in each case, at −9.0 and −6.5 ppm for the thiocyanate complex and −9.0, −5.7 ppm for the azide complex. Lowering the

temperature to 223 K does not produce any new peaks in both cases and only increases the separation between the peaks present. The addition of excess dppe (2.5 equiv.) changes the solution equilibrium as indicated by new broad signals, which are barely distinguishable from the base line at room temperature. While at room temperature these new signals appear at −6 ppm for thiocyanate and at −2 ppm for the azide complex, lowering the temperature to 223 K shifts these broad signals downfield with well-defined peak positions. At the low temperature limit, with excess dppe, the SCN complex shows a clear peak at 6.6 ppm and the azide complex at 7.5 ppm indicative of the formation of the bis chelated complex in rapid equilibrium with the non-chelated form.

2.5. ^1H NMR spectroscopy

All the compounds prepared in this study indicate temperature dependent chemical shifts in the ^1H NMR spectra. The room temperature NMR spectrum of complex **1** indicates two broad resonances at 2.3 and 2.0 ppm for methylene protons. A broad multiplet is observed for aromatic protons in the range 6.6–7.8 ppm. Upon lowering the temperature, the methylene signals start splitting, and at 223 K two clear signals are obtained centered at 2.0 and 1.8 ppm. Likewise, the aromatic protons also exhibit temperature dependence, and at 223 K they show a complex multiplet in the range 6.4–8.0 ppm.

Complexes **2** and **4** show nearly identical temperature dependence and differ slightly from complex **1**. At room temperature, the methylene protons show two broad peaks, 2.2 and 2.1 ppm for the thiocyanate complex and for the azide complex they are 2.3 and 2.1 ppm. Gradual lowering of the temperature splits the methylene resonances into three clear signals at the low temperature limit (2.2, 2.0, and 1.8 ppm for thiocyanate complex and for azide complex they are 2.2, 2.1, and 1.9 ppm). Similarly, the aromatic signals observed in the range 7.3–6.8 for both complexes **2** and **4** undergo further splitting at 223 K in the range 7.7–6.6 ppm. Although complex **3** shows changes with temperature, the changes are distinctly different. Both methylene (2.4, 2.1 ppm) and aromatic protons (7.3–7.1 ppm) do not show fine structure but do show slight changes in their chemical shift on lowering the temperature.

3. Discussion

3.1. Solution behavior

The solution behavior of complexes **1**, **2**, and **4** are significantly different from **3** and those studied earlier with counterions, Cl^-, ClO_4^-, or I^-. The elegant work of Sadler and coworkers [13f] has shown that a bis chelated form $[Cu(dppe)_2]^+$ is the major species with a ^{31}P resonance at 10.0 ppm when Cl^- is the counter anion. In the presence of excess dppe the intensity of this peak increased. The temperature dependent ^1H NMR studies were also consistent with the observation of dissociative equilibria with the 2.42 ppm peak assignable to $[Cu(dppe)_2]^+$, present over the entire range of temperature and more predominant at lower temperatures. A similar temperature dependent behavior has been observed in two other complexes. In solutions of $[Cu_2(dppe)_3(CH_3CN)_2]^{2+}$, Vijayashree et al. [14] have noted a similar equilibrium. More recently, Comba et al. [13a] have studied the iodo complex $Cu_2(dppe)_3I_2$ in solution and reached the same conclusion. The observed low temperature ^{31}P NMR signals of the reported complexes and those of the present study are collected in Table 2.

Based on the ^{31}P, ^1H NMR and IR spectra, the three complexes **1**, **2** and **4** appear to be unique in not forming the bis chelated complex of Cu(I) at any temperature. Further, complex **1** is different from **2** and **4**. Even the deliberate addition of excess dppe aimed to produce $[Cu(dppe)_2]CN$ species (in analogy with the chloride complex), was not successful. These results suggest that the binding of the cyanide group to the metal is quite strong and the anion is retained in the cavity even in the presence of excess dppe. The formation of a species with an ionic cyanide such as $[Cu(dppe)_2]CN$ is not favored. The solution behavior can thus be described by a fluxional processes involving breaking and closing of the chelate ring and retention of the bridging coordination in the ^{31}P NMR time scale. Chelation is normally a stable coordination mode for five member rings, but the angle subtended at the metal center (90°), is much smaller than what is required for an ideal tetrahedron. This would cause bond weakening in this family of complexes. Since there are two chelate rings, solution equilibrium will naturally involve a number of species. As a result of rapid equilibrium, only two sets of phosphorous resonances are observed. A signal at −3.5 ppm could be assigned to the P atoms of bridging dppe. The other peak at −1.5 ppm could be assigned to the P atoms present in the partially broken chelating ligand that undergoes exchange with the coordinated arm. The broad nature of this signal is probably due to many magnetically inequivalent P atoms in equilibrium. On decreasing the temperature, a slowing down of the exchange process leads to reduced line broadening and increased intensity of the signals. The tenacious nature of CN^- is revealed by the absence of $[Cu(dppe)_2]^+$ even at the low temperature limit.

Likewise, the ^{31}P NMR of complexes **2** and **4** do not indicate the presence of the $[Cu(dppe)_2]^+$cation in significant concentrations. The IR spectra are also very clear that the free anions are not involved in

Table 2
Summary of low temperature ^{31}P NMR data for copper dppe complexes

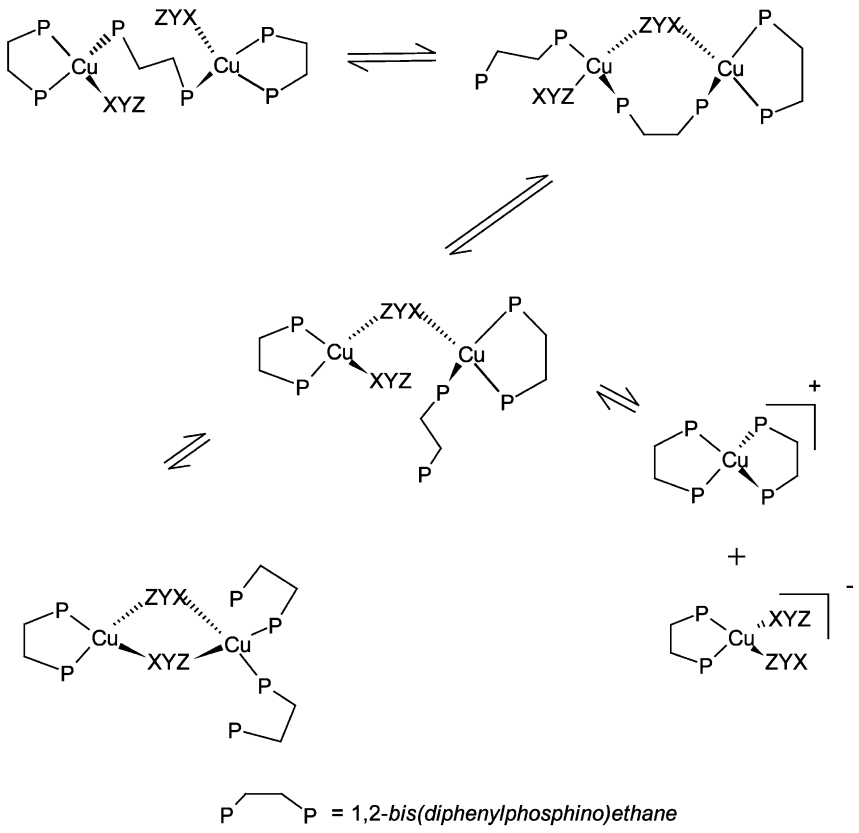
Complex	T (K)	$[Cu(dppe)_2]^{2+}$ form (ppm)	Various forms of monodentate dppe (ppm)				References
$Cu(dppe)_2BF_4$ in CD_2Cl_2	198	+7.5					[13a]
$Cu(dppe)_2I$ in CD_2Cl_2		+7.5				−9.5	[13a]
$Cu(dppe)(CH_3)_2C_2B_4H_5$ in CD_2Cl_2	173	+8.5		−3.4		−9.2	[26]
$Cu_2(dppe)_3Cl_2$ in CD_2Cl_2	188	+10.5	+3.2	−4.3		−9.1	[13f]
$Cu_2(dppe)_3(CH_3CN)_2(ClO_4)_2$ in acetone-d_6	233	+7.7	−1.5	−3.0		−8.7	[14]
1 in $CDCl_3$	223	absent	−1.5	−3.5			this work
2 in $CDCl_3$	223	absent			−6.5	−8.6	this work
4 in $CDCl_3$	223	absent			−5.7	−9.0	this work
3 in $CDCl_3$	223	+5.0				−9.0, −9.7	this work

significant concentrations as in the case of complex **1**. But in the presence of added dppe there are differences in the IR spectrum and the ^{31}P NMR pattern. This suggests a different kind of solution processes from what is observed for **1**. The solution ^{31}P NMR indicates a very broad singlet in both cases (a major difference from the cyano complex), at room temperature. These anions are long enough for bridging the metal centers. This might result in a breaking of the bridging/chelated dppe. Rapid equilibration through the intermediacy of anion bridged structures in solution could result in a single broad peak. In other words, the dissociation in the case of the thiocyanate and azide complexes could be promoted by the extra bridging ability of the anion. First the anion attacks the metal center resulting in a partially bonded chelated/bridging dppe unit. These processes lead to the formation of a weakly bound intermediate (S bound SCN complex for example), which dissociates to give $[Cu(dppe)_2]^+$. As a result, in the presence of excess dppe, the equilibrium is shifted towards the bis chelated complex. In this series, the nitrate complex **3** alone, behaves similar to the chloride complex. The anion is not held firmly in the cavity or coordinated to the copper in solution. However, in the solid state, there is no difference between the three complexes. Given the choice between ambidentate anions and dppe, the latter is preferred for bridging the metal centers.

These results including the ^1H NMR spectra are best understood on the basis of varying degree of lability exhibited by these anions. They point out that the cyanide complex **1** represents one extreme where the anion remains completely coordinated to the copper. Even in the presence of excess dppe, there is no hint of formation of the bis chelated complex. The nitrate complex **3** is the other extreme, typical of most complexes in this series. Complexes **2** and **4** are intermediate cases and represent unique examples where additional anion bridged structures exist. The formation of $[Cu(dppe)_2]^+$ species only in the presence of added dppe indicates that the SCN^- or N_3^- is less labile than the complexes studied earlier but more labile compared to the cyanide. The predominance of the bis chelated form at low temperatures is similar to what is observed in the chloride complex and is a reflection of the thermodynamic stability of this form. The solution equilibrium unique to **2** and **4** is shown in Scheme 1.

On the basis of these results it is clear that the solid state structure is not retained in solution in these complexes except in the case of the cyanide. The cyanide remains coordinated to the copper while most anions are labile. The π accepting and soft nature of the cyanide favors an inert complex. However, if these were the only factors, one is hard put to explain the structure of the nitrate and thiocyanate complexes. Binding with the nitrate anion appears to be quite strong judging from the distance between Cu and O, a hard donor. The ambidentate SCN anion prefers to have nitrogen coordination rather than sulfur, despite Cu(I) being soft and thiophillic [22]. However, all these results are consisent with the tendency of Cu(I) to balance the number of soft donors and hard donors in its coordination sphere [23]. This tendency, along with favorable short contacts (vide infra) with anions might be responsible for the coordination of hard donors like N and O to Cu in the solid state. The $Cu–ONO_2$ bond in complex **3** is expected to be strong (on the basis of solid state results), it succumbs to competition from the soft centers in solution and is not coordinated to Cu(I) in their presence leading to the formation of $Cu(dppe)_2^+$.

What makes the $[Cu_2(dppe)_3]^{2+}$ core capable of accepting large anions? The steric demands of aryl phosphines and their relationship to the stability of their metal complexes are quite well known. Usually the cone angles of phosphines are the best criteria to assess the steric demands of phosphines. The cone angles of PPh_2Me, and PPh_3 are 136°, and 145°, respectively. Since the dppe ligand is structurally very similar to PPh_2Me (differs only in the methyl group) one would have expected a similar cone angle at the P center. However, covalent tying of methylene units results in significant reduction of cone angle and the cone angle of dppe has been estimated to be 125° [11]. This significant



Scheme 1. Equilibria unique to complexes **2** and **4**.

reduction of steric demand around phosphorus atoms upon chelation to the metal offers sufficient space for a fourth coordination site involving rather bulky ligands.

3.2. Analysis of the solid state structures

We now discuss why this framework is flexible making it an universal host for anions. Using the programs PREQUEST and VISTA available in CSD [24] we have analyzed the bond distances, angles and torsion angles associated with this framework in the present and reported structures. It is clear that the torsion angles about the C–C bond (t_1) (see Fig. 4) of the chelating dppe are not very different for different anions. This is in accord with the theoretical studies on five member chelates. It was shown that the energy of the chelate critically depends on the torsion angles about the C–C bond rather than any other conformational change within the chelate ring [25]. Accordingly, the torsion angles t_1 are found to be invariant in all the structures of the $Cu_2(dppe)_3$ series.

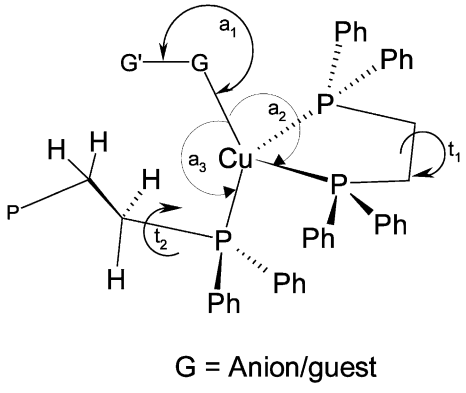


Fig. 4. The flexible torsion and bond angles of the host frame work.

The conformation associated with the bridging dppe varies significantly. The torsion angles associated with the bridging dppe (involving small anions) are listed in Table 3. Gaughan et al. have found the torsion angle (t_2) of the bridging dppe (Cu–P–C–C) as a key parameter for describing the overall conformation of the molecule [13i]. An increase in t_2 (rotation about the P–C bond) is expected to minimize intramolecular bumping. In the case of small anions, an increase is observed in the torsion angles of the bridging dppe (Cu–P–C–C) on increasing the size requirements of the anion. It is interesting to note that the changes in this torsion angle correlates with the coordination angle a_1 rather than the size indicated by the thermochemical radii. If one considers the solid angle swept away by the anion rather than the volume occupied by the anion, the coordination angle at the metal is a critical factor. The solid angle

Table 3
Steric and conformational parameters in $[Cu_2(dppe)_3X_2]$ complexes

Anions X	Thermochemical radius (pm)	Torsion angle (°) t_2 (Cu–P–C–C_{br})	a_1 (°)	a_3 (°)	a_2 (°)
NO_3^-	165	64.8	121.7	109.86	116.25
Cl^-	167	51.3		102.23	115.65
CN^-	177	56.3	174.3	107.05	111.43
N_3^-	181	61.9	134.4	99.87	117.48
SCN^-	199	54.9	161.7	108.78	111.45
I^-	206	61.2		109.80	113.9

spanned by a bent anion is more. Hence the steric requirement of the anions are dictated by the coordination angles rather than the thermochemical radii. In addition to this, the angles a_2 and a_3, which involve the anion and the host frame work, show an inverse correlation.

The steric demands of bulkier anions are more difficult to interpret since a major portion of the anion is outside the cavity formed by dppe ligands. Unlike small anions, factors other than the coordination angles influence the bridging dppe angles. This is understandable as there are aromatic rings in these anions which are capable of interacting with the aromatic rings of dppe. The deviation of the torsion angles in the case of bulkier guests were attributed by Gaughan et al. to several non-bonded interactions [13i].

Further modulation of cavity size can be achieved by changing the spatial arrangement of the six phenyl rings surrounding each metal center. Four hydrogens on these phenyl rings roughly demarcate the cavity size. Some of the aromatic hydrogen atoms are found to interact with the anion through C–H π interactions. A list of short contacts with explanatory figures is given in the supporting material. These short contacts were also noticed by Albano et al. in the case of $Cu_2(dppe)_3Cl_2$ [13h]. It is the N and/or O atom of the anions that exhibit weak interactions with the aromatic hydrogen atoms. Thus the short contacts observed in the case of the thiocyanate are between the N of SCN^- and the aromatic hydrogen atoms. The bent coordination geometry of the thiocyanate localizes the charge on the more electronegative nitrogen end of the ligand resulting in a lone pair being available for short contacts. It also causes a deviation from the correlation between the coordination angle with the torsion angle t_2 in the solid state.

4. Conclusion

In the present study, direct reactions between dppe and Cu(I) salts with different bidentate anions have been explored. The resulting complexes have very similar solid state structures and conform to the structural motif that has been characterized for this stoichiometry. The variation in the size of the cavity produced by the three PPh_2 units coordinated to the Cu^+ to accommodate anions is a result of several factors. The flexibility associated with the rotation of phenyl rings, the torsion angles associated with the bridging dppe and the possibility of different coordination angles around Cu(I) lead to a fairly flexible host for anions. The bond distances around copper and the metrical parameters associated with the chelating dppe remain constant. The IR, and NMR spectra of these compounds in solution suggest a complex solution behavior very much dependant on the anion. A new process involving a bridging anion rather than one bridged through dppe is suggested to explain the behavior of azide and thiocyanate complexes. A bis chelated dppe complex is observed only in the presence of added dppe in these systems. However, the cyanide ion is distinctly different and is the only one, which is kinetically inert. The $[Cu_2(dppe)_3]^{2+}$ core is indeed unique in accommodating a variety of anions of different shapes and sizes making it an ideal universal host for anions.

5. Experimental

5.1. General remarks

Dichloromethane, petroleum ether (b.p. 60°–80°), and MeCN were purified and dried by conventional methods. They were distilled under N_2 and deoxygenated before use. All manipulations were carried out under an atmosphere of purified N_2 Standard Schlenk techniques were used. CuCN was obtained locally and CuSCN, was freshly prepared before use [27]. Cupric nitrate was obtained from Ranbaxy, India. The complex $Cu_2(dppe)_3(N_3)_2$ (**4**) was synthesized using the reported procedure [13j]. ^1H NMR spectra were recorded on a Bruker ACF 200 MHz or on a Bruker AMX 400 MHz spectrometer with TMS as the internal reference. $^{31}P\{^1H\}$ NMR spectra were recorded on a Bruker AMX 400 MHz spectrometer operating at 162 MHz. IR spectra were recorded either in solid state as KBr pellets or as $CHCl_3$ solution on a Bruker spectrometer.

Table 4
Summary of crystallographic information for compounds **1**–**3**

Crystal data	**1**	**2**	**3**
Empirical formula	$C_{80}H_{72}Cu_2N_2P_6\cdot 2H_2O$	$C_{80}H_{72}Cu_2N_2P_6S_2$	$C_{78}H_{72}Cu_2N_2O_6P_6$
Formula weight	1410.32	1438.42	1446.28
Crystal system	monoclinic	monoclinic	monoclinic
Space group	$C2/c$	$P2_1/n$	$P2_1/n$
a (Å)	23.290(2)	12.817(1)	12.806(2)
b (Å)	17.662(1)	19.404(2)	17.377(3)
c (Å)	17.597(2)	15.508(3)	16.910(2)
β (°)	92.02(1)	103.85(1)	105.66(1)
V (Å^3)	7234.0(11)	3744.7(9)	3623.3(9)
Z	4	2	2
ρ_{calc} (Mg m^{-3})	1.295	1.276	1.326
Absorption coefficient (mm^{-1})	0.768	0.795	0.773
$F(000)$	2936	1492	1500
Crystal size (mm)	0.31 × 0.24 × 0.17	0.27 × 0.25 × 0.24	0.29 × 0.27 × 0.21
θ Range (°)	1.83–23.50	1.86–24.01	1.78–24.00
Reflections collected	5492	6128	5952
Independent reflections	5345 [$R_{int} = 0.0260$]	5844 [$R_{int} = 0.0155$]	5673 [$R_{int} = 0.0174$]
Data/restraints/parameters	5345/0/415	5844/0/415	5673/0/424
Final R indices [$I > 2\sigma(I)$]	R_1 [a] = 0.0367, wR_2 [b] = 0.0848	R_1 [a] = 0.0408, wR_2 [b] = 0.0953	R_1 [a] = 0.0451, wR_2 [b] = 0.0997
Final R indices (all data)	R_1 [a] = 0.0536, wR_2 [b] = 0.0931	R_1 [a] = 0.0585, wR_2 [b] = 0.1042	R_1 [a] = 0.0743, wR_2 [b] = 0.1091
Goodness-of-fit on F^2	1.032	1.042	1.022
Residual ρ (e Å^{-3})	0.343 and −0.216	0.280 and −0.237	0.285 and −0.349

[a] $R_1 = (\Sigma||F_0|-|F_c||)/(\Sigma|F_0|)$.
[b] $wR_2 = [\Sigma\ w(|F_0|^2-|F_c|^2)^2]/\Sigma|w|F_0|^2)^2]^{1/2}$.

5.2. Syntheses of complexes

5.2.1. $Cu_2(dppe)_3(CN)_2$ (**1**)

To a slurry of CuCN (0.02 g, 0.2 mmol) in CH_2Cl_2 (10 ml), 1.5 equiv. of dppe (0.133 g) was added and stirred for 1 h. After complete dissolution of CuCN, the solvent was removed under vacuum. The residue was then washed with Et_2O and dried in vacuum to give complex **1** in quantitative yield. *Anal*. Calc. for $[Cu_2(C_{26}H_{24}P_2)_3(CN)_2]\cdot CH_2Cl_2$: C, 66.66; H, 5.07; N, 1.92. Found: C, 66.91; H, 5.19; N, 2.11%. Suitable crystals for X-ray diffraction were grown from CH_2Cl_2 on layering with petroleum ether.

5.2.2. $Cu_2(dppe)_3(SCN)_2$ (**2**)

A similar procedure was adopted with 0.03 g of CuSCN and 0.15 g (1.5 equiv.) of dppe and the yields were quantitative. *Anal*. Calc. for $[Cu_2(C_{26}H_{24}P_2)_3(SCN)_2]\cdot 0.5CH_2Cl_2$: C, 65.29; H 4.93; N, 1.89. Found: C, 64.81; H, 4.95; N, 1.91%. Suitable crystals for X-ray diffraction were grown from CH_2Cl_2 on layering with petroleum ether.

5.2.3. $Cu_2(dppe)_3(NO_3)_2$ (**3**)

To a solution of $Cu(NO_3)_2$ (0.03 g) in distilled MeCN (15 ml), few strips of Cu foil were added and stirred. After complete reduction of $Cu(NO_3)_2$ (as indicated by the disappearance of blue color), 0.15 g of dppe was added to the same solution and stirred for 20 min. After filtration, the solvent was removed under vacuum. The white residue was washed with ether, and dried in vacuum to get **3** in quantitative yield. *Anal*. Calc. for $[Cu_2(C_{26}H_{24}P_2)_3(NO_3)_2]\cdot 0.5CH_2Cl_2$: C, 63.32; H, 4.90; N, 1.88. Found: C, 63.70; H, 4.95; N, 1.95%. Suitable crystals for X-ray diffraction studies were grown from CH_2Cl_2 on layering with petroleum ether.

5.3. X-ray crystallographic study

Crystals were mounted along the largest dimension and used for data collection. The intensity data were collected on a Siemens P4 single crystal diffractometer equipped with Mo source ($\lambda = 0.71073$ Å) and highly oriented graphite monochromator. The lattice parameters and standard deviations were obtained by least-squares fit to 40 reflections. The data were collected by $2\theta-\theta$ scan mode with a variable scan speed ranging from 2.0° to a maximum of 60.0° min^{-1}. Three reflections were used to monitor the stability and orientation of the crystal and were re-measured after every 97 reflections. Their intensities did not change significantly during the data collection. The data were corrected for LP factors and an empirical absorption correction based on ψ scan method was also applied.

The structure was solved by direct methods using SHELX-97 package [28] and also refined using the same. All the non-hydrogen atoms were refined anisotropically. The hydrogen atoms were included in the ideal positions with fixed isotropic U values and were riding with their respective non-hydrogen atoms. The hydro-

gen atoms of the water molecule were located from the difference Fourier and included as such in the refinement and were riding with water oxygen. A summary of the details of structure determination is given in Table 4.

6. Supplementary material

Crystallographic data for the crystal structures have been deposited with the Cambridge Crystallographic Data Centre, CCDC NOS. 183692–183694 for compounds **1**, **2** and **3**, respectively. Copies of this information may be obtained free of charge from The Director, CCDC, 12 Union Road, Cambridge, CB2 1EZ, UK (fax: (internet) +44-1223-336033; e-mail: deposit@ccdc.cam.ac.uk or http://www.ccdc.cam.ac.uk/conts/retrieving.html).

Acknowledgements

We wish to thank CSIR, New Delhi for financial assistance and the Chairman, Bioinformatics Center, and Sophisticated Instrumentation Facility, Indian Institute of Science, Bangalore, India for the data from CSD and the NMR spectrometer, respectively.

References

[1] (a) P.D. Beer, P.A Gale, Angew. Chem., Int. Ed. Engl. 40 (2001) 486;
(b) P.A. Gale, Coord. Chem. Rev. 199 (2000) 181.
[2] (a) B. Moss, Chem. Ind. (1996) 407;
(b) C. Glidewell, Chem. Br. 26 (1990) 137.
[3] (a) P.J. Chakrabarti, J. Mol. Biol. 234 (1993) 463;
(b) H. Luecke, F.A. Quiocho, Nature 347 (1990) 402;
(c) J.J. He, F.A. Quiocho, Science 251 (1991) 1479.
[4] S.R. Gadre, C. Kölmel, I.H. Shrivastava, Inorg. Chem. 31 (1992) 2279.
[5] (a) J.A. Atwood, K.T. Holman, J.W. Steed, Chem. Commun. (1996) 1401;
(b) P.D. Beer, Acc. Chem. Res. 31 (1998) 71.
[6] (a) G.S. Papaefstathiou, S.P. Perlepes, A. Escuer, R. Vicente, M. Font-Bardia, X. Solans, Angew. Chem., Int. Ed. Engl. 40 (2001) 884;
(b) V. Amendola, E. Bastianello, L. Fabbrizzi, C. Mangano, P. Pallavicini, A. Perotti, A.M. Lanfredi, F. Ugozzoli, Angew. Chem., Int. Ed. Engl. 39 (2000) 2917;
(c) R.-D. Schnebeck, E. Freisinger, B. Lippert, Angew. Chem., Int. Ed. Engl. 38 (1999) 168;
(d) A. Knoepfler-Muhlecker, B. Scheffter, H. Kopacka, K. Wurst, P. Peringer, J. Chem. Soc., Dalton Trans. (1999) 2525;
(e) S. Warzeska, R. Krämer, Chem. Commun. (1996) 499;
(f) B. Hämmerle, E.P. Müller, D.L. Wilkinson, G. Muller, P. Peringer, J. Chem. Soc., Chem. Commun. (1989) 1527;
(g) L. Fabbrizzi, P. Pallvicini, L. Parodi, A. Taglietti, Inorg. Chim. Acta 238 (1995) 5.
[7] (a) T. Okubo, S. Kitagawa, M. Kondo, H. Matsuzaka, T. Ishii, Angew. Chem., Int. Ed. Engl. 38 (1990) 931;
(b) K.T. Holman, G.W. Orr, J.W. Steed, J.L. Atwood, Chem. Commun. (1998) 2109;
(c) P.L. Jones, K.J. Byrom, J.C. Jeffery, J.A. McCleverty, M.D. Ward, Chem. Commun. (1997) 1361;
(d) K.T. Holman, M.M. Halihan, J.W. Steed, S.S. Juisson, J.L. Atwood, J. Am. Chem. Soc. 117 (1995) 7848.
[8] (a) J.K. Bera, M. Nethaji, A.G. Samuelson, Inorg. Chem. 38 (1999) 218;
(b) J.K. Bera, M. Nethaji, A.G. Samuelson, Inorg. Chem. 38 (1999) 1725.
[9] B.J. Hathaway, in: G. Wilkinson, R.D. Gillard, J.A. McCleverty (Eds.), Comprehensive Coordination Chemistry, vol. 5, Pergamon Press, Oxford, 1987, pp. 534–593.
[10] S. Kitagawa, M. Kondo, S. Kawata, S. Wada, M. Maekawa, M. Munakata, Inorg. Chem. 34 (1995) 1445.
[11] C.A. McAuliffe, in: G. Wilkinson, R.D. Gillard, J.A. McCleverty (Eds.), Comprehensive Coordination Chemistry, vol. 2, Pergamon Press, Oxford, 1987, pp. 984–1066.
[12] N. Vijayashree, Ph.D. Thesis, Indian Institute of Science, 1993.
[13] (a) P. Comba, C. Katsichtis, B. Nuber, H. Pritzkow, Eur. J. Inorg. Chem. (1999) 777;
(b) M. Biagini-Cingi, Anna-Maria Manotti-Lanfredi, F. Ugozzoli, A. Camus, N. Marsich, Inorg. Chim. Acta 262 (1997) 69;
(c) J. Romero, J.A. Garcia-Vazquez, A. Sousa, Y.D. Chang, J. Zubieta, Inorg. Chim. Acta 245 (1996) 119;
(d) E.W. Ainscough, E.N. Baker, M.L. Brader, A.M. Brodie, S.l. Ingham, J.M. Waters, J.V. Hanna, P.C. Healy, J. Chem. Soc., Dalton Trans. (1991) 1243;
(e) E.W. Ainscough, E.N. Baker, A.G. Bingham, A.M. Brodie, C.A. Smith, J. Chem. Soc., Dalton Trans. (1989) 2167;
(f) S.J. Berners-Price, R.K. Johnson, C.K. Mirabelli, L.F. Faucette, F.L. McCabe, P.J. Sadler, Inorg. Chem. 26 (1987) 3383;
(g) P. Fiaschi, C. Floriani, M. Pasquali, A. Chiesi-Villa, C. Guastini, Inorg. Chem. 25 (1986) 462;
(h) V.G. Albano, P.L. Bellon, G. Ciani, J. Chem. Soc., Dalton Trans. (1972) 1938;
(i) A.P. Gaughan, K.S. Bowman, Z. Dori, Inorg. Chem. 11 (1972) 601;
(j) A.P. Gaughan, R.F. Ziolo, Z. Dori, Inorg. Chem. 12 (1971) 2776.
[14] N. Vijayashree, A.G. Samuelson, M. Nethaji, Curr. Sci. 65 (1993) 57.
[15] (a) Y. Zhao, M. Hong, W. Su, R. Cao, Z. Zhou, A.S.C. Chan, J. Chem. Soc., Dalton Trans. (2000) 1685;
(b) D.J. Chesnut, J. Zubieta, Chem. Commun. (1998) 1707;
(c) D.J. Chesnut, A. Kusnetzow, J. Zubieta, J. Chem. Soc., Dalton Trans. (1998) 4801;
(d) M. Kabesová, R. Boca, M. Melník, D. Valigura, M. Dunaj-Jurco, Coord. Chem. Rev. 140 (1995) 115.
[16] J. Ellermann, F.A. Knoch, K.J. Meier, M. Moll, J. Organomet. Chem. 428 (1992) C44.
[17] (a) A.P. Gaughan, R.F. Ziolo, Z. Dori, Inorg. Chem. Acta 4 (1970) 640;
(b) N.K. Homsy, M. Noltemeyer, H.W. Roesky, H.-G. Schmidt, G.M. Sheldrick, Inorg. Chem. Acta 90 (1984) L59.
[18] J.C. Dyason, L.M. Engelhardt, P.C. Healy, H.L. Klich, A.H. White, Aust. J. Chem. 39 (1986) 2003.
[19] M. Mathew, G.J. Palenik, A.J. Carty, Can. J. Chem. 49 (1971) 4119.
[20] K. Nakamato, Infrared Spectroscopy of Inorganic and Coordination Compounds, 2nd ed., Wiley, New York, 1978, p. 178.
[21] A.J. Carty, A. Efraty, Inorg. Chem. 8 (1969) 543.
[22] (a) R.G. Pearson, Chemical Hardness: Applications from Molecules to Solids, Wiley-VCH, Weinheim, 1997, p. 3;
(b) R.G. Pearson, J. Chem. Edu. 45 (1968) 581.

[23] G. Pilloni, B. Corain, M. Degano, B. Longato, G. Zanotti, J. Chem. Soc., Dalton Trans. (1993) 1777.
[24] Cambridge Structural Database, Version 5.21 Release, April 2001.
[25] J.R. Gollogly, C.J. Hawkins, Inorg. Chem. 8 (1969) 1168.
[26] L. Barton, P.K. Rush, Inorg. Chem. 24 (1985) 3413.
[27] G.H. Jeffery, J. Bassett, J. Mendham, R.C. Denney, Vogel's Textbook of Quantitative Chemical Analysis, 5th ed., Longman UK, London, 1989, p. 495.
[28] G.M. Sheldrick, SHELX-97, Fortran Program for Crystal Structure Refinement, 1997.

C_6H_2) [13] have been structurally characterised. Such compounds should be useful precursors for dianionic bifunctional ligands in transition metal chemistry. In addition, the presence of a P-containing group is advantageous for reactivity studies by ^{31}P NMR spectroscopy.

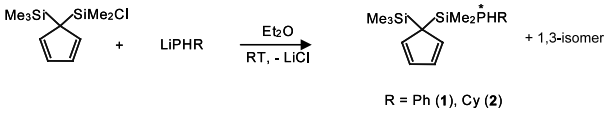
We have previously reported the synthesis of the PH-functionalised ferrocene derivatives *rac*-[Fe{(η^5-C_5H_4)CMe_2PHR}$_2$] (R = Ph, Mes) [14] and the metallocene derivatives [{(η^5-C_5H_4)CMe_2PHR}$_2ZrCl_2$] and [{(η^5-C_5H_4)CMe_2PHR}$_2$TiCl] (R = Ph, ^{t}Bu). The latter slowly decompose on recrystallisation from THF, Et_2O or toluene with formation of [{(η^5-C_5H_4)$_2CMe_2$}MCl_2] (M = Zr, Ti) and $(PR)_n$ (R = Ph, n = 4–6; R = ^{t}Bu, n = 4) and PH_2R [15].

We now report the synthesis of the first stable monosubstituted PH-functionalised phosphanylalkyl- and phosphanylsilylcyclopentadienyl complexes of Group 4 metals, namely, [{(η^5-C_5H_4)$SiMe_2PHR$}$ZrCl_3$] [R = Ph (**4**), Cy (**5**)] and [{(η^5-C_5H_4)CMe_2PH^tBu}MCl_3] [M = Ti (**6**), Zr (**7**)] and their activity in the polymerisation of ethene and propene. Recently, Erker et al. reported the synthesis and catalytic properties in the polymerisation of olefins of the constrained-geometry catalysts [{(η^5-C_5H_4)CMe_2PCy}$M(NR_2)_2$] (M = Ti, R = Me; M = Zr, R = Et) [16]. Hou et al. reported the synthesis of [{(η^5-C_5Me_4)$SiMe_2PMes^*$}$Ln(L)_n$] (Ln = Sm: L = THF, n = 1 or 3; L = $MeOCH_2CH_2OMe$, n = 2; L = $PO(NMe_2)_3$, n = 2; Ln = Yb, L = THF, n = 3) and the polymerisation of ethene, ε-caprolactone and 1,3-butadiene with the Sm^{II}–mono-THF complex [13].

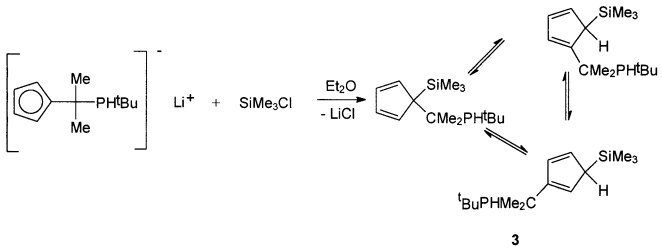
2. Results and discussion

2.1. Synthesis

The general synthetic method for the preparation of a monocyclopentadienyl metal trichloride complex of Group 4 metals is the elimination of $SiMe_3Cl$ [17]. Occasionally, this method can also be employed for the synthesis of metallocene derivatives. We therefore prepared the silylated phosphanylsilyl- and phosphanylalkylcyclopentadienes 1- and 3-$SiMe_3$–1-$SiMe_2PHRC_5H_4$ [R = Ph (**1**), Cy (**2**)] and 1-, 2- and 3-CMe_2PH^tBu–1-$SiMe_3C_5H_4$ (**3**) from LiPHR and 1-$SiMe_3$–1-$SiMe_2ClC_5H_4$ [18] (Eq. (1)) and Li[1-$PH^tBuCMe_2C_5H_4$] and $SiMe_3Cl$ (Eq. (2)), respectively.



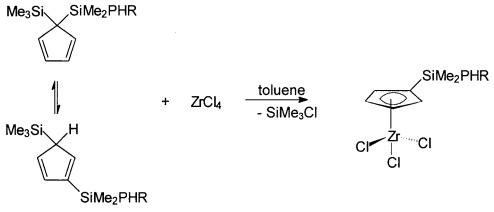
(1)



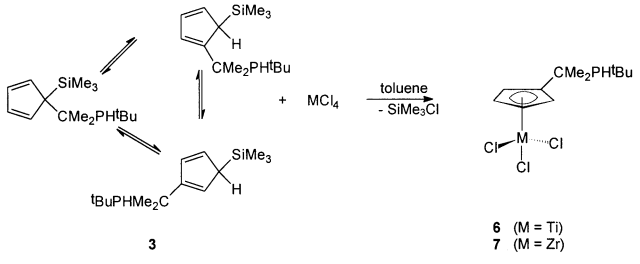
(2)

Work-up yielded **1**–**3** as colourless (**1**, **2**) or yellow (**3**) oil. The different constitutional isomers could not be separated by distillation [19]. Compounds **1**–**3** were characterised by NMR (^1H, ^{31}P) and IR spectroscopy and mass spectrometry. In the MS, molecular-ion peaks were observed, and the peak of 100% intensity was due to $m/z = M^+ - PHR$ (R = Ph, Cy, ^{t}Bu).

Compounds **1** and **2** react with $ZrCl_4$ in toluene to give [{(η^5-C_5H_4)$SiMe_2PHR$}$ZrCl_3$] [R = Ph (**4**), Cy (**5**); Eq. (3)], and **3** reacts with MCl_4 with formation of [{(η^5-C_5H_4)CMe_2PH^tBu}MCl_3] [M = Ti (**6**), Zr (**7**); Eq. (4)]. As $SiMe_3Cl$ is eliminated, the mixture of constitutional isomers (see Eqs. (1) and (2)) can be employed in these reactions. Compounds **4**–**7** can be recrystallised from dichloromethane or THF; the complexes are almost insoluble in non-coordinating and non-polar solvents, and this indicates association in the solid state (presumably by chloro bridges, cf. [{(η^5-C_5H_4)$_2CH_2CH_2PPh_2$}$ZrCl_3$] [20]) and adduct formation in THF (cf. [{(η^5-C_5Me_4)$_2CH_2CH_2PPh_2$}$ZrCl_3$(THF)] [21]). Compounds **4**–**7** are obtained as yellow (**4**), white (**5**, **6**) or red (**7**) microcrystalline powders in good to moderate yields (45–80%). Compounds **4** and **5** are only moderately air sensitive, while **6** and **7** are more so, and all complexes decompose with formation of phosphine



(3)



(4)

(PH_2R).

Compounds **4**–**7** were characterised by NMR (^1H, ^{13}C, ^{31}P) and IR spectroscopy and mass spectrometry. Compounds **4**, **5** and **7** [**4**: −117.1 ($^1J_{P-H} = 200.9$ Hz); **5**: −121.6 ($^1J_{P-H} = 201.0$ Hz); **7**: 36.7 ppm ($^1J_{P-H} = 213.4$ Hz)] exhibit a doublet in the ^{31}P NMR spectrum (in [D_8]THF), which is shifted to low field by approximately 1–12 ppm relative to the starting materials **1**–**3** [**1**: −121.6 ($^1J_{P-H} = 201.0$ Hz) and −122.3 ppm ($^1J_{P-H} = 204.1$ Hz); **2**: −124.9 ($^1J_{P-H} = 191.2$ Hz) and −127.6 ppm ($^1J_{P-H} = 189.5$ Hz); **3**: 25.2 (d of dec, $^1J_{P-H} = 196.7$ Hz, $^3J_{P-H} = 12.1$ Hz), 19.2 (d, $^1J_{P-H} = 198.4$ Hz) and 13.1 ppm (d of dec, $^1J_{P-H} = 199.5$ Hz, $^3J_{P-H} = 12.2$ Hz)]. This indicates that there is no interaction between the phosphanyl group and the transition metal. In contrast, **6** [−6.8 ppm ($^1J_{P-H} = 282.5$ Hz)] exhibits a doublet in the ^{31}P NMR spectrum (in [D_8]THF) which is shifted to high field relative to the starting material **3**, and the coupling constant increased by approximately 85 Hz.

For **4**–**7**, only peaks for the monomeric complexes were observed in the mass spectra. While the formation of monomeric molecules is rather unlikely, this suggests that readily cleavable dimers are probably present rather than oligomers.

3. Polymerisation studies

The complexes **4**–**7** were studied in the catalytic polymerisation of ethene, propene and styrene with activation by MAO (1000-fold excess, in toluene) as cocatalyst. No reaction was observed with styrene, which was rather unexpected as related side-chain-functionalised monocyclopentadienyl complexes of Ti exhibit good catalytic properties [22]. Presumably, complexes **4**–**7** are destroyed by MAO (attack at the P–Si or P–C bond with concomitant decomposition of the complexes) at the elevated temperatures employed (60 °C). However, ethene and propene are readily polymerised with formation of high-density polyethylene and polypropylene (Table 1); the elastomeric properties of the latter indicate a P–M interaction during the polymerisation process. Similar behaviour was already observed for related constrained-geometry catalysts with *N*-functionalised side-chains [6e].

Table 1
Activity of **4**–**7** in the polymerisation of propene

Complex	Ratio MAO:cat.	Activity for polypropylene (g mol^{-1} h^{-1})
4	300	0.86×10^3
5	300	2.61×10^3
6	300	0.84×10^3
7	300	8.20×10^3

The activities of complexes **4** and **7** are slightly higher than those of the constrained-geometry complexes and on the same order of magnitude as those of the Cp/phosphanido Group 4 complexes [14]. Regarding propene, the activity attained by complexes **4**–**7** is far lower than that observed with metallocene complexes [2,6e].

4. Experimental

All experiments were carried out under purified dry Ar. Solvents were dried and freshly distilled under Ar. The NMR spectra were recorded at 25 °C in C_6D_6 or [D_8]THF with an AVANCE DRX 400 spectrometer (Bruker): ^1H NMR: internal standard solvent (C_6H_6 or THF), external standard $SiMe_4$; ^{13}C NMR: external standard $SiMe_4$, internal standard solvent; ^{31}P NMR: external standard 85% H_3PO_4. The IR spectra were recorded on a Perkin–Elmer System 2000 FT-IR spectrometer in the range 350–4000 cm^{-1}. The mass spectra were recorded with an MAT-212 (Finnigan), EI MS, 70 eV. The m.p. were determined in sealed capillaries under Ar and are uncorrected.

LiPHPh [23], LiPHCy [24], Li[1-PH^{t}BuCMe$_2$C$_5$H$_4$] [15], and 1-SiMe$_3$–1-SiMe$_2$ClC$_5$H$_4$ [18] were prepared according to literature procedures.

4.1. 1- and 3-SiMe$_3$–1-SiMe$_2$PHPhC$_5$H$_4$ (1)

LiPHPh (4.10 g, 35 mmol) was suspended in *n*-C_6H_{14} (150 ml) and cooled to −20 °C. Then 1-SiMe$_3$–1-SiMe$_2$ClC$_5$H$_4$ (8.10 g, 35 mmol) was added, and the reaction mixture warmed to ambient temperature. The mixture was stirred for 1 day, filtered, the solvent evaporated in vacuo and the resulting yellow oil distilled under reduced pressure (65–75 °C, 2×10^{-2} Torr) to give 6.5 g (61%) of **1** as a colourless oil.

^1H NMR (C_6D_6): $\delta = -0.05$ (s, 18H, C*H*$_3$ in SiMe$_3$, 2 isomers), 0.01 (d, 6H, C*H*$_3$ in SiMe$_2$, $^3J_{P-H} = 2.4$, 2 isomers), 0.02 (d, 6H, C*H*$_3$ in SiMe$_2$, $^3J_{P-H} = 2.8$ Hz, 2 isomers), 3.10 (br s, 1H, C*H* in C_5H_4, 1 isomer), 3.20 (d, 2H, P*H*, $^1J_{P-H} = 192.6$ Hz, 2 isomers), 6.44 (m, 2H, C*H* in C_5H_4, 2 isomers), 6.48 (m, 1H, C*H* in C_5H_4, 1 isomer), 6.75 (m, 4H, C*H* in C_5H_4, 2 isomers), 7.01 (m, 6H, *o*- and *p*-C*H* in Ph, 2 isomers), 7.26 (t, 4H, *m*-C*H* in Ph, $^3J_{H-H} = 5.4$ Hz, 2 isomers).—^{31}P NMR (C_6D_6): $\delta = -121.6$, d, $^1J_{P-H} = 201$ Hz; −122.3, d, $^1J_{P-H} = 204$ Hz.—EI MS: *m*/*z* 304 (45%, [M^+]), 195 (100%, [M^+ − PHPh]), 73 (65%, $SiMe_3$), and fragmentation products thereof.—IR (KBr): $\tilde{\nu}$ (cm^{-1}): 2352 st (νPH), 1622 m, 1484 m (νC=C).—*Anal*. Calc. for $C_{16}H_{25}PSi_2$ (304.51): C 63.1, H 8.3, P 10.2; Found: C 56.8 (due to silicon carbide formation), H 8.1, P 9.3%.

4.2. 1- and 3-$SiMe_3$–1-$SiMe_2PHCy$–C_5H_4 (**2**)

LiPHCy (3.80 g, 31 mmol) was suspended in n-C_6H_{14} (150 ml) and cooled to −50 °C. Then 1-$SiMe_3$–1-$SiMe_2ClC_5H_4$ (8.00 g, 34 mmol) was added, and the reaction mixture warmed to ambient temperature. The mixture was stirred for 1 day, filtered, the solvent evaporated in vacuo and the resulting yellow oil distilled under reduced pressure (50–55 °C, 1×10^{-2} Torr) to give 4.1 g (43%) of **2** as a colourless oil.

^{1}H NMR (C_6D_6): $\delta = -0.01$ (s, 18H, CH_3 in $SiMe_3$, 2 isomers), 0.03 (d, 6H, CH_3 in $SiMe_2$, $^3J_{P-H} = 3.0$ Hz, 2 isomers), 0.04 (d, 6H, CH_3 in $SiMe_2$, $^3J_{P-H} = 3.3$ Hz, 2 isomers), 1.2–2.1 (m, 22H, Cy, 2 isomers), 2.60 (d of d, 2H, PH, $^1J_{P-H} = 191.0$, $^3J_{P-H} = 6.4$ Hz, 2 isomers), 2.91 (br s, 1H, CH in C_5H_4, 1 isomer), 6.50 (m, 3H, CH in C_5H_4, 2 isomers), 6.62 (m, 4H, CH in C_5H_4, 2 isomers).—^{31}P NMR (C_6D_6): $\delta = -124.9$, d, $^1J_{P-H} =$ 191.2 Hz; −127.6, d, $^1J_{P-H} = 189.5$ Hz.—EI MS: m/z 360 (27%, [M^+]), 209 (100%, [$M^+ -$PHCy]), 73 (100%, $SiMe_3$) and fragmentation products thereof.—IR (KBr): $\bar{\nu}$ (cm^{-1}): 2327 st (νPH), 1635 m, 1625 m (νC=C).—*Anal*. Calc. for $C_{20}H_{33}PSi_2$ (360.62): C 61.9, H 10.1, P 10.0; Found: C 56.9 (due to silicon carbide formation), H 9.5, P 8.9%.

4.3. 1-, 2- and 3-CMe_2PH^tBu–1-$SiMe_3C_5H_4$ (**3**)

Li[1-$PH^tBuCMe_2C_5H_4$] (1.00 g, 4.5 mmol) was dissolved in Et_2O (25 ml), $SiMe_3Cl$ (0.6 ml, 5 mmol) was added and the reaction mixture stirred for 12 h. LiCl was filtered off, the solvent evaporated in vacuo and the resulting yellow oil distilled under reduced pressure (55 °C, 3×10^{-3} Torr) to give 1.1 g (91%) of **3** as a yellow oil.

^{1}H NMR (C_6D_6): $\delta = -0.09$ (br s, 27H, CH_3 in $SiMe_3$, 3 isomers), 0.98 (d, 9H, CH_3 in ^{t}Bu, $^3J_{P-H} = 8.5$ Hz, 1 isomer), 1.07 (d, 9H, CH_3 in ^{t}Bu, $^3J_{P-H} = 8.7$ Hz, 1 isomer), 1.10 (d, 9H, CH_3 in ^{t}Bu, $^3J_{P-H} = 13.2$ Hz, 1 isomer), 1.34 (d, 3H, CH_3 in CMe_2, $^3J_{P-H} = 16.6$ Hz, 1 isomer), 1.36 (d, 3H, CH_3 in CMe_2, $^3J_{P-H} = 16.6$ Hz, 1 isomer), 1.43 (d, 3H, CH_3 in CMe_2, $^3J_{P-H} = 13.6$ Hz, 1 isomer), 1.45 (d, 3H, CH_3 in CMe_2, $^3J_{P-H} = 10.1$ Hz, 1 isomer), 1.48 (d, 3H, CH_3 in CMe_2, $^3J_{P-H} = 12.3$ Hz, 1 isomer), 1.56 (d, 3H, CH_3 in CMe_2, $^3J_{P-H} = 7.6$ Hz, 1 isomer), 3.08 (br s, 2H, CH in C_5H_4, 2 isomers), 3.31 (d, 2H, PH, $^1J_{P-H} = 197.4$ Hz, 2 isomers), 3.49 (d, 1H, PH, $^1J_{P-H} = 199.5$ Hz, 1 isomer), 5.98 (s, 2H, CH in C_5H_4, 1 isomer), 6.05 (s, 1H, CH in C_5H_4, 1 isomer), 6.15 (s, 1H, CH in C_5H_4, 1 isomer), 6.36 (s, 2H, CH in C_5H_4, 1 isomer), 6.63 (s, 1H, CH in C_5H_4, 1 isomer), 6.65 (s, 1H, CH in C_5H_4, 1 isomer), 6.80 (s, 1H, CH in C_5H_4, 1 isomer), 6.81 (s, 1H, CH in C_5H_4, 1 isomer).—^{31}P NMR (C_6D_6): $\delta = 25.2$, d of dec, $^1J_{P-H} = 196.7$ Hz, $^3J_{P-H} = 12.1$ Hz; 19.2, d, $^1J_{P-H} = 198.4$ Hz; 13.1, d of dec, $^1J_{P-H} = 199.5$ Hz, $^3J_{P-H} = 12.2$ Hz.—EI MS: m/z 268 (25%, [M^+]), 179 (100%, [$M^+ -$PH^{t}Bu]), 73 (100%, $SiMe_3$), and fragmentation products thereof.—IR (KBr): $\bar{\nu}$ (cm^{-1}): 2345 m (νPH), 1625 m, 1503 m (νC=C).—*Anal*. Calc. for $C_{15}H_{29}PSi$ (268.45): C 67.1, H 10.9, P 11.5; Found: C 65.9, H 9.9, P 10.9%.

4.4. [{(η^5-C_5H_4)$SiMe_2PHPh$}$ZrCl_3$] (**4**)

$ZrCl_4$ (1.33 g, 5.7 mmol) was suspended in $C_6H_5CH_3$ (30 ml), and a solution of **1** (1.75 g, 5.8 mmol) in $C_6H_5CH_3$ (20 ml) was added dropwise. The reaction mixture was stirred for 1 day, then the solvent was evaporated in vacuo and the resulting residue washed with n-C_5H_{12} (30 ml) and extracted with THF to give 2.0 g (80%) of **4** as a yellow microcrystalline solid. M.p.: 150–155 °C. ^{1}H NMR ([D$_8$]THF): $\delta = 0.54$ (d, 3H, CH_3 in $SiMe_2$, $^3J_{P-H} = 4.9$ Hz), 0.55 (d, 3H, CH_3 in $SiMe_2$, $^3J_{P-H} = 3.9$ Hz), 2.62 (d, 1H, PH, $^1J_{P-H} = 200.9$ Hz), 6.52 (m, 1H, CH in C_5H_4), 6.55 (m, 1H, CH in C_5H_4), 6.58 (m, 1H, CH in C_5H_4), 6.61 (m, 1H, CH in C_5H_4), 7.10 (m, 3H, CH in Ph), 7.11 (m, 2H, CH in Ph).—^{13}C NMR ([D$_8$]THF): $\delta = -1.09$ (d, 1C, CH_3Si, $^2J_{P-C} = 2.9$ Hz), −1.00 (d, 1C, CH_3Si, $^2J_{P-C} = 5.5$), 119.34 (s, 2C, C in C_5H_4), 121.95 (d, 2C, C in C_5H_4, $^3J_{P-C} = 6.2$ Hz), 126.32 (d, 1C, *ipso*-C in Ph, $^1J_{P-C} =$ 22.0 Hz), 126.70 (d, 1C, C1 in C_5H_4, $^2J_{P-C} = 12.8$ Hz), 127.00 (s, 1C, *p*-C in Ph), 128.66 (d, 2C, *m*-C in Ph, $^3J_{P-C} = 5.8$ Hz), 134.45 (d, 2C, *o*-C in Ph, $^2J_{P-C} = 14.4$ Hz).—^{31}P NMR ([D$_8$]THF): $\delta = -117.1$, d, $^1J_{P-H} =$ 200.9 Hz.—EI MS: m/z 428 (2%, [M^+]), 319 (32%, [$M^+ -$PHPh]), 122 (100%, $C_5H_4SiMe_2^+$), 109 (52%, $PHPh^+$), and fragmentation products thereof.—IR (KBr): $\bar{\nu}$ (cm^{-1}): 2351 s (νPH).—*Anal*. Calc. for $C_{13}H_{16}Cl_3PSiZr$ (428.9): C 36.4, H 3.8, P 7.2; Found: C 26.4 (due to silicon carbide formation), H 4.0, P 7.1%.

4.5. [{(η^5-C_5H_4)$SiMe_2PHCy$}$ZrCl_3$] (**5**)

$ZrCl_4$ (1.80 g, 7.7 mmol) was suspended in $C_6H_5CH_3$ (50 ml), and a solution of **2** (2.79 g, 7.8 mmol) in $C_6H_5CH_3$ (50 ml) was added dropwise. The reaction mixture was stirred for 1 day, then the solvent was evaporated in vacuo and the resulting residue washed with n-C_5H_{12} (30 ml) and extracted with THF to give 2.0 g (58%) of **5** as white microcrystalline solid. M.p.: 145 °C. ^{1}H NMR ([D$_8$]THF): $\delta = 0.63$ (d, 3H, CH_3 in $SiMe_2$, $^3J_{P-H} = 4.3$ Hz), 0.64 (d, 3H, CH_3 in $SiMe_2$, $^3J_{P-H} = 6.1$ Hz), 1.18–1.85 (m, 11H, Cy), 2.59 (d, 1H, PH, $^1J_{P-H} = 191.1$ Hz), 6.57 (m, 2H, CH in C_5H_4), 6.64 (m, 2H, CH in C_5H_4).—^{31}P NMR ([D$_8$]THF): $\delta =$ −121.6, d, $^1J_{P-H} = 201.0$ Hz.—EI MS: m/z 434 (7%, [M^+]), 319 (45%, [$M^+ -$PHCy]), 122 (100%, $C_5H_4SiMe_2^+$), 115 (82%, $PHCy^+$), and fragmentation products thereof.—IR (KBr): $\bar{\nu}$ (cm^{-1}): 2403 m (νPH).—*Anal*. Calc. for $C_{13}H_{22}Cl_3PSiZr$ (434.95): C

35.9, H 5.1, P 7.1; Found: C 27.3 (due to silicon carbide formation), H 4.9, P 6.5%.

4.6. [{(η^5-C_5H_4)CMe_2PH^tBu}$ZrCl_3$] (6)

$ZrCl_4$ (1.00 g, 4.3 mmol) was suspended in $C_6H_5CH_3$ (50 ml), and a solution of **3** (1.15 g, 4.3 mmol) in $C_6H_5CH_3$ (10 ml) was added dropwise. The reaction mixture was stirred for 12 h, then the solvent was evaporated in vacuo and the resulting residue washed with n-C_5H_{12} (30 ml) and extracted with THF to give 0.76 g (45%) of **6** as white microcrystalline solid. M.p.: 105 °C. ^{1}H NMR ([D$_8$]THF): $\delta = 1.03$ (d, 9H, CH_3 in ^{t}Bu, $^3J_{H-H} = 13.2$ Hz), 1.46 (d, 3H, CH_3C, $^3J_{P-H} = 8.1$ Hz), 1.54 (d, 3H, CH_3C, $^3J_{P-H} = 11.2$ Hz), 3.54 (d, 1H, PH, $^1J_{P-H} = 294.9$ Hz), 6.31 (m, 1H, CH in C_5H_4), 6.53 (m, 1H, CH in C_5H_4), 6.55 (m, 1H, CH in C_5H_4), 6.63 (m, 1H, CH in C_5H_4).—^{13}C NMR ([D$_8$]THF): $\delta =$ 30.04 (d, 3C, CH$_3$ in ^{t}Bu, $^2J_{P-C} = 5.5$ Hz), 33.02 (d, 1C, $C(CH_3)_2$, $^1J_{P-C} = 8.1$ Hz), 33.20 (d, 1C, $C(CH_3)_3$, $^1J_{P-C} = 11.9$ Hz), 33.64 (d, CH$_3$C, $^2J_{P-C} = 4.3$ Hz), 34.30 (d, CH$_3$C, $^2J_{P-C} = 5.8$ Hz), 115.39 (s, 1C, C in C_5H_4), 119.01 (s, 1C, C in C_5H_4), 119.78 (s, 1C, C in C_5H_4), 119.82 (s, 1C, C in C_5H_4), 129.71 (d, 1C, C1 in C_5H_4, $^2J_{P-C} = 10.2$ Hz).—^{31}P NMR (d$_8$-THF): $\delta = -$ 6.8, d, $^1J_{P-H} = 282.5$ Hz.—EI MS: m/z 392 (3%, [M^+]), 303 (11%, [$M^+ - PH^tBu$]), 107 (80%, $C_5H_4CMe_2^+$), and fragmentation products thereof.—IR (KBr): $\tilde{\nu}$ (cm^{-1}): 2379 m (νPH).—*Anal*. Calc. for $C_{12}H_{20}Cl_3PZr$ (392.84): C 36.7, H 5.1, P 7.9; Found: C 34.3, H 4.9, P 7.5%.

4.7. [{(η^5-C_5H_4)CMe_2PH^tBu}$TiCl_3$] (7)

$TiCl_4$ (1.50 g, 7.9 mmol) was suspended in $C_6H_5CH_3$ (50 ml), and a solution of **3** (2.11 g, 7.9 mmol) in $C_6H_5CH_3$ (20 ml) was added dropwise. The reaction mixture was stirred for 12 h, then the solvent was evaporated in vacuo and the resulting residue washed with n-C_5H_{12} (30 ml) and extracted with $C_6H_5CH_3$ to give 1.85 g (67%) of **7** as a red microcrystalline solid. M.p.: 82–86 °C. ^{1}H NMR ([D$_8$]THF): $\delta = 0.92$ (d, 9H, CH_3 in ^{t}Bu, $^3J_{H-H} = 12.0$ Hz), 1.69 (m, 6H, CH_3C), 3.50 (d, 1H, PH, $^1J_{P-H} = 212.6$ Hz), 6.26 (m, 2H, CH in C_5H_4), 6.93 (m, 2H, CH in C_5H_4).—^{13}C NMR ([D$_8$]THF): $\delta = 31.07$ (d, 3C, CH$_3$ in ^{t}Bu, $^2J_{P-C} = 12.8$ Hz), 31.45 (d, 1C, $C(CH_3)_2$, $^1J_{P-C} = 19.2$ Hz), 33.12 (d, 1C, $C(CH_3)_3$, $^1J_{P-C} = 10.1$ Hz), 35.37 (s, CH$_3$C), 37.20 (s, CH$_3$C), 121.09 (s, 2C, C in C_5H_4), 122.64 (d, 1C, C1 in C_5H_4, $^2J_{P-C} = 27.7$ Hz), 130.88 (s, 2C, C in C_5H_4).—^{31}P NMR ([D$_8$]THF): $\delta = 36.7$, d, $^1J_{P-H} =$ 213.4 Hz.—EI MS: m/z 348 (5%, [M^+]), 224 (26%, [$M^+ - Cl-PH^tBu$]), 107 (20%, $C_5H_4CMe_2^+$), and fragmentation products thereof.—IR (KBr): $\tilde{\nu}$ (cm^{-1}): 2324 m (νPH).—*Anal*. Calc. for $C_{12}H_{20}Cl_3PTi$ (349.5): C 41.2, H 5.8, P 8.9; Found: C 39.8, H 5.5, P 8.4%.

4.8. Polymerisation experiments

All manipulations of air-sensitive materials were performed with the rigorous exclusion of oxygen and moisture in flamed Schlenk-type glassware on a dual-manifold Schlenk line, or interfaced to a high vacuum (10^{-5} Torr) line, or in a nitrogen-filled Vacuum Atmospheres glove box with a medium-capacity recirculator (1–2 ppm O_2). Argon, ethene, propene and nitrogen gases were purified by passage through a MnO oxygen-removal column and a Davison 4 Å molecular sieve column. Styrene (Spectrum) was freshly distilled under vacuum from CaO. All solvents for vacuum-line manipulations were stored in vacuo over Na/K alloy in resealable bulbs.

The polymerisation experiments were conducted in a 100 ml flamed heavy-wall glass round-bottom reaction flask attached to a high-vacuum line. In a typical experiment, 10 mg of **4**–**7** and the corresponding amount of MAO (MAO:cat. = 1:300) were charged to the flask containing a magnetic stir bar. The reaction vessel was connected to a high-vacuum line, pumped down and back-filled three times with Ar. Then the flask was re-evacuated, and a measured quantity of $C_6H_5CH_3$ (5 ml) was vacuum transferred into the reaction flask from Na/K. Then gaseous ethene or propene was condensed into the vessel through a gas-purification column. The flask was warmed to room temperature, and the pressure was continuously measured by means of a manometer. Rapid stirring of the solution was initiated, and after a measured time interval (2 h), the polymerisation was quenched by releasing the excess pressure of ethene or propene and immediately injecting a methanol/HCl mixture. The polymer product was collected by filtration, washed with C_6H_{14} and C_3H_6O and dried under vacuum for several hours.

Acknowledgements

We gratefully acknowledge financial support from the Deutsche Forschungsgemeinschaft, the German-Israeli-Foundation grant no. I-142/95 and the Fonds der Chemischen Industrie.

References

[1] K. Ziegler, E. Holzkamp, H. Breil, H. Martin, Angew. Chem. 67 (1955) 541.
[2] (a) N. Schneider, M.E. Huttenloch, U. Stehling, R. Kirsten, F. Schaper, H.H. Brintzinger, Organometallics 16 (1997) 3413 (and references therein);
(b) E.Y.-X. Chen, T.J. Marks, Chem. Rev. 100 (2000) 1391;
(c) T.J. Marks, J.C. Stevens (Eds.), Top. Catal. 7 (1999) 1 (special issue on 'Advances in Polymerization Catalysis. Catalysts and Processes');

(d) W. Kaminsky, Metalorganic Catalysts for Synthesis and Polymerization: Recent Results by Ziegler-Natta and Metallocene Investigations, Springer-Verlag, Berlin, 1999;
(e) G.J.P. Britovsek, V.C. Gibson, D.F. Wass, Angew. Chem., Int. Ed. Engl. 38 (1999) 428;
(f) J.A. Gladysz (Ed.), Chem. Rev. 100 (2000) (special issue devoted to the polymerisation of α-olefins).
[3] W. Kaminsky, O. Rabe, A.-M. Schauwienold, G.U. Schupfner, J. Hanss, J. Kopf, J. Organomet. Chem. 497 (1995) 181.
[4] S.T. Chacon, E.B. Coughlin, L.M. Henling, J.E. Bercaw, J. Organomet. Chem. 497 (1995) 171.
[5] (a) W. Kaminsky, K. Külper, H.H. Brintzinger, F.R.W.P. Wild, Angew. Chem. 97 (1985) 507; Angew. Chem., Int. Ed. Engl. 24 (1985) 507;
(b) H.H. Brintzinger, D. Fischer, R. Mülhaupt, B. Rieger, R. Waymouth, Angew. Chem. 107 (1995) 1255; Angew. Chem., Int. Ed. Engl. 34 (1995) 1143;
(c) G. Fink, R. Mülhaupt, H.H. Brintzinger, Ziegler Catalysts—Recent Scientific Innovations and Technological Improvements, Springer-Verlag, Berlin, 1995.
[6] (a) P.J. Shapiro, E. Bunel, W.P. Schaefer, J.E. Bercaw, Organometallics 9 (1990) 867;
(b) P.J. Shapiro, W.D. Cotter, W.P. Schaefer, J.A. Labinger, J.E. Bercaw, J. Am. Chem. Soc. 116 (1994) 4623;
(c) J.C. Flores, J.C.W. Chien, M.D. Rausch, Organometallics 13 (1994) 4140;
(d) H.G. Alt, K. Föttinger, W. Milius, J. Organomet. Chem. 572 (1999) 21;
(e) M. Galan-Fereres, T. Koch, E. Hey-Hawkins, M.S. Eisen, J. Organomet. Chem. 580 (1999) 145;
(f) A.L. McKnight, R.M. Waymouth, Chem. Rev. 98 (1998) 2587;
(g) J.A.M. Canich, Eur. Patent 420 436, 1991;
(h) G.F. Schmidt, F.J. Timmers, G.W. Knight, S.-Y. Lai, P.N. Nickias, R.K. Rosen, J.C. Stevens, D.R. Wilson, Eur. Patent 416 815, 1991;
(i) G. Lanza, I.L. Fragala, T.J. Marks, J. Am. Chem. Soc. 122 (2000) 12764 (and references therein).
[7] (a) S.J. Brown, X. Gao, D.G. Harrison, L. Koch, R.E.v.H. Spence, G.P.A. Yap, Organometallics 17 (1998) 5445;
(b) F. Mathey, Chem. Rev. 88 (1988) 429;
(c) C. Janiak, K.C.H. Lange, U. Versteeg, D. Lentz, P.H.M. Budzelaar, Chem. Ber. 129 (1996) 1517;
(d) C. Janiak, U. Versteeg, K.C.H. Lange, R. Weimann, E. Hahn, J. Organomet. Chem. 501 (1995) 219.
[8] H. Butenschön, Chem. Rev. 100 (2000) 1527 (and references cited therein).
[9] T. Koch, E. Hey-Hawkins, Polyhedron 18 (1999) 2113 (and references therein).
[10] C.S. Slone, D.A. Weinberger, C.A. Mirkin, Prog. Inorg. Chem. 48 (1999) 233.
[11] U.J. Bildmann, G. Müller, Z. Naturforsch., Teil B 55 (2000) 895.
[12] U.J. Bildmann, M. Winkler, G. Müller, Z. Naturforsch., Teil B 55 (2000) 1005.
[13] O. Tardif, Z. Hou, M. Nishiura, Take-aki Koizumi, Y. Wakatsuki, Organometallics 20 (2001) 4565.
[14] T. Höcher, S. Blaurock, E. Hey-Hawkins, Eur. J. Inorg. Chem. (2002) 1174.
[15] T. Koch, S. Blaurock, F.B. Somoza, Jr., A. Voigt, R. Kirmse, E. Hey-Hawkins, Organometallics 19 (2000) 2556.
[16] K. Kunz, G. Erker, S. Döring, R. Fröhlich, G. Kehr, J. Am. Chem. Soc. 123 (2001) 6181.
[17] J. Jubb, J. Song, D. Richeson, S. Gambarotta, in: E.W. Ebel, F.G.A. Stone, G. Wilkinson (Eds.), Comprehensive Organometallic Chemistry II, vol. 4, Pergamon Press, Oxford, 1995, p. 543ff.
[18] S. Ciruelos, T. Cuenca, P. Gómez-Sal, A. Manzanero, P. Royo, Organometallics 14 (1995) 177.
[19] I. Dorado, J.C. Flores, M. Galakhov, P.G. Sal, A. Martin, P. Royo, J. Organomet. Chem. 563 (1998) 7.
[20] D.P. Krut'ko, M.V. Borzov, E.N. Veksler, A.V. Churakov, J.A.K. Howard, Polyhedron 17 (1998) 3889.
[21] D.P. Krut'ko, M.V. Borzov, E.N. Veksler, R.S. Kirsanov, A.V. Churakov, Eur. J. Inorg. Chem. (1999) 1973.
[22] (a) N. Ishihara, M. Kuramoto, M. Uoi, Macromolecules 21 (1988) 3356;
(b) N. Ishihara, Macromol. Symp. 89 (1995) 553;
(c) W. Kaminsky, S. Lenk, V. Scholz, Macromolecules 30 (1997) 7647.
[23] C. Frenzel, E. Hey-Hawkins, Phosphorus Sulfur 143 (1998) 1.
[24] E. Hey-Hawkins, S. Kurz, Phosphorus Sulfur 90 (1994) 281.

to heavier alkali metal compounds. In this work "[Li(PyNSiMe$_3$)(15C5)]", which could only be isolated as a viscous red oil, was employed. Despite numerous attempts, no crystalline material could be isolated; this implies an ill-defined complex, reflecting the poor host–guest fit of lithium with 15C5. Metathesis of "[Li(PyNSiMe$_3$)(15C5)]" with potassium *tert*-butoxide or rubidium 2-ethylhexoxide affords **3** and **4**, respectively, as red oils, in essentially quantitative yields (Eq. (1)). Recrystallisation of these oils from solutions of methylcyclohexane containing THF yields crystals of **3** and **4** suitable for X-ray crystallographic study.

$$\text{"[Li(PyNSiMe}_3\text{)15C5)]"} + \text{MOR} \rightarrow 1/2[\{\text{M(PyNSiMe}_3\text{)(15C5)}\}_2] + \text{LiOR}$$

$$\text{M} = \text{K};\ \text{R} = \text{Bu}^t$$

$$\text{M} = \text{Rb};\ \text{R} = \text{CH}_3(\text{CH}_2)_3\text{CH}(\text{CH}_2\text{CH}_3)\text{CH}_2 \qquad (1)$$

The ^{1}H and ^{13}C NMR spectra of **3** and **4** exhibit the expected signals in accord with the solid state structures (see below). The ^{29}Si NMR spectra exhibit signals at −19.03 and −18.97 ppm, respectively, reflecting the similarity of potassium and rubidium in terms of Pauling electronegativities, and are commensurate with the soft polarisable nature of higher alkali metals leading to increased shielding at the amido centre.

An X-ray crystallographic study reveals that **3** crystallises as a 'slipped' dimer with no significant intermolecular interactions (Fig. 1). Selected bond lengths and angles are given in Table 1. The coordination sphere of each potassium ion is dominated by the 15C5, which bridges via one oxygen centre to the other potassium centre, forming a $(KO)_2$ ring that lies on a crystallographic inversion centre. This bridging nature of crown ethers with alkali metals is rare, but some examples have been reported with lithium [10,11], sodium [12] and potassium [13–15]. The coordination

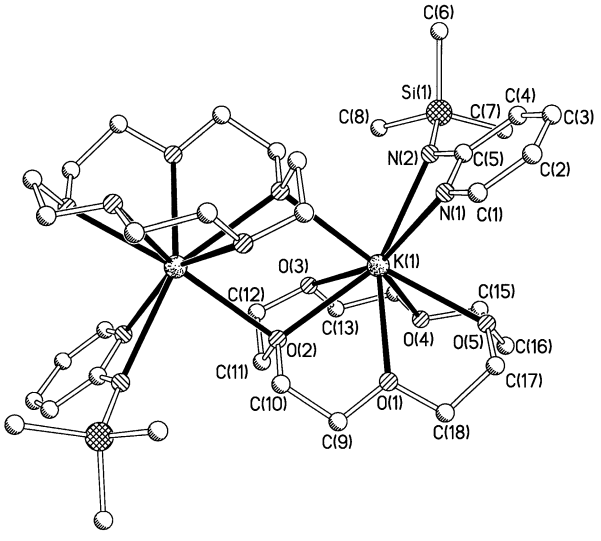


Fig. 1. The molecular structure of **3**, without H atoms.

Table 1
Selected bond lengths (Å) and angles (°) for **3** and **4**

3 [a]			
Bond lengths			
K(1)–N(1)	2.7930(11)	K(1)–N(2)	2.8001(11)
K(1)–O(1)	2.8747(11)	K(1)–O(2)	2.8289(10)
K(1)–O(2A)	2.9510(10)	K(1)–O(3)	2.8658(10)
K(1)–O(4)	2.8365(10)	K(1)–O(5)	2.7758(10)
Bond angles			
N(1)–K(1)–N(2)	48.87(3)	N(1)–K(1)–O(2A)	79.37(3)
N(2)–K(1)–O(2A)	81.12(3)	O(1)–K(1)–O(2)	59.91(3)
O(2)–K(1)–O(3)	61.30(3)	O(3)–K(1)–O(4)	59.15(3)
O(4)–K(1)–O(5)	60.16(3)	O(5)–K(1)–O(1)	59.67(3)
O(2)–K(1)–O(2A)	72.06(3)	K(1)–O(2)–K(1A)	107.94(3)
4 [b]			
Bond lengths			
Rb(1)–N(1)	3.143(2)	Rb(1)–N(1A)	3.036(2)
Rb(1)–N(2)	2.979(2)	Rb(1)–N(2A)	3.174(2)
Rb(1)–O(1)	3.119(2)	Rb(1)–O(2)	2.970(2)
Rb(1)–O(3)	3.063(2)	Rb(1)–O(4)	3.019(2)
Rb(1)–O(5)	3.177(2)		
Bond angles			
N(1)–Rb(1)–N(1A)	105.48(5)	N(1)–Rb(1)–N(2)	44.07(6)
N(1A)–Rb(1)–N(2)	92.08(6)	N(1A)–Rb(1)–N(2A)	43.45(6)
N(1)–Rb(1)–N(2A)	86.52(6)	N(2)–Rb(1)–N(2A)	105.18(5)
O(1)–Rb(1)–O(2)	54.57(6)	O(2)–Rb(1)–O(3)	57.61(6)
O(4)–Rb(1)–O(5)	54.64(5)	O(5)–Rb(1)–O(1)	53.77(5)
Rb(1)–N(1)–Rb(1A)	74.52(5)	Rb(1)–N(2)–Rb(1A)	74.82(5)

[a] Symmetry operations for equivalent atoms (A): $-x, -y+1, -z$.
[b] Symmetry operations for equivalent atoms (A): $-x+1, -y+1, -z+1$.

sphere of each potassium cation is completed by the amide, which is relegated to a terminal chelating role. This bonding mode illustrates the strength of the macrocyclic effect; clearly the potassium cation is not large enough to accommodate bridging amide with a capping 15C5 molecule as with the previously reported dimer **1** [9], so the dimer 'slips'.

The five terminal K–O bond lengths span the narrow range 2.776(2)–2.875(2) Å, a smaller range than observed in **1**, reflecting the better host–guest fit of 15C5 than 12C4 with potassium. This range also compares well with other previously reported examples of K(15C5) complexes [16,17]. Thus, each potassium resides 1.558 Å from the mean plane of the oxygen atoms of the crown, a smaller deviation than in **1**. The bridging K–O bond length of 2.951(2) Å is longer, as would be expected for a bridging oxygen centre. The K–N(2) bond length of 2.880(2) Å is somewhat longer than the K–N(1) bond length of 2.793(2) Å. It might be expected that the amido N(2) centre would have the shorter bond length. However, inspection of a space-filling plot reveals that the amido centre is pushed away to relieve steric strain by the bulky trimethylsilyl group. Nevertheless, the observed K–N bond lengths fall within ranges previously reported [9,18]. The ligand bite angle of 48.87(3)° is substantially smaller than those observed

in the compound [{Na(12C4)$_2$}{Na(PyNSiMe$_3$)$_2$(THF)}] [9], reflecting the larger ionic radius of potassium compared to sodium (effective ionic radii for coordination number 6 are given as 1.02, 1.38, and 1.52 Å for Na^+, K^+, and Rb^+, respectively [19]). The amides exhibit a hinge angle of 157.8°, defined as the dihedral angle between the mean plane of the pyridyl ring and amido N(2), and the KN_2 plane; this would be 180° if the potassium ion lay exactly in the plane of the ligand. This hinge angle results in a deviation from planarity at N(2) [sum of bond angles = 356.83(9)°]. The trimethylsilyl groups are staggered with respect to the pyridyl ring to minimise steric strain.

The molecular structure of **4** is illustrated in Fig. 2 and selected bond lengths and angles are given in Table 1. The complex crystallises as a contact ion pair dimer constructed around a transoid $(RbN)_2$ ring involving the amido nitrogen centres, with additional coordination by bridging pyridyl groups, and capped on each end by a molecule of 15C5. The molecule is centrosymmetric, the $(RbN)_2$ ring lying on a crystallographic inversion centre. The larger ionic radius of rubidium compared to potassium is demonstrated by the retention of the bridged amide dimer core observed in **1** and **2**, instead of 'slipping' to the dimer architecture observed in **3**. The Rb–O bond lengths span the range 2.970(2)–3.177(2) Å, reflecting the increased ionic radius of rubidium compared to potassium and agreeing well with previous examples [20,21]. Consequently the rubidium cation resides 1.943 Å above the oxygen mean plane of the crown, reflecting not only the larger ionic radius of rubidium, but also the more congested coordination sphere of the metal. For the amido ligand, the Rb–N bond lengths span the ranges 2.979(2)–3.174(2) Å (amide) and 3.036(2)–3.143(2) Å (pyridyl). Whilst the lower value for the Rb–N(amide) is in good agreement with bond lengths observed in **2**, the other three bond lengths are at the higher end of bond lengths associated with tertiary amines coordinated to rubidium. For example, Rb–N bond lengths in the ranges 3.022–3.099 and 3.092–3.131 Å have been observed in the complexes [{Rb(fluorenyl)(PMDETA)}$_8$] [22] and [{RbC(H)(SiMe$_3$)$_2$(PMDETA)}$_2$] [23] (PMDETA = *N*,*N*′,*N*″,*N*″-pentamethyldiethylenetriamine), respectively. This is, perhaps, an indication of the crowding in this dimer as a result of increasing the size of the crown. Whereas potassium cannot accommodate the complete coordination environment and gives a 'slipped' dimer, rubidium is just large enough, but at the expense of a long Rb–N bond as the macrocyclic effect dominates. The trimethylsilyl groups are again staggered with respect to the pyridyl rings minimising steric strain. The pyridyl rings are tilted from the normal of the Rb(1)···Rb(1A) vector. The N(1) pyridyl ring tilts towards Rb(1A) (hinge angles of 143.9° to the plane of N(1)/N(2)/Rb(1) and 134.7° to the plane of N(1)/N(2)/Rb(1A)). This is a smaller degree of tilt than observed in **1** or **2**, reflecting the increased coordination number of rubidium, and hence a diminished requirement of electron density from the π system of the pyridyl ring.

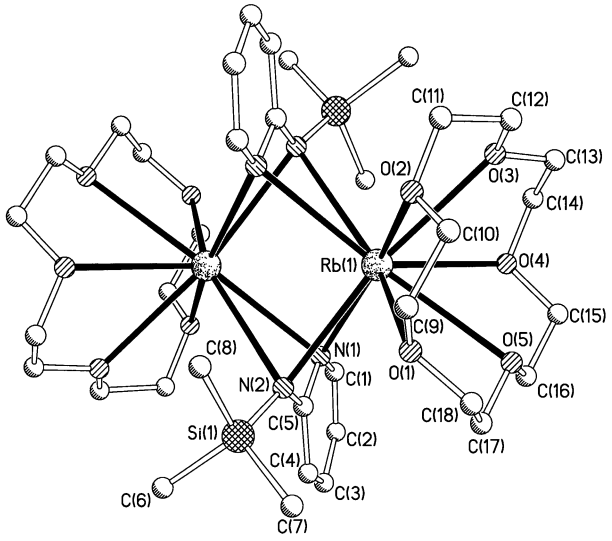


Fig. 2. The molecular structure of **4**, without H atoms.

3. Conclusion

The new potassium and rubidium amides are readily prepared by a metathesis protocol in excellent yields. The structures adopted in the solid state are cation dictated; in **3** a slipped dimer is formed by bridging crowns, giving a $(KO)_2$ ring with terminal chelating amides, whereas for **4** a dimer with a $(RbN)_2$ ring is formed, with additional coordination by bridging pyridyl groups and capping crowns, as a consequence of the larger size of rubidium compared to potassium.

4. Experimental

4.1. General comments

All manipulations were carried out using standard Schlenk techniques under an atmosphere of dry nitrogen. Methylcyclohexane and THF were distilled from sodium–benzophenone ketyl radical under an atmosphere of dry nitrogen and stored over activated 4A molecular sieves. 15-Crown-5 ether was dried by, and stored over activated 4A molecular sieves. 2-Trimethylsilylaminopyridine was prepared as described previously [9]. Butyllithium was purchased from Aldrich as a 2.5 M solution in hexanes. Potassium *tert*-butoxide was purchased from Aldrich and was baked at 100 °C (10^{-2} mmHg) and stored under an atmosphere of dry nitrogen prior to use. Rubidium-2-ethylhexoxide was prepared by

a literature method [24]. Deuteriated solvents were distilled from a potassium mirror, deoxygenated by three freeze–pump–thaw cycles, and stored over activated 4A molecular sieves.

The ^{1}H and ^{13}C NMR spectra were recorded on a Bruker AC200 spectrometer and ^{29}Si spectra on a Bruker WM300 operating at 200.1, 50.3 and 59.6 MHz, respectively, and chemical shifts are quoted in ppm relative to tetramethylsilane. Elemental analyses were obtained by Elemental Microanalysis Ltd., Okehampton, UK.

4.2. Preparation of [{K(PyNSiMe$_3$)(μ-15C5)}$_2$] (3)

Bu^{n}Li (1.28 ml, 3.19 mmol) was added dropwise to a solution of 2-trimethylsilylaminopyridine (0.53 g, 3.19 mmol) and 15-crown-5 (0.63 ml, 3.19 mmol) in THF (40 ml) and stirred for 1 h to afford a yellow solution. Dropwise addition of this solution to Bu^{t}OK (0.36 g, 3.19 mmol) gave a dark orange solution. Removal of volatiles in vacuo yielded a viscous red oil; recrystallisation from methylcyclohexane/THF solution at 5 °C gave crystals of **3** suitable for X-ray crystallography (0.98 g, 72.3%). Microanalysis for **3**: C, 50.68; H, 8.21; N, 6.31. $C_{36}H_{66}K_2N_4O_{10}Si_2$ requires C, 50.91; H, 7.83; N, 6.60%. Spectroscopic data for **3**: δ_H ([^{2}H]$_8$ THF) 0.10 (18H, s, SiMe$_3$), 3.67 (40H, s, 15C5), 5.68 (2H, t, β-H-Py), 6.05 (2H, d, β′-H-Py), 6.78 (2H, t, γ-H-Py) and 7.68 (2H, d, α-H-Py). δ_C ([^{2}H]$_8$ THF) 2.79 (SiMe$_3$), 69.64 (15C5), 103.01 (β-C-Py), 115.27 (β′-C-Py), 134.66 (γ-C-Py), 149.53 (α-C-Py) and 170.47 (α′-C-Py). δ_{Si} ([^{2}H]$_8$ THF) −19.03 (s, SiMe$_3$).

4.3. Preparation of [{Rb(μ-PyNSiMe$_3$)(15C5)}$_2$] (4)

Bu^{n}Li (1.35 ml, 3.37 mmol) was added dropwise to a solution of 2-trimethylsilylaminopyridine (0.56 g, 3.37 mmol) and 15-crown-5 (0.67 ml, 3.37 mmol) in THF (40 ml) and stirred for 1 h to afford a yellow solution. Addition of this solution to rubidium-2-ethylhexoxide (0.72 g, 3.37 mmol) gave a dark orange solution. Removal of volatiles in vacuo yielded a viscous red oil; recrystallisation from a methylcyclohexane/THF solution at 5 °C gave crystals of **4** suitable for X-ray crystallography (1.15 g, 72.4%). Microanalysis for **4**: C, 46.25; H, 7.40; N, 5.65. $C_{36}H_{66}N_4O_{10}Rb_2Si_2$ requires C, 45.90; H, 7.06; N, 5.95%. Spectroscopic data for **4**: δ_H ([^{2}H]$_8$ THF) 0.10 (18H, s, SiMe$_3$), 3.62 (40H, s, 15C5), 5.72 (2H, t, β-H-Py), 6.04 (2H, d, β′-H-Py), 6.79 (2H, t, γ-H-Py) and 7.73 (2H, d, α-H-Py). δ_C ([^{2}H]$_8$ THF) 2.77 (SiMe$_3$), 69.90 (15C5), 103.11 (β-C-Py), 115.60 (β′-C-Py), 134.75 (γ-C-Py), 149.65 (α-C-Py) and 170.16 (α′-C-Py). δ_{Si} ([^{2}H]$_8$ THF) −18.97 (s, SiMe$_3$).

4.4. X-ray crystallography

Crystal data for complexes **3** and **4** are listed in Table 2. Crystals were examined on a Bruker AXS SMART CCD area detector with graphite-monochromated Mo Kα radiation ($\lambda = 0.70173$ Å) at 160 K with an Oxford Cryostream low-temperature device. Cell parameters were refined from positions of all strong reflections in each data set. Intensities were corrected semi-empirically for absorption, based on symmetry-equivalent and repeated reflections. The structures were solved by direct methods and refined on F^2 values for all unique data. All non-hydrogen atoms were refined anisotropically. All hydrogen atoms were placed in geometrically calculated positions and constrained with a riding model; U(H) was set at 1.2 (1.5 for methyl groups) times U_{eq} for the parent atom. Programs were Bruker AXS SMART (control) and SAINT (integration) [25], and SHELXTL for structure solution, refinement and molecular graphics [26].

Table 2
Crystal data and structure refinement parameters for **3** and **4**

Compound	**3**	**4**
Formula	$C_{36}H_{66}K_2N_4O_{10}Si_2$	$C_{36}H_{66}N_4O_{10}Rb_2Si_2$
Formula weight	849.3	942.1
Temperature (K)	160	160
Crystal system	monoclinic	triclinic
Space group	$P2_1/c$	$P\bar{1}$
Unit cell dimensions		
a (Å)	12.7950(6)	10.6890(7)
b (Å)	9.4632(4)	11.2629(7)
c (Å)	18.5977(8)	11.7875(8)
α (°)		103.220(2)
β (°)	92.661(2)	112.535(2)
γ (°)		108.048(2)
V (Å^3)	2249.41(17)	1144.57(13)
Z	2	1
Absorption coefficient (mm^{-1})	0.32	2.24
Crystal size (mm)	0.76 × 0.48 × 0.36	0.80 × 0.80 × 0.38
θ_{max} (°)	28.6	28.6
Reflections measured	18968	9981
Unique reflections	5377	5226
Reflections with $F^2 > 2\sigma(F^2)$	4410	3813
Transmission factors	0.754–0.881	0.176–0.361
R_{int}	0.0185	0.0396
Number of parameters	247	248
R [a] [$F^2 > 2\sigma(F^2)$]	0.0318	0.0358
R_w [b] (all data)	0.0922	0.0840
Goodness-of-fit [c] (S)	1.084	0.851
Largest difference peak and hole (e Å^{-3})	0.65 and −0.26	1.06 and −0.86

[a] Conventional $R = \Sigma||F_o| - |F_c||/\Sigma|F_o|$ for 'observed' reflections having $F^2 > 2\sigma(F^2)$.

[b] $R_w = [\Sigma w(F_o^2 - F_c^2)^2/\Sigma w(F_o^2)^2]^{1/2}$ for all data.

[c] $S = [\Sigma w(F_o^2 - F_c^2)^2/(\text{no. of unique reflections} - \text{no. of parameters})]^{1/2}$.

5. Supplementary information

Crystallographic data for the structural analysis of compounds **3** and **4** have been deposited with the Cambridge Crystallographic Data Centre, CCDC Nos. 179632 and 179631 for compounds **3** and **4**, respectively. Copies of this information may be obtained free of charge from The Director, CCDC, 12 Union Road, Cambridge, CB2 1EZ, UK (fax: +44-1223-336033; e-mail: deposit@ccdc.cam.ac.uk or www: http://www.ccdc.cam.ac.uk).

Acknowledgements

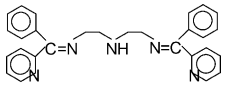
We thank the EPSRC for partial funding of diffractometer equipment.

References

[1] W.N. Setzer, P. von, R. Schleyer, Adv. Organomet. Chem. 24 (1985) 353.
[2] C. Schade, P. von, R. Schleyer, Adv. Organomet. Chem. 27 (1987) 169.
[3] K. Gregory, P. von, R. Schleyer, R. Snaith, Adv. Inorg. Chem. 37 (1991) 47.
[4] R.E. Mulvey, Chem. Soc. Rev. 20 (1991) 167.
[5] M.A. Beswick, D.S. Wright, in: E.W. Abel, F.G.A. Stone, G. Wilkinson (Eds.), Comprehensive Organometallic Chemistry II, Pergamon Press, Oxford, 1995, p. 1.
[6] J.D. Smith, Adv. Organomet. Chem. 43 (1999) 267.
[7] M.F. Lappert, P.P. Power, A.R. Sanger, R.C. Srivastava, Metal and Metalloid Amides, Horwood-Wiley, Chichester, 1980, p. 24.
[8] A.M. Sapse, P. von R. Schleyer (Eds.), Lithium Chemistry. A Theoretical and Experimental Overview, Wiley Interscience, New York, 1995.
[9] S.T. Liddle, W. Clegg, J. Chem. Soc., Dalton Trans. (2001) 402.
[10] A. Dietrich, B. Neumuller, K. Dehnicke, Z. Anorg. Allg. Chem. 625 (1999) 619.
[11] M.P. Murchie, J.W. Bovenkamp, A. Rodrigue, K.A. Watson, S. Fortier, Can. J. Chem. 66 (1988) 2515.
[12] K.A. Watson, S. Fortier, M.P. Murchie, J.W. Bovenkamp, Can. J. Chem. 69 (1991) 687.
[13] S. Chadwick, K.R. Senge, Chem. Eur. J. 4 (1998) 1768.
[14] M.E. Fraser, S. Fortier, A. Rodrigue, J.W. Bovenkamp, Can. J. Chem. 64 (1986) 816.
[15] G. Krauter, F. Weller, K. Dehnicke, Z. Naturforsch. 44 (1989) 444.
[16] T.E. Waldman, B. Waltermire, A.L. Rheingold, R.D. Ernst, Organometallics 12 (1993) 4161.
[17] B. Borgsen, F. Weller, K. Dehnicke, Z. Anorg. Allg. Chem. 596 (1991) 55.
[18] P.C. Andrews, D.R. Baker, W. Clegg, R.E. Mulvey, P.A. O'Neil, Polyhedron 10 (1991) 1839.
[19] R.D. Shannon, Acta Crystallogr., Sect. A 32 (1976) 751.
[20] D.L. Ward, S.B. Dawes, O. Fussa, J.L. Dye, Am. Cryst. Assoc., Abstr. Papers (Winter) 13 (1985) 25.
[21] N.S. Fender, S.S. Finegan, D. Miller, M. Mitchell, I.A. Kahwa, F.R. Fronczek, Inorg. Chem. 33 (1994) 4002.
[22] D. Hoffmann, F. Hampel, P. von, R. Schleyer, J. Organomet. Chem. 456 (1993) 13.
[23] P.B. Hitchcock, M.F. Lappert, W.P. Leung, L. Diansheng, T. Shun, J. Chem. Soc., Chem. Commun. (1993) 1386.
[24] M.H. Chisholm, S.R. Drake, A.A. Naiini, W.E. Streib, Polyhedron 10 (1991) 337.
[25] SMART and SAINT software for CCD diffractometers, Bruker AXS Inc., Madison, WI, USA, 1997.
[26] G.M. Sheldrick, SHELXTL user manual, version 5.1, Bruker AXS Inc., Madison, WI, USA, 1997.

2.2. Synthesis of ligand

The pentadentate ligand was made adopting a modified procedure of similar type of ligand as reported [6]. Diethylene triamine (0.515 g, 5 mmol) and 2-benzoyl pyridine (1.83 g, 10 mmol) was refluxed in 15 cm^3 dehydrated alcohol for 4 h. The pentadentate ligand was isolated after evaporating the solvent and purified from alcohol. The product was isolated as a brown semisolid mass after dried in vacuum over P_4O_{10}: yield 1.86 g ($\sim$86%). *Anal*. Found: C, 77.4; H, 6.2; N, 15.9. Calc. for $C_{28}H_{27}N_5$: C, 77.6; H, 6.3; N, 16.2%.



L

2.3. Preparation of $[Ni_2L_2(NCS)_2](ClO_4)_2$ (1)

The MeCN solution (10 cm^3) of the ligand (L) (0.217 g, 0.5 mmol) was added to an MeCN solution (5 cm^3) of $Ni(ClO_4)_2\cdot 6H_2O$ (0.183 g, 0.5 mmol). To the resulting brown–red solution, an aqueous solution (0.038 g, 0.5 mmol, 2 cm^3 H_2O) of ammonium thiocyanate was added slowly with constant stirring. The clear red solution was left for slow evaporation and after 3–4 days deep red needle crystals of **1** were obtained (0.142 g, 44%). *Anal*. Found: C, 53.9; H, 4.0; N, 12.8; Ni, 9.0. Calc. for $C_{58}H_{54}Cl_2N_{12}Ni_2O_8S_2$: C, 53.6; H, 4.2; N, 12.9, Ni, 9.0%.

2.4. Preparation of $[Ni_2L_2(NCO)_2](ClO_4)_2$ (2)

This compound was synthesized following the same procedure as illustrated above for **1** except that ammonuim thiocyanate was replaced with equimolar quantity of sodium cyanate. Red crystals of composition $[Ni_2L_2(NCO)_2](ClO_4)_2\cdot 4CH_3CN$ suitable for X-ray study was isolated after about 5 days (yield of the dried product was 0.085 g, 27%). *Anal*. Found: C, 54.9; H, 4.1; N, 13.2; Ni, 9.1. Calc. for $C_{58}H_{54}Cl_2N_{12}Ni_2O_{10}$ (without MeCN solvent of crystallization): C, 55.0; H, 4.3; N, 13.3; Ni, 9.3%.

Caution: Perchlorate complexes are potentially explosive especially in presence of organic ligands. Therefore, preparation and handling of these compounds deserve special attention.

2.5. Physical measurements

Elemental analysis for carbon, hydrogen and nitrogen were performed using a Perkin–Elmer 2400II elemental analyzer. Nickel contents was determined by atomic absorption spectrophotometric measurements (A GBC Model-Avanta was used). Variable temperature magnetic susceptibility data were obtained with a Quantum Design MPMS5 SQUID spectrophotometer. Pascal's constants were utilized to estimate diamagnetic correction, this value was subtracted from the experimental susceptibility data to give molar magnetic susceptibility (χ_M). IR spectra (4000–400 cm^{-1}) were taken at 298 K using JASCO FT/IR-420 spectrometer.

2.6. Crystal structures determination and refinement

Single crystals suitable for X-ray crystallographic analysis were selected following examination under a microscope. Crystals of $[Ni_2L_2(NCO)_2](ClO_4)_2\cdot 4CH_3CN$ were not stable outside mother liquor and were quickly coated with an inert oil to prevent solvent loss before collecting the relevant data at 200 K. Single crystal X-ray diffraction data for the compounds were collected on a Bruker-AXS SMART APEX/CCD diffractometer using Mo Kα radiation ($\lambda = 0.71073$ Å) in an $\omega-2\theta$ scan mode. Diffracted data were corrected for Lp effects [7] and for absorption using the SADABS program. The structures were solved by direct methods and the structure solution and refinement was based on $|F|^2$. All non-hydrogen atoms were refined with anisotropic displacement parameters whereas hydrogen atoms were placed in calculated positions when possible and given isotropic U values 1.2 times that of the atom to which they are bonded. Hydrogen atoms bonded to heteroatoms were located in the Fourier map and their coordinates fixed to ride on the bonded atom with isotropic U values 1.2 times that of the atom to which they are bonded. All crystallographic calculations were conducted with the SHELXTL program package. The crystal data and data collection details are collected in Table 1.

3. Results and discussion

3.1. Synthesis

The ligand was synthesized by refluxing diethylene triamine and 2-benzoyl pyridine in 1:2 mol ratio in dehydrated alcohol. It reacted with nickel(II) perchlorate hexahydrate and ammonium thiocyanate/sodium cyanate using a ratio of $L–Ni^{II}–NCS^-/NCO^- = 1:1:1$ in aqueous acetonitrile medium affording red crystalline products suitable of X-ray crystallographic work having composition $[Ni_2L_2(NCS)_2](ClO_4)_2$ (**1**) and $[Ni_2L_2(NCO)_2](ClO_4)_2\cdot 4CH_3CN$ (**2**), respectively. It is also interesting to note that by changing ratio of $L–Ni^{II}–NCS^-/NCO^- = 1:1:0.5$, which is usual ratio to make binuclear compound of the usual type $[Ni_2L_2(X)]^{3+}$ (where $X^- = NCS^-$ or NCO^-) lead to the same

Table 1
The crystal data and data collection summary for **1** and **2**

Empirical formula	$C_{58}H_{54}Cl_2N_{12}Ni_2O_8S_2$	$C_{66}H_{66}Cl_2N_{16}Ni_2O_{10}$
Formula weight	1299.57	1431.67
Temperature (K)	200	200
λ (Å)	0.71073	0.71073
Space group	$P2_1/n$ (no. 14)	$P2_1/n$ (no. 14)
a (Å)	8.9713(11)	12.0581(11)
b (Å)	15.611(2)	13.8567(12)
c (Å)	20.239(3)	19.7526(17)
α (°)	90	90
β (°)	92.483(4)	95.444(2)
γ (°)	90	90
V (Å^3)	2831.9(6)	3285.5(5)
Z	2	2
D_{calc} (g cm^{-3})	1.524	1.447
μ(Mo Kα) (mm^{-1})	0.901	0.727
F(000)	1344	1488
Crystal size (mm)	0.20 × 0.20 × 0.10	0.20 × 0.15 × 0.10
$2\theta_{max}$ (°)	56.5	56.6
Reflections collected	6282	20 101
Reflections observed [$I > 2.0\sigma(I)$]	4065	7747
Independent reflections	4065 [$R_{int} = 0.0365$]	7747 [$R_{int} = 0.0471$]
R; wR	0.0414; 0.0746	0.0404; 0.0637
Goodness-of-fit on F^2	0.798	0.778
Largest difference peak and hole (e Å^{-3})	0.378 and −0.355	0.619 and −0.392

compound as **1** and **2**, respectively. These two complexes **1** and **2** were insoluble in all common solvents.

3.2. IR spectroscopy

The IR spectrum of **1** exhibits a very strong absorption at 2036 cm^{-1} and that of **2** at 2225 cm^{-1} corresponds to the asymmetric stretching vibrations of thiocyanate and cyanate ions, respectively. The stretching vibrations of C=N bond of Schiff base at 1637 and 1590 cm^{-1} and 1643 and 1595 cm^{-1} for compounds **1** and **2**, respectively [8].

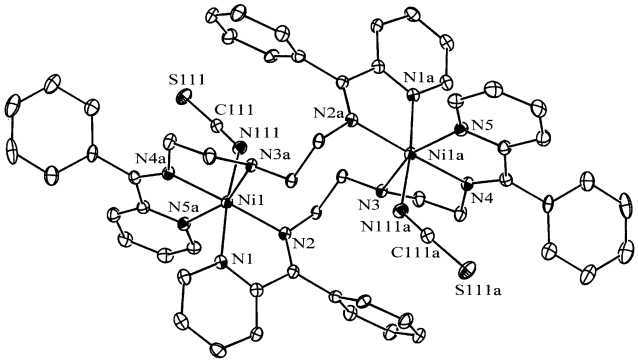


Fig. 1. ORTEP drawing of $[Ni_2L_2(NCS)_2]^{2+}$ with atom labeling scheme.

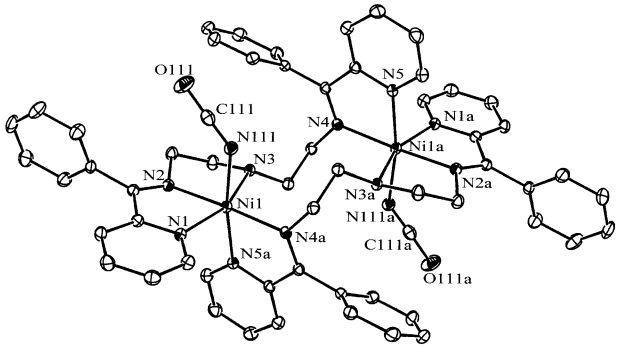


Fig. 2. ORTEP drawing of $[Ni_2L_2(NCO)_2]^{2+}$ with atom labeling scheme.

3.3. Crystal structures of $[Ni_2L_2(NCS)_2](ClO_4)_2$ and $[Ni_2L_2(NCO)_2](ClO_4)_2\cdot 4CH_3CN$

The ORTEP drawing of the dimeric cations $[Ni_2L_2(NCS)_2]^{2+}$ of **1** and $[Ni_2L_2(NCO)_2]^{2+}$ of **2** are shown, respectively in Figs. 1 and 2, and the selected bond distances and angles are listed in Tables 2 and 3. In both the complexes each nickel(II) is in a distorted octahedral (NiN_6) coordination environment consisting

Table 2
Selected bond distances (Å) and angles (°) for the complex **1**

Bond distances			
Ni(1)–N(1)	2.066(3)	Ni(1)–N(2)	2.061(3)
Ni(1)–N(3)#1	2.150(3)	Ni(1)–N(4)#1	2.021(3)
Ni(1)–N(5)#1	2.087(3)	Ni(1)–N(111)	2.088(3)
N(111)–C(111)	1.171(4)	S(111)–C(111)	1.623(4)
N(2)–C(6)	1.292(4)	N(2)–C(7)	1.475(4)
Bond angles			
N(1)–Ni(1)–N(2)	78.50(12)	N(1)–Ni(1)–N(3)#1	93.32(11)
N(1)–Ni(1)–N(4)#1	99.12(12)	N(1)–Ni(1)–N(5)#1	91.46(11)
N(1)–Ni(1)–N(111)	172.43(13)	N(2)–Ni(1)–N(3)#1	99.30(11)
N(2)–Ni(1)–N(4)#1	177.61(11)	N(2)–Ni(1)–N(111)	94.12(12)
N(3)#1–Ni(1)–N(4)#1	80.97(12)	N(3)#1–Ni(1)–N(5)#1	158.88(13)
N(3)#1–Ni(1)–N(111)	89.51(11)	N(4)#1–Ni(1)–N(5)#1	77.97(12)
N(4)#1–Ni(1)–N(111)	88.25(12)	N(5)#1–Ni(1)–N(111)	88.39(12)
N(111)–C(111)–S(111)	177.5(4)		

Table 3
Selected bond distances (Å) and angles (°) for the complex **2**

Bond distances			
Ni(1)–N(1)	2.0953(18)	Ni(1)–N(2)	2.0313(17)
Ni(1)–N(3)	2.1604(17)	Ni(1)–N(4)#1	2.0791(16)
Ni(1)–N(5)#1	2.0610(18)	Ni(1)–N(111)	2.0731(19)
N(111)–C(111)	1.147(3)	O(111)–C(111)	1.219(3)
N(2)–C(6)	1.277(2)	N(2)–C(7)	1.472(3)
Bond angles			
N(1)–Ni(1)–N(2)	78.54(7)	N(1)–Ni(1)–N(3)	159.21(6)
N(1)–Ni(1)–N(4)#1	98.99(7)	N(1)–Ni(1)–N(5)#1	94.01(7)
N(1)–Ni(1)–N(111)	91.47(7)	N(2)–Ni(1)–N(3)	80.70(7)
N(2)–Ni(1)–N(4)#1	176.72(7)	N(2)–Ni(1)–N(111)	88.60(7)
N(3)–Ni(1)–N(4)#1	101.80(6)	N(3)–Ni(1)–N(5)#1	90.42(7)
N(3)–Ni(1)–N(111)	87.10(7)	N(4)#1–Ni(1)–N(5)#1	78.08(7)
N(4)#1–Ni(1)–N(111)	93.63(7)	N(5)#1–Ni(1)–N(111)	170.68(7)
N(111)–C(111)–O(111)	178.4(3)		

of three nitrogen atoms from one, two nitrogen atoms from another pentadentate ligand and the last one from terminal ion. In these molecules each flexible ligand shows a very unusual [5] type of binding mode and distributed its coordination potential to two different nickel(II) centers thereby forms the dimer. Usually bivalent nickel reacts with a linear pentadentate or macrocyclic ligand (L) to form complexes of the type $[Ni^{II}L(X)]^{n+}$ (where X = neutral or anionic donor) or $[Ni_2^{II}(L)_2(Y)]^{3+}$ (where Y = monoanionic bridging ligand) [5], but in the present case the linear pentadentate ligand itself act like a bridge between two nickel ions forming the complexes $[Ni_2L_2(NCS)_2]^{2+}$ (**1**) and $[Ni_2L_2(NCO)_2]^{2+}$ (**2**) with thiocyanate and cyanate as terminal ligands. The Ni–N distances are ranging from 2.021(3) to 2.150(3) Å for **1** and 2.0313(17) to 2.1604(17) Å for **2**. These Ni–N distances are consistent with corresponding values of analogous NiN_6 chromophores [2,9]. The Ni1···Ni1a distances for **1** and **2** are, respectively 5.809(1) and 5.695(1) Å. The *cis* and *trans* angles are varied from 77.97(12)° to 101.81(12)° and 158.88(13)° to 177.61(11)° for **1** and 78.08(7)° to 101.80(6)° and 159.21(6)° to 176.72(7)° for **2**, respectively, indicating the nature of distortion in the coordination sphere. The crystals of compound **1** contains no solvent of crystallization, but there are four acetonitrile solvent of crystallization in the molecule **2**, the loss of which explains the deterioration of these crystals outside mother liquor. Both compounds **1** and **2** consist of isolated binuclear unit in the crystal lattice and is consistent with their magnetic properties (vide infra).

3.4. Magnetic properties

A variable temperature magnetic susceptibility study was performed on polycrystalline sample of **1** and **2**. The magnetic susceptibilities (χ_M) of these two compounds were examined in a 10.0 kG field in the temperature range 2.0–300.0 K. The $\chi_M T$ versus T plot indicates a very weak intramolecular interaction between two nickel atoms. Inspite of our best effort we were unable to get good fit for magnetic data to determine exchange parameters. The plausible reason is that the nickel centers are so far apart (Ni1···Ni1a distances are 5.809(1) and 5.695(1) Å for compounds **1** and **2**, respectively) and bridged by a ligand that involves a long pathway for exchange interaction and also containing saturated $-CH_2-CH_2-$ links that are further weakening the magnetic interaction [10]. As a result intermolecular interactions and zero-field splittings become just as important as the intramolecular interactions, and thereby fitting becomes in applicable. So, although we have described here a very unusual coordination behavior of a flexible pentadentate ligand to produce a binuclear nickel complex, but to achieve reasonably good interactions between two metal atoms we have to modify the ligand pathways as well as suitable linkages (such as unsaturated linkages instead of saturated one) that are able to propagate magnetic exchange interactions in a better way.

4. Supplementary material

Crystallographic data for the structural analysis have been deposited with the Cambridge Crystallographic Data Centre, CCDC nos. 183183 and 183182 for compounds **1** and **2**, respectively. Copies of this information may be obtained free of charge from The Director, CCDC, 12 Union Road, Cambridge, CB2 1EZ, UK (fax: 44-1223-336033; email: deposit@ccdc.cam.ac.uk or www: http://www.ccdc.cam.ac.uk).

Acknowledgements

The project was financially supported by the Council of Scientific and Industrial Research and University Grants Commission (under DSA program), New Delhi, India. One of the authors (S.D.) is thankful for the fellowship provided by The University of Burdwan. We are also grateful to Professor A.K. Das and B.C. Mondal of our department for help regarding atomic absorption data. The authors are indebted to Professor George Christou and M. Soler for the magnetic results.

References

[1] P. Dapporto, M. Formica, V. Fusi, M. Mivchaloni, P. Paoli, R. Pontellini, P. Rossi, Inorg. Chem. 39 (2000) 4663.
[2] J. Ribas, M. Monfort, C. Diaz, C. Bartos, X. Solans, Inorg. Chem. 32 (1993) 3557.
[3] E. Ruiz, J. Cano, S. Alvarej, P. Alemany, J. Am. Chem. Soc. 120 (1998) 11122.
[4] F.F. de Biani, E. Ruiz, J. Cano, J.J. Novoa, S. Alvarej, Inorg. Chem. 39 (2000) 3221.
[5] M.D. Vaira, F. Mani, P. Stoppioni, Inorg. Chim. Acta 303 (2000) 61.
[6] C. Jubert, A. Mahamadou, J. Marrot, J.-P. Barbier, J. Chem. Soc., Dalton Trans. (2001) 1230.
[7] A.C.T. North, D.C. Phillips, F.S. Mathews, Acta Crystallogr., Sect. A 24 (1968) 351.
[8] K. Nakamoto, Infrared Spectra of Inorganic and Coordination Compounds, Wiley, New York, 1997.
[9] I.R. Laskar, T.K. Maji, S. Chaudhuri, A. Ghosh, N.R. Chaudhuri, Polyhedron 19 (2000) 1803.
[10] S.J. Brudenell, L. Spiccia, A.M. Bond, G.D. Fallon, D.C.R. Hockless, G. Lazarev, P.J. Mahon, E.R.T. Tiekink, Inorg. Chem. 39 (2000) 881.

(photobleaching) of the phthalocyanines are also important for determining the stability of the MPc complexes during PDT action. We report on the singlet oxygen quantum yields and the photobleaching studies of a series of unsymmetrically and symmetrically substituted zinc phthalocyanines (Scheme 1).

2. Experimental

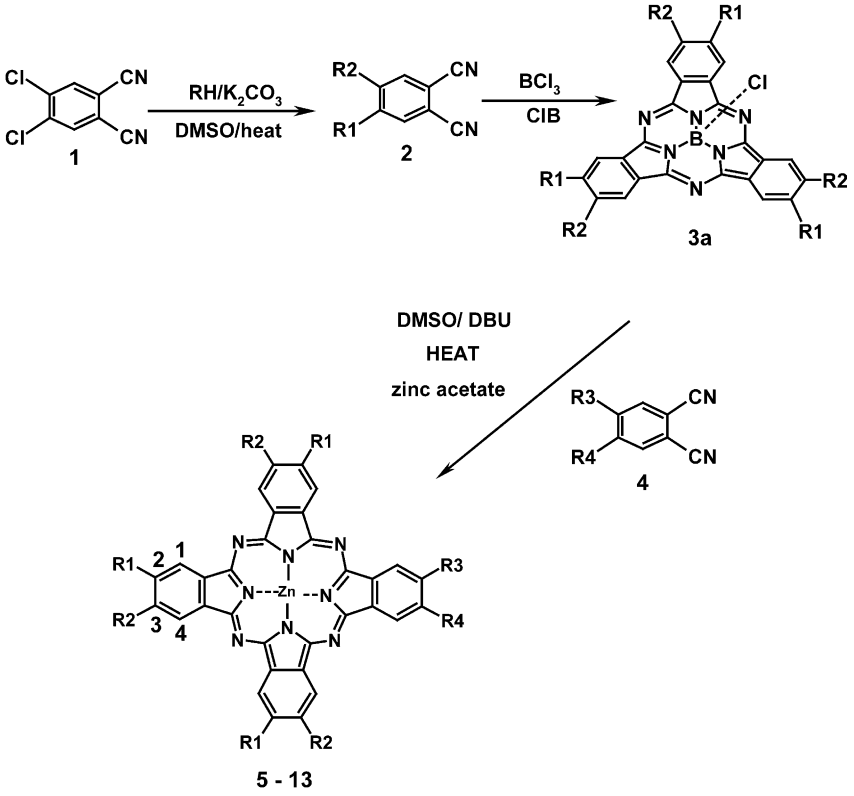
2.1. Materials

N,*N*′-dimethylformamide (DMF) used for electrochemical studies was freshly distilled. Dimethylsulfoxide (DMSO) was dried over alumina before use. Thionyl chloride, potassium carbonate, nitrophthalimide, dichlorophthalic anhydride, dicarboxynaphthalene, 2-naphthol, 4-*tert*-butylphenol, 4-hydroxybenzoic acid, 1,8-diazabicyclo[5.4.0]undec-7-ene (DBU), diazabicyclooctane (DABCO), 1,3-diphenylisobenzofuran (DPBF) and chlorobenzene (ClB) were purchased either from Aldrich or Merck and were used as received. Tetrabutylammonium perchlorate (TBAP) was recrystallized from ethanol and used as an electrolyte for electrochemical studies.

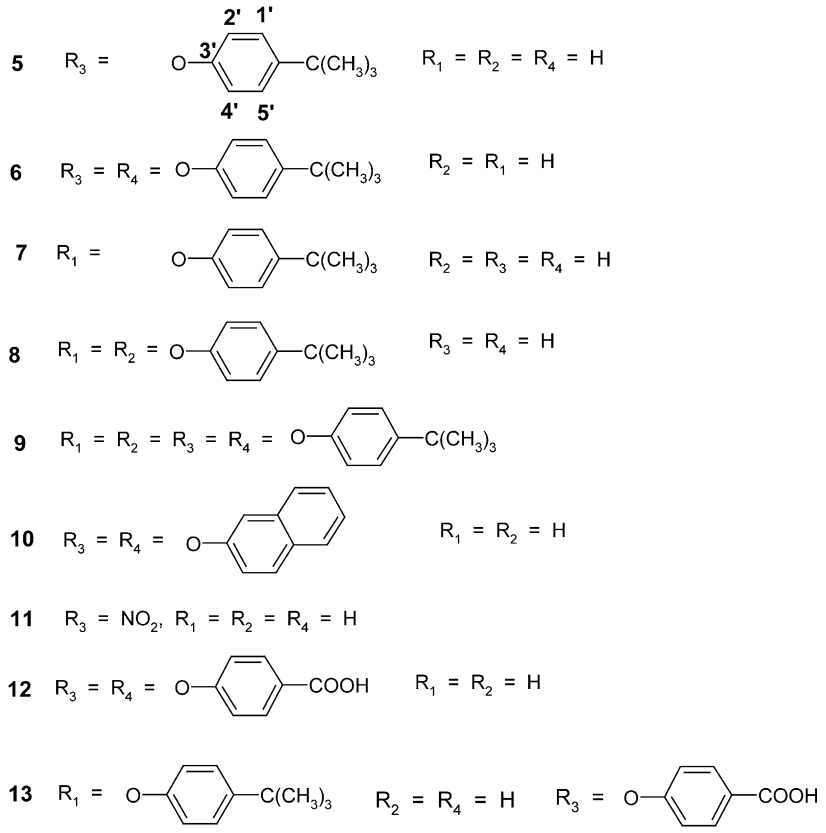
2.2. Synthesis

2.2.1. Substituted dicyanobenzene (*2* and *4*)

4,5-Dichlorodicyanobenzene (**1**) was synthesized from dichlorophthalic anhydride according to a reported procedure [21]. The disubstituted dicyanobenzenes ($\mathbf{R_1} = \mathbf{R_2}$ (for **2**) or $\mathbf{R_3} = \mathbf{R_4}$ for **4**) were then synthesized from 4,5-dichlorodicyanobenzene using the general procedure reported before [21] as follows: dry potassium carbonate (0.64 g, 0.0046 mol) was suspended in DMSO under nitrogen. To this suspension, 4,5-dichlorodicyanobenzene and the appropriate amount of the respective phenoxy substituent (2-naphthol, 4-*tert*-butylphenol or 4-hydroxybenzoic acid) were added. See Table 1 for the amounts of reagents used. Further aliquots of potassium carbonate were added after 4 h, and 24 h of stirring at room temperature (r.t.), giving total amounts shown in Table 1. The mixture was further stirred at r.t. and under nitrogen atmosphere for the total time shown in Table 1. The product was purified following literature methods [21]. Monosubstituted dicyanobenzenes ($\mathbf{R_2} = \mathbf{H}$ (for **2**) or $\mathbf{R_3} = \mathbf{H}$ (for **4**)) were synthesized by the procedure outlined above for the disubstituted derivatives using nitrophthalonitrile instead of dichlorodicyanobenzene. The amounts for the synthesis are shown in Table 1. 4-Nitrophthalonitrile was synthesized from 4-nitrophthalimide using reported procedures [22].



Scheme 1.



Scheme 1 (*continued*).

Dicyanonaphthalonitrile was synthesized from dicarboxynaphthalene following reported procedures [21].

2.2.2. Sub-phthalocyanines(*3a*)

The unsubstituted, tri- or hexa-substituted subphthalocyanines were synthesized by following reported procedures [15,16] as follows. The respective dichlorocyanobenzene (**1**), di- or mono-substituted dicyanobenzene (**2**, 0.4 g, 0.003 mol), was suspended in 1-chloronaphthalene (6 ml), stirred at r.t. in an atmosphere of nitrogen and in the presence of 0.001 mol (0.12 g) BCl_3. The reaction mixture was heated to 220 °C for 0.5 h. The products were purified according to reference [16], and characterized by UV–Vis, infrared and ^1H NMR spectroscopies.

2.2.3. Sub-naphthalocyanine (Sub-NPc, *3b*)

Sub-naphthalocyanine was synthesized from dicyanonaphthalonitrile following the procedure outlined above for Sub-Pc, by replacing **2** with dicyanonaphthalonitrile.

2.2.4. Symmetrically (*9*) and unsymmetrically (*5–8, 10–14*) substituted zincphthalocyanines (Scheme 1)

These complexes were synthesized according to literature methods [23] by dissolving (0.25 g, 0.00092 mol) the unsubstituted or substituted dicyanobenzene (**4**) to

Table 1
Amounts of reagents used for synthesis of substituted dicyanobenzenes

Substituent	Amount of substituent added (g, mol)	4,5-Dichloro-dicyanobenzene (g, mol)	Total K_2CO_3 added (g, mol)	Total stirring time
Di-substituted				
4-Hydroxy benzoic acid	0.21, 0.00021	0.36, 0.0021	1.92, 0.0138	28 h
4-*tert*-Butylphenol	2.2, 0.015	1.0, 0.005	4.1, 0.12	28 h
2-Naphthol	8.6, 0.06	2.0, 0.0095	8.2, 0.24	28 h
Mono-substituted				
4-Dihydroxy benzoic acid	0.43, 0.0031	0.36, 0.0021	1.92, 0.0138	5 days
4-*tert*-Butylphenol	4.4, 0.03	3.4, 0.02	16.5, 0.12	48 h
2-Naphthol	1.3, 0.009	1.0, 0.0059	5.4, 0.039	5 days

be used for ring expansion in a mixture of freshly distilled DMSO–1-chloronaphthalane (4/2 ml) in the presence of DBU (0.1 g, 0.00065 mol). The reaction mixture was heated to 130 °C, then a suspension of the appropriate unsubstituted or substituted Sub-Pc (**3a**) or the sub-naphthacyanine (**3b**) (0.2 g, 0.00046 mol) and zinc(II) acetate dihydrate (0.11 g, 0.0005 mol) in the DMSO–1-chloronaphthalene solvent mixture was added drop-wise to the heated mixture over a period of 1 h. After cooling, glacial acetic acid (0.04 g, 0.65 mol) was added and the solvents evaporated. For complex **9**, there was no need for ring expansion of Sub-Pc, hence the complex was synthesized by reacting dicyanobenzene disubstituted with *tert*-butylphenol directly with zinc (II) acetate dihydrate. For all complexes, methanol was added and the product was separated by centrifugation. The product was further purified by thin layer chromatography (TLC), using ethyl acetate and toluene for elution.

2.2.5. 2-Mono(tert-butylphenoxy) phthalocyanato zinc (**5**)

Yield 35%. *Anal.* Calc. for $C_{42}H_{28}N_8O_1Zn\cdot 6(C_4H_8O_2)$: C, 63.16; H, 6.06; N, 8.93. Found: C, 63.99; H, 6.24; N, 8.14%.

IR (KBr), ν (cm^{-1}). 3962, 3056, 1715, 1602, 1558, 1507 (C–H); 1471, 1394, 1363, 1336, 1262 (C–O–C); 1235, 1174, 1091, 1046, 946, 803. ^{1}H NMR (*d*-DMSO, 400 Hz): 8.90 (s, 8H, 1,4-Pc); 8.85 (s, 7H, 2,3-Pc); 8.10 (d, 2H, 1′,5′-H); 7.40 (d, 2H, 2′,4′-H); 1.30 (s, 9H, CH_3). λ_{max} (nm) (log ε) in DMF: 675 (5.09), 609 (3.71), 348 (3.96).

2.2.6. 2,3-Bis(tert-butylphenoxy) phthalocyanato zinc (**6**)

Yield 40%. *Anal.* Calc. for $C_{52}H_{40}N_8O_2Zn\cdot 6H_2O$: C, 63.58; H, 5.30; N, 11.41. Found: C, 61.54; H, 3.54; N, 13.41%. IR (KBr), ν (cm^{-1}): 3403, 2964 (C–H); 1601, 1508 (C–H); 1392, 1247, 1106, 994, 895 (C–O–C); 831, 745, 726, 477. ^{1}H NMR (*d*-DMSO, 400 Hz): 9.20 (s, 6H, 1,4-Pc); 8.50 (s, 2H, 1,4-Pc); 8.17 (s, 6H, 2,3-Pc); 8.00 (d, 4H, 1′,5′-H); 7.93 (d, 4H, 2′,4′-H); 1.45 (s, 18H, CH_3). λ_{max} (nm) (log ε) in DMF: 678 (4.47), 611 (3.74), 359 (4.00).

2.2.7. 2,9,16-Tri(tert-butylphenoxy) phthalocyanato zinc (**7**)

Yield 43%. IR (KBr), ν (cm^{-1}): 3385, 2931 (C–H); 1709, 1625, 1485, 1331, 1250 (C–O–C); 1185, 1092, 887, 776, 751, 725, 467. ^{1}H NMR (*d*-DMSO, 400 Hz): 9.48 (s, 8H, 1,4-Pc); 8.54 (m, 2H, 2,3-Pc); 8.10 (m, 3H, 2,3-Pc); 7.60 (d, 6H, 1′, 5′-H); 7.30 (d, 6H, 2′, 4′-H); 1.3 (s, 27H, CH_3). λ_{max} (nm) (log ε) in DMF: 669 (4.57), 604 (3.82), 335 (4.24).

2.2.8. 2,3,9,10,16,17-Hexa(tert-butylphenoxy) phthalocyanato zinc (**8**)

Yield 30%. IR (KBr), ν (cm^{-1}): 2946 (C–H); 1699, 1486, 1409, 1332, 1273 (C–O–C); 1091, 889, 774, 752, 467. ^{1}H NMR (*d*-DMSO, 400 Hz): 9.80 (s, 8H, 1,4-Pc); 8.75 (s, 2H, 2,3-Pc); 8.00 (d, 12H, 1′,5′-H); 7.70 (d, 12H, 2′,4′-H); 1.3 (s, 54H, CH_3). λ_{max} (nm) (log ε) in DMF: 670 (4.75), 605 (3.91), 342 (4.09).

2.2.9. 2,3,9,10,16,17,23,24-Octa(tert-butylphenoxy) phthalocyanato zinc (**9**)

Yield 38%. IR (KBr), ν (cm^{-1}): 3056, 2959 (C–H); 2622, 2550, 2433, 1954, 1719, 1607, 1506, 1484, 1456, 1407, 1331, 1283 (C–O–C); 1244, 1209, 1164, 1114, 1092, 1059, 950, 886, 829, 794, 774, 751, 728, 634, 570, 499, 435. ^{1}H NMR (*d*-DMSO, 400 Hz): 9.5 (s, 8H, 1,4-Pc); 7.5 (d, 16H, 1′,5′-H); 7.0 (d, 16H, 2′,4′-H); 1.2 (s, 72H, CH_3). λ_{max} (nm) (log ε) in DMF: 670 (4.73), 605 (4.20), 335 (4.48).

2.2.10. 2,3-Bis(naphthoxy) phthalocyanato zinc(II) (**10**)

Yield 20%. *Anal.* Calc. for $C_{42}H_{28}N_8O_1Zn\cdot 2(H_2O)$: C, 69.60; H, 3.57; N, 12.50. Found: C, 68.78; H, 2.70; N, 14.17%. IR (KBr), ν (cm^{-1}): 3053, 2930 (C–H); 2859, 2625, 2547, 1957, 1713, 1600, 1484, 1408, 1334, 1285 (C–O–C); 1210, 1165, 1059, 962, 913, 887, 809, 771, 752, 721, 634, 571, 500, 471, 433. ^{1}H NMR (*d*-DMSO, 400 Hz): 9.25 (s, 8H, 1,4-Pc); 8.25 (s, 6H, 2,3-Pc); 8.8–7.5 (m, 14H, naphthoxy). λ_{max} (nm) (log ε) in DMF: 670 (4.97), 605(4.24), 335 (4.69).

2.2.11. 2-Mono-nitro phthalocyanato zinc(II) (**11**)

Yield 41%. *Anal.* Calc. for $C_{32}H_{15}N_9O_2Zn\cdot 2(C_4H_8O_2)$: C, 60.15; H, 3.88; N, 15.79. Found: C, 59.67; H, 3.18; N, 16.28%. IR (KBr), ν (cm^{-1}): 3931, 3332, 1950, 1702, 1652, 1458, 1322 (NO_2); 1162, 1055, 885, 724, 632, 567, 495, 433. ^{1}H NMR (*d*-DMSO, 400 Hz): 9.70 (s, 8H, 1,4-Pc); 8.60 (s, 6H, 2,3-H). λ_{max} (nm) (log ε) in DMF: 670 (4.00), 605 (3.50), 343 (4.10).

2.2.12. 2,3-Bis(carboxyphenoxy) phthalocyanato zinc(II) (**12**)

Yield 48%. *Anal.* Calc. for $C_{46}H_{24}N_8O_6Zn\cdot 5H_2O$: C, 57.68; H, 3.76; N, 11.70. Found: C, 59.76; H, 3.58; N, 11.85%. IR (KBr), ν (cm^{-1}): 3437, 3050 (OH); 1602, 1502, 1403, 1271 (C–O–C); 1213, 1165, 1013, 951, 889, 858, 782, 745, 699, 618, 495, 433. ^{1}H NMR (*d*-DMSO, 400 Hz): 9.4–9.6 (s, 8H, 1,4-Pc); 8.35 (d, 6H, 2,3-Pc); 7.95 (d, 4H, 1′,5′-H); 7.50 (d, 4H, 2′,4′-H); 2H from COOH are not seen as their peak is too weak compared with that of the Pc ring and the phenoxy ring. λ_{max} (nm) (log ε) in DMF: 671 (6.05), 606 (4.32), 357 (3.71), 284 (4.57).

*2.2.13. 2,9,16-Tri(tert-butylphenoxy)-23-mono(carboxyphenoxy) phthalocyanato zinc(II) (**13**)*

Yield 20%. *Anal.* Calc. for $C_{42}H_{28}N_8O_1Zn\cdot 2(H_2O)$: C, 66.19; H, 4.20; N, 14.71. Found: C, 66.57; H, 4.21; N, 16.36%. IR (KBr), ν (cm^{-1}): 3056, 2946 (C–H); 1716, 1658, 1597, 1499, 1453, 1270 (C–O–C); 1218, 1162, 1107, 1015, 883, 759, 690, 619, 486. ^{1}H NMR (*d*-DMSO, 400 Hz): 9.40 (s, 8H, 1,4-Pc); 9.00 (s, 4H, 2,3-Pc); 7.55 (d, 8H, 2′,4′-H); 7.42 (d, 8H, 1′,5′,-H); 1.28 (t, 27H, CH_3). λ_{max} (nm) (log ε) in DMF: 682 (4.97), 614 (4.24), 346 (4.69).

*2.2.14. 2,3-Tribenzo phthalocyanato zinc(II) (**14**)*

Yield 38%. *Anal.* Calc. for $C_{44}H_{22}N_8Zn\cdot 8H_2O$: C, 60.45; H, 4.35; N, 12.82. Found: C, 60.77; H, 5.67; N, 14.71%. IR (KBr), ν (cm^{-1}): 3389, 3180, 3056 (C–H); 1720, 1440, 1255, 1009, 797, 752, 615, 468. ^{1}H NMR (*d*-DMSO, 400 Hz): 9.45 (d, 8H, 1,4-Pc); 8.30 (d, 6H, 6,7-H); 7.90 (d, 6H, 5,8-H). λ_{max} (nm) (log ε) in DMF: 672 (4.76), 607 (4.07), 344 (4.69).

2.3. Electrochemical methods

Electrochemical data were collected with the BioAnalytical Systems (BAS) model 100 B/W electrochemical workstation. For cyclic and square wave voltammetries, a platinum disk (3.0 mm diameter) was used as a working electrode. Platinum wire auxiliary and Ag wire pseudo-reference electrodes were employed for all electrochemical experiments. DMF containing $\sim$0.5 mol dm^{-3} TBAP was employed as an electrolyte. Nitrogen gas was bubbled through the solutions prior to recording cyclic voltammograms, and a nitrogen atmosphere was maintained throughout the cyclic voltammogram scans. The ferrocinium–ferrocene (Fc^+–Fc) couple was employed as an internal standard, and potentials were referenced versus saturated calomel electrode (SCE) using the reported [24] potential of 0.46 V (vs. SCE) for the Fc^+–Fc couple in DMF. The cathodic to anodic peak separation was found to be 80 mV for the Fc^+–Fc couple. Prior to cyclic voltammetry (CV) scans, the platinum working electrode was polished with alumina (<10 μm) on a Buehler felt pad, followed by washing with deionized water and rinsing with methanol and DMF. For cyclic and square wave voltammetry studies concentrations were of the order of 10^{-4} mol dm^{-3}.

2.4. Photodegradation and determination of singlet oxygen studies

Photodegradation and singlet oxygen quantum yield determinations were carried out using experimental setup which has been described in detail somewhere else [19,25]. Experiments were performed in air. Typically a 2 ml DMSO solution of the complex (about 1×10^{-5} mol l^{-1}) was introduced to a 1 cm pathlength UV–Vis cell and photolyzed in the Q band region with a General Electric Quartz line lamp (300 W). For singlet oxygen quantum yield studies, photolysis was performed in the presence of DPBF as a singlet oxygen quencher. To avoid chain reactions induced by DPBF in the presence of singlet oxygen [26] the concentration of DPBF was lowered to $\sim3\times10^{-5}$ mol l^{-1}. The DPBF decay at 417 nm was monitored. A 600 nm glass cut off filter (Schott) and a water filter were used to filter off ultraviolet and far infrared radiation. And an interference filter (Intor, 670 nm with a bandwidth of 20 nm) was placed in the light path before the sample. The light intensity at 670 nm was measured with a power meter (Lasermate) and was found to be 5×10^{16} photons s^{-1} cm^{-2}.

Quantum yields of singlet oxygen (Φ_Δ) photogeneration were determined using the relative method with unsubstituted zinc phthalocyanine (ZnPc) as reference, using the following relationship Eq. (1).

$$\Phi_\Delta = \Phi_\Delta^{PcZn}\frac{W\times I_{abs}^{PcZn}}{W^{PcZn}\times I_{abs}} \quad (1)$$

where, Φ_Δ^{PcZn} is the singlet oxygen quantum yield in the presence of unsubstituted ZnPc as a standard. For ZnPc standard, Φ_Δ^{PcZn} in DMSO is 0.67 [27]. W and W^{ZnPc} are the DPBF photobleaching rates in the presence of substituted ZnPc derivatives under investigation and unsubstituted ZnPc standard, respectively. I_{abs} and I_{abs}^{ZnPc} are the rates of light absorption by the substituted ZnPc derivatives and ZnPc standard, respectively. The initial DPBF concentrations were kept the same for both the ZnPc reference and the samples. No significant changes in the absorbance of the substituted ZnPc derivatives was observed during the singlet oxygen studies. All the experiments were carried out at r.t.

The quantum yields for photobleaching were determined using Eq. (2).

$$\Phi = -\frac{(C_t - C_0)\times V\times N_A}{I_{abs}\times S\times t} \quad (2)$$

where C_t and C_0 in mole l^{-1} are the concentrations of the substituted ZnPc derivatives after and prior to irradiation, respectively, the changes in concentration of the dyes was about 15% for these studies. Values of C_t and C_0 were obtained in DMF using the Q band extinction coefficient given in the Section 2. V is the reaction volume, S the irradiated area of the cell, t the irradiation time, N_A is the Avogadro's number and I_{abs} the overlap integral of the radiation source light intensity and the absorption of the substituted ZnPc derivatives (the action spectrum) in the region of the interference filter transmittance and is defined by Eq. (3).

$$I_{abs} = \int (1 - 10^{A_\lambda}) I_\lambda d\lambda \quad (3)$$

where I_λ is the intensity of light and A_λ is the absorbance of the ZnPc derivative at wavelength, λ. Experiments were performed also whereby the solutions were deaerated with N_2 gas or saturated with O_2 in order to study the role of oxygen in the photodegradation process.

Triplet state life times were determined for complexes **5**, **7** and **8** using a flash photolysis system. The excitation pulse was provided by a Nd-Yag (in frequency-doubled mode, providing 160 mJ, 8 ns pulses of laser light at 0–10 Hz), pumping a Lambda-Physik FL2002 dye laser. Single laser pulse energies used ranged from 0.001 to 2 mJ. A 75 W xenon arc lamp provided the analyzing light. Triplet state quantum yields (ϕ_T) were calculated by a comparative method using zinc phthalocyanine as a standard (ϕ_T ZnPc = 0.25 [28]).

UV–Vis spectra were recorded on a Varian 500 UV–Vis–NIR spectrophotometer. IR spectra (KBr pellets) were recorded on a Perkin–Elmer Spectrum 2000 FTIR spectrometer. ^{1}H nuclear magnetic resonance (NMR, 400 MHz) spectra were obtained in $CDCl_3$ and d_6-DMSO using the Bruker EMX 400 NMR spectrometer.

3. Results and discussion

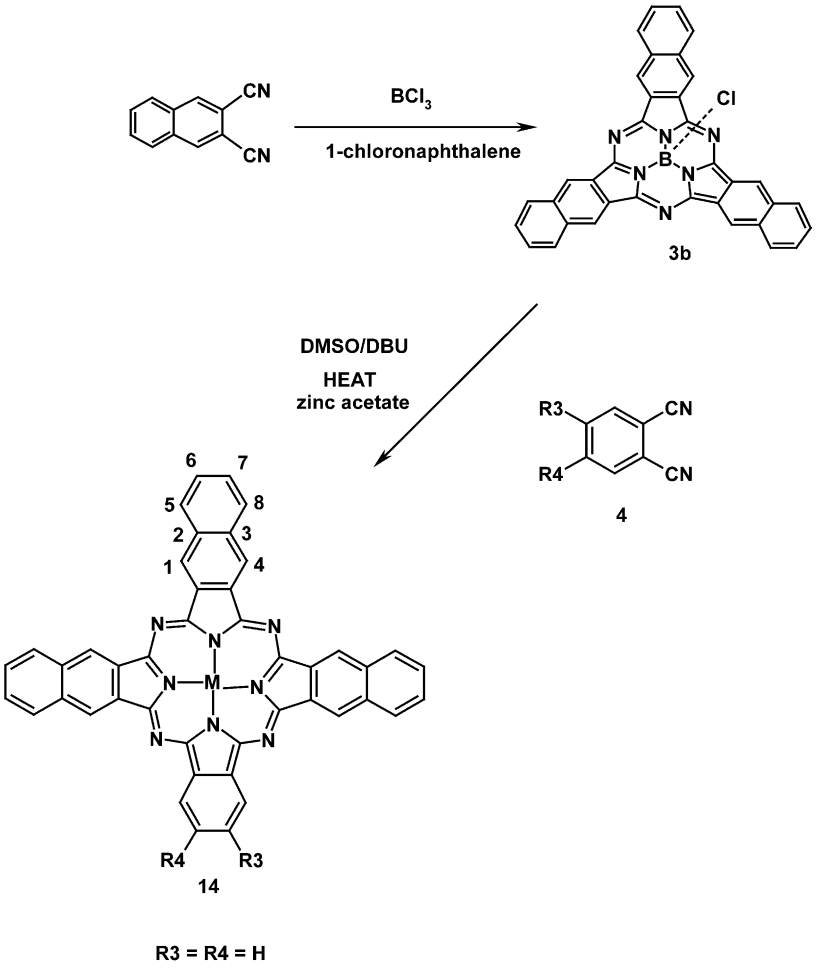
3.1. Synthesis and characterization

Synthesis of unsubstituted and substituted Sub-Pcs has been reported by several researchers [15,16,29–31]. The Sub-Pc complexes have been employed as starting materials for the formation of unsymetrically substituted MPc complexes by ring expansion using substituted or unsubstituted phthalonitriles. The use of Sub-Pcs as intermediates for the synthesis of unsymmtrically substituted phthalocyanines has gained popularity over using statistical condensation of two differently substituted phthalonitrile derivatives. The later results in a complex mixture of products. However, using the reaction mixture containing phthalonitriles and boron trihalide, gives ring-halogenated Sub-Pc, in addition to the desired products. The halogenated Sub-Pcs is difficult to separate. The Sub-Pc complexes were used to prepare the unsymmetrically substituted zinc phthalocyanines according to Schemes 1 and 2. The product mixture will inevitably contain halogenated Pc derivatives and the desired products were separated using preparative TLC.

The ZnPc derivatives (**5**, **6**, **10**–**12**) were synthesized using unsubstituted Sub-Pc and ring expanding using dicyanobenzene which was mono-substituted with *tert*-butylphenol (**5**) or nitro (**11**); and dicyanobenzene disubstituted with *tert*-butylphenol (**6**), naphthol (**10**) or hydroxybenzoic acid (**12**). Complexes **7**, and **13** were synthesized using Sub-Pc substituted with three *tert*-butylphenol groups and ring expanding with unsubstituted dicyanobenzene (**7**) or hydroxybenzoic acid (**13**). Complex **8** was synthesized using Sub-Pc substituted with six *tert*-butylphenol groups and ring expanding with unsubstituted dicyanobenzene (**8**). Complex **9** was sythesized from dicyanobenzene disubstituted with *tert*-butylphenol. Complex **14** was synthesized from subnaphthalocyanine (Sub-NPc, **3b**, Scheme 2) and ring expanding with dicyanobenzene (**4**). In all cases an excess of the dicyanobenzene (over the Sub-Pc or Sub-NPc) was employed. The complexes gave satisfactory spectroscopic analyses, confirming the absence of chlorinated derivatives. The formation of the ZnPc derivatives was monitored using UV–Vis spectroscopy, Fig. 1. An expected decrease in the absorption band of the Sub-Pc in the 570 nm region and the simultaneous formation of the Q and B bands of the phthalocyanine was observed. The reaction was complete within 1–4 h depending on the complex. Complex **5** required only 1 h, while the rest of the complexes needed 2–4 h. Reaction times much longer than these have been reported for these types of reactions [29]. The lack of clear isosbestic points in Fig. 1, could be due to the presence of differently ring substituted isomers.

Yields of the ZnPc derivatives were comparable or higher than those reported in the literature [29] for synthesis of Pcs from Sub-Pcs. The complexes were soluble in DMF or DMSO to a varying degree. Complexes containing *tert*-butylphenol substituents or hydroxybenzoic acid were found to be more soluble. Complexes **1**–**9**, **12** and **13** were soluble in chloroform. Elemental analysis was not obtained for some of the complexes because of the difficulty in obtaining reliable results due to the presence of differently ring substituted isomers.

In general the spectra of the complexes was typical of non-aggregated species at concentrations lower than 1×10^{-5} mol dm^{-3}, as judged the fact that Beer's law was obeyed, Fig. 2. The Q band wavelengths of complexes under discussion ranged from 669 (complex **7**) to 682 nm (complex **13**) in DMF, Table 2. The Q band maximum for complex **13** is shifted to longer wavelengths compared with the rest of the complexes. This complex contains two different type of substituents: *tert*-butylphenol and hydroxybenzoic acid on the phthalocyanine ring, while the rest of the complexes contain one type of substituent. It is well known [30] that the Q band shifts to longer wavelengths with enlargement of π-conjugated system and that the shifts became less, the larger the molecules. On going from complex **5**–**9**, the bulkiness of the molecule increases as the number of *tert*-butylphenol groups is increased from 1 (**5**) to 8 (for **9**). For these complexes, the wavelength of the Q band increases as follows: **6** (678) > **5** (675) > **8** (670) = **9**



Scheme 2.

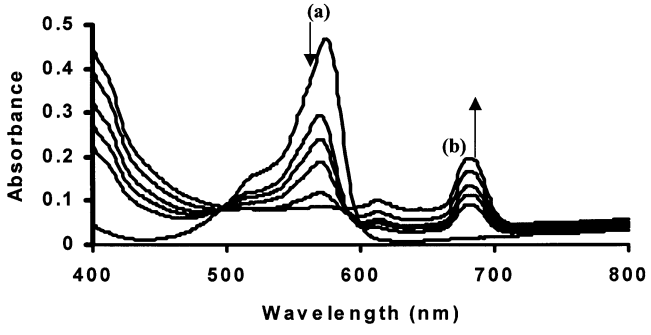


Fig. 1. Changes in UV–Vis spectra during the formation of ZnPc derivatives from Sub-Pc. Spectra at the start (a), and at the end (b), of the reaction. Solvent, DMF.

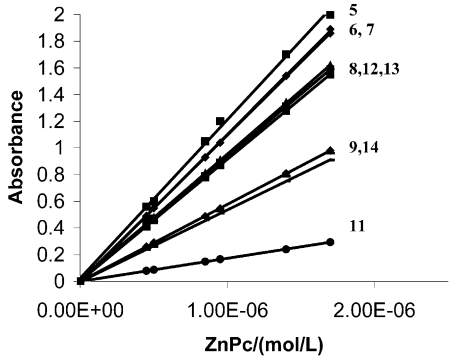


Fig. 2. Beer's law dependence of the ZnPc derivatives in DMF.

(670) ~ **7** (669 nm). Thus the Q band wavelength is shorter for the more bulky molecules (complexes **7**, **8** and **9**) and longer for less bulky molecules (complexes **5** and **6**), in agreement with the literature [30]. The shift to longer wavelength could be due to either the destabilization of the highest occupied molecular orbital (HOMO) or the stabilization of the lowest unoccupied molecular orbital (LUMO). It has been observed that the shifting of the Q band observed on increasing the π-system, is due mainly to the destabilization of the HOMO. Lack of symmetry in phthalocyanines results in the splitting in the Q band [29]. Fig. 3 shows a representative spectra of the complexes, and no split in the Q band was observed showing that the complexes still have some symmetry.

Infrared spectra observed for the phthalocyanine complexes are all very similar. All the compounds with the exception of **11** and **14**, show a band at ~1200 cm^{-1} (C–O–C vibration) which is characteristic of a phenyl ether functionality.

Table 2
Quantum yields for singlet oxygen and photobleaching for the ZnPc derivatives in DMSO

Complex	$\lambda_{Q\ band}$ (nm)	Φ_{Δ} [a]	$10^5\ \Phi_{photobleaching}$
5	675	0.68 (114)	3.9
6	678	0.49	4.1
7	669	0.57 (240)	5.8
8	670	0.51 (129)	6.5
9	670	0.52	3.3
10	670	0.43	4.1
11	670	0.49	3.8
12	671	0.40	3.7
13	682	0.22	3.3
14	672	0.32	3.0

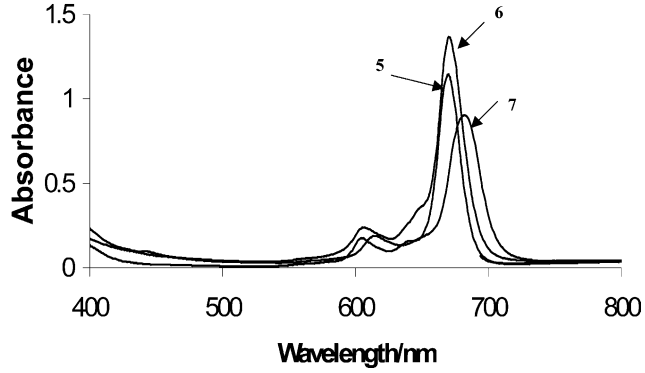


Fig. 3. Electronic absorption spectra of selected complexes (**5**–**7**) in DMF. Concentration = 5×10^{-6} mol dm^{-3}.

^{1}H NMR spectra of the complexes was recorded in *d*-DMSO. Characteristic resonances due to the peripheral (1,4 positions, see Schemes 1 and 2 for numbering) protons of the phthalocyanes were observed as mainly singlets between 8.5 and 9.8 ppm, integrating for a total of eight protons. A doublet was observed for these protons for complex **14**. In addition, 2,3 protons for the phthalocyanine ring were observed at resonances ranging from 8.0 to 9.0. For mono-substituted ZnPc derivatives (**5** and **11**) a singlet integrating for a total of seven protons (2,3 protons) was observed for each complex. For di-substituted ZnPc derivatives (**6**, **10** and **12**), singlets or doublets integrating for six protons was observed for each complex. Tri-substituted complex (**7**) gave a multiplets integrating for a total of five protons, and for the hexasubstituted complex (**8**), a singlet integrating for two protons was observed as expected. Tetrasubstituted complex **13** gave a singlet for the 2,3 protons of the phthalocyanine ring, integrating for a total of four protons, Complex **9** is octasubstituted hence contained no 2,3 protons.

The substituents on the phthalocyanine ring showed resonances due to the aromatic rings and these integrated correctly. In the Section 2, the ring protons of the substituents are denoted as 2′,4′-H or 1′,5′-H, and the numbering is shown for complex **5** in Scheme 1.

3.2. Voltammetric studies

The redox properties of the ZnPc derivatives were studied using both CV and Osteryoung square wave voltammetry (OSWV) in DMF containing TBAP. Figs. 4 and 5 show the cyclic voltammogram and square wave voltammograms for complexes **8** and **5**, respectively. Two reduction couples labeled **II** and **III** was observed, and oxidation couple(s) (labeled as **I** or **Ia** and **Ib**) were also observed. The cyclic voltammograms for the first scan were similar to those of the second and subsequent scans, suggesting that no complicated reactions occurs following oxidation or reduction. For all couples, the cathodic to anodic peak currents (ip_c/ip_a) were near unity, and cathodic to anodic peak separation ranged from 80 to 150 mV, suggesting reversible to quasi-reversible behavior. The cathodic to anodic peak separation was found to be 80 mV for the Fc^+–Fc couple. The peak currents increased linearly with the square root of scan rates, for scan rates ranging from 5 to 800 mV s^{-1}, indicating that the electrode reactions are purely diffusion-controlled. The broadness of some of the redox couples could be a result of the presence of isomers.

All processes are ring based since the central Zn metal is electroinactive [32]. Using controlled potential coulometry, couples **II** and **III** are assigned to ring reduction in ZnPc derivatives and the formation of Pc^{-3}–Pc^{-2} and Pc^{-4}–Pc^{-3}, respectively. The separation between the first and second ring reductions was found to range between 0.4 and 0.5 V in agreement with the separation reported [32] for ring based reductions in non-transition metal phthalocyanines. For complex **5**, Fig. 5, two closely spaced couples (**Ia** and **Ib**) were observed for the oxidation process. For complex **8**, the splitting was more easily observed in the SWV, Fig. 4. The splitting

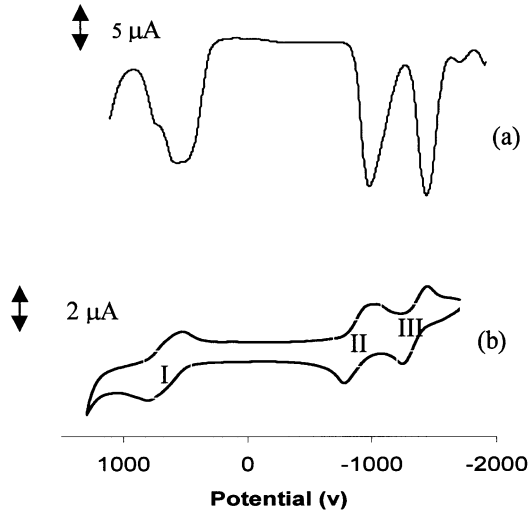


Fig. 4. Osteryoung square wave voltammogram (a) and cyclic voltammogram (b) of 1×10^{-4} mol dm^{-3} of complex **8** in DMF containing 0.1 mol dm^{-3} TBAP. Scan rate = 100 mV s^{-1}.

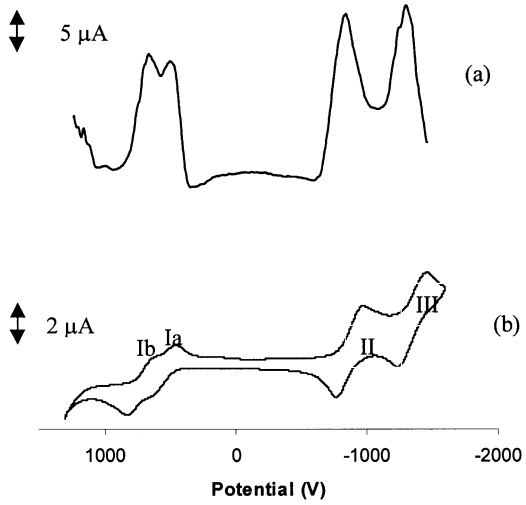


Fig. 5. Osteryoung square wave voltammogram (a) and cyclic voltammogram (b) of 1×10^{-4} mol dm^{-3} of complex **5** in DMF containing 0.1 mol dm^{-3} TBAP. Scan rate = 100 mV s^{-1}.

was observed to varying extents for the ZnPc derivatives. The observation of two closely spaced oxidation peaks has been attributed to the presence of both the aggregated and unaggregated substituted ZnPc complexes in solution [32]. At the concentrations employed for voltammetric studies in this work ($\sim 10^{-4}$ mol dm^{-3}), aggregation of the ZnPc derivatives is expected and was confirmed by the broadening of the spectra at these concentrations. The observation of two closely spaced oxidation peaks could also be a result of the presence of isomers. Thus the two couples observed for the oxidation process in Fig. 5, are attributed to the ring oxidation of the aggregated and non-aggregated species. Table 3 compares the half-wave potentials ($E_{1/2}$) for complexes **5**, **7**, **8** and **9** containing increasing number of *tert*-butyl phenol substituents. The Pc ring becomes easier to reduce and more difficult to oxidize as the number of *tert*-butyl phenol substituents increase from 1 (complex **5**) to 8 (complex **9**), Table 3. The presence of electron donating methyl groups is expected to make the ring more difficult to reduce and easier to oxidize. Thus it is expected that as the number of *tert*-butyl phenol substituents increases, the ring should be more difficult to reduce and easier to oxidize. The reverse is observed in Table 3.

3.3. Photobleaching and singlet oxygen studies

Photobleaching of complexes is characterised by complete disappearance of the spectra due to the degradation of the phthalocyanine ring. Photobleaching studies were undertaken in order to determine the effects of the different substituents on the stability of the ZnPc derivatives in the presence of light.

Photobleaching studies were performed in DMSO and the quantum yields for photobleaching are listed in Table 2. Photobleaching quantum yields were of the order of 10^{-5} for all the complexes. Photodecomposition of phthalocyanine complexes usually occurs through oxidative cleavage [33]. Comparing complexes which contain an increasing number of the *tert*-butyl phenol substituents (**5**–**9**), we observe a low photobleaching quantum yield (hence higher stability) for complex **9** which was shown to be more difficult to oxidize by electrochemical methods, hence confirming that oxidative degradation occurs for these complexes. Complex **5** was easier to oxidize electrochemically, but is relatively stable, suggesting that it is not only the oxidative mechanism which plays a part in the degradation of the ring in these ZnPc derivatives. It is normally accepted [33] that during photodegradation of MPc complexes O_2 ($^1\Delta_g$) is generated which attacks the phthalocyanine ring. However, the attack of O_2 ($^1\Delta_g$) on the Pc ring may also be affected by the shielding effects of the ring substituents [34]. It has been shown [33,34] that the singlet oxygen interacts with the phthalocyanine, resulting in the macrocycle destruction and formation of phthalimide as the product of photodegradation.

Quantum yields of photobleaching increased when oxygen was bubbled to solutions, confirming that oxidative degradation occurs. Inhibition of the photobleaching process in the presence of the singlet oxygen quencher, DABCO, Fig. 6 is in agreement with the involvement of singlet oxygen in the degradation of the phthalocyanine macrocycle.

Quantum yields of singlet oxygen photogeneration (Φ_Δ) of compounds **5**–**14** are listed in Table 2. These values range from 0.22 to 0.68. No photobleaching of the complexes was observed during the determination of singlet oxygen quantum yields, since these processes

Table 3
Comparison of redox potentials for complexes **5**, **7**, **8** and **9** substituted with varying numbers of *tert*-butyl phenol substituents

Complex	Number of *tert*-butyl phenol substituents	$E_{1/2}$ (V vs. SCE)		
		I Pc^{-1}–Pc^{-2}	**II** Pc^{-2}/Pc^{-3}	**III** Pc^{-3}–Pc^{-4}
5	1	0.35, 0.55	−1.08	−1.56
7	3	0.75	−0.82	−1.32
8	6	0.70	−0.84	−1.32
9	8	0.97	−0.68	−1.12

Solvent, DMF containing TBAP. Pc(−2), phthalocyanine dianion.

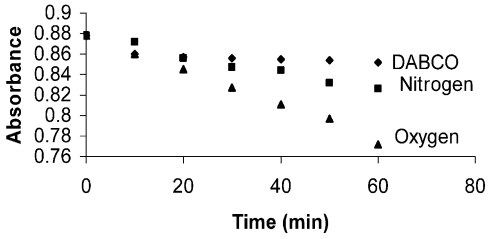


Fig. 6. Kinetic curves for the photobleaching of complex **5** in DMSO saturated with oxygen and nitrogen, and containing DABCO (2×10^{-3} mol dm^{-3}).

occur much slower than singlet oxygen production. It is well known that aggregation of the phthalocyanine complexes results in decreased photochemical activity due to enhanced probability of radiationless decay of excited states. The concentration employed for Φ_Δ and photobleaching studies was 1×10^{-6} mol dm^{-3}, hence no aggregation is expected according to Fig. 2. Comparing complexes which, contain an increasing number of the *tert*-butyl phenol substituents (**5**–**9**), complex **5** with one substituent gave the largest value for Φ_Δ. Triplet life times (τ_T) were determined for complexes **5**, **7** and **8** and are listed in Table 3. Of the three complexes, the largest τ_T value was observed for complex **7** and the lowest for **5** even though the later has the highest Φ_Δ value. A direct correlation between Φ_Δ, and τ_T or Φ_Δ was also not evident for substituted MPc complexes reported in the literature [3]. The lowest Φ_Δ value was observed for complex **14** containing naphthalene units.

In conclusion voltammetric behavior of the substituted ZnPc derivatives under discussion show that as the number of *tert*-butyl substituents increase, the complexes become more difficult to oxidize and easier to reduce. The complexes are relatively stable to photodegradation with quantum yields of photobleaching of the order of 10^{-5}. The majority of the complexes have singlet oxygen quantum yields in the 0.4 and 0.5 region, hence show promise as candidates for PDT.

Acknowledgements

This work is supported by Rhodes University and by the Foundation of Research Development in South Africa. We wish Imperial College (Professor David Phillips) for use of Photolysis equipment.

References

[1] I. Rosenthal, E. Ben-Hur, in: C.C. Leznoff, A.B.P. Lever (Eds.), Phthalocyanines: Properties and Applications, vol. 1 (Chapter 6), VCH, New York, 1989.
[2] S. Nalwa, J.S. Shirk, in: C.C. Leznoff, A.B.P. Lever (Eds.), Phthalocyanines: Properties and Applications, vol. 4 (Chapter 4), VCH, New York, 1996.
[3] K. Hanabusa, H. Shirai, in: C.C. Leznoff, A.B.P. Lever (Eds.), Phthalocyanines: Properties and Applications, vol. 2 (Chapter 4), VCH, New York, 1993.
[4] J. Simon, P. Bassoul, in: C.C. Leznoff, A.B.P. Lever (Eds.), Phthalocyanines: Properties and Applications, vol. 2 (Chapter 5), VCH, New York, 1993.
[5] N.B. McKeown, Phthalocyanine Materials: Synthesis, Structure and Function, Cambridge University Press, Cambridge, 1998.
[6] E. Lukyanets, J. Porphyrins Phthalocyanines 3 (1999) 424.
[7] R. Bonnett, Chem. Soc. Rev. 24 (1995) 19.
[8] I. Rosenthal, Photochem. Photobiol. 53 (1991) 859.
[9] K. Tabata, K. Fukushima, I. Okura, J. Porphyrins Phthalocyanines 4 (2000) 278.
[10] L.R. Milgrom, Colours of Life, Oxford University Press, Oxford, 1977.
[11] V. Iliev, V. Alexiev, L. Bilyarska, J. Mol. Catal. A Chem. 137 (1999) 15.
[12] P.C. Martin, M. Gouterman, B.V. Pepich, G.E. Renzeoni, D.C. Schindele, Inorg. Chem. 30 (1991) 3305.
[13] K. Lang, D.M. Wagnerova, J. Brodilova, J. Photochem. Photobiol. A: Chem 72 (1993) 9.
[14] R.W. Boyle, D. Dolphin, Photochem. Photobiol. 64 (1996) 469.
[15] M. Geyer, F. Plenzig, J. Rausechnabel, M. Hanach, B. del Rey, A. Sastre, T. Torres, Synthesis (1996) 1139.
[16] H. Ali, S.K. Sim, J.E. van Lier, J. Chem. Res. (S) (1999) 496.
[17] N. Kobayashi, R. Kondo, S.-I. Nakajima, T. Osa, J. Am. Chem. Soc. 112 (1990) 9640.
[18] C.G. Claessens, T. Torres, Chem. Eur. J. 6 (2000) 2168.
[19] I. Seotsanyana-Mokhosi, N. Kuznetsova, T. Nyokong, J. Photochem. Photobiol. A: Chem. 140 (2001) 215.
[20] S.B. Brown, T.G. Truscott, Chem. Br. (1993) 955.
[21] D. Wöhrle, M. Eskes, K. Shigehara, A. Yamada, Synthesis (1993) 194.
[22] H. Kliesch, A. Weitemeyer, S. Müller, D. Wöhrle, D. Liebig. Ann. (1995) 1272.
[23] A. Weitermeyer, H. Kliesch, D. Wöhrle, J. Org. Chem. 60 (1995) 4900.
[24] M. Sekota, T. Nyokong, Polyhedron 15 (1996) 2901.
[25] D.M. Maree, N. Kuznetsova, T. Nyokong, J. Photochem. Photobiol. A: Chem. 140 (2001) 117.
[26] W. Spiller, H. Kliesch, D. Wöhrle, S. Hackbarth, B. Roder, G. Schnurpfeil, J. Porphyrins Phthalocyanines 2 (1998) 145.
[27] N. Kuznetsova, E. Makarova, S. Dashkevich, N. Gretsova, V. Negrimovsky, O. Kaliya, E. Luk'yanets, Zh. Obshch. Khim. 70 (2000) 140.
[28] P. Jacques, A.M. Braun, Helv. Chim. Acta 64 (1981) 1800.
[29] N. Kobayashi, T. Ishizaki, K. Ishii, H. Konami, J. Am. Chem. Soc. 121 (1999) 9096.
[30] N. Kobayashi, H. Konami, in: C.C. Leznoff, A.B.P. Lever (Eds.), Phthalocyanines: Properties and Applications, vol. 4 (Chapter 9), VCH, New York, 1999.
[31] G. Schmid, M. Sommerauer, M. Hanack, in: C.C. Leznoff, A.B.P. Lever (Eds.), Phthalocyanines: Properties and Applications, vol. 4 (Chapter 1), VCH, New York, 1996.
[32] A.B.P. Lever, E.R. Milaeva, G. Speier, in: C.C. Leznoff, A.B.P. Lever (Eds.), Phthalocyanines: Properties and Applications, vol. 3 (Chapter 1), VCH, New York, 1993.
[33] G. Winter, H. Heckmann, P. Haisch, W. Eberhardt, M. Hanack, L. Lüer, H.J. Egelhaaf, D. Oelkrug, J. Am. Chem. Soc. 120 (1998) 11663.
[34] G. Schnurpfeil, A. Sobbi, W. Spiller, H. Kliesch, D. Wöhrle, J. Porphyrins Phthalocyanines 1 (1997) 159.

X-ray diffraction were grown after several hours. They were filtered and washed thoroughly with water. *Anal*. Calc.: C, 52.17; N, 12.17; H, 4.78. Found: C, 51.97; N, 12.20; H, 4.78%. The yield for the preparation of **I** and **II** was 49.5% and 49.7%, respectively.

2.2. X-ray crystallography

2.2.1. Crystal data

$C_{20}H_{20}CuN_4O_5$, $M_r = 459.94$, monoclinic, space group $C2/c$, $a = 14.6748(7)$, $b = 18.0138(9)$, $c = 8.3678(4)$ Å, $\beta = 115.946(5)^\circ$, $V = 1989.1(2)$ Å^3, $Z = 4$ (cell parameters from 7810 reflections).

2.2.2. Data collection

A blue, prismatic crystal of dimensions $0.4 \times 0.3 \times 0.2$ mm was used for data collection at 293 K on a Kuma KM4CCD diffractometer [7] with graphite monochromated Mo Kα radiation ($\lambda = 0.71073$ Å) using ω scans, $3.73^\circ < \theta < 27.50^\circ$, $-19 \le h \le 18$, $-23 \le k \le 23$, $-9 \le l \le 10$, 11 174 measured reflections, 2272 independent reflections, 2228 reflections with $I > 2\sigma(I)$, $R_{int} = 0.0177$. Extinction coefficient 0.0020(3). No significant decay. Numerical absorption correction, min./max. transmission 0.598/0.701 [8,9].

2.2.3. Structure analysis and refinement

The title structures were solved by the conventional Patterson method and refined by full-matrix least-squares calculations on F^2 using programs SHELXS-97 and SHELXL-97 [10,11]. The large displacement factors of two central C atoms of the dicarboxylate ion indicated disordered localization of the aliphatic chain. Two different positions (a and b) of C12 were established with occupancy factors of 0.725 and 0.275, respectively. All non-H atoms were refined anisotropically. A weighting scheme of the form $w = 1/[\sigma^2(F_o^2) + (0.0223P)^2 + 2.3576P]$, where $P = (F_o^2 + 2F_c^2)/3$ was applied. The H atom connected to the C12b atom was included in a calculated position with C–H = 0.93 Å and refined using a riding model, with a fixed isotropic displacement factor taken as $1.2U_{eq}$ of the bonded C12b atom. All other H atoms were located from a difference synthesis and refined isotropically. The largest difference peak was 0.293 e Å^{-3}, largest hole −0.287 e Å^{-3}. The final data: parameter ratio was 12.0:1, goodness-of-fit = 1.097, $R[F^2 > 2\sigma(F^2)] = 0.0248$, $wR(F^2) = 0.0596$.

2.3. Magnetism

Magnetic susceptibility measurements in the temperature range 1.7–300 K were carried out on powdered samples of the complexes, at a magnetic field of 5 kG using a Quantum Design SQUID magnetometer (type MPMS-5). Powdered samples used for magnetic measurements were prepared from the single crystals. They were measured twice from different samples using the Faraday method and SQUID, the results were the same in each case. This is the confirmation of the magnetic purity of the samples. Corrections for diamagnetism of the constituent atoms were calculated using Pascal constants [12].

The value 60×10^{-6} cm^3 mol^{-1} was used as the temperature-independent paramagnetism of the Cu(II) ion. The effective magnetic moment was calculated per Cu atom from the equation $\mu = 2.83\sqrt{\chi_M T}$ B.M., where χ_M is the molar magnetic susceptibility corrected for diamagnetism of the constituent atoms.

EPR spectra were recorded at room temperature and 77 K on a Bruker ESP 300 spectrometer operating at X-band equipped with an ER 035M Bruker NMR gaussmeter and a HP 5350B Hewlett–Packard microwave frequency counter.

Reflectance d–d spectra of undiluted compounds were measured on a Beckmann UV5240 spectrophotometer in the 250–2000 nm range.

3. Results and discussion

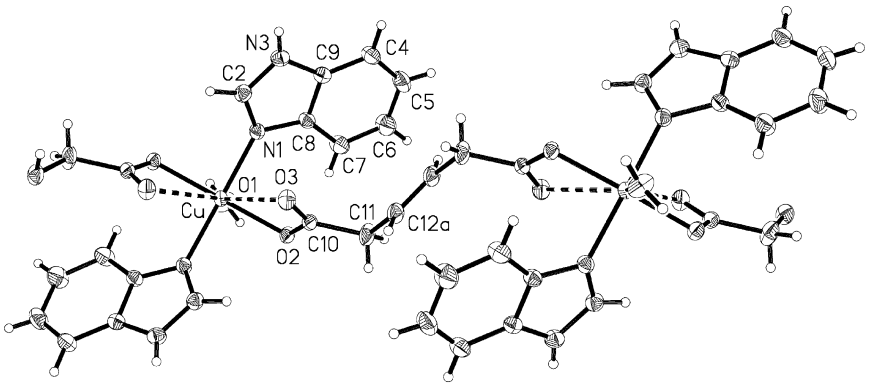
3.1. Crystal structure

A fragment of the polymeric structure of the title compound **I** is shown in Fig. 1(a). It is isostructural with μ-adipato complex **II** [2]. The Cu atom and H_2O molecule are located on the twofold axis. The Cu atoms are connected by bridging tetradentate *trans*-2-butene-

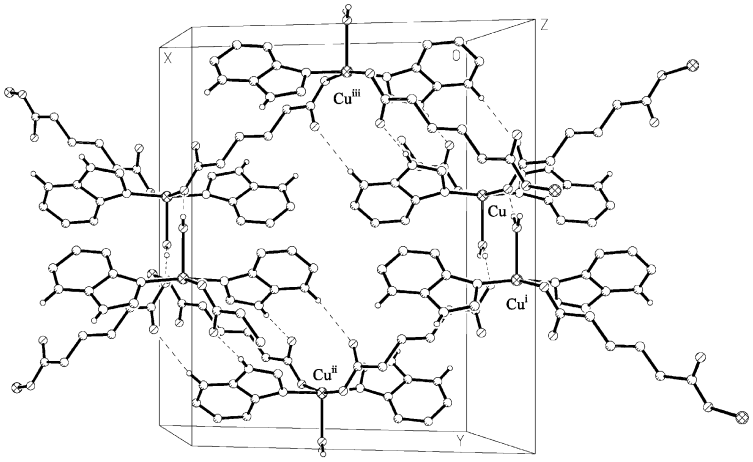
Table 1
Selected geometric parameters

Bond lengths (Å)			
Cu–O1	2.230(2)	O3–C10	1.234(2)
Cu–O2	2.0152(10)	N1–C2	1.319(2)
Cu–O3	2.9078(11)	N1–C8	1.397(2)
Cu–N1	2.0065(13)	N3–C2	1.333(2)
O2–C10	1.282(2)	N3–C9	1.381(2)
Bond angles (°)			
O1–Cu–O2	96.98(3)	N1–Cu–O3	72.56(4)
O1–Cu–O3	142.49(2)	N1^i–Cu–O3	101.35(4)
O2^i–Cu–O2	166.03(6)	N1^i–Cu–N1	172.56(7)
O2–Cu–O3	49.66(4)	Cu–O2–C10	112.89(9)
O2^i–Cu–O3	117.02(4)	Cu–O3–C10	71.60(8)
N1–Cu–O1	93.72(4)	C2–N1–Cu	121.67(11)
N1–Cu–O2	89.73(5)	C8–N1–Cu	129.30(10)
N1^i–Cu–O2	89.36(5)		

Symmetry code: i $-x, -y, -z+1/2$.



(a)



(b)

		(I)	(II)
interchain	$Cu\cdots Cu^{i}$ (Å)	5.5896(3)	5.6109(8)
interchain	$Cu\cdots Cu^{iii}$ (Å)	8.5190(5)	8.494(1)
interchain	$Cu\cdots Cu^{iv}$ (Å)	8.3678(4)	8.535(1)
intrachain	$Cu^{i}\cdots Cu^{ii}$ (Å)	11.2389(6)	10.926(1)

symmetry codes: ^{i} *-x, -y+1, -z+1;* ^{ii} *x+1/2, y+1/2, z;* ^{iii} *-x+1/2, -y+1/2, -z+1;* ^{iv} *x, y, z+1*

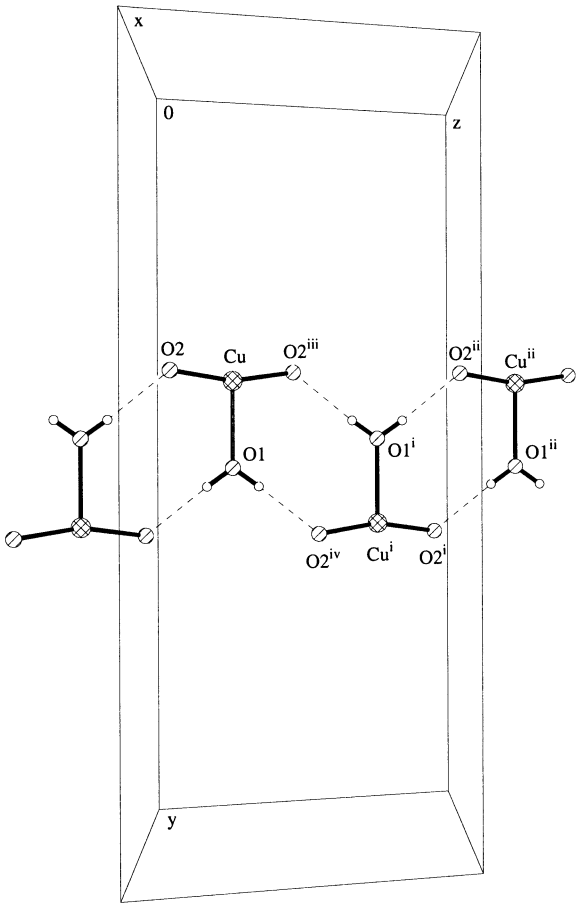
Fig. 1. (a) A fragment of the polymeric structure of **I**. Displacement ellipsoids are drawn at the 30% probability level. (b) The arrangement of the polymeric chains, the hydrogen bonds and Cu···Cu contacts. H atoms not involved in the hydrogen bonding and Cu···O3 semicoordinate bonds are omitted for clarity.

1,4-dicarboxylate ions to form polymeric chains, which are extended in a zigzag form along [10$\bar{1}$]. Fig. 1(b) shows the arrangement of the polymeric chains, interchain hydrogen bonds and Cu···Cu contacts. Selected bond lengths and angles are given in Table 1.

Two N1 atoms (one from each benzimidazole group) and two O2 atoms (one from each carboxylate group) form Cu–N1 and Cu–O2 bonds of lengths 2.0065(13) and 2.0152(10) Å, respectively. The Cu–H_2O bond of 2.230(2) Å completes the coordination to an elongated pyramid, which is completed to a pyramid with a double-capped base by two long, semicoordinate Cu–O3 bonds of 2.9078(11) Å.

The bidentate carboxylic group is not in the ideal coplanar position with the Cu atom, giving a Cu–O2–C10–O3 torsion angle of 17.6(2)°, distinctly more than the value of 10.2(2)° in the adipato complex **II**.

The neighbouring $[Cu(H_2O)(C_7H_6N_2)_2(C_6H_6O_4)]_\infty$ chains are connected by a hydrogen bond system formed by O–H···O, O···H–N and O···H–C contacts (Table



symmetry codes: ^{i} *-x, -y+1, -z+1;* ^{ii} *x, y, z+1;* ^{iii} *-x, y, -z+1/2;* ^{iv} *x, -y+1, z+1/2*

Fig. 2. The ribbon of condensed centrosymmetric rings formed by the O2···H–O1–H···O2 hydrogen bonds between the shortest separated Cu atoms in the structures **I** and **II**.

2, Figs. 1(b) and 2). In **I** the O1–H1···O2 and C4–H4···O3 bonds are shorter than in **II**. The distances O1···O2 and C4···O3 are 2.860(1) and 3.413(2) Å in **I** and 2.917(3) and 3.460(3) Å in **II**, respectively.

In **I** and **II** the Cu···Cu spacing between neighbouring atoms in the polymeric chains are 11.2383(6) and 10.926(1) Å, respectively. The shorter Cu···Cu distances (5.5896(3) Å in **I** and 5.6109(8) Å in **II**) are observed between the interchain Cu atoms located on the $x = 0$ plane of the unit cell. As it is shown on Fig. 2, they are closed by two hydrogen bonds in eight-membered centrosymmetric condensed rings, which form a continuous nearly planar ribbon extended along the z axis. In the continuous –Cu–O2···H1–O1–H1···O2–Cu– chain along the translation vector c, Cu···Cu distances are 8.3678(4) and 8.535(1) Å in **I** and **II**, respectively.

The N3–H3···O3 and C4–H4···O3 hydrogen bonds (see Fig. 1(b)) are formed between the Cu-semicoordinated O3 atoms and a benzimidazole molecule of the neighbouring polymeric chain. The interchain Cu···Cu separations are of 8.5190(5) and 8.494(1) Å in **I** and **II**, respectively. In the 12-membered rings the H3···O3 distances of 1.93(2) and 2.03(3) Å in **I** and **II**, respectively, are comparatively short.

To compare the relative importance of Cu–N and Cu–O bonds of Cu(II) polyhedra in **I** and **II** and to check the assumed Cu(II) coordination numbers, the

Table 2
Hydrogen-bonding geometry

	D–H (Å)	H···A (Å)	H···A (Å)	D–H···A (°)
O1–H1···O2^{i}	0.82(2)	2.05(2)	2.860(1)	175(2)
N3–H3···O3^{ii}	0.85(2)	1.93(2)	2.763(2)	165(2)
C4–H4···O3^{iii}	0.91(2)	2.58(2)	3.413(2)	152(2)

Symmetry codes: i: $-x$, $-y+1$, $-z$; ii: $-x+1/2$, $-y+1/2$, $-z+1$; iii: $x+1/2$, $-y+1/2$, $z-1/2$.

Table 3
Valence sums around the Cu atoms in **I** and **II**

Cu–j	**I**		**II**	
	d_{Cu-j} (Å)	v_{Cu-j} (v.u.)	d_{Cu-j} (Å)	v_{Cu-j} (v.u.)
Cu–N1	2.005(2)	0.454 [a]	2.007(2)	0.452 [a]
Cu–O1	2.229(2)	0.226	2.245(4)	0.217
Cu–O2	2.013(1)	0.405 [a]	2.010(2)	0.409 [a]
Cu–O3	2.907(1)	0.036 [a]	2.930(2)	0.034 [a]
V_{Cu}	2.016		2.007	

d_{Cu-j} are the observed bond lengths between Cu and j atoms, v_{Cu-j} is the computed bond valence (v.u.) and $V_{Cu} = \Sigma\ v_{Cu-j}$.
[a] Occurs twice around the Cu atom.

valences of Cu bonds (v_{Cu-j}) and of Cu atoms (V_{Cu}) were computed (Table 3). The bond valences were computed according to Brown [13,14] and O'Keeffe and Brese [15], as $v_{Cu-j} = \exp[(R_{Cu-j} - d_{Cu-j})/0.37]$, where R_{Cu-j} are the bond valence parameters (in the formal sense R_{Cu-j} is the bond length between Cu and j atoms for $v_{Cu-j} = 1$); d_{Cu-j} are the Cu–j bond lengths. R_{Cu-N} was determined by us from the Cambridge Structural Database [16] as 1.713 Å [5]. R_{Cu-O}, according to Brese and O'Keeffe [17], was taken as 1.679 Å. In both structures the valences of the Cu atoms are consistent with the valence-sum rule ($V_i = \Sigma\ v_{ij}$), which gives $V_{Cu} = 2.016$ and 2.007 v.u. (v.u., valence unit) for **I** and **II**, respectively.

In the Cu(II) polyhedra, the Cu–N bonds are stronger than the short Cu–O2 bonds (average $v_{Cu-N} = 0.453$ v.u. and average $v_{Cu-O2} = 0.407$ v.u.). The average valence of the longer axial Cu–O1 bond is 0.221 v.u., distinctly greater than usually observed in Cu(II) square-pyramidal complexes. The average valences of the two very long Cu–O3 bonds are only 0.035 v.u., but neglect of these bonds disturbs the valence sum rule.

3.2. Magnetism

Both complexes present quantitatively similar magnetic properties. The results of susceptibility measurements are illustrated in Figs. 3 and 4 in the form $\chi_{Cu}T$ versus T (χ_{Cu} being the corrected molar magnetic susceptibility per Cu(II) and T the absolute temperature).

The room temperature $\chi_{Cu}T$ values (0.429 and 0.418 $cm^3\ K\ mol^{-1}$ for **I** and **II**, respectively) correspond well to that expected for isolated, magnetic Cu(II) centres. The $\chi_{Cu}T$ value is constant up to 10 K and then with lowering temperature decreases rapidly and reaches values 0.304 $cm^3\ K\ mol^{-1}$ in **I** and 0.318 $cm^3\ K\ mol^{-1}$ in complex **II** at 1.72 K. It suggests a weak antiferromagnetic interaction between the Cu(II) centres in the crystal lattice.

The crystal structure in both cases is composed of polymeric chains where Cu centres are connected by bridging of tetradentate 2-butane-l,4-dicarboxylate ions in **I** and tetradentate μ-adipate ligands in **II**. An interesting feature of these structures is three-dimensional hydrogen bond system (Fig. 1(b), Fig. 2).

It is well known that a bridging moiety is most effective in supporting an antiferromagnetic exchange interaction between two transition magnetic ions if the bridge has available molecular orbitals that can interact with the bonding combination of two metal d orbitals [18,19]. It was shown earlier that the adipate bridging unit will not propagate any interaction due to the small and incomplete effective overlap at the chain C–C

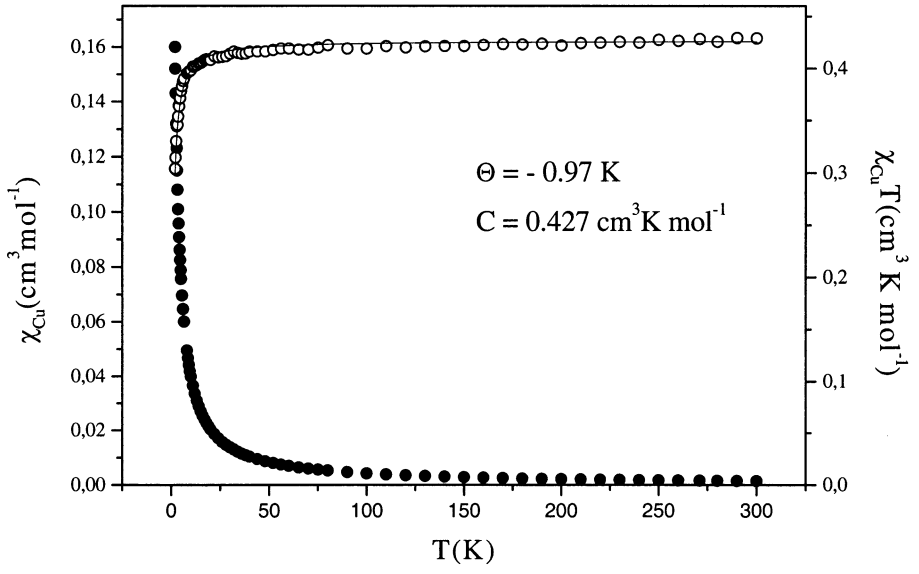


Fig. 4. Plots of χ_{Cu} and $\chi_{Cu}T$ vs. T for **II**. Solid line: theoretical fit of the data with the parameters listed in the text.

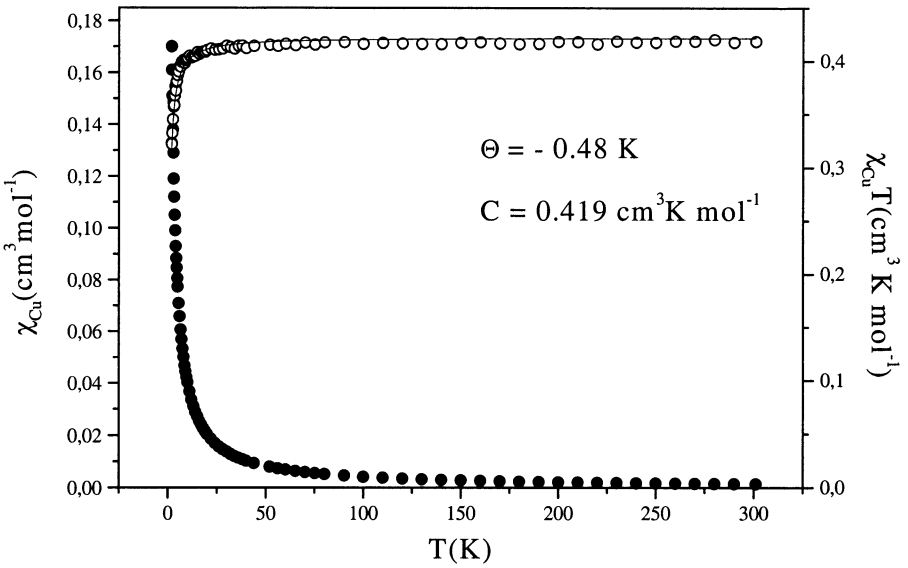


Fig. 3. Plots of χ_{Cu} and $\chi_{Cu}T$ vs. T for **I**. Solid line: theoretical fit of the data with the parameters listed in the text.

interactions [20,21]. Nevertheless, the capability of both hydrogen bonds and carboxylate groups will be examined.

Magnetic data were analyzed using the Ising expression:

$$\chi_M = \frac{Ng^2\beta^2}{4kT}\exp\left(-\frac{J}{kT}\right)$$

for infinite chains of Cu ions [19], the J value characterizes intrachain interactions, the spin Hamiltonian is defined as $H = -J\,\Sigma\, S_iS_{i+1}$.

A molecular field term was added to describe interchain interactions:

$$\chi_M^{mf} = \frac{\chi_M}{1 - \dfrac{2zJ' - \chi_M}{Ng^2\beta^2}}$$

where χ_M is the molar susceptibility given by Ising's

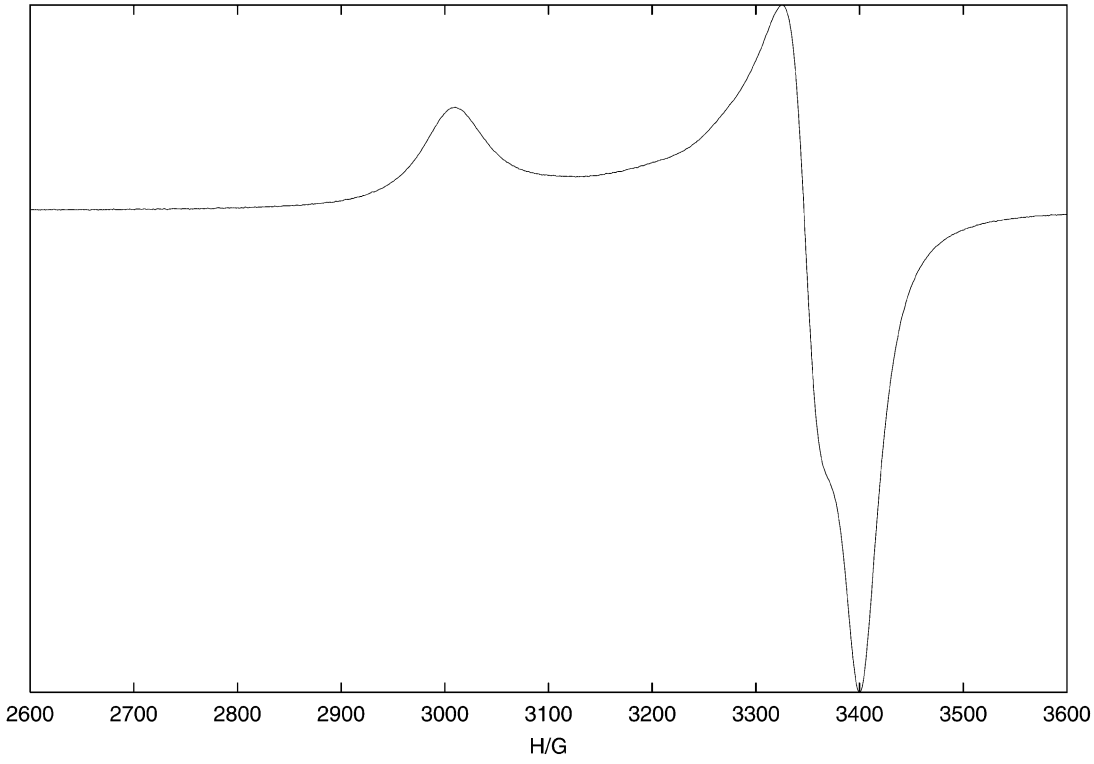


Fig. 5. Polycrystalline powder EPR spectrum of **I**, at 77 K. Compound **II** presents the same type of spectrum, parameters are listed in the text.

expression, J' characterizes interchain interaction between z Cu(II) neighbours.

A least-squares fit of the data leads to the values of $J = -0.58$ cm^{-1}, $zJ' = +0.38$ cm^{-1}, $g = 2.13$ and $R = 1.8 \times 10^{-5}$ for **I** and $J = -0.63$ cm^{-1}, $zJ' = +0.80$ cm^{-1}, $g = 2.12$ and $R = 1.8 \times 10^{-5}$ for **II**. R is the agreement factor defined as $R = \Sigma_i [(\chi_{Cu}T)_{obs}(i) - (\chi_{Cu}T)_{calc}(i)]^2/\Sigma_i [(\chi_{Cu}T)_{obs}(i)]^2$. Intrachain antiferromagnetic interaction, although weak, compensates ferromagnetic interchain contribution and is dominant in both complexes.

The temperature dependence of χ_{Cu}^{-1} is represented by a Curie–Weiss law with $\theta = -0.97$ K and $C = 0.427$ cm^3 K mol^{-1} for **I** and $\theta = -0.48$ K and $C = 0.419$ cm^3 K mol^{-1} for complex **II**, and confirms weak antiferromagnetic interaction between Cu(II) centres in the crystal lattice.

Average spectroscopic splitting parameters obtained from the EPR spectra and from the fitting process are in good agreement. The EPR spectra of the polycrystalline samples of both complexes **I** and **II** are temperature independent and show a pseudorhombic pattern (Fig. 5), consisting of three g values: **I**, 2.32_4, 2.08_8, 2.05_7 ($g_{av} = 2.15_3$) and **II**, 2.31_7, 2.08_8, 2.05_3 ($g_{av} = 2.15_2$). It is a result of the existence of partial mixing of the d_{z^2} orbital into the $d_{x^2-y^2}$ magnetic orbital [22]. This EPR aspect is in fairly good agreement with the Cu geometries obtained from the crystal structures.

The d–d spectra of complexes **I** and **II** consist of broad bands, centered at 655 nm in **I** and at 705 nm in **II**. The shift toward lower energy can be related to a lower ligand field in complex **II** with the adipate anion.

4. Supplementary material

Further details of the crystal structure investigation are available from the Cambridge Crystallographic Data Centre, CCDC no. 172444 (compound catena-((μ2-*trans*-2-butene-1,4-dicarboxylato-O,O′:O″,O‴)-aquabis-(benzimidazole-N^3)copper(II)). Copies of this information may be obtained free of charge on request from The Director, CCDC, 12 Union Road, Cambridge, CB2 1EZ, UK (fax: +44-1223-336033; e-mail: deposit@ccdc.cam.ac.uk or www: http://www.ccdc.cam.ac.uk).

Acknowledgements

This work was financially supported by the State Committee for Scientific Research (Poland) Grant No. 3T09A 03915 and Grant I17/Dz.St./49 from the Technical University of Łódź.

References

[1] A. Tosik, M. Bukowska-Strzyżewska, J. Crystallogr. Spectrosc. Res. 22 (1992) 225.
[2] A. Tosik, L. Sieroń, M. Bukowska-Strzyżewska, Acta Crystallogr., Sect. C 51 (1995) 1985.
[3] A. Tosik, L. Sieroń, M. Bukowska-Strzyżewska, Acta Crystallogr., Sect. C 51 (1995) 1987.
[4] L. Sieroń, M. Bukowska-Strzyżewska, Acta Crystallogr., Sect. C 54 (1998) 1431.
[5] L. Sieroń, M. Bukowska-Strzyżewska, Acta Crystallogr., Sect. C 55 (1999) 1230.
[6] L. Sieroń, M. Bukowska-Strzyżewska, Acta Crystallogr., Sect. C 56 (2000) 19.
[7] KM4CCD Software, Data Collection and Reduction Program, Version 1.163, UNIL IC & KUMA Diffraction Instruments GmbH, 2000.
[8] Stoe & Cie, X-RED, Version 1.18, Data Reduction Program, Stoe & Cie GmbH, Darmstadt, Germany, 1999.
[9] Stoe & Cie, X-SHAPE, Version 1.05, Crystal Optimisation for Numerical Absorption Correction, Stoe & Cie GmbH, Darmstadt, Germany, 1999.
[10] G.M. Sheldrick, SHELXS-97, Program for the Solution of Crystal Structures, University of Göttingen, Germany, 1997.
[11] G.M. Sheldrick, SHELXL-97, Program for the Refinement of Crystal Structures, University of Göttingen, Germany, 1997.
[12] E. König, Magnetic Properties of Coordination and Organometallic Transition Metal Compounds, Springer-Verlag, Berlin, 1966.
[13] I.D. Brown, Acta Crystallogr., Sect. B 48 (1992) 553.
[14] I.D. Brown, Bond-Length–Bond-Valence Relationships in Inorganic Solids (in Structure Correlation part III by H.-B. Burgi and J.D. Dunitz), 1994, pp. 405–429.
[15] M. O'Keeffe, N.E. Brese, J. Am. Chem. Soc. 113 (1991) 3226.
[16] Cambridge Structural Database, Cambridge Crystallographic Data Centre, 12 Union Road, Cambridge, UK, 1998.
[17] N.E. Brese, M. O'Keeffe, Acta Crystallogr., Sect. B 47 (1991) 192.
[18] P.J. Hay, J.C. Thibeault, R. Hoffmann, J. Am. Chem. Soc. 97 (1995) 4884.
[19] O. Kahn, Molecular Magnetism, VCH, Weinheim, Germany, 1993.
[20] M.S. Haddad, D.N. Hendrickson, J.P. Cannady, R.S. Drago, D.S. Bieksza, J. Am. Chem. Soc. 101 (1979) 898.
[21] E.G. Bakalbassis, M. Korabik, A. Michailides, J. Mroziński, C. Raptopoulou, S. Skoulika, A. Terzis, D. Tsaousis, J. Chem. Soc., Dalton Trans. (2001) 850.
[22] S. Kawata, S. Kitagawa, H. Kumagai, Ch. Kudo, H. Kamesaki, T. Ishiyama, R. Suzuki, M. Kondo, M. Katada, Inorg. Chem. 35 (1996) 4449.

As compared to the bridged dinuclear ruthenium(II) complexes, studies made with the diosmium(II) analogues are less numerous; still less studies have been reported for heterodinuclear $Os^{II}Ru^{II}$ complexes. In two previous publications [14,15] we have reported the structures, spectroscopic properties and proton-coupled electron transfer reactions of diastereoisomerically pure diruthenium(II) polypyridal complexes involving pyrazole-3,5-bis(benzimidazole) [H_3pzbzim] and pyrazole-3,5-bis(benzothiazole) [Hpzbzth] as the bridging ligands. To extend this study for the homo- and heterodinuclear osmium(II) complexes, we report here the synthesis and compare the properties of the mononuclear osmium(II) complexes of H_3pzbzim with the ruthenium(II) analogues.

2. Experimental

2.1. Materials

All chemicals were obtained from commercial sources and used as received. Pyrazole-3,5-bis(benzimidazole) [15] and $[Os(bpy)_2Cl_2]$ [16] were prepared by the literature methods. Robinson–Britton [17] buffer solutions of pH range 2–12 were used. The supporting electrolyte tetraethylammonium perchlorate (TEAP) was prepared according to the reported method [18] and recrystallized thrice from hot water.

2.2. Preparation of the complexes

2.2.1. $[(bpy)_2Os(H_3pzbzim)](ClO_4)_2\cdot 2H_2O$ (1)

A mixture of $[Os(bpy)_2Cl_2]$ (0.29 g, 0.5 mmol) and H_3pzbzim (0.30 g, 1.2 mmol) in 50 cm^3 of EtOH–water (1:1) mixture was heated under reflux in nitrogen atmosphere with constant stirring for 60 h. After removal of the unreacted ligand, the dark red filtrate was rotary evaporated to approximately 20 cm^3 and to it was then added an aqueous solution (5 cm^3) of $NaClO_4$ (1 g). A dark microcrystalline product that separated was filtered and recrystallized from MeOH–water (1:1) containing a few drops of $HClO_4$ (1 mmol dm^{-3}). Yield: 0.21 g, 40%. *Anal.* Found: C, 42.7; H, 3.15; N, 13.6. $C_{37}H_{32}Cl_2N_{10}O_{10}Os$ requires: C, 42.8; H, 3.1; N, 13.5%. IR (KBr): 3400br, 1640s, 1600s, 1485m, 1470s, 1430m, 1390w, 1290m, 1270w, 1240w, 1100s, br, 785s, 760s, 740m, 675m, 650w, 630s, 600w cm^{-1}.

2.2.2. $[(bpy)_2Os(Hpzbzim)]\cdot 2H_2O$ (2)

To a stirred MeOH solution (20 cm^3) of (**1**) (0.12 g) was added a piece of freshly cut sodium metal (approximately 0.05 g). In a few minutes, a dark red microcrystalline product deposited. This was collected by filtration and thoroughly washed with MeOH. Yield: 0.08 g, almost quantitative. *Anal.* Found: C, 53.25; H, 3.5; N, 16.65. $C_{37}H_{30}N_{10}O_2Os$ requires: C, 53.1; H, 3.6; N, 16.75%. IR (KBr): 3400br, 1610m, 1575w, 1470s, 1460s, 1420m, 1380w, 1320w, 1280m, 1220w, 1050w, 1010m, 750s, 735w, 680m cm^{-1}.

$[(bpy)_2Ru(H_3pzbzim)](ClO_4)_2\cdot 2H_2O$ (**3**) and $[(bpy)_2Ru(Hpzbzim)]\cdot 2H_2O$ (**4**) were prepared according to the earlier reported procedures [15].

CAUTION! The perchlorate salts reported in this study are potentially explosive and therefore should be handled with care.

2.3. Physical measurements

The C, H and N analyses were performed on a Perkin–Elmer 2400II elemental analyzer. Infrared spectra were recorded on a Perkin–Elmer 783 spectrophotometer using KBr discs. ^1H and $\{^1H$–$^1H\}$COSY NMR spectra were recorded on a Bruker Avance DPX 300 spectrometer using $(CD_3)_2SO$ solutions.

The electrochemical measurements were carried out with a BAS 100B electrochemistry system. A three-electrode assembly comprising a Pt or glassy carbon working electrode, Pt auxiliary electrode, and an aqueous Ag/AgCl reference electrode were used. The cyclic voltammetric (CV) and differential pulse voltammetric (DPV) measurements were carried out at 25 °C in MeCN solution of the complexes (approximately 1 mmol dm^{-3}) with TEAP (0.1 mol dm^{-3}) as the supporting electrolyte. The electrochemical measurements were carried out with oxygen-free solutions made by purging with purified nitrogen. The reference electrode was separated from the bulk electrolyte by a salt bridge containing TEAP (0.1 mol dm^{-3}) in MeCN–water (1:1). The potentials measured were compensated for the *iR* drop in the cell. Under the experimental condition used the reversible oxidation of the ferrocene/ferrocenium ion was observed at 0.36 V.

For variable-pH electrochemical measurements, MeCN–aqueous (3:2) solutions of the complexes were used. The pH measurements were made with a Beckman Research Model pH meter. The pH meter responded reproducibly to the variation of hydrogen ion concentration and as such, the pH meter readings were referred to as pH. The $E_{1/2}$ value of the ferrocene/ferrocenium couple in the above solvent mixture at approximately pH 7 is 0.26 V.

Electronic spectra were recorded on a Shimadzu UV-2100 spectrophotometer. To determine the pK_a values of the complexes spectrophotometric titrations were carried out with a series of MeCN–aqueous buffer (3:2) solutions containing the same amount (10^{-5} mol dm^{-3}) of complex and pH adjusted in the range 2–12. The oxidative titrations were also followed spectrophotometrically by incremental addition of a solution of ceric(IV) ammonium nitrate in MeCN–water (3:2) to a solution of the complex in the same solvent mixture. Emission

spectra were recorded on a Hitachi F-4500 fluorescence spectrophotometer using MeOH–EtOH (1:4) solution of the complex (at 300 K) and glass (at 77 K).

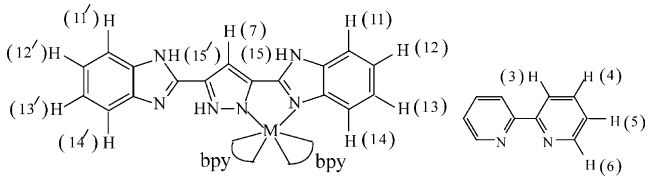
3. Results and discussion

The reaction between one equivalent each of *cis*-$[(bpy)_2OsCl_2]$ and pyrazole-3,5-bis(benzimidazole) [H_3pzbzim] leading to the substitution of the two chloride ions by the two imine nitrogen donors of the incoming ligand is kinetically slow. The product was isolated as $[(bpy)_2Os(H_3pzbzim)](ClO_4)_2\cdot 2H_2O$ (**1**) (in 40% yield) after 60 h reaction. Complex (**1**) is asymmetric because only one part of the bridging ligand H_3pzbzim is involved in metal binding, while the other part remains free. As will be seen, consequent to complexation, the NH groups in closer proximity to the metal centre in (**1**) become considerably more acidic relative to those in the free ligand. In particular, the pyrazole NH gets partially deprotonated in solution, thus, requiring recrystallization of (**1**) to be carried out in mildly acidic solution. Complex (**1**) gets deprotonated to $[(bpy)_2Os(Hpzbzim)]\cdot 2H_2O$ (**2**) on treatment with sodium alkoxide or triethylamine. As reported earlier [15], compared to (**1**), the formation of $[(bpy)_2Ru(H_3pzbzim)](ClO_4)_2\cdot 2H_2O$ (**3**) takes place more readily.

3.1. ^1H NMR spectra

The ^1H and $\{^1H–^1H\}$COSY NMR spectra for complexes $[(bpy)_2Os(H_3pzbzim)](ClO_4)_2\cdot 2H_2O$ (**1**), $[(bpy)_2Os(Hpzbzim)]\cdot 2H_2O$ (**2**), $[(bpy)_2Ru(H_3pzbzim)](ClO_4)_2\cdot 2H_2O$ (**3**) and $[(bpy)_2Ru(Hpzbzim)]\cdot 2H_2O$ (**4**) have been recorded in $(CD_3)_2SO$ solutions at room temperature. The numbering scheme used to assign the observed resonances is given in Scheme 1.

The ^1H NMR spectra for complexes (**1**)–(**4**) are shown in Figs. 1–4, respectively. The asymmetric nature of the complexes are evident from the occurrence of fairly large number of resonances, many of which, especially in (**1**), are overlapped with each other. The COSY spectra have been particularly useful to locate spin couplings in the aromatic protons of the benzimidazole moiety bound to the metal as against the uncoordinated one. The assignments of the bipyridine protons were facilitated by taking into consideration of



Scheme 1.

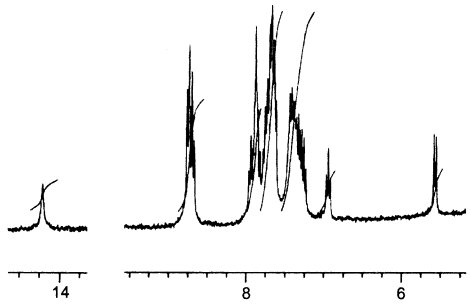


Fig. 1. ^1H NMR spectrum of $[(bpy)_2Os(H_3pzbzim)]^{2+}$ ($\mathbf{1}^{2+}$) in $(CD_3)_2SO$.

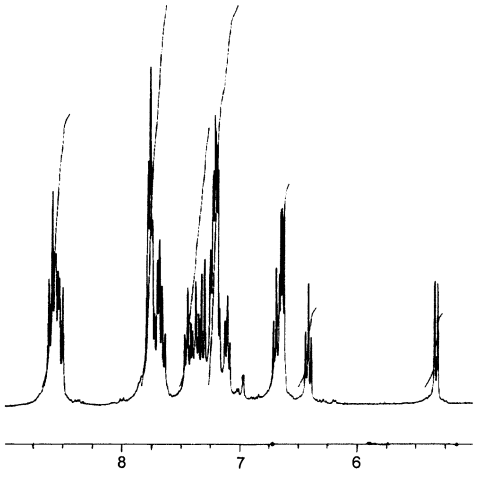


Fig. 2. ^1H NMR spectrum of $[(bpy)_2Os(Hpzbzim)]$ (**2**) in $(CD_3)_2SO$.

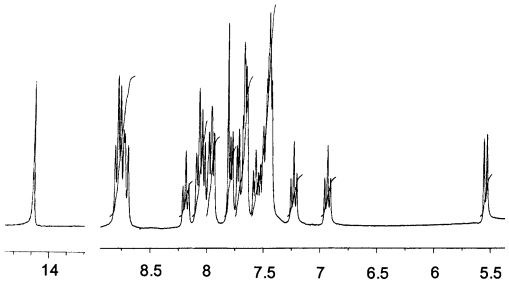


Fig. 3. ^1H NMR spectrum of $[(bpy)_2Ru(H_3pzbzim)]^{2+}$ ($\mathbf{3}^{2+}$) in $(CD_3)_2SO$.

the following facts [19]. The usual decreased order of chemical shifts is H(3) > H(4) ≥ H(5) > H(6); $J_{3,4}/J_{4,5} \approx 8$ Hz, $J_{5,6} \approx 5$ Hz and $J_{3,5}/J_{4,6} \approx 1.2$ Hz; the protons H(3) and H(6) are normally observed as doublets, while H(4) and H(5) appear either as triplet or doublet of doublet.

As may be seen in Figs. 1–4, for each of the complexes all the resonances, barring two, occur in the range 6.4–8.8 ppm. Of the two disparate signals, the one which is most shielded amongst all appears as a doublet between 5.3 and 5.5 ppm. The doublet accounts for a single proton and is clearly due to H(14) (see Scheme 1 for proton labelling) since this proton experiences maximum diamagnetic shielding by the anisotropic

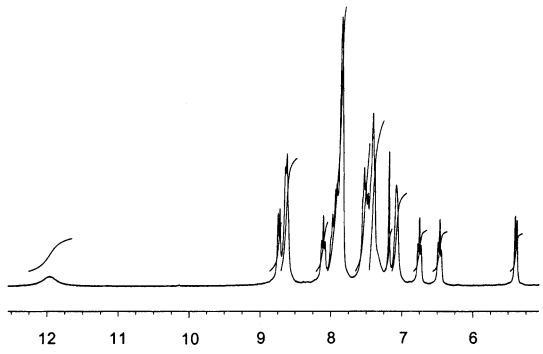


Fig. 4. ^{1}H NMR spectrum of $[(bpy)_2Ru(Hpzbzim)]$ (**4**) in $(CD_3)_2SO$.

ring current of the adjacent bipyridine rings. The second distinct signal, which is most downfield-shifted, is observed either as a sharp singlet at 14.2 ppm for (**1**) and (**3**) or as a broad feature at approximately 12.0 ppm for (**2**) and (**4**). The singlet observed for (**1**) and (**3**) is due to the two benzimidazole NH protons (H(15) and H(15′)), while the broad signal observed in (**2**) and (**4**) is due to the single NH group (H(15′)) in these compounds. The relative higher field shift of this signal in (**2**)/(**4**) with respect to (**1**)/(**3**) is consistent with the augmentation of electronic charge in (**2**)/(**4**).

Table 1 summarizes spectral assignments made for complexes (**1**)–(**4**). It would be of interest to compare the chemical shifts of some of the pertinent resonances in the osmium(II) complexes with their ruthenium(II) analogues and also to examine the influence of deprotonation on chemical shifts. It may be noted that, the chemical shift due to H(14) proton of the osmium(II) complex (**1**) (5.57 ppm) is almost identical to that of the ruthenium(II) complex (**3**) (5.55 ppm). The same is more or less true for the other phenyl ring protons of the two compounds. Interestingly, the singlet due to pyrazole H(7) is observed at 7.85 ppm for (**1**) as against 7.82 ppm for (**3**). Similarly, the singlet due to the NH protons occurs almost at the same place for (**1**) (14.21 ppm) and (**3**) (14.23 ppm). When the two deprotonated complexes (**2**) and (**4**) are compared, again a similar trend is observed.

On deprotonation of the NH groups belonging to the pyrazole and one of the benzimidazole moieties of (**1**) and (**3**), significant upfield shifts occur for the aromatic protons H(11)–H(14), which are in the vicinity of the deprotonated sites. Specifically, H(7) pyrazolate ring proton of (**2**) and (**4**) gets more shielded relative to (**1**) and (**3**) by 0.64 ppm.

3.2. Redox properties

The redox activities of complexes (**1**)–(**4**) have been studied in acetonitrile solution and the relevant electrochemical data are given in Table 2. In all the cases metal-centred oxidation (M^{II}/M^{III}) take place reversibly as borne out by their strict adherence to the usual criteria of reversibility. Fig. 5 shows the cyclic voltammograms of $[(bpy)_2Os(H_3pzbzim)]^{2+}$ ($\mathbf{1}^{2+}$) and $[(bpy)_2Ru(H_3pzbzim)]^{2+}$ ($\mathbf{3}^{2+}$) over the potential range +1.2– −2.2 V (vs. Ag/AgCl). It may be noted that the redox

Table 1
NMR spectral data[a] for complexes (**1**)–(**4**) in $(CD_3)_2SO$

Proton[b]	(**1**)	(**2**)	(**3**)	(**4**)
15	14, 21(s), 2H	11.98(s,br), 1H	14.23(s), 2H	11.96(s,br), 1H
15′				
14	5.57(d), 1H, 8.3	5.32(d), 1H, 7.9	5.55(d), 1H, 8.2	5.39(d), 1H, 7.8
13	6.94(t), 1H, 7.7	6.41(t), 1H, 7.8	6.94(t), 1H, 7.7	6.47(t), 1H, 7.4
12		6.68(t), 1H, 7.6	7.23(t), 1H, 7.7	6.76(t), 1H, 7.3
11		6.62–6.66, 2H	7.57(d), 1H, 8.0	7.08[c], 2H
14			7.78(d), 1H, 7.8	
13′	7.22–7.44[c], 6H	7.11(t), 1H, 7.8	8.19(t), 2H, 7.4	7.43–7.53[c], 3H
12′		7.66(t), 1H, 6.1		
11′		7.68(d), 1H, 6.2	8.09(d), 1H, 7.6	
7	7.85(s), 1H	7.22(s), 1H	7.82(s), 1H	7.18(s), 1H
6	7.62–7.78[c], 8H	7.16–7.26[c], 4H	7.43–7.53[c], 4H	7.30–7.42[c], 4H
		7.33(t), 2H, 6.7		
5		7.38(t), 1H, 6.8	7.60–7.74[c], 4H	7.75–7.88[c], 4H
		7.44(t), 1H, 7.0		
4	7.78–7.98[c], 4H	7.76(t), 2H, 5.5	7.96(t), 2, 5.8	7.90–8.05[c], 3H
		7.70(t), 2H, 5.6	8.04(t), 2, 5.6	8.11(t), 1H, 5.6
3	8.68(d), 2H, 8.5	8.52(d), 1H, 8.3	8.71(d), 1H, 7.8	8.63[c], 3H
	8.75(d), 2H, 8.5	8.55(d), 1H, 8.3	8.75(d), 1H, 7.7	8.73(d), 1H, 7.6
		8.58(d), 1H, 8.4	8.78(d), 1H, 7.8	
		8.62(d), 1H, 8.4	8.80(d), 1H, 8.0	

[a] For ^{1}H NMR data, respectively: chemical shift (ppm), number of protons, J(Hz).
[b] For proton numbering see Scheme 1.
[c] Unresolved signals.

Table 2
Electrochemical data for the complexes[a]

Complex	Oxidation		Reduction			
	$E_{1/2}$ (V)	ΔE_p (mV)[b]	$E_{1/2}{}^1$ (V)	ΔE_p (mV)[b]	$E_{1/2}{}^2$ (V)	ΔE_p (mV)[b]
1	0.48	65	−1.56	65	−1.88	75
2	0.14	70	−1.58	75	−1.92	80
3	0.89	65	−1.62	70	−1.90	75
4	0.60	80	−1.60	80	−1.93	85

[a] Scan rate, 100 mV s^{-1}. Potentials are referenced to Ag/AgCl.
[b] Separation of peak potentials.

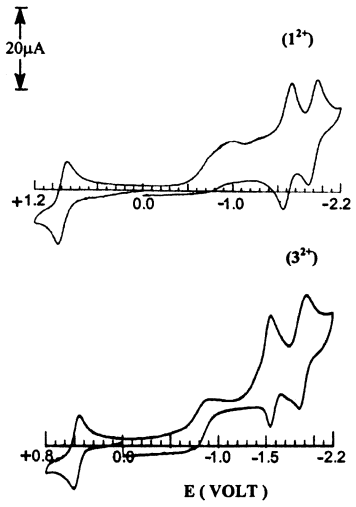


Fig. 5. Cyclic voltammograms of $[(bpy)_2Os(H_3pzbzim)]^{2+}$ ($\mathbf{1}^{2+}$) and $[(bpy)_2Ru(H_3pzbzim)]^{2+}$ ($\mathbf{3}^{2+}$) in acetonitrile.

potential of the Os^{II}/Os^{III} couple in (**1**) ($E^{ox}_{1/2} = 0.48$ V) is 0.41 V less positive as compared to the Ru^{II}/Ru^{III} couple in (**3**) ($E^{ox}_{1/2} = 0.89$ V). In the deprotonated state, the removal of an electron from the metal centre becomes more facile. Thus, the $E^{ox}_{1/2}$ values of (**2**) and (**4**) 0.14 and 0.60 V, respectively, are appreciably less relative to those of (**1**) and (**3**). On the other hand, the electrochemical responses for all the four complexes are similar in the negative potential regime upto −2.2 V, where electrons are added to the unoccupied acceptor orbitals of bipyridine. As may be seen in Fig. 5, both for ($\mathbf{1}^{2+}$) and ($\mathbf{3}^{2+}$), two reversible one electron reduction processes occur at about −1.65 and −1.90 V. Interestingly, Fig. 5 also shows the presence of a broad irreversible feature around −1 V for both ($\mathbf{1}^{2+}$) and ($\mathbf{3}^{2+}$). The origin of this reduction process is not clear at this stage. However, it could be due to the reduction of an acidic ligand proton $H^+ + e^- \rightarrow 0.5H_2$.

3.3. Equilibrium constants involving electroprotic reactions

The coupled electron and proton transfer reactions of $[(bpy)_2Os(H_3pzbzim)]^{2+}$ ($\mathbf{1}^{2+}$) in acetonitrile–water (3:2) have been studied over the pH range 1–12 in the same way as reported earlier [14] for $[(bpy)_2Ru(H_3pzbzim)]^{2+}$ ($\mathbf{3}^{2+}$). It should be noted that while in pure acetonitrile the $E_{1/2}$ value for the ferrocene/ferrocenium couple was found to be 0.36 V, in acetonitrile–water (3:2) it is 0.26 V. Thus, while comparing the $E_{1/2}$ values in the two solvent media the normalizing factor 0.10 V should be applied.

The variation of $E_{1/2}$ as a function of pH for ($\mathbf{1}^{2+}$) is shown in Fig. 6. It may be noted that in strongly acidic medium (pH < 2) as well as in strongly basic medium (pH > 10), the $E_{1/2}$ values remain pH independent, indicating that in these two regions the electron transfer is not accompanied by proton transfer. In the intermediate range, 2 < pH < 10, steady decrease of $E_{1/2}$ with the increase of pH occurs in two steps. The slopes of the $E_{1/2}$ versus pH plots in these two regions are close to −60 mV/pH, indicating that both the steps are associated with one-electron–one-proton transfer reactions. The observed electro-protic reactions are illustrated in Scheme 2.

Further dissociation of the benzimidazole proton away from the metal site does not occur even at pH 12. It should be noted that the dissociation constants K_1 and K_2 refer to the species involving osmium(II), while K_3 and K_4 refer to osmium(III) containing species.

As the electron transfer reactions occur reversibly, the observed $E_{1/2}$ can be related to the acid dissociation

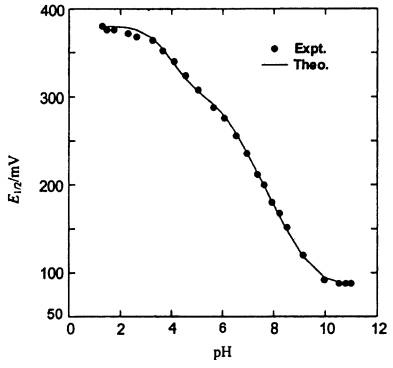
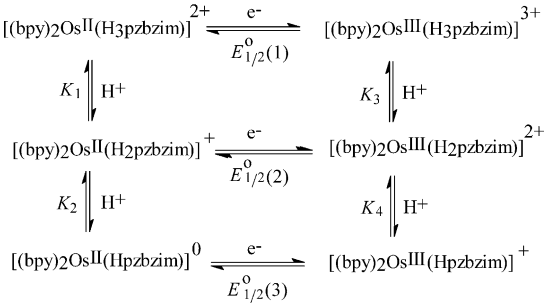


Fig. 6. Variation of $E_{1/2}$ for the Os^{II}/Os^{III} couple in $[(bpy)_2Os(H_3pzbzim)]^{2+}$ ($\mathbf{1}^{2+}$) as a function of pH in acetonitrile–water (3:2).



Scheme 2.

constants of the complexes by Eq. (1)

$$E_{1/2} = E^{\circ}_{1/2} + 0.059 \log \frac{[H^+]^2 + K_1[H^+] + K_1K_2}{[H^+]^2 + K_3[H^+] + K_3K_4} \qquad (1)$$

where $E^{\circ}_{1/2}$ is the standard redox potential of the Os^{II}/Os^{III} couple at pH 0 and at 25 °C. As shown in Fig. 6, nonlinear least-squares analysis of the 25 experimental data points has provided the best fit curve with the following pK values: $pK_1 = 4.7$, $pK_2 = 9.5$, $pK_3 = 3.3$ and $pK_4 = 5.9$. These values may be compared with those of the corresponding ruthenium species for which $pK_1 = 5.4$, $pK_2 = 10.0$, $pK_3 = 3.0$ and $pK_4 = 6.3$ [14]. The results indicate: (i) as compared to the ruthenium species, the azole protons are more acidic in the osmium species. (ii) The acid dissociation constant for a given ligand site is considerably greater when the metal ion is in +3 state relative to that in +2 state. For the metal-free H_3pzbzim, the pK value of the pyrazolyl proton is 10.5, while for the benzimidazolyl protons these are well above 12.

The $E^{\circ}_{1/2}$ values of all the protonated and deprotonated redox couples for the osmium and ruthenium complex species in acetonitrile–water (3:2) are given below for comparision

$E^{\circ}_{1/2}(1) = 0.38$ V(Os), 0.78 V(Ru)

$E^{\circ}_{1/2}(2) = 0.33$ V(Os), 0.66 V(Ru)

$E^{\circ}_{1/2}(3) = 0.09$ V(Os), 0.44 V(Ru)

These results show the expected trend of progressive shifts of the redox potentials to less positive values. The extent of shift in potentials on passing from the fully protonated state to the fully deprotonated state, that is $E^{\circ}_{1/2}(1) - E^{\circ}_{1/2}(3)$, is 0.29 V for osmium and 0.34 V for ruthenium. On the other hand, at every state of protonation the osmium species get more easily oxidized relative to the corresponding ruthenium species by a margin of 0.33–0.40 V.

A comparison of the redox potentials for complexes (**1**)–(**4**) in acetonitrile, as given in Table 2, vis-à-vis those in acetonitrile–water (3:2) show some differences even by taking into account the shift of the $E_{1/2}$ value for the ferrocene/ferrocenium couple from 0.36 V in acetonitrile to 0.26 V in acetonitrile–water (3:2). For instance, $E^{\circ}_{1/2}(3)$ for Os at 0.09 V in acetonitrile–water is somewhat more positively shifted relative to the Os^{II}/Os^{III} couple of (**2**) observed at 0.14 V. Further, the difference between $E^{\circ}_{1/2}(1)$ and $E^{\circ}_{1/2}(3)$ is 0.29 V for Os and 0.34 V for Ru, while the corresponding differences in redox potentials given in Table 2 for the protonated and deprotonated species are 0.34 and 0.29 V, respectively. We attribute these deviations to non-specific solvent effects.

3.4. Absorption spectral studies of proton and electron transfer reactions

The absorption spectrum of $[(bpy)_2Os(H_3pzbzim)]^{2+}$ ($\mathbf{1}^{2+}$) in acetonitrile recorded over the range 300–900 nm exhibit three bands at 345 (29 400), 515 (11 600) and 685 nm (2800) with their molar absorptivities (ε/dm^3 mol^{-1} cm^{-1}) given in parentheses. The band at 345 nm seems to be due to intraligand (H_3pzbzim) π–π^* transition, while the other two bands are due to $Os(d\pi) \rightarrow bpy(\pi^*)$ charge transfer transitions. In the deprotonated complex $[(bpy)_2Os(Hpzbzim)]$ (**2**), substantial red shift of the MLCT bands take place with their peaks occurring at 560 (11 100) and 780 nm (2900). On the other hand, the band due to intraligand transition is nominally shifted to 340 nm (28 300).

The influence of pH on the absorption spectral behavior of ($\mathbf{1}^{2+}$) in acetonitrile–water (3:2) over the pH range 2–12 is shown in Fig. 7. As may be noted, with the increase of pH, the two MLCT bands in the successive absorption curves undergo redshifts during which they pass through four isosbestic points at 457, 525, 628 and 700 nm. These observations along with the analysis of the spectrophotometric titration data by a graphical method [20] suggest the occurrence of the

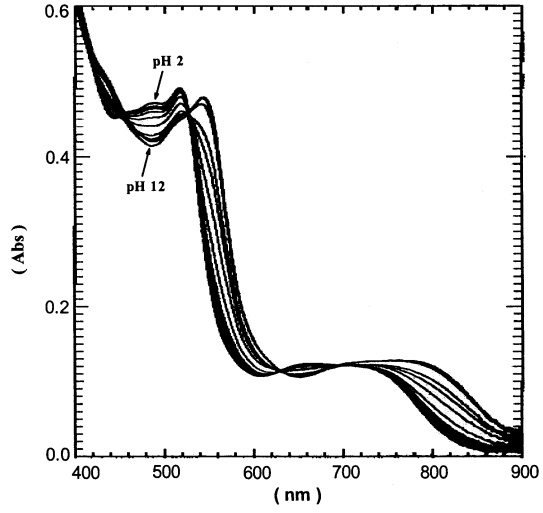


Fig. 7. Changes in the absorption spectrum of $[(bpy)_2Os(H_3pzbzim)]^{2+}$ ($\mathbf{1}^{2+}$) with the variation of pH in acetonitrile–water (3:2).

following acid–base equilibria.

$$[(bpy)_2Os(H_3pzbzim)]^{2+} \overset{K_1}{\rightleftharpoons} [(bpy)_2Os(H_2pzbzim)]^{+} + H^{+} \quad (2)$$

$$[(bpy)_2Os(H_2pzbzim)]^{+} \overset{K_2}{\rightleftharpoons} [(bpy)_2Os(Hpzbzim)] + H^{+} \quad (3)$$

The pK_I values have been evaluated from the absorption data pertaining to the pH ranges 2–7 and 7–12 of Fig. 7 using Eq. (4)

$$pH = pK_1 - \log\frac{A - A_o}{A_f - A} \quad (4)$$

where A_o, A_f and A refer to the absorbances at the initial, final and intermediate pH values at a given wavelength. The results thus obtained, $pK_1 = 4.75(5)$ and $pK_2 = 9.40(5)$, are in good agreement with those obtained by the electrochemical method ($pK_1 = 4.7$ and $pK_2 = 9.5$).

The redox equilibrium involving the generation of the osmium(III) species by the chemical oxidation of ($\mathbf{1}^{2+}$) with cerium(IV) ammonium nitrate in acetonitrile–water (3:2) has also been studied spectrophotometrically. The spectral changes that occur during the redox titration is shown in Fig. 8. It may be noted that the more intense MLCT band of ($\mathbf{1}^{2+}$) at 515 nm gradually gets depleted and undergoes red shift till the oxidation is complete, when the MLCT band is replaced by the LMCT ($H_3pzbzim \rightarrow Os^{III}$) band with its peak at 530 nm ($\varepsilon = 4100$ dm^3 mol^{-1} cm^{-1}). Further, the second MLCT band at 680 nm gradually disappears during oxidation.

Fig. 8 shows that the one-electron chemical oxidation reaction takes place smoothly and quantitatively as the successive absorption curves pass through two isosbestic points at 365 and 795 nm.

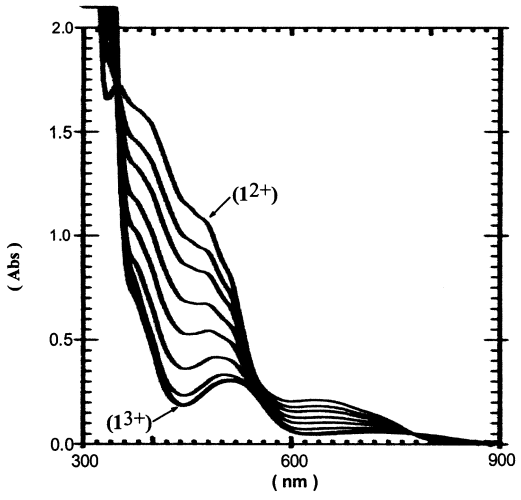


Fig. 8. Changes in the absorption spectrum of $[(bpy)_2Os(H_3pzbzim)]^{2+}$ ($\mathbf{1}^{2+}$) on oxidation with cerium(IV) in acetonitrile–water (3:2).

3.5. Luminiscence spectra

The emission spectral behavior of complexes (**1**) and (**2**) have been studied at 300 and 77 K in methanol–ethanol (1:4) solutions and glass, respectively. The osmium complex (**1**) does not luminescent at room temperature in solution. However, in frozen glass at 77 K a very weak and broad luminiscence with its peak around 760 nm. In contrast, the ruthenium(II) complex (**3**) exhibits fairly strong luminiscence both at 300 and 77 K with quantum yield 3.5×10^{-3} and 7.2×10^{-2}, respectively. It should be noted that for a given ligand, ^{3}MLCT energy decreases for osmium(II) relative to that of ruthenium(II). Consequently, quenching to the ground state takes place more efficiently for a osmium(II) compound [21]. In the case of the deprotonated osmium(II) compound (**2**) further lowering of ^{3}MLCT energy occurs and as a result (**2**) does not luminescent even at 77 K.

Acknowledgements

K.N. is thankful to the Council of Scientific and Industrial Research, India for funding this work.

References

[1] V. Balzani, A. Juris, M. Venturi, S. Campagna, S. Serroni, Chem. Rev. 96 (1996) 759.
[2] J.-P. Sauvage, J.-P. Collin, J.-C. Chambron, S. Gullierez, C. Coudret, V. Balzani, F. Barigelletti, L. DeCola, L. Flamigni, Chem. Rev. 94 (1994) 993.
[3] A. Harriman, R. Ziessel, Chem. Commun. (1996) 1707.
[4] M.D. Ward, Chem. Soc. Rev. 24 (1995) 121.
[5] E.C. Constable, Prog. Inorg. Chem. 42 (1994) 67.
[6] F.R. Keene, Chem. Soc. Rev. 27 (1998) 185.
[7] (a) F.M. MacDonnell, M.-J. Kim, S. Bodige, Coord. Chem. Rev. 185/186 (1999) 535;
(b) S. Campagna, S. Serroni, S. Bodige, F.M. MacDonnell, Inorg. Chem. 38 (1999) 692;
(c) D.J. Maloney, D. Tate, G.R. Kinsel, A.K. Walker, F.M. MacDonnell, J. Am. Chem. Soc. 119 (1997) 10364.
[8] (a) B.T. Patterson, F.R. Keene, Inorg. Chem. 37 (1998) 645;
(b) N.C. Fletcher, F.R. Keene, J. Chem. Soc., Dalton Trans. (1999) 683.
[9] (a) U. Knof, A. von Zelewsky, Angew. Chem., Int. Ed. Engl. 38 (1999) 302;
(b) N.C. Fletcher, F.R. Keene, H. Viebrock, A. von Zelewsky, Inorg. Chem. 36 (1997) 1113;
(c) H. Muerner, P. Belser, A. von Zelewsky, J. Am. Chem. Soc. 118 (1996) 7989.
[10] (a) G. Giuffrida, S. Campagna, Coord. Chem. Rev. 135/136 (1994) 517;
(b) J.T. Hupp, J. Am. Chem. Soc. 112 (1990) 1563;
(c) W. Kaim, V. Kasack, Inorg. Chem. 29 (1990) 4696;

(d) R. Hage, J.G. Haasnoot, H.A. Nieuwenhuis, J. Reedijk, D.J.A. DeRidder, J.G. Vos, J. Am. Chem. Soc. 112 (1990) 9245.
[11] (a) R. Hage, J.G. Haasnoot, D.J. Stufkens, T.L. Snoeck, J. Reedijk, J.G. Vos, Inorg. Chem. 28 (1989) 1413;
(b) R. Hage, J.G. Haasnoot, H.A. Nieuwenhuis, J. Reedijk, D.J.A. de Ridder, J.G. Vos, J. Am. Chem. Soc. 112 (1990) 9245;
(c) F. Barigletti, L. DeCola, U. Balzani, R. Hage, J.G. Haasnoot, J. Reedijk, J.G. Vos, Inorg. Chem. 30 (1991) 641;
(d) J.H. van Dieman, R. Hage, J.G. Haasnoot, H.E.B. Lempers, J. Reedijk, J.G. Vos, L. DeCola, F. Barigelletti, V. Balzani, Inorg. Chem. 31 (1992) 3518;
(e) S. Serroni, S. Campagna, G. Denti, T.E. Keyes, J.G. Vos, Inorg. Chem. 35 (1996) 4513.
[12] D.P. Rillema, R. Sahai, P. Matthews, A.K. Edwards, R.J. Shaver, L. Morgan, Inorg. Chem. 29 (1990) 167.
[13] (a) M. Haga, M.M. Ali, H. Macgawa, K. Nozaki, A. Yoshimura, T. Ohno, Coord. Chem. Rev. 132 (1994) 99;
(b) M. Haga, T. Ano, T. Ishazaki, K. Kano, K. Nazaki, T. Ohno, J. Chem. Soc., Dalton Trans. (1994) 263;
(c) M. Haga, M.M. Ali, S. Koeski, A. Yoshimura, K. Nozaki, T. Ohno, Inorg. Chim. Acta 226 (1994) 17;
(d) T. Ohno, K. Nozaki, M. Haga, Inorg. Chem. 31 (1992) 4256;
(e) M. Haga, T. Ano, K. Kano, S. Yambe, Inorg. Chem. 30 (1991) 3843;
(f) M. Haga, A.M. Bond, Inorg. Chem. 30 (1991) 475.
[14] S. Baitalik, U. Flörke, K. Nag, J. Chem. Soc., Dalton Trans. (1999) 719.
[15] S. Baitalik, U. Flörke, K. Nag, Inorg. Chem. 38 (1999) 3296.
[16] P.A. Lay, A.M. Sargeson, H. Taube, Inorg. Synth. 24 (1986) 291.
[17] D.D. Perrin, B. Dempsey, Buffers for pH and Metal Ion Control, Chapman and Hall, London, 1974.
[18] A.J. Fry, W.E. Britton, in: P.T. Kissinger, W.R. Heineman (Eds.), Laboratory Techniques in Electroanalytical Chemistry, Marcel Dekker, New York, 1984.
[19] (a) E.C. Constable, K.R. Seddon, J. Chem. Soc., Chem. Commun. (1982) 34;
(b) P.J. Steel, F. Lahousse, D. Lerner, C. Marzin, Inorg. Chem. 22 (1983) 1488;
(c) R. Hage, J.G. Haasnoot, J. Reedijk, J.G. Vos, Inorg. Chim. Acta 118 (1986) 73;
(d) L.S. Kelso, D.A. Reitsma, F.R. Keene, Inorg. Chem. 35 (1996) 5144.
[20] J.S. Coleman, L.P. Varge, S.H. Mastin, Inorg. Chem. 9 (1970) 1013.
[21] J.N. Demas, B.A. DeGraff, Anal. Chem. 63 (1991) 8294.

special interest as certain ferric cytochromes having a FeS_6 moiety are associated with electron transport in biological systems and these are involved in spin equilibrium suggesting that spin state conversion is coupled to electron transport [11].

Thermal decomposition studies of iron(III) dithiocarbamates and related compounds have also attracted the attention of several workers [12,13]. Thermogravimetric studies of $[Fe(S_2CNEt_2)_3]$ by D'Ascenzo and Wendlendt [14] have shown this to be completely volatile, whereas Lanjewar and Garg [15] have reported volatile, non-volatile and partially volatile natures depending on symmetrical and unsymmetrical substituents. Earlier we had reported Mössbauer spectral, magnetic moment and thermal decomposition studies of some tris(*N*,*N*′-dialkyldithiocarbamato) iron(III) complexes wherein $Fe(SCN)_3$ was formed as an intermediate product [16].

In this paper we have reported the synthesis, IR spectral, variable temperature magnetic moment, Mössbauer spectral and thermal decomposition studies of the four unsymmetrically substituted complexes $[(OHCH_2CH_2)RNCS_2]_3Fe$ with R = CH_3, C_2H_5, *n*-C_3H_7 and *n*-C_4H_9. Also from the TGA plots, the kinetic and thermodynamic parameters were calculated using a Freeman and Carroll method [17].

2. Experimental

All the chemicals used were of analytical/guaranteed or high purity grade.

2.1. Preparation of the complexes

First the dithiocarbamate ligands were prepared as sodium salts by the reaction of the respective secondary amine in tetrahydrofuran with CS_2 and adding sodium hydroxide solution in equal mole ratio with vigorous stirring for 5–6 h at room temperature [16]. The crude product was recrystallized from methanol. The purity of ligands was checked by determining m.p. which matched well with the literature values. 4 g of ferric nitrate was dissolved in a minimum amount of absolute ethanol and then a calculated amount of sodium *N*-alkyl,*N*′-hydroxyethyldithiocarbamate was added with thorough stirring for 1–2 h at room temperature as described earlier [16]. In all cases a black coloured complex was formed. These were washed with water and dried diethyl ether and then dried over fused calcium chloride in a vacuum desiccator overnight. Elemental analysis of the complexes is given in Table 1.

2.2. Physical measurements

Mössbauer spectra were recorded using a constant acceleration transducer driven Mössbauer spectrometer (ECIL, Hyderabad) in conjunction with 1024 MCA (Canberra). A 25 mCi $^{57}Co(Rh)$ source procured from Amersham, UK was used. The spectrometer was calibrated using a natural iron foil as well as recrystallized sodium nitroprusside dihydrate (SNP) as standards at 295 K. The spectral data were least-square fitted. Magnetic moments were measured at room temperature (295 K) using a Vibrating Sample Magnetometer (VSM Model 155, Princeton Applied Research, USA). Thermograms were recorded on a thermogravimetric analyser system, STA-780 series (Stanton Redcroft, UK) at a heating rate of 10 °C min^{-1}. All the measurements were carried out in static air atmosphere using Al_2O_3 as reference material. IR spectra in the range 4000–400 cm^{-1} were recorded in KBr medium on a Perkin–Elmer 1600, FT-IR Spectrophotometer. Further spectra were also recorded down to 50 cm^{-1} at the RSIC, IIT-Madras.

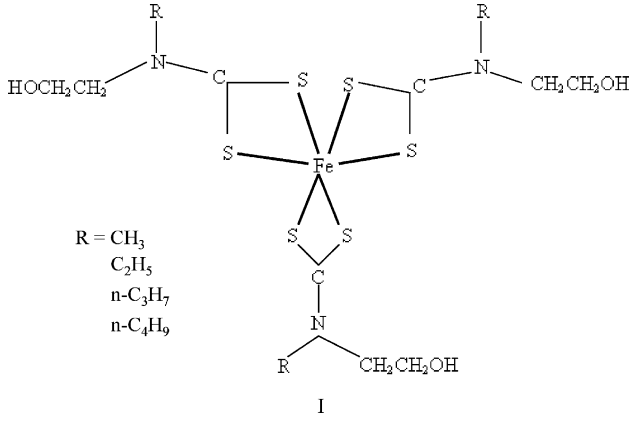
3. Results and discussion

All the four complexes were black solids, which are stable under normal atmospheric conditions. Typical Mössbauer spectra of the (*N*-methyl,*N*′-hydroxyethyldithiocarbamato) iron(III) complex from room temperature (295 K) down to liquid nitrogen temperature (77 K) are shown in Fig. 1. Mössbauer parameters derived from these spectra after fitting are listed in Table 2. Variation of magnetic moment with temperature in the 77–295 K range for all the complexes, are shown in Fig. 2. Typical thermograms (TG, DTG and DTA) of the complexes, $[(HOCH_2CH_2)RNCS_2]_3Fe$ having R = CH_3 and C_2H_5 are shown in Fig. 3. Thermogravimetric data and the kinetic and thermodynamic parameters for all the complexes are listed in Table 3.

Tris(*N*,*N*′-dialkyldithiocarbamato) iron(III) complexes have trigonally distorted octahedral geometry with six sulfur donor atoms surrounding the central iron(III) in D_3 symmetry with a twist angle φ varying from about 33° to 40°, depending on the nature of the alkyl group [18]. Earlier we had studied the crystal structure of the tris(*N*,*N*′-diallyl dithiocarbamato) iron(III) complex and confirmed that the crystals are monoclinic with space group $C2/c$ where $a = 18.737(5)$ Å, $b = 10.229(3)$ Å and $c = 15.571(3)$ Å and the angles $\alpha = 90°$, $\beta = 106.13°$ and $\gamma = 90°$. The bond lengths of Fe–S were found to be 2.3262, 2.3657 and 2.3488 Å and bond angles S–Fe–S were 74.25°, 90.48°, 94.58°, 97.99°, 98.93° and 160.09° [19]. Since the basic nature of the ligands remains the same, the molecular structure of the presently studied unsymmetrically substituted complexes is likely to remain similar and the possible structure may be represented as I.

Table 1
Analytical and infrared spectral data of tris(*N*-alkyl-*N*′-hydroxyethyldithiocarbamato) iron(III) complexes

Complex $[Fe(S_2CNR_1R_2)_3]$ $R_1 = CH_2CH_2OH$ and $R_2 =$	Analytical					Infrared				
	C (calc.)	H (calc.)	N (calc.)	S (calc.)	Fe (calc.)	$\nu_{(N=C)}$	$\nu_{(N\cdots C_2)}$	$\nu_{(C\cdots S)}$	$\nu_{(Fe-S)}$	
									HS	LS
$-CH_3$	28.46	4.74	8.30	37.94	11.07	1499	1190	985	233	332
	(27.98)	(4.71)	(8.38)	(36.54)	(10.89)			1279		
$-C_2H_5$	32.80	5.77	7.66	35.03	10.22	1492	1180	987	232	353
	(32.85)	(5.70)	(7.45)	(34.30)	(10.34)			1238		
n-C_3H_7	36.61	6.10	7.11	32.54	9.49	1493	1171	981	227	342
	(35.91)	(6.23)	(6.98)	(31.12)	(9.53)			1224		
n-C_4H_9	39.87	6.64	6.64	30.37	8.86	1496	1165	992	226	348
	(40.05)	(6.51)	(6.72)	(32.42)	(8.79)			1327		



I

3.1. Magnetic moment

Magnetic moment studies of dialkyldithiocarbamato iron(III) complexes have been reported by several workers [3–6]. On the basis of the room temperature magnetic moments, all the complexes are in a mixed spin state though these are predominantly in high spin state ($^6A_{1g}$). This suggests that the complexes exhibit high spin(HS)⇌low spin(LS) equilibria at room temperature. As the temperature is lowered it is converted more and more towards the low spin state ($^2T_{2g}$). This is quite evident from the plots of variation of magnetic moment with temperature as shown in Fig. 2. Also an interesting relationship seems to exist between the nature of alkyl group and the magnetic moment. Evidently as the carbon chain length increases from methyl to *n*-butyl, it tends to shift more towards a high spin state and the same trend is observed at all temperatures. Apparently this is due to an increase in the electron density on the Fe atom due to the positive inductive effect of the alkyl group.

3.2. IR spectra

The metal–ligand stretching band appearing in the far IR region provides information about the strength of the metal–ligand bond and the spin state of the system [20,21]. Ewald et al. [3] proposed the 300–400 cm^{-1} region for both the high and low spin states of the Fe–S stretching band. Butcher et al. [20] examined the far IR spectra of $Fe(R_2dtc)_3$ complexes using isotopic substitution, and assigned the high spin ν_{Fe-S} at a lower energy than that for the low spin mode, keeping both in the 300–400 cm^{-1} region. In a further investigation of far IR spectra of tris(*N*,*N*′-dialkyldithiocarbamato) iron(III) complexes using ^{54}Fe and ^{57}Fe isotopes, Hutchinson et al. [21] showed that high spin ν_{Fe-S} appears at 205–250 cm^{-1}, the low spin at 305–350 cm^{-1} and the intermediate spin ν_{Fe-S} in both regions. Various assignments for the IR stretching bands are listed in Table 1. On the basis of literature reports the ν_{Fe-S} stretching band in the 226–233 cm^{-1} region corresponds to the high spin state and another strong band in the 332–353 cm^{-1} region is attributed to the low spin state. Interestingly, intensities of the two bands corresponding to high and low spin states also vary depending on their contributions in the equilibrium mixture.

Besides ν_{Fe-S}, IR spectral assignments of other bands are also reported. Chatt et al. [22] suggested resonance structures on the basis of an intense band in the region 1550–1480 cm^{-1} due to a C···N stretching vibration. Bradley and Gitlitz [23] studied IR bands in several metal *N*,*N*′-dialkyldithiocarbamates and reported the thioureide (N···C) band near 1500 cm^{-1} as a characteristic of the ligand indicating considerable double bond character in the $(S_2)C\cdots N(R_2)$ bond. We have observed $\nu_{(N\cdots C)}$ in the 1492–1496 cm^{-1} region, which matches well with the literature value. Another strong band in the 1165–1190 cm^{-1} region may be attributed to $N-C_2$

for all the complexes. Strong bands at 981–992 cm^{-1} and 1224–1327 cm^{-1} due to $\nu_{(C_S)}$ are suggestive of the chelating character of the dithiocarbamate ligand in all cases [24].

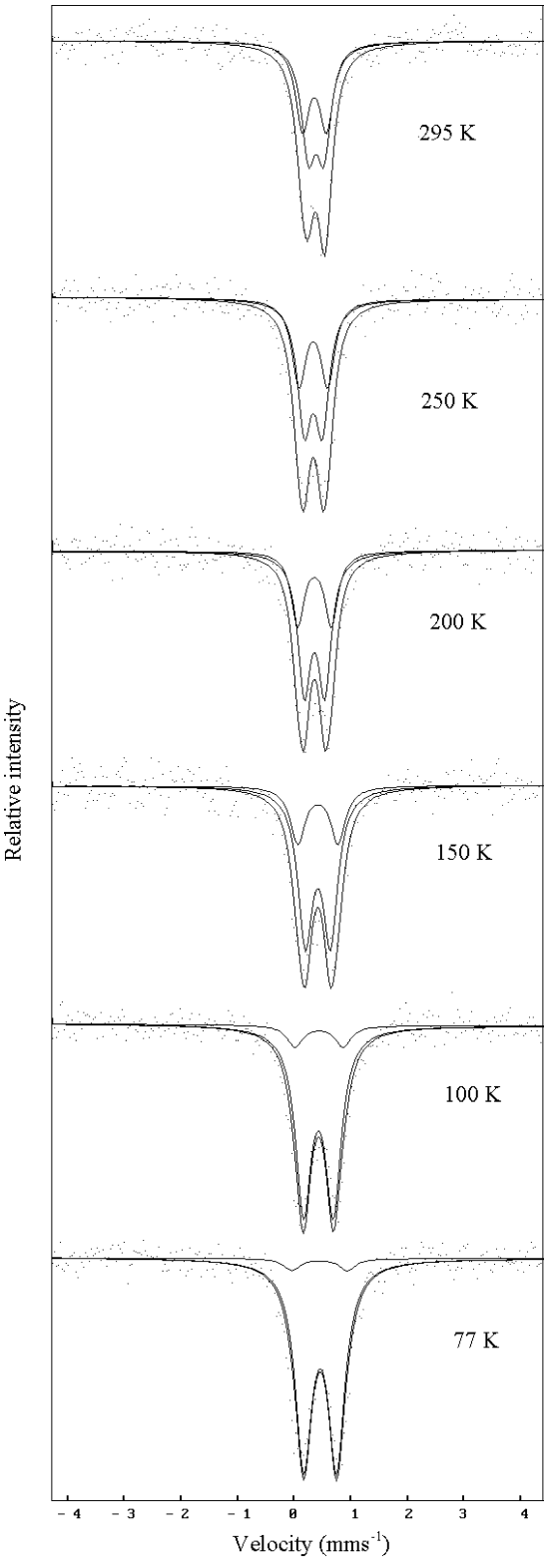


Fig. 1. Mössbauer spectra of the tris(*N*-methyl,*N*′-hydroxyethyldithiocarbamato) iron(III) complex at different temperatures.

An electronic spectrum of the complexes in acetone exhibits a strong band at 28 600 cm^{-1} which corresponds to charge transfer ($^2T_2 \rightarrow {}^4T_1$). Another weak band at 19 600 cm^{-1} is due to a spin forbidden *d*–*d* transition ($^2T_2 \rightarrow {}^2T_1$). These observations are in accordance with the literature [3].

3.3. Mössbauer spectra

Mössbauer spectra for all the complexes at 295 K exhibit an asymmetric doublet, which can be resolved into two doublets corresponding to low and high spin states. However, at temperatures ≤ 250 K the spectra become increasingly symmetric with large line widths. Typical Mössbauer spectra of tris(*N*-methyl,*N*′-hydroxyethyldithiocarbamato) iron(III) complex at various temperatures in Fig. 1 indicate two doublets corresponding to high and low spin states in equilibrium at 295 K and then the contribution of the HS state continuously decreases with the lowering of temperature. The isomer shift (δ) values for both spin states do not vary significantly. However, the quadrupole splitting (ΔE_Q) values for the low spin state are somewhat lower (0.27–0.44 mm s^{-1}) compared to that for the high spin state (0.42–0.59 mm s^{-1}). In general, the ΔE_Q value increases with decreasing temperature and on increasing the number of carbon atoms in the alkyl group attached to the N-atom of the ligand. Pandeya et al. [7] have claimed the largest ever reported $\Delta E_Q = 0.716$ mm s^{-1} at 300 K in the complex tris[bis(hydroxyethyl)dithiocarbamato)]iron(III) suggesting a large asymmetry of the ligand field. In the present study, since one of the hydroxyethyl groups has been replaced by alkyl groups, still larger asymmetry was expected. However, in Table 2 the largest value of ΔE_Q is 0.59 mm s^{-1} for tris(*N*-butyl,*N*′-hydroxyethyldithiocarbamato) iron(III) at 295 K which increases to 1.28 mm s^{-1} at 77 K. It seems asymmetric substitution at N-atoms does not necessarily mean more asymmetry at the central Fe atom.

In order to find out the correlation, ΔE_Q was plotted with the molecular weight of the alkyl group and it shows a linear increase in Fig. 4. Surprisingly ΔE_Q for both the spin states increases linearly with temperature. It is well known that by increasing the carbon chain length, the positive inductive effect of the alkyl group increases. This will result in an increase in *s*-electron density at the Fe nucleus by way of donation. On going down to 77 K all the complexes exhibit increasing tendency towards low spin state ($^2T_{2g}$). In fact Mössbauer spectral results confirm our observation of increasing contribution of the HS state with increasing carbon chain length. However, an opposite trend is observed for the LS state. Magnetic moments were also calculated on the basis of estimated percent contribu-

Table 2
Mössbauer parameters of high spin and low spin states in tris(*N*-alkyl,*N*′-hydroxyethyldithiocarbamato) iron(III) complexes and calculated magnetic moments

Complex $[Fe(S_2CNR_1R_2)_3]$ $R_1 = CH_2CH_2OH$ and $R_2 =$		High spin		Low spin		Estimated percentage of spin state		Magnetic moment [a] μ_{eff} (B.M.)
		δ [b] (mm s^{-1})	ΔE_Q (mm s^{-1})	δ [b] (mm s^{-1})	ΔE_Q (mm s^{-1})	HS	LS	
$-CH_3$	r.t.	0.39	0.42	0.42	0.27	45	55	3.53(3.61)
	150 K	0.45	0.71	0.45	0.44	27	73	2.80(2.86)
	77 K	0.48	0.98	0.49	0.58	6	94	1.87(1.98)
$-C_2H_5$	r.t.	0.37	0.48	0.39	0.31	61	39	4.17(4.28)
	150 K	0.43	0.82	0.43	0.56	29	71	2.87(2.94)
	77 K	0.45	1.11	0.45	0.75	17	83	2.37(2.44)
$-n$-C_3H_7	r.t.	0.36	0.52	0.32	0.38	65	35	4.37(4.45)
	150 K	0.44	0.88	0.45	0.58	34	66	3.02(3.15)
	77 K	0.46	1.21	0.46	0.81	22	78	2.57(2.65)
$-n$-C_4H_9	r.t.	0.36	0.59	0.34	0.44	70	30	4.58(4.66)
	150 K	0.45	0.92	0.45	0.61	37	63	3.18(3.28)
	77 K	0.47	1.28	0.47	0.84	26	74	2.78(2.82)

[a] In parentheses is μ_{eff} calculated on the basis of percent contributions of high and low spin states.
[b] With respect to iron as standard, ± 0.02 mm s^{-1}.

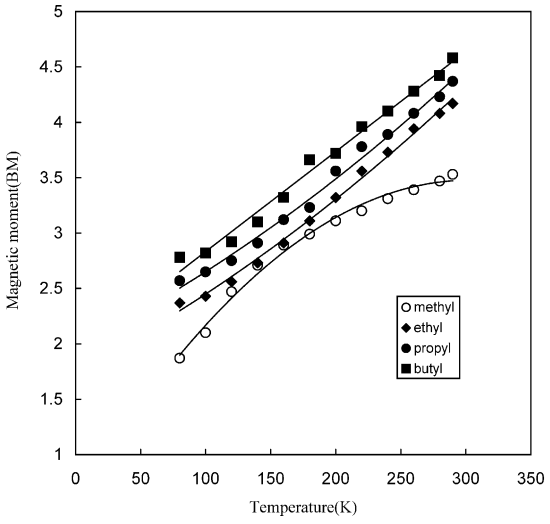


Fig. 2. Variation of magnetic moment with temperature for tris(*N*-alkyl,*N*′-hydroxyethyl-dithiocarbamato) iron(III) complexes.

tions of high and low spin states. The magnetic moments so calculated compare well with the experimentally determined values showing good agreement between Mössbauer spectral and magnetic moment data (Table 2).

3.4. Thermogravimetric studies

Thermogravimetric studies suggest that all the complexes, are stable up to ~140 °C, after which decomposition starts and the whole process is completed at ~650 °C in two stages. In all cases the first step is very fast, corresponding to 65–70% weight loss and it is completed up to ~350 °C, as can be seen in Fig. 3.

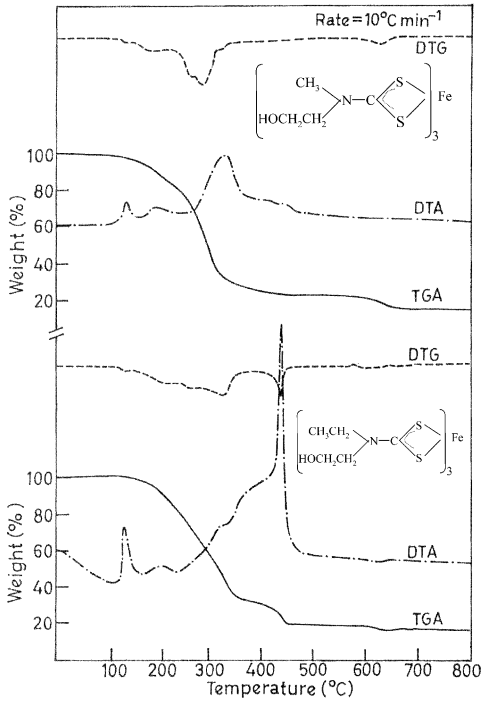


Fig. 3. TGA (—), DTG (-----) and DTA (- · · · -) plots for some typical iron(III) complexes.

Further decomposition takes place at ~550 °C and a constant weight is obtained at 610–650 °C (Table 3). In all the complexes, the final weight matches well with the expected weight of Fe_2O_3 and hence all the complexes can be grouped as non-volatile. In earlier reports there have been speculations about the formation of Fe_2S_3 [13,14] or a partially non-volatile group of complexes yielding 70–80% residual weight at 900 °C [15]. In the present studies no Fe_2S_3 is formed. Incidentally melting

Table 3
Thermogravimetric characteristics of tris(*N*-alkyl,*N*′-hydroxyethyldithiocarbamato) iron(III) complexes

Complex $[Fe(S_2CNR_1R_2)_3]$ $R_1 = CH_2CH_2OH$ and $R_2 =$	Initial decomposition temperature (°C)	DTA peak (°C)	Const. weight temperature (°C)	Final wt. [a] (%)	Activation energy (E_a) (kJ mol^{-1})	Order of reaction (n)	Rate constant ($k \times 10^3$) (s^{-1})	ΔH (kJ mol^{-1})	ΔG (kJ mol^{-1})	ΔS (J K^{-1} mol^{-1})
$-CH_3$	140	300, 169, 94	650	14.2 (15.8)	22.98	0.28	1.14	21.70	168.4	−266.7
C_2H_5	150	409, 192, 96	610	14.8 (14.6)	29.06	0.64	1.42	26.13	167.5	−257.0
C_3H_7	150	310, 237	640	13.8 (13.6)	55.48	0.99	5.68	50.92	160.9	−200.8
C_4H_9	170	428, 215	630	14.0 (12.7)	78.50	1.48	13.56	71.27	157.0	−155.1

[a] In parentheses is the expected weight % of Fe_2O_3 on the basis of formula weight.

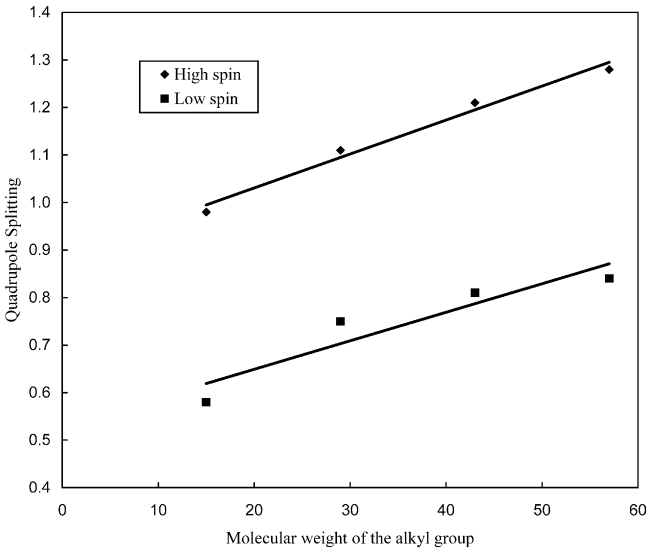


Fig. 4. Variation of quadrupole splitting with molecular weight of alkyl group for tris(*N*-alkyl,*N*′-hydroxyethyldithiocarbamato) iron(III) complexes.

points of all the complexes were observed in the range 170–240 °C whereas the first exothermic DTA peak is also observed in this temperature range only (Fig. 3). It suggests that the first stage of decomposition involves melting of the complex. In addition, another broad exotherm is observed at ~350 °C. Kaushik et al. [25] have attributed this to the conversion of iron sulfate to iron oxide. However, we could not identify the formation of iron sulfate as an intermediate though we had earlier confirmed the formation of $Fe(SCN)_3$ in some dithiocarbamates [16].

In order to identify the intermediate and final products, Mössbauer spectra were recorded after heating the complexes at 500 and 700 °C. Typical Mössbauer spectra for the tris(*N*-ethyl,*N*′-hydroxyethyldithiocarbamato) iron(III) complex after heating at these temperatures in Fig. 5 show that α-Fe_2O_3 starts forming at 500 °C as indicated by the appearance of a sextet with $H_{eff} = 517$ kOe and $\delta = 0.37$ mm s^{-1}. A centrally located doublet is also observed having $\delta = 0.39$ mm s^{-1} and $\Delta E_Q = 0.51$ mm s^{-1}. It suggests primarily an undecomposed compound in a high spin state. After further heating up to 700 °C the centrally located doublet disappears and a pure sextet is observed with $H_{eff} = 514$ kOe and $\delta = 0.39$ mm s^{-1}. These parameters correspond to that for α-Fe_2O_3 [26]. Therefore, no evidence was found for the formation of Fe_2S_3. Undoubtedly the decomposition of unsymmetrically substituted tris(*N*-alkyl,*N*′-hydroxyethyldithiocarbamato)iron(III) complexes is affected by the nature of alkyl substituents. However, intermediate products seem to be different although we had earlier confirmed it to be $Fe(SCN)_3$ [16]. Finally α-Fe_2O_3 is formed in all cases.

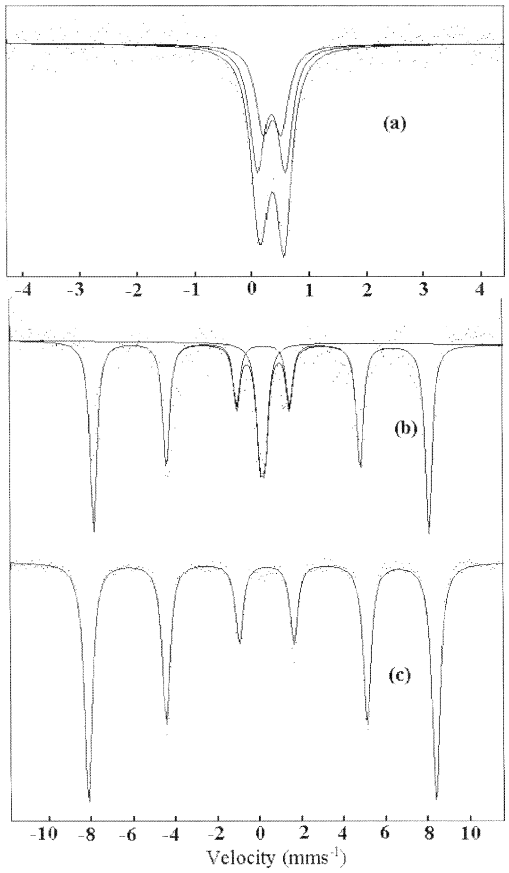


Fig. 5. Mössbauer spectra of the tris(*N*-ethyl,*N*′-hydroxyethyldithiocarbamato) iron(III) complex at r.t., after heating at (b) 500 °C and (c) 700 °C for 1 h.

From the thermograms of the complexes various kinetic and thermodynamic parameters were calculated using the Freeman and Carroll [17] method and these are given in Table 3. From the linear plots of [$\Delta\log(dw/dt)/\Delta\log w_r$] vs. $\Delta(1/T)/\Delta\log w_r$, the activation energy (E_a) and order of the reaction were calculated. The

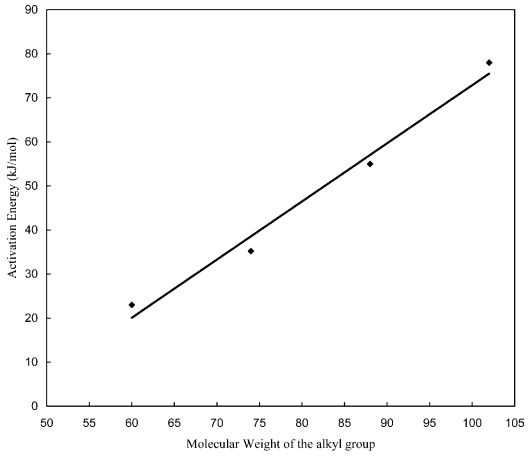


Fig. 6. Variation of the activation energy with molecular weight of alkyl group for tris(*N*-alkyl,*N*′-hydroxyethyldithiocarbamato) iron(III) complexes.

frequency factor ($\ln A$) was calculated from the intercept using the relationship:

$$\ln \frac{d\alpha/dt}{(1-\alpha)^n} = \ln A - \frac{E_a}{RT}$$

and then the rate constant was calculated. It is observed that all these parameters vary with the nature of the alkyl substituent suggesting strong dependence on the nature of the substituent. A perusal of data in Table 3 shows that the activation energy varies in a wide range of 22.98–78.50 kJ $mol^{-1}$and a linear correlation is observed between E_a and the molecular weight of the alkyl group as shown in Fig. 6. Incidentally these do not correlate with the spin state of the complexes. The order of the reaction of the complexes is in the range 0.28–1.48, well within unity suggesting intramolecular rearrangement. Similarly the rate of the reaction decreases as the molecular weight is increased as shown in Table 3. As the number of carbon atoms in the alkyl group is increased the electron density at the iron atom increases so that more energy is required to break the bond and the reaction becomes slower. Possibly this is due to positive inductive effect of the alkyl group causing increased polarity in the molecule. In other words as we move from CH_3 to the bulkier n-C_4H_9 group, the ionic character increases so that the Fe–S bond becomes stronger.

The activation thermodynamic parameters, namely enthalpy (ΔH), entropy (ΔS) and free energy (ΔG), were also evaluated (Table 3). The values of ΔS in all cases were found in the range -155.1 to -266.7 J K^{-1} mol^{-1}. This suggests that the decomposition process involves molecular rearrangement whereby a significant restriction is exerted on the vibrational degrees of freedom. However, during these processes an intermediate is likely to be formed which ultimately decomposes into α-Fe_2O_3 at ~ 700 °C in air atmosphere.

Acknowledgements

Grateful thanks are due to the Council of Scientific and Industrial Research, New Delhi for the award of a Senior Research Fellowship to S.S.

References

[1] P. Gütlich, J. Jung, Nuovo Cimento 18D (1996) 107.
[2] E. Konig, G. Ritter, S.K. Kulshershtha, Chem. Rev. 85 (1985) 219.
[3] A.H. Ewald, R.L. Martin, E. Sinn, A.H. White, Inorg. Chem. 8 (1969) 1837.
[4] R. Rickards, C.E. Johnson, H.A.O. Hill, J. Chem. Phys. 48 (1968) 5231.
[5] J.G. Leipoldt, P. Coppens, Inorg. Chem. 12 (1973) 2260.
[6] G.R. Hall, D.N. Hendrickson, Inorg. Chem. 15 (1976) 607.
[7] K.B. Pandeya, R. Singh, C. Prakash, J.S. Baijal, Inorg. Chem. 26 (1987) 3216.
[8] M. Kopf, D. Varech, J. Tuchagues, D. Mansuy, I. Artaud, J. Chem. Soc., Dalton Trans. 991 (1998).
[9] P.J.V. Koningsbruggen, Y. Garcia, O. Kahn, L. Fournes, H. Kooijman, A.L. Spek, J.G. Haasnoot, J. Moscovici, K. Provost, A. Michalowicz, F. Renz, P. Gutlich, Inorg. Chem. 39 (2000) 1891.
[10] P. Manikandan, K. Padmakumar, K.R. Justin Thomas, B. Varghese, H. Onodera, P.T. Manoharan, Inorg. Chem. 40 (2001) 6930.
[11] I. Morishima, T. Jizaka, J. Am. Chem. Soc. 96 (1974) 5239.
[12] J.O. Hill, R.J. Magee, Rev. Inorg. Chem. 4 (1981) 141.
[13] A.K. Sharma, Thermochim. Acta 104 (1986) 339.
[14] G. D'Ascenzo, W.W. Wendlendt, J. Inorg. Nucl. Chem. 32 (1970) 2431.
[15] R.B. Lanjewar, A.N. Garg, Polyhedron 12 (1993) 2619.
[16] S. Singhal, C.L. Sharma, A.N. Garg, K. Chandra, Transition Met. Chem. 26 (2001) 81.
[17] E.S. Freeman, B. Carroll, J. Phys. Chem. 62 (1958) 394.
[18] R.L. Martin, N.M. Rohde, G.B. Robertson, D. Taylor, J. Am. Chem. Soc. 96 (1974) 3647.
[19] S. Singhal, C.L. Sharma, A.N. Garg, K. Chandra, Eur. J. Inorg. Chem., submitted for publication.
[20] R.J. Butcher, J.R. Ferraro, E. Sinn, Inorg. Chem. 15 (1976) 2077.
[21] B. Hutchinson, P. Neill, A. Finkelstein, J. Takemato, Inorg. Chem. 20 (1981) 2000.
[22] J. Chatt, L.A. Puncanson, L.M. Veranzi, Nature 177 (1956) 1042.
[23] D.C. Bradley, M.H. Gitlitz, J. Chem. Soc., A 1152 (1969).
[24] F. Bonati, R. Ugo, J. Organomet. Chem. 10 (1967) 257.
[25] N.K. Kaushik, G.R. Chattwal, A.K. Sharma, J. Thermal. Anal. 26 (1983) 309.
[26] V.I. Gol'danskii, V.F. Belov, M.N. Devisheva, V.A. Trukhtanov, Soviet Phys.-JETP 22 (1966) 1149.

which are also used to build selective sensors [15]. In addition, many examples of alkali metal ion complexation by calix[4]arenes bearing complexing arms on the lower rim (particularly carbonyl derivatives) are known [16] as well as complexes uniting transition metal and alkali metal ions [17] and complexes with *p*-sulfonato derivatives of calix[4,5]arenes [18] and calix[6]arenes [19]. Considering the relative scarcity of simple calix[4]arenes (unsubstituted on the lower rim) used for the structural characterization of such complexes, these being reduced to *p-tert*-butylcalix[4]arene, *p-tert*-butyldihomooxacalix[4]arene and *p-tert*-butyltetrathiacalix[4]arene, we decided to investigate the complexes formed by the simplest member of this family, calix[4]arene, denoted LH_4 hereafter, in its anionic state and we report herein the synthesis and crystal structures of one sodium and two caesium ion complexes obtained in the course of this work. In the case of caesium, novel arrangements result from the absence of *para* substituents in the ligand.

2. Experimental

2.1. Synthesis

Calix[4]arene was synthesized as previously published [20].

2.1.1. $\{Na_2(LH_3)_2[(CH_3)_2CO]_3\}\cdot 2CHCl_3\cdot 2H_2O$ (**1**)

Calix[4]arene (500 mg, 1.18 mmol) was dissolved in a mixture of $CHCl_3$ (120 ml) and aq. NaOH 6 M (120 ml). After stirring for half an hour at room temperature (r.t.) a sevenfold excess of $NaNO_3$ (700 mg, 8.24 mmol) was added and the resulting mixture stirred for 2 h. The organic phase was then separated, evaporated to dryness and the product recrystallized from hot acetone, resulting in colourless crystals suitable for X-ray crystallography.

2.1.2. $[Cs(LH_3)(py)]$ (**2**)

Calix[4]arene (100 mg, 0.24 mmol) was dissolved in CH_3CN (100 ml) in the presence of a large excess of NaOH (1.5 g). The solution became light pink on refluxing. Cs_2CO_3 in excess (200 mg, 0.61 mmol) was then added and the resulting pink solution was further stirred for 1 h at r.t., then filtered. The solution was evaporated to dryness and recrystallized from pyridine, giving colourless single crystals suitable for X-ray crystallography on slow evaporation.

2.1.3. $[Cs_2(LH_3)_2(H_2O)]\cdot CH_3CN$ (**3**)

Calix[4]arene (110 mg, 0.26 mmol) was dissolved in $CHCl_3$ (50 ml) with a large excess of NEt_3 (4 ml). Cs_2CO_3 in excess (330 mg, 1.01 mmol) was then added and the resulting cloudy whitish solution was stirred for 1 h at r.t., then filtered. The solution was evaporated to dryness and recrystallized from CH_3CN, giving colourless single crystals suitable for X-ray crystallography on slow evaporation.

2.2. Crystallography

The data were collected on a Nonius Kappa-CCD area detector diffractometer [21] using graphite-monochromated Mo Kα radiation (0.71073 Å). The crystals were introduced in Lindemann glass capillaries with a protecting 'Paratone' oil (Exxon Chemical Ltd.) coating. The unit cell parameters were determined from the reflections collected on 10 frames and were then refined on all data. The data were processed with DENZO-SMN [22]. The structures were solved by direct methods with SHELXS-97 [23] and subsequent Fourier-difference synthesis and refined by full-matrix (compounds **2** and **3**) or blocked full-matrix (compound **1**) least-squares on F^2 with SHELXL-97 [24]. Absorption effects were empirically corrected with the program DELABS from PLATON [25]. All non-hydrogen atoms were refined with anisotropic displacement parameters. Special details for each compound are as follows.

2.2.1. Compound *1*

Some constraints have been applied, particularly on the badly resolved chloroform molecules. Phenolic and water protons were not found, nor introduced. All other protons were introduced at calculated positions as riding atoms, with an isotropic displacement parameter equal to 1.2 (CH, CH_2) or 1.5 (CH_3) times that of the parent atom.

2.2.2. Compound *2*

Constraints on displacement parameters have been applied for some atoms behaving badly on refinement. The phenolic protons were not found, nor introduced. All other protons were introduced at calculated positions as riding atoms, with an isotropic displacement parameter equal to 1.2 times that of the parent atom.

2.2.3. Compound *3*

The protons bound to the phenolic oxygen atoms have been found on the Fourier-difference map and introduced as riding atoms with an isotropic displacement parameter equal to 1.2 times that of the parent atom. All other protons (except those of the water molecule) were introduced at calculated positions as riding atoms, with an isotropic displacement parameter equal to 1.2 (CH, CH_2) or 1.5 (CH_3) times that of the parent atom.

Crystal data and refinement details are reported in Table 1. The molecular plots were drawn with SHELXTL [26]. All calculations were performed on a Silicon Graphics R5000 workstation.

Table 1
Crystal data and structure refinement details

	1	2	3
Empirical formula	$C_{67}H_{70}Cl_6Na_2O_{13}$	$C_{33}H_{28}CsNO_4$	$C_{58}H_{51}Cs_2NO_9$
M (g mol^{-1})	1341.91	635.47	1171.82
Temperature (K)	100(2)	100(2)	100(2)
Crystal system	triclinic	orthorhombic	monoclinic
Space group	$P\bar{1}$	$P2_12_12_1$	Cc
a (Å)	17.2328(17)	7.1288(10)	26.3258(18)
b (Å)	19.5644(13)	18.5462(17)	11.1154(8)
c (Å)	21.1940(18)	20.032(2)	17.7265(9)
α (°)	105.926(5)	90	90
β (°)	99.702(4)	90	111.824(4)
γ (°)	101.258(5)	90	90
V (Å^3)	6550(1)	2648.5(5)	4815.4(5)
Z	4	4	4
μ (mm^{-1})	0.338	1.439	1.576
Reflections collected	43 164	14 461	16 213
Observed reflections [$I > 2\sigma(I)$]	8718	1721	6746
Independent reflections	22 079	4599	8109
R_{int}	0.088	0.052	0.058
Parameters refined	1643	353	632
R_1	0.102	0.083	0.045
wR_2	0.234	0.153	0.090

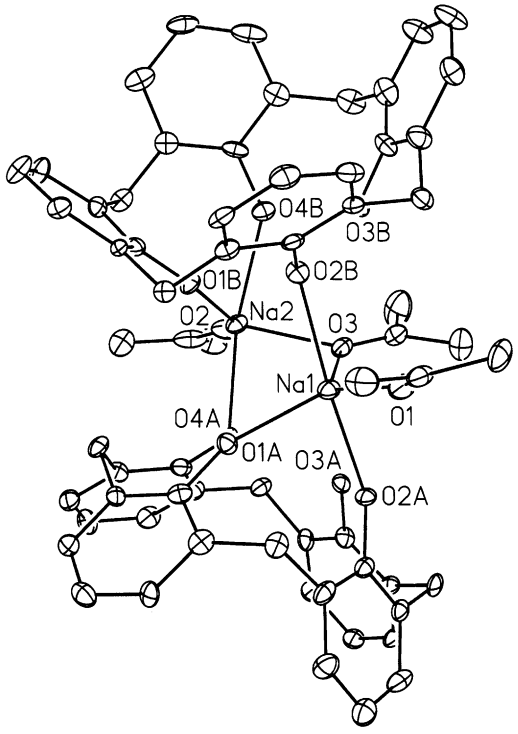


Fig. 1. View of one of the dimers in complex **1**. Hydrogen atoms and solvent molecules have been omitted for clarity. Thermal ellipsoids are drawn at the 30% probability level.

3. Discussion

The asymmetric unit in $\{Na_2(LH_3)_2[(CH_3)_2CO]_3\}\cdot 2CHCl_3\cdot 2H_2O$ (**1**) corresponds to two independent and nearly identical dimeric complexes, with calixarene molecules denoted A–B and C–D in the two dimers, respectively. As represented in Fig. 1 in the case of the A–B dimer, two mono-anionic calixarenes in *cone* conformation are bridged by two sodium ions, the coordination sphere of the latter being completed by three acetone molecules located in the median plane, two of them monodentate and one bridging. Each calixarene acts as a bidentate ligand towards one sodium ion and monodentate towards the other, the situation respective to each cation being reversed in the two calixarenes. In each molecule, the phenolic atom O3 is not bound to the cation, which results in the two calixarenes not being parallel to each other. The plane defined by the four oxygen atoms being taken as a reference plane the dihedral angles between these two planes in each dimer are 50.1(2) and 48.9(2)°, respectively, the distance between the two planes being the largest where they are separated by the bridging acetone molecule. The protons were not located in this rather large structure due to the limited data quality and it cannot be ascertained where the phenoxides are located. The Na–$O_{calixarene}$ distances, reported in Table 2, do not provide any clear-cut clue in this respect, being in the range 2.280(5)–2.518(6) [mean value 2.34(7)] Å, in agreement with published values. The O···O separations between adjacent phenolic groups are in the range 2.472(8)–2.905(8) Å, with however a difference between the O···O separations relative to the oxygen atoms coordinated to the same cation (O1 and O2 in molecules A and C, O1 and O4 in B and D) and all the other distances. The former are significantly larger, with a range 2.849(8)–2.905(8) Å and a mean value of 2.87(3) Å, than the latter, which are in the range 2.472(8)–2.684(8) [mean value 2.56(6)] Å. When taking in consideration the corresponding distances in complex **3**, in which the protons were located (vide infra), it can be concluded that the two atoms corresponding to the largest separation are both protonated and involved in strong hydrogen bonds with their other two neighbours, the phenoxide atom among the latter being probably the coordinated one. The dihedral angles between the reference O_4 planes and the mean planes defined by the aromatic rings are in the range 43.1(2)–72.4(2)°. The largest values, associated to the more 'vertical' aromatic rings, correspond in the four calixarenes to coordinated groups, and particularly to those bound to the same cation, while the lowest values, in all but one case, correspond to the uncoordinated group. It may be that the latter adopts a more 'horizontal' position due to the vicinity of the bridging acetone molecule. The three acetone molecules are located so that the three donating

Table 2
Selected distances (Å) and angles (°) in complexes **1**–**3**

1							
Na1–O1A	2.284(5)	Na2–O4A	2.339(5)	Na3–O1C	2.280(5)	Na4–O4C	2.309(5)
Na1–O2A	2.327(5)	Na2–O1B	2.320(5)	Na3–O2C	2.518(6)	Na4–O1D	2.308(5)
Na1–O2B	2.337(5)	Na2–O4B	2.391(5)	Na3–O2D	2.298(5)	Na4–O4D	2.375(5)
Na1–O1	2.206(6)	Na2–O2	2.234(5)	Na3–O4	2.300(5)	Na4–O5	2.334(5)
Na1–O3	2.394(5)	Na2–O3	2.368(5)	Na3–O6	2.357(5)	Na4–O6	2.457(5)
Na1···Na2	3.857(3)			Na3···Na4	4.001(4)		
O1A···O2A	2.876(8)	O1B···O2B	2.533(8)	O1C···O2C	2.849(9)	O1D···O2D	2.559(8)
O2A···O3A	2.602(8)	O2B···O3B	2.472(8)	O2C···O3C	2.684(8)	O2D···O3D	2.519(8)
O3A···O4A	2.481(8)	O3B···O4B	2.590(8)	O3C···O4C	2.520(9)	O3D···O4D	2.645(8)
O4A···O1A	2.523(7)	O4B···O1B	2.905(8)	O4C···O1C	2.541(8)	O4D···O1D	2.849(8)
2							
Cs–O1′ [a]	3.169(12)	Cs–O3	3.704(16)	Cs–N	3.098(16)		
O1···O2	2.56(2)	O2···O3	2.56(2)	O3···O4	2.77(2)	O4···O1	2.86(2)
3							
Cs1–O1B′ [b]	3.065(5)	Cs1–O1	2.97(3)	Cs2–O2A	3.361(6)	Cs2–O4A	3.283(8)
Cs1–O4B′ [b]	3.079(5)	Cs2–O1A	3.396(6)	Cs2–O3A	3.233(7)	Cs2–O2B	3.673(5)
O3A···O4A	2.91(1)	O1B···O4B	2.994(7)	O1′ [b]···O3B	2.71(1)		
O1A···O2A	2.491(9)	O1A–H1A	1.05	H1A···O2A	1.49	O1A–H1A···O2A	158.2
O3A···O2A	2.507(9)	O3A–H3A	0.76	H3A···O2A	1.76	O3A–H3A···O2A	170.9
O4A···O1A	2.819(10)	O4A–H4A	1.29	H4A···O1A	1.60	O4A–H4A···O1A	153.5
O1B···O2B	2.585(7)	O1B–H1B	1.06	H1B···O2B	1.54	O1B–H1B···O2B	169.5
O3B···O2B	2.457(6)	O3B–H3B	1.16	H3B···O2B	1.41	O3B–H3B···O2B	145.8
O4B···O3B	2.627(7)	O4B–H4B	0.89	H4B···O3B	1.75	O4B–H4B···O3B	169.2

[a] Symmetry code: $x-1, y, z$.
[b] Symmetry code: $x+0.5, 2.5-y, z+0.5$.

oxygen atoms are roughly located in a plane bisecting the two calixarene mean planes, with Na–O distances larger for the bridging species [mean value 2.39(4) Å] than for the other ones [mean value 2.27(6) Å]. The coordination geometry of the cation can be described as distorted trigonal bipyramidal, with, in the case of Na1 for instance, O1, O3 and O1A defining the equatorial plane and O2A and O2B the axial positions, with an O2A–Na1–O2B angle of 169.3(2)° (Fig. 1). The location of the solvent molecules is unremarkable, the water molecules being hydrogen bonded to each other, but not to the calixarene phenol/phenoxide oxygen atoms.

It is worth comparing this structure to those of sodium complexes of simple, parent calix[4]arenes and tetrathiacalix[4]arenes previously reported. In the presence of sodium hydride [4] or triethylamine [12] as deprotonating agent, mono-deprotonation of these ligands is always observed in the case of sodium complexation (the dianion has however been reported in the case of the 1,3-dimethyl ether derivative of *p-tert*-butylcalix[4]arene in the presence of sodium hydride [6]). All other conditions being equal, LiH leads to twofold deprotonation of *p-tert*-butylcalix[4]arene and NaH to mono-deprotonation [4]. This observation has been discussed on the basis of structural arguments [4] (see also Ref. [12]). The present result, with concentrated NaOH as a deprotonating agent, does not differ from the previous cases in this respect. It is however possible to generate higher deprotonation degrees, up to three and fourfold ones, in the presence of lithium amide [5] and butyl-lithium [7,8], respectively. The sodium cation/calixarene system appears to give very different complexes depending on the calixarene and conditions used. Central coordination by all four oxygen atoms is observed with the tetramethyl ether derivative of *p-tert*-butylcalix[4]arene [3] and *exo* coordination to two oxygen atoms with the parent *p-tert*-butylcalix[4]arene [4] and *p-tert*-butyltetrathiacalix[4]arene [12], with additional loose coordination to sulfur in the latter. Complex **1** is closer to the sodium-fused calixarene systems obtained with the 1,3-dimethyl ether derivative of *p-tert*-butylcalix[4]arene [6] or some mixed transition metal ion/sodium ion complexes of *p-tert*-butylcalix[4]arene [17]. The closest relative to **1** is however to be found in the potassium ion complex of *p-tert*-butyltetrathiacalix[4]arene [12], which is also a $M_2(LH_3)_2$ binuclear 'sandwich', with one singly coordinating, two chelating and one uncomplexed oxygen atoms in each calixarene and two coordinated diethylether and one bridging water molecules near the bisecting plane. Similar arrangements are thus obtained with either the smallest or the largest cation/calixarene pair (tetrathiacalix[4]arene being significantly more spacious than its methylene-linked counterpart), with however the difference of a higher coordination number in the case of K^+ ensured by bonding to sulfur.

The isolation of the complex [Cs(LH$_3$)(py)] **2** from a solution highly concentrated in sodium ions evidences a selectivity for caesium which has been demonstrated in the related case of *p-tert*-butylcalix[4]arene [2]. Compound **2** crystallizes with only one complex molecule in the asymmetric unit, but it appears to be a polymeric compound, as represented in Fig. 2. As in complex **1**, the calixarene in **2** is a mono-anion. As a common feature with the caesium complex of *p-tert*-butylcalix[4]arene, in which caesium π-bonding by a calixarene was structurally evidenced for the first time and in which the calixarene is also mono-anionic [10], the cation in **2** is complexed in an *endo* fashion, with likely π-bonding to the aromatic rings, but the absence of bulky *para* substituents results in novel features and overall arrangement. Whereas Cs^+ was located on the fourfold symmetry axis of *p-tert*-butylcalix[4]arene, it is located off-centre in **2**, the interactions with the four aromatic rings being quite dissymetric, with mean Cs···C distances of 4.3(4), 3.6(1), 4.0(4) and 3.6(1) Å and Cs···centroid distances of 4.14, 3.30, 3.79 and 3.35 Å for the four rings, respectively. The shortest Cs···C contacts for each ring are 3.78(2), 3.42(2), 3.55(2) and 3.45(2) Å, respectively, and they involve the carbon atoms bound to oxygen in rings 1 and 3 and either *ortho* or *meta* carbon atoms in rings 2 and 4. On the basis of these distances, the interactions with rings 2 and 4 at least can be considered as strong π-bonds (in the possible range of interactions from η_1 to η_6, these are closer to the latter). For comparison, the Cs···C distances were 3.545(3)–4.121(4) and 3.53(1)–4.17(1) Å and the Cs···centroid distances 3.57 and 3.61 Å in the complexes of *p-tert*-butylcalix[4]arene and *p-tert*-butyldihomooxacalix[4]arene, respectively (two aromatic rings only being involved in the latter). The cation in **2** is also bound to one phenolic (or phenoxide) oxygen atom of the calixarene in which it is included, with a Cs–O3 distance of 3.704(16) Å, larger than that observed for bonding to two oxygen atoms in the *p-tert*-butyldihomooxacalix[4]arene complex [3.422(7) Å], which may be due to the smaller cavity size and less shallow conformation of calix[4]arene preventing the cation from going deeper in the cavity, i.e. closer to the coordinated oxygen atom. However, a peculiar feature of complex **2** is that the cation is bound to one phenolic (or phenoxide) oxygen atom of the neighbouring molecule along the *a* axis, with a shorter Cs–O1′ distance of 3.169(12) Å. The cation coordination sphere is completed by a pyridine molecule located between the calixarene moieties. By contrast with the observation that solvents with high cation solvating ability, such as acetone or acetonitrile, are likely to withdraw Cs^+ from the calixarene cavity [11], acetonitrile has been used as the reaction solvent in the present case and pyridine, used for recrystallization, completes the coordination sphere, which suggests that **2** is a highly stable species. The resulting structure consists of polymeric chains directed along the *a* axis, the calixarenes being tilted with respect to this axis. The O···O separations, as in complex **1**, seem to indicate that O1 and O4 are both protonated, the phenoxide group corresponding either to O2 or O3, both involved in strong hydrogen bonds with all their neighbours. The dihedral angles between the four mean planes defined by the aromatic rings and the reference O_4 plane are 46.5(5), 58.4(5), 42.3(7) and 76.2(5)°, the two rings more strongly involved in π-bonding being more 'vertical' than the other ones. These dihedral angles are 57.4(1)° in the *p-tert*-butylcalix[4]arene complex and 25.4(3) (O-coordinated rings) and 68.7(3)° (polyhapto-coordinated rings) in the *p-tert*-butyldihomooxacalix[4]arene one.

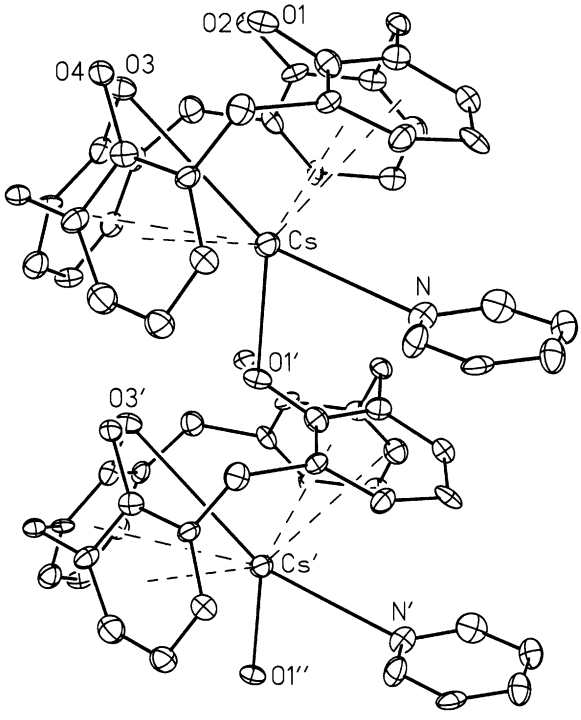


Fig. 2. Partial view of the columnar arrangement in complex **2**, *a* axis vertical. π-Bonding is indicated by dashed lines joining the cation and the aromatic ring centroids. Hydrogen atoms have been omitted for clarity. Thermal ellipsoids are drawn at the 10% probability level. Symmetry codes: $' = x-1, y, z$; $'' = x-2, y, z$.

Comparison of complex **2** with the two other caesium complexes of simple and small calixarenes, *p-tert*-butylcalix[4]arene and *p-tert*-butyldihomooxacalix[4]arene, evidences some interesting features (*p-tert*-butyltetrathiacalix[4]arene does not provide a relevant comparison since it complexes Cs^+ in an *exo* fashion, the soft sulfur donors being prefered to π-electrons). The distance between the cation and the O_4 reference plane can be taken as a measure of the depth of cation inclusion. This value is virtually identical in calix[4]arene and its *p-tert*-butyl derivative (3.56 and 3.57 Å, respectively) and it is significantly shorter in the homo-

oxacalixarene (3.06 Å), allowing for a stronger intramolecular O-coordination in the latter. Slight differences in conformation probably account for O-coordination by calix[4]arene and its absence in the *p*-*tert*-butyl derivative. O-coordination to a neighbouring calixarene in **2**, which can be seen as 'intermolecular' O-coordination for the sake of clarity, notwithstanding the ambiguity of this term in the present case, is very likely related to the absence of *p*-*tert*-butyl substituents, which enables a closer approach of the second anion. In the *p*-*tert*-butyl derivative, an acetonitrile molecule is located on the main axis of the calixarene, near its upper rim, and is coordinated to Cs^+. The distance between the cation and the mean plane defining (approximately) the border of the upper rim (aromatic carbon atoms in *para* position in **2**, terminal *tert*-butyl carbon atoms in the other complexes) is a parameter which gives some information on the accessibility of the cation towards *'intermolecular'* coordination. This parameter amounts to 0.23 Å in **2**, to be compared to 2.29 and 1.83 Å in the other two compounds. The cation is thus far more accessible in the former case, with approximately a free half-coordination sphere.

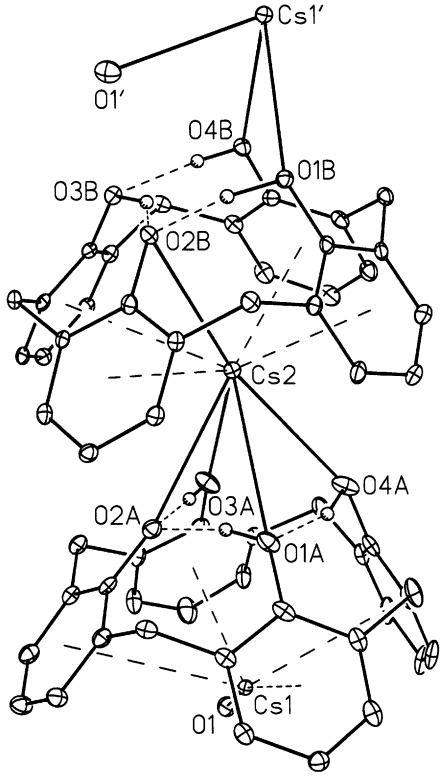


Fig. 3. Partial view of the columnar arrangement parallel to the (101) direction in complex **3**. π-Bonding is indicated by dashed lines joining the cation and the aromatic ring centroids. Hydrogen bonds are represented as dashed lines and phenolic protons as small spheres of arbitrary radii. Other hydrogen atoms and solvent molecules are omitted for clarity. Thermal ellipsoids are drawn at the 10% probability level. Symmetry code: $' = x-0.5, 2.5-y, z-0.5$.

A similar situation arises in $[Cs_2(LH_3)_2(H_2O)]\cdot CH_3CN$ (**3**). This complex, obtained with triethylamine as a deprotonating agent, crystallizes with two independent caesium ions and two calixarene mono-anions, denoted A and B, in the repeat unit (it may be noted that in its triethylammonium ion complexes, calix[4]arene is also mono-deprotonated [27]). As shown in Fig. 3, the overall shape, with formation of polymeric chains parallel to the (101) direction from units related by the glide plane perpendicular to the *b* axis, is roughly analogous to that of complex **2**, but the details are quite different. The two caesium ions are not equivalent in what concerns their environment. Both of them are located in the cavity of a calixarene moiety and are involved in polyhapto bonding. The mean Cs···C distances are 3.9(3), 4.0(3), 3.9(2) and 3.7(4) Å in the case of Cs1 and the four aromatic rings of calixarene A, with the corresponding shortest contacts of 3.530(7), 3.540(7), 3.652(7) and 3.637(8) Å and Cs···centroid distances of 3.61, 3.73, 3.69 and 3.41 Å. In the case of Cs2 and the four aromatic rings of calixarene B, the mean distances are 3.74(9), 4.1(4), 4.0(3) and 3.71(8) Å, the shortest contacts 3.639(7), 3.518(7), 3.558(6) and 3.596(7) Å and the Cs···centroid distances 3.47, 3.89, 3.71 and 3.44 Å. π-Bonding is obvious in both cases, the four rings being differently involved, as in compound **2**. Cs1 is further bound to two phenolic oxygen atoms of a neighbouring calixarene, with a mean Cs–O distance of 3.07(1) Å, slightly shorter than its counterpart in complex **2** and it is also bound to a water molecule (O1) located in a similar manner as the pyridine molecule in **2**. No bond between Cs1 and the oxygen atoms of the calixarene in which it is included is observed, at variance with the previous complex. By contrast, Cs2 is bound to one such oxygen atom, with a bond length of 3.673(5) Å comparable to its equivalent in **2**, and it is also bound to the four oxygen atoms of the neighbouring calixarene, with a much larger mean Cs–O bond length of 3.9(3) Å. The distances between caesium ions and the mean planes defining the borders of the lower and upper rims (O_4 in the first case) are 3.559(3) and 0.144(5) Å for Cs1 and calixarene A and 3.520(3) and 0.145(4) Å for Cs2 and calixarene B, i.e. in both cases the cation is even closer to the upper rim than in complex **2**. The dihedral angles between the aromatic rings and the reference O_4 plane are 52.9(2), 44.3(3), 58.8(3) and 73.7(2)° in calixarene A and 68.2(2), 37.4(3), 48.1(2) and 70.8(2)° in calixarene B, both sets of values indicating a distorsion of the *cone* conformation analogous to that in complex **2**. The dihedral angle between the two reference O_4 planes is 13.0(4)°, indicating a slight deviation of the calixarene units with respect to parallelism. By contrast with the structures of complexes **1** and **2**, the phenolic protons can be located in that of **3**. In both molecules A and B, the phenoxide oxygen atom is O2, which is involved in strong hydrogen bonds with

its two neighbours (Table 2). A possible hydrogen bond links the water molecule and O3B of the neighbouring calixarene.

Apart from the differences between complexes **2** and **3** with regards to O-coordination, the same polymeric structure is found, with a stacking of alternate cations and anions, the latter all pointing towards the same direction. To the best of our knowledge, this peculiar arrangement has never been observed in alkali metal ion complexes of *p*-*R*-calix[4]arene and its derivatives. The lack of *p*-alkyl substituents in the present cases enables the cation enclosed in the calixarene cavity to be easily complexed through the upper rim aperture by a bulky species such as a second calixarene moiety. Although stacking of uncomplexed calixarenes in columns held by feeble interactions is known, the present results show that novel tightly linked polymeric chain assemblages can be obtained from alkali-metal ions and one of the simplest calixarenes.

4. Supplementary material

Crystallographic data for the structural analysis have been deposited with the Cambridge Crystallographic Data Centre, CCDC no. 187709–187711 for compounds **1**, **2** and **3**, respectively. Copies of this information may be obtained free of charge from The Director, CCDC, 12 Union Road, Cambridge CB2 1EZ, UK (Fax: +44-1223-336033; e-mail: deposit@ccdc.cam.ac.uk or www: http://www.ccdc.cam.ac.uk).

References

[1] C.D. Gutsche, in: Z. Asfari, V. Böhmer, J. Harrowfield, J. Vicens (Eds.), Calixarenes 2001 (Chapter 1), Kluwer Academic Publishers, Dordrecht, 2001, pp. 1–25.

[2] R.M. Izatt, J.D. Lamb, R.T. Hawkins, P.R. Brown, S.R. Izatt, J.J. Christensen, J. Am. Chem. Soc. 105 (1983) 1782.

[3] S.G. Bott, A.W. Coleman, J.L. Atwood, J. Am. Chem. Soc. 108 (1986) 1709.

[4] F. Hamada, K.D. Robinson, G.W. Orr, J.L. Atwood, Supra. Chem. 2 (1993) 19.

[5] H. Bock, A. John, C. Näther, Z. Havlas, J. Am. Chem. Soc. 117 (1995) 9367.

[6] S.R. Dubberley, A.J. Blake, P. Mountford, Chem. Commun. (1997) 1603.

[7] M.G. Davidson, J.A.K. Howard, S. Lamb, C.W. Lehmann, Chem. Commun. (1997) 1607.

[8] G. Guillemot, E. Solari, C. Rizzoli, C. Floriani, Chem. Eur. J. 8 (2002) 2072.

[9] N.P. Clague, W. Clegg, S.J. Coles, J.D. Crane, D.J. Moreton, E. Sinn, S.J. Teat, N.A. Young, Chem. Commun. (1999) 379.

[10] J.M. Harrowfield, M.I. Ogden, W.R. Richmond, A.H. White, J. Chem. Soc., Chem. Commun. (1991) 1159.

[11] R. Assmus, V. Böhmer, J.M. Harrowfield, M.I. Ogden, W.R. Richmond, B.W. Skelton, A.H. White, J. Chem. Soc., Dalton Trans. (1993) 2427.

[12] A. Bilyk, A.K. Hall, J.M. Harrowfield, M.W. Hosseini, B.W. Skelton, A.H. White, Inorg. Chem. 40 (2001) 672.

[13] B.W.F. Gordon, M.J. Scott, Inorg. Chim. Acta 297 (2000) 206.

[14] For reviews on this topic, see: (a) P. Thuéry, M. Nierlich, V. Lamare, J.F. Dozol, Z. Asfari, J. Vicens, J. Incl. Phenom. 36 (2000) 375;
(b) A. Casnati, R. Ungaro, Z. Asfari, J. Vicens, in: Z. Asfari, V. Böhmer, J. Harrowfield, J. Vicens (Eds.), Calixarenes 2001, Kluwer Academic Publishers, Dordrecht, 2001 (Chapter 20), pp. 365–384;
(c) F. Arnaud-Neu, M.J. Schwing-Weill, J.F. Dozol, in: Z. Asfari, V. Böhmer, J. Harrowfield, J. Vicens (Eds.), Calixarenes 2001, Kluwer Academic Publishers, Dordrecht, 2001 (Chapter 35), pp. 642–662.

[15] H.F. Ji, R. Dabestani, G.M. Brown, R.L. Hettich, J. Chem. Soc., Perkin Trans. 2 (2001) 585 (and references therein).

[16] F. Arnaud-Neu, M.A. McKervey, M.J. Schwing-Weill, in: Z. Asfari, V. Böhmer, J. Harrowfield, J. Vicens (Eds.), Calixarenes 2001 (Chapter 21, and references therein), Kluwer Academic Publishers, Dordrecht, 2001, pp. 385–406.

[17] C. Floriani, R. Floriani-Moro, in: Z. Asfari, V. Böhmer, J. Harrowfield, J. Vicens (Eds.), Calixarenes 2001 (Chapter 29, and references therein), Kluwer Academic Publishers, Dordrecht, 2001, pp. 536–560.

[18] J.L. Atwood, L.J. Barbour, M.J. Hardie, C.L. Raston, Coord. Chem. Rev. 222 (2001) 3 (and references therein).

[19] Z. Asfari, J. Harrowfield, P. Thuéry, J. Vicens, Supra. Chem., in the press.

[20] R. Ungaro, A. Pochini, J. Chem. Soc., Perkin Trans. 2 (1984) 1979.

[21] Kappa-CCD Software, Nonius B.V., Delft, 1998.

[22] Z. Otwinowski, W. Minor, Methods Enzymol. 276 (1997) 307.

[23] G.M. Sheldrick, Acta Crystallogr., Sect. A 46 (1990) 467.

[24] G.M. Sheldrick, SHELXL-97, Program for the Refinement of Crystal Structures, University of Göttingen, 1997.

[25] A.L. Spek, PLATON, University of Utrecht, 2000.

[26] G.M. Sheldrick, SHELXTL, Version 5.1, University of Göttingen, distributed by Bruker AXS Inc., Madison, WI, 1999.

[27] P. Thuéry, Z. Asfari, M. Nierlich, J. Vicens, Acta Crystallogr., Sect. C 58 (2002) o223.

products but others are also formed in variable amounts, as was shown by IR and NMR investigation of the reaction mixture. From this mixture one new compound was isolated in crystalline form. This prompted us to conduct a structural examination of this novel norbornadiene complex, [Mo(μ-Cl)($SnCl_3$)$(CO)_2$(η^4-C_7H_8)(NCMe)] (**3**). To the best of our knowledge, up to now only three molybdenum(II) compounds containing norbornadiene ligands, [$MoBr_2$(CO)(η^4-C_7H_8)(bpy)] [9], [MoBr(CO)(η^4-C_7H_8)(terpy)]SbF_6 [10] and [Mo(μ-Cl)($SnCl_3$)$(CO)_3$(η^4-C_7H_8)] (**2**) [7], have been analysed by X-ray diffraction studies.

Additionally, we were especially intrigued by the possibility that the seven-coordinate molybdenum(II) and tungsten(II) compounds containing norbornadiene ligands could initiate ROMP of cyclic olefins and the rearrangement mechanism of the coordinated alkene to the alkylidene species initiating the catalytic reaction.

2. Experimental

2.1. General data

All reactions were carried out under nitrogen by standard Schlenk line techniques. The solvents and reagents applied were dried, distilled and stored in air-tight solvent bulbs with Teflon closures. Solution IR spectra were obtained using KBr or NaCl plates whereas solid samples were recorded using KBr pellets on a Nicolet model-400 FT-IR instrument. ^{1}H, ^{13}C, ^{13}C{^{1}H} and two-dimensional correlation ^{1}H–^{1}H, and ^{1}H–^{13}C NMR spectra were recorded on an AMX 300 and 500 MHz Brucker spectrometer. All chemical shifts are referenced to solvent signals. In ^{1}H NMR spectra $\delta_H = 1.98$ for CD_3CN, $\delta_H = 5.32$ for CD_2Cl_2 and $\delta_H = 7.24$ for $CDCl_3$. In ^{13}C NMR spectra $\delta_C = 118.00$ for CD_3CN, $\delta_C = 54.00$ for CD_2Cl_2 and $\delta_C = 77.00$ for $CDCl_3$.

2.2. Synthesis of [Mo(μ-Cl)($SnCl_3$)$(CO)_2$(η^4-C_7H_8)(NCMe)] (3)

A solution of the complex [Mo(μ-Cl)($SnCl_3$)$(CO)_3$($NCMe)_2$] (**1**) [11] (0.25 g, 0.48 mmol) and NBD (0.1 cm^3, 0.9 mmol) in CH_2Cl_2 (50 cm^3) was stirred under an atmosphere of nitrogen at room temperature (r.t.) for 96 h. The orange–yellow solution was layered with $C_6H_5CH_3$ (2 cm^3) and n-C_7H_{16} (12 cm^3) and put into a refrigerator. After 2 weeks orange crystals of [Mo(μ-Cl)($SnCl_3$)$(CO)_2$(η^4-C_7H_8)(NCMe)] (**3**) were obtained (0.16 g, 60%). The solution was removed and the crystals were washed several times with n-C_7H_{16} to separate a greenish–yellow powder of other molybdenum compound.

Anal. Calc. for $C_{11}H_{11}Cl_4MoNO_2Sn$: C, 24.21; H, 2.03; N, 2.57%. Found: C, 24.18; H, 2.10; N, 2.50%. IR (cm^{-1}, KBr disc): 2291 (vw) ν(CN), 2012 (s), 1963 (s) ν(CO); ^{1}H NMR (δ_H, ppm, CD_2Cl_2, 293 K): 5.43 (t, $J_{HH} = 3.7$ Hz, $^1J_{CH} = 182$ Hz, =C*H*), 4.84 (t, $J_{HH} = 4.0$ Hz, $^1J_{CH} = 182$ Hz, =C*H*), 4.00 (t, $J_{HH} = 4.5$ Hz, $^1J_{CH} = 180$ Hz, =C*H*), 3.91 (t, $J_{HH} = 4.6$ Hz, =C*H*), 3.81 (broad s, C*H*), 3.76 (broad s, C*H*), 2.46 (CH_3CN), 1.77 (m, CH_2); ^{13}C{^{1}H} NMR (δ_C, ppm, CD_2Cl_2, 293 K): 219.67, 214.17 (*C*O), 128.45 (CH_3*C*N), 96.00, 94.07, 53.86, 52.31 (=*C*H), 62.09 (*C*H_2), 45.67, 45.42 (*C*H), 4.83 (*C*H_3CN).

2.3. Synthesis of [Mo($SnCl_3$)$_2$(CO)(η^4-C_7H_8)($NCMe)_2$] (4)

A solution of complex **1** (0.20 g, 0.38 mmol) and NBD (0.1 cm^3, 0.9 mmol) in CH_2Cl_2 (25 cm^3) was stirred under an atmosphere of nitrogen at r.t. for 1 week. During that time a greenish–yellow precipitate was settled out. It was separated by filtration, washed with CH_2Cl_2 and dried. After crystallisation from MeCN, the compound was identified as [Mo($SnCl_3$)$_2$(CO)(η^4-C_7H_8)($NCMe)_2$] (**4**) (0.1 g, 35%). *Anal*. Calc. for $C_{12}H_{14}Cl_6MoN_2OSn_2$ C, 19.26; H, 1.89; N, 3.74. Found: C, 18.94; H, 2.05; N, 4.07%. IR (cm^{-1}, KBr disc): 2320 (w), 2291 (w), ν(CN), 1961 (s) ν(CO); ^{1}H NMR (δ_H, ppm, CD_3CN, 293 K): 4.43 (t, $J_{HH} = 4.3$ Hz, =C*H*), 4.04 (t, $J_{HH} = 4.3$ Hz, =C*H*), 3.72 (broad s, C*H*), 3.65 (broad s, C*H*), 2.45, 2.42 (CH_3CN), 1.67 (CH_2); ^{13}C NMR (δ_C, ppm, CD_3CN, 293 K): 215.23 (*C*O), 129.45, 126.39 (CH_3*C*N), 70.31 (dt, $^1J_{CH} = 186$ Hz, $^3J_{CH} = 6$ Hz, =*C*H), 68.31 (dt, $^1J_{CH} = 185$ Hz, $^3J_{CH} = 6$ Hz, =*C*H), 60.29 (t, $^1J_{CH} = 135$ Hz, *C*H_2), 43.52 (d, $^1J_{CH} = 155$ Hz, *C*H), 42.73 (d, $^1J_{CH} = 155$ Hz, *C*H), 4.74 (*C*H_3CN).

2.4. Crystal and refinement data for compound 3

Crystal data and relevant refinement details are presented in Table 1. The orange–yellow crystals of **3** were grown from a CH_2Cl_2–$C_6H_5CH_3$–n-C_7H_{16} (5:0.2:1.2) solution. The crystals were stable enough when handled in an inert atmosphere or coated with a light-hydrocarbon oil to protect them from the atmosphere.

Crystal data for **3** were collected on a Kuma KM4CCD κ-axis diffractometer with graphite-monochromated Mo Kα radiation, μ(Mo Kα) = 2.848 mm^{-1}. The data were corrected for Lp effects. After refinement with isotropic displacement parameters for all atoms, an absorption correction based on the least-squares filled against $|F_c| - |F_o|$ differences was also applied [12]. Minimum and maximum value of the absorption correction factors ranging between 0.7875 and 1.1842. Data reduction and analysis were carried out with

Table 1
Crystal data and structure refinement for [Mo(μ-Cl)($SnCl_3$)(CO)$_2$(η^4-C_7H_8)(NCMe)] (**3**)

Chemical formula	$C_{11}H_{11}Cl_4MoNO_2Sn$
Molecular weight	545.64
Temperature (K)	100(1)
λ(Mo Kα) (Å)	0.71073
Crystal system	monoclinic
Space group	$P2_1/c$
Unit cell dimensions	
a (Å)	8.773(2)
b (Å)	7.538(2)
c (Å)	25.596(5)
β (°)	92.50(3)
V (Å^3)	1691.1(6)
Z	4
D_{calc} (g cm^{-3})	2.143
μ(Mo Kα) (mm^{-1})	2.848
F(000)	1040
Crystal size (mm)	0.10 × 0.10 × 0.13
Method of collection	$\omega-2\theta$ scan
2θ Range for data collection (°)	$7.3 < 2\theta < 50.0$
Index ranges	$-9 \le h \le 10$, $-8 \le k \le 7$, $-29 \le l \le 30$
Collected/unique data	9299/2953
Data with [$I \le 2\sigma(I)$]	2676/225
Absorption correction factors, min/max	0.7875/1.1842
Refinement method	Full-matrix least-squares on F^2
Residuals R_1, wR_2	0.0613, 0.0704
Goodness-of-fit on F^2	1.320
Final ($\Delta\rho$) (e Å^{-3})	0.789/−0.779

KUMA DIFFRACTION (Wrocław) programs. The structure was solved by heavy-atom methods using the SHELXS-97 program [13] and refined by the full-matrix least-squares method on all F^2 data using the SHELXL-97 program [14] to $R_1 = 0.0613$, $wR_2 = 0.0704$. Hydrogen atoms were included from geometry of molecules. During the refinement they were treated as rigid groups with fixed interatomic distances.

2.5. Reactions in NMR tubes

2.5.1. Decomposition of compound 3 in $CDCl_3$

The solution of compound **3** (0.01 g, 0.018 mmol) in $CDCl_3$ (0.5 cm^3) was periodically analysed by ^{1}H NMR spectroscopy over a period of several days at r.t. The decay of signals due to compound **3** and the formation of an amorphous greenish–yellow precipitate were observed. The ^{1}H NMR spectrum of this solid in CD_3CN solution shows signals due to compound **4** (see Section 2.3) and other proton signals at $\delta_H = 4.12$, 3.79 (t, $J_{HH} = 4.4$ Hz, =C*H*), 3.63, 3.56 (broad s, C*H*), 1.62 (CH_2) assigned to the compound [$MoCl_2$(CO)(η^4-C_7H_8)(NCMe)$_2$] (**5**). In the ^{13}C{^{1}H} NMR spectrum, carbon signals at 68.31, 43.00 (=*C*H), 59.21 (*C*H$_2$), 42.80, 41.88 (*C*H) due to compound **5** were detected. The proper assignment of these resonances was possible due to the correlation of ^{1}H–^{1}H and ^{1}H–^{13}C NMR spectra.

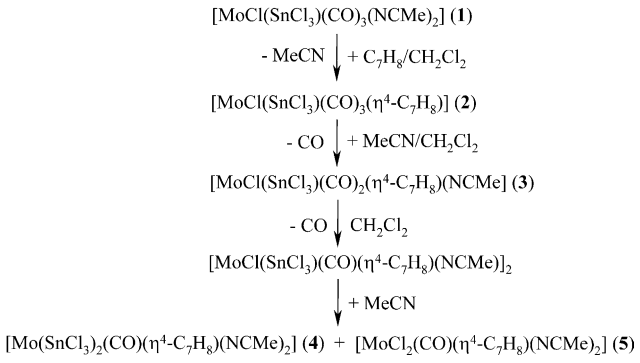
2.5.2. Reaction of compound 3 with NBD in CD_2Cl_2

To the NMR tube containing the solution of compound **3** (0.04 g, 0.073 mmol) in CD_2Cl_2 (0.5 cm^3) were added 10 equiv. of NBD (0.06 cm^3, 0.73 mmol) by means of a syringe and a sample was periodically analysed by ^{1}H NMR spectroscopy at r.t. A decrease in the intensity of proton signals due to **3** and increase in the intensity of proton signals due to polynorbornadiene (poly-NBD) at $\delta_H = 5.60$, 5.57, 5.37, 5.20 (=C*H*), 3.64, 3.24 (C*H*), 2.33 and 1.23 (CH_2) was parallel with the appearance of signals at $\delta_H = 10.49$ (broad s), 6.21 (dd, $J_{HH} = 5.6$ and 3.0 Hz), 5.99 (dd, $J_{HH} = 5.6$ and 3.0 Hz), 2.94 (broad s) and 2.86 (broad s), which can be assigned to an alkylidene ligand deriving from the transformation of an NBD ligand.

3. Results and discussion

3.1. Reaction of [Mo(μ-Cl)($SnCl_3$)(CO)$_3$(NCMe)$_2$] (1) with NBD

In reaction of [Mo(μ-Cl)($SnCl_3$)(CO)$_3$(NCMe)$_2$] (**1**) with NBD monitored by IR spectra in dichloromethane solution, the formation of [Mo(μ-Cl)($SnCl_3$)(CO)$_3$(η^4-C_7H_8)] (**2**) is observed due to a characteristic weak ν(CO) band at approximately 2090 cm^{-1} [7] from the beginning of the reaction. After prolonged reaction time this band decays and other ν(CO) bands appear at lower frequencies and increase. During a slow crystallisation process the compound [Mo(μ-Cl)($SnCl_3$)(CO)$_2$(η^4-C_7H_8)(NCMe)] (**3**) is separated from the reaction mixture in a pure crystalline form. In the IR spectrum of **3** two equal-intensity ν(CO) bands at 2012 and 1963 cm^{-1} are observed, indicating the *cis* arrangement of the two CO ligands. Compound **3** is the first example of a Group 6 metal(II), a norbornadiene complex, in which such an arrangement of two CO groups is observed. Up to now only compounds with two mutually *trans* CO groups, such as [WBr_2(CO)$_2$(η^4-C_7H_8)] [15], [WBr(SC_6F_5)(CO)$_2$(η^4-C_7H_8)] [16] and [WBr_2(CO)$_2$(η^4-C_7H_8)(PMePh_2)] [17], have been characterised by X-ray diffraction studies. In the IR spectra of these and other bis(carbonyl) compounds one weak and one strong ν(CO) band has been observed [9,15–17]. However, compound **3** is unstable in CH_2Cl_2 solution and decomposes losing the CO ligand. This process is accompanied by the decay of the ν(CO) bands characteristic for **3** and an increase in one strong band at about 1970 cm^{-1} in CH_2Cl_2 solution. Simultaneously, a greenish–yellow precipitate is formed. It is soluble only in coordinating solvents such as acetonitrile. After recrystallisation from MeCN, a new compound was



Scheme 1.

isolated with one characteristic ν(CO) band at 1961 cm^{-1} (KBr) and elemental analysis for C, H and N indicating the presence of $[Mo(SnCl_3)_2(CO)(\eta^4\text{-}C_7H_8)(NCMe)_2]$ (**4**). The reaction course and the pathway leading to the formation of compound **4** are proposed in Scheme 1. This involves the CO loss in CH_2Cl_2 solution and the formation of a dimeric compound containing chloride bridges. In acetonitrile solution the redistribution of anionic ligands between two molybdenum atoms occurs to give bis(stannyl) and bis(chloride) complexes **4** and **5**. Such a process were observed earlier during the preparation of $[Mo(SnCl_3)_2(CO)_2(NCMe)_3]$ from compound **1** [11].

3.2. NMR identification of new compounds containing NBD ligand

The ^{1}H NMR spectrum of **3** shows seven well-separated signals due to the protons of the norbornadiene ligand. Four peaks at $\delta_H = 5.43$, 4.84, 4.00 and 3.91, which appear as pseudo-triplets with approximately $J_{HH} = 4$ Hz, are due to protons attached to the double C=C bonds, while the broad peaks at $\delta_H = 3.81$ and 3.76 are due to protons attached to the bridgehead methine carbons. The signal at $\delta_H = 1.77$ appears as a pseudo-quartet, i.e. two doublets with second-order distortion, and can be assigned to two protons of the bridge methylene group. Four resonances of the olefin protons of **3** are at a higher field than that of the free NBD by 1.22–2.74 ppm. Thus, the ^{1}H NMR data for **3** suggest that the NBD ligand coordinates unsymmetrically to the metal centre.

For the previously investigated compound **2**, with a more symmetrically coordinated NBD ligand, only two olefinic proton signals at $\delta_H = 5.27$ and 4.02 were observed in the ^{1}H NMR spectrum [7]. The lower-field norbornadiene signal of **2** was assigned to the protons of the HC=CH unit in *trans* position to the CO group and the signal at a higher field to the protons of the double bond *trans* to the chlorine ligand. By analogy, for **3**, two lower-field resonances can be assigned to protons of the olefinic bond *trans* to CO and two higher-field resonances to protons of the olefinic bond *trans* to an anionic ligand. However, in dichloromethane solution compound **3** slowly decomposes to give the complex $[MoCl(SnCl_3)(CO)(\eta^4\text{-}C_7H_8)(NCMe)]_2$, insoluble in this solution and most probably dimeric. The latter compound in acetonitrile solution gives two different monomeric compounds, **4** and **5** (Scheme 1), both characterised by five proton signals in the integration ratio 2:2:1:1:2 in ^{1}H NMR spectra. Only two olefinic proton signals at δ_H 4.43 and 4.04 are observed in the ^{1}H NMR spectrum of compound **4**. However, from the ^{1}H–^{1}H NMR correlation spectrum it can be seen that each of them is coupled with different bridgehead methine protons ($\delta_H = 3.65$ and 3.72, respectively), thus both signals are due to protons belonging to the same olefinic unit. The high value of the coordination shift ($\Delta\delta_H$) of these signals ($\Delta\delta_H = 2.22$ and 2.61) suggests that both olefinic units are in *trans* position to the same, most probably anionic ligands. A similar set of NBD resonances as for **4** has been reported by Daniel et al. for $[MoBr_2(CO)(\eta^4\text{-}C_7H_8)(bpy)]$ ($\delta_H = 4.48$, 3.92 (=C*H*), 3.96, 3.65 (C*H*) and 1.76 (CH_2) [9]). Proton signals due to $[MoCl_2(CO)(\eta^4\text{-}C_7H_8)(NCMe)_2]$ (**5**), which is formed alongside compound **4** in the CH_3CN solution of the decarbonylation product of compound **3** (Scheme 1), were observed at $\delta_H = 4.12$, 3.79 (=C*H*), 3.63, 3.56 (C*H*) and 1.62 (CH_2). Such a ^{1}H NMR spectrum was always observed immediately after the dissolution in CD_3CN of the precipitate formed in CH_2Cl_2 solution of compound **3** (Scheme 1). Compound **5** is more labile than **4** and decays during the isolation process.

The $^{13}C\{^1H\}$ NMR spectrum of **3** shows four olefinic carbon resonances. The detection of two higher-field signals in CD_2Cl_2 solution was possible due to the measurement of two-dimensional heteronuclear correlation spectra (^{1}H–^{13}C NMR). The chemical shifts of the olefinic carbon signals for compound **4** are at a higher field than for **2** [7] and **3**. The greater coordination shift of the olefinic protons and the olefinic carbon signals for **4** indicate a stronger interaction of the NBD ligand with the Mo centre in the latter complex than in **2** or **3**. The carbon resonances for the norbornadiene ligand in compound **5** are at higher field, than for the other molybdenum compounds **2**–**4**. The higher-field shifts of the olefinic proton and the carbon signals suggest a stronger interaction of the NBD ligand with the molybdenum centre for **5** than for **2**, **3** and **4**. This correlates with π acidity of the ligands in *trans* position to the olefinic bonds, which decreases in the order $CO > SnCl_3^- > Cl^-$.

3.3. Solid state structure of 3

The results of an X-ray investigation of compound **3** are shown in Figs. 1 and 2 and Tables 1 and 2. The

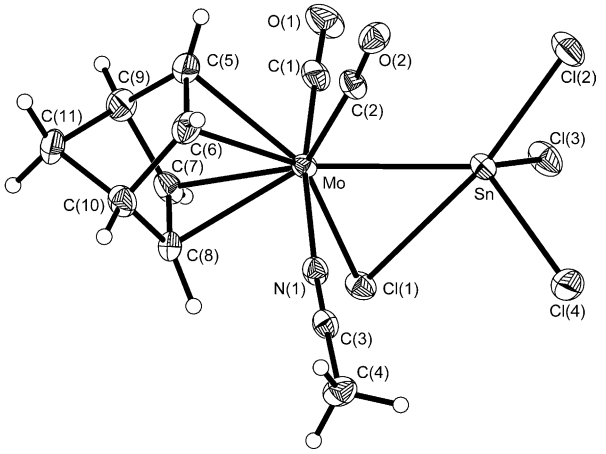


Fig. 1. Molecular structure of $[Mo(\mu\text{-}Cl)(SnCl_3)(CO)_2(\eta^4\text{-}C_7H_8)(NCMe)]$ (**3**).

molecule $[Mo(\mu\text{-}Cl)(SnCl_3)(CO)_2(\eta^4\text{-}C_7H_8)(NCMe)]$ (**3**), is shown in Fig. 1 together with the atomic numbering scheme. Table 2 contains selected bond distances and angles. The molybdenum atom is seven-coordinate and the tin atom is five-coordinate, with one chlorine atom occupying a bridging position between the two metal atoms. The environment of the molybdenum atom in **3** is a distorted pentagonal bipyramid (Fig. 2). In the pentagonal plane there are two olefinic bonds of the NBD ligand, carbonyl, $SnCl_3^-$ and chloride ligands. The Mo–Sn bond of 2.739(1) Å is supported by a chlorine bridge.

The angles subtended at the molybdenum atom by the five atoms determining the pentagonal plane are in the 63.1°–82.1° range (Fig. 2). The greatest distortions from the regularity of the pentagonal bipyramid appear to be associated with the presence of the chelating NBD ligand. The angles between the two alkene bonds are approximately 63° while those between the alkene bonds and the neighbouring ligands are approximately 80°.

The two axial sites are occupied by CO and acetonitrile ligands with a C(1)–Mo–N(1) angle of 170.2(2)°. The CO group *trans* to the nitrile ligand is a shorter distance from the Mo atom, at 1.989(7) Å, than the CO group *trans* to the olefinic ligand, at 2.010(6) Å.

The most significant feature of complex **3** is the fact that the arrangement of the coordination of the norbornadiene ligand is of two types. One of the olefinic bonds is approximately *trans* to CO and the other *trans* to Cl. This gives rise to a slight difference between the Mo–C distances; such that Mo–C(5) = 2.288(7) and Mo–C(6) = 2.338(7) Å are almost 0.12 Å shorter than Mo–C(8) = 2.403(6) and Mo–C(7) = 2.455(6) Å, whereas the difference between the shortest and the longest Mo–C(olefinic) bond is 0.167 Å. The above bond lengths are in excellent agreement with the degree of electron back-donation from the dπ-orbitals of molybdenum to the ligands whose π acidity is taken into account. As CO is a better π acid than the olefinic bond, back-donation to CO is much preferred. For the C=C and its *trans* Cl ligand, the electron density due to back-donation is almost completely accepted by C=C, resulting in shortened Mo–C(5) and Mo–C(6) and in lengthened C(5)–C(6) distances compared to Mo–C(7) and Mo–C(8) and C(7)–C(8) distances. Thus the

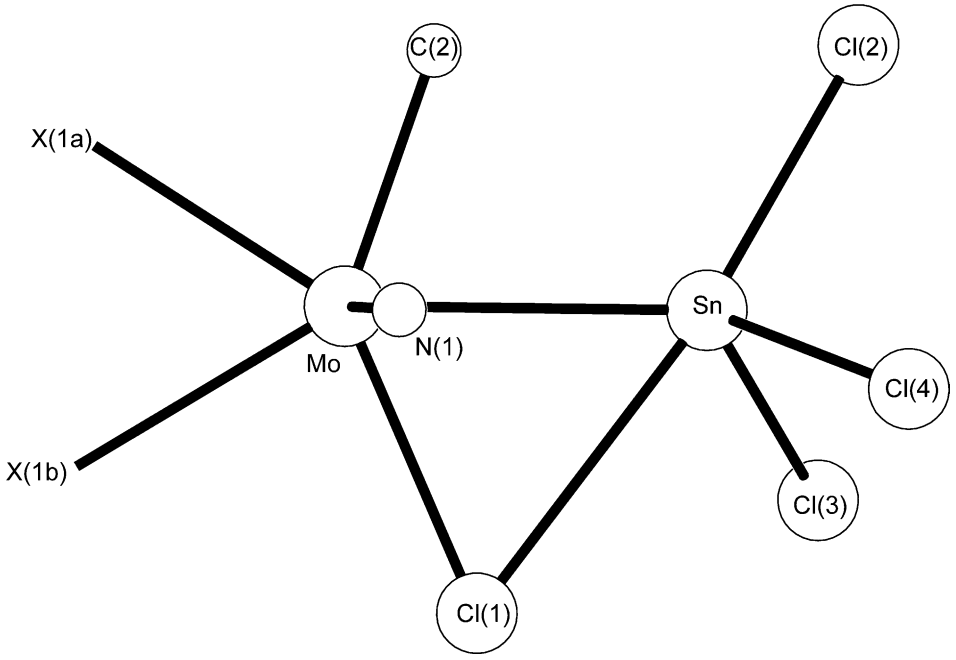


Fig. 2. Projection of the coordination sphere of Mo on the pentagonal plane illustrating the pentagonal bipyramid geometry of **3**. X(1a) and X(1b) represents the midpoint of the C=C linkage.

Table 2
Selected bond lengths (Å) and angles (°) for [Mo(μ-Cl)($SnCl_3$)$(CO)_2$(η^4-C_7H_8)(NCMe)] (**3**)

Bond lengths			
Mo–C(1)	1.989(7)	Sn–Cl(4)	2.352(2)
Mo–C(2)	2.010(6)	Sn–Cl(3)	2.354(2)
Mo–N(1)	2.198(5)	Sn–Cl(2)	2.393(2)
Mo–C(6)	2.288(7)	Sn–Cl(1)	2.897(2)
Mo–C(5)	2.338(7)	O(1)–C(1)	1.150(7)
Mo–C(8)	2.403(6)	O(2)–C(2)	1.145(7)
Mo–C(7)	2.455(6)	N(1)–C(3)	1.135(7)
Mo–Cl(1)	2.484(2)	C(5)–C(6)	1.397(10)
Mo–Sn	2.739(1)	C(7)–C(8)	1.359(9)
Bond angles			
C(1)–Mo–C(2)	92.1(2)	C(7)–Mo–Cl(1)	83.25(18)
C(1)–Mo–N(1)	170.2(2)	C(1)–Mo–Sn	81.42(18)
C(2)–Mo–N(1)	86.7(2)	C(2)–Mo–Sn	71.58(17)
C(1)–Mo–C(6)	107.9(3)	N(1)–Mo–Sn	88.97(12)
C(2)–Mo–C(6)	74.9(2)	C(6)–Mo–Sn	145.56(17)
N(1)–Mo–C(6)	81.3(2)	C(5)–Mo–Sn	140.68(17)
C(1)–Mo–C(5)	73.0(3)	C(8)–Mo–Sn	147.50(17)
C(2)–Mo–C(5)	80.0(2)	C(7)–Mo–Sn	142.96(17)
N(1)–Mo–C(5)	116.3(2)	Cl(1)–Mo–Sn	67.06(4)
C(6)–Mo–C(5)	35.1(2)	Cl(4)–Sn–Cl(3)	98.73(6)
C(1)–Mo–C(8)	110.8(2)	Cl(4)–Sn–Cl(2)	97.64(6)
C(2)–Mo–C(8)	134.8(2)	Cl(3)–Sn–Cl(2)	95.50(6)
N(1)–Mo–C(8)	76.50(19)	Cl(4)–Sn–Mo	120.73(4)
C(6)–Mo–C(8)	61.3(2)	Cl(3)–Sn–Mo	118.29(4)
C(5)–Mo–C(8)	71.1(2)	Cl(2)–Sn–Mo	120.68(5)
C(1)–Mo–C(7)	78.3(2)	Sn–Cl(1)–Mo	60.4(2)
C(2)–Mo–C(7)	139.4(3)	C(3)–N(1)–Mo	176.7(4)
N(1)–Mo–C(7)	108.74(19)	O(1)–C(1)–Mo	177.0(5)
C(6)–Mo–C(7)	70.9(2)	O(2)–C(2)–Mo	174.6(5)
C(5)–Mo–C(7)	59.4(2)	C(6)–C(5)–Mo	70.5(4)
C(8)–Mo–C(7)	32.5(2)	C(9)–C(5)–Mo	101.3(5)
C(1)–Mo–Cl(1)	92.76(19)	C(5)–C(6)–Mo	74.4(4)
C(2)–Mo–Cl(1)	137.04(18)	C(10)–C(6)–Mo	100.0(4)
N(1)–Mo–Cl(1)	81.56(14)	C(8)–C(7)–Mo	71.7(3)
C(6)–Mo–Cl(1)	142.19(17)	C(9)–C(7)–Mo	96.6(4)
C(5)–Mo–Cl(1)	141.75(17)	C(7)–C(8)–Mo	75.9(3)
C(8)–Mo–Cl(1)	81.97(17)	C(10)–C(8)–Mo	95.6(4)

structure of **3** provides a good model for comparing the effect of the relative position of alkene and CO ligands on the Mo–C bond distance. Regarding the mutual position of the olefinic carbons and the two ligands (CO and NCMe) in an axial position to the pentagonal plane, it should be noted that the olefinic carbon which is closer to the CO ligand is more strongly coordinated to the metal, with the Mo–C distance 0.05 Å shorter than that closer to the nitrile group (Fig. 2).

The tin atom is five-coordinate in **3** with a geometry that is best described as distorted trigonal bipyramid with the two chlorine atoms occupying the axial sites. In the trigonal plane there are two chlorine atoms and the Mo atom. The tin-to-bridging-chlorine distance is 2.897(2) Å, being considerably longer than the Sn–Cl distances in the trigonal plane (av. 2.35 Å). The molybdenum-to-bridging-chlorine distance is 2.484(1) Å and indicates that the bridging chlorine forms a stronger bond with the molybdenum whereas the Sn–Cl bond is weakened.

3.4. Searching for the catalytically active species

The reaction between **3** and an excess of NBD was followed by ^{1}H NMR spectroscopy, which confirmed the formation of polynorbornadiene with characteristic signals of the olefinic protons above 5 ppm (Fig. 3). The ROMP of NBD starts immediately after reagents are mixed. At the beginning of a reaction the olefinic proton signals of the coordinated NBD in **3** decrease in intensity. Simultaneously the signal of an alkylidene species at $\delta_H = 10.49$ appears and grows. Parallel with the latter signal, other, very low-intensity signals appear at $\delta_H = 6.21$, 5.99, 2.99 and 2.91. These can be assigned to protons of a cyclopentadienyl moiety formed after the rearrangement of the NBD ligand (Scheme 2). The coupling between protons observed at $\delta_H = 6.21$ and 5.99 was confirmed by two-dimensional correlation ^{1}H–^{1}H NMR spectra. After a prolonged reaction time (7 days), signals due to **3** decrease in intensity by approximately 60% and the intensity of signals due to poly-NBD increases considerably. However, only a small part of compound **3** rearranges to species initiating the polymerisation reaction. The intensity of the signal due to the proton of the alkylidene ligand at $\delta_H =$ 10.49 reaches a value of 0.5–5% of the intensity of the signal due to the starting compound **3** at $\delta_H = 4.84$ (Fig. 3a–d). Although the polymerisation reaction is stopped due to a gelation process, at least 10 molecules of NBD were polymerised by one molecule of compound **3**.

In the observed ^{13}C{^{1}H} NMR spectrum (Fig. 4) of the above reaction mixture the microstructure of the poly-NBD formed can be analysed [18]. From the intensity ratio of the signal due to methine carbons denoted 1,4 at $\delta_C = 48.38$ (*trans* double bond) and 43.65 (*cis* double bond), the value of the *cis* double bond content was calculated to be approximately 42%. This spectrum was measured during a reaction in the NMR tube, so carbon signals due to free NBD and the NBD ligand in the residual compound **3** could still be observed.

Although the mechanism of the transformation of compound **3** to the alkylidene species initiating the ROMP is not clear at present, three possible ways of norbornadiene ligand rearrangement can be considered. One of the possible reaction routes may involve first, the formation of metallacyclobutane species (due to the valence isomerisation and the creation of the cyclopropane ring) and next alkylidene containing a cyclopentadienyl fragment as the end group (Scheme 2A). The rearrangement of two norbornadiene molecules to a

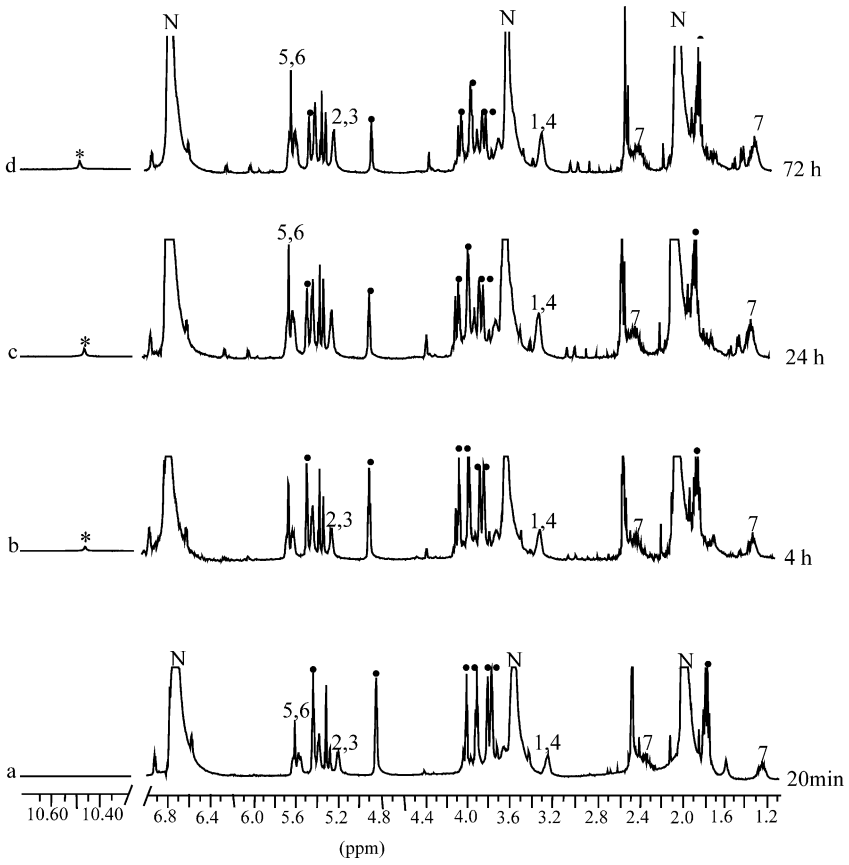
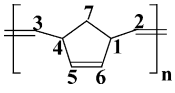
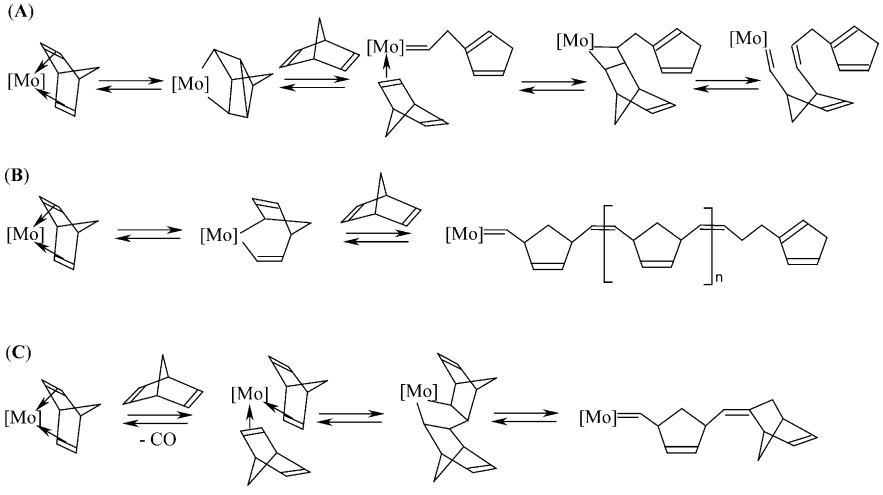


Fig. 3. The olefinic proton region of the ^{1}H NMR spectra recorded at 500 MHz during reaction of **3** and NBD (N) at 293 K in CD_2Cl_2 after (a) 20 min, (b) 4 h, (c) 24 h, (d) 72 h. The resonances denoted by (●) are due to protons of the NBD ligand in **3**. Signals assigned to an alkylidene signal at $\delta_H = 10.49$, 6.21, 5.98, 2.96 and 2.89 are marked with an asterisk (*). Proton signals in the poly-NBD are labelled as follows:



nortricyclyl–norbornenyl group was first observed by Itoh et al. [19], in reduction reaction of $[RuCl_2(C_7H_8)]_n$ by means of zinc powder in the presence of NBD. Other pathway for the conversion of coordinated NBD in **3** is



Scheme 2.

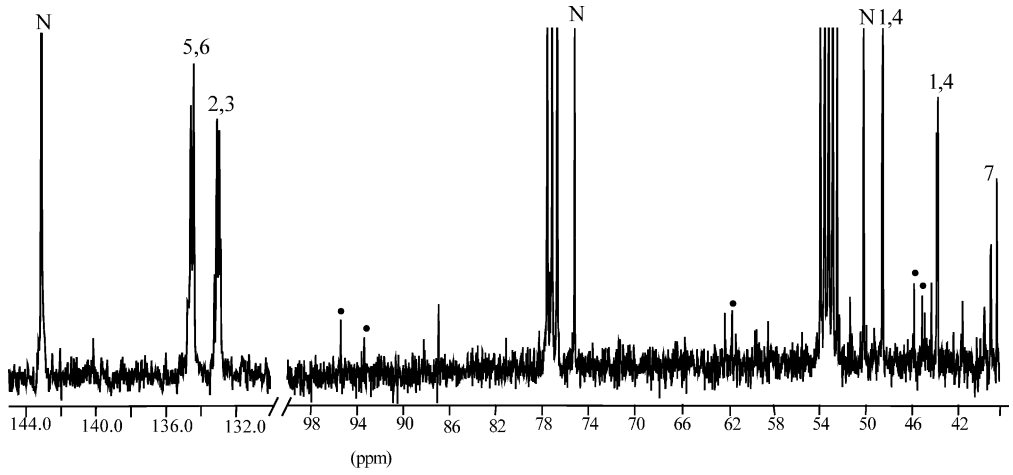
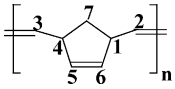


Fig. 4. $^{13}C\{^{1}H\}$ NMR spectrum recorded at 300 MHz in CD_2Cl_2–$CDCl_3$ = 5:2, after reaction of **3** (●) and NBD (N) at 293 K. Carbon signals in the poly-NBD are labelled as follows:



the cleavage of C–C bond and the formation of vinylcyclopantadiene species (Scheme 2B). This type of transformation was observed in reaction of several ruthenium complexes containing norbornadiene ligand [20–25]. Such a transformation can result first from the asymmetry shown by the NBD ligand and a very weak interaction of one of the olefinic bond with the metal centre. Another reason for the high reactivity of compound **3** towards NBD is that the carbonyl ligand in *trans* position to the olefinic bond is very labile. Thus, in the presence of an excess of NBD, the weakly coordinating alkene bond or CO ligand in **3** can be substituted by the olefinic bond of the NBD molecule leading to the formation of a metallacyclopentane (Scheme 2C). Such intermediates were considered by Grubbs and Miyashita [26], Schrock and coworkers [27] and Rooney [28,29]. However, our results have only shown the formation of an alkylidene ligand from the olefin coordinated to molybdenum(II). Hopefully further DFT calculation on the transformation of the model compounds **2** and **3** to the alkylidene complex could established this mechanistic proposal.

4. Conclusions

In this work the reactivity and catalytic application of a heterobimetallic Mo–Sn complex **1** in metathesis polymerisation of norbornadiene have been studied. It is shown that the labile nitrile ligands in **1** can be substituted under mild conditions by norbornadiene to give $[Mo(\mu\text{-}Cl)(SnCl_3)(CO)_3(\eta^4\text{-}C_7H_8)]$ (**2**). Next, the CO ligand in complex **2** very easily undergoes substitution by nitrile to give $[Mo(\mu\text{-}Cl)(SnCl_3)(CO)_2(\eta^4\text{-}C_7H_8)(NCMe)]$ (**3**).

The results presented here conclusively establish the existence of a very unsymmetrically coordinated norbornadiene ligand in **3**. We also outline how these structural features relate to the alkylidene ligand formation observed in the presence of an excess of norbornadiene, and the initiation of norbornadiene polymerisation.

To the best of our knowledge this paper presents the first study that has simultaneously detected the alkylidene ligand formation from olefin coordinated to metal and the initiation of ROMP by this catalytically active species.

Studies aiming at a better understanding of the formation mechanism as well as further applications of this new compound in catalysis will be continued.

5. Supplementary material

Crystallographic data for the structural analysis have been deposited with the Cambridge Crystallographic Data Centre, CCDC No. 182154 for compound **3**. Copies of this information may be obtained free of charge from The Director, CCDC, 12 Union Road, Cambridge, CB2 1EZ, UK (fax: +44-1223-336033; e-mail: deposit@ccdc.cam.ac.uk or www: http://www.ccdc.cam.ac.uk).

Acknowledgements

Financial support from the Polish State Committee for Scientific Research (grant No. 3T09A 059 17 and 3T09A 068 19) is gratefully acknowledged.

References

[1] P.K. Baker, Adv. Organomet. Chem. 40 (1996) 45.
[2] P.K. Baker, Chem. Soc. Rev. 27 (1998) 125.
[3] L. Bencze, G. Szalai, J.G. Hamilton, J.J. Rooney, J. Mol. Catal. A: Chem. 115 (1997) 193.
[4] M.A. Jahdali, P.K. Baker, A.J. Lavery, M.M. Meehan, D.J. Muldoon, J. Mol. Catal. A: Chem. 159 (2000) 51.
[5] T. Szymańska-Buzar, in: E. Khosravi, T. Szymańska-Buzar (Eds.), Ring Opening Metathesis Polymerisation and Related Chemistry, NATO ASI Series, Kluwer Academic, Dordrecht, 2002, p. 349.
[6] I. Czeluśniak, T. Szymańska-Buzar, J. Mol. Catal. A: Chem. in press.
[7] T. Szymańska-Buzar, T. Głowiak, I. Czeluśniak, J. Organomet. Chem. 640 (2001) 72.
[8] T. Szymańska-Buzar, T. Głowiak, Polyhedron 16 (1997) 1599.
[9] T. Daniel, H. Nagao, K. Tanaka, A. Nakamura, Chem. Ber. 128 (1995) 1007.
[10] T. Daniel, H. Nagao, H. Nakajima, K. Tanaka, A. Nakamura, J. Organomet. Chem. 509 (1996) 225.
[11] T. Szymańska-Buzar, T. Głowiak, J. Organomet. Chem. 575 (1999) 98.
[12] P. Starynowicz, COSABS-99, Program for Absorption Correction, University of Wrocław, Wrocław, Poland, 1999.
[13] G.M. Sheldrick, SHELXS-97, Program for Solution of Crystal Structures, University of Göttingen, Göttingen, Germany, 1997.
[14] G.M. Sheldrick, SHELXS-97, Program for Crystal Structure Refinement, University of Göttingen, Göttingen, Germany, 1997.
[15] F.A. Cotton, J.H. Meadows, Inorg. Chem. 23 (1984) 4688.
[16] L. Carlton, J.L. Davidson, G. Vasapollo, G. Douglas, K.W. Muir, J. Chem. Soc., Dalton Trans. (1993) 3341.
[17] J.L. Davidson, H. Richtzenhein, B.J.S. Thiebaut, K. Landskron, G.M. Rosair, J. Organomet. Chem. 592 (1999) 168.
[18] B. Bell, J.G. Hamilton, O.N.D. Mackey, J.J. Ronney, J. Mol. Catal. 77 (1992) 61.
[19] K. Itoh, N. Oshima, G.B. Jameson, H.C. Lewis, J.A. Ibers, J. Am. Chem. Soc. 103 (1981) 3041.
[20] H. Suzuki, T. Kakigano, H. Fukui, M. Tanaka, Y. Moro-oka, J. Organomet. Chem. 473 (1994) 295.
[21] G. Jia, W.S. Ng, C.P. Lau, Organometallics 17 (1998) 4538.
[22] J.L. Brumaghim, G.S. Girolami, J. Organomet. Chem. 586 (1999) 258.
[23] T. Mitsudo, T. Suzuki, S.-W. Zhang, D. Imai, K. Fujita, T. Manabe, M. Shiotsuki, Y. Watanabe, K. Wada, T. Kondo, J. Am. Chem. Soc. 121 (1999) 1839.
[24] Y. Ohki, H. Suzuki, Angew. Chem., Int. Ed. Engl. 39 (2000) 3463.
[25] S.H. Liu, W.S. Ng, H.S. Chu, T.B. Wen, H. Xia, Z.Y. zhou, C.P. Lau, G. Jia, Angew. Chem., Int. Ed. Engl. 41 (2002) 1589.
[26] H. Grubbs, A. Miyashita, J. Am. Chem. Soc. 100 (1978) 1300.
[27] S.J. McLain, J. Sancho, R.R. Schrock, J. Am. Chem. Soc. 101 (1979) 5451.
[28] J.J. Rooney, J. Mol. Catal. 31 (1985) 147.
[29] D.T. Laverty, J.J. Rooney, J. Chem. Soc., Faraday Trans. 79 (1983) 869.

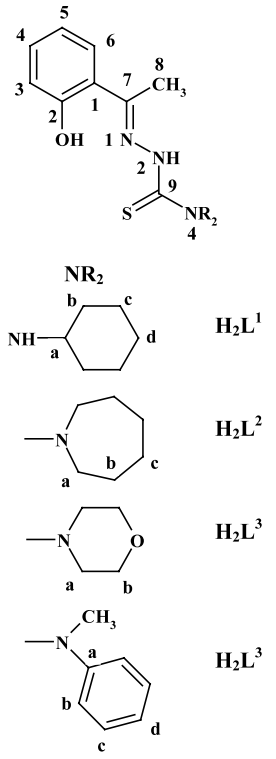


Fig. 1. Structures of thiosemicarbazones.

2. Results and discussion

2.1. Synthesis of complexes

It has been found that the Co(II) ion undergoes oxidation in the presence of methanol or chloroform unlike in ethanol [15]. All the complexes are found to be brown in colour but the crystalline nature may vary depending on their mode of formation. Complexes of H_2L^4 were found to give fine crystals on keeping while compounds of H_2L^1 and H_2L^2 were found to give the products more readily.

The elemental analysis data (Table 1) of all compounds suggests a formulation of [$MLBN_3$]. This along with the conductance data indicates that the azide ion is coordinated to the metal. However, for the compound **1** the elemental data matches with a stochiometry containing 0.5 molecule of water of crystallization/lattice water. The compounds **2** and **4** each contain one molecule of uncoordinated water and compound **6** contains three molecules of water. Compound **8** is obtained in two different colours, viz. brown (**8a**) and green (**8b**). The elemental data indicate that **8a** is having one molecule of water, while the later **8b** is devoid of it. The elemental data of compound **8b** is reported here. Both give similar IR and UV spectra. The slight variations found in the elemental data for some of the compounds are due to the presence of non-stochiometric amount of water of crystallization present. All the complexes are found to be diamagnetic confirming that the cobalt is in the +3 oxidation state and hence corresponds to d^6 ion in strong field.

The thermal analysis of the compounds **1**, **2**, **4** and **6** showed that the non-stochiometric water of crystallization begins to leave in the 220–260 °C range. The loss is gradual in **1**, **4** and in **5** but a sharp change at 250 °C is found in the case of compound **2**. All the complexes started decomposing at 310 °C and the changes are sharp at 330 °C.

The FAB mass spectrum of the compound **6** gives a molecular ion [M^+] peak at m/z 613 (15) corresponding to trihydrated formulation. The next major peak at m/z 558 (20) corresponds to the non-hydrated formulation. The next lower but major fraction appears at m/z 516 (78) corresponding to a fraction stripped off its azido group.

2.2. Crystal structure of CoL^4bipyN_3

Dark brown X-ray quality single crystals of compound **7** (CoL^4bipyN_3) were grown by slow diffusion of ethanol into a solution of the compound in chloroform. The compound crystallized into a monoclinic lattice with space group symmetry $P2_1/a$ with one molecule per asymmetric unit. The molecular structure of the compound was found to be distorted octahedral. The

Table 1
Elemental analyses data of Co(III) complexes

Compound	Formulae	Colour	Found (Calc.) %			
			C	H	N	Co
CoL^1bipyN_3 (**1**)	$C_{25}H_{28}CoN_8OS\cdot 0.5H_2O$	pale brown	57.77 (57.09)	4.93 (5.09)	19.93 (20.20)	10.52 (10.54)
CoL^1phenN_3 (**2**)	$C_{27}H_{28}CoN_8OS\cdot H_2O$	brown	54.86 (55.00)	5.03 (5.13)	19.20 (19.01)	10.26 (10.00)
CoL^2bipyN_3 (**3**)	$C_{25}H_{28}CoN_8OS$	light brown	54.62 (54.94)	4.89 (4.98)	20.42 (20.50)	10.79 (10.78)
CoL^2phenN_3 (**4**)	$C_{27}H_{28}CoN_8OS\cdot H_2O$	brown	54.86 (55.00)	4.97 (5.13)	18.94 (19.01)	10.03 (10.00)
CoL^3bipyN_3 (**5**)	$C_{23}H_{24}CoN_8O_2S$	light brown	51.96 (51.59)	4.42 (4.52)	21.23 (20.93)	11.07 (11.0)
CoL^3phenN_3 (**6**)	$C_{25}H_{24}CoN_8O_2S\cdot 3H_2O$	brown	48.87 (48.94)	4.96 (4.93)	18.29 (18.26)	9.56 (9.61)
CoL^4bipN_3 (**7**)	$C_{26}H_{24}CoN_8OS$	reddish brown	55.99 (56.21)	4.14 (4.35)	19.97 (20.17)	10.67 (10.61)
CoL^4phenN_3 (**8a**)	$C_{28}H_{24}CoN_8OS$	brown	58.10 (58.03)	4.32 (4.17)	19.20 (19.33)	10.07 (10.17)

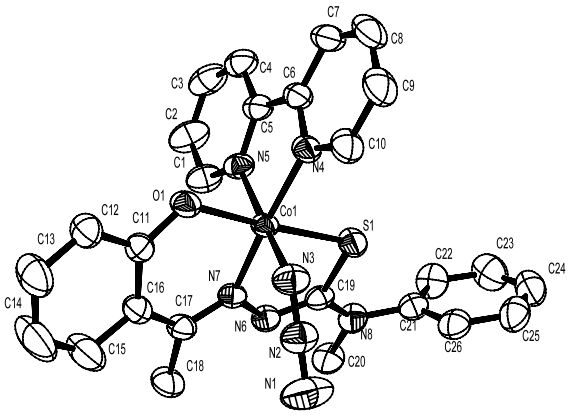


Fig. 2. ORTEP diagram for compound **7** (CoL^4bipyN_3), displacement ellipsoids are drawn at the 54% probability level and hydrogen atoms are omitted for clarity.

perspective view of the complex CoL^4bipyN_3 (Fig. 2) shows that the thiosemicarbazone is functioning as an ONS donor ligand and it is coordinated in a meridonal arrangement along with bipy and a terminal azido group. The selected bond lengths and angles are presented in Table 2. As observed the thiosemicarbazone moiety is in the same plane of the Co atom indicated by the bond angles O1–Co1–N3 (89.51°) and N7–Co1–O1 (94.9°). The apical positions of the octahedron are occupied by one of the nitrogen N3 of the azido group and N5 of the bipy with bond lengths 1.946 Å (Co–N3) and 1.963 Å (Co–N5). The bond angles N3–Co1–N5 (172.3°) and N5–Co1–N4 (82°) are quiet far from a perfect octahedron indicating distortion in the geometry. Coordination lengthens the thiosemicarbazone moiety's C19–S1 bond from 1.699 to 1.743 Å [12] and shortens C19–N6 bond from 1.358 to 1.294 Å, which is consistent with the C19–S1 acquiring a partial single bond and C19–N6 a partial double bond. Short bond length of Co–N4 (1.948 Å) compared to Co–N5 (1.963 Å) indicates strong bonding due to equatorial bipy nitrogen. Strong coordination of azomethine nitrogen is indicated by much shorter Co–N7 (1.900 Å) bond length. The N(4) methyl group (C20) is on the same side of the thiosemicarbazone moiety as the methyl group C18 of the azomethine function (i.e. *trans* to the sulfur and *Z* isomer). The Co–N3–N2 bond angle is 121.36° and shows the azido coordination is bent but N3–N2–N1 (177.2°) is nearly linear.

Table 2
Selected bond lengths (Å) and angles (°) for compound **7**

Bond lengths			
Co(1)–N(7)	1.9008(18)	Co(1)–O(1)	1.9072(16)
Co(1)–N(3)	1.946(2)	Co(1)–N(4)	1.9482(19)
Co(1)–N(5)	1.963(2)	Co(1)–S(1)	2.2126(7)
S(1)–C(19)	1.743(2)	N(7)–C(17)	1.307(3)
N(7)–N(6)	1.404(3)	N(4)–C(10)	1.335(3)
N(4)–C(6)	1.358(3)	N(5)–C(1)	1.333(3)
N(5)–C(5)	1.355(3)	N(6)–C(19)	1.294(3)
O(1)–C(11)	1.311(3)	C(19)–N(8)	1.376(3)
N(3)–N(2)	1.196(3)	N(2)–N(1)	1.151(3)
C(21)–N(8)	1.426(3)	N(8)–C(20)	1.470(3)
C(17)–C(16)	1.462(3)	C(17)–C(18)	1.508(3)
Bond angles			
N(7)–Co(1)–O(1)	94.90(8)	N(7)–Co(1)–N(3)	90.77(8)
O(1)–Co(1)–N(3)	89.51(9)	N(7)–Co(1)–N(4)	174.01(8)
O(1)–Co(1)–N(5)	85.85(8)	N(3)–Co(1)–N(5)	172.31(8)
N(4)–Co(1)–N(5)	82.18(9)	N(7)–Co(1)–S(1)	87.68(6)
O(1)–Co(1)–S(1)	176.66(5)	N(3)–Co(1)–S(1)	92.57(7)
N(4)–Co(1)–S(1)	86.77(6)	N(5)–Co(1)–S(1)	91.79(6)
C(19)–S(1)–Co(1)	93.64(8)	C(17)–N(7)–N(6)	115.00(18)
C(17)–N(7)–Co(1)	126.21(16)	N(6)–N(7)–Co(1)	118.65(14)
C(19)–N(6)–N(7)	114.21(18)	N(6)–C(19)–N(8)	118.1(2)
N(2)–N(3)–Co(1)	121.36(17)	N(7)–C(17)–C(18)	118.5(2)
N(7)–Co(1)–O(1)	94.90(8)	N(7)–Co(1)–N(3)	90.77(8)
O(1)–Co(1)–N(3)	89.51(9)	N(7)–Co(1)–N(4)	174.01(8)
N(1)–N(2)–N(3)	177.7(3)		

2.3. Electronic and IR spectra

The electronic spectra (Table 3) of Co(III) complexes have four d–d bands: $^1A_{1g}\rightarrow{}^1T_{1g}$; $^1A_{1g}\rightarrow{}^1T_{2g}$; $^1A_{1g}\rightarrow{}^3T_{1g}$ and $^1A_{1g}\rightarrow{}^3T_{2g}$ [16,17]. We have assigned $^1A_{1g}\rightarrow{}^1T_{1g}$ approximately 20 620 cm^{-1}, $^1A_{1g}\rightarrow{}^1T_{2g}$ approximately 25 000 cm^{-1}, and $^1A_{1g}\rightarrow{}^3T_{2g}$ approximately 16 870 cm^{-1}. Assignment of the two high energy bands is complicated by overlap of inter ligand and charge transfer transitions. $^1A_{1g}\rightarrow{}^3T_{2g}$ was most difficult to assign because this weak spin forbidden band is always at the onset of other high-energy intense bands. The CT band is rather too broad and is explained as a combination of two bands resulting from the S→Co(III) and O→Co(III) LMCT transitions. Compounds **8a** and **8b** dissolve to give a reddish brown solution in CH_2Cl_2 and give similar IR and UV spectra.

Compounds **1**, **4**, **5** and **6** show broad IR bands (Table 4) approximately 3400 cm^{-1}, which is due to the O–H stretching modes of the uncoordinated water molecules. The IR spectrum of the complexes show peaks approximately 1595 cm^{-1} due to the newly formed $^2N{=}^9C$ bond indicating that the coordination of the thiosemicarbazone takes place in the form of thiol rather than as thione. The lowering of the band approximately 1602 cm^{-1} ($^7C{=}^1N$) by 30–50 cm^{-1} is an explicit evidence for the coordination of the thiosemicarbazone through the azomethine nitrogen. The spectra of the complexes exhibit a systematic shift in the position of the bands in the region 1600–1350 cm^{-1} due to ν(C=C) and ν(C=N) vibrational modes, and their mixing patterns are different from those present in the ligand spectrum. Coordination of the bases is indicated by the presence of weak bands in the 410–485 cm^{-1} region due to Co–N stretching vibration. Weak bands in the region 510–565 cm^{-1} indicate the presence of Co–O bond resulting from coordination of phenolic oxygen. Besides the shifting of the band due to Ar–O group to lower

Table 3
Electronic spectral assignments, λ/cm^{-1} (log ε [a]) for compounds **1**–**8**

Compound	d–d	LMCT	n → π*	π → π*
H_2L^1			30 300 (4.05), 32 342 sh (4.32)	35 000 (4.26)
CoL^1bipyN_3 (**1**)	17 094 (2.49), 20 583 (3.18)	24 937 (3.82), 29 154 sh (4.10)	33 003 (4.43)	39 525 (4.48), 37 453 (4.47)
CoL^1phenN_3 (**2**)	16 528 (2.42), 20 202 (2.80)	24 691 sh (3.90)	32 520 (4.52)	43 478 (4.22), 39 604 (4.54)
H_2L^2			30 581 (4.19), 32 372 (4.23)	35 587 (4.48)
CoL^2bipyN_3 (**3**)	16 949 (2.20), 20 000 (2.76)	24 570 (4.01)	32 573 (4.56), 33 333 sh (4.45)	40 241 (4.52), 36 630 (4.62)
CoL^2phenN_3 (**4**)	16 530 (2.47), 20 408 (3.22)	24 937 (4.02)	32 051 (4.50), 34 722 sh (4.55)	37 313 (4.75), 43 197 (4.72)
H_2L^3			30 030 (4.43), 32 895 (4.41)	42 370 (4.25)
CoL^3bipyN_3 (**5**)	16 758 (2.70), 20 636 (3.23)	24 498 (3.80)	29 485 sh (4.12), 32 786 (4.40)	39 683 (4.44)
CoL^3phenN_3 (**6**)	16 474 (2.71), 20 080 (2.82)	24 938 (4.02)	32 258 (4.49), 34 222 sh (4.57)	38 168 (4.75), 42 735 (4.63)
H_2L^4			30 211 (4.19), 35 524 sh (4.40)	42 371 (4.32)
CoL^4bipyN_3 (**7**)	17 035 (2.74), 20 202 (3.25)	24 570 (3.75)	29 762 sh (4.10), 32 679 (4.35)	40 322 (4.34), 36 630 (4.29)
CoL^4phenN_3 (**8**)	16 612 (2.55), 20 325 (3.07)	24 570 (4.00)	32 363 (4.35), 34 628 sh (4.47)	37 453 (4.62), 43 290 (4.58)

[a] ε is expressed in (l mol^{-1} cm^{-1}).

frequencies indicates the weakening of the Ar–O bond due to coordination. The presence of the azide group in the coordination sphere is evidenced from the very strong and sharp absorption peak approximately 2022 cm^{-1}. The azido group is bound to cobalt as terminal indicated by a strong absorption at 2030 cm^{-1} characteristic of a terminal azido group [18]. The slight lowering in values is assumed to the result of its coordination to the metal [19]. The coordination via the thiolate sulfur is evidenced from the lowering of band due to the C–S stretching vibration approximately 1365 cm^{-1}, and C–S bending vibration approximately 864 cm^{-1}. The two very intense bands at 1495 and 1465 cm^{-1} show presence of different delocalised ligand molecules linked to the metal through the imine nitrogen.

2.4. ^1H NMR spectra

^1H NMR spectral measurements (Table 5) show disappearance of the peaks corresponding to the phenolic and proton attached to the ^2N of the thiosemicarbazone moiety. This supports the evidence from IR spectra that the thiosemicarbazone coordinate as dibasic tridentate ligand existing in the thiol form. The signals corresponding to the phenoxy group are shifted up field by 0.2–0.6 ppm in the complex. This is due to the electron withdrawal from the aromatic ring due to coordination with the metal. The protons corresponding to the heterocyclic base show separate signals, which indicate loss of symmetry for the base on coordination due to imposition of rigid geometry around the metal ion. This suggests that the complexes indicate signals corresponding to the heterocyclic bases and the thiosemicarbazone moiety. The resonance absorptions of some of the protons near to the coordinated nitrogens are shifted downfield. This unusual position of the signal viz. δ 9.4 of the aromatic system of the bipyridine can be attributed to the proximity to the azide group that cause polar interaction. The coordinated phenoxy oxygen is weekly bound to the closely lying bipyridine/phenanthroline proton via intramolecular hydrogen

Table 4
Infrared spectral assignment for compounds **1**–**8**

Compound	$\nu(^7C{=}N^1)$	$\nu(^2N{=}C^9)$	$\nu(N_3)$	ν(Co–N)	ν/δ(C=S)	ν(C–O)	ν(Co–O)	Bands due to heterocyclic bases
H_2L^1	1599 s				1365 s, 864 m	1219 s		
CoL^1bipyN_3 (**1**) [a]	1564 m	1593 s	2029 s	482 w, 413 w	1329 s, 762 m	1154 s	525 w	1492 m, 1435 s, 730 m
CoL^1phenN_3 (**2**) [a]	1562 m	1590 s	2022 s	479 w, 415 w	1335 s, 766 m	1135 s	571 w	1497 s, 1439 s, 1367 m, 868 w
H_2L^2	1603 s				1383 s, 839 m	1252 s		
CoL^2bipyN_3 (**3**)	1562 m	1588	2018 s	479 w, 416 w	1334 s, 765 m	1203 m	541 w	1498 m, 1438 m, 1367 m, 866 m
CoL^2phenN_3 (**4**)	1564 m	1594 s	2018 s	414 w, 443 w	1339 s, 753 m	1195 m	542 w	1495 m, 1438 m, 1366 m, 845 m
H_2L^3	1605 s				1374 s, 835 m	1219 s		
CoL^3bipyN_3 (**5**)	1560 m	1594 s	2022 s	412 m, 403 w	1342 m, 761	1156 m	545 w	1497 s, 1440 s, 1387 m, 727 m
CoL^3phenN_3 (**6**)	1563 m	1595 s	2024 s	443 w, 410 w	1342 m, 751 m	1145 m	542 w	1469 s, 1436 s, 1356 m, 761 m, 849 w, 642 m
H_2L^4	1601 s				1375 s, 791 m	1222 s		
CoL^4bipN_3 (**7**)	1563 m	1596 s	2025 s	411 w, 441 w	1340 m, 771 m	1123	567 w	1463 s, 1409 s, 1351 m, 856 m, 705 m
CoL^4phenN_3 (**8**)	1562 m	1594 s	2022 s	442 m, 412 w	1344 s, 756 m	1125 s	552 w	1494 m, 1432 m, 846 m, 727 m, 700 w

[a] Peak 3338 sh, due to ^4NH vibration.

Table 5
^{1}H NMR assignments of ligands and complexes **1**–**8**

Compound	H^3	H^4	H^5	H^6	H(Me)	H^a	H^b	H^c	^{4}NH/NCH$_3$	OH	^{2}NH
H_2L^1	6.97 d	7.31 dd	6.93 dd	7.46 d	2.38 s	1.69 m	1.22–2.19 [d]	6.72	10.89	08.74	
$[CoL^1(bipy)N_3]\cdot 0.5\ H_2O$	6.70 d	6.95 t	6.55 t	7.59 d	3.14 s	4.83 m	2.09 m	1.17–1.40 m	3.71 m		
$[CoL^2(phen)N_3]\cdot H_2O$	6.71 d	6.96 t	6.57 t	7.62 m	3.13 s	1.75 m	1.61, 1.48 m	3.70 s			
H_2L^2	7.00 d	7.25 t	6.81 t	7.32 d	2.24 s	3.76 s	1.79 s	1.55 s		12.75	08.36
$[CoL^2(bipy)N_3]$	6.45 d	6.87 t	6.47 t	7.52 d	3.06 s	3.63 m	1.69 m	1.42 m			
$[CoL^2(phen)N_3]\cdot H_2O$	6.57 d	6.86 t	6.49 t	7.55 d	3.12 s	3.61 q	1.68 m	1.42 m			
H_2L^3	6.88 d	7.28 t	6.88 d	7.60 d	3.35 s	3.66 t	3.91 t			12.90	10.38
$[CoL^3(bipy)N_3]$	6.69 d	6.94 t	6.54 t	7.59 d	3.14 s	3.72 s (br)					
$[CoL^3(phen)N_3]\cdot 3H_2O$	6.61 d	6.89 t	6.56 t	7.63 d	3.19 s	3.70 s					
H_2L^4	7.00 d	7.23 m	6.81 t	7.56 t	1.79 s	7.34 d	7.28 m	7.49 t	3.70 s	12.64	08.31
$[CoL^4(bipy)N_3]$	6.70 d	6.94 t	6.53 t	7.58 t	3.16 s	7.30 m	7.16 d	3.58 s			
$[CoL^4(phen)N_3]$	6.61 d	6.91 t	6.56 t	7.64 m	3.23 s	7.29 d	7.24 t	7.11 t	3.58 s		

[a,b,c] Corresponds to protons of N(4) substituents.
[d] Multiplet due to aliphatic CH_2 of the cyclohexyl group.

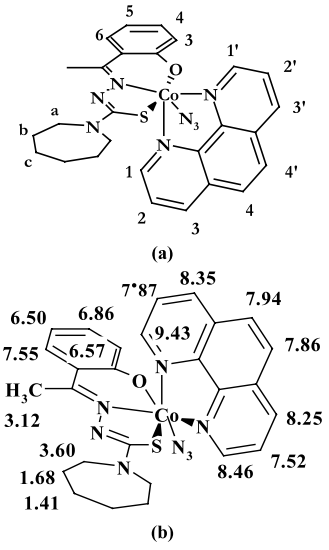


Fig. 3. Atom labeling scheme (a) and approximate ^{1}H NMR assignments (b) for the compound **4** (CoL^2phenN_3).

bonding. Fig. 3 shows the atom labeling and approximate ^{1}H NMR assignments for compound **4**.

3. Experimental

3.1. Synthesis of ligands

The thiosemicarbazones were obtained as per reported procedure of Scovill et al. [1b] from 2-hydroxyacetophenone and N(4)-substituted thiosemicarbazide (1:1 molar ratio) in MeCN or MeOH. The mixture was refluxed for 20–40 min and then cooled, filtered and recrystallised. All analytical and spectroscopic data are in good agreement with the expected values. Sodium azide (Merck) and heterocyclic bases, viz. bipyridine and phenanthroline were of reagent grade (Merck), and were used as supplied. Cobalt acetate tetrahydrate (BDH) was purified by recrystallisation before complexation.

3.2. Synthesis of complexes

The thiosemicarbazone (0.5 mmol) was dissolved in 20 ml of EtOH, to which was added 0.5 mmol of the heterocyclic base in the solid form. The mixture was slightly warmed to ensure complete dissolution of the ligands. To the above mixture was added about 10 ml of methanolic solution of cobalt(II) acetate tetrahydrate (0.5 mmol), with stirring. When a deep brown solution resulted, solid sodium azide (0.75 mmol) was added. Stirring was continued for about an hour. The solution was kept aside overnight for crystallization to occur. The compound was filtered washed with EtOH, water, and ether, respectively. It was then dried over P_4O_{10} in vacuo.

3.3. Physical measurements

Elemental analyses were carried out using a Heraeus Elemental Analyzer at CDRI, Lucknow, India. Cobalt was estimated on a Perkin–Elmer AAnalyst 700 spectrophotometer, after decomposing the compounds by standard methods. FAB mass spectrum was recorded on a JEOL SX-102 FAB mass spectrometer. IR spectra were recorded on a Shimadzu DR 8001 series FTIR instrument as KBr pellets and electronic spectra were recorded on Shimadzu 160A UV–Vis Spectrophotometer from a solution in CH_2Cl_2/DMF. ^{1}H NMR spectra were recorded in an AMX 400 MHz FT NMR Spectrometer using $CDCl_3$ as a solvent and TMS and an internal standard at Sophisticated Instrumental Facility, IISc, Bangalore, India.

Table 6
Crystal data and structure refinement for $CoL^4(N_3)$bipy (compound **7**)

Empirical formula	$C_{26}H_{23}CoN_8OS$
Formula weight (M)	554.51
Temperature (T) K	293(2)
Wavelength (Mo Kα) (Å)	0.70930 Å
Crystal system	monoclinic
Space group	$P2_1/a$
Unit cell dimensions	
a (Å)	13.625(2)
b (Å)	10.610(14)
c (Å)	17.8410(19)
α (°)	90.000(10)
β (°)	107.355(10)
γ (°)	90.000(10)
Volume (V) (Å^3)	2461.9(6)
Z	4
Calculated density (ρ) (mg m^{-3})	1.496
Absorption coefficient (μ) (mm^{-1})	0.820
$F(000)$	1144
Crystal size (mm)	0.4 × 0.4 × 0.4
θ Range for data collection (°)	1.19–24.92
Limiting indices	$0 \le h \le 16$, $0 \le k \le 12$, $-21 \le l \le 20$
Reflections collected	4069
Unique reflections	4069 [$R_{int} = 0.000$]
Completeness to θ	24.92 (88.7%)
Max. and min. transmission	1.000 and 0.952
Refinement method	full-matrix least-squares on F^2
Data/restraints/parameters	4069/0/426
Final R indices [$I > 2\sigma(I)$]	$R_1 = 0.0347$, $wR_2 = 0.0962$
R indices (all data)	$R_1 = 0.0380$, $wR_2 = 0.0996$
Goodness-of-fit on F^2	1.102
Largest difference peak and hole (e Å^{-3})	0.494 and −0.342

3.4. X-ray crystallography

A dark brown monoclinic crystal of the CoL^4bipyN_3 (**7**) having approximate dimensions 0.4 × 0.4 × 0.4 mm was sealed in a glass capillary, and intensity data were measured at room temperature (293 K) on an Nonius MACH3 diffractometer equipped with graphite-monochromated Mo Kα ($\lambda = 0.71073$ Å) radiation. The crystallographic data along with details of structure solution refinements are given in Table 6. Unit cell dimensions were obtained using 25 centered reflections in the θ range 5.53°–12.15°. The intensity data were collected by ω-scan mode within $1.190° < \theta < 24.92°$ for hkl ($0 \le h \le 16$, $0 \le k \le 12$, $-21 \le l \le 20$) in monoclinic system. The trial structure was obtained by direct methods using SHELXS-97 [20] and refined by full-matrix least-squares on F^2 (SHELXL-97) [21]. The non-hydrogen atoms were refined with anisotropic thermal parameters. All the hydrogen atoms were geometrically fixed and allowed to refine using a riding model. Absorption corrections were employed using ψ-scan ($T_{max} = 1.000$ and $T_{min} = 0.952$).

4. Supplementary material

Crystallographic data for the structural analysis has been deposited with the Cambridge Crystallographic Data Center, CCDC No. 182200 for compound CoL^4-bipyN_3. Copies of this information may be obtained free of charge from The Director, CCDC, 12 Union Road, Cambridge, CB2 1EZ, UK (fax: +44-1223-336033; e-mail: deposit@ccdc.cam.ac.uk or www: http://www.ccdc.cam.ac.uk).

Acknowledgements

R.P.J. thanks the Council of Scientific and Industrial Research (CSIR), Government of India for the award of research fellowship. The authors are also thankful to RSIC, CDRI, Lucknow for the elemental analysis, SIF, IISc Bangalore for NMR measurements, National Single Crystal X-ray Diffraction Facility, IIT Bombay for the X-ray crystallographic data.

References

[1] (a) M.J.M. Campbell, Coord. Chem. Rev 15 (1975) 279; (b) J.P. Scovill, D.L. Klayman, C.F. Franchino, J. Med. Chem. 25 (1982) 1261.
[2] A.C. Sartorelli, K.C. Agrawal, A.S. Tsiftsoglou, E.C. Moore, Adv. Enzyme Reg. 15 (1977) 117.
[3] P. Bindu, M.R.P. Kurup, T.R. Satyakeerthy, National Seminar on Metal ions in Biological Sciences, Department of Chemistry, IIT, Chennai, India, March 1997.
[4] P. Bindu, M.R.P. Kurup, Transition Met. Chem. 22 (1997) 578.
[5] P. Bindu, M.R.P. Kurup, T.R. Satyakeerthy, Polyhedron 18 (1998) 321.
[6] P. Bindu, M.R.P. Kurup, Indian J. Chem., Sect. A 36 (1997) 1094.
[7] P. Bindu, M.R.P. Kurup, Indian J. Chem., Sect. A 38 (1999) 388.
[8] R.K. Parashar, R.C. Sharma, A. Kumar, G. Mohan, Inorg. Chim. Acta 151 (1988) 201.
[9] H. Chen, D. Han, H. Yan, W. Tang, Y. Yang, H. Wang, Polyhedron 12 (1993) 1097.
[10] J.P. Costes, G. Cros, M.H. Darbieu, J.P. Laurent, Inorg. Chim. Acta 60 (1982) 111.
[11] A. Bottcher, T. Takeuchi, K.I. Hardcastle, T.J. Meade, H.B. Gray, D.C. Wickel, M. Kapon, Z. Dori, Inorg. Chem. 36 (1997) 2498.
[12] (a) M.B. Ferrari, G.G. Fava, C. Pelizzi, P. Tarasconi, J. Chem. Soc., Dalton Trans. (1992) 2153; (b) M.B. Ferrari, G.G. Fava, C. Pelosi, M.C. Rodriguez-Argűelles, P. Tarasconi, J. Chem. Soc., Dalton. Trans. (1995) 3035.
[13] N. Mondal, D.K. Dey, S. Mitra, K.M. Abdul Malik, Polyhedron 19 (2000) 2707.
[14] J. Ribas, A. Escuer, M. Monfort, R. Vincente, R. Corte, Luis Lezama, T. Rojo, Coord. Chem. Rev. 193–195 (1999) 1027.
[15] M.B. Ferrari, G.G. Fava, M. Lanfranchi, C. Pelizzi, A. Tarasconi, J. Chem. Soc., Dalton. Trans. (1991) 1951.
[16] D.X. West, P.M. Ahrweiler, G. Ertem, J.P. Scovill, D.L. Klayman, J.S. Flippen-Anderson, R. Gilardi, C. George, L.K. Pannel, Transition Met. Chem. 10 (1985) 264.

[17] D.X. West, J.K. Swearingen, J. Vades-Martinez, S. Hernandez-Ortega, A.K. El-Sawaf, F. van Meurs, A. Castineiras, I. Garcia, E. Bermejo, Polyhedron 18 (1999) 2919.
[18] A.L. Balch, L.A. Fosset, R.R. Guimerans, M.M. Olmstead, P.E. Reed, F.E. Wood, Inorg. Chem. 25 (1986) 1248.
[19] K. Nakamoto, Infrared and Raman Spectra of Inorganic and Coordination Compounds, 5th ed., Wiley, New York, 1978, p. 124.
[20] G.M. Sheldrick, SHELXL-97, Program for the Solution of Crystal Structures, University of Göttingen, Göttingen, Germany, 1997.
[21] G.M. Sheldrick, SHELXS-97, Program for the Solution of Crystal Structures, University of Göttingen, Göttingen, Germany, 1997.

2.1. Carbonylation products of $(Et_4N)_2[(Cl_4\text{-}cat)Mo(MeCN)Fe_3S_4Cl_3]$ (**I**) in the presence of $Fe(PEt_3)_2Cl_2$

The $(Et_4N)_2[(Cl_4\text{-cat})Mo(MeCN)Fe_3S_4Cl_3]$ cluster (**I**) (2.5 g, 2.39 mmol) and 3 equiv. of $Fe(PEt_3)_2Cl_2$ (2.6 g, 7.16 mmol) were dissolved in MeCN (50 ml) and the solution was put into the high pressure reactor. CO gas (500 psi) was introduced and the reaction mixture was stirred under CO pressure for 2 days. The CO was vented by releasing pressure and the solvent was removed by purging with nitrogen. The residue was subjected to flash column chromatography using *n*-pentane, hexanes and CH_2Cl_2 eluents on TLC silica gel. The reaction products from each fraction have been crystallized and identified by FT-IR spectroscopy.

2.1.1. $(Cl_4\text{-cat})Mo(CO)_2(PEt_3)_2$ (**II**)

$(Cl_4\text{-cat})Mo(CO)_2(PEt_3)_2$ (**II**) was eluted with *n*-pentane. Slow evaporation of the pentane solution produced a dark purple crystalline material (130 mg, 0.2 mmol, 8.36% yield). FAB (positive, NBA), (*m*/*z*, relative intensity) 633.9($[M]^+$, 44.9), 577.9 ($[M-2(CO)]^+$, 69.3), 460.2($[M-\{2(CO)+(PEt_3)\}]^+$, base peak); FT-IR (KBr, cm^{-1}) 2969(w), 2937(w), 2875(w), 1928(s), 1843(vs), 1421(s), 1266(m), 1032(m), 985(m), 809(w), 788(w), 770(w), 759(w), 622(w), 567(w).

2.1.2. $(Cl_4\text{-cat})Mo(PEt_3)Fe_3S_4(SPEt_3)_2Cl$ (**III**)

$(Cl_4\text{-cat})Mo(PEt_3)Fe_3S_4(SPEt_3)_2Cl$ (**III**) was eluted using 25–50% of CH_2Cl_2–hexanes. Black crystalline material (500 mg, 0.458 mmol) was isolated, after standing for 5–7 days in 19% yield. *Anal*. Calc. for $MoFe_3Cl_5S_6P_3O_2C_{24}H_{45}$ (MW 1091.67): C, 26.41; H, 4.15. Found: C, 27.05; H, 4.15%. FT-IR (KBr, cm^{-1}) 2971, 2935, 2903, 2878, 1432(s), 1251(m), 1037, 976(m), 773(m), 537. UV–Vis (CH_2Cl_2, nm) 314(sh), 470. EPR (CH_2Cl_2, 17 K) $g = 5.46$, 5.15, 4.38, 2.12, 2.06, 1.99. Mössbauer (125 K, mm s^{-1}) $\delta = 0.420$, 0.441, 0.370. $\Delta E_Q = 0.659$, 0.934, 1.144.

2.2. Carbonylation products of $(Et_4N)_2[(Cl_4\text{-}cat)Mo(MeCN)Fe_3S_4Cl_3]$ (**I**) in the presence of PEt_3–$NaBPh_4$

$(Et_4N)_2[(Cl_4\text{-cat})(MeCN)MoFe_3S_4Cl_3]$ (1.0 g, 0.96 mmol) (**I**) was dissolved in 60 ml of MeCN in the high pressure reactor vessel and 4.3 equiv. of PEt_3(0.6 ml, 4.11 mmol) and 3 equiv. of $NaBPh_4$ (1.0 g, 2.92 mmol) were added into the solution. The reactor was charged with CO at a pressure of 500 psi. After 3 days, the reaction mixture was transferred to a Schlenk flask to reduce the volume. The concentrated solution was loaded on the preparative silica gel TLC and developed using a 1:1 mixture of hexanes and CH_2Cl_2. The major product, isolated from the dark red band on the preparative TLC, was the known $(Cl_4\text{-cat})Mo(O)Fe_3S_3(PEt_3)_3(CO)_5$ cluster (200 mg, 0.179 mmol, 19% yield) [4b].

2.3. $(Cl_4\text{-cat})_2MoFe_2S_2(CO)_4(PEt_3)_2$ (**IV**)

Elution of the bright red band with CH_2Cl_2 and slow evaporation of this solution produced 20 mg (18 μmol, 1.9% yield) of purple rhombic crystals of **IV**. FT-IR (KBr, cm^{-1}) 2963(w), 2952(w), 2925(w), 2883(w), 2022(s), 1999(vs), 1970(s), 1965(s), 1960(s), 1455(s), 1274(s), 1033(m), 1001(m), 990(m), 813(m), 791(m), 569(m), 478(m), 449(s), 414(s), 377(s), 362(m). Microprobe. Calculated for $C_{28}H_{30}Cl_8Fe_2MoO_8P_2S_2$ (MW 1111.86): Mo, 8.63; Fe, 10.05; Cl, 25.51; S, 5.77; P, 5.57. Found: Mo, 9.92(19); Fe, 10.31(14); Cl, 25.86(36); S, 6.36(76); P, 5.23(42)%.

2.4. X-ray crystallography

The crystals isolated from the chromatographic fractions were attached to glass fibers and diffraction data were collected at 158(2) K using a Siemens SMART area diffractometer. The empirical absorption correction SADABS has been applied to the data. The crystal data and structural parameters for the compound **II**, **III** and **IV** are listed in Table 1. The structures were determined by direct methods to locate heavy atoms. The non-hydrogen atoms were located through subsequent difference Fourier syntheses. Structural refinements were carried out by full-matrix least-squares on F^2. Hydrogen atoms were assigned idealized positions. All non-hydrogen atoms were refined with anisotropic thermal parameters and all hydrogen atoms were refined isotropically. All calculations were performed using SHELXTL-NT V. 5.1 software.

3. Results and discussion

In previous reports we have described the reactivity of cluster-bound R_3P ligands cluster manifested in the concomitant formation of $P_3P{=}S$ and depletion of μ_3 sulfido ligands. Thus, under a pressure of CO the $(Cl_4\text{-cat})_2Mo_2Fe_6S_8(PR_3)_6$ [R = Et [10], ^{n}Pr [3]] fused-cubane clusters afford new, reduced, FeMoS clusters that contain CO and R_3P terminal ligands and the rare, sulfur-voided $[MoFe_3S_3]^{2+,4+}$ cores. In these reactions, non-polar solvent soluble, alkali metal salts of non-coordinating anions such as BPh_4^- or PF_6^-. were used to remove the halide ligands. The latter readily precipitate as insoluble alkali metal chloride salts.

The cluster reduction, and removal of terminal halide and bridging sulfide ligands also can be achieved using the $Fe(PR_3)_2Cl_2$ (R = alkyl) 'reagent'. The latter both provides PR_3 and removes halide ligands to form

Table 1
Data collection and crystal parameters for the (Cl_4-cat)Mo(PEt_3)$_2$(CO)$_2$ (**II**), the (Cl_4-cat)Mo(PEt_3)Fe_3S_4(SPEt_3)$_2$Cl (**III**), and the (Cl_4-cat)$_2$MoFe_2S_2(Pet$_3$)$_2$(CO)$_4$ (**IV**) compounds

Compound	II	III	IV
Empirical formula	$C_{20}H_{30}Cl_4MoO_4P_2$	$C_{24}H_{45}Cl_5Fe_3MoO_2P_3S_6$	$C_{28}H_{30}Cl_8Fe_2MoO_8P_2S_2$
Formula weight	634.12	1091.61	1111.82
Wavelength (Å)	0.71073	0.71073	0.71073
Crystal system	triclinic	orthorhombic	Monoclinic
Space group	$P\bar{1}$	$Cmc2(l)$	$C2/c$
Unit cell dimensions			
a (Å)	10.5554(6)	16.659(3)	24.610(4)
b (Å)	11.1415(7)	12.598(2)	10.3487(17)
c (Å)	12.9264(8)	20.405(4)	15.965(3)
α (°)	0.5070(10)		
β (°)	103.0450(10)		98.461(3)
γ (°)	105.0010(10)		
Volume (Å^3)	1288.48(14)	4282.4(13)	4021.9(11)
Z	2	4	4
Calculated density (Mg m^3)	1.634	1.693	1.836
Absorption coefficient (mm^{-1})	1.073	2.022	1.779
$F(000)$	644	2204	2216
Crystal size (mm)	0.18 × 0.18 × 0.04	0.52 × 0.32 × 0.30	0.20 × 0.08 × 0.06
θ Range for data collection (°)	1.80–26.39	2.00–26.43	1.67–26.41
Limiting indices	$-12 \le h \le 13$	$-20 \le h \le 20$	$-30 \le h \le 30$
	$-13 \le k \le 13$	$-15 \le k \le 15$	$-12 \le k \le 12$
	$-16 \le l \le 16$	$-25 \le l \le 25$	$-19 \le l \le 19$
Reflections collected/unique	13 582/5239	20 348/4545	18 996/4118
R_{int}	0.0258	0.0238	0.0647
Data/restraints/parameters	5239/0/280	4545/1/211	4118/0/246
Goodness-of-fit on F^2	1.006	1.091	1.026
Final R indices	$R_1 = 0.0243$, $wR_2 = 0.0591$	$R_1 = 0.0309$, $wR_2 = 0.0813$	$R_1 = 0.0361$, $wR_2 = 0.0712$
$[I > 2\sigma(I)]$	0.0591	0.0813	0.0712
R indices (all data)	$R_1 = 0.0337$, $wR_2 = 0.0611$	$R_1 = 0.0315$, $wR_2 = 0.0817$	$R_1 = 0.0575$, $wR_2 = 0.0777$

[Fe(PEt_3)Cl_2X]$^-$ or [$FeCl_2X_2$]$^{2-}$ [3]. The reaction of the Fe(PR_3)$_2Cl_2$ reagent with **I** affords the mononuclear(Cl_4-cat)Mo(CO)$_2$(PEt_3)$_2$, (**II**) and the neutral cubane (Cl_4-cat)Mo(PEt_3)Fe_3S_4(SPEt_3)$_2$Cl (**III**). In the latter the generated P_3P=S byproduct serves as a terminal ligand to the Fe atoms.

The reaction of **I** with CO in the presence of R_3P and $NaBPh_4$ in CH_3CN solution also proceeds with the removal of Cl^- ligands as NaCl and formation of P_3P=S. However, the products isolated by this route are the known (Cl_4-cat)Mo(O)Fe_3S_3(PEt_3)$_3$(CO)$_5$ cluster and the trinuclear cluster (Cl_4-cat)$_2$MoFe_2S_2(CO)$_4$(PEt_3)$_2$ (**IV**).

3.1. Structures

3.1.1. (Cl_4-cat)Mo(PEt_3)$_2$(CO)$_2$ (II)

The monomeric, **II**, is a six-coordinate 16-electron Mo(II) complex (Fig. 1) with a distorted trigonal prismatic coordination geometry. In the coordination sphere of the Mo atom, the triangular, coordination polyhedron faces, P(1)–C(7)–O(2) and P(2)–C(8)–O(1) are rotated approximately 25° from being trigonal prismatic and they are roughly parallel to each other. There are a few structurally characterized six-coordinate 16-electron MoX_2(PR_3)$_2$(CO)$_2$ [X = halide] complexes [11] and several seven-coordinate 18-electron complexes [12], such as Mo(O_2CR')$_2$(PR_3)$_2$(CO)$_2$ and MoX(O_2CR')(PR_3)$_2$(CO)$_2$ [R, R′ = H, Me, Et, Ph]. All of these compounds have the (PR_3)$_2$(CO)$_2$ ligand unit in common with **II**. A comparison of selected bond distances in **II** with other Mo(II) complex is available in Table 2. The Mo–C distances of 1.951(2) and 1.961(2) Å in **II** are similar to those found in (O_2CH)$_2$Mo(PEt_3)$_2$(CO)$_2$ (1.951(3) and 1.954(3) Å). The latter [12c] is an 18-electron complex adopting a 3:4 'piano stool' configuration. The three oxygen atoms of the two formato ligands, with the forth free oxygen atom, occupy the triangular cap. The CO and PEt_3 ligands form the rectangular base of the molecule. The ν(C≡O)'s also are similar at 1928 and 1843 cm^{-1} and at 1929 and 1833 cm^{-1} for **II** and (O_2CH)$_2$Mo(PEt_3)$_2$(CO)$_2$), respectively.

The 18-electron, (acac)MoI(PEt_3)$_2$(CO)$_2$ [12a], shows relatively different bond length distributions where two Mo–C bonds have different distances (1.950(10) and 1.994(11) Å) and the Mo–P bonds (2.541(2) and 2.543(3) Å) are longer than those of the 16-electron complexes. This probably is due to the bulky iodide ligand in the Mo(II) coordination sphere. It should be

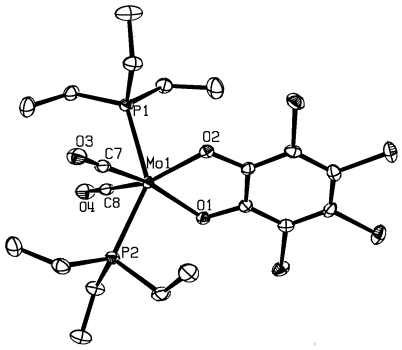


Fig. 1. The crystallographic structure of the $(Cl_4\text{-cat})Mo(PEt_3)_2(CO)_2$ (**II**) compound.

noted that compound **II** could also be described as an 18-electron complex if the Cl_4-cat (tetrachlorocatecholate) ligand is internally oxidized to a tetrachloroquinone ligand (and the Mo atom is now Mo(0)). The assignment of the ligand as $Cl_4\text{-cat}^{2-}$ is based on the low energy ν(C=O) in the IR spectrum at 1421 cm^{-1} and the rather long C–O bonds of 1.331(3) and 1.325(3) Å. Generally, distances of C–O for benzoquinones, semiquinonates and catecholates are 1.23, 1.29, and 1.35 Å, respectively [13].

3.1.2. $(Cl_4\text{-cat})Mo(PEt_3)Fe_3S_4(SPEt_3)_2Cl$ (*III*)

The new $(Cl_4\text{-cat})Mo(PEt_3)Fe_3S_4(SPEt_3)_2Cl$ cluster (**III**) is the first example of a site-differentiated $MoFe_3S_3$ cluster with a $[MoFe_3S_4]^{3+}$ core and two different terminal ligands on the Fe atoms (Fig. 2). The structure of **III** shows a core geometry similar to that in **I**, but has shorter M–M distances (Table 3). There is a crystallographic mirror plane within the molecule that contains P(1), Mo(1), Fe(2), S(3), S(1), and Cl(3). The Mo(1) atom has distorted octahedral coordination geometry and the crystllographically independent P(1), O(1), S(2), and S(3) atoms are found at distances of 2.5918(15),

Table 2
Selected bond distances (Å) of the $(Cl_4\text{-cat})Mo(PEt_3)_2(CO)_2$ (**II**), the $(O_2CH)_2Mo(PEt_3)_2(CO)_2$, and the $(acac)MoI(PEt_3)_2(CO)_2$ compounds

Compound	**II**	$(O_2CH)_2Mo(PEt_3)_2(CO)_2$	$(acac)MoI(Pet_3)_2(CO)_2$
Mo(1)–C(7)	1.951(2)	1.951(3)	1.950(11)
Mo(1)–C(8)	1.961(2)	1.954(3)	1.994(10)
Mo(1)–O(2)	2.063(2)	2.281(2)	2.158(6)
Mo(1)–O(1)	2.075(2)	2,218(2)	2.167(6)
Mo–O		2.148(2)	
Mo(1)–P(1)	2.4636(6)	2.472(1)	2.541(2)
Mo(1)–P(2)	2.4775(6)	2.516(1)	2.543(3)
O(1)–C(1)	1.331(3)	1.263(4)	
O(2)–C(6)	1.325(3)	1.252(4)	
O–C	1.210(4)		
O(3)–C(7)	1.168(3)	1.160(4)	
O(4)–C(8)	1,165(3)	1.155(4)	
–(C≡O) (cm^{-1})	1928, 1843	1929, 1833	1921, 1809
Reference	this work	[12(c)]	[12(a)]

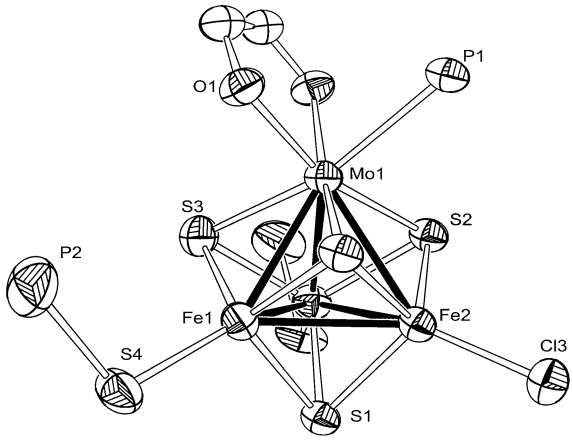


Fig. 2. The crystallographic structure of the $(Cl_4\text{-cat})Mo(PEt_3)Fe_3S_4(SPEt_3)_2Cl$ (**III**) cluster.

2.076(3), 2.3565(10), and 2.4006(17) Å, respectively. The Mo(1)–P(1) distance of 2.5918(15) Å in **III** is slightly shorter than that in the $(Cl_4\text{-cat})_2Mo_2Fe_6S_8(PEt_3)_6$ cluster at 2.602(3) Å. The latter has a reduced $[MoFe_3S_4]^{2+}$ core. The Mo(1)–P(1) bond in **III** also is within the range found for the Mo–P bonds in the $(Cl_4\text{-cat})_2Mo_2Fe_6S_8(PR_3)_6$ [R = Et, ^{n}Pr, ^{n}Bu] clusters (2.602(3)–2.575(2) Å) [3]. The only $[MoFe_3S_4]^{3+}$ (oxidized) cluster with a phophine ligand bound to the Mo atom is $(Et_4N)[Mo(dmpe)Fe_3S_4Cl_4]$ [14]. The two P atoms in the latter are found at distances of 2.562(3) and 2.545(3) Å from the Mo atom.

The tetrahedrally coordinated Fe(1) atom has four ligands, S(1), S(2), S(3) and S(4) at distances of 2.2787(13), 2.2543(11), 2.2543(14), and 2.3020(13) Å, respectively. The ligands of the tetrahedrally coordinated Fe(2) atom, S(1), S(2), S(2)#, and Cl(3), are found at 2.2776(15), 2.2730(17), 2.2730(17), and 2.2030(17) Å, respectively. As shown in Table 3, the average Mo–Fe distance in **III** at 2.71(2) Å is shorter than that of **I** [15] at 2.754(5) Å, and slightly longer than those in other $[MoFe_3S_4]^{2+}$ clusters. The Mo(1)–Fe(2) distance of 2.7512(10) Å in **III** is significantly longer than the other Mo(1)–Fe(1) distance of 2.6894(8) Å. A recent report [16] on the reduced $[MoFe_3S_4]^{2+}$ clusters shows average Mo–Fe and Fe–Fe distances that range from 2.67(1) to 2.71(1) and 2.62(1) to 2.693(3) Å, respectively. The average Fe–Fe distance in **III** (2.692(9) Å) is shorter than that in **I** (2.733(5) Å) and is the shortest among $[MoFe_3S_4]^{3+}$ clusters [17]. Indeed, the Mo–Fe and Fe–Fe distance comparison shows **III** with metric details closer to the reduced $[MoFe_3S_4]^{2+}$ clusters. The average Mo–S distance of 2.371(15) Å in **III** is slightly longer than that of 2.354(9) Å in **I** and the average Fe–S distance of 2.266(4) Å in **III** also is the shortest among $[MoFe_3S_4]^{3+}$ clusters.

At present the origin of the shorter distances intracluster M–M and M–S distances in **III** is difficult to ascertain. It may be due to the σ/π donor (reducing)

Table 3
Selected bond distances (Å) of the $(Cl_4\text{-cat})Mo(PEt_3)Fe_3S_4(SPEt_3)_2Cl$ (**III**), the $(Et_4N)_2[(Cl_4\text{-cat})Mo(MeCN)Fe_3S_4Cl_3]$ (**I**), the $(Cl_4\text{-cat})_2Mo_2Fe_6S_8(Pet_3)_6$, and the $(Cl_4\text{-cat})Mo(MeCN)Fe_3S_4(P^iPr_3)_3$ clusters

Bond	III	I	$(Cl_4\text{-cat})_2Mo_2Fe_6S_8(Pet_3)_6$ [a]	$(Cl_4\text{-cat})Mo(MeCN)Fe_3S_4(P^iPr_3)_3$ [b]
Mo(1)–Fe(1)	2.6894(8)	2.749(3)	2.671(2)	2.696(4)
			2.658(2)	2.667(4)
Mo(1)–Fe(2)	2.7512(10)	2.765(4)	2.684(2)	2.681(1)
Average Mo–Fe	2.71(2)	2.754(5)	2.677(5)	
Fe(1)–Fe(2)	2.7013(9)	2.734(4)	2.632(2)	2.632(5)
			2.639(3)	2.596(5)
Fe(1)–Fe(1)#	2.6742(13)	2.732(5)	2.632(2)	2.628(2)
Average Fe–Fe	2.692(9)	2.733(5)	2.639(3)	2.619(11)
Mo(1)–P(1)	2.5918(15)	2.29(3) (N–MeCN)	2.602(3) (P–PEt_3)	2.280(9) (N–MeCN)
Mo(1)–O(1)	2.076(3)	2.052(12)	2.098(7)	2.14(2)
			2.093(7)	2.05(2)
Mo(1)–S(2)	2.3565(10)	2.364(5)	2.366(3)	2.344(7)
			2.362(3)	2.398(8)
Mo(1)–S(3)	2.4006(17)	2.335(7)	2.434(3)	2.356(2)
Average Mo–S	2.371(15)	2.354(9)	2.387(13)	2.36(3)
Fe(1)–S(3)	2.2543(14)	2.276(6)	2.247(4)	2.254(7)
			2.236(4)	2.229(6)
Fe(2)–S(2)	2.2730(11)	2.269(5)	2.257(4)	2.236(8)
			2.236(4)	2.278(9)
Average Fe–S	2.266(4)	2.275(8)	2.29(2)	2.25(2)
Fe(1)–S(4)	2.3020(13)	2.749(3) (Cl)	2.355(4) (P–Pet_3)	2.344(9) (P–Pet_3)
			2.323(5) (P–Pet_3)	2.368(2) (P–Pet_3)
Fe(2)–Cl(3)	2.2030(17)	2.190(8)	2.277(3) ($_4\mu_5$–S)	2.380(2) (P–Pet_3)

[a] Ref. [2].
[b] Ref. [14].

properties of the $SPEt_3$ ligands but also it could be due to the neutral nature of the cluster. In general, charged clusters may have longer bonds than the neutral ones because of net intra-molecular repulsions among the atoms. It is reasonable to assume that both electronic and charge effects contribute to the short M–M and M–L distances in **III**.

The Mössbauer spectrum [18] of **III** can be fit by three Fe sites with isomer shifts of $\delta = 0.420$, 0.441, 0.370 and quadrupole splittings of $\Delta E_Q = 0.659$, 0.934, 1.144, respectively (Fig. 3). As the Fe centers in **III** has non-thiolate ligands, the empirical equation ($\delta = 1.44–0.43$ s) between isomer shift and mean oxidation state [19] is not applicable. Generally, the average isomer shifts of $[MoFe_3S_4]^{3+}$ clusters [20] are found between 0.29–0.40 mm s^{-1} and those of the $[MoFe_3S_4]^{2+}$ clusters [21] are found between 0.41 and 0.52 mm s^{-1}. The average isomer shift of **III** at $\delta = 0.41$mm s^{-1} which is close to a $Fe^{+2.33}$ formal mean oxidation state for a $[MoFe_3S_4]^{2+}$ cluster. By Mössbauer spectroscopic criteria, the electronic structure of the core in **III** is closer to that in the $[MoFe_3S_4]^{2+}$ clusters. The Mössbauer spectroscopy and structural results suggest that the oxidation states of the metal atoms in **III** could best be assigned as Mo(IV)Fe(II)$_2$Fe(III).

3.1.3. $(Cl_4\text{-cat})_2MoFe_2S_2(PEt_3)_2(CO)_4$ (**IV**)

There are several known organometallic clusters [22] with the $[MFe_2E_2]$ cores, [M = Pt, Pd, Mo, Co, Ni, Ti, Fe, Sn, Ge, and E = S, Se, Te]. They are mainly synthesized from the reaction of (μ-dithio)bis(tricarbonyliron) with coordinatively unsaturated low-valent transition metal compounds. Among them, only a few have been structurally characterized [23]. Their syntheses require the reduced $[Fe_2S_2(CO)_6]^{2-}$ unit and a Mo(II) reagent. These compounds, which contain the $MoFe_2S_2$ moiety as a subunit., include: The $Fe_3S_4(PEt_3)_3MoFe_2S_2(CO)_6$ cluster [24], clusters that contain the $[Mo_2O_2(\mu\text{-}E)_2]^{2+}$ (E = O or S) cores bound by $[Fe_2S_2(CO)_6]^{2-}$ units [25], a compound with two $[Fe_2S_2(CO)_6]$ units bound to a central $[(O)Mo(\mu\text{-}S)_2Fe]$

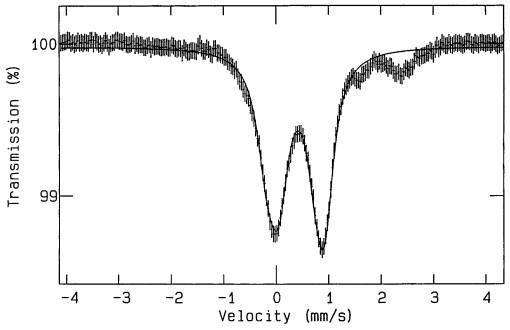


Fig. 3. ^{57}Fe Mössbauer spectrum of the $(Cl_4\text{-cat})Mo(PEt_3)Fe_3S_4(SPEt_3)_2Cl$ (**III**) cluster measured at 125 K in zero applied magnetic field. The source was ^{57}Co in a Rh matrix and the isomer shift was reported vs. Fe metal at room temperature. The solid lines show the fitted spectra as described in the text.

core [26] and a compound with three $[Fe_2S_2(CO)_6]$ units bound to central Mo atom [27].

The isolation of products, **II**, **III**, and **IV** from the reaction of **I** with CO can be rationalized in terms of the pathway shown in Scheme 1. Addition of CO ligands on the Fe atoms of **I** (probably following μ_3-S^{2-} abstraction by trialkylphosphine) initiates the oxidative cleavage of the $[MoFe_3S_4]$ core [28] into $[Fe_2S_2(PEt_3)_2(CO)_4]$ and $[(Cl_4\text{-cat})Mo(PEt_3)FeS_2L_n]$ units. Further cleavage of the $[(Cl_4\text{-cat})Mo(PEt_3)FeS_2L_n]$ unit in the presence of CO may produce **II** and $S{=}PEt_3$. The latter substitutes for the PEt_3 ligands on the Fe atoms of $[(Cl_4\text{-cat})Mo(PEt_3)Fe_3S_4(PEt_3)_2Cl]$ cluster to produce **III**. The addition of **II** to the $[Fe_2S_2(PEt_3)_2(CO)_4]$ unit with dissociation of CO ligands results in the $[(Cl_4\text{-cat})Mo(PEt_3)_2Fe_2S_2(PEt_3)_2(CO)_4]$ cluster which is further oxidized to **IV** while the PEt_3 ligand on the Mo atom is substituted by $Cl_4\text{-cat}^{2-}$.

The compound **IV** has been structurally characterized (Table 1) [29] and the structure has a crystallographic C_2 axis. The rotation axis contains the Mo(1) atom and passes through the center of the Fe–Fe# bond (Fig. 4). The Fe(1)–Fe(1#) distance of 2.6642(10) Å is short and indicative of M–M bonding. The Mo(1) shows weaker M–M interactions with the two Fe atoms (Mo(1)–Fe(1); 2.8515(7) Å). The Mo(1) atom's coordination geometry can be defined as trigonal prismatic brought about by four O atoms and two S atoms (Mo(1)–O(1); 1.995(2) Å, Mo(1)–O(2); 2.042(2) Å, Mo(1)–S(1); 2.3351(9) Å). The Fe(1) atom has a trigonal bipyramidal coordination geometry with axial S(1) (2.2216(10) Å) and P(1) (2.2649(10) Å) ligands and equatorial S(2) (2.2172(10) Å), C(7) (1.775(4) Å) and C(8) (1.798(4) Å) ligands. The S atoms on the equatorial position have shorter Fe–S distances compared with those on the axial position.

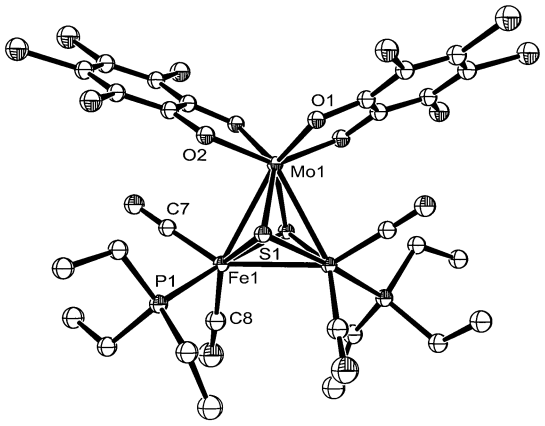
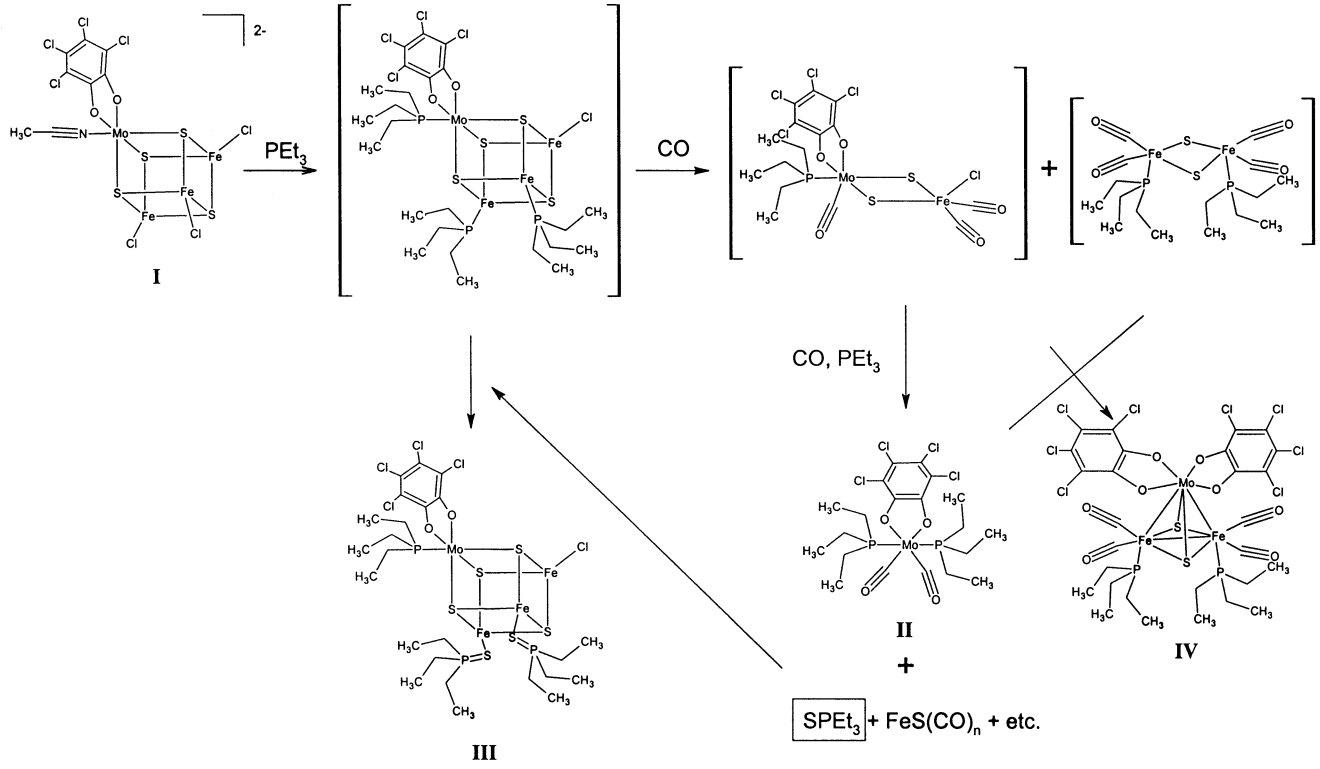


Fig. 4. The crystallographic structure of the $(Cl_4\text{-cat})_2MoFe_2S_2(PEt_3)_2(CO)_4$ (**IV**) cluster. Selected distances (Å) and angles (°): Mo1–Fe1, 2.8515(7); Fe1–Fe1#, 2.6642(10); Mo1–S1, 23351(9); Fe1–S1, 2.2172(10); Fe1–S1#, 2.2216(10); Fe1–P1, 22649(10); Fe1–C7,1.775(4); Fe1–C8, 1.798(4). S1–Mo1–S1# 85.33(5); Fe1–Mo1–Fe1#, 55.70(2); S1–Fe1–S1#, 90.97(4); Fel–Sl–Fel#, 73.77(3).



Scheme 1. Proposed reaction pathways for the $(Cl_4\text{-cat})Mo(PEt_3)_2(CO)_2$ (**II**), the $(Cl_4\text{-cat})Mo(PEt_3)Fe_3S_4(SPEt_3)_2Cl$ (**III**), and the $(Cl_4\text{-cat})_2MoFe_2S_2(PEt_3)_2(CO)_4$ (**IV**) clusters from the $(Et_4N)_2[(Cl_4\text{-cat})Mo(MeCN)Fe_3S_4Cl_3]$ (**I**) cluster.

The $(Cl_4\text{-cat})_2MoFe_2S_2(PEt_3)_2(CO)_4$ (**IV**) cluster contains the $[MoFe_2]^{8+}$ core and is a 46-electron cluster. The oxidation states of the metal atoms in **IV** can be assigned as Mo(IV) and 2Fe(II). The Mo(IV) atom is considered as a 14-electron center with two $Cl_4\text{-cat}^{2-}$ and two μ_3-S ligands. The two Fe(II) atoms are considered as 16-electron centers coordinated by two CO, a PEt_3 and two μ_3-S ligands. The addition of three M–M bonds between the Mo and Fe atoms results in a 16-electron Mo center and two 18-electron Fe centers.

4. Supplementary data

Crystallographic data for the structural analysis have been deposited with the Cambridge Crystallographic Data Centre, CCDC No. 168354 for compound **II**, CCDC No. 168353 for compound **III**, and CCDC No. 168352 for compound **IV**. Copies of this information may be obtained free of charge from The Director, CCDC, 12 Union Road, Cambridge, CB2 1EZ, UK (fax: +44-1223-336066; e-mail: deposit@ccdc.cam.ac.uk or www: http://www.ccdc.cam.ac.uk).

Acknowledgements

The authors acknowledge the support of this work by a grant from the National Institutes of Health (GM 33080). Dr. Namdoo Moon in the Biophysics Department at the University of Michigan is greatly appreciated for his Mössbauer and EPR measurements and helpful discussion.

References

[1] (a) J.B. Howard, D.C. Rees, Chem. Rev. 96 (1996) 2965 (and references therein);
(b) J.W. Peters, M.H.B. Stowell, S.M. Soltis, M.G. Finnegan, M.K. Johnson, D.C. Rees, Biochemistry 36 (1997) 1181;
(c) S.M. Mayer, D.M. Lawson, C.A. Gormal, S.M. Roe, B.E.J. Smith, Mol. Biol. 292 (1999) 871.
[2] K.D. Demadis, C.F. Campana, D. Coucouvanis, J. Am. Chem. Soc. 117 (1995) 7832.
[3] J. Han, M. Koutmos, S. Al-Ahmad, D. Coucouvanis, Inorg. Chem. 40 (2001) 5985.
[4] (a) J. Han, K. Beck, N. Ockwig, D. Coucouvanis, J. Am. Chem. Soc. 121 (1999) 10448;
(b) M.A. Tyson, D. Coucouvanis, Inorg. Chem. 36 (1997) 3808.
[5] D. Coucouvanis, J. Han, N. Moon, Inorg. Chem. 124 (2001) 216.
[6] J. Han, D. Coucouvanis, J. Am. Chem. Soc. 123 (2001) 11304.
[7] R.E. Palermo, R. Singh, J.K. Bashkin, R.H. Holm, J. Am. Chem. Soc. 106 (1984) 2600.
[8] P.R. Challen, Ph.D. thesis, University of Michigan, 1990.
[9] G. Booth, J. Chatt, J. Chem. Soc. (1962) 2099.
[10] K.D. Demadis, C.F. Campana, D. Coucouvanis, J. Am. Chem. Soc. 117 (1995) 7832.
[11] J.R. Moss, B.L. Shaw, J. Chem. Soc. A (1970) 595.
[12] (a) P.K. Baker, A.I. Clark, M.G.B. Drew, M.C. Durrant, R.L. Richards, J. Organomet. Chem. 549 (1997) 193;
(b) B.J. Brisdon, A.G.W. Hodson, M.F. Mahon, K.C. Molloy, J. Chem. Soc., Dalton Trans. (1993) 245;
(c) D.C. Brower, P.B. Winston, T.L. Tonker, J.L. Templeton, Inorg. Chem. 25 (1986) 2883.
[13] C.G. Pierpont, R.M. Buchanan, Coord. Chem. Rev. 38 (1981) 45.
[14] (a) dmpe = 1,2-bis(dimethylphosphino)ethane;
(b) Y.-P. Zhang, J.K. Bashkin, R.H. Holm, Inorg. Chem. 26 (1987) 694.
[15] The average Mo–Fe distance among the $(Et_4N)_2[(Cl_4\text{-cat})Mo(L)Fe_3S_4Cl_3]$ (L = THF, $MeNHNH_2$, $MeNH_2$), the $(Et_4N)_2[(al\text{-cat})Mo(THF)Fe_3S_4Cl_3]$ (al-cat = 3,6-diallylcatecholate), and the $(Et_4N)_3[(Cl_4\text{-cat})Mo(Cl)Fe_3S_4Cl_3]$ cluster are shown at 2.742(6) , 2.729(11), 2.735(9), 2.775(9), and 2.749(10) Å, respectively.
[16] F. Osterloh, B.M. Segal, C. Achim, R.H. Holm, Inorg. Chem. 39 (2000) 980.
[17] The average Fe–Fe distance among the $(Et_4N)_2[(Cl_4\text{-cat})Mo(L)Fe_3S_4Cl_3]$ (L = THF, $MeNHNH_2$, $MeNH_2$), the $(Et_4N)_2[(al\text{-cat})Mo(THF)Fe_3S_4Cl_3]$ (al-cat = 3,6-diallylcatecholate), and the $(Et_4N)_3[(Cl_4\text{-cat})Mo(Cl)Fe_3S_4Cl_3]$ cluster are shown at 2.716(7) , 2.722(10), 2.724(14), 2.728(3), and 2.707(19) Å, respectively.
[18] For the experimental conditions, N. Moon, C.T. Coffin, D.C. Steinke, R.H. Sands, W.R. Dunham, Nucl. Inst. Meth. Phys. Res. B. 119 (1996) 555.
[19] G. Christou, P.K. Mascharak, W.H. Armstrong, G.C. Papaefthymiou, R.B. Frankel, R.H. Holm, J. Am. Chem. Soc. 104 (1982) 2820.
[20] The average isomer shifts of $(Et_4N)_3[(al_2cat)MoFe_3S_4(S\text{-}p\text{-}C_6H_4Me)_4]$, $(Et_4N)[(dmpe)MoFe_3S_4(SEt)_4]$, $(Et_4N)_2[(al_2cat)Mo(THF)Fe_3S_4Cl_3]\cdot 1/2Me_2CO$, and $(Et_4N)[(dmpe)MoFe_3S_4Cl_4]$ are found at 0.30, 0.29, 0.40, and 0.38 mm s^{-1}, respectively. M.J. Carney, J.A. Kovacs, Y.-P. Zhang, G.C. Papaefthymiou, K. Spartalian, R.B. Frankel, R.H. Holm, Inorg. Chem. 26 (1987) 719.
[21] Most of the $[MoFe_3S_4]^{2+}$ clusters have phosphine ligands and their isomer shifts primarily depend on the alkyl group of the ligand. The $(Cl_4\text{-cat})_2Mo_2Fe_6S_8(PEt_3)_6$ cluster shows an isomer shift at 0.47 mm s^{-1} and its P^nPr_3 analog shows at 0.41 mm s^{-1}. The $(Cl_4\text{-cat})Mo(MeCN)Fe_3S_4(P^tBu_3)_3$ cluster and the $(Cl_4\text{-cat})Mo(MeCN)Fe_3S_4(P^iPr_3)_3$ cluster show the isomer shifts at 0.52 and 0.46 mm s^{-1}, respectively.
[22] (a) P. Mathur, I.J. Mavunkal, V. Rugmini, J. Organomet. Chem. 367 (1989) 243;
(b) M. Cowie, R.L. DeKock, T.R. Wagenmaker, D. Seyferth, R.S. Henderson, M.K. Gallagher, Organometallics 8 (1989) 119;
(c) Y. Wakatsuki, H. Yamazaki, G. Cheng, J. Organomet. Chem. 347 (1988) 151;
(d) D. Seyferth, R.S. Henderson, L.-C. Song, Organometallics 1 (1982) 125;
(e) D.A. Lesch, T.B. Rauchfuss, J. Organomet. Chem. 199 (1980) C6;
(f) D. Seyferth, R.S. Henderson, M.K. Gallagher, J. Organomet. Chem. 193 (1980) C75.
[23] (a) B. Zhuang, P. Chen, L. Huang, J. Lu, Polyhedron 11 (1992) 127;
(b) P.T. Bishop, J.R. Dilworth, S. Morton, J.A. Zubieta, J. Organomet. Chem. 341 (1988) 373;
(c) J.R. Dilworth, S. Morton, J. Organomet. Chem. 314 (1986) C25.
[24] K.S. Bose, S.A. Chmielewski, P.A. Eldredge, E. Sinn, B.A. Averill, J. Am. Chem. Soc. 111 (1989) 8953.
[25] D.E. Barber, R.F. Bryan, M. Sabat, K.S. Bose, B.A. Averill, Inorg. Chem. 35 (1996) 4635.

[26] K.S. Bose, P.E. Lamberty, J.E. Kovacs, E. Sinn, B.A. Averill, Polyhedron 5 (1986) 393.
[27] P.A. Eldredge, R.F. Bryan, E. Sinn, B.A. Averill, J. Am. Chem. Soc. 110 (1988) 5573.
[28] Such a reductive cleavage of the $[MoFe_3S_4]$ cuboidal core has been reported by us in reference [5].
[29] Compound **IV** was also crystallized with a CH_2Cl_2 molecule in the orthorhombic cell system. Space group was *Pcnb* and $R_1 = 0.0577$ (for $I > 2\sigma(I)$).

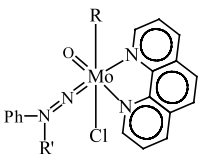
zido-molybdenum complexes [*trans*-$R_2MoO(NNPhR')(o\text{-phen})$], R = R′ = Me (**1**), R = Me, R′ = Ph (**2**), R = Ph, R′ = Me (**3**), R = R′ = Ph (**4**) toward (i) neutral hydrazines: $R'PhNNH_2$ and (ii) organohydrazine hydrochlorides: $R'PhNNH_2 \cdot HCl$, R′ = Me, Ph. These studies provide a convenient access to the synthesis of new coordination complexes containing the *trans*-[RMoCl] fragments (R = Me, Ph). The new coordination compounds, formulated as [*trans*-$RClMoO(NNPhR')(o\text{-phen})$], R = R′ = Me (**5**), R = Me, R′ = Ph (**6**), R = Ph, R′ = Me, (**7**)·MeCN, R = R′ = Ph, (**8**)·MeCN, and [*trans*-$Cl_2MoO(NNPhR')(o\text{-phen})$], R′ = Me (**9**), Ph (**10**), were characterised by IR, UV–Vis and ^{1}H NMR spectroscopies and, in the case of complex **6**, by X-ray diffraction analysis.

2. Results and discussion

2.1. Synthesis and spectroscopic characterisation

The organometallic compounds previously described by us [17] as [*trans*-$Me_2MoO(NNPhR)(o\text{-phen})$], R = Me (**1**), Ph (**2**) and [*trans*-$Ph_2MoO(NNPhR)(o\text{-phen})$], R = Me (**3**), Ph (**4**), were synthesised in two steps: firstly, the mono-functionalisation of complex [$MoO_2Br_2(o\text{-phen})$] with neutral 1,1-disubstituted hydrazines and then alkylation or arylation of the resultant mono-functionalised complexes [$MoO(NNPhR')Br_2(o\text{-phen})$] with an excess of the appropriate Grignard reagents. In order to study the functionalisation of the residual oxo group in complexes **1**–**4**, we examined their reactivity toward (i) an excess of neutral 1,1-disubstituted hydrazines, $RPhNNH_2$, R = Me, Ph, and (ii) 1,1-disubstituted hydrazine hydrochlorides, $RPhNNH_2 \cdot HCl$, R = Me, Ph, at room temperature and using acetonitrile as a solvent.

In the first experimental case, the complexes **1**–**4** were inert toward the neutral 1,1-disubstituted hydrazines whatever the experimental conditions used (reflux, excess of hydrazine, time of reaction, etc.). On the other hand, in the second case, the reactions of precursors **1**–**4** with the 1,1-disubstituted hydrazine hydrochlorides, in a 1:1 molar ratio, did not afford the expected bis(organohydrazido) complexes [$R_2Mo(NNPhR')_2(o\text{-phen})$] but they afforded *trans*-MeCl–molybdenum complexes **5** and **6**, and *trans*-PhCl–molybdenum complexes **7**·MeCN and **8**·MeCN (Scheme 1). Finally, when the precursors **1**–**4** were reacted with 1,1-disubstituted hydrazine hydrochlorides in MeCN using a 1:2 molar ratio, the known dichloro-complexes of formula [*trans*-$Cl_2MoO(NNPhMe)(o\text{-phen})$] (**9**) and [*trans*-$Cl_2MoO(NNPh_2)(o\text{-phen})$] (**10**) were obtained [14].



Scheme 1.

The reactions can be rationalised considering an acid–base reaction between the organohydrazinium acid, $RPhNNH_3^+$, and the basic methyl- and phenyl-transition metal complexes [18]. Although the mechanism is unknown, one can reasonably put a proton on the metal centre followed by a reductive elimination of the methyl or phenyl ligands as methane or benzene, respectively, and by a coordination of the chloride ion. Nevertheless, these reactions are a useful synthetic route to the *trans*-MeCl–molybdenum complexes **5**–**6**, and *trans*-PhCl–molybdenum complexes (**7**–**8**)·MeCN. To produce compounds **9** and **10**, this process must operate with twice the amount of 1,1-disubstituted hydrazine hydrochlorides.

The four new organometallic complexes **5**–**6** and (**7**–**8**)·MeCN were obtained as red–orange air stable microcrystalline solids in yields ranging from 21 to 70%, and were characterised by elemental analyses, ^{1}H NMR, IR and UV–Vis spectroscopy (see Section 4). The crystalline and molecular structure of **6** was determined by single crystal X-ray diffraction analysis (vide infra).

For all the compounds, the ^{1}H NMR spectra showed a complex resonance pattern in the 8.00–10.20 ppm range, assigned to the eight non-equivalent protons of the *o*-phenanthroline ligand. The phenyl proton resonances also exhibited a complicated pattern at the upper field in the 6.60–8.00 ppm range. Moreover, the spectra of the compounds (**7**–**8**)·MeCN are more complex than those of **5** and **6** due to the overlapping of the proton resonances of the phenyl ligands bonded to the molybdenum centre. The spectra of the compounds **5** and **7**·MeCN also showed methyl proton resonances attributable to the NNMePh ligand at 4.23 and 4.31 ppm, respectively. In addition to this, the compounds **5** and **6** exhibited methyl proton resonances at 0.56 and 0.63 ppm which is a characteristic of methyl ligands bonded to the molybdenum centre. These signals shifted downfield compared to the signals of the methyl groups in the starting complexes **1** and **2** ($\delta = 0.17$ and 0.19, respectively), which is indicative of a less electron-rich metal centre in **5** and **6**. Both spectra of compounds **7**·MeCN and **8**·MeCN, which crystallise with a CH_3CN solvent molecule, exhibit a methyl proton resonance at 2.50 ppm. The IR spectra of these organometallic compounds show a characteristic medium intensity band in the 1586–1592 cm^{-1} range, which was attributed to the ν(NN) vibration [19] and a strong band in the 880–900 cm^{-1} region corresponding to the ν(MoO) mode [20]. Finally, the electronic spectra of compounds **5**–**6** and (**7**–**8**)·MeCN, recorded in CH_2Cl_2, exhibit three absorp-

tion bands in the 260–520 nm region. The bands observed in the 260–300 and 300–390 nm regions were attributed to the *cis*-MoO(NNPhR) chromophore [21] while the band observed above 400 nm could be assigned to a L–Mo charge transition [22].

2.2. Structural study

A single crystal X-ray diffraction study was undertaken on a selected good quality block-shaped crystal of [*trans*-MeClMoO(NNPh$_2$)(*o*-phen)] (**6**), and its crystal structure was determined as outlined in Section 4. The ORTEP view of [*trans*-MeClMoO(NNPh$_2$)(*o*-phen)] is presented in Fig. 1. The molybdenum centre displays a distorted octahedral geometry, with the methyl and chloro ligands occupying *trans* positions, and with the equatorial plane which is defined by the oxo group, the N(1) atom of the diphenylhydrazido ligand and the N(3) and N(4) atoms of the *o*-phenanthroline. The geometric parameters observed in the *cis*-[MoO(NNPh$_2$)]$^{2+}$ core of this complex (Table 1) are similar to those reported in the literature for other (organohydrazido)oxomolybdenum complexes [13,23]. An extensive delocalisation of the electron density throughout the Mo(NNPh$_2$) unit is supported by (i) the short Mo–N(1) and N(1)–N(2) bond lengths of 1.787(9) and 1.30(1) Å, (ii) the Mo–N(1)–N(2) bond angle of 172.5(8)° which is practically linear and (iii) the Mo–N(1)–N(2)C(1)C(7) moiety, which is almost planar, being the sum of the bond angles around the N(2) atom 360°. Similar to what is observed with its precursor **2** [17], the *trans* influence exerted by the oxo group is clearly far more important than that exerted by the organohydrazido ligand, e.g. Mo–N(3) = 2.346(9) Å versus Mo–N(4) = 2.30(1) Å.

One of the most remarkable features of the structure of this compound is the preferential inclination of the methyl and the chloro ligands toward the N(3) atom of the *o*-phenanthroline ligand; thus, the C(25)–Mo–N(3) and Cl–Mo–N(3) bond angles are 78.5(4)° and 79.1(3)°, respectively, while the C(25)–Mo–N(4) and Cl–Mo–N(4) bond angles are 84.7(4)° and 84.2(3)°, respectively.

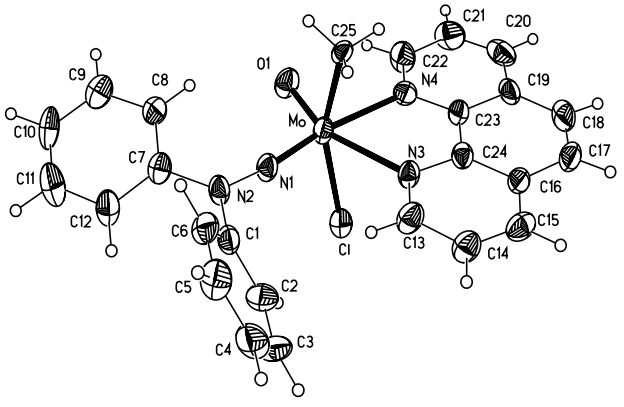


Fig. 1. ORTEP view of complex **6** with the atom-labelling scheme.

Table 1
Selected bond lengths (Å) and angles (°) of complex **6**

Bond distances			
Mo–O(1)	1.712(8)	Mo–Cl	2.472(4)
Mo–N(1)	1.787(9)	N(1)–N(2)	1.30(1)
Mo–N(4)	2.30(1)	N(2)–C(7)	1.44(2)
Mo–C(25)	2.29(1)	N(2)–C(1)	1.46(2)
Mo–N(3)	2.346(9)		
Bond angles			
O(1)–Mo–N(1)	105.1(4)	Cl–Mo–N(1)	95.5(3)
N(1)–Mo–N(3)	98.8(4)	Cl–Mo–N(3)	79.1(3)
N(3)–Mo–N(4)	69.7(3)	Cl–Mo–N(4)	84.2(3)
N(4)–Mo–O(1)	86.2(4)	C(25)–Mo–Cl	157.2(3)
N(1)–Mo–C(25)	91.5(4)	O(1)–Mo–N(3)	155.8(4)
C(25)–Mo–O(1)	97.1(4)	N(1)–Mo–N(4)	168.4(4)
C(25)–Mo–N(1)	91.5(4)	Mo–N(1)–N(2)	172.5(8)
C(25)–Mo–N(3)	78.5(4)	N(1)–N(2)–C(1)	117.0(1)
C(25)–Mo–N(4)	84.7(4)	N(1)–N(2)–C(7)	120.0(1)
Cl–Mo–O(1)	101.9(3)		

These differences can be mainly ascribed, as it has been observed in the parent compound, [*trans*-Me$_2$MoO(NNPh$_2$)(*o*-phen)] [17], to repulsions between the methyl and chloro ligands and the oxo group. As a further consequence of these repulsions, the C(25)–Mo–Cl bond angle is 157.2°, approximately 7.3° greater than that of the precursor [17].

3. Conclusion

The present study provides a convenient access to the preparation of organometallic molybdenum compounds containing the *trans*-[RMoCl] fragment (R = Me, Ph) which could be further functionalised with a variety of monodentate ligands via Mo–Cl substitution reaction. The new organometallic compounds **5**–**6** and (**7**–**8**)·MeCN cannot be directly synthesised by a reaction of [*trans*-X$_2$MoO(NNPhR)(*o*-phen)], X = Cl, Br, with an equimolar amount of Grignard reagents.

4. Experimental

All manipulations were carried out under inert atmosphere using standard vacuum/dinitrogen line (Schlenk) techniques. Organometallic molybdenum compounds, [*trans*-Me$_2$MoO(NNPhR)(*o*-phen)], R = Me (**1**), Ph (**2**) and [*trans*-Ph$_2$MoO(NNPhR)(*o*-phen)], R = Me (**3**), Ph (**4**) were synthesised as was previously described [17]. 1,1-Diphenylhydrazine hydrochloride, Ph$_2$NNH$_2$·HCl, was obtained from commercial sources and used without further purification. 1-Methyl-1-phenylhydrazine hydrochloride, MePhNNH$_2$·HCl was prepared as described in Ref. [14c]. Solvents were dried and distilled under dinitrogen by standard methods prior to use. Electronic spectra were recorded in a CH$_2$Cl$_2$ solution

on a Hewlett–Packard 8452A spectrophotometer. IR spectra were obtained as KBr disks on a Perkin–Elmer model 1600 FT-IR spectrophotometer. ^{1}H NMR spectra were recorded in $CDCl_3$ or DMSO-d_6 on a Bruker FT AC/200P spectrometer; chemical shifts were reported in ppm related to tetramethylsilane, with the residual solvent proton resonance as internal standards. Microanalytical data were obtained on a Perkin–Elmer model 2400 elemental analyser. Melting points were determined by using a Kofler apparatus.

4.1. Preparation of complexes 5–8

4.1.1. [trans-MeClMoO(NNPhMe)(o-phen)] (5)

51.0 mg (0.322 mmol) of $MePhNNH_2 \cdot HCl$ dissolved in 10 ml of dry MeCN were added dropwise to 142 mg (0.322 mmol) of **1** dissolved in 30 ml of dry MeCN under dinitrogen at room temperature. The solution was vigorously stirred for 1 day at room temperature giving an orange solid. Then, the suspension was filtered and washed with MeCN and recrystallised from Me_2CO. Yield: 122 mg (38%). M.p.: 125 °C dec. *Anal*. Calc. for $C_{20}H_{19}ClMoN_4O$: C, 51.91; H, 4.14. Found: C, 51.62; H, 4.06%. UV–Vis [(CH_2Cl_2), λ_{max}, nm (log ε)]: 270 (6.25); 282 (6.27); 292 (6.29); 332 (6.34); 382 (6.41); 472 (6.50). IR (cm^{-1}, KBr): 3074 (w), ν(CH); 2961 (m), ν(CH); 2899 (w), ν(CH); 1624 (m), 1592(m), ν(NN); 897(s), ν(Mo=O). ^{1}H NMR ($CDCl_3$), δ (ppm), TMS. *o*-Phen resonances: 10.14 (d, 1H, $J = 4.8$ Hz); 9.17 (d, 1H, $J = 5.0$ Hz); 8.61 (d, 1H, $J = 6.7$ Hz); 8.47 (d, 1H, $J = 8.3$ Hz); 8.09–8.01 (m, 4H). Phenyl resonances: 7.80–7.68 (m, 3H); 7.47 (pseudo-t, 2H). Methyl resonances: 4.23 (3H, NCH_3); 0.56 (s, 3H, MoCH_3).

4.1.2. [trans-MeClMoO(NNPh$_2$)(o-phen)] (6)

The procedure adopted was similar to that described for the preparation of **5**, using in this case 72.4 mg (0.328 mmol) of $Ph_2NNH_2 \cdot HCl$ and 165 mg (0.328 mmol) of **2**. The product was obtained as a red orange solid. Yield: 239 mg (70%). M.p.: 113 °C dec. *Anal*. Calc. for $C_{25}H_{21}ClMoN_4O$: C, 57.21; H, 4.03. Found: C, 57.02; H, 3.98%. UV–Vis [(CH_2Cl_2), λ_{max}, nm (log ε)]: 278 (6.24); 296 (6.27); 388 (6.38); 514 (6.51). IR (cm^{-1}, KBr): 3063 (m), ν(CH); 2899 (w), ν(CH); 2834 (w), ν(CH); 2684 (w), ν(C=N); 1627 (m), ν(C=N); 1587 (m), ν(NN); 900 (s), ν(Mo=O). ^{1}H NMR ($CDCl_3$), δ (ppm), TMS. *o*-Phen resonances: 10.18 (dd, 1H, $J = 5.0$; 1.5 Hz); 8.58 (dd, 1H, $J = 8.2$;1.5 Hz); 8.30 (dd, 1H, $J = 8.2$; 1.4 Hz); 8.08–7.89 (m, 5H). Phenyl resonances: 7.73 (pseudo-t, 4H); 7.53 (t, 4H, $J = 7.4$ Hz); 7.42–7.29 (m, 2H). Methyl resonance: 0.63 (s, 3H, MoCH_3). Suitable single crystals for X-ray diffraction studies were obtained from acetone.

4.1.3. [trans-PhClMoO(NNPhMe)(o-phen)]·MeCN (7·MeCN)

53.3 mg (0.340 mmol) of $MePhNNH_2 \cdot HCl$ dissolved in 10 ml of dry MeCN were added dropwise to 190 mg (0.335 mmol) of **3** dissolved in 35 ml of dry MeCN under nitrogen. The solution was vigorously stirred for 1 day at room temperature giving a dark red solid. Then, the suspension was filtered and washed with MeCN and recrystallised from Me_2CO. Yield: 133 mg (40%). M.p.: 218 °C dec. *Anal*. Calc. for $C_{27}H_{24}ClMoN_5O$: C, 57.30; H, 4.27. Found: C, 57.02; H, 4.12%. UV–Vis [(CH_2Cl_2), λ_{max}, nm (log ε)]: 268 (6.17); 298 (6.22); 334 (6.27); 390 (6.33); 478 (6.42). IR (cm^{-1}, KBr): 3041 (w), ν(CH); 2954 (m), ν(CH); 1627 (m), ν(C=N);1586 (w), ν(NN); 899 (s), ν(Mo=O). ^{1}H NMR ($CDCl_3$), δ (ppm), TMS. *o*-Phen resonances: 10.12 (d, 1H, $J = 4.0$ Hz); 9.38 (d, 1H, $J = 4.5$ Hz); 8.98 (d, 1H, $J = 7.8$ Hz); 8.79 (d, 1H, $J = 7.8$ Hz); 8.35–8.04 (m, 4H). Phenyl resonances: 7.89 (d, 2H, $J = 6.9$ Hz); 7.47 (t, 2H, $J = 7.8$ Hz); 7.19–7.15 (m, 3H); 6.62 (pseudo-d, 3H). Methyl resonances: 4.31 (s, 3H, NCH_3); 2.50 (s, 3H, CH_3CN).

4.1.4. [trans-PhClMoO(NNPh$_2$)(o-phen)]·MeCN (8·MeCN)

The procedure adopted was similar to that described for the preparation of **7**, using in this case 25.0 mg (0.117 mmol) of $Ph_2NNH_2 \cdot HCl$ and 71.5 mg (0.114 mmol) of **4**. The product was obtained as an orange solid. Yield: 24 mg (21%). M.p.: 158 °C dec. *Anal*. Calc. for $C_{32}H_{26}ClMoN_5O$: C, 61.20; H, 4.17. Found: C, 60.96; H, 4.14%. UV–Vis [(CH_2Cl_2), λ_{max}, nm (log ε)]: 278 (6.36); 294 (6.39); 300 (6.40); 366 (6.48); 500 (6.62). IR (cm^{-1}, KBr): 3052(m), ν(CH); 2899 (s), ν(CH); 2848(s), ν(CH); 2673(s), ν(C=N); 1624 (m), ν(C=N); 1587(s), ν(NN); 901(m), ν(Mo=O). ^{1}H NMR (DMSO-d_6), δ (ppm), TMS. *o*-Phen resonances: 10.14 (d, 1H, $J = 3.8$ Hz); 9.00 (d, 1H, $J = 7.2$ Hz); 8.66 (d, 1H, $J = 8.1$ Hz); 8.38–8.12 (m, 4H); 8.02 (d, 1H, $J = 4.0$ Hz). Phenyl resonances: 7.92–7.50 (m, 9H); 7.20–7.16 (m, 3H); 7.03–6.65 (pseudo-d, 3H). Methyl resonance: 2.50 (s, 3H, CH_3CN).

4.1.5. [trans-Cl$_2$MoO(NNPhR′)(o-phen)], R = Me (9), Ph (10)

Similar reactions to those described for the preparation of complexes **5** and **6** were studied in MeCN using $MePhNNH_2 \cdot HCl$ with **1**, and $Ph_2NNH_2 \cdot HCl$ with **4**, in a 2:1 molar ratio. Complexes formulated as [*trans*-$Cl_2MoO(NNPhMe)(o\text{-phen})$] (**9**), and [*trans*-$Cl_2MoO(NNPh_2)(o\text{-phen})$]·MeCN (**10**), were authenticated by comparing their IR and ^{1}H NMR data with those presented in Ref. [14h].

4.2. X-ray structure determination of **6**

4.2.1. Data collection

$C_{25}H_{21}ClMoN_4O$, $M_r = 524.85$ g mol^{-1}, unit cell dimensions: $a = 8.733(6)$, $b = 9.013(7)$, $c = 16.368(9)$ Å, $\alpha = 101.04(6)$, $\beta = 92.10(5)$, $\gamma = 111.98(6)^\circ$, $V = 1164(1)$ Å^3, triclinic, $P\bar{1}$, $Z = 2$, $D_{calc} = 1.494$ g cm^{-3}, μ(Mo Kα) = 0.702 mm^{-1}, $F(000) = 530$, crystal size (mm): $0.16 \times 0.14 \times 0.04$. Siemens R3m/V four circle diffractometer; Mo Kα radiation ($\lambda = 0.71073$, graphite monochromator), 2θ range 5.00°–50.10° at 298 K, scan type $\theta-2\theta$, reflections collected 4133, observed reflections 2214 [$F_o^2 > 2\sigma(F_o^2)$]. Convergence at $R_1 = 0.081$, $wR_2 = 0.136$. Cell parameters were determined from least-squares fits of 25 reflections with $5.00^\circ \leq 2\theta \leq 50.10^\circ$. Two standard reflections, monitored every 98 reflections, showed no significant variation of intensity during data collection. Intensities were corrected for Lorentz and polarisation effects, and semiempirical corrections based on ψ scans were applied for absorption.

4.2.2. Structure refinement

The structure was solved by direct methods and refined on F by full-matrix least-squares calculations. The function minimised was $\Sigma w(F_o - F_c)^2$. All non-hydrogen atoms were refined anisotropically. A riding model was applied to H atoms, which were placed at calculated positions with C–H = 0.96 Å, with the equivalent isotropic thermal parameters of their parent C atoms. All calculations were performed with the Siemens SHELXTL-PLUS system of programs [24].

5. Supplementary material

Crystallographic data (excluding structure factors) for the structure of **6** reported in this paper were deposited with the Cambridge Crystallographic Data Centre, CCDC No. 178505. Copies of this information may be obtained free of charge from The Director, CCDC, 12 Union Road, Cambridge, CB2 1EZ, UK (fax: +44-1223-336033; e-mail: deposit@ccdc.cam.ac.uk or www: http://www.ccdc.cam.ac.uk)].

Acknowledgements

This work was supported by "Fondo Nacional de Desarrollo Científico y Tecnológico", FONDECYT-CHILE, Grant No. 1951088 and "Dirección General de Investigación y Postgrado, Universidad Católica de Valparaíso-Chile" (D.C. and C.M.). A.M.G. thanks Instituto de Cooperación Iberoamericana, Spain, for their granting of a graduate fellowship.

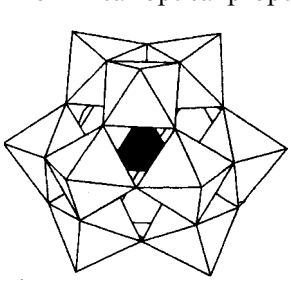
References

[1] D.J. Evans, R.A. Henderson, B.E. Smith, in: J. De Reedijk (Ed.), Bioinorganic Catalysis, Marcel Dekker, New York, 1993, pp. 89–130.
[2] M. Hidai, Y. Mizobe, Chem. Rev. 95 (1995) 1115 (and references cited therein).
[3] R.A. Henderson, G.J. Leigh, C.J. Pickett, J. Chem. Soc., Dalton Trans. (1989) 425.
[4] P.J. Walsh, M.J. Carney, R.G. Bergman, J. Am. Chem. Soc. 113 (1991) 6343.
[5] J.R. DeBord, T.A. George, Y. Chang, Q. Chen, J. Zubieta, Inorg. Chem. 32 (1993) 785.
[6] M.G. Vale, R.R. Schrock, Inorg. Chem. 32 (1993) 2767.
[7] M. Retboll, E.R. Möller, R.G. Hazell, A. Jörgensen, Acta Chem. Scand. 49 (1995) 278.
[8] J.D. Niemoth-Anderson, J.R.D. Debord, T.A. George, C.R. Ross, II, J.J. Stezowski, Polyhedron 15 (1996) 4031.
[9] R.A. Henderson, K.E. Oglieve, J. Chem. Soc., Dalton Trans. (1990) 1093.
[10] C. Bustos, C. Manzur, D. Carrillo, F. Robert, P. Gouzerh, Inorg. Chem. 33 (1994) 4937.
[11] C. Bustos, M. Matamala, D. Boys, D. Carrillo, Bol. Soc. Chil. Quím. 47 (2002) in press.
[12] C. Manzur, C. Bustos, D. Carrillo, D. Boys, J.-R. Hamon, Inorg. Chim. Acta 255 (1997) 73.
[13] S. Kahlal, J.-Y. Saillard, J.-R. Hamon, C. Manzur, D. Carrillo, J. Chem. Soc., Dalton Trans. (1998) 1229.
[14] (a) C. Bustos, C. Manzur, H. Gonzalez, R. Schrebler, D. Carrillo, C. Bois, Y. Jeannin, P. Gouzerh, Inorg. Chim. Acta 185 (1991) 25;
(b) D. Carrillo, F. Robert, P. Gouzerh, Inorg. Chim. Acta 197 (1992) 209;
(c) C. Bustos, C. Manzur, D. Carrillo, F. Robert, P. Gouzerh, Inorg. Chem. 33 (1994) 1427;
(d) J. Li-Kao, O. Gonzalez, R. Mariezcurreña, R. Baggio, M.T. Garland, D. Carrillo, Acta Crystallogr., Sect. C 51 (1995) 2486;
(e) C. Manzur, C. Bustos, D. Carrillo, F. Robert, P. Gouzerh, Inorg. Chim. Acta 249 (1996) 245;
(f) C. Manzur, D. Carrillo, R. Baggio, M.T. Garland, J. Chem. Crystallogr. 27 (1997) 339;
(g) C. Manzur, D. Carrillo, D. Boys, Acta Crystallogr., Sect. C 53 (1997) 1401;
(h) C. Manzur, D. Carrillo, D. Boys, P. Hamon, J.-R. Hamon, Inorg. Chim. Acta 268 (1998) 199;
(i) C. Manzur, D. Carrillo, A. Vega, M.T. Garland, Bol. Soc. Chil. Quím. 44 (1999) 5.
[15] D. Carrillo, C.R. Acad. Sci. Paris, Série IIc 3 (2000) 175.
[16] C. Manzur, D. Carrillo, F. Robert, P. Gouzerh, J.-R. Hamon, Organometallics 17 (1998) 3728.
[17] A.M. Galindo, C. Manzur, J.-R. Hamon, D. Carrillo, Eur. J. Inorg. Chem. (1999) 387.
[18] M.G. Vale, R.R. Schrock, Inorg. Chem. 32 (1993) 2767.
[19] T. Nicholson, J. Zubieta, J. Chem. Soc., Chem. Commun. (1985) 367.
[20] P.W. Schneider, D.C. Bravard, J.W. McDonald, W.E. Newton, J. Am. Chem. Soc. 94 (1972) 8640.
[21] S.N. Shaik, J. Zubieta, Inorg. Chem. 25 (1986) 4613.
[22] C. Pickett, S. Kumar, P.A. Vella, J. Zubieta, Inorg. Chem. 21 (1982) 908.
[23] W.A. Nugent, J.M. Mayer, Metal–Ligand Multiple Bonds, Wiley-Interscience, New York, 1988.
[24] G.M. Sheldrick, SHELLXTL-Plus, Release 4.2 for Siemens Crystallographic research Systems, Siemens Analytical X-ray Instruments, Madison, WI, 1992.

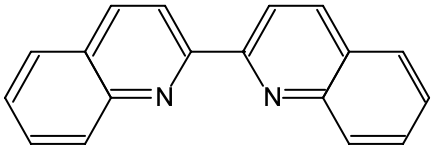
Photochromic properties of these compounds are closely related to the reduction potential of the polyoxoanion and to the donor properties of the organic molecules. Structural factors can also be important although no correlations have been found, so far, between the electronic or photochromic properties and the structure of charge transfer compounds based on Keggin anions [20,22–27,29,31,33,35–38]. For application in technological devices reversible photocromism is desirable [15]. Many photochromic polyoxoanion salts are reported in literature, but they generally do not meet the above condition, showing irreversible photo-redox processes [15,39].

Charge transfer salts based on polyoxometalates have also been studied on account of their non-linear optical properties. A few compounds combining Keggin-type anions with organic molecules of high dipole moments, leading to second-order harmonic generation (SHG), have been reported [26,30]. The highest SHG was obtained with the compound $(4\text{-DMSP})_4(NH_2Me_2)_2[HSiFeMo_{11}O_{40}]\cdot 3H_2O$, 4-DMSP = 4-[(*p*-(dimethylamino)styril]pyridine, with an efficiency 1.2 times that of KH_2PO_4 under the same conditions [30]. Until now, the second-order non-linear optical responses of those compounds are not comparable to those of some organic molecules, but the chemical and thermal instability or the weak mechanical resistance that are a drawback to the application of the organic crystals in non-linear optical devices [40,41] can possibly be overcome with the polyoxometalates. Polyoxometalate compounds with third-order non-linear optical properties were described as well [26,28,32].

Our interest has been focused on the preparation of charge transfer salts by co-crystallization of electron-rich heterocyclic aromatic amines like 2,2′-bipiridine, 1,10-phenantroline, or 2,2′-biquinoline with the Keggin anions $\alpha\text{-}[XM_{12}O_{40}]^{m-}$ (**1**), X = P, Si, M = Mo, W (abbreviated as XM_{12}. The α-isomers were used in all studies and the prefix α- will be omitted subsequently). Of the prepared compounds, only those obtained from 2,2′-biquinoline (**2**) showed significant charge transfer properties. Their synthesis and characterization in the solid state and in solution will be presented here, with special attention to the electronic properties. Studies of the photochromic properties of some of the prepared compounds under visible radiation will be presented. Second-order non-linear optical properties were studied, but significant SHG of 1064 nm radiation was only found for one compound.



(I)



(II)

2. Experimental

2.1. Synthesis

2.1.1. $(Hbiqui)_3[PM_{12}O_{40}]$ and $(Hbiqui)_4[SiM_{12}O_{40}]\cdot nH_2O$, M = W, Mo

A solution of 2,2′-biquinoline (0.234 g, 0.91 mmol) in 30 cm^3 of boiling acetonitrile was added, with vigorous stirring, to a solution of $H_3[PW_{12}O_{40}]\cdot 23H_2O$ (1.00 g, 0.30 mmol) in 5 cm^3 of water, at the same temperature. A yellow precipitate was formed immediately. The solid was filtered, washed with warm acetonitrile and dried in an evacuated desiccator. The same procedure was applied for the synthesis of the other compounds, starting with the acids $H_3[PMo_{12}O_{40}]\cdot nH_2O$ and $H_4[SiM_{12}O_{40}]\cdot nH_2O$, M = Mo, W. In all cases a molar proportion of organic base/Keggin anion equal to the polyanion charge was used. The compounds with Mo must be protected from light during preparation as they are photosensitive.

$(HC_{18}N_2H_{12})_3[PW_{12}O_{40}]$ *Anal*. (%). Found (Calc.): C, 17.31 (17.77); N, 2.23 (2.30); H, 1.01 (1.08). IR (cm^{-1}): ν_{as}(P–O_a) 1080 (vs), ν_{as}(W–O_d) 978 (vs), ν_{as}(W–O_b–W) 897 (s), ν_{as}(W–O_c–W) 810 (vs).

$(HC_{18}N_2H_{12})_4[SiW_{12}O_{40}]\cdot 3H_2O$ *Anal.* (%). Found (Calc.): C, 21.15 (21.85); N, 2.70 (2.83); H, 1.56 (1.48); H_2O, 1.5 (1.4). IR (cm^{-1}): ν_{as}(W–O_d) 970 (s), ν_{as}(Si–O_a) 921 (vs), ν_{as}(W–O_b–W) 885 (m), ν_{as}(W–O_c–W) 796 (vs).

$(HC_{18}N_2H_{12})_3[PMo_{12}O_{40}]$ *Anal.* (%). Found (Calc.): C, 25.16 (25.00); N, 3.28 (3.24); H, 1.54 (1.51). IR (cm^{-1}): ν_{as}(P–O_a) 1063 (vs), ν_{as}(Mo–O_d) 960 (vs), ν_{as}(Mo–O_b–Mo) 882 (s), ν_{as}(Mo–O_c–Mo) 802 (vs).

$(HC_{18}N_2H_{12})_4[SiMo_{12}O_{40}]\cdot 4H_2O$ *Anal.* (%). Found (Calc.): C, 30.04 (29.61); N, 4.00 (3.84); H, 2.14 (2.07); H_2O, 2.3 (2.5). IR (cm^{-1}): ν_{as}(Mo–O_d) 947 (s), ν_{as}(Si–O_a) 903 (vs), ν_{as}(Mo–O_b–Mo) 864 (m), ν_{as}(Mo–O_c–Mo) 795 (vs).

^{1}H NMR spectra of all compounds in deuterated dimethylsulfoxide (dmso-d_6) were similar to that of 2,2′-biquinoline. ^{1}H NMR spectra of 2,2′-biquinoline in dmso-d_6: δ (ppm), 8.81 H3 (d, $^3J_{34} = 8.6$ Hz), 8.59 H4 (d, $^3J_{34} = 8.6$ Hz), 8.19 H8 (dd, $^3J_{78} = 8.3$ Hz, $^5J_{68} = 0.9$ Hz), 8.09 H5 (dd, $^3J_{56} = 8.2$ Hz, $^5J_{57} = 1.3$ Hz), 7.86 H7,

(dddd, $^3J_{67} = 6.9$ Hz, $^3J_{78} = 8.4$ Hz, $^5J_{57} = 1.5$ Hz), 7.69 H6, (dtd $^3J_{67} = 6.9$ Hz, $^3J_{56} = 8.1$ Hz, $^5J_{68} = 1.2$ Hz).

2.1.2. *(Hbiqui)$_3$[PM$_{12}$O$_{40}$]·3dmf and (Hbiqui)$_4$[SiM$_{12}$O$_{40}$]·3dmf, M = W, Mo*

All compounds obtained by the procedure described above were dissolved in *N*,*N*-dimethylformamide (saturated solutions) and re-crystallized by diethylether diffusion, at room temperature. The small crystals formed were filtered and washed with ether. Experiments were performed in light protected conditions.

$(HC_{18}N_2H_{12})_3[PW_{12}O_{40}]\cdot 3dmf$ *Anal.* (%). Found (Calc.): C, 19.69 (19.56); N, 3.19 (3.26); H, 1.66 (1.56); dmf, 5.6 (5.7). IR (cm^{-1}): ν_{as}(P–O$_a$) 1079 (vs), ν_{as}(W–O$_d$) 976 (vs), ν_{as}(W–O$_b$–W) 896 (s), ν_{as}(W–O$_c$–W) 812 (vs).

$(HC_{18}N_2H_{12})_4[SiW_{12}O_{40}]\cdot 3dmf$ *Anal.* (%). Found (Calc.): C, 23.46 (23.60); N, 3.72 (3.74); H, 2.00 (1.78); dmf, 5.7 (5.3). IR (cm^{-1}): ν_{as}(W–O$_d$) 969 (s), ν_{as}(Si–O$_a$) 919 (vs), ν_{as}(W–O$_b$–W) 884 (m), ν_{as}(W–O$_c$–W) 798 (vs).

$(HC_{18}N_2H_{12})_3[PMo_{12}O_{40}]\cdot 3dmf$ *Anal.* (%). Found (Calc.): C, 27.27 (26.90); N, 4.38 (4.48); H, 2.36 (2.15); dmf, 7.4 (7.8). IR (cm^{-1}): ν_{as}(P–O$_a$) 1061 (vs), ν_{as}(Mo–O$_d$) 954 (vs), ν_{as}(Mo–O$_b$–Mo) 880 (vs), ν_{as}(Mo–O$_c$–Mo) 803 (vs).

$(HC_{18}N_2H_{12})_4[SiMo_{12}O_{40}]\cdot 3dmf$ *Anal.* (%). Found (Calc.): C, 31.37 (31.71); N, 5.26 (5.02); H, 2.25 (2.40); dmf, 6.7 (7.1). IR (cm^{-1}): ν_{as}(Mo–O$_d$) 944 (s), ν_{as}(Si–O$_a$) 901 (vs), ν_{as}(Mo–O$_b$–Mo) 865 (m), ν_{as}(Mo–O$_c$–Mo) 796 (vs).

^{1}H NMR spectra in dmso-d_6 showed, besides the spectra of 2,2′-biquinoline, three additional singlets at 2.73, 2.89 and 7.95 ppm, of relative intensities 3:3:1, assigned to the CH_3 and CH protons of the dmf molecules. Integration of the signals corresponding to the methyl protons and to the aromatic protons of 2,2′-biquinoline confirms the number of dmf molecules in the formula determined by thermogravimetric analyses.

2.2. Reagents and methods

All chemicals were used as received from suppliers. Elemental analyses (C, H, N) were performed on a Leco CHNS-932. Thermogravimetric analyses were carried out in air between 30 and 700 °C at a heating rate of 5 °C min^{-1}, on a Mettler M3 thermobalance equipped with a TC 10A microprocessor.

Electronic absorption spectra (visible/UV) were recorded on a JASCO V-560 spectrophotometer using solutions approximately 0.005 mol dm^{-3}. Diffuse reflectance spectra (UV/visible/near infrared) were registered on a Shimadzu 3100 spectrophotometer, using MgO as reference. Infrared absorption spectra were recorded on a Mattson 7000 FTIR spectrometer, using KBr pellets.

^{1}H and ^{31}P NMR spectra (in dmso-d_6) were carried out in 5 mm tubes on a Bruker AMX 300 spectrometer. ^{31}P spectra were recorded using 85% aqueous H_3PO_4 as external reference.

Powder EPR spectra were recorded with a Bruker ESP 300E spectrometer at 120 K. Typical experimental conditions used: microwave frequency, 9.53 GHz; modulation frequency, 100 KHz, modulation amplitude, 0.1–0.5 mT, microwave power, 5 mW.

Powder XRD at room temperature data were collected on a X'Pert MPD Philips diffractometer (Cu Kα X-radiation) with a curved graphite monochromator, a fix incident area of 10 mm^2, and a flat plate sample holder, in a Bragg–Brentano para-focusing optics configuration. Intensity data were collected by the step counting method (step 0.02° and time 5 s) in the range $2\theta = 5°–50°$.

Second-order non-linear optical properties were estimated by the following procedure. Powder samples of determined average grain sizes were prepared with the aid of standard sieves and were used to fill round glass cells of 16 mm diameter. The fundamental beam of a Nd:YAG laser (1064 nm), pulse duration of 7 ns and a 10 Hz-repetition rate, was weakly focused on the sample. The second harmonic was separated from the incident fundamental beam using dichroic mirrors and then sent into a monochromator. The signal was detected using a photomultiplier tube (type 1P28 at 900 V bias) and read using a fast digital oscilloscope (Tektronix TDS 520 with a bandwidth of 500 MHz). Averages over 100 laser shots were acquired in order to reduce the influence of the shot-to-shot variations in laser power.

Photochromism experiences were performed as follows: samples of each compound (100 mg, finely ground) were exposed to sunlight or placed under a tungsten lamp (40W Osram Concentra R80), for the chosen period of time. Those powders that evidenced photosensitivity were, after irradiation, placed in the dark for a determined period of time or introduced in an autoclave and kept under O_2 (5 atm) for 24 h. Changes were monitored by reflectance and EPR spectroscopy.

3. Results and discussion

3.1. Synthesis and characterization of new compounds

Solids with cations formed by protonation of the organic base 2,2′-biquinoline (**2**) and Keggin polyoxoanions (**1**) were easily obtained by addition of a solution of the former in acetonitrile to an aqueous solution of the heteropolyacid of interest. The chemical formula of all obtained compounds presented the molar proportion organic cation/Keggin anion equal to the polyanion charge. Re-crystallization of the prepared solids in *N*,*N*-

dimethylformamide yielded new dmf solvated compounds.

The infrared spectra of all compounds presented the characteristic peaks corresponding to the Keggin anions in the 790–1100 cm^{-1} region, at frequencies near to those of tetra-*n*-butylammonium salts of XM_{12} [42]. Bands corresponding to the organic molecules were observed at frequencies higher than 1100 cm^{-1}.

All compounds were soluble in dimethylsulfoxide (dmso) and these solutions were used to obtain ^{31}P and ^{1}H NMR spectra. One peak was observed at −14.5 ppm in the ^{31}P NMR spectra of compounds with PW_{12} and at −2.95 ppm for those with PMo_{12} (chemical shifts identical to the observed for $H_3[PW_{12}O_{40}]$ and $H_3[PMo_{12}O_{40}]$ in the same solvent, respectively), indicating that the $[PM_{12}O_{40}]^{3-}$ anions are present in solution. The ^{1}H NMR spectrum of 2,2′-biquinoline in dmso showed several signals that were assigned to the protons of the molecule by comparison with published studies [43,44]. The proton spectra of the prepared compounds showed the peaks corresponding to the organic base with a slight change (0.02–0.05 ppm) in chemical shifts (except H3) to higher frequencies and almost no variation on coupling constants. The largest differences were observed for protons H4 and H8. Additionally, signals corresponding to dmf were observed in the spectra of dmf-solvated compounds.

The methods of preparation used and the molecular formula obtained suggested that the 2,2′-biquinoline molecules should be protonated in the solids. However, extensive dissociation must take place in solution, and no evidence could be found in the ^{1}H NMR spectra to corroborate that fact. The slight chemical shift variation observed in the spectra of the prepared compounds in comparison with that of free base was reproduced by addition of adequate stoichiometric quantities of trifluoroacetic acid to the dmso-d_6 solutions of 2,2′-biquinoline. Larger differences could only be observed when a much larger excess of acid was added to the solutions.

By means of thermogravimetric analyses, it was found that the crystallization solvent (when present) was lost below 100 °C (water) or in a narrow range around 150–160 °C (dmf). The decomposition of 2,2′-biquinolinium (after loss of solvent, when present) started at temperatures around 280–330 °C, with the exception of compounds with PW_{12}, in which it was stable up to 410 °C (Table 1).

Single crystals were developed for the compounds solvated with dmf, but single crystal X-ray diffraction measurements could only be made for the $(Hbiqui)_4[SiW_{12}O_{40}]\cdot 3dmf$ compound. However, the analyses of X-ray data revealed disordered Keggin anions and disordered 2,2′-biquinoline molecules and the structure could not be resolved with adequate refinement. Nevertheless, there is no evidence of a close contact (that would indicate covalent interaction) between the organic base molecules and the SiW_{12} anions [45]. This means that the charge transfer properties observed by electronic spectroscopy and described below are not associated with direct interactions but may result from induced-dipole effects as it has been reported for analogous charge transfer compounds [24,26].

Table 1
Temperature (°C) interval of decomposition of 2,2′-biquinolinium in the prepared compounds

Anion	Anhydrous or hydrated compounds [a]	dmf-solvated compounds [a]
PW_{12}	410–620	412–624
SiW_{12}	331–624	311–553
PMo_{12}	318–528	318–451
$SiMo_{12}$	286–522	309–509

[a] Values obtained by thermogravimetric analysis: first value, beginning of weight loss due to decomposition of 2,2′-biquinolinium; second value: end of thermal decomposition of the compound.

Samples of other compounds but $(Hbiqui)_4[SiW_{12}O_{40}]\cdot 3dmf$ had, generally, low crystallinity, as shown by X-ray powder diffraction. By comparison of the diffraction patterns of the various compounds it was apparent that some pairs of compounds, like $(Hbiqui)_3[PMo_{12}O_{40}]\cdot 3dmf$ and $(Hbiqui)_3[PW_{12}O_{40}]\cdot 3dmf$ or $(Hbiqui)_4[SiMo_{12}O_{40}]\cdot 4H_2O$ and $(Hbiqui)_4[SiW_{12}O_{40}]\cdot 3H_2O$, were isomorphous and that compounds with formula that differ only on solvation, like $(Hbiqui)_4[SiW_{12}O_{40}]\cdot 3H_2O$ and $(Hbiqui)_4[SiW_{12}O_{40}]\cdot 3dmf$ or $(Hbiqui)_3[PW_{12}O_{40}]$ and $(Hbiqui)_3[PW_{12}O_{40}]\cdot 3dmf$, had different crystal structures.

3.2. Electronic spectra and charge transfer properties

Diffuse reflectance spectra of the prepared compounds were compared with those of 2,2′-biquinoline and of the heteropolyacids used as starting materials. Two maxima were observed in the spectrum of 2,2′-biquinoline at 248 and 350 nm (Fig. 1). $H_3[PW_{12}O_{40}]\cdot nH_2O$ and $H_4[SiW_{12}O_{40}]\cdot nH_2O$ absorbed in the same region (PW_{12}: 259 and 331 nm; SiW_{12}: 259 and 341 nm). The reflectance spectra of $(Hbiqui)_3[PW_{12}O_{40}]$ and $(Hbiqui)_4[SiW_{12}O_{40}]\cdot 3H_2O$ presented in Fig. 1(A and B) also have two bands with maxima at about 250 and 350 nm, mainly due to the presence of 2,2′-biquinoline (as a consequence of compounds stoichiometry). However, an additional band at about 410–420 nm, with intensity close to that of the UV bands, was observed in each spectrum. This band is characteristic of the synthesized compounds and is responsible for their yellow colour. It is not observed in the spectra of 2,2′-biquinoline, $H_3[PW_{12}O_{40}]$ or $H_4[SiW_{12}O_{40}]$ (all white)

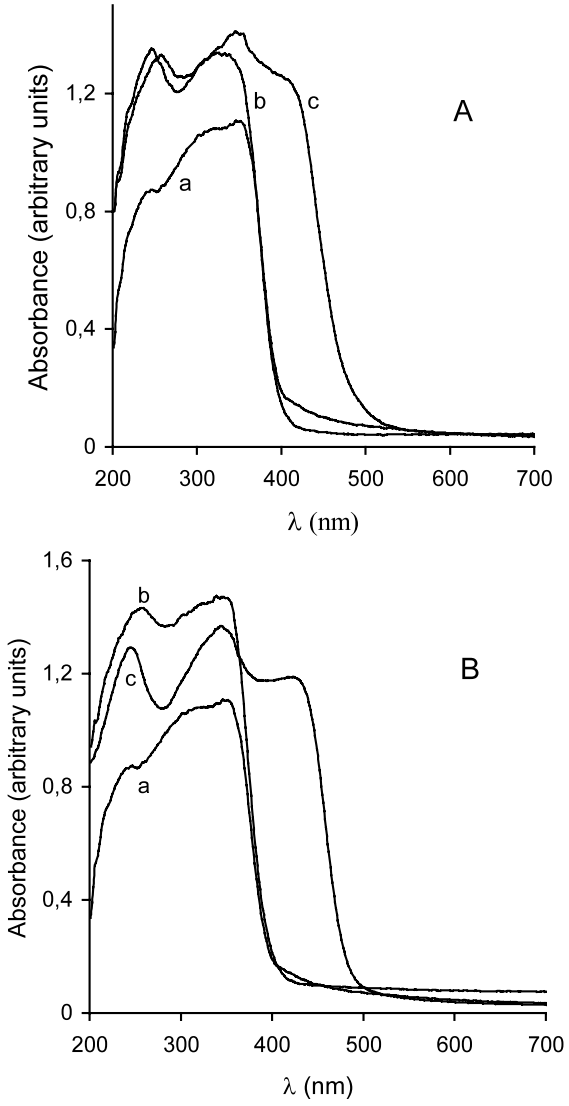


Fig. 1. (A) Diffuse reflectance spectra of 2,2′-biquinoline (a), $H_3[PW_{12}O_{40}]\cdot nH_2O$ (b), $(Hbiqui)_3[PW_{12}O_{40}]$ (c). (B) Diffuse reflectance spectra of 2,2′-biquinoline (a), $H_4[SiW_{12}O_{40}]\cdot nH_2O$ (b), $(Hbiqui)_4[SiW_{12}O_{40}]\cdot 4H_2O$ (c).

and was assigned to charge transfer between the organic base and the Keggin anions [26,27].

Similar spectra were obtained for other prepared compounds, often with the absorption around 410 nm being observed as a shoulder. These results gave evidence of strong intermolecular electronic interactions between the organic moiety and any of the Keggin anions in the solids. In the case of $(Hbiqui)_3[PMo_{12}O_{40}]\cdot 3dmf$, the spectrum showed also a large band with low intensity centred around 750 nm, which was attributed to an electronic transition $Mo^{V}\rightarrow Mo^{VI}$ in the Keggin anion [1]. This implies the occurrence of reduction of the Keggin anion (Section 3.3) and could, possibly, be due to the difficulty of keeping compounds in the dark during synthesis and manipulation.

Electronic absorption spectra in dmso (0.005 mol dm^{-3}) were registered for $\lambda > 350$ nm, with the purpose of finding if the electronic interaction exhibited in the solids was retained in solution. This solvent is not possibly the most convenient for this type of studies, as it is known to be involved in electronic interaction with Keggin anions [25], but the choice of solvent was limited by the solubility of the different compounds. The organic base (in dmso) does not absorb in this range of λ and the spectra of the prepared compounds were, thus, compared with those of the corresponding heteropolyacid in the same solvent. Changes in the electronic spectra were more pronounced for compounds with the polyanion SiW_{12} (Fig. 2). In this case the tail of the lowest energy absorption band moved to significantly higher wavelengths (red shift of about 40 nm) in comparison with the spectra of the corresponding heteropolyacid. Changes were less obvious in the case of compounds with PW_{12} and negligible for other anions (Fig. 2). Spectra of the dmf-solvated compounds were identical to those of the non-solvated or hydrated compounds.

These results indicate that there is a strong electronic interaction between the 2,2′-biquinoline and $[SiW_{12}O_{40}]^{4-}$, in the studied solutions. This result is quite unusual. For other charge transfer compounds with Keggin polyanions reported in literature, it has always been shown that the electronic interactions observed in the solid are insignificant or weak in solution, unless there is a large excess of the organic base relative to the Keggin anion [23–27,29,35,36].

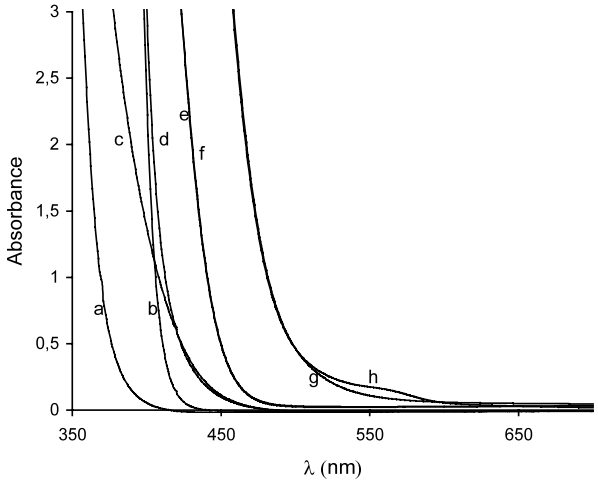


Fig. 2. Electronic absorption spectra of compounds in dimethylsulfoxide solutions (0.005 mol dm^{-3}): (a) $H_4[SiW_{12}O_{40}]\cdot nH_2O$; (b) $(Hbiqui)_4[SiW_{12}O_{40}]\cdot 3H_2O$; (c) $H_3[PW_{12}O_{40}]\cdot nH_2O$; (d) $(Hbiqui)_3[PW_{12}O_{40}]$; (e) $H_4[SiMo_{12}O_{40}]\cdot nH_2O$; (f) $(Hbiqui)_4[SiMo_{12}O_{40}]\cdot 4H_2O$; (g) $H_3[PMo_{12}O_{40}]\cdot nH_2O$; (h) $(Hbiqui)_3[PMo_{12}O_{40}]$.

3.3. Photochromism of molybdenum compounds under sunlight or visible radiation

Studies concerning photochemistry of charge transfer compounds based on Keggin polyoxoanions have been, in most of cases, performed in solution [23,25,46]. Photosensitivity of solid compounds to radiation from UV sources [26,27,29] or sunlight [36–38] has been referred, but no detailed studies were presented. In this work we report studies on the photochromism of solid compounds under exposure to sunlight or under irradiation of a tungsten lamp (visible region).

Compounds with the XMo_{12} anions showed significant alterations in colour and in the spectroscopic properties (diffuse reflectance and EPR spectra) after irradiation with sunlight or with the tungsten lamp. The former were more pronounced and will be described below. The experiences conducted under the W lamp provided comparable results but only after longer periods of time (more than 48 h to reach the largest change in colour, compared with 2–10 h under sunlight, depending upon the compound).

Under sunlight, the compounds $(Hbiqui)_3[PMo_{12}O_{40}]$ and $(Hbiqui)_4[SiMo_{12}O_{40}]\cdot 4H_2O$ changed from yellow or yellow–green to green and the corresponding solvates with dmf changed from yellow–green to dark green or green, respectively (Fig. 3). The corresponding reflectance spectra showed an electronic band around 750 nm that, for each compound, increased up to a limit, with irradiation time (Table 2). EPR spectra of the irradiated solids had one isotropic signal at $g = 1.95$ (Fig. 4). These facts indicate the presence of Mo(V) in the Keggin anion [1,22,28,31,33] and suggest that the exposure to sunlight has induced the reduction of $[XMo_{12}^{VI}O_{40}]^{m-}$ to $[XMo_{11}^{VI}Mo^{V}O_{40}]^{(m+1)-}$, possibly as a result of charge transfer between 2,2′-biquinolinium and the anions. No decomposition was detected by spectroscopic techniques

Table 2
Intensities of selected bands in the diffuse reflectance spectra of compounds

Compound	Conditions	A_{750} [a]	A_{350} [b]	A_{750}/A_{350}
$(Hbiqui)_3[PMo_{12}O_{40}]$	[c]	0.501	1.602	0.313
$(Hbiqui)_3[PMo_{12}O_{40}]\cdot 3dmf$	[d]	0.167	1.660	0.101
$(Hbiqui)_3[PMo_{12}O_{40}]\cdot 3dmf$	[c]	1.149	1.687	0.681
$(Hbiqui)_4[SiMo_{12}O_{40}]\cdot 4H_2O$	[c]	0.452	1.647	0.274
$(Hbiqui)_4[SiMo_{12}O_{40}]\cdot 4H_2O$	[e]	0.280	1.640	0.171
$(Hbiqui)_4[SiMo_{12}O_{40}]\cdot 3dmf$	[c]	0.762	1.737	0.438
$(Hbiqui)_4[SiMo_{12}O_{40}]\cdot 3dmf$	[f]	0.291	1.675	0.174

[a] Absorbance (in arbitrary units) of the maximum near 750 nm. This band is not present in the spectra of non-irradiated compounds, except for $(Hbiqui)_3[PMo_{12}O_{40}]\cdot 3dmf$.
[b] Absorbance (in arbitrary units) of the maximum near 350 nm.
[c] After exposure to sunlight for 10 h.
[d] Without irradiation.
[e] After 1 month in the dark after previous exposure.
[f] After 3 months in the dark after previous exposure.

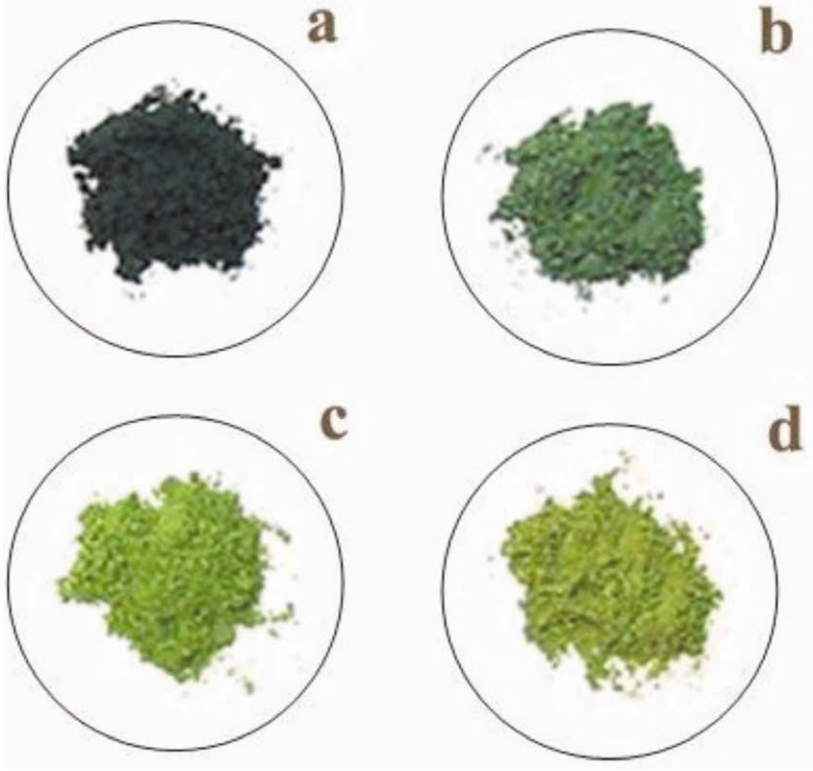


Fig. 3. Samples irradiated with sunlight for 10 h: (a) $(Hbiqui)_3[PMo_{12}O_{40}]\cdot 3dmf$; (b) $(Hbiqui)_4[SiMo_{12}O_{40}]\cdot 3dmf$; (c) $(Hbiqui)_3[PMo_{12}O_{40}]$; (d) $(Hbiqui)_4[SiMo_{12}O_{40}]\cdot 4H_2O$.

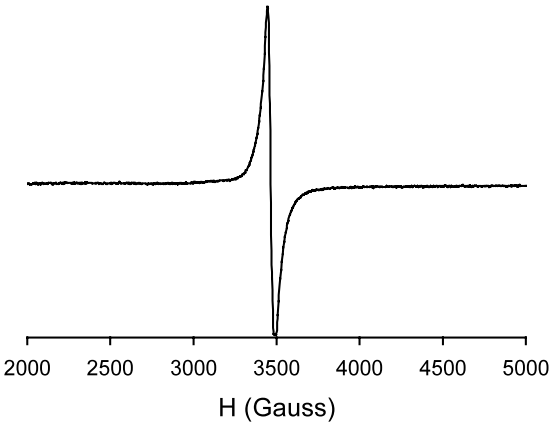


Fig. 4. Powder EPR spectrum ($T = 120$ K) of $(Hbiqui)_3[PMo_{12}O_{40}]\cdot 3dmf$ after exposure to sunlight for 10 h.

of the protonated organic base or of the Keggin anions on the solid compounds after exposure to light.

When similar experiments were performed with the XW_{12} compounds, no significative alterations in colour or in the spectra were observed. This is not unexpected, since the respective anions have lower reduction potentials than the molybdenum counterparts [1,47–49].

It was possible to make a semi-quantitative evaluation of the extension of reduction of the Keggin anions in the photosensitive compounds by comparing the intensities of the maxima in the reflectance spectra near 750 nm (a band corresponding to the reduced Keggin anion, A_{750}) and 350 nm (mainly an absorption band of 2,2′-biquinolinium, A_{350}). Based on the values of the ratio A_{750}/A_{350}, after irradiation for 10 h (Table 2), the following order of photosensitivity was found (that corresponds to the colour changes of Fig. 3): $(Hbiqui)_3[PMo_{12}O_{40}]\cdot 3dmf > (Hbiqui)_4[SiMo_{12}O_{40}]\cdot 3dmf > (Hbiqui)_3[PMo_{12}O_{40}] > (Hbiqui)_4[SiMo_{12}O_{40}]\cdot 4H_2O$. The variation of A_{750}/A_{350} with irradiation time (Fig. 5) showed that the compounds with $SiMo_{12}$ reached faster a state for which no further alteration was observed (less than 2 h for the hydrated salt). For compounds with PMo_{12} very little evolution could be detected after irradiation for more than 10 h.

The two compounds of XMo_{12} crystallizing with dmf molecules were found to be more photosensitive than any of the others studied, for any time of irradiation considered. This means that the dmf molecules also play a role in the charge transfer that leads to the reduction of the anions. The existence of charge transfer between amides and Keggin anions is known [23–26,46] and the compound $[(dma)_2H]_3[PMo_{12}O_{40}]\cdot CH_3CN\cdot 0.5H_2O$ (dma = *N*,*N*-dimethylacetamide) was reported to be light sensitive [24]. For comparison, $[(dmf)_2H]_3[PMo_{12}O_{40}]$ was isolated using a similar procedure [24] and was found to be photosensitive in the conditions used in this work [50]. This does not prove that dmf is directly involved as an electron donor, but there is no

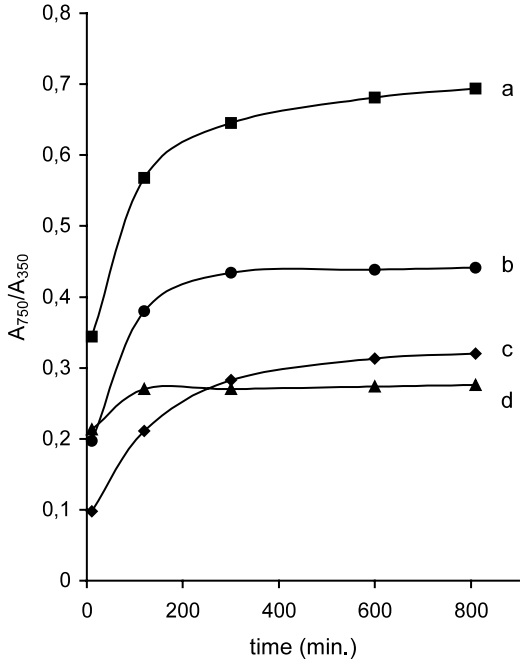


Fig. 5. Time dependence of A_{750}/A_{350}: (a) $(Hbiqui)_3[PMo_{12}O_{40}]\cdot 3dmf$; (b) $(Hbiqui)_4[SiMo_{12}O_{40}]\cdot 3dmf$; (c) $(Hbiqui)_3[PMo_{12}O_{40}]$; (d) $(Hbiqui)_4[SiMo_{12}O_{40}]\cdot 4H_2O$.

doubt that the compounds $(Hbiqui)_3[PMo_{12}O_{40}]\cdot 3dmf$ and $(Hbiqui)_4[SiMo_{12}O_{40}]\cdot 3dmf$ were more photosensitive than those that have only 2,2′-biquinolinium or dmf. The simultaneous combination of these organic molecules with the molybdenum Keggin anions leads to an enhancement of the response to sunlight or W-lamp visible light. Other dmf-solvated charge transfer compounds with Keggin anions have been reported [29,31,35], but the influence of this solvent in the photosensitivity has not been considered.

Some of the studied photosensitive compounds recovered partially the original colours (and reflectance spectra) when left in the dark, at room temperature, under aerobic conditions, during a comparatively long period of time after previous exposure to light (Table 2, Fig. 6). Only $(Hbiqui)_3[PMo_{12}O_{40}]$ did not show any degree of recovering. In the spectra of compounds with $SiMo_{12}$, the visible band around 750 nm decreased 50–70% after about 1–3 months in the dark (Fig. 6). Attempts to accelerate the recovery by the use of O_2 (5 atm, 24 h) did not yield different results. To use these compounds as photochromic materials the recovery of the original colours, after removal of the light source, should occur faster. Until now, truly reversible photochromism has been well established for a few alkylammonium salts of isopolymolybdates [39,51]. Concerning charge transfer compounds with Keggin anions, reversible photochromic properties have only been briefly mentioned for some solids with the $[(CH_2OH)_3CNH_3]^+$ cation [36].

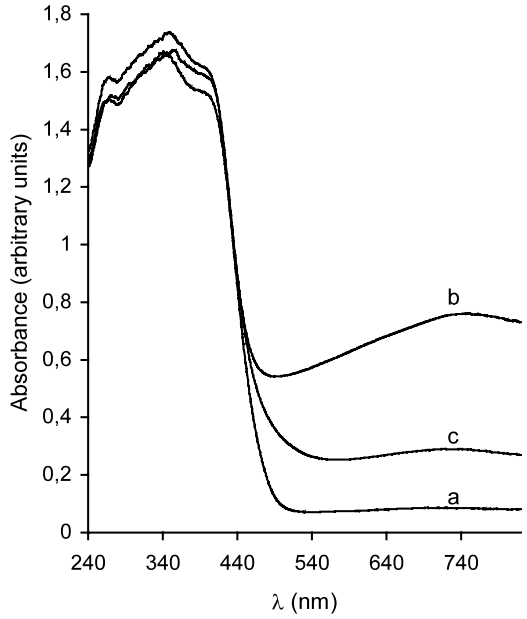


Fig. 6. Diffuse reflectance spectra of $(Hbiqui)_4[SiMo_{12}O_{40}]\cdot 3dmf$: (a) without irradiation; (b) after irradiation with sunlight (5 h); (c) after 3 months in the dark following previous light exposure.

3.4. Non-linear optical properties

The Kurtz powder test set-up [52] was used to characterize the intensity of the optical second harmonic signal. Several samples were prepared, each consisting of crystal grains with an average size of 30, 50, 65, 90 and 100 μm measured on standard sieves. Upon irradiation with Nd:YAG laser light ($\lambda = 1064$ nm), the intensity of the green light from the powder samples was measured in $(Hbiqui)_4[SiW_{12}O_{40}]\cdot 3H_2O$ and urea under the same conditions and its values compared. It was found that the SHG signal intensity was about 15% that of urea. This value is comparable to that obtained with the compound $(hmpaH)_4[SiW_{12}O_{40}]\cdot 2H_2O$, hmpa = hexamethylphosphoramide [26]. Preliminary tests on the other prepared compounds have provided negligible responses. Future work on the design of polyoxometalate-based materials in order to obtain more intense SHG is required. The study of third-order non-linear properties is in progress and will be presented elsewhere.

3.5. Concluding remarks

Reaction of the electron donor 2,2′-biquinoline with heteropolyacids originated novel compounds of general formula $(Hbiqui)_m[XM_{12}O_{40}]\cdot n$solv, X = P ($m = 3$), Si ($m = 4$); M = Mo, W. These were coloured yellow or yellow–green due to charge transfer between protonated 2,2′-biquinoline and the anions. Electronic spectroscopy corroborated this fact. The salt $(Hbiqui)_4[SiW_{12}O_{40}]\cdot 3H_2O$ is particularly interesting, since it exhibited intense charge transfer in the solid state, intermolecular electronic interaction in solution and second-order non-linear optical properties. Some of the prepared compounds are potential candidates for third-order non-linear optics.

Compounds with molybdenum proved to be photochromic under sunlight and, to a smaller extent, under visible light from a tungsten lamp. Change in colour accompanied reduction of the Keggin anions. Solids crystallized with dmf were more photosensitive than others. None of the studied compounds exhibited a truly reversible photochromism, but for some of them partial recovery of the initial colours and spectra were observed.

Acknowledgements

Thanks are due to the University of Aveiro and FCT (project PRAXIS/2/2.1Q/419/94 and PhD grant of J.A.F.G.) for financial support of this work.

References

[1] M.T. Pope, Heteropoly and Isopoly Oxometalates, Springer-Verlag, Berlin, 1983.
[2] L.C.W. Baker, D.C. Glick, Chem. Rev. 98 (1998) 3.
[3] M.T. Pope, in: G. Wilkinson (Ed.), Comprehensive Coordination Chemistry, vol. 3, Pergamon Press, Oxford, 1987, p. 1023.
[4] M.T. Pope, A. Muller, Angew. Chem., Int. Ed. Engl. 30 (1991) 34.
[5] M.T. Pope, A. Muller (Eds.), Polyoxometalates: From Platonic Solids to Anti-retroviral Activity, Kluwer Academic Publishers, Dordrecht, 1994.
[6] C.L. Hill (guest editor), Chem. Rev. 98 (1998) no. 1, thematic issue.
[7] C.L. Hill, C.M. Prosser-McCartha, Coord. Chem. Rev. 143 (1995) 407.
[8] R. Neumann, Prog. Inorg. Chem. 47 (1998) 317.
[9] I.V. Kozhevnikov, Chem. Rev. 98 (1998) 171.
[10] N. Mizuno, M. Misono, Chem. Rev. 98 (1998) 199.
[11] C.L. Hill, J. Mol. Catal. A 114 (1996) no. 1–3, thematic issue.
[12] M. Misono, Chem. Commun. (2001) 1141.
[13] J.T. Rhule, C.L. Hill, D.A. Judd, Chem. Rev. 98 (1998) 327.
[14] E. Coronado, C.J. Gomez-Garcia, Comments Inorg. Chem. 17 (1995) 255.
[15] E. Coronado, C.J. Gomez-Garcia, Chem. Rev. 98 (1998) 273.
[16] L. Ouahab, Chem. Mater. 9 (1997) 1909.
[17] J.M. Clemente-Juan, E. Coronado, Coord. Chem. Rev. 193–195 (1999) 361.
[18] L. Ouahab, Coord. Chem. Rev. 178–180 (1998) 1501.
[19] D.E. Katsoulis, Chem. Rev. 98 (1998) 359.
[20] P. Le Maguerès, L. Ouahab, S. Golhen, D. Grandjean, O. Pena, J. Jegaden, C.J. Gomez-Garcia, P. Delhaes, Inorg. Chem. 33 (1994) 5180.
[21] S. Golhen, L. Ouahab, D. Grandjean, P. Molinié, Inorg. Chem. 37 (1998) 1499.
[22] D. Attanasio, F. Bachechi, Adv. Mater. 6 (1994) 145.
[23] C.M. Prosser-McCartha, M. Kadkhodayan, M. Williamson, D.A. Bouchard, C.L. Hill, J. Chem. Soc., Chem. Commun. (1986) 1747.
[24] M. Williamson, D.A. Bouchard, C.L. Hill, Inorg. Chem. 26 (1987) 1436.

[25] C.L. Hill, D.A. Bouchard, M. Kadkhodayan, M. Williamson, J.A. Schmidt, E.F. Hilinski, J. Am. Chem. Soc. 110 (1988) 5471.
[26] J. Niu, X. You, C. Duan, H. Fun, Z. Zhou, Inorg. Chem. 35 (1996) 4211.
[27] D. Attanasio, M. Bonamico, V. Fares, P. Imperatori, L. Suber, J. Chem. Soc., Dalton Trans. (1990) 3221.
[28] E. Wang, Y. Zhou, Z. Wang, L. Zhang, Transition Met. Chem. 21 (1996) 447.
[29] X. Zhang, B. Shan, X. You, Z. Zhong-Yuan, Z. Xiang-Ge, Polyhedron 16 (1997) 713.
[30] X. Zhang, B. Shan, C. Duan, X. You, Chem. Commun. (1997) 1131.
[31] X. Zhang, B. Shan, X. You, Polyhedron 16 (1997) 95.
[32] Y. Zhou, E. Wang, J. Peng, J. Liu, C. Hu, R. Huang, X. You, Polyhedron 18 (1999) 1419.
[33] J. Niu, B. Shan, X. You, H. Fun, B. Yip, Transition Met. Chem. 24 (1999) 108.
[34] P. Maguerès, S.M. Hubig, S.V. Lindeman, P. Veya, J.K. Kochi, J. Am. Chem. Soc. 122 (2000) 10073.
[35] L. Zhang, Y. Zhou, Z. Yu, G. Fang, X. You, J. Mol. Struct. 570 (2001) 83.
[36] L. Bi, E. Wang, L. Xu, R. Huang, Inorg. Chim. Acta 305 (2000) 163.
[37] B. Lihua, H. Oizhuang, J. Quiong, W. Enbo, J. Mol. Struct. 597 (2001) 83.
[38] Z. Han, E. Wang, G. Luan, Y. Li, H. Zhang, Y. Duan, C. Hu, N. Hu, J. Mater. Chem. 12 (2002) 1169.
[39] T. Yamase, Chem. Rev. 98 (1998) 307.
[40] J. Pécaut, R. Masse, J. Mater. Chem. 4 (1994) 1851.
[41] Y. Fur, M. Bagieu-Beucher, R. Masse, J. Nicond, J. Lévy, Chem. Mater. 8 (1996) 68.
[42] C. Rocchiccioli–Deltcheff, M. Fournier, R. Franck, R. Thouvenot, Inorg. Chem. 22 (1983) 207.
[43] J.A.G. Drake, D.W. Jones, Org. Magn. Res. 18 (1982) 42.
[44] A.G. Osborne, R. Greene, I.H. Sadler, D. Reed, Magn. Res. Chem. 27 (1989) 4.
[45] Crystal structure analysis on $(Hbiqui)_4[SiW_{12}O_{40}]\cdot 3dmf$: orthorhombic, space group *Fddd*, $a = 1796.9(2)$, $b = 2124.1(2)$, $c = 5275.4(2)$ pm, $V = 20135(4) \times 10^6$ pm^3, $Z = 8$. Preliminary examination and data collection were carried out on a Nonius κ-CCD device attached to a rotating anode (NONIUS FR591) and graphite monochromator Mo Kα radiation. Data collection was performed at 143 K. A total of 19 778 reflections were collected. After merging ($R_{int} = 0.093$), 4203 independent reflections remained and were used for all calculations. Data were corrected for Lorentz and polarization effects. The structure was solved by a combination of direct methods and difference-Fourier syntheses. Due to the presence of highly disordered 2,2′-biquinoline molecules and $[SiW_{12}O_{40}]^{4-}$ anions the *dmf* molecules could not be resolved and we decided to stop the calculations at $R_1 = 0.1177$. Nevertheless these results are exact enough for the statements given in Section 3.
[46] C.L. Hill, D.A. Bouchard, J. Am. Chem. Soc. 107 (1985) 5148.
[47] K. Unoura, N. Tanaka, Inorg. Chem. 22 (1983) 2963.
[48] B. Keita, L. Nadjo, J. Electroanal. Chem. 227 (1987) 77.
[49] M. Sadakane, E. Steckhan, Chem. Rev. 98 (1998) 219.
[50] $[(dmf)_2H]_3[PMo_{12}O_{40}]$ was obtained by adding dmf to a concentrated aqueous solution of $H_3[PMo_{12}O_{40}]$ (molar ratio of 6:1). A yellow solid was collected and dried in vacuum. Its characterization by thermogravimetric analyses, infrared and NMR (^{31}P and ^{1}H) spectroscopy was consistent with the chemical formula indicated above. Exposure to sunlight changed the colour of this compound to green. The reduction of $[PMo_{12}O_{40}]^{3-}$ was evidenced by EPR and diffuse reflectance spectroscopy.
[51] T. Yamase, T. Ikawa, Bull. Chem. Soc. Jpn. 50 (1977) 746.
[52] S.K. Kurtz, T.T. Perry, J. Appl. Phys. 39 (1968) 2798.

intriguing observation that the pharmacological activity has been found to be highly dependent on the identity of the metal and the donor sequence of the ligands with different ligands showing widely different biological properties although they may vary only slightly in their molecular structure [20,24]. However, no pattern has emerged to enable the activity to be predicted on the basis of the structure of this type of compound, their substituents or their metal complexes [27]. Apart from their biological activity, nitrogen–sulfur donor ligands of thiosemicarbazides and thiosemicarbazones and their metal complexes generate intriguing stereochemical, electrochemical and electronic properties. Current research is probing into the electron-transfer behaviors of these complexes as well [28–30].

We continue our work in this area to supplement available information and thus contribute to the effort to elucidate the selectivity pattern of these Schiff base ligands. Our recent observations have shown that antimony and cobalt complexes with NNS donor sequence Schiff bases exhibited very low CD_{50} values of 0.35–1.6 μg cm^{-3} [31] while a number of transition metal complexes of methyl-3-[1-(2-pyridyl)ethylidene]carbodithioate have been reported to have antitumor activity [2] and palladium(II) complexes containing the dithiocarbazate moiety showed positive in vitro antiamoebic activity against *E. histolytica* [32]. Encouraged by these results, we have extended our study to new bidentate NS Schiff bases derived from the condensation of SBDTC with 5-methyl-2-furyldehyde (NS) and 2-furyl-methylketone (NS′). In addition, we report herein the bioactivity of a previously reported tridentate NNS Schiff base (SBD1) [33] derived from SBDTC with pyrrole-2-carboxaldehyde and its nickel(II) and copper(II) complexes.

2. Experimental

All the chemicals and solvents were of reagent grade, and were used as received.

2.1. Preparation of S-benzyldithiocarbazate and its Schiff bases

SBDTC was prepared as previously reported [3]. The yield was 35 g (85%), m.p. 124 °C (Lit. 125 °C). All the Schiff bases were prepared by adding a solution of SBDTC (0.1 mol) in absolute EtOH (40 cm^3) to an equimolar solution of aldehyde or ketone in 50 cm^3 of the same solvent. The mixture was heated on a steam bath for 10 min and then cooled to 0 °C in an ice bath until the Schiff base precipitated. After being filtered, washed with cold EtOH and dried in vacuo over silica gel, the yield of each product was measured and its m.p. was recorded.

2.2. General method for the preparation of metal complexes

Schiff base (0.0076 mol) prepared as outlined in Section 2.1 was dissolved in EtOH (50 cm^3) in the presence of an equimolar amount of KOH (0.4 g). The clear solution was treated with a solution containing a stoichiometric amount of metal salt in the same solvent (approximately 50 cm^3). The mixture was heated to 100 °C for 5 min and then kept in an ice-salt bath. The product was isolated, washed with EtOH and dried in a vacuum desiccator over P_2O_5. The metal salts used were $Cu(NO_3)_2 \cdot 2.5H_2O$, $NiCl_2 \cdot 6H_2O$, $Cd(CH_3COO)_2 \cdot 2H_2O$ and $ZnCl_2$.

2.3. Physical measurements

The analyses for carbon, hydrogen and nitrogen were carried out at *Mikroanalytisches Labor Pascher*, Remagen-Bandorf, Germany. The IR spectra in KBr pellets were recorded (4000–400 cm^{-1}) using a Perkin–Elmer FTIR 1750X spectrophotometer. The molar conductance of a 10^{-3} M solution of each metal complex in DMSO was measured at 29 °C using a Jenway 4310 conductivity meter and a dip-type cell with platinised electrode. M.p. were determined using an Electrothermal digital m.p. apparatus while the UV–Vis spectra were recorded on a Shimadzu UV-2501 PC spectrophotometer (800–200 nm).

2.4. X-ray structure determination of [Cd(NS)$_2$]

A selected crystal of the recrystallized Cd(II) complex was mounted on a SMART CCD diffractometer. Reflection data were measured at 20 °C using graphite monochromated Mo Kα ($\lambda = 0.71073$ Å) radiation with a detector distance of 4 cm and swing angle of −35°. The collected data were reduced using the program SAINT [34] and an empirical absorption correction was carried out using SADABS [35]. The structure was solved by direct methods and refined using the full-matrix least-squares method on F^2_{obs} using the SHELXTL [36] software package. All non-H atoms were anisotropically refined. The hydrogen atoms were located by different syntheses and refined isotropically, using SHELXTL created the molecular graphics. Atomic scattering factors and anomalous dispersions corrections were taken from the International Table for X-ray crystallography [37].

2.5. Target microorganisms

Eight pathogenic microbes were used to test the biological potentials of the ligands and their complexes. They were *Methicillin resistant sthaphylococcus* (MRSA), *Bacillus subtilis* wild type (B29), *Subtilis*

mutant (mutant defective DNA repair-B28), *Pseudomonas aeruginosa* (60690), *Candida albicans* (C.A.), *Aspergillus ochraceous* (398), *Saccaromyces ceciricaee* (20341) and *Candida lypolytica* (2075).

2.5.1. Qualitative antimicrobial assay

Antimicrobial activity of each sample was qualitatively determined by a modified disc diffusion method as previously reported [31,38].

2.5.2. Quantitative antimicrobial assay

Compounds that showed positive antimicrobial activities with the modified disc diffusion assay were subjected to the broth dilution method for the quantitative measurement of microbiostatic (inhibitory) activity as described by Hufford and Clark [39]. The lowest concentration that completely inhibited visible microbial growth was recorded as the minimum inhibitory concentration (MIC, μg cm^{-3}). Streptomycin and nystatin were used as positive controls for bacteria and fungi, respectively.

2.5.3. Cytotoxic assay

CEM-SS (Human T-lymphoblastic leukemia cell line) obtained from the National Cancer Institute, USA and HT-29 (Human colon adenocarcinoma cell line) obtained from American Type Culture Collection were used. The cells were cultured in RPMI-1640 medium supplemented with 10% fetal calf serum. Cytotoxicity was determined using the microtitration of 3-(4,5-dimethylthiazol-2-yl)-2,5-diphenyltetrazolium bromide assay (MTT) (Sigma, USA) as reported by Mosmann [40]. The solutions of compounds of different concentrations were prepared from the stock solutions (10 mg cm^{-3}) by serial dilution in RPMI-1640 to give a volume of 0.1 cm^3 in each well of a microtiter plate as described previously [19]. Each well was filled with 0.1 cm^3 of cell suspension in complete growth medium (CGM) at 1–2×10^5 cells cm^{-3}. Controls that contained only cells were included for each sample. Doxorubicin and tamoxifen were used as control cytotoxins.

3. Results and discussion

The condensation of SBDTC with 5-methyl-2-furfural and 2-furyl-methylketone yielded the isomeric Schiff bases, **1** and **2**, respectively. The CHNS elemental analyses results are in full agreement with the calculated values (Table 1). The Schiff bases **1** and **2** have protons adjacent to the thione groups. The thione groups are relatively unstable in the monomeric forms and tend to turn to the more stable thiol forms by enethiolization in solution [3] (Figs. 1a,b and 2a,b). The absence of ν(SH) modes at approximately 2570 cm^{-1}, in the solid state, indicates that thione (**1a**) and (**2a**) was the major tautomer in each case. However, in the presence of KOH, the Schiff bases can quickly form the thiolate anions in solution [3]. This enhances the nucleophilicity of the ligand thus affording bidentate uninegative chelation with metal ions. The results of elemental analyses, the melting points, UV–Vis spectra, IR spectra and molar conductance values are given in Tables 1 and 2. The IR spectra of the Schiff bases **1** and **2** display strong bands at approximately 1000 cm^{-1} which can be assigned to the asymmetric stretching mode of CSS. Upon coordination, these bands were found either to split or to give well-defined shoulders, indicating the presence of unidentate sulfur coordination [41]. The ν(C=S) modes of **1** and **2**, at approximately 1100 cm^{-1}, were lost in all the metal complexes (Table 2), confirming that the Schiff bases were coordinated through the thiolo sulfur. The ν(C=N) modes of **1** and **2** observed at 1620 and 1599 cm^{-1}, respectively, were shifted to lower (approximately 50 cm^{-1}) frequencies (Table 2) in the complexes, indicating coordination by the azomethine nitrogen. The ν(N–N) modes of all the free ligands were shifted to higher wave numbers on complexation as a result of a reduction in the repulsion between the lone pairs of electrons on the nitrogen atoms due to coordination through the azomethine nitrogen atom [42]. The disappearances of the ν(NH) modes of the free Schiff bases **1** and **2**, at 3200 and 3210 cm^{-1}, upon complexation (Table 2), evidences coordination through

Table 1
Analytical data and physical properties of the Schiff bases and their complexes

Compound	Color	M.p (°C)	Found (Calc.) (%)			Molar conductance (Ω^{-1} cm^2 mol^{-1})
			C	H	N	
NS (**1**)	orange	134.4				
NS′ (**2**)	dark orange	133.3	57.70 (57.93)	5.01 (4.83)	10.02 (9.66)	
$[Ni(NS)_2]\cdot 4H_2O$ (**3**)	dark orange	198.2	46.40 (47.41)	4.31 (4.79)	7.90 (7.90)	22
$[Cu(NS)_2]\cdot 2H_2O$ (**4**)	brown	176.0	49.13 (50.94)	4.13 (4.24)	8.66 (8.49)	19
$[Zn(NS)Cl\cdot H_2O]\cdot H_2O$ (**5**)	yellow	233.9	38.44 (39.45)	3.32 (3.99)	6.74 (6.57)	33
$[Ni(NS')_2]\cdot 4H_2O$ (**6**)	dark green	210.0	47.96 (48.65)	4.26 (4.63)	8.12 (8.11)	19
$[Cd(NS)_2]$	orange	186.5	48.37 (48.67)	4.43 (3.76)	8.18 (8.11)	

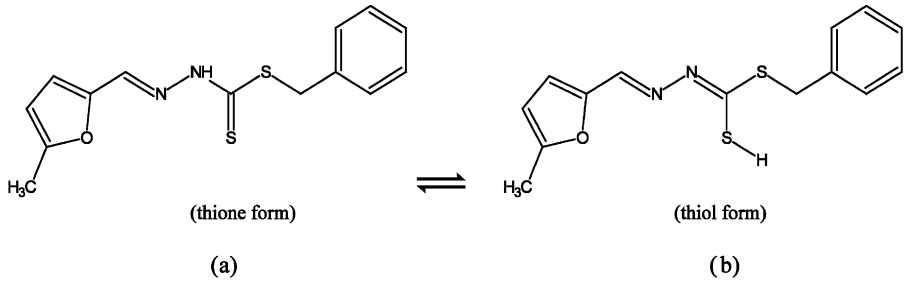


Fig. 1. The Schiff base **1**, thione form turning to thiol form.

the thiolate anions generated as a result of enethiolization.

The zinc complex, **5**, has a molar conductance of 33 Ω^{-1} cm^2 mol^{-1}, in DMSO, characteristic of 1:1 electrolytes [43]. Other metal complexes have molar conductance values <25.0 Ω^{-1} cm^2 mol^{-1} indicating covalent bonding in each case.

The band maxima in the UV–Vis spectra of the dark orange nickel complex, **3** at 485, 420, 357 nm and its dark green nickel complex, **6**, at 510, 420, 315 nm were characteristic of a square-planar Ni(II) configuration [3]. The bands may be attributed to the $^1A_1g \rightarrow {}^1A_2g$, $^1A_1g \rightarrow {}^1B_1g$ and $^1A_1g \rightarrow {}^1Eg$ transitions, respectively [44]. The UV–Vis spectra for the copper(II) complex, **4**, displays two bands corresponding to $^2B_1g \rightarrow {}^2A_1g$ (380–375 nm) and $^2B_1g \rightarrow {}^2E_1g$ (350–345 nm) transitions, presumably arising from a square-planar Cu(II) [3]. The very low solubility of the yellow zinc(II) complex, **5**, in most organic solvents indicates a polymeric structure. A bridged dimeric square-planar structure is very unlikely since zinc(II) ion generally forms tetrahedral complexes because of its d^{10} electronic configuration. The absorption maxima at 360, 340 and 300 nm can be attributed to intra-ligand transitions only [44].

3.1. X-ray crystal and molecular structure study of [Cd(NS)$_2$]

Recrystallization of [Cd(NS)$_2$] from DMF gave beautiful dark yellow transparent crystals after a week. Fig. 3 shows the perspective view and the atomic numbering scheme of the complex. The summary of crystallographic data, as well as the solution and refinement information for the complex are given in Table 6. Selected bond lengths and angles are listed in Table 7. The complex, of composition [$CdC_{28}H_{26}N_4S_4O_2$], is composed of discrete molecules (Fig. 3). The central cadmium atom of the complex molecule adopts a distorted tetrahedral geometry with N–Cd–N, N–Cd–S and S–Cd–S angles between 79.07(8)° and 130.15(8)°. The C–N bond distances of the bi-chelated ligands of 1.279(5)–1.293(5) Å are typical for double bond Schiff base compounds [45,46]. The C–S bond distances of 1.741(4)–1.798(5) Å indicate single bond character which supports the suggestion that the complex formation involves the ligand in its thiol form. Both the Cd–N (2.267(3) and 2.286(4) Å) and Cd–S (2.4807(11) and 2.4819(11) Å) bond lengths are slightly shorter than those found in complexes of octahedral symmetry where Cd–N bond lengths of between 2.349(3) and 2.578(4) Å [28] and Cd–S bond length of 2.640(1) Å in the Cd(II) complex containing 1,4,7,10-tetrakis(pyrazol-1-ylmethyl)-1,4,7,10-tetraazacyclododecane ligand [25,47] have been reported. The methylfurylmethylenedithiocarbazate moieties C7/S2/C8/N1/N2/S1/C9/C10/C11/C12/C13/C14/O1/Cd and C21/S4/C22/N3/N4/S3/C23/C24/C25/C26/C27/C28/O2/Cd are essentially planar but almost perpendicular to each other about the central Cd atom with a dihedral angle of 75.76(3)°. The phenyl rings, C1/C2/C3/C4/C5/C6 and C15/C16/C17/C18/C19, are out of plane with their respective methylfurylmethylenedithiocarbazate groups with dihedral angles of 73.0(1)° and 76.4(1)°, respectively. A weak intramole-

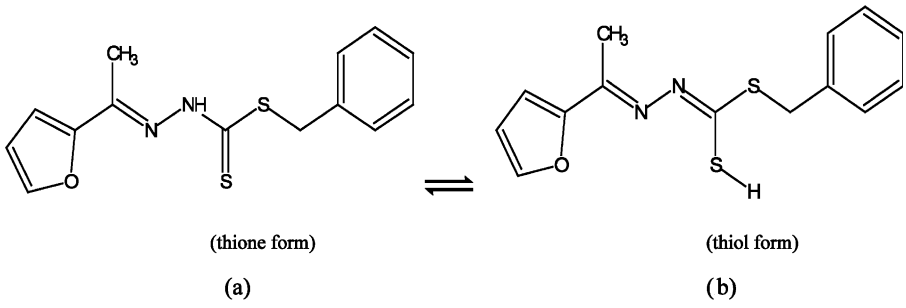


Fig. 2. The Schiff base **2**, thione form turning to thiol form.

Table 2
Spectral data (band maxima)

Compound	Infrared absorption bands (frequency, cm^{-1})					UV–Vis spectra [a] (λ_{max}, nm)
	ν(C=S)	ν(C=N)	ν(C=O)	ν(NH)	ν(N–N)	
1	1100	1620	–	3200	1023	
2	1180	1599	–	3210	1036	
3	–	1599	–	–	–1038	357 (4.4), 420 (4.2), 485 (3.9)
4	–	1600	–	–	–1032	345 (4.3), 380 (4.3)
5	–	1615	–	–	–1039	300 (4.2), 340 (3.9), 360 (3.7)
6	–	1636	–	–	–1035	315 (4.3), 420 (3.9), 510 (3.4)

–, lost.
[a] Log ε ($l\ cm^{-1}\ mol^{-1}$) are given in parentheses.

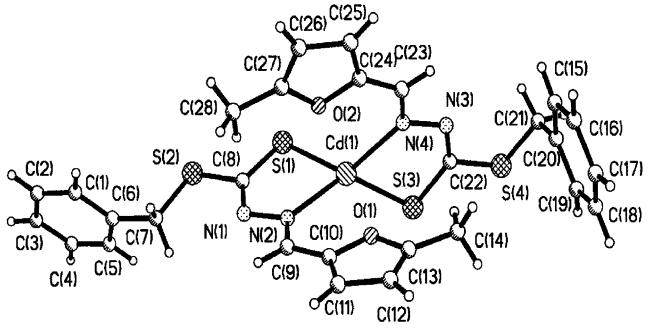


Fig. 3. Molecular structure of $[Cd(NS)_2]$ with 50% probability displacement ellipsoids.

cular interaction involving C28–H28···N1 is present in the molecule with H28···N1 bond length of 2.555 Å and C28–H28···N1 bond angle of 169.9°.

3.2. Cytotoxic activity

Compounds having CD_{50} values of less than 5 μg cm^{-3} are considered highly active, 5–10 μg cm^{-3}, moderately active, 10–20 μg cm^{-3}, weak and more than 20 μg cm^{-3}, inactive [19]. Screening results against CEM-SS (Human T-lymphoblastic leukemia cell line) cells are shown in Table 3. The NNS Schiff base, SBD1, reported by Ali et al. [33] and the new NS Schiff base, **1**, were highly active with the same CD_{50} values of 3.10 μg cm^{-3}, while **2** showed weak activity with a CD_{50} value of 12.00 μg cm^{-3}. The complexes, SBD1·Cu, **5** and **6**, were active against CEM-SS cells. Compound **5** showed strong activity with a CD_{50} value of 2.0 μg cm^{-3} while the CD_{50} value for **6** was 3.4 μg cm^{-3}. $[Cd(NS)_2]$ was also strongly active against CEM-SS with a CD_{50} value of 4.95 μg cm^{-3}. This cadmium complex was also tested against HELA (Cervical Cancer Cells) and was found to be very active with a CD_{50} value of 4.0 μg cm^{-3}. Epoxide was used as standard in the screening against HELA. The previously reported complex, SBD1·Cu [33], showed weak activity against CEM-SS cells (CD_{50} value of 19.5 μg cm^{-3}). All Schiff bases reported herein were inactive towards HT-29 while the complexes, SBD1·Cu and **5** showed weak activities against HT-29 with CD_{50} values of 12.0 and 13.0 μg cm^{-3}, respectively. Cytotoxicity of the simple metal salts is included in Table 3 for comparison. The selectivity of the Schiff bases and their complexes is of particular interest and is undoubtedly related to the mode of interaction between them and the target organisms. A study on the mechanism of chelation/binding has therefore been initiated.

3.3. Qualitative and quantitative antimicrobial assay results

Qualitative results for antimicrobial assays are given in Table 4. The SBD1 Schiff base showed a clear inhibition zone of 15 mm and above with all fungi,

Table 3
Screening test against leukemic (CEM-SS) and colon cancer cells (HT-29)

Compound	CD_{50} (μg cm^{-3})	
	CEM-SS	HT-29
1	3.10	–
2	12.00	–
3	–	–
4	–	–
5	2.0	13.00
6	3.4	–
$[Cd(NS)_2]$	4.95	not available
SBD1	3.10	–
SBD1·Cu	19.50	12.00
SBD1·Ni	–	–
Metal salt		
$ZnCl_2$	16.20	–
$NiCl_2$	–	–
$CuCl_2$	–	29.5
$CdBr_2$	14.00	3.5
Standard		
Doxorubicin	0.10	6.00
Tamoxifen	36.00	36.00

SBD1 = SBDTC + pyrole-2-carboxaldehyde; –, inactive.

Table 4
Qualitative antimicrobial assay results [a] (diameter in mm)

Compound	MRSA	B29	B28	60690	C.A.	398	20341	2075
1	–	–	–	–	–	17	–	16
5	16	22	24	21	–	18	–	–
6	–	14	26	–	18	18	18	20
$[Cd(NS)_2]$	21	19	22	20	26	15	18	–
SBD 1	–	–	–	–	15	21	15	20
Streptomysin (antibacterial control)	31	30	30	30	–	–	–	–
Nystatin (antifungal control)	–	–	–	–	21	25	24	27

Methicillin resistant sthaphylococcus (MRSA); *B. subtilis* wild type (B29); *S. mutant* (mutant defective DNA repair-B28); *P. aeruginosa* (60690); *C. albicans* (C.A.); *A. ochraceous* (398); *S. ceciricaee* (20341); *C. lypolytica* (2075). –, inactive.
[a] Diameter of 15 mm and above considered active.

Table 5
Quantitative antimicrobial assay results (MIC values in μg cm^{-3})

Compound	MRSA	B29	B28	60690	C.A.	398	20341	2075
1	–	–	–	–	–	25 000	–	25 000
5	1250	3125	1563	3125	–	3125	–	–
6	–	–	3250	–	6250	6250	6250	6250
$[Cd(NS)_2]$	12 500	25 000	50 000	781	n.a.	50 000	25 000	–
SBD 1	–	–	–	–	25 000	6250	2500	2500
Streptomysin (antibacterial control)	12.2	48.8	48.8	12.2	–	–	–	–
Nystatin (antifungal control)	–	–	–	–	3125	3125	6250	6250

n.a., not available; –, inactive.

while **1** showed clear inhibition of 15 mm and above with *A. ochraceous* (398) and *C. lypolytica* (2075). Compound **5** showed clear inhibition (> 15 mm) against all bacteria and *A. ochraceous* (398), while **6**, showed a clear inhibition zone against all fungi and *S. mutant* (mutant defective DNA repair-B28). $[Cd(NS)_2]$ complex was active against all bacteria and fungi used in our qualitative screening.

The quantitative antimicrobial results (Table 5) showed that the Schiff base, SBD1 was very effective against *S. ceciricaee* (20341) with a MIC value of 2500 μg cm^{-3}, while the MIC values for SBD1 against *C. lypolytica* (2075) were comparable to the antifungal control (Table 5).

4. Supplementary material

Crystallographic data for the structural analysis have been deposited with the Cambridge Crystallographic Data Centre, CCDC No. 163829 for the compound $[Cd(NS)_2]$. Copies of this information may be obtained free of charge from The Director, CCDC, 12 Union Road, Cambridge, CB2 1EZ, UK (fax: +44-1223-336033; e-mail: deposit@ccdc.cam.ac.uk or www: http://www.ccdc.cam.ac.uk).

Table 6
Summary of crystal data and structure refinement parameters for $[Cd(NS)_2]$

Compound	$[Cd(NS)_2]$
Chemical formula	$C_{28}H_{26}CdN_4O_2S_4$
Formula weight	691.17
Temperature (K)	293(2)
Mo Kα (Å)	0.71073
Crystal class	triclinic
Space group	$P\bar{1}$
a (Å)	9.1037(1)
b (Å)	12.2239(1)
c (Å)	14.5941(1)
α (°)	86.073(1)
β (°)	81.450(1)
γ (°)	72.411(1)
V ($Å^3$)	1530.46(2)
Z	2
ρ_{calc} (Mg m^{-3})	1.500
μ (mm^{-1})	1.018
$F(000)$	700
Sample dimension (mm)	0.34 × 0.22 × 0.18
Reflections collected	10 950
Independent reflections	7165 [$R_{int} = 0.0565$]
Data used for refinement	7165
Parameters refined	352
Correction	
Residuals	
Final R indices [$I > 2\sigma(I)$]	$R_1 = 0.0558$, $wR_2 = 0.1355$
R indices (all data)	$R_1 = 0.0751$, $wR_2 = 0.1433$
Goodness-of-fit on F^2	0.917
Largest and smallest peak (e $Å^{-3}$)	0.882 and −1.553

Table 7
Selected bond lengths (Å) and angles (°) for $[Cd(NS)_2]$

Bond lengths	
Cd(1)–N(2)	2.267(3)
O(2)–C(24)	1.367(5)
O(2)–C(27)	1.376(5)
N(1)–C(8)	1.281(5)
N(1)–N(2)	1.402(4)
C(4)–C(5)	1.366(8)
N(2)–C(9)	1.279(5)
N(3)–C(22)	1.292(5)
N(3)–N(4)	1.392(4)
N(4)–C(23)	1.293(5)
C(9)–C(10)	1.420(6)
Cd(1)–N(4)	2.286(3)
Cd(1)–S(3)	2.4807(11)
Cd(1)–S(1)	2.4819(11)
S(1)–C(8)	1.733(4)
S(2)–C(8)	1.757(4)
S(2)–C(7)	1.798(5)
S(3)–C(22)	1.741(4)
S(4)–C(22)	1.753(4)
S(4)–C(21)	1.806(6)
O(1)–C(10)	1.372(5)
O(1)–C(13)	1.376(5)
Bond angles	
N(2)–Cd(1)–N(4)	128.62(11)
N(2)–Cd(1)–S(3)	130.15(8)
N(4)–Cd(1)–S(3)	79.35(8)
N(2)–Cd(1)–S(1)	79.07(8)
N(4)–Cd(1)–S(1)	126.21(9)
S(3)–Cd(1)–S(1)	120.28(4)
C(8)–S(1)–Cd(1)	95.07(13)
C(8)–S(2)–C(7)	102.2(2)
C(22)–S(3)–Cd(1)	94.62(14)
C(6)–C(7)–S(2)	109.0(4)
C(6)–C(7)–H(7A)	109.9
S(2)–C(7)–H(7A)	109.9
C(6)–C(7)–H(7B)	109.9
S(2)–C(7)–H(7B)	109.9
H(7A)–C(7)–H(7B)	108.3
N(1)–C(8)–S(1)	131.6(3)
N(1)–C(8)–S(2)	118.2(3)
S(1)–C(8)–S(2)	110.2(2)
N(2)–C(9)–C(10)	123.1(4)
N(2)–C(9)–H(9A)	118.4
C(10)–C(9)–H(9A)	118.4
S(4)–C(21)–H(21B)	108.2
H(21A)–C(21)–H(21B)	107.3
N(3)–C(22)–S(3)	131.6(3)
N(3)–C(22)–S(4)	117.0(3)
S(3)–C(22)–S(4)	111.4(2)
N(4)–C(23)–C(24)	124.1(4)
N(4)–C(23)–H(23A)	117.9
C(24)–C(23)–H(23A)	117.9
C(25)–C(24)–O(2)	109.5(4)
C(25)–C(24)–C(23)	132.0(4)
O(2)–C(24)–C(23)	118.5(4)

Acknowledgements

We thank the Department of Chemistry, Universiti Putra Malaysia, for the provision of laboratory facilities. This research was funded by a grant from the Ministry of Science and Environment, Malaysia, under the Intensification of Research in Priority Areas (IRPA) program (Grant No. 09-02-04-0083).

References

[1] M.A. Ali, R. Bose, J. Inorg. Nucl. Chem. 39 (1977) 265.
[2] M.A. Ali, S.E. Livingstone, Coord. Chem. Rev. 13 (1974) 101.
[3] M.A. Ali, M.T.H. Tarafder, J. Inorg. Nucl. Chem. 39 (1977) 1785.
[4] M.T.H. Tarafder, M.A. Ali, Can. J. Chem. 56 (1978) 2000.
[5] M.A. Ali, S.M.G. Hossain, S.M.M.H. Majumder, M. Nazimuddin, M.T.H. Tarafder, Polyhedron 6 (1987) 1653.
[6] A.K. Saxena, J.K. Koacher, J.P. Tandom, S.R. Das, J. Toxicol. Environ. Health 10 (1982) 709.
[7] M.A. Ali, M.H. Kadir, M. Nazimuddin, S.M.H. Majumder, M.T.H. Tarafder, M.A. Khair, Indian J. Chem., Sect. A 27 (1988) 1064.
[8] M.T.H. Tarafder, M. Rahim, Indian J. Chem., Sect. A 28 (1989) 1105.
[9] M.A. Ali, C.M. Haroon, M. Nazimuddin, S.M.M.H. Majumder, M.T.H. Tarafder, M.A. Khair, Transition Met. Chem. 17 (1992) 133.
[10] M.E. Hossain, M.N. Alam, M.A. Ali, M. Nazimuddin, F.E. Smith, R.C. Hynes, Polyhedron 15 (1996) 973.
[11] H.K. Fun, K. Sivakumar, Y.P. Tian, C.Y. Duan, Z.L. Lu, X.Z. You, Acta Crystallogr., Sect. C 52 (1996) 1143.
[12] C.Y. Duan, Y.P. Tian, X.Z. Yu, T.C.W. Mak, Polyhedron 16 (1997) 4097.
[13] X.H. Zhu, S.H. Liu, Y.J. Liu, J. Ma, C.Y. Duan, X.Z. You, Y.P. Tian, F.X. Xie, S.S. Ni, Polyhedron 19 (1998) 181.
[14] M.A. Ali, N.E. Ibrahim, R.J. Butcher, J.P. Jasinski, J.M. Jasinski, J.C. Bryan, Polyhedron 17 (1998) 1803.
[15] H.L. Singh, S. Varshney, A.K. Varshney, Appl. Organomet. Chem. 13 (1999) 637.
[16] H.L. Singh, S. Varshney, A.K. Varshney, Appl. Organomet. Chem. 14 (2000) 212.
[17] H.L. Singh, A.K. Varshney, Appl. Organomet. Chem. 15 (2001) 762.
[18] H.L. Singh, B. Khunger, U.D. Triphathi, A.K. Varshney, Main Group Met. Chem. 24 (2001) 5.
[19] M.T.H. Tarafder, A. Kasbollah, K.A. Crouse, A.M. Ali, B.M. Yamin, H.-K. Fun, Polyhedron 20 (2001) 2363.
[20] M.T.H. Tarafder, A. Asmadi, S.M.S. Talib, A.M. Ali, K.A. Crouse, Transition Met. Chem. 26 (2001) 170 (and references therein).
[21] M.B. Ferrari, S. Capacchi, G. Pelosi, G. Reffo, P. Tarasconi, R. Albertini, S. Pinelli, P. Lunghi, Inorg. Chim. Acta 286 (1999) 134.
[22] D.L. Klaymen, J.P. Scovill, J. Bruce, J.F. Bartosevich, J. Med. Chem. 27 (1984) 87.
[23] J.P. Scovill, D.L. Klayman, D.L. Franchino, J. Med. Chem. 25 (1982) 1261.
[24] G.M. de Lima, J.L. Neto, H. Beraldo, H.G.L. Siebald, D.J. Duncalf, J. Mol. Struct. 604 (2002) 287 (and references therein).
[25] (a) C. Klofutar, S. Paljk, F. Krasovec, P. Suhae, Kem. Ind. 24 (1975) 361;
(b) C. Klofutar, S. Paljk, F. Krasovec, P. Suhae, Chem. Abstr. 84 (1976) 84739.
[26] R.A. Sanchez-Delgado, K. Lazardi, L. Rincon, J.A. Urbina, J. Med. Chem. 36 (1993) 2041.
[27] L. Mishra, J. Indian Chem. Soc. 76 (1999) 175.
[28] M. Maji, S. Ghosh, S.K. Chattopadhyay, T.C.W. Mak, Inorg. Chem. 36 (1997) 2938.

[29] Y.P. Tian, C.Y. Duan, C.Y. Zhao, X.Z. You, T.C.W. Mak, Z.Y. Zhang, Inorg. Chem. 36 (1997) 1247.
[30] X. Wang, Z. Deng, B. Jin, Y. Tian, X. Lin, Electrochim. Acta 47 (2002) 1537.
[31] M.T.H. Tarafder, M.A. Ali, N. Saravanan, W.Y. Weng, S. Kumar, N. Umar-Tsafe, K.A. Crouse, Transition Met. Chem. 25 (2000) 295.
[32] N. Bharti, R.M. Maurya, F. Naqvi, A. Bhattacharya, S. Bhattacharya, A. Azam, Eur. J. Med. Chem. 35 (2000) 481.
[33] M.A. Ali, K.R. Fernando, D. Palit, M. Nazimuddin, Transition Met. Chem. 20 (1995) 19.
[34] G.M. Sheldrick, SAINT V4 Software Reference Manual, Siemens Analytical X-ray Systems, Madison, WI, 1996.
[35] G.M. Sheldrick, SADABS, Program for Empirical Absorption Correction of Area Detector *Data*, University of Göttingen, Germany, 1996.
[36] G.M. Sheldrick, SHELXTL V5.1 Software Reference manual, Bruker AXS, Inc., Madison, WI, USA, 1997.
[37] A.L. Spek, PLATON, An integrated tool for the analysis of the results of a single crystal structure determination, Acta Crystallogr., Sect. A 46 (1996).
[38] A.W. Bauer, M.D.K. Kirny, J.C. Sherries, M. Turck, Am. J. Clin. Pathol. 45 (1966) 493.
[39] C.D. Hufford, A.M. Clark, Discovery and development in new drugs for systemic opportunistic infections, in: Atta-ur-Rahman (Ed.), Studies in Natural Product Chemistry, vol. 2, Elsevier, Amsterdam, 1988, pp. 421.
[40] T. Mosmann, J. Immunol. Methods 65 (1983) 55.
[41] N. Koji, H.S. Philippa, Infrared Absorption Spectroscopy, 2nd ed., Holden-Day Inc, San Francisco, 1977, p. 33.
[42] M.A. Ali, R.J. Butcher, J.C. Bryan, Inorg. Chim. Acta 287 (1998) 8.
[43] W.J. Geary, Coord. Chem. Rev. 7 (1971) 81.
[44] H.B. Gray, C.J. Ballhausen, J. Am. Chem. Soc. 85 (1963) 260.
[45] Q. Hao, X. Yang, F. Jian, L. Lu, X. Wang, I.A. Razak, S. Chantrapromma, H.K. Fun, Acta Crystallogr., Sect. C 57 (2001) 42.
[46] C.Y. Duan, Y.P. Tian, C.Y. Zhao, X.Z. You, T.C.W. Mak, Polyhedron 16 (1997) 2857.
[47] M.D. Vaira, F. Mani, M. Menicatti, R. Morassi, P. Stoppioni, Polyhedron 16 (1997) 3585.

the present paper, we want to show the nature of adducts formed between thallium(I) nitrate and 3-nitrophenoxide, 2,4-dinitrophenoxide and 4-nitrobenzoate ligands.

2. Experimental

2.1. Physical measurements

IR spectra were recorded as Nujol mulls using Perkin–Elmer 597 and Nicolet 510P spectrophotometers. Microanalyses were carried out using a Heraeus CHN-O-Rapid analyzer.

2.2. Preparation of Tl(3-np)

The complex Tl(3-np) was prepared by dissolving 0.266 g (1 mmol) thallium(I) nitrate in distilled water and adding a mixture of 3-nitrophenol (0.139 g, 1 mmol) and potassium hydroxide (0.057 g, 1 mmol) in ethanol (10 ml). The resulting solution was stirred for 1 h at room temperature, then it was allowed to stand for 2–3 days in a refrigerator. Yellow crystals of the desired product precipitated, were filtered off, washed with acetone and ether and air dried (0.239 g, yield 70%), m.p. 190 °C.

Anal. Found: C, 19.65; H, 1.29; N, 4.31. Calc. for $C_{12}H_8N_2O_6Tl_2$: C, 21.05; H, 1.17; N, 4.05%.

IR (cm^{-1}) selected bands: 720(s), 850(s), 1380(vs), 1590(s), 1612(s), 2980(w), 3140(w).

2.3. Preparation of Tl(2,4-dnp)

An ethanolic solution of 2,4-dinitrophenol (0.368 g, 2 mmol) and potassium hydroxide (0.114 g, 2 mmol) was added to a solution of thallium(I) nitrate (0.532 g, 2 mmol) in water. The resulting solution was concentrated on a water bath at 80 °C and cooled to room temperature (~ 25 °C), when a red microcrystalline compound was separated. The compound was filtered off, washed with cold ethanol and dried over silica gel (0.387 g, yield 50%). The red single crystals were isolated by the following branch tube method. The complex (0.3 g) was placed in one arm of the branched tube. Methanol was carefully added to fill both arms, then the tube was sealed and the complex-containing arm immersed in a bath at 60 °C while the other was at ambient temperature. After 10 days, red crystals (m.p. 240 °C) had deposited in the cooler arm. *Anal*. Found: C, 18.3; H, 0.9; N, 7.3. Calc. for $C_6H_3N_2O_5Tl$: C, 18.59; H, 0.77; N, 7.23%.

IR(cm^{-1}) selected bands: 720(w), 850(w), 1180(s), 1350(vs), 1385(vs), 1560(s), 1590(s), 1640(vs), 3030(w).

2.4. Preparation of Tl(4-nb)

The complex Tl(4-nb) was prepared by dissolving 0.266 g (1 mmol) thallium(I) nitrate in distilled water and adding an ethanolic solution of 3-nitrobenzoic acid (0.167 g, 1 mmol) and potassium hydroxide (0.057 g, 1 mmol). The resulting solution was stirred for 2 h at room temperature, and then it was allowed to stand for 3–4 days in a refrigerator. A white powder of the desired product precipitated, which was filtered off, washed with acetone and ether and air dried (0.230 g, yield 55%), m.p. 208 °C.

Anal. Found: C, 22.15; H, 1.13; N, 3.82. Calc. for $C_7H_4NO_4Tl$: C, 22.67; H, 1.08; N, 3.78%.

IR(cm^{-1}) selected bands: 717(vs), 817(s), 1331(vs), 1375(vs), 1507(vs), 1544(s), 2980(w), 3045(w).

2.5. Crystallography

2.5.1. Crystal data and refinement details

[Tl(3-np)]. $C_{12}H_8N_2O_6Tl_2$, M 684.94, triclinic, space group $P\bar{1}$, $a = 3.7649(15)$, $b = 9.400(4)$, $c = 10.068(4)$ Å, $\alpha = 85.159(8)^\circ$, $\beta = 86.133(8)^\circ$, $\gamma = 78.749(7)^\circ$, $V = 347.8(2)$ Å^3, D_{calc} ($Z = 1$ f.u.) 3.271 Mg m^{-3}, $F(000)$ 304. Specimen: $0.10 \times 0.1 \times 0.20$ mm; $T_{max,min}$ 0.761, 0.265, N 2891, N_0 1359, R 0.0468, R_w 0.0835.

Tl(2,4-dnp)]. $C_6H_3N_2O_5Tl$, M 387.47, monoclinic, space group $P2(1)/c$, $a = 5.7649(15)$, $b = 19.261(11)$, $c = 7.636(4)$ Å, $\alpha = 90^\circ$, $\beta = 91.857(11)^\circ$, $\gamma = 90^\circ$, $V = 802.4(8)$ Å^3, D_{calc} ($Z = 4$ f.u.) 3.208 Mg m^{-3}, $F(000)$ 696. Specimen: $0.05 \times 0.2 \times 0.30$ mm; $T_{max,min}$ 0.1553, 0.0294, N 9196, N_0 2339, R 0.0500, R_w 0.1046.

2.5.2. Determination of the structures

Crystallographic measurements were made at 140(2) K for [Tl(3-np)] and 120(2) K for [Tl(2,4-dnp)] using a Siemens R3m/V diffractometer. The intensity data were collected within the range $2.03^\circ \le \theta \le 27.03^\circ$ for [Tl(3-np)] and $3.41^\circ \le \theta \le 30.06^\circ$ for [Tl(2,4-dnp)] using graphite monochromated Mo Kα radiation ($\lambda =$ 0.71073 Å). Accurate unit cell parameters and an orientation matrix for data collection were obtained from least-squares refinement. Intensities of 2891 and 9196 unique reflections were measured, from which 1359 and 2339 with $I > 2\sigma(I)$ were used in the refinement for [Tl(3-np)] and [Tl(2,4-dnp)], respectively. The structures have been solved by direct methods and refined by full-matrix least-squares techniques on F^2.

The positions of hydrogen atoms were idealized and included in the calculations of the structure factors as fixed contributions. Each hydrogen atom was assigned an isotropic thermal parameter. R, R_w, with goodness-of-fit on F^2 0.897 and 0.754 are 0.0468, 0.0835 and 00.0385, 0.0962 for [Tl(3-np)] and [Tl(2,4-dnp)], respectively. The final difference density map showed a maximum peak and hole of 1.992, −1.495 e Å^{-3} for

[Tl(3-np)] and 2.507, −2.103 e Å^{-3} for [Tl(2,4-dnp)]. Corrections for Lorentz and polarization effects as well as the empirical correction for absorption using the SADABS programs were applied. All structural calculations were carried out with a PDP−11/23+ computer using the SDP-PLUS program package [17,18].

Crystal data and structure refinement are given in Tables 1 and 2. Selected bond lengths and angles are given in Tables 3 and 4. Anisotropic thermal parameters, observed and calculated structure factors, full lists of bond distances, bond angles and torsion angles are given in the supplementary material. ORTEP diagrams and a perspective view of the packing in the unit cells are shown in Figs. 1–4.

3. Discussion

3.1. Synthesis

Reaction between 3-nitrophenoxide, 4-nitrobenzoate and 2,4-dinitrophenoxide ligands provided powdered

Table 1
Crystal data and structure refinement for Tl(3-$NO_2C_6H_4O$)

Identification code	Tl(3-$NO_2C_6H_4O$)
Empirical formula	$C_{12}H_8N_2O_6T_{12}$
Formula weight	684.94
Temperature (K)	140(2)
Wavelength (Å)	0.71073
Crystal system	triclinic
Space group	$P\bar{1}$
Unit cell dimensions	
a (Å)	3.7649(15)
b (Å)	9.400(4)
c (Å)	10.068(4)
α (°)	85.159(8)
β (°)	86.133(8)
γ (°)	78.749(7)
V (Å^3)	347.8(2)
Z	1
D_{calc} (Mg m^{-3})	3.271
Absorption coefficient (mm^{-1})	23.171
$F(000)$	304
Crystal size (mm)	0.1 × 0.1 × 0.2
Theta range for data collection (°)	2.03–27.03
Index ranges	$-4 \le h \le 4$, $-12 \le k \le 12$, $-12 \le l \le 12$
Reflections collected	2891
Independent reflections	1359 [$R_{int} = 0.0708$]
Completeness to theta = 27.03°	89.6%
Absorption correction	SADABS program
T_{min}/T_{max}	0.265/0.761
Refinement method	full-matrix least-squares on F^2
Data/restraints/parameters	1359/0/100
Goodness-of-fit on F^2	0.897
Final R indices [for 1008 reflections with $I > 2\sigma(I)$]	$R_1 = 0.0468$, $wR_2 = 0.0835$
R indices (all data)	$R_1 = 0.0661$, $wR_2 = 0.0877$
Largest difference peak and hole (e Å^{-3})	1.992 and −1.495

Table 2
Crystal data and structure refinement for Tl(2,4-dnp)

Empirical formula	$C_6H_3N_2O_5Tl$
Formula weight	387.47
Temperature (K)	120(2)
Wavelength (Å)	0.71073
Crystal system	monoclinic
Space group	$P2(1)/c$
Unit cell dimensions	
a (Å)	5.458(3)
b (Å)	19.261(11)
c (Å)	7.636(4)
α (°)	90
β (°)	91.857(11)
γ (°)	90
V (Å^3)	802.4(8)
Z	4
D_{calc} (Mg m^{-3})	3.208
Absorption coefficient (mm^{-1})	20.126
$F(000)$	696
Crystal size (mm)	0.05 × 0.2 × 0.3
Theta range for data collection (°)	3.41–30.06
Limiting indices	$-7 \le h \le 7$, $-27 \le k \le 27$, $-10 \le l \le 10$
Reflections collected/unique	9196/2339 [$R_{int} = 0.0637$]
Completeness to $\theta = 30.06°$	99.3%
Absorption correction	Semi-empirical from equivalents
Max/min transmission	0.1553, 0.0294
Refinement method	Full-matrix least-squares on F^2
Data/restraints/parameters	2339/0/127
Goodness-of-fit on F^2	0.754
Final R indices [for 1862 reflections with $1.2\sigma(I)$]	$R_1 = 0.0385$, $wR_2 = 0.0962$
R indices (all data)	$R_1 = 0.0500$, $wR_2 = 0.1046$
Largest difference peak and hole (e Å^{-3})	2.507 and −2.103

Table 3
Selected bond lengths (Å) and angles (°) for Tl(3-np)

Bond lengths		Bond angles	
Tl(1)–O(1)	2.499(8)	O(1)–Tl(1)–O(1)#1	73.0(3)
Tl(1)–O(1)#1	2.562(7)	O(1)–Tl(1)–O(1)#2	82.3(3)
Tl(1)–O(1)#2	2.717(10)	O(1)#1–Tl(1)–O(1)#2	90.9(3)
Tl(1)–O(2)#3	3.005(8)	O(1)–Tl(1)–Tl(1)#5	95.88(19)
Tl(1)–O(1)#4	3.396(11)	O(1)#1–Tl(1)–Tl(1)#5	133.8(2)
Tl(1)–O(3)#3	3.515(10)	O(1)#2–Tl(1)–Tl(1)#5	42.88(16)
Tl(1)–O(2)#4	3.554(9)	O(1)–Tl(1)–Tl(1)#6	84.12(19)
Tl(1)–Tl(1)#2	3.9308(14)	O(1)#1–Tl(1)–Tl(1)#6	46.2(2)
Tl(1)–Tl(1)#1	4.0696(14)	O(1)#2–Tl(1)–Tl(1)#6	137.12(16)
Tl(1)–Tl(1)#5	3.7649(15)	C(1)–O(1)–Tl(1)	126.0(7)
Tl(1)–Tl(1)#6	3.7649(15)	C(1)–O(1)–Tl(1)#1	123.7(7)
O(1)–Tl(1)#1	2.562(7)	C(1)–O(1)–Tl(1)#2	98.7(7)
O(1)–Tl(1)#2	2.717(10)	Tl(1)–O(1)–Tl(1)#1	107.0(3)
		Tl(1)–O(1)–Tl(1)#2	97.7(3)
		Tl(1)#1–O(1)–Tl(1)#2	90.9(3)

Symmetry transformations used to generate equivalent atoms: #1 $-x+1, y+2, -z$, #2 $-x, -y+2, -z$, #3 $-x+1, -y+1, -z$, #4 $-x, -y+1, -z$, #5 $x+1, y, z$; #6 $x-1, y, z$.

Table 4
Selected bond lengths (Å) and angles (°) for Tl (2,4-dnp)

Bond lengths		Bond angles	
Tl(1)–O(1)	2.601(5)	O(1)–Tl(1)–O(1)#1	75.41(18)
Tl(1)–O(1)#1	2.626(5)	O(1)–Tl(1)–Tl(1)#2	127.69(11)
Tl(1)–Tl(1)#2		O(1)#–Tl(1)–Tl(1)#2	141.24(11)
		C(1)–O(1)–Tl(1)	124.6(4)
		C(1)#–O(1)–Tl(1)#1	130.6(4)
		Tl(1)–O(1)–Tl(1)#1	104.59(18)

Symmetry transformations used to generate equivalent atoms: #1 $-x+1, -y+1, -z+2$, #2 $-x+1, -y+1, -z+1$.

materials analyzing as [Tl(3-np)], [Tl(4-nb)] and [Tl(2,4-dnp)], respectively. Attempts to isolate suitable single crystals for X-ray crystallography for [Tl(4-nb)] were not successful and each time the powdered compound was isolated.

3.2. Crystal structure of [Tl(3-np)]

Determination of the structure of [Tl(3-np] by X-ray crystallography (Table 1) showed the complex in the solid state (Fig. 2) to be a polymeric species with various similarities to the polymeric structures of [Tl(2-np)] and [Tl(4-np)], and it is really a novel one-dimensional polymer. The thallium atoms are linked within a classical 'stair-polymer' array by phenoxide oxygen atoms, each Tl(μ-O)$_2$Tl unit having an inversion point at its center, and a pair of them making up the unit b component of the polymer.

Thus, each thallium atom can be considered to be three-coordinate with an O_3 donor atom array (three

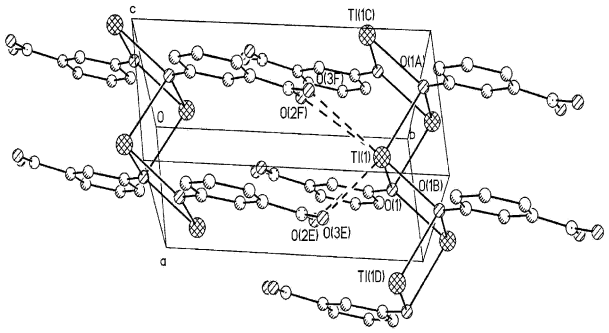


Fig. 2. A view perpendicular to a polymeric strand of the solid showing the chelating and bridging functions of the 3-nitrophenoxide ligand and the full donor atom environment of the Tl atoms in Tl(3-np).

oxygen atoms of the 3-nitrophenoxide ligand with Tl–O distances of Tl1···O1 = 2.499, Tl1···O1 $(-x+1, -y+2, -z)$ = 2.562 and Tl1···O $(-x, -y+2, -z)$ = 2.717 Å), and the weak interaction of thallium(I) with oxygen atoms of an adjacent molecule produces polymer units in the solid state. In fact each Tl atom in this structure alone with three normal bonds forms four "weak" Tl···O bonds and the exact distances are Tl1···O2 $(-x+1, -y+1, -z)$ = 3.005, Tl1···O3 $(-x, -y+1, -z)$ = 3.396 Å, Tl1···O3 $(-x+1, -y+1, -z)$ = 3.515 and Tl1···O2 $(-x, -y+1, -z)$ = 3.554 Å (Table 3). The presence of a lone pair of electron on the thallium atom is apparently the reason that the bridging interactions cannot come closer together. If the stereochemically active lone pair was not present, it might create more interaction between the bridging atoms of thallium(I) with the neighboring oxygen atoms

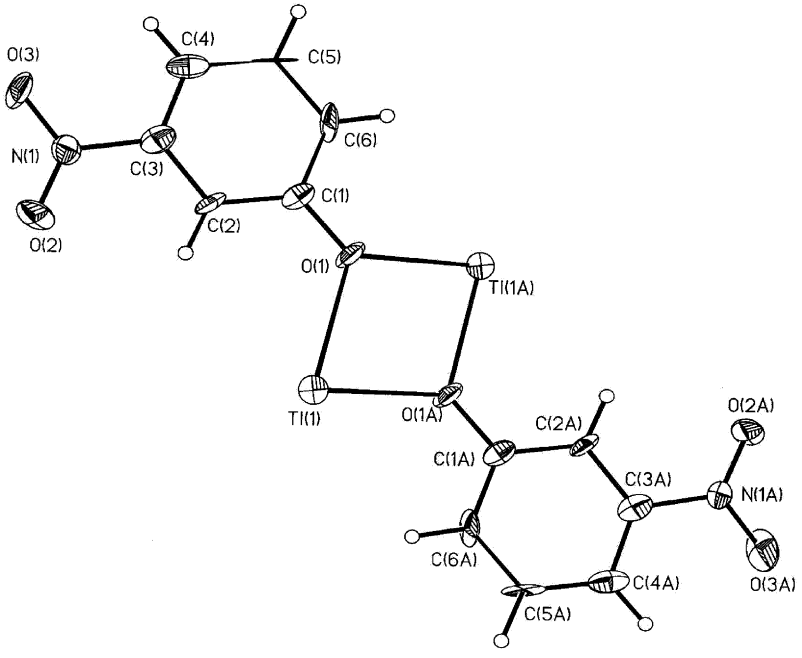


Fig. 1. The ORTEP diagram of the Tl_2O_2 rhomb forming the basic link of the polymeric structure of [Tl(3-np)]$_2$.

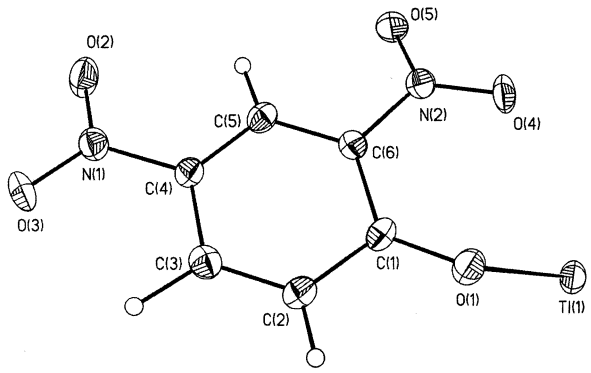


Fig. 3. The ORTEP diagram of Tl(2,4-dnp).

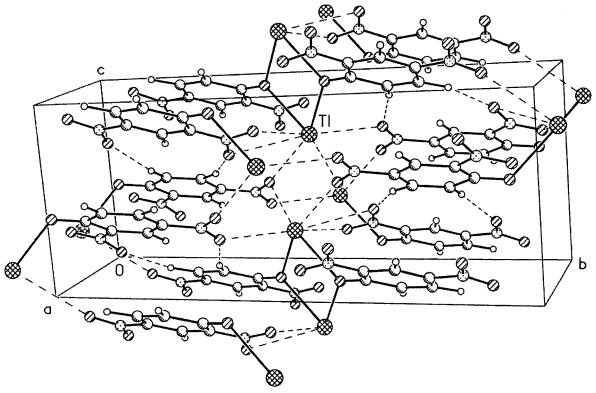


Fig. 4. A view perpendicular to a polymeric strand of the solid showing the chelating and bridging functions of the 2,4-dinitrophenoxide ligand and the full donor atom environment of the Tl atoms in Tl(2,4-dnp).

of nitrophenoxide. Consequently, this phenomenon could lead to more symmetry.

The arrangement of the oxygen atoms of nitrophenoxide suggest a gap or hole in the coordination geometry around the metal ion, occupied possibly by a stereoactive lone pair of electrons on thallium(I). The observed shortening of the Tl–O bond on the side of the Tl(I) ion opposite to the putative lone pair (2.499 compared with 2.717 Å adjacent to the lone pair) supports the presence of this feature. There are some "weak" Tl···Tl bonds in the polymeric state and the exact distances are Tl1···Tl1 $(-x, -y+2, -z) =$ 3.9308 Å, Tl1···Tl1 $(-x+1, -y+2, -z) = 4.0696$ Å, Tl1···Tl1 $(x+1, y, z) = 3.7649$ Å and Tl1···Tl1 $(x-1, y, z) = 3.7649$ Å (Table 3). The Tl···Tl across the rhomb (3.7649 Å) is appreciably shorter than the normal of approximately 4.0696 Å proposed as typical of Tl···Tl in Tl(μ-O_2)Tl rhomb. The nakedness of the resulting thallium environment possibly suggests a stereochemically active lone pair.

3.3. Crystal structure of [Tl(2,4-dnp)]

Determination of the structure of [Tl(2,4-dnp] by X-ray crystallography (Table 2) showed the complex in the solid state (Fig. 4) to be a polymeric species with various similarities to the polymeric structures of [Tl(2-np)], [Tl(4-dnp)] and [Tl(3-dnp)], and it is really a novel three-dimensional polymer. The thallium atoms are linked within a classical 'stair-polymer' array by phenoxide oxygen atoms. Each thallium atom can be considered to be two-coordinate with an O_2 donor atom array (two oxygen atoms of the 2,4-nitrophenoxide ligand) with Tl–O distances of Tl1···O1 = 2.601, and Tl1···O1 $(-x+1, -y+2, -z+2) = 2.626$, and the weak interaction of thallium(I) with oxygen atoms of the nitro group of an adjacent molecule produces polymer units in the solid state (Table 4). There are "weak" Tl···Tl bonds in the polymeric state and the exact distances are Tl1···Tl1 $(-x+1, -y+1, -z+1) = 3.740$ Å (Table 4). The presence of a lone pair of electrons on the thallium atom is apparently the reason that the bridging interactions cannot come closer together. The arrangement of oxygen atoms of nitrophenoxide suggest a gap or hole in the coordination geometry around the metal ion, occupied possibly by a stereoactive lone pair of electrons on thallium(I). If the stereochemically active lone pair was not present, it might create more interaction between the bridging atoms of thallium(I) with the neighboring oxygen atoms of nitrophenoxide. Consequently, this phenomenon could lead to more symmetry.

The strikingly similar feature of the $[Tl(3\text{-np})]_n$ complex with the $[Tl(2,4\text{-dnp})]_n$ complex is that there is a π–π stacking [19,20] interaction between the parallel aromatic rings belonging to adjacent chains in the two compounds. The question is, does the π–π stacking between the parallel aromatic rings help to increase the "gap" in coordination geometry around the metal ion or does the 'gap' arise from the "stereochemical activity" of valence shell lone electron pairs that then help to form π–π stacking.

The strikingly different feature of the $[Tl(3\text{-np})]_n$ complex with the $[Tl(2,4\text{-dnp})]_n$ complex is that the $[Tl(3\text{-np})]_n$ complex is a one-dimensional polymer whereas the $[Tl(2,4\text{-dnp})]_n$ complex is a three-dimensional polymer. This point must relate to the additional nitro group in the nitrophenoxide ligand. The $[Tl(2\text{-np})]_n$ and $[Tl(4\text{-np})]_n$ complexes [8] are one-dimensional polymers and support the presence of this feature.

Crystallographic data, selected bond lengths and angles are given in Tables 1–4. Atomic coordinates, anisotropic thermal parameters, observed and calculated structure factors, full lists of bond distances, bond angles and torsion angles are given in the supplementary material. A perspective view of the ORTEP diagram and the packing in the unit cell are shown in Figs. 1–4.

4. Supplementary material

Complete bond lengths and angles, co-ordinates and displacement parameters have been deposited with the Cambridge Crystallography Data Centre, CCDC Nos. 174597 for [Tl(3-np)] and 183434 for [Tl(2,4-dnp)]. Copies of this information may be obtained free of charge from The Director, CCDC, 12 Union Road, Cambridge, CB2 1EZ, UK (fax: +44-1223-336033; e-mail: deposit@cdc.cam.ac.uk or www: http://www.ccdc.cam.ac.uk).

Acknowledgements

The Tarbiat Modarres University Research Council supported this work. We thank the Institute of Organoelement Compounds of the Russian Academy of Science for determining the crystal structure by X-ray crystallography.

References

[1] M.J. Taylor, P.J. Brothers, in: A.J. Downs (Ed.), Chemistry of Gallium, Indium and Thallium (Ch. 3, see pp. 209–210, in particular), Blackie, London, 1993, p. 110.
[2] D.G. Tuck, in: R.D. Gillard, J.A. McCleverty, G. Wilkinson (Eds.), Comprehensive Coordination Chemistry, vol. 3 (Chapter 25.2), Pergamon, Oxford, 1987, p. 153.
[3] (a) J.M. Harrowfield, H. Miyamae, B.W. Skelton, A.A. Soudi, A.H. White, Aust. J. Chem. 49 (1996) 1029;
(b) J.M. Harrowfield, Miyamae H, T.M. Shand, B.W. Skelton, A.A. Soudi, A.H. White, Aust. J. Chem. 49 (1996) 1043;
(c) J.M. Harrowfield, H. Miyamae, T.M. Shand, B.W. Skelton, A.A. Soudi, A.H. White, Aust. J. Chem. 49 (1996) 1051;
(d) J.M. Harrowfield, H. Miyamae, B.W. Skelton, A.A. Soudi, A.H. White, Aust. J. Chem. 49 (1996) 1067;
(e) J.M. Harrowfield, H. Miyamae, B.W. Skelton, A.A. Soudi, A.H. White, Aust. J. Chem. 49 (1996) 1081;
(f) G.A. Bowmaker, J.M. Harrowfield, H. Miyamae, B.W. Skelton, A.A. Soudi, A.H. White, Aust. J. Chem. 49 (1996) 1089;
(g) I. Bytheway, L.M. Engelhardt, J.M. Harrowfield, D.L. Kepert, H. Miyamae, J.M. Patrick, B.W. Skelton, A.A. Soudi, A.H. White, Aust. J. Chem. 49 (1996) 1099;
(h) L.M. Engelhardt, J.M. Harrowfield, D.L. Kepert, H. Miyamae, J.M. Patrick, B.W. Skelton, A.A. Soudi, A.H. White, Aust. J. Chem. 49 (1996) 111;
(i) J.M. Harrowfield, H. Miyamae, B.W. Skelton, A.A. Soudi, A.H. White, Aust. J. Chem. 49 (1996) 1121;
(j) J.M. Harrowfield, H. Miyamae, B.W. Skelton, A.A. Soudi, A.H. White, Aust. J. Chem. 49 (1996) 1127;
(k) L.M. Engelhardt, J.M. Harrowfield, D.L. Kepert, H. Miyamae, J.M. Patrick, B.W. Skelton, A.A. Soudi, A.H. White, Aust. J. Chem. 49 (1996) 1135;
(l) J.M. Harrowfield, D.L. Kepert, H. Miyamae, B.W. Skelton, A.A. Soudi, A.H. White, Aust. J. Chem. 49 (1996) 1147;
(m) J.M. Harrowfield, H. Miyamae, B.W. Skelton, A.A. Soudi, A.H. White, Aust. J. Chem. 49 (1996) 1157;
(n) J.M. Harrowfield, H. Miyamae, B.W. Skelton, J.M. Harrowfield, H. Miyamae, B.W. Skelton, A.A. Soudi, A.H. White, Aust. J. Chem. 49 (1996) 1165.
[4] A. Morsali, M. Payheghader, M.S. Salehi, Z. Anorg. Allg. Chem. 628 (2002) 12.
[5] A.R. Mahjoub, A. Morsali, Chem. Lett. 1234 (2001).
[6] A.R. Mahjoub, A. Morsali, Z. Kristallogr. NCS 216, 601 (2001).
[7] A.R. Mahjoub, A. Morsali, Polyhedron, 21 (2002) 1223.
[8] J.M. Harrowfield, R.P. Sharma, B.W. Skelton, A.H. White, Aust. J. Chem. 51 (1998) 735 (and references cited therein).
[9] A. Schouten, J.A. Kanters, N.S. Poonia, Acta Crystallogr. Sect. C 46 (1990) 61.
[10] M. Botoshansky, F.H. Herbstein, M. Kapon, Acta Crystallogr. Sect. B 50 (1994) 589.
[11] G.A. Bowmaker, F.M.M. Hannaway, P.C. Junk, A.M. Lee, B.W. Shelton, A.H. White, Aust. J. Chem. 51 (1998) 331 (and references cited therein).
[12] L.J. Barbour, S.J. Belfield, P.C. Junk, M.K. Smith, Aust. J. Chem. 51 (1998) 337.
[13] A. Morsali, A. Tadjarodi, R. Mohammadi, A.R. Mahjoub, Z. Kristallogr. NCS 216 (2001) 379.
[14] L. Shimonni- Livny, J.P. Glusker, C.W. Bock, Inorg. Chem. 37 (1998) 1853.
[15] N.S. Poonia, A.V. Bajaj, Chem. Rev. 79 (1979) 389.
[16] J.C. Speakman, Struct. Bonding (Berlin) 12 (1972) 141.
[17] G. Ferguson, C. Glidewell, E.S. Lavender, Acta Crystallogr. Sect. B B55 (1999) 591.
[18] G.M. Sheldrick, SHELXTL-97 V5.10, 1997, Bruker AXS Inc., Madison, WI 53719, USA.
[19] R.D. Hancock, M.S. Shaikjee, S.M. Dobson, J.C.A. Boeyens, Inorg. Chim. Acta 154 (1988) 229.
[20] R. Foster (Ed.), Molecular Complexes, Paul Elek (Scientific Books), London, 1973.

tetrachlorocuprate(II) monohydrate is thermochromic and the crystal structure of its hydrated green phase was reported [11]. For a clear understanding of the mechanism of thermochromism one needs the crystal structure analysis of both the phases.

In this paper, we report the synthesis and crystal structure of the anhydrous yellow phase; the role of the water molecule in the thermochromism is also explored.

2. Experimental

2.1. Materials and measurements

High purity (98%) benzimidazole and copper(II) chloride, dihydrate were purchased from Emerck Germany and used as received. Elemental analyses (carbon, hydrogen and nitrogen) were performed using a Perkin–Elmer 240C elemental analyzer and the Cu contents in all the complexes were estimated spectrophotometrically [12]. IR spectra in KBr (4500–500 cm^{-1}) were recorded using a Perkin–Elmer RXI FT-IR spectrophotometer. Electronic spectra of mulls (1200–350 nm) were recorded with a Hitachi U-3501 spectrophotometer where Nujol was used as a medium as well as a reference. The effective magnetic moments were calculated from magnetic susceptibility measurements with an EG&G PAR vibrating sample magnetometer model 155 at room temperature (r.t.) and diamagnetic corrections were made using Pascal's constants [13]. The thermal analyses (TG–DTA) were carried out on a Metler Toledo TGA/SDTA 851 thermal analyzer in a dynamic atmosphere of dinitrogen (flow rate: 30 cm^3 min^{-1}). The sample was heated in an alumina crucible at a rate of 5 °C min^{-1}. The X-ray powder diffraction experiments were carried out using a Philips PW 3710 diffractometer with a Cu tube anode.

2.2. Preparations

2.2.1. $(HBz)_2CuCl_4$ (yellow) (1)

$CuCl_2 \cdot 2H_2O$ (5 mmol) was dissolved in a minimum volume of water. To this solution was mixed benzimidazole (10 mmol) dissolved in 5 ml of 10 (M) HCl. The resulting solution was concentrated in a water bath to approximately 3 ml and kept in a desiccator. After a few days yellow crystals suitable for X-ray diffraction were obtained. *Anal*. Found (Calc.): C, 38.0 (37.9); H, 3.8 (3.6); Cu, 14.5 (14.3); N, 12.5 (12.6)%. μ_{eff} 1.73 BM at 278 K. λ_{max} 22 222, 8734 cm^{-1}.

2.2.2. $(HBz)_2[CuCl_4] \cdot H_2O$ (green) (2)

The green crystals of the compound were prepared according to the reported method [11]. *Anal*. Found (Calc.): C, 36.2 (36.4); H, 4.2 (3.9); Cu, 13.6 (13.8); N, 12.3 (12.1)%. μ_{eff} 1.80 BM at 278 K. λ_{max} 24 155 (sh), 12 500 cm^{-1}.

The concentration of HCl in the reaction medium plays an important role in the synthesis of compound **1** or **2**. The green needle shaped crystals of **2** are readily obtained if the acidity of the reaction mixture is less than 6 M, whereas yellow crystals of **1** is the only product when the acidity is 9–12 M. Both the green and yellow compounds can be isolated from the 6 to 9 M acid solutions depending upon the experimental conditions. For instances, **2** is always resulted on cooling (10–12 °C) of a dilute solution (10 mmol benzimidazole, 5 mmol $CuCl_2 \cdot 2H_2O$ in 10 ml of 6–9 M HCl). If the solution is more concentrated (approximately 5 ml) and the temperature is higher (approximately 25 °C), yellow crystals of **1** are obtained on keeping the solution overnight without stirring. On stirring, however, **2** crystallizes immediately. It is very interesting to observe that the seeding of green or yellow crystals in this solution produce solely the respective crystals at r.t.

2.3. X-ray crystallography

A suitable single crystal of the complex **1** was mounted on a Bruker AXS CCD area detector system for data collection. The crystal data of the complex was collected at 293(2) K. Intensity data were collected in the

Table 1
Crystal data and structure refinement details

Empirical formula	$C_7H_7Cl_2Cu_{0.5}N_2$
Formula weight	221.89
Crystal system	monoclinic
Space group	$C2/c$
Unit cell dimensions	
a (Å)	14.903(2)
b (Å)	7.815(3)
c (Å)	16.130(3)
β (°)	92.93(3)
Volume (Å^3)	1876.2(8)
Z	8
D_{calc} (Mg m^{-3})	1.563
Absorption coefficient (mm^{-1})	1.735
$F(000)$	884
Crystal dimensions (mm)	0.26 × 0.19 × 0.14
Crystal colour	yellow
θ Range for data collection (°)	3.18–27.00
Limiting indices	$-19 \le h \le 19$, $0 \le k \le 9$, $0 \le l \le 20$
Reflections collected	11 396
Unique reflections	2038 [$R_{int} = 0.0226$]
Completeness to $\theta = 28.09°$	92.2%
Refinement method	full-matrix least-squares on F^2
Data/restraints/parameters	2038/0/135
Final R indices [$I > 2\sigma(I)$]	$R_1 = 0.0376$, $wR_2 = 0.0701$
R indices (all data)	$R_1 = 0.0992$, $wR_2 = 0.0801$
Goodness-of-fit on F^2	0.758
Extinction coefficient	0.0003(2)
Largest difference peak and hole (e Å^{-3})	0.453 and −0.422

ω–2θ scan mode using graphite monochromated Mo Kα radiation (0.71073 Å). The empirical absorption corrections were based on ψ scans. The structure was solved by direct method using SIR-97 [14]. The derived atomic coordinates were put through the full-matrix least-squares method of refinement by the SHELXL-97 [15] program. The structure was first refined isotropically varying the positional parameters and isotropic thermal parameters of the non-hydrogen atoms together with the overall scale factor. Further least-square refinements of the coordinates of non-hydrogen atoms were done using anisotropic temperature factors. The hydrogen atoms were placed geometrically and refined in the 'riding' model with isotropic thermal parameters 1.2 times U_{eq} of the atom to which they were attached and were treated as fixed contributors to the final structure factor calculations. Complex neutral atom scattering factors were used throughout the refinement. All calculations were carried out using SHELX-97 [15], PLATON-99 [16] and ORTEP [17] programs. Selected crystallographic data for compound **1** are displayed in Table 1 while selected bond lengths and angles of the compound are presented in Table 2. The H- and non-bonding contacts of **1** are listed in Table 3.

3. Results and discussion

3.1. Description of the structure

An ORTEP view of compound **1** with the atom numbering scheme is shown in Fig. 1. The crystal structure of $(HBz)_2[CuCl_4]$ (Bz = benzimidazole) consists of a discrete tetrachlorocuprate anion and two benzimidazolium cations. The Cu atom, Cu1, occupies the special position on the twofold axis of the *C*2/*c* space group. The $CuCl_4^{2-}$ anion assumes a distorted tetrahedral geometry of D_{2d} symmetry, consistent with the anticipated distortions predicted by the Jahn–Teller effect. These distortions are typically measured by the value of the *trans* Cl–Cu–Cl angle, which is 132.89° [8] in the present compound. The observed yellow colour of compound **1** is also consistent with the value of the *trans* angle [9]. In the organic cation, both the benzene and imidazole rings are almost planar with deviations ranging between −0.0071 and 0.0073 Å and are fused to lie in the same plane. Here, both the hydrogen atoms H1 and H3 attached to nitrogen atoms N1 and N3, respectively play an important role in forming the extended molecular association through hydrogen bonding where only one Cl atom, Cl1, acts as an acceptor of these N–H···Cl hydrogen bonds (Fig. 2). It is interesting to note that the other Cl atom, Cl2, is not participating in the hydrogen bonding network. The

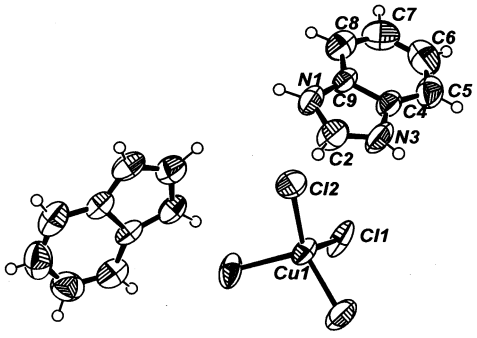


Fig. 1. ORTEP drawing of complex **1** showing the atom numbering scheme.

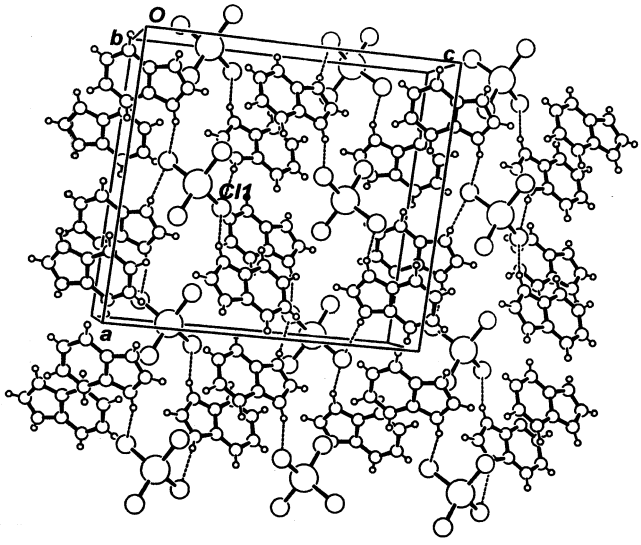


Fig. 2. Crystal packing arrangement showing the hydrogen bonding scheme and the stacking of benzimidazolium moieties. The dotted lines indicate hydrogen bonds.

Table 2
Bond lengths (Å) and angles (°) with e.s.d.'s in parentheses

Bond lengths	
Cu(1)–Cl(2)	2.1951(10)
Cu(1)–Cl(1)	2.3040(11)
Bond angles	
$Cl(2)^{(1)}$–Cu(1)–Cl(2)	132.86(7)
$Cl(2)^{(1)}$–Cu(1)–Cl(1)	99.04(4)
Cl(2)–Cu(1)–Cl(1)	108.42(4)
Cl(1)–Cu(1)–$Cl(1)^{(1)}$	107.47(7)

Symmetry transformation used to generate equivalent atoms: (1) $-x+1, y, -z+1/2$.

Table 3
Hydrogen bonding distances (Å) and angles (°)

D–H···A	D–H	D···A	H···A	∠ D–H···A
N(1)–H(1)···Cl(1)	0.909	3.186(3)	2.324	158.17
N(3)–H(3)···$Cl(1)^{(1)}$	0.716	3.169(4)	2.458	172.27

Symmetry equivalents: (1) $x-1/2, y+1/2, z$.

Cu–Cl distances differ appreciably (0.109 Å) with the longer Cu–Cl distance associated with the Cl atom, Cl1, which is engaged in hydrogen bonding and is consistent with those found in other chlorocuprates [2]. Molecular packing and stacking interaction plays the major role in structural association. Cohesion of the crystal occurs due to van der Waals' interaction. An intermolecular stacking is observed between the planes containing the fused aromatic rings. The imidazole ring of one cationic moiety is stacked with the benzene ring of two other cationic moieties ($1/2-x$, $1/2-y$, $-z$; $-x$, $1-y$, $-z$) where the perpendicular distances between the stacked rings are 3.429 and 3.166 Å, respectively. The benzene ring of the same cationic moiety was found to be stacked with the imidazole rings of two other likewise symmetry-related cations with the same intervals. Thus one cationic moiety forms antiparallel stacking with both the symmetry related cations. The shortest C–H···Cl distance is more than 3.75 Å, which excludes any C–H···Cl interactions [10].

Since compound **1** can be obtained by solid state transformation of **2**, a structural comparison between them is relevant. The crystal structure of compound **2** consists of alternating polymeric $[CuCl_4^{2-}]_\infty$ and $[CuCl_2(H_2O)_2]_\infty$ chains along the y-axis [11]. The structure of both chains may be described as elongated square bipyramids with four very short Cu–Cl(H_2O) bonds and two very long Cu–Cl bonds of 3.154(1) and 3.330(1) Å. The four cationic columns surrounding each polymeric chain form an extensive net of hydrogen bonds. Unlike the yellow phase, here all the Cl atoms of the $CuCl_4^{2-}$ units as well as the coordinated water molecules participate in the hydrogen bonding. The H atom of the imidazole carbon (C_2) is also involved significantly in the hydrogen bonding network in addition to both the hydrogens attached to the N atoms. The extensive hydrogen bonding stabilises the square bipyramid geometry and makes the aromatic ring much more puckered compared to that of **1**. Bezimidazolium cations are stacked in parallel one upon another (compared to the antiparallel stacking in the yellow phase) along the y-axis. The colour of the square bipyramidal tetrachlorocuprate is also found to be green in other similar types of complexes [9].

3.2. Thermal analysis and mechanism of thermochromism

The simultaneous TG–DTA curves of compound **2** (Fig. 3) show that it loses the coordinated water molecule in two steps. The first step starts rather abruptly at approximately 43 °C and continues up to approximately 60 °C (obs. loss = 1.4 ± 0.1%). The remaining portion of water is lost gradually up to approximately 145 °C (obs. loss = 2.5 ± 0.1%). The observed total loss in the two steps (3.9 ± 0.1%) corresponds to the calculated loss of one molecule of water (4.06%). The colour of **2**, however, changes from green to yellow at approximately 43 °C. This yellow compound (and compound **1** also) on keeping in open atmosphere at room temperature for several hours absorbs exactly one molecule of water and transforms to the green compound. The X-ray powder diffraction pattern and the thermal profile of this transformed species are found to be identical to those of **2**.

In the hydrated green phase (**2**), an extended copper halide network exists along with the extensive hydrogen bonding network. In such a structure, usually, there is a competition between the hydrogen bonding interaction and the bridging Cu–Cl–Cu interaction. At higher temperature, the increased thermal vibration of the water molecules and organic cations weaken the hydrogen bonding which in turn increases the electrostatic repulsion between the chloride ions [8]. Consequently, the Cl–Cu–Cl angles which are close to 90° in the square bipyramid structure tend to increase causing changes in the coordination number and geometry around Cu(II). The results of thermal analysis suggest that the sequence of events starts at 43 °C with the loss of one water molecule per Cu in the hydrated chain (leaving the chain intact), followed by slow break up of the hydrated chain at higher temperature corroborating the gradual loss of water molecule until 145 °C. Alternatively, both the water molecules of the hydrated chlorocuprate chain may be thrown out of the coordination sphere at 43 °C leading to the formation of discrete $CuCl_4^{2-}$. For water molecules, the temperature 43 °C is too low to be evaporated instantly. Moreover, at least part of the water molecules should remain in the crystal lattice by forming hydrogen bonds with the $CuCl_4^{2-}$. As a result, in the TG curve a partial weight loss, approximately 1.4% is recorded at 43–60 °C and

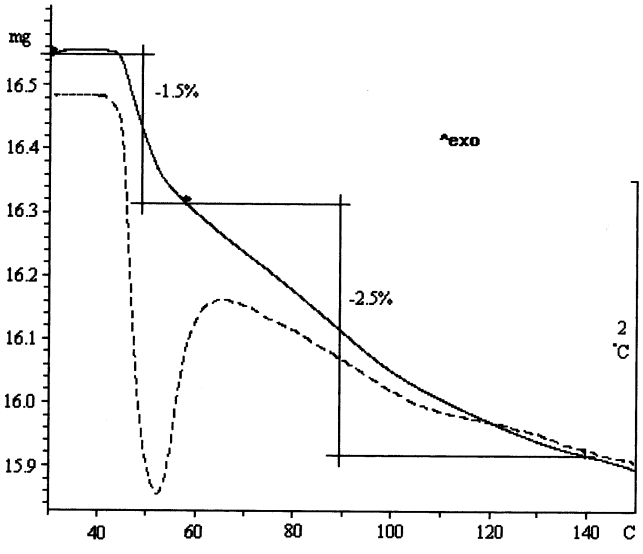


Fig. 3. The simultaneous TG (—) and DTA (----) curves for compound **2** (sample mass 16.4 mg).

the rest water is lost slowly upon heating. The different structural parameters of the green and yellow phases suggest that a phase transition should be accompanied with the colour change as in related systems [4]. The endothermic peak, found in the DTA curve at approximately 51 °C, is probably a combined effect of phase transition and loss of water. This is further supported by the fact that the compound **2** turns completely yellow at approximately 43 °C, the temperature where the loss of water just begins. The loss of water molecule is therefore not the cause of the colour change, rather it is the effect of some thermochromic phase transitions at this temperature. On the other hand, compound **2** on keeping in a desiccator at room temperature turns slowly into yellow. The complete transformation takes place over several days in a P_2O_5 desiccator. The proportion of yellow phase increases gradually with the loss of water from compound **2** at this temperature indicating that the bridging copper chloride framework is stabilized only in the presence of coordinated water molecule. The loss of water molecule is therefore the cause of the green to yellow transformation at any temperature below 43 °C. The mechanism of the reversal of the yellow to green phase is also very interesting. One discrete tetrachlorocuprate of compound **1** absorbs two molecules of water and selectively forms a one dimensional polymeric $[CuCl_2(H_2O)_2]_\infty$ chain with the similarly hydrated species. As a requirement of the crystal lattice of compound **2**, another chloro bridged chain of anhydrous tetrachlorocuprates, $[CuCl_4^{2-}]_\infty$, should also be formed simultaneously. In thermochromic chlorocuprates, thermally induced change of coordination number and consequent changes in the connectivity of the extended copper halide framework is known [1]. To our knowledge, to date the present system is the only example of thermochromic tetrachlorocuprates containing cations of organic base where deaquation–aquation is connected with monomeric⇋polymeric transformation associated with thermochromism.

4. Supplementary material

Crystallographic data for the structural analysis have been deposited with the Cambridge Crystallographic Data Centre, CCDC No. 181606 ($C_{14}H_{14}Cl_4CuN_4$). Copies of this information may be obtained free of charge from The Director, CCDC, 12 Union Road, Cambridge, CB2 1EZ, UK (fax: +44-1223-336033; e-mail: deposit@ccdc.cam.ac.uk or www: http://www.ccdc.cam.ac.uk).

Acknowledgements

We would like to thank the University Grant Commission, India, for the financial support (Sanction No. UGC/2976/GRW(UNG) 99-00).

References

[1] (a) S.A. Roberts, D.R. Bloomquist, R.D. Willett, H.W. Dodgen, J. Am. Chem. Soc. 103 (1981) 2603;
(b) D.R. Bloomquist, M.R. Pressprich, R.D. Willett, J. Am. Chem. Soc. 110 (1988) 7391.
[2] (a) R.L. Harlow, W.J. Wells, G.W. Watt, S.H. Simonsen, Inorg. Chem. 13 (1974) 2106;
(b) M. Wei, R.D. Willett, Inorg. Chem. 35 (1996) 6381;
(c) D.W. Smith, Coord. Chem. Rev. 21 (1976) 93.
[3] D.R. Bloomquist, R.D. Willett, H.W. Dodgen, J. Am. Chem. Soc. 103 (1981) 2610.
[4] R.D. Willett, D.R. Bloomquist, Coord. Chem. Rev. 47 (1982) 125.
[5] D.R. Bloomquist, R.D. Willett, J. Am. Chem. Soc. 103 (1981) 2615.
[6] R.D. Willett, J.A. Haugen, J. Lebsack, J. Morrey, Inorg. Chem. 13 (1974) 2510.
[7] R.D. Willett, H. Place, M. Middleton, J. Am. Chem. Soc. 110 (1988) 8639.
[8] G.S. Long, M. Wei, R.D. Willett, Inorg. Chem. 36 (1997) 3102.
[9] R.D. Willett, P. Zanchini, Inorg. Chem. 29 (1990) 3027.
[10] S. Haddad, R.D. Willett, Inorg. Chem. 40 (2001) 2457.
[11] M. Bukowska-Strzyzewska, J. Skoweranda, Acta Crystallogr., Sect. C 43 (1987) 2290.
[12] A.I. Vogel, A Text book of Quantitative Inorganic Analysis, 4th ed., Longman, New York, 1978, p. 842.
[13] B.N. Figgis, J. Lewis, in: J. Lewis, R.C. Wilkins (Eds.), Modern Coordination Chemistry, Interscience, New York, 1960, p. 403.
[14] A. Altomare, G. Cascarano, C. Giacovazzo, A. Guagliardi, A.G.G. Moliterni, M.C. Burla, G. Polidori, M. Camalli, R. Spagna, Private Communication, 1997.
[15] G.M. Sheldrick, SHELX-97, Program for the Refinement of Crystal Structure, University of Göttingen, Göttingen, Germany.
[16] A.L. Spek, PLATON, A Multipurpose Crystallographic Tool, University of Utrecht, Utrecht, The Netherlands, 2001.
[17] L.J. Farrugia, ORTEP-3, J. Appl. Crystallogr. 30 (1997) 565.

catalytic oxygenation and the ring contraction of 3-substituted 5-(2′-pyridyl)-1,4-benzodiazepin-2-one derivatives [19]. Here we report on the preparation and structural characterisation of the Zn^{II} and Pd^{II} complexes with ligands (+)-**L1** and (±)-**L2** (Scheme 1) as well as on biological properties of free benzodiazepine ligands and their complexes. To our knowledge, compounds Zn**L1**Cl_2 (**1**) and Zn**L2**Cl_2 (**3**) are the first Zn^{II} complexes of benzodiazepines reported so far.

2. Experimental

2.1. Materials and instrumentation

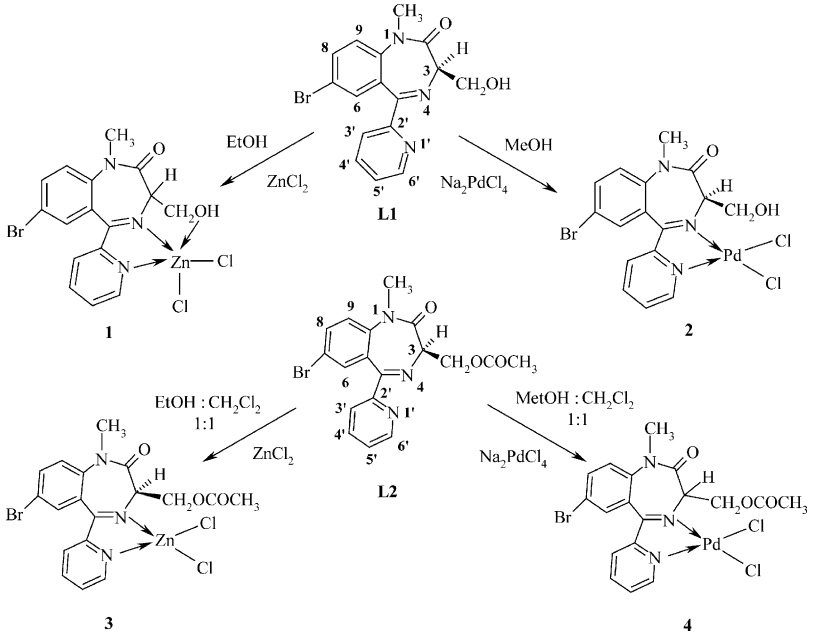
(+)-7-Bromo-1,3-dihydro-3-hydroxymethyl-1-methyl-5-(2′-pyridyl)-2*H*-1,4-benzodiazepin-2-one ((+)-**L1**) was prepared by lipase catalysed kinetic resolution [15] whereas *rac*-3-acetoxymethyl-7-bromo-2,3-dihydro-1-methyl-5-(2′-pyridyl)-2*H*-1,4-benzodiazepin-2-one ((±)-**L2**) was prepared according to the reported method [11]. All other reagents and solvents were analytical grade products and were used without further purification. FTIR spectra were recorded on a Perkin–Elmer 2000 spectrophotometer using KBr (4000–400 cm^{-1}) and polyethylene (400–200 cm^{-1}) pellets. ^1H NMR spectra were performed with a Varian broadband Gemini 300 spectrometer in $CDCl_3$ and DMSO-d_6 containing Me_4Si as an internal standard. Two-dimensional experiments were performed by standard pulse sequences, using Gemini Data System software Version 6.3. Elemental analyses were performed with a Perkin–Elmer Elemental Analyser E-2400 Series 2 (CHN) and thermogravimetric analyses with a Cahn RG electromicrobalance in an air atmosphere.

2.2. Zn[*L1*]Cl_2 (*1*)

A solution of (+)-**L1** (0.072 g, 0.20 mmol) in absolute EtOH (1.0 ml) was added dropwise to a stirred solution of $ZnCl_2 \cdot 2H_2O$ (0.035 g, 0.20 mmol) in absolute EtOH (2.0 ml). The reaction mixture was stirred for 1 h at room temperature (r.t.), the yellow hygroscopic precipitate formed was separated, washed with absolute cold EtOH and stored overnight in vacuum. Yield: 0.031 g (30%). Crystals for X-ray analysis were obtained from absolute EtOH by slow evaporation in a desiccator over silica gel. *Anal*. Calc. for $C_{16}H_{14}BrCl_2N_3O_2Zn \cdot 2H_2O$ (532.53): C, 36.09; H, 3.41; N, 7.89. Found: C, 36.29; H, 3.28; N, 7.32%. IR (cm^{-1} KBr disc): 3369 w br [ν(OH], 1677 vs br [ν(C=O)], 1625 m, 1592 s and 1560 w [δ(OH), ν(C=N), ν(C=C)], 1496 s, 1485 s, 1444 m, 1403 m, 1337 s, 1300 sh, 1265 sh, 1253 m, 1190 w, 1125 m-s, 1102 m, 1050 w, 1020 m, 978 w, 889 w, 834 m-s, 801 m-s, 756 w, 724 w, 678 m and 642 w-m; IR (cm^{-1}, polyethylene): 314 m-s br.

2.3. Pd[*L1*]Cl_2 (*2*)

A solution of (+)-**L1** (0.053 g, 0.15 mmol) in MeOH (1.0 ml) was added dropwise to a stirred solution of $Na_2PdCl_4 \cdot 3H_2O$ (0.055 g, 0.15 mmol) in MeOH (3.0 ml). The reaction mixture was stirred for 2 h at r.t., the yellow precipitate formed was filtered off, washed with cold MeOH and dried in vacuum over P_2O_5. Yield: 0.070 g (87%). Single crystals were obtained from DMF.



Scheme 1. Chemical diagrams of ligands and complexes.

Anal. Calc. for $C_{16}H_{14}BrCl_2N_3O_2Pd$ (537.73): C, 35.80; H, 2.44; N, 7.87. Found: C, 36.17; H, 2.75; N, 7.61%. IR (cm^{-1} KBr disc): 3427 m-s [ν(OH)], 1669 vs [ν(C=O)], 1590 s, 1561 m and 1541 w [δ(OH), ν(C=N), ν(C=C)], 1489 s, 1479 s, 1442 m, 1443 w, 1400 m, 1352 m, 1321 m-s, 1255 m-s, 1187 w, 1140 w-m, 1125 w, 1068 m, 1034 m-s, 97 w, 924 w, 889 w, 826 s, 791 m, 751 w-m, 745 w-m, 677 w-m and 659 w; IR (cm^{-1}, polyethylene): 373 w, 345 w, 328 w-m and 299 w.

2.4. *Zn[**L2**]Cl$_2$ (**3**)*

A solution of **L2** (0.100 g, 0.25 mmol) in a 1:1 mixture of absolute EtOH and CH_2Cl_2 (2 ml) was added dropwise to a stirred solution of $ZnCl_2 \cdot 2H_2O$ (0.050 g, 0.29 mmol) in the same mixture of solvents (2 ml). After complete addition, the reaction mixture was continuously stirred for 24 h at ambient temperature and left at 277 K for another 48 h. Yellow crystals were obtained (yield: 0.070 g, 52%). *Anal.* Calc. for $C_{18}H_{16}BrCl_2N_3O_3Zn \cdot H_2O$ (556.77): C, 38.82; H 3.26; N 7.58. Found: C, 39.28; H, 3.12; N, 7.15%. IR (cm^{-1} KBr disc): 3508 w br [ν(OH)], 1742 vs [ν(C=O) acetate], 1691 vs br [ν(C=O) lactam, ν_{as}(COO)], 1599 m, 1589 s, 1568 m and 1556 s [δ(OH),ν(C=N), ν(C=C)], 1480 s, 1470 s, 1439 s, 1427 m, 1395 m-s, 1364 m-s, 1334 s, 1301 m, 1261 s, 1221 vs br, 1186 m, 1125 m, 1120 m, 1102 s, 1054 m, 1023 s, 973 w, 932 w-m, 920 w-m, 892 w, 830 s, 802 s, 745 m-s, 720 w-m, 710 w, 678 s, 643 m and 619 w; IR (cm^{-1}, polyethylene): 335 s br, 313 m-s and 326 w br.

2.5. *Pd[**L2**]Cl$_2$ (**4**)*

A mixture of **L2** (0.100 g, 0.25 mmol) and $Na_2[PdCl_4] \cdot 3H_2O$ (0.084 g, 0.25 mmol) in a 1:1 mixture of MeOH and CH_2Cl_2 (3.0 ml) was stirred for 3 h at ambient temperature. The yellow precipitate formed was filtered off, washed with cold MeOH and CH_2Cl_2, and dried in vacuum over P_2O_5. Yield: 0.120 g (80%). *Anal*. Calc. for $C_{18}H_{16}BrCl_2N_3O_3Pd$ (579.77): C, 37.28; H, 2.78; N, 7.28. Found: C, 36.81; H, 3.00; N, 6.71%; IR (cm^{-1} KBr disc): 1742 s [ν(C=O) acetate], 1683 vs and 1668 vs [ν(C=O) lactam, ν_{as}(COO)], 1593 m, 1564 w and 1539 w [ν(C=N), ν(C=C)], 1489 m, 1472 m, 1441 w, 1403 w, 1368 w-m, 1340 m, 1257 s, 1247 m-s, 1214 s, 1190 w, 1126 w, 1105 w-m, 1040 sh, 1034 m-s, 980 w, 920 w, 874 w, 842 w, 822 w, 798 w, 760 w, 709 w, 679 w, 642 w and 616 w-m; IR (cm^{-1}, polyethylene): 353 m-s, 343 m, 328 m, 313 m and 280 w-m.

2.6. *X-ray structure analysis*

Suitable single crystals were obtained by a slow evaporation from different solvents listed in Table 1, which also summarises crystal data, experimental details of data collection and refinement. Data were collected on an Enraf–Nonius CAD4 diffractometer for complex **3**, and on a Nonius Kappa CCD 2000 diffractometer for **1** and **2**. Data were corrected for Lp effects [20]. Structures of **1** and **3** were solved using the package SIR-97 [21], whereas the structure of **2** was solved with SHELXS-86 [22]. Complex **2** was refined with a racemic twin model. The occupation of the component with opposite chirality from that shown in Fig. 2 refined to 0.007(9), indicating that the crystal is enantiopure and has strong inversion distinguishing power [23]. All data were refined using the package SHELXL-97 [24]. Molecular geometry calculations and illustrations were prepared with PLATON [25]. Atomic scattering factors were those included in SHELXL-97. The H-atom coordinates were calculated geometrically and refined using the SHELXL-97 riding model.

2.7. *In vitro cytostatic assays*

The cytostatic activity of the free benzodiazepine ligands and their metal complexes was assayed in vitro on the murine leukemia L1210/0 cell line as well as on the human T-lymphoblast Molt4/C8 and CEM/0 cell lines, according to previously described methods [26,27]. The activity was expressed as the concentration (in μg ml^{-1}) of the compound at which tumour cell growth showed 50% inhibition (IC_{50}).

2.8. *In vitro antiviral assays*

The antiviral and cytotoxicity assays of compounds were carried out in either Vero, HEL or HeLa cell cultures, following previously established procedures [28]. The inhibitory effects of the test compounds on the replication of parainfluenza-3 virus, reovirus type 1, Sindbis virus, Coxsackie virus B4 and Punta Toro virus was evaluated in Vero cells, on herpes simplex virus type 1 (KOS), herpes simplex virus type 2(G), vaccinia virus, vesicular stomatitis virus and herpes simplex virus type 1 (TK^- KOS ACV) in HEL cells, and on vesicular stomatitis, Coxsackie virus B4 and respiratory syncytial virus in HeLa cells. The antiviral activity was expressed as concentration of the compound required to reduce virus-induced cytopathogenicity by 50%.

3. Results and discussion

3.1. *Preparation of the complexes*

The reaction of benzodiazepine ligands **L1** and **L2** with the appropriate zinc and palladium salt yielded dichloro adducts as depicted in Scheme 1. The enantiomerically pure (+)-**L1** gave with $ZnCl_2$ in absolute ethanol the pale yellow complex dichloro-[7-bromo-1,3-dihydro-3-hydroxymethyl-1-methyl-5-(2′-pyridyl)-2*H*-

Table 1
Crystallographic data, crystallisation details, structure solution and refinement of compounds **1**, **2** and **3**

Compound	**1**	**2**	**3**
Empirical formula	$C_{16}H_{14}BrCl_2N_3O_2Zn\cdot CH_3CH_2OH$	$C_{16}H_{14}BrCl_2N_3O_2Pd\cdot C_3H_7NO$	$C_{18}H_{16}BrCl_2N_3O_3Zn$
M_r	496.50	610.62	538.53
Temperature during data collection (K)	293(2)	150	293(2)
Wavelength (Å)	1.54183	0.71073	0.71073
Crystal system	Monoclinic	orthorhombic	orthorhombic
Space group	$P2_1/n$	$P2_12_12_1$	$P2_12_12_1$
a (Å)	9.894(1)	7.1411(10)	10.008(2)
b (Å)	12.709(2)	17.081(4)	10.859(3)
c (Å)	16.747(5)	18.161(5)	37.998(7)
β (°)	90.703(1)		
V (Å^3)	2105.6(7)	2215.2(9)	4128(3)
Z	4	4	8
D_{calc} (Mg m^{-3})	1.712	1.831	1.7325
Crystallisation solvent(s)	Ethanol	DMF, DMSO	ethanol, dichloromethane
Crystal colour	Colourless	yellow	yellow
Absorption correction	None	none	Ψ-scan
Θ_{max}	36.2	27.4	26.3
Index ranges	$-8 \le h \le 8$, $-10 \le k \le 10$, $-13 \le l \le 13$	$-9 \le h \le 9$, $-22 \le k \le 22$, $-23 \le l \le 23$	$-12 \le h \le 0$, $0 \le k \le 13$, $0 \le l \le 47$
Total data collected	1905	47 954	4754
Unique data	969	5052	4721
Observed data $[(I > 2\sigma(I)]$	814	3640	1643
R_1 $[F_o > 4\sigma(F_o)]$	0.0771	0.0416	0.0892
wR_2 (F^2)	0.2295	0.0623	0.2834
S	1.089	1.022	1.206
Parameters	195	278	289
$\Delta\rho_{max}$, $\Delta\rho_{min}$ (e Å^{-3})	0.84, −0.56	0.50, −0.52	1.23, −1.71

1,4-benzodiazepin-2-one-*N*,*N*,*O*]zinc(II) (**1**). The reaction of 60% enantiomerically pure **L2** [19] and $ZnCl_2$ in a 1:1 mixture of ethanol and dichloromethane yielded the enantiomerically pure complex dichloro-[3-acetoxymethyl-7-bromo-1,3-dihydro-1-methyl-5-(2′-pyridyl)-2*H*-1,4-benzodiazepin-2-one-*N*,*N*]zinc(II) (**3**), which reversibly changes its colour from pale-yellow to pink. In the mother liquor, crystals are yellow-coloured, whereas exposed to air they quickly change their colour to pink. Hygroscopic properties of the compound might be related to this effect. The reaction of benzodiazepine ligands with Na_2PdCl_4 in methanol (**L1**) and in a mixture of methanol and dichloromethane 1:1 (**L2**), yielded the yellow square-planar complex *cis*-dichloro-[7-bromo-1,3-dihydro-3-hydroxymethyl-1-methyl-5-(2′-pyridyl)-2*H*-1,4-benzodiazepin-2-one-*N*,*N*]palladium(II) (**2**) and *cis*-dichloro-[7-bromo-1,3-dihydro-3-acetoxymethyl-1-methyl-5-(2′-pyridyl)-2*H*-1,4-benzodiazepin-2-one-*N*,*N*]palladium(II) (**4**), respectively. No racemisation was observed during the formation of the Pd^{II} complexes.

3.2. The crystal structures

ORTEP [29] drawings of **1** and **2** are given in Figs. 1 and 2, respectively. A PLUTON drawing of the molecular structure of **3** is given in Fig. 3. The crystal structure of **2** is depicted in Fig. 4. The selected geometry for all structures is summarised in Tables 2 and 3. Hydrogen bonds are listed in Table 4.

In the molecular structure of **1**, Zn^{II} is five-coordinated. **L1** acts as a tridentate ligand, through two azomethine nitrogens, N4 and N15, and hydroxy oxygen O13 (Fig. 1). Fivefold coordination of Zn^{II} is completed with two chlorine atoms. Bond distances Zn–O and Zn–N (Table 3) are in accordance with the previously reported values for five-coordinated Zn^{II} complexes found in the *CSD* [30]. The molecule of **1** displays a strongly distorted trigonal bipyramidal coordination, with Cl1, Cl2 and N4 in an equatorial plane, whereas the Zn atom is slightly above it [0.045(2) Å]. The distortion from the regular trigonal bipyramidal coordination has been introduced by the angle N15–Zn–O13 of 145.8(5)° (that differs considerably from the required 180°). Molecular structure of **1** exhibits the usual *boat* conformation [31]. There are no significant differences in values of geometrical parameters inside the diazepin ring of complex **1** (Table 2) and its Cu^{II} analogue described in our previous paper [19]. Thus, the metal coordination has a minor influence on the conformation of the diazepine ring. In **2**, Pd^{II} is, as expected, in a fourfold square-planar coordination

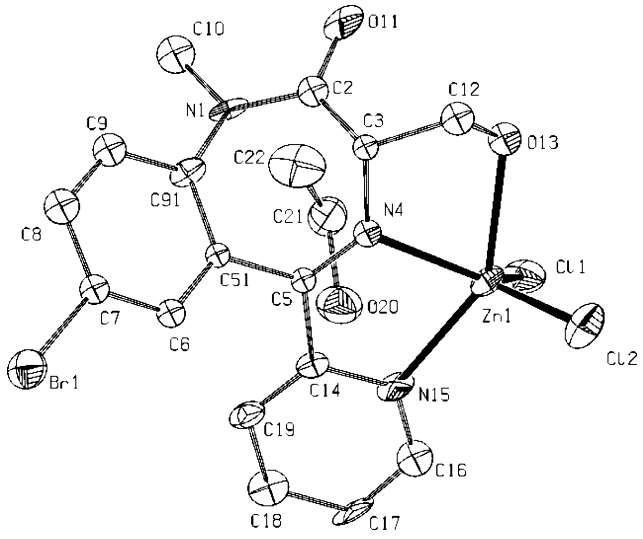


Fig. 1. ORTEP drawing of complex **1** with atom numbering. Thermal ellipsoids are scaled at the 30% probability level. Hydrogen atoms are omitted for clarity.

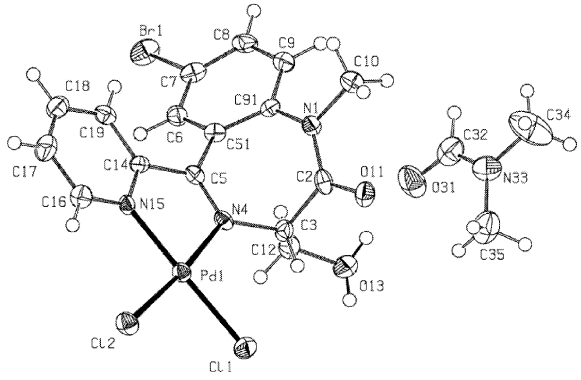


Fig. 2. ORTEP drawing of complex **2** with atom numbering. Thermal ellipsoids are scaled at the 50% probability level.

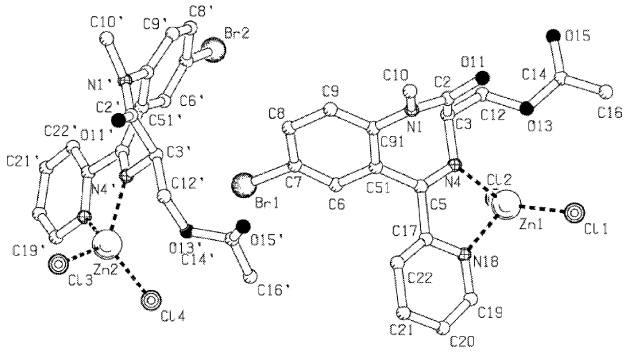


Fig. 3. PLUTON drawing of complex **3**. Hydrogen atoms are omitted for clarity.

[deviations from the least-squares plane ranging from −0.038(4) Å for N15 to 0.0300(14) Å for Cl2] (Fig. 2). In this complex, **L1** acts as a bidentate ligand to Pd^{II} through the pyridine and diazepine nitrogens. The fourfold coordination is completed by two chlorine

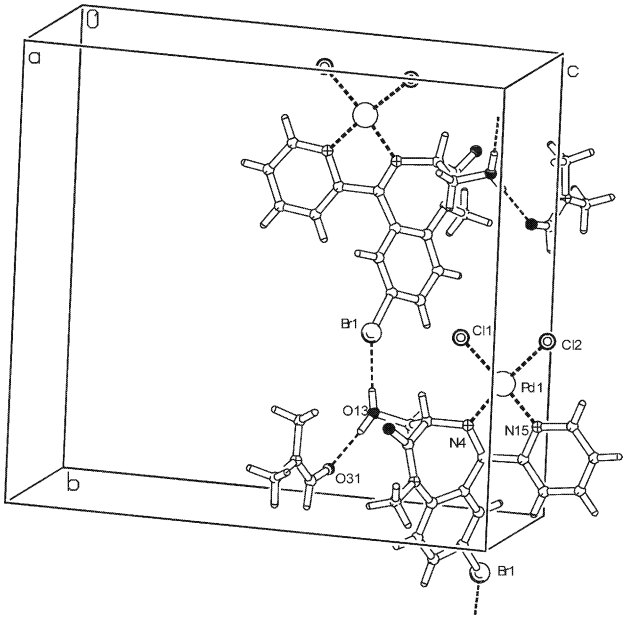


Fig. 4. Crystal packing of the complex **2**. The complex molecules are connected via an O13–H···Br interaction. This interaction has half site occupancy, the other half being occupied by an O13–H···O31 hydrogen bond which connects the complex molecule with a solvent.

atoms. X-ray structure analysis has revealed *S*-configuration at the C3 stereogenic centre. Significant conformational changes in the ligand upon coordination were not observed; hence the *boat* conformation of the seven-membered diazepine ring is retained. In **3**, **L2** acts as an *N*,*N*-bidentate ligand chelating Zn^{II} through diazepine and pyridyl nitrogen atoms (Fig. 3). The fourfold coordination is completed by two chlorine atoms. Severely distorted tetrahedra were observed; bond angles involving Zn^{II} ranged from 79.1(7)° to 125.3(5)° in molecule **A**, and from 76.5(8)° to 119.9(6)° in molecule **B** (Table 3). Unlike in **1**, hydroxy oxygen O13 is not coordinated to Zn^{II}. Complex **3** crystallises in the non-centrosymmetric space group $P2_12_12_1$ with two independent molecules in an asymmetric unit. The *R*-absolute configuration at the stereogenic centres C3 and C3′ was determined by X-ray structure analysis. Comparison of the coordination details in Cu^{II} complexes of **L1** and **L2**, and in their Zn^{II} analogues, reveals significant differences, related to their electronic configuration [32]. Both Cu^{II} and Zn^{II} form with **L1** five-coordinated complexes, and **L1** acts as an *N*,*N*,*O*-tridentate ligand. In **L2**, instead of an hydroxymethyl group at C3, there is a bulky acetoxymethyl group, and for steric reasons O13 is not involved in the metal coordination. Therefore, copper forms five-coordinated species using lactame oxygen from the neighbouring molecule to complete the fivefold coordination in the shape of square-planar pyramide with a long apical Cu^{II}–O bond, whereas Zn^{II} retains the fourfold coordination sphere [22]. However, in the active sites of zinc-

Table 2
Selected bond lengths (Å), angles (°) and torsion angles (°) in **L2**, **1**, **2** and **3**

	1	**2**	**3(A)**	**3(B)**	**L2** [a]
Bond lengths					
Br1–C7	1.92(2)	1.895(5)	1.86(2)	1.90(2)	1.901(6)
N1–C2	1.35(2)	1.367(6)	1.36(3)	1.28(3)	1.366(6)
C2–C3	1.45(2)	1.524(7)	1.48(3)	1.52(3)	1.512(8)
C3–N4	1.47(2)	1.486(7)	1.50(3)	1.57(3)	1.457(7)
N4–C5	1.23(2)	1.297(6)	1.24(2)	1.23(3)	1.274(6)
C5–C51	1.50(2)	1.472(7)	1.48(3)	1.45(3)	1.465(6)
C51–C91	1.38(2)	1.394(7)	1.37(3)	1.45(3)	1.404(8)
N1–C10	1.46(2)	1.471(6)	1.48(3)	1.49(3)	1.471(9)
C2–O11	1.28(2)	1.220(6)	1.29(3)	1.22(3)	1.211(6)
C3–C12	1.49(2)	1.511(7)	1.47(3)	1.58(4)	1.510(7)
C5–C1′ [b]	1.50(3)	1.472(7)	1.55(3)	1.61(3)	1.506(8)
Bond angles					
N1–C2–C3	121.2(16)	119.8(4)	118.5(19)	116.0(19)	115.7(4)
C2–C3–N4	107.4(14)	110.2(4)	106.0(19)	110.2(18)	108.0(4)
C3–N4–C5	122.6(14)	120.9(4)	114.4(16)	115.3(19)	118.1(4)
N4–C5–C51	122.4(15)	124.4(5)	125.4(18)	128.0(19)	124.4(5)
C5–C51–C91	118.3(14)	121.6(4)	120.5(17)	124.0(19)	122.4(4)
C51–C91–N1	125.0(15)	122.0(4)	121.4(18)	116.7(19)	121.9(4)
C91–N1–C2	118.9(14)	125.3(4)	116.9(18)	126.0(19)	123.8(4)
Torsion angles					
C2–N1–C91–C51	−53(2)	44.6(7)	58(3)	57(3)	−45.6(7)
N4–C5–C51–C91	45(2)	−50.4(7)	−44(3)	−37(4)	42.2(8)
C91–N1–C2–C3	13(2)	−12.4(7)	−12(3)	−14(3)	5.0(7)
C3–N4–C5–C51	−2(2)	6.0(6)	2(3)	1(3)	1.1(8)
N1–C2–C3–N4	61(2)	−57.7(6)	−70(2)	−66(2)	70.2(5)
C5–N4–C3–C2	−69(2)	62.4(5)	74(2)	69(2)	−74.1(6)

[a] Geometric parameters of the structure of **L2** are taken from our previous paper [19].
[b] C1′ is a pyridyl C-atom bonded to the C5 of a diazepine ring (C14 in **1** and **2**, C17 in **L2** and **3**).

Table 3
Bond lengths (Å) and angles (°) in the M^{II} coordination spheres of **1**, **2** and **3**

	1	**2**	**3(A)**	**3(B)**
Bond lengths				
M–Cl1	2.255(5)	2.2788(14)	2.183(7)	2.180(9)
M–Cl2	2.211(6)	2.2905(14)	2.191(8)	2.23(1)
M–N4	2.11(1)	2.027(4)	2.09(2)	2.11(2)
M–N2′ [a]	2.17(2)	2.004(3)	2.08(2)	2.03(2)
M–O13	2.22(1)			
Bond angles				
Cl1–M–Cl2	119.0(2)	90.50(4)	121.2(3)	115.4(4)
Cl1–M–N4	122.0(4)	95.42(11)	125.3(5)	112.3(6)
Cl1–M–N2′	94.6(4)	174.25(10)	108.9(5)	119.9(6)
Cl1–M–O13	94.2(3)			
Cl2–M–N4	118.7(4)	174.08(11)	103.9(5)	125.2(6)
Cl2–M–N2′	106.0(4)	94.12(10)	110.2(5)	101.1(7)
Cl2–M–O13	98.3(3)			
N4–M–N2′	74.3(5)	79.97(14)	79.1(7)	76.5(8)
N4–M–O13	73.0(5)			
N2′–M–O13	145.8(5)			

[a] N2′ is a pyridyl nitrogen (N15 in **1** and **2**, N18 in **3**).

containing enzymes, Zn^{II} is mostly four-coordinated [33].

The crystal structure of **1** is characterised by the hydrogen bond O13–H···O20 which connects the complex with ethanol as the solvent molecule. In the crystal structure of **2**, two equally populated positions of the hydrogen atom at O13 were observed. As a consequence of this structural disorder, O13 is (as a donor) involved in two different hydrogen bonds; with the carbonyl oxygen of the solvent molecule and with the bromine from a neighbouring molecule (Table 4, Fig. 4). In the crystal structure of **3** only weak van der Waals interactions were observed.

3.3. Infrared spectra

The IR spectra of the free benzodiazepine ligands and their complexes are complicated with significant vibrational coupling and overlapping of absorption bands. Upon metal coordination, the marked changes of ligand bands may be noticed between 1700 and 1500 cm^{-1} where the azomethine and pyridine C=N, lactam and acetate C=O, and aromatic C=C stretching vibrations are found [19,34]. In the spectra of complexes with *N*,*N*-chelatation (complexes **2**, **3** and **4**), most of these bands are shifted to lower frequencies, while in Zn^{II} complex **1** in which **L1** acts as a *N*,*N*,*O*-tridentate ligand, they are

Table 4
Hydrogen bonds in complexes **1** and **2**

	D–H···*A* (Å)	D–H (Å)	H···*A* (Å)	D–H···*A* (°)	Symmetry operation on *A*
1					
O13–H···O20	2.71	1.12	1.63	162	$-x, y-0.5, 0.5-z$
2					
O13–H···O31	2.628	0.84	1.79	172	
O13–H···Br	3.060	0.80	2.30	160	$-x, 0.5+y, 0.5-z$

shifted slightly to the higher frequency region. The similar spectral pattern was observed in the Cu^{II} complex of this ligand with the similar fivefold metal–ligand coordination [19].

The far-IR spectra (400–200 cm^{-1}) of complexes give insight into the metal–ligand vibrations. In complex **1**, a very broad band of weak to medium intensity between 350 and 240 cm^{-1} covers the whole region expected for stretching modes of the zinc–oxygen/halogen/nitrogen vibrations for this kind of complex [35,36]. The absence of highly characterised zinc-specific vibrations may be ascribed to low symmetry of this complex and to the presence of a mixture of conformers. A complicated spectral pattern was found also in **3** and **4**, where the internal deformation modes of the acetate ligand are superimposed on the metal–ligand vibrations. The spectrum of **2** shows four rather sharp bands in this frequency region, as expected for the *N*,*N*-bonded dichloro *cis*-square-planar Pd^{II} complexes [22].

3.4. ^1H NMR spectra

The ^1H NMR data of the free ligands **L1** and **L2**, their Zn^{II} complexes in $CDCl_3$ and Pd^{II} complexes in DMSO-d_6, are summarised in Table 5 according to the numbering scheme shown in Scheme 1. The spectral studies have shown that Pd^{II} complexes retain their integrity in DMSO solution, while this solvent with strong complexing ability initiates dissociation of Zn^{II} complexes by displacing the benzodiazepine ligands. This is in accordance with the assumption that zinc complexes generally show low stability [37].

The NMR spectral patterns of the aromatic region of free ligands **L1** and **L2** are in general similar to those obtained for various benzodiazepine derivatives [25,38–41]. The 3-H proton of the heterocyclic diazepine ring in both ligands appears as a triplet, while absorptions of the 3-CH_2 and OH protons are solvent-dependent. In **L1** two non-equivalent diastereotopic methylene protons in DMSO-d_6 give two separated multiplets due to geminal coupling and couplings with H-3 and OH protons, while two broad singlets (partly split) could be observed in chloroform solution. In **L2** these protons in $CDCl_3$ resonate as two distinctive doublet of doublets, while in DMSO-d_6 signals are overlapped giving a multiplet pattern. The OH signal in **L1** appears as a triplet (DMSO-d_6) or as a broad singlet ($CDCl_3$). The assignment of proton resonances was ascertained by connectivities in COSY spectra. The *N*,*N*-metal bonding in all the complexes through the azomethine and pyridine nitrogens brings about similar spectral changes for the aromatic protons. The pyridine protons, apart from H-3′, show a downfield shift (0.30–0.70 ppm), which may be related to the deshielding effect of the metal atom due to its magnetic anisotropy and to the lowering in the electron density in this aromatic ring following the electron-withdrawing effect of complexation. The upfield shift of H-3′ comes from two opposite phenomena, a downfield shift produced by the metal inductive effect and a prevalent upfield shift produced by the disappearance of the N-4 paramagnetic effect upon complexation [27,29]. The same two effects may also be expected to influence the H-6′ signal, but due to closer proximity of this proton to the metal, the latter effect is predominant. This situation could be explained by the fact that free ligands are characterised by *anti* orientation of the nitrogen atoms N-1′ and N-4, as two centres of high electron density, while in complexes the α-diimine system is in the *syn* orientation due to *N*,*N*-bidentate ligand coordination. For this reason, great changes could also be observed in absorptions of the H-3 and 3-CH_2 protons (Fig. 5). In complex **1**, a downfield shift of OH ($\sim$1 ppm) and 3-CH_2 ($\sim$3 ppm) signals supports the ligand coordination also through the hydroxy oxygen (Fig. 1). The absorption of the H-3 proton with a downfield shift ($\sim$0.40 ppm) and that of OH with an upfield shift ($\sim$0.70 ppm) are overlapped in complex **2**, giving a very broad signal at about 4 ppm. Not visible is the coupling with the adjacent 3-CH_2 protons, which appeared as two separate singlets with downfield shifts of approximately 1.35 ppm with respect to the free ligand. The second set of signals observed for the pyridine H-3′ and H-6′ protons (in a ratio $\sim$1:8) may be ascribed to the presence of two isomeric forms caused by restricted rotation within the Pd^{II} coordination sphere. In complexes **3** and **4**, the H-3 proton shows a downfield shift of 0.32 and 2.14 ppm, respectively. There are also differences in the 3-CH_2 resonances. In **4**, signals of diastereotopic methylene protons show upfield shifts of 0.78 and 0.98 ppm, while in **3** one of them

Table 5
^{1}H NMR spectral data [a]

Compound Solvent Proton	**L1** $CDCl_3$	**1** $CDCl_3$	**L1** DMSO-d_6	**2** DMSO-d_6	**L2** $CDCl_3$	**3** $CDCl_3$	**L2** DMSO-d_6	**4** $CDCl_3$
N–CH_3	3.41 (s)	3.46 (s)	3.27 (s)	3.31 (s)	3.42 (s)	3.43 (s)	3.29 (s)	3.28 (s)
H-3	3.83 (t) $^3J_{HH}$ = 7.2 Hz	4.23 (t) $^3J_{HH}$ = 5.9 Hz	3.63 (t) $^3J_{HH}$ = 6.3 Hz	3.95 [b]	3.95 (t) $^3J_{HH}$ = 6.5 Hz	4.27 (t) $^3J_{HH}$ = 4.3 Hz	3.95 (t) $^3J_{HH}$ = 6.3 Hz	6.09 (t) $^3J_{HH}$ = 6.5 Hz
3-CH_2	4.21, 4.44 (2 br s)	7.54; 7.72 (2 dd) $^3J_{HH}$ = 6.5 Hz J_{gem} = 9.8 Hz	3.97, 4.15 (2 m)	5.33, 5.80 (2 s)	4.83, 4.96 (2 dd) $^3J_{HH}$ = 6.6 Hz J_{gem} = 11.2 Hz	4.72, 5.14 (2 dd) $^3J_{HH}$ = 4.4 Hz J_{gem} = 12.2 Hz	4.63 (m) [c]	3.65, 3.85 (2 dd) $^3J_{HH}$ = 6.6 Hz J_{gem} = 11.6 Hz
OH (3b) [d]	3.02 br s	4.03 br s	4.71 t $^3J_{HH}$ = 5.4 Hz	~4.0 (br s) [e]				
$COCH_3$					2.08 (s)	2.36 (s)	1.99 (s)	1.94 (s)
H-6	7.52 (d) $^4J_{HH}$ = 2.1 Hz	7.88 (d) $^4J_{HH}$ = 2.2 Hz	7.53 (d) $^4J_{HH}$ = 2.0 Hz	8.00 (s)	7.55 (d) $^4J_{HH}$ = 2.2 Hz	7.80 (d) $^4J_{HH}$ = 2.2 Hz	7.53 (s)	7.95 (d) $^4J_{HH}$ = 2.1 Hz
H-8	7.66 (dd) $^3J_{HH}$ = 8.5 Hz $^4J_{HH}$ = 2.1 Hz	7.92 (dd) $^3J_{HH}$ = 8.8 Hz $^4J_{HH}$ = 2.4 Hz	7.79 (dd) $^3J_{HH}$ = 8.8 Hz $^4J_{HH}$ = 2.0 Hz	7.98 [f]	7.67 (dd) $^3J_{HH}$ = 8.8 Hz $^4J_{HH}$ = 2.5 Hz	7.95 (dd) $^3J_{HH}$ = 8.7 Hz $^4J_{HH}$ = 2.1 Hz	7.81 (dd) $^3J_{HH}$ = 8.6 Hz $^4J_{HH}$ = 2.0 Hz	8.01 (dd) $^3J_{HH}$ = 9.0 Hz $^4J_{HH}$ = 2.0 Hz
H-9	7.24 (d) $^3J_{HH}$ = 8.5 Hz	7.44 (d) $^3J_{HH}$ = 8.8 Hz	7.51 [g]	7.58 (d) $^3J_{HH}$ = 9.2 Hz	7.27 (d) $^3J_{HH}$ = 8.8 Hz	7.43 (d) $^3J_{HH}$ = 9.1 Hz	7.53 (d) $^3J_{HH}$ = 8.4 Hz	7.57 (d) $^3J_{HH}$ = 9.0 Hz
H-3′	8.14 (d) $^3J_{HH}$ = 7.5 Hz	7.89 [h]	8.13 (d) $^3J_{HH}$ = 7.5 Hz	7.87 (7.78) (d) [i] $^3J_{HH}$ = 8.1 Hz	8.18 (d) $^3J_{HH}$ = 7.9 Hz	7.88 [c]	8.06 (d) $^3J_{HH}$ = 8.0 Hz	7.79 (d) $^3J_{HH}$ = 7.7 Hz
H-4′	7.83 (td) $^3J_{HH}$ = 7.5 Hz $^4J_{HH}$ = 1.1 Hz	8.13 (td) $^3J_{HH}$ = 8.0 Hz $^4J_{HH}$ = 1.5 Hz	7.93 (t) $^3J_{HH}$ = 7.6 Hz	8.34 (t) $^3J_{HH}$ = 8.0 Hz	7.86 (td) $^3J_{HH}$ = 7.8 Hz $^4J_{HH}$ = 1.5 Hz	8.22 (t) $^3J_{HH}$ = 8.1 Hz	7.95 (t) $^3J_{HH}$ = 7.6 Hz	8.30 (t) $^3J_{HH}$ = 7.5 Hz
H-5′	7.40 (ddd) $^3J_{HH}$ = 7.5 Hz $^3J_{HH}$ = 4.5 Hz $^4J_{HH}$ = 1.1 Hz	7.81 (dd) $^3J_{HH}$ = 7.3 Hz $^3J_{HH}$ = 5.4 Hz	7.49 [j]	7.96 [k]	7.41 (t) $^3J_{HH}$ = 6.9 Hz	7.90 [l]	7.51 [m]	7.92 (t) [h] $^3J_{HH}$ = 7.3 Hz
H-6′	8.64 (d) $^3J_{HH}$ = 4.5 Hz	9.02 (d) $^3J_{HH}$ = 4.4 Hz	8.53 (d) $^3J_{HH}$ = 4.2 Hz	9.23 (9.15) (d) [i] $^3J_{HH}$ = 5.7 Hz	8.64 (d) $^3J_{HH}$ = 4.2 Hz	8.98 (d) $^3J_{HH}$ = 4.1 Hz	8.57 (d) $^3J_{HH}$ = 4.7 Hz	9.14 (d) $^3J_{HH}$ = 5.3 Hz

[a] Chemical shifts in ppm relative to TMS coupling constants in Hz. Multiplicities: s, singlet; d, doublet; dd, doublet of doublet; t, triplet; m, multiplet; br, broad signal.
[b] Overlapped with OH. Tentative value obtained from a ^{1}H–^{1}H COSY experiment.
[c] Visible as a sextet with $J(H^3H^{3a}) \sim 6.3$ and $J_{gem} \sim 12$ Hz.
[d] D_2O exchangeable proton.
[e] Overlapped with H-3.
[f] Partly overlapped with H-5′. Tentative value obtained from a COSY experiment.
[g] Overlapped with H-5′ and H-6. Tentative value obtained from a COSY experiment.
[h] Partly overlapped with H-6. Tentative value obtained from a COSY experiment.
[i] Value for the minor isomer is given in parenthesis.
[j] Partly overlapped with H-9. Tentative value obtained from a COSY experiment.
[k] Partly overlapped with H-6 and H-8. Tentative value obtained from a COSY experiment.
[l] Partly overlapped with H-3′. Tentative value obtained from a COSY experiment.
[m] Overlapped with H-6 and H-9. Tentative value obtained from a COSY experiment.

shows a slight downfield shift and the second one a slight upfield shift. In both complexes the separation between the two sets of signals becomes larger (up to 0.30 ppm) than in free ligand **L2**. This variation in spectral patterns of methylene protons indicates their different proximity to the metal centre. The proton chemical shifts of the remote $N–CH_3$ and $COCH_3$ groups, as well as of H-8 and H-9 of the second aromatic ring, are practically unchanged in comparison to the free ligands. The H-6 proton shows a downfield shift of 0.25–0.47 ppm.

3.5. In vitro cytostatic activity

The cytostatic activity of the free benzodiazepine ligands **L1** and **L2** and their Zn^{II}, Pd^{II} and Cu^{II} complexes was determined in vitro against the murine leukemia L1210/0 cell line as well as the human T-lymphoblast Molt4/C8 and CEM/0 cell lines. The data, expressed as concentration of the compound required to inhibit tumour cell growth by 50% (IC_{50}), are summarised in Table 6. None of the examined compounds were found to exhibit cytostatic activity at therapeutically meaningful concentrations (1–10 μg ml^{-1}). Their activity varied widely from 40 to >500 μg ml^{-1}, and the most active is the Pd^{II} complex **2** with IC_{50} values within 40–60 μg ml^{-1}. There were no significant differences in response between the three cell lines used.

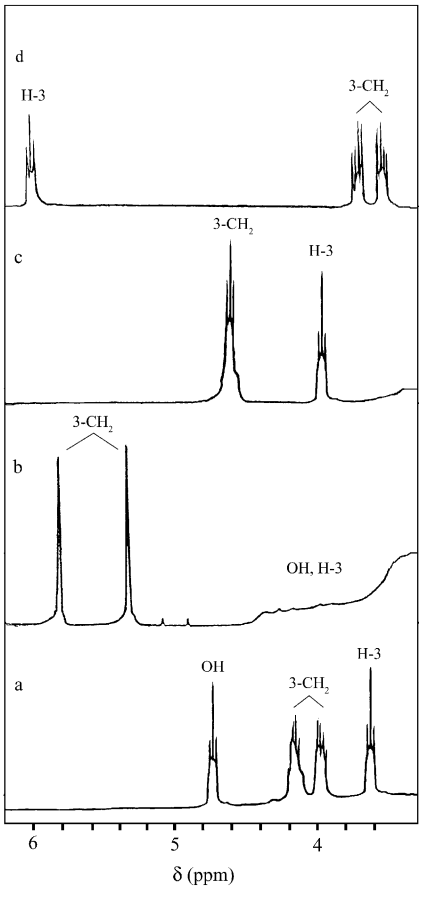


Fig. 5. Selected portions of ^1H NMR spectra of **L1** (a), **2** (b), **L2** (c) and **4** (d).

Table 6
In vitro cytostatic activity of **L1** and **L2** and their Zn^{II}, Pd^{II} and Cu^{II} complexes

Compound	IC_{50} (μg l^{-1}) [a]		
	L1210/0 [b]	Molt4/C8 [c]	CEM/0 [c]
L1	430±100	384±116	>500
1	194±40	168±19	213±6
2	44±5	51±15	45±7
Cu**L1**Cl_2	220±5	174±3	190±6
L2	90±38	51±10	51±4
3	206±5	164±9	208±9
4	210±37	154±82	169±18
Cu**L2**Cl_2	102±82	86±44	49±6

[a] 50% inhibitory concentration.
[b] L1210 murine leukemia cell line.
[c] Molt4/C8 and CEM/0-human T-lymphoblast cell lines.

3.6. In vitro antiviral activity

The antiviral assays of free benzodiazepine ligands and their complexes were based on an inhibition of virus-induced cytopathogenicity in Vero, HEL or HeLa cell cultures against a variety of DNA and RNA viruses. The antiviral activity expressed as concentration of the compound required to reduce virus-induced cytopathogenicity by 50% as well as their cytotoxicity expressed as a concentration of the compound required to cause a microscopically detectable alteration of normal cell morphology, obtained in Vero cell cultures are summarised in Table 7, together with bromovinyldeoxyuridine (BVDU), (*S*)-9-(2,3-dihydroxypropyl)adenine [(*S*)-DHPA] and ribavirin as the control test compounds. The results obtained in HEL and HeLa cells are given as Supplementary Material available from the authors upon request. The compounds showed no or only marginal antiviral activity. No antiviral effects were noted for any of the compounds against any of the viruses evaluated at concentrations that were at least fivefold below the cytotoxic concentrations. The latter ranged from 40 to 200 μg ml^{-1}.

4. Supplementary material

Crystallographic data for the structures reported in this paper have been deposited with the Cambridge Crystallographic Data Centre, CCDC Nos. 177526–177528 for compounds **1**, **3**, **2**. Copies of the data may be obtained free of charge on application to The Director, CCDC, 12 Union Road, Cambridge, CB2

Table 7
In vitro cytotoxicity and antiviral activity of **L1** and **L2** and their Zn^{II}, Pd^{II} and Cu^{II} complexes in Vero cell cultures

Compound	Minimum cytotoxic concentration (μg ml^{-1}) [a]	Minimum inhibitory concentration (μg ml^{-1}) [b]				
		Parainfluenza-3 virus	Reovirus-1	Sindbis	Coxsackie virus B4	Punta toro virus
L1	≥ 200	> 200	> 200	> 200	> 200	> 200
1	200	> 40	> 40	> 40	> 40	> 40
2	≥ 40	> 40	> 40	> 40	> 40	> 40
Cu**L1**Cl_2	200	> 40	> 40	> 40	> 40	> 40
L2	200	> 40	> 40	> 40	> 40	> 40
3	200	> 40	> 40	> 40	> 40	> 40
4	≥ 40	> 40	> 40	> 40	> 40	> 40
Cu**L2**Cl_2	200	> 40	> 40	> 40	> 40	> 40
BVDU	> 400	> 400	> 400	> 400	> 400	> 400
(*S*)-DHPA	> 400	80	240	> 400	> 400	> 400
Ribavirin	> 400	48	48	> 400	> 400	48

[a] Required to cause a microscopically detectable alteration of normal cell morphology.
[b] Required to reduce virus-induced cytopathogenicity by 50%.

1EZ, UK (fax: +44-1223-336033; e-mail: deposit@ccdc.cam.ac.uk or www: http://www.ccdc.cam.ac.uk).

Acknowledgements

This work was kindly supported by the grants 0098035, 0098036 and 0098050 from the Ministry of science and technology of the Republic of Croatia. The authors also thank Dr Bram Schierbeck, Bruker Nonius, Delft, The Netherlands, for the data collection of compound **1**.

References

[1] H.J. Roth, A. Kleemann, T. Besswenger, Pharmaceutical Chemistry, vol. 1, Wiley, New York, 1997, pp. 312–323.
[2] N.E. Kohl, S.C. Mosser, S.J. deSolms, E.A. Giuliani, D.L. Pompliano, S.L. Graham, R.L. Smith, E.M. Scolnick, A. Oliff, J.B. Gibbs, Science 260 (1993) 1934.
[3] R.F. Squires, C. Braestrup, Nature 266 (1977) 732.
[4] H. Mohler, T. Okada, Science 198 (1977) 849.
[5] C. Braestrup, R.F. Squires, Proc. Natl. Acad. Sci. USA 74 (1977) 3805.
[6] D. Hadjipavlou-Litina, C. Hansch, Chem. Rev. 94 (1994) 1483.
[7] N. Langlois, A. Rojas-Rousseau, C. Gaspard, G.H. Werner, F. Darro, R. Kiss, J. Med. Chem. 44 (2001) 3754.
[8] E. De Clercq, Actual. Chim. Thér. 18 (1991) 133.
[9] I.A. O'Neal, C.L. Murray, R.C. Hunter, S.B. Kalindjian, T.C. Jenkins, Synlett (1997) 78.
[10] A. Marchi, L. Marvelli, R. Rossi, V. Bertolasi, V. Ferretti, Inorg. Chim. Acta 272 (1998) 267.
[11] M.C. Aversa, P. Giannetto, G. Bruno, M. Cusumano, A. Giannetto, S. Geremia, J. Chem. Soc., Dalton Trans. (1990) 2433.
[12] P. Bombicz, E. Forizs, J. Madarasz, A. Deak, A. Kalman, Inorg. Chim. Acta 315 (2001) 229 (and the references therein).
[13] A. Avdagić, V. Šunjić, Helv. Chim. Acta 81 (1998) 85.
[14] P. Čudić, B. Klaić, Z. Raza, D. Šepac, V. Šunjic, Tetrahedron 47 (1991) 5295.
[15] M. Majerić-Elenkov, D. Žiher, A. Višnjevac, Z. Hameršak, B. Kojić-Prodić, V. Šunjić, Croat. Chem. Acta 74 (2001) 707.
[16] A. Avdagić, A. Lesac, Z. Majer, M. Hollosi, V. Šunjić, Helv. Chim. Acta 81 (1998) 1567.
[17] V. Vinković, Z. Raza, V. Šunjić, Spectrosc. Lett. 27 (1994) 269.
[18] E. Decorte, R. Toso, A. Šega, V. Šunjić, Ž. Ružić-Toroš, B. Kojić-Prodić, Helv. Chim. Acta 64 (1981) 1145.
[19] A. Višnjevac, Lj. Tušek-Bozić, M. Majerić-Elenkov, V. Šunjić, B. Kojić-Prodić, Eur. J. Inorg. Chem. (2001) 2647.
[20] L. Spek, HELENA, Program for Data Reduction, University of Utrecht, Utrecht, The Netherlands, 1993.
[21] A. Altomare[1], G. Cascarano[1], C. Giacovazzo[1], A. Guagliardi[1], A.G.G. Moliterni[1], M.C. Burla[2], G. Polidori[2], M. Camalli[3], R. Spagna[3], SIR-97: A Package for Crystal Structure Solution by Direct Methods and Refinement, [1]Istituto di Ricerca per lo Sviluppo di Metodologie Cristallografiche, Bari, [2]Dipartimento di Scienze della Terra, Perugia, [3]Istituto di Strutturistica Chimica 'G. Giacomello', Roma, Italy, 1997.
[22] G.M. Sheldrick, SHELXS-86: Program for the Solution of Crystal Structures, Universität Göttingen, Germany, 1986.
[23] H.D. Flack, G. Bernardinelli, J. Appl. Crystallogr. 11 (2000) 43.
[24] G.M. Sheldrick, SHELX-97: Program for the Refinement of Crystal Structures, Universität Göttingen, Germany, 1997.
[25] T. Spek, PLATON-98: A Multipurpose Crystallographic Tool, 120398 Version, University of Utrecht, Utrecht, The Netherlands, 1998.
[26] E. De Clercq, J. Balzarini, P.F. Torrence, M.P. Mertes, C.L. Schmidt, D. Shugar, P.J. Barr, A.S. Jones, G. Verhelst, R.T. Walker, Mol. Pharmacol. 19 (1981) 321.
[27] Lj. Tušek-Bozić, A. Furlani, V. Scarcia, E. De Clercq, J. Balzarini, J. Inorg. Biochem. 72 (1998) 201.
[28] E. De Clercq, In vitro and ex vivo test systems to rationalize drug design and delivery, in: D. Crommelin, P. Couvreur, D. Duchene (Eds.), Editions de Santé, Paris, France, 1994, pp. 108–125.
[29] C.K. Johnson, ORTEP-II, Report ORNL-5138, Oak Ridge National Laboratory, TN, 1976.
[30] F.H. Allen, O. Kennard, Chem. Des. Automation News 8 (1993) 1.
[31] A. Višnjevac, Stereochemistry of the chiral 1,4-benzodiazepin-2-ones and their metal complexes, PhD Thesis, University of Zagreb, Zagreb, Croatia, 2001.
[32] G. Parkin, Chem. Commun. 20 (2000) 1971.
[33] I.L. Alberts, K. Nadassy, S.J. Wodak, Protein Sci. 7 (1998) 1700.
[34] M.A. Cinellu, M.L. Ganadu, G. Minghetti, F. Cariati, F. Demartin, M. Manassero, Inorg. Chim. Acta 143 (1988) 197.

[35] K. Nakamoto, Infrared and Raman Spectra of Inorganic and Coordination Compounds, Part B: Applications in Coordination, Organometallic and Bioinorganic Chemistry, 5th ed., Willey-Interscience, New York, 1997, pp. 24 and 59.
[36] S. Gourbatsis, S.P. Perlepes, J.S. Butler, N. Hadjiliadis, Polyhedron 18 (1999) 2369.
[37] A. Abufarag, H. Vahrenkamp, Inorg. Chem. 34 (1995) 2207.
[38] M.C. Aversa, P. Bonaccorsi, M. Cusumano, P. Gianneto, D. Minniti, J. Chem. Soc., Dalton Trans. (1991) 3431.
[39] S. Stoccoro, M.A. Cinellu, A. Zucca, G. Minghetti, Inorg. Chim. Acta 215 (1994) 17.
[40] M. Cusumano, A. Giannetto, D. Minniti, Inorg. Chim. Acta 215 (1994) 41.
[41] M.J. Mphahlele, P. Kaye, Magn. Reson. Chem. 38 (2000) 207.

to deal with these other cases. Thus, we have tried to provide IR and NMR spectroscopic data leading to general observations that may be useful for the characterization of other phosphazene polymers with organometallic complexes.

2. Experimental

2.1. General considerations

All the reactions were carried out under dry nitrogen. K_2CO_3 and Cs_2CO_3 were dried at 140 °C prior to use. The C_3H_6O used as solvent was predistilled from $KMnO_4$, and distilled twice from anhydrous $CaSO_4$. The MeOH was distilled from CaH_2. The THF was treated with KOH and distilled twice from Na in the presence of benzophenone. Petroleum ether refers to that fraction with boiling point in the range 60–65 °C. The hexachlorocyclotriphosphazene $[N_3P_3Cl_6]$ (Fluka) was purified from hot petroleum ether and dried in vacuum. The cyclic $[N_3P_3(O_2C_{12}H_8)_2Cl_2]$ [11], and $[N_3P_3(O_2C_{12}H_8)_2(OC_6H_4PPh_2)]$ [8], were prepared as described elsewhere. The polymer $[NPCl_2]_n$ was prepared by heating the $[N_3P_3Cl_6]$ in solution as described by Magill and coworkers [26]. The phosphine $[PPh_2(C_6H_4–OH)]$ was prepared as described in the experimental part (a slight modified version of the reported in Ref. [8]).

The IR spectra were recorded with a Perkin–Elmer FT Paragon 1000 spectrometer. NMR spectra were recorded on Bruker AC-200, AC-300 and DPX 300 instruments, using $CDCl_3$ as solvent. ^1H and $^{13}C\{^1H\}$ NMR are given in δ relative to TMS. $^{31}P\{^1H\}$ NMR are given in δ relative to external 85% aqueous H_3PO_4. Coupling constants are in Hz. C, H, N analyses were performed with a Perkin–Elmer 2400 microanalyzer. The chlorine, Mn and P elemental analyses were performed by Galbraith laboratories. GPC were measured with a Perkin–Elmer equipment with a model LC 250 pump, a model LC 290 UV, and a model LC 30 refractive index detector. The samples were eluted with a 0.1% by weight solution of tetra-*n*-butylammonium bromide in THF through Perkin–Elmer PLGel (Guard, 10^5, 10^4 and 10^3 Å) at 30 °C. Approximate molecular weight calibration were obtained using narrow molecular weight distribution polystyrene standards. T_g values were measured with a Mettler DSC 300 differential scanning calorimeter equipped with a TA 1100 computer, at 10 °C min^{-1}. Thermal gravimetric analyses were performed on a Mettler TA 4000 instrument. The polymer samples were heated at a rate of 10 °C min^{-1} from ambient temperature to 800 °C under constant flow of nitrogen.

2.2. Preparation of $PPh_2(C_6H_4–OH)$

A mixture of *p*-bromophenol (12.5 g, 72.2 mmol), 2-methoxypropene (13.8 ml, 144.5 mmol) and a drop of $POCl_3$ was stirred in the absence of light for 1 h. Four drops of Et_3N were added and the volatiles were evaporated in vacuo. The resulting pale yellow oil (very light sensitive) was dissolved in petroleum ether (80 ml). To this solution was added dropwise and with stirring a solution of LiBu 2.5 M (31.8 ml, 79.42 mmol) in petroleum ether (30 ml). The stirring was continued for 4 h to give a white precipitate that was filtered and dried in vacuo. The resulting solid was dissolved at −70 °C in THF (70 ml) and to the solution was added dropwise a solution of $PClPPh_2$ (8.4 ml, 47.04 mmol) in THF (30 ml). The mixture was allowed to reach room temperature (r.t.) and stirred overnight. Then, 20% aqueous HCl (36 mL) was added and, after stirring for 3 h, the mixture was extracted with Et_2O (4 × 50 ml). The extracts were stirred with an excess of solid Na_2CO_3, washed with water (3 × 50 ml), dried over Na_2SO_4, and filtered. The solvent was evaporated in vacuo to give an orange oily residue that was dissolved in CH_2Cl_2, filtered through silica-gel, concentrated by evaporation in vacuo, and mixed with petroleum ether to obtain two layers. This mixture was then kept into a freezer until crystallization and then the white microcrystals were dried in vacuo. Yield: 6 g (46%).

Anal. Found: C, 77.3; H, 5.5. Calc.: C, 77.7; H, 5.4%.

^1H NMR ($CDCl_3$): 7.4–6.7 (m.br., 14H, aromatic rings); 5.3 (s.br., 1H, OH). ^{31}P NMR ($CDCl_3$): −6.6. ^{13}C NMR ($CDCl_3$): 157.4 s, 136.5 {d, J ($^{31}P–^{13}C$) = 21.6}, 128.5 {d, J ($^{31}P–^{13}C$) = 8}, 116.4 {d, J ($^{31}P–^{13}C$) = 8.3}, [P–C_6H_4]; 138.2 {d, J ($^{31}P–^{13}C$) = 9.2}, 134.1 {d, J ($^{31}P–^{13}C$) = 19.3}, 129.1 {d, J ($^{31}P–^{13}C$) = 10.6}, 129.0 [PPh_2].

2.3. Preparation of $\{Mn(CO)_2(\eta^5\text{-}C_5H_4Me)[PPh_2(C_6H_4–OH)]\}$ (1)

To a solution of $PPh_2(C_6H_4–OH)$ (1.85 g, 6.65 mmol) in THF (40 ml) cooled at −30 °C was added the complex $[Mn(THF)(CO)_2(\eta^5\text{-}C_5H_4Me)]$, obtained by irradiating with UV light a solution of $[Mn(CO)_3(\eta^5\text{-}C_5H_4Me)]$ (1.88 g, 8.62 mmol) in THF (45 ml) at −30 °C until the carbonyl band at 2018 cm^{-1} could not longer be observed (approximately 3.5 h). The mixture was stirred at r.t. overnight and the volatiles were removed in vacuo. The residue was chromatographed in silica–gel eluting first with petroleum ether and then with CH_2Cl_2. The CH_2Cl_2 fraction was evaporated to give $\{Mn(CO)_2(\eta^5\text{-}C_5H_4Me)[PPh_2\text{-}(C_6H_4–OH)]\}$ as a brown solid. Yield: 2.2 g, 71%.

Anal. Found: C, 66.6; H, 4.6. Calc.: C, 66.7; H, 4.7%.

IR (ν-CO-region): (CH_2Cl_2) 1926s, 1859s; (THF) 1930s, 1867s.

IR (KBr): 3509s (ν-OH), 3056w (ν-CH, aryl rings), 2922vw (ν-CH, C_5H_4–Me), 1912vs, 1893m, 1850s, 1828vs (ν-CO), 1600m, 1582m, 1560w, 1498m, 1482w, 1458vw, 1434m, 1420w (OC_6H_4–PPh_2) 1399vw, 1375vw (δ-CH_3, C_5H_4–Me), 1328w, 1273m, 1191w, 1174m, 1094s, 1029w, 829s, 748m, 696s (OC_6H_4–PPh_2), 667m, 634w, 622m (δ-MnCO), 524s.

^{1}H NMR ($CDCl_3$): 7.3–6.8 (m.br., 14H, aromatic rings); 5.3 (s.br., 1H, OH); 4.2, 4.0 (m., 4H, C_5H_4); 1.9 (s, 3H, CH_3). ^{31}P NMR ($CDCl_3$): 91.3. ^{13}C NMR ($CDCl_3$): 234.0 {d, J (^{31}P–^{13}C) = 23, CO}; 157.3, 139.4 {d, J (^{31}P–^{13}C) = 40}, 135.6 {d, J (^{31}P–^{13}C) = 11}, 133.2 {d, J (^{31}P–^{13}C) = 9}, 129.9, 129.3br., 128.7 {d, J (^{31}P–^{13}C) = 7.5}, 115.8 {d, J (^{31}P–^{13}C) = 9} (aromatic carbons); 99.7, 83.9, 82.6 (C_5H_4Me), 14.5 (Me).

2.4. Preparation of {N_3P_3[$OC_6H_4PPh_2$–$Mn(CO)_2(\eta^5$-$C_5H_4Me)]_6$} (**2**)

A mixture of [$N_3P_3Cl_6$] (0.1 g, 0.29 mmol) and [$Mn(CO)_2(\eta^5$-$C_5H_4Me)$[$PPh_2(C_6H_4$–OH)]} (0.84 g, 1.8 mmol) and Cs_2CO_3 (1.13 g, 3.47 mmol) in THF (20 ml) was refluxed for 3 h. The solvent was removed in vacuo and the residue was extracted with CH_2Cl_2 (5 × 20 ml). The solution was filtered and evaporated to dryness. The residue was washed with MeOH (3 × 30 ml) to give **5** as a yellow solid. Yield: 0.72 g, 85%.

Anal. Found: C, 62.9; H, 4.4; N: 1.4. Calc.: C, 63.7; H, 4.3; N, 1.4%.

IR (ν-CO-region): (CH_2Cl_2) 1926s, 1859s; (THF) 1929s, 1866s.

IR (KBr): 3056w (ν-CH, aryl rings), 2961w, 2922w (ν-CH, C_5H_4–Me), 1927vs, 1859vs (ν-CO), 1587m, 1483s, 1434m (aryl rings), 1376w (δ-CH_3, C_5H_4–Me), 1267m (ν-C–OP), 1204s, 1189s, 1163vs (ν-PN), 1091s (ν-P–OC), 953m, 940m (δ-POC), 884m, 833m, 745m, 696s (aryl rings and δ-PNP), 662m, 619m, 596m (δ-MnCO), 524m,br.

^{1}H NMR ($CDCl_3$): 7.3–7.2–7.0 (m.br., 84H, aromatic rings); 4.1, 3.9 (m., 24H, C_5H_4); 1.9 (s, 18H, CH_3). ^{31}P NMR ($CDCl_3$): 92.9 (s, PPh_2); 8.0 (s, P_3N_3). ^{13}C NMR ($CDCl_3$): 233.4 {d, J (^{31}P–^{13}C) = 24, CO}; 151.8, 138.7 {d, J (^{31}P–^{13}C) = 40}, 135.9 {d, J (^{31}P–^{13}C) = 40}, 135.0 {d, J (^{31}P–^{13}C) = 11.5}, 133.3 {d, J (^{31}P–^{13}C) = 10.5}, 130.1, 128.8 {d, J (^{31}P–^{13}C) = 9), 121 {d, J (^{31}P–^{13}C) = 8}, (aromatic carbons); 99.6, 83.7, 82.4 (C_5H_4Me), 14.4 (Me).

2.5. Preparation of {$N_3P_3(O_2C_{12}H_8)_2$[$OC_6H_4PPh_2$–$Mn(CO)_2(\eta^5$-$C_5H_4Me)]_2$} (**3**)

2.5.1. Method a

To a solution of [$N_3P_3(O_2C_{12}H_8)_2(OC_6H_4PPh_2)_2$] (**2**) (0.2 g, 0.19 mmol) in THF (30 ml) cooled at −30 °C was added the complex [$Mn(THF)(CO)_2(\eta^5$-$C_5H_4Me)$], obtained by irradiating with UV light a solution of [$Mn(CO)_3(\eta^5$-$C_5H_4Me)$] (0.11 g, 0.50 mmol) in THF (30 ml) at −30 °C until the carbonyl band at 2018 cm^{-1} could no longer be observed (approximately 1.5 h). The mixture was allowed to reach r.t. and stirred for 6 h. The volatiles were removed in vacuo, and the oily residue was chromatographed in silica–gel eluting first with petroleum ether and then with CH_2Cl_2. The CH_2Cl_2 fraction was evaporated to give **6** as a yellow solid. Yield: 0.17 g, 62%.

Anal. Found: C, 63.4; H, 4.0; N, 2.7. Calc.: C, 63.5; H, 4.1; N, 2.9%.

IR (ν-CO-region): (CH_2Cl_2) 1928s, 1861s; (THF) 1929s, 1866s.

IR (KBr): 3058w (ν-CH, aryl rings), 2961w, 2922w (ν-CH, C_5H_4–Me), 1927vs, 1859vs (ν-CO), 1587m, 1478m, 1435m, 1396w (aryl rings), 1376w (δ-CH_3, C_5H_4–Me), 1273m (ν-C–OP), 1229m, 1170vs (ν-PN), 1093s (ν-P–OC), 936s,br. (δ-POC), 885s, 837w, 786m, 752m (aryl rings and δ-PNP), 718w, 695m, 662m, 617sh, 608m, 590sh (aryl-rings and δ-MnCO), 524m.

^{1}H NMR ($CDCl_3$): 7.3–7.1 (m.br., 44H, aromatic rings); 4.2, 4.0 (m., 8H, C_5H_4); 1.9 (s, 6H. CH_3). ^{31}P NMR ($CDCl_3$): 92.9 (s., PPh_2), 25.7 [d, $P(O_2C_{12}H_8)$] 9.7 [dd, $P(OC_6H_4PP_2)_2$]{M_2X spin system, J (P–P) = 93}. ^{13}C NMR ($CDCl_3$): 233.5 {d, J (^{31}P–^{13}C) = 24, CO}; 152.1m, 138.9 {d, J (^{31}P–^{13}C) = 40.5}, 136.5 {d, J (^{31}P–^{13}C) = 40.5}, 135.1 (d, J (^{31}P–^{13}C) = 11.5}, 133.4 (d, J (^{31}P–^{13}C) = 10.5), 130.1, 128.8 (d, J (^{31}P–^{13}C) = 9), 121.4m, ($OC_6H_4PPh_2$); 148.6, 130.4, 130.3, 129.3, 126.8, 122.5 ($OC_{12}H_8$); 99.7, 83.8, 82.5 (C_5H_4Me); 14.5 (Me).

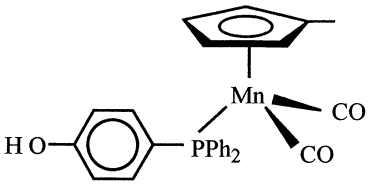
2.5.2. Method b

A mixture of [$N_3P_3(O_2C_{12}H_8)_2Cl_2$] (0.2 g, 0.35 mmol) and [$Mn(CO)_2(\eta^5$-$C_5H_4Me)$[$PPh_2(C_6H_4$–OH)]} (0.35 g, 0.75 mmol) and Cs_2CO_3 (0.46 g, 1.4 mmol) in THF (25 ml) was refluxed for 2 h. The solvent was removed in vacuo and the residue was extracted with CH_2Cl_2 (5 × 20 ml). The solution was filtered and evaporated to dryness to give **6** as a yellow solid that was washed with methanol (2 × 40 ml) and dried in vacuo. Yield: 0.45 g, 90%.

Anal. Found: C, 62.9; H, 4.2; N, 2.7. Calc.: C, 63.5; H,4.1; N, 2.9%.

2.6. Preparation of [{$NP(O_2C_{12}H_8)$}$_{0.6}${NP[OC_6H_4P-Ph_2–$Mn(CO)_2(\eta^5$-$C_5H_4Me]_2$}$_{0.4}$·$0.5(OC_4H_8)$]$_n$ (**4**)

A mixture of [$NPCl_2$]$_n$ (1.0 g, 8.63 mmol), 2,2′-HO–C_6H_4–C_6H_4–OH (0.965 g, 5.18 mmol) and K_2CO_3 (2.86 g, 20.69 mmol) in THF (130 ml) was refluxed with mechanical stirring for 10 h. Then, the complex {[$Mn(CO)_2(\eta^5$-$C_5H_4Me)$][$PPh_2(C_6H_4$–OH)]} (4.85 g, 10.35 mmol) and Cs_2CO_3 (3.37 g, 10.34 mmol) were added, and the reaction was continued for another 131



1

Chart 1.

h. The resulting mixture was poured into water (1.5 l) to give a precipitate that was washed twice with water (1 l) and dissolved in THF (200 ml). The solution was filtered and concentrated until a viscous liquid was formed that was precipitated slowly into water (1.5 l). The reprecipitation procedure was repeated in the same way from THF/isopropyl alcohol, and THF/petroleum ether to give a yellow solid that was dried in vacuo at r.t. for a week. Yield: 3.3 g, 68%.

Anal. Found: C, 62.9; H, 4.7; N, 2.6; P, 10.8; Mn, 7.5. Calc.: C, 63.7; H, 4.6; N, 2.5; P, 9.9; Mn, 7.8. Chlorine content: 0.03%.

IR (ν-CO-region): (CH_2Cl_2) 1927s, 1860s; (THF) 1929s, 1866s.

IR (KBr): 3058w (ν-CH, aryl rings), 2927w, 2857w (ν-CH, PTHF), 1928vs, 1861vs(ν-CO), 1588w, 1480m,br., 1435m, (aryl rings), 1376w (δ-CH_3, C_5H_4–Me), 1263m (ν-C–OP), 1246m, 1198vs (ν-PN), 1170m, 1095m (ν-P–OC), 940s,br. (δ-POC), 832w, 786m, 752m (aryl rings and δ-PNP), 696m, 663m, 617m, 598m (aryl-rings and δ-MnCO), 526m.

^{1}H NMR ($CDCl_3$): 7.1–6.7 (m.br., 16H, aromatic rings); 3.9, 3.7(m., 3.2H, C_5H_4); 3.4m, 1.6m (4H, OC_4H_8); 1.8 (s, 2.4H, CH_3). ^{31}P NMR ($CDCl_3$): 92.1 (s., PPh_2); −6.4 [m., $P(O_2C_{12}H_8]$; −23.6 [m., $P(OC_6H_4PPh_2)_2$]. ^{13}C NMR ($CDCl_3$): 234 {d, J ($^{31}P-^{13}C$) = 23, CO}; 153, 139, 134, 133, 130, 129, 121, [(all broad, OC_6H_4–$P(C_6H_5)_2$], 150, 126, 121 (all broad, $O_2C_{12}H_8$); 100.0, 83.7, 82.4 (C_5H_4Me); 71.3, 27.2, (OC_4H_8); 14.1 (Me).

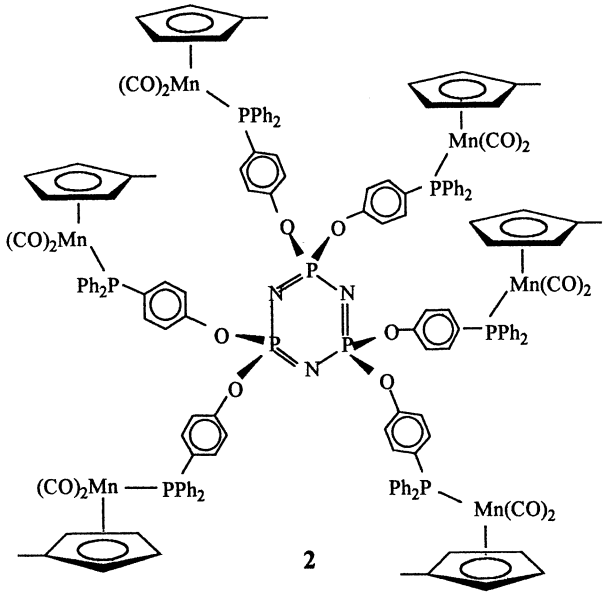
M_w (GPC): 1,100,000 ($M_w/M_n = 4$). T_g (DSC): 128 °C ($\Delta C_p = 0.16$ J g^{-1} K^{-1}. TGA: −22% (350 °C), −36% (425 °C). Residue at 800 °C: 41%.

3. Results and discussion

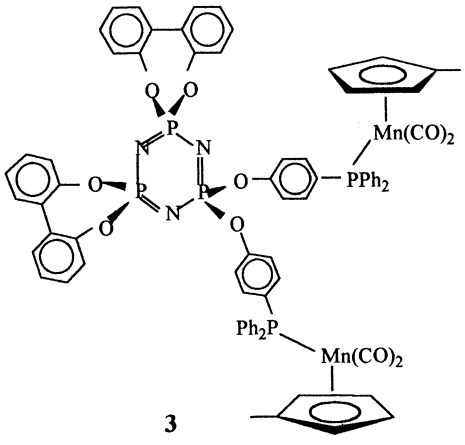
Following a method previously described by us for other phosphazene phosphine complexes [8], the hexachlorocyclotriphosphazene [$N_3P_3Cl_6$] was reacted with 6 equiv. of the phenolic phosphine complex {$Mn(CO)_2(\eta^5$-$C_5H_4Me)[PPh_2(C_6H_4$–$OH)]$} (**1**) (Chart 1) in acetone in the presence of Cs_2CO_3 to give the hexametallic phosphazene complex {$N_3P_3[OC_6H_4PPh_2$–$Mn(CO)_2(\eta^5$-$C_5H_4Me)]_6$} (**2**) in good yield and analytically pure (Chart 2).

This result is interesting, because it has been reported [12] that the direct substitution reaction of the cyclophosphazene–hexaphosphine {$N_3P_3[OC_6H_4PPh_2]_6$} with the precursor [$Mn(THF)(CO)_2(\eta^5$-$C_5H_5)$] in THF gives a mixture of complexes with $OC_6H_4PPh_2$–$Mn(CO)_2(\eta^5$-$C_5H_5)$ units, and the saturation of all the PPh_2 sites required the presence of an important excess of the organometallic manganese precursor. Thus, the synthesis of the pure totally substituted complex analogous to (**2**) was not reported.

In a similar manner, the cyclic chorophosphazene [$N_3P_3(O_2C_{12}H_8)_2Cl_2$] where ($O_2C_{12}H_8$ = 2,2′-dioxybiphenyl) was reacted with (**1**) to give the bimetallic cyclic



2



3

Chart 2.

phosphazene complex $\{N_3P_3(O_2C_{12}H_8)_2[OC_6H_4PPh_2–Mn(CO)_2(\eta^5\text{-}C_5H_4Me)]_2\}$ (**3**), also in good yield. We observed that, in this case, the same complex **3** could be also prepared by ligand replacement reaction from the diphosphine $\{N_3P_3(O_2C_{12}H_8)_2[OC_6H_4PPh_2]_2\}$ [8] and $[Mn(THF)(CO)_2(\eta^5\text{-}C_5H_4Me)]$ in THF.

The reactions of the phenolic complex **1** with the cyclic models could be successfully extended to the partially substituted phosphazene copolymer $\{[NP(O_2C_{12}H_8)]_{0.6}[NPCl_2]_{0.4}\}_n$, which is a polymeric counterpart of the cyclic bis-spirophosphazene $[N_3P_3(O_2C_{12}H_8)_2Cl_2]$. Thus, the reaction of this latter with **1** in THF in the presence of Cs_2CO_3 gave the high molecular weight polymeric complex $[\{NP(O_2C_{12}H_8)\}_{0.6}\{NP[OC_6H_4PPh_2–Mn(CO)_2(\eta^5\text{-}C_5H_4Me)]_2\}_{0.4}\cdot 0.5(OC_4H_8)]_n$ (**4**) (Scheme 1). The yield (68%) was good and much higher than for the analogous polymer with $W(CO)_5$ fragments [8], and the effectiveness of the substitution reaction was very high, as shown by the very low residual chorine content in the isolated polymer (0.03% in weight). This shows that the method in Scheme 1 may be of wide application provided that the necessary phenolic complex OH–C_6H_4–L–MLn is stable under refluxing THF for several hours.

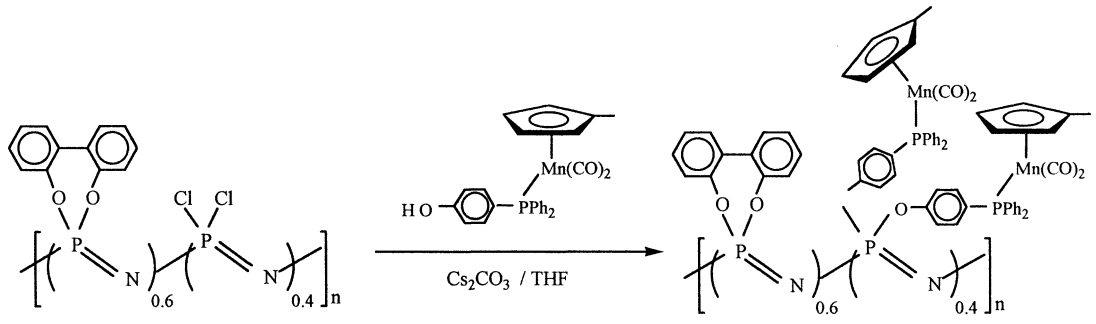
The polymer **4** was very stable and could be stored in the solid state for years unaltered. The M_w (by GPC) was 1,100,000 (polydispersity index = 4). Taking into account that the weight of the chain units is 529.4, the weight-averaged degree of polymerization is approximately 2000 units per chain, a value which is only slightly low for that type of phosphazene random copolymer [11]. The presence of some polytetrahydrofuran (PTHF) in this copolymer, that is expected when using THF as solvent in the substitution reaction from $[NPCl_2]_n$ [11,13], was detected and measured as described below. The PTHF, that can be minimized if necessary [13], represents approximately 6% in weight of the isolated material and does not alter the efficacy of the synthesis of **4**.

The successful preparation of polymer **4** from $\{[NP(O_2C_{12}H_8)]_{0.6}[NPCl_2]_{0.4}\}_n$ is valuable considering that it could not be prepared by the ligand substitution reaction from the precursor $[Mn(THF)(CO)_2(\eta^5\text{-}C_5H_4Me)]$, using the known phosphine containing polymer $[\{NP(O_2C_{12}H_8)\}_{0.6}\{NP[OC_6H_4PPh_2]_2\}_{0.4}]_n$ [8,14]. Thus, even using a large excess of the organometallic precursor the product isolated by this method had only 50% of the available PPh_2 ligands coordinated to $Mn(CO)_2(\eta^5\text{-}C_5H_4Me)$ fragments (as measured by ^{31}P NMR), and the elemental analysis showed a Mn content of 9.6%, much larger than the expected (4.4%), indicating the presence of uncharacterized contaminating Mn species. Considering the stability of **4**, this shows that the difficulty in completing the coordination of the PPh_2 groups in the $[\{NP(O_2C_{12}H_8)\}_{0.6}\{NP[OC_6H_4PPh_2]_2\}_{0.4}]_n$ by the THF substitution of $[Mn(THF)(CO)_2(\eta^5\text{-}C_5H_4Me)]$ is mainly due to the large steric effects imposed to the entering $Mn(CO)_2(\eta^5\text{-}C_5H_4Me)$ fragments by those already present in the polymeric chain.

All the spectroscopic data (see Section 2) were in accord with the structure proposed for the new compounds and provided further useful experimental evidences to characterize polymeric complexes of the transition metals.

The IR spectra (cm^{-1}) in CH_2Cl_2 or THF solutions of **1** to **4** (Section 2) showed the expected two strong stretching carbonyl absorptions of the $Mn(CO)_2(C_5H_4CH_3)$ groups at 1927, 1860. The solid state spectra (KBr pellets) showed several helpful features. In Section 2 are quoted all the signals observed with appreciable intensity. However, the assignments given (see the discussion below) correspond only to those more relevant absorptions, and in the region 800–600, where various significant frequencies appear among other from the vibrations of the aromatic rings, they have been quoted under a general assignment.

The IR of the cyclic phosphazene models **2** and **3**, showed the presence of the organometallic fragment by the two carbonyl absortions and also by two of the expected bands of the Mn–$C_5H_4CH_3$ ring [15], that were clearly distinguished at 2922w (ν-CH, CH_3) and 1376vw



4

Scheme 1.

(δ-CH_3), and by three conspicuous bands at 662m, 618m and 596m, that are related to δ-MnCO modes [15]. All those bands were absent in the spectra of the uncoordinated phosphazene phosphines $\{N_3P_3[OC_6H_4PPh_2]_6\}$ and $\{N_3P_3(O_2C_{12}H_8)_2[OC_6H_4PPh_2]_2\}$. However, in the region from 1600 to 680, that could be potentially useful to study P-aryl compounds [16], the IR spectra of **2** and **3** (Section 2) appear almost identical to those of the corresponding free ligands. Thus, except for the commented weak band at 1376, the only significant difference was observed in a pair of very closed but well resolved peaks at 950–940, because, in the case of the metal complexes, the later, that is assignable to δ-POC modes [17], is much stronger than the former. As this feature is also observed for the analogous $W(CO)_5$ complexes, it suggests a decrease intensity of the band at 950 after the complexation of a MLn fragment to the PPh_2 group that could be useful to denote it. However, although all the differences commented between the spectra of the cyclic phosphazene phosphines and its complexes were also found in the spectra of the polymeric complex **4** and its corresponding free ligand $[\{NP(O_2C_{12}H_8)\}_{0.6}\{NP[OC_6H_4PPh_2]_2\}_{0.4}]_n$, in this case, the 950–940 band was too broad to unambiguously show the coordination of a metallic fragment.

A couple of bands at 2927w, 2857w in the IR of the polymer **4**, evidenced the presence of the PTHF, that was expected in this synthesis [13].

Finally, the broad band near 525 cm^{-1}, that is observed in the spectra of **2**, **3** and **4**, may be attributed to the aryloxyphosphazene scheleton (δ-NPO modes) [17], but similar bands are also present in the spectra of the phosphine **1**, therefore is was not assigned in Section 2.

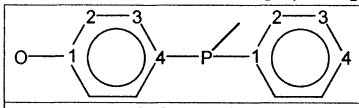
The ^{31}P NMR spectra was specially significant showing the very large deshielding of the phosphorus of the PPh_2 coordinated to the manganese dicarbonyl fragment as compared with those of the free phosphines. Thus, in the free phenolic phosphine $HOC_6H_4PPh_2$, in the cyclic phosphazene hexaphosphine $\{N_3P_3[OC_6H_4PPh_2]_6\}$, and in the spyro-phosphazene bis-phosphine $\{N_3P_3(O_2C_{12}H_8)_2[OC_6H_4PPh_2]_2\}$, the chemical shift is circa -6 ppm, while in their $Mn(CO)_2(C_5H_4{-}CH_3)$ complexes **1**, **2** and **3**, the value is near 93 ppm. Consistently, the ^{31}P NMR of the polymer **4** showed three peaks at 92.1(PPh_2), −6.4 [$NP(O_2C_{12}H_8)$] and −23.6 [$P(OC_6H_4PPh_2Mn(CO)_2(C_5H_4{-}CH_3)$], and the intensity of the latter two were in accord with the ratio of the units present in the proposed formula. By comparing the chemical shift of the phosphorus of the phosphazene rings in $\{N_3P_3[OC_6H_4PPh_2]_6\}$ (8.8 ppm) $\{N_3P_3(O_2C_{12}H_8)_2\ [OC_6H_4PPh_2]_2\}$ (25.8 for the $NP(O_2C_{12}H_8)$, and 10.0 for the $NP[OC_6H_4PPh_2]_2$) [8], with those in **2** (8.0) and **3** (25.7 and 9.7, respectively), it can be noticed how they are sensitive to the presence of the coordinated metallic fragment. This has been repeatedly observed in cyclic and polymeric phosphazenes having pendant complexes with other ligands, such as $OC_6H_4{-}CN$ [18], or OC_5H_4N [9,19,20]. This effect is also noted in the chemical shifts of the phosphorus atoms baring the groups $OC_6H_4PPh_2{-}Mn(CO)_2(\eta^5\text{-}C_5H_4Me)$ in polymer **4**, that are 1.6 ppm lower than in the free phosphine polymer $[\{NP(O_2C_{12}H_8)\}_{0.6}\{NP[OC_6H_4PPh_2]_2\}_{0.4}$ [8].

The ^1H NMR of all the Mn complexes showed the ($C_5H_4CH_3$) ring as two multiplets at 4.2 and 4.0, and a singlet at 1.9 (CH_3). In the case of the polymer **4**, those peaks appeared at slightly lower frequencies (3.9, 3.7 and 1.8 ppm). This is usually observed by comparing the NMR signals of different groups when free and when pendant from long spyro-phosphazene copolymeric chains [9]. On the other hand, the relative intensities of those signals with those of the aromatic protons (broad signals between 7.5 and 6.7 ppm) gave a ratio of 0.62/0.38 for the two phosphazene units in the copolymer, very close to the idealized value given in the proposed formula. The ^1H spectra of polymer **4** also showed the presence of PTHF (peaks at 3.4 and 1.6) the intensity of which corresponded to an amount of 0.5 OC_4H_8 units per NP unit, representing 6.4% in weight.

The ^{13}C NMR of the models **2** and **3** and the polymer **4**, showed the two carbonyls $Mn(CO)_2$ as a doublet at 234 ppm with a coupling constant $^{13}C{-}^{31}P$ of 24 Hz, and the ($C_5H_4CH_3$) ring as four singlets at nearly 100, 84, 82 and 14 (CH_3) ppm. Other peaks in the ^{13}C NMR spectra corresponded to the $O_2C_{12}H_8$ rings (148.6, 130.4, 130.3, 129.3, 126.8, 122.5) [11], and to the $OC_6H_4{-}PPh_3$ units (in Table 1 are given the assignments, that may be useful for the characterization of similar phosphazenes with transition metal phosphine complexes). As can be noticed, some peaks of the two types of aromatic rings may interfere, as happens in the polymer **4**, where some assignments may be ambiguous, specially those near the 130 ppm region. However, the data in Table 1 clearly show that, in agreement with a general rule noted by us [21], when the phenol $HOC_6H_4{-}PPh_2Mn(CO)_2(C_5H_4CH_3)$ is transformed into $NP{-}OC_6H_4{-}PPh_2Mn(CO)_2(C_5H_4CH_3)$ groups pendant from cyclic or polymeric phosphazene units, the chemical shift of the C1 carbon of the $OC_6H_4{-}$ ring is shifted approximately 5 ppm to lower frequencies, that of the C4 increases by nearly the same amount, that of C2 also increases, and that of the C3 remains almost unaffected. On the other hand, the carbons of the $P(C_6H_5)_2$ rings shift very little upon the coordination of a metallic fragment to the phosphorus atom, although a large increase in the $^{13}C{-}^{31}P$ coupling constant (from 10 to 40 Hz) is clearly observed.

In the case of polymer **4**, the spectrum was rather broad, and the peaks at 130–129 corresponding to the C6, C4 and C1 carbons of the $O_2C_{12}H_8$ rings are hidden

Table 1
^{13}C NMR data for the O–C_6H_4–PPh_2 groups in phosphazenes [a]

	OC_6H_4P C_1	OC_6H_4P C_2	OC_6H_4P C_3	OC_6H_4P C_4	$(C_6H_5)_2P$ C_1	$(C_6H_5)_2P$ C_2	$(C_6H_5)_2P$ C_3	$(C_6H_5)_2P$ C_4	Ref
HO-C_6H_4-PPh_2	157.4	116.4 (8)	136.5 (21.5)	128.5 (8)	138.2 (9)	134.1 (19)	129.1 (10.5)	129	8
N_3P_3(O-C_6H_4-PPh_2)$_6$	151.6	121.8 (broad)	135.7 (20.5)	134.6 (12)	137.6 (11)	134.2 (19.5)	129.2 (7)	129.5	8
N_3P_3(O-C_6H_4-$PPh_2W(CO)_6$)$_6$	152.4	121.4 (10)	135 (13)	132.7 (34)	136 (40)	133.5 (12)	129.4 (10)	131.2	8
HO-C_6H_4-$PPh_2Mn(CO)_2$ (η^5-C_5H_4Me) (**1**)	157.3	115.8 (9)	135.6 (11)	129.3 (not seen)	139.4 (40)	133.2 (9)	128.7 (7.5)	129.9	This work
N_3P_3(O-C_6H_4-PPh_2-$Mn(CO)_2(\eta^5$-$C_5H_4Me)$)$_6$ (**2**)	151.8	121 (8)	135 (11.5)	135.9 (40)	138.7 (40)	133.3 (10.5)	128.8 (9)	130.1	This work
$N_3P_3(O_2C_{12}H_8)_2$(O-C_6H_4-PPh_2-$Mn(CO)_2(\eta^5$-$C_5H_4Me)$)$_2$ (**3**)	152.1	121.4	135.1 (11.5)	136.5 (40.5)	138.9 (40.5)	133.4 (10.5)	128.8 (9)	130.1	This work
{[NP($O_2C_{12}H_8$)]$_{0.65}$ [NP (O-C_6H_4-PPh_2]$_{0.35}$ }$_n$	152	121.7 (broad)	135.2 (19)	(hidden)	138 (broad)	134.1 (19)	129 (broad)	129 (broad)	8
{[NP($O_2C_{12}H_8$)]$_{0.65}$ [NP ((O-C_6H_4-PPh_2-$W(O)_5$)$_2$]$_{0.35}$ }$_n$	152	121 (broad)	134 (broad)	(hidden)	136 (broad)	133. (broad)	129	131 (broad)	8
{[NP($O_2C_{12}H_8$)]$_{0.6}$[NP ((O-$C_6H_4PPh_2$-$Mn(CO)_2(\eta^5$-$C_5H_4Me)$)$_2$]$_{0.4}$ }$_n$ (**4**)	153	121	134 (broad)	(hidden)	139 (broad)	133 (broad)	129 (broad)	130 (broad)	This work

[a] δ in ppm, J in Hz, $CDCl_3$ as solvent.

under the intense signals of the C3 and C4 of the $P(C_6H_5)_2$ groups (see Table 1). The ^{13}C NMR spectra of polymer **4** also confirmed the presence of PTHF (71.3, 27.2 ppm).

The thermal stability of the polymeric complex **4**, as measured by TGA at a heating rate of 10 °C min^{-1}, was only moderate. Surprisingly, the initial loss of weigh below 150[a]C expected for the depolymerization of PTHF (6%) and evaporation of the resulting THF, was reduced to 1.25% between 0 and 250 °C. A first important loss (22%) was centered at 350 °C, followed by another one of 36% at 450 °C. At 800 °C the residue was of the order of 41%. The loss of 350 °C is probably due to the volatilisation of organic molecules arising from the organometallic ligands, while the loss at higher temperature correspond to the formation of volatiles after the decomposition of the aryloxypolyphosphazene units to give a crosslinked pyrolitic residue [22].

The DSC curve for **4**, scanned from −50 to 250 °C, showed a clear heat capacity jump corresponding to a glass transition with $T_g = 128$ °C ($\Delta C_p = 0.16$ J g^{-1} K^{-1}). This T_g is higher than that of the free phosphine polymer [{NP($O_2C_{12}H_8$)}$_{0.6}${NP[$OC_6H_4PPh_2$]$_2$}$_{0.4}$·0.7[OC_4H_8]$_n$ ($M_w = 800.000$, $T_g = 96$ °C), made by the same method [14], a difference due to the presence of voluminous transition metal-ligand fragments in **4** [23–25] (for the similar phosphine polymer with higher M_w the value is 115 °C, and for its $W(CO)_5$ complex is 127 °C [8]).

Acknowledgements

We are grateful to the DGICYT (Project PB-1997-1276), CSIC(Project 2001Cl0008), and to the FONDECYT (Projects 7000672 and 1000672) for financial support.

References

[1] F. Ciardelli, E. Tsuchida, D. Wöhrle, Macromolecule—Metal Complexes, Springer, Berlin, 1996.
[2] P.E. Garrou, B.C. Gates, in: D.C. Sherrington, P. Hodge (Eds.), Syntheses and Separations using Functional Polymers (chapter 3), Wiley, New York, 1988, p. 123.
[3] C.U. Pittman, Jr., in: G. Wilkinson, F.G.A. Stone, E.W. Abel (Eds.), Comprehensive Organometallic Chemistry, vol. 8 (chapter 55), Pergamon, London, 1982, p. 553.
[4] J.E. Sheats, C.E. Carraher, Jr., C.U. Pittman, Jr., M. Zeldin, B. Currell (Eds.), Inorganic and Metal-Containing Polymeric Materials, Plenum, New York, 1990.
[5] H.R. Allcock, J.L. Desorcie, G.H. Riding, Polyhedron 6 (1987) 119.
[6] H.R. Allcock, I. Manners, M.N. Mang, M. Parvez, Inorg. Chem. 29 (1990) 522.
[7] R.A. Dubois, P.E. Garrou, K.D. Lavin, H.R. Allcock, Organometallics 5 (1986) 460.
[8] G.A. Carriedo, F.J. García Alonso, P.A. González, P. Gómez Elipe, Polyhedron 18 (1999) 2853.
[9] G.A. Carriedo, F.J. García Alonso, J.L. García Alvarez, C. Díaz Valenzuela, N. Yutronic Sáez, Polyhedron 21 (2002) 2587.
[10] G.A. Carriedo, F.J. García Alonso, P.A. González, Macromol. Rapid Commun. 18 (1997) 371.

[11] G.A. Carriedo, L. Fernández-Catuxo, F.J. García Alonso, P. Gómez Elipe, P.A. González, Macromolecules 29 (1996) 5320.
[12] H.R. Allcock, K.D. Lavin, N.M. Tollefson, T.L. Evans, Organometalics. 2 (1983) 267.
[13] G.A. Carriedo, F.J. García Alonso, P. Gómez Elipe, P.A. González, C. Marco, M.A. Gómez, G. Ellis, J. Appl. Polym. Sci. 77 (2000) 568.
[14] G.A. Carriedo, F.J. García Alonso, P.A. González, A. Presa, work in preparation.
[15] D.M. Adams, A. Squire, J. Organomet. Chem. 63 (1973) 381.
[16] L.J. Bellamy, The Infrared Spectra of Complex Molecules, vol. 1, Chapman and Hall, London, 1975, p. 358.
[17] G.A. Carriedo, F.J. García-Alonso, P.A. González, J.R. Menéndez, J. Raman Spectr. 29 (1998) 327.
[18] G.A. Carriedo, L. Fernández-Catuxo, F.J. García Alonso, P. Gómez Elipe, J. Organomet. Chem. 503 (1995) 59.
[19] G.A. Carriedo, P. Gómez Elipe, F.J. García Alonso, L. Fernández-Catuxo, M.R. Díaz, S. García Granda, J. Organomet. Chem. 498 (1995) 207.
[20] G.A. Carriedo, F.J. García Alonso, J.L. García, R.J. Carbajo, F. López Ortiz, Eur. J. Inorg. Chem. (1999) 1015.
[21] G.A. Carriedo, J.I. Fidalgo-Martínez, F.J. García Alonso, E. Rodicio González, A. Presa Soto, Eur. J. Inorg. Chem. (2002) 1502.
[22] H.R. Allcock, G.S. McDonnell, G.H. Riding, I. Manners, Chem. Mater. 2 (1990) 425.
[23] H.R. Allcock, J.T. Connolly, S. Sisco, S. Al-Shali, Macromolecules 21 (1988) 323.
[24] H.R. Allcock, A.A. Dembek, E.H. Klingenberg, Macromolecules 24 (1991) 5208.
[25] A.L. Crumbliss, D. Coobe, J. Castillo, P. Wisian-Neilson, Inorg. Chem. 32 (1993) 6088.
[26] A.N. Mujumdar, S.G. Young, R.L. Merker, J.H. Magill, Macromolecules 23 (1990) 14.

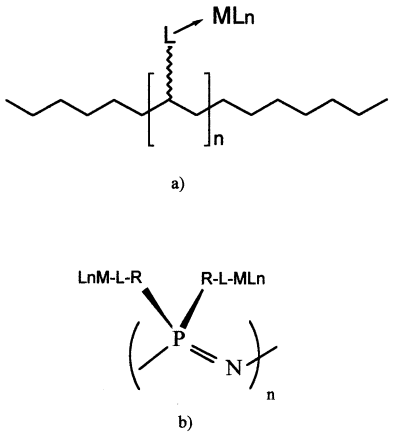


Chart 1.

The 2,2′-dihydroxybiphenyl, HO–C_6H_4–C_6H_4–OH, the 4-hydroxypyridine HOC_5H_4N and the *N*-methyl-piyrrolidinone (NMP) were used as purchased (Aldrich). The hexachlorocyclotriphosphazene $[N_3P_3Cl_6]$ (Fluka) was purified from hot petroleum ether and dried in vacuum. The starting polymer $[NPCl_2]_n$ was prepared as described by Magill and coworkers [11]. The complex $[W(HOMe)(CO)_5]$ was prepared as described in the literature [12]. All the reactions were carried out under dry nitrogen.

The IR spectra were recorded with a Perkin–Elmer Paragon 1000 spectrometer. wavenumbers are in cm^{-1}. NMR spectra were recorded on Bruker AC-200, AC-300 and DPX-300 instruments. ^1H and $^{13}C\{^1H\}$ NMR are given in δ relative to TMS. $^{31}P\{^1H\}$ NMR are given in δ relative to external 85% aqueous H_3PO_4. Coupling constants are in Hz. C, H, N analyses were performed with a Perkin–Elmer 240 microanalyzer. Cl analyses were performed by Galbraith Laboratories. GPC were measured with a Perkin–Elmer equipment with a model LC 250 pump, a model LC 290 UV, and a model LC 30 refractive index detector. The samples were eluted with a 0.1% by weight solution of tetra-*n*-butylammonium bromide in THF through Perkin–Elmer PLGel (Guard, 10^5, 10^4 and 10^3 Å) at 30 °C. Approximate molecular weight calibration was obtained using narrow molecular weight distribution polystyrene standards. T_g values were measured with a Mettler DSC 300 differential scanning calorimeter equipped with a TA 1100 computer. Thermal gravimetric analysis were performed on a Mettler TA 4000 instrument. The polymer samples were heated at a rate of 10 °C min^{-1} from ambient temperature to 800 °C under constant flow of nitrogen.

2.2. Synthesis of $\{[NP(O_2C_{12}H_8)]_{0.7}[NP(OC_5H_4N)_2]_{0.3}\}_n$ (**2**)

To a solution of $[NPCl_2]_n$ (3.2 g, 27.6 mmol) in THF (95 ml), HO–C_6H_4–C_6H_4–OH (3.43 g, 18.4 mmol), K_2CO_3 (15.26 g, 110.6 mmol) and more THF (150 ml) were added and the mixture was refluxed and mechanically stirred for 12 h. The ^{31}P NMR of the mixture showed two groups of signals, one at −6.2 ppm ($[NP(O_2C_{12}H_8)]$, approximately 73%), and other at −23.3 ($NPCl_2$, approximately 27%). To the mixture, HOC_5H_4N (1.77 g, 18.6 mmol) and more THF (50 ml) was added, and the refluxing with stirring was continued for another 74 h. The mixture was poured into water (1.5 l) and the precipitate was washed with more water and dissolved in THF (300 ml). The resulting solution was concentrated until viscous and poured dropwise into water (1.5 l) with stirring. The precipitated product was purified twice by dissolving it in THF, concentrating the solution, and precipitating dropwise first into isopropanol, and finally into petroleum ether. The resulting lentil-shaped white powder was dried at 70 °C in the vacuum for 7 days. Yield: 3.7 g (58.1%).

$(C_{11.4}H_8N_{1.6}O_2P)_n$ (230.23)$_n$: *Anal.* Calc.: C, 59.4; H, 3.50; N, 9.73; Found: C, 57.4; H, 3.56; N, 8.70. Chlorine content $< 0.5\%$.

IR (KBr): 3060 (m, νCH, $O_2C_{12}H_8$), 3029 (m, νCH, OC_5H_4N), 2940w, 2862w (νCH, PTHF); 1635m, 1582vs, 1500s (νCC, νCN, OC_5H_4N), 1477(s, νCC, $O_2C_{12}H_8$); 1244vs, 1190vs (νPN), 1267 (sh, νC–OP), 1095 (s, νP–OC), 923 (vs, br, δPOC), 785 s, 751s, 716m (δCH, $O_2C_{12}H_8$ and δPNP).

$^{31}P\{^1H\}$ NMR ($CDCl_3$): $\delta = -4.32$ [m, $NP(O_2C_{12}H_8)$], −24.12 [m, $NP(OC_5H_4N)_2$]. $^{31}P\{^1H\}$ NMR (NMP/D_2O): $\delta = -5.06$ [m, $NP(O_2C_{12}H_8)$], −24.20 [m, $NP(OC_5H_4N)_2$].

^1H NMR ($CDCl_3$): $\delta = 7.9$ (o-H, OC_5H_4N), 7.27–7.2–6.59 (m, br, $O_2C_{12}H_8$), 3.42, 1.63 (OC_4H_8). ^1H NMR (NMP/D_2O): $\delta = 8.15$ (o-H, OC_5H_4N), 7.48–7.19–6.81 (m, br, $O_2C_{12}H_8$).

$^{13}C\{^1H\}$ NMR ($CDCl_3$): $\delta = 148.1$ (C2), 129.1, 129.0, 128.8 (C1,C6,C4), 125.4 (C5), 121.8 (C3) [$O_2C_{12}H_8$], 157.3 (C4), 150.7 (C2), 115.5 (C3) [OC_5H_4N], 70.5, 26.4 [OC_4H_8]$_n$.

M_w (GPC): 560.000, $M_w/M_n = 7.0$.

TGA: −2% beginning at 75 °C (evaporation of the THF), fast loss centred at 450 °C to give a residue at 800 °C of 42%. Continuing the heating at 800 °C for 20 min gave a final residue of 35.7%.

DSC: $T_g = 174$ °C ($\Delta C_p = 0.10$ J g^{-1} K^{-1}).

2.3. Synthesis of $\{[NP(O_2C_{12}H_8)]_{0.7}[NP(OC_5H_4N-W(CO)_5)_2]_{0.3}\}_n$ (**4**)

A solution of $[W(CO)_6]$ (0.65 g, 1.86 mmol) in MeOH (75 ml) was stirred under UV irradiation until the disappearance of the 1977 cm^{-1} IR absorption (approximately 1 h), to give an orange solution of $[W(HOMe)(CO)_5]$ (IR: 2075w, 1932s, 1887m.,br.). To this solution, another solution of the polymer **2** (0.65 g, 2.83 mmol = 1.7 mmol OC_5H_4N) in CH_2Cl_2 (250 ml)

was added and the mixture was stirred at room temperature for 2.5. The volatiles were evaporated and the resulting solid was washed with C_6H_{14} (4 × 50 ml) and CH_2Cl_2, and dried in vacuum for 24 h to give complex **4** as a yellow solid. Yield: 0.86 g (72%).

$(C_{14.4}H_8N_{1.6}O_5PW_{0.6})_n$ $(424.59)_n$: *Anal.* Calc.: C, 40.7; H, 1.90; N, 5.28. Found: C, 39.5; H, 1.98; N 5.25%.

IR (KBr): 3067 (m, br, νCH, OC_5H_4N, $O_2C_{12}H_8$), 2071w, 1977m, 1925s,br [ν(CO)], 1636m, 1605m, 1500s (νCC, νCN, OC_5H_4N), 1477s (νCC, $O_2C_{12}H_8$); 1246vs, 1193vs (νPN), 1096s (νP–OC), 927vs,br. (δPOC), 785s, 751s, 716m (δCH, $O_2C_{12}H_8$ and δPNP). IR (NMP, solnt.): 2069w, 1973m, 1927s, 1887m.

$^{31}P\{^1H\}$ NMR (NMP/D_2O): $\delta = -3.8$ br [$NP(O_2C_{12}H_8]$, −25.3 vbr [$NP(OC_5H_4N)_2$].

^1H NMR (NMP/D_2O): $\delta = 8.8$–8.4 (m, vbr, *o*-H, OC_5H_4N), 7.5–7.3–6.9 (m, br, $O_2C_{12}H_8$).

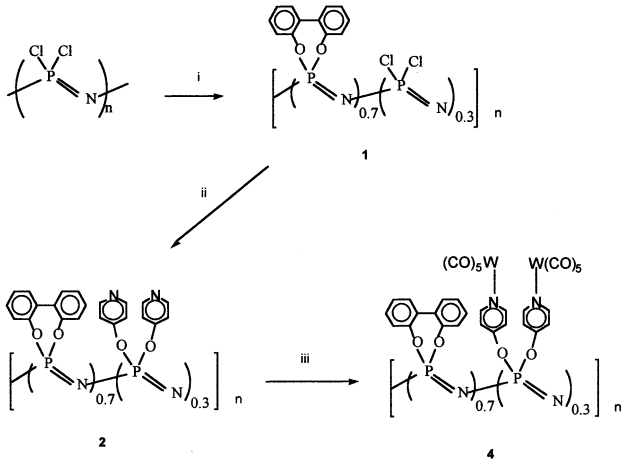
^{13}C $\{^1H\}$ NMR (NMP/D_2O): $\delta = 199.7$, 192.9 [$W(CO)_5$], 149br (C2), 130 vbr (C1,C6,C4), 127br (C5), 123br (C3) [$O_2C_{12}H_8$], 159br (C4), 149br (C2), 118br (C3) [OC_5H_4N], 70.5, 26.4 [OC_4H_8]$_n$.

TGA: continuous loss beginning at 75 °C to give a residue at 800 °C of 72.2% that decreased to 71% after 20 min at this temperature.

DSC: No glass transition detected below 250 °C.

3. Results and discussion

Using a method earlier described by us [13], the reaction of the parent polydichoro–phosphazene $[NPCl_2]_n$ with 0.7 equiv. of the bifunctional biphenol 2,2′-dihydroxybiphenyl (HO–C_6H_4–C_6H_4–OH) and K_2CO_3 in (THF) gave a solution of the uncrosslinked linear polymer $\{[NP(O_2C_{12}H_8)]_{0.7}[NPCl_2]_{0.3}\}_n$ (**1**) ((i) in Scheme 1). The addition of 4-hydroxypyridine to complete the substitution of the chlorine atoms gave the stable phosphazene copolymer $\{[NP(O_2C_{12}H_8)]_{0.7}$-$[NP(OC_5H_4N)_2]_{0.3}\}_n$ (**2**), that carries pyridine ligands as side groups ((ii) in Scheme 1).



Scheme 1. (i) HO–C_6H_4–C_6H_4–OH/K_2CO_3/THF; (ii) HOC_5H_4N/K_2CO_3/THF; (iii) [W(HOMe)$(CO)_5$].

The average M_w, as measured by GPC was 560.000 (polydispersity ratio of 7.0), which is smaller that those found for other analogous polyspirophosphazene copolymers [13] suggesting some degree of chain degradation during the substitution step with the hydroxypyridine.

All the analytical and spectroscopic data for (**2**) were in accord with its formulation. First of all, the IR spectrum (cm^{-1}) in KBr (Fig. 1 and Section 2) showed, the signals for the CH stretching vibrations at 3060m ($O_2C_{12}H_8$ groups) and 3029m (OC_5H_4N ring). Other CH stretching at 2940w, 2862w revealed the presence of some polytetrahydrofuran (PTHF) [14], a product that can be anticipated in some polyphosphazenes obtained from $[NPCl_2]_n$ dissolved in THF [13,14]. The CC and CN stretching frequencies corresponding to the aromatic rings appeared at 1635m, 1582vs and 1500s (OC_5H_4N) and 1477s ($O_2C_{12}H_8$, the other absorption predicted at 1500 is hidden by the strong one of the pyridinoxy group). The expected bands for the poly-p(aryloxy)phosphazene skeleton [15] appeared at 1244vs, 1190vs (νPN), 1267sh (νC–OP), 1095s (νP–OC), 923vs,br (δPOC). The spectrum shows other peaks at 785s, 751s and 716m, that may be assigned to the deformation PNP modes, and also to the expected CH deformation modes for the $O_2C_{12}H_8$ rings [15].

The ^{31}P NMR showed two broad signals, one at −4.32 ppm, corresponding to the cyclic $[NP(O_2C_{12}H_8]$ units, and other at −24.12 ppm, corresponding to the $[NP(OC_5H_4N)_2]$ units. Another weak single peak at −19.18 ppm indicated the presence of a small fraction of $[NPCl(OC_5H_4N)]$ units. The relative intensities showed that the actual formula of the polymer was $\{[NP(O_2C_{12}H_8)]_{0.68}[NP(OC_5H_4N)_2]_{0.3}$ $[NPCl(OC_5H_4N)]_{0.02}\}_n$, which is in accord with the residual chlorine content found (less than 0.5% in weight).

The ^1H NMR spectrum showed the complex pattern expected for the presence of $[NP(O_2C_{12}H_8)]$ and $[NP(OC_5H_4N)]$ groups. Thus, only the doublet (not resolved) of the *ortho*-hydrogens of the AB spin system of the oxypyridines was observed separately (7.9 ppm), the other one (expected at 6.9 ppm) being masked by one of the signals of the dioxy-biphenyl groups. It is interesting to note that the *ortho*-hydrogens of the oxypyridine appear 0.75 ppm to lower field than in the model spyrocyclic compound $[N_3P_3(O_2C_{12}H_8)_2$-$(OC_5H_4N)_2]$ (**3**), previously reported by us [8]. This may be attributed to the fact that the oxypyridines are present in a long polymeric chain. Again the relative intensities of the signals were in accord with the proposed chemical formula.

The ^1H NMR spectrum also showed two multiplets at 3.42 and 1.63 ppm, showing the presence of a small amount of PTHF. Their integration gave a ratio of 0.06

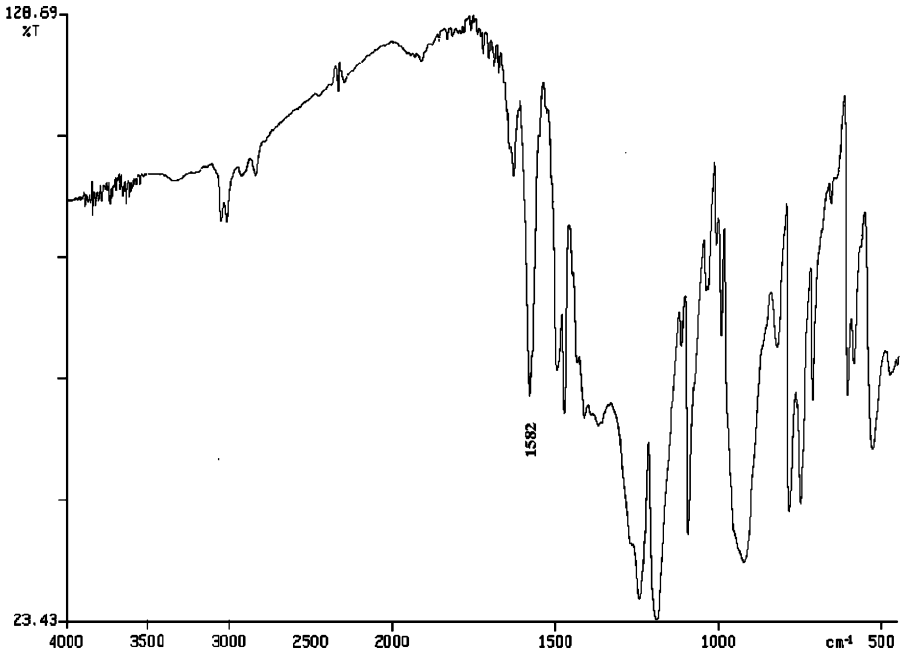


Fig. 1. 4000–500 cm^{-1} IR spectrum of polymer **2** in KBr pellets.

(OC_4H_8) units per formula unit of the polymer (a PTHF content of 1.85% in weight), which is low, as observed in other polyspirophosphazene copolymers prepared by the same experimental procedure [13]. Therefore, the composition of the product (**2**) can be adjusted, without significant error, to the proposed ideal formula $\{[NP(O_2C_{12}H_8)]_{0.7}[NP(OC_5H_4N)_2]_{0.3}\}_n$.

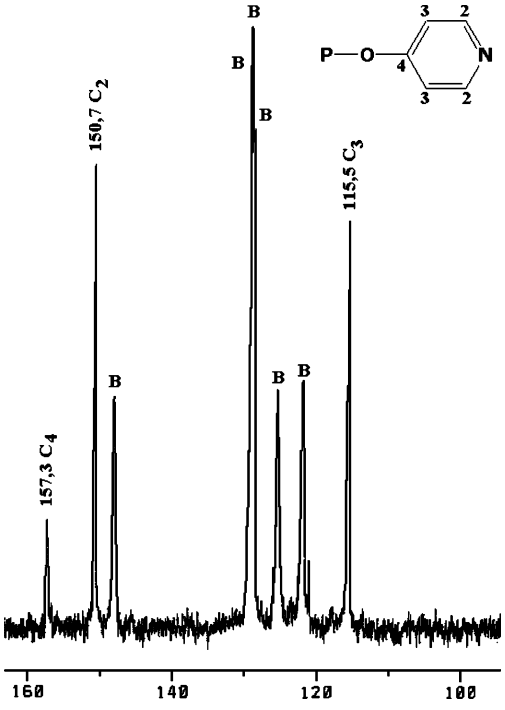


Fig. 2. 200 MHz ^{31}C NMR spectrum ($CDCl_3$ solution) of polymer **2**. B = peaks corresponding to the diphenoxybiphenyl rings (see text).

The ^{13}C NMR of (**2**) (Fig. 2) further confirmed its structure, showing the expected peaks for the dioxybiphenyl rings carbons at 148.1 (C2), 129.1, 129.0, 128.8 (C1,C6,C4), 125.4 (C5) and 121.8 (C3), and those of the OC_5H_4N ring at 157.3 (C4), 150.7 (C2), and 115.5 (C3) ppm (for the free HOC_5H_4N, the peaks appear at 180.0, 139.0 and 117.5 in $CHCl_3$). Other peaks at 70.5 and 26.4 corresponded to the PTHF carbons.

The values observed for the pyridinoxy rings in **2** are consistent with those found for the cyclic triphosphazene $[N_3P_3(OC_5H_4N)_6]$ (157.1, 152.6 and 116.4) [7] and show that the shielding of the C4 carbon of the hydroxypiridine HOC_5H_4N following its transformation into a $NP–OC_5H_4N$ group is rather large (22.7 ppm).

The thermal stability of the polymer was estimated by the TGA curve, that showed a first mass loss of approximately 2% beginning at 75 °C, due to the depolymerization of the PTHF and evaporation of the resulting THF, followed by a fast loss centred at 450 °C. After reaching 800 °C the residue was 42%, but it was further decreased (to 35.7%) after 20 min of heating at 800 °C. The final residue corresponds to the crosslinked pyrolitic material, that, similarly to other polyaryloxyphosphazenes [16], is formed in the decomposition.

The thermal stability allowed an study of the DSC curves from −50 to 250 °C, which showed a well defined glass transition with a $T_g = 174$ °C and a $\Delta C_p = 0.1$ J g^{-1} K^{-1}. This T_g is very high for a polyphosphazene and is consistent with the contribution of the rigid $[NP(O_2C_{12}H_8)]$ units. However, as the value for the homopolymer $[NP(O_2C_{12}H_8)]_n$ is 160 °C [13], it is apparent that the presence of the $[NP(OC_5H_4N)_2]$

units makes a positive contribution to the T_g. This is important in order to design high glass transition temperature polymers, useful in NLO [17].

The presence of the pyridine side groups in (**2**) suggested the possibility of using it as a ligand to coordinate transition metal complexes. In fact, we have previously shown that the model compound (**3**) is able to coordinate $W(CO)_5$ fragments [8].

Therefore, we reacted a CH_2Cl_2 solution of polymer (**2**) with a solution of [W(HOMe)$(CO)_5$] in methanol [ν(CO) absorptions at 2075w, 1932s, 1887m,br] to give the complex $\{[NP(O_2C_{12}H_8)]_{0.7}[NP(OC_5H_4N–W(CO)_5)_2]_{0.3}\}_n$ (**4**) as a yellow solid, that was only sparingly soluble in THF (Scheme 1).

The IR spectrum of the solid in KBr (Fig. 3) clearly evidenced the coordination of the $W(CO)_5$ fragment to the pendant pyridines. Thus, apart from the ν(CO) pentacarbonyl absorptions [8] at 2071vw, 1978m, 1918 vs, br, it was evident the absence of the strong oxypyridine band at 1582 cm^{-1} and the appearance of a new weak band at 1604 cm^{-1}, a fact also noted in the IR spectra of the cyclic model (**3**) and its bis-$W(CO)_5$ complex [8]. We believed that this observation could be very useful in the detection of this coordination in pyridine complexes.

Although the product (**4**) was almost insoluble in THF and CH_2Cl_2, it was very soluble in NMP, to give a deep yellow solution, the IR spectrum of which showed four carbonyl absorptions for the $W(CO)_5$ fragment [18] at 2069vw (A1), 1973w (B2), 1927s,br (E), and 1887m (A1). The ^1H and ^{31}P NMR spectra (see Section 2), and the comparison with those of the parent polymer **2** in the same solvent, are consistent with the coordination of the $W(CO)_5$ fragments to the N atoms of the pendant $–OC_5H_4N$ ligands. Of special significance was the effect on the chemical shift of the *o*-H of the pyridinoxy groups that increased from 8.15 in **2** to 8.8–8.5 in **4**. The broadness of this latter signal is due to the polymeric nature of the complex **4**. This fact is totally consistent with the ^1H NMR spectra of the cyclic model (**3**) and their $W(CO)_5$ complexes. The ^{13}C NMR of **4**, taken in NMP overnight, showed very broad unresolved peaks but also indicated the presence of the $W(CO)_5$ fragments. A signal assigned to the four CO ligands cis to the pyridine appeared at δ 199.7 whereas the CO trans to the pyridine (and trans location making it more sensitive to the heteroligand) gave a signal at δ 193. No ^{183}W satellites could be unambiguously measured.

The solutions of **4** are only moderately stable. Thus, although the polymeric complex can be recovered almost unaffected by dropwise reprecipitation into water of a freshly prepared solution, the metallic content decreases slowly on standing, which is consistent with the behaviour of the analogous cyclic models [8]. In fact, heating for several hours a suspension of **4** in THF in the presence of NCMe or pyridine, and precipitating it into water gave a derivative having much less content of $W(CO)_5$ fragments.

The thermal stability of **4** was low as compared with that of the free polymeric ligand (**2**), decomposing from 75 °C. However, the final residue above 800 °C was very high (70.8%), due to the contribution of the metal (26.0%) that may be involved in the ultimate cross-linking degradation process to form a pyrolitic material. No glass transition could be identified in the DSC curves in the range −50 to 250 °C (a larger interval would be

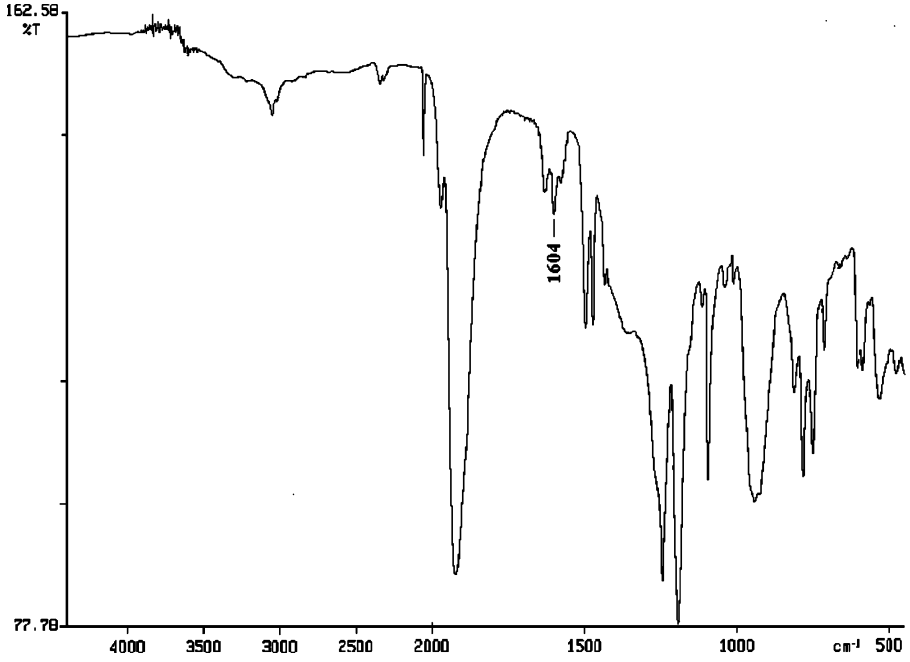


Fig. 3. 4000–500 cm^{-1} IR spectrum of polymer **4** in KBr pellets.

influenced by the decomposition of the copolymer), which could indicate a T_g higher that 250 °C, as expected by the presence of a transition metal [19–21].

Acknowledgements

We are grateful to the CSIC (Project 2001Cl0008), and to the FONDECYT (Projects 7000672 and 1000672) for financial support.

References

[1] F. Ciardelli, E. Tsuchida, D. Wöhrle, Macromolecule-Metal Complexes, 1st ed., Springer, Berlin, 1996.
[2] (a) P.E. Garrou, B.C. Gates, in: D.C. Sherrington, P. Hodge (Eds.), Polymer Bound Transition Metal Complex Catalysts, Synthesis and Separation using Functional Polymers, 1st ed. (chapter 3), Wiley, New York, 1988, p. 123 ff;
(b) C.U. Pittman, Jr., in: G. Wilkinson, F.G.A. Stone, E.W. Abel (Eds.), Polymer Supported Catalysts Comprehensive Organometallic Chemistry, vol. 8, 1st ed. (chapter 55), Pergamon, London, 1982, p. 553 ff.
[3] H.R. Allcock, J.L. Desorcie, G.H. Riding, Polyhedron 6 (1987) 119.
[4] G.A. Carriedo, F.J. García Alonso, P.A. González, P. Gómez Elipe, Polyhedron 18 (1999) 2853 (and references therein).
[5] U. Diefenbach, H.R. Allcock, Inorg. Chem. 33 (1994) 4562.
[6] V. Chandrasekhar, S. Nagendran, Chem. Soc. Rev. 30 (2001) 193.
[7] G.A. Carriedo, P. Gómez Elipe, F.J. García Alonso, L. Fernández-Catuxo, M.R. Díaz, S. García Granda, J. Organomet. Chem. 498 (1995) 207.
[8] G.A. Carriedo, F.J. García Alonso, J.L. García, R.J. Carbajo, F. López Ortiz, Eur. J. Inorg. Chem. (1999) 1015.
[9] P.G. Lacroix, W. Lin, G.K. Wong, Chem. Mater. 7 (1995) 1293.
[10] H.R. Allcock, C.J. Nelson, W.D. Coggio, Chem. Mater. 6 (1994) 516.
[11] A.N. Mujumdar, S.G. Young, R.L. Merker, J.H. Magill, Macromolecules 23 (1990) 14.
[12] D.J. Darensbourg, C.J. Bishoff, J.H. Reibenspies, Inorg. Chem. 30 (1991) 1144.
[13] G.A. Carriedo, L. Fernández Catuxo, F.J. García Alonso, P. Gómez Elipe, P.A. González, Macromolecules 29 (1996) 5320.
[14] G.A. Carriedo, F.J. García Alonso, P. Gómez Elipe, P.A. González, C. Marco, M.A. Gómez, G. Ellis, J. Appl. Polym. Sci. 77 (2000) 568.
[15] G.A. Carriedo, F.J. García Alonso, P.A. González, J.R. Menéndez, J. Raman Spect. 29 (1998) 327.
[16] H.R. Allcock, G.S. McDonnell, G.H. Riding, I. Manners, Chem. Mater. 2 (1990) 425.
[17] G. Rojo, G. Martin, F. Agulló López, G.A. Carriedo, F.J. García Alonso, J.I. Fidalgo Martinez, Chem. Mater. 12 (2000) 3603.
[18] R.J. Angelici, M.D. Malone, Inorg. Chem. 6 (1967) 1731.
[19] H.R. Allcock, J.T. Connolly, S. Sisco, S. Al-Shali, Macromolecules 21 (1988) 323.
[20] H.R. Allcock, A.A. Dembek, E.H. Klingenberg, Macromolecules 24 (1991) 5208.
[21] A.L. Crumbliss, D. Coobe, J. Castillo, P. Wisian-Neilson, Inorg. Chem. 32 (1993) 6088.

2.1. Synthesis of compounds

The ligand was obtained from *N*-methylisatin and thiosemicarbazide (1:1 molar ratio) in EtOH–water as previously reported for other thiosemicarbazones [6]. M.p. 257 °C. *Anal.* Found: C, 51.3; H, 4.1; N, 23.3; S, 13.4. Calc. for $C_{10}H_{10}N_4OS$: C, 51.3; H, 4.3; N, 23.9; S, 13.7%. Mass spectrum (*m*/*z*, 235 (M^+, 50%), 218 (M^+-NH_2, 30), 176 (M^+-NH_2-CS, 35), 79 (C_4NO, 100). ν_{max}/cm^{-1} (KBr): 3426s, 3247m,br, 3150m (NH_2+NH); 1676s (C=O); 1607s,br (C=N); 832m (C=S). NMR data (see Fig. 1 for numbering scheme): ^1H: δ[N(2)H] 12.39 s(1); δ[N(1)H_2] 9.05 s(1), 8.70 s(1); δ[C(4)H] 7.68d(1); δ[C(5)H] 7.44 t(1); δ[C(6,7)H] 7.15 m(2); δ[C(10)H_3] 3.21 s(3); ^{13}C: δ[C(1)] 178.7, δ[C(9)] 160.7, δ[C(8)] 143.6, δ[C(2)] 131.2, δ[C(6)] 130.9, δ[C(5)] 122.9, δ[C(4)] 120.6, δ[C(3)] 119.3, δ[C(7)] 109.8, δ[C(10)] 25.7 ppm.

All complexes were prepared by the following general procedure: a hot EtOH solution of the ligand was added to the chlorides (1:1 molar ratio) or acetates (1:2 molar ratio) of Cu(II), Ni(II), Co(II) dissolved in EtOH. The solution was refluxed for 3–6 h and after cooling a solid was formed that was isolated and dried under vacuum.

2.1.1. $CuL_2\cdot 2H_2O$

Anal. Found for green solid: C, 41.7; H, 3.4; N, 18.7; S, 11.9. $C_{20}H_{22}CuN_8O_3S_2$ requires: C, 42.4; H, 3.9; N, 19.7; S, 11.3%, m.p. 202 °C. ν_{max}/cm^{-1} (KBr): 3418m,vbr, 3287m,vbr, 3165w,br (NH_2+NH); 1688m (C=O); 1655m,br, 1608s,br (C=N); 779m (C=S).

2.1.2. CuClL

Anal. Found: C, 36.2; H, 2.6; N, 15.7; S, 9.7. $C_{10}H_9ClCuN_4OS$ requires: C, 36.1; H, 2.7; N, 16.9; S, 9.6%, m.p. 187 °C. ν_{max}/cm^{-1} (KBr): 3398m,br, 3289m, 3167w (NH_2+NH); 1658m (C=O); 1627w, 1604s (C=N); 778m (C=S).

In the mother liquor brown crystals suitable for X-ray studies were isolated and the structural analysis revealed that the complex shows a polymeric nature corresponding to the formula $[CuClL]_n$ (**1**).

2.1.3. NiL_2

Anal. Found: C, 45.3; H, 3.3; N, 20.6; S, 12.5. Calc. for $C_{20}H_{18}N_8NiO_2S_2$: C, 45.7; H, 3.4; N, 21.3; S, 12.2%, m.p. >300 °C. ν_{max}/cm^{-1} (KBr): 3428w, 3320m,br, 3171vw (NH_2+NH); 1654m (C=O); 1609s (C=N); 772m (C=S).

The same complex was obtained as a garnet powder both starting from the chloride and from the acetate. When the garnet solid was dissolved in *N*,*N*′-dimethylformamide, after several days, a crystalline product of formula $[NiL_2]$ (**2**) was isolated.

2.1.4. CoL_2

Anal. Found for garnet solid: C, 45.3; H, 3.3; N, 20.4; S, 12.8. Calc. for $C_{20}H_{20}CoN_8O_2S_2$: C, 45.7; H, 3.4; N, 21.3; S, 12.2%, m.p. >300 °C. ν_{max}/cm^{-1} (KBr): 3432m, 3264m,vbr, 3167w (NH_2+NH); 1658sh(C=O); 1643s, 1607s,br (C=N); 781m (C=S).

2.1.5. $CoClL\cdot 0.5H_2O$

Anal. Found for garnet solid: C, 36.4; H, 3.3; N, 17.0; S, 10.1. Calc. for $C_{10}H_{10}ClCoN_4O_{1.5}S$: C, 35.7; H, 3.0; N, 16.6; S, 9.5%, m.p. 248 °C. ν_{max}/cm^{-1} (KBr): 3363m,vbr, 3270m, 3057w (NH_2+NH); 1639s (C=O); 1605sh, 1590s (C=N); 774m (C=S). When the mother liquor was slowly evaporated in the air, it afforded few red crystals that were suitable for X-ray diffraction studies and later identified as $[CoL_2]_2[CoCl_4]\cdot 2EtOH$ (**3**).

2.2. X-ray crystallography

The crystal and instrumental parameters used in the unit-cell determination and data collection for all three compounds are summarized in Table 1. The intensity data were collected with a Siemens AED, on a Philips and with a CAD4 single-crystal diffractometer for compounds **1**, **2** and **3**, respectively using the $\theta-2\theta$ scan technique. Data were corrected for Lp, but no correction for absorption was applied. The structures of **1** and **2** were solved using SIR-92 [7a] and structure of **3** using SIR-97 [7b]. Refinements were carried out by full-matrix least-squares using the SHELXL-97 [8] program. All non-hydrogen atoms were refined anisotropically. The hydrogen atoms, located on a difference map, were refined isotropically only for complex **2**. In complex **1** and **3**, the poor data quality has limited the accuracy of the refinement. Several crystals were used in the attempt to improve the accuracy of the results, but all sets of data suffered from the same problems. The hydrogen atoms were placed in calculated positions 'riding' on their C atoms; in **1** only the aminic nitrogen hydrogens were located on a difference map. All atomic scattering factors were taken from Ref. [9]. All calculations were performed on an ENCORE 91 computer at the Centro di Studio per la Strutturistica Diffrattometrica del CNR (Parma). Molecular geometry calculations were carried out by using the computer program PARST [10] and the structure drawings by using the ORTEP [11] and PLUTO [12] programs.

3. Results and discussion

The coordinating properties of 1-methylisatin 3-thiosemicarbazone (HL) have been investigated towards cobalt, nickel and copper ions in presence of chloride or acetate anions. All the complexes were isolated as solid products and with high yield, performing the reaction at

Table 1
Experimental data for crystallographic analyses

Compound	(1)	(2)	(3)
Empirical formula	$C_{10}H_9ClCuN_4OS$	$C_{20}H_{18}N_8NiO_2S_2$	$C_{44}H_{48}Cl_4Co_3N_{16}O_6S_4$
Molecular weight	334.28	525.24	1343.82
λ (Å)	1.54178	0.71069	1.54178
Space group	$P2_1/n$	$C2/c$	$C2/c$
a (Å)	8.721(3)	14.927(4)	13.573(3)
b (Å)	7.688(2)	8.483(3)	24.325(4)
c (Å)	18.184(5)	19.301(5)	16.712(3)
β (°)	91.01(2)	117.51(5)	99.84(1)
V (Å^3)	1219.0(6)	2168(1)	5436(2)
Z	4	4	4
F (000)	676	1080	2740
D_{calc} (Mg m^{-3})	1.82	1.61	1.64
μ (mm^{-1})	6.10	11.25	10.86
Radiation	Cu Kα	Mo Kα	Cu Kα
θ Range (°)	3–70	3–30	3–70
Index ranges	$-10 \le h \le 10$; $0 \le k \le 9$; $0 \le l \le 22$	$-20 \le h \le 18$; $0 \le k \le 11$; $0 \le l \le 27$	$-15 \le h \le 15$, $0 \le k \le 27$, $0 \le l \le 18$
Crystal size (mm)	0.61 × 0.51 × 0.23	0.94 × 0.23 × 0.05	0.41 × 0.23 × 0.24
Measured reflections	2563	6848	8363
Unique reflections	689	3141	3927
Refined parameters	300	245	350
Max and min height in final ΔF map (e Å^{-3})	2.04–0.91	1.05–1.10	0.62–0.83
$R = \Sigma \|\|F_o\| - \|F_c\|\|/\Sigma\|F_o\|$	0.0890 [a]	0.0656 [a]	0.0914 [a]
wR	0.3302	0.1988	0.2987
Weights	$1/[\sigma^2(F_o^2)+(0.1033P)^2+0.31P]$	$1/[\sigma^2(F_o^2)+(0.1971P)^2+0.0P]$	$1/[\sigma^2(F_o^2)+(0.1371P)^2+0.0P]$

$P = (\max(F_o^2, 0)+2F_c^2)/3$.
[a] The data were corrected for absorption following Sheldrick's method [8].

room temperature; they are soluble in dmso and dmf, but insoluble in water and common organic solvents, except for CuClL and CoClL, which are soluble in EtOH. The analytical data show different stoichiometries, mainly influenced by the nature of the inorganic anion. In fact all the metal acetates give complexes of formula ML_2 in spite of the molar ratio M:L, while using the metal chlorides, with the exception of the nickel derivative, the formula $MClL \cdot xH_2O$ is found.

3.1. Description of the structures

The molecular structure of complex $[CuClL]_n$ (**1**) is shown in Fig. 1. The copper atom presents a penta-coordination (square-pyramidal). The SNO terdentate ligand and a chlorine atom constitute the square base, while a sulphur atom belonging to a molecule in the $1/2-x, y-1/2, 1/2-z$ position occupies the axial site, Cu–S′ = 2.825(8) Å. In this way sulphur-bridged polymeric chains are formed along the y axis (Fig. 2), joined through longer interactions [Cu···C6 $(-x, 1-y, -z) = 3.26$ Å] and these generate sheets of polyhedra parallel to the (1 0 −1) planes. This last weak contact completes the copper coordination to a very elongated square-bipyramid. The pyramid basal plane shows a slight tetrahedral distortion and the copper atom lies 0.18 Å out of the same plane towards the S′ atom. The angles formed by Cu–S′ and Cu–C6 lines and the normal to the coordination plane are 12.3° and 0.85°, respectively. In the basal plane the Cu–S, Cu–N and Cu–Cl bond distances (Table 2) agree well with those found in other copper(II) complexes with thiosemicarbazones; the Cu–O(carbonyl) [2.21(1) Å] is longer than Cu–O (carboxylate) [13] or Cu–O (phenol) [14] where a negative charge is present which probably determines the observed bond shortening. In comparison with other Cu–O (carbonyl) distances reported in literature [15] this fairly long distance is probably mainly imposed by the rigidity of the ligand backbone which affects the geometry of the chelation ring. The endocyclic angle C9–C2–N3 in the five-membered chelation ring Cu–

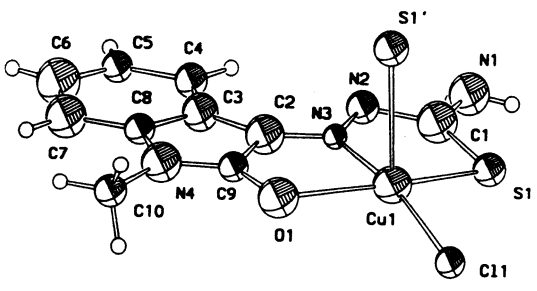


Fig. 1. Perspective view of the copper complex [CuClL] in **1**.

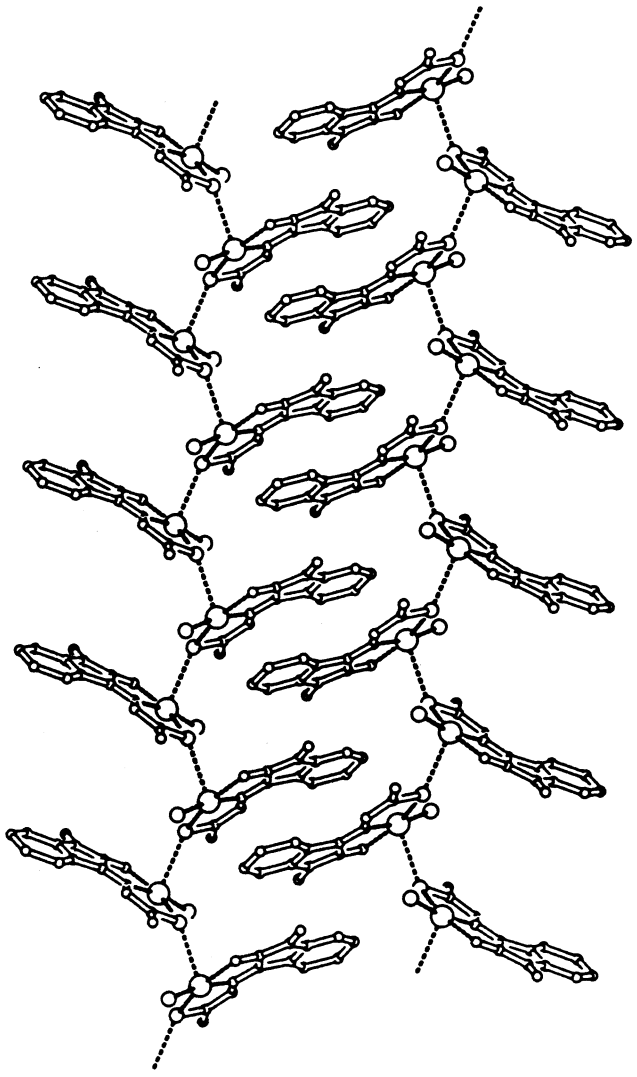


Fig. 2. Polymeric chains of sulfur bridged complexes along the y-axis in compound **1**.

N3–C2–C9–O1 is 119(2)°, while in uncoordinated isatin thiosemicarbazones the corresponding value is larger [128.3(4)°, 127.2(4)°, 127.6(4)° in Ref. [16] and 127.1(4)° in Ref. [17]. The two five-membered chelate rings are nearly planar and the dihedral angle between the mean planes is 7.0(3)°.

In the packing hydrogen bonds N1···Cl ($1/2-x$, $1/2+y$, $1/2-z$) = 3.33(2) Å and N1···Cl ($x-1$, y, z) = 3.43(2) Å link the layers of polyhedra. Weak charge transfer interactions are present between the aromatic rings (C4···C9 ($-x$, $1-y$, $-z$) = 3.36(3) Å, C3···C3 ($-x$, $1-y$, $-z$) = 3.53(3) Å).

The crystal structure of compound [NiL_2] (**2**) is shown in Fig. 3. The nickel atom lies on a crystallographic twofold axis and the two ligands, symmetrically related, are coordinated by the metal via the sulphur, the nitrogen from the hydrazine chain and the carbonyl oxygen of the isatin moiety in a distorted octahedral

Table 2
Selected bond distances (Å) and angles (°) for compound **1**

Bond distances			
Cu1–Cl1	2.197(6)	N4–C8	1.38(3)
Cu1–S1	2.266(7)	N4–C9	1.33(3)
Cu1–S1′	2.825(8)	N4–C10	1.45(3)
Cu1–O1	2.217(15)	C2–C3	1.46(3)
Cu1–N3	1.941(14)	C2–C9	1.49(3)
S1–C1	1.73(3)	C3–C4	1.36(3)
O1–C9	1.29(3)	C3–C8	1.39(3)
N1–C1	1.35(4)	C4–C5	1.43(3)
N2–N3	1.32(2)	C5–C6	1.36(3)
N2–C1	1.33(3)	C6–C7	1.43(4)
N3–C2	1.27(3)	C7–C8	1.40(3)
Bond angles			
Cl1–Cu1–S1	97.6(2)	S1–Cu1–O1	163.2(5)
Cl1–Cu1–S1′	98.1(2)	S1–Cu1–N3	83.0(5)
Cl1–Cu1–O1	96.1(5)	S1′–Cu1–O1	81.9(4)
Cl1–Cu1–N3	168.7(5)	S1′–Cu1–N3	92.6(5)
S1–Cu1–S1′	105.6(3)	O1–Cu1–N3	81.7(7)

fashion. The ligands are in a meridional configuration with S and O atoms *cis* to each other and N atoms *trans*. The coordination distances Ni–S = 2.367(2), Ni–N = 2.005(6), Ni–O = 2.264(4) Å (Table 3) are similar to those found in nickel complexes with not methylated

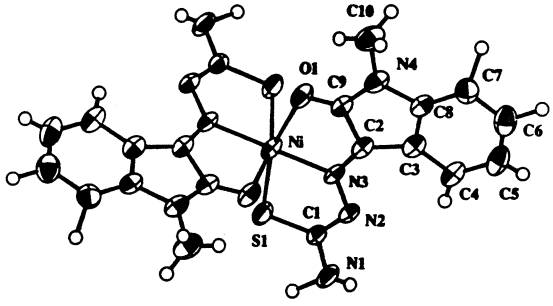


Fig. 3. Molecular structure of [NiL_2] **2**.

Table 3
Selected bond distances (Å) and angles (°) for compound **2**

Bond distances			
Ni–S1	2.367(2)	N4–C9	1.345(7)
Ni–O1	2.264(4)	N4–C10	1.470(9)
Ni–N3	2.005(6)	C2–C9	1.482(8)
S1–C1	1.719(7)	C2–C3	1.442(9)
O1–C9	1.243(8)	C3–C4	1.402(11)
N1–C1	1.331(8)	C3–C8	1.380(7)
N2–N3	1.332(7)	C4–C5	1.369(10)
N2–C1	1.365(7)	C5–C6	1.374(9)
N3–C2	1.320(6)	C6–C7	1.406(12)
N4–C8	1.424(9)	C7–C8	1.379(8)
Bond angles			
S1–Ni–O1	161.9(1)	S1–Ni–S1′	96.5(1)
S1–Ni–N3	81.3(1)	O1–Ni–N3	80.7(2)
S1–Ni–O1′	90.4(1)	S1–Ni–N3′	105.6(1)
O1–Ni–O1′	88.2(1)	O1–Ni–N3′	92.0(2)
N3–Ni–N3′	169.9(2)		

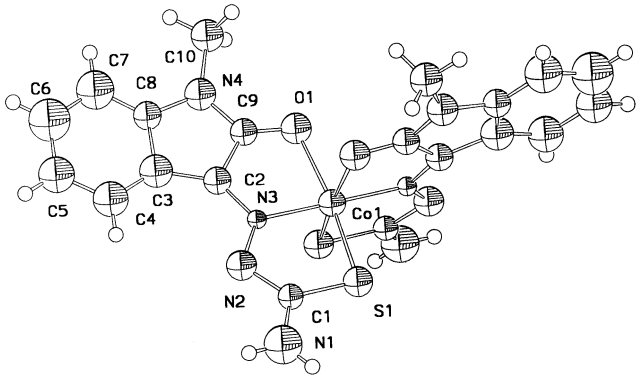


Fig. 4. ORTEP drawing of the $[CoL_2]^+$ cation.

isatin and acenaphthenequinone thiosemicarbazones [2,18]. Also in this complex the Ni–O bond is particularly long in comparison with the sum of the Pauling covalent radii, 2.05 Å. This lengthening is probably caused by the rigidity of the methylisatin moiety which affects the geometry of the chelation ring. In the five-membered chelation ring Ni–N3–C2–C9–O1 the endocyclic angle C9–C2–N3 is 115.6(5)°, similar to that found in Ref. [2].

The pair of five-membered chelate rings are only approximately planar (maximum dev. 0.07 Å), the dihedral angle between them being 3.5(1)°. The Ni–O1–C9–C2–N3 ring assumes an *envelope* conformation (puckering parameters: $q_2 = 0.109(4)$ Å, $\phi_2 = -179(3)°$), while the Ni–N3–N2–C1–S1 one shows a *twist* conformation with a twofold axis passing through the Ni atom [$q_2 = 0.057(4)$ Å, $\phi_2 = -17(5)°$] [19]. The packing is determined by hydrogen bonds involving the aminic nitrogen N1, N1···O1 ($x-1/2$, $y-1/2$, z) = 3.029(8) and N1···N2 ($-x-1/2$, $y-1/2$, $1/2-z$) = 3.197(7) Å.

In the crystals of (**3**) the asymmetric unit contains three cobalt atoms lying on binary axes, and therefore with site occupation factors of 0.5; in two of them the metal atom results to be surrounded by two ligands chelating in a SNO fashion and giving the metal a octahedral coordination (Fig. 4) while the third cobalt is part of a tetrachlorocobaltate(II) anion. The compound is an ionic complex, of formula $[CoL_2]_2[CoCl_4]\cdot 2C_2H_5OH$, formed by $[CoL_2]^+$ cations, $[CoCl_4]^{2-}$ anions and ethanol as crystallization solvent (Fig. 5). As the ligands can undergo a single deprotonation the only combination of oxidation states that can justify the stoichiometry is that the two complexes, that have the 1-methylisatin 3-thiosemicarbazone as a ligand, contain Co(III), while the $[CoCl_4]^{2-}$ unit contains a Co(II). This assignment is corroborated by typical bond lengths Co–S, Co–N and Co–O reported in the literature [15] for Co(III) that differ significantly from those present in analogous compounds of Co(II) (Table 4). The packing (Fig. 5) is determined by a complex network of hydrogen bonds involving the terminal amino groups of both cobalt complexes in the asymmetric unit, two of the chlorides belonging to the $[CoCl_4]^{2-}$ unit and the hydroxyl groups of the ethanol molecules.

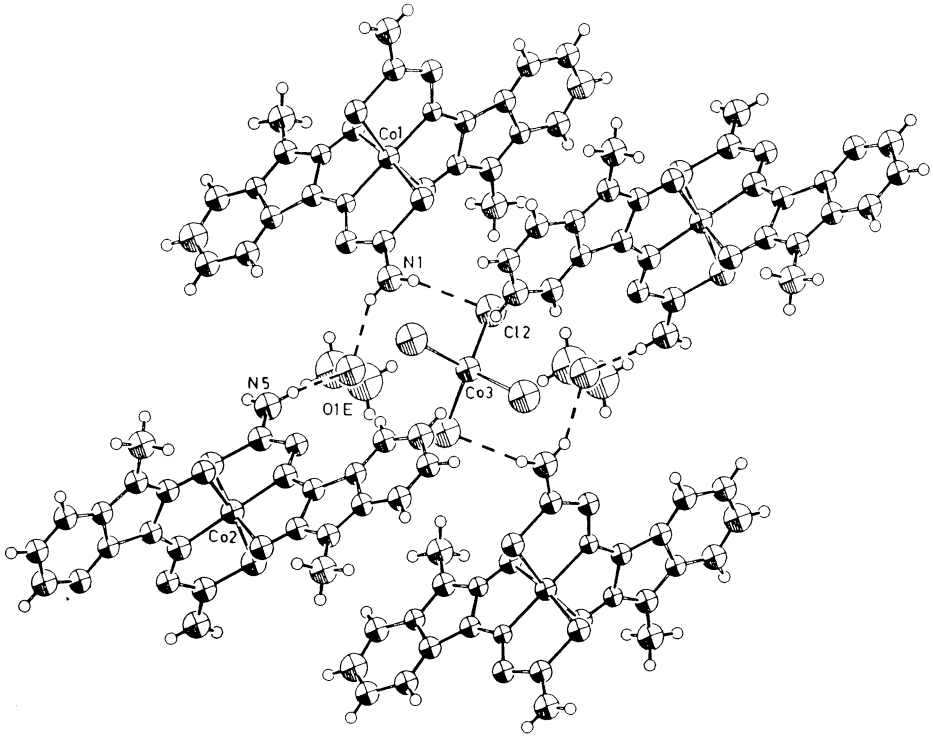


Fig. 5. Hydrogen bonds present between $[CoL_2]^+$ cations, $[CoCl_4]^{2-}$ anions and ethanol in complex **3**.

Table 4
Selected bond distances (Å) and angles (°) for compound **3**

Bond distances			
Co1–S1	2.196(5)	N7–C12	1.39(2)
Co1–O1	2.034(10)	N8–C18	1.39(2)
Co1–N3	1.867(13)	N8–C19	1.35(2)
Co2–S2	2.202(6)	N8–C20	1.47(2)
Co2–O2	2.061(11)	C2–C3	1.44(2)
Co2–N7	1.894(14)	C2–C9	1.46(2)
Co3–Cl1	2.237(6)	C3–C4	1.34(3)
Co3–Cl2	2.280(6)	C3–C8	1.44(2)
S1–C1	1.69(2)	C4–C5	1.37(2)
S2–C11	1.67(2)	C5–C6	1.38(3)
O1–C9	1.23(2)	C6–C7	1.39(3)
O2–C19	1.23(2)	C7–C8	1.34(2)
N1–C1	1.35(2)	C12–C13	1.47(2)
N2–N3	1.39(2)	C12–C19	1.48(3)
N2–C1	1.36(2)	C13–C14	1.37(2)
N3–C2	1.34(2)	C13–C18	1.45(2)
N4–C8	1.40(2)	C14–C15	1.36(3)
N4–C9	1.34(2)	C15–C16	1.40(3)
N4–C10	1.46(2)	C16–C17	1.36(3)
N5–C11	1.36(2)	C17–C18	1.37(2)
N6–N7	1.30(2)	O1E–C1E	1.42(4)
N6–C11	1.39(2)	C1E–C2E	1.48(4)
Bond angles			
S1–Co1–O1	169.8(3)	S2–Co2–N7	82.5(4)
S1–Co1–N3	94.7(4)	O2–Co2–N7	87.6(5)
O1–Co1–N3	94.5(5)	S2–Co2–S2′	91.2(2)
S1–Co1–S1′	95.3(2)	S2–Co2–O2′	91.9(3)
S1–Co1–O1′	90.0(3)	S2–Co2–N7′	96.2(4)
S1–Co1–N3′	85.3(4)	O2–Co2–O2′	86.6(4)
O1–Co1–O1′	86.2(4)	O2–Co2–N7′	93.8(5)
O1–Co1–N3′	85.6(5)	N7–Co2–N7′	178.2(6)
N3–Co1–N3′	179.9(5)	Cl1–Co3–Cl2	103.1(2)
S2–Co2–O2	169.9(3)		

In all three complexes the deprotonated 1-methylisatin 3-thiosemicarbazone moiety adopts the *Z* conformation with respect to the C1–N2 bond to facilitate the coordination to the metal, as already found in other isatin 3-thiosemicarbazone complexes [2,17,20]. An *E* conformation about this bond was instead present in the free ligand isatin 3-thiosemicarbazone [17] and in N(4)-substituted isatin 3-thiosemicarbazones [16].

In nickel complex **2** the bond distances and angles in the thiosemicarbazone and 1-methylisatin moieties (Table 3) are similar to that found in nickel complexes with the not methylated ligand [2], while the greatest difference in comparison with the free isatin-3-thiosemicarbazone [17] can be noticed in C1–S1 bond [1.719(7) vs. 1.663(4) Å] and in N2–N3 bond [1.332(7) vs. 1.356(5) Å]. For the copper and cobalt complexes **1** and **3** as a consequence of the poor data quality we are unable to discuss the ligand bonds in detail. The dihedral angles between the methylisatin and the thiosemicarbazide moieties are 10.1(6)° and 11.2(1)° in complexes **1** and **2**, respectively and 4.6(4)°, 10.0(5)° in the two Co1 and Co2 cation complexes of compound **3**. The six- and five-membered rings of methylisatin moiety are nearly coplanar in all three compounds. The dihedral angles between the mean planes are only 1.7(1)° in **1**, 1.3(2)° in **2** and 1.1(5)°, 0.2(5)° in **3**.

3.2. IR spectra

The infrared spectra of the ligand and the metal complexes are mainly characterized by the vibrational modes of the NH_2, NH, C=O and C=S groups.

The IR spectrum of HL shows three bands at 3426s, 3247m, 3150m cm^{-1} attributed to $\nu(NH_2)$ and $\nu(NH)$; while in the spectra of the complexes the monodeprotonated nature of the ligand justifies the presence of only two absorption bands.

The coordination of the carbonyl oxygen of the isatin moiety is related to the value of the $\nu(CO)$ band in the 1700–1650 cm^{-1} range; the $\nu(CO)$ values in the spectra of $CuL_2{\cdot}2H_2O$ (1688 cm^{-1}) agree well with an uncoordinated carbonyl oxygen; on the contrary the negative shift observed in the spectra of CoL_2 (1658 cm^{-1}), NiL_2 (1654 cm^{-1}), CuClL (1658 cm^{-1}) is consistent with a participation of the carbonyl oxygen in the coordination to the metal. A stronger metal–oxygen interaction seems to be present in the $CoClL{\cdot}0.5H_2O$ complex, since a more negative shift (1639 cm^{-1}) is observed in the spectrum. The attribution of the thioamide band, which has a substantial contribution from the $\nu(C{=}S)$ is at 832 cm^{-1} in the spectrum of the free ligand and shifts to lower energies in the spectra of all the complexes (see Section 2) [5a].

Taking into account the assignments of the vibrational absorptions, the following considerations on the ligand behaviour in the metal complexes can be made:

i) a N, S bidentate ligand behaviour can be proposed in the $CuL_2{\cdot}2H_2O$ with a probable tetracoordination around the metal atom;
ii) an O, N, S tridentate ligand behaviour is suggested in the other complexes.

4. Supplementary data

Crystallographic data (excluding structure factors) for the structure reported in this paper have been deposited with the Cambridge Crystallographic Data Centre, CCDC no. 179029 (**1**), 179030 (**2**) and 179031 (**3**). Copies of the data can be obtained free of charge from The Director, CCDC, 12 Union Road, Cambridge, CB2 1EZ, UK (fax: +44-1223-336033; e-mail: deposit@ccdc.cam.ac.uk or www: http://www.ccdc.cam.ac.uk).

Acknowledgements

M.C.R.A. thanks Xunta de Galicia (Spain) for a grant and Ministero dell'Università e della Ricerca Scientifica e Tecnologica (Murst) of Italy for financial support.

References

[1] S.N. Pandeya, D. Siram, G. Nath, E. DeClercq, Eur. J. Pharm. Sci. 9 (1999) 25 (and references therein).
[2] M.C. Rodríguez-Argüelles, A. Sánchez, M. Belicchi Ferrari, G. Gasparri Fava, C. Pelizzi, G. Pelosi, R. Albertini, P. Lunghi, S. Pinelli, J. Inorg. Biochem. 73 (1999) 7.
[3] R. Boon, Antiviral Chem. Chemother. 8 (1997) 5.
[4] S.N. Pandeya, J.R. Dimmock, Pharmazie 48 (1993) 659.
[5] (a) D.X. West, A.K. El-Sawaf, G.A. Bain, Transition Met. Chem. 23 (1998) 1;
(b) E. Labisbal, A. Sousa, A. Castiñeiras, J.A. García-Vázquez, J. Romero, D.X. West, Polyhedron 19 (2000) 1255;
(c) E. Labisbal, A. Sousa, A. Castiñeiras, J.A. García Vázquez, J. Romero, G.A. Bain, D.X. West, Z. Naturforsch., Teil. B 55 (2000) 162.
[6] F.E. Anderson, C.J. Duca, J.V. Scudi, J. Am. Chem. Soc. 73 (1951) 4967.
[7] (a) A. Altomare, G. Cascarano, C. Giacovazzo, A. Guagliardi, M.C. Burla, G. Polidori, M. Camalli, SIR 92, J. Appl. Cryst. 27 (1994) 435.;
(b) A. Altomare, M.C. Burla, M. Camalli, G.L. Cascarano, C. Giacovazzo, A. Guagliardi, A.G.G. Moliterni, G. Polidori, R. Spagna, SIR97, J. Appl. Cryst. 32 (1999) 115.
[8] G. Sheldrick, SHELXL 97, A Program for Structure Refinement, University of Göttingen, Germany, 1997.
[9] International Tables for X-Ray Crystallography, vol. 4, Kynoch Press, Birmingham, UK, 1974.
[10] M. Nardelli, PARST95, An update to PARST: a system of Fortran routines for calculating molecular structure parameters from the results of crystal structure analyses, J. Appl. Cryst. 28 (1995) 659.
[11] C.K. Johnson, M.N. Burnett, ORTEPIII, Report ORNL-6895, Oak Ridge National Laboratory, TN, USA, 1996.
[12] A.L. Spek, PLATON, A multipurpose crystallographic tool, Utrecht University, Utrecht, NL, 1999.
[13] M. Belicchi Ferrari, G. Gasparri Fava, P. Tarasconi, C. Pelizzi, J. Chem. Soc., Dalton Trans. (1989) 361.
[14] M. Belicchi Ferrari, G. Gasparri Fava, P. Tarasconi, R. Albertini, S. Pinelli, R. Starcich, J. Inorg. Biochem. 53 (1994) 13.
[15] F.H. Allen, O. Kennard, Chemical Des. Automation News 8 (1993) 31.
[16] G.A. Bain, D.X. West, J. Krejci, J. Valdés-Martinez, S. Hernandez-Ortega, R.A. Toscano, Polyhedron 16 (1997) 855.
[17] J.S. Casas, A. Castiñeiras, M.C. Rodríguez-Argüelles, A. Sánchez, J. Sordo, A. Vázquez-López, E.M. Vázquez-López, J. Chem. Soc., Dalton Trans. (2000) 4056.
[18] M.C. Rodríguez-Argüelles, M. Belicchi Ferrari, G. Gasparri Fava, C. Pelizzi, G. Pelosi, R. Albertini, A. Bonati, P.P. Dall'Aglio, P. Lunghi, S. Pinelli, J. Inorg. Biochem. 66 (1997) 7.
[19] D. Cremer, J.A. Pople, J. Am. Chem. Soc. 97 (1975) 1354.
[20] J.S. Casas, E.E. Castellano, M.S. Garcia Tasende, A. Sánchez, J. Sordo, Inorg. Chim. Acta 304 (2000) 283.

crystal structures of three new organic–inorganic hybrid polyoxovanadates: $[Ni(1,10'\text{-phen})_3]_2[V_{10}O_{26}]$ (**1**), containing an unusual empty ellipsoidal mixed-valent polyoxoanion $[V_{10}O_{26}]^{4-}$ 'host' cage; $[Zn(2,2'\text{-bipy})_3]_3[V_{15}O_{36}Cl]\cdot 3H_2O$ (**2**) and $[Co(2,2'\text{-bipy})_3]_3\ [V_{15}O_{36}Cl]\cdot 3H_2O$ (**3**), both containing a spherical mixed-valent oxovanadate cluster $[V_{15}O_{36}]$ 'host' shell with a Cl^- 'guest' encapsulated. To our knowledge, the organic–inorganic hybrid polyoxovanadate **1** has been isolated for the first time from aqueous solution with the help of a hydrothermal technique. The polyoxoanions of **2** and **3**, cocrystallized with transitional metal coordination complex cations, are also isolated for the first time. The role of organic templates (1,10′-phen and 2,2′-bipy) on the structures of polyoxoanions is discussed.

2. Experimental

2.1. Materials and measurements

All chemicals purchased were of reagent grade and used without further purification. Elemental analyses (C, H and N) were performed on a Perkin–Elmer 2400 CHN Elemental Analyzer. V, Co, Ni, Zn were determined by a Leeman inductively coupled plasma (ICP) spectrometer. Cl was determined by a DX-300 ion chromatograph (IC) equipped with a conductivity detector and an AS4A-SC anion column. IR spectra were recorded in the range 400–4000 cm^{-1} on an Alpha Centaurt FT/IR Spectrometer using KBr pellets. EPR spectra were obtained on a Japanese JES-FE3AX spectrometer at 293 K. TG analyses were performed on a Perkin–Elmer TGA7 instrument in flowing N_2 with a heating rate of 10 °C min^{-1}.

2.2. Hydrothermal syntheses

2.2.1. Synthesis of $[Ni(1,10'\text{-phen})_3]_2[V_{10}O_{26}]$ (1)

A mixture of NH_4VO_3, $NiCl_2\cdot 6H_2O$, 1,10′-phenanthroline and H_2O in the mole ratio 1:1:2:444 was sealed in a 20 ml Teflon-lined autoclave, adjusted by 1 mol l^{-1} HCl to pH 5.0 and heated to 155 °C for 3 days. After cooling to room temperature (r.t.), dark-red column crystals of **1** were obtained. The compound was filtered, washed with distilled water and dried in air (65% yield based on V). *Anal*. Found: C, 40.63; H, 2.32; N, 7.84; V, 23.87; Ni, 5.44. Calc. for $C_{72}H_{48}N_{12}Ni_2O_{26}V_{10}$: C, 40.71; H, 2.28; N, 7.92; V, 23.98; Ni, 5.53%.

2.2.2. Synthesis of $[Zn(2,2'\text{-bipy})_3]_3[V_{15}O_{36}Cl]\cdot 3H_2O$ (2)

A mixture of NH_4VO_3, $ZnCl_2$, 2,2′-bipyridine and H_2O in the mole ratio 1:1:2:444 was sealed in a 20 ml Teflon-lined autoclave, adjusted by 1 mol l^{-1} HCl to pH 5.0 and heated to 155 °C for 4 days. After cooling to r.t., deep-red block crystals of **2** were obtained. The product was filtered, washed with distilled water and dried in air (70% yield based on V). *Anal*. Found: C, 36.59; H, 2.64; N, 8.45; Cl, 1.25; V, 25.34; Zn, 6.39. Calc. for $C_{90}H_{78}ClN_{18}O_{39}V_{15}Zn_3$: C, 35.66; H, 2.59; N, 8.32; Cl, 1.17; V, 25.21; Zn, 6.47%.

2.2.3. Synthesis of $[Co(2,2'\text{-bipy})_3]_3[V_{15}O_{36}Cl]\cdot 3H_2O$ (3)

When $ZnCl_2$ was substituted by $CoCl_2\cdot 6H_2O$ while the other reaction conditions remained the same, dark-brown block crystals of **3** were obtained (60% yield based on V). *Anal*. Found: C, 36.28; H, 2.62; N, 8.87; Cl, 1.27; Co, 5.78; V, 25.74. Calc. for $C_{90}H_{78}ClCo_3N_{18}O_{39}V_{15}$: C, 35.89; H, 2.61; N, 8.37; Cl, 1.18; Co, 5.87; V, 25.37%.

When $ZnCl_2$ was substituted by $NiCl_2\cdot 6H_2O$ with the same synthetic conditions, dark green crystals of **4** were obtained. The IR spectrum of **4** exhibits the similar characteristic peaks as **2** and **3**. However, owing to the poor quality of the crystals, no precise structure was determined by single crystal X-ray diffraction.

2.3. X-ray crystallography

Data for **1** were collected on a Siemens P4 four-circle diffractometer with Mo Kα radiation ($\lambda = 0.71073$ Å) at 293 K using the ω-scan technique. Empirical absorption correction (ψ scan) was applied. Data for compound **2** were collected at 293 K on a Bruker CCD diffractometer employing graphite-monochromated Mo Kα radiation ($\lambda = 0.71073$ Å). Empirical absorption correction was applied. Data for **3** were collected at 293 K on a *R*-axis RAPID diffractometer with the IP technique. Empirical absorption correction was applied.

All structures were solved by direct methods and refined by full-matrix least-squares on F^2 using the SHELXL-97 software [21]. All of the non-hydrogen atoms were refined anisotropically. All the hydrogen atoms were located from difference Fourier maps. Atomic coordinates, bond lengths and angles, and anisotropic displacement parameters of **1**, **2** and **3** are available in the supplementary crystallographic data. A summary of crystal data and structure refinement for compounds **1**, **2** and **3** is provided in Table 1. Selected bond lengths and angles of **1**, **2** and **3** are listed in Tables 2 and 3.

3. Results and discussion

3.1. Hydrothermal syntheses of 1–3

The isolation of **1**–**3** relies on hydrothermal techniques. Hydrothermal synthesis has recently been proved a useful technique in preparation of organic–inorganic hybrid materials [2,11–15,18–20]. In the hydrothermal

Table 1
Crystal data and structure refinement of compounds **1**–**3**

	1	**2**	**3**
Formula	$C_{72}H_{48}N_{12}Ni_2O_{26}V_{10}$	$C_{90}H_{78}ClN_{18}O_{39}V_{15}Zn_3$	$C_{90}H_{78}ClCo_3N_{18}O_{39}V_{15}$
M	2124.04	3031.36	3012.04
Crystal system	orthorhombic	Trigonal	Trigonal
Space group	*Pbcn*	*R*-3*c*	*R*-3*c*
a (Å)	13.629(3)	17.596(3)	17.547(3)
b (Å)	22.156(4)	17.596(3)	17.547(3)
c (Å)	25.712(4)	64.75(1)	64.23(1)
γ (°)		120	120
V (Å^3)	7764(2)	17361(5)	17126(5)
Z	4	6	6
D_{calc} (g cm^{-3})	1.817	1.740	1.752
μ(Mo Kα) (mm^{-1})	1.704	1.865	1.696
θ Range (°)	1.75–25.00	1.84–25.08	2.32–27.48
Reflections collected	8536	19126	45756
Independent reflections	6842	3418	4355
Data/parameters	6842/552	3418/229	4355/282
$R_1(wR_2)$ [a]	0.0403(0.0446)	0.0682(0.1612)	0.0672(0.1649)
Goodness-of-fit on F^2	0.694	1.102	0.994

[a] $\{R_1 = \Sigma\ ||F_o|-|F_c||/\Sigma\ |F_o|;\ wR_2 = \Sigma\ [w(F_o^2-F_c^2)^2]/\Sigma\ [w(F_o^2)^2]^{1/2}\}$.

Table 2
Selected bond lengths (Å) and angles (°) for **1**

Bond lengths			
V(1)–O(13)	1.597(3)	V(1)–O(2)	1.681(3)
V(1)–O(10)	1.800(3)	V(2)–O(5)	1.601(3)
V(2)–O(3)	1.680(3)	V(2)–O(10)	1.786(3)
V(2)–O(8)	1.790(3)	V(3)–O(7)	1.617(3)
V(3)–O(9)	1.775(3)	V(3)–O(4)	1.779(3)
V(4)–O(14)	1.582(4)	V(4)–O(3)	1.941(3)
V(4)–O(1)	1.949(4)	V(6)–O(12)	1.585(4)
V(6)–O(2)	1.933(3)	V(6)–O(6)	1.943(3)
Ni–N(3)	2.044(4)	Ni–N(2)	2.073(4)
Ni–N(1)	2.080(4)	Ni–N(5)	2.087(4)
Ni–N(4)	2.086(4)	Ni–N(6)	2.098(5)
Bond angles			
O(13)–V(1)–O(2)	109.9(2)	O(13)–V(1)–O(10)	107.5(2)
O(5)–V(2)–O(10)	109.0(2)	O(3)–V(2)–O(8)	111.0(2)
O(7)–V(3)–O(9)	106.8(2)	O(11)–V(5)–O(9)	105.5(2)
O(3)–V(4)–O(1)	86.9(2)	O(14)–V(4)–O(1)	104.5 (1)
O(2)–V(6)–O(6)#1	83.8(1)	O(1)–V(4)–O(1)#1	151.0(2)

#1, $-x$, y, $-z+1/2$.

Table 3
Selected bond lengths (Å) and angles (°) for **2** and **3**

	2	**3**
Bond lengths		
V(1)–O(4)	1.604(5)	1.597(4)
V(1)–O(1)	1.892(5)	1.898(4)
V(1)–O(6)	1.810(3)	1.824(2)
V(1)–O(3)	1.910(5)	1.902(4)
V(2)–O(2)	1.603(6)	1.603(4)
V(2)–O(3)	1.925(5)	1.922(4)
V(2)–O(5)	1.879(5)	1.883(4)
V(3)–O(7)	1.596(7)	1.537(6)
V(3)–O(3)	1.992(5)	2.010(4)
M(1)–N(2)	2.179(7)	2.103(5)
M(1)–N(1) [a]	2.124(7)	2.097(5)
M(2)–N(3)	2.188(13)	2.183(8)
M(2)–N(4)	2.156(13)	2.111(10)
Bond angles		
O(4)–V(1)–O(6)	104.0(3)	103.7(2)
O(4)–V(1)–O(1)	110.1(2)	109.8(2)
O(4)–V(1)–O(3)	109.9(2)	110.0(2)
O(1)–V(1)–O(3)	138.4(2)	138.86(17)
O(2)–V(2)–O(3)	108.4(2)	108.73(19)
O(6)–V(1)–O(1)	91.10(17)	90.64(14)
O(6)–V(1)–O(3)	90.27(17)	89.87(13)
O(2)–V(2)–O(5)	106.9(2)	106.81(19)
O(5)–V(2)–O(3)	144.1(2)	143.97(17)

[a] M = Zn (in **1**) or Co (in **2**).

environment, the reduced viscosity of the solvent results in enhanced rates of solvent extraction of solids and crystal growth from solution. Furthermore, since different solubility problems are minimized, a variety of simple organic and/or inorganic templating agents can be introduced. [14,15,22,23]. However, hydrothermal synthesis is still a relatively complex process because many factors can effect the reaction, such as initial reactants, concentration, pH and crystallization temperature.

To investigate the influence of ligands on the formation of cage-like polyoxovanadates, we selected two bidentate N-containing ligands (1,10-phen and 2,2′-bipy) and kept the other synthetic conditions the same. It is noteworthy that the introduction of different organic structure-directing agents leads to two kinds of polyoxovanadate structures during the preparations of **1**–**3**. The geometry of organic templating agents in this case may be one of the important factors that influence the self-assembly of the oxovanadate clusters. Further-

more, the prolonged reaction time is probably another factor, which leads to higher polymerization of polyoxovanadate clusters.

3.2. Crystal structures of *1–3*

Single crystal X-ray analysis reveals that **1** consists of an unusual oblate spherical mixed-valent polyoxoanion $[V_{10}O_{26}]^{4-}$ and two $[Ni(1,10\text{-phen})_3]^{2+}$ cations. The polyoxoanion of **1** (Fig. 1(a)) exhibits two independent vanadium coordination environments, that is, the distorted $\{VO_4\}$ tetrahedron and the distorted $\{VO_5\}$ square pyramid (Fig. 1(b)). In the $\{VO_4\}$ tetrahedron, the vanadium center is coordinated with three bridging oxygen (O_b) atoms and one terminal oxygen (O_t) atom with V–O_b distances in the range of 1.662(4)–1.800(3) Å and V–O_t distances 1.586(3)–1.617(3) Å. The bond angles at V atoms range from 105.50(12)° to 110.95(16)°. In the $\{VO_5\}$ square pyramid, the vanadium center is connected with four O_b atoms and one O_t atom with V–O_b lengths in the range 1.933(3)–1.949(4) Å and V–O_t lengths 1.582(4)–1.585(4) Å. The bond angles at V atoms vary from 83.75(13)° to 151.0(2)°.

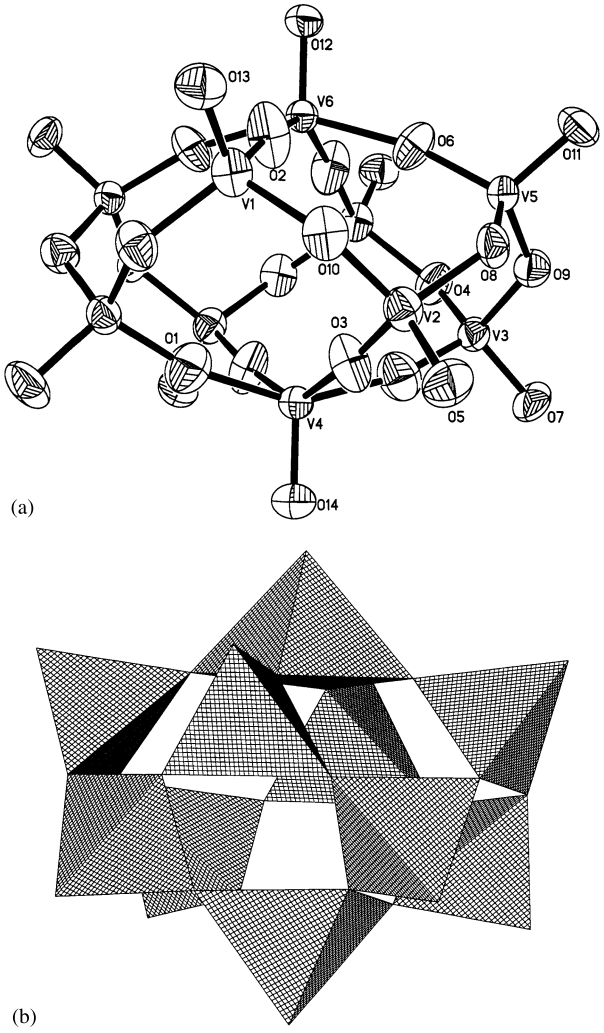


Fig. 1. (a) The structure of $[V_2^{IV}\ V_8^{V}\ O_{26}]^{4-}$ in **1**; (b) The polyhedron representative of $[V_2^{IV}\ V_8^{V}\ O_{26}]^{4-}$ in **1**.

It is interesting that eight $\{VO_4\}$ tetrahedra are connected with one another via the corner-sharing mode to form a puckered 16-member ring with an average diameter of 6.68 Å. Two $\{VO_5\}$ units are capped on both sides of the ring to form an empty ellipsoidal 'host' cage. The distance between two $\{VO_5\}$ moieties is 4.69 Å.

Valence sum calculations [24] (see Table 4) show that the eight vanadium centers in $\{VO_4\}$ tetrahedral environments are in the 5+ oxidation state, while the other two vanadium centers in the $\{VO_5\}$ units are in the 4+ oxidation state. Therefore, the detailed formula of the cluster can formally be described as $[V_2^{IV}\ V_8^{V}\ O_{26}]^{4-}$.

In compound **1**, two coordination complexes $[Ni(1,10'\text{-phen})_3]^{2+}$ act as counter cations. The Ni^{2+} ion is coordinated with six N atoms in three phen groups to form a chiral cationic unit with an average Ni–N length of 2.078 Å. In the unit cell of **1**, weak π–π interactions (with an average distance 3.42 Å) exist between the $[Ni(1,10\text{-phen})_3]^{2+}$ cations, while the $[V_{10}O_{26}]^{4-}$ anions are connected with these cations via electrostatic attraction. The packing arrangement of **1** along the *b* axis is shown in Fig. 2.

Compound **2** consists of a spherical mixed-valent polyoxoanion $[V_{15}O_{36}Cl]^{6-}$ (see Fig. 3(a)), three $[Zn(2,2'\text{-bipy})_3]^{2+}$ cations and three lattice water molecules. The polyoxoanion $[V_{15}O_{36}Cl]^{6-}$ can be described as a nearly spherical oxo-vanadium cluster formed by 15 $\{VO_5\}$ square pyramids via the cornering-sharing mode as shown in Fig. 3(b). A 'guest' Cl^- ion was encapsulated in the $[V_{15}O_{36}]$ 'host' shell. In the distorted $\{VO_5\}$ square pyramid, V–O_b lengths are in the range of 1.810(3)–1.992(5) Å, V–O_t lengths 1.596(7)–1.604(5) Å, and the bond angles of O–V–O vary from 90.27(7)° to 144.1(2)°. The average radius (the distance from V atom to Cl^- ion) of the cage is 3.41 Å.

The $[V_{15}O_{36}Cl]^{6-}$ cluster is closely related to those found in alkali–vanadium oxide–halide systems described by Müller et al. [4,5]. Valence sum calculations (see Table 4) of **2** give an average value of 4.51 for calculated oxidation states of V. The calculations show

Table 4
Sums of the bond valences [a] for the V atoms of **1**, **2** and **3**

	1	2	3
V(1)	4.91	4.79	4.79
V(2)	4.94	4.77	4.76
V(3)	5.00	3.98	4.15
V(4)	4.31		
V(6)	4.35		

[a] The results refer to the equation $V_i = \Sigma_j \exp((r_0 - r_{ij})/B)$ (Ref. [24]).

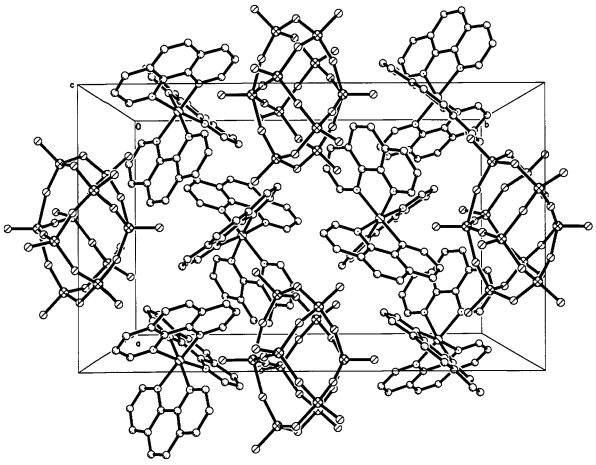


Fig. 2. Packing arrangement of compound **1** along the *c* axis.

that eight vanadium centers are in the 4+ oxidation state, while the other seven vanadium centers are in the 5+ oxidation state, which confirms the molecular formula of **2** and is consistent with the previous reports [4,5,25]. Therefore, the detailed formula of the polyoxoanion can be described as $[V_8^{IV}\ V_7^{V}\ O_{36}Cl]^{6-}$.

In compound **2**, three coordination complexes $[Zn(2,2'\text{-bipy})_3]^{2+}$ act as counter cations. The Zn^{2+} ion is coordinated with six N atoms in three 2,2′-bipy groups to form a chiral cationic unit with an average Zn–N distance of 2.162 Å. Every four $[Zn(2,2'\text{-bipy})_3]^{2+}$ groups in **2** lie in the same plane. The polyoxoanions are located above and below this plane and are connected with the $[Zn(2,2'\text{-bipy})_3]^{2+}$ groups via electrostatic attraction. The packing arrangement of **1** along the *b* axis is shown in Fig. 4.

Compound **3** is isostructural with **2** and needs no further discussion.

3.3. IR and EPR spectra

In the IR spectrum of **1** (see Fig. 5), the strong bands at 965, 888, 844, 721 and 665 cm^{-1} are due to the ν(V=O) or ν(V–O–V) vibrations. Bands in the 1626–1099 cm^{-1} regions are attributed to extending vibrations of the 1,10′-phen groups. The IR spectra of compounds **2**, **3** and **4** exhibit similar characteristic peaks**.** The strong bands at 981, 769, 732 and 660 cm^{-1} are ascribed to the ν(V=O) or ν(V–O–V) vibrations. Bands in the range of 1632–1017 cm^{-1} are characteristic of C=C and/or C–N bonds of the 2,2′-bipy groups.

The EPR spectrum of **1** (Fig. 6(a)) at room temperature shows a V^{4+} signal with $g = 1.9884$. No fine signals were recorded for **1** owing to the high concentrations of vanadium. The EPR spectrum of **2** (Fig. 6(b)) at room temperature shows fine V^{4+} signals with $g_{\perp} = 1.997$, $g_{\parallel} = 1.934$, $A_{\perp} = 1.875$, and $A_{\parallel} = 1.668$. All these results are in accordance with the valence sum calculations,

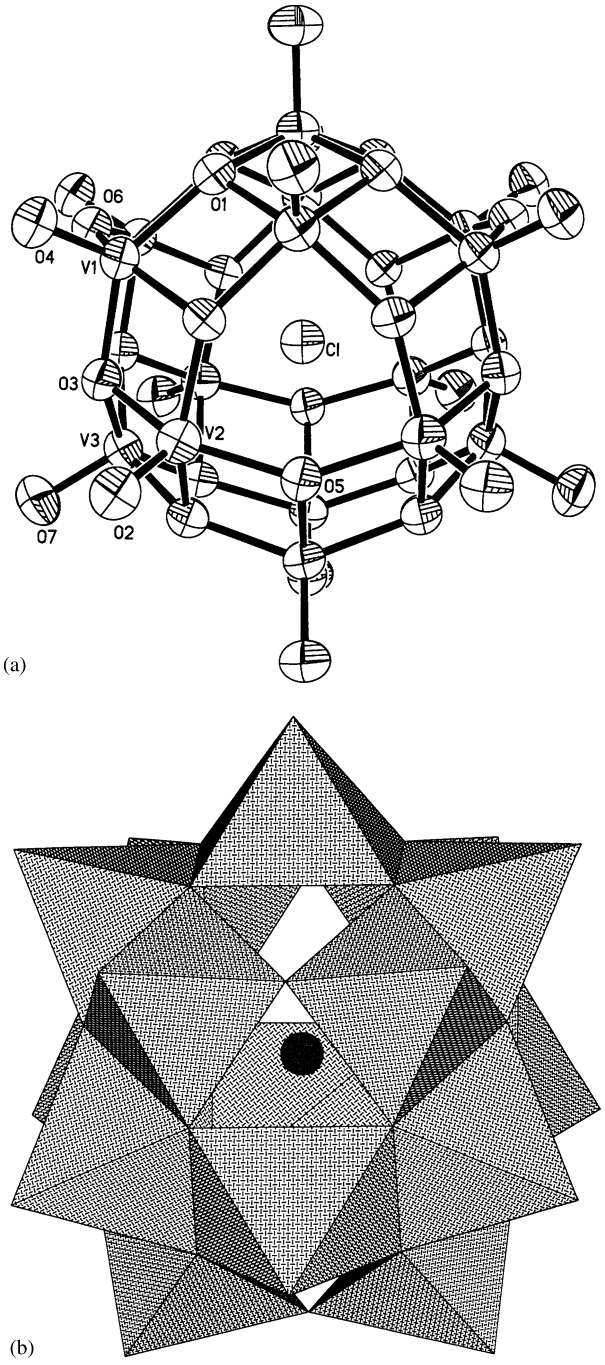


Fig. 3. (a) The structure of $[V_8^{IV}\ V_7^{V}\ O_{36}Cl]^{6-}$ in **2**; (b) The polyhedron representative of $[V_8^{IV}\ V_7^{V}\ O_{36}Cl]^{6-}$ in **2**.

further confirming that compounds **1**–**3** all possess mixed V^{4+}/V^{5+} oxidation states.

3.4. Thermal analyses of *1*–*3*

The TG curve of compound **1** (Fig. 7(a)) is divided into three continuous stages. The first weight loss is 5.49% in the temperature range 498–518 °C. The second weight loss is 27.32% from 530 to 650 °C and the third is 15.61% in the range 655–755 °C. These

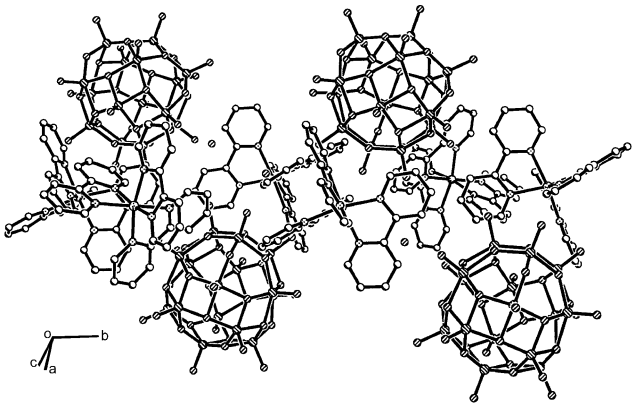


Fig. 4. Packing arrangement of compound **2** along the *b* axis.

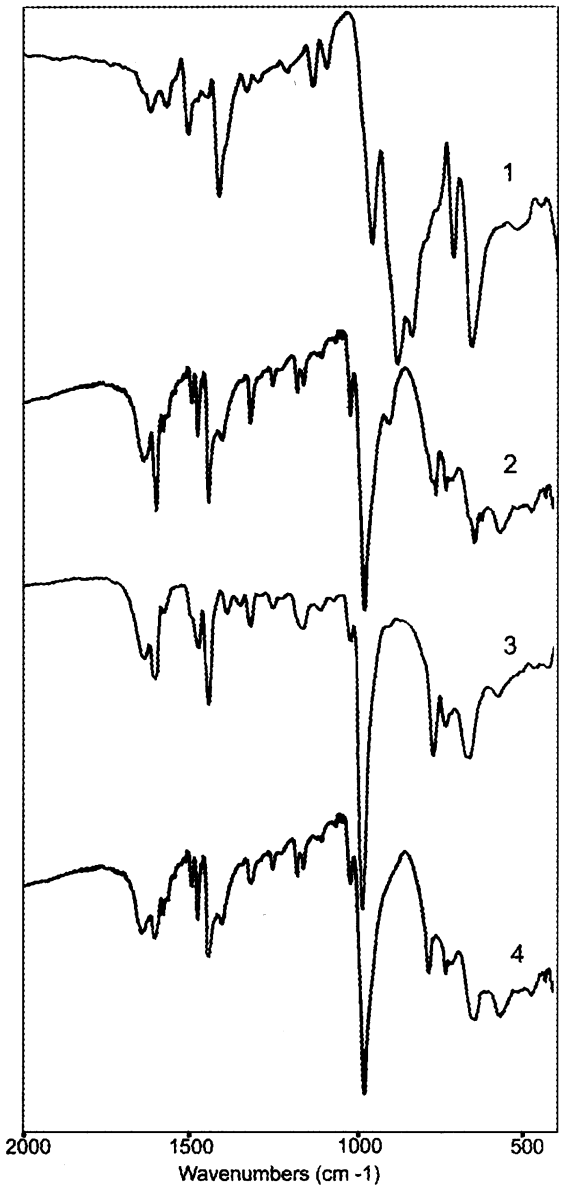


Fig. 5. IR spectra of compounds **1**, **2**, **3** and **4**.

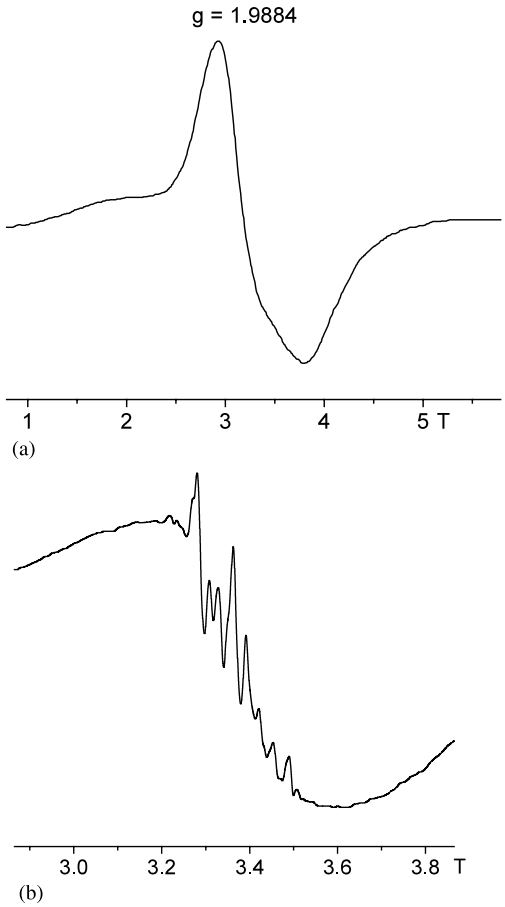


Fig. 6. (a) EPR spectrum of **1**; (b) EPR spectrum of **2**.

three continuous weight losses are ascribed to the release of the 1,10′-phen groups. The whole weight loss (48.41%) is in good agreement with the calculated value (50.84%). The sample does not lose weight at temperatures higher than 760 °C.

The TG curve of compound **2** (Fig. 7(b)) exhibits four steps of weight losses. The first weight loss is 2.91% in the temperature range 25–120 °C, corresponding to the release of crystal water. The second weight loss is 5.59% from 195 to 345 °C, the third is 31.50% in the range 345–485 °C, and the fourth is 7.01% in 485–570 °C, all assigned to the release of 2,2′-bipy groups. The whole weight loss (47.01%) is consistent with the calculated value (48.10%). The sample does not lose weight at temperatures higher than 570 °C.

The TG curve of compound **3** (see Fig. 7(c)) exhibits similar weight loss stages compared with **2**. The first weight loss is 2.03% in the temperature range 25–180 °C, corresponding to the release of crystal water. The remaining three weight losses amount to 44.45% from 180 to 570 °C, and are ascribed to the release of 2,2′-bipy groups. The whole weight loss (46.48%) agrees well with the calculated value (48.41%).

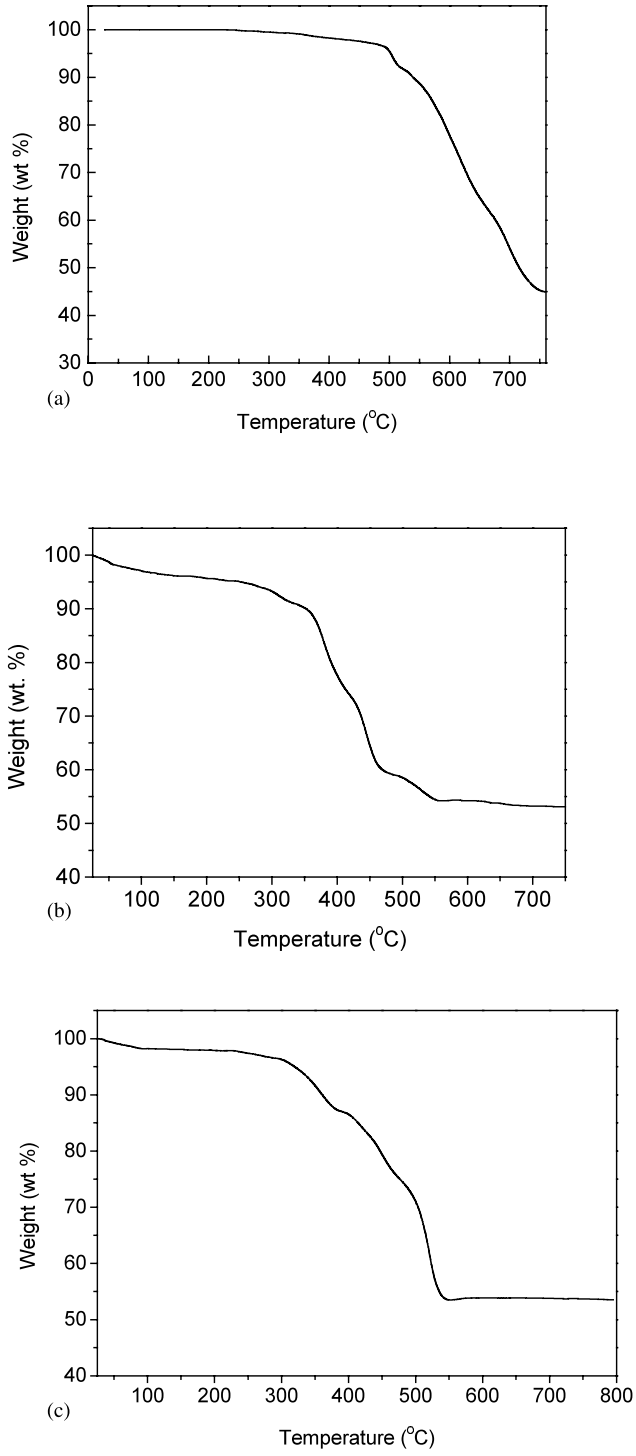


Fig. 7. (a) The TG curve of compound **1**; (b) the TG curve of compound **2**; (c) the TG curve of compound **3**.

4. Conclusions

In this paper, three new organic–inorganic hybrid materials based on the spherical mixed-valent polyoxovanadates have been hydrothermally synthesized. Under similar synthetic conditions, the introduction of different organic N-containing ligands leads to various self-assembly of polyoxovanadate clusters. The geometry of these organic templating agents may be one of the important factors that influence the growth and self-assembly of the oxovanadate clusters. Studies are going on in order to provide more structural information of such organic–inorganic hybrid complexes and reveal structural relationships between N-containing ligands and the polyoxoanions.

5. Supplementary material

Crystallographic data for the structural analysis have been deposited with the Cambridge Crystallographic Data Centre, CCDC No. 182191–182193 for compounds **1**, **2** and **3**, respectively. Copies of this information may be obtained free of charge from The Director, CCDC, 12 Union Road, Cambridge, CB2 1EZ, UK (fax: +44-1223-336033; e-mail: deposit@ccdc.cam.ac.uk or www: http://www.ccdc.cam.ac.uk).

Acknowledgements

This work was financially supported by the National Natural Science Foundation of China (20171010).

References

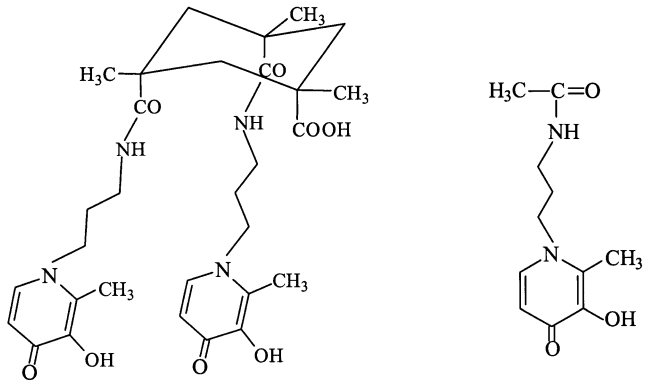
[1] (a) W. Li, J.R. Dahn, D.S. Wainwright, Science 264 (1994) 1115; (b) D.W. Murphy, P.A. Christian, Science 205 (1979) 651.
[2] Y.P. Zhang, C.J. O'Connor, A. Clearfield, R.C. Haushalter, Chem. Mater. 8 (1996) 595.
[3] W.G. Kemperer, T.A. Marquart, O.M. Yaghi, Angew. Chem., Int. Ed. Engl. 31 (1992) 49.
[4] A. Müller, E. Krickemeyer, M. Penk, R. Rohlfing, A. Armatage, H. Bögge, Angew. Chem., Int. Ed. Engl. 42 (1991) 1674.
[5] A. Müller, M. Penk, R. Rohlfing, E. Krickemeyer, J. Döring, Angew. Chem., Int. Ed. Engl. 8 (1990) 926.
[6] A. Müller, H. Renter, S. Dillinger, Angew. Chem., Int. Ed. Engl. 34 (1995) 2328.
[7] A. Müller, J. Mol. Struct. 325 (1994) 13.
[8] T. Yamase, M. Suzuki, K. Ohtaka, J. Chem. Soc., Dalton Trans. (1997) 2463.
[9] T. Yamase, K. Ohtaka, M. Suzuki, J. Chem. Soc., Dalton Trans. (1996) 283.
[10] G.B. Karet, Z.M. Sun, W.E. Streib, J.C. Bollinger, D.N. Hendrickson, G. Christou, Chem. Commun. (1999) 2249.
[11] Y.G. Li, E.B. Wang, H. Zhang, G.Y. Luan, C.W. Hu, N.H. Hu, H.Q. Jia, J. Solid State Chem. 163 (2002) 10.
[12] T. Duraisamy, N. Ojha, A. Ramanan, J.J. Vittal, Chem. Mater. 11 (1999) 2339.
[13] Y.P. Zhang, R.C. Haushalter, A. Clearfield, Inorg. Chem. 35 (1996) 4950.
[14] P.J. Hagrman, J. Zubieta, Inorg. Chem. 39 (2000) 3252.
[15] Y.P. Zhang, R.C. Haushalter, J. Zubieta, Inorg. Chim. Acta 277 (1998) 263.
[16] A. Müller, R. Sessoli, E. Krickemeyer, H. Bögge, J. Meyer, D. Gatteschi, Inorg. Chem. 36 (1997) 5239.

[17] (a) C. Heitner-Wirguin, J. Selbin, J. Inorg. Nucl. Chem. 30 (1968) 3181;
(b) A. Bino, S. Cohen, C. Heitner-Wirguin, Inorg. Chem. 21 (1981) 429.
[18] L. Xu, Y.Q. Sun, E.B. Wang, E.H. Shen, Z.R. Liu, C.W. Hu, New J. Chem. 23 (1999) 1041.
[19] L. Xu, Y.Q. Sun, E.B. Wang, E.H. Shen, Z.R. Liu, C.W. Hu, J. Solid State Chem. 146 (1999) 533.
[20] Y.G. Li, E.B. Wang, S.T. Wang, Y.B. Duan, C.W. Hu, N.H. Hu, H.Q. Jia, J. Mol. Struct. 611 (2002) 185.
[21] (a) G.M. Sheldrick, SHELXS-97, Program for Crystal Structure Solution, University of Göttingen, 1997.;
(b) G.M. Sheldrick, SHELXL-97, Program for Crystal Structure Refinement, University of Göttingen, 1997.
[22] A. Stein, S.W. Keller, T.G. Mallouk, Science 259 (1993) 1558.
[23] J. Gopalakrishnan, Chem. Mater. 7 (1995) 1265.
[24] I.D. Brown, D. Altermatt, Acta Crystallogr., Sect. B 41 (1985) 244.
[25] T. Drezen, O. Joubert, M. Ganne, L. Brohan, J. Solid State Chem. 136 (1998) 298.

nones), has been recently proposed a special role on the increase of the bone uptake of ^{67}Ga, thus, conferring to carboxyl–hydroxypyridonate derivatives a potential interest in bone tumour radiodiagnosis [11,12]. On the other hand, there is a large number of biological active MMP enzyme inhibitors which have a hydroxamate chelating group, as well as a carboxylate extra-functional group [13]. Some hydroxypyridinones, such as mimosine (β-*N*-(3-hydroxy-4-pyridone)-α-aminopropionic acid, herein named as H_2L^4), which has been also implicated in the inhibitory activity of various M(II)-containing enzymes (M = Cu, Zn) and other biological systems, possess also a 'free' carboxylate group [2].

Accordingly, this new ligand could be thought as a candidate for potential radiopharmaceutical, in relation to its chelation either with $^{64,67}Cu$, to be used in PET analysis [14], or with other M^{2+} metal ions, for metalloenzyme inhibition.

In this paper, we report the study of a tetradentate bifunctional ligand, *cis*,*cis*-1,3-di-[1′-(3″-carboxyaminopropyl)-3′-hydroxy-2′-methyl-4′-pyridinone-yl]-5-carboxyl-1,3,5-trimethylcyclohexane, hereafter named as KEMP(NPrHP)$_2$ or H_3L^1 (Scheme 1). It is a bis(3-hydroxy-4-pyridinonate)-monocarboxylate ligand and so, herein, sometimes it is referred as a 'bis-chelator', in comparison with the corresponding 'mono-chelator' pendant unit, 1-(3′-methylcarboxyaminopropyl)-3-hydroxy-2-methyl-4-pyridinone), hereafter named AcNPrHP or HL^2, which was also studied. Each 3,4-HP unit is linked to an aminoalkylic chain, which acts both as a spacer and also a way of attachment to the cyclic backbone via its carboxylate groups. Besides the preparation and characterization of the ligands (acid–base and lipo-hydrophilic properties), their complexation ability towards the first transition series of divalent metal ions [Cu(II), Zn(II) and Ni(II)] as well as the corresponding speciation are described and discussed herein. The equilibrium studies were carried out in aqueous media and were based on potentiometric and spectrophotometric measurements. A brief molecular mechanics simulation was also carried out to get an insight on the ability of this new 'bis-chelator' to wrap this type of metal ions.



KEMP(NPrHP)$_2$, H_3L^1 AcNPrHP, HL^2

Scheme 1.

2. Results and discussion

2.1. Synthesis

The synthesis of this bis(hydroxypyridinonate)-carboxylate ligand involved a preliminary protection of one of the carboxylic functions of the starting material, the *cis*–*cis*-1,3,5-trimethylcyclohexane-1,3,5-tricarboxilic acid (KEMP acid), by its convertion into the intermediate cyclic anhydride [5-(chloroformyl)-*cis*,*cis*-1,3,5-trimethylcyclohexane-1,3-dicarboxilic anhydride], by standard methods [15]. This reaction takes advantage of the proximity between the carboxylic groups in the starting material and so it was performed with high yield. This intermediate was then coupled to 1-(3′-propylamine)-3-benzyloxy-4-pyridinone, to give the *O*-benzyl protected bis-hydroxypyridinone-mono-carboxylic acid derivative. To afford the final product, H_3L^1, the deprotection of the hydroxypyridinonate hydroxyl groups was performed by standard methods of hydrogenolysis [11]. The synthesis of the 'mono-chelator' compound, HL^2, involved a condensation of 1-(3′-propylamine)-3-benzyloxy-4-pyridinone with acethyl chloride.

2.2. Acid–base properties of the ligands

The bis- and the mono-hydroxypyridonate ligands, in their neutral form (H_3L^1 and HL^2), have only three and one labile protons, respectively, due to the carboxylic/phenolic groups, whereas, in their fully protonated form, they have the extra dissociable pyridinium protons. From the fitting analysis of potentiometric titration curves of the ligands (Fig. 1) with the SUPERQUAD program [16], five and two protonation constants were determined, respectively. Table 1 shows the calculated stepwise protonation constants together with the corresponding values for some representative 3-hydroxy-4-pyridinone analogues, such as 1,2-dimethyl-3-hydroxy-2-methyl-4-pyridinone (HL^3) [17] and mimosine (H_2L^4) [2]. Based on chemical evidences, the first two protonation constants of H_3L^1 ($\log K_a = 10.17$; 9.43) and the first one of HL^2 ($\log K_{a1} = 9.61$) are undoubtedly attributed to the phenolic groups. The three remaining $\log K_a$ values (4.70; 3.64; 2.96) of H_3L^1 are attributed to the carboxylic group and to the pyridinium groups. Although these three processes overlap each other, comparison between these stepwise protonation constants and the corresponding values for the pyridinium group of HL^2 (3.37) and other analogous compounds

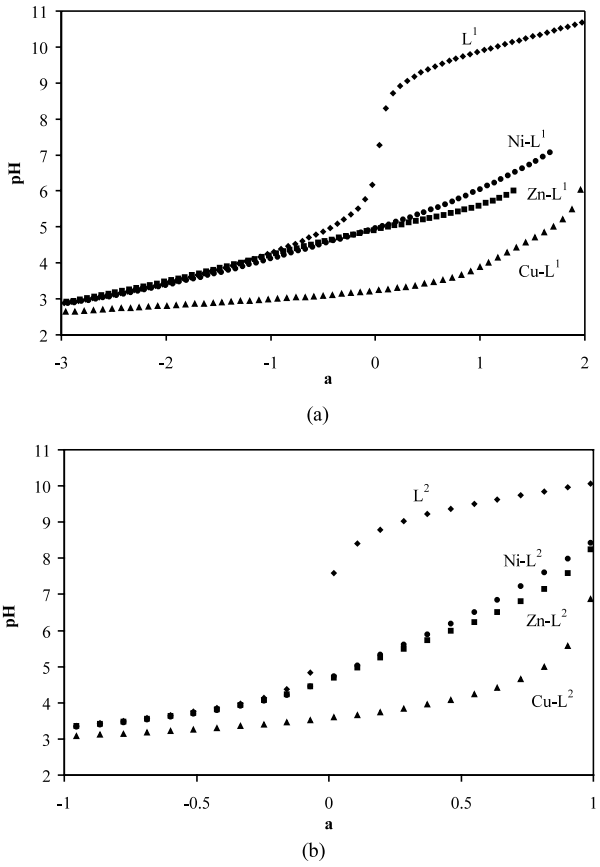


Fig. 1. Potentiometric titration curves for the ligands alone and in the presence of each M(II) metal ion (M = Cu, Ni, Zn): H_3L^1, at 1:1 metal to ligand molar ratio ($C_L = 2.9 \times 10^{-3}$ M, $I = 0.2$ M (KCl)) (a); HL^2, at 1:2 metal to ligand molar ratio. ($C_L = 1.6 \times 10^{-3}$ M, $I = 0.1$ M (KNO_3)) (b). $T = 25.0 \pm 0.1$ °C; a = mols of base added per mol of ligand.

(see Table 1) suggests that the two lower values (3.64; 2.96) should be mainly attributed to the pyridinium groups. Besides, the higher value (4.70), attributed to the carboxylic group, is comparable to the log K_a values of other tertiary carboxylic groups (ex. 2,2-dimethylpropanoic acid, log $K_a = 4.8$) [18]. Analysis of the speciation plots related to the calculated log K_a values shows that the mono-anion $[H_2L^1]^-$ dominates over the pH range 5.5–8.5. Thus, this tetradentate ligand is expected to have a considerably higher hydrophilic character at the physiological conditions than the neutral bidentate derivative (HL^2).

2.3. Complexation studies

Complexation behaviour of these di- and mono-hydroxypyridinonate ligands ($H_3L^1$and HL^2) with the first transition series of metal ions [Cu(II), Ni(II) and Zn(II)] was studied by potentiometry and the interpretation of these results was aided by UV–Vis spectrophotometry. Precipitation was not observed in the samples containing some ligand excess but appeared at 1:1 ratio or at metal ion excess. The titrations were finished if precipitation occurred. Representative titration curves of these two ligands in the presence of each of those metal ions studied are shown in Fig. 1(a) (H_3L^1) and (b) (HL^2), for the 1:1 and in 2:1 ligand to metal molar ratios, respectively. Some species distribution diagrams for the complexation with the di-hydroxypyridonate ligand (H_3L^1) are presented in Fig. 2.

Analysis of the titration curves indicates that the metal complexation of both the ligands starts at a quite lower pH (approximately 2.5) with copper(II) than with nickel(II) and zinc(II) (approximately pH 4), thus, indicating a stronger interaction with copper(II). The experimental data presented good fittings for the complexation models having 1:1 and 1:2 stoichiometry for H_3L^1 and HL^2, respectively, with different protonation degrees. Comparison between the formation constants calculated for the complexes with H_3L^1 (Table 1) shows that log β_{ML} is higher for Cu(II) than for Zn(II) and Ni(II) by a factor of 5.6 and 7.0 logarithmic units, respectively. Identical difference was found between the log $\beta_{ML_2^1}$ of the complexes of these metal ions with the monomeric derivatives, HL^2 and HL^3 (deferiprone) [17] (see Table 1).

Comparative analysis of the chelating abilities of H_3L^1 and the other analogues has to be made with care, mainly due to differences in the acid–base properties of the ligands and the stoichiometry of the complexes. Therefore, the pM values ($pM = -\log[M^{2+}]$) were also calculated for the different metal ions, at the physiological conditions (pH 7.4, Table 1) and for Cu(II), along a large range of pH (Fig. 3). A brief comparison of the complexing behaviour of the di-hydroxypyridinone and the mono-analogue suggests that the same binding sites (the 3-hydroxy-4-pyridinone portions) should be involved in the co-ordination of the ligands to each metal ion. In fact, for each metal ion, the profiles of the titration curves are very similar. The overall formation constants (log β_{ML}) calculated for the (1:1) complexes of this di-hydroxypyridinonate ligand with copper(II), nickel(II) and zinc(II) (17.42, 10.41, 11.78) are close to, albeit slightly lower than, the values (log β_{ML_2}) for the corresponding (1:2) complexes with the mono-hydroxypyridinonate ligands: HL^2, (18.99, 12.38, 13.70) and HL^3, (19.61, 12.13, 13.53) [17]. However, at conditions of 10-fold excess of the ligand and mM or μM concentrations, the pM values are higher for the dihydroxypyridinone, H_3L^1, (ex.: for $C_{Cu} = 10^{-4}$ M, pCu = 13.5; for $C_{Cu} = 10^{-6}$ M, pCu = 13.6) then the monohydroxypyridinone, HL^2, (ex.: for $C_{Cu} = 10^{-4}$ M, pCu = 12.4; for $C_{Cu} = 10^{-6}$ M, pCu = 10.4). Fig. 3 presents a graphical illustration of the higher copper binding ability of the bischelator KEMP(NPrHP)$_2$ (H_3L^1) over the monochelators (HL^2 and HL^3), along a range of pH above 4.

Table 1
Stepwise protonation constants of KEMP(NPrHP)$_2$ (H_3L^1) and relevant analogous; overall formation constants of their metal complexes (M = Cu, Ni, Zn) and the corresponding pM values * ($T = 25$ °C, $I = 0.2$ M (KCl))

Ligand	H_3L^1 (KEMP2NPrHP)	HL^2 (AcNPrHP) [a]	HL^3 (3,4-DMHP) [b]	H_2L^4 (Mimosine) [c]
log *K*i	10.17(2)	9.61(2)	9.86	8.86
	9.43(2)	3.57(3)	3.70	7.00
	4.70(2)			2.62
	3.64(1)			1.1
	2.96(3)			
log $\beta_{Cu_pH_qL_r}$	(1, 1, 1) = 22.05(2)	(1, 0, 1) = 10.29(1)	(1, 0, 1) = 10.62	(1, 1, 1) = 16.36
	(1, 0, 1) = 17.42(2)	(1, 0, 2) = 18.99(2)	(1, 0, 2) = 19.61	(1, 0, 1) = 9.48
				(1, 1, 2) = 24.40
				(1, 0, 2) = 16.81
pCu	13.6	10.4	10.5	9.9
log $\beta_{Ni_pH_qL_r}$	(1, 1, 1) = 17.07(1)	(1, 0, 1) = 6.99(5)	(1, 0, 1) = 6.92	
	(1, 0, 1) = 10.41(2)	(1, 0, 2) = 12.38(9)	(1, 0, 2) = 12.13	
pNi	7.9	6.2	6.3	
log $\beta_{Zn_pH_qL_r}$	(1, 1, 1) = 17.39(1)	(1, 0, 1) = 7.19(9)	(1, 0, 1) = 7.19	(1, 1, 1) = 13.84
	(1, 0, 1) = 11.78(1)	(1, 0, 2) = 13.70(9)	(1, 0, 2) = 13.53	(1, 0, 1) = 6.50
				(1, 1, 2) = 19.76
				(1, 0, 2) = 12.27
pZn	7.9	6.3	6.2	6.4

* The equilibrium process to which the overall stability constant (log β) relates is: $pM + qH + rL \rightleftarrows M_pH_qL_r$; $\beta = [M_pH_qL_r]/[M]^p[H]^q[L]^r$; the (p, q, r) symbolism means a species with stoichiometry ($M_pH_qL_r$); $pM = -\log[M^{2+}]$ with $C_L/C_M = 10$, $C_M = 10^{-6}$ M) and at pH 7.4.
[a] $I = 0.1$ M, KNO_3.
[b] According to Ref. [17].
[c] According to Ref. [2].

The stability constants of the di-hydroxypyridone (H_3L^1) complexes with this set of bivalent metal ions seem to follow the proposed Irving–Williams order Ni < Cu > Zn [19], as it happens with hydroxamate complexes [20].

Regarding the type of binding modes in MHL^1 species, two different possibilities can be admitted. As a first possibility, two hydroxypyridinonate groups could be involved in the co-ordination to the metal ion, leaving the dissociable proton in the carboxylic group. Such a co-ordination mode could be favourable if the complex species was formed when the carboxylic moiety is protonated (below pH 4, as happens with the copper complexes, see Figs. 1 and 2(a)). As a second possibility, one of the hydroxypyridinonate groups is in the co-ordinated form while the other one is in protonated form; this complex would be favoured in the pH-range where the carboxylic moiety is already deprotonated (above pH 4, as happens for the nickel and zinc complexes, see Figs. 1 and 2(b)).

In order to get some insight into the co-ordination modes involved in the copper(II) complexes with the di-hydroxypyridonate ligand, UV–Vis absorption spectra of solutions containing this metal ion in the presence of H_3L^1 or HL^2 were registered at different pH (Fig. 4), for comparison purpose. Analysis of Fig. 4 confirms that, in both the systems, complexation has already started at approximately pH 2.5, in accordance with the species distribution diagram (Fig. 2(a)). At pH 3.5, the samples containing the copper(II)–H_3L^1complexes exhibit a *d*–*d* transition band centred at 680 nm ($\varepsilon = 43$ M^{-1} cm^{-1}) and a charge transfer transition ($\lambda_{max} = 377$ nm, $\varepsilon = 250$ M^{-1} cm^{-1}). From the species distribution diagram, it can be mostly assigned to the CuL^1H species. The similarity between the *d*–*d* transition band of this complex and the corresponding bands for the 1:2 complexes with HL^2 ($\lambda_{max} = 675$ nm, $\varepsilon = 59$ M^{-1} cm^{-1}, at pH 5.56), HL^3 ($\lambda_{max} = 692$ nm, $\varepsilon = 31$ M^{-1} cm^{-1}) [17] and H_2L^4 ($\lambda_{max} = 690$ nm, $\varepsilon = 33$ M^{-1} cm^{-1}) [2] gives support to the assumption made on the binding mode through the hydroxypyridinonate moieties. For higher pH values ($3.5 < pH < 5.3$), there is a small blue shift of λ_{max} to 665 nm ($\varepsilon = 51$ M^{-1} cm^{-1}) which may be associated with some formation of the CuL^1 species and some strengthening of metal–ligand bond in these species.

Above pH 5.3, more than 80% of the copper complex is in the neutral form (CuL^1) (see Fig. 2(b)) and precipitation starts in our experimental conditions.

Concerning the nickel(II) complexes, at pH 6.7, the UV–Vis spectra presented a charge transfer transition ($\lambda_{max} = 392$ nm, $\varepsilon = 66$ M^{-1} cm^{-1}) and a very week band in the *d*–*d* region ($\lambda_{max} = 673$ nm, $\varepsilon = 15$ M^{-1} cm^{-1}). This should correspond to the neutral bis-chelated species (NiL, approximately 50%) which started to precipitate with increasing concentration (at pH ≥ 7). According to the spectra, octahedral or pseudo-octahedral geometry around the metal ion is suggested. Since only four coordination sites are occupied by two hydroxypyridinonate moieties, probably

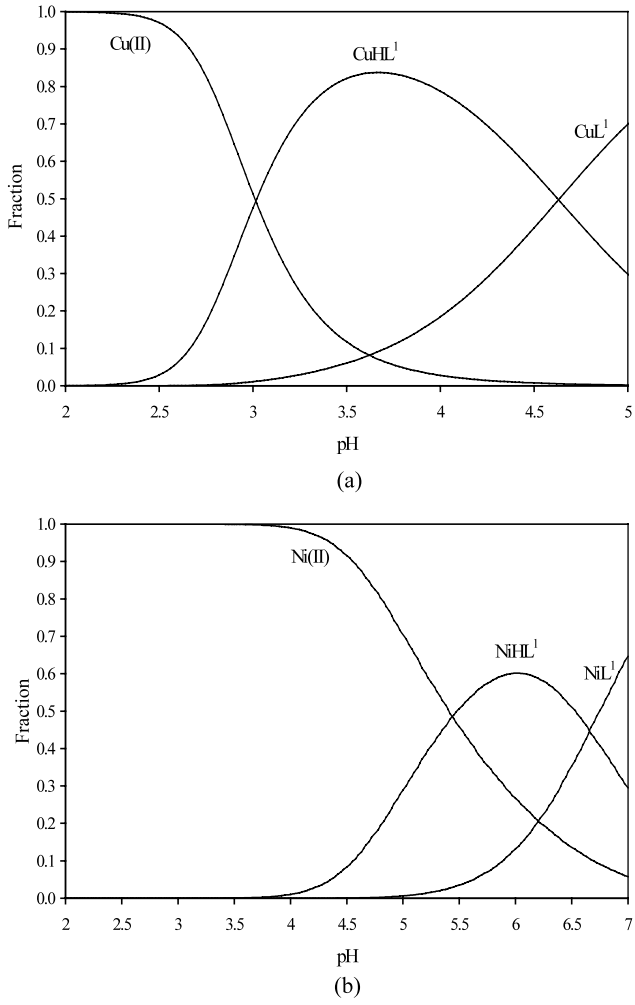


Fig. 2. Concentration distribution curves calculated for the Cu–H_3L^1 complexes (a) and Ni–H_3L^1 complexes (b), at 1:1 metal to ligand ratio and $C_L = 2.9 \times 10^{-3}$ M.

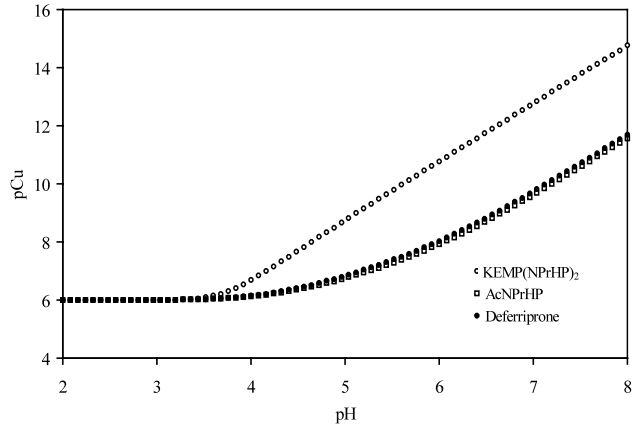


Fig. 3. Copper complexation strength for H_3L^1 ($KEMP(NPrHP)_2$), HL^2 (AcNPrHP) and HL^3 (Deferiprone), reported as pCu vs. pH ($pCu = -\log[Cu^{2+}]$ with $C_L/C_{Cu} = 10$ and $C_{Cu} = 10^{-6}$ M).

two water molecules are also involved to complete the co-ordination around the metal centre. The involvement

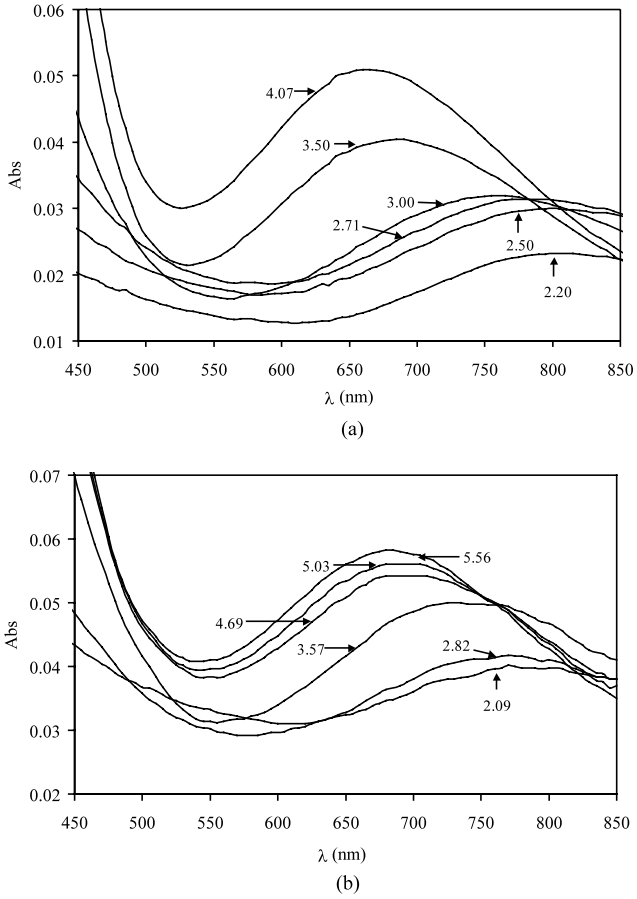


Fig. 4. Absorption spectra registered at various pH values for: the Cu(II)–H_3L^1 system ($C_L = 1.5 \times 10^{-3}$ M, $C_L/C_M = 1.5$) (a); the Cu(II)–HL^2 system ($C_L = 2.0 \times 10^{-3}$ M, $C_L/C_M = 2$).

of the carboxylate group in the coordination can hardly be assumed, due to steric demands.

Regarding the zinc(II) complexes, a brief comparative analysis of the ^1H NMR spectra was performed for complex and ligand solutions in the pH range 4–6. These results showed that the highest deviations in the chemical shifts, $\Delta\delta = -(0.2–0.4)$ ppm, were observed for the two hydroxypyridinone ring protons, thus suggesting the involvement of the hydroxypyridinonate moieties in the co-ordination to the metal centre.

Furthermore, as stated above, the hydroxypyridonate coordination in the metal complexes is also supported by the similarity between the potentiometric titration profiles and also between the overall formation constants obtained for the 1:1 complexes and the 1:2 complexes with H_3L^1 and HL^2, respectively.

Finaly, aimed at giving some contribution to the interpretation of the complexation behaviour of the dihydroxypyridonate ligand, a brief molecular modelling calculation was performed for this ligand (using MOPAC program included in the INSIGHT package [21]) and the Cu–L^1 complex (using molecular mechanics, with the CERIUS2 [22] program and the default force

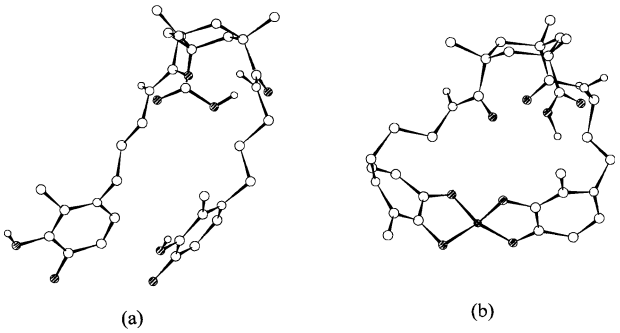


Fig. 5. Structure diagrams calculated for: the ligand H_3L^1, KEMP(NPrHP)$_2$, (a) and the CuL^1 complex (b). The metal ions are doubly hatched; the oxygen atoms are hatched; hydrogen atoms bonded to carbon atoms are omitted.

fields [23]). The simulated structure of the ligand (Fig. 5(a)) suggested a *chair* conformation for the cyclohexane backbone with the alkylamide-hydroxypyridinonate and the carboxylate pendant arms in axial position, thus, pre-orientated to wrap the metal ion. That conformation is apparently supported by some hydrogen-bond interaction between the neighbouring pendant arms. Concerning the Cu–L^1 complex, a distorted square-planar coordination geometry seems probable, with no significant interaction between the carboxylate group and the metal ion, due to steric demands. The coordination of the ligand towards the Cu(II) ion requires the disruption of the hydrogen-bond network found in the ligand, although the *chair* conformation was kept in the minimum energy conformer (Fig. 5(b)).

2.4. Distribution coefficient

The distribution coefficient of the free ligand between the aqueous phase (buffered at pH 7.4 with Tris) and octanol showed that, at physiological pH, the 'dimeric' ligand ($\log D = -1.96 \pm 0.02$) is much more hydrophilic than the corresponding monomeric species ($\log D = -1.04 \pm 0.02$). This is due to the fact that, at this pH, the 'dimeric' ligand is mono-charged $[H_2L^1]^-$ as a result of the dissociation of the carboxylic proton. Even so, it is much less hydrophilic than other (carboxyalkyl)hydroxypyridinones [$\log D = -(2.8–2.9)$] [12] due to some hydrophobicity induced by the higher ratio between the number of hydroxypyridinonate and carboxylate groups (2:1 instead of 1:1).

3. Conclusions

This new heteropodant bis-hydroxypyridonate ligand forms quite stable 1:1 complexes with the bivalent metal ions of the first transition series. The metal co-ordination environment is dominated by the hydroxypyridinonate moieties, thus leaving the extra carboxylic group for further eventual interaction with biological ligands (e.g. proteins). It has proved a good lipo-hydrophilic balance. So, important biological roles may be admitted for this ligand, probably as an enzymatic inhibitor, related to its affinity for Ni(II) and Zn(II), or as a good chelating agent for radio-diagnosis (PET) due to its high affinity for ^{64,67}Cu(II).

4. Experimental

4.1. Chemicals

Analytical grade reagents were used as supplied. Whenever necessary, solvents were dried according to standard methods [24]. All the chemical reactions were TLC controlled.

4.1.1. Synthesis of the ligand, H_3L^1 (or KEMP(NPrHP)$_2$) (**1**)

*4.1.1.1. 1-(3′-Aminopropyl)-3-benzyloxy-2-methyl-4-pyridinone (**3**).* 3-Benzyloxy-2-methyl-4-pyrone (2.3 g, 10.7 mmol), obtained according to previously described [11], and 1,3-diaminopropane (1.1 ml, 13.2 mmol) were left refluxing in water (30 ml) for 6 h. Evaporation of water and excess of 1,3-diaminopropane in vacuum gave an oil which was then dissolved in MeOH. Acidification of that solution until pH 2 with HCl saturated MeOH gave a white precipitate which was recrystallized from dry MeOH–MeCN to give the pure product ($\eta = 40\%$). M.p. 186–189 °C; IR (cm^{-1}, KBr) 1630 ($\nu_{C=O}$). ^{1}H NMR ($CDCl_3$) 8.14 (1H, d, 6-HPy), 7.42 (5H, s, Ph), 7.11 (1H, d, 5-HPy), 5.13 (2H, s, CH_2Ph), 4.31 (2H, t, CH_2N–Pyr), 3.03 (2H, t, CH_2N), 2.36 (2H, t, CH_2CH_2-CH_2), 2.12 (3H, s, Me). *m/z* (FAB) 273 ($M+1$).

*4.1.1.2. 5-(Ch1oroformyl)-cis,cis-1,3,5-trimethylcyclohexane-1,3-dicarboxilic anhydride (**4**).* To a solution of 1,3,5-trimethyl-1,3,5-cyclohexane-tricarboxylic acid (1.95 g, 7.4 mmol) in dry CH_2Cl_2 (50 ml), oxalyl chloride (0.8 ml) was added as well as one drop of dry dimethylformamide (DMF). The mixture was left refluxing under dry nitrogen atmosphere for 4 h. Excess of oxalyl chloride was removed by rota-evaporation. Two 10 ml batches of dry $CHCl_3$ were subsequently added to the residue and then removed by vacuum distillation, giving a white solid. Recrystallisation from dry toluene gave the pure product ($\eta = 85\%$). M.p. 254–258 °C (255–260 °C) [15]. IR (KBr): 1790 cm^{-1} ($\nu_{C=O}$). ^{1}H NMR (C_6D_6) δ: 0.11, 0.77 (2H, 2 × d, $J =$ 14.1 Hz, CH_2Cy); 0.32, 2.33 (4H, 2 × d, $J = 14.1$ Hz, CH_2Cy); 0.86 (6H, s, CH_3), 0.59 (3H, s, CH_3). *m/z* (FAB): 260 ($M+1$).

4.1.1.3. Cis,cis-1,3-di-(1′-(3″-carboxyaminopropyl)-3′-benzyloxy-2′-methyl-4′-pyridinone-yl)-5-carboxyl-1,3,5-

*trimethyl-cyclohexane (**5**)*. To a solution of **3** (1.7 g; 6.25 mmol) and Et_3N (2.6 ml, 18.8 mmol) in dry CH_2Cl_2 (50 ml), under a nitrogen atmosphere and in ice-water bath, a freshly prepared solution of **4** (0.572 g, 2.21 mmol) in dry CH_2Cl_2 (15 ml) was drop-wise added. The reaction mixture was then stirred at room temperature (r.t.) for 6 h. The solvent was removed under reduced pressure and the solid residue was purified by column chromatography on silica gel with CH_2Cl_2–MeOH (30/8) as the eluent. The isolated product was recrystallized from dry MeOH–MeCN ($\eta = 48\%$). M.p. 189–191 °C. IR (cm^{-1}, KBr): 2374 (ν_{NH+}); 1626, 1558 ($\nu_{C=O}$). ^1H NMR (CD_3OD) δ: 7.74 (2H, d, 6-HPy), 7.30 (10H, s, Ph), 6.31 (2H, d, 5-HPy), 5.01 (4H, s, CH_2Ph), 3.96 (4H, t, CH_2NPy); 3.07, 2.82 (4H, 2 × m, CH_2NCO), 2.72 (4H, d, CH_2Cy), 2.12 (6H, s, Me–Py), 1.72 (4H, t, $CH_2CH_2CH_2$), 1.17 (3H, s, CH_3), 1.08 (6H, s, CH_3Cy), 0.85 (2H, d, CH_2Cy). *m/z* (FAB): 767 ($M+1$).

*4.1.1.4. cis,cis-1,3-Di-(1′-(3″-carboxyaminopropyl)-3′-hydroxy-2′-methyl-4′-pyridinonyl)-5-carboxyl-1,3,5-trimethyl-cyclohexane, H_3L^1 (**1**)*. To a solution of **5** (0.2 g, 0.26 mmol) in dry MeOH (50 ml) was added 10% Pd/C (0.05 g) and the mixture was stirred under H_2 (1 atm) for 5 h at r.t. After filtration of the solid residue, the solvent was evaporated under reduced pressure and the product was obtained as a white powder, which was then recrystallized from MeOH–MeCN ($\eta = 80\%$). M.p. 180–182 °C. IR (cm^{-1}, KBr): 3285 (ν_{OH}), 2361 (ν_{NH+}); 1629, 1568 ($\nu_{C=O}$). ^1H NMR (MeOD) δ: 7.65 (2H, d, 6-HPy), 6.31 (2H, d, 5-HPy), 3.95 (4H, t, CH_2NPy), 3.04, 2.86 (2 × 2H, 2 × m, CH_2NCO), 2.72 (4H, d, CH_2Cy), 2.343 (6H, s, Me–Py), 1.77 (4H, t, $CH_2CH_2CH_2$), 1.17 (3H, s, CH_3Cy), 1.08 (6H, s, CH_3Cy), 0.85 (2H, d, CH_2Cy). *m/z* (FAB): 587 ($M+1$). *Anal.* Calc. for $C_{30}N_4H_{42}O_8 \cdot 3H_2O$: C, 56.27; H, 7.50; N, 8.75. Found: C, 56.6; H, 7.58; N, 8.42%.

*4.1.2. Synthesis of the ligand HL^2 (or AcNPrHP) (**2**)*

*4.1.2.1. 1-(3′-Methylcarboxyaminopropyl)-3-benzyloxy-2-methyl-4-pyridinone (**6**)*. To a solution of 1-(3′-aminopropyl)-3-benzyloxy-2-methyl-4-pyridinone (0.46 g; 1.69 mmol) and *N*-methylmorpholine (0.17 g; 1.69 mmol) in dry MeOH (15 ml), cooled in a ice-water bath, was dropwise added a solution of acethylchloride (0.17 g; 2.20 mmol) in dry THF (10 ml). After the addition, the reactional mixture was left under stirring at r.t. for 3 h. The *N*-methylmorpholinium salt, formed during the reaction, was filtered off and the solvents were removed under reduced pressure. The obtained product was than purified by flash column chromatography on silicagel with CH_2Cl_2–MeOH (30:7) as the eluent. The pure product was isolated as a pale oil ($\eta =$ 47%). ^1H NMR (CD_3OD) δ: 7.63 (1H, d, 6-HPy), 7.26 (5H, s, Ph), 6.39 (1H, d, 5-HPy), 5.00 (2H, s, CH_2Bz), 3.90 (2H, t, CH_2NPy), 3.10 (2H, t, CH_2NH), 2.09 (3H, s, CH_3Py), 1.86 (3H, s, $CH_3C{=}O$), 1.76 (2H, q, $CH_2CH_2CH_2$). *m/z* (FAB): 315 ($M+1$).

*4.1.2.2. 1-(3′-Methylcarboxyaminopropyl)-3-hydroxy-2-methyl-4-pyridinone, HL^2 (**2**)*. To a solution of **6** (0.25 g; 0.80 mmol) in dry MeOH (10 ml) was added 10% Pd/C (0.08 g) and the mixture was stirred under H_2 (1.4 atm) for 4 h at r.t. After the solid residue filtration, the solvent was evaporated under reduced pressure and product was obtained as a pale solid. Recrystallization from dry MeOH–MeCN afforded the pure product as pale crystals ($\eta = 84\%$). M.p. = 135–136 °C. ^1H NMR (CD_3OD) δ: 7.53 (1H, d, 6-HPy), 6.30 (1H, d, 5-HPy), 3.98 (2H, t, CH_2NPy), 3.14 (2H, t, CH_2NH), 2.34 (3H, s, CH_3Py), 1.85 (3H, s, $CH_3C{=}O$), 1.79 (2H, q, $CH_2CH_2CH_2$). *m/z* (FAB): 225 ($M+1$). *Anal.* Calc. for $C_{11}N_2H_{16}O_3 \cdot 1.3H_2O$: C, 53.34; H, 7.57; N, 11.31. Found: C, 53.59; H, 7.69; N, 10.82%.

4.2. Potentiometric measurements

The potentiometric measurements were performed at 25 ± 0.1 °C with a MOLSPIN pH-Meter equipped with a Metrohm combined electrode and Mol-ACS microburette controlled by computer. The electrode system was calibrated by the method of Irving et al. [25], so that the pH-meter readings could be converted into hydrogen ion concentrations. Atmospheric CO_2 was excluded from the system with a purging stream of argon gas. The ligand concentration in the sample was 2.9×10^{-3} M (H_3L^1) and 1.6×10^{-3} M (HL^2) with ionic strength of 0.2 M (KCl) and 0.1 M (KNO_3), respectively. The concentration of the ligand stock solutions together with the protonation constants was determined from the potentiometric data by the use of the SUPERQUAD computer program [16].

The complexation studies were performed for each metal ion by potentiometric titrations, with 1:1 and 1:2 metal-ion:ligand ratios. The metal ions were provided from metal-ion stock solutions of the corresponding chloride or nitrate salts. The stability constants were determined using the computer program PSEQUAD [26].

The selection of the equilibrium models was based on the critical analysis of the weighted residuals and the statistical parameters (χ^2 and σ for the SUPERQUAD [27] and the fitting parameter for the PSEQUAD) as well as on graphical comparisons between the experimental and simulated potentiometric curves.. The fitting parameters obtained for the equilibrium models of each ligand–metal ion system were less than 2×10^{-3}.

4.3. Spectrophotometric measurements

All spectra were measured on a HP 8453 and a Lambda 9 Perkin–Elmer spectrophotometer at 25 °C

and at constant ionic strengths. Solutions of the metal complexes were generated in situ by addition of a standard metal ion solution to the ligand solution. The pH measurements were carried out using a 420A Orion pH-meter, equipped with an Orion 91-03 glass calomel combination electrode.

4.4. Partition coefficients

Octanol–water partition coefficients of the ligands were determined at physiological pH, at approximately 25 °C, as described previously [11]. Equal volumes (3 ml) of 2×10^{-4} M ligand solutions in octanol and water (2×10^{-3} M tris buffered solution, pH 7.4) were placed in a 20 ml screw-cap vial. The mixture was stirred for 18 h, allowed to stand for 3 h and then poured into an extraction funnel to separate the two phases. After adequate dilution of the samples, the species concentration was evaluated by UV spectrophotometry (using the 285–295 nm λ_{max} bands). The partition coefficients, D (or $\log D$), were obtained as the ratio of the ligand concentrations in the organic phase to that in the aqueous phase. Both the solvents used in all determinations (octanol and buffered water solution) were previously saturated in each other, by stirring the mixture for 18 h.

4.5. Other measurements

The ^{1}H NMR spectra were recorded on a Varian Unity 300 spectrometer at 25 °C. Chemical shifts are reported in ppm (δ) from internal reference tetramethylsilane (TMS) in organic solvents and sodium 3-(trimethylsilyl)-[2,2,3,3-$^2H_4$]propionate in D_2O solutions (DSS). The following abbreviations are used: d, duplet; s, singlet; t, triplet. Melting temperatures were measured with a Leica Galen III hot stage apparatus and are uncorrected. Elemental analysis was performed on a Fisons EA1108 CHNF/O instrument. Mass spectra were recorded on a VG TRIO-2000 GC/MS instrument.

Acknowledgements

The authors thank to the Portuguese *Fundação para a Ciência e Tecnologia* (FCT) (project POCTI/35344/99), to the Hungarian Scientific Research Fund (OTKA T034674) and COST D21/001 program for financial support.

References

[1] (a) R.L.N. Harris, Aust. J. Chem. 29 (1976) 1329;
(b) R.L. Harris, T. Teitei, Aust. J. Chem. 30 (1977) 649;
(c) H. Stunzi, R.L.N. Harris, D.D. Perrin, T. Tritei, Aust. J. Chem. 33 (1980) 2207.
[2] H. Stunzi, D.D. Perrin, T. Teitei, R.L.N. Harris, Aust. J. Chem. 32 (1979) 21.
[3] R.C. Hider, G.J. Kontoghiorghes, J. Silver, U.K. Patent, G.B. 2118176, 1982.
[4] P.S. Dobbin, R.C. Hider, A.D. Hall, P.D. Taylor, P. Sarpong, J.B. Porter, G. Xiao, D. van der Helm, J. Med. Chem. 36 (1993) 2448.
[5] Z.D. Liu, H.H. Khodr, D.Y. Liu, S.L. Lu, R.C. Hider, J. Med. Chem. 42 (1999) 4814.
[6] G.J. Kontoghiorghes, The Lancet (1985) 817.
[7] (a) Z.D. Liu, H.H. Khodr, S.L. Lu, R.C. Hider, Pharm. Pharmacol. 52 (2000) 263;
(b) Z.D. Liu, R. Hider, Med. Res. Rev. 22 (2002) 26.
[8] M.A. Santos, Coord. Chem. Rev. 228 (2002) 187.
[9] (a) B.L. Ellis, A.K. Duhme, R.C. Hider, M.B. Hossain, S. Rizvi, D. van der Helm, J. Med. Chem. 39 (1996) 3659;
(b) Z. Zang, D.M. Lyster, G.A. Webb, C. Orvig, Nucl. Med. Biol. 19 (1992) 327.
[10] (a) R. Kayyali, J.B. Porter, Z.D. Liu, N.A. Davies, J.H. Nugent, C.E. Cooper, R.C. Hider, J. Biol. Chem. 276 (2001) 48814;
(b) Z.D. Liu, R. Kayyali, R.C. Hider, J.B. Porter, A.E. Theobald, J. Med Chem. 45 (2002) 631.
[11] M.A. Santos, R. Grazina, A.Q. Neto, G. Cantinho, L. Gano, L. Patrício, J. Inorg. Biochem. 78 (2000) 303.
[12] M.A. Santos, M. Gil, S. Marques, L. Gano, G. Cantinho and S. Chaves, J. Inorg. Biochem. 92 (2002) 43.
[13] H.J. Smith, H. Williams, in: H.J. Smith (Ed.), Introduction to the Principles of Drug Design and Action, Harwood, Amsterdam, 1988, pp. 299–309.
[14] S.V. Smith, P.F. Schmidt, N. Di Bartolo, J. Label. Comp. Radiopharm. 40 (1998) 479.
[15] D.S. Kemp, K.S. Petrakis, J. Org. Chem. 46 (1981) 5140.
[16] P. Gans, A. Sabatini, A. Vacca, J. Chem. Soc., Dalton Trans. (1985) 1195.
[17] E.T. Clarke, A.E. Martell, Inorg. Chim. Acta 191 (1992) 57.
[18] A.E. Martell, R.J. Motekaitis, Determination and Use of Stability Constants, vol. 3, VCH, New York, 1988, p. 13.
[19] H. Irving, R.J.P. Williams, J. Chem. Soc. (1953) 3192.
[20] (a) M.A. Santos, R. Grazina, M. Pinto, E. Farkas, Inorg. Chim. Acta 321 (2001) 42;
(b) M.A. Santos, M. Gaspar, M.T. Amorim, Inorg. Chim. Acta 284 (1999) 20.
[21] INSIGHT program, Version 97.2, Molecular Simulations Inc, Cambridge, 1997.
[22] CERIUS2 Program, Version 3.5, Molecular Simulations Inc., Cambridge, 1998.
[23] A.K. Rappe, C.J. Casewit, K.S. Colwell, W.A. Goddard, W.M. Skiff, J. Am. Chem. Soc. 114 (1992) 10024.
[24] W.L.F. Armarego, D.D. Perring, Purification of Laboratory Chemicals, 4th ed., Butterworth-Heinemann, Oxford, 1999.
[25] H. Irving, M.G. Miles, L.D. Pettit, Anal. Chim. Acta 38 (1967) 475.
[26] L. Zékány, I. Nagypál, in: D. Legget (Ed.), Computational Methods for the Determination of Stability Constants, Plenum, New York, 1985.
[27] A. Sabatini, A. Vacca, P. Gans, Talanta 21 (1974) 53.

Now we are extending our studies to the reactivity of the compounds $[ReOX_3(AsPh_3)_2]$ (X = Cl, Br) towards NO and here we present our results of the synthesis, spectroscopic and structural characterisation of the following complexes: $[ReBr_3(NO)(OAsPh_3)_2]$ (**1**), $[ReCl_3(NO)(OAsPh_3)_2]$ (**2**), $[ReCl_3(NO)(AsPh_3)_2]$-$[ReCl_4(AsPh_3)_2]$ (**3**) and $[ReCl_4(OAsPh_3)_2]$ (**4**).

We have also carried out the reactions of $[NBu_4]_2$-$[ReX_5(NO)]$ (X = Cl, Br) with an excess of triphenylarsine, which lead to $[ReCl_3(NO)(AsPh_3)_2][ReCl_4$-$(AsPh_3)_2]$ (**3**) and $[ReBr_3(NO)(AsPh_3)_2]$ (**5**), respectively.

Considering that $AsPh_3$ and $OAsPh_3$ molecules are replaced more readily than P- and N-donor ligands, these complexes are predicted to be very useful starting material in the synthesis of new rhenium nitrosyls [17–22].

2. Experimental

Triphenylarsine and NH_4ReO_4 were purchased from Aldrich Chemical Co. and used without further purification. The $[ReOX_3(AsPh_3)_2]$ and $[NBu_4]_2[ReX_5(NO)]$ (X = Cl, Br) complexes were synthesised according to the literature methods [23,24]. Gaseous NO, obtained in the reaction: $2NaNO_2 + 3H_2SO_4 + 2FeSO_4 \rightarrow 2NO + 2NaHSO_4 + Fe_2(SO_4)_3 + 2H_2O$, was purified by passing through washers with concentrated KOH solution and over solid NaOH. Solvents were dried and deoxygenated prior to use in the usual way. The reaction, all preparations and the recrystallisation were performed under argon atmosphere.

2.1. Synthesis of *1*

NO was passed through a vigorously stirred and refluxing solution of $[ReOBr_3(AsPh_3)_2]$ (1.05 g, 1 mmol) in CH_2Cl_2, tetrahydrofurane or C_6H_6 (40 cm^3).

The reaction was carried out for 4–5 h. The colour changed gradually from bright green to dark green. Then the resulting solution was evaporated to the volume of 10 cm^3. The green precipitate was formed by an addition of 40 cm^3 of EtOH and after 15 min it was filtered off. The product was washed with cold ether and dried in vacuo. The yield of **1** does not depend on sort of solution and it equals to 0.88 g (0.80 mmol).

Anal. Calc. for $C_{36}H_{30}As_2Br_3O_3NRe$ (**1**): C, 39.29; H, 2.75; N, 1.27. Found: C, 39.24; H, 2.72; N, 1.29%.

2.2. Synthesis of *2, 3 and 4*

The reaction of gaseous NO with $[ReOCl_3(AsPh_3)_2]$ (0.92 g, 1 mmol) in a CH_2Cl_2, tetrahydrofurane or C_6H_6 solution (40 cm^3) was carried out in the same manner as for **1**, but a mixture of the three products was isolated and the complexes **2**, **3** and **4** were separated by recrystallisation. At room temperature complex **3** does not dissolve in MeCN but **2** and **4** compounds dissolve in CH_3CN readily and **4** precipitates from the solution first. Compound **3** was recrystallised from CH_2Cl_2. The yield of **2**, **3** and **4** depends on the kind of the reaction solution; in CH_2Cl_2 and tetrahydrofurane—**2** (75%), **3** and **4** (3%); in C_6H_6—**2** (70%), **3** and **4** (5%).

Anal. Calc. for $C_{36}H_{30}As_2Cl_3O_3NRe$ (**2**): C, 44.71; H, 3.13; N, 1.45. Found: C, 44.64; H, 3.16; N, 1.41%. Calc. for $C_{72}H_{60}As_4Cl_7ONRe_2$ (**3**): C, 46.11; H, 3.22; N, 0.75. Found: C, 46.24; H, 3.25; N, 0.87%. Calc. for $C_{36}H_{30}$-$As_2Cl_4O_2Re$ (**4**): C, 44.46; H, 3.11. Found: C, 44.57; H, 3.15%.

2.3. Synthesis of *3*

A mixture of $[NBu_4]_2[Re(NO)Cl_5]$ (1 g, 1.14 mmol) and $AsPh_3$ (5 g, 0.016 mol) in EtOH (30 cm^3) was refluxed for 6 h. The formed dark red precipitate was filtered and washed with ether. Yield: 65%.

2.4. Synthesis of *5*

A mixture of $[NBu_4]_2[Re(NO)Br_5]$ (1 g, 0.91 mmol) and $AsPh_3$ (5 g, 0.016 mol) in EtOH (30 cm^3) was refluxed for 6 h. The formed dark red precipitate was filtered and washed with ether. Yield: 70%.

Anal. Calc. for $C_{36}H_{30}As_2Br_3ONRe$ (**5**): C, 40.47; H, 2.83; N, 1.31. Found: C, 40.41; H, 2.87; N, 1.34%.

2.5. Physical measurements

Infrared spectra were recorded on a Nicolet Magna 560 spectrophotometer in the spectral range 4000–400 cm^{-1} with the samples in the form of potassium bromide pellets. Electronic spectra were measured on a Beckman 5240 spectrophotometer in the range 800–220 nm in deoxygenated CH_2Cl_2 solution.

EPR spectra in the X-band ($\nu \approx 9.5$ GHz) at $T = 295$ K have been recorded for CH_2Cl_2 solutions of complexes **1** and **5** and for **5** in the solid state, using a Bruker EMX spectrometer. About 10^{-3} M solutions of **1** and **5** in CH_2Cl_2 were used.

Magnetic susceptibilities were measured at 296 K by the Faraday method.

Elemental analyses (C H N) were performed on a Perkin–Elmer CHN-2400 analyzer.

2.6. Crystal structure determination and refinement

The crystals of **1**, **3**–**5** suitable for X-ray structure determination were obtained by slow evaporation from MeCN solutions. The X-ray intensity data were collected on a Kuma KM-4 diffractometer (compounds **3** and **5**) with ω–2θ scan mode and on a KM-4-CCD automatic diffractometer equipped with CCD detector

Table 1
Crystal data and structure refinement for **1**, **3**, **4** and **5**

	1	**3**	**4**	**5**
Empirical formula	$C_{36}H_{30}As_2Br_3O_3NRe$	$C_{36}H_{30}As_2Cl_{3.33}O_{0.67}N_{0.67}Re$	$C_{36}H_{30}As_2Cl_4O_2Re$	$C_{36}H_{30}As_2Br_3ONRe$
Formula weight	1100.38	936.81	972.44	1068.38
Temperature (K)	293(2)	293(2)	293(2)	293(2)
Crystal system	monoclinic	triclinic	monoclinic	monoclinic
Space group	$P2_1/n$	$P\bar{1}$	$C2/c$	$C2/c$
Unit cell dimensions				
a (Å)	10.2800(3)	12.077(3)	14.077(3)	25.044(5)
b (Å)	20.8840(8)	14.143(3)	13.271(3)	9.664(5)
c (Å)	17.3947(6)	16.605(3)	19.376(4)	16.225(8)
α (°)	90	65.56(2)	90	90
β (°)	93.559(3)	83.34(2)	95.00(3)	116.77(5)
γ (°)	90	87.88(2)	90	90
Volume (Å^3)	3727.2(2)	2564.5(10)	3606.0(13)	3506(3)
Z	4	3	4	4
D_{calc} (Mg m^{-3})	1.961	1.820	1.791	2.024
Absolute coefficient (mm^{-1})	8.273	5.763	5.519	8.788
$F(000)$	2092	1361	1884	2028
Crystal dimensions (mm)	0.25 × 0.09 × 0.09	0.11 × 0.32 × 0.45	0.17 × 0.11 × 0.04	0.08 × 0.20 × 0.20
θ Range for data collection (°)	3.15–25.05	1.36–25.05	3.44–28.83	1.82–25.05
Index ranges	$-12 \le h \le 12$, $0 \le k \le 24$, $-20 \le l \le 0$	$-14 \le h \le 14$, $0 \le k \le 15$, $-18 \le l \le 18$	$-19 \le h \le 19$, $0 \le k \le 17$, $0 \le l \le 25$	$-18 \le h \le 29$, $-2 \le k \le 11$, $-18 \le l \le 19$
Reflections collected	6587	8833	4435	3906
Independent reflections	6587 ($R_{int} = 0.00$)	8535 ($R_{int} = 0.0207$)	4435 ($R_{int} = 0.00$)	3059 ($R_{int} = 0.0394$)
Data/restraints/parameters	6587/0/445	8535/1/593	4435/0/205	3059/0/202
Goodness-of-fit on F^2	1.061	1.152	1.148	1.134
Final R indices [$I > 2\sigma(I)$]	$R_1 = 0.0348$ $wR_2 = 0.0874$	$R_1 = 0.0512$ $wR_2 = 0.1081$	$R_1 = 0.0684$ $wR_2 = 0.1064$	$R_1 = 0.0416$ $wR_2 = 0.0948$
R indices (all data)	$R_1 = 0.0464$ $wR_2 = 0.0946$	$R_1 = 0.0750$ $wR_2 = 0.1200$	$R_1 = 0.0883$ $wR_2 = 0.1152$	$R_1 = 0.0619$ $wR_2 = 0.1085$
Largest difference peak and hole (e Å^{-3})	0.841 and −0.936	2.109 and −1.448	2.017 and −1.567	1.328 and −0.870

(compounds **1** and **4**), with ω scan mode, 30 s exposure time was used and a half of the Ewald sphere was collected. The unit cell parameters were determined from least-squares refinement of the setting angles from a number of the strongest reflections. Details concerning crystal data and refinement are given in Table 1. Lorentz, polarization, empirical absorption corrections (compounds **3** and **5**) and numerical absorption corrections [25] (compounds **1** and **4**) were applied. The structures were solved by means of the Patterson and direct methods and subsequently completed by difference Fourier recycling. All the non-hydrogen atoms were refined anisotropically using full-matrix, least-squares technique. The hydrogen atoms of the phenyl rings were treated as 'riding' on their parent carbon atoms [d(C–H) = 0.96 Å] and assigned isotropic temperature factors equal to 1.2 times the value of the equivalent temperature factor of the parent carbon atom. SHELXS-97 [26a], SHELXL-97 [26b] and SHELXTL [27] programs were used for all the calculations. Atomic scattering factors were those incorporated in the computer programs.

3. Results and discussion

It is known that reactions of high oxidation state metal halides with gaseous nitric oxide usually lead to low-valent nitrosyl complexes and it is accompanied with the elimination of nitrosyl halides [28,29].

The reaction of $[ReOCl_3(AsPh_3)_2]$ with NO leads to the complex **2** (the main product) and two by-products (**3** and **4**), whereas only one compound (complex **1**) was isolated in the reaction of the bromine oxocomplex with nitric oxide.

The difference in the course of the reactions $[ReOX_3(AsPh_3)_2]$ (X = Cl, Br) with NO depending on the kind of halogen in the starting oxocomplex can be explained considering that NOX are relatively unstable

gaseous compounds under normal conditions and that NOBr is much less stable than NOCl.

The suggested course of the main (**2**) and minor (**3** and **4**) product formation is given in the following scheme:

$$[ReOCl_3(AsPh_3)_2] + 3NO \rightarrow [ReCl_3(NO)(OAsPh_3)_2] + N_2O \quad (1)$$

$$[ReOCl_3(AsPh_3)_2] + 4NO \rightarrow [ReCl_2(NO)_2(AsPh_3)_2] + NOCl + NO_2 \quad (2)$$

$$[ReCl_2(NO)_2(AsPh_3)_2] + 2NOCl \rightarrow [ReCl_4(OAsPh_3)_2] + 2N_2O \quad (3)$$

$$2[ReOCl_3(AsPh_3)_2] + NOCl \rightarrow [ReCl_3(NO)(AsPh_3)_2] \; [ReCl_4(AsPh_3)_2] + O_2 \quad (4)$$

The $[ReCl_2(NO)_2(AsPh_3)_2]$ compound has not been isolated, but the analogous dinitrosyl $[ReCl_2(NO)_2(PPh_3)_2]$, obtained in the reaction of $[ReOCl_3(PPh_3)_2]$ with nitric oxide, has been characterised [7].

The proposed above mechanism of the reaction of $[ReOCl_3(AsPh_3)_2]$ with NO can be confirmed by the higher yields of by-products in benzene solution than in CH_2Cl_2 or THF. Due to the formation of the $ClNO \cdot C_6H_6$ complex, the concentration of nitrosyl chloride in benzene is much higher than in dichloromethane or tetrahydrofurane, where $ClNO \cdot CH_2Cl_2$ and $ClNO \cdot THF$ are not formed [30,31].

As in the reaction of $[ReOBr_3(AsPh_3)_2]$ with NO only one product has been isolated—$[ReBr_3(NO)(OAsPh_3)_2]$ (**1**)—it can be assumed that the unstable NOBr is not formed and the reactions similar to Eqs. (2)–(4) do not occur.

The reaction equation explains the formation of complex **5**:

$$[NBu_4]_2[ReBr_5(NO)] + 2AsPh_3 \rightarrow [ReBr_3(NO)(AsPh_3)_2] + 2[NBu_4]Br$$

whereas the reaction of $[NBu_4]_2[ReCl_5(NO)]$ with triphenylarsine goes as follows:

$$2[NBu_4]_2[ReCl_5(NO)] + 4AsPh_3 \rightarrow [ReCl_3(NO)(AsPh_3)_2] \; [ReCl_4(AsPh_3)_2] + NOCl + 2[NBu_4]Cl$$

The yield of the product in the reactions of $[NBu_4]_2$-$[ReX_5(NO)]$ with $AsPh_3$ depends on:

- mass ratio of $[NBu_4]_2[ReX_5(NO)]$ to triphenylarsine and it is the highest when it is equal to 1:5.
- reaction time; the yield drops considerably when the reaction is carried out for a time shorter than 6 h.

The complex **1** crystallises in the monoclinic space group $P2_1/n$ and its structure consists of discrete and well-separated monomers. Fig. 1 shows the molecular structure of this compound. The rhenium atom is in a distorted octahedral environment with a linear N–O group *trans* to one of the $OAsPh_3$ ligands, two mutually

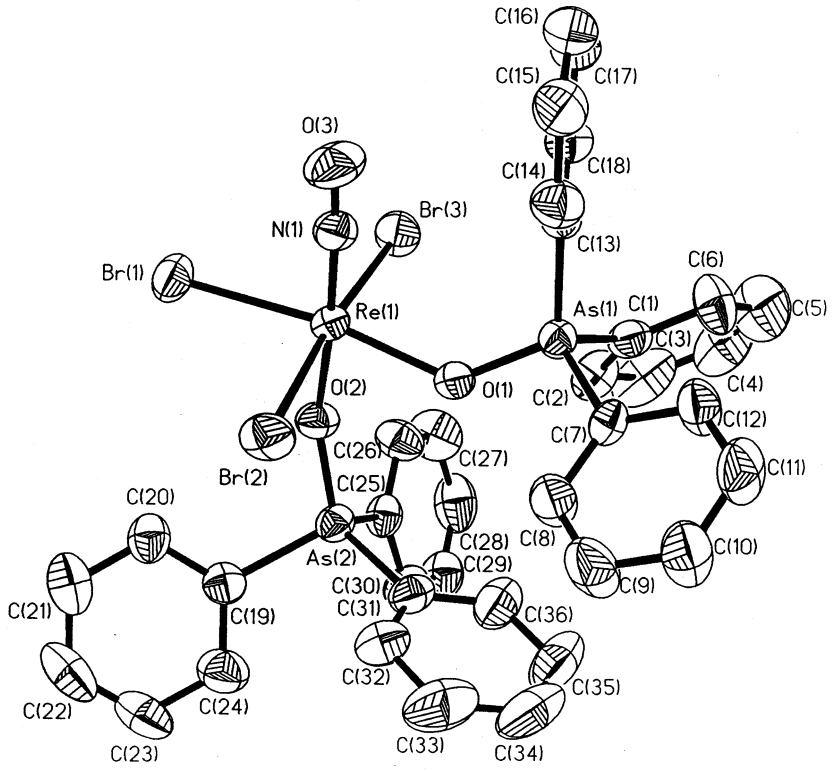


Fig. 1. The molecular structure of **1**. The thermal ellipsoids are drawn at the 50% probability level.

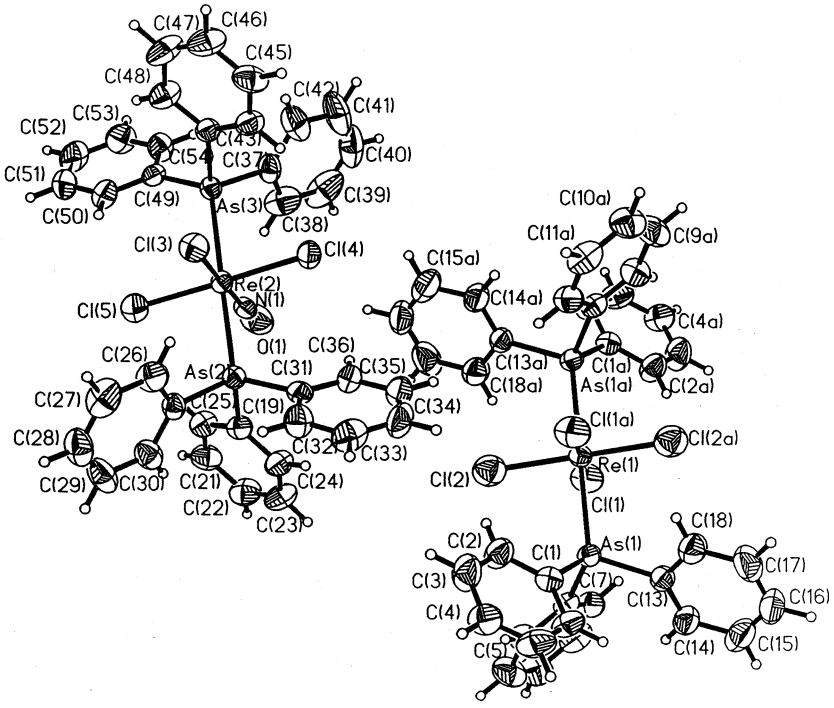


Fig. 2. The molecular structure of **3**.

cis $OAsPh_3$ molecules and three bromine ligands in *meridional* geometry. The major distortion in the geometry, which is an increase in the N(1)–Re(1)–O(1) angle, is caused by the presence of a multiply bonding ligand (Re–NO) and sizeable steric interactions of two mutually *cis* $OAsPh_3$ molecules.

The asymmetric unit of **3**, which crystallises in the triclinic space group $P\bar{1}$, consists of one molecule—$[ReCl_3(NO)(AsPh_3)_2]$—with all atoms in general positions and half the $[ReCl_4(AsPh_3)_2]$ molecule with the rhenium atom on a centre of symmetry. Due to the requirements of the symmetry, the atoms Re(1), Cl(1), Cl(2) and the symmetry equivalents of the two chlorine atoms of the $[ReCl_4(AsPh_3)_2]$ complex lie in one plane and the coordination around the central atom is a square bipyramid extended along the Re–As bonds. Three mutually meridional chlorine atoms, two $AsPh_3$ ligands *trans* to each other and the linear nitrosyl group octahedrally surround the rhenium atom in the $[ReCl_3(NO)(AsPh_3)_2]$ complex. The departure from the ideal octahedron—the angles between *cis*-ligands vary between 85.31° and 95.38°, and the *trans*-angles are between 175.17° and 178.31°—appears to be due to the electronic factors and steric interactions with the NO ligand and it is commonly observed in octahedral complexes containing a multiply bonding ligand [32–34]. The relative orientation of the $[ReCl_4(AsPh_3)_2]$ and $[ReCl_3(NO)(AsPh_3)_2]$ molecules is depicted in Fig. 2.

The complex **4** belongs to the *C*2/*c* space group and the molecular structure of **4** is shown in Fig. 3. The rhenium atom in **4** occupies a special position *e* of the space group *C*2/*c* with multiplicity 4 and site symmetry 2. Atom O(1) shows signs of disorder with a particularly high value of one of the displacement parameters, but all attempts to model the disorder failed. It can be suggested that the disorder is dynamical in character. The atom Cl(2) shows multipositional disorder, but invoking this model did not improve the quality of refinement, therefore the model was not applied. The chlorine atoms Cl(2) and its symmetry equivalent Cl(2A) and two *cis*-oxo atoms of OAsPh3 molecules, O(1) and O(1A) hold the equatorial positions. The Cl(1) and its symmetry equivalent Cl(1A) ions occupy the apical positions. The deviations from an ideal octahedron (the angles between *cis*-ligands vary between 84.1° and 95.06°, and the *trans*-angles are between 171.33° and 178.4°) are caused by steric interactions of two mutually *cis* $OAsPh_3$ molecules.

The structure of **5** consists of discrete and well-separated monomers. The numbering scheme of **5** is shown in Fig. 4. The complex has pseudooctahedral geometry with *trans* arsine ligands, *meridional* bromo ligands and a linear nitrosyl group. The rhenium, NO and bromine species are sited on a crystallographic twofold axis, therefore only half of the molecule is independently located in the asymmetric unit. The three mutually perpendicular coordination planes are well defined and there are no significant intermolecular contacts. The angles between *cis*-ligands vary between 87.83° and 92.14° (Table 2), and the *trans*-angles are between 177.88° and 180°.

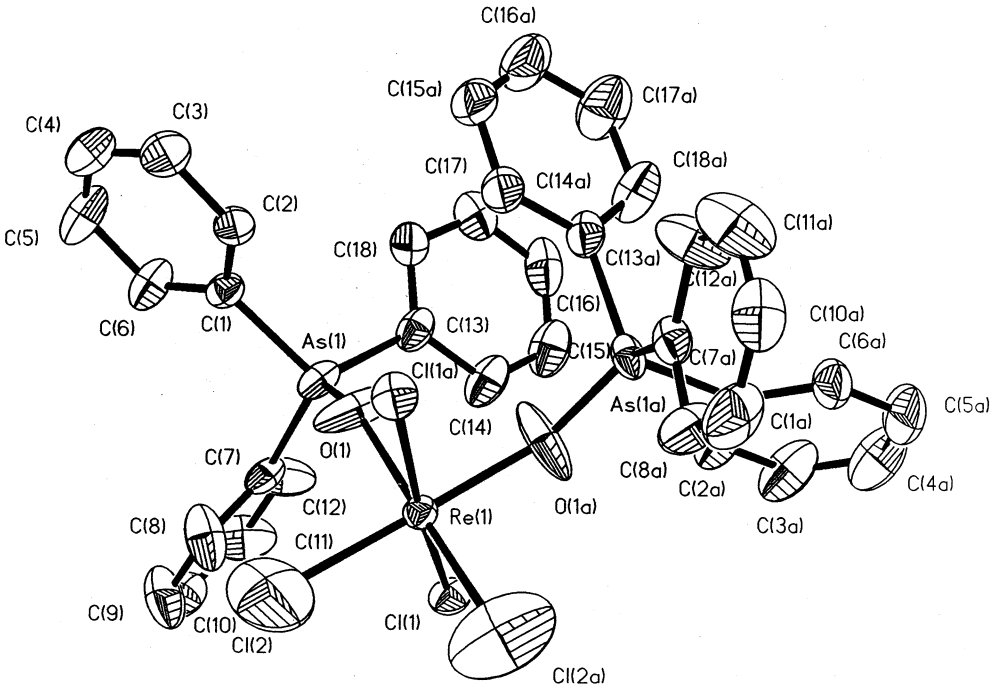


Fig. 3. The molecular structure of **4**.

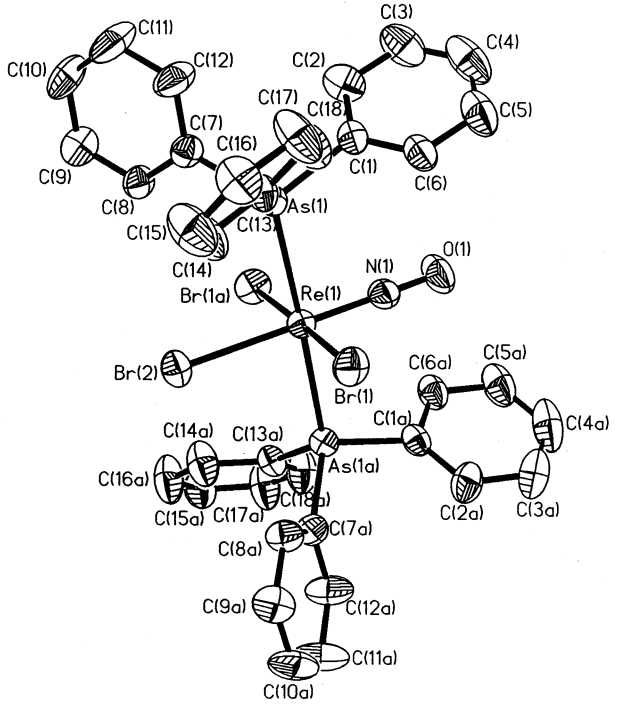


Fig. 4. The molecular structure of **5**.

The complex **5** is isomorphous with $[ReX_3(NO)(PPh_3)_2]$ (X = Cl and Br) [14,16], $[ReOCl_3(PPh_3)_2]$ [35] and several similar ruthenium nitrosyl compounds [36,37]. The packing of the two bulky triphenylarsine or triphenylphosphine ligands, which are *trans* to each other, seems to govern the solid-state structure of these complexes. In fact, the *C*2/*c* space group with four formula units per unit cell is the preferred one for such neutral pseudooctahedral bis(triphenylphosphine) or bis(triphenylarsine) complexes when the co-ordination plane perpendicular to the P–P or As–As vector contains three or four ligands of low steric bulk, which will not cause unusual intermolecular interactions.

The *trans*-arrangement of the two bulky triphenylarsine molecules in **3** and **5** complexes, connected with sterically demanding nature of the arsine ligands, causes the *cis*-location of the nitrosyl group, with respect to the $AsPh_3$ molecules (π-acid ligands). This is also supported by the electronic influence of the multiply bonded ligand, which forces the metal nonbonding d electrons to lie in the plane perpendicular to the M–NO bond axis. This general rule appears to hold for isonitrile, carbonyl, olefin, acetylene, thioether and often phosphine ligands [38–40].

Table 1 presents crystal data and structural refinement for compounds **1**, **3**, **4** and **5**. The most important bond lengths and angles for compounds **1**, **3**, **4** and **5** are reported in Table 2. The Re–NO and N–O bond lengths and the values of Re–N–O angles for complexes **1**, **3** and **5**, summarised in Table 3, confirm the linear coordination of the nitrosyl group and are comparable with values previously found by others (Table 3). For nitrosyl complexes containing two *trans* triphenylarsine molecules, elongation of the Re–halogen bond *trans* to the linear nitrosyl group is observed: the Re–Br(2) bond length at 2.5578(19) Å in **5** is longer than Re–Br(1) by about 0.05 Å and in $[ReCl_3(NO)(AsPh_3)_2]$ the Re–Cl(3)

Table 2
Selected bond lengths (Å) and angles (°) for **1**, **3**, **4** and **5**

1		**3**		**4**		**5**	
Bond lengths							
Re(1)–N(1)	1.749(5)	Re(1)–Cl(2)	2.329(3)	Re(1)–O(1)	2.000(7)	Re(1)–N(1)	1.740(11)
Re(1)–O(1)	2.050(4)	Re(1)–Cl(1)	2.358(3)	Re(1)–Cl(2)	2.292(7)	Re(1)–Br(1)	2.5034(19)
Re(1)–O(2)	2.059(4)	Re(1)–As(1)	2.6023(10)	Re(1)–Cl(1)	2.370(2)	Re(1)–Br(2)	2.5578(19)
Re(1)–Br(2)	2.5117(7)	Re(2)–N(1)	1.816(10)	As(1)–O(1)	1.640(7)	Re(1)–As(1)	2.5946(9)
Re(1)–Br(1)	2.5180(7)	Re(2)–Cl(5)	2.338(3)			N(1)–O(1)	1.177(13)
Re(1)–Br(3)	2.5263(7)	Re(2)–Cl(4)	2.339(2)				
N(1)–O(3)	1.156(6)	Re(2)–Cl(3)	2.376(2)				
O(1)–As(1)	1.680(4)	Re(2)–As(2)	2.6060(11)				
O(2)–As(2)	1.662(4)	Re(2)–As(3)	2.6186(11)				
		N(1)–O(1)	1.092(2)				
Bond angles							
N(1)–Re(1)–O(1)	100.6(2)	Cl(2)#1–Re(1)–Cl(2)	180.0	O(1)#2–Re(1)–O(1)	84.8(7)	N(1)–Re(1)–Br(1)	90.88(2)
N(1)–Re(1)–O(2)	175.98(19)	Cl(2)#1–Re(1)–Cl(1)	91.08(11)	O(1)#2–Re(1)–Cl(2)	178.4(4)	Br(1)–Re(1)–Br(1)#3	178.25(5)
O(1)–Re(1)–O(2)	83.24(16)	Cl(2)–Re(1)–Cl(1)	88.92(11)	O(1)–Re(1)–Cl(2)	93.8(4)	N(1)–Re(1)–Br(2)	180.000(1)
N(1)–Re(1)–Br(2)	93.30(17)	Cl(1)–Re(1)–Cl(1)#1	180.0	Cl(2)–Re(1)–Cl(2)#2	87.6(4)	Br(1)–Re(1)–Br(2)	89.12(2)
O(1)–Re(1)–Br(2)	86.59(12)	Cl(2)–Re(1)–As(1)#1	92.40(8)	O(1)#2–Re(1)–Cl(1)	84.1(2)	N(1)–Re(1)–As(1)	91.07(2)
O(2)–Re(1)–Br(2)	88.06(12)	Cl(1)–Re(1)–As(1)#1	87.10(8)	O(1)–Re(1)–Cl(1)	89.5(2)	Br(1)–Re(1)–As(1)	87.82(6)
N(1)–Re(1)–Br(1)	89.90(16)	Cl(2)–Re(1)–As(1)	87.60(8)	Cl(2)–Re(1)–Cl(1)	95.06(14)	Br(1)#3–Re(1)–As(1)	92.15(6)
O(1)–Re(1)–Br(1)	169.43(11)	Cl(1)–Re(1)–As(1)	92.90(8)	Cl(2)#2–Re(1)–Cl(1)	91.20(13)	Br(2)–Re(1)–As(1)	88.93(2)
O(2)–Re(1)–Br(1)	86.27(12)	As(1)#1–Re(1)–As(1)	180.0	Cl(1)–Re(1)–Cl(1)#2	171.33(12)	As(1)–Re(1)–As(1)#3	177.87(4)
Br(2)–Re(1)–Br(1)	91.76(3)	N(1)–Re(2)–Cl(5)	93.9(3)	O(1)–As(1)–C(1)	104.0(4)	O(1)–N(1)–Re(1)	180.000(2)
N(1)–Re(1)–Br(3)	92.22(17)	N(1)–Re(2)–Cl(4)	90.8(3)	O(1)–As(1)–C(13)	110.8(5)	C(7)–As(1)–C(1)	106.4(4)
O(1)–Re(1)–Br(3)	88.03(12)	Cl(5)–Re(2)–Cl(4)	175.17(9)	C(1)–As(1)–C(13)	110.7(4)	C(7)–As(1)–C(13)	100.3(3)
O(2)–Re(1)–Br(3)	86.73(12)	N(1)–Re(2)–Cl(3)	178.2(3)	O(1)–As(1)–C(7)	115.8(4)	C(1)–As(1)–C(13)	104.3(3)
Br(2)–Re(1)–Br(3)	172.92(2)	Cl(5)–Re(2)–Cl(3)	87.90(9)	C(1)–As(1)–C(7)	107.4(4)	C(7)–As(1)–Re(1)	119.9(3)
Br(1)–Re(1)–Br(3)	92.68(2)	Cl(4)–Re(2)–Cl(3)	87.34(9)	C(13)–As(1)–C(7)	108.1(4)	C(1)–As(1)–Re(1)	107.2(2)
O(3)–N(1)–Re(1)	176.8(5)	N(1)–Re(2)–As(2)	89.5(3)	As(1)–O(1)–Re(1)	147.5(4)	C(13)–As(1)–Re(1)	117.3(3)
As(1)–O(1)–Re(1)	132.9(2)	Cl(5)–Re(2)–As(2)	85.49(7)				
O(1)–As(1)–C(13)	116.7(2)	Cl(4)–Re(2)–As(2)	93.71(7)				
O(1)–As(1)–C(7)	107.2(2)	Cl(3)–Re(2)–As(2)	90.29(7)				
C(13)–As(1)–C(7)	105.9(3)	N(1)–Re(2)–As(3)	91.9(3)				
O(1)–As(1)–C(1)	107.2(2)	Cl(5)–Re(2)–As(3)	95.38(7)				
C(13)–As(1)–C(1)	109.1(3)	Cl(4)–Re(2)–As(3)	85.31(7)				
C(7)–As(1)–C(1)	110.6(3)	Cl(3)–Re(2)–As(3)	88.29(7)				
		As(2)–Re(2)–As(3)	178.31(3)				
		O(1)–N(1)–Re(2)	176.0(9)				
		C(7)–As(1)–C(13)	103.9(4)				
		C(7)–As(1)–C(1)	103.7(4)				
		C(13)–As(1)–C(1)	102.2(4)				
		C(7)–As(1)–Re(1)	114.1(3)				
		C(13)–As(1)–Re(1)	114.6(3)				
		C(1)–As(1)–Re(1)	116.8(3)				

Table 3
Relevant structural data for selected rhenium nitrosyl complexes

Complex	Re–NO bond length (Å)	N–O bond length (Å)	Re–N–O angle (°)
$[ReBr_3(NO)(AsPh_3)_2]$	1.740(11)	1.177(13)	180.000(2)
$[ReCl_3(NO)(AsPh_3)_2]$	1.816(10)	1.092(2)	176.0(9)
$[ReBr_3(NO)(OAsPh_3)_2]$	1.749(5)	1.156(6)	176.8(5)
$[ReCl_3(NO)(OPPh_3)_2]$ [13]	1.72(3)	1.21(3)	172.0(4)
$[ReCl_3(NO)(PPh_3)_2]$ [14]	1.765(9)	1.200(11)	180.000(2)
$[ReBr_3(NO)(OPPh_3)_2]$ [16]	1.757(12)	1.261(13)	172.6(13)
$[ReBr_3(NO)(PPh_3)_2]$ [16]	1.769(12)	1.12(2)	180.000(2)
$[NEt_4][ReBr_4(NO)(MeCN)]$ [41]	1.771(11)	0.99(2)	178.0(6)
$[NEt_4][ReBr_4(NO)(EtOH)]$ [41]	1.723(15)	1.19(2)	169.0(3)
$[ReCl_3(NO)(NPPh_3)(OPPh_3)]$ [42]	1.734(10)	1.183(13)	174.1(9)

Table 4
Band position (cm^{-1}) in IR range for complexes **1**–**5**

1	2	3	4	5	Assignment
1733	1721	1738		1773	ν(NO)
1483	1481	1482	1482	1481	δ(C–CH in the plane)
1439	1439	1435	1436	1435	ν(As–C_6H_5)
1085	1085	1077	1080	1076	δ(C–H in the plane)
1023	1024	1024	1024	1034	δ(C–H in the plane)
893	888		890		ν(As=O)
837	850		840		ν(As=O)
739	739	741	740	737	δ(C–C out of the plane)
688	689	692	690	691	δ(C–C in the plane)
628	625				δ(C–C in the plane)
480	481	471		474	ν(Re–N)

bond length at 2.376(2) Å is longer than Re–Cl(4) and Re–Cl(5) by about 0.04 Å. A similar trend is observed in $[ReX_3(NO)(PPh_3)_2]$ (X = Cl, Br) complexes [14,16].

The Re–As distances 2.6023(10) Å in $[ReCl_4(AsPh_3)_2]$, 2.6060(11) and 2.6186(11) Å in $[ReCl_3(NO)(AsPh_3)_2]$ and 2.5946(9) Å in **5** are considerable longer than those found in the rhenium complexes with a *cis* arrangement of arsine ligands: 2.557(2) and 2.541(2)Å in $[ReO_2(dadpe)_2]^+$ and 2.532(1), 2.552(1), 2.541(1) and 2.546(1) Å in $[ReN(dpae)_2Cl]^+$ [43].

The Re–$OAsPh_3$ and the As–O bond lengths in complexes **1** and **4** (Table 2) are in good agreement with values found for $[ReOBr_3(AsPh_3)(OAsPh_3)]$ (Re–O = 2.010(7), As–O = 1.675(7) Å) and $[ReOCl_3(AsPh_3)(OAsPh_3)]$ (Re–O = 2.019(8), As–O = 1.643(9) Å [44]). In complex **4**, the Re–Cl(2) distance at 2.292(7) Å is shorter than Re–Cl(1) by about 0.08 Å as a result of its *trans* position to the $OAsPh_3$ molecule.

The bond valences were computed as $v_{ij} = \exp[(R_{ij} - d_{ij})/0.37]$ [47–49], where R_{ij} is the bond-valence parameter (in the formal sense R_{ij} is the single-bond length between *i* and *j* atoms) [50]. The R_{Re-O}, R_{Re-N}, R_{Re-Br}, R_{Re-Cl} values were taken as 1.97, 2.06, 2.45 and 2.23 [47], respectively. The computed bond valences of rhenium in compound **1** are $v_{Re-O} = 0.79$, 0.80, $v_{Re-Br} = 0.80$, 0.81, 0.85; $v_{Re-N} = 2.32$ v.u. (valence units), in compound **3** are $v_{Re-As} = 0.81$, 0.84, $v_{Re-Cl} =$ 0.67, 0.71, 0.75, 0.74, 0.76, 0.81, 0.85; $v_{Re-N} = 1.93$ v.u., in compound **4** are $v_{Re-O} = 0.92$, $v_{Re-Cl} = 0.68$, 1.04 v.u. and in compound **5** are $v_{Re-As} = 0.86$, $v_{Re-Br} = 0.74$, 0.86; $v_{Re-N} = 2.37$ v.u. The weakest bonds are Re–Cl bonds in compound **3** and the strongest are Re–N bonds (formally these bonds can be considered as double bonds).

The molecules of **1** are linked to form dimers via C(10)–H(10A)···Br(2#$-x$, $-y+2$, $-z+1$) intermolecular weak hydrogen bonds [51] (D···A distance equals 3.603(8) Å and D–H···A angle 137.4°). One more C(26)–H(26A)···O(2) weak intramolecular hydrogen bond (D···A distance equals 2.992(8) Å and D–H···A angle 112.9°) exists in the molecule, which provides additional conformational stabilisation. The conformations of molecules of compound **3** are stabilised by six C–H···Cl weak intramolecular hydrogen bonds (D···A distances vary from 3.31(1) to 3.67(1) Å and D–H···A angles vary from 112.9° to 149.9°) and one C(38)–H(38A)···N(1) weak intramolecular hydrogen bond (D···A distance equals 3.34(1) Å and D–H···A angle 127.2°). The molecules of **4** are assembled via C(11)–H(11A)···Cl($1-x+1/2$, $-y+1/2$, $-z+1$) weak intermolecular hydrogen bonds (D···A distance equal to 3.59(1) Å and D–H···A angle 145.9°) to give an infinite hydrogen bonded chain created by perpendicular rings in a spiro arrangement. Only one weak intramolecular hydrogen bond, C(8)–H(8A)···Br($1-x$, y, $-z+1/2$) with a D···A distance equal to 3.507(9) Å and D–H···A angle 133.1°, can be found in compound **5**, providing slight stabilisation to the molecule.

Table 4 contains assignments of characteristic bands in the IR range for **1**–**5** compounds.

For $[ReX_3(NO)L_2]$ complexes with an identical ligand L, the NO stretching frequency of the chloro-compounds is lower than that of the corresponding bromo-complexes, which is in accordance with the greater π-acceptor character of the bromo ion than the chloro one. A neutral group, L, also causes a variation in the NO stretching frequency. The higher frequencies are found for complexes containing $AsPh_3$ than $OAsPh_3$. The difference between ν_{NO} of bromo- and chloronitrosyl is much higher for complexes containing arsines (**3** and **5**) than for complexes containing arsine oxides (**1** and **2**), which results from the different ligands' arrangement around the rhenium atom in these complexes. The presence of two strong bands at about 890 and 840 cm^{-1} in the IR spectra of complexes **1**, **2** and **4** confirms the *cis* geometry of the two coordinated $OAsPh_3$ molecules.

Complexes **1**, **2**, **4** and **5** are paramagnetic compounds with a magnetic moment corresponding to one unpaired electron.

Table 5
Band positions, molar absorption coefficients and assignments for complexes **1**–**5**

$[ReBr_3(NO)(OAsPh_3)_2]$ (**1**)			$[ReCl_3(NO)(OAsPh_3)_2]$ (**2**)			$[ReCl_3(NO)(AsPh_3)_2][ReCl_4(AsPh_3)_2]$ (**3**)			$[ReCl_4(OAsPh_3)_2]$ (**4**)			$[ReBr_3(NO)(AsPh_3)_2]$ (**5**)		
Band position (cm^{-1})	ε	Assignment	Band position (cm^{-1})	ε	Assignment	Band position (cm^{-1})	ε	Assignment	Band position (cm^{-1})	ε	Assignment	Band position (cm^{-1})	ε	Assignment
14 925	150	$d_{xy} \rightarrow d_{xz}$	14 150	30	$d_{xy} \rightarrow d_{xz}$	18 800	320	$d_{xy} \rightarrow d_{yz}$	15 100	13	$d_{xy} \rightarrow d_{yz}$	14 700	200	$d_{xz} \rightarrow \pi^*_{NO}$
23 900	2050	$d_{xz} \rightarrow d_{x^2-y^2}$, $d_{yz} \rightarrow \pi^*_{O=As}$	23 000	410	$d_{yz} \rightarrow d_{x^2-y^2}$	25 850	280	$d_{xy} \rightarrow d_{xz}$	25 300	300	$d_{xy} \rightarrow d_{xz}$	15 550	270	$d_{yz} \rightarrow \pi^*_{NO}$
27 740	4800	$d_{xy} \rightarrow \pi^*_{NO}$, $d_{yz} \rightarrow d_{x^2-y^2}$	25 125	960	$\pi^o_{O=As} \rightarrow d_{xz}$	36 100	5180	$d_{xy} \rightarrow d_{x^2-y^2}$, $\pi^b_{Re-Cl} \rightarrow d_{xz}$, $(d_{xy} \rightarrow \pi^*_{NO})$ [a]	34 000	6400	$d_{xy} \rightarrow d_{x^2-y^2}$, $d_{xy} \rightarrow \pi^*_{O=As}$	17 850	2050	$d_{xy} \rightarrow d_{xz}$
31 850	2400	$d_{xy} \rightarrow \pi^*_{O=As}$	29 750	1390	$d_{xy} \rightarrow \pi^*_{NO}$	42 920	7400	$\pi^b_{C6H5} \rightarrow 4d_{As}$	43 700	47 000	$\pi^b_{C6H5} \rightarrow 4d_{As}$	21 600	15 090	$\pi^o_{Br-} \rightarrow d_{xz}$
36 900	14 500	$d_{xy} \rightarrow d_{x^2-y^2}$, $\pi^o_{Br} \rightarrow \pi^*_{NO}$	36 900	6400	$d_{xy} \rightarrow d_{x^2-y^2}$, $d_{xy} \rightarrow \pi^*_{O=As}$							35 200	16 080	$d_{xy} \rightarrow d_{x^2-y^2}$, $d_{xy} \rightarrow \pi^*_{NO}$
37 900	17 000	$\pi^b_{Re-Br} \rightarrow d_{xz}$	37 900	6850	$\pi^b_{Re-Cl} \rightarrow d_{xz}$							38 750	17 640	$\pi^b_{Re-Br} \rightarrow d_{xz}$
43 300	75 000	$\pi^b_{C6H5} \rightarrow 4d_{As}$	43 300	43 000	$\pi^b_{C6H5} \rightarrow 4d_{As}$							42 900	17 930	$\pi^b_{C6H5} \rightarrow 4d_{As}$

ε = molar absorption coefficient ($dm^3\ mol^{-1}\ cm^{-1}$).
[a] Covered by $\pi^b_{Re-Cl} \rightarrow d_{xz}$ transition.

Table 6
Values of ligand field parameters for **1**, **2**, **4** and **5**

Complex	Ligand field parameter		
	Dq (cm^{-1})	Ds (cm^{-1})	Dt (cm^{-1})
$[ReBr_3(NO)(OAsPh_3)_2]$	3690	−3741	−449
$[ReCl_3(NO)(OAsPh_3)_2]$	3690	−5104	−111
$[ReCl_4(OAsPh_3)_2]$	3400	−5272	−143
$[ReBr_3(NO)(AsPh_3)_2]$	3521	−5952	1

The positions and molar absorption coefficients of electronic bands for complexes **1**–**5** and the electronic transitions assigned to the bands are shown in Table 5. Based on the data of Table 5, the values of the ligand field parameters Dq, Ds and Dt have been defined and the energies of molecular orbitals for the complexes have been estimated. The values of ligand field parameters are listed in Table 6, and simplified MO diagrams for complexes **1**, **2**, **4** and **5** are presented in Fig. 5.

Intensities of $\pi^{b}_{C6H5} \rightarrow 4d_{As}$ transitions in complexes containing arsine oxides are significantly higher in

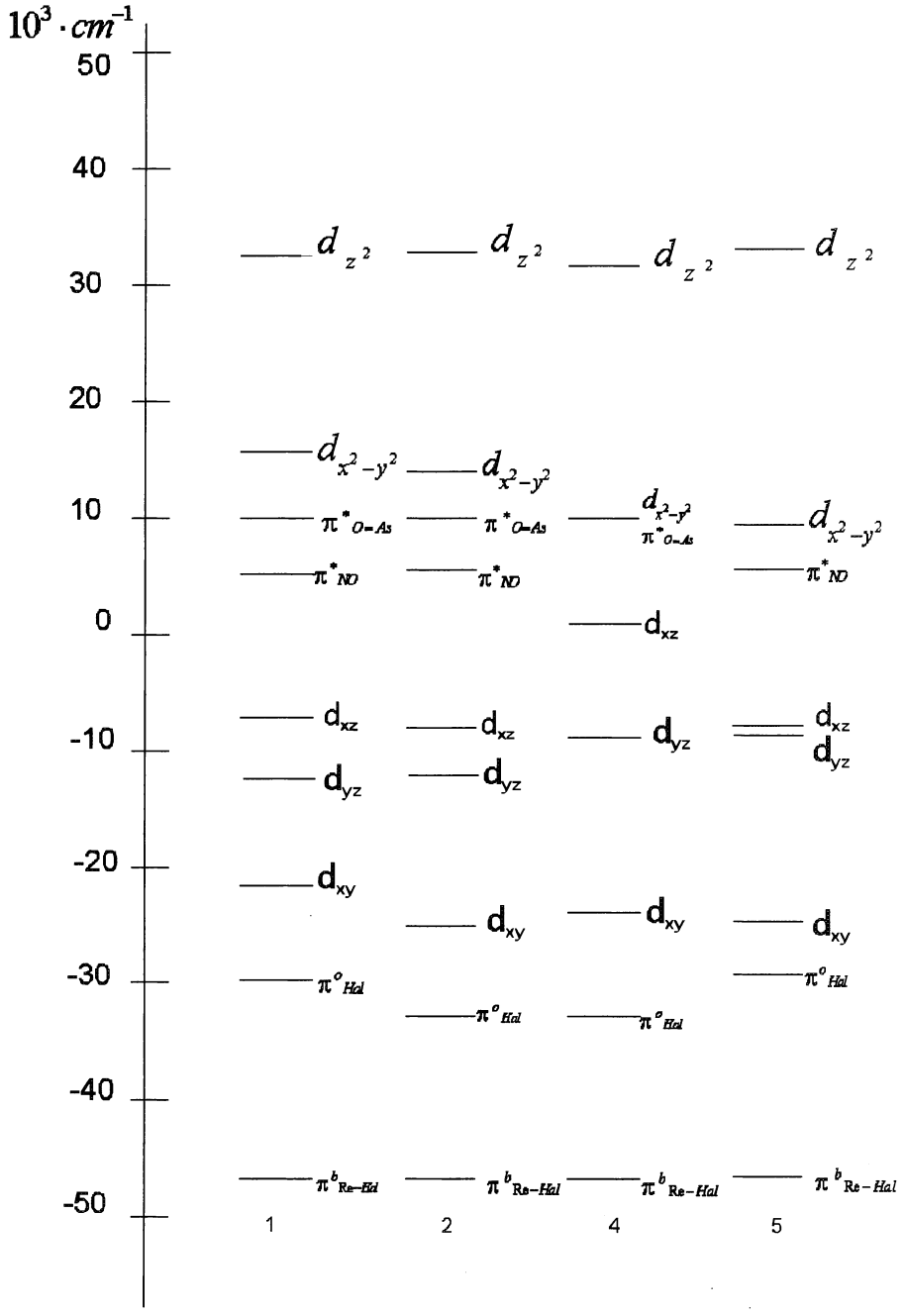


Fig. 5. The simplified molecular orbitals diagrams for **1**, **2**, **4** and **5**.

comparison with complexes containing arsines, which is connected to:

- As⇒O electron density transfer,
- lack of a Re→As transition, which leads to an increase in As acceptor ability towards π_{C6H5} electrons.

Significant intensities of bands:

- at 23 900, 27 740, 36 900 and 37 900 cm^{-1} in **1**,
- at 36 900 cm^{-1} in **2**
- at 36 100 cm^{-1} in **3**
- at 34 000 cm^{-1} in **4**

result from a superposition of charge transfer transitions and d→d transitions.

The lower intensity of the $d_{xy} \rightarrow \pi^*_{NO}$ transition in complexes containing arsine oxides in comparison with complexes containing arsines results from the presence of an O=As acceptor group in the *xy* plane, which is competitive towards NO. That is why in complexes containing an O=As group, the N–O bond is shorter and the Re–N bond is longer than in complexes containing $AsPh_3$. High electron density on oxygen atoms from the O–As group also results in an effective σ_{Re-O} bonding and simultaneously an increase in electron density on the Re^{II} ion. The last fact increases its π-donor ability towards Br(1), resulting in a shortening of the Re–Br(1) bond in comparison with the Re–Br(3) bond.

The comparatively high intensity of the bands attributed to the $d_{xy} \rightarrow \pi^*_{NO}$ transition proves the linear NO coordination (lack of electron density in π^*_{NO}). The low intensity of the $d_{yz} \rightarrow \pi^*_{NO}$ and $d_{xz} \rightarrow \pi^*_{NO}$ transition is caused by the symmetry of these orbitals and NO to each other. Based on the presented simplified MO diagrams and absorption band analysis, one can conclude that complexes **1**, **2** and **5** have electron configurations $(d_{xy})^2(d_{yz})^2(d_{xz})^1$, and complex **4**—$(d_{xy})^2(d_{yz})^1$. In **3** both these configurations exist simultaneously.

The Dq parameter for the $[ReBr_3(NO)(AsPh_3)_2]$ complex is slightly higher (by 2638 cm^{-1}) than Dq for the $[ReBr_3(NO)(PPh_3)_2]$ complex. This increase in its value is connected with the increase in the degree of covalency of the Re–As bonds (higher π-acceptor ability of As compared to P) and Re–N bonds. The higher π-acceptor ability of As manifests also in an increase in molar extinction coefficient of the band resulting from $\pi^b_{C_6H_5} \rightarrow 4d_{As}$ and in consequence in an elongation of C–C bonds in $AsPh_3$ compared to PPh_3. The small elongation of the Re–As bond (by only 0.054 Å) compared to the Re–P bond, in spite of the fact that $r_{As^{-3}}$ is longer (by 0.1 Å) also proves the higher acceptor ability of As in comparison to P. The decrease in electron density at the rhenium atom, connected with $5d_{xz,yz} \rightarrow 4d_{As}$ electron transitions, increases the probability of charge transfer from Br^- to $5d_{Re}$ (the band at 21 598 cm^{-1}; other authors observed the $Br^- \rightarrow Re$ transition at 23 830 cm^{-1}) [45,46]. Therefore, it leads to an increase in the probability of the $d_{xy} \rightarrow \pi^*_{NO}$ electron transition and causes an abridgement of the Re–N bond (by 0.015 Å) and an elongation of the N–O bond (by 0.057 Å) in the $[ReBr_3(NO)(AsPh_3)_2]$ complex compared to the $[ReBr_3(NO)(PPh_3)_2]$ complex. Replacing PPh_3 with $AsPh_3$ in nitrosyl Re(II) complexes causes a change in charge distribution in complex molecules.

Spectroscopic data confirm EPR signals in the solid phase of **5** and in methylene chloride solutions of **1** and **5** (Figs. 6–8). The solid phase signal clearly confirms the axial symmetry of complex **5**, characterised by $g_{\|} =$

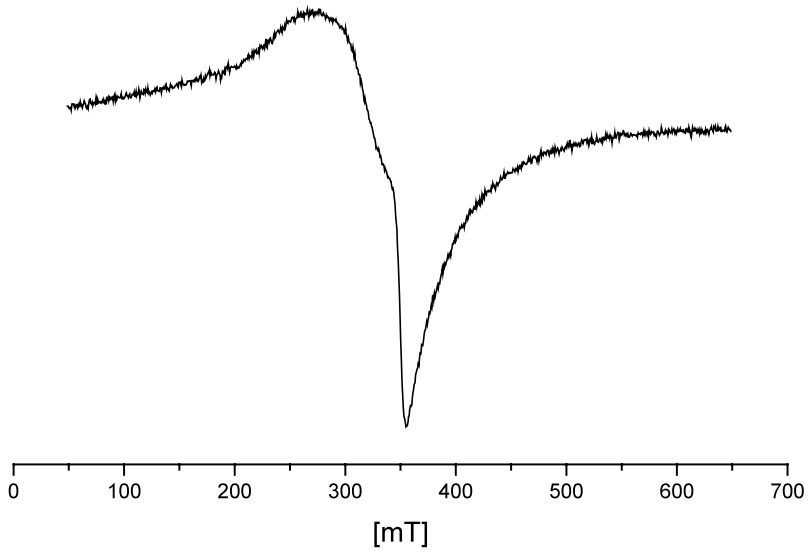


Fig. 6. Experimental X-band EPR spectrum of **5** in the solid phase at $T = 295$ K.

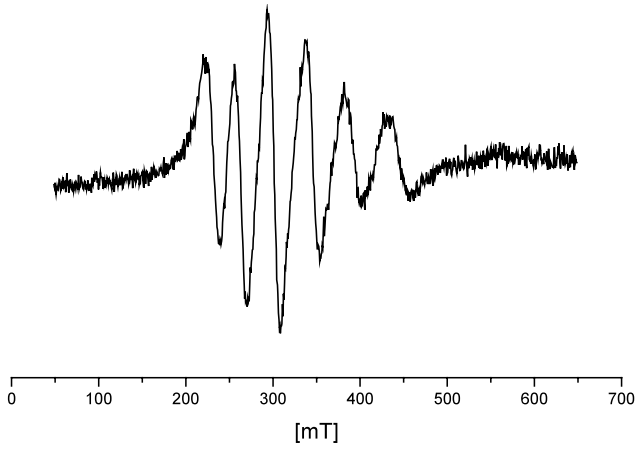


Fig. 7. Experimental X-band EPR spectrum of **3** in CH_2Cl_2 at $T = 295$ K.

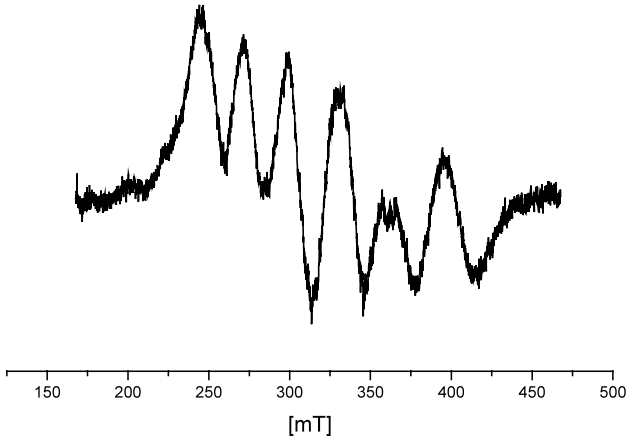


Fig. 8. Experimental X-band EPR spectrum of **5** in CH_2Cl_2 at $T = 295$ K.

2.4057, $g_{\perp} = 2.0412$ and $g_{av} = 2.1624$ values. EPR signals of methylene chloride solutions of **1** and **5** also have axial symmetry. Complex **5** is characterised by $g_{av} = 2.1942$ and $A_{av} = 31.3$ mT values, and complex **1**—by $g_{av} = 2.2192$ and $A_{av} = 26.7$ mT values. These facts confirm an interaction of an unpaired electron $(d_{xz})^1$ with the axial ligands. If the unpaired electron was on the d_{xy} orbital, the values of g_{av} in complexes **1** and **5** would be in reverse relation. The higher g_{av} value in **1** results from a higher spin-orbital contribution of axial Br^- ligands ($\lambda_{Br^-} = 2460\ cm^{-1}$) into $g_{||}$, compared to $AsPh_3$ ligands with significantly lower λ_{As} value. The lower A_{av} value of complex **1** results from covalency of the Re–Br bond, confirmed by $r_{Re-Br} = 0.251$ nm. The Re–Br distance is shorter than the sum of the ion radii $r_{Re}^{2+} + r_{Br^-}$ by 0.041 nm.

The sextet signal of complexes **1** and **5**, resulting from an interaction of the unpaired electron with the nuclear spins of ^{185}Re and ^{187}Re, indicates a small delocalisation of this electron towards the ligands. Quadruple moments of ^{14}N, ^{75}As, ^{79}Br, ^{81}Br, ^{185}Re and ^{187}Re, broadening the signals, cause superposition of hyperfine structure components.

4. Supplementary material

Crystallographic data for the structural analysis have been deposited with the Cambridge Crystallographic Data Centre, CCDC Nos. 188153–56 for compounds $[ReBr_3(NO)(AsPh_3)_2]$, $[ReCl_3(NO)(AsPh_3)_2]$-$[ReCl_4(AsPh_3)_2]$, $[ReCl_4(OAsPh_3)_2]$, $[ReBr_3(NO)$-$(OAsPh_3)_2]$. Copies of this information may be obtained free of charge from The Director, CCDC, 12 Union Road, Cambridge, CB2 1EZ, UK (fax: +44-1223-336033; e-mail: deposit@ccdc.cam.ac.uk or www: http://www.ccdc.cam.ac.uk).

Acknowledgements

We wish to express our thanks to Danuta Kwapulińska for recording EPR spectra. X-ray crystallography of compounds **1** and **4** was financed by statutory funds allocated by the State Committee for Scientific Research to the Institute of General and Ecological Chemistry, Technical University of Łódź.

References

[1] R.M.J. Palmer, A.G. Ferrige, S. Moncada, Nature 327 (1987) 524.
[2] S. Moncada, R.M.J. Palmer, E.A. Higgs, Pharmacol. Rev. 43 (1991) 109.
[3] P.L. Feldman, O.W. Griffith, D.J. Stuehr, Chem. Eng. News 71 (1993) 26.
[4] M. Feeelish, J.S. Stamler (Eds.), Methods in Nitric Oxide Research, Wiley, Chichester, England, 1996.
[5] W. Volkert, W.F. Goeckeler, G.J. Ehrhardt, A.R. Ketring, J. Nucl. Med. 32 (1991) 174.
[6] E.A. Deutsch, K. Libson, J.L. Vanderheyden, Technetium and Rhenium in Chemistry and Nuclear Medicine, Raven Press, New York, 1990.
[7] J.O. Dzięgielewski, K. Filipek, B. Machura, Polyhedron 14 (1995) 555.
[8] J.O. Dzięgielewski, B. Machura, T. Kupka, in: J.C. Merlin, S. Turrell, J.P. Huvenne (Eds.), Spectroscopy of Biological Molecules, Kluver Academic Publishers, Dordrecht, 1995, p. 589.
[9] J.O. Dzięgielewski, B. Machura, J. Marek, Polyhedron 15 (1996) 3713.
[10] J.O. Dzięgielewski, B. Machura, T.J. Bartczak, Polyhedron 15 (1996) 2813.
[11] T.J. Bartczak, W. Czurak, J.O. Dzięgielewski, B. Machura, Polish J. Chem. 72 (1998) 633.
[12] J.O. Dzięgielewski, B. Machura, T. Kupka, T.J. Bartczak, W. Czurak, Polish J. Chem. 72 (1998) 1009.
[13] J.O. Dzięgielewski, B. Machura, T.J. Bartczak, W. Czurak, J. Kusz, J. Warczewski, J. Coord. Chem. 48 (1999) 125.
[14] T.J. Bartczak, W. Czurak, J.O. Dzięgielewski, B. Machura, A. Jankowska, J. Kusz, J. Warczewski, Polyhedron 18 (1999) 2313.
[15] T.J. Bartczak, W. Czurak, J.O. Dzięgielewski, B. Machura, J. Kusz, J. Warczewski, Polish J. Chem. 74 (2000) 265.

[16] T.J. Bartczak, W. Czurak, J.O. Dzięgielewski, B. Machura, A. Jankowska, J. Kusz, J. Warczewski, J. Coord. Chem. 52 (2001) 361.
[17] S.G. Fontán, A. Marchi, L. Marvelli, R. Rossi, S. Antoniutti, G. Albertin, J. Chem. Soc., Dalton Trans. (1996) 2779.
[18] C. Bolzati, F. Tisato, F. Refosco, G. Bandali, A. Dolmella, Inorg. Chem. 35 (1996) 6221.
[19] F. Connac, Y. Lucchese, M. Dartiguenave, A.L. Beauchamp, Inorg. Chem. 36 (1997) 256.
[20] R.G. Cavell, R.W. Hilts, H. Luo, R. McDonald, Inorg. Chem. 38 (1999) 897.
[21] R. Rossi, A. Marchi, A. Duatti, L. Magon, U. Casellato, R. Graziani, J. Chem. Soc., Dalton Trans. (1998) 1857.
[22] M.F.N.N. Carvalho, A.J.L. Pombeiro, D.L. Hughes, R.L. Richards, J. Organomet. Chem. 335 (1987) C23.
[23] N.P. Johnson, C.J.L. Lock, G. Wilkinson, J. Chem. Soc. (1964) 1054.
[24] D. Giusto, G. Cova, Gazz. Chem. Ital. 102 (1972) 265.
[25] STOE & Cie (1999). X-RED. Version 1.18. STOE & Cie GmbH, Darmstadt, Germany.
[26] (a) G.M. Sheldrick, Acta Crystallgr., Sect. A 46 (1990) 467–473; (b) G.M. Sheldrick, SHELXL-97, Program for the Solution and Refinement of Crystal Structures, University of Göttingen, Germany, 1997.
[27] G.M. Sheldrick, SHELXTL: release 4.1 for Siemens Crystallographic Research Systems, 1990.
[28] W.B. Hughes, E.A. Zeuch, Inorg. Chem. 12 (1973) 471.
[29] L. Bencze, J. Kohan, Inorg. Chim. Acta 65 (1982) L17.
[30] D.L.H. Williams, Nitrosation, Cambridge University Press, New York, 1988.
[31] R.P. Mueller, S. Murata, J.R. Huber, Chem. Phys. 66 (1982) 237.
[32] P.W.R. Corfield, R.J. Doedens, J.A. Ibers, Inorg. Chem. 6 (1967) 197.
[33] G. La Monica, S. Cenini, J. Chem. Soc., Dalton Trans. (1980) 1145.
[34] D.C. Bradley, M.B. Hursthouse, K.M.A. Malik, A.J. Nielson, R.L. Short, J. Chem. Soc., Dalton Trans. (1983) 2651.
[35] A.M. Lebuis, A.L. Beauchamp, Can. J. Chem. 71 (1993) 441.
[36] D. Bright, J.A. Ibers, Inorg. Chem. 8 (1969) 1078.
[37] D.H.F. Souza, G. Oliva, A. Teixeira, A.A. Batista, Polyhedron 14 (1995) 1031.
[38] T. Lis, Acta Crystallogr., Sect. B 33 (1977) 944.
[39] V.S. Sergienko, M.A. Porai-Koshits, V.E. Mistryukov, K.V. Kotegov, Koord. Khim. 8 (1982) 230.
[40] J.M. Mayer, D.L. Thorn, T.H. Tulip, J. Am. Chem. Soc. 107 (1985) 7454.
[41] G. Ciani, D. Giusto, M. Manassero, M. Sansoni, J. Chem. Soc., Dalton Trans. (1975) 2156.
[42] N. Mronga, F. Weller, K. Dehnicke, Z. Anorg. Allg. Chem. 502 (1983) 35.
[43] M.T. Castello, P.E. Farwick, M.A. Green, R.A. Walton, Inorg. Chem. 30 (1991) 861.
[44] J.O. Dzięgielewski, B. Machura, T.J. Bartczak, J. Kusz, J. Warczewski, submitted to J. Coord. Chem.
[45] A.P. Mortala, J.W. Moskowitz, N. Rooch, C.D. Cousman, H.B. Gray, Chem. Phys. Lett. 32 (1975) 283.
[46] F.A. Cotton, E.P. Edersen, J. Am. Chem. Soc. 97 (1975) 303.
[47] I.D. Brown, Acta Crystallogr., Sect. B 48 (1992) 553.
[48] I.D. Brown, Acta Crystallogr., Sect. B 53 (1997) 381.
[49] M. O'Keeffe, N.E. Brese, J. Am. Chem. Soc. 113 (1991) 3226.
[50] L. Sieron, M. Bukowska-Strzyzewska, Acta Crystallogr., Sect. C 55 (1999) 1230.
[51] G.R. Desiraju, T. Steiner, The Weak Hydrogen Bond in Structural Chemistry and Biology, Oxford University Press, Oxford, 1999.

We have employed as starting material the nickel binuclear compound $[\{Ni(dien)(H_2O)\}_2(\mu\text{-ox})](PF_6)_2\cdot 2H_2O$ owing to the lability of their water molecules, which may be replaced by a plethora of ligands, such as the pseudohalide ligands: N_3^-, NCO^-, NCS^-, and, due to the attractiveness of polymers comprised of M–CN–M′ units, CN^- and the cyanocomplexes $[M(CN)_n]^{y-}$, M: Ni, Pd, Pt, Cu, and Au. In this paper we report the synthesis, crystal structure, magnetic properties and DFT calculations of the molecular complexes of type $[\{Ni(dien)\}_2(\mu\text{-ox})\{(\mu\text{-}M(CN)_4)\}]$ where M = Ni(II) [7a], Pd(II) and Pt(II).

2. Experimental

Microanalyses of carbon, nitrogen and hydrogen were performed on a LECO CHNS-932 analyser. IR spectra were recorded on a Nicolet 740 FTIR spectrometer using KBr pellets. All reagents were commercial grade chemicals and were used without further purification. The $[\{Ni(dien)(H_2O)\}_2(\mu\text{-ox})](PF_6)_2\cdot 2H_2O$ complex was synthesised according to the literature method [7g].

2.1. Synthesis

A general procedure was followed in the synthesis of the three compounds: two aqueous solutions of $K_2[M(CN)_4]$ (0.06 mmol) and $[\{Ni(dien)(H_2O)\}_2(\mu\text{-ox})](PF_6)_2\cdot 2H_2O$ (0.06 mmol) were mixed. The initially formed pink precipitate was removed by filtration, and the concentrated solution was allowed to cool slowly to room temperature to obtain blue single crystals of the corresponding compounds, yield 15% for **1**, 25% for **2** and 40% for **3**.

2.1.1. $[\{Ni(dien)\}_2(\mu\text{-ox})\{(\mu\text{-}Pd(CN)_4)\}]$ (**2**)

FTIR (KBr disk, cm^{-1}): ν(C≡N) 2132m, 2159w. *Anal*. Found C, 26.9; H, 4.0; N, 22.3. Calc. for $C_{14}H_{26}N_{10}Ni_2O_4Pd$: C, 27.02; H, 4.21; N, 22.51%.

2.1.2. $[\{Ni(dien)\}_2(\mu\text{-ox})\{(\mu\text{-}Pt(CN)_4)\}]$ (**3**)

FTIR (KBr disk, cm^{-1}): ν(C≡N) 2132m, 2163w, 2173w. *Anal*. Found C, 23.4; H, 3.5; N, 19.2. Calc. for $C_{14}H_{26}N_{10}Ni_2O_4Pt$: C, 23.65; H, 3.69; N, 19.70%.

2.2. X-ray crystallography

Data collection for prismatic blue single crystals of **2** and **3** were performed on a STOE IPDS diffractometer, equipped with graphite monochromated Mo Kα radiation ($\lambda = 0.71073$ Å). Indexes and unit-cell refinement were based on all observed reflections from 10 frames collected with an oscillation range of 1°/frame and exposure time of 3 min/frame. Experimental details and crystal data for both compounds are listed in Table 1. The atomic scattering factors were taken from the International Tables for X-ray Crystallography [8]. The data were processed and corrected for Lp effects. Analytical absorption corrections were applied. Both structures were solved by direct methods (DIRDIF-96) [9] and refined by full-matrix least-squares refinement of F^2 [10]. All non-hydrogen atoms were anisotropically refined except cyanide atoms in compound **3**. Hydrogen atoms were placed in calculated positions and refined with a riding model. The calculations were performed using the WINGX crystallographic software package [11].

Table 1
Crystallographic data for compounds **2** and **3** [a]

Compound	**2**	**3**
Empirical formula	$C_{14}H_{26}N_{10}Ni_2O_4Pd$	$C_{14}H_{26}N_{10}Ni_2O_4Pt$
Formula weight	622.27	710.96
Radiation Mo Kα (Å)	0.71073	0.71073
Space group	*I2/a*	*I2/a*
a (Å)	13.252(5)	13.221(2)
b (Å)	11.806(3)	11.770(1)
c (Å)	14.183(4)	14.185(2)
β	96.93(3)	96.81(2)
V (Å^3)	2202.8(1)	2191.8(5)
Z	4	4
D_{calc} (g cm^{-3})	1.876	2.155
F(000)	1256	1384
μ (mm^{-1})	2.543	8.111
Crystal size (mm)	0.60 × 0.10 × 0.05	0.14 × 0.11 × 0.07
Crystal colour, habit	blue, plaque	blue, prism
Observed reflections	1125, $I \geq 2\sigma(I)$	1195, $I \geq 2\sigma(I)$
Independent reflections	1386	2093
Number of parameters	141	122
R	0.0379	0.0493
wR	0.1189	0.1104
Goodness-of-fit	1.093	0.799

[a] Relevant data from Ref. [7a] for compound **1**: space group *I2/a*, $a = 13.133(1)$, $b = 11.644(1)$, $c = 14.154(1)$ Å, $\beta = 97.13(1)°$, $V = 2147.7(5)$ Å^3.

2.3. Magnetic susceptibility measurements

Magnetic susceptibility measurements were carried out on polycrystalline samples in the temperature range 4.2–300 K, with a pendulum type susceptometer/magnetometer (Manicsd DSM8) equipped with a helium continuous flow cryostat. The diamagnetic contribution was calculated from Pascal's constants.

2.4. Computational details

Single point energy calculation at the experimental geometry for compound **1** in C_2 symmetry was performed at the B3PW91 level of theory [12]. The Los Alamos effective core potential combined with a DZ basis (LANL2DZ) [13] was chosen for the transition metals, as a compromise between accuracy and computational power available. For the remaining atoms, the

D95V [14] basis was used. All calculations were performed using the GAUSSIAN-98W program [15]. The MO figures were done with MOLEKEL 4.2 [16].

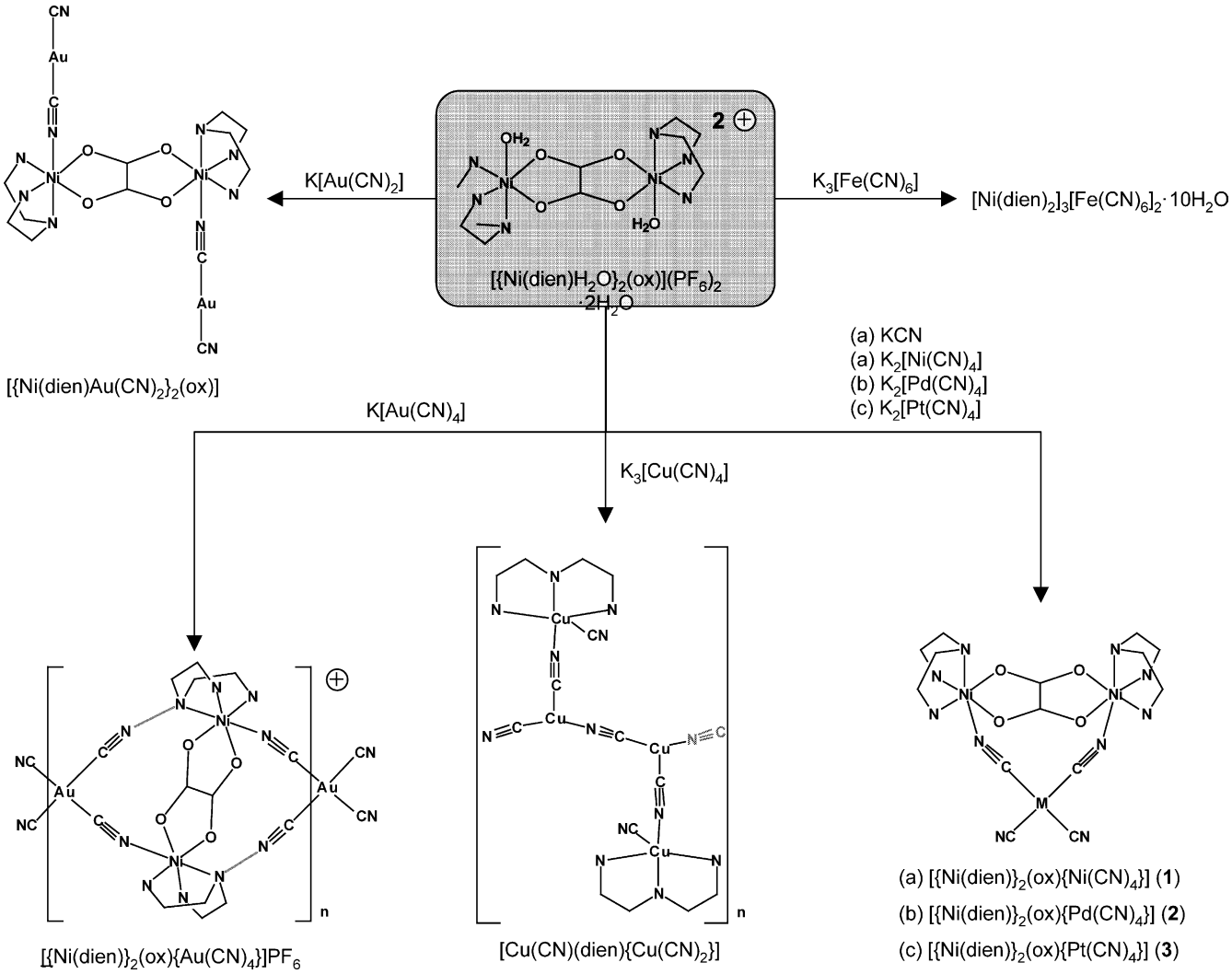
3. Results and discussion

3.1. Synthesis

In the synthesis of the three compounds, the binuclear complex $[\{Ni(dien)(H_2O)\}_2(\mu\text{-}ox)]^{2+}$ was used as precursor owing to the lability of their water molecules which may be substituted by a plethora of ligands. As can be seen in Scheme 1, reaction of the precursor with different cyanometallates gives complexes with a high structural diversity. Thus, when tetracyanocuprate(I) or tetracyanoaurate(III) is employed polynuclear complexes are obtained. In the case of tetracyanometallates of Group 10 trinuclear species are obtained, where dien ligands are *cis* respect to the oxalate plane. Water substitution in the precursor occurs when dicyanoaurate(I) is used.

3.2. Crystal structure of compounds [{Ni(dien)}$_2$(μ-ox){(μ-M(CN)$_4$)}], M = Ni (1), Pd (2) and Pt (3)

The three compounds crystallise in the same monoclinic space group *I2/a* and are isostructural. Single crystal structure analyses reveals the presence of a neutral trinuclear complex with C_2 crystallographic symmetry. The twofold axis passes through the tetracoordinated metal atom and the middle point of the C1–C1′ bond of the oxalate ligand, which is coordinated in a bis (bidentate) fashion to the twofold related Ni1 atoms. The distorted octahedral environment of each Ni1 atom is completed by three nitrogen atoms from a diethylenetriamine ligand in *fac* arrangement and one nitrogen atom from a bridging cyanide ligand, which belongs to the square-plane coordination M atom (Fig. 1). Thus, the $M(CN)_4^{2-}$ group act as a *cis*



Scheme 1.

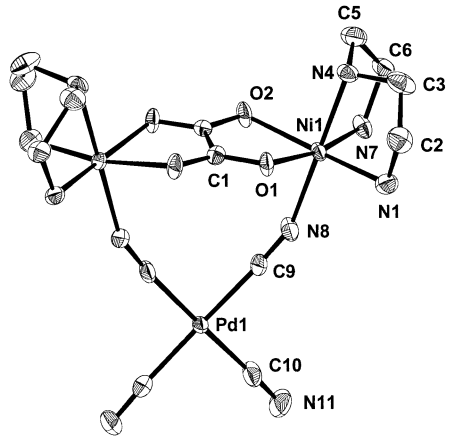


Fig. 1. ORTEP view of compound **2** with atom labelling.

Table 2
Selected bond distances (Å) and angles (°) for compounds **2** and **3**

Compound	**2**	**3**
*Ni*1 *coordination sphere*		
Bond distances		
Ni1–O1	2.091(4)	2.093(9)
Ni1–O2	2.102(5)	2.083(9)
Ni1–N1	2.107(6)	2.085(12)
Ni1–N4	2.100(5)	2.097(10)
Ni1–N7	2.078(5)	2.077(11)
Ni1–N8	2.110(6)	2.112(10)
Bond angles		
O1–Ni1–O2	80.3(2)	79.9(3)
O1–Ni1–N1	88.8(2)	88.9(4)
O1–Ni1–N4	93.0(2)	92.6(4)
O1–Ni1–N7	170.1(2)	170.1(4)
O1–Ni1–N8	88.2(2)	88.2(4)
O2–Ni1–N1	167.9(2)	167.6(4)
O2–Ni1–N4	91.5(2)	91.6(4)
O2–Ni1–N7	91.2(2)	91.8(4)
O2–Ni1–N8	87.9(2)	87.1(4)
N1–Ni1–N4	83.7(2)	83.3(4)
N1–Ni1–N7	99.1(2)	98.1(5)
N1–Ni1–N8	96.5(2)	98.0(4)
N4–Ni1–N7	82.1(2)	82.1(4)
N4–Ni1–N8	178.5(2)	178.3(4)
N7–Ni1–N8	96.5(2)	96.8(4)
M coordination plane		
Bond distances		
M–C9	2.012(7)	1.984(12)
M–C10	2.007(7)	1.992(13)
Bond angles		
C9–M–C10	175.8(3)	176.5(6)
C9–M–C9^{I}	86.1(3)	85.9(7)
C9–M–C10^{I}	93.0(3)	92.9(4)
C10–M–C10^{I}	88.1(3)	88.4(7)
Hydrogen contacts		
N4···N11^{II}	3.346(8)	3.331(16)
N7···N11^{III}	3.194(9)	3.168(16)
N7···O2^{IV}	3.005(7)	3.011(15)

Symmetry codes: (I) $1/2-x$, y, $1-z$; (II) $1/2-x$, $y-1$, $1-z$; (III) $x-1/2$, $y-1/2$, $z-1/2$; (IV) $1/2-x$, $1/2-y$, $1/2-z$.

bidentate-bridging unit between both octahedrically coordinated nickel atoms. The bridging *cis* coordination of the tetracyanometallate anion is very unusual. The *cis* disposition implies the substitution and rupture, during the synthesis process, of the starting binuclear complex in which the two water molecules were in *trans* disposition with respect to the oxalate plane. Bond lengths and angles involving non-hydrogen atoms are listed in Table 2. The *cis* coordination of $M(CN)_4^{2-}$ group also induces a significant distortion around octahedral Ni centres, forcing the Ni–oxalato–Ni fragment to adopt a boat conformation which produces a shortening in the Ni1···Ni1 distance. The dihedral angle between the oxalate plane and the equatorial coordination Ni1 plane is around 10.5° for the three compounds.

The crystal structure of these compounds has a pronounced two-dimensional character and can be viewed as a succession along the [1 0 −1] direction of antiparallel layers of molecular complexes. Inside the layers each trinuclear complex is linked to its neighbours through hydrogen bonds of type N–H···N≡C (Fig. 2). The amino groups of *dien* as donors and oxygen atoms of the oxalate as acceptors are involved in the connection between layers (Table 2).

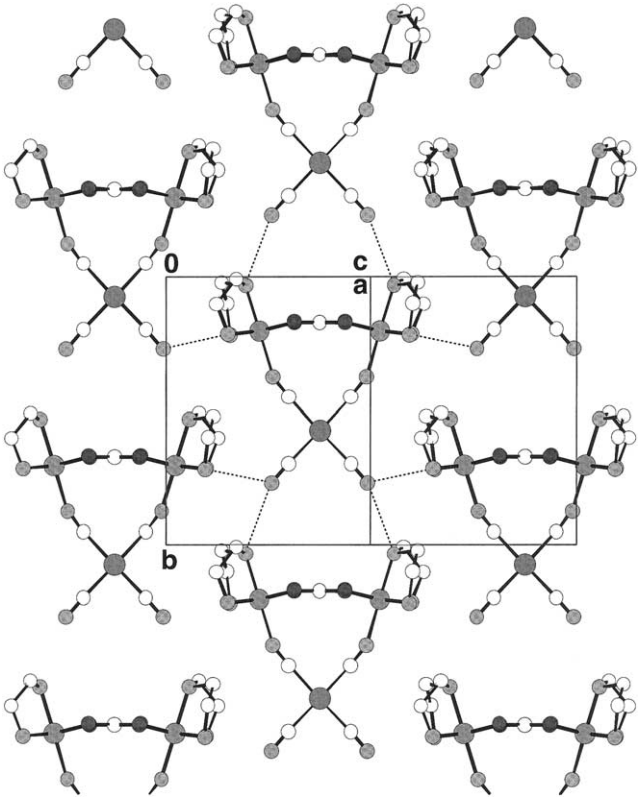


Fig. 2. Two-dimensional arrangement along the *xy* plane. Dotted lines mean all hydrogen bonds of one molecule.

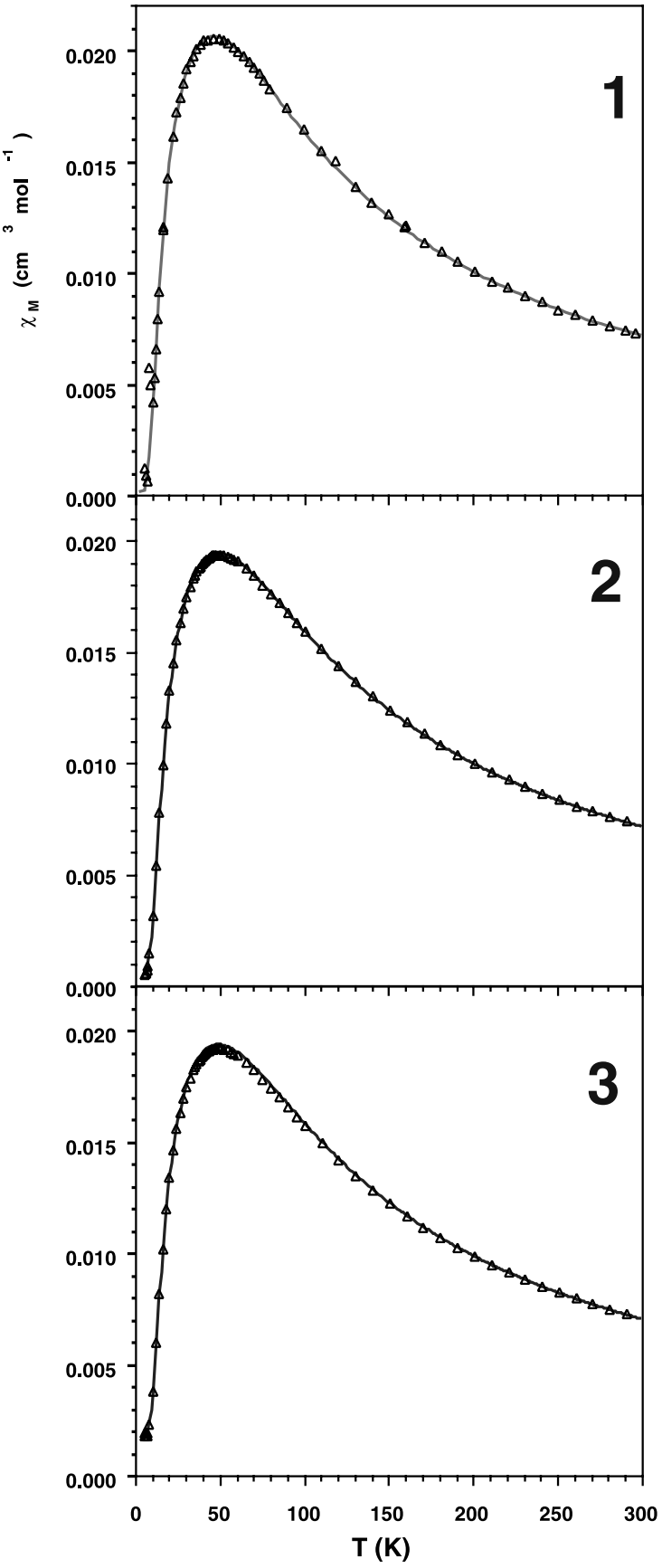


Fig. 3. Thermal dependence of the molar magnetic susceptibility for compounds **1**–**3**.

Table 3
Selected magnetostructural parameters (Å, °) for compounds of type [{Ni(dien)}$_2$(μ-ox){μ-M(CN)$_4$}] related to cyanogold complexes

Compound	$-J$	g	Ni–O$_{ox}$	Ni–N$_{eq}$	Ni–N$_{ap}$	Ni–N′$_{ap}$	O–Ni–O	Ni···Ni	h(Ni)	Reference
[{Ni(dien)}$_2$(μ-ox)(μ-Ni(CN)$_4$)]	31.2	2.15	2.088	2.073/2.094	2.092	2.105	80.3	5.324	0.391	[7a]
[{Ni(dien)}$_2$(μ-ox)(μ-Pd(CN)$_4$)]	33.5	2.17	2.091/2.102	2.107/2.078	2.100	2.110	80.3	5.352	0.387	This work
[{Ni(dien)}$_2$(μ-ox)(μ-Pt(CN)$_4$)]	33.6	2.18	2.085/2.095	2.085/2.077	2.097	2.112	79.9	5.355	0.386	This work
[{Ni(dien)(Au(CN)$_2$)}$_2$(μ-ox)]	30.7	2.17	2.104	2.083	2.075		79.3	5.397	0.021	[7h]
[{Ni(dien)}$_2$(μ-ox)(μ-Au(CN)$_4$)]·PF$_6$	33.8	2.17	2.080/2.087	2.067/2.089	2.089	2.096	80.3	5.419	0.129	[7h]

Abbreviations used: dien = diethylenetriamine. J in cm^{-1}, Ni–O$_{ox}$: distance Ni–O(oxalato); Ni–N$_{eq}$: distance Ni–N(dien-equatorial); Ni–N$_{ap}$: distance Ni–N(dien-apical); Ni–N′$_{ap}$: distance Ni–N(cyanide); d(Ni···Ni): nickel–nickel separation across the oxalato ligand; O–Ni–O: bite angle; h(Ni): metal height from the oxalate mean plane.

3.3. Magnetic properties

The substantially flat square-planar coordination of the $M(CN)_4^{2-}$ diamagnetic units permits that, from a magnetic point of view, the compounds can be treated as a dimeric complexes in which the two octahedrically coordinated Ni(II) ions are linked by two different bridging ligands. The magnetic coupling between the two nickel atoms might propagate through both bridges, but the length of the exchange pathway through the bidentate tetracyanometallate(II) ligand is large enough to predict that the magnetic interaction may take place mainly through the oxalate ligand, which is known to be very effective in mediating antiferromagnetic coupling between first-row transition metal ions separated by around 5.5 Å in homo- [17] and heteropolynuclear compounds [18]. The thermal dependence of the molar magnetic susceptibility, χ_M, of the complexes is characteristic of an antiferromagnetic interaction between the two single ion triplet states (Fig. 3). The susceptibility curve for these complexes increases when the compound is cooled until a maximum is reached, T_{max} 46 (**1**), 49 (**2**) and 49 K (**3**), and then decreases very quickly. The ground state of a nickel(II) ion in an

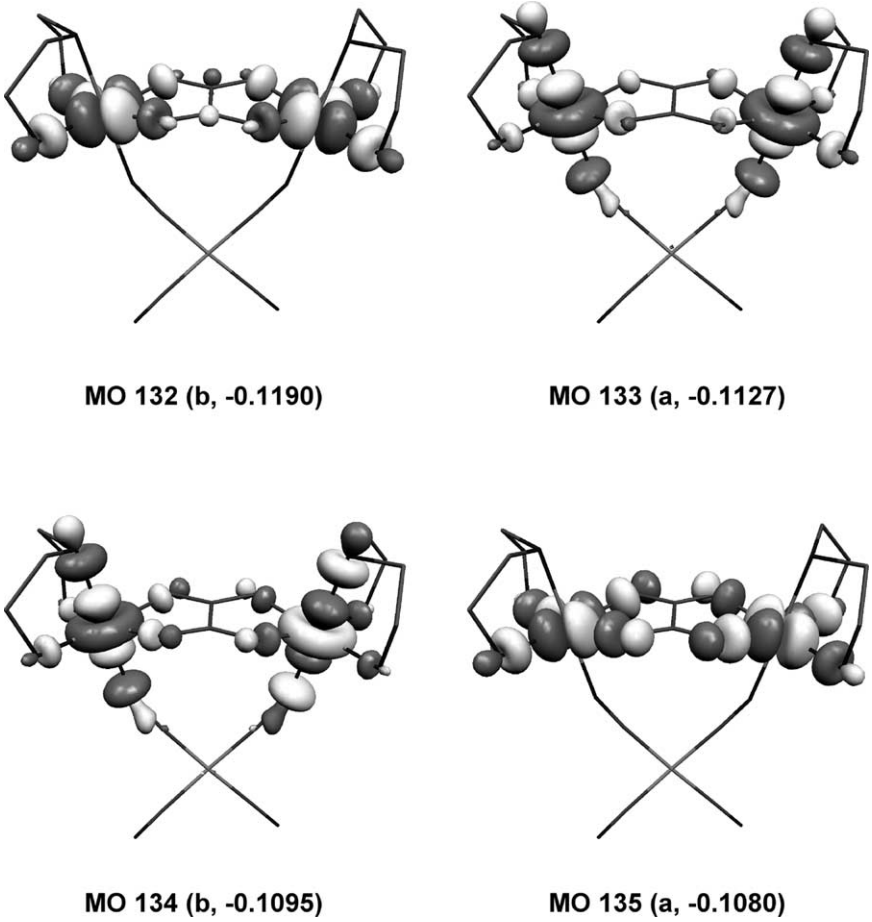


Fig. 4. Magnetic orbitals for compound **1** (symmetry, energy).

octahedral environment is orbitally non-degenerate, and as such, it is possible to represent the intradimer magnetic interaction, J, with the isotropic spin Hamiltonian $H = -JS_A \cdot S_B$. The molar magnetic susceptibility for a nickel(II) dimer (local spins $S_A = S_B = 1$) may be expressed by Eq. (1):

$$\chi_M = \frac{2N\beta^2 g^2}{kT} \times \frac{\exp(J/kT) + 5\exp(3J/kT)}{1 + 3\exp(J/kT) + 5\exp(3J/kT)} \quad (1)$$

Previously reported J values for compounds containing the $[\{Ni(dien)(H_2O)\}_2(\mu\text{-ox})]^{2+}$ building block are close to those of compounds **1**–**3**. This information is summarised in Table 3 for Ni^{II}-oxalate systems in NiO_2N_4 environments containing cyanometal complexes as axial ligands. It is well-known that structural distortions (distance Ni–O_{ox}, bite angle O–Ni–O, deviation from the planarity of the nickel ion respect to mean plane of the oxalate bridging ligand) can play a key role on the fine tuning of exchange coupling.

A graphical representation of the four DFT magnetic orbitals, obtained with restricted open formalism (RODFT) for the high spin state ($S = 2$), of compound **1** are given in Fig. 4, with those for compound **2** and **3** being very similar. As expected for the case of octahedral nickel centres, the unpaired electrons are mainly located in the d_{z^2} and d_{xy} orbitals, with a noticeable contribution to the d_{z^2} magnetic orbital of the nitrogen lone pairs which belong to the bridging cyanide ligands.

4. Supplementary material

Crystallographic data (excluding structure factors) for the structures reported in this paper have been deposited with the Cambridge Crystallographic Data Centre, CCDC No. 188643–188644 for compounds **2** and **3**, respectively. Copies of this information may be obtained free of charge from The Director, CCDC, 12 Union Road, Cambridge, CB2 1EZ, UK (fax: +44-1223-336033; or e-mail: deposit@ccdc.cam.ac.uk or www: http://www.ccdc.cam.ac.uk).

Acknowledgements

This work was supported by MEC (Grant No. PB98/0238).

References

[1] (a) D. Gatteschi, O. Khan, J.S. Miller, F. Palacio, D. Reidel (Eds.), Magnetic Molecular Materials, Kluwer Academic, Dordrecht, 1991;
(b) O. Khan, Molecular Magnetism, VCH, New York, 1993;
(c) M. Verdaguer, Polyhedron 20 (1991) 1115.

[2] (a) A. Bencini, A. Bianchi, P. Paoli, E. Garcia-España, M. Julve, M. Marcelino, J. Chem. Soc., Dalton Trans. (1990) 2213;
(b) A. Escuer, R. Vicente, J. Ribas, J. Jaud, B. Raynaud, Inorg. Chim. Acta 216 (1994) 139;
(c) J. Glerup, P.A. Goodson, D.J. Hodgson, K. Michelsen, Inorg. Chem. 34 (1995) 6255.

[3] (a) G. De Munno, M. Julve, F. Nicolo, F. Lloret, J. Faus, R. Ruiz, E. Sinn, Angew. Chem., Int. Ed. Engl. 32 (1993) 613;
(b) A. Escuer, R. Vicente, X. Solans, M. Font-Bardia, Inorg. Chem. 33 (1994) 6007;
(c) S. Kitagawa, T. Okubo, S. Kawata, M. Kondo, M. Katada, H. Kobayashi, Inorg. Chem. 34 (1995) 4790;
(d) S. Decurtins, H.W. Schmalle, R. Pellaux, P. Schneuwly, A. Hauser, Inorg. Chem. 35 (1996) 1451 (and references therein);
(e) Z. Travnicek, Z. Smekal, J. Marek, Z. Kristallogr. 212 (1997) 123;
(f) I. Castro, M.L. Calatayud, J. Sletten, F. Lloret, M. Julve, J. Chem. Soc., Dalton Trans. (1997) 811.

[4] (a) O. Kahn, Angew. Chem., Int. Ed. Engl. 24 (1985) 834;
(b) M. Julve, M. Verdaguer, O. Kahn, A. Gleizes, O. Philoche–Levisalles, Inorg. Chem. 22 (1983) 368;
(c) M. Julve, M. Verdaguer, O. Kahn, A. Gleizes, O. Philoche–Levisalles, Inorg. Chem. 23 (1984) 3808;
(d) J. Glerup, P.A. Goodson, D.J. Hodgson, K. Michelsen, Inorg. Chem. 34 (1995) 6255.

[5] (a) J. Cabrero, N. Ben Amor, C. de Graaf, F. Illas, R. Caballol, J. Phys. Chem., Sect. A 104 (2000) 9983;
(b) S. Alvarez, M. Julve, M. Verdaguer, Inorg. Chem. 29 (1990) 4500;
(c) J. Cano, P. Alemany, S. Alvarez, M. Verdaguer, E. Ruiz, Chem. Eur. J. 4 (1998) 476;
(d) A. Escuer, R. Vicente, J. Ribas, J. Jaud, B. Raynaud, Inorg. Chim. Acta 216 (1994) 139;
(e) A. Escuer, R. Vicente, M.S. El Fallah, J. Jaud, Inorg. Chim. Acta 232 (1995) 151;
(f) P. Román, C. Guzmán-Miralles, A. Luque, J.I. Beitia, J. Cano, F. Lloret, M. Julve, S. Alvarez, Inorg. Chem. 35 (1996) 3741.

[6] (a) J. Cernak, M. Orendac, I. Potocnak, J. Chomic, A. Orendacova, J. Skorsepa, A. Feher, Coord. Chem. Rev. 224 (2002) 51;
(b) M. Ohba, N. Maruono, H. Okawa, T. Enoki, J. Latour, J. Am. Chem. Soc. 116 (1994) 11566;
(c) W.R. Entley, G.S. Girolami, Science 268 (1995) 397;
(d) O. Sato, T. Iyoda, A. Fujishima, K. Hashimoto, Science 271 (1996) 49;
(e) H. Miyasaka, N. Matsumoto, H. Okawa, N. Re, E. Gallo, C. Floriani, J. Am. Chem. Soc. 118 (1996) 981;
(f) T. Mallah, S. Thiebaut, M. Verdaguer, P. Veillet, Science 262 (1993) 1554;
(g) H. Vahrenkamp, A. Geiss, G.N. Richardson, J. Chem. Soc., Dalton Trans. (1997) 3643;
(h) H. Zhang, J. Cai, X.-L. Feng, H.-Y. Sang, J.-Z. Liu, X.-Y. Li, L.-N. Ji, Polyhedron 21 (2002) 721.

[7] (a) I. Muga, J.M. Gutiérrez-Zorrilla, A. Luque, P. Román, F. Lloret, Inorg. Chem. 36 (1997) 743;
(b) O. Castillo, I. Muga, A. Luque, J.M. Gutiérrez-Zorrilla, J. Sertucha, P. Vitoria, P. Román, Polyhedron 18 (1999) 1235;
(c) I. Muga, J.M. Gutiérrez-Zorrilla, P. Vitoria, A. Luque, M. Insausti, P. Román, F. Lloret, Eur. J. Inorg. Chem. 12 (2000) 2541;
(d) O. Castillo, A. Luque, F. Lloret, P. Román, Inorg. Chim. Acta 324 (2001) 141;
(e) O. Castillo, A. Luque, P. Roman, F. Lloret, M. Julve, Inorg. Chem. 40 (2001) 5526;
(f) C. Guzmán-Miralles, O. Castillo, A. Luque, J.I. Beitia, P. Román, Acta Crystallogr., Sect. E 57 (2001) m407;
(g) I. Muga, P. Vitoria, J.M. Gutiérrez-Zorrilla, A. Luque, C. Guzmán-Miralles, P. Román, Acta Crystallogr., Sect. C 58 (2002)

m81;
(h) I. Muga, P. Vitoria, J.M. Gutiérrez-Zorrilla, A. Luque, P. Román, L. Lezama, F.J. Zúniga, J.I. Beitia, Inorg. Chem. (2002), in press.
[8] International Tables for X-Ray Crystallography, vol. IV, Kynoch Press, Birminghan, 1974.
[9] P.T. Beurskens, G. Beurskens, W.P. Bosman, R. de Gelder, S. García-Granda, R.O. Gould, R. Israel, J.M.M. Smits, J.M.M. The DIRDIF-96 Program System, Technic., 1996.
[10] G.M. Sheldrick, SHELX-97. Programs for Crystal Structure Analysis (Release 97-2), University of Göttingen, Germany, 1997.
[11] L.J. Farrugia, WINGX, a Windows Program for Crystal Structure Analysis, University of Glasgow, 1999.
[12] (a) A.D. Becke, J. Chem. Phys. 98 (1993) 5648;
(b) K. Burke, J.P. Perdew, Y. Wang, in: J.F. Dobson, G. Vignale, M.P. Das (Eds.), Electronic Density Functional Theory: Recent Progress and New Directions, Plenum, New York, 1998;
(c) J.P. Perdew, in: P. Ziesche, H. Eschrig (Eds.), Electronic Structure of Solids '91, Akademie Verlag, Berlin, 1991;
(d) J.P. Perdew, Y. Wang, Phys. Rev. B 45 (1992) 13244;
(e) J.P. Perdew, J.A. Chevary, S.H. Vosko, K.A. Jackson, M.R. Pederson, D.J. Singh, C. Fiolhais, Phys. Rev. B 46 (1992) 6671;
(f) J.P. Perdew, J.A. Chevary, S.H. Vosko, K.A. Jackson, M.-R. Pederson, D.J. Singh, C. Fiolhais, Phys. Rev. B 48 (1993) 4978;
(g) J.P. Perdew, K. Burke, Y. Wang, Phys. Rev. B 54 (1996) 16533.
[13] (a) P.J. Hay, W.R. Wadt, J. Chem. Phys. 82 (1985) 270;
(b) W.R. Wadt, P.J. Hay, Chem. Phys. 82 (1985) 284;
(c) P.J. Hay, W.R. Wadt, J. Chem. Phys. 82 (1985) 299.
[14] T.H. Dunning, P.J. Hay, in: H.F. Schaefer (Ed.), Modern Theoretical Chemistry, Plenum, New York, 1976.
[15] M.J. Frisch, G.W. Trucks, H.B. Schlegel, G.E. Scuseria, M.A. Robb, J.R. Cheeseman, V.G. Zakrzewski, J.A. Montgomery, R.E. Stratmann, J.C. Burant, S. Dapprich, J.M. Millam, A.D. Daniels, K.N. Kudin, M.C. Strain, O. Farkas, J. Tomasi, V. Barone, M. Cossi, R. Cammi, B. Mennucci, C. Pomelli, C. Adamo, S. Clifford, J. Ochterski, G.A. Petersson, P.Y. Ayala, Q. Cui, K. Morokuma, D.K. Malick, A.D. Rabuck, K. Raghavachari, J.B. Foresman, J. Cioslowski, J., Ortiz, B.B. Stefanov, G. Liu, A. Liashenko, P. Piskorz, I. Komaromi, R. Gomperts, R.L. Martin, D.J. Fox, T. Keith, M.A. Al-Laham, C.Y. Peng, A. Nanayakkara, C. Gonzalez, M. Challacombe, P.M.W. Gill, B.G. Johnson, W. Chen, M.W. Wong, J.L. Andres, M. Head-Gordon, E.S. Replogle, J.A. Pople, GAUSSIAN-98W (Revision A.7), Gaussian, Inc., Pittsburgh, PA, 1998.
[16] (a) P. Flükiger, H.P. Lüthi, S. Portmann, J. Weber, Swiss Center for Scientific Computing, Manno (Switzerland), 2000–2002;
(b) S. Portmann, H.P. Lüthi, Chimia 54 (2000) 766.
[17] (a) F. Lloret, M. Julve, J. Faus, X. Solans, Y. Journaux, I. Morgenstern-Badarau, Inorg. Chem. 29 (1990) 2232;
(b) S. Decurtins, H.W. Schmalle, P. Schneuwly, H.R. Oswald, Inorg. Chem. 32 (1993) 1888;
(c) C. Mathonière, S.G. Carling, D. Yusheng, P. Day, J. Chem. Soc., Chem. Commun. (1994) 1551;
(d) G. De Munno, R. Ruiz, F. Lloret, J. Faus, R. Sessoli, M. Julve, Inorg. Chem. 34 (1995) 408.
[18] (a) M. Verdaguer, M. Julve, A. Michalowicz, O. Kahn, Inorg. Chem. 22 (1983) 2624;
(b) M. Julve, M. Verdaguer, M.F. Charlot, R. Claude, Inorg. Chim. Acta 82 (1984) 5;
(c) Y. Pei, Y. Journaux, O. Kahn, Inorg. Chem. 28 (1989) 100;
(d) H. Tamaki, Z.J. Zhong, N. Matsumoto, S. Kida, M. Koikawa, N. Achiwa, Y. Hashimoto, H. Okawa, J. Am. Chem. Soc. 114 (1992) 6974;
(e) M. Ohba, H. Tamaki, N. Matsumoto, H. Okawa, Inorg. Chem. 32 (1993) 5385;
(f) S. Decurtins, H.W. Schmalle, H.R. Oswald, A. Linden, J. Ensling, P. Gütlich, A. Hauser, Inorg. Chim. Acta 216 (1994) 65;
(g) R. Cortés, M.K. Urtiaga, L. Lezama, M.I. Arriortua, T. Rojo, Inorg. Chim. Acta 33 (1994) 829;
(h) S.G. Carling, C. Mathonière, P. Day, K.M. Abdul Malik, S.J. Coles, M.B. Hursthouse, J. Chem. Soc., Dalton Trans. 1 (1996) 1839.

2. Experimental

2.1. General

Unless otherwise stated, all reactions were carried out under an oxygen-free nitrogen atmosphere using standard Schlenk techniques. Diethyl ether and thf were purified by reflux over sodium-benzophenone and distillation under nitrogen. Dichloromethane and MeCN were heated to reflux over CaH_2 and distilled under nitrogen. ClP^iPr_2 was from Aldrich. 2-(Diphenylphosphino)ethylamine [11] and 3-(diphenylphosphino)-1-propylamine [12], $MCl_2(PhCN)_2$ (M = Pt, Pd) [13] and PtMeX(cod) (X = Me, Cl) [14] were prepared according to literature methods. IR spectra were recorded as either KBr discs or solutions in the range 4000–200 cm^{-1} on a Perkin–Elmer 2000 FT spectrometer. NMR spectra were recorded on a Gemini 2000 spectrometer (operating at 121.4 MHz for ^{31}P and 300 MHz for ^{1}H). Microanalyses were performed by the St. Andrews University service and EI/FAB mass spectra by the Swansea Mass Spectrometer Service.

2.1.1. $Ph_2PCH_2CH_2NHPPr^i_2$ (1)

Chlorodiisopropyl phosphine (1.04 cm^3, 0.998 g, 6.54 mmol) was added dropwise over a period of 20 min to a stirred solution of $Ph_2PCH_2CH_2NH_2$ (1.5 g, 6.54 mmol) and Et_3N (1.09 cm^3, 0.794 g, 7.85 mmol) in Et_2O (50 cm^3). The mixture was stirred at room temperature (r.t.) for 1 h. The white precipitate (triethylamine hydrogen chloride) was filtered off and the solvent removed in vacuo to produce a clear, viscous liquid. Yield: 2.03 g, 90%. $^{31}P\{H\}$ NMR ($CDCl_3$): $\delta(P_A)$ −20.2(s) ppm; $\delta(P_X)$ 66.0(s) ppm. ^{1}H NMR ($CDCl_3$): δ 7.56–7.45 (m, 10H, aromatics), 3.23 (m, 2H, CH_2), 2.41 (m, 2H, CH_2), 1.30 (m, 1H, NH), 1.34 (m, 2H, CH), 1.15 (m, 12H, CH_3) ppm. MS: m/z 345 [M^+].

2.1.2. $Ph_2PCH_2CH_2CH_2NHPPr^i$ (2)

Chlorodiisopropyl phosphine (1.01 cm^3, 0.971 g, 6.37 mmol) was added dropwise over a period of 20 min to a stirred solution of $Ph_2PCH_2CH_2CH_3NH_2$ (1.548 g, 6.36 mmol) and Et_3N (1.01 cm^3, 0.773 g, 7.59 mmol) in Et_2O (50 cm^3). The mixture was stirred at r.t. for 1 h. The white precipitate (triethylamine hydrogen chloride) was filtered off and the solvent removed in vacuo to produce a white solid. Yield: 1.359 g, 60%. $^{31}P\{H\}$ NMR ($CDCl_3$): $\delta(P_A)$ −14.7(s) ppm; $\delta(P_X)$ 66.9(s) ppm. ^{1}H NMR ($CDCl_3$): δ 7.52–7.43 (m, 10H, aromatics), 3.13 (m, 2H, CH_2), 2.17 (m, 2H, CH_2), 1.67 (m, 2H, CH_2), 1.10 (m, 12H, CH_3) ppm.

2.1.3. $PdCl_2(Ph_2PCH_2CH_2NHPPr^i_2)$ (3)

$Ph_2PCH_2CH_2NH_2$ (1) (0.113 g, 0.327 mmol) and $PdCl_2(PhCN)_2$ (0.125 g, 0.327 mmol) were stirred in CH_2Cl_2 (10 cm^3) for 20 min. A cream precipitate started to form. The solvent was removed in vacuo until about 2 cm^3 remained. Diethyl ether was added dropwise to fully precipitate the cream solid which was collected by suction filtration. Yield: 0.093 g, 54%. *Anal*. Found (Calc. for $C_{20}H_{29}Cl_2NP_2Pd$): C, 45.67 (45.95); H, 5.51 (5.59); N, 2.65 (2.68)%. $^{31}P\{H\}$NMR ($CDCl_3$): $\delta(P_A)$ 20.9(d) ppm; $\delta(P_X)$ 90.3(d) ppm, $^{2}J(^{31}P-^{31}P) = 7$ Hz. MS: m/z 545 [$M+Na$]$^+$, 487 [$M-Cl$]$^+$. IR (KBr): 3244s (νNH), 3072w, 1638w, 287m, 217s cm^{-1}.

2.1.4. $PtCl_2(Ph_2PCH_2CH_2NHPPr^i_2)$ (4)

$Ph_2PCH_2CH_2NHPPr^i_2$ (1) (0.079 g, 0.22 mmol) and $PtCl_2(PhCN)_2$ (0.108 g, 0.22 mmol) were stirred in CH_2Cl_2 (10 cm^3) for 20 min. The solvent was removed in vacuo until product just started to precipitate; ether (10 cm^3) was added dropwise to aid precipitation. The cream solid was collected by suction filtration. Yield: 0.105 g, 75%. *Anal*. Found (Calc. for $C_{20}H_{29}Cl_2NP_2Pt$): C, 39.60 (39.29); H, 4.53 (4.78); N, 2.25 (2.29)%. $^{31}P\{H\}$ NMR ($CDCl_3$): $\delta(P_A)$ −1.4(d) ppm, $^{1}J(^{195}Pt-^{31}P_A) =$ 3584 Hz; $\delta(P_X)$ 57.8(d) ppm, $^{1}J(^{195}Pt-^{31}P) = 3595$ Hz, $^{2}J(^{31}P_A-^{31}P_X) = 17$ Hz. MS: m/z 576 [$M-Cl$]$^+$. IR (KBr): 3273s (νNH), 3027w, 303w, 278w cm^{-1}.

2.1.5. $PtMe_2(Ph_2PCH_2CH_2NHPPr^i_2)$ (5)

$Ph_2PCH_2CH_2NH_2$ (1) (0.117 g, 0.34 mmol) and $PtMe_2$(cod) (0.113 g, 0.34 mmol) were stirred in CH_2Cl_2 (10 cm^3) for 20 min. The solvent was removed in vacuo until a white solid started to precipitate; then Et_2O was added dropwise to aid precipitation. The solid was collected by suction filtration. Yield: 0.061 g, 32%. *Anal*. Found (Calc. for $C_{22}H_{35}NP_2Pt$): C, 46.06 (46.36); H, 6.03 (6.18); N, 2.30 (2.45)%. $^{31}P\{H\}$ NMR ($CDCl_3$): $\delta(P_A)$ 7.1(d) ppm, $^{1}J(^{195}Pt-^{31}P_A) = 1849$ Hz; $\delta(P_X)$ 68.3(d) ppm, $^{1}J(^{195}Pt-^{31}P_X) = 1990$ Hz, $^{2}J(^{31}P_A-^{31}P_X) = 22$ Hz. ^{1}H NMR ($CDCl_3$): δ 7.69–7.39 (m, 10H, aromatics), 3.20 (m, 2H, CH_2), 2.35 (m, 2H, CH_2), 2.19 (m, 2H, CH_2), 1.29–1.03 (m, 12H, CH_3), 0.78–0.67 (m, 6H, CH_3) ppm. MS: m/z 555 [$M-Me$]$^+$. IR (KBr): 3384s (νNH), 3070w, 2959s, 2864s, 1589w, 1098s cm^{-1}.

2.1.6. $PtClMe(Ph_2PCH_2CH_2NHPPr^i_2)$ (6)

$Ph_2PCH_2CH_2NH_2$ (1) (0.113 g, 0.33 mmol) and PtClMe(cod) (0.116 g, 0.33 mmol) were stirred in CH_2Cl_2 (10 cm^3) for 20 min. The solvent was removed in vacuo until a white solid started to precipitate. Diethyl ether was added dropwise to aid precipitation. The solid was collected by suction filtration. Yield: 0.141 g, 73%. *Anal*. Found (Calc. for $C_{21}H_{32}ClNP_2Pt$): C, 42.31 (42.68); H, 5.53 (5.46); N, 2.09 (2.37)%. $^{31}P\{H\}$ NMR ($CDCl_3$): $\delta(P_A)$ 6.4(d) ppm, $^{1}J(^{195}Pt-^{31}P_A) =$ 1879 Hz; $\delta(P_X)$ 63.8(d) ppm, $^{1}J(^{195}Pt-^{31}P_X) = 4626$ Hz, $^{2}J(^{31}P_A-^{31}P_X) = 18$ Hz. ^{1}H NMR ($CDCl_3$): δ 7.85–7.38 (m, 10H, aromatics), 3.45 (m, 2H, CH_2), 2.25 (m, 2H, CH_2), 1.38 (m, 2H, CH), 1.2 (m, 12H,

CH_3), 0.76 (m, 3H, CH_3) ppm. MS: *m/z* 555 $[M-Cl]^+$. IR (KBr): 3277s (*v*NH), 3052w, 2962s, 2867s, 1435s, 1100s, 274w cm^{-1}.

2.1.7. $Fe(CO)(\eta^5\text{-}C_5H_5)(Ph_2PCH_2CH_2NHPPr^i_2)I$ (7)

$Ph_2PCH_2CH_2NHPr_2$ (**1**) (0.114 g, 0.33 mmol), $Fe(CO)_2(\eta^5\text{-}C_5H_5)I$ (0.091 g, 0.30 mmol) and catalyst $Fe(CO)_2(\eta^5\text{-}C_5H_5)$ (0.010 g, 0.057 mmol) were refluxed in MeCN (15 cm^3). Reaction followed by IR to completion. The reaction mixture was allowed to cool to r.t., before the solvent was removed in vacuo, producing a green precipitate. The precipitate was re-dissolved in CH_2Cl_2 and precipitated with 60–80 pet ether. The solid was collected by suction filtration. Yield: 0.107 g, 57%. *Anal*. Found (Calc. for $C_{26}H_{34}FeINOP_2$): C, 50.59 (50.27); H, 5.65 (5.52); N, 2.30 (2.25)%. $^{31}P\{H\}$ NMR ($CDCl_3$): $\delta(P_A)$ 53.0(d) ppm; $\delta(P_X)$ 119.8(d) ppm, $^2J(^{31}P_A-^{31}P_X) = 67$ Hz. ^1H NMR ($CDCl_3$): δ 7.96–7.37 (m, 10H, aromatics), 4.99 (m, 5H, Cp), 3.57 (m, 2H, CH_2), 2.73 (m, 2H, CH_2), 2.27 (m, 2H, CH), 1.50–1.21 (m, 12H, CH_3) ppm. MS: *m/z* 494 $[M^+]$. IR (KBr): 3179m (*v*NH), 3048m, 1954s.

2.1.8. $NiCl_2(Ph_2PCH_2CH_2NHPPr^i_2)$ (8)

$Ph_2PCH_2CH_2NHPr_2$ (**1**) (0.273 g, 0.79 mmol) and $NiCl_2\cdot 6H_2O$ (0.188 g, 0.79 mmol) were stirred in thf (10 cm^3) at r.t. for 20 min. A dark orange solid started to precipitate. The solvent was removed in vacuo and Et_2O added dropwise to aid precipitation. The orange solid was collected by suction filtration. Yield: 0.263 g, 70%. *Anal*. Found (Calc. for $C_{20}H_{29}Cl_2NNiP_2$): C, 50.22 (50.57); H, 6.65 (6.15); N, 2.94 (2.95)%. IR (KBr): 3263s (*v*NH), 326m, 287m.

2.1.9. $PdCl_2[Ph_2P(CH_2)_3NHPPr^i_2]$ (9)

$Ph_2P(CH_2)_3NHPPr^i_2$ (**2**) (0.125 g, 0.45 mmol) and $PdCl_2(PhCN)_2$ (0.133 g, 0.45 mmol) were stirred at r.t. in CH_2Cl_2 (10 cm^3) for 20 min. Cream solid started to precipitate. Solvent was removed in vacuo until approximately 2 cm^3 remained. Diethyl ether was added dropwise to fully precipitate solid. The solid was collected by suction filtration. Yield: 0.159 g, 85%. *Anal*. Found (Calc. for $C_{21}H_{31}Cl_2NP_2Pd$): C, 47.03 (47.14); H, 5.61 (5.84); N, 2.78 (2.62)%. No NMR as very insoluble. MS: *m/z* 500 $[M-Cl]^+$, 463 $[M-2Cl]^{2+}$. IR (KBr): 3262s (*v*NH), 3052w, 1435s, 297m, 282m cm^{-1}.

2.1.10. $PtCl_2[Ph_2P(CH_2)_3NHPPr^i_2]$ (10)

$Ph_2P(CH_2)_3NHPPr^i_2$ (**2**) (0.248 g, 0.69 mmol) and $PtCl_2(PhCN)_2$ (0.326 g, 0.69 mmol) were stirred at r.t. in CH_2Cl_2 (10 cm^3) for 20 min. The solvent was removed in vacuo until a white solid started to precipitate. Diethyl ether was added dropwise to precipitate the white solid. The solid was collected by suction filtration. Yield: 0.356 g, 92%. *Anal*. Found (Calc. for $C_{21}H_{31}Cl_2NP_2Pt$): C, 40.24 (40.41); H, 4.42 (5.01); N, 2.58 (2.24)%. MS: *m/z* 590 $[M-Cl]^+$, 552 $[M-2Cl]^+$. IR (KBr): 3330s (*v*NH), 3053w, 1700w, 1653w, 304m, 297, 282 *v*(M–Cl) cm^{-1}.

2.1.11. $PtMe_2[Ph_2P(CH_2)_3NHPPr^i_2]$ (11)

$Ph_2P(CH_2)_3NHPPr^i_2$ (**2**) (0.105 g, 0.29 mmol) and $PtMe_2$(cod) (0.097 g, 0.29 mmol) were stirred at r.t. in CH_2Cl_2 (10 cm^3) for 60 min. Solvent was removed in vacuo until precipitate started to form. Diethyl ether was added to aid precipitation. White solid was collected by suction filtration. Yield: 0.122 g, 71%. *Anal*. Found (Calc. for $C_{23}H_{37}NP_2Pt$): C, 47.05 (47.29); H, 6.12 (6.38); N, 2.48 (2.4)%. $^{31}P\{H\}$ NMR ($CDCl_3$): $\delta(P_A)$ 7.3 ppm, $^1J(^{195}Pt-^{31}P_A) = 1823$ Hz; $\delta(P_X)$ 94.4 ppm, $^1J(^{195}Pt-^{31}P_X) = 2164$ Hz, $^2J(^{31}P_A-^{31}P_X) = 15$ Hz. ^1H NMR ($CDCl_3$): δ 7.83–7.46 (m, 10H, aromatics), 3.31–3.22 (m, 2H, CH_2), 2.88–2.75 (m, 2H, CH_2), 2.41–2.26 (m, 2H, CH_2), 1.65–1.52 (m, 2H, CH), 1.35–1.24 (m, 12H, CH_3), 0.77–0.48 (m, 3H, CH_3), 0.37–0.08 (m, 3H, CH_3) ppm. MS: *m/z* 584 $[M]^+$, 569 $[M-Me]^+$, 554 $[M-2Me]^+$. IR (KBr): 3377s (*v*NH), 3073w, 1434s.

2.1.12. $PtMeCl[Ph_2P(CH_2)_3NHPPr^i_2]$ (12)

$Ph_2P(CH_2)_3NHPPr^i_2$ (**2**) (0.126 g, 0.49 mmol) and PtMeCl(cod) (0.124 g, 0.49 mmol) were stirred at r.t. in CH_2Cl_2 (10 cm^3) for 60 min. Solvent was removed in vacuo until a precipitate started to form. Diethyl ether was added dropwise to fully precipitate solid. The white solid was collected by suction filtration. Yield: 0.155 g, 73%. *Anal*. Found (Calc. for $C_{22}H_{34}ClNP_2Pt$): C, 43.75 (43.74); H, 5.51 (5.67); N, 2.41 (2.32)%. $^{31}P\{H\}$ NMR ($CDCl_3$): δ 8.8 ppm, $^1J(^{195}Pt-^{31}P) = 1655$ Hz, $^2J(^{31}P-^{31}P) = 12$ Hz; δ 23.2 ppm, $^1J(^{195}Pt-^{31}P) = 3042$ Hz; δ 67.5 ppm, $^1J(^{195}Pt-^{31}P) = 2945$ Hz; δ 82.2 ppm, $^1J(^{195}Pt-^{31}P) = 4575$ Hz, $^2J(^{31}P-^{31}P) = 13$ Hz. MS: *m/z* 604 $[M]^+$, 569 $[M-Cl]^+$. IR (KBr): 3280s (*v*NH), 3052m, 1588w, 279w cm^{-1}.

2.2. Crystallography

X-ray diffraction studies were performed at 293 K using a Rigaku Mercury CCD for **8** and a Bruker SMART diffractometer for **11** with graphite-monochromated Mo Kα radiation ($\lambda = 0.71073$ Å). The structures were solved by direct methods, non-hydrogen atoms were refined with anisotropic displacement parameters; hydrogen atoms bound to carbon were idealised and fixed (C–H 0.95 Å), the NH protons were located by ΔF map. Structural refinements were by the full-matrix least-squares method on F^2 using SHELXTL [15]. Compound **8** was only obtained as poorly diffracting very thin plates.

*2.2.1. $NiCl_2(Ph_2PCH_2CH_2NHPPr^i_2)$ (**8**)*

$C_{20}H_{29}Cl_2N_1Ni_1P_2$, $M = 474.99$, monoclinic, space group $P2_1/n$, $a = 8.979(3)$, $b = 15.115(6)$, $c = 16.688(6)$ Å, $\beta = 91.903(5)^\circ$, $U = 2264(1)$ Å^3, $Z = 4$, $D_{calc} = 1.394$ Mg m^{-3}, $\mu = 1.239$ mm^{-1}, $F(000) = 992$, crystal size = $0.23 \times 0.10 \times 0.02$ mm. Of 14 456 measured data, 4774 were unique ($R_{int} = 0.0517$) and observed to give R_1 [$I > 2\sigma(I)$] = 0.1153.

*2.2.2. $PtMe_2[Ph_2P(CH_2)_3NHPPr^i_2]$ (**11**)*

$C_{23}H_{37}N_1P_2Pt$, $M = 584.57$, monoclinic, space group $P2_1/c$, $a = 9.4476(2)$, $b = 15.5972(3)$, $c = 16.1970(1)$ Å, $\beta = 91.161(1)^\circ$, $U = 2386(1)$ Å^3, $Z = 4$, $D_{calc} = 1.627$ Mg m^{-3}, $\mu = 6.022$ mm^{-1}, $F(000) = 1160$, crystal size = $0.10 \times 0.10 \times 0.13$ mm. Of 10 219 measured data, 2965 were unique ($R_{int} = 0.0192$) and observed to give R_1 [$I > 2\sigma(I)$] = 0.0159.

3. Results and discussion

Surprisingly, there are relatively few examples of unsymmetrical diphosphines in which the two phosphorus atoms have different substituents. One limiting factor in the synthesis has been the inconvenient routes involving highly air sensitive intermediates. Grim et al. [15–18] have synthesised a number of diphosphines of the types $RPhP(CH_2)_nPPh_2$ ($n = 1$–3, R = Me, Et, Pr, Pr^i, Bu^t, Bu) and $R_2P(CH_2)_nPPh_2$ ($n = 1$, R = Me, Pr^i, $n = 3$, R = Me), but their route is experimentally difficult. Briggs and coworkers [19] reported an easier synthesis of diphosphines of the type $RPhP(CH_2)_nPPh_2$ ($n = 3$–6, R = Me, Et, c-C_6H_{11}) via the stepwise formation of the mono- and di-phosphonium salts, using a non-polar solvent in the first stage and a polar solvent for the second stage, and on the loss of phenyl in preference to alkyl at the hydrolysis stage. More recently a one-pot synthesis to unsymmetrical 1,2-bis(phosphanyl)ethanes has been developed [20]. We have been interested in the use of P–N bond forming reactions for phosphine synthesis and have developed strategies for the synthesis of unsymmetrical aryl backbone phosphines from amines [21–26]. Here we have extended our methods to alkyl backbone systems. Thus $Ph_2PCH_2CH_2NHPPr^i_2$ (**1**) and $Ph_2P(CH_2)_3NHPPr^i_2$ (**2**), were obtained by direct reaction of the appropriate amine, and chlorodiisopropylphosphine. The presence of slightly more than 1 M equivalent of triethylamine ensures complete removal of the hydrogen chloride by-product (Eq. (1)).

$$Ph_2P(CH_2)_nNH_2 + {}^iPr_2PCl + Et_3N \rightarrow Ph_2P(CH_2)_nNHP^iPr_2 + NEt_3HCl \quad (1)$$

$n = 2$ (**1**); 3 (**2**)

The structure of **1** was confirmed by mass spectrometry and $^{31}P\{H\}$ and ^1H NMR. MS gave a M^+ peak at 345. $^{31}P\{H\}$ NMR revealed the predicted AX spectrum. The peak at $\delta(P_A)$ −20.2 ppm was assigned to the diphenyl phosphorus, as the peak in the starting material was at −20.5 ppm and $\delta(P_X)$ 65.9 ppm was assigned to the di-isopropyl phosphorus. There is no observable coupling between the 2 inequivalent. phosphorus nuclei. Compound **2** is a white solid whilst **1** is a clear, viscous liquid. In **2** the P_A peak corresponding to the diphenyl phosphorus is at −14 ppm [similar to the starting material at −14.6 ppm]; the $\delta(P_X)$ peak assigned to the di-isopropyl phosphorus, like that of **1**, occurs at $\delta(P)$ 67 ppm.

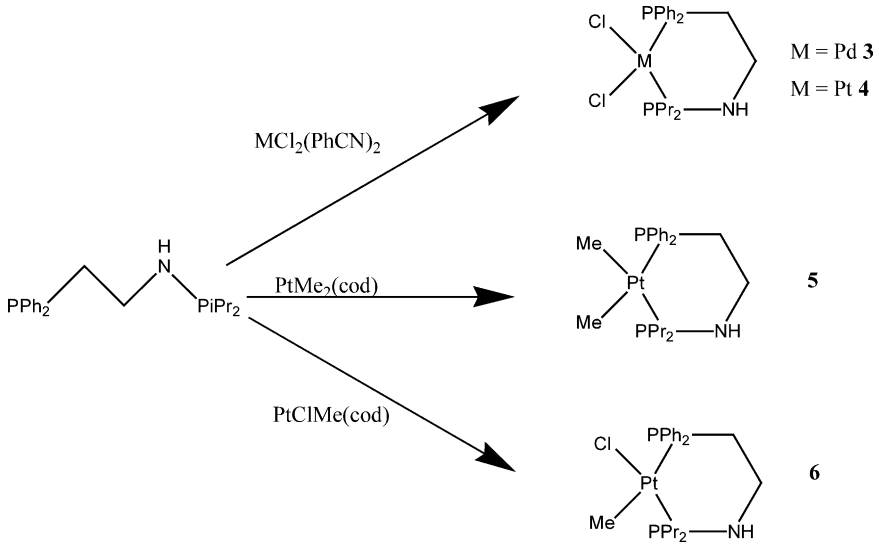
Further evidence for the above assignment is that **1** reacts with 1 equiv. of elemental selenium at the most basic and therefore most reactive phosphorus atom, the di-isopropyl phosphorus atom since $\delta(P_A)$ −20 ppm remains in the same place, whilst $\delta(P_X)$ 65.9 ppm in **1** shifts to 89 ppm in $Ph_2PCH_2CH_2NHP(Se)Pr^i_2$.

We examined some simple coordination chemistry of **1** and **2**. Complexation reactions were straightforward, with coordination to platinum, palladium and nickel all being carried out at room temperature. Coordination to iron required refluxing in acetonitrile in the presence of a catalyst. All complexes were formed as fine powders. The spectroscopic data for the complexes are readily interpreted and consistent with chelate monomeric systems though we noted some weak high value m/z peaks in some of the mass spectra which could suggest dimer formation in the mass spectrometer at least.

The palladium dichloride complex **3** was formed by direct reaction of **1** with $PdCl_2(PhCN)_2$. Mass spectroscopy gave the $M+Na^+$ peak at 545, corresponding to a monomeric complex and microanalysis was in good agreement with the proposed structure. In its $^{31}P\{^1H\}$ NMR the diphenyl phosphorus group is observed at $\delta(P_A)$ 20.9 ppm whilst $\delta(P_X)$ 90.3 ppm, the coupling constant, $^2J(P_X–P_A) = 7$ Hz, is very small. The two peaks in the IR spectrum assigned as ν(M−Cl) 297, 282 cm^{-1} suggest the ligand coordinates in a *cis*-geometry and therefore the complex has a six-membered PdP_2NC_2 chelate ring. The dichloro-, dimethyl- and chloromethylplatinum complexes were all formed by similar ligand substitution reactions (Scheme 1).

The geometry of complexes **4**–**6** was confirmed by examination of the Pt–P coupling constants in their $^{31}P\{H\}$ NMR summarised below (Table 1). The mass spectrum of **4** has a major peak at 576 corresponding to $[M-Cl]^+$. The $^{31}P\{H\}$ NMR of complex **6** has $\delta(P_A)$ 6.4 ppm, $^1J(Pt–P_A) = 1879$ Hz and $\delta(P_X)$ 63.8 ppm, $^1J(Pt–P_X) = 4626$ Hz. The $\delta(P_A)$ peak is assigned to the diphenyl phosphorus group *trans* to methyl with the PPr^i_2 group is *trans* to chloride.

Coville et al. [27] found $[(\eta^5\text{-}C_5H_5)Fe(CO)_2I]$ reacts with diphosphines (L–L) in the presence of $[(\eta^5\text{-}C_5H_5)Fe(CO)_2]_2$ catalyst to produce $[(\eta^5\text{-}C_5H_5)Fe(CO)(L–$



Scheme 1. Formation of palladium and platinum complexes of **1**.

L)]I. The reaction for each of the diphosphines, L–L = $Ph_2P(CH_2)_nPPh_2$ ($n = 1$–4), was followed by IR and in each case $[(\eta^5\text{-}C_5H_5)Fe(CO)_2(L\text{–}L)]I$ was readily identified by the characteristic ν(CO) at 2050, 2000 cm^{-1}. We have found that reaction of **1** under the same conditions as above gives $[(\eta^5\text{-}C_5H_5)Fe(CO)(Ph_2PCH_2CH_2NHPPr^i_2)]I$ (**7**) identified by ν(CO) 1954 cm^{-1}, microanalysis and mass spectrometry. The ^{31}P NMR of **7** contains the expected AX spectrum, with a large change in chemical shift on coordination to the iron ($\delta(P_A)$ 53.0 ppm, $\delta(P_X)$ 119.8 ppm) compared to the free ligand values of $\delta(P_A)$ −20.2 ppm and $\delta(P_X)$ 66.0 ppm. The spectrum also shows a large P–P coupling, $^2J(P_X\text{–}P_A) = 67$ Hz. In a separate experiment in which no catalyst was used, the intermediate $[(\eta^5\text{-}C_5H_5)Fe(CO)_2(Ph_2PCH_2CH_2NHPPr^i_2)]I$ was observed after 16 h [ν(CO) 2951, 2006 cm^{-1}] which is consistent with Coville's work [27].

$NiCl_2\cdot 6H_2O$ reacts with **1** to give $NiCl_2(Ph_2PCH_2CH_2NHPPr^i_2)$ (**8**). Microanalyses are consistent with this formulation and its IR spectrum contains peaks at 287 and 326 cm^{-1}, confirming the presence of *cis* Ni–Cl bonds. We were unable to obtain a satisfactory NMR spectrum of **8** since it is poorly soluble and appears to be paramagnetic in solution which suggests at least some tetrahedral character in solution. X-ray crystallography reveals the solid state structure of **8** (Fig. 1) with the nickel in an approximate square planar geometry and the two phosphorus atoms coordinating in a *cis* fashion. The diphosphine ligand forms a six-membered metallacycle, which can best be described as having a half-boat conformation, $NiP_2NC(13)$ are approximately coplanar with C(14) at the prow of the boat. Hydrogen bonding between the amine proton N(2) and Cl(2) of the adjacent complex [Cl···H 2.40, Cl···N 3.37 Å, N–H···Cl 170°) results in an infinite chain motif (Fig. 2).

As with **1** complexation of $Ph_2P(CH_2)_3NHPPr^i_2$ (**2**) involves straight forward ligand substitution reactions, we established coordination to platinum and palladium for illustrative purposes. All complexes were produced as fine powders. In the ^{31}P NMR of **11** the spectrum is again the expected AX type, with satellites due to coupling to platinum. $\delta(P_A)$ 7.3 ppm is assigned to

Table 1
$^{31}P\{H\}$ NMR data

	δP_A (PPh_2) (ppm)	δP_B (PPr_2) (ppm)	$^1J(P_A\text{–Pt})$ (Hz)	$^1J(P_X\text{–Pt})$ (Hz)	$^2J(P_A\text{–}P_X)$ (Hz)
$Ph_2PCH_2CH_2NHPPr^i_2$ (**1**)	−20.2	66.0			0
$Ph_2PCH_3CH_3CH_3NHPPr^i$ (**2**)	−14.7	66.9			0
$PdCl_2(Ph_2PCH_2CH_2NHPPr^i_2)$ (**3**)	20.9	90.3			7
$PtCl_2(Ph_2PCH_2CH_2NHPPr^i_2)$ (**4**)	−1.4	57.8	3584	3595	17
$PtMe_2(Ph_2PCH_2CH_2NHPPr^i_2)$ (**5**)	7.1	68.3	1849	1990	22
$PtClMe(Ph_2PCH_2CH_2NHPPr^i_2)$ (**6**)	6.4	63.8	1879	4626	18
$Fe(CO)(\eta^5\text{-}C_5H_5)(Ph_2PCH_2CH_2NHPPr^i_2)I$ (**7**)	53.0	119.8			67
$PtMe_2[Ph_2P(CH_2)_3NHPPr^i_2]$ (**11**)	7.3	94.4	1823	2164	15
$PtMeCl[Ph_2P(CH_2)_3PPr^i_2]$ (**12A**)	8.8	82.2	1655	4575	12
$PtMeCl[Ph_2P(CH_2)_3PPr^i_2]$ (**12B**)	23.2	67.5	3042	2945	13

No spectra were obtained for **8**, **9** and **10** because of insolubility.

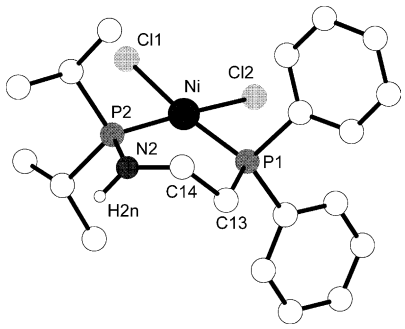


Fig. 1. X-ray structure of $NiCl_2(PH_2PCH_2CH_2NHPPr^i_2)$ (**8**). Selected bond lengths (Å) and angles (°) Ni–P(1) 2.173(2), Ni–P(2) 2.186(2), Ni–Cl(1) 2.196(2), Ni–Cl(2) 2.226(2), P(1)–C(13) 1.822(6), C(13)–C(14) 1.524(9), C(14)–N(2) 1.448(8), N(2)–P(2) 1.668(6); P(1)–Ni–P(2) 96.1(1), Cl(1)–Ni–Cl(2) 90.1(8), N(2)–P(2)–Ni 117.3(2), C(14)–Ni–P(2) 125.7(4).

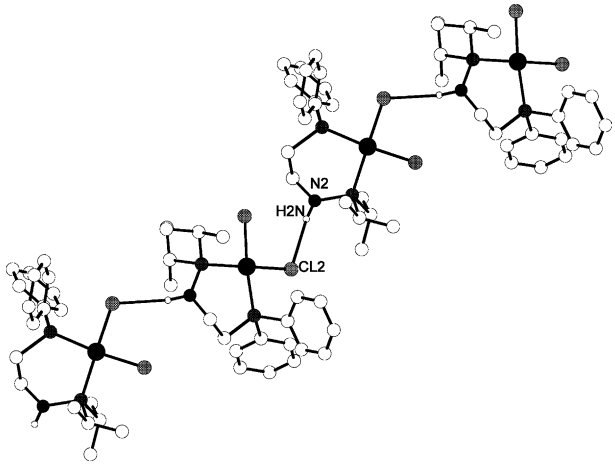


Fig. 2. Hydrogen bonding between the amine proton and chloride of the adjacent complex resulting in an infinite chain motif in $NiCl_2(PH_2PCH_2CH_2NHPPr^i_2)$ (**8**).

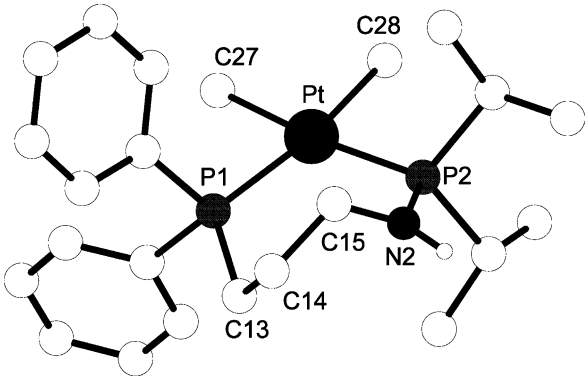


Fig. 3. The X-ray structure of $PtMe_2[Ph_2P(CH_2)_3NHPPr^i_2]$ (**11**). Selected bond lengths (Å) and angles (°) Pt–P(1) 2.285(1), Pt–P(2) 2.285(1), Pt–C(27) 2.124(3), Pt–C(28) 2.110(3), P(1)–C–(!3) 1.844(3), C(13)–C(14) 1.524(5), C(14)–C(15) 1.508(5), C(15)–N(2) 1.455(4), N(2)–P(2) 1.684(3); P(1)–Pt–P(2) 100.0(1), C(27)–Pt–C(28) 82.8(1), N(2)–P(2)–Pt 115.5(1), C(15)–N(6)–P(2) 123.8(2).

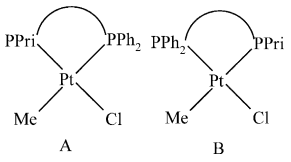


Fig. 4. Different isomers of **12**.

PPh_2 and $\delta(P_X)$ 94.4 ppm is assigned to PPr^i_2. The proton NMR clearly shows the different environments of the two methyl groups on the platinum, both methyl groups are coupled to the phosphorus to give an apparent quartet $J(^1H–^{31}P) = 7.7$ Hz with satellite peaks either side due to coupling to the platinum. Crystallography confirmed the structure of **11** (Fig. 3) to be monomeric with the diphosphine ligand coordinating as a chelate. The geometry around the platinum is distorted square planar, [P(1)–Pt(1)–P(2) 100.0(1)° and C(28)–Pt(1)–C(27) 82.8(1)°] with the ligand displaying a significantly larger bite angle than **1** in **8** as a consequence of the extra methylene group in the backbone here and since the *trans* methyl groups are less sterically demanding than the chlorides in **8**. The conformation of the ring is a distorted 'chaise longue'.

Complex **12** was formed by reaction of ligand **2** with PtMeCl(cod). ^{31}P NMR (Table 1) shows the presence of equal proportions of two isomers (Fig. 4). If $\delta(P_A)$ is assigned to PPh_2 and $\delta(P_X)$ is assigned to PPr^i_2 then in isomer A the PPh_2 moiety is *trans* to methyl and has a small coupling constant to platinum, $^1J(^{31}P_A–^{195}Pt) =$ 1665 Hz, and the PPr^i_2 moiety is *trans* to chloride and therefore has a large coupling constant with platinum, $^1J(^{31}P_X–^{195}Pt) = 4575$ Hz.

This work clearly illustrates the ease of formation of unsymmetrical phosphines and should allow the effect of variation of the two phosphorus centres on a range of catalytic processes to be studied.

4. Supplementary material

Full lists of structure refinement data, atomic coordinates, bond lengths and angles, anisotropic displacement parameters and hydrogen atom parameters have been deposited with the Cambridge Crystallographic Data Centre, CCDC Nos. 188819 (**8**), 188820 (**11**). Copies of this information may be obtained free of charge from The Director, CCDC, 12 Union Road, Cambridge, CB2 1EZ, UK (fax: +44-1223-336033; e-mail: deposit@ccdc.cam.ac.uk or www: http://www.ccdc.cam.ac.uk).

References

[1] C.A. McAuliffe, Comprehensive Coordination Chemistry, vol. 2, Pergamon, Oxford, 1987, p. 989.

[2] E. Drent, J.A.M. van-Brockhoven, M.J. Doyle, J. Organomet. Chem. 417 (1991) 235.
[3] M.J. Joshi, J.S. Thornburn, S.J. Rettig, B.R. James, Inorg. Chim. Acta 198–200 (1992) 283.
[4] Y.B. Kang, M. Pabel, D.D. Pathak, A.C. Willis, S.B. Wild, Main Group Chem. 1 (1995) 89.
[5] R. Ugo, Aspects of Homogenous Catalysis; A Series of Advances, Reidel, Dordrecht, 1974.
[6] S. Ittel, G. Parshall, Homogeneous Catalysis: The Applications and Chemistry of Catalysis by Soluble Transition Metal Complexes, Wiley, New York, 1992.
[7] S.M. Aucott, A.M.Z. Slawin, J.D. Woollins, J. Organomet. Chem. 582 (1999) 83–89.
[8] Q. Zhang, S.M. Aucott, A.M.Z. Slawin, J.D. Woollins, Eur. J. Inorg. Chem. (2002) 1635.
[9] Y. Ben-David, M. Portnoy, D. Milstein, J. Chem. Soc., Chem. Commun. (1989) 1816.
[10] E. Lindner, M. Schmid, J. Wald, J.A. Queisser, M. Geprags, P. Wegner, C. Nachtigal, J. Organomet. Chem. 602 (2000) 173.
[11] K. Kashiwabara, I. Kinoshita, T. Ito, J. Fujita, Bull. Chem. Soc. Jpn. 54 (1981) 725.
[12] K. Kashiwabara, M. Jung, J. Fujita, Bull. Chem. Soc. Jpn. 64 (1991) 2372.
[13] G.K. Anderson, M. Lin, Inorg. Synth. 28 (1990) 60.
[14] H.C. Clarke, L.E. Manzer, J. Organomet. Chem. 59 (1973) 411.
[15] SHELXTL, Version 5.10, Bruker AXS, 1998.
[16] S.O. Grim, R.C. Barth, J. Organomet. Chem. 94 (1975) 327.
[17] S.O. Grim, J.D. Mitchell, Inorg. Chem. 16 (1977) 1762.
[18] S.O. Grim, J.D. Mitchell, Inorg. Chem. 16 (1977) 1770.
[19] F.R. Benn, J.C. Briggs, C.A. McAuliffe, J. Chem. Soc., Dalton Trans. (1984) 293.
[20] G. Fries, J. Wolf, M. Pfeiffer, D. Stalke, H. Werner, Angew. Chem., Int. Ed. Engl. 3 (2000) 564.
[21] A.M.Z. Slawin, M. Wainwright, J.D. Woollins, New J. Chem. 24 (2000) 69.
[22] A.M.Z. Slawin, J.D. Woollins, Q. Zhang, Inorg. Chem. Commun. 2 (1999) 386.
[23] S.M. Aucott, A.M.Z. Slawin, J.D. Woollins, J. Chem. Soc., Dalton Trans. (2000) 2559.
[24] M.L. Clarke, G.L. Holliday, A.M.Z. Slawin, J.D. Woollins, Inorg. Chem. Commun. 4 (2001) 115.
[25] S.M. Aucott, M.L. Clarke, A.M.Z. Slawin, J.D. Woollins, J. Chem. Soc., Dalton Trans. (2001) 972.
[26] S.M. Aucott, A.M.Z. Slawin, J.D. Woollins, J. Chem. Soc., Dalton Trans. (2001) 2279.
[27] N.J. Coville, E.A. Darling, A.W. Hearn, P. Johnston, J. Organomet. Chem. 328 (1987) 375.

preconcentration [12], and stationary phases for chromatography [13], and as well as in the use of these new materials to immobilize agrochemical compounds in order to anchor pesticides [14].

The present investigation is focused on the silylant agent 3-glycidoxypropyltrimethoxysilane (GPTS), taking into account its ability to react by considering epoxide group opening, in the presence of nucleophiles. This enhanced reactivity leads to ring opening allowing facile introduction of nucleophiles like amines, as represented here by the bifunctional molecule, propane-1,3-diamimine.

2. Experimental

2.1. Chemicals

Reagent grade solvents were purified and distilled just before use. Silica gel, with particle size in the range 70–230 mesh, average pore diameter 60 Å and pore volume 0.75 $cm^3\ g^{-1}$, was treated and activated as before [7,8]. The silylant agent GPTS was used without further purification; propane-1,3-diamine and triethylamine were distilled under reduced pressure.

2.2. Heterogeneous process

The heterogeneous route consisted in suspending 20.0 g of activated silica gel in 100.0 cm^3 of dry toluene, followed by addition of 20.0 cm^3 (91.0 mmol) of GPTS. The mixture was mechanically stirred under reflux of the solvent in an inert dry nitrogen atmosphere for 72 h [7,8]. The mixture was filtered and the solid was washed with toluene and methanol. The white product (SiG) was dried in vacuo for 24 h at 323 K. In sequence, 5.0 g of this modified silica was suspended in 100.0 cm^3 of toluene. This suspension was heated to solvent reflux with mechanical stirring when 8.5 cm^3 (102.0 mmol) of propane-1,3-diamine was added, under a dry atmosphere, and maintained at reflux for another 48 h. After cooling, the solid was filtered, washed and dried as described before, obtaining the product, SiHT [7,8].

2.3. Homogeneous process

This method comprised in reacting 5.0 cm^3 (23.0 mmol) of GPTS with 1.9 cm^3 (23.0 mmol) of the diamine in 100 cm^3 of dry methanol. The mixture was refluxed under a dry atmosphere of nitrogen for 48 h. The solution was concentrated to approximately 40 cm^3 and added to 5.0 g of silica suspended in 100.0 cm^3 of dry toluene. After refluxing for 72 h under a dry nitrogen atmosphere, the solid was filtered, washed with toluene and methanol and dried as described for the heterogeneous route, to obtain the product, SiHM [14,15].

2.4. Characterization

The anchored surfaces, SiG, SiHT and SiHM, had their elemental compositions analyzed with a Perkin–Elmer 2400 Series II microelemental analyzer. The values obtained reflect the degree of organofunctionalization of both kinds of these matrices.

The surface area of the silicas was obtained by using the BET equation, through nitrogen adsorption isotherms at 77 K, by means of a Flowsorb 2300 analyzer. Before starting the analysis, the samples were dried at 373 K and each surface was purged in a stream of dry nitrogen [7,8].

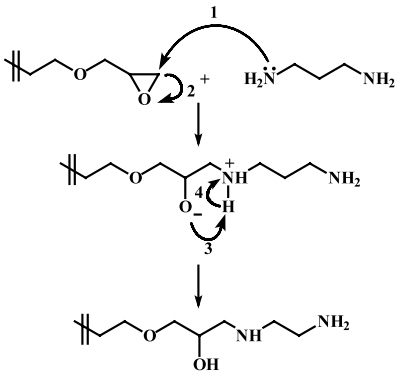
The mass loss determinations were performed on a DuPont instrument, Model 951, using 8.0–12.0 mg of the sample under nitrogen at a heating rate of 0.17 K s^{-1}. Infrared spectra of the compounds were obtained in the 4000–400 cm^{-1} region with a resolution of 4 cm^{-1}, by accumulating 32 scans using a MB-Bomem FTIR spectrophotometer; KBr pellets were used for solid samples and NaCl windows for liquid samples [7,8].

Nuclear magnetic resonance spectra of the solid samples were obtained on an AC 300/P Bruker spectrometer at room temperature. For each run, approximately 1 g of each modified silica was compacted into a 7 mm zirconium oxide rotor. The measurements were obtained for carbon and silicon with frequencies at 75.47 and 59.61 MHz, respectively, with a magic-angle spinning speed of 4 Hz. In order to increase the signal to noise ratio of the solid-state spectra, the CP/MAS technique was used for ^{13}C and ^{29}Si nuclei. The spectra were obtained with pulse repetitions of 1 and 3 s and contact times were 1 and 3 ms, with number of the scans 19 000 and 22 000 for carbon and silicon, respectively [7,8].

3. Results and discussion

The reaction between the epoxy moiety attached to the silylant agent GPTS, with a diamine molecule is based on a typical nucleophilic attack of the basic nitrogen atom on the strained acidic carbon atom of the ring [16], as represented in Scheme 1 when the propane-1,3-diamine is involved.

The non-bonded electron pair on the nitrogen of propane-1,3-diamine interacts initially with the acidic carbon atom of the epoxy ring (1); consequently the electrons of the bond between the carbon and oxygen of the epoxy ring are transferred to oxygen, opening the ring as represented in step (2). The excess of charge on the oxygen atom attracts the nearby hydrogen atom,



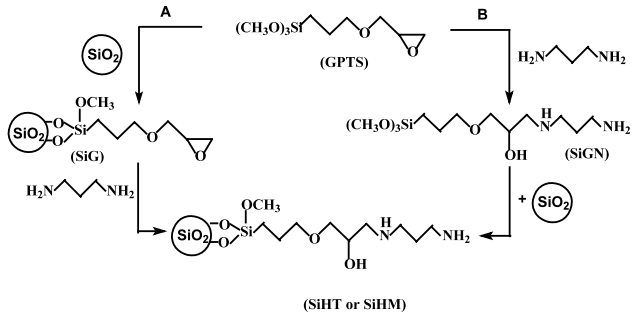
Scheme 1. Proposed mechanism of the reaction between the epoxy moiety of the silylant agent and propane-1,3-diamine.

once bonded to nitrogen, to form an oxygen–hydrogen bond (3), permitting electronic rearrangement (4) and producing the final, neutral product.

Taking this into account, epoxy ring reactivity in the presence of an amine molecule causes the incorporation of propane-1,3-diamine onto the silylant agent chain, to give a new silylant agent, which can be immobilized in two distinct ways, that is, by homogeneous and heterogeneous processes, as represented in Scheme 2.

The heterogeneous route was based on the prior immobilization of the silylant agent GPTS onto silica gel to form a SiG surface. This reaction is followed by incorporation of propane-1,3-diamine to give the final product, SiHT. When the silylant agent GPTS reacted with the diamine, a new silylant agent, SiGN, is formed, which was then anchored onto silica gel to yield the SiHM surface.

The contents of carbon, nitrogen and hydrogen for the anchored surfaces are listed in Table 1. These elemental analysis data are in agreement with propane-1,3-diamine molecule incorporation into GTPS and its immobilization onto the silica gel surface, as proposed. Taking into account the percentages of these elements, it is easy to conclude that the amount of the propane-1,3-diamine immobilized onto the silica gel surface by the homogeneous route is much higher than the amount immobilized by the heterogeneous route. Thus, based on



Scheme 2. Incorporation of the propane-1,3-diamine molecule into the epoxy moiety by using heterogeneous (A) and homogeneous (B) processes.

Table 1
Percentages of carbon (C), hydrogen (H) and nitrogen (N) and the anchored amount (n) of groups per gram of silica

Surface	C (%)	H (%)	N (%)	n (mmol g^{-1})
SiG	8.62±0.01	1.75±0.01		1.03±0.01
SiHT	11.59±0.02	2.46±0.04	2.22±0.01	0.80±0.01
SiHM	20.76±0.53	4.39±0.08	4.28±0.24	1.53±0.09

the nitrogen content, the values of 0.80 and 1.53 mmol of pendant groups were calculated, respectively.

The surface areas for SiHT and SiHM silicas were determined through the BET equation and the results obtained were 154.8±12.2 and 133.2±1.4 m^2 g^{-1}, respectively, values which differ from that of the original silica, 420.8±3.4 m^2 g^{-1}. This decrease in the surface area after functionalization is due to the presence of pendant groups, which partially block the adsorption of nitrogen molecules on the surface.

The infrared spectra of liquid samples obtained for reagents propane-1,3-diamine and GPTS, and the liquid silylant agent, SiGN, corroborate the nucleophilic reaction between the amine and the epoxy groups. Evidence of the progress of reaction involving SiGN is its spectrum, that showed the disappearance of a peak at a 1254 cm^{-1}, which is characteristic of the presence of the epoxy group. This fact confirms that the epoxy ring is opened to form the GPTS silylant agent, after reacting with the amine group of the propane-1,3-diamine compound. In the SiGN spectrum, another important band is related to nitrogen–hydrogen stretching of an aliphatic amine at 3360 cm^{-1}, whose appearance denotes the immobilization [17]. These spectra are shown in Fig. 1.

The infrared spectra obtained for solid samples are presented in Fig. 2. The main features of all silica spectra are related to the similarity of bands associated with the inorganic backbone such as (i) a large broad

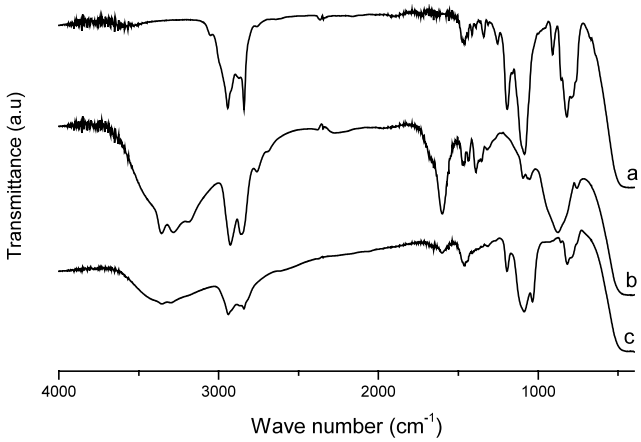


Fig. 1. Infrared spectra of liquid samples: GPTS (a), propane-1,3-diamine (b), and the new synthesized silylant agent, SiGN (c).

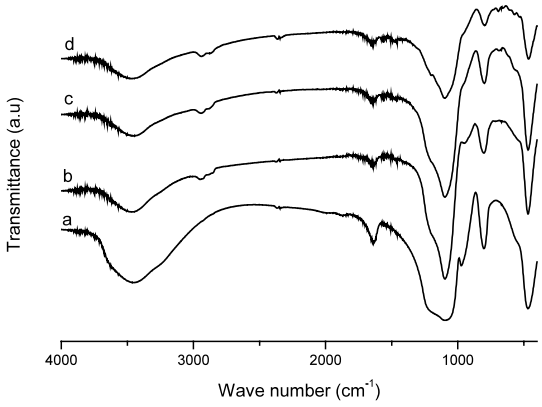


Fig. 2. Infrared spectra of solid samples: silica gel (a), SiG (b), SiHT (c) and SiHM (d).

band between 3400 and 3200 cm^{-1}, which is attributed to the presence of the O–H stretching frequency of silanol groups and also to the remaining adsorbed water, (ii) the intense band related to siloxane stretching of these groups at 1100 cm^{-1}, (iii) a band assigned to Si–O stretching frequency for silanol groups at 900 cm^{-1} and (iv) the band around 1650 cm^{-1}, assigned to angular vibration of water molecules. Moreover, SiG, SiHT and SiHM spectra showed the characteristic peak assigned to tetrahedron carbon at 2950 cm^{-1}, which confirms the presence of the organic groups immobilized onto the silica gel surface [7,8].

The thermogravimetric curves for crude and immobilized silicas are shown in Fig. 3. The profiles indicate that the anchored silicas have similar thermal stability, with distinct mass losses, as a consequence of the quantity of the pendant groups covalently bonded to the inorganic backbone.

Physically adsorbed water initially bonded on silica was lost at a low temperature in a first step. An increase in temperature caused condensation of surface silanol groups that gives a second mass loss step. The functionalized surfaces showed a mass loss due to the physically adsorbed water in the first step, near the same range as observed for the original silica. An abrupt loss in mass was detected in the second step, which included loss of the anchored molecules and also loss of water from the condensing surface silanol groups. In examining the degree of mass loss, which reflects the amount of silylant agent anchored onto the silica gel surface, it is clearly observed that the curve of SiHM presented a mass loss twice as high as that found for SiHT or SiG surfaces, indicating that the homogeneous route encourages the anchoring process.

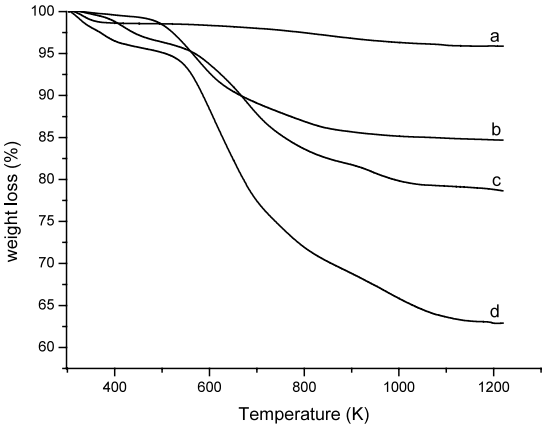


Fig. 3. Thermogravimetric curves for silica gel (a), SiG (b), SiHT (c) and SiHM (d) surfaces.

Important features related to the information about the attachment of the pendant group on the inorganic structure of the hybrid formed can be obtained through ^{13}C NMR spectra in solid state. Thus, spectra for hybrids SiG, SiHT and SiHM are shown in Fig. 4. For the SiG spectrum, four well-formed peaks, at 4, 32, 51 and 75 ppm, are observed. A similar sequence of four peaks is also observed for SiHT and SiHM. The first surface presented peaks at 4, 37, 50, 73 ppm and the second one at 4, 27, 43, 50, 73 ppm. These peaks are assigned to carbons of the pendant groups that conform to the numbers on the structure shown on the spectrum. These peaks show that both materials were obtained as expected, due to the fact that the sequence of peaks are related to the carbon of the pendant groups of the organic part of these synthesized hybrids and confirm the success of the preparation of these materials [18,19].

These silicas were easily synthesized, based on the nucleophilic attack of a compound having an amine group on an epoxy group and showed that this kind of reaction yields new silylant agents, available to graft to a

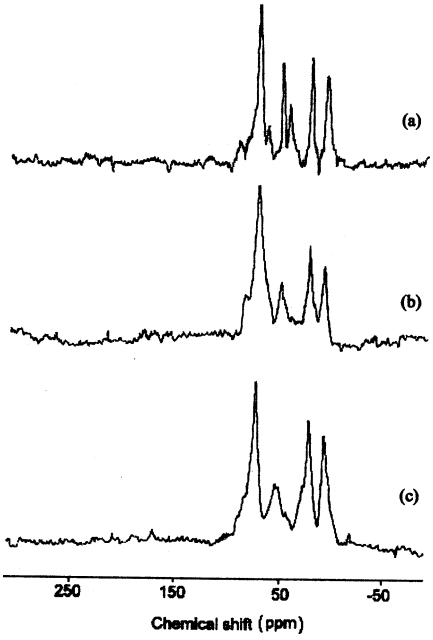


Fig. 4. ^{13}C NMR spectra of anchored SiG (A); SiHT (B) and SiHM (C).

silica surface having basic centers. Such reaction systems should be further explored, due to this rapid and quantitative reaction for the opening of an epoxy ring. The known ability of these attached basic centers in removing and preconcentrating cations and other contaminants from water and other solvents merits further investigations [20].

4. Conclusions

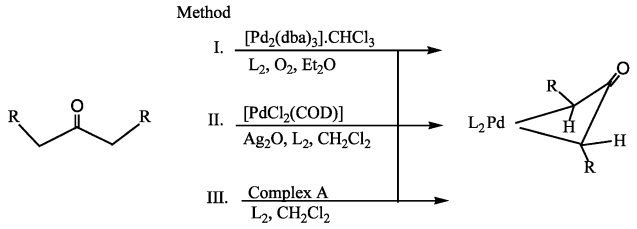
Incorporation of propane-1,3-diamine molecules on free or anchored silylant agent, GPTS, through homogeneous or heterogeneous routes, enabled the production of the same kind of immobilized surface. However, the efficiency in covalently attaching the desired pendant groups manifested with the homogeneous route is nearly twice that for the heterogeneous route. This fact suggests a better applicability of such a surface in extracting cations from solution, through the basic center atoms bonded on the pendant groups.

Acknowledgements

The authors are indebted to CNPq for fellowships to J.A.A.S. and C.A. and to FAPESP for financial support and a fellowship to A.G.S.P.

References

[1] J. Thornton, Pure Appl. Chem. 93 (2001) 1231.
[2] A.G.S. Prado, L.N.H. Arakaki, C. Airoldi, J. Chem. Soc., Dalton Trans. (2001) 2206.
[3] D.L. Hjeresen, D.L. Schutt, J.M. Boese, J. Chem. Educ. 77 (2000) 1543.
[4] N. Winterton, Green Chem. 3 (2001) 73.
[5] A.G.S. Prado, C. Airoldi, Anal. Chim. Acta 432 (2001) 201.
[6] J.H. Clark, D.J. Macquarrie, Chem. Soc. Rev. (1996) 303.
[7] A.G.S. Prado, C. Airoldi, J. Colloid Interface Sci. 236 (2001) 161.
[8] A.G.S. Prado, C. Airoldi, Pest Manag. Sci. 56 (2000) 419.
[9] K. Wilson, J.H. Clark, Pure Appl. Chem. 72 (2000) 1313.
[10] P.M. Padilha, L.A. de Melo Gomes, C.C.F. Padilha, J.C. Moreira, N.L. Dias Filho, Anal. Lett. 32 (1999) 1807.
[11] A. Goswani, A.K. Singh, Anal.Chim. Acta 454 (2002) 229.
[12] A.G.S. Prado, C. Airoldi, Fresenius J. Anal. Chem. 371 (2001) 1028.
[13] C.R. Silva, I.C.S.F. Jardim, C. Airoldi, J. Chromatogr. A 913 (2001) 65.
[14] A.G.S. Prado, C. Airoldi, Green Chem., 4 (2002) 288.
[15] L.N.H. Arakaki, C. Airoldi, Polyhedron 20 (2001) 929.
[16] T.W.G. Solomons, Fundamentals of Organic Chemistry, 4th ed., Wiley, New York, 1994.
[17] A. Tuel, H. Hommel, A.P. Legrand, M.F. Gonnord, E. Mincsovics, A.M. Siouffi, J. Chim. Phys. 89 (1992) 477.
[18] K.D. Behringer, J. Blumel, J. Liq. Chromatogr. Rel. Technol. 19 (1996) 2753.
[19] C. Merckle, J. Blumel, Chem. Mater. 13 (2001) 3617.
[20] A.G.S. Prado, L.N.H. Arakaki, C. Airoldi, Green Chem. 4 (2002) 42.



Complex A: $[Pd(\eta^3\text{-}CH\{CO_2Me\}COCH\{CO_2Me\})(L')_2]$ ($L' = PPh_3$ or $AsPh_3$)

Method	L_2	R = CO_2Me	R = CO_2Et
I.	dppe	**3a**	
	dppp	**3b**	
	dppb	**3c**	
	dppf	**3d**	
II.	dppe	**3a**	**4a**
	dppp	**3b**	
	dppb	**3c**	
	dppf	**3d**	
III. $L' = PPh_3$	dppe	**3a**	
	dppp	**3b**	
$L' = AsPh_3$	dppe	**3a**	
	dppp	**3b**	
	dppb	**3c**	
	dppf	**3d**	

Scheme 1. Complex A: $[Pd(\eta^3\text{-}CH\{CO_2Me\}COCH\{CO_2Me\})(L')_2]$ ($L' = PPh_3$ or $AsPh_3$).

The room temperature ^1H NMR spectra of complexes, $[Pd(\eta^3\text{-}CH\{CO_2Me\}COCH\{CO_2Me\})L_2]$ (**3**), showed the expected features, with a singlet resonance at low frequency for methyl protons of the CO_2Me groups and one doublet for the CH protons of the oxodimethylenemethane ligand. The ^1H NMR spectra of the palladium complex $[Pd(\eta^3\text{-}CH\{CO_2Et\}COCH\{CO_2Et\})(dppe)]$ (**4a**), exhibited a triplet resonance at low frequency for the methyl protons, a quartet for the methylene protons of the CO_2Et groups, and one doublet for the CH protons of the oxodimethylenemethane ligand.

The room temperature $^{31}P\{^1H\}$ NMR spectra for all the bidentate phosphorus complexes of oxodimethylenemethane consist of two sets of resonances, in a 5:1 or 4:1 ratio. This is thought to be due to the presence of both the equatorial–equatorial and more favourable axial–equatorial isomers. In order to identify the presence of both isomers, various low temperature ^1H NMR experiments were performed. The ^1H NMR spectrum of **3a** measured at −86 °C at 300 MHz, showed the expected features for the axial–equatorial static structure, with two signals for the methyl protons of the CO_2Me groups on the oxodimethylenemethane, and two signals for the CH protons. The two signals for the CH protons can be assigned on the basis of previous work [6]. The equatorial hydrogen, the lower frequency signal, couples to both the *cis*-phosphorus and *trans*-phosphorus, and appears as a broad signal. The higher frequency signal is assigned to the axial hydrogen, showing no discernible coupling to its *cis*-phosphorus ligand and appears as a doublet ($^3J(PH) = 8.53$ Hz) due to *trans*-phosphorus coupling only. In addition to these signals there is a methyl resonance at δ 2.84 ppm and a doublet at δ 3.20 ppm due to the CH protons of a small amount of the equatorial–equatorial isomer, which is also present.

Previous studies on oxodimethylenemethane metal complexes have shown that the complexes undergo ring inversion in solution at room temperature and that the complexes exhibited temperature dependent ^1H NMR spectra. Activation energies for ring inversion have been determined. Examination of the ^1H NMR spectra of **3a** showed that the CH protons of the palladium complex appeared as a doublet (δ 4.34) at room temperature which split into a doublet at δ 4.68 and a broad singlet at δ 3.97 ppm. These signals are assigned to the axial and equatorial protons of **3a**, respectively, by analogy with related systems [6]. The coalescence temperature for the complex **3a**, was found to be −48 °C and application of the Gutowsky–Holm equations [12] gave a value for barrier to ring inversion of 43.1 kJ mol^{-1}. This value is very similar to those observed for the reported palladacyclobutan-3-ones [6]. A coalescence temperature for the methyl resonances in **3a** could not be observed.

The CH protons of the palladium complex **3d** appeared as a doublet (δ 4.34) at room temperature which collapsed to a broad signal at −34 °C. At lower temperature the complex began to crystallise from the solution.

The IR spectra of the oxodimethylenemethane metal complexes normally exhibit five maxima in the 1705–1550 cm^{-1} region. For the complexes with methyl ester groups, two bands are observed in the region 1705–1660 cm^{-1} and are assigned to ν(CO) of the ester carbonyls. The carbonyl of the oxodimethylenemethane ligand gives a band in the region of 1595–1580 cm^{-1}. The observed frequencies for the ring carbonyl are lower than that found for the analogous platinum complexes which occurs in the region of 1625–1635 cm^{-1} [2,11]. The lower values for the ring carbonyls of palladium complexes suggest that the metal–CO interactions in palladium complexes are stronger than those in platinum complexes.

The FAB MS spectra indicate the presence of parent ions and fragmentation patterns due to loss of the dialkyl ester and the donor ligand.

3. Experimental

Microanalytical results, melting points (m.p.), IR, mass spectral and NMR data are presented for the new complexes. Microanalysis were carried out by Butterworth Laboratories Ltd., 54-56 Waldegrave Rd., Teddington, Middlessex, TW11 8LG. M.p. were measured on a Gallenkamp apparatus and are uncorrected. The FAB MS spectrum of the solid complexes were obtained on a Kratos Concept Double Focusing Sector Mass Spectrometer. The ^{1}H NMR spectra were recorded at room temperature in [$^2H_1$]chloroform on a Bruker AM300 spectrometer operating at 300.13 MHz or on a Bruker ARX 250 spectrometer at 250.13 MHz with $SiMe_4$ (0.0 ppm) as internal reference. Coupling constants J are in Hz. The $^{31}P\{^1H\}$ NMR spectra were recorded at room temperature in dichloromethane on a JEOL JNM-FX90 spectrometer operating at 36.2 MHz, with $[P(OH)_4]^+$ in [$^2H_2$]water (0.0 ppm) as external reference. The IR spectra were recorded on a Perkin–Elmer 580B spectrophotometer in Nujol mulls between NaCl plates in the range 2000–1400 cm^{-1}.

All reactions were performed under a dry, oxygen-free, nitrogen atmosphere unless otherwise stated, using solvents which were dried and distilled under nitrogen just prior to use. The following drying agents were used: dichloromethane (calcium hydride) and diethyl ether (sodium–benzophenone). Light petroleum refers to the fraction that boils in the 40–60 °C range. The compounds triphenylphosphine (Lancaster), silver(I) oxide, 1,3-dimethylacetonedicarboxylate, triphenylarsine, 1,3-diethylacetone-dicarboxylate 1,2-bis(diphenylphosphino)ethane, 1,3-bis(diphenylphosphino)propane, 1,4-bis(diphenylphosphino)butane, 1,1′-bis(diphenylphosphino)-ferrocene (Aldrich) were used as supplied by commercial sources. The complexes $[Pd_2(dba)_3]\cdot CHCl_3$ [13], $[PdCl_2(COD)]$ [14], and $[Pd\{\eta^3\text{-}CH(CO_2Me)CO\text{-}CH(CO_2Me)\}(L')_2]$ ($L' = PPh_3$ or $AsPh_3$) [6] were all prepared as described in the literature. Precious metal salts were obtained on loan from Johnson Matthey plc.

3.1. Method I

An excess of the appropriate diphosphine was added to a stirred suspension of $[Pd_2(dba)_3]\cdot CHCl_3$ (0.5 g, 0.48 mmol) in diethyl ether (50 cm^3) containing the required 3-oxopentanedioic acid dialkyl ester (1 cm^3) under oxygen for 24–96 h. The resulting pale yellow solid was collected, recrystallised from dichloromethane–diethyl ether and dried in vacuo.

3.1.1. Preparation of [Pd{η^3-CH(CO_2Me)COCH(CO_2Me)}(dppe)] (**3a**)

A mixture of $[Pd_2(dba)_3]\cdot CHCl_3$, dppe (0.4 g, 1 mmol) and 3-oxopentanedioic acid dimethyl ester was stirred for 24 h. Recrystallisation from dichloromethane–diethyl ether gave a pale yellow solid, **3a** (0.250 g, 38%). Found: C, 59.0; H, 5.0; P, 8.9. $C_{33}H_{32}O_5P_2Pd$ requires C, 58.6; H, 4.7; P, 9.2%. M.p. 180–182 °C (dec.); IR: 1705, 1668, 1595 ν(CO) cm^{-1}. ^{1}H NMR (250 MHz, [$^2H_1$]chloroform), $\delta = 7.85$–7.32 (20H, m, Ph), 4.34 [2H, d, CH, $|^3J(PH)_{trans} + {}^3J(PH)_{cis}|$ 8.53], 2.94 (6H, s, CH_3), 2.50–2.20 (4H, m, CH_2); ^{1}H NMR (300 MHz, [$^2H_1$] dichloromethane, −86 °C), $\delta = 7.80$–7.18 (20H, m, Ph), 4.68 [1H, d, CH, ^3J(PH) 10.8], 3.97 (1H, bs, CH), 2.68 (3H, s, CH_3), 2.65 (3H, s, CH_3), 2.13–2.0 (4H, m, CH_2CH_2) ppm. $^{31}P\{^1H\}$ NMR (24 MHz, CD_2Cl_2), $\delta = 49.8$ ppm (s), 48.3 ppm (s) (5:1 ratio). Mass spectrum (FAB), $[MH]^+$ 677.

3.1.2. Preparation of [Pd{η^3-CH(CO_2Me)COCH(CO_2Me)}(dppp)] (**3b**)

A mixture of $[Pd_2(dba)_3]\cdot CHCl_3$, dppp (1 g, 2.4 mmol) and 3-oxopentanedioic acid dimethyl ester was stirred for 72 h. Recrystallisation from dichloromethane–diethyl ether gave a pale yellow solid, **3b** (0.5 g, 75%). Found: C, 59.3; H, 5.2; P, 8.3. $C_{34}H_{34}O_5P_2Pd$ requires C, 59.1; H, 5.0; P, 9.0%. IR: 1705, 1665, 1592 ν(CO), cm^{-1}. ^{1}H NMR (250 MHz, [$^2H_1$]chloroform), $\delta = 7.70$–7.22 (20H, m, Ph), 3.6 (2H, m, CH), 2.78 (6H, s, CH_3), 2.35–1.92(6H, m, CH_2CH_2) ppm. $^{31}P\{^1H\}$ NMR (24 MHz, CH_2Cl_2), $\delta = 6.7$ ppm (s), 5.5 ppm (5:1 ratio). Mass spectrum (FAB), $[MH]^+$ 691.

3.1.3. Preparation of [Pd{η^3-CH(CO_2Me)COCH(CO_2Me)}(dppb)] (**3c**)

A mixture of $[Pd_2(dba)_3]\cdot CHCl_3$, dppb (0.93 g, 2 mmol) and 3-oxopentanedioic acid dimethyl ester was stirred for 96 h. Recrystallisation from dichloromethane–diethyl ether gave a pale yellow solid, **3c** (0.7 g, 90%). Found: C, 59.2; H, 5.6; P, 8.5. $C_{35}H_{36}O_5P_2Pd$ requires C, 59.6; H, 5.1; P, 8.8%. M.p. 220–222 °C (dec.). IR: 1705, 1670, 1556 ν(CO), cm^{-1}. ^{1}H NMR (250 MHz, [$^2H_1$]chloroform), $\delta = 7.8$–7.24 (20H, m, Ph), 4.2 (2H, br, CH), 3.0 (3H, s, CH_3), 2.9 (3H, s, CH_3), 2.50–2.20 (8H, m, CH_2CH_2) ppm. $^{31}P\{^1H\}$ NMR (24 MHz, $CDCl_3$), $\delta = 19.5$ ppm (s). Mass spectrum (FAB), $[MH]^+$ 705.

3.1.4. Preparation of [Pd{η^3-CH(CO_2Me)COCH(CO_2Me)}(dppf)] (**3d**)

A mixture of $[Pd_2(dba)_3]\cdot CHCl_3$ (0.3 g, 0.3 mmol), dppf (0.28 g, 0.5 mmol) and 3-oxopentanedioic acid dimethyl ester was stirred for 48 h. Recrystallisation from dichloromethane–diethyl ether gave a solid, **3d** (0.420 g, 84%). Found: C, 59.5; H, 4.2; P, 7.9. $C_{41}H_{36}FeO_5P_2Pd$ requires C, 59.1; H, 4.4; P, 7.4%. M.p. 178–180 °C (dec.). IR: 1690, 1660, 1590 ν(CO), cm^{-1}. ^{1}H NMR (300 MHz, [$^2H_1$]chloroform), $\delta = 7.74$–7.08 (20H, m, Ph), 4.34 [2H, d, CH, $|^3J(PH)_{trans} + {}^3J(PH)_{cis}|$ | 10.6], 4.63–3.83 (8H, m, Cp), 2.98 (6H, s, CH_3) ppm.

$^{31}P\{^{1}H\}$ NMR (24 MHz, $CDCl_3$), $\delta = 28.2$ (s) and 24.4 ppm (s) (1:4 ratio). Mass spectrum (FAB), $[MH]^+$ 833.

3.2. Method II

An excess of ligand was added to a stirred solution of [$PdCl_2$(COD)] (0.5 g, 1.75 mmol) in dichloromethane (25 cm^3) containing the required 1,3-dialkylacetone dicarboxylate (1 cm^3) and an excess of silver(I) oxide (0.7 g) under nitrogen and was refluxed for 5 h. Filtration to remove silver salts afforded a pale yellow solution which was evaporated to dryness under reduced pressure and redissolved in dichloromethane (5 cm^3) followed by the addition of diethyl ether or petroleum ether to give a pale yellow solid. Removing the solid by filtration afforded the complex which was dried in vacuo.

3.2.1. Preparation of [Pd{η^3-CH(CO_2Me)COCH(CO_2Me)}(dppe)] (**3a**)

A mixture of [$PdCl_2$(COD)], dppe (0.7 g, 1.75 mmol), 1,3-dimethylacetone dicarboxylate and an excess of silver(I) oxide in dichloromethane gave a pale yellow solid which was identified as **3a** (0.210 g, 18%) by comparison of its IR and ^1H NMR spectra with an authentic sample.

3.2.2. Preparation of [Pd{η^3-CH(CO_2Me)COCH(CO_2Me)}(dppp)] (**3b**)

A mixture of [$PdCl_2$(COD)] (0.2 g, 0.7 mmol), dppp (0.43 g, 1 mmol), 1,3-dimethylacetone dicarboxylate and an excess of silver(I) oxide in dichloromethane gave an oily residue of **3b** which was identified by comparison of its IR, ^1H and $^{31}P\{^1H\}$ NMR spectra with that of an authentic sample.

3.2.3. Preparation of [Pd{η^3-CH(CO_2Me)COCH(CO_2Me)}(dppb)] (**3c**)

A mixture of [$PdCl_2$(COD)] (0.2 g, 0.7 mmol), dppb (0.45 g, 1.1 mmol), 1,3-dimethylacetone dicarboxylate and an excess of silver(I) oxide in dichloromethane gave a pale yellow solid of **3c** (0.325 g, 66%) which was identified by comparison of its IR, ^1H and $^{31}P\{^1H\}$ NMR spectra with that of an authentic sample.

3.2.4. Preparation of [Pd{η^3-CH(CO_2Me)COCH(CO_2Me)}(dppf)] (**3d**)

A mixture of [$PdCl_2$(COD)], dppf (0.195 g, 0.35 mmol), 1,3-dimethylacetone dicarboxylate and an excess of silver(I) oxide in dichloromethane gave a solid of **3d** (0.280 g, 96%) which was identified by comparison of its IR, ^1H and $^{31}P\{^1H\}$ NMR spectra with that of an authentic sample.

3.2.5. Preparation of [Pd{η^3-CH(CO_2Et)COCH(CO_2Et)}(dppe)] (**4a**)

A mixture of [$PdCl_2$(COD)] (0.2 g, 0.7 mmol), dppe (0.3 g, 0.75 mmol), 1,3-diethylacetone dicarboxylate and an excess of silver(I) oxide in dichloromethane gave a pale yellow solid, **4a** (0.25 g, 50%). Found: C, 59.5; H, 4.7; P, 9.0. $C_{33}H_{32}O_5P_2Pd$ requires C, 59.7; H, 5.1; P, 8.8%. M.p. 170–172 °C (dec.). IR: 1730, 1700, 1668, 1580, ν(CO), cm^{-1}. ^1H NMR (250 MHz, [$^2H_1$]chloroform), $\delta = 7.98$–7.54 (20H, m, Ph), 4.74 (2H, d, CH), 3.85 (4H, q, CH_2CH_3), 2.48 (4H, m, CH_2CH_2), 1.0 (6H, t, CH_2CH_3) ppm. $^{31}P\{^1H\}$ NMR (24 MHz, CH_2Cl_2), $\delta = 49.2$ ppm (s), 48.8 ppm (s) (5:1 ratio). Mass spectrum (FAB), $[MH]^+$ 705.

3.3. Method III

A mixture of [Pd(η^3-CH{CO_2Me}COCH{CO_2Me})(L′)$_2$], (L′ = PPh_3 (**2a**) or $AsPh_3$ (**2b**)) and the appropriate ligand was refluxed in dichloromethane for several hours. The resulting mixture was evaporated to 1–2 cm^3 volume under reduced pressure and addition of diethyl ether afforded a pale yellow solid which was filtered and washed with diethyl ether and then dried in vacuo.

3.3.1. Preparation of [Pd{η^3-CH(CO_2Me)COCH(CO_2Me)}(dppe)] (**3a**)

A mixture of **2a** (0.085 g, 0.1 mmol) and dppe (0.06 g, 1.5 mmol) in dichloromethane gave a pale yellow solid, **3a** (0.070 g, 98%) which was identified by comparison of its IR, ^1H and $^{31}P\{^1H\}$ NMR spectra with that of an authentic sample.

3.3.2. Preparation of [Pd{η^3-CH(CO_2Me)COCH(CO_2Me)}(dppp)] (**3b**)

A mixture of **2a** (0.1 g, 0.125 mmol) and dppp (0.1 g, 0.24 mmol) in dichloromethane gave a pale yellow solid, **3b** (0.04 g, 50%) which was identified by comparison of its IR, ^1H and $^{31}P\{^1H\}$ NMR spectra with that of an authentic sample.

3.3.3. Preparation of [Pd{η^3-CH(CO_2Me)COCH(CO_2Me)}(dppe)] (**3a**)

A mixture of **2b** (0.2 g, 0.225 mmol) and dppe (0.1 g, 0.25 mmol) in dichloromethane gave a pale yellow solid, **3a** (0.140 g, 92%) which was identified by comparison of its IR, ^1H and $^{31}P\{^1H\}$ NMR spectra with that of an authentic sample.

3.3.4. Preparation of [Pd{η^3-CH(CO_2Me)COCH(CO_2Me)}(dppp)] (**3b**)

A mixture of **2b** (0.1 g, 0.11 mmol) and dppp (0.7 g, 1.7 mmol) in dichloromethane gave pale yellow solid, **3b** (0.025 g, 33%) which was identified by comparison of its

IR, ^{1}H and $^{31}P\{^{1}H\}$ NMR spectra with that of an authentic sample.

3.3.5. Preparation of [Pd{η^3-CH(CO_2Me)COCH(CO_2Me)}(dppb)] (**3c**)

A mixture of **2b** (0.1 g, 0.11 mmol) and dppb (0.1 g, 0.24 mmol) in dichloromethane gave a pale yellow solid of **3c** (0.021 g, 26%) which was identified by comparison of its IR, ^{1}H and $^{31}P\{^{1}H\}$ NMR spectra with that of an authentic sample.

3.3.6. Preparation of [Pd{η^3-CH(CO_2Me)COCH(CO_2Me)}(dppf)] (**3d**)

A mixture of **2b** (0.17 g, 0.18 mmol) and dppf (0.1 g, 0.19 mmol) in dichloromethane gave a pale yellow solid, **3d** (0.090 g, 60%) which was identified by comparison of its IR, ^{1}H and $^{31}P\{^{1}H\}$ NMR spectra with that of an authentic sample.

Acknowledgements

The Zonguldak Karaelmas University, Turkey, is thanked for financial support, the University of Leicester, UK, for laboratory facilities, and Johnson Matthey plc. for the supply of palladium metal salts.

References

[1] J. Mann, Tetrahedron 42 (1986) 4611.
[2] D.A. Clarke, R.D.W. Kemmitt, M.A. Mazid, D.R. Russell, M.D. Schilling, J.L.S. Sherry, J. Chem. Soc., Dalton Trans. (1984) 1993.
[3] J. Fawcett, W. Henderson, M.D. Jones, R.D.W. Kemmitt, D.R. Russell, B. Lam, S.K. Kang, T.A. Albright, Organometallics 8 (1989) 1991.
[4] D.A. Clarke, R.D.W. Kemmitt, M.A. Mazid, D.R. Russell, M.D. Schilling, J. Chem. Soc., Chem. Commun. (1978) 744.
[5] P. McKenna, Ph.D. thesis, University of Leicester, 1983.
[6] R.D.W. Kemmitt, P. McKenna, D.R. Russell, L.J.S. Sherry, J. Chem. Soc., Dalton Trans. (1985) 259.
[7] A. Imran, R.D.W. Kemmitt, A.J. Markwick, P. McKenna, D.R. Russell, L.J.S. Sherry, J. Chem. Soc., Dalton Trans. (1985) 549.
[8] K.W. Chiu, W. Henderson, R.D.W. Kemmitt, L.J.S. Prouse, D.R. Russell, J. Chem. Soc., Dalton Trans. (1988) 427.
[9] A. Ohsuka, T. Hirao, H. Kurosawa, I. Ikeda, Organometallics 14 (1995) 2538.
[10] R.D.W. Kemmitt, P. McKenna, D.R. Russell, L.J.S. Prouse, J. Chem. Soc., Dalton Trans. (1989) 345.
[11] C. Proctor, Ph.D. thesis, University of Leicester, 1994.
[12] H.S. Gutowsky, C.H. Holm, J. Chem. Phys. 25 (1956) 1228.
[13] T. Ukai, H. Kawazura, Y. Ishii, J.J. Bonnet, J.A. Ibers, J. Organomet. Chem. 65 (1974) 253.
[14] D. Drew, J.R. Dogl, Inorg. Synth. 13 (1972) 52.

bend toward the major groove and a widening and flattening of the minor groove. Studies showing significant differences in the effectiveness of EN–Pt (EN = 1,2-ethylenediamine) and DACH–Pt (DACH = 1,2-diaminocyclohexane) adducts in inhibiting transformation efficiency in a repair-deficient strain of *Escherichia coli* suggest that some carrier ligand effects on resistant cell lines arise from differences in the ability of certain Pt–DNA adducts to inhibit other processes like replication or transcription [5,6,12–14]. These structural distortions and differences in carrier ligand effects in turn likely affect the ability of the platinum drugs to block DNA replication and transcription [15,16].

A series of compounds with 1,2-DACH, 1,4-DACH and homopiperazine as carrier ligands have been synthesized in our laboratory [17,18]. Here at the M.D. Anderson Cancer Center, DACH–acetate–Pt(IV) complexes have been identified as circumventing cisplatin resistance [19]. This led us to design and synthesize platinum complexes of a monodentate seven-member hexamethyleneimine (HMI) ligand as a stable amine with different leaving groups. We wish to report here the synthesis, and characterization of new platinum complexes and the crystal structure of [Pt^{II}(hexamethyleneimmine)$_2$(cyclobutanedicarboxylato)]·H_2O complex.

2. Experimental

2.1. Chemicals

K_2PtCl_4 and silver sulfate were purchased from Johnson Matthey, Seabrook, NH. HMI, 1,1-cyclobutanedicarboxylic acid (CBDCA), sodium oxalate, malonic acid disodium salt, and acetic anhydride were purchased from Aldrich Chemical Co., Milwaukee, WI. Silver nitrate and HCl were obtained from Fisher Scientific Co., Houston, TX. All chemicals obtained from commercial sources were used as supplied.

2.2. Physical measurements

Elemental analyses of the complexes were performed by Robertson Laboratory Inc., Madison, NJ. Infrared (IR) spectra in the range of 600–4000 cm^{-1} and far-IR spectra in the range of 150–600 cm^{-1} were recorded in KBr and polyethylene pellets, respectively, on a Perkin–Elmer 2000 spectrophotometer. ^{13}C and ^{195}Pt NMR spectra in methanol were recorded using a Bruker Advance 300 spectrometer. ^{13}C spectra were recorded with a 5 mm tunable probe at 75.13 MHz, ^{195}Pt spectra were recorded at 43.055 MHz, and the shifts were measured relative to an external standard of 2.2 M Na_2PtCl_6 in D_2O at 0.00 ppm.

2.3. Synthesis

2.3.1. Preparation of [Pt(HMI)$_2$Cl$_2$] (complex 1)

K_2PtCl_4 (20.00 g, 48.19 mmol) was dissolved in 300 ml of deionized water and filtered. A solution of KI (63.99 g, 385.54 mol) in 150 ml of water was added to it, and the reaction mixture was stirred for 10 min. Next, HMI (9.55 g, 96.38 mmol) was added dropwise to the mixture while stirring to obtain a yellow precipitate of [Pt(HMI)$_2$I$_2$] (**1a**). The stirring was continued for a further 30 min, and the precipitate was then collected by filtration. This compound was stirred in 100 ml of dimethylformamide, filtered, washed with water, ethanol, and acetone, and dried under vacuum (yield, 95%). [Pt(HMI)$_2$I$_2$] (13.00 g, 20.08 mmol) was suspended in an aqueous solution of silver nitrate (6.87 g, 40.16 mmol) in 400 ml of water. The reaction mixture was stirred for 24 h at room temperature (r.t.) in the dark. The AgI precipitate was filtered off, and a solution of 1:1 concentrated HCl was added to the filtrate with constant stirring until a yellow precipitate of **1** formed. It was filtered washed with water and acetone and dried under vacuum. Complex **1** was used as a precursor for Pt(IV) complexes **7**–**9** (see below).

2.3.2. [Pt^{II}(HMI)$_2$(OSO_3)H_2O] (complex 2)

To a suspension of **1a** (3.1 g, 4.79 mmol) in 250 ml of water Ag_2SO_4 (1.49, 4.79 mmol) was added. The reaction mixture was then stirred in the dark at r.t. for 24 h. The dark yellow precipitate was filtered off, and the filtrate was evaporated to dryness under reduced pressure at 35 °C. A pale yellow solid was obtained. The product was recrystallized from water, to yield a white compound. Complex **2** was used as a precursor for Pt(II) complexes **3**–**6** (see below).

2.3.3. [Pt^{II}(HMI)$_2$(CBDCA)]·H_2O (complex 3)

Complex **2** (0.40 g, 0.84 mmol) was dissolved in 50 ml of water and then added to 50 ml of sodium salt of CBDCA (0.067 g, 1.68 mmol) prepared in situ. The reaction mixture was stirred for 24 h, filtered, and evaporated to 10 ml under reduced pressure. It was cooled at 0 °C for 24 h in a refrigerator. A white precipitate of **3** was obtained. The final product was filtered, washed with cold water, and dried in vacuum. Recrystallization of **3** was achieved by dissolving 0.025 g of the compound in 100 ml of methanol, after which the volume of the solution was reduced to 50 ml and filtered. The filtrate was allowed to evaporate slowly at r.t. Within 2 weeks, colorless needle-shaped crystals were separated from the solution and used for single-crystal X-ray diffraction.

Complexes **4**–**6** were prepared by the same procedure as described for the complex **3**.

2.3.4. [$Pt^{IV}(HMI)_2$trans-$(OH)_2Cl_2$] (complex 7)

To a suspension of **1** (2.00 g, 4.30 mmol) in 200 ml of water was added 30 ml of 30% H_2O_2. The reaction mixture was then stirred for 3 h at 70 °C and thereafter continuously stirred for 24 h at r.t. It was filtered and evaporated to dryness and precipitated with acetone. A pale yellow precipitate of **7** formed and was filtered, washed with acetone, and dried in vacuo.

2.3.5. [$Pt^{IV}(HMI)_2$trans-(acetato)$_2Cl_2$] (complex **8**)

Complex **7** (1.00 g, 2.00 mmol) was suspended in 25 ml of acetic anhydride and stirred at r.t. for 24 h. Methanol (25 ml) was added to the reaction mixture and stirred. A clear solution formed, which was filtered and evaporated to dryness. The crude product was dissolved in acetone, supplemented with activated carbon, and filtered. The resulting solution was then evaporated to dryness. A pale yellow compound was obtained and dried in vacuo.

2.3.6. [$Pt^{IV}(HMI)_2Cl_4$] (complex **9**)

Complex **7** (1.00 g, 2.20 mmol) was suspended in 20 ml of water supplemented with 15 ml of concentrated HCl. A clear solution was obtained. The stirring was continued for 4 days at r.t. to obtain a yellow crystalline compound. This was filtered and washed with water. The solid was recrystallized from acetone and dried in vacuo.

2.4. Single-crystal X-ray crystallographic study

The experimental details of the X-ray data collection, the structure solution, and refinement of the title compound are compiled in Table 1. A single-crystal of $[Pt^{II}(HMI)_2(CBDCA)]\cdot H_2O$ was coated with a thin layer of epoxy cement and mounted on the goniometer of a Bruker SMART 1K diffractometer equipped with a CCD area detector. The data was corrected for Lorentz and polarization effects. An empirical absorption correction was applied using the program SADABS [20]. No appreciable decay of the crystal was detected during data collection.

The structure was solved using direct methods with the SHELXTL software package [20]. Scattering factors were taken from the literature [21]. Heavy atoms were located initially to set the correct phases for the model. All other atoms were located by successive Fourier maps and were refined using the full-matrix least-squares method on F^2. Two complete molecules were found to occupy the asymmetric unit of the crystal lattice. Attempts to transform the crystallographic data to a space group that possessed higher symmetry and would presumably only contain a single molecule in the asymmetric unit, did not result in successful solution of the data. The choice of the space group *Pc* was confirmed through symmetry software in the PLATON crystallographic package [22]. Hydrogen atoms were placed in calculated positions and allowed to ride on the adjacent atom. Toward the end of the refinement it was discovered that one of the amine ligands on each platinum atom was disordered over two positions. The disorder was modeled and the structure was refined accordingly. Carbon–carbon bonds in the disordered ligands were constrained to the same distances. Disordered atoms were allowed to refine isotropically. All other non-hydrogen atoms were refined anisotropically. Refinement of positional and anisotropic parameters led to convergence.

Table 1
Crystal data and structure refinement for $[Pt^{II}(HMI)_2(CBDCA)]\cdot H_2O$

Empirical formula	$C_{18}H_{32}N_2O_4Pt\cdot H_2O$
Formula weight	552.54
Temperature (K)	293(2)
Wavelength (Å)	0.71073
Crystal system	monoclinic
Space group	*Pc*
Unit cell dimensions	
a (Å)	13.144(3)
b (Å)	11.285(2)
c (Å)	14.483(3)
β (°)	98.42(3)
V (Å^3)	2125.3(7)
Z	4
D_{calc} (Mg m^{-3})	1.724
Absorption coefficient	6.630
F(000) (mm^{-1})	1084
Crystal size (mm)	0.30 × 0.27 × 0.25
θ Range for data collection (°)	1.57–23.29
Limiting indices	$-14 \le h \le 14$, $-12 \le k \le 9$, $-16 \le l \le 16$
Reflections collected	8948
Independent reflections	5697 [$R_{int} = 0.0305$]
Completeness to θ	23.29°, 99.4%
Absorption correction	empirical
Max/min transmission	1.000000, 0.603765
Refinement method	full-matrix least-squares on F^2
Data/restraints/parameters	5697/53/438
Goodness-of-fit on F^2	1.040
Final *R* indices [$I > 2\sigma(I)$]	$R_1 = 0.0348$, $wR_2 = 0.0916$
R indices (all data)	$R_1 = 0.0367$, $wR_2 = 0.0927$
Absolute structure parameter	0.017(13)
Largest difference peak and hole (e Å^{-3})	1.480 and −1.411

3. Results and discussion

3.1. Synthesis of platinum complexes

The steps involved in the synthesis of platinum(II) and platinum(IV) complexes are shown in Schemes 1 and 2. Compound **1** was prepared according to the method described by Dhara [23], which was adopted because it is rapid and easy and provides a much higher yield than when K_2PtCl_4 is treated directly with HMI.

Pt^{II} Complexes

$K_2PtCl_4 + 8KI \longrightarrow K_2PtI_4 + 4KI + 4KCl$ (A)

$K_2PtI_4 + 2(HMI) \longrightarrow [Pt^{II}(HMI)_2I_2] + 2KI$ (B)

$[Pt^{II}(HMI)_2I_2] + 2AgNO_3 \longrightarrow [Pt^{II}(HMI)_2(H_2O)_2](NO_3)_2 + 2AgI$ (C)

$[Pt^{II}(HMI)_2(H_2O)_2](NO_3)_2 + 2HCl \longrightarrow [Pt^{II}(HMI)_2Cl_2] + 2HNO_3 + 2H_2O$ (D)

$[Pt^{II}(HMI)_2Cl_2] + 2AgSO_4 \longrightarrow [Pt^{II}(HMI)_2(OSO_3)H_2O] + 2AgCl$ (E)

$[Pt^{II}(HMI)_2(OSO_3)H_2O] + Na_2X \longrightarrow [Pt^{II}(HMI)_2X] + Na_2SO_4$ (F)

Scheme 1. Where HMI = hexamethyleneimine; X = 1,1-cyclobutyldicarboxylato (CBDCA), methylmalonato, oxalato, or tartronato; Y = chloro or acetato.

Pt^{IV} Complexes

$[Pt^{II}(HMI)_2Cl_2] \xrightarrow{30\%\ H_2O_2} [Pt^{IV}(HMI)_2trans\text{-}(OH)_2Cl_2]$ (G)

$[Pt^{IV}(HMI)_2trans\text{-}(OH)_2Cl_2] \xrightarrow{\text{acetic anhydride}} [Pt^{IV}(HMI)_2trans\text{-}(Y)_2Cl_2]$ (H)

$[Pt^{IV}(HMI)_2trans\text{-}(OH)_2Cl_2] \xrightarrow{\text{conc. HCl}} [Pt^{IV}(HMI)_2trans\text{-}(Y)_2Cl_2]$ (I)

Scheme 2. Where HMI = hexamethyleneimine; X = 1,1-cyclobutyldicarboxylato (CBDCA), methylmalonato, oxalato, or tartronato; Y = chloro or acetato.

Complexes **1** and **2** were used as precursors for both $[Pt^{II}(HMI)_2X]$- and $[Pt^{IV}(HMI)_2trans\text{-}(Y)_2Cl_2]$-type complexes.

In Scheme 1, K_2PtCl_4 mixed with an excess of KI produced K_2PtI_4 in solution. K_2PtI_4 was then treated with 2 equiv. of HMI to precipitate $[Pt^{II}(HMI)_2I_2]$. The reaction of $[Pt^{II}(HMI)_2I_2]$ with $AgNO_3$ led to the formation of $[Pt^{II}(HMI)_2(H_2O)_2](NO_3)_2$ in solution, which was further converted to $[Pt^{II}(HMI)_2Cl_2]$ by treating it with a concentrated 1:1 HCl solution. The reaction of $[Pt^{II}(HMI)_2Cl_2]$ with Ag_2SO_4 formed $[Pt^{II}(HMI)_2(OSO_3)H_2O]$. The reaction of $[Pt^{II}(HMI)_2(OSO_3)H_2O]$ with 1 equiv. of corresponding sodium salt of dicarboxylic acids in methanol produced $[Pt^{II}(HMI)_2X]$ type complexes (complexes **3**–**6**).

In Scheme 2, Pt(II) complexes of the type $[Pt^{II}(HMI)_2X]$ were oxidized with 30% H_2O_2 to form corresponding axial dihydroxyplatinum(IV) complex **7** $[Pt^{IV}(HMI)_2trans\text{-}(OH)_2Cl_2]$. By substitution of the hydroxo group with acetate using acetic anhydride, complex **8** $[Pt^{IV}(HMI)_2trans\text{-}(acetato)_2Cl_2]$ was produced. Hydroxide was substituted with chloride by reacting *trans*-hydroxy complex with conc. HCl to form complex **9** $[Pt^{IV}(HMI)_2Cl_4]$.

3.2. Characterization of platinum complexes

The complexes were characterized by elemental analysis and IR, ^{13}C NMR, and ^{195}Pt NMR spectroscopy. The composition of each complex as determined by elemental analysis showed good agreement between the theoretical and actual values. The analytical results are summarized in Table 2. The results of characterization by IR, ^{13}C NMR, and ^{195}Pt NMR are shown in Table 3. These values are close to the values reported for similar types of platinum complexes [18,24–27].

The IR spectra of the complexes in general showed a broad absorption between 3204 and 3009 cm^{-1}, which was due to the ν_{N-H} stretching vibrations of coordinated HMI. The carboxyl groups in complexes **3**–**6** displayed a band in the range of 1580–1610 cm^{-1} corresponding to the $\nu_{as}(COO^-)$ band. The $\nu_s(COO^-)$ band appeared in the range of 1360–1390 cm^{-1}. Two intense bands at 620 and 1130 cm^{-1} in complex **2** indicated the presence of an SO_4 group in the complex. The Pt–N, Pt–Cl, and Pt–O stretching frequencies showed peaks in the range of 520–525, 325–360, and 420–430 cm^{-1}, respectively.

The proton-decoupled ^{13}C NMR spectra showed a signal in the range of 180–190 ppm for magnetically equivalent carbonyl carbons in complexes **3**–**7**. The values of the free acids and platinum complexes are shown in the Table 3. Complexation shifts ($\Delta C = \delta$[complex] $- \delta$[ligand]) fell between 1.8 and 2.5 ppm.

The ^{195}Pt NMR data shown in Table 3 further confirmed the structures of these platinum complexes. $[Pt^{II}(HMI)_2Cl_2]$ showed a signal at −2210 ppm, which is characteristic of the square planar platinum(II) complex in which the two adjacent corners are occupied by two nitrogen and the other two positions by two chlorides. Two peaks were observed at −1623 and −1666 ppm in the spectrum of complex **2**. Complexes **3**–**7** showed signals in the range of −1802 through −1821 ppm. Such chemical shifts are characteristic of square planar platinum(II) complexes having two nitrogens and two oxygen atoms as donor ligands. As oxidation of platinum(II) to platinum(IV) leads to a large shift, complex **7** showed a singlet at 1069 ppm and complex **8** a singlet at 1150 ppm. These values are close to those of the related platinum(IV) complexes having two nitrogen atoms, two oxygen atoms, and two chloride ions as donor ligands. In these complexes (**7** and **8**), the chloride ions occupied the equatorial positions. Complex **9** showed a signal at −150 ppm, consistent with the values of platinum(IV) complexes having two nitrogen atoms and four chloride ions as donor ligands. Figs. 1 and 2 show the general structure of the complexes.

3.3. Crystal structure

Fig. 3 shows a view of the crystal structure of $[Pt^{II}(HMI)_2(CBDCA)]\cdot H_2O$. Selected bond lengths and bond angles are given in Table 4. In this molecule, the coordination environment around the platinum atom is a slightly distorted square plane, with the angles ranging from 88.0(4)° to 92.9(4)°. The distortion is caused by limitation in the bite distances of the chelating ligand.

Table 2
Elemental analysis of platinum complexes

Complex	Complex name	Observed (calculated)				Yield (%)
		C	H	N	Cl	
1	$[Pt^{II}(HMI)_2Cl_2]$	31.62 (32.77)	5.70 (5.46)	6.00 (5.88)	14.88 (14.91)	61.53
2	$[Pt^{II}(HMI)_2(OSO_3)H_2O]$	27.50 (28.04)	5.47 (5.52)	5.41 (5.52)		90.90
3	$[Pt^{II}(HMI)_2(CBDCA)]\cdot H_2O$	39.04 (39.05)	5.99 (6.14)	5.05 (5.06)		64.22
4	$[Pt(HMI)_2$(methylmalonato)]	36.27 (36.42)	5.58 (6.07)	5.44 (5.31)		52.00
5	$[Pt^{II}(HMI)_2$(oxalato)]	34.45 (34.92)	5.30 (5.40)	5.64 (5.82)		46.00
6	$[Pt^{II}(HMI)_2$(tartronato)]	35.04 (35.22)	5.47 (5.47)	5.31 (5.47)		53.84
7	$[Pt^{II}(HMI)_2$(*trans*-$(OH)_2Cl_2$]	28.64 (28.91)	5.70 (5.62)	5.35 (5.62)	14.00(14.25)	48.00
8	$[Pt^{II}(HMI)_2$*trans*-(acetato)$_2)Cl_2$]	32.54 (32.(98)	5.51 (5.49)	4.72 (4.81)	21.32 (21.19)	36.45
9	$[Pt^{IV}(HMI)_2Cl_4]$	26.76 (26.91)	4.98 (4.85)	4.83 (5.23)	26.90 (26.54)	87.00

HMI, hexamethlyeneimine.

Table 3
IR, ^{13}C NMR, and ^{195}Pt NMR spectroscopic data for platinum complexes [a]

Complex	IR (cm^{-1})						^{13}C (C=O)			^{195}Pt
	ν(N–H)	ν_a(C=O)	ν_s(C–O)	ν(Pt–N)	ν(Pt–O)	ν(Pt–Cl)	Ligand	Complex	ΔC	
1	3182			525		327				−2267[b]
2	3165			518	448					−1666, −1623[c]
3	3076	1610	1367	560	465		177.3	180.8	3.5	−1802[c]
4	3170	1644	1374	578	466		175.8	179.7	3.8	−1821[c]
5	3189	1637	1371	553	445		176.4	181.4	5.0	−1872[c]
6	3180	1655	1380	536	440		172.7	177.0	4.3	−1890[c]
7	3168			565	471	332				1069[c]
8	3180	1649	1382	545	457	341	178.2	181.6	3.4	1245[d]
9	3145			530		320, 334				−150[d]

[a] See Figs. 1 and 2 for structures.
[b] Recorded in *N*,*N*-dimethylformamide.
[c] Recorded in methanol.
[d] Recorded in acetone; $\Delta C = \delta$[complex] $- \delta$[ligand].

The platinum coordination environment contains two adjacent corners occupied by the two nitrogen atoms of the HMI ligand, whereas the remaining two *cis* positions are coordinated with two of the oxygen atoms of the CBDCA. All Pt–N and Pt–O bond lengths are in the range normally observed for platinum(II) complexes. The average Pt–N bond length of 2.06(9) Å is consistent with the length of those found in other monodentate and bidentate amine ligand-containing complexes. For instance, this length is 1.99(2) Å in $[Pt^{II}$(1-methylhomopiperazine)(methylmalonato)]$\cdot 2H_2O$ [18], 2.02(10) Å in $[Pt^{II}$(hpip)(pentadecanoato)$_2]$ [25], 2.038(8) Å in $[Pt^{II}$(3-methylpiperidine)(malonato)]$\cdot H_2O$ [28], 2.03 Å in [Pt(*trans*-*l*-1,2-DACH)(CBDCA)]$\cdot H_2O$ [29], 2.043(2) Å in [Pt(*cis*-1,4-DACH)(CBDCA)] [30], and 2.02 Å in [Pt(*cis*-1,4-DACH)(malonato)] [31].

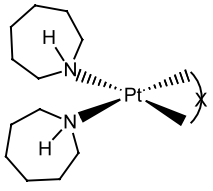


Fig. 1. Structure of $[Pt^{II}(HMI)_2X]$; HMI = hexamethyleneimine; X = dichloro in complex **1**; sulfato in complex **2**; CBDCA, methylmalonato, oxalato, or tatronato in complexes **3**–**6**, respectively.

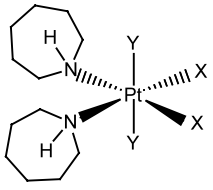


Fig. 2. Structure of $[Pt^{II}(HMI)_2(CBDCA)]\cdot H_2O$; X = chloro in complexes **7**–**9**; Y = OH in complex **7**, acetato in complex **8**, and chloro in complex **9**.

The average Pt–O bond length of 2.02 Å is normal as compared with the values observed in other Pt(II) carboxylate complexes, e.g. 2.01(9) Å in [Pt(*trans*-*l*-1,2-DACH)(CBDCA)]$\cdot H_2O$ [29], 2.02(2) Å in $[Pt^{II}$(1-methylhomopiperazine)(methylmalonato)]$\cdot 2H_2O$ [18], 2.014(7) Å in [Pt(3-methylpiperidine)$_2$(malonato)]$\cdot H_2O$ [28], and 2.038(10) Å in $[Pt^{II}$(hpip)(pentadecanoato)$_2]$ [25].

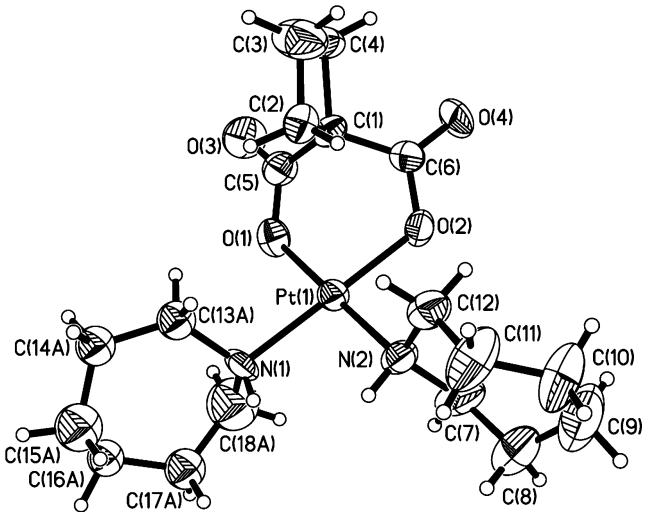


Fig. 3. ORTEP representation of the structure of $[Pt^{II}(HMI)_2(CBDCA)]\cdot H_2O$ with atom numbering scheme.

Table 4
Selected bond lengths (Å) and angles (°) for $[Pt^{II}(HMI)_2(CBDCA)]\cdot H_2O$

Bond lengths	
Pt(1)–O(2)	2.015(8)
Pt(1)–O(1)	2.033(9)
Pt(1)–N(2)	2.036(10)
Pt(1)–N(1)	2.067(8)
Pt(2)–O(22)	2.013(8)
Pt(2)–O(21)	2.028(8)
Pt(2)–N(22A)	2.054(9)
Pt(2)–N(21)	2.059(10)
Bond angles	
O(2)–Pt(1)–O(1)	89.9(3)
O(2)–Pt(1)–N(2)	89.3(4)
O(1)–Pt(1)–N(2)	178.8(4)
O(2)–Pt(1)–N(1)	177.0(4)
O(1)–Pt(1)–N(1)	87.8(4)
N(2)–Pt(1)–N(1)	93.0(4)
C(18A)–N(1)–Pt(1)	109.3(8)
C(13A)–N(1)–Pt(1)	108.3(6)
C(5)–O(1)–Pt(1)	119.2(8)
C(6)–O(2)–Pt(1)	119.5(7)
C(7)–N(2)–Pt(1)	111.7(7)
C(12)–N(2)–Pt(1)	112.2(6)
O(22)–Pt(2)–O(21)	88.3(3)
O(22)–Pt(2)–N(22A)	89.1(4)
O(21)–Pt(2)–N(22A)	177.1(4)
O(22)–Pt(2)–N(21)	176.6(4)
O(21)–Pt(2)–N(21)	89.6(4)
N(22A)–Pt(2)–N(21)	93.0(4)
C(32)–N(21)–Pt(2)	110.8(8)
C(27)–N(21)–Pt(2)	111.3(8)
C(25)–O(21)–Pt(2)	119.3(7)
C(26)–O(22)-Pt(2)	121.5(8)
C(38)–N(22A)–Pt(2)	109.7(8)
C(33A)–N(22A)–Pt(2)	109.5(8)

The coordination structure of the platinum complex with two ring nitrogens of HMI is considerably strained. The N(2)–Pt(1)–N(1) bond angle is expanded to an average value of 93.0° due to geometric constraints imposed by the ligand. These angles are close to the 98.8(4)° reported for [Pt(*cis*-1,4-DACH)(CBDCA)] [30] and the 100.0(2)° reported for [Pt(*cis*-1,4-DACH)(malonato)] [31]. The bond between HMI and the metal ion are also considerably strained as evidenced by the average C–N–Pt angle of 109.1(8)°. These angles are 112.1(9)°, 114.2(7)°, and 122.3(7)° in [Pt(*trans*-*l*-1,2-DACH)(CBDCA)] [29], [Pt(3-methylpiperidine)$_2$(malonato)]·H_2O [28], and [Pt(*cis*-1,4-DACH)(CBDCA)] [30], respectively. The expansion of the N(2)–Pt(1)–N(1) bond angle was compensated for by the contraction of the O(1)–Pt(1)–O(2) angle to 89.9(3)° and the O(21)–Pt(2)–O(22) angle to 88.3(3)°. The molecules in the crystal show a system of N–H···O hydrogen bonds (Fig. 4). The hydrogen bond interactions were examined using the program CRYSTALS [32]. The hydrogen bond lengths were found to range from 2.039 to 2.413 Å, with the average N–H···O interaction being 2.207 Å in length and possessing a bond angle of approximately 158.3°.

In summary, we have synthesized and characterized a series of new platinum(II) and (IV) complexes containing HMI as nonleaving amine ligands and different groups as leaving ligands. The crystal structure of $[Pt^{II}(HMI)_2(CBDCA)]\cdot H_2O$ was determined by X-ray crystallography.

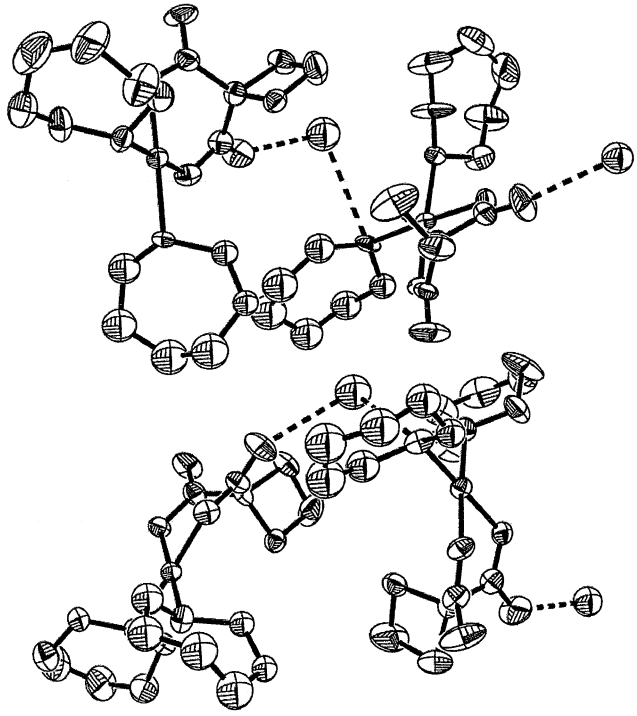


Fig. 4. Packing diagram of $[Pt^{II}(HMI)_2(CBDCA)]\cdot H_2O$ Hydrogen bonds are shown by dashed lines.

4. Supplementary material

Full lists of bond lengths and bond angles, atomic coordinates and equivalent isotropic displacement parameters, anisotropic displacement parameters, and hydrogen coordinates have been deposited at the Cambridge Crystallographic Data Centre (CCDC). Supporting information is available from The Director, CCDC, 12 Union Road, Cambridge, CB2 1EZ, UK (fax: +44-1223-336033; e-mail: deposit@ccdc.cam.ac.uk or www: http://www.ccdc.cam.ac.uk) on request, quoting the deposition number 181721. Any request to the CCDC for this material should quote the full literature citation.

Acknowledgements

This work was supported by grants by CA-77332 and CA-82361 from National Cancer Institute, Robert A. Welch Foundation (C-0976), and the National Science Foundation (CHE9983352).

References

[1] R.F. Ozoles, Hematol. Oncol. Clin. North Am. 6 (1992) 879.
[2] O. Rixe, W. Ortuzar, M. Alvarez, R. Parker, E. Reed, K. Paull, T. Fojo, Biochem. Pharmacol. 52 (1996) 1855.
[3] P.A. Andrews, H.B. Howell, Cancer Cell (Cold Spring Harbor) 2 (1990) 35.
[4] W. Schmidt, S.G. Chaney, Cancer Res. 53 (1993) 799.
[5] A. Vaisman, S.E. Lim, S.M. Patrick, W.C. Copeland, D.C. Hinkle, J.J. Terchi, S.G. Chaney, Biochemistry 38 (1999) 11026.
[6] J.D. Page, I. Husain, A. Sancar, S.G. Chaney, Biochemistry 29 (1990) 1016.
[7] A.R. Khokhar, S. Al-Baker, R. Perez-Soler, Anticancer Drugs 3 (1992) 95.
[8] M.C. Christinan, E. Kohn, G. Sarosy, C. Link, P. Davis, D. Adamo, R.B. Weiss, L. Brewster, F. Lombardo, E. Reed, Proc. Am. Soc. Clin. Oncol. 11 (1992) 117.
[9] J.M. Extra, M. Espie, F. Calvo, C. Ferme, L. Mignot, M. Marty, Cancer Chemother. Pharmacol. 25 (1990) 299.
[10] R. Perez-Soler, G. Lopez-Berestein, J. Luthersztain, S. Al-Baker, K. Francis, D. Macias-Kiger, M.N. Raber, A.R. Khokhar, Cancer Res. 50 (1990) 4254.
[11] L.R. Kelland, in: S.P. Fricke (Ed.), Metal Compounds in Cancer Therapy: Platinum Anticancer Drugs, Chapman & Hall, London, 1994, p. 32.
[12] G.R. Gibbons, J.D. Page, S.K. Mauldin, I. Hussain, S.G. Chaney, Cancer Res. 50 (1990) 6497.
[13] P.M. Takahara, C.A. Fredrick, S.J. Lippard, J. Am. Chem. Soc. 118 (1996) 12309.
[14] A. Gelasco, S.J. Lippard, Biochemistry 37 (1998) 9230.
[15] S.U. Dunham, C.J. Turner, S.J. Lippard, J. Am. Chem. Soc. 120 (1998) 5395.
[16] E.D. Scheef, S.B. Howell, Proc. Am. Assoc. Cancer Res. 39 (1998) 158 (Abstract).
[17] S. Shamsuddin, M.S. Ali, A.R. Khokhar, J. Coord. Chem. 49 (2000) 291.
[18] M.S. Ali, K.H. Whitmire, T. Toyomasu, Z.H. Siddik, A.R. Khokhar, J. Inorg. Biochem. 77 (1999) 231.
[19] Z.H. Siddik, G.S. Hagopian, G. Thai, S. Tomisaki, T. Toyomasu, A.R. Khokhar, J. Inorg. Biochem. 77 (1999) 65.
[20] G. Scheldrick, SHELXTL. 6.10, Göttingen, Göttingen, Germany, 2001.
[21] The scattering factors are part of the SHELXTL package and can be found in the international Tables for X-ray Crystallography, vol. C, Kluwer, Dordrecht, The Netherlands, 1992.
[22] A.L. Spek, PLATON—A Multipurpose Crystallographic Tool, Utrecht, The Netherlands, 2002.
[23] S.C. Dhara, Indian J. Chem. 8 (1970) 193.
[24] S. Shamsuddin, I. Takahashi, Z.H. Siddik, A.R. Khokhar, J. Inorg. Biochem. 61 (1996) 291.
[25] M.S. Ali, C.A. Powers, K.H. Whitmire, I. Guzman-Jimenez, A.R. Khokhar, J. Coord. Chem. 52 (2001) 273.
[26] S.R. Ali Khan, A.R. Khokhar, J. Coord. Chem. 52 (2000) 119.
[27] S.R. Ali Khan, S. Shamsuddin, S. Inutsuka, K.H. Whitmire, Z.H. Siddik, A.R. Khokhar, Bioorg. Med. Chem. 8 (2000) 515.
[28] S.R. Ali Khan, I. Guzman-Jimenez, K.H. Whitmire, A.R. Khokhar, Polyhedron 19 (2000) 983.
[29] P. Bitha, G.O. Morton, T.S. Dunne, E.F. Delos Santos, Y. Lin, S.T. Boone, R.C. Haltwanger, C.G. Pierpont, Inorg. Chem. 29 (1990) 645.
[30] S. Shamsuddin, A.R. Khokhar, J. Coord. Chem. 33 (1994) 83.
[31] J.D. Hoeshele, H.D. Hollis Showalter, A.J. Krakar, W.L. Illiott, B.J. Roberts, J.W. Kamp, J. Med. Chem. 37 (1994) 2630.
[32] D.J. Watkin, C.K. Prout, J.R. Carruthers, P.W. Betterridge, R.I. Cooper, CRYSTALS, Issue 11, Chemical Crystallography Laboratory, University of Oxford, Oxford, 2002.

ences in the bond lengths (M–N and M–O), ring strain and the ligand configuration [1–5,8–19,21–29].

The edta-like ligands [diamine-*N*,*N*′-diacetate-*N*,*N*′-di-3-propionate ions (eddadp or 1,3-pddadp)], differing only in the length of the diamine chain, can form a maximum of three geometrical isomers on hexadentate coordination: *trans*(O_5) (I), *trans*(O_5O_6) (II) and *trans*(O_6) (III) (Fig. 1) (O_5 and O_6 refer to the five- and six-membered N–O rings, respectively). The six-membered β-alaninate rings serve better for the formation of less-strained G rings favoring the *trans*(O_5) isomers of $[M(eddadp)]^{n-}$ complexes [6–15]. Only one of two *trans*(O5) isomers was also prepared with the optically active *SS*-edds ligand (*SS*-ethylenediamine-*N*,*N*′-disuccinate ion) which produces metal complexes stereospecifically with the Λ configuration [6,7,15–18]. Contrary to this, all possible isomers of $[M(1,3\text{-pddadp})]^{n-}$ have been reported for Cr(III) [19], but only two isomers (*trans*(O_5O_6) and *trans*(O_6) for Co(III) [20,21] and *trans*(O_5) and *trans*(O_5O_6) for Rh(III) [22]) have been isolated and characterized. In addition, only one dominant isomer of the same complex *trans*(O_6) of Cu(II) [23] has been established.

This paper deals with the preparation and characterization of the two geometrical isomers (*trans*(O_5) (**1**) and *trans*(O_5O_6) (**2**)) of the $[Ni(1,3\text{-pddadp})]^{2-}$ complex. The X-ray data are reported for the binuclear complex *trans*(O_5)-$[Ni_2(1,3\text{-pddadp})(H_2O)_4]\cdot 4H_2O$ (**1**). Structural parameters and strain analysis data of this complex and the other related complexes are compared and discussed in relation to the structure of the ligand, geometry of complexes and their octahedral distortion. The results presented for isomers **1** and **2**, based upon IR (carboxylate region) and electronic absorption spectroscopy, are compared with earlier results obtained for related complexes.

2. Experimental

All commercially obtained reagent-grade chemicals were used as supplied. The 1,3-propanediamine-*N*,*N*′-diacetic-*N*,*N*′-di-3-propionic acid ($H_4$1,3-pddadp) was prepared using a previously described procedure [20].

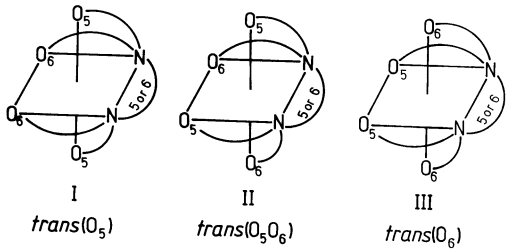


Fig. 1. Three possible geometrical isomers of hexadentate $[M(eddadp)]^{n-}$ and $[M(1,3\text{-pddadp})]^{n-}$ complexes.

2.1. Preparation and separation of complexes: *trans*(O_5) geometrical isomer of sodium (1,3-propanediamine-*N*,*N*′-diacetato-*N*,*N*′-di-3-propionato)nickelate(II) dihydrate, *trans*(O_5)-$Na_2[Ni(1,3\text{-pddadp})]\cdot 2H_2O$ (**1**) and *trans*(O_5O_6) geometrical isomer of sodium (1,3-propanediamine-*N*,*N*′-diacetato-*N*,*N*′-di-3-propionato)nickelate(II) trihydrate, *trans*(O_5O_6)-$Na_2[Ni(1,3\text{-pddadp})]\cdot 3H_2O$ (**2**)

A solution of nickel(II) chloride hexahydrate, $NiCl_2\cdot 6H_2O$ (2.38 g, 0.0100 mol in 25 cm^3 of water) was added to solution of $H_4$1,3-pddadp (3.34 g, 0.0100 mol) and $NaHCO_3$ (1.68 g, 0.0200 mol) in 25 cm^3 of water with heating (65 °C) and stirring. Heating with stirring at the same temperature was continued for 1 h. After the pH of the mixture was adjusted to approximately 7 by gradual addition of $NaHCO_3$, the blue solution was then heated (80 °C) with stirring for a further 2 h (the volume of the solution was maintained by periodic addition of hot water). The solution was then reduced to approximately 15 cm^3 and desalted by passing it through a G-10 Sephadex column, eluting with distilled water. The obtained eluate was introduced into a 5 × 60 cm column containing Dowex 1-X8 (200–400 mesh) anion-exchange resin in the Cl^- form. After the column was washed with water, the charged complexes were eluted with a 0.1 M NaCl solution at a rate of 0.3 $cm^3\ min^{-1}$. Two bands appeared on the column. The obtained eluate of each band was reduced to a small volume and then desalted. The eluate of the first band (*trans*(O_5) isomer (**1**)) was reduced to a volume of 4 cm^3 and stored in a desiccator over methanol for several days. The light blue crystals of *trans*(O_5)-$Na_2[Ni(1,3\text{-pddadp})]\cdot 2H_2O$ (**1**) were collected, washed with methanol and then ether, and air-dried (2.5 g). The second eluate (*trans*(O_5O_6) isomer (**2**)) was reduced to 2 cm^3 and stored in a desiccator over $CaCl_2$ for several days. The light blue crystal powder of *trans*(O_5O_6)-$Na_2[Ni(1,3\text{-pddadp})]\cdot 3H_2O$ (**2**) was collected (0.2 g). Found: Ni, 12.40; C, 32.82; H, 4.76; N, 5.85; H_2O, 8.02%. Calc. for *trans*(O_5)-$Na_2[Ni(1,3\text{-pddadp})]\cdot 2H_2O$ (**1**), $Na_2NiC_{13}H_{22}N_2O_{10}$ (FW = 471.00): Ni, 12.46; C, 33.15; H, 4.71; N, 5.95; H_2O, 7.65%. Found: Ni, 12.20; C, 31.84; H, 4.96; N, 5.70; H_2O, 11.32%. Calc. for *trans*(O_5O_6)-$Na_2[Ni(1,3\text{-pddadp})]\cdot 3H_2O$ (**2**), $Na_2NiC_{13}H_{24}N_2O_{11}$ (FW = 489.01): Ni, 12.00; C, 31.93; H, 4.95; N, 5.73; H_2O, 11.05%.

Complex **1** in the form of the nickel(II) salt was obtained using the ion-exchange column technique. The eluate was reduced to a small volume and allowed to stand at room temperature (r.t.) to crystallize the complex $[Ni_2(1,3\text{-pddadp})(H_2O)_4]\cdot 4H_2O$ (**1**). Found: Ni, 19.74; C, 26.50; H, 5.74; N, 4.80%. Calc. for $[Ni_2(1,3\text{-pddadp})(H_2O)_4]\cdot 4H_2O$ (**1**), $Ni_2C_{13}H_{34}N_2O_{16}$ (FW = 591.80): Ni, 19.83; C, 26.38; H, 5.79; N, 4.73%.

The suitable crystal for X-ray analysis of this complex was obtained from an aqueous solution.

2.2. Physical measurements

2.2.1. $[Ni_2(1,3\text{-pddadp})(H_2O)_4]\cdot 4H_2O$ (**1**)

A pale blue crystal with approximate dimensions of $0.39 \times 0.47 \times 0.54$ mm was used for X-ray data collection. Intensity measurements were made on a Siemens AED single-crystal diffractometer using graphite-monochromated Mo Kα radiation ($\lambda = 0.71073$ Å) at 293 K.

Crystal data: $Ni_2C_{13}H_{34}N_2O_{16}$ (FW = 591.80), triclinic, space group $P\bar{1}$, $a = 14.065(4)$, $b = 10.070(2)$, $c = 9.408(1)$ Å, $\alpha = 63.21(6)^\circ$, $\beta = 74.11(5)^\circ$, $\gamma = 79.41(4)^\circ$, $V = 1141.2(8)$ Å^3, $Z = 2$, $D_c = 1.722$ g cm^{-3}, $D_m = 1.68$ g cm^{-3}, $F(000) = 620$, μ(Mo Kα) = 17.30 cm^{-1}.

The unit-cell dimensions were obtained from the setting angles of 28 accurately measured reflections with $14.7^\circ < \theta < 19.9^\circ$. No decay in the intensity of the standard reflection was noticed over the course of data collections. The intensity data were corrected for Lorentz and polarization effects but not for absorption. The structure was solved by direct methods using SIR-92 [30] and refined by full-matrix least-squares techniques based on F^2. The refinement converged to $R = 0.0521$ ($wR(F^2) = 0.1725$) for 5210 reflections ($F_o > 2\sigma(F_o)$) of 6629 collected in the range $6^\circ < 2\theta < 60^\circ$. Anisotropic thermal parameters were employed for non-hydrogen atoms, the hydrogen atoms being put in calculated positions and refined isotropically. Neutral scattering factors [31] were employed and the anomalous dispersion terms for all atoms were included in F_c. All calculations were performed on an ENCORE-91 computer using the programs SHELXL-93 [32], PARST [33] and ORTEP [34].

IR spectra were recorded on a Perkin–Elmer FT-IR 1725X spectrophotometer using KBr pellets. Aqueous solution spectra were obtained in D_2O.

Electronic absorption spectra were recorded on a Varian Cary 17D spectro-photometer. For these measurements, about 8×10^{-2} M aqueous solutions were used.

Elemental microanalyses for carbon, hydrogen, nitrogen and nickel were performed by the Microanalytical Laboratory, Faculty of Chemistry, University of Belgrade (Serbia, YU).

3. Results and discussion

The geometrical isomers of the complex $[M(1,3\text{-pddadp})]^{n-}$ have been chromatographically separated following the order: *trans*(O_5) (first), *trans*(O_5O_6) (second) and *trans*(O_6) (third) (Fig. 1). This order was established for the corresponding three isomers of Cr(III) [19], two isomers of Co(III) [20,21] and the two isomers of Rh(III) [22]. The two isomers of the $[Ni(1,3\text{-pddadp})]^{2-}$ complex [*trans*(O_5) (**1**) (C_2 molecular symmetry) and *trans*(O_5O_6) (**2**) (C_1 molecular symmetry)] have been prepared at pH ∼ 7 and all carboxylate groups are expected to be coordinated. The *trans*(O_5) configuration was verified in the molecular structure of (**1**) presented here. Following the order of elution, the complex (**2**) (second band) is expected to represent the *trans*(O_5O_6) isomer of the same complex. Spectral data reported for **1** and **2** are in agreement with the geometry of the complexes.

3.1. Description of the molecular structure of *trans*(O_5)-$[Ni_2(1,3\text{-pddadp})\text{-}(H_2O)_4]\cdot 4H_2O$ (**1**)

An ORTEP drawing of the *trans*(O_5)-$[Ni_2(1,3\text{-pddadp})(H_2O)_4]\cdot 4H_2O$ (**1**) is shown in Fig. 2, where the numbering scheme adopted for the respective atoms is also given. The bond lengths and selected bond angles are listed in Table 1.

The crystals of **1** are built up from binuclear homometallic complexes. The structural unit consists of $[Ni(1,3\text{-pddadp})]^{2-}$ and $[Ni(H_2O)_4(O_G\text{-carbox.})_2]^{2+}$ octahedra and four water solvent molecules (Fig. 2). In the complex anion, the Ni1 atom is surrounded by all of the donating atoms (2N and 4O) of the 1,3-pddadp ligand acting in a hexadentate. The complex anion represents a *trans*(O_5) isomer with the two glycinate (R_1 and R_2) rings in the *trans* positions and the two β-alaninate (G_1 and G_2) rings coordinated in the equatorial position forming a 6–6–6 ring system in the G-plane. The Ni2 atom is coordinated to four water molecules and two bridging carboxylate oxygen atoms, O(1) and O(3) of the G_1 and G_2 β-alaninate rings, respectively, resulting

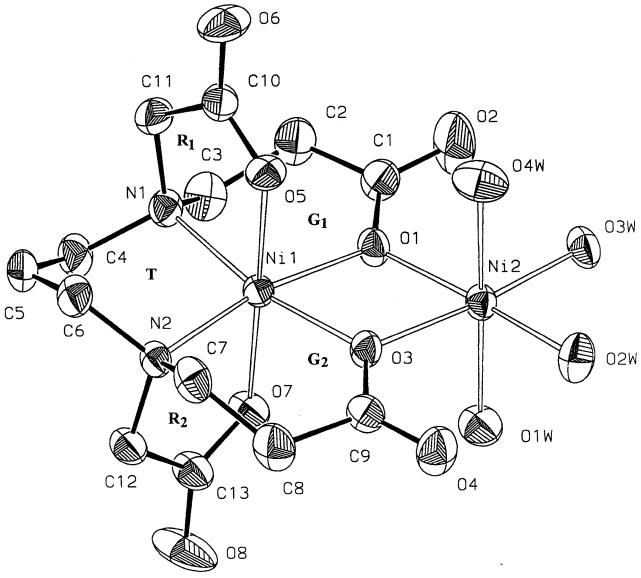


Fig. 2. The molecular structure (ORTEP) of the binuclear complex, *trans*(O_5)-$[Ni_2(1,3\text{-pddadp})(H_2O)_4]\cdot 4H_2O$ (**1**).

Table 1
Bond distances (Å) and selected bond angles (°) with e.s.d.'s in parentheses for *trans*(O_5)-[Ni_2(1,3-pddadp)(H_2O)$_4$]·4H_2O (**1**)

Bond distances			
Ni(1)–O(1)	2.089(2)	O(6)–C(10)	1.243(5)
Ni(1)–O(3)	2.074(3)	O(7)–C(13)	1.266(4)
Ni(1)–O(5)	2.060(3)	O(8)–C(13)	1.243(5)
Ni(1)–0(7)	2.060(3)	N(1)–C(3)	1.502(5)
Ni(1)–N(l)	2.090(3)	N(1)–C(4)	1.488(6)
Ni(1)–N(2)	2.109(3)	N(1)–C(11)	1.489(4)
Ni(2)–O(1)	2.073(3)	N(2)–C(6)	1.484(5)
Ni(2)–O(3)	2.083(2)	N(2)–C(7)	1.487(6)
Ni(2)–O(1W)	2.095(3)	N(2)–C(12)	1.483(5)
Ni(2)–O(2W)	2.044(4)	C(1)–C(2)	1.497(6)
Ni(2)–O(3W)	2.056(3)	C(2)–C(3)	1.528(7)
Ni(2)–O(4W)	2.072(3)	C(4)–C(5)	1.529(5)
O(1)–C(1)	1.285(4)	C(5)–C(6)	1.517(7)
O(2)–C(1)	1.235(5)	C(7)–C(8)	1.514(6)
O(3)–C(9)	1.283(4)	C(8)–C(9)	1.511(5)
O(4)–C(9)	1.236(5)	C(10)–C(11)	1.516(7)
O(5)–C(10)	1.272(4)	C(12)–C(13)	1.524(5)
Bond angles			
N(l)–Ni(1)–N(2)	95.7(1)	O(2W)–Ni(2)–O(4W)	89.1(1)
O(7)–Ni(1)–N(2)	81.7(1)	O(2W)–Ni(2)–O(3W)	91.7(1)
O(7)–Ni(1)–N(l)	98.1(1)	O(1W)–Ni(2)–O(4W)	179.3(1)
O(5)–Ni(1)–N(2)	97.7(1)	O(1W)–Ni(2)–O(3W)	91.7(1)
O(5)–Ni(1)–N(1)	81.7(1)	O(1W)–Ni(2)–O(2W)	90.6(1)
O(5)–Ni(1)–0(7)	179.3(1)	O(3)–Ni(2)–O(4W)	90.6(1)
O(3)–Ni(1)–N(2)	93.4(1)	O(3)–Ni(2)–O(3W)	172.8(1)
O(3)–Ni(1)–N(l)	168.2(1)	O(3)–Ni(2)–O(2W)	95.5(1)
O(3)–Ni(1)–O(7)	90.6(1)	O(3)–Ni(2)–O(lW)	88.8(1)
O(3)–Ni(1)–0(5)	89.7(1)	O(l)–Ni(2)–O(4W)	88.7(1)
O(l)–Ni(1)–N(2)	169.1(1)	O(l)–Ni(2)–O(3W)	94.5(1)
O(l)–Ni(1)–N(l)	93.6(1)	O(l)–Ni(2)–O(2W)	173.4(1)
O(l)–Ni(1)–O(7)	91.3(1)	O(l)–Ni(2)–O(lW)	91.5(1)
O(l)–Ni(1)–O(5)	89.3(1)	O(l)–Ni(2)–O(3)	78.3(1)
O(l)–Ni(1)–O(3)	78.2(1)	Ni(1)–O(l)–Ni(2)	101.7(1)
O(3W)–Ni(2)–O(4W)	88.9(1)	Ni(l)–0(3)–Ni(2)	101.8(1)

in a four terms ring and making a discrete binuclear unit (Fig. 2). Both octahedra formed around the central atoms are irregular in shape and their octahedral *cis* angles (Table 1) range from 78.2(1)° to 98.1(1)° (for Ni1) and from 78.3(1)° to 95.5(1)° (for Ni2) while the *trans* ones in the complex anion are 179.3(1)°, 168.2(1)° and 169.1(1)°.

The conformations of the chelate rings in the complex anion (Fig. 2) are those usually expected for these kinds of chelates. The two five-membered glycinate rings show a relatively small puckering (R_1 in a twist conformation with puckering parameters of $q_2 = 0.081(4)$ Å and $\varphi_2 = 88(2)°$ and R_2 in an envelope conformation with puckering parameters of $q_2 = 0.105(4)$ Å and $\varphi_2 = 71(2)°$). The six-membered diamine (T) ring adopts a twist-boat conformation (λ, as expected for the complex anion presented in Fig. 2 having Δ configuration) with puckering parameters of QT = 0.781(4) Å and $\theta_2 = 90.5(3)°$. Two β-alaninate (G) rings adopting an envelope-like conformation show a similar degree of puckering (puckering parameters: QT = 0.566(4) Å, $\theta_2 = 63.7(4)°$ for G_1 ring and QT = 0.544(4) Å, $\theta_2 = 59.1(3)°$ for G_2 ring). The binuclear unit is stabilized by the two coordination bonds (Ni2–O(1), 2.073(3) Å; Ni2–O(3), 2.083(2) Å) and also by an extended hydrogen bonding network involving prevalently the oxygen atoms of the carboxylic groups and the hydrogen atoms of the coordinated and crystal water molecules.

3.2. Structural parameters of edta-type chelates and their octahedral distortion in relation to the structure of the ligand and geometry of the complex

The mean Ni–L bond distances and some bond angles of binuclear complex **1** and the corresponding values of some other Ni(II) complexes containing various edta-type ligands eddadp (**3**) [13], edds (**4**) [16–18], 1,3-pdta (1,3-propane-diaminetetraacetate ion) (**5**) [24] and edta (**6**) [3–5]) are given in Table 2. The presence of the two carboxylic atoms (O(1) and O(3)) bridging the two metal centers and the resulting four terms ring (Fig. 2) is responsible for both the lengthening of the Ni–O(G) distances compared with the Ni–O(R) distances (mean: 2.082 vs. 2.060 Å) and the narrowing of the corresponding O(1)–Ni–O(3) angle (78.2(1)° for Ni1 and 78.3(1)° for Ni2) (Tables 1 and 2). These two values are limited in a series of complexes listed in Table 2. The values for complexes **4** [16–18] and **6** [3–5] (Table 2) are not significantly changed by variation of counter ions.

As was expected [8,13–15,24–26], the mean Ni–O(R) distances are on average shorter than the mean Ni–O(G) distances (Table 2), with an exception for **4** and **5**, where the equatorial Ni–O(G) bonds are shorter than the Ni–O(R) bonds. However, the mean Ni–O distances of complexes listed are shorter than the mean Ni–N distances. The values given (Table 2) indicate that the mean Ni–O distances (mean Ni–O range, 2.044–2.071 Å) and the mean Ni–N distances (mean Ni–N range, 2.058–2.105 Å) are less sensitive to the structure of the ligand than was the case for the corresponding distances of M(III) complexes [8,13,22,25,26]. The complexes considered (Table 2) attain octahedral symmetry with varying degrees of distortion, reflecting the structure of the ligand and geometry of the complex. Octahedral distortion of these complexes slightly decreases with an increasing number of six-membered rings in the G-plane. Among the complexes listed (Table 2) the greatest deviation of the O(G_1)–Ni–O(G_2) angle was realized for **1**, **5** and **6** and vice versa for the O(R_1)–Ni–O(R_2) and N(1)–Ni–N(2) angles. For complexes **3** and **4**, having a 6–5–6 ring system in the G-plane, these angles are closer to the ideal values and these complexes attain higher octahedral symmetry. We observe that an increase in number of six-membered rings in the G-plane, going from **6** to **1**, causes a steady decrease in the

Table 2
Comparison of Ni–L bond distances (Å) and some bond angles (°) for $[Ni(edta\text{-}type)]^{2-}$ complexes

Complex (ligand) [a]	Mean Ni–L bond distances (Å)				Reference
	Ni–N	Ni–O(G)	Ni–O(R)	Ni–O	
(1,3-pddadp) (**1**)	2.100	2.082	2.060	2.071	This work
(eddadp) (**3**)	2.104	2.048	2.041	2.044	[13]
(edds) (**4**)	2.105	2.045	2.090	2.068	[16]
	2.060	2.051	2.069	2.060	[17]
	2.058	2.044	2.062	2.053	[18]
(1,3-pdta) (**5**)	2.073	2.026	2.078	2.052	[24]
(edta) (**6**)	2.084	2.066	2.056	2.061	[3]
	2.072	2.058	2.054	2.056	[4]
	2.100	2.040	2.065	2.053	[5]
	Rings in G-plane	Angles (°)			
		N(1)–Ni-N(2)	O(R1)–Ni–O(R2)	O(G1)–Ni–O(G2)	
(1,3-pddadp) (**1**)	6–6–6	95.7(1)	180.7(1)	78.2(1)	This work
(eddadp) (**3**)	6–5–6	86.4(2)	184.5(2)	92.8(2)	
(edds) (**4**)	6–5–6	83.5(6)	183.0	93.5(6)	
		86.2(3)	181.4(3)	95.5(3)	
		86.3(3)	183.0	93.0(3)	
(1,3-pdta) (**5**)	5–6–5	96.3(3)	184.9(3)	99.4(3)	
(edta) (**6**)	5–5–5	87.	181.3	12.7	
		87.5(1)	183.3(1)	12.0(1)	
		84.3(3)	180.7(3)	15.3(3)	

[a] For complexes **1**, **3** and **4** the values are given for *trans*(O_5) isomer.

$O(G_1)$–Ni–$O(G_2)$ *cis* angle. This angle for the group of Ni(II) complexes decreases in the order: 112.0(1)°-115.3(3)° (**6**) > 99.4(3)° (**5**) > 93.0(3)°-95.5(3)° (**4**) > 92.8(2)° (**3**) > 78.2(1)° (**1**). The same trend is observed for the N(1)–Ni–N(2) bond angle, although, it fits better for a series of complexes forming the diamine (T) or the diamine (E) ring only. For both *cis* angles similar trend was recently observed for a series of Rh(III) and Co(III) edta-type complexes [22].

Strain analysis data are available for the *trans*(O_6)-$[M(1,3\text{-}pddadp)]^{n-}$ complexes (M=Co(III) [14,25], Cr(III) [14,26] or Cu(II) [23]). The corresponding data are reported here for the two isomers (the *trans*(O_5) and *trans*(O_5O_6)) of Rh(III) [22] and the *trans*(O_5) isomer of the investigated Ni(II) complex (complexes **1** and **7**–**11**, Table 3). The total deviation of the octahedral angles of these complexes varies reflecting their large ionic radii [35] and the geometry of the complex (the ring system in the G-plane). These values vary from 38° for **7** [14,25] to 43° for **9** [23] (*trans*(O_6) isomers) and from 42° for **11** (*trans*(O_5O_6) isomer) to 55° for **10** and 60° for **1** (*trans*(O_5) isomers). The values are less for complexes **7**–**9** (5–6–5 ring system) and the complex **11** (5–6–6 ring system) and these complexes attain higher octahedral symmetry. The Rh(III) complex **11** (C_1 molecular symmetry) with respect to **10** (having 6–6–6 ring system in the G-plane and C_2 molecular symmetry) attains higher octahedral symmetry ($\Sigma\Delta(O_h)$, 42° vs. 55°, Table 3). For metal ions of the size comparable with Rh(III), as was reported [22], the best combination of the rings that can span the girdle plane seems to be the 5–6–6 system (**11**) which allows the diamine ring to adopt the energetically favored twist conformation and brings the $O(G_1)$–Rh–$O(G_2)$ *cis* angle close to 90°. The total deviation of the octahedral angles sums 60° for **1** indicating a greater octahedral distortion with respect to the size of the ionic radii [35] than among the other complexes listed. This value is expected because of the structure of the binuclear complex unit (**1**) (the presence of the two oxygen atoms (O(1) and O(3)) bridging the two metal centers by forming a four-membered ring) (Fig. 2). The six octahedral angles of **1** show very large deviations (Table 1).

The bond angle chelate-ring sums for the R, G, and diamine (T) rings are as expected for these kinds of chelates [13–15,23–26] (Table 3). The bond angle chelate-ring sums for the R glycinate rings are closer to the ideal values (538.5°). The total deviations are 0° for **1** and +1° for **11**, but unusually a large negative deviation (of −6°) was observed for **10** [22]. The bond angle chelatering sums for the G glycinate rings, as expected, are less than the ideal values (the negative total deviation varies from −10° to −11°). The larger deviations are positive for all six-membered rings (Table 3). The diamine (T) rings are in a twist-boat conformation and show positive total deviation (from +26° for **8**

Table 3
Strain analysis of $[M(l,3\text{-pddadp})]^{n-}$ chelates

M (isomer)	r_M (Å)[a]	ΣΔ [b]		ΣΔ [c]		Δ(M–O–C) [d]		ΣΔ [e]	
		(O_h)	T	R	G	R	G	N	Reference
Co(III) (**7**)	0.685	38	+28	+33	−11	+17	+4	16	[14,21,25]
Cr(III) (**8**)	0.755	42	+26	+33	−11	+19	+5	15	[14,19,26]
Cu(II) (*trans*(O_6)) (**9**)	0.870	43	+27	+14	−11	0	+5	17	[23]
Rh(III) (*trans* (O_5)) (**10**)	0.805	55	+37	−6	+27	+5	+14	7	[22] and this work
Rh(III)[f] (*trans* (O_5O_6)) (**11**)	0.805	42	+33	+1 (+32)	−10 (+41)	+5 (+14)	+4 (+21)	13	[22] and this work
Ni (II) (*trans*(O_5)) (**1**)	0.830	60	+28	0	+36	+7	+20	8	This work

[a] Ionic radius for C.N. = 6 [35].
[b] $\Sigma\Delta(O_h)$ is the sum of the absolute values of the deviations from 90° of the L–M–L' bite angles. All values rounded off to the nearest degree.
[c] $\Delta\Sigma$(ring) is the deviation from the ideal of the corresponding chelate rings' bond angle sum. A mean value of the two rings (R or G) is reported for complexes having in approx. C_2 molecular symmetry.
[d] Δ(M–O–C) (ring) is the mean value of the deviation of the corresponding rings' M–O–C bond angle from 109.5°.
[e] ΣΔ(N) is the sum of the absolute values of the deviations from 109.5° of the six bond angles made by the nitrogen atoms. A mean value for the two nitrogens is reported.
[f] For this complex having C_1 molecular symmetry the two values are reported. The values in parentheses are given for six-membered rings.

to +37° for **10**). The total deviations of the β-alaninate rings vary from +14° to +33° (for the R rings) and from +27° to +41° (for the G rings). An extremely large deviation of the G ring for **11** (+41°, ca. 6.8° per angle) is comparable with those observed for some related M(III) complexes [14,25,26]. All complexes considered (Table 3) show positive deviation of the M–O–C(R,G) bond angles (except for tetragonally elongated complex **9**, Cu–O–C(R) = 109.0 [23]). These deviations, as expected [13,14,25,26], are less for the glycinate rings (from +5° to +7° and from +4° to +5° for the R and G rings, respectively) than for the β-alaninate rings (from +14° to +19° for the R rings (except for **9** [23]) and from +14° to +21° for the G rings, Table 3).

When each of the deviations for the six angles made by the nitrogen atoms is summed, the total deviations (absolute values) for each complex were obtained (Table 3). Total deviation about the chelating N atoms sums to roughly 16° (for **7**) [14,25], 15° (for **8**) [14,26], 17° (for **9**) [23], 17° (for **10**), 13° (for **11**) and 8° (for **1**). These complexes, having N atoms connecting mixed (one acetate and one β-alaninate) rings, with respect to those containing N atoms connecting two acetate or two β-alaninate rings [25,26], show less total deviations about the N atoms. Among the complexes listed, the least deviation was observed for complex **1** (8°). This complex, compared with those of **7**–**11**, contains N atoms with less strained bonds.

3.3. Spectral characteristics of complexes

In the expected IR carboxylate region [6,7,13,23–25] the complexes **1** and **2** show absorption in agreement with their molecular symmetries (C_2 for **1** and C_1 for **2**). Infrared spectra for these complexes were taken both in the solid state and in D_2O (to eliminate interference from OH) and data obtained support fully coordinated carboxylates in both states. Complex **1** (having two pairs of equivalent rings, R and G) exhibits two very strong bands [at 1640sh cm^{-1} (1600 cm^{-1} in D_2O) and at 1591 cm^{-1} (1580 cm^{-1} in D_2O)] assigned to the asymmetric stretch of five-membered carboxylate moieties at higher energy (R rings) and six-membered carboxylate moieties at lower energy (G rings). In the same region, complex **2** having four non-equivalent rings, instead of four, exhibits three absorption bands [at 1635sh and 1610 cm^{-1} (1606 and 1590 cm^{-1} in D_2O) at higher energy and at 1588 cm^{-1} (1570 cm^{-1} in D_2O) at lower energy]. These data are in agreement with its C_1 molecular symmetry and the two bands appearing at higher energy correspond to the asymmetric stretch of coordinated carboxylates contained in a glycinate residue (R and G rings) and the one at lower energy was assigned to the moieties of the six-membered carboxylate arms. The bands appearing in the symmetric frequency region (at 1409 and 1337 cm^{-1} for **1** and at 1393, 1366 and 1330 cm^{-1} for **2**) can be assigned tentatively to the symmetric

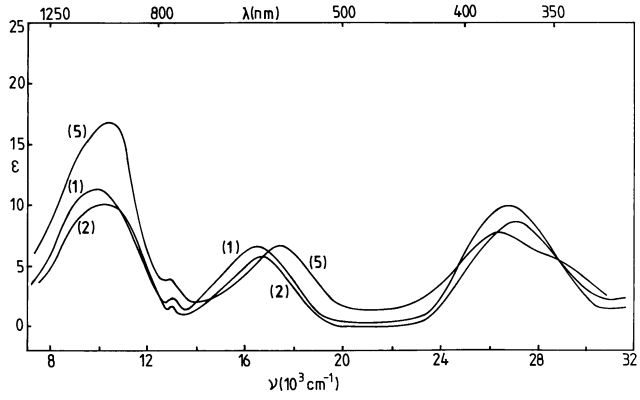


Fig. 3. Electronic absorption spectra of: (**1**) *trans*(O_5)-[Ni(1,3-pddadp)]$^{2-}$ (**2**) *trans*(O_5O_6)-[Ni(1,3-pddadp)]$^{2-}$ and (**5**) [Ni(1,3-pdta)]$^{2-}$.

Table 4
Absorption data for [Ni(edta-type)]$^{2-}$ complexes forming six-membered diamine rings

Complex		Absorption [a]			Assignments	Reference
		ν_{obs}	ε	ν_{calc}	O_h	
Trans(O_5)-[Ni(1,3-pddadp)]$^{2-}$ (**1**)	I	10.18	11.3		$^3A_{2g} \rightarrow {}^3T_{2g}(F)$	This work
	II	13.00	2.3		$\rightarrow {}^1E_g(D)$	
	III	16.55	6.5	16.39	$\rightarrow {}^3T_{1g}(F)$	
	IV	26.88	10.0	26.88	$\rightarrow {}^3T_{1g}(P)$	
Trans(O_5O_6)-[Ni(1,3-pddadp)]$^{2-}$ (**2**)	I	10.27	10.0		$^3A_{2g} \rightarrow {}^3T_{2g}(F)$	This work
	II	13.02	1.8		$\rightarrow {}^1E_g(D)$	
	III	16.75	5.7	16.54	$\rightarrow {}^3T_{1g}(F)$	
	IV	27.17	8.8	27.17	$\rightarrow {}^3T_{1g}(P)$	
[Ni(1,3-pdta)]$^{2-}$ (**5**)	I	10.50	16.6		$^3A_{2g} \rightarrow {}^3T_{2g}(F)$	[24]
	II	12.98	3.9		$\rightarrow {}^1E_g(D)$	
	III	17.54	6.8		$\rightarrow {}^3T_{1g}(F)$	
	IV	26.37–28.57sh	7.6		$\rightarrow {}^3T_{1g}(P)$	

[a] In units of $cm^{-1} \times 10^3$ for the absorption maxima and mol^{-1} dm^3 cm^{-1} for the molar absorbance (ε).

stretching vibrations of the corresponding carboxylate groups.

The ligand field absorption spectra for complexes **1** and **2** and the spectrum of complex [Ni(1,3-pdta)]$^{2-}$ (**5**) of known structure [24], taken for comparison, are given in Fig. 3 (Table 4). All of these complexes forming diamine (T) rings, with respect to those of related complexes forming diamine (E) rings [13], show broadening of the first absorption band (lower energy side, Fig. 3) due to the influence of tetragonality on the spectrochemical behavior of these complexes (D_{4h} model). Apparently, if the equatorial N_2O_2 ligand field is smaller than the one imposed by two axially coordinated oxygen atoms, the D_{4h} model is consistent with the pattern, the lower energy peak being $^3B_{1g} \rightarrow {}^3B_{2g}$ (D_{4h}) and the higher energy peak being $^3B_{1g} \rightarrow {}^3E_g$ (D_{4h}), both of which are derived from the same $^3T_{2g}(O_h)$ state [36]. However, the noncubic field components are small compared with the approximately cubic field and spectra of these complexes, as established for edta-type [13,24] and most other Ni(II) complexes [37–40], can best be interpreted by using an octahedral model: $^3A_{2g} \rightarrow {}^3T_{2g}(F)$ (band I); $^3A_{2g} \rightarrow {}^3T_{1g}(F)$ (band III) and $^3A_{2g} \rightarrow {}^3T_{1g}(P)$ (band IV) (Table 4). In each of the spectra a shoulder at approximately 13 000 cm^{-1} (band II, Table 4) occurs on the higher-energy side of the spin-allowed band. This band probably arises from a spin-forbiden triplet to singlet transition.

The spectrochemical behavior of Ni(II) complexes often reflects the average coordination geometry. That such is the case for complexes **1** and **2** is demonstrated by the calculation of the energies of the $^3A_{2g} \rightarrow {}^3T_{1g}(F)$ and $^3A_{2g} \rightarrow {}^3T_{1g}(P)$ transitions from the $^3A_{2g} \rightarrow {}^3T_{2g}(F)$ transition which has an energy of $10Dq$ [39]. The close agreement (within 2%) between the observed and calculated values (Table 4) gives strong support for the expected octahedral geometry of these complexes. The absorption maxima of **1** and **2** (bands I and III) are located at lower energies than those found for complex **5** [24]. The ligand field strength (LFS) for these complexes (Fig. 3, Table 4) increases in the order: **1** < **2** < **5** with the decreasing number of six-membered rings in the G-plane.

4. Supplementary data

Crystallographic data for the structural analysis have been deposited with the Cambridge Crystallographic Data Centre, CCDC No. 182490 for compound **1**. Copies of this information may be obtained free of charge from The Director, CCDC, 12 Union Road, Cambridge, CB2 1EZ, UK (fax: +44-1223-336033; e-mail: deposit@ccdc.cam.ac.uk or www: http://www.ccdc.cam.ac.uk).

Acknowledgements

The authors are grateful to the Serbian Ministry for Science and Technology for financial support (Project No. II1315).

References

[1] H.A. Weakliem, J.L. Hoard, J. Am Chem. Soc. 81 (1959) 549.
[2] E.F.K. McCandlish, T.K. Michael, J.A. Neal, E.C. Lingafelter, N.J. Rose, Inorg. Chem. 17 (1978) 1383 (and references therein).
[3] E. Coronado, M. Drillon, A. Fuertes, D. Beltran, A. Mosset, J. Galy, J. Am. Chem. Soc. 108 (1986) 900.
[4] J.M. Nesterova, M.A. Porai-Koshits, Koord. Khim. 10 (1984) 129.
[5] M.V. Leont'eva, A. Ya. Fridman, N.M. Dyatlova, V.M. Agre, T.F. Sysoeva, Zh. Neorg. Khim. 32 (1987) 2494.

[6] D.J. Radanović, Coord. Chem. Rev. 54 (1984) 159 (and references therein).
[7] D.J. Radanović, B.E. Douglas, J. Coord. Chem. 4 (1975) 191.
[8] T. Mizuta, T. Yamamoto, N. Shibata, K. Miyoshi, Inorg. Chim. Acta 169 (1990) 257.
[9] R. Herak, Lj. Manojlović-Muir, M.I. Djuran, D.J. Radanović, J. Chem. Soc., Dalton Trans. (1985) 861.
[10] F.T. Helm, W.H. Watson, D.J. Radanović, B.E. Douglas, Inorg. Chem. 16 (1977) 2351.
[11] T. Yamamoto, K. Mikata, K. Miyoshi, H. Yoneda, Inorg. Chim. Acta 150 (1988) 237.
[12] K. Kanamori, J. Kumada, M. Yamamoto, T. Okayasu, K. Okamoto, Bull. Chem. Soc. Jpn. 68 (1995) 3445.
[13] D.J. Radanović, S. Ianelli, G. Pelosi, Z.D. Matović, S. Tasić-Stojanović, B.E. Douglas, Inorg. Chim. Acta 278 (1998) 66.
[14] M. Parvez, C. Maricondi, D.J. Radanović, M.I. Djuran, B.E. Douglas, Inorg. Chim. Acta 182 (1991) 177.
[15] B.E. Douglas, D.J. Radanović, Coord. Chem. Rev. 128 (1993) 139 (and references therein).
[16] F. Pavelčik, V. Kettmann, J. Majer, Collect. Czech. Chem. Commun. 44 (1979) 1070.
[17] I.M. Bezrukavnikova, T.N. Polynova, M.A. Porai-Koshits, I.B. Kovaleva, N.D. Mitrofanova, Koord. Khim. 17 (1991) 770.
[18] I.M. Bezrukavnikova, T.N. Polynova, I.B. Kovaleva, N.D. Mitrofanova, M.A. Porai-Koshits, Koord. Khim. 18 (1992) 150.
[19] S. Kaizaki, M. Byakuno, M. Hayashi, J.I. Legg, K. Umakoshi, S. Ooi, Inorg. Chem. 26 (1987) 2395.
[20] D.J. Radanović, S.R. Trifunović, M.S. Cvijović, C. Maricondi, B.E. Douglas, Inorg. Chim. Acta 196 (1992) 161.
[21] M. Parvez, C. Maricondi, D.J. Radanović, S.R. Trifunović, V.D. Miletić, B.E. Douglas, Inorg. Chim. Acta 248 (1996) 89.
[22] U. Rychlewska, M.I. Djuran, M.M. Vasojević, D.D. Radanović, V.M. Ristanović, D.J. Radanović, Inorg. Chim. Acta 328 (2002) 218.
[23] D.J. Radanović, B.V. Prelesnik, D.D. Radanović, Z.D. Matović, B.E. Douglas, Inorg. Chim. Acta 262 (1997) 203.
[24] D.J. Radanović, T. Ama, H. Kawaguchi, N.S. Drašković, D.M. Ristanović, S. Janićijević, Bull. Chem. Soc. Jpn. 74 (2001) 701 (and references therein).
[25] D.J. Radanović, V.D. Miletić, T. Ama, H. Kawaguchi, Bull. Chem. Soc. Jpn. 71 (1998) 1605.
[26] D.J. Radanović, N. Sakagami, V.M. Ristanović, S. Kaizaki, Inorg. Chim. Acta 292 (1999) 16.
[27] R.H. Nuttall, D.M. Stalker, Talanta 24 (1977) 355.
[28] J.J. Stezowski, R. Countryman, J.L. Hoard, Inorg. Chem. 12 (1973) 1749.
[29] J.P. Fackler, Jr., F.J. Kristine, A.M. Mazany, T.J. Moyer, R.E. Shepherd, Inorg. Chem. 24 (1985) 1857.
[30] A. Altomare, G. Cascarano, C. Giacovazzo, A. Guagliardi, M.C. Burla, G. Polidori, M. Camalli, J. Appl. Crystallogr. 27 (1994) 435.
[31] International Tables for X-ray Crystallography, vol. 4, Kynoch Press, Birmingham, UK, 1974.
[32] G.M. Sheldrick, SHELXL-93, Program for the Refinement of Crystal Structures, University of Göttingen, Germany, 1993.
[33] M. Nardelli, Comput. Chem. 7 (1983) 95.
[34] C.K. Johnson, ORTEP Report ORNL-3794, Oak Ridge National Laboratory, Oak Ridge, TN, 1965.
[35] R.D. Shannon, Acta Crystallogr., Sect. A 32 (1976) 751.
[36] A.B.P. Lever, Coord. Chem. Rev. 3 (1968) 119.
[37] C.K. Jørgensen, Acta Chem. Scand. 9 (1955) 1362; 10 (1956) 887.
[38] N.J. Rose, C.A. Root, D.H. Busch, Inorg. Chem. 6 (1967) 1431.
[39] W.C.E. Higginson, S.C. Nyburg, J.S. Wood, Inorg. Chem. 3 (1964) 463.
[40] O. Bostrup, C.K. Jørgensen, Acta Chem. Scand. 11 (1957) 1223.

Academy of Sciences. IR spectra were recorded on a Nicolet AVATAR-360IR spectrophotometer in KBr pellets. Electronic spectra were recorded on a Shimadzu UV 240 spectrometer in CH_2Cl_2. X-ray photoelectron spectral (XPS) data were measured on a Perkin–Elmer PHI 5000C ESCA System, calibrated by carbon (C1s = 284.6 eV).

2.2. Synthesis of $(NH_4)_2WO_2Se_2$ and $(NH_4)_2WOSe_3$

Activated $WO_3 \cdot H_2O$ was synthesized as described in the literature [5]. The vessels used in the reaction were flushed with dinitrogen beforehand. The reaction mixture was prepared under nitrogen atmosphere by dissolving 5 g of activated $WO_3 \cdot H_2O$ in 25 ml of concentrated NH_3 aqueous solution and then stirred under 0 °C. H_2Se was generated by hydrolysis of Al_2Se_3 in dilute hydrochloric acid and was introduced to the reaction mixture by a stream of N_2. The reaction was monitored via the electronic spectrum of the reaction mixture. H_2Se addition was halted when the characteristic band of $(NH_4)_2WO_2Se_2$ reached a maximum but before the appearance of that of $(NH_4)_2WOSe_3$ [6]. An equal volume of cold absolute ethanol was slowly added to the stirred reaction mixture and the same volume of ether was then added. An orange–red solid was precipitated and separated by a glass frit, washed with a small amount of ethyl ether, and dried in vacuum. Solid (2.1 g) were obtained with about 25% yield. It was confirmed as $(NH_4)_2WO_2Se_2$ by its electronic and IR spectra. It can be used for synthesis purposes without further purification.

When excess H_2Se was introduced into the reaction mixture of 5 g of activated $WO_3 \cdot H_2O$ and 25 ml of concentrated NH_3 aqueous solution, after the maximum absorption band of $(NH_4)_2WOSe_3$ was observed, cold absolute ethanol and ether were added successively as described above. After filtering off the formed $(NH_4)_2WO_2Se_2$, the filtrate was allowed to stand overnight. A red crystalline solid settled down in the filtrate. The solid (2.9 g) was separated by a glass frit and washed with a small amount of ethyl ether, dried in vacuum, yield 31%. It was confirmed by its electronic and IR spectra as $(NH_4)_2WOSe_3$. It also can be used for synthesis purposes without further purification.

Both dried $(NH_4)_2WO_2Se_2$ and $(NH_4)_2WOSe_3$ are stable in the desiccator.

2.3. Synthesis of $[(C_4H_9)_4N]_2[WOSe_3Cu_3Br_{1.67}Cl_{1.33}]$ (**1**)

$(NH_4)_2WO_2Se_2$ (0.266 g, 0.646 mmol), CuCl (0.126 g, 1.29 mmol) and $(C_4H_9)_4NBr$ (0.422 g, 1.31 mmol) were mixed and well grounded under N_2 atmosphere and then sealed in a glass tube filled with N_2. The glass tube was heated to about 95 °C for 10 h. The reaction mixture was extracted with 2×8 ml of methylene chloride. The extracting solvent was combined and 8 ml of isopropanol was added under stirring. The mixed solution was filtered through celite. 0.35 g of violet red crystals were obtained from the solution under ventilation. Yield 42%. *Anal.* Found: C, 30.32; H, 5.70; N, 2.41%. Calc. for $C_{32}H_{72}N_2WOSe_3Cu_3Br_{1.67}Cl_{1.33}$ C, 29.73; H, 5.61; N, 2.17%. UV–Vis λ_{max} (nm) (CH_2Cl_2): 445 (ε dm^3 mol^{-1} 1.75×10^3), 365 (4.80×10^3), 286 (8.45×10^3), 255 (1.39×10^4), 229 (1.77×10^4). IR (KBr pellet), ν_{max} cm^{-1} 910 (W=O), 540 (W–Se), 440 (W–Se). Raman ν_{max} cm^{-1} 910 (W=O), 276 (Cu–Se)vs, 153 $\delta(WSe_2)$vs. Single crystals suitable for X-ray analysis were obtained from the methylene chloride extractant by layering isopropanol on the top and storing in a refrigerator for several weeks.

2.4. Synthesis of $[(C_4H_9)_4N]_3[WSe_4Cu_3Br_2Cl_2]$ (**2**)

The synthesis method is similar to that described for $[(C_4H_9)_4N]_2[WOSe_3Cu_3BrCl_2]$. $(NH_4)_2WOSe_3$ was used as starting material instead of $(NH_4)_2WO_2Se_2$. The crystalline product was a mixture of **1** and **2**, which could be identified from the feature and color of the crystals. Brick red crystals of **2** were separated and a single crystal suitable for X-ray analysis was selected.

Other cluster compounds of the type $[(C_4H_9)_4N]_2[MOS_3Cu_3X_3]$ (M = Mo, W; X = Cl, Br) were similarly synthesized by the above procedure. For example $[(C_4H_9)_4N]_2[MoOS_3Cu_3Cl_3]$ was synthesized with $(NH_4)_2MoO_2S_2$, CuCl and $(C_4H_9)_4NCl$, and

Table 1
Elemental analysis of some clusters

		Calculated (Found)		
	FM	C (%)	H (%)	N (%)
$[(C_4H_9)_4N]_2[MoOS_3Cu_3BrCl_2]$	1034.51	37.2(36.8)	7.0(6.8)	2.7(2.5)
$[(C_4H_9)_4N]_2[MoOS_3Cu_3Br_3]$	1123.42	34.2(33.7)	6.5(6.4)	2.5(2.3)
$[(C_4H_9)_4N]_2[MoOS_3Cu_3Cl_3]$	1262.11	30.4(30.8)	5.7(5.7)	2.2(2.5)
$[(C_4H_9)_4N]_2[WOSe_3Cu_3Br_{1.67}Cl_{1.33}]$	1292.72	29.8(30.3)	5.6(5.7)	2.2(2.4)

Table 2
Electronic spectra data of clusters in methylene chloride

	λ_{max} (nm)/(ε dm^3 mol^{-1} 1.75 × 10^3)					a
$[(C_4H_9)_4N]_2[MoOS_3Cu_3BrCl_2]$	227(22.0)	238(19.2)	280(11.9)	400(7.89)	488(1.74)	532(0.88)
$[(C_4H_9)_4N]_2[MoOS_3Cu_3Cl_3]$	231(15.6)	255(14.8)	286(8.73)	366(5.87)	446(1.94)	532(0.20)
$[(C_4H_9)_4N]_2[MoOS_3Cu_3Br_3]$	231(18.0)	256(16.8)	287(9.83)	367(6.16)	448(2.21)	532(0.21)
$[(C_4H_9)_4N]_2[WOSe_3Cu_3Br_{1.67}Cl_{1.33}]$	229(17.7)	255(13.9)	286(8.45)	365(4.80)	445(1.75)	532(0.88)

a, molar extinction coefficient at the wavelength of the laser source.

Table 3
Infrared data of clusters

	ν(M=O)		ν(M–S or Se)
$[(C_4H_9)_4N]_2[MoOS_3Cu_3BrCl_2]$	920	802	443
$[(C_4H_9)_4N]_2[MoOS_3Cu_3Br_3]$	939	803	447
$[(C_4H_9)_4N]_2[MoOS_3Cu_3Cl_3]$	938	815	446
$[(C_4H_9)_4N]_2[WOSe_3Cu_3Br_{1.67}Cl_{1.33}]$	911	805	444, 419

$[(C_4H_9)_4N]_2[MoOS_3Cu_3Br_3]$ was synthesized with $(NH_4)_2MoO_2S_2$, CuBr and $(C_4H_9)_4NBr$. Characterization data of these products are summarized in Tables 1–3.

Table 4
Crystal data and structure refinement for $[(C_4H_9)_4N]_2[WOSe_3Cu_3Br_{1.67}Cl_{1.33}]$ (**1**)

Empirical formula	$C_{32}H_{72}Br_{1.67}Cl_{1.33}Cu_3N_2OSe_3W$
Formula weight	1292.72
Temperature (K)	293(2)
Crystal system	monoclinic
Space group	$P2_1/c$
Unit cell dimensions	
a (Å)	21.983(3)
b (Å)	11.282(2)
c (Å)	22.211(4)
α (°)	90.00(1)
β (°)	120.00(2)
γ (°)	90.00(2)
Volume (Å^3)	4770.6(14)
Z	4
D_{calc} (Mg m^{-3})	1.759
Absorption coefficient (mm^{-1})	6.985
F(000)	2520
Crystal size (mm)	0.32 × 0.12 × 0.10
θ Range for data collection (°)	1.07–25.29
Index ranges	$0 \le h \le 26$, $0 \le k \le 13$, $-26 \le l \le 23$
Reflections collected/unique	8466/8466 [$R_{int} = 0.0000$]
Completeness to $2\theta = 25.29$ (%)	92.3
Max/min transmission	0.5418 and 0.2134
Refinement method	full-matrix least-squares on F^2
Data/restraints/parameters	8466/0/254
Goodness-of-fit on F^2	1.012
Final R indices [$I > 2\sigma(I)$]	$R_1 = 0.0726$, $wR_2 = 0.1873$
R indices (all data)	$R_1 = 0.3463$, $wR_2 = 0.3143$
Extinction coefficient	0.00031(14)
Largest difference peak and hole (e Å^{-3})	2.649 and −1.571

2.5. Crystal structure analysis

The molecular structure of $[(C_4H_9)_4N]_2[WOSe_3Cu_3Br_{1.67}Cl_{1.33}]$ (**1**) and $[(C_4H_9)_4N]_3[WSe_4Cu_3Br_2Cl_2]$ (**2**) were determined on an Enraf-Nonius CAD4 X-ray diffractometer equipped with a graphite monochromator. Data collection was performed with Mo Kα radiation ($\lambda = 0.71073$ Å).

Table 5
Crystal data and structure refinement for $[(C_4H_9)_4N]_3[WSe_4Cu_3Br_2Cl_2]$ (**2**)

Empirical formula	$C_{48}H_{108}Br_2Cl_2Cu_3N_3Se_4W$
Formula weight	1648.40
Temperature (K)	293(2)
Crystal system	rhombohedral
Space group	$R3c$
Unit cell dimensions	
a (Å)	17.162(2)
b (Å)	17.162(7)
c (Å)	38.788(3)
α (°)	90.00 (3)
β (°)	90.00 (3)
γ (°)	120.00 (3)
Volume (Å^3)	9894(4)
Z	6
Calculated density (Mg m^{-3})	1.660
Absorption coefficient (mm^{-1})	6.223
F(000)	4908
Crystal size (mm)	0.30 × 0.21 × 0.20
θ Range for data collection (°)	2.37–25.03
Index range	$-17 \le h \le 17$, $0 \le k \le 20$, $0 \le l \le 46$
Reflections collected/unique	3845/1981 [$R_{int} = 0.1008$]
Completeness to $2\theta = 25.03$ (%)	33.3
Absorption correction	empirical absorption correction
Max/min transmission	1.0000, 0.6235
Refinement method	full-matrix least-squares on F^2
Data/restraints/parameters	1981/1/191
Goodness-of-fit on F^2	1.066
Final R indices [$I > 2\sigma(I)$]	$R_1 = 0.0707$, $wR_2 = 0.1739$
R indices (all data)	$R_1 = 0.1109$, $wR_2 = 0.1945$
Absolute structure parameter	−0.03(7)
Extinction coefficient	0.00014(6)
Largest difference peak and hole (e Å^{-3})	1.506 and −1.029

The positions of Cl(1) and Cl(2) are statistically occupied by Br(1) and Br(2) atoms with a 50% occupancy factor. C(12), C(17) and C(22) shown two possible positions due to their high thermal vibrational effect.

The structures of the clusters were solved by direct methods and expanded using Fourier techniques. The non-hydrogen atoms were refined anisotropically with full-matrix least-squares. Hydrogen atoms were not included in the refinement. The crystal data and structure refinement parameters are given in Tables 4 and 5.

2.6. Optical limiting measurements

The optical limiting properties of these clusters were measured with 8 ns and 35 ps duration laser pulses at 532 nm in methylene chloride solution. The nanosecond laser pulses were generated from a Q-switched, frequency-doubled Nd-YAG laser and the picosecond laser pulses were generated from a mode-locked and frequency-doubled Nd-YAG laser. In our experiments, the 35 ps pulsed laser was operated at 10 Hz repetition rate, but the 8 ns pulsed laser was maintained at a low repeatability of 2 Hz in order to reduce the influence of thermal effects. The laser beams were focused by a 13 cm focal length lens into the methylene chloride solution of the clusters placed in a 5 mm thick quartz cuvette. The laser power was adjusted by neutral attenuators. The incident and transmitted pulse energies were measured simultaneously by two 5×5 mm^2 Si photoelectric diode detectors. The signals were averaged by a Boxcar and then recorded by a PC computer.

3. Results and discussion

3.1. Synthesis

Traditionally, Cu–Mo(W)–S clusters were synthesized via reactions in solution [7]. However, a versatile method has been devised to synthesize the Cu–Mo–S clusters by heating a solid mixture of $(NH_4)_2MO_2S_2$, CuX and a suitable cation such as $(C_4H_9)_4NX$ (M = Mo, W; X = halogen or pseudohalogen such as CN) under dinitrogen. Due to the strong coordination ability of sulfur atoms, cage or nest-shaped clusters can be synthesized starting from a $MO_2S_2^{2-}$ anion with CuX and $(C_4H_9)_4NX$ (X can be halogen or pseudohalogen) in different molecular ratios. The Cu atom can be replaced by Ag and Mo can be replaced by W or both. In our study, compounds $[(C_4H_9)_4N]_2[MoOS_3Cu_3BrCl_2]$, $[(C_4H_9)_4N]_2[MoOS_3Cu_3Br_3]$ and $[(C_4H_9)_4N]_2[MoOS_3Cu_3Cl_3]$ were all synthesized by this method. Their similar structure can be deduced from their electronic spectra, which was attributed to the common chromophore $MoOS_3^{2-}$. The products maintained similar structure when Mo was replaced by W and S was replaced by Se. But if all the skeleton atoms were replaced by heavier atoms, that is Mo, S, Cu by W, Se, Ag, respectively, the product obtained was not the expected compound $[(C_4H_9)_4N]_2[WOSe_3Ag_3X_3]$. For example, $(NH_4)_2WO_2Se_2$, AgBr and $(C_4H_9)_4NBr$ were mixed and well grounded under N_2 atmosphere and then heated to about 95 °C for 10 h under N_2. The product obtained from the methylene chloride extractant showed a very different electronic spectrum (λ_{max} at 227 and 279 nm). Its IR (KBr pellet) gave peaks at 2962s, 2874s, 974s, 814s, 668s, 578m and 447s cm^{-1}, also indicating a different skeleton with $[(C_4H_9)_4N]_2[WOSe_3Cu_3Br_{1.67}Cl_{1.33}]$ (**1**). The Ag-containing product decomposed slowly in solution but remained stable in the solid state for several days.

In the synthesis process, rearrangement of the terminal M–S bond of $(NH_4)_2MO_2S_2$ must have occurred during heating because the nest shape product contains a MOS_3 molecular fragment. In the case of $(NH_4)_2MO_2Se_2$, the Se atom should be more labile than the S atom on heating. However, it seems that only one of the terminal oxygen atoms can be replaced by the Se atom to form $WOSe_3^{2-}$, which is found as a molecular fragment in cluster compound **1**. It was reported recently that MSe_4^{2-} as a synthesis precursor remained as a building block in its products [8]. In our synthesis, some MSe_4^{2-} might form. One of the labile terminal Se atoms in MSe_4^{2-} was replaced by Br or Cl, forming a W–Br or W–Cl bond as in cluster **2**.

3.2. Description of structures

The cluster structure of molecule $[(C_4H_9)_4N]_2[WOSe_3Cu_3Br_{1.67}Cl_{1.33}]$ (**1**) is shown in Fig. 1. Selected bond lengths and bond angles are collected in Table 6. The skeleton of the cluster anion, $[WOSe_3Cu_3Br_{1.67}Cl_{1.33}]^{2-}$, consisting of one W atom, three μ_3-Se atoms and three Cu atoms, is in a nest shape, similar to that of its analogue compound $[(C_4H_9)_4N]_2[MoOS_3Cu_3BrCl_2]$ [9]. The W atom has an ideal tetrahedral geometry, being

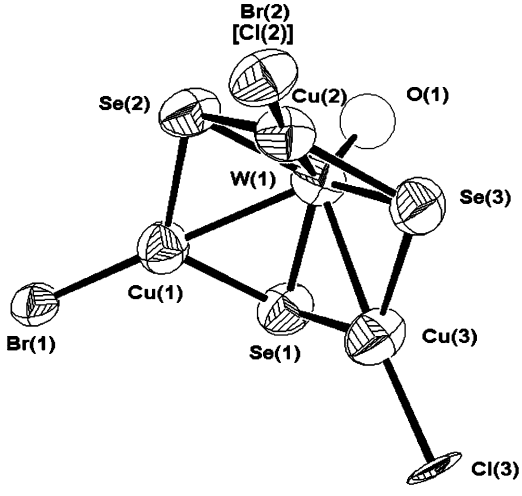


Fig. 1. ORTEP diagram of the cluster anion of $[(C_4H_9)_4N]_2[WOSe_3Cu_3Br_{1.67}Cl_{1.33}]$.

Table 6
Selected bond lengths (Å) and bond angles (°) for $[(C_4H_9)_4N]_2[WOSe_3Cu_3Br_{1.67}Cl_{1.33}]$ (**1**) [a]

Bond lengths			
W(1)–O(1)	1.721(9)	Se(1)–Cu(1)	2.357(2)
W(1)–Se(2)	2.382(2)	Se(2)–Cu(2)	2.347(3)
W(1)–Se(1)	2.394(2)	Se(2)–Cu(1)	2.364(3)
W(1)–Se(3)	2.403(2)	Se(3)–Cu(2)	2.343(3)
W(1)–Cu(2)	2.674(2)	Se(3)–Cu(3)	2.359(3)
W(1)–Cu(3)	2.692(2)	Cu(1)–Cl(1)	2.268(3)
W(1)–Cu(1)	2.693(2)	Cu(2)–Cl(2)	2.244(3)
Se(1)–Cu(3)	2.335(3)	Cu(3)–Cl(3)	2.252(4)
Bond angles			
O(1)–W(1)–Se(2)	110.9(4)	Cu(2)–Se(2)–Cu(1)	106.0(1)
O(1)–W(1)–Se(1)	108.5(4)	Cu(2)–Se(2)–W(1)	68.9(1)
Se(2)–W(1)–Se(1)	109.9(1)	Cu(1)–Se(2)–W(1)	69.1(1)
O(1)–W(1)–Se(3)	108.8(4)	Cu(2)–Se(3)–Cu(3)	107.8(1)
Se(2)–W(1)–Se(3)	109.6(1)	Cu(2)–Se(3)–W(1)	68.6(1)
Se(1)–W(1)–Se(3)	109.1(1)	Cu(3)–Se(3)–W(1)	68.8(1)
O(1)–W(1)–Cu(2)	125.6(4)	Cl(1)–Cu(1)–Se(2)	122.8(1)
Se(2)–W(1)–Cu(2)	55.0(1)	Cl(1)–Cu(1)–Se(1)	125.3(1)
Se(1)–W(1)–Cu(2)	125.9(1)	Se(2)–Cu(1)–Se(1)	111.8(1)
Se(3)–W(1)–Cu(2)	54.7(1)	Cl(1)–Cu(1)–W(1)	178.3(1)
O(1)–W(1)–Cu(3)	124.1(4)	Se(2)–Cu(1)–W(1)	56.1(1)
Se(2)–W(1)–Cu(3)	125.0(1)	Se(1)–Cu(1)–W(1)	55.8(1)
Se(1)–W(1)–Cu(3)	54.3(1)	Cl(2)–Cu(2)–Se(3)	121.4(1)
Se(3)–W(1)–Cu(3)	54.8(1)	Cl(2)–Cu(2)–Se(2)	125.4(1)
Cu(2)–W(1)–Cu(3)	90.1(1)	Se(3)–Cu(2)–Se(2)	113.0(1)
O(1)–W(1)–Cu(1)	128.4(4)	Cl(2)–Cu(2)–W(1)	174.7(1)
Se(2)–W(1)–Cu(1)	55.1(1)	Se(3)–Cu(2)–W(1)	56.8(1)
Se(1)–W(1)–Cu(1)	54.8(1)	Se(2)–Cu(2)–W(1)	56.2(1)
Se(3)–W(1)–Cu(1)	122.8(1)	Cl(3)–Cu(3)–Se(1)	126.9(1)
Cu(2)–W(1)–Cu(1)	89.0(1)	Cl(3)–Cu(3)–Se(3)	120.4(1)
Cu(3)–W(1)–Cu(1)	87.7(1)	Se(1)–Cu(3)–Se(3)	112.7(1)
Cu(3)–Se(1)–Cu(1)	105.2(1)	Cl(3)–Cu(3)–W(1)	176.1(1)
Cu(3)–Se(1)–W(1)	69.4(1)	Se(1)–Cu(3)–W(1)	56.3(1)
Cu(1)–Se(1)–W(1)	69.0(1)	Se(3)–Cu(3)–W(1)	56.4(1)

[a] Numbers in parentheses are e.s.d. in the least significant digits.

surrounded by three bridging Se atoms and one terminal O atom with Se–W–Se angles of 109.5° and O–W–Se angles of 109.4°, respectively. In its Mo–S analogue anion $[MoOS_3Cu_3BrCl_2]^{2-}$, the Mo atom has a distorted tetrahedral geometry in which the corresponding bond angles S–Mo–S and O–Mo–S are 107.5° and 112.0°, respectively. In its W–S analogue anion $[WOS_3Cu_3Cl_3]^{2-}$, the average S–W–S bond angle is 108.1° [9]. The larger Se–W–Se angle in cluster **1** is evidently due to the larger volume and weaker electronegativity of Se atoms comparing to S atoms in the anion skeleton. As a result, cluster **1** has a larger opening in its nest shaped structure of the anion than that of $[MoOS_3Cu_3BrCl_2]^{2-}$ and $[WOS_3Cu_3Cl_3]^{2-}$. The three W–Se bond distances in the cluster **1**, ranging from 2.382(2) to 2.403(2) Å, are in the range of single bonds. The W–O bond length of 1.721(9) Å is typical for a double bond. All three Cu atoms in the cluster **1** adopt trigonal planar coordination geometry. The Cu atoms are linked to W through symmetrical $Cu(Se)_2$ bridges with all Cu–Se distances in a range from 2.335(3) to 2.364(3) Å. All three W–Cu–X (X = Cl, Br) bond angles range from 174.7° to 178.3°; this allows formation of stronger π-bonding over the $W(Se)_2Cu$ ring. In its Mo–S analogue, the Mo–Cu–Cl bond angles are 167.3° and 166.9° and only the Mo–Cu–Br bond angle is close to linearity. In **1**, the terminal ligand site of Cu–X was statistically occupied by a Br atom with five-ninths occupancy factor and by a Cl atom with four-ninths occupancy factor.

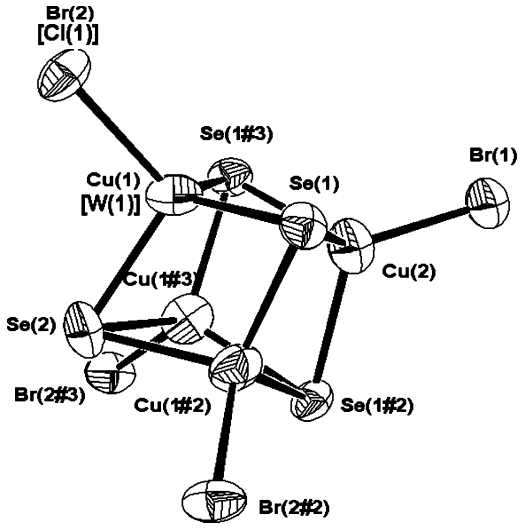


Fig. 2. An ORTEP diagram of the cluster anion of $[(C_4H_9)_4N]_3[WSe_4Cu_3Br_2Cl_2]$. The W(1) atom statistically occupies the position of the Cu(1) atom and has one third of the occupancy factor. The Cl(1) atom statistically occupies the position of the Br(2) atom and has two third of the occupancy factor.

Table 7
Selected bond lengths (Å) and bond angles (°) for $[(C_4H_9)_4N]_3[WSe_4Cu_3Br_2Cl_2]$ (**2**) [a]

Bond lengths			
Se(1)–W(1)	2.402(3)	W(1)–Se(1)#2	2.438(3)
Se(1)–Cu(1)#1	2.438(3)	W(1)–Cl(1)	2.501(4)
Se(1)–Cu(2)	2.531(4)	Cu(2)–Br(1)	2.344(7)
Se(2)–W(1)	2.464(4)	Cu(2)–Se(1)#1	2.531(4)
Bond angles			
W(1)–Se(1)–Cu(1)#1	71.0(1)	Se(1)–W(1)–Se(2)	107.1(1)
W(1)–Se(1)–Cu(2)	75.1(1)	Se(1)#2–W(1)–Se(2)	106.0(1)
Cu(1)#1–Se(1)–Cu(2)	74.5(1)	Se(1)–W(1)–Cl(1)	116.9(1)
W(1)–Se(2)–Cu(1)#2	69.5(1)	Se(1)#2–W(1)–Cl(1)	115.8(1)
W(1)–Se(2)–W(1)#1	69.5(1)	Se(2)–W(1)–Cl(1)	103.5(2)
Cu(1)#2–Se(2)–Cu(1)#1	69.5(1)	Br(1)–Cu(2)–Se(1)	117.7(1)
Se(1)–W(1)–Se(1)#2	106.6(1)	Se(1)#1–Cu(2)–Se(1)	100.1(2)

[a] Numbers in parentheses are e.s.d. in the least significant digits. Symmetry transformations used to generate equivalent atoms; #1 $-y+1, x-y-1, z$; #2 $-x+y+2, -x+1, z$.

The cluster structure of compound $[(C_4H_9)_4N]_3[WSe_4Cu_3Br_2Cl_2]$ (**2**) is shown in Fig. 2. Selected bond lengths and bond angles are collected in Table 7. The anion of cluster **2** has a distorted cubane structure with trigonal symmetry. Four Se atoms and four Cu (or W) atoms

alternatively compose the vertexes of the closed cage. Atoms Br(1), Cu(2) and Se(2) are aligned on a threefold axis. Different from cluster **1**, all the Cu atoms in cluster **2** are in tetrahedral geometry. The coordination environment of Cu(2) atom contains three Se atoms and one Br atom. The three metal positions off the threefold axis are statistically occupied by Cu atom with two-thirds occupancy factor and W atom with one-third occupancy factor. The terminal M–X bonds are statistically occupied by Br atom with one-third occupancy factor and by Cl atom with two-thirds occupancy factor. The cage has an obtuse vertex at Cu(2) with a Se(1)–Cu(2)–Se(1, #2) angle of 100.09° and an acute vertex at Se(2) with a Cu(1)-Se(2)-Cu(1, #2) angle of 69.52°. In its analogue compound $[MAg_3Se_3I(PPh_3)_3Se]$ (M = W, Mo) and $[MoCu_3Se_3Cl(PPh_3)_3Se]$ [8], all have distorted cage shaped cubane structures. The former analogue cubane structure has an obtuse vertex angle of about 107.3° and an acute vertex at the I atom of about 68.7°, and the later has an obtuse vertex angle of about 108.6° and an acute vertex at the Cl atom of about 74.6°. The statistical arrangement of Cu–W and Cl–Br in cluster **2** is supported by the X-ray photoelectron spectrum data and the composition also agrees with the X-ray photoelectron spectrum measurement (Table 8).

3.3. Electronic spectrum

Fig. 3 gives the linear absorption spectrum of cluster **1**, showing characteristic absorption bands similar to that of $[(C_4H_9)_4N]_2[MoOS_3Cu_3BrCl_2]$. There is no absorbency above 550 nm until near the IR region. Its absorption maxima at 445, 365 and 290 nm, showing clearly blue shift in the visible region compared with the values of 488, 400 and 280 nm found in the spectrum of $[(C_4H_9)_4N]_2[MoOS_3Cu_3BrCl_2]$ under the same conditions, are comparable to the values found in the spectrum of $WOSe_3^{2-}$, which are 452, 385 and 293 nm, respectively [10].

The dominant features of the electronic spectra of $[(C_4H_9)_4N]_2[MoOS_3Cu_3Br_3]$ and $[(C_4H_9)_4N]_2[MoOS_3Cu_3Cl_3]$ is that they are more like $[(C_4H_9)_4N]_2[WOSe_3Cu_3BrCl_2]$ than their analogue $[(C_4H_9)_4N]_2[MoOS_3Cu_3BrCl_2]$. From the data listed in Table 2, it is noticed that all compounds have relatively low linear absorptivity at 532 nm [11].

Table 8
Binding energies (eV) of elements in the anion of cluster **2**

$[WSe_4Cu_3Br_2Cl_2]^{3-}$	W	Se	Cu	Cl	Br
	$4f_{7/2}$	$3d_{5/2}$	$2p_{3/2}$	2p	3d
	35.9	53.8	932.7	199.0	68.6
Relative ratio	0.47	1.3	1	0.86	0.75

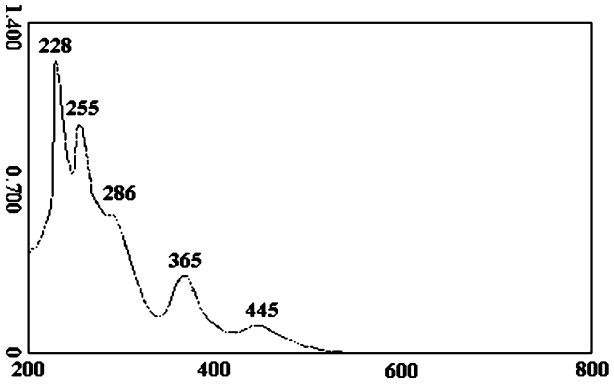


Fig. 3. The electronic spectrum of $[(C_4H_9)_4N]_2[WOSe_3Cu_3Br_{1.67}Cl_{1.33}]$ in CH_2Cl_2 with a concentration of 5.90×10^{-5} M. The optical path is 1 cm.

3.4. Optical limiting properties

A common problem with many inorganic semiconductors is their large linear absorption (α_o) and hence small optical limiting figure of merit $\chi^{(3)}/\alpha_o$ in the visible region (especially the blue–green region) of the spectrum. There has been considerable interest in clusters that exhibit strong reverse saturable absorption (RSA) in the visible spectral region. The skeletal atoms of these clusters are believed to be critical to their nonlinear optical properties [12].

Experimental results obtained in acetonitrile solution with a 7 ns pulsed laser at 532 nm show that cage shaped clusters $[MS_4M'_3BrX_3]^{3-}$ (M = Mo W; M′ = Cu, Ag; X = Cl, Br, I) exhibit strong NLO absorption and weak light self-focusing effects [13], whereas nest-shaped clusters $[MoOS_3(CuNCS)_3]^{4-}$ $[MoOS_3(CuCl)_2(CuBr)]^{4-}$ and $[Mo_2O_2S_2(CuI)_4(CuBr)_2]^{4-}$ exhibit both strong NLO absorption and strong self-defocusing effects [14].

The nanosecond and picosecond optical limiting effects of the nest-shaped cluster **1** and $[(C_4H_9)_4N]_2[MoOS_3Cu_3BrCl_2]$ are depicted in Fig. 4. At very low light fluence they respond linearly to the incident light in accordance with Beer's law. The output energy deviates from the linear response when the incident laser pulse energy exceeds 30 μJ. The materials become increasingly less transparent as the light fluence rises. It is interesting to note that under the same transmitting conditions, cluster **1** shows a poorer optical limiting property than $[(C_4H_9)_4N]_2[MoOS_3Cu_3BrCl_2]$ under 35 ps laser pulses. However, under 8 ns laser pulses, cluster **1** shows a better optical limiting property than $[(C_4H_9)_4N]_2[MoOS_3Cu_3BrCl_2]$. The heavy atoms effect cannot adequately explain the different optical limiting properties of $[(C_4H_9)_4N]_2[MoOS_3Cu_3BrCl_2]$ and $[(C_4H_9)_4N]_2[WOSe_3Cu_3BrCl_2]$ under different durations of the laser pulses. It was noticed that two structural differences of the clusters might be related to their different response to the duration of the laser pulses.

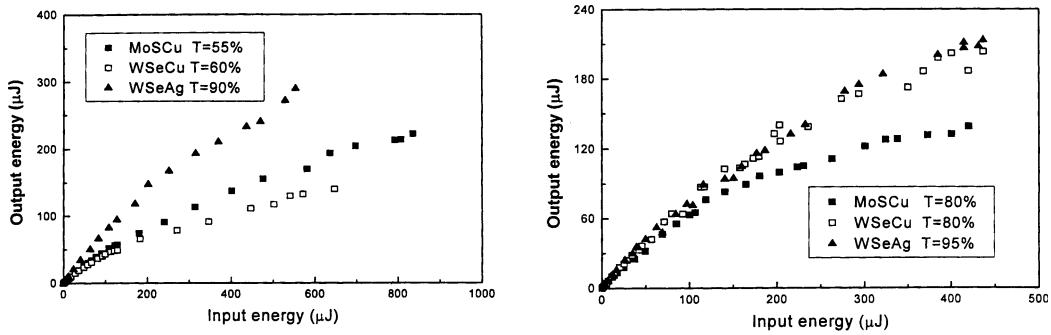


Fig. 4. Optical limiting properties of different nest-shaped clusters in nanoseconds (a) and picosecond (b). MoSCu, $[(C_4H_9)_4N]_2[MoOS_3Cu_3BrCl_2]$; WSeCu, cluster **1** and WSeAg, silver containing compound.

One of the structural differences is the heavier atoms of W (molecular weight 184) and Se (79) compared with Mo (96) and S (32) in the skeleton of the two clusters. It is believed that heavier atoms in the skeleton of the clusters may introduce large numbers of excited states positioned close to the ground state, which, therefore, will help to enhance the singlet–triplet intersystem crossing under excitation. The contribution of the excited triplet states to optical limiting properties towards a nanosecond pulsed laser may then be enhanced. The other structural difference is the larger opening of the nest-shaped structure of cluster **1** compared with $[(C_4H_9)_4N]_2[MoOS_3Cu_3BrCl_2]$. We are not sure whether the shape of the skeleton may play any important role in optical limiting behavior. Although the Ag-containing product shows some optical limiting property, its solubility in methylene chloride solution is too low and it decomposed in solution slowly.

In W–Se–Cu and Mo–S–Cu clusters, the influence of the peripheral ligands on the optical limiting properties is trivial. However, we found that a larger peripheral ligand (Br) showed better optical limiting properties compared with the smaller ligand (Cl) in W–Se–Ag complexes.

4. Supplementary data

Crystallographic data have been deposited with the CCDC, 12 Union Road, Cambridge, CB2 1EZ, UK (fax: +44-1223-336033; e-mail: deposit@ccdc.cam.ac.uk or www: http://www.ccdc.cam.ac.uk) and are available on request quoting the deposition number 162956 for $[(C_4H_9)_4N]_2[WOSe_3Cu_3Br_{1.67}Cl_{1.33}]$ (**1**) and 162683 for $[(C_4H_9)_4N]_3[WSe_4Cu_3Br_2Cl_2]$ (**2**).

Acknowledgements

This work was supported by the National Natural Science Foundation of China.

References

[1] M.C.R. Devray, Hebd. Seances Acad. Sci. 96 (1883) 1616.
[2] (a) R.H. Holm, Chem. Soc. Rev. 10 (1981) 455;
(b) C.F. Millis, Philos. Trans. R. Soc. London, Ser. B 288 (1979) 51;
(c) E.D. Simhon, N.C. Baenziger, M. Kanatzidis, M. Draganjic, D. Coucouvanis, J. Am. Chem. Soc. 103 (1981) 1218.
[3] (a) S. Shi, W. Ji, S.H. Tang, J.L. Lang, X.Q. Xin, J. Am. Chem. Soc. 116 (1994) 3615;
(b) S. Shi, W. Ji, J.P. Lang, X.Q. Xin, J. Phys. Chem. 98 (1994) 3570;
(c) S. Banerjee, G.R. Kumar, P. Mathur, P. Sekar, Chem. Commun. (1997) 299.;
(d) G. Sakane, T. Shibahare, H.W. Hou, X.Q. Xin, S. Shi, Inorg. Chem. 34 (1995) 4785.
[4] W.L. Jolly, The Synthesis and Characterization of Inorganic Compounds, Waveland Press, Prospect Heights, IL, 1991, pp. 116–121.
[5] A.R. Jiang, Z. Pang, T.D. Gu, Chem. J. Chin. Univ. 5 (1987) 403.
[6] A. Müller, A.C. Ranade, W. Rittner, Z. Anorg. Allg. Chem. Bd. 380 (1971) 76.
[7] (a) M. Minelli, J.H. Enemark, J.R. Nicholson, C.D. Garner, Inorg. Chem. 23 (1984) 4385;
(b) J.M. Mandi, C. Potvin, F. Secheresse, S. Marzak, Inorg. Chim. Acta 150 (1988) 257.
[8] (a) Q.F. Zhang, W.H. Leung, X.Q. Xin, H.K. Fun, Inorg. Chem. 39 (2000) 417;
(b) Q. Zhang, M. Hong, W. Su, R. Cao, H. Liu, Polyhedron 16 (1997) 1433;
(c) S. Du, X. Wu, J. Lu, Polyhedron 13 (1994) 841.
[9] H. Hou, X. Ye, X. Xin, J. Liu, M. Chen, S. Shi, Chem. Mater. 7 (1995) 472.
[10] A. Müller, A.C. Ranade, W. Rittner, Z. Anorg. Allg. Chemie. Bd. (1971) 380.
[11] Molecular extinction coefficient at 532 nm is 1.33×10^2 dm^3 mol^{-1} per cm for $[(C_4H_9)_4N]_2[MoOS_3Cu_3BrCl_2]$.
[12] S. Shi, W. Ji, L.P. Lang, X.Q. Xin, J. Phys. Chem. 98 (1994) 3570.
[13] Z.R. Chen, H.W. Hou, X.Q. Xin, K.B. Yu, S. Shi, J. Phys. Chem. 99 (1995) 8717.
[14] (a) M. Sheik-Bahae, A.A. Said, E.W. Van Struyland, Opt. Lett. 14 (1989) 955;
(b) M. Sheik-Bahae, A.A. Said, T.H. Wei, D.J. Hagan, E.W. Van Struyland, IEEE J. Quantum Electron. 26 (1990) 760.

interesting series of ligands whose properties can be greatly modified by introducing organic substitutents thereby inducing different stereochemistries in the resultant metal complexes. Some of the metal complexes may be expected to be biologically active. Indeed, carcinostatic activities have already been found for some metal complexes of dithiocarbazic acid and some Schiff bases derived from its *S*-methyl ester [20]. The synthesis of these complexes continues to be of interest in order to evaluate their coordination chemistry and their potential as anti-microbial and anti-cancer agents.

2. Experimental

2.1. Physical measurements

Carbon, hydrogen, nitrogen and sulfur analyses were carried out at Mikroanalytisches Labor Pascher, Remagen-Bandorf, Germany or at the Department of Chemistry, University Putra Malaysia. The IR spectra were recorded as KBr pellets, in the 4000–400 cm^{-1} region, on a Perkin–Elmer 1750X FTIR spectrometer. Metal determinations were carried out using a Perkin–Elmer Plasma 1000 Emission Spectrometer. ^1H NMR spectra were recorded on an Hitachi R1200 (60 MHz) NMR spectrometer. The molar conductance of 10^{-3} M solutions of the metal complexes in DMSO was measured at 30 °C using a Jenway 4310 conductivity meter and a dip-type cell with platinized electrode. The UV–Vis spectra were run on a Shimadzu UV-2501 PC spectrophotometer (900–200 nm). Melting points (m.p.) were determined using an electrothermal digital m.p. apparatus. Magnetic susceptibility measurements were carried out using a Sherwood Auto MSB at 298 K. All susceptibilities were corrected for the diamagnetic contribution using Pascal's constant. All measurements were carried out at the Department of Chemistry, University Putra Malaysia unless otherwise mentioned.

2.2. Preparation of S-methyldithiocarbazate (SMDTC)

SMDTC was prepared as previously reported [21].

Potassium hydroxide (22.8 g, 0.4 mol) was dissolved completely in 90% ethanol (114 ml) and the mixture was cooled in ice. To the mixture, hydrazine hydrate (20 g, 0.4 mol) was added slowly with stirring. Carbon disulfide (30.4 g, 0.4 mol) was then added dropwise with vigorous stirring. The temperature of the reaction mixture was not allowed to rise above 6 °C during the period of addition of carbon disulfide. The resulting yellow oil was separated by means of a separatory funnel and dissolved in 40% ethanol (40 ml) and the solution was cooled in ice. Methyl iodide (58 g, 0.4 mol) was added slowly with vigorous stirring. The white product was separated by filtration, washed with water and dried in air. The crude product was recrystallized from ethanol; yield, 20 g (40%); the m.p. was 81 °C (Lit. 81–82 °C) [21].

2.3. General method for preparation of the Schiff bases

SMDTC (2.44 g, 0.02 mol) dissolved in hot absolute ethanol (30–40 ml) was added to the solution of an equimolar amount of carbonyl compound in hot absolute ethanol (20 ml). The mixture was heated for 10 min and then cooled to 0 °C in an ice-bath. The products were filtered, washed with absolute ethanol, recrystallized from absolute ethanol, and then dried over silica gel. The carbonyl compounds used were 2-furylmethylketone and 5-methyl-2-furaldehyde. The yield and m.p. were recorded for each product.

2.4. General method for preparation of the metal complexes

To 0.1 mol of metal salt dissolved in absolute ethanol (40 ml) was added Schiff base (0.2 mol) in 40 ml of absolute ethanol. The mixture was heated while being stirred. The precipitate was filtered, washed with ice-cold ethanol and dried over silica gel. The yield and m.p. were recorded for each product. The metal salts used for synthesis were copper(II) acetate, nickel(II) acetate tetrahydrate and zinc(II) acetate dihydrate.

2.5. X-ray structure determination

The selected crystal of the Zn(II) complex was mounted on a SMART CCD diffractometer. Reflection data were measured at 20 °C using graphite monochromated Mo Kα ($\lambda = 0.71073$ Å) radiation with a detector distance of 4 cm and a swing angle of $-35°$. The data collected were reduced using the program SAINT [22] and an empirical absorption correction was carried out using SADABS [23]. The structure was solved using direct methods and refined using the full-matrix least-square method on F_{obs}^2 using the SHELTXL [24] software package. All non-H atoms were anisotropically refined. The hydrogen atoms were located by difference syntheses and refined isotropically. The molecular graphics were created using SHELXTL. Atomic scattering factors and anomalous dispersion correction were taken from the International Table for X-Ray Crystallography [25].

2.6. Bioactivity

Antimicrobial and cytotoxic activities were evaluated at the Animal Cell and Tissue Culture Laboratory, Department of Biotechnology, University Putra Malaysia.

2.6.1. Qualitative antimicrobial assay

Eight pathogenic microbials were used to test the biological potential of the compounds: (i) Methicillin resistant *Staphylococcus* (MRSA), (ii) *Bacillus subtilis* wild type (B29), (iii) *Bacillus subtilis* mutant defective DNA repair (B28), (iv) *Pseudomonas aeruginosa* (60690), (v) *Candida albicans*, (vi) *Aspergillus ochraceous* (398), (vii) *Saccharomyces cereviceae* (20341) and (viii) *Candida lypolytica* (2075). The sources of microbes and culture maintenance were as previously described [26]. The antimicrobial activity of the extracts was qualitatively determined by a modified disc diffusion method [27]. A lawn of microorganisms was prepared by pipetting and evenly spreading inoculum (10^{-4} cm^3, adjusted turbidometrically to 10^5–10^6 cfu cm^3 (cfu, colony forming units) on to agar set in petri dishes, using nutrient agar (NA) for the bacteria and potato dextrose agar (PDA) for fungi. Whatman No. 1 filter paper discs of 6 mm diameter were impregnated with stock solution of the compound (100 mg cm^{-3}) and dried under sterile conditions. The dried discs were then placed on the previously inoculated agar surface. The plates were inverted and incubated for 24 h at 30 °C for bacteria and 37 °C for fungi. Antimicrobial activity was indicated by the presence of clear inhibition zones around the discs. Commercially available streptomycin was used for antibacterial control while nystatin was used as antifungal control.

2.6.2. Quantitative antimicrobial assay

Substances showing positive antimicrobial activity via the disc diffusion assay were subjected to the broth dilution method for the quantitative measurement of microbiostatic (inhibitory) activity as described by Hufford and Clark [28]. The lowest concentration that completely inhibited visible microbial growth was recorded as the minimum inhibitory concentration (MIC, μg cm^{-3}). Streptomycin and nystatin (Sigma, USA) were used as positive controls for bacteria and fungi, respectively.

2.6.3. Cytotoxic assay

Three types of cell lines were used, CEM-SS (human cell T-lymphoblastic leukemia), HT-29 (human colon andenocarcinoma cells) and HELA (cervical cancer cells). The CEM-SS and HELA cell lines were obtained from the National Cancer Institute, USA while the HT-29 cell line was obtained from American Type Culture Collection (ATCC). The cells were cultured in RPMI-1640 (Sigma) medium supplemented with 10% fetal calf serum. Cytotoxicity was determined using the MTT (3-[4,5-dimethylthiozol-2-yl]-2,5-diphenyltetrazolium bromide) assay following Mosmann's report [26]. Solutions of compounds of different concentrations were prepared from the stock solutions (10 mg cm^{-3}) by serial dilution in RPMI-1640. About 10^{-4} cm^3 was placed in each well of a microtiter plate as described before by Ali et al. [11]. Each well was filled with 10^{-4} cm^3 of cell suspension in complete growth medium (CGM) at $(1–2) \times 10^5$ cells cm^{-3}. Controls that contained only cells were included for each sample.

The assay for each concentration of extract was performed in triplicate. The culture plates were kept at 37 °C under 5% (v/v) CO_2 for 3 days. After 72 h of incubation, 10^{-4} cm^3 of the medium was removed from each well. Subsequently, 20×10^{-3} cm^3 of 50% w/v MTT dissolved in phosphate buffered saline solution was added to each well and incubated for a further 4 h. All supernatants were then carefully discarded from each well of the microtiter plate and 10^{-4} cm^3 of pure spectral grade DMSO was added to each well and vigorously mixed to dissolve the formazan crystals. Absorbance values were measured with a microplate reader (Bio Tek EL 340, USA) at 550 nm. Cytotoxicity was expressed as CD_{50}, i.e. the concentration, which reduced the absorbance of treated cells by 50% with reference to the control (untreated cells). Doxorubicin and tamoxifen were used as cytotoxic standards.

3. Results and discussion

In a neutral medium, condensation of SMDTC with 2-furyl-methylketone and 5-methyl-2-furaldehyde gave the isomeric Schiff bases **1** and **2**, in high yield. The Schiff bases exist in tautomeric forms through the loss of thiolo protons as shown in Fig. 1. Both Schiff bases behaved as uninegatively charged bidentate ligands by coordinating through the thiolo sulfur and the azo-

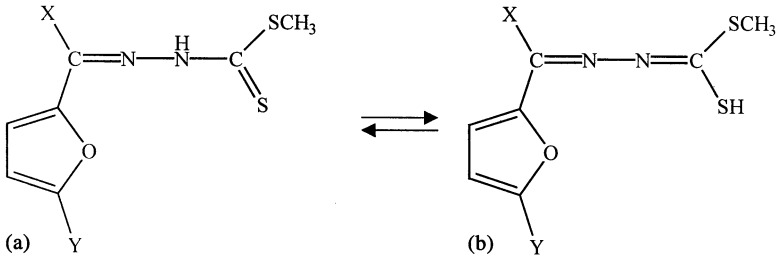


Fig. 1. Tautomeric forms. (a) Thione form. (b) Thiolo form. NS′: X = CH_3, Y = H; NS″: X = H, Y = CH_3.

Table 1
Analytical data for the Schiff bases and their complexes

Compound	Color	M.p. (°C)	Found (calculated, %)					Yields (%)
			C	H	N	S	M	
1 NS′	orange	123.7	44.71 (44.86)	4.86 (4.67)	13.55 (13.08)	29.75 (29.91)		80.6
2 NS″	light yellow	130.4	44.80 (44.86)	4.89 (4.67)	13.60 (13.08)	29.46 (29.91)		85.3
3 $Cu(NS')_2$	dark green	176.5	39.51 (39.21)	3.60 (3.70)	11.39 (11.43)	26.41 (26.16)	12.58 (12.97)	60.7
4 $Cu(NS'')_2$	light brown	240.0	39.13 (39.21)	3.66 (3.70)	12.10 (11.43)	25.86 (26.16)	12.62 (12.97)	72.9
5 $Ni(NS')_2$	dark brown	225.9	39.02 (39.60)	3.46 (3.74)	11.01 (11.55)	25.76 (26.43)	11.78 (12.10)	69.6
6 $Ni(NS'')_2$	brown	245.0	39.36 (39.60)	3.76 (3.74)	11.60 (11.55)	25.93 (26.43)	12.36 (12.10)	76.8
7 $Zn(NS')_2$	yellow	162.4	39.11 (39.06)	3.64 (3.69)	11.12 (11.39)	26.03 (26.07)	12.96 (13.29)	68.8
8 $Zn(NS'')_2$	yellow	158.8	39.32 (39.06)	3.77 (3.69)	11.07 (11.39)	26.20 (26.07)	13.13 (13.29)	73.5

Table 2
^{1}H NMR data for the Schiff bases

Compound	^{1}H NMR				
	CH	CH_3	SCH_3	NH	Aromatic
1		2.312 2.508	3.331	8.512	6.652–7.084
2	3.512	2.361 2.522	3.333	8.835	6.290–6.960

Table 3
Infrared data for Schiff bases and their complexes

Compound	Frequency (cm^{-1})			
	ν(N–H)	ν(C=N)	ν(C=S)	ν(C–S)
1	3210	1572	1064	
2	3114	1618	1094	
3		1553		1011
4		1578		1003
5		1555		1008
6		1572		1016
7		1588		1008
8		1568		1026

methine nitrogen. The melting point, elemental analyses and percentage yield for each are given in Table 1.

The ^{1}H NMR data for the Schiff bases are given in Table 2. The assignments shown are based on those for closely similar Schiff bases [29]. The ^{1}H NMR spectra of the Schiff bases do not show any peak at approximately δ 4.0 ppm attributable to the S–H proton [30], indicating that they exist in the thioketo tautomeric form in solution. The **1** and **2** Schiff bases containing a methyl group on the aliphatic carbon atom and furanic ring, respectively, showed a peak at approximately δ 2.3–2.5 ppm attributed to the methyl hydrogen while the peak at approximately (3.33 ppm may be assigned to the methyl groups attached to a sulfur atom. Meanwhile, **1** Schiff base does not has methine (C–H) group on the aliphatic carbon atom while the signal at 8.542 ppm is attributed to the N–H group. However, the signals at 3.512 and 8.835 ppm are attributed to the methine (C–H) and N–H group, respectively. The aromatic groups are observed in the range approximately δ 6.2–7.1 ppm.

The IR spectra (Table 3) of the **1** and **2** Schiff bases showed strong bands at 3210 and 3114 cm^{-1}, respectively. These are attributed to the secondary amine ν(N–H) mode of the free ligands. The thione groups are relatively unstable in the monomeric form and tend to turn to the more stable thiolo forms by enethiolization in solution [3] (Fig. 1). The absence of ν(S–H) absorbance at approximately 2570 cm^{-1}, indicates that in the solid state, the bases exist primarily in the thione form. The disappearance of ν(N–H) bands the IR spectra of the metal complexes suggests deprotonation and consequent coordination through the thiolate anions. The **1** and **2** Schiff bases also showed strong bands at 1572 and 1618 cm^{-1}, respectively. These are assigned to the ν(C=N) modes for the free ligands. In the metal complexes, this stretching band shifted to lower frequencies, due to the lowering of the C=N bond order as a result of the metal–nitrogen bond formation. The **1** and **2** Schiff bases also showed ν(C=S) modes at 1064 and 1098 cm^{-1}, respectively. The ν(C=S) mode observed in the free ligand disappeared in the complexes, thus supporting the above contention of thiolate bonding with metal ions. Consequently the ν(C–S) mode is observed in the spectra of the complexes confirming that complexation occurred.

The molar conductance data (Table 4) indicated that all complexes were non-electrolytes, suggesting that the two molecules of Schiff bases were covalently bonded with the metal ions. The magnetic susceptibility measurements (Table 4) show that the **3** and **4** complexes were paramagnetic at room temperature. The magnetic moments of 1.75 and 1.79 B.M. for **3** and **4** are consistent with a square-planar structure [31]. The remaining complexes **5**, **6**, **7** and **8** were diamagnetic.

Table 4
The physical properties of the metal complexes

Compound	UV–Vis spectra (λ_{max} (nm)) [a]	Molar conductance (Ω^{-1} cm^2 mol^{-1})	μ_{eff} (B.M.)
3	308 (4.3), 370 (3.2)	2.35	1.75
4	298 (3.3), 374 (2.3)	3.69	1.79
5	312 (4.2), 355 (3.4), 412 (2.5)	1.60	diamagnetic
6	320 (3.3), 357 (2.3), 421 (1.2)	4.32	diamagnetic
7	312 (2.3), 359 (1.4)	2.78	diamagnetic
8	369(3.4)	3.56	diamagnetic

[a] log ε (cm^{-1} mol^{-1} l) are given in parentheses.

For the electronic spectra, the diamagnetic nature of complexes **5** and **6** (Table 4) indicate a singlet ground state term characteristic of square-planar Ni(II). Three bands corresponding to the transitions $^1A_{1g} \rightarrow {}^1A_{2g}$ (312–320 nm), $^1A_{1g} \rightarrow {}^1B_{1g}$ (355–357 nm), and $^1A_{1g} \rightarrow {}^1E_g$ (412–421 nm) are observed in the electronic spectra of such square-planar nickel(II) complexes as expected [27]. The **3** and **4** complexes display two bands corresponding to $^2B_{1g} \rightarrow {}^2A_{1g}$ (298–308 nm) and $^2B_{1g} \rightarrow {}^2E_{1g}$ (370–374 nm) transitions, presumably arising from a square-planar copper(II) configuration. The **7** and **8** complexes gave only bands in the electronic spectra region, which are attributed to charge transfer.

3.1. Description of the structure

The crystal system of bis[*S*-methyl-β-*N*-(2-furylmethyl)methylenedithiocarbazato]zinc(II) is monoclinic with space group of *C*2/*c*, $a = 13.2778(2)$ Å, $b = 12.0398(2)$ Å, $c = 27.1919(3)$ Å, $\alpha = 90°$, $\beta = 99.1186(11)°$ and $\gamma = 90°$. The crystal data and structure refinement parameters are shown in Table 5. The ORTEP diagram of the molecule with the atomic numbering scheme is shown in Fig. 2 and the selected bond lengths and bond angles are listed in Table 6. The two bidentate ligands are coordinated to the zinc atom through an azomethine nitrogen and thiolo sulfur in a distorted tetrahedral environment around zinc atom with S–Zn–N angles between 85.98(13)° and 126.16(16)°. The coordinated sulfur and nitrogen atoms in the two ligands are in opposite positions The C1–N2, N1–C5, C11–N3 and N4–C3 bond distances of 1.274(7), 1.300(5), 1.299(6) and 1.307(7) Å, respectively, indicate a strong electron delocalization in the conjugation of the C–N–N–C moiety compared with the tridentate complex of zinc with *S*-benzyl-β-*N*-(2-pyridyl)methylenedithiocarbazate, $[Zn(C_{14}H_{22}N_3S_2)_2]$ [32]. The coordinated Zn–S and Zn–N bond lengths of 2.30(16) and 2.0(4) Å are also shorter than similar bonds in the tridentate complex (2.34(1) and 2.45(1) Å, respectively). The Zn1S1C1N2N1 and Zn1S3C3N4N3 planes are essentially planar but bisect each other by 86.96(16)°. The furyl O1C6C7C8C9 and O2C12C13C14C15 planes are also planar with the angle between the planes of 61.1(4)°. The dihedral angle between the furyl ring O1C6C7C8C9 and the five-membered ring Zn1S1C1N2N1 of 11.79(19)° is smaller than the dihedral angle between O2C12C13C14C15 and Zn1S3C3N4N3 of 30.4(3)°.

Table 5
Crystal data, data collection and structure refinement parameters for the $[Zn(NS')_2]$ complex

Compound	$[Zn(C_8H_9N_2O_lS_2)_2]$
Empirical formula	$C_{16}H_{18}N_4O_2S_4Zn$
Formula weight	491.95
Temperature (K)	293 (2)
Wavelength (Å)	0.71073
Crystal system	monoclinic
Space group	*C*2/*c*
Unit cell dimensions	
a (Å)	13.2778 (2)
b (Å)	12.0398 (2)
c (Å)	27.1919 (3)
α (°)	90
β (°)	99.1186 (11)
γ (°)	90
Volume (Å^3)	4292.02 (11)
Z	8
Calculated density (Mg m^{-3})	1.523
Absorption coefficient (mm^{-1})	1.552
F(000)	2016
Crystal size (mm)	0.50 × 0.30 × 0.24
θ Range (°)	2.61–25.00
Limiting indices	$-15 \le h \le 12$, $-14 \le k \le 13$, $-32 \le l \le 31$
Reflections collected/unique	10 108/3767 [$R_{int} = 0.1021$]
Completeness to $\theta = 25.00$	99.3%
Absorption correction	empirical
Max/min transmission	0.7070/0.5108
Refinement method	full-matrix least-squares on F^2
Data/restraints/parameters	3767/0/245
Goodness-of-fit on F^2	0.940
Final *R* indices [$I > 2\sigma(I)$]	$R_1 = 0.0601$, $wR_2 = 0.1441$
R indices (all data)	$R_1 = 0.0878$, $wR_2 = 0.1550$
Extinction coefficient	0.00067 (19)
Largest difference peak and hole (e Å^{-3})	0.724 and −0.865

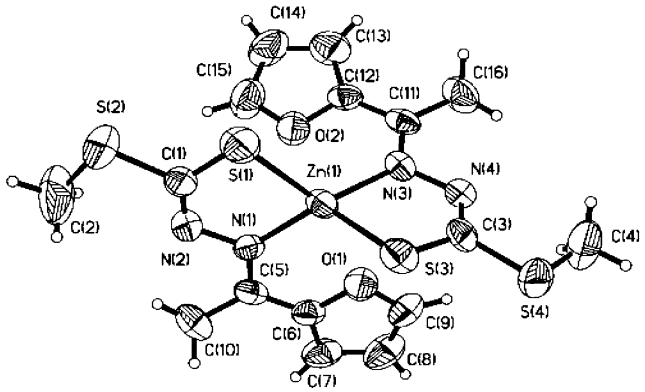


Fig. 2. Crystal structure of $Zn(NS')_2$ with atomic numbering scheme.

Table 6
Selected bond lengths (Å) and bond angles (°) for the $[Zn(NS')_2]$ complex

Bond lengths			
Zn(1)–N(1)	2.050(4)	Zn(1)–N(3)	2.061(4)
Zn(1)–S(1)	2.3027(16)	Zn(1)–S(3)	2.3037(15)
N(1)–N(2)	1.402(6)	N(3)–N(4)	1.411(6)
N(1)–C(5)	1-300(6)	N(3)–C(11)	1.299(6)
N(2)–C(1)	1.274(7)	N(4)–C(3)	1.307(7)
S(1)–C(1)	1.738(6)	S(2)–C(1)	1.763(6)
S(2)–C(2)	1.812(9)	S(3)–C(3)	1.737(6)
S(4)–C(3)	1.729(6)	S(4)–C(4)	1.792(7)
O(1)–C(9)	1.357(6)	O(1)–C(6)	1.364(6)
O(2)–C(15)	1.334(7)	O(2)–C(12)	1.358(6)
C(5)–C(6)	1.421(7)	C(5)–C(10)	1.503(7)
C(6)–C(7)	1.339(7)	C(7)–C(8)	1.418(9)
C(8)–C(9)	1.322(9)	C(11)–C(12)	1.454(7)
C(11)–C(16)	1.498(7)	C(12)–C(13)	1.351(8)
C(13)–C(14)	1.396(9)	C(14)–C(15)	1.375(9)
Bond angles			
N(1)–Zn(1)–N(3)	126.16(16)	N(1)–Zn(1)–S(1)	86.99(12)
N(3)–Zn(1)–S(1)	123.53(12)	N(1)–Zn(1)–S(3)	122.90(12)
N(3)–Zn(1)–S(3)	85.98(13)	S(1)–Zn(1)–S(3)	115.00(6)
C(1)–S(1)–Zn(1)	91.2(2)	C(1)–S(2)–C(2)	102.1(4)
C(3)–S(3)–Zn(1)	91.97(18)	C(3)–S(4)–C(4)	103.0(3)
C(9)–O(1)–C(6)	106.7(4)	C(15)–O(2)–C(12)	108.2(5)
C(5)–N(1)–N(2)	113.6(4)	C(5)–N(1)–Zn(1)	130.7(4)
N(2)–N(1)–Zn(1)	115.7(3)	C(1)–N(2)–N(1)	115.1(4)
C(11)–N(3)–N(4)	113.8(4)	C(11)–N(3)–Zn(1)	130.5(4)
N(4)–N(3)–Zn(1)	115.7(3)	C(3)–N(4)–N(3)	114.5(4)
N(2)–C(1)–S(1)	130.6(4)	N(2)–C(1)–S(2)	116.8(5)
S(1)–C(1)–S(2)	112.6(4)	N(4)–C(3)–S(4)	117.8(4)
N(4)–C(3)–S(3)	128.6(4)	S(4)–C(3)–S(3)	113.5(3)
N(1)–C(5)–C(6)	119.8(5)	N(1)–C(5)–C(10)	122.2(5)
C(6)–C(5)–C(10)	118.0(5)	C(7)–C(6)–O(1)	109.1(5)
C(7–C(6)–C(5)	132.7(5)	O(1)–C(6)–C(5)	118.1(4)
C(6)–C(7)–C(8)	107.2(5)	C(9)–C(8)–C(7)	106.2(6)
C(8)–C(9)–O(1)	110.8(6)	N(3)–C(11)–C(12)	117.6(5)
N(3)–C(11)–C(16)	125.0(5)	C(12)–C(11)–C(16)	117.5(5)
C(13)–C(12)–O(2)	108.4(5)	C(13)–C(12)–C(11)	134.4(6)
0(2)–C(12)–C(11)	117.2(4)	C(12)–C(13)–C(14)	108.2(6)
C(15)–C(14)–C(13)	105.2(6)	O(2)–C(15)–C(14)	109.9(6)

3.2. Biological activities

3.2.1. Antimicrobial activity

All the Schiff bases and metal complexes were tested for antimicrobial activity. The disc diffusion technique was employed [33]. Only the **3** complex showed clear inhibition of the bacteria, *B. subtilis* mutant-defective DNA repair (B28), while both Schiff bases **1** and **2** showed strong activity against all fungi. Complexes **3** and **5** showed clear inhibition of *C. albicans* and *S. cereviceae* (20341), respectively. Qualitative antimicrobial results are shown in Table 7. Quantitative measurements (Table 8) were done to determine the MIC values. The Schiff bases and complexes showed antifungal activity comparable to the standard drug, nystatin, but, the compounds **2** and **5** showed MIC values higher than that of nystatin (MIC = 25 000–50 000 μg cm^{-3}) for *S. cereviceae* (20341). Only **3** showed a MIC value higher than that of streptomycin.

3.2.2. Cytotoxic activity

The **3**, **5** and **7** complexes showed very good activity against the leukemic cell (CEM-SS) line with CD_{50} values of 1.6, 2.1 and 3.0 μg ml^{-1}, respectively. The remainder of the Schiff bases and complexes were inactive towards CEM-SS cells. None of the compounds showed any activity towards colon cancer cells (HT-29). Only complexes **3** and **7** were highly active against cervical cancer cells (HELA cells) with CD_{50} values of 1.5 and 2.1 μg ml^{-1}, respectively, while complex **5** was weakly active against these cells (HELA cells) with a CD_{50} value of 23.0 μg ml^{-1}. The compounds mentioned were more active than their uncomplexed metal salts. The results of cytotoxic assays are shown in Table 9.

4. Supplementary material

Crystallographic data for the structural analysis have been deposited with the Cambridge Crystallographic Data Center, CCDC No. 184218. Copies of this information may be obtained free of charge from The Director, CCDC, 12 Union Road, Cambridge, CB2 1EZ, UK (fax: +44-1223-336033; email: deposit@ccdc.cam.ac.uk. or www: http://www.ccdc.cam.ac.uk.

Acknowledgements

We thank the Department of Chemistry and the Department of Biotechnology, at UPM, for the provision of laboratory facilities. We also wish to thank the Ministry of Science, Technology and Environment, Malaysia, for funding this research under the Intensification of Research in Priority Areas scheme (IRPA grant No. 09-02-04-0296).

Table 7
Qualitative antimicrobial assay (100 mg cm^{-3}) [a]

Compound	*B. subtilis* (mutant-defective DNA repair, B28)	*P. aeruginosa* (60690)	Methicillin resistant *Staphylococcus* (MRSA)	*B. subtilis* (wild type, B29)	*S. cereviceae* (20341)	*C. albicans*	*C. lypolytica* (2075)	*A. ochraceous* (398)
1	6	8	10	6	22	17	21	22
2	7	8	7	6	16	12	24	22
3	15	10	13	14	6	19	6	8
4	6	6	6	8	7	8	6	7
5	6.5	9	9	6.5	15	13	11	13
6	10	7	7	13	13	7	8	12
7	6	6	9	6.5	6	8	6	6
8	6.5	6.5	6	7	6	6	14	8
Streptomycin (control)	30	30	31	30				
Nystatin (control)					24	21	27	25

[a] Inhibition diameter in mm. Inhibition diameter >15 mm—strongly active.

Table 8
Quantitative antimicrobial assay (MIC value, μg ml^{-3}) [a]

Compound	*B. subtilis* (mutant-defective DNA repair, B28)	*P. aeruginosa* (60690)	Methicillin resistant *Staphylococcus* (MRSA)	*B. subtilis* (wild type, B29)	*S. cereviceae* (20341)	*C. albicans*	*C. lypolytica* (2075)	*A. ochraceous* (398)
1					6250	6250	6250	3125
2					25 000		3125	3125
3	390				6250			
5					50 000			
Streptomycin (control)	48.8	12.2	12.2	48.8				
Nystatin (control)					6250	3125	6250	3125

[a] MIC (μg ml^{-3}), minimum inhibitory concentration, i.e. the lowest concentration to completely inhibit microbial growth.

Table 9
Cytotoxic activity

Compound	CD_{50} (μg ml^{-1})		
	T-lymphoblastic leukemic cells (CEM-SS)	Colon cancer cells (HT-29)	Cervical cells (HELA)
1	–	–	na
2	–	–	na
3	1.6	na	1.5
4	–	–	na
5	2.1	na	23.0
6	–	–	na
7	3.0	na	2.1
8	–	na	–
$Cu(NO_3)_2 2.5H_2O$	–	29.5	na
$NiCl \cdot 6H_2O$	–	–	na
$ZnCl_2$	16.2	–	na
Doxorubicin (standard)	0.10	6.0	na
Tamoxifen (standard)	36.0	36.0	na

na, not available. –, not active. CD_{50}, < 5.0 ng ml^{-1}—strongly active. CD_{50}, 5.0 to < 10.0 μg ml^{-1}—moderately active. CD_{50}, 10.0–25.0 μg ml^{-1}—weakly active. CD_{50}, > 25.0 μg ml^{-1}—not active.

References

[1] M.A. Ali, N.E. Ibrahim, R.J. Butcher, J.P. Jasinski, J.M. Jasinski, J.C. Bryan, Polyhedron 17 (1998) 1803.
[2] M.A. Ali, C.M. Haroon, M.N. Uddin, S.M. Majumder, M.T.H. Tarafder, M.A. Khair, Transition Met. Chem. 17 (1992) 133.
[3] M.A. Ali, M.T.H. Tarafder, J. Inorg. Nucl. Chem. 39 (1977) 1785.
[4] M.A. Ali, S.M.G. Hossain, S.M.M.H. Majumder, M.N. Uddin, M.T.H. Tarafder, Polyhedron 6 (1987) 1653.
[5] M.A. Ali, I. Intan-Safinar, M.M. Mackeen, S.H. El-Sharkawy, K. Takahata, H. Kanzaki, K. Kawazu, Natural Product Sci. 4 (1998) 10.
[6] M.A. Ali, S.E. Livingstone, Coord. Chem. Rev. 13 (1974) 101.
[7] M.A. Ali, S.M.M.H. Majumder, R.J. Butcher, J.P. Jasinski, J.M. Jasinski, Polyhedron 16 (1997) 2749.
[8] M.A. Ali, K.K. Dey, M.N. Uddin, F.E. Smith, R.J. Butcher, J.P. Jasinski, J.M. Jasinski, Polyhedron 15 (1996) 3331.
[9] M.A. Ali, M.H. Kadir, M. Nazimuddin, S.M.M.H. Majumder, M.T.H. Tarafder, M.A. Khair, Indian J. Chem. 27A (1988) 1064.
[10] M.A. Ali, M. Uddin, M.N. Uddin, D.A. Chowdhury, M.T.H. Tarafder, Indian J. Chem. 25A (1986) 238.
[11] M.A. Ali, A.H. Mirza, R.J. Butcher, M.T.H. Tarafder, M.A. Ali, Inorg. Chim. Acta 320 (2001) 1.
[12] M.T.H. Tarafder, M.A. Ali, D.J. Wee, K. Azahari, S. Silong, K.A. Crouse, Transition Met. Chem. 25 (2000) 456.
[13] M.T.H. Tarafder, M.A. Ali, N. Saravanan, W.Y. Weng, S. Kumar, N. Umar-Tsafe, K.A. Crouse, Transition Met. Chem. 25 (2000) 295.
[14] M.E. Hossain, M.N. Alam, J. Begum, M.A. Ali, M.N. Uddin, F.E. Smith, R.C. Hynes, Inorg. Chim. Acta 249 (1996) 207.
[15] M.T.H. Tarafder, M.A. Ali, Can. J. Chem. 56 (1978) 2000.
[16] M.T.H. Tarafder, S. Roy, Indian J. Chem. 27A (1988) 407.
[17] M.T.H. Tarafder, Indian J. Chem. 28A (1989) 531.
[18] M.T.H. Tarafder, M.A.J. Miah, R.N. Bose, M.A. Ali, J. Inorg. Nucl. Chem. 43 (1981) 3151.
[19] M.T.H. Tarafder, M. Rahim, Indian J. Chem. 28A (1989) 1105.
[20] S.M.M.H. Majumder, M.A. Ali, F.E. Smith, M.A.U. Mridha, Polyhedron 7 (1988) 2183.
[21] M. Das, S.E. Livingstone, Inorg. Chim. Acta 19 (1976) 5.
[22] G.M. Sheldrick, SAINT V4, Software Reference Manual, Siemens Analytical X-ray Systems, Madison, WI, USA, 1996.
[23] G.M. Sheldrick, SADABS, Program for Empirical Absorption Correction of Area Detector Data, University of Göttingen, Göttingen, Germany, 1996.
[24] G.M. Sheldrick, SHELXTL V5.1, Software Reference Manual, Bruker AXS Inc, Madison, WI, USA, 1997.
[25] A.L. Spek, Acta Crystallogr., A 46 (1996) C34.
[26] T. Mosmann, J. Immunol. Meth. 65 (1983) 55.
[27] A.W. Bauer, M.D.K. Kirny, J.C. Sherries, M. Turck, Am. J. Clin. Pathol. 45 (1966) 493.
[28] C.D. Hufford, A.M. Clark, Discovery and Development in the New Drugs for Systematic Opportunistic Infections, Studies in Natural Product Chemistry, vol. 2, Elsevier, Amsterdam, 1988, pp. 421–452.
[29] J.P. Costes, Inorg. Chim. Acta 82 (1984) 101.
[30] D. Gattegno, A.M. Giuliani, Tetrahedron 30 (1974) 701.
[31] L. Sacconi, M. Ciampolini, H. Campigli, Inorg. Chem. 4 (1965) 407.
[32] M.T.H. Tarafder, A. Kasbollah, K.A. Crouse, A.M. Ali, B.M. Yamin, H.-K. Fun, Polyhedron 20 (2001) 2363.
[33] H.B. Gray, J. Ballhausen, J. Am. Chem. Soc. 85 (1963) 260.

study on ligands derived from *S*-benzyldithiocarbazate (SBDTC), we report herein the synthesis, characterization and bioactivity of some transition metal (Fe^{2+} and Co^{2+}) and non-transition metal (Cd^{2+}, Pb^{2+} and Sn^{2+}) complexes of isomeric nitrogen–sulfur donor ligands formed between SBDTC with 5-methyl-2-furaldehyde (NS), (Fig. 1) and 2-furaldehyde (NS′), (Fig. 2). The structures of *S*-benzyl-β-*N*-(5-methyl-2-furyl methylene)dithiocarbazate, NS, free ligand and bis[*S*-benzyl-β-*N*-(2-furylmethylketone) dithiocarbazato] cadmium(II), $[Cd(NS')_2]$, as determined by X-ray analysis of single crystals are also given.

2. Experimental

All chemicals and solvents were of analytical grade and were used as received.

2.1. Preparation of S-benzyldithiocarbazate (SBDTC)

SBDTC was prepared as previously reported [9].

2.2. General method for synthesizing Schiff bases

A solution of SBDTC (1.98 g, 0.1 mol) in absolute ethanol (40 cm^3) was added to an equimolar solution of 5-methyl-2-furyladehyde or 2-furylmethylketone in 50 cm^3 of the same solvent. The mixture was heated on a steam bath for 10 min and then cooled to 0 °C in an ice bath. Precipitated Schiff bases were filtered, washed with cold ethanol and dried in vacuo over silica gel. The yield and melting point were recorded for each product.

2.3. General method for synthesis of metal complexes

Schiff base (0.0076 mol) prepared as outlined in Section 2.2 was dissolved in ethanol (50 cm^3) in the presence of an equimolar amount of potassium hydroxide (0.4 g). The clear solution was treated with a solution containing a stoichiometric amount of metal salt in the same solvent ($\sim$50 cm^3). The mixture was heated at 90 °C for 5 min and subsequently cooled in an ice–salt bath. The product was isolated and washed with ethanol. It was dried in a vacuum desiccator over P_2O_5. The metal salts used were $SnCl_2$, $FeCl_3$, $CoCl_2$, $Pb(CH_3COO)_2\cdot 3H_2O$ and $Cd(CH_3COO)_2\cdot 2H_2O$.

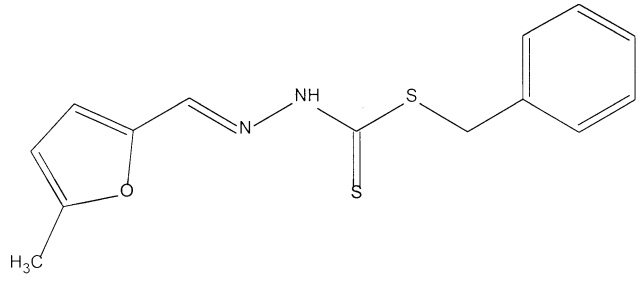


Fig. 1. Chemical structure of *S*-benzyl-β-*N*-(5-methyl-2-furylmethylene) dithiocarbazate.

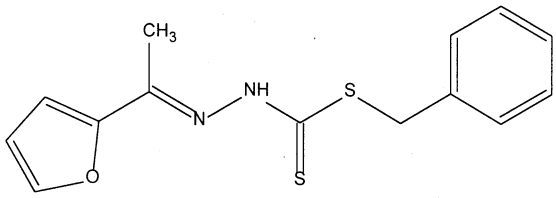


Fig. 2. Chemical structure of *S*-benzyl-β-*N*-(2-furylmethylketone) dithiocarbazate.

2.4. Physical measurements

The analyses for carbon, hydrogen, nitrogen and sulfur were carried out using a LECO CHNS-932 instrument. The IR spectra in KBr pellets were recorded using a Perkin–Elmer FT IR 1750X spectrophotometer (4000–400 cm^{-1}). The molar conductance of 10^{-3} M solutions of the metal complexes in dimethyl sulfoxide (DMSO) were measured at 29 °C using a Jenway 4310 conductivity meter and a dip-type cell with platinized electrode. Magnetic susceptibilities at room temperature were measured using a Sherwood Scientific MSB-AUTO magnetic susceptibility balance. The UV–Vis spectra were run on a Shimadzu UV-2501 PC Recording Spectrophotometer (900–200 nm). All these measurements were done at the Chemistry Department, UPM.

2.5. X-ray structure determination of NS and $[Cd(NS')_2]$

Beautiful dark-yellow crystals of the NS ligand and $[Cd(NS')_2]$ complex were formed after the DMF solutions were allowed to slowly evaporate for a few weeks. A selected crystal was mounted on a SMART CCD diffractometer in each case. Reflection data were measured at 20 °C using graphite monochromated Mo Kα ($\lambda = 0.71073$ Å) radiation with a detector distance of 4 cm and swing angle of $-35°$. The collected data were reduced using the program SAINT [10] and an empirical absorption correction was carried out using SADABS [11]. The structure was solved by direct methods and refined by using the full-matrix least-squares method on F^2_{obs} using the SHELXTL [12] software package. All non-H atoms were anisotropically refined. The hydrogen atoms were located by difference syntheses and refined isotropically. The molecular graphics were created using SHELXTL. Atomic scattering factors and anomalous dispersion correction were taken from the International Table for X-ray Crystallography [13].

2.6. Target microorganisms

Eight pathogenic microbials were used to test the biological potential of the ligands and their complexes. They were *Methicillin resistant sthaphylococcus* (MRSA), *Bacillus subtilis wild type* (B29), *Subtilis mutant* (mutant defective DNA repair-B28), *Pseudomonas aeruginosa* (60690), *Candida albicans* (C.A.), *Aspergillus ochraceous* (398), *Saccaromyces ceciricaee* (20341) and *Candida lypolytica* (2075).

2.6.1. Qualitative antimicrobial assay

Antimicrobial activity of each sample was qualitatively determined by a modified disc diffusion method as previously reported [14]. Antimicrobial activity was indicated by the presence of clear inhibition zones around the discs. Commercially available streptomysin (Sigma, USA) was used for antibacterial control while nystatin (Sigma, USA) was used as antifungal control.

2.6.2. Quantitative antimicrobial assay

Compounds that showed positive (>15 mm) antimicrobial activities with the disc diffusion assay were subjected to the broth dilution method for the quantitative measurement of microbiostatic (inhibitory) activity as described by Hufford and Clark [15]. The lowest concentration that completely inhibited visible microbial growth was recorded as the minimum inhibitory concentration (MIC, μg cm^{-3}). Both streptomycin and nystatin were used as positive controls for bacteria and fungi, respectively.

2.6.3. Cytotoxic assay

The CEM-SS (Human T-lymphoblastic leukemia) cell line was obtained from the National Cancer Institute, USA. The cells were cultured in RPMI-1640 medium supplemented with 10% fetal calf serum. Cytotoxicity was determined using the microtitration of 3-(4,5-dimethylthiazol-2-yl)-2,5-diphenyltetrazolium bromide (MTT) assay (Sigma, USA) as reported by Mosmann [16]. Controls that contained only cells were included for each sample.

Cytotoxicity was expressed as CD_{50}, i.e. the concentration that reduced the absorbance of treated cells by 50% with reference to the control (untreated cells). Doxorubicin and tamoxifen were used as control cytotoxins.

3. Results and discussion

The physical and analytical data for the metal complexes are given in Table 1. All the analytical data obtained are in agreement with the proposed empirical formulae. The characterized ligands are soluble in all organic solvents tested and all compounds are stable in air. For both the NS and NS′ free ligands, the physical and analytical data have been reported earlier [17].

3.1. Infrared spectra

Major vibration bands of the free ligands and metal complexes are given in Table 2. For complexation to occur, the free ligand must exibit thiol–thione tautomers which is brought about by the presence of thioamide –NH–C=S functional group [18,19]. The ν(C=S) band at 1096 cm^{-1} and the ν(NH) band at approximately 3150 cm^{-1} were present, indicating that the free ligands remain as the thione tautomer in the solid state. The ν(NH) band present in the free ligand was not observed in any metal complex, indicating deprotonation of the ligand in situ to form the thiol tautomers for the formation of metal complexes to take place.

The ν(C=S) bands at 1096 and 1026 cm^{-1} for NS and NS′ free ligand were also not observed in the metal complexes, thus supporting the suggestion of coordination through the thione sulfur. Sharp bands observed in the spectrum of the free ligand at approximately 1600 cm^{-1} are assigned to ν(C=N) [20]. In the metal complexes this absorption was shifted to lower frequencies indicating coordination of the azomethine nitrogen to the central metal atoms [21,22]. The lowering in frequency of the ν(N–N) band in all the metal complexes is another clear indication that the coordination involves azomethine nitrogen. There was no

Table 1
Analytical data and physical properties of NS and NS′ complexes

Compound	Color	M.p. (°C)	Found (Calc.) (%)				Yield (%)
			C	H	N	S	
$[Pb(NS)_2]\cdot H_2O$	yellow	198.0	41.79(41.83)	3.66(3.24)	6.99(6.97)		75
$[Sn(NS)_2]Cl_2\cdot 2H_2O$	dark yellow	172.0	41.69(41.81)	3.23(3.73)	6.99(6.97)	16.00(15.93)	80
$[Fe(NS)_2]Cl_2\cdot H_2O$	dark brown	173.5	51.25(51.55)	4.18(4.29)	8.62(8.60)	19.68(19.54)	68
$[Co(NS)_2]\cdot Cl$	brown	222.0	54.70(52.75)	4.18(4.38)	8.94(8.80)	20.40(20.10)	65
$[Pb(NS')_2]$	yellow	228.0	42.65(42.79)	3.59(3.31)	7.23(7.13)		72
$[Cd(NS')_2]$	yellow	217.0	48.94(48.67)	3.85(3.77)	8.12(8.11)	19.17(18.54)	70

Table 2
Infrared spectral data (band maxima) and molar conductance

Compound	Absorption bands (frequency, cm^{-1})					Molar conductance (Ω^{-1} cm^2 mol^{-1})	Ion ratio
	ν(NH)	ν(C=N)	ν(C=S)	ν(N–N)	ν(C–O–C)		
NS	3102	1618	1096	1023	1232 [17,24]		
NS′	3200	1600	1026	1062	1232 [17,24]		
$[Pb(NS)_2]\cdot H_2O$		1612		934	1234	18	
$[Sn(NS)_2]Cl_2\cdot 2H_2O$		1612		936	1234	85	2:1
$[Fe(NS)_2]Cl_2\cdot H_2O$		1592		962	1236	88	2:1
$[Co(NS)_2]\cdot Cl$		1598		962	1230	20	
$[Pb(NS')_2]$		1584		990	1230	22	
$[Cd(NS')_2]$		1590		998	1230	20	

significant displacement of the frequency of the ring breathing and ν(C–O–C) vibrations at 1230 cm^{-1} [7] and no presence of metal oxygen bond stretching observed at 440–450 cm^{-1} [8] in any complex. This shows that there was no coordination by the furanic oxygen. Indeed there is no indication of oxygen bonding to the central metal atom in the crystal structure of the $[Cd(NS)_2]$ complex.

3.2. Magnetic and conductivity data and electronic spectra

At room temperature, magnetic susceptibility (Table 3) measurements show that all the complexes are diamagnetic and low spin except for $[Fe(NS)_2]Cl_2\cdot H_2O$ which has paramagnetic properties with μ_{eff} of 1.77 B.M., characteristic of a square planar structure. All the diamagnetic complexes are four-coordinated and expected to be distorted tetrahedral, as proved for our cadmium complex by its crystal structure. For the iron(II) ion which has a $3d^6$ electron configuration, the magnetic moment (1.77 B.M.) suggests that the iron(II) ion is in a low-spin iron(II) state.

The complexes $[Sn(NS)_2]Cl_2\cdot H_2O$ and $[Fe(NS)_2]Cl_2\cdot H_2O$ exhibit molar conductance values corresponding to 2:1 electrolytes in DMSO. The conductivity presumably arises from solvation according to the following scheme:

$$[Sn(NS)_2]Cl_2\cdot H_2O + DMSO \rightarrow [Sn(NS)_2](DMSO)_2\cdot H_2O + 2Cl^-$$

and

$$[Fe(NS)_2]Cl_2\cdot H_2O + DMSO \rightarrow [Fe(NS)_2](DMSO)_2\cdot H_2O + 2Cl^-$$

The electronic spectrum of the $[Co(NS)_2]$ complex displays two diagnostic absorptions at 393 and 339 nm corresponding to $^1A_{1g}\rightarrow{}^1T_{1g}$ and $^1A_{1g}\rightarrow{}^1T_{2g}$ transitions. The remaining compounds showed bands that are caused by charge transfer.

3.3. Crystal structure studies

3.3.1. Crystal structure of NS (see Table 6)

A perspective view of the ligand with the numbering scheme is shown in Fig. 3. The relevant bond distances and bond angles are given in Table 7. The asymmetric unit consists of two independent *S*-benzyl-β-*N*(5-methyl-2-furylmethylene)dithiocarbazate molecules. The methylfurylmethylenedithiocarbazate moiety of the two molecules are not exactly planar. The methylfuryl plane of (O1–C10–C11–C12–C13–C9) is planar with C14 atom deviated by only −0.030(3) Å. This plane makes a dihedral angle of 11.33(9)° with the S1–S2–N1–N2–C7–C8 plane. Similarly, in the second molecule the methylfuryl O2–C24–C25–C26–C27–C28 is planar with maximum deviation of 0.04(2) Å at the C28

Table 3
UV–Vis spectral of band maxima (λ, nm (log ε)) and magnetic susceptibility of metal complexes

Compound	λ_{max} (nm)	μ_{eff} (B.M.) [a]
$[Pb(NS)_2]\cdot H_2O$	355.5(4.817), 588.0(4.738)	diamagnetic
$[Sn(NS)_2]Cl_2\cdot 2H_2O$	357.5(4.821), 295.5(4.056), 585.0(1.523)	diamagnetic
$[Fe(NS)_2]Cl_2\cdot H_2O$	354.5(6.045), 418.0(5.574), 587.0(5.097)	1.77
$[Co(NS)_2]\cdot Cl$	339.0(4.402), 393.0(4.385)	diamagnetic
$[Pb(NS')_2]$	303.5(4.434), 347.5(4.569)	diamagnetic
$[Cd(NS')_2]$	307.5(4.320), 359.5(4.420)	diamagnetic

Beer's law: $A = \varepsilon bc$ where A, absorption, $b = 1$ cm and c, concentration (M), log ε (cm^{-1} mol^{-1} l) are given in parentheses.
[a] Tetrahedral complex, 1.94–2.00 B.M.; distorted square-planar, 1.90–1.93 B.M.; square-planar, 1.85–1.89 B.M.

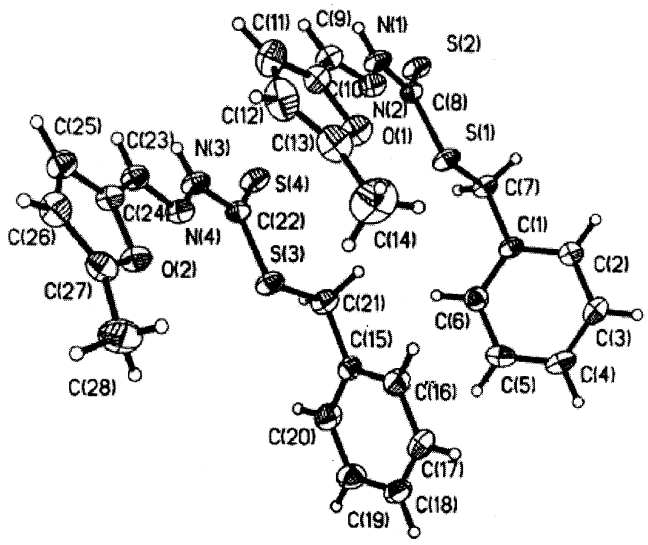


Fig. 3. Molecular structure and atom numbering scheme of (NS).

atom. However, the S3–S4–N3–N4–C4–C5–C6–C7 plane showed large deviation from the planar S3–N3–C21–C22 group at the S4 and N4 atoms of 0.126(1) and −0.119(1) Å, respectively. The dihedral angle between the methylfurfuryl O2–C24–C25–C26–C27–C28 plane and S3–N3–C21–C22 is 6.41(16)° which is smaller than in the first molecule. The phenyl ring C1–C2–C3–C4–C5–C6–C7 is nearly perpendicular to the methylene-dithiocarbazate S1–S2–N1–N2–C7–C8 of 80.21(6)°. In the second molecule, the phenyl ring C15–C16–C17–C18–C19–C20 makes a dihedral angle of 74.12(9)° with the S3–N3–C21–C22 plane.

The C8–S2 and C22–S4 bond lengths in the two molecules of 1.6669(15) and 1.6667(15) Å, respectively, are intermediate between 1.82 Å for C–S single bond and 1.56 Å for C=S double bond [23] and is in agreement with the reported value in SBDTC [24]. Thus, the compound exits as a thioketo tautomeric form. The furylmethylene and benzyl groups are *trans* and *cis* with respect to the ion about the the C–N and C–S bonds, respectively. A similar configuration was also reported for SBDTC [24]. The N1–N2 and N3–N4

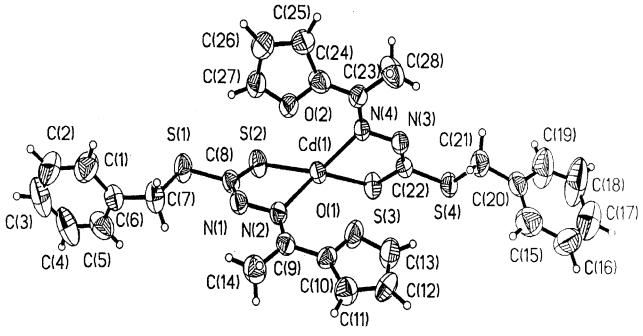


Fig. 4. Molecular structure and atom numbering scheme of $[Cd(NS')_2]$.

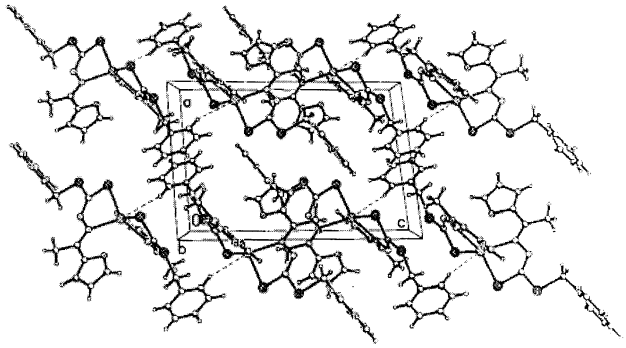


Fig. 5. Packing arrangement of $[Cd(NS')_2]$.

bond distances of 1.3820(16) and 1.3824(17) Å are slightly shorter than the corresponding bond lengths in unsubstituted SBDTC (1.406(3) Å) [24] due to the delocalised electrons of the furan ring. The two molecules are connected by hydrogen bondings, N1–H1A···S4 (H1A···S4 2.578 Å) and N3–H3A···S2 (H3A···S2 2.589 Å), and therefore, are arranged as dimers parallel to the *b* and *c* axes in the lattice.

3.3.2. Crystal structure of the $[Cd(NS')_2]$ complex

The molecular structure of the $[Cd(NS')_2]$ complex is shown in Fig. 4, while Fig. 5 shows the packing arrangement of the molecules on the ac plane. The central cadmium atom is bis-chelated by the uninegatively charged bidentate ligand through the azomethine nitrogen atoms, N2 and N4, and the thiolate sulfur atoms, S2 and S3. Both nitrogen atoms (N2, N4) and sulfur atoms (S2 and S3) from the two ligands are coordinated at opposite positions. The formation of this complex gives a distorted tetrahedral geometry about the central cadmium atom with angles of 78.89(10)°–137.72(11)°. The bond lengths of the complex are comparable to the analogous complex bis[*S*-benzyl-β-*N*(5-methyl-2-furylmethylene)dithiocarbazato]cadmium(II) reported earlier [17]. Both complexes show non-participation of the furanic oxygen in the coordination to the central cadmium atom. This observation, however, is in contrast to the one proposed by Jouad et al. [25]. There is slight variation in corresponding bond lengths in the C9–N2–N1–C8–S1–C17 and C23–N4–N3–C22–S4–C21 moieties in the complex. The largest variation is shown by the C9–C10 and C23–C24 of 1.466(6) and 1.419(7) Å, respectively. The C8–N1 and C22–N3 bond lengths of 1.257(6) and 1.300(7) Å clearly indicate the complexation involves deprotonation at N1 and N3 atoms of the ligand. The conjugation system of the moieties is influenced by the coordination with the metal as shown by the slight bond lengthenings compared with the uncomplexed ligand. The N1–N2 and N3–N4 distances of of 1.424(5) and 1.417(5) Å are slightly longer than the normal values of about 1.36–1.38 Å [22,26]. The corresponding bond lengths in

octahedral tridentate bis[*S*-benzyl-β-*N*(2-pyridylmethylene)dithiocarbazato]zinc(II) are 1.379(4) and 1.374(4) Å, respectively [1]. The cadmium atom makes a linear plane with the furyl groups Cd1–O1–N1–N2–C9–C10–C11–C12–C13–C14, with maximum deviation of 0.048(4) Å at C11, and Cd1–O2–N3–N4–C23–C24–C25–C26–C27 with maximum deviation of 0.032(7) Å at N4, respectively. The cadmium-bidentate rings are less planar. The Cd1–S2–N1–N2–C8 has a minimum deviation of 0.085(5) Å at the N1 atom and maximum deviation of 0.181(4) Å at the S4 atom. For the Cd1–S3–N3–N4–C22 plane the minimum deviation is 0.096(5) Å at the N3 atom and the maximum deviation is 0.219(9) Å at the N4 atom. The dihedral angles between the planar benzyl planes C1–C2–C3–C4–C5–C6–C7 and C15–C16–C17–C18–C19–C20–C21 with their corresponding furyl planes O1–C10–C11–C12–C13–C14 (maximum deviation at C9, 0.021(5) Å) and O2–C32–C24–C25–C26–C27 (maximum deviation at C24, 0.047(6) Å) are quite different with values of 83.9(4)° and 67.7(4)°, respectively. The intramolecular interaction of C14–H14A···N1 (H14A···N1, 2.259 Å) and C28–H28A···N3 (H28A···N3, 2.248 Å) result in the formation of six-membered rings in the ligand moieties and may contribute to the planarity of the furyl-Schiff base group of the complex.

3.4. Biological activity

3.4.1. Cytotoxic activity

$PbNO_3$ salt is inactive, but chelation by the NS is active, but chelation by Nsfree ligand gives $[Pb(NS)_2]\cdot H_2O$ complex of high cytoxicity against CEM-SS with a CD_{50} of 3.25 μg cm^{-1}. Most of our recent research on cadmium(II) complexes [17] showed high cytotoxic activity on all of the cell lines, but the activity of the $[Cd(NS')_2]$ complex was greatly reduced and was even much lower than the simple cadmium(II) salt. The remainder of the complexes investigated do not possess any significant activity against CEM-SS, with the exception of $[Sn(NS)_2]Cl_2\cdot 2H_2O$ and $[Pb(NS')_2]$ complexes which are toxic at higher concentrations. Detailed results against CEM-SS cell lines are shown in Table 4.

Table 4
Results of screening against leukemic cells (CEM-SS)

Compound	CD_{50} (μg cm^{-3}) [a] CEM-SS
$[Fe(NS)_2]Cl_2\cdot H_2O$	–
$[Sn(NS)_2]Cl_2\cdot 2H_2O$	29
$[Co(NS)_2]\cdot Cl$	–
$[Pb(NS)_2]\cdot H_2O$	3.25
$[Cd(NS')_2]$	–
$[Pb(NS')_2]$	29.7
Metal salts	
$SnCl_2$	–
$FeCl_2$	–
$PbNO_3$	–
$CoCl_3$	12.00
$CdBr_2$	14.00
Standard	
Doxorubicin	0.10
Tamoxifen	36.00

–, inactive.
[a] CD_{50} (μg cm^{-3}), cytotoxic dose at 50%, i.e. the concentration to reduce growth of cancer cells by 50%.

3.4.2. Antimicrobial assay

Preliminary screening for antimicrobial activity was done on all compounds. All the compounds showed clear inhibition zones of 10 mm and above against *A. ochraceous* except the $[Cd(NS')_2]$ complex. $[Fe(NS)_2]Cl_2\cdot H_2O$ was active against *A. ochraceous* with a clear inhibition zone of 21 mm. The qualitative screening results are shown in Table 5.

Only $[Fe(NS)_2]Cl_2\cdot H_2O$ was used for quantitative measurement of MIC. Its MIC value of 100 000 μg cm^{-3} towards *A. ochraceous* is higher than that for the standard drug nystatin (3125 μg cm^{-3}).

Table 5
Qualitative antimicrobial assay results [a] (diameter in mm)

Compound	MRSA	B29	B28	60690	C.A.	398	20341	2075
$[Fe(NS)_2]Cl_2\cdot H_2O$	8	7	8	8	13.5	21	11	11
$[Pb(NS)_2]\cdot H_2O$	–	8	7	–	–	12	–	–
$[Sn(NS)_2]Cl_2\cdot 2H_2O$	8	8	9		8	12	8	–
$[Cd(NS')_2]$	–	–	–	–	11	8	11	–
$[Pb(NS')_2]$	8	7	8	8	7	12	–	8
Streptomysin (antibacterial control)	31	30	30	30	–	–	–	–
Nystatin (antifungal control)	–	–	–	–	21	25	24	27

Methicillin resistant sthaphylococcus (MRSA); *Bacillus subtilis wild* type (B29); *Subtilis mutant* (mutant defective DNA repair-B28); *P. aeruginosa* (60690); *C. albicans* (C.A); *A. ochraceous* (398); *S. ceciricaee* (20341); *C. lypolytica* (2075); '–', inactive.
[a] Diameter of 15 mm and above considered active.

Table 6
Summary of crystal data and structure refinement parameters for NS and $[Cd(NS')_2]$

Compound	NS	$[Cd(NS')_2]$
Chemical formula	$C_{14}H_{14}N_2OS_2$	$C_{28}H_{26}CdN_4O_2S_4$
Formula weight	290.39	691.17
Crystal class	Monoclinic	triclinic
Space group	$P2_1/n$	$P\bar{1}$
a (Å)	9.7144(2)	10.5620(2)
b (Å)	23.26670(10)	10.5926(2)
c (Å)	12.93790(10)	14.9458(3)
α (°)	90	95.377(1)
β (°)	97.2500(10)	93.468(1)
γ (°)	90	114.156(1)
V (Å^3)	2900.87(7)	1509.97(5)
Z	8	2
Mo Kα (Å)	0.71073	0.71073
T (K)	293(2)	293(2)
ρ_{calc} (Mg m^{-3})	1.330	1.520
μ (mm^{-1})	0.360	1.032
Sample dimension (mm)	0.48 × 0.46 × 0.42	0.46 × 0.34 × 0.32
$F(000)$	1216	700
Total number of reflections collected	19 747	10 658
Independent reflections	6962 [$R_{int} = 0.0669$]	7007 [$R_{int} = 0.0845$]
Number of data used for refinement	6962	7007
Number of parameters refined	346	353
Goodness-of-fit on F^2	0.944	0.970
Correction	empirical	empirical
Final R indices $[I > 2\sigma(I)]$	$R_1 = 0.0416$, $wR_2 = 0.1090$	$R_1 = 0.0716$, $wR_2 = 0.1670$
R indices (all data)	$R_1 = 0.0643$, $wR_2 = 0.1184$	$R_1 = 0.0919$, $wR_2 = 0.1845$
Largest and smallest peak (e Å^{-3})	0.326 and −0.265	1.259 and −1.990

Table 7
Selected bond lengths (Å) and bond angles (°) for NS and $[Cd(NS')_2]$

NS		$[Cd(NS')_2]$	
Bond lengths			
S(1)–C(8)	1.7506(14)	Cd(1)–N(4)	2.285(4)
S(1)–C(7)	1.8197(17)	Cd(1)–N(2)	2.315(4)
S(2)–C(8)	1.6669(195)	Cd(1)–S(2)	2.4813(13)
S(3)–C(22)	1.7528(15)	Cd(1)–S(3)	2.4827(13)
S(3)–C(21)	1.8149(18)	S(1)–C(8)	1.770(5)
S(4)–C(22)	1.6667(15)	S(1)–C(7)	1.812(6)
N(1)–C(8)	1.3348(19)	S(2)–C(8)	1.747(6)
N(1)–N(2)	1.3820(16)	S(3)–C(22)	1.755(6)
N(2)–C(9)	1.275(2)	S(4)–C(22)	1.730(5)
N(3)–C(22)	1.337(2)	S(4)–C(21)	1.837(6)
N(3)–N(4)	1.3824(17)	N(1)–C(8)	1.257(6)
N(4)–C(23)	1.285(2)	N(1)–N(2)	1.424(5)
		N(2)–C(9)	1.261(6)
		N(3)–C(22)	1.300(7)
		N(3)–N(4)	1.417(5)
		N(4)–C(23)	1.292(7)
Bond angles			
C(8)–S(1)–C(7)	102.37(7)	N(4)–Cd(1)–N(2)	115.98(15)
C(22)–S(3)–C(21)	101.91(8)	N(4)–Cd(1)–S(2)	137.20(11)
C(8)–N(1)–N(2)	119.36(12)	N(2)–Cd(1)–S(2)	79.11(10)
C(9)–N(2)–N(1)	115.86(13)	N(4)–Cd(1)–S(3)	78.89(10)
C(10)–O(1)–C(13)	106.65(15)	N(2)–Cd(1)–S(3)	136.04(11)
C(27)–O(2)–C(24)	106.23(13)	S(2)–Cd(1)–S(3)	119.26(5)
C(8)–N(1)–N(2)	119.36(12)	C(8)–S(1)–C(7)	104.6(3)
C(9)–N(2)–N(1)	115.86(13)	C(8)–S(2)–Cd(1)	93.15(17)
C(22)–N(3)–N(4)	120.74(13)	C(22)–S(3)–Cd(1)	93.15(17)
C(23)–N(4)–N(3)	114.38(13)	C(22)–S(4)–C(21)	104.5(3)
C(1)–C(7)–S(1)	106.30(10)	C(10)–O(1)–C(13)	106.3(4)
N(1)–C(8)–S(2)	121.75(11)	C(27)–O(2)–C(24)	107.8(4)
N(1)–C(8)–S(1)	112.96(11)	C(8)–N(1)–N(2)	115.3(4)
S(2)–C(8)–S(1)	125.29(9)	C(9)–N(2)–N(1)	114.3(4)
N(2)–C(9)–C(10)	121.32(15)	C(9)–N(2)–Cd(1)	131.3(3)
C(11)–C(10)–O(1)	109.51(15)	N(1)–N(2)–Cd(1)	114.4(3)
N(3)–C(22)–S(4)	121.48(12)	C(22)–N(3)–N(4)	114.6(4)
S(4)–C(22)–S(3)	125.23(10)	C(23)–N(4)–N(3)	113.6(4)
N(4)–C(23)–C(24)	123.11(15)	C(23)–N(4)–Cd(1)	130.7(3)
		N(3)–N(4)–Cd(1)	115.3(3)

4. Supplementary material

Crystallographic data for the structural analyses of NS ligand and $[Cd(NS')_2]$ complex have been deposited with the Cambridge Crystallographic Data Center, CCDC 164801 and CCDC 164800. Copies of this information may be obtained free of charge from: The Director, CCDC, 12 Union Road, Cambridge, CB2 1EZ, UK (fax: +44-1223-336033; e-mail: deposit@ccdc.cam.ac.uk or www: http://www.ccdc.cam.ac.uk).

Acknowledgements

The authors would like to thank the Department of Chemistry, Universiti Putra Malaysia, for the provision of laboratory facilities. This research was funded by a grant from the Ministry of Science and Environment, Malaysia, under the Intensification of Research in Priority Areas (IRPA) program (Grant No. 09-02-04-0296).

References

[1] M.T.H. Tarafder, A. Kasbollah, K.A. Crouse, A.M. Ali, B.M. Yamin, H.-K. Fun, Polyhedron 20 (2001) 2363.
[2] M.T.H. Tarafder, A. Asmadi, S.M.S. Talib, A.M. Ali, K.A. Crouse, Transition Met. Chem. 26 (2001) 170.
[3] M.A. Ali, S.E. Livingstone, Coord. Chem. Rev. 13 (1974) 101.
[4] M.A. Ali, C.M. Haroon, M. Nazimuddin, S.M.M.H. Majumder, M.T.H. Tarafder, M.A. Khair, Transition Met. Chem. 17 (1992) 133.
[5] M.A. Ali, N.E. Ibrahim, R.J. Butcher, J.P. Jasinski, J.M. Jasinski, J.C. Bryan, Polyhedron 17 (1998) 1803.
[6] M.A. Ali, S.M.G. Hossain, S.M.M.H. Majumder, M. Nazimuddin, M.T.H. Tarafder, Polyhedron 6 (1987) 1653.
[7] M.A. Ali, R.N. Bose, J. Inorg. Nucl. Chem. 39 (1977) 265.
[8] M.A. Ali, R.N. Bose, Polyhedron 3 (1984) 517.

[9] M.A. Ali, M.T.H. Tarafder, J. Inorg. Nucl. Chem. 39 (1977) 1785.
[10] G.M. Sheldrick, SAINT V4 Software Reference Manual, Siemens Analytical X-ray Systems, Madison, WI, 1996.
[11] G.M. Sheldrick, SADABS. Program for Empirical Absorption Correction of Area Detector Data, University of Göttingen, Göttingen, Germany, 1996.
[12] G.M. Sheldrick, SHELXTL V5.1 Software Reference Manual, Bruker AXS, Madison, WI, USA, 1997.
[13] A.L. Spek, PLATON, an integrated tool for the analysis of the results of a single crystal structure determination, Acta Crystallogr., Sect. A (1996) 46.
[14] M.T.H. Tarafder, M.A. Ali, N. Saravanan, W.Y. Weng, S. Kumar, N. Umar-Tsafe, K.A. Crouse, Transition Met. Chem. 25 (2000) 295.
[15] C.D. Hufford, A.M. Clark, Discovery and development in new drugs for systemic opportunistic infections, in: A. ur-Rahman (Ed.), Studies in Natural Product Chemistry, vol. 2, Elsevier, Amsterdam, 1988, p. 421.
[16] T. Mosmann, J. Immunol. Methods 65 (1983) 55.
[17] M.T.H. Tarafder, T.J. Khoo, K.A. Crouse, A.M. Ali, B.M. Yamin, H.-K. Fun, Polyhedron 21 (2002) 2547.
[18] M.T.H. Tarafder, M. Rahim, Indian J. Chem. 28A (1989) 1105.
[19] M.T.H. Tarafder, M.A. Ali, Can. J. Chem. 56 (1978) 2000.
[20] M.E. Hossain, M.N. Alam, M.A. Ali, M. Nazimuddin, F.E. Smith, R.C. Hynes, Polyhedron 15 (1996) 973.
[21] M.A. Ali, K.R. Fernando, D. Palit, M. Nazimuddin, Transition Met. Chem. 20 (1995) 19.
[22] N. Koji, H.S. Philippa, Infrared Absorption Spectroscopy, 2nd ed., Holden-Day, San Francisco, CA, 1977, p. 33.
[23] L.E. Sutton, Table of Interatomic Distances and Configurations in Molecules and Ions (Supplement), The Chemical Society, London, 1965.
[24] S.S.S. Raj, B.M. Yamin, Y.A. Yussof, M.T.H. Tarafder, H.-K. Fun, K.A. Crouse, Acta Crystallogr., Sect. C 56 (2000) 1236.
[25] E.M. Jouad, A. Riou, M. Allain, M.A. Khan, M.B. Gilles, Polyhedron 20 (2001) 67.
[26] F.H. Allen, O. Kennard, D.G. Watson, L. Brammer, A.G. Orpen, R. Taylor, J. Chem. Soc., Perkin Trans. 2 (1987) S1.

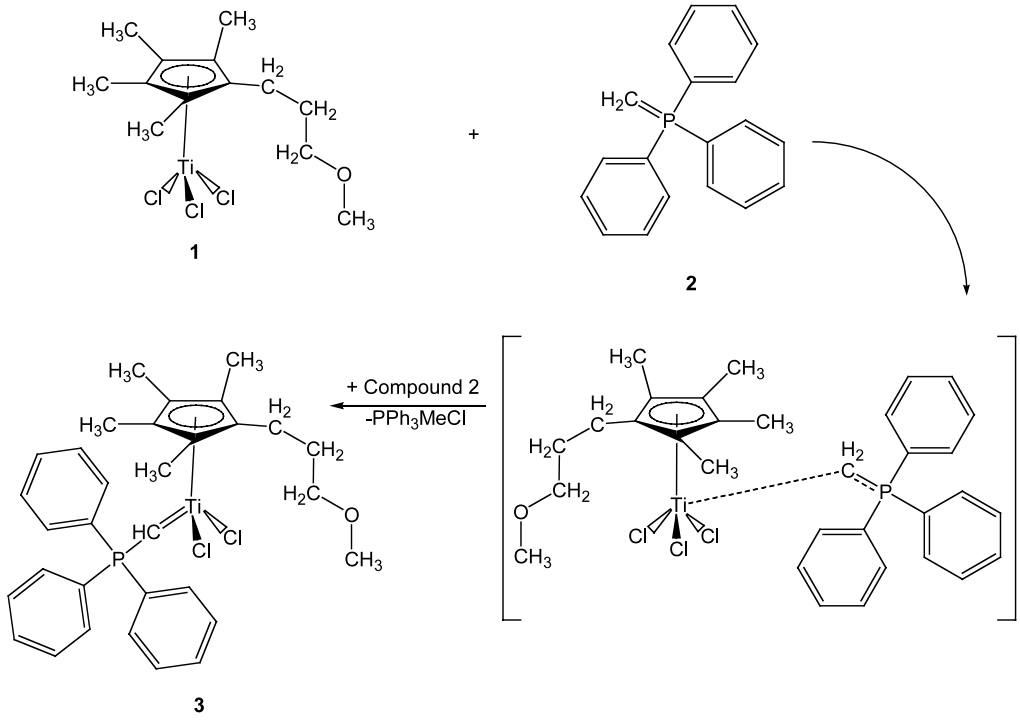


Fig. 1. First step in the two-step synthesis of the title complex.

energy than the dissociated singlet carbene and neutral phosphine [8,9].

From a structural point of view, in a phosporonium ylid the phosphorous atom is in a pseudo-tetrahedral environment, while the carbon atom has a pseudo-trigonal planar geometry. In addition, one of the H–P–C angles is slightly larger than the other two; the respective H–P bond length is also longer [6]. These features are characteristics of phosphorous ylids.

In a phosphorus ylid, the formally cationic phosphorus group has very stable unoccupied molecular orbitals (UMOs), including phosphorus 3d and P–H σ^* orbitals. The anionic carbon's highest occupied molecular orbital (HOMO) is of very high energy and can donate electron density into the UMOs on the phosphorus in a back-bonding manner. This back-bonding results in two strongly polarized τ (banana) bonds between phosphorous and carbon. Repulsion between the τ bonds and the P–H σ bond is responsible for the larger C–P–H bond angle and corresponding P–H bond length [7].

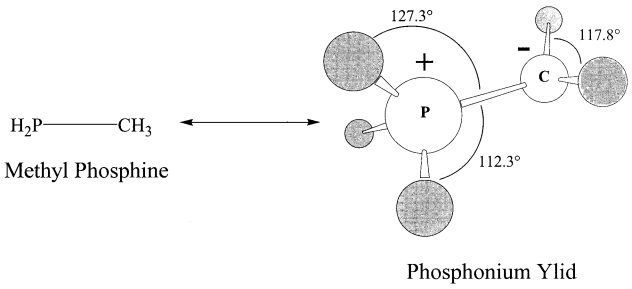


Fig. 3. Structural characteristics of the simplest phosphorus ylid [6].

Phosphorus ylids are Brønsted bases with phosphonium salts as conjugate acids. This basicity permits

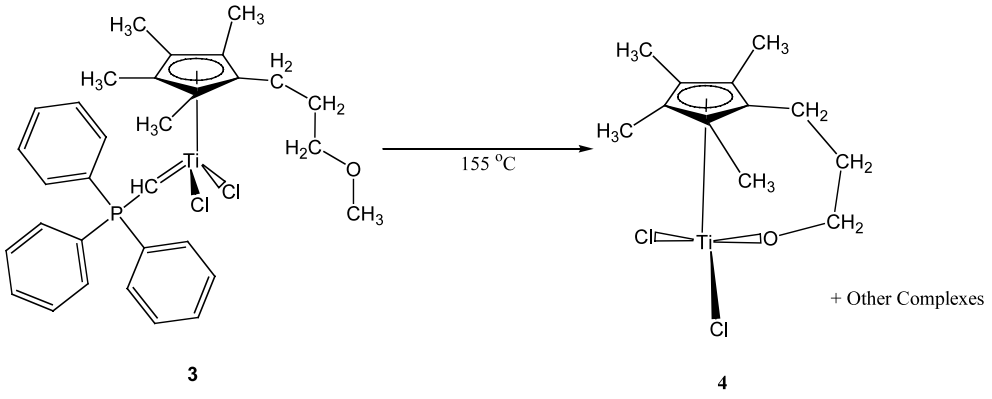


Fig. 2. Second step in the two-step synthesis of the title complex.

strong acid phosphonium salts and strong base phosphorus ylids to undergo transylidation reactions, such as the one shown in Fig. 1 [10]. As a ligand, the ylid can be either neutral or anionic which in turn leads to a plethora of ylid-metal coordination modes. A few of these modes, relevant to this work, are depicted in Fig. 4. The coordination modes illustrate the utility of ylids in forming metal carbon bonds. Another advantage ylids maintain is the presence of a β onium group that stays in the product after attachment to the metal center(s).

2. Details of the calculations

The structure of complex **4** was obtained by optimizing [12] crystal structure parameters for this molecule [1]. The optimized structure of **4** was then used to construct the initial coordinates in the optimization of all compounds via the Gaussian 98^{TM} [11] geometry optimization algorithm [12]. The Gaussian 98^{TM} [11] suite of programs were employed to solve Schrödinger's equation using the Hartree–Fock–Roothaan Self-Consistent-Field method [13]. The triple zeta basis set, 6-311G, successfully represents titanium but lacks the required polarization functions for carbon and phosphorus [7]. Therefore, all reported values were calculated from restricted Hartree–Fock optimized structures using the 6-311G(d) basis set provided in Gaussian [14–21].

In order to increase the speed of the calculations and simplify the analysis of the results, the methyl groups on the substituted cyclopentadienyl ligand (Cp*) were replaced by hydrogen atoms (Cp). The results shown in Table 1 indicate that the substitution had negligible effects on the results of the calculations.

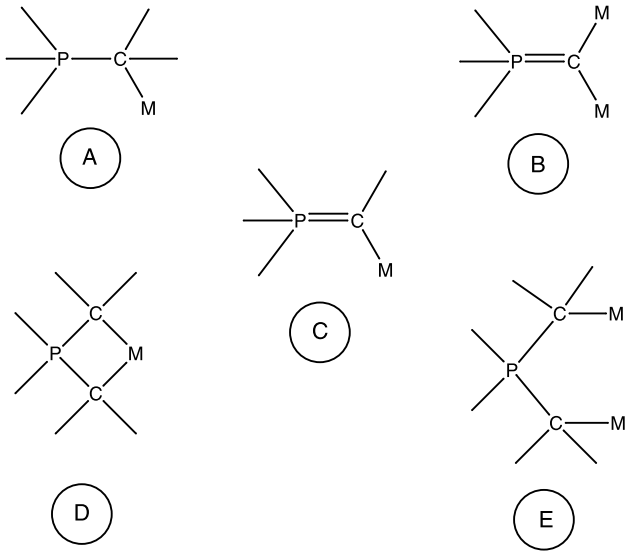


Fig. 4. A sample of possible coordination modes between the phosphorus ylid ligand and transition metals [10].

Table 1
A comparison of the energy (in hartrees) of selected molecular orbitals of complex **4**

Molecular orbital	Complex **4** with Cp	Complex **4** with Cp*
LUMO	0.0507	0.0726
HOMO	−0.3708	−0.3457
SHOMO	−0.3748	−0.3472
HOMO–LUMO gap	0.3201	0.2731

Gaussian 98^{TM} was executed on either a Gateway^{TM} E-5200 computer or the National Computational Science Alliance's HP-Convex Exemplar X-Class Scalable Supercomputer located at the University of Kentucky.

3. Results and discussion

Discussion of the data begins with an analysis of the role of the phosphorus ylid in the two-step synthesis. We turn first to the phosphonium ylid: this molecule is known to have one larger H–P–C bond angle and one longer H–P bond length. It also displays pseudo-tetrahedral geometry at the phosphorus center and pseudo-trigonal planar geometry at the carbon. Table 2 shows that **2**, the free ylid in the synthesis, diplays these structural characteristics. This is also evident in Fig. 3.

When bonded in complex **3**, methylenetriphenylphosphorane, **2** exhibits structural characteristics similar to those of the free ylid, except that the unique bond angle and length are smaller than their counterparts in the free ylid. The longer P–X bond lengths are expected, due to the increased steric requirement of the phenyl substituents. The C–H bond length remains almost exactly the same as in the free ylid, while the C–P bond length increases to accommodate the larger Ti group on the ylidic carbon. Zwitterionic character persists between the carbon and phosphorus atoms in **3**, as evident in Table 2. As expected the phosphorus ylid structural trends reappear in methylated **2**, one of the side products of the second synthetic reaction.

Titanium-ylid bonding in **3** can be described by the two resonance structures in Fig. 5. Teuben and associates reported form B as the major contributor [1], but this implies a partial negative charge on the titanium atom, which does not agree with the results of the calculations. These indicate that form A is the major contributor, as specified by the partially positive titanium atom and partially negative ylidic carbon in Table 3.

The site of attack in Reaction 2 is now considered, where an intramolecular nucleophilic attack was proposed as the probable mechanism [1]. Intramolecular

Table 2
Selected ylid structural characteristics

	Phosphonium ylid	Compound **2** [22]	Complex **3**	Methylated compound **2**
Bond lengths (Å)				
C_{ylid}–P	1.668	1.672	1.722	1.671
P–X	1.392, 1.392, 1.420	1.827, 1.855, 1.831	1.836, 1.835, 1.816	1.833, 1.859, 1.831
C_{ylid}–H	1.076, 1.076	1.076, 1.077	1.079	1.079
C_{ylid}–X			(Ti) 1.945	(Me) 1.515
Bond angles (°)				
C_{ylid}–P–X	112.3, 112.3, 127.9	109.8, 109.6, 121.0	110.8, 113.8, 114.8	111.8, 108.3, 120.7
H–C_{ylid}–P	117.7, 117.7	118.0, 118.6	107.8	113.8
X–C_{ylid}–P			(Ti) 133.5	(Me) 124.9

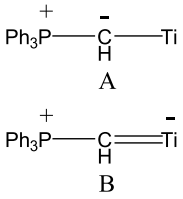


Fig. 5. The two resonance structures representing titanium–ylid bonding in complex **3**.

nucleophilic attacks can be orbital or charge controlled. If the attack is orbital controlled, the nucleophilic site is expected to be at the HOMO of complex **3**, while its LUMO would be localized at the electrophilic site. In this reaction, the HOMO should be on the ylidic carbon and the LUMO on the methoxy group. From Figs. 6 and 7 we discern that this is not the case. Although **3**'s HOMO does exhibit electron density at the ylidic carbon there is a complete absence of the LUMO on the methoxy group.

On the other hand, a charge-controlled reaction is one in which the nucleophilic site carries the largest negative charge and the electrophilic site carries the largest positive charge. For **3** we would expect the ylidic carbon to carry a partial negative charge and the methoxy carbon to carry a partial positive charge. Reaction 2 does appear to be charge controlled as portrayed by Table 3 data. We now turn to the bonding characteristics of **4**.

When investigating bonding in an organometallic complex containing a Cp ring, hapticity can not be

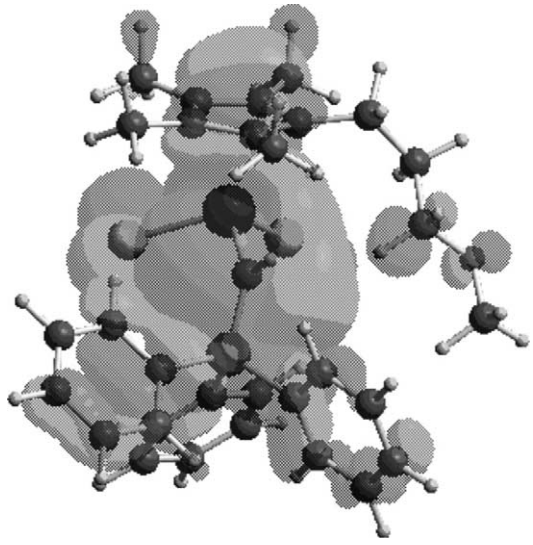


Fig. 6. The HOMO of complex **3**.

ignored. Cp rings commonly display η^5 hapticity but have been known to exhibit η^1 or η^3 bonding [23]. The Mulliken overlap population analysis of **4** contained in Table 4, indicates that the amount of electron density between the titanium atom and each of the cyclopentadienyl carbons is not exactly equal, as predicted for true η^5-type bonding. The Cp ring exhibits ring slippage as expected due to the constraining propoxy chain as seen in Fig. 8.

Another bond of interest in **4** is the titanium–oxygen bond. We know the titanium–chlorine bond in **4** is a

Table 3
Mulliken net atomic charges, with hydrogen's net atomic charge summed into heavy atoms, for selected atoms

Compound	Ti	C_{ylid}	P	O	$C_{methoxy}$
1	1.50			−0.45	0.22
2 [23]		−0.62	1.24		
3	1.67	−1.05	1.42	−0.45	0.21
4	1.68			−0.73	
Methylated **2**		−0.60	1.28		−0.01
Phosphonium ylid		−0.55	0.55		
Methylated phosphonium ylid		−0.55	0.54		

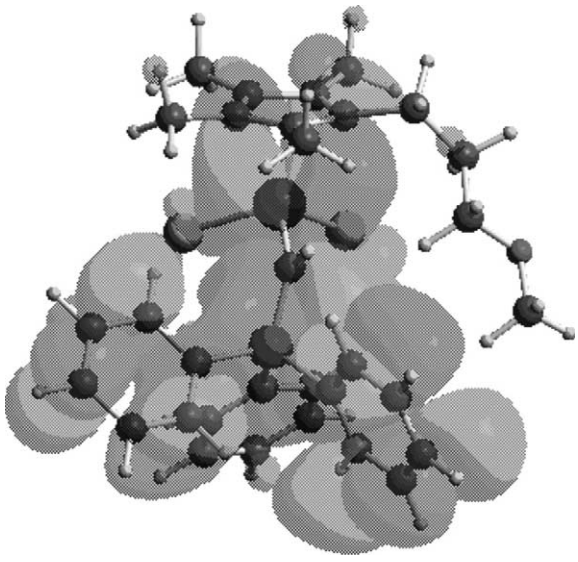


Fig. 7. The LUMO of complex **3**.

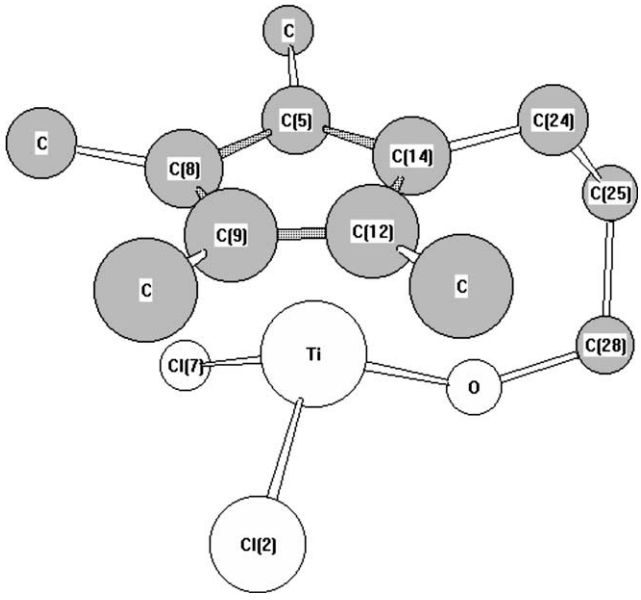


Fig. 8. Structure of complex **4**. Hydrogen atoms are not shown for clarity.

Table 4
Mulliken overlap populations for relevant bonds in **4**

Bond	Overlap population
Ti–Cl(2)	0.1954
Ti–Cl(7)	0.1960
Ti–O	0.1594
O–C(28)	0.1827
C(28)–C(25)	0.3221
C(25)–C(24)	0.2838
C(24)–C(14)	0.2313
Ti–C(14)	0.0297
Ti–C(12)	0.0419
Ti–C(9)	0.0559
Ti–C(8)	0.0617
Ti–C(5)	0.0461

single bond with an overlap density of about 0.20 electrons. **4**'s titanium–oxygen bond exhibits an overlap of 0.13 electrons and can, therefore, also be considered a single bond.

4. Conclusion

The bonding and reactivity of Complex **3** and **4** in Reactions 1 and 2 were investigated via ab initio Hartree–Fock calculations at the 6-311G(d) basis set level. Results of the calculations indicate that methylenetriphenylphosphorane continues to exhibit structural and electronic properties characteristic of ylids when bonded to the titanium center in **3**. In addition, the Ti–O bond in **4** is a single bond, while the cyclopentadienyl ring exhibits a slight degree of ring slippage, due to constraints imposed by the linking propoxy arm. The titanium–ylid bonding in **4** can be described by two resonance structures. Of these two structures, the predominant form has a partial positive charge on the phosphorus atom, a partial negative charge on the ylidic carbon, and a single bond between the ylidic carbon atom and the titanium center.

The intramolecular nucleophilic attack occurring in the second step of the synthesis is charge controlled. In this step, **3**'s partially negative ylidic carbon attacks the partially positive carbon of the dangling methoxy group.

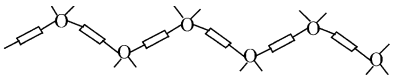
Acknowledgements

The authors acknowledge generous support from the National Computational Science Alliance in the form of supercomputer reseources. J.L.S. also acknowledges support from the University Honors Program and the Office of the Provost at Eastern Michigan University. Special thanks are extended to Hrant P. Hratchian and Shaun B. Beier for helpful and insightful discussions throughout this project.

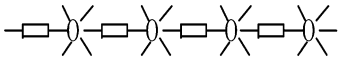
References

[1] R. Fandos, A. Meetsma, J.H. Teuben, Organometallics (1991) 59.
[2] H. Staudinger, J. Meyer, Helv. Chim. Acta 2 (1919) 619.
[3] A.W. Johnson, Ylides and Imines of Phosphorus, Wiley, New York, 1993.
[4] W.C. Kaska, Coord. Chem. Rev. 48 (1983) 1.
[5] H. Schmidbaur, Angewandte Chemie Int. Edn. 22 (1983) 907 (English).
[6] T.H. Dunning Jr., P.J. Hay, in: H.F.S. (Ed.), Methods of Electronic Structure Theory III, Plenum, New York, 1977, Chapter 1.

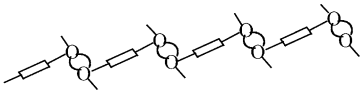
[7] D.A. Dixon, Theoretical description of the bonding in ylides, in: A.W. Johnson (Ed.), Ylides and Imines of Phosphorus, Wiley, New York, 1993.
[8] B.F. Yates, W.J. Bouma, L.J. Radom, J. Am. Chem. Soc. 106 (1984) 5805.
[9] B.F. Yates, W.J. Bouma, L.J. Radom, J. Am. Chem. Soc. 109 (1987) 2250.
[10] H.J. Bestmann, Chem. Ber. 95 (1962) 58.
[11] M.J. Frisch, G.W. Trucks, H.B. Schlegel, G.E. Scuseria, M.A. Robb, J.R. Cheeseman, V.G. Zakrzewski, J.A. Montgomery, R.E. Stratmann, J.C. Burant, S. Dapprich, J.M. Millam, A.D. Daniels, K.N. Kudin, M.C. Strain, O. Farkas, J. Tomasi, V. Barone, M. Cossi, R. Cammi, B. Mennucci, C. Pomelli, C. Adamo, S. Clifford, J. Ochterski, G.A. Petersson, P.Y. Ayala, Q. Cui, K. Morokuma, D.K. Malick, A.D. Rabuck, K. Raghavachari, J.B. Foresman, J. Cioslowski, J.V. Ortiz, B.B. Stefanov, G. Liu, A. Liashenko, P. Piskorz, I. Komaromi, R. Gomperts, R.L. Martin, D.J. Fox, T. Keith, M.A. Al-Laham, C.Y. Peng, A. Nanayakkara, C. Gonzalez, M. Challacombe, P.M.W. Gill, B. Johnson, W. Chen, M.W. Wong, J.L. Andres, C. Gonzalez, M. Head-Gordon, E.S. Replogle, J.A. Pople, Gaussian 98^{TM}; Revision A, seventh ed, Gaussian, Pittsburgh, PA, 1998.
[12] C.Y. Peng, P.Y. Ayala, H.B. Schlegel, M.J. Frisch, J. Comput. Chem. 17 (1996) 49.
[13] C.C.J. Roothaan, Rev. Mod. Phys. 23 (1951) 68.
[14] A.D. McLean, G.S. Chandler, J. Chem. Phys. 72 (1980) 5639.
[15] R. Krishnan, J.S. Binkley, R. Seeger, J.A. Pople, J. Chem. Phys. 72 (1980) 650.
[16] A.J.H. Wachters, J. Chem. Phys. 52 (1970) 1033.
[17] P.J. Hay, J. Chem. Phys. 66 (1977) 4377.
[18] K. Raghavachari, G.W. Trucks, J. Chem. Phys. 91 (1989) 1062.
[19] R.C.J. Binning, L.A. Curtiss, J. Comp. Chem. 11 (1990) 1206.
[20] L.A. Curtiss, M.P. McGrath, J.P. Blaudeau, N.E. Davis, R.C. Binning, L. Radom, J. Chem. Phys. 103 (1995) 6104.
[21] M.P. McGrath, L. Radom, J. Chem. Phys. 94 (1991) 511.
[22] S.B. Beier, Unpublished work.
[23] G.L. Miessler, D.A. Tarr, Inorganic Chemistry, 2nd ed, Prentice Hall, Upper Saddle River, NJ, 1999.



(a) 1-D zigzag-chain structures



(b) 1-D straight-chain structures



(c) 1-D stair-step structures

Fig. 1. Kinds of 1-D polymer chain.

2.2. Starting material

The complexes $Zn(NO_3)_2\cdot 6H_2O$ and $CoCl_2\cdot 6H_2O$ were used as obtained from commercial sources without further purification. The reagent PPz hexahydrate (PPz = piperazine) was purchased from Aldrich.

2.3. $[Zn(NCS)_2(PPz)]_n$ (1)

Compound **1** was obtained upon carefully laying a solution of $Zn(NO_3)_2\cdot 4H_2O$ (0.19 g, 1 mmol) and NH_4SCN (0.15 mg, 2 mmol) in methanol (5 ml) onto a solution of PPz (0.19 mg, 1 mmol) in methanol (5 ml). Large pale crystals formed and were collected by filtration to give a yield of 0.17 g (65%). *Anal*. Calc. for $C_{10}H_{20}N_6S_2Zn$ C, 26.89; H, 3.74; N, 20.92. Found: C, 26.79; H, 3.72; N, 21.27%. IR (KBr disk): 3218(m), 3127(m), 2987(s), 2928(s), 2858(s), 2077(m), 1426(m), 1319(m), 1265(s), 1190(s), 1141(s), 1103(m), 1077(s), 1017(m), 990(m), 872(m), 667(s), 625(s), 474(m).

2.4. $[CoCl_2(PPz)]_n$ (2)

Compound **2** was obtained upon carefully laying a solution of $CoCl_2\cdot 4H_2O$ (0.24 g, 1 mmol) in methanol (5 ml) onto a solution of PPz (0.19 g, 1mmol) in methanol (5 ml). Large blue crystals formed and were collected by filtration to give a yield of 0.11 g (52%). *Anal*. Calc. for $C_4H_{10}N_2Cl_2Co$ C, 26.89; H, 4.63; N, 20.92. Found: C, 26.61; H, 4.53; N, 20.13%. IR (KBr disk): 3203(br), 2976(m), 2949(s), 2825(s), 2373(m), 1658(s), 1572(s), 1464(s), 1421(s), 1125(s), 1098(m), 1071(s), 883(m), 641(s), 528(s).

3. X-ray crystallography

The diffraction data of each compound was collected on a Siemens P4 diffractometer using graphite-monochromated Mo Kα ($\lambda_\alpha = 0.71073$ Å) radiation. Data reduction was carried out by standard methods [12].

The positions of the heavy atoms, including zinc atoms, were located by the direct method. The remaining atoms were found in a series of alternating difference Fourier maps and least-square refinements [13]. Basic information pertaining to crystal parameters and structure refinement is summarized in Table 1, selected bond distances and angles are listed in Table 2 for **1** and Table 3 for **2**.

Table 1
Crystal data for $[Zn(NCS)_2(PPz)]_n$, **1**, and $[CoCl_2(PPz)]_n$, **2**

	1	**2**
Formula	$C_6H_{10}N_4S_2Zn$	$C_4H_{10}N_2Cl_2Co$
FW	267.67	215.97
Crystal system	triclinic	monoclinic
Space group	$P\bar{1}$	$P2(1)/n$
a (Å)	7.4145(4)	6.3612(6)
b (Å)	8.1805(9)	10.223(1)
c (Å)	9.5248(7)	12.125(1)
α (°)	92.839(7)	90
β (°)	110.263(6)	103.531(7)
γ (°)	92.162(7)	90
V (Å^3)	540.37(8)	766.6(1)
Z	2	4
d_{calc} (g cm^{-3})	1.645	1.871
Crystal size (mm)	0.24 × 0.4 × 0.8	0.16 × 0.22 × 0.42
μ (Mo Kα) (mm^{-1})	2.620	2.847
Radiation monochromated in incident beam (λ (Mo Kα) (Å))	0.71073	0.71073
Range (2θ) for data collection (°)	$4.56 \le 2\theta \le 55.00$	$5.28 \le 2\theta \le 55.00$
Reflections collected	8036	2471
Independent reflections	2467 [$R_{int} = 0.0084$]	1762 [$R_{int} = 0.0255$]
Data/restraints /parameters	2464/0/159	1762/0/114
Quality-of-fit indicator [c]	1.136	1.078
Final R indices [$I > 2\sigma(I)$] [a,b]	$R_1 = 0.0294$, $wR_2 = 0.0697$	$R_1 = 0.0268$, $wR_2 = 0.0576$
R indices (all data)	$R_1 = 0.0355$, $wR_2 = 0.0755$	$R_1 = 0.0395$, $wR_2 = 0.0787$
Largest difference peak and hole (e Å^{-3})	0.446 and −0.468	0.899 and −0.449

[a] $R_1 = \Sigma||F_o| - |F_c||/\Sigma|F_o|$.

[b] $wR_2 = [\Sigma\, w(F_o^2 - F_c^2)^2/\Sigma\, w(F_o^2)^2]^{1/2}$. $w = 1/[\sigma^2(F_o^2) + (ap)^2 + (bp)]$, $p = [\max(F_o^2 \text{ or } 0) + 2(F_c^2)]/3$. $a = 0.0292$, $b = 0.3885$ for **1**; $a = 0.0314$, $b = 0.0990$ for **2**.

[c] Quality-of-fit = $[\Sigma\, w(|F_o^2| - |F_c^2|)^2/(N_{observed} - N_{parameters})]^{1/2}$.

Table 2
Selected bond distances (Å) and angles (°) for $[Zn(NCS)_2(PPz)]_n$

Bond distances			
Zn(1)–N(1)	1.940(3)	Zn(1)–N(2)	1.953(3)
Zn(1)–N(4)	2.037(2)	Zn(1)–N(3)	2.039(2)
S(1)–C(1)	1.619(3)	S(2)–C(2)	1.615(3)
N(1)–C(1)	1.147(4)	N(2)–C(2)	1.149(4)
N(3)–C(3)	1.480(3)	N(3)–C(4)	1.485(3)
N(4)–C(6)	1.477(3)	N(4)–C(5)	1.485(4)
Bond angles			
N(1)–Zn(1)–N(2)	108.7(1)	N(1)–Zn(1)–N(4)	105.8(1)
N(2)–Zn(1)–N(4)	110.6(1)	N(1)–Zn(1)–N(3)	114.5(1)
N(2)–Zn(1)–N(3)	108.3(1)	N(4)–Zn(1)–N(3)	108.94(8)
C(1)–N(1)–Zn(1)	162.1(3)	C(2)–N(2)–Zn(1)	161.4(3)
C(3)–N(3)–C(4)	110.2(2)	C(3)–N(3)–Zn(1)	112.4(2)
C(4)–N(3)–Zn(1)	112.7(2)	C(6)–N(4)–C(5)	109.6(2)
C(6)–N(4)–Zn(1)	112.1(2)	C(5)–N(4)–Zn(1)	113.7(2)
N(1)–C(1)–S(1)	178.7(3)	N(2)–C(2)–S(2)	178.3(3)
N(3)–C(3)–C(4A)	111.6(2)	N(3)–C(4)–C(3A)	112.5(2)
N(4)–C(5)–C(6A)	112.1(3)	N(4)–C(6)–C(5A)	112.2(2)

Table 3
Selected bond distances (Å) and angles (°) for $[CoCl_2(PPz)]_n$

Bond distances			
Co(1)–N(2)	2.042(2)	Co(1)–N(1)	2.064(2)
Co(1)–Cl(1)	2.2467(8)	Co(1)–Cl(2)	2.2470(8)
N(1)–C(2)	1.484(3)	N(1)–C(1)	1.486(4)
N(2)–C(4)	1.488(3)	N(2)–C(3)	1.488(3)
Bond angles			
N(2)–Co(1)–N(1)	108.86(9)	N(2)–Co(1)–Cl(1)	111.55(7)
N(1)–Co(1)–Cl(1)	111.65(7)	N(2)–Co(1)–Cl(2)	107.29(7)
N(1)–Co(1)–Cl(2)	112.22(7)	Cl(1)–Co(1)–Cl(2)	105.18(3)
C(2)–N(1)–C(1)	109.7(2)	C(2)–N(1)–Co(1)	109.5(2)
C(1)–N(1)–Co(1)	112.5(2)	C(4)–N(2)–C(3)	109.3(2)
C(4)–N(2)–Co(1)	113.4(2)	C(3)–N(2)–Co(1)	108.3(2)

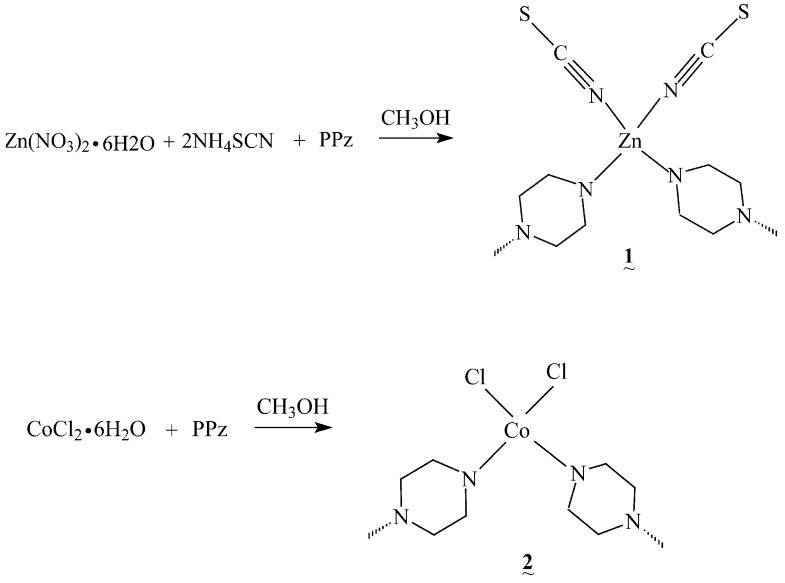
4. Results and discussion

4.1. Syntheses and spectroscopic studies

The reaction pathways are shown in Scheme 1. The IR spectrum of the complex **1** clearly shows the existence of PPz and thiocyanate molecules. The absorption bands at 2077, 872 and 474 cm^{-1} correspond to ν(C≡N), ν(C–S) and δ(N≡C–S), respectively, consistent with terminally nitrogen-bonded NCS^- group [14]. The complexes **1**–**2** contain characteristic C–N and C–C vibrational frequencies of the ligand PPz. There is a shift of approximately 15 cm^{-1} of the absorption bands to higher frequencies as compared with those of the free PPz molecule.

4.2. Structure

The complex of **1** belongs to type a in Fig. 1 and forms a 1-D zigzag Zn–PPz–Zn chain. Fig. 2(a) shows the local coordination of the zinc center, and Fig. 2(b) shows an infinite one-dimensional chain. The distorted tetrahedral Zn(II) metal center is achieved by means of a single bridging PPz ligands and two terminal N-bonded NCS^- anions. There are one long Zn–N(PPz) bond (2.039(2) Å) and two short Zn–N (NCS) bonds (1.940(3) and 1.953(3) Å), again consistent with corresponding bond length in, for $[Zn(NCS)_2(PPz)]$ [15] molecules. The NCS^- groups are almost linear with an N–C–S angle of 178.7(3) Å. The connection between Zn atoms and NCS^- groups are bent with a C(1)–N(1)–Zn(1) angle of 162.1(3)°. The $[Zn(NCS)_2(PPz)]_n$ structures are linked into three-dimensional structure through NCS···H–N (S···H = 2.58(3) and 2.68(3)) interactions, which are formed between adjacent chains



Scheme 1. Reaction pathways for $[Zn(NCS)_2(PPz)]_n$ and $[CoCl_2(PPz)]_n$.

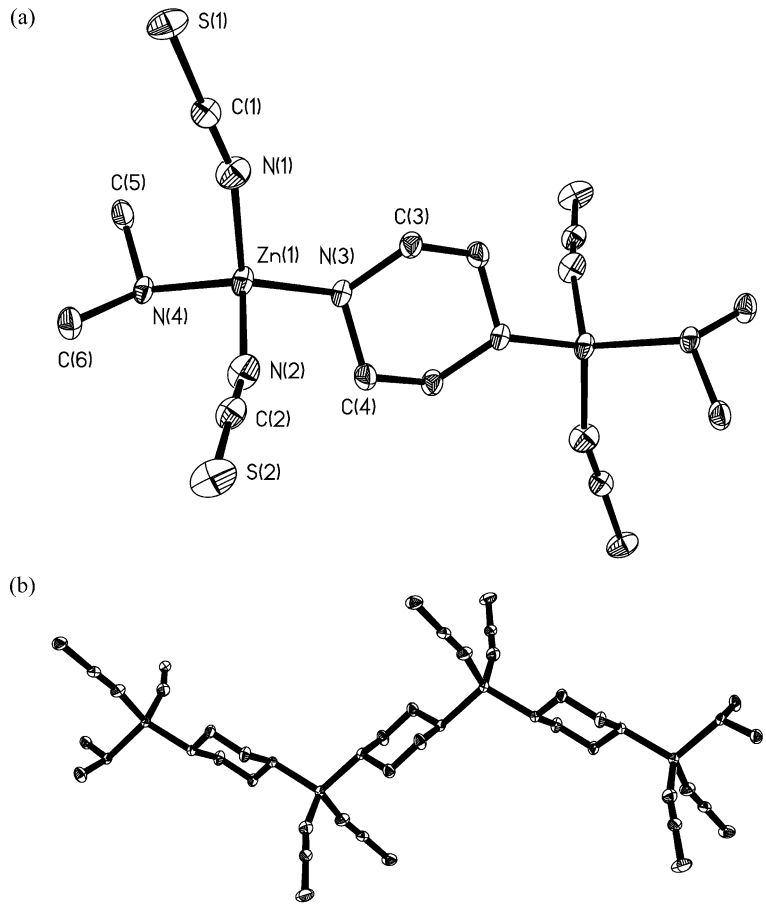


Fig. 2. (a) ORTEP drawing of the local coordination of Zn in **1**. (b) An infinite one-dimensional chain.

through the sulfur atoms and the amine hydrogen atoms of PPz molecules (Fig. 3).

In the structure of **2**, the Co center is coordinated to one PPz ligands and two Cl anions. Fig. 4(a) shows the

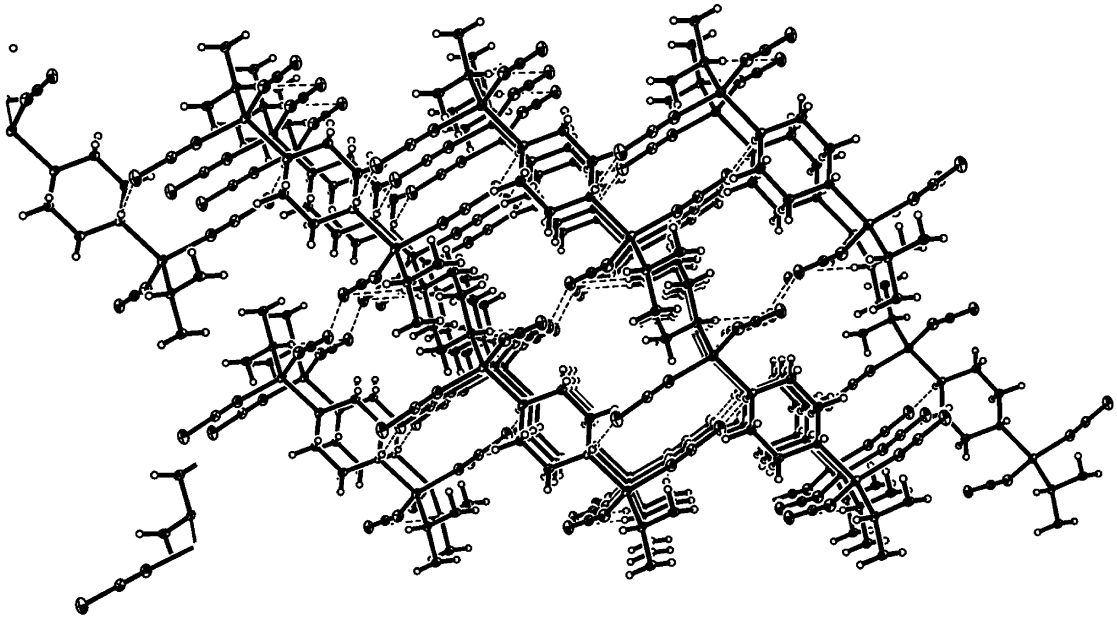


Fig. 3. Packing diagram of **1**, showing the crystal structures are linked via NCS···H–N interactions.

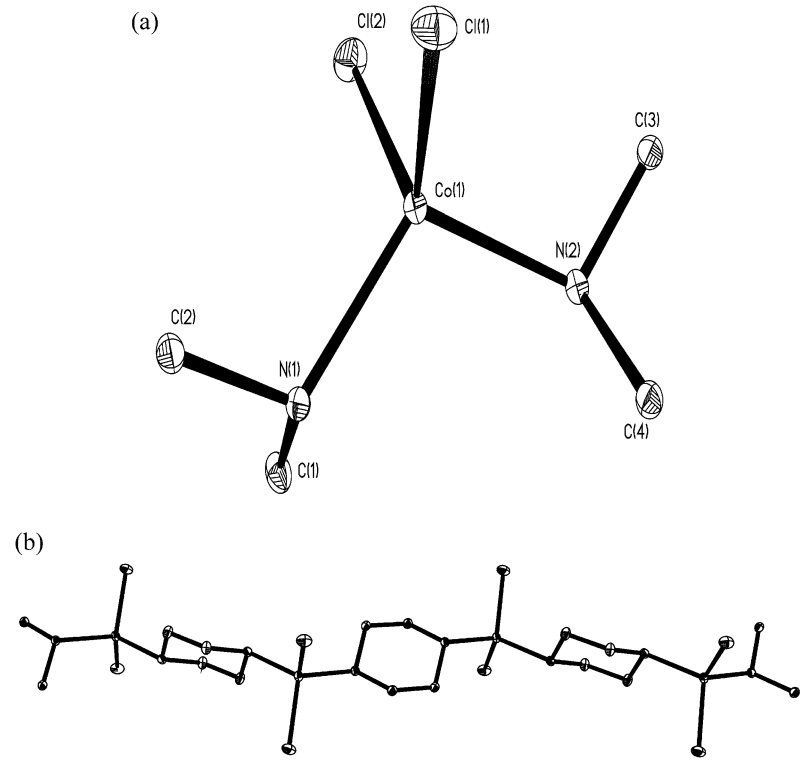


Fig. 4. (a) ORTEP drawing of the local coordination of Co in **2**. (b) An infinite one-dimensional chain.

local coordination of the zinc center, and Fig. 4(b) shows an infinite one-dimensional chain. The Co–Cl distances, which are 2.2467(8) and 2.2470(8) Å, respectively, are significantly shorter than those of molecular $Co_4Cl_8(C_4H_8O)_6$ (av. Co–(μ_2-Cl) = 2.400 Å) [16], $Co_3Cl_8(C_4H_8O)_2$ (av. Co–(μ_2-Cl) = 2.403 Å) [17] and polymeric $[CoCl_2(H_2O)_2][HN(CH_3)_3Cl]$ (av. Co–(μ_2-Cl) = 2.480 Å) [18], $CoCl_2(DMSO)_2$(4,4-bipy) (Co–Cl = 2.4707(5)) [19] and $CoCl_2(Pyz)_2$ [20]. The Cl–Co–Cl angle is 105.18(3)° and the N(2)–Co–N(1) angle is 108.86(9)°.

The ability of metal chloride complexes to act as hydrogen bond acceptors has been investigated and designed structures have been successfully prepared [21]. The existence and structural importance of weak C–H···X hydrogen-bonding interaction are now well

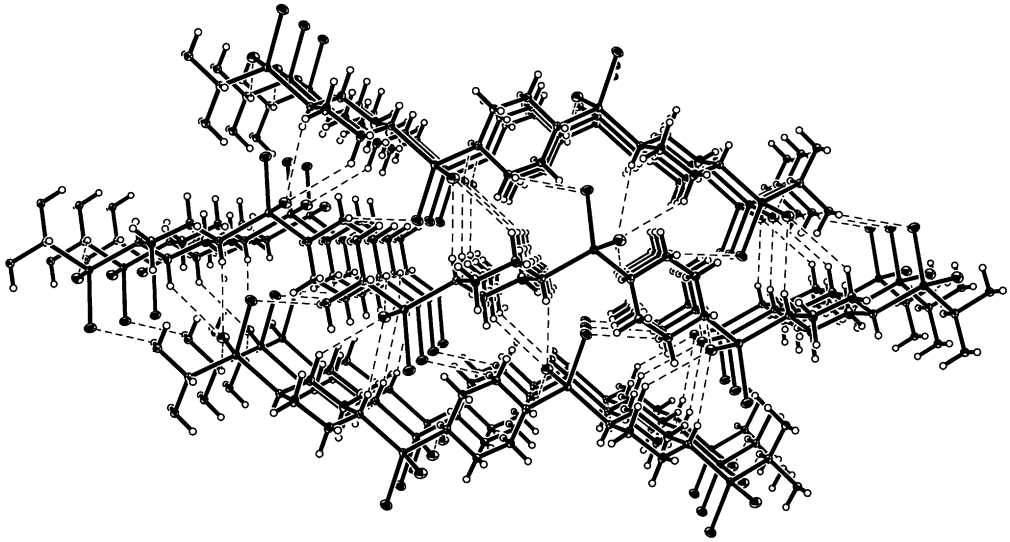


Fig. 5. Packing diagram of **2**, showing the crystal structures are linked via N–H···Cl–M and C–H···Cl–M interactions.

established [22] and are observed in many compounds, such as the N···H–C interaction in 1,3,5-tricyanobenzene-hexamethylbenzene [23], the O···H–C interaction in $(C_{14}H_{12}N_2)[Cu(opba)]\cdot 3H_2O$ and $Na_2C_{12}H_{12}N_2[Cu(opba)]_2\cdot 4H_2O$ (opba = *o*-phenylenebis(oxamate)) [24], and the Cl···H–C interaction in CuCl(Pyz) [25], $CdCl_2$(Pyz) [26] and Cu_2Cl_2(Pyz) [27]. In complex **2**, linkage into a three-dimensional structure is achieved through three N–H···Cl–M (H···Cl = 2.75(2), 2.83(3) and 2.87(2) Å ∠ N–H···Cl = 57(2)°, 142(2)° and 152(1)°) and one C–H···Cl–M (H···Cl = 2.82(2) Å, ∠ C–H···Cl = 72.2(4)°) hydrogen bonds (Fig. 5).

5. Supplementary material

Crystallographic data (excluding structure factors) for the structures in this paper has been deposited with the Cambridge Crystallographic Data Center as CCDC Nos. 187495 and 187496. Copies of the data can be obtained free of charge on application to The Director, CCDC, 12 Union Road, Cambridge, CB2 1EZ, UK (fax: +44-1223-336033 or e-mail: deposit@ccdc.cam.ac.uk or www: http://www.ccdc.cam.ac.uk).

Acknowledgements

The researchers wish to thank the Nanya Institute of Technology of the Republic of China for support.

References

[1] M. Maekawa, K. Sugimoto, T. Kuroda-Sowa, Y. Sucenaga, M. Munakata, J. Chem. Soc., Dalton Trans. (1999) 4357.
[2] (a) M. Li, Z. Xu, X. You, Z. Dong, G. Guo, Polyhedron 12 (1993) 921;
(b) A.S. Batsanov, M.J. Begley, P. Hubberstey, J. Stroud, J. Chem. Soc., Dalton Trans. (1996) 1947;
(c) A.J. Blake, S.J. Hill, P. Hubberstey, W.-S. Li, J. Chem. Soc., Dalton Trans. (1998) 909;
(d) B.F. Abraham, B.F. Hoskins, G. Winter, Aust. J. Chem. 43 (1990) 1759.
[3] M. Andruh, H.W. Roesky, M. Noltemeyer, H.-G. Schmidt, Z. Naturfosch., Teil. B 49 (1994) 31.
[4] R.-G. Xiong, Z. Yu, C.-M. Liu, X.-Z. You, Polyhedron 15 (1997) 2667.
[5] (a) D.-L. Zhu, Y.-P. Yu, G.-C. Guo, H.-J. Zhuang, J.-S. Huang, O. Liu, Z. Xu, X.-Z. You, Acta Crystallogr., Sect. C 52 (1996) 1963;
(b) J.T. Sampanthar, J.J. Vittal, J. Chem. Soc., Dalton Trans. (1999) 1993.
[6] (a) F. Kubel, J. Strahle, Z. Naturforsch., Teil. B 37 (1982) 272;
(b) J. Lu, C. Yu, T. Niu, T. Paliwale, G. Crisci, F. Somosa, A. Jacobson, Inorg. Chem. 37 (1999) 4637.
[7] R.W. Gable, B.F. Hoskins, G. Winter, Inorg. Chim. Acta 96 (1985) 151.
[8] I. Lange, E. Wieland, P.G. Jones, A. Blaschette, J. Organomet. Chem. 458 (1993) 57.
[9] K.-B. Yu, S.-H. Gou, X.-Z. You, Z. Xu, Z. Naturforsch., Teil. C 47 (1991) 2653.
[10] B.F. Abraham, B.F. Hoskins, G. Winter, Aust. J. Chem. 43 (1990) 175.
[11] (a) P.-J. Prest, J.S. Moore, Acta Crystallogr., Sect. C 52 (1996) 2176;
(b) J. Lu, G. Crisic, T. Niu, A.J. Jacobson, Inorg. Chem. 36 (1997) 5140;
(c) P.M. Slangen, P.J.V. Koningsbruggen, J.G. Haasnoot, J. Jansen, S. Gorter, J. Reedijk, H. Kooijman, W.J.J. Smeels, A.L. Spek, Inorg. Chim. Acta 212 (1993) 289.
[12] XSCANS, Release 2.10b, Siemens Energy and Automation Inc., Madison, WI, 1994.
[13] G.M. Sheldrick, SHELXTL, Release 5.03, Siemens Analytical X-ray Instruments, Karlsruche, Germany, 1993.
[14] I.S. Ahuja, R. Singh, C.L. Yadava, J. Molec. Struct. 74 (1981) 143.
[15] V.N. Kokozey, S.R. Petrusenko, A.V. Sinkevich, Y.A. Simonov, Ukra. Khim. Zhur. 59 (1993) 236.
[16] P. Sobota, Z. Olejnik, J. Utko, T. Lis, Polyhedron 12 (1993) 613.
[17] C. Von Hamisch, D. Fenske, F. Weigend, R. Ahlrichs, J. Chem. 3 (1997) 1494.
[18] D.B. Losee, J.N. Mceleaney, G.E. Shankle, R.L. Carlin, Phys. Rev. B 8 (1973) 2185.
[19] J. Lu, C. Yu, T. Niu, T. Paliwala, G. Crisci, F. Somosa, A.J. Jacobson, Inorg. Chem. 37 (1998) 4637.
[20] P.W. Carreck, M. Goldstein, E.M. McPartlin, W.D. Unsworth, Chem. Commun. (1971) 164.
[21] (a) G. Aullon, D. Bellamy, L. Brammer, E.A. Bruton, A.G. Orpen, Chem. Commun. (1998) 653;
(b) A.L. Gillon, G.R. Lewis, A.G. Orpen, S. Rotter, J. Starbuck, X.-M. Wang, Y. Rodriguez-Martin, C. Ruiz-Perez, J. Chem. Soc. Dalton Trans. (2000) 3897.
[22] G.R. Desiraju, Acc. Chem. Res. 29 (1996) 441.
[23] D.S. Reddy, B.S. Goud, K. Panneersel, G.R. Desiraju, J. Chem. Soc. Chem. Commun. (1993) 663.
[24] I. Unamuno, J.M. Guterrez-Zorrilla, A. Luque, P. Roman, L. Lezama, R. Calvo, T. Rojo, Inorg. Chem. 37 (1998) 6452.
[25] R. Kuhlman, G.L. Schimek, J.W. Kolis, Polyhedron 18 (1999) 1379.
[26] R.D. Balley, W.T. Pennington, Polyhedron 16 (1997) 417.
[27] S. Kawata, S. Kitagawa, H. Kumagai, S. Iwabuchi, M. Katada, Inorg. Chim. Acta 267 (1998) 143.

by an unusual conformation of the puckered chelate ring where the methyl group will occupy an axial position. The structure of analogous coordination compounds can be understood or predicted on this basis. X-ray structure of Cu(II) complexes with Schiff base derived from propanediamine and salicylaldehyde [8] reveals that Cu(II) is five-coordinated with water molecule in axial position, but others [9,10] found Cu(II) in the complex with the same Schiff base in six-coordination. However, there is an evidence of the essentially four-coordinated nearly planar copper(II) in the discussed type of Schiff bases complexes [11,12]. The diversity of structures and properties of the Cu(II) complexes with Schiff bases derived from acetylacetone or salicylaldehyde depends on the donors field strength and thus to view that the p- and π*-orbitals of the ligand are important but there is also a stereochemical impact on the geometry of Cu(II) coordination sphere.

The structure of Schiff base coordination compounds derived from substituted 1,2-cyclohexanediamines and 2-hydroxy-3- and 2-hydroxy-5-methylbenzaldehyde have not been studied and it is presently not possible to predict how the ligands orient themselves around the metal ion. The electronic structure of a benzylaldimine is less suited for stereochemical studies, by means of CD, because of the low effective symmetry so that the internal $\pi \rightarrow \pi^*$ transition moments are found to have directions far from the N–O line or its perpendicular order in the plane of the molecule. Thus an earlier study on such salicylaldimine copper(II) compounds has not tried to relate CD to electronic or geometric structure. In a series of the studied metal complexes containing π–π conjugated ligand the reactivity of the complexes and the redox potential of the central metal are sensitive to the nature of the substituents on the chelate ring [13]. CD spectra of transition metal complexes have been extensively studied in recent years as their interpretation can yield valuable information concerning the origin of absorption bands in the electronic spectra of complexes [14–17]. The sensitivity of CD on a molecular structure makes the technique valuable for investigation of the chelate ring conformation and configuration and these will be discussed in the present work.

2. Experimental

2.1. Materials

$Cu(AcO)_2 \cdot H_2O$, $Co(AcO)_2 \cdot 4H_2O$, $Ni(AcO)_2 \cdot 4H_2O$ (analytical grade) were purchased from POCh (Gliwice, Poland); 2-hydroxy-3-methylbenzaldehyde (98%), 2-hydroxy-5-methylbenzaldehyde (99%) were purchased from Aldrich. *trans*-(1*R*,2*R*)-(−)-1,2-cyclohexanediammonium $(+)_D$-tartrate [(−)-chxn(+)tart], was prepared according to Galsbol et al. [18] and employed to obtain (1*R*,2*R*)-*trans*-(−)-cyclohexanediamine (−)-chxn, which was used in situ or isolated for Schiff bases synthesis.

2.2. Instrumentation

UV–Vis absorption spectra were recorded on a Milton Roy Spectronic 1201 in CH_3CN (1×10^{-5} M) solution and with a Specord M-40 (Carl Zeiss Jena) spectrophotometer as Nujol mulls. IR spectra were performed on a Spectrum 2000 Perkin–Elmer FT IR using KBr pellets in the range 400–4000 cm^{-1} and PE discs in 400–200 cm^{-1}. ^1H NMR spectra were collected with a Varian Gem. 1200 MHz in $CDCl_3$ for diamagnetic and paramagnetic complexes. Paramagnetic complexes spectra were measured in 0.003 M solution, data block size 8K, acquisition time 0.256 s and relaxation delay (RD) 0 s at 295 K. CD spectra were measured with a JASCO 715 spectropolarimeter in 800–180 nm range for the same solution as for UV–Vis.

2.3. Synthesis

2.3.1. Syntheses of Schiff bases

(−)-Chxn 1.82 g (16 mmol) and 2-hydroxy-5-methylbenzaldehyde 4.35 g (32 mmol) or 2-hydroxy-3-methylbenzaldehyde (32 mmol) in EtOH solutions were stirred under reflux for 2 h. The yellow solution of the Schiff base was evaporated to the dryness on a rotary evaporator and recrystallized from ethanol. Schiff bases were characterized with ^1H NMR (−)-chxn-(3-methylbaH)$_2$: 1.4–1.9 (m-8H), 3.29, 3.31, 3.34 (t-2H) 8.24 (s-4H), 2.24 (s-6H), 13.6 (s-2H), 6.67–7.14 (m-8H), (−)-chxn-(5-methylbaH)$_2$ 1.25–1.96 (m-8H), 3.27, 3.29, 3.31 (t-2H), 8.19 (s-2H), 2.21 (s-6H), 13.05 (s-2H), 6.77–7.07 (m-8H) ppm. IR (−)-chxn-(3-methylbaH)$_2$: 1624 cm^{-1} ν(CN), 3437 cm^{-1} ν(OH), (−)-chxn-(5-methylbaH)$_2$: 1628 cm^{-1} ν(CN), 3433 cm^{-1} ν(OH).

2.3.2. Syntheses of complexes

Cobalt(II), copper(II) and nickel(II) complexes were obtained as follows: $Co(AcO)_2 \cdot H_2O$ 1.95 g (10 mmol) was dissolved in hot MeOH and added to the stirred deoxygenated ligand 3.5 g (10 mmol) solution in *n*-PrOH, under argon. The precipitate appeared immediately and the reaction mixture was stirred and heated under reflux for 30 min, to complete the reaction. The complex was filtered, washed and dried on a vacuum line. $Ni(AcO)_2 \cdot 4H_2O$ (2.5 g–10 mmols) or $Cu(AcO)_2 \cdot H_2O$ (2 g–10 mmols) were dissolved in ethanol and stirred under reflux for 10 min, followed by the addition of the Schiff base 3.5 g (10 mmol) in ethanol and reaction mixtures were stirred upon heating for 1 h. Obtained precipitates were filtered, washed with methanol and dried in the air. Besides many attempts (chloromethane–benzene, dichloromethane–benzene,

acetonitrile–benzene) we were unable to obtain crystals suitable for X-ray analysis. Results of elemental analyses: [(Co(−)-chxn-(3-methylba)$_2$] (**1**) (Calc./Found) C (64.9/65.2); H (5.94/6.14); Co (14.5/14.7); N (6.9/6.53)%. [(Co(−)-chxn-(5-methylba)$_2$] (**2**) (Calc./Found) C (64.9/64.5); H (5.94/5.4); Co (14.5/14.2); N (6.9/6.4)%. [(Cu(−)-chxn-(3-methylba)$_2$] (**3**) (Calc./Found) C (64.2/64.5); H (5.9/5.5); Cu (15.4/15.1); N (6.8/6.2)%. [(Cu(−)-chxn-(5-methylba)$_2$] (**4**) (Calc./Found) C (64.2/64.5); H (5.9/6.0); Cu (15.4/15.6); N (6.8/6.7)%. [(Ni(−)-chxn-(3-methylba)$_2$] (**5**) (Calc./Found) C (64.9/65.1); H (5.9/6.3); N (6.9/6.7); Ni (14.4/14.6)%. [(Ni(−)-chxn-(5-methylba)$_2$] (**6**) (Calc./Found) C (64.9/65.3); H (5.9/5.8); N (6.9/6.3); Ni (14.4/14.3)%.

3. Results and discussion

3.1. CD and UV–Vis absorption spectra

The free ligand absorption spectra in acetonitrile revealed bands at 222 and 255 nm for (−)-chxn-(5-methylbaH)$_2$ and at 217 and 255 nm for (−)-chxn-(3-methylba)$_2$, which can be assigned to π–π* type transitions of the benzene ring. These bands in the spectra of **1**–**6** were detected in 220–230 and 242–270 nm ranges. The band from π–π* transition, which involves molecular orbital of C=N chromophore was detected for (−)-chxn-(5-methylbaH)$_2$ at 325 nm, whereas for (−)-chxn-(3-methylbaH)$_2$ at 321 nm [19–21]. Upon coordination the latter ones, in the spectra of **3**, **4** are shifted towards lower energies (372 nm), whereas for **1**, **2**, **5**, **6** in the range 320–410 nm several coinciding bands were observed.

CD spectra of [Co(−)-chxn-(3-methylba)$_2$] (**1**) and [Co(−)-chxn-(5-methylba)$_2$] (**2**) revealed bands at 578 (+0.33), 485.5 nm (−0.11), 463 nm (+0.10), and 415.5 (−2.89) nm for **1** and at 565.5 nm (+0.47), 412.5 nm (−1.63) for **2**, which derived from d–d transitions from xz, yz or z^2 to x^2-y^2 (Fig. 1). The higher energy CD components at 355.5 nm (−1.33) and 294 nm (+0.2), for **1**, and at 336.5 nm (−0.76) and 289.5 nm (+0.07) for **2** are all assigned to π→π* and ligand to metal charge transfer transitions. Bands from the π–π* transition of the benzene ring are localized at 244 nm (−4.66) and 217.5 nm (+2.01) for **1** and at 251 nm (−2.09) and 219 nm (+1.36) for **2** and the dominating sign of these bands is negative (Fig. 1). The Cotton effects observed as a minimum CD at 251 nm and a maximum CD at 219 nm come out from the exciton coupled π–π* type transitions [14]. The wing shape of the CD components was typical for the exciton-coupled transitions. The two CD constituents of the π→π* transitions in (−)-chxn-(salH)$_2$ system have approximately the same rotational strength and can, therefore, be considered to represent a relatively pure exciton couplet. The above results can be concluded, that in (1*R*,2*R*)-(−)-cyclohexanediamine Schiff base Co(II) chelates, the cyclohexane ring is transfused to the central chelate ring, forming a rigid structure in which the metalated ring is locked stereospecifically in the λ-conformation similar to the observed previously [1,7,14–17].

In CD spectra of **3** and **4** the band from π→π* transition is split into 360.5 nm (**3** +2.42), 361.5 nm (**4** +2.56) and 399.5 nm (**3** −4.21), and 400 nm (**4** −3.94) components (Fig. 1). The exciton interaction can be related to the molecular geometry of the complex, where two azomethene groups are not planar but produce the tetrahedral distortion. CD bands observed for **3** at 478 nm (+0.50); 595 nm (−0.11) and for **4** at 480 nm (+0.44) can be assigned to d–d transitions from xz, yz, zx to x^2-y^2 [17].

The CD spectrum of [Ni(−)-chxn-(5-methylba)$_2$] exhibited an absorption in the range 400–700 nm with components at 413 nm (−0.99), whereas for [(Ni(−)-chxn-(3-methylba)$_2$] at 415.5 (−0.80) (Fig. 1). These transitions give rise to the CD bands, which most probably are from the non-bonding, the π-antibonding and the weakly σ antibonding 3d-orbitals to strongly σ antibonding 3d-orbitals (x^2-y^2, when O, N, N, O are placed at the x- and y-axes). The π→d transitions obtain an electric transition moment, **P**, which is defined from the atomic arrangement in the mean coordination plane. The magnetic transition moment, **M**, associated with the same transition is mainly from the tetrahedral out of plane distortion as a charge rotation during the transition. To produce a negative rotational strength $\mathbf{R} = \mathbf{P} \times \mathbf{M}$ the distortion has to take the shape shown in Fig. 2, and not its mirror image [7]. The higher energy bands at 348.5 (−0.67) nm in the spectrum of [(Ni(−)-chxn-(3-methylba)$_2$] and 346 nm (−0.89) in [(Ni(−)-chxn-(5-methylba)$_2$] are all considered to be ligand metal charge transfer (LMCT) bands [14]. Observed transitions can be rationalized as a result of the λ-conformation of bridging cyclohexylene carbons. Similar observations were noted for [Ni(−)chxn-(sal)$_2$] and [Ni(−)-chxn-(hacphen)$_2$] [7,14], where the slight distortion from planarity was detected both in the solid state (X-ray structures) and solution.

3.2. NMR studies of diamagnetic Ni(II) and paramagnetic Co(II) complexes

The ^{1}H NMR spectra of [Ni(−)-chxn-(3-methylba)$_2$] and [(Ni(−)-chxn-(5-methylba)$_2$] revealed signals from methyl group at C-3′ and C-5′ at 2.20 ppm (singlet), phenyl hydrogens in the region from 6.8 to 7.1 ppm, a singlet centered at 3.09 ppm from methine hydrogens in cyclohexyl ring and 7.25 ppm from C-4 hydrogen (Fig. 3). The largest coordination shift $\Delta = \delta_{comp} - \delta_{lig}$ (0.9 ppm) was observed for azomethine hydrogen, which is

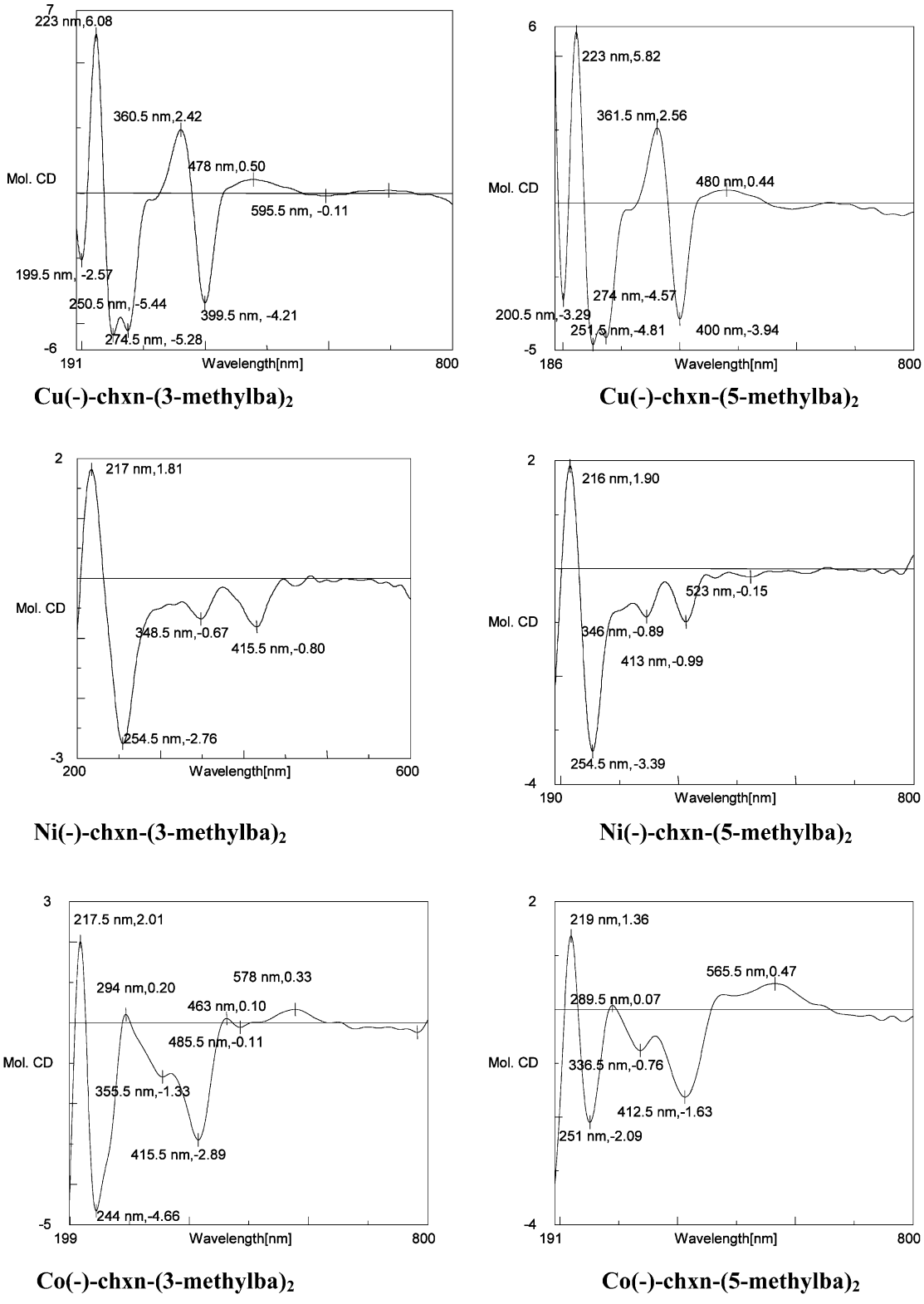


Fig. 1. CD spectra of the complexes.

close to coordination center. In the latter complex the interactions via space between methyl and C-4 hydrogens were indicative and the same distortion can be postulated for the complexes studied for imine and methine hydrogens [14]. Due to the lack of the X-ray structure we cannot suggest the umbrella form but rather tetrahedral distortion as it was found in X-ray structure of [Ni(−)-chxn-(salal)$_2$] [14]. Unfortunately

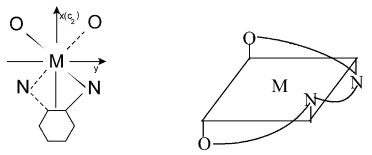


Fig. 2. A schematic structure of [M(−)-chxn-(3-methylba)$_2$] and [M(−)-chxn-(5-methylba)$_2$] complexes and tetrahedral distortion of coordination plane.

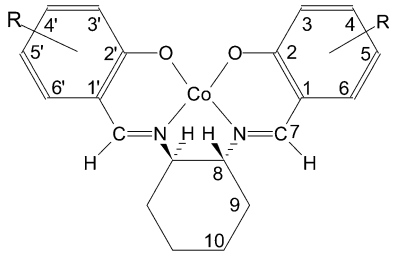


Fig. 3. Ni(II), Cu(II) and Co(II) complexes with Schiff bases derived from (1*R*,2*R*)-(−)-1,2-cyclohexylenediamine and 2-hydroxy-3-methylbenzaldehyde or 2-hydroxy-5-methylbenzaldehyde.

due to the poor solubility of complexes we were unable to obtain ^{13}C NMR spectra where these effects could be observed.

^{1}H NMR spectroscopy has not been applied extensively to Co(II) coordination complexes because of their paramagnetism, which complicates spectra acquisition and interpretation. Chemical shift assignments were made for ligand hydrogens detected outside what is typically considered as the diamagnetic region (0–14 ppm), through systematic substitution of the aromatic hydrogens [C(3′) and C(5′) phenyl ring] in **1** and **2**. It has been shown that the ligand geometry markedly affected the chemical shift pattern of hydrogens. The ^{1}H NMR paramagnetic spectra of [Co(−)-chxn-(5-methylba)$_2$] and [Co(−)-chxn-(3-methylba)$_2$] (Fig. 4), were measured in the range from +250 to −250 ppm. The most upfield shifted resonance at −60 ppm, which is extremely broad and weak, can be assigned to the hydrogen in –CH=N– group. This signal was registered after more than 1000 scans, that is the fivefold longer acquisition time as compared with the remainder of the spectrum. Similarly large upfield shift ($\sim$400 ppm) was observed for azomethine proton for Mn(III) complexes [22,23]. On the other hand for [Co(−)-chxn-(salen)$_2$] complexes this signal was registered in the 'diamagnetic' part of the spectrum. In order to show that CH=N gives rise to the most upfield resonance, selectively deuterated compounds should be used in NMR experiments. The broad signal detected at −28 ppm for [Co(−)-chxn-(3-methylba)$_2$] can be assigned to the hydrogen atom in position 5′ of phenyl ring, because for the [Co(−)-chxn-(5-methylba)$_2$], in which hydrogen atom is replaced by –CH$_3$ group and there is no other signal between −50 and 0 ppm. In the spectrum of [Co(−)-chxn-(3-methylba)$_2$], a pair of signals was observed at 21.58 and 23.83 ppm, which can be assigned to the cyclohexane methine bridge hydrogens (at CH–CH). These resonances are from the hydrogens, which are in the closest proximity to the paramagnetic center. For [Co(−)-chxn-(5-methylba)$_2$] the same hydrogen atoms give rise to signals at 20.94 and 24.7 ppm. The resonances of these hydrogens most probably are affected by the distortion in the N_2O_2 coordination plane that results in their magnetic unequivalency and detected different chemical shifts and relaxation times. The assignment of all signals, which appeared in the paramagnetic part of the spectrum, is impossible due to the lack of the subsequently substituted Schiff bases. Presented analysis of the paramagnetic spectra of Co(II) complexes confirms the influence of the steric distortions in the coordination sphere on the chemical shift of hydrogens in the closest distance to Co(II), similar to the observed for [Co(−)-chxn-(sal)$_2$] [24–28]. The paramagnetic and diamagnetic spectra of Co(II) and Ni(II) revealed the most significant changes in the resonances of the CH–CH and CH=N hydrogens which are in the nearest neighborhood to the coordination center and can be moved outside the coordination plane due to the pseudotetrahedral distortion from the planarity.

3.3. Infrared studies

Upon complexation characteristic C=N stretching absorption band in 1620–1640 cm^{-1} range for Schiff bases, is shifted towards lower energies (1601–1634 cm^{-1}). Another absorption band which is sensitive on ligand coordination origins from (Ph)C–O vibrations (1270–1300 cm^{-1} in Schiff base) is also shifted upon coordination towards higher energies (ca. 50 cm^{-1}). Assuming C_{2v} symmetry for the nearest surrounding of the central ion (N_2O_2), one can expect two M–O (A_1+B_1) and two M–N (A_1+B_1) stretching vibrations active in IR [29]. Literature data revealed that M–O vibrations should appear between 270 and 330 cm^{-1}, whereas M–N in 410–450 cm^{-1} range [30–33]. In the spectra of **1** and **2** bands noted at 313 cm^{-1} (B_1) and 279 cm^{-1} (A_1) can be assigned to ν(Co–O), whereas at 422 cm^{-1} (A_1) and 444 cm^{-1} (B_1) to ν(Co–N) stretching vibrations. In the case of **3**–**6** metal–ligand vibrations appeared at the following frequencies: Ni–N: 441 cm^{-1} (B_1), 403 cm^{-1} (A_1), Cu–N: 416 cm^{-1} (A_1), 441 cm^{-1} (B_1), Ni–O: 323 cm^{-1} (B_1), 294 cm^{-1} (A_1) and Cu–O: 316 cm^{-1} (B_1), 275 cm^{-1} (A_1). Hence the IR data are in favor of the chelating mode of Schiff bases and four-coordinated central ions (N_2O_2 chromophore).

4. Conclusions

Spectroscopic results (CD) confirmed the square planar tetrahedrally distorted geometry of the coordina-

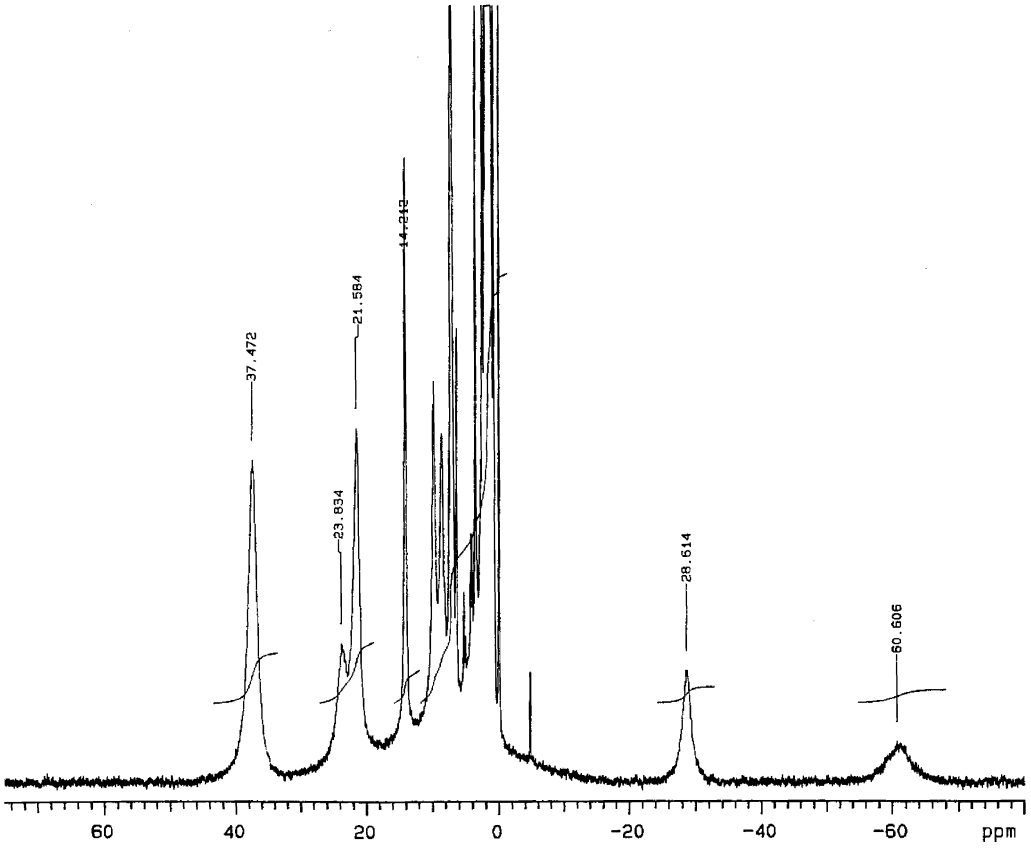


Fig. 4. ^{1}H NMR spectrum of [Co(−)-chxn-(3-methylba)$_2$].

tion center. Distortion has further evidence in Ni(II) diamagnetic and paramagnetic ^{1}H NMR spectra of Co(II) complexes, which revealed significant coordination shifts of the hydrogen atoms in the closest proximity to the coordination center. Hydrogen atoms of the imine carbon are shifted upfields, whereas those from C-1 are split upon coordination that suggests unequivalency of these atoms coming out from the ligand coordination to the metal center.

Acknowledgements

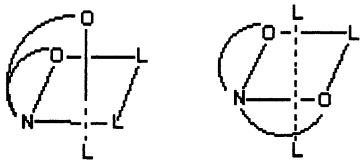
Financial support for M. Barwiolek from the Polish State Committee for Scientific Research grant 3T09A 04821 is gratefully acknowledged.

References

[1] R.S. Downing, F.L. Urbach, J. Am. Chem. Soc. 91 (1969) 5977.
[2] P.A. Ganeshpure, G.L. Tembe, S. Satish, J. Mol. Catal. A113 (1996) 1423.
[3] B. Bosnich, J. Am. Chem. Soc. 90 (1968) 627.
[4] J.P. Costes, J.M. Dominiguez-vera, J.P. Laurent, Polyhedron 14 (1995) 2179.
[5] E.N. Jacobsen, F. Kakiuchi, R.G. Konsler, J.F. Larrow, M. Tokunaga, Tetrahedron Lett. 38 (1997) 773.
[6] M.B. Ferrari, G.G. Fava, C. Pelizi, Acta Crystallogr., Sect. B 32 (1976) 901.
[7] A. Wojtczak, E. Szłyk, M. Jaskólski, E. Larsen, Acta Chem. Scand. 51 (1997) 274.
[8] J. Llewellyn, T.N. Waters, J. Chem. Soc. Dalton (1960) 2639.
[9] J.M. Epstein, B. Figgis, A.H. White, A.C. Willis, J. Chem. Soc. Dalton 4 (1974) 1954.
[10] E.N. Baker, D. Hall., T.N. Waters, J. Chem. Soc. (1970) 400.
[11] H. Milburn, M.R. Truter, B.L. Vickery, J. Chem. Soc. (1974) 841.
[12] M.B. Ferrari, G.G. Fava, C. Pelizi, Acta Crystallogr., B 32 (1976) 901.
[13] K. Bernardo, S. Leppard, A. Robert, G. Commenges, F. Dahan, B. Meunier, Inorg. Chem. 35 (1996) 387.
[14] E. Szłyk, A. Wojtczak, E. Larsen, A. Surdykowski, J. Neumann, Inorg. Chim. Acta 293 (1999) 239.
[15] S.M. Crawford, Spectrochim. Acta 19 (1963) 255.
[16] C.J. Hipp, W.A. Baker, J. Am. Chem. Soc. 92 (1970) 792.
[17] E. Larsen, Acta Chem. Scand. 23 (1969) 2158.
[18] F. Galsbol, P. Steenbol, B.S. Sorensen, Acta Chem. Scand. 26 (1972) 962.
[19] O. Signorini, E.R. Dokal, G. Castellano, G. Oliva, Polyhedron 15 (1996) 245.
[20] J.R. Zamian, E.R. Dockal, Transition Met. Chem. 21 (1996) 370.
[21] R.C. Felicio, G.A. da Silva, L.F. Ceridorio, E.R. Dokal, Synth. React. Met. Org. Chem. 29 (1999) 171.
[22] C. Srivanavit, D.G. Brown, J. Am. Chem. Soc. (1976) 4447.
[23] Y. Ciringh, S.W. Gordon-Wylie, R.E. Norman, G.R. Clark, S.T. Weintraub, C.P. Horwitz, Inorg. Chem. 36 (1997) 4968.
[24] G.C. La Mar, F.A. Walker, J. Am. Chem. Soc. 95 (1973) 6950.

[25] G.C. La Mar, F.A. Walker, J. Am. Soc. 97 (1975) 5103.
[26] G.N. La Mar, W.D. Horrocks, R.H. Holm, NMR of Paramagnetic Molecules, Academic Press, New York, 1973.
[27] E. Kwiatkowski, M. Klein, G. Romanowski, Inorg. Chim. Acta 293 (1999) 115.
[28] E. Szlyk, A. Surdykowski, M. Barwiolek, Pol. J. Chem. 74 (4) (2000) 595.
[29] K. Nakamoto, Infrared and Raman Spectra of Inorganic Compounds, Wiley, New York, 1997.
[30] P. Gluvchinsky, G.M. Mockler, Spectrochim. Acta, Part A 33 (1997) 1073.
[31] J.H.S. Green, D.J. Harrison, Spectrochim. Acta, Part A 32 (1976) 1279.
[32] K. Nakamoto, C. Udovich, J. Takemoto, J. Am. Chem. Soc. (1970) 3973.
[33] A.E. Martel, K. Cleno, J. Phys. Chem. 19 (1956) 1407.

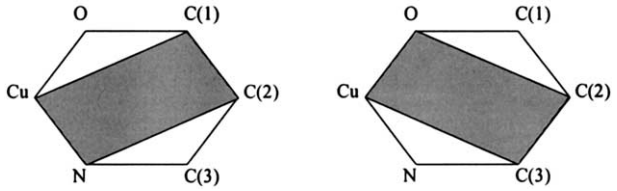
Cu(II)–Ida ratio, the Cu(II) exhibits either distorted square pyramidal coordination (type 4+1) or an octahedral coordination (type 4+2 or 4+1+1) or, more rarely, a square planar one (type 4). The Ida or Ida-like ligand acts as a tridentate ligand exhibiting a *trans*-conformation (forming two nearly coplanar five-membered chelate rings) or a *cis*-conformation (forming two nearly perpendicular chelate rings):



cis- *trans-*

In the absence of additional ligands, with the exception of water molecules, the structurally characterized Cu(II) complexes with Ida have a polymeric chain structure and a *cis*-conformation [9–11]. On the other hand, in all known Cu(II) complexes with the *N*-aryliminodiacetates a *trans*-conformation has been observed [12–19], most of them having a monomeric structure. Only in the [Cu(*p*-Cl–Phida)] and [Cu(*p*-OH–Phida)H_2O] complexes (*p*-Cl–Phida = *N*-(*p*-chlorophenyl)iminodiacetate, *p*-OH–Phida = *N*-(*p*-hydroxyphenyl)iminodiacetate) does the Ida-group act as a bridge between two metal centers via carboxylate binding [17,18]. In the presence of an *ortho*-substituent, the dihedral angle between the benzene plane and the mean equatorial plane around the Cu atom is nearly perpendicular [12–15], otherwise it is close to 109.5° (sp^3-hybridization of the N atom) [16–19].

There are many structural data about the conformations of glycinate chelate rings. However, information about β-alaninate A-rings is relatively scarce and only a few Cu(II) complexes containing A-rings without peptide bonds are known [20–33]. According to Ilyukhin et al. [34], A-rings can be divided into two groups due to the magnitudes of the dihedral angle O–Cu–N–C(3) (ϕ). In the case of $\phi < 40°$, a plane CuNC(2)C(1) is observed. If ϕ is higher than 40°, the base plane is OCuC(3)C(2):



In the present work, the Cu(II) complex of *p*-Tdp was synthesized and characterized by XRD, IR and UV–Vis spectroscopy with the purpose of studying the selectivity of arylamino-di-3-propionates towards copper(II) ions. It seems to be the first structurally characterized complex with an Idp-like ligand.

2. Experimental

2.1. Preparation of the complex $[Cu(p\text{-}Tdp)(H_2O)_2]\cdot 2H_2O$

H_2(*p*-Tdp) was prepared as follows: 17 ml (0.25 mol) of acrylic acid (Aldrich 14,723-0) was added to a solution of 10.7 g (0.10 mol) *p*-toluidine (Fluka 89632) in 40 ml of 1,2-dichloroethane. The mixture was heated at boiling temperature for 7 h. After 2 h H_2(*p*-Tdp) precipitated as a polycrystalline powder. Then H_2(*p*-Tdp) was filtered, washed and recrystallized three times from 1,2-dichloroethane. Yield after recrystallization was 14.5 g (57.7 %). The purity of the acid H_2(*p*-Tdp) ($\geq$99.5%) was checked by pH-titration with a standard carbonate-free solution of KOH. *Anal*. Calc. for $C_{13}H_{17}NO_4$: C, 62.14; H, 6.82; N, 5.57. Found: C, 62.27; H, 6.79; N, 5.57%. ^{1}H NMR (δ, ppm): 2.17 (s; 3H; $-CH_3$), 2.42 (t; 4H; $-CH_2-COOH$; $J = 7.2$ Hz), 3.51 (t; 4H; $=N-CH_2-$; $J = 7.2$ Hz), 6.60 (d; 2H; H_{Ph} 3.5; $J = 8.4$ Hz), 6.99 (d; 2H; H_{Ph} 2.6; $J = 8.4$ Hz), 12.22 (sbr; 2H; –COOH).

The Cu(II) complex of *N*,*N*-di(2-carboxyethyl)-*p*-toluidine was prepared by mixing a hot saturated aq. solution of H_2(*p*-Tdp) with $(CuOH)_2CO_3$ until CO_2 is removed. After filtration, crystals suitable for X-ray crystallography were obtained by slow evaporation at room temperature (r.t.) over a few days. *Anal*. Calc. for $C_{13}H_{23}CuNO_8$: C, 40.57; H, 6.02; N, 3.64; Cu, 16.51. Found: C, 40.47; H, 6.25; N, 3.68; Cu, 16.49%.

2.2. X-ray structure analysis

The experimental data for a deep-blue crystal with dimensions 0.76 × 0.70 × 0.34 mm was measured using a CAD4 diffractometer (λ (Mo Kα) = 0.71073 Å, graphite monochromator, $T = 293(2)$ K).

Crystal data: $C_{13}H_{23}CuNO_8$ (FW 384.86), triclinic, space group $P\bar{1}$, $a = 11.522(1)$, $b = 12.563(2)$, $c = 19.304(2)$ Å, $\alpha = 95.982(9)°$, $\beta = 106.789(7)°$, $\gamma = 99.526(8)°$, $V = 2603.9(5)$ Å^3, $Z = 6$, $D_{calc} = 1.473$ g cm^{-3}, $\mu = 1.296$ mm^{-1}.

The $\theta/2\theta$ scan technique was employed to measure the intensities for 6133 reflections in the range $1.85° < \theta < 22.50°$. The structure was solved by direct methods and refined by the full-matrix least-squares method in an anisotropic approximation for all non-hydrogen atoms and isotropically for H atoms with positions located on a difference electron density map. The final *R* indices are $R_1 = 0.0431$ and $wR_2 = 0.1127$ for 5724 non-zero unique I_{hkl} (899 parameters) with ($I > 2\sigma$); goodness-of-fit = 0.992. All calculations were performed with the SHELX-97 program package.

2.3. Spectral measurements

IR spectra were recorded in the 4000–400 cm^{-1} range on a Specord 75IR spectrophotometer (Carl Zeiss, Germany) as KBr pellets. Electronic absorption spectra were recorded on a SF-46 spectrophotometer (LOMO, Russia) at r.t. An electronic reflectance spectrum was run on a Shimadzu UV-3101PC spectrophotometer. The ^1H NMR spectrum was realized on an Avance 400 spectrometer from Brucker in DMSO-d_6 at a frequency of 400 MHz, the internal standard was TMS.

2.4. pH measurements

Potentiometric titrations were carried out with a PC-controlled system assembled with a Crison MicropH 2002 pH meter, a Crison MicroBU 2030 micro burette, an Orion 90-02-00 (double junction AgCl/Ag) reference electrode and a Russel SWL/S7 glass electrode. The titrations were conducted under an atmosphere of CO_2 and O_2-free nitrogen at 25.0(1) °C in a Metrohm EA880T double wall glass cell with a Metrohm E649 stirrer. The control program was written in QuickBasic (Microsoft Corporation, version 7.0) to control the titration system, via an RS232C interface. The glass electrode was calibrated in terms of hydrogen ion concentration with buffers: 0.01 M borax, phosphate (0.025 M KH_2PO_4 and 0.025 M Na_2HPO_4) and 0.05 M potassium hydrogen phthalate with ionic strength adjusted to 0.1 M with potassium nitrate in a procedure recommended by Vasconcelos and Machado [35].

A *p*-Tdp concentration range of 1–10 mM was studied, varying the concentration of Cu(II) ($Cu(NO_3)_2$ 0.1000 M Orion standard solution no. 942906) in the ligand–metal ratios 1:1, 1:2, 2:1. CO_2-free KOH 0.1 M was used as a titrant. All acid–base and metal–ligand complexation parameters were calculated and refined with the SUPERQUAD program [36].

3. Results and discussion

3.1. Crystal structure

The crystal structure of [Cu(*p*-Tdp)(H_2O)$_2$]·2H_2O consists of neutral [Cu(*p*-Tdp)(H_2O)$_2$] complexes and water molecules. Three crystallographically independent [Cu(*p*-Tdp)(H_2O)$_2$] complex molecules have a similar structure. A generalized numbering system is shown in Fig. 1, while selected bond lengths and angles are given in Table 1.

The coordination polyhedron of each Cu atom is a square pyramid (type 4+1) with a slight trigonal bipyramidal distortion, and is formed by the donor atoms of the tridentate *p*-Tdp ligand, the O atom of the water molecule in the base plane and by another water molecule in the apex of the pyramid. The percentage of trigonal distortion from the idealized square pyramidal coordination, $\tau = 100(\beta - \alpha)/60$ (where β is the largest *trans* angle and α is the second one [37]), is 12.92%, 13.28% and 0.9% for each of three crystallographically independent molecules. The Cu–O2 apical bonds (2.216–2.297 Å) are longer than the bond lengths in the plane, but significantly shorter than usually obtained for square pyramidal Cu(II) complexes. The *ortho*-H atom in benzene ring blocks up the sixth coordination position in the Cu polyhedron (Cu–H distances are 2.54–2.57 Å). The basal planes are tetrahedrally dis-

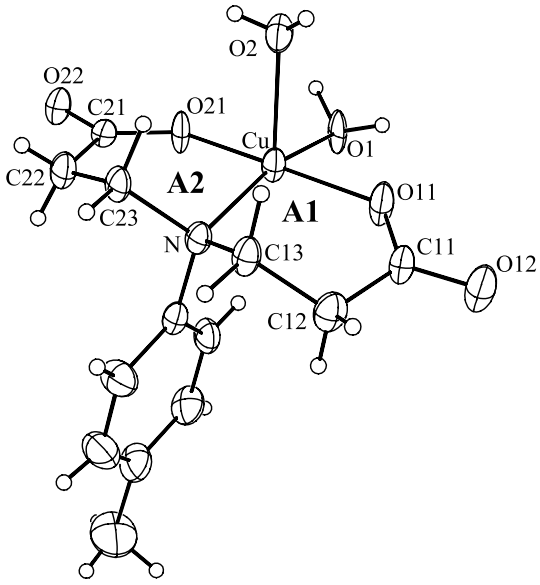


Fig. 1. Generalized numbering scheme of atoms and rings in [Cu(*p*-Tdp)(H_2O)$_2$] molecule.

Table 1
Selected bond lengths (Å) and angles (°) with e.s.d.s. for three crystallographically independent Cu(*p*-Tdp)(H_2O)$_2$ molecules in [Cu(*p*-Tdp)(H_2O)$_2$]·2H_2O

	1	2	3
Bond lengths			
Cu–O11	1.927(1)	1.925(1)	1.920(1)
Cu–O21	1.941(1)	1.925(1)	1.914(1)
Cu–O1	1.966(1)	2.013(1)	2.022(1)
Cu–O2	2.292(1)	2.216(1)	2.297(1)
Cu–N	2.027(1)	2.034(1)	2.024(1)
Bond angles			
O11–Cu–O21	168.72(4)	167.22(5)	166.15(4)
O11–Cu–O1	84.82(4)	82.53(5)	82.93(4)
O21–Cu–O1	85.28(4)	85.82(4)	86.38(5)
O11–Cu–N	95.59(4)	94.25(5)	95.42(5)
O21–Cu–N	92.01(4)	94.81(5)	92.97(5)
O1–Cu–N	160.96(4)	159.25(5)	166.69(4)
O11–Cu–O2	93.80(4)	91.93(4)	96.37(5)
O21–Cu–O2	92.68(4)	94.41(4)	92.16(5)
O1–Cu–O2	96.47(4)	95.56(5)	88.79(4)
N–Cu–O2	102.49(4)	105.05(5)	104.52(4)

torted (0.105, 0.120 and 0.034 Å). The Cu atoms are located out of the mean planes of the four basal atoms (0.20–0.30 Å) toward the O2 atoms.

The tridentate function of the *p*-Tdp ligand is realized by the formation of two β-alaninate rings (A1 and A2, Fig. 1), which are located practically in one plane, dihedral angles between A1/A2 mean planes are 9.87°, 6.13° and 6.82°. Thus, the ligand in the complex has a *trans*-conformation in contrast with the *cis*-conformation of Ida [9–11]. The benzene ring is arranged almost perpendicularly to the base plane of the copper pyramid (82.2°–87.1°), opposite to Cu(II) complexes with *meta*- or/and *para*-substituted *N*-phenyliminodiacetates [16–19], in which the equatorial plane of the coordinating polyhedron is placed with an angle of about 109.5°.

The crystal structure of $[Cu(p\text{-Tdp})(H_2O)_2]\cdot 2H_2O$ exhibits six non-equivalent A-rings. Puckering parameters of the A-rings are given in Table 2. The dihedral angle ϕ varies in a wide range from 28.3° to 45.8° that gives the possibility of tracking the chelate ring conformation changes as a function of ϕ magnitude. In four A-rings with $\phi < 40°$, a plane defined by CuNC(2)C(1) is observed, the plane in the two others being OCuC(3)C(2). The lowest $\phi = 28.3°$ is observed in the A1(**1**)-ring, in which the conformation of a strongly plane boat B_{25} at the oxygen atom is implemented. The oxygen atom is deviated only 0.076 Å from the average plane defined by CuNC(2)C(1). Therefore, the most approximate conformation may be considered as the sofa S_5 (half-boat, envelope). With the following increase of ϕ, A1(**3**)-ring would have an intermediate form between the sofa S_5 and the half-chair H_{56}, then A1(**2**), A2(**2**), A2(**3**)-rings ($\phi = 36.8°$–$42.7°$) adopt a shape close to the half-chair H_{56}, and finally A2(**1**)-ring ($\phi = 45.8°$) has the intermediate form between the half-chair H_{56} and the sofa S_6. The reason for such a large deviation of ϕ resides in the significant dependence of the coordinated oxygen atom O_c position in the crystal packing.

For evaluation of the ring stress level capacity, the deviation of the sum of the internal angles from the 'ideal' value $648 = 120 + (109.5 \times 4) + 90$ was applied [38]. One can see from Table 5 that all A-rings present a positive deviation and have a stress resulting in the flattering (decreasing of goffering). The greatest deviation was observed for Cu–O–C (+21.2°–24.5°) and O–C–C (+7.6°–11.2°) angles.

The bond lengths and angles in the coordination polyhedra (Table 1) are comparable with the corresponding values of Cu(II) complexes containing A-rings [20–33]. In all A-rings internal angles N–Cu–O are higher than 90° in contrast with glycinate rings [9–19]. The sum of internal angles is higher than the ideal magnitude of 20°–40°. The distinction in the C–N bond lengths towards the benzene ring (1.465–1.474 Å) and side branches (1.497–1.512 Å) is induced by a negative mesomeric effect of the benzene ring.

Complex molecules and non-coordinated water molecules are joined in a three-dimensional framework by H-bonds with O···O distances ranging from 2.692 to 2.913 Å.

3.2. IR spectra

The IR spectrum shows a zwitterionic structure of $H_2(p\text{-Tdp})$ that is confirmed by the existence of a N^+–H band and carboxylate group bands. The 'ammonium' stretching band $\nu(N^+–H) = 2700–2400\ cm^{-1}$ has a characteristic position for the $R_3N^+–H$ group [39] and it is observed as a group of weak bands. The existence of $\nu(C{=}O) = 1705$ and $\delta(O–H) = 1290\ cm^{-1}$ bands that are specific for a carboxyl group as well as carboxylate bands $\nu_s(COO^-) = 1385$ and $\nu_{as}(COO^-) = 1605\ cm^{-1}$ points out for the zwitterionic structure of $H_2(p\text{-Tdp})$.

The IR spectrum of $[Cu(p\text{-Tdp})(H_2O)_2]\cdot 2H_2O$ differs significantly from the $H_2(p\text{-Tdp})$ spectrum. The absence of absorption bands corresponding to the carboxyl group $\nu(C{=}O)$ and $\delta(OH)$ and to the ammonium group

Table 2
Sum of internal angles, dihedral angles ϕ and Cremer–Pople parameters of β-alaninate chelate rings in $[Cu(p\text{-Tdp})(H_2O)_2]\cdot 2H_2O$

Ring	Sum of internal angles (°)	ϕ (°)	Cremer–Pople parameters [a]			Conformation [b]
			Q (Å)	θ (°)	φ (°)	
A1(**1**)	682.7	28.31(7)	0.560	57.4	244.6	S_5
A1(**2**)	684.5	36.78(9)	0.555	54.3	262.9	H_{56}
A1(**3**)	686.2	33.80(8)	0.533	53.1	257.2	S_5/H_{56}
A2(**1**)	684.0	45.79(8)	0.569	46.6	281.0	H_{56}/S_6
A2(**2**)	683.7	38.46(9)	0.572	56.0	268.5	H_{56}
A2(**3**)	682.5	42.8(1)	0.564	46.9	273.6	H_{56}

[a] Ref. [34].

[b] According to Ref. [35]. *B*, boat; *S*, sofa; *H*, half-chair. The subscripts show the numbers of atoms responsible for conformation: in *B*, they are atoms in the *trans* position deviating in the same direction; in *H* adjacent atoms deviating in opposite directions. The numeration order is Cu–O–C–C–C–N.

$\nu(N^+–H)$ must be mentioned. These variations were caused by the participation of the carboxylate and amino groups in the coordination with the Cu(II) cation. In the range of stretching bands ν(O–H) of water molecules 3390 and 3250 cm^{-1} bands were registered that corresponds to the non-coordinated and coordinated water molecules, respectively. For crystal water molecules, the absorption band δ(O–H) at 1630–1600 cm^{-1} is equally typical [40], however it is overlapped with a $\nu_{as}(COO^-)$ band giving a multiplet in the range 1595–1555 cm^{-1}. Absorption band $\nu_s(COO^-)$ is located at 1380 cm^{-1} (Fig. 2).

3.3. Electronic spectra

The electronic absorption spectra of aqueous solutions of *p*-Tdp versus pH value confirmed the assumption about the existence of two groups that absorb light species: one group contains all the protonated forms having a betaine-like structure {H_3(*p*-Tdp)$^+$, H_2(*p*-Tdp) and H(*p*-Tdp)$^-$—Fig. 3, curve *1*}, whereas the other contains only the deprotonated form {(*p*-Tdp)$^{2-}$, Fig. 3, curve *2*}. The corresponding numeric data for these spectra are summarized in Table 3. The absorption bands were assigned by comparing the spectra of benzene, aniline, and the anilinium cation [41].

The electronic absorption spectra of aqueous solutions of the Cu(*p*-Tdp) complex in the pH range 1–8 have been studied. In more alkaline solutions, precipitation is observed. The spectrum of the complex at the optimal pH range is displayed in Fig. 3 (curves *3* and *4*).

In the visible spectrum, one wide asymmetric absorption band (Fig. 3, curve *4*) is observed. This band is interpreted as an envelope of the three bands caused by electron transitions $E_1(z^2 \rightarrow x^2-y^2)$, $E_2(xy \rightarrow x^2-y^2)$, $E_3(xz, yz \rightarrow x^2-y^2)$ [42]. The complex compound formation is developed in hypsochromic shift ($\lambda = 740$ nm)

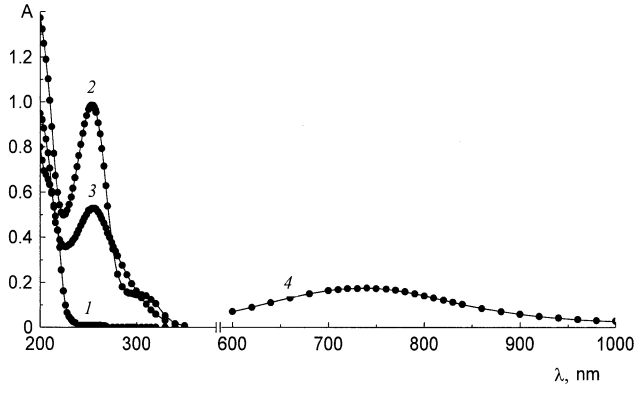


Fig. 2. Electronic absorption spectra of the aqueous solutions of *p*-Tdp and Cu(*p*-Tdp): (1) pH 1.88, $c(p\text{-Tdp}) = 1.10 \times 10^{-4}$ mol l^{-1} (protonated form); (2) pH 9.50, $c(p\text{-Tdp}) = 1.10 \times 10^{-4}$ mol l^{-1} (deprotonated form); (3) pH 7.0, $c(p\text{-Tdp}) = c(CuSO_4) = 1.10 \times 10^{-4}$ mol l^{-1}; (4) pH 7.0, $c(p\text{-Tdp}) = c(CuSO_4) = 2.00 \times 10^{-3}$ mol l^{-1}.

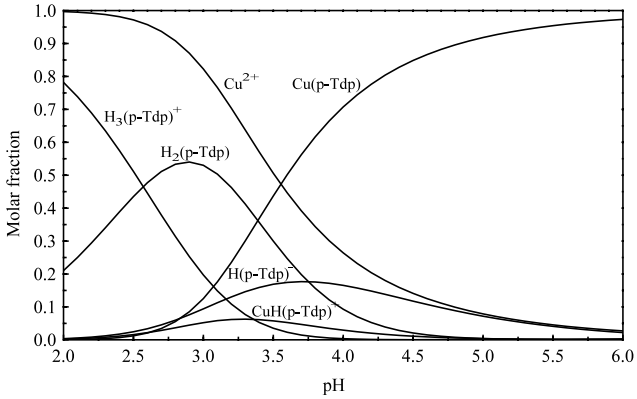


Fig. 3. Species distribution diagram as a function of pH for the Cu(II)–(*p*-Tdp) system, $c(Cu^{2+}) = c(p\text{-Tdp}) = 5.0 \times 10^{-3}$ mol l^{-1} ($I = 0.1$ M KNO_3, 25 °C).

Table 3
Electronic spectra of aqueous solutions of *N*,*N*-di(2-carboxyethyl)-*p*-toluidine

Band	ν (cm^{-1})	ε (l mol^{-1} cm^{-1})	$\nu_{1/2}$ (cm^{-1})
H_3(p-Tdp)$^+$, H_2(p-Tdp), H(p-Tdp)$^-$			
$^1B_{1u}$	> 50 000	–	–
$^1B_{2u}$	39 280(80)	220(5)	1650(90)
(p-Tdp)$^{2-}$			
$^1B_{1u}$	39 570(60)	9160(90)	230(80)
$^1B_{2u}$	32 540(230)	1300(150)	1530(280)

and hyperchromy ($\varepsilon = 98$ l mol^{-1} cm^{-1}) of the absorption band in comparison with the spectrum of the hexaaquacation $[Cu(H_2O)_6]^{2+}$.

Studies applying the method of continuous variation (Job's method) showed that the maximum deviation from absorbance additivity is observed at the 1:1 molar ratio. Similar results were obtained by a molar-ratio method for the variable concentration of one of the components.

The similarity of the reflectance spectra of the crystal $[Cu(p\text{-Tdp})(H_2O)_2]\cdot 2H_2O$ ($\lambda = 262$, 735 nm) and those taken from the solution shows that the complex has the same square pyramidal geometry in both states.

3.4. Protonation and stability constants

The protonation constants of *p*-Tdp and stability constants of its Cu(II) complex were determined in our previous work [2,6] at room temperature 20(1) °C and $I = 0.1$ M KCl with calibration of a glass electrode in terms of proton activity. Therefore, the mixed constants were obtained. In this work, these constants were determined using more accurate procedures and both types of glass electrode calibration (Table 4).

The mixed protonation constants of *p*-Tdp are in good agreement (Table 4) in spite of the different

Table 4
Protonation constants of *p*-Tdp and stability constants of its Cu(II) complexes

Log *K*					*I* (M)	*T* (°C)	Type of constants [a]	Reference
$H(p\text{-Tdp})^-$	$H_2(p\text{-Tdp})$	$H_3(p\text{-Tdp})^+$	$CuH(p\text{-Tdp})^+$	$Cu(p\text{-Tdp})$				
6.96(6)	3.93(6)	2.99(5)	–	6.75(7)	0.1 KCl	20(1)	*m*	[2,6]
6.96(2)	3.87(2)	2.90(2)	2.20(5)	6.36(3)	0.1 KNO_3	25.0(1)	*m*	this work
6.87(2)	3.75(2)	2.57(2)	2.13(5)	6.38(3)	0.1 KNO_3	25.0(1)	*c*	this work

[a] *m*, mixed; or *c*, concentration constants.

temperature and media used. Hence, the difference between mixed and concentration protonation constants mainly depends on the type of calibration.

The model of complex formation that best fits the experimental results consists as $CuH(p\text{-Tdp})^+$ and $Cu(p\text{-Tdp})$ complexes. The stability constants slightly depend on the type of glass electrode calibration but are sparingly compared, as they were determined in different conditions (Table 4). The species distribution diagram (Fig. 3) was calculated taking into account the values of the protonation constants of the ligand and stability constants of the complexes. The diagram indicates that the protonated complex $CuH(p\text{-Tdp})$ has an important contribution in the pH range 2.5–4.5.

4. Supplementary data

Crystallographic data for the structural analysis have been deposited with the Cambridge Crystallographic Data Centre, CCDC No. 143764. Copies of this information may be obtained free of charge from The Director, CCDC, 12 Union Road, Cambridge, CB2 1EZ, UK (fax: +44-1223-336033; e-mail: deposit@ccdc.cam.ac.uk or www: http://www.ccdc.cam.ac.uk).

Acknowledgements

The Post-Doctoral scholarship of Yu.A. Skorik (SFRH/BPD/3628/2000) was funded by Fundação para a Ciência e a Tecnologia. This work was partially supported by the Ministry of education of RF (grant no. UR.05.01.007) and by the Urals Research and Education Center for Advanced Materials (grant no. CRDF REC-005). We are grateful to C.M.R. Almeida and Dr E.A. Filonova for help in preparation of the manuscript.

References

[1] J. Colonge, G. Descotes, G. Frenay, Bull. Soc. Chim. France 10 (1963) 2264.
[2] V.P. Melkozerov, L.K. Neudachina, A.A. Vshivkov, Russ. J. Gen. Chem. 67 (1997) 92.
[3] M. Farahani, J.M. Antonucci, L.R. Karam, J. Appl. Polym. Sci. 67 (1998) 1545.
[4] Yu.A. Skorik, L.K. Neudachina, A.A. Vshivkov, L.A. Pasechnik, N.V. Legkikh, Izv. Vyssh. Uchebn. Zaved., Khim. Khim. Tekhnol. 41 (1998) 119.
[5] Yu.A. Skorik, L.K. Neudachina, A.A. Vshivkov, Russ. J. Phys. Chem. 72 (1998) 1191.
[6] Yu.A. Skorik, L.K. Neudachina, A.A. Vshivkov, Russ. J. Gen. Chem. 69 (1999) 285.
[7] Yu.A. Skorik, L.K. Neudachina, A.A. Vshivkov, Yu.G. Yatluk, N.V. Gert, Russ. J. Phys. Chem. 73 (1999) 2055.
[8] Yu.A. Skorik, L.K. Neudachina, A.A. Vshivkov, V.Kh. Mursalimova, Russ. J. Inorg. Chem. 46 (2001) 132.
[9] F.G. Kramarenko, T.N. Polynova, M.A. Porai-Koshits, V.P. Chalyi, G.N. Kupriyanova, L.I. Martynenko, Zh. Strukt. Khim. 14 (1973) 744.
[10] A. Podder, J.K. Dattagupta, N.N. Saha, W. Saenger, Acta Crystallogr., Sect. B 35 (1979) 53.
[11] M.J. Román-Alpiste, J.D. Martín-Ramos, A. Castiñeiras-Campos, E. Bugella-Altamirano, A.G. Sicilia-Zafra, J.M. González-Pérez, J. Niclós-Gutiérrez, Polyhedron 18 (1999) 3341.
[12] M.A. Hidalgo, A. Romerosa, J. Suárez-Varela, J.C. Avila-Rosón, J.D. Martín-Ramos, Acta Crystallogr., Sect. C 51 (1995) 1510.
[13] M.A. Hidalgo, J. Romero, J. Suárez-Varela, J.C. Avila-Rosón, J.D. Martín-Ramos, Acta Crystallogr., Sect. C 51 (1995) 1512.
[14] J. Suárez-Varela, E. Colacio, A. Romerosa, J.C. Avila-Rosón, M.A. Hidalgo, J. Romero, Inorg. Chim. Acta 217 (1994) 39.
[15] Y.-T. Chen, H.-Q. Liu, J.-J. Liu, X.-H. Bu, J.-L. Wang, L.-G. Zhang, F.M. Miao, J. Coord. Chem. 25 (1992) 43.
[16] X.-L. Liu, L.-G. Zhang, F.M. Miao, H.-Q. Liu, Y.-M. Rong, C.-Y. Jin, Y.-T. Chen, Chin. Chem. Lett. 2 (1991) 463.
[17] J.-L. Wang, G.-H. Tian, F.M. Miao, H.-Q. Liu, R.-T. Chen, Acta Crystallogr., Sect. C 47 (1991) 2205.
[18] A.Ye. Obodovskaya, L.M. Shkol'nikova, N.M. Dyatlova, Koord. Khim. 10 (1984) 161.
[19] J.-L. Wang, G.-H. Tian, F.-M. Miao, H.-Q. Liu, R.-T. Chen, Jiegou Huaxue 11 (1992) 384.
[20] K. Tomita, Bull. Chem. Soc. Jpn. 34 (1961) 297.
[21] Y. Mitsui, Y. Iitaka, H. Sakaguchi, Acta Crystallogr., Sect. B 32 (1976) 1634.
[22] M.V. Kamwaya, S.G. Teoh, J. Fiz. Malays. 5 (1984) 1.
[23] S.-B. Teo, C.-H. Ng, S.-G. Teoh, H.-K. Fun, J. Coord. Chem. 24 (1991) 151.
[24] A.B. Ilyukhin, L.M. Shkol'nikova, A.L. Poznyak, S.S. Makarevich, Kristallographiya 36 (1991) 1155.
[25] A.Ye. Obodovskaya, L.M. Shkol'nikova, A.L. Poznyak, Russ. J. Inorg. Chem. 40 (1995) 1229.
[26] I.N. Polyakova, V.S. Sergienko, A.L. Poznyak, Russ. J. Inorg. Chem. 40 (1995) 1744.
[27] D.J. Radanović, B.V. Prelesnik, D.D. Radanović, Z.D. Matović, B.E. Douglas, Inorg. Chim. Acta 262 (1997) 203.
[28] A.L. Poznyak, A.C. Antsyshkina, G.G. Sadikov, V.S. Sergienko, L.V. Stopolyaskaya, Russ. J. Inorg. Chem. 43 (1998) 875.

[29] I.F. Burshtein, A.L. Poznyak, Russ. J. Inorg. Chem. 43 (1998) 1053.
[30] Z.D. Matović, G. Pelosi, S. Ianelly, G. Ponticelli, D.D. Radanović, D.J. Radanović, Inorg. Chim. Acta 268 (1998) 221.
[31] I.F. Burshtein, A.L. Poznyak, L.V. Stopolyaskaya, Russ. J. Inorg. Chem. 44 (1999) 1179.
[32] Yu.A. Skorik, G.V. Romanenko, L.K. Neudachina, A.A. Vshivkov, Russ. J. Coord. Chem. 27 (2001) 796.
[33] U. Rychlewska, D.D. Radanović, M.D. Dimitrijević, D.M. Ristanović, M.M. Vasoević, D.J. Radanović, Polyhedron 20 (2001) 2523.
[34] A.B. Ilyukhin, L.M. Shkol'nikova, A.L. Poznyak, Koord. Khim. 16 (1990) 1597.
[35] M.T.S.D. Vasconcelos, A.A.S.C. Machado, Rev. Port. Quim. 28 (1986) 120.
[36] P. Gans, A. Sabatini, A. Vacca, J. Chem. Soc., Dalton Trans. (1985) 1195.
[37] A.W. Addison, T.W. Rao, J. Reedijk, J. Van Rijn, G.C. Verscher, J. Chem. Soc., Dalton Trans. (1984) 1349.
[38] H.A. Weakliem, J.L. Hoard, J. Am. Chem. Soc. 81 (1959) 549.
[39] L.J. Bellamy, The Infrared Spectra of Complex Molecules, Wiley, London, 1963.
[40] K. Nakamoto, Infrared and Raman Spectra of Inorganic and Coordination Compounds, 4th ed., A Wiley-Interscience Publication, Wiley, New York, 1986.
[41] E.S. Stern, C.J. Timmons, Gillam and Stern's Introduction to Electronic Absorption Spectroscopy in Organic Chemistry, 3rd ed., Edward Arnold, London, 1970.
[42] A.B.P. Lever, Inorganic Electronic Spectroscopy, Elsevier, Amsterdam, 1984.

Table 1
Selected crystal data, bond distances, bond angles and ^{15}N chemical shifts for adducts, $[Zn_2(Py)(S_2CNEt_2)_2]$, and the clathrate, $[Zn_2(Py)(S_2CNEt_2)_2]\cdot Py$

	Compound **2**[1]		Compound **4**[2]	Compound **3**[5]
Space group	$P2_12_12_1$ (No. 19)		$P2_1/c$	$P2_1$
Crystal system	orthorhombic		monoclinic	monoclinic
Unit cell dimensions				
a (Å)	10.2119(8)		10.140(2)	11.188(5)
b (Å)	16.3000(12)		31.794(5)	8.225(5)
c (Å)	25.354(3)		13.480(1)	14.0010(13)
α (°)	90		90	90
β (°)	90		107.17(1)	102.57(6)
γ (°)	90		90	90
Formula units per unit cell, Z	8		8	2
Temperature (K)	291(1)		293(2)	170(1)
	Compound **2**[1]		Compound 4[2]	Compound **3**[5]
	α-**2**	β-**2**		
Selected bond lengths (Å)				
Zn–N	2.072(5)	2.079(5)	2.072(4)	2.060(3)
Zn–S(1) [a]	2.323(2)	2.330(2)	2.3561(17)	2.331(2)
Zn–S(2) [a]	2.334(2)	2.335(2)	2.3691(17)	2.352(2)
Zn–S(3) [a]	2.590(2)	2.556(2)	2.5292(17)	2.565(2)
Zn–S(4) [a]	2.616(2)	2.609(2)	2.5566(18)	2.597(2)
Selected bond angles (°)				
N–Zn–S(1)	112.10(15)	111.23(15)	109.32(14)	118.1(1)
N–Zn–S(2)	112.54(14)	112.81(15)	110.38(14)	119.3(1)
N–Zn–S(3)	96.90(15)	96.79(15)	96.53(14)	97.2(1)
N–Zn–S(4)	97.96(14)	96.96(15)	95.53(14)	90.8(1)
S(1)–Zn–N–C(1) [b]	−55.2(5)	+59.5(5)	−54.6(5) [c]	5.0(4)
S(3)–Zn–N–C(1) [b]	+48.5(5)	−47.7(5)	+51.5(5) [c]	−103.7(4)
S(2)–Zn–N–C(2) [b]	−53.8(6)	+57.5(5)	−49.3(5) [c]	6.1(4)
S(4)–Zn–N–C(2) [b]	+52.7(6)	−45.6(5)	+55.2(5) [c]	−98.6(4)
	Compound **1**[7]	Compound **2**[1]	Compound **4** [d]	Compound **3**[5]
^{15}N isotropic chemical shifts (ppm) [relative to NH_4Cl (0 ppm)]				
$(Et)_2\mathbf{N}CS_2^-$	136.6	131.3	130.6	132.7
	149.6	132.2	131.1	134.9
		133.9	130.6	
$C_5H_5\mathbf{N}$–Zn		228.9	230.8	227.1
		231.7		
$C_5H_5\mathbf{N}$ (guest)				279.7

[a] Nomenclature S(i), $i = 1, 2, 3, 4$, is chosen with the Zn–S bond length increasing.
[b] C(1) and C(2) are the C–N carbon atoms in the pyridine molecule which lies between S(1) and S(3), and between S(2) and S(4) atoms, respectively, when projected parallel to the Zn–N bond.
[c] Measured from data on compound 103200 deposited at the Cambridge Crystallographic Data Center.
[d] This work.

tate of **1** was collected, filtered off, washed with water, dried in vacuo over phosphorus pentoxide and recrystallized two times from toluene. The adduct, $[Zn(Py)(S_2CNEt_2)_2]$ (**2**) (see Fig. 1), was prepared by dissolving equimolar quantities of pyridine and the initial zinc(II) complex in a minute volume of toluene and isolated by means of slow evaporation of the solvent. In contrast, O'Brien et al. have prepared $[Zn(Py)(S_2CNEt_2)_2]$, by the reaction of 2,4,6-$C_6H_2Me_3SZnS_2CNEt_2$ with an excess of pyridine. The mixture was heated to obtain a clear solution, concentrated under vacuum, and left in the fridge to crystallize [2]. Recently, we also reported the formation of the solvated form of the discussed adduct with the outer-sphere Py molecule, $[Zn(Py)(S_2CNEt_2)_2]\cdot Py$ (compound **3** in Fig. 1), from the initial complex **1**, which is either recrystallized from pure pyridine or if Py is absorbed by **1** in the molar ratio 2:1, respectively [5]. Clathrated adduct, $[Zn(Py)(S_2CNEt_2)_2]\cdot Py$ (**3**), crystallizes in the same monoclinic space group, $P2_1$ [5], as $[Zn(Py)(S_2CNEt_2)_2]$ reported by O'Brien et al. One pyridine molecule of **3** has a covalent bond, N–Zn, in adduct molecules while the other pyridine molecule is the outer-sphere one and only held by van der Waals forces

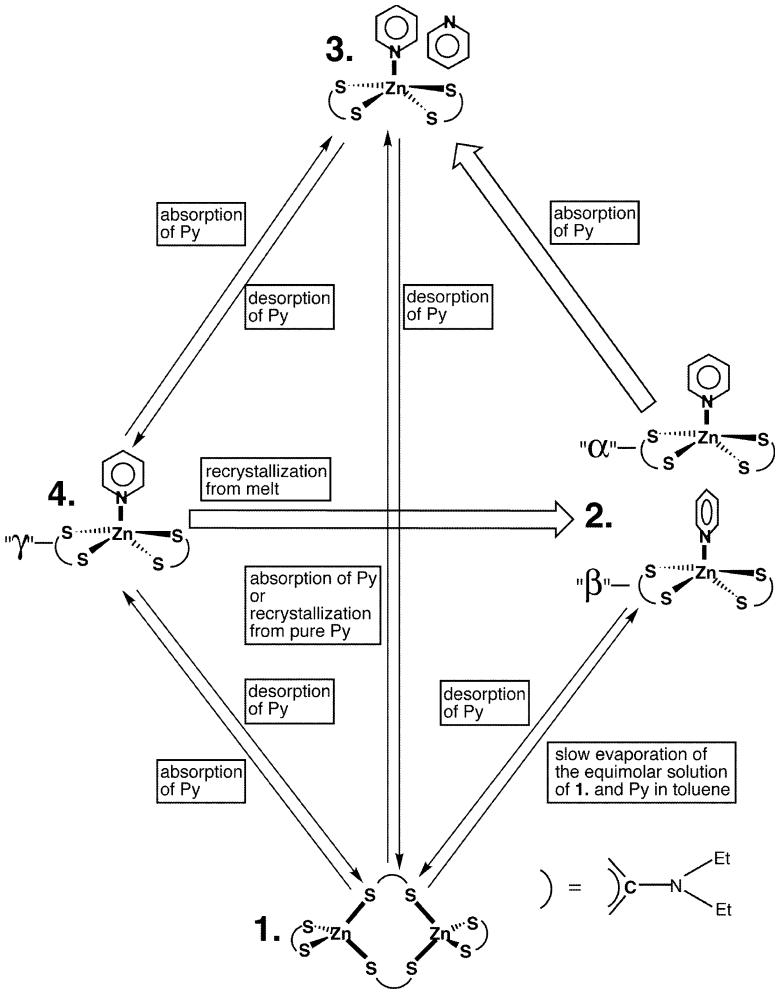


Fig. 1. Chemical pathways for bis(diethyldithiocarbamato)zinc(II), **1**; its adduct with pyridine, $[Zn_2(Py)(S_2CNEt_2)_2]$ (**2**), (α- and β- are two isomorphs of **2**); the solvated form of the adduct with guest molecules of pyridine, $[Zn_2(Py)(S_2CNEt_2)_2]\cdot Py$ (**3**); and the metastable state of the adduct, γ-$[Zn_2(Py)(S_2CNEt_2)_2]$ (**4**).

in the system of channels formed by $[Zn(Py)(S_2CNEt_2)_2]$ molecules [5]. The solvated form **3** is not very stable and slow desorption of guest Py molecules cannot be avoided at room temperature, if crystals of the clathrate are not protected by a thin film of glue during X-ray data collection. The single crystal structure of **3** has been resolved from X-ray measurements at 170(1) K with crystals protected by films of an epoxy glue [5]. On the contrary, O'Brien et al. performed their X-ray measurements at 293(2) K without any particular protection of the crystals [2]. We suggest that $[Zn(Py)(S_2CNEt_2)_2]$ reported by this group is, in fact, a special structural state of the adduct formed from the clathrate **3**, which has lost either a large part of or all of its guest pyridine molecules. The symmetry of the single crystal, and most of the unit cell dimensions of **3**, are retained after desorption of guest Py molecules (see Table 1). Here we abbreviate this state of the adduct as γ-$[Zn(Py)(S_2CNEt_2)_2]$ (**4**) (see Fig. 1).

In order to check this hypothesis, we used natural abundance solid-state ^{15}N cross-polarization/magic-angle-spinning NMR spectroscopy with high-power ^{1}H-decoupling [6]. Recently, we pointed out that the ^{15}N chemical shifts of nitrogen sites have extremely high sensitivity to structural variations in polycrystalline thioorgano-metallic compounds, such as dithiocarbamate complexes of Ni and Zn [7], dithiocarbamatezinc adducts with nitrogen bases, [1,8–11] and solvated forms of these adducts with pyridine [5], morpholine [9–12], benzene [8–11,13], and various chlorcarbohydrates [14–17].

Owing to the low natural abundance of the ^{15}N isotope (0.365%) and a low resonance frequency of 36.48 MHz at the magnetic field of 8.46 T (Chemagnetics CMX-360 NMR spectrometer), large quantities of samples were needed for obtaining a reasonable signal-to-noise ratio during 24–72 h of total accumulation time with a pulse delay of 2 s. Polycrystalline samples of approximately 300–400 mg were packed in 7.5 mm Chemagnetics ZnO_2 rotors and spun at either 6 or 5.5 kHz. Generally, from 15 000 to 75 000 signal acquisitions were sufficient to obtain signal intensities with

signal-to-noise ratio (S/N) > 5 for all resonances. The cross-polarization contact time was varied from 1.2 to 3.5 ms for different samples in order to achieve a maximum cross-polarization efficiency for the weakest resonance line in the spectrum (usually nitrogen sites of pyridine molecules). The proton π/2 pulse duration was either 3.2 or 5 μs. The dipole-dipole $^{1}H-^{15}N$ interactions, which broaden resonance lines in the solid state, were suppressed by high power ^{1}H-continuous-wave-decoupling at the proton resonance frequency with a nutation frequency of the rf-field from 48.8 to 85 kHz for different samples. The isotropic ^{15}N chemical shifts (ppm) were referenced to external crystalline NH_4Cl (0 ppm; −341 ppm on the absolute scale [18,19]). No special B_0-field stabilization was used, since the magnetic-field drift for the ^{15}N nuclei was only 0.016 Hz h^{-1}.

Fig. 2 shows ^{15}N CP/MAS NMR spectra of the polycrystalline zinc(II) diethyldithiocarbamate complex, its adducts and the clathrated form with pyridine. Fig. 2(a) represents the spectrum of the initial polycrystalline

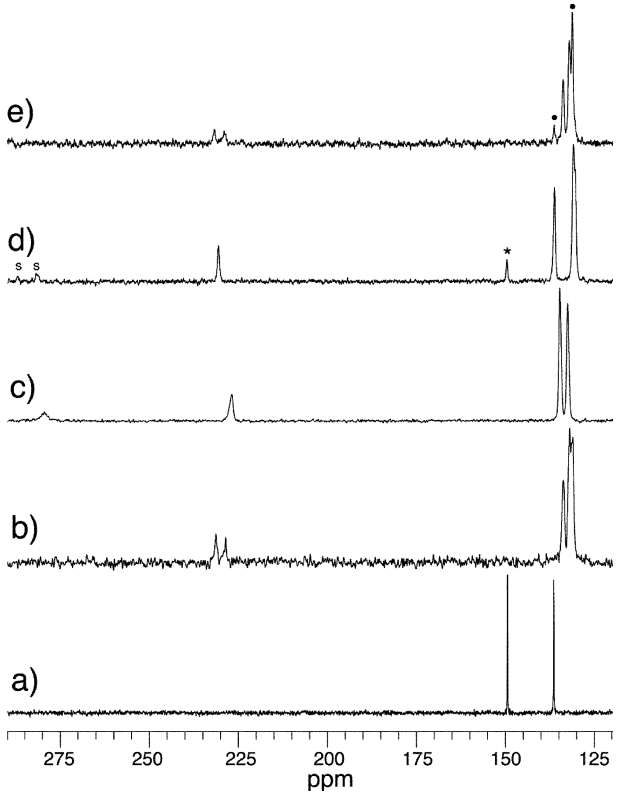


Fig. 2. ^{15}N CP/MAS NMR (36.46 MHz) spectra of powder samples of **1** (a), **2** (b), **3** (c), **3** after a partial desorption of pyridine (d) and following recrystallization from the melt (e). The MAS frequency was 6.0 kHz in (a), (b), (c) and (e) or 5.5 kHz in (d). The number of transients and cross-polarization times were, respectively: (3740, 1.25 ms) (a); (17 600, 3.5 ms) (b); (25 000, 3.5 ms) (c); (77 702, 1.2 ms) (d); and a sum of two spectra with (50 000, 1.2 ms) and (25 000, 2.4 ms) (e). An admixture of the initial complex **1** in (d) and the adduct **4** in (e) are labeled as (*) and (●), respectively. 's' in (d) denotes spinning sidebands.

dinuclear diethyldithiocarbamate zinc(II) complex, $[Zn_2(S_2CNEt_2)_4]$. Two resonances have been assigned previously to two pairs of magnetically equivalent nitrogen sites in bridging (149.6 ppm) and terminal (136.6 ppm) diethyldithiocarbamate ligands [7]. The adduct **2**, $[Zn(Py)(S_2CNEt_2)_2]$, recrystallized from toluene has only terminal ligands (131.3, 132.2 and 133.9 ppm) and two distinct resonances of the adduct pyridine molecules (231.7 and 228.9 ppm), which correspond to two different isomers of **2** in the asymmetric unit cell (see Fig. 2(b)) [1]. The latter resonances are weaker than those of nitrogen sites in dithiocarbamate ligands because of differences in both cross-polarization efficiency and in $T_{1\rho}$ relaxation times. After further adsorption of pyridine molecules by **2** (or by recrystallization of **1** from pure pyridine), up to a molar ratio of $Zn(S_2CNEt_2)_2$: Py equal to 1:2, the solvated species of the adduct, $[Zn(Py)(S_2CNEt_2)_2]\cdot Py$ (**3**), is formed. Fig. 2(c) shows the spectrum of **3** with four well resolved nitrogen resonances at 132.7, 134.9 ppm (nitrogen sites in the two terminal diethyldithiocarbamate groups which are structurally slightly different), 227.1 ppm (coordinated pyridine molecules) and at 279.7 ppm (solvating Py molecules held by van der Waals forces in the system of channels formed by adduct molecules) [5]. X-ray diffraction analysis revealed only one adduct molecule in the unit cell that faithfully correlates with the ^{15}N CP/MAS NMR spectrum of **3** (a single resonance for the coordinated Py molecule) [5]. Fig. 2(d) depicts the spectrum of a sample of **3** after partial desorption of Py, which was achieved by gentle heating of the sample. The resonance of solvating pyridine molecules at 279.7 ppm has disappeared, and the resonance line of the other (coordinated by Zn) pyridine molecule is shifted from 227.1 to 230.8 ppm. The latter is close to the mean value of chemical shifts of nitrogen sites in Py of the two isomers of the adduct **2** (compare with Fig. 2(b) and Table 1). Furthermore, the chemical shifts of nitrogen sites in diethyldithiocarbamate groups after the desorption of Py are substantially different from those for both the adduct **2** and the clathrated form **3**. It can be also seen that, in a part of the sample, the desorption of Py proceeded even further to the initial complex **1** (a small peak labeled (*) at 149.6 ppm and a part of the resonance at 136.4 ppm). We suggest that the spectrum shown in Fig. 2(d) corresponds to the adduct **4**, γ-$[Zn(Py)(S_2CNEt_2)_2]$, with the X-ray diffraction structure reported earlier by O'Brien and co-workers [2]. The presence of a single nitrogen resonance of adduct Py in this ^{15}N NMR spectrum suggests a single rotation isomer of $[Zn(Py)(S_2CNEt_2)_2]$ in the unit cell [2], with a slightly different structure from the other two, so called α- and β-isomers of this adduct **2** discussed in [1] (see Table 1). It is noteworthy that, an almost identical ^{15}N NMR spectrum (as in Fig. 2(d)) is produced by a sample of **1** after equimolar absorption

of pyridine from the gas phase, suggesting that the same compound **4** is formed (spectrum not shown). That the state of the adduct **4** is a meta-stable one can be proved by a simple recrystallization of **4** from the melt. This procedure gives rise to a more stable state of the adduct, i.e. **2**, with the two isomers discussed above, as can be seen in Fig. 2(e). This spectrum is very similar to that of the adduct **2** (compare with Fig. 2(b)) apart from a small admixture of the residual adduct form **4** (marked with (●)).

These results can be summarized in the diagram shown in Fig. 1. The metastable state of the adduct, **4**, is formed by either absorption of Py by the initial complex **1** or by desorption of guest molecules of pyridine from the solvated form **3**. In contrast, the other state of the adduct, **2**, can be prepared by either slow evaporation of an equimolar solution of **1** and pyridine from toluene or by the recrystallization of **4** from the melt. The latter process, **4**→**2** (as well as **2**→**3**) is not directly reversible, since **4** can be obtained from **2** only through the clathrated form **3** (or through the initial complex **1**). This points to chemical hysteresis in the adduct formation of $[Zn(Py)(S_2CNEt_2)_2]$.

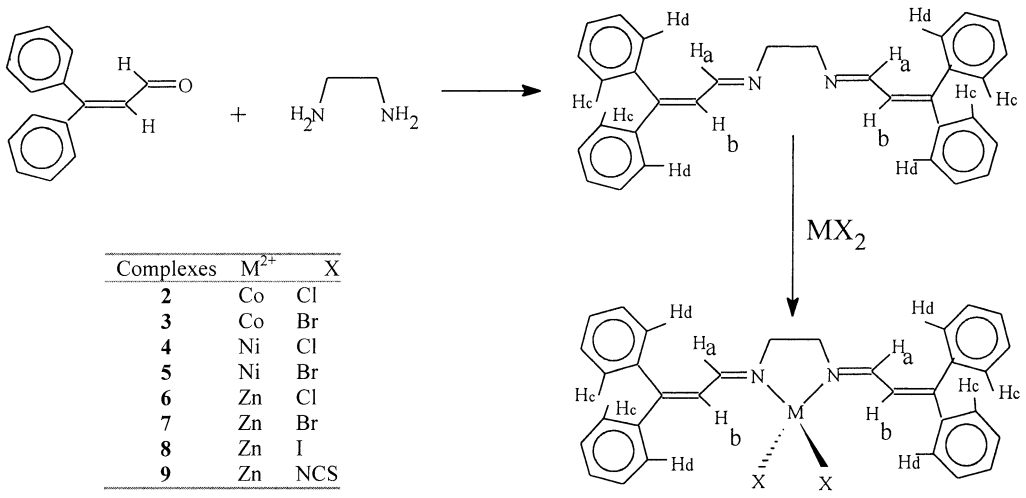
In conclusion, this work illustrates the chemical hysteresis in which the structure of an adduct depends on the pathway of physico-chemical conditions during the preparation of metastable compounds, such as adducts or clathrates of alkyldithiocarbamates of transition metals. We anticipate that similar types of polymorphism of adducts of other thio- and selenocarbamate complexes reported earlier by O'Brien et al. [2] can occur. Therefore, special precautions are needed during the synthesis, preparation and analysis of these compounds.

Acknowledgements

One of the authors (A.V.I.) acknowledges the financial support from Luleå University of Technology. The CMX-360 spectrometer was purchased with a grant from the Swedish Council for Planning and Coordination of Research (FRN). We express our gratitude to Dr. M. Kritikos for loading and recalculating data on **4** from the CCDC and to Dr. D. Baxter for comments on the manuscript.

References

[1] A.V. Ivanov, V.I. Mitrofanova, M. Kritikos, O.N. Antzutkin, Polyhedron 18 (1999) 2069.
[2] M. Azad Malik, M. Motevalli, P. O'Brien, Polyhedron 18 (1999) 1259.
[3] P. O'Brien, Precursors for electronic materials, in: D.W. Bruce, D. O'Hare (Eds.), Inorganic Materials, Wiley, New York, 1992, p. 491.
[4] M. Bonamico, G. Mazzone, A. Vaciago, L. Zambonelli, Acta Crystallogr. 19 (1965) 898.
[5] A.V. Ivanov, M. Kritikos, O.N. Antzutkin, A. Lund, V.I. Mitrofanova, Russ. J. Coord. Chem. (Engl. Transl.) 24 (1998) 645.
[6] A. Pines, M.G. Gibby, J.S. Waugh, J. Chem. Phys. 56 (1972) 1776.
[7] A.V. Ivanov, T.A. Rodyna, O.N. Antzutkin, Polyhedron 17 (1998) 3101.
[8] A.V. Ivanov, I.A. Lutsenko, W. Forsling, Russ. J. Coord. Chem. (Engl. Transl.) 28 (2002) 57.
[9] A.V. Ivanov, M. Kritikos, O.N. Antzutkin, W. Forsling, Inorg. Chim. Acta 321 (2001) 63.
[10] A.V. Ivanov, W. Forsling, M. Kritikos, O.N. Antzutkin, E.V. Novikova, Doklady Chem. (Proc. Russ. Acad. Sci.) (Engl. Transl.) 369 (1999) 268.
[11] A.V. Ivanov, W. Forsling, O.N. Antzutkin, E.V. Novikova, Russ. J. Coord. Chem. (Engl. Transl.) 27 (2001) 158.
[12] A.V. Ivanov, E.V. Novikova, O.N. Antzutkin, W. Forsling, Russ. J. Inorg. Chem. (Engl. Transl.) 46 (2001) 2019.
[13] A.V. Ivanov, M. Kritikos, A. Lund, O.N. Antzutkin, T.A. Rodina, Russ. J. Inorg. Chem. (Engl. Transl.) 43 (1998) 1377.
[14] A.V. Ivanov, M. Kritikos, O.N. Antzutkin, A. Lund, Russ. J. Inorg. Chem. (Engl. Transl.) 44 (1999) 1605.
[15] A.V. Ivanov, M. Kritikos, O.N. Antzutkin, W. Forsling, A. Lund, I.A. Lutsenko, Russ. J. Coord. Chem. (Engl. Transl.) 25 (1999) 543.
[16] A.V. Ivanov, W. Forsling, O.N. Antzutkin, M. Kritikos, T.A. Rodyna, I.A. Lutsenko, Doklady Chem. (Proc. Russ. Acad. Sci.) (Engl. Transl.) 366 (1999) 142.
[17] A.V. Ivanov, W. Forsling, M. Kritikos, O.N. Antzutkin, Russ. J. Coord. Chem. (Engl. Transl.) 26 (2000) 53.
[18] C.I. Ratcliffe, J.A. Ripmeester, J.S. Tse, Chem. Phys. Lett. 99 (1983) 177.
[19] J. Mason, in: D.M. Grant, R.K. Harris (Eds.), Encyclopedia of Nuclear Magnetic Resonance, vol. 5, Wiley, New York, 1996, p. 3222.



Complexes	M^{2+}	X
2	Co	Cl
3	Co	Br
4	Ni	Cl
5	Ni	Br
6	Zn	Cl
7	Zn	Br
8	Zn	I
9	Zn	NCS

Scheme 1.

reactions were purified and dried by conventional methods [18].

2.1. Physical measurements

NMR spectra were obtained on a BRUKER AVANCE DRX500 (500 MHz) spectrometer. Proton chemical shifts δ are reported in part per million (ppm) relative to an internal standard of Me_4Si, and the J values are reported in Hertz. The UV–Vis spectra were recorded on a Perkin–Elmer Lambda 9 spectrophotometer with quartz cells (1 cm path length). Elemental analyses were performed by using Heraeus CHN-O-RAPID elemental analyzer. IR spectra were recorded as KBr pellets on a Shimadzu 435 spectrophotometer.

2.2. Synthesis

2.2.1. *N,N′-bis(β-phenylcinnamaldehyde)-1,2-diiminoethane, Phca$_2$en (**1**)*

To a solution of 2.08 g (10 mmol) β-phenylcinnamaldehyde in 25 ml ethanol, cooled in an ice bath, was added dropwise 300 mg (5 mmol) of ethylenediamine. The mixture was then stirred for an additional 2 h. *N*,*N*′-bis(β-phenylcinnamaldehyde)-1,2-diiminoethane (Phca$_2$en) was obtained as a white microcrystalline precipitate. The precipitate was filtered off, washed with 5 ml cold absolute ethanol. Yield: 3.960 g (90%). *Anal*. Calc. for $C_{32}H_{28}N_2$: C, 87.28; H, 6.36; N, 6.36. Found: C, 87.30; H, 6.35; N, 6.38%. IR (KBr, cm^{-1}): ν_{max} 1614 (s, C=N). ^{1}H NMR: δ 3.68 (s, 4H, –C*H*$_2$–C*H*$_2$–), 6.82 (d, 2H, Ph_2C=C*H*–), 7.31 (m, 20H, Ar*H*), 7.85 (d, 2H, –C*H*=N–). ^{13}C NMR: δ 61.52 (=N^{13}CH$_2^{13}$CH$_2$N=), 126.72, 127.87, 128.15, 128.23, 128.35, 128.72, 130.31, 140.95, 151.73 (Ph^{13}CH–), 163.01 (–^{13}C=N–).

2.2.2. *[Co(Phca$_2$en)Cl$_2$] (**2**)*

To a solution of Phca$_2$en (440 mg, 1 mmol) in 10 ml CH_2Cl_2 was added 130 mg (1 mmol) of anhydrous $CoCl_2$, and stirred at room temperature (r.t.) for 3 h under nitrogen atmosphere. The reaction mixture was filtered off. The volume of the solvent was reduced under vacuum to about 1 ml. The diffusion of diethyl ether vapor into the concentrated solution gave needle like blue crystals suitable for X-ray studies. The crystals were filtered off and washed with a mixture of diethyl ether–dichloromethane (9:1 v/v), and dried in vacuo. Yield: 456 mg (80%). *Anal*. Calc. for $C_{32}H_{28}N_2Cl_2Co$: C, 67.41; H, 4.91; N, 4.91. Found: C, 67.42; H, 4.93; N, 4.90%. IR (KBr, cm^{-1}): ν_{max} 1603 (s, C=N).

2.2.3. *[Co(Phca$_2$en)Br$_2$] (**3**)*

This complex was prepared in a similar manner to **2** using $CoBr_2$ (218 mg, 1 mmol). Deep green crystals were collected by filtration and dried in vacuo. Yield: 514 mg (82%). *Anal.* Calc. for $C_{32}H_{28}N_2Br_2Co$: C, 58.31; H, 4.25; N, 4.25. Found: C, 58.33; H, 4.27; N, 4.26%. IR (KBr, cm^{-1}): ν_{max} 1600 (s, C=N).

2.2.4. *[Ni(Phca$_2$en)Cl$_2$] (**4**)*

To a stirring solution of 129 mg (1 mmol) of anhydrous $NiCl_2$ in 20 ml acetonitrile was added dropwise a solution of 440 mg (1 mmol) Phca$_2$en in 10 ml acetonitrile, and refluxed for 30 min. The solvent was evaporated on a rotatory evaporator at 40 °C under reduced pressure. The solid residue was dissolved in 20 ml acetonitrile and filtered off. The filtrate was left overnight under diffusion of diethyl ether to give pink–red crystals. Yield: 415 mg (73%). *Anal.* Calc. for $C_{32}H_{28}N_2Cl_2Ni$: C, 67.43; H, 4.91; N, 4.91. Found: C, 67.49; H, 4.90; N, 4.95%. IR (KBr, cm^{-1}): ν_{max} 1603 (s, C=N).

2.2.5. [Ni(Phca$_2$en)Br$_2$] (5)

This complex was prepared in a similar manner to **4** using $NiBr_2$ (218 mg, 1 mmol). Deep pink crystals were collected by filtration and dried in vacuo. Yield: 501 mg (76%). *Anal*. Calc. for $C_{32}H_{28}N_2Br_2Ni$: C, 58.34; H, 4.25; N, 4.25. Found: C, 58.37; H, 4.27; N, 4.26%. IR (KBr, cm^{-1}): ν_{max} 1604(s, C=N).

2.2.6. [Zn(Phca$_2$en)Cl$_2$] (6)

To a solution of 136 mg (1 mmol) $ZnCl_2$ in 10 ml methanol was added a solution of 440 mg (1 mmol) Phca$_2$en in 5 ml methanol and stirred at r.t. for 3 h. The product precipitated as a white microcrystalline powder and collected by filtration. The crude product was recrystallized from acetone to give white needle-shape crystals. The crystals were collected by filtration and dried in vacou. Yield: 529 mg (92%). *Anal*. Calc. for $C_{32}H_{28}N_2Cl_2Zn$: C, 66.65; H, 4.85; N, 4.85. Found: C, 66.68; H, 4.86; N, 4.86%. IR (KBr, cm^{-1}): ν_{max} 1616(s, C=N). ^{1}H NMR: δ 3.72 (s, 4H, $-CH_2-CH_2-$), 7.35 (m, 22H, $Ph_2C{=}CH-$, Ar*H*), 8.0 (d, 2H, $J_{HH} = 9.78$ Hz, $-CH{=}N-$). ^{13}C NMR: δ 58.72 ($=N^{13}CH_2^{13}CH_2N=$), 124.45, 129.75, 129.86, 130.14, 130.47, 131.52, 131.72, 138.39,140.45, 161.48 ($Ph^{13}CH-$), 168.91 ($-^{13}C{=}N-$).

2.2.7. [Zn(Phca$_2$en)Br$_2$] (7)

This complex was prepared in a similar manner to **6** using $ZnBr_2$ (225 mg, 1 mmol). Yield: 578 mg (87%). *Anal.* Calc. for $C_{32}H_{28}N_2Br_2Zn$: C, 57.75; H, 4.21; N, 4.21. Found: C, 57.77; H, 4.20; N, 4.21%. IR (KBr, cm^{-1}): ν_{max} 1615 (s, C=N). ^{1}H NMR: δ 3.72 (s, 4H, $-CH_2-CH_2-$), 7.36 (m, 22H, $Ph_2C{=}CH-$, Ar*H*), 8.01(d, 2H, $J_{HH} = 9.82$ Hz, $-CH{=}N-$). ^{13}C NMR: δ 58.65 ($=N^{13}CH_2^{13}CH_2N=$), 124.37, 129.75, 129.89, 130.19, 130.48, 131.54, 131.75, 138.38, 140.48, 161.53 ($Ph^{13}CH-$), 168.80 ($-^{13}C{=}N-$).

2.2.8. [Zn(Phca$_2$en)I$_2$] (8)

This complex was prepared in a similar manner to **6** using ZnI_2 (319 mg, 1 mmol). Yield: 637 mg (84%). *Anal*. Calc. for $C_{32}H_{28}N_2I_2Zn$: C, 50.60; H, 3.69; N, 6.39. Found: C, 50.48; H, 6.37; N, 6.37%. IR (KBr, cm^{-1}): ν_{max} 1614 (s, C=N). ^{1}H NMR: δ 3.72 (s, 4H, $-CH_2-CH_2-$), 7.37 (m, 20H, Ar*H*), 7.57 (d, 2H, $J_{HH} = 9.83$ Hz, $Ph_2C{=}CH-$), 8.02 (d, 2H, $J_{HH} = 9.83$ Hz, $-CH{=}N-$). ^{13}C NMR: δ 58.49 ($=N^{13}CH_2^{13}CH_2N=$), 124.28, 129.77, 129.93, 130.29, 130.53, 131.55, 131.78, 138.35, 140.60, 161.39 ($Ph^{13}CH-$), 168.51 ($-^{13}C{=}N-$).

2.2.9. [Zn(Phca$_2$en)(NCS)$_2$] (9)

To a solution of 261 mg (1 mmol) $Zn(NO_3)_2$ in 10 ml ethanol was added a solution of 194 mg (2 mmol) of KSCN in 5 ml ethanol and stirred for 20 min. The resulting white KNO_3 salt was filtered off and a solution of 440 mg (1 mmol) of Phca$_2$en in 5 ml methanol was added to the filtrate and stirred for 30 min. The product was precipitated as a white microcrystalline powder and collected by filtration and dried in air. Yield: 528 mg (85%). *Anal*. Calc. for $C_{34}H_{28}N_4S_2Zn$: C, 61.80; H, 4.50; N, 4.50. Found: C, 61.85; H, 4.52; N, 4.51%. IR (KBr, cm^{-1}): ν_{max} 1603 (s, C=N), 2055 (s, NCS). ^{1}H NMR: δ 3.67 (s, 4H, $-CH_2-CH_2-$), 6.99 (d, 2H, $J_{HH} = 9.80$ Hz, $Ph_2C{=}CH-$) 7.36 (m, 20H, Ar*H*), 8.02 (d, 2H, $J_{HH} = 9.80$ Hz, $-CH{=}N-$). ^{13}C NMR: δ 58.75 ($=N^{13}CH_2^{13}CH_2N=$), 123.47, 129.88, 130.00, 130.12, 130.44, 130.95, 131.65, 132.26, 138.12, 140.15, 163.75 ($Ph^{13}CH-$), 170.07 ($-^{13}C{=}N-$).

2.3. X-ray crystallography

Suitable single crystals of [Co(Phca$_2$en)Cl$_2$] (**2**), [Ni(Phca$_2$en)Br$_2$] (**5**), and [Zn(Phca$_2$en)Cl$_2$] (**6**), were obtained by diffusion of diethyl ether vapor into the dichloromethane solution of **2** and acetonitrile solution of **5** or by slow evaporation of an acetone solution of **6** at r.t. Data were collected on a Siemens SMART CCD diffractometer using graphite-monochromated Mo Kα ($\lambda = 0.71073$ Å) radiation. For each crystals, a full sphere of reciprocal lattice was scanned by 0.3° steps in ω with a crystal-to-detector distance of 3.97 cm. Preliminary orientation matrices were obtained from the first frames using SMART [19]. The data were empirically corrected for absorption and other effects using SADABS [20]. The structures were solved by direct methods and refined by the full-matrix least-squares method on F^2 data using the SHELXTL [21]. All non-H atoms were refined anisotropically. The H atoms were constrained to idealized geometries and refined isotropically.

3. Results and discussion

3.1. Synthesis

Phca$_2$en was prepared by the condensation of β-Phenylcinnamaldhyde with ethylenediamine. The product, as a white solid material, was characterized by IR, UV–Vis and ^{1}H, ^{13}C NMR spectroscopy.

The cobalt complexes were prepared by reacting equimolar quantities of the anhydrous cobalt halides salts and Phca$_2$en in dichloromethane. These complexes are stable in air in the solid state. The stability of cobalt complexes in solution depends on the solvent used. The compounds are stable in dichloromethane for at least 24 h, while they are much less stable in methanol. A methanolic solution in open air slowly turns brown in 6 h. To avoid any oxidation of the cobalt complexes, the synthesis of **2** and **3** were carried out under nitrogen atmosphere.

The nickel complexes were prepared by reacting equimolar quantities of the anhydrous nickel halides salts and Phca$_2$en in boiling acetonitrile. The zinc

complexes were prepared by reacting equimolar quantities of anhydrous zinc salts and $Phca_2en$ in dichloromethane. The zinc complexes are colorless solids dissolving in chloroform, methanol, ethanol and acetone and they are stable at ambient conditions.

3.2. Spectral studies

All complexes show similar IR spectral features, exhibiting a strong band between 1600 and 1616 cm^{-1} corresponding to ν(C=N). This band is shifted to the lower frequencies by 6–20 cm^{-1} relative to the free ligand upon the coordination of the nitrogen atoms. The observation of a strong band at 2065 cm^{-1} in the IR spectrum of complex **9** indicates that the NCS ligand in this complex is most probably N-bonded [22].

The ^{1}H NMR data of the $Phca_2en$ suggest that the ligand has a symmetrical structure with H_a and H_b protons (Scheme 1) in *trans* positions ($J = 9.5$ Hz). The four methylene protons appear as a singlet at 3.68 ppm. The two vinyl C*H* protons (H_b) are observed as a doublet centered at 6.82 ppm, and the multiplet centered at 7.31 ppm is assigned to the phenyl protons. The two *H*–C=N protons (H_b) appear as a doublet at 7.85 ppm.

In the ^{1}H NMR spectra of compounds **6**–**9**, the hydrogen of the imine C*H* groups (H_a) exhibits a downfield shift relative to the free ligand and shows no significant difference by changing the anion. Nevertheless, the signals due to H_b protons appear at 7.35, 7.36, 7.57 and 6.99 ppm for $ZnLCl_2$, $ZnLBr_2$, $ZnLI_2$ and $ZnL(NCS)_2$, respectively (Fig. 1). In search for an explanation for this behavior, we have found no interaction between H_b and the chloride atoms in $ZnLCl_2$. However, the observed variation in the H_b chemical shifts could be attributed to an intramolecular interaction with metal atom in the form of C–H···Zn weak hydrogen bonds (see more details in the crystal structures). Such interactions have also been reported by others [23,24]. The extent of interaction depends on the steric restrictions imposed by the coordinated anion and the electron density of metal atom. The shielding effect resulting from this intramolecular interaction is strongest for Cl followed by Br and I and to a greater extent for NCS coordinated to the metal atom.

The ^{13}C NMR spectrum of the free ligand exhibits 12 signals due to the fact that the two phenyl rings (*exo* and *endo*) are in different position relative to the ethylenic protons (*trans* and *cis*), and each phenyl ring has the its own characteristic signals. In the ^{13}C NMR spectra of the complexes **6**–**9**, the carbon atoms adjacent to the donor nitrogen atoms show downfield shift in their positions as compared with the free ligand, clearly indicating the coordination of the ligand and retention of the structure in the chloroform solutions.

The UV–Vis spectral data of $M(Phca_2en)X_2$ complexes are presented in Table 1. The $Co(Phca_2en)Cl_2$ show three closely spaced weak bands in the visible region and a very intense band in the UV region. In the regular tetrahedral and near-tetrahedral Co(II) complexes only one d–d transition [$^4A_2(F) \rightarrow {}^4T_1(P)$, assigned as υ_3] is observed in the visible region. This transition has been reported for the tetrahedral $[Co(NCS)_4]^{2-}$ at 615 nm and for the pseudotetrahedral $[Co(morpholine)_2(NCS)_2]$ at 616 nm [25]. The three

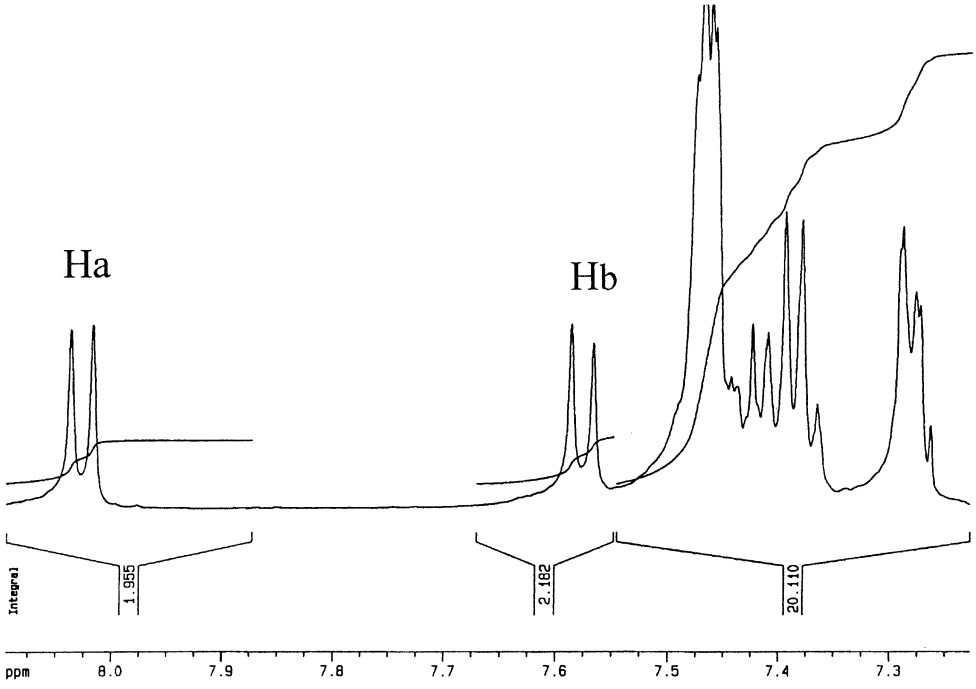


Fig. 1. ^{1}H NMR spectrum of $[Zn(Phca_2en)I_2]$ (**8**).

Table 1
UV–Vis spectral data of M(Phca$_2$en)X$_2$ complexes

Compound	Solvent	UV–Vis λ_{max} (nm) (log ε (M^{-1} cm^{-1}))
Phca$_2$en (**1**)	chloroform	330(4.73)
Co(Phca$_2$en)Cl$_2$ (**2**)	chloroform	651(2.77), 633(2.79), 580(3.08), 342(4.59)
Co(Phca$_2$en)Br$_2$ (**3**)	chloroform	649(3.00), 602(3.00), 578(2.67), 350(4.57)
Ni(Phca$_2$en)Cl$_2$ (**4**)	chloroform	499(2.20), 320(4.65)
Ni(Phca$_2$en)Br$_2$ (**5**)	chloroform	514(2.29), 330(4.68)
Zn(Phca$_2$en)Cl$_2$ (**6**)	chloroform	329.5(4.75)
Zn(Phca$_2$en)Br$_2$ (**7**)	chloroform	331(4.71)
Zn(Phca$_2$en)I$_2$ (**8**)	chloroform	332(4.72)
Zn(Phca$_2$en)(NCS)$_2$ (**9**)	chloroform	335(4.70)

closely spaced transitions in the spectrum of Co(Phca$_2$en)X$_2$ complexes arise from the distortion in the tetrahedral symmetry around the metal center. This splitting originates from the reduction of the orbital degeneracy due to the difference in the ligand field strength of imine and halides donor atoms and the restricted bite angle of the N(1)–M–N(2) chelating ligand [25,26]. The intensity of the UV-band is consistent with its being a ligand-centered $\pi \rightarrow \pi^*$ transition or/and a charge-transfer transition.

The $^3T_1(F) \rightarrow {}^3T_1(P)$ transition [27] in Ni(Phca$_2$en)X$_2$ complexes (**4**, **5**), appears as a low intensity band at 514 nm which is similar to that reported for Ni(Me$_4$propylenediamine)$_2$Cl$_2$ (512 nm) [25]. A strong band at 330 nm is assigned to a ligand-centered $\pi \rightarrow \pi^*$ transition or/and a charge-transfer transition. The electronic spectral data conform with the structures determined by X-ray crystallography for cobalt and nickel complexes.

The electronic absorption spectra of the Zn(Phca$_2$en)X$_2$ complexes (**6**–**9**) in chloroform, are dominated by the broad band in the region 320 nm corresponding to the intra-ligand transition of Phca$_2$en or/and a charge-transfer transition. No d–d transition are expected for d^{10} Zn(II) complexes.

3.3. Crystal and molecular structure of *2*, *5* and *6*

The crystallographic and refinement data are summarized in Table 2 and the selected bond distances and angles are given in Table 3. The molecular structures of **2**, **5** and **6** are illustrated in Figs. 2 and 3, respectively, where metal atoms are coordinated by the bidentate Schiff base ligand and two halogen atoms. Our results show that **2** and **6** are isomorph and isostructure. While a tetrahedral geometry might be expected for a four-coordinated M(II) center, the geometry about M(II) in **2**, **5** and **6** is distorted by the restricting bite of chelating ligand. Considering a low structural preference energy for other geometries of d^7 and d^{10} ions, a distorted tetrahedral structure can be inferred for other Co(Phca$_2$en)X$_2$ and Zn(Phca$_2$en)X$_2$ complexes and most probably for Ni(Phca$_2$en)X$_2$ complexes as well.

For **2** (see Fig. 2), the N(1)–Co–N(2) angle is only 84.07(15)° being in the range of 82°–89° found for ethylenediamine chelated complexes [28–30]. This angle is fixed by the bite size of the ligand (N(1)···N(2) = 2.737(1) Å). The Cl(1)–Co–Cl(2) angle is 110.17(6)° but the Cl(1)–Co–N(2) angle, 117.27(12)°, is larger than the tetrahedral values. The average Co–Cl bond length of 2.22 Å agrees well with the same distance in other tetrahedral cobalt complexes: Co(ethylenedimorpholine)Cl$_2$, 2.23 Å; Co(*p*-toluidine)$_2$Cl$_2$, 2.26 Å; Co(bdmpab)Cl$_2$, 2.23 Å. The Co–N$_{av}$ of 2.0483 Å is being normal [29–33]. The Co(II) complexes with bidentate Schiff bases showing a distorted tetrahedral structure, are common both in solid state and in solution (of non-coordinating solvents) [34–36] and the observed pseudotetrahedral structure for Co(Phca$_2$en)Cl$_2$ (**2**) is in accordance with this expectation.

The compound Ni(Phca$_2$en)Br$_2$ crystallizes with two molecules per asymmetric unit (molecule A and B) showing some conformational differences (see Fig. 3). Nickel complexes with bidentate chelating ligands including Schiff-bases often prefer tetragonal geometries [29,30]. However, the steric effects from Phca$_2$en distort the geometry at Ni(II) in Ni(Phca$_2$en)Br$_2$, (**5**), to pseudotetrahedral (Fig. 4). The angles N(1)–Ni–N(2), 84.63(9)° (A) and 85.08(9)° (B), and Br(1)–Ni–Br(2), 122.645(18)° (A) and 125.729(18)° (B), are indicative of a large deviation from idealized tetrahedral symmetry that is similar to those found in Ni($C_{20}H_{24}N_2$)Br$_2$ [23] and Ni(biq)Br$_2$ [37].

The Ni–Br average bond length of 2.34 Å agrees with those reported for other tetrahedral nickel complexes: [Ni(PPh$_3$)$_2$Br$_2$], 2.34 Å [38,39]; [(*n*-C_4H_9)$_4$N]-[Ni(C_9H_7N)Br$_3$], 2.38 Å [25] and Ni(biq)$_2$Br$_2$, 2.34 Å [37]. The average Ni–N distances of 1.99 Å are similar to those found in the pseudotetrahedral bis(*N*-isopropylsalicylaldiminato)nickel(II), 1.97 Å [40,41] and Ni(II) imine complexes, (Ni(biq)$_2$Br$_2$ 1.99 Å [37] and [Ni(TC-6,6)] 1.95 Å), [42], but they are approximately 0.07 Å longer than those for tetragonal Ni(II) analogues [43,44]. In the tetragonal case, the dx^2-y^2 orbital is vacant, allowing ligands to approach to the metal along the *x* and *y* axes.

The Zn(II) in **6** adopts a pseudotetrahedral coordination (see Fig. 2), where the tetrahedron is somewhat distorted by a small N(1)–Zn–N(2) angle being 83.45(16)°. The Cl(1)–Zn–Cl(2) angle has opened up to 112.02(6)°. The average Cl–Zn–N angle of 114.67° is also larger than the tetrahedral value. The Zn–N distance ranging from 2.078(4) to 2.066(4) Å are considered normal and comparable for those for **2** and **5**. The average Zn–Cl distance of 2.22 Å agree well with normal Zn–Cl bond distances [24].

Table 2
Crystallographic data for compound **2**, **5** and **6**

Compound	$Co(Phca_2en)Cl_2$ (**2**)	$Ni(Phca_2en)Br_2$ (**5**)	$Zn(Phca_2en)Cl_2$ (**6**)
Empirical formula	$C_{32}H_{28}Cl_2N_2Co$	$C_{32}H_{28}Br_2N_2Ni$	$C_{32}H_{28}Cl_2N_2Zn$
Formula weight	570.39	659.09	576.83
T (K)	297(2)	183(2)	183(2)
Crystal system	monoclinic	triclinic	monoclinic
Space group	$P2_1/n$ (No. 14)	$P\bar{1}$ (No. 2)	$P2_1/n$ (No. 14)
a (Å)	10.4102(3)	7.9336(1)	10.3083(1)
b (Å)	15.3333(4)	15.9184(1)	15.3555(1)
c (Å)	18.6290(4)	23.9192(1)	18.5743(2)
α (°)	90	96.802(1)	90
β (°)	101.149(1)	96.106(1)	101.460(1)
γ (°)	90	100.166(1)	90
V (Å^3)	2917.49(13)	2927.27(4)	2881.49(5)
Z, D_{calc} (g cm^{-3})	4, 1.299	4, 1.496	4, 1.330
μ (mm^{-1})	0.794	3.415	1.061
F(000)	1180	1328	1192
Index ranges	$-11 \le h \le 11$; $-17 \le k \le 17$; $-20 \le l \le 20$	$-9 \le h \le 9$; $-19 \le k \le 19$; $-29 \le l \le 26$	$-12 \le h \le 12$; $-18 \le k \le 18$; $-22 \le l \le 22$
Reflections collected	18 181	34 184	30 770
Independent reflection	4176	11 921	5266
R(int)	0.037	0.038	0.080
Data/parameters	4176/334	11 921/667	5266/334
Good-of-fit on F	1.147	1.064	1.042
R_1/wR_2 [a] for observed reflection $[I > 2\sigma(I)]$	0.062/0.168	0.033/0.080	0.062/0.137
R_1/wR_2 for all data	0.072/0.175	0.050/0.092	0.094/0.154
Largest resolution peak/hole (e Å^{-3})	1.314/−0.290	0.525/−0.721	1.453/−1.092

[a] $R_1 = \Sigma||F_o|-|F_c||/\Sigma|F_o|$, $wR_2 = \{\Sigma[w(F_o^2-F_c^2)^2]/\Sigma[w(F_o^2)^2]\}^{1/2}$.

Table 3
Selected bond distances (Å) and angles (°) for compound **2**, **5** and **6**

	2	**5**		**6**
M, X	Co, Cl	Ni, Br		Zn, Cl
		Molecule A	Molecule B	
Bond distances				
M–N1	2.047(4)	2.007(2)	1.998(8)	2.078(4)
M–N2	2.048(4)	1.985(2)	1.988(2)	2.066(4)
M–X1	2.2187(15)	2.3673(4)	2.3578(4)	2.2168(14)
M–X2	2.2358(14)	2.3264(4)	2.3325(4)	2.2310(14)
Bond angles				
N1–M–N2	84.07(15)	84.63(9)	85.08(9)	83.45(16)
N1–M–X1	110.66(12)	105.42(6)	102.89(7)	110.66(12)
N2–M–X1	117.27(12)	104.45(7)	105.89(6)	115.85(11)
N1–M–X2	119.83(12)	114.81(7)	116.81(7)	118.52(11)
N2–M–X2	113.02(12)	117.89(6)	112.63(9)	113.68(12)
X1–M–X2	110.17(6)	122.645(18)	125.729(18)	112.02(6)
C3–N1–M	134.7(3)	132.53(19)	130.44(19)	135.0(4)
C4–N1–M	107.8(3)	107.90(16)	109.51(16)	107.6(3)
C6–N2–M	135.5(4)	129.85(19)	132.08(19)	135.0(4)
C5–N2–M	107.5(3)	110.37(16)	109.28(16)	107.6(3)

The ligand adopts a Z,Z configuration in these complexes. The mean value for dihedral angles N=C–C=C is about 177.5° indicating the planarity of this moiety for the complexes studied here. However, the N=C–C=C moieties in each complex are not coplanar, but showing parallel configuration. The single bond distance C(2)–C(3) in **2**, **5**, and **6** (1.42, 1.43–1.44 and 1.42 Å, respectively) being slightly shorter than C(4)–C(5) in **2**, **5** and **6** (1.518, 1.523–1.528 and 1.524 Å, respectively) indicating an extended electron delocalization in these complexes. Torsion angles in the chelating ring and the stiryl moieties are listed in Table 4. In comparison to the *exo*-phenyl rings, the planes of the *endo*-phenyl rings are more parallel to the planes defined by the C–C=N groups. This result demonstrates that π delocalization in the stiryl moiety is solely between the *endo*-phenyl rings and the chain connecting the rings to the coordinated nitrogen atoms.

Despite the fact that the donor nitrogen atoms are sp^2 hybridized, the chelate ring is significantly puckered in all three complexes and some strain in the chelate ring is suggested by the deviation from 120° angle about the nitrogen, Co–N(1)–C(3) (134.7(3)°) and Co–N(1)–C(4) (107.8(3)°) in **2**; Ni–N(1)–C(3) (132.53(19)°, 130.44(19)°) and Ni–N(1)–C(4) (107.90(16)°, 109.51(16)°) in **5**; Zn–N(1)–C(3) (135.0 (4)°) and Zn–N(1)–C(4) (107.6(3)°) in **6**. The dihedral angles N(1)–C(4)–C(5)–N(2) are −56.8(5)° in **2**, −51.9(3)° and 50.1(3)° in **5** and −56.3(5)° in **6** that is typical for diamine chelate [30,45,46].

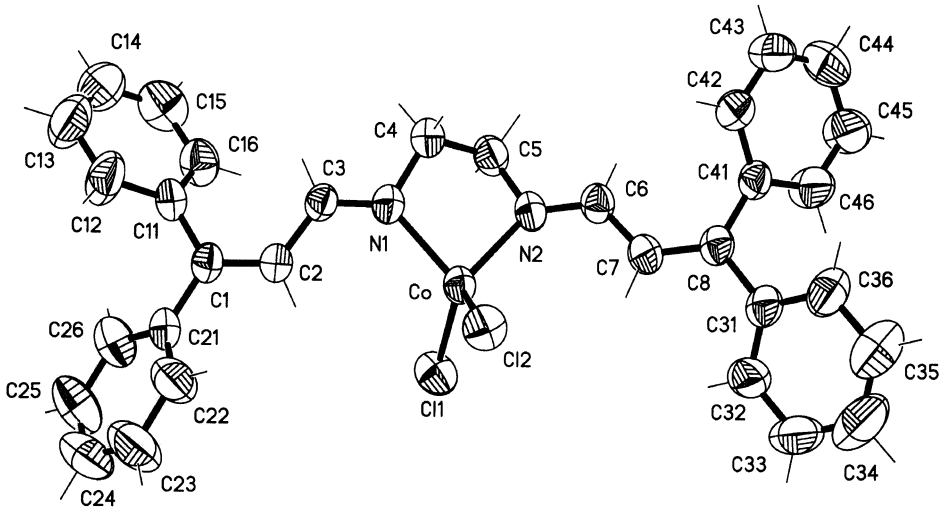


Fig. 2. Representation of molecular structure of **2** with atom-labeling scheme. Atomic displacement parameters are shown at 50% probability level. The crystal structure of $[ZnCl_2(Phca_2en)]$ (**6**) is visually indistinguishable from that of the cobalt compound and uses an identical atom numbering scheme, but with 'Co' replaced by 'Zn'.

The geometry of hydrogen bonds are given in Table 5. Complexes **2** and **6** exhibit similar hydrogen bonding patterns built up from the C–H···Cl hydrogen bonds. Chains of $MLCl_2$ molecules arranged along *a* axis are linked together via C–H···Cl hydrogen bonds to form three-dimensional networks (Fig. 4(a and b)). The H···Cl contacts range from 2.63 to 2.83 Å with the C–H···Cl angles of 134°–167°. For complex **5**, the C–H···Br hydrogen bonds have minor impact on crystal packing, though a three-dimensional hydrogen bonding network exists. The H···Br contacts are as large as 3.01 Å and the mean C–H···Br angle being 139° reflecting the weakness of such intermolecular interactions in the solid state.

Due to the geometrical restrictions in **2**, **5** and **6**, the H_b atoms, i.e. H(2) and H(7), lie in the vicinity of the metal atoms making intramolecular interactions possible in the form of weak C–H···M hydrogen bonds. This type of interaction is somewhat similar to the agostic interactions found in many organometallic complexes [47,48], although a $C-H^{\delta+}\cdots M^{\delta-}$ charge-assisted hydrogen bonding could be encountered here. As a matter of fact, the involvement of the metal centers in hydrogen bonding is now well established and known as non-traditional hydrogen bonds [49,50]. A recent survey by Desiraju and Steiner [51], gives the range 2.5–3.2 Å for the weak (C–)H···M hydrogen bonds. Our structural data reveals that the (C–)H···M interactions ranging from 2.9 to 3.13 Å in **2**, **5** and **6** would meet the above criteria and can be regarded as intramolecular weak hydrogen bonds. Consequently, the H_b atoms are influenced by the change in the electron density on the central metal atom and this can be followed easily by ^1H NMR spectroscopy. Our results from ^1H NMR study of $Zn(Phca_2en)X_2$ complexes, in which X = Cl, Br, I and NCS, clearly give further evidence to the existence of

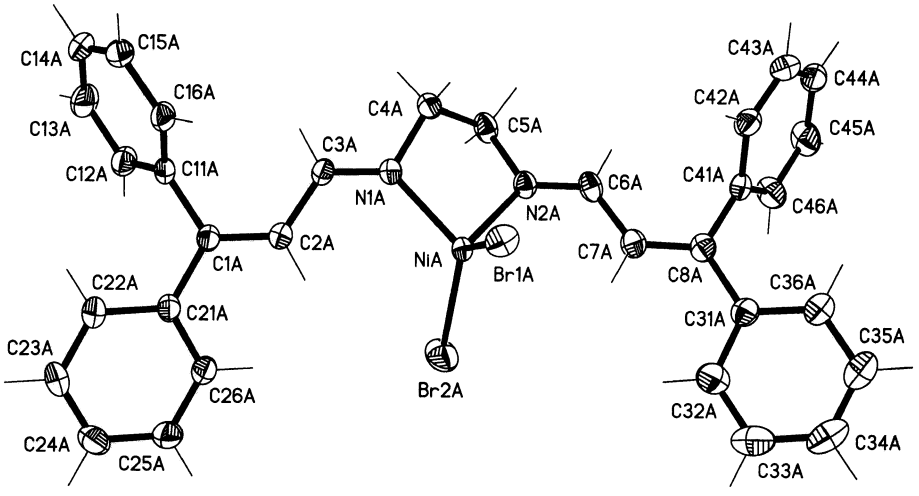


Fig. 3. Representation of molecular structure of **5** with atom-labeling scheme. Atomic displacement parameters are shown at 50% probability level.

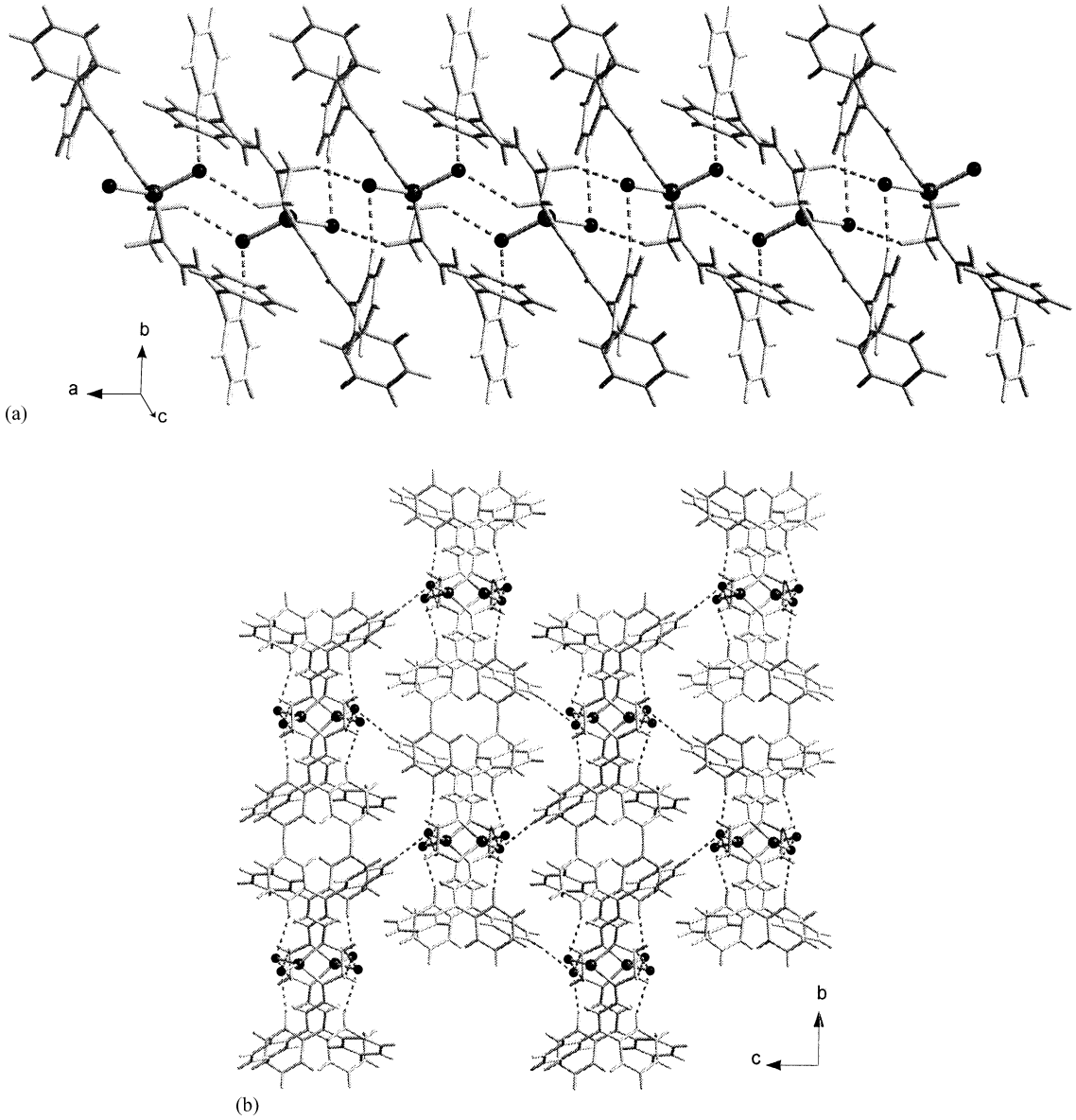


Fig. 4. The C–H···Cl hydrogen bonds are forming chains (a) of $CoLCl_2$ (or $ZnLCl_2$) molecules along *a* axis in the crystal structure of **2** (or **6**) and a three-dimensional network (b) is built up from linking chains.

Table 4
Torsion angles for chelating ring and stiryl groups

	2	**5**		**6**
		Molecule A	Molecule B	
N1–C4–C5–N2	−56.3(5)	−51.9(3)	50.1(3)	−56.8(5)
N1–C3–C2–C1	−178.4(5)	178.9(3)	−178.9(3)	−177.5(5)
N2–C6–C7–C8	−175.5(5)	−179.3(3)	174.7(3)	−176.6(5)
C2–C1–C21–C22	35.4(8)	157.2(3)	36.4(4)	34.9(8)
C2–C1–C11–C12	−129.3(6)	121.6(3)	−129.7(3)	−133.6(7)
C7–C8–C31–C32	39.5(7)	18.9(4)	−40.4(4)	39.3(7)
C7–C8–C41–C42	48.1(8)	63.7(4)	−43.3(4)	48.0(8)

such (C–)H···Zn intramolecular interactions, although being weak but can be significant. This type of interaction has also been reported by others [52,24] for closely related structures.

4. Supplementary material

Crystallographic data (excluding structure factors) for the structures reported in this paper have been deposited with the Cambridge Crystallographic Centre as supplementary publication no. CCDC- 182874 (**2**), 182875 (**5**) and 182876 (**6**). Copies of the data can be obtained free of charge on application to The Director, CCDC, 12 Union Road, Cambridge, CB2 1EZ, UK (fax: +44-1223-336033; e-mail: deposit@ccdc.cam.ac.uk or www: http://www.ccdc.cam.ac.uk).

Table 5
Intra- and intermolecular hydrogen bonds for **2**, **5** and **6** (Å, °)

D–H···A	d(D–H)	d(H···A)	d(D···A)	< (DHA)
2				
C2–H2···Co	0.95	3.13	3.538(1)	103
C7–H7···Co	0.95	3.13	3.538(1)	103
C5–H5A···Cl1[a]	0.97	2.79	3.593(5)	141
C16–H16···Cl1[a]	0.93	2.65	3.560(6)	166
C34–H34···Cl1[b]	0.93	2.78	3.587(8)	145
C4–H4A···Cl2[c]	0.97	2.83	3.585(5)	136
C42–H42···Cl2[c]	0.93	2.81	3.685(6)	157
5				
C2A–H2A···NiA	0.95	3.00	3.427(2)	106
C7A–H7A···NiA	0.95	2.92	3.357(2)	144
C2B–H2B···NiB	0.95	2.91	3.361(2)	142
C7B–H7B···NiB	0.95	3.02	3.430(2)	142
C12B–H12B···Br2A[a]	0.95	2.93	3.703(3)	140
C42B–H42B···Br1A	0.95	2.90	3.695(3)	142
C12A–H12A···Br2B[b]	0.95	3.01	3.736(3)	135
6				
C2–H2···Zn	0.95	3.12	3.547(1)	102
C7–H7···Zn	0.95	3.13	3.550(1)	103
C4–H4a···Cl2[a]	0.99	2.80	3.552(5)	134
C5–H5A···Cl1[b]	0.99	2.76	3.564(5)	139
C16–H16···Cl1[b]	0.95	2.63	3.561(6)	167
C34–H34···Cl1[c]	0.95	2.77	3.580(7)	143
C42–H42···Cl2[a]	0.95	2.76	3.658(5)	157

Symmetry codes: (**2**); a) $-x+1, -y, -z$, b) $-x+1/2, y+1/2, -z+1/2$; (**5**); a) $x, y+1, z$, b) $x, y-1, z$; (**6**); a) $-x+1, -y+1, -z$, b) $-x+2, -y+1, -z$, c) $-x+3/2, y+1/2, -z+1/2$.

Acknowledgements

Authors wish to thank the Division of Inorganic Chemistry, Department of Chemistry, Göteborg University for providing X-ray structure determination facilities. M.A. and S.D. would like to acknowledge the Isfahan University of Technology and Tarbiat Modarres University Research Council for partial support of this work.

References

[1] S. Yamada, Coord. Chem. Rev. 190–192 (1999) 537.
[2] S. Chang, L. Jones, C.M. Wang, L.M. Henling, R.H. Gruubbs, Organometallics 17 (1998) 3460.
[3] K.K. Chaturvedl, J. Inorg. Nucl. Chem. 39 (1977) 901.
[4] R.D. Archer, B. Wang, Inorg. Chem. 29 (1990) 39.
[5] J. Costamagna, J. Vargas, R. Latorre, A. Alvarado, G. Mena, Coord. Chem. Rev. 119 (1992) 67.
[6] S.C. Bhatia, J.M. Bindlish, A.R. Saini, P.C. Jain, J. Chem. Soc., Dalton Trans. (1981) 1773.
[7] J.M. Bindlish, S.C. Bhatia, P.C. Jain, Indian J. Chem. 13 (1975) 18.
[8] J.M. Bindlish, S.C. Bhatia, P. Gautam, P.C. Jain, Indian J. Chem., Sect. A 16 (1978) 279.
[9] M.T. Miller, P.K. Gantzel, T.B. Karpishin, Inorg. Chem. 38 (1999) 3414.
[10] R.J. Butcher, E. Sinn, Inorg. Chem. 16 (1977) 2334.
[11] S.S. Tandon, S. Chander, L.K. Thompson, Inorg. Chim. Acta 300-302 (2000) 638.
[12] E. Quiroz-Castro, S. Bernes, N. Barba-Behrens, R. Tapia-Benavids, R. Contreras, H. Noth, Polyhedron 19 (2000) 1479.
[13] H.L. Blonk, W.L. Driessen, J. Reedijk, J. Chem. Soc., Dalton Trans. (1985) 1699.
[14] A.G. Orpen, L. Brammer, F.H. Allen, O. Kennard, D.G. Watson, R. Taylor, J. Chem. Soc., Dalton Trans. (1985) S1.
[15] Z. Dori, H.B. Gray, J. Am. Chem. Soc. 88 (1966) 1394.
[16] M. Amirnasr, K.J. Schenk, A. Gorji, R. Vafazadeh, Polyhedron 20 (2001) 695.
[17] M. Amirnasr, R. Vafazadeh, Sci. Iranica 4 (1997) 35.
[18] D.D. Perrin, W.L. Armarego, D.R. Perrin, Purification of Laboratory Chemicals, 2nd ed., Pergamon, New York, 1990.
[19] 'SMART and SAINT: Area Detector Control and Integration Software', Siemens Analytical X-ray Instruments Inc., Madison, WI, 1995.
[20] G.M. Sheldrick, SADABS: Program for Empirical Absorption Correction of Area Detectors, University of Göttingen, Germany, 1996.
[21] 'SHELXTL (Version 5.10)', Bruker AXS Inc., Madison, WI, 1997.
[22] K. Nakamoto, Infrared and Raman Spectra of Inorganic and Coordination Complexes, fourth ed., Wiley, New York, 1992.
[23] D. Johnston, W.L. Rohrbuagh, W.D. Horrockas, Jr., Inorg. Chem. 10 (1971) 574.
[24] P. Li, I.J. Scowen, J.E. Davies, M.A. Halcrow, J. Chem. Soc., Dalton Trans. (1998) 3791.
[25] A.B.P. Lever, Inorganic Electronic Spectroscopy, 2nd ed., Elsevier, Amsterdam, 1984, p. 496.
[26] N. Greenwood, A. Earnshaw, Chemistry of the Elements (Chapter 26), Pergamon, Oxford, 1984.
[27] C.A. Otter, S.M. Couchman, J.C. Jeffery, K.L.V. Mann, E. Psillakis, M.D. Ward, Inorg. Chim. Acta 278 (1998) 178.
[28] W.D. Horrocks, Jr., D.H. Templeton, A. Zalkin, Inorg. Chem. 7 (1968) 2303.
[29] J.R. Wiesner, E.C. Lingafelter, Inorg. Chem. 5 (1966) 1770.
[30] W.R. Scheidt, J.C. Hanson, P.G. Rasmussen, Inorg. Chem. 8 (1969) 2398.
[31] H.I. Blonk, W.L. Driessen, J. Reedijk, J. Chem. Soc., Dalton Trans. (1985), 1699.
[32] Y. Yamamoto, T. Suzuki, S. Kaizaki, J. Chem. Soc., Dalton Trans. (2001) 1566.
[33] Y. Yamamoto, T. Suzuki, S. Kaizaki, J. Chem. Soc., Dalton Trans. (2001) 2943.
[34] B.O. West, J. Chem. Soc. (1962) 1374.
[35] L. Sacconi, M. Ciampolini, F.P. Cavasino, J. Am. Chem. Soc. 84 (1962) 3246.
[36] R.H. Holm, G.W. Evervtt, A. Chakravorty, Prog. Inorg. Chem. 7 (1966).
[37] R.J. Butcher, E. Sinn, Inorg. Chem. 16 (1977) 2334.
[38] Y.P. Tian, C.Y. Duan, Z.L. Lu, X.Z. You, X.Y. Huang, J. Coord. Chem. 38 (1996) 219.
[39] J.A.J. Jarvis, R.H.B. Mais, P.G. Owston, J. Chem. Soc. A (1968) 1473.
[40] J.L. deBoer, D. Rogers, A.C. Skapski, P.G.H. Troughton, Chem. Commun. (1966) 756.
[41] M.R. Fox, P.L. Orioli, E.C. Lingafelter, L. Sacconi, Acta Crystallogr. 17 (1964) 1159.
[42] W.M. Davis, M.M. Roberts, A. Zask, K. Nakanishi, T. Nozoe, S.J. Lipard, J. Am. Chem. Soc. 107 (1985) 3864.
[43] S. Knapp, T.P. Keenan, X. Zhang, R. Fikar, J.A. Potenza, H.J. Schugar, J. Am. Chem. Soc. 112 (1990) 3452.
[44] Y. Elerman, A. Elmali, I. Svoboda, H. Fuess, Acta Crystallogr., Sect. C 54 (1998) 1076.
[45] Y. Satio, H. Iwasaki, Bull. Chem. Soc. Jpn. 39 (1966) 92.
[46] C.F. Liu, J.A. Ibers, Inorg. Chem. 9 (1962) 773.

[47] M. Brookhart, M.L.H. Green, L.L. Wang, Prog. Inorg. Chem. 30 (1988) 1.
[48] R.H. Crabtree, Angew. Chem., Int. Ed. Engl. 32 (1993) 789.
[49] D. Braga, F. Grepioni, G.R. Desiraju, Chem. Rev. 98 (1988) 1375.
[50] D. Braga, F. Grepioni, E. Tedesco, K. Biradha, G.R. Desiraju, Organometallics 16 (1987) 1846.
[51] G.R. Desiraju, T. Steiner, The Weak Hydrogen Bonds in Structural Chemistry and Biology, Oxford University Press, New York, 1999.
[52] D.L. Johnston, W.L. Rohrbaugh, W.D. Horrocks, Jr., Inorg. Chem. 10 (1971) 547.

NMR spectroscopy was successfully used as an analytical and structural method for those high-spin cobalt(II) complexes from the early beginning [11–17].

In case of homo- or heteroscorpionate tris(pyrazolyl)borate ligands of low or medium steric hindrance both bis-ligand Tp'_2M or mono-ligand Tp′MX complexes are formed depending on the method of synthesis (X, an anion disregarded as a ligand in this case). Here we report on the synthesis and structures of mono- and bis-ligand complexes with tris(pyrazolyl)borates obtained from 3(5)-phenyl,5(3)-methylpyrazole and 3,5-dimethylpyrazole. We also describe the unexpected reactivity of hydrobis(3-phenyl,5-methylpyrazolyl)(3,5-dimethylpyrazolyl)boratocobalt(II)(L) complexes, where L = $[OOCCH(OH)CH_3]^-$ (Lac), $[OOCC(O)CH_3]^-$ (Pyr), and $[OOCCH(OH)CH_2CH_3]^-$ (Hbu).

2. Experimental

2.1. Syntheses

2.1.1. General synthetic and analytical procedures

Sodium hydrotris(3-phenyl,5-methylpyrazolyl)borate (Na[HB(3-Ph,5-Mepz)$_3$]) and sodium hydrobis(3-phenyl,5-methylpyrazolyl)(3-methyl,5-phenylpyrazolyl)borate (Na[HB(3-Ph,5-Mepz)$_2$(3-Me,5-Phpz)]) as well as hydrobis(3-phenyl,5-methylpyrazolyl)(3,5-dimethylpyrazolyl)borate (Na[HB(3-Ph,5-Mepz)$_2$(3,5-diMepz)]) and its high-spin cobalt(II) complex-[HB(3-Ph,5-Mepz)$_2$(3,5-diMepz)]Co(NCS) have been synthesized before [7,12]. Here we have described the optimized protocols of synthesis of heteroscorpionate Na[HB(3-Ph,5-Mepz)$_2$(3-Me,5-Phpz) in which the homoscorpionate Na[HB(3-Ph,5-Mepz)$_3$] is obtained as side-product and that for Na[HB(3-Ph,5-Mepz)$_2$(3,5-diMepz)].

The general procedure of synthesis of Tp′CoX complexes (X = thiocyanate or carboxylate anion) used here was based on addition of solution of NaTp′ in tetrahydrofuran (THF) to an excess of the metal ion salt (0.1 M) and additional excess of potassium thiocyanate or sodium carboxylate (0.5 M, unless otherwise stated) in water, and subsequent extraction of the product(s) into methylene dichloride. In some cases a mixture of NaTp′ salts was used and separation of ligands as Tp′Co(NCS) complexes was applied. The composition of mixtures of Tp′Co(NCS) at every step of both the synthesis and separation was controlled by means of ^{1}H NMR spectroscopy.

2.1.2. Optimized protocol for the synthesis of Na[HB(3-Ph,5-Mepz)$_2$(3-Me,5-Phpz)] and Na[HB(3-Ph,5-Mepz)$_3$]

The synthesis of the sodium salts of ligands and Tp′Co(NCS) complexes have been described before [7]. An optimized large-scale protocol of the synthesis of Na[HB(3-Ph,5-Mepz)$_3$] and Na[HB(3-Ph,5-Mepz)$_2$(3-Me,5-Phpz)] is given as follows: 1.1368 g $NaBH_4$ (30 mmol) was heated with 3(5)-phenyl,5(3)-methylpyrazole (14.2378 g, 90 mmol) in octadecane (40 cm^3). The temperature of the mixture was gradually increased up to boiling point of the solvent and the reaction mixture was heated until hydrogen evolution ceased (2.3 dm^3 were collected within a period of 20 min). Heptane (100 cm^3) was added to the pre-cooled mixture, which was then slowly cooled down with continuous stirring for next 12 h. The solid residue was filtered off, washed with petroleum ether and dried under high vacuum. White solid (13.7 g) was isolated. The precipitate was heated three times in boiling heptane (100 cm^3, 20 min) and filtered off while hot. Then the heating was repeated with 500 cm^3 heptane. Finally, 9.56 g of pure Na[HB(3-Ph,5-Mepz)$_2$(3-Me,5-Phpz)] was isolated as a heptane-insoluble compound (18.9 mmol, 62.9% yield). From the first three combined filtrates 0.81 g of pure Na[HB(3-Ph,5-Mepz)$_3$] was isolated as colorless crystals (1.6 mmol, 5.3% yield).

2.1.3. Optimized protocol for the synthesis of Na[HB(3-Ph,5-Mepz)$_2$(3,5-diMepz)] and [HB(3-Ph,5-Mepz)$_2$(3,5-diMepz)]Co(NCS)

Syntheses of Na[HB(3-Ph,5-Mepz)$_2$(3,5-diMepz)] and [HB(3-Ph,5-Mepz)$_2$(3,5-diMepz)]Co(NCS) have been described previously [12].

In the optimized protocol the sodium salt of [HB(3-Ph,5-Mepz)$_2$(3,5-diMepz)]$^-$ was obtained by condensation of $NaBH_4$ (0.7684 g, 20.3 mmol) with 3,5-dimethylpyrazole (2.1189 g, 22.0 mmol) and 3(5)-phenyl,5(3)-methylpyrazole (6.0116 g, 38.0 mmol) in heptadecane (40 cm^3) gradually heated up to boiling point; 1430 cm^3 of hydrogen evolved. The reaction mixture was cooled to approximately 100 °C and 50 cm^3 of heptane was added. After storage at room temperature for 12 h the white precipitate formed, which was filtered off, washed with approximately 100 cm^3 of petroleum ether and dried under reduced pressure. Yield of crude product (calculated for the desired compound): 6.29 g (69.7%).

Further purification has been done by heating the crude product under refluxing heptane (150 cm^3) twice for 20 min and separation of the insoluble product by filtration. Finally, 2.6 g of solid sodium salt was isolated (28.8% yield).

The [HB(3-Ph,5-Mepz)$_2$(3,5-diMepz)]Co(NCS) complex was obtained by the described procedure [12], i.e. typically by dropwise addition of 1.0 g of NaTp′ in THF (35 cm^3) into 0.1 M $Co(NO_3)_2$ and 0.5 M KNCS water solution (200 cm^3). The product was extracted into dichloromethane (300 cm^3), the organic phase was washed twice with 300 cm^3 water, and dichloromethane was removed on a rotary evaporator keeping the temperature of bath at 30 °C. Formation of a white precipitate was observed (about 0.15 g), which was later

identified as a mixture of bis-ligand Tp′CoTp″ complexes (vide infra). These were insoluble in cold THF. Thus, the violet [HB(3-Ph,5-Mepz)$_2$(3,5-diMepz)]Co(NCS) was easily separated by dissolving in THF.

The solvent was removed under high vacuum and the complex was found to be pure as analyzed by its ^{1}H NMR spectrum. However, it has been found that prolonged storage of the complex in polar solvents like methanol or tetrahydrofuran was accompanied by formation of a white precipitate. When [HB(3-Ph,5-Mepz)$_2$(3,5-diMepz)]Co(NCS) was heated to the boiling point of the solvents, vast side reactions took place.

2.1.4. Pyruvato hydrotris(3-phenyl,5-methylpyrazolyl)boratocobalt(II) ($Tp^{Ph,Me}Co(Pyr)$, (**1**))

The $NaTp^{Ph,Me}$ and $Tp^{Ph,Me}Co(NCS)$ complexes were prepared as described before [7]. The $Tp^{Ph,Me}Co(Pyr)$ complex was obtained by metathesis of $Tp^{Ph,Me}$-Co(NCS)(THF) (100 mg, 0.149 mmol). The starting compound was dissolved in 100 cm^3 dichloromethane and vigorously stirred three times with 0.5 M water solution of sodium pyruvate for 2 h. After separation of the organic phase, the dichloromethane was stripped out on a rotary evaporator and the solid residue was recrystallized twice from tetrahydrofuran–hexane mixture to give pink needles of $Tp^{Ph,Me}Co(Pyr)$ (20 mg, 21.3% yield). One of the collected crystals was analyzed crystallographically (Table 1).

2.1.4.1. Analytical data for **1**.

Elemental analysis: Calc. for $C_{33}H_{31}N_6O_3BCo$ (M.W. 629.38): C, 62.97; H, 4.96; N, 13.35. Found: C, 63.15; H, 4.86; N, 13.28%.

^{1}H NMR ($CDCl_3$, 298K); δ (intensity, assignment): −10.1 (3H, CH_3(Pyr)); 4.4 (6H, broad, *o*-H(3-Ph)); 7.1 (4H, *p*-H(3-Ph)); 8.9 (6H, *m*-H(3-Ph)); 12.6 (1H, B-*H*); 18.9 (9H, 5-CH_3); 64.5 (3H, 4-H).

(CD_3OD, 298K); δ (intensity, assignment): −21.4 (6H, *o*-H(3-Ph)); 9.4 (3H, CH_3(Pyr)); 27.5 (9H, 5-CH_3); 40.0 (1H, B-*H*); 57.8 (3H, 4-H). IR (KBr) $\nu_{(BH)}$ 2561 cm^{-1}.

2.1.5. Bis[hydrobis(3-phenyl,5-methylpyrazolyl)(3-methyl,5-phenylpyrazolyl)borato]cobalt(II) ([HB(3-Ph,5-Mepz)$_2$(3-Me,5-Phpz)]$_2$Co(II) (**2**))

Cobalt(II) nitrate (3.8 cm^3, 0.05 M, 0.19 mmol) was added dropwise to a vigorously stirred THF solution (30 cm^3) containing 200 mg Na[HB(3-Ph,5-Mepz)$_2$(3-Me,5-Phpz)] (0.39 mmols). A yellow precipitate formed, which dissolved upon addition of chloroform (100 cm^3). The organic phase was separated and washed twice with water (100 cm^3), solvents were removed on a rotary evaporator and the solid residue was dried under high vacuum. The product was recrystallized from THF–hexane mixture to give 193 mg of yellow crystals of [HB(3-Ph,5-Mepz)$_2$(3-Me,5-Phpz)]$_2$Co(II) (0.17 mmol, 97% yield). One of the crystals was analyzed crystallographically.

2.1.5.1. Analytical data for **2**.

Elemental analysis: Calc. for $C_{60}H_{56}N_{12}B_2Co$ (M.W. 1025.72): C, 70.26; H, 5.50; N, 16.39. Found: C, 69.95; H, 5.69; N, 16.52%.

^{1}H NMR (two rotational isomers were observed). Temperature dependent spectra were taken in toluene-d_8. (see Section 3).

IR (KBr) $\nu_{(BH)}$ 2555 cm^{-1}.

Mass spectrum (ESI, positive polarization) *m*/*e*: (**2**)$^+$ 1025.7 (3%); (**1**-$C_{10}N_2H_9$, corresponding to 3(5)-Me,5(3)-PhpzH) 868.8 (100%).

2.1.6. Bis[hydrotris(3-phenyl,5-methylpyrazolyl)borato]cobalt(II) ($Tp_2^{Ph,Me}Co(II)$ (**3**))

Cobalt(II) nitrate (3.8 cm^3, 0.05 M, 0.19 mmol) was added dropwise to a vigorously stirred THF solution (30 cm^3) containing 204 mg $NaTp^{Ph,Me}$ (0.40 mmol). A pink precipitate formed, which dissolved upon addition of chloroform (100 cm^3). The organic phase was washed twice with water (100 cm^3), solvents were removed on rotary evaporator and the solid residue was dried under high vacuum. The product was recrystallized from THF–hexane.

After 1 week of co-diffusion of solvents 162 mg of pink crystals of **3** were obtained (0.158 mmol, 83% yield). One of the crystals was analyzed crystallographically (Table 1).

2.1.6.1. Analytical data for **3**.

Elemental analysis: Calc. for $C_{60}H_{56}N_{12}B_2Co$ (M.W. 1025.72): C, 70.26; H, 5.50; N, 16.39. Found: C, 70.15; H, 5.63; N, 16.56%.

^{1}H NMR ($CDCl_3$, 298K); δ (intensity, assignment): −39.5 (12H, *o*-H(3-Ph)); 0.5 (6H, *p*-H(3-Ph)); 0.8 (12H, *m*-H(3-Ph)); 36.1 (18H, 5-CH_3); 50.2 (6H, 4-H); 87.9 (2H, B–H).

IR (KBr): $\nu_{(BH)}$ 2547 cm^{-1}.

2.1.7. Bis[hydrobis(3-phenyl,5-methylpyrazolyl)(3-methyl,5-phenylpyrazolyl)borato]copper(II) ([HB(3-Ph,5-Mepz)$_2$(3-Me,5-Phpz)]$_2$Cu(II) (**4**))

Na[HB(3-Ph,5-Mepz)$_2$(3-Me,5-Phpz)] (200 mg, 0.39 mmols) dissolved in 5 cm^3 THF was added dropwise to a vigorously stirred 0.14 M water solution of cobalt(II) nitrate and 1.5 M sodium pyruvate (30 cm^3). A yellow precipitate formed, which dissolved upon addition of chloroform (80 cm^3). The organic phase was separated and washed twice with water (100 cm^3), the solvents were removed on a rotary evaporator and the solid residue was dried under high vacuum. The product was recrystallized from THF–hexane to give 120 mg of **4** as reddish–amber crystals (0.116 mmol, 59.7% yield). One

Table 1
Crystal data and structure refinement

Compound	1	2	3	4
Empirical formula	$C_{33}H_{31}BN_6O_3Co$	$C_{60}H_{56}B_2N_{12}Co$	$C_{60}H_{56}B_2N_{12}Co$	$C_{60}H_{56}B_2N_{12}Cu$
Formula weight	629.38	1025.72	1025.72	1030.33
Temperature (K)	100(2)	100(2)	100(2)	100(2)
λ (Å)	0.71073	0.71073	0.71073	0.71073
Crystal system	triclinic	triclinic	monoclinic	triclinic
Space group	$P\bar{1}$	$P\bar{1}$	$C2/c$	$P\bar{1}$
a (Å)	10.1405(19)	10.663(2)	17.9951(18)	10.664(2)
b (Å)	15.932(3)	12.064(2)	13.7117(18)	12.118(2)
c (Å)	18.974(3)	20.848(4)	22.101(4)	20.891(4)
α (°)	89.654(14)	101.57(3)		101.74(3)
β (°)	86.715(14)	96.89(3)	112.03(2)	96.90(3)
γ (°)	89.504(15)	95.34(3)		95.38(3)
V (Å^3)	3060.1(10)	2589.4(8)	5055.1(12)	2604.6(8)
Z	4	2	4	2
D_c (Mg m^{-3})	1.366	1.316	1.348	1.314
μ (mm^{-1})	0.605	0.385	0.394	0.473
F (000)	1308	1074	2148	1078
Crystal size (mm)	0.45 × 0.27 × 0.13	0.23 × 0.18 × 0.15	0.25 × 0.18 × 0.15	0.25 × 0.17 × 0.15
θ Range for data collection (°)	3.23–25.00	3.40–28.42	3.58–28.48	3.35–28.40
Ranges of h, k, l	−12/12, −18/18, −22/22	−13/14, −13/15, −27/26	−23/23, −18/17, −29/23	−14/14, −15/13, −24/27
Reflections collected	32 607	17 902	17 005	18 046
Independent reflections (R_{int})	10 738 (0.0530)	11 399 (0.0355)	5876 (0.0730)	11 459 (0.0292)
Data/parameters	10 738/1042	11 399/842	5876/343	11 459/903
Goodness-of-fit on F^2	1.170	1.179	1.167	1.074
Final R_1/wR_2 indices ($I > 2\sigma(I)$)	0.0547/0.1018	0.0790/0.1781	0.1277/0.3246	0.0527/0.1470
Extinction coefficient	0.0012(2)	0.0033(4)	0.0062(8)	
Largest difference peak and hole (e Å^{-3})	0.418 and −0.397	1.016 and −0.409	2.424 and −1.001	0.464 and −1.027

of the crystals was examined crystallographically (Table 1).

*2.1.7.1. Analytical data for **4**.* Elemental analysis: Calc. for $C_{60}H_{56}N_{12}B_2Cu$ (M.W. 1030.33): C, 69.94; H, 5.48; N, 16.31. Found: C, 69.80; H, 5.29; N, 16.20%.

IR (KBr): $\nu_{(BH)}$ 2559 cm^{-1}.

2.1.8. Conversion of [HB(3-Ph,5-Mepz)$_2$(3,5-diMepz)]Co(X) upon addition of sodium carboxylates (X = thiocyanate, lactate, pyruvate and 2-hydroxybutyrate)

In an attempted synthesis of [HB(3-Ph,5-Mepz)$_2$(3,5-diMepz)]Co(Lac), which was previously obtained in situ by addition of sodium lactate to [HB(3-Ph,5-Mepz)$_2$(3,5-diMepz)]Co(NCS) [12], Na[HB(3-Ph,5-Mepz)$_2$(3,5-diMepz)] (100 mg, 0.225 mmol) dissolved in 5 cm^3 THF was added dropwise to 50 cm^3 0.1 M cobalt(II) nitrate and 2M sodium lactate with vigorous stirring. The reddish-pink product was extracted with 100 cm^3 of dichloromethane. The organic layer was washed twice with 100 cm^3 water. Formation of a white precipitate, which was insoluble in cold THF, accompanied evaporation of organic solvents. The reddish product(s) was dissolved in THF and left for crystallization from THF–heptane. Again, the formation of a white precipitate upon standing in co-diffusing solvents was observed. Totally, 65 mg of white products were collected by filtration and analyzed by ^{1}H NMR spectroscopy and mass spectra. The isolated solid products turned out to be a mixture of bis-ligand homo- and heteroleptic complexes:

[HB(Ph,Mepz)$_2$(Me$_2$pz)]Co[HB(Ph,Mepz)$_3$] (*m/e* 964.2, 1%) [HB(Ph,Mepz)$_2$(Me$_2$pz)]$_2$Co (and/or [HB(Ph,Mepz)(Me$_2$pz)$_2$]Co[HB(3-Ph,5-Mepz)$_3$]) (*m/e* 901.2, 20%); [HB(Ph,Mepz)$_2$(Me$_2$pz)]Co[HB(Ph,Mepz)-(Me$_2$pz)$_2$] (*m/e* 839.0, 100%); [HB(Ph,Mepz)-(Me$_2$pz)$_2$]$_2$Co (and/or [HB(Ph,Mepz)$_2$(Me$_2$pz)]Co[HB-(Me$_2$pz)$_3$) (*m/e* 777.1, 45%); [HB(Ph,Mepz)(Me$_2$pz)$_2$]-Co[HB(Me$_2$pz)$_3$] (*m/e* 715.2, 2%); [HB(Me$_2$pz)$_3$]$_2$Co (*m/e* 653.4, 18%).

The solvents were removed from the filtrate in a stream of nitrogen and the solid residue was examined by ^{1}H NMR spectroscopy in CD$_3$OD solution. The identified products were: [HB(3-Ph,5-Mepz)$_2$(3,5-di-Mepz)]Co(Lac),Tp^{Ph,Me}Co(Lac), and [HB(3-Ph,5-Mepz)$_2$(3-Me,5-Phpz)]Co(Lac) [12,7].

Metathesis of thiocyanate into carboxylate anions were performed by stirring a THF and/or methanol solution of [HB(3-Ph,5-Mepz)$_2$(3,5-diMepz)]Co(NCS) (at ca. 0.16 mmol scale) with aqueous sodium lactate (1 M), sodium pyruvate (1 M) or sodium 2-hydroxybutyrate (0.2 M), followed by extraction of the product into CH$_2$Cl$_2$. The procedure was repeated three times.

The products were crystallized from THF–hexane or THF–heptane. The formation of bis-ligand complexes as white precipitates was observed in every case. The white compounds were analyzed as before by MS and ^{1}H NMR spectroscopy giving analogous results as those described above.

2.2. Methods and instruments

^{1}H NMR spectra were obtained with a Bruker AMX300 spectrometer operating in the quadrature mode at 300 MHz. The residual peaks of deuterated solvents were used as internal standards. The FT IR spectra were recorded on a Perkin–Elmer 1725X instrument.

Mass spectra were obtained on a Finnigan MAT TSQ 700 spectrometer by the ESI method at 4.5 kV ionization potential and 250 °C capillary temperature in chloroform.

Crystal data are given in Table 1, together with refinement details. All measurements of crystals **1**–**4** were performed at low temperature using an Oxford Cryosystem device on a Kuma KM4CCD κ-axis diffractometer with graphite-monochromated Mo Kα radiation. Crystals were positioned at 65 mm from the CCD camera. 612 frames were measured at 0.75° intervals with a counting time of 10–15 s. Accurate cell parameters were determined and refined by a least-squares fit of 1800 for **3** to 6200 for **1** strongest reflections. The data were corrected for Lorentz and polarization effects. No absorption correction was applied. Data reduction and analysis were carried out with the Oxford Diffraction (Poland) Sp. Z o.o. (formerly Kuma Diffraction Wroclaw, Poland) programs. Structures were solved by direct methods (program SHELXS-97 [18]) and refined by the full-matrix least-squares method on all F^2 data using the SHELXL-97 [19] programs. Non-hydrogen atoms were refined with anisotropic displacement parameters; hydrogen atoms were included from geometry of molecules and $\Delta\rho$ maps. They were refined with isotropic displacement parameters for **1** and **4**, and fixed for **2** and **3**.

3. Results and discussion

The unsubstituted Tp ligand forms bis-ligand Tp_2M complexes (M = Fe(II), Co(II), Ni(II), Cu(II), Zn(II)) even in the presence of excess of metal ion [20]. In the case of Tp′ ligands of medium steric demands (bearing for instance *i*Pr, *neo* Pent, Ph substituents attached to C-3), the protocol for synthesis of Tp′CoX complexes (where $X = NCS^-$, Cl^-, NCO^-, N_3^- and others) requires the use of metal ion in excess and sometimes additional excess of X^-. The series of homo- and heteroscorpionate Tp″CoX complexes have been prepared previously according to this method [2,3,7–9,11–15].

3.1. Synthesis and structure of hydrotris(3-phenyl,5-methylpyrazolylborate)cobalt(II) pyruvate ($Tp^{Ph,Me}Co(Pyr)$ (**1**))

The $Tp^{Ph,Me}Co(Pyr)$ complex was obtained by metathesis of the anion achieved in a two-phase system: methylene dichloride (containing starting $Tp^{Ph,Me}$-Co(NCS)) and water (saturated with sodium pyruvate). The conversion was completed after threefold extraction and the resulting product was obtained without substantial loss of $Tp^{Ph,Me}Co$(II). The **1** was recrystallized from THF–hexane mixture and subjected to X-ray crystallographic analysis. Two crystallographically independent molecules were found in the solid state. The details of the molecular structure are presented in Table 2 and Fig. 1. The pyruvate anion is coordinated to the central metal ion via two atoms: the oxygen from the carboxylate group and the second one from the carbonyl group. Thus, a five-membered chelate ring is formed and the molecule is stable enough to be isolated. Relatively large bite angles of $Tp^{Ph,Me}$ ligands in **1** (boron-centered bite angles, 75.1° and 74.9°; cobalt-centered bite angles, 135.4° and 135.0°) renders the cobalt(II) central ion available for two oxygen donors from the pyruvate ligand. In comparison, when nitrogen from thiocyanate and oxygen from tetrahydrofuran complete the coordination sphere of pentacoordinate $Tp^{Ph,Me}$-Co(NCS)(THF) the boron-centered and cobalt-centered bite angles are 76.5° and 140.3°, respectively [12]. Although carboxylate $Tp^{Ph}Co(X)$ complexes were synthesized before (where X = OAc, OBz, OBz-4-NO_2, OBz-4-F and OBz-2-NH_2; OBz = benzoate) structural data were not available due to difficulties in crystallization of complexes [21]. It has been found for example that attempted crystallization of $Tp^{Ph}Co$(anthranilate) from THF led to dismutation of the starting complex into insoluble Co(anthranilate)$_2$ and $(Tp^{Ph})_2Co$ [21]. The only complex of $Tp^{Ph,Me}$ and a carboxylate ancillary ligand that was characterized structurally was pentacoordinate $Tp^{Ph,Me}Cu$(OBz)(3-Ph,5-MepzH) [22].

3.2. Properties of thiocyanato hydrobis(3-phenyl, 5-methylpyrazolyl)(3,5-dimethylpyrazolyl)boratocobalt(II) ([HB(3-Ph,5-Mepz)$_2$(3,5-diMepz)]Co(NCS)) in presence of sodium carboxylates

Previously we have demonstrated that the heteroscorpionate ligand in [HB(3-Ph,5-Mepz)$_2$(3,5-diMepz)]Co(NCS) is stable enough to survive the demanding procedure of thermal conversion to form [HB(3-Ph,5-Mepz)(3-Me,5-Phpz)(3,5-diMepz)]Co(NCS) with approximately 30% yield accompanied with for-

Table 2
Selected bond lengths (Å) and angles (°) in **1**–**4**

Compound	M–N and M–O distances (Å)		N–M–N and O–M–N angles (°) [a]	
$Tp^{Ph,Me}Co(Pyr)$ (**1**) (two independent molecules)	Co(1)–O(1)	1.946(2)	O(1)–Co(1)–N(4)	127.75(10)
	Co(1)–N(4)	2.037(3)	O(1)–Co(1)–N(6)	131.26(11)
	Co(1)–N(6)	2.040(3)	N(4)–Co(1)–N(6)	97.44(11)
	Co(1)–N(2)	2.111(3)	O(1)–Co(1)–N(2)	103.27(10)
	Co(1)–O(3)	2.264(2)	N(4)–Co(1)–N(2)	90.61(11)
	Co(2)–O(21)	1.940(2)	N(6)–Co(1)–N(2)	92.11(11)
	Co(2)–N(22)	2.031(3)	O(1)–Co(1)–O(3)	77.43(9)
	Co(2)–N(24)	2.043(3)	N(4)–Co(1)–O(3)	87.21(10)
	Co(2)–N(26)	2.109(3)	N(6)–Co(1)–O(3)	89.05(10)
	Co(2)–O(23)	2.265(2)	N(2)–Co(1)–O(3)	177.65(9)
			O(21)–Co(2)–N(22)	127.63(10)
			O(21)–Co(2)–N(24)	131.70(11)
			N(22)–Co(2)–N(24)	97.37(11)
			O(21)–Co(2)–N(26)	103.40(10)
			N(22)–Co(2)–N(26)	90.40(11)
			N(24)–Co(2)–N(26)	91.39(10)
			O(21)–Co(2)–O(23)	77.43(9)
			N(22)–Co(2)–O(23)	87.95(10)
			N(24)–Co(2)–O(23)	89.10(9)
			N(26)–Co(2)–O(23)	178.32(9)
$[HB(3\text{-}Ph,5\text{-}Mepz)_2(3\text{-}Me,5\text{-}Phpz)]_2Co$ (**2**) (two independent molecules)	Co(1)–N(2)	2.260(4)	N(6)–Co(1)–N(4)	89.91(13)
	Co(1)–N(4)	2.206(4)	N(6)–Co(1)–N(2)	89.45(13)
	Co(1)–N(6)	2.113(4)	N(4)–Co(1)–N(2)	81.93(13)
	Co(2)–N(8)	2.148(4)	N(8)–Co(2)–N(12)	89.90(14)
	Co(2)–N(10)	2.239(4)	N(8)–Co(2)–N(10)	90.94(13)
	Co(2)–N(12)	2.172(4)	N(12)–Co(2)–N(10)	82.47(13)
$[HB(3\text{-}Ph,5\text{-}Mepz)_3]_2Co$ (**3**)	Co(1)–N(2)	2.169(6)	N(2)–Co(1)–N(6)	89.2(2)
	Co(1)–N(6)	2.200(5)	N(2)–Co(1)–N(4)	90.9(2)
	Co(1)–N(4)	2.271(6)	N(6)–Co(1)–N(4)	88.0(2)
$[HB(3\text{-}Ph,5\text{-}Mepz)_2(3\text{-}Me,5\text{-}Phpz)]_2Cu$ (**4**) (two independent molecules)	Cu(1)–N(4)	2.158(2)	N(4)–Cu(1)–N(2)	90.08(8)
	Cu(1)–N(2)	2.180(2)	N(4)–Cu(1)–N(6)	90.73(8)
	Cu(1)–N(6)	2.240(2)	N(2)–Cu(1)–N(6)	82.25(8)
	Cu(2)–N(12)	2.118(2)	N(12)–Cu(2)–N(10)	89.92(8)
	Cu(2)–N(10)	2.216(2)	N(12)–Cu(2)–N(8)	89.39(8)
	Cu(2)–N(8)	2.255(2)	N(10)–Cu(2)–N(8)	81.94(8)

[a] Both nitrogens from the same Tp′ ligand.

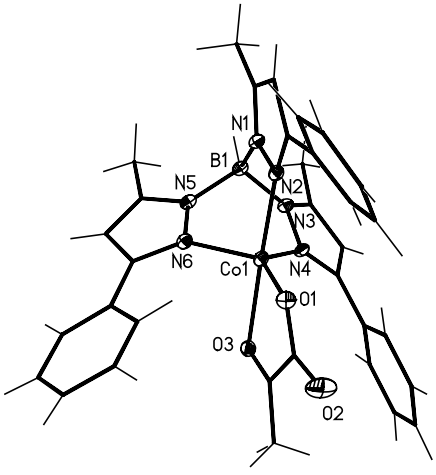


Fig. 1. View of one of two independent molecules of **1**.

mation of a not-identified side-product with about 10% yield [12]. On the other hand, the [HB(3-Ph,5-Mepz)$_2$(3,5-diMepz)]Co(NCS) undergoes slow conversion into not identified bis-ligand complexes, when stored in polar solvents like methanol or tetrahydrofuran. The heteroscorpionate [HB(3-Ph,5-Mepz)$_2$(3,5-diMepz)]Co(NCS) was also demonstrated to convert into [HB(3-Ph,5-Mepz)$_2$(3,5-diMepz)]Co(Lac) in situ upon addition of sodium lactate in methanol-d_4 solution. Encouraged with those results we have attempted to obtain [HB(3-Ph,5-Mepz)$_2$(3,5-diMepz)]Co(Lac) by large scale metathesis with excess sodium lactate. Surprisingly, we have isolated a colorless precipitate, which was a mixture of bis-ligand complexes. Reproducible mass spectral data have demonstrated that mixture composes of:

$[HB(Ph,Mepz)_2(Me_2pz)]Co[HB(Ph,Mepz)(Me_2pz)_2]$, $[HB(Ph,Mepz)(Me_2pz)_2]_2Co$, $[HB(Ph,Mepz)(Me_2pz)_2]$-$Co[HB(Me_2pz)_3]$ and $[HB(Me_2pz)_3]_2Co$, whereas the filtrate indicated the presence of mostly $[HB(3\text{-}Ph,5\text{-}Mepz)_3]Co(Lac)$, easily identified by its ^1H NMR spectrum [7]. In order to answer the question whether the conversion results from alkyl (methyl of lactate) versus aryl (3-phenyl of pyrazolyl moiety) cross-transfer, we have performed an additional experiment using sodium α-hydroxybutyrate instead of sodium lactate. The mass spectrum taken for bis-ligand cobalt(II) complexes was identical with that obtained previously. The same result was obtained with sodium pyruvate. Thus, we have concluded that cross-exchange of pyrazolyl moieties between two molecules of Tp′Co(L) complexes took place. Two questions desired answering, (i) is the formation of bis-ligand complexes (heteroleptic Tp′CoTp″ ones, containing sterically non-demanding $[HB(Ph,Mepz)(Me_2pz)_2]^-$ and $[HB(Me_2pz)_3]^-$ anions) a driving force for the observed conversions; and (ii) does the cross-exchange of other pyrazoles, able to form less sterically demanding Tp′ ligands, occur in a similar fashion.

Several attempts to prepare the crystals of mono-ligand Tp′M(carboxylate) complexes both by a preparative way, starting from M(II) carboxylates (M(II) = Co(II) or Cu(II)) and by metathesis of the corresponding Tp′Co(NCS) failed and the products isolated were bis-ligand complexes containing unconverted Tp′ ligands (Tp′ = $[HB(3\text{-}Ph,5\text{-}Mepz)_2(3\text{-}Me,5\text{-}Phpz)]^-$ and $[HB(3\text{-}Ph,5\text{-}Mepz)_3]^-$). The only example of a carboxylate complex of the Tp′Co(carboxylate) type isolated by crystallization from concentrate solution was **1** (vide supra).

3.3. Structure of bis-ligand homoleptic complexes: $[HB(3\text{-}Ph,5\text{-}Mepz)_2(3\text{-}Me,5\text{-}Phpz)]_2Co$ (**2**), $Tp_2^{Ph,Me}Co$ (**3**), and $[HB(3\text{-}Ph,5\text{-}Mepz)_2(3\text{-}Me,5\text{-}Phpz)]_2Cu$ (**4**)

Bis-ligand homoleptic Co(II) and Cu(II) complexes with Tp′ ligands composed of 3(5)-phenyl-5(3)-methylpyrazoles form spontaneously from the corresponding Tp′Co(carboxylate) counterparts via dismutation. In order to establish if the ligands bound in the bis-ligand complexes undergo interconversion we have synthesized **2** and **3** by a deliberate synthetic pathway using an excess of the sodium salt of the corresponding homo- and heteroscorpionates and cobalt(II) nitrate. The compounds were isolated with good yields and their structures have been elucidated crystallographically. Both complexes were stable both in solution when heated in refluxing toluene-d_8 and in the solid state. However, they were unstable in conditions used for mass spectral examination. Only **2** gave reliable results although the relative intensity of the peak of the molecular cation was low in comparison to the fragment **1**-3(5)-Me,5(3)-PhpzH. For other complexes studied here further fragementation took place.

In the case of **3** the Tp^{PhMe} ligands are bound to cobalt(II) central ion less tightly than heteroscorpionate Tp′ ligands in **2** and probably even in the solid state some percentage of the molecules of **3** contain Tp′ ligands bound in a $\eta^3\eta^2$ manner resulting in a lower value of R_f. The tight packing of two ligands in **3** causes a 2.7° deviation of the B···Co···B angle from linearity. Consistently, the $\nu_{(BH)}$ stretching vibration is less shifted towards higher wavenumbers in **3** in comparison with that in **2**.

The molecular structures of **2** and **3** are presented in Figs. 2 and 3. Selected bond lengths and angles are collected in Table 2. The Tp′ ligands are η^3 coordinated via three pyrazolyl nitrogen atoms. Thus, the cobalt central metal ions are hexacoordinate in both complexes. There are two slightly different molecules of **2**, with boron-centered (α) and cobalt-centered angles (β) of 85.5°; 85.9° and 154.7°; 154.5°, respectively (entry 1 in Table 3). However, both molecules have only slightly distorted octahedral environments around metal ion; all N_t–Co–N_t angles are ideally 180° (where N_t are *trans*-nitrogen donors). Also the B···Co···B axes are collinear ($\gamma = 180°$, column 6 in Table 3). The cobalt(II) ion in **3** is more distorted from the octahedral environment; N_t–Co–N_t angles are equal to 169.0°, 169.0°, and 171.5° resulting from considerably smaller bite angles of the homoscorpionate ligand (entry 2 in Table 3). Consequently, as one can see from Table 3, γ is smaller than 180° in **3**, which is a general trend observed for Tp′ ligands with α lower than 83°, with only a few exceptions.

The heteroscorpionate bis-ligand complex $[HB(3\text{-}Ph,5\text{-}Mepz)_2(3\text{-}Me,5\text{-}Phpz)]_2Cu$ (**4**) was obtained during the attempted synthesis of a mono-ligand copper(II)

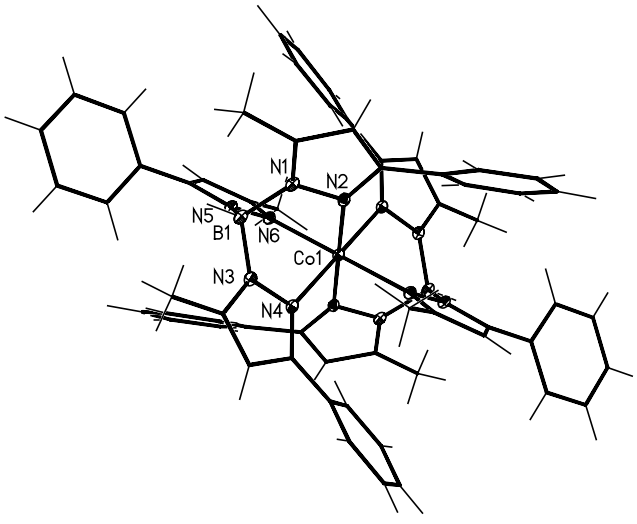


Fig. 2. View of one of two independent molecules of **2**.

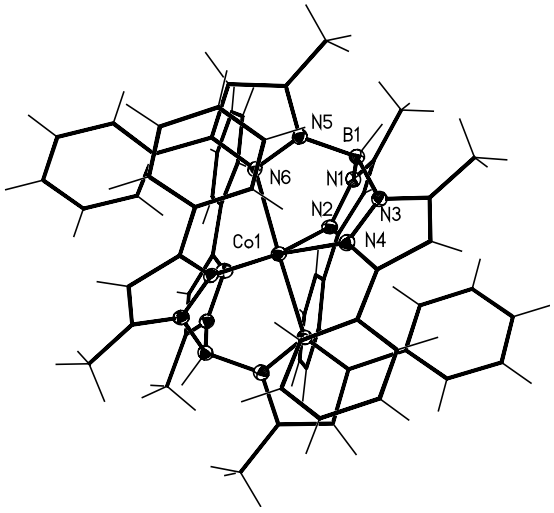


Fig. 3. View of **3**.

complex with a lactate auxiliary ligand. The molecular structure in **4** is presented in Fig. 4. Relevant bond lengths and angles are collected in Table 2. Both ligands are η^3 coordinated via three pyrazolyl nitrogen atoms. The boron-centered and copper-centered bite angles in two crystallographically different centrosymmetric molecules are, 86.0°; 87.3° and 155.0°; 154.8°, respectively, which are slightly larger than the corresponding ones in the cobalt(II) analogue (see entries 15 and 1 in Table 3). Generally, the Tp′ ligands are less tightly bound to Cu(II) in comparison with Co(II) Tp′MTp″ analogues; bite angles are larger and B–B distances are also slightly longer in the case of copper analogues (see entries 3 vs. 16, 6 vs. 21 and 1 vs. 15). Undoubtedly it results from the Jahn–Teller effect in octahedral Cu(II) complexes, which is clearly pronounced for almost all considered Tp′CuTp″ complexes (entries 16–21). As one can see, for smaller bite angles (larger steric hindrance of Tp′), smaller Jahn–Teller distortion is observed. Thus, the effect is almost negligible in **4**.

Table 3
Relevant bond lengths, angles and geometric factors describing Tp′MTp″ complexes (M = Co(II), Cu(II))

Entry (reference)	Compound [b]	M–N (Å) [e]	α (°) [e]	β (°) [e]	γ (°) [f]	B–B (Å) [g]
1 [a]	[HB(3-Ph,5-Mepz)$_2$(3-Me,5-Phpz)]$_2$Co (**2**)	2.21, 2.26, 2.11 [h], 2.17, 2.24, 2.15 [h]	85.5, 85.9	154.7, 154.5	180.0	6.31, 6.30
2 [a]	$Tp_2^{Ph,Me}$ Co (**3**)	2.17, 2.20, 2.27	83.0	147.7	177.3	6.19
3 [23]	Tp_2Co	2.13, 2.12, 2.12, 2.13, 2.13, 2.14	111.8, 111.4	222.8, 222.8	178.8	6.39
4 [24]	Tp_2^{Tn} Co	2.16, 2.15, 2.15	78.2	137.1	180.0	6.13
5 [24]	Tp_2^{Tn*} Co[c]	2.18, 2.19, 2.14 [h]	78.8	138.2	180.0	6.18
6 [25]	Tp_2^{4Bo} Co	2.12, 2.12, 2.14, 2.10, 2.10, 2.12	110.0, 109.0	220.8, 219.7	180.0	6.39, 6.37
7 [26]	$Tp_2^{iPr,Me}$ Co	2.26, 2.22, 2.16	81.8	145.8	174.3	6.23
8 [2]	[HB(3-*i*Prpz)$_2$(5-*i*Prpz)]$_2$Co	2.17, 2.16, 2.10 [h]	103.0	191.5	180.0	6.30
9 [2]	[HB(3-*i*Pr-4-Brpz)$_2$(5-*i*Pr-4Brpz)]$_2$Co	2.21, 2.15, 2.09 [h]	102.1	190.8	180.0	6.30
10 [27]	$Tp^{cPr}CoTp^{Ph}$	2.13, 2.12, 2.12, 2.20, 2.21, 2.26	95.5, 83.0	174.4, 146.9	171.4	6.23
11 [28]	$Tp^{Np}CoTp^{Me,(4,5\text{-}CH2)3)}$	2.14, 2.13, 2.14, 2.23, 2.25, 2.23	95.8, 82.3	173.9, 145.2	177.8	6.24
12 [29]	$Tp^{Np}CoTp^{3Bo,7Me}$	2.17, 2.17, 2.19, 2.15, 2.15, 2.15	94.4, 95.6	174.2, 174.0	175.7	6.37
13 [29]	$Tp^{Np}CoTp^{a*,3Me}$	2.12, 2.17, 2.17, 2.19, 2.20, 2.23	96.1, 78.9	173.1, 142.5	179.6	6.35
14 [9]	$Tp^{Ph,Me,Ph}CoTp^{Het}$ [d]	2.20, 2.21, 2.17, 2.21, 2.15, 2.11 [h]	83.7, 88.8	145.6, 157.5	167.0	6.20
15 [a]	[HB(3-Ph,5-Mepz)$_2$(3-Me,5-Phpz)]$_2$Cu **4**	2.16, 2.18, 2.24 [h], 2.13, 2.20, 2.25 [h]	86.0, 87.3	155.0, 154.8	180.0	6.30, 6.32
16 [30]	Tp_2Cu	2.00, 2.02, 2.53, 1.97, 2.09, 2.36	114.2, 112.4	224.3, 223.5	180.0	6.42
17 [31]	Tp_2^{4Me} Cu	2.00, 2.03, 2.47, 2.11, 2.06, 2.28	113.6, 113.3	223.5, 223.6	180.0	6.40, 6.37
18 [31]	Tp_2^{Me} Cu	2.02, 2.11, 2.34, 2.06, 2.06, 2.39	97.0, 98.2	175.3, 177.7	180.0	6.30, 6.35
19 [32]	Tp_2^{Me2} Cu	2.14, 2.02, 2.28	96.1	173.7	180.0	6.30
20 [31]	$Tp_2^{Me,Me,Cl}$ Cu	2.26, 2.12, 2.09, 2.25, 2.11, 2.13	97.3, 97.3	175.5, 175.6	178.1	6.31
21 [25]	Tp_2^{4Bo} Cu	2.02, 2.00, 2.45, 2.02, 2.01, 2.36, 2.02, 2.01, 2.41	111.6, 110.0, 111.1	221.9, 220.6, 220.9	180.0	6.40, 6.40, 6.37

[a] This paper.
[b] Names according to nomenclature in [1].
[c] Rotational heteroscorpionate, with 2′-sulfur directed towards cobalt metal ion.
[d] Tp^{Het} = hydrobis(3,4-diphenyl,5-methylpyrazolyl)(3-methyl,4,5-diphenylpyrazolyl)borate.
[e] Boron-centered (α) and metal ion centered (β) bite angles defined as in [7]. Sets of bond lengths and angles are given in rows corresponding to Tp′ ligands in sequence of appearance in the formula described in column 2 or corresponding to crystallographically distinguished molecules of complexes.
[f] The angle between lines connecting boron atoms of Tp′ ligands and central metal ion.
[g] Intramolecular boron–boron distance.
[h] Distinguished pyrazolyl moiety.

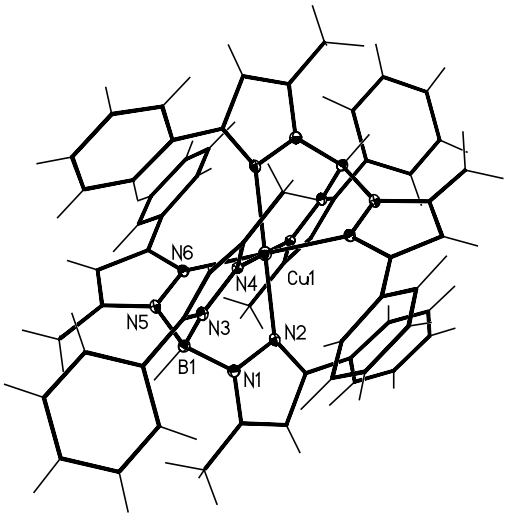
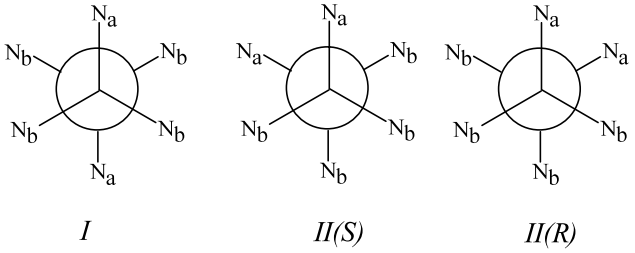


Fig. 4. View of one of two independent molecules of **4**.

3.4. The ^{1}H NMR studies of [HB(3-Ph,5-Mepz)$_2$(3-Me,5-Phpz)]$_2$Co

The temperature dependent ^{1}H NMR spectra of [HB(3-Ph,5-Mepz)$_2$(3-Me,5-Phpz)]$_2$Co have shown that two rotational isomers are present in solution (Fig. 5).

It is reasonable to assume that population of anti-periplanar isomer (*I*) in solution is higher than that of any of two enantiomeric synclinal isomers (*II*(*S*) and *II*(*R*)).



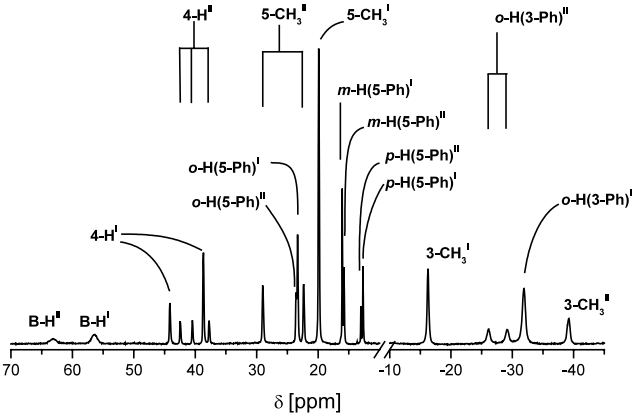


Fig. 5. ^{1}H NMR spectrum of **2** in toluene-d_8 at 350K. The corresponding resonances of isomer *I* and isomer *I* are labelled with $^{I,\ II}$ superscripts, respectively. The −10–10 ppm region was omitted for the sake of clarity.

Isomer *I* was found to be the only one existing at 100 K in the solid state by crystallographic measurement. It has a the plane of symmetry passing through the 3-methyl,5-phenylpyrazolyl rings (the donor atom is depicted as N_a in rotational isomer *I*) and a center of inversion at the metal ion. Thus, both 3-CH_3 groups and *o*-H(5-Ph) hydrogens give one resonance each, shifted upfield (−16 ppm) and downfield (23 ppm), respectively (Fig. 5). Also both 3-phenyl,5-methylpyrazolyl entities are equivalent resulting in presence of one *o*-H(3-Ph) and one 5-CH_3 resonances at −32 and 20 ppm, respectively. The pyrazolyl 4-H resonances of 4:2 intensity ratio are downfield shifted to about 40–45 ppm at 350 K. The spectrum of isomer *II* is much more complicated, though absolutely clear; the diastereotopic Tp′ ligands give three pyrazolyl 4-H, and pairs of both of *o*-H(3-Ph) and 5-CH_3 signals, as shown at Fig. 5. The spectrum presented in Fig. 5 was recorded at 350 K; at this temperature the resonances from *II* have relatively high intensity. Furthermore, no overlapping of resonances is observed. From integral intensity of the corresponding resonances of isomers *I* and *II* in the ^{1}H NMR variable temperature spectra the concentration ratio of *I* and *II*, and thus the equilibrium constant were estimated. The van't Hoff plot revealed considerable curvature, suggesting the involvement of additional species, undistinguishable by ^{1}H NMR spectroscopy. One of the possible explanations may be the presence of Tp′η^3Coη^2CoTp″ species being in fast equilibrium with *I* and *II*. Also the Curie plots for both isomers reveal a substantial curvature (Fig. 6). It has been evidenced that the hyperfine shift for hexacoordinate Tp$_2$Co complexes is dominated by a dipolar shift [16]. Thus, rather the involvement of the above mentioned Tp′η^3Coη^2Tp″ species in the averaged spectral picture should be considered instead of a large contribution of contact shift into isotropic shift [33]. Indeed, even in the solid state a medium sterically hindered Tp^{Ph} ligand produces a stable Tp$^{Ph}\eta^3$Coη^2Tp^{Ph} complex [21].

4. Conclusions

Carboxylate anions (OOCR = lactate, pyruvate and 2-hydroxybutyrate) induce conversion of [HB(3-Ph,5-Mepz)$_2$(3-Me,5-Phpz)]Co(OOCR) and [HB(3-Ph,5-Mepz)$_2$(3-Me,5-Phpz)]Cu(OOCR) into [HB(3-Ph,5-Mepz)$_2$(3-Me,5-Phpz)]$_2$Co and [HB(3-Ph,5-Mepz)$_2$(3-Me,5-Phpz)]$_2$Cu. In the case of [HB(3-Ph,5-Mepz)$_2$(3,5-diMepz)]Co(OOCR) the scrambling of pyrazoles takes place accompanied by formation of bis-ligand complexes of the Tp′CoTp″ type with Tp′ (Tp″) ligands of lower steric hindrance. This property of the [HB(3-Ph,5-Mepz)$_2$(3,5-diMepz)]$^-$ heteroscorpionate is rather unique; other two Tp′ ligands; the more hindered

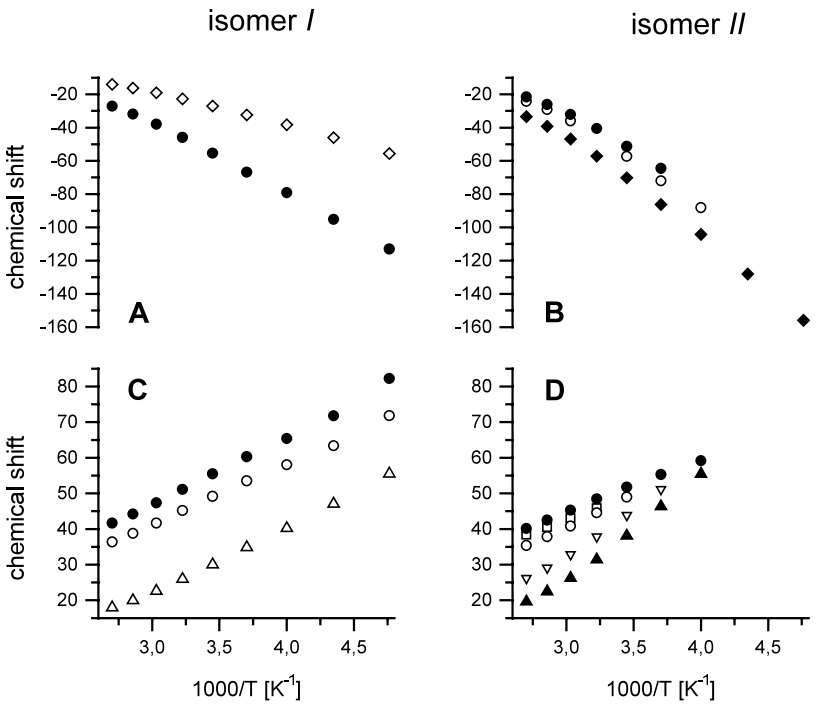


Fig. 6. Curie plots for isomers *I* and *II* of **2**. The *o*-H(Ph) and 3-CH_3 resonances are denoted as circles and diamonds, respectively, at traces A and B. The 4-H(pz) and 5-CH_3 resonances are denoted as circles and triangles, respectively, at traces C and D.

$[HB(3\text{-}Ph,5\text{-}Mepz)_2(3\text{-}Me,5\text{-}Phpz)]^-$ and $[HB(3\text{-}Ph,5\text{-}Mepz)_3]^-$ do not interconvert into their Tp'_2Co complexes. The only stable Tp′Co(carboxylate) complex was $Tp^{Ph,Me}Co(OOCC(O)CH_3)$ whose molecular structure was determined crystallographically.

5. Supplementary data

Crystallographic data for the structures reported in this paper (excluding structure factors) have been deposited with the Cambridge Crystallographic Data Centre, CCDC no. 182947 for compound **1**, CCDC no. 182945 for **2**, CCDC no. 182946 for **3** and CCDC no. 182947 for **4**. Copies of this information may be obtained free of charge from the Director, CCDC, 12 Union Road, Cambridge, CB2 1EZ, UK (fax: +44-1223-336033; e-mail: deposit@ccdc.cam.ac.uk or www: http://www.ccdc.cam.ac.uk).

Acknowledgements

T.R., Z.C. and S.W. kindly acknowledge the financial support from the State Committee for Scientific Research KBN (Grant number 3 T09A 05219).

References

[1] S. Trofimenko, Scorpionates: the Coordination Chemistry of Polypyrazolylborate Ligands, Imperial College Press, London, 1999.
[2] S. Trofimenko, J.C. Calabrese, P.J. Domaille, G.S. Thompson, Inorg. Chem. 28 (1989) 1091.
[3] J.C. Calabrese, S. Trofimenko, Inorg. Chem. 31 (1992) 4810.
[4] U.E. Bucher, A. Currao, R. Nesper, H. Rüegger, M.L. Venanzi, E. Younger, Inorg. Chem. 34 (1995) 66.
[5] D.J. Darensbourg, E.L. Maynard, M.W. Holtcamp, K.K. Klausmeyer, J.H. Reibenspies, Inorg. Chem. 35 (1996) 2682.
[6] A. Albinati, M. Bovens, H. Rüegger, M.L. Venanzi, Inorg. Chem. 36 (1997) 5991.
[7] M. Łukasiewicz, Z. Ciunik, R. Ruman, M. Skóra, S. Wołowiec, Polyhedron 20 (2001) 237.
[8] A.L. Rheingold, C.B. White, S. Trofimenko, Inorg. Chem. 32 (1993) 3471.
[9] J. Huang, L. Lee, B.S. Haggerty, A.L. Rheingold, M.A. Walters, Inorg. Chem. 34 (1995) 4268.
[10] P. Ghosh, D.G. Churchill, K. Rubinstein, G. Parkin, New J. Chem. 23 (1999) 961.
[11] M. Łukasiewicz, Z. Ciunik, S. Wołowiec, Polyhedron 19 (2000) 2119.
[12] T. Ruman, M. Łukasiewicz, Z. Ciunik, S. Wołowiec, Polyhedron 20 (2001) 2551.
[13] T. Ruman, Z. Ciunik, J. Mazurek, S. Wołowiec, Eur. J. Inorg. Chem. (2002) 754.
[14] T. Ruman, Z. Ciunik, A. Goclan, M. Łukasiewicz, S. Wołowiec, Polyhedron 20 (2001) 2965.
[15] T. Ruman, Z. Ciunik, S. Wołowiec, Angew. Chem., submitted.
[16] J.P. Jesson, J. Chem. Phys. 47 (1967) 582.
[17] J.C. Calabrese, P.J. Domaille, G. Thompson, S. Trofimenko, Inorg. Chem. 29 (1990) 4429.

[18] G.M. Sheldrick, SHELXS-97, Program for Solution of Crystal Structures, University of Göttingen, 1997.
[19] G.M. Sheldrick, SHELXL-97, Program for Crystal Structure Refinement, University of Göttingen, 1997.
[20] S. Trofimenko, J. Am. Chem. Soc. 89 (1967) 3170.
[21] A. Kremer-Aach, W. Kläui, R. Bell, A. Strerath, H. Wunderlich, D. Mootz, Inorg. Chem. 36 (1997) 1552.
[22] S. Guo, E. Ding, Y. Yin, K. Yu, Polyhedron 17 (1998) 3841.
[23] M.R. Churchill, K. Gold, C.E. Maw, Inorg. Chem. 9 (1970) 1597.
[24] J.C. Calabrese, P.J. Domaille, S. Trofimenko, G.J. Long, Inorg. Chem. 30 (1991) 2795.
[25] C. Janiak, S. Temizdemir, S. Dechert, W. Deck, F. Girgsdies, J. Heinze, M.J. Kolm, T.G. Scharmann, O.M. Zipffel, Eur. J. Inorg. Chem. (2000) 1229.
[26] M. Ruf, B.C. Noll, M. Groner, G.T. Yee, C.G. Pierpont, Inorg. Chem. 36 (1997) 4860.
[27] A.L. Rheingold, G.P. Yap, M.L. Liable-Sands, I.A. Guzei, S. Trofimenko, Inorg. Chem. 36 (1997) 6261.
[28] A.L. Rheingold, M.L. Liable-Sands, S. Trofimenko, Inorg. Chem. 39 (2000) 1333.
[29] A.L. Rheingold, B.S. Haggerty, G.P.A. Yap, S. Trofimenko, Inorg. Chem. 36 (1997) 5097.
[30] A. Murphy, B.J. Hathaway, T.J. King, J. Chem. Soc., Dalton Trans. (1979) 1646.
[31] C. Santini, C. Pettinari, M. Pellei, G. Gioia Lobbia, A. Pifferi, M. Camalli, A. Mele, Polyhedron 18 (1999) 2255.
[32] N. Kitajima, Y. Moro-Oka, A. Uchida, Y. Sasada, Y. Ohashi, Acta Crystallogr., Sect. C 44 (1988) 1876.
[33] F.A. Walker, U. Simonis, Biological magnetic resonance, in: L.J. Berliner, J. Reuben (Eds.), NMR of Paramagnetic Molecules, vol. 12, Plenum Press, New York, 1993.

Unity Inova-400 spectrometer (400 MHz for ^{1}H and 161.92 MHz for ^{31}P). Chemical shifts are relative to TMS (^{1}H), or external 85% H_3PO_4 (^{31}P), with downfield values reported as positive. Coupling constants J are given in Hertz.

2.2. Preparation of the complexes

2.2.1. Preparation of $UO_2Br_2 \cdot xH_2O$

Uranyl acetate was quantitatively transformed to uranyl bromide as follows: $UO_2(CH_3CO_2)_2 \cdot 2H_2O$ (0.5 g, 1.18 mmol) was dissolved in a mixture of methanol (5 ml) and 47% hydrobromic acid (2 ml). The solution was concentrated to dryness in a bath at approx. 100 °C leading to an orange residue of composition $UO_2Br_2 \cdot xH_2O$ ($2 < x < 3$).

2.2.2. Preparation of $[UO_2L_4](Br_3)_2$ ($L = HMPA$, $OPPh_3$, $OAsPh_3$)

The orange residue above obtained (ca. 1.15 mmol of $UO_2Br_2 \cdot xH_2O$) was dissolved in methanol (2 ml) and 0.5 g (3.13 mmol) of Br_2 was added with stirring. Then a solution of L (6.27 mmol) in methanol (15 ml) was added. After stirring the resulting mixture for 10 min at room temperature (r.t.), the orange microcrystalline precipitate was filtered, washed with diethyl ether (3 × 2 ml), and dried under vacuum.

2.2.2.1. $[UO_2(HMPA)_4](Br_3)_2$. Yield 1.477 g (85.5%). IR (cm^{-1}): ν(U=O) 917; ν(P=O) 1068. *Anal*. Found: C, 19.47; H, 4.70; N, 11.65; U, 16.01. Calc. for $C_{24}H_{72}Br_6N_{12}O_6P_4U$: C, 19.66; H, 4.95; N, 11.46; U, 16.23%.

2.2.2.2. $[UO_2(OPPh_3)_4](Br_3)_2$. Yield 1.623 g (75.8%). IR (cm^{-1}): ν(U=O) 925; ν(P=O) 1050. *Anal*. Found: C, 44.05; H, 3.15; U, 12.55. Calc. for $C_{72}H_{60}Br_6O_6P_4U$: C, 46.43; H, 3.25; U, 12.78%.

2.2.2.3. $[UO_2(OAsPh_3)_4](Br_3)_2$. Yield 2.27 g (94.4%). IR (cm^{-1}): ν(U=O) 901; ν(As=O) 840, 858. *Anal*. Found: C, 41.62; H, 2.94; U, 11.81. Calc. for $C_{72}H_{60}As_4Br_6O_6U$: C, 42.43; H, 2.97; U, 11.68%.

2.2.3. Preparation of a solution of UO_2I_2 in acetonitrile

Uranyl acetate was quantitatively transformed to $UO_2Cl_2 \cdot xH_2O$ by heating to dryness a solution of $UO_2(CH_3CO_2)_2 \cdot 2H_2O$ (0.5 g, 1.18 mmol) in a mixture of methanol (5 ml) and 35% hydrochloric acid (2 ml). The resulting $UO_2Cl_2 \cdot xH_2O$ was dissolved in acetonitrile (2 ml) and then a solution of 1.4 g (6.6 mmol) of NaI in acetonitrile (6 ml) was added. After stirring the mixture for 10 min the NaCl precipitated was filtered and washed with acetonitrile (2 × 1 ml). The clear red filtrate, consisting of a solution of UO_2I_2 and NaI in acetonitrile with some residual water, was used to prepare the polyiodides.

2.2.4. Preparation of $[UO_2L_4](I_3)_2$ ($L = HMPA$, $OPPh_3$, $OAsPh_3$)

The solution above prepared, containing about 1.15 mmol of UO_2I_2 in 10 ml of acetonitrile was treated with 1.21 g (4.76 mmol) of I_2 dissolved in 15 ml of acetonitrile. Then, 5 mmol of L in acetonitrile (15 ml) was added. After stirring the resulting mixture for 10 min the brown microcrystalline precipitate was filtered, washed with diethyl ether (3 × 2 ml) and dried under vacuum.

2.2.4.1. $[UO_2(HMPA)_4](I_3)_2$. Yield 1.858 g (90.06%). IR (cm^{-1}): ν(U=O) 917; ν(P=O) 1072. *Anal*. Found: C, 16.31; H, 4.02; N, 9.71; U, 13.39. Calc. for $C_{24}H_{72}I_6N_{12}O_6P_4U$: C, 16.49; H, 4.15; N, 9.61; U, 13.62%.

2.2.4.2. $[UO_2(OPPh_3)_4](I_3)_2$. Yield 1.75 g (69.14%). IR (cm^{-1}): ν(U=O) 920; ν(P=O) 1065. *Anal*. Found: C, 39.95; H, 2.83; U, 11.22. Calc. for $C_{72}H_{60}I_6O_6P_4U$: C, 40.32; H, 2.82; U, 11.10%.

2.2.4.3. $[UO_2(OAsPh_3)_4](I_3)_2$. Yield 2.588 g (93.42%). IR (cm^{-1}): ν(U=O) 890; ν(As=O) 850. *Anal*. Found: C, 36.76; H, 2.59; U, 10.08. Calc. for $C_{72}H_{60}As_4I_6O_6U$: C, 37.27; H, 2.61; U, 10.26%.

2.2.5. Preparation of $[UO_2L_4](I_7)_2$ ($L = HMPA$, $OPPh_3$, $OAsPh_3$)

A solution of UO_2I_2 in acetonitrile containing about 1.15 mmol of UO_2I_2 was treated successively with 16 g (18.9 mmol) of I_2 in acetonitrile (20 ml) and 5 mmol of L in acetonitrile (15 ml) at r.t. After stirring the resulting mixture for 10 min, the microcrystalline precipitate was filtered and dried under vacuum.

2.2.5.1. $[UO_2(HMPA)_4](I_7)_2$. Yield 2.941 g (90.19%). Blue black. IR (cm^{-1}): ν(U=O) 922; ν(P=O) 1065. *Anal*. Found: C, 10.96; H, 2.85; N, 6.72; U, 8.57. Calc. for $C_{24}H_{72}I_{14}N_{12}O_6P_4U$: C, 10.43; H, 2.63; N, 6.08; U, 8.61%.

2.2.5.2. $[UO_2(OPPh_3)_4](I_7)_2$. Yield 3.178 g (85.22%). Blue black. IR (cm^{-1}): ν(U=O) 918; ν(P=O) 1054. *Anal*. Found: C, 27.19; H, 1.87; U, 7.66. Calc. for $C_{72}H_{60}I_{14}O_6P_4U$: C, 27.37; H, 1.91; U, 7.53%.

2.2.5.3. $[UO_2(OAsPh_3)_4](I_7)_2$. Yield 3.784 g (96.138%). Brown black. IR (cm^{-1}): ν(U=O) 898; ν(As=O) 850, 858. *Anal*. Found: C, 39.38; H, 2.85; U, 7.07. Calc. for $C_{72}H_{60}As_4I_{14}O_6U$: C, 25.93; H, 1.81; U, 7.14%.

2.3. Crystal-structure determinations

Suitable single crystals were grown at r.t. by slow evaporation of saturated solutions in acetonitrile. Crystal data for $[UO_2(OAsPh_3)_4](Br_3)_2$: monoclinic, $P2_1/n$, $a = 9.383(1)$, $b = 15.150(1)$, $c = 26.358(1)$ Å, $\alpha = 90°$, $\beta = 94.668(1)°$, $\gamma = 90°$, $V = 3734.8(1)$ Å^3, $Z = 2$. Crystal data for $[UO_2(OPPh_3)_4](I_3)_2$: monoclinic, $P2_1/n$, $a = 9.407(1)$, $b = 15.739(1)$, $c = 26.189(1)$ Å, $\alpha = 90°$, $\beta = 98.366(1)°$, $\gamma = 90°$, $V = 3836.4(1)$ Å^3, $Z = 2$.

Crystals of $[UO_2(OAsPh_3)_4](Br_3)_2$ (block, orange, dimensions $0.50 \times 0.15 \times 0.10$ mm) and for $[UO_2(OPPh_3)_4](I_3)$ (block, orange, dimensions $0.20 \times 0.10 \times 0.05$ mm) were used for the structure determination. X-ray data were collected using a Bruker SMART CCD area detector single-crystal diffractometer with graphite monochromatized Mo Kα radiation ($\lambda = 0.71073$ Å) by the phi-omega scan method. A total of 1271 frames of intensity data were collected for each compound. The first 50 frames were recollected at the end of data collection to monitor for decay. The integration processes yield a total 25 322 for $[UO_2(OAsPh_3)_4](Br_3)_2$ and 20 468 for $[UO_2(OPPh_3)_4](I_3)$, of which 9182 and 6782, respectively, were independent. Absorption corrections were applied using SADABS program (maximum and minimum transmission coefficients 0.5334 and 0.1235 for $[UO_2(OAsPh_3)_4](Br_3)_2$; and 0.8004 and 0.4559 for $[UO_2(OPPh_3)_4](I_3)$). The structures were solved using the Bruker SHELXTL-PC software by direct methods and refined by full-matrix least-squares methods on F^2. Hydrogen atoms were included in calculated positions and refined in the riding mode. For $[UO_2(OAsPh_3)_4](Br_3)_2$ convergence was reached at a final $R_1 = 0.0440$ [for $I > 2\sigma(I)$], $wR_2 = 0.0910$ (for all data), 403 parameters, with allowance for the thermal anisotropy for all non-hydrogen atoms. Residual electron densities extremes were 1.253 and -0.919 e Å^{-3} and the goodness-of-fit on F^2 was 1.047 for all observed reflections. For $[UO_2(OPPh_3)_4](I_3)$ convergence was reached at a final $R_1 = 0.0553$ [for $I > 2\sigma(I)$], $wR_2 = 0.1204$ (for all data), 403 parameters, with allowance for the thermal anisotropy for all non-hydrogen atoms. Residual electron densities extremes were 1.476 and -1.622 e Å^{-3} and the goodness-of-fit on F^2 was 1.031 for all observed reflections. Crystal data and details on the data collection and refinement are given in the supplementary material.

3. Results and discussion

3.1. Synthesis and characterization of the complexes

The first evidence of the facile formation of uranyl tribromide complexes was obtained during the preparation of addition compounds of UO_2Br_2 (**4**). Thus, when 30% H_2O_2 was added to a solution consisting of UO_2Br_2, HBr, CH_3OH and $AsPh_3$ a product consistent with the formulation $[UO_2(OAsPh_3)_4](Br_3)_2$ was obtained. This was attributed to the simultaneous formation of $OAsPh_3$ and Br_2, and the subsequent rearrangement of the species in solution to form the tribromide complex. Following a more rational procedure—treatment of a solution of $UO_2Br_2 \cdot x H_2O$ in CH_3OH with Br_2 and then with $OAsPh_3$—we were able to prepare the same product in good yield. The tribromides containing $OPPh_3$ and HMPA were similarly isolated. The addition of bromine to the solution of uranyl bromide prior to the organic ligand is advisable. This way the precipitation of neutral $UO_2Br_2L_2$ adducts is avoided. However, to minimize side reactions of bromine with the organic ligands these should be added soon after the addition of bromine is completed.

In a similar manner a number of polyiodides can be easily isolated. The ability of iodide ions to form triiodides but also higher polyiodides allowed the isolation of a variety of compounds with the same uranyl cation and variable amount of iodine. Among them only the triiodides and 'heptaiodides' could be prepared in an accurate and reproducible manner. The triiodides could be obtained even with a significant excess of iodine above the stoichiometric. In this regard it is to note that the starting UO_2I_2 solution is rich in NaI so that a considerable excess of iodine is required to form species beyond I_3^-; and also that neither NaI nor NaI_n lead to precipitation with the organic ligands in these conditions. The 'heptaiodides' are formed with a large excess of iodine and likely they are authentic heptaiodides having in mind that the anion I_7^- is well known in many compounds [11]; however, at present we have been unable to obtain crystals of quality for the structural characterization.

All compounds are insoluble in water and diethyl ether, somewhat soluble in acetone and methanol, and very soluble in dimethyl formamide and dimethyl sulfoxide. Care should be exercised in the washing of the precipitates with diethyl ether, and in drying by pumping, as the halogen is easily removed from the polyhalide ions. They decompose before melting with liberation of the halogen.

The IR spectra of the compounds in the region 4000–400 cm^{-1} characterize by a strong band around 900 cm^{-1} characteristic for $\nu_{as}(UO_2)$ along with several bands attributable to the organic ligand. It is to note that $\nu_{as}(UO_2)$ shifts slight but regularly to lower energies, for each set of compounds with the same anion, in the sequence $OPPh_3 > HMPA > OAsPh_3$. This suggests that the basicity of the ligands [12] plays same role (*cis*-effect) on the strength of the U–O multiple bond, the more basic the ligand ($OAsPh_3$) the lower $\nu_{as}(UO_2)$. However, the nature of the anion also affects the position of this band as for compounds with the

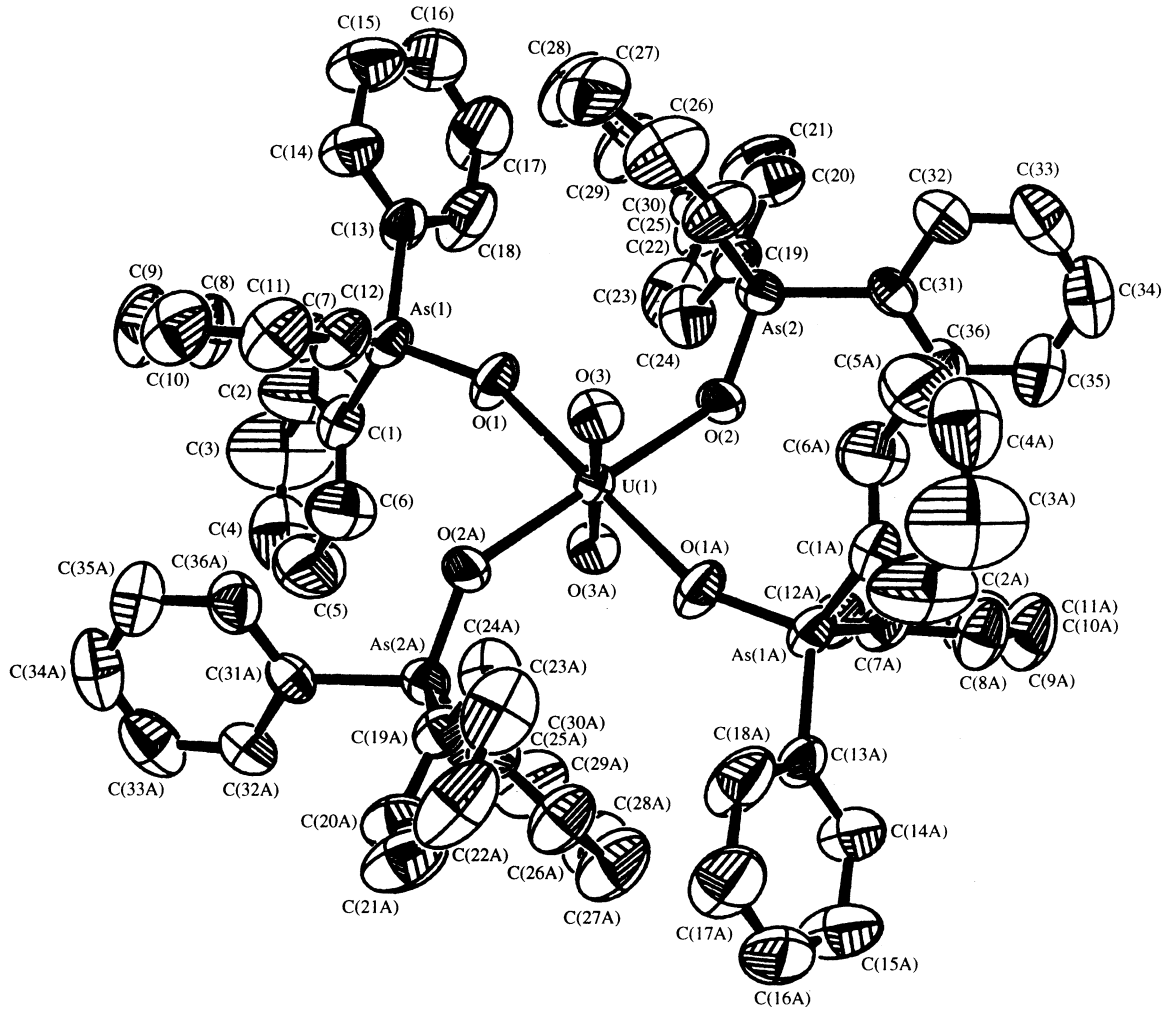


Fig. 1. Molecular structure and atom-labeling scheme for $[UO_2(OAsPh_3)_4](Br_3)_2$, (50% probability ellipsoids); hydrogen atoms are omitted.

same cation $\nu_{as}(UO_2)$ are only occasionally coincident. The bands assigned to ν(O=P) and ν(O=As) occur at lower frequencies in the complexes than in the free ligands as expected [13]. In this regard, it is worth noting that we have obtained products of composition $[UO_2(OAsPh_3)_4](Br_3)_2$ with three slightly different IR spectra (data reported in the experimental part belong to the product structurally characterized). This suggests the existence of conformational isomers for the cation, what can be extended to the other cations having in mind the steric requirements of these ligands and the precedent for all *trans*-$[UO_2Cl_2(OPPh_3)_2]$ [14].

Full characterization of the complexes through NMR is difficult. ^{31}P NMR spectra show that in solvents in which they are more soluble, DMF and DMSO, the ligands $OPPh_3$ and HMPA are totally displaced from the coordination sphere of uranium. The same occurs in methanol, despite the tribromides are prepared in this solvent. In acetone-d_6, at 20 °C, the ^{1}H NMR spectrum of $[UO_2(HMPA)_4](Br_3)_2$ shows two signals at $\delta = 2.92$ and 2.78 ppm (d, $J_{P-H} = 9.8$ Hz, intensity ratio = 5/6) that shift at $\delta = 2.88$ and 2.66 ppm (d, $J_{P-H} = 9.8$ Hz, intensity ratio = 3/2) at −70 °C. The ^{31}P NMR spectrum shows a broad signal at $\delta = 35.6$ ppm at 20 °C, and two signals at $\delta = 35.5$ and 29.7 ppm at −70 °C, far from the position for the free ligand ($\delta = 25.1$ ppm at 20 °C). Similar superior complexity was observed in the NMR of the other HMPA and $OPPh_3$ compounds. These findings are also consistent with the existence of conformational isomers for the cations in solution. However, this assumption should be regarded with caution as the polyhalide ions react with the solvent, and the reaction by-products may react with the cationic complexes.

3.2. Molecular structures

The molecular structures for the cations in $[UO_2(OAsPh_3)_4](Br_3)_2$ (**1**) and $[UO_2(OPPh_3)_4](I_3)_2$ (**2**) are shown in Figs. 1 and 2, respectively. Selected bond lengths and angles are listed in Table 1.

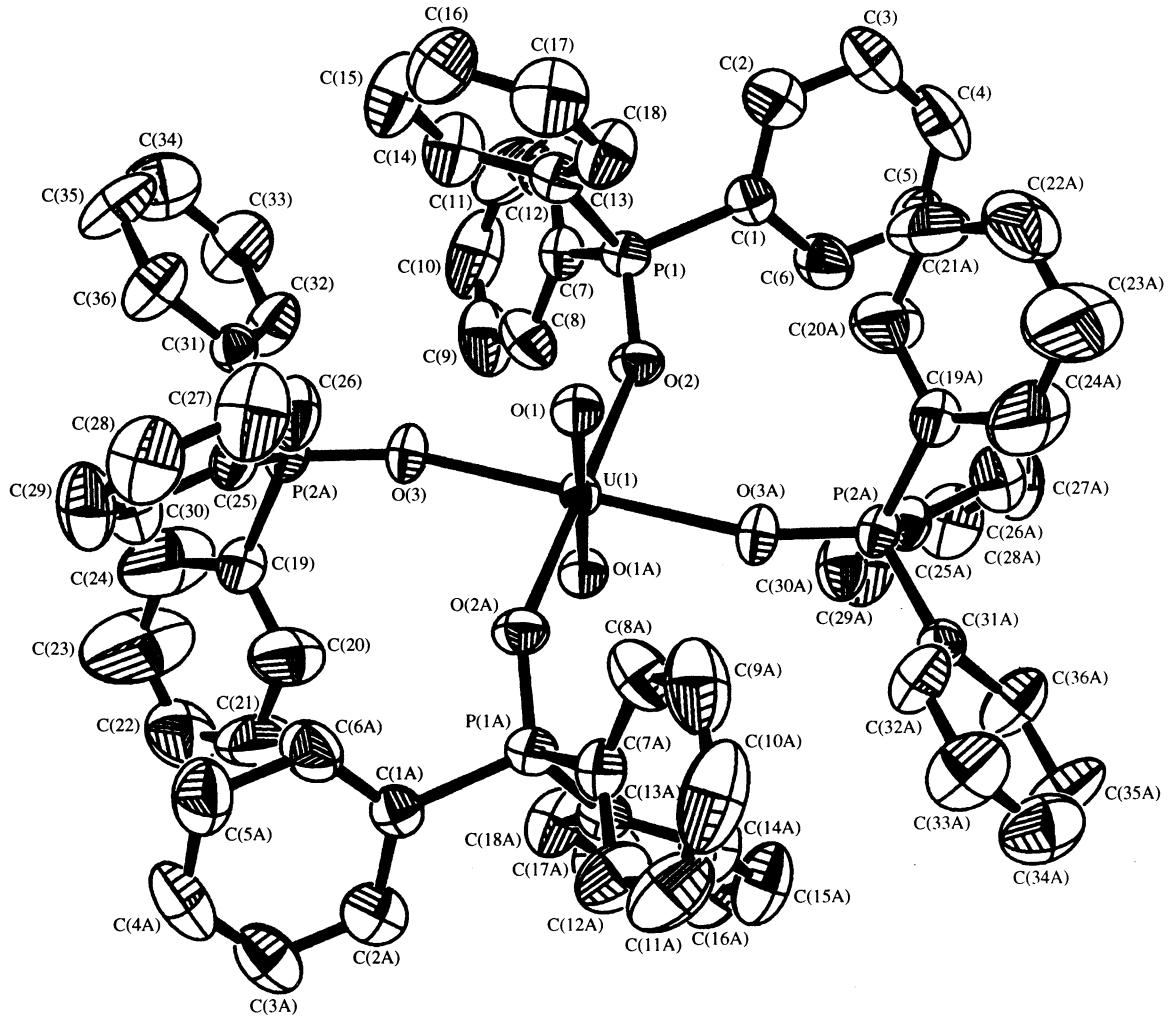


Fig. 2. Molecular structure and atom-labeling scheme for $[UO_2(OPPh_3)_4](I_3)_2$, (50% probability ellipsoids); hydrogen atoms are omitted.

Table 1
Selected bond lengths (Å) and angles (°) for $[UO_2(OAsPh_3)_4](Br_3)_2$ and $[UO_2(OPPh_3)_4](I_3)_2$

$[UO_2(OAsPh_3)_4](Br_3)_2$ (**1**)		$[UO_2(OPPh_3)_4](I_3)_2$ (**2**)	
Bond lengths			
U(1)–O(3)	1.772(3)	U(1)–O(1)	1.753(5)
U(1)–O(1)	2.265(3)	U(1)–O(2)	2.302(6)
U(1)–O(2)	2.284(3)	U(1)–O(3)	2.308(5)
As(1)–O(1)	1.670(3)	P(2)–O(3)	1.513(6)
As(2)–O(2)	1.678(3)	P(1)–O(2)	1.521(6)
Br(2)–Br(3)	2.531(2)	I(1)–I(2)	2.919(13)
Br(1)–Br(2)	2.550(2)	I(2)–I(3)	2.901(13)
Bond angles			
O(3)–U(1)–O(3)	180.0(3)	O(1)–U(1)–O(1)	180.0(5)
O(3)–U(1)–O(1)	89.78(16)	O(1)–U(1)–O(2)	90.9(2)
O(1)–U(1)–O(2)	89.49(13)	O(2)–U(1)–O(3)	90.8(2)
As(1)–O(1)–U(1)	154.2(2)	U(1)–O(3)–P(2)	159.2(4)
As(2)–O(2)–U(1)	140.4(2)	U(1)–O(2)–P(1)	146.9(4)
Br(3)–Br(2)–Br(1)	179.06(6)	I(3)–I(2)–I(1)	179.75(5)

As expected, the uranium is coordinated in a pseudo-octahedral fashion by two *trans*-oxo and four O-donor ligands in the equatorial plane. Comparison with related complexes is difficult, as these are the unique uranyl tribromides structurally identified, and only one uranyl triiodide has been fully characterized [8]. In **1** there are three couples of identical U-ligand distances associated to each pair of *trans*-ligands. In **2** the four U–O distances in the equatorial plane are virtually identical. The trihalide ions in **1** and **2** are almost linear and symmetrical, with distances and angles in the range of other trihalides [11].

The distances U–O(oxo) in **1** (1.772) and **2** (1.753) are typical for uranyl compounds [15]. The somewhat larger distance in **1** might be derived from the superior basicity of $OAsPh_3$ respect to $OPPh_3$. This may cause reduction in π-donation from the oxo ligands to the uranium with concomitant decreasing in the strength of the bonds within the uranyl entity. Consistent with this assumption are the distances U–O(P,As), shorter in **1** than in **2**, and the position of $\nu_{as}(UO_2)$ before commented. The ex-

istence of two pairs of slightly different distances in **1** may be due only to packing forces. Indeed, several uranyl complexes of composition UO_2L_4 as for example $[UO_2Br_4]^{2-}$ in $(NMe_4)_2[UO_2Br_4]$ [16] and $[UO_2(HMPA)_4]^{2+}$ in $[UO_2(HMPA)_4](ClO_4)_2$ [10] display two and four different U–L distances, respectively, despite the counterions possess high symmetry. It is to note that the mean U–O(P) distance in **2**, 2.305, is slightly superior to that in the closely related $[UO_2(HMPA)_4](I_3)_2$, 2.292 [8], as expected from the lower basicity of $OPPh_3$ with regard to HMPA.

The angles O(oxo)–U–O(oxo), O(oxo)–U–O(P,As) and O(P,As)–U–O(P,As) are close to 180°, 90° and 90°, respectively, in both cations. In **1** the angles U–O–As, 154.2° and 140.4°, are identical for each pair of *trans*-ligands, both within the wide range of values found in UO_2–$OAsPh_3$ complexes [4,17–19]. The same is applicable to the angles U–O–P in **2**, 146.0° and 159.2°, also in the range of other UO_2–$OPPh_3$ complexes (for example in $[UO_2(NCS)_2(OPPh_3)_2(Me_2CO)]$ the angles are 143.3° and 163.3° [20]).

Finally, the orientation of the equatorial ligands is similar in both complexes. The cations are centrosymmetric with regard to the $UO_2(OX)_4$ (X = P, As) group. Two of opposite X atoms are oriented toward the bisection of adjacent O(oxo)–U–O(X) angles while the other two X atoms lye close to the equatorial plane (dihedral angles for As(2)–O(2)–U(1)–O(3) = 42.92°, for As(1)–O(1)–U(1)–O(2) = 5.57°, for P(1)–O(2)–U(1)–O(1) = 43.13°, for P(2)–O(3)–U(1)–O(2) = 7.29°). We believe there are several possible conformations of similar energy for the group $U(OX)_4$ (square planar UO_4, non-linear U–O–X). The adoption of a particular conformation is likely determined by packing forces. However, the steric demand of these ligands may lead to restraints in free rotation and consequently to the existence of stable conformers for these cations no only as solid salts but also in solution. Studies to get further insight on this possibility are in progress with salts involving anions more stable than polyhalides.

4. Supplementary material

Crystallographic data for the structural analysis have been deposited with the Cambridge Crystallographic Data Centre, CCDC Nos. 186697 and 186698 for $[UO_2(OAsPh_3)_4][Br_3]_2$ and $[UO_2(OPPh_3)_4][I_3]_2$, respectively. Copies of this information may be obtained free of charge from The Director, CCDC, 12 Union Road, Cambridge, CB2 1EZ, UK (fax: +44-1223-336033; e-mail: deposit@ccdc.cam.ac.uk or www: http://www.ccdc.cam.ac.uk).

Acknowledgements

This work was supported by the Junta de Castilla y Leon (Grant BU14/98).

References

[1] C.J. Burns, D.C. Smith, A.P. Sattelberger, H.B. Gray, Inorg. Chem. 31 (1992) 3724.
[2] D.M. Barnhart, C.J. Burns, N.N. Sauer, J.G. Watkin, Inorg. Chem. 34 (1995) 4079.
[3] M.P. Wilkerson, C.J. Burns, R.T. Paine, B.L. Scott, Inorg. Chem. 38 (1999) 4156.
[4] F.J. Arnáiz, M.J. Miranda, R. Aguado, J. Mahía, M.A. Maestro, Polyhedron 20 (2001) 3295.
[5] J.H. Burns, in: J.J. Katz, G.T. Seaborg, L.R. Mors (Eds.), The Chemistry of the Actinide Elements, Chapman and Hall, New York, 1986.
[6] L. Deshayes, N. Keller, M. Lance, M. Nierlich, D. Vigner, Acta Crystallogr., Sect. C 48 (1992) 1660.
[7] L. Deshayes, N. Keller, M. Lance, M. Nierlich, D. Vigner, Acta Crystallogr., Sect. C 48 (1992) 2209.
[8] M.R. Caira, J.F. De Wet, J.G.H. Du Preez, B. Busch, H.E. Rohwer, Inorg. Chim. Acta 77 (1983) L73.
[9] Y.K. Gusev, Radiokhim 27 (1985) 412.
[10] L.R. Nassimbeni, A.L. Rodgers, Cryst. Struct. Commun. 5 (1976) 301.
[11] See e.g.: (a) K.F. Tebbe, I. Dombrowski, Z. Anorg. Allg. Che. 625 (1999) 167.(b) M.W. Renner, K.M. Barkigia, Y. Zhang, C.J. Medforth, K.M. Smith, J. Fajer, J. Am. Chem. Soc. 116 (1994) 8582.(c) P.C. Junk, L.R. MacGillivray, M.T. May, K.D. Robinson, J.L. Atwood, Inorg. Chem. 34 (1995) 5395.
[12] J. Leciejewicz, N.W. Alcock, T.J. Kemp, Struct. Bonding 82 (1995) 43.
[13] See, e.g.: K. Nakamoto, Infrared and Raman Spectra of Inorganic and Coordination Compounds, 5th ed., Wiley, New York, 1997.
[14] S.B. Akona, J. Fawcett, J.H. Holloway, D.R. Russel, I. Leban, Acta Crystallogr., Sect. C 47 (1991) 45.
[15] K.W. Bagnal, in: G. Wilkinson, R.D. Gillard, J.A. McCleverty (Eds.), Comprehensive Coordination Chemistry, vol. 3, Pergamon Press, Oxford, 1987.
[16] (a) G. Ingletto, L. Di Sipio, E. Tondello, G. Pelizzi, A. Montero, Cryst. Struct. Commun. 3 (1974) 297;
(b) W. Jensen, D. Dickerson, Q. Johnson, Acta Crystallogr., Sect. B 30 (1974) 840.
[17] C. Panattoni, R. Graziani, U. Croatto, B. Zarli, G. Bombieri, Inorg. Chim. Acta 2 (1968) 43.
[18] R. Graziani, B. Zarli, A. Cassol, G. Bombieri, E. Forsellini, E. Tondello, Inorg. Chem. 9 (1970) 2116.
[19] B. Zarli, R. Graziani, U. Croatto, G. Bombieri, E. Forsellini, Chem. Commun. (1971) 1501.
[20] G. Bombieri, E. Forsellini, G. De Paoli, D. Brown, T.C. Tso, J. Chem. Soc., Dalton Trans. 26 (1979) 2042.

MeCN, 0.1 M TEAP) was done at a platinum electrode under nitrogen atmosphere on a PAR model 370-4 electrochemistry system [10]. EPR measurements were made at X-band using Varian E-109C spectrometer fitted with a quartz dewar. The relevant parameters are: microwave frequency, 9.1–9.2 GHz; modulation, 100 kHz; power 30 dB; sweep center 3300 G; sweep width 250 G; sweep time, 240 s. Microanalyses (C, H, N) were done by using a Perkin–Elmer 2400C Series II elemental analyzer. Magnetic moments were measured by using a PAR-155 vibrating sample magnetometer.

2.2. Synthesis of chlorocarbonyl(3,5-ditertiarybutyl-o-benzosemiquinone)bis (triphenylphosphine)ruthenium(II), [Ru(dbsq)(Cl)(CO)(PPh$_3$)$_2$] (**5**)

A solution of dbq (89 mg, 0.40 mmol) in ethanol (20 ml) was purged with N_2 for 15 min. To it was added [Ru(H)(Cl)(CO)(PPh3)3] (100 mg, 0.10 mmol) and the reaction mixture was heated to reflux under nitrogen for 2 h. The resulting greenish blue solution was allowed to cool to room temperature (r.t.) affording a dark solid which was filtered off and washed with a little *n*-hexane and then dried in air. The solid was recrystallized from ethanol and then from dichloromethane–hexane solution. Yield: (51 mg, 53%). *Anal*. Calc. for $C_{51}H_{50}ClO_3P_2Ru$: C, 67.36; H, 5.54. Found: C, 67.52; H, 5.42%. UV–Vis [λ_{max}, nm (ε, M^{-1} cm^{-1})]: 238(28 890), 256(23 590), 502(1985), 642(2390), 878(820), 1002(sh)(615). IR (KBr, cm^{-1}): 1939 (CO), 1410 (sq).

2.3. Synthesis of chlorocarbonyl(tetrachloro-o-benzosemiquinone)bis(triphenylphosphine)-ruthenium(II), [Ru(tcsq)(Cl)(CO)(PPh$_3$)$_2$] (**6**)

The quinone tcq (99 mg, 0.40 mmol) was dissolved in dry benzene (20 ml) and purged with nitrogen for 15 min. To this solution was added [Ru(H)(Cl)(CO)(PPh$_3$)$_3$] (100 mg, 0.10 mmol) and the mixture was heated to reflux under nitrogen for 4 h. The initial bluish green colour changed to dark blue. The solution was then cooled to r.t. and filtered to remove unreacted starting materials. The solvent was stripped from the filtrate under reduced pressure. The residue thus obtained was extracted with hexane. The extract was subjected to chromatography on silica gel. The [Ru(tcsq)(Cl)(CO)(PPh$_3$)$_2$] complex moved as a blue band with benzene. The solid obtained by stripping benzene was recrystallized from dichloromethane–hexane to yield the blue complex in pure form. Yield: (52 mg, 53%). *Anal*. Calc. for $C_{43}H_{30}Cl_5O_3P_2Ru$: C, 55.24; H, 3.23. Found: C, 55.57; H, 3.60%. UV–Vis [λ_{max}, nm (ε, M^{-1} cm^{-1})]: 230(45 030), 370(3630), 502(sh)(1240), 608(2150), 674(2120), 744(2425), 934(940), 1058(940). IR (KBr, cm^{-1}): 1959 (CO), 1422 (sq).

2.4. Synthesis of carbonyl(tetrachloro-o-benzosemiquinone)hydridobis(triphenylphosphine)-ruthenium(II), [Ru(tcsq)(H)(CO)(PPh$_3$)$_2$] (7)

The quinone tcq (107 mg, 0.44 mmol) was dissolved in dry benzene (20 ml) and purged with nitrogen for 15 min. To this solution was added [Ru(H)$_2$(CO)(PPh$_3$)$_3$] (100 mg, 0.11 mmol) and the mixture was heated to reflux under nitrogen for 2 h. The reaction mixture was then cooled to r.t. and the solvent removed under reduced pressure. The residue was extracted with dichloromethane and subjected to chromatography on silica gel followed by further recrystallization in the same manner as in the case of (**6**). Yield: (56 mg, 57%). *Anal*. Calc. for $C_{43}H_{31}Cl_4O_3P_2Ru$: C, 57.35; H, 3.47. Found: C, 56.81; H, 3.38%. UV–Vis [λ_{max}, nm (ε, M^{-1} cm^{-1})]: 230(49 020), 272(23 455), 336(4190), 368(3830), 496(sh)(1135), 610(2180), 754(2790), 1060(1260). IR (KBr, cm^{-1}): 1961(CO), 1421(sq), 2050 (hydride).

2.5. X-ray crystallography

Single crystals of compound [Ru(dbsq)(Cl)(CO)-(PPh$_3$)$_2$] were grown by slow diffusion of hexane into dichloromethane solution of the complex. Cell parameters were determined by the least-squares fit of 30 machine-centered reflections ($14^\circ \le 2\theta \le 28^\circ$). Data were collected by the ω-scan technique on a Siemens R3m/V four circle diffractometer with graphite monochromated Mo Kα ($\lambda = 0.71073$ Å) radiation at 25 °C in the range $3^\circ \le 2\theta \le 48^\circ$. Two check reflections measured after every 198 reflections showed no significant intensity reduction. All data were corrected for Lorentz-polarization effects, an empirical absorption correction was done on the basis of azimuthal scan of six reflections [11]. The metal atom was located from a Patterson map and the rest of the non-hydrogen atoms emerged from successive Fourier synthesis. The structure was refined by full-matrix least-squares procedure on F^2. All non-hydrogen atoms were refined anisotropically and hydrogen atoms added at calculated positions. All calculations for data reduction and structure solution and refinement were done by using the SHELXTL V5.03 [12] Program package. Significant crystal data are listed in Table 1.

3. Results and discussion

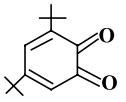
3.1. Synthesis

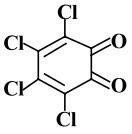
The starting materials for synthesis are quinones and hydridic carbonyl ruthenium(II) species. Specific items and the isolated semiquinone radical species are listed and numbered in Scheme 1. The semiquinone complexes [Ru(dbsq)(Cl)(CO)(PPh$_3$)$_2$] and [Ru(tcsq)(Cl)(CO)-(PPh$_3$)$_2$] were synthesized by reacting [Ru(H)(Cl)(CO)-

Table 1
Crystallographic data for [Ru(dbsq)(Cl)(CO)(PPh$_3$)$_2$] (**5**)

Empirical formula	$C_{51}H_{50}ClO_3P_2Ru$
Formula weight	909.37
Crystal system	monoclinic
Space group	$P2_1/c$
a (Å)	16.599(6)
b (Å)	12.180(5)
c (Å)	22.615(6)
β (°)	100.93(3)
V (Å^3)	4489(3)
Z	4
ρ_{calc} (Mg m^{-3})	1.345
Reflections collected	7407
Independent reflections	7022 [$R_{int} = 0.0263$]
μ (mm^{-1})	0.522
θ Range (°)	1.83–24.00
Final R indices [$I > 2\sigma(I)$]	$R = 0.0434$ [a], $wR_2 = 0.1047$ [b]
Goodness-of-fit on F^2	1.061

[a] $R = \Sigma||F_o| - |F_c||/\Sigma|F_o|$.
[b] $wR_2 = [\Sigma\, w(F_o^2 - F_c^2)^2/\Sigma(F_o^2)^2]^{1/2}$.

(1)  **(dbq)**

(2)  **(tcq)**

(3) **Ru(H)(Cl)(CO)(PPh$_3$)$_3$**

(4) **Ru(H)$_2$(CO)(PPh$_3$)$_3$**

(5) **Ru(dbsq)(Cl)(CO)(PPh$_3$)$_2$**

(6) **Ru(tcsq)(Cl)(CO)(PPh$_3$)$_2$**

(7) **Ru(tcsq)(H)(CO)(PPh$_3$)$_2$**

Scheme 1.

(PPh$_3$)$_3$] with fourfold excess of quinones in dry solvents under an inert atmosphere. The dihydride [Ru(H)$_2$(CO)(PPh$_3$)$_3$] similarly afforded the semiquinone complex [Ru(tcsq)(H)(CO)(PPh$_3$)$_2$] which is unusual in having hydride as a coligand. The basic synthetic reaction is stated in Eq. (2). The

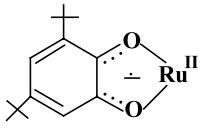
$$\text{Ru–H} + \text{q} \rightarrow \text{Ru(sq)} + 1/2\text{H}_2 \qquad (2)$$

semiquinone chelates occur as dark colored solids which afford blue solutions in organic solvents. The present work adds a notable dimension in Ru^{II}(sq) chemistry [13] in terms of the new synthetic method and in terms of realization of model semiquinone binding, vide infra. The reported methods for the synthesis of ruthenium semiquinonates include chelation of preformed semiquinone salts [14], oxidation of preformed catecholate complexes [15–17], oxidative addition of quinones [18–20] and reductive addition of catechols [18]. Structurally characterized semiquinone species include two monochelates viz. [Ru^{II}(dbsq)(bpy)$_2$]$^+$ and [Ru^{III}(dbsq)(PPh$_3$)$_2$Cl$_2$] and a few bis-chelates having the Ru(sq)$_2$ fragment [18,20–23].

3.2. Structure

The chelate [Ru(dbsq)(Cl)(CO)(PPh$_3$)$_2$] (**5**) afforded good single crystals and a molecular view in shown in Fig. 1. Selected bond parameters are listed in Table 2. In the pseudooctahedral RuCClO$_2$P$_2$ coordination sphere the *trans* RuP$_2$ fragment defines a nearly linear axis (P(2)–Ru–P(1) ~ 177.81(5)°). The metal and the donors O1, O2, C51 and Cl make a satisfactory equatorial plane of mean deviation 0.04 Å. The Ru(dbsq) fragment minus the *t*-butyl groups is approximately planar (mean deviation of 0.04 Å) and it makes a dihedral angle of 7.2° with the virtually perfect Ru(CO)(Cl) plane.

In the Ru(dbsq) fragment, the two C–O lengths, 1.291(6) and 1.296(6) Å, are equal within experimental error. The C37–C38, C39–C40, C40–C41 and C37–C42 distances are significantly longer (average, 1.43 Å) than the C39–C40 and C41–C42 distances (average, 1.36 Å). These bond length trends are diagnostic of model semiquinonoid binding as in **8** [13,24]. To our knowledge the only other structurally characterized semiquinone monochelate of bivalent ruthenium is [Ru^{II}(dbsq)(bpy)$_2$]$^+$ wherein the bonding is complicated by two unequal C–O distances [25].



8

It is instructive to compare metal–ligand bond distances of **5** with that of the trivalent complex [Ru^{III}(dbsq)(PPh$_3$)$_2$Cl$_2$] (**9**) [18] which is formally related to **5** via substitution of the carbon monoxide ligand by a chloride ligand with concomitant increase of the metal oxidation level by one unit. Since the Ru–O and Ru–Cl bonds are primarily σ in character, their average lengths in **5** are larger than those in **9** by ~0.05 Å reflecting the logical σ-radius trend Ru^{II} > Ru^{III}. On the other hand, the average Ru–P length in **5** is shorter than that in **9** by 0.02 Å. This is attributed to Ru^{II}–P back bonding in **5**. The bonding is evidently strong enough to more than offset the above noted σ-trend. Trivalent ruthenium (as in **9**) can at best be a very weak π-base [26,27].

3.3. Magnetism and spectra

The semiquinone chelates are paramagnetic ($s = 1/2$), (Table 3) and in the microcrystalline state display an EPR line at $g \sim 2.00$. In fluid solution a three-line

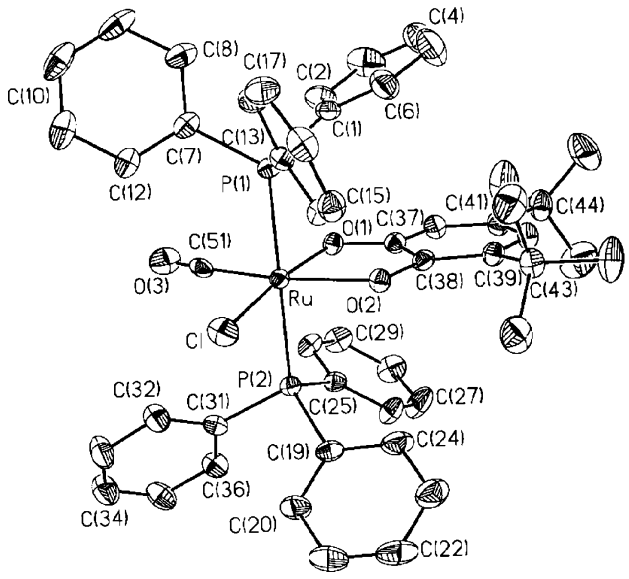


Fig. 1. ORTEP plot (30% probability ellipsoids) and atom labelling scheme for $[Ru(dbsq)(Cl)(CO)(PPh_3)_2]$ (**5**).

superhyperfine structure ($A_{iso} \sim 17$ G) due to coupling with two *trans*-^{31}P atoms is resolved [28]. EPR spectral parameters are listed in Table 3 and a representative spectrum is shown in Fig. 2. IR and electronic spectral data are listed in the Section 2. In IR a semiquinone CO stretch [17] occurs in the region 1410–1425 cm^{-1}. In $[Ru(tcsq)(H)(CO)(PPh_3)_2]$, the Ru–H stretch is clearly observed as a weak but sharp band at 2050 cm^{-1}. The stretching frequency of the carbon monoxide ligand increases from 1939 to 1959 cm^{-1} in going from $[Ru(dbsq)(Cl)(CO)(PPh_3)_2]$ to $[Ru(tcsq)(Cl)(CO)(PPh_3)_2]$, consistent with electron withdrawal by chloro substituents in tcsq. All the semiquinone complexes display a few bands of moderate intensity in the region 500–1100 nm presumably due to CT transitions from split t_2 components of the metal to sq π*-orbitals [17,29].

Table 2
Selected bond distances (Å) and angles (°) for $Ru(dbsq)(Cl)(CO)(PPh_3)_2$ (**5**)

Bond distances			
Ru–O1	2.026(3)	O2–C38	1.296(6)
Ru–O2	2.145(3)	C37–C42	1.394(7)
Ru–P1	2.397(2)	C37–C38	1.460(7)
Ru–P2	2.395(2)	C38–C39	1.426(7)
Ru–Cl	2.401(2)	C39–C40	1.368(7)
Ru–C51	1.909(7)	C40–C41	1.427(7)
O3–C51	0.969(6)	C41–C42	1.350(7)
O1–C37	1.291(6)		
Bond angles			
C51–Ru–O1	91.3(2)	O1–Ru–Cl	172.45(9)
C51–Ru–O2	169.1(2)	O2–Ru–Cl	95.22(9)
C51–Ru–P1	92.7(2)	P2–Ru–P1	177.81(5)
C51–Ru–P2	88.7(2)	P2–Ru–Cl	87.90(5)
C51–Ru–Cl	95.6(2)	O1–Ru–O2	78.00(12)
O1–Ru–P1	92.42(10)	C37–O1–Ru	115.8(3)
O1–Ru–P2	89.16(10)	C38–O2–Ru	112.4(3)
O2–Ru–P1	85.58(9)	P1–Ru–Cl	90.35(5)
O2–Ru–P2	93.28(9)		

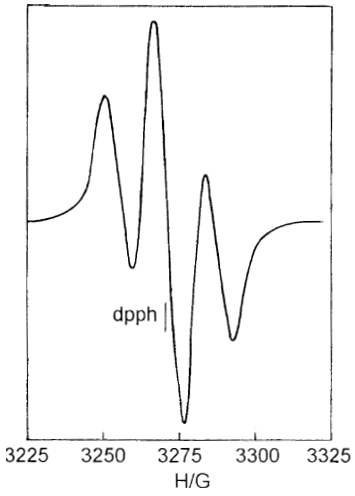


Fig. 2. Solution EPR spectrum of $[Ru(dbsq)(Cl)(CO)(PPh_3)_2]$ (**5**) in the X-band (9.1 GHz) at 298 K.

3.4. Electrochemistry

Two one-electron cyclic responses are observed for each complex in acetonitrile solution. The responses at higher and lower potentials are, respectively, assigned to the coordinated q–sq and sq–cat couples (cat is catechloate). Reduction potential data are given in Table 4 and representative voltammograms are shown

Table 3
Bulk magnetic moments and EPR g values at 298 K

Compound	Polycrystalline		Solution	
	μ_{eff} (μ_B)	g (ΔH_{pp} [a](G))	g_{iso}	A_{iso}
$[Ru(dbsq)(Cl)(CO)(PPh_3)_2]$	1.90	2.003(25)	2.002	17
$[Ru(tcsq)(Cl)(CO)(PPh_3)_2]$	1.84	2.002(30)	2.004	16.5
$[Ru(tcsq)(H)(CO)(PPh_3)_2]$	1.89	2.006(20)	2.005	16.5

[a] ΔH_{pp}, peak-to-peak line width.

Table 4
Cyclic voltammetric data in acetonitrile solution (0.1 M TEAP) [a]

Compound	$E_{1/2}$ (V) (ΔE_P (mV))	
	q/sq	sq/cat
$[Ru(dbsq)(Cl)(CO)(PPh_3)_2]$	0.42 (80)	−0.55 (140)
$[Ru(tcsq)(Cl)(CO)(PPh_3)_2]$	0.87 (60)	+0.05 (60)
$[Ru(tcsq)(H)(CO)(PPh_3)_2]$	1.00 (60)	+0.15 (80)

[a] Conditions: working electrode, platinum; reference electrode, SCE; scan rate 50 mV s^{-1}. $E_{1/2} = 1/2(E_{pa} + E_{pc})$, where E_{pa} and E_{pc} are the anodic and cathodic peak potentials, respectively; $\Delta E_p = E_{pa} - E_{pc}$.

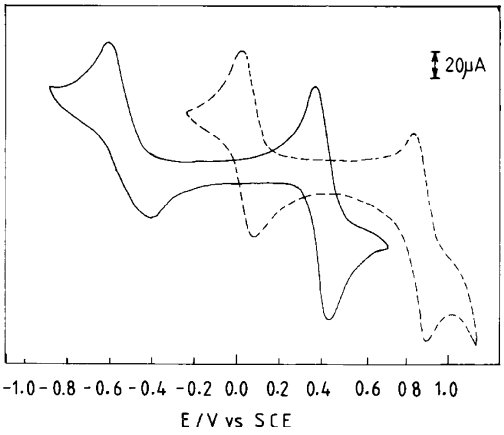


Fig. 3. Cyclic voltammograms of [Ru(dbsq)(Cl)(CO)(PPh_3)$_2$] (**5**) (—) and [Ru(tcsq)(Cl)(CO)(PPh_3)$_2$] (**6**) (– – –) in acetonitrile solution.

in Fig. 3. The $E_{1/2}$ values undergo a shift of $\sim$500 mV to higher potentials in going from **5** to **6** consistent with effects of substituents (*t*-Bu vs. Cl) [30]. Upon replacement of the chloride ligand by hydride (**6**→**7**), the $E_{1/2}$ values move further to higher potentials by $\sim$100 mV due to weaker *trans*-metal electron donation by hydride compared with chloride.

4. Conclusion

It is demonstrated that homolytic cleavage of an Ru–H bond by *o*-quinones constitute an excellent method for synthesis of semiquinone monochelates of carbonylruthenium(II) (**5**–**7**). Structure determination of **5** has revealed model semiquinone character of the chelating ligand which has four long and two short ring C–C bonds and two equal C–O bonds.

Solution EPR spectra of **5**–**7** are characterized by the presence of superhyperfine coupling of the radical anion electron with ^{31}P atoms. The q/sq and sq/cat $E_{1/2}$ values are more positive in [Ru(tcsq)(Cl)(CO)(PPh_3)$_2$], and [Ru(tcsq)(H)(CO)(PPh_3)$_2$] than in [Ru(dbsq)(Cl)(CO)-(PPh_3)$_2$]. Correspondingly, the carbon monoxide stretching frequency is lower in **5**.

5. Supplementary material

Crystallographic data for the structural analysis have been deposited with the Cambridge Crystallographic Data Centre, CCDC No. 169368 for compound **5**. Copies of this information may be obtained free of charge from The Director, CCDC, 12 Union Road, Cambridge, CB2 1EZ, UK (fax: +44-1223-336033; e-mail: deposit@ccdc.cam.ac.uk or www: http://www.ccdc.cam.ac.uk).

Acknowledgements

We are grateful to the Department of Science and Technology, New Delhi, India, and the Council of Scientific and Industrial Research, New Delhi, India for financial support.

References

[1] M. Shivakumar, K. Pramanik, I. Bhattacharyya, A. Chakravorty, Inorg. Chem. 39 (2000) 4332 (and references therein).
[2] S. Kimura, E. Bill, E. Bothe, T. Weyhermuller, K. Wieghardt, J. Am. Chem. Soc. 123 (2001) 6025 (and references therein).
[3] M. Shivakumar, K. Pramanik, P. Ghosh, A. Chakravorty, Chem. Commun. (1998) 2103.
[4] M. Shivakumar, K. Pramanik, P. Ghosh, A. Chakravorty, Inorg. Chem. 37 (1998) 5968.
[5] K. Pramanik, M. Shivakumar, P. Ghosh, A. Chakravorty, Inorg. Chem. 31 (2000) 195.
[6] P. Ghosh, K. Pramanik, M. Shivakumar, A. Chakravorty, J. Indian Chem. Soc. 77 (2000) 547.
[7] N. Ahmad, J.J. Levison, S.D. Robinson, M.F. Uttley, Inorg. Synth. 15 (1975) 45.
[8] G.K. Lahiri, S. Bhattacharya, B.K. Ghosh, A. Chakravorty, Inorg. Chem. 26 (1987) 4324.
[9] S.K. Chandra, P. Basu, D. Ray, S. Pal, A. Chakravorty, Inorg. Chem. 29 (1990) 2423.
[10] P. Ghosh, A. Pramanik, N. Bag, G.K. Lahiri, A. Chakravorty, J. Organomet. Chem. 454 (1993) 2327.
[11] A.C.T. North, D.C. Philips, F.S. Mathews, Acta Crystallogr., Sect. A 24 (1968) 351.
[12] G.M. Sheldrick, SHELXTL™, Version 5.03, Structure Determination Software Programs, Siemens Analytical X-Ray Instruments, Madison, WI, 1994.
[13] C.G. Pierpont, C.W. Lange, Prog. Inorg. Chem. 41 (1994) 331.
[14] V.K. Cherkasov, K.G. Shal'nova, G.A. Abakumov, G.A. Razuvaev, Izv. Akad. Nauk SSR, Ser. Khim. 12 (1984) 2830.
[15] N.G. Connelly, I. Manners, J.R.C. Protheroe, W.M. Whiteley, J. Chem. Soc., Dalton Trans. (1984) 2713.
[16] N. Bag, A. Pramanik, G.K. Lahiri, A. Chakravorty, Inorg. Chem. 31 (1992) 40.
[17] M.A. Haga, E.S. Dodsworth, A.B.P. Lever, Inorg. Chem. 25 (1986) 447.
[18] S. Bhattacharya, C.G. Pierpont, Inorg. Chem. 30 (1991) 1511.
[19] S. Bhattacharya, C.G. Pierpont, Inorg. Chem. 30 (1991) 2906.
[20] S. Bhattacharya, C.G. Pierpont, Inorg. Chem. 33 (1994) 6038.
[21] N. Bag, G.K. Lahiri, P. Basu, A. Chakravorty, J. Chem. Soc., Dalton Trans. (1992) 113.
[22] S.R. Boone, C.G. Pierpont, Polyhedron 9 (1990) 2267.
[23] M.A. Haga, E.S. Dodsworth, A.B.P. Lever, S.R. Boone, C.G. Pierpont, J. Am. Chem. Soc. 108 (1986) 7413.
[24] O. Carngo, C.B. Castellani, K. Djinovic, M. Rizzi, J. Chem. Soc., Dalton Trans. (1992) 837.
[25] S.R. Boone, C.G. Pierpont, Inorg. Chem. 26 (1987) 1769.
[26] A. Pramanik, N. Bag, D. Ray, G.K. Lahiri, A. Chakravorty, Inorg. Chem. 30 (1991) 410.
[27] J.F. Wishart, A. Bino, H. Taube, Inorg. Chem. 25 (1986) 3318.
[28] W. Kaim, Coord. Chem. Rev. 76 (1987) 187.
[29] A.B.P. Lever, P.R. Auburn, E.S. Dodsworth, M. Haga, W. Liu, M. Melnik, W.A. Nevin, J. Am. Chem. Soc. 110 (1988) 8076.
[30] M.D. Stallings, M.M. Morrison, D.T. Sawyer, Inorg. Chem. 20 (1981) 2655.

using FX-80-Q Fourier transform NMR spectrometer. Electronic spectra were recorded on a Hewlett–Packard 8452 A spectrophotometer in the range 250–820 nm. The IR spectra were recorded on a Hitachi 270-50 spectrophotometer in the range 400–4000 cm^{-1}. The cyclic voltammograms were obtained on an apparatus comprising a PAR model 173 potentiostat/galvanostat, 175 universal programmer, 176 current follower and 179 coulometer. Conductivity measurements of the complexes were determined on an Elico model SX80 conductivity bridge using freshly prepared solutions of the complexes in DMF. For cyclic voltammetry three electrode systems were used in which the counter and working electrodes were platinum foils (1 cm^2) and the reference electrode was Ag/AgCl. Ferrocene/ferrocenium(1+) couple was used as an internal standard. All potentials are reported relative to the Ag/AgCl reference electrode. The $E_{1/2}$ of the ferrocenium/ferrocene (Fc^+/Fc) couple under the experimental condition is 470 mV in DMF and ΔE_p for Fc^+/Fc is 70 mV. IR compensation was not applied. All electrochemical measurements were carried out in solutions purged with analor nitrogen gas for 30 min prior to each experiment. Variable-temperature magnetic studies were performed on a PAR model 155 vibrating-sample magnetometer in the temperature range 77–300 K, and the instrument was calibrated using metallic nickel. Room temperature magnetic moments of the complexes were determined using a Guoy balance. $Hg[Co(SCN)_4]$ was used as the reference. X-band EPR spectra were recorded on a Varian EPR-E 112 spectrometer using diphenylpicrylhydrazine (DPPH) as the reference.

2.2. Materials

5-Methylsalicylaldehyde and 6,6′-piperazine-1,4-diyl-dimethylenebis(4-methyl-2-formyl-phenol) (P.C-I) was prepared by following the literature method [11]. Tetrabutylammoniumperchlorate (TBAP) was obtained from Fluka and recrystallized from methanol. (**Caution**! All perchlorate salts are explosive and hence care should be taken while handling). DMF (HPLC) was obtained from Qualigens and used as such. All other chemicals and solvents were of reagent grade and used as received.

2.3. Synthesis of complexes

All the oxime binuclear complexes were prepared [12] by a stepwise synthesis. Reaction of P.C-I with M(II) (M = Ni or Cu) acetate led to the isolation of mononuclear complex. Further reaction with 1 equiv. of the appropriate divalent metal ion, hydroxylamine hydrochloride and triethylamine gave the binuclear complex Scheme 1.

2.4. Synthesis of mononuclear complexes

2.4.1. [NiL]

Nickel(II) acetate (2.48 g, 10 mmol) dissolved in methanol (25 ml) was added to P.C-I (3.82 g, 10 mmol) dissolved in $CHCl_3$–MeOH(40 ml, 1:1) under boiling condition and refluxed for 1 h. The orange coloured precipitate formed was collected by filtration, washed with $CHCl_3$ followed by MeOH and dried. *Anal*. for $C_{22}H_{24}N_2O_4Ni$: Found: C, 60.12; H, 5.39; N, 6.54; Ni, 13.25. Calc. C, 60.17; H, 5.47; N, 6.39; Ni, 13.37%. Selected IR data (ν cm^{-1} using KBr): 3320(br), 1670(s) cm^{-1} (br, broad, str, strong, s, sharp, m, medium).

2.4.2. [CuL]

Copper(II) acetate (1.99 g, 10 mmol) dissolved in methanol (25 ml) was added to P.C-I (3.82 g, 10 mmol) dissolved in $CHCl_3$–MeOH (40 ml, 1:1) under boiling condition and refluxed for 1 h. The orange coloured precipitate formed was collected by filtration, washed with $CHCl_3$ followed by MeOH and dried. *Anal*. for $C_{22}H_{24}N_2O_4Cu$: Found: C, 60.01; Cu, 14.64; H, 5.21; N, 6.41. Calc. C, 59.52; Cu, 14.32; H, 5.41; N, 6.31%. Selected IR data (ν cm^{-1} using KBr): 3310(br), 1665(s) cm^{-1}.

2.5. Synthesis of binuclear complexes

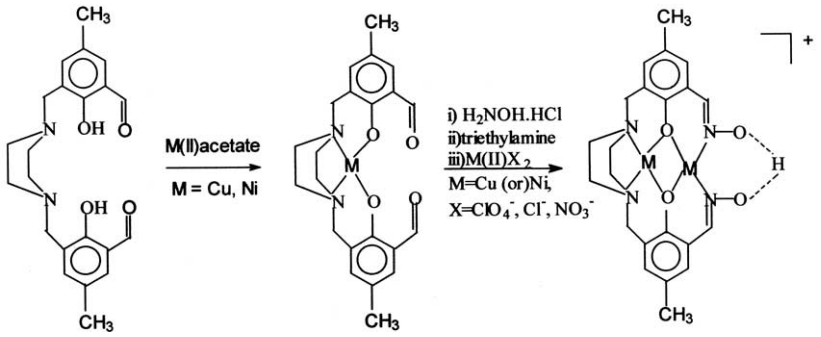
2.5.1. $[Ni_2L](ClO_4)\cdot CH_3OH$ (1)

$Ni(ClO_4)_2\cdot 6H_2O$ (0.91 g, 2 mmol) in methanol (30 ml) was added to a suspension of [NiL] (0.87 g, 2 mmol) in MeOH (30 ml) and hydroxyl amine hydrochloride (0.14 g, 2 mmol) in the presence of triethylamine (2 mmol) with stirring. The resulting orange colored product was obtained by evaporation of the solvent and collected by filtration, washed with methanol and recrystallized from DMF–MeOH. *Anal*. for $C_{22}H_{25}N_4O_4Ni_2(ClO_4)\cdot CH_3OH$: Found: C, 41.39; H, 4.14; N, 8.62; Ni, 17.80. Calc. C, 41.95; H, 4.40; N, 8.51; Ni, 17.84%. Selected IR (KBr disc, ν cm^{-1}): 3320(br), 2350(str), 1630(str), 1586, 1112, 1070(s), 620(s). UV–Vis [λ_{max} nm (ε M^{-1} cm^{-1})] in DMF: 670(250), 417(sh), 302(6190), 270(8880). Molar conductance [Λ_M S (cm^2 Ω^{-1} mol^{-1})] in DMF: 78.

The above procedure was used for the following oxime complexes by varying the metal(II) salt (salt = chloride, nitrate, perchlorate).

2.5.2. $[Ni_2L(Cl)]H_2O$ (2)

Orange colored solid. *Anal*. for $C_{22}H_{25}N_4O_4Ni_2(Cl)\cdot H_2O$: Found: C, 45.72; H, 4.45; N, 9.52; Ni, 20.12. Calc. C, 45.53; H, 4.65; N, 9.65; Ni, 20.24%. Selected IR (KBr disc, ν cm^{-1}): 3450(br), 2360(m), 1625(str), 1556, 1152(s), 1112(s) 762. UV–Vis [λ_{max} nm (ε M^{-1} cm^{-1})] in DMF: 740(sh), 620(206), 328(5910),



Scheme 1.

270(10 000). Molar conductance [Λ_M S (cm^2 Ω^{-1} mol^{-1})] in DMF: 84.

2.5.3. $[Cu_2L](ClO_4)\cdot CH_3OH$ (3)

Dark green colored solid. *Anal*. for $C_{22}H_{25}N_4O_4Cu_2(ClO_4)\cdot CH_3OH$: Found: C, 41.13; Cu, 19.12; H, 4.24; N, 8.65. Calc. C, 41.37; Cu, 19.04; H, 4.34; N, 8.39%. Selected IR (ν cm^{-1} using KBr): 3423(br), 2374(m), 1630(str), 1593, 1096(s), 620. UV–Vis [λ_{max} nm (ε M^{-1} cm^{-1})] in DMF: 600(286), 326(3760), 268(8070). Molar conductance [Λ_M S (cm^2 Ω^{-1} mol^{-1})] in DMF: 71.

2.5.4. $[Cu_2L(Cl)]H_2O$ (4)

Green colored solid. *Anal*. for $C_{22}H_{25}N_4O_4Cu_2Cl\cdot H_2O$: Found: C, 44.73; Cu, 21.28; H, 4.52; N, 8.98. Calc. C, 44.78; Cu, 21.54; H, 4.58; N, 9.50%. Selected IR (ν cm^{-1} using KBr): 3410(br), 2335(m), 1625(str), 1556, 1124(s), 1020(s) 762. UV–Vis [λ_{max} nm (ε M^{-1} cm^{-1})] in DMF: 680(sh), 614(304), 324(2780), 266(7870). Molar conductance [Λ_M S (cm^2 Ω^{-1} mol^{-1})] in DMF: 86.

2.5.5. $[Cu_2L(NO_3)]\cdot H_2O$ (5)

Green colored solid. *Anal*. for $C_{22}H_{25}N_4O_4Cu_2(NO_3)\cdot H_2O$: Found: C, 42.68; Cu, 20.35; H, 4.58; N, 11.61. Calc. C, 42.85; Cu, 20.61; H, 4.38; N, 11.36%. Selected IR (ν cm^{-1} using KBr): 3250(br), 2362(m), 1625(str), 1745, 1703(s), 1158, 1124(s). UV–Vis [λ_{max} nm (ε M^{-1} cm^{-1})] in DMF: 720(sh), 620(206), 384(5980), 307(8460). Molar conductance [Λ_M S (cm^2 Ω^{-1} mol^{-1})] in DMF: 75.

3. Results and discussion

All the oxime complexes were prepared by stepwise synthetic method. The IR spectral data of the mononuclear complexes M(II) (M = Ni or Cu) show a peak around 1670 cm^{-1} due to –CHO group. This peak disappears and a new peak due to ν(C=N) [13,14] appears around 1625 cm^{-1} for binuclear complexes. Binuclear complexes show a peak observed around 2350 cm^{-1} attributed to O···H···O hydrogen-bond fragment. A peak due to N–O bond [15,16] is observed around 1112–1280 cm^{-1}.

The complexes $[Ni_2L](ClO_4)$ (**1**) and $[Cu_2L](ClO_4)$ (**3**) show a broad peak due to uncoordinated perchlorate ion [17] around 1090 and 620 cm^{-1}. For $[Cu_2L(NO_3)]$ (**5**) two peaks have been observed at 1703 and 1745 cm^{-1} due to coordinated nitrate ion [18,19].

The electronic spectra were recorded in DMF solvent in the region 260–820 nm. The nickel complexes $[Ni_2L](ClO_4)$ complex shows a single weak d–d band at 670 nm ($\varepsilon = 250$ M^{-1} cm^{-1}) due to $^1A_1g \rightarrow {}^1A_2g$ transition [20,21] associated with square planar geometry. The two compartments in the binuclear complexes have N_2O_2 coordinating sites in the equatorial position. So, the d–d transition of the two Ni(II) ions in square planar geometry absorbs more or less same region. The two peaks are very close to each other and give rise to a single broad spectrum. The complex $[Cu_2L](ClO_4)$ shows a single weak d–d transition [600 nm ($\varepsilon = 486$ M^{-1} cm^{-1})] associated with square planar geometry. The complex $[Cu_2L(Cl)]$, $[Cu_2L(NO_3)]$, $[Ni_2L(Cl)]$ shows two d–d transition. This shows the coordination of counter ion to one of the copper(II) ion and has square pyramidal geometry. Moderately intense band observed in the region 320–400 nm ($\varepsilon = 1580$–5910 M^{-1} cm^{-1}) is associated with ligand to metal charge transfer transition while intense transition observed around 290 nm ($\varepsilon = 7860$–$10\,000$ M^{-1} cm^{-1}) is due to ligand to ligand charge transfer transition.

3.1. Electrochemistry of the complexes

The electrochemical properties of the binuclear complexes were studied by using cyclic voltammetry in DMF solution containing TBAP as supporting electrolyte in the potential range +1.3 to −1.3 V. The electrochemical data are given in Tables 1 and 2. The cyclic voltammogram of the complexes is shown in Figs. 1 and 2.

Generally the electrochemical properties of the complexes depend on a number of factors such as chelate ring/size [22,23] axial ligation [24,25], degree and distribution of unsaturation [26] and substitution pattern [27] in the chelate ring.

Table 1
Electrochemical data of nickel(II) and copper(II) oxime complexes (reduction at cathodic potential)

Number	Complex	E^{1}_{pc} (V)	E^{1}_{pa} (V)	ΔE^{1}_{p} (mV)	$E^{1}_{1/2}$ (V)	E^{2}_{pc} (V)	E^{2}_{pa} (V)	ΔE^{2}_{p} (mV)	$E^{2}_{1/2}$ (V)
1	$[Ni_2L](ClO_4)\cdot CH_3OH$	−0.63	−0.48	150	−0.56	−1.08	−0.92	160	−1.00
2	$[Ni_2L(Cl)]\cdot H_2O$	−0.40	−0.25	150	−0.32	−1.10	−0.93	170	−1.01
3	$[Cu_2L](ClO_4)\cdot CH_3OH$	−0.62	−0.48	140	−0.55	−1.25	−1.06	190	−1.15
4	$[Cu_2L(Cl)]\cdot H_2O$	−0.28	−0.10	180	−0.19	−1.20	−0.98	220	−1.09
5	$[Cu_2L(NO_3)]\cdot H_2O$	−0.18	−0.08	100	−0.13	−1.18	−0.95	230	−1.06

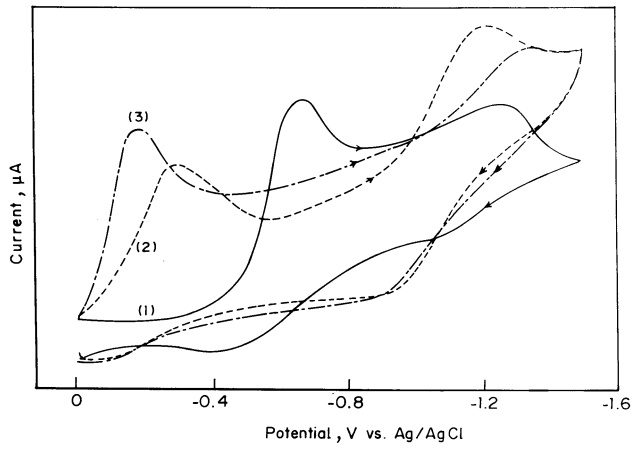


Fig. 1. Cyclic voltammograms of the copper complexes: $[Cu_2L](ClO_4)$ (**3**), $[Cu_2L(Cl)]$ (**4**), $[Cu_2L(NO_3)]$ (**5**) in dmf, scan rate 50 mV s^{-1}. Potential are given in V vs. Ag/AgCl; platinum working and Ag/AgCl reference electrodes; supporting electrolyte TBAP; concentration of complex 1×10^{-3} M, concentration of TBAP 1×10^{-1} M.

3.1.1. Reduction process

All the complexes show a quasi-reversible two step single electron transfer process as it is evidenced from the criteria: the $E_{1/2}$ values are independent of scan rate; the ΔE_p increases with increasing scan rate and is always greater than 60 mV. The peak currents i_{pc} and i_{pa} are not equal. Controlled potential electrolysis carried out at 100 mV more negative than the first reduction wave confirms the consumption of one electron per molecule ($n = 0.95$). Controlled potential electrolysis conducted at 100 mV more negative than second reduction wave confirmed the consumption of two electrons per molecule.

$[Cu_2L(Cl)]$ ($E_{pc} = -0.28$ V) and $[Cu_2L(NO_3)]$ ($E_{pc} = -0.18$ V) reduces at less negative potential compared with $[Cu_2L](ClO_4)$ ($E_{pc} = -0.62$ V) (Fig. 1). Similarly, $[Ni_2L(Cl)]$ (**2**) ($E_{pc} = -0.40$ V) reduces at less negative potential compared with $[Ni_2L](ClO_4)$ ($E_{pc} = -0.63$ V). This may be due to distortion [28–30] in geometry that arises due to axial coordination of the anions (chloride and nitrate) to the copper and nickel ion. $E_{1/2}$ value for $[Cu_2L](ClO_4)$ is −0.55, $[Cu_2L(Cl)]$ is −0.19 and $[Cu_2L(NO_3)]$ is −0.13. For nickel complexes also the change in redox potential observed with change in geometry. $E_{1/2}$ value for $[Ni_2L](ClO_4)$ is −0.56, $[Ni_2L(Cl)]$ is −0.32. The coordination site influence is less than geometrical distortion effect in the redox potential of the complexes. Since the difference in $E_{1/2}$ value between chloro complex and nitrato complex is less when compared with these two $E_{1/2}$ values with respect to perchlorato complex.

3.1.2. Oxidation process

The cyclic voltammogram of nickel complexes at positive potential show two step single electron transfer

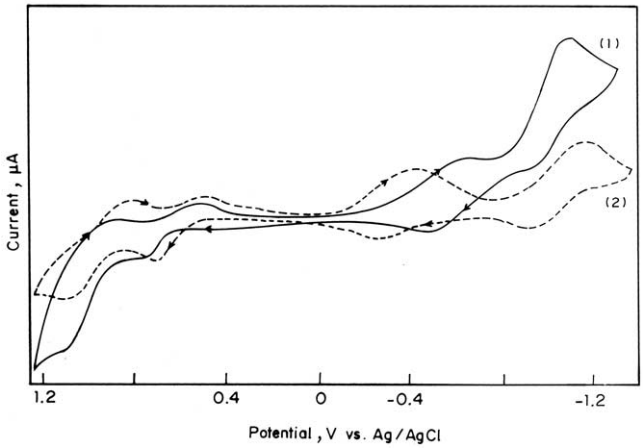


Fig. 2. Cyclic voltammograms of the nickel complexes $[Ni_2L](ClO_4)$ (**1**), $[Ni_2L(Cl)]$ (**2**) in dmf, scan rate 50 mV s^{-1}. Potential are given in V vs. Ag/AgCl; platinum working and Ag/AgCl reference electrodes; supporting electrolyte TBAP; concentration of complex 1×10^{-3} M, concentration of TBAP 1×10^{-1} M.

Table 2
Electrochemical data of the nickel(II) oxime complexes (oxidation at anodic potential)

Number	Complex	E^{1}_{pa} (V)	E^{1}_{pc} (V)	ΔE^{1}_{p} (mV)	$E^{1}_{1/2}$ (V)	E^{2}_{pa} (V)	E^{2}_{pc} (V)	ΔE^{2}_{p} (mV)	$E^{2}_{1/2}$ (V)
1	$[Ni_2L](ClO_4)\cdot CH_3OH$	0.78	0.55	230	0.66	1.13	0.93	200	1.03
2	$[Ni_2L(Cl)]\cdot H_2O$	0.75	0.52	230	0.63	1.10	0.88	220	0.99

Table 3
ESR spectral data of the copper(II) oxime complexes

Number	Complex	$g_{\|}$	$g_{\perp}$	$-2J$, cm^{-1}	ρ	μ_{eff} (B.M) (RT)
3	$[Cu_2L](ClO_4)\cdot CH_3OH$	2.18	2.04	172	0.001	1.59
4	$[Cu_2L(Cl)]\cdot H_2O$	2.11	2.03			1.55
5	$[Cu_2L(NO_3)]\cdot H_2O$	2.21	2.09			1.49

processes in the potential range 0–1.15 V. The electrochemical data for the complexes at positive potential region is given in Table 2. The cyclic voltammogram of the nickel complexes in cathodic and anodic potential region is given in Fig. 2. The redox process is quasi-reversible in nature. The $E_{1/2}$ values for nickel complex $[Ni_2L](ClO_4)$ is $E_{1/2} = +0.66$ V and for the complex $[Ni_2L(Cl)]$ is $E_{1/2} = +0.63$ V. This shows that the chloride complex oxidised easily than the perchlorate complex, but the difference in $E_{1/2}$ value is very small (0.03 V).

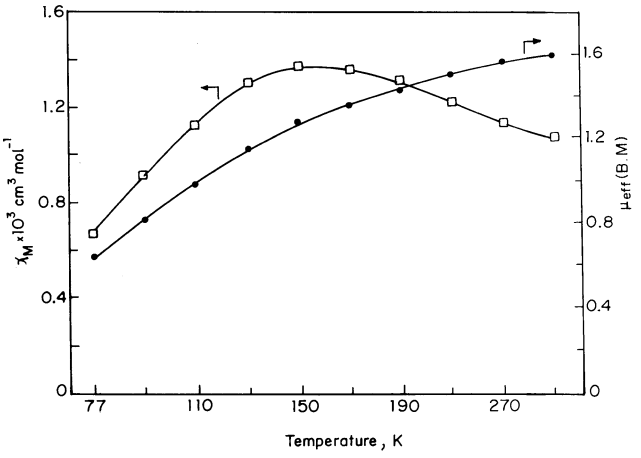


Fig. 3. Temperature dependence of magnetic susceptibility (χ_{cu}) and effective magnetic moment (μ_{eff}) for complex $[Cu_2L](ClO_4)$.

3.2. Magnetic properties of the complex

The nickel complexes are EPR inactive, which evinces that the nickel complexes are diamagnetic and have square planar geometry. The EPR spectra of the mononuclear copper complexes show four line with hyperfine splitting and binuclear complexes show a broad signal at $g = 2.1$ and room temperature (at 298 K) magnetic moment studies of the complex $[Cu_2L](ClO_4)$ show μ_{eff} value of 1.59 B.M, which is less than the spin only value of single copper(II) ion. These indicate that the presence of coupling between two copper(II) centers. So, to evaluate the singlet–triplet energy separation ($-2J$), variable temperature magnetic susceptibility measurement (77–300 K) was carried out for complex $[Cu_2L](ClO_4)$. The magnetic susceptibility measurement data for the complex $[Cu_2L](ClO_4)$ was fitted to the modified form of Bleaney–Bowers equation.

$$\chi_{cu} = (Ng^2\beta^2)/(kT)[3 + \exp(-2J/kT)]^{-1}(1-\rho) + N_{\alpha}$$

where χ_{cu} is the paramagnetic susceptibility per metal atom after the correction for the diamagnetism, N is Avagadro number, β Boltzman constant, g is the

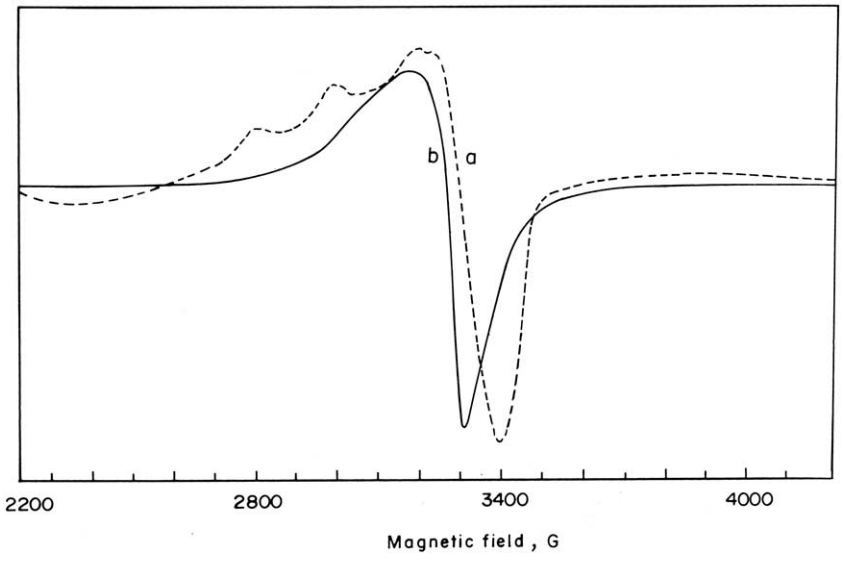


Fig. 4. ESR spectra of the complexes: (a) [CuL]; (b) $[Cu_2L](ClO_4)$.

average gyromagnetic ratio and ρ is the fraction of the monomeric copper(II) impurities, $-J$ the singlet–triplet separation, N_α is the temperature independent paramagnetism (60×10^{-6} cgs units) per copper(II) complexes. A nonlinear least-square fitting programme was employed to calculate $-J$, g and ρ. The best fit parameters are tabulated in Table 3. Temperature dependence of the magnetic properties for complexes $[Cu_2L](ClO_4)$ is given in Figs. 3 and 4. The antiferromagnetic exchange interaction ($-2J = 172$ cm^{-1}) observed for the complex $[Cu_2L]ClO_4$ is similar to that of analogous unsymmetrical macrocyclic complex ($-2J = 170$ cm^{-1}) reported by Kandaswamy et al. [28]. This is in agreement with the results reported by Busch et al. [12] for unsymmetrical schiff base oxime complexes and analogous unsymmetrical macrocyclic complexes.

4. Summary

The binuclear unsymmetrical compartmental oxime ligands and their mono, binuclear nickel(II) and copper(II) complexes have been synthesized and characterized. The electrochemical and magnetic properties of the complexes are discussed.

References

[1] C.J. Cairns, D.H. Busch, Coord. Chem. Rev. 69 (1986) 1.
[2] A.J. Atkins, D. Black, A.J. Black, A. Marin-Bacerra, S. Parsons, L. Ruiz-Ramirez, M. Schroder, Chem. Commun. (1996) 457.
[3] O. Kahn, Struct. Bonding (Berlin) 68 (1987) 89.
[4] P. Guerriero, S. Tamburini, P.A. Vigato, Coord. Chem. Rev. 139 (1995) 17.
[5] N.H. Pilkington, R. Robson, Aust. J. Chem. 23 (1970) 2225.
[6] U. Casellato, D. Fregona, S. Sitran, S. Tamburini, P.A. Vigato, Inorg. Chem. Acta 110 (1985) 181.
[7] G.A. Lawrence, M. Maeder, E.N. Wilkes, Inorg. Chem. 13 (1993) 199.
[8] M. Yonemura, Y. Matsumura, H. Furutachi, M. Ohba, H. Okawa, D.E. Fenton, Inorg. Chem. 36 (1997) 2711.
[9] M. Lubben, B.L. Feringa, J. Org. Chem. 59 (1994) 2227.
[10] A.V. Bordunov, N.G. Lukyanenko, V.N. Pastushok, K.E. Krakowiak, J.S. Bradshaw, N.K. Dalley, X. Kou, J. Org. Chem. 60 (1995) 4912.
[11] J.C. Duff, J. Chem. Soc. (1941) 547.
[12] E.V. Rybak-Akimova, D.H. Busch, P.K. Kahol, N. Pinto, N.W. Alcock, H.J. Clase, Inorg. Chem. 36 (1997) 510.
[13] K. Nakomoto, Infrared and Raman Spectra of Inorganic and Coordination Compounds, Wiley-Interscience, New York, 1970.
[14] G. Das, R. Shukla, S. Mandal, R. Singh, P.K. Bharadwaj, J.V. Hall, K.H. Whitmire, Inorg. Chem. 36 (1997) 323.
[15] E.V. Rybak-Akimova, N.W. Alcock, D.H. Daryle, H. Busch, Inorg. Chem 37 (1998) 1563.
[16] B. Egenus, Talanta 19 (1972) 1387.
[17] M. Lachkar, R. Guilard, A. Atmani, A. De. Cian, J. Fischer, R. Weiss, Inorg. Chem. 37 (1998) 1575.
[18] S.S. Tandon, L.K. Thompson, J.N. Bridson, M. Bubenik, Inorg. Chem. 32 (1993) 4621.
[19] L. Chen, L.K. Thompson, J.N. Bridson, Can. J. Chem. 70 (1992) 1886.
[20] A.B.P. Lever, Inorganic Electronic Spectroscopy, 2nd ed., Elsevier, Amsterdam, 1984.
[21] S. Bhattacharyya, T.J.R. Weakley, M. Chaudhury, Inorg. Chem. 38 (1999) 633.
[22] F.V. Lovecchio, E.S. Gore, D.H. Busch, J. Am. Chem. Soc. 96 (1974) 3104.
[23] G.K. Barefield, G.M. Freeman, D.G. van Derveer, Inorg. Chem. 25 (1986) 552.
[24] C. Kratky, R. Tschatka, C. Angst, J.E. Johanson Plaquevent, Helv. Chim. Acta 68 (1985) 1312.
[25] P.A. Connick, K.A. Macor, Inorg. Chem. 30 (1991) 4654.
[26] A.M. Tait, F.V. Lovecchio, D.H. Busch, Inorg. Chem. 16 (1977) 2206.
[27] J.A. Streeky, D.G. Pilsbury, D.H. Busch, Inorg. Chem. 19 (1980) 3148.
[28] S. Karunakaran, M. Kandaswamy, J. Chem. Soc., Dalton Trans. (1995) 1851.
[29] M. Marrapan, M. Kandaswamy, V. Narayanan, J. Chem. Soc., Dalton Trans. (1998) 3405.
[30] A. Bottcher, T. Takeuchi, K.I. Hardcastle, T.J. Meade, H.B. Gray, D. Cwikel, M. Kapon, Z. Dori, Inorg. Chem. 36 (1997) 2498.

Thus, besides the great number of investigations, the challenge to find the 'ideal antenna molecule' still remains.

The choice of ruthenium metal is of particular interest because of its octahedral geometry since one can introduce specific ligands in a controlled manner [4]. More specifically, by introducing different donor/acceptor/functional groups it is possible to 'fine tune' the spectral properties of the complex. In the family of Ru(II) polypyridine complexes few molecules with terpy derivatives are known. The complexes with the bdmpp ligand exhibit significantly different electronic properties from their terpy analogs [5]. Very recently it has been demonstrated that they can also be used for the sensitization process [6]. The topic of this work is to present the synthesis and characterization of a new Ru(II) dye molecule, [Ru(II)(dcbpyH_2)(bdmpp)NCS](PF_6) (**1**), and evaluate the performance of the corresponding dye-sensitized solar cell. The complex is of theoretical interest because it contains two chromophore units (bpy and bdmpp). The first ligand (dcbpyH_2 = 2,2′-bipyridine-4,4′-dicarboxylic acid) bears a carboxylic acid functional moiety, which serves as interlocking agent. The second ligand [bdmpp = 2,6-bis(3,5-dimethyl-*N*-pyrazoyl)pyridine] can be considered as a terpyridine derivative, exhibiting significantly different electronic properties. The complex is also endowed with a monodentate thiocyanato ligand, –N=C=S. The role of this ligand is to tune the metal t_{2g}-orbitals of Ru(II) and possibly to stabilize the hole that is being generated on the metal, after having injected an electron into the TiO_2 conduction band [7].

2. Experimental

2.1. Materials

$RuCl_3 \cdot 3H_2O$, 2,2′-bipyridine-4,4′-dicarboxylic acid (dcbpyH_2), sodium thiocyanate (NaSCN) were purchased from Riedel-de Haën, Fluka and Carlo Erba, respectively, and were used as received without additional purification. The bdmpp ligand was prepared by Prof. V.J. Catalano. Ammonium hexafluorophosphate (NH_4PF_6) and tetrabutyl ammonium hexafluorophosphate (Bu_4PF_6) were purchased from Aldrich. The solvents ethanol, toluene, acetonitrile and diethyl ether were from Riedel-de Haën, Panreac and Merck, respectively. MeOH-d_4 was from Riedel-de Haën.

2.2. Methods

2.2.1. Analytical measurements

The mass spectra were obtained on a TSQ 7000 Finnigan Mat spectrometer using the ESI (electrospray) technique. All the m/z values are based on ^{102}Ru, which is the most abundant isotope. UV–Vis spectra were recorded using a Perkin–Elmer Lambda 19 spectrometer using Teflon-stoppered quartz cells having a path length of 1 cm. ^{1}H and ^{13}C NMR spectra 1D and 2D were measured in CD_3OD solution with a Bruker Avance 500 MHz spectrometer. The reported chemical shifts were against TMS. The IR spectra were measured using a Nicolet 550 Magna-IR^{TM} spectrometer. The spectra are the average of 16 accumulated scans.

Cyclic voltammetry measurements were performed in a 5×10^{-4} M solution of the complex in acetonitrile (CH_3CN) in the presence of 0.1 M $TBAPF_6$ supporting electrolyte, using a Vinci Technologies P/G STAT Z1 potentiostat, operating in conjunction with a 33120 A Hewlett–Packard function/arbitrary waveform generator with a Linseis LY 18100 X-Y recorder. A three-electrode electrochemical cell was used, with a Metrohm dot platinum working electrode (WE), a Metrohm planar platinum counter electrode (CE) and a Metrohm 6.0726.100 Ag/AgCl reference electrode containing 0.1 M Bu_4NCl in CH_3CN as the inner electrolyte and the outer electrolyte. The experiments were performed in deoxygenated solutions by passing purified Ar gas (99.9%) through the solutions. During the experiment the Ar was passed over the solution surface. Under these conditions the ferrocenium/ferrocene couple has an $E_{1/2}$ of 0.343 V versus AgCl with $E_{pa} - E_{pc} = 111$ mV.

2.3. Synthesis of [Ru(dcbpyH_2)(bdmpp)NCS](PF_6)

To prepare the Ru(bdmpp)Cl_3 precursor, $RuCl_3 \cdot 3H_2O$ (260 mg, 1.26 mmol) and bdmpp (267 mg, 1.0 mmol) were dissolved in absolute ethanol and the mixture was refluxed for 3 h under stirring. The solution was then cooled at room temperature (r.t.), filtered and the resulting brown powder was washed with absolute ethanol and ether and air-dried, Fig. 1, reaction (1). The precursor [Ru(bdmpp)Cl_3] thus prepared (without any purification) and the dcbpyH_2 ligand (1/1 molar ratio) were refluxed for 8 h in EtOH–H_2O (3/1:v/v) containing LiCl and triethylamine as a reductant. The hot solution was filtered through celite and evaporated to dryness. After dissolving the crude product in EtOH, a saturated methanol solution of NH_4PF_6 ($\sim$10 ml) was added (Fig. 1, reaction (2)). The solution was left at 0 °C for a

$$RuCl_3 \cdot H_2O + bdmpp \xrightarrow{EtOH,reflux} Ru(bdmpp)Cl_3 \quad (1)$$

$$Ru(bdmpp)Cl_3 + dcbpyH_2 \xrightarrow{NEt_3,EtOH/H_2O,reflux} [Ru(bdmpp)(dcbpyH_2)Cl]^+ \quad (2)$$

$$[Ru(bdmpp)(dcbpyH_2)Cl]^+ \xrightarrow{NaNCS,EtOH/H_2O,reflux} [Ru(bdmpp)(dcbpyH_2)NCS]^+ \quad (3)$$

Fig. 1. Schematic diagram of the synthesis of [Ru(dcbpyH_2)(bdmpp)(NCS)](PF_6) complex.

day. The resulting deep brown precipitate corresponding to [Ru(dcbpyH$_2$)(bdmpp)Cl](PF$_6$) [6,8] was collected on a sintered glass funnel and washed with cold water then with ether (yields 76.2 mg, 24%). The complex is soluble in EtOH, MeOH, AcCN, aceton, moderably soluble in $CHCl_3$.

A suspension of [Ru(dcbpyH$_2$)(bdmpp)Cl](PF$_6$) (60 mg, 0.076 mmol) and NaNCS (25.4 mg, 0.31 mmol) in (10 ml) of ethanol–water (1:1) mixture was refluxed under Ar for 4 h in the dark. After cooling, a saturated aqueous solution of ammonium hexafluorophosphate (12 ml) was added dropwise to the reaction mixture. The black precipitate formed was filtered and washed successively with water (2×5 ml), toluene (2×5 ml) and ether (2×12 ml) to yield the title compound **1** as a dark powder (59 mg, 95%), Fig. 1, reaction (3). The complex is soluble in carbon tetrachloride, toluene, ethanol, methanol and acetonitrile. It is insoluble in cyclohexane. Melting point (m.p.): above 250 °C.

3. Results and discussion

3.1. FT-IR spectroscopy

The most direct evidence for the presence of N-coordinated NCS comes from the FT-IR spectrum of complex **1**, recorded in a KBr pellet in the 4000–400 cm^{-1} region (see supplementary information Fig. 8). The strong absorption band at 2109 cm^{-1} is assigned as to the N-bonded NCS^- ligand ν(C=N) stretching vibration. The presence of band at 771 cm^{-1} is assigned to the ν(C=S) stretching vibration. For the complex **1** at 2856–2927 cm^{-1} (w) there are the C–H stretch vibrations for the CH_3 groups. The 1713 cm^{-1} (m) vibration is characteristic of the C=O bond stretching on the carboxylate group. Ring stretching vibrations occur in the region between 1613 and 1317 cm^{-1} (m). The C–O stretch occurs at 1262–1232 cm^{-1} (w). At 846 cm^{-1} (s) appears the characteristic band of multinuclear aromatics from the C–H out of plane bend. The C–H stretch vibrations of the heteroaromatic pyridines expected about 3100 cm^{-1} are weak because of a very strong moisture background.

3.2. Mass spectrometry

The identity of complex **1** was ascertained by mass spectrometry (ESI), Fig. 2. Both parent ion peaks and expected fragments of the complex were detected. In fact, in the case of the +Q1MS mode (positive region), a strong peak at $m/z = 671.2$ was observed and was attributed to the $(Ru(dcbpy)(bdmpp)NCS)^+$ cation. In −Q1MS mode (see supplementary information Fig. 9), a peak at $m/z = 144.8$ characteristic of the (PF_6^-) anion was obtained. The m/z value is based on ^{102}Ru, which is the most abundant isotope.

3.3. Molecular confuguration and ^{1}H NMR spectroscopy

On the basis of the IR analysis, the electrospray MS data and taking into account that the presence of the

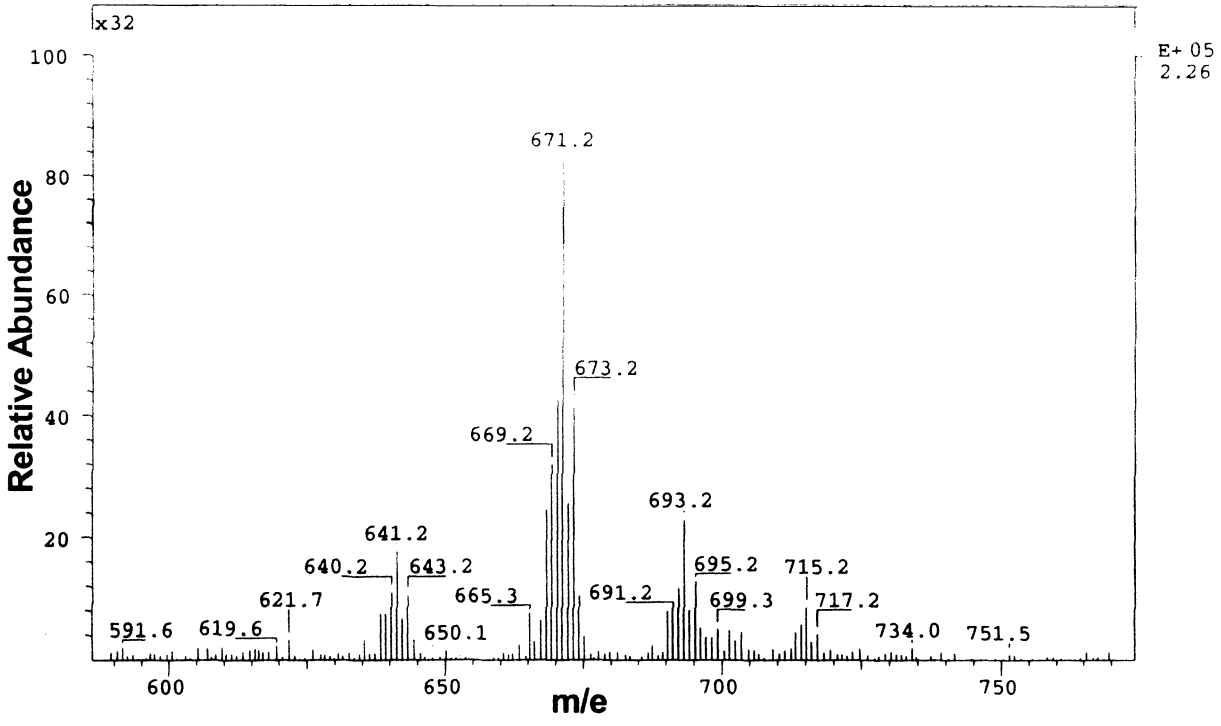


Fig. 2. Ionization electrospray ESI MS spectra of complex **1**: +Q1MS.

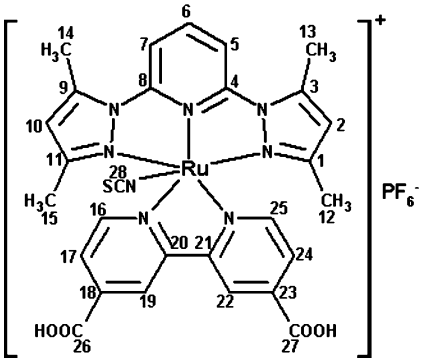


Fig. 3. Proposed molecular configuration for the [Ru(II)(dcbpyH$_2$)(bdmpp)NCS](PF$_6$) complex.

carboxylic acid moieties on the bipyridine ligand can not essentially modify the structure of the obtained species, a molecular configuration similar to that obtained for the [Ru-(bdmpp-bpy)Cl]$^+$ complex [6] can be proposed, Fig. 3.

The NMR data (the 1D and 2D NMR spectra) strongly support the above molecular configuration for the [Ru(dcbpy)(bdmpp)NCS)](PF$_6$) (**1**). In complex **1**, the proton assignments of the bdmpp and the 2,2′-bipyridine-4,4′-dicarboxylic acid ligands were made on the basis of peak integration, coupling constants and ^{1}H–^{1}H COSY and NOESY experiments (see supplementary information, Fig. 10). The chemical shift data and corresponding assignments are presented on Table 1.

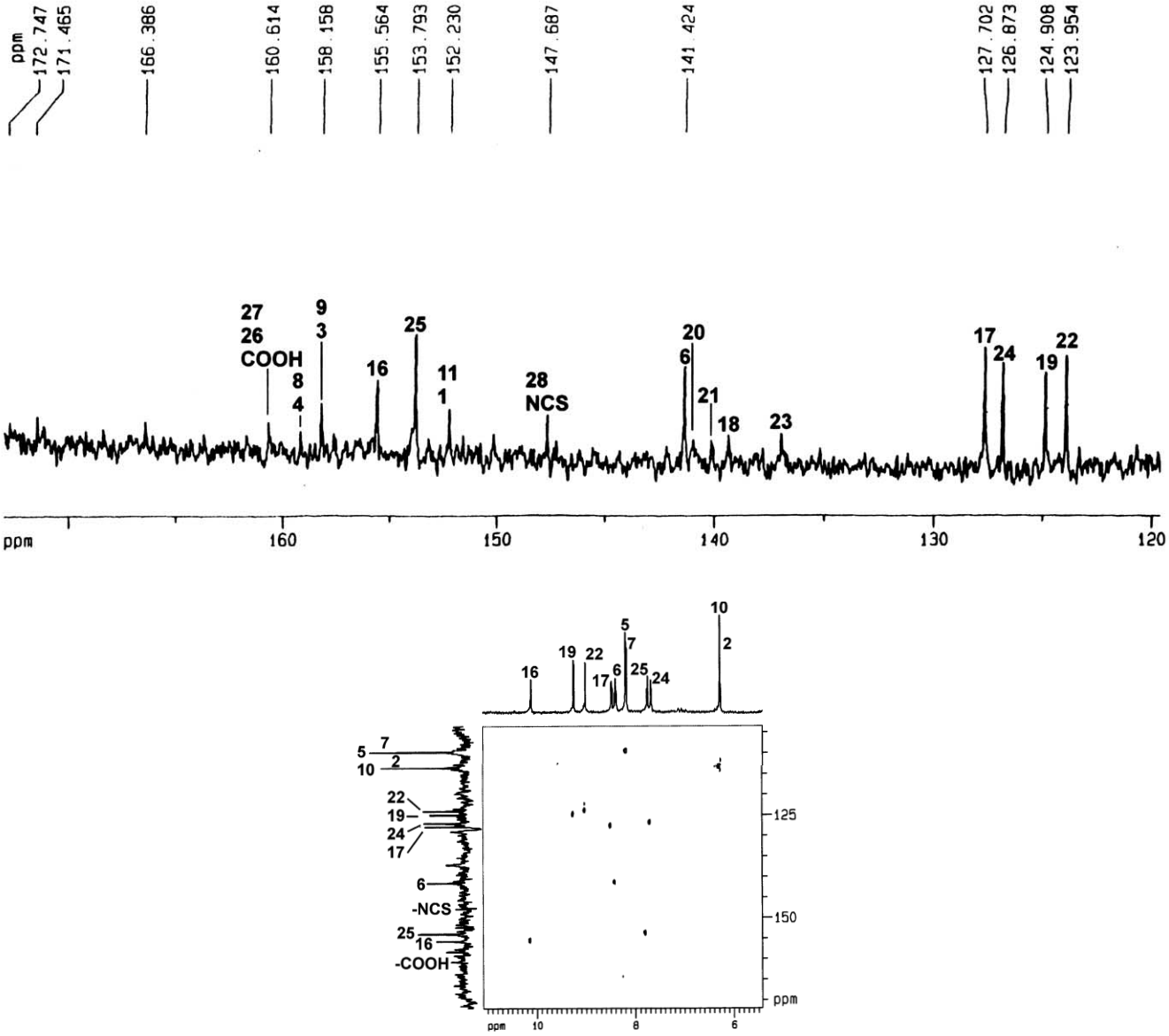


Fig. 4. ^{13}C NMR spectra of the [Ru(II)(dcbpyH$_2$)(bdmpp)NCS](PF$_6$) complex (a); the corresponding two-dimensional ^{1}H–^{13}C NMR (HSQC) spectra (b).

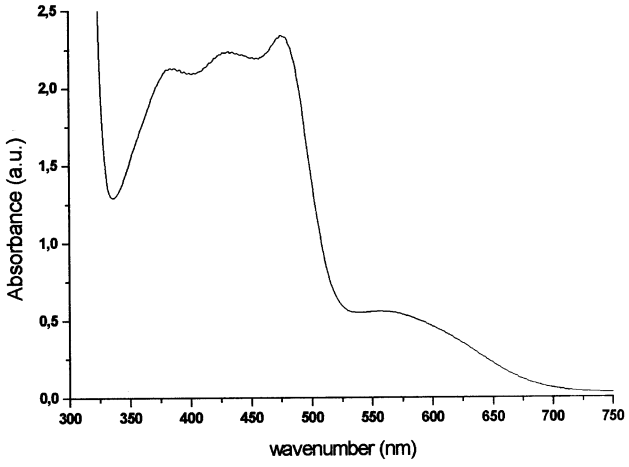


Fig. 5. UV–Vis spectrum of the complex **1** (10^{-4} M) in MeOH.

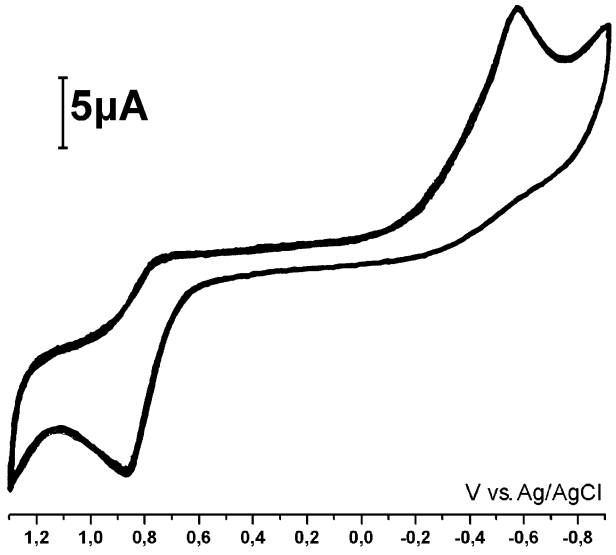


Fig. 6. Cyclic voltammogram of 5×10^{-4} M [Ru(II)(dcbpyH$_2$)(bdmpp)NCS](PF$_6$) complex in CH_3CN; supporting electrolyte 0.1 M Bu_4NPF_6; scan rate: 100 mV s^{-1}.

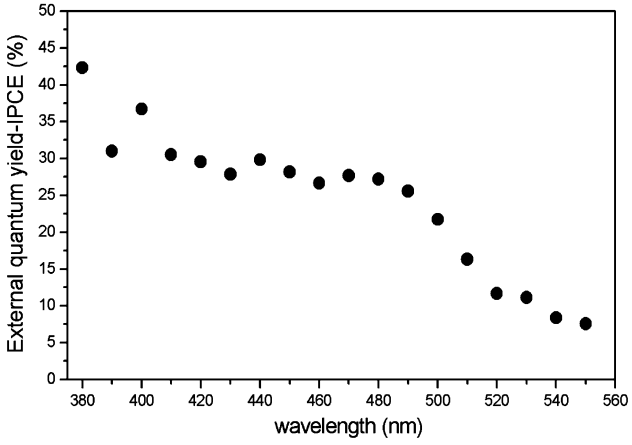


Fig. 7. Photocurrent action spectrum of TiO_2–[Ru(dcbpyH$_2$)(bdmpp)(NCS)](PF$_6$) dye-sensitized solar cell using the PEO–TiO_2(I^-/I_3^-) composite PEO/titania redox electrolyte.

Table 1
^{1}H (δ_H, ppm) and ^{13}C (δ_C, ppm) chemical shifts for complex **1** in CD_3OD at 298 K

H-2/H-10	6.28
H-5/H-7 [a]	8.19
H-6 [b]	8.40
H-12/H-15	1.55
H-13/H-14	2.98
H-16 [c]	10.12
H-17 [d]	8.48
H-19	9.25
H-22	9.01
H-24 [e]	7.68
H-25 [f]	7.76
C-1/C-11	152.23
C-2/C-10	113.41
C-3/C-9	158.16
C-4/C-8	159.09
C-5/C-7	109.66
C-6	141.42
C-12/C-15	12.13
C-13/C-14	14.69
C-16	155.56
C-17	127.70
C-18	139.35
C-19	124.91
C-20	140.89
C-21	140.12
C-22	123.95
C-23	136.99
C-24	126.87
C-25	153.79
C-26/C-27	160.61
C-28	147.69

[a] $^3J = 8.72$ Hz.
[b] $^3J = 8.36$ Hz.
[c] $^3J = 5.80$ Hz.
[d] $^3J = 5.80$ Hz, $^4J = 1.45$ Hz.
[e] $^3J = 5.81$ Hz, $^4J = 1.45$ Hz.
[f] $^3J = 5.81$ Hz.

Table 2
Extinction coefficient values of [Ru(II)(dcbpyH$_2$)(bdmpp)NCS](PF$_6$) (**1**) complex

λ^{abs} (nm) [a]	$10^{-4}\varepsilon_{max}$ (M^{-1} cm^{-1}) [b]
650	0.22
620	0.38
569	0.55
475	2.34
432	2.24
383	2.13
293	6.00

[a] Absorption spectra acquired at room temperature.
[b] In MeOH.

3.4. ^{13}C NMR spectroscopy

The 1D ^{13}C NMR spectrum of complex (**1**) in CD_3OD, Fig. 4(a)), shows 19 resonance signals in the

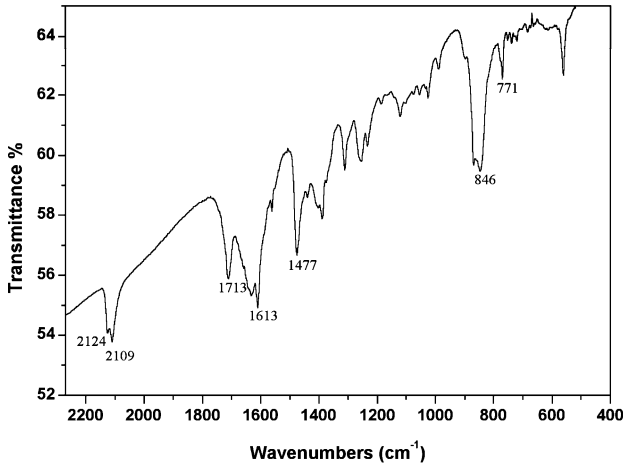


Fig. 8. FT-IR spectrum of [Ru(II)(dcbpyH$_2$)(bdmpp)NCS](PF$_6$) (1) in a KBr pellet.

aromatic region (δ 109–161 ppm) corresponding to 2,2′-bipyridine-4,4′-dicarboxylic acid, bdmpp and NCS^-. The assignment of the peaks (listed in Table 1) is based on the 2D HSQC spectrum, Fig. 4(b) as well as on chemical reasoning.

The two resonance peaks in the aliphatic region, at δ 14.69 and 12.13 ppm, correspond to 2 nonequiv. methyl carbon atom groups of the coordinated bdmpp ligand. The downfield resonance at 160.61 ppm is assigned to the carboxylate carbons of the 2,2′-bipyridine-4,4′-dicarboxylic acid ligand. The peak at 159.09 ppm is assigned to quaternary C4 and C8 carbons, which are near to two electron withdrawing nitrogens of the coordinated bdmpp ligand. The more intense peak at 158.16 ppm is due to quaternary C3, C9 carbons which are near to one electron withdrawing nitrogen but also are near to the electron withdrawing nitrogen of the central coordinated pyridine. More upfield there is an intense peak at 152.23 ppm, which is assigned to quaternary C1, C11 carbons. The C20, C21 carbons are observed at 140.89 and 140.12 ppm, respectively. The peaks at 139.35 and 136.99 are due to quaternary C18 and C23 carbons. The peak at 147.69 ppm is assigned to the carbon of the NCS^- ligand [9]. The most likely reason for such a downfield shift could be that this carbon is *trans* to one ring of the bidentate ligand dcbpyH$_2$ [8].

3.5. Electronic spectra

The electronic absorption spectra of **1** (10^{-4} M in MeOH), Fig. 5, is typical of Ru(II) diimine systems. The complex presents an intense and composite broad band in the visible attributed to a MLCT process. The band consists of three absorption maxima of very high intensity appearing at 383 nm ($\varepsilon = 21\,274$ M^{-1} cm^{-1}), 432 nm ($\varepsilon = 22\,353$ M^{-1} cm^{-1}) and 475 nm ($\varepsilon = 23\,397$ M^{-1} cm^{-1}), respectively (Table 2). The visible absorption spectrum of the new complex shows that it absorbs over the most of the visible, with a significant degree of

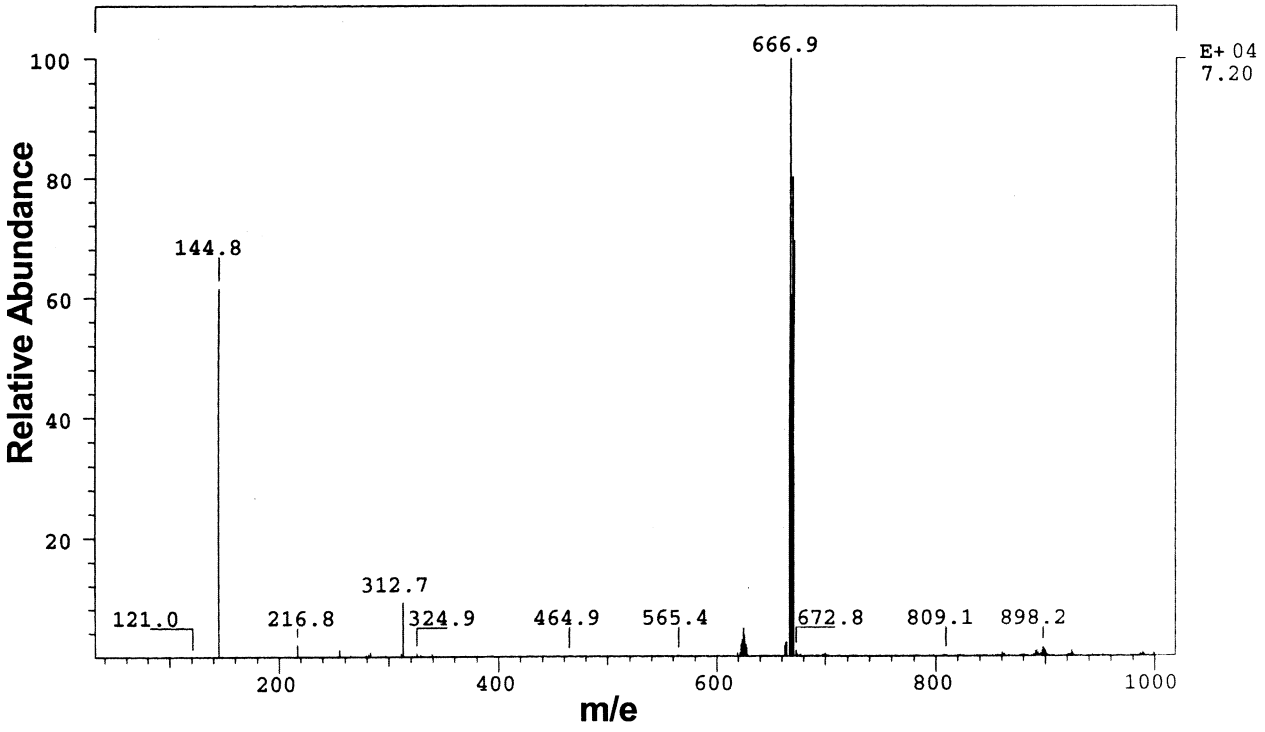


Fig. 9. Ionization electrospray ESI MS spectra of complex **1**: −Q1MS.

absorption into the low energy region greater than 525 nm. It is worth mentioning the presence of an absorption hump at 569 nm (5481 M^{-1} cm^{-1}) and the fact that even at 620 nm, the extinction coefficient is still high ($\varepsilon = 3768$ M^{-1} cm^{-1}). This is very important point for the photosensitization purpose [10].

3.6. Electrochemistry

The cyclic voltammogram of the complex was similar with those of other typical dyes containing bipyridine, phenanthroline and terpyridine ligands which have been used as sensitizers in regenerative photoelectrochemical cells. It was obtained in CH_3CN containing 0.1 M TBAH at a sweep rate of 100 mV s^{-1}, Fig. 6, and shows a well defined reversible oxidation–reduction wave attributed to the Ru(II)/Ru(III) redox couple, with a half-wave potential ($E_{1/2}$) of +0.795 V versus Ag/AgCl and $E_{pa} - E_{pc} = 120$ mV; the peak observed at −0.612 V can be assigned to the first ligand centred reduction.

3.7. Sensitizing ability

Rough, high surface area nanostructured TiO_2 thin film electrodes prepared using the doctor-blade technique on TEC 15 conductive glass substrates [11] developed a deep yellow–brown color following overnight immersion in a 10^{-4} ethanolic solution of the complex. The complex is chemically adsorbed on TiO_2 via an ester-like linkage formed between the carboxylic acid functional groups (–COOH) of the bipyridine ligand and the hydroxyl moieties (–OH) present on the semiconductor surface [12]. To check the sensitizing ability of the complex, the derivatized electrodes (active surface size 0.4 cm^2) were then incorporated in a solid-state dye-sensitized solar cell using a composite electrolyte consisting of polyethylene oxide (PEO) with an

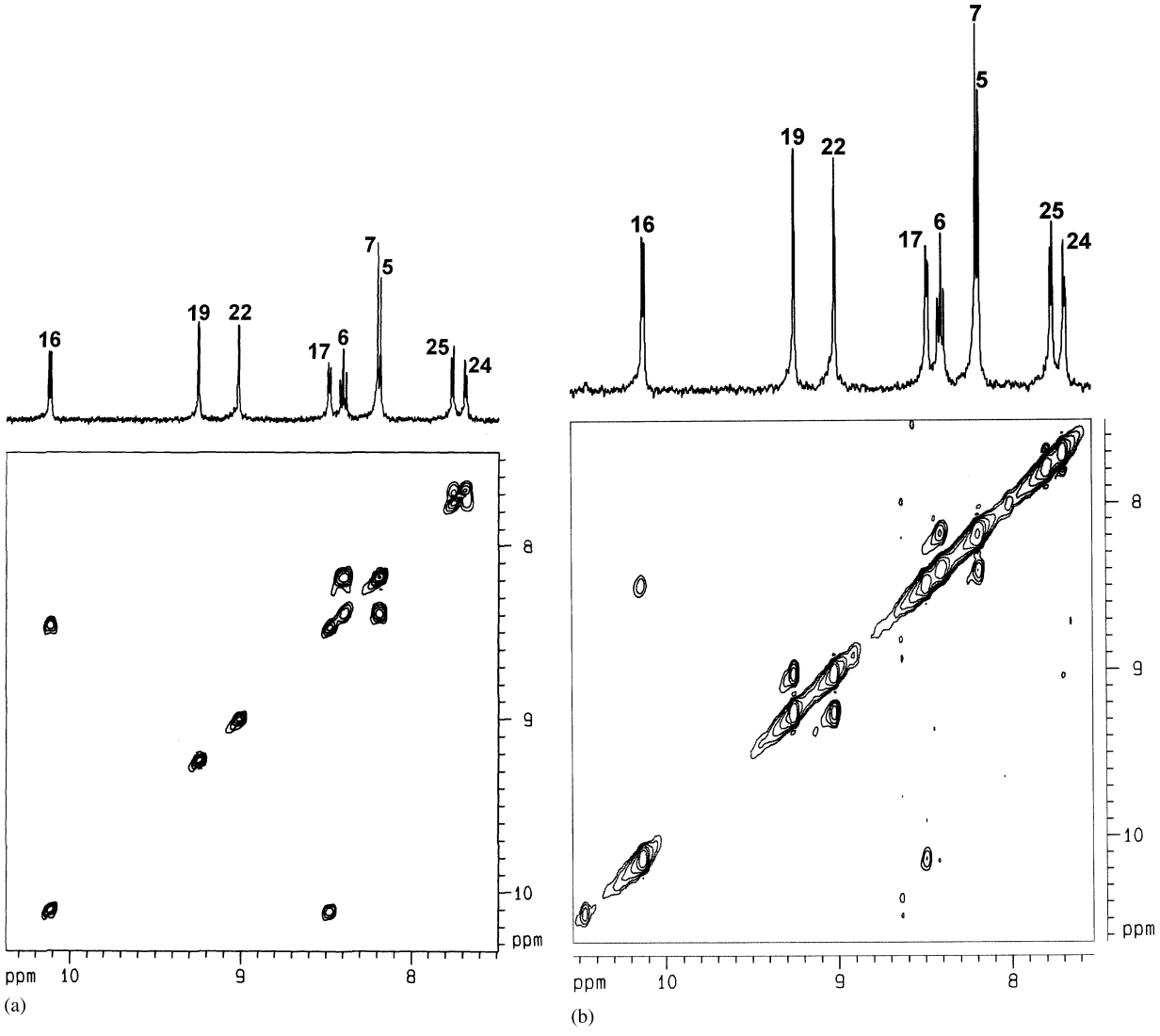


Fig. 10. Two-dimensional ^1H–^1H NMR spectra of complex **1**: COSY (a); NOESY aromatic region (b); NOESY aromatic vs. aliphatic region (c).

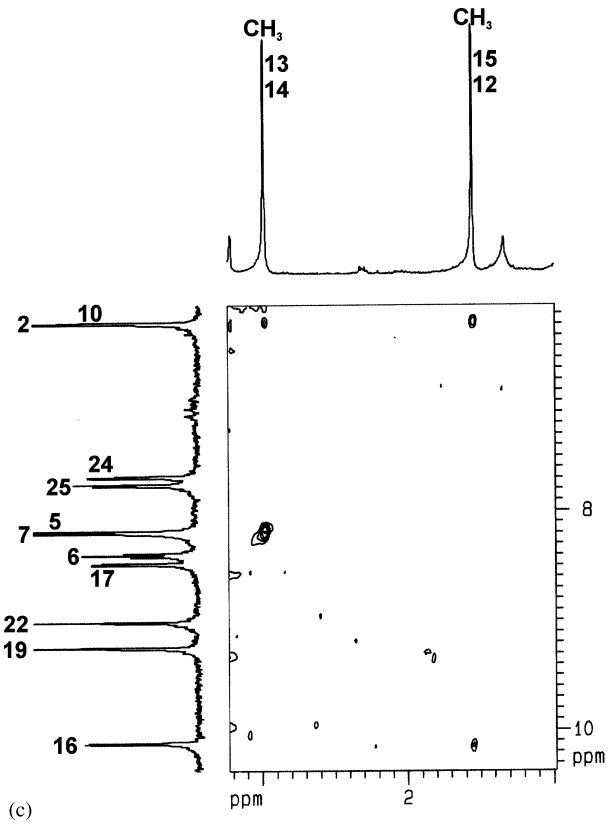


Fig. 10 (*Continued*)

inorganic oxide (TiO_2 Degussa P25) as the filler, in the presence of the I^-/I_3^- redox couple [13,14]. The electrolyte was sandwiched between the photoelectrode and a TEC 8 transparent conductive glass on which very small platinum layer was deposited. An adhesive tape was placed between the photoelectrode and the CE to avoid short-circuiting. This solid-state dye-sensitized solar cell gave high incident monochromatic photon-to-current conversion efficiency (IPCE) values. Under short circuit conditions, in the wavelength region between 400 and 500 nm, the IPCE values (number of electrons generated, divided by the number of incident photons) exceed 30%, Fig. 7. At higher wavelengths, significantly lower IPCE values were obtained and this is attributed to a low light harvesting ability, as the absorption spectrum indicates.

Under direct sunlight illumination (solar irradiance was 600 W m^{-2}), the cell produced a continuous photocurrent as high as 4.3 mA cm^{-2}, and a photovoltage of 600 mV. The corresponding overall energy conversion efficiency (electric power produced to incident solar irradiance ratio) was as high as 1.7%. This sounds particularly optimistic, especially when one takes into account the solid-state nature of the cell. It is well known that dye-sensitized solar cells using a liquid electrolyte present expressively higher conversion efficiencies (at least three times) that the corresponding solid-state modules using room temperature molten salts, inorganic p-type semiconductors, ionic conducting polymers or organic hole transport materials [2,15,16].

The idea that bdmpp is potentially useful in complexes capable of solar energy conversion has been recently reported [6]. However, the incorporation of the monodentate thiocyanato (NCS^-) ligand (replacing the Cl^- moiety) into the complex aims at generating a new dye with superior properties to those of the Cl-complex. Moreover, the coexistence of bdmpp, bpy and NCS^- ligands is believed to affect the ability of the complex to function as a charge transfer sensitizer for solar energy conversion. In fact, the corresponding solid-state solar cell using the $[Ru(bdmpp)(dcbpy)Cl]^+$ complex shows clearly lower performance (IPCE values of about 23% and overall energy conversion efficiency of 0.5%). Such a difference can be attributed to NCS^- ligand, which is able to better stabilize the oxidized complex form following electron injection [7].

4. Conclusions

We have succeeded in developing a new sensitizer based on a ruthenium(II) complex having two chromophore groups, 2,6-bis(3,5-dimethyl-*N*-pyrazoyl)pyridine, and 2,2′-bipyridine-4,4′-dicarboxylic acid as well

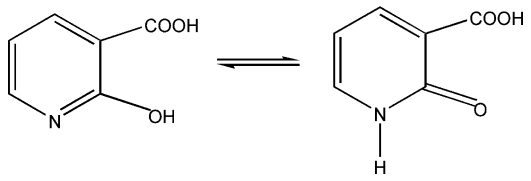
as one thiocyanate group as ligands. The synthesis of the $[Ru(dcbpyH_2)(bdmpp)NCS](PF_6)$ complex (*trans*-isothiocyanate species with respect to one ring of the bidentate ligand $dcbpyH_2$) was performed by reaction of the $[Ru(dcbpyH_2)(bdmpp)Cl](PF_6)$ precursor with the monodentate ligand NCS^- in ethanol–water (1:1) mixture. The complex was characterized and identified by IR, ES MS and NMR and its molecular configuration is proposed on the basis of the spectroscopic data. The electronic spectrum is consistent with very interesting light harvesting properties. The effectiveness of the complex in sensitizing the titanium dioxide was evaluated in a solid-state dye-sensitized solar cell, thus confirming its molecular antenna character.

Acknowledgements

Thanks must be addressed to Professor V.J. Catalano for providing the bdmpp ligand, to Degussa AG Frankfurt-Germany/Dellis AE-Greece for generously providing the TiO_2 Degussa P25 and to I.M. Arabatzis and G. Katsaros for their precious help and assistance. Financial support from NCSR 'Demokritos' (Dimoerevna 598 project) and General Secretariat for Research and Technology of Greece (EPET II, 98AΔ86 project) is also greatly acknowledged.

References

[1] S.M. Zakeeruddin, M.K. Nazeeruddin, P. Pechy, F.P. Rotzinger, R. Humphry-Baker, K. Kalyanasundaran, M. Grätzel, V. Shklover, T. Haibach, Inorg. Chem. 36 (1997) 5937.
[2] B. O' Regan, M. Grätzel, Nature 353 (1991) 737.
[3] K. Kalyanasundaram, M. Grätzel, Coord. Chem. Rev. 77 (1998) 347.
[4] S.M. Zakeeruddin, M.K. Nazeeruddin, R. Humphry-Baker, M. Grätzel, V. Shklover, Inorg. Chem. 37 (1998) 5251.
[5] V.J. Catalano, R. Kurtaran, R.A. Heck, A. Öhman, M.G. Hill, Inorg. Chim. Acta 286 (1999) 181.
[6] K. Chryssou, V.J. Catalano, R. Kurtaran, P. Falaras, Inorg. Chim. Acta 328 (2002) 204.
[7] M.K. Nazeeruddin, M. Grätzel, J. Photochem. Photobiol. A: Chem. 145 (2001) 79.
[8] B.-W. Jing, W.-Q. Wang, M.-H. Zhang, T. Shen, Dyes Pigments 37 (1998) 177.
[9] J.A. Kargol, R.W. Crecely, J.L. Burmeister, Inorg. Chem. 18 (1979) 2532.
[10] M.K. Nazeeruddin, P. Péchy, M.Grätzel, Chem. Commun. (1997) 1705.
[11] A. Provata, P. Falaras, A. Xagas, Chem. Phys. Lett. 297 (1998) 484.
[12] P. Falaras, Solar Energy Mater. Solar Cells 53 (1998) 163.
[13] G. Katsaros, T. Stergiopoulos, I.M. Arabatzis, K.G. Papadokostaki, P. Falaras, J. Photochem. Photobiol. A: Chem. 149 (2002) 237.
[14] P. Falaras, K. Chryssou, T. Stergiopoulos, I.M. Arabatzis, G. Katsaros, V.J. Catalano, R. Kurtaran, A. Hugot-Le Goff, M.-C. Bernard, SPIE Proc. 4801 (2002) 23.
[15] A.F. Nogueira, J.R. Durrant, M.-A. De Paoli, Adv. Mater. 11 (2001) 826.
[16] U. Bach, D. Lupo, P. Comte, J.E. Moser, F. Weissörtel, J. Salbeck, H. Spreitzer, M. Grätzel, Nature 395 (1998) 583.



Scheme 1.

through the nitrogen atom only. Spectroscopic results are in agreement with the crystallographic data, showing preferential coordination of the $HnicO^-$ ligand through the nitrogen atom of the pyridine ring, and in the case of rhenium, molybdenum and tungsten, a possible *N*,*O*-chelation with the adjacent oxygen atom.

2. Results and discussion

2.1. Preparations

Suspensions of *trans*-$[Pd(PPh_3)_2Cl_2]$ or *cis*-$[Pt(PPh_3)_2Cl_2]$ and H_2nicO in an ethanol–methanol mixture were stirred for several days in the presence of triethylamine to give the complexes *trans*-$[PdCl(HnicO)(PPh_3)_2]\cdot 0.75CH_3OH$ (**1**) and *cis*-$[PtCl(HnicO)(PPh_3)_2]\cdot 0.75CH_3OH\cdot 0.5H_2O$ (**4**). When $K_2[PdCl_4]$ was used as starting material, the compound obtained was $K[PdCl(HnicO)_2]\cdot H_2O$ (**2**). The reaction of the 2,2′-bipyridine (bipy) complexes $[M(bipy)Cl_2]$ (M = Pd, Pt) with H_2nicO gave the complexes $[Pd(HnicO)_2(bipy)]$ (**3**) and $[PtCl(HnicO)(bipy)]$ (**5**). The complex *cis*-$[ReOI_2(HnicO)(PPh_3)]$ (**6**) was synthesised by refluxing *trans*-$[ReOI_2(OEt)(PPh_3)_2]$ with H_2nicO in acetone. The reaction of $Na_2[MO_4]\cdot 2H_2O$ (M = Mo or W) and H_2nicO in water, under reflux, produced the complexes $Na_2[M_2O_6(HnicO)_2]\cdot 5H_2O$ (M = Mo **7** or W **9**) and $Na_2[Mo_4O_{12}(HnicO)_2]\cdot 2H_2O$ (**8**). Suitable crystals of complexes **1** and **4** for X-ray diffraction studies were obtained by vapour diffusion of diethyl ether into acetonitrile solutions of the complexes.

2.2. Crystal structures

The crystals structures of *trans*-$[PdCl(HnicO)(PPh_3)_2]\cdot 0.75CH_3OH$ (**1**) and *cis*-$[PtCl(HnicO)(PPh_3)_2]\cdot 0.75CH_3OH\cdot 0.5H_2O$ (**4**) were determined by single crystal X-ray diffraction. ORTEP diagrams of the complexes **1** and **4** with the labeling scheme adopted are shown in Figs. 1 and 2, respectively. Selected bond lengths and angles are listed in Table 2 and indicate that both metal centers display distorted square coordination spheres composed of two phosphorus from two PPh_3 ligands, one chlorine and one nitrogen from the $HnicO^-$ ligand. However, the ligands adopt different spacial dispositions in these two complexes. In **4** the two PPh_3 ligands provide a *trans* geometric arrangement with a P(1)–Pt–P(2) angle of 172.2(1)° and in **1** they are mutually *cis* with a P(1)–Pd–P(2) angle of 97.2(1)°. In addition, in **4** the $HnicO^-$ ligand is almost perpendicular to the equatorial coordination plane intersecting at 88.3(1)° while in **1** that ligand is sandwiched between two phenyl rings of the PPh_3 ligands and intersecting the equatorial P_2NCl coordination plane at 77.2(1)°.

In both complexes the coordination of the $HnicO^-$ ligand, through the nitrogen donor, forces the phenol group to be directed towards the metal centre, leading to similar Pd···O and Pt···O distances of 3.009 and 3.047 Å, respectively. This structural feature was also found in the related complexes [1] $[PdCl(picOH)(PPh_3)_2]$ (HpicOH = 3-hydroxypicolinic acid) and $[PtCl(picOH)(PPh_3)_2]$ in which the ligands display a NP_2Cl coordination sphere with identical disposition of the ligands to the corresponding complexes reported here. However, in those $picOH^-$ complexes, the oxygen that is directed towards the metal centre belongs to a carboxylate group rather than a phenol group giving Pd···O and Pt···O distances of 2.773(5) and 2.734(4) Å, respectively, which are substantially shorter than those found for **1** and **4**. On the other hand the dimensions of bonds and angles subtended at the metal centres in **1** and **4** are similar to those found for the respective $picOH^-$ complexes. In the latter two complexes, the $picOH^-$ ligand is also nearly perpendicular to the N_4Cl_2 coordination plane, intersecting at angles of 88.8° and 84.2° for the Pd and Pt complexes, respectively. Therefore, this comparison suggests that the specific orientation of the aromatic ligand is determined in each structure by the minimisation of the steric interactions between the bulky PPh_3 ligands and the $HnicO^-$ anion. As would be expected in the *cis* complex **4** a slight *trans* differential effect is apparent from the M–P bond lengths. Thus, the length of the Pt–P(1) bond [2.266(3) Å] *trans* to the Pt–Cl bond [2.353(4) Å] is slightly shorter than that of the Pt–P(2) bond [2.293(4) Å], which is *trans* to the Pt–N bond [2.104(10) Å].

2.3. Vibrational spectra

Infrared and Raman data for H_2nicO and its complexes are shown in Table 3. Tentative assignments are based on those found in the literature for complexes of 3-hydroxypicolinc acid, [1,2] salicylic acid [13] and 2-hydroxypyridines [14,15]. Only the bands more sensitive to metal coordination are reported.

In both infrared and Raman spectra of the free ligand, the bands corresponding to the hydroxyl group vibrations seem to be absent, namely, the ν(O–H) stretch (missing at ca. 3400 cm^{-1}) [16] and the in-plane $\beta(C_2$–OH) bend (missing at ca. 1280 cm^{-1}); [14] also, the strong band around 1023 cm^{-1}, indicative of the pyridine structrure, [14] is not seen in the vibrational

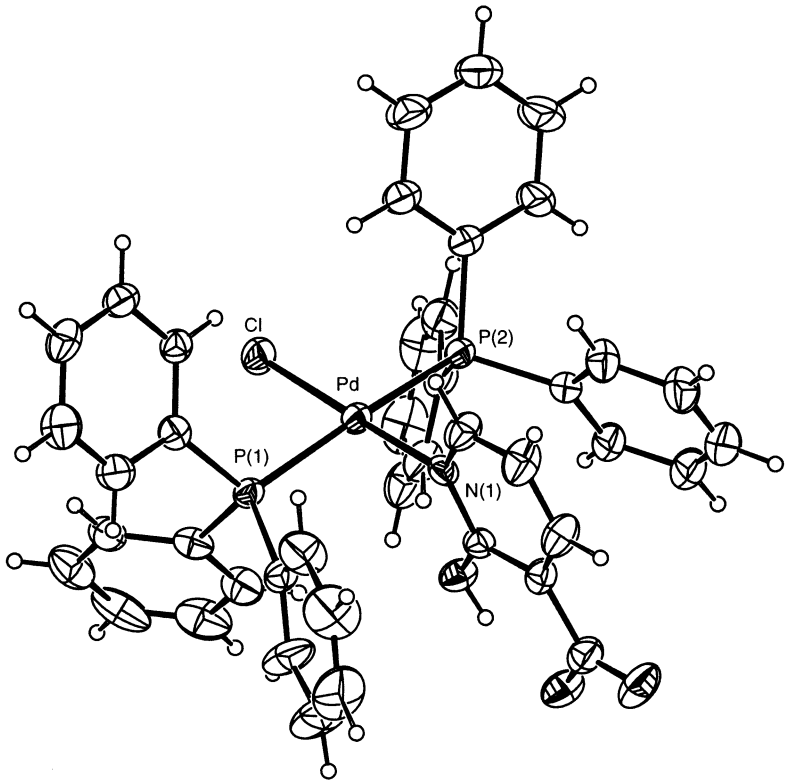


Fig. 1. ORTEP diagrams of *trans*-[PdCl(HnicO)(PPh_3)$_2$] **1**, with thermal ellipsoids drawn at 30% probability showing the overall structure.

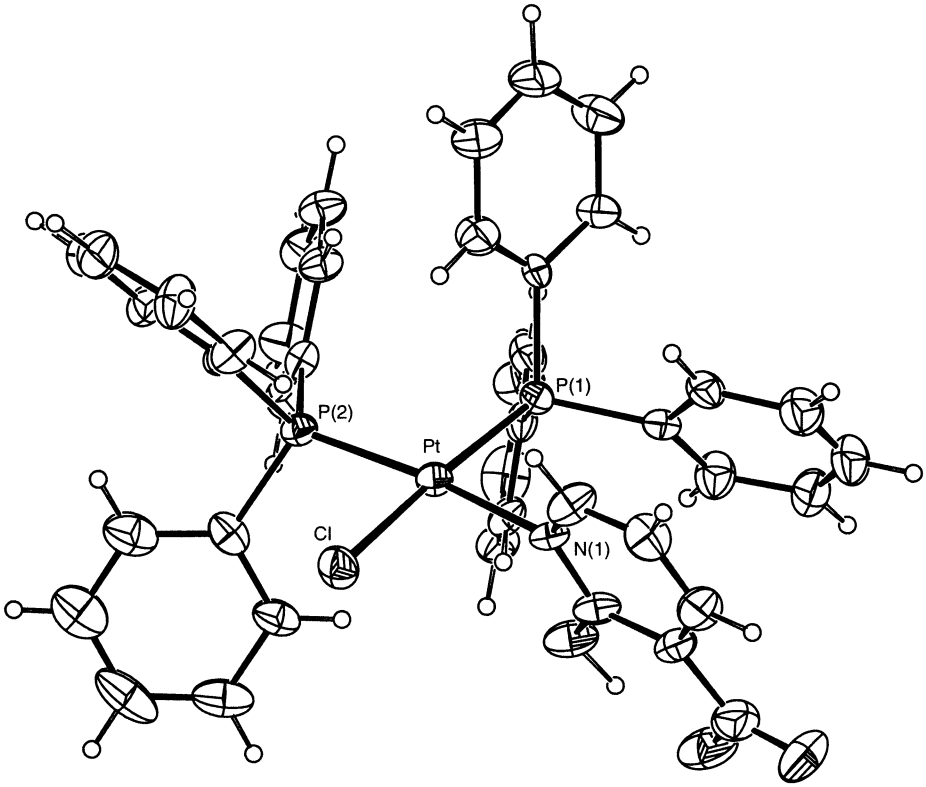


Fig. 2. ORTEP diagrams of *cis*-[PtCl(HnicO)(PPh_3)$_2$] **4**, with thermal ellipsoids drawn at 30% probability showing the overall structure.

Table 1
Crystal data and pertinent refinement details for complexes **1** and **4**

Compound	**1**	**4**
Empirical formula	$C_{43.50}H_{36.25}ClN_{1.75}O_3P_2Pd$	$C_{42.75}H_{37.25}ClO_{4.25}P_2Pt$
Formula weight	835.28	911.49
Crystal system	monoclinic	monoclinic
Space group	$P2_1/n$	$P2_1/n$
Unit cell dimensions		
a (Å)	16.143(22)	12.514(17)
b (Å)	14.873(21)	12.591(17)
c (Å)	16.974(25)	26.156(33)
β (°)	92.57(1)	99.54(1)
Volume (Å^3)	4071.3	4064.2
Z	4	4
D_{calc} (Mg m^{-3})	1.363	1.512
$F(000)$	1706	1839
Absorption coefficient (mm^{-1})	0.640	3.639
Independent reflections collected	7117	7130
Data/restraints/parameters	7117/1/470	7130/1/470
Final R indices [$I > 2\sigma(I)$]	$R_1 = 0.0675$, $wR_2 = 0.1394$	$R_1 = 0.0781$, $wR_2 = 0.1607$
R indices (all data)	$R_1 = 0.1055$, $wR_2 = 0.1576$	$R_1 = 0.1081$, $wR_2 = 0.1722$

Table 2
Selected bond lengths (Å) and angles (°) for complexes **1** and **4**

Complex	**1**; [M = Pd(II)]	**4**; [M = Pt(II)]
Bond lengths		
M–N(1)	2.055(5)	2.104(10)
M–P(1)	2.336 (3)	2.266(3)
M–P(2)	2.337(3)	2.293(4)
M–Cl(1)	2.311(3)	2.353(4)
Bond angles		
N(1)–M–P(1)	92.0(2)	88.8(3)
N(1)–M–P(2)	91.6(1)	173.9(3)
P(1)–M–P(2)	172.2(1)	97.2(1)
N(1)–M–Cl(1)	178.0(1)	86.6(3)
P(1)–M–Cl(1)	88.1(1)	175.39(1)
P(2)–M–Cl(1)	88.5(1)	87.5(1)

spectra. These features suggest that the ligand is possibly in the ketone rather than the hydroxy form. Furthermore, the presence of the stretching vibrations ν(C2=O) at 1740 cm^{-1} and ν(N–H) at 3229 cm^{-1}, the in-plane β(NH) bend at 1608 cm^{-1} and the out-of-plane π(NH) bend at 538 cm^{-1}, in the IR and Raman spectra of free ligand, suggest that the ketone form predominates in the solid state [14].

The C=O stretch of the carboxylic group, $\nu(C{=}O)_c$, in the IR and Raman spectra of the free ligand, is seen at 1630 and 1628 cm^{-1}, respectively. These bands shift to higher wavenumbers (in the range 1640–1702 cm^{-1}) in the spectra of complexes **1**, **2**, **4**, **5** and **7**–**9**. These shifts are possibly due to the destruction of the hydrogen bond between the COOH and C=O groups on coordination, with the carboxyl group not bound to the metals [17]. The C–O stretch of the carboxyl group, $\nu(C{-}O)_c$, shows small shifts in the complexes spectra.

The ν(C2=O) band shifts to lower wavenumbers on coordination; the smallest shifts are possibly observed in the spectra of the complexes where the HnicO$^-$ ligand coordinates only through the nitrogen atom, as can be suggested for complexes **1**–**5** (and according to the crystal structures of **1** and **4**). For complexes **6**–**9**, the shifts in the ν(C2=O) bands are the highest, up to 80 cm^{-1}, and the coordination to metals through the oxygen atom also (in a orto position to the ring nitrogen) can be suggested.

In the spectra of the Mo(VI) and W(VI) complexes the MoO_2 stretches, $\nu_s(MoO_2)$ and $\nu_{as}(MoO_2)$, provide two strong bands at approximately 930 and 880 cm^{-1}, respectively. In the IR spectrum of the rhenium complex a very strong band characteristic of the Re=O stretch is observed at 989 cm^{-1}. In addition PPh_3 and bipy bands were observed in all the applicable spectra.

The proposed formula for complexes **2**, **3** and **5**–**9** are based on elemental analysis and spectroscopic data, considering analogous complexes that have been reported [1,2,4,17] for similar bidentate ligands. In complex **2**, two HnicO$^-$ ligands are coordinated to palladium together with a chlorine ligand, as shown in the infrared and Raman spectra by the presence of a band assigned to the ν(Pd–Cl) stretch; a similar compound was reported with 3-hydroxypicolinc acid (picOH$^-$ ligand) [1]. For the palladium and platinum complexes containing 2,2′-bipyridine, two HnicO$^-$ ligands are coordinated to palladium in **3** while only one is coordinated to platinum in **5**; the latter complex keeps one chlorine ligand from the starting [Pt(bipy)Cl_2] compound, as shown in the infrared and Raman spectra by the presence of a band assigned to the Pt–Cl stretching vibration. Complex **6** is analogous to a reported rhenium complex with the picOH$^-$ ligand [1]. Compounds **7**–**9** are analogous to the polynuclear molybdenum and tungsten complexes of HpicOH previously reported, [2] having possibly similar structures, though with a four membered *N*,*O*-chelate ring in the HnicO$^-$ ligand (instead of the six-membered *N*,*O*-chelate ring that is formed with the picOH$^-$ ligand).

2.4. ^1H and $^{13}C\{^1H\}$ NMR spectra

^{1}H and ^{13}C NMR data and tentative assignments for H_2nicO (see Plate 1 for labelling) and complexes **1**, **2**, **4**–

Table 3
Analytical [a] and vibrational data [b] for 2-hydroxynicotinic acid and its complexes

Compound	Analysis (%)			ν(C2=O)	ν(C=O)$_c$	ν(CC),ν(CN)	ν(C–O)$_c$	ν_s(MO$_2$)	ν_{as}(MO$_2$)	ν(M–N)	ν(M–Cl)
	C	H	N								
2-hydroxynicotinic acid				1740 vs	1630 vs	1548 s	1414 s				
				1740 (4)	*1628(1)*	*1554 (10)*	*1422(1)*				
trans-[PdCl(HnicO)(PPh$_3$)$_2$]·0.75CH$_3$OH (**1**)	61.1	4.7	2.3	1719 vs	1702 vs	1540 s	1407 sh			389 m	342 m
	62.5	*4.4*	*2.9*	*1711 (1)*	*1701 (1)*	*1552 (2)*				*391 (1)*	*344 (1)*
K[PdCl(HnicO)$_2$]·H$_2$O (**2**)	29.4	1.9	5.7	1733 sh	1683 sh	1561 vs	1383 s			417 w	356 m
	30.3	*2.1*	*5.9*	*1740 (1)*	*1677 (1)*	*1553 (2)*				*397 (1)*	*353 (1)*
[Pd(HnicO)$_2$(bipy)] (**3**)	48.2	3.4	10.2	Sh	1618 vs	1575 s	1374 sh				
	49.0	*3.0*	*10.4*	*1709 (3)*	*vw*	*1568 (4)*	*1370(1)*			*375 (3)*	
cis-[PtCl(HnicO)(PPh$_3$)$_2$]·0.75CH$_3$OH·0.5H$_2$O (**4**)	54.8	3.9	2.6	1706 s	1698 sh	1546 F	1387 sh			390 m	313 sh
	55.4	*4.1*	*1.5*	*1709 (1)*	*vw*	*1544 (1)*				*394 (2)*	*316 (5)*
[PtCl(HnicO)(bipy)] (**5**)	34.0	2.4	8.1	1710 vs	1695 sh	1550 s	1421 sh			350 m	336 m
	36.6	*2.3*	*8.0*	*1706 (1)*	*vw*	*1563 (2)*	*1426(1)*				*336 (1)*
cis-[ReOI$_2$(HnicO)(PPh$_3$)] (**6**)	33.4	3.1	1.7	1644 vs	1627 s	1551 s	1420 s			454 m	
	33.7	*2.2*	*1.6*								
Na$_2$[Mo$_2$O$_6$(HnicO)$_2$]·5H$_2$O (**7**)	21.2	2.3	4.0	1659 vs	1640 vs	1567 vs	1383 s	931 vs	879 vs	455 m	
	20.6	*2.6*	*4.0*	*Vw*	*vw*	*1556 (1)*	*1378 (1)*	*927 (10)*	*890 (2)*	*453 (1)*	
Na$_2$[Mo$_4$O$_{12}$(HnicO)$_2$]·2H$_2$O (**8**)	15.7	1.9	2.9	1659 vs	1641 vs	1567 s	1383 s	929 s	875 m	452 w	
	15.4	*1.3*	*3.0*	*Vw*	*vw*	*1556 (1)*	*1378 (1)*	*927(10)*	*881 (2)*	*450 (1)*	
Na$_2$[W$_2$O$_6$(HnicO)$_2$]·5H$_2$O (**9**)	15.8	1.8	3.1	1655 vs	1643 vs	1573 vs	1382 s	929 vs	879 vs	444 w	
	16.5	*2.1*	*3.2*	*1654 (1)*	*1643 (1)*	*1575 (1)*	*1382 (2)*	*929 (10)*	*874 (2)*	445 (1)	

[a] Calculated values in italics.
[b] Infrared and Raman (in italics) data; vs, very strong; s, strong; m, medium; w, weak; vw, very weak; sh, shoulder.

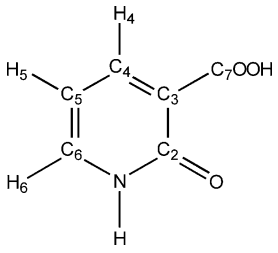


Plate 1.

7 in solution are given in Tables 4 and 5. Complexes **2**, **3**, **5**, **8** and **9** were not sufficiently soluble in the common NMR solvents for ^{13}C NMR measurements; for **8** and **9** ^{1}H NMR measurements were also not possible. CP-MAS ^{13}C NMR spectra of the free ligand and of some of the solid complexes were recorded (Table 5). Tentative assignments of the NMR spectra are based on those found in the literature for complexes of mercaptonicotinic acid, [4,18,19] 3-hydroxypyridin-2-one, [20] 1,2-dimetil-3-hydroxypyridin-2-one [20] and salicylic acid [13].

The ^{1}H NMR spectrum of the ligand in dmso-d_6 shows a triplet at 6.69 ppm assigned to the H_5 proton, a doublet–doublet at 7.96 ppm assigned to the H_4 proton and another doublet–doublet at 8.39 ppm assigned to the H_6 proton. The NH proton gives rise to a broad signal at about 13.4 ppm and another broad signal at 14.79 ppm is assigned to the COOH proton. In all complexes, only one signal is present in the range 17.5–13.4 ppm assigned to the latter proton. In general, the resonance of the ring protons of the coordinated ligand shifts upfield in all complexes. The chemical shift of C2 in the free ligand (164.66 ppm in dmso-d_6 solution and 166.10 ppm in solid state) is consistent with the ketonic form of H_2nicO [1,20]. The major downfield chemical shifts are observed in the ^{13}C NMR spectra of the complexes where the $HnicO^-$ ligand coordinates via monodentate-*N*, for the C2 and C6 carbon atoms. In the complexes where the ligand coordinates via bidentate-*N*,*O*, there is an upfield shift in the chemical shift of C2 due to the reduction of the bonding order from double to single [21]. Small shifts are observed for the other carbons. In the spectra of complexes **1** and **4**, two signals are observed for each carbon. In the CP-MAS ^{13}C NMR spectra of **2**, **8** and **10**, the major downfield chemical shifts (4–6 ppm) are observed for C2 and C6 as was also observed in the solution spectra of the other complexes.

2.5. FAB mass spectra

Positive-ion FAB mass spectra were recorded for complexes **1**, **4** and **6** in the appropriate solvents and in a *p*-nitrobenzyl alcohol matrix. In all cases, a molecular ion [MH^+] peak confirms the molecular structure of the complexes. In the positive-ion FAB mass spectra of **1** the [MH^+] peak was observed at *m*/*z* 806. Other peaks resulting from the fragmentation of **1** are observed at *m*/*z* 768, 665 and 506, assigned to $[Pd(HnicO)(PPh_3)_2]^+$, $[PdCl(PPh_3)_2]^+$ and $[Pd(HnicO)(PPh_3)]^+$, respectively. Similar peaks are found in the ion-positive FAB mass spectra of **4**, the molecular ion being observed at *m*/*z* 894, with peaks at *m*/*z* 858 and 754 assigned to $[Pt(HnicO)(PPh_3)_2]^+$ and $[PtCl(PPh_3)_2]^+$, respectively. In the mass spectra of **6** the molecular ion appears at *m*/*z* 858 and peaks at *m*/*z* 730 and 719 are assigned to $[ReOI(HnicO)(PPh_3)]^+$ following loss of I^- and $[ReOI_2(PPh_3)]^+$ following subsequent loss of $HnicO^-$.

3. Experimental

3.1. Preparation of complexes

All chemicals were of at least reagent grade and used as supplied by Aldrich. The starting complexes, *trans*-

Table 4
^{1}H NMR spectroscopic data for 2-hydroxyonicotinic acid and its complexes in solution

Compound	Chemical shift (ppm) [a]				
	H4	H5	H6	H(NH)	H(COOH)
2-hydroxynicotinic acid [b]	7.96 dd (2.1)	6.69 t (6.6)	8.39 dd (2.1)	13.4 b	14.8 b
2-hydroxynicotinic acid [c]	8.01 dd (2.0)	6.75 t (6.7)	8.48 dd (2.1)	12.1 b	14.4 b
trans-$[PdCl(HnicO)(PPh_3)_2]\cdot 0.75CH_3OH$ (**1**) [d]	7.23 dd (1.9)	5.76 m	7.49 dd (1.9)		16.40 s
$K[PdCl(HnicO)_2]\cdot H_2O$ (**2**) [b]	7.82 dd (2.1)	6.42 m	8.57 dd (2.1)		17.50 s 17.06 s
cis-$[PtCl(HnicO)(PPh_3)_2]\cdot 0.75CH_3OH\cdot 0.5H_2O$ (**4**) [d]	7.82 dd (1.9)	6.25 m	7.87 m		16.69 s
[PtCl(HnicO)(bipy)] (**5**) [d]	8.41 dd (2.0)	6.52 t (6.7)	9.56 d (5.3)		16.30 s
cis-$[ReOI_2(HnicO)(PPh_3)]$ (**6**) [b]	7.98 dd (2.2)	6.70 t (6.7)	8.40 dd (2.2)		13.4 b
$Na_2[Mo_2O_6(HnicO)_2]\cdot 5H_2O$ (**7**) [b]	8.00 dd (2.0)	6.68 t (6.4)	8.19 dd (2.0)		

[a] *J* values in parentheses (Hz).
[b] In dmso-d_6.
[c] In acetone-d_6.
[d] In $CDCl_3$; dd, doblet–doblet; t, triplet; m, multiplet; s, singulet; b, broad.

Table 5
^{13}C NMR spectroscopic data for 2-hydroxynicotinic acid and its complexes [a]

Compound	Chemical shift (ppm)					
	C2	C3	C4	C5	C6	C7
2-hydroxynicotinic acid [b]	164.66	116.68	141.58	108.75	146.29	165.08
	166.10	*116.12*	*144.05*	*110.78*	*146.71*	*166.10*
trans-[PdCl(HnicO)(PPh_3)$_2$]·0.75CH_3OH **1** [c]	169.24	114.31	141.04	110.59	151.24	168.02
	168.55		140.11	110.43	150.77	167.69
	169.63	*114.93*	*142.84*	*112.34*	*153.34*	*168.03*
		113.80	*140.32*	*110.74*	*151.04*	*166.62*
K[PdCl(HnicO)$_2$]·H_2O (**2**)	*167.0*	*113.0*	*140.0*	*109.8*	*155.0*	*170.3*
cis-[PtCl(HnicO)(PPh_3)$_2$]·0.75CH_3OH·0.5H_2O (**4**) [c]	168.55	115.42	140.98	110.23	150.66	168.48
		115.37		110.18		
cis-[$ReOI_2$(HnicO)(PPh_3)] (**6**) [b]	*160.86*	*C*	*142.23*	*112.22*	*149.03*	*163.13*
Na_2[Mo_2O_6(HnicO)$_2$]·5H_2O (**7**) [b]	166.34	115.65	142.69	110.97	145.74	167.58
	163.61	*118.88*	*144.44*	*112.80*	*148.43*	*172.02*
Na_2[W_2O_6(HnicO)$_2$]·5H_2O (**9**)	162.07	117.72	142.94	113.72	147.21	171.89

Overlapped with C5 signal.
[a] CP-MAS data in italics.
[b] In dmso-d_6.
[c] In $CDCl_3$.

[$PdCl_2$(PPh_3)$_2$], [16] *cis*-[$PtCl_2$(PPh_3)$_2$], [22] [MCl_2(bipy)] [20] (M = Pd, Pt) and *trans*-[$ReOI_2$(EtO)(PPh_3)$_2$] [23] were prepared by the relevant literature procedures.

3.1.1. *trans*-[PdCl(HnicO)(PPh_3)$_2$]·0.75CH_3CN (**1**)

To a stirred suspension of *trans*-[$PdCl_2$(PPh_3)$_2$] (0.35 g, 0.5 mmol) in ethanol (10 cm^3) was added a methanolic suspension (4 cm^3) of 2-hydroxynicotinic acid (0.14 g, 1 mmol) and triethylamine (0.28 cm^3, 2 mmol) giving a beige suspension. This suspension was stirred during 1 week and then centrifuged and a yellow solid isolated. It was washed with ethanol and dried over silica gel. Yield: 0.38 g, 0.47 mmol, 94%. Yellow X-ray quality crystals of **1** were obtained by vapour diffusion of diethyl ether into a solution of the compound in CH_3CN.

3.1.2. K[PdCl(HnicO)$_2$]·H_2O (**2**)

A suspension of 2-hydroxynicotinic (0.14 g, 1 mmol) in methanol (4 cm^3) was added to an aqueous solution (5 cm^3) of K_2[$PdCl_4$] (0.14 g, 0.5 mmol). The resulting suspension was stirred for 1 day. It was centrifuged and a pale yellow solid was isolated, washed with ethanol and dried over silica gel. Yield: 0.13 g, 0.27 mmol, 54%.

3.1.3. [Pd(HnicO)$_2$(bipy)] (**3**)

To a stirred suspension of [Pd(bipy)Cl_2] (0.05 g, 0.15 mmol) in ethanol (5 cm^3) was added a methanolic suspension (5 cm^3) of 2-hydroxynicotinic acid (0.04 g, 0.3 mmol) and triethylamine (0.08 cm^3, 0.6 mmol). The resulting orange suspension was stirred for 1 day. It was centrifuged and an off white solid was isolated, washed with ethanol and dried over silica gel. Yield: 0.08 g, 0.148 mmol, 99%.

3.1.4. *cis*-[PtCl(HnicO)(PPh_3)$_2$]·0.75CH_3OH·0.5H_2O (**4**)

To a stirred suspension of *cis*-[$PtCl_2$(PPh_3)$_2$] (0.40 g, 0.5 mmol) in ethanol (10 cm^3) was added a methanolic suspension (4 cm^3) of 2-hydroxynicotinic acid (0.14 g, 0.5 mmol) and triethylamine (0.28 cm^3, 2 mmol). The resulting off white suspension was stirred during 2 weeks. It was centrifuged and an off white solid was isolated, washed with ethanol and dried over silica gel. Yield: 0.29 g, 0.32 mmol, 64%. Off-white X-ray quality crystals of **4** were obtained by vapour diffusion of diethyl ether into a solution of the compound in CH_3CN.

3.1.5. [PtCl(HnicO)(bipy)] (**5**)

To a stirred suspension of [Pt(bipy)Cl_2] (0.06 g, 0.15 mmol) in ethanol (5 cm^3) was added a methanolic suspension (5 cm^3) of 2-hydroxynicotinic acid (0.04 g, 0.3 mmol) and triethylamine (0.08 cm^3, 0.6 mmol). The resulting suspension was stirred for 2 weeks. It was centrifuged and a yellow solid was isolated, washed with ethanol and dried over silica gel. Yield: 0.07 g, 0.13 mmol, 87%.

3.1.6. *cis*-[$ReOI_2$(HnicO)(PPh_3)] (**6**)

To a suspension in acetone (20 cm^3) of *trans*-[$ReOI_2$(EtO)(PPh_3)$_2$] (0.31 g, 0.3 mmol) was added 2-hydroxynicotinic acid (0.08 g, 0.6 mmol). The suspension was refluxed by 5 h. Some of the solvent was evaporated until a solid formed. To the dark solution obtained was added ether and a dark suspension was obtained. It was centrifuged and a dark green solid was isolated, washed with ether and dried over silica gel. Yield: 0.05 g, 0.064 mmol, 21%.

3.1.7. $Na_2[Mo_2O_6(HnicO)_2]\cdot 5H_2O$ (7)

2-Hydroxynicotinic acid (1.39 g, 10 mmol) was added to an aqueous solution (20 cm^3) of $Na_2MoO_4\cdot 2H_2O$ (1.21 g, 5 mmol). The resulting suspension was refluxed for 6 h and then filtered off. A white solid was isolated, washed with water and dried over silica gel. Yield: 1.59 g, 2.3 mmol, 91%.

3.1.8. $Na_2[Mo_4O_{12}(HnicO)_2]\cdot 2H_2O$ (8)

A suspension of 2-hydroxynicotinic acid (0.28 g, 2 mmol) was added to an aqueous solution (5 cm^3) of $Na_2MoO_4\cdot 2H_2O$ (0.24 g, 1 mmol). The resulting suspension was refluxed for 3 h and then filtered off. The white solid was washed with hot CH_3CN and dried over silica gel. Yield: 0.20 g, 0.21 mmol, 84%.

3.1.9. $Na_2[W_2O_6(HnicO)_2]\cdot 5H_2O$ (9)

2-Hydroxynicotinic acid (1.39 g, 10 mmol) was added to an aqueous solution (20 cm^3) of $Na_2WO_4\cdot 2H_2O$ (1.65 g, 5 mmol). The resulting suspension was refluxed for 7 h and then filtered off. Some solvent was evaporated and a white solid was formed. It was isolated, washed with water and dried over silica gel. Yield: 0.8 g, 0.91 mmol, 37%.

3.2. Crystallography

The crystal data of the complexes **1** and **2** are given in Table 1, together with refinement details. The X-ray data for all three complexes were collected on a MAR research plate system using graphite Mo Kα radiation at Reading University. The crystals were positioned at 70 mm from the image plate. 95 frames were measured at 2° intervals using an adequate counting time between 2 and 5 min. Data analysis was carried out with the XDS program [24].

The structures were solved by direct methods with the SHELXS program. All non-hydrogen atoms were refined with anisotropic thermal parameters. The hydrogen atoms were introduced in the refinement at the geometric idealised positions and given isotropic thermal parameters equal 1.2 times those of the carbon atom they were attached. An empirical absorption correction was applied to intensities of both complexes using version of the DIFABS program modified for image plate geometry [25]. The two structures were then refined by full-matrix least-squares on F^2 until convergence with the SHELXL [26]. ORTEP plots were drawn with the PLATON graphical interface [27].

3.3. Instrumentation

Infrared spectra were measured as KBr pellets on a Mattson 7000 FT instrument. Raman spectra were measured on a Bruker RFS100/S FT instrument (Nd:YAG laser, 1064 nm excitation). ^1H and ^{13}C NMR spectra were recorded on a Bruker AMX300 spectrometer (^1H, 300 MHz; ^{13}C, 75.4 MHz) referenced to $SiMe_4$ or to the solvent. CPMAS ^{13}C NMR spectra were recorded on a Bruker MSL 400P spectrometer at 100.6 MHz with a 4.5 μs 90° pulse, contact time of 2 ms. Mass spectra were recorded on a VG Autospec spectrometer (Micromass, Manchester). Microanalyses (C, H and N) were measured at the Department of Chemistry, University of Aveiro.

4. Supplementary material

Supplementary data are available from the Director, CCDC, 12 Union Road, Cambridge, CB2 1EZ, UK (fax: +44-1223-336033; e-mail: deposit@ccdc.cam.ac.uk or www: http://www.ccdc.cam.ac.uk) on request, quoting the deposition numbers 188751 and 188752.

Acknowledgements

The authors would like to acknowledge Fundação para a Ciência e a Tecnologia (FCT) for financial support. S.M.O. Quintal thanks the FCT for a postgraduate grant. We also thank EPSRC (UK) and the University of Reading (UK) for funds for the Image Plate System and A.W. Johans for his assistance with the crystallography.

References

[1] S.M.O. Quintal, H.I.S. Nogueira, V. Félix, M.G.B. Drew, New J. Chem. 24 (2000) 511.
[2] S.M.O. Quintal, H.I.S. Nogueira, H. Carapuça, V. Félix, M.G.B. Drew, J. Chem. Soc., Dalton Trans. (2001) 3196.
[3] A.J. Boulton, A. McKillop, Comprehensive Heterocyclic Chemistry: the Structure, Reactions, Synthesis and Uses of Heterocyclic Compounds, vol. 2, Pergamon, Oxford, 1984.
[4] S.M.O. Quintal, H.I.S. Nogueira, V. Félix, M.G.B. Drew, J. Chem. Soc., Dalton Trans., in press.
[5] M.S. Saleh, K.A. Idriss, M.S. Abu-Bakr, E.Y. Hashem, Analyst 117 (1992) 1003.
[6] R. Bertani, G.G. Bombi, A. Tapparo, Rapid Commun. Mass Spectrosc. 13 (1999) 1878.
[7] V.B. Di Marco, A. Tapparo, G.G. Bombi, Annali Chim. 89 (1999) 535.
[8] A.K.W. Stephens, C. Orvig, Inorg. Chim. Acta 273 (1998) 47.
[9] K.A. Idriss, M.S. Saleh, E.Y. Hashem, Bull. Pol. Ac. Sci. 43 (1995) 67.
[10] M.S. Saleh, J. Indian Chem. Soc. 70 (1993) 202.
[11] K.A. Idriss, M.S. Saleh, H. Sedaira, Monat. Chem. 122 (1991) 507.
[12] E. Kiss, K. Petrohan, D. Sanna, E. Garriba, G. Micera, T. Kiss, Polyhedron 19 (2000) 55.
[13] C.F. Edwards, W.P. Griffith, A.J.P. White, D.J. Williams, J. Chem. Soc., Dalton Trans. (1993) 3813.
[14] K.M. Mukherjee, T.N. Misra, J. Raman Spectrosc. 27 (1996) 595.
[15] J.S. Kwiatkowski, J. Leszczynski, J. Mol. Struct. 376 (1996) 325.

[16] R.C. Cookson, D.W. Jones, J. Chem. Soc. (1965) 1881.
[17] W.P. Griffith, H.I.S. Nogueira, B.C. Parkin, R.N. Sheppard, A.J.P. White, D.J. Williams, J. Chem. Soc., Dalton Trans. (1995) 1775.
[18] K. Nomiya, S. Takahashi, R. Noguchi, J. Chem. Soc., Dalton Trans. (2000) 2091.
[19] K. Nomiya, R. Noguchi, T. Shigeta, Y. Kondoh, K. Tsuda, K. Ohsawa, N.C. Kasuga, M. Oda, Bull. Chem. Soc. Jpn. 73 (2000) 1143.
[20] W.P. Griffith, S.I. Mostafa, Polyhedron 11 (1992) 2997.
[21] P.A.P. Lourido, J.A.G. Vásquez, J. Romero, M.S. Louro, A. Sousa, Q. Chen, Y. Chang, J. Zubieta, J. Chem. Soc., Dalton Trans. (1996) 2047.
[22] J.C. Bailar, Jr., H. Itatani, Inorg. Chem. 4 (1965) 1618.
[23] G.F. Ciani, G. D'Alfonso, P.F. Romiti, A. Sironi, M. Freni, Inorg. Chim. Acta 72 (1983) 29.
[24] W. Kabsch, J. Appl. Crystallogr. 21 (1988) 916.
[25] N. Walker, D. Stuart, Acta Crystallogr., Sect. A 39 (1983) 158.
[26] (a) G.M. Sheldrick, Acta Crystallogr., Sect. A 46 (1990) 467; (b) G.M. Sheldrick, SHELX-97, University of Göttingen, 1997.
[27] A.L. Spek, PLATON A Multipurpose Crystallographic tool, Utrecht University, Utrecht, The Netherlands, 1999.

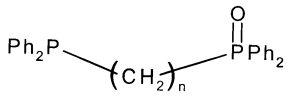


Fig. 1. Bis(phosphine) monoxide.

have been studied. We report spectroscopic and electrochemical studies on the complexes with phosphine and phosphine oxide coordination, along with structural characterization of the dppeo complex. The solvent and anion dependent lability of P=O coordination in solution has also been studied.

2. Experimental

All the reactions were carried out under an atmosphere of purified nitrogen, and the solvent chloroform was dried with P_2O_5 and distilled prior to the reaction. Diethyl ether and petroleum ether were distilled before use. The ligands were synthesized according to the reported procedure [9].

2.1. Physical measurements

^{1}H NMR spectra were recorded on a Bruker ACF 200 MHz spectrometer with tetramethylsilane as the internal reference. ^{31}P $\{^1$H$\}$ NMR spectra were recorded on a Bruker AMX 400 MHz spectrometer operating at 162 MHz. H_3PO_4 was used as external reference. FT-IR spectra were recorded in the solid state dispersed in KBr pellets on a Bruker (EQUINOX 55) spectrometer. The MALDI mass spectra were recorded on a Kratos PCKompact spectrometer using an α-cyanocinnamic acid matrix prepared from methanol solutions of the complexes with a laser power of 120. A CH Instruments 600A potentiostat was used for the electrochemical measurements. Elemental analyses were performed on a Carlo–Erba elemental analyzer model 1106.

2.2. Preparation of the complexes

2.2.1. $Cu(dppeo)_2ClO_4$ (1)

About 0.02 g of $[Cu(CH_3CN)_4]ClO_4$ was mixed with 0.05 g (2 equiv.) of the ligand in chloroform (5 ml) and stirred for 20 min. Completion of reaction was ascertained by the absence of free ligand using TLC (eluant: diethyl ether: chloroform, 50:50). During this time, a white turbidity appeared in the reaction mixture. Addition of excess of diethyl ether precipitated complex **1** as a white powder in 83% yield. *Anal*. Calc. for $C_{52}H_{48}P_4O_6ClCu\cdot CHCl_3$ C 57.22, H 4.41. Found: C, 57.8; H, 4.62%. ^{1}H NMR (δ, $CDC1_3$, 293 K): 7.26–7.72 (40H, m), 2.59 (8H, br). ^{31}P NMR (δ, $CDC1_3$, 293 K): −9 (br), +42 (br) ppm. MS (MALDI): *m/z* 893.0 (100) ($[C_{52}H_{48}P_4O_2Cu]^+$, Calc. 891.2.

2.2.2. $Cu(dppmo)_2ClO_4$ (2)

Synthesis of complex **2** was carried out following the procedure used for complex **1**. After 2 h of stirring, the reaction was complete and the complex was precipitated with diethyl ether in 69% yield. *Anal*. Calc. for $C_{50}H_{44}P_4O_6ClCu\cdot 0.5CHC1_3$: C, 59.24; H, 4.35. Found: C, 58.44; H, 4.41%. ^{1}H NMR (δ, $CDC1_3$, 293 K): 7.20–7.75 (40H, m), 3.52 (4H, d, $J_{HH} = 6$). ^{31}P NMR (δ, $CDC1_3$, 293 K): −21 (br), +38 (br) ppm. MS (MALDI): *m/z* 864.7 (100) ($[C_{50}H_{44}P_4O_2Cu]^+$, Calc. 863.15.

2.3. Crystallographic structure determinations

Single crystals were grown from a dichloromethane solution of complex **1** by layering with diethyl ether. Although most of them were opaque, a moderately formed single crystal ($0.3 \times 0.2 \times 0.3$ mm) was sealed in a Lindemann capillary along with the mother liquor and used for data collection. The intensity data were collected on an Enraf–Nonius CAD4 single crystal diffractometer equipped with graphite-monochromatized Mo Kα radiation. The lattice parameters and standard deviations were obtained by least-squares refinements of 25 well orientated reflections in the range $12^\circ \leq 2\theta \leq 24^\circ$. Three reflections were used to monitor the stability and orientation of the crystal during the time of data collection. All computations were performed using the WINGX [12a] package. Data collected at 25 °C were corrected for Lorentz, polarization and absorption effects using DIFABS [12b]. The positions of the heavy atoms were determined by SHELS-86 [12c,12d]. The remaining atoms were located from difference Fourier analysis using SHELXL-97 [12c,12d]. Hydrogen atoms were included in the final stage of the refinement on calculated positions bonded on their carrier atoms.

3. Results and discussion

Copper(I) complexes were made by mixing the BPMO ligand with $[Cu(CH_3CN)_4]ClO_4$ in the appropriate ratio. Since this source of copper(I) has labile acetonitrile ligands, it has been used effectively for the preparation of several complexes with less volatile ligands [1]. In this case, completion of reaction could be confirmed by the absence of free ligand. Once complexation of the ligand was complete, the reaction mixture was treated with a solvent in which the complex was less soluble such as diethyl ether or petroleum ether. In the case of complex **1**, single crystals suitable for X-ray diffraction studies could be obtained. A brief summary of the crystal structure determination is given in Table 1.

Table 1
Brief summary of the crystal structure determination

Crystal data	Complex **1**
Empirical formula	$C_{52}H_{48}ClCuO_6P_4 \cdot CH_2Cl_2$
Formula weight	1076.4
Crystal system	monoclinic
Space group	*C*2/*c*
a (Å)	23.041(11)
b (Å)	10.047(3)
c (Å)	24.683(11)
α (°)	90
β (°)	105.66(4)
δ (°)	90
V (Å^3)	5502(4)
Z	4
ρ_{calc} (Mg m^{-3})	1.178
Absorption coefficient (mm^{-1})	0.603
θ	1.7–24.97
F(000)	2224
Independent reflections	4984
Data/restraints/parameters	4827/0/312
Final [$I > 2\sigma(I)$]	$R_1 = 0.0950$ [a], $wR_2 = 0.1981$ [b]
Final (all data)	$R_1 = 0.2420$ [a], $wR_2 = 0.2571$ [b]
Goodness-of-fit	0.933
Largest differences peak and hole (e Å^{-3})	0.669 and −0.601

[a] $R_1 = (\Sigma||F_o| - |F_c||)/(\Sigma|F_o|)$.
[b] $wR_2 = [\Sigma w(|F_o|^2 - |F_c|^2)^2]/\Sigma w[F(|F_o|^2)^2]^{1/2}$.

3.1. Molecular structure of *1*

The molecular structure of $Cu(dppeo)_2ClO_4$ consists of a cation containing Cu(I) coordinated to two ligands and a non-coordinating perchlorate anion. Fig. 2 shows the cationic part of the molecular structure, and the selected bond distances and angles are given in Table 2.

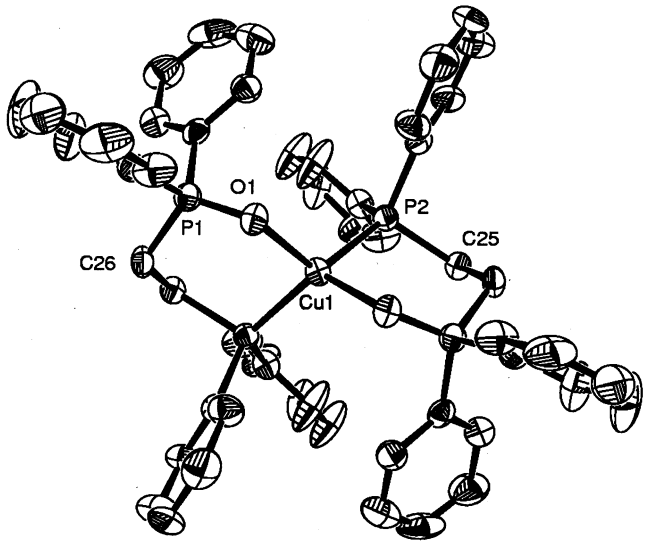


Fig. 2. ORTEP diagram of complex **1** at the 30% probability level. The hydrogen atoms and the disordered counter anion are omitted for clarity.

Table 2
Selected bond lengths (Å) and angles (°) for complex **1**

Bond lengths (Å)	
Cu(1)–O(1)	2.117(6)
Cu(1)–P(2)	2.225(3)
P(1)–O(1)	1.495(6)
Bond angles (°)	
O(1)–Cu(1)–P(2)	120.32(19)
O(1)#1–Cu(1)–O(1)	98.3(4)
O(1)–Cu(1)–P(2)#1	99.03(18)
P(2)#1–Cu(1)–P(2)	119.19(16)

Two dppeo ligands are in chelating mode. The central copper atom adopts a severely distorted tetrahedral geometry with two P atoms and two O atoms coordinating to it, thus confirming phosphine oxide coordination. The Cu–P distances (2.225 Å) and Cu–O distances (2.117 Å) are in the usual ranges expected for Cu(I) complexes. Chelation produces two six-membered rings which are present in a chair conformation very similar to the reported six-membered chelate structure found in $Cu(dppp)_2ClO_4$, where dppp is bis(diphenylphosphino)propane [13]. The molecule possesses a twofold axis passing through the central metal ion. The angles involving O–Cu–P atoms are symmetry related. The chelate angles O–Cu–P are each 99.0° and the non-chelating O–Cu–P angles are 120.3°. The other angles comprising of O–Cu–O and P–Cu–P are 98.3° and 119.2°, respectively. In the case of copper(II) complexes with PPh_3O, the P=O–Cu (II) [6] unit has an angle of 180° whereas in the present case an angle of 119.9° is observed.

A perchlorate anion, and a solvent molecule were also located in the structure. The perchlorate group remains non-coordinating. As observed in other systems [14], the non-bonded anion is disordered with the chloride atom in a special position, and oxygen atoms exhibiting positional disorder with huge thermal parameters. Modeling the perchlorate ion as two intermeshed tetrahedra with partial occupancies did not improve the fit. The error observed in bond lengths, and angles might be due to the poor quality of the crystal examined.

3.2. IR spectroscopy

In the absence of a crystal structure for complex **2**, IR spectroscopy appears suitable for characterization of the compound. The coordination of aromatic phosphine oxides to metal complexes is identified by a shift in the $\nu_{(P=O)}$ stretch. This characteristic band is moderately intense and occurs around 1180, and 1183 cm^{-1} in the free ligands, dppeo and dppmo, respectively. IR spectroscopy thus offers the quickest means of proving oxygen atom coordination to Cu. Bonding to Cu(I) results in a significant shift of the P=O stretching frequency to

lower values in complexes **1**, and **2**. Structurally characterized phosphine oxide complexes show broadening of the $\nu_{(P=O)}$ vibration in some cases. Cotton et al. [15], have explained the line broadening to the coupling of two P=O vibrations via the metal atom. In complex **1** no broadening of the P=O stretching frequency could be observed, although, complex **2** exhibited a slight broadening. The bands due to perchlorate anions present in complex **1** and **2** are similar and occur at 1090 cm^{-1} as expected for a non-coordinating perchlorate anion [16].

3.3. ^{31}P NMR studies

The lability of copper(I) complexes in solution is well known [17]. In order to examine the solution behavior of these complexes, the ^{31}P NMR spectra were recorded for the complexes and the free ligand. The free dppeo ligand is soluble in chloroform and slightly soluble in acetone, whereas the complex is sparingly soluble in chloroform and freely soluble in acetone. As a result spectroscopic studies on the free ligand were carried out in acetone-d_6 or when greater concentrations were required, as in ^{31}P NMR, in a mixture of acetone-d_6 and $CDCl_3$. No significant solvent effect was found for the ^{31}P NMR chemical shifts on increasing $CDCl_3$ content. The spectrum exhibits a signal at -12 ppm for the P(III) center, and another peak at $+33$ ppm for the phosphine oxide group (Fig. 3). Similarly, for dppmo, the signals are at -28 ppm for the P(III) center and at $+28$ ppm for the phosphine oxide center. These signals are doublets due to P–P coupling with the values of 53 and 55 Hz for dppmo and dppeo, respectively [9].

An acetone-d_6 solution of complex **1** displays a broad peak at -9 ppm, $\Delta\delta = 3$ ppm, (δ complex$-\delta$ ligand), attributable to coordinated phosphine and a relatively more intense peak at 42 ppm ($\Delta\delta = 9$ ppm) for the phosphine oxide group. A noteworthy feature of the ^{31}P NMR of complex **1** is the disappearance of the doublet pattern observable in the free ligand (Fig. 3). The solution ^{31}P NMR of complex **1** illustrates that the solid state structure is predominantly retained in solution. However, Cu–P coupling is not observed and only broad signals are observable at RT suggesting, an exchange process involving breaking of Cu–P and Cu–O bonds. The peaks are significantly narrower at low temperature. The solution NMR of Cu(dppmo)$_2$$ClO_4$ obtained in $CDCl_3$ and in acetone-d_6, is similar to that of **1** in terms of upfield shifts of the signals ($\Delta\delta_{P=O} = 10$ ppm, $\Delta\delta_P = 7$ ppm) and the line broadening due to an exchange process involving an equilibria where chelation is lost.

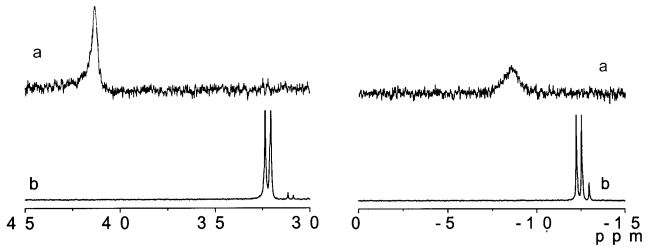
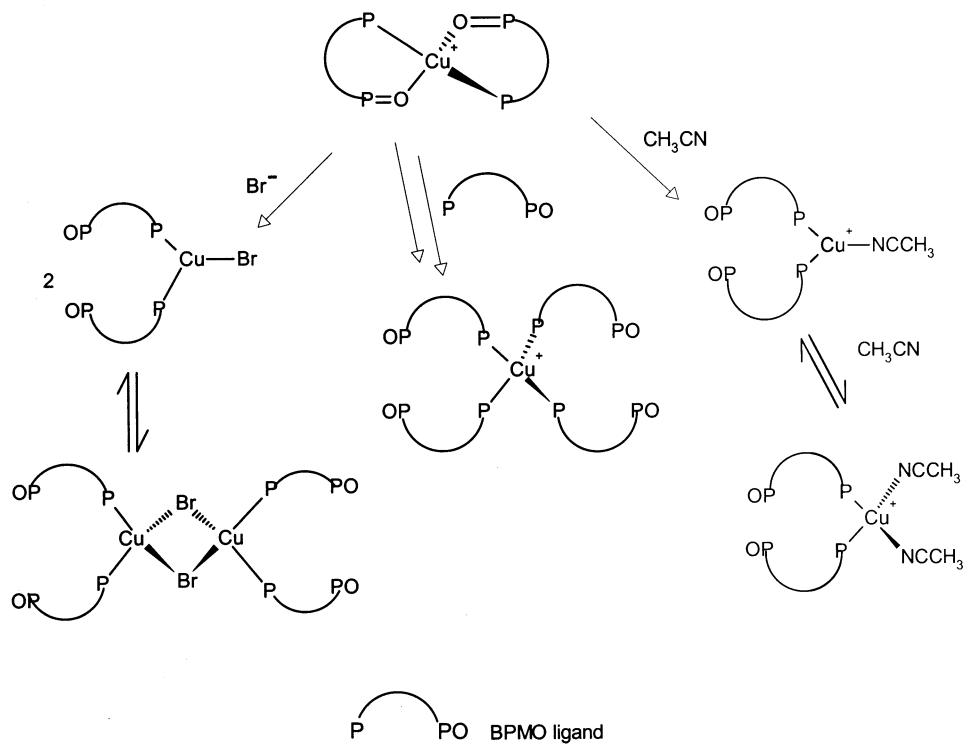


Fig. 3. The ^{31}P NMR of (a) complex **1**, and (b) dppeo.

The two different methylene protons of the dppeo framework are degenerate in ^1H NMR and appear as a broad singlet in the free ligand. The accidental degeneracy is almost removed in the ^1H NMR of **1** and a slight upfield shift (0.31 ppm) of the peaks is observed. Hence it is certain that **1** and **2** possess the expected phosphine oxide coordination in non-coordinating solvents like aetone-d_6 and $CDCl_3$. Based on these evidences we suggest similar solution and solid state structures for **1** and **2** in which only equilibria with non-chelated forms is occurring.

Since rapid equilibria with the non-coordinated forms are involved, it is of interest to examine the relative strengths of the Cu–O/Cu–P bonds through competition experiments. The ability of the P=O group relative to acetonitrile to coordinate to copper(I), which is a moderate π-acceptor was examined by recording the NMR spectrum of complex **1** in CD_3CN as the solvent. The influence of solvent is quite pronounced on the signal for the phosphine oxide group. The P=O group now resonates at $+33$ ppm very close to that of free phosphine oxide group. Interestingly, the signal appears as a doublet and resembles the signal for free P=O present in the ligand. On the contrary, the signal due to phosphine group shows little difference in CD_3CN and retains the position ($\delta = 8.8$ ppm) and line shape observed in acetone-d_6. The spectrum of complex **2** in CD_3CN produces similar results as well. The phosphine moiety shows binding ($\Delta\delta_P = 8$ ppm), while the phosphine oxide signal occurs close to the free ligand with a doublet pattern, ($\Delta\delta_{P=O} = 1$ ppm). These results are in accord with the preference of copper(I) for acetonitrile, a moderate π-acceptor rather than the oxygen of P=O when the former is present in excess.

In another experiment, 4 equiv. of the ligand were added to [Cu(CH_3CN)$_4$]ClO_4 in $CDCl_3$. The presence of 4 equiv. of the dppeo ligand with respect to the copper(I) source, leads to a competition between the chelated structure (CuP_2O_2) and a complex with all four phosphine centers coordinated to Cu(I), with uncoordinated P=O centers. The spectrum indicates the presence of free P=O group and bound phosphine moiety with signals at $+33$ and -9 ppm, respectively. The reappearance of the doublet near the free ligand value for the P(V) center is clearly due to loss of Cu–O bonding. The NMR results indicate that the intermolecular P(III) center is more acceptable to the Cu(I) center than intramolecular interaction from P(V) (see Scheme 1). Thus the CuP_2O_2 unit is stable only in the absence of competitive interactions from soft donors.



Scheme 1.

In a separate experiment, tetrabutylammonium bromide was added to the complex **1** in 1:1 ratio. Addition of bromide increases the solubility of 1 in $CDCl_3$, the phosphine signal in ^{31}P NMR is shifted downfield, where as the P=O signal is close to the free ligand value. The shifts in the ^{31}P NMR spectrum illustrate that the bromide ion retards the coordination of P=O moiety. The accidental degeneracy of the ^{1}H NMR signal in the free ligand is lifted on coordination. Two sets of broad peaks are observed in the ^{1}H NMR spectrum (2.34 and 2.58 ppm) and thus different from what is observed for complex **1**. The $\nu_{(P=O)}$ stretch of the product in this reaction, also occurs close to the free ligand and the IR studies are consistent with what is expected on the basis of NMR studies. When 2 equiv. of the ligand dppeo are mixed with CuBr in $CDCl_3$, similar observations were made in ^{31}P NMR and ^{1}H NMR spectra.

An attempt was made to isolate the complex $(CuBr)(dppeo)_2$ formed in the reaction of CuBr with dppeo following the procedure used for making **1** and **2**. The IR spectral changes for the complex generated in this fashion closely resembles the free ligand spectrum in the $\nu_{(P=O)}$ region. It is to be noted that the ^{31}P resonance of the P=O moiety occurs close to the δ value for free P=O and is different from that in the perchlorate complex, and the resulting NMR matches that observed in the in situ generation of the complex. In addition, the doublet pattern reappears for the P=O signal as in the case of non-coordinating phosphine oxides. However, the white complex isolated in this reaction was relatively unstable and became colored precluding complete characterization.

3.4. Electrochemical studies

Electrochemical studies were performed in chloroform solution using Pt as working electrode and Ag/AgCl as the reference electrode. Tetrabutylammonium perchlorate was used as the supporting electrolyte (0.08 M). All the complexes examined had an electrochemical event in the potential window of 1.4–0 V where the Cu(I)/Cu(II) redox couple is usually observed for copper(I) phosphine complexes [18]. A clean background was ascertained in each experiment prior to the addition of the complex. The results from cyclic voltammograms at 50 mV S^{-1} are reproduced in Fig. 4 and the details of cyclic voltammograms at other scan speeds are summarized in Table 3.

The cyclic voltammogram of $Cu(dppeo)_2ClO_4$ (0.1 mM solution in chloroform) displays well-defined anodic and cathodic peaks (Fig. 4(a)). However, the process is only quasi reversible, as indicated by ΔE_P values and I_p^a/I_p^c, at different scan rates. The electrochemical behavior of complex **2**, $Cu(dppmo)_2ClO_4$ was also examined under identical conditions. Although the $E_{1/2}$ values at different scan rates are comparable to that of **1**, the cathodic process in complex **2** is suppressed and

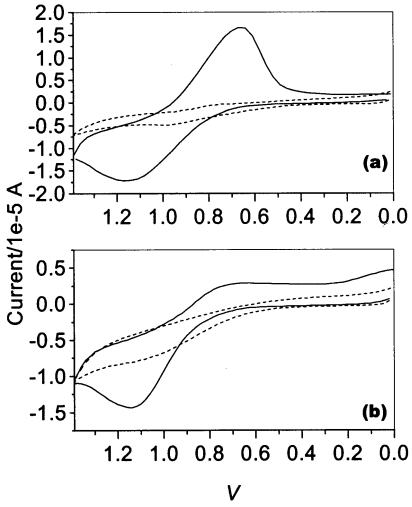


Fig. 4. Cyclic voltammogram of (a) complex **1**, and (b) complex **2**. The broken line traces are for the respective free ligands (scan rate: 50 mV S^{-1}).

I_p^a/I_p^c values at different scan rates are quite large (Fig. 4(b)). The electrochemical behavior of the BPMO derived complexes are dependent on the chain length. The influence of chain length on electrochemical processes in chelate complexes has been noted quite often [19]. The I_p^a/I_p^c values indicate that complex **1** with dppeo shuttles between two oxidation states more readily than complex **2**.

The complex $Cu(dppe)_2ClO_4$ with all soft phosphorus centers in the coordination sphere was also studied for comparison. Unlike complexes **1** and **2**, the $Cu(dppe)_2ClO_4$ shows a broad oxidation wave, while the reduction wave is well-defined and occurs at more positive potentials than for BPMO complexes. The broad anodic peak precludes accurate measurement of an E_{pa} value, and was calculated from the derivative of the cyclic voltammogram. The electrochemical behavior of the relevant ligands was also probed in order to confirm the origin of electrochemical processes. In the potential window studied, the ligands are inactive and the complexes are clearly distinguishable from the ligands due to the presence of the Cu(I)/Cu(II) couple.

The results of the electrochemical studies on BPMO complexes with a mixed coordination sphere are compared with the results from studies on the dppe complex, which possesses only soft ligands in the coordination sphere. The reduction potential values are well-defined in all three complexes, and indicate that the phosphine complex is more easy to reduce (more positive potential), than complex **1** and **2**. Similarly the broad anodic wave of the dppe complex illustrates a less favorable, slower oxidation processes than the BPMO analogues. This trend is also supported by the observation that the addition of excess dppeo (2 equiv.) to the complex **1** shifts the redox processes anodically by 50 mV and approaches the behavior of the CuP_4 complex. The addition of bromide to the complex to generate the bromide complex, complicates the oxidation event with multiple processes presumably due to the presence of an equilibrium in solution as illustrated in the Scheme 1. However, at least one of the processes requires a more positive potential than the CuP_2O_2 system. This can be reasonably attributed to the dimeric species, while the other wave might originate from the three-coordinated monomer. As expected, the reduction potential of the bromide complex is more positive than the BPMO complexes.

Hence the electrochemical results are suggestive of the fact that the CuP_2O_2 system is relatively easier to oxidize to the copper(II) complex. Whereas, a complex with an all soft coordination environment, is more difficult to oxidize. Complexes with the P_2O_2 ligand set are readily synthesized and stable enough for isolation when copper(I) is not given a choice to coordinate to soft ligands.

4. Summary

The present study indicates that bis(phosphine) monooxides are suitable ligands for Cu(I) and form stable copper(I) complexes. It is also clear that the Cu–O bond and Cu–P bonds are quite labile. Unlike the Cu–P bond the Cu–O bond requires a non-coordinat-

Table 3
Cyclic voltammetry data

Complex	Scan rate mV S^{-1}	E_{pa}	E_{pc}	$E_{1/2}$	I_p^a/I_p^c
$Cu(dppeo)_2ClO_4$	20	1.19	0.70	0.94	0.6
	50	1.17	0.67	0.92	0.6
	100	1.30	0.48	0.89	
$Cu(dppmo)_2ClO_4$	20	1.06	0.68	0.87	4
	50	1.14	0.65	0.89	3.8
	100	1.20	0.56	0.88	
$Cu(dppe)_2ClO_4$	50	1.25	0.80	1.02	
$Cu(dppeO)_2ClO_4$+2 equiv. of dppeo	50	1.24	0.73	0.98	
$CuBr(dppeo)_2$	50	1.25, 1.08	0.78		

ing counter anion or solvent to remain in the coordination sphere of copper(I). Spectroscopic studies show that copper(I) would favor soft donors to O, a hard donor in its coordination sphere. In a situation where 4 equiv. of the BPMO ligand are made available for copper(I), the coordination of four P atoms to Cu is favored. Even entropy driven stabilization of the CuP_2O_2 coordination fails to win over the CuP_4 coordination. The electrochemical behavior of the complexes illustrates that the mismatched coordination environment leads to a copper(I) center that is more easily oxidized. Thus the four phosphine-coordinated complex is more difficult to oxidize than the complex with two O and two P atoms. The greater stability Cu(I) complexes with a complement of soft ligands is evident from these competition experiments.

5. Supplementary material

Crystallographic data for the crystal structure of **1** has been deposited at the Cambridge Crystallographic Data center as CCDC-175552. These data can be obtained free of charge at www: http://www.ccdc.cam.ac.uk/conts/retrieving.html or from the Director, CCDC, 12 Union Road, Cambridge, CB2 1EZ, UK (fax: +44-1223-336033; e-mail: deposit@ccdc.cam.ac.uk.

Acknowledgements

We wish to acknowledge the generous financial support of the Council for Scientific and Industrial Research, New Delhi for this work and SIF at the Indian Institute of Science, Bangalore for NMR spectra.

References

[1] B.J. Hathaway, in: G. Wilkinson, R.D. Gillard, J.A. McCleverty (Eds.), Comprehensive Coordination Chemistry, vol. 5, Pergamon Press, Oxford, 1987, p. 534.
[2] J.D. Lee, Concise Inorganic Chemistry, 4th ed., Chapman & Hall, London, 1991, p. 822.
[3] R.G. Pearson, J. Chem. Educ. 45 (1968) 581.
[4] (a) P.L. Goggin in Ref. [1], vol. 2, p. 497;
(b) S.S. Krishnamurthy, Proc. Indian Acad. Sci. Chem. Sci. 108 (1996) 111;
(c) N. Burford, Coord. Chem. Rev. 112 (1992) 1.
[5] (a) J.G.H. Du Preez Bernardus, J.A.M. Van Brecht, I. Warden, Inorg. Chim. Acta 131 (1987) 259;
(b) D. Jin, R. Yang, B. Xue, K. Kozawa, T. Uchida, J. Coord. Chem. 26 (1992) 321.
[6] (a) J.A. Bertrand, Inorg. Chem. 6 (1967) 495;
(b) M.R. Churchill, B.G. DeBoer, S.J. Mendak, Inorg. Chem. 14 (1975) 2496.
[7] (a) J.C. Dyason, L.M. Engelhardt, P.C. Healy, H.L. Klich, A.W. White, Aust. J. Chem. 39 (1986) 2003;
(b) R.D. Hart, P.C. Healy, G.A. Hope, D.W. Turner, A.H. White, J. Chem. Soc., Dalton Trans. (1994) 773;
(c) A.P. Gaughan, Z. Dori, J.A. Ibers, Inorg. Chem. 13 (1974) 1657;
(d) G.G. Messmer, G.J. Palenik, Inorg. Chem. 8 (1969) 2750;
(e) R.J. Restivo, A. Costin, G. Ferguson, A. Carty, Can. J. Chem. 53 (1975) 1949;
(f) D.J. Darensbourg, M.W. Holtcamp, B. Khandelwal, J.H. Reibenspies, Inorg. Chem. 34 (1995) 5390;
(g) C. Lopes, M. Håkansson, S. Jagner, Inorg. Chim. Acta 254 (1997) 361;
(h) B. Jung, K.D. Karlin, A.D. Zuberbühler, J. Am. Chem. Soc. 118 (1996) 3763.
[8] G. Pilloni, B. Corain, M. Degano, B. Longato, G. Zanotti, J. Chem. Soc., Dalton Trans. (1993) 1777.
[9] (a) V.V. Grushin, J. Am. Chem. Soc. 121 (1999) 5831;
(b) V.V. Grushin, Organometallics 20 (2001) 3950.
[10] (a) R.J. Coyle, Y.L. Slovokhotov, M.Y. Antipin, V.V. Grushin, Polyhedron 17 (1998) 3059;
(b) I. Brassat, U. Engelert, W. Keim, D.P. Keitel, S. Killat, G.-P. Suranna, R. Wang, Inorg. Chim. Acta 280 (1998) 150;
(c) T.C. Blagborough, R. Davis, P. Ivison, J. Organomet. Chem. 467 (1994) 85;
(d) S.J. Higgins, R. Taylor, B.L. Shaw, J. Organomet. Chem. 325 (1987) 285;
(e) Q.-B. Bao, S.J. Landon, A.L. Rheingold, T.M. Haller, T.B. Brill, Inorg. Chem. 24 (1985) 900;
(f) S.O. Grim, L.C. Satek, C.A. Tolman, J.P. Jesson, Inorg. Chem. 14 (1975) 656.
[11] (a) C. Abu-Gnim, I. Amer, J. Organomet. Chem. 516 (1996) 235;
(b) R.W. Wegman, A.G. Abatjoglou, A.M. Hasrrison, J. Chem. Soc., Chem. Commun. (1987) 1891.
[12] (a) L.J. Farrugia, WinGX (1.63.02), An Integrated System of Windows Program for the Solution, Refinement, and Analysis of Single Crystal X-Ray Diffraction;
(b) N. Walker, D. Stuart, Acta Crystallogr., Sect. A 39 (1983) 158;
(c) G.M. Sheldrick, SHELXS-86, Program for Crystal Structure Determination, University of Cambridge, Cambridge, 1986;
(d) G.M. Sheldrick, SHELXL-97, Program For Crystal Structure Refinement, University of Göttingen, Göttingen, Germany, 1997.
[13] (a) S. Kitagawa, M. Kondo, S. Kawata, S. Wada, M. Maekawa, M. Munakata, Inorg. Chem. 34 (1995) 1445;
(b) P. Comba, C. Katsichtis, B. Nuber, H. Pritzkow, Eur. J. Inorg. Chem. (1999) 777.
[14] (a) L.M. Engelhardt, C. Pakawatchai, A.H. White, J. Chem. Soc., Dalton Trans. (1985) 125;
(b) M.G.B. Drew, J. Nelson, S.M. Nelson, J. Chem. Soc., Dalton Trans. (1981) 1685;
(c) N.A. Bailey, M.M. Eddy, D.E. Fenton, S. Moss, A. Mukhopadhyay, G. Jones, J. Chem. Soc., Dalton Trans. (1984) 2281;
(d) G.D. Brayer, M.N.G. James, Acta Crystallogr., Sect. B 38 (1982) 654;
(e) M.F. Richardson, R.E. Sievers, J. Am. Chem. Soc. 94 (1972) 4134;
(f) K. Bechgaard, K. Carneiro, F.B. Rasmussen, M. Olsen, G. Rindorf, C.S. Jacobsen, H.J. Pedersen, J.C. Scott, J. Am. Chem. Soc. 103 (1981) 2440;
(g) P.K. Coughlin, S.J. Lippard, J. Am. Chem. Soc. 106 (1984) 2328;
(h) W. Fitzgerald, B. Hathaway, C.J. Simmons, J. Chem. Soc., Dalton Trans. (1985) 141;
(i) G. Kolks, S.J. Lippard, Acta Crystallogr., Sect. C (Cr. Str. Commun.) 40 (1984) 261.
[15] F.A. Cotton, R.D. Barnes, E. Bannister, J. Chem. Soc. (1960) 2119.
[16] K. Nakamato, Infrared Spectroscopy of Inorganic and Coordination Compounds, 3rd ed., Wiley, New York, 1978.

[17] (a) S.J. Berners-Price, R.K. Johnson, C.K. Mirabelli, L.F. Faucette, F.L. McCabe, P.J. Sadler, Inorg. Chem. 26 (1987) 3383;
(b) N. Vijayashree, A.G. Samuelson, M. Nethaji, Curr. Sci. 65 (1993) 57;
(c) L. Barton, P. Rush, Inorg. Chem. 24 (1985) 3413.
[18] (a) A.M. Leiva, L. Rivera, B. Loeb, Polyhedron 10 (1991) 347;
(b) V.W.-W. Yam, W.K.-M. Fung, M.-T. Wong, Organometallics 16 (1997) 1772;
(c) V.W.-W. Yam, W.K.-M. Fung, K.-K. Cheung, Organometallics 17 (1998) 3293.
[19] (a) E.A. Ambundo, M.-V. Deydier, A.J. Grall, N. Aguera-Vega, L.T. Dressel, T.H. Cooper, M.J. Heeg, L.A. Ochrymowycz, D.B. Rorabacher, Inorg. Chem. 38 (1999) 4233;
(b) M. Schatz, M. Becker, F. Thaler, F. Hampel, S. Schindler, R.R. Jacobson, Z. Tyeklár, N.N. Murthy, P. Ghosh, Q. Chen, J. Zubieta, K.D. Karlin, Inorg. Chem. 40 (2001) 2312.

metal ion binding sites as well as conformational changes that occur on the ligand by chelation. In a first time, the complexation mechanism with Al(III) of 3-hydroxyflavone, 5-hydroxyflavone and 3′4′-dihydroxyflavone have been studied by spectroscopy and quantum chemical calculations [17–19], these molecules possess only one chelating site. In a second time, the quercetin molecule, that presents three potential sites for the coordination of Al(III), has been investigated in order to compare the chelating power of the different sites in competition [20]. As a continuation of this work, we report, in this paper, the study of the complexation of Al(III) by isoquercitrin (2-(3,4-dihydroxyphenyl)-3-(β-D-glucofuranosyloxy)-5,7-dihydroxy-4H-1-benzopyran-4-one). Isoquercitrin (Fig. 1) presents two chelating sites: the 5-hydroxy-4-keto and the 3′,4′dihydroxyl (catechol) groups in competition towards aluminium ion. The aim of this study is to determine the first site implicated in the complex formation with Al(III), the stoichiometry and formation constants of complexes. Due to the very low solubility of isoquercitrin in water, study in methanol solution was performed. The pH influence upon the complexation has been investigated by adding sodium acetate or methanoate to the solution. The molecular geometry of the free ligand and of the formed complexes has been optimized by semiempirical molecular orbital calculations (AM1 method) in order to observe the conformational changes engendered by the chelation. Recent advances both in computational chemistry and in rapidity of computers make it possible to optimize structures of medium-size molecules by density functional theory (DFT). So, from geometrical parameters obtained by the AM1 method, the structures have been re-optimized by DFT. Electronic and vibrational spectroscopies were used to confirm the theoretical models.

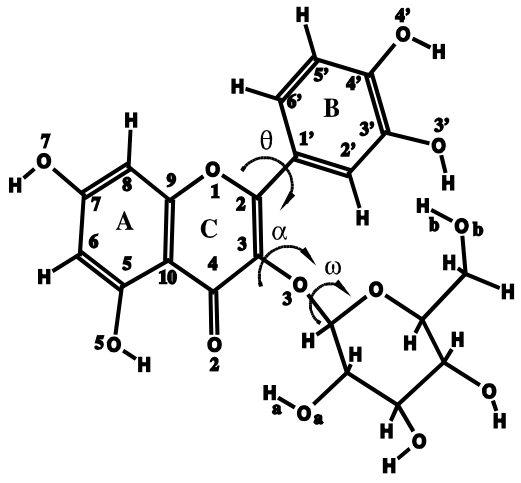


Fig. 1. Scheme and atomic numbering of isoquercitrin.

2. Experimental

2.1. Solution preparation for spectrophotometric methods

Isoquercitrin was obtained commercially from Extrasynthèse (France). Anhydrous aluminium chloride, hydrochloric acid, sodium acetate, sodium methanoate and spectroscopic grade methanol were used without purification.

The molar ratio method, introduced by Yoe and Jones [21] permits to deduce the composition of complexes in solution from spectrophotometric spectra. For this method, solutions containing a constant concentration (4×10^{-5} M) of isoquercitrin in methanol and variable concentration of $AlCl_3$ (from 4×10^{-7} to 4×10^{-2} M) were prepared. In order to verify the results of the first method, the complex stoichiometry has also been determined by the method of continuous variation (Job's method). For the study in alkaline solution, isoquercitrin solutions were successively prepared in methanol containing sodium acetate 10^{-1} M, and in methanol with 5×10^{-3} M of sodium methanoate. The molar ratio method was used for the determination of complex stoichiometry. In acidic medium, the solutions consist in a mixture of 90% methanol–10% water where the ionic strength has been adjusted to 0.1 with sodium chloride. The aqueous solution contains hydrochloric acid 3.2×10^{-2} M (apparent pH 2.5).

2.2. Instrumentation

The UV–Vis spectra were recorded on a Cary-1 (Varian) spectrophotometer with cells of 1 cm path length. FT-Raman spectra of isoquercitrin (10^{-2} M) and of its complexes with Al(III) were recorded with a Bruker IFS 88W spectrometer connected to a Raman module (Bruker, FRA-106). Radiation of 1064 nm from an Nd:Yag laser was used for excitation with a laser power of 300 mW. An excitation in the near-infrared range allows the collection of fluorescence-free spectra.

2.3. Calculations

The formation constants of the complexes of isoquercitrin were estimated by using a multivariate data analysis program for modelling and fitting equilibrium titration 3D data sets obtained from the spectrophotometric measurements. The UV–Vis spectra were refined using the SPECFIT software (version 3.0) [22]. The set of spectra obtained at variable Al(III) concentration were treated by evolving factor analysis (EFA) [23] in order to determine the number of absorbing species in the system and the pure electronic spectrum of each complex. The SPECFIT software has also been used to estimate the stability constants (β) of the complexes and the standard deviation (σ) of each value. In order to obtain

the best fit between the complexation model and the experimental data, several models of complexes with different stoichiometries and with different initial constant values have been envisaged for the refinement of the stability constants.

The free isoquercitrin molecule was previously studied by us [24] using the Austin Model 1 (AM1) quantum mechanical semiempirical method [25] with the HYPERCHEM program [26]. Three stable conformers (noted Ia, Ib and Ic) with equivalent energy have been found for the molecule. Their molecular structures only differ by the torsional angle of the B ring and by the glucose orientation. These three conformers are stabilized by seven or eight intramolecular hydrogen bonds involving both aglycon and sugar moities. In this study, only the conformer Ib, with a θ angle value of -14.3° has been considered for DFT calculations.

The DFT calculations with the hybrid functional method (B3LYP) [27,28] were carried out by using the GAUSSIAN 98 program package [29] implemented on a IBM RS/6000 SP computer. We performed full structural optimizations of the free isoquercitrin and of the more predominant complexed forms starting from geometrical data first obtained by the quantum semiempirical treatment. Due to the size of the molecular system, the 6-31G* basis set was used for all the calculations. In order to reduce the computational time, the SCF convergence criterion has been set to 10^{-6}. For the complexes, water molecules have been added to aluminium atoms to obtain an octahedral environment of this ion and thus to respect its valence. Previous studies indicated that the substitution of water by methanol has only little influence on the calculated structure of aglycon.

The wavelengths of electronic transitions observed in the UV–Vis spectra of isoquercitrin and of its complexes have been calculated with HYPERCHEM program using a configuration interaction treatment. This calculation only takes into account the contribution of the singly excited configurations involving the 11 highest occupied and the 11 lowest unoccupied molecular orbitals.

3. Results and discussion

3.1. Stoichiometry and formation constants of complexes in neutral methanol

The electronic spectrum of free isoquercitrin in methanoic solution is mainly characterised by an important absorption band (band I) at 359 nm. The addition of anhydrous $AlCl_3$ to an isoquercitrin solution in methanol results in important modifications of the UV–Vis spectrum of the flavonoid, with the appearance of a new band centred on 406 nm for $[AlCl_3]$–[Iso] ratios comprised between 0 and 0.5. For these ratios, an isobestic point is observed at 380 nm, indicating an equilibrium between the free molecule and a first complexed form (complex I). For ratios $0.5 < [AlCl_3]$–$[Iso] < 1$, bathochromic shifts of the band at 406 nm are observed with the increase of added $AlCl_3$ amount, no isobestic point is then observed, and let presume the presence of at least three different absorbing species in solution. For ratios superior to 1, a new isobestic point appears at 409 nm, indicating a novel equilibrium between two complexed forms of isoquercitrin and the absorption maximum of the second complex is centered on 436 nm. The fact that a certain number of spectra do not cross at one of the two possible isobestic points provides evidence that the second complex formation begins before a complete chelation of the first site of free isoquercitrin. So, for ratios $0.5 < [AlCl_3]$–$[Iso] < 1$, one can simultaneously observed the formation of the two complexes. The UV–Vis spectra on Fig. 2 illustrate the different steps occurring in the chelation process of isoquercitrin with Al(III) according to the $[AlCl_3]$–[Iso] ratio.

The molar ratio method was used to determine the stoichiometry of the complexes of isoquercitrin with aluminium(III). In this method ideally two straight lines are obtained when the absorbance at one wavelength is plotted versus the Al(III) to flavonoid ratio, and the point of intersection of these two lines corresponds to the stoichiometric ratio upon interpolation to the molar ratio axis. The molar ratio plots at 406 nm (λ_{max} of the first complex: complex I) and at 436 nm (λ_{max} of the second complex: complex II) are presented on Fig. 3(b), respectively. The curve of absorbance versus $[AlCl_3]$–[Iso] molar ratio plotted at 406 nm (Fig. 3(a)) clearly shows a stoichiometry of 1:1 for complex I. The presence of more than one complexed forms in the

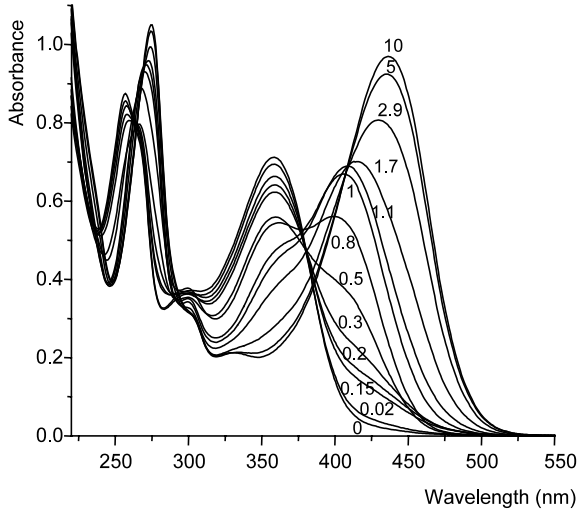


Fig. 2. Evolution of UV–Vis spectra of isoquercitrin in neutral methanol in presence of $AlCl_3$. The molar ratio [Al(III)]–[Iso] is indicated on each spectrum.

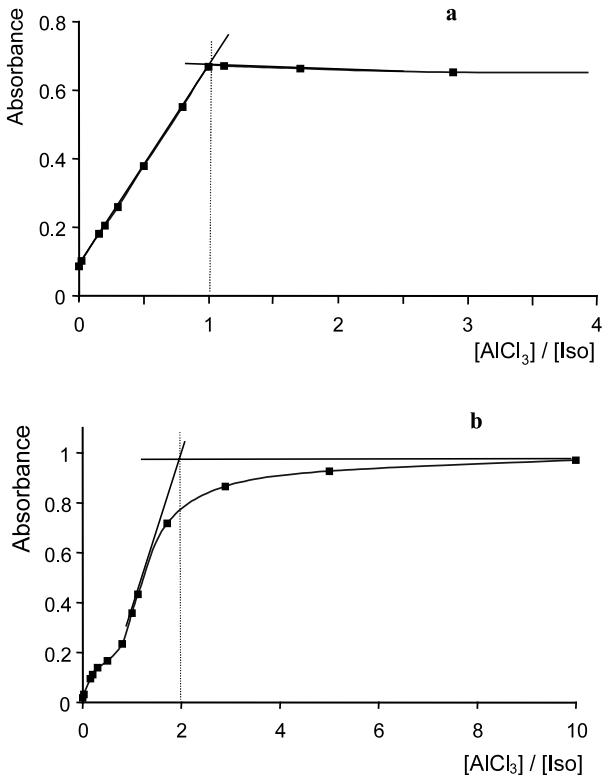


Fig. 3. Absorbance vs. $[AlCl_3]$–[Iso] molar ratio plots at 406 nm (a) and 436 nm (b).

system simultaneously, is reflected on the shape of the curve shown in Fig. 3(b). For the second complex, one can deduce from this curve that two aluminium ions are coordinated to the ligand, and so a Al(III)–Iso = 2:1 stoichiometry. However, one can notice that a tenfold excess of aluminium(III) is necessary to obtain a complete complexation of isoquercitrin. The stoichiometries of the two complexed species have been confirmed by the Job's method or continual variations method (results not shown). Similar results were obtained by Porter et al. concerning rutin (3,5,7,3′,4′-pentahydroxy-flavone-3-*O*-rutinoside), a parent of isoquercitrin, where the sugar at position 3 is not a glucose but a rutinose [30]. These authors have found, in neutral methanol solution, the formation of two complexes of stoichiometry Al(III)–rutin = 1:1 and 2:1.

In order to know the potential site involves in formation of the first complex, pH conditions were changed by adding concentrate HCl to the complex II solution. The acid addition has led to a complete vanishing of the electronic absorption band relative to complex II, whereas the absorption band of complex I was not modified. Our previous works, concerning notably the complexation of 3′4′-dihydroxy-flavone and quercetin, have shown that *ortho*-dihydroxyl group does not complex aluminium(III) in very acidic medium. This fact allows to conclude that the catechol group is only involved in the second step of the complexation of isoquercetin, and consequently it could be predicted that, in complex I, the coordination of isoquercitrin with Al(III) in neutral methanol solution takes place through the carbonyl and hydroxyl group in position 5 of the molecule. So, for low concentration of aluminium in methanol, Al ion coordinates with the 5-hydroxychromone group to lead to the formation of $Al(Iso)^{2+}$ complex, and for larger amount of aluminium ($[AlCl_3]$–[Iso] > 0.5) a second atom of Al(III) coordinates to the catechol group to give the complex II $(Al_2Iso)^{3+}$. In pure methanol, only hydroxyls involving in chelate are deprotonated.

From electronic spectra obtained by varying the $[AlCl_3]$–[Iso] molar ratio, the determination of the number of spectroscopically distinct species was estimated by the EFA method. Three principal components were found corresponding, respectively, to spectra of free ligand, $Al(Iso)^{2+}$ and $Al_2(Iso)^{3+}$ complexes. A fourth component can be also detected only in the first spectra and with a very low contribution. However, it is worth noting that the electronic spectrum of a specie only existing in very minor concentration is poorly defined. Further, spectral changes due to the coordination of one, two or three ligands on the Al(III) atom are rather similar insofar as the same chelating site is implicated, and thus difficult to differentiate. In order to estimate the formation constants and with regard to our previous observations, a numerical treatment of the electronic spectra has been carried out starting from a simple model containing species with stoichiometry 0:1, 1:1 and 2:1 (metal–ligand). The relatively large deviation of this model from the experimental data, reflected by the σ values, led us to introduce new species. Several ratios and initial formation constants were tested, introducing the model or the species that yield more reasonable fittings. The model which provides the best fit to the experimental spectra is composed of the complexes of stoichiometry (metal:ligand) 1:1 ($\log \beta = 6.49 \pm 0.16$), 1:2 ($\log \beta = 10.50 \pm 0.19$) and 2:1 ($\log \beta = 11.24 \pm 0.17$). This result comes from the following reaction equation:

$$a\mathrm{Al} + b\mathrm{Iso} \Leftrightarrow \mathrm{Al}_a\mathrm{Iso}_b$$

with the corresponding stability constant:

$$\beta = \frac{[\mathrm{Al}_a\mathrm{Iso}_b]}{[\mathrm{Al}]^a[\mathrm{Iso}]^b}$$

The deprotonation of the oxygen atoms at the level of the chelating site has not been taking into account in the constant calculation insofar as the pH notion has no much sense in methanoic medium. Moreover, no deprotonated form of the ligand exits in this medium. The minor participation of the complex $Al(Iso)_2^{+}$ is illustrated on Fig. 4 which shows the concentration variations of the different species versus the added

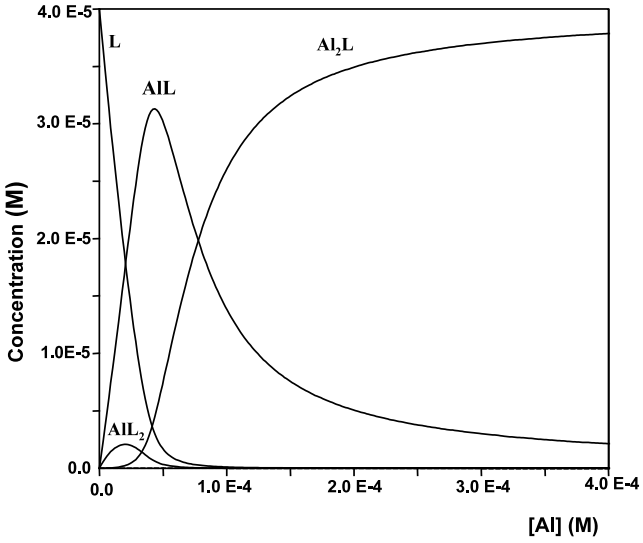


Fig. 4. Distribution curves of the aluminium complexes with isoquercitrin in methanol as a function of Al(III) concentration.

quantity of aluminium. These curves well confirm that the chelation of the second site (catechol), with the formation of $Al_2(Iso)^{3+}$, occurs before a complete formation of the first complex $Al(Iso)^{2+}$. For purpose of comparison, the complexation of Al(III) by quercetin shows that two consecutively steps occur. The chelation at the level of the catechol group only starts when the totality of ligands is already involved in the first complex implicating the 3-hydroxychromone group.

3.2. Conformational analysis of complexes

The most relevant structure parameters of isoquercitrin, complex I $Al(Iso)(H_2O)_4^{2+}$ and complex II $Al_2(Iso)(H_2O)_8^{3+}$ determined with both the semiempirical AM1 and B3LYP/6-31G* DFT methods are given in Tables 1–3. Only bond lengths and valence angles of the aglycon have been reported, and the main torsion angles have been selected. Concerning the free ligand, the bond lengths and valence angles of the γ-pyrone ring calculated with DFT are slightly different than those obtained from AM1 calculations, whereas the valence bonds and angles of both A and B rings show minor differences. The comparison of the torsional angle values obtained with the two methods reveals small discrepancy in the sugar orientation (α and ω angles), while the position and the orientation of the B ring are similarly calculated. The C–O distances relative to the hydroxyl groups calculated at the DFT level are a little bit smaller than those obtained by the AM1 method.

With regard to isoquercitrin, the geometrical parameters of complexes I and II, vary in the same way and commonly with the same magnitude for both methods of calculations. By coordination of Al(III) on the 5-hydroxy-4-keto site, the structure of the ligand is profoundly modified as well for bond lengths as for valence angles. The γ-pyrone ring is the most affected part of the molecule. A clear decrease of the values of C(3)C(4), C(4)C(10) and of the inter-ring bond C(2)C(1′) is observed associated to an increase of the C(2)C(3) bond length that takes a single bond character. The B ring geometry is also modified, the C(1′)C(2′), C(3′)C(4′), C(4′)C(5′) and C(6′)C(1′) bond lengths increase whereas C(2′)C(3′) and C(5′)C(6′) are calculated shorter than in the free ligand. These observations let assume a preponderant participation of a mesomeric cynnamoyl form (Fig. 5(a)). This is confirmed by the shortening of 0.02 Å of the C(4′)O(4′) bond that is more influenced than the C(3′)O(3′) one. The participation of a benzoyle mesomeric form (Fig. 5(b)) to the resonance of the system is manifested by the reduction of the C(5)C(6), C(8)C(9) and C(7)O(7) and the augmentation of the C(10)C(5), C(6)C(7), C(7)C(8) and C(9)C(10) bond lengths. In spite of the increase of the electronic conjugation over the chromone part and the B ring, through the inter-ring bond, the aglycon is not planar and the θ value is very weakly reduced. The strong intra-molecular hydrogen bonds established between the glucose and the B ring should certainly prevent its rotation. At the level of the chelating site, the six-membered ring obtained with the coordination of Al(III) is slightly puckered with the metallic ion out of plane. For purpose of comparison, the chelation of the quercetin molecule with aluminium on the 3-hydroxyl-4-keto site led to a structure mainly stabilised by a pyronium mesomeric form [20].

The chelation of the entity $Al(H_2O)_4^{3+}$ on the catechol group, to form the complex II, leads to an important steric hindrance with the sugar moiety. The consequence is a rotation of the B-ring that adopts a θ value of 27° (−13° for the free ligand) and a reorientation of the glucose with a modification of α and ω angle values. The electronic delocalisation between the B ring and the γ-pyrone is reduced and then the inter-ring bond length increases with respect to complex I. In this second complex, the contribution of the benzoyle form to the stabilisation of the aglycon structure is reinforced, whereas the cynnamoyl form becomes insignificant.

3.3. Model validation by FT-Raman and UV–Vis spectroscopies

Changes in the vibrational spectra caused by the coordination of a Al(III) ion to isoquercitrin have been used to confirm that the first site implied in the complexation mechanism is the 5-hydroxyl-4-keto group. A complexation at the level of the 3-hydroxyl-4-keto group must result in a considerable modification of the carbonyl vibration band. The FT-Raman spectrum of isoquercitrin in methanol solution exhibits lines at 1657 and 1617 cm^{-1} (shoulder) which can be,

Table 1
Bond lengths (Å) of isoquercitrin and complexes $Al(Iso)(H_2O)_4^{2+}$ and $Al_2(Iso)(H_2O)_8^{3+}$ calculated by AM1 and DFT methods

	Isoquercitrin		Complex I		Complex II	
	AM1	DFT	AM1	DFT	AM1	DFT
O(1)–C(2)	1.389	1.367	1.377	1.360	1.373	1.357
O(1)–C(9)	1.382	1.363	1.383	1.363	1.385	1.367
C(2)–C(3)	1.367	1.380	1.414	1.412	1.397	1.396
C(3)–C(4)	1.469	1.449	1.413	1.404	1.427	1.413
C(4)–C(10)	1.455	1.442	1.429	1.424	1.424	1.417
C(5)–C(10)	1.418	1.425	1.429	1.431	1.432	1.434
C(5)–C(6)	1.404	1.392	1.399	1.388	1.399	1.387
C(6)–C(7)	1.400	1.403	1.407	1.411	1.408	1.413
C(7)–C(8)	1.404	1.399	1.410	1.402	1.414	1.404
C(8)–C(9)	1.398	1.388	1.391	1.382	1.387	1.380
C(9)–C(10)	1.410	1.405	1.420	1.415	1.424	1.418
C(2)–C(1′)	1.462	1.467	1.429	1.436	1.446	1.449
C(1′)–C(2′)	1.402	1.413	1.416	1.422	1.413	1.419
C(2′)–C(3′)	1.395	1.384	1.385	1.377	1.387	1.382
C(3′)–C(4′)	1.413	1.410	1.424	1.420	1.436	1.428
C(4′)–C(5′)	1.402	1.394	1.412	1.403	1.398	1.397
C(5′)–C(6′)	1.390	1.391	1.379	1.382	1.390	1.389
C(6′)–C(1′)	1.407	1.410	1.423	1.422	1.411	1.414
C(4)–O(2)	1.248	1.265	1.329	1.323	1.318	1.309
C(3)–O(3)	1.388	1.376	1.385	1.381	1.385	1.380
C(5)–O(5)	1.361	1.339	1.347	1.353	1.344	1.350
C(7)–O(7)	1.369	1.359	1.356	1.342	1.353	1.338
C(3′)–O(3′)	1.379	1.368	1.376	1.358	1.363	1.362
C(4′)–O(4′)	1.369	1.355	1.350	1.333	1.349	1.349
O(2)–Al			1.768	1.799	1.771	1;800
O(5)–Al			1.754	1.785	1.751	1;787
O(3′)–Al					1.778	1;793
O(4′)–Al					1.782	1;810

respectively, assigned to C(4)=O(2) and C(2)=C(3) stretching modes. However, ours previous studies have shown that for such flavonoids, the carbonyl stretching is partially coupled with the C(2)=C(3) stretching vibration. Thus, the frequency generally assigned to the carbonyl function involves a participation of the C(2)=C(3) vibrator, and consequently the vibrational normal mode attributed to C(2)=C(3) stretching also implicates the carbonyl vibration. The addition of aluminium to the isoquercitrin solution (with [Al(III)]–[Iso] ratio < 1) significantly modifies the spectrum both in wavenumbers and intensity, notably in the spectral range 1200–1700 cm^{-1}. The Raman line previously assigned to the carbonyl vibration disappears, whereas the C(2)=C(3) stretching mode shifts to 1635 cm^{-1}. The high frequency shift observed for the C(2)=C(3) vibration might seem incoherent with an increase of the C(2)=C(3) bond length in complex I with respect to isoquercitrin and a displacement to lower frequencies of this mode would be expected. This fact can be easily explained by the mechanical coupling between the C(4)=O(2) and C(2)=C(3) vibration modes in isoquercitrin. This coupling increases the carbonyl frequency and decreases the C=C frequency, whereas in complex I, the line at 1635 cm^{-1} corresponds to a pure C(2)=C(3) stretching vibration. Two new intense bands located at 1548 and 1426 cm^{-1} appear in the Raman spectrum of complex I. These lines can be, respectively, assigned to the anti-symmetric and symmetric C–O stretching modes involving the C(4)–O(2) and C(3)–O(3) bonds. In the same time, the line at 1501 cm^{-1} attributed to the C(3)–O(3) stretching mode in the isoquercitrin Raman spectrum, has totally vanished of the complex spectrum. All these observations validate the hypothesis that chelation between Al(III) and isoquercitrin firstly occurs with the 5-hydroxyl-4-keto site. Nevertheless, the complex FT-Raman spectrum does not allow to observe and to differentiate the two forms: $Al(Iso)^{2+}$ and $Al(Iso)_2^{+}$, certainly because of the low concentration of this last one.

In order to obtain additional arguments for the structural modifications of the ligand engendered by the complexation with Al(III) and to certain of the presence of the $Al(Iso)_2^{+}$ complex, the electronic spectra of the different forms have been calculated and compared with the experimental ones. Due to the size of studied systems (more than hundred atoms for $Al(Iso)_2^{+}$), only semiempirical calculations could be envisaged. From optimised structures, the electronic spectra of isoquercitrin and of its three complexed forms

Table 2
Valence angles (°) of isoquercitrin and complexes $Al(Iso)(H_2O)_4^{2+}$ and $Al_2(Iso)(H_2O)_8^{3+}$ calculated by AM1 and DFT methods

	Isoquercitrin		Complex I		Complex II	
	AM1	DFT	AM1	DFT	AM1	DFT
C(9)–O(1)–C(2)	119.1	123.1	121.2	124.9	120.4	124.4
O(1)–C(2)–C(3)	121.1	118.9	118.9	117.0	120.4	117.9
C(2)–C(3)–C(4)	122.5	121.7	121.2	120.5	120.6	120.4
C(3)–C(4)–C(10)	115.1	116.4	119.5	120.6	119.0	120.3
C(4)–C(10)–C(9)	119.1	119.5	117.2	117.1	117.8	117.3
C(4)–C(10)–C(5)	123.5	122.2	125.7	124.6	125.2	124.1
C(10)–C(5)–C(6)	120.9	119.7	120.6	119.2	120.6	118.9
C(5)–C(6)–C(7)	119.3	119.8	119.8	120.6	119.9	120.6
C(6)–C(7)–C(8)	121.7	121.8	121.4	121.3	121.4	121.5
C(7)–C(8)–C(9)	117.7	117.6	117.7	117.7	117.8	117.6
C(8)–C(9)–C(10)	123.0	122.8	123.3	122.9	123.3	122.8
C(3)–C(2)–C(1′)	129.1	129.8	130.0	130.0	128.3	128.8
C2–C(1′)–C(6′)	119.7	119.4	119.6	119.4	119.3	118.6
C(6′)–C(5′)–C(4′)	119.7	120.2	119.7	120.1	118.5	119.3
C(5′)–C(4′)–C(3′)	119.6	119.4	119.2	119.8	120.4	120.4
C(4′)–C(3′)–C(2′)	120.5	120.5	120.8	120.1	120.8	120.2
C(3′)–C(2′)–C(1′)	119.7	120.5	120.1	120.6	118.3	119.5
C(2′)–C(1′)–C(6′)	119.8	118.4	118.5	118.5	120.5	119.7
C(10)–C(4)–O(2)	123.5	121.8	122.8	121.6	123.2	122.5
C(4)–C(3)–O(3)	116.2	116.4	118.1	117.3	117.8	116.1
C(6)–C(5)–O(5)	114.7	119.4	116.5	119.3	116.6	119.8
C(8)–C(7)–O(7)	116.1	116.6	115.7	116.3	115.6	116.0
C(8)–C(9)–O(1)	114.0	116.9	114.6	117.2	114.9	117.5
C(10)–C(9)–O(1)	123.0	120.2	122.1	119.8	121.8	119.7
O(1)–C(2)–C(1′)	109.8	111.3	111.1	113.0	111.3	113.2
C(2)–C(3)–O(3)	120.5	121.3	120.2	121.5	121.3	123.4
C(10)–C(5)–O(5)	124.3	120.8	122.9	121.4	122.8	121.3
C(6)–C(7)–O(7)	122.2	121.6	122.9	122.4	123.1	122.5
C(4')–C(3')–O(3′)	116.0	114.8	115.4	114.7	115.8	115.4
C(5′)–C(4′)–O(4′)	117.7	120.8	117.8	120.0	123.7	123.9
C(3)–O(3)–C	115.4	119.0	115.4	119.4	115.5	117.9
C(4)–O(2)–Al			120.8	126.7	122.0	127.1
C(5)–O(5)–Al			120.7	126.2	121.7	126.7
O(2)–Al–O(5)			105.8	98.3	105.2	97.9
C(3′)–O(3′)–Al					106.4	108.2
C(4′)–O(4′)–Al					106.8	108.1
O(3′)–Al–O(4′)					94.7	92.3

have been calculated with the AM1 method using configuration interaction treatment. On Fig. 6, the UV–Vis spectra of the different forms as well as the positions of the calculated electronic transitions are represented. The $Al_2(Iso)^{3+}$ experimental spectrum has been recorded from a solution containing $AlCl_3$ and

Table 3
Main dihedral angles (°) of isoquercitrin and complexes $Al(Iso)(H_2O)_4^{2+}$ and $Al_2(Iso)(H_2O)_8^{3+}$ calculated by AM1 and DFT methods

	Isoquercitrin		Complex I		Complex II	
	AM1	DFT	AM1	DFT	AM1	DFT
C(2)–C(3)–O(3)–C = α	124.2	116.9	118.4	116.7	103.3	95.9
C(3)–O(3)–C–O = ω	−94.2	−102.9	−93.4	−95.4	−89.5	−93.9
O(1)–C(2)–C(1′)–C(6′) = θ	−14.3	−12.7	−6.3	−11.9	27.8	26.5
C(2)–C(3)–C(4)–O(2)	175.9	175.8	176.7	175.5	−179.0	−177.7
O(1)–C(2)–C(3)–O(3)	174.6	173.6	172.8	171.1	173.4	178.0
C(4)–C(3)–C(2)–C(1′)	−174.68	−175.4	−177.2	−178.1	179.2	179.3
C(3)–C(4)–O(2)–Al			171.1	169.1	−179.4	−173.3
C(2′)–C(3′)–O(3′)–Al					−172.5	−174.7

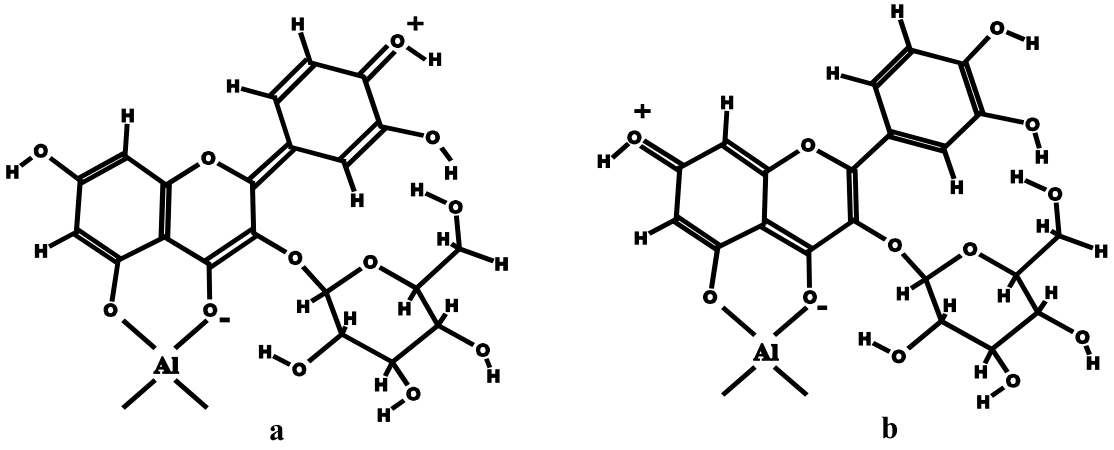


Fig. 5. Cinnamoyl (a) and benzoyle (b) mesomeric forms participating in the resonance of $Al(Iso)(H_2O)_4^{2+}$. Water molecules have been omitted.

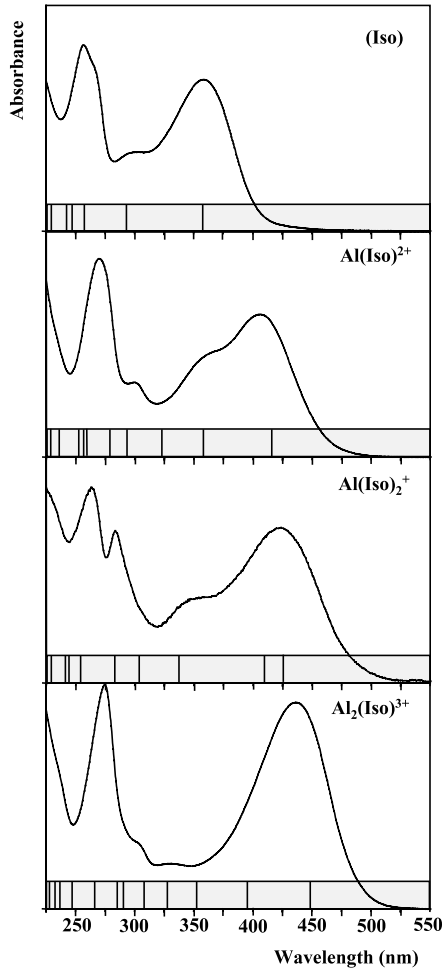


Fig. 6. UV–Vis spectra of isoquercitrin and its complexes with aluminium(III) in methanol. Vertical lines correspond to allowed calculated transitions.

isoquercitrin with a [Al(III)]–[Iso] ratio of 10, whereas the UV–Vis spectra of $Al(Iso)^{2+}$ and $Al(Iso)_2^{+}$ have been extracted using the SPECTFIT program. For all the compounds, a rather good accord is observed between the experimental spectra and the calculated allowed electronic transitions. Notably, excellent agreement of the experimental and calculated longest-wavelength band positions is obtained. This transition mainly involves the HOMO→LUMO contribution and presents a $\pi \rightarrow \pi^*$ character. Moreover, the bathochromic shift of the band I observed by addition of Al(III) to isoquercitrin is well reproduced by the CI calculations. The calculated electronic spectrum of complex $Al(Iso)_2^{+}$ is consistent with the extracted spectrum by SPECTFIT program and proves the existence of this form despite its low contribution. The accuracy found in the electronic spectra of isoquercitrin and of its complexes validates the geometries of these different forms obtained by the quantum chemical calculations.

3.4. Influence of the deprotonation state of isoquercitrin upon complexation

As previously explained, the *ortho*-dihydroxyl group cannot be involved in a complex with Al(III) in acidic medium. The voltammetric studies of Downard et al. [31] concerning the catechol–Al(III) system have shown that no complex is formed for pH below 4, whereas chelates of high stoichiometry particularly dominate in alkaline solution. We have studied the complexation of isoquercitrin in a mixture methanol (90%)–water (10%), in presence of HCl (3.2×10^{-2} M). The addition of $AlCl_3$ to the isoquercitrin solution leads to the formation of a complex of stoichiometry 1:1 involving the 5-hydroxyl-4-keto site, this complexed form is the same as this obtained in neutral methanol.

The complexation of isoquercitrin has also been investigated in alkaline medium, by adding to the methanol solution either sodium acetate (10^{-1} M) or sodium methanoate (5×10^{-3}). Generally, the flavonols are decomposed in alkaline medium. Dechene has shown that the unprotrected hydroxyl on position 3 contributes to the instability of flavonols, and conse-

quently the glycosilation on position 3 increases the stability of these compounds [32]. Thus, isoquercitrin is stable in presence of MeO^-, whereas the quercetin molecule is decomposed. The presence of sodium acetate or methanoate ionizes only the most acidic hydroxyl group in flavonoids and these ions compete with the potential sites of the molecule for complexing the metal ion. In flavonoids, the weakest acidic hydroxyl groups are generally in position 3, 7 and 4′ [33], in the case of isoquercitrin, only 7-hydroxyl and 4′-hydroxyl groups are susceptible to be deprotonated. The protonation constants of rutin have been spectroscopically determined by Escalar et al. [34], they estimated the two first pK_a at 7.1 and 8.3 but these last values have not be assigned to particular hydroxyl groups. As rutin only differs from isoquercitrin by the nature of the sugar, it is reasonable to think that the pK_a values of isoquercitrin are very close to those of rutin. The works of Jurd et al. [35] suggest that the hydroxyl function on position 7 of flavones and flavonols is more acidic than the other hydroxyls present in compounds, and that the presence of a free 7-hydroxyl group is observed by a bathochromic shift of the low wavelength band in alcoholic sodium acetate medium. On the other hand, for quercetin, Sauerwald et al. [36] propose pK_a values of 7.0 for the 3′ or 4′ positions and 9.1 for the hydroxyl on position 7, implicating that the 4′-hydroxyl is more acidic than the 7-hydroxyl. Nevertheless, these values are dubious and in complete disagreement with earlier studies concerning this kind of flavonoids such as morin (3,5,7,2′,4′-pentahydroxyflavone) [34,37]. Finally, the quercetin monoanion may be a mixture of tautomer species formed upon deprotonation of the most acidic 4′-hydroxyl and 7-hydroxyl group [38,39].

The UV–Vis spectrum of isoquercitrin in presence of acetate (Fig. 7(b)) exhibits a bathochromic shift of both the two absorption bands (band I: $\lambda_{max} = 378$ nm) with respect to the isoquercitrin in pure methanol spectrum (band I: $\lambda_{max} = 359$ nm) (Fig. 7(a)). This spectrum could be mainly assigned to the mono-deprotonated molecule involving two forms with deprotonation of the 4′-OH and 7-OH groups. Whereas the spectrum of isoquercitrin in presence of methanoate (band I: $\lambda_{max} = 407$ nm; Fig. 7(c)) could be attributed to a bi-deprotonated form with deprotonation both in 4′ and 7 positions. The addition of aluminium to the solution in presence of AcO^- leads to the formation of a first complex of stoichiometry 1:1. The spectrum (Fig. 7(d)) (band I: $\lambda_{max} = 425$ nm) of this chelate totally differs of the spectrum of complex 1:1 obtained in pure methanol. Therefore, the site implicates in this chelate is the catechol group and the formed complex is $Al(Iso)^+$. In a same way, the catechol group is involved in the complex obtained with isoquercitrin in presence of MeO^- (Fig. 7(e)) but with a stoichiometry Al(III):Iso = 1:2. Both with AcO^- or MeO^-, a large amount of added $AlCl_3$, with $[AlCl_3]$–[Iso] > 1 leads to the formation of a same complex (band I: $\lambda_{max} = 436$ nm) of stoichiometry Al(III)–Iso = 2:1, where the two potential sites are involved.

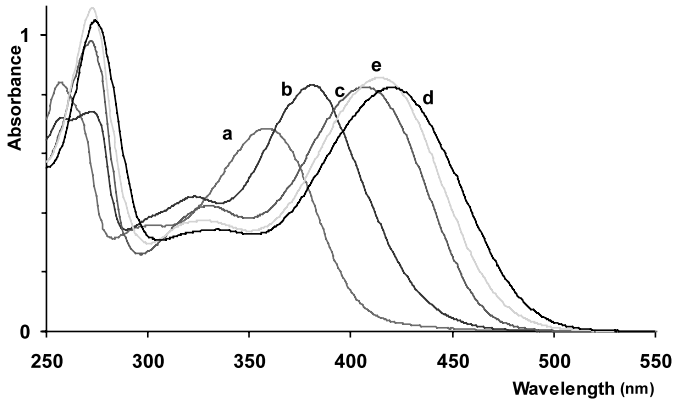


Fig. 7. UV–Vis spectra of: (a) isoquercitrin in pure methanol, (b) in pure methanol in presence of acetate, (c) in methanol in presence of methanoate, (d) of the complex in methanol in presence of acetate, (e) of the complex in methanol in presence of methanoate.

4. Conclusion

UV–Vis and Raman spectroscopies have permitted to determine the composition and the involved chelating sites of complexes of Al(III) with isoquercitrin molecule. Table 4 resumes the complexed species observed in different media and the chelating group involved in each form. It is worth noting that the formation of complexes simultaneously involving the two potential chelating sites necessitate a great amount of aluminium, and reasonably only the first formed specie present an interest. In acidic and in neutral conditions, the 5-hydroxy-4-keto group has a chelating power superior to the catechol group, whereas the complexation in alkaline medium occurs in the reverse order.

Table 4
Complex composition of Al(III) with isoquercitrin in different media

Medium	Complex	Chelating site
Neutral methanol	$Al(Iso)^{2+}$	5OH
	$Al(Iso)_2{}^+$	5OH
	$Al_2(Iso)^{3+}$	5OH + cat
Methanol + H_2O + HCl	$Al(Iso)^{2+}$	5OH
Methanol + AcO^-	$Al(Iso)^+$	cat
	$Al_2(Iso)^{3+}$	5OH + cat
Methanol + MeO^-	$Al(Iso)_2{}^-$	cat
	$Al_2(Iso)^{3+}$	5OH + cat

The last column present the group(s) involved in each complex. 5OH is relative to 5-hydroxy-4-keto group and cat to the catechol group.

References

[1] E. Middelton, C. Kandaswami, in: J.B. Harborne (Ed.), The Flavonoids: Advances in Research Since 1986, Chapman & Hall, London, 1994.
[2] L. Bravo, Nutr. Rev. 56 (1998) 317.
[3] E. Middelton, C. Kandaswami, T.C. Theoharides, Pharmacol. Rev. 52 (2000) 673.
[4] J. Kühnau, Wld. Rev. Nutr. Diet 24 (1976) 117.
[5] W. Bors, W. Heller, C. Michel, K. Stettmaier, Flavonoids and polyphenols: chemistry and biology, in: E. Cadenas, L. Parker (Eds.), Handbook of Antioxydants, Marcel Dekker, New York, 1996, p. 409.
[6] J.V. Formica, W. Regelson, Food Chem. Toxicol. 33 (1995) 1061.
[7] P.C. Hollman, M.B. Katan, Food Chem. Toxicol. 37 (1999) 937.
[8] G.G. Duthie, S.J. Duthie, J.A. Kyle, Nutr. Res. Rev. 13 (2000) 79.
[9] P.C. Hollman, J.M.B. Van Trijp, M.N.C. Buysman, M.S.V. Gaag, M.J.B. Mengelers, J.H. de Vries, M.B. Katan, FEBS Lett. 418 (1997) 152.
[10] Y. Masataka, K. Murakami, Anal. Biochem. 257 (1998) 40.
[11] J.E. Brown, H. Khodr, R.C. Hider, C.A. Rice-Evans, Biochem. J. 330 (1998) 1173.
[12] M.M. Krunz, T.J. Janjic, L.B. Pfendt, Mikrochim. Acta (1982) 417.
[13] Z. Radovic, D. Malesev, Mikrochim. Acta (1985) 247.
[14] D. Malesev, Z. Radovic, M. Jelikic-Stankov, M. Bogavac, Anal. Lett. 24 (1991) 1159.
[15] R. Dass, J.R. Mehta, J. Indian Chem. Soc. 72 (1995) 285.
[16] M. Katyal, Talanta 15 (1968) 95.
[17] A.C. Boudet, J.P. Cornard, J.C. Merlin, Spectrochim. Acta 56 (2000) 829.
[18] J.P. Cornard, A.C. Boudet, J.C. Merlin, Spectrochim. Acta 57 (2001) 591.
[19] J.P. Cornard, J.C. Merlin, J. Mol. Struct. 569 (2001) 129.
[20] J.P. Cornard, J.C. Merlin, J. Inorg. Biochem. (2002), in press.
[21] J.H. Yoe, L. Jones, Ind. Eng. Chem. Anal. Ed. 16 (1944) 11.
[22] Specfit Global Analysis System, Spectrum software Associates, Marlborough, MA, USA.
[23] H. Gampp, M. Maeder, C.J. Meyer, A. Zuberbühler, Talanta 33 (1986) 943.
[24] J.P. Cornard, A.C. Boudet, J.C. Merlin, J. Mol. Struct. 508 (1999) 37.
[25] M.J. Dewar, E.G. Zoebisch, E.F. Healy, J.J. Stewart, J. Am. Chem. Soc. 107 (1985) 3902.
[26] Hypercube Inc., Gainesville, FL, USA.
[27] A.D. Becke, J. Chem. Phys. 98 (1993) 5648.
[28] C. Lee, W. Yang, R.G. Parr, Phys. Rev. B 37 (1988) 785.
[29] M.J. Frisch, G.W. Trucks, H.B. Schlegel, G.E. Scuseria, M.A. Robb, J.R. Cheeseman, V.G. Zakrzewski, J.A. Montgomery, Jr., R.E. Stratmann, J.C. Burant, S. Dapprich, J.M. Millam, A.D. Daniels, K.N. Kudin, M.C. Strain, O. Farkas, J. Tomasi, V. Barone, M. Cossi, R. Cammi, B. Mennucci, C. Pomelli, C. Adamo, S. Clifford, J. Ochterski, G.A. Petersson, P.Y. Ayala, Q. Cui, K. Morokuma, D.K. Malick, A.D. Rabuck, K. Raghavachari, J.B. Foresman, J. Cioslowski, J.V. Ortiz, A.G. Baboul, B.B. Stefanov, G. Liu, A. Liashenko, P. Piskorz, I. Komaromi, R. Gomperts, R.L. Martin, D.J. Fox, T. Keith, M.A. Al-Laham, C.Y. Peng, A. Nanayakkara, C. Gonzalez, M. Challacombe, P.M.W. Gill, B. Johnson, W. Chen, M.W. Wong, J.L. Andres, C. Gonzalez, M. Head-Gordon, E.S. Replogle, J.A. Pople, GAUSSIAN 98, Revision A.7, Gaussian, Pittsburgh, PA, 1998.
[30] L.J. Porter, K.R. Markham, J. Chem. Soc. (1970) 1309.
[31] A.J. Downard, B. O'Sullivan, K.J. Powell, Polyhedron 15 (1996) 3469.
[32] E.B. Dechene, J. Am. Pharm. Assoc. 40 (1951) 495.
[33] K.H. Rosler, D.P. Wong, T.J. Mabry, J. Nat. Prod. 48 (1985) 837.
[34] G.M. Escalar, L.F. Sala, Can. J. Chem. 69 (1991) 1994.
[35] L. Jurd, R.M. Horowitz, J. Org. Chem. 22 (1957) 1618.
[36] N. Sauerwald, M. Schwenk, J. Polster, E. Bengsch, Z. Naturforsch. Teil. B 53 (1998) 315.
[37] B.A. Browne, J.G. McColl, C.T. Driscoll, J. Environ. Qual. 19 (1990) 65.
[38] P.K. Agrawal, H.J. Schneider, Tetrahedron Lett. 24 (1983) 177.
[39] O. Dangles, C. Dufour, S. Bret, J. Chem. Soc, Perkin Trans. 2 (1999) 737.

Table 1
Crystal and structure refinement data

Compound	**1** (−65 °C)	**1** (20 °C)	**2**	**3a** (−50 °C)	**3a** (20 °C)
Empirical formula	$C_{16}H_{22}N_2O_8Cu$	$C_{16}H_{22}N_2O_8Cu$	$C_{18}H_{24}N_2O_7Cu$	$C_{46}H_{41}N_5O_9Cu$	$C_{46}H_{41}N_5O_9Cu$
Formula weight	433.90	433.90	443.93	871.38	871.38
T (K)	208(2)	293(2)	293(2)	223(2)	293(2)
Crystal system	triclinic	triclinic	tetragonal	monoclinic	monoclinic
Space group	$P\bar{1}$ (no. 2)	$P\bar{1}$ (no. 2)	$I4_1/a$ (no. 88)	Cc (no. 9)	Cc (no. 9)
Unit cell dimensions					
a (Å)	7.9796(12)	8.0143(9)	30.6801(15)	19.9376(11)	19.969(4)
b (Å)	8.6175(17)	8.6833(10)	30.6801(15)	14.6957(11)	14.752(2)
c (Å)	14.639(2)	14.7608(17)	9.9339(6)	15.1213(7)	15.129(2)
α (°)	73.64(2)	73.371(2)	90.00	90.00	90.00
β (°)	84.728(15)	84.341(2)	90.00	109.281(6)	109.393(6)
γ (°)	73.005(13)	72.445(2)	90.00	90.00	90.00
V (Å^3)	923.7(3)	938.33(19)	9350.5(9)	4182.0(4)	4203.8(11)
Z	2	2	16	4	4
ρ_{calc} (g cm^{-3})	1.560	1.536	1.261	1.384	1.377
Abs. coeff. (mm^{-1})	1.229	1.210	0.970	0.586	1.259
F(000)	450	450	3693	1812	1812
Crystal size (mm)	0.45 × 0.30 × 0.25	0.39 × 0.18 × 0.07	0.63 × 0.14 × 0.12	0.25 × 0.10 × 0.10	0.28 × 0.28 × 0.16
θ Range (°)	3.02–30.92	1.44–23.20	1.33–28.03	2.48–25.78	3.81–70.00
Index ranges	$-1 \le h \le 11$, $-12 \le k \le 12$, $-21 \le l \le 12$	$-8 \le h \le 4$, $-9 \le k \le 9$, $-16 \le l \le 16$	$-25 \le h \le 40$, $-39 \le k \le 40$, $-12 \le l \le 13$	$-24 \le h \le 21$, $-17 \le k \le 17$, $-17 \le l \le 16$	$-24 \le h \le 0$, $0 \le k \le 17$, $-17 \le l \le 18$
Reflections collected	6092	4195	25973	12845	4104
Independent reflections	5293 [$R_{int} = 0.050$]	2688 [$R_{int} = 0.060$]	5600 [$R_{int} = 0.087$]	6466 [$R_{int} = 0.038$]	4104 [$R_{int} = 0.000$]
Absorption correction	Ψ-scans	SADABS	SADABS	Ψ-scans	Ψ-scans
Max/min transmission	0.915/0.875	1.000/0.657	1.000/0.786	0.944/0.867	0.824/0.719
Data/parameters	5293/244	2688/252	5600/257	6466/665	4104/551
Goodness-of-fit	0.994	0.973	0.973	0.970	1.017
Final R indices [$I > 2\sigma(I)$]	$R_1 = 0.0493$, $wR_2 = 0.1230$	$R_1 = 0.0515$, $wR_2 = 0.1244$	$R_1 = 0.0639$, $wR_2 = 0.1898$	$R_1 = 0.0427$, $wR_2 = 0.0912$	$R_1 = 0.0402$, $wR_2 = 0.102$

attempt to recrystallize **3** from CH_3CN, afforded single crystals of a compound of formula [Cu(HMANO)-(bipy)$_2$](HMANO)·H_2MANO·CH_3CN (**3a**).

In the 3000–3500 cm^{-1} region, the IR spectra of **1**–**3** show two bands, generally of medium intensity, corresponding to OH stretching vibrations. The strong band around 1590 cm^{-1} is attributable to ν_{asym}(OCO), and the band between 1330 and 1390 cm^{-1} to ν_{sym}(OCO). The values of $\Delta\nu = \nu_{asym}(OCO) - \nu_{sym}(OCO)$, 209–258 cm^{-1}, are typical of monodentate carboxylato groups [8] and very similar to those found in copper(II)/α-hydroxycarboxylato/1,10-phenanthroline systems [9]. The bands around 1490 and 1450 cm^{-1} are due to the C=C and C=N stretching modes of the coordinated 2,2′-bipyridine molecules. A weak band around 400 cm^{-1} is assignable to ν(CuO), and the band between 250 and 300 cm^{-1} is tentatively identified as due to ν(CuN) [10].

The three compounds have similar diffuse reflectance spectra (Table 2). They consist of an intense charge transfer band between 26600 and 28600 cm^{-1} together with a broad d–d band centred at wavenumbers typical of octahedral copper(II) complexes with tetragonal distortion, 14200–12800 cm^{-1} [11].

Table 2
UV–Vis spectra, EPR and magnetic moment data for complexes **1**–**3**

Complex	UV–Vis (cm^{-1})	$G_{\|\|}$	$g_\perp$	$g_{av.}$	μ_{eff} (BM)
1	26 600, 14 200	2.29		2.06	1.47
2	27 030, 12 850	2.30	2.04	2.08	1.67
3	28 570, 12 800	2.25	2.03	2.09	1.56

The magnetic moments of **1** and **3** fall as temperatures rises. At room temperature μ_{eff} is only 1.47 BM for **1**, 1.67 BM for **2** and 1.56 BM for **3**. Such low values suggest the possibility of antiferromagnetic coupling between metal centres [12,13], although low magnetic moments are also displayed by mixed complexes of Cu^{II} with 1,10-phenanthroline and glycolic or mandelic acid in which there is no antiferromagnetic coupling [9]. At low temperatures (79–200 K for **1** and 79–250 K for **3**), the magnetic moments are within the range reported for copper(II) complexes lacking Cu–Cu interaction, 1.7–2.2 BM [14].

The room temperature EPR spectrum of polycrystalline **1** (Table 2) is typical of axially symmetric coordination, with $g_{||} > g_{\perp}$. The symmetry of the copper atom is thus approximately C_{4v}, and the unpaired electron occupies a $3d x^2-y^2$ orbital. The value of 2.29 for g suggests octahedral coordination with a tetragonal distortion [12,15]. Similar spectra are displayed by complexes of copper(II) with α-hydroxycarboxylato ligands and 1,10-phenanthroline [9]. The EPR spectra of **2** and **3** (Table 2) are typical of rhombic systems with g values consistent with compressed rhombic-octahedral or *cis*-distorted octahedral stereochemystries [15].

The thermogravimetric behaviour of compounds **1** and **3** (Table 3) is similar to that of mixed complexes containing 1,10-phenanthroline and α-hydroxycarboxylato ligands [9]. Weakly bound lattice water is largely lost during stabilization of the balance. Decomposition of the ligands begins at 200 °C and in the case of **3** continues up to 400 °C. In **1**, ligand decomposition over the range 200–250 °C, is followed by a stable region up to 400 °C and by further weight loss between 400 and 450 °C. For **2**, one water molecule is lost between 75 and 150 °C, and the ligands decompose over the range 150–225 °C. No further weight loss was suffered by any of the compounds. The ratios of final to initial weights (19.48% for **1**, 16.41% for **2** and 17.77% for **3**) approximated the values expected for CuO (20.51% for **1**, 17.91% for **2** and 15.24% for **3**).

Table 3
Thermogravimetric analyses for the complexes **1**–**3**

Compound	Temperature range (°C)	% Weight loss	Corresponding to
1	RT–200	stable	
	200–250	76.22	bipy + HLACO
	250–400	stable	
	400–450	4.25	
	450–600	stable	
2	RT–75	stable	
	75–150	6.06	1 H_2O
	150–225	76.82	bipy + HMLACO
	225–700	stable	
3	RT–200	stable	
	200–225	70.80	bipy + HMANO
	225–300	6.12	
	300–400	5.20	
	400–600	stable	

3. Structural analysis

Selected interatomic distances and angles are listed in Table 4, and the main hydrogen bonds in Table 5. Figs. 1–3 show drawings of the structures of compounds **1**, **2** and **3a**, respectively, together with the atom-numbering schemes used.

The structure of **1** and **3a** are essentially the same at −65 °C (**1**) or −50 °C (**3a**) as at 20 °C, the only marginally significant differences being that at room temperature the unit cell volume is slightly greater and the axes slightly longer (Table 1). In what follows, the bond lenghts and angles cited (Table 4) are the values measured at low temperature.

The crystals of **1** and **2** are based on neutral complexes of the form $[Cu(HL)_2(2,2'\text{-bipy})]\cdot n H_2O$, where HL is a monoanionic O,O′-bidentate α-hydroxycarboxylato li-

Table 4
Selected interatomic bond lengths (Å) and bond angles (°) for complexes **1**–**3**

	1	**2**	**3a**
Bond lengths			
Cu–O11	1.963(2)	1.956(4)	2.047(3)
Cu–O21	1.969(2)	1.952(4)	
Cu–N1	2.013(3)	2.015(4)	1.988(4)
Cu–N2	2.001(3)	1.995(4)	2.057(4)
Cu–N3			2.157(4)
Cu–N4			2.003(4)
Cu–O13	2.384(3)	2.291(4)	
Cu–O23	2.302(2)	2.310(4)	
Bond angles			
O11–Cu–O21	93.06(11)	91.72(18)	
O11–Cu–N2	93.23(11)	93.27(18)	147.94(14)
O21–Cu–N2	168.54(11)	166.69(18)	
O11–Cu–N1	168.81(11)	166.48(18)	91.97(15)
O21–Cu–N1	94.47(10)	96.57(18)	
N2–Cu–N1	80.80(11)	81.01(18)	80.80(18)
O11–Cu–O23	94.47(10)	99.76(15)	
O21–Cu–O23	74.92(9)	76.10(15)	
N2–Cu–O23	95.04(10)	90.88(15)	
N1–Cu–O23	95.48(9)	92.61(16)	
O11–Cu–O13	75.03(9)	75.90(15)	
O21–Cu–O13	87.59(10)	98.47(17)	
N2–Cu–O13	103.30(10)	94.72(16)	
N1–Cu–O13	97.02(9)	92.28(16)	
O23–Cu–O13	159.21(8)	173.08(13)	
N3–Cu–N1			99.27(16)
N4–Cu–N1			177.28(13)
N3–Cu–N2			113.63(11)
N4–Cu–N2			97.68(17)
N3–Cu–O11			98.32(14)
N4–Cu–O11			90.50(14)
N4–Cu–N3			79.23(17)

Table 5
Main hydrogen bonds in the complexes **1**–**3**

D–H···A	*d*(D–H) (Å)	*d*(H···A) (Å)	*d*(D···A) (Å)	∠(DHA) (°)
Compound ***1*** [a]				
O13–H13···O2	0.62	2.16	2.766(4)	164.2
O23–H23···O1	0.68	1.99	2.643(3)	160.5
O1–H1A···O12^{i}	0.88	1.90	2.748(4)	162.0
O1–H1B···O12^{ii}	0.96	1.85	2.779(3)	162.1
O2–H2A···O2^{iii}	0.91	1.91	2.794(7)	164.5
O2–H2B···O22^{iii}	1.09	1.90	2.993(4)	178.2
C10–H10···O11	0.97	2.41	3.033(4)	121.4
C3–H3···O22^{iv}	0.84	2.58	3.338(4)	150.9
C7–H7···O22^{v}	0.80	2.55	3.307(5)	157.8
C9–H9···O12^{vi}	0.88	2.73	3.335(5)	127.1
Compound ***2*** [b]				
O13–H13···O22^{i}	0.94(6)	1.72(6)	2.657(6)	173(5)
O23–23···O12^{ii}	0.93	2.06	2.721(5)	126.8
O22···O1			2.958(8)	
O1···O1^{i}			3.086(5)	
C7–H7···O12^{iii}	0.93	2.33	3.256(7)	173.2
C10–H10···O11	0.93	2.53	3.023(7)	113.7
Compound ***3a*** [c]				
O21–H21A···O31^{i}	1.25	1.23	2.437(4)	159.2
O13–H13A···O32	1.43	1.39	2.765 (7)	157.7
O23–H23A···O22	0.74	2.05	2.612(6)	134.0
O33–H33A···O12	0.79	2.09	2.755(5)	142.0
O33–H33A···O32	0.79	2.26	2.694(5)	115.7
C24–H24···O13	0.89	2.36	3.196(6)	158.5
C60–H60···O33	0.93	2.34	3.255(7)	166.2
C47–H47···O11^{ii}	0.82	2.58	3.306(7)	147.7

[a] Symmetry transformations: i, $-x$, $-y+1$, $-z$; ii, x, $y-1$, z; iii, $-x$, $-y+1$, $-z+1$; iv, $-x$, $-y$, $-z+1$; v, $x+1$, $y-1$, z; vi, $-x+1$, $-y+1$, $-z$.

[b] Symmetry transformations: i, $y+3/4$, $-x+3/4$, $z-1/4$; ii; $-x+3/2$, $-y+1/2$, $-z+1/2$; iii, x, y, $z-1$.

[c] Symmetry transformations: i, x, $-y+1$, $z+1/2$; ii, x, $-y$, $z-1/2$.

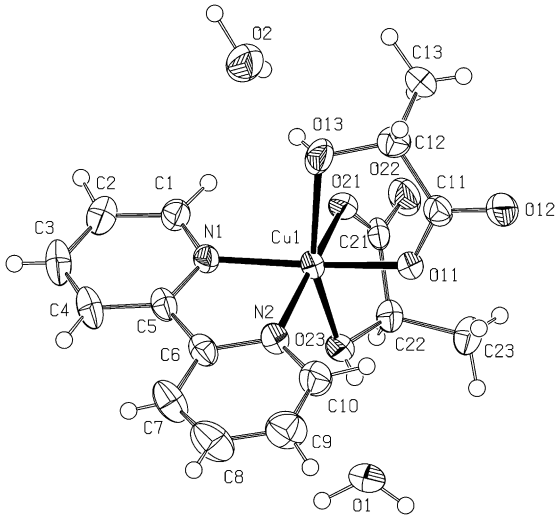


Fig. 1. Molecular structure of [Cu(HLACO)$_2$(bip*y*)]·2H$_2$O (**1**).

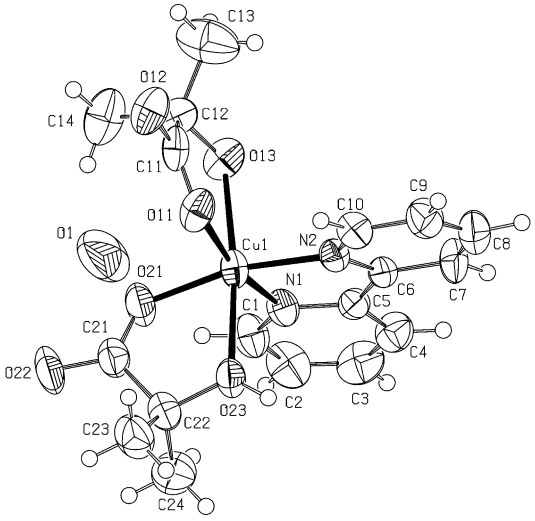


Fig. 2. Molecular structure of [Cu(HMLACO)$_2$(bipy)]·H$_2$O (**2**).

gand (lactato in **1**, 2-methyllactato in **2**). The copper ions are six-coordinate, being bound to the nitrogen atoms of the 2,2′-bipyridine molecule and to one carboxy and one hydroxyl oxygen of each of two α-hydroxycarboxylato anions. There are thus three five-membered chelate rings. In both **1** and **2** the copper atom has elongated octahedral coordination geometry with the two nitrogen atoms and the mutually *cis* $O_{carboxy}$ atoms equatorial and the two α-hydroxyl oxygen atoms axial, the difference between the average equatorial and axial bond lengths being 0.356 Å in **1** and 0.301 Å in **2**. This elongation of the coordination polyhedron, due to a Jahn–Teller effect, is also observed in polymeric complexes containing lactato or 2-methyllactato ligands and 4,4′-bipyridine [16]. Additional deviation from ideal octahedral geometry is shown by the chelating angles ranging from 74.92° to 80.80° in **1** and from 75.90° to 81.01° in **2** (Table 4) and by some of the *trans* angles, such as $O_{hydroxyl}$–Cu–$O_{hydroxyl}$ in **1** [159.21(8)°] and $O_{carboxy}$–Cu–N in **2** [166.69(18)° and 166.48(18)°]. The Cu–$O_{carboxy}$ distances fall within the range usually observed in similar copper(II) complexes (1.90–1.97 Å) [16–19], as do the Cu–$O_{hydroxyl}$ distances [16], and as in other complexes with a CuN_2O_4 core [16,17,20] the values of the latter depend on their involvement in hydrogen bonds, the hydroxyl oxygens with the shorter Cu–$O_{hydroxyl}$ bonds having the shorter hydrogen bond (Table 5). The Cu–N distances, 1.995–2.015 Å, are within the normal range for complexes with N,N-chelating ligands [17,18] but are slightly shorter

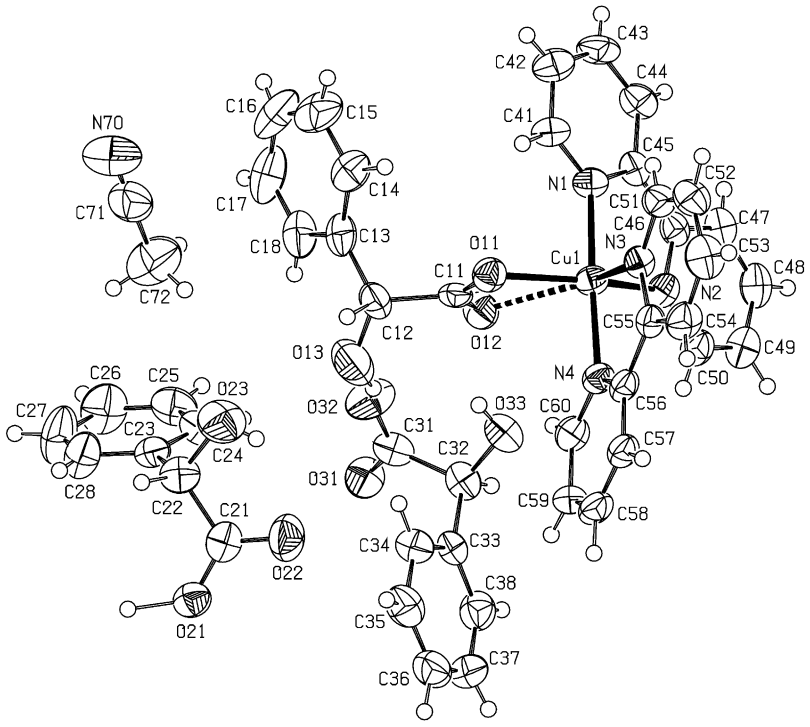


Fig. 3. Structure of $[Cu(HMANO)(bipy)_2](HMANO)(H_2MANO)\cdot CH_3CN$ (**3a**).

than in polymeric copper(II) complexes containing 4,4′-bipyridine [16].

In compound **3a** the asymmetric unit is composed of the cationic complex $[Cu(HMANO)(bipy)_2]^+$ and, in the outer coordination sphere, an $HMANO^-$ counterion, a nondeprotonated neutral H_2MANO molecule, and a solvating acetonitrile molecule. α-Hydroxycarboxylic acids have been reported to show similarly diverse behaviour in mixed complexes containing other diamines [9,21,22], without there apparently being any relation between this behaviour and the bulk of the α-hydroxycarboxylic acid. The copper atom in **3a** is five-coordinated to the four 2,2′-bipyridine nitrogens and to one of the carboxylato oxygens of the monodentate, monodeprotonated mandelic acid; the second carboxylato oxygen, O12, is too far from the metal [2.673(3) Å] for coordination. The Cu–N and Cu–O distances are within the usual ranges for this kind of copper(II) complex [9,13,23]. The coordination polyhedron cannot be described as either a square pyramid or a trigonal bipyramid, having a trigonality index $\tau = 0.49$ ($\tau = (\beta - \alpha)/60°$, where β and α are the largest angles in the coordination sphere [24]; its value is zero for a perfect square pyramid and unit for a perfect trigonal bipyramid).

The C–O distances of the coordinated α-hydroxycarboxylato oxygen atoms are similar in the three complexes (between 1.256 and 1.267 Å) and only slightly longer than those of the uncoordinated oxygen atoms (1.226–1.246 Å). The O–C–O angles are also very similar, 122.5°–125.1°. As expected, the individual pyridine rings of the bipy ligands are all planar. The bipy ligand as a whole is also planar in **1**, but in **2** and **3a** there are dihedral angles between the pyridyl rings of each bipy: 7.2(2)° in **2**, and 2.3(3)° and 8.0(3)° in **3a**. Twisting around the 2-2′ bond is normal in coordinated bipy [25].

All three compounds have both intra- and intermolecular hydrogen bonds (Table 5). In **1** the two solvating water molecules play a key role in the formation of a 2D network, bridging between neighbouring molecules of **1** (Fig. 4). Each water molecule accepts the hydroxyl

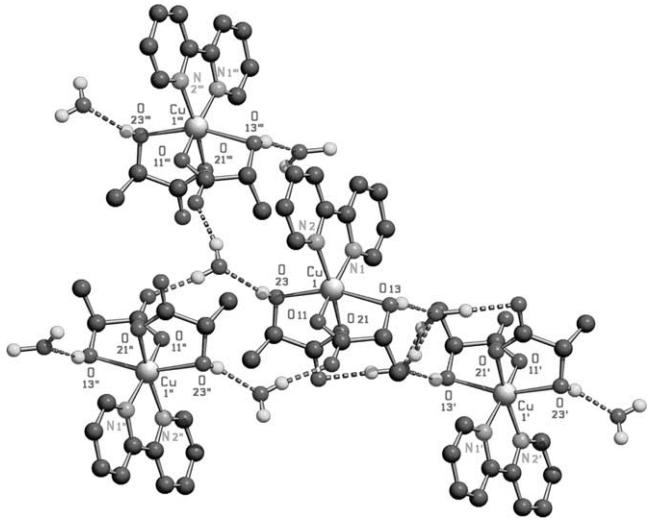


Fig. 4. View of the hydrogen bonding linkage in **1**.

hydrogen of one of the α-hydroxycarboxylato ions of its 'own' molecule, and donates hydrogens to the uncoordinated O atoms of neighbouring molecules (and, in the case of H_2O (**2**), to another O2 oxygen). The O···O hydrogen bond distances and angles are in the ranges 2.643(3)–2.993(4) Å and 160.5°–178.2°, respectively. In **2** the salient feature of the crystal packing is the three-dimensional supramolecular arrangement of the molecules around a fourfold screw axis, which is stabilized by hydrogen bonds between the hydroxyl groups and the uncoordinated carboxylato O atoms (Table 5 and Fig. 5). The channels so generated run through the crystal in the direction of the c axis with the water molecules inside them. The O···O hydrogen bond distances are in the range 2.657(6)–2.958(8) Å.

In all three complexes there are also C–H···O interactions, mainly involving bipy carbons and $O_{carboxy}$ atoms (Table 5). In **3a**, in which these hydrogen bonds play a decisive role in the crystal packing (Fig. 6), there are also C–H···O interactions between the mandelic acid and the mandelato anion of the outer sphere. The C···O distances and C–H···O angles of these bonds have values indicating significant interactions [26], 3.023–3.338 Å and 113.7°–173.2°, respectively (Table 5), the strongest of these bonds being intramolecular.

The shortest centroid-to-centroid distances between pyridyl rings belonging to different bipy ligands are 3.655 Å in **1** and **3a** and 3.913 Å in **2** [27]. The latter distance is too large for a π stacking interaction [28], but both are similar to those observed in copper(II) complexes of 1,10-phenanthroline [9,29]

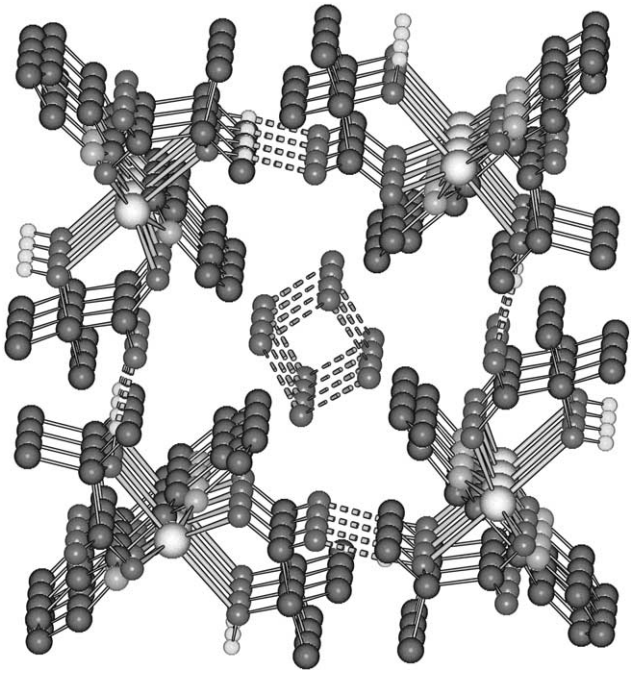


Fig. 5. View of the packing in **2**, showing the channel formation along *c* with the water molecules inside them.

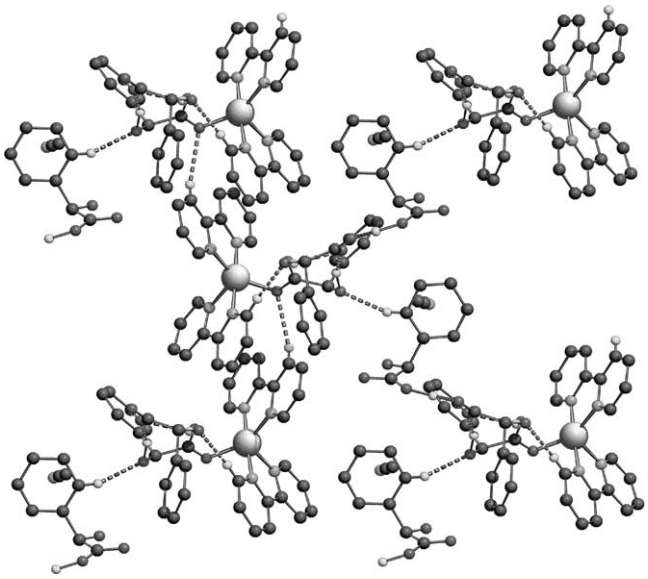


Fig. 6. View of the hydrogen bonding linkage in **3a**.

4. Experimental

4.1. Materials and instruments

Chemicals were purchased from commercial sources and used without further purification. Elemental analyses (C, H, N) were performed in a Carlo Erba 1108 microanalyser. Melting points were measured in a Büchi melting point apparatus and are uncorrected. The IR spectra of samples incorporated in KBr discs (4000–400 cm^{-1}) or polyethylene-sandwiched Nujol mulls (500–100 cm^{-1}) were recorded on a Bruker IFS66v spectrophotometer. A Shimadzu UV-3101PC spectrophotometer was used to obtain electronic spectra in the region 900–350 nm. Magnetic susceptibility measurements were made at room temperature using a Johnson Matthey magnetic susceptibility balance (for **2**) or at variable temperature with a DSM-10 magnetometer (for **1** and **3**). X-band (9300 MHz) EPR spectra were obtained at room temperature with a Bruker ESP 300E spectrometer. Thermogravimetric analyses were performed on a Shimadzu TGA-DGT-50H instrument coupled to a Nicolet Magma 550 FT-IR spectrophotometer.

4.2. Preparation of the complexes

A mixture of $CuCO_3 \cdot Cu(OH)_2$ (2.26 mmol) and the appropriate α-hydroxycarboxylic acid (9.10 mmol) in 35 mL of ethanol was refluxed for 4 h at 75 °C. 2,2′-Bipyridine (4.52 mmol) was added, and refluxing was continued for 2 h, after which the mixture was stirred for several days. The blue solids formed were filtered out, washed with ethanol and dried over $CaCl_2$.

4.3. [Cu(HLACO)$_2$(bipy)]·2H$_2$O (1)

Yield: 55%. M.p.: 206 °C. *Anal.* Found: C, 44.5; H, 5.2; N, 6.6. Calc. for $C_{16}H_{22}N_2O_8Cu$ (433.9): C, 44.3; H, 5.1; N, 6.5%. IR (ν cm^{-1}): 3407, 3115, ν(OH); 1607, ν(CC); 1595, ν_{asym}(OCO); 1386, ν_{sym}(OCO); 1497, 1450, ν(CC, CN); 1084, ν(CO); 1049, ring breathing; 733, γ(CH); 396, ν(CuO); 310, ν(CuN).

Single crystals of **1** were obtained by slow concentration of the mother liquor at room temperature (r.t.).

4.4. [Cu(HMLACO)$_2$(bipy)]·H$_2$O (2)

Yield: 65%. M.p.: 190 °C. *Anal.* Found: C, 47.9; H, 5.6; N, 6.2. Calc. for $C_{18}H_{24}N_2O_7Cu$ (443.9): C, 48.7; H, 5.4; N, 6.3%. IR (ν cm^{-1}): 3442, 3205, ν(OH); 1642, ν(CC); 1593, ν_{asym}(OCO); 1359, ν_{sym}(OCO); 1492, 1459, ν(CC, CN); 1176, ν(CO); 1059, ring breathing; 734, γ(CH); 393, ν(CuO); 296, ν(CuN).

Crystals of **2** were grown at room temperature by slow diffusion of *n*-hexane into a solution of the compound in acetone.

4.5. [Cu(HMANO)$_2$(bipy)]·4H$_2$O (3)

Yield: 75%. M.p.: 199 °C. *Anal.* Found: C, 52.3; H, 4.2; N, 4.7. Calc. for $C_{26}H_{30}N_2O_{10}Cu$ (594.0): C, 52.6; H, 5.1; N, 4.7%. IR (ν cm^{-1}): 3410, 3110, ν(OH); 1607, ν(CC); 1597, ν_{asym}(OCO); 1339, ν_{sym}(OCO); 1490, 1445, ν(CC, CN); 1082, ν(CO); 1058, ring breathing; 731, γ(CH); 406, ν(CuO); 272, ν(CuN).

Slow concentration of the mother liquor yielded a blue oil that upon attempted recrystallization from CH_3CN afforded blue single crystals of formula [Cu(HMANO)(bipy)$_2$](HMANO)(H$_2$MANO)·CH_3CN (**3a**).

4.6. X-ray crystallography

Data collection and refinement parameters are listed in Table 1. The diffraction data were collected on an Enraf–Nonius CAD4 (complex **1** at −65 °C and complex **3a** at 20 °C), on a Bruker SMART CCD (complexes **1** and **2** at r.t.) and on a STOE-IPDS diffractometer (complex **3a** at −50 °C). Graphite-monochromated Mo Kα radiation ($\lambda = 0.71073$ Å) or Cu Kα radiation ($\lambda = 1.54184$ Å) were used and the data were corrected for Lorentz and polarization effects for absorption [30,31]. The structures were solved by direct methods and subsequent Fourier difference techniques (SHELXS [32]), and were refined on F^2 using SHELXL [33]. Hydrogen atoms were inserted at calculated positions and constrained with isotropic thermal parameters, except for those hydroxyl and water H atoms that it was possible to locate from a Fourier difference map, which were refined isotropically. Complex **3a** crystallizes in the chiral space group *Cc*, and the analysis unambiguously established its absolute stereochemistry [Flack parameter 0.000(14)]. Neutral atom scattering factors and anomalous dispersion corrections were taken from International Tables for X-ray Crystallography [34]. Geometrical calculations and illustrations were performed or generated with the SHELXL-97 [33], SCHAKAL-97 [35] and PLATON [27] packages.

5. Supplementary material

Crystallographic data for the structural analysis have been deposited with the Cambridge Crystallographic Data Centre, CCDC nos. 182331 for **1** (20 °C), 182332 for **1** (−65 °C), 182333 for **2**, 182334 for **3a** (−50 °C) and 194598 for **3a** (20 °C). Copies of this information may be obtained free of charge from The Director, CCDC, 12 Union Road, Cambridge CB2 1EZ, UK (Fax: +44-1223-336033; e-mail: deposit@ccdc.cam.ac.uk or www: http://www.ccdc.cam.ac.uk).

Acknowledgements

We thank the DGESIC and Xunta de Galicia for financial support (Refs. BQU202-04523-C02, BQU2002-03543 and PGIDT00PXI20302PN).

References

[1] R.B. King, Encyclopedia of Inorganic Chemistry, Wiley, New York, 1994.
[2] N. Farrel, Transition Metal Complexes as Drugs and Chemotherapeutic Agents, Kluwer Academic, Dordrecht, 1989.
[3] M. Biagioli, L. Strinna-Erre, G. Micela, A. Panzanelli, M. Zema, Inorg. Chim. Acta 310 (2000) 1.
[4] P. Kiprof, W. Scherer, L. Pajdla, E. Herdtweck, W.A. Herrmann, Chem. Ber. 125 (1992) 43.
[5] G.G. Bombi, B. Corain, A.A. Sheikh-Osman, G.C. Valle, Inorg. Chim. Acta 171 (1990) 79.
[6] Z. Guo, P.J. Sadler, Angew. Chem., Int. Edn. Engl. 38 (1999) 1512.
[7] H. Sigel, Inorg. Chem. 19 (1980) 1411.
[8] G.B. Deacon, R.J. Phillips, Coord. Chem. Rev. 33 (1980) 227.
[9] R. Carballo, B. Covelo, S. Balboa, A. Castiñeiras, J. Niclós, Z. Anorg. Allg. Chem. 627 (2001) 948.
[10] K. Nakamoto, Infrared and Raman Spectra of Inorganic and Coordination Compounds, 3rd ed., Wiley, New York, 1978.
[11] A.B.P. Lever, Inorganic Electronic Spectroscopy, 2nd ed., Elsevier, Amsterdam, 1986.
[12] R.C. Mehrotra, R. Bohra, Metal Carboxylates (and references therein), Academic Press, New York, 1983.
[13] M. McCann, J.F. Cronin, M. Devereaux, G. Ferguson, Polyhedron 14 (1995) 2379.
[14] F.A. Cotton, G. Wilkinson, Advanced Inorganic Chemistry, 5th ed., Wiley, New York, 1988.

[15] B.J. Hathaway, in: G. Wilkinson, R.D. Gillard, J.A. McClevarty (Eds.), Comprehensive Coordination Chemistry, vol. 5, Pergamon Press, Oxford, 1987.
[16] R. Carballo, A. Castiñeiras, B. Covelo, E.M. Vázquez-López, Polyhedron 20 (2001) 899.
[17] M. Saladini, M. Candini, D. Iacopino, L. Menabue, Inorg. Chim. Acta 292 (1999) 189.
[18] M. McCann, F. Humphreys, V. Mckee, Polyhedron 16 (1997) 3655.
[19] J. Fawcett, S.H. Laurie, C. Simpson, M.C.R. Symons, F.A. Taiwo, L. Hawkins, Inorg. Chim. Acta 312 (2001) 245.
[20] K. Prout, V.S.B. Mtetwa, F.J.C. Rossoti, Acta Crystallogr., Sect. B B49 (1993) 73.
[21] M. Ahlgrén, R. Hämäläinen, Finn. Chem. Lett. (1975) 211.
[22] M. Ahlgrén, U. Turpeinen, R. Hämäläinen, Acta Chem. Scand. A36 (1982) 841.
[23] M. Devereux, M. McCann, J.F. Cronin, G. Ferguson, V. McKee, Polyhedron 18 (1999) 2141.
[24] A.W. Addison, T.N. Rao, J. Reedijk, J. Van Rijn, G.C. Verschoor, J. Chem. Soc., Dalton Trans. (1984) 1349.
[25] P. Román, A. Luque, C. Guzmán-Miralles, J.I. Beitia, Polyhedron 14 (1995) 2863.
[26] G.R. Desiraju, Acc. Chem. Res. 29 (1996) 441.
[27] A.L. Spek, PLATON. A Multipurpose Crystallographic Tool, University of Utrecht, 2000.
[28] C. Janiak, J. Chem. Soc., Dalton Trans. (2000) 3885.
[29] G. Mendoza-Diaz, L.M.R. Martínez-Aguilera, R. Moreno-Esparza, K.H. Pannell, F. Cervantes-Lee, J. Inorg. Biochem. 50 (1993) 65.
[30] A.C.T. North, D.C. Phillips, F.S. Mathews, Acta Crystallogr., Sect. A 24 (1968) 351.
[31] SMART (control) and SAINT (integration) software. Bruker Analytical X-ray Systems, Madison, WI, 1994.
[32] G.M. Sheldrick, Acta Crystallogr., Sect. A 46 (1990) 467.
[33] G.M. Sheldrick, SHELXL-97, Universität Göttingen, Göttingen, Germany, 1997.
[34] A.J.C. Wilson, International Tables for Crystallography, vol. C, Kluwer Academic, Dordrecht, 1992.
[35] E. Keller, SCHAKAL-97, A Computer Program for the Graphic Representation of Molecular and Crystallographic Models, University of Freiburg, Freiburg, Germany, 1997.

were washed with methanol and dried on air. (Found: C, 32.23; H, 3.61; N, 15.04; $C_{10}H_{13}N_4O_5ClZn$ Calc. C, 32.46; H, 3.54; N, 15.14%; melting point (m.p.) 172 °C).

2.2. Instrumental

IR spectra were recorded on Perkin–Elmer FTIR 1600 spectrometer using standard KBr pellet technique. Raman data were collected on a Bruker RFS100 spectrometer equipped with Nd laser excitation. The UV–Vis reflectance spectrum was obtained on a CARY 500 UV–Vis NIR instrument, however, the complex spectrum was very similar to that of the ligand sodium salt and will not be discussed here.

2.3. Crystal structure determination

Crystal data together with refinement details are given in Table 1. All measurements on the crystal were performed on a KUMA KM4CCD κ-axis diffractometer with graphite-monochromated Mo Kα radiation. The data were corrected for Lorentz and polarisation effects. No absorption correction was applied. The structure was solved by direct methods (program SHELXS-97 [11]) and refined by the full-matrix least-squares method on all F^2 data using the SHELXL-97 [12] program. Non-hydrogen atoms were refined with anisotropic thermal parameters; hydrogen atoms were included from the $\Delta\rho$ maps and refined with isotropic thermal parameters. Crystal structures were drawn with help of the ORTEP [13].

Table 1
Crystallographic details

Empirical formula	$C_{10}H_{13}N_4O_5ClZn$
Formula weight	370.06
Temperature (K)	293(2)
Wavelength (Å)	1.54180
Crystal system	triclinic
Space group	$P\bar{1}$
Unit cell dimensions	
a (Å)	7.7090(15)
b (Å)	7.8920(16)
c (Å)	11.496(2)
α (°)	97.95(3)
β (°)	93.35(3)
γ (°)	100.60(3)
Volume (Å^3)	678.3(2)
Z	2
D_{calc} (Mg m^{-3})	1.812
Absorption coefficient (mm^{-1})	4.614
$F(000)$	376
Crystal size (mm)	0.10 × 0.12 × 0.15
θ Range for data collection (°)	3.90–80.21
Index ranges	$-9 \le h \le 9$, $-10 \le k \le 10$, $-14 \le l \le 14$
Reflections collected/unique	6074/2764 [$R_{int} = 0.0398$]
Refinement method	full-matrix least-squares on F^2
Data [$I > 2\sigma(I)$]/parameters	2302/242
Goodness-of-fit on F^2	1.088
Final R indices [$I > 2\sigma(I)$]	$R_1 = 0.0375$, $wR_2 = 0.0853$
R indices (all data)	$R_1 = 0.0517$, $wR_2 = 0.1000$
Largest difference peak and hole (e Å^{-3})	0.368 and −1.304

2.4. Density functional calculations

The theoretical studies presented in this work were performed using the GAUSSIAN-98 package [14] and applying the density functional theory (DFT) [15] methods. The DFT approach utilised the Becke's three-parameter hybrid functional (B3LYP) [16] and the LanL2DZ [17,18] basis set. The vibrational analyses were carried out on the optimised structures and applying the harmonic oscillator approximation.

3. Results and discussion

3.1. Description of the structure

The imidazole-4-acetic acid is a complexing agent offering several co-ordination centres as both imidazole ring nitrogen and carboxylate oxygen atoms (Fig. 1) Taking into account the stability of the chelate complexes, the anionic form **IV** seems to by the most suitable for metal binding. This chelating ability has been postulated in equilibrium analysis [19,20] and has been found in the X-ray studies [21,22] where copper(II) ions were chelated by one of the carboxylate oxygen atoms and N_3 atom of the imidazole ring.

Quite different co-ordination mode of imidazole-4-acetic acid is observed in the present work, where two ligand forms are engaged in complex formation. One half of the ligand acts as bidentate, but not chelating agent. Prior to complexation, the 'chelating' form **IV** is converted into tautomeric form **V** by translating the N_1 proton to the N_3 atom. Thus, the zinc(II) ions are bonded via carboxylate oxygen and N_1 nitrogen atoms leading to the one-dimensional polymeric structure of the complex (Fig. 2). The polymeric pattern extends along the b axis of the crystal unit cell. The metal co-ordination sphere is completed by one chloride anion and carboxylate oxygen of second, neutral ligand molecule being in form **III**. This 'zwitterion' form is

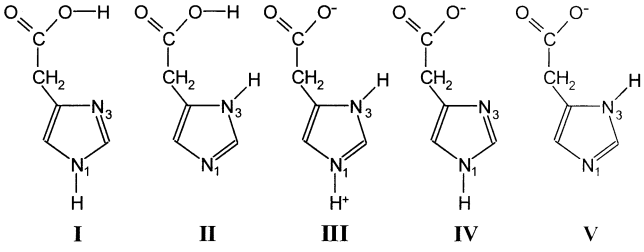


Fig. 1. Neutral and ionic forms of the ligand.

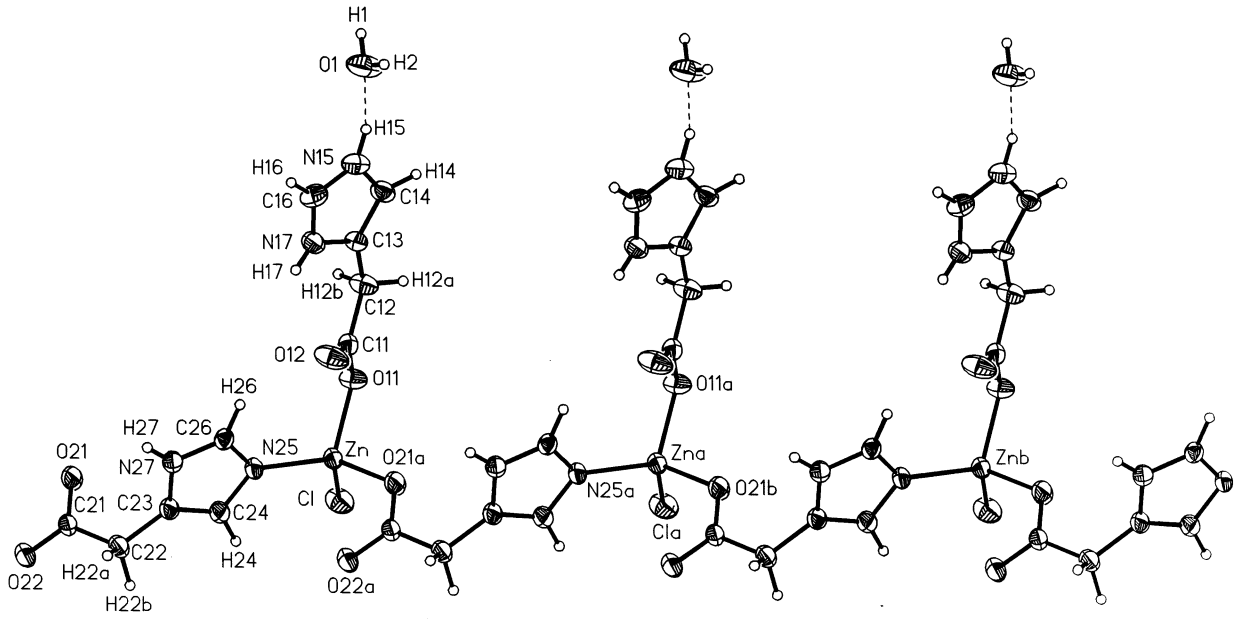


Fig. 2. View of [ZnCl(ia)(Hia)]·H_2O polymer with atom numbering scheme and 50% probability thermal ellipsoids.

typical for pure ligand in solid state, as has been found in the crystal structure of the imidazole-4-acetic acid monohydrate [23]. The same investigation revealed that imidazole ring and adjacent carbon atom of methylene group are planar. Such planarity is also preserved in the studied complex, for both forms of the ligand. The difference between free and co-ordinating ligand was found for the orientation of the carboxylate group with respect to the imidazole ring. In the Hia·H_2O structure [23], these subunits are nearly perpendicular. In the present complex structure, the carboxylate group is less twisted forming with the imidazole plane an angle 77.2(3)° found for bridging form **V** and 31.6(3)° for side ligand described as tautomer **III**. In the ligand form **V**, one of the imidazole ring nitrogen atoms is involved in metal bonding, whereas in the form **III** is not. It is interesting to check how much the imidazole skeleton is altered by Zn–N bond formation. The comparison of the respective structural data (Table 2) shows that co-ordination effects are relatively small: only one, C26–N27 bond is 0.036 Å longer when imidazole ring is co-ordinating. The differences in the remaining bond lengths of the imidazole moiety are comparable with their standard deviations. Also the 'in-plane' imidazole ring angles are altered less than 3°.

The metal surrounding is quasi-tetrahedral. The maximum deviation from the ideal tetrahedron angles is observed for the N25–Zn–O21a angle equal to 119.2(1)°. Metal–nitrogen and metal–oxygen bond lengths are very similar (1.987(2) and 1.981(2), 1.979(2) Å, respectively), whereas the metal–chlorine bond, being 2.258(1) Å, is markedly longer. The two Zn–O bond distances are comparable with those frequently

Table 2
Selected interatomic distances (Å) and angles (°)

Metal surrounding			
Interatomic distances			
Zn–O11	1.981(2)	Zn–O21a	1.979(2)
Zn–Cl	2.258(1)	Zn–N25	1.987(2)
Interatomic angles			
O11–Zn–O21a	102.6(1)	O21a–Zn–Cl	111.1(1)
O11–Zn–N25	113.6(1)	N25–Zn–O21a	119.2(1)
O11–Zn–Cl	103.1(1)	N25–Zn–Cl	106.2(1)
Monodentate ligand		Bidentate ligand	
Interatomic distances			
O11–C11	1.266(4)	O21–C21	1.255(4)
O12–C11	1.222(4)	O22–C21	1.243(4)
C11–C12	1.524(4)	C21–C22	1.524(4)
C12–C13	1.487(5)	C22–C23	1.496(4)
C13–C14	1.347(4)	C23–C24	1.343(4)
C14–N15	1.376(5)	C24–N25	1.381(4)
N15–C16	1.316(5)	N25–C26	1.316(4)
C16–N17	1.306(5)	C26–N27	1.342(4)
N17–C13	1.381(4)	N27–C23	1.376(5)
Interatomic angles			
O11–C11–C12	113.9(3)	O21–C21–C22	118.0(3)
C11–C12–C13	116.5(3)	C21–C22–C23	117.3(3)
C12–C13–C14	129.8(3)	C22–C23–C24	131.5(3)
C13–C14–N15	107.1(3)	C23–C24–N25	109.7(3)
C14–N15–C16	109.0(3)	C24–N25–C26	106.3(3)
N15–C16–N17	108.3(3)	N25–C26–N27	110.1(3)
C16–N17–C13	109.9(3)	C26–N27–C23	108.3(3)
N17–C13–C14	105.8(3)	N27–C23–C24	105.6(3)
C24–N25–Zn	123.6(2)	C26–N25–Zn	130.0(2)
Zn–O11–C11	116.0(2)	Zn–O21a–C21a	119.0(2)

Atom numbering is given in Fig. 2. Symmetry transformation used to generate equivalent atoms; a: $x, y-1, z$.

observed for carboxylato complexes [24,25]. The distances between pendant carboxylic oxygen atoms and the zinc(II) ion are much longer (2.929(3) and 3.013(2) Å), indicating the monodentate configuration of the carboxylato groups. The length of co-ordination bond between zinc and imidazole N_1 (N25) atom is similar to these found in tetrahedral zinc complexes of neutral imidazole as co-ligand [26], but slightly shorter than those of the imidazole derivatives [25,27].

The zinc(II) environment can partially be compared with the active site of the native carboxypeptidase A, where the metal is bonded to two imidazole rings (His69 and His196) and carboxylic oxygen (Glu72) [28,29]. The metal–nitrogen distance found here is almost the same as the Zn–His69 (1.98 Å) and 0.1 Å shorter than the Zn–His196 (2.08 Å) [29]. The metal–oxygen bond lengths in carboxypeptidase A are longer being 2.17 Å [28] and 2.24 Å [29].

The complex polymer chains are linked in a three-dimensional manner by hydrogen bonds. The side, monodentate ligand subunits of parallel chains are intercalated (Fig. 3), which provides many ineratomic contacts suitable for hydrogen bonding. In these interactions the water molecules are fully engaged, joining three polymer chains via N15–H15···O1, O1–H1···O22e and O1–H2···O12f bonds (equivalent oxygen atoms are generated by symmetry transformations e: $x-1$, $y-1$, $z+1$; f: $-x-1$, $-y$, $-z+1$). The respective donor–acceptor distances are 2.663(5), 2.780(4) and 2.818(5) Å indicating the strong H-bonding and the significant role of the water molecules in the stabilisation of the crystal structure. Additional hydrogen bonds are formed by remaining N–H groups. The monodentate ligand shows an intramolecular N17–H17···O12 interaction with N17···O12 distance equal 2.805(4) Å. In the bidentate ligand moiety, similar distance N27···O22 is much longer being 4.458(4) Å, as a result of much more twisted orientation of the carboxylate group with respect to the imidazole ring. However, an interchain bonding is observed between N27–H27 group and O22d (d: $-x$, $-y+2$, $-z$) atom with 2.884(4) Å donor–acceptor distance. In addition, the weak interaction of the mentioned N17–H17 group and chlorine atom has also be considered since the respective N17···Clc distance is 3.239(3) Å (c: $x-1$, y, z).

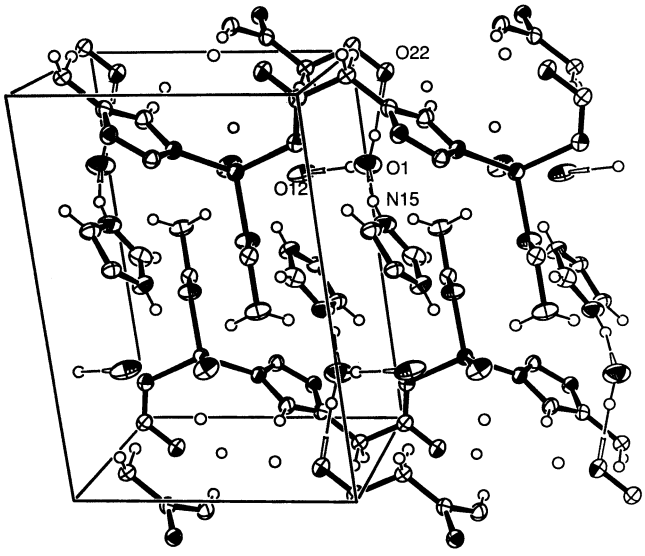


Fig. 3. View of the unit cell content demonstrating the intercalation of polymer chains and H-bonding of water molecule. In order to complete the polymeric pattern, atoms in the range $0 \le a \le 1$, $0 \le b \le 2$, $-0.9 \le c \le 1.1$ are presented.

3.2. Vibrational spectra

Since two different forms of the ligand are present in the complex, it is interesting how this phenomenon is reflected in the vibrational spectra. First evidence is the higher number of bands observed for the complex in the middle-infrared region in comparison with the spectra of copper(II) imidazole-4-acetate complexes where only one, chelating form of the ligand is present [21,22]. However, this number of bands is not twice higher, which suggests that only some ligand vibrations of mono- and bidentate ligand forms have significantly different frequencies. The main difference between these forms is the co-ordination Zn–N bond instead of the N–H bond. Thus, the differences between respective vibrations of imidazole rings are expected to be the most significant. As results from the X-ray data, the geometry of imidazole rings is almost the same, which means that the electron density and respective force constants are of similar values. Considering also the H–Zn mass effect, it is difficult to predict simply the vibrational effects caused by imidazole–zinc(II) bond formation. In order to solve this problem, the vibrations of two subunits (Fig. 4), representing both ligand forms were predicted from density functional calculations.

In such theoretical attempts there is always a problem of model simplification, necessary in case of polymeric

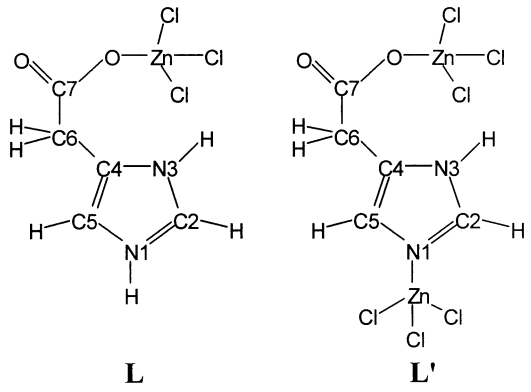


Fig. 4. Models of the mono- and bidentate ligand forms.

compounds. In present work, the calculations were carried out for two molecular ions shown in Fig. 4. The quasi-tetrahedral surrounding of the zinc(II) ions was mimic by additional chloride ions, which produced additional vibrations but of low frequencies and not interfering with the imidazole ring or carboxylate group modes. The attempts to use only zinc(II) ions as terminal ones gave the optimised geometry too much differing from that found in the X-ray investigation. For applied models, the geometry of the imidazole ring was

Table 3
Selected vibrations of zinc(II) complex with imidazole-4-acetic acid

Calculated		Observed			Assignment with PED (%) [a]
L	**L′**	IR	*R*	IR deut.	
1665		1628s	1623w		ν(C4–C5)-47 + δ(N3–H)-13 + ν(C4–C6)-11 + δ(N3–H)-17
1639				**1618s**	**ν(C4–C5)-59 + ν(C4–C6)-14**
	1626	1605vs	1610s		ν(C–O)-23 + ν(C=O)-22 + ν(C4–C5)-18
1607		1593vs	1602sh [b]	1593vs	ν(C–O)-40 + ν(C=O)-39
1595				**1593vs**	**ν(C–O)-33 + ν(C=O)-30 + ν(C4–C5)-15**
	1574	1550sh	n.o. [c]	1550sh	ν(C4–C5)-29 + ν(C–O)-17 + ν(C=O)-16
1550		1538w	n.o.	1520w	ν(C2–N3)-36 + δ(C2–H)-26 + ν(N1–C2)-24
	1492	1495m	1494s	1495w	δ(C2–H)-26 + ν(N1–C2)-23 + ν(C2–N3)-20
1480		1445sh	1443s		δ(N1–H)-49 + ν(N1–C2)-20
1400				**n.o.**	**ν(N1–C2)-34 + ν(N1–C5)-15 + δ(N1–D)-14**
1415		1403m	1403s	1413m	δ(N3–H)-31 + ν(C2–N3)-16 + ν(N3–C4)-14
1383				**1387vs**	**ν(N3–C4)-26 + ν(N3–C2)-21**
	1403	1387vs	1386s		ν(N3–C4)-29 + ν(C2–N3)-13 + ν(C4–C5)-12
	1379	1364sh	1364s		ν(N1–C2)-28 + δ(N3–H)-20 + ν(C2–N3)-11
	1334			**1345m**	**ν(N1–C2)-25 + ν(C2–N3)-21 + ν(C=O)-16**
	1337	1306vs	1306s	1305sh	ν(C=O)-35 + ν(C–O)-24 + ν(C6–C7)-13
1308		1295sh	1295s	1297s	ν(C=O)-28 + ν(C–O)-27
1271		1268m	1268s	1256m	ν(C4–C6)-21 + ν(N3–C4)-13 + ν(N1–C5)-10
	1259	1239m	1241s	1233m	ν(N1–C5)-31 + δ(C5–H)-16
1214		1200w	1200s	1197w	δ(C2–H)-41 + δ(C5–H)-15 + δ(N1–H)-15
	1159	1160sh	1163m		δ(N3–H)-30 + ν(C2–N3)-24 + δ2(im)-13
1154		1149s	1150s		δ(N3–H)-30 + ν(N1–C2)-24 + ν(C2–N3)-16
	1123	1110s	1109s	1110s	ν(N1–C5)-50 + δ(C5–H)-21 + ν(N1–C2)-12
1095		1095w	1097m	1095sh	ν(N1–C5)-52 + δ(C5–H)-17
	1066	1029m	1026w		π(N3–H)-88
1021		971m	973m		π(N3–H)-35 + δ2(im)-29 + ν(N3–C4)-11
	999	1008m	1008s	1001m	δ2(im)-35 + ν(N3–C4)-12 + ν(C4–C6)-11
	981	989s	989m		δ1(im)-72 + ν(N3–C4)-14
956		937m	n.o.		δ1(im)-54 + ν(N3–C4)-25
934		805s	n.o.	690sh	π(N3–H)-51 + δ1(im)-20
	901	887m	887w		ν(C6–C7)-45 + δ(C=O)-16 + ν(C=O)-14
	886			**890m**	**δ(N3–D)-36 + ν(C6–C7)-12**
883				**890m**	**δ(N1–D)-47**
	873	852m	851w	848m	π(C2–H)-99
872		852m	851w	848m	ν(C6–C7)-52
	844	840m	n.o.	837sh	π(C5–H)-94
841		840m	n.o.	837sh	π(C5–H)-42 + π(C2–H)-19
807		n.o.	790w	789m	π(C2–H)-50 + δ(C–O)-17
789		775m	775m		π(C5–H)-53 + π(C2–H)-23 + δ(C–O)-14
	776			**n.o.**	**π(N3–D)-91**
714				**n.o.**	**π(N3–D)-65**
684		715s	710m		τ1(im)-22 + τ2(im)-18 + δ2(im)-14
	677	657m		659m	τ1(im)-93
	676	657m	660m	659m	τ2(im)-86
667		560m	560w		π(N1–H)-81
634		635sh	636w	635m	τ1(im)-37
612		632m	n.o.	630m	τ2(im)-70 + τ1(im)-29

Data for N-deuterated isotopomer differing significantly in energy from those of natural molecule are listed separately and boldfaced.

[a] ν, stretching; δ, in-plane bending; π, out-of-plane bending; δ(im), in-plane bending of imidazole ring; τ(im), out-of-plane bending of imidazole ring. Atom numbering is given in Fig. 4.

[b] Shoulder.

[c] Not observed.

very well reproduced. All calculated bond lengths were slightly overestimated, but no more than 4%. For ring angles the agreement was excellent, the maximum deviation was 0.9° (0.8%).

Normal vibrations, calculated by GAUSSIAN-98 program in Cartesian co-ordinates, were converted into internal co-ordinates defined as recommended by Pulay et al. [30]. Using these co-ordinates, a potential energy distribution (PED) has been calculated for all normal modes of natural and N-deuterated species.

Table 3 lists the wavenumbers of selected normal vibrations characterised by predominant PED terms contributing more than 10% to the vibrational energies. Observed IR and Raman bands were correlated with calculated modes on the basis of similar frequencies, relative intensities and deuteration effects. Comparing both ligand subunits, one may expect that imidazole stretching vibrations of the N1–C2 and N1–C5 bonds (Fig. 4) should be the most affected by zinc(II) co-ordination. The performed calculations do not support such assumption. The vibrations of predominant ν(N1–C5) character are observed at close frequencies (1110 and 1095 cm^{-1}) for both ligand forms. The ν(N1–C2) vibration is strongly coupled with other modes and cannot be similarly compared. It contributes, together with the ν(C2–N3) vibration, to two normal modes observed for **L** at 1538 and 1149 cm^{-1} and for **L′** at 1495 and 1364 cm^{-1}. In addition, the ν(N1–C2) vibration is involved in the 1445 cm^{-1} mode, predominantly due to δ(N1–H) vibration of monodentate form **L**. The last vibration is not present in **L′** and in consequence the ν(N1–C2) vibration additionally appears in the 1110 cm^{-1} mode. Different distribution of the ν(N1–C2) vibration causes changes in the ν(C2–N3) contributions and further, in the PEDs and frequencies of most imidazole 'in plane' vibrations, being strongly coupled. For example, the ν(C4–C5) vibration contributes mainly to the normal modes observed for **L** at 1628 cm^{-1} and at much lower wavenumber (1550 cm^{-1}) for **L′**. The stretching of the fifth imidazole bond, namely ν(N3–C4) vibration, dominates in only one normal mode observed for **L′** at 1387 cm^{-1}, and it is coupled with imidazole bending modes δ1(im), δ2(im) which also have considerably different frequencies 989 and 937 cm^{-1} for **L** and **L′** subunits, respectively.

The aforementioned coupling between imidazole ring vibrations is partially extended on side, acetic chain vibrations, causing the differences in their frequencies as it is noted for ν(CC) and ν(CO) vibrations. According to PED, the ν(C6–C7) vibration has a dominating contribution to 887 and 852 cm^{-1} modes related to **L′** and **L** ligands. The ν(C4–C6) vibration is strongly mixed with imidazole ring vibrations and cannot be definitely attributed to any of observed bands. The asymmetric ν(CO) vibrations, calculated for **L′** and **L** at 1626 and 1607 cm^{-1}, were attributed to local maxima of an intense band centred in the IR spectrum at about 1600 cm^{-1}. The symmetric counterparts were localised at about 1300 cm^{-1}, giving approximately 300 cm^{-1} separation from the asymmetric modes, which confirms the monodentate co-ordination of the carboxylate groups.

The above results suggest the conclusion that the discussed differences between **L** and **L′** vibrations are rather due to the detachment of the N1 proton than the imidazole–zinc(II) bond formation. As has been predicted by calculations, the wavenumbers of many corresponding vibrational modes of **L** and **L′** are different enough to be observed as separate bands or shoulders. This also explains the higher number of observed IR and Raman transitions, mentioned at the beginning of the present section.

4. Conclusions

The chelating ability of the imidazole-4-acetic acid has been previously documented. In the presence study, we have unambiguously demonstrated for the first time that this compound in its deprotonated form is also capable of acting as bridging ligand. Such co-ordination mode leads to the 1D polymeric structure of the metal complex. Moreover, at each metal centre we have found another, neutral ligand molecule co-ordinating the zinc(II) ion via carboxylate oxygen atom. The use of the carboxylate group for metal co-ordination, instead of imidazole ring nitrogen atoms may be explained by general tendency of the imidazole-4-acetic acid to adopt the 'zwitterionic' structure, as has been observed in its crystalline state [23]. This tautomer preference is also confirmed by the respective values of the acidity constants equal $pK_{COOH} = 3.188(2)$ for the carboxylic group and $pK_{im} = 7.336(1)$ for the NH group [19].

5. Supplementary data

Crystallographic data for the structural analysis have been deposited with the Cambridge Crystallographic Data Centre, CCDC No. 189497. Copies of this information may be obtained free of charge from The Director, CCDC, 12 Union Road, Cambridge, CB2 1EZ, UK (fax: +44-1223-336033); e-mail: deposit@ccdc.cam.ac.uk or www: http://www.ccdc.cam.ac.uk.

Acknowledgements

This work was supported by Wroclaw University of Technology. Thanks are due to Poznan Supercomputing and Networking Centre for the generous allotment of computer time.

References

[1] I. Bertini, H.B. Gray, S.J. Lippard, J.S. Valentine, Bioinorganic Chemistry, University Science Books, Mill Valley, CA, 1994.
[2] L.D. Pettit, Pure Appl. Chem. 56 (1994) 247.
[3] S. Sjöberg, Pure Appl. Chem. 69 (1997) 1549.
[4] C.I.H. Ashby, C.P. Cheng, E.N. Duesler, T.L. Brown, J. Am. Chem. Soc. 30 (1978) 6063.
[5] E. Kimura, Y. Kurogi, M. Shionoya, M. Shira, Inorg. Chem. 30 (1991) 4524.
[6] R.W. Schayer, J. Biol. Chem. 196 (1952) 469.
[7] R.C. Baldridge, C.D. Tourtellotte, J. Biol. Chem. 233 (1958) 125.
[8] M. Chebib, K.N. Mewett, G.A.R. Johnston, Eur. J. Pharmacol. 357 (1998) 227.
[9] J.K. Khandelwal, G.D. Prell, A.M. Morrishow, J.P. Green, J. Neurochem. 52 (1989) 1107.
[10] D.E. Wilcox, Chem. Rev. 96 (1996) 2435.
[11] G.M. Sheldrick, SHELXS-97, Program for Solution of Crystal Structures, University of Göttingen, Göttingen, Germany, 1997.
[12] G.M. Sheldrick, SHELXL-97, Program for Crystal Structure Refinement, University of Göttingen, Göttingen, Germany, 1997.
[13] L.J. Farrugia, J. Appl. Crystallogr. 30 (1997) 565.
[14] M.J. Frisch, G.W. Trucks, H.B. Schlegel, G.E. Scuseria, M.A. Robb, J.R. Cheeseman, V.G. Zakrzewski, J.A. Montgomery, Jr., R.E. Stratmann, J.C. Burant, S. Dapprich, J.M. Millam, A.D. Daniels, K.N. Kudin, M.C. Strain, O. Farkas, J. Tomasi, V. Barone, M. Cossi, R. Cammi, B. Mennucci, C. Pomelli, C. Adamo, S. Clifford, J. Ochterski, G.A. Petersson, P.Y. Ayala, Q. Cui, K. Morokuma, D.K. Malick, A.D. Rabuck, K. Raghavachari, J.B. Foresman, J. Cioslowski, J.V. Ortiz, A.G. Baboul, B.B. Stefanov, G. Liu, A. Liashenko, P. Piskorz, I. Komaromi, R. Gomperts, R.L. Martin, D.J. Fox, T. Keith, M.A. Al-Laham, C.Y. Peng, A. Nanayakkara, M. Challacombe, P.M.W. Gill, B. Johnson, W. Chen, M.W. Wong, J.L. Andres, C. Gonzalez, M. Head-Gordon, E.S. Replogle, J.A. Pople, GAUSSIAN-98, Revision A.9, Gaussian, Pittsburgh, PA, 1998.
[15] R.G. Parr, W. Wang, Density Functional Theory of Atoms and Molecules, Oxford University Press, Oxford, 1989.
[16] A.D. Becke, J. Chem. Phys. 104 (1996) 1040.
[17] P.J. Hay, W.R. Wadt, J. Chem. Phys. 82 (1985) 270.
[18] T.H. Dunning, Jr., P.J. Hay, in: H.F. Schaefer, III (Ed.), Modern Theoretical Chemistry, vol. 3, Plenum, New York, 1976, p. 1.
[19] I. Török, P. Surdy, A. Rockenbauer, L. Korecz, Jr., G.J. Anthony, A. Koolhaas, T. Gajda, J. Inorg. Biochem. 71 (1998) 7.
[20] H. Sigel, A. Saha, N. Saha, P. Carloni, L.E. Kapinos, R. Griesser, J. Inorg. Biochem. 78 (2000) 129.
[21] P. Drożdżewski, B. Pawlak, T. Głowiak, Pol. J. Chem. 75 (2001) 1711.
[22] P. Drożdżewski, B. Pawlak, T. Głowiak, J. Coord. Chem. 55 (2002) 735.
[23] N. Okabe, T. Hayashi, Acta Crystallogr., Sect. C 55 (1999) 1142.
[24] T.J. Otto, K.A. Wheeler, Acta Crystallogr., Sect. C 57 (2001) 704.
[25] T.A. Zevaco, G. Görls, E. Dinjus, Inorg. Chem. Commun. 1 (1998) 170.
[26] R. Baggio, M.T. Garland, M. Perec, D. Vega, Inorg. Chim. Acta 284 (1999) 49.
[27] T.A. Zevaco, G. Görls, E. Dinjus, Inorg. Chem. Acta 269 (1998) 283.
[28] D.C. Rees, M. Lewis, W.N. Lipscomb, J. Mol. Biol. 168 (1983) 367.
[29] J.T. Bukrinsky, M.J. Bjerrum, A. Kadziola, Biochemistry 37 (1998) 16555.
[30] P. Pulay, G. Fogarasi, F. Pang, J.E. Boggs, J. Am. Chem. Soc. 101 (1979) 2550.

2.2. Preparations

2.2.1. Preparation of 1-bromo-2,6-bis(bromomethyl)benzene

To a stirred solution of 2-bromometaxylene (24.95 g, 0.135 mol) in CCl_4 (150 ml) were added 2 equiv. of *N*-bromosuccinimide (NBS) (48.01 g, 0.270 mol) and a catalytic amount of 2,2′-azobis-(2-methylpropionitrile) (AIBN). The reaction mixture was heated to reflux and stirred for 6 h. The succinimide formed was then filtered off and the orange filtrate evaporated to dryness. A solid was obtained and recrystallized in hexane (150 ml) affording white needles. Yield: 21.11 g (46%). M.p.: 95 °C (literature: 97–98 °C [3a]); ^{1}H NMR ($CDCl_3$, 250.1 MHz, δ ppm): 4.65 (s, 4H, CH_2), 7.29 (t, $^3J_{H/H}$ = 6.7 Hz, 1H, 4-aryl-H), 7.42 (d, $^3J_{H/H}$ = 6.7 Hz, 2H, 3,5-aryl-H); ^{13}C NMR ($CDCl_3$, 50.3 MHz, δ ppm): 33.92 (CH_2Br), 126.69 (1-aryl-C), 128.08 (4-aryl-C), 131.45 (3,5-aryl-C), 138.52 (2,6-aryl-C). EI MS (70 eV, *m*/*z* %): 342 (M^+, 11); 263 ($M^+ - Br$, 100), 182 ($M^+ - Br_2$, 35), 103 ($M^+ - Br_3$, 32).

2.2.2. Preparation of 1-bromo-2,6-bis[(diethylamino)methyl]benzene

To a stirred solution of 1-bromo-2,6-bis(bromomethyl)benzene (21.11 g, 0.062 mol) dissolved in 150 ml of toluene was added dropwise a solution of diethylamine (21.67 g, 0.296 mol, 31 ml) in 50 ml of toluene for 1 h. After 10 min a white precipitate of diethylammonium bromide was formed. The reaction mixture was stirred for 18 h and the solid filtered off. The filtrate was evaporated to dryness to lead to a yellow oil, which was purified by distillation affording a colorless oil (132 °C/0.25 mmHg (literature: 150 °C/0.5 mmHg [4b]b)). Yield: 12.95 g (64%). ^{1}H NMR ($CDCl_3$, 80.1 MHz, δ ppm): 1.07 (t, $^3J_{H/H}$ = 7.0 Hz, 12H, CH_3(Et)), 2.61 (q, $^3J_{H/H}$ = 7.0 Hz, 8H, CH_2(Et)), 3.69 (s, 4H, CH_2N); 7.16–7.52 (m, 3H, 3,4,5-aryl-H); ^{13}C NMR ($CDCl_3$, 50.3 MHz, δ ppm): 12.07 (CH_3(Et)), 47.30 (CH_2(Et)), 57.90 (CH_2N), 125.92 (1-aryl-C), 126.66 (4-aryl-C), 128.66 (3,5-aryl-C), 139.71 (2,6-aryl-C); EI MS (70 eV, *m*/*z* %): 326 (M^+, 19), 311 (M^+ − Me, 100), 254 ($M^+ - NEt_2$, 29), 240 ($M^+ - CH_2NEt_2$, 28).

Anal. Found: C, 58.84; H, 8.42. Calc. for $C_{16}H_{27}N_2Br$: C, 58.71; H, 8.31%.

2.2.3. Preparation of 1-bromo-2,6-bis[(diisopropylamino)methyl]benzene

A solution of diisopropylamine (29.98 g, 0.296 mol, 42 ml) and 1-bromo-2,6-bis(bromomethyl)benzene (21.11 g, 0.062 mol) in toluene (250 ml) was heated to reflux for 48 h. The white diisopropylamine bromide solid was then removed by filtration; the filtrate was concentrated in vacuum and the crude product recrystallized from pentane at −20 °C affording white crystals. Yield: 22.70 g, 96%. M.p.: 76 °C. ^{1}H NMR (C_6D_6, 250.1 MHz, δ ppm): 0.95 (d, $^3J_{H/H}$ = 6.5 Hz, 24H, CH_3(*i*-Pr)), 2.95 (sept, $^3J_{H/H}$ = 6.5 Hz, 4H, CH(*i*-Pr)), 3.88 (s, 4H, CH_2N), 7.28 (t, $^3J_{H/H}$ = 7.6 Hz, 1H, 4-aryl-H), 7.77 (d, $^3J_{H/H}$ = 7.6 Hz, 2H, 3,5-aryl-H); ^{13}C NMR (C_6D_6, 50.3 MHz, δ ppm): 20.91 (CH_3(*i*-Pr)), 49.00 (CH(*i*-Pr)), 50.17 (CH_2N), 124.80 (1-aryl-C), 126.96 (4-aryl-C), 128.59 (3,5-aryl-C), 142.12 (2,6-aryl-C); EI MS (70 eV, *m*/*z* %): 382 (M^+, 18), 367 (M^+ − Me, 100), 282 ($M^+ - N$*i*-Pr_2, 26), 182 ($M^+ - 2(N$*i*-$Pr_2)$, 56).

2.2.4. Preparation of chloro[2,6-bis[(diethylamino)methyl]phenyl]germylene (**1**)

A solution of 1-bromo-2,6-bis[(diethylamino)methyl]benzene (2.0 g, 6.1 mmol) in Et_2O (15 ml) was treated by a stoichiometric amount of *n*-butyllithium (4.2 ml, 1.6 M in hexane) at 0 °C, and the mixture was stirred for 30 min. After removal of the solvents in vacuum, 15 ml of THF was added. The 1-lithio-2,6-bis[(diethylamino)methyl])benzene was then added dropwise to a solution of $GeCl_2$·dioxane (1.41 g, 6.1 mmol) in THF (15 ml) at −78 °C. The solution was allowed to warm to room temperature (r.t.) and stirred for 30 min. Volatile materials were removed in vacuum and the residue was treated in pentane. The mixture was filtered to remove LiCl and concentrated under reduced pressure. After several hours in pentane at r.t., X-ray quality crystals of **1** were obtained. Yield: 1.84 g, 85%. M.p.: 70 °C. ^{1}H NMR (C_7D_8, 400.1 MHz, δ ppm): 1.18 (t, $^3J_{H/H}$ = 7.1 Hz, 12H, CH_3(Et)), 2.85, 2.86 (2q, $^3J_{H/H}$ = 7.1 Hz, 8H, CH_2(Et)), 3.62, 3.91 (AB system, $^2J_{H/H}$ = 14.3 Hz, 4H, CH_2N), 7.25–7.46 (m, 3H, 3,4,5-aryl-H); ^{13}C NMR (C_7D_8, 100.6 MHz, δ ppm): 9.72 (CH_3(Et)), 44.94 (CH_2(Et)), 58.68 (CH_2N), 123.93 (3,5-aryl-C), 127.60 (4-aryl-C), 145.04 (2,6-aryl-C), 157.48 (1-aryl-C); EI MS (70 eV, *m*/*z* %):356 (M^+, 24), 327 (M^+ − Et, 22), 291 (M^+ − 2Me − Cl, 18), 217 (Ar − 2Me, 100).

Anal. Found: C, 54.19; H, 7.76. Calc. for $C_{16}H_{27}N_2GeCl$: C, 54.07; H, 7.66%.

2.2.5. Preparation of chloro[2,6-bis[(diisopropylamino)methyl]phenyl]germylene (**2**)

A solution of 1-bromo-2,6-bis[(diisopropylamino)methyl]benzene (1.30 g, 3.4 mmol) in THF (15 ml) was treated with a stoichiometric amount of *n*-butyllithium (2.3 ml, 1.6 M in hexane) at −78 °C. The mixture was stirred for 20 min at −78 °C and slowly added to a solution of $GeCl_2$·dioxane (0.79 g, 3.4 mmol) in THF (15 ml) at the same temperature. The solution was then allowed to warm up to r.t. and stirred for 30 min. Solvents were evaporated in vacuum and the residue was treated with pentane. The mixture was filtered to remove LiCl and a yellow solid was obtained after evaporation to dryness. Yield: 1.26 g, 90%. M.p. (dec.): 77 °C. ^{1}H NMR (C_6D_6, 250.1 MHz, δ ppm): 1.03

(d, $^3J_{H/H} = 6.7$ Hz, 12H, CH_3(*i*-Pr)), 1.08 (d, $^3J_{H/H} = 6.7$ Hz, 12H, CH_3(*i*-Pr)), 3.42 (sept, $^3J_{H/H} = 6.7$ Hz, 4H, CH(*i*-Pr)), 3.70, 3.99 (AB system, $^2J_{H/H} = 15.0$ Hz, 4H, CH_2N), 6.96 (d, $^3J_{H/H} = 7.4$ Hz, 2H, 3,5-aryl-H), 7.15 (t, $^3J_{H/H} = 7.4$ Hz, 1H, 4-aryl-H); ^{13}C NMR (C_6D_6, 50.3 MHz, δ ppm): 20.33, 21.00 (CH_3(*i*-Pr)), 51.25 (CH(*i*-Pr)), 53.64 (CH_2N), 123.15 (3,5-aryl-C), 128.19 (4-aryl-C), 147.70 (2,6-aryl-C), 158.86 (1-aryl-C); IE MS (70 eV, *m*/*z* %): 412 (M^+, 26), 377 ($M^+ - Cl$, 26), 369 ($M^+ - i$-Pr, 100).

Anal. Found: C, 58.51; H, 8.69. Calc. for $C_{16}H_{27}N_2GeCl$: C, 58.37; H, 8.57%.

2.2.6. Preparation of chlorobis[2,4,6-tris(trifluoromethyl)phenyl]germane Ar'_2GeHCl

A diethyl ether solution of [2,4,6-tris(trifluoromethyl)phenyl]lithium [5] (2.14 mmol) was added dropwise to a 0 °C diethyl ether solution of $GeCl_2$·dioxane (196 mg, 0.85 mmol). The mixture was allowed to warm to r.t. and stirred for 2 h. All volatiles were removed in vacuum, 10 ml of pentane was added to filter the insoluble salts. A yellow powder precipitated after 24 h at −20 °C in pentane. Yield: 0.11 g, 8%. M.p. (dec.): 160 °C. ^{1}H NMR (C_6D_6, 250.1 MHz, δ ppm): 7.16 (13 peaks, $^5J_{H/F} = 4.5$ Hz, 1H, Ge–H), 7.75 (s, 4H, 3,5-aryl-H); ^{13}C NMR (C_6D_6, 62.9 MHz, δ ppm): 122.48 (q, $^1J_{C/F} = 273.7$ Hz, *p*-CF_3), 123.27 (q, $^1J_{C/F} = 275.7$ Hz, *o*-CF_3), 127.32 (s, 3,5-aryl-C), 133.57 (q, $^2J_{C/F} = 34.8$ Hz, 2,6-aryl-C), 136.87 (q, $^1J_{C/F} = 34.1$ Hz, 4-aryl-C), 165.41 (s, 1-aryl-C); ^{19}F NMR (C_6D_6, 188.3 MHz, δ ppm): 11.96 (s, 6F, *p*-CF_3), 20.15 (s, 12F, *o*-CF_3); IE MS (70 eV, *m*/*z* %): 671 ($M^+ - H^+$, 1), 653 ($M^+ - F$, 2), 637 ($M^+ - Cl$, 2), 391 ($M^+ - Ar$, 100), 355 (ArGe, 5); IR (C_6D_6, cm^{-1}): 2187.0 (ν(GeH)).

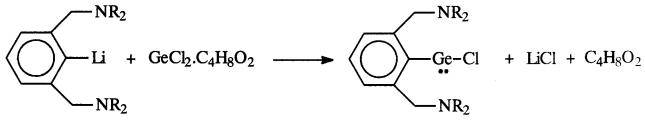
2.2.7. Preparation of chlorobis[2,6-bis(trifluoromethyl)phenyl]germane Ar''_2GeHCl

A solution of [2,6-bis(trifluoromethyl)phenyl]lithium [6] (50.61 mmol) in THF (100 ml) was added dropwise to a solution of $GeCl_2$·dioxane (2.34 g, 10.11 mmol) in THF (100 ml) at −78 °C during a period of 1 h. The mixture was allowed to warm up to r.t. and stirred for 8 h. All volatiles were removed in vacuum, 100 ml of pentane was added to filter the insoluble salts. A orange powder precipitated at −20 °C in pentane. Yield: 0.54 g, 10%. M.p.: 132 °C. ^{1}H NMR (C_6D_6, 250.1 MHz, δ ppm): 6.64 (t, $^3J_{H/H} = 7.9$ Hz, 2H, 4-aryl-H), 7.27 (d, $^3J_{H/H} = 7.9$ Hz, 2H, 3,5-aryl-H), 7.38 (13 peaks, $^5J_{H/F} = 4.2$ Hz, 1H, Ge–H). ^{13}C NMR (C_6D_6, 62.9 MHz, δ ppm): 124.33 (q, $^1J_{C/F} = 274.9$ Hz, *o*-CF_3), 130.50 (s, 4-aryl-C), 130.73 (s, 3,5-aryl-C), 135.51 (q, $^2J_{C/F} = 33.1$ Hz, 2,6-aryl-C), 169.02 (s, 1-aryl-C); ^{19}F NMR (C_6D_6, 188.3 MHz, δ ppm): 20.54 (s); IE MS (70 eV, *m*/*z* %): 535 ($M^+ - H^+$, 3), 501 ($M^+ - Cl$, 7), 323 ($M^+ - Ar$, 100); IR (C_6D_6, cm^{-1}): 2167.9 (ν(GeH)).

3. Results and discussion

3.1. The arylchlorogermylenes 1 and 2

The reaction of ArLi with $GeCl_2$·dioxane in THF in 1:1 molar ratio at −78 °C affords germylenes ArGeCl in good yield (Eq. (1)). Single crystals of **1**, suitable for an X-ray structure determination were grown from pentane at room temperature. The structure determination and refinement [7] show a monomeric structure in the solid state (Fig. 1). Significant bond lengths and angles are presented in Table 1.



1: R = Et, **2**: R = *i*Pr

(1)

In this complex, the Ar ligand is tridentate to germanium: σ-bonded through *ipso*-carbon C(1) and also bis-orthochelated by intramolecular N→Ge coordinations. In solid state, the observed Ge–N distances are quite different, 2.337(11) Å for the coordinated bond N(2)→Ge and 2.570(10) Å for the other distance Ge–N(1). This latter is the longest coordination bond of all known chlorogermylenes with substituents bearing nitrogen donors in a side-chain. At the opposite, the Ge–Cl bond (2.309(4) Å), oriented almost orthogonal to the plane of the aryl ligand, lies in the range of chlorogermylenes coordinated by a side-chain nitrogen atom (see Table 2). The geometry at the germanium center may show us that the degree of hybridization of the metal is quite low. Indeed, the angles (Table 1) C(1)–Ge(1)–Cl(1), C(1)–Ge(1)–N(2), N(2)–Ge(1)–Cl(1), C(1)–Ge(1)–N(1) are in the range of 90° (74.2(4)°–97.2(4)°). This seems indicate that the bonds to the ligands are involving p-orbitals at the germanium atom. So, the nitrogen atoms of the side-chains can interact easily with the vacant p-orbital on the germanium; the lone pair is

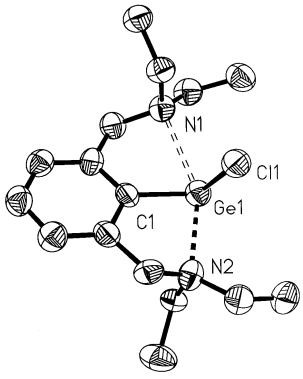
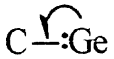


Fig. 1. Thermal ellipsoid plot (30%) of **1**. Hydrogen atoms are not shown. Important structural data are given in Table 1.

Table 1
Selected bond length (Å) and angles (°) for **1**

Bond lengths			
Ge(1)–N(2)	2.337(11)	Ge(1)–N(1)	2.570(10)
Ge(1)–Cl(1)	2.309(4)	Ge(1)–C(1)	1.941(11)
Bond angles			
C(1)–Ge(1)–Cl(1)	97.2(4)	N(2)–Ge(1)–Cl(1)	89.2(3)
C(1)–Ge(1)–N(2)	76.9(4)	C(1)–Ge(1)–N(1)	74.2(4)

localized in an orbital with high s character. On the other hand, **1** exhibits a surprisingly short Ge–C(1) bond length (1.941(11) Å) appreciably shorter than in the other halogermylenes (1.989(5)–2.402(3) Å) (Table 2). This value seems to indicate a back bonding donation  of the germanium to the *ipso*-carbon arising from consequent electronic effects of the two side-chain ligands: donation N→Ge and withdrawing inductive effect of the two *ortho* CH_2NEt_2 moieties, increasing the electrophilic character of the *ipso*-carbon. Removal of the back bonding by complexation of the germanium atom, for example in the recently described complex $ArGeOH{\cdot}W(CO)_5$, leads as expected to a lengthening of the Ge–C(1) bond (1.975(3) Å) [8]. This explanation can also be supported regarding the ^{13}C NMR chemical shift of the *ipso*-carbons C(1). Indeed, in the above complex, the C(1) appears at 153.44 ppm [8], much more shielded than in **1** (157.48 ppm) or in **2** (158.86 ppm). The ^1H NMR spectra (80 MHz) of **1** and **2** at room temperature show that, in solution, the chelate side-chains are equivalent due to a rapid exchange of the coordination sites. The signal of the two inequivalent benzyl hydrogen atoms appears as an AB pattern; moreover, in the case of **1**, we can also observe two resonances for the methylenic protons of the ethyl groups due to the chirality of the germanium atom and for **2**, two resonances for the methyl protons of the isopropyl groups.

3.2. Comparison of *1* and *2* with reviewed halogermylenes

Fruitful comments can be made from a study of known stable and isolated halogermylenes (Table 2). Non hindered halogermylenes such as ethylchlorogermylene EtGeCl and phenylchlorogermylene PhGeCl were the first representatives of halogermylenes [9,10]. These chlorogermylenes are 'associated' by intermolecular germanium–chlorine bonds but without Ge–Ge bonds. All phenylhalogermylenes PhGeX (X = F, Cl, Br, I) have been synthesized [11]. Later, were described the most interesting halogermylenes stabilized as monomeric species by hindered substituents or by donor ligands. Chlorogermylenes RGeCl are the most numerous owing to the easy available and most often used dichlorogermylene $GeCl_2{\cdot}C_4H_8O_2$ complex precursor. Known so far stable and isolated halogermylenes are chronologically reported in Table 2. We can distinguish alkyl or arylhalogermylenes with C–Ge–X linkage (compounds **1**–**2**, **9**–**11**, **13**, **16**–**19**, **23**, **25**–**26**, **35**) and heterohalogermylenes with Y–Ge–X (Y = N, O, P) moieties (compounds **3**–**8**, **12**, **14**–**15**, **20**–**22**, **24**, **27**–**34**). As expected, a comparison of different coordinated and non coordinated derivatives shows that intramolecular coordination of the amino functionality in the side-chain makes longer and so weakens drastically the Ge–Cl bond. Accordingly, such derivatives are suitable synthons for easy nucleophilic substitutions at the divalent metal to access to many heteroleptic germylenes. In our group, a recent example showed that diazogermylenes $RGeC(N_2)R'$, precursors of germynes RGe≡CR′, have been obtained from correspondent chlorogermylenes **1** or **2** and a lithiodiazo compound [12].

If many halogermylenes are stabilized by donor ligands (cf. Table 2), none monohalogermylene bearing strong electron-withdrawing effect substituent is known yet. In this area, only the symmetric diarylgermylene Ar'_2Ge: [Ar′ = 2,4,6-tris(trifluoromethyl)phenyl] has been described [13]. In order to have suitable synthons to access to electron poor low coordinated species of germanium, we attempted to synthesize the two chlorogermylenes Ar′GeCl and Ar″GeCl (Ar″ = 2,6-bis(trifluoromethyl)phenyl).

3.3. New chlorodiarylgermanes

Surprisingly, the classic reaction using stoichiometric amounts of lithio-derivatives Ar′Li [5] or Ar″Li [6] with complex $GeCl_2{\cdot}$dioxane, did not lead to the expected chlorogermylenes but beside unidentified products to chlorodiarylgermanes Ar'_2GeHCl and Ar''_2GeHCl in low yields. In these compounds, the hydrogen atom bonded to germanium exhibits an exceptional acidic character because of the strong withdrawing effects of two aryl groups 14 and of the chlorine atom. Thus, in the ^1H NMR spectra, the deshielded Ge–H signal appears at 7.16 ppm for Ar'_2GeHCl and at 7.38 ppm for Ar''_2GeHCl and in the Infra-Red spectra, we can observe characteristic ν_{Ge-H} at 2187.0 cm^{-1} for Ar'_2GeHCl and at 2167.9 cm^{-1} for Ar''_2GeHCl. These results evidenced the instability of these chlorogermylenes in our experimental conditions. Formation of chlorodiarylgermanes remains difficult to explain; we can postulate that creation of a Ge–H linkage probably arises from a radical process. Is this result in relation with a triplet structure of germylenes bearing strong electron-withdrawing groups such as Ar′ or Ar″ and Cl? This question is now in study.

Table 2
Stable and isolated halogermylenes (chronological order)

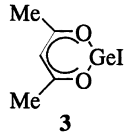
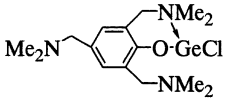
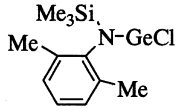
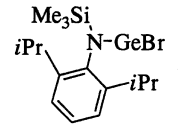
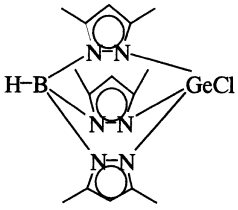
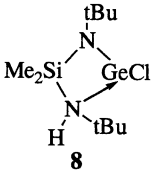
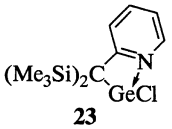
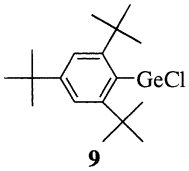
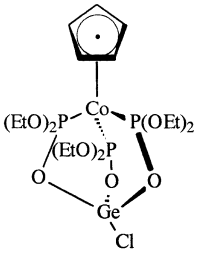
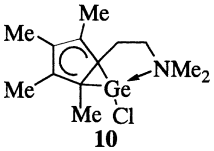
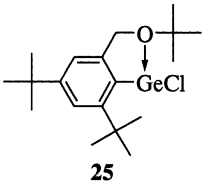
R-Ge-X	**d Ge-X (Å)** d Ge-C (Å) *d Ge-Y (Å)* *Y = N, O, P, Ge*	Ref	R-Ge-X	**d Ge-X (Å)** [d Ge-C (Å)] *d Ge-Y (Å)* *Y = N, O, P, Ge*	Ref
 **3**	**2.736(1)** *Ge-O: 1.931(5)-1.914(5)*	15	 **20**	**	27
 **4**  **5**	**	16	 **21**	**2.536(1)** *Ge-N:* *2.013(4)-* *2.023(3)-* *2.379(3)*	28
*t*BuNHGeCl* **6** *t*BuOGeCl* **7**	** **2.262(2)** *Ge-O: 1.986(6)* *Ge-O coord: 2.028(6)*	17	*t*Bu$_2$P-GeCl* **22**	**2.270(4)** *GeP: 2.487(7)* *GeP coord:* *2.492(7)*	29
 **8**	**2.374(1)** *Ge-N: 1.894(3)* *Ge-N coord: 2.096(3)*	17	 **23**	**2.294(8)** 2.138(5) *Ge-N coord:* *2.082(4)*	30
 **9**	**2.281** Ge-C: not given	18	 **24**	**2.419(4)** *Ge-O:* *1.918(6)-* *1.929(4)-* *2.494(9)*	31
 **10**	**2.369(1)** 2.180(3)-2.402(3) *Ge-N coord: 2.286(3)*	19	 **25**	**2.333(1)** 2.009(3) *Ge-O coord:* *2.073(2)*	32

Table 2 *(continued)*

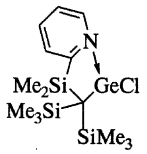
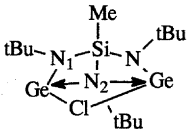
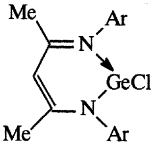
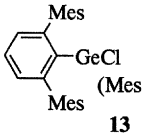
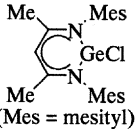
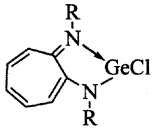
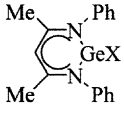
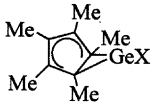
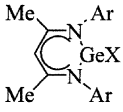
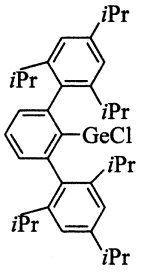
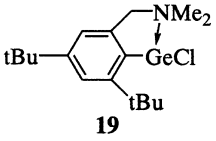
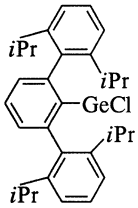
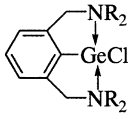
$(Me_3Si)_3C$-GeCl **11**	**	20	 **26**	**2.321(7)** 2.060(1) *Ge-N coord: 2.081(4)*	33
 **12**	**2.563(4)** *Ge-N_1: 1.892(9)* *Ge-N_2 coord: 2.022(7)*	21	 Ar = 2,6-iPr$_2$C$_6$H$_3$ **27**	**2.295(1)** *Ge-N: 1.988(2)* *Ge-N coord: 1.997(3)*	34
*  (Mes = mesityl) **13**	**2.120(2)** 2.000(6) *Ge-Ge: 2.443(2)*	22	 (Mes = mesityl) **28**	**2.328(1)** *Ge-N: 1.958(2)-1.980(2)*	35
R = Me **14**  R = iPr **15**	**2.377(4)** *Ge-N: 1.937(3)-1.938(3)* **2.368(2)** *Ge-N: 1.956(4)*	23	X = Cl **29**  X = I **30**	**	36
X = Cl **16**  X = Br* **17**	X = Cl: **2.384(2)** 2.214(3)-2.221(2) X = Br: **2.706(1)** 2.201(5)-2.292(5) *GeBr assoc.: 3.133(1)*	24	 **31** X = F Ar = 2,6-iPr$_2$C$_6$H$_3$ **32** X = F 2,6-Me$_2$C$_6$H$_3$ **33** X = Cl Ar = 2,6-Me$_2$C$_6$H$_3$	**1.805(2)** *Ge-N: 1.977(2)-1.978(2)* ** **	37

Table 2 *(continued)*

 **18**	**2.202(6)** 1.989(5) **Ge-Ge: 2.363(2)*	25	$[Me_2Si(OtBu)]_2N$-Ge-Cl **34**	**	38
 **19**	**2.328(3)** 2.015(6) *Ge-N coord:2.093(6)*	26	 **35**	**	39
			1: R = Et  **2**: R = *i*Pr	R = Et: **2.309(4)** 1.941(1) *Ge-N coord: 2.337(1)-2.570(1)* R = *i*Pr: **	This work

* dimeric structure.
** no structure.

4. Supplementary material

Crystallographic data for the structural analysis of **1** have been deposited with the Cambridge Crystallographic Data Centre, CCDC No. 189943. Copies of this information may be obtained free of charge from The Director, CCDC, 12 Union Road, Cambridge, CB2 1EZ, UK (fax: +44-1223-336033; e-mail: deposit@ccdc.cam.ac.uk or www: http://www.ccdc.cam.ac.uk).

References

[1] (a) N. Tokitoh, R. Okazaki, Coord. Chem. Rev. 210 (2000) 251; (b) J. Barrau, G. Rima, Coord. Chem. Rev. 178 (1998) 593.

[2] T. Fjeldberg, A. Haaland, B.E.R. Schilling, M.F. Lappert, A.J. Thorne, J. Chem. Soc., Dalton Trans. (1986) 1551.

[3] (a) F. Vögtle, Chem. Ber. 102 (1969) 1784; (b) L.A. van de Kuil, H. Luitjes, D.M. Grove, J.W. Zwikker, J.G.M. van der Linden, A.M. Roelofsen, L.W. Jenneskens, W. Drenth, G. van Koten, Organometallics 13 (1994) 468.

[4] (a) H. Schumann, W. Wassermann, A. Dietrich, J. Organomet. Chem. 365 (1989) 11; (b) J.A.M. van Beek, G. van Koten, G.P.C.M. Dekker, E. Wissing, M.C. Zoutberg, C.H. Stam, J. Organomet. Chem. 394 (1990) 659; (c) H. Schumann, U. Hartmann, W. Wassermann, Chem. Ber. 124 (1991) 1567.

[5] G.E. Carr, R.D. Chambers, T.F. Holmes, D.G. Parker, J. Organomet. Chem. 325 (1987) 13.

[6] M.P. Bigwood, P.J. Corvan, J.J. Zuckermann, J. Am. Chem. Soc. 103 (1981) 7643.

[7] Crystal data for **1**: $C_{16}H_{27}ClGeN_2$, $M_r = 355.44$, monoclinic, space group $P2_1/c$, $a = 7.342(1)$, $b = 19.215(4)$, $c = 25.244(4)$ Å, $\beta = 92.42(2)^\circ$, $V = 3558.2(10)$ Å^3, $Z = 8$, $\rho_{calcd} = 1.327$ Mg m^{-3}, $F(000) = 1488$, $\lambda = 0.71073$ Å, $T = 293(2)$ K, μ (Mo Kα) = 1.866 mm^{-1}, crystal dimensions $0.6 \times 0.2 \times 0.1$ mm, $1.93^\circ \leq \Theta \leq 21.49^\circ$, 27 345 reflections ($R_{int} = 0.1339$) were collected on a STOE-IPDS diffractometer. A semi-empirical absorption correction was employed. The structure was solved by direct methods (SHELXS-97) [40] and 362 parameters were refined using the least-squares method on F^2 [41]. Maximum residual electron density residue: 0.594 e Å^{-3}, R_1 (for $I > 2\sigma(I)$) = 0.0729 and $wR_2 = 0.2143$ (all data) with $R_1 = \Sigma||F_o| - |F_c||/\Sigma|F_o|$ and $wR_2 = (\Sigma\, w(F_o^2 - F_c^2)^2/\Sigma\, w(F_o^2)^2)^{0.5}$.

[8] C. Bibal, S. Mazières, H. Gornitzka, C. Couret, Organometallics 21 (2002) 2940.

[9] J. Satgé, M. Massol, P. Rivière, J. Organomet. Chem. 56 (1973) 1 (and references therein).
[10] P. Rivière, M. Rivière-Baudet, J. Satgé, Comprehensive Organometallic Chemistry, vol. 2, 1982, p. 478.
[11] P. Rivière, M. Rivière-Baudet, J. Satgé, J. Organomet. Chem. 96 (1975) C7.
[12] C. Bibal, S. Mazières, H. Gornitzka, C. Couret, Angew. Chem. Int. Ed. 40 (2001) 952.
[13] J.E. Bender, IV, M.M. Banaszak Holl, J.W. Kampf, Organometallics 16 (1997) 2743.
[14] Ar′ and Ar″ exhibit an ideal combination of electronic and steric characteristics, since they can withdraw electrons from the metal inductively but can donate electron density to the metal from the fluorine atoms of the o-CF_3 substituents on the aryl ligand: F.T. Edelmann, Comments Inorg. Chem. 12 (1992) 259.
[15] S.R. Stobart, M.R. Churchill, F.J. Hollander, W.J. Youngs, J. Chem. Soc., Chem. Commun. (1979) 911.
[16] A. Meller, C.-P. Gräbe, Chem. Ber. 118 (1985) 2020.
[17] M. Veith, P. Hobein, R. Rösler, Z. Naturforsch., Teil. B 44 (1989) 1067.
[18] P. Jutzi, C. Leue, Organometallics 13 (1994) 2898.
[19] P. Jutzi, H. Schmidt, B. Neumann, H.-G. Stammler, J. Organomet. Chem. 499 (1995) 7.
[20] T. Ohtaki, W. Ando, Organometallics 15 (1996) 3103.
[21] M. Veith, M. Zimmer, Z. Anorg. Allg. Chem. 622 (1996) 1471.
[22] R.S. Simons, L. Pu, M.M. Olmstead, P.P. Power, Organometallics 16 (1997) 1920.
[23] H.V. Rasika Dias, Z. Wang, J. Am. Chem. Soc. 119 (1997) 4650.
[24] (a) F.X. Kohl, P. Jutzi, J. Organomet. Chem. 243 (1983) 31;
(b) J.G. Winter, P. Portius, G. Kociok-Köhn, R. Steck, A.C. Filippou, Organometallics 17 (1998) 4176.
[25] (a) L. Pu, M.M. Olmstead, P.P. Power, Organometallics 17 (1998) 5602;
(b) 18 crystallizes simultaneously as both monomer and weakly Ge–Ge bonded dimer: M. Stender, L. Pu, P.P. Power, Organometallics 20 (2001) 1820.
[26] H. Schmidt, S. Keitemeyer, B. Neumann, H.-G. Stammler, W.W. Schoeller, P. Jutzi, Organometallics 17 (1998) 2149.
[27] J. Barrau, G. Rima, T. El-Amraoui, J. Organomet. Chem. 561 (1998) 167.
[28] A.C. Filippou, P. Portius, G. Kociok-Köhn, J. Chem. Soc., Chem. Commun. (1998) 2327.
[29] C. Druckenbrodt, W.-W. du Mont, F. Ruthe, P.G. Jones, Z. Anorg. Allg. Chem. 624 (1998) 590.
[30] S. Benet, C.J. Cardin, D.J. Cardin, S.P. Constantine, P. Heath, H. Rashid, S. Teixeira, J.H. Thorpe, A.K. Todd, Organometallics 18 (1999) 389.
[31] A.C. Filippou, P. Portius, G. Kociok-Köhn, V. Albrecht, J. Chem. Soc., Dalton Trans. (2000) 1759.
[32] P. Jutzi, S. Keitemeyer, B. Neumann, A. Stammler, H.-G. Stammler, Organometallics 20 (2001) 42.
[33] S.S. Al-Juaid, A.G. Avent, C. Eaborn, M.S. Hill, P.B. Hitchcock, D.J. Patel, J.D. Smith, Organometallics 20 (2001) 1223.
[34] Y. Ding, H.W. Roesky, M. Noltemeyer, H.-G. Schmidt, P.P. Power, Organometallics 20 (2001) 1190.
[35] A.E. Ayers, T.M. Klapötke, H.V. Rasika Dias, Inorg. Chem. 40 (2001) 1000.
[36] A. Akkari, J.J. Byrne, I. Saur, G. Rima, H. Gornitzka, J. Barrau, J. Organomet. Chem. 622 (2001) 190.
[37] Y. Ding, H. Hao, H.W. Roesky, M. Noltemeyer, H.-G. Schmidt, Organometallics 20 (2001) 4806.
[38] M. Veith, A. Rammo, Z. Anorg. Allg. Chem. 627 (2001) 662.
[39] M. Stender, A.D. Phillips, R.J. Wright, P.P. Power, Angew. Chem. Int. Ed. 41 (2002) 1785.
[40] G.M. Sheldrick, Acta Crystallogr., Sect. A 46 (1990) 467.
[41] G.M. Sheldrick, SHELXL-97, Program for Crystal Structure Refinement, University of Göttingen, 1997.

Available online at www.sciencedirect.com
SCIENCE DIRECT®
Polyhedron 21 (2002) 2835–2854
POLYHEDRON
www.elsevier.com/locate/poly

Author Index to Volume 21

Abboud, K.A., see Mills, R.C., 1051
Abdul Malik, K.M., see Azam, K.A., 885
Abdul Malik, K.M., see Azam, K.A., 381
Abdul Malik, K.M., see Johns, C.A., 395
Abel Lozano, A., see Santana, M.D., 1935
Abiko, S.-i., see Kita, M., 843
Abram, U., see de Figueiredo, A.T., 2351
Abu-Surrah, A.S., Kettunen, M., Lappalainen, K., Piironen, U., Klinga, M. and Leskelä, M., Synthesis of new chiral diimine palladium(II) and nickel(II) complexes bearing oxazoline- and myrtanyl-based nitrogen ligands. Crystal structure of the C_2-symmetric complex [{(1*R*,2*S*)-*inda-box*}$PdCl_2$], 27
Acuña, V., see Manzur, J., 181
Acuña-Cueva, E.R., Faure, R., Illán-Cabeza, N.A., Jiménez-Pulido, S.B. and Moreno-Carretero, M.N., Spectral and XRD studies on perchlorate salts of several Co(II), Ni(II), Cu(II), Zn(II), Cd(II) and Hg(II) complexes from 1-methyllumazine and 1,6,7-trimethyllumazine, 1961
Adams, H., Bradshaw, D. and Fenton, D.E., A co-ordination number asymmetric dinuclear zinc(II) complex of an unsymmetrical compartmental proligand, 1957
Adeyga, A.M., see Benetollo, F., 425
Adrover, B., see García-Raso, A., 1197
Agnoletto, P., see Albertin, G., 1755
Aguado, R., see Arnáiz, F.J., 2755
Aguado, R., see Arnáiz, F.J., 1635
Aguirre, A., see Domínguez, M., 1429
Ahmad, S., Isab, A.A., Al-Arfaj, A.R. and Arnold, A.P., Synthesis of cyano(selenone)gold(I) complexes and investigation of their scrambling reactions using ^{13}C and ^{15}N NMR spectroscopy, 2099
Ahmad, S., see Isab, A.A., 1267
Airoldi, C., see Sales, J.A.A., 2647
Airoldi, C., see de Farias, R.F., 1677
Alam, T.M., see Boyle, T.J., 2333
Alan Howie, R., see Aupers, J.H., 2107
Alan Howie, R., see Bomfim, J.A.S., 1667
Al-Arfaj, A.R., see Ahmad, S., 2099
Alberdi, G., see Ares, R., 2309
Alberti, G., see Pesavento, M., 1343
Albertin, G., Agnoletto, P. and Antoniutti, S., Preparation of acetylide and propadienylidene complexes of iron(II), 1755
Ali, A.M., see Tarafder, M.T.H., 2683
Ali, A.M., see Tarafder, M.T.H., 2691
Ali, M.S., Thurston, J.H., Whitmire, K.H. and Khokhar, A.R., Synthesis and characterization of platinum(II) and (IV) complexes containing hexamethyleneimine ligand: crystal structure of [Pt^{II}(hexamethyleneimine)$_2$(cyclobutanedicarboxylato)]·H_2O, 2659
Ali, A.M., see Tarafder, M.T.H., 2547
Ali, M.S., Mukhopadhyay, U., Shirvani, S.M., Thurston, J., Whitmire, K.H. and Khokhar, A.R., Homopiperazine platinum(II) complexes containing substituted disulfide groups: crystal structure of [Pt^{II}(homopiperazine)(diphenylsulfide)Cl]NO_3, 125
Al-Jahdali, M., see Baker, P.K., 2301
Alp, H., see Kantekin, H., 1865
Al-Salem, N.A., see Goher, M.A.S., 1871
Alstrum-Acevedo, J.H., see Valdés-Martínez, J., 409
Alzuet, G., see Cejudo, R., 1057
Amélia Santos, M., Grazina, R., Buglyó, P., Gama, S. and Farkas, E., A new bipodal carboxy-bis(hydroxypyridinonate) ligand. Synthesis and complexation with copper(II), nickel(II) and zinc(II) in aqueous solution, 2609
Amirkhanov, V.M., see Gubina, K.E., 963
Amirnasr, M., Mahmoudkhani, A.H., Gorji, A., Dehghanpour, S. and Bijanzadeh, H.R., Cobalt(II), nickel(II), and zinc(II) complexes with bidentate *N*,*N*′-bis(β-phenylcinnamaldehyde)-1,2-diiminoethane Schiff base: synthesis and structures, 2733
Amorello, D., Gambino, V., Romano, V. and Zingales, R., The determination of mineral acidity excess in solutions containing Ga(III), Al(III), Bi(III), 1369
Andac, O., see Yilmaz, V.T., 2393
Andrews, N.L., see Boyle, T.J., 2333
Andy Hor, T.S., see Wang, W., 1991
Annibale, G., see Pitteri, B., 2283
Anticó, E., see Domínguez, M., 1429
Antoniutti, S., see Albertin, G., 1755
Antus, S., see Ősz, K., 2149
Antzutkin, O.N., see Ivanov, A.V., 2727
Aoyama, T., see Kameta, N., 805
Apostilco, L., see Binions, R., 1943
Appleby, T., Aucott, S.M., Clarke, M.L., Slawin, A.M.Z. and Derek Woollins, J., Preparation and coordination chemistry of $Ph_2P(CH_2)_nNHP^iPr_2$ ($n = 2$, 3), 2639
Aquino, M.A.S., see Cooke, M.W., 1235
Arab, M., see Isab, A.A., 1267
Araujo, M.L., see Armas, M.T., 1513
Ares, R., López-Torres, M., Fernández, A., Castro-Juiz, S., Suarez, A., Alberdi, G., Fernández, J.J. and Vila, J.M., Cyclopalladated compounds with bridging and chelating diphosphine ligands. Effect of ring size. Crystal and molecular structure of [{Pd[4-(COH)C_6H_3C(H)=N(Cy)-*C2*,*N*](Cl)}$_2$(μ-$Ph_2PCH_2PPh_2$)], 2309
Armas, M.T., Mederos, A., Gili, P., Domínguez, S., Hernández-Molina, R., Lorenzo, P., Vaz-Júnior, S., Baran, E.J., Araujo, M.L., Lubes, V. and Brito, F., Speciation in oxovanadium(IV)–carnosine system, 1513
Arnáiz, F.J., Miranda, M.J., Aguado, R., Mahía, J. and Maestro, M.A., Uranyl polyhalides. Molecular structure of $[UO_2(OAsPh_3)_4](Br_3)_2$ and $[UO_2(OPPh_3)_4](I_3)_2$, 2755
Arnáiz, F.J., see Gómez-Saiz, P., 2257
Arnáiz, F.J., Aguado, R., Pedrosa, M.R., Mahía, J. and Maestro, M.A., Addition compounds of MoO_2Br_2 from $MoO_2Br_2(H_2O)_2$. Molecular structure of $MoO_2Br_2\{OP[N(CH_3)_2]_3\}_2$ and $MoO_2Br_2\{CH_2[P(O)(C_6H_5)_2]_2\}$, 1635
Arnold, A.P., see Ahmad, S., 2099
Arnold, D.P., see Pan, N., 1905
Aromí, G., Bhaduri, S., Artús, P., Huffman, J.C., Hendrickson, D.N. and Christou, G., A tetranuclear manganese carboxylate cluster with bis(2-pyridyl)amine ligation: $[Mn_4O_2(O_2CEt)_7(bpya)_2](ClO_4)$, 1779
Arrington, D.L., see Royer, A.C., 155
Artús, P., see Aromí, G., 1779
Asada, H., Ozeki, M., Fujiwara, M. and Matsushita, T., Structures of

Elsevier Science Ltd.
PII: S0277-5387(02)01350-5

four types of novel high-valent manganese complexes obtained by the reactions of $KMnO_4$ with tridentate Schiff base ligands, 1139
Asadi, M., Zabardasti, A., Karimivand, V.A. and Ghasemi, J., The thermodynamic studies of the molecular interactions of methyltin(IV) tribromide with free base *meso*-tetraarylporphyrins, 1255
Asadi, M., Zabardasti, A. and Ghasemi, J., The thermodynamic studies of the molecular interactions of dimethyltin(IV) dichloride with free base *meso*-tetraarylporphyrins, 683
Asaji, T., Tajima, F. and Hashimoto, M., On the crystal structures of some protonic complexes of oxo-ligands with tetrachloroauric acid, $[(RO)_nH][AuCl_4]$ (R: Py, Ph_3As; n: 1, 2), prepared from deuterated and non-deuterated solvent systems, 2207
Asfari, Z., see Thuéry, P., 2497
Asfari, Z., see Thuéry, P., 1949
Atwood, D., see Kim, C.-H., 225
Aucott, S.M., see Appleby, T., 2639
Aupers, J.H., Chohan, Z.H., Comerlato, N.M., Alan Howie, R., Silvino, A.C., Wardell, J.L. and Wardell, S.M.S.V., Bis(1,3-dithiole-2-one-4,5-dithiolato)antimonate(1-) salts, $[Q][Sb(dmio)_2]$. Structural comparisons of $[Q][Sb(dmio)_2]$ and bis(1,3-dithiole-2-thione-4,5-dithiolato)antimonate(1-) salts, $[Q][Sb(dmit)_2]$, 2107
Ávila Terra, L.H.S., Guekezian, M., Gaubeur, I., Matos, J.R. and Suárez-Iha, M.E.V., Synthesis, characterization, properties and thermal study of nickel(II)/di-2-pyridyl ketone benzoylhydrazone complex, 2375
Ayers, A.E., see Dias, H.V.R., 611
Aymonino, P.J., see Soria, D.B., 1767
Azam, K.A., Hanif, K.M., Ghosh, A.C., Kabir, S.E., Karmakar, S.R., Abdul Malik, K.M., Parvin, S. and Rosenberg, E., Triosmium and triruthenium clusters containing deprotonated 2-mercapto-1-methylimidazole ligand: X-ray structures of $[(\mu\text{-}H)Os_3(CO)_{10}\{\mu\text{-}SC{=}NCH{=}CHN(CH_3)\}]$, $[(\mu\text{-}H)Ru_3(CO)_9\{(\mu_3\text{-}\eta^2\text{-}SC{=}NCH{=}CHN(CH_3)\}]$ and $[(\mu\text{-}H)Os_3(CO)_8\{\mu\text{-}SC{=}NCH{=}CHN(CH_3)\}(\mu\text{-}dppm)]$, 885
Azam, K.A., Golzar Hossain, G.M., Kabir, S.E., Abdul Malik, K.M., Mottalib, M.A., Perven, S. and Sarker, N.C., Sulfido triosmium clusters containing bridging dppm ligand: crystal structures of $[Os_3(CO)_7(\mu_3\text{-}CO)(\mu_3\text{-}S)(\mu\text{-}dppm)]$ and the two isomers of $[Os_3(CO)_7(\mu_3\text{-}S)_2(\mu\text{-}dppm)]$, 381
Azevedo, F., Freire, C. and de Castro, B., Reductive electrochemical study of Ni(II) complexes with N_2O_2 Schiff base complexes and spectroscopic characterisation of the reduced species. Reactivity towards CO, 1695
Azócar-Guzmán, I., see Moya, S.A., 439

Báča, J., see Plešek, J., 975
Bag, P., see Baitalik, S., 2481
Bagherzadeh, H., see Mahjoub, A.R., 2555
Bahgat, K. and Orabi, A.S., Physical characteristics, vibrational spectroscopy and normal-coordinate analysis of 2-aminophenol and 2-phenylenediamine complexes, 987
Baitalik, S., Bag, P. and Nag, K., Synthesis, spectroscopic properties and proton-coupled redox activities of mononuclear osmium(II) mixed-chelates derived from pyrazole-3,5-bis(benzimidazole) and 2,2′-bipyridine, 2481
Baker, P.K. and Al-Jahdali, M., The reactions of the monodentate organometallic phosphines $[MI_2(CO)_3\{MeC(CH_2PPh_2)_3\text{-}P,P'\}]$ (M = Mo, W) with π-allyl molybdenum(II) complexes and iron(O) and iron(II) carbonyl complexes, 2301
Balboa, S., see Carballo, R., 2811
Ball, R.J., see Devereux, M., 1063
Bandyopadhyay, P. and Mukhopadhyay, S., Kinetics of oxidation of hydroxylamine by [ethylenebis(biguanide)]silver(III) in aqueous media, 1893
Banger, K.K., see Ngo, S.C., 1289
Baran, P., Boča, R., Breza, M., Elias, H., Fuess, H., Jorík, V., Klement, R. and Svoboda, I., The spectroscopic and structural properties of copper(II) complexes of the novel tridentate (ONO) pyridine N-oxide ligand Hpoxap, 1561
Baran, E.J., see Armas, M.T., 1513
Barfield, M.E., see Vohs, J.K., 531
Barman, R.K., Chakrabarty, R. and Das, B.K., Structure and properties of tetraaquabis(hydrogenmaleato)iron(II), 1189
Barret, M.C., Mahon, M.F., Molloy, K.C., Wright, P. and Creeth, J.E., The structural chemistry of copper(II) hinokitiol and its adducts, 1761
Barron, A.R., see van Poppel, L.H., 1877
Bartczak, T.J., see Machura, B., 2617
Bartoszak-Adamska, E., Bregier-Jarzebowska, R. and Lomozik, L., Crystal and molecular structures of cadmium(II) nitrate complexes with triamines: 1,5-diamino-3-azapentane, 1,6-diamino-3-azahexane and 1,7-diamino-4-azaheptane, 739
Barwiolek, M., see Szlyk, E., 2711
Basosi, R., see Noethig-Laslo, V., 1643
Batista, A.A., see Von Poelhsitz, G., 2221
Beck, E.J., see Cooke, M.W., 1235
Beer, R.H., see Torzilli, M.A., 697
Beer, R.H., see Torzilli, M.A., 705
Beheshti, A., Clegg, W., Hyvadi, R. and Fereshteh Hekmat, H., Synthesis and structures of the $WOS_3Cu_3Pz_3Cl$ and $[PPh_4]_4[\{WOS_3(CuNCSe)_3\}_2]$ clusters (Pz = pyrazole), and structure of $[PPh_4]_2[Cu(NCS)_4]$, 1547
Bekaroğlu, Ö., see Kandaz, M., 255
Bell, N.A., Coles, S.J., Constable, C.P., Hursthouse, M.B., Light, M.E., Mansor, R. and Salvin, N.J., Mercury(II) halide complexes of tertiary phosphines. Part XVII. Complexes of the very basic and sterically demanding ligand, tris(2,4,6-trimethoxyphenyl)phosphine (TMPP) of stoichiometry $(TMPP)_x(HgX_2)_y$ (X = Cl, Br, I; $x = 1, 2$; $y = 1$: $x = 2$, $y = 3$: X = I; $x = 1$, $y = 2$). Crystal structures of the monomeric 1:1 complexes $(TMPP)HgX_2$ (X = Br, I) and $(TMPP)(HgI_2)_2$, 1845
Bell, N.A., Brooks, J.S., Forder, S.D., Robinson, J.K. and Thorpe, S.C., Backscatter Fe-57 Mössbauer studies of iron(II) phthalocyanine, 115
Belokon', A.I., see Kessler, V.G., 1629
Belsley, M., see Gamelas, J.A.F., 2537
Bencini, A., Berni, E., Chuburu, F., Giorgi, C., Handel, H., Le Baccon, M., Paoletti, P. and Valtancoli, B., Basicity and coordination ability of linear hexa-amines in relation to $N\text{-}(CH_2)_n\text{-}N$ chain-link lengths. A solution study, 1459
Bencini, A., Bianchi, A., Fornasari, P., Giorgi, C., Paoletti, P. and Valtancoli, B., Cd(II) complexation in aqueous solution with dipyridine- and phenanthroline-containing polyamine macrocycles, 1329
Benetollo, F., see Clemente, D.A., 2161
Benetollo, F., Bombieri, G., Adeyga, A.M., Fonda, K.K., Gootee, W.A., Samaria, K.M. and Vallarino, L.M., Lanthanide(III) complexes of six-nitrogen-donor macrocyclic ligands with benzyl-type peripheral substituents, and crystal structure of $[La(NO_3)_2(H_2O)(C_{36}H_{38}N_6)](NO_3)(H_2O)$, 425
Benniston, A.C., Ellis, D., Farrugia, L.J., Kennedy, R., Peacock, R.D. and Walker, S., The synthesis of small azamacrocycles bearing pendant aromatic functionalities. The crystal structures of $[Cu(\mathbf{L}_1)_2](PF_6)_2$, $[(\mathbf{L}_1)CuCl_2]$, $[Cu(\mathbf{L}_6)(NO_3)_2]$ and $[Cu_2(\mathbf{L}_7{-}H)_2(OH_2)_2](PF_6)_2\cdot 3H_2O$ ($\mathbf{L}_1$ = *N*-(mesitylethyl)-1,4,7-triazacyclononane, $\mathbf{L}_6$ = *N*-(4-hydroxymethylbenzyl)-1,4,7-triazacylcononane, $\mathbf{L}_7$ = *N*-(4-benzylcarboxylic acid)-1,4,7-triazacylcononane), 333
Bentiss, F., Lagrenée, M., Wignacourt, J.P. and Holt, E.M., Complexes of cobalt(II), nickel(II) and copper(II) with a thia ligand; 2,5-bis(2-pyridyl)-1,3,4-thiadiazole: structural identification, 403
Bera, S.K., see Deoghoria, S., 2457
Bera, P., Butcher, R.J., Chaudhuri, S. and Saha, N., Synthesis and spectroscopic characterisation of cobalt(III) complexes with *S*-benzyl-β-*N*-(5-methylpyrazole-3-yl)methylenedithiocarbazate

(H_2L): X-ray structures of $[Co(HL)_2]NO_3 \cdot EtOH$ (**1**) and $[Co(HL)(L)] \cdot H_2O$ (**2**), 1
Bermejo, E., see Ketcham, K.A., 859
Bermejo, E., see García, I., 729
Bernal, I., see Cai, J., 817
Bernès, S., see Gasque, L., 935
Berni, E., see Bencini, A., 1459
Bertolasi, V., see Pitteri, B., 2283
Bessler, K.E., see de Figueiredo, A.T., 2351
Beyer, L., see Domínguez, M., 1429
Bhaduri, S., see Aromí, G., 1779
Bharara, M., see Kim, C.-H., 225
Bhattacharya, R., Sinha Ray, M., Dey, R., Righi, L., Bocelli, G. and Ghosh, A., Synthesis, crystal structure and thermochromism of benzimidazolium tetrachlorocuprate: $(C_7H_7N_2)_2[CuCl_4]$, 2561
Bhattacharyya, I., Shivakumar, M. and Chakravorty, A., Chemistry of a family of semiquinone monochelates of carbonyl ruthenium(II) generated by reacting quinones with hydridic species, 2761
Bhattacharyya, S., see Chakraborty, I., 1597
Bian, Z.-Q., Wang, K.-Z. and Jin, L.-P., Syntheses, spectroscopic and crystal structural studies of novel imidazo[4,5-f]1,10-phenanthroline derivatives and their Eu(III) ternary complexes with dibenzoylmethane, 313
Bianchi, A., see Bencini, A., 1329
Bibal, C., Mazières, S., Gornitzka, H. and Couret, C., New arylchlorogermylenes stabilized by two *ortho* side-chain donor ligands, 2827
Biesuz, R., see Pesavento, M., 1343
Bijanzadeh, H.R., see Amirnasr, M., 2733
Binions, R., Blackman, C.S., Carmalt, C.J., O'Neill, S.A., Parkin, I.P., Molloy, K. and Apostilco, L., Tin phosphide coatings from the atmospheric pressure chemical vapour deposition of SnX_4 (X = Cl or Br) and PR_xH_{3-x} (R = Cyc^{hex} or phenyl), 1943
Bismondo, A., Di Bernardo, P., Portanova, R., Tolazzi, M. and Zanonato, P.L., Complexation of lanthanide(III) with a tripodal polyaza polycatecholate ligand, 1393
Blackman, C.S., see Binions, R., 1943
Blacque, O., see Boni, G., 371
Blanco, L.M., see Kharisov, B.I., 2081
Bobev, S. and Sevov, S.C., Isolated deltahedral clusters of lead in the solid state: synthesis and characterization of Rb_4Pb_9 and $Cs_{10}K_6Pb_{36}$ with Pb_9^{4-}, and $A_3A'Pb_4$ (A = Cs, Rb, K; A′ = Na, Li) with Pb_4^{4-}, 641
Boča, R., see Baran, P., 1561
Bocelli, G., see Bhattacharya, R., 2561
Bocheńska, M., Zielińska, A., Kravtsov, V.C., Gdaniec, M., Luks, E. and Radecka-Paryzek, W., Lower rim substituted *tert*-butylcalix[4]arenes (II). Complexing ability of 5,11,17,23-tetra-*tert*-butyl-25,26,27,28-tetrakis-*O*-(piperidinylcarbonyl)methylenecalix[4]arene. The crystal structures of the ligand and its sodium complex, 763
Bogusz, K., see Kroczewska, D., 295
Bohra, R., see Gupta, A., 2387
Bóka, B., see Ősz, K., 2149
Bombieri, G., see Benetollo, F., 425
Bomfim, J.A.S., Filgueiras, C.A.L., Alan Howie, R., Low, J.N., Skakle, J.M.S., Wardell, J.L. and Wardell, S.M.S.V., Tris(2-methyl-2-phenylpropyl)stannane derivatives, $(Neo)_3SnX$, revisited. Comparison of crystal structures of $(Neo)_3SnX$ (X = Cl, Br, I, N_3, NCS and OAc), 1667
Boncella, J.M., see Mills, R.C., 1051
Bondarenko, G.I., see Kharisov, B.I., 2081
Boni, G., Blacque, O., Sauvageot, P., Poujaud, N., Moïse, C. and Kubicki, M.M., Tantalocene–hydride–phosphorus chemistry. Some new complexes and crystal structures of $[CpCp'TaH_2(PMe_2H)]PF_6$ (Cp = C_5H_5, Cp′ = $C_5H_2^tBu(Me)_2$) and $Cp_2Ta(H)(\mu\text{-}PPh_2,H)Fe(CO)_3$, 371
Booncoon, S., see Youngme, S., 1279
Borda, E., see Smieja, J.A., 1889
Borneman, M., see Smieja, J.A., 1889
Borrás, J., see Macías, B., 1899
Borrás, J., see Macías, B., 1229
Borrás, J., see Cejudo, R., 1057
Bosque, R., see López, C., 2361
Bott, S.G., see van Poppel, L.H., 1877
Boyle, T.J., Andrews, N.L., Alam, T.M., Rodriguez, M.A., Santana, J.M. and Scott, B.L., Crystallographic characterization of the esterification pathway of Group V alkoxides, 2333
Bradshaw, D., see Adams, H., 1957
Braibanti, A., see Compari, C., 1503
Braibanti, A., Molecular energy parameters by solution thermodynamics, 1439
Bregier-Jarzebowska, R., see Bartoszak-Adamska, E., 739
Breza, M., see Baran, P., 1561
Bridgeman, A.J. and Cavigliasso, G., Bonding in $[W_4O_{16}]^{8-}$ isopolyanions, 2201
Brito, H.F., see Teotonio, E.E.S., 1837
Brito, F., see Armas, M.T., 1513
Brombacher, H., see Craven, E., 553
Bronowska, W., Staszak, Z., Daszkiewicz, M., Cieślak-Golonka, M. and Wojciechowska, A., Systematic investigation of the $[Ni^{2+}$–phen–$CrO_4^{2-}]$ system; dichromate species isolated from alkaline solutions, 997
Brooks, J.S., see Bell, N.A., 115
Brown, S.T., Petraco, N.D.K., Yamaguchi, Y. and Schaefer, H.F., III, $\tilde{X}\ ^3\Sigma^-$ and $\tilde{A}\ ^3\Pi$ electronic states of linear disilaketenylidene (SiSiO): analysis of the Renner effect in the $\tilde{A}\ ^3\Pi$ state. Comparison with the analogous multiple bonded systems SiCO, CSiO, and CCO, 599
Bu, X.R., see Liang, S., 2021
Budiu, T., see Rațiu, C., 353
Bugella-Altamirano, E., see Serrano-Padial, E., 1451
Buglyó, P., see Amélia Santos, M., 2609
Bukowska-Strzyżewska, M., see Sieroń, L., 2473
Bunel, S., see Parada, J., 2215
Bunton, C.A., see Parada, J., 2215
Burlov, A.S., see Kharisov, B.I., 2081
Bushuev, M.B., Virovets, A.V., Garcia, Y., Gieck, C., Sheludyakova, L.A., Ikorskii, V.N., Tremel, W., Gütlich, P. and Lavrenova, L.G., Mononuclear coordination compounds based on a novel chelating triazole ligand: 1-vinyl-3-acetylamino-1,2,4-triazole, 797
Butcher, R.J., see Saha, N.C., 779
Butcher, R.J., see Singh, A.K., 667
Butcher, R.J., see Bera, P., 1
Byun, J.C., see Na, H.G., 917

Cai, Z.-G., see Tian, Y.-P., 1217
Cai, J., Hu, X., Bernal, I. and Ji, L.-N., Nickel(II) complexes of amino acids in comparison with the cobalt(III) analogues: interesting structural aspects relative to intermolecular hydrogen bonds and chiral recognition, 817
Cai, J., see Chen, C.-H., 689
Cai, J., see Zhang, H., 721
Cameron, T.S., see Cooke, M.W., 1235
Cao, R., see Luo, J.-H., 893
Carballo, R., Castiñeiras, A., Balboa, S., Covelo, B. and Niclós, J., Solid state coordination chemistry of copper(II)/α-hydroxycarboxylato/2,2′-bipyridine systems, 2811
Carballo, R., see Serrano-Padial, E., 1451
Carlton, L., see Cîrcu, V., 1775
Carmalt, C.J., see Binions, R., 1943
Carrasco, A.L., see Zuno-Cruz, F.J., 1105
Carriedo, G.A., García Alonso, F.J., Luis García Álvarez, J., Valenzuela, C.D. and Sáez, N.Y., Synthesis and spectroscopic properties of a new high molecular weight poly-spirophosphazene–oxypyridine copolymer and its complexes with $W(CO)_5$ fragments, 2587

Carriedo, G.A., García Alonso, F.J., González, P.A., Díaz Valenzuela, C. and Yutronic Sáez, N., Synthesis and spectroscopic characterization of cyclic and polymeric phosphazenes bearing phosphine complexes, 2579
Carrillo, D., see Galindo, A.M., 2531
Carunchio, V., Metal complexes: from pioneers to the GTC, 1313
Casas, J.S., Castaño, M.V., Cifuentes, M.C., Sánchez, A. and Sordo, J., Synthesis and structures of acetylferrocene thiosemicarbazones and their dimethylthallium(III) complexes, which have four- or five-membered chelate rings, 1651
Čáslavský, J., see Plešek, J., 975
Castanheira, R., see Delgado, R., 2265
Castaño, M.V., see Casas, J.S., 1651
Castellano, E.E., see Von Poelhsitz, G., 2221
Castillo, O., see Luque, A., 19
Castiñeiras, A., see Carballo, R., 2811
Castiñeiras, A., see Macías, B., 1899
Castiñeiras, A., see Labisbal, E., 1553
Castineiras, A., see Lobana, T.S., 1603
Castiñeiras, A., see Choquesillo-Lazarte, D., 1485
Castiñeiras, A., see Serrano-Padial, E., 1451
Castiñeiras, A., see Macías, B., 1229
Castiñeiras, A., see Ketcham, K.A., 859
Castiñeiras, A., see García, I., 729
Castineiras, A., see Lobana, T.S., 205
Castro-Juiz, S., see Ares, R., 2309
Cataldo, F. and Keheyan, Y., About a new class of inorganic polymers: the polythiocyanogens $[S_z(CN)_2]_x$, 1825
Caubet, A., see López, C., 2361
Caubet, A., see García-Raso, A., 1197
Cavaleiro, A.M.V., see Gamelas, J.A.F., 2537
Cavaleiro, A.M.V., see Santos, I.C.M.S., 2009
Cavigliasso, G., see Bridgeman, A.J., 2201
Cecconi, F., Frassineti, C., Gans, P., Iotti, S., Midollini, S., Sabatini, A. and Vacca, A., Complex formation equilibria of phosphocreatine with sodium, potassium and magnesium ions, 1481
Cejudo, R., Alzuet, G., Borrás, J., Liu-González, M. and Sanz-Ruiz, F., Crystal structure, magnetic and spectroscopic properties of copper(II) formato dimethylformamide: a new tetracarboxylato-bridged copper(II) dimer, 1057
Cesar, A., see de Moura, C.V.R., 2227
Chacón Villalba, M.E., see Soria, D.B., 1767
Chaichit, N., see Youngme, S., 1279
Chaichit, N., see Youngme, S., 943
Chaichit, N., see Youngme, S., 247
Chakrabarty, R., see Barman, R.K., 1189
Chakraborty, I., Bhattacharyya, S. and Chakravorty, A., The first family of trigonal prismatic M(bidentate)$_2$(monodentate)$_2$ complexes: synthesis and characterization of halobis(2-amidothiophenolato)triphenylphosphinerhenium(V), 1597
Chakravarty, A.R., see Rath, R.K., 1929
Chakravorty, A., see Bhattacharyya, I., 2761
Chakravorty, A., see Chakraborty, I., 1597
Chakravorty, A., see Panda, B.K., 899
Chanda, N., Mondal, B., Puranik, V.G. and Lahiri, G.K., Ruthenium monoterpyridine complexes incorporating α,α′-diimine based ancillary functions. Synthesis, crystal structure, spectroelectrochemical properties and catalytic aspect, 2033
Chandra, K., see Singhal, S., 2489
Chandra, S.K., see Deoghoria, S., 2457
Chang, H.-C., see Yu, X.-Y., 1613
Chang, F., see Liu, S.-T., 1073
Charsley, S.M., Jones, C.J., Neaves, B.D., Kresiński, R.A., McWhinnie, S.L.W., McCleverty, J.A. and Yellowlees, L.J., Synthesis, electrochemistry and spectroelectrochemistry of hydrazido(2-) bridged bimetallic molybdenum species, and the X-ray crystal structure of $[Mo\{HB(3,5\text{-}Me_2pz)_3\}(NO)Cl]_2(\mu\text{-}NHNH)$ in solid solution, 849
Chattopadhyay, S., see Panda, B.K., 899
Chaudhuri, N.R., see Sain, S., 2293
Chaudhuri, S., see Saha, N.C., 779
Chaudhuri, S., see Bera, P., 1
Chen, M.-Q., see Pang, Z., 2675
Chen, L.-H., see Misra, T.K., 2045
Chen, Y.S., see Zeng, W.F., 1081
Chen, X.-M., see Chen, C.-H., 689
Chen, C.-H., Cai, J., Feng, X.-L. and Chen, X.-M., Assembly via H-bonds and Ag–Ag attractions of one-dimensional silver(I) complexes of nicotinamide and nicotinic acid with sulfonate counteranions, 689
Cheng, C.P., see Zeng, W.F., 1081
Chern, S.S., see Zeng, W.F., 1081
Chew, K.-B., see Tarafder, M.T.H., 2683
Chiang, M.Y., see Sain, S., 2293
Chiang, M.Y., see Zeng, W.F., 1081
Chicote, E., see Macías, B., 1899
Cho, H.Y., Roh, S.-G. and Jeong, J.H., Syntheses and reactivities of new bis(imido)Mo(VI) complexes of hydrotris(3,5-dimethyl-1-pyrazolyl)borate and X-ray molecular structures of $[\{HB(3,5\text{-}Me_2C_3N_2H)_3\}Mo(Nmes)_2X]$ (X = Cl or OH; mes = 2,4,6-trimethylphenyl), 1211
Chohan, Z.H., see Aupers, J.H., 2107
Choi, K.-Y., Chun, K.-M., Lee, K.-C. and Kim, J., Synthesis and characterization of nickel(II) complexes of hexaazamacrotetracyclic ligand containing organic ligands, 1913
Choi, J.H., see Na, H.G., 917
Choi, M.-G., see Park, Y.J., 33
Choquesillo-Lazarte, D., Covelo, B., González-Pérez, J.M., Castiñeiras, A. and Niclós-Gutiérrez, J., Metal chelates of *N*-(2-pyridylmethyl)iminodiacetate(2-) ion (pmda). Part I. Two mixed-ligand copper(II) complexes of pmda with *N*,*N*-chelating bases. Synthesis, crystal structure and properties of $H_2pmda\cdot 0.5H_2O$, $[Cu(pmda)(pca)]\cdot 3H_2O$ (pca = α-picolylamine) and $[Cu(pmda)(Hpb)]\cdot 5H_2O$ (Hpb = 2-(2′-pyridyl)benzimidazole), 1485
Choquesillo-Lazarte, D., see Serrano-Padial, E., 1451
Christou, G., see Aromí, G., 1779
Chryssou, K., Stergiopoulos, T. and Falaras, P., Synthesis and spectroscopic properties of a new bipyridine-bipyrazoyl(pyridine)-thiocyanato-ruthenium(II) complex, 2773
Chu, S.-Y., see Lai, C.-H., 579
Chuburu, F., see Bencini, A., 1459
Chun, K.-M., see Choi, K.-Y., 1913
Chung, C.-S., see Misra, T.K., 2045
Cieślak-Golonka, M., see Bronowska, W., 997
Cifuentes, M.C., see Casas, J.S., 1651
Cindrić, M., see Korpar-Čolig, B., 147
Ciunik, Z., see Ruman, T., 2743
Clarke, M.L., see Appleby, T., 2639
Clegg, W., see Liddle, S.T., 2451
Clegg, W., see Beheshti, A., 1547
Clemente, D.A., Marzotto, A. and Benetollo, F., Synthesis, crystal and molecular structure of pseudotetrahedral Zn(II) zwitterionic complexes: trichloro(1-methylpiperazin-1-ium-N^4)zinc(II) and trichloro(1,4-dimethylpiperazin-1-ium-N^4)zinc(II), 2161
Coles, S.J., see Bell, N.A., 1845
Collison, D., see Zhang, Y., 81
Collison, D., see Zhang, Y., 69
Colquhoun, S., see Torzilli, M.A., 697
Colquhoun, S., see Torzilli, M.A., 705
Comerlato, N.M., see Aupers, J.H., 2107
Compari, C., Fisicaro, E. and Braibanti, A., Cooperativity effects in the protonation of aliphatic polyamines, 1503
Compari, C., see Fisicaro, E., 1497
Comuzzi, C., Novelli, V., Portanova, R. and Tolazzi, M., The influence of *N*-alkylation and chain length in the coordination ability of

diamines towards silver(I) in dimethylsulfoxide, 1337
Comuzzi, C., Di Bernardo, P., Portanova, R., Tolazzi, M. and Zanonato, P., Affinity of lanthanide(III) ions for oxygen- and mixed oxygen–nitrogen-donor ligands in dimethylsulfoxide: a thermodynamic and spectroscopic investigation, 1385
Conato, C., Kozłowski, H., Młynarz, P., Pulidori, F. and Remelli, M., Copper and nickel complex-formation equilibria with Lys–Gly–His–Lys, a fragment of the matricellular protein SPARC, 1469
Concolino, T., see Reger, D.L., 1795
Constable, C.P., see Bell, N.A., 1845
Cooke, M.W., Murphy, C.A., Cameron, T.S., Beck, E.J., Vamvounis, G. and Aquino, M.A.S., Synthesis and crystal structures of urea and thiourea derivatives of diruthenium(II,III) tetraacetate, 1235
Cordopatis, P., see Tiliakos, M., 229
Córdova, C., see Manzur, J., 181
Cornard, J.P. and Merlin, J.C., Complexes of aluminium(III) with isoquercitrin: spectroscopic characterization and quantum chemical calculations, 2801
Cornu, D., Hitchcock, P.B., Lappert, M.F. and Uiterweerd, P.G.H., Some 2,6-bis(dimethylamino)phenyl–mercury(II) and –boron complexes, 635
Cotton, S.A., Franckevicius, V. and Fawcett, J., Syntheses and structures of iron(III) complexes of simple N-donor ligands, 2055
Coucouvanis, D., see Han, J., 2523
Couret, C., see Bibal, C., 2827
Covelo, B., see Carballo, R., 2811
Covelo, B., see Choquesillo-Lazarte, D., 1485
Crans, D.C., see Rosu, C., 959
Craven, E., Mutlu, E., Lundberg, D., Temizdemir, S., Dechert, S., Brombacher, H. and Janiak, C., Thallium(I) complexes with modified poly(pyrazolyl)borate ligands—metal-ligand coordination and crystal packing, 553
Cîrcu, V., Fernandes, M.A. and Carlton, L., Reactivity of a rhodium(I) complex towards oxygen enhanced by a cyano ligand. Structure of $[Rh(CN)(O_2)(PPh_3)_2(XNC)]$ (XNC = xylyl isocyanide), 1775
Creeth, J.E., see Barret, M.C., 1761
Crespo, M., Font-Bardía, M. and Solans, X., Formation and cleavage of platinacycles containing a fluorinated imine. Crystal structure of $[PtMe(3,4,5\text{-}C_6HF_3CH{=}NCH_2C_6H_5)PPh_3]$, 105
Crisponi, G., Diaz, A., Nurchi, V.M., Pivetta, T. and Tapia Estévez, M.J., Equilibrium study on Cd(II) and Zn(II) chelates of mercapto carboxylic acids, 1319
Cristiani, F., see Villaescusa, I., 1363
Crouse, K.A., see Tarafder, M.T.H., 2683
Crouse, K.A., see Tarafder, M.T.H., 2691
Crouse, K.A., see Tarafder, M.T.H., 2547
Císařová, I., see Plešek, J., 975
Cui, C.-P., Dai, J.-C., Du, W.-X., Fu, Z.-Y., Hu, S.-M., Wu, L.-M. and Wu, X.-T., Synthesis, structure and fluorescence of a 3-D polymer $\{(Mo_4O_{12})(4,4'\text{-bipy})_2\}_n$, 175
Cuypers, L., see Uhl, W., 511
Czeluśniak, I., see Szymańska-Buzar, T., 2505
Czeluśniak, I., see Szymańska-Buzar, T., 1817

Dai, J.-C., see Cui, C.-P., 175
Damnatara, K., see Youngme, S., 943
Daniele, S., Hubert-Pfalzgraf, L.G. and Perrin, M., Molecular structures of volatile Ce(IV) tetrafluoroisopropoxide complexes with TMEDA and diglyme. CVD experiments, 1985
Darensbourg, M.Y., see de Moura, C.V.R., 2227
Das, B.K., see Barman, R.K., 1189
Das, C., see Saha, A., 97
Daszkiewicz, M., see Bronowska, W., 997
Datta, A., Karan, N.K., Mitra, S. and Tiekink, E.R.T., A novel trinuclear cyano-bridged calcium(II)–iron(III) complex; $[(phen)_2(H_2O)_2CaNC(NC)_4FeCNCa(OH_2)(Phen)_2NO_3]\cdot H_2O$, 2237
Díaz, P., Doménech, A., García-España, E. and Soriano, C., Synthesis, acid–base behaviour, co-ordination and electrochemistry studies on new open-chain bithiophene receptors, 1523
Díaz, C. and Valenzuela, M.L., Transition metal containing dendrimers based on cyclophosphazene units, 909
Díaz Valenzuela, C., see Carriedo, G.A., 2579
de Araujo, M.P., see Von Poelhsitz, G., 2221
De Bellis, V.M., see Oliveira, M.R.L., 2243
de Castro, B., see Azevedo, F., 1695
Dechert, S., see Craven, E., 553
Decinti, A., see Zolezzi, S., 55
De Clercq, E., see Višnjevac, A., 2567
de Faria, D.L.A., see Teotonio, E.E.S., 1837
de Farias, R.F., Airoldi, C. and Scatena, H., Jr., Empirical correlations involving calorimetric, thermogravimetric and infrared data for zinc halides adducts, 1677
de Fátima Cabral, M., see Delgado, R., 2265
de Figueiredo, A.T., Deflon, V.M., Bessler, K.E., Maichle-Mössmer, C. and Abram, U., Hydroximato complexes of boron—the X-ray crystal structures of dicyclohexylammonium bis(benzohydroximato)borate chloroform solvate and tetra-*n*-propylammonium bis(benzohydroximato)borate, 2351
Deflon, V.M., see de Figueiredo, A.T., 2351
Dehghanpour, S., see Amirnasr, M., 2733
Delgado, R., de Fátima Cabral, M., Castanheira, R., Zhang, A. and Herrmann, R., Metal complexes of edta-derived macrocyclic ether bis(lactones). Hydrolysis of the macrocycles and the metal catalysis effect, 2265
de Lima, G.M., see Moura, E.M., 2323
de Matos Gomes, E., see Gamelas, J.A.F., 2537
de Moura, C.V.R., Silva, R.M., Cesar, A., Darensbourg, M.Y. and Reibenspies, J., X-ray structure of $[Nb(\eta^5\text{-}C_5H_5)_2(SCH_2CH_2CH_2S]$. ECP quantum chemistry of niobium five and six metallacycle complexes, 2227
Deng, Y.-F., see Zhou, Z.-H., 787
Deoghoria, S., Sain, S., Moulton, B., Zaworotko, M.J., Bera, S.K. and Chandra, S.K., Synthesis, crystal structure and magnetic behavior of two new binuclear complexes bridged by a pentadentate ligand: $[Ni_2L_2(NCS)_2](ClO_4)_2$ and $[Ni_2L_2(NCO)_2](ClO_4)_2$ [L = pentadentate ligand], 2457
de Oliveira, L.A.A., see Von Poelhsitz, G., 2221
Derek Woollins, J., see Appleby, T., 2639
Derveer, D.V., see Liang, S., 2021
Descalzo, A.B., see Sancenón, F., 1397
de Sousa, A.S. and Fernandes, M.A., The synthesis and low-temperature X-ray study of bis[*N*,*N*,*N*′,*N*′-tetrakis-(2-hydroxyethyl)ethylenediamine]copper(II) perchlorate, 1883
de Sousa, G.F., see Fernandes, R.M., 1149
Devereux, M., McCann, M., Leon, V., McKee, V. and Ball, R.J., Synthesis and catalytic activity of manganese(II) complexes of heterocyclic carboxylic acids: X-ray crystal structures of $[Mn(pyr)_2]_n$, $[Mn(dipic)(bipy)_2]\cdot 4.5H_2O$ and $[Mn(chedam)(bipy)]\cdot H_2O$ (pyr = 2-pyrazinecarboxylic acid; dipic = pyridine-2,6-dicarboxylic acid; chedam = chelidamic acid(4-hydroxypyridine-2,6-dicarboxylic acid); bipy = 2,2-bipyridine), 1063
Dey, R., see Bhattacharya, R., 2561
Diamantopoulou, E., Raptopoulou, C.P., Terzis, A., Tangoulis, V. and Perlepes, S.P., Heptanuclearity in nickel(II) chemistry: preparation, characterization, crystal structure and magnetic properties of $[Ni_7(OH)_2(acac)_8(btaO)_4(H_2O)_2]$ ($btaO^-$ = the 1-hydroxybenzotriazolate ion), 2117
Dias, H.V.R. and Ayers, A.E., Reactions of divalent group 14 compounds containing an azide functionality: synthesis and characterization of $[HB(3,5\text{-}(CF_3)_2Pz)_3]AgGe(N_3)[(n\text{-}Pr)_2ATI]$ and $[HB(3,5\text{-}(CF_3)_2Pz)_3]AgSn(N_3)[(n\text{-}Pr)_2ATI]$, 611
Diaz, A., see Crisponi, G., 1319
Di Bernardo, P., see Bismondo, A., 1393
Di Bernardo, P., see Comuzzi, C., 1385

Dinda, R., see Rana, A., 1023
Ding, E.-R., see Liu, S.-T., 1073
Do, Y., see Yoo, J., 715
Do, Y., see Park, Y.J., 33
Dobrzyńska, D., Duczmal, M., Jezierska, J. and Jerzykiewicz, L.B., Synthesis and structure of the mixed ligand complex of copper(II), bis(9,10-dihydro-9-oxo-10-acridineacetato)bis(imidazole)copper(II) tetrahydrate, 2381
Dolmella, A., Intini, F.P., Pacifico, C., Padovano, G. and Natile, G., Structural characterization of the 'lantern-shaped' platinum(III) complex $[Pt_2Cl_2\{N(H)C(Bu^t)O\}_4]$, 275
Domasevitch, K.V., see Gubina, K.E., 963
Domasevitch, K.V., see Lysenko, A.B., 769
Doménech, A., see Díaz, P., 1523
Domínguez, S., see Armas, M.T., 1513
Domínguez, M., Anticó, E., Beyer, L., Aguirre, A., García-Granda, S. and Salvadó, V., Liquid–liquid extraction of palladium(II) and gold(III) with *N*-benzoyl-*N*′,*N*′-diethylthiourea and the synthesis of a palladium benzoylthiourea complex, 1429
Doucet, D., see Torzilli, M.A., 697
Doufou, P., see Mills, R.C., 1051
Downs, A.J., Himmel, H.-J. and Manceron, L., Low valent and would-be multiply bonded derivatives of the Group 13 metals Al, Ga and In revealed through matrix isolation, 473
Downs, L.E., see Vohs, J.K., 531
Dozol, J.-F., see Thuéry, P., 2497
Drake, J.E., see Gupta, A., 2387
Drake, J.E., see Singh, A.K., 667
Drew, M.G.B., see Quintal, S.M.O., 2783
Drobot, D.V., see Shcheglov, P., 2317
Drożdżewski, P., Pawlak, B. and Głowiak, T., Unusual co-ordination behaviour of imidazole-4-acetic acid. Synthesis, crystal structure and vibrational studies of one-dimensional co-ordination polymer of zinc(II) with two different ligand forms, 2819
Du, W.-X., see Cui, C.-P., 175
Duan, Y.-B., see Li, Y.-G., 2601
Duczmal, M., see Dobrzyńska, D., 2381
Dutta, D.P., Jain, V.K., Knoedler, A. and Kaim, W., Dithiocarbamates of gallium(III) and indium(III): syntheses, spectroscopy, and structures, 239
Dyrda, G., see Słota, R., 677
Dzięgielewski, J.O., see Machura, B., 2617

Eccles, H., see Zhang, Y., 81
Eccles, H., see Zhang, Y., 69
Edwards, D., see Smieja, J.A., 1889
Eilmes, J., Ptaszek, M. and Wozniak, K., Synthesis, reactivity, crystal and molecular structure of [5,14-dihydro-7,16-bis(2-oxo-3*H*-furan-5-yl)-6,8,15,17-tetramethyldibenzo[b,i][1,4,8,11]tetraazacyclotetradecinato(2-)-κ^4N]nickel(II), 7
Eisen, M.S., see Koch, T., 2445
Elerman, Y., see Kavlakoglu, E., 1539
Elias, H., see Baran, P., 1561
Elizondo, N.V., see Kharisov, B.I., 2081
Ellena, J., see Von Poelhsitz, G., 2221
Ellis, D., see Benniston, A.C., 333
Elmali, A., see Kavlakoglu, E., 1539
El-Sawaf, A.K., see Ketcham, K.A., 859
El Sawaf, A.K., see García, I., 729
Þentürk, O.S., see Hogarth, G., 791
Escuer, A., see Papaefstathiou, G.S., 2027
Escuer, A., see Goher, M.A.S., 1871
Espinosa, E., see García-Raso, A., 1197
Espinosa-Pérez, G., see Valdés-Martínez, J., 409
Espínola, J.G.P., see Teotonio, E.E.S., 1837
Evans, D.J., Junk, P.C. and Smith, M.K., The effect of coordinated solvent ligands on the solid-state structures of compounds involving uranyl nitrate and Schiff bases, 2421
Evans, W.J., Fujimoto, C.H. and Ziller, J.W., Synthesis and structure of inorganic and organometallic *N*,*N*′-bis(3, 5-di-*tert*-butylsalicylidene)ethylenediamine yttrium complexes, 1683

Falaras, P., see Chryssou, K., 2773
Falaras, P., see Raţiu, C., 353
Falvello, L.R., see Rana, A., 1023
Farkas, E., see Amélia Santos, M., 2609
Farková, M., see Havel, J., 1375
Farrugia, L.J., see Benniston, A.C., 333
Faure, R., see Acuña-Cueva, E.R., 1961
Fawcett, J., see Cotton, S.A., 2055
Fawcett, J., Platt, A.W.G. and Russell, D.R., Structures and catalytic properties of triphenylphosphine oxide complexes of scandium and lanthanide triflates, 287
Félix, V., see Quintal, S.M.O., 2783
Feng, X.-L., see Chen, C.-H., 689
Feng, X.-L., see Zhang, H., 721
Fenton, D.E., see Adams, H., 1957
Fereshteh Hekmat, H., see Beheshti, A., 1547
Fernandes, M.A., see de Sousa, A.S., 1883
Fernandes, M.A., see Cîrcu, V., 1775
Fernandes, R.M., Lang, E.S., López, E.M.V. and de Sousa, G.F., Organotin(IV) complexes of 4,6-dimethylpyrimidine-2-thione, Me_2-PymtH. Preparation, characterization and crystal structure determination of *cis*-$[Ph_2Sn(Me_2Pymt)_2]$ and $[Ph_3Sn(Me_2Pymt)]$, 1149
Fernández, J.J., see Ares, R., 2309
Fernández, A., see Ares, R., 2309
Fernández, A., see López-Torres, M., 2063
Fernández, J.J., see López-Torres, M., 2063
Fernández, J.J., see Fernández, A., 39
Fernández, A., Pereira, E., Fernández, J.J., López-Torres, M., Suárez, A., Mosteiro, R. and Vila, J.M., Cyclopalladated compounds derived from [C,N,O] terdentate ligands: synthesis, characterization and reactivity, 39
Feroci, G., see Fini, A., 1421
Ferrari, M.B., Pelizzi, C., Pelosi, G. and Rodríguez-Argüelles, M.C., Preparation, characterization and X-ray structures of 1-methylisatin 3-thiosemicarbazone copper, nickel and cobalt complexes, 2593
Ferrari, R., see Gasque, L., 935
Ferreira, A.G., see Von Poelhsitz, G., 2221
Ferrer, E.G., see Williams, P.A.M., 1979
Ferretti, V., see Pitteri, B., 2283
Fidalgo, E.G., Neels, A., Stoeckli-Evans, H. and Süss-Fink, G., New iso and heteropolyoxomolybdates: synthesis and molecular structure of the anions $[Mo_8^{VI}O_{26}(OH)]^{5-}$, $[HAs^{III}As^{V}Mo^{V}Mo_8^{VI}O_{34}]^{6-}$ and $[HAs^{III}As^{V}Mo^{V}Mo_8^{VI}O_{34}\{Co(C_5H_5N)_2(H_2O)_3\}]^{4-}$, 1921
Field, L.D., He, T., Masters, A.F. and Turner, P., The synthesis and X-ray structural characterisation of the decaphenylmolybdenocenium cation as its tetrafluoroborate salt, 1707
Filgueiras, C.A.L., see Bomfim, J.A.S., 1667
Fini, A., Feroci, G. and Roda, A., Acidity in bile acid systems, 1421
Fiol, N., see Villaescusa, I., 1363
Fiol, J.J., see García-Raso, A., 1197
Fischer, R.A., see Weiß, D., 535
Fisicaro, E., see Compari, C., 1503
Fisicaro, E., Compari, C. and Moroi, Y., Apparent and partial molar enthalpies of some potassium *p*-*n*-alkyl-benzoate aqueous solutions, 1497
Floris, C., see Villaescusa, I., 1363
Foley, S.R., Yap, G.P.A. and Richeson, D.S., Synthesis and structural characterization of the first trialkylguanidinate and hexahydropyramidopyramidinate complexes of tin, 619
Fonda, K.K., see Benetollo, F., 425
Font-Bardía, M., see López, C., 2361
Font-Bardía, M., see Papaefstathiou, G.S., 2027

Font-Bardía, M., see Crespo, M., 105
Forder, S.D., see Bell, N.A., 115
Formica, M., Giorgi, L., Fusi, V., Micheloni, M. and Pontellini, R., Two triaza-polyamine units linked together by different aromatic spacers, coordination properties towards metal cations of a new compartmental ligand, 1351
Fornasari, P., see Bencini, A., 1329
Foster, C.L., Kilner, C.A., Thornton-Pett, M. and Halcrow, M.A., Steric effects on the stereochemistry of copper complexes of 2,6-bis(pyrazol-1-ylmethyl)pyridines, 1031
Franckevicius, V., see Cotton, S.A., 2055
Frassineti, C., see Cecconi, F., 1481
Freire, C., see Azevedo, F., 1695
Frenking, G., see Weiß, D., 535
Fröhlich, N., see Weiß, D., 535
Fu, Z.-Y., see Cui, C.-P., 175
Fuess, H., see Baran, P., 1561
Fujimoto, C.H., see Evans, W.J., 1683
Fujisawa, K., see Yamada, Y., 2143
Fujisawa, K., see Mahboob, N., 1809
Fujiwara, M., see Asada, H., 1139
Fun, H.-K., see Tarafder, M.T.H., 2683
Fun, H.-K., see Tarafder, M.T.H., 2691
Fun, H.-K., see Tarafder, M.T.H., 2547
Fun, H.K., see Kannan, S., 2403
Fusi, V., see Formica, M., 1351
Fuyuhiro, A., see Kita, M., 843

Gabrielli, M., see Masci, B., 1125
Gade, L.H., see Haller, I., 629
Galan-Fereres, M., see Koch, T., 2445
Galas, D.F., see Grant, G.J., 879
Galindo, A.M., Mardones, M., Manzur, C., Hamon, J.-R., Vega, A., Garland, M.T. and Carrillo, D., Reactivity of [*trans*-$R_2MoO(NNPhR')$(*o*-phen)] toward $R'PhNNH_2$ and $R'PhNNH_3^+Cl^-$, R = Me, Ph and R′ = Me, Ph. X-ray structure of [*trans*-MeCl-$MoO(NNPh_2)$(*o*-phen)], 2531
Galli, A., Ghezzi, L., Raspi, G., Secco, F. and Spinetti, M., Detection of heterologous bovine pancreatic trypsin inhibitor by capillary zone electrophoresis, 1405
Gama, S., see Amélia Santos, M., 2609
Gambino, V., see Amorello, D., 1369
Gamelas, J.A.F., Cavaleiro, A.M.V., de Matos Gomes, E., Belsley, M. and Herdtweck, E., Synthesis, properties and photochromism of novel charge transfer compounds with Keggin anions and protonated 2,2′-biquinoline, 2537
Gans, P., see Cecconi, F., 1481
Gao, S., see Liu, Q.-D., 1097
Gao, J.-X., see Zhou, Z.-H., 787
Gao, E.-Q., Sun, H.-Y., Liao, D.-Z., Jiang, Z.-H. and Yan, S.-P., Synthesis of and magnetic interactions in binuclear Cu(II)–M(II) (M = Cu, Ni and Mn) complexes of macrocyclic oxamido ligands, 359
García, L., see Santana, M.D., 1935
García, G., see Santana, M.D., 1935
García, L., see Serrano, J.L., 1589
García, I., see Macías, B., 1229
García, I., Bermejo, E., El Sawaf, A.K., Castiñeiras, A. and West, D.X., Structural studies of metal complexes of 2-pyridineformamide N(4)-methylthiosemicarbazone, 729
García, A.M., see Manzur, J., 181
García Alonso, F.J., see Carriedo, G.A., 2587
García Alonso, F.J., see Carriedo, G.A., 2579
García-España, E., see Díaz, P., 1523
García-Granda, S., see Domínguez, M., 1429
García-Raso, A., Fiol, J.J., Adrover, B., Caubet, A., Espinosa, E., Mata, I. and Molins, E., Synthesis and structure of peptide–copper(II)–isocytosine ternary complexes, 1197
García-Tojal, J., see Gómez-Saiz, P., 2257
Garcia, I., see Ketcham, K.A., 859
Garcia, Y., see Bushuev, M.B., 797
Garg, A.N., see Singhal, S., 2489
Garland, M.T., see Galindo, A.M., 2531
Garnovskii, A.D., see Kharisov, B.I., 2081
Gasowska, A. and Lomozik, L., Spectroscopic and potentiometric investigation of the solution structure and stability of Ni(II) and Co(II) complexes with adenosine 5′-monophosphate and 1,12-diamino-4,9-diazadodecane (spermine) or 1,11-diamino-4,8-diazaundecane, 745
Gasque, L., Bernès, S., Ferrari, R. and Mendoza-Díaz, G., Cadmium complexation by aspartate. NMR studies and crystal structure of polymeric $Cd(AspH)NO_3$, 935
Gaubeur, I., see Ávila Terra, L.H.S., 2375
Gdaniec, M., see Bocheńska, M., 763
Ge, Q.-C., see Guo, Y.-H., 1005
Ghasemi, J., see Asadi, M., 1255
Ghasemi, J., see Asadi, M., 683
Ghezzi, L., see Galli, A., 1405
Ghosh, A., see Bhattacharya, R., 2561
Ghosh, S., see Rana, A., 1023
Ghosh, A.C., see Azam, K.A., 885
Ghosh, K., see Panda, B.K., 899
Gieck, C., see Bushuev, M.B., 797
Gili, P., see Armas, M.T., 1513
Gillitt, N.D., see Parada, J., 2215
Giorgi, C., see Bencini, A., 1459
Giorgi, C., see Bencini, A., 1329
Giorgi, L., see Formica, M., 1351
Głowiak, T., see Drożdżewski, P., 2819
Głowiak, T., see Szymańska-Buzar, T., 2505
Głowiak, T., see Szłyk, E., 2001
Głowiak, T., see Kurdziel, K., 1857
Głowiak, T., see Szymańska-Buzar, T., 1817
Glowiak, T., see Moncol', J., 365
Glowiak, T., see Szlyk, E., 343
Glueck, D.S., see Pelczar, E.M., 2409
Goeta, A.E., Lawrence, S.E., Meehan, M.M., O'Dowd, A. and Spalding, T.R., Synthesis, crystal and molecular structures of three triphenylsilanol amine adducts, 1689
Goher, M.A.S., Escuer, A., Mautner, F.A. and Al-Salem, N.A., A new series of 1D polymeric nickel(II) complex cations of pyridine derivative ligands with a single μ-1,3 azide bridge and X-ray crystal structure and magnetic properties of polymeric $\{[Ni(4\text{-ethylpyridine})_4(N_3)_n](PF_6)_n\}$, 1871
Gohil, S., see Shcheglov, P., 2317
Gök, Y., see Kantekin, H., 1865
Goldberg, I., see Patra, G.K., 2195
Golzar Hossain, G.M., see Azam, K.A., 381
Gomes, C.A.R., see Skorik, Y.A., 2719
Gómez-Saiz, P., García-Tojal, J., Maestro, M.A., Mahía, J., Arnáiz, F.J. and Rojo, T., Synthesis, crystal structure and spectroscopic properties of copper(II) complexes derived from 2-methylamino-5-pyridin-2-yl-1,3,4-oxadiazole, 2257
González, P.A., see Carriedo, G.A., 2579
González Baró, A.C., see Williams, P.A.M., 1979
González Garmendia, M.J., see Seco, J.M., 457
González-Pérez, J.M., see Choquesillo-Lazarte, D., 1485
Goodwin, S.D., see Vohs, J.K., 531
Gootee, W.A., see Benetollo, F., 425
Gorji, A., see Amirnasr, M., 2733
Görls, H., see Scholz, J., 305
Gornitzka, H., see Bibal, C., 2827
Goswami, S., see Saha, A., 97
Grant, G.J., Galas, D.F. and VanDerveer, D.G., Heteroleptic platinu-

m(II) complexes with crown thioether and phosphine ligands: the crystal structures of $[Pt(9S3)(PPh_3)Cl](PF_6)\cdot CH_3NO_2$ and $[Pt(10S3)(PPh_3)Cl](PF_6)$, 879
Grazina, R., see Amélia Santos, M., 2609
Grüner, B., see Plešek, J., 975
Gubina, K.E., Ovchynnikov, V.A., Swiatek-Kozlowska, J., Amirkhanov, V.M., Sliva, T.Y. and Domasevitch, K.V., Novel tetranuclear cubane-like Co(II) complexes involving chelate phosphoramide ligands, 963
Guekezian, M., see Ávila Terra, L.H.S., 2375
Guerrero, J., see Moya, S.A., 439
Guney, S., see Yilmaz, V.T., 2393
Guo, Y.-H., Ge, Q.-C., Lin, H., Lin, H.-K. and Zhu, S.-R., Thermodynamic studies on supramolecular interactions of metal ions with nucleotides/tripods ligands, 1005
Gupta, A., Sharma, R.K., Bohra, R., Jain, V.K., Drake, J.E., Hursthouse, M.B. and Light, M.E., Synthetic, spectroscopic and structural aspects of triphenylantimony(V) complexes with internally functionalized oximes: crystal and molecular structure of $[Ph_3Sb\{ON{=}C(Me)C_5H_4N\text{-}2\}_2]$, 2387
Gupta, S.K., Hitchcock, P.B. and Kushwah, Y.S., The crystal structure of 4-methyl-2,6-dibenzoylphenol and its conversion into a mononuclear cobalt(III) complex by treatment with cobalt(II) chloride and propane-1,3-diamine, 1787
Gupta, R., Lal, T.K. and Mukherjee, R., Synthesis and properties of $[Cu(L^5)_2][ClO_4]_2\cdot H_2O$ having square planar and pseudo-octahedral geometries in the same unit cell, and anion-bound complexes $[Cu(L^5)_2X][ClO_4]$ ($X = Cl^-$, NCS^-, N_3^-) [L^5 = 2-(3,5-dimethylpyrazol-1-ylmethyl)pyridine], 1245
Gutiérrez-Zorrilla, J.M., see Muga, I., 2631
Gütlich, P., see Bushuev, M.B., 797
Guzei, I.A., see Nelson, K.J., 2017

Halcrow, M.A., see Foster, C.L., 1031
Hall, I.H., see Wang, W., 1991
Haller, I., Renner, P. and Gade, L.H., A C_3-chiral lithium triamidostannate(II) containing a Sn–Li bond, 629
Hameršak, Z., see Višnjevac, A., 2567
Hamon, J.-R., see Galindo, A.M., 2531
Hampel, S., see Ruck, M., 651
Han, J., Huang, M. and Coucouvanis, D., New heteronuclear Mo/Fe/S clusters. The syntheses and structures of $(Cl_4\text{-cat})Mo(PEt_3)Fe_3S_4(SPEt_3)_2Cl$ and $(Cl_4\text{-cat})_2MoFe_2S_2(PEt_3)_2(CO)_4$ clusters, 2523
Han, Y.-K., see Yoo, J., 715
Handel, H., see Bencini, A., 1459
Hanif, K.M., see Azam, K.A., 885
Harms, K., see Uhl, W., 511
Harrison, W.T.A., see Yilmaz, V.T., 2393
Hashimoto, M., see Asaji, T., 2207
Hashimoto, M., see Shen, X., 969
Havel, J., Soto-Guerrero, J. and Lubal, P., Spectrophotometric study of uranyl–oxalate complexation in solution, 1411
Havel, J., Lubal, P. and Farková, M., Evaluation of chemical equilibria with the use of artificial neural networks, 1375
Hazarika, P., see Sarmah, S., 389
He, T., see Field, L.D., 1707
Heatley, F., see Zhang, Y., 81
Heatley, F., see Zhang, Y., 69
Heeg, M.J., see Yu, Z., 1117
Helfrich, B., see Valdés-Martínez, J., 409
Helliwell, M., see Zhang, Y., 81
Helliwell, M., see Zhang, Y., 69
Hendrickson, D.N., see Aromí, G., 1779
Herdtweck, E., see Gamelas, J.A.F., 2537
Herdtweck, E., see Zhang, G., 1737
Heřmánek, S., see Plešek, J., 975
Hernández-Molina, R., see Armas, M.T., 1513
Hernández-Ortega, S., see Valdés-Martínez, J., 409
Herrmann, R., see Delgado, R., 2265
Hey-Hawkins, E., see Koch, T., 2445
Hey-Hawkins, E., see Karasik, A.A., 2251
Hill, N.J., Levason, W., Popham, M.C., Reid, G. and Webster, M., Scandium halide complexes of phosphine- and arsine-oxides: synthesis, structures and ^{45}Sc NMR studies, 1579
Hill, N.J., Levason, W., Popham, M.C., Reid, G. and Webster, M., Yttrium halide complexes of phosphine- and arsine oxides: synthesis, multinuclear NMR and structural studies, 445
Himmel, H.-J., see Downs, A.J., 473
Hitchcock, P.B., see Gupta, S.K., 1787
Hitchcock, P.B., see Cornu, D., 635
Hoffmann, N., see Streubel, R., 119
Hogarth, G., Sarýkahya, F. and Þentürk, O.S., Thermal reactions of dimanganese decacarbonyl with tetraalkyldiphosphine disulfides (R = Me, Et, Pr^n, Bu^n) and crystal structure of $[Mn_2(CO)_8(\mu\text{-}PBu^n_2)_2]$, 791
Holt, E.M., see Bentiss, F., 403
Holub, K., see Plešek, J., 975
Hong, M.-C., see Luo, J.-H., 893
Hu, N.-H., see Li, Y.-G., 2601
Hu, C.-W., see Li, Y.-G., 2601
Hu, X., see Liu, S.-T., 1073
Hu, X., see Cai, J., 817
Hu, S.-M., see Cui, C.-P., 175
Huang, M., see Han, J., 2523
Hubert-Pfalzgraf, L.G., see Daniele, S., 1985
Huffman, J.C., see Aromí, G., 1779
Huffman, J.C., see Martins, M.A.C., 421
Hughes, R.P., Overby, J.S., Lam, K.-C., Incarvito, C.D. and Rheingold, A.L., Oxidative addition reaction of perfluoro-*n*-butyl iodide to (COD)$PtMe_2$ to give (COD)$PtMe(^nC_4F_9)$. The molecular structure of (COD)$PtMe_2$, 2357
Hursthouse, M.B., see Gupta, A., 2387
Hursthouse, M.B., see Bell, N.A., 1845
Hursthouse, M.B., see Singh, A.K., 667
Hyvadi, R., see Beheshti, A., 1547

Ianelli, S., see Matović, Z.D., 2667
Ibarra, C., see Parada, J., 2215
Ikorskii, V.N., see Bushuev, M.B., 797
Illán-Cabeza, N.A., see Acuña-Cueva, E.R., 1961
Illingsworth, M.L., Schwartz, L.J., Jensen, A.J., Zhu, T., Knappenberger, E.J., Sweet, J.E., Wilkinson, P.S., Waltermire, B.E. and Rheingold, A.L., Synthesis, structure, and reactivity of bis(*N*,*N*′-bis(2-hydroxybenzylidene)-2-hydroxyphenylmethanediaminato)zirconium(IV), a Schiff base complex with 6,4,6-membered chelate rings, 211
Imamura, T., see Suzuki, T., 835
Imura, H., see Kameta, N., 805
Incarvito, C.D., see Hughes, R.P., 2357
Incarvito, C.D., see Pelczar, E.M., 2409
Inoue, K., see Itaya, T., 1573
Intini, F.P., see Dolmella, A., 275
Iotti, S., see Cecconi, F., 1481
Isab, A.A., see Ahmad, S., 2099
Isab, A.A., Ahmad, S. and Arab, M., Synthesis of silver(I) complexes of thiones and their characterization by ^{13}C, ^{15}N and ^{107}Ag NMR spectroscopy, 1267
Ishii, Y., see Konno, H., 61
Ishitani, O., see Konno, H., 61
Islam, N.S., see Sarmah, S., 389
Itaya, T. and Inoue, K., Construction of hairy-rod coordination polymers with lamellar structure by self-assembling of hexakis(4-pyridylmethoxy)cyclotriphosphazene and silver alkylsulfonates, 1573

Ivanov, A.V. and Antzutkin, O.N., Isomorphism of bis(diethyldithiocarbamato)zinc(II) adduct with pyridine, $[Zn(Py)(EDtc)_2]$: hysteresis in the reaction of the adduct formation, 2727
Izumi, C.M.S., see Teotonio, E.E.S., 1837

Jain, V.K., see Gupta, A., 2387
Jain, V.K., see Dutta, D.P., 239
Jänchenová, J., see Plešek, J., 975
Janczak, J. and Kubiak, R., Synthesis and characterisation of dipyridinated magnesium phthalocyaninato(2-) complex, 265
Janezak, J., see Oliveira, M.R.L., 2243
Janiak, C., see Craven, E., 553
Janićijević, S.K., see Matović, Z.D., 2667
Jeffery, J.C., Leedham, A.P. and Russell, C.A., Synthesis and X-ray structure of a complex containing the trisimido borate trianion—the imido analogue of the orthoborate trianion, 549
Jeffery Leigh, G., see Luiz, J.B., 2137
Jensen, A.J., see Illingsworth, M.L., 211
Jeong, J.H., see Cho, H.Y., 1211
Jerzykiewicz, L.B., see Dobrzyńska, D., 2381
Jezierska, J., see Dobrzyńska, D., 2381
Jezierska, J., see Kurdziel, K., 1857
Jezierska, J., see Kroczewska, D., 295
Ji, L.-N., see Cai, J., 817
Ji, L.-N., see Zhang, H., 721
Jia, H.-Q., see Li, Y.-G., 2601
Jia, W.-L., see Wang, Z.-H., 873
Jiang, J., see Pan, N., 1905
Jiang, M.-H., see Tian, Y.-P., 1217
Jiang, L. and Mao, X.-A., Conformation of adenosine-5′-triphosphate in the presence of Mg^{2+} at different pH, 435
Jiang, Z.-H., see Gao, E.-Q., 359
Jiménez-Cruz, F., see Nieto-Alvarez, D.A., 417
Jiménez-Pulido, S.B., see Acuña-Cueva, E.R., 1961
Jin, G.-X., see Yu, X.-Y., 1613
Jin, L.-P., see Bian, Z.-Q., 313
John, R.P., Sreekanth, A., Prathapachandra Kurup, M.R. and Mobin, S.M., Synthesis and structural studies of novel Co(III) ternary complexes containing N(4)-substituted thiosemicarbazones of 2-hydroxyacetophenone and heterocyclic bases, 2515
Johns, C.A. and Abdul Malik, K.M., Synthesis and structural studies of the dien complexes of metal saccharinates, $[M(dien)_2]\cdot 2(sac)\cdot H_2O$ [M(II) = Ni(II), Cu(II) and Zn(II); dien = diethylenetriamine, $C_4H_{13}N_3$; sac = saccharinate, $C_7H_4NO_3S^-$], and $[Cd(dien)_2]\cdot 2(sac)$, 2(sac), 395
Jones, C.J., see Charsley, S.M., 849
Jones, P.G., see Streubel, R., 119
Jorík, V., see Baran, P., 1561
Juanatey, P., see López-Torres, M., 2063
Jun, M.-J., see Park, J.S., 1273
Jun, M.-J., see Park, Y.J., 33
Junk, P.C., see Evans, D.J., 2421

Kabir, S.E., see Azam, K.A., 885
Kabir, S.E., see Azam, K.A., 381
Kadarkaraisamy, M., see Singh, A.K., 667
Kafarski, P., see Matczak-Jon, E., 321
Kaim, W., see Dutta, D.P., 239
Kaizaki, S., see Suzuki, T., 835
Kaluđerović, G.N. and Sabo, T.J., Synthesis and characterization of the cobalt(III) complexes with ethylenediamine-*N,N′*-di-3-propanoate ligand and its esters, 2277
Kamecka, A., see Matczak-Jon, E., 321
Kamenar, B., see Korpar-Čolig, B., 147
Kameníček, J., see Smékal, Z., 1203
Kameta, N., Imura, H., Ohashi, K. and Aoyama, T., Stability constants of inner- and outer-sphere complexes of hydrated tris(1-(2-thienyl)-4,4,4-trifluoro-1,3-butanedionato) lanthanide(III) with tris(2,4-pentanedionato) cobalt(III), 805
Kandaswamy, M., see Sengottuvelan, N., 2767
Kandaz, M., Yılmaz, İ., Keskin, S. and Koca, A., Synthesis, spectroscopy and redox properties of a novel (*E*–*E*) *vic*-dioxime and its mono-, di- and trinuclear complexes bearing an 18-membered $N_2O_2S_2$ macrocyle, 825
Kandaz, M., Yaraşir, M.N.U., Koca, A. and Bekaroğlu, Ö., Synthesis, characterization and electrochemistry of novel differently octasubstituted phthalocyanines, 255
Kannan, S., Usman, A. and Fun, H.K., Synthesis and characterization of [bis(β-diketonato)uranium(VI)]nitrone compounds. The crystal and molecular structure of $[UO_2(TTA)_2\cdot p\text{-}NO_2\text{–}C_5H_4NO]$, 2403
Kano, N., Xing, J.-H., Kawa, S. and Kawashima, T., Cycloaddition reactions of an iminophosphorane bearing the Martin ligand with some double-bond compounds: syntheses, structures and thermolyses of a $1,3,2\lambda^5$-oxazaphosphetidine and a $1,3,2\lambda^5$-diazaphosphetidine-4-thione, 657
Kantekin, H., Ocak, Ü., Gök, Y. and Alp, H., Synthesis and characterization of new (*E*,*E*)-dioxime and its homo and heterotrinuclear complexes containing dioxadithiadiazamacrobicycle moiety, 1865
Karan, N.K., see Datta, A., 2237
Karasik, A.A., Naumov, R.N., Sommer, R., Sinyashin, O.G. and Hey-Hawkins, E., Water-soluble aminomethyl(ferrocenylmethyl)phosphines and their trinuclear transition metal complexes, 2251
Karimivand, V.A., see Asadi, M., 1255
Karmakar, S.R., see Azam, K.A., 885
Karvembu, R. and Natarajan, K., Synthetic, catalytic and biological studies of new binuclear ruthenium(II) complexes containing thiobis(β-diketones) and triphenylphosphine, 1721
Karvembu, R. and Natarajan, K., Synthesis and spectral studies of binuclear ruthenium(II) carbonyl complexes containing bis(β-diketone) and their applications, 219
Kashiwabara, K., see Suzuki, T., 835
Kassel, S., see Reger, D.L., 1795
Kavlakoglu, E., Elmali, A., Elerman, Y. and Svoboda, I., Magnetostructural characterization of tetranuclear copper(II) complex $[Cu_4(pz)_4L_2]\cdot(ClO_4)$ (LH = 1,3-diamino-2-propanol, Hpz = pyrapyrazole), 1539
Kawa, S., see Kano, N., 657
Kawashima, T., see Kano, N., 657
Keheyan, Y., see Cataldo, F., 1825
Kemmitt, R.D.W., see Mentes, A., 2653
Keng, T.-C., see Suen, M.-C., 2705
Kennedy, R., see Benniston, A.C., 333
Keskin, S., see Kandaz, M., 825
Kessler, V.G., see Shcheglov, P., 2317
Kessler, V.G., Turevskaya, E.P., Belokon', A.I. and Turova, N.Y., Interaction of magnesium and niobium methoxides. X-ray single crystal study of $Mg_2Nb_2O_2(OMe)_{10}(MeOH)_4$, 1629
Ketcham, K.A., Garcia, I., Swearingen, J.K., El-Sawaf, A.K., Bermejo, E., Castiñeiras, A. and West, D.X., Spectral studies and X-ray crystal structures of three nickel(II) complexes of 2-pyridineformamide 3-piperidylthiosemicarbazone, 859
Kettunen, M., see Abu-Surrah, A.S., 27
Kharisov, B.I., Blanco, L.M., Burlov, A.S., Kuznetsova, L.I., Elizondo, N.V., Uraev, A.I., Kurbatov, V.P., Bondarenko, G.I. and Garnovskii, A.D., Trinuclear metal chelates of β-aminovinylimines, 2081
Khokhar, A.R., see Ali, M.S., 2659
Khokhar, A.R., see Mukhopadhyay, U., 2369
Khokhar, A.R., see Ali, M.S., 125
Khoo, T.-J., see Tarafder, M.T.H., 2547
Khoo, T.-J., see Tarafder, M.T.H., 2691
Kilner, C.A., see Foster, C.L., 1031
Kim, J., see Choi, K.-Y., 1913
Kim, J., see Torzilli, M.A., 705

Kim, C.-H., Parkin, S., Bharara, M. and Atwood, D., Linear coordination of Hg(II) by cysteamine, 225
Kim, C., see Park, Y.J., 33
Kim, K.M., see Park, Y.J., 33
King, R.B., Chemical bonding topology of superconductors. 5. The similarities between magnesium diboride and cuprate superconductors and the role of subvalent magnesium, 2347
Kishikawa, K., see Tokitoh, N., 563
Kita, M., Abiko, S.-i., Fuyuhiro, A., Yamanari, K., Murata, K. and Yamashita, S., Synthesis and crystal structures of palladium(II) complexes containing benzyl 8-quinolyl sulfide and phenethyl 8-quinolyl sulfide, 843
Kitagawa, S., see Yu, X.-Y., 1613
Kittilstved, K., see Smieja, J.A., 1889
Kivekäs, R., see Lehtonen, A., 1133
Klasová, P., see Smékal, Z., 1203
Klement, R., see Baran, P., 1561
Klinga, M., see Abu-Surrah, A.S., 27
Klinkhammer, K., Dihypersilylstannylene and dihypersilylplumbylene—two Lewis-amphoteric carbene homologues, 587
Kloo, L., Rosdahl, J. and Taylor, M.J., The nature of subvalent gallium and indium in aqueous media, 519
Knappenberger, E.J., see Illingsworth, M.L., 211
Knoedler, A., see Dutta, D.P., 239
Knüfer, A., see Weiß, D., 535
Kobe, J., see Szłyk, E., 2001
Koca, A., see Kandaz, M., 825
Koca, A., see Kandaz, M., 255
Koch, T., Hey-Hawkins, E., Galan-Fereres, M. and Eisen, M.S., PH-functionalised phosphanylalkyl(silyl)cyclopentadienyl ligands: Synthesis and catalytic properties of [{(η^5-C_5H_4)CMe_2PH^t-Bu}MCl_3] (M = Ti, Zr) and [{(η^5-C_5H_4)$SiMe_2PHR$}$ZrCl_3$] (R = Ph, Ph, Cy), 2445
Köhnlein, H., see Schnöckel, H., 489
Kojić-Prodić, B., see Višnjevac, A., 2567
Koman, M., see Moncol', J., 365
Kong, Z.-P., see Wei, D.-Y., 1621
Konno, H., Ishii, Y., Sakamoto, K. and Ishitani, O., Synthesis, spectroscopic characterization, electrochemical and photochemical properties of ruthenium(II) polypyridyl complexes with a tertiary amine ligand, 61
Kooijman, H., see Višnjevac, A., 2567
Kopel, P., see Smékal, Z., 1203
Korabik, M., see Sieroń, L., 2473
Korolev, A.V., see Yu, Z., 1117
Korpar-Čolig, B., Cindrić, M., Matković-Čalogović, D., Vrdoljak, V. and Kamenar, B., Synthesis and characterization of some new acetato complexes of molybdenum(IV), (V) and (VI). Crystal structures of $Na_2[Mo_2O_4(OCOCH_3)_6]\cdot NaOCOCH_3\cdot CH_3COOH$ and $K[MoO_2(OCOCH_3)_3]\cdot CH_3COOH$, 147
Koutsodimou, A., see Raţiu, C., 353
Kozerski, L., see Szlyk, E., 343
Kozłowski, H., see Conato, C., 1469
Krannich, L.K., see Styron, E.K., 1747
Kravtsov, V.C., see Bocheńska, M., 763
Kresiński, R.A., see Charsley, S.M., 849
Kroczewska, D., Kurzak, B. and Matczak-Jon, E., Mixed-ligand zinc(II) complexes with diethylenetriamine (or triethylenetetramine) and α-(or β-) alaninehydroxamic acids in water solution. Potentiometric and NMR studies, 2183
Kroczewska, D., Bogusz, K., Kurzak, B. and Jezierska, J., Potentiometric and spectroscopic study of mixed-ligand copper(II) complexes with *N*,*N*′,*N*″,*N*‴-pentamethyldiethylenetriamine and α- (or β-) alaninehydroxamic acids in water solution, 295
Kruszynski, R., see Machura, B., 2617
Kubiak, R., see Janczak, J., 265
Kubicki, M., see Maciejewski, H., 1261
Kubicki, M.M., see Boni, G., 371
Kühn, F.E., see Zhang, G., 1737
Kujundžić, N., see Nigović, B., 1661
Kumara Swamy, K.C., see Kumaraswamy, S., 1155
Kumaraswamy, S. and Kumara Swamy, K.C., A spirocyclic tetraoxyphosphorane with an apically located chlorine in a trigonal bipyramid and its hydrolysis product, 1155
Kun Fun, H., see Tian, Y.-P., 1217
Kurbatov, V.P., see Kharisov, B.I., 2081
Kurdziel, K., Głowiak, T. and Jezierska, J., *Trans* hexaco-ordinate complexes of copper(II) and nickel(II) with 4(5)-hydroxymethyl-5(4)-methylimidazole—crystal structure and physico-chemical properties, 1857
Kurtán, T., see Ősz, K., 2149
Kurzak, B., see Kroczewska, D., 2183
Kurzak, B., see Kroczewska, D., 295
Kurzak, B., see Matczak-Jon, E., 321
Kushwah, Y.S., see Gupta, S.K., 1787
Kusz, J., see Machura, B., 2617
Kuznetsova, L.I., see Kharisov, B.I., 2081
Kwiatkowski, E., Romanowski, G. and Suwińska, K., Nickel(II) and palladium(II) complexes with singly condensed diprimary triamines and 2-aminobenzaldehyde, 2071

Labisbal, E., Sousa-Pedrares, A., Castiñeiras, A., Swearingen, J.K. and West, D.X., Structural studies of pyrazineformamide N4-methylthiosemicarbazone and its zinc(II) and cadmium(II) complexes formed by electrochemical oxidation, 1553
Lagrenée, M., see Bentiss, F., 403
Lahiri, G.K., see Chanda, N., 2033
Lai, S., see Villaescusa, I., 1363
Lai, C.-H., Su, M.-D. and Chu, S.-Y., Relative stability of multiple bonds between germanium and arsenic. A theoretical study, 579
Laitinen, R.S., see Pietikäinen, J., 1089
Lake, C.H., see Styron, E.K., 1747
Lakomska, I., see Szłyk, E., 2001
Lakomska, I., see Szlyk, E., 343
Lal, T.K., see Gupta, R., 1245
Lam, K.-C., see Hughes, R.P., 2357
Lam, W.H. and Lin, Z., Understanding the electron counts of aluminum metalloid clusters, 503
Lamare, V., see Thuéry, P., 2497
Lampeka, R.D., see Lysenko, A.B., 769
Lang, E.S., see Fernandes, R.M., 1149
Lappalainen, K., see Abu-Surrah, A.S., 27
Lappert, M.F., see Cornu, D., 635
Larrazabal, G., see Parada, J., 2215
Larsen, E., see Szlyk, E., 2711
Lavrenova, L.G., see Bushuev, M.B., 797
Lawrence, S.E., see Goeta, A.E., 1689
Le Baccon, M., see Bencini, A., 1459
Lee, K.-C., see Choi, K.-Y., 1913
Lee, D.C., see Na, H.G., 917
Lee, Y.S., see Yoo, J., 715
Lee, G.H., see Saha, A., 97
Leedham, A.P., see Jeffery, J.C., 549
Lehtonen, A., Kivekäs, R. and Sillanpää, R., The separation of *cis*- and *trans*-1,3-cyclohexanediol isomers by copper complexation. Crystal structures of *cis*-1,3-cyclohexanediol and copper(II) chloride *cis*-1,3-cyclohexanediol complex, 1133
Lehtonen, A. and Sillanpää, R., Mononuclear tungsten(VI) complexes with bis(phenolato) ligands: syntheses, characterisations and activity in ROMP reaction, 1017
Lehtonen, A. and Sillanpää, R., Preparation and crystal structures of new phenoxide derivatives of tungsten(VI) oxytetrachloride, 349
Leon, V., see Devereux, M., 1063
Leskelä, M., see Abu-Surrah, A.S., 27

Levason, W., see Hill, N.J., 1579
Levason, W., see Hill, N.J., 445
Lhotský, A., see Plešek, J., 975
Li, Y.-F., see Pang, Z., 2675
Li, Y.-G., Lu, Y., Luan, G.-Y., Wang, E.-B., Duan, Y.-B., Hu, C.-W., Hu, N.-H. and Jia, H.-Q., Hydrothermal syntheses and crystal structures of new cage-like mixed-valent polyoxovanadates, 2601
Li, J.-R., see Liu, Q.-D., 1097
Li, X.-Y., see Zhang, H., 721
Liang, S., Derveer, D.V., Qian, S.Y., Sturgeon, B. and Bu, X.R., A chiral salen vanadyl complex with two significantly different configurations in solid state: synthesis, characterization, and molecular structure, 2021
Liang, Y.-C., see Luo, J.-H., 893
Liao, D.-Z., see Gao, E.-Q., 359
Liddle, S.T. and Clegg, W., Synthesis and crystal structures of the 15-crown-5 solvates of potassium- and rubidium-2-trimethylsilylamidopyridine, 2451
Light, M.E., see Gupta, A., 2387
Light, M.E., see Bell, N.A., 1845
Light, M.E., see Singh, A.K., 667
Lim, J.W., see Na, H.G., 917
Lin, Y.-C., see Misra, T.K., 2045
Lin, H.-K., see Guo, Y.-H., 1005
Lin, H., see Guo, Y.-H., 1005
Lin, Z., see Lam, W.H., 503
Lisowski, J. and Mazurek, J., Chiral macrocyclic La(III), Ce(III), Pr(III) and Eu(III) complexes with chloride anions, 811
Liu, Q.-D., Gao, S., Li, J.-R., Ma, B.-Q., Zhou, Q.-Z. and Yu, K.-B., Lanthanide contraction and anions-controlled dimensional diversity in Ln–Cu–NTA (Ln = lanthanide, H_3NTA = nitrilotriacetic acid) coordination polymers: crystal structure and magnetic properties, 1097
Liu, Y.-C., see Liu, S.-T., 1073
Liu, S.-T., Hu, X., Chang, F., Liu, Y.-C., Ding, E.-R., Wu, B.-F. and Zhao, Z.-R., Substituted boat-shaped Co_6 carbonyl cluster derivatives containing a semi-interstitial P atom and both bridging dithiolate and heterocyclic phosphido ligands, 1073
Liu, Y., see Xu, Y.-K., 867
Liu, J.-Z., see Zhang, H., 721
Liu-González, M., see Cejudo, R., 1057
Livens, F.R., see Zhang, Y., 81
Livens, F.R., see Zhang, Y., 69
Lloret, F., see Muga, I., 2631
Lloris, J.M., see Sancenón, F., 1397
Lobana, T.S. and Castineiras, A., Metal–heterocyclic thione interactions. 13. Pyridine-2-thione derivatives of copper(I): crystal structure of dinuclear [bromo(pyridine-2-thione)(tri-*p*-tolylphosphine)copper(I)]$_2$ complex, 1603
Lobana, T.S., Verma, R., Singh, A., Shikha, M. and Castineiras, A., Metal-phosphine chalcogenide interactions. Crystal structures of palladium(II)/mercury(II) complexes with 1,2-bis(diphenylthiophosphinyl)ethane containing seven-membered metallacyclic rings, 205
Lomozik, L., see Gasowska, A., 745
Lomozik, L., see Bartoszak-Adamska, E., 739
López, C., Caubet, A., Pérez, S., Bosque, R., Solans, X. and Font-Bardía, M., Synthesis, X-ray crystal structure and solution behaviour of $[Zn\{(\eta^5\text{-}C_5H_5)Fe[(\eta^5\text{-}C_5H_4)-CH=N-(CH_2)_3-NMe_2]\}Cl_2]$, 2361
López, G., see Santana, M.D., 1935
López, G., see Serrano, J.L., 1589
López, E.M.V., see Fernandes, R.M., 1149
López-Ortiz, F., see Lysenko, A.B., 769
López-Torres, M., see Ares, R., 2309
López-Torres, M., Juanatey, P., Fernández, J.J., Fernández, A., Suárez, A., Vázquez-García, D. and Vila, J.M., Reactivity of cyclometallated palladium(II) compounds derived from *N*-(benzylidene)xylylendiamines, 2063
López-Torres, M., see Fernández, A., 39
Lorenzo, P., see Armas, M.T., 1513
Loureiro, L.H., see Santos, I.C.M.S., 2009
Lovell, T., see Stranger, R., 1969
Low, J.N., see Bomfim, J.A.S., 1667
Lu, Y., see Li, Y.-G., 2601
Lu, T.-H., see Sain, S., 2293
Luan, G.-Y., see Li, Y.-G., 2601
Lubal, P., see Havel, J., 1411
Lubal, P., see Havel, J., 1375
Lubes, V., see Armas, M.T., 1513
Luis García Álvarez, J., see Carriedo, G.A., 2587
Luiz, J.B., Jeffery Leigh, G. and Nunes, F.S., 2-Mercaptobenzoxazole pentacyanoferrate(II/III) complexes—kinetics of formation, substitution and the thermodynamic cycle, 2137
Luks, E., see Bocheńska, M., 763
Lund, G.S., see Nelson, K.J., 2017
Lundberg, D., see Craven, E., 553
Luo, J.-H., Hong, M.-C., Cao, R., Liang, Y.-C., Zhao, Y.-J., Wang, R.-H. and Weng, J.-B., Syntheses and crystal structures of cadmium(II) coordination polymers with end-to-end dicyanamide bridges, 893
Luque, A., Sertucha, J., Castillo, O. and Román, P., Magneto-structural studies and thermal analysis of *n*-ethylpyridinium ($n = 2$, 3, 4) tetrabromocuprate(II) complexes, 19
Lysenko, A.B., Domasevitch, K.V., Peralta-Pérez, E., López-Ortiz, F., Steed, J.W. and Lampeka, R.D., Complexation of 3-(2-pyridyl)substituted *N*-methyl isoxazolidine with Pd(II), Zn(II) and Cu(II): stereochemistry of co-ordination compounds in solution and solid-state, 769

Ma, B.-Q., see Liu, Q.-D., 1097
Maaninen, A., see Pietikäinen, J., 1089
Macías, B., Villa, M.V., Chicote, E., Martín-Velasco, S., Castiñeiras, A. and Borrás, J., Copper complexes with dithiocarbamates derived from natural occurring amino acids. Crystal and molecular structure of [Cu(en)(EtOH)$(H_2O)_3$][Cu(dtc-pro)$_2$], 1899
Macías, B., García, I., Villa, M.V., Borrás, J., Castiñeiras, A. and Sanz, F., Synthesis and characterization of sulfonamides containing 8-aminoquinoline and their Ni(II) complexes. Crystalline structures of the Ni complexes, 1229
Maccarrone, G., Rizzarelli, E. and Vecchio, G., Synthesis and coordination properties of functionalized β-cyclodextrins. Thermodynamic of proton and copper(II) complexes of 3A-deoxy-3A-(2-methylaminopyridine)-2A(*S*),3A(*R*)-β-cyclodextrin in aqueous solution, 1531
Machura, B., Dzięgielewski, J.O., Michalik, S., Bartczak, T.J., Kruszynski, R. and Kusz, J., Reactivity of $[ReOX_3(AsPh_3)_2]$ (X = Cl, Cl, Br) complexes towards gaseous nitric oxide. Crystal, molecular and electronic structure of $[ReBr_3(NO)(OAsPh_3)_2]$, $[ReCl_3(NO)(AsPh_3)_2][ReCl_4(AsPh_3)_2]$, $[ReCl_4(OAsPh_3)_2]$ and $[ReBr_3(NO)(AsPh_3)_2]$, 2617
Maciejewski, H., Kubicki, M., Marciniec, B. and Sydor, A., Phosphine nickel(0) π-complexes with vinylcyclosilazane—synthesis and structure, 1261
Maekawa, M., see Yu, X.-Y., 1613
Maestro, M.A., see Arnáiz, F.J., 2755
Maestro, M.A., see Gómez-Saiz, P., 2257
Maestro, M.A., see Arnáiz, F.J., 1635
Mahía, J., see Arnáiz, F.J., 2755
Mahía, J., see Gómez-Saiz, P., 2257
Mahía, J., see Arnáiz, F.J., 1635
Mahboob, N., Miyashita, Y., Yamada, Y., Fujisawa, K. and Okamoto, K.-i., Characterization and electrochemical properties for rhenium(III) ion incorporated into linear-type S-bridged trinuclear complexes. Crystal structures of ΔΛ- and ΔΔ/ΛΛ-$[Re\{Ir(aet)_3\}_2]^{3+}$

(aet = 2-aminoethanethiolate), 1809
Mahjoub, A.R., Morsali, A. and Bagherzadeh, H., Syntheses and characterization of thallium(I) complexes with 3-nitrophenoxide [Tl(3-np)], 4-nitrobenzoate [Tl(4-nb)] and 2,4-dinitrophenoxide [Tl(2,4-dnp)]: X-ray crystal structures of $[Tl(3\text{-}np)]_n$ and Tl(2,4-dnp) (two new polymeric compounds), 2555
Mahjoub, A.R. and Morsali, A., Direct synthesis of a dimeric mixed-anion lead(II) complex, crystal structure of $[Pb(phen)(_2OCCH_3)(NCS)]_2$, 1223
Mahjoub, A.R. and Morsali, A., Syntheses and characterization of lead(II) salts with 4,4′-bithiazole ligand: X-ray crystal structures of $[(BTZ)_2Pb(NO_3)_2]$ and $[(BTZ)Pb(SCN)_2]_n$ (a new polymeric compound), 197
Mahmoudkhani, A.H., see Amirnasr, M., 2733
Mahon, M.F., see Barret, M.C., 1761
Maichle-Mössmer, C., see de Figueiredo, A.T., 2351
Majerić-Elenkov, M., see Višnjevac, A., 2567
Maji, T.K., see Sain, S., 2293
Mak, T.C.W., see Song, H.-B., 1043
Malta, O.L., see Teotonio, E.E.S., 1837
Manceron, L., see Downs, A.J., 473
Mancilla, T., see Nieto-Alvarez, D.A., 417
Manessi-Zoupa, E., see Tiliakos, M., 229
Mangayarkarasi, N., Prabhakar, M. and Zacharias, P.S., Synthesis and structural characterization of complexes from the NOS ligating Schiff base of dfp: structurally different molecules in the unit cell of the manganese complex, 925
Manonmani, J., see Sengottuvelan, N., 2767
Mansor, R., see Bell, N.A., 1845
Manzur, C., see Galindo, A.M., 2531
Manzur, J., García, A.M., Córdova, C., Pizarro, O., Acuña, V. and Spodine, E., Oxidation of 3,5-di-*tert*-butylcatechol by molecular oxygen catalysed by a copper(I) complex, $Cu_2(bdpdz)Cl_2$, bdpdz = 3,6-bis-(di-2-pyridilmethyl) pyridazine, 181
Mao, X.-A., see Jiang, L., 435
Marangoni, G., see Pitteri, B., 2283
Marciniec, B., see Maciejewski, H., 1261
Mardones, M., see Galindo, A.M., 2531
Mareček, V., see Plešek, J., 975
Martins, M.A.C., Silva, R.M. and Huffman, J.C., Syntheses and characterization of nickel thiolate complexes: X-ray structure of $[Ni(SCH_2CH_2S)(PPh_2CH{=}CHPPh_2)]$, 421
Martínez-Máñez, R., see Sancenón, F., 1397
Martín-Velasco, S., see Macías, B., 1899
Marzotto, A., see Clemente, D.A., 2161
Masci, B., see Thuéry, P., 1949
Masci, B., Gabrielli, M., Mortera, S.L., Nierlich, M. and Thuéry, P., Hydrogen bonded supramolecular assemblies from uranyl ion complexes of tetrahomodioxacalix[4]arenes with various counterions, 1125
Masters, A.F., see Field, L.D., 1707
Mata, I., see García-Raso, A., 1197
Matczak-Jon, E., see Kroczewska, D., 2183
Matczak-Jon, E., Kurzak, B., Kamecka, A. and Kafarski, P., Interactions of zinc(II), magnesium(II) and calcium(II) with aminomethane-1,1-diphosphonic acids in aqueous solutions, 321
Matković-Čalogović, D., see Korpar-Čolig, B., 147
Matlaba, P. and Nyokong, T., Synthesis, electrochemical and photochemical properties of unsymmetrically substituted zinc phthalocyanine complexes, 2463
Matos, J.R., see Ávila Terra, L.H.S., 2375
Matović, Z.D., Ianelli, S., Pelosi, G., Janićijević, S.K., Ristanović, V.M., Ponticelli, G. and Radanović, D.J., Characterization of the two geometrical isomers of (1,3-propanediamine-*N*,*N*′-diacetato-*N*,*N*′-di-3-propionato)-nickelate(II). X-ray structure of the binuclear complex *trans*(O_5)-$[Ni_2(1,3\text{-}pddadp)(H_2O)_4]\cdot 4H_2O$ and octahedral distortion of edta-type chelates, 2667
Matsushita, T., see Asada, H., 1139
Mautner, F.A., see Goher, M.A.S., 1871
Mazières, S., see Bibal, C., 2827
Mazurek, J., see Lisowski, J., 811
McCann, M., see Devereux, M., 1063
McCleverty, J.A., see Charsley, S.M., 849
McGaff, R.W., see Nelson, K.J., 2017
McGrady, J.E., see Stranger, R., 1969
McKee, V., see Devereux, M., 1063
McWhinnie, S.L.W., see Charsley, S.M., 849
Mederos, A., see Armas, M.T., 1513
Meehan, M.M., see Goeta, A.E., 1689
Melník, M., see Moncol', J., 365
Mendoza-Díaz, G., see Gasque, L., 935
Mentes, A. and Kemmitt, R.D.W., Bidentate phosphorus complexes of oxodimethylenemethanepalladium(II), 2653
Merlin, J.C., see Cornard, J.P., 2801
Merz, K., see Weiß, D., 535
Michalik, S., see Machura, B., 2617
Micheloni, M., see Formica, M., 1351
Midollini, S., see Cecconi, F., 1481
Migchielsen, S., Publishing Editor Inorganic Chemistry, Professor Achim Müller awarded 2001 Sir Geoffrey Wilkinson Prize, 905
Mikel, C. and Potvin, P.G., Synthesis and enhanced photosensitization ability of a 4-carboxy-2,2′:6′,2″-terpyridine complex of rutheniu-m(II), 49
Miller, D.O., see Xu, Z., 1715
Milletti, M.C., see Sonnenberg, J.L., 2699
Mills, R.C., Doufou, P., Abboud, K.A. and Boncella, J.M., Synthesis and characterization of tantalum(V) complexes containing bis-sulfamide ligands: X-ray crystal structure of $Ta[N(Me)_2]_3[SO_2(NCMe_3)_2]$, 1051
Miranda, M.J., see Arnáiz, F.J., 2755
Misra, T.K., Chen, L.-H., Lin, Y.-C. and Chung, C.-S., Synthesis, X-ray structures and ternary complex formation kinetics of (2,2′,2″-triaminotriethylamine)nickel(II) with bidentate ligands, 2045
Mitra, S., see Datta, A., 2237
Mitra, K.N., see Saha, A., 97
Miyamoto, R., Sugai, T. and Sudoh, S., Spectroscopic study of the coordination sphere of Gd(III) in Gd(III)–M(II) complexes with a compartmental ligand, where the local environment around Gd(III) is controlled by (M(II) M(II) = Ni(II), Zn(II) and a vacancy), 2127
Miyashita, Y., see Yamada, Y., 2143
Miyashita, Y., see Mahboob, N., 1809
Miyazaki, Y., see Nakamoto, T., 1299
Młynarz, P., see Conato, C., 1469
Mobin, S.M., see John, R.P., 2515
Mohamed, M.M.A. and Shoukry, M.M., Complex formation equilibria of palladium(II) complexes involving *N*,*N*′-dimethylethylenediamine, DNA constituents and cyclobutane dicarboxylic acid. The catalysis of glycine methyl ester hydrolysis through complex formation, 167
Molins, E., see Serrano, J.L., 1589
Molins, E., see García-Raso, A., 1197
Molloy, K., see Binions, R., 1943
Molloy, K.C., see Barret, M.C., 1761
Moncol', J., Palicová, M., Segl'a, P., Koman, M., Melník, M., Valko, M. and Glowiak, T., Structure and spectral study of copper(II) pyridinecarboxylates: crystal and molecular structure of *trans*-diaqua-bis(*N*,*N*-diethylnicotinamide-*N*)bis(2-chloronicotinate-*O*)copper(II), 365
Mondal, B., see Chanda, N., 2033
Monika, see Saravanabharathi, D., 2433
Moreno-Carretero, M.N., see Acuña-Cueva, E.R., 1961
Morita, T., see Yu, X.-Y., 1613
Moroi, Y., see Fisicaro, E., 1497
Morris, S., see Reglinski, J., 2175

Morris, S., see Reglinski, J., 2167
Morsali, A., see Mahjoub, A.R., 2555
Morsali, A., see Mahjoub, A.R., 1223
Morsali, A., see Mahjoub, A.R., 197
Mortera, S.L., see Masci, B., 1125
Moïse, C., see Boni, G., 371
Mostafa, G., see Sain, S., 2293
Mosteiro, R., see Fernández, A., 39
Mottalib, M.A., see Azam, K.A., 381
Moulton, B., see Deoghoria, S., 2457
Moura, E.M., Siebald, H.G.L. and de Lima, G.M., Synthesis, characterisation and molecular structure of Ru–Sn(II) containing derivatives, 2323
Moya, S.A., Guerrero, J., Pastene, R., Azócar-Guzmán, I. and Pardey, A.J., Metal carbonyl complexes containing heterocyclic nitrogen ligands: Part IX. $MnBr(CO)_3$(3,3′-R-2,2′-biquinoline) compounds, 439
Mroziński, J., see Sieroń, L., 2473
Mu, Y., see Xu, Y.-K., 867
Muga, I., Gutiérrez-Zorrilla, J.M., Vitoria, P., Román, P. and Lloret, F., Binuclear Ni(II) complexes based on bridging oxalate and tetracyanometallates. Synthesis, crystal structure and magnetic properties, 2631
Mukherjee, R., see Gupta, R., 1245
Mukhopadhyay, U., Thurston, J.H., Whitmire, K.H. and Khokhar, A.R., Synthesis and characterization of *cis*-bis-heptamethyleneimine platinum(II) dicarboxylate complexes: crystal structure of *cis*-[Pt(heptamethyleneimine)$_2$(malonate)]$\cdot H_2O$, 2369
Mukhopadhyay, S., see Bandyopadhyay, P., 1893
Mukhopadhyay, U., see Ali, M.S., 125
Murata, K., see Kita, M., 843
Murphy, C.A., see Cooke, M.W., 1235
Mutikainen, I., see van Albada, G.A., 141
Mutlu, E., see Craven, E., 553

Na, H.G., Lee, D.C., Lim, J.W., Choi, J.H., Byun, J.C. and Park, Y.C., Synthesis of 14-π nickel(II) complexes with disubstituted benzoN_4 macrocycles and electrochemical studies of 14-π nickel(II) complexes with monosubstituted benzoN_4 macrocycles, 917
Nag, K., see Baitalik, S., 2481
Nakamoto, T., Wang, Q., Miyazaki, Y. and Sorai, M., Crystal structure and heat capacity of the mixed-valence trinuclear iron monoiodoacetate complex, $[Fe(III)_2Fe(II)O(O_2CCH_2I)_6(H_2O)_3][Fe(III)_3O(O_2CCH_2I)_6(H_2O)_3]I$, 1299
Nakata, N., see Tokitoh, N., 563
Nartowski, A.M. and Parkin, I.P., Solid state metathesis synthesis of metal silicides; reactions of calcium and magnesium silicide with metal oxides, 187
Natarajan, K., see Karvembu, R., 1721
Natarajan, K., see Karvembu, R., 219
Natile, G., see Dolmella, A., 275
Naumov, R.N., see Karasik, A.A., 2251
Navarro, C.M., see Santana, M.D., 1935
Neaves, B.D., see Charsley, S.M., 849
Neels, A., see Fidalgo, E.G., 1921
Nelson, K.J., Guzei, I.A., Lund, G.S. and McGaff, R.W., Copper(II) methoxide: direct solventothermal synthesis and X-ray crystal structure, 2017
Nethaji, M., see Saravanabharathi, D., 2793
Nethaji, M., see Rath, R.K., 1929
Neudachina, L.K., see Skorik, Y.A., 2719
Ngo, S.C., Banger, K.K., Toscano, P.J. and Welch, J.T., Synthesis and physical and structural characterization of Ag(I) complexes supported by non-fluorinated β-diketonate and related ancillary ligands, 1289
Niclós, J., see Carballo, R., 2811
Niclós-Gutiérrez, J., see Choquesillo-Lazarte, D., 1485
Niclós-Gutiérrez, J., see Serrano-Padial, E., 1451
Nierlich, M., see Thuéry, P., 1949
Nierlich, M., see Masci, B., 1125
Nieto-Alvarez, D.A., Jiménez-Cruz, F. and Mancilla, T., Synthesis and characterization of new di-*n*-butylhydroxytin(IV) derived compounds from 1,3-diketone malonates, 417
Nigović, B. and Kujundžić, N., Electrochemical behavior of iron(III) complexes with aminohydroxamic acids, 1661
Noethig-Laslo, V., Paulić, N., Basosi, R. and Pogni, R., Role of apically bound water molecule on aliphatic–aliphatic side-chain interactions in bis[*N*,*N*-dimethyl-L-α-isoleucinato]copper(II) studied by EPR spectroscopy, 1643
Nogueira, H.I.S., see Quintal, S.M.O., 2783
Norman, N.C., see Pardoe, J.A.J., 543
Novelli, V., see Comuzzi, C., 1337
Nunes, F.S., see Luiz, J.B., 2137
Nurchi, V.M., see Crisponi, G., 1319
Nurchi, V.M., see Villaescusa, I., 1363
Nyokong, T., see Matlaba, P., 2463
Nyokong, T., see Thamae, M., 133
Nytko, E.A., see Pelczar, E.M., 2409

Ocak, Ü., see Kantekin, H., 1865
O'Dowd, A., see Goeta, A.E., 1689
Ohashi, K., see Kameta, N., 805
Oilunkaniemi, R., see Pietikäinen, J., 1089
Okamoto, K.-i., see Yamada, Y., 2143
Okamoto, K.-i., see Mahboob, N., 1809
Okazaki, R., see Tokitoh, N., 563
Oliveira, M.R.L., Vieira, H.P., Perpétuo, G.J., Janezak, J. and De Bellis, V.M., Syntheses, crystal structure and spectroscopic characterization of novel *N*-R-sulfonyldithiocarbimate and triphenylphosphine nickel(II) complexes, 2243
Oliveira, S.F., see Teotonio, E.E.S., 1837
O'Neill, S.A., see Binions, R., 1943
Orabi, A.S., see Bahgat, K., 987
Orpen, A.G., see Serrano, J.L., 1589
Ősz, K., Bóka, B., Várnagy, K., Sóvágó, I., Kurtán, T. and Antus, S., The application of circular dichroism spectroscopy for the determination of metal ion speciation and coordination modes of peptide complexes, 2149
Ovchynnikov, V.A., see Gubina, K.E., 963
Overby, J.S., see Hughes, R.P., 2357
Ozeki, M., see Asada, H., 1139

Pacifico, C., see Dolmella, A., 275
Padovano, G., see Dolmella, A., 275
Pakawatchai, C., see Youngme, S., 1279
Palicová, M., see Moncol', J., 365
Pan, N., Rintoul, L., Arnold, D.P. and Jiang, J., Raman spectroscopic characteristics of phthalocyanine and naphthalocyanine in sandwich-type phthalocyaninato and porphyrinato rare earth complexes. Part 3. The effect of rare earth ionic size on the Raman characteristics of naphthalocyanine in bis(naphthalocyaninato) rare earth complexes, 1905
Panda, B.K., Chattopadhyay, S., Ghosh, K. and Chakravorty, A., Synthesis and structure of pyridine-2-thiolato ruthenium aryls bearing a pendant imine–phenol function, 899
Pang, Z., Zhao, L., Chen, M.-Q., Wang, J.-Y. and Li, Y.-F., Synthesis, crystal structure and optical limiting properties of some W–Se–Cu clusters, 2675
Paoletti, P., see Bencini, A., 1459
Paoletti, P., see Bencini, A., 1329
Papaefstathiou, G.S., Escuer, A., Font-Bardía, M., Perlepes, S.P., Solans, X. and Vicente, R., Benzoate as terminal ligand in the defective double-cubane, tetranuclear cobalt(II) complex $[Co_4(N_3)_2(O_2CPh)_2\{(py)_2C(OH)O\}_4]\cdot 2DMF$ with simultaneous

$\mu_{1,1}$-azido and μ-O bridges [$(py)_2C(OH)O$ = the monoanion of the hydrated, *gem*-diol form of di-2-pyridyl ketone], 2027
Parada, J., Bunel, S., Ibarra, C., Larrazabal, G., Gillitt, N.D. and Bunton, C.A., Sucrose bis(1,10-phenanthroline)cobalt (III). Predicted distortion at the octahedral center, 2215
Pardey, A.J., see Moya, S.A., 439
Pardo, T., see Sancenón, F., 1397
Pardoe, J.A.J., Norman, N.C. and Timms, P.L., Studies on BCl and on the exchange reaction of BCl_3 with polyboron fluorides, 543
Park, J.S., Youm, K.-T. and Jun, M.-J., Copper(II) complexes of 1,3-dithian-2-ylidenemalonate: doubly layered 2D sheet induced by alkali metal ions, 1273
Park, Y.C., see Na, H.G., 917
Park, Y.J., Do, Y., Kim, K.M., Choi, M.-G., Jun, M.-J. and Kim, C., Design and properties of mixed-metal multinuclear molecules. Part II. Novel heterotrinuclear complexes of $[Ag(PPh_3)_2]_2[Cu(mtm)_2]$ and $[Ag_2(dppm)_2][Cu(mtm)_2]$ (mtm = [bis(methylthio)methylene]malo-o)methylene]malonate and dppm = bis(diphenylphosphi-bis(diphenylphosphino)methane), 33
Parkin, I.P., see Binions, R., 1943
Parkin, G., Polyhedron Symposia-in-Print, number 24: Subvalent and multiply bonded compounds of the p-block elements, 465
Parkin, S., see Kim, C.-H., 225
Parkin, I.P., see Nartowski, A.M., 187
Parvin, S., see Azam, K.A., 885
Pastene, R., see Moya, S.A., 439
Patra, G.K. and Goldberg, I., Mercury(II)–dien complexes (dien ≡ diethylene triamine). First example of dien-bridged Hg(II) dimer. Syntheses, characterization and X-ray crystal structures of $[Hg_2(dien)_3](ClO_4)_4$ and $[Hg(dien)(H_2O)](PF_6)_2$, 2195
Paulić, N., see Noethig-Laslo, V., 1643
Pawlak, B., see Drożdżewski, P., 2819
Pazderski, L., see Szlyk, E., 343
Peacock, R.D., see Benniston, A.C., 333
Pedrosa, M.R., see Arnáiz, F.J., 1635
Pelczar, E.M., Nytko, E.A., Zhuravel, M.A., Smith, J.M., Glueck, D.S., Sommer, R., Incarvito, C.D. and Rheingold, A.L., Synthesis and structure of platinum and palladium complexes of dimesitylphosphine, 2409
Pelizzi, C., see Ferrari, M.B., 2593
Pelosi, G., see Matović, Z.D., 2667
Pelosi, G., see Ferrari, M.B., 2593
Peng, S.-M., see Saha, A., 97
Peralta-Pérez, E., see Lysenko, A.B., 769
Pereira, E., see Fernández, A., 39
Pérez, S., see López, C., 2361
Pérez, J., see Santana, M.D., 1935
Pérez, E., see Serrano, J.L., 1589
Pérez, J., see Serrano, J.L., 1589
Perlepes, S.P., see Diamantopoulou, E., 2117
Perlepes, S.P., see Papaefstathiou, G.S., 2027
Perpétuo, G.J., see Oliveira, M.R.L., 2243
Perrin, M., see Daniele, S., 1985
Perven, S., see Azam, K.A., 381
Pesavento, M., Biesuz, R., Riva, F.D. and Alberti, G., Investigation of the complexation properties of a natural water towards copper(II), manganese(II) and aluminium(III), based on sorption of metal ions on a complexing resin, 1343
Petraco, N.D.K., see Brown, S.T., 599
Petrie, S. and Stranger, R., Metal–metal bonding trends in mixed-group, face-shared d^3d^3 bioctahedral dimer systems, $M'M''Cl_9^{n-}$, 1163
Pietikäinen, J., Maaninen, A., Laitinen, R.S., Oilunkaniemi, R. and Valkonen, J., Halogenation of tellurium by SO_2Cl_2. Formation and crystal structures of $(H_3O)[Te_3Cl_{13}]\cdot 1/2SO_2$, $[(C_4H_8O)_2H][TeCl_5]\cdot(C_4H_8O)$, $[(Me_2SO)_2H]_2[TeCl_6]$, and $[Ni(NCCH_3)_6][Te_2Cl_{10}]$, 1089
Piironen, U., see Abu-Surrah, A.S., 27
Pinilla, E., see Seco, J.M., 457
Piro, O.E., see Soria, D.B., 1767
Pitteri, B., Annibale, G., Marangoni, G., Bertolasi, V. and Ferretti, V., Base hydrolysis kinetics and equilibria of [bis(2-pyridylmethyl)amine]chloroplatinum(II) and crystal and molecular structures of $[Pt(bpma)Cl]Cl\cdot H_2O$ and $[Pt(bpma)(OH_2)](ClO_4)_2\cdot 2H_2O$, 2283
Pivetta, T., see Crisponi, G., 1319
Pizarro, O., see Manzur, J., 181
Platt, A.W.G., see Fawcett, J., 287
Plešek, J., Grüner, B., Heřmánek, S., Báča, J., Mareček, V., Jänchenová, J., Lhotský, A., Holub, K., Selucký, P., Rais, J., Císařová, I. and Čáslavský, J., Synthesis of functionalized cobaltacarboranes based on the *closo*-$[(1,2\text{-}C_2B_9H_{11})_2\text{-}3,3'\text{-}Co]^-$ ion bearing polydentate ligands for separation of M^{3+} cations from nuclear waste solutions. Electrochemical and liquid–liquid extraction study of selective transfer of M^{3+} metal cations to an organic phase. Molecular structure of the *closo*-[(8-(2-CH_3O–C_6H_4–O)-$(CH_2CH_2O)_2$-1,2-$C_2B_9H_{10}$)-(1′,2′-$C_2B_9H_{11}$)-3,3′-Co]Na determined by X-ray diffraction analysis, 975
Pogni, R., see Noethig-Laslo, V., 1643
Pontellini, R., see Formica, M., 1351
Ponticelli, G., see Matović, Z.D., 2667
Popham, M.C., see Hill, N.J., 1579
Popham, M.C., see Hill, N.J., 445
Portanova, R., see Bismondo, A., 1393
Portanova, R., see Comuzzi, C., 1337
Portanova, R., see Comuzzi, C., 1385
Potvin, P.G., see Mikel, C., 49
Poujaud, N., see Boni, G., 371
Powell, D.H., see Styron, E.K., 1747
Powell, A.K., see Zhang, Y., 81
Powell, A.K., see Zhang, Y., 69
Power, P.P., see Stender, M., 525
Prabhakar, M., see Mangayarkarasi, N., 925
Prado, A.G.S., see Sales, J.A.A., 2647
Prathapachandra Kurup, M.R., see John, R.P., 2515
Prött, M., see Uhl, W., 511
Ptaszek, M., see Eilmes, J., 7
Pulidori, F., see Conato, C., 1469
Puranik, V.G., see Chanda, N., 2033

Qian, S.Y., see Liang, S., 2021
Qu, Z.-W., see Xu, Y.-K., 867
Queiroz, S.L., see Von Poelhsitz, G., 2221
Quintal, S.M.O., Nogueira, H.I.S., Félix, V. and Drew, M.G.B., Coordination modes of 2-hydroxynicotinic acid in second- and third-row transition metal complexes, 2783

Radanović, D.J., see Matović, Z.D., 2667
Radecka-Paryzek, W., see Bocheńska, M., 763
Rais, J., see Plešek, J., 975
Rajendiran, N. and Santhanalakshmi, J., Interaction of sulfur dioxide with zinc(II)tetrasulfophthalocyanine in aqueous medium: steady state fluorescence quenching studies, 951
Rana, A., Dinda, R., Sengupta, P., Ghosh, S. and Falvello, L.R., Synthesis, characterisation and crystal structure of *cis*-dioxomolybdenum(VI) complexes of some potentially pentadentate but functionally tridentate (ONS) donor ligands, 1023
Raptis, D., see Tiliakos, M., 229
Raptopoulou, C.P., see Diamantopoulou, E., 2117
Raptopoulou, C.P., see Tiliakos, M., 229
Raspi, G., see Sbrana, E., 1475
Raspi, G., see Galli, A., 1405
Rath, R.K., Nethaji, M. and Chakravarty, A.R., Synthesis, crystal structure and solution properties of a diastereomeric (*p*-cymene)ruthenium(II) chiral Schiff base complex, 1929
Rațiu, C., Tomșa, A.-R., Koutsodimou, A., Falaras, P. and Budiu, T.,

Synthesis and characterization of $K_6[Ti(H_2O)P_2MoW_{16}O_{61}]\cdot 17H_2O$, a Ti(IV) derivative of monolacunary Wells-Dawson 16-tungstomolybdo-2-phosphate, 353
Raudaschl-Sieber, G., see Zhang, G., 1737
Ray, U.S., see Senapoti, S., 753
Reedijk, J., see van Albada, G.A., 141
Reger, D.L., Wright, T.D., Smith, M.D., Rheingold, A.L., Kassel, S., Concolino, T. and Rhagitan, B., Syntheses and structures of monothiocyanate complexes of cadmium(II) and lead(II) containing bulky nitrogen based polydentate ligands, 1795
Reglinski, J., Morris, S. and Stevenson, D.E., Supporting conformational change at metal centres. Part 2: four and five coordinate geometry, 2175
Reglinski, J., Morris, S. and Stevenson, D.E., Supporting conformational change at metal centres. Part 1: octahedral systems, 2167
Reibenspies, J., see de Moura, C.V.R., 2227
Reid, G., see Hill, N.J., 1579
Reid, G., see Hill, N.J., 445
Remelli, M., see Conato, C., 1469
Renner, P., see Haller, I., 629
Rhagitan, B., see Reger, D.L., 1795
Rheingold, A.L., see Hughes, R.P., 2357
Rheingold, A.L., see Pelczar, E.M., 2409
Rheingold, A.L., see Reger, D.L., 1795
Rheingold, A.L., see Illingsworth, M.L., 211
Richeson, D.S., see Foley, S.R., 619
Riggio, I., see van Albada, G.A., 141
Righi, L., see Bhattacharya, R., 2561
Rintoul, L., see Pan, N., 1905
Ristanović, V.M., see Matović, Z.D., 2667
Riva, F.D., see Pesavento, M., 1343
Rizzarelli, E., see Maccarrone, G., 1531
Robinson, G.H., see Vohs, J.K., 531
Robinson, J.K., see Bell, N.A., 115
Rocha, R.C. and Toma, H.E., Benzotriazolate-bridged ruthenium dinuclear and trinuclear complexes, 2089
Roda, A., see Fini, A., 1421
Rodríguez-Argüelles, M.C., see Ferrari, M.B., 2593
Rodriguez, M.A., see Boyle, T.J., 2333
Rodriguez i Zubiri, M., Slawin, A.M.Z., Wainwright, M. and Woollins, J.D., The preparation and coordination chemistry of phosphorus-(III) derivatives of piperazine and homopiperazine, 1729
Rogers, R.D., see Royer, A.C., 155
Roh, S.-G., see Cho, H.Y., 1211
Rojo, T., see Gómez-Saiz, P., 2257
Román, P., see Muga, I., 2631
Román, P., see Luque, A., 19
Romanenko, G.V., see Skorik, Y.A., 2719
Romano, V., see Amorello, D., 1369
Romanowski, G., see Kwiatkowski, E., 2071
Rosales-Hoz, M.J., see Zuno-Cruz, F.J., 1105
Rosdahl, J., see Kloo, L., 519
Rosenberg, E., see Azam, K.A., 885
Rosu, C., Crans, D.C. and Weakley, T.J.R., Rational synthesis and X-ray structure of $[Mn_4^{II}(H_2O)_2(As^VW_9O_{34})_2]^{10-}$ from $[As_4^{III}W_{40}O_{140}]^{28-}$, MnO_4^- and Mn^{2+}, 959
Royer, A.C., Rogers, R.D., Arrington, D.L., Street, S.C. and Vincent, J.B., Spectroscopic studies of the dodecanuclear chromium complex $Cr_{12}O_9(OH)_3(pivalate)_{15}$: confirmation of the presence of twelve Cr(III) centers and the crystal structure of $Cr_{12}O_9(OH)_3(pivalate)_{15}\cdot 2PrOH\cdot 9H_2O$, 155
Ruck, M. and Hampel, S., Stabilization of homonuclear Bi_5^+ and Bi_6^{2+} polycations by cluster anions in the crystal structures of $Bi_{12-x}IrCl_{13-x}$, $Bi_{12-x}RhCl_{13-x}$ and $Bi_{12-x}RhBr_{13-x}$, 651
Ruman, T., Ciunik, Z., Szklanny, E. and Wołowiec, S., Complexes of heteroscorpionate trispyrazolylborate ligands. Part VI. Carboxylate induced conversion of mono-ligand Tp′M(L) into bis-ligand Tp'_2M complexes (M = Co(II) and Cu(II)), 2743
Russell, C.A., see Jeffery, J.C., 549
Russell, D.R., see Fawcett, J., 287
Ruthe, F., see Streubel, R., 119

Sabatini, A., see Cecconi, F., 1481
Sabo, T.J., see Kaluđerović, G.N., 2277
Sáez, N.Y., see Carriedo, G.A., 2587
Saha, N., see Saha, N.C., 779
Saha, N.C., Butcher, R.J., Chaudhuri, S. and Saha, N., Synthesis and spectroscopic studies of cobalt(III) complexes with 5-methyl-3-formylpyrazole-N(4)-diethylthiosemicarbazone (HMP_zNEt_2): X-ray crystallography of $[Co(MP_zNEt_2)_2]ClO_4\cdot 2H_2O$ (**I**) and $[Co(MP_z-NEt_2)_2]BF_4\cdot 2H_2O$ (**II**), 779
Saha, A., Das, C., Mitra, K.N., Peng, S.-M., Lee, G.H. and Goswami, S., Synthesis, structure and redox properties of isomeric $[RuCl_2(L)_2]$ (L = *N*-aryl-1,2-arylenediimine) complexes formed by the oxidative dimerization of coordinated aromatic amines, 97
Saha, N., see Bera, P., 1
Sain, S., see Deoghoria, S., 2457
Sain, S., Maji, T.K., Mostafa, G., Lu, T.-H., Chiang, M.Y. and Chaudhuri, N.R., Self assembly towards the construction of molecular ladder and rectangular grid of cadmium(II)-selenocyanate, 2293
Sakamoto, K., see Konno, H., 61
Sakata, K., see Shen, X., 969
Sakurai, H., see Yamada, Y., 2143
Sales, J.A.A., Prado, A.G.S. and Airoldi, C., The incorporation of propane-1,3-diamine into silylant epoxide group through homogeneous and heterogeneous routes, 2647
Salvadó, V., see Domínguez, M., 1429
Salvin, N.J., see Bell, N.A., 1845
Samaria, K.M., see Benetollo, F., 425
Samuelson, A.G., see Saravanabharathi, D., 2793
Samuelson, A.G., see Saravanabharathi, D., 2433
Sancenón, F., Descalzo, A.B., Lloris, J.M., Martínez-Máñez, R., Pardo, T., Seguí, M.J. and Soto, J., Open-chain polyazaalkanes functionalised with pyrene groups as sensing fluorogenic receptors for metal ions, 1397
Sánchez, G., see Serrano, J.L., 1589
Sánchez, A., see Casas, J.S., 1651
Sang, H.-Y., see Zhang, H., 721
Santana, J.M., see Boyle, T.J., 2333
Santana, M.D., García, G., Navarro, C.M., Abel Lozano, A., Pérez, J., García, L. and López, G., Dithiophosphate and dithiophosphonate complexes of pentacoordinate nickel(II) containing the macrocycle 2,4,4-trimethyl-1,5,9-triazacyclododec-1-ene ([12]aneN_3-mc1) or its 9-methyl derivative ([12]aneN_3-mc2). Crystal structures of $[Ni([12]aneN_3\text{-}mc1)\{S_2P(OEt)_2\}][PF_6]$ and $[Ni([12]aneN_3\text{-}mc1)\{S_2P(p\text{-}CH_3OPh)(O^iPr)\}][PF_6]$, 1935
Santhanalakshmi, J., see Rajendiran, N., 951
Santos, I.C.M.S., Loureiro, L.H., Silva, M.F.P. and Cavaleiro, A.M.V., Studies on the hydrothermal synthesis of niobium oxides, 2009
Santra, P.K., see Senapoti, S., 753
Sanz, F., see Macías, B., 1229
Sanz-Ruiz, F., see Cejudo, R., 1057
Saravanabharathi, D., Nethaji, M. and Samuelson, A.G., The first bis(phosphine) monoxide (BPMO) complexes of copper(I), 2793
Saravanabharathi, D., Monika, Venugopalan, P. and Samuelson, A.G., Solid state structural and solution studies on the formation of a flexible cavity for anions by copper(I) and 1,2-bis(diphenylphosphino)ethane, 2433
Sarker, N.C., see Azam, K.A., 381
Sarmah, S., Hazarika, P. and Islam, N.S., Reaction of diperoxovanadate with vanadyl sulphate in presence of EDTA as an access to dinuclear peroxovanadates(V), 389
Sarýkahya, F., see Hogarth, G., 791

Sasamori, T., see Tokitoh, N., 563
Sauvageot, P., see Boni, G., 371
Sbrana, E., Spinetti, M., Secco, F. and Raspi, G., Bubble extraction and affinity chromatography techniques for human trypsin inhibitors enrichment and purification, 1475
Scatena, H., Jr., see de Farias, R.F., 1677
Schaefer, H.F., III, see Brown, S.T., 599
Schnöckel, H. and Köhnlein, H., Synthesis and structure of metalloid aluminum clusters—intermediates on the way to the elements, 489
Scholz, J. and Görls, H., 1,4-Diaza-1,3-diene niobium chlorides: syntheses and X-ray crystal structures of (*t*-Bu-DAD)$NbCl_3$(THF), (*t*-Bu-DAD)$_2$NbCl, and [(*t*-Bu-DAD)$NbCl_4$](H_3N*t*-Bu), 305
Schwartz, L.J., see Illingsworth, M.L., 211
Scott, B.L., see Boyle, T.J., 2333
Secco, F., see Sbrana, E., 1475
Secco, F., see Galli, A., 1405
Seco, J.M., González Garmendia, M.J., Pinilla, E. and Torres, M.R., 2-Anilinopyridinate of Cu(I) and adducts of 2-anilinopyridine and metal acetates. Crystal structure of $Cu_2(\mu\text{-}OAc)_4(PhNHpy)_2$, 457
Segl'a, P., see Moncol', J., 365
Seguí, M.J., see Sancenón, F., 1397
Seisenbaeva, G.A., see Shcheglov, P., 2317
Selucký, P., see Plešek, J., 975
Senapoti, S., Ray, U.S., Santra, P.K., Sinha, C., Slawin, A.M.Z. and Woollins, J.D., Osmium–azopyrimidine chemistry. Part VII: synthesis, structural characterisation and electrochemistry, 753
Sengottuvelan, N., Manonmani, J. and Kandaswamy, M., Synthesis of unsymmetrical compartmental oxime nickel(II) and copper(II) complexes: spectral, electrochemical and magnetic studies, 2767
Sengupta, P., see Rana, A., 1023
Serrano, J.L., García, L., Pérez, J., Pérez, E., Vives, J., Sánchez, G., López, G., Molins, E. and Orpen, A.G., Synthesis and characterization of new cyclometallated Pd(II) complexes with bridging or terminal imidato ligands. Crystal structures of [{Pd(μ-succinimide)(phpy)}$_2$] and [Pd(azb)(succinimide)(PPh_3)] (phpy = 2-phenylpyridine; azb = azobenzene), 1589
Serrano-Padial, E., Choquesillo-Lazarte, D., Bugella-Altamirano, E., Castiñeiras, A., Carballo, R. and Niclós-Gutiérrez, J., New copper(II) compound having protonated forms of ethylenediaminetetraacetate(4−) ion (EDTA) and adenine (AdeH): synthesis, crystal structure, molecular recognition and physical properties of ($AdeH_2$)[Cu(HEDTA)(H_2O)]·$2H_2O$, 1451
Sertucha, J., see Luque, A., 19
Sevov, S.C., see Bobev, S., 641
Sharma, C.L., see Singhal, S., 2489
Sharma, R.K., see Gupta, A., 2387
Sharp, P.R., see Xia, A., 1305
Shcheglov, P., Seisenbaeva, G.A., Gohil, S., Drobot, D.V. and Kessler, V.G., Preparation of trimetallic alkoxide complexes exploiting the isomorphous substitution approach. Synthesis, X-ray single crystal and mass-spectrometric study of $NbTa(OMe)_8(ReO_4)_2$ and $Nb_2Ta_2O_2(OMe)_{14}(ReO_4)_2$, 2317
Sheludyakova, L.A., see Bushuev, M.B., 797
Shen, X., Sakata, K. and Hashimoto, M., Syntheses and characterization of di- and mono-thiocyanato germanium (**IV**) complexes with 5,14-dihydro-6,8,15,17-tetra-methyldibenzo[*b*,*i*][1,4,8,11]tetraazacyclotetradecine, 969
Shikha, M., see Lobana, T.S., 205
Shirvani, S.M., see Ali, M.S., 125
Shivakumar, M., see Bhattacharyya, I., 2761
Shoukry, M.M., see Mohamed, M.M.A., 167
Siebald, H.G.L., see Moura, E.M., 2323
Sieroń, L., Bukowska-Strzyżewska, M., Korabik, M. and Mroziński, J., X-ray structure of poly[aquabis(benzimidazole-N^3)copper(II)-μ-*trans*-2-butene-1,4-dicarboxylato-O,O′:O″,O‴] (**I**) and magnetic and spectroscopic characterization of **I** and the isostructural copper(II)-μ-adipato complex **II**, 2473
Sillanpää, R., see Lehtonen, A., 1133
Sillanpää, R., see Lehtonen, A., 1017
Sillanpää, R., see Lehtonen, A., 349
Silva, R.M., see de Moura, C.V.R., 2227
Silva, M.F.P., see Santos, I.C.M.S., 2009
Silva, R.M., see Martins, M.A.C., 421
Silvino, A.C., see Aupers, J.H., 2107
Šindelář, Z., see Smékal, Z., 1203
Singh, A.K., Sooriyakumar, J., Kadarkaraisamy, M., Drake, J.E., Hursthouse, M.B., Light, M.E. and Butcher, R.J., *N*-[2-(4-Methoxyphenyltelluro)ethyl]benzamide (**L**^{1}) and *N*-[2-(4-methoxyphenyl telluro)propyl]phthalimide (**L**^{2}): synthesis and ligation with palladium(II), platinum(II) and ruthenium(II). Crystal structures of **L**^{1} and **L**^{2}, the latter as a mixed crystal with **L**$^2H_2$, 667
Singh, A., see Lobana, T.S., 205
Singhal, S., Sharma, C.L., Garg, A.N. and Chandra, K., Mössbauer spectral, magnetic moment and thermal decomposition studies of unsymmetrically substituted (*N*-alkyl,*N*′-hydroxyethyldithiocarbamato) iron(III) complexes, 2489
Sinha, C., see Senapoti, S., 753
Sinha Ray, M., see Bhattacharya, R., 2561
Sinyashin, O.G., see Karasik, A.A., 2251
Sitkowski, J., see Szłyk, E., 2001
Sitkowski, J., see Szlyk, E., 343
Skakle, J.M.S., see Bomfim, J.A.S., 1667
Skorik, Y.A., Romanenko, G.V., Gomes, C.A.R., Neudachina, L.K. and Vshivkov, A.A., Synthesis, XRD structure and properties of diaqua(*p*-toluidine-*N*,*N*-di-3-propionato)copper(II) dihydrate [Cu(*p*-Tdp)(H_2O)$_2$]·$2H_2O$, 2719
Slawin, A.M.Z., see Appleby, T., 2639
Slawin, A.M.Z., see Rodriguez i Zubiri, M., 1729
Slawin, A.M.Z., see Senapoti, S., 753
Sliva, T.Y., see Gubina, K.E., 963
Słota, R., Dyrda, G. and Wacławek, W., Investigation of phthalocyanine crystals exposed to NO_2 ambient gas, 677
Smékal, Z., Kameníček, J., Klasová, P., Wrzeszcz, G., Šindelář, Z., Kopel, P. and Žák, Z., Oxalato complexes of copper(II) with chelating diamines. Crystal structure of [Cu(dmen)ox(H_2O)]$_2$[Cu(dmen)$_2$](ClO_4)$_2$, 1203
Smieja, J.A., Borneman, M., Kittilstved, K., Edwards, D. and Borda, E., Reactivity of Os(TTP)($NC_6H_4NO_2$)$_2$ (TTP = dianion of 5,10,15,20-tetra(*p*-tolyl)porphyrin) including a kinetic study of imido ligand transfer to phosphines, 1889
Smith, J.M., see Pelczar, E.M., 2409
Smith, M.K., see Evans, D.J., 2421
Smith, M.D., see Reger, D.L., 1795
Solans, X., see López, C., 2361
Solans, X., see Papaefstathiou, G.S., 2027
Solans, X., see Crespo, M., 105
Sommer, R., see Pelczar, E.M., 2409
Sommer, R., see Karasik, A.A., 2251
Song, H.-B., Zhang, Z.-Z. and Mak, T.C.W., Synthesis and structural characterization of palladium(II) and platinum(II) complexes containing a chiral *P*,*N*-donor iminophosphine ligand, 1043
Sonnenberg, J.L. and Milletti, M.C., Ab initio investigation of the synthesis of (3-(2,3,4,5-tetramethylcyclopentadienyl)propoxy)titanium dichloride, 2699
Sooriyakumar, J., see Singh, A.K., 667
Sorai, M., see Nakamoto, T., 1299
Sordo, J., see Casas, J.S., 1651
Soria, D.B., Chacón Villalba, M.E., Piro, O.E. and Aymonino, P.J., Crystal and molecular structure and photoisomerization of nitropentaamminecobalt(III) nitroprusside sesquihydrate, [Co(NH_3)$_5NO_2$][Fe(CN)$_5$NO]·$1.5H_2O$, 1767
Soriano, C., see Díaz, P., 1523
Soto, J., see Sancenón, F., 1397
Soto-Guerrero, J., see Havel, J., 1411

Sousa-Pedrares, A., see Labisbal, E., 1553
Sóvágó, I., see Ősz, K., 2149
Spalding, T.R., see Goeta, A.E., 1689
Spinetti, M., see Sbrana, E., 1475
Spinetti, M., see Galli, A., 1405
Spodine, E., see Manzur, J., 181
Spodine, E., see Zolezzi, S., 55
Sreekanth, A., see John, R.P., 2515
Starikova, Z.A., Turevskaya, E.P., Turova, N.Y. and Yanovsky, A.I., On the structure of heterometallic methoxide $Li_2(WO)_2(OMe)_{10}\cdot MeOH$, 193
Staszak, Z., see Bronowska, W., 997
Steed, J.W., see Lysenko, A.B., 769
Stender, M. and Power, P.P., Reaction of {HC(CMeNAr)$_2$}Li (Ar = 2,6-*i*-$Pr_2C_6H_3$) with indium monochloride to yield the In–In bonded dimer [{HC(CMeNAr)$_2$}InCl]$_2$ and the hydroxide [{HC(CMeNAr)$_2$}InCl(μ-OH)]$_2$, 525
Stergiopoulos, T., see Chryssou, K., 2773
Stevenson, D.E., see Reglinski, J., 2175
Stevenson, D.E., see Reglinski, J., 2167
Stoeckli-Evans, H., see Fidalgo, E.G., 1921
Stoeckli-Evans, H., see Vallina, A.T., 1177
Stranger, R., Lovell, T. and McGrady, J.E., Quantifying the effect of high-spin/low-spin crossover on electron delocalization in d^5d^5 $M_2Cl_9^{3-}$ (M = Fe, Ru, Os) dimers, 1969
Stranger, R., see Petrie, S., 1163
Street, S.C., see Royer, A.C., 155
Streubel, R., Hoffmann, N., Ruthe, F. and Jones, P.G., Determining substrate selectivity and regiochemistry of nitrilium phosphanylid tungsten complexes in cycloaddition reactions with terminal alkynes, 119
Sturgeon, B., see Liang, S., 2021
Styron, E.K., Lake, C.H., Powell, D.H., Watkins, C.L. and Krannich, L.K., A comparison of the NMR, mass spectral, and molecular structure data for [$R_2AlN(CH_2Ph)_2]_2$, where R = Me, Et, Pr^n, Bu^n, and Bu^i, 1747
Su, M.-D., see Lai, C.-H., 579
Suarez, A., see Ares, R., 2309
Suárez, A., see López-Torres, M., 2063
Suárez, A., see Fernández, A., 39
Suárez-Iha, M.E.V., see Ávila Terra, L.H.S., 2375
Sudoh, S., see Miyamoto, R., 2127
Suen, M.-C., Keng, T.-C. and Wang, J.-C., One-dimensional structures of zinc(II) and cobalt(II) coordination complexes [$Zn(NCS)_2(PPz)]_n$ and [$CoCl_2(PPz)]_n$ (PPz = piperazine), 2705
Sugai, T., see Miyamoto, R., 2127
Sun, H., see Xu, Y.-K., 867
Sun, H.-Y., see Gao, E.-Q., 359
Surdykowski, A., see Szlyk, E., 2711
Surdykowski, A., see Szłyk, E., 2001
Surdykowski, A., see Szlyk, E., 343
Süss-Fink, G., see Fidalgo, E.G., 1921
Suwińska, K., see Kwiatkowski, E., 2071
Suzuki, T., Imamura, T., Kaizaki, S. and Kashiwabara, K., Preparation, crystal structures and spectroscopic properties of chloro(pentane-2,4-dionato){1,1,1-tris(dimethylphosphinomethyl)ethane}chromium(III), –cobalt(III) and –rhodium(III) hexafluorophosphate: comparison of the M–P, M–Cl and M–O (M = Cr, Co and Rh) bond lengths among the three M^{III} complexes, 835
Svoboda, I., see Kavlakoglu, E., 1539
Svoboda, I., see Baran, P., 1561
Swearingen, J.K., see Labisbal, E., 1553
Swearingen, J.K., see Ketcham, K.A., 859
Sweet, J.E., see Illingsworth, M.L., 211
Swiatek-Kozlowska, J., see Gubina, K.E., 963
Sydor, A., see Maciejewski, H., 1261
Szklanny, E., see Ruman, T., 2743
Szlyk, E., Surdykowski, A., Barwiolek, M. and Larsen, E., Spectroscopy and stereochemistry of the optically active copper(II), cobalt(II) and nickel(II) complexes with Schiff bases *N*,*N*′-(1*R*,2*R*)-(−)-1,2-cyclohexylenebis(3-methylbenzylideneiminato) and *N*,*N*′-(1*R*,2*R*)-(−)-1,2-cyclohexylenebis(5-methylbenzylideneiminato), 2711
Szłyk, E., Łakomska, I., Kobe, J., Surdykowski, A., Głowiak, T. and Sitkowski, J., The bonding of ribavirin to platinum(II) ion. The X-ray and spectroscopy of Pt(II) complexes with 1-β-D-ribofuranosyl-1,2,4-triazole-3-carboxamide and dimethylsulfoxide, 2001
Szlyk, E., Pazderski, L., Lakomska, I., Surdykowski, A., Glowiak, T., Sitkowski, J. and Kozerski, L., The X-ray structure of bis(5,7-dimethyl-1,2,4-triazolo-[1,5α]-pyrimidinium) hexachloroplatinate(IV) and spectroscopic properties of Pt(II) and Pt(IV) chloride complexes with 1,2,4-triazolo-[1,5α]-pyrimidines, 343
Szymańska-Buzar, T., Głowiak, T. and Czeluśniak, I., Reactivity of [$Mo(\mu\text{-}Cl)(SnCl_3)(CO)_3(NCMe)_2$] towards norbornadiene. X-ray crystal structure of [$Mo(\mu\text{-}Cl)(SnCl_3)(CO)_2(\eta^4\text{-}C_7H_8)(NCMe)$], 2505
Szymańska-Buzar, T., Głowiak, T. and Czeluśniak, I., The oxidative addition of $SnCl_4$ to [$W(CO)_4(NCMe)(PPh_3)$]. The X-ray crystal structure of [$WH(CO)_3(NCMe)(PPh_3)_2$][$SnCl_5\cdot MeOH$], 1817

Tajima, F., see Asaji, T., 2207
Takeda, N., see Tokitoh, N., 563
Tang, L.-F., see Wang, Z.-H., 873
Tangoulis, V., see Diamantopoulou, E., 2117
Tapia Estévez, M.J., see Crisponi, G., 1319
Tarafder, M.T.H., Chew, K.-B., Crouse, K.A., Ali, A.M., Yamin, B.M. and Fun, H.-K., Synthesis and characterization of Cu(II), Ni(II) and Zn(II) metal complexes of bidentate NS isomeric Schiff bases derived from S-methyldithiocarbazate (SMDTC): bioactivity of the bidentate NS isomeric Schiff bases, some of their Cu(II), Ni(II) and Zn(II) complexes and the X-ray structure of the bis[*S*-methyl-β-*N*-(2-furyl-methyl)methylenedithiocarbazato]zinc(II) complex, 2683
Tarafder, M.T.H., Khoo, T.-J., Crouse, K.A., Ali, A.M., Yamin, B.M. and Fun, H.-K., Coordination chemistry and bioactivity of some metal complexes containing two isomeric bidentate NS Schiff bases derived from *S*-benzyldithiocarbazate and the X-ray crystal structures of *S*-benzyl-β-*N*-(5-methyl-2-furylmethylene)dithiocarbazate and bis[*S*-benzyl-β-*N*-(2-furylmethylketone)dithiocarbazato]cadmium(II), 2691
Tarafder, M.T.H., Khoo, T.-J., Crouse, K.A., Ali, A.M., Yamin, B.M. and Fun, H.-K., Coordination chemistry and bioactivity of Ni^{2+}, Cu^{2+}, Cd^{2+} and Zn^{2+} complexes containing bidentate Schiff bases derived from *S*-benzyldithiocarbazate and the X-ray crystal structure of bis[*S*-benzyl-β-*N*-(5-methyl-2-furylmethylene)dithiocarbazato]cadmium(II), 2547
Taylor, M.J., see Kloo, L., 519
Temizdemir, S., see Craven, E., 553
Teotonio, E.E.S., Espínola, J.G.P., Brito, H.F., Malta, O.L., Oliveira, S.F., de Faria, D.L.A. and Izumi, C.M.S., Influence of the *N*-[methylpyridyl]acetamide ligands on the photoluminescent properties of Eu(III)-perchlorate complexes, 1837
Terzis, A., see Diamantopoulou, E., 2117
Terzis, A., see Tiliakos, M., 229
Thamae, M. and Nyokong, T., Interaction of sulfur dioxide and cyanide with cobalt(II) tetrasulfophthalocyanine in aqueous media, 133
Thompson, L.K., see Xu, Z., 1715
Thornton-Pett, M., see Foster, C.L., 1031
Thorpe, S.C., see Bell, N.A., 115
Thuéry, P., Asfari, Z., Vicens, J., Lamare, V. and Dozol, J.-F., Synthesis and crystal structure of sodium and caesium ion complexes of unsubstituted calix[4]arene. New polymeric chain arrangements, 2497
Thuéry, P., Asfari, Z., Nierlich, M., Vicens, J. and Masci, B., *ortho*-Methylene linked di- and triphenols and their uranyl ion complexes:

a crystallographic investigation, 1949
Thuéry, P., see Masci, B., 1125
Thurston, J.H., see Ali, M.S., 2659
Thurston, J.H., see Mukhopadhyay, U., 2369
Thurston, J., see Ali, M.S., 125
Tian, Y.-P., Yu, W.-T., Zhao, C.-Y., Jiang, M.-H., Cai, Z.-G. and Kun Fun, H., Structural characterization and second-order nonlinear optical properties of zinc halide thiosemicarbazone complexes, 1217
Tiekink, E.R.T., see Datta, A., 2237
Tiliakos, M., Raptis, D., Terzis, A., Raptopoulou, C.P., Cordopatis, P. and Manessi-Zoupa, E., Metal complexes of dipeptides containing the α-aminoisobutyric residue (Aib): preparation, characterization and crystal structures of copper(II) complexes with H–Aib–Aib–OH, 229
Timms, P.L., see Pardoe, J.A.J., 543
Tokitoh, N., Kishikawa, K., Okazaki, R., Sasamori, T., Nakata, N. and Takeda, N., Synthesis and characterization of an extremely hindered tetraaryl-substituted digermene and its unique properties in the solid state and in solution, 563
Tolazzi, M., see Bismondo, A., 1393
Tolazzi, M., see Comuzzi, C., 1337
Tolazzi, M., see Comuzzi, C., 1385
Toma, H.E., see Rocha, R.C., 2089
Tomşa, A.-R., see Raţiu, C., 353
Torrens, F., Calculation of organic solvent–water partition coefficients of iron–sulfur protein models, 1357
Torres, M.R., see Seco, J.M., 457
Torzilli, M.A., Colquhoun, S., Doucet, D. and Beer, R.H., The interconversion of dichlorobis(*N*-*n*-propylsalicylaldimine)zinc(II) and bis(*N*-*n*-propylsalicylaldiminato)zinc(II), 697
Torzilli, M.A., Colquhoun, S., Kim, J. and Beer, R.H., Structural and ^{1}H NMR spectroscopic characterization of bis(*N*-isopropylsalicylaldiminato)iron(II), 705
Toscano, P.J., see Ngo, S.C., 1289
Toscano, R.A., see Valdés-Martínez, J., 409
Tremel, W., see Bushuev, M.B., 797
Turevskaya, E.P., see Kessler, V.G., 1629
Turevskaya, E.P., see Starikova, Z.A., 193
Turner, P., see Field, L.D., 1707
Turova, N.Y., see Kessler, V.G., 1629
Turova, N.Y., see Starikova, Z.A., 193
Turpeinen, U., see van Albada, G.A., 141
Tušek-Božić, L., see Višnjevac, A., 2567

Uhl, W., Cuypers, L., Prött, M. and Harms, K., Molecular self-assembly controlled by gallium–gallium single bonds—facile syntheses of macrocyclic octagallium compounds, 511
Uiterweerd, P.G.H., see Cornu, D., 635
Uraev, A.I., see Kharisov, B.I., 2081
Usman, A., see Kannan, S., 2403

Vacca, A., see Cecconi, F., 1481
Valdés-Martínez, J., Alstrum-Acevedo, J.H., Toscano, R.A., Hernández-Ortega, S., Espinosa-Pérez, G., West, D.X. and Helfrich, B., Tetrachlorocuprate(II) salts of heterocyclic aminoguanidonium (guanylhydrazonium) ions, 409
Valenzuela, C.D., see Carriedo, G.A., 2587
Valenzuela, M.L., see Díaz, C., 909
Valko, M., see Moncol', J., 365
Valkonen, J., see Pietikäinen, J., 1089
Vallarino, L.M., see Benetollo, F., 425
Vallina, A.T. and Stoeckli-Evans, H., Coordination chemistry of a new imine-ether ligand, *N*,*N*′-bis(2-pyridylmethylene)-2,2′-(ethylenedioxy)bis(ethylamine): mono-helical and single-helical-strand coordination modes identified by X-ray crystallography, 1177
Valtancoli, B., see Bencini, A., 1459
Valtancoli, B., see Bencini, A., 1329
Vamvounis, G., see Cooke, M.W., 1235
van Albada, G.A., Mutikainen, I., Riggio, I., Turpeinen, U. and Reedijk, J., X-ray crystal structures, spectroscopic and magnetic measurements of dinuclear alkoxo-bridged copper(II) compounds with substituted bis(2-benzimidazolyl)alkane ligands. First X-ray structure of a copper(II) dinuclear propoxo-bridged compound, 141
VanDerveer, D.G., see Grant, G.J., 879
van Poppel, L.H., Bott, S.G. and Barron, A.R., Molecular structures of $Ga(^{t}Bu)_2(OPh)(pyz)\cdot PhOH$ and $[(^{t}Bu)_2Ga(H_2O)(\mu\text{-}OH)Ga(^{t}Bu)_2]_2(\mu\text{-}OC_6H_4O)\cdot 4(2\text{-Mepy})$: intra- and inter-molecular hydrogen bonding to gallium aryloxides, 1877
Várnagy, K., see Ősz, K., 2149
Vaz-Júnior, S., see Armas, M.T., 1513
Vázquez-García, D., see López-Torres, M., 2063
Vecchio, G., see Maccarrone, G., 1531
Vega, A., see Galindo, A.M., 2531
Venugopalan, P., see Saravanabharathi, D., 2433
Verma, R., see Lobana, T.S., 205
Vicens, J., see Thuéry, P., 2497
Vicens, J., see Thuéry, P., 1949
Vicente, R., see Papaefstathiou, G.S., 2027
Vieira, H.P., see Oliveira, M.R.L., 2243
Vila, J.M., see Ares, R., 2309
Vila, J.M., see López-Torres, M., 2063
Vila, J.M., see Fernández, A., 39
Villa, M.V., see Macías, B., 1899
Villa, M.V., see Macías, B., 1229
Villaescusa, I., Fiol, N., Cristiani, F., Floris, C., Lai, S. and Nurchi, V.M., Copper(II) and nickel(II) uptake from aqueous solutions by cork wastes: a NMR and potentiometric study, 1363
Vincent, J.B., see Royer, A.C., 155
Virovets, A.V., see Bushuev, M.B., 797
Višnjevac, A., Tušek-Božić, L., Majerić-Elenkov, M., Hameršak, Z., Kooijman, H., De Clercq, E. and Kojić-Prodić, B., Synthesis, structural characterisation and biological activity of Zn(II) and Pd(II) complexes of 3-substituted 5-(2′-pyridyl)-1,4-benzodiazepin-2-one derivatives, 2567
Vitoria, P., see Muga, I., 2631
Vittal, J.J., see Wang, W., 1991
Vives, J., see Serrano, J.L., 1589
Vohs, J.K., Downs, L.E., Barfield, M.E., Goodwin, S.D. and Robinson, G.H., Synthesis and molecular structure of tris(pentamethylphenyl)gallium, 531
Von Poelhsitz, G., de Araujo, M.P., de Oliveira, L.A.A., Queiroz, S.L., Ellena, J., Castellano, E.E., Ferreira, A.G. and Batista, A.A., *fac*-$[RuCl_3(NO)(dppb)]$ (**I**) and *mer*-$[RuCl_3(NO)(diop)]$ (**II**) complexes: syntheses, characterization and X-ray structures, 2221
Vrdoljak, V., see Korpar-Čolig, B., 147
Vshivkov, A.A., see Skorik, Y.A., 2719

Wacławek, W., see Słota, R., 677
Wainwright, M., see Rodriguez i Zubiri, M., 1729
Walker, S., see Benniston, A.C., 333
Waltermire, B.E., see Illingsworth, M.L., 211
Wan, H.-L., see Zhou, Z.-H., 787
Wang, J.-C., see Suen, M.-C., 2705
Wang, J.-Y., see Pang, Z., 2675
Wang, E.-B., see Li, Y.-G., 2601
Wang, W., Yan, Y.K., Andy Hor, T.S., Vittal, J.J., Wheaton, J.R. and Hall, I.H., Synthesis, X-ray structures, and cytotoxicity of rhenium-(I) carbonyl 2-(dimethylamino)ethoxide complexes, 1991
Wang, Q., see Nakamoto, T., 1299
Wang, R.-H., see Luo, J.-H., 893
Wang, H.-G., see Wang, Z.-H., 873
Wang, J.-T., see Wang, Z.-H., 873
Wang, Z.-H., Tang, L.-F., Jia, W.-L., Wang, J.-T. and Wang, H.-G., Synthesis and characterization of bidentate organotin Lewis acid

derivatives containing bis(pyrazol-1-yl)alkanes: X-ray crystal structure of $PhBr_2(L)SnCH_2SnPhBr_2$ (L = bis(4-chloropyrazol-1-yl)-methane), 873
Wang, G., see Zhou, Z.-H., 787
Wang, K.-Z., see Bian, Z.-Q., 313
Wardell, S.M.S.V., see Aupers, J.H., 2107
Wardell, J.L., see Aupers, J.H., 2107
Wardell, S.M.S.V., see Bomfim, J.A.S., 1667
Wardell, J.L., see Bomfim, J.A.S., 1667
Watkins, C.L., see Styron, E.K., 1747
Weakley, T.J.R., see Rosu, C., 959
Webster, M., see Hill, N.J., 1579
Webster, M., see Hill, N.J., 445
Wei, D.-Y., Kong, Z.-P. and Zheng, Y.-Q., Sebacato-bridged Cu(II) phen complexes: syntheses and crystal structures of $^2_\infty[Cu_2(phen)_2L_{4/2}](H_2O)_6$ and $[(phen)_2Cu(\mu\text{-}L)Cu(phen)_2](HL)_2(H_2L)(H_2O)_4$ (H_2L = sebacic acid; phen = 1,10-phenanthroline), 1621
Weiß, D., Winter, M., Merz, K., Knüfer, A., Fischer, R.A., Fröhlich, N. and Frenking, G., Synthesis, structure and bonding situation of [(dcpe)Pt(InCp*)$_2$] and {(dcpe)Pt[GaC(SiMe$_3$)$_3$]$_2$}—two novel examples of platinum complexes of low valent Group 13 metal species, 535
Welch, J.T., see Ngo, S.C., 1289
Weng, J.-B., see Luo, J.-H., 893
West, D.X., see Labisbal, E., 1553
West, D.X., see Ketcham, K.A., 859
West, D.X., see García, I., 729
West, R., Multiple bonds to silicon: 20 years later, 467
West, D.X., see Valdés-Martínez, J., 409
Wheaton, J.R., see Wang, W., 1991
Whitmire, K.H., see Ali, M.S., 2659
Whitmire, K.H., see Mukhopadhyay, U., 2369
Whitmire, K.H., see Ali, M.S., 125
Wignacourt, J.P., see Bentiss, F., 403
Wilkinson, P.S., see Illingsworth, M.L., 211
Williams, P.A.M., González Baró, A.C. and Ferrer, E.G., Study of the interaction of oxovanadium(IV) with a plant component (caffeic acid). Synthesis and characterization of a solid compound, 1979
Winter, C.H., see Yu, Z., 1117
Winter, M., see Weiß, D., 535
Wocadlo, S., see Zhang, Y., 81
Wocadlo, S., see Zhang, Y., 69
Wojciechowska, A., see Bronowska, W., 997
Wołowiec, S., see Ruman, T., 2743
Woollins, J.D., see Rodriguez i Zubiri, M., 1729
Woollins, J.D., see Senapoti, S., 753
Wozniak, K., see Eilmes, J., 7
Wright, T.D., see Reger, D.L., 1795
Wright, P., see Barret, M.C., 1761
Wrzeszcz, G., see Smékal, Z., 1203
Wu, B.-F., see Liu, S.-T., 1073
Wu, X.-T., see Cui, C.-P., 175
Wu, L.-M., see Cui, C.-P., 175

Xia, A. and Sharp, P.R., Diphosphazane supported platinum(II) triflate, amine, and amido complexes: synthesis and X-ray crystal structures, 1305
Xing, J.-H., see Kano, N., 657
Xu, Z., Thompson, L.K. and Miller, D.O., A non-homoleptic Cu_9 [3 × 3] mixed ligand grid—structural and magnetic properties, 1715
Xu, Y.-K., Mu, Y., Sun, H., Qu, Z.-W., Zhang, F., Zhang, Y.-T. and Liu, Y., Synthesis, crystal structure and catalysis for polyethylene of a paramagnetic chromium complex $[(\eta^5\text{-}Cp^{Si})Cr(\mu\text{-}Cl)Cl]_2$ [$Cp^{Si} = (C_5H_4)Si(CH_3)_2(C_6H_5)$], 867

Yamada, Y., Sakurai, H., Miyashita, Y., Fujisawa, K. and Okamoto, K.-i., Crystal structures, electronic absorption and reflectance spectral behaviors, and electrochemical properties of five-coordinated chlorocopper(II) complexes with 5,6-disubstituted-1,10-phenanthroline, 2143
Yamada, Y., see Mahboob, N., 1809
Yamaguchi, Y., see Brown, S.T., 599
Yamanari, K., see Kita, M., 843
Yamashita, S., see Kita, M., 843
Yamin, B.M., see Tarafder, M.T.H., 2683
Yamin, B.M., see Tarafder, M.T.H., 2691
Yamin, B.M., see Tarafder, M.T.H., 2547
Yan, Y.K., see Wang, W., 1991
Yan, S.-P., see Gao, E.-Q., 359
Yanovsky, A.I., see Starikova, Z.A., 193
Yap, G.P.A., see Foley, S.R., 619
Yaraşir, M.N.U., see Kandaz, M., 255
Ye, J.-J., see Zhou, Z.-H., 787
Yellowlees, L.J., see Charsley, S.M., 849
Yilmaz, V.T., Guney, S., Andac, O. and Harrison, W.T.A., Different coordination modes of saccharin in the metal complexes with 2-pyridylmethanol: synthesis, spectroscopic, thermal and structural characterization, 2393
Yılmaz, İ., see Kandaz, M., 825
Yoo, J., Han, Y.-K., Lee, Y.S. and Do, Y., Cocrystallization of a dinuclear platinum complex as a monomer and a one-dimensional polymer, 715
Youm, K.-T., see Park, J.S., 1273
Youngme, S., Chaichit, N., Pakawatchai, C. and Booncoon, S., The coordination chemistry of mono and bis(di-2-pyridylamine)copper(II) complexes: preparation, characterization and crystal structures of $[Cu(L)(NO_2)_2]$, $[Cu(L)(H_2O)_2(SO_4)]$, $[Cu(L)_2(NCS)](SCN)\cdot 0.5DMSO$ and $[Cu(L)_2(SCN)_2]$, 1279
Youngme, S., Chaichit, N. and Damnatara, K., The coordination chemistry of dinitrato-di-2-pyridylamine copper(II). Crystal structures of *catena*-poly[[(di-2-pyridylamine)(nitrato-*O*,*O*′)copper(II)]-μ-nitrato-*O*:*O*′] and bis(nitrato-*O*,*O*′)(di-2-pyridylamine)copper(II) dihydrate, 943
Youngme, S. and Chaichit, N., Coordination geometries in bis(di-2-pyridylamine)copper(II) complexes. Crystal structures and spectroscopic properties of $[CuL_2(H_2O)_2](S_4O_6)$, $[CuL_2(CF_3SO_3)_2]$ and $[CuL_2(SO_4)]_2[CuL_2(H_2O)_2](PF_6)_2\cdot 2H_2O$ (L = Di-2-pyridylamine), 247
Yu, X.-Y., Maekawa, M., Morita, T., Chang, H.-C., Kitagawa, S. and Jin, G.-X., Syntheses and crystal structures of mononuclear rhodium hydrido complexes from the reactions of $[Rh(H)_2(PPh_3)_2(EtOH)_2]ClO_4$ with various nitrogen ligands, 1613
Yu, W.-T., see Tian, Y.-P., 1217
Yu, Z., Korolev, A.V., Heeg, M.J. and Winter, C.H., Synthesis and structural characterization of complexes derived from treatment of gallium trichloride with 3,5-diphenylpyrazole, 1117
Yu, K.-B., see Liu, Q.-D., 1097
Yutronic Sáez, N., see Carriedo, G.A., 2579

Zabardasti, A., see Asadi, M., 1255
Zabardasti, A., see Asadi, M., 683
Zacharias, P.S., see Mangayarkarasi, N., 925
Žák, Z., see Smékal, Z., 1203
Zanonato, P.L., see Bismondo, A., 1393
Zanonato, P., see Comuzzi, C., 1385
Zaworotko, M.J., see Deoghoria, S., 2457
Zeng, W.F., Chen, Y.S., Chiang, M.Y., Chern, S.S. and Cheng, C.P., Preparation and structures of complexes of titanium(IV) and 8-hydroxyquinoline: $TiQ_2(Opr^i)_2$ and $[TiQ_2(\mu\text{-}O)]_4\cdot 6H_2O$, 1081
Zhang, A., see Delgado, R., 2265
Zhang, G., Zhao, J., Raudaschl-Sieber, G., Herdtweck, E. and Kühn, F.E., Syntheses and characterization of dimolybdenum and dirhodium complexes containing 2-pyridylphosphine ligands, 1737
Zhang, Z.-Z., see Song, H.-B., 1043

Zhang, Y.-T., see Xu, Y.-K., 867
Zhang, F., see Xu, Y.-K., 867
Zhang, H., Cai, J., Feng, X.-L., Sang, H.-Y., Liu, J.-Z., Li, X.-Y. and Ji, L.-N., Assembly chemistry of a cadmium(II) complex with cyanometalate anions $[Fe(CN)_5NO]^{2-}$, $[Pd(CN)_4]^{2-}$ and $[Pt(CN)_6]^{2-}$, 721
Zhang, Y., Collison, D., Livens, F.R., Helliwell, M., Heatley, F., Powell, A.K., Wocadlo, S. and Eccles, H., Synthesis and characterisation of uranyl substituted malonato complexes: Part II: ^{13}C CPMAS NMR spectroscopy related to structural diversity, 81
Zhang, Y., Livens, F.R., Collison, D., Helliwell, M., Heatley, F., Powell, A.K., Wocadlo, S. and Eccles, H., Synthesis and characterisation of uranyl substituted malonato complexes: Part I. Structural diversity with dimethylmalonate and different counter-cations, 69
Zhao, L., see Pang, Z., 2675
Zhao, J., see Zhang, G., 1737
Zhao, C.-Y., see Tian, Y.-P., 1217
Zhao, Z.-R., see Liu, S.-T., 1073
Zhao, Y.-J., see Luo, J.-H., 893
Zheng, Y.-Q., see Wei, D.-Y., 1621
Zhou, Q.-Z., see Liu, Q.-D., 1097
Zhou, Z.-H., Ye, J.-J., Deng, Y.-F., Wang, G., Gao, J.-X. and Wan, H.-L., Monomeric and polymeric nickel complexes of malate: X-ray crystal structure of polymeric homochiral *S*-malato nickel(II), $[\Delta\text{-}Ni(S\text{-}Hmal)(H_2O)_2]_n \cdot nH_2O$, 787
Zhu, S.-R., see Guo, Y.-H., 1005
Zhu, T., see Illingsworth, M.L., 211
Zhuravel, M.A., see Pelczar, E.M., 2409
Zielińska, A., see Bocheńska, M., 763
Ziemkowska, W., Alkylaluminium derivatives of 2,2′-di(hydroxymethyl)biphenyl: structural characterization of trinuclear complexes, 281
Ziller, J.W., see Evans, W.J., 1683
Zingales, R., see Amorello, D., 1369
Zolezzi, S., Spodine, E. and Decinti, A., Electrochemical studies of copper(II) complexes with Schiff-base ligands, 55
Zuno-Cruz, F.J., Carrasco, A.L. and Rosales-Hoz, M.J., ^{1}H, ^{13}C and ^{29}Si NMR study of acetylide and parallel alkyne substituted Ru_3 and Os_3 clusters derived from HC≡CR (R = $SiMe_3$, $SiPh_3$ and CMe_3). X-ray crystallographic study of $[(\mu\text{-}H)M_3(CO)_9(CCR)]$ (M = Ru, R = $SiMe_3$, $SiPh_3$; M = Os, R = $SiPh_3$, CMe_3) and $[Ru_3(\mu\text{-}CO)(CO)_9(HCCR)]$ (R = CMe_3), 1105

Available online at www.sciencedirect.com
SCIENCE DIRECT®
Polyhedron 21 (2002) 2855–2885
POLYHEDRON
www.elsevier.com/locate/poly

Subject Index to Volume 21

Ab initio
Molecular orbital, Mechanism, Intermolecular nucleophilic attack, Titanium, Ylid, 2699
Absolute configuration
Arene ruthenium, Crystal structures, CH–π interaction, 2D NMR, 1929
Absorption and EPR spectra
2-(3,5-Dimethylpyrazol-1-ylmethyl)pyridine, Bis-ligand and anion-bound copper(II) complexes, X-ray structure, Cyclic voltammetry, 1245
Acetate
Organotin, Crystal structures, Halides, *N*-Thiocyanate, Azide, 1667
Acetates
Molybdenum, Crystal structures, Cluster complexes, Reduction, 147
Acetylacetonate complexes
1-Hydroxybenzotriazolate complexes, Magnetic properties, Nickel(II), 2117
Acetylacetonate complexes
Trans influence, Crystal structures, Ligand-field strength, Tripodal tridentate phosphine, Chromium(III) complexes, 835
Acetylide
Iron, Vinylidene, Propadienylidene, 1755
Acetylide
Ruthenium, Osmium, Alkyne, Clusters, 1105
Acidity parameter
Aqueous solution, Hydroxy groups, Glycine-conjugated bile acids, 1421
Acridine
Hydrogen-bonding, Silanol, Amine, Adducts, 4,4′-bipyridine, Phenylpyridine, 1689
Actinides
Dioxouranium(VI) polyhalides, Uranyl polyhalides, Polybromides, Polyiodides, 2755
Acyclic
Binuclear, Pyrazole bridged, Asymmetric unit, Pentagonal bipyramidal, 925
Adduct compounds
N-oxides, Uranyl bis(β-diketonates), X-ray structures, 2403
Adduct
Copper, Hinokitiol, X-ray, 1761
Adduct formation
Thermodynamics, Tin compounds, Porphyrins, Equilibrium constant, Spectral method, 683
Adducts
Hydrogen-bonding, Silanol, Amine, Acridine, 4,4′-bipyridine, Phenylpyridine, 1689
Adeninium
Copper(II) complex, Crystal structures, EDTA, Ion pair, Molecular recognition, 1451
Adenosine 5′-monophosphate
Ni(II), Co(II), Tetramines, Mixed-ligand complexes, 745
Adenosine-5′-triphosphate (ATP)
Mg(II), NOESY, Torsion angle (χ), 435
Affinity chromatography
Urinary trypsin inhibitors, Bubble extraction, RP-HPLC, 1475
Ag–Ag interaction
Silver(I), Nicotinamide, Nicotinic acid, Sulfonate, Hydrogen bond, Assembly chemistry, 689
Al(III) complexes
Isoquercitrin, Stoichiometry, UV–Vis Spectroscopy, DFT calculations, FT Raman, 2801
Alkali metal ions
Doubly layered 2D sheet, Copper(II) complexes, 1273
Alkali metal ions
Sodium ion, Caesium ion, Calix[4]arene, Crystal structures, 2497
Alkoxides
Crystal structures, Lithium, Tungsten, Methoxide, 193
Alkoxides
Magnesium, Niobium, Oxoalkoxides, Mass-spectra, Crystal structures, 1629
Alkoxo-bridged
Copper(II), Magnetism, Benzimidazoles, Crystal structures, 141
Alkylaluminium diolates
Aluminium, Diols, Trinuclear complexes, 2,2′-Di(hydroxymethyl)biphenyl, Crystal structures, 281
Alkyne
Ruthenium, Osmium, Acetylide, Clusters, 1105
π-Allyl molybdenum
Organometallic phosphine, Multimetallic, Iron carbonyl complexes, Cyclopentadienyl iron complexes, 2301
Aluminium
Diols, Trinuclear complexes, 2,2′-Di(hydroxymethyl)biphenyl, Crystal structures, Alkylaluminium diolates, 281
Aluminum
Electron counts, Metalloid clusters, 503
Aluminum(I) halides
Metalloid clusters, Nanosized clusters, Intermediates, Metal lattice, X-ray structural analysis, 489
Amidate bridging ligands
Platinum(III) compounds, Lantern-type complexes, X-ray structure, 275
Amide ligands
Potassium, Rubidium, 15-Crown-5, Crystal structures, 2451
Amides
C_3-chiral triamidostannate, Tin, Lithium, 629
Amide
tert-Butylcalix[4]arenes, Sodium complexes, Yttrium(III) complexes, Lanthanide(III) complexes, X-ray structures, 763
Amide
Yttrium, Salen, Aryloxide, Organometallic, 1683
Amido
Amine, Triflate, Platinum, Diphosphazane, Cyclometalation, 1305
2-Amidothiophenolato complexes
Rhenium complexes, Trigonal prismatic geometry, 1597
Amine
Amido, Triflate, Platinum, Diphosphazane, Cyclometalation, 1305
Amine
Hydrogen-bonding, Silanol, Adducts, Acridine, 4,4′-bipyridine, Phenylpyridine, 1689
Amino acid
Nickel(II), Coordination chemistry, Hydrogen bond, Chiral recognition, 817
Amino acids
Electron paramagnetic resonance (EPR) spectroscopy, Copper(II) complexes, *N*,*N*-dimethyl-L-α-isoleucine, 1643
Aminoalane
Trialkylaluminum, Dibenzylamine, NMR, Mass spectrometry, Molecular structure, 1747
Aminoalcohol
Rhenium(I), Carbonyl, Cytotoxicity, Oxidative-alkoxylation, Hydrogen-bonding, 1991
Aminoguanidonium
Copper(II) halides, Crystal structures, Tetrachlorocuprate(II), 409
Aminohydroxamate complexes
Iron complexes, Electrochemical reduction, Cyclic voltammetry, EC mechanism, 1661
Aminohydroxamic acids
Copper(II) complexes, Mixed-ligand com-

Elsevier Science Ltd.
PII: S0277-5387(02)01351-7

plexes, Five-coordinate complexes, EPR spectra, Vis spectra, 295
Aminohydroxamic acids
Zinc(II) complexes, Mixed-ligand complexes, Polyamines, NMR spectra, Potentiometry, 2183
α-Aminoisobutyryl-α-aminoisobutyric acid (H–Aib–Aib–OH)
Copper(II) peptide complexes, Spectroscopic characterization, X-ray crystal structures, 229
Aminomethane-1,1-diphosphonic acids
Zinc(II) complexes, Magnesium(II) complexes, Calcium(II) complexes, Potentiometry, NMR, 321
2-(Aminomethyl)pyridine
Copper(II), *N*-(2-Pyridylmethyl)iminodiacetic acid, *N*-(2-Pyridylmethyl)iminodiacetate(2-) ion, α-Picolylamine, 2-(2′-Pyridyl)benzimidazole, Crystal structures, Mixed-ligand complexes, Aromatic π,π-staking interactions, Molecular recognition, Thermal stability, Spectral and magnetic properties, 1485
2-Aminophenol
Cd(II) and Hg(II) complexes, Spectroscopic properties, Normal coordinate, Force constant, 2-Phenylenediamine, 987
8-Aminoquinoline
Nickel complexes, Sulfonamide complexes, X-ray crystal structures, 1229
Aminotroponimine
Azide, Germanium, Tin, Silver, Tris(pyrazolyl)borate, 611
β-Aminovinylimines
Trinuclear metal chelates, Chemical and electrochemical synthesis, 2081
Analogous multiple bonded systems
Electronic states, Linear disilaketenylidene (SiSiO), Renner effect, 599
Ancillary functions
Ruthenium monoterpyridine complexes, Crystal structures, 2033
2-Anilinopyridine
Crystal structures, Antiferromagnetic dimers, Dinuclear acetates, Copper(I), 457
Anion controlled assembly
Lanthanide contraction, Crystal structures, Magnetic properties, 1097
Anions
Copper(I), Dppe, Coordination mode, Solid state structures, 2433
Antibacterial activity
Binuclear, Ruthenium(II) complexes, Thiobis(β-diketone), Syntheses, Catalytic oxidation, 1721
Antibacterial activity
Ruthenium(II), Binuclear, Bis(β-diketone), Triphenylarsine, Syntheses, Catalytic study, 219
Antiferromagnetic
Copper, Formato, Dinuclear complexes, EPR, 1057
Antiferromagnetic coupling
Density functional theory, Face-shared dimers, Metal–metal bonding, High spin/low spin crossover, Electron delocalization, Broken-symmetry, 1969
Antiferromagnetic coupling
Tetranuclear copper(II) complexes, Crystal structures, Magnetism, Molecular orbital calculation, 1539
Antiferromagnetic dimers
2-Anilinopyridine, Crystal structures, Dinuclear acetates, Copper(I), 457
Antimony(III)
1,3-Dithiole-2-thione-4,5-dithiolates, 1,3-Dithiole-2-one-4,5-dithiolates, Crystal structures, 2107
APCVD
Tin phosphide, Thin film, 1943
Apparent molar enthalpies of
Potassium *p*-*n*-hexylbenzoate, Potassium *p*-*n*-heptylbenzoate, Potassium *p*-*n*-octylbenzoate, Partial molar enthalpies of, Micellization enthalpy, Methylene group contribution, 1497
Aqueous solution
Acidity parameter, Hydroxy groups, Glycine-conjugated bile acids, 1421
Aqueous solutions
Uranyl oxalates, Oxalic acid, UV–Vis spectrophotometry, Speciation, Stability constants, 1411
Arene ruthenium
Absolute configuration, Crystal structures, CH–π interaction, 2D NMR, 1929
Aromatic pendant arms
Azamacrocycles, Coordination compounds, Metallic polymer, 333
Aromatic π,π-staking interactions
Copper(II), *N*-(2-Pyridylmethyl)iminodiacetic acid, *N*-(2-Pyridylmethyl)iminodiacetate(2-) ion, 2-(Aminomethyl)pyridine, α-Picolylamine, 2-(2′-Pyridyl)benzimidazole, Crystal structures, Mixed-ligand complexes, Molecular recognition, Thermal stability, Spectral and magnetic properties, 1485
Arsenic
B3LYP, CCSD(T), Germanium, 579
Arsenic
Heteropolyoxometalate, Tungstate, Lacunary, Synthesis, Redox chemistry, 959
Arsine oxide
Scandium, Phosphine oxide, X-ray structures, ^{45}Sc NMR, 1579
Arsine oxide
Yttrium, Phosphine oxide, X-ray structures, 445
Artificial neural networks
Experimental design, Stability constants, Metal complexes, Ion selective electrodes, Metal–ligand equilibria, 1375
Arylazopyrimidines
Osmium(II) complexes, Geometrical isomers, X-ray structures, MLCT transitions, Redox property, 753
Arylmetal complexes
Mercury(II), Boron, The 2,6-bis(dimethylamino)phenyl ligand, 635
Aryloxide
Gallium, Hydrogen bonding, Hydrolysis, 1877
Aryloxide
Yttrium, Salen, Amide, Organometallic, 1683
Aspartate
Cadmium(II), Structures, ^{111}Cd NMR, 935
Assembly chemistry
Silver(I), Nicotinamide, Nicotinic acid, Sulfonate, Hydrogen bond, Ag–Ag interaction, 689
Association constants
Zinc(II)tetrasulfophthalocyanine, Sulfur dioxide, Fluorescence quenching, 951
Asymmetric catalysis
Nickel, Malic acid, Malate, Coordination polymer, Crystal structures, Electroplating, 787
Asymmetric 14-π nickel(II) tetraazaannulene
Synthesis and electrochemistry, Hammett plot, Electrocatalysis, 917
Asymmetric unit
Acyclic, Binuclear, Pyrazole bridged, Pentagonal bipyramidal, 925
Autoxidation
Copper(I) complexes, Kinetic data, Catalytic activity, 181
Azamacrocycles
Aromatic pendant arms, Coordination compounds, Metallic polymer, 333
Aza-Wittig reaction
Iminophosphorane, Cycloaddition, Four-membered ring compounds, Thermolysis, X-ray analysis, 657
Azide
Germanium, Tin, Silver, Tris(pyrazolyl)borate, Aminotroponimine, 611
Azide
Organotin, Crystal structures, Halides, *N*-Thiocyanate, Acetate, 1667

Backscatter Mössbauer spectroscopy
Iron(II) phthalocyanine, Gas sensing, 115
Base hydrolysis kinetics
Equilibria, Crystal and molecular structures, 2283
bdmpp
Ru(II) complexes, dcbpy, Thiocyanato ligands, Sensitizing ability, 2773
Benzimidazoles
Copper(II), Alkoxo-bridged, Magnetism, Crystal structures, 141
Benzimidazolium
Thermochromism, Crystal structures, Tetrachlorocuprate, 2561
Benzoate ligands
Cobalt(II) complexes, Di-2-pyridyl ketone complexes, End-on azide ligands, Magnetic properties, 2027
Benzohydroximate anion
Boron complexes, Synthesis, Crystal structures, 2351
Benzotriazole
Ruthenium-ammine, Polynuclear complexes, Mixed-valence, Electron transfer, Molecular wires, 2089
Benzyl 8-quinolyl sulfide
Palladium(II) complexes, Phenethyl 8-qui-

nolyl, Crystal structures, 843
BF_2^+-capped complexes
Nickel(II) complexes, Heterotrinuclear complexes, Dioxadithiadiazamacrobicycle, Template effect, *vic*-Dioxime, 1865
Bidentate ligands
Cobalt(III) complexes, Tetradentate ligands, Eddp, 2277
Bidentate nitrogen ligands
Palladium, Nickel, Chirality, Crystal structures, 27
Bifunctional ligand
Hydroxypyridinones, Hydroxypyridinonate complexes, Chelating agents, 2609
Bimetallics
Tantalum, Metallocenes, Hydrides, Metallophosphines, X-ray structures, 371
Binuclear
Acyclic, Pyrazole bridged, Asymmetric unit, Pentagonal bipyramidal, 925
Binuclear complexes
Lanthanide(III) chelate, Cobalt(III) chelate, Inner-sphere coordination, Outer-sphere coordination, Stability constant, 805
Binuclear complexes
Macrocyclic compound, Magnetic properties, 359
Binuclear complexes
Synthesis, Equilibria, Polyamines, 1351
Binuclear nickel(II) complexes
Crystal structures, Magnetic properties, Terminal thiocyanato ion complexes, Terminal cyanato ion complexes, Pentadentate ligands, 2457
Binuclear
Ruthenium(II), Bis(β-diketone), Triphenylarsine, Syntheses, Antibacterial activity, Catalytic study, 219
Binuclear
Ruthenium(II) complexes, Thiobis(β-diketone), Syntheses, Catalytic oxidation, Antibacterial activity, 1721
Binucleating ligand
Copper(II) complexes, Nickel(II) complexes, Electrochemistry, Magnetic properties, 2767
Bioactivity of metal complexes
Metal complexes, *S*-Benzyldithiocarbazate, Bioactivity of Schiff bases, Crystal structure of Cd(II) complexes, 2547
Bioactivity of Schiff bases
Metal complexes, *S*-Benzyldithiocarbazate, Bioactivity of metal complexes, Crystal structure of Cd(II) complexes, 2547
Bioactivity
Schiff base ligands, Cadmium(II) complexes, Crystal structures, Dithiocarbazate Schiff base crystal structures, Metal complexes, 2691
Bioligands
Palladium(II) complexes, Glycine methyl ester hydrolysis, 167
2,2′-Bipyridine complexes
Mixed-ligand complexes, Copper(II) complexes, Lactic acid, 2-Methyllactic acid, Mandelic acid, Crystal structures, 2811
4,4′-bipyridine
Hydrogen-bonding, Silanol, Amine, Adducts, Acridine, Phenylpyridine, 1689
Bis(β-diketone)
Ruthenium(II), Binuclear, Triphenylarsine, Syntheses, Antibacterial activity, Catalytic study, 219
bis(diphenylthiophosphinyl)ethane
Phosphine chalcogenide, Seven-membered, Palladium(II), Mercury(II), Metallacyclic rings, 205
Bis-ligand and anion-bound copper(II) complexes
2-(3,5-Dimethylpyrazol-1-ylmethyl)pyridine, X-ray structure, Absorption and EPR spectra, Cyclic voltammetry, 1245
Bismuth
Polycations, Cluster compounds, Crystal structures, Iridium, Rhodium, 651
Bis(phosphine) monoxides
Cu(I), Chelates, NMR, Electrochemistry, Hard–soft acids and bases, 2793
Bis(pyrazol-1-yl)alkane
Organotin(IV), X-ray structures, 873
Bis-sulfamide
Tantalum(V), Diamide, Crystal structures, 1051
Bithiophene
Polyamine, Coordination, Cu(II)-electrochemical pattern, Potentiometry, 1523
B3LYP
CCSD(T), Germanium, Arsenic, 579
Bond dissociation energy
Digermene, Germylene, X-ray crystallographic analysis, Dissociation, Equilibrium, Dioxadigermetane, Terminal tungsten complexes, 563
Boron
Arylmetal complexes, Mercury(II), The 2,6-bis(dimethylamino)phenyl ligand, 635
Boron complexes
Benzohydroximate anion, Synthesis, Crystal structures, 2351
Boron
Lithium, Imido, Complexes, X-ray, 549
Boron monochloride
Halogen exchange, Polyboron halides, 543
BPTI
Capillary electrophoresis, Hydrophobic interaction chromatography, Heterologous protein, *Saccharomyces cerevisiae*, 1405
Broken-symmetry
Density functional theory, Face-shared dimers, Metal–metal bonding, High spin/low spin crossover, Electron delocalization, Antiferromagnetic coupling, 1969
BTZ ligands
X-ray crystallography, Pb(II) salts, π–π stacking interaction, 197
Bubble extraction
Urinary trypsin inhibitors, Affinity chromatography, RP-HPLC, 1475
Buffer capacity
Partition function, Equilibria in solution, Cooperativity, Site affinity, Heat capacity, 1439
Bulky ligands
β-Diketiminate, Low valent indium, Metal–metal bonds, 525

Cadmium complexes
Dca ligand, Double end-to-end, Zigzag chain, π–π interaction, 893
Cadmium(II)
Aspartate, Structures, ^{111}Cd NMR, 935
Cadmium(II) complexes
Coordination polymers, Crystal structures, Symbiosis, 2293
Cadmium(II) complexes
Cyanometalate, Coordination polymers, Crystal structures, 721
Cadmium(II) complexes
Polyamines, X-ray structures, 739
Cadmium(II) complexes
Schiff base ligands, Crystal structures, Dithiocarbazate Schiff base crystal structures, Metal complexes, Bioactivity, 2691
Cadmium(II)
2-Pyridineformamide, Thiosemicarbazone, Nickel(II), Zinc(II), Crystal structures, 729
Cadmium(II)
Tris(pyrazolyl)borate and 2,6-pyridyl-diimine ligands, Thiocyanate, Lead(II), 1795
Cadmium
Macrocycles, Polyamines, Dipyridine, Phenanthroline, 1329
Cadmium
Nickel, Copper, Zinc, Saccharinate, X-ray structures, 395
Cadmium
Pyrazineformamide, Thiosemicarbazone, Zinc, Crystal structures, Electrochemical synthesis, 1553
Caesium ion
Alkali metal ions, Sodium ion, Calix[4]arene, Crystal structures, 2497
Caffeic acid complexes
Vanadium complexes, IR spectra, UV–Vis spectra, Potentiometric titrations, Catecholate-like ligand, 1979
Cage-like structure
Polyoxovanadates, Organic–inorganic hybrid, Mixed-valence, Hydrothermal synthesis, 2601
Calcium(II) complexes
Aminomethane-1,1-diphosphonic acids, Zinc(II) complexes, Magnesium(II) complexes, Potentiometry, NMR, 321
Calix[4]arene
Alkali metal ions, Sodium ion, Caesium ion, Crystal structures, 2497
Calixarenes
Uranyl ion, Homooxacalixarenes, Supramolecular assembly, Crystal structures, 1125
Calorimetry
Zinc adducts, Emprirical correlations, Infrared spectroscopy, 1677
^{13}C and ^{15}N NMR spectroscopy
Synthesis, Cyano(selenone)gold(I) complexes, 2099
Capillary electrophoresis

Hydrophobic interaction chromatography, Heterologous protein, BPTI, *Saccharomyces cerevisiae*, 1405
Carbacylamidophosphates
Cobalt(II), Cubane complexes, X-ray data, 963
Carba metallaboranes
Carboranes, Dicarbollides, Cyclic voltammetry, Liquid–liquid extraction, Lanthanide and actinide extaction, 975
Carbohydrates
Cobalt complexes, Circular dichroism, Sucrose complexes, ^{1}H NMR, Semi-empirical calculations, 2215
Carbonyl
Rhenium(I), Aminoalcohol, Cytotoxicity, Oxidative-alkoxylation, Hydrogen-bonding, 1991
Carbonyls
Cyclophosphazenes, Polyphosphazenes, Phenolic phosphine, Macromolecular complexes, Spectroscopic characterization, 2579
Carboranes
Carba metallaboranes, Dicarbollides, Cyclic voltammetry, Liquid–liquid extraction, Lanthanide and actinide extaction, 975
Carboxylate
Trinuclear complexes, Single crystal structures, Copper(II), Silver(I), Thioether, 33
Carnosine
Oxovanadium(IV) complexes, Potentiometric and spectrophotometric studies, Stability constants, 1513
Catalase resistance
Diperoxovanadate, Vanadyl, EDTA inhibition, EDTA bridged heteroligand peroxovanadates, Oxo-bridged peroxovanadates containing sulphate, 389
Catalysis
Organometallics, Heterobimetallics, Organoruthenium, Mössbauer, NMR, 2323
Catalysis
Silver, Hydroxylamine, Kinetics, Mechanism, Redox, 1893
Catalysis
Triflates, Triphenylphosphine oxide complexes, Single crystal X-ray diffraction, Scandium and lanthanide, 287
Catalytic activity
Copper(I) complexes, Autoxidation, Kinetic data, 181
Catalytic disproportionation
Manganese(II) complexes, 2-Pyrazine carboxylic acid, 2,6-Pyridinedicarboxylic acid, Chelidamic acid, Crystal structures, Hydrogen peroxide, 1063
Catalytic oxidation
Binuclear, Ruthenium(II) complexes, Thiobis(β-diketone), Syntheses, Antibacterial activity, 1721
Catalytic study
Ruthenium(II), Binuclear, Bis(β-diketone), Triphenylarsine, Syntheses, Antibacterial activity, 219
Catecholate ligands
Lanthanide, Polyaza ligands, Stability constants, Potentiometry, 1393
Catecholate-like ligand
Vanadium complexes, Caffeic acid complexes, IR spectra, UV–Vis spectra, Potentiometric titrations, 1979
Cation–π interaction
Thallium(I) complexes, Scorpionate ligands, Crystal packing, π-Stacking, 553
Cations
Solutions, Equilibria, Hydrolysis, Titration, Masking, 1369
C_3-chiral triamidostannate
Amides, Tin, Lithium, 629
CCSD(T)
B3LYP, Germanium, Arsenic, 579
Cd(II) and Hg(II) complexes
Spectroscopic properties, Normal coordinate, Force constant, 2-Phenylenediamine, 2-Aminophenol, 987
^{111}Cd NMR
Cadmium(II), Aspartate, Structures, 935
CD spectra
Optically active Schiff bases, Co(II), Cu(II) and Ni(II) complexes, Co(II) paramagnetic ^{1}H NMR, 2711
CD spectroscopy
Copper(II), Nickel(II), Palladium(II), Peptides, Methionine, 2149
Cerium
Fluoroalkoxides, Structures, Complexes, MOCVD, Films, 1985
C–H activation
Cyclometallation, Phosphorus ligands, Schiff bases, Palladium, 39
Chain complex
Crystal structures, Nickel(II) complexes, Hexaazamacrocycle, Organic ligands, 1913
Charge transfer
Polyoxometalates, Keggin, Photochromism, 2537
Chelate complexes
$Ph_2P(CH_2)_nNHP^iPr_2$, Diphosphine ligands, 2639
Chelates
Bis(phosphine) monoxides, Cu(I), NMR, Electrochemistry, Hard–soft acids and bases, 2793
Chelate
Titanium, Coordination chemistry, Structure elucidation, 8-Hydroxyquinolinate, 1081
Chelating agents
Hydroxypyridinones, Hydroxypyridinonate complexes, Bifunctional ligand, 2609
Chelex 100
Natural metal complexes, Natural ligands, Resin titration, Ligand titration, 1343
Chelidamic acid
Manganese(II) complexes, 2-Pyrazine carboxylic acid, 2,6-Pyridinedicarboxylic acid, Crystal structures, Catalytic disproportionation, Hydrogen peroxide, 1063
Chemical and electrochemical synthesis
Trinuclear metal chelates, β-Aminovinylimines, 2081
Chemical bonding
Polyoxometalates, Transition metals, Molecular orbitals, Density–functional theory, 2201
Chemical bonding topology
Superconductors, Magnesium diboride, Cuprate superconductors, 2347
Chemical vapor deposition
Silver(I) complexes, Non-fluorinated β-diketonate ligands, Monothio-β-ketonate, β-Ketoiminate, Crystal structures, 1289
Chemosensors
Polyazaalkanes ligand, Fluorogenic receptors, 1397
CH–π interaction
Arene ruthenium, Absolute configuration, Crystal structures, 2D NMR, 1929
Chiral benzodiazepine ligands
Zinc complexes, Palladium complexes, Spectroscopy, X-ray structure analysis, Cytostatic and antiviral activity, 2567
Chiral complexes
Macrocycles, Lanthanide complexes, Crystal structures, NMR of paramagnetic compounds, 811
Chiral complexes
Vanadyl complexes, Schiff bases, EPR, X-ray structures, 2021
Chiral iminophosphine ligand
Palladium complexes, Platinum complexes, 1043
Chirality
Palladium, Nickel, Bidentate nitrogen ligands, Crystal structures, 27
Chiral recognition
Nickel(II), Amino acid, Coordination chemistry, Hydrogen bond, 817
Chloride ligands
Oxo ligands, Phenolates, Tungsten, 349
Chloridotellurate anions
Tellurium dichloride, X-ray crystallography, NMR spectroscopy, 1089
Chloro-bridged complexes
Cyclometallated palladium(II) compounds, *N*-(Benzylidene)xylylendiamines, 2063
$C_{10}H_{20}N_2S_4Zn\cdot C_5H_5N$
Isomorphism, Structures, ^{15}N CP/MAS NMR spectroscopy, 2727
Chromium
Crystal structures, Homogeneous catalyst, Electron spin resonance, Polyethylene, 867
Chromium(III) complexes
Trans influence, Crystal structures, Ligand-field strength, Tripodal tridentate phosphine, Acetylacetonate complexes, 835
Chromium
Pivalate, Mass spectrometry, Paramagnetic, NMR, X-ray photoelectron spectroscopy, 155
Circular dichroism
Carbohydrates, Cobalt complexes, Sucrose complexes, ^{1}H NMR, Semi-empirical calculations, 2215
cis-1,2-Bis(diphenylphosphino)ethene
Nickel, Thiolate, X-ray structures, 421
Cluster complexes
Molybdenum, Crystal structures, Acetates,

Reduction, 147
Cluster compounds
Polycations, Crystal structures, Bismuth, Iridium, Rhodium, 651
Cluster
Optical limiting properties, Crystal structures, 2675
Clusters
Crystal structures, Intermetallic compounds, Lead, Zintl phases, 641
Clusters
Ruthenium, Osmium, Acetylide, Alkyne, 1105
^{13}C NMR spectra
Dimethylthallium(III), Thiosemicarbazones, Crystal structures, IR spectra, ^{1}H, 1651
^{13}C NMR spectroscopy
Sulfur dicyanide $S_y(CN)_2$, Polythiocyanogens, Paracyanogen $(CN)_x$, 1825
Cobalt complexes
Carbohydrates, Circular dichroism, Sucrose complexes, ^{1}H NMR, Semi-empirical calculations, 2215
Cobalt complexes
Isopolyoxomolybdates, Heteropolyoxomolybdates, Hydrothermal synthesis, 1921
Cobalt(I) clusters
Crystal structures, Interstitial phosphorus atom, Heterocyclic phosphide, Semi-bridging carbonyl, Substituted site, 1073
Cobalt(II) complexes
Benzoate ligands, Di-2-pyridyl ketone complexes, End-on azide ligands, Magnetic properties, 2027
Cobalt(II)
Cubane complexes, Carbacylamidophosphates, X-ray data, 963
Cobalt(III) chelate
Lanthanide(III) chelate, Binuclear complexes, Inner-sphere coordination, Outer-sphere coordination, Stability constant, 805
Cobalt(III) complexes
Synthesis, 4-Methyl-2,6-dibenzoylphenol, NMR, TGA, Cyclic voltammetry, X-ray structures, 1787
Cobalt(III) complexes
Tetradentate ligands, Bidentate ligands, Eddp, 2277
Cobalt(III)
Pyrazolylthiosemicarbazone, ^{1}H NMR, X-ray crystallography, 779
Cobalt(III)
Thiosemicarbazone, X-ray crystal studies, ^{1}H NMR, IR, Electronic spectra, 2515
Cobalt(II)
One-dimensional structures, Zinc(II), Coordination complexes, 2705
Cobalt(II)
Schiff base complexes, Nickel(II), Zinc(II), Tetrahedral, Crystal structures, 2733
Cobalt
Phthalocyanine, Cyanide, Sulfur dioxide, Kinetics, Equilibria, 133
Cobalt
Phthalocyanines, Phthalonitrile derivatives, Electrochemistry, Nickel, Zinc, 255
Cocrystallization
Dinuclear platinum complexes, One-dimensional polymers, 715
Co(II), Cu(II) and Ni(II) complexes
Optically active Schiff bases, CD spectra, Co(II) paramagnetic ^{1}H NMR, 2711
Co(III) complexes
Pyrazole, Dithiocarbazate, Synthesis, Spectroscopy, X-ray crystal structures, 1
Co(II)
Ni(II), Tetramines, Adenosine 5′-monophosphate, Mixed-ligand complexes, 745
Co(II) paramagnetic ^{1}H NMR
Optically active Schiff bases, Co(II), Cu(II) and Ni(II) complexes, CD spectra, 2711
Complexes
Boron, Lithium, Imido, X-ray, 549
Complexes
Cerium, Fluoroalkoxides, Structures, MOCVD, Films, 1985
Complexes
Lanthanides(III), Oxygen donors, 2,2′-Oxydiethylamine, Dimethylsulfoxide, Thermodynamics, 1385
Complexes
N-[2-(4-Methoxyphenyltelluro)ethyl]benzamide, *N*-[2-(4-Methoxyphenyl telluro)-propyl]phthalimide, Palladium(II), Platinum(II), Ruthenium(II), Crystal structures, 667
Complexes
Silver(I), *N*-methylated polyamines, Dimethylsulfoxide, Thermodynamics, 1337
Complex-formation equilibria
Copper complexes, Nickel complexes, Lysyl–glycyl–histidyl–lysine, 1469
Complex history
Complex pioneers, Thermodynamics group, Coordination chemistry, 1313
Complex pioneers
Complex history, Thermodynamics group, Coordination chemistry, 1313
Cone angle
Dimesitylphosphine, Secondary phosphine, X-ray crystallography, NMR, Fluxional, 2409
Conformational change
Four or five coordinate geometry, Metal centre, Transition metals, 2175
Conformational change
Schiff's base ligands, Octahedral systems, Transition metals, 2167
Cooperativity effect
Statistical thermodynamic model, Site constant, Cooperativity potential, Polyamines, 1503
Cooperativity
Partition function, Equilibria in solution, Site affinity, Buffer capacity, Heat capacity, 1439
Cooperativity potential
Statistical thermodynamic model, Cooperativity effect, Site constant, Polyamines, 1503
Coordination bonding
Cyclophosphazene, Supramolecular polymer, Hairy-rod structure, Lamellar packing, 1573
Coordination chemistry
Complex history, Complex pioneers, Thermodynamics group, 1313
Coordination chemistry
Crystal structures, Piperazine, Homopiperazine, 1729
Coordination chemistry
Mono-helical, Single-helical-strand, Mono-bridged species, Transition metals, X-ray crystallography, 1177
Coordination chemistry
Nickel(II), Amino acid, Hydrogen bond, Chiral recognition, 817
Coordination chemistry
Titanium, Chelate, Structure elucidation, 8-Hydroxyquinolinate, 1081
Coordination complexes
One-dimensional structures, Zinc(II), Cobalt(II), 2705
Coordination compounds
Azamacrocycles, Aromatic pendant arms, Metallic polymer, 333
Coordination mode
Copper(I), Anions, Dppe, Solid state structures, 2433
Co-ordination number asymmetry
Crystal structures, Zinc(II) complexes, 1957
Coordination
Polyamine, Bithiophene, Cu(II)-electrochemical pattern, Potentiometry, 1523
Coordination polymer
Nickel, Malic acid, Malate, Asymmetric catalysis, Crystal structures, Electroplating, 787
Coordination polymers
Cadmium(II) complexes, Crystal structures, Symbiosis, 2293
Coordination polymers
Cyanometalate, Crystal structures, Cadmium(II) complexes, 721
Coordination polymers
Solventothermal synthesis, Crystal structures, Copper methoxide, Single crystals, 2017
Coordination structures
EPR spectroscopy, Rare earth complexes, 4f-Electron, 2127
Copper complexes
Crystal structures, Di-2-pyridylamine complexes, Tetrathionate complexes, Trifluoromethanesulfonate complexes, Sulfate complexes, Hexafluorophosphate complexes, 247
Copper complexes
Crystal structures, Lumazine complexes, Zinc complexes, 1961
Copper complexes
Crystal structures, Nitrate complexes, Di-2-pyridylamine complexes, 943
Copper complexes
Crystal structures, Tungsten complexes, Pyrazole, 1547
Copper complexes

Nickel complexes, Complex-formation equilibria, Lysyl–glycyl–histidyl–lysine, 1469
Copper complexes
Stereochemistry, X-ray structures, Steric properties, 1031
Copper complexes
Structures, Spectroscopic properties, Oxadiazole complexes, 2257
Copper
Cork, Solid state ^{13}C MAS and CP-MAS NMR, Nickel, Potentiometric titration, Metal uptake, 1363
Copper
Formato, Dinuclear complexes, Antiferromagnetic, EPR, 1057
Copper
Hinokitiol, X-ray, Adduct, 1761
Copper(I)
2-Anilinopyridine, Crystal structures, Antiferromagnetic dimers, Dinuclear acetates, 457
Copper(I)
Anions, Dppe, Coordination mode, Solid state structures, 2433
Copper(I) complexes
Autoxidation, Kinetic data, Catalytic activity, 181
Copper(I) complexes
Pyridine-2-thione, Tri-*p*-tolylphosphine, Triphenylphosphine, Sulfur-bridged dimer, 1603
Copper(II)
Alkoxo-bridged, Magnetism, Benzimidazoles, Crystal structures, 141
Copper(II)
CD spectroscopy, Nickel(II), Palladium(II), Peptides, Methionine, 2149
Copper(II) complex
Crystal structures, EDTA, Adeninium, Ion pair, Molecular recognition, 1451
Copper(II) complexes
Alkali metal ions, Doubly layered 2D sheet, 1273
Copper(II) complexes
Binucleating ligand, Nickel(II) complexes, Electrochemistry, Magnetic properties, 2767
Copper(II) complexes
Crystal structures, Cyclohexanediols, Separation of isomers, 1133
Copper(II) complexes
Crystal structures, Nitrite complexes, Sulfate complexes, di-2-Pyridylamine complexes, Thiocyanato complexes, 1279
Copper(II) complexes
Cyclodextrins, 2-Methylaminopyridine, 1531
Copper(II) complexes
Electron paramagnetic resonance (EPR) spectroscopy, Amino acids, *N*,*N*-dimethyl-L-α-isoleucine, 1643
Copper(II) complexes
Imidazole, 9,10-dihydro-9-oxo-10-acridineacetate, Crystal structures, Spectra, Magnetic measurements, 2381
Copper(II) complexes
Mixed-ligand complexes, 2,2′-Bipyridine complexes, Lactic acid, 2-Methyllactic acid, Mandelic acid, Crystal structures, 2811
Copper(II) complexes
Mixed-ligand complexes, Five-coordinate complexes, Aminohydroxamic acids, EPR spectra, Vis spectra, 295
Copper(II) complexes
Oxalato complexes, Oxalato-bridged complexes, Magnetic properties, Crystal structures, 1203
Copper(II) complexes
Spectral properties, Crystal structures, Pyridinecarboxylate complexes, Mononuclear complexes, 365
Copper(II) halides
Aminoguanidonium, Crystal structures, Tetrachlorocuprate(II), 409
Copper(II)
N-(2-Pyridylmethyl)iminodiacetic acid, *N*-(2-Pyridylmethyl)iminodiacetate(2-) ion, 2-(Aminomethyl)pyridine, α-Picolylamine, 2-(2′-Pyridyl)benzimidazole, Crystal structures, Mixed-ligand complexes, Aromatic π,π-staking interactions, Molecular recognition, Thermal stability, Spectral and magnetic properties, 1485
Copper(II) peptide complexes
α-Aminoisobutyryl-α-aminoisobutyric acid (H–Aib–Aib–OH), Spectroscopic characterization, X-ray crystal structures, 229
Copper(II)
Trinuclear complexes, Single crystal structures, Silver(I), Carboxylate, Thioether, 33
Copper methoxide
Solventothermal synthesis, Crystal structures, Coordination polymers, Single crystals, 2017
Copper
Nickel, Zinc, Cadmium, Saccharinate, X-ray structures, 395
Copper
Self-assembly, Supramolecules, X-ray structures, 1621
Cork
Solid state ^{13}C MAS and CP-MAS NMR, Copper, Nickel, Potentiometric titration, Metal uptake, 1363
CO
Synthesis, Mo/Fe/S cluster, Structures, $S{=}PEt_3$ ligand, 2523
Counter-cation
Uranyl, Dimethylmelonate, CPMAS ^{13}C NMR, X-ray crystallography, 69
CPMAS ^{13}C NMR
Uranyl, Dimethylmelonate, Counter-cation, X-ray crystallography, 69
CPMAS ^{13}C NMR
Uranyl, Malonato complexes, X-ray crystallography, 81
15-Crown-5
Potassium, Rubidium, Amide ligands, Crystal structures, 2451
Crown thioethers
Thioether complexes, Platinum complexes, Trithiacyclononane, Platinum nuclear magnetic resonance, Phosphine complexes, 879
Crystal and molecular structure
N-Benzoylthiourea derivatives, Gold, Palladium, Solvent extraction, Ion selective electrode, 1429
Crystal and molecular structures
Base hydrolysis kinetics, Equilibria, 2283
Crystal packing
Thallium(I) complexes, Scorpionate ligands, π-Stacking, Cation–π interaction, 553
Crystal structure
Nickel(0), Vinylcyclosilazane complexes, 1261
Crystal structure of Cd(II) complexes
Metal complexes, *S*-Benzyldithiocarbazate, Bioactivity of Schiff bases, Bioactivity of metal complexes, 2547
Crystal structure
Platinum, Hexamethyleneimine, 1,1-Cyclobutanedicarboxylato, Synthesis, 2659
Crystal structure
Platinum(II), Homopiperazines, Disubstituted sulfides, Synthesis, 125
Crystal structures
Alkali metal ions, Sodium ion, Caesium ion, Calix[4]arene, 2497
Crystal structures
Alkoxides, Lithium, Tungsten, Methoxide, 193
Crystal structures
Aluminium, Diols, Trinuclear complexes, 2,2′-Di(hydroxymethyl)biphenyl, Alkylaluminium diolates, 281
Crystal structures
Aminoguanidonium, Copper(II) halides, Tetrachlorocuprate(II), 409
Crystal structures
2-Anilinopyridine, Antiferromagnetic dimers, Dinuclear acetates, Copper(I), 457
Crystal structures
Arene ruthenium, Absolute configuration, CH–π interaction, 2D NMR, 1929
Crystal structures
Binuclear nickel(II) complexes, Magnetic properties, Terminal thiocyanato ion complexes, Terminal cyanato ion complexes, Pentadentate ligands, 2457
Crystal structures
Bis-sulfamide, Tantalum(V), Diamide, 1051
Crystal structures
Boron complexes, Benzohydroximate anion, Synthesis, 2351
Crystal structures
Cadmium(II) complexes, Coordination polymers, Symbiosis, 2293
Crystal structures
Chromium, Homogeneous catalyst, Electron spin resonance, Polyethylene, 867
Crystal structures
Clusters, Intermetallic compounds, Lead, Zintl phases, 641
Crystal structures
Cobalt(I) clusters, Interstitial phosphorus

atom, Heterocyclic phosphide, Semi-bridging carbonyl, Substituted site, 1073
Crystal structures
Coordination chemistry, Piperazine, Homopiperazine, 1729
Crystal structures
Copper complexes, Di-2-pyridylamine complexes, Tetrathionate complexes, Trifluoromethanesulfonate complexes, Sulfate complexes, Hexafluorophosphate complexes, 247
Crystal structures
Copper complexes, Lumazine complexes, Zinc complexes, 1961
Crystal structures
Copper complexes, Nitrate complexes, Di-2-pyridylamine complexes, 943
Crystal structures
Copper(II), Alkoxo-bridged, Magnetism, Benzimidazoles, 141
Crystal structures
Copper(II) complex, EDTA, Adeninium, Ion pair, Molecular recognition, 1451
Crystal structures
Copper(II) complexes, Cyclohexanediols, Separation of isomers, 1133
Crystal structures
Copper(II) complexes, Imidazole, 9,10-dihydro-9-oxo-10-acridineacetate, Spectra, Magnetic measurements, 2381
Crystal structures
Copper(II) complexes, Nitrite complexes, Sulfate complexes, di-2-Pyridylamine complexes, Thiocyanato complexes, 1279
Crystal structures
Copper(II) complexes, Oxalato complexes, Oxalato-bridged complexes, Magnetic properties, 1203
Crystal structures
Copper(II) complexes, Spectral properties, Pyridinecarboxylate complexes, Mononuclear complexes, 365
Crystal structures
Copper(II), *N*-(2-Pyridylmethyl)iminodiacetic acid, *N*-(2-Pyridylmethyl)iminodiacetate(2-) ion, 2-(Aminomethyl)pyridine, α-Picolylamine, 2-(2′-Pyridyl)benzimidazole, Mixed-ligand complexes, Aromatic π,π-staking interactions, Molecular recognition, Thermal stability, Spectral and magnetic properties, 1485
Crystal structures
Cyanometalate, Coordination polymers, Cadmium(II) complexes, 721
Crystal structures
Dibenzotetraaza[14]annulenes, Macrocyclic Ni(II) complexes, Succinyl dichloride, Solid state supramolecular complexes, 7
Crystal structures
Dimethylthallium(III), Thiosemicarbazones, IR spectra, ^{1}H, ^{13}C NMR spectra, 1651
Crystal structures
Diruthenium carboxylates, Urea and thiourea derivatives, Infrared spectroscopy, 1235
Crystal structures
Dithiocarbamates, Cu(II) complexes, Ethylenediamine, Mixed-ligands Cu(II) chelates, 1899
Crystal structures
Dithiocarbimates, Triphenylphosphine, Nickel complexes, 2243
Crystal structures
1,3-Dithiole-2-thione-4,5-dithiolates, 1,3-Dithiole-2-one-4,5-dithiolates, Antimony(III), 2107
Crystal structures
Dithiophosphate complexes, Dithiophosphonate complexes, Macrocycle complexes, Pentacoordinate nickel(II) complexes, 1935
Crystal structures
1D nickel(II) azido complexes, Pyridine derivative complexes, Preparation, Magnetic data, Spectra, 1871
Crystal structures
Hemidirected, Lead(II) complexes, Thiocyanate ligands, 1223
Crystal structures
Idp-type ligand, *N*,*N*-Di(2-carboxyethyl)-*p*-toluidine, *p*-Toluidine-*N*,*N*-di-3-propionic acid, Square pyramidal copper(II) complexes, 2719
Crystal structures
Imidato complexes, Cyclometallated palladium(II) complexes, 1589
Crystal structures
Imidazole-4-acetic acid, Polymeric zinc(II) complexes, Vibrational spectra, Density functional calculations, 2819
Crystal structures
Iron(II) complexes, Hydrogen-bonded network, Hydrogen maleate, 1189
Crystal structures
Isotope effect, Hydrogen bond, Dimer, NQR, Tetrachloroaurate(III), 2207
Crystal structures
Lanthanide contraction, Anion controlled assembly, Magnetic properties, 1097
Crystal structures
Macrocycles, Germanium(IV) tmtaa complexes, Six-coordinate geometry, *Trans*-positions, 969
Crystal structures
Macrocycles, Lanthanide complexes, Chiral complexes, NMR of paramagnetic compounds, 811
Crystal structures
Magnesium, Niobium, Alkoxides, Oxoalkoxides, Mass-spectra, 1629
Crystal structures
Magnesium phthalocyanines, Magnesium complexes, IR spectroscopy, Raman spectroscopy, UV–Vis spectroscopy, 265
Crystal structures
Magnetic properties, Thermal properties, Tetrabromocuprate(II), *n*-Ethylpyridinium, 19
Crystal structures
Manganese(II) complexes, 2-Pyrazine carboxylic acid, 2,6-Pyridinedicarboxylic acid, Chelidamic acid, Catalytic disproportionation, Hydrogen peroxide, 1063
Crystal structures
Mercury(II) halides, Phosphine complexes, 1845
Crystal structures
Metal-organic frameworks (MOF), Synthesis, TGA–DTA, 175
Crystal structures
Mixed-ligand complexes, Copper(II) complexes, 2,2′-Bipyridine complexes, Lactic acid, 2-Methyllactic acid, Mandelic acid, 2811
Crystal structures
Molybdenum, Cluster complexes, Acetates, Reduction, 147
Crystal structures
Molybdenum, Tin, Metathesis, Polymerisation, Norbornadiene, NMR spectra, 2505
Crystal structures
Mononuclear complexes, Rhodium complexes, Hydrido complexes, Nitrogen ligands, 1613
Crystal structures
Mononuclear complexes, Triazole derivatives, 797
Crystal structures
Nickel complexes, Palladium complexes, 2071
Crystal structures
Nickel(II) chromate and dichromate complexes of phenanthroline, Monodentate coordination of CrO_4^{2-}, IR and UV–Vis–NIR band analysis, 997
Crystal structures
Nickel(II) complexes, Hexaazamacrocycle, Organic ligands, Chain complex, 1913
Crystal structures
Nickel, Malic acid, Malate, Coordination polymer, Asymmetric catalysis, Electroplating, 787
Crystal structures
Nickel, Palladium, Platinum, Oxalate, Magnetic properties, DFT calculations, 2631
Crystal structures
Nitrogenase, Hydrazido(2-), Molybdenum, Spectroelectrochemistry, 849
Crystal structures
N-[2-(4-Methoxyphenyltelluro)ethyl]benzamide, *N*-[2-(4-Methoxyphenyl telluro)propyl]phthalimide, Palladium(II), Platinum(II), Ruthenium(II), Complexes, 667
Crystal structures of Zn(II) complexes
S-methyldithiocarbazate (SMDTC), NS Schiff base, Cu(II), Ni(II), Zn(II) complexes, 2683
Crystal structures
Optical limiting properties, Cluster, 2675
Crystal structures
Organotin, Halides, *N*-Thiocyanate, Azide, Acetate, 1667
Crystal structures
Organotin(IV) complexes, Dimethylpyrimidinethione, 1149
Crystal structures
Palladium(II) complexes, Benzyl 8-quino-

lyl sulfide, Phenethyl 8-quinolyl, 843
Crystal structures
Palladium, Nickel, Chirality, Bidentate nitrogen ligands, 27
Crystal structures
Physico-chemical properties, Spectroscopy, X-ray diffraction, Imidiazole complexes, 1857
Crystal structures
3-Piperidine, Thiosemicarbazone, 2-Pyridineformamide, Nickel(II), Spectra, 859
Crystal structures
Platinum, Cyclometallation, Imine, Fluorine, Phosphine, 105
Crystal structures
Platinum(II) complexes, Heptamethyleneimine, Synthesis, 2369
Crystal structures
Polycations, Cluster compounds, Bismuth, Iridium, Rhodium, 651
Crystal structures
Polydentate Ni(II) edta-type complexes, 2667
Crystal structures
Potassium, Rubidium, Amide ligands, 15-Crown-5, 2451
Crystal structures
Pyrazineformamide, Thiosemicarbazone, Zinc, Cadmium, Electrochemical synthesis, 1553
Crystal structures
2-Pyridineformamide, Thiosemicarbazone, Nickel(II), Zinc(II), Cadmium(II), 729
Crystal structures
Rhenium(III) complexes, Iridium(III) complexes, S-bridged polynuclear complexes, UV–Vis absorption spectra, Cyclic voltammetry, 1809
Crystal structures
Ruthenium monoterpyridine complexes, Ancillary functions, 2033
Crystal structures
Schiff base complexes, Cobalt(II), Nickel(II), Zinc(II), Tetrahedral, 2733
Crystal structures
Schiff base ligands, Cadmium(II) complexes, Dithiocarbazate Schiff base crystal structures, Metal complexes, Bioactivity, 2691
Crystal structures
Silver(I) complexes, Non-fluorinated β-diketonate ligands, Monothio-β-ketonate, β-Ketoiminate, Chemical vapor deposition, 1289
Crystal structures
Solventothermal synthesis, Coordination polymers, Copper methoxide, Single crystals, 2017
Crystal structures
Synthesis, X-ray diffraction, 1883
Crystal structures
Ternary complexes, Kinetic studies, 2045
Crystal structures
Tetranuclear copper(II) complexes, Magnetism, Antiferromagnetic coupling, Molecular orbital calculation, 1539
Crystal structures
Thermochromism, Benzimidazolium, Tetrachlorocuprate, 2561
Crystal structures
Thiadiazole, M = Co, M = Ni, M = Cu, Monomeric complexes, 403
Crystal structures
Trans influence, Ligand-field strength, Tripodal tridentate phosphine, Acetylacetonate complexes, Chromium(III) complexes, 835
Crystal structures
Trinuclear complexes, Cyano-bridge, Spectroscopic study, 2237
Crystal structures
Tungsten complexes, Pyrazole, Copper complexes, 1547
Crystal structures
Tungsten, Tin, Oxidative addition, Hydride, NMR, 1817
Crystal structures
Uranyl ion, Calixarenes, Homooxacalixarenes, Supramolecular assembly, 1125
Crystal structures
Uranyl ion, Polyphenols, Oligophenols, 1949
Crystal structures
Zinc(II) complexes, Co-ordination number asymmetry, 1957
Crystal structures
Zn(II)–N bonds, Zn(II) complexes, Piperazine and piperazin-1-ium ligands, 2161
Crystal structure
Thallium(I) complexes, Nitrophenoxide complexes, 2555
Cubane complexes
Cobalt(II), Carbacylamidophosphates, X-ray data, 963
Cu(I)
Bis(phosphine) monoxides, Chelates, NMR, Electrochemistry, Hard–soft acids and bases, 2793
Cu(II) complexes
Dithiocarbamates, Ethylenediamine, Mixed-ligands Cu(II) chelates, Crystal structures, 1899
Cu(II) complexes
Ternary complexes, Peptide–Cu(II)–isocytosine complexes, Isocytosine complexes, 1197
Cu(II)-electrochemical pattern
Polyamine, Bithiophene, Coordination, Potentiometry, 1523
Cu(II), Ni(II), Zn(II) complexes
S-methyldithiocarbazate (SMDTC), NS Schiff base, Crystal structures of Zn(II) complexes, 2683
Cu(II) stereochemistry
X-ray structures, Magnetism, EPR spectra, 2473
Cuprate superconductors
Chemical bonding topology, Superconductors, Magnesium diboride, 2347
Cyanide
Cobalt, Phthalocyanine, Sulfur dioxide, Kinetics, Equilibria, 133
Cyano-bridge
Trinuclear complexes, Crystal structures, Spectroscopic study, 2237
Cyanometalate
Coordination polymers, Crystal structures, Cadmium(II) complexes, 721
Cyano
Rhodium, Dioxygen, Enhanced reactivity, Structures, 1775
Cyano(selenone)gold(I) complexes
Synthesis, ^{13}C and ^{15}N NMR spectroscopy, 2099
Cyclic voltammetry
Carboranes, Carba metallaboranes, Dicarbollides, Liquid–liquid extraction, Lanthanide and actinide extaction, 975
Cyclic voltammetry
2-(3,5-Dimethylpyrazol-1-ylmethyl)pyridine, Bis-ligand and anion-bound copper(II) complexes, X-ray structure, Absorption and EPR spectra, 1245
Cyclic voltammetry
Five-coordinated chlorocopper(II) complexes, 1,10-Phenanthroline and its 5,6-disubstituted derivatives, X-ray structures, Electronic absorption and diffuse reflectance spectra, 2143
Cyclic voltammetry
Iron complexes, Aminohydroxamate complexes, Electrochemical reduction, EC mechanism, 1661
Cyclic voltammetry
Photoinduced electron transfer, Supramolecular pre-association, Ruthenium(II) complexes, 2,2′:6′,2″-Terpyridine, 4′-*p*-Tolyl-2,2′:6′,2″-terpyridine-4-carboxylic acid, 49
Cyclic voltammetry
Rhenium(III) complexes, Iridium(III) complexes, S-bridged polynuclear complexes, Crystal structures, UV–Vis absorption spectra, 1809
Cyclic voltammetry
Salen Cu(II) complexes, Schiff-base ligands, Hammett substituent constants, 55
Cyclic voltammetry
Synthesis, Cobalt(III) complexes, 4-Methyl-2,6-dibenzoylphenol, NMR, TGA, X-ray structures, 1787
Cyclisation
P-Ligands, 2*H*-Azaphosphirene complexes, 2*H*-1,2-Azaphosphole complexes, 1,3-Dipoles, 119
Cycloaddition
Iminophosphorane, Four-membered ring compounds, Thermolysis, Aza-Wittig reaction, X-ray analysis, 657
Cyclo-addition
Metallacycles, oxo ligands, P ligands, Palladium, Structure elucidation, 2653
1,1-Cyclobutanedicarboxylato
Platinum, Hexamethyleneimine, Synthesis, Crystal structure, 2659
Cyclodextrins
Copper(II) complexes, 2-Methylaminopyridine, 1531
Cyclohexanediols
Crystal structures, Copper(II) complexes,

Separation of isomers, 1133
Cyclometalation
Amido, Amine, Triflate, Platinum, Diphosphazane, 1305
Cyclometallated paladium(II) complexes
Imidato complexes, Crystal structures, 1589
Cyclometallated palladium(II) compounds
N-(Benzylidene)xylylendiamines, Chloro-bridged complexes, 2063
Cyclometallation
C–H activation, Phosphorus ligands, Schiff bases, Palladium, 39
Cyclometallation
Platinum, Imine, Fluorine, Phosphine, Crystal structures, 105
1,5-Cyclooctadiene
Oxidative addition reaction, Perfluoro-*n*-butyl iodide, Fluoroalkyls, 2357
Cyclopentadienyl iron complexes
Organometallic phosphine, Multimetallic, π-Allyl molybdenum, Iron carbonyl complexes, 2301
Cyclophosphazene
Dendrimers, Metal–nitrile complexes, 909
Cyclophosphazenes
Polyphosphazenes, Phenolic phosphine, Macromolecular complexes, Carbonyls, Spectroscopic characterization, 2579
Cyclophosphazene
Supramolecular polymer, Coordination bonding, Hairy-rod structure, Lamellar packing, 1573
Cysteamine
Cysteine, Sulfur, Hydrogen bonding, 225
Cysteine
Cysteamine, Sulfur, Hydrogen bonding, 225
Cysteine ligand
Solvation parameter model, Partition coefficient, Hydrophobic moment, Iron–sulfur protein, Mixed-valence non-integer oxidation number, 1357
Cytostatic and antiviral activity
Chiral benzodiazepine ligands, Zinc complexes, Palladium complexes, Spectroscopy, X-ray structure analysis, 2567
Cytotoxicity
Rhenium(I), Carbonyl, Aminoalcohol, Oxidative-alkoxylation, Hydrogen-bonding, 1991

Dca ligand
Cadmium complexes, Double end-to-end, Zigzag chain, π–π interaction, 893
dcbpy
Ru(II) complexes, bdmpp, Thiocyanato ligands, Sensitizing ability, 2773
Dendrimers
Cyclophosphazene, Metal–nitrile complexes, 909
Density functional calculations
Imidazole-4-acetic acid, Polymeric zinc(II) complexes, Crystal structures, Vibrational spectra, 2819
Density functional theory
Face-shared dimers, Metal–metal bonding, High spin/low spin crossover, Electron delocalization, Broken-symmetry, Antiferromagnetic coupling, 1969
Density–functional theory
Polyoxometalates, Transition metals, Chemical bonding, Molecular orbitals, 2201
Desulfurization
Triosmium cluster, Tetramethylthiourea, Sulfido, X-ray structures, 381
DFT calculations
Dinuclear transition metal complexes, Electron transfer, Magnetic coupling, Metal–metal bonding, Spin polarization, 1163
DFT calculations
Ferrocenyl Schiff bases, Isomerism, 2361
DFT calculations
Isoquercitrin, Al(III) complexes, Stoichiometry, UV–Vis Spectroscopy, FT Raman, 2801
DFT calculations
Nickel, Palladium, Platinum, Oxalate, Crystal structures, Magnetic properties, 2631
2,6-Diacetylpyridine
Lanthanide(III) complexes, Macrocyclic ligands, 3-Substituted-1,2-diaminopropanes, 425
Dialkyldithiophosphates
Gallium, Indium, Dithiocarbamates, ^{71}Ga NMR, Structures, 239
Diamide
Bis-sulfamide, Tantalum(V), Crystal structures, 1051
Diarylchlorogermanes
Halogermylenes, Donor side-chain, Intramolecular coordination, 2827
1,4-Diaza-1,3-diene
Niobium complexes, Heterodiene, X-ray crystal structures, 305
1,5-Diaza-3,7-diphosphacyclooctane
Ferrocenylmethylphosphine, Phosphino amino acids, 1,3-Diaza-5-phosphacyclohexane, Water-soluble complexes, Trinuclear complexes, 2251
1,3-Diaza-5-phosphacyclohexane
Ferrocenylmethylphosphine, Phosphino amino acids, 1,5-Diaza-3,7-diphosphacyclooctane, Water-soluble complexes, Trinuclear complexes, 2251
Dibenzotetraaza[14]annulenes
Macrocyclic Ni(II) complexes, Succinyl dichloride, Crystal structures, Solid state supramolecular complexes, 7
Dibenzoylmethane
Europium complexes, X-ray crystallography, Luminescence property, 2-(4′-Dimethylaminophenyl)imidazo[4,5-f]1,10-phenanthroline, 3-Ethyl-2-(4′-dimethylaminophenyl)imidazo[4,5-f]1,10-phenanthroline, 313
Dibenzylamine
Trialkylaluminum, Aminoalane, NMR, Mass spectrometry, Molecular structure, 1747
Dicarbollides
Carboranes, Carba metallaboranes, Cyclic voltammetry, Liquid–liquid extraction, Lanthanide and actinide extaction, 975
Diethylene triamine
Hg(II) complexes, Dimer, X-ray crystal structures, 2195
Digermene
Germylene, X-ray crystallographic analysis, Dissociation, Equilibrium, Bond dissociation energy, Dioxadigermetane, Terminal tungsten complexes, 563
2,2′-Di(hydroxymethyl)biphenyl
Aluminium, Diols, Trinuclear complexes, Crystal structures, Alkylaluminium diolates, 281
Diimine
Molybdenum complexes, oxo-Hydrazido complexes, Methyl-molybdenum complexes, Phenyl-molybdenum complexes, X-ray structures, 2531
1,2-Diimine
Ruthenium promoted reactions, Dimerization of aromatic amines, Structures, Redox, 97
β-Diketiminate
Low valent indium, Bulky ligands, Metal–metal bonds, 525
Dimanganese decacarbonyl
Diphosphine disulfide, Phosphido, Phosphidosulfide, 791
Dimer
Hg(II) complexes, Diethylene triamine, X-ray crystal structures, 2195
Dimer
Isotope effect, Hydrogen bond, Crystal structures, NQR, Tetrachloroaurate(III), 2207
Dimerization of aromatic amines
Ruthenium promoted reactions, 1,2-Diimine, Structures, Redox, 97
Dimesitylphosphine
Secondary phosphine, X-ray crystallography, NMR, Cone angle, Fluxional, 2409
2-(4′-Dimethylaminophenyl)imidazo[4,5-f]1,10-phenanthroline
Europium complexes, X-ray crystallography, Luminescence property, Dibenzoylmethane, 3-Ethyl-2-(4′-dimethylaminophenyl)imidazo[4,5-f]1,10-phenanthroline, 313
Dimethylmelonate
Uranyl, Counter-cation, CPMAS ^{13}C NMR, X-ray crystallography, 69
2-(3,5-Dimethylpyrazol-1-ylmethyl)pyridine
Bis-ligand and anion-bound copper(II) complexes, X-ray structure, Absorption and EPR spectra, Cyclic voltammetry, 1245
Dimethylpyrimidinethione
Organotin(IV) complexes, Crystal structures, 1149
Dimethylsulfoxide
Lanthanides(III), Oxygen donors, 2,2′-Oxydiethylamine, Complexes, Thermodynamics, 1385
Dimethylsulfoxide
Silver(I), *N*-methylated polyamines, Complexes, Thermodynamics, 1337

Dimethylthallium(III)
Thiosemicarbazones, Crystal structures, IR spectra, ^{1}H, ^{13}C NMR spectra, 1651
Di-*n*-butylhydroxytin(IV)
Tin enolates, Diorganohydroxytin, Diorganotin, Sn(IV) complexes, Malonates, 417
Dinuclear acetates
2-Anilinopyridine, Crystal structures, Antiferromagnetic dimers, Copper(I), 457
Dinuclear complexes
Copper, Formato, Antiferromagnetic, EPR, 1057
Dinuclear
Guanidinate, 1,3,4,6,7,8-Hexahydro-2*H*-pyramido[1,2-*a*]pyramidinate, Tin, Mononuclear, 619
Dinuclear platinum complexes
Cocrystallization, One-dimensional polymers, 715
Dinuclear transition metal complexes
DFT calculations, Electron transfer, Magnetic coupling, Metal–metal bonding, Spin polarization, 1163
Diols
Aluminium, Trinuclear complexes, 2,2′-Di(hydroxymethyl)biphenyl, Crystal structures, Alkylaluminium diolates, 281
Diop
Nitrosyl complexes, Ruthenium(II), NMR spectra, X-ray structures, Dppb, 2221
Diorganohydroxytin
Tin enolates, Diorganotin, Sn(IV) complexes, Malonates, Di-*n*-butylhydroxytin(IV), 417
Diorganotin
Tin enolates, Diorganohydroxytin, Sn(IV) complexes, Malonates, Di-*n*-butylhydroxytin(IV), 417
Dioxadigermetane
Digermene, Germylene, X-ray crystallographic analysis, Dissociation, Equilibrium, Bond dissociation energy, Terminal tungsten complexes, 563
Dioxadithiadiazamacrobicycle
Nickel(II) complexes, Heterotrinuclear complexes, BF_2^+-capped complexes, Template effect, *vic*-Dioxime, 1865
Dioxomolybdenum(VI) bromides
Oxotransfer catalysts, Thiol oxidation, 1635
Dioxomolybdenum(VI) complexes
Thiocarbodihydrazone Schiff base, X-ray structures, 1023
Dioxouranium(VI) polyhalides
Actinides, Uranyl polyhalides, Polybromides, Polyiodides, 2755
Dioxygen reactivity
Iron(II), Zinc(II), Schiff base, X-ray crystal structures, ^{1}H NMR spectroscopy, 705
Dioxygen
Rhodium, Cyano, Enhanced reactivity, Structures, 1775
Diperoxovanadate
Vanadyl, EDTA inhibition, EDTA bridged heteroligand peroxovanadates, Catalase resistance, Oxo-bridged peroxovanadates containing sulphate, 389
3,5-diphenylpyrazole
Gallium pyrazole complexes, Tetrachlorogallate salt, Gallium trichloride, 1117
Diphosphazane
Amido, Amine, Triflate, Platinum, Cyclometalation, 1305
Diphosphine disulfide
Dimanganese decacarbonyl, Phosphido, Phosphidosulfide, 791
Diphosphine ligands
$Ph_2P(CH_2)_nNHP^iPr_2$, Chelate complexes, 2639
Diplumbenes
Stannylenes, Plumbylenes, Distannenes, Lewis-amphoteric behavior, 587
1,3-Dipoles
P-Ligands, 2*H*-Azaphosphirene complexes, 2*H*-1,2-Azaphosphole complexes, Cyclisation, 119
Dipyridine
Macrocycles, Cadmium, Polyamines, Phenanthroline, 1329
Di-2-pyridylamine complexes
Crystal structures, Copper complexes, Tetrathionate complexes, Trifluoromethanesulfonate complexes, Sulfate complexes, Hexafluorophosphate complexes, 247
di-2-Pyridylamine complexes
Crystal structures, Copper(II) complexes, Nitrite complexes, Sulfate complexes, Thiocyanato complexes, 1279
Di-2-pyridyl ketone benzoylhydrazone
Nickel(II) complexes, Spectroscopy, Thermal analyses, 2375
Di-2-pyridyl ketone complexes
Benzoate ligands, Cobalt(II) complexes, End-on azide ligands, Magnetic properties, 2027
Diruthenium carboxylates
Urea and thiourea derivatives, Crystal structures, Infrared spectroscopy, 1235
Disilenes
Silenes, Silanones, Matrix isolation, Photolysis, 467
Dissociation
Digermene, Germylene, X-ray crystallographic analysis, Equilibrium, Bond dissociation energy, Dioxadigermetane, Terminal tungsten complexes, 563
Distannenes
Stannylenes, Plumbylenes, Diplumbenes, Lewis-amphoteric behavior, 587
Disubstituted sulfides
Platinum(II), Homopiperazines, Synthesis, Crystal structure, 125
Dithiocarbamates
Cu(II) complexes, Ethylenediamine, Mixed-ligands Cu(II) chelates, Crystal structures, 1899
Dithiocarbamates
Gallium, Indium, Dialkyldithiophosphates, ^{71}Ga NMR, Structures, 239
Dithiocarbazate
Co(III) complexes, Pyrazole, Synthesis, Spectroscopy, X-ray crystal structures, 1
Dithiocarbazate Schiff base crystal structures
Schiff base ligands, Cadmium(II) complexes, Crystal structures, Metal complexes, Bioactivity, 2691
Dithiocarbimates
Triphenylphosphine, Nickel complexes, Crystal structures, 2243
1,3-Dithiole-2-one-4,5-dithiolates
1,3-Dithiole-2-thione-4,5-dithiolates, Antimony(III), Crystal structures, 2107
1,3-Dithiole-2-thione-4,5-dithiolates
1,3-Dithiole-2-one-4,5-dithiolates, Antimony(III), Crystal structures, 2107
Dithiophosphate complexes
Dithiophosphonate complexes, Macrocycle complexes, Pentacoordinate nickel(II) complexes, Crystal structures, 1935
Dithiophosphonate complexes
Dithiophosphate complexes, Macrocycle complexes, Pentacoordinate nickel(II) complexes, Crystal structures, 1935
1D nickel(II) azido complexes
Pyridine derivative complexes, Preparation, Crystal structures, Magnetic data, Spectra, 1871
2D NMR
Arene ruthenium, Absolute configuration, Crystal structures, CH–π interaction, 1929
Donor side-chain
Halogermylenes, Intramolecular coordination, Diarylchlorogermanes, 2827
Double end-to-end
Cadmium complexes, Dca ligand, Zigzag chain, π–π interaction, 893
Doubly layered 2D sheet
Alkali metal ions, Copper(II) complexes, 1273
Dppb
Nitrosyl complexes, Ruthenium(II), NMR spectra, X-ray structures, Diop, 2221
Dppe
Copper(I), Anions, Coordination mode, Solid state structures, 2433
DTA
Pentacyaninotrosylferrate(2−) ion, Metastable excited states, X-ray diffraction, FIRRS, TGA, 1767

EC mechanism
Iron complexes, Aminohydroxamate complexes, Electrochemical reduction, Cyclic voltammetry, 1661
Eddp
Cobalt(III) complexes, Tetradentate ligands, Bidentate ligands, 2277
EDTA bridged heteroligand peroxovanadates
Diperoxovanadate, Vanadyl, EDTA inhibition, Catalase resistance, Oxo-bridged peroxovanadates containing sulphate, 389
EDTA
Copper(II) complex, Crystal structures, Adeninium, Ion pair, Molecular recognition, 1451
Edta-derived macrocycles
Macrocyclic ether bis(lactones), Stability constants, EPR of Cu(II) complexes, EPR of dinuclear Cu–Cu complexes, Hydro-

lysis of macrocycles, 2265
EDTA inhibition
Diperoxovanadate, Vanadyl, EDTA bridged heteroligand peroxovanadates, Catalase resistance, Oxo-bridged peroxovanadates containing sulphate, 389
Eight-coordinate
Schiff base, Zirconium complexes, X-ray crystal structure, Synthon, Heteroleptic, 211
Electrocatalysis
Synthesis and electrochemistry, Asymmetric 14-π nickel(II) tetraazaannulene, Hammett plot, 917
Electrochemical reduction
Iron complexes, Aminohydroxamate complexes, Cyclic voltammetry, EC mechanism, 1661
Electrochemical synthesis
Pyrazineformamide, Thiosemicarbazone, Zinc, Cadmium, Crystal structures, 1553
Electrochemistry
Binucleating ligand, Copper(II) complexes, Nickel(II) complexes, Magnetic properties, 2767
Electrochemistry
Bis(phosphine) monoxides, Cu(I), Chelates, NMR, Hard–soft acids and bases, 2793
Electrochemistry
2-Mercaptobenzoxazole, Pentacyanoferrate, Kinetics, Equilibrium constants, 2137
Electrochemistry
Phthalocyanines, Phthalonitrile derivatives, Nickel, Zinc, Cobalt, 255
Electrochemistry
Tertiary amines, Ruthenium complexes, Photochemistry, 61
Electron counts
Aluminum, Metalloid clusters, 503
Electron delocalization
Density functional theory, Face-shared dimers, Metal–metal bonding, High spin/low spin crossover, Broken-symmetry, Antiferromagnetic coupling, 1969
Electronic absorption and diffuse reflectance spectra
Five-coordinated chlorocopper(II) complexes, 1,10-Phenanthroline and its 5,6-disubstituted derivatives, X-ray structures, Cyclic voltammetry, 2143
Electronic spectra
Cobalt(III), Thiosemicarbazone, X-ray crystal studies, ^{1}H NMR, IR, 2515
Electronic states
Linear disilaketenylidene (SiSiO), Renner effect, Analogous multiple bonded systems, 599
Electronic structures
Rhenium, Nitrosyl, X-ray structures, Nitric oxide, 2617
Electron paramagnetic resonance (EPR) spectroscopy
Copper(II) complexes, Amino acids, *N*,*N*-dimethyl-L-α-isoleucine, 1643
Electron spin resonance
Chromium, Crystal structures, Homogeneous catalyst, Polyethylene, 867
Electron transfer
DFT calculations, Dinuclear transition metal complexes, Magnetic coupling, Metal–metal bonding, Spin polarization, 1163
Electron transfer
Mixed-valence compound, Iron, Trinuclear, Iodoacetate, Heat capacity, 1299
Electron transfer
Ruthenium-ammine, Benzotriazole, Polynuclear complexes, Mixed-valence, Molecular wires, 2089
Electroplating
Nickel, Malic acid, Malate, Coordination polymer, Asymmetric catalysis, Crystal structures, 787
Elemental analyses
Tris(pentamethylphenyl)gallium, Pentamethylphenylmagnesium bromide, Single crystal X-ray diffraction, 531
Emprirical correlations
Zinc adducts, Calorimetry, Infrared spectroscopy, 1677
End-on azide ligands
Benzoate ligands, Cobalt(II) complexes, Di-2-pyridyl ketone complexes, Magnetic properties, 2027
Enhanced reactivity
Rhodium, Cyano, Dioxygen, Structures, 1775
Epoxide
Silica gel, Immobilization, Propane-1,3-diamine, 2647
EPR
Copper, Formato, Dinuclear complexes, Antiferromagnetic, 1057
EPR of Cu(II) complexes
Edta-derived macrocycles, Macrocyclic ether bis(lactones), Stability constants, EPR of dinuclear Cu–Cu complexes, Hydrolysis of macrocycles, 2265
EPR of dinuclear Cu–Cu complexes
Edta-derived macrocycles, Macrocyclic ether bis(lactones), Stability constants, EPR of Cu(II) complexes, Hydrolysis of macrocycles, 2265
EPR
Salen ligands, Ni(I) complexes, Nickel(II) complexes, 1695
EPR spectra
Copper(II) complexes, Mixed-ligand complexes, Five-coordinate complexes, Aminohydroxamic acids, Vis spectra, 295
EPR spectra
Cu(II) stereochemistry, X-ray structures, Magnetism, 2473
EPR spectroscopy
Rare earth complexes, Coordination structures, 4f-Electron, 2127
EPR
Vanadyl complexes, Schiff bases, Chiral complexes, X-ray structures, 2021
Equilibria
Base hydrolysis kinetics, Crystal and molecular structures, 2283
Equilibria
Cobalt, Phthalocyanine, Cyanide, Sulfur dioxide, Kinetics, 133
Equilibria in solution
Partition function, Cooperativity, Site affinity, Buffer capacity, Heat capacity, 1439
Equilibria
Solutions, Cations, Hydrolysis, Titration, Masking, 1369
Equilibria
Synthesis, Binuclear complexes, Polyamines, 1351
Equilibrium constant
Adduct formation, Thermodynamics, Tin compounds, Porphyrins, Spectral method, 683
Equilibrium constants
2-Mercaptobenzoxazole, Pentacyanoferrate, Kinetics, Electrochemistry, 2137
Equilibrium
Digermene, Germylene, X-ray crystallographic analysis, Dissociation, Bond dissociation energy, Dioxadigermetane, Terminal tungsten complexes, 563
Esterification
Metal alkoxides, Single-crystal X-ray, Group V, Tantalum, Niobium, 2333
3-Ethyl-2-(4′-dimethylaminophenyl)imidazo[4,5-f]1,10-phenanthroline
Europium complexes, X-ray crystallography, Luminescence property, Dibenzoylmethane, 2-(4′-Dimethylaminophenyl)-imidazo[4,5-f]1,10-phenanthroline, 313
Ethylenediamine
Dithiocarbamates, Cu(II) complexes, Mixed-ligands Cu(II) chelates, Crystal structures, 1899
Europium complexes
X-ray crystallography, Luminescence property, Dibenzoylmethane, 2-(4′-Dimethylaminophenyl)imidazo[4,5-f]1,10-phenanthroline, 3-Ethyl-2-(4′-dimethylaminophenyl)imidazo[4,5-f]1,10-phenanthroline, 313
Europium
Photoluminescence, Perchlorate, Methylpyridylacetamide, Intensity parameters, 1837
Experimental design
Artificial neural networks, Stability constants, Metal complexes, Ion selective electrodes, Metal–ligand equilibria, 1375

Face-shared dimers
Density functional theory, Metal–metal bonding, High spin/low spin crossover, Electron delocalization, Broken-symmetry, Antiferromagnetic coupling, 1969
4f-Electron
EPR spectroscopy, Rare earth complexes, Coordination structures, 2127
Ferrocenylmethylphosphine
Phosphino amino acids, 1,3-Diaza-5-phosphacyclohexane, 1,5-Diaza-3,7-diphosphacyclooctane, Water-soluble complexes, Trinuclear complexes, 2251
Ferrocenyl Schiff bases

Isomerism, DFT calculations, 2361
Films
Cerium, Fluoroalkoxides, Structures, Complexes, MOCVD, 1985
FIRRS
Pentacyaninotrosylferrate(2−) ion, Metastable excited states, X-ray diffraction, TGA, DTA, 1767
Five-coordinate complexes
Copper(II) complexes, Mixed-ligand complexes, Aminohydroxamic acids, EPR spectra, Vis spectra, 295
Five-coordinated chlorocopper(II) complexes
1,10-Phenanthroline and its 5,6-disubstituted derivatives, X-ray structures, Electronic absorption and diffuse reflectance spectra, Cyclic voltammetry, 2143
Fluorescence quenching
Zinc(II)tetrasulfophthalocyanine, Sulfur dioxide, Association constants, 951
Fluorine
Platinum, Cyclometallation, Imine, Phosphine, Crystal structures, 105
Fluoroalkoxides
Cerium, Structures, Complexes, MOCVD, Films, 1985
Fluoroalkyls
Oxidative addition reaction, Perfluoro-*n*-butyl iodide, 1,5-Cyclooctadiene, 2357
Fluorogenic receptors
Polyazaalkanes ligand, Chemosensors, 1397
Fluxional
Dimesitylphosphine, Secondary phosphine, X-ray crystallography, NMR, Cone angle, 2409
Force constant
Cd(II) and Hg(II) complexes, Spectroscopic properties, Normal coordinate, 2-Phenylenediamine, 2-Aminophenol, 987
Formation constants
Mercapto-carboxylic acid, Potentiometry, IR, Ionisation constants, 1319
Formato
Copper, Dinuclear complexes, Antiferromagnetic, EPR, 1057
Four-membered ring compounds
Iminophosphorane, Cycloaddition, Thermolysis, Aza-Wittig reaction, X-ray analysis, 657
Four or five coordinate geometry
Conformational change, Metal centre, Transition metals, 2175
FT Raman
Isoquercitrin, Al(III) complexes, Stoichiometry, UV–Vis Spectroscopy, DFT calculations, 2801

Gallium
Aryloxide, Hydrogen bonding, Hydrolysis, 1877
Gallium–gallium bonds
Macrocycles, Supramolecular chemistry, 511
Gallium(II)
Subvalent indium and gallium, Indium(I), Indium(II), Halide complexes, Raman spectra, 519
Gallium
Indium, Dithiocarbamates, Dialkyldithiophosphates, ^{71}Ga NMR, Structures, 239
Gallium
Indium, Platinum, Heterobimetallic complexes, X-ray structure analysis, Quantum chemical calculations, 535
Gallium pyrazole complexes
Tetrachlorogallate salt, Gallium trichloride, 3,5-diphenylpyrazole, 1117
Gallium trichloride
Gallium pyrazole complexes, Tetrachlorogallate salt, 3,5-diphenylpyrazole, 1117
^{71}Ga NMR
Gallium, Indium, Dithiocarbamates, Dialkyldithiophosphates, Structures, 239
Gas sensing
Iron(II) phthalocyanine, Backscatter Mössbauer spectroscopy, 115
Geometrical isomers
Arylazopyrimidines, Osmium(II) complexes, X-ray structures, MLCT transitions, Redox property, 753
Germanium
Azide, Tin, Silver, Tris(pyrazolyl)borate, Aminotroponimine, 611
Germanium
B3LYP, CCSD(T), Arsenic, 579
Germanium(IV) tmtaa complexes
Macrocycles, Crystal structures, Six-coordinate geometry, *Trans*-positions, 969
Germylene
Digermene, X-ray crystallographic analysis, Dissociation, Equilibrium, Bond dissociation energy, Dioxadigermetane, Terminal tungsten complexes, 563
Glycine-conjugated bile acids
Acidity parameter, Aqueous solution, Hydroxy groups, 1421
Glycine methyl ester hydrolysis
Palladium(II) complexes, Bioligands, 167
Gold
N-Benzoylthiourea derivatives, Palladium, Solvent extraction, Ion selective electrode, Crystal and molecular structure, 1429
Group 13 metals
Low valent, Multiply bonded derivatives, Matrix isolation, 473
Group V
Metal alkoxides, Esterification, Single-crystal X-ray, Tantalum, Niobium, 2333
Guanidinate
1,3,4,6,7,8-Hexahydro-2*H*-pyramido[1,2-*a*]pyramidinate, Tin, Mononuclear, Dinuclear, 619

Hairy-rod structure
Cyclophosphazene, Supramolecular polymer, Coordination bonding, Lamellar packing, 1573
Halide complexes
Subvalent indium and gallium, Gallium(II), Indium(I), Indium(II), Raman spectra, 519
Halide complexes
Zinc, Thiosemicarbazones, Ligand, 1217
Halides
Organotin, Crystal structures, *N*-Thiocyanate, Azide, Acetate, 1667
Halogen exchange
Boron monochloride, Polyboron halides, 543
Halogermylenes
Donor side-chain, Intramolecular coordination, Diarylchlorogermanes, 2827
Hammett plot
Synthesis and electrochemistry, Asymmetric 14-π nickel(II) tetraazaannulene, Electrocatalysis, 917
Hammett substituent constants
Salen Cu(II) complexes, Schiff-base ligands, Cyclic voltammetry, 55
Hard–soft acids and bases
Bis(phosphine) monoxides, Cu(I), Chelates, NMR, Electrochemistry, 2793
2*H*-Azaphosphirene complexes
P-Ligands, 2*H*-1,2-Azaphosphole complexes, Cyclisation, 1,3-Dipoles, 119
2*H*-1,2-Azaphosphole complexes
P-Ligands, 2*H*-Azaphosphirene complexes, Cyclisation, 1,3-Dipoles, 119
^{1}H
Dimethylthallium(III), Thiosemicarbazones, Crystal structures, IR spectra, ^{13}C NMR spectra, 1651
Heat capacity
Mixed-valence compound, Electron transfer, Iron, Trinuclear, Iodoacetate, 1299
Heat capacity
Partition function, Equilibria in solution, Cooperativity, Site affinity, Buffer capacity, 1439
Hemidirected
Lead(II) complexes, Thiocyanate ligands, Crystal structures, 1223
Heptamethyleneimine
Platinum(II) complexes, Synthesis, Crystal structures, 2369
Heterobimetallic complexes
Gallium, Indium, Platinum, X-ray structure analysis, Quantum chemical calculations, 535
Heterobimetallics
Organometallics, Organoruthenium, Catalysis, Mössbauer, NMR, 2323
Heterocyclic nitrogen ligands
Metallic carbonyl complexes, Manganese, 439
Heterocyclic phosphide
Crystal structures, Cobalt(I) clusters, Interstitial phosphorus atom, Semi-bridging carbonyl, Substituted site, 1073
Heterocyclic thioamides
Osmium, Ruthenium, 2-Mercapto-1-methylimidazole, X-ray structures, 885
Heterodiene
Niobium complexes, 1,4-Diaza-1,3-diene, X-ray crystal structures, 305
Heteroleptic
Eight-coordinate, Schiff base, Zirconium complexes, X-ray crystal structure, Synthon, 211

Heteroleptic
X-ray, Mononuclear tungsten(VI) complexes, Ligand, 1017
Heterologous protein
Capillary electrophoresis, Hydrophobic interaction chromatography, BPTI, *Saccharomyces cerevisiae*, 1405
Heteropolyanions
Polyoxometalates, Ti(IV) complex, Wells-Dawson structure, 353
Heteropolyoxometalate
Arsenic, Tungstate, Lacunary, Synthesis, Redox chemistry, 959
Heteropolyoxomolybdates
Isopolyoxomolybdates, Hydrothermal synthesis, Cobalt complexes, 1921
Heterotrinuclear complexes
Nickel(II) complexes, BF_2^+-capped complexes, Dioxadithiadiazamacrobicycle, Template effect, *vic*-Dioxime, 1865
Hexaazamacrocycle
Crystal structures, Nickel(II) complexes, Organic ligands, Chain complex, 1913
Hexafluorophosphate complexes
Crystal structures, Copper complexes, Di-2-pyridylamine complexes, Tetrathionate complexes, Trifluoromethanesulfonate complexes, Sulfate complexes, 247
1,3,4,6,7,8-Hexahydro-2*H*-pyramido[1,2-*a*]pyramidinate
Guanidinate, Tin, Mononuclear, Dinuclear, 619
Hexamethyleneimine
Platinum, 1,1-Cyclobutanedicarboxylato, Synthesis, Crystal structure, 2659
Hexaniobate
Niobates, Hydrothermal synthesis, $NaNbO_3$, 2009
HF/ECP calculations
Niobium sulphide metallacycles, X-ray structures, 2227
Hg(II) complexes
Dimer, Diethylene triamine, X-ray crystal structures, 2195
High spin/low spin crossover
Density functional theory, Face-shared dimers, Metal–metal bonding, Electron delocalization, Broken-symmetry, Antiferromagnetic coupling, 1969
Hinokitiol
Copper, X-ray, Adduct, 1761
^{1}H NMR
Carbohydrates, Cobalt complexes, Circular dichroism, Sucrose complexes, Semi-empirical calculations, 2215
^{1}H NMR
Cobalt(III), Pyrazolylthiosemicarbazone, X-ray crystallography, 779
^{1}H NMR
Cobalt(III), Thiosemicarbazone, X-ray crystal studies, IR, Electronic spectra, 2515
^{1}H NMR spectroscopy
Iron(II), Zinc(II), Schiff base, X-ray crystal structures, Dioxygen reactivity, 705
Homogeneous catalyst
Chromium, Crystal structures, Electron spin resonance, Polyethylene, 867
Homolytic hydride cleavage
Ruthenium(II) complexes, Semiquinone monochelates, 2761
Homooxacalixarenes
Uranyl ion, Calixarenes, Supramolecular assembly, Crystal structures, 1125
Homopiperazine
Coordination chemistry, Crystal structures, Piperazine, 1729
Homopiperazines
Platinum(II), Disubstituted sulfides, Synthesis, Crystal structure, 125
Hydrazido(2-)
Nitrogenase, Molybdenum, Crystal structures, Spectroelectrochemistry, 849
Hydrides
Tantalum, Metallocenes, Metallophosphines, Bimetallics, X-ray structures, 371
Hydride
Tungsten, Tin, Oxidative addition, Crystal structures, NMR, 1817
Hydrido complexes
Mononuclear complexes, Rhodium complexes, Nitrogen ligands, Crystal structures, 1613
Hydrogen-bonded network
Crystal structures, Iron(II) complexes, Hydrogen maleate, 1189
Hydrogen bonding
Aryloxide, Gallium, Hydrolysis, 1877
Hydrogen bonding
Cysteamine, Cysteine, Sulfur, 225
Hydrogen bonding
Phosphoranes, Pentacoordinated, X-ray structures, 1155
Hydrogen bonding
Pyridine N-oxide ligands, copper(II) complexes, X-ray structures, Magnetism, 1561
Hydrogen-bonding
Rhenium(I), Carbonyl, Aminoalcohol, Cytotoxicity, Oxidative-alkoxylation, 1991
Hydrogen-bonding
Silanol, Amine, Adducts, Acridine, 4,4′-bipyridine, Phenylpyridine, 1689
Hydrogen bond
Isotope effect, Dimer, Crystal structures, NQR, Tetrachloroaurate(III), 2207
Hydrogen bond
Nickel(II), Amino acid, Coordination chemistry, Chiral recognition, 817
Hydrogen bond
Silver(I), Nicotinamide, Nicotinic acid, Sulfonate, Ag–Ag interaction, Assembly chemistry, 689
Hydrogen maleate
Crystal structures, Iron(II) complexes, Hydrogen-bonded network, 1189
Hydrogen peroxide
Manganese(II) complexes, 2-Pyrazine carboxylic acid, 2,6-Pyridinedicarboxylic acid, Chelidamic acid, Crystal structures, Catalytic disproportionation, 1063
Hydrolysis
Aryloxide, Gallium, Hydrogen bonding, 1877
Hydrolysis of macrocycles
Edta-derived macrocycles, Macrocyclic ether bis(lactones), Stability constants, EPR of Cu(II) complexes, EPR of dinuclear Cu–Cu complexes, 2265
Hydrolysis
Solutions, Equilibria, Cations, Titration, Masking, 1369
Hydrophobic interaction chromatography
Capillary electrophoresis, Heterologous protein, BPTI, *Saccharomyces cerevisiae*, 1405
Hydrophobic moment
Solvation parameter model, Partition coefficient, Iron–sulfur protein, Mixed-valence non-integer oxidation number, Cysteine ligand, 1357
Hydrothermal synthesis
Isopolyoxomolybdates, Heteropolyoxomolybdates, Cobalt complexes, 1921
Hydrothermal synthesis
Niobates, $NaNbO_3$, Hexaniobate, 2009
Hydrothermal synthesis
Polyoxovanadates, Organic–inorganic hybrid, Mixed-valence, Cage-like structure, 2601
1-Hydroxybenzotriazolate complexes
Acetylacetonate complexes, Magnetic properties, Nickel(II), 2117
Hydroxy groups
Acidity parameter, Aqueous solution, Glycine-conjugated bile acids, 1421
Hydroxylamine
Silver, Kinetics, Mechanism, Redox, Catalysis, 1893
2-Hydroxynicotinic acid
Palladium, Platinum, X-ray crystal structures, Raman spectra, 2783
Hydroxypyridinonate complexes
Hydroxypyridinones, Chelating agents, Bifunctional ligand, 2609
Hydroxypyridinones
Hydroxypyridinonate complexes, Chelating agents, Bifunctional ligand, 2609
8-Hydroxyquinolinate
Titanium, Chelate, Coordination chemistry, Structure elucidation, 1081

Idp-type ligand
N,*N*-Di(2-carboxyethyl)-*p*-toluidine, *p*-Toluidine-*N*,*N*-di-3-propionic acid, Square pyramidal copper(II) complexes, Crystal structures, 2719
Imidato complexes
Cyclometallated paladium(II) complexes, Crystal structures, 1589
Imidazole-4-acetic acid
Polymeric zinc(II) complexes, Crystal structures, Vibrational spectra, Density functional calculations, 2819
Imidazole, 9,10-dihydro-9-oxo-10-acridineacetate
Copper(II) complexes, Crystal structures, Spectra, Magnetic measurements, 2381
Imidiazole complexes
Crystal structures, Physico-chemical properties, Spectroscopy, X-ray diffraction, 1857

Imido
Boron, Lithium, Complexes, X-ray, 549
Imido transfer
Osmium porphyrin, Phosphines, Kinetics, 1889
Imine–phenol function
Ruthenium aryls, Pyridine-2-thiolates of ruthenium, 899
Imine
Platinum, Cyclometallation, Fluorine, Phosphine, Crystal structures, 105
Iminophosphorane
Cycloaddition, Four-membered ring compounds, Thermolysis, Aza-Wittig reaction, X-ray analysis, 657
Immobilization
Silica gel, Epoxide, Propane-1,3-diamine, 2647
Indium
Gallium, Dithiocarbamates, Dialkyldithiophosphates, ^{71}Ga NMR, Structures, 239
Indium
Gallium, Platinum, Heterobimetallic complexes, X-ray structure analysis, Quantum chemical calculations, 535
Indium(II)
Subvalent indium and gallium, Gallium(II), Indium(I), Halide complexes, Raman spectra, 519
Indium(I)
Subvalent indium and gallium, Gallium(II), Indium(II), Halide complexes, Raman spectra, 519
Infrared spectroscopy
Diruthenium carboxylates, Urea and thiourea derivatives, Crystal structures, 1235
Infrared spectroscopy
Zinc adducts, Emprirical correlations, Calorimetry, 1677
Inner-sphere coordination
Lanthanide(III) chelate, Cobalt(III) chelate, Binuclear complexes, Outer-sphere coordination, Stability constant, 805
Inorganic polymer
Polyphosphazene, Metal–polymer complexes, 2587
Intensity parameters
Europium, Photoluminescence, Perchlorate, Methylpyridylacetamide, 1837
π–π interaction
Cadmium complexes, Dca ligand, Double end-to-end, Zigzag chain, 893
Interconversion
Schiff bases, Salicylaldimine adducts, X-ray crystal structures, Zinc complexes, Zwitterion, 697
Intermediates
Aluminum(I) halides, Metalloid clusters, Nanosized clusters, Metal lattice, X-ray structural analysis, 489
Intermetallic compounds
Clusters, Crystal structures, Lead, Zintl phases, 641
Intermolecular nucleophilic attack
Molecular orbital, Ab initio, Mechanism, Titanium, Ylid, 2699
Interstitial phosphorus atom
Crystal structures, Cobalt(I) clusters, Heterocyclic phosphide, Semi-bridging carbonyl, Substituted site, 1073
Intramolecular coordination
Halogermylenes, Donor side-chain, Diarylchlorogermanes, 2827
Iodoacetate
Mixed-valence compound, Electron transfer, Iron, Trinuclear, Heat capacity, 1299
Ionisation constants
Mercapto-carboxylic acid, Potentiometry, IR, Formation constants, 1319
Ion pair
Copper(II) complex, Crystal structures, EDTA, Adeninium, Molecular recognition, 1451
Ion selective electrode
N-Benzoylthiourea derivatives, Gold, Palladium, Solvent extraction, Crystal and molecular structure, 1429
Ion selective electrodes
Artificial neural networks, Experimental design, Stability constants, Metal complexes, Metal–ligand equilibria, 1375
IR and UV–Vis–NIR band analysis
Nickel(II) chromate and dichromate complexes of phenanthroline, Monodentate coordination of CrO_4^{2-}, Crystal structures, 997
IR
Cobalt(III), Thiosemicarbazone, X-ray crystal studies, ^{1}H NMR, Electronic spectra, 2515
Iridium(III) complexes
Rhenium(III) complexes, S-bridged polynuclear complexes, Crystal structures, UV–Vis absorption spectra, Cyclic voltammetry, 1809
Iridium
Polycations, Cluster compounds, Crystal structures, Bismuth, Rhodium, 651
IR
Mercapto-carboxylic acid, Potentiometry, Formation constants, Ionisation constants, 1319
Iron
Acetylide, Vinylidene, Propadienylidene, 1755
Iron carbonyl complexes
Organometallic phosphine, Multimetallic, π-Allyl molybdenum, Cyclopentadienyl iron complexes, 2301
Iron complexes
Aminohydroxamate complexes, Electrochemical reduction, Cyclic voltammetry, EC mechanism, 1661
Iron(II) complexes
Crystal structures, Hydrogen-bonded network, Hydrogen maleate, 1189
Iron(III) dialkyldithiocarbamates
Mössbauer spectra, Magnetic moment, Thermal decomposition, Spin crossover, 2489
Iron(III)
Single-crystal X-ray, N-donor, Terpyridyl, 2055
Iron(II) phthalocyanine
Backscatter Mössbauer spectroscopy, Gas sensing, 115
Iron(II)
Zinc(II), Schiff base, X-ray crystal structures, ^{1}H NMR spectroscopy, Dioxygen reactivity, 705
Iron
Mixed-valence compound, Electron transfer, Trinuclear, Iodoacetate, Heat capacity, 1299
Iron–sulfur protein
Solvation parameter model, Partition coefficient, Hydrophobic moment, Mixed-valence non-integer oxidation number, Cysteine ligand, 1357
IR spectra
Dimethylthallium(III), Thiosemicarbazones, Crystal structures, ^{1}H, ^{13}C NMR spectra, 1651
IR spectra
Vanadium complexes, Caffeic acid complexes, UV–Vis spectra, Potentiometric titrations, Catecholate-like ligand, 1979
IR spectroscopy
Magnesium phthalocyanines, Magnesium complexes, Crystal structures, Raman spectroscopy, UV–Vis spectroscopy, 265
Isatin
X-ray, Thiosemicarbazone, Metal complexes, 2593
Isocytosine complexes
Cu(II) complexes, Ternary complexes, Peptide–Cu(II)–isocytosine complexes, 1197
Isomerism
Ferrocenyl Schiff bases, DFT calculations, 2361
Isomorphism
$C_{10}H_{20}N_2S_4Zn\cdot C_5H_5N$, Structures, ^{15}N CP/MAS NMR spectroscopy, 2727
Isopolyoxomolybdates
Heteropolyoxomolybdates, Hydrothermal synthesis, Cobalt complexes, 1921
Isoquercitrin
Al(III) complexes, Stoichiometry, UV–Vis Spectroscopy, DFT calculations, FT Raman, 2801
Isotope effect
Hydrogen bond, Dimer, Crystal structures, NQR, Tetrachloroaurate(III), 2207
Isoxazolidines
Pd-, Zn-, Cu-complexes, Syntheses, X-ray, NMR, 769

Keggin
Polyoxometalates, Charge transfer, Photochromism, 2537
β-Ketoiminate
Silver(I) complexes, Non-fluorinated β-diketonate ligands, Monothio-β-ketonate, Chemical vapor deposition, Crystal structures, 1289
Kinetic data
Copper(I) complexes, Autoxidation, Catalytic activity, 181

Kinetics
Cobalt, Phthalocyanine, Cyanide, Sulfur dioxide, Equilibria, 133
Kinetics
2-Mercaptobenzoxazole, Pentacyanoferrate, Equilibrium constants, Electrochemistry, 2137
Kinetics
Osmium porphyrin, Imido transfer, Phosphines, 1889
Kinetics
Silver, Hydroxylamine, Mechanism, Redox, Catalysis, 1893
Kinetic studies
Ternary complexes, Crystal structures, 2045

Lactic acid
Mixed-ligand complexes, Copper(II) complexes, 2,2′-Bipyridine complexes, 2-Methyllactic acid, Mandelic acid, Crystal structures, 2811
Lacunary
Heteropolyoxometalate, Arsenic, Tungstate, Synthesis, Redox chemistry, 959
Lamellar packing
Cyclophosphazene, Supramolecular polymer, Coordination bonding, Hairy-rod structure, 1573
Lantern-type complexes
Platinum(III) compounds, Amidate bridging ligands, X-ray structure, 275
Lanthanide and actinide extaction
Carboranes, Carba metallaboranes, Dicarbollides, Cyclic voltammetry, Liquid–liquid extraction, 975
Lanthanide complexes
Macrocycles, Crystal structures, Chiral complexes, NMR of paramagnetic compounds, 811
Lanthanide contraction
Anion controlled assembly, Crystal structures, Magnetic properties, 1097
Lanthanide(III) chelate
Cobalt(III) chelate, Binuclear complexes, Inner-sphere coordination, Outer-sphere coordination, Stability constant, 805
Lanthanide(III) complexes
Macrocyclic ligands, 2,6-Diacetylpyridine, 3-Substituted-1,2-diaminopropanes, 425
Lanthanide(III) complexes
tert-Butylcalix[4]arenes, Amide, Sodium complexes, Yttrium(III) complexes, X-ray structures, 763
Lanthanide
Polyaza ligands, Catecholate ligands, Stability constants, Potentiometry, 1393
Lanthanides(III)
Oxygen donors, 2,2′-Oxydiethylamine, Dimethylsulfoxide, Complexes, Thermodynamics, 1385
Lead
Clusters, Crystal structures, Intermetallic compounds, Zintl phases, 641
Lead(II) complexes
Hemidirected, Thiocyanate ligands, Crystal structures, 1223
Lead(II)
Tris(pyrazolyl)borate and 2,6-pyridyl-diimine ligands, Thiocyanate, Cadmium(II), 1795
Lewis-amphoteric behavior
Stannylenes, Plumbylenes, Distannenes, Diplumbenes, 587
LH_4
vic-Dioxime, Nickel(II), Cobalt(II), Copper(II), Iron(II), Uranyl(IV), Electrochemistry, $N_2O_2S_2$ macrocyle, 825
Ligand-field strength
Trans influence, Crystal structures, Tripodal tridentate phosphine, Acetylacetonate complexes, Chromium(III) complexes, 835
Ligand titration
Natural metal complexes, Natural ligands, Resin titration, Chelex 100, 1343
Ligand
X-ray, Mononuclear tungsten(VI) complexes, Heteroleptic, 1017
Ligand
Zinc, Halide complexes, Thiosemicarbazones, 1217
Linear disilaketenylidene (SiSiO)
Electronic states, Renner effect, Analogous multiple bonded systems, 599
Linear polyamines
Metal complexes, Polyamine complexes, 1459
Liquid–liquid extraction
Carboranes, Carba metallaboranes, Dicarbollides, Cyclic voltammetry, Lanthanide and actinide extaction, 975
Lithium
Alkoxides, Crystal structures, Tungsten, Methoxide, 193
Lithium
Boron, Imido, Complexes, X-ray, 549
Lithium
C_3-chiral triamidostannate, Amides, Tin, 629
Low valent indium
β-Diketiminate, Bulky ligands, Metal–metal bonds, 525
Low valent
Multiply bonded derivatives, Group 13 metals, Matrix isolation, 473
Lumazine complexes
Crystal structures, Copper complexes, Zinc complexes, 1961
Luminescence property
Europium complexes, X-ray crystallography, Dibenzoylmethane, 2-(4′-Dimethylaminophenyl)imidazo[4,5-f]1,10-phenanthroline, 3-Ethyl-2-(4′-dimethylaminophenyl)imidazo[4,5-f]1,10-phenanthroline, 313
Lysyl–glycyl–histidyl–lysine
Copper complexes, Nickel complexes, Complex-formation equilibria, 1469

Macrocycle complexes
Dithiophosphate complexes, Dithiophosphonate complexes, Pentacoordinate nickel(II) complexes, Crystal structures, 1935
Macrocycles
Cadmium, Polyamines, Dipyridine, Phenanthroline, 1329
Macrocycles
Gallium–gallium bonds, Supramolecular chemistry, 511
Macrocycles
Germanium(IV) tmtaa complexes, Crystal structures, Six-coordinate geometry, *Trans*-positions, 969
Macrocycles
Lanthanide complexes, Crystal structures, Chiral complexes, NMR of paramagnetic compounds, 811
Macrocyclic compound
Binuclear complexes, Magnetic properties, 359
Macrocyclic ether bis(lactones)
Edta-derived macrocycles, Stability constants, EPR of Cu(II) complexes, EPR of dinuclear Cu–Cu complexes, Hydrolysis of macrocycles, 2265
Macrocyclic ligands
Lanthanide(III) complexes, 2,6-Diacetylpyridine, 3-Substituted-1,2-diaminopropanes, 425
Macrocyclic Ni(II) complexes
Dibenzotetraaza[14]annulenes, Succinyl dichloride, Crystal structures, Solid state supramolecular complexes, 7
Macromolecular complexes
Cyclophosphazenes, Polyphosphazenes, Phenolic phosphine, Carbonyls, Spectroscopic characterization, 2579
Magnesium complexes
Magnesium phthalocyanines, Crystal structures, IR spectroscopy, Raman spectroscopy, UV–Vis spectroscopy, 265
Magnesium complexes
Phoshocreatine, ^{31}P NMR spectroscopy, Sodium complexes, Potassium complexes, 1481
Magnesium diboride
Chemical bonding topology, Superconductors, Cuprate superconductors, 2347
Magnesium(II) complexes
Aminomethane-1,1-diphosphonic acids, Zinc(II) complexes, Calcium(II) complexes, Potentiometry, NMR, 321
Magnesium
Niobium, Alkoxides, Oxoalkoxides, Mass-spectra, Crystal structures, 1629
Magnesium phthalocyanines
Magnesium complexes, Crystal structures, IR spectroscopy, Raman spectroscopy, UV–Vis spectroscopy, 265
Magnetic coupling
DFT calculations, Dinuclear transition metal complexes, Electron transfer, Metal–metal bonding, Spin polarization, 1163
Magnetic data
1D nickel(II) azido complexes, Pyridine derivative complexes, Preparation, Crystal structures, Spectra, 1871
Magnetic measurements

Copper(II) complexes, Imidazole, 9,10-dihydro-9-oxo-10-acridineacetate, Crystal structures, Spectra, 2381
Magnetic moment
Iron(III) dialkyldithiocarbamates, Mössbauer spectra, Thermal decomposition, Spin crossover, 2489
Magnetic properties
Acetylacetonate complexes, 1-Hydroxybenzotriazolate complexes, Nickel(II), 2117
Magnetic properties
Benzoate ligands, Cobalt(II) complexes, Di-2-pyridyl ketone complexes, End-on azide ligands, 2027
Magnetic properties
Binuclear nickel(II) complexes, Crystal structures, Terminal thiocyanato ion complexes, Terminal cyanato ion complexes, Pentadentate ligands, 2457
Magnetic properties
Binucleating ligand, Copper(II) complexes, Nickel(II) complexes, Electrochemistry, 2767
Magnetic properties
Copper(II) complexes, Oxalato complexes, Oxalato-bridged complexes, Crystal structures, 1203
Magnetic properties
Crystal structures, Thermal properties, Tetrabromocuprate(II), *n*-Ethylpyridinium, 19
Magnetic properties
Lanthanide contraction, Anion controlled assembly, Crystal structures, 1097
Magnetic properties
Macrocyclic compound, Binuclear complexes, 359
Magnetic properties
Nickel, Palladium, Platinum, Oxalate, Crystal structures, DFT calculations, 2631
Magnetism
Copper(II), Alkoxo-bridged, Benzimidazoles, Crystal structures, 141
Magnetism
Cu(II) stereochemistry, X-ray structures, EPR spectra, 2473
Magnetism
Pyridine N-oxide ligands, copper(II) complexes, X-ray structures, Hydrogen bonding, 1561
Magnetism
Tetranuclear copper(II) complexes, Crystal structures, Antiferromagnetic coupling, Molecular orbital calculation, 1539
Magnetochemical studies
X-ray crystallography, Manganese oxide clusters, 1779
Malate
Nickel, Malic acid, Coordination polymer, Asymmetric catalysis, Crystal structures, Electroplating, 787
Malic acid
Nickel, Malate, Coordination polymer, Asymmetric catalysis, Crystal structures, Electroplating, 787
Malonates
Tin enolates, Diorganohydroxytin, Diorganotin, Sn(IV) complexes, Di-*n*-butylhydroxytin(IV), 417
Malonato complexes
Uranyl, CPMAS ^{13}C NMR, X-ray crystallography, 81
Mandelic acid
Mixed-ligand complexes, Copper(II) complexes, 2,2′-Bipyridine complexes, Lactic acid, 2-Methyllactic acid, Crystal structures, 2811
Manganese(II) complexes
2-Pyrazine carboxylic acid, 2,6-Pyridinedicarboxylic acid, Chelidamic acid, Crystal structures, Catalytic disproportionation, Hydrogen peroxide, 1063
Manganese
Metallic carbonyl complexes, Heterocyclic nitrogen ligands, 439
Manganese oxide clusters
X-ray crystallography, Magnetochemical studies, 1779
Masking
Solutions, Equilibria, Cations, Hydrolysis, Titration, 1369
Mass-spectra
Magnesium, Niobium, Alkoxides, Oxoalkoxides, Crystal structures, 1629
Mass-spectrometric study
Trimetallic alkoxides, Molecular structure, X-ray study, Rhenium methoxides, Niobium methoxide, Tantalum methoxide, 2317
Mass spectrometry
Chromium, Pivalate, Paramagnetic, NMR, X-ray photoelectron spectroscopy, 155
Mass spectrometry
Trialkylaluminum, Aminoalane, Dibenzylamine, NMR, Molecular structure, 1747
Matrix isolation
Disilenes, Silenes, Silanones, Photolysis, 467
Matrix isolation
Low valent, Multiply bonded derivatives, Group 13 metals, 473
M = Co
Thiadiazole, M = Ni, M = Cu, Crystal structures, Monomeric complexes, 403
M = Cu
Thiadiazole, M = Co, M = Ni, Crystal structures, Monomeric complexes, 403
Mechanism
Molecular orbital, Ab initio, Intermolecular nucleophilic attack, Titanium, Ylid, 2699
Mechanism
Silver, Hydroxylamine, Kinetics, Redox, Catalysis, 1893
2-Mercaptobenzoxazole
Pentacyanoferrate, Kinetics, Equilibrium constants, Electrochemistry, 2137
Mercapto-carboxylic acid
Potentiometry, IR, Formation constants, Ionisation constants, 1319
2-Mercapto-1-methylimidazole
Heterocyclic thioamides, Osmium, Ruthenium, X-ray structures, 885
Mercury(II)
Arylmetal complexes, Boron, The 2,6-bis(dimethylamino)phenyl ligand, 635
Mercury(II) halides
Phosphine complexes, Crystal structures, 1845
Mercury(II)
Phosphine chalcogenide, Seven-membered, Palladium(II), Metallacyclic rings, bis(diphenylthiophosphinyl)ethane, 205
Metal alkoxides
Esterification, Single-crystal X-ray, Group V, Tantalum, Niobium, 2333
Metal centre
Conformational change, Four or five coordinate geometry, Transition metals, 2175
Metal complexes
Artificial neural networks, Experimental design, Stability constants, Ion selective electrodes, Metal–ligand equilibria, 1375
Metal complexes
Linear polyamines, Polyamine complexes, 1459
Metal complexes
S-Benzyldithiocarbazate, Bioactivity of Schiff bases, Bioactivity of metal complexes, Crystal structure of Cd(II) complexes, 2547
Metal complexes
Schiff base ligands, Cadmium(II) complexes, Crystal structures, Dithiocarbazate Schiff base crystal structures, Bioactivity, 2691
Metal complexes
X-ray, Thiosemicarbazone, Isatin, 2593
Metallacycles, oxo ligands
Cyclo-addition, P ligands, Palladium, Structure elucidation, 2653
Metallacyclic rings
Phosphine chalcogenide, Seven-membered, Palladium(II), Mercury(II), bis(diphenylthiophosphinyl)ethane, 205
Metallation
Palladium, Schiff base, Phosphorus ligands, X-ray diffraction, 2309
Metal lattice
Aluminum(I) halides, Metalloid clusters, Nanosized clusters, Intermediates, X-ray structural analysis, 489
Metallic carbonyl complexes
Manganese, Heterocyclic nitrogen ligands, 439
Metallic polymer
Azamacrocycles, Aromatic pendant arms, Coordination compounds, 333
Metal–ligand equilibria
Artificial neural networks, Experimental design, Stability constants, Metal complexes, Ion selective electrodes, 1375
Metallocene
Molybdenum, Metallocenium, Pentaphenylcyclopentadienyl, 1707
Metallocenes
Tantalum, Hydrides, Metallophosphines, Bimetallics, X-ray structures, 371

Metallocenium
Molybdenum, Metallocene, Pentaphenylcyclopentadienyl, 1707
Metalloid clusters
Aluminum(I) halides, Nanosized clusters, Intermediates, Metal lattice, X-ray structural analysis, 489
Metalloid clusters
Electron counts, Aluminum, 503
Metallophosphines
Tantalum, Metallocenes, Hydrides, Bimetallics, X-ray structures, 371
Metal–metal bonding
Density functional theory, Face-shared dimers, High spin/low spin crossover, Electron delocalization, Broken-symmetry, Antiferromagnetic coupling, 1969
Metal–metal bonding
DFT calculations, Dinuclear transition metal complexes, Electron transfer, Magnetic coupling, Spin polarization, 1163
Metal–metal bonds
β-Diketiminate, Low valent indium, Bulky ligands, 525
Metal–metal interactions
Molybdenum, Pyridylphosphines, Rhodium, 1737
Metal–nitrile complexes
Dendrimers, Cyclophosphazene, 909
Metal-organic frameworks (MOF)
Synthesis, Crystal structures, TGA–DTA, 175
Metal–polymer complexes
Inorganic polymer, Polyphosphazene, 2587
Metal uptake
Cork, Solid state ^{13}C MAS and CP-MAS NMR, Copper, Nickel, Potentiometric titration, 1363
Metastable excited states
Pentacyaninotrosylferrate(2−) ion, X-ray diffraction, FIRRS, TGA, DTA, 1767
Metathesis
Molybdenum, Tin, Crystal structures, Polymerisation, Norbornadiene, NMR spectra, 2505
Methionine
CD spectroscopy, Copper(II), Nickel(II), Palladium(II), Peptides, 2149
Methoxide
Alkoxides, Crystal structures, Lithium, Tungsten, 193
2-Methylaminopyridine
Cyclodextrins, Copper(II) complexes, 1531
4-Methyl-2,6-dibenzoylphenol
Synthesis, Cobalt(III) complexes, NMR, TGA, Cyclic voltammetry, X-ray structures, 1787
Methylene group contribution
Potassium *p*-*n*-hexylbenzoate, Potassium *p*-*n*-heptylbenzoate, Potassium *p*-*n*-octylbenzoate, Apparent molar enthalpies of, Partial molar enthalpies of, Micellization enthalpy, 1497
2-Methyllactic acid
Mixed-ligand complexes, Copper(II) complexes, 2,2′-Bipyridine complexes, Lactic acid, Mandelic acid, Crystal structures, 2811
Methyl-molybdenum complexes
Molybdenum complexes, oxo-Hydrazido complexes, Phenyl-molybdenum complexes, Diimine, X-ray structures, 2531
Methylpyridylacetamide
Europium, Photoluminescence, Perchlorate, Intensity parameters, 1837
Methyltin(IV) tribromide
Porphyrins, Sitting–Atop complexes, Organotin(IV) halide adducts, Tin compounds, Spectral method, 1255
Mg(II)
Adenosine-5′-triphosphate (ATP), NOESY, Torsion angle (χ), 435
Micellization enthalpy
Potassium *p*-*n*-hexylbenzoate, Potassium *p*-*n*-heptylbenzoate, Potassium *p*-*n*-octylbenzoate, Apparent molar enthalpies of, Partial molar enthalpies of, Methylene group contribution, 1497
Mixed-ligand complexes
Copper(II) complexes, 2,2′-Bipyridine complexes, Lactic acid, 2-Methyllactic acid, Mandelic acid, Crystal structures, 2811
Mixed-ligand complexes
Copper(II) complexes, Five-coordinate complexes, Aminohydroxamic acids, EPR spectra, Vis spectra, 295
Mixed-ligand complexes
Copper(II), *N*-(2-Pyridylmethyl)iminodiacetic acid, *N*-(2-Pyridylmethyl)iminodiacetate(2-) ion, 2-(Aminomethyl)pyridine, α-Picolylamine, 2-(2′-Pyridyl)benzimidazole, Crystal structures, Aromatic π,π-staking interactions, Molecular recognition, Thermal stability, Spectral and magnetic properties, 1485
Mixed-ligand complexes
Ni(II), Co(II), Tetramines, Adenosine 5′-monophosphate, 745
Mixed-ligand complexes
Zinc(II) complexes, Aminohydroxamic acids, Polyamines, NMR spectra, Potentiometry, 2183
Mixed-ligands Cu(II) chelates
Dithiocarbamates, Cu(II) complexes, Ethylenediamine, Crystal structures, 1899
Mixed-valence compound
Electron transfer, Iron, Trinuclear, Iodoacetate, Heat capacity, 1299
Mixed-valence non-integer oxidation number
Solvation parameter model, Partition coefficient, Hydrophobic moment, Iron–sulfur protein, Cysteine ligand, 1357
Mixed-valence
Polyoxovanadates, Organic–inorganic hybrid, Hydrothermal synthesis, Cage-like structure, 2601
Mixed-valence
Ruthenium-ammine, Benzotriazole, Polynuclear complexes, Electron transfer, Molecular wires, 2089
MLCT transitions
Arylazopyrimidines, Osmium(II) complexes, Geometrical isomers, X-ray structures, Redox property, 753
M = Ni
Thiadiazole, M = Co, M = Cu, Crystal structures, Monomeric complexes, 403
MOCVD
Cerium, Fluoroalkoxides, Structures, Complexes, Films, 1985
Mo/Fe/S cluster
Synthesis, Structures, S=PEt_3 ligand, CO, 2523
Molecular orbital
Ab initio, Mechanism, Intermolecular nucleophilic attack, Titanium, Ylid, 2699
Molecular orbital calculation
Tetranuclear copper(II) complexes, Crystal structures, Magnetism, Antiferromagnetic coupling, 1539
Molecular orbitals
Polyoxometalates, Transition metals, Chemical bonding, Density–functional theory, 2201
Molecular recognition
Copper(II) complex, Crystal structures, EDTA, Adeninium, Ion pair, 1451
Molecular recognition
Copper(II), *N*-(2-Pyridylmethyl)iminodiacetic acid, *N*-(2-Pyridylmethyl)iminodiacetate(2-) ion, 2-(Aminomethyl)pyridine, α-Picolylamine, 2-(2′-Pyridyl)benzimidazole, Crystal structures, Mixed-ligand complexes, Aromatic π,π-staking interactions, Thermal stability, Spectral and magnetic properties, 1485
Molecular structures
Tridentate Schiff base ligand, Potassium permanganate, Photosystem II, 1139
Molecular structure
Trialkylaluminum, Aminoalane, Dibenzylamine, NMR, Mass spectrometry, 1747
Molecular structure
Trimetallic alkoxides, X-ray study, Mass-spectrometric study, Rhenium methoxides, Niobium methoxide, Tantalum methoxide, 2317
Molecular wires
Ruthenium-ammine, Benzotriazole, Polynuclear complexes, Mixed-valence, Electron transfer, 2089
Molybdenum complexes
oxo-Hydrazido complexes, Methyl-molybdenum complexes, Phenyl-molybdenum complexes, Diimine, X-ray structures, 2531
Molybdenum
Crystal structures, Cluster complexes, Acetates, Reduction, 147
Molybdenum
Metallocene, Metallocenium, Pentaphenylcyclopentadienyl, 1707
Molybdenum
Metal–metal interactions, Pyridylphosphines, Rhodium, 1737
Molybdenum
Nitrogenase, Hydrazido(2-), Crystal structures, Spectroelectrochemistry, 849
Molybdenum

Tin, Crystal structures, Metathesis, Polymerisation, Norbornadiene, NMR spectra, 2505
Mono-bridged species
Mono-helical, Single-helical-strand, Coordination chemistry, Transition metals, X-ray crystallography, 1177
Monodentate coordination of CrO_4^{2-}
Nickel(II) chromate and dichromate complexes of phenanthroline, Crystal structures, IR and UV–Vis–NIR band analysis, 997
Mono-helical
Single-helical-strand, Mono-bridged species, Coordination chemistry, Transition metals, X-ray crystallography, 1177
Monomeric complexes
Thiadiazole, M = Co, M = Ni, M = Cu, Crystal structures, 403
Mononuclear bis(imido) Mo(VI) complexes
Pyrazole, X-ray crystal structures, 1211
Mononuclear complexes
Copper(II) complexes, Spectral properties, Crystal structures, Pyridinecarboxylate complexes, 365
Mononuclear complexes
Rhodium complexes, Hydrido complexes, Nitrogen ligands, Crystal structures, 1613
Mononuclear complexes
Triazole derivatives, Crystal structures, 797
Mononuclear
Guanidinate, 1,3,4,6,7,8-Hexahydro-2*H*-pyramido[1,2-*a*]pyramidinate, Tin, Dinuclear, 619
Mononuclear tungsten(VI) complexes
X-ray, Ligand, Heteroleptic, 1017
Monothio-β-ketonate
Silver(I) complexes, Non-fluorinated β-diketonate ligands, β-Ketoiminate, Chemical vapor deposition, Crystal structures, 1289
Morphologies
Uranyl complexes, Schiff base ligand, 2421
Mössbauer
Organometallics, Heterobimetallics, Organoruthenium, Catalysis, NMR, 2323
Mössbauer spectra
Iron(III) dialkyldithiocarbamates, Magnetic moment, Thermal decomposition, Spin crossover, 2489
Multimetallic
Organometallic phosphine, π-Allyl molybdenum, Iron carbonyl complexes, Cyclopentadienyl iron complexes, 2301
Multiply bonded derivatives
Low valent, Group 13 metals, Matrix isolation, 473

$NaNbO_3$
Niobates, Hydrothermal synthesis, Hexaniobate, 2009
Nanosized clusters
Aluminum(I) halides, Metalloid clusters, Intermediates, Metal lattice, X-ray structural analysis, 489
Naphthalocyanine
Raman, Rare earth, Sandwich complexes, 1905
Natural ligands
Natural metal complexes, Resin titration, Ligand titration, Chelex 100, 1343
Natural metal complexes
Natural ligands, Resin titration, Ligand titration, Chelex 100, 1343
N-Benzoylthiourea derivatives
Gold, Palladium, Solvent extraction, Ion selective electrode, Crystal and molecular structure, 1429
N-(Benzylidene)xylylendiamines
Cyclometallated palladium(II) compounds, Chloro-bridged complexes, 2063
^{15}N CP/MAS NMR spectroscopy
$C_{10}H_{20}N_2S_4Zn \cdot C_5H_5N$, Isomorphism, Structures, 2727
N-donor
Iron(III), Single-crystal X-ray, Terpyridyl, 2055
N-donor ligands
Platinum chloride complexes, X-ray structures, ^{15}N NMR, 1,2,4-Triazolo-[1,5α]-pyrimidines, 343
n-Ethylpyridinium
Crystal structures, Magnetic properties, Thermal properties, Tetrabromocuprate(II), 19
Nickel complexes
Copper complexes, Complex-formation equilibria, Lysyl–glycyl–histidyl–lysine, 1469
Nickel complexes
Crystal structures, Palladium complexes, 2071
Nickel complexes
Dithiocarbimates, Triphenylphosphine, Crystal structures, 2243
Nickel complexes
Sulfonamide complexes, 8-Aminoquinoline, X-ray crystal structures, 1229
Nickel
Copper, Zinc, Cadmium, Saccharinate, X-ray structures, 395
Nickel
Cork, Solid state ^{13}C MAS and CP-MAS NMR, Copper, Potentiometric titration, Metal uptake, 1363
Nickel(II)
Acetylacetonate complexes, 1-Hydroxybenzotriazolate complexes, Magnetic properties, 2117
Nickel(II)
Amino acid, Coordination chemistry, Hydrogen bond, Chiral recognition, 817
Nickel(II)
CD spectroscopy, Copper(II), Palladium(II), Peptides, Methionine, 2149
Nickel(II) chromate and dichromate complexes of phenanthroline
Monodentate coordination of CrO_4^{2-}, Crystal structures, IR and UV–Vis–NIR band analysis, 997
Nickel(II), Cobalt(II), Copper(II), Iron(II), Uranyl(IV), Electrochemistry
vic-Dioxime, LH_4, $N_2O_2S_2$ macrocyle, 825
Nickel(II) complexes
Binucleating ligand, Copper(II) complexes, Electrochemistry, Magnetic properties, 2767
Nickel(II) complexes
Crystal structures, Hexaazamacrocycle, Organic ligands, Chain complex, 1913
Nickel(II) complexes
Di-2-pyridyl ketone benzoylhydrazone, Spectroscopy, Thermal analyses, 2375
Nickel(II) complexes
Heterotrinuclear complexes, BF_2^+-capped complexes, Dioxadithiadiazamacrobicycle, Template effect, *vic*-Dioxime, 1865
Nickel(II) complexes
Salen ligands, Ni(I) complexes, EPR, 1695
Nickel(II)
Crystal structures, 3-Piperidine, Thiosemicarbazone, 2-Pyridineformamide, Spectra, 859
Nickel(II)
2-Pyridineformamide, Thiosemicarbazone, Zinc(II), Cadmium(II), Crystal structures, 729
Nickel(II)
Schiff base complexes, Cobalt(II), Zinc(II), Tetrahedral, Crystal structures, 2733
Nickel
Malic acid, Malate, Coordination polymer, Asymmetric catalysis, Crystal structures, Electroplating, 787
Nickel
Palladium, Chirality, Bidentate nitrogen ligands, Crystal structures, 27
Nickel
Palladium, Platinum, Oxalate, Crystal structures, Magnetic properties, DFT calculations, 2631
Nickel
Phthalocyanines, Phthalonitrile derivatives, Electrochemistry, Zinc, Cobalt, 255
Nickel
Thiolate, *cis*-1,2-Bis(diphenylphosphino)ethene, X-ray structures, 421
Nickel(0)
Vinylcyclosilazane complexes, Crystal structure, 1261
Nicotinamide
Silver(I), Nicotinic acid, Sulfonate, Hydrogen bond, Ag–Ag interaction, Assembly chemistry, 689
Nicotinic acid
Silver(I), Nicotinamide, Sulfonate, Hydrogen bond, Ag–Ag interaction, Assembly chemistry, 689
Ni(I) complexes
Salen ligands, Nickel(II) complexes, EPR, 1695
Ni(II)
Co(II), Tetramines, Adenosine 5′-monophosphate, Mixed-ligand complexes, 745
Niobates
Hydrothermal synthesis, $NaNbO_3$, Hexaniobate, 2009
Niobium complexes
Heterodiene, 1,4-Diaza-1,3-diene, X-ray crystal structures, 305

Niobium
Magnesium, Alkoxides, Oxoalkoxides, Mass-spectra, Crystal structures, 1629
Niobium
Metal alkoxides, Esterification, Single-crystal X-ray, Group V, Tantalum, 2333
Niobium methoxide
Trimetallic alkoxides, Molecular structure, X-ray study, Mass-spectrometric study, Rhenium methoxides, Tantalum methoxide, 2317
Niobium sulphide metallacycles
X-ray structures, HF/ECP calculations, 2227
Nitrate complexes, Di-2-pyridylamine complexes
Crystal structures, Copper complexes, 943
Nitric oxide
Rhenium, Nitrosyl, X-ray structures, Electronic structures, 2617
Nitrite complexes
Crystal structures, Copper(II) complexes, Sulfate complexes, di-2-Pyridylamine complexes, Thiocyanato complexes, 1279
Nitrogenase
Hydrazido(2-), Molybdenum, Crystal structures, Spectroelectrochemistry, 849
Nitrogen dioxide
Phthalocyanines, Scanning electron microscopy, X-ray microprobe, UV–Vis and FTIR spectroscopy, X-ray powder diffractometry, 677
Nitrogen ligands
Mononuclear complexes, Rhodium complexes, Hydrido complexes, Crystal structures, 1613
Nitrophenoxide complexes
Thallium(I) complexes, Crystal structure, 2555
Nitrosyl complexes
Ruthenium(II), NMR spectra, X-ray structures, Diop, Dppb, 2221
Nitrosyl
Rhenium, X-ray structures, Electronic structures, Nitric oxide, 2617
N-[2-(4-Methoxyphenyltelluro)ethyl]benzamide
N-[2-(4-Methoxyphenyl telluro)propyl]phthalimide, Palladium(II), Platinum(II), Ruthenium(II), Complexes, Crystal structures, 667
N-[2-(4-Methoxyphenyl telluro)propyl]phthalimide
N-[2-(4-Methoxyphenyltelluro)ethyl]benzamide, Palladium(II), Platinum(II), Ruthenium(II), Complexes, Crystal structures, 667
N-methylated polyamines
Silver(I), Complexes, Dimethylsulfoxide, Thermodynamics, 1337
NMR
Aminomethane-1,1-diphosphonic acids, Zinc(II) complexes, Magnesium(II) complexes, Calcium(II) complexes, Potentiometry, 321
NMR and IR analysis
Platinum(II) complexes, Ribavirin, X-ray structures, 2001
NMR
Bis(phosphine) monoxides, Cu(I), Chelates, Electrochemistry, Hard–soft acids and bases, 2793
NMR
Chromium, Pivalate, Mass spectrometry, Paramagnetic, X-ray photoelectron spectroscopy, 155
NMR
Dimesitylphosphine, Secondary phosphine, X-ray crystallography, Cone angle, Fluxional, 2409
NMR
Isoxazolidines, Pd-, Zn-, Cu-complexes, Syntheses, X-ray, 769
NMR of paramagnetic compounds
Macrocycles, Lanthanide complexes, Crystal structures, Chiral complexes, 811
NMR
Organometallics, Heterobimetallics, Organoruthenium, Catalysis, Mössbauer, 2323
NMR
Poly(3-Rpyrazolyl)borate cobalt(II) complexes, Structures, 2743
NMR spectra
Molybdenum, Tin, Crystal structures, Metathesis, Polymerisation, Norbornadiene, 2505
NMR spectra
Nitrosyl complexes, Ruthenium(II), X-ray structures, Diop, Dppb, 2221
NMR spectra
Zinc(II) complexes, Mixed-ligand complexes, Aminohydroxamic acids, Polyamines, Potentiometry, 2183
NMR spectroscopy
Tellurium dichloride, Chloridotellurate anions, X-ray crystallography, 1089
NMR studies
Silver(I) complexes, Thiones, 1267
NMR
Synthesis, Cobalt(III) complexes, 4-Methyl-2,6-dibenzoylphenol, TGA, Cyclic voltammetry, X-ray structures, 1787
NMR
Trialkylaluminum, Aminoalane, Dibenzylamine, Mass spectrometry, Molecular structure, 1747
NMR
Triphenylantimony(V), Oximes, X-ray, 2387
NMR
Tungsten, Tin, Oxidative addition, Crystal structures, Hydride, 1817
N,*N*-Di(2-carboxyethyl)-*p*-toluidine
Idp-type ligand, *p*-Toluidine-*N*,*N*-di-3-propionic acid, Square pyramidal copper(II) complexes, Crystal structures, 2719
N,*N*-dimethyl-L-α-isoleucine
Electron paramagnetic resonance (EPR) spectroscopy, Copper(II) complexes, Amino acids, 1643
^{15}N NMR
Platinum chloride complexes, X-ray structures, N-donor ligands, 1,2,4-Triazolo-[1,5α]-pyrimidines, 343
NOESY
Adenosine-5′-triphosphate (ATP), Mg(II), Torsion angle (χ), 435
Nona-nuclear copper complex
Trinuclear copper complex, Structural and magnetic properties, 1715
Non-fluorinated β-diketonate ligands
Silver(I) complexes, Monothio-β-ketonate, β-Ketoiminate, Chemical vapor deposition, Crystal structures, 1289
Norbornadiene
Molybdenum, Tin, Crystal structures, Metathesis, Polymerisation, NMR spectra, 2505
Normal coordinate
Cd(II) and Hg(II) complexes, Spectroscopic properties, Force constant, 2-Phenylenediamine, 2-Aminophenol, 987
$N_2O_2S_2$ macrocyle
vic-Dioxime, Nickel(II), Cobalt(II), Copper(II), Iron(II), Uranyl(IV), Electrochemistry, LH_4, 825
N-oxides
Uranyl bis(β-diketonates), Adduct compounds, X-ray structures, 2403
N-(2-Pyridylmethyl)iminodiacetate(2-) ion
Copper(II), *N*-(2-Pyridylmethyl)iminodiacetic acid, 2-(Aminomethyl)pyridine, α-Picolylamine, 2-(2′-Pyridyl)benzimidazole, Crystal structures, Mixed-ligand complexes, Aromatic π,π-staking interactions, Molecular recognition, Thermal stability, Spectral and magnetic properties, 1485
N-(2-Pyridylmethyl)iminodiacetic acid
Copper(II), *N*-(2-Pyridylmethyl)iminodiacetate(2-) ion, 2-(Aminomethyl)pyridine, α-Picolylamine, 2-(2′-Pyridyl)benzimidazole, Crystal structures, Mixed-ligand complexes, Aromatic π,π-staking interactions, Molecular recognition, Thermal stability, Spectral and magnetic properties, 1485
NQR
Isotope effect, Hydrogen bond, Dimer, Crystal structures, Tetrachloroaurate(III), 2207
NS Schiff base
S-methyldithiocarbazate (SMDTC), Cu(II), Ni(II), Zn(II) complexes, Crystal structures of Zn(II) complexes, 2683
N-Thiocyanate
Organotin, Crystal structures, Halides, Azide, Acetate, 1667
Nucleotides
Supramolecular interactions, Tripodal ammonium, Ternary complexes, Zn(II), 1005

Octahedral systems
Conformational change, Schiff's base ligands, Transition metals, 2167
Oligophenols
Uranyl ion, Polyphenols, Crystal structures, 1949
One-dimensional polymers
Cocrystallization, Dinuclear platinum complexes, 715
One-dimensional structures

Zinc(II), Cobalt(II), Coordination complexes, 2705
Optical limiting properties
Crystal structures, Cluster, 2675
Optically active Schiff bases
Co(II), Cu(II) and Ni(II) complexes, CD spectra, Co(II) paramagnetic ^{1}H NMR, 2711
Organic–inorganic hybrid
Polyoxovanadates, Mixed-valence, Hydrothermal synthesis, Cage-like structure, 2601
Organic ligands
Crystal structures, Nickel(II) complexes, Hexaazamacrocycle, Chain complex, 1913
Organometallic phosphine
Multimetallic, π-Allyl molybdenum, Iron carbonyl complexes, Cyclopentadienyl iron complexes, 2301
Organometallics
Heterobimetallics, Organoruthenium, Catalysis, Mössbauer, NMR, 2323
Organometallic
Yttrium, Salen, Amide, Aryloxide, 1683
Organoruthenium
Organometallics, Heterobimetallics, Catalysis, Mössbauer, NMR, 2323
Organotin
Crystal structures, Halides, *N*-Thiocyanate, Azide, Acetate, 1667
Organotin(IV)
Bis(pyrazol-1-yl)alkane, X-ray structures, 873
Organotin(IV) complexes
Dimethylpyrimidinethione, Crystal structures, 1149
Organotin(IV) halide adducts
Porphyrins, Sitting–Atop complexes, Methyltin(IV) tribromide, Tin compounds, Spectral method, 1255
Osmium
Heterocyclic thioamides, Ruthenium, 2-Mercapto-1-methylimidazole, X-ray structures, 885
Osmium(II) complexes
Arylazopyrimidines, Geometrical isomers, X-ray structures, MLCT transitions, Redox property, 753
Osmium(II) complex
Redox activity, Proton-coupled redox process, Pyrazole-3,5-bis(benzimidazole), 2481
Osmium porphyrin
Imido transfer, Phosphines, Kinetics, 1889
Osmium
Ruthenium, Acetylide, Alkyne, Clusters, 1105
Outer-sphere coordination
Lanthanide(III) chelate, Cobalt(III) chelate, Binuclear complexes, Inner-sphere coordination, Stability constant, 805
Oxadiazole complexes
Copper complexes, Structures, Spectroscopic properties, 2257
Oxalate
Nickel, Palladium, Platinum, Crystal structures, Magnetic properties, DFT calculations, 2631
Oxalato-bridged complexes
Copper(II) complexes, Oxalato complexes, Magnetic properties, Crystal structures, 1203
Oxalato complexes
Copper(II) complexes, Oxalato-bridged complexes, Magnetic properties, Crystal structures, 1203
Oxalic acid
Uranyl oxalates, UV–Vis spectrophotometry, Speciation, Stability constants, Aqueous solutions, 1411
Oxidative addition reaction
Perfluoro-*n*-butyl iodide, 1,5-Cyclooctadiene, Fluoroalkyls, 2357
Oxidative addition
Tungsten, Tin, Crystal structures, Hydride, NMR, 1817
Oxidative-alkoxylation
Rhenium(I), Carbonyl, Aminoalcohol, Cytotoxicity, Hydrogen-bonding, 1991
Oximes
Triphenylantimony(V), NMR, X-ray, 2387
Oxoalkoxides
Magnesium, Niobium, Alkoxides, Mass-spectra, Crystal structures, 1629
Oxo-bridged peroxovanadates containing sulphate
Diperoxovanadate, Vanadyl, EDTA inhibition, EDTA bridged heteroligand peroxovanadates, Catalase resistance, 389
oxo-Hydrazido complexes
Molybdenum complexes, Methyl-molybdenum complexes, Phenyl-molybdenum complexes, Diimine, X-ray structures, 2531
Oxo ligands
Chloride ligands, Phenolates, Tungsten, 349
Oxotransfer catalysts
Dioxomolybdenum(VI) bromides, Thiol oxidation, 1635
Oxovanadium(IV) complexes
Carnosine, Potentiometric and spectrophotometric studies, Stability constants, 1513
2,2′-Oxydiethylamine
Lanthanides(III), Oxygen donors, Dimethylsulfoxide, Complexes, Thermodynamics, 1385
Oxygen donors
Lanthanides(III), 2,2′-Oxydiethylamine, Dimethylsulfoxide, Complexes, Thermodynamics, 1385

Palladium
C–H activation, Cyclometallation, Phosphorus ligands, Schiff bases, 39
Palladium complexes
Chiral benzodiazepine ligands, Zinc complexes, Spectroscopy, X-ray structure analysis, Cytostatic and antiviral activity, 2567
Palladium complexes
Crystal structures, Nickel complexes, 2071
Palladium complexes
Platinum complexes, Chiral iminophosphine ligand, 1043
Palladium
Cyclo-addition, Metallacycles, oxo ligands, P ligands, Structure elucidation, 2653
Palladium
2-Hydroxynicotinic acid, Platinum, X-ray crystal structures, Raman spectra, 2783
Palladium(II)
CD spectroscopy, Copper(II), Nickel(II), Peptides, Methionine, 2149
Palladium(II) complexes
Benzyl 8-quinolyl sulfide, Phenethyl 8-quinolyl, Crystal structures, 843
Palladium(II) complexes
Bioligands, Glycine methyl ester hydrolysis, 167
Palladium(II)
N-[2-(4-Methoxyphenyltelluro)ethyl]benzamide, *N*-[2-(4-Methoxyphenyl telluro)-propyl]phthalimide, Platinum(II), Ruthenium(II), Complexes, Crystal structures, 667
Palladium(II)
Phosphine chalcogenide, Seven-membered, Mercury(II), Metallacyclic rings, bis(diphenylthiophosphinyl)ethane, 205
Palladium
Metallation, Schiff base, Phosphorus ligands, X-ray diffraction, 2309
Palladium
N-Benzoylthiourea derivatives, Gold, Solvent extraction, Ion selective electrode, Crystal and molecular structure, 1429
Palladium
Nickel, Chirality, Bidentate nitrogen ligands, Crystal structures, 27
Palladium
Nickel, Platinum, Oxalate, Crystal structures, Magnetic properties, DFT calculations, 2631
Paracyanogen $(CN)_x$
Sulfur dicyanide $S_y(CN)_2$, Polythiocyanogens, ^{13}C NMR spectroscopy, 1825
Paramagnetic
Chromium, Pivalate, Mass spectrometry, NMR, X-ray photoelectron spectroscopy, 155
Partial molar enthalpies of
Potassium *p*-*n*-hexylbenzoate, Potassium *p*-*n*-heptylbenzoate, Potassium *p*-*n*-octylbenzoate, Apparent molar enthalpies of, Micellization enthalpy, Methylene group contribution, 1497
Partition coefficient
Solvation parameter model, Hydrophobic moment, Iron–sulfur protein, Mixed-valence non-integer oxidation number, Cysteine ligand, 1357
Partition function
Equilibria in solution, Cooperativity, Site affinity, Buffer capacity, Heat capacity, 1439
Pb(II) salts
BTZ ligands, X-ray crystallography, π–π stacking interaction, 197
Pd-, Zn-, Cu-complexes

Isoxazolidines, Syntheses, X-ray, NMR, 769
Pentacoordinated
Phosphoranes, X-ray structures, Hydrogen bonding, 1155
Pentacoordinate nickel(II) complexes
Dithiophosphate complexes, Dithiophosphonate complexes, Macrocycle complexes, Crystal structures, 1935
Pentacyaninotrosylferrate(2−) ion
Metastable excited states, X-ray diffraction, FIRRS, TGA, DTA, 1767
Pentacyanoferrate
2-Mercaptobenzoxazole, Kinetics, Equilibrium constants, Electrochemistry, 2137
Pentadentate ligands
Binuclear nickel(II) complexes, Crystal structures, Magnetic properties, Terminal thiocyanato ion complexes, Terminal cyanato ion complexes, 2457
Pentagonal bipyramidal
Acyclic, Binuclear, Pyrazole bridged, Asymmetric unit, 925
Pentamethylphenylmagnesium bromide
Tris(pentamethylphenyl)gallium, Elemental analyses, Single crystal X-ray diffraction, 531
Pentaphenylcyclopentadienyl
Molybdenum, Metallocene, Metallocenium, 1707
Peptide–Cu(II)–isocytosine complexes
Cu(II) complexes, Ternary complexes, Isocytosine complexes, 1197
Peptides
CD spectroscopy, Copper(II), Nickel(II), Palladium(II), Methionine, 2149
Perchlorate
Europium, Photoluminescence, Methylpyridylacetamide, Intensity parameters, 1837
Perfluoro-*n*-butyl iodide
Oxidative addition reaction, 1,5-Cyclooctadiene, Fluoroalkyls, 2357
1,10-Phenanthroline and its 5,6-disubstituted derivatives
Five-coordinated chlorocopper(II) complexes, X-ray structures, Electronic absorption and diffuse reflectance spectra, Cyclic voltammetry, 2143
Phenanthroline
Macrocycles, Cadmium, Polyamines, Dipyridine, 1329
Phenethyl 8-quinolyl
Palladium(II) complexes, Benzyl 8-quinolyl sulfide, Crystal structures, 843
Phenolates
Chloride ligands, Oxo ligands, Tungsten, 349
Phenolic phosphine
Cyclophosphazenes, Polyphosphazenes, Macromolecular complexes, Carbonyls, Spectroscopic characterization, 2579
2-Phenylenediamine
Cd(II) and Hg(II) complexes, Spectroscopic properties, Normal coordinate, Force constant, 2-Aminophenol, 987
Phenyl-molybdenum complexes
Molybdenum complexes, oxo-Hydrazido complexes, Methyl-molybdenum complexes, Diimine, X-ray structures, 2531
Phenylpyridine
Hydrogen-bonding, Silanol, Amine, Adducts, Acridine, 4,4′-bipyridine, 1689
PH-functionalised phosphanylalkyl(silyl)cyclopentadienyl ligands
Zirconium complexes, Titanium complexes, Polymerisation studies, 2445
Phoshocreatine
^{31}P NMR spectroscopy, Sodium complexes, Potassium complexes, Magnesium complexes, 1481
Phosphido
Diphosphine disulfide, Dimanganese decacarbonyl, Phosphidosulfide, 791
Phosphidosulfide
Diphosphine disulfide, Dimanganese decacarbonyl, Phosphido, 791
Phosphine chalcogenide
Seven-membered, Palladium(II), Mercury(II), Metallacyclic rings, bis(diphenylthiophosphinyl)ethane, 205
Phosphine complexes
Mercury(II) halides, Crystal structures, 1845
Phosphine complexes
Thioether complexes, Platinum complexes, Trithiacyclononane, Platinum nuclear magnetic resonance, Crown thioethers, 879
Phosphine oxide
Scandium, Arsine oxide, X-ray structures, ^{45}Sc NMR, 1579
Phosphine oxide
Yttrium, Arsine oxide, X-ray structures, 445
Phosphine
Platinum, Cyclometallation, Imine, Fluorine, Crystal structures, 105
Phosphines
Osmium porphyrin, Imido transfer, Kinetics, 1889
Phosphino amino acids
Ferrocenylmethylphosphine, 1,3-Diaza-5-phosphacyclohexane, 1,5-Diaza-3,7-diphosphacyclooctane, Water-soluble complexes, Trinuclear complexes, 2251
Phosphoranes
Pentacoordinated, X-ray structures, Hydrogen bonding, 1155
Phosphorus ligands
C–H activation, Cyclometallation, Schiff bases, Palladium, 39
Phosphorus ligands
Palladium, Metallation, Schiff base, X-ray diffraction, 2309
Photobleaching
Zinc phthalocyanine, Sensitizer, Singlet oxygen, 2463
Photochemistry
Tertiary amines, Ruthenium complexes, Electrochemistry, 61
Photochromism
Polyoxometalates, Keggin, Charge transfer, 2537
Photoinduced electron transfer
Cyclic voltammetry, Supramolecular preassociation, Ruthenium(II) complexes, 2,2′:6′,2″-Terpyridine, 4′-*p*-Tolyl-2,2′:6′,2″-terpyridine-4-carboxylic acid, 49
Photoluminescence
Europium, Perchlorate, Methylpyridylacetamide, Intensity parameters, 1837
Photolysis
Disilenes, Silenes, Silanones, Matrix isolation, 467
Photosystem II
Tridentate Schiff base ligand, Potassium permanganate, Molecular structures, 1139
$Ph_2P(CH_2)_nNHP^iPr_2$
Diphosphine ligands, Chelate complexes, 2639
Phthalocyanine
Cobalt, Cyanide, Sulfur dioxide, Kinetics, Equilibria, 133
Phthalocyanines
Nitrogen dioxide, Scanning electron microscopy, X-ray microprobe, UV–Vis and FTIR spectroscopy, X-ray powder diffractometry, 677
Phthalocyanines
Phthalonitrile derivatives, Electrochemistry, Nickel, Zinc, Cobalt, 255
Phthalonitrile derivatives
Phthalocyanines, Electrochemistry, Nickel, Zinc, Cobalt, 255
Physico-chemical properties
Crystal structures, Spectroscopy, X-ray diffraction, Imidiazole complexes, 1857
α-Picolylamine
Copper(II), *N*-(2-Pyridylmethyl)iminodiacetic acid, *N*-(2-Pyridylmethyl)iminodiacetate(2-) ion, 2-(Aminomethyl)pyridine, 2-(2′-Pyridyl)benzimidazole, Crystal structures, Mixed-ligand complexes, Aromatic π,π-staking interactions, Molecular recognition, Thermal stability, Spectral and magnetic properties, 1485
Piperazine and piperazin-1-ium ligands
Zn(II)–N bonds, Crystal structures, Zn(II) complexes, 2161
Piperazine
Coordination chemistry, Crystal structures, Homopiperazine, 1729
3-Piperidine
Crystal structures, Thiosemicarbazone, 2-Pyridineformamide, Nickel(II), Spectra, 859
Pivalate
Chromium, Mass spectrometry, Paramagnetic, NMR, X-ray photoelectron spectroscopy, 155
Platinum
Amido, Amine, Triflate, Diphosphazane, Cyclometalation, 1305
Platinum chloride complexes
X-ray structures, N-donor ligands, ^{15}N NMR, 1,2,4-Triazolo-[1,5α]-pyrimidines, 343
Platinum complexes
Palladium complexes, Chiral iminophosphine ligand, 1043

Platinum complexes
Thioether complexes, Trithiacyclononane, Platinum nuclear magnetic resonance, Phosphine complexes, Crown thioethers, 879
Platinum
Cyclometallation, Imine, Fluorine, Phosphine, Crystal structures, 105
Platinum
Gallium, Indium, Heterobimetallic complexes, X-ray structure analysis, Quantum chemical calculations, 535
Platinum
Hexamethyleneimine, 1,1-Cyclobutanedicarboxylato, Synthesis, Crystal structure, 2659
Platinum
2-Hydroxynicotinic acid, Palladium, X-ray crystal structures, Raman spectra, 2783
Platinum(II) complexes
Heptamethyleneimine, Synthesis, Crystal structures, 2369
Platinum(II) complexes
Ribavirin, X-ray structures, NMR and IR analysis, 2001
Platinum(II)
Homopiperazines, Disubstituted sulfides, Synthesis, Crystal structure, 125
Platinum(III) compounds
Lantern-type complexes, Amidate bridging ligands, X-ray structure, 275
Platinum(II)
N-[2-(4-Methoxyphenyltelluro)ethyl]benzamide, *N*-[2-(4-Methoxyphenyl telluro)propyl]phthalimide, Palladium(II), Ruthenium(II), Complexes, Crystal structures, 667
Platinum
Nickel, Palladium, Oxalate, Crystal structures, Magnetic properties, DFT calculations, 2631
Platinum nuclear magnetic resonance
Thioether complexes, Platinum complexes, Trithiacyclononane, Phosphine complexes, Crown thioethers, 879
P ligands
Cyclo-addition, Metallacycles, oxo ligands, Palladium, Structure elucidation, 2653
P-Ligands
2*H*-Azaphosphirene complexes, 2*H*-1,2-Azaphosphole complexes, Cyclisation, 1,3-Dipoles, 119
Plumbylenes
Stannylenes, Distannenes, Diplumbenes, Lewis-amphoteric behavior, 587
^{31}P NMR spectroscopy
Phoshocreatine, Sodium complexes, Potassium complexes, Magnesium complexes, 1481
Polyamine
Bithiophene, Coordination, Cu(II)-electrochemical pattern, Potentiometry, 1523
Polyamine complexes
Linear polyamines, Metal complexes, 1459
Polyamines
Cadmium(II) complexes, X-ray structures, 739
Polyamines
Macrocycles, Cadmium, Dipyridine, Phenanthroline, 1329
Polyamines
Statistical thermodynamic model, Cooperativity effect, Site constant, Cooperativity potential, 1503
Polyamines
Synthesis, Equilibria, Binuclear complexes, 1351
Polyamines
Zinc(II) complexes, Mixed-ligand complexes, Aminohydroxamic acids, NMR spectra, Potentiometry, 2183
Polyazaalkanes ligand
Fluorogenic receptors, Chemosensors, 1397
Polyaza ligands
Lanthanide, Catecholate ligands, Stability constants, Potentiometry, 1393
Polyboron halides
Boron monochloride, Halogen exchange, 543
Polybromides
Actinides, Dioxouranium(VI) polyhalides, Uranyl polyhalides, Polyiodides, 2755
Polycations
Cluster compounds, Crystal structures, Bismuth, Iridium, Rhodium, 651
Polydentate Ni(II) edta-type complexes
Crystal structures, 2667
Polyethylene
Chromium, Crystal structures, Homogeneous catalyst, Electron spin resonance, 867
Polyiodides
Actinides, Dioxouranium(VI) polyhalides, Uranyl polyhalides, Polybromides, 2755
Polymeric zinc(II) complexes
Imidazole-4-acetic acid, Crystal structures, Vibrational spectra, Density functional calculations, 2819
Polymerisation
Molybdenum, Tin, Crystal structures, Metathesis, Norbornadiene, NMR spectra, 2505
Polymerisation studies
PH-functionalised phosphanylalkyl(silyl)cyclopentadienyl ligands, Zirconium complexes, Titanium complexes, 2445
Polynuclear complexes
Ruthenium-ammine, Benzotriazole, Mixed-valence, Electron transfer, Molecular wires, 2089
Polyoxometalates
Heteropolyanions, Ti(IV) complex, Wells-Dawson structure, 353
Polyoxometalates
Keggin, Charge transfer, Photochromism, 2537
Polyoxometalates
Transition metals, Chemical bonding, Molecular orbitals, Density–functional theory, 2201
Polyoxovanadates
Organic–inorganic hybrid, Mixed-valence, Hydrothermal synthesis, Cage-like structure, 2601
Polyphenols
Uranyl ion, Oligophenols, Crystal structures, 1949
Polyphosphazene
Inorganic polymer, Metal–polymer complexes, 2587
Polyphosphazenes
Cyclophosphazenes, Phenolic phosphine, Macromolecular complexes, Carbonyls, Spectroscopic characterization, 2579
Poly(3-Rpyrazolyl)borate cobalt(II) complexes
Structures, NMR, 2743
Polythiocyanogens
Sulfur dicyanide $S_y(CN)_2$, ^{13}C NMR spectroscopy, Paracyanogen $(CN)_x$, 1825
Porphyrins
Adduct formation, Thermodynamics, Tin compounds, Equilibrium constant, Spectral method, 683
Porphyrins
Sitting–Atop complexes, Methyltin(IV) tribromide, Organotin(IV) halide adducts, Tin compounds, Spectral method, 1255
Potassium complexes
Phoshocreatine, ^{31}P NMR spectroscopy, Sodium complexes, Magnesium complexes, 1481
Potassium permanganate
Tridentate Schiff base ligand, Molecular structures, Photosystem II, 1139
Potassium *p*-*n*-heptylbenzoate
Potassium *p*-*n*-hexylbenzoate, Potassium *p*-*n*-octylbenzoate, Apparent molar enthalpies of, Partial molar enthalpies of, Micellization enthalpy, Methylene group contribution, 1497
Potassium *p*-*n*-hexylbenzoate
Potassium *p*-*n*-heptylbenzoate, Potassium *p*-*n*-octylbenzoate, Apparent molar enthalpies of, Partial molar enthalpies of, Micellization enthalpy, Methylene group contribution, 1497
Potassium *p*-*n*-octylbenzoate
Potassium *p*-*n*-hexylbenzoate, Potassium *p*-*n*-heptylbenzoate, Apparent molar enthalpies of, Partial molar enthalpies of, Micellization enthalpy, Methylene group contribution, 1497
Potassium
Rubidium, Amide ligands, 15-Crown-5, Crystal structures, 2451
Potentiometric and spectrophotometric studies
Oxovanadium(IV) complexes, Carnosine, Stability constants, 1513
Potentiometric titration
Cork, Solid state ^{13}C MAS and CP-MAS NMR, Copper, Nickel, Metal uptake, 1363
Potentiometric titrations
Vanadium complexes, Caffeic acid complexes, IR spectra, UV–Vis spectra, Catecholate-like ligand, 1979

Potentiometry
Aminomethane-1,1-diphosphonic acids, Zinc(II) complexes, Magnesium(II) complexes, Calcium(II) complexes, NMR, 321
Potentiometry
Lanthanide, Polyaza ligands, Catecholate ligands, Stability constants, 1393
Potentiometry
Mercapto-carboxylic acid, IR, Formation constants, Ionisation constants, 1319
Potentiometry
Polyamine, Bithiophene, Coordination, Cu(II)-electrochemical pattern, 1523
Potentiometry
Zinc(II) complexes, Mixed-ligand complexes, Aminohydroxamic acids, Polyamines, NMR spectra, 2183
Preparation
1D nickel(II) azido complexes, Pyridine derivative complexes, Crystal structures, Magnetic data, Spectra, 1871
Propadienylidene
Iron, Acetylide, Vinylidene, 1755
Propane-1,3-diamine
Silica gel, Immobilization, Epoxide, 2647
Proton-coupled redox process
Osmium(II) complex, Redox activity, Pyrazole-3,5-bis(benzimidazole), 2481
p-Toluidine-*N*,*N*-di-3-propionic acid
Idp-type ligand, *N*,*N*-Di(2-carboxyethyl)-*p*-toluidine, Square pyramidal copper(II) complexes, Crystal structures, 2719
4′-*p*-Tolyl-2,2′:6′,2″-terpyridine-4-carboxylic acid
Photoinduced electron transfer, Cyclic voltammetry, Supramolecular pre-association, Ruthenium(II) complexes, 2,2′:6′,2″-Terpyridine, 49
2-Pyrazine carboxylic acid
Manganese(II) complexes, 2,6-Pyridinedicarboxylic acid, Chelidamic acid, Crystal structures, Catalytic disproportionation, Hydrogen peroxide, 1063
Pyrazineformamide
Thiosemicarbazone, Zinc, Cadmium, Crystal structures, Electrochemical synthesis, 1553
Pyrazole-3,5-bis(benzimidazole)
Osmium(II) complex, Redox activity, Proton-coupled redox process, 2481
Pyrazole bridged
Acyclic, Binuclear, Asymmetric unit, Pentagonal bipyramidal, 925
Pyrazole
Co(III) complexes, Dithiocarbazate, Synthesis, Spectroscopy, X-ray crystal structures, 1
Pyrazole
Crystal structures, Tungsten complexes, Copper complexes, 1547
Pyrazole
Mononuclear bis(imido) Mo(VI) complexes, X-ray crystal structures, 1211
Pyrazolylthiosemicarbazone
Cobalt(III), ^{1}H NMR, X-ray crystallography, 779
Pyridinecarboxylate complexes
Copper(II) complexes, Spectral properties, Crystal structures, Mononuclear complexes, 365
Pyridine derivative complexes
1D nickel(II) azido complexes, Preparation, Crystal structures, Magnetic data, Spectra, 1871
2,6-Pyridinedicarboxylic acid
Manganese(II) complexes, 2-Pyrazine carboxylic acid, Chelidamic acid, Crystal structures, Catalytic disproportionation, Hydrogen peroxide, 1063
2-Pyridineformamide
Crystal structures, 3-Piperidine, Thiosemicarbazone, Nickel(II), Spectra, 859
2-Pyridineformamide
Thiosemicarbazone, Nickel(II), Zinc(II), Cadmium(II), Crystal structures, 729
Pyridine N-oxide ligands, copper(II) complexes
X-ray structures, Hydrogen bonding, Magnetism, 1561
Pyridine-2-thiolates of ruthenium
Ruthenium aryls, Imine–phenol function, 899
Pyridine-2-thione
Tri-*p*-tolylphosphine, Triphenylphosphine, Sulfur-bridged dimer, Copper(I) complexes, 1603
2-(2′-Pyridyl)benzimidazole
Copper(II), *N*-(2-Pyridylmethyl)iminodiacetic acid, *N*-(2-Pyridylmethyl)iminodiacetate(2-) ion, 2-(Aminomethyl)pyridine, α-Picolylamine, Crystal structures, Mixed-ligand complexes, Aromatic π,π-staking interactions, Molecular recognition, Thermal stability, Spectral and magnetic properties, 1485
2-Pyridylmethanol
Saccharin complexes, Single crystal structures, Thermal analysis, 2393
Pyridylphosphines
Metal–metal interactions, Molybdenum, Rhodium, 1737

Quantum chemical calculations
Gallium, Indium, Platinum, Heterobimetallic complexes, X-ray structure analysis, 535

Raman
Naphthalocyanine, Rare earth, Sandwich complexes, 1905
Raman spectra
2-Hydroxynicotinic acid, Palladium, Platinum, X-ray crystal structures, 2783
Raman spectra
Subvalent indium and gallium, Gallium(II), Indium(I), Indium(II), Halide complexes, 519
Raman spectroscopy
Magnesium phthalocyanines, Magnesium complexes, Crystal structures, IR spectroscopy, UV–Vis spectroscopy, 265
Rare earth complexes
EPR spectroscopy, Coordination structures, 4f-Electron, 2127
Rare earth
Naphthalocyanine, Raman, Sandwich complexes, 1905
Redox activity
Osmium(II) complex, Proton-coupled redox process, Pyrazole-3,5-bis(benzimidazole), 2481
Redox chemistry
Heteropolyoxometalate, Arsenic, Tungstate, Lacunary, Synthesis, 959
Redox property
Arylazopyrimidines, Osmium(II) complexes, Geometrical isomers, X-ray structures, MLCT transitions, 753
Redox
Ruthenium promoted reactions, Dimerization of aromatic amines, 1,2-Diimine, Structures, 97
Redox
Silver, Hydroxylamine, Kinetics, Mechanism, Catalysis, 1893
Reduction
Molybdenum, Crystal structures, Cluster complexes, Acetates, 147
Renner effect
Electronic states, Linear disilaketenylidene (SiSiO), Analogous multiple bonded systems, 599
Resin titration
Natural metal complexes, Natural ligands, Ligand titration, Chelex 100, 1343
Rhenium complexes
Trigonal prismatic geometry, 2-Amidothiophenolato complexes, 1597
Rhenium(I)
Carbonyl, Aminoalcohol, Cytotoxicity, Oxidative-alkoxylation, Hydrogen-bonding, 1991
Rhenium(III) complexes
Iridium(III) complexes, S-bridged polynuclear complexes, Crystal structures, UV–Vis absorption spectra, Cyclic voltammetry, 1809
Rhenium methoxides
Trimetallic alkoxides, Molecular structure, X-ray study, Mass-spectrometric study, Niobium methoxide, Tantalum methoxide, 2317
Rhenium
Nitrosyl, X-ray structures, Electronic structures, Nitric oxide, 2617
Rhodium complexes
Mononuclear complexes, Hydrido complexes, Nitrogen ligands, Crystal structures, 1613
Rhodium
Cyano, Dioxygen, Enhanced reactivity, Structures, 1775
Rhodium
Metal–metal interactions, Molybdenum, Pyridylphosphines, 1737
Rhodium
Polycations, Cluster compounds, Crystal structures, Bismuth, Iridium, 651
Ribavirin
Platinum(II) complexes, X-ray structures, NMR and IR analysis, 2001

RP-HPLC
Urinary trypsin inhibitors, Bubble extraction, Affinity chromatography, 1475
Rubidium
Potassium, Amide ligands, 15-Crown-5, Crystal structures, 2451
Ru(II) complexes
dcbpy, bdmpp, Thiocyanato ligands, Sensitizing ability, 2773
Ruthenium-ammine
Benzotriazole, Polynuclear complexes, Mixed-valence, Electron transfer, Molecular wires, 2089
Ruthenium aryls
Pyridine-2-thiolates of ruthenium, Imine–phenol function, 899
Ruthenium complexes
Tertiary amines, Photochemistry, Electrochemistry, 61
Ruthenium
Heterocyclic thioamides, Osmium, 2-Mercapto-1-methylimidazole, X-ray structures, 885
Ruthenium(II)
Binuclear, Bis(β-diketone), Triphenylarsine, Syntheses, Antibacterial activity, Catalytic study, 219
Ruthenium(II) complexes
Binuclear, Thiobis(β-diketone), Syntheses, Catalytic oxidation, Antibacterial activity, 1721
Ruthenium(II) complexes
Photoinduced electron transfer, Cyclic voltammetry, Supramolecular pre-association, 2,2′:6′,2″-Terpyridine, 4′-*p*-Tolyl-2,2′:6′,2″-terpyridine-4-carboxylic acid, 49
Ruthenium(II) complexes
Semiquinone monochelates, Homolytic hydride cleavage, 2761
Ruthenium(II)
Nitrosyl complexes, NMR spectra, X-ray structures, Diop, Dppb, 2221
Ruthenium(II)
N-[2-(4-Methoxyphenyltelluro)ethyl]benzamide, *N*-[2-(4-Methoxyphenyl telluro)-propyl]phthalimide, Palladium(II), Platinum(II), Complexes, Crystal structures, 667
Ruthenium monoterpyridine complexes
Ancillary functions, Crystal structures, 2033
Ruthenium
Osmium, Acetylide, Alkyne, Clusters, 1105
Ruthenium promoted reactions
Dimerization of aromatic amines, 1,2-Diimine, Structures, Redox, 97

Saccharinate
Nickel, Copper, Zinc, Cadmium, X-ray structures, 395
Saccharin complexes
2-Pyridylmethanol, Single crystal structures, Thermal analysis, 2393
Saccharomyces cerevisiae
Capillary electrophoresis, Hydrophobic interaction chromatography, Heterologous protein, BPTI, 1405
Salen Cu(II) complexes
Schiff-base ligands, Cyclic voltammetry, Hammett substituent constants, 55
Salen ligands
Ni(I) complexes, Nickel(II) complexes, EPR, 1695
Salen
Yttrium, Amide, Aryloxide, Organometallic, 1683
Salicylaldimine adducts
Schiff bases, Interconversion, X-ray crystal structures, Zinc complexes, Zwitterion, 697
Sandwich complexes
Naphthalocyanine, Raman, Rare earth, 1905
S-Benzyldithiocarbazate
Metal complexes, Bioactivity of Schiff bases, Bioactivity of metal complexes, Crystal structure of Cd(II) complexes, 2547
S-bridged polynuclear complexes
Rhenium(III) complexes, Iridium(III) complexes, Crystal structures, UV–Vis absorption spectra, Cyclic voltammetry, 1809
Scandium and lanthanide
Triflates, Triphenylphosphine oxide complexes, Single crystal X-ray diffraction, Catalysis, 287
Scandium
Phosphine oxide, Arsine oxide, X-ray structures, ^{45}Sc NMR, 1579
Scanning electron microscopy
Phthalocyanines, Nitrogen dioxide, X-ray microprobe, UV–Vis and FTIR spectroscopy, X-ray powder diffractometry, 677
Schiff base complexes
Cobalt(II), Nickel(II), Zinc(II), Tetrahedral, Crystal structures, 2733
Schiff base
Eight-coordinate, Zirconium complexes, X-ray crystal structure, Synthon, Heteroleptic, 211
Schiff base
Iron(II), Zinc(II), X-ray crystal structures, ^{1}H NMR spectroscopy, Dioxygen reactivity, 705
Schiff base ligands
Cadmium(II) complexes, Crystal structures, Dithiocarbazate Schiff base crystal structures, Metal complexes, Bioactivity, 2691
Schiff-base ligands
Salen Cu(II) complexes, Cyclic voltammetry, Hammett substituent constants, 55
Schiff base ligand
Uranyl complexes, Morphologies, 2421
Schiff base
Palladium, Metallation, Phosphorus ligands, X-ray diffraction, 2309
Schiff bases
C–H activation, Cyclometallation, Phosphorus ligands, Palladium, 39
Schiff bases
Salicylaldimine adducts, Interconversion, X-ray crystal structures, Zinc complexes, Zwitterion, 697
Schiff bases
Vanadyl complexes, Chiral complexes, EPR, X-ray structures, 2021
Schiff's base ligands
Conformational change, Octahedral systems, Transition metals, 2167
^{45}Sc NMR
Scandium, Phosphine oxide, Arsine oxide, X-ray structures, 1579
Scorpionate ligands
Thallium(I) complexes, Crystal packing, π-Stacking, Cation–π interaction, 553
Secondary phosphine
Dimesitylphosphine, X-ray crystallography, NMR, Cone angle, Fluxional, 2409
Self-assembly
Copper, Supramolecules, X-ray structures, 1621
Self-propagating
Silicides, Solid state metathesis, 187
Semi-bridging carbonyl
Crystal structures, Cobalt(I) clusters, Interstitial phosphorus atom, Heterocyclic phosphide, Substituted site, 1073
Semi-empirical calculations
Carbohydrates, Cobalt complexes, Circular dichroism, Sucrose complexes, ^{1}H NMR, 2215
Semiquinone monochelates
Ruthenium(II) complexes, Homolytic hydride cleavage, 2761
Sensitizer
Zinc phthalocyanine, Singlet oxygen, Photobleaching, 2463
Sensitizing ability
Ru(II) complexes, dcbpy, bdmpp, Thiocyanato ligands, 2773
Separation of isomers
Crystal structures, Copper(II) complexes, Cyclohexanediols, 1133
Seven-membered
Phosphine chalcogenide, Palladium(II), Mercury(II), Metallacyclic rings, bis(diphenylthiophosphinyl)ethane, 205
Silanol
Hydrogen-bonding, Amine, Adducts, Acridine, 4,4′-bipyridine, Phenylpyridine, 1689
Silanones
Disilenes, Silenes, Matrix isolation, Photolysis, 467
Silenes
Disilenes, Silanones, Matrix isolation, Photolysis, 467
Silica gel
Immobilization, Epoxide, Propane-1,3-diamine, 2647
Silicides
Solid state metathesis, Self-propagating, 187
Silver
Azide, Germanium, Tin, Tris(pyrazolyl)borate, Aminotroponimine, 611
Silver
Hydroxylamine, Kinetics, Mechanism, Redox, Catalysis, 1893

Silver(I) complexes
Non-fluorinated β-diketonate ligands, Monothio-β-ketonate, β-Ketoiminate, Chemical vapor deposition, Crystal structures, 1289
Silver(I) complexes
Thiones, NMR studies, 1267
Silver(I)
Nicotinamide, Nicotinic acid, Sulfonate, Hydrogen bond, Ag–Ag interaction, Assembly chemistry, 689
Silver(I)
N-methylated polyamines, Complexes, Dimethylsulfoxide, Thermodynamics, 1337
Silver(I)
Trinuclear complexes, Single crystal structures, Copper(II), Carboxylate, Thioether, 33
Single crystals
Solventothermal synthesis, Crystal structures, Coordination polymers, Copper methoxide, 2017
Single crystal structures
2-Pyridylmethanol, Saccharin complexes, Thermal analysis, 2393
Single crystal structures
Trinuclear complexes, Copper(II), Silver(I), Carboxylate, Thioether, 33
Single crystal X-ray diffraction
Triflates, Triphenylphosphine oxide complexes, Scandium and lanthanide, Catalysis, 287
Single crystal X-ray diffraction
Tris(pentamethylphenyl)gallium, Pentamethylphenylmagnesium bromide, Elemental analyses, 531
Single-crystal X-ray
Iron(III), N-donor, Terpyridyl, 2055
Single-crystal X-ray
Metal alkoxides, Esterification, Group V, Tantalum, Niobium, 2333
Single-helical-strand
Mono-helical, Mono-bridged species, Coordination chemistry, Transition metals, X-ray crystallography, 1177
Singlet oxygen
Zinc phthalocyanine, Sensitizer, Photobleaching, 2463
Site affinity
Partition function, Equilibria in solution, Cooperativity, Buffer capacity, Heat capacity, 1439
Site constant
Statistical thermodynamic model, Cooperativity effect, Cooperativity potential, Polyamines, 1503
Sitting–Atop complexes
Porphyrins, Methyltin(IV) tribromide, Organotin(IV) halide adducts, Tin compounds, Spectral method, 1255
Six-coordinate geometry
Macrocycles, Germanium(IV) tmtaa complexes, Crystal structures, *Trans*-positions, 969
S-methyldithiocarbazate (SMDTC)
NS Schiff base, Cu(II), Ni(II), Zn(II) complexes, Crystal structures of Zn(II) complexes, 2683
Sn(IV) complexes
Tin enolates, Diorganohydroxytin, Diorganotin, Malonates, Di-*n*-butylhydroxytin(IV), 417
Sodium complexes
Phoshocreatine, ^{31}P NMR spectroscopy, Potassium complexes, Magnesium complexes, 1481
Sodium complexes
tert-Butylcalix[4]arenes, Amide, Yttrium(III) complexes, Lanthanide(III) complexes, X-ray structures, 763
Sodium ion
Alkali metal ions, Caesium ion, Calix[4]arene, Crystal structures, 2497
Solid state ^{13}C MAS and CP-MAS NMR
Cork, Copper, Nickel, Potentiometric titration, Metal uptake, 1363
Solid state metathesis
Silicides, Self-propagating, 187
Solid state structures
Copper(I), Anions, Dppe, Coordination mode, 2433
Solid state supramolecular complexes
Dibenzotetraaza[14]annulenes, Macrocyclic Ni(II) complexes, Succinyl dichloride, Crystal structures, 7
Solutions
Equilibria, Cations, Hydrolysis, Titration, Masking, 1369
Solvation parameter model
Partition coefficient, Hydrophobic moment, Iron–sulfur protein, Mixed-valence non-integer oxidation number, Cysteine ligand, 1357
Solvent extraction
N-Benzoylthiourea derivatives, Gold, Palladium, Ion selective electrode, Crystal and molecular structure, 1429
Solventothermal synthesis
Crystal structures, Coordination polymers, Copper methoxide, Single crystals, 2017
Speciation
Uranyl oxalates, Oxalic acid, UV–Vis spectrophotometry, Stability constants, Aqueous solutions, 1411
Spectra
Copper(II) complexes, Imidazole, 9,10-dihydro-9-oxo-10-acridineacetate, Crystal structures, Magnetic measurements, 2381
Spectra
Crystal structures, 3-Piperidine, Thiosemicarbazone, 2-Pyridineformamide, Nickel(II), 859
Spectra
1D nickel(II) azido complexes, Pyridine derivative complexes, Preparation, Crystal structures, Magnetic data, 1871
Spectral and magnetic properties
Copper(II), *N*-(2-Pyridylmethyl)iminodiacetic acid, *N*-(2-Pyridylmethyl)iminodiacetate(2-) ion, 2-(Aminomethyl)pyridine, α-Picolylamine, 2-(2′-Pyridyl)benzimidazole, Crystal structures, Mixed-ligand complexes, Aromatic π,π-staking interactions, Molecular recognition, Thermal stability, 1485
Spectral method
Adduct formation, Thermodynamics, Tin compounds, Porphyrins, Equilibrium constant, 683
Spectral method
Porphyrins, Sitting–Atop complexes, Methyltin(IV) tribromide, Organotin(IV) halide adducts, Tin compounds, 1255
Spectral properties
Copper(II) complexes, Crystal structures, Pyridinecarboxylate complexes, Mononuclear complexes, 365
Spectroelectrochemistry
Nitrogenase, Hydrazido(2-), Molybdenum, Crystal structures, 849
Spectroscopic characterization
α-Aminoisobutyryl-α-aminoisobutyric acid (H–Aib–Aib–OH), Copper(II) peptide complexes, X-ray crystal structures, 229
Spectroscopic characterization
Cyclophosphazenes, Polyphosphazenes, Phenolic phosphine, Macromolecular complexes, Carbonyls, 2579
Spectroscopic properties
Cd(II) and Hg(II) complexes, Normal coordinate, Force constant, 2-Phenylenediamine, 2-Aminophenol, 987
Spectroscopic properties
Copper complexes, Structures, Oxadiazole complexes, 2257
Spectroscopic study
Trinuclear complexes, Cyano-bridge, Crystal structures, 2237
Spectroscopy
Chiral benzodiazepine ligands, Zinc complexes, Palladium complexes, X-ray structure analysis, Cytostatic and antiviral activity, 2567
Spectroscopy
Co(III) complexes, Pyrazole, Dithiocarbazate, Synthesis, X-ray crystal structures, 1
Spectroscopy
Crystal structures, Physico-chemical properties, X-ray diffraction, Imidiazole complexes, 1857
Spectroscopy
Di-2-pyridyl ketone benzoylhydrazone, Nickel(II) complexes, Thermal analyses, 2375
S=PEt$_3$ ligand
Synthesis, Mo/Fe/S cluster, Structures, CO, 2523
Spin crossover
Iron(III) dialkyldithiocarbamates, Mössbauer spectra, Magnetic moment, Thermal decomposition, 2489
Spin polarization
DFT calculations, Dinuclear transition metal complexes, Electron transfer, Magnetic coupling, Metal–metal bonding, 1163
Square pyramidal copper(II) complexes
Idp-type ligand, *N*,*N*-Di(2-carboxyethyl)-

p-toluidine, *p*-Toluidine-*N*,*N*-di-3-propionic acid, Crystal structures, 2719
Stability constant
Lanthanide(III) chelate, Cobalt(III) chelate, Binuclear complexes, Inner-sphere coordination, Outer-sphere coordination, 805
Stability constants
Artificial neural networks, Experimental design, Metal complexes, Ion selective electrodes, Metal–ligand equilibria, 1375
Stability constants
Edta-derived macrocycles, Macrocyclic ether bis(lactones), EPR of Cu(II) complexes, EPR of dinuclear Cu–Cu complexes, Hydrolysis of macrocycles, 2265
Stability constants
Lanthanide, Polyaza ligands, Catecholate ligands, Potentiometry, 1393
Stability constants
Oxovanadium(IV) complexes, Carnosine, Potentiometric and spectrophotometric studies, 1513
Stability constants
Uranyl oxalates, Oxalic acid, UV–Vis spectrophotometry, Speciation, Aqueous solutions, 1411
π–π stacking interaction
BTZ ligands, X-ray crystallography, Pb(II) salts, 197
π-Stacking
Thallium(I) complexes, Scorpionate ligands, Crystal packing, Cation–π interaction, 553
Stannylenes
Plumbylenes, Distannenes, Diplumbenes, Lewis-amphoteric behavior, 587
Statistical thermodynamic model
Cooperativity effect, Site constant, Cooperativity potential, Polyamines, 1503
Stereochemistry
Copper complexes, X-ray structures, Steric properties, 1031
Steric properties
Copper complexes, Stereochemistry, X-ray structures, 1031
Stoichiometry
Isoquercitrin, Al(III) complexes, UV–Vis Spectroscopy, DFT calculations, FT Raman, 2801
Structural and magnetic properties
Nona-nuclear copper complex, Trinuclear copper complex, 1715
Structure elucidation
Cyclo-addition, Metallacycles, oxo ligands, P ligands, Palladium, 2653
Structure elucidation
Titanium, Chelate, Coordination chemistry, 8-Hydroxyquinolinate, 1081
Structures
Cadmium(II), Aspartate, ^{111}Cd NMR, 935
Structures
Cerium, Fluoroalkoxides, Complexes, MOCVD, Films, 1985
Structures
$C_{10}H_{20}N_2S_4Zn\cdot C_5H_5N$, Isomorphism, ^{15}N CP/MAS NMR spectroscopy, 2727
Structures
Copper complexes, Spectroscopic properties, Oxadiazole complexes, 2257
Structures
Gallium, Indium, Dithiocarbamates, Dialkyldithiophosphates, ^{71}Ga NMR, 239
Structures
Poly(3-Rpyrazolyl)borate cobalt(II) complexes, NMR, 2743
Structures
Rhodium, Cyano, Dioxygen, Enhanced reactivity, 1775
Structures
Ruthenium promoted reactions, Dimerization of aromatic amines, 1,2-Diimine, Redox, 97
Structures
Synthesis, Mo/Fe/S cluster, S=PEt$_3$ ligand, CO, 2523
3-Substituted-1,2-diaminopropanes
Lanthanide(III) complexes, Macrocyclic ligands, 2,6-Diacetylpyridine, 425
Substituted site
Crystal structures, Cobalt(I) clusters, Interstitial phosphorus atom, Heterocyclic phosphide, Semi-bridging carbonyl, 1073
Subvalent indium and gallium
Gallium(II), Indium(I), Indium(II), Halide complexes, Raman spectra, 519
Succinyl dichloride
Dibenzotetraaza[14]annulenes, Macrocyclic Ni(II) complexes, Crystal structures, Solid state supramolecular complexes, 7
Sucrose complexes
Carbohydrates, Cobalt complexes, Circular dichroism, ^{1}H NMR, Semi-empirical calculations, 2215
Sulfate complexes
Crystal structures, Copper complexes, Di-2-pyridylamine complexes, Tetrathionate complexes, Trifluoromethanesulfonate complexes, Hexafluorophosphate complexes, 247
Sulfate complexes
Crystal structures, Copper(II) complexes, Nitrite complexes, di-2-Pyridylamine complexes, Thiocyanato complexes, 1279
Sulfido
Triosmium cluster, Tetramethylthiourea, Desulfurization, X-ray structures, 381
Sulfonamide complexes
Nickel complexes, 8-Aminoquinoline, X-ray crystal structures, 1229
Sulfonate
Silver(I), Nicotinamide, Nicotinic acid, Hydrogen bond, Ag–Ag interaction, Assembly chemistry, 689
Sulfur-bridged dimer
Pyridine-2-thione, Tri-*p*-tolylphosphine, Triphenylphosphine, Copper(I) complexes, 1603
Sulfur
Cysteamine, Cysteine, Hydrogen bonding, 225
Sulfur dicyanide $S_y(CN)_2$
Polythiocyanogens, ^{13}C NMR spectroscopy, Paracyanogen $(CN)_x$, 1825
Sulfur dioxide
Cobalt, Phthalocyanine, Cyanide, Kinetics, Equilibria, 133
Sulfur dioxide
Zinc(II)tetrasulfophthalocyanine, Fluorescence quenching, Association constants, 951
Superconductors
Chemical bonding topology, Magnesium diboride, Cuprate superconductors, 2347
Supramolecular assembly
Uranyl ion, Calixarenes, Homooxacalixarenes, Crystal structures, 1125
Supramolecular chemistry
Gallium–gallium bonds, Macrocycles, 511
Supramolecular interactions
Tripodal ammonium, Nucleotides, Ternary complexes, Zn(II), 1005
Supramolecular polymer
Cyclophosphazene, Coordination bonding, Hairy-rod structure, Lamellar packing, 1573
Supramolecular pre-association
Photoinduced electron transfer, Cyclic voltammetry, Ruthenium(II) complexes, 2,2′:6′,2″-Terpyridine, 4′-*p*-Tolyl-2,2′:6′,2″-terpyridine-4-carboxylic acid, 49
Supramolecules
Copper, Self-assembly, X-ray structures, 1621
Symbiosis
Cadmium(II) complexes, Coordination polymers, Crystal structures, 2293
Syntheses
Binuclear, Ruthenium(II) complexes, Thiobis(β-diketone), Catalytic oxidation, Antibacterial activity, 1721
Syntheses
Isoxazolidines, Pd-, Zn-, Cu-complexes, X-ray, NMR, 769
Syntheses
Ruthenium(II), Binuclear, Bis(β-diketone), Triphenylarsine, Antibacterial activity, Catalytic study, 219
Synthesis and electrochemistry
Asymmetric 14-π nickel(II) tetraazaannulene, Hammett plot, Electrocatalysis, 917
Synthesis
Boron complexes, Benzohydroximate anion, Crystal structures, 2351
Synthesis
Cobalt(III) complexes, 4-Methyl-2,6-dibenzoylphenol, NMR, TGA, Cyclic voltammetry, X-ray structures, 1787
Synthesis
Co(III) complexes, Pyrazole, Dithiocarbazate, Spectroscopy, X-ray crystal structures, 1
Synthesis
Crystal structures, X-ray diffraction, 1883
Synthesis
Cyano(selenone)gold(I) complexes, ^{13}C and ^{15}N NMR spectroscopy, 2099
Synthesis
Equilibria, Binuclear complexes, Polyamines, 1351
Synthesis

Heteropolyoxometalate, Arsenic, Tungstate, Lacunary, Redox chemistry, 959
Synthesis
Metal-organic frameworks (MOF), Crystal structures, TGA–DTA, 175
Synthesis
Mo/Fe/S cluster, Structures, S=PEt$_3$ ligand, CO, 2523
Synthesis
Platinum, Hexamethyleneimine, 1,1-Cyclobutanedicarboxylato, Crystal structure, 2659
Synthesis
Platinum(II) complexes, Heptamethyleneimine, Crystal structures, 2369
Synthesis
Platinum(II), Homopiperazines, Disubstituted sulfides, Crystal structure, 125
Synthon
Eight-coordinate, Schiff base, Zirconium complexes, X-ray crystal structure, Heteroleptic, 211

Tantalum
Metal alkoxides, Esterification, Single-crystal X-ray, Group V, Niobium, 2333
Tantalum
Metallocenes, Hydrides, Metallophosphines, Bimetallics, X-ray structures, 371
Tantalum methoxide
Trimetallic alkoxides, Molecular structure, X-ray study, Mass-spectrometric study, Rhenium methoxides, Niobium methoxide, 2317
Tantalum(V)
Bis-sulfamide, Diamide, Crystal structures, 1051
Tellurium dichloride
Chloridotellurate anions, X-ray crystallography, NMR spectroscopy, 1089
Template effect
Nickel(II) complexes, Heterotrinuclear complexes, BF_2^+-capped complexes, Dioxadithiadiazamacrobicycle, *vic*-Dioxime, 1865
Terminal cyanato ion complexes
Binuclear nickel(II) complexes, Crystal structures, Magnetic properties, Terminal thiocyanato ion complexes, Pentadentate ligands, 2457
Terminal thiocyanato ion complexes
Binuclear nickel(II) complexes, Crystal structures, Magnetic properties, Terminal cyanato ion complexes, Pentadentate ligands, 2457
Terminal tungsten complexes
Digermene, Germylene, X-ray crystallographic analysis, Dissociation, Equilibrium, Bond dissociation energy, Dioxadigermetane, 563
Ternary complexes
Crystal structures, Kinetic studies, 2045
Ternary complexes
Cu(II) complexes, Peptide–Cu(II)–isocytosine complexes, Isocytosine complexes, 1197
Ternary complexes
Supramolecular interactions, Tripodal ammonium, Nucleotides, Zn(II), 1005
2,2′:6′,2″-Terpyridine
Photoinduced electron transfer, Cyclic voltammetry, Supramolecular pre-association, Ruthenium(II) complexes, 4′-*p*-Tolyl-2,2′:6′,2″-terpyridine-4-carboxylic acid, 49
Terpyridyl
Iron(III), Single-crystal X-ray, N-donor, 2055
tert-Butylcalix[4]arenes
Amide, Sodium complexes, Yttrium(III) complexes, Lanthanide(III) complexes, X-ray structures, 763
Tertiary amines
Ruthenium complexes, Photochemistry, Electrochemistry, 61
Tetrabromocuprate(II)
Crystal structures, Magnetic properties, Thermal properties, *n*-Ethylpyridinium, 19
Tetrachloroaurate(III)
Isotope effect, Hydrogen bond, Dimer, Crystal structures, NQR, 2207
Tetrachlorocuprate(II)
Aminoguanidonium, Copper(II) halides, Crystal structures, 409
Tetrachlorocuprate
Thermochromism, Crystal structures, Benzimidazolium, 2561
Tetrachlorogallate salt
Gallium pyrazole complexes, Gallium trichloride, 3,5-diphenylpyrazole, 1117
Tetradentate ligands
Cobalt(III) complexes, Bidentate ligands, Eddp, 2277
Tetrahedral
Schiff base complexes, Cobalt(II), Nickel(II), Zinc(II), Crystal structures, 2733
Tetramethylthiourea
Triosmium cluster, Desulfurization, Sulfido, X-ray structures, 381
Tetramines
Ni(II), Co(II), Adenosine 5′-monophosphate, Mixed-ligand complexes, 745
Tetranuclear copper(II) complexes
Crystal structures, Magnetism, Antiferromagnetic coupling, Molecular orbital calculation, 1539
Tetrathionate complexes
Crystal structures, Copper complexes, Di-2-pyridylamine complexes, Trifluoromethanesulfonate complexes, Sulfate complexes, Hexafluorophosphate complexes, 247
TGA–DTA
Metal-organic frameworks (MOF), Synthesis, Crystal structures, 175
TGA
Pentacyaninotrosylferrate(2−) ion, Metastable excited states, X-ray diffraction, FIRRS, DTA, 1767
TGA
Synthesis, Cobalt(III) complexes, 4-Methyl-2,6-dibenzoylphenol, NMR, Cyclic voltammetry, X-ray structures, 1787
Thallium(I) complexes
Crystal structure, Nitrophenoxide complexes, 2555
Thallium(I) complexes
Scorpionate ligands, Crystal packing, π-Stacking, Cation–π interaction, 553
The 2,6-bis(dimethylamino)phenyl ligand
Arylmetal complexes, Mercury(II), Boron, 635
Thermal analyses
Di-2-pyridyl ketone benzoylhydrazone, Nickel(II) complexes, Spectroscopy, 2375
Thermal analysis
2-Pyridylmethanol, Saccharin complexes, Single crystal structures, 2393
Thermal decomposition
Iron(III) dialkyldithiocarbamates, Mössbauer spectra, Magnetic moment, Spin crossover, 2489
Thermal properties
Crystal structures, Magnetic properties, Tetrabromocuprate(II), *n*-Ethylpyridinium, 19
Thermal stability
Copper(II), *N*-(2-Pyridylmethyl)iminodiacetic acid, *N*-(2-Pyridylmethyl)iminodiacetate(2-) ion, 2-(Aminomethyl)pyridine, α-Picolylamine, 2-(2′-Pyridyl)benzimidazole, Crystal structures, Mixed-ligand complexes, Aromatic π,π-staking interactions, Molecular recognition, Spectral and magnetic properties, 1485
Thermochromism
Crystal structures, Benzimidazolium, Tetrachlorocuprate, 2561
Thermodynamics
Adduct formation, Tin compounds, Porphyrins, Equilibrium constant, Spectral method, 683
Thermodynamics group
Complex history, Complex pioneers, Coordination chemistry, 1313
Thermodynamics
Lanthanides(III), Oxygen donors, 2,2′-Oxydiethylamine, Dimethylsulfoxide, Complexes, 1385
Thermodynamics
Silver(I), *N*-methylated polyamines, Complexes, Dimethylsulfoxide, 1337
Thermolysis
Iminophosphorane, Cycloaddition, Four-membered ring compounds, Aza-Wittig reaction, X-ray analysis, 657
Thiadiazole
M = Co, M = Ni, M = Cu, Crystal structures, Monomeric complexes, 403
Thin film
Tin phosphide, APCVD, 1943
Thiobis(β-diketone)
Binuclear, Ruthenium(II) complexes, Syntheses, Catalytic oxidation, Antibacterial activity, 1721
Thiocarbodihydrazone Schiff base
Dioxomolybdenum(VI) complexes, X-ray structures, 1023
Thiocyanate ligands
Hemidirected, Lead(II) complexes, Crystal

structures, 1223
Thiocyanate
Tris(pyrazolyl)borate and 2,6-pyridyl-diimine ligands, Cadmium(II), Lead(II), 1795
Thiocyanato complexes
Crystal structures, Copper(II) complexes, Nitrite complexes, Sulfate complexes, di-2-Pyridylamine complexes, 1279
Thiocyanato ligands
Ru(II) complexes, dcbpy, bdmpp, Sensitizing ability, 2773
Thioether complexes
Platinum complexes, Trithiacyclononane, Platinum nuclear magnetic resonance, Phosphine complexes, Crown thioethers, 879
Thioether
Trinuclear complexes, Single crystal structures, Copper(II), Silver(I), Carboxylate, 33
Thiolate
Nickel, *cis*-1,2-Bis(diphenylphosphino)-ethene, X-ray structures, 421
Thiol oxidation
Dioxomolybdenum(VI) bromides, Oxo-transfer catalysts, 1635
Thiones
Silver(I) complexes, NMR studies, 1267
Thiosemicarbazone
Cobalt(III), X-ray crystal studies, ^{1}H NMR, IR, Electronic spectra, 2515
Thiosemicarbazone
Crystal structures, 3-Piperidine, 2-Pyridineformamide, Nickel(II), Spectra, 859
Thiosemicarbazone
Pyrazineformamide, Zinc, Cadmium, Crystal structures, Electrochemical synthesis, 1553
Thiosemicarbazone
2-Pyridineformamide, Nickel(II), Zinc(II), Cadmium(II), Crystal structures, 729
Thiosemicarbazones
Dimethylthallium(III), Crystal structures, IR spectra, ^{1}H, ^{13}C NMR spectra, 1651
Thiosemicarbazones
Zinc, Halide complexes, Ligand, 1217
Thiosemicarbazone
X-ray, Isatin, Metal complexes, 2593
Ti(IV) complex
Polyoxometalates, Heteropolyanions, Wells-Dawson structure, 353
Tin
Azide, Germanium, Silver, Tris(pyrazolyl)borate, Aminotroponimine, 611
Tin
C_3-chiral triamidostannate, Amides, Lithium, 629
Tin compounds
Adduct formation, Thermodynamics, Porphyrins, Equilibrium constant, Spectral method, 683
Tin compounds
Porphyrins, Sitting–Atop complexes, Methyltin(IV) tribromide, Organotin(IV) halide adducts, Spectral method, 1255
Tin enolates
Diorganohydroxytin, Diorganotin, Sn(IV) complexes, Malonates, Di-*n*-butylhydroxytin(IV), 417
Tin
Guanidinate, 1,3,4,6,7,8-Hexahydro-2*H*-pyramido[1,2-*a*]pyramidinate, Mononuclear, Dinuclear, 619
Tin
Molybdenum, Crystal structures, Metathesis, Polymerisation, Norbornadiene, NMR spectra, 2505
Tin phosphide
Thin film, APCVD, 1943
Tin
Tungsten, Oxidative addition, Crystal structures, Hydride, NMR, 1817
Titanium
Chelate, Coordination chemistry, Structure elucidation, 8-Hydroxyquinolinate, 1081
Titanium complexes
PH-functionalised phosphanylalkyl(silyl)cyclopentadienyl ligands, Zirconium complexes, Polymerisation studies, 2445
Titanium
Molecular orbital, Ab initio, Mechanism, Intermolecular nucleophilic attack, Ylid, 2699
Titration
Solutions, Equilibria, Cations, Hydrolysis, Masking, 1369
Torsion angle (χ)
Adenosine-5′-triphosphate (ATP), Mg(II), NOESY, 435
Trans influence
Crystal structures, Ligand-field strength, Tripodal tridentate phosphine, Acetylacetonate complexes, Chromium(III) complexes, 835
Transition metals
Conformational change, Four or five coordinate geometry, Metal centre, 2175
Transition metals
Conformational change, Schiff's base ligands, Octahedral systems, 2167
Transition metals
Mono-helical, Single-helical-strand, Mono-bridged species, Coordination chemistry, X-ray crystallography, 1177
Transition metals
Polyoxometalates, Chemical bonding, Molecular orbitals, Density–functional theory, 2201
Trans-positions
Macrocycles, Germanium(IV) tmtaa complexes, Crystal structures, Six-coordinate geometry, 969
Trialkylaluminum
Aminoalane, Dibenzylamine, NMR, Mass spectrometry, Molecular structure, 1747
Triazole derivatives
Mononuclear complexes, Crystal structures, 797
1,2,4-Triazolo-[1,5α]-pyrimidines
Platinum chloride complexes, X-ray structures, N-donor ligands, ^{15}N NMR, 343
Tridentate Schiff base ligand
Potassium permanganate, Molecular structures, Photosystem II, 1139
Triflate
Amido, Amine, Platinum, Diphosphazane, Cyclometalation, 1305
Triflates
Triphenylphosphine oxide complexes, Single crystal X-ray diffraction, Scandium and lanthanide, Catalysis, 287
Trifluoromethanesulfonate complexes
Crystal structures, Copper complexes, Di-2-pyridylamine complexes, Tetrathionate complexes, Sulfate complexes, Hexafluorophosphate complexes, 247
Trigonal prismatic geometry
Rhenium complexes, 2-Amidothiophenolato complexes, 1597
Trimetallic alkoxides
Molecular structure, X-ray study, Mass-spectrometric study, Rhenium methoxides, Niobium methoxide, Tantalum methoxide, 2317
Trinuclear complexes
Aluminium, Diols, 2,2′-Di(hydroxymethyl)biphenyl, Crystal structures, Alkylaluminium diolates, 281
Trinuclear complexes
Cyano-bridge, Crystal structures, Spectroscopic study, 2237
Trinuclear complexes
Ferrocenylmethylphosphine, Phosphino amino acids, 1,3-Diaza-5-phosphacyclohexane, 1,5-Diaza-3,7-diphosphacyclooctane, Water-soluble complexes, 2251
Trinuclear complexes
Single crystal structures, Copper(II), Silver(I), Carboxylate, Thioether, 33
Trinuclear copper complex
Nona-nuclear copper complex, Structural and magnetic properties, 1715
Trinuclear metal chelates
β-Aminovinylimines, Chemical and electrochemical synthesis, 2081
Trinuclear
Mixed-valence compound, Electron transfer, Iron, Iodoacetate, Heat capacity, 1299
Triosmium cluster
Tetramethylthiourea, Desulfurization, Sulfido, X-ray structures, 381
Triphenylantimony(V)
Oximes, NMR, X-ray, 2387
Triphenylarsine
Ruthenium(II), Binuclear, Bis(β-diketone), Syntheses, Antibacterial activity, Catalytic study, 219
Triphenylphosphine
Dithiocarbimates, Nickel complexes, Crystal structures, 2243
Triphenylphosphine oxide complexes
Triflates, Single crystal X-ray diffraction, Scandium and lanthanide, Catalysis, 287
Triphenylphosphine
Pyridine-2-thione, Tri-*p*-tolylphosphine, Sulfur-bridged dimer, Copper(I) complexes, 1603
Tripodal ammonium
Supramolecular interactions, Nucleotides,

Ternary complexes, Zn(II), 1005
Tripodal tridentate phosphine
Trans influence, Crystal structures, Ligand-field strength, Acetylacetonate complexes, Chromium(III) complexes, 835
Tri-*p*-tolylphosphine
Pyridine-2-thione, Triphenylphosphine, Sulfur-bridged dimer, Copper(I) complexes, 1603
Tris(pentamethylphenyl)gallium
Pentamethylphenylmagnesium bromide, Elemental analyses, Single crystal X-ray diffraction, 531
Tris(pyrazolyl)borate and 2,6-pyridyl-diimine ligands
Thiocyanate, Cadmium(II), Lead(II), 1795
Tris(pyrazolyl)borate
Azide, Germanium, Tin, Silver, Aminotroponimine, 611
Trithiacyclononane
Thioether complexes, Platinum complexes, Platinum nuclear magnetic resonance, Phosphine complexes, Crown thioethers, 879
Tungstate
Heteropolyoxometalate, Arsenic, Lacunary, Synthesis, Redox chemistry, 959
Tungsten
Alkoxides, Crystal structures, Lithium, Methoxide, 193
Tungsten
Chloride ligands, Oxo ligands, Phenolates, 349
Tungsten complexes
Crystal structures, Pyrazole, Copper complexes, 1547
Tungsten
Tin, Oxidative addition, Crystal structures, Hydride, NMR, 1817

Uranyl bis(β-diketonates)
N-oxides, Adduct compounds, X-ray structures, 2403
Uranyl complexes
Morphologies, Schiff base ligand, 2421
Uranyl
Dimethylmelonate, Counter-cation, CPMAS ^{13}C NMR, X-ray crystallography, 69
Uranyl ion
Calixarenes, Homooxacalixarenes, Supramolecular assembly, Crystal structures, 1125
Uranyl ion
Polyphenols, Oligophenols, Crystal structures, 1949
Uranyl
Malonato complexes, CPMAS ^{13}C NMR, X-ray crystallography, 81
Uranyl oxalates
Oxalic acid, UV–Vis spectrophotometry, Speciation, Stability constants, Aqueous solutions, 1411
Uranyl polyhalides
Actinides, Dioxouranium(VI) polyhalides, Polybromides, Polyiodides, 2755
Urea and thiourea derivatives
Diruthenium carboxylates, Crystal structures, Infrared spectroscopy, 1235
Urinary trypsin inhibitors
Bubble extraction, Affinity chromatography, RP-HPLC, 1475
UV–Vis absorption spectra
Rhenium(III) complexes, Iridium(III) complexes, S-bridged polynuclear complexes, Crystal structures, Cyclic voltammetry, 1809
UV–Vis and FTIR spectroscopy
Phthalocyanines, Nitrogen dioxide, Scanning electron microscopy, X-ray microprobe, X-ray powder diffractometry, 677
UV–Vis spectra
Vanadium complexes, Caffeic acid complexes, IR spectra, Potentiometric titrations, Catecholate-like ligand, 1979
UV–Vis spectrophotometry
Uranyl oxalates, Oxalic acid, Speciation, Stability constants, Aqueous solutions, 1411
UV–Vis Spectroscopy
Isoquercitrin, Al(III) complexes, Stoichiometry, DFT calculations, FT Raman, 2801
UV–Vis spectroscopy
Magnesium phthalocyanines, Magnesium complexes, Crystal structures, IR spectroscopy, Raman spectroscopy, 265

Vanadium complexes
Caffeic acid complexes, IR spectra, UV–Vis spectra, Potentiometric titrations, Catecholate-like ligand, 1979
Vanadyl complexes
Schiff bases, Chiral complexes, EPR, X-ray structures, 2021
Vanadyl
Diperoxovanadate, EDTA inhibition, EDTA bridged heteroligand peroxovanadates, Catalase resistance, Oxo-bridged peroxovanadates containing sulphate, 389
Vibrational spectra
Imidazole-4-acetic acid, Polymeric zinc(II) complexes, Crystal structures, Density functional calculations, 2819
vic-Dioxime
Nickel(II), Cobalt(II), Copper(II), Iron(II), Uranyl(IV), Electrochemistry, LH_4, $N_2O_2S_2$ macrocyle, 825
vic-Dioxime
Nickel(II) complexes, Heterotrinuclear complexes, BF_2^+-capped complexes, Dioxadithiadiazamacrobicycle, Template effect, 1865
Vinylcyclosilazane complexes
Nickel(0), Crystal structure, 1261
Vinylidene
Iron, Acetylide, Propadienylidene, 1755
Vis spectra
Copper(II) complexes, Mixed-ligand complexes, Five-coordinate complexes, Aminohydroxamic acids, EPR spectra, 295

Water-soluble complexes
Ferrocenylmethylphosphine, Phosphino amino acids, 1,3-Diaza-5-phosphacyclohexane, 1,5-Diaza-3,7-diphosphacyclooctane, Trinuclear complexes, 2251
Wells-Dawson structure
Polyoxometalates, Heteropolyanions, Ti(IV) complex, 353

X-ray analysis
Iminophosphorane, Cycloaddition, Four-membered ring compounds, Thermolysis, Aza-Wittig reaction, 657
X-ray
Boron, Lithium, Imido, Complexes, 549
X-ray
Copper, Hinokitiol, Adduct, 1761
X-ray crystallographic analysis
Digermene, Germylene, Dissociation, Equilibrium, Bond dissociation energy, Dioxadigermetane, Terminal tungsten complexes, 563
X-ray crystallography
BTZ ligands, Pb(II) salts, π–π stacking interaction, 197
X-ray crystallography
Cobalt(III), Pyrazolylthiosemicarbazone, ^1H NMR, 779
X-ray crystallography
Dimesitylphosphine, Secondary phosphine, NMR, Cone angle, Fluxional, 2409
X-ray crystallography
Europium complexes, Luminescence property, Dibenzoylmethane, 2-(4′-Dimethylaminophenyl)imidazo[4,5-f]1,10-phenanthroline, 3-Ethyl-2-(4′-dimethylaminophenyl)imidazo[4,5-f]1,10-phenanthroline, 313
X-ray crystallography
Magnetochemical studies, Manganese oxide clusters, 1779
X-ray crystallography
Mono-helical, Single-helical-strand, Mono-bridged species, Coordination chemistry, Transition metals, 1177
X-ray crystallography
Tellurium dichloride, Chloridotellurate anions, NMR spectroscopy, 1089
X-ray crystallography
Uranyl, Dimethylmelonate, Counter-cation, CPMAS ^{13}C NMR, 69
X-ray crystallography
Uranyl, Malonato complexes, CPMAS ^{13}C NMR, 81
X-ray crystal structure
Eight-coordinate, Schiff base, Zirconium complexes, Synthon, Heteroleptic, 211
X-ray crystal structures
α-Aminoisobutyryl-α-aminoisobutyric acid (H–Aib–Aib–OH), Copper(II) peptide complexes, Spectroscopic characterization, 229
X-ray crystal structures
Co(III) complexes, Pyrazole, Dithiocarbazate, Synthesis, Spectroscopy, 1
X-ray crystal structures
Hg(II) complexes, Dimer, Diethylene triamine, 2195
X-ray crystal structures
2-Hydroxynicotinic acid, Palladium, Pla-

tinum, Raman spectra, 2783
X-ray crystal structures
Iron(II), Zinc(II), Schiff base, ^{1}H NMR spectroscopy, Dioxygen reactivity, 705
X-ray crystal structures
Nickel complexes, Sulfonamide complexes, 8-Aminoquinoline, 1229
X-ray crystal structures
Niobium complexes, Heterodiene, 1,4-Diaza-1,3-diene, 305
X-ray crystal structures
Pyrazole, Mononuclear bis(imido) Mo(VI) complexes, 1211
X-ray crystal structures
Schiff bases, Salicylaldimine adducts, Interconversion, Zinc complexes, Zwitterion, 697
X-ray crystal studies
Cobalt(III), Thiosemicarbazone, ^{1}H NMR, IR, Electronic spectra, 2515
X-ray data
Cobalt(II), Cubane complexes, Carbacylamidophosphates, 963
X-ray diffraction
Crystal structures, Physico-chemical properties, Spectroscopy, Imidiazole complexes, 1857
X-ray diffraction
Palladium, Metallation, Schiff base, Phosphorus ligands, 2309
X-ray diffraction
Pentacyaninotrosylferrate(2−) ion, Metastable excited states, FIRRS, TGA, DTA, 1767
X-ray diffraction
Synthesis, Crystal structures, 1883
X-ray
Isoxazolidines, Pd-, Zn-, Cu-complexes, Syntheses, NMR, 769
X-ray microprobe
Phthalocyanines, Nitrogen dioxide, Scanning electron microscopy, UV–Vis and FTIR spectroscopy, X-ray powder diffractometry, 677
X-ray
Mononuclear tungsten(VI) complexes, Ligand, Heteroleptic, 1017
X-ray photoelectron spectroscopy
Chromium, Pivalate, Mass spectrometry, Paramagnetic, NMR, 155
X-ray powder diffractometry
Phthalocyanines, Nitrogen dioxide, Scanning electron microscopy, X-ray microprobe, UV–Vis and FTIR spectroscopy, 677
X-ray structural analysis
Aluminum(I) halides, Metalloid clusters, Nanosized clusters, Intermediates, Metal lattice, 489
X-ray structure analysis
Chiral benzodiazepine ligands, Zinc complexes, Palladium complexes, Spectroscopy, Cytostatic and antiviral activity, 2567
X-ray structure analysis
Gallium, Indium, Platinum, Heterobimetallic complexes, Quantum chemical calculations, 535
X-ray structure
2-(3,5-Dimethylpyrazol-1-ylmethyl)pyridine, Bis-ligand and anion-bound copper(II) complexes, Absorption and EPR spectra, Cyclic voltammetry, 1245
X-ray structure
Platinum(III) compounds, Lantern-type complexes, Amidate bridging ligands, 275
X-ray structures
Arylazopyrimidines, Osmium(II) complexes, Geometrical isomers, MLCT transitions, Redox property, 753
X-ray structures
Bis(pyrazol-1-yl)alkane, Organotin(IV), 873
X-ray structures
Cadmium(II) complexes, Polyamines, 739
X-ray structures
Copper complexes, Stereochemistry, Steric properties, 1031
X-ray structures
Copper, Self-assembly, Supramolecules, 1621
X-ray structures
Cu(II) stereochemistry, Magnetism, EPR spectra, 2473
X-ray structures
Dioxomolybdenum(VI) complexes, Thiocarbodihydrazone Schiff base, 1023
X-ray structures
Five-coordinated chlorocopper(II) complexes, 1,10-Phenanthroline and its 5,6-disubstituted derivatives, Electronic absorption and diffuse reflectance spectra, Cyclic voltammetry, 2143
X-ray structures
Heterocyclic thioamides, Osmium, Ruthenium, 2-Mercapto-1-methylimidazole, 885
X-ray structures
Molybdenum complexes, oxo-Hydrazido complexes, Methyl-molybdenum complexes, Phenyl-molybdenum complexes, Diimine, 2531
X-ray structures
Nickel, Copper, Zinc, Cadmium, Saccharinate, 395
X-ray structures
Nickel, Thiolate, *cis*-1,2-Bis(diphenylphosphino)ethene, 421
X-ray structures
Niobium sulphide metallacycles, HF/ECP calculations, 2227
X-ray structures
Nitrosyl complexes, Ruthenium(II), NMR spectra, Diop, Dppb, 2221
X-ray structures
N-oxides, Uranyl bis(β-diketonates), Adduct compounds, 2403
X-ray structures
Phosphoranes, Pentacoordinated, Hydrogen bonding, 1155
X-ray structures
Platinum chloride complexes, N-donor ligands, ^{15}N NMR, 1,2,4-Triazolo-[1,5α]-pyrimidines, 343
X-ray structures
Platinum(II) complexes, Ribavirin, NMR and IR analysis, 2001
X-ray structures
Pyridine N-oxide ligands, copper(II) complexes, Hydrogen bonding, Magnetism, 1561
X-ray structures
Rhenium, Nitrosyl, Electronic structures, Nitric oxide, 2617
X-ray structures
Scandium, Phosphine oxide, Arsine oxide, ^{45}Sc NMR, 1579
X-ray structures
Synthesis, Cobalt(III) complexes, 4-Methyl-2,6-dibenzoylphenol, NMR, TGA, Cyclic voltammetry, 1787
X-ray structures
Tantalum, Metallocenes, Hydrides, Metallophosphines, Bimetallics, 371
X-ray structures
tert-Butylcalix[4]arenes, Amide, Sodium complexes, Yttrium(III) complexes, Lanthanide(III) complexes, 763
X-ray structures
Triosmium cluster, Tetramethylthiourea, Desulfurization, Sulfido, 381
X-ray structures
Vanadyl complexes, Schiff bases, Chiral complexes, EPR, 2021
X-ray structures
Yttrium, Phosphine oxide, Arsine oxide, 445
X-ray study
Trimetallic alkoxides, Molecular structure, Mass-spectrometric study, Rhenium methoxides, Niobium methoxide, Tantalum methoxide, 2317
X-ray
Thiosemicarbazone, Isatin, Metal complexes, 2593
X-ray
Triphenylantimony(V), Oximes, NMR, 2387

Ylid
Molecular orbital, Ab initio, Mechanism, Intermolecular nucleophilic attack, Titanium, 2699
Yttrium(III) complexes
tert-Butylcalix[4]arenes, Amide, Sodium complexes, Lanthanide(III) complexes, X-ray structures, 763
Yttrium
Phosphine oxide, Arsine oxide, X-ray structures, 445
Yttrium
Salen, Amide, Aryloxide, Organometallic, 1683

Zigzag chain
Cadmium complexes, Dca ligand, Double end-to-end, π–π interaction, 893
Zinc adducts
Emprirical correlations, Calorimetry, Infrared spectroscopy, 1677
Zinc complexes
Chiral benzodiazepine ligands, Palladium

complexes, Spectroscopy, X-ray structure analysis, Cytostatic and antiviral activity, 2567
Zinc complexes
Crystal structures, Copper complexes, Lumazine complexes, 1961
Zinc complexes
Schiff bases, Salicylaldimine adducts, Interconversion, X-ray crystal structures, Zwitterion, 697
Zinc
Halide complexes, Thiosemicarbazones, Ligand, 1217
Zinc(II) complexes
Aminomethane-1,1-diphosphonic acids, Magnesium(II) complexes, Calcium(II) complexes, Potentiometry, NMR, 321
Zinc(II) complexes
Crystal structures, Co-ordination number asymmetry, 1957
Zinc(II) complexes
Mixed-ligand complexes, Aminohydroxamic acids, Polyamines, NMR spectra, Potentiometry, 2183
Zinc(II)
Iron(II), Schiff base, X-ray crystal structures, ^{1}H NMR spectroscopy, Dioxygen reactivity, 705
Zinc(II)
One-dimensional structures, Cobalt(II), Coordination complexes, 2705
Zinc(II)
2-Pyridineformamide, Thiosemicarbazone, Nickel(II), Cadmium(II), Crystal structures, 729
Zinc(II)
Schiff base complexes, Cobalt(II), Nickel(II), Tetrahedral, Crystal structures, 2733
Zinc(II)tetrasulfophthalocyanine
Sulfur dioxide, Fluorescence quenching, Association constants, 951
Zinc
Nickel, Copper, Cadmium, Saccharinate, X-ray structures, 395
Zinc phthalocyanine
Sensitizer, Singlet oxygen, Photobleaching, 2463
Zinc
Phthalocyanines, Phthalonitrile derivatives, Electrochemistry, Nickel, Cobalt, 255
Zinc
Pyrazineformamide, Thiosemicarbazone, Cadmium, Crystal structures, Electrochemical synthesis, 1553
Zintl phases
Clusters, Crystal structures, Intermetallic compounds, Lead, 641
Zirconium complexes
Eight-coordinate, Schiff base, X-ray crystal structure, Synthon, Heteroleptic, 211
Zirconium complexes
PH-functionalised phosphanylalkyl(silyl)cyclopentadienyl ligands, Titanium complexes, Polymerisation studies, 2445
Zn(II) complexes
Zn(II)–N bonds, Crystal structures, Piperazine and piperazin-1-ium ligands, 2161
Zn(II)–N bonds
Crystal structures, Zn(II) complexes, Piperazine and piperazin-1-ium ligands, 2161
Zn(II)
Supramolecular interactions, Tripodal ammonium, Nucleotides, Ternary complexes, 1005
Zwitterion
Schiff bases, Salicylaldimine adducts, Interconversion, X-ray crystal structures, Zinc complexes, 697